An MO Study on the Hydrogen Bond System of H_2O-HF

Shinichi YAMABE, Shigeki KATO, Hiroshi FUJIMOTO, and Kenichi FUKUI

Department of Hydrocarbon Chemistry, Faculty of Engineering, Kyoto University, Sakyo-ku, Kyoto 606

(Received Fcbruary 12, 1974)

An LCAO MO SCF calculation has been carried out on H_2O–HF system with a minimal STO-3G basis set, with respect to three assumed models, *i.e.* SIGMA, PI, and BIFURCATED models. A configuration analysis of the wave function has shown that charge-transferred electron configurations weakly mix into the original electron configuration in the SIGMA and PI models, while the contribution of charge-transferred configurations is negligibly small in the BIFURCATED model. The SIGMA model has been found to be most stable mainly due to the Coulombic attraction energy between the two species. The intermolecular electron density between the two interacting systems has been investigated by means of a concept of orbital interaction, leading to a conclusion that the mixing-in of the occupied MO's of H_2O with the unoccupied MO's of HF contributes slightly to the hydrogen bond in the SIGMA and PI models.

Over the last two decades, hydrogen bonding has been of increasing interest to both experimental and theoretical chemists.[1–14] Recent *ab initio* calculations by the use of LCAO MO SCF methods on several hydrogen-bonding systems have given satisfactory results in explaining the physical and chemical properties of those systems, such as the stable geometries, hydrogen-bonding energy and charge-transfer along the bond formation.[15–26] In these studies, the quantities which describe the hydrogen bonding are usually defined as the differences between those of a composite system and those of the isolated systems. Then, we should note that the resultant differences are far smaller than the corresponding quantities of normal chemical bonds. Therefore, they may depend, to some extent, upon the basis set adopted to construct the MO's. Morokuma and Winick pointed out, however, the addition of p-type functions to hydrogen and of d-type functions to oxygen in the calculation of water dimer would yield an excess stabilization, unless the MO's of monomers were of the Hartree-Fock limit.[17] Hence, we should be careful about the inclusion of the polarization functions.

Apart from these works on the Hartree-Fock level, there have been several theoretical ways to approach hydrogen-bonding. For instance, Coulson and Danielsson studied the hydrogen bond in water dimer on the basis of the valence-bond theory.[27] These theories could present chemically graspable pictures of hydrogen bond between a proton donor (A–H) and a proton acceptor (B). Although these approaches are only qualitative in comparison with the works performed by accurate MO calculations a partitioning of the interaction energies,[28–36] and the calculation of the weights of various electron configurations[37] will supply us some valuable information for an understanding of the basic feature of hydrogen bond.

Here, we take a simple hydrogen-bonding system composed of H_2O and HF[19] and analyze the wave function of the system, calculated by an *ab initio* MO method, into several important electron configurations by the aid of a configuration analysis procedure.[38–40]

Results of Calculation

The SCF MO's, ϕ_i, were constructed by linear combinations of the basis atomic orbitals (AO), χ_r,[41]

$$\phi_i = \sum_r c_r{}^i \chi_r$$

In this work, we employed the minimal set of the Slater type orbitals (STO's), which were expanded into three Gaussian type orbitals (GTO's).[42,43] In this STO-3G expansion, the values of the exponents (α_m) and the coefficients (d_m) of the GTO were taken after Stewart.[44]

$$\chi_r = \mathrm{STO}(\zeta) = \sum_{m=1}^{3} d_m \mathrm{GTO}(\alpha_m)$$

The exponents of the STO's, ζ, were taken to be the optimized values in regard to the two monomers, H_2O and HF, obtained by Hehre, Stewart, and Pople.[45] They are given in Table 1.

TABLE 1. THE EXPONENTS ζ OF THE STO'S

Molecule	Type of STO	Value
HF	H_{1s}	1.33 (1.00)[a]
	F_{1s}	8.65 (8.70)
	F_{2s}	2.55 (2.60)
	F_{2p}	
H_2O	H_{1s}	1.28 (1.00)
	O_{1s}	7.66 (7.70)
	O_{2s}	2.25 (2.275)
	O_{2p}	

a) Calculated by the Slater rule as a reference.

As for the hydrogen-bonding system, we considered three different geometries, SIGMA, PI, and BIFURCATED, as illustrated in Fig. 1. The geometrical parameters are given in Fig. 1 with respect to the SIGMA model. In the three models of H_2O–HF, the distance from the oxygen atom of H_2O to the fluorine atom of HF, R(O–F), was taken to be 2.72 Å. It may be natural here to suppose that the O–H and H–F bond distances will vary, depending on the type of interaction. Therefore, the most stable geometry of the hydrogen-bonding system will be determined by a delicate balance between the stabilization due to the intermolecular interaction and the destabilization due to the deformation of the two species from the most stable geometries in an isolated state. Accordingly, our assumption of the fixed nuclei of H_2O and HF in interacting states might involve an un-

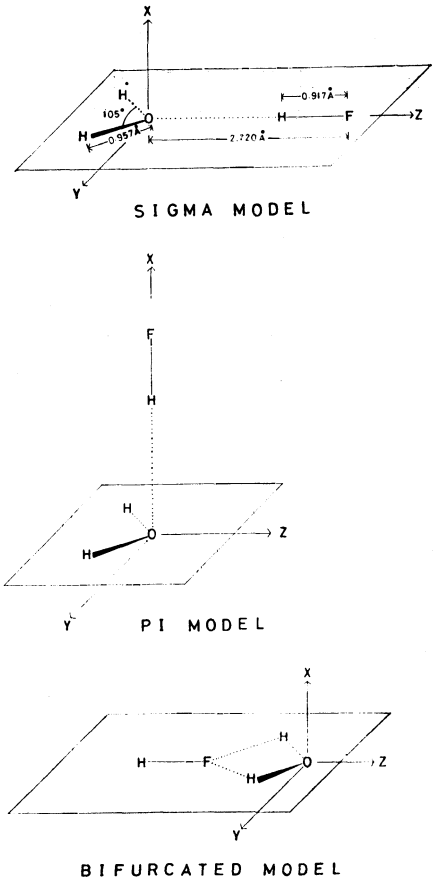

Fig. 1. The assumed models of hydrogen bonding in H_2O and HF.

certainty in studying this weakly interacting system. However, the deformations of the interacting species are usually small[19] and we hope that an approach based on an isolated molecule approximation would provide us some chemically important information on hydrogen bond.

Under the assumption mentioned above, the energy of hydrogen bond may be defined as,

$$E = E_T(H_2O\text{-}HF) - E_T(H_2O) - E_T(HF)$$

where $E_T(X)$ is the total energy of the system X (the electronic energy plus the nuclear repulsion in the fixed nuclei).

The results of the MO calculation on H_2O, HF, and H_2O–HF systems are given in Table 2. The calculation of $(-V/2T)$ (V is the potential energy and T is the kinetic energy) indicates that the assumption of the same ζ values for the composite system as those for the isolated species is not so poor. So, it seems likely that ζ's are not so sensitive to the change in the electron distribution arising from hydrogen bond formation.

The atomic populations on the three hydrogen-bonding systems calculated here show that the amount of charge transferred from H_2O to HF (ΔQ) is 0.029 in SIGMA, 0.038 in PI and −0.004 in BIFURCATED respectively. In the last model with the negative value of ΔQ, HF serves as an electron donor and H_2O as an electron acceptor. Among the three models, the PI model gives the largest ΔQ. This seems to come from the fact that the PI model contains the most effective charge-transfer interaction. This point will be discussed later in detail.

Examining $E_T(H_2O\text{–}HF)$, we see that the SIGMA model is most stable among the three models, in agreement with the result of Kollman and Allen (the linear structure in their notation).[19]

As shown in Table 2, the SIGMA model has a larger dipole moment (3.69 D) than the sum of the moments of the monomers (3.15D=1.39D+1.76D). The increase in the dipole moment comes mainly from

Table 2. Results of MO calculation on HF, H_2O and H_2O·HF at the optimized ζ of STO-3G. The values in the parenthesis are by other MO works or experimental (exptl.) ones.

Molecule	Total energy E_T(a.u.)	Test of virial theorem $(-V/2T)$	Atomic population	Dipole moment (D)	The orbital energy of the HOMO (eV)
HF	−98.5577 (−98.5274)[45] (−100.0708)[46]	1.0019	H——F 0.7768 9.2232	1.39 $(1.82)^{[48]}_{exptl.}$	−12.11 (15.77)[50]
H_2O	−74.9515 (−75.7050)[17] (−76.0594)[47]	1.0006	H O 8.3718 0.8141 H	1.76 $(1.85)^{[49]}_{exptl.}$	−10.27 (12.59)[51]
H_2O·HF SIGMA model	−173.5210 (−175.9840)[19]	1.0011	H 8.3810 9.2746 O···H—F 0.7542 H 0.7951	3.69	
H_2O·HF PI model	−173.5173	1.0011	F 9.2681 H 0.7656 0.7977 H O 8.3709 H	2.60	
H_2O·HF BIFURCATED model	−173.5124	1.0013	H 9.2297 H—F O 8.3822 0.7659 H 0.8111	3.27	

Table 3. The weights of some electronic structures of the three H_2O–HF hydrogen bond models

Electronic structures	Weights (%) SIGMA model	PI model	BIFURCATED model
$H_2O \cdot HF$	96.8740	96.5512	99.4809
$H_2O^- \cdot HF^+$	0.0636	0.0038	0.4701
$H_2O^+ \cdot HF^-$	2.8572	3.2888	0.0355
$H_2O \cdot HF^*$	0.0922	0.0584	0.0059
$H_2O^* \cdot HF$	0.0272	0.0364	0.0045
$H_2O^{-2} \cdot HF^{+2}$	0.0000	0.0000	0.0004
$H_2O^{+2} \cdot HF^{-2}$	0.0114	0.0145	0.0000
$H_2O^{+-} \cdot HF^{-+}$	0.0011	0.0001	0.0001
$H_2O^* \cdot HF^*$	0.0001	0.0000	0.0000
Total	99.9268	99.9532	99.9975

the charge-transfer from H_2O to HF. The enhancement of the moment, however, would also arise from the polarization interaction between the two monomers.

Configuration Analysis

The result of the configuration analysis of the wave function of the composite system in terms of the electron configurations of the two isolated species is given in Table 3. There, the first electronic structure ($H_2O \cdot$ HF) stands for the original electron configuration without any electron shifting. In addition to this dominant configuration, several important charge-transferred and locally excited terms are presented. Here, ($H_2O^- \cdot HF^+$) indicates mono-transferred configurations with one electron migrated from HF to H_2O, and ($H_2O^* \cdot HF$) locally mono-excited configurations in H_2O. The other terms in Table 3 may be understood in a similar way.[52] In these three models, the total weight covered by only these rather simple electron configurations is very close to 100%. This suggests that the other configurations omitted in Table 3, *i.e.* highly-transferred and highly-excited configurations can be neglected without a serious loss of accuracy.

As for the SIGMA and the PI models, the mono-transferred term ($H_2O^+ \cdot HF^-$) plays an important role, with the larger weight in the PI model (3.29%) than in the SIGMA model (2.86%). This superiority of the PI model to the SIGMA model in ($H_2O^+ \cdot HF^-$) arises from the more efficient charge-transfer interaction in the former than in the latter, as has been expected from the calculation of ΔQ. The next important term in these models is ($H_2O \cdot HF^*$), having a larger weight in the SIGMA model (0.09%) than in the PI model (0.06%). Considering the contributions of various electron configurations, we can approximately describe the electronic structure of H_2O–HF solely by the two terms, ($H_2O \cdot HF$) and ($H_2O^+ \cdot HF^-$).[53] This calculation seems to support our insistence mentioned before

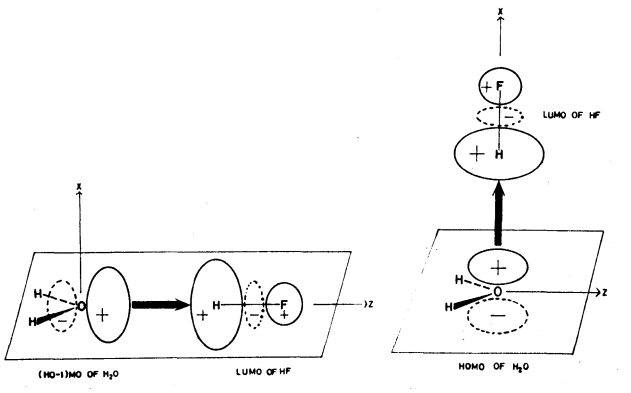

Fig. 2. A schematic representation of the dominant orbital interaction in the SIGMA and the PI models.

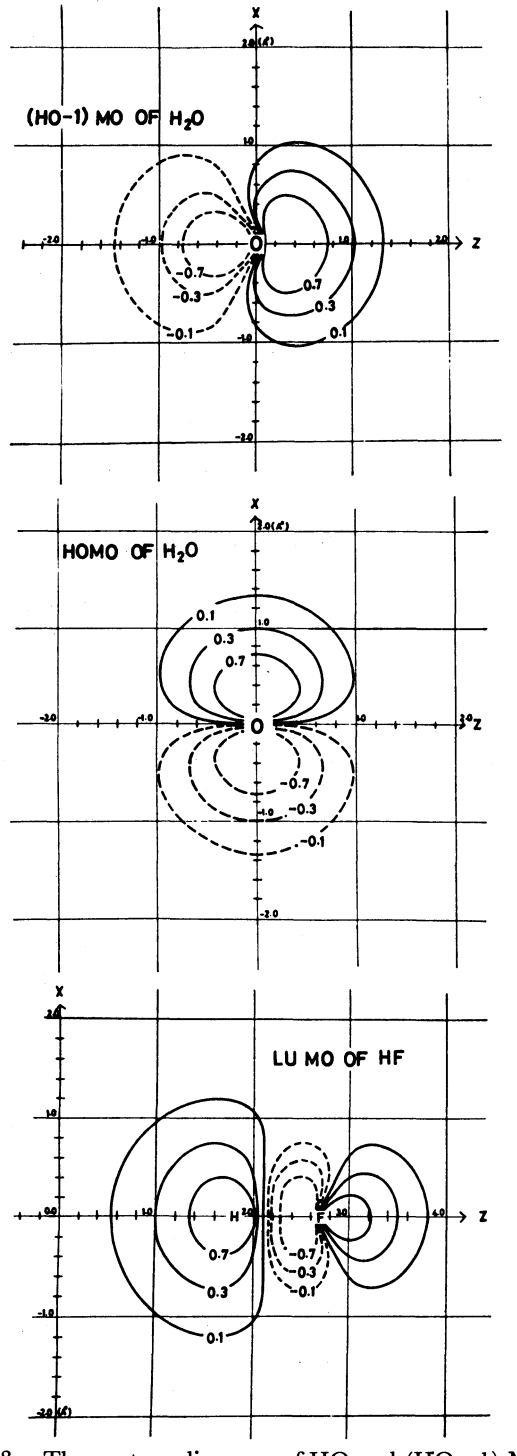

Fig. 3. The contour diagrams of HO and (HO−1) MO's of H_2O and the LUMO of HF.

that this simple hydrogen-bonding system can be regarded as an electrostatic and exchange model with a minor charge-transfer effect.

In order to examine this point a little more in detail, we evaluated the Coulomb interaction energy (E_Q) and the delocalization energy (E_D) with respect to the SIGMA and the PI models, obtaining E_Q(SIGMA)$=-0.398$ eV, E_Q(PI)$=-0.325$ eV, E_D(SIGMA)$=-0.027$ eV, and E_D(PI)$=-0.034$ eV.[54] This calculation indicates that the SIGMA model is more stabilized than the PI model through the electrostatic interaction, although the delocalization interaction is stronger in the PI model than in the SIGMA model as has been expected from the configuration analysis of the wave function. Figure 2 illustrates schematically the dominant charge-transfer interaction in the SIGMA and the PI models. The shapes of the highest occupied (HO) MO and the next highest occupied (HO–1)MO of H_2O and the lowest unoccupied (LU) MO (taken real) are shown in Fig. 3.

In the BIFURCATED model, the extremely large weight of the original configuration (99.48%) allows us one-term approximation by ($H_2O\cdot HF$). In this model, HF is an electron donor and H_2O serves as an acceptor with ($H_2O^-\cdot HF^+$)$=0.47\%$ and ($H_2O^+\cdot HF^-$)$=0.04\%$ in accordance with the calculation of ΔQ. The delocalization energy of the BIFURCATED model was found to be as small as -0.002 eV.

Chemical Binding between H_2O and HF

In the above, we found that relative orientation of H_2O and HF is mostly determined by the Coulombic and exchange interactions. However, if the hydrogen-bonding is purely electrostatic, the increase of the electron density in the region between H_2O and HF would not be yielded. The result of the present calculation, on the contrary, shows the considerable increase in the density in the intermolecular region. In order to detect the origin of this change in the electron distribution, we partition the total intermolecular electron density which is termed here $\rho(1|1)_{\text{total}}$ into the following four terms.[55,56]

$$\rho(1|1)_{\text{total}} = \rho(1|1)_{\text{exchange}} + \rho(1|1)_{\text{CT}} + \rho(1|1)_{\text{back CT}} + \rho(1|1)_{j,l}$$

$$\rho(1|1)_{\text{exchange}} = 2\sum_{g=1}^{10}\sum_{i=1}^{5}\sum_{k=1}^{5} C_i^{(g)} C_{k+7}^{(g)} \{a_i(1)b_k(1) + b_k(1)a_i(1)\}$$

$$\rho(1|1)_{\text{CT}} = 2\sum_{g=1}^{10}\sum_{i=1}^{5} C_i^{(g)} C_{l+7}^{(g)} \{a_i(1)b_l(1) + b_l(1)a_i(1)\} \quad (l=6)$$

$$\rho(1|1)_{\text{back CT}} = 2\sum_{g=1}^{10}\sum_{k=1}^{5}\sum_{j=6}^{7} C_j^{(g)} C_{k+7}^{(g)} \{a_j(1)b_k(1) + b_k(1)a_j(1)\}$$

$$\rho(1|1)_{j,l} = 2\sum_{g=1}^{10}\sum_{j=6}^{7} C_j^{(g)} C_{l+7}^{(g)} \{a_j(1)b_l(1) + b_l(1)a_j(1)\} \quad (l=6)$$

In the above equations, a_i and a_j stand for the occupied and unoccupied MO's of H_2O, and b_k and b_l ($l=6$) are the occupied and unoccupied MO's of HF. The expansion coefficients, $C_i^{(g)}$, are defined in the following way.

$$\phi_g = \sum_{i=1}^{5} C_i^{(g)} a_i + \sum_{j=6}^{7} C_j^{(g)} a_j + \sum_{k=1}^{5} C_{k+7}^{(g)} b_k + C_{l+7}^{(g)} b_l$$

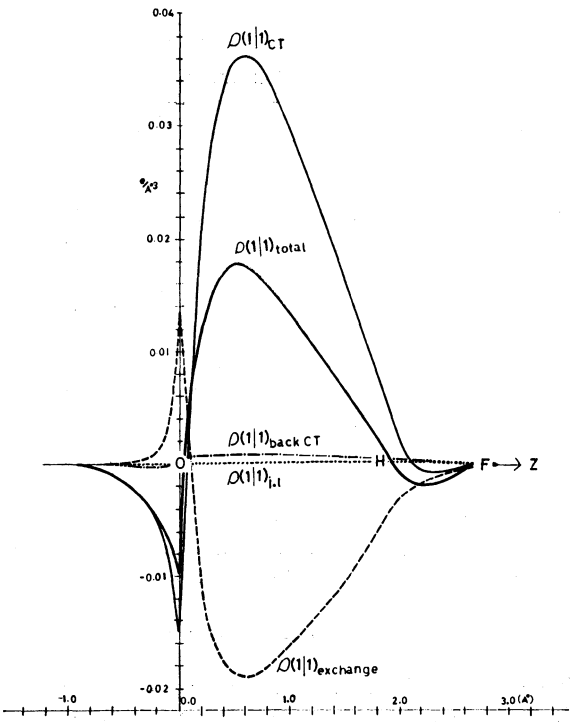

Fig. 4. The intermolecular densities in the SIGMA model.

We must mention here that the partitioning of $\rho(1|1)$ and the classification of the terms are made in an approximate sense. The density $\rho(1|1)_{\text{exchange}}$ is the intermolecular density accumulated between H_2O and HF through the overlapping of a_i with b_k (both of them are occupied MO's), $\rho(1|1)_{\text{CT}}$ comes from the interaction between the occupied MO's of H_2O and the unoccupied MO of HF, and $\rho(1|1)_{\text{back CT}}$ is due to the interaction between the unoccupied MO's of H_2O and the occupied MO's of HF. The density $\rho(1|1)_{j,l}$ stands for the density change in the intermolecular region through the overlapping of the unoccupied MO's of the two monomers. The sum $\rho(1|1)_{\text{total}}$ of these partitioned electron densities creates the usual intermolecular bond-order density. In Fig. 4, the profile of the contour map of these components with respect to the SIGMA model is illustrated. We see the change in the intermolecular electron density is composed almost exclusively of $\rho(1|1)_{\text{exchange}}$ and $\rho(1|1)_{\text{CT}}$.

$$\rho(1|1)_{\text{back CT}} < 0.0009\ \text{e/Å}^3$$

$$\rho(1|1)_{j,l} < 0.0001\ \text{e/Å}^3$$

The electron density $\rho(1|1)_{\text{exchange}}$ is negative, contributing to $\rho(1|1)_{\text{total}}$ in an antibonding way. On the contrary, $\rho(1|1)_{\text{CT}}$ presents a positive electron density in the intermolecular region, and it overcomes the negative $\rho(1|1)_{\text{exchange}}$ yielding the positive $\rho(1|1)_{\text{total}}$. This $\rho(1|1)_{\text{CT}}$ comes almost solely from the mixing of the ionic configuration ($H_2O^+\cdot HF^-$) into the original electron configuration. Therefore, the charge-transfer interaction, though small as a whole, has an important role to enforce the hydrogen bond, in addition to the purely electrostatic interaction between the two monomers. Among the terms appearing in $\rho(1|1)_{\text{CT}}$, the charge-transfer interaction between the

(HO−1) MO of H_2O and the LUMO of HF shown in Fig. 2 contributes dominantly to the electronic structure of the SIGMA model.

By means of a highly accurate MO calculation, Kollman and Allen showed that $\rho(1|1)_{total}$ was negative.[19] It seems likely that the bond-order density (or the Mulliken overlap population[57]) depends on the basis set. However, no matter whether $\rho(1|1)_{total}$ is positive or negative, $\rho(1|1)_{exchange}$ and $\rho(1|1)_{CT}$ will play their characteristic roles as mentioned above to weaken or reinforce the intermolecular chemical binding.

One of the present authors (S. Y.) thanks Mr. K. Ishida for his advice in making the computer program.

References

1) D. Hadzi, "Hydrogen Bonding," Pergamon Press, New York (1959).
2) G. C. Pimentel and A. L. McClellan, "The Hydrogen Bond," W. H. Freeman, San Francisco, Calif. (1960).
3) N. D. Sokolov and V. M. Tschulanovskii, "Vodorondnaya Svyaz," Nauka, Moscow (1964).
4) W. C. Hamilton and J. Ibers, "Hydrogen Bonding in Solids," W. A. Benjamin, New York (1968).
5) A. S. N. Murthy and C. N. R. Rao, *Appl. Spectrosc. Rev.*, **2**, 1 (1968).
6) A. S. N. Murthy and C. N. R. Rao, *J. Mol. Struct.*, **6**, 253 (1970).
7) H. Ratajczak and W. J. Orville-Thomas, *ibid.*, **1**, 449 (1968).
8) J. C. Davis and K. K. Deb., *Advan. Magn. Resonance*, **4**, 201 (1970).
9) S. Bratoz, *Advan. Quantum Chem.*, **3**, 209 (1967).
10) J. W. Smith, *Sci. Progr.*, **52**, 97 (1964).
11) S. H. Lin, "Physical Chemistry—An Advanced Treatise," H. Eyring, D. Henderson, and W. Jost, Eds., Academic Press, New York (1970), p. 439.
12) P. A. Kollman and L. C. Allen, *Chem. Rev.*, **72**, 283 (1972).
13) C. G. Prettre and A. Pullman, *Theoret. Chim. Acta*, **25**, 83 (1972).
14) R. Bonaccorsi, C. Petrongolo, E. Scrocco, and J. Tomasi, *ibid.*, **20**, 331 (1971).
15) M. Weissmann and N. V. Cohan, *J. Chem. Phys.*, **43**, 119 (1965).
16) K. Morokuma and L. Pedersen, *ibid.*, **48**, 3275 (1968).
17) K. Morokuma and J. R. Winick, *ibid.*, **52**, 1301 (1970).
18) G. H. F. Diercksen, *Chem. Phys. Lett.*, **4**, 373 (1969).
19) P. A. Kollman and L. C. Allen, *J. Chem. Phys.*, **52**, 5085 (1970).
20) Y. Fang and J. R. De La Vega, *Chem. Phys. Lett.*, **6**, 117 (1970).
21) G. H. F. Diercksen and W. P. Kraemer, *ibid.*, **5**, 570 (1970).
22) W. P. Kraemer and G. H. F. Diercksen, *ibid.*, **5**, 463 (1970).
23) P. A. Kollman and L. C. Allen, *J. Amer. Chem. Soc.*, **93**, 4991 (1971).
24) E. Clementi, *J. Chem. Phys.*, **46**, 3851 (1967).
25) A. Johansson, P. Kollman, and S. Rothenberg, *Chem. Phys. Lett.*, **16**, 123 (1972).
26) J. E. Del Bene and F. T. Marchese, *J. Chem. Phys.*, **58**, 926 (1973).
27) C. A. Coulson and U. Danielsson, *Arkiv. Fysik*, **8**, 239, 245 (1954).
28) C. A. Coulson, *Research*, **10**, 149 (1957).
29) F. B. van Duijneveldt and J. N. Murrell, *J. Chem. Phys.*, **46**, 1759 (1967).
30) J. G. C. M. van Duijneveldt-van de Rijdt and F. B. van Duijneveldt, *Theoret. Chim. Acta*, **19**, 83 (1970).
31) P. A. Kollman and L. C. Allen, *ibid.*, **18**, 399 (1970).
32) M. Dreyfus and A. Pullman, *ibid.*, **19**, 20 (1970).
33) K. Morokuma, *J. Chem. Phys.*, **55**, 1236 (1971).
34) D. P. Santry, *J. Amer. Chem. Soc.*, **94**, 8311 (1972).
35) H. Berthod and A. Pullman, *Chem. Phys. Lett.*, **14**, 217 (1972).
36) R. Sustmann and F. Vahrenholt, *Theoret. Chim. Acta*, **29**, 305 (1973).
37) H. Tsubomura, This Bulletin, **27**, 445 (1954).
38) H. Baba, S. Suzuki, and T. Takemura, *J. Chem. Phys.*, **50**, 2078 (1969).
39) H. Morita and S. Nagakura, *Theoret. Chim. Acta*, **27**, 325 (1972).
40) H. Fujimoto, S. Kato, S. Yamabe, and K. Fukui, *J. Chem. Phys.*, **60**, 572 (1974).
41) C. C. J. Roothaan, *Rev. Mod. Phys.*, **23**, 69 (1951).
42) K. O-ohata, H. Taketa, and S. Huzinaga, *J. Phys. Soc. Jap.*, **21**, 2306 (1966).
43) H. Taketa, S. Huzinaga, and K. O-ohata, *ibid.*, **21**, 2313 (1966).
44) R. F. Stewart, *J. Chem. Phys.*, **52**, 431 (1970).
45) W. J. Hehre, R. F. Stewart, and J. A. Pople, *ibid.*, **51**, 2657 (1969).
46) P. E. Cade and W. M. Fuo, *ibid.*, **47**, 614 (1967).
47) D. Neumann and J. W. Moskowitz, *ibid.*, **49**, 2056 (1968).
48) R. Weiss, *Phys. Rev.*, **131**, 659 (1963).
49) G. Birnbaum and S. K. Chatterjie, *J. Appl. Phys.*, **23**, 220 (1952).
50) J. A. R. Coope, D. C. Frost, and C. A. McDowell, *Nature*, **179**, 1186 (1957).
51) K. Watanabe, *J. Chem. Phys.*, **26**, 542 (1957).
52) We have three singlet wave functions for a configuration with four electrons in four different orbitals, two of which belonging to H_2O and the other two to HF. They can formally be partitioned into a locally excited state and a mutual charge-transferred state, by factoring the coefficients.
53) The weights of the charge-transferred configurations will decrease in case of the inclusion of configuration interaction.
54) K. Fukui and H. Fujimoto, This Bulletin, **41**, 1989 (1968).
55) S. Yamabe, T. Minato, H. Fujimoto, and K. Fukui, *Theoret. Chim. Acta*, **32**, 187 (1974).
56) S. Yamabe, S. Kato, H. Fujimoto, and K. Fukui, This Bulletin, **46**, 3619 (1973).
57) R. S. Mulliken, *J. Chem. Phys.*, **23**, 1833, 1841, 2338, 2343 (1955).

An MO-Theoretical Treatment of the Cationic Ring-Opening Polymerisation. I. Ethylene Oxide

Gernot FRENKING, Hiroshi KATO,* and Kenichi FUKUI

Department of Hydrocarbon Chemistry, Faculty of Engineering, Kyoto University, Sakyo-ku, Kyoto 606
**College of General Education, Nagoya University, Chikusa-ku, Nagoya 464*

(Received July 26, 1974)

The stereochemical course of the acid-catalyzed ring-opening polymerisation of ethylene oxide (e.o.) has been investigated on the basis of the CNDO/2 method. By the calculation of the total energy of the interacting system of e.o. and protonated e.o. the most favored reaction path is indicated. The activation energy is found to consist only of the desolvation process. The effect of the deformation of the molecular geometry upon the net charge, the total energy, and the shape of particular MO's is discussed. It is concluded that the ring strain does not influence the rate. By means of configuration analysis, the dominance of the HOMO–LUMO interaction in the later stage of the reaction has been established. The initiation and propagation reactions follow the same reaction mechanism.

Extensive experimental studies in the field of ring-opening polymerisation (ROP) have been made.[1] In contrast to numerous papers reporting those results, however, there have been very few theoretical treatments of this field.[2] The experimental results concerning the reaction path of the acid-catalyzed ROP of cyclic ethers can be summarized as follows:[3] The initiator is first formed by a reversible protonation:

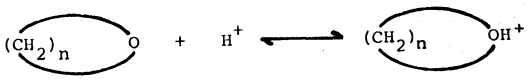

The initiation is considered to be the addition of a monomer to this protonated monomer. There is much evidence that the process of the ring-opening addition takes place as an S_N2-like backside attack. The propagation step is essentially constructed by a succession of similar processes at the terminal monomeric unit of a polymer chain:

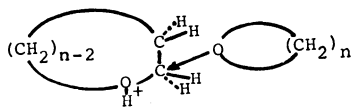

The backside attack is indicated by an inversion at the attacked carbon atom. However, still remains some doubt about the sequence of the bond interchange and the transition state. There has been discussed a "borderline S_N2-mechanism,"[4] where the old C–O bond is already partly broken at a rather early stage of the attack. Recent kinetic studies of the cationic ROP of some four-membered cyclic ethers show that the entropy of activation is the dominating factor in the reactivity.[5]

In the present and forthcoming papers, we want to report the results of our MO-theoretical treatment of various aspects of the reactivity and stereochemistry of heterocyclic-ring compounds in ROP. We start with ethylene oxide (e.o.), since it may serve as a simple model case for other, more complicated compounds.[6] Using the CNDO/2 method, we treat the isolated e.o. and its protonated compound, and also their interacting system. In order to determine the most favored geometries and reaction path, we examine the effect of changes in several geometrical parameters. Furthermore, utilizing the frontier theory[8] and configuration analysis,[9] the mechanisms of cationic ROP are investigated.

Calculations and Used Geometries

All our MO-calculations were based upon the CNDO/2 model of Pople *et al.*[7]

Figure 1(a) shows the energy levels of the MO's of e.o. and protonated e.o., together with the chosen geometry. Figure 1(b) shows the resulting net charges.

We calculated the total energy of the combined system of e.o. and protonated e.o. with different geometries. Figure 2 shows the geometries which gave the energy minimum at the fixed C–O′ distance for each of the frontside and backside attacks.[16] Further-

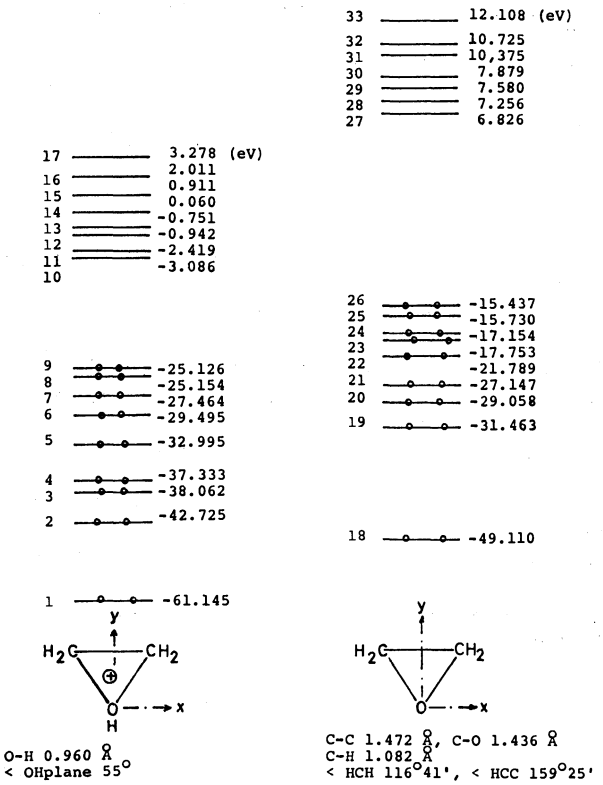

Fig. 1(a). MO energy levels and geometry of ethylene oxide and protonated ethylene oxide.

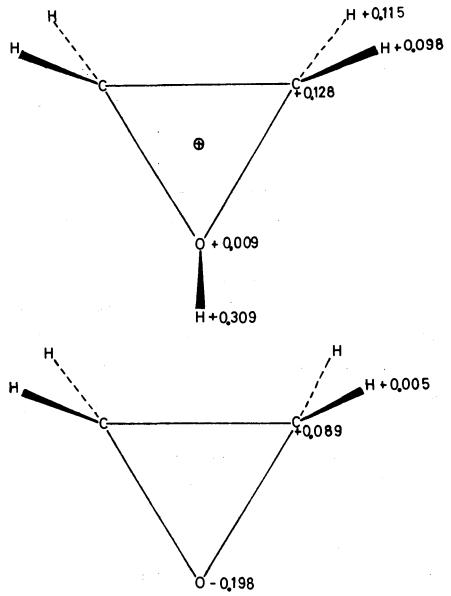

Fig. 1(b). Net charges of ethylene oxide and protonated ethylene oxide.

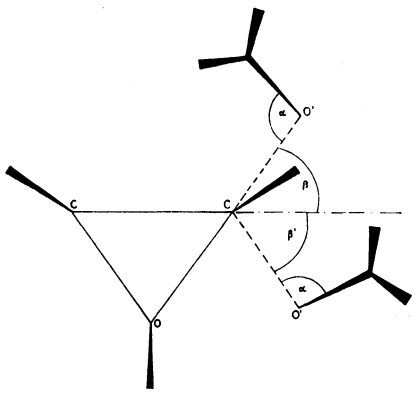

Fig. 2. Geometry of the molecules in the two attacking directions, the backside attack upper and the frontside attack lower.
$\alpha=110°$, $\beta=60°$, $\beta'=60°$.

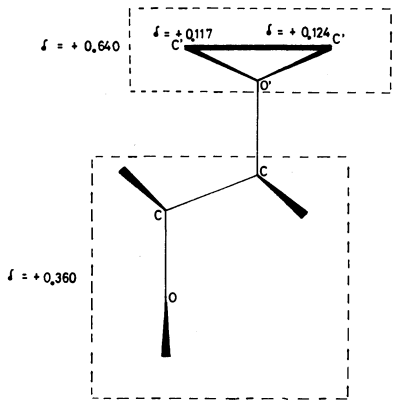

Fig. 3. Geometry of the final product of the initiation reaction and net charge distribution. The ring has the same geometry as e.o. (see Fig. 1).
O'–C 1.430 Å; C–C 1.540 Å; C–O 1.430 Å; C–H 1.090 Å; O–H 0.960 Å; $<$O'CC 110°; $<$HC plane $=<$OC plane 55°.

Table 1. Values of total energy, energy between the attacking oxygen (O') and the attacked carbon (C), and the net charge transfer with different geometries

$r_{C-O'}$ [Å]	Stretching of r_{C-O} [Å]	Bending of C–H bond γ [degree]	E_{tot} [a.u.]	$E_{C-O'}$ [a.u.]	Transferred charge
		Attack along the y-axis			
2.5	0	0	−71.8140	−0.013	0.002
		$\beta=60°$ (backside attack)			
2.5	0	0	−71.8068	−0.012	0.005
		−30	−71.8100	−0.019	0.009
	0.2	0	−71.7529	−0.018	0.012
		−60	−71.7463	−0.032	0.019
2.0	0	0	−71.8114	−0.064	0.047
		−30	−71.8302	−0.104	0.061
		−60	−71.8017	−0.134	0.084
	0.2	0	−71.7709	−0.095	0.083
		−30	−71.8031	−0.140	0.095
		−60	−71.7962	−0.177	0.125
1.5	0	0	−71.7323	−0.341	0.246
		−30	−71.8262	−0.462	0.290
		−60	−71.8528	−0.548	0.352
	0.2	0	−71.7412	−0.434	0.354
		−30	−71.8445	−0.546	0.376
		−60	−71.8951	−0.632	0.424
		$\beta'=60°$ (frontside attack)			
2.5	0	0	−71.8146	−0.019	0.009
	0.2	0	−71.7583	−0.027	0.012
		30	−71.7185	−0.026	0.014
2.0	0	0	−71.8245	−0.094	0.048
		30	−71.7973	−0.099	0.052
	0.2	0	−71.7880	−0.151	0.089
		30	−71.7561	−0.161	0.109
1.5	0	0	−71.7833	−0.493	0.250
		30	−71.7929	−0.538	0.285
	0.2	0	−71.8460	−0.645	0.408
		30	−71.8595	−0.697	0.451
		final product of the initiation reaction			
			−71.9441	−0.890	0.640

more, the neutral e.o. has been placed in a planar and perpendicular position to the protonated e.o. plane. Among all of these calculations, the geometries adapted in Fig. 2 gave the lowest energy values with regard to the above-mentioned parameters (see Table 1).

In the next step, we examine the energy minimum as to the attacking direction with the two C–O' distances of 2.0 and 2.5 Å. We also calculate the energy of the final product of this reaction of ROP. Its geometry is shown in Fig. 3, while the resulting energy is listed in Table 1.

Finally, we investigate the deformation of the ring of protonated e.o., since the geometry of the attacked protonated e.o. changes toward the geometry of the final product throughout the reaction. The considered deformations are indicated in Fig. 4, where the deformations of 1 and/or 4 are taken in the frontside attack course and those of 2, 3, and/or 4 for the backside attack.

The results are listed in Table 1. The table also

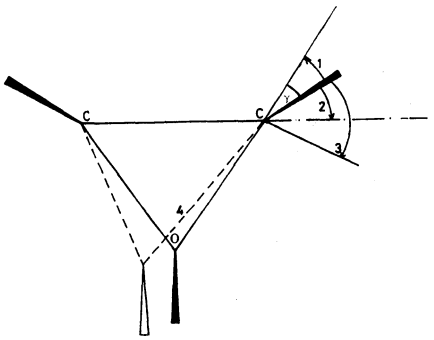

Fig. 4. Assumed deformations of the protonated ethylene oxide during the attack of the neutral molecule.
1: Hydrogens shifted up to $\gamma=30°$
2: Hydrogens shifted down to $\gamma=-30°$
3: Hydrogens shifted down to $\gamma=-60°$
4: One C–O bond length stretched by 0.2 Å.

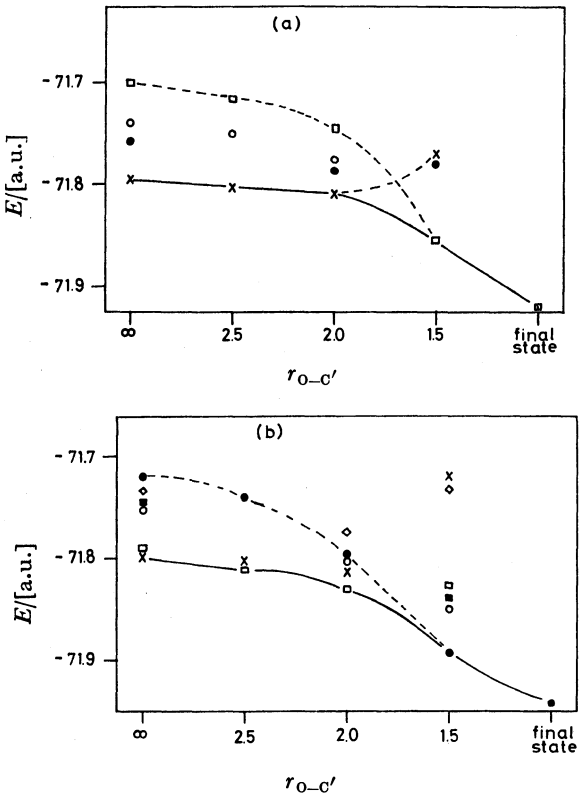

Fig. 5. The changes of energy levels along the two paths of attacking with the change of geometry indicated.
(a): Frontside attack
C–O bond length normal γ: 0° (×), γ: 30° (●)
C–O bond length +0.2 Å δ: 0° (○), δ: 30° (□)
(b): Backside attack
C–O bond length normal γ: 0° (×), γ: −30° (□), γ: −60° (○).
C–O bond length +0.2 Å γ: 0° (◇), γ: −30° (■), γ: −60° (●).

gives the values of the transferred charge from the neutral to the protonated compound and the values of the energy of the C–O′ bonding (E_{AB} in CNDO/2). Figures 5(a) and 5(b) show the total energies in relation to the C–O′ distance. The datum for $r=\infty$ is the simple sum of the values for the separated molecules.

Discussion

In spite of the use of many approximations, the results give interesting insights into the reaction path. Comparing the frontside and the backside attacks with the energy values shown in Fig. 5(a) and 5(b), it can be seen that there is not much difference with $r_{C-O'}$ values larger than 2.0 Å. After this stage, the backside attack is strongly favored from an energetic point of view.

It has been proposed in several papers by Fukui *et al.*[8] that "a majority of chemical reactions should take place at the position and in the direction of the maximum overlapping of the HOMO (Highest Occupied MO's) and the LUMO (Lowest Unoccupied MO's)." The HOMO of e.o., which is not shown here, is indeed mainly localized on the lone-pair oxygen p_z orbital (AO coefficient 0.88). There are two nearly degenerated LUMO's of the protonated e.o. (a' at −3.086 eV and a'' at −2.419 eV, with the point group C_s). They correspond to the a_1 and b_2 LUMO's of e.o. (point group C_{2v}). The consideration of both of them has previously been emphasized in the calculations of the anionic ROP of e.o.[10] The shapes of

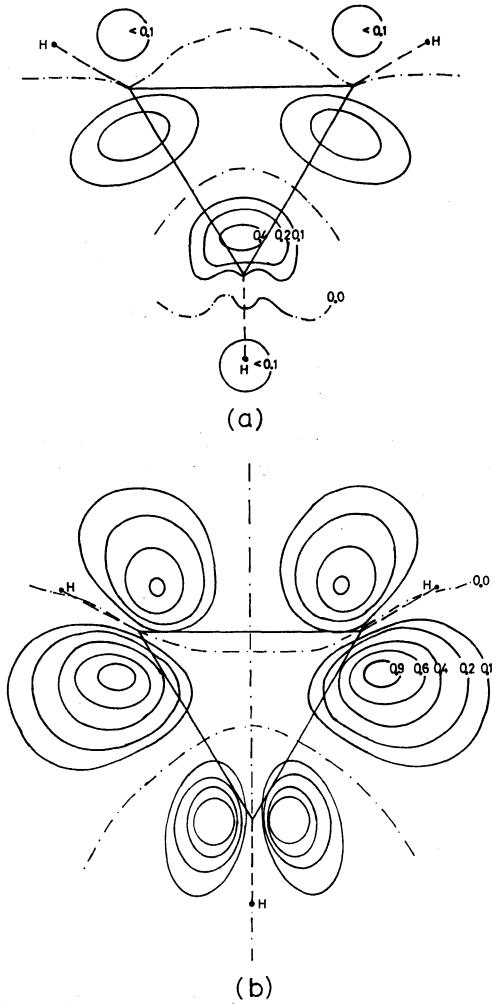

Fig. 6. The LUMO's of protonated e.o. The figures indicate the values of the real MO's in the molecular plane. The contour lines correspond to the density values indicated.
(a): a' LUMO (b): a'' LUMO

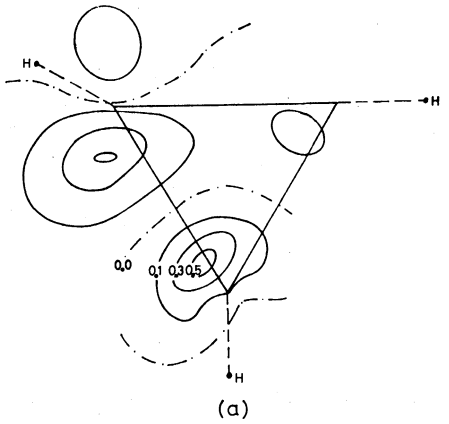

(a): a' LUMO at normal C–O bond length, H-shift with $\gamma = -30°$.

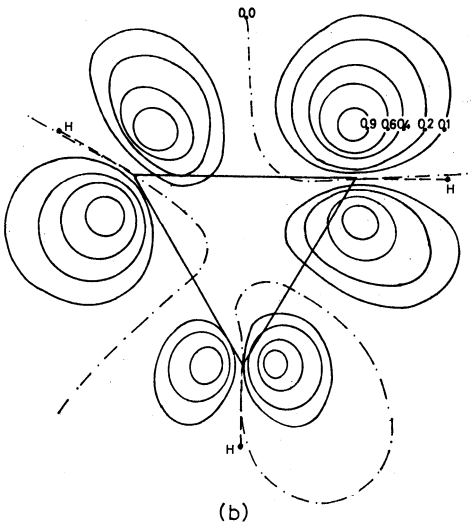

(b): a'' LUMO at normal C–O bond length, H-shift with $\gamma = -30°$.

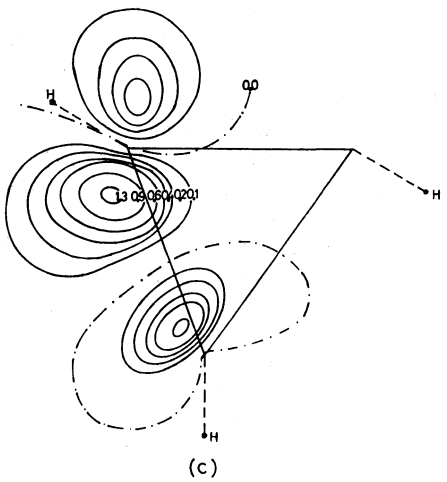

(c): a' LUMO at C–O bond length $+0.2$ Å, H-shift with $\gamma = -60°$.

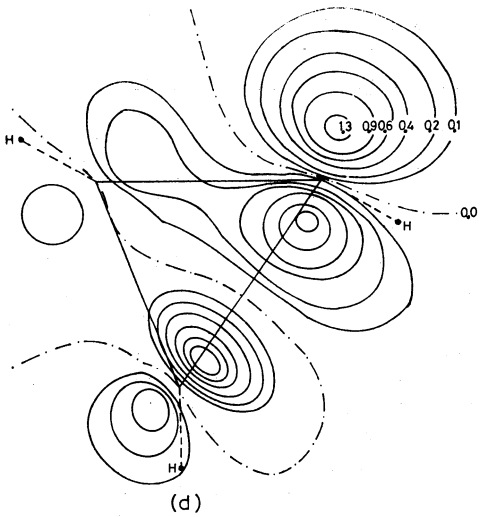

(d): a'' LUMO at C–O bond length $+0.2$ Å, H-shift with $\gamma = -60°$.

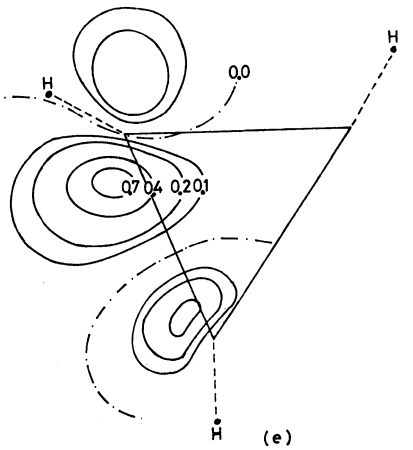

(e): a' LUMO at C–O bond length $+0.2$ Å, H-shift with $\gamma = 30°$.

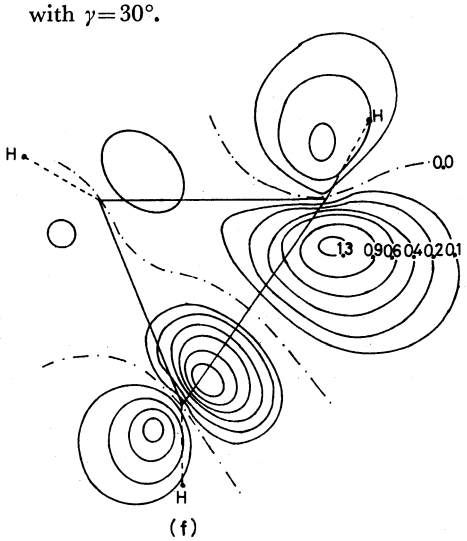

(f): a'' LUMO at C–O bond length $\times 0.2$ Å, H-shift with $\gamma = 30°$.

Fig. 7. Change of the two LUMO's under some deformations of the geometry of protonated e.o.

these LUMO's in the molecular plane are shown in Figs. 6(a) and 6(b). Both of them have a node between oxygen and carbon, but the a' LUMO has its main extension in an antibonding region between oxygen and hydrogen. (In Fig. 6(a) the contour lines not on the molecular plane do not appear.) Therefore, it may be presumed that it is the a'' LUMO which plays the dominant role in the ring cleavage.

This LUMO mainly extends in the initial geometry at the frontside. However, it is noticed that the shapes and energies of these LUMO's may vary with the geometry. Figures 7(a)—(f) collect the shapes of the LUMO's with various geometries which give the local minima for the respective $r_{C-O'}$ values, as given in Table 1. With these geometries, the notations a' and a'' lose their exact meaning because of the loss of symmetry, but they are still kept for the sake of convenience. Figure 7(b) clearly indicates that the shift of the hydrogens, which is expected to occur at an earlier stage of the reaction, as is shown in Table 1 and Fig. 5, results in a reversal of the maximum extension of the a'' LUMO from the frontside to the backside direction, whereas the extension of the a' LUMO at the attacked carbon atom is reduced. This tendency is even more accelerated with the deformation of the ring frame and a further hydrogen shift, as is shown in Figs. 7(c) and 7(d). Figures 7(e) and 7(f) show a similar trend for the frontside reaction.

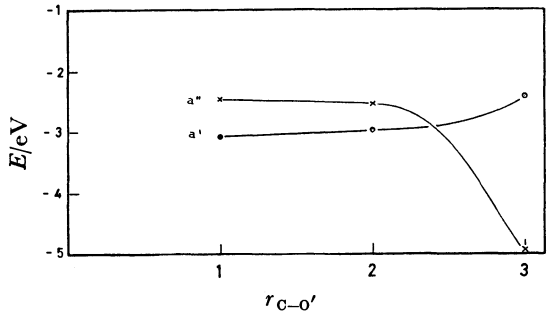

Fig. 8. Change of the energy level of the two LUMO's of protonated e.o. with some deformations which correspond to the reaction path of the backside attack (see Fig. 5(b)).
1: initial geometry, 2: C–O bond length normal, H-shift γ −30°, 3: C–O bond length +0.2 Å, H-shift γ −60°.

That it is the a'' LUMO and not the a' LUMO which is dominating in the HOMO–LUMO interaction can also be seen from the change in the energy level along with the change in the geometry, as is indicated for the backside attack in Fig. 8. The narrowing of the frontier orbitals has already been pointed out by Fukui *et al.*[8]

Some additional calculations have been carried out for the backside attack. We calculated the composed system by placing the neutral e.o. at a $r_{C-O'}$ distance of 2.5 Å along the y-axis in a planar arrangement to the protonated compound, as the Coulomb attraction should be the dominating force in this case. The numerical results, given in Table 1, show a greater stabilisation than the corresponding value for the assumed backside path. Furthermore, we varied the geometry parameters with a $r_{C-O'}$ distance of 1.5 Å. The values for β (see Fig. 2) have been taken as 75 and 45°, and the hydrogen shift with $\gamma=-45°$ (see Fig. 4). However, all these calculations gave no further stabilisation compared to the values for $\beta=60°$ and $\gamma=-60°$ (see Table 1). As our results for the principal reaction mechanism are independent of the exact location, we did not make any further calculations concerning the exact reaction path.

Additional information is given by the results of the configuration analysis[9,11] listed in Table 2, where some absolute values of coefficients for the ground state, monotransferred (delocalized), and intramolecular monoexcited (polarized) configurations are presented. The large value of the coefficient of the ground-state configuration at the early stage of the reaction indicates the dominance of the Coulomb interaction. However, the dramatically increasing value of the monotransferred configuration at $r_{C-O'}=1.5$ Å, especially that corresponding to the transfer from of e.o. the HOMO to the LUMO of protonated e.o.,[12] shows the importance of this kind of interaction at the final stage of the reaction.

From Table 1 it can be seen that the values for $E_{C-O'}$ and the quantities of charge transfer show no remarkable parallelism with the total energy, nor is there any interdependence between them. Roughly speaking, both values increase with the lowering of the total energy. It is interesting that, with the distance $r_{C-O'}$ of 1.5 Å, the backside attack shows a significantly lower total energy, but smaller $E_{C-O'}$ and transferred charge, than the frontside attack.

It is worthwhile to examine the charge transfer in more detail. Table 3 shows the change in the net charge of each atom at the different reaction stages for the local minimum energy (see Fig. 5). The numbers represent the differences from the net charge calculated for the isolated molecules with the respective geometry, where the + sign refers to the decrease in the atomic electron density caused by the interaction, and the — sign, to its increase. In contradiction to the whole protonated e.o. molecule coming more negative (less positive), the attacked carbon atom, 2, be-

Table 2. Absolute values of the coeeficients for the ground state, some monotransferred and monoexcited configurations along the backside and frontside paths
only the one or two largest values are indicated

Attacking-direction	$r_{C-O'}$ [Å]	Ψ_0	Coefficients for monotransferred configurations	Coefficients for monoexcited configurations
Backside ($\beta=60°$)	2.5	0.999	$0.06(\Psi_{26\to11})$; $0.03(\Psi_{21\to11})$	$0.02(\Psi_{24\to27})$
	2.0	0.960	$0.17(\Psi_{36\to11})$; $0.08(\Psi_{21\to11})$	$0.03(\Psi_{6\to11})$; $0.03(\Psi_{23\to27})$
	1.5	0.690	$0.39(\Psi_{26\to10})$; $0.18(\Psi_{21\to10})$	$0.19(\Psi_{8\to10})$; $0.13(\Psi_{5\to10})$
Frontside ($\beta'=60°$)	2.5	0.992	$0.04(\Psi_{36\to11})$; $0.04(\Psi_{26\to10})$	$0.03(\Psi_{23\to27})$
	2.0	0.959	$0.13(\Psi_{36\to11})$; $0.07(\Psi_{26\to10})$	$0.04(\Psi_{23\to27})$
	1.5	0.598	$0.39(\Psi_{36\to10})$; $0.18(\Psi_{21\to10})$	$0.33(\Psi_{9\to10})$; $0.14(\Psi_{5\to10})$

TABLE 3. DIFFERENCE OF THE NET CHARGES AT EACH ATOM BETWEEN THE COMBINED SYSTEM AND ISOLATED MOLECULES WITH THE RESPECTIVE GEOMETRY. THE GEOMETRIES ARE THOSE ONES WHICH GAVE MINIMA IN THE ENERGY CALCULATIONS (see Table 1)

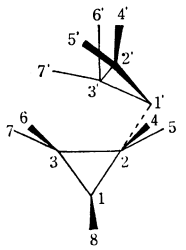

Atom	$r_{C-O'}$=2.5Å	$r_{C-O'}$=2.0Å	$r_{C-O'}$=1.5Å
1	−0.007	−0.029	−0.128
2	+0.011	+0.042	+0.084
3	−0.004	−0.021	−0.094
4	+0.003	−0.008	−0.064
5	+0.002	−0.010	−0.066
6	−0.004	−0.011	−0.046
7	−0.004	−0.010	−0.043
8	−0.003	−0.013	−0.073
1′	−0.027	−0.018	+0.132
2′	+0.003	+0.006	+0.021
3′	+0.003	+0.005	+0.020
4′	+0.030	+0.042	+0.079
5′	−0.014	−0.007	+0.046
6′	+0.030	+0.042	+0.079
7′	−0.015	−0.008	+0.045

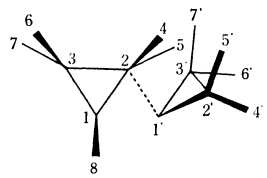

1	+0.003	−0.014	−0.173
2	+0.014	+0.061	+0.184
3	−0.010	−0.037	−0.102
4	−0.006	−0.017	−0.084
5	−0.007	−0.019	−0.056
6	−0.004	−0.009	−0.035
7	−0.005	−0.011	−0.100
8	+0.005	−0.001	−0.086
1′	−0.058	−0.053	+0.160
2′	+0.009	+0.011	+0.016
3′	+0.001	0.0	+0.008
4′	+0.030	+0.039	+0.080
5′	−0.001	+0.007	+0.055
6′	+0.030	+0.038	+0.078
7′	−0.003	+0.006	+0.054

comes more positive. Similarly, the oxygen atom, 1′, of the neutral molecule is still at $r_{C-O'}$=2.0 Å, more negative than in the isolated molecule, before it becomes more positive at $r_{C-O'}$=1.5 Å.

The potential curve of the reaction path anticipated from Fig. 5 indicates the absence of an energy barrier. This can easily be understood in view of the important role played by the solvent in ionic reactions. It has been found that this is particularly important for the reactivity of cyclic ethers in ROP.[13] Polar solvents stabilizing the monomers much better bring about a remarkable decrease in the reactivity of the monomers in ROP, compared with less polar solvents. Our calculations indicate that the activation energy originates only from the desolvation process. Therefore, the location of the transition state along the reaction path of Fig. 5(a) remains rather uncertain, however, the facts that the deformation of the ring frame occurs rather late ($r_{C-O'}$ <2.0 Å) and is accompanied by a rapid decrease in the total energy suggest that the transition state is placed somewhere earlier, with a geometry where the ring frame of the protonated e.o. is not yet deformed. If this is true, it follows that, in kinetically-controlled reactions where the activation energy determines the reaction rate, the ring strain is not influential on the rate. This has already been pointed out by Saegusa *et al.*[14] in reporting on their kinetic studies of 4-, 5-, and 7-membered cyclic ethers in cationic ROP. They found that the activation entropy is the most important factor in determining the reactivity.

There remains one problem. So far we have dealt only with the initiation step, but it has been stressed that the propagation step is quite different in its reaction rate, the latter being faster than the former.[15] The difference is as follows: in the propagation step, e.o. attacks an oxyethylated e.o. cation instead of a protonated one, and the length of the substituent chain is supposed to be not very important in connection with the reaction rate. Accordingly, we calculated the LUMO of the product of the initiation step. Figure 9 shows its shape in the ring plane. As the AO coefficients of this MO at atoms not placed in the ring plane are smaller than 0.03, it can be thought that the charges are located only in this plane. A comparison with the *a″* LUMO of the protonated e.o. (Fig. 6(b)) shows a great similarity. In the case of alkylated e.o., however, the LUMO is not degenerated, being the lowest one not undergoing deformation due to the interaction. Also, the charge distributions (Fig. 3) of

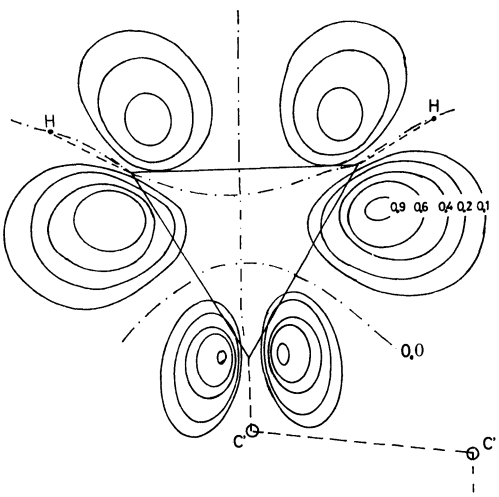

Fig. 9. The LUMO of the final product of the initiation reaction with the geometry of Fig. 3, indicating the values in the ring plane.

the atoms located at the ring are nearly the same as those of the protonated e.o. (Fig. 1(b)). From those facts, it can be expected that the mechanisms of the propagation reaction is not very different from the initiation.

The question is left why the rate of the propagation reaction is higher than the initiation reaction. The orbital energies of the LUMO's of the respective cations lead us to the opposite results. The LUMO of protonated e.o. (−3.086 eV) is lower than the LUMO of the oxyethylated e.o. (−1.629 eV). However, our results have shown that the bond breaking is more important than the bond making. The E_{AB} values for the C–O bond which is going to break during the reaction indicate a weaker bond for the oxyethylated e.o. (−0.816 eV) than for the protonated e.o. (−0.829 eV). This gives an explanation of the difference in the reaction rate.

From these calculations, the stereochemical course can be summarized as follows: the attack of the e.o. starts along the y-axis and is, in the beginning, governed by the Coulomb attraction only. The approach toward one carbon atom is accompanied by a shift of the connected hydrogens at a rather early stage of the reaction and produces a change in the a'' LUMO extension towards the attacking oxygen. This in turn accelerates the reaction by an increase in the charge transfer resulting from better HOMO–LUMO interaction. The deformation of the ring frame at a later stage accelerates this process still more and causes remarkable decreases in the total energy and also the C_2–O_1 bonding energy and increases in the amount of charge transfer and the C–O′ bonding energy. In this way, the deformation of the protonated compound leads to a reaction path with a lower energy for the backside attack than for the frontside attack.

One of the authors (G.F.) wishes to express his gratitude to Professor Takeo Saegusa and Dr. Shiro Kobayashi for a valuable discussion; he is also indebted to Dr. Hiroshi Fujimoto, Mr. Satoshi Inagaki, Mr. Tsutomu Minato, and Mr. Shigeki Kato for making avalaible the computer programs.

All three authors wish to express their appreciation to the Data Processing Center of Kyoto University for the generous permission to use the FACOM 230-60 computer there.

Thank is given to the Japanese Minister of Education and the Deutscher Akademischer Austauschdienst for giving grant to one of the authors (G.F.).

References

1) a) R. E. Parker and N. S. Isaacs, *Chem. Rev.*, **59**, 737 (1959); b) Y. Ishii and S. Sakai, "Ring Opening Polymerisation," ed. by K. C. Frisch and S. L. Reegen, Marcel Dekker, (1969), pp. 13—109.

2) K. Fukui, H. Kato, T. Yonezawa, and S. Okamura, This Bulletin, **37**, 904 (1964).

3) See Ref. 1b), p. 16.

4) See Ref. 1a), p. 746.

5) T. Saegusa and S. Kobayashi, *Progr. Polym. Sci.*, **6**, 107 (1973).

6) a) J. Koskikallio and E. Whalley, *Trans. Faraday. Soc.*, **59**, 815 (1959); b) C. C. Price and R. Spector, *J. Amer. Chem. Soc.*, **88**, 4171 (1966).

7) J. A. Pople, D. P. Santry, and G. A. Segal, *J. Chem. Phys.*, **43**, 129 (1965).

8) See *e.g.* K. Fukui, *Fortschr. Chem. Forsch.*, **15**, 1 (1970) and literatures cited therein.

9) See *e.g.* H. Baba, S. Suzuki, and T. Takemura, *J. Chem. Phys.*, **50**, 2028 (1969); H. Fujimoto, S. Kato, S. Yamabe, and K. Fukui, *ibid.*, **60**, 572 (1974).

10) H. Fujimoto, M. Katata, S. Yamabe, and K. Fukui, This Bulletin, **45**, 1320 (1971); note the choice of a different principal axis in the determination of the symmetry group.

11) S. Yamabe, T. Minato, H. Fujimoto, and K. Fukui, *Theor. Chim. Acta*, **32**, 187 (1974).

12) The reader is reminded that the succession of the orbitals denoted for the initial geometry in Fig. 1(a) changes in part because of the change in geometry. Therefore, the a'' LUMO of the protonated e.o., which plays the dominating part in the HOMO–LUMO interaction, is (in the succession of Fig. 1(a)) in the beginning the 11, but later the 10. See also Fig. 8.

13) See Ref. 5, p. 114, Table 1.

14) See Ref. 5, p. 145, Table 8.

15) See Ref. 5, p. 129.

16) The calculations where geometrical data are not listed have been carried out for the C–O′ distance of 1.5 Å and for the values for $\beta=30$, 60, 90°; $\beta'=30$, 60, and 90°, where β refers to the angle of backside attack, and β', to the frontside attack, as is indicated in Fig. 2.

The Catalytic Action of Fe(III) in the U(IV)-U(VI) Electron Exchange Reaction

Hiroshi TOMIYASU and Hiroshi FUKUTOMI*

Department of Chemistry, Faculty of Science, Shinshu University, Asahi, Matsumoto 390
**Research Laboratory for Nuclear Reactors, Tokyo Institute of Technology, Meguro-ku, Tokyo 152*

(Received September 8, 1973)

The catalytic action of ferric ions in the U(IV)–U(VI) electron exchange reaction has been studied in the presence of a high concentration of hydrochloric acid. The exchange rate is found to be accelerated by the addition of ferric ions; the observed rate law is given by:

$$R = k_0[\mathrm{U(IV)}][\mathrm{U(VI)}] + k_c[\mathrm{Fe(III)}]_0\sqrt{[\mathrm{U(IV)}][\mathrm{U(VI)}]}$$

An activation energy of 19.7 kcal/mol was calculated for the iron-catalyzed reaction in the U(IV)–U(VI) electron exchange reaction. This value is much smaller than that of 32.2 kcal/mol, which was found in the non-catalytic reaction. The kinetics and equilibrium of the reaction between Fe(III) and U(IV) have also been studied in order to investigate in detail the mechanism of the catalytic reaction. A one-electron-transfer mechanism producing U(V) as an intermediate is estimated from the rate law and supported by the kinetics and equilibrium studies of the Fe(III)–U(IV) reaction.

In the earlier papers dealing with the electron exchange reaction between U(IV) and U(VI) in concentrated hydrochloric acid,[1–4] it was shown that the rate of the electron exchange reaction (1) markedly increased with the acidity;

$$^{235}\mathrm{U(IV)} + {}^{238}\mathrm{U(VI)} \rightleftharpoons {}^{238}\mathrm{U(IV)} + {}^{235}\mathrm{U(VI)} \quad (1)$$

The present investigation was undertaken in order to determine the electron exchange rate between U(IV) and U(VI) in the presence of the smallest amount of Fe(III) and in order to observe the catalytic action of Fe(III).

Experimental

All of the chemicals used in this work were analytical reagent grade. The preparation and analysis of materials for the exchange reaction and the procedure in the kinetic experiment have been described in detail elsewhere.[2,3] The concentration of the Fe(III) stock solution was standardized for the potassium dichromate solution by passing an aliquot through a column of zinc amalgam. The desired concentrations of U(IV), U(VI), Fe(III), and hydrogen ions were obtained by adding appropriate amounts of hydrochloric acid and triply-distilled water. An aqueous solution of Fe(III) has an intense absorption maximum (*i.e.*, a molar extinction coefficient of 3.5×10^3 in 8M HCl) at 370 nm, whilst a negligibly small absorption and a weak absorption were observed at this wavelength in the solutions of Fe(II) and U(IV) and in U(VI) respectively. Therefore, the spectrophotometric determination of Fe(III) in the reaction mixtures was performed at 370 nm, using as a reference solution U(VI) which has the same concentration of U(VI) as the reaction mixtures. The spectrophotometric measurement was carried out by using a Shimadzu-50L recording spectrophotometer. The cell used for the measurement was filled with nitrogen gas and hermetically sealed to prevent the air oxidation of U(IV) and Fe(II). The electron exchange rate was measured by a mass-spectrometric analysis of the uranium isotope in U(VI).[2,3]

Results and Discussion

Kinetics and Equiliblium of the Reaction between U(IV) and Fe(III). Betts studied the kinetics of the oxidation of U(IV) by Fe(III) at a low acidity[5] and showed that the reaction proceeded *via* the following two steps:

$$\mathrm{U(IV)} + \mathrm{Fe(III)} \xrightarrow{k_2} \mathrm{U(V)} + \mathrm{Fe(II)} \quad (2)$$

$$\mathrm{U(V)} + \mathrm{Fe(III)} \xrightarrow{k_3} \mathrm{U(VI)} + \mathrm{Fe(II)} \quad (3)$$

Reaction (2) was found to be the rate-determining step, with a rate constant of 12.3 $M^{-1}\,s^{-1}$ in 1M HCl at 24 °C.

In an attempt to gain a better understanding of the interaction between U(IV) and Fe(III), several investigations have been conducted in our laboratory in concentrated hydrochloric acid solutions. Since the concentration of U(IV), [U(IV)], was large enough in the kinetic run compared with the Fe(III) concentration, [Fe(III)], [U(IV)] may be regarded as constant during the reaction. If Reaction (2) is the rate-determining step, the rate law may be written as a first-order rate equation with respect to [Fe(III)]:

$$\ln\{[\mathrm{Fe(III)}]/[\mathrm{Fe(III)}]_0\} = -2k_2[\mathrm{U(IV)}] \quad (4)$$

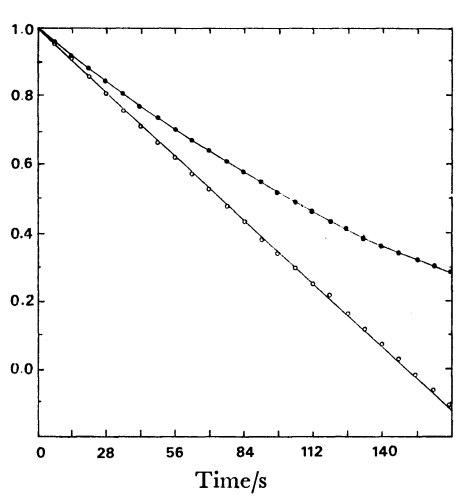

Fig. 1. Typical kinetic run for the oxidation of U(IV) by Fe(III) at 25 °C in 8 M HCl solution.
●: log {[Fe(III)]/[Fe(III)]$_0$} *vs.* time, *t*
○: Left-hand side of Eq. (7) *vs.* time, *t*
[Fe(III)]$_0$=2.9×10^{-4} M, [U(IV)]=1.88×10^{-2} M

where $[Fe(III)]_0$ denotes the initial concentration of Fe(III). As is shown in Fig. 1, a plot of $\log\{[Fe(III)]/Fe(III)]_0\}$ against time, t, indicates a gradual departure from linearity. This fact suggests that the above-mentioned mechanism was unsuccessful under these conditions and leads us to assume that Reaction (2) is reversible:

$$U(IV) + Fe(III) \underset{k_{-2}}{\overset{k_2}{\rightleftarrows}} U(V) + Fe(II) \qquad (2')$$

Therefore, we may now write the following differential equation:

$$-\frac{d[Fe(III)]}{dt} = k_2[U(IV)][Fe(III)] - k_{-2}[U(V)][Fe(II)] + k_3[U(V)][Fe(III)] \qquad (5)$$

The application of a steady-state approximation to [U(V)] gives:

$$[U(V)] = \frac{k_2[Fe(III)][U(IV)]}{k_{-2}[Fe(II)]+k_3[Fe(III)]} \qquad (6)$$

The substitution of Eq. (6) into Eq. (5) and integration yields:

$$\log\left(\frac{[Fe(III)]}{[Fe(III)]_0}\right) - \frac{1}{2.303(k_3/k_{-2}-1)}\left(\frac{[Fe(III)]_0}{[Fe(III)]}-1\right) = -\frac{2k_2[U(IV)]}{2.303(1-k_{-2}/k_3)}t \qquad (7)$$

Although the values of k_2, k_{-2}, and k_3 in Eq. (7) are not known, the left-hand side of Eq. (7) can be calculated for an arbitrary value of k_3/k_{-2}. If the assumptions are valid, a plot of the value of the left-hand side in Eq. (7) against t should give a straight line for some value of k_3/k_{-2}. As may be seen in Fig. 1, a straight line was obtained by introducing the value of $k_3/k_{-2}=5.83$, which was computed by the least-square method. From the slope, k_2 was calculated at 0.32 $M^{-1}\,s^{-1}$. It should be noted that the linear correlation was kept, even when U(VI) had previously been added to the reaction mixture, and that the value of k_2 was independent of the U(VI) concentration. This fact reveals that the backward reaction in Eq. (3) is so slow that it makes no appreciable contribution to Eq. (7).

The value of k_2 obtained in 8M HCl is much smaller than that of 12.3 $M^{-1}\,s^{-1}$ which was reported by Betts in 1M HCl. Some experiments were made in an 8M $HClO_4$ solution in order to investigate why the rate is reduced in 8M HCl as compared with that in 1M HCl. Unlike in 8M HCl, a plot of $\log\{[Fe(III)]/Fe(III)]_0\}$ *vs.* t gave a straight line under the conditions of $[U(IV)]=7.7\times10^{-3}$ M, $[Fe(III)]_0=3.8\times10^{-4}$ M and 8M $HClO_4$, and a much larger value of 2.4 $M^{-1}\,s^{-1}$ was obtained for k_2. Although this value is still smaller than that in 1M HCl, the effect of the hydrogen ion itself on the rate appears to be not very large, since the hydrolyzed species of U(IV) is more reactive with Fe(III) than U^{4+} at a low acidity.[12] Therefore, the high concentration of chloride ions seems to play a major role in reducing the reaction rate in 8M HCl. This is consistent with the findings in previous studies[13,14] that U(IV) is stabilized by forming a chloro complex in concentrated hydrochloric acid and that the oxidation rate by molecular oxygen is very slow compared with that in low acid concentrations. In addition, the redox potential between Fe(III) and Fe(II) may be changed in the presence of a high concentration of chloride ions. This change would influence the rate of the reaction between U(IV) and Fe(III) and would also play an important role in the mechanism where the reaction does not proceed by a simple first order with respect to Fe(III).

In the course of a kinetic study of the reaction between U(IV) and Fe(III), it has become apparent that the reduction of Fe(III) by U(IV) did not proceed to completion, no matter how large an excess of U(IV) was present. This can be seen in Fig. 2, where the absorption spectra were measured after the reaction between U(IV) and Fe(III) had reached equilibrium. The maximum peak at about 370 nm shows that trace amounts of Fe(III) are able to exist under the conditions mentioned above. The equilibrium concentration of Fe(III), $[Fe(III)]_{eq}$,* was estimated from the

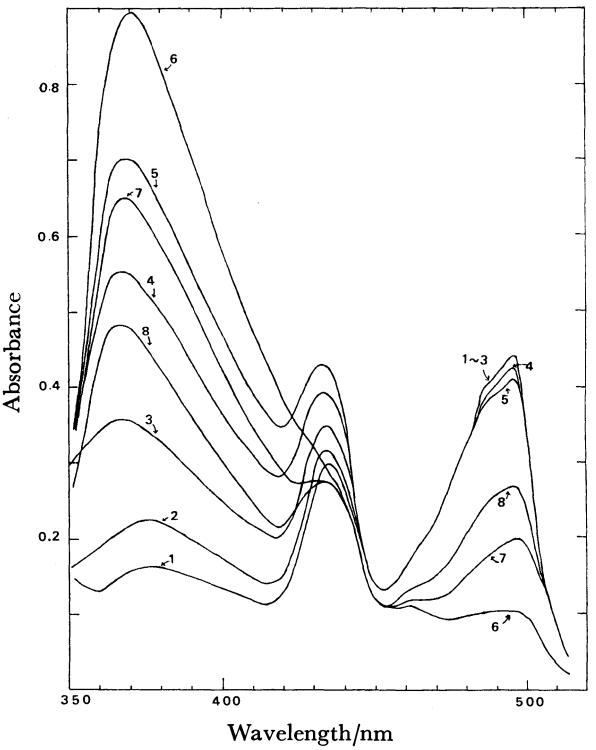

Fig. 2. Absorption spectra in the solution including Fe(III), Fe(II), U(IV), and U(VI) in 8 M HCl at 25 °C.
As reference solution, U(VI) which was the same concentration as in sample solution was used.
$[Fe(III)]_0$ is: (1) 1.40×10^{-3} M, (2) 1.96×10^{-3} M, (3) 2.80×10^{-3} M, (4) 4.20×10^{-3} M, (5) 5.60×10^{-3} M, while [U(IV)] and [U(VI)] are kept constant at 1.9×10^{-2} M and 2.1×10^{-2} M respectively.
[U(IV)] is: (6) 3.71×10^{-3} M, (7) 7.72×10^{-3} M, (8) 1.09×10^{-3} M, while $[Fe(III)]_0$ and [U(VI)] are kept constant at 3.6×10^{-3} M and 1.6×10^{-2} M respectively.

* In the equations from (9) to (16), [ ] shows the equilibrium concentrations. However, in order to distinguish the equilibrium concentration of Fe(III) from the time-dependent concentration, [Fe(III)], in Eq. (7) or Fig. 1, inferior letters, eq, will be used, as in $[Fe(III)]_{eq}$.

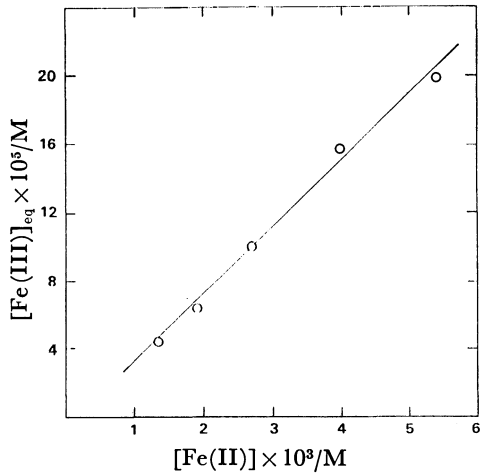

Fig. 3. Plot of $[Fe(III)]_{eq}$ *vs.* [Fe(II)] in Fe(III), Fe(II), U(IV), and U(VI) mixture.
[U(IV)] and [U(VI)] are kept constant at 1.8×10^{-2} M and 2.2×10^{-2} M respectively.

absorbance at this wavelength and was found to be associated with $[Fe(III)]_0$ and [U(IV)]. In Fig. 3, $[Fe(III)]_{eq}$ is plotted against [Fe(II)], which was calculated from the difference between $[Fe(III)]_0$ and $[Fe(III)]_{eq}$; a linear relationship is obtained. This might be explained stoichiometrically by the following reaction:

$$U(IV) + 2Fe(III) = U(VI) + 2Fe(II) \quad (8)$$

If these species are in equilibrium, the equilibrium constant, K, is given by:

$$K = \frac{[U(VI)][Fe(II)]^2}{[U(IV)][Fe(III)]^2_{eq}} \quad (9)$$

or

$$[Fe(III)]_{eq} = \frac{1}{\sqrt{K}}[Fe(II)]\sqrt{\frac{[U(VI)]}{[U(IV)]}} \quad (10)$$

As is shown in Fig, 4, the concentration of Fe(III) yields a stright line when plotted as a function of $1/\sqrt{[U(IV)]}$, keeping the value of $[Fe(III)]_0$ constant; the intercept of the straight line is found to be 0, within the limits of experimental error. These results are

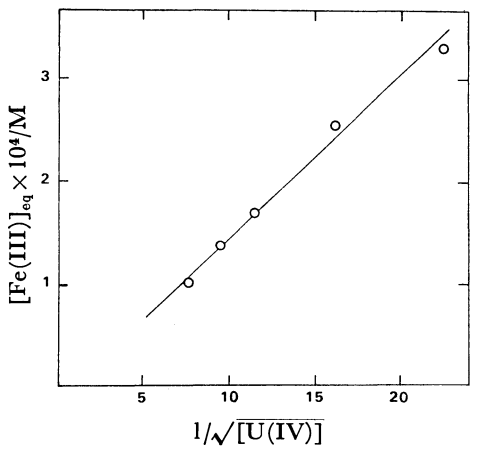

Fig. 4. Plot of $[Fe(III)]_{eq}$ *vs.* $1/\sqrt{[U(IV)]}$ in Fe(III), Fe(II), U(IV) and U(VI) mixture.
$[Fe(III)]_0$ and [U(VI)] are kept constant at 3.6×10^{-3} M and 1.6×10^{-2} M.

evidence in support of Eq. (10). Unfortunately, the relationship between $[Fe(III)]_{eq}$ and [U(VI)] could not be experimentally examined, because Fe(III) seems to interact with U(VI) and the absorption peak of Fe(III) shifts slightly depending upon the U(VI) concentration. However, there seems no doubt that Eq. (10) can be used for a solution containing Fe(III), Fe(II), U(IV), and U(VI). The values of $\sqrt{K}$ calculated from Eq. (10) are listed in Table 1, with the concentrations of these species.

Table 1. Equilibrium concentrations and equilibrium constant in Fe(III), Fe(II), U(IV), and U(VI) mixture at 25 °C in 8 M HCl solution

$[Fe(III)]_0$ $\times10^3$ M	$[Fe(III)]_{eq}$ $\times10^4$ M	[Fe(II)] $\times10^3$ M	[U(IV)] $\times10^2$ M	[U(VI)] $\times10^2$ M	$\sqrt{K}$
5.60	1.99	5.40	1.73	2.27	31.2
4.20	1.57	4.04	1.80	2.20	28.5
2.80	1.00	2.70	1.86	2.14	29.0
1.96	0.63	1.90	1.90	2.10	31.6
1.40	0.44	1.36	1.93	2.07	32.0
3.63	3.30	3.30	0.195	1.64	30.4
3.63	2.54	3.38	0.371	1.63	29.3
3.63	1.74	3.46	0.727	1.63	31.2
3.63	1.37	3.49	1.09	1.63	32.9
3.63	1.00	3.53	1.62	1.62	37.2
1.13	0.83	1.05	0.308	1.80	30.7
2.26	1.73	2.09	0.255	1.88	31.9
				Average	31.3

Table 2. Rate constants for the Fe(III)-catalyzed U(IV)–U(VI) electron exchange reaction at 30 °C in 8M HCl solution

[U(IV)] $\times10^2$ M	[U(VI)] $\times10^2$ M	$[Fe(III)]_0$ $\times10^5$ M	k $\times10^5$ M^{-1} s^{-1}	k_c $\times10^2$ M^{-1} s^{-1}
2.79	2.59	0	3.0	—
2.79	2.59	1.54	4.5	2.6_2
2.79	2.59	4.64	6.7	2.1_3
2.79	2.59	9.25	10.7	2.2_3
			Average	2.3_3

U(IV)–U(VI) Electron Exchange Reaction in the Presence of Fe(III). The U(IV)–U(VI) electron exchange reaction in the presence of Fe(III) was measured by the mass-spectrometric analysis described before, and the results were treated by using the McKay equation.[6] The rate constants in the presence of Fe(III) are listed in Table 2, along with various $[Fe(III)]_0$ values. It can be seen from Table 2 that the rate constants increase with $[Fe(III)]_0$. A plot of the rate constant, k, *versus* $[Fe(III)]_0$ yields a straight line (Fig. 5). The intercept of the line should give the rate constant in the absence of Fe(III); it agrees very closely with the value of 3.0×10^{-5} M^{-1} s^{-1} obtained in the previous paper. In Fig. 6, a plot of k *versus* $1/\sqrt{[U(VI)]}$ is shown under the conditions of constant $[Fe(III)]_0$ and [U(IV)] values; it gives a straight line. These results lead to the following rate law, although the [U(IV)] dependence on the rate has not yet been shown:

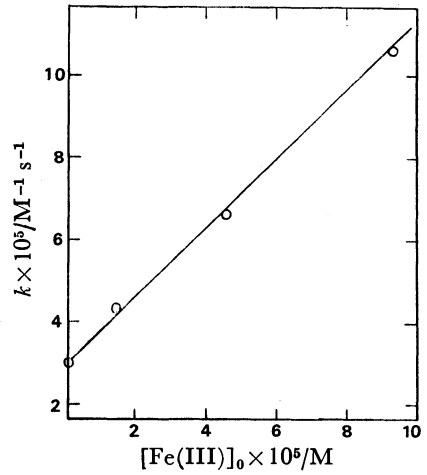

Fig. 5. Rate constant, k, as a function of $[Fe(III)]_0$ at 30 °C in 8 M HCl solution.
$[U(IV)]=2.79\times10^{-2}$ M, $[U(VI)]=2.59\times10^{-2}$ M.

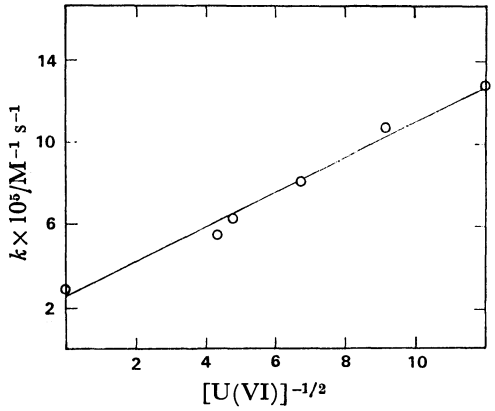

Fig. 6. Plot of k *vs.* $[U(VI)]^{-1/2}$.

Table 3. Rate constants

$[U(IV)]$ $\times10^2$ M	$[U(VI)]$ $\times10^2$ M	$[Fe(III)]_0$ $\times10^5$ M	k $\times10^5$ M^{-1} s^{-1}	k_c $\times10^2$ M^{-1} s^{-1}
2.78	2.59	6.30	8.3	2.2_8
1.67	1.56	6.30	12.0	2.3_0

$$k = k_0 + \frac{k_c[Fe(III)]_0}{\sqrt{[U(IV)][U(VI)]}} \qquad (11)$$

where k_0 and k represent the rate constants for the noncatalytic and catalytic paths respectively. In Table 3, the rate constants obtained from the kinetic runs under two different conditions are listed. As may be seen in Table 3, the two values of k_c are nearly equal and are in good agreement with those listed in Table 2. It thus appears that the kinetic order with respect to [U(IV)] in Eq. (11) well explains the experimental results.

The temperature dependence of k, ranging from 20 to 70 °C, is shown in Fig. 7. As may be seen in Fig. 7, the plots show a slight deviation from the linear relationship in the range of low temperatures. This result also implies that the U(IV)–U(VI) electron exchange, in which the least amount of Fe(III) is involved, consists of at least two reaction paths. A graph of

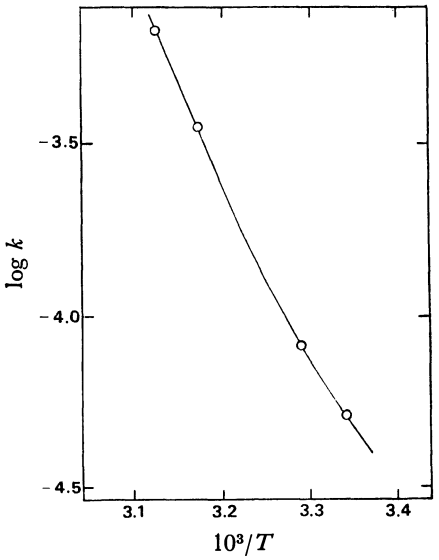

Fig. 7. Temperature dependence of k.

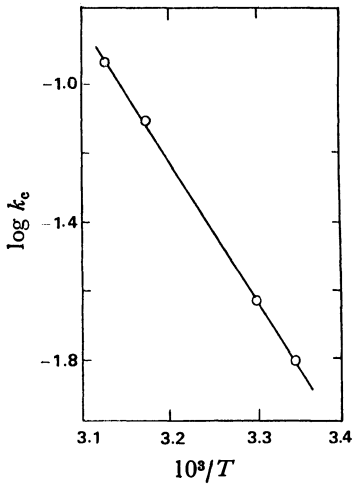

Fig. 8. Temperature dependence of k_c.

log k_c *versus* $1/T$ gives a straight line (Fig. 8), and the activation energy of 19.7 kcal/mol is calculated for the catalytic reaction. This value is much smaller than that of the non-catalytic reaction, that is, 32.2 kcal/mol.[2]

From the results mentioned above, the most probable mechanism for a catalytic reaction is seemed to be a one-electron transfer reaction through the formation of U(V). The initiation step might be the oxidation of U(IV) by Fe(III) (k_2 path), followed by a faster reaction (k_3 path):

$$U(IV) + Fe(III) \rightleftarrows U(V) + Fe(II) \qquad (2)$$

$$U(V) + Fe(III) \rightleftarrows U(VI) + Fe(II) \qquad (3)$$

Gordon and Taube studied the electron exchange reaction between U(V) and U(VI):

$$U(V) + U(VI) \rightleftarrows U(VI) + U(V) \qquad (12)$$

and estimated that the rate constant was 52.0 M^{-1} s^{-1} in a 1.0 M $HClO_4$ solution.[7] This value is much larger than that of k_2 (0.32 M^{-1} s^{-1}) obtained in a concentrated hydrochloric acid solution, as has been

described above. Therefore, it would be reasonable to assume that Reaction (12) proceeds much faster than Reaction (2), so that the electron exchange (12) occurs immediately after the formation of U(V) by Reaction (2) (k_2 path).

On the basis of this assumption, the rate law for the Fe(III)-catalyzed reaction may be given by:

$$R_c = k_2[\mathrm{U(IV)}][\mathrm{Fe(III)}] \tag{13}$$

where R_c is the rate of the Fe(III)-catalyzed reaction. The substitution of Eq. (10) into Eq. (13) gives:

$$R_c = \frac{k_2}{\sqrt{K}}[\mathrm{Fe(II)}]\sqrt{[\mathrm{U(IV)}][\mathrm{U(VI)}]} \tag{14}$$

Hence, the overall exchange rate, R, and the rate constant, k, may be expressed by:

$$R = k_0[\mathrm{U(IV)}][\mathrm{U(VI)}] + \frac{k_2}{\sqrt{K}}[\mathrm{Fe(II)}]\sqrt{[\mathrm{U(IV)}][\mathrm{U(VI)}]} \tag{15}$$

and:

$$k = k_0 + \frac{k_2}{\sqrt{K}}\frac{[\mathrm{Fe(II)}]}{\sqrt{[\mathrm{U(IV)}][\mathrm{U(VI)}]}} \tag{16}$$

The disproportionation of U(V) may make some contribution to the U(IV)–U(VI) electron exchange reaction.[8–11]

$$2\mathrm{U(V)} \rightleftarrows \mathrm{U(IV)} + \mathrm{U(VI)} \tag{17}$$

The rate law, however, is valid even if the disproportionation is faster than Reaction (12). In the course of a kinetic study of the oxidation of U(IV) by Fe(III), it may be clear that the disproportionation of U(V) is slow compared with Reaction (3) (k_3 path). This is because, if the disproportionation of U(V) were very fast, the reaction between U(IV) and Fe(III) would proceed simply by first-order with [Fe(III)], a plot of $\log\{[\mathrm{Fe(III)}]/[\mathrm{Fe(III)}]_0\}$ against t should give a straight line, and the linear relationship with respect to Eq. (7) as in Fig. 1 would not be obtained.

Since $[\mathrm{Fe(III)}]_0$ in Eq. (11) is nearly equal to [Fe(II)], as may be seen in Table 1, Eq. (16) is completely consistent with Eq. (11). This leads to the following relation:

$$k_c = k_2/\sqrt{K} \tag{18}$$

From the Fe(III)-catalyzed U(IV)–U(VI) electron exchange reaction, k_c can be obtained experimentally as 1.3×10^{-2} M^{-1} s^{-1} at 25 °C. On the other hand, k_2 and $\sqrt{K}$ were 0.32 M^{-1} s^{-1} and 31.3 respectively at 25 °C, as is shown in Fig. 1 and Table 1. From these results, $k_2/\sqrt{K}$ was calculated to be 1.0×10^{-2} M^{-1} s^{-1}. The $k_2/\sqrt{K}$ ratio gives the estimated rate constant for the Fe(III)-catalyzed U(IV)–U(VI) electron exchange reaction, assuming the rate law (16) and assuming that the value of 1.0×10^{-2} M^{-1} s^{-1} is in satisfactory agreement, within the limits of experimental error, with that of 1.3×10^{-2} M^{-1} s^{-1} obtained by the direct measurement of the U(IV)–U(VI) electron exchange reaction. This final result supports very strongly the mechanism we have discussed in this paper.

References

1) H. Kakihana, H. Fukutomi, K. Gonda, and H. Tomiyasu, Proceedings of the 9th International Conference on Coordination Chemistry, p. 275, St. Moritz, Switzerland, (1966).

2) H. Tomiyasu, H. Fukutomi, and H. Kakihana, *J. Inorg. Nucl. Chem.*, **30**, 2501 (1968).

3) Y. Kato and H. Fukutomi, *Bull. Tokyo Inst. Tech.*, No. 90, 1 (1969).

4) Y. Kato, K. Suzuki, H. Fukutomi, H. Tomiyasu, and G. Gordon, *ibid.*, No. 96, 133 (1970).

5) R. E. Betts, *Can. J. Chem.*, **26**, 702 (1948).

6) H. A. McKay, *Nature*, **142**, 997 (1938).

7) G. Gordon and H. Taube, *J. Inorg. Nucl. Chem.*, **16**, 272 (1961).

8) H. Iami, This Bulletin, **30**, 873 (1957).

9) D. M. Kern and E. F. Orleman, *J. Amer. Chem. Soc.*, **71**, 2102 (1946).

10) B. J. Masters and L. Schwartz, *ibid.*, **83**, 2620 (1961).

11) T. W. Newton and F. B. Baker, *Inorg. Chem.*, **8**, 1166 (1965).

12) A. G. Sykes, "Kinetics of Inorganic Reactions," Pergamon Press, Oxford (1966).

13) H. Tomiyasu, Ph. D Thesis, Tokyo Institute of Technology, 1968.

14) T. Kojima, H. Fukutomi, and H. Kakihana, *Bull. Tokyo Inst. Tech.*, No. 83, 87 (1968).

NH_2 Radicals Trapped on the Surface of Porous Vycor Glass at 77 K*

Norio SHIMAMOTO,** Keiichiro HATANO,*** Takashi KATSU, and Yuzaburo FUJITA
Faculty of Pharmaceutical Sciences, The University of Tokyo, Hongo, Bunkyo-ku, Tokyo 113
(Received January 26, 1974)

The results of ESR studies of the amino radicals produced by the photolysis of ammonia adsorbed on the surface of porous Vycor glass at 77 K are described. The observed ESR signal patterns of the amino radicals were remarkably affected by the amount of ammonia on the surface. The isotropic and anisotropic spectra were analyzed by the use of isotopically-substituted amino radicals.

Although several ESR studies have been devoted to the formation of NH_2 radicals by the irradiation of ionizing radiation on ammonia in various matrices[1-3] and on solid surfaces,[4-6] there are few studies of the photolysis of ammonia on solid surfaces. In this report, the results of ESR studies of the amino radicals produced by the photolysis of ammonia adsorbed on the surface of porous Vycor glass (PVG) at 77 K will be presented, in connection with a previous study of methylamino radicals.[7]

Experimental

PVG rods (Corning code No. 7930; 4 mm in diameter; 2 cm in length; surface area of 75 m^2/sample) were used. After the pretreatment of the PVG rod with oxygen at 550—600 °C and evacuation for a few hours in a quartz sample tube attached to a conventional high-vacuum system, a specified amount of ammonia was introduced into the sample tube at room temperature. The sample tube was then gradually cooled to the temperature of liquid nitrogen and then submitted to irradiation and ESR measurements. Gaseous ammonia from a concentrated aqueous solution was dried by passing it through a column packed with potassium hydroxide tablets; it was subsequently purified by vacuum distillation. Gaseous $^{15}NH_3$ was prepared from a $(^{15}NH_4)_2SO_4$ (99.8 ^{15}N atomic %) solution by alkalifying with KOH. The ESR spectra were recorded at 77 K with a JEOL P-10 spectrometer. The irradiation of the sample was carried out with a low-pressure mercury lamp (UL2-2HQ, 200W, Ushio Electric Inc.) at 77 K without any filters.

Results and Discussion

The observed ESR signal patterns of the amino radicals were greatly affected by the preadsorbed amount of ammonia on the surface of PVG.

Larger than the Monolayer Amount. An isotropic spectrum of apparent seven lines such as is shown in Fig. 1a was observed after irradiation with the full light of a low-pressure mercury lamp for 5 min at 77 K. A similar spectrum of the NH_2 radical produced by γ-irradiation on anhydrous ammonia at 77 K has been reported by Al-Naimy *et al.*[2] The spectrum can be assigned to the freely tumbling NH_2 radicals, free from any interaction with the surface. Further irradiation caused a selective growth of a particular triplet with an anisotropic nature, as can be seen from the dotted line spectrum in Fig. 1a. On slight warming, the isotropic spectrum decayed faster than the remaining triplet. Hereafter, the radicals with the isotropic and anisotropic natures will be denoted as A-type and B-type radicals respectively. The A-type

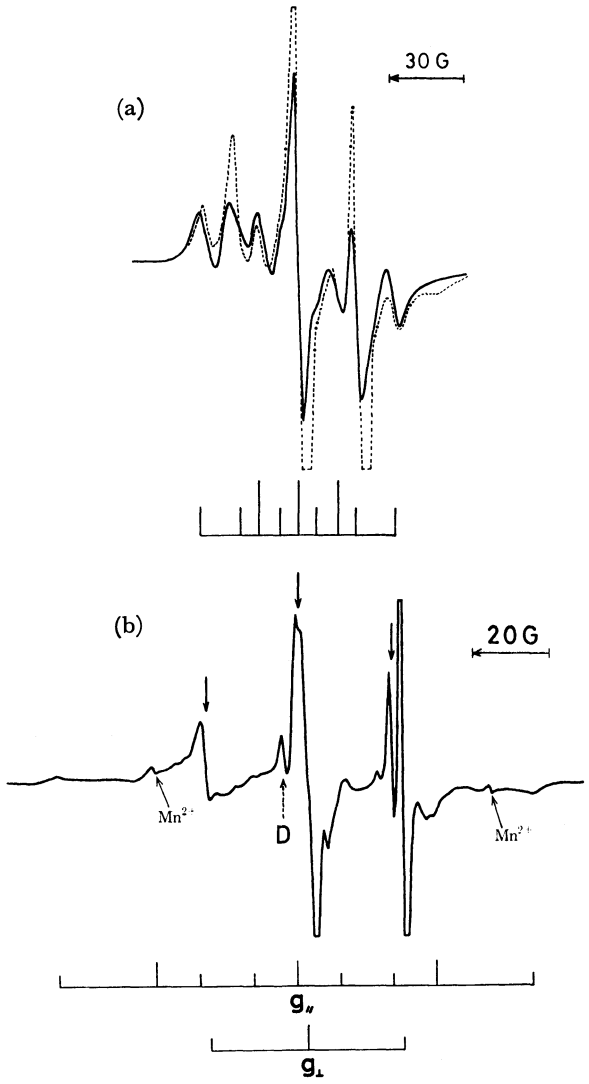

Fig. 1. ESR spectra of $^{14}NH_2$ radicals trapped on PVG surface at 77 K. (a): isotropic spectrum. solid line spectrum: irradiated for 5 min, dotted line spectrum: irradiated for 20 min. (b): anisotropic spectrum. Mn^{2+}: Mn^{2+} signal, D: defect signal, arrows: signal of R_3 radical.

* A part of this work was presented at The 10th Symposium on ESR, Osaka, October, 1971, Preprint p. 44.

** Present address: Central Research Division, Takeda Chemical Industries, Ltd., Higashiyodogawa-ku, Osaka.

*** Present address: Faculty of Pharmaceutical Sciences, Nagoya City University, Mizuho-ku, Nagoya.

spectrum of the ND_2 radical is shown in Fig. 2a. The ratio of the hf constants of the H and D nuclei in the NH_2 and ND_2 radicals, $A^H/A^D=6.5$, is exactly in agreement with the theoretical ratio, supporting the above assignment. The A-type spectrum of $^{15}NH_2$ is shown in Fig. 3a; in this case the linewidth is too broad for the hf constants of H and ^{15}N to be determined separately. However, the total spreading of the spectrum, 72 G, coincides well with the expected value of $(A^{15N}+2A^H)=(A^{14N}\times g^{15N}/g^{14N}+2A^H)=71$ G, where $A^H=25$ G, $A^{14N}=15$ G of $^{14}NH_2$, and $g^{15N}/g^{14N}=1.4$ were used. Thus, the hf constants of the A-type of $^{15}NH_2$ radical can reasonably be evaluated as is shown in Table 1.

Less than 1/10 of the Monolayer Amount. When the adsorbed amount was in the range $1>\theta>1/10$, a similar ESR spectrum of the triplet, such as is shown in Fig. 1a, was observed even after short irradiation.

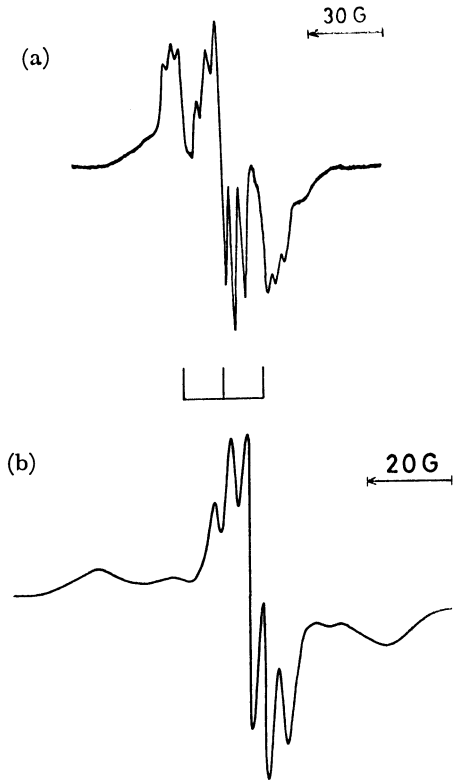

Fig. 2. ESR spectra of $^{14}ND_2$ radicals trapped on PVG surface at 77 K. (a): isotropic spectrum. (b): anisotropic spectrum.

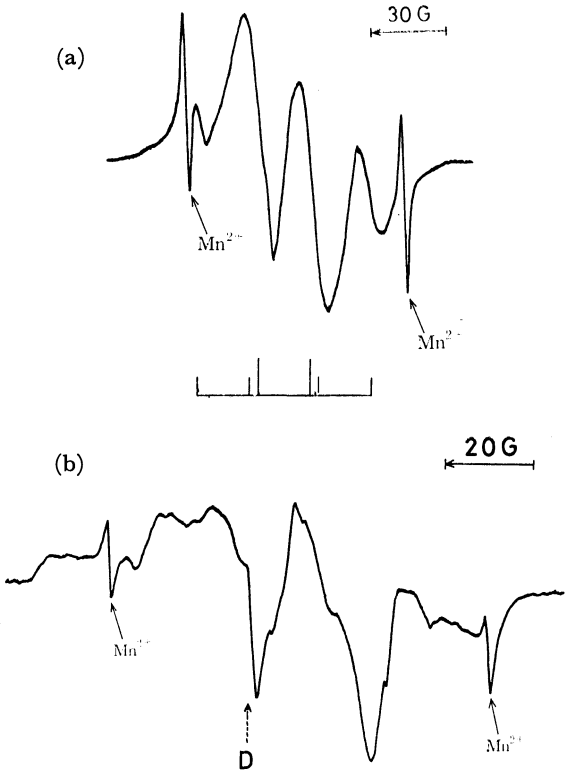

Fig. 3. ESR spectra of $^{15}NH_2$ radicals trapped on PVG surface at 77 K. (a): isotropic spectrum. (b): anisotropic spectrum. Mn^{2+}: Mn^{2+} signal, D: defect signal.

Table 1. ESR data for amino radicals in various matrices

Matrix	Radical	T/K	$A_{//}^{14N}$/G	$A_{\perp}^{14N}$/G	A_{iso}^{14N}/G	A^H/G	Ref.
Argon	NH_2	4.2			10.4	23.8	11
NH_3	NH_2	77			15.0	24.5	1
NH_3	NH_2	77			16.5	23.4	9
NH_3	NH_2	118			15.2	25.4	3
NH_3 on PVG	NH_2 (A-type)	77			15	25	This work
ND_3	ND_2	118			15.2	3.9 (D)	3
ND_3 on PVG	ND_2 (A-type)	77			15	~4 (D)	This work
NH_3	$^{15}NH_2$	77			21.3 (^{15}N)	25.4	3
NH_3 on PVG	$^{15}NH_2$ (A-type)	77			21 (^{15}N)[a]	25[a]	This work
NH_3 on PVG	NH_2 (B-type)	77	36	~0		25	This work
NH_3 on SiO_2	NH_2	77	37.5	3		24	4
NH_3 on MS	NH_2	77	35	3		26	5
NH_3 on SiO_2	NH_2	77	32	—		25	6
NH_3–H_2O	NH_2	77	41	0		24	9
NaN_3–H_2O	NH_2	77	39	3		24	12
ND_3 on PVG	ND_2 (B-type)	77	36	~0		~4 (D)	This work
NH_3 on PVG	$^{15}NH_2$ (B-type)	77	50 (^{15}N)[a]	5[a]		25[a]	This work

a) The values are evaluated from the total spreading of the spectra.

A further decrease in the adsorbed amount, $\theta<1/10$, resulted in the appearance of a well-resolved complicated spectrum, as is shown in Fig. 1b. The photolysis of ND_3 ($1>\theta>1/10$) was also carried out to ascertain whether the extra triplet in Fig. 1a or 1b is caused by two protons or a single ^{14}N nucleus in the radical. Since the triplet was replaced by a quintet in the case of ND_3 photolysis, as is shown in Fig. 2b, and since the ratio of the hf constants between both radical species coincided with the expected value, the triplet is attributable to the proton hf splitting of the NH_2 radical.

In general, the ^{14}N hf splitting has an anisotropic nature in adsorbed states; this is the reason why the deuteron hf splitting on $m_I=\pm1$ lines of nitrogen is only partially resolved. Morton *et al.*[8] have reported a large anisotropy in the ^{15}N hf splitting of the $^{15}NH_2$ radical trapped in γ-irradiated $K^{15}NH_2SO_3$ single crystals: the principal values of the ^{14}N hf splitting calculated from their data by using the nuclear g-factor ratio are $A_{xx}^{^{14}N}=38.3$, $A_{yy}^{^{14}N}=1.4$, and $A_{zz}^{^{14}N}=0.2$ G, where the x-axis is taken along the $2p\pi$ orbital of the nitrogen atom. Assuming an axial symmetry of ^{14}N hf splitting and a nearly isotropic splitting for the proton in the NH_2 radical rotating about the unpaired spin orbital,[9] the hf constants of ^{14}N and H were determined to be as is shown in Table 1.

Although almost all the ESR lines in Fig. 1b can thus be assigned to the NH_2 radical of the B-type, there exist some other lines which are not due to this radical species, indicating the existence of other radical species. Recently, Brotikovskii *et al.*[4] have observed spectra due to the overlap of three different radical species in γ-irradiated NH_3–SiO_2 systems at 77 K; namely, the R_1, R_2, and R_3 radicals in their notation. Among these radicals, the R_1 radical obviously corresponds to the B-type radical in our case: the hf constants of the R_1 radical are $A_{//}^{^{14}N}=37.5$, $A_{\perp}^{^{14}N}=3$, and $A^{H}=24$ G, values which almost coincide with those of our B-type radical. The three lines marked with arrows in Fig. 1b correspond to those of the R_3 radical, which can probably be assigned to another NH_2 radical species interacting more strongly with a different site from that of the R_1 or B-type radical species, resulting in an apparent quenching of the ^{14}N hf splitting as a result of a strong interaction with the surface. The spectrum corresponding to the R_2 radical, which has been tentatively assigned by Brotikovskii *et al.* to the S–NH radical (S denotes a surface site), was perceptible only at an initial stage of irradiation on a sample evacuated at higher temperatures; this is in accordance with their results, where the R_2 radical was the predominant species on the surface of SiO_2 preheated at 800 °C *in vacuo*.

When $^{15}NH_3$ was photolyzed under the same conditions as are shown in Fig. 1b, the ESR spectrum shown in Fig. 3b was observed. The total spreading of the $^{15}NH_2$ spectrum should be equal to $(A_{//}^{^{14}N}+2A^{H})=(A_{//}^{^{14}N}\times g^{^{14}N}/g^{^{14}N}+2A^{H})=100.5$ G, which is exactly in agreement with the observed total spreading of 100 G.

From the above results, it may be concluded that the primary radical of the photodecomposition of ammonia adsorbed on the surface of PVG with the light of a low-pressure mercury lamp is the NH_2 radical, and that the spectral pattern of the NH_2 radical depends remarkably on the amount of ammonia preadsorbed on the surface.

For comparison, the ESR data for NH_2 radicals trapped in various matrices are listed in Table 1, along with those for the photoproduced NH_2 radicals on the surface of PVG.

The isotropic ^{14}N and H hf constants of NH_2 trapped in anhydrous NH_3 and on PVG are nearly in accordance with each other, while the $A_{iso}^{^{14}N}$ of NH_2 trapped in an argon matrix is significantly smaller than the others. The latter change in the hf constants is a common phenomenon arising from the different radical environment. Rao and Symons[9] have discussed their observation of various values of $A_{iso}^{^{14}N}$ with changes in the medium. The change in $A_{iso}^{^{14}N}$ observed with the change of medium from argon to anhydrous NH_3 or NH_3 adsorbed on PVG may be due to a weak hydrogen-bonding interaction between the radical and host NH_3 molecules. However, this hydrogen bond is considered to be not strong enough to prevent the free tumbling of the radical, since the observed ESR signal pattern shows an isotropic nature even at 77 K. Nearly constant values of $A_{iso}^{^{14}N}$ both in anhydrous ammonia and on PVG indicate that the A-type NH_2 radical is trapped in a condensed phase of ammonia free from any interaction with the PVG surface. Accordingly, the A-type radical may be said to decay rapidly by means of the radical recombination due to the softening of the matrix on slight warming.

The values of $A_{//}^{^{14}N}$ scatter slightly depending on the radical environments, as is shown in Table 1. This may be partly due to an ambiguous estimation of the value from the positions of the outermost humps of the powder-pattern spectra, and partly to different interaction forces with the surfaces, as in the case of methyl radicals trapped on the PVG surfaces.[10] The radicals of the B-type with an axially symmetric hf tensor of ^{14}N, interacting strongly with the surface silanol group through the $2p\pi$ orbital of the radical rather than the hydrogen bond, are immobilized on the surface and, consequently, are allowed to rotate only around the $2p\pi$ orbital. Thus, the translational motion of the radical is so restricted to prevent the radical recombination that the B-type NH_2 radical was observed even at −20 °C in a thermal-decay experiment.

The authors wish to express their thanks to Professor Masamichi Tsuboi and Dr. Akiko Hirakawa of this faculty for their kind gift of ^{15}N-ammonium sulfate.

References

1) V. I. Tupikov, V. I. Tsivenko, S. Ya. Pshezhetskii, A. G. Kotov, and V. K. Milinchuk, *Russ. J. Phys. Chem.*, **37**, 65 (1963).

2) B. S. Al-Naimy, P. N. Moorthy, and J. J. Weiss, *J. Phys. Chem.*, **70**, 3654 (1966).

3) D. R. Smith and W. A. Seddon, *Can. J. Chem.*, **48**, 1938 (1970).

4) O. I. Brotikovskii, G. M. Zhidomirov, V. B. Kazanskii,

A. I. Mashchenko, and B. N. Shelimov, *Kinet. Katal.*, **12**, 700 (1971).

5) E. F. Vansant and J. H. Lunsford, *J. Phys. Chem.*, **76**, 2716 (1972).

6) S. Nagai, This Bulletin, **46**, 1144 (1973).

7) K. Hatano, N. Shimamoto, T. Katsu, and Y. Fujita, *ibid.*, **47**, 4 (1974).

8) J. R. Morton and D. R. Smith, *Can. J. Chem.*, **44**, 1951 (1966).

9) K. V. S. Rao and M. C. R. Symons, *J. Chem. Soc., A*, **1971**, 2163.

10) Y. Fujita, T. Katsu, M. Sato, and K. Takahashi, *J. Chem. Phys.*, **61**, 4307 (1974).

11) S. N. Foner, E. L. Cochran, V. A. Bowers, and C. K. Jen, *Phys. Rev. Lett.*, **1**, 91 (1958); E. L. Cochran, F. J. Adrian, and V. A. Bowers, *J. Chem. Phys.*, **51**, 2759 (1969).

12) I. S. Ginns and M. C. R. Symons, *J. Chem. Soc. Faraday II*, **68**, 631 (1972).

The Electronic Structures of Several Aliphatic Carbonyls. The Effects of Polar Substituents

Yoshiro YONEZAWA* and Takayuki FUENO

Department of Chemistry, Faculty of Engineering Science, Osaka University, Toyonaka, Osaka 560

(Received February 13, 1974)

The electronic structures of several aliphatic carbonyls, X_2CO, CH_3COX, and $(XCO)_2$ (X=H, F, CN, CH_3), have been investigated by the INDO method. Variations in the calculated electron density, the $n\pi^*$-excitation energy, the electron affinity, and the ionization potential with α-X substitution are explained qualitatively in terms of the σ-attracting and π-donating character of F, the π-attracting nature of CN and XCO, and the σ,π-donating property of CH_3. The lowest $^3n\pi^*$ excitation energies and ionization potentials calculated by the UHF method are in reasonable agreement with the experimental values in most cases. The partitioning of the total energy suggests that the C–O bonds of X_2CO compounds in the lowest $^3n\pi^*$ state and the radical anions derived from them are somewhat longer than those of the parent molecules, primarily because of the decrease in the electron-core attraction. The C–C bonds in some $(XCO)_2$ compounds appear to be cloven as easily as the C–X one on thermal activation and electron impact.

The structural and photochemical properties of aliphatic carbonyls in the excited state have already received considerable attention.[1,2] However, no all-valence-electron study of the electronic structure has yet been carried out. We thus applied the INDO method to several aliphatic carbonyls, X_2CO, CH_3COX, and $(XCO)_2$ (X=H, F, CN, CH_3), in the ground and excited states, as well as to the radical anions and cations derived from them. The total energies were partitioned into one- and two-atom terms,[3,4] and we tried to determine how the interatomic interactions influence the electronic excitation, ionization, and electron attachment.

Method of Calculation

The INDO calculations of the closed- and open-shell configurations were carried out by the usual procedure.[3] The total energy of the molecule is written as a sum of one- and two-atom terms:[3,4]

$$E_{\text{total}} = \sum_{A} E_A + \sum_{A<B}\sum E_{A-B} \tag{1}$$

$$E_{A-B} = E^1_{A-B} + E^2_{A-B} + E^3_{A-B} \tag{2}$$

where the two-atom terms are given by:

$$E^1_{A-B} = 2\sum_{r}^{A}\sum_{s}^{B} P_{rs}S_{rs}\beta^{\circ}_{AB} \tag{3}$$

$$E^2_{A-B} = -\frac{1}{2}\sum_{r}^{A}\sum_{s}^{B} P^2_{rs}\gamma_{AB} \tag{4}$$

$$E^3_{A-B} = (P_{AA}P_{BB} - P_{AA}Z_B - P_{BB}Z_A)\gamma_{AB} + Z_AZ_B/R_{AB} \tag{5}$$

Here, P_{rs} and S_{rs} are the bond order and the overlap integral between the r and s atomic orbitals; β°_{AB}, γ_{AB}, and R_{AB} are the empirical bonding parameter, the two-center repulsion integral, and the distance between the A and B atoms respectively, and P_{AA} and Z_A are the electron density and the core charge at the atom A respectively. When wavefunctions of the unrestricted Hartree-Fock (UHF) type are used, Eq. (4) takes this form:

$$E^2_{A-B} = -\sum_{r}^{A}\sum_{s}^{B}[(P^{\alpha}_{rs})^2 + (P^{\beta}_{rs})^2]\gamma_{AB} \tag{6}$$

where P^{α}_{rs} (P^{β}_{rs}) is the bond order between the r and s atomic orbitals of the α- (β-) spin electron. We have used the original INDO parameters of Pople *et al.*[3] throughout this work.

Most of the molecular geometries employed were taken from the literature.[5,6] No experimental data are available for the geometries of carbonyl cyanide and oxalyl cyanide;[7] the former was assumed to be $\overline{CO}$=1.20 Å, $\overline{CC}$=1.47 Å, $\overline{CN}$=1.16 Å, and $\angle CCC=120°$, and the latter, to be $\overline{CO}$=1.22 Å, $\overline{C(CN)}$=1.47 Å, $\overline{CC}$=1.50 Å, $\overline{CN}$=1.16 Å, $\angle CCC=120°$, and $\angle OCC=123°$. The same geometries were employed for $^3n\pi^*$ molecules and for radical ions. All the oxalyl compounds were assumed to be in the *s-trans* conformation.

Results and Discussion

Ground State. The electron densities on the carbonyl group of X_2CO compounds are given in Table 1. It is expected, from the values of the Hammett's substituent constants, that the F atom has a σ-attracting and π-donating character, that the CN and XCO groups have σ,π-attracting nature, and that the CH_3 group has a σ,π-donating property.[8] As to the electron density at the carbonyl oxygen, it is noticeable that the population of the 2pz atomic orbital (perpendicular to the molecular plane) increases

TABLE 1. ELECTRON DENSITIES ON THE CARBONYL GROUP OF THE GROUND-STATE X_2CO MOLECULES

Molecule	Atom	Electron densities				
		Total	2s	$2p_x$	$2p_y$	$2p_z$
H_2CO	C	3.66	1.09	0.87	0.90	0.80
	O	6.23	1.76	1.37	1.90	1.20
F_2CO	C	3.18	0.97	0.76	0.69	0.76
	O	6.33	1.75	1.33	1.85	1.40
$(CN)_2CO$	C	3.66	1.00	0.87	0.94	0.85
	O	6.24	1.76	1.36	1.94	1.18
$(CH_3)_2CO$	C	3.69	1.04	0.88	0.96	0.81
	O	6.31	1.78	1.33	1.95	1.25

* Present address: Department of Industrial Chemistry, Faculty of Engineering, Kyoto University, Yoshida, Kyoto 606.

Table 2. Orbital energies,[a] total energies and dipole moments of the ground-state molecules

Molecule	Orbital energy (eV) E_n	Orbital energy (eV) E_{π^*}	Total energy (eV) E_{total}	Dipole moment (D) Calcd	Dipole moment (D) Obsd
H_2CO	−13.69	4.42	−700.35	1.88	2.31[b]
F_2CO	−16.59	4.03	−2098.71	0.77	0.95[c]
$(CN)_2CO$	−13.57	1.69	−1626.10	0.02	—
$(CH_3)_2CO$	−12.28	4.04	−1160.07	2.84	2.90[d]
CH_3COH	−12.83	4.41	−930.09	2.31	2.70[e]
CH_3COF	−14.14	4.31	−1628.89	2.61	2.96[e]
CH_3COCN	−12.98	2.71	−1393.33	3.12	3.45[e]
$(HCO)_2$	−12.45	1.76	−1361.80	0.0	—
$(FCO)_2$	−13.55	1.51	−2758.80	0.0	—
$(CNCO)_2$	−12.75	0.45	−2287.86	0.0	—
$(CH_3CO)_2$	−11.29	2.22	−1821.36	0.0	1.05[f]

a) The symbols E_n and E_{π^*} denote the highest occupied n and lowest vacant π^* orbital energies respectively. b) J. N. Shoolery and A. H. Sharbaugh, *Phys. Rev.*, **82**, 95 (1951). c) V. W. Laurie and D. T. Pense, *J. Chem. Phys.*, **37**, 2995 (1962). d) J. D. Swalen and C. C. Costain, *ibid.*, **31**, 1562 (1959). e) L. C. Krisher and E. B. Wilson, Jr., *ibid.*, **31**, 882 (1959). f) At 328.45 K, G. I. M. Bloom and L. E. Sutton, *J. Chem. Soc.*, **1941**, 727.

with an increase in the π-donating ability of the substituents.

The frontier orbital energies, total energies, and dipole moments are summarized in Table 2. The calculated dipole moments show a good agreement with the experimental values except for the oxalyl compounds, which will take both *cis* and *trans* conformations under the present experimental conditions.

The orbital energies of the highest occupied and lowest vacant levels are correlated with the first ionization potential and the electron affinity respectively. The highest occupied orbital of each molecule is an n orbital localized almost completely at the carbonyl oxygen, *i.e.*, the $2p_y$ atomic orbital (perpendicular to the molecular axis). The energy levels of this orbital rise in this order: F$\ll$H, CN$<$$CH_3$, XCO. The F substituent lowers this level because of its σ-attracting character. On the other hand, the lowest vacant orbital is essentially a π^* orbital. The energy levels rise in this order: CN, XCO$\ll$F, $CH_3<$H. The CN and XCO substituents lower the π^* level because of their π-attracting nature.

The Lowest Excited State. The lowest nπ^* singlet and triplet excitation energies, $\Delta E^V(^1n\pi^*)$ and $\Delta E^V(^3n\pi^*)$, as calculated by the virtual-orbital approximation without configuration interaction, are given in Table 3. These energies are expressed by:

$$\Delta E^V(^1n\pi^*) = (E_{\pi^*}-E_n) - J_{n\pi^*} + 2K_{n\pi^*} \quad (7)$$

and;

$$\Delta E^V(^3n\pi^*) = (E_{\pi^*}-E_n) - J_{n\pi^*} \quad (8)$$

where $(E_{\pi^*}-E_n)$ is the frontier orbital energy gap and where $J_{n\pi^*}$ and $K_{n\pi^*}$ are the interorbital Coulomb and exchange integrals respectively. $J_{n\pi^*}$ decreases with the replacement of the H atom by the CH_3, CN, and XCO groups as a result of the expansion of the π^* orbital of the carbonyl group. $K_{n\pi^*}$ is small because of the different symmetries of the n and π^* orbitals.

The nπ^* energy change caused by α-X substitution will be discussed qualitatively on the basis of the orbital energies alone, because the variation in $(E_{\pi^*}-E_n)$ with the substituents is generally greater than the changes in $J_{n\pi^*}$ and $K_{n\pi^*}$. Thus, an inspection of the relative heights of the frontier orbitals as discussed in the preceding section suggests that the nπ^* excitation energies increase in this order: XCO$<$CN, $CH_3<$H$<$F. Such energy shifts show a reasonable agreement with the experimental data (Table 3).

The nπ^* excitation energies from Eqs. (7) and (8) are 1—2 eV greater than experimental values. Although there are some obvious ways to improve the

Table 3. The lowest singlet and triplet nπ^* excitation energies (eV)

Molecule	Singlet transition Calcd $\Delta E^V(^1n\pi^*)$	Singlet transition Obsd	Triplet transition[a] Calcd $\Delta E^V(^3n\pi^*)$	Triplet transition[a] $\Delta E^U(^3n\pi^*)$	Triplet transition[a] Obsd
H_2CO	4.98	3.54—5.43[b]	4.50	3.43	3.15—3.47[b]
F_2CO	8.01	—	7.60	6.06	—
$(CN)_2CO$	5.55	2.92—4.77[c]	5.16	2.74	—
$(CH_3)_2CO$	5.34	3.54—4.45[d]	4.92	2.77	3.39[b]
CH_3COH	5.47	3.54—5.28[d]	5.05	3.30	2.48—3.65[d]
CH_3COF	7.39	6.04[e]	7.00	4.98	—
CH_3COCN	5.32	4.01[f]	4.90	2.40	—
$(HCO)_2$	4.34	2.72[g]	3.99	3.08	2.42[g]
$(FCO)_2$	5.40	4.02[h]	5.05	4.17	3.71[h]
$(CNCO)_2$	4.60	—	4.30	2.86	—
$(CH_3CO)_2$	4.35	2.83[i]	4.05	3.02	2.45[i]

a) ΔE^V and ΔE^U obtained from Eqs. (7), (8), and (9), respectively. b) G. Herzberg, "Molecular Spectra and Molecular Structure III. Electronic Spectra and Electronic Structure of Polyatomic Molecules," Van Nostrand, New York, N.Y. (1966), Appendix. c) J. Prochorow, A. Tramer, and K. L. Wierzchowski, *J. Mol. Spectrosc.*, **19**, 45 (1966). d) Ref. 1. e) K. Yates, S. L. Klemenko, and I. G. Csizmadia, *Spectrochim. Acta*, **25A**, 765 (1969). f) B. E. Tate and P. D. Bartlett, *J. Amer. Chem. Soc.*, **78**, 5575 (1956). g) J. W. Sidman, *J. Chem. Phys.*, **27**, 429 (1957). h) W. J. Balfour and G. W. King, *J. Mol. Spectrosc.*, **25**, 132 (1968). i) H. Shimada and Y. Kanda, This Bulletin, **40**, 2742 (1967).

correlation, we did not attempt to do so. Instead, we dealt with the lowest $^3n\pi^*$ excited state by the UHF method, retaining the original INDO parametrization.

The triplet excitation energies, $\Delta E^U(^3n\pi^*)$, in the UHF method are defined as:

$$\Delta E^U(^3n\pi^*) = E^U_{total}(^3n\pi^*) - E_{total}(\text{ground}) \quad (9)$$

These values are generally in better agreement with the experimental values than $\Delta E^V(^3n\pi^*)$.

Radical Ions. The radical anions and cations derived from the parent molecules were treated by the UHF method. The electron affinities, E_A, and ionization potentials, I_D, were obtained from:

$$E_A = E_{total}(\text{ground}) - E^U_{total}(\text{anion}) \quad (10)$$

$$I_D = E^U_{total}(\text{cation}) - E_{total}(\text{ground}) \quad (11)$$

and are summarized in Table 4.

The calculated electron affinities are 0.5—1.0 eV greater than the $(-E_{\pi^*})$ obtained from Table 2, but still appear to be much smaller than the experimental ones. The E_A values increase in this order: H, F< CH_3<XCO<CN. The oxalyl compounds might have as large electron affinities as carbonyl cyanide.

The ionization potentials calculated from Eq. (11) are 1—3 eV smaller than the $(-E_n)$ from Table 2 and compare well with the experimental values. In both the X_2CO and CH_3COX compounds, they show this ordering: CH_3<XCO, H, CN<F. It should be noted that the effects of α-X substitution on E_A and I_D given here are almost identical with those already mentioned for the π^* and n orbital energies in the ground state.

Partitioning of the Energy. The two-atom terms for several X_2CO and $(XCO)_2$ compounds in the ground state (G), and lowest $^3n\pi^*$ state (T), as well as those for radical anions (A) and cations (C) derived

Table 4. Electron affinities and ionization potentials (eV)

Molecule	Electron affinity		Ionization potential	
	Calcd	Obsd	Calcd	Obsd
H_2CO	−3.7	—	12.2	10.9[c]
F_2CO	−3.6	—	14.7	—
$(CN)_2CO$	−0.8	1.2[a]	11.9	—
$(CH_3)_2CO$	−2.9	—	9.8	9.7[c]
CH_3COH	−3.5	—	10.9	10.2[c]
CH_3COF	−3.5	—	12.4	—
CH_3COCN	−1.7	—	10.5	—
$(HCO)_2$	−1.0	—	12.0	11.4[d]
$(FCO)_2$	−1.0	—	13.0	—
$(CNCO)_2$	0.7	—	12.3	—
$(CH_3CO)_2$	−1.2	1.1[b]	10.5	9.5[e]

a) T. Fueno and Y. Yonezawa, This Bulletin, **45**, 52 (1972). b) R. N. Compton, L. G. Christophrou, G. S. Hurst, and P. W. Reinhardt, *J. Chem. Phys.*, **45**, 4634 (1966). c) K. Watanabe, *ibid.*, **26**, 542 (1957). d) Monog. Ser. Res. Instit. Appl. Elect. Hokkaido Univ., No. 4, (1954—1957), Appendix. e) H. Neuert, *Z. Naturforsch.*, **7a**, 293 (1952).

Table 5. Two-atom terms in the total energies of some X_2CO and $(XCO)_2$ compounds (eV)

Molecule	State[b]	Bonded atoms			Non-bonded atoms	Sum[a]
		E_{C-O}	E_{C-X}	E_{C-C}	E_{X-X}	$\sum\sum_{A<B} E_{A-B}$
H_2CO	G	−46.06	−20.42	—	0.40	−85.55
	T	−35.95	−19.96	—	0.15	−75.86
	A	−38.23	−19.18	—	0.74	−73.43
	C	−43.01	−18.55	—	0.32	−79.44
F_2CO	G	−47.18	−29.93	—	0.83	−104.58
	T	−32.46	−28.66	—	0.60	−88.88
	A	−39.94	−26.29	—	1.38	−87.52
	C	−36.94	−30.72	—	0.32	−98.14
$(CN)_2CO$	G	−42.46	−31.17	—	−0.06	−222.26
	T	−33.78	−31.83	—	−0.51	−214.64
	A	−35.60	−32.33	—	0.15	−213.19
	C	−38.59	−30.57	—	−0.40	−217.23
$(HCO)_2$	G	−44.04	−20.07	−30.58	−0.08	−156.93
	T	−41.39	−19.60	−31.15	−0.04	−152.83
	A	−39.17	−19.40	−35.43	0.03	−148.23
	C	−46.15	−18.99	−25.80	0.03	−154.85
$(FCO)_2$	G	−44.98	−28.16	−27.76	0.21	−172.85
	T	−41.49	−27.88	−27.96	0.16	−166.96
	A	−40.58	−25.95	−33.10	0.46	−161.64
	C	−45.42	−29.30	−21.98	0.02	−171.79
$(CNCO)_2$	G	−42.25	−31.26	−29.27	−0.07	−293.41
	T	−45.54	−33.30	−29.30	−0.02	−289.95
	A	−37.54	−31.28	−33.14	0.00	−285.33
	C	−44.03	−30.70	−24.57	0.04	−291.57

a) The value $\sum\sum_{A<B} E_{A-B}$ in Eq. (1) is given. b) The symbols G, T, A, and C denote the ground state, the lowest triplet state, radical anion, and radical cation, respectively.

from the parent molecules, are summarized in Table 5. The E_{C-X} of X_2CO changes markedly with the α-X substitution. The E_{C-C} of $(XCO)_2$ compounds also varies with the substituents and is either greater or smaller in magnitude than E_{C-X}. This must be related at least in part to the ease of thermal decomposition of both C–X and C–C bonds for oxalyl compounds.[9] The non-bonded two-atom terms, E_{X-X}, increase in this order: CN–CN<H–H<F–F. This suggests a small steric repulsion between the CN groups.

Table 6. Partitionings of the two-atom terms E_{C-O} for X_2CO and E_{C-C} for $(XCO)_2$ compounds (eV)

Molecule	State[a]	E^1_{A-B}	E^2_{A-B}	E^3_{A-B}
		E_{C-O} Terms		
H_2CO	G	−49.91	−11.52	15.37
	T	−43.95	−8.27	16.27
	A	−45.45	−9.30	16.52
	C	−49.45	−10.86	17.30
F_2CO	G	−51.85	−10.98	15.65
	T	−43.67	−7.22	18.43
	A	−47.13	−9.16	16.35
	C	−48.44	−8.84	20.34
		E_{C-C} Terms		
$(HCO)_2$	G	−33.37	−4.85	7.64
	T	−32.90	−5.56	7.31
	A	−36.16	−6.38	7.11
	C	−29.97	−3.94	8.11
$(FCO)_2$	G	−31.70	−4.50	8.44
	T	−30.78	−5.01	7.83
	A	−34.33	−5.90	7.13
	C	−27.93	−3.53	9.48

a) The symbols G, T, A, and C denote the ground state, the lowest triplet state, radical anion, and radical cation, respectively.

The various types of two-atom terms, Eqs. (3)—(5), for the E_{C-O} values of several X_2CO compounds in the G, T, A, and C states are summarized in Table 6, together with those for the E_{C-C} of $(XCO)_2$ compounds. It has been established that formaldehyde is non-planar, with a somewhat lengthened carbonyl bond, in the lowest $^3n\pi^*$ state.[10] The E_{C-O} of X_2CO in the T state is considerably decreased in magnitude from the parent molecules. Most of the decrease originates from E^1_{C-O}, which corresponds to the off-diagonal core matrix elements, while the decreases in the electron-exchange term, E^2_{C-O}, and the electrostatic term, E^3_{C-O}, are both relatively immaterial. At any rate, the large decrease in $|E_{C-O}|$ upon excitation suggests a drastic reorganization of electrons in the carbonyl moiety. This, in turn, is probably related to the fact that these molecules have longer carbonyl bonds in the excited state. The increases in the E_{C-O} and E_{C-C} values of $(XCO)_2$ are not so great as that of the E_{C-O} of X_2CO.

As for the radical anion (A), E_{C-O} is decreased by 7—8 eV in magnitude from the parent molecules. As was true in the case of the T state, most of the decrease originates from E^1_{C-O}. Probably, these radical anions will also have a longer carbonyl bond than the parent molecules. In oxalyl compounds, the decrease in $|E_{C-O}|$ is rather small and is nearly counterbalanced by the increase in $|E_{C-C}|$.

The change in the sum of two-atom terms, $\sum\sum_{A<B} E_{A-B}$, from the parent molecule is rather small for radical cations. However, it is noticeable that the $|E_{C-C}|$ values of some oxalyl compounds are decreased by 5—6 eV upon ionization, primarily as a result of the decrease in $|E^1_{C-C}|$. Thus, it is likely that the C–C bond is cloven as easily as the C–X bond in such cases.

References

1) R. B. Cundall and A. S. Davies, *Progr. Reaction Kinetics*, **4**, 149 (1967).
2) N. J. Turro, "Technique of Organic Chemistry, XIV," A. Weissberger (ed.), Interscience Publishers, New York (1969), p. 133.
3) J. A. Pople and D. L. Beveridge, "Approximate Molecular Orbital Theory," McGraw-Hill Inc., New York (1970).
4) M. S. Gordon, *J. Amer. Chem. Soc.*, **91**, 3122 (1969).
5) A. D. Mitchell, ed., "Table of Interatomic Distances and Configuration in Molecules and Ions," The Chemical Society, London (1958).
6) J. L. Hencher and G. W. King, *J. Mol. Spectrosc.*, **16**, 168 (1965).
7) R. W. Begland, A. Cairncross, D. S. Donald, D. R. Hartter, W. A. Sheppard, and O. W. Webster, *J. Amer. Chem. Soc.*, **93**, 4953 (1971).
8) K. B. Wiberg, "Physical Organic Chemistry," John Wiley & Sons Inc., New York (1963), p. 278.
9) Z. G. Szabo, D. Kiraly, and I. Bardi, *Z. Phys. Chem. (N.F.)*, **27**, 127 (1961).
10) J. C. D. Brand, *J. Chem. Soc.*, **1956**, 858.

Investigation of the Concept of Free Volume by Means of a Correlation Function Method

Kiyoshi ARAKAWA and Kazumitsu KOJIMA

Research Institute of Applied Electricity, Hokkaido University, Sapporo 060

(Received March 6, 1974)

An investigation of the validity of the free volume theory of liquid has been undertaken on the basis of the theory of correlation functions. A formula for free volume without use of a geometrical model has been proposed and discussed. The magnitude of equivalent free volumes obtained from the formula has been found to be nearly equal to that calculated from the entropy of vaporization by means of the free volume theory. The results give support to the physical reality of the concept of free volumes. The communal entropy deduced agrees with that obtained by an expansion formula to the first order of density. A formula for compressibility has also been derived, which gives satisfactory results in comparison with observed data.

The Lennard-Jones and Devonshire (LJD) theory and the Yvon-Born-Green-Kirkwood (YBGK) theory were the starting points of extensive researches in the field of the theory of liquids.[1] The free volume theory originated from the LJD theory has been applied extensively to liquids[2] and solutions[3,4] as an approximate representation of their thermodynamic properties.

On the semi-emprical basis of the free volume theory, several critical studies have been carried out, among which those by Kirkwood[5] and by Hildebrand[6] are the most important. Concerning Kirkwood's critique (1950) with respect to the formulation of the theory, several improvements have been made.[7-9] The problem of communal entropy was also investigated by Hoover and Ree[10] and others by means of the Monte Carlo method.

Hildebrand proposed a serious question on the physical reality of the concept of free volume from results showing that free volumes calculated from identical thermodynamical data showed a marked discrepancy among the models adopted.[6] Thus it seems worth-while to attempt to place the concept of free volume on a sounder theoretical basis and to give a difinite explanation.

Since the proposition of Percus-Yevick and H N C equations in 1958—1960, development in the equilibrium theory of liquids using correlation functions is remarkable.[11-16] Some noticeable results from model experiments by Bernal and King[17] have been obtained, as well as those from computer experiments[18] by means of the Monte Carlo method and molecular dynamics.

At present, the application of these new theories to real liquids is limited except for that to liquid argon and liquid metals, model theories such as the free volume theory of liquids still playing an important role for the explanation of various properties of fluids.

We have examined the theoretical basis of the free volume theory according to recent liquid theories using correlation functions, with the purpose of elucidating the physical meaning of the concept of free volume.

Theoretical

Theoretical Consideration on the Nature of Free Volume. The Percus-Yevick integral equation is expressed as follows.[11-16]

$$h(r) = c(r) + \rho\int c(|\boldsymbol{r}-\boldsymbol{r}'|)h(|\boldsymbol{r}'|)\mathrm{d}\boldsymbol{r}' \tag{1}$$

$$c(r) = g(r)\exp(u(r)/kT)[\exp(-u(r)/kT)-1], \tag{2}$$

where $c(r)$ is the direct correlation function, $h(r)=g(r)-1$ the total correlation function, $g(r)$ the radial distribution function, and $u(r)$ the two body potential.

The equation has been solved analytically by Wertheim[19] and Thiele[20] for the fluid of hard spheres. The equation of state obtained has been found to be identical with that deduced from the scaled particle theory by Reiss *et al.*,[21] which is expressed as

$$p = \rho kT(1+y+y^2)/(1-y)^3, \quad y = \pi\rho a^3/6, \tag{3}$$

where ρ is the number density, a the diameter of a hard sphere and y the volume fraction of hard sphere molecules.

The partition function Z for a hard sphere fluid is derived from Eq. (3) to be

$$Z = \left[\frac{V}{N}(1-y)\exp\left(1-\frac{3y(2-y)}{2(1-y)^2}\right)\right]^N\left(\frac{2\pi mkT}{h^2}\right)^{3/2N}. \tag{4}$$

For a hard sphere fluid with an internal potential V_N, it is expressed as

$$Z = \left[\frac{V}{N}(1-y)\exp\left(1-\frac{3y(2-y)}{2(1-y)^2}\right)\right]^N\left(\frac{2\pi mkT}{h^2}\right)^{3/2N} \times \exp(-\langle V_N\rangle_{\mathrm{av.}}/kT). \tag{5}$$

A formula similar to this expression was first introduced by Longuet-Higgins and Widom[22] and also given by Miller.[23] We have given an explanation of its theoretical basis in connection with the mean spherical model (MSM) approximation proposed by Lebowitz *et al.*[24] (see Appendix).

The free volume fraction f is defined as follows.

$$f \equiv (1-y)\exp\left(-\frac{3y(2-y)}{2(1-y)^2}\right). \tag{6}$$

From Eq. (5), we then have

$$Z = \left[\left(\frac{2\pi mkT}{h^2}\right)^{3/2} efv\right]^N \exp(-\langle V_N\rangle_{\mathrm{av.}}), \tag{7}$$

where $v=V/N$ is the volume per molecule in liquid.

According to the free volume theory of liquid,[5] the partition function is expressed as a function of free volume, independent of the above theory as follows.

$$Z = \left[\left(\frac{2\pi mkT}{h^2}\right)^{3/2} ev_f\right]^N \exp(-\langle V_N\rangle_{\mathrm{av.}}/kT) \tag{8}$$

where $v_f = V_f/N$ is the free volume (fluctuational volume[25]) per molecule.

Equating Eqs. (7) and (8), we have

$$f = v_f/v \quad \text{or} \quad f = V_f/V \tag{9}$$

from which the nomenclature of f comes.

From Eqs. (6) and (7) we can calculate the values of V_f. Values of the free volume fraction f as a function of y, together with the values of V_f calculated for two liquids CCl_4, $c\text{-}C_6F_{11}CF_3$ are given in Table 1.

Table 1. Free volume fraction and free volume

y		0.50	0.51	0.52	0.54	0.60	0.64
$f\times 10^3$		5.55	4.25	3.20	1.72	0.152	0.0152
V(cm³/mol)	CCl_4	0.54	0.41	0.31	0.17	0.015	0.0015
	$c\text{-}C_6F_{11}CF_3$	1.09	0.83	0.63	0.34	0.030	0.0030

Determination of the Equilibrium Values of Volume Fraction y and Free Volume V_f in Liquids. In the case of the face-centered cubic packing of hard sphere molecules, where all molecules are in contact with each other, the magnitude of y is $\sqrt{2}\pi/6 = 0.74$, which is the maximum value of y.

Bernal and King proposed the "random network model" for the structure of liquid state on the basis of a series of model experiments,[17] giving the magnitude of y to be 0.64 for the liquid state at its triple point.

For determination of the equilibrium values of y, the equation of state derived from Eq. (5) is used.

$$pV = NkT\left(\frac{1+y+y^2}{(1-y)^3}\right) - V\frac{\partial\langle V_N\rangle_{av.}}{\partial V} \tag{10}$$

When $\langle V_N\rangle_{av.}$ is taken to be propotional to the n-th power of volume V as usual, we have

$$pV = NkT\left(\frac{1+y+y^2}{(1-y)^3}\right) + n\langle V_N\rangle_{av.}. \tag{11}$$

For the determination of y the equation of state at vanishing pressure,[4,26] which is obtained by equating the right-hand side of Eq. (11) to zero, is used, together with the relation $-\langle V_N\rangle_{av.} = \Delta H_{vap.} - RT$ ($\Delta H_{vap.}$; the heat of vaporization). Thus, we get

$$RT\left(\frac{1+y+y^2}{(1-y)^3}\right) = n(\Delta H_{vap.} - RT). \tag{12}$$

The equilibrium values of y thus determined using the experimental data[27] of n and $\Delta H_{vap.}$ for CCl_4 and $c\text{-}C_6F_{11}CF_3$ are 0.50 and 0.54 at 25 °C, respectively. In the case of CCl_4 the magnitude of y determined by the consideration of compressibility is 0.51, in line with that determined by Eq. (12).

The values of V_f for CCl_4 and $c\text{-}C_6F_{11}CF_3$ at 25 °C are thus determined to be 0.41 and 0.34 cm³/mol, respectively, from the values of y given in Table 1. The values are nearly equal to those for "$\Delta S_{vap.}$" given by Hildebrand (Table 2). This shows that the values of V_f obtained directly from $\Delta S_{vap.}$ by means of the free volume theory are consistent with those of the "equivalent free volume" determined here as a statistical average by use of correlation functions (Eqs. (6), (9), and (12)).

For deriving Eqs. (1)—(9) (except Eq. (8)), no approximation based on a geometrical model was introduced. The free volume fraction defined by Eq. (6) consists of a factor $1-y$ and an exponential factor $\exp(-3y(2-y)/2(1-y)^2)$. The former factor is equal to the fraction of void space for the total volume V, and the latter is supposed to come from the volume exclusion effect of hard sphere molecules in their thermal motions. The free volume V_f is thus regarded as a statistical average of fluctuational void space. This brings the free volume fraction f as a function of y only. Agreement of the values of V_f for $\Delta S_{vap.}$ with those determined through f (Eq. (6)) gives a comfirmative support of the concept of free volume calculated from $\Delta S_{vap.}$ as a thermodynamic parameter.

Table 2. Free volumes at 25 °C (cm³/mol)[a]

	V	V_f				
		van der Waals[b]	$\Delta S_{vap.}$[c]	Cage[d]	Cubic[e]	This work
CCl_4	96	7.7	0.24	0.042	0.34	0.41
$c\text{-}C_6F_{11}CF_3$	196	10.9	0.36	0.034	0.27	0.34

a) The values of V_f for models b)—e) are cited from Table 1 in the note by Hildebrand.[6] They were calculated from identical data[27] on the basis of the relation $\partial S/\partial V = R(\partial \ln V_f/\partial V)$. The difference between the values is ascribed to the geometrical feature of each model.[6] b) Calculated from the definition $V_f = V - b$. c) Calculated from $\Delta S_{vap.}$ using the relation $\Delta S_{vap.} = R\ \ln(V_g/V_f)$, where V_g is the volume of gaseous state in equilibrium. d) The fluctuational volume for a cage model; $(V_f)_{cage} = [R/V^{2/3}(\partial S/\partial V)]^3$. e) The fluctuational volume for simple cubic packing.

Communal Entropy. The communal entropy ΔS is obtained as

$$\Delta S = k \ln (ef)^N. \tag{13}$$

Inserting Eq. (6) into Eq. (13), we get

$$\Delta S = Nk\left[1 + \ln(1-y) - \frac{3y(2-y)}{2(1-y)^2}\right]. \tag{14}$$

The volume fraction y is expressed by (ρ/ρ_0), where ρ_0 is the closest number density at face-centerd cubic packing.

$$\rho_0 = \sqrt{2}/a^3$$

and

$$y = \frac{\pi}{6}\rho a^3 = \frac{\sqrt{2}\pi}{6}\left(\frac{\rho}{\rho_0}\right) = 0.740475\left(\frac{\rho}{\rho_0}\right).$$

Thus the communal entropy ΔS is expressed by the power of (ρ/ρ_0) as follows.

$$\Delta S/Nk = 1 - 2.9619(\rho/\rho_0) - 2.741515(\rho/\rho_0)^2 \tag{15}$$

The expansion of $\Delta S/Nk$ by (ρ/ρ_0) agrees to the first order term with the formula obtained by Hoover and Ree[28] by means of the Mayer f function expansion. The linear dependence of the communal entropy at small density has been confirmed by means of a Monte Carlo calculation.[10]

Compressibility. From Eqs. (6) and (10), we can derive the following formula for the isothermal compressibility κ_T of liquid, using the relation

$$\langle V_N\rangle_{av.} = \Delta H_{vap.} - RT = \frac{\text{Const.}}{V^n} \tag{16}$$

$$\kappa_T = \left[\frac{1}{\kappa_0} - \frac{n(n+1)}{V}(\Delta H_{vap.} - RT)\right]^{-1}, \quad (17)$$

where κ_0 is the isothermal compressibility for the fluid of hard spheres and expressed by

$$\kappa_0 = \left(\frac{V}{NkT}\right)\left[\frac{(1-y)^2}{(1+2y)}\right]^2. \quad (18)$$

The first term in $(\kappa_T)^{-1}$ in Eq. (17) comes from the repulsion of hard spheres in thermal motions and the second term from the attraction between molecules.

Using Eqs. (17) and (18), we have calculated the values of compressibility of various liquids and the results are given in Table 3. As the values of a we have used those estimated from the results of studies of X-ray diffraction,[29,30] second virial coefficient,[2] viscosity[2] and molecular structure theory,[31] noting that the estimated values of a should be consistent with the values of y determined through Eq. (12). The agreement between calculated and observed values is very good. Equations (17) and (18) could therefore be used for determination of the equivalent hard sphere diameter of molecules.

Table 3. Compressibility

	a (Å)	n	T (K)	y	$\kappa_{obs.}$ (10^{-12} dyn^{-1} cm^2)	$\kappa_{calc.}$ (10^{-12} dyn^{-1} cm^2)
Ar	3.40	1.00	87.3	0.43	215.2	226.8
CCl_4	5.40	1.09	298	0.51	106.7	90.9
C_6H_6	5.20	1.05	293	0.50	101.5	101.1
C_6H_{12}	5.60	1.00	298	0.51	116.0	95.1

Appendix

A similar equation to Eq. (5) has been used by Longuet-Higgins and Widom[22] and also by Miller[23] for a discussion of thermodynamic properties of fluids. We have undertaken here to give a theoretical basis for the approximation.

Using the exact solution of Percus-Yevick equation for the fluid of hard spheres together with the mean spherical model (MSM) approximation,[24] we postulate as follows as regards the direct correlation function $c(r)$,

$$\begin{aligned} c(r) &= c_0(r) \quad \text{for } r \leq a \\ c(r) &= -u(r)/kT \quad \text{for } r > a, \end{aligned} \quad (A1)$$

where $c_0(r)$ is Wertheim-Thiele's analytical solution.

The MSM approximation assumes (1) the Ornstein-Zernike equation, (2) $g(r)=0$ for $r<a$ and (3) $c(r)=-u(r)/kT$ for $r>a$. When $u(r)\to 0$, the MSM approximation is reduced to the Percus-Yevick equation for the fluid of hard spheres with no attraction. Thus the direct introduction of Wertheim-Thiele's solution to MSM as in Eq. (A1) is reasonable as a zeroth order approximation, if $u(r)$ is not much larger than kT. In the approximation Eq. (A1), the change of $c(r)$ from $c_0(r)$ for $r \leq a$ which results from the presence of $u(r)$ for $r>a$ is ignored.

The compressibility equation is expressed as

$$\partial(p/kT)/\partial\rho = 1 - \rho\int c(r)\mathrm{d}r. \quad (A2)$$

Inserting Eq. (A1) into Eq. (A2), we obtain

$$\begin{aligned} \partial(p/kT)/\partial\rho &= 1 - \rho\int_0^a c_0(r)4\pi r^2\mathrm{d}r + \frac{\rho}{kT}\int_a^\infty u(r)4\pi r^2\mathrm{d}r \\ &= \frac{(1+2y)^2}{(1-y)^4} + \frac{\rho}{kT}\int_a^\infty u(r)4\pi r^2\mathrm{d}r. \end{aligned} \quad (A3)$$

Integrating with respect to ρ, we have

$$p/\rho kT = \frac{1+y+y^2}{(1-y)^3} + \frac{2\pi\rho}{kT}\int_a^\infty u(r)4\pi r^2\mathrm{d}r. \quad (A3)$$

If we put $(2\pi/kT)\int_a^\infty u(r)4\pi r^2\mathrm{d}r \equiv$ const.

Eq. (A4) becomes identical with that used by Longuet-Higgins & Widom, and also by Miller.

References

1) A. Harashima, "Theory of Liquids," Iwanami, Tokyo (1954); T. L. Hill, "Statistical Mechanics," McGraw-Hill, New York (1956).
2) J. O. Hirshfelder, C. F. Curtiss, and R. B. Bird, "Molecular Theory of Gases and Liquids," Wiley, New York (1954).
3) I. Prigogine, A. Bellemans, and V. Mathot, "The Molecular Theory of Solutions," North Holland Pub., Amsterdam (1957).
4) K. Arakawa and O. Kiyohara, This Bulletin, **43**, 975 (1970).
5) J. G. Kirkwood, *J. Chem. Phys.*, **18**, 380 (1950).
6) J. H. Hildebrand, *ibid.*, **31**, 1423 (1959).
7) J. E. Mayer and G. Careri, *ibid.*, **20**, 1001 (1952).
8) J. S. Dahler and J. G. Hirshfelder, *ibid.*, **32**, 330 (1960); H. S. Chung and J. S. Dahler, *ibid.*, **40**, 2868 (1964).
9) J. Fisher, F. Kohler, and F. Weissenböck, *ibid.*, **53**, 2004 (1970).
10) W. G. Hoover and F. H. Ree, *ibid.*, **49**, 3609 (1968).
11) H. L. Frisch and J. L. Lebowitz, "The Equilibrium Theory of Classical Fluids," Benjamin, New York (1964).
12) S. A. Rice and P. Gray, "The Statistical Mechanics of Simple Liquids," Interscience, New York (1965).
13) H. L. Frisch and Z. W. Salsburg, "Simple Dense Fluids," Academic Press, New York (1968).
14) H. N. V. Temperley, J. S. Rowlinson, and G. S. Rushbrooke, ed., "Physics of Simple Liquids," North-Holland, Amsterdam (1968).
15) J. S. Rowlinson, "Liquids and Liquid Mixtures," 2nd ed. Butterworth, London (1969).
16) K. Kojima and K. Arakawa, *Bull. Res. Inst. Appl. Elec.* (Hokkaido Univ.), **25**, 1 (1973).
17) J. D. Bernal and S. V. King, Ref. 14), chapt. 6.
18) W. W. Wood, Ref. 14), chapt. 5; L. Verlet, *Phys. Rev.*, **159**, 98 (1967), **165**, 201 (1968).
19) M. S. Wertheim, *Phys. Rev. Lett.*, **10**, 321 (1963); *J. Math. Phys.*, **5**, 643 (1964).
20) E. Thiele, *J. Chem. Phys.*, **39**, 474 (1963).
21) H. Reiss, H. L. Frish, and J. L. Lebowitz, *ibid.*, **31**, 369 (1956); H. Reiss, *Advan. Chem. Phys.*, **9**, 1 (1964).
22) H. C. Longuet-Higgins and B. Widom, *Mol. Phys.*, **8**, 549 (1964).
23) R. C. Miller, *J. Chem. Phys.*, **55**, 1613 (1971).
24) J. L. Lebowitz and J. K. Percus, *Phys. Rev.*, **144**, 251 (1966); M. S. Wertheim, *J. Chem. Phys.*, **55**, 4291 (1971); E. Waisman and J. L. Lebowitz, *ibid.*, **56**, 3086 (1972).
25) A. Bondi, *J. Phys. Chem.*, **58**, 929 (1954).
26) I. Prigogine and A. Bellemans, *Discuss. Faraday Soc.*, **15**, 80 (1953).
27) E. B. Smith and J. H. Hildebrand, *J. Chem. Phys.*, **31**, 145 (1959).
28) W. G. Hoover and F. H. Ree, *ibid.*, **47**, 4873 (1967).
29) P. G. Mikolaj and C. J. Pings, *ibid.*, **46**, 1401 (1967).
30) A. H. Narten, M. D. Danford, and H. A. Levy, *ibid.*, **46**, 4895 (1967).
31) L. Pauling, "The Nature of the Chemical Bond," 3rd Ed., Cornell University Press, Ithaca, New York (1960).

Circular Dichroism in Lyotropic Liquid Crystals of Polyglutamate Solutions

Nobuaki TSUCHIHASHI*, Hiroyuki NOMORI, Masahiro HATANO, and Shigeo MORI**

Chemical Research Institute of Non-Aqueous Solutions, Tohoku University, Katahira, Sendai 980

**Faculty of Engineering, Tohoku University, Aramaki, Sendai 980*

***Central Research Laboratories, Ajinomoto Co., Inc., Suzuki-cho, Kawasaki, Kanagawa 210*

(Received March 14, 1974)

A poly-γ-ethyl-L-glutamate solution with a cholesteric color exhibits a circular dichroism due to the selective reflection of circularly polarized light of one sense by the cholesteric helical structure existing in the solution. On the other hand, an induced circular dichroism is observed in the wavelength region corresponding to the absorption bands of an achiral dye molecule when the molecule is dissolved in the poly-γ-benzyl-D-glutamate liquid crystalline phase. The two modes of circular dichroism are correlated to the structure and the chirality of the cholesteric phase of concentrated polyglutamate solutions.

Polyglutamate having α-helical conformation forms a lyotropic liquid crystalline phase when dissolved in various organic solvents in concentrations exceeding a critical value.[1,2] Robinson *et al.*[2] have extensively studied the structure of the liquid crystalline phase, and suggested two types of supramolecular structure, cholesteric and nematic, for the lyotropic liquid crystalline phase of a polyglutamate solution.

The cholesteric structure, which is the most common for the liquid crystalline phase of the polyglutamate solution, has been described as follows. In any given domain of the solution, rigid rod-like polyglutamate molecules are packed in a set of equispaced parallel planes in which the polyglutamate molecules lie parallel to one another. The molecules in one plane have a slight twist relative to those in adjacent planes about an axis of torsion perpendicular to the set of planes. Incorporation of successive layers of appropriately oriented polyglutamate molecules results in a helical structure, causing an extraordinarily high optical rotatory power to the solution. The sign of the optical rotation changes with variation of the solvent specics, reflecting the inversion of the helical sense by the variation of the solvent species.[2a,2e] Robinson *et al.* presumed this optical rotation to be due to the selective reflection of circularly polarized light of one sense by the helical structure. They demonstrated by their experiment using a quarter-plate that the light reflected by the concentrated poly-γ-ethyl-L-glutamate solution in ethyl acetate is right circularly polarized.[2e]

The nematic structure has been elucidated as the untwisted array of equispaced parallel planes in which polyglutamate molecules are packed parallel to one another; the nematic structure is regarded as the cholesteric structure where the pitch of the helix is expanded to infinity, no optical rotatory power being caused. The nematic structure can be realized by dissolving polyglutamate in a particular solvent mixture[2d] or by untwisting the cholesteric structure by the application of magnetic field.[3]

Saeva and Wysocki[4,5] reported that the achiral dye molecule becomes optically active when the dye molecule is dissolved in a thermotropic cholesteric phase, and in this case, a strong circular dichroism (CD) is induced in the wavelength region of the absorption (AB) bands of the dye molecule. Saeva[6] also indicated that the induced circular dichroism of the achiral molecule in the thermotropic liquid crystalline phase can be used as a probe to determine the existence and the chirality of the cholesteric liquid crystalline phase.

We detected the circular dichroism corresponding to the optical rotation due to the selective reflection of circularly polarized light of one sense by the cholesteric helical structure in the liquid crystalline phase of the polyglutamate solution. We found the induced circular dichroism due to the achiral molecule dissolved in the lyotropic liquid crystalline phase of the polyglutamate solution. The two modes of circular dichroism are discussed in relation to the structure and the chirality of the cholesteric liquid crystalline phase of the concentrated polyglutamate solution.

Experimental

Materials. A lyotropic liquid crystal with a cholesteric color was obtained by the polymerization of 27 g of *N*-carboxyanhydride of γ-ethyl-L-glutamate in 50 ml of vinyl acetate using a mixture of triethylamine and β-dimethylaminoethanol (95 : 5 in molar ratio) as an initiator. The resulting solution was directly used for CD measurement.

Poly-γ-benzyl-D-glutamate (PBDG) was obtained by the polymerization of *N*-carboxyanhydride of γ-benzyl-D-glutamate, the degree of polymerization of the resultant polymer being 910. The liquid crystalline phase of the PBDG solution was formed when PBDG was dissolved in dichloromethane, chloroform or 1,1,2,2-tetrachloroethane at a concentration of 0.75 M of the glutamyl residue. Achiral dyes were added to this concentrated PBDG solution. Acridine orange (AO) was purified by the method described elsewhere.[7] The solvents used were spectral grade ones and used without further purification.

Methods. The CD measurement of the poly-γ-ethyl-L-glutamate (PELG) solution was carried out with a JASCO MOE-7 magnetorotatory dispersion spectropolarimeter with a CD attachment. The CD and the AB spectra of the systems of the dyes dissolved in the PBDG solution were recorded on a JASCO J-20A or J-15 spectropolarimeter. In all cases, the sample solutions were slowly introduced into a quartz cell having a 0.5 mm path length.

Results and Discussion

Circular Dichroism Due to the Selective Reflection by the Cholesteric Structure. Robinson *et al.* found a cholesteric color in the PELG solution in ethyl acetate, where the cholesteric pitch is comparable with the

wavelength of the visible light. They demonstrated that the origin of this cholesteric color is the selective reflection of circularly polarized light of one sense by the cholesteric pitch.[2d,2e]

We found a brilliant iridescent color also for the PELG solution in vinyl acetate. This gives evidence to the existence of a cholesteric structure in this solution. The solution was thus expected to exhibit a circular dichroism due to the selective reflection by the cholesteric structure. A positive CD band was observed for the PELG solution in the visible region with a peak around 800 nm (Fig. 1). This is attributable to the selective reflection of circularly polarized light of one sense by the cholesteric pitch since no AB band exists in this wavelength region for any component of the PELG solution.

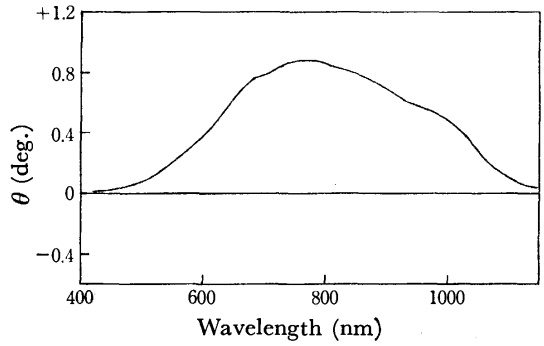

Fig. 1. CD spectrum due to the selective reflection of the lyotropic cholesteric phase of the PELG solution in vinyl acetate.

The circular dichroism due to the selective reflection by the cholesteric structure for the lyotropic liquid crystalline phase enables us to determine the cholesteric helical sense on the basis of the observed CD sign in comparison with the results of Saeva and Wysocki[4-6] concerning the thermotropic liquid crystalline phase, where the sign of the circular dichroism due to the selective reflection by the cholesteric structure is positive for the right-handed cholesteric helical sense and negative for the left-handed one. The PELG solution in vinyl acetate is concluded to be the cholesteric phase of right-handed helical sense, since the solution displays a positive CD band due to the selective reflection by the cholesteric structure.

The magnitude of a CD band is defined as the absorbance for the left circularly polarized light minus that for the right circularly polarized light. The sample in the Robinson experiment would thus exhibit a negative CD band, since the light reflected by their sample was right circularly polarized, indicating that the apparent absorbance for the right circularly polarized light is larger in their sample. The CD sign, the cholesteric helical sense of the PELG solution in vinyl acetate, is opposite to that of the Robinson sample, while polyglutamate in both studies is the same in configuration. It has been confirmed by observation of the circular dichroism due to the selective reflection of circularly polarized light of one sense by the cholesteric helical structure that the helical sense of the lyotropic cholesteric structure in the PELG solution depends on the solvent in which polyglutamate is dissolved. An analogous situation has already been shown by the optical rotatory measurements for the PBLG cholesteric phase.[2a,2e]

We have the well-known relationship between the cholesteric pitch P and the wavelength of the maximum reflectivity λ_m:

$$\lambda_m = n \times P$$

where n is the average refractive index of the cholesteric phase. The value of λ_m can be determined from the wavelength of the CD peak due to the selective reflection by the cholesteric structure. Thus, the cholesteric structure in the PELG solution in vinyl acetate is found to have a cholesteric pitch *ca.* 570 nm, the value of n being 1.4.

Induced Circular Dichroism of Dye Molecules in PBDG Liquid Crystalline Phase. We found that achiral dye molecules become optically active when they are dissolved in the PBDG liquid crystalline phase and that definite CD bands appear in the wavelength region where the AB bands of the dyes exist. Acridine orange gave a large positive circular dichroism around 500 nm when dissolved in the concentrated solution of PBDG in 1,1,2,2-tetrachloroethane. Positive CD peaks were also observed for *N*-ethylcarbazole in the solution of PBDG in tetrachloroethane in near ultraviolet region. Typical CD spectra of the systems of AO and *N*-ethylcarbazole dissolved in the concentrated PBDG solution are given in Figs. 2 and 3, respectively, together with their AB spectra. Due to the existence of many strong AB bands in the systems, CD measurement in a wavelength region shorter than 280 nm could not be carried out successfully.

It was confirmed by CD measurements for the concentrated PBDG solution without dye molecules that no CD band due to the selective reflection exists in the wavelength region in which the CD bands due to the

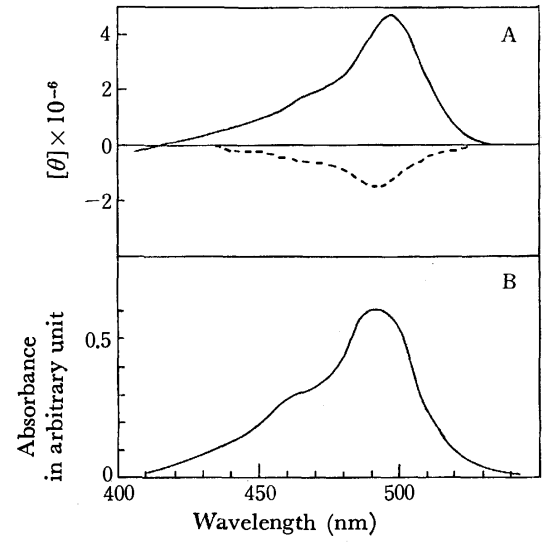

Fig. 2. (A) CD spectra of AO induced in the cholesteric phases of the PBDG solutions in tetrachloroethane (——), and in dichloromethane (------) and (B) absorption spectrum of AO in the PBDG solution in tetrachloroethane. [θ] was calculated on the basis of the concentration of AO.

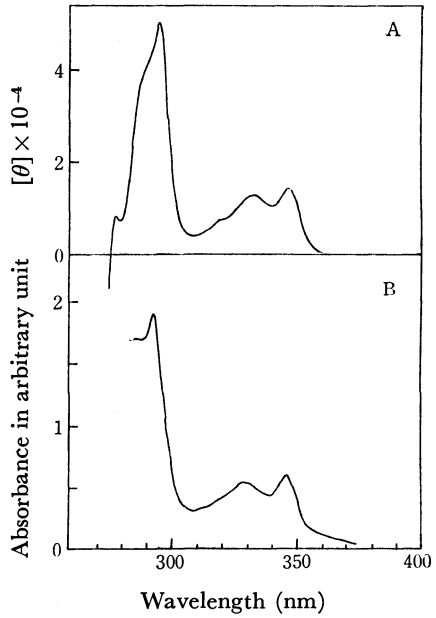

Fig. 3. (A) CD spectrum of *N*-ethylcarbazole induced in the cholesteric phase of the PBDG solution in tetrachloroethane and (B) absorption spectrum of *N*-ethylcarbazole in the PBDG solution in tetrachloroethane. $[\theta]$ was calculated on the basis of the concentration of *N*-ethylcarbazole.

dye molecules appear. No CD band could be detected in the dilute solution of PBDG containing AO. The circular dichroism observed for the system of AO dissolved in the cholesteric liquid crystalline phase of the PBDG solution in dichloromethane or tetrachloroethane disappeared when the cholesteric structure in this system was untwisted to the nematic structure by the application of magnetic field.

The possibility that the dissymmetric field of the α-helix constituting the cholesteric phase causes the circular dichroism can be eliminated. We see that the circular dichroism observed for the achiral dyes dissolved in the concentrated solution of PBDG are induced by the dissymmetric field effect of the cholesteric helical structure formed in these systems on the electronic transitions of the dyes. This is similar to cases of dyes buried in thermotropic liquid crystalline phases.[4-6,8]

Thus, the achiral dyes in the cholesteric liquid crystalline phase of the PBDG solution are intercalated in the helical structure in this phase and are oriented relative to this helical structure. As a result, they appear in the dissymmetric field due to the cholesteric helical structure.

The CD bands observed for *N*-ethylcarbazole in the PBDG solution in tetrachloroethane is simply positive in sign in the wavelength region 280—370 nm (Fig. 3). This is not the case in Saeva's results[5] where the CD curve for *N*-ethylcarbazole in the thermotropic liquid crystalline phase consists of two regions with opposite signs. As Sackmann and Voss[8] indicated, the CD sign depends on the polarization character of the corresponding electronic transition of the dye molecule only when the helical arrangement of the dye molecule along the cholesteric helical axis is realized. Our results show that such a helical arrangement is absent for the dye molecule in the lyotropic liquid crystalline phase.

A similar induced circular dichroism was reported recently by Saeva and Olin,[9] their results agreeing with ours.

Relations between the CD Profile and the PBDG Cholesteric Structure. The CD spectra of AO were observed not only in the solution of PBDG in tetrachloroethane but also in the solutions of PBDG in dichloromethane and in chloroform. The CD sign observed for AO around 500 nm changed with solvent, being negative in the dichloromethane solution and positive in the tetrachloroethane solution. The CD sign in the region for the chloroform solution turns positive from negative with time. For all the cases investigated, the CD magnitude around 500 nm increased when the solution was left to stand after being introduced into the observation cell. It took several hours or even days for the equilibration of the CD magnitude. Figure 4 shows the change of the CD magnitude with time for AO in the solution of PBDG in tetrachloroethane. Such a time dependent character of the circular dichroism was also observed for the system containing *N*-ethylcarbazole.

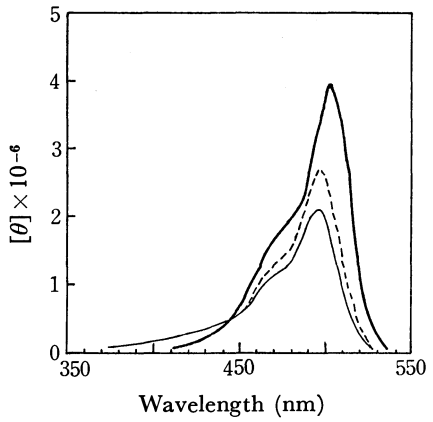

Fig. 4. Change in the CD magnitude observed for AO in the cholesteric phase of the PBDG solution in tetrachloroethane; (——) recorded immediately after the introduction of the sample into the observation cell, (------) 1 hour after and (——) 2 days after. $[\theta]$ was calculated on the basis of the concentration of AO.

In the course of maturation of the PBDG cholesteric phase in the observation cell, the microscopic observation showed that the cholesteric phase which had been disturbed through the introduction into the cell attained to its equilibrated state, exhibiting the retardation lines characteristic of the cholesteric phase on a time scale comparable with that of the change in CD magnitude. It is assumed that the recovery of the PBDG cholesteric structure to its equilibrium state increases the CD magnitude of the bands. Such a long relaxation is observed also in the NMR studies[3] on the magnetic field induced reorientation of the PBLG liquid crystalline phase and regarded as characteristic of polyglutamate liquid crystalline solutions.

We postulate that the circular dichroism is brought

about by the dissymmetric field of the cholesteric helix. The sign of the dissymmetric perturbation from the helical structure is known to change by the inversion of the helical sense. Thus, the fact that the sign of the circular dichroism induced for the dye molecule in the solution of PBDG in dichloromethane is opposite to that in tetrachloroethane leads to the conclusion that the helical sense of the cholesteric structure is inversed by the change of the solvent from dichloromethane to tetrachloroethane. The cholesteric helical sense is determined not only by the steric isomerism of polyglutamate in the solution but also by the mode of the interaction of polyglutamate with the solvent. Inversion of the CD sign with time for AO in the solution of PBDG in chloroform suggests that the interaction between PBDG and chloroform reduces the energy difference between the cholesteric helical senses in this system.

We could detect no circular dichroism due to the selective reflection for the PBDG cholesteric phase as a result of very large cholesteric pitch in this phase. Robinson *et al.* reported that the sign of the optical rotation is positive for the cholesteric liquid crystalline phase of the solution of PBLG in dichloromethane.[2a,2e] This might show that there exists a negative Cotton effect at the longer wavelength region corresponding to the cholesteric pitch band. If so, the sense of the cholesteric helix for the solution of PBLG in dichloromethane is left-handed. We can therefore expect the right-handed helical sense to exist in the PBDG cholesteric phase in dichloromethane. On combining this and the above-mentioned result concerning the induced circular dichroism, the negative sign of the circular dichroism induced for the dye in the PBDG cholesteric phase in dichloromethane is taken as diagnostic of the right-handed cholesteric helical sense in this system.

Thus, the inversion of the cholesteric helical sense is demonstrated again by the observation of the sign of the induced circular dichroism for the achiral dyes dissolved in the cholesteric liquid crystalline phase of polyglutamate.

The authors are grateful to Professor Kunio Seto for his encouragement throughout this investigation and to Professors Hiroshi Kojima and Kimiyoshi Goto for the measurements of circular dichroism with a JASCO MOE-7 magnetorotatory dispersion spectropolarimeter. They are also indebted to Mr. Yukio Sato for the purification of AO and for valuable discussions.

References

1) A. Elliott and E. J. Ambrose, *Discuss. Faraday Soc.*, **9**, 246 (1950).
2) a) C. Robinson, *Trans. Faraday Soc.*, **52**, 571 (1956); b) C. Robinson and J. C. Ward, *Nature*, **180**, 1183 (1957); c) C. Robinson, J. C. Ward, and R. B. Beevers, *Discuss. Faraday Soc.*, **25**, 29 (1958); d) C. Robinson, *Tetrahedron*, **13**, 219 (1961); e) *idem*, *Mol. Cryst.*, **1**, 467 (1966).
3) a) S. Sobajima, *J. Phys. Soc. Japan*, **23**, 1070 (1967); b) M. Panar and W. D. Phillips, *J. Amer. Chem. Soc.*, **90**, 3880 (1968); c) E. T. Samulski and A. V. Tobolsky, *Mol. Cryst. Liq. Cryst.*, **7**, 433 (1969).
4) F. D. Saeva and J. J. Wysocki, *J. Amer. Chem. Soc.*, **93**, 5928 (1971).
5) F. D. Saeva, *ibid.*, **94**, 5135 (1972).
6) F. D. Saeva, *Mol. Cryst. Liq. Cryst.*, **18**, 375 (1972).
7) M. Hatano, M. Yoneyama, and Y. Sato, *Biopolymers*, **12**, 895 (1973).
8) E. Sackmann and J. Voss, *Chem. Phys. Lett.*, **14**, 528 (1972).
9) F. D. Saeva and G. R. Olin, *J. Amer. Chem. Soc.*, **95**, 7882 (1973).

An MO Theoretical Investigations of the Electronic Spectra of Divalent Sulfur Compounds

Hideki SAKAI, Tokio YAMABE, Hiroshi KATO*, Shinichi NAGATA, and Kenichi FUKUI

Department of Hydrocarbon Chemistry, Faculty of Engineering, Kyoto University, Kyoto 606

**College of General Education, Nagoya University, Nagoya 464*

(Received March 20, 1974)

The singlet transition energies and oscillator strengths of several divalent sulfur compounds are calculated by the semi-empirical ASMO–SCF method. It is shown that the UV absorption bands with transition energies of 5—6 eV observed in these sulfur compounds can be assigned to n-σ_1*, n-σ_2*, or σ-σ_1*, implying that the 3d orbitals of the sulfur atom do not play an important role in these electronic transitions or may contribute absorption bands with higher transition energies.

It is well known that a number of divalent sulfur compounds have characteristic electronic absorption bands in the near-ultraviolet region; they have often been identified as n-σ*, σ-σ*, n-3d, n-4s, *etc.* In 1965, Clark *et al.*[1] obtained satisfactory vacuum-ultraviolet spectra of several divalent sulfur compounds, *i.e.*, hydrogen sulfide, alkyl sulfides, cyclic alkyl sulfides, and thiols, and tried to give their assignments on the basis of a simple schematic molecular orbital (MO) diagram according to the Walsh rule. Subsequently, several calculations of their assignments have been carried out by semi-empirical MO methods.[2–4] The results obtained, however, show disagreement with each other in their assignments, as will be shown in this text.

In the present paper, we intend to describe some investigations concerning the singlet transition energies and the assignments of some saturated divalent sulfur compounds based on the MO calculations of the semi-empirical ASMO–SCF method.

Method

The calculations are carried out by the semi-empirical ASMO–SCF method,[5] where the approximation of the zero differential overlap is adopted for valence electron system; the contributions of the 3d atomic orbitals of the sulfur atom are also included. In parametrizing the core resonance integrals,

$$H_{rs} = -KS_{rs}(I_r+I_s)/2,$$

where the notations are the same as those in Ref. 5; we adopted a value of 0.8 for the K constant.

The compounds treated in this work are H_2S, CH_3SH, $(CH_3)_2S$, C_2H_4S, and C_3H_6S. Their geometries are shown in Table 1, where tetrahedral angles are assumed for the alkyl groups. The ultraviolet (UV) absorption spectra of these compounds observed by Clark *et al.*[1] are referred for the sake of comparison with the calculated values.

TABLE 1. MOLECULAR STRUCTURE OF SULFUR COMPOUNDS USED FOR CALCULATIONS

Compound	Bond angle RSR′ (deg)	Bond distance H–S (Å)	Bond distance C–S (Å)
H_2S	92.2	1.35	
CH_3SH	100.0	1.33	1.82
CH_3SCH_3	100.0		1.82
C_2H_4S	48.4		1.82
C_3H_6S	78.0		1.82

Results and Discussion

H_2S. The results of H_2S are presented in Fig. 1. According to the present calculations, the lowest singlet transition, $^1A_2$ (b_1—b_2*), is symmetry-forbidden and may not be detectable by UV spectroscopy, while the next one, $^1B_1$ (b_1—a_1*), with the transition energy (ΔE) of 6.54 eV and the oscillator strength (f) of 0.037 may be reasonably identified as the first absorption band of H_2S (ΔE=6.32 eV, f=0.04) observed by Clark *et al.*[1] At first they assigned it to the $^1A_1$ (a_1—a_1*) transition according to the Walsh diagram; subsequently, though, Thompson *et al.*[3] calculated the transition energy by their own semi-empirical method and predicted that the excitation must be that of an electron from the lone-pair orbital to either the 3d or the 4s orbital to be significantly atomic in nature (*i.e.*, the Rydberg state). However, their oscillator strengths are quite small ($f=4\times10^{-6}$ for the 3d and 0.006 for the 4s orbital) compared with the observed value (f=0.04), whereas our calculation gives a reasonable oscillator strength (0.037).

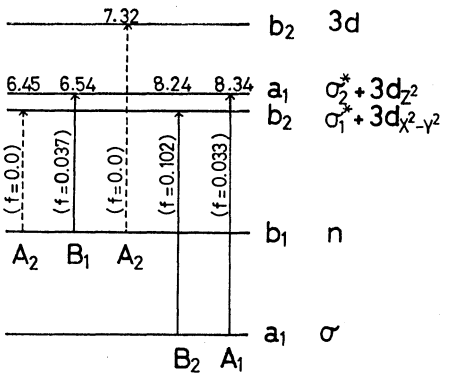

Fig. 1. Singlet transitions of H_2S. Observed values;[1] 6.32 eV (f=0.04), 7.85, 8.02.

The orbital (a_1*) to which the excitation occurs shows an antibonding character, although it includes a 33% contribution from the 3d orbital. Indeed, preliminary calculations excluding 3d orbitals show no significant change for this transition in its transition energy (0.14 eV) and its oscillator strength, implying

that the 3d orbitals do not essentially change the antibonding nature of the σ* level.

On the other hand, in their non-empirical calculations Polezzo *et al.*[6] and Hillier *et al.*[7] assigned the lowest forbidden transition, $^1A_2$, with excitation energies of 6.70 and 6.51 eV respectively, to the observed lowest transition of 6.32 eV. It may be more reasonable, however, to assign it to $^1B_1$ (b_1—a_1*), because the $^1A_2$ transition is forbidden and, therefore, is not expected to be observed, while the oscillator strength of $^1B_1$ (f=0.037) is in good agreement with the observed one (f=0.04).

It is well known that there exists a vibrational structure in this absorption band; from their analysis of the vibrational structure, Thompson *et al.*[3] concluded that it is due to the symmetrical bending mode and that the band is the transition from the lone-pair orbital to the 3d or the 4s orbital because of a slight anharmonicity. Moreover, they have insisted that if the transition were one to the antibonding orbital, there would be more anharmonicity and other stretching modes in the vibrational structure. Such would also be expected if the transition were from the bonding orbital to the antibonding orbital. However, there is evidence that the structure of the excited H_2S molecule (H_2S*), which corresponds approximately to the transition from the lone-pair orbital, is not altered so much as to give a considerable anharmonicity in comparison with the ground-state H_2S molecule. That is, the structure of the ground-state H_2S^+ cation radical,[8] which is probably similar to H_2S* with respect to its molecular structure, is almost unchanged from that of H_2S, showing that a large anharmonicity in the vibrational structure is unnecessary.

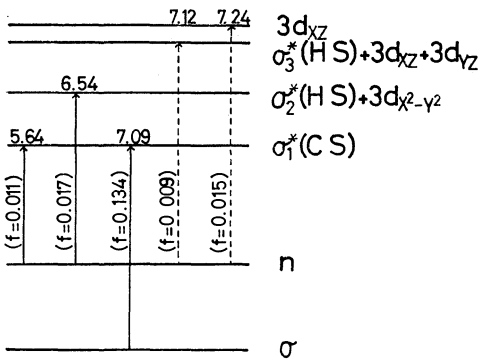

Fig. 2. Singlet transitions of CH_3SH. Observed values;[1] 5.21 (log ε=2.30), 6.08 (3.45), 6.74 (3.30).

CH_3SH. The results for CH_3SH are presented in Fig. 2. According to our calculations, CH_3SH has three low-lying singlet transitions; they are, in the order of increasing energy: n-σ_1* (from the lone pair to the C–S antibonding orbital), n-σ_2* (from the lone pair to the S–H antibonding orbital), and σ-σ_1* (C–S excitation). The lower n-σ_1* transition with a CH_3SH value of 5.64 eV corresponds to the forbidden transition, $^1A_2$ (b_1—b_2*), of H_2S. Clark *et al.* assigned the observed three lowest transitions of CH_3SH, 5.21, 6.08, and 6.70 eV, to the n-σ* type, the intramolecular charge transfer (from the C–S bonding orbital to the H–S antibonding orbital), and the C–S excitation respectively. Their assignments for the first and the third transitions are in agreement with ours. The second, however, is not in agreement; *i.e.*, our result shows that the C–T band has a higher energy (ΔE= 7.87 eV) than the C–S excitation and that in addition, another n-σ* (H–S) transition exists (ΔE=6.54 eV) between them. On the other hand, the calculations excluding the 3d orbitals showed almost no change in the first and the third transitions, though the second one is changed in the ordering of the energy levels; the calculations show an energy shift of some extent (ΔE=7.47 eV, f=0.067). It can easily be seen from these results that the σ-σ* transition seems not to be affected considerably by the basis set of calculations with respect to the energy and the intensity, so it may be reasonabe to assign the σ-σ_1* and the n-σ_2* transitions to the second or the third band of the observed spectra of CH_3SH.

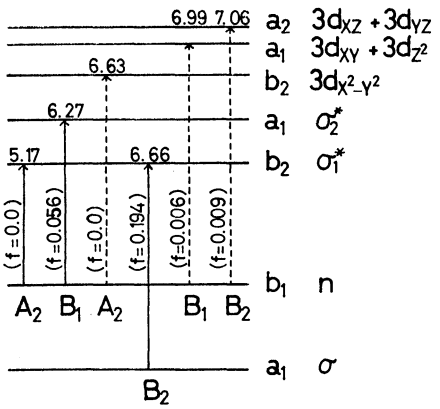

Fig. 3. Singlet transitions of $(CH_3)_2S$. Observed values;[1] 5.20 (very weak), 5.61 (f=0.016), 6.14 (f=0.06).

Alkyl Sulfide. Recently, Rosenfield *et al.*[9] have reported their studies of the rotational strengths of the alkyl sulfides, and before their work there were a few discussions of the transitions of the alkyl sulfides (*e.g.*, Carroll *et al.*[2] and Clark *et al.*);[1] their results are minutely discussed in the paper of Rosenfield *et al.* Our results for $(CH_3)_2S$ are presented in Fig. 3. According to our calculations, it can be seen that the assignments for the first two bands, which are the b_1—b_2* (n-σ_1*) transition and the b_1—a_1* (n-σ_2*) transition, are in agreement with those of Rosenfield *et al.* Furthermore, they have assigned the third band to the n-3d transition on the basis of the optical-active data and the oscillator strength. According to our results, the third is the b_1—b_2* (n-3d) transition at 6.63 eV; this is, however, symmetry-forbidden, so the third band in the UV spectrum of this compound may be assigned to the next strong a_1—b_2* (σ—σ_1*) transition. Moreover, it is clear from the studies of Rosenfield *et al.* of the electric and magnetic moments of the transitions that the a_1—b_2* transition may be optical-active when the sulfide chromophore is in a dissymmetrical field. Therefore, it seems that the observed moderately strong absorption band at 6.14 eV can reasonably be assigned to the a_1—b_2*, but not the n—3d, transition.

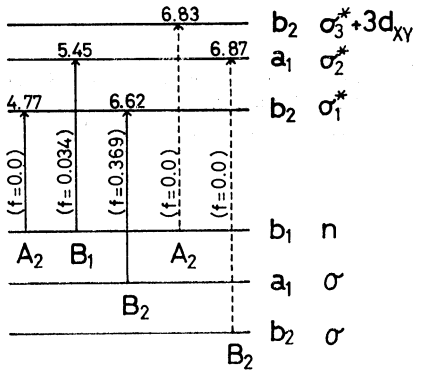

Fig. 4. Singlet transitions of C_2H_4S. Observed values;[1] 4.80 ($\log \varepsilon = 1.30$), 5.10 (1.32), 5.69 (2.30), 5.85 (3.60), 5.99 (3.60), 6.11 (3.60).

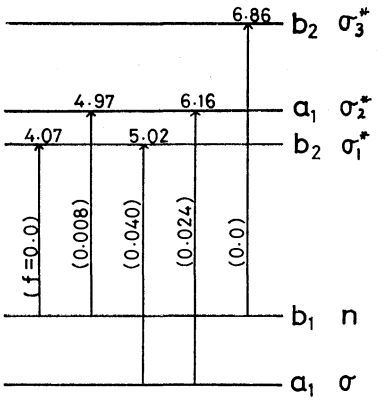

Fig. 5. Singlet transitions of C_3H_6S. Observed values;[1] 4.46 ($\log \varepsilon = 1.00$), 4.71 (1.11), 5.58 (3.30), 5.83 (3.11), 6.20 (3.45).

Cyclic Sulfides. The results of C_2H_4S are presented in Fig. 4. The calculated lowest singlet transition energies are 4.77, 5.45, and 6.62 eV, which correspond to the b_1—b_2* (n—σ_1*), b_1—a_1* (n—σ_2*), and a_1—b_2* (σ—σ_1*) transitions respectively. Those σ* levels (b_2* and a_1*) at which the transitions occur bear little d-character. The calculated transitions can reasonably be assigned to the absorption spectrum of C_2H_4S; *i.e.*, the first band, which is characterized by the transition energy of 5.1 eV with a very weak intensity ($\log \varepsilon_{max} = 1.3$) in solution, may be assigned to the b_1—b_2* (n—σ_1*) transition, because, although the transition is apparently symmetry-forbidden, the ring distortion, which may occur as a result of excitation in such a strained molecule, has little effect on the oscillator strength. According to our additional MO calculations, in which the CSC ring is distorted by changing the length of one S–C bond only, the oscillator strength of the n—σ_1* transition is about 10^{-4}; this value does not change greatly with the extent of distortion. The vapor-phase UV spectrum of this transition band, however, shows two broad peaks at 4.80 and 5.10 eV, while in the solution spectrum[14] only one is observed in the same region. For these two peaks, Williams *et al.*[4] have assigned two different transitions based on their CNDO/2 calculation including 3d orbitals. However, it is obvious from the CD and ORD spectra of the optical-active steroidal episulfides[12,13] that there is only one electronic transition band in this region. The splitting of this band in the vapor-phase UV spectrum is probably due to the non-vertical transition, as was recently pointed out by Strausz *et al.*[10] based on the non-empirical MO calculations. The second lowest transition, b_1—a_1* (n—σ_2*), may be easily assigned to the observed absorption of 5.69 eV. The third transition, a_1—b_2* (σ—σ_1*), might be assigned to the three observed peaks, 5.85, 5.99, and 6.11 eV, which are probably the vibrational splittings corresponding to the CH_2 bending (1120 cm^{-1} in the Raman spectrum[11]) or the ring deformation (1040 cm^{-1} in the Raman spectrum).

The results for C_3H_6S are presented in Fig. 5. The two lowest observed absorption bands, 4.46 and 4.71 eV, can also be assigned to the symmetry-forbidden b_1—b_2* (n—σ_1*) transition of 4.07 eV, while the other transitions may be assigned to the b_1—a_1* (n—σ_2*), a_1—b_2* (σ—σ_1*), and a_1—a_1* (σ—σ_2*) transitions in the order of increasing energy. The σ* levels (b_1* and a_1*) at which these transitions occur have little d-character. For this compound, Williams *et al.*[4] have also given assignments which are different from the situation with C_2H_4S; *i.e.*, they assigned the first two absorption bands as one electronic transition. Their result for the first transition is equivalent to ours, but they seem to overestimate the role of the 3d orbitals; *i.e.*, their result for the lowest vacant orbital shows 30% of the 3d orbital contribution. The discrepancy is due to the difference in the parametrizations adopted for the MO calculations.

Conclusion

It has been shown that the saturated divalent sulfur compounds have similar electronic transitions in the lower-energy region. They are usually the n—σ_1*, the n—σ_2*, and the σ—σ_1* transitions, although there are a few exceptions caused by the substituents on the sulfur atom or the molecular symmetries. The 3d orbitals of the sulfur atom may not play an important role in the lower-energy transitions.

The authors are indebted to the Data Processing Center of Kyoto University, where the numerical calculations have been performed.

References

1) L. B. Clark and W. T. Simpson, *J. Chem. Phys.*, **43**, 3666 (1965).
2) D. G. Carroll, A. T. Armstrong, and S. P. McGlynn, *ibid.*, **44**, 1865 (1966).
3) S. D. Thompson, D. G. Carroll, F. Watson, M. O'Donnell, and S. P. McGlynn, *ibid.*, **45**, 1367 (1966).
4) D. R. Williams and L. T. Kontnik, *J. Chem. Soc. B*, **1971**, 312.
5) T. Yonezawa, H. Konishi, and H. Kato, This Bulletin, **42**, 933 (1969).
6) S. Polezzo, M. P. Stabilini, and M. Simonetta, *Mol. Phys.*, **17**, 609 (1969).
7) I. H. Hillier and V. R. Saunders, *Chem. Phys. Lett.*, **5**, 384 (1970).
8) G. Duxbury, M. Horani, and J. Rostas, *Proc. Roy. Soc. Ser. A*, **331**, 1109 (1972).

9) J. S. Rosenfield and A. Moscowitz, *J. Amer. Chem. Soc.*, **94**, 4797 (1972).
10) O. P. Strausz, H. E. Gunning, A. S. Denes, and I. G. Csizmadia, *ibid.*, **94**, 8317 (1972).
11) H. W. Thompson and D. J. Dupre, *Trans. Faraday Soc.*, **36**, 805 (1940).
12) K. Kuriyama, T. Komeno, and K. Takeda, *Tetrahedron*, **22**, 1039 (1966).
13) D. E. Bays, R. C. Cookson, R. R. Hill, J. F. McGhi, and G. E. Usher, *J. Chem. Soc.*, **1964**, 1563.
14) R. E. Davis, *J. Org. Chem.*, **23**, 1380 (1958).

Charge-transfer and Proton-transfer in the Formation of Molecular Complexes. XI.[1] Phase Transitions in Hertel's Picric Acid Complexes

Yoshio MATSUNAGA, Eiji OSAWA, and RYUZO OSAWA*

Department of Chemistry, Faculty of Science, Hokkaido University, Sapporo 060

(Received May 9, 1974)

The isomerization from true phenolates to charge-transfer complexes by phase transitions in Hertel's five amine–picric acid complexes was confirmed by spectroscopic examinations. The amines and the estimated heats of transition were as follows: *o*-bromoaniline, 6.7; *o*-iodoaniline, 6.2; 1-chloro-2-naphthylamine, 8.0; 1-bromo-2-naphthylamine, 8.2; 1,6-dibromo-2-naphthylamine, 3.3 kcal/mol. The transition temperatures and/or the heats in the naphthylamine complexes were shown to be markedly reduced by crushing the crystals. The charge-transfer complexes have electrical resistivities lower by a factor of many decades than the isomeric phenolates. Phase transitions without isomerization were found in the metastable 1-halo-2-naphthylamine complexes of the charge-transfer type.

In connection with our work on new complex isomers,[1–3] a physicochemical study of the isomeric pairs of Hertel's five picric acid complexes has been undertaken. Phase transitions accompanied by a color change from yellow to red in the solid phase were found by Hertel in the complexes with *o*-bromo- and *o*-iodoanilines and 1-chloro-, 1-bromo-, and 1,6-dibromo-2-naphthylamines.[4] Some years ago, Briegleb and Delle carried out spectroscopic studies of the isomeric pairs in the complexes of the last two amines.[5,6] Their conclusions that the yellow low-temperature forms are true phenolates and that the red high-temperature forms are charge-transfer (CT) complexes are in accordance with ours for some new complex isomers. However, the vibrational spectra of the low-temperature forms presented by Briegleb and Delle show patterns due to the NH_2 groups which one would not expect in true phenolates. Consequently, spectroscopic examinations of all the above-mentioned pairs were performed in the present work. Then, changes in the enthalpy and in the electrical resistivity by the transitions were studied in order to find additional manifestations of the complex isomerization. Anomalous changes in the electrical resistivity have been found at the transition temperatures of a number of organic materials—*e.g.*, hexamethylbenzene,[7,8] phenanthrene,[9,10] phenanthrene–picric acid,[11] and some tetracyanoquinodimethane anion-radical salts.[12–14] As it has been recognized that a lowering of resistivity is generally associated with complex formation,[15] the change at the transition accompanied by the isomerization from a true phenolate to a CT complex might be quite drastic.

Experimental

Materials. The picric acid and the *o*-haloanilines were commercially obtained. The derivatives of 2-naphthylamine were prepared as has been described in a previous paper of ours.[3] The complexes were precipitated by mixing component compounds which had been separately dissolved in chloroform or methanol. The 1,6-dibromo-2-naphthylamine complex was obtained as yellow fine crystals, but it slowly turned reddish brown upon filtration, as has been reported by Hertel.[4] The complex was redissolved in methanol, and then the solution was slowly evaporated to dryness by letting it stand at room temperature. In this way, the yellow form could be isolated.

Measurements. The spectroscopic, calorimetric, and X-ray measurements were made as has been reported in previous papers of the present series.[2,3] The procedure used for recording the electrical resistivity curve has been described in a paper by Koizumi and Matsunaga.[11]

Results and Discussion

Vibrational Spectra. As an example, Fig. 1 presents the spectra of two forms of the *o*-bromoaniline complex. The red form was obtained by the solidification of the fused sample between rocksalt plates. The presence of the NH_3^+ group in the yellow form is clearly indicated by broad bands appearing at 2575 and 2825 cm^{-1}. Upon transition, they are replaced by rather sharp bands located at 3375 and 3475 cm^{-1}. The latter pattern arises from the stretching vibration of the NH_2 group.

The spectra of the 1-bromo-2-naphthylamine complex are shown in Fig. 2. Unlike the spectrum of the yellow form reported by Briegleb and Delle, our spectrum

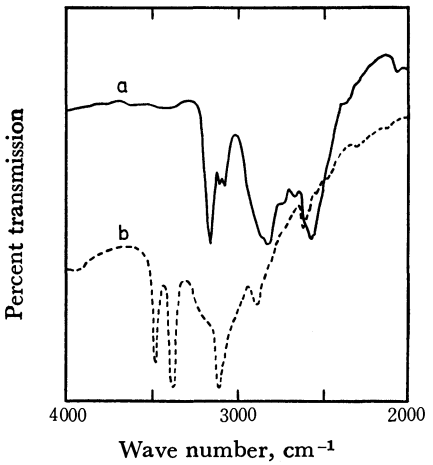

Fig. 1. Vibrational spectra of a) the yellow form and b) the red form of the *o*-bromoaniline–picric acid complex.

* Present address: Bridgestone Tire Co., Kodaira, Tokyo.

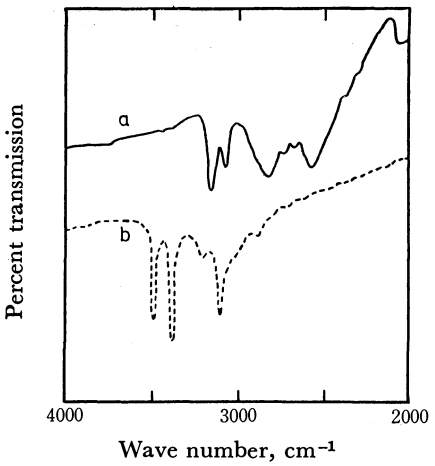

Fig. 2. Vibrational spectra of a) the yellow form and b) the reddish brown form of the 1-bromo-2-naphthylamine–picric acid complex.

shows no band assignable to the NH_2 group. This disagreement may be attributed to the extent of dissociation of the complex on the surface of the alkali halides. One may suppose that the complex in a potassium bromide disc employed by the German workers was well dispersed; therefore, an appreciable amount of the free amine might exist in equilibrium. On the other hand, the complex examined by our technique may be essentially free from such a complication because of its small surface area. It must be added that no color change could be observed upon heating above the transition temperatures when we examined the *o*-haloaniline complexes by the KBr disc technique. The presence of the proton-transfer from picric acid to the amine molecule in the low-temperature form and its absence in the high-temperature form were similarly confirmed for the other combinations.

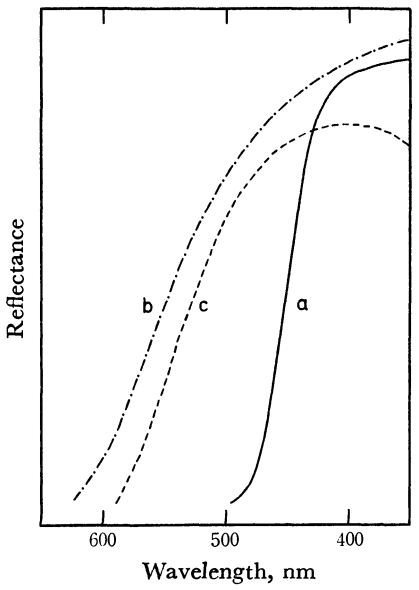

Fig. 3. Reflectance spectra of a) the yellow form and b) the red form of the *o*-bromoaniline–picric acid complex and c) the corresponding *s*-trinitrobenzene complex.

Electronic Spectra. Briegleb and Delle have shown that the absorption bands characteristic of the high-temperature forms of the bromo- and dibromo-naphthylamine complexes are similar to the CT absorption bands in the corresponding *s*-trinitrobenzene complexes. As the electron-acceptor strength of picric acid is nearly the same as that of *s*-trinitrobenzene, the similarity in the spectrum has been considered as evidence that the high-temperature forms of the picric acid complexes are of the CT type. In Fig. 3, the spectra of the yellow and red forms of the bromoaniline-picric acid are compared with that of the trinitrobenzene complex. Here again, the absorption band which appears when the complex is heated above the transition temperature is located close to that of the CT absorption band in the trinitrobenzene complex. In the same way, the appearance of CT absorption in the high-temperature forms was firmly established for all the complexes.

TABLE 1. TRANSITION TEMPERATURES AND ENTHALPY CHANGES IN THE PICRIC ACID COMPLEXES

Amine	Temp. (°C)		ΔH (kcal/mol)
	This work	Hertel	
o-Bromoaniline	103—110	95	6.7
o-Iodoaniline	100—107	90	6.2
1-Chloro-2-naphthylamine	128—138	130	8.0
	74—76[a)]	—	1.4[a)]
1-Bromo-2-naphthylamine	118—125	114	8.2
	76—79[a)]	—	0.8[a)]
1,6-Dibromo-2-naphthylamine	99—108	96	3.4

a) Transitions in the charge-transfer complexes.

Calorimetric Data. The transition temperatures and enthalpy changes are listed in Table 1. These values were for polycrystalline samples as deposited from solutions. It must be noted that the endothermic peaks recorded at a heating rate of 3 °C/min are anomalously broad. The temperature intervals defined by the points of departure from and return to the baseline of the calorimetric curves in Table 1 are several times broader than those of the ordinary transitions—*e.g.*, that in hexamethylbenzene used for the calibration. Moreover, our temperatures tend to be higher than those reported by Hertel.[4)] Especially in

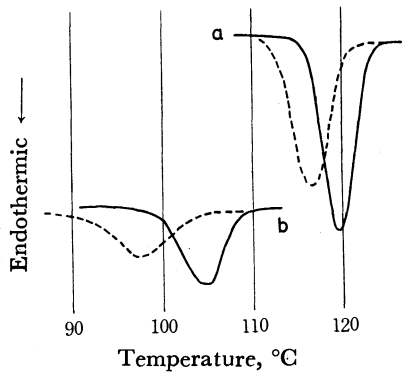

Fig. 4. DSC thermograms of the picric acid complexes of a) 1-bromo-2-naphthylamine and b) 1,6-dibromo-2-naphthylamine before grinding (——) and after grinding (------).

the case of the haloaniline complexes, even the lower limit of the interval is as much as 10 °C higher. When the polycrystalline samples of the bromo- and dibromonaphthylamine complexes were crushed, all the peaks were found to shift significantly to lower temperatures (see Fig. 4). Only a few minutes were enough to produce these changes by grinding. The points of departure from the baseline in the calorimetric curves of the ground samples are located below the transition temperatures reported by Hertel. In addition, the endothermic peaks become a little broader and the amounts of heat of the transition become as much as 20% less than the values given in Table 1. In the case of the chloronaphthylamine complex, the peak was found at almost the same temperature interval before and after grinding; however, the decrease in the heat was comparable with those in the other two naphthylamine complexes. On the other hand, grinding for a short time does not seem to affect much the transitions in the haloaniline complexes. Although small shifts in the transition to lower temperatures were observed, grinding did not result in any observable change in the amount of the heat. These observations suggest that the behavior in complex isomerization is more or less modified by the imperfections incorporated into the crystals by grinding.

The high-temperature forms of the naphthylamine complexes can be cooled to room temperature without any color change. Nevertheless, X-ray examinations revealed that the 1-halonaphthylamine complexes of the CT type at room temperature are different from those obtained by heating the salts above the transition temperature. The existence of phase transitions without complex isomerization between these two forms could be established by the calorimetric method, as is indicated in Table 1. It may be added that the corresponding trinitrobenzene complexes also exhibit phase transitions a little below the transition temperatures in the picric acid complexes of the CT type; that is, they are at 0.9 kcal/mol at 65 °C in the chloronaphthylamine complex and at 1.4 kcal/mol at 60 °C in the bromonaphthylamine complex. All the heats of transition accompanied by complex isomerization listed in Table 1 are appreciably larger than those without isomerization. Such a relation may be recognized as a general tendency, but it is not always true. The heat of transition with isomerization can be as small as 2.2 kcal/mol, as has been found in *o*-chloroaniline–trinitrobenzoic acid,[3] while that without isomerization can be as large as 3.5 kcal/mol, as has been reported for anthracene–picric acid.[11]

Electrical Resistivity. The logarithm of the resistivity of the *o*-haloaniline complexes recorded at ascending temperatures is plotted against the reciprocal temperature in Fig. 5. In the first run, the slope becomes progressively steeper. The activation energy for semiconduction (E), defined by $\rho=\rho_0\exp(E/kT)$, is about 2.25 eV at 60 °C and 4.0 eV at 95 °C in the case of the bromoaniline complex, while the values for the iodoaniline complex are 2.55 and 7.2 eV. At the end of the run, the samples were found to be dark red. Therefore, no anomaly locating the lower limit of transition temperature interval in these complexes was found by our resistivity measurements. On the other hand, the upper limit in the bromoaniline complex may be located in the vicinity of 100 °C. This marked lowering of the upper limit compared to the value in Table 1 may be attributed to the effect of imperfections incorporated by compression to as much as 3 ton/cm^2 employed in the preparation of the sample rod. After the first run, the samples were quickly cooled and the second run was immediately recorded. The slopes in the range from 60 to 80 °C are nearly constant—that is, 1.6 and 2.0 eV. The resistivity values at room temperature may be estimated as 10^{13}—10^{14} ohm cm by extrapolation; they are in good agreement with that of a closely-related CT complex, the 5×10^{13} ohm cm value of the *p*-chloroaniline–*s*-trinitrobenzene.[16] Nevertheless, the activation energies in this temperature range can hardly be considered those

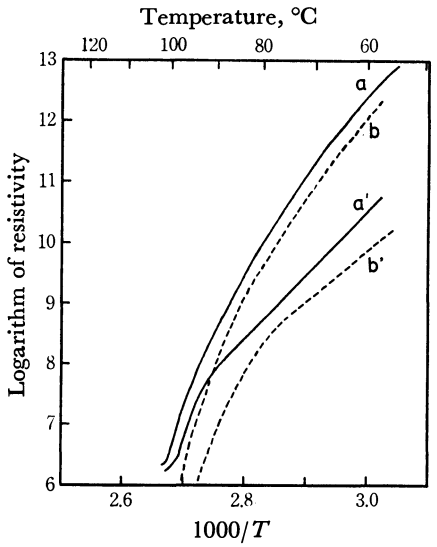

Fig. 5. Electrical resistivities of the picric acid complexes of a) *o*-bromoaniline and b) *o*-iodoaniline. a′ and b′ are the second runs.

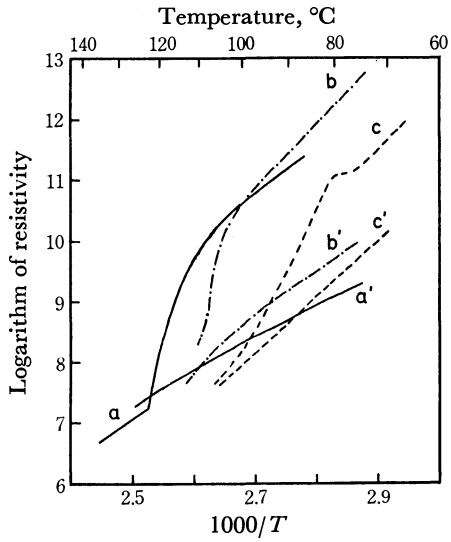

Fig. 6. Electrical resistivities of the picric acid complexes of a) 1-chloro-2-naphthylamine, b) 1-bromo-2-naphthylamine, and c) 1.6-dibromo-2-naphthylamine. a′, b′, and c′ are the second runs.

of the CT complexes. At room temperature, standing overnight is enough for the red form of the *o*-haloaniline complex to return to the stable yellow form. The rate can, of course, be expected to be very much faster in the measured temperature range. Moreover, the slope becomes as steep as that in the first run at high temperatures. Such behavior may suggest that a part of the sample changes into the yellow form during the process of reheating. The transition in the reverse direction in the naphthylamine complexes is slower than those in the aniline complexes. Therefore, the electrical behavior shown in Fig. 6 seems easily explainable. The yellow form of the chloronaphthylamine complex shows an activation energy of 1.5 eV below 100 °C. Then, the slope becomes gradually steeper. The completion of the isomerization may account for the constancy of activation energy above 123 °C. In the second run, the average of the activation energy is about 1.1 eV and the extrapolation to higher temperature almost coincides with the linear part of the first run. As might be expected, the CT complex is more conducting by two orders of magnitude at the beginning of the transition, which may be located around 100 °C. The resistivity extrapolated to room temperature is 10^{16} ohm cm in the yellow form and 10^{12} ohm cm in the red form. Similar anomalous behavior in the transition-temperature interval and a large difference in the electrical resistivity between the complex isomers can also be noted in the other two complexes (see Fig. 6). The activation energy for semiconduction in the yellow form of the bromonaphthylamine complex is 2.2 eV, and that in the red form, 1.4—1.9 eV. The corresponding values in the dibromonaphthylamine complex are 2.1 and 1.8 eV respectively. According to the resistivity measurements, the transformation in the latter complex occurs in the interval from 85 to 100 °C. The large shift to the lower-temperature side and the great breadth in the compressed sample compared to the values given in Table 1 seem to be in accord with the observation of the grinding effects made by the calorimetric method; however, the general tendency here is more pronounced than that demonstrated by the calorimetric curve.

The authors wish to express their thanks to Professor Toshio Yokokawa for letting them use the X-ray diffractometer.

References

1) Part X: Y. Matsunaga, G. Saito, and N. Sakai, This Bulletin, **47**, 2873 (1974).
2) N. Inoue and Y. Matsunaga, *ibid.*, **46**, 3345 (1973).
3) Y. Matsunaga and R. Osawa, *ibid.*, **47**, 1589 (1974).
4) E. Hertel, *Ann.*, **451**, 179 (1926).
5) G. Briegleb and H. Delle, *Z. Elektrochem.*, **64**, 347 (1960).
6) G. Briegleb and H. Delle, *Z. Phys. Chem. (N. F.)*, **24**, 359 (1960).
7) H. Chojnacki, *Acta Phys. Polon.*, **30**, 715 (1966).
8) K. Kurematsu, N. Kaneko, and S. Matsumoto, This Bulletin, **44**, 2845 (1971).
9) R. A. Arndt and A. C. Damask, *J. Chem. Phys.*, **45**, 4627 (1966).
10) S. Matsumoto, This Bulletin, **40**, 2749 (1967).
11) S. Koizumi and Y. Matsunaga, *ibid.*, **47**, 9 (1974).
12) Y. Iida, M. Kinoshita, M. Sano, and H. Akamatu, *ibid.*, **37**, 428 (1964).
13) J. G. Vegter, T. Hibma, and J. Kommandeur, *Chem. Phys. Lett.*, **3**, 427 (1969).
14) N. Sakai, I. Shirotani, and S. Minomura, This Bulletin, **45**, 3321 (1972).
15) M. M. Labes, R. Sehr, and M. Bose, *J. Chem. Phys.*, **33**, 868 (1960).
16) H. Kuroda, K. Yoshihara, and H. Akamatu, This Bulletin, **35**, 1604 (1962).

Anomalous Phosphorescence of *p*-Methylacetophenone in Nonpolar Solvent at 77 K

Yoshifumi TANIMOTO, Noboru HIROTA,* and Saburo NAGAKURA

The Institute for Solid State Physics, The University of Tokyo, Roppongi, Minato-ku, Tokyo 106

(Received May 29, 1974)

Absorption and phosphorescence spectra were studied for *p*-methylacetophenone in 3-methylpentane–isopentane mixed solvent at low temperature. From the concentration and temperature dependencies of the absorption spectrum, it is concluded that the monomer-dimer equilibrium exists in the solution of the *p*-methylacetophenone at low temperature. The phosphorescence of *p*-methylacetophenone in the mixed solvent at low temperature was found to be composed of two components, with lifetimes of 23 and 42 ms at 77 K. They are ascribed to the π,π^* triplet states of the monomer and dimer, respectively.

A number of aromatic carbonyl compounds exhibit anomalous phosphorescence with non-exponential decay.[1-9] Yang and Murov[1] studied phosphorescence for a series of aromatic carbonyl compounds and found that 1-indanone exhibits two phosphorescences with different lifetimes at 77 K, the short-lived one being assigned to the n,π^* triplet state, but the assignment of the long-lived one was open to question. They reported that simple aryl alkyl ketones like acetophenone and propiophenone also show a similar phenomenon.

Callis and Wilson[5] studied the absorption and emission spectra of Michler's ketone in glassy solutions at 77 K. They concluded that, in most commonly used glasses, the solute molecules are surrounded by two or three different types of environments and consequently anomalous luminescence appears. Wagner, May, and Haug[6] analyzed the viscosity dependence of dual phosphorescence of phenyl alkyl ketones at 77 K and ascribed the higher and lower frequency emissions to the n,π^* triplet state of the rigidly held molecule and to that of the conformationally relaxed one, respectively.

Griffin[4] explained anomalous phosphorescence of some acetophenone derivatives in terms of coexistent n,π^*, π,π^*, and charge-transfer triplet states. This explanation, however, is doubtful in view of the fact that, since the molecular relaxation time is of the order of 10^{-12} s,[10] a thermal equilibrium among the nearby triplet states is established within their decay and their phosphorescence decay times must be equal to each other, as was formulated by Mao and Hirota.[11a]

The mechanism of the anomalous phosphorescence observed with aromatic carbonyl compounds is still open to question. Hirota[12] found that the phosphorescence of *p*-methylacetophenone shows non-exponential decay and its apparent decay time changes with the concentration of the solution. In the present study, we have undertaken a study of the mechanism of the anomalous phosphorescence observed with this molecule in nonpolar solvent.

Experimental

p-Methylacetophenone (Tokyo Kasei, EP Grade) was purified with a Perkin-Elmer F21 gaschromatograph. Isopentane and 3-methylpentane were treated with active alumina column, dried with calcium chloride, and finally distilled over sodium metal. 3-Methylpentane–isopentane (1:6 volume ratio) mixed solvent (hereafter abbreviated to 3MP–P solvent) was used as nonpolar solvent.

Low temperature absorption spectra were measured with a Cary spectrophotometer model 14, quartz cells of 1 and 10 mm light-path lengths being used. Temperatures between 97 and 300 K were obtained by controlling a flow of cold nitrogen gas from an evaporation vessel containing liquid nitrogen.

Phosphorescence excitation spectra (PE spectra) were measured at 77 K with a phosphoroscope by exciting samples at various wavelengths with the aid of a 500 W xenon lamp and a Spex 1700-II monochromator. In order to eliminate the effect of stray light, an interference filter (λ_{max}=422 nm, transmittance 30%) was set in front of an EMI 6256S photomultiplier used as a detector.

Phosphorescence spectra were measured at 77 K with the Spex monochromator by exciting samples with an Avco Everett model C950 pulsed nitrogen gas laser. The excitation-wavelength dependence of phosphorescence was observed with an Avco Everett model 1000 tunable wavelength laser as a monochromatized excitation source and a PAR model 121 lock-in amplifier. Time-resolved phosphorescence spectra and phosphorescence decay times were measured with a combination of the pulsed nitrogen gas laser and a PAR model 160 boxcar integrator.

Results and Discussion

Absorption Spectra. Three absorption bands were observed with *p*-methylacetophenone in 3MP–P solvent; the n,π^* transition band at ~360 nm, the π,π^* transition band at ~290 nm corresponding to the α band of benzene, and the π,π^* transition band with the charge-transfer character (the CT transition band) at ~260 nm.

Figure 1 shows the absorption spectra in the 290 nm region measured at 100 K with solutions of various concentrations of *p*-methylacetophenone. Since 3MP–P solvent is not rigid at 100 K, the system can rapidly attain equilibrium. For the solution with a concentration of 2.7×10^{-4} M, a band maximum appears at 288.1 nm. With increasing concentration of the solution its intensity decreases and a new band appears at 291.2 nm. The intensity of the new band increases with increasing concentration and isosbestic points appear at 287.5 and 288.7 nm.

* On sabbatical leave from the Department of Chemistry, State University of New York at Stony Brook.

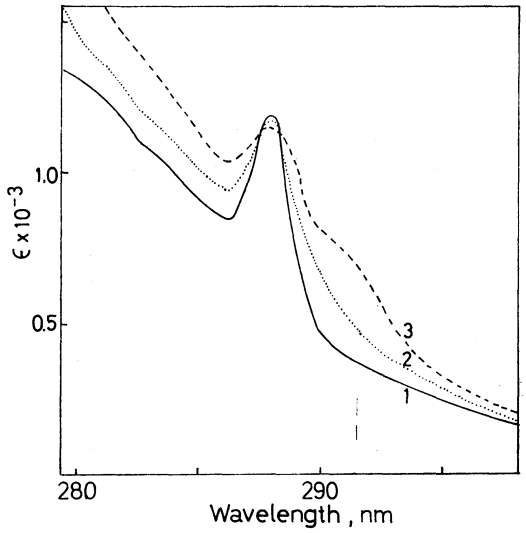

Fig. 1. Absorption spectra (280 nm—300 nm) observed at 100 K with 3MP–P solutions with various concentrations of *p*-methylacetophenone: the concentrations of *p*-methylacetophenone are 2.7×10^{-4}, 5.4×10^{-4}, and and 1.1×10^{-3} M for curves 1, 2, and 3, respectively.

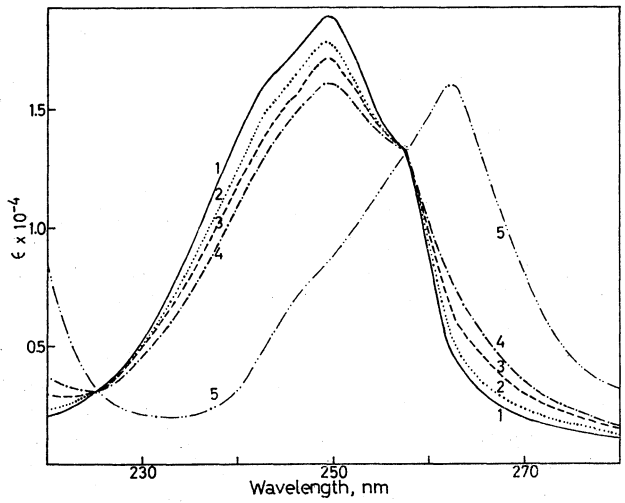

Fig. 2. Absorption spectra (220 nm—280 nm) observed at various temperatures with the 3MP–P solution of *p*-methylacetophenone (5.4×10^{-4} M): curve 1 at 120 K; curve 2 at 110 K; curve 3 at 107 K; curve 4 at 97 K. In this figure, the absorption spectrum of the dimer obtained with the aid of the observed spectrum at 97 K and the equilibrium constant is shown for the purpose of comparison (curve 5).

Figure 2 shows the temperature effect on the absorption spectrum in the range 280—220 nm observed for the solution with a concentration of 5.4×10^{-4} M. The spectra shown in this figure were observed in the temperature range 120—97 K.[13] The intensity of the band at 249 nm decreases with decreasing temperature. On the other hand, the absorption intensity at ~263 nm increases with decreasing temperature and isosbestic points appear at 225 and 258 nm.

The n,π^* transition band at ~360 nm was obtained through the PE spectrum. Figure 3 shows the observed concentration dependence of the band. *p*-Methylacetophenone has a band maximum at 360 nm in the solu-

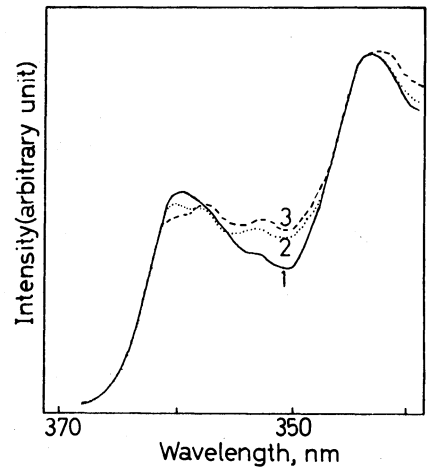

Fig. 3. The phosphorescence excitation spectra (340 nm —370 nm) of *p*-methylacetophenone observed at 77 K in 3MP–P solutions: the concentrations of *p*-methylacetophenone are 1.0×10^{-5}, 1.0×10^{-4}, and 1.0×10^{-3} M for curves 1, 2, and 3, respectively.

tion with a concentration of 1×10^{-5} M. With increasing concentration of the solution, the intensity of the 360 nm band decreases, and a new band at 357 nm gradually grows.

The results show that an equilibrium exists between the monomer and associated species and the new bands at 357, 291.2, and ~263 nm which appear in the relatively concentrated solutions are due to the associated species, most probably the dimer.

From the results shown in Fig. 2, we tried to obtain the monomer-dimer equilibrium constant and the enthalpy (ΔH) and entropy (ΔS) changes for the dimer formation. In view of the fact that the isosbestic points appear at 225 and 258 nm and that the absorption spectrum of the dimer has a peak at about 261—264 nm and its intensity increases with decreasing wavelength below 225 nm, we assumed that the apparent molar extinction coefficient of the dimer around 240 nm is equal to that at the isosbestic point at 225 nm. We further assumed that the absorption spectrum measured at 120 K is entirely due to the monomer. This might be reasonable since the intensity of the monomer band remains constant above this temperature, while below this temperature it increases with a

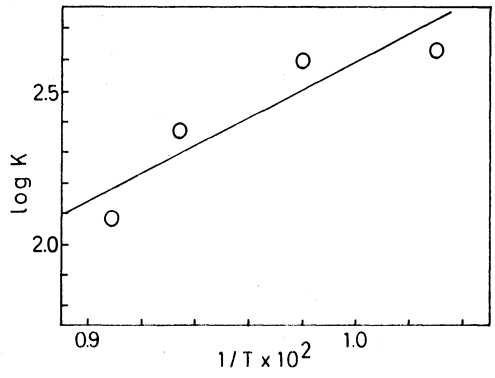

Fig. 4. Temperature dependence of the monomer-dimer equilibrium constant (K) of *p*-methylacetophenone.

rise in temperature. Thus we achieved a rough estimate of the concentrations of the monomer and dimer, C_M and C_D, and the equilibrium constant $K=C_D/C_M^2$ from the absorption intensity around 240 nm observed with a solution of a fixed concentration of *p*-methylacetophenone.[14] In actuality, K was obtained at 242.5, 240.0, and 237.5 nm. The values obtained at these wavelengths are in good agreement with each other at a fixed temperature. The logarithm of the average value of K's obtained at the three wavelengths is plotted against the reciprocal of temperature ($1/T$) in Fig. 4. From this plot, we obtained ΔH and ΔS to be -2 kcal/mol and -10 e.u., respectively. These values are very rough but reasonable for weak association.[15]

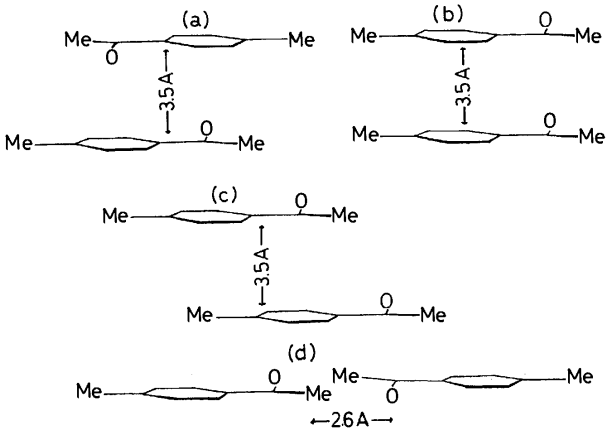

Fig. 5. Geometries of the *p*-methylacetophenone dimer taken for the CNDO/2 calculation.

Let us consider the geometry of the dimer. Using the MO's evaluated by the CNDO/2 method,[16] we calculated the band shifts due to the dimer formation considering interaction between permanent dipole moments in both the ground state and the appropriate excited states and also interaction between transition dipoles.[17] Figure 5 shows the dimer conformations which were used. Figure 5(a) shows the geometry of the dimer which best reproduces the observed band shifts. The experimental observation that the π,π^* and CT bands showed red shift by dimer formation while the n,π^* band showed blue shift can be explained qualitatively by this dimer conformation. This geometry may be reasonable in view of the fact that the stabilization due to the dipole-dipole interaction in the ground state of the dimer is conceivably large for this conformation.

Phosphorescence Spectra. Figures 6(a) and 6(b) show the integrated and time-resolved phosphorescence spectra of *p*-methylacetophenone in 3MP–P solvent at 77 K. The integrated phosphorescence has band maxima at 393.8, 420.8, and 451.8 nm, and the phosphorescence shows non-exponential decay. The time resolved spectra measured 1 and 70 ns after the excitation by the nitrogen gas laser have peaks at 393.0, 420.3, and 450.8 nm, and at 395.8, 420.9, and 453.2 nm, respectively. Thus, we interpret the phosphorescence spectrum as having two components: the band maxima for the longer-lived component lie at slightly

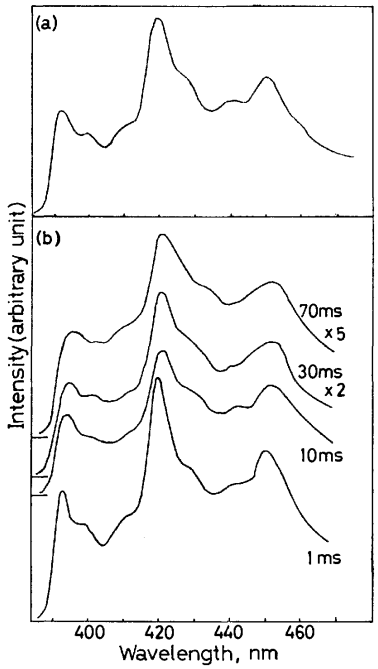

Fig. 6. Integrated (a) and time-resolved (b) phosphorescence spectra observed at 77 K with the 3MP–P solution of *p*-methylacetophenone (1.4×10^{-3} M).

lower energy. The phosphorescence decay curve observed at 420 nm at 77 K is shown in Fig. 7. From the analysis of this curve, the lifetimes of the short- and long-lived components were determined to be 23 and 42 ms, respectively. This indicates that two kinds of molecular species exist in the 3MP–P solution of *p*-methylacetophenone at 77 K.

It is reasonable to ascribe the short- and long-lived phosphorescences to the monomer and dimer of *p*-methylacetophenone, which exist in equilibrium in solution as concluded from the absorption measurement.

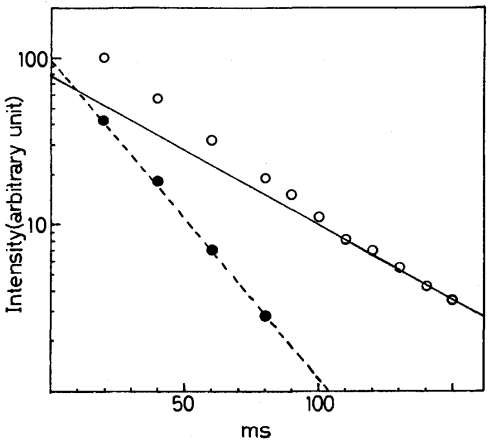

Fig. 7. Analysis of the phosphorescence (420 nm) decay curve observed at 77 K with the 3MP–P solution of *p*-methylacetophenone (8.4×10^{-4} M):
○; the observed decay curve
—; the long-lived component with the lifetime of 42 ms
●; the short-lived component, the difference between the observed decay curve and the long-lived component.

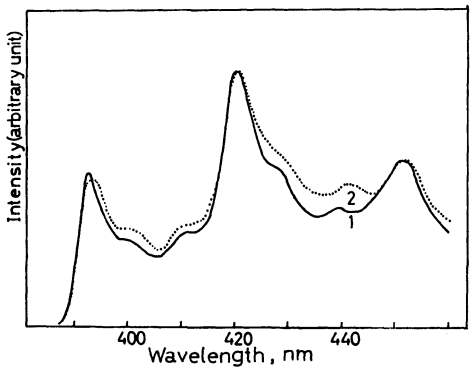

Fig. 8. Phosphorescence spectra observed at 77 K with the 3MP–P solution of *p*-methylacetophenone (1.4×10^{-3} M): excitation was made at 360 nm for curve 1 and at 357 nm for curve 2.

This is supported by the fact that the phosphorescence decay with the short- and long-lived components can be observed only in the low temperature region in which a considerable amount of the dimer exists in solution.[18]

In order to check this mechanism of the anomalous phosphorescence observed with *p*-methylacetophenone and also to determine which of the long-lived and short-lived components corresponds to the monomer or dimer, we measured the excitation-wavelength dependence of the phosphorescence spectrum.

Figure 8 shows the phosphorescence spectra obtained by the excitation at 360 and 357 nm at which the absorptions of the monomer and dimer mainly occur, respectively (Fig. 3). Although both spectra are similar to each other, the band maxima of the spectrum excited at 360 nm appear at slightly higher frequencies than the corresponding maxima of the spectrum excited at 357 nm. It is therfore, concluded that the dimer phosphorescence appears in lower frequencies than the monomer one. Combining this result with the time-resolved phosphorescence, we are led to the conclusion that the higher frequency phosphorescence with the lifetime of 23 ms and the lower energy one with the lifetime of 42 ms are ascribed to the monomer and dimer, respectively. The assignment is supported by the observed tendency that the band positions in the phosphorescence spectrum observed with *p*-methylacetophenone in 3MP–P shift to longer wavelengths with decreasing temperature in the range 90—80 K and also with increasing concentration of *p*-methylacetophenone.[19]

The phosphorescent states of the monomer and dimer of *p*-methylacetophenone may be regarded as π,π^* triplet states, since both lifetimes are too long to be ascribed to the n,π^* triplet state.[11b]

Cheng and Hirota[11b] presented a linear relationship between $k_z^{1/2}$ and ΔE_T^{-1} for aromatic carbonyl compounds. Here, k_z and ΔE_T are the decay rate constant of the T_z sublevel and the energy difference between the n,π^* and π,π^* triplet states, respectively. Since $1/\tau=k=\sum_i n_i k_i$, we can calculate the ΔE_T from the observed lifetime, if we assume $k_x=k_y=0$.[20] Here, τ and k are the mean lifetime and the mean decay rate constant, respectively, and k_i and n_i the decay rate constant and population fraction of the T_i sublevel, respectively. At 77 K $n_i=1/3$ is used. Thus, ΔE_T's are calculated to be 348 and 475 cm^{-1} for the monomer and dimer, respectively.

The authors would like to express their sincere thanks to Dr. Michiya Ito, Faculty of Pharmaceutical Sciences, The University of Tokyo, for valuable suggestions and discussions. N. H. acknowledges support from the National Science Foundation (U.S.) during his stay in Japan under the U.S.-Japan Scientific Collaboration Program.

References and Notes

1) N. C. Yang and S. Murov, *J. Chem. Phys.*, **45**, 4358 (1966).
2) G. Yamaguchi, Y. Kakinoki, and H. Tsubomura, This Bulletin, **40**, 426 (1967).
3) P. Gacoin and Y. Meyer, *C. R. Acad. Sci., Paris, Ser. B*, **267**, 149 (1968).
4) R. N. Griffin, *Photochem. Photobiol.*, **7**, 159 (1968).
5) P. R. Callis and R. W. Wilson, *Chem. Phys. Lett.*, **13**, 417 (1972).
6) P. G. Wagner, M. May, and A. Haug, *ibid.*, **13**, 545 (1972).
7) P. Gacoin, *J. Chem. Phys.*, **57**, 1418 (1972).
8) M. E. Long and E. C. Lim, *Chem. Phys. Lett.*, **20**, 413 (1973).
9) E. Malawer and C. Marzzacco, *J. Mol. Spectrosc.*, **46**, 341 (1973).
10) P. M. Rentzepis, *Chem. Phys. Lett.*, **3**, 717 (1969).
11) a) S. W. Mao and N. Hirota, *Mol. Phys.*, **27**, 327 (1974); b) T. H. Cheng and N. Hirota, *ibid.*, **27**, 281 (1974).
12) N. Hirota, *Chem. Phys. Lett.*, **4**, 305 (1969).
13) The spectrum measured at room temperature does not cross the isosbestic points and the absorption peak shifts slightly toward shorter wavelengths. This shift may be due to the difference in the environment between room temperature and ~100 K.
14) We determined the K value roughly on the assumption that the molar extinction coefficient of the dimer band at 291.2 nm is equal to that of the monomer band at 288.1 nm. The value thus obtained is 200 M^{-1} l at 100 K—almost half the corresponding value 400 M^{-1} l at 102 K obtained by the method given in the text. This discrepancy seems to be unavoidable because of the roughness of both methods, in particular the method mentioned here. Importance should be attached to the fact that both methods give values of the same order of magnitude.
15) J. A. Katul and A. B. Zahlan, *J. Chem. Phys.*, **47**, 1012 (1967).
16) J. A. Pople and G. A. Segal, *ibid.*, **44**, 3289 (1966).
17) H. Hosoya, J. Tanaka, and S. Nagakura, *J. Mol. Spectrosc.*, **8**, 257 (1962).
18) By extrapolating the straight line in Fig. 4, we can estimate the equilibrium constants at 90 and 80 K to be 1280 and 5480 M^{-1} l, respectively. By the use of these values, the concentration ratio of the dimer to the monomer is evaluated for the *p*-methylacetophenone solution of 1×10^{-3} M to be 3: 5 and 4: 3 at 90 and 80 K, respectively. Furthermore, considering the fact that the lifetimes of the two components are rather close to each other, we may explain the observation that the phosphorescence decay of

the 3MP–P solution containing 8.4×10^{-4} M *p*-methylacetophenone fits considerably well into a single exponential curve at 87 K but deviates from it at 77 K.

19) The phosphorescence of *p*-methylacetophenone in 3MP–P is weak, particularly above 90 K. It is therefore difficult to measure its intensity in a wide temperature range accurately enough for the monomer-dimer equilibrium and the temperature dependence of the phosphorescence intensity to be treated quantitatively.

20) This assumption is reasonable since k_x for most aromatic carbonyl compounds is predominantly large among the three decay rate constants.[11b)]

Polarized Reflection and Absorption Spectra of the [2.2]-Paracyclophane Crystal

Kiyokazu FUKE* and Saburo NAGAKURA*,**

*The Institute for Solid State Physics, The University of Tokyo, Roppongi, Minato, Tokyo 106
**The Institute of Physical and Chemical Research, Wako, Saitama 351

(Received June 18, 1974)

The reflection spectra of a [2.2]-paracyclophane crystal were measured in the 17000—62000 cm^{-1} region with incident light polarized parallel and perpendicular to the a-axis. From analysis of the reflection spectra by the Kramers-Kronig method, the a-axis and c-axis polarized absorption spectra in the 38000—60000 cm^{-1} region were obtained. The c-axis polarized spectrum was obtained for the first time. The 43000 cm^{-1} band in the c-axis spectrum was assigned to the transitions to the $^1B_{1u}$ (p) and $^1B_{1u}$ (CT) states. The band around 48000 cm^{-1} was assigned to the transition to the $^1B_{3u}^-$ state, corresponding to the transition to the $^1E_{2g}^-$ state in benzene.

The electronic absorption spectra of [2.2]-paracyclophane (abbreviated hereafter to PC) in single crystal and in solution together with those of tetramethyl [2.2]-paracyclophane and multilayered cyclophanes in solution were reported previously.[1] Comparing the observed transition energies, oscillator strengths, and directions of transition moments with those obtained theoretically by considering the interaction between the ground, locally excited, and charge-transfer configurations, better assignments than those by others[2-4] were made.

It was difficult in the previous study,[1] however, to obtain the c-axis polarized absorption spectrum of the PC crystal in the region higher than 38000 cm^{-1} since the intensity was too strong for direct absorption measurement. In order to overcome this difficulty, we have undertaken to obtain polarized absorption spectra of PC single crystals by reflection measurement in the 17000—62000 cm^{-1} region and to verify our previous assignments by analysis of accurately determined polarization ratios.

Experimental

PC was purified by column chromatography on silica gel and then sublimed *in vacuo*. Single crystals were obtained by recrystallization from chloroform solution. The (011) faces of the crystals, on which reflection spectra were measured, were identified by optical conoscopy and X-ray analysis.

Reflection spectra at room temperature were measured with a reflection spectrophotometer.[5] Since PC sublimes gradually in high vacuum even at room temperature, reflection measurements in the vacuum ultraviolet region were performed under one atmosphere of dry nitrogen. The spectra shown in Fig. 1 are the averages of six determinations. Actual measurements of reflection spectra were made with the incident light polarized parallel and perpendicular to the a-axis. The refractive index, n, and the absorption index, k, were calculated by the Kramers-Kronig method.[6] The molar absorption coefficient, ε, for light polarized parallel or perpendicular to the a-axis was calculated with the formula

$$\varepsilon = \frac{4\pi nkv}{2.303M}$$

where v is the frequency in cm^{-1} and M the molarity of the crystal (5.91 mol/l for PC). The c-axis polarized spectrum was obtained from the ε values for the light polarized paralell and perpendicular to the a-axis in the (011) plane,

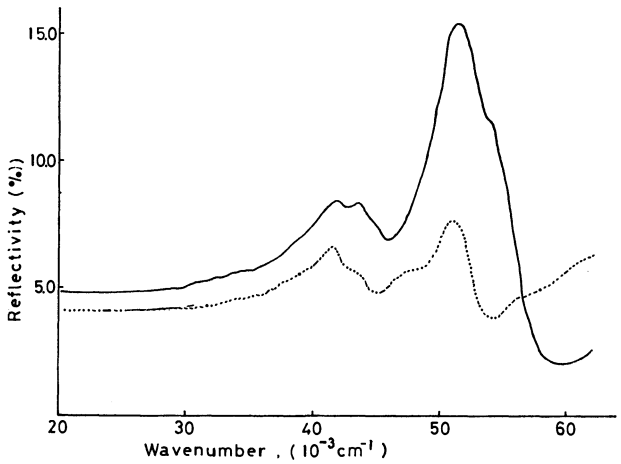

Fig. 1. Reflection spectra observed on the (011) face of the PC crystal. The solid and dotted cruves were obtained with the incident light polarized perpendicular and parallel to the a-axis, respectively.

the orientation of molecules in a unit cell being considered. In the actual evaluation the following equation was used:

$$\varepsilon_c = \frac{\varepsilon_{\perp a} - \cos^2 49°14' \, \varepsilon_a}{\cos^2 40°46'}$$

Results

Absorption spectra derived from the reflection spectra at room temperature are shown in Fig. 2. These spectra correspond fairly well to the absorption spectrum in solution. Here we are not concerned with the weak bands (bands I and II[1]) which appear in the 29500—38000 cm^{-1} region in solution but with bands III—VII which appear in the 38000—59400 cm^{-1} region.

The a-axis spectrum in the 38000—50000 cm^{-1} region agrees with the spectrum of the (001) face obtained by direct absorption measurement.[1] In the region above 56000 cm^{-1}, the intensity of the a-axis spectrum is slightly increased with increasing wave number. The reliability of this result was confirmed by varying the trial reflection curve[7] for the frequency region higher than our experimental limit. With all the trial curves, we found an a-axis polarized transition band in this region.

The c-axis spectrum in the wave number region higher than 38000 cm^{-1} was obtained for the first time.

The absorption intensity in this region is too strong to be measured directly. The observed band positions and the oscillator strengths in solution and in crystal are listed in Table 1.

Discussion

The PC crystal belongs to the D_{4h}^{14} space group (tetragonal) and has two molecules per unit cell.[8] The molecular point group and the molecular site group are both D_{2h}. PC is thus an example in which the site symmetry is the same as the full molecular point group symmetry. The unique symmetry axis of two molecules in a unit cell and their benzene-ring planes are perpendicular to each other. Therefore, a Davydov splitting is expected neither for the transition to the $^1B_{2u}$ state polarized parallel to the y molecular axis nor for the transition to the $^1B_{3u}$ state polarized parallel to the x molecular axis. Both transition bands are expected to appear in the spectra polarized along the a and b crystal axes, while the band corresponding to the transition to the $^1B_{1u}$ state polarized parallel to the z molecular axis is expected to appear in the spectrum polarized along the c crystal axis.

In the a-axis component of the crystal spectrum derived from the observed reflection spectrum, a weak band appears at 39400 cm^{-1}, in agreement with the direct absorption measurement.[1] The oscillator strength of this band was roughly estimated to be 0.01_5 in the present study. These results support the previous assignment[1] that the band at 39400 cm^{-1} is due to the transition to the $^1B_{2u}$ (α-parentage) excited state.

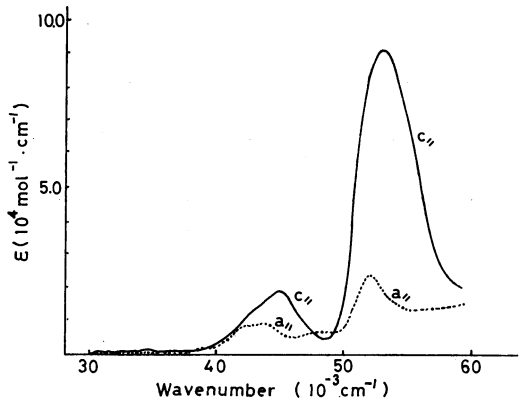

Fig. 2. Polarized absorption spectra of PC derived from the reflection spectra.

The 43000 cm^{-1} band in the a-axis spectrum and the 45000 cm^{-1} band in the c-axis spectrum (Fig. 2), correspond to the 44500 cm^{-1} band in solution. Two bands polarized along the long molecular axis are expected to appear in this region of the c-axis spectrum;[1] one of them corresponds to the *p*-band of *p*-xylene which is strongly polarized along the long molecular axis[9-11] and the other is due to the transition to the charge-transfer (CT) state stabilized by interaction with a locally excited configuration corresponding to the β-band of *p*-xylene. The former band is theoretically predicted to appear at 41400 cm^{-1} (f=0.220) and the latter at 46930 cm^{-1} (f=0.327). The band observed at 45000 cm^{-1} in the c-axis spectrum can be separated into two bands; a stronger band at higher frequencies and a weaker band at lower frequencies. Thus, the observed c-axis spectrum supports the prediction.

Let us consider the 43000 cm^{-1} band in the a-axis spectrum. From the polarization, this band can be ascribed to a transition to the $^1B_{2u}$ or $^1B_{3u}^-$ state. Two bands polarized along the a-axis are theoretically predicted to appear in this region. They are due to transitions to the $^1B_{3u}^-$ and $^1B_{2u}$ (CT) states. The transition energies and oscillator strengths are calculated to be as follows: 46680 cm^{-1}, 0.425 for the transition to the $^1B_{2u}$ state and 45300 cm^{-1}, 0 for the transition to the $^1B_{3u}^-$ state. The observed spectrum (Fig. 2) shows that another band (band V in the previous paper) polarized along the a-axis appears at 48700 cm^{-1} as a shoulder. It is therefore reasonable to consider that the a-axis polarized bands at 43000 and 48700 cm^{-1} are due to the predicted transitions to the $^1B_{2u}$ and $^1B_{3u}^-$ states. Since the calculated transition energies are close to each other for both transitions, it is difficult to determine which transition corresponds to the 43000 cm^{-1} band. By comparing the observed and predicted intensities, however, it is more probable that the 43000 and 48700 cm^{-1} bands are due to the transitions to the $^1B_{2u}$ and $^1B_{3u}^-$ states, respectively.

The $^1B_{3u}^-$ state is mainly composed of a locally excited configuration corresponding to the excitation to the $^1E_{2g}^-$ state of benzene. A number of studies have been made on the band corresponding to the transition to the $^1E_{2g}^-$ state which is forbidden for benzene.[12-21] Quite recently, a band at 46300 cm^{-1} was assigned to this transition.[19,20] Thus it is reasonable to assign the 48700 cm^{-1} band of PC to the $^1B_{3u}^- \leftarrow {}^1A_{1g}$ transition.

The 52000 and 53200 cm^{-1} bands polarized along the a- and c-axis, respectively, correspond to the 53000 cm^{-1} band in solution. From the consideration of the absorption intensities and polarizations, the 52000 cm^{-1} band can be assigned to a transition to a $^1B_{2u}$ state (theoretically at 62380 cm^{-1} and β-parentage) and the 53200 cm^{-1} band to a $^1B_{1u}$ state (theoretically at 62610 cm^{-1} and β-parentage). Both bands correspond to the strong β bands of *p*-xylene.

The a-axis spectrum has an absorption band at 59000 cm^{-1}. This band may correspond to a shoulder at 58000 cm^{-1} in solution. In view of the polarization, the 59000 cm^{-1} band is tentatively assigned to a transition to a $^1B_{3u}^+$ excited state (theoretically predicted to appear at 62270 cm^{-1}). This transition band corresponds to the $^1E_{2g}^+ \leftarrow {}^1A_{1g}^-$ transition band of benzene which appears at 169—172 nm.[19] In the crystal, however, a transition to the conduction band is also possible in the region above 55000 cm^{-1}. This makes the assignment of the 59000 cm^{-1} band ambiguous.

All the assignments are listed in Table 1. The transition energies for observed bands in the crystal show consistent trends; the bands of the a-axis spectrum show a red shift, while those of the c-axis spectrum show no shift or a small blue shift compared with those of the solution spectrum. These results can be qualitatively

Table 1. Observed and calculated transition energies (ΔE in 10^3 cm^{-1}), oscillator strengths (f), and polarizations of PC

Band[a]	Obsd: Soln ΔE_{soln}	Obsd: Soln f	Obsd: Cryst ΔE_{cryst}	Obsd: Cryst Pol	Obsd: Cryst f[b]	Calcd[d] $\Delta\nu$[c]	Calcd[d] ΔE_{calcd}	Calcd[d] f[f]	Upper state
III	41.0	0.05	39.4	*a*	0.02[e]	1.6	34.3	0.010 (y)	$^1B_{2u}(\alpha)$
IV	44.5	0.26	43.0	*a*	0.12[e]	1.5	46.7	0.425 (y)	$^1B_{2u}$(CT)[g]
			44.8	*c*	0.13	−0.3	41.3	0.220 (z)	$^1B_{1u}(p)$
							46.9	0.327 (z)	$^1B_{1u}$(CT)[g]
V	48.7	0.12	48.0	*a*	0.07[e]	0.7	45.3	0.0 (x)	$^1B_{3u}^-$
VI	53.3	1.07	52.0	*a*	0.26[e]	1.3	63.0	0.619 (y)	$^1B_{2u}(\beta)$
			53.2	*c*	0.72	0.1	63.0	0.667 (z)	$^1B_{1u}(\beta)$
VII	57.8	0.20	~58.0	*a*	0.16[e]	—	62.4	0.0 (x)	$^1B_{3u}^+$

a) We are concerned here with absorption bands in the frequency region higher than 38000 cm^{-1}, so bands I and II have been omitted from this table. b) For comparison with the solution values, these values were obtained by multiplying observed oscillator strengths of the c- and a-axes polarized bands by 1/3 and 2/3, respectively. c) $\Delta\nu=\Delta E_{soln}-\Delta E_{cryst}$. d) Theoretical values taken from Ref. 1. e) Roughly estimated because of overlapping of the corresponding bands. f) Polarization direction is indicated in parentheses:

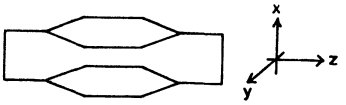

g) Transitions to these states are mainly caused by intensity borrowing from the β states of the benzene ring.

interpreted by the simple exciton theory of molecular crystals[20] as follows.

In the case of the PC crystal, there are two translationally nonequivalent molecules per unit cell located at (0,0,0) and (1/2, 1/2, 1/2). Exciton states are given by the following linear combinations of $\mathbf{k}=0$:

$$\Psi_i^f = (2N)^{-1/2} \quad (\varphi_1^f \pm \varphi_2^f) \tag{1}$$

where i refers to the irreducible representation in the factor group ($i=1$ and 2 refer to E_u and A_u, respectively). φ_i^f is a one-site exciton function of Site i and State f. To first order, the energy of the i-th factor group component of the f-th electronic state of the crystal is given by:

$$E_i^f - E_0 = \varepsilon^f + D^f + J_i^{ff}(\mathbf{k}). \tag{2}$$

ε^f is the excitation energy of the free molecule from the ground state to the f-th excited state, D^f the environmental shift, and J_i^{ff} the sum of intermolecular excitation exchange integrals usually taken to be a sum of dipole-dipole interactions. In the case of the PC crystal, we have $J_i^{B_{2u},B_{2u}}=J_i^{B_{3u},B_{3u}}=0$, and $J_i^{B_{1u},B_{1u}}\neq 0$ because of the orientation of the two molecules in the unit cell. The calculated excitation exchange integrals are listed in Table 2. We see that the crystal states from the B_{2u} and B_{3u} excited states of the free molecule have zero Davydov splittings. The band shifts between solution and crystal are interpreted by the second term of Eq. (2). The B_{1u} molecular excited state splits in the crystal into the A_u and E_u exciton states with an energy difference of 325 cm^{-1}/Å^2. However, since the unique symmetry axis of the crystal (c-axis) is parallel to the long axis of all molecules, only the transition to the A_u state is optically allowed (c-axis polarized). The D^f term usually has a negative value for a crystal of an aromatic compound. This is easily seen from the a-axis spectrum. Thus the shift of each absorption band in the c-axis spectrum results from cancellation of the second and third terms in Eq. (2).

Table 2. Excitation exchange integrals (J_i^{fg}, cm^{-1}/Å^2)

	$^1B_{1u}$	$^1B_{2u}$	$^1B_{3u}$
$^1B_{1u}$	163	0	0
$^1B_{2u}$	0	0	−75
$^1B_{3u}$	0	−75	0

These values were obtained by the summation of dipole-dipole interaction terms within 50 Å spheres.

We are greatly indebted to Drs. Junko Nakamura and Suehiro Iwata, The Institute of Physical and Chemical Research, and to Dr. Koji Kaya, Tohoku University, for their helpful advice.

References

1) S. Iwata, K. Fuke, M. Sasaki, S. Nagakura, T. Otsubo, and S. Misumi, *J. Mol. Spectrosc.*, **46**, 1 (1973).

2) J. Koutécký and J. Paldus, *Collect. Czech. Chem. Commu.*, **27**, 599, 2139 (1962); J. Paldus, *ibid.*, **28**, 1110 (1963); J. Koutécký and J. Paldus, *Tetrahedron*, **19**, Suppl. 2, 201 (1963).

3) M. T. Vala, Jr., I. H. Hillier, S. A. Rice, and J. Jortner, *J. Chem. Phys.*, **44**, 23 (1966).

4) A. Ron and O. Schnepp, *ibid.*, **37**, 2540 (1962); **44**, 19 (1966).

5) K. Fuke, K. Kaya, T. Kajiwara, and S. Nagakura, *J. Mol. Spectrosc.*, in press.

6) T. S. Robinson, *Proc. Phys. Soc. Ser., B*, **65**, 910 (1952); D. M. Roessler, *Brit. J. Appl. Phys.*, **16**, 1193 (1965).

7) L. B. Clark and M. R. Philpott, *J. Phys. Chem.*, **53**, 3790 (1970).

8) C. J. Brown, *J. Chem. Soc.*, **1953**, 3265; K. Lonsdale, H. J. Milledge, and K. V. K. Rao, *Proc. Roy. Soc. Ser. A*, **255**, 82 (1960).

9) A. C. Albrecht and W. T. Simpson, *J. Chem. Phys.*, **23**, 1480 (1955).
10) E. W. Thulstrup, M. Vala, and J. H. Eggers, *Chem. Phys. Lett.*, **7**, 31 (1970).
11) K. Kaya, K. Fuke, and S. Nagakura, This Bulletin, **47**, 438 (1974).
12) J. N. Murrel and J. A. Pople, *Proc. Roy. Soc. Ser. A*, **69**, 245 (1956).
13) M. Dunn and C. K. Ingold, *Nature*, **176**, 65 (1955).
14) J. N. Murrel and K. L. McEwen, *J. Chem. Phys.*, **25**, 1143 (1956).
15) W. E. Donath, *ibid.*, **40**, 77 (1964).
16) D. P. Craig and L. E. Lyons, *Nature*, **169**, 1102 (1952).
17) B. Katz, M. Brith, A. Ron, B. Sharf, and J. Jortner, *Chem. Phys. Lett.*, **2**, 189 (1968).
18) M. Brith, R. Lubart, and I. T. Steinberger, *J. Chem. Phys.*, **54**, 5104 (1971).
19) A. M. Taleh, I. H. Munro, and J. B. Birks, *Chem. Phys. Lett.*, **21**, 454 (1973).
20) G. C. Morris and J. G. Angus, *J. Mol. Spectrosc.*, **45**, 271 (1973).
21) E. N. Lassetre, A. Skerbele, M. A. Dillon, and K. J. Ross, *J. Chem. Phys.*, **48**, 5066 (1968).

The Crystal Absorption Spectra of Some Hexachloroiridate(IV) Salts

Akio URUSHIYAMA, Masayoshi NAKAHARA, and Yukio KONDO

Department of Chemistry, Faculty of Science, Rikkyo University, Nishi-Ikebukuro, Toshima-ku, Tokyo 171

(Received June 24, 1974)

The absorption spectra of the single-crystals of several hexachloroiridate(IV) salts and the doped crystals of the hexachlorostannate(IV) salts and the hexachloroplatinate(IV) salt with the $IrCl_6^{2-}$ anion were measured. Distinct dichroisms appeared in the polarized absorption spectra of all the anisotropic crystals studied. The splittings of the bands and the dichroisms of the spectra were interpreted in terms of the lowering of the symmetry of the $IrCl_6^{2-}$ anions in the crystal. The absorption bands at 19760 and 20000 cm^{-1} in the spectra of $(CH_3NH_3)_2Sn(Ir)Cl_6$ could be assigned to the $E'_g \rightarrow E''_u$ and $E'_g \rightarrow E'_u$ transitions respectively from their polarizations in the double group, D_{3d}*. Similarly, the bands at 23100, 23500, and 24500 cm^{-1} were assigned to the $E'_g \rightarrow E'_u$, $E'_g \rightarrow E''_u$, and $E'_g \rightarrow E'_u$ transitions respectively. The polarized absorption spectra of $Na_2IrCl_6 \cdot 6H_2O$ and $Na_2Pt(Ir)Cl_6 \cdot 6H_2O$ were also interpreted, assuming that the $IrCl_6^{2-}$ anions in these crystals were of the D_{4d} symmetry.

The nature of the electronic absorption spectra of the transition-metal hexahalogenocomplexes was first discussed by Jørgensen,[1] and since then many reports have appeared in this field, especially concerned with Ir(IV) complexes.[2] In these studies the absorption spectra and the magnetic circular dichroisms of the complexes have been measured in solution or by means of the doped crystals because of their large molar extinction coefficients ($\log \varepsilon > 3$). The hexahalogenostannate(IV) salts and the hexahalogenozirconate(IV) salts have been frequently employed as the host lattice. However, π(halogen)$\rightarrow t_{2g}$(metal) electron-transfer absorption bands of the complexes have been known to change considerably in their shapes and positions according to their matrices.[3] In fact, different absorption spectra have been obtained in these studies of Ir(IV) complexes doped into various host lattices and in solution.

One of the present authors (Y. K.) has previously measured the single-crystal polarized absorption spectra of $Na_2IrCl_6 \cdot 6H_2O$, and observed its remarkably distinct dichroism. This dichroism evidently indicates that the complexes are fairly much distorted from O_h in this anisotropic crystal. Therefore, for a detailed discussion of the absorption spectra, it seems important to study the absorption bands under a reduced symmetry of the complex, especially in the anisotropic crystals.

In the present work, the single-crystal absorption spectra of several hexachloroiridate(IV) salts and the doped crystals of the hexachlorostannate(IV) salts and of the hexachloroplatinate(IV) salt with $IrCl_6^{2-}$ anion were measured. The spectra thus measured were interpreted in terms of the lowering of the symmetry of the complexes in the crystal.

Experimental

The visible absorption spectra of the crystalline samples were measured by means of a microspectrophotometer composed of a Hitachi EPS-3T spectrophotometer and a specially-designed stainless-steel box containing a microscope. For the low-temperature studies, the box could be evacuated and was equipped with a stainless-steel cylinder that could hold *ca.* 500 ml of liquid nitrogen. The liquid nitrogen flowed from this cylinder to a specially-designed cooling stage of the microscope through a copper tube. Depending on the cross-section of the crystalline sample, a condenser and an objective with an appropriate power (×4, ×10: ordinary glass objective, ×20, ×40: reflection type optics; Zeiss-Jena) were used. The slit image of the spectrophotometer on the stage of the microscope was about 0.15 mm, as the ×4 lens system was employed, while the ×40 lens system could condense it to about 15 μm in length. The crystalline sample should be large enough to cover the slit image on the stage completely for the measurement. For some doped crystals, the low-temperature absorption spectra were measured. These doped crystals were mounted over a hole in an aluminum plate, which was then placed on the cooling stage of the microscope. Apiezon N grease ensured good thermal contact between the crystal, the aluminum plate, and the cooling stage. The thermocouple indicated that the samples were cooled to about 90 K.

Excellent single-crystals of the hexachloroiridate(IV) salts were obtained when one drop of the 6M HCl solution of the salt was put between two plates of the quartz slide and the plates were then allowed to stand overnight in air in order to evaporate the solvent. The crystals thus obtained were examined under a polarizing microscope, and the absorption spectra of the appropriate samples were measured. The thickness of the samples was not measured in the present studies. However, it could be estimated to be less than 1 μm, assuming that the molar extinction coefficient of the complexes in solution does not change in the crystal. Doped crystals of various hexachlorostannate(IV) salts and sodium hexachloroplatinate(IV) with the $IrCl_6^{2-}$ anion were grown from a slowly-evaporating solution of the salts in 6M HCl containing small quantities (*ca.* 0.05%) of the $IrCl_6^{2-}$ anion. It was found that, in most cases, the $IrCl_6^{2-}$ anions were condensed into the host crystals to some extent. Crystals about 0.5 mm thick were selected and used for the measurements. The polarized absorption spectra of the anisotropic crystals were measured on their extinction directions using a Rochon polarizer. The Raman spectra of the solid powder of the hexachlorostannate(IV) salts were obtained by a laser excited Raman spectrometer. The X-ray crystallographic studies were done with a Weissenberg camera.

Results and Discussion

K_2IrCl_6, $(NH_4)_2IrCl_6$, $K_2Sn(Ir)Cl_6$, $(NH_4)_2Sn(Ir)Cl_6$. These crystals of the hexachloroiridate(IV) salts and the host hexachlorostannate(IV) salts belong to the cubic crystal system, with the space group *Fm3m*.[6] The crystallographically-required symmetry of the complexes in these crystals is O_h. The absorption spectra

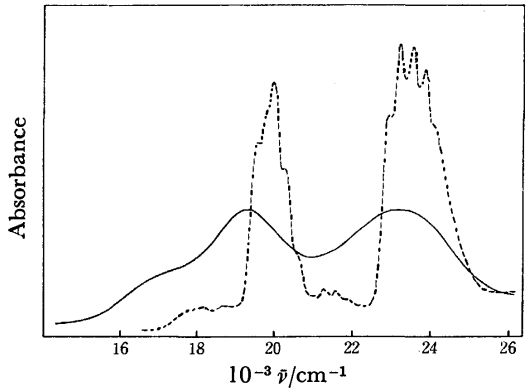

Fig. 1. Crystal absorption spectra of K_2IrCl_6 (——), and $K_2Sn(Ir)Cl_6$ at 90 K (------).

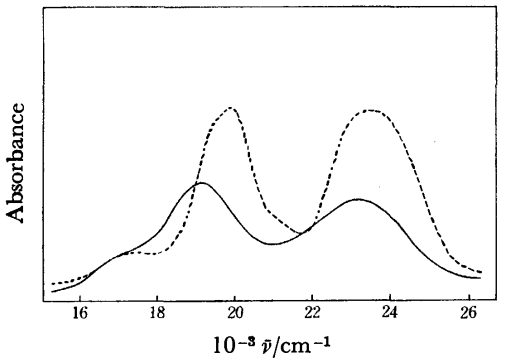

Fig. 2. Crystal absorption spectra of $(NH_4)_2IrCl_6$ (——), and $(NH_4)_2Sn(Ir)Cl_6$ (------).

of the single-crystals and the doped crystals are shown in Figs. 1 and 2. The familiar intense absorption bands of the $IrCl_6^{2-}$ anion were observed in the 20000 and 23500 cm^{-1} regions in all the cases; also, in some cases, there were weak absorption bands in the 17000 and 21500 cm^{-1} regions. Schatz *et al.*[7-9] investigated the absorption spectra and the magnetic circular dichroisms of π(halogen)$\rightarrow t_{2g}$(metal) electron-transfer absorption bands of the $IrCl_6^{2-}$ anion and concluded that the intense absorption bands in the 20000 and 23500 cm^{-1} regions could be assigned to the $^2T_{2g}\rightarrow{}^2T_{1u}$ and $^2T_{2g}\rightarrow{}^2T_{2u}$ transitions respectively, assuming the $IrCl_6^{2-}$ anion

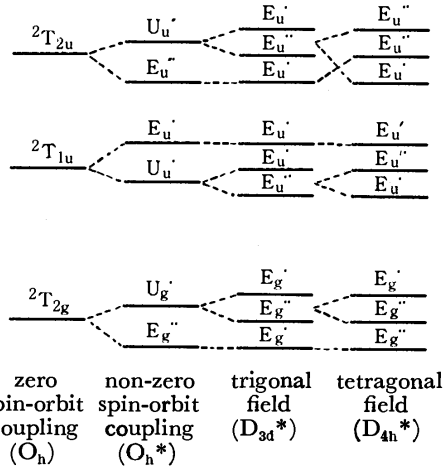

Fig. 3. Schematic energy level diagram of the electron transfer configurations of d^5 complex.

to have the O_h symmetry. Figure 3 shows the schematic energy levels of the electron-transfer configurations of the d^5 complex. It was found that the band maximum of the $^2T_{2g}\rightarrow{}^2T_{1u}$ transition of the pure crystals was always located at a lower wave number than that of the doped crystals. This fact has already been interpreted by Jørgensen in terms of the compression effect in the pure crystals. The absorption spectrum of $K_2Sn(Ir)Cl_6$ in Fig. 1 is consistent with that reported by Sleight[10] in 1968. That is, in the $^2T_{2g}\rightarrow{}^2T_{1u}$ absorption region, five components—at (1) 19570 cm^{-1}, (2) 19880(sh) cm^{-1}, (3) 20040 cm^{-1}, (4) 20350 cm^{-1}, and (5) 20650(sh) cm^{-1}—can be found. It can be considered that the (1) and (2) components form one set of vibrational fine structures, while the (3), (4), and (5) components form another set of vibrational structures. On the other hand, in the $^2T_{2g}\rightarrow{}^2T_{2u}$ absorption region, only one component, with its vibrational fine structures beginning at 22990 cm^{-1}, was observed. Sufficient evidence for the splitting of this band could not be obtained. However, it may be noted by a careful observation of the absorption spectra in Figs. 1 and 2 that each $^2T_{2g}\rightarrow{}^2T_{2u}$ band seems to have a shoulder on the higher-wave number side of the band. Measurements with higher resolution are necessary for any discussion of the band splittings of the complexes in the crystallographically-required O_h.

$(CH_3NH_3)_2IrCl_6$, $(CH_3NH_3)_2Sn(Ir)Cl_6$. The structure of $(CH_3NH_3)_2SnCl_6$ was determined by Wyckoff.[11] The crystals of $(CH_3NH_3)_2SnCl_6$ belong to the trigonal crystal system, with the space group *R3m*. The crystallographically-required symmetry of the complex is D_{3d}. The three-fold axis (z axis) of the complex should be normal to the well-developed face of the thin hexagonal plate of the crystal, in accord with the unique axis of the crystal. The crystals of $(CH_3NH_3)_2IrCl_6$, which also grow as thin hexagonal plates, must be isomorphous to $(CH_3NH_3)_2SnCl_6$, since they showed a similar Debye-Scherrer pattern in this work. The low-temperature absorption spectrum of $(CH_3NH_3)_2Sn(Ir)Cl_6$, with the light propagated along the unique axis of the crystal, has already been studied by Bird *et al.*[12] In the present work, using a carefully selected crystal, the polarized absorption spectra by

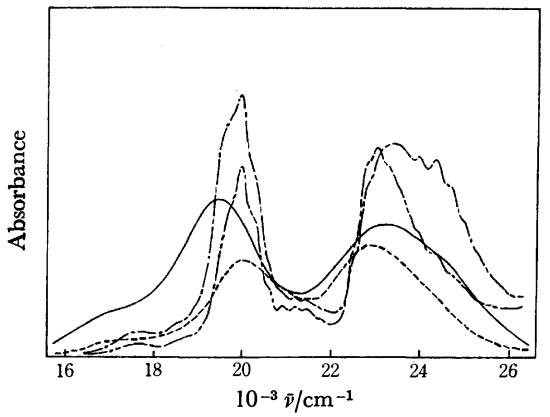

Fig. 4. Polarized absorption spectra of $(CH_3NH_3)_2IrCl_6$ (—— $\perp C_3$, ------ $//C_3$), and $(CH_3NH_3)_2Sn(Ir)Cl_6$ at 90 K (----- $\perp$ C_3, —— // C_3).

light propagated perpendicular to the unique axis of the crystal could be obtained. Figure 4 shows the polarized absorption spectra of $(CH_3NH_3)_2IrCl_6$ and $(CH_3NH_3)_2Sn(Ir)Cl_6$. It was found that the two crystals showed distinct dichroisms with similar patterns, although $(CH_3NH_3)_2IrCl_6$ was studied at room temperature. This reasonably indicates that the $IrCl_6^{2-}$ anions are appreciably distorted in these crystals. Bird *et al.* considered that the $IrCl_6^{2-}$ anion doped into $(CH_3NH_3)_2SnCl_6$ does not suffer any appreciable distortion from O_h symmetry, since the splitting of the $\nu_5(t_{2g})$ line of the $SnCl_6^{2-}$ anion in the crystal could not actually be observed in their Raman studies. However, in the present work, the measurements of the Raman spectra of the powdered host stannate(IV) salts showed that the $\nu_5(t_{2g})$ line of the $SnCl_6^{2-}$ anion in $(CH_3NH_3)_2SnCl_6$ has a small shoulder. This fact also suggests that the symmetry of the $IrCl_6^{2-}$ anion doped into $(CH_3NH_3)_2SnCl_6$ is reduced from O_h. The Raman lines of the solid stannate(IV) salts are listed in Table 1.

TABLE 1. VIBRATIONAL FREQUENCIES (Raman active)

	$\nu_1(a_{1g})$	$\nu_2(e_g)$	$\nu_5(t_{2g})$
K_2SnCl_6	325.6 cm^{-1}	246.2 cm^{-1}	147.2 cm^{-1}
$(CH_3NH_3)_2SnCl_6$	316.0	241.1	174.0
			161.7 sh
$\{(CH_3)_2NH_2\}_2SnCl_6$	313.9	245.4	173.2
		236.7	159.3
$\{(CH_3)_3NH\}_2SnCl_6$	306.4	241.8	171.3
		232.1	162.7

The absorption spectrum of $(CH_3NH_3)_2Sn(Ir)Cl_6$, measured with polarized light whose electric vector was perpendicular to the unique axis, was essentially consistent with that given by Bird *et al.* However, as the crystal was cooled to 4 K in their studies, their spectrum appeared in a better resolution than ours, particularly in the $^2T_{2g}\rightarrow{}^2T_{1u}$ absorption region. They noted that the absorption band in this region consisted of three peaks centered at 19760, 20000, and 20300 cm^{-1}, but they considered that the peak at 20300 cm^{-1} belonged to the member of the vibrational fine structure of the component at 20000 cm^{-1}. Thus, they concluded that the spectrum contained two absorption components in this region, and they identified these two components arising from the excited state spin-orbit splitting in the O_h* double group. However, in the polarized absorption spectrum with its electric vector parallel to the three-fold axis of the complex, the component at 19760 cm^{-1} seemed to be considerably reduced in intensity compared with that at 20000 cm^{-1}. As is shown in Fig. 3, the $^2T_{1u}$ state is split into three levels, which transform as E_u', E_u'', and E_u' respectively in the D_{3d}*, double group while the ground state must still be E_g' because of the large spin-orbit coupling constant (ξ_{Ir}—3000 cm^{-1}). The Laporte allowed transitions of $E_g'\rightarrow E_u''$ and $E_g'\rightarrow E_u'$ should have their transition moments directed along xy and xyz respectively in the D_{3d}* double group. Therefore, the absorption component at 19760 cm^{-1}, the intensity of which along the z axis of the complex was remarkably reduced, must be due to the $E_g'\rightarrow E_u''$ transition. The component at

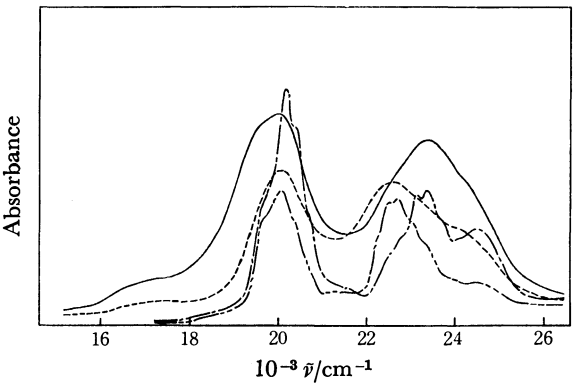

Fig. 5. Polarized absorption spectra of $\{(CH_3)_2NH_2\}_2IrCl_6$ (——, -----), and $\{(CH_3)_2NH_2\}_2Sn(Ir)Cl_6$ at 90 K (-----, ——).

20000 cm^{-1} must be assigned to $E_g'\rightarrow E_u'$, as it has the transition moment also along the z axis. Two E_u' levels arise from $^2T_{1u}$, but it cannot be determined easily which E_u' level corresponds to this component. However, according to the calculations by Piepho *et al.*,[13] the $E_g'\rightarrow E_u'(D_{3d}^*)[U_u'(O_h^*)]$ must have a dipole strength of $D=1/4$. Therefore, this electronic transition must contribute largely to the absorption band at 20000 cm^{-1}.

The intense absorption-band group between 22500 and 26000 cm^{-1} has been considered to be due to the $^2T_{2g}\rightarrow{}^2T_{2u}$ transition in O_h. There have been several discussions concerning the composition of the band group in this region.[8,12] However, the absorption spectrum with the light polarized parallel to the unique axis of the crystal clearly revealed an absorption maximum at 23100 cm^{-1}, while this maximum did not appear in the spectrum with the light propagated along the unique axis. Thus, the band group in this region seems to consist of three components—namely, a band with some vibrational fine structures centered at 23100 cm^{-1}, a structureless band at 23500 cm^{-1}, and a band representing the extensive vibrational structures centered at 24500 cm^{-1}. The component appearing clearly at 23100 cm^{-1} in the z spectrum seems to have its intensity also in the xy direction; therefore, it could be considered to be of the xyz polarization. The vibrational fine structures centered at 24500 cm^{-1} could be seen also in the z spectrum; this component was overlapped with the slope of the band at 23500cm^{-1} to increase its intensity apparently in the xy spectrum. Therefore, the component centered at 24500 cm^{-1} could be regarded as the xyz polarization. Three levels which transform as E_u', E_u'', and E_u' in the D_{3d}* double group arise from the $^2T_{2u}$ state. The present polarization studies suggest the following assignments: the bands centered at 23100, 23500, and 24500 cm^{-1} are the components due to $E_g'\rightarrow E_u'$ (xyz polarization), $E_g'\rightarrow E_u''$ (xy polarization), and $E_g'\rightarrow E_u'$ (xyz polarization) respectively. Referring again to the dipole strength (D) calculated by Piepho *et al.*, the band at 23100 cm^{-1} can further be assigned to $E_g'\rightarrow E_u'(D_{3h}^*)[E_u''(O_h^*)]$-$(D=2/3)$, and that at 24500 cm^{-1}, to $E_g'\rightarrow E_u'(D_{3h}^*)$-$[U_u'(O_h^*)](D=1/12)$. McCaffery *et al.*[8] studied the MCD spectra of this doped crystal with the light

propagated along the unique axis of the crystal. These spectra showed two negative $[\theta]_M$ maxima, at 23000 and 24500 cm^{-1}, and may be interpreted in terms of the overlapping of the peaks corresponding to $E_g' \rightarrow E_u'$-(C=0.60), $E_g' \rightarrow E_u''$(C=−0.225), and $E_g' \rightarrow E_u'$(C=0.075) respectively in the D_{3d}* double group.

The single-crystal of $(CH_3NH_3)_2IrCl_6$ showed polarized absorption spectra with a pattern similar to that of the doped crystal. As the crystal is isomorphous to the host one, the same statements can be made concerning these spectra.

$\{(CH_3)_2NH_2\}_2IrCl_6$, $\{(CH_3)_2NH_2\}_2Sn(Ir)Cl_6$.

Figure 5 shows the polarized absorption spectra of $\{(CH_3)_2NH_2\}_2IrCl_6$ and $\{(CH_3)_2NH_2\}_2Sn(Ir)Cl_6$. The crystals of $\{(CH_3)_2NH_2\}_2SnCl_6$ belong to the orthorhombic crystal system, with the space group of Pnn2 or Pnnm. The complex in this crystal is crystallographically required to possess one of three symmetries, C_1, C_s, or C_2. Solid $\{(CH_3)_2NH_2\}_2IrCl_6$ gave a Debye-Scherrer pattern similar to that of $\{(CH_3)_2NH_2\}_2SnCl_6$. Both Raman lines, $\nu_2(e_g)$ and $\nu_5(t_{2g})$, of the $SnCl_6^{2-}$ anion in the $\{(CH_3)_2NH_2\}_2SnCl_6$ were found to be clearly split, as is shown in Table 1. This suggests that the complex must have suffered a severe distortion force in the crystal to convert it to a low symmetry. The single-crystal and the doped crystal showed polarized absorption spectra with similar patterns. It was found that the $^2T_{2g} \rightarrow {}^2T_{2u}$ absorption band was clearly split into three components in the spectra of the doped crystal at 90 K. However, a detailed discussion of the polarized absorption spectra is not possible because the actual symmetry of the complex is not known.

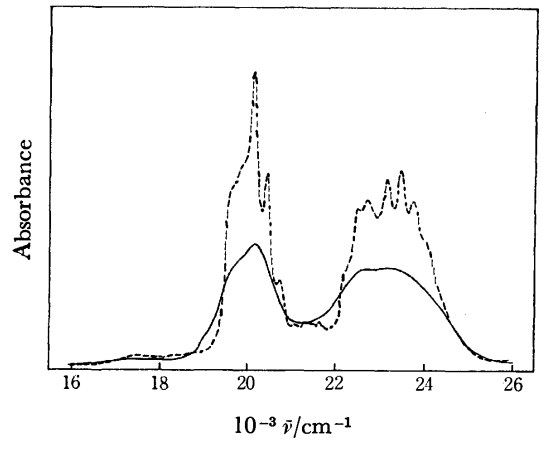

Fig. 6. Crystal absorption spectra of $\{(CH_3)_3NH\}_2IrCl_6$ (——), and $\{(CH_3)_3NH)\}_2Sn(Ir)Cl_6$ at 90 K (------).

$\{(CH_3)_3NH\}_2IrCl_6$, $\{(CH_3)_3NH\}_2Sn(Ir)Cl_6$.

Figure 6 shows the absorption spectra of $\{(CH_3)_3NH\}_2IrCl_6$ and $\{(CH_3)_3NH\}_2Sn(Ir)Cl_6$. The host crystal of $\{(CH_3)_3NH\}_2SnCl_6$ belongs to the cubic crystal system with the space group *Pa3*.[6] The crystallographically-required symmetry of the complex is D_{3d}. The Debye-Scherrer photograph of $\{(CH_3)_3NH\}_2IrCl_6$ is similar to that of $\{(CH_3)_3NH\}_2SnCl_6$. As is shown in Table 1, not only the $\nu_5(t_{2g})$ but also $\nu_2(e_g)$ Raman lines of $SnCl_6^{2-}$ in the host crystal were found to be split. This indicates that the complex in this crystal may have a lower symmetry than D_{3d}, contrary to the results of the X-ray studies. It was found in the spectrum of the doped crystal that the bands due to both $^2T_{2g} \rightarrow {}^2T_{1u}$ and $^2T_{2g} \rightarrow {}^2T_{2u}$ were split into two components with clear vibrational structures. The absorption spectrum of $\{(CH_3)_3NH\}_2IrCl_6$ appeared to be almost the same as that of the doped crystal at room temperature. However, as the crystals belong to the cubic crystal system, polarized absorption studies were not possible.

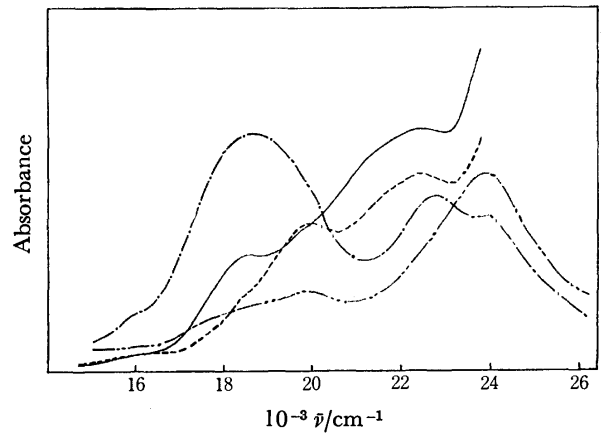

Fig. 7. Polarized absorption spectra of $Na_2IrCl_6 \cdot 6H_2O$ (-----: A direction, ——: B direction), and $Na_2Pt(Ir)Cl_6 \cdot 6H_2O$ (——: A direction, ------: B direction).

$Na_2IrCl_6 \cdot 6H_2O$, $Na_2Pt(Ir)Cl_6 \cdot 6H_2O$. Figure 7 shows the polarized absorption spectra of $Na_2IrCl_6 \cdot 6H_2O$ and $Na_2Pt(Ir)Cl_6 \cdot 6H_2O$. The crystals of $Na_2IrCl_6 \cdot 6H_2O$ and $Na_2PtCl_6 \cdot 6H_2O$ belong to the triclinic crystal system, being isomorphous with each other.[14] For both samples, the polarized absorption spectra measured were not related to their crystal axes. However, although, in the absorption spectra of the doped crystal, the $^2T_{2g} \rightarrow {}^2T_{2u}$ absorption region was overlapped with the slope of the strong absorption band of the $PtCl_6^{2-}$ anion, the patterns of the absorption spectra appeared to be comparable to that of $Na_2IrCl_6 \cdot 6H_2O$ in the $^2T_{2g} \rightarrow {}^2T_{1u}$ region. That is, the $^2T_{2g} \rightarrow {}^2T_{1u}$ absorption bands were split into two components, with strong dichroisms for both samples.

One of the present authors (Y. K.)[4] had previously measured the polarized absorption spectra of $Na_2IrCl_6 \cdot 6H_2O$, and had found a remarkably strong dichroism; hence, there has been a doubt as to the chemical composition of the fine crystals studied. Therefore, the sample crystals used in the course of this work were prepared by the evaporation of a 6M HCl solution of the salts in order to avoid any aquation of the complexes. Since all the crystals of $Na_2IrCl_6 \cdot 6H_2O$ thus obtained exhibited a distinct dichroism under the polarizing microscope, and since all the doped crystals of $Na_2Pt(Ir)Cl_6 \cdot 6H_2O$ prepared also showed a clear dichroism, it seems reasonable to say that the sample crystals certainly consist of $IrCl_6^{2-}$ anions. Griffith *et al.*[15] reported, on the basis of their ESR studies, that the $IrCl_6^{2-}$ anion doped into $Na_2PtCl_6 \cdot 6H_2O$

could be considered to be approximately of a D_{4h} symmetry. $Na_2IrCl_6 \cdot 6H_2O$ is isomorphous to $Na_2PtCl_6 \cdot 6H_2O$, and it showed polarized absorption spectra similar to those of $Na_2Pt(Ir)Cl_6 \cdot 6H_2O$, as has been described already. This suggests that the $IrCl_6^{2-}$ anion in the $Na_2IrCl_6 \cdot 6H_2O$ crystal can be considered to be approximately of a D_{4h} symmetry. The schematic energy levels in the D_{4h}* double group are shown in Fig. 3.

The bands at 18750 cm^{-1} ($Na_2IrCl_6 \cdot 6H_2O$) and at 18600 cm^{-1} ($Na_2Pt(Ir)Cl_6 \cdot 6H_2O$) which appeared in one polarization direction (the A direction in Fig. 7) would correspond to $E_g'' \rightarrow E_u'(D_{4h}^*)[U_h'(O_h^*)]$ (xy polarization). These distinct dichroisms observed in this region indicate that the $IrCl_6^{2-}$ anions of the D_{4h} symmetry lie in an ordering in the crystals favorable for the polarization studies. The band at 19850 cm^{-1} ($Na_2IrCl_6 \cdot 6H_2O$), which appeared as a shoulder in the spectrum of the A direction, almost covered by the slope of the band at 18750 cm^{-1}, could be considered to have its transition moment in either polarization direction of the spectra. The band at 19900 cm^{-1} ($Na_2Pt(Ir)Cl_6 \cdot 6H_2O$) clearly appeared in two directions of the spectra. These two bands can naturally be assigned to $E_g'' \rightarrow E_u''(D_{4h}^*)[U_u'(O_h^*)]$ (xyz polarization). On the basis of the evidence, the band at 22800 cm^{-1} ($Na_2IrCl_6 \cdot 6H_2O$) was considered to be of the xy polarization. Hence, it corresponds to $E_g'' \rightarrow E_u'(D_{4h}^*)[U_u'(O_h^*)]$. Different absorption maxima could be observed at 23950 cm^{-1} in the B direction and at 24040 cm^{-1} in the A direction of the polarized absorption spectra of $Na_2IrCl_6 \cdot 6H_2O$ shown in Fig. 7. This observation indicates that the actual symmetry of the complex in the crystal is reduced further than D_{4h}. However, assuming that the complexes are in the D_{4h} symmetry, these bands must correspond to the $E_g'' \rightarrow E_u''$ (xyz polarization) transitions arising from the $^2T_{2u}$ excited state.

The authors wish to express their thanks to Professor C. K. Jørgensen and American Cyanamid Company for the gift of some samples. Special thanks are due to Dr. Teruo Nomura for his valuable suggestions in the X-ray studies, Mr. Hiroshi Saito for his help with the Raman measurements, and Professor Gene S. Lehman for his kindness in reading the original manuscript.

References

1) C. K. Jørgensen, *Mol. Phys.*, **2**, 309 (1959); C. K. Jørgensen, "Absorption Spectra and Chemical Bonding in Complexes," Pergamon Press, Inc., New York (1962).

2) Von E. Blasius and W. Preetz, *Z. Anorg. Allgem. Chem.*, *B*, **335**, 16 (1965); W. Preetz, *ibid.*, *B*, **348**, 151 (1966); C. K. Jørgensen and W. Preetz, *Z. Naturforschg*, **22a**, 945 (1967); I. N. Douglous, *J. Chem. Phys.*, **51**, 3066 (1969); G. C. Allen, R. Al-Mobarak, G. A. M. El-Sharkawy, and K. D. Warren, *Inorg. Chem.*, **11**, 787 (1972); M. D. Rowe, A. J. McCaffery, R. Gale, and D. N. Copsey, *ibid.*, **11**, 3090 (1972); A. J. McCaffery, M. D. Rowe, and D. A. Rice, *J. Chem. Soc., Dalton*, **1973**, 1605.

3) C. K. Jørgensen, *Acta Chem. Scand.*, **17**, 1034 (1963).

4) Y. Kondo and C. K. Jørgensen, Proc. 10th Int. Conf. on Coord. Chem., Nikko, Japan 1967.

5) A. Urushiyama, Y. Itoh, M. Nakahara, and Y. Kondo, *Bunko Kenkyu*, **22**, 151 (1973).

6) R. G. Dickinson, *J. Amer. Chem. Soc.*, **44**, 276 (1922); R. W. G. Wyckoff and R. B. Corey, *Amer. J. Sci.*, **18**, 437 (1929); G. B. Bokii and P. I. Usikov, *Compt. Rend. Acad. Sci. URSS*, **26**, 782 (1940).

7) G. N. Henning, A. J. McCaffery, and P. N. Schatz, *J. Chem. Phys.*, **48**, 5656 (1968).

8) A. J. McCaffery, P. N. Schatz, and T. E. Lester, *ibid.*, **50**, 379 (1969).

9) S. B. Piepho, J. R. Dickinson, A. J. Spencer, and P. N. Schatz, *ibid.*, **57**, 982 (1972).

10) T. P. Sleight and C. R. Hare, *J. Phys. Chem.*, **72**, 2207 (1968).

11) R. W. G. Wyckoff, *Amer. J. Sci.*, **16**, 349 (1928).

12) B. D. Bird, P. Day, and E. A. Grant, *J. Chem. Soc.*, *A*, **1970**, 100.

13) S. B. Piepho, T. E. Lester, A. J. McCaffery, J. R. Dickinson, and P. N. Schatz, *Mol. Phys.*, **19**, 781 (1970).

14) Gmelin Handbuch 67, "Iridium," p. 92.

15) J. H. E. Griffith and J. Owen, *Proc. Roy. Soc. Ser. A*, **226**, 96 (1954).

ESR Studies of Reduced Molybdovanadophosphoric Heteropoly Acids. II. Homogeneous Reduction

Masayuki OTAKE and Tadaaki OTAKI

The Central Research Laboratories, Mitsubishi Chemical Industries Ltd., Hisamoto 290, Takatsu-ku, Kawasaki 213

(Received January 31, 1974)

ESR spectra of the chemically reduced molybdovanadophosphoric heteropoly acids ($H_{3+x}Mo_{12-x}V_xPO_{40}\cdot nH_2O$, where $x=1$ and 2) were observed in the solution and glassy state in various organic solvents. On addition of equimolar amounts of reductants such as $SnCl_2\cdot 2H_2O$, $HSCH_2CH_2SH$, and CH_3SCH_3, a transient ESR signal(B) appeared with eight hfs lines referred to as V(IV), $I=7/2$, and with $\langle g\rangle=1.96$ and $\langle T\rangle=-0.83\times10^{-2}$ cm^{-1}. However, it disappeared within *ca.* 5 hr at 20 °C and another signal(C) with $\langle g\rangle=1.962$ and $\langle T\rangle=-1.00\times10^{-2}$ cm^{-1} gradually increased in intensity. The hyperfine coupling constant of the transient species was thus unusually small as compared with that of the ordinary V(IV) species and the C species. The mechanistic pathways of the reduction were discussed. The splitting observed in the low-field parallel components of the B signal was satisfactorily explained by a "geometrical charge isomerism" characteristic of the structure of the heteropoly anion. The origin of the unusually small hfs constant was discussed in the light of its molecular structure.

In a previous paper,[1] it was demonstrated that partial substitution by vanadium ions for the molybdenum in molybdophosphoric acid is effective for clarifying the mechanism of the reduction and the nature of the reduced species. The results might be summarized as follows:

A) Localization of an electron on the vanadium ions giving rise to an ESR signal was confirmed.

B) In the low stage of reduction, only one paramagnetic center exists in the heteropoly cage, *i.e.*, Mo(V) for molybdophosphoric and V(IV) for vanadium substituted heteropoly acids.

C) As with usual vanadyl complexes, the terminal oxygen of the octahedral oxyanions in the heteropoly cage plays an important part in the localization of the electron on the V=O moiety.

D) As a reduction mechanism, a modified Pottkamp and Umland scheme[2] was proposed, in which almost all the reduced molybdenum ions are tetravalent, Mo(IV)–OH.

The present study was undertaken to obtain more advanced knowledge on the mechanism of the reduction. The polarographic reduction of the above compounds has been extensively studied.[3] However, discrepancies were observed in the results, apparently arising from failure to take into account the hydrolytic instability of the heteropoly anion in the dilute aqueous solution. In order to prevent hydrolysis we chose several organic compounds. Reduction was carried out at room temperature in various organic solvents, using stannous chloride, ethylene dithioglycol and several other sulfur compounds as reducing agents. The difference in the redox potential and the functional groups was expected to allow the formation of a different reduced state corresponding to the individual reductant. Large coupling constants and the strong anisotropic nature of the vanadium(IV) ion, introduced in the cage structure, were useful in the present study.

Experimental

Molybdovanadophosphoric acids $H_{3+x}Mo_{12-x}V_xPO_{40}$, where $x=1$ and 2, were prepared as reported[1] according to the method of Tsigdinos and Hallada.[4] The acids are soluble in organic compounds such as nitrile (acetonitrile), ketones (acetone and methyl ethyl ketone) and esters (methyl isobutyrate and *n*-butyl acetate). In order to avoid contamination with water, the heteropoly acids were evacuated at 100 °C to less than 10^{-3} mmHg, most of the water being removed. Commercial reagents of guaranteed grade were used without further purification. Contamination of the solvents with water was estimated to be less than 0.1%. The reductant solution was added to a solution of the heteropoly acid with the aid of a calibrated microsyringe. An X-band ESR spectrometer, JES-P-10, Japan Electron Optics Lab. Co., was used. Measurements were carried out both at 293 and 77 K. Analysis of the spectra was carried out as described.[1]

Results

Reduction with $SnCl_2\cdot 2H_2O$ in Acetonitrile. The original molybdovanadophosphoric acids gave weak ESR signals both in their solid state and in solution. When a solution of the heteropoly acid and the reductant were mixed, the original orange solution turned blue and a new ESR signal(B), consisting of eight hfs lines referred to as vanadium(IV) ion with $I=7/2$, appeared with remarkably enhanced intensity. How-

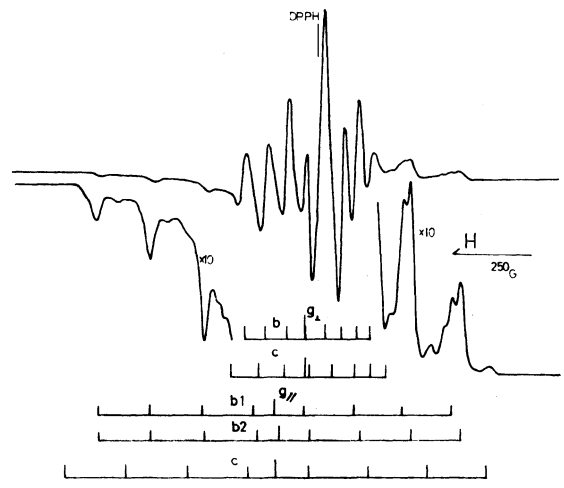

Fig. 1. ESR spectrum (1st derivative, 77 K) of $H_4Mo_{11}V_1PO_{40}$ reduced with $SnCl_2$ in acetonitrile, 0.1 M.

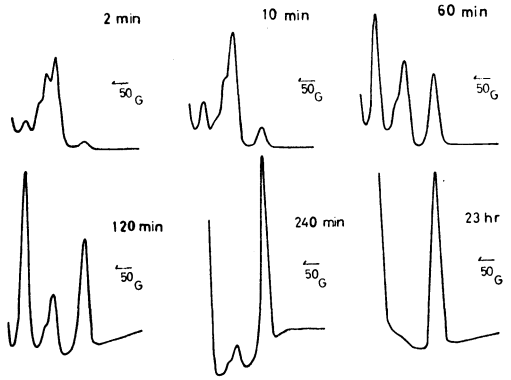

Fig. 2. The change with time of the ESR spectrum (1st derivative, 77 K) of $H_4Mo_{11}VPO_{40}$ reduced with $SnCl_2$ in acetonitrile ($m_n=-7/2$ and a part of $m_n=-5/2$, parallel hfs components)

ever, the spectral pattern changed with time, and another signal(C) gradually grew in intensity, superimposing on the former one which finally disappeared in *ca.* 5 hr at 20 °C. An illustration of the first-derivative spectrum ($x=1$ acid) is given in Fig. 1, in which both signals B and C are superimposed on each other. Splittings are observed in the low-field parallel components of signal B, which indicates that there are at least two kinds of B species. Its hfs coupling constants differ from those of C, while the *g*-values of both signals are almost the same. Signal C was found to be identical with that of a solution of the heteropoly acid reduced in a stream of hydrogen at 280 °C. The rate of formation and decay of the transient species B were measured more precisely by freezing the solution at liquid nitrogen temperature, after keeping the mixture for several minutes at 20 °C. Figure 2 shows how the parallel $m_n=-7/2$ hfs components of signals B and C change with time. The splitting of the parallel component of signal B is most remarkable in this spectral region. Results of the analysis of the spectrum are summarized in Table 1.

Reduction with $HSCH_2CH_2SH$ in Acetonitrile. Various amounts of ethylene dithioglycol were added to a 0.1 M solution of the $x=1$ acid in acetonitrile, but the effect of the quantity of reductant on the ESR spectral pattern was almost negligible except for that on signal intensity. The spectrum, like that in Fig. 1, indicates again the spontaneous formation of species B which disappears within a few hours. The line shape changed gradually, leaving only eight hfs lines of species C. Results of the analysis are given in Table 1. No Mo(V) signal, such as that of dithioglycol-Mo(V) complex ($\langle g\rangle=2.002$, $\langle T\rangle=32$ G)[5] was detected.

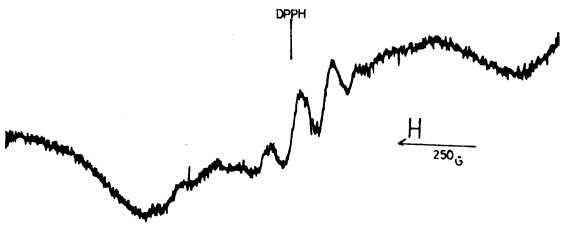

Fig. 3. ESR Spectrum (1st derivative, 20 °C) of $H_5Mo_{10}V_2PO_{40}$ reduced heterogeneously with hydrogen at 280 °C, *n*-butyl acetate solution, 0.1 M.

Other Sulfur Compounds as Reductant. Dimethyl sulfide and thiomalic acid dissolved in acetonitrile caused reduction of the $x=1$ heteropoly acid, giving ESR spectra similar to the spectrum of dithioglycol. The ESR parameters obtained are listed in Table 1.

Reduction with $SnCl_2\cdot 2H_2O$ in Other Solvents. Reduction in a solution of acetone and methyl ethyl ketone gave ESR signals similar to those in Fig. 1. However, the splitting of low-field parallel components of signal B was not so marked as in the case of the spectrum in the acetonitrile solution. Figure 3 illustrates an effect of the solvents on the ESR spectrum of the reduced $x=2$ heteropoly acid, in which the partly reduced acid is dissolved in *n*-butyl acetate. Separation of the hfs components is obviously incomplete.

Discussion

The reduction of molybdovanadophosphoric heteropoly acids with chemical reagents was found to proceed *via* a two step reaction. A number of polarographic studies of molybdophosphoric or other heteropoly acids have been reported[2,3] but not dealing with the forma-

TABLE 1. ESR PARAMETERS OF THE REDUCED $x=1$ HETEROPOLY ACID[a]

Reductants	Species	$g_\perp$	$g_{//}$	$\langle g\rangle$	$T_\perp$[b]	$T_{//}$[b]	$\langle T\rangle$[b]
$SnCl_2$	B_1	1.978	1.932	(1.963)	−0.520	−1.467	(−0.836)
	B_2	1.978	1.926	(1.961)	−0.520	−1.424	(−0.821)
	C	1.982	1.930	(1.964)	−0.648	−1.707	(−1.001)
DSH[c]	B_1	1.978	1.931	(1.962)	−0.525	−1.473	(−0.841)
	B_2	1.978	1.925	(1.960)	−0.525	−1.429	(−0.827)
	C	1.981	1.923	(1.962)	−0.662	−1.731	(−1.018)
DMS[c]	B_1	1.979	1.930	(1.963)	−0.532	−1.473	(−0.845)
	B_2	1.979	1.923	(1.960)	−0.532	−1.432	(−0.832)
	C	1.981	1.923	(1.962)	−0.654	−1.715	(−1.008)
TMA[c]	B_1	1.978	1.940	(1.966)	−0.537	−1.440	(−0.838)
	B_2	1.978	1.934	(1.963)	−0.537	−1.394	(−0.822)
	C	1.981	1.934	(1.965)	−0.657	−1.701	(−1.005)

a) acetonitrile solution, 0.1 M, 77 K, b) unit in $10^{-2}cm^{-1}$ c) DSH; ethylene dithioglycol, DMS; dimethyl sulfide, TMA; thiomalic acid, ( ) indicates calculated values.

tion and decay of transient species. Pottkamp and Umland[2] reported a very slow change in the polarogram of 12-molybdophosphoric acid in *n*-butyl acetate. However, their observation in the polarogram seems to have no connection with ours in ESR, since the rate of appearance of signal B was very fast, and the signal was retained for *ca.* 5 hr at 20 °C.

If the reaction is assumed to follow the first-order kinetics, and $k_1 \gg k_2$, as follows,

$$\underset{\substack{\text{(non-reduced)}\\\text{Diamagnetic}}}{A} \xrightarrow{k_1} \underset{\substack{\text{(Transient)}\\\text{Paramagnetic}}}{B} \xrightarrow{k_2} \underset{\substack{\text{(Final)}\\\text{Paramagnetic}}}{C} \qquad (1)$$

then we obtain the relation

$$C_B/(C_C - C_0 + C_B) = \exp(-k_2 \cdot t) \qquad (2)$$

where C_B and C_C are the concentration of species B and C, respectively, at time t, and C_0 is the initial concentration of C. The time-dependency of $C_B/(C_C - C_0 + C_B)$, determined from the peak heights of each $m_n = -7/2$ parallel line (Fig. 2) is plotted in Fig. 4. The linear relation apparently supports Scheme (1).

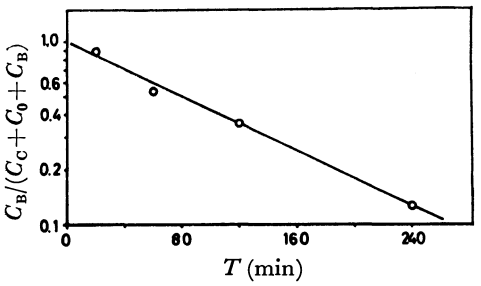

Fig. 4. The change with time of the relative peak heights of the transient (B) and the final (C) species, see text.

The mechanism for satisfying the present observation can be explained as follows.

(a) Species B is assigned as a reduced heteropoly acid and species C as a hydrolysed product from B with such a form as $[VO(H_2O)_x(Solvent)_y]^{2+}$. According to Flynn and Pope,[6] hydrolysis of 5-tungstovanadate(IV) occurs in an aqueous solution to form hydrated vanadyl ion, $[VO(H_2O)_5]^{2+}$. The T value of the hydrate (-1.06×10^{-2} cm^{-1}) is somewhat larger than that of the original heteropoly anion (-0.94×10^{-2} cm^{-1}). The T value of signal C in the present study ($\approx -1.00 \times 10^{-2}$ cm^{-1}) is close to but difinitely smaller than that of the hydrated vanadyl ion. Assumption of the solvation to form $[VO(H_2O)_x(Solvent)_y]^{2+}$ may explain, even partly, such a shift of T. However, the remarkably small $g_{//}$ of species C is closer to that of both B and 11-tungstovanado(IV)phosphate polyanion[7] rather than to that of the usual VO^{2+} complexes whose $g_{//}$ lies in the range 1.93—1.96 (Table 2). Smith and Pope[8] further disclosed the "hydrolytic disproportionation" of the $x=1$ tungstovanadophosphate anion into the $x=0$ and $x=2$ anions. This model partly supports the present observation that g-values of B ($x=1$, in this model) and C ($x=2$) are nearly the same, but it is not suitable for kinetics or for explaining the large difference in the hfs constants. Another contradiction in this decomposition scheme is that ESR spectra of the heteropoly acids reduced with a variety of chemical reagents show a formation of species B with similar rates of formation and similar ESR parameters and its decay into species C. The ESR signal of this species is identical with that of a fresh solution of the heterogeneously reduced heteropoly acid, while reduction with hydrogen at 280 °C never causes decomposition of the compounds.

(b) Another explanation is to assign species B as an intermediate of the reduction and C as the final reduced state of the heteropoly acid in scheme (1), which can remove the contradictions of the first mechanism. It is very probable that the rate of heterogeneous reduction is too fast for the intermediate B to coexist with the final reaction product C, and thus only signal C is observed in the ESR of the reduced mass or its solution. It is of interest to investigate how the two species differ structurally or electronically from each other. If the McConnel linear relation between the hfs parameters and the electron density is also applicable in the present compounds, the hfs constant of signal B, unusually smaller than that of the ordinary vanadyl(IV) compounds as exemplified in Table 2, would indicate that the electrons are much more delocalized over the entire species. There are at least two or three isomers in each of species B and C as is obvious in the low-field splitting of their ESR spectra (Fig. 1 and Figs. 1 and 2 of the previous paper.[1]). They give a hint to elucidating the structure of the two species. An abbreviated scheme of the Keggin-type heteropoly anion structure is given in Fig. 5. Part A represents how the corner-sharing[12] bonds constitute the tetrahedral environment of the central phosphate anion with $(Mo_3O_9)^E$, meaning an edge-sharing unit[12] whose structure is illustrated in part B. Each molybdenum oxyanion has one terminal oxygen with double-bond nature that serves as the main site for the electron-exchange in the chemical redox reactions. Thus we can count and characterize the

Table 2. ESR parameters of several vanadium(IV) compounds

Compounds	$g_\perp$	$g_{//}$	$\langle g \rangle$	$T_\perp$[a]	$T_{//}$[a]	$\langle T \rangle$[a]
$H_4Mo_{11}VPO_{40}$[b] B	1.978	1.928	(1.96)	52.5	145.0	(83.0)
C	1.981	1.923	(1.962)	66.2	173.1	(101.8)
$H_4W_{11}VPO_{40}$[c]	1.968	1.9232	(1.953)	59.6	169.3	(96.2)
$VOCl_2$[d]	1.981	1.932	1.965	71.8	182.6	106.3
$VO(acac)_2$[e]	1.981	1.945	1.967	61.8	169.0	97.5
VOPC[f]	1.985	1.966	(1.979)	55.0	161.0	(109.0)

a) In unit 10^{-4}cm^{-1}, negative signs were omitted. b) Present result, dithioglycol reduction in acetonitrile. c) Authentic sample, Ref. 7. d) In 3M HCl solution, Ref. 11. e) Vanadyl acetylacetonate in tetrahydrofuran solution, Ref. 11. f) Vanadylphthalocyanine in H_2SO_4 solution, Ref. 11.

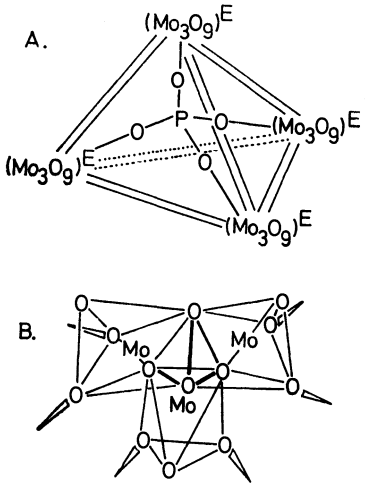

Fig. 5. Skeletal model of the Keggin structure for a) corner sharing bonds, and b) edge-sharing trimer unit, $(Mo_3O_9)^E$.

neighboring oxyanions for one molybdenum (or vanadium substituting for it) ion as is given in Table 3. Since every Mo–O bond is of highly covalent nature as is understandable from their IR spectra,[13] it is reasonable to expect that all the oxyanions are bound by the electron delocalization through the edge- and corner-sharing oxygen ions. In this respect, the edge-sharing oxyanions can make greater contribution to the delocalization of the electron brought into the heteropoly anion by reduction, since they share the d_{z^2} atomic orbital of the molybdenum ions which is directly connected with the terminal oxygen ion contributing to the electron exchange reaction. Intermediate B would then have the same molecular structure as the original heteropoly anion A, but with one reduced molybdenum(V) or vanadium(IV) ions, and one or two molybdenum(IV) ions in the neighboring positions. The difference in the position and nature of the reduced ions in relation to the paramagnetic ion can cause a different contribution to the delocalization of the paramagnetic electron. This can be regarded as the geometrical charge isomerism in the heteropoly anion. In the final reduced species C, the localization of the electron on the paramagnetic ion is more marked and its electronic state is similar to the vanadyl(IV) ion. Such a decrease in the delocalization of electron is understandable if we assume the protonation of the molybdenum(V or IV) ions coexisting in the heteropoly cage with V(IV) ion. The protonation or abstraction of hydrogen can occur at the terminal oxygen ion with double-bond nature, so that delocalization of the electron in the neighbouring ions is disturbed. This model for species C is what was proposed previously. However, a theoretical investigation based on the molecular orbital describing the heteropoly anion seems necessary for a more complete explanation for the difference in hfs parameters of the two species.

TABLE 3. CONSTRUCTION OF A HETEROPOLY CAGE IN KEGGIN STRUCTURE

Type of connection[a]	Number of neighbors
Nearest neighbor	
Edge-sharing	2
Corner-sharing	2
Next nearest neighbor	
Edge—Corner	4 or 2
Corner—Edge	2 or 4
Third neighbor	
Edge—Corner—Edge	1

a) Shortest path from one molybdenum oxyanion.

The low-field parallel lines of species B were found to be split into two or three components. The splitting (≈35 G) is nearly twice as large in magnitude as that in the reduced species in the solid spectrum (≈15 G).[1] In the solution, however, the splitting of signal C disappears, since it is not large enough for detection due to the line broadening of the solution spectrum. In the ESR spectrum of the authentic tungstovanado(IV)phosphate anion,[7] the splittings are not observed. They are thus characteristic of the chemically reduced heteropoly anion in which both V(IV) and Mo(IV) ions coexist in the heteropoly cage. The splittings are completely due to the "geometrical charge isomerism", the larger splitting in species B being related to the larger electron delocalization.

Organic solvents have been found to show an interesting effect on the spectrum. All the line-widths were somewhat larger than that of the solid. The spectrum in Fig. 3 differs from that in Fig. 1, particularly in the line-width. The line-width of the former is estimated to be *ca.* 150 G[9] and that of the latter *ca.* 25 G. This increase (solvents being *n*-butyl acetate and acetonitrile, respectively) is much larger than that in the solvent viscosity, 0.732 and 0.359 cp, respectively. This is related to the specific interaction of the heteropoly acids with esters,[10] in which hydrogen-bonding between the carboxyl group and the heteropoly acid forms a strongly solvated species.

Conclusion

Homogeneous reduction of the molybdovanadophosphoric heteropoly acids dissolved in organic solvents was investigated in order to clarify the mechanism of the reduction. Two kinds of ESR signals, B and C, were observed with a substantially different hfs parameter but with nearly equal *g*-tensor. The first-order kinetics of the decay and formation of these species was observed. A mechanism based on the assignment of species C to be some decomposition product from B had several contradiction. Signal B, which appeared just after mixing the reductant and disappeared within *ca.* 5 hr, had unusually small *T*-tensor values and was assigned to be the intermediate of the reduction. Signal C, whose intensity increased gradually, was assigned to be the final reduced species. A small structural difference in the heteropoly cage of the two species was assumed.

There are at least two isomers in both species B and C, which gave a complicated splitting in the low-field ESR spectra. This observation was characteristic of the chemically reduced heteropoly anion and was explained by the "geometrical charge isomerism".

The authors are indebted to the director of the Central Research Laboratories, Mitsubishi Chemical Industries Ltd., for permitting publication of this paper, to Dr. K. Wada for helpful discussions, and to Miss Y. Komiyama for her help in the measurement of the ESR spectra.

References

1) M. Otake, Y. Komiyama, and T. Otaki, *J. Phys. Chem.*, **24**, 2896 (1973).
2) F. Pottkamp and F. Umland, *Z. Anal. Chem.*, **260**, 185 (1972).
3) G. A. Tsigdinos, Molybdenum Chemicals Bulletin Cdb-12a (Revised), Climax Molybdenum Co., November, 1969.
4) a) G. A. Tsigdinos and C. J. Hallada, *Inorg. Chem.*, **7**, 437 (1968); b) *Inorg. Syn.*, **1**, 127 (1939).
5) T. J. Huang and G. P. Haight Jr., *J. Amer. Chem. Soc.*, **92**, 2236 (1970).
6) C. M. Flynn, Jr. and M. T. Pope, *Inorg. Chem.*, **12**, 1626 (1973).
7) D. P. Smith, H. So, J. Bender, and M. T. Pope, *ibid.*, **12**, 685 (1973).
8) D. P. Smith and M. T. Pope, *ibid.*, **12**, 331 (1973).
9) H. Takahashi, M. Shiotani, H. Kobayashi, and J. Sohma, *J. Catal.*, **14**, 134 (1969).
10) E. M. Ivashkovich, *Ukr. Khim. Zh.*, **38**, 185 (1972).
11) B. A. Goodman and J. B. Raynor, *Advan. Inorg. Radiochem.*, **13**, 135 (1970).
12) P. C. Mitchell and F. Trifiro, *J. Chem. Soc. A*, **1970**, 3183.
13) G. Lange, H. Hahn, and K. Dehnicke, *Z. Naturforsch.*, **24b**, 1498 (1969).

The Extraction of Alkali Metal Picrates with Dibenzo-18-Crown-6

Akira SADAKANE, Tadashi IWACHIDO,* and Kyoji TÔEI

Department of Chemistry, Faculty of Science, Okayama University, Tsushima, Okayama 700
**College of Liberal Arts, Okayama University, Tsushima, Okayama 700*

(Received May 2, 1974)

The distribution of alkali metal picrate complexes of macrocyclic polyether (dibenzo-18-crown-6) between water and benzene was investigated. The polyether-cation complexes were found to be of a 1:1 stoichiometry. The formation of 2:1 complexes was recognized for Rb and Cs in a large excess of the polyether. The extractability of complex cation-picrate ion-pairs decreases in this sequence: K>Rb>Cs>Na>Li. The values of the extraction constants ($\log K_{ex}$) were determined to be 4.65, 3.75, and 3.07 for K, Rb, and Cs compounds respectively. The thermodynamic quantities for the extraction process were calculated from the change in the extraction constants with the temperature. The extraction reactions are all exothermic, accompanied by an entropy decrease.

Macrocyclic polyethers, widely investigated by Pedersen[1] in the last decade, are known as ligands which can form fairly stable stoichiometric complexes with certain cations. It is quite noteworthy that some of these compounds have a great affinity even for alkali metals, though non-cyclic polyethers are commonly not considered strong complexing agents. The most stable complex is formed with a cation which fits well into the molecular cavity of a given ligand, whereas a stable complex is not formed if the ion is too large or too small to lie in the cavity. For instance, polyethers such as 18-crown-6 and its analogues, containing six oxygen atoms linked by six ethylene groups, have ether rings 2.6—3.2 Å[2] in diameter; therfore, they complex with the potassium ion (ionic diameter, 2.66 Å) selectively. X-Ray analyses[3-5] of crystalline complexes show that the metal cation is located in the center of the ether ring. Cations larger than the optimum size can not be accommodated well into the molecular hole, so they tend to form a 2:1 or 3:2 polyether-cation complex of a sandwich type.[2,6-8]

As regards the extraction of an ion-pair species, it has been widely accepted that the extractability of the ion-pair increases with the bulkiness, indicating that the concept of water structure-enforced ion-pairing[9] is applicable. Accordingly, a complex ion-pair species formed by the association of a complexed cation and a large anion, which is considered more hydrophobic and bulkier than an uncomplexed one, is expected to be more extractable.

The present work was undertaken in order to investigate the distribution equilibria and the dependence of the extractability on the size of the alkali metal picrate complexes.

Dibenzo-18-crown-6 was chosen as the complexing agent, since the properties of the polyether and the complexes formed with alkali metals had been well characterized.[1] The picrate anion was chosen as the counter ion so that the ion-pair formed could be determined colorimetrically. Benzene was chosen as the solvent for its non-ionizing property, though it was not necessarily the best solvent. The analysis of the extraction equilibria may be facilitated by the use of non-ionizing solvents, since uncomplexed alkali metal picrates are scarcely extracted into the solvents and the complex ion-pairs do not dissociate in the solvents.

Experimental

Materials. Dibenzo-18-crown-6 was synthesized by the method of Pedersen[1] from catechol and bis(2-chloroethyl)-ether. Recrystallization from benzene gave white, fibrous crystals. The polyether thus obtained had a melting point and an infrared spectrum identical with those of an authentic sample. The alkali metal picrates were prepared by adding a corresponding carbonate solution to an aqueous solution of picric acid; the resulting precipitates of caesium, rubidium, and potassium picrates were recrystallized from water, and the precipitates of sodium picrate, from a water-ethanol (1:3) mixture. The sodium picrate was found to be monohydrate by means of a thermogravimetric method. Benzene of a guaranteed-grade was washed with a sodium hydroxide solution and then water, distilled, and saturated with water. The resulting water-saturated benzene was stored so as to prevent any dissolution of the carbon dioxide. Deionized water was carefully decarbonated by boiling and was saturated with benzene just before each experimental run in order to minimize the volume change on mixing.

Extraction Procedure. An aliquot of an aqueous alkali metal picrate solution and a lithium hydroxide solution (5×10^{-5} M) were transferred into a 50 ml centrifuge tube equipped with a well-grounded stopper and diluted to 20 ml with water (to give these final concentrations: Na and K$<10^{-2}$ M, Rb$<3\times10^{-3}$ M, and Cs$<5\times10^{-3}$ M). 20 ml of a benzene solution containing the polyether ($<10^{-2}$ M) was then added. The resulting mixture was shaken in a thermostated water bath (10—30$\pm$0.1 °C) for 20 min and subsequently allowed to stand for 20 min to complete the phase separation. All the extractions were carried out at pH>6.7.

Determination of the Picrates. The concentrations of the picrates in the organic and aqueous phases were determined spectrophotometrically (Hitachi Spectrophotometer, Type 124) at 425 and 353 nm respectively with appropriate quartz cells 2—50 mm in length. The molar extinction coefficients, ε, of the complex ion-pairs in the organic phase were determined to be 9930, 9800, and 9600 for caesium, rubidium, and potassium compounds respectively. The ε values of the 2:1 polyether-cation complexes for rubidium and caesium were virtually identical with those of the 1:1 complexes. The ε value of the picrate ion in the aqueous phase was also determined to be 14400.

The Distribution Coefficient of the Polyether. A benzene solution containing the polyether ($<5\times10^{-3}$ M) was shaken with pure water under the conditions described above. The aqueous phase thus separated was concentrated by evaporation

to less than one-third of its original volume in order to remove any dissolved benzene. The concentration of the polyether was then determined spectrophotometrically at 272 nm (ε= 5050). Measurements were carried out at five different temperatures, ranging from 10 to 30 °C.

Results and Discussion

Extraction Equilibria. The equilibrium between an aqueous solution containing the alkali metal cation, M^+, and the picrate anion A^-, and an organic solution containing dibenzo-18-crown-6, L, can be written as:

$$M_a^+ + L_o + A_a^- \rightleftarrows MLA_o$$

$$K_{ex} = \frac{[MLA]_o}{[M^+]_a[L]_o[A^-]_a} \quad (1)$$

where MLA denotes the complex ion-pair extracted in the organic phase; the molar concentrations are given in brackets. The overall extraction equilibrium can be analyzed in terms of the following four constituent equilibria.

i) Transfer of the uncomplexed polyether from the organic to the aqueous phase:

$$L_a \rightleftarrows L_o \qquad D^L = \frac{[L]_o}{[L]_a} \quad (2)$$

ii) Complexation of alkali metals with the polyether:

$$L_a + M_a^+ \rightleftarrows ML_a^+ \qquad K_a^{ML} = \frac{[ML^+]_a}{[L]_a[M^+]_a} \quad (3)$$

iii) Association of the complexed cations with the picrate anion:

$$ML_a^+ + A_a^- \rightleftarrows MLA_a \quad K_a^{MLA} = \frac{[MLA]_a}{[ML^+]_a[A^-]_a} \quad (4)$$

iv) Transfer of the complex ion-pairs from the aqueous to the organic phase:

$$MLA_a \rightleftarrows MLA_o \qquad D^{MLA} = \frac{[MLA]_o}{[MLA]_a} \quad (5)$$

Distribution Ratios of the Picrates. The distribution ratios of the picrates, q^A, was calculated from either the concentration in the organic phase, A, or that in the aqueous phase, $A^\circ - A$:

$$q^A = \frac{A}{A^\circ - A} \quad (6)$$

where the superscript o denotes the initial concentration. From the mass balances, the following relations can be obtained:

$$[A^-]_a = A^\circ - A - \frac{A}{D^{MLA}} = f(A) \quad (7)$$

$$[M^+]_a = M^\circ - A - g(A) \quad (8)$$

$$g(A) = \frac{A}{D^{MLA}}\left(\frac{1}{f(A)K_a^{MLA}} + 1\right)$$

$$[L]_o = \frac{L^\circ - A - g(A)}{1 + 1/D^L} \quad (9)$$

The substitution of Eqs. (7)—(9) into Eq. (5) gives:

$$q' = \frac{A}{A^\circ - A - A/D^{MLA}} = \frac{K_{ex}(L^\circ - A - g(A))(M^\circ - A - g(A))}{1 + 1/D^L} \quad (10)$$

The q' is related to q^A by the following equation:

$$\frac{1}{q'} = \frac{1}{q^A} - \frac{1}{D^{MLA}} \quad (11)$$

Assuming that $A^\circ - A \gg A/D^{MLA}$, $D^L \gg 1$, and $M^\circ - A$, $L^\circ - A \gg g(A)$, Eq. (11) can be reduced to:

$$q^A = K_{ex}(M^\circ - A)(L^\circ - A) \quad (12)$$

In the above formulations, complexes with other than the 1 : 1 stoichiometry are not considered; this exclusion is supported by the method of continuous variation (Fig. 1). The theory indicates that the maximum

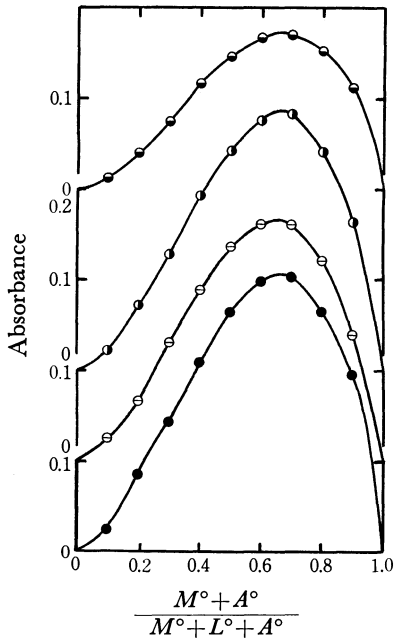

Fig. 1. The method of continuous variation.
Alkali metalpicrate complexes of dibenzo-18-crown-6,
●: Na, $M^\circ + L^\circ + A^\circ = 3 \times 10^{-2}$ M, 50 mm cell.
◒: K, $M^\circ + L^\circ + A^\circ = 1.5 \times 10^{-2}$ M, 2 mm cell.
◑: Rb, $M^\circ + L^\circ + A^\circ = 9 \times 10^{-3}$ M, 50 mm cell.
⊖: Cs, $M^\circ + L^\circ + A^\circ = 1.5 \times 10^{-2}$ M, 50 mm cell.
Temp.: 25 °C. Absorbances: org. phase, at 425 nm.

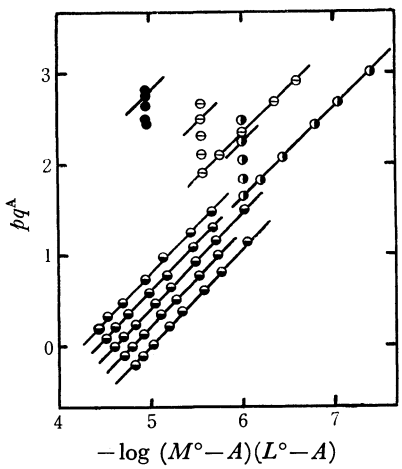

Fig. 2. Plots of pq^A against $-\log (M^\circ - A)(L^\circ - A)$. The symbols used are identical with those in Fig. 1. The vertically-arrayed five points are those obtained at the different temperatures: 30, 25, 20, 15, and 10 °C (from top to bottom).

extraction occurs when equimolar solutions of alkail metal salts and the polyether are added to a system. The equimolar composition corresponds to the point of 2/3 on the abscissa of Fig. 1. As can be expected from Eq. (12), a linear relationship exists between pq^{A} and $-\log(M^{\circ}-A)(L^{\circ}-A)$ values (Fig. 2), indicating that each ion-pair is of the 1:1 stoichiometry. The values of the extraction constants, K_{ex}, calculated from the plots in Fig. 2 are given in Table 1. Since the extractability of the complex sodium ion-pair was so small that the molar extinction coefficient could not be determined, it was assumed that $\varepsilon=9800$, the average value of the other alkali metal compounds.

TABLE 1. EXTRACTION CONSTANTS AND THERMODYNAMIC QUANTITIES

MLA	L	NaLA	KLA	RbLA	CsLA
$\log K_{ex}$	2.9[a]	2.2[b]	4.65	3.75	3.07
ΔH°(kcal/mol)	2.0	−8.9[b]	−16.3	−16.4	−16.0
ΔS°(e.u.)	20	−20[b]	−33.4	−37.8	−39.6

a) $\log D^{L}$ value. b) Estimated value.

The value of K_{ex} for the potassium compound shows that about a half of the potassium is transferred into the benzene phase, when the same volumes of the polyether (10^{-2} M) and the picrate (10^{-2} M) solutions are equilibrated at 25 °C. Figure 3 shows that dibenzo-18-crown-6 is highly selective for potassium, as had been expected.

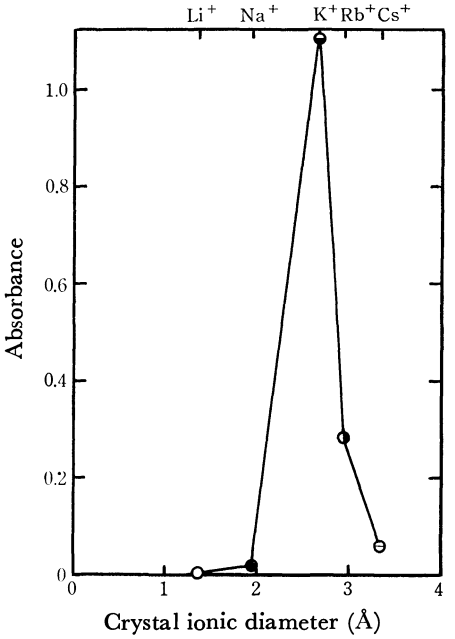

Fig. 3. Extractabilities of alkali metal picrate complexes of dibenzo-18-crown-6 at 25 °C.
M°, L°, $A^{\circ}=10^{-3}$ M. Absorbances: org. phase, at 425 nm with 50 mm cell.

When the polyether was present in excess ($L^{\circ}/M^{\circ}>5$), a plot of pq^{A} against $-\log(M^{\circ}-A)(L^{\circ}-2A)^{2}$ was found to be linear for rubidium and caesium. The implication of such a relationship can easily be understood by assuming a further complexation of complex ion-pair with the polyether:

$$L_o + MLA_o \rightleftarrows ML_2A_o \quad K_o^{ML,A} = \frac{[ML_2A]_o}{[L]_o[MLA]_o} \qquad (13)$$

The existence of such an ion-pair has been demonstrated with some polyethers in the solid state[2,6-8] or in a methanol solution.[10] This may support, though not directly, the above assumption. The overall extraction equilibrium can also be formulated as:

$$M_a^{+} + 2L_o + A_a^{-} \rightleftarrows ML_2A_o$$

$$K_{ex}' = \frac{[ML_2A]_o}{[M^{+}]_a[L]_o^{2}[A^{-}]_a} \qquad (14)$$

The values of $\log K_{ex}'$ were determined from the plots to be 6.5 and 5.6 for the rubidium and caesium compounds respectively. The corresponding association constants, $K_o^{ML,A}$, of the rubidium and caesium ion-pairs can be calculated to be $10^{2.7}$ and $10^{2.5}$ respectively by dividing K_{ex}' by K_{ex}. These values are of a magnitude similar to that of the stability constant obtained by Frensdorff[10] in methanol ($[CsL_2]/[CsL][L]=10^{2.92}$).

No ion-pair of the ML_2A type was found with potassium, not even in a large excess of the polyether ($L^{\circ}/M^{\circ}<18$).

Since the umcomplexed polyether is sparingly soluble in water (about 10^{-5} M at room temperature), it seems reasonable to assume that the ion-pair of ML_2A type can not exist in the aqueous phase, not even when the polyether is present in a large excess in the organic phase.

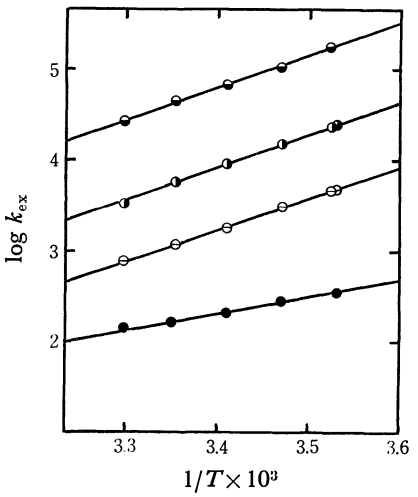

Fig. 4. Plots of $\log K_{ex}$ against $1/T$.
The symbols used are identical with those in Fig. 1.

Thermodynamic Quantities. The values of the extraction constants increase monotonously with a decrease in the temperature. A plot of $\log K_{ex}$ against $1/T$ shows a straight line for each alkali metal (Fig. 4). The value of the enthalpy change, ΔH°, was calculated from the slope. The value of the entropy change, ΔS°, was calculated from the corresponding ΔH° and K_{ex} values by using these thermodynamic relations: $\Delta G^{\circ}=-RT\ln K_{ex}$ and $\Delta G^{\circ}=\Delta H^{\circ}-T\Delta S^{\circ}$.

It can be seen that the entropy contribution, $T\Delta S^{\circ}$, to the free energy change, ΔG°, is smaller than the thermal effect and has the same sign. There is no

significant difference in $\Delta H°$, but the negative values in $\Delta S°$ apparently increase in going from sodium to caesium compounds. The thermodynamic quantities, $\Delta H°_{(15)}$ and $\Delta S°_{(15)}$, for the

$$M_a^+ + L_a + A_a^- \rightleftarrows MLA_o \qquad (15)$$

process were obtained by subtracting the $-\Delta H°_{(2)}$ and $-\Delta S°_{(2)}$ values from the corresponding $\Delta H°$ and $\Delta S°$ values: K, $\Delta H°_{(15)} = -14.3$ kcal/mol and $\Delta S°_{(15)} = -13.4$ e.u.; Rb, -14.4 and -17.8; and Cs, -14.0 and -19.6. The values of $\Delta H°_{(5)}$ and $\Delta S°_{(5)}$ can also be calculated in a similar way if the quantities of the association processes in the aqueous phase represented by Eqs. (3) and (4), $\Delta H°_{ass}$ and $\Delta S°_{ass}$, are known, or *vice versa*, but neither of the quantities is easy to obtain because of the very low solubility of the polyether in water. The thermodynamic quantities for the association processes of dicyclohexyl-18-crown-6 have been reported by Izatt *et al.*:[11] K, $\Delta H°_{ass} = -3.88$ kcal/mol and $\Delta S°_{ass} = -3.8$ e.u.; Rb, -3.33 and -4.2; and Cs, -2.41 and -3.7. If the values of $\Delta H°_{ass}$ and $\Delta S°_{ass}$ for dibenzo-18-crown-6 are assumed to be identical with dicyclohexyl-18-crown-6, the values of $\Delta H°_{(5)}$ and $\Delta S°_{(5)}$ may be calculated to be about -11 kcal/mol and -10——16 e.u. respectively for each alkali metal.

From the above discussion, it follows that the association processes in the aqueous phase play only a minor role in determining the magnitude of the entropy change associated with the overall extraction process, and that the difference in $\Delta S°$ values is determined to a large extent by the difference in $\Delta S°_{(5)}$ values. A plot of $\Delta S°_{(15)}$ against the reciprocal of the cation radius was found to be linear, indicating that the magnitude of $\Delta S°_{(15)}$ is a result largely of electrostatic interaction as well as the relative hydration and number of product and reactant species. The trend in $\Delta S°_{(15)}$ values is consistent with Krasnov's observation:[12] for the extraction of triphenylmethane dye salts by chloroform, the larger the cationic radius, the more negative the distribution entropy becomes.

Though the effect of solvent polarity on the extractability of complex ion-pairs was not investigated systematically, a preliminary test has shown that polar solvents, such as isobutyl methyl ketone and nitrobenzene, give rise to an enhanced extractability. This observation is consistent with the results obtained by Frensdorff:[13] the extractability of the potassium picrate complex of dicyclohexyl-18-crown-6 decreases in this solvent sequence: methylene chloride>trichlorotrifluoroethane>*n*-hexane. Methylene chloride ($K_{ex} = 10^{5.85}$)[13] is found to be better than benzene ($K_{ex} = 10^{4.65}$) as a solvent of the potassium picrate complex of dibenzo-18-crown-6.

Thus, dibenzo-18-crown-6 and its analogues will be considered promising reagents for the separation and extraction of potassium.

References

1) C. J. Pedersen, *J. Amer. Chem. Soc.*, **89**, 7017 (1967).
2) C. J. Pedersen, *ibid.*, **92**, 386 (1970).
3) D. Bright and M. R. Truter, *Nature*, **225**, 176 (1970).
4) M. A. Bush and M. R. Truter, *J. Chem. Soc., B*, **1971**, 1440.
5) P. Groth, *Acta Chem. Scand.*, **25**, 3189 (1971).
6) J. J. Christensen, J. O. Hill, and R. M. Izatt, *Science*, **174**, 459 (1971).
7) L. T. Taylor, S. C. Vergez, and D. H. Busch, *J. Amer. Chem. Soc.*, **88**, 3170 (1966).
8) A. C. L. Su and J. F. Weiher, *Inorg. Chem.*, **7**, 176 (1968).
9) R. M. Diamond, *J. Phys. Chem.*, **67**, 2513 (1963).
10) H. K. Frensdorff, *J. Amer. Chem. Soc.*, **93**, 600 (1971).
11) R. M. Izatt, D. P. Nelson, J. H. Rytting, B. L. Haymore, and J. J. Christensen, *ibid.*, **93**, 1619 (1971).
12) K. S. Krasnov, "Solvent Extraction," Vol. 2, ed. by J. G. Gregory, B. Evans, and P. C. Weston, Society of Chemical Industry, London, (1971), p. 1204.
13) H. K. Frensdorff, *J. Amer. Chem. Soc.*, **93**, 4687 (1971).

Binuclear Metal Complexes. X.[1] Preparation and Magnetism of Mononuclear and Binuclear Copper(II) Complexes of Schiff Bases Derived from 4,6-Diacetylresorcine and Polyamines

Noriaki MANADA, Hisashi OKAWA, and Sigeo KIDA

Department of Chemistry, Faculty of Science, Kyushu University, Hakozaki, Higashi-ku, Fukuoka 812

(Received May 10, 1974)

New binuclear complexes $Cu_2X_2dar(en\text{-}R)_2$ and $[Cu_2dar(dien)_2](ClO_4)_2\cdot H_2O$ were synthesized, $H_2dar(A)_2$ being a Schiff base prepared from 4,6-diacetylresorcinol and an amine A; A stands for *N,N*-dialkylethylenediamine-(=en-R, R=C_2H_5 or *iso*-C_3H_7) or diethylenetriamine(=dien). Mononuclear complexes CuXHdar(en-R) were also prepared for comparison. Two copper(II) ions of the binuclear complexes are separated from each other by the benzene ring. Magnetic susceptibilities of the compounds were measured in the temperature range 77.4~300 K. It was found by means of the plots of χ_A^{-1} *versus* T that all the compounds obey the Curie-Weiss law. The Weiss constants for the binuclear complexes (−10~−34 K) indicate the presence of antiferromagnetic interactions between copper(II) ions through the conjugated π-system of 4,6-diacetylresorcinol moiety, whereas those of the mononuclear complexes are practically zero, showing that the intermolecular interaction is negligibly small.

A number of reports[2-4] have appeared on polynuclear copper(II) complexes which exhibit subnormal magnetic moments. In most of them the copper(II) ions are kept in close proximity by bridging groups.

Some polynuclear copper(II) complexes which exhibit magnetic moments lower than 1.73 B.M., in spite of the considerably long distance between the metal ions, are polymeric copper(II) complexes formed by a catena-μ-group such as pyrazine,[5] quinoxaline[6] and their derivatives,[7,8] and binuclear copper(II) complexes of complicated ligands such as 1,2,4,5-tetraaminobenzene-derivatives[9] and oxamide-derivatives.[10] The magnetic behaviors of these complexes could be explained on the basis of antiferromagnetic exchange interaction between the copper(II) ions through the π-conjugated system of the ligand. In order to obtain an additional information on long distance spin-coupling in binuclear copper(II) complexes, we have prepared a new class of binuclear copper(II) complexes with the use of di-Schiff bases of 4,6-diacetylresorcinol. The complexes obtained are $Cu_2X_2dar(en\text{-}R)_2$ (X=Cl or Br and R=C_2H_5(Et) or *iso*-C_3H_7(*i*-Pr)) and $[Cu_2dar(dien)_2](ClO_4)_2\cdot H_2O$, where $H_2dar(en\text{-}R)_2$ and $H_2dar(dien)_2$ are the di-Schiff bases of 4,6-diacetylresorcine with *N,N*-dialkylethylenediamines and diethylenetriamine, respectively. Two copper(II) ions are separated from each other by 4,6-diacetylresorcinol moiety.

The mononuclear copper(II) complexes CuXHdar-(en-R) (X=Cl or Br and R=Me, Et or *i*-Pr) were prepared, $H_2dar(en\text{-}R)$ denoting the mono-Schiff bases prepared from 4,6-diacetylresorcinol and *N,N*-dialkylethylenediamine. The new compounds were characterized on the basis of elemental analyses, and IR and visible spectra. Magnetic properties of the binuclear complexes were discussed in comparison with those of the mononuclear complexes.

Experimental

Syntheses. 4,6-Diacetylresorcinol was synthesized according to Baker's method.[11]

$Cu_2X_2dar(en\text{-}R)_2$ Complexes. These complexes were prepared by practically the same method. A typical procedure is as follows for $Cu_2Cl_2dar(en\text{-}Et)_2$. *N,N*-Diethylethylenediamine (232 mg, 2 mmol) and 2,2-dimethoxypropane (1 g) were added to an anhydrous methanolic solution (50 ml) of 4,6-diacetylresorcinol (194 mg, 1 mmol) and the reaction mixture was refluxed for 4~5 hr. To this solution were added anhydrous copper(II) chloride (268 mg, 2 mmol) and triethylamine (202 mg, 2 mmol), and the mixture was refluxed for 1~2 hr. Triethylamine was added as a proton-acceptor, without which the binuclear complexes could not be obtained probably due to the decomposition of the Schiff base. The brown needles separated were collected and washed with anhydrous methanol.

$[Cu_2dar(dien)_2](ClO_4)_2\cdot H_2O$. To an anhydrous methanolic solution (50 ml) of 4,6-diacetylresorcinol (194 mg) were added $[Cu(dien)H_2O](ClO_4)_2$ (750 mg), 2,2-dimethoxypropane (1 g) and triethylamine (202 mg). The mixture was heated under stirring for 2 hr and concentrated to 20 ml to give pink prisms which were filtered and recrystallized from methanol.

CuXHdar(en-Me) and CuXHdar(en-Et) Complexes. These complexes were prepared by practically the same method. A typical procedure is as follows for CuClHdar(en-Me). *N,N*-Dimethylethylenediamine (88 mg, 1 mmol) and 2,2-dimethoxypropane (1 g) were added to an anhydrous ethanolic solution (50 ml) of 4,6-diacetylresorcinol (194 mg, 1 mmol) and the reaction mixture was refluxed for 2~3 hr. Anhydrous copper(II) chloride (134 mg, 1 mmol) and triethylamine (101 mg, 1 mmol) were added to the solution which was refluxed for 1 hr and allowed to stand at room temperature overnight. The blue prisms separated were collected and washed with anhydrous ethanol.

CuClHdar(en-i-Pr). *N,N*-di(*iso*-propyl)ethylenediamine (144 mg, 1 mmol) and 2,2-dimethoxypropane (1 g) were added to an anhydrous methanolic solution (50 ml) of 4,6-diacetylresorcinol (194 mg, 1 mmol), and the reaction mixture was refluxed for 2~3 hr. Anhydrous copper(II) chloride (134 mg, 1 mmol) and triethylamine (101 mg, 1 mmol) were added to the solution which was refluxed for 1 hr. The hot solution gave the binuclear complex $Cu_2Cl_2dar(en\text{-}i\text{-}Pr)_2$ as brown crystals, which were filtered and the filtrate was allowed to stand overnight. The brown needles obtained from the filtrate were collected and washed with anhydrous methanol.

Analytical data are given in Table 1.

Measurements. Infrared spectra were measured with a

Table 1. Elemental analyses of complexes

Complex	C(%)		H(%)		N(%)	
	Calcd	Found	Calcd	Found	Calcd	Found
$Cu_2Cl_2dar(en\text{-}Et)_2$	45.05	45.00	6.19	6.17	9.55	9.46
$Cu_2Br_2dar(en\text{-}Et)_2$	39.12	39.17	5.37	5.27	8.29	8.21
$Cu_2Cl_2dar(en\text{-}i\text{-}Pr)_2\cdot MeOH$	48.06	47.59	7.17	7.00	8.30	8.04
$Cu_2Br_2dar(en\text{-}i\text{-}Pr)_2$	42.69	43.20	6.06	6.17	7.66	7.41
$[Cu_2dar(dien)_2](ClO_4)_2\cdot H_2O$	30.60	30.36	4.57	4.50	11.89	11.79
CuClHdar(en-Me)	46.41	46.36	5.28	5.29	7.73	7.75
CuBrHdar(en-Me)	41.43	41.52	4.71	4.88	6.89	6.55
CuClHdar(en-Et)	49.23	48.96	5.91	6.15	7.16	6.93
CuBrHdar(en-Et)	44.20	43.99	5.33	5.79	6.44	6.19
CuClHdar(en-*i*-Pr)·1/2MeOH	51.15	51.49	6.72	7.00	6.45	6.39

Hitachi Grating Infrared Spectrometer model 215 in the region 4000~650 cm^{-1} on a KBr disk. Reflectance spectra were measured with a Shimadzu Multipurpose Spectrometer model MPS-50L at room temperature. Magnetic susceptibilities were determined by the Faraday method in the range from liquid nitrogen temperature to room temperature. Effective magnetic moments μ_{eff} were calculated by the equation

$$\mu_{eff} = 2.828\sqrt{(\chi_A - N\alpha)T}$$

where χ_A is the atomic susceptibility corrected for diamagnetism by the use of Pascal's constants[12] and $N\alpha$ denotes the temperature independent paramagnetism of copper(II) ions.

Results and Discussion

The yield of the binuclear complex $Cu_2X_2dar(en\text{-}R)_2$ is highly dependent on the substituent R. We were successful in obtaining $Cu_2X_2dar(en\text{-}i\text{-}Pr)_2$ in a high yield and $Cu_2X_2(en\text{-}Et)_2$ in a low yield, all the attempts to obtain $Cu_2X_2(en\text{-}Me)_2$ being unsuccessful. Attempts to prepare the binuclear complexes, $[Cu_2dar(en\text{-}R)_2Sol_2](ClO_4)_2$ (Sol denotes a solvent molecule, such as water, methanol or ethanol) were unsuccessful. This is probably because the desired compounds decompose in the solvent into monomeric species. On the other hand, $[Cu_2dar(dien)_2](ClO_4)_2\cdot H_2O$ was easily obtainable. It seems that the larger chelate effect operates for $[Cu_2dar(dien)_2](ClO_4)_2\cdot H_2O$ as compared with $[Cu_2dar(en\text{-}R)_2Sol_2](ClO_4)_2$. The ligand field effect can contribute to the stabilization of $[Cu_2dar(dien)_2](ClO_4)_2\cdot H_2O$.

Table 2. IR and visible spectral data of complexes

Complex	IR (cm^{-1})		Reflectance ($\times 10^3$ cm^{-1})	
	C=O	C=N	d-d	C.T.
$Cu_2Cl_2dar(en\text{-}Et)_2$	—	1590	16.1	20.9
$Cu_2Br_2dar(en\text{-}Et)_2$	—	1595	16.0	20.6
$Cu_2Cl_2dar(en\text{-}i\text{-}Pr)_2\cdot MeOH$	—	1595	15.7	20.8
$Cu_2Br_2dar(en\text{-}i\text{-}Pr)_2$	—	1595	15.4	20.0
$[Cu_2dar(dien)_2](ClO_4)_2\cdot H_2O$	—	1580	17.9	—
CuClHdar(en-Me)	1650	1600	15.6	22.5
CuBrHdar(en-Me)	1650	1600	15.7	22.0
CuClHdar(en-Et)	1630	1580	15.6	22.2
CuBrHdar(en-Et)	1630	1595	15.7	21.4
CuClHdar(en-*i*-Pr)·1/2MeOH	1650~1620	1600~1580	16.1	21.6

The infrared and visible spectral data of the binuclear and the mononuclear complexes are given in Table 2. In the binuclear copper(II) complexes no absorption band was found in the region 1700~1600 cm^{-1}, while in the mononuclear copper(II) complexes a strong band due to the C=O stretching vibration of free acetyl group was found near 1630 cm^{-1}. The absorption band which is attributable to the C=N stretching vibration is observed in the region 1600~1580 cm^{-1}. This band is superposed by the skeletal vibration of the aromatic ring. The broad and strong band around 1100 cm^{-1} in $[Cu_2dar(dien)_2](ClO_4)_2\cdot H_2O$ is attributable to the non-coordinated perchlorate ion. The reflectance spectra of $Cu_2X_2dar(en\text{-}R)_2$ and CuXHdar(en-R) show a ligand field band in the region 16.1~15.4 kK. A band was observed at 20~22.5 kK in addition to the d-d band. Since no such a band is present in the spectrum of $[Cu_2dar(dien)_2](ClO_4)_2\cdot H_2O$, and the bands for $Cu_2Cl_2dar(en\text{-}R)_2$ and CuClHdar(en-R) are located at higher energy region as com-

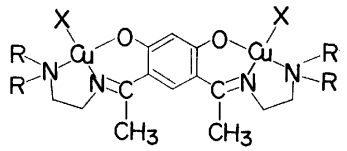

$Cu_2X_2dar(en\text{-}R)_2$ X=Cl, Br R=Et, *i*-Pr

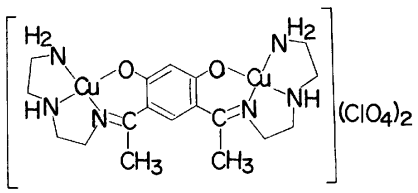

$[Cu_2dar(dien)_2](ClO_4)_2$

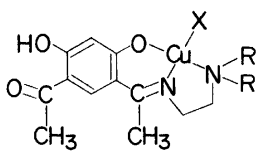

CuXHdar(en-R) X=Cl, Br
R=Me, Et, *i*-Pr

Fig. 1. Proposed structures of complexes.

TABLE 3. MAGNETIC DATA OF COMPLEXES

Complex	θ(K)	μ_{eff}(T)	
$Cu_2Cl_2dar(en\text{-}Et)_2$	−20	1.66 (78.1)	1.80 (288.0)
$Cu_2Br_2dar(en\text{-}Et)_2$	−12	1.66 (83.7)	1.75 (290.0)
$Cu_2Cl_2dar(en\text{-}i\text{-}Pr)_2 \cdot MeOH$	−34	1.66 (81.0)	1.85 (297.8)
$Cu_2Br_2dar(en\text{-}i\text{-}Pr)_2$	−10	1.62 (80.6)	1.75 (297.8)
$[Cu_2dar(dien)_2](ClO_4)_2 \cdot H_2O$	−17	1.69 (83.9)	1.75 (297.8)
CuClHdar(en-Me)	−1	1.76 (83.6)	1.78 (297.8)
CuBrHdar(en-Me)	−2	1.75 (78.3)	1.79 (297.8)
CuClHdar(en-Et)	−2	1.73 (86.0)	1.76 (293.0)
CuBrHdar(en-Et)	0	1.74 (84.1)	1.78 (295.4)
CuClHdar(en-*i*-Pr)·1/2MeOH	0	1.74 (81.2)	1.74 (297.8)

pared with those for the bromo homologues, it is natural to assign the band to the charge transfer band from the halogen ion to the copper(II) ion. This implies that the halogen ion is coordinated to the copper(II) ion. It is thus concluded that the complexes have the structures given in Fig. 1.

The magnetic susceptibilities of the binuclear and mononuclear copper(II) complexes were measured over the temperature range 77.4~300 K. The effective magnetic moments at room temperature and near liquid nitrogen temperature are given in Table 3. The effective magnetic moments of the binuclear copper(II) complexes and those of the mononuclear

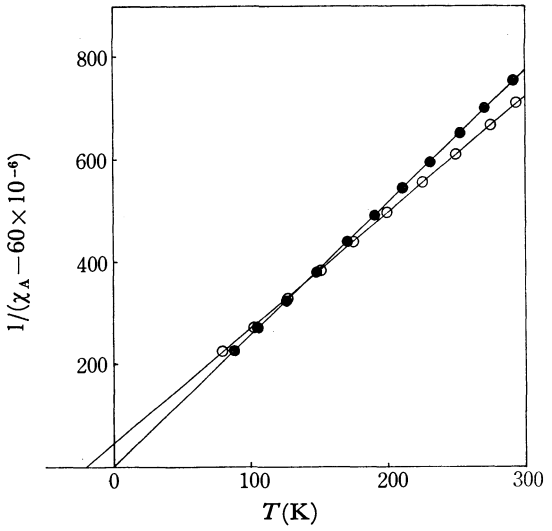

Fig. 2. Plots of reciprocal atomic susceptibilities of (○) $Cu_2Cl_2dar(en\text{-}Et)_2$ and (●) CuClHdar(en-Et) as a function of temperature.

copper(II) complexes show nearly the same values; all the values being larger than the spin-only value, 1.73 B.M. Although the magnetic moment of each mononuclear copper(II) complex near liquid-nitrogen temperature is nearly equal to that at room temperature, the magnetic moments of the binuclear copper(II) complexes are considerably lower than those at room temperature. The reciprocal of $\chi_A - 60\times10^{-6}$ was plotted against temperature. Typical examples for the binuclear and the mononuclear complexes are shown in Fig. 2. The magnetism for the complexes is interpreted in terms of the Curie-Weiss law, $\chi_A = C/(T-\theta)$. The Weiss constants of the complexes are also given in Table 3. The Weiss constants of the mononuclear complexes are nearly zero. This fact clearly indicates that the intermolecular magnetic spin-exchange interaction is negligibly small. On the other hand, the Weiss constants of binuclear copper(II) complexes are in the range −10~−34 K. In comparison with the magnetic properties of mononuclear copper(II) complexes, the antiferromagnetisms of the binuclear copper(II) complexes are attributable to an intramolecular spin-exchange interaction through the π-pathway of 4,6-diacetylresorcine moiety.

The expenses of the research were defrayed by a grant from the Ministry of Education.

References

1) Part IX: M. Tanaka, H. Okawa, T. Tamura, and S. Kida, This Bulletin, **47**, 1669 (1974).
2) M. Kato, H. B. Jonassen, and J. C. Fanning, *Chem. Rev.*, **64**, 99 (1964).
3) E. Sinn and C. M. Harris, *Coord. Chem. Rev.*, **4**, 391 (1969).
4) H. Okawa, T. Tokii, Y. Muto, and S. Kida, This Bulletin, **46**, 2464 (1973).
5) J. F. Villa and W. E. Hatfield, *J. Amer. Chem. Soc.*, **93**, 4081 (1971).
6) H. W. Richardson, W. E. Hatfield, H. J. Stocklosa, and J. R. Wasson, *Inorg. Chem.*, **12**, 2051 (1973).
7) G. W. Inman and W. E. Hatfield, *ibid.*, **11**, 3085 (1972).
8) G. W. Inman, J. A. Barnes, and W. E. Hatfield, *ibid.*, **11**, 764 (1972).
9) E. F. Hasty, T. J. Colburn, and D. N. Hendrickson, *ibid.*, **12**, 2414 (1973).
10) H. Ojima and K. Nonoyama, *Z. Anorg. Allg. Chem.*, **389**, 75 (1972).
11) W. Baker, *J. Chem. Soc.*, **1934**, 71.
12) P. W. Selwood, "Magnetochemistry," Interscience Publishers, New York (1956), pp. 78, 91.

Reaction of Iron(III)-Form Ion Exchanger with Acetylacetone

Kunio Ohzeki, Mayumi Ikeuchi, and Tomihito Kambara
Department of Chemistry, Faculty of Science, Hokkaido University, Sapporo 060
(Received May 16, 1974)

It was found that ferric ions are removed from resin by acetylacetone(Hacac) to form trisacetylacetonatoiron-(III), $Fe(acac)_3$. By the addition of a small amount of pyridine-water mixture to the iron(III)-form resin in acetylacetone milieu, the ferric ions are quantitatively removed from the resin, and in their place the pyridinium ions are adsorbed onto it. The reaction was successfully applied to the synthesis of $Fe(acac)_3$ in over 95% yield.

The conversion of a metallic ion on the cation exchanger into a chelate compound based on the ion exchange reaction in organic medium was investigated.

It was anticipated that if the resin suspended in an organic solvent is brought in contact with a chelating reagent such as β-diketone, the metal ions on the resin will be pulled out into the solvent in the form of metal chelate and the protons liberated from the β-diketone are adsorbed on the resin in place of the metal ions, as shown by

$$(RSO_3)_3Fe + 3Hacac = 3RSO_3H + Fe(acac)_3 \quad (1)$$

where R denotes the resin matrix.

In this paper the reaction of iron(III)-form Amberlyst 15 with acetylacetone is described.

Experimental

Apparatus and Reagents. Absorption measurements were carried out on a Shimadzu QV-50 spectrophotometer and a Hitachi 356 two-wavelength double-beam spectrophotometer with 10 mm cells. A Hitachi 063 type gas chromatograph with a thermal conductivity detector was used. Acetylacetone and pyridine (analytical grade, Wako Pure Chemical Inc.) were used without further purification.

Preparation of Iron(III)-Form Resin. The sulfonic acid cation exchanger, Amberlyst 15,[1] with a macroreticular structure was used, Commercial Amberlyst 15 was crushed and sieved to a fraction of 60—80 mesh. The resin was first washed with ethyl alcohol to remove impregnated toluene, and then with water, and treated with 4 M hydrochloric acid. The water-washed hydrogenform resin was treated with 0.1 M ferric nitrate. The resulting iron(III)-form resin is washed with water until the washings showed no color reaction with potassium ferrocyanide,[2] air dried, and then stored in a desiccator.

A part of ferric ion on the resin might be expected to coordinate hydroxyl ion, *e.g.*, $(RSO_3)_2FeOH$. In this case, the corresponding ion exchange reaction would proceed as follows,

$$(RSO_3)_2FeOH + 3Hacac = 2RSO_3H + Fe(acac)_3 + H_2O \quad (2)$$

Determination of Ferric Ions on the Iron(III)-Form Resin. The ferric ions on the 100 mg portion of the dried iron(III)-form resin were eluted with 2 M hydrochloric acid and determined spectrophotometrically with *o*-phenanthroline method. It was found that the 4.52 ± 0.10 meq of ferric ions are adsorbed per 1 g of the dried iron(III)-form resin.

Conversion of Ferric Ion on the Resin into Acetylacetonate. A test tube containing 5 mg of dried iron(III)-form resin and 3 ml of acetylacetone was dipped into the water bath kept at 70 ± 1 °C and shaken by hand for 5 min. A pyridine-water mixture was then added and warmed again for 5 min. After filtration, the resin was washed with ethyl alcohol and then with water. The ferric ions remaining on the resin were eluted by 2 M hydrochloric acid, and determined spectrophotometrically by the *o*-phenanthroline method.

Results and Discussion

Reaction of Ferric-Form Resin with Acetylacetone. In the course of the reaction, the color of the solution turned red as a result of the formation of tris(acetylacetonato)iron(III) complex identified by spectrophotometry. It was found that although the reaction shown by Eqs. (1) and/or (2) occurs, a considerable amount of iron is firmly retained on the resin. The phenomenon has not bee clarified.

Effect of Pyridine and Water. Conditions were studied for the complete liberation of iron from the resin. Addition of a pyridine-water mixture was found to be highly effective (Figs. 1 and 2). Addition of an appropriate amount of pyridine or water was effective to some extent, but a mixture of the two was the most effective, more than 99% of iron ions being removed from the resin by addition of the 2:1 to 1:5 pyridine-water mixture, 5—7% of the volume of acetylacetone employed. In the presence of the pyridine-water mixture, the dissociation of Hacac takes place as follows.

$$py + H_2O = pyH^+ + OH^-$$

$$Hacac + OH^- = acac^- + H_2O$$

The resulting acetylacetonate anion attacks the ferric

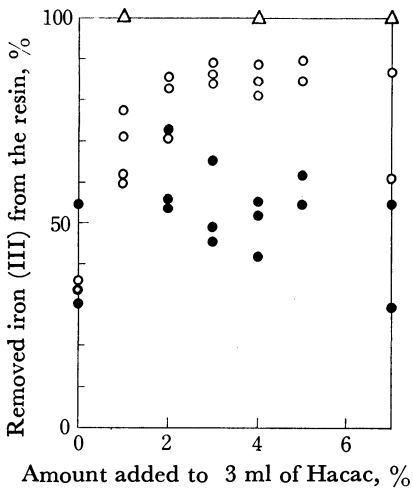

Fig. 1. Effect of the addition of pyridine (●), H_2O (○), and their 1:2 mixture (△) on the removal of the iron-(III) from the 5 mg of the resin with 3 ml of Hacac.

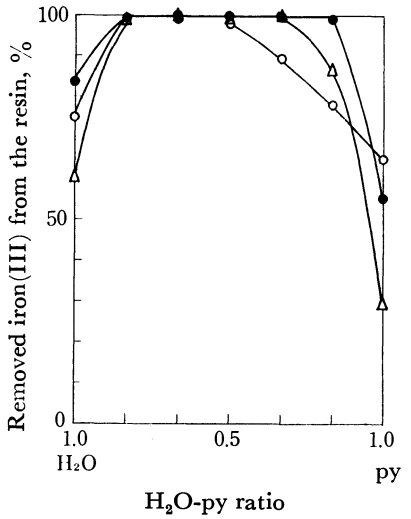

Fig. 2. Effect of the pyridine-water mixture with various ratio on the removal of the iron(III) from the 5 mg of the resin with 3 ml of Hacac. The ratio of the pyridine-water mixture added to Hacac is 1% (○), 5% (●), 7% (△) in Hacac, respectively.

ion on the resin, while the pyridinium ion competes with the ferric ion for the site, namely, the former withdraws the ferric ion from the resin and the latter is adsorbed on the resin in place of the ferric ion. One reaction predicted is shown by

$$(RSO_3)_3Fe + 3Hacac + 3py \xrightarrow{H_2O} 3RSO_3Hpy + Fe(acac)_3 \quad (3)$$

It was necessary to analyze the $Fe(acac)_3$ in the resulting solution and to detect the pyridinium ion on the resin.

Absorption Spectra of the Resulting Solution. After completion of the above procedure, the resin was filtered and washed with acetylacetone, all the washings being collected into a 20 ml volumetric flask, and then a 5 ml portion of the solution was taken out and the flask was filled up to 10 ml with Hacac. A comparison of the absorption spectra of the solution and that of synthesized one in which the corresponding amount of $Fe(acac)_3$ is dissolved in Hacac is shown in Fig. 3. The synthesis of $Fe(acac)_3$ is described later. It may be said that the compound is formed quantitatively by the reaction of iron(III)-form resin with Hacac.

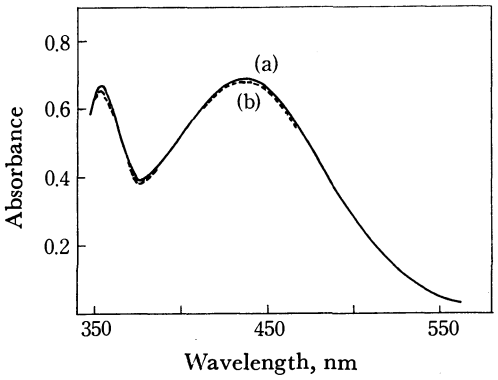

Fig. 3. Comparison of absorption spectra of $Fe(acac)_3$ in Hacac. (a) Synthesized chelate, 1.888×10^{-4} M, (b) Solution obtained by present method *vs.* Hacac.

Test for Pyridinium Ion on the Resin. The resin separated by filtration was further washed with ethyl alcohol and then with water until the washings gave no pyridine odor. A small amount of the 1 M sodium hydroxide was poured onto the resulting resin to elute the presumed pyridinium ion on the resin. The eluate having a strong pyridine odor was analyzed by gas chromatograph on the 1 m column packed with 30% PEG 4000 on 80—100 mesh Chromosorb W, at 90 °C. A pyridine peak appeared on the chromatogram indicating that the pyridinium ion had been adsorbed on the resin. The desorption of iron might proceed according to scheme (3). The sequence of addition of reagents is important, because if pyridine and water are present at the beginning of the reaction, they are adsorbed onto the metal ions on the resin and hinder the contact of Hacac with metal ions as confirmed experimentally.

Application to the Synthesis of the Chelate Compound. Treat 500 mg of iron(III)-form resin with 10 ml of Hacac and then add 0.5 ml of pyridine-water (1 : 2) solution. After the reaction, separate the resin by filtration and wash it with a small amount of Hacac, and collect the filtrate into a test tube. Heat to 130 °C and boil off the excess Hacac and pyridine by bubbling nitrogen gas. Collect the crude $Fe(acac)_3$ at the bottom of the test tube, and press it with glass wool. Narrow the neck of the test tube, and put it into a vessel connected to a vacuum pump, by heating the bottom of the tube to 190 °C at 1 Torr. The chelate deposits at the neck of the test tube. The mp of the chelate 181—183 °C (reported,[3] 181.3—182.3 °C); results of elemental analysis: Found: C, 50.98; H, 5.94%. Calcd for $Fe(C_5H_7O_2)_3$: C, 51.01; H, 5.99%. The yield of duplicate synthesis was 96 and 97%, respectively.

The reaction may commonly occur between the metallic form ion exchanger and chelating agent. Recently Higgins[4] applied the method to the preparation of cesium lanthanoid hexafluoroacetylacetonates. A reaction of this kind might have a wide applicability.

References

1) R. Kunin, E. Meitzner, and N. Bortnick, *J. Amer. Chem. Soc.*, **84**, 305 (1962).
2) F. Feigl, "Spot Tests in Inorganic Analysis," Elsevier, Maruzen Co. Ltd. (1958), p. 161.
3) A. E. Finn, G. C. Hampson, and L. E. Sutton, *J. Chem. Soc.*, **1938**, 1256.
4) C. E. Higgins, *J. Inorg. Nucl. Chem.*, **35**, 1941 (1973).

A-Subustituted 5β-Steroids. VI.[1] *trans*-S_N2' Reaction in Acylolysis of 4β-Bromo-3-keto-5β-steroids

T. Tomoyoshi TAKAHASHI and J. Yasuo SATOH*

Department of Chemistry, The Jikei University School of Medicine, Kokuryo, Chofu, Tokyo 182
**Department of Chemistry, Faculty of Science St. Paul's University, Nishi-Ikebukuro, Toshima-ku Tokyo 171*

(Received February 26, 1974)

A new type of S_N2' reaction in which the nucleophile enters to the leaving group occurs in the acylolysis of 4β-bromo-3-keto-5β-steroids (**1**) to give 2α-acyloxy-3-keto-5β-steroids (**2**) as a product. This reaction pathway was observed by NMR and by tlc.

During the course of our studies on the chemistry of A-substituted 5β-steroids, we have found that the substitution reaction of 4β-bromo-3-keto-5β-steroid (**1a**) with potassium salts of organic acids under refluxing conditions is accompanied with a new rearrangement of a substituent from C_4 to C_2 resulting in the 2β-acyloxy-3-keto-derivative (**3a**) in good yield.[2] A rearrangement in the substitution reaction of steroidal α-halogenoketone has been investigated by several groups in recent years. For example, on acetolysis of 2α-bromo-5α-cholestan-3-one, Fieser and Romero[3] obtained 2α-acetoxy- and 4α-acetoxy-5α-cholestan-3-ones in a 1 to 1 ratio (40%). The fact that 4α-acetoxy-5α-cholestan-3-one was obtained proved that the rearrangement in the substitution reaction from C_2 to C_4 had partially taken place. Under the same condition, 2α-acetoxy-cholest-4-en-3-one was also obtained through the rearrangement from C_6 to C_2 in the substitution reaction of 6β-bromo-cholest-4-en-3-one in 17% yield.[3] Fieser and Romero suggested the following sequence as a possible mechanism for this rearrangement: enolization→allylic isomerization of the bromine atom→substitution with acetoxy-ion. This mechanism was also applied implicitly to the rearrangement from C_2 to C_4. Clarke *et al.* reported that when this reaction was carried out with 6β-bromotestosterone acetate as the reactant, the 2β-acetoxy-derivative was obtained, not the 2α-derivative.[4] They stated that the 2β-acetoxy-group epimerized to the α-acetoxy-derivative, which is a more stable form under the conditions. As a result, they concluded that the primary product was the 2β-acetoxy-derivative.

From the fact that halogeno-ketones as well as allylic halides undergo rearrangement in the substitution reaction, Newman suggested that the substitution reactions of a halogeno-ketone system also belong to the S_N2' reaction.[5] That is to say, these reactions are considered to involve nucleophilic substitution in the enolic form of the ketone; hence an allylic mechanism is reasonable. In these reactions the nucleophile has a *cis*-relationship to the leaving group when it attacks a γ-carbon (allylic position).[6] This consideration for the transition state seems consistent with the previous investigations of the S_N2' reactions in cyclic allylic compounds, in which only *cis*-substitutions have been investigated.[6] In the cases of the steroidal α-bromo-ketones,[3,4] mentioned above, the entering and the leaving groups are in *cis*-relationship to each other, also. In a recent communication, however, we reported a new type of S_N2' reaction in which the nucleophile enters *trans* to the leaving group.[7]

That is to say, when the 4β-bromo-3-keto-5β-steroid (**1a**) were treated with (a) potassium acetate–acetic acid, (b) potassium acetate–dioxane–water, (c) acetic acid–triethylamine and (d) potassium pivalate–dioxane–water at 90—95 °C, and with (e) tetramethylammonium acetate–dioxane at room temperature, the 2α-acyloxy-3-keto-derivatives (**2a, b, c**) was formed as a primary product.

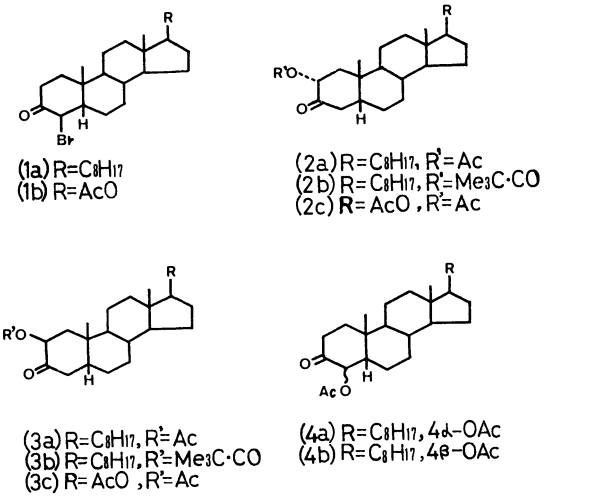

Fig. 1.

In the present paper, we wish to describe in full the details of the mechanism of the new reaction.

Results and Discussion

In each case above, 2α-acyloxy-5β-cholestan-3-ones (**2a, b**) was produced first. Since the isomerization of the 2α-acyloxy- to the 2β-acyloxy-derivative (**3a**) is relatively fast for cases (a) and (c), it was impossible to isolate the intial product, 2α-acyloxy-5β-cholestan-3-one, in high yield, but the 2α-acyloxy-derivative was obtained almost stereospecifically in 5 hr by reaction (b) and in 5 days by reaction (e).

In order to examine the stereochemical pathway of this reaction, **1a** was treated with potassium acetate in acetic acid (reaction (a)). The progress of the reaction was followed by tlc at certain time intervals. It could be observed that only the initial product (**2a**) was formed during the first 0.5 hr; and then during the next 0.5 hr, this initial product began to isomerize to the **3a**. This isomerization gradually continued, and the ratio of **2a** to **3a** became 1 : 1 at 3 hr. After 6.5 hr,

the **2a** completely disappeared.

In reaction (d), the NMR spectrum of the reactant, terminated after 1 hr, had peaks at 5.20 ppm (t, J= 9.5 Hz, which probably is in a boat conformation due to the severe interaction of the 2α-pivaloyloxy group with C_9–H and C_9–C_{10} in the chair conformation) and 4.80 ppm (d, J=11.5 Hz) due to the 2β-H in the 2α-pivaloyloxy-derivative and the 4α-H in the starting material respectively. When the reaction, which had once been terminated, was continued for 8 hr, the NMR spectrum of the reactant showed peaks at 5.04 ppm (dd, J=6.0 and 14.5 Hz) and 5.20 ppm, due to the 2β- (**3b**) and 2α-pivaloyloxy-derivatives (**2b**), respectively. In the NMR spectrum of the reactant after 30 hr, the triplet at 5.20 ppm disappeared and the quartet at 5.04 ppm remained. This suggested that an α-side attack is also possible for such a bulky nucleophile as Me_3CCOO^-. These NMR spectra are shown in Fig. 2. Such a phenomenon was already observed in reaction (b) by using a 220 MHz spectrometer to observe the change in the signals due to the methyl protons of the 2α- and 2β-acetoxy groups.[7]

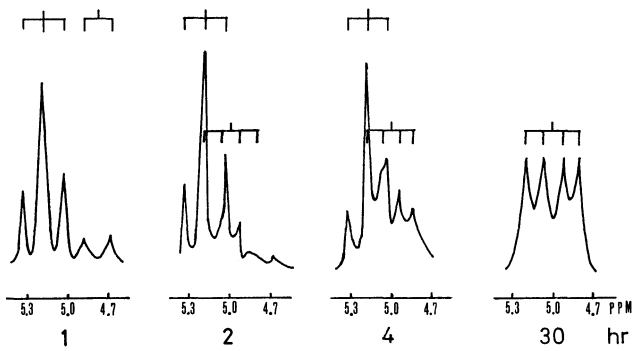

Fig. 2. 60 MHz NMR signals due to C_2H in the case of reaction (d) at intervals. Starting material: 4.80 ppm; α-Isomer: 5.20 ppm; β-Isomer: 5.04 ppm.

As the mechanism of the acylolysis, it is possible to consider that normal substitution occurs at C_4 with acyloxy-ion, and subsequently the acyloxy group formed rearranges to C_2.

Therefore, the 4α-acetoxy-derivative (**4a**) was synthesized from 5β-cholestan-3-one to find out whether or not the acetoxy-derivative changes to the 2α-acetoxy-isomer. Because this 4α-acetoxy-derivative contaminated with a trace of 4β-acetoxy-derivative, the crystallization of **4a** was unsuccessful. The structure of **4a** was confirmed by the comparison of NMR spectral data with the three other isomers (2α-, 2β-, and 4β-acetoxy-derivatives). When the 4α-acetoxy-derivative without further purification was treated with potassium acetate–acetic acid under the same conditions for the acetolysis described above, the 4β-acetoxy-derivative (**4b**) formed quantitatively. A parallel study[11] on 4α,17β-diacetoxy-5β-androstan-3-one found essentially the same behaviour. On the other hand, when the 4β-acetoxy-derivative was treated under the same conditions, the starting material was recovered.[8] From these results, it was ascertained that, in the acylolysis of 4β-bromo-5β-cholestan-3-one, the possibility of normal substitution products rearranging to give the 2-acyloxy-isomer is eliminated.

There is a further possibility that the substitution reaction by acyloxy ion takes place after a rearrangement of the bromine from C_4 to C_2 in the 4β-bromo-3-keto-derivative (**1**). Recently, one of the authors reported the first example of rearrangement of a halogen in an α-halogeno-ketone from the α- to the α′-carbon in such acylolysis.[9] That is, in the acetolysis of 1β-halogeno-5β-cholestan-2-one with potassium acetate–acetic acid at 98 °C, 3-halogeno-ketones could be isolated along with the 3-acetoxy-2-keto-derivative. But in the case of the reaction of 4β-halogeno-3-keto-5β-steroids, the 2-halogeno-3-keto-derivatives were not obtained, nor could they be observed by following the reaction with NMR and tlc. The foregoing facts would suggest that the rearrangement of 4β-halogeno-3-keto-5β-steroids to 2-halogeno-derivatives does not occur under our conditions. This result was identical with Liston's observation that 2β- and 4β-bromo-17β-acetoxy-5β-androstan-3-ones are not interchanged or equilibrated.[10]

While this report was being prepared, Wareneboldt and Weiler reported that the reaction of 17β-acetoxy-4β-bromo-5β-androstan-3-one (**1b**) with sodium acetate–acetic acid gave 2β,17β-diacetoxy-5β-androstan-3-one (**3c**) under refluxing conditions.[11] They did not observe formation of the 2α-acetoxy-isomer (**2c**), but they discussed the mechanism of the acetolysis by reference to the possible pathways for the reaction of *cis*-S_N2' type catalogued by Bordwell.[12] That is to say, in the acetolysis of 17β-acetoxy-2β-bromo-5β-androstan-3-one, it is cleanly converted to the 2β-acetoxy derivative in refluxing acetic acid–sodium acetate at a rate comparable to the 4β-bromo-derivative. From this finding, they suggested a carbonium ion pathway for this reaction. Thus both bromoketones give the same intermediate. If the acetolysis proceeds by such a mechanism, it can be considered that, for acetoxy ion attack, the steric environment at C_2 is not so different from that at C_4. From the conception of "product development control",[13] moreover, a 4β-substituted product may be anticipated from the carbonium ion. However, Weiler's product was only the

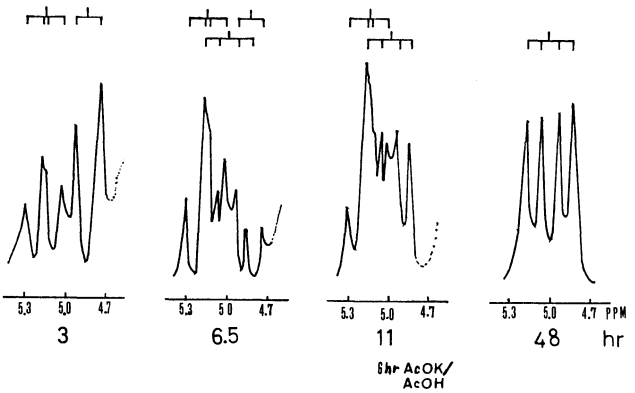

Fig. 3. 60 MHz NMR signals due to C_2H in the case of **1b**–potassium acetate–dioxane–water (100 mg/500 mg/7 ml/0.5 ml). Starting material: 4.80 ppm: α-Isomer: 5.14 ppm; β-Isomer: 5.02 ppm.

2β-acetoxy-derivative, not the 4-isomer. Therefore, we examined the acetolysis of 17β-acetoxy-4β-bromo-5β-androstan-3-one under our conditions. In both the case of reaction (a) and (b), the 2α-acetoxy-derivative (**2c**) was also formed as a primary product. In the former, however, the 2α-acetoxy-derivative was converted rapidly to the 2β-isomer (**3c**). In the latter case, it could be observed that the initial product was isomerized gradually to the 2β-isomer by the NMR spectra in each reaction step (Fig. 3).

According to these results, it is inferred that the acetolysis of 17β-acetoxy-4β-bromo-5β-androstan-3-one (**1b**) belongs to the *trans*-S_N2' reaction, and the primary product is the 2α-acetoxy-derivative (**2c**). Therefore, it does not seem reasonable that the carbonium ion pathway can be applied to the S_N2' reaction of the *trans* type. However, it seems reasonable that the acetolysis of 2α-bromo-5α-cholestan-3-one[3] proceeds by a carbonium ion pathway. To make sure that the reaction proceeded by such a pathway, the acetolysis of 2α-bromo-5α-cholestan-3-one was followed by taking NMR spectra at certain intervals. From these results, it turned out that 2α- and 4α-acetoxy-5α-cholestan-3-one in one to one proportion was already produced at an early stage. The ratio was retained during the acetolysis. The same results were also obtained in the case of 4α-bromo-5α-cholestan-3-one. Thus, it can be considered that with the 5α-series, this reaction proceeds by a carbonium ion pathway.

The *trans*-S_N2' reaction proceeded perfectly without allowing the normal substitution to take place, that is, the reaction of 4β-bromo-3-keto-5β-steroids with nucleophilic reagents gave 2-substituted 3-keto-5β-steroids only. Therefore, the acetoxy-ion present at high concentration in the reaction system is likely to attack the C_2-position directly by the S_N2' reaction mechanism. On the α-side attack at C_2, the enolization of the 3-keto group by acylolysis of **1** allows ring A to be a relatively flat with respect to ring B.[7] This conformation provides a favorable environment for nucleophile to attack at C_2. Furthermore, α-attack occurs more readily than β-attack at this position, because of the steric effect of the 10-methyl group. The 2α-acyloxy-derivative (**2**) was, therefore, formed as the product of the *trans*-S_N2' reaction and then was isomerized to the more stable 2β-isomer. Whether the nucleophile enters *trans* or *cis* to the leaving group depends on the stereochemistry of the reactant.

On the basis of these results, we conclude that in the S_N2' reaction of the α-halogeno-ketone, the entering group is not always *cis* to the leaving group.

Experimental

Thin-layer chromatography was carried out on Wakogel B-5 (Wako Pure Chemical Industries Ltd.), and detected by sulfuric acid. IR spectra were measured (KBr) with a Hitachi model 215 infrared spectrophotometer. ORD spectra were obtained in dioxane with JASCO model ORD/UV-5 instrument. NMR spectra were recorded in carbon tetrachloride with tetramethylsilane as an internal standard using a Hitachi-Perkin Elmer R-20A and Varian HR-220 instruments.

Acetoxylation of 5β-Cholestan-3-one. The synthesis was carried out following the procedure of Henbest *et al.*[14] for the synthesis of 2α-acetoxy-5α-cholestan-3-one from 5α-cholestan-3-one. A solution of 5β-cholestan-3-one (5 g) and lead tetraacetate (6.4 g) in benzene (150 ml) containing boron trifluoride–ether complex (1 ml) was stirred at room temperature in a nitrogen atmosphere for 4 hr. The reaction mixture was washed with water, dried and evaporated. The resultant oily product was chromatographed on silica gel and elution with benzene–light petroleum (2: 3) gave 4β-acetoxy-5β-cholestan-3-one (**4b**) (1.7 g), which crystallized from ethanol as needles, mp 104—106 °C, IR: ν_{max} 1745, 1725, and 1225 cm^{-1}; ORD (*c* 0.4, dioxane) at 21 °C: $[\alpha]_{389}$ +67.5°, $[\alpha]_{321}$ +247.5°, $[\alpha]_{306}$ +170°, $[\alpha]_{301}$ +185°, $[\alpha]_{299}$ +170°, and $[\alpha]_{280}$ +450; NMR: 5.33 ppm (d, J=12 Hz, 1H); Found: C, 78.27; H, 10.92, $C_{29}H_{48}O_3$ requires C, 78.37; H, 10.88%.

Reaction of 4β-Acetoxy-5β-cholestan-3-one (4b) with Potassium Acetate–Acetic Acid. A mixture of **4b** (22 mg), potassium acetate (20 mg) and acetic acid (2 ml) was refluxed for 6 hr. After the usual work-up, the starting material was recovered from the reaction mixture.

3β,4β-Oxido-3α-acetoxy-5β-cholestane. The synthesis was carried out following the procedure of Williamson and Johnson.[15] A solution of 3-acetoxy-5β-cholest-3-ene (4.5 g) in dichloromethane (70 ml) was treated with *m*-chloroperbenzoic acid (3.0 g) at room temperature for 24 hr. The reaction mixture was poured into water and the dichloromethane layer was worked up in the usual manner. Crystallization of the resulting oil from acetone gave 3β,4β-oxido-3α-acetoxy-5β-cholestane (844 mg), mp 135—138 °C, IR cm^{-1}: ν_{max} 1745, 1225, and 1052; NMR: 2.86 ppm (s, 1H); Found: C, 78.33; H, 10.88, $C_{29}H_{48}O_3$ requires C, 78.26; H, 10.97%.

4α-Acetoxy-5β-cholestan-3-one (4a). A sample of 3β,4β-oxido-3α-acetoxy-5β-cholestane (636 mg), mp 135—138 °C, was placed in a 20 ml Erlenmeyer flask which was immersed for 5 min in an oil bath maintained at 160 °C. The resulting oil which failed to crystallize; IR: ν_{max} 1750, 1727, and 1235 cm^{-1}; NMR: 5.25 ppm (d, J=8.6 Hz, 1H). The synthesis was carried out following the procedure of Williamson and Johnson.[15]

Reaction of 4α-Acetoxy-5β-cholestan-3-one (4a) with Potassium Acetate–Acetic Acid. A mixture of (**4a**, oil) (22 mg), potassium acetate (20 mg) and acetic acid (2 ml) was refluxed for 6 hr. The NMR indicated that 4α-acetoxyderivative completely isomerized to the corresponding 4β-acetoxy-derivative (**4b**).

Acetolysis of 1a with Tetramethylammonium Acetate in Dioxane. A mixture consisting of **1a** (50 mg), tetramethylammonium acetate (210 mg) and dioxane (2.5 ml) was stirred at room temperature. After 5 days, the reaction mixture was poured into water and extracted with ether. The ether extracts were washed with water, dried and evaporated. Crystallization of the residue from ethanol gave (**2a**) (23 mg) as needles, mp 138—139 °C. The product was identical in infrared spectrum with authentic 2α-acetoxy-5β-cholestan-3-one.[2]

2β-Trimethylacetoxy-5β-cholestan-3-one (3b). A solution of **1a** (100 mg) in dioxane (5 ml) was stirred with pivalic acid (521 mg), potassium hydroxide (286 mg), and water (1 ml) at refluxing temperature. After 18 hr, the reaction mixture was poured into water, and extracted with ether. After the usual work up, crystallization from ethanol afforded needles (258 mg), mp 125—126 °C, IR: ν_{max} 1746, 1728, and 1158 cm^{-1}; ORD (*c* 0.96, dioxane) at 25 °C: $[\alpha]_{330}$ −31.3°, $[\alpha]_{310}$ −146°, $[\alpha]_{275}$ +407°; NMR: 5.04 ppm (q, J=6.0 and 13.5 Hz, 1H); Found: C, 79.19; H, 11.23, $C_{32}H_{54}O_3$ requires C, 78.96; H, 11.18%.

Followings of the Progress in Acylolysis of 1a. Each

amount (100 mg) of 4β-bromo-5β-cholestan-3-one (**1a**) was treated with (a) potassium acetate–acetic acid (500 mg/6 ml), (b) potassium acetate–dioxane–water (500 mg/7 ml/0.5 ml), (c) triethyl amine–acetic acid (3 ml/7 ml), (d) pivalic acid–potassium hydroxide–dioxane–water (521 mg/286 mg/5 ml/1 ml) at 90—95 °C, and (e) tetramethylammonium acetate–dioxane (420 mg/5 ml) at room temperature. Each reaction was stopped at certain time intervals. After the usual work up, the progress of the reaction was followed by tlc and by using NMR spectrometer. R_f values of the starting material (**1a**) and the resultant α-acyloxy-ketones in benzene–ether system (19: 1) are as follows; 4β-bromo- (**1a**): 0.77, 2α-acetoxy- (**2a**): 0.46, 2β-acetoxy- (**3a**): 0.61, 2α-pivaloxy- (**2b**): 0.45, and 2β-pivaloyloxy-5β-cholestan-3-one (**3b**): 0.64. The NMR spectra of method (b), as an example for the acetolysis, and method (d) are shown in Figs. 3 and 2, respectively.

Epimerization of 2α-Acetoxy-5β-cholestan-3-one. (i) A solution of **2a** (50 mg) in acetic acid (2 ml) was refluxed with potassium acetate (35 mg) for 3 hr. The tlc indicated that the 2α-acetoxy-derivative (**2a**) completely epimerized to the corresponding 2β-acetoxy-isomer (**3a**). (ii) Instead of using acetic acid as a solvent, dioxane was used. The epimerization was completed in 6 hr refluxing conditions.

*Acetolysis of 17β-Acetoxy-4β-bromo-5β-androstan-3-one (**1b**).* This method was identical with reaction (b), described above. 2α,17β-Diacetoxy- and 2β,17β-diacetoxy-5β-androstan-3-one formed could not be identified on the tlc. The NMR spectra of the reaction mixture at certain time intervals are shown in Fig. 3.

The authors wish to thank Professors Jisaku Kuroda, Machiko Tozawa, and Tunetaka Kushimoto for their many supports during this work.

References

1) Part V: J. Y. Satoh, K. Misawa, T. T. Takahashi, M. Hirose, C. A. Horiuchi, S. Tsujii, and A. Hagitani, This Bulletin, **46**, 3155 (1973).
2) J. Y. Satoh, T. T. Takahashi, M. Mukoh, Y. Ogaki, C. T. Kimura, H. Aoki, and A. Hagitani, *ibid.*, **39**, 855 (1966); T. T. Takahashi, J. Y. Satoh, and A. Hagitani, *Nippon Kagaku Zasshi*, **89**, 974 (1968).
3) L. F. Fieser and M. Romero, *J. Amer. Chem. Soc.*, **75**, 4716 (1953).
4) R. L. Clarke, K. Dobriner, A. Mooradian, and M. Martini, *ibid.*, **77**, 661 (1955).
5) M. S. Newman, "Steric Effects in Organic Chemistry," John Wiley & Sons, Inc., New York, N.Y. (1959), p. 97.
6) P. de Mayo, "Molecular Rearrangements," Interscience, London (1963), p. 27.
7) J. Y. Satoh and T. T. Takahashi, *Chem. Commun.*, **1970**, 1714.
8) D. Sc. Thesis of T. T. Takahashi, St. Paul's University, March, 1971.
9) J. Y. Satoh, C. A. Horiuchi, and A. Hagitani, *Chem. Lett.*, **1972**, 995.
10) A. J. Liston, *J. Org. Chem.*, **31**, 2105 (1966).
11) R. B. Warneboldt and L. Weiler, *Tetrahedron Lett.*, **1971**, 3413.
12) F. G. Bordwell, *Accounts Chem. Res.*, **3**, 281 (1970).
13) W. G. Dauben, G. T. Fonken, and D. S. Noyce, *J. Amer. Chem. Soc.*, **78**, 2579 (1956).
14) H. B. Henbest, D. N. Jones, and G. P. Slater, *J. Chem. Soc.*, **1961**, 4472.
15) K. L. Williamson and W. S. Johnson, *J. Org. Chem.*, **26**, 4563 (1961).

Reaction of 1,3-Oxazinium Salt with Active Methylene Compounds

Isao SHIBUYA and Masahiro KURABAYASHI
National Chemical Laboratory for Industry, Mita, Meguro-ku, Tokyo 153
(Received March 7, 1974)

2,4,6-Triphenyl-1,3-oxazinium perchlorate reacts with active methylene compounds to give several butadiene derivatives and various pyridine derivatives. The reactions seem to proceed as follows: The carbanion from an active methylene compound attacks the 6-position of the oxazinium ring, and opens the ring to form a butadiene as an intermediate, which is then recyclized to a pyridine derivative according to a characteristic mode. The mode of recyclization differs with the constituent of each active methylene. There are five modes characteristic of cyano-, ester-, amido- and benzoyl constituents and nitromethane. A compound containing two different constituents usually follows either of the two possible modes.

Pyrylium, 1,3-oxazinium, and 1,3,5-oxadiazinium salts constitute a homologous series with respect to the number of nitrogen atoms in their rings. It was found that 1,3-oxazinium[1,2] and 1,3,5-oxadiazinium salts,[2-5] as well as pyrylium salt, are 6π-cation compounds. The high reactivity of the salts toward many kinds of nucleophiles is known, in particular that of pyrylium salt.[6-9] Active methylene compounds are nucleophiles which introduce a carbon atom with one or two nucleophilic substituents. Dimroth and Neubauer showed that active methylene compounds react with 2,4,6-triphenylpyrylium salt (**1**) to produce various benzenes.[10,11] Schmidt *et al.* reported that 2,4,6-triphenyl-1,3-oxazinium perchlorate (**2**) gives 2-benzoylamino-3-cyano-4,6-diphenylpyridine (**4**) on reaction with malononitrile.[12,13] We showed that 2,4,6-triphenyl-1,3,5-oxadiazinium salt (**3**) reacts with several active methylenes to give pyrimidine derivatives.[14,15] It was found that an active methylene does not always behave in the same manner in reacting with **1** and **3**; for example, benzoylacetonitrile reacts with **1** to give 2,4,6-triphenylbenzonitrile, and with **3** to give 5-cyano-2,4,6-triphenylpyrimidine and 5-benzoyl-4-benzoylamino-2,6-diphenylpyrimidine; methyl cyanoacetate reacts with **1** to give 2,4,6-triphenylbenzonitrile and with **3** to give 4-benzoylamino-5-methoxycarbonyl-2,6-diphenylpyrimidine. In order to clarify the behavior of active methylenes reacting with **1**, **2**, and **3**, the reactions of **2** with these methylene were studied. The results are discussed together with those dealing with **1** and **3**.

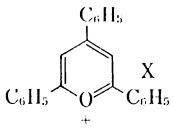
1

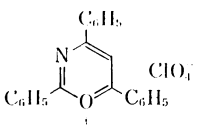
2

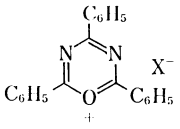
3

Results and Discussion

Methyl Cyanoacetate. Since methyl cyanoacetate reacts with **1** and **3** in different ways,[10,14] its reaction with **2** was examined. **5** was obtained in a good yield on refluxing this compound and **2** in dioxane in the presence of a 1.5 molar amount of triethylamine. The molecular weight of **5** was determined by mass spectroscopy to be 376. **5** has a cyano group (2205 cm^{-1}) and an ester group (1756, 1229 cm^{-1}). On the other hand, when 2-chloro-3-cyano-4,6-diphenylpyridine[13,16] was treated with benzoic acid in pyridine, the product was the same as **5**. Thus, **5** was identified to be 2-benzoyloxy-3-cyano-4,6-diphenylpyridine. It was found that this compound reacts with **1**, **2**, and **3** in different ways.

Diethyl Malonate. Diethyl malonate did not react on refluxing with **2**, but after treatment at room temperature it produced **6** which was determined to be an adduct of the oxazinium cation and the carbanion from this compound. Schmidt reported that **2** reacting with some active methylenes gives some adducts with butadiene structures.[13] It is assumed that **6** is a butadiene derivative. When **6** was heated above its melting point, **7** was derived. The molecular weight of **7** was determined to be 423. Its IR spectrum resembles that of **5** very closely, and shows the presence of two kinds of ester groups (1757, 1720, 1265, 1232 cm^{-1}). This and the results of elemental analysis indicate that **7** is 2-benzoyloxy-3-ethoxycarbonyl-4,6-diphenylpyridine. The type of reaction which gives **7** is thought to be the same as that for **5**. For **3**, this compound gives 4-benzoyloxy-5-ethoxycarbonyl-2,6-diphenylpyrimidine with the liberation of ethanol followed by benzoyl migration.[15] Therefore, this compound is regarded to react in the same way with **2** and **3** to give benzoyl-pyridine and -pyrimidine, respectively.

Cyanoacetamide and Ethyl Carbamoylacetate. When **2** was refluxed with cyanoacetamide in dioxane, **8** was obtained. Its IR spectrum coincided with that of 2-hydroxy-3-cyano-4,6-diphenylpyridine which was derived from dibenzoylmethane and this compound.[13] However, ethyl carbamoylacetate reacting with **2** gave **9** when left to stand at room temperature. This product is regarded as a butadiene derivative from its IR and NMR spectra. When heated above its melting point, **9** was converted into **10**. **10** is weakly acidic. Its IR spectrum has no absorption assigned to an amide group, but closely resembles that of **8**. Thus, **10** was determined to be 2-hydroxy-3-ethoxycarbonyl-4,6-diphenylpyridine. Since these two compounds possessing a carbamoyl group produce 2-hydroxypyridines, it may be certain that cyanoacetamide forms a butadiene derivative as an intermediate.

Dibenzoylmethane, Benzoylacetonitrile, Benzoylacetamide, Nitromethane, p-Chlorobenzoylacetonitrile, and Bis(p-chlorobenzoyl)methane. **11**, **12**, and **14** were obtained, respectively when dibenzoylmethane, benzoylaceto-

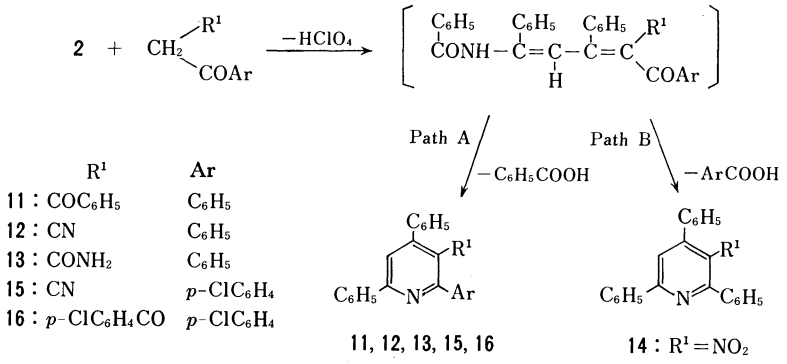

Scheme 1.

nitrile and nitromethane were refluxed with **2**, whereas treatment of **2** with benzoylacetamide at room temperature gave **13**. Their molecular weights were determined to be 411, 332, 350, and 352, respectively, the values being equal to the sums of the mass of the 2,4,6-triphenylpyridyl group (306) and that of each constituent, *i.e.*, the benzoyl (105), cyano (26), carbamoyl (44), and nitro groups (46), respectively. Their IR spectra were regarded as essentially the same except for the absorptions assigned to each group described above. On the other hand, **11** is identified to be 3-benzoyl-2,4,6-triphenylpyridine[17] with an authentic sample. Thus, **12**, **13**, and **14** were confirmed to be 3-cyano-, 3-carbamoyl-, and 3-nitro-2,4,6-triphenylpyridines. Two cyclization schemes can be assumed for the formation of **11**, **12**, or **13** as Scheme 1.

In order to determine which path is correct, the reaction of *p*-chlorobenzoylacetonitrile and bis(*p*-chlorobenzoyl)methane with **2** were examined. The resulting pyridines, **15** and **16**, respectively, have a *p*-chlorophenyl group in the 2-position. It is thus evident that these compounds possessing a benzoyl as well as a *p*-chlorobenzoyl group produce pyridines *via* path A. However, nitromethane gives **14** *via* path B. For benzoylacetamide, another product, **17**, was obtained together with **13** upon refluxing. **17** was confirmed to be 2-hydroxy-3-benzoyl-4,6-diphenylpyridine, since the IR spectrum of **17** closely resembles those of **8** and **10**.

Ethyl Benzoylacetate. This gave an adduct, **18**, upon treatment with **2** at room temperature. **18** was confirmed to be a butadiene similar to **6** and **9**. **18** was expected to give 3-ethoxycarbonyl-2,4,6-triphenylpyridine or 2-benzoyloxy-3-benzoyl-4,6-diphenylpyridine or both. However, heating of **18** above its melting point resulted in the recovery of **18**. This may be caused by the fact that bulky constituents such as benzoyl and ethoxycarbonyl groups sterically hinder the cyclization of **18**.

All the compounds employed in this investigation, except for ethyl benzoylacetate, gave various pyridines when treated with **2** as well as malononitrile. These reactions are thought to proceed as Scheme 2.

The carbanion from active methylene attacks the 6-position of the oxazinium ring, and opens the ring to form a butadiene as an intermediate, which then recyclizes to a pyridine derivative according to a characteristic mode. From the relation between the reagents employed and the constituents, which are parts of the pyridines produced, the cyclization processes can be classified into five modes. The first mode, **C**, is characteristic of the compound possessing a cyano group, and produces 2-benzoylaminopyridine with the migration of a benzoyl group. Malononitrile is of this mode. The second, **E**, takes in an ester group, *i.e.*, diethyl malonate and methyl cyanoacetate, and is characterized by the formation of 2-benzoyloxypyridines with

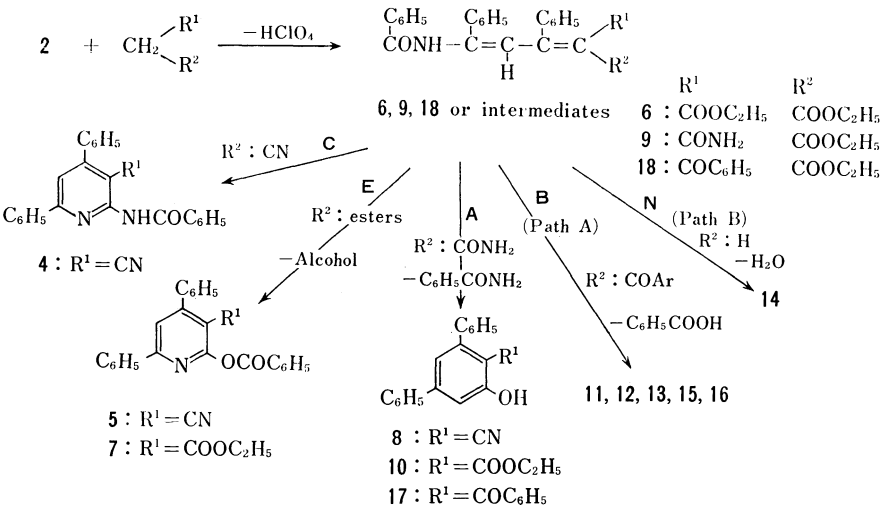

Scheme 2.

the liberation of an alcohol followed by the benzoyl migration. The third, **A**, takes place in cyanoacetamide, ethyl carbamoylacetate, and benzoylacetamide, and these derive 2-hydroxypyridines with the liberation of benzamide. The fourth, **B**, occurs in dibenzoylmethane, benzoylacetonitrile, and benzoylacetamide. This mode is characteristic of path A with the liberation of benzoic acid. For these four modes, the phenyl group in the 2-position of **2** is mobile, that is, on the cyclization to pyridines it migrates as a benzoyl group (**C**, **E**) or escapes as a benzoic acid (**B**) or a benzamide (**A**). However, nitromethane is considered to follow the fifth mode (**N**), and the phenyl group is introduced into the 2-position of **14** as such.

The compounds possessing the same two constituents follow this mode characterized by their own constituents. However, the compounds possessing two different constituents have two possible modes, and in practice, with the exception of benzoylacetamide, take either of the two. If we suppose that each compound follows the easiest mode, the relation **B**$\gtrsim$**A**>**E**>**C**, is observed between the four modes. However, for the same supposition, a different relation, **A**>**C**$\gtrsim$**B**>**E**, is derived from the results obtained from reactions of **3** with several active methylenes.[14,15] The most important factor characterizing the mode still remains undetermined. However, the reactions of **2** and **3** with active methylenes are useful for synthesizing pyridine or pyrimidine derivatives.

Experimental

The melting points of all products were measured in capillary tubes with a Mettler FPI apparatus at the rate 2 °C/min. The IR spectra were measured in KBr pellets with a JASCO DS-403G spectrometer. The molecular

Table 1. Pyridine derivatives (**5**, **7**, **8**, and **10—17**)

Compound	Reaction conditions[a]	Solvent for recrystn.	Mp (°C)	Yield (%)	Mol. wt	Elemental analysis Found (Calcd) (%) C	H	N	Cl	IR (cm^{-1})
5	A	EtOH	144.5	73	376	79.68	4.18	7.54		2205, 1756, 1592, 1576,
						(79.77	4.29	7.52)		1531, 1431, 1229, 1111.
7	C	EtOH	141.8	70	423	75.21	4.73	3.30		1757, 1720, 1593, 1576,
						(75.58	5.00	3.31)		1527, 1265, 1232, 1102.
8	A	DMF	>300	57		79.24	4.32	10.26		3020, 2800, 2210, 1640,
						(79.38	4.45	10.29)		1573, 1530, 1499, 1222.
10	C	NaOH–HCl[b]	183.9	82		75.13	5.24	4.36		3050, 2700, 1721, 1621,
						(75.22	5.37	4.39)		1570, 1530, 1246, 1108.
11	A	AcOH	172.6	35	411	87.42	5.24	3.36		1663, 1570, 1530, 1492,
						(87.56	5.15	3.40)		1441, 1261.
12	A	AcOH	225.6	78	332	87.03	4.96	8.33		2210, 1569, 1532, 1491,
						(86.70	4.86	8.50)		1374.
13	B	MeCN	233.0	92	350	82.35	5.09	7.88		3469, 3278, 3156, 1648,
						(82.26	5.17	7.99)		1570, 1532, 1492, 1366.
14	A	AcOH	195.0	46	352	76.24	4.53	7.59		1587, 1577, 1540, 1491,
						(76.39	4.58	7.95)		1363.
15	A	MeCN	250.3	68		78.38	3.91	7.85	9.65	2212, 1582, 1566, 1529,
						(78.58	4.12	7.61	9.66)	1490, 1088, 1012, 836.
16	A	MeCN	195.4	40		75.01	3.99	2.92	14.76	1674, 1582, 1529, 1493,
						(75.07	3.97	3.08	14.47)	1090, 1011, 924, 833.
17	A	NaOH–HCl	266.5	10		81.95	4.88	3.99		3020, 2700, 1665, 1615,
						(82.03	4.88	3.99)		1570, 1525, 1497, 1257.

a) A: Under refluxing, B: Left to stand at room temp., C: Conversion of the butadiene. b) Reprecipitated by pouring the solution in aqueous sodium hydroxide into dilute hydrochloric acid.

Table 2. 1-Benzoylamino-1,3-diphenyl-4,4-disubstituted butadienes (**6**, **9**, and **18**)

Compound	Substituent	Mp (°C)	Yield (%)	Elemental analysis Found (Calcd) (%) C	H	N	IR (cm^{-1})	NMR (δ)
6	$COOC_2H_5$	115.3	46	74.35	5.97	3.01	3380, 1720, 1676, 1601,	0.94(t, 3H), 1.29(t, 3H),
	$COOC_2H_5$			(74.18	5.80	2.98)	1470, 1217, 1104.	3.96(q, 2H), 4.30(q, 2H),
								7.30(m, 17H).
9	$COOC_2H_5$	187.2	35	73.52	5.52	6.36	3430, 3160, 1716, 1663,	0.81(t, 3H), 3.28(s, 1H),
	$CONH_2$			(73.79	5.27	6.37)	1484, 1232, 1056.	3.82(q, 2H), 6.80(s, 1H),
								7.30(m, 15H), 9.43(s, 2H).
18	$COOC_2H_5$	128.4	53	79.27	5.54	3.01	3430, 1713, 1695, 1600,	1.08(t, 3H), 4.14(q, 2H),
	COC_6H_5			(79.02	5.43	2.79)	1466, 1219, 1112.	6.90(s, 1H), 7.30(m, 21H).

weights were determined with a Hitachi RMU6E mass spectrometer equipped with a direct inlet and operating at an ionization electron energy of 70 eV. The NMR spectra were obtained in deuteriochloroform with a Varian XL-100 spectrometer with tetramethylsilane as an internal standard.

Genaral Procedures for the Reaction of **2** *with Active Methylene Compounds.* 2 mmol of **2** was added to a solution of 2 mmol of an active methylene compound and 3 mmol of triethylamine in 10 ml of dioxane. The mixture was stirred for ten minutes, and then either (A): refluxed for an hour, or (B): allowed to stand for a week at room temperature. The resulting mixture was poured into dilute hydrochloric acid. The precipitate was collected by filtration, and purified by recrystallization from an appropriate solvent. Results for the pyridine derivatives (**5**, **7**, **8**, and **10**—**17**) are given in Table 1. The butadienes were always obtained under the reaction conditions, B, and purified by recrystallization from methanol. Results for the butadienes are given in Table 2.

*Conversion of Butadienes to Pyridines (***7** *and* **10***).* 0.50 g of **6** was heated to above its melting point, *i.e.*, 140—150 °C for 20 min, and 0.5 g of **9** was treated at 180—190 °C for 2 hr (Table 1). **18** was treated in a similar way to that given above, at 150—160 °C for 4 hr, but recovered as such.

*2-Benzoyloxy-3-cyano-4,6-diphenylpyridine (***5***) from 2-Chloro-3-cyano-4,6-diphenylpyridine.* A solution of 1.00 g of 2-chloro-3-cyano-4,6-diphenylpyridine and 1.00 g of benzoic acid in 5 ml of pyridine was allowed to stand at room temperature for two days. The solvent was evaporated *in vacuo*, and the residue was washed with dilute hydrochloric acid and aqueous sodium hydroxide, and then recrystallized from ethanol to yield 0.22 g (16%) of **5**; mp 144.4 °C. The IR spectrum and molecular weight agreed completely with those of **5** derived from **2** with methyl cyanoacetate. Found: C, 79.83; H, 4.39; N, 7.53%. Calcd for $C_{25}H_{18}N_2O_2$: C, 79.77; H, 4.29; N, 7.53%.

References

1) S. Hünig and K. Hübner, *Chem. Ber.*, **95**, 937 (1962).
2) R. R. Schmidt, *ibid.*, **98**, 334 (1965).
3) H. Meerwein, P. Laasch, R. Mersch, and J. Spille, *ibid.*, **89**, 209 (1956).
4) K. Bredereck and R. Richter, *ibid.*, **99**, 2454 (1966).
5) D. Martin and A. Weise, *ibid.*, **100**, 3736 (1967).
6) A. Balaban and C. D. Nenitzescu, *Ann. Chem.*, **625**, 74 (1959).
7) G. Märkl, *Angew. Chem.*, **74**, 696 (1962).
8) K. Hafner and H. Kaiser, *Ann. Chem.*, **618**, 140 (1958).
9) G. Märkl, F. Lieb, and A. Merz, *Angew. Chem.*, **79**, 475 (1959).
10) K. Dimroth and G. Neubauer, *Chem. Ber.*, **92**, 2042 (1959).
11) K. Dimroth and G. Neubauer, *ibid.*, **92**, 2046 (1959).
12) R. R. Schimidt, D. Schwill, and U. Sommer, *Ann. Chem.*, **723**, 111 (1969).
13) R. R. Schmidt, *Chem. Ber.*, **98**, 3892 (1965).
14) I. Shibuya and M. Kurabayashi, This Bulletin, **42**, 2382 (1969).
15) I. Shibuya and M. Kurabayashi, *ibid.*, **46**,3902 (1973).
16) R. R. Schmidt, *Chem. Ber.*, **98**, 346 (1965).
17) D. E. Piper and G. F. Wright, *J. Amer. Chem. Soc.*, **72**, 1669 (1950).

Nucleophilic Substitution on Trivalent Nitrogen Atom.[1] Menschutkin Type Reaction of *O*-2,4-Dinitrophenylhydroxylamine with Uncharged Nucleophiles

Fumio YAMAMOTO and Shigeru OAE*

Department of Applied Chemistry, Faculty of Engineering, Osaka City University, Sugimoto-cho, Sumiyoshi-ku, Osaka 558

**Department of Chemistry, University of Tsukuba, Sakura-mura, Niihari-gun, Ibaraki 300-31*

(Received May 27, 1974)

Kinetic investigation carried out on the reaction between *O*-2,4-dinitrophenylhydroxylamine and neutral nucleophiles revealed that the reaction is a typical S_N2 reaction on the trivalent nitrogen atom. Moreover, the order of reactivities of common nucleophiles was found to be somewhat similar to that of the nucleophilicities toward sp^3 carbon atom. However, unlike the S_N2 reaction on sp^3 carbon atom, the S_N2 reaction on the trivalent nitrogen atom found to be not very sensitive to the steric effect of substituted pyridine.

Nitrogen and carbon are adjacent elements in the periodic table and, as such, share certain common chemical properties, such as the ability to form trigonal and tetrahedral bonding skeletons, the octet electronic environment, *etc.* While the nucleophilic substitutions on carbon atom have been studied systematically in the past three decades, those on nitrogen atom have been investigated very little except for a few fragmental examples.[2,3] Those studied were chloramine[2] and hydroxylamine-*O*-sulfonic acid[3] which are too unstable to be subjected to the kinetic experiments, reacting only under the limited conditions, *e.g.*, in liq. ammonia solution.

Recently, Sheradsky[4] first observed the following reactions shown in Eqs. (1) and (2).

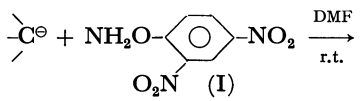

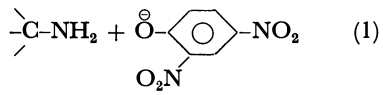

(1)

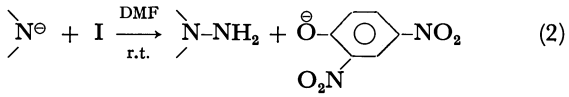

(2)

These reactions appear to be the most suitable for examining the nature of the S_N2 reaction on the nitrogen atom if the starting compound (I) can be made in pure form. Fortunately, the hydroxylamine (I) was able to be made in crystalline form, mp 113 °C.

We have therefore undertaken a kinetic study of Menschutkin type reactions with *O*-2,4-dinitrophenylhydroxylamine (I). Pyridine derivatives, aryl alkyl sulfide and triphenylphosphine were chosen as representative uncharged nucleophiles.

Results and Discussion

All these nucleophiles react smoothly with the hydroxylamine (I) in dioxane at room temperature and gave the readily isolable products, which are summarized in Table 1. The structures of the reaction products were determined on the basis of the spectral data and elemental analyses, details of which are given in the experimental section. These results indicate undoubtedly that the nucleophilic displacement takes place only at the nitrogen atom.

TABLE 1. REACTION PRODUCTS OF THE HYDROXYLAMINE (I) WITH SOME NUCLEOPHILES

Nucleophile	Product[a]		Mp °C	Yield (%)
Pyridine	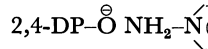	(Ia)	158—159	95
2-Picoline	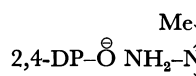	(Ib)	160—161	90
2,6-Lutidine		(Ic)	143—144	80
$PhSCH_3$	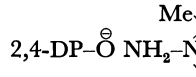	(Id)	106—107	85
Ph_3P	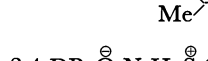	(Ie)	140—141	95

a) 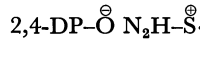

Kinetic measurements were carried out by following the UV spectra of 2,4-dinitrophenolate ion formed during the reaction.

Figure 1 shows the plot of pseudo-first-order rate

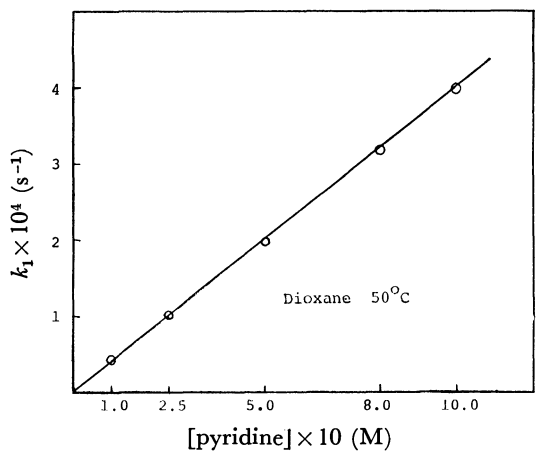

Fig. 1. Plot of pseud-first-order rate constant *vs.* pyridine concentration.

TABLE 2. THERMODYNAMIC DATA FOR THE REACTION OF THE HYDROXYLAMINE (I) WITH PYRIDINE IN DIOXANE

Temp. (°C)	$k_2(M^{-1}s^{-1}) \times 10^4$	
35	1.20	
40	1.87	$E_a = 15.5$ kcal/mol
45	2.90	$\Delta S^{\ddagger}_{40} = -28.1$ e.u.
50	3.83	$\Delta H^{\ddagger}_{40} = 14.9$ kcal/mol

constants against the initial concentration of pyridine in large excess, *e.g.*, from 10 to 100 times, over that of the hydroxylamine (I). Dioxane was employed as the solvent while temperature was set at 50 °C. From the slope of the line the second order nature of the reaction is apparent with $k_2 = 3.83 \times 10^{-4}$ M^{-1} s^{-1}. The observed second-order rate constants are listed in Table 2 along with the calculated activation parameters. Obviously, these values also suggest the reaction to proceed *via* the S_N2 path at the nitrogen atom. The values of the activation parameters are quite similar to and only somewhat smaller than that of Menschutkin reaction ($E_a = 13.6$ kcal/mol, $\Delta S^{\ddagger} = -33.1$ e.u., $\Delta H^{\ddagger} = 13.0$ kcal/mol)[5] of methyl iodide and the same base.

TABLE 3. SOLVENT EFFECTS FOR THE REACTION OF THE HYDROXYLAMINE(I) WITH PYRIDINE AT 40 °C

Solvent	D.C.	$k_2 \times 10^4$ ($M^{-1}s^{-1}$)
Dioxane	2.21	1.87
$CHCl_3$	4.81	3.30
Acetone	20.5	6.68
CH_3CN	37.5	7.32
DMF	36.7	14.01
CH_3OH	32.6	2.09
C_2H_5OH	24.3	2.52
H_2O–Dioxane (25%v/v)		5.00
H_2O–Dioxane (50%v/v)		7.16
H_2O–Dioxane (75%v/v)		7.66

Table 3 shows solvent effect for the reaction of the hydroxylamine(I) with pyridine at 40 °C. All these values indicate the same tendency as that of the Menschutkin reaction.[6] As the polarity of the solvent and the solvation of the leaving group, *i.e.*, 2,4-dinitrophenolate ion, increases with increasing water content, the reaction rate also increases.

Relative reactivites of a few representative nucleophiles are listed in Table 4.

Inspection of the data in Table 4 indicates that the reactivity order of these common nucleophiles lie in somewhat similar order with those of the nucleophilicities toward sp^3 carbon atom.[7] However, unlike in the S_N2 reaction on sp^3 carbon atom, the rate of 2-picoline is somewhat higher than that of pyridine. Even for 2,6-lutidine bearing two methyl groups on both side of the nucleophilic center, the rate constant is not much smaller than pyridine. These observations clearly show that the S_N2 reaction on the trivalent nitrogen atom is not very sensitive to the steric effect of methyl substitution as compared to that on the sp^3 carbon atom.

TABLE 4. RELATIVE RATIOS OF S_N2 REACTIONS ON NITROGEN AND CARBON ATOMS

Compound	Nucleophiles				
	Pyridine	2-Picoline	2,6-Lutidine	$PhSCH_3$	Ph_3P
I	1[a]	1.1	0.3	8	60
CH_3I[c]	1[b]	0.3	0.02	3	58

a) $3.38 \times 10^{-4} M^{-1}s^{-1}$ at 50 °C. b) $2.20 \times 10^{-5} M^{-1}s^{-1}$ at 25 °C. c) Reference 7.

As the lone pair of the trivalent nitrogen atom of the substrate (I) is considered to bear a substantial s-character,[8] it is much more vulnerable to distortion than the C–H sigma bond at the transition state as shown below.

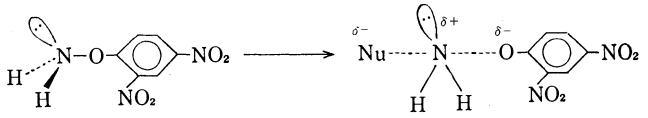

sp^2 transition state

The lone pair would not be solvated much in an aprotic solvent, but in a protic solvent it would be solvated markedly due to the hydrogen bonding.[9]

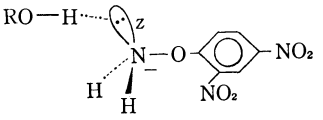

TABLE 5. STERIC EFFECT OF PYRIDINE DERIVATIVES IN VARIOUS SOLVENTS AT 40 °C

Solvent	Pyridine[a]	2-Picoline	2,6-Lutidine
Dioxane	1	1.10	0.29
CH_3CN	1	0.98	0.24
CH_3OH	1	0.79	0.19
H_2O–Dioxane (25%v/v)	1	0.89	0.20
H_2O–Dioxane (75%v/v)	1	0.77	0.19

a) The each value of k_2 are shown in Table 3.

Table 5 shows the magnitude of the steric effect of these substituted pyridines in both aprotic and protic solvents. On account of the hydrogen bonding as shown below, the steric effect increases by changing the solvent from aprotic to protic solvent. Since these nucleophiles are also solvated in protic solvents the reaction becomes more sensitive to the steric effect in protic solvent, and the order of reactivities approaches to that on the sp^3 carbon atom.

Experimental

Pyridine derivatives were purified according to the Coetzee and Padmanabhan's method.[10] Other nucleophiles were purified by distillation or by recrystallization of the commercial products. *O*-2,4-Dinitrophenylhydroxylamine(I) was prepared by the reaction of ethyl *O*-2,4-dinitrophenyl-acetohydroxamate with 70% perchloric acid in dioxane,[11] mp 113 °C (lt,[12] 112 °C). Found: C, 36.10; H, 2.64; N, 21.04%. Calcd for $C_6H_5N_3O_5$: C, 36.17; H, 2.54; N, 21.19%.

An equimolar mixture of the hydroxylamine(I) and nucleophile dissolved in dioxane was allowed to stand at room

temperature for a few hours. After evapolation of solvent the residual crystals were washed with hot benzene and recrystallized from ethanol or chloroform. The products were identified by elemental analysis and by comparing the NMR and IR spectra with those of the hydroxylamine(I) and nucleophilies.

Table 6. Elemental analysis data

Compound	Calcd (%)			Found (%)		
	C	H	N	C	H	N
Ia	47.49	3.62	20.14	47.41	3.61	20.30
Ib	49.32	4.14	19.17	49.46	4.05	19.50
Ic	50.98	4.61	18.29	50.90	4.60	18.31
Id	48.29	4.05	13.00	48.21	3.97	13.40
Ie	62.47	4.37	9.11	62.14	4.35	8.45

Kinetic Measurement. All kinetic runs were followed by pipetting 1 ml aliquots from 20 ml glass-stopped flask into 50 ml of ice water or ethanol a portion of which was subjected to measurement of the absorption spectra of 2,4-dinitrophenolate ion (λ_{max} 360 nm, ε 11000) by UV spectrometer. All the rate constants were determined from the pseudo-first-rate equation as follows.

$k=(2.303/bt)\log(a_\infty-a_0)/(a_\infty-a_t)$

a_∞: the final intensity of produced phenolate ion.

a_0: the initial intensity of produced phenolate ion.

a_t: the intensity of produced phenolate ion after t.

b: the initial concentration of nucleophile.

A typical run is shown in Table 7. (50 °C).

Table 7.

Time (min)	a_t	$\log(a_\infty-a_0)/(a_\infty-a_t)$	$k_1(s^{-1})\times10^4$
0	0.35		
3	0.51	0.0290	3.72
6	0.66	0.0577	3.70
9	0.82	0.0909	3.87
12	0.96	0.1219	3.89
18	1.21	0.1840	3.90
24	1.40	0.2377	3.83
30	1.59	0.2993	3.83
	2.86		

Hydroxylamine(I) $=1\times10^{-2}$M. Mean of k_1s.; 3.83 $\pm0.06\times10^{-4}$ $M^{-1}s^{-1}$. Pyridine(b)=1 M.

References

1) S. Oae and F. Yamamoto, *Tetrahedron Lett.*, **1973**, 5143.

2) R. E. Corbett, W. S. Metcalf, and F. G. Soper, *J. Chem. Soc.*, **1953**, 1927; R. E. McCoy, *J. Amer. Chem. Soc.*, **76**, 2829 (1954); F. N. Collier Jr., W. W. Horner, P. M. Dickens, J. G. Hull, and W. T. Layton, *ibid.*, **83**, 2235 (1961); M. Anbar and G. Yagil, *ibid.*, **84**, 1790 (1962).

3) P. A. S. Smith, H. R. Alul, and R. L. Baymgarten, *ibid.*, **86**, 1139 (1964).

4) T. Sheradsky, *Tetrahedron Lett.*, **1968**, 1909; T. Sheradsky and Z. Nir, *ibid.*, **1969**, 77.

5) N. J. T. Pickles and C. N. Hinshelwood, *J. Chem. Soc.*, **1936**, 1353; R. A. Fairelough and C. N. Hinshelwood, *ibid.*, **1937**, 1573.

6) E. L. Eliel and M. S. Newman, "Steric Effects in Organic Chemistry", ed. by M. S. Newman, John Wiley & Sons, Inc., New York (1956), p. 70; N. Tokura and Y. Kondo, This Bulletin, **36**, 200 (1963).

7) R. G. Pearson, H. Sobel, and J. Songstad, *J. Amer. Chem. Soc.*, **90**, 319 (1968).

8) T. A. Claxton, *Chem. & Ind.* (London), **1964**, 1713.

9) K. Brown, A. R. Katritzky, and A. J. Waring, *Proc. Chem. Soc.*, **1964**, 257.

10) J. F. Coetzee and G. R. Padmanabhan, *J. Amer. Chem. Soc.*, **87**, 5005 (1965).

11) Y. Tamura, J. Minamikawa, K. Sumoto, S. Fuji, and M. Ikeda, *J. Org. Chem.*, **38**, 1239 (1973).

12) T. Sheradsky, *J. Heterocycl. Chem.*, **4**, 413 (1967).

The Syntheses of Ripariochromene A and Methylripariochromene A[1]

Masao TSUKAYAMA

Department of Applied Chemistry, Faculty of Engineering, University of Tokushima, Tokushima 770

(Received August 9, 1974)

7,8-Dimethoxy-2,2-dimethylchroman was obtained from pyrogallol trimethyl ether and β,β-dimethylacrylyl chloride *via* the corresponding chroman-4-one. The Friedel-Crafts reaction of the chroman with acetyl chloride yielded 6-acetyl-7-hydroxy-8-methoxy-2,2-dimethylchroman. The dehydrogenation of the acetylchroman with DDQ in anhydrous benzene afforded ripariochromene A. Ripariochromene A was converted into methylripariochromene A

Ripariochromene A has recently been isolated, along with several chromenes, from Australian *Eupatorium riparium* Regel.[2] Its structure has been shown to be 6-acetyl-7-hydroxy-8-methoxy-2,2-dimethylchromene (I), with an unique 1,2,3-trioxygenated pattern, on the basis of the spectral evidence.[2] Methylripariochromene A (the methyl ether of I) (II) also has been isolated from Australian[2] and Jamaican *E. riparium* Regel.[3] The present paper will describe the syntheses of I[4] and II from 7,8-dimethoxy-2,2-dimethylchroman (III).

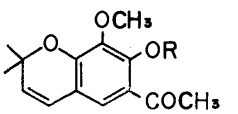

I R=H
II R=CH_3
X R=CH_3CO

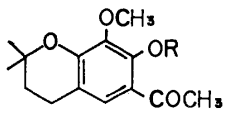

VIII R=H
IX R=CH_3CO

The condensation of pyrogallol trimethyl ether (IV) and β,β-dimethylacrylyl chloride (V) in the presence of anhydrous aluminum chloride over a 52 hr period gave 7,8-dimethoxy-2,2-dimethylchroman-4-one (VI). When the above condensation was allowed to proceed for a relatively short period of time, 2-hydroxy-3,4-dimethoxyphenyl 2-methyl-1-propenyl ketone (VII) was obtained, along with a small amount of VI. The NMR spectra of VI and VII showed the presence of one methylene group (δ 2.68 ppm) and one hydrogen-bonded hydroxyl group (δ 13.13 ppm) respectively. The ketone (VII) was easily converted into the chromanone (VI) when heated with ethanolic hydrochloric acid or acetic acid. The Clemmensen-reduction of VI or the hydrogenolysis of the thioketal of VI with Raney nickel gave the chroman (III).[5] The hydrogenolysis afforded III in a better yield than did the Clemmensen-reduction. The Friedel-Crafts reaction of III with acetyl chloride gave 6-acetyl-7-hydroxy-8-methoxy-2,2-dimethylchroman (VIII) (δ 2.52 ppm). The dehydrogenation[6-8] of VIII with 2,3-dichloro-5,6-dicyano-*p*-quinone (DDQ) in anhydrous benzene gave the desired chromene (I) (mp 89.5—90.5 °C),[1] which was shown to be identical with natural ripariochromene A on the basis of a mixed-melting-point determination and by NMR, infrared, and ultraviolet spectral comparisons.

The chromene (I) was easily converted into the methyl ether (II) (colorless liquid).[2] The properties of this synthetic chromene (II) were in full accord with those of natural methylripariochromene A.

Experimental[9]

2-Hydroxy-3,4-dimethoxyphenyl 2-Methyl-1-propenyl Ketone (VII). With stirring and cooling at 0 °C, β,β-dimethylacrylyl chloride (5.2 g) was added, drop by drop, to a solution of anhydrous aluminum chloride (6.5 g), pyrogallol trimethyl ether (5.6 g), and anhydrous ether (100 ml). After stirring at room temperature for 6 hr, the mixture was poured into a mixture of ice and dilute hydrochloric acid, and extracted with ether. The ethereal extract was washed with aqueous sodium bicarbonate and water, dried, and evaporated. The residue was recrystallized from a mixture of acetone and *n*-hexane to give yellow needles (mp 66.5—67 °C), which gave a dark green ferric chloride reaction in ethanol; yield, 5.5 g (70%). IR: 1642 cm^{-1}. NMR: ($CDCl_3$) 2.03_s, 2.19_s ($2\times CH_3$); 3.88_s, 3.90_s ($2\times CH_3O$); 6.46_d (C_5–H), 7.55_d (C_6–H) (each J=9 Hz); 6.70_{bs} (CH=C); 13.13_s (OH).

Found: C, 65.93; H, 6.88%. Calcd for $C_{13}H_{16}O_4$: C, 66.08; H, 6.83%.

7,8-Dimethoxy-2,2-dimethylchroman-4-one (VI). The ketone (VII) (3 g) was heated under reflux with ethanol containing 2 M hydrochloric acid (100 ml) for 3 hr. After removing the ethanol under reduced pressure, the residue was poured into cold water (50 ml) and extracted with ether. The ethereal extract was washed with 5% aqueous sodium carbonate and water, dried, and evaporated. The residue was then recrystallized from aqueous ethanol to give colorless needles; mp 75—75.5 °C; yield, 2.7 g (90%). IR: 1693 cm^{-1} (Nujol). NMR: ($CDCl_3$) 1.44_s ($2\times CH_3$); 2.68_s (CH_2); 3.80_s, 3.89_s ($2\times CH_3O$); 6.55_d (C_6–H), 7.61_d (C_5–H) (each J=9 Hz).

Found: C, 66.14; H, 6.77%. Calcd for $C_{13}H_{16}O_4$: C, 66.08; H, 6.83%.

The ketone (VII) was also converted into the chroman-4-one (VI) in boiling glacial acetic acid containing a small amount of concentrated hydrochloric acid.

The chromanone (VI) was also obtained along with a small amount of the ketone (VII) by the Friedel-Crafts reaction of pyrogallol trimethyl ether with β,β-dimethylacrylyl chloride in anhydrous ether at room temperature for 52 hr. It gave a mp of 75—75.5 °C and a mixed mp of 75—75.5 °C with the above chromanone.

7,8-Dimethoxy-2,2-dimethylchroman (III). A mixture of the chromanone (VI) (2.7 g), anhydrous sodium sulfate (2 g), freshly-fused zinc chloride (2.5 g), and ethyl mercaptan (20 ml) was allowed to stand overnight in a refrigerator, and then for 3 hr at room temperature. The mixture was subsequently poured into cold water (50 ml) and extracted with ether. The ethereal layer was washed with 10% aqueous sodium hydroxide, water, dried, and evaporated. The residue gave a thioketal (colorless liquid) (3.8 g). The crude thioketal (3.8 g) was refluxed with Rany nickel (80 g) in ethanol (100 ml) for 3 hr to give III (colorless liquid) (2 g, 72%),

which was purified by column chromatography on silica gel with chloroform. IR: 1498, 1582, 1613 cm^{-1} (liquid). NMR: ($CDCl_3$) 1.35_s ($2\times CH_3$); 1.78_t (C_3–H), 2.72_t (C_4–H) (each 2H, $J=7$ Hz); 3.80_s ($2\times CH_3O$); 6.40_d (C_6–H), 6.74_d (C_5–H) (each $J=9$ Hz).

The chroman (III) was also prepared by the Clemmensen-reduction described by Schwarz *et al.* (yield, 22%).[5]

6-Acetyl-7-hydroxy-8-methoxy-2,2-dimethylchroman (VIII). The acetylation of the chroman (III) (2.5 g) with acetyl chloride (3 g) and anhydrous aluminum chloride (4 g) in anhydrous ether (50 ml) at room temperature gave, in the course of 6 hr, the desired acetyl chroman, VIII. It was then recrystallized from aqueous ethanol to give colorless needles (2.3 g; 45%; mp 97—98 °C) and gave a brown ferric chloride reaction in ethanol. IR: 1640 cm^{-1}. UV: λ_{max}^{EtOH} nm(log ε); 222.5 (4.30), 238 (4.00), 288 (4.22), 327 (3.66). NMR: ($CDCl_3$) 1.40_s ($2\times CH_3$); 1.83_t (C_3–H), 2.76_t (C_4–H) (each 2H, $J=7$ Hz); 2.52_s (CH_3CO); 3.84_s (CH_3O); 7.26_s (C_5–H); 12.40_s (OH).

Found: C, 67.19; H, 7.03%. Calcd for $C_{14}H_{18}O_4$: C, 67.18; H, 7.25%.

Acetate (IX). The acetic anhydride–pyridine method; mp 143—144 °C (colorless needles from aqueous ethanol); a negative ferric chloride reaction. IR: 1670, 1762 cm^{-1}. NMR: ($CDCl_3$) 1.39_s ($2\times CH_3$); 1.83_t (C_3–H), 2.83_t (C_4–H) (each 2H, $J=7$ Hz); 2.37_s, 2.48_s ($2\times CH_3CO$); 3.80_s (CH_3O); 7.38_s (C_5–H).

Found: C, 65.92; H, 6.97%. Calcd for $C_{16}H_{20}O_5$: C, 65.74; H, 6.90%.

6-Acetyl-7-hydroxy-8-methoxy-2,2-dimethylchromene (Ripariochromene A) (I). The chroman (VIII) (0.3 g) and DDQ (0.32 g) in anhydrous benzene (60 ml) were heated under reflux for 3 hr, and then the benzene was removed under reduced pressure. The residue was purified by column chromatography on silica gel with petroleum ether–ethyl acetate (9: 1) to give the desired chromene. It was recrystallized from petroleum ether to give colorless needles (mp 89.5—90.5 °C, not depressed by mixture with nautral riperiochromene A (lit, mp 88.5 °C[2])) and gave a light blue ferric chloride reaction in ethanol; yield, 0.11 g (37%). IR: 1635 cm^{-1}. UV: λ_{max}^{EtOH} nm(log ε); 258 (4.57), 293 (3.89), 348 (3.64). NMR: ($CDCl_3$) 1.47_s ($2\times CH_3$); 2.52_s (CH_3CO); 3.88_s (CH_3O); 5.58_d (C_3–H), 6.27_d (C_4–H) (each $J=9$ Hz); 7.10_s (C_5–H); 12.80_s (OH).

Found: C, 67.65; H, 6.35%. Calcd for $C_{14}H_{16}O_4$: C, 67.73; H, 6.50%.

6-Acetyl-7,8-dimethoxy-2,2-dimethylchromene (Methylripariochromene A) (II). The chromene (I) (49 mg) was refluxed with dimethyl sulfate (0.4 g) and anhydrous potassium carbonate (0.6 g) in anhydrous acetone (30 ml) for 24 hr, and then the acetone was removed. The mixture was extracted with ether, and the ethereal extract was washed with dilute hydrochloric acid and water, dried, and evaporated. The residue was purified by column chromatography on silica gel with chloroform to give the methyl ether[2] (colorless liquid) (48 mg, 92%), which gave a negative ferric chloride reaction. IR: 1673 cm^{-1} (CCl_4). UV: λ_{max}^{EtOH} nm(log ε); 255 (4.24), 290 (3.68). NMR: ($CDCl_3$) 1.47_s ($2\times CH_3$); 2.57_s (CH_3CO); 3.85_s, 3.94_s ($2\times CH_3O$); 5.57_d (C_3–H), 6.28_d (C_4–H) (each $J=9$ Hz); 7.20_s (C_5–H).

Found: C, 68.60; H, 7.22%. Calcd for $C_{15}H_{18}O_4$: C, 68.68; H, 6.93%.

Acetate (X). The acetic anhydride–pyridine method; colorless liquid; a negative ferric chloride reaction. IR: 1676, 1767 cm^{-1}. NMR: ($CDCl_3$) 1.48_s ($2\times CH_3$); 2.35_s, 2.45_s ($2\times CH_3CO$); 3.82_s (CH_3O); 5.63_d (C_3–H), 6.30_d (C_4–H) (each $J=9$ Hz); 7.29_s (C_5–H).

Found: C, 66.26; H, 6.26%. Calcd for $C_{16}H_{18}O_5$: C, 66.19; H, 6.25%.

The author wishes to express his deep gratitude to Professor Shûichi Hayashi and Dr. Mitsuru Nakayama, Hiroshima University, for their guidance and encouragement throughout the course of this work, and also to Dr. Thorleif Anthonsen, Norway Institute of Technology, for supplying the natural ripariochromene A and methylripariochromene A.

References

1) This has previously been reported in a preliminary form: M. Nakayama, S. Hayashi, M. Tsukayama, T. Horie, and M. Masumura, *Chem. Lett.*, **1972**, 315.

2) T. Anthonsen, *Acta Chem. Scand.*, **23**, 3605 (1969).

3) D. R. Taylor and J. A. Wright, *Phytochemistry*, **10**, 1665 (1971).

4) A new synthesis of ripariochromene A has recently reported: B. S. Bajwa, Pyare Lal Khanna, and T. R. Seshadri, *Indian J. Chem.*, **11**, 100 (1973).

5) J. S. P. Schwarz, A. I. Cohen, W. D. Ollis, E. A. Kaczka, and L. M. Jackman, *Tetrahedron*, **20**, 1330 (1964).

6) M. Nakayama, M. Ohno, S. Hayashi, and K. Fukui, This Bulletin, **43**, 3311 (1970).

7) M. Nakayama, S. Nishimura, T. Matsui, S. Hayashi, and K. Fukui, *Nippon Kagaku Zasshi*, **91**, 1092 (1970).

8) M. Nakayama, S. Nishimura, T. Matsui, S. Hayashi, and K. Fukui, *Experientia*, **27**, 875 (1971).

9) All the melting points are uncorrected. The NMR spectra were measured with a Hitachi R-20 spectrometer (60 MHz), using tetramethylsilane as the internal standard (δ, ppm): s, singlet; d, doublet; t, triplet; b, broad; bs, broad singlet.

Reactions of 1-Azaazulan-2-one and Its 3-Substituted Derivatives[1]

Takashi TODA, Shoji RYU,* Yohichi HAGIWARA,** and Tetsuo NOZOE***

Department of Chemistry, Faculty of Science, Tohoku University, Aoba, Aramaki, Sendai 980

(Received February 12, 1974)

Chemical properties of 1-azaazulan-2-one (I) and its 3-substituted derivatives such as 3-acetyl, 3-cycloheptatrienyl and 3-ethoxycarbonyl were investigated. It was shown that the electrophilic substitution reactions take place at the 3-position, replacement of the substituents occuring in some cases by the reactions with cationoid reagents. The Beckmann rearrangement, Curtius rearrangement, Hofmann degradation reaction, Stevens-McFadyen reaction, *etc.* of these compounds are described.

Since 1-azaazulan-2-one (I) (cyclohepta[*b*]pyrrol-2-one) and its 3-ethoxycarbonyl derivative (II) were synthesized,[2,3] new synthetic methods,[4] and some electrophilic and nucleophilic substitution reactions[2,3,5] of I and its derivatives have been investigated. However, the chemical properties of 3-substituted derivatives of I have not been published, except for its 3-formyl (III)[6] and 3-dimethylamino[7] derivatives. In some cases[2,8] abnormal reactions are known to take place on the seven-membered ring moiety of an azulene skeleton during the reactions of functional groups on the five-membered ring moiety. We have thus prepared 3-acetyl and 3-cycloheptatrienyl derivatives of I by means of cationoid reactions of I and investigated their chemical properties.

The reaction of I and 7-tropyl ethyl ether in the presence of a small amount of hydrochloric acid gave 3-(cycloheptatrien-7-yl)-1-azaazulan-2-one (IV). When IV was treated with mineral acids, bromine and *p*-tolyldiazonium chloride, compound (I), 3-bromo-1-azaazulan-2-one isolated as its *N*-acetate, and 3-(*p*-tolylazo)-1-azaazulan-2-one (VI) were obtained, respectively.

The Vilsmeyer reaction of I by means of dimethylacetamide afforded 3-acetyl-1-azaazulan-2-one (VII).[4a] The reaction of VII with iodine and pyridine gave 3*N*-pyridiniummethylcarbonyl-1-azaazulan-2-one and subsequent base treatment afforded 3-carboxy-1-azaazulan-2-one (VIII).[3] However, VIII could not be obtained by the usual iodoform reaction of VII. The catalytic reduction and Clemensen reduction of VII gave only resinous substances.[9]

Although VII gave the corresponding oxime (IX) and hydrazone (X), large excess hydrazine was necessary for the formation of X. When an equivalent amount of hydrazine was used, sparingly soluble azine derivative (XI) was formed as the sole product. In the Beckmann rearrangement of IX, the use of sulfuric acid caused only elimination of the substituent at the 3-position to give I, but the rearrangement proceeded smoothly and gave *N*-acetyl-3-acetylamino-1-azaazulan-2-one (XII)[3] when acetic anhydride was employed. The Wolff-Kishner reduction of X with potassium hydroxide in ethylene glycol gave only resinous substances, but with sodium ethoxide in absolute alcohol or potassium hydroxide in alcohol, it afforded *ca.* 40% of VII.

Treatment of 3-ethoxycarbonyl-1-azaazulan-2-one (II) with ammonia and hydrazine gave the corresponding 3-carbamoyl (XIII) and 3-hydrazidocarbonyl (XIV) derivatives, respectively. Reaction of XIII with bromine in methanol and subsequent acetylation gave XII. Diazotization of XIV afforded an unstable azidocarbonyl derivative (XV) which shows a strong characteristic absorption band at 2120 cm^{-1}.[10] Although XV could not be isolated in the pure state, heating in acetic anhydride caused the Curtius rearrangement to give 3-acetamido derivative (XII). The Stevens-McFadyen degradation of XIV by the reaction with tosyl chloride gave the expected 3-formyl derivative (III) in a good yield.

The electron density of I is high at the 3-position with a contribution of canonical formula such as Ia.[2,11] Thus, electrophilic substitution reactions of I proceed readily to give IV and VII in good yields.

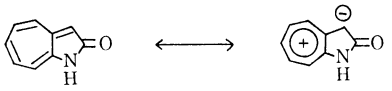

I Ia

If substituents at the 3-position of I can be eliminated as stable cations such as tropylium ion, the exchange reaction of substituents takes place by attack of the second electrophilic reagents as shown below. This is the case of the reactions of IV with other electrophiles. The elimination reaction of acetyl oxime group of IX may be explained analogously.

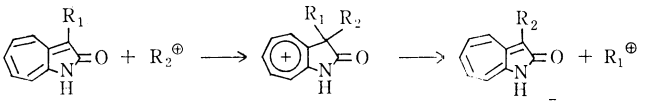

In the case of the Hofmann and Curtius reactions of XIII and XV, an intramolecular reaction takes place between the electron rich center (C_3) and the electron deficient center (nitrogen) and the rearrangements proceed smoothly. Analogous elimination reactions at the 3-position of azulenes[12] and azaazulanes[5] have been observed.

All the compounds obtained are listed in the following table.

* Present address: Hitachi Chemical Co., Tokyo.

** Present address: Central Research Laboratory, Toray Co., Ohtsu, Shiga.

*** Present address: Kamiyoga, 2-501-811, Setagaya-ku, Tokyo.

Table

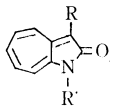

R	R′
III: CHO	H
IV:	H
V: Br	Ac
VI: *p*-$MeC_6H_4N_2$–	H
VII: Ac	H
VIII: COOH	H
IX: MeC=NOH	H
X: $MeC{=}NNH_2$	H
XI: 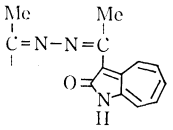	H
XII: NHAc	Ac
XIII: $CONH_2$	H
XIV: $CONHNH_2$	H
XV: CON_3	H

Experimental[13]

3-(Cycloheptatrien-7-yl)-1-azaazulan-2-one (IV). To a solution of 1.45 g of I in 30 ml of ethanol and 20 ml of benzene containing a few drops of concd. hydrochloric acid was added 2.95 g of tropyl ethyl ether with stirring and the reaction mixture was allowed to stand at room temperature for 3 hr. The precipitates formed were collected by filtration to give 2.10 g of orange scales of IV, mp 213—215 °C from dioxane.

Found: C, 81.68; H, 5.57; N, 5.95%. Calcd for $C_{16}H_{13}ON$: C, 82.21; H, 5.83; N, 5.79%.

Acetate of IV. A solution of 470 mg of IV in 10 ml of acetic anhydride was heated at 120 °C for 3 hr, and the solvent was removed under reduced pressure. The residue was recrystallized from cyclohexane to give 360 mg of orange yellow needles, mp 132—133 °C.

Found: N, 4.75%. Calcd for $C_{18}H_{15}O_2N$: N, 5.05%.

Bromination of IV. A solution of 235 mg of IV and 180 mg of bromine in 5 ml of acetic acid was stirred for one hr. After the solvent had been removed under reduced pressure, the residue was heated with 1 ml of acetic anhydride for 1 hr. Excess acetic anhydride was removed and the residue was recrystallized from ethyl acetate to give 200 mg of orange yellow needles, mp 245—247 °C which was identical with the authentic sample of *N*-acetyl-3-bromo-1-azaazulan-2-one.[3]

Azo-coupling Reaction of IV. *p*-Tolyldiazonium chloride prepared from 110 mg of *p*-toluidine was added with stirring to a solution of 235 mg of IV in 5 ml of dioxane cooled in an ice bath. After 3 hr, the precipitates formed were collected by filtration and recrystallized from cyclohexane–acetone to give 200 mg of 3-(*p*-tolylazo)-1-azaazulan-2-one, mp 153—154 °C which was identical with the authentic sample of the azo compound.[3]

3-Acetyl-1-azaazulan-2-one (VII). To a solution of 500 mg of I in 3 ml of dimethylacetamide cooled in an ice bath was added 1.0 g of phosphorus oxychloride with stirring. The reaction mixture was allowed to stand for 4 days at room temperature, and was then poured into crushed ice containing 1.0 g of sodium acetate and extracted with chloroform. The combined chloroform layer was washed with saturated sodium bicarbonate, water, dried over sodium sulfate, and then concentrated. The residue was chromatographed on alumina. Benzene–ether (1: 1) elutes afforded 380 mg of yellow needles of VII, mp 297—299 °C from cyclohexane–acetone.

1-Azaazulan-2-on-3-carboxylic Acid (VIII). A solution of 500 mg of VII and 800 mg of iodine in 5 ml of pyridine was stirred for 24 hr. To this was added 20 ml of 10% of sodium hydroxide and heated for 4 hr on a water bath. The solution was then acidified with 1 M hydrochloric acid to give precipitates. Recrystallization of the precipitates from methanol gave 260 mg of VIII, mp 200—202 °C (decomp.), which was identical with the authentic sample.[3]

Oxime of VII (IX). An equivalent of VII, two equivalents of hydroxylamine and of sodium acetate in alcohol were refluxed for 5 hr. After the alcohol had been removed, the residue was washed with water and recrystallized from alcohol to give the oxime in a quantitative yield, mp 241 °C (decomp.).

Found: C, 62.84; H, 5.24; N, 13.53%. Calcd for $C_{11}H_{10}O_2N_2 \cdot 1/2H_2O$: C, 62.55; H, 5.25; N, 13.26%.

Beckmann Rearrangement of IX. a) A solution of 290 mg of IX in 9 M sulfuric acid was heated on a water bath for 2.5 hr. After being cooled the reaction mixture was poured onto crushed ice, and the resulting precipitates were collected by filtration. Recrystallization from alcohol gave 157 mg of I.

b) A solution of 700 mg of IX in 10 ml of acetic anhydride was heated under reflux for 4 hr, and excess acetic anhydride was removed under reduced pressure. The residues were recrystallized from alcohol to give 420 mg of XII, mp 265—267 °C.

Found: C, 63.68; H, 4.45; N, 11.64%. Calcd for $C_{13}H_{12}O_3N_2$: C, 63.92; H, 4.95; N, 11.47%.

Hydrazone of VII (X). A solution of 1.13 g of VII and 12 equivalents of hydrazine hydrate and 0.5 ml of 6 M hydrochloric acid in 100 ml of alcohol was refluxed for 6 hr. The precipitates formed were collected by filtration. Recrystallization from alcohol containing hydrazine gave dark red needles of X, mp 270 °C; yield 986 mg.

Found: C, 65.76; H, 5.74; N, 20.23%. Calcd for $C_{11}H_{11}ON_3$: C, 65.67; H, 5.51; N, 20.88%.

When the reaction was carried out with 1.2 equivalent moles of hydrazine, the azine (XI) of VII was formed quantitatively. The azine is hard to purify and did not give good analysis.

Diacetate of XI. A solution of 242 mg of XI and 1 ml of acetic anhydride in 10 ml of pyridine was refluxed for 7 hr. The usual treatment gave 208 mg of diacetate of XI, mp 270 °C (decomp.); orange yellow needles from ethyl acetate.

Found: C, 68.09; H, 4.73; N, 11.99%. Calcd for $C_{26}H_{22}O_4N_4$: C, 68.71; H, 4.88; N, 12.33%.

Wolff-Kishner Reduction of X. A solution of 178 mg of X and 525 mg of potassium hydroxide in 200 ml of alcohol was refluxed for 8 hr. Alcohol was then removed under reduced pressure. The residue was washed with 1 M hydrochloric acid and water, and recrystallization from alcohol gave 124 mg of VII.

When the reaction was carried out with 2.4 equivalent moles of sodium ethoxide in absolute alcohol and treated as above, 40% of VII and 6.5% of XI were obtained together with some resinous substances. The reaction in boiling ethylene glycol gave only intractable resinous substances.

3-Carbamoyl-1-azaazulan-2-one (XIII). A solution of 500 mg of II in 10 ml of alcohol cooled in an ice bath was saturated with ammonia gas and allowed to stand for 6 hr at room temperature, and then heated on a water bath for 1 hr. After excess alcohol was removed, the residue obtained was recrystallized from cyclohexane–acetone to give yellow prisms of XIII, mp 186—187 °C; yield, 420 mg.

Found: C, 64.25; H, 4.71; N, 15.14%. Calcd for $C_{10}H_8O_2N_2$: C, 63.82; H, 4.29; N, 14.89%.

3-Hydrazinocarbonyl-1-azaazulan-2-one (XIV). A solution of 500 mg of II and 350 mg of hydrazine hydrate in 10 ml of alcohol was heated on a water bath for 1 hr and then concentrated. The residue formed was recrystallized from alcohol to give 450 mg of orange yellow needles of XIV, mp 198—200 °C.

Found: C, 59.03; H, 4.20; N, 20.55%. Calcd for $C_{10}H_9O_2N_3$: C, 59.10; H, 4.46; N, 20.68%.

Hofmann Degradation of XIII. A solution of 320 mg of XIII, 270 mg of bromine in 10 ml of absolute methanol containing 80 mg of sodium was refluxed for 1 hr, and excess reagents and the solvent were removed under reduced pressure. The residue was treated with 5 ml of boiling acetic anhydride for 3 hr, concentrated, and extracted with benzene. The combined benzene extracts were washed with water, dried over sodium sulfate and concentrated. The residue obtained was recrystallized from cyclohexane–acetone to give 270 mg of orange scales of XII, mp 265—267 °C, which was identical with the authentic sample of 1-acetyl-3-acetylamino-1-azaazulan-2-one.[3]

Curtius Rearrangement of XIV. A solution of 600 mg of XIV and 250 mg of sodium nitrate in 10 ml of dimethylformamide was stirred at room temperature. To this was added dropwise 2 ml of acetic acid and stirring was continued for 24 hr. Crystalline substances precipitated were collected by filtration, washed with water, and dried in a desiccator to give the acid azide (XV), mp 280—285 °C (decomp.); yield, 520 mg. ν_{KBr}: 2120, 1670, and 1590 cm^{-1}.

Five hundred mg of XV was heated under reflux for 5 hr in 5 ml of acetic anhydride, and acetic anhydride was removed under reduced pressure. The residue was recrystallized from acetone–cyclohexane to give 340 mg of XII, mp 263—265 °C.

Stevens-McFadyen Reaction of XIV. Five hundred mg of tosyl chloride was added in small portions with stirring to a solution of 500 mg of XIV in 5 ml of pyridine and 10 ml of dimethylformamide. The reaction was continued for 48 hr at room temperature. The precipitate formed was then collected by filtration and recrystallized from acetone–cyclohexane to give 360 mg of yellow needles, mp 283—285 °C, which was identical with the authentic sample of 3-formyl-1-azaazulan-2-one.[6]

This research was supported by grants from the Ministry of Education and Sankyo Co. Ltd.

References

1) Part of thesis, S. Ryu, 1966, Tohoku University.
2) T. Nozoe and K. Kikuchi, "Dai Yuki Kagaku." Vol. 13, ed. by M. Kotake, Asakura Shoten, Tokyo (1960), pp. 519—572.
3) T. Nozoe, S. Seto, S. Matsumura, and T. Terasawa, *Chem. Ind.* (London), **1954**, 1356, 1357.
4) a) K. Ogura, H. Sasaki, and S. Seto, This Bulletin, **38**, 306 (1965); b) H. Nakao, N. Soma, and G. Sunagawa, *Chem. Pharm. Bull.* (Tokyo), **13**, 828 (1965).
5) T. Toda, S. Seto, and T. Nozoe, This Bulletin, **41**, 2102 (1968).
6) T. Toda, *ibid.*, **40**, 590 (1967).
7) A. Sato, S. Nozoe, T. Toda, S. Seto, and T. Nozoe, *ibid.*, **46**, 3530 (1973).
8) T. Nozoe, T. Asao, H. Susumago, and M. Ando, *ibid.*, **47**, 1471 (1974).
9) The catalytic reduction of 3-chloro and 3-nitro derivatives of I gave I and 3-amino derivative, respectively, in good yields. Ethylbenzene was obtained from acetophenone under the same Clemensen reduction conditions.
10) L. J. Bellamy, "Infra-red Spectra of Complex Molecules," 2nd ed., Methuen, London (1958), p. 273.
11) H. Kon, *Sci. Repts. Tohoku Univ., I*, **38**, 67 (1954).
12) T. Nozoe, T. Toda, T. Asao, and A. Yamanouchi, This Bulletin, **41**, 2935 (1968).
13) All melting points are uncorrected.

Catalytic Activity of Metal Polyphthalocyanines in Autoxidation Reactions[1]

Takao HARA, Yasukazu OHKATSU,* and Tetsuo OSA*

Department of Chemistry, Faculty of Engineering, Yokohama National University, Ohoka, Minami-ku, Yokohama 233

**Department of Industrial Chemistry, Faculty of Engineering, The University of Tokyo, Hongo, Bunkyo-ku, Tokyo 113*

(Received April 30, 1974)

The oxidation of cumene and acrolein was carried out using metal polyphthalocyanines as a catalyst. The catalyst activated an oxygen molecule to form a phthalocyanine–O_2 complex, which then abstracted the hydrogen atom of a reactant to initiate the oxidation. The catalyst had no effects on the decomposition of cumene hydroperoxide, formed selectively in the oxidation of cumene. The addition of a small amount of pyridine induced a drastic shortening of the induction period as well as a considerable increase in the oxidation rate. The initiation mechanism assumed on the basis of findings on the desorption of oxygen from the catalyst and on the effect of pyridine was confirmed by a kinetic study of the homogeneous liquid-phase oxidation of acrolein.

Metal phthalocyanines have been used as catalysts in the autoxidation of such hydrocarbons as cumene.[2–6] Kropf proposed that, in the oxidation of cumene below 100 °C, copper phthalocyanine activated a molecular oxygen through its coordination with the metal ion to form a phthalocyanine–O_2 complex, which then abstracted the tertiary hydrogen of cumene to initiate the oxidation.[2] However, Min'kov and Keier reported that a unimolecular decomposition of cumene hydroperoxide occurred at 40—70 °C, whereas a higher-order decomposition occurred at 90—110 °C; they concluded that the catalytic activity of copper phthalocyanine was associated not with the activation of oxygen, but with the decomposition of the hydroperoxide, over both temperature ranges.[3] Furthermore, a polymeric metal phthalocyanine (metal polyphthalocyanine, Me-polyPc) was also used as a catalyst in the liquid-phase autoxidation.[5,6] Inoue *et al.* presumed, in the oxidation of acetaldehyde ethylene acetal, that metal ions, especially Fe(II) ions, located in the conjugated system of phthalocyanines might act as active sites for the activation of oxygen as well as for the decomposition of the hydroperoxide. From the above description, it can be understood that the role of a phthalocyanine catalyst in an autoxidation reaction has not yet been clarified univocally.

In this investigation, many kinds of metal polyphthalocyanines were synthesized and used as catalysts for the decomposition of cumene hydroperoxide and the liquid-phase oxidation of cumene; this was done in order to elucidate how the catalyst affects the activation of oxygen and/or the decomposition of the hydroperoxide. Besides, the results obtained by the kinetic study of the homogeneous liquid-phase oxidation of acrolein supported the proposed initiation mechanism; that is, a phthalocyanine–O_2 complex abstracts the hydrogen atom of a reactant to initiate the oxidation.

Experimental

Materials. The metal polyphthalocyanines were synthesized according to the method reported by Epstein and Wildi.[7] Copper–Iron polyphthalocyanine, for example, was prepared in the following manner. A mixture of 1,2,4,5-tetracyanobenzene (4.00 g), $CuCl_2$ (0.80 g), $FeCl_2$ (0.70 g), and urea (0.25 g) was ground sufficiently and was then heated at 300 °C under a nitrogen atmosphere for 18 hr. The mixture was then heated for two additional hours at 350 °C. The resulting solid was washed with methanol to remove the unchanged metal chlorides; the catalyst thus obtained will be called a "crude" polyphthalocyanine below. Then the solid was extracted with boiling pyridine until the greenish color of the extract faded out, resulting in the removal of not only monomeric but also oligomeric metal phthalocyanine. The residue was dried and heated at 350 °C/ 10^{-1} mmHg for 30 hr; this will be called a "purified" polyphthalocyanine.

TABLE 1. ELEMENTAL ANALYSIS OF METAL POLYPHTHALOCYANINES

Me–polyPc	C	H	N
Cu–polyPc			
Found:	57.5%	1.53%	24.4%
Calcd 1:	57.1	1.0	26.7
Calcd 2:	61.9	1.0	28.8
Co–polyPc			
Found:	53.3	1.96	27.1
Calcd 1:	57.8	1.0	27.1
Calcd 2:	61.8	1.0	29.0

Calcd 1 and 2 are obtained as the structure of Me–polyPc is $[Me(C_6H_2(CN)_4)_2]_n$ and $Me(C_6H_2(CN)_4)_4$, respectively.

Eleven kinds of catalysts were obtained as a dark solid-powder and were not dissolved in any organic solvents. No data have been obtained on the molecular weight of the catalysts. Considering that when a monomeric phthalocyanine and a polymeric one in which the degree of polymerization remain low are slightly dissolved in boiling pyridine they assume a characteristic color, the molecular weight of the "purified" catalyst may be quite large. This was also presumed because the IR absorption peak ascribed to the terminal -CN group in the catalysts was not observed.[8] The results of the elemental analyses of some catalysts are shown in Table 1. If the structure of a Me-polyPc thus obtained is similar to that of a monomeric phthalocyanine, its molecular formula can be expressed as $Me(C_6H_2(CN)_4)_4$. When the degree of polymerization becomes sufficiently large, the expression may be transformed to $[Me(C_6H_2(CN)_4)_2]_n$. The

results shown in Table 1 also indicate that the prepared catalysts are highly-polymerized phthalocyanines. The metal contents in Cu–Fe polyPc were measured by the spectrophotometric method reported by Underwood.[9] Copper and iron ions existed in the catalyst in the ratio of 2.7:4.1, an iron-rich catalyst being thus prepared. The total contents of metal ions in Cu–Fe polyPc were 86 and 160% of the theoretical values when calculated by means of the molecular formulae of $[Me(C_6H_2(CN)_4)_2]_n$ and $Me(C_6H_2(CN)_4)_4$ respectively. However, no data have yet been obtained with respect to the disposition of the two kinds of metal ions in the enlarged conjugated system.

Procedure. The catalytic decomposition of cumene hydroperoxide and the oxidation of cumene were carried out using the apparatus and the procedure described in a previous paper.[10]

The kinetic study of the homogeneous liquid-phase oxidation of acrolein was carried out according to a new method using an oxygen analyzer, model 777, manufactured by the Toshiba-Beckman Co.[11] A 22 ml reactor equipped with a sensor of the analyzer was filled with benzene as a solvent and a certain amount of a catalyst. A solution containing a desirable concentration of oxygen was prepared by bubbling of the corresponding gaseous mixture of oxygen and nitrogen. Immediately after a certain amount of acrolein has been charged into the reactor, the reaction system filled with the solution was closed. The continuous change in the concentration of dissolved oxygen corresponding to the amount of oxygen absorbed was recorded by the analyzer.

The behavior of oxygen on metal polyphthalocyanines was examined in the following manner. A "purified" metal polyphthalocyanine stored under a nitrogen atmosphere was charged into a 100 ml flask and heated at 350 °C/10^{-2} Torr for 5 hr. The catalyst was then cooled to room temperature and allowed to be in contact with pure oxygen for 24 hr. Then the atmosphere was removed again, and the inner pressure was strictly maintained at 2.1×10^{-2} Torr for 3 hr. The temperature was then raised to about 350 °C at a constant rate of 2 °C per min, and the increase in the inner pressure was measured.

Results and Discussion

The decomposition reaction of cumene hydroperoxide was carried out at 82 °C in a *p*-xylene solution. As is illustrated in Fig. 1, cumene hydroperoxide was not decomposed within 4 hr in the presence of "purified" Cu–Fe polyPc, Cu–polyPc, or Fe–polyPc, whereas it was almost completely decomposed after 4 hr using the "crude" Cu–Fe polyPc catalyst. The valency of a transition metal ion or ions can be changed in the conjugated-ring system of a phthalocyanine. When cumene hydroperoxide is catalytically decomposed through the Haber-Weiss mechanism,[12] the catalytic activity generally depends on the redox potential of a metal ion. The redox potentials of monomeric phthalocyanines were obtained in a pyridine solution as −0.98 and −0.49 V *vs.* SCE with regard to iron and cobalt phthalocyanine respectively.[13] Considering that the reduction potential of a hydroperoxide is −0.7 to −0.8 V,[14] a monomeric phthalocyanine, especially iron phthalocyanine, can possibly decompose the hydroperoxide. On the other hand, the potential of a polymeric phthalocyanine may be decreased with the enlargement of the π-electrons conjugated ring system;

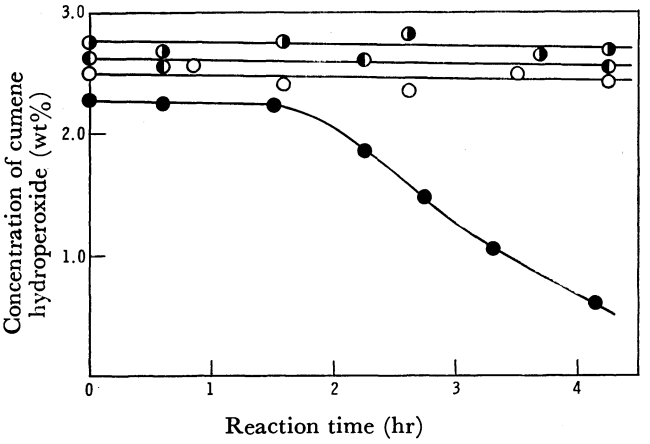

Fig. 1. The decomposition of cumene hydroperoxide by metal polyphthalocyanines. Reaction conditions; Me-polyPc 4.9×10^{-3} M, solvent *p*-xylene, at 81.5°C. ○ Cu–Fe polyPc, ◑ Cu–polyPc, ◐ Fe–polyPc, ● crude Cu–Fe polyPc.

chelation is recognized to make a metal ion stable and, consequently, to lower the potential. The "purified" metal polyphthalocyanine is considered not to decompose cumene hydroperoxide because of its lower redox potential. The opposite results mentioned above relating to the decomposition of a hydroperoxide may be ascribed to the degree of purification of a metal polyphthalocyanine.

The behavior of oxygen on a metal polyphthalocyanine was examined in order to confirm the mechanism of the activation of oxygen. Oxygen was desorbed from a metal polyphthalocyanine as the temperature rose. The differential pressure per centigrade of the desorbed oxygen is plotted against the temperature in Fig. 2. The first peak of Cu–Fe polyPc was also observed either in the case of Cu–polyPc or Fe–polyPc in the temperature range of 80—150 °C, but the second peak was characteristic of Cu–Fe polyPc. In addition, the first peak of Cu–polyPc existed over a higher temperature range than that of Fe–polyPc. These results imply that a strongly-chemisorbed oxygen existed on a

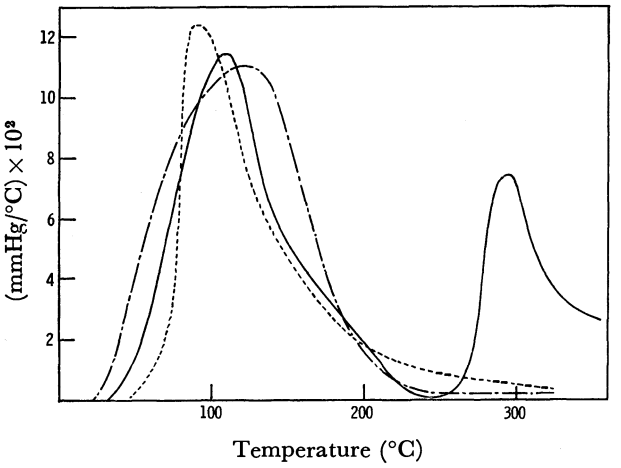

Fig. 2. Desorption of oxygen on metal polyphthalocyanines Me-polyPc 180 mg, —— Cu–Fe polyPc, —·— Cu–polyPc, ------ Fe–polyPc.

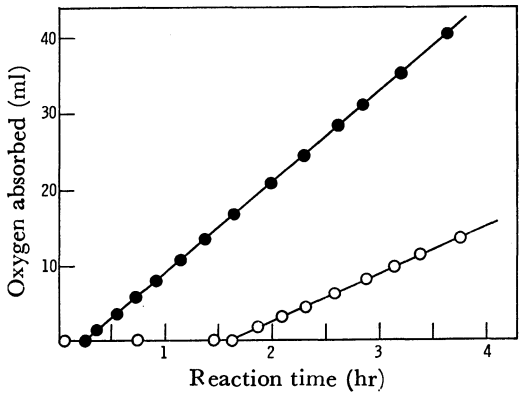

Fig. 3. The oxidation of cumene with Cu–Fe polyPc. Reaction conditions; cumene 0.652 M, Cu–Fe polyPc 4.82×10^{-3} M, in *p*-xylene at 81.5 °C. ● with pyridine, 2.25×10^{-1} M.

metal polyphthalocyanine catalyst, especially on Cu–Fe polyPc; that is, the catalyst activates a molecular oxygen, as has been described by Inoue *et al.*[5]

It was examined in the oxidation of cumene whether or not the activated oxygen could abstract a hydrogen atom to initiate the oxidation. The oxidation of cumene in *p*-xylene was carried out at 82 °C using a metal polyphthalocyanine in the presence and in the absence of pyridine. No oxygen was absorbed without the catalyst for 6 hr, while in the presence of Cu–Fe polyPc the uptake of oxygen started at a steady rate after an induction period of 100 min (Fig. 3). A drastic shortening of the induction period as well as a considerable increase in the oxidation rate were induced by the presence of a small amount of pyridine. A similar absorption curve of oxygen was also obtained when pyridine was added after one hour. The oxidation under the reaction conditions shown in Fig. 3 gave cumene hydroperoxide as the only product. The active oxygen in the hydroperoxide was estimated to be 1.9×10^{-3} mol after a 4 hr reaction time; this amount corresponded to 108% of the amount of oxygen absorbed. This means that a "purified" metal polyphthalocyanine can produce cumene hydroperoxide selectively without its decomposition.

Table 2. Effect of metal ions in polyphthalocyanines

Metal	$-dO_2/dt$ $\times10^6$ M s^{-1}	Induction period, min
Cu–Fe	2.36	14
Cu–Fe[a]	2.38	10
Cu–Co	1.76	12
Cu–Mn	1.69	17
Cu	1.51	0
Co	1.41	18
Cr	1.30	8
Fe–Co	1.27	19
Mn	1.26	23
Fe	1.17	5
Co–Mn	1.13	33
Fe–Mn	0.57	16

Reaction conditions were the same as in Fig. 4.
a) under the same reaction condition

Table 2 illustrates the effects of metal ions in polyphthalocyanines on the rate of oxidation and shows that metal polyphthalocyanines including a copper ion are more effective; the order of activity is different from that reported in the oxidation of acetaldehyde ethylene acetal.[5] The active order of copper, iron, and copper–iron polyphthalocyanines is found to correspond to the order of the peak temperature based on the desorption of oxygen from the catalysts, as is shown in Fig. 2. That is to say, the catalysts on which oxygen is chemisorbed more strongly may be active in initiating the oxidation, resulting in an increase in the oxidation rate. This suggests that the metal ion, particularly the copper ion, is effective in forming its complex with oxygen, which may abstract the tertiary hydrogen of cumene.

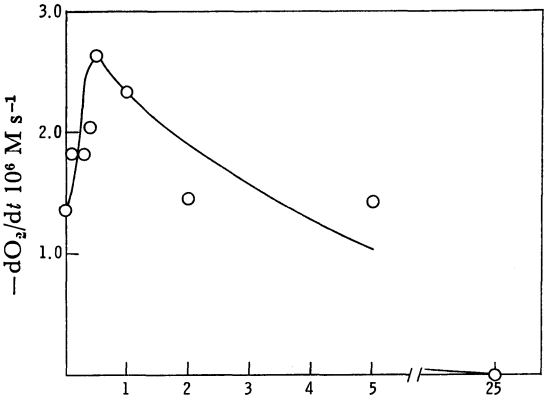

Fig. 4. Effect of pyridine on the rate of oxidation. Reaction conditions; cumene 0.652 M, Cu–Fe polyPc 4.80×10^{-3} M, in *p*-xylene at 81.5 °C, total volume of the solution 55 ml.

The effect of pyridine on the oxidation rate was also examined (Fig. 4). The absorption rate of oxygen varied considerably depending on the amount of pyridine added, though Inoue *et al.* related only a negative effect of added pyridine. The maximum rate was obtained when 0.5 ml of pyridine was added to 55 ml of the total volume of the oxidation solution; this rate was 2.1 times that in the absence of pyridine. The excess addition showed rather a negative effect on the rate, and the oxidation did not proceed over 6 hr in the presence of more than 25 ml of pyridine. Though almost the same absorption rate was given in the case of the addition of 5.0 ml as that observed in the absence of pyridine, the induction period was shortened to 9 min.

With respect to pyridine, Elvidge and Lever found that manganese phthalocyanine could carry an oxygen molecule reversibly in a pyridine solution.[15] Calvin *et al.* explained this oxygen-carrying mechanism by a spectrophotometric method and pointed out the activation of oxygen by the coordination of pyridine at the *trans*-position. The effect of pyridine on this oxidation of cumene, consequently, may also be related to the initiation mechanism with which a metal polyphthalocyanine is concerned. However, the activation mechanism by Calvin *et al.* cannot be applied to a metal

polyphthalocyanine, because it is completely insoluble in the reaction solution. As the distance between the layers of the planar crystalline of a monomeric phthalocyanine was reported to be 3.38 Å,[17] there is no room for pyridine to enter between the layers of the catalyst to activate a molecular oxygen at the *trans*-position.

On the other hand, Barret *et al.* reported that iron phthalocyanine formed a 1 : 6 adduct with aniline, four molecules of aniline being coordinated with the conjugated system, and two, with the central metal, iron.[18] This explanation may make it possible to consider that an adequate amount of pyridine is coordinated with the conjugated-ring system of a metal polyphthalocyanine and acts in the same manner as that at the *trans*-position to facilitate the activation of oxygen at the central metal ions on the surface of the catalyst by moving electrons through the ring system. This can lead to the shortening of the induction periods to approximately 10 min. The excess amount of pyridine may occupy all the coordination sites including metal ions to deactivate the catalyst. The decrease in the oxidation rate upon the addition of more than 5.0 ml of pyridine may be ascribed to the decrease in the amount of available activated oxygen. This consideration is supported by the result that the oxidation did not occur in such solvents as DMF and DMSO, which have higher coordination strengths. Besides, the negative effect of pyridine may be partly attributed to the formation of a charge-transfer complex between the cumylperoxy radical and pyridine, as has been reported by Thomas.[19]

The assumed initiation mechanism involving the activation of oxygen by the catalyst is confirmed by the kinetic study. The method of the homogeneous liquid-phase oxidation is suitable for the investigation of the effect of oxygen on the rate of oxidation, because the transfer-process of oxygen from the gas phase to the liquid phase is not involved in the measurement of the absorption rate of oxygen.[11] The oxidation of acrolein was studied instead of that of cumene, as the reaction temperature was limited below 45 °C by the use of the oxygen analyzer.

Acrolein was not oxidized even in the presence of Cu–Fe polyPc at 40 °C in benzene; the concentration of dissolved oxygen remained constant over 24 hr. When a small amount of pyridine was added, the concentration of oxygen began to decrease and assymptotically became zero towards the end of the reaction. The effect of pyridine was similar to that described in the oxidation of cumene, and it should be noticed in the case of acrolein that the presence of pyridine was indispensable to the initiation of the oxidation. The kinetic study was carried out with pyridine (5.6×10^{-1} M), where the accelerating effect on the rate was observed.

Assuming that the autoxidation proceeds through the known chain mechanism including the assumed initiation step, the stationary-state treatment gives the following theoretical rate equation:

$$\mathrm{RH} + \mathrm{cat} + \mathrm{O_2} \xrightarrow{k_1} \mathrm{R}\cdot$$

$$\mathrm{R}\cdot + \mathrm{O_2} \xrightarrow{k_2} \mathrm{RO_2}\cdot$$

$$\mathrm{RO_2}\cdot + \mathrm{RH} \xrightarrow{k_3} \mathrm{RO_2H} + \mathrm{R}\cdot$$

$$\left.\begin{array}{l} 2\mathrm{R}\cdot \xrightarrow{k_4} \\ \mathrm{R}\cdot + \mathrm{RO_2}\cdot \xrightarrow{k_5} \\ 2\mathrm{RO_2}\cdot \xrightarrow{k_6} \end{array}\right\} \text{non-radical products}$$

where RH denotes the acrolein molecule

$$-\mathrm{dO_2/d}t = [k_1(\mathrm{RH})(\mathrm{cat})(\mathrm{O_2})]^{1/2} \times \frac{k_2k_4^{-1/2}(\mathrm{RH})(\mathrm{O_2})}{(\mathrm{RH}) + (k_2k_4^{-1/2}/k_3k_6^{-1/2})(\mathrm{O_2})}$$

The rate constant, $k_2k_4^{-1/2}$ and $k_3k_6^{-1/2}$, have been reported to be 3.7×10 and 5.5×10^{-2} ($\mathrm{M^{-1/2}\,s^{-1/2}}$) respectively in the oxidation initiated by di-*t*-butyl diperoxyoxalate in benzene at 40 °C.[20] Consequently, the k_1 constant can be calculated under various reaction conditions (Table 3). Runs 1—4 show the effect of the catalyst concentration. The decrease in the chain length with the increase in the catalyst concentration may be partly ascribed to the termination of radicals by the catalyst, considering that a negative catalyst effect[21] was observed at higher concentrations of the catalyst. Runs 1 and 5—7 show the dependence on the concentration of acrolein. In the case of a constant concentration of the catalyst, the chain length was given as close to 30. The k_1 constant is given as $(6.3\pm0.3)\times10^{-2}\,\mathrm{M^{-2}\,s^{-1}}$ under all the reaction conditions.

Table 3. Effect of the concentration of acrolein and the catalyst on the rate of oxidation

Run	$-\mathrm{dO_2/d}t$ $\times10^6$ M s^{-1}	(RH) M	$(\mathrm{O_2})^{a)}$ $\times10^3$ M	(cat) $\times10^3$ M	R_i $\times10^8$ M s^{-1}	Chain length	k_1 $\times10^2$ $\mathrm{M^{-2}\,s^{-1}}$
1	5.10	0.34	1.39	4.72	13.7	37	6.1
2	3.55	0.34	1.39	2.31	6.6	54	6.1
3	2.64	0.34	1.39	1.22	3.7	72	6.3
4	1.85	0.34	1.20	0.76	2.0	94	6.3
5	14.3	0.48	3.05	4.72	45.1	32	6.6
6	3.00	0.20	1.63	4.72	10.0	30	6.4
7	1.49	0.14	1.30	4.72	5.3	28	6.3

a) The concentration of oxygen at which the rate of oxidation reached maximum. Reaction conditions: amount of pyridine added, 1.0 ml; 40 °C in benzene; initial concentrations of oxygen were set as about 2.0×10^{-3} M except the case of the run 5.

The influence of the concentration of oxygen can be determined in an experiment in the homogeneous liquid-phase oxidation. In Run 5, the oxidation rate decreased with the decrease in the concentration of oxygen after a certain induction period. During the oxidation, the change in the concentration of acrolein was negligible because the ratio of the concentration of acrolein to that of oxygen was set as about 10^2. The theoretical rate equation can be transformed as follows:

$$-\mathrm{dO_2/d}t = \frac{k_1^{1/2}k_2k_4^{-1/2}A^{3/2}B^{1/2}(\mathrm{O_2})^{3/2}}{A + (k_2k_4^{-1/2}/k_3k_6^{-1/2})(\mathrm{O_2})}$$

where A and B denote the concentrations of acrolein (0.48 M) and the catalyst (4.72×10^{-3} M) respectively. Then k_1 can be calculated from the differential value

Table 4. Effect of the concentration of oxygen on the rate of oxidation

(O_2) $\times 10^3$ M	$-dO_2/dt$ [a] $\times 10^6$ M s^{-1}	R_i $\times 10^8$ M s^{-1}	Chain length	k_1 $\times 10^2$ M^{-2} s^{-2}
3.05	14.3	45.1	32	6.6
2.67	13.1	39.7	33	6.6
2.29	11.6	33.6	33	6.5
1.91	10.2	28.5	36	6.6
1.53	8.57	22.9	37	6.7
1.14	6.67	17.0	39	6.6
0.76	4.50	11.0	41	6.4
0.38	2.21	5.8	38	6.8

a) The rate of oxidation at each concentration of oxygen. Reaction conditions: initial concentration of acrolein, 0.48 M; of the catalyst, 4.7×10^{-3} M; and of oxygen, 6.8×10^{-3} M (0.89 atm. of partial pressure of oxygen); pyridine added, 1.0 ml; 40 °C in benzene.

of the decreasing curve of oxygen (rate of oxidation) at each concentration of oxygen (Table 4). The k_1 constant is given as $(6.6\pm0.2)\times10^{-2}$ M^{-2} s^{-1} over the range of concentration of oxygen from 0.38 to 3.05×10^{-3} M.

The value of k_1 did not change with the change in the concentrations of the catalyst, acrolein and oxygen, which supported the initiation mechanism: a phthalocyanine–O_2 complex abstracts the hydrogen of a reactant to initiate the oxidation.

References

1) Partly contributed to *Chem. Lett.*, **1973**, 103; *ibid.*, **1973**, 953.
2) H. Kropf, *Ann. Chem.*, **637**, 73 (1960).
3) A. I. Min'kov and N. P. Keier, *Kinet. Katal.*, **8**, 160 (1967).
4) Y. Kamiya, *Tetrahedron Lett.*, **1968**, 4965.
5) H. Inoue, Y. Kida, and E. Imoto, This Bulletin, **40**, 184 (1967).
6) R. V. Norton, American Chemical Society Chicago Meeting, September 1970, Session of Petrochem. B. 18.
7) A. Epstein and B. S. Wildi, *J. Chem. Phys.*, **32**, 324 (1960).
8) S. Z. Roginskii, A. A. Berlin, O. A. Golovina, E. S. Dokukina, M. M. Sakharov, and L. G. Cherkaskina, *Kinet. Katal.*, **4**, 431 (1963).
9) A. L. Underwood, *Anal. Chem.*, **25**, 1910 (1953).
10) Y. Ohkatsu, T. Hara, T. Osa, and A. Misono, This Bulletin, **40**, 1893 (1967).
11) T. Takeuchi and T. Osa, *Nippon Kagaku Kaishi*, **1972**, 2374.
12) F. Haber and J. Weiss, *Angew. Chem.*, **46**, 51 (1953).
13) T. Osa, Y. Ohkatsu, and M. Tezuka, *Chem. Lett.*, **1973**, 98.
14) A. J. Chalk and J. F. Smith, *Trans. Faraday Soc.*, **53**, 1214 (1957).
15) J. A. Elvidge and A. B. P. Lever, *Proc. Chem. Soc.*, **1958**, 195.
16) A. Yamamoto, L. K. Philips, and M. Calvin, *Inorg. Chem.*, **7**, 847 (1968).
17) J. M. Robertson and I. Woodward, *J. Chem. Soc.*, **1937**, 219.
18) P. A. Barret, D. A. Frye, and R. P. Linstead, *ibid.*, **1938**, 1157.
19) J. R. Thomas, *J. Amer. Chem. Soc.*, **85**, 591 (1963).
20) T. Hara, Y. Ohkatsu, and T. Osa, This Bulletin, **47**, 156 (1974).
21) Y. Kamiya and K. U. Ingold, *Can. J. Chem.*, **42**, 1027 (1964).

Chlorination of Methylcyclohexane in Molten Salt Media

Shōichi KIKKAWA, Takatoshi HAYASHI*, Masakatsu NOMURA, and Noboru ŌTSU
Department of Applied Chemistry, Faculty of Engineering, Osaka University, Yamadakami, Suita, Osaka 565
(Received June 6, 1974)

The chlorination of methylcyclohexane in several molten metal chloride mixtures ($ZnCl_2$/KCl/NaCl, CuCl/KCl/NaCl, $AlCl_3$/KCl/NaCl, and $CuCl_2$/KCl/NaCl) has been carried out, using nitrogen gas as a diluent, at three levels of temperature (250, 350, and 450 °C). The reactions in both $ZnCl_2$ and CuCl melts were studied extensively, the former representing the molecular-type melt and the latter standing for the partially-ionic-type one. These reactions gave 1-, 2-, 3-, and 4-chloro-methylcyclohexanes and 1-, 3-, and 4-methylcyclohexenes as primary products, along with smaller amounts of toluene and methylcyclohexadiene. The formation of these olefins were interpreted by the subsequent elimination (by a carbonium-ion mechanism) of HCl catalytically enhanced by these melts from the methyl-chlorocyclohexane derivatives. The difference observed in the product distributions between $ZnCl_2$ and CuCl melts was also explained by the studies of the effect of hydrogen chloride produced in these reactions over molten salts.

A great many studies have been carried out on the chlorination of hydrocarbons in the liquid and gas phases, and many detailed data on the reactivities and reaction mechanism are available. However, the chlorination employing molten salts as a reaction medium[1] has been investigated much less systematically. Melts have the advantages of a high solubility of chlorine and of good thermal conductivity, which effects the removal of the local heat, accompanied by exothermic chlorinations.

The present authors have carried out the chlorinations of ethylbenzene,[2] alicyclic hydrocarbons (C_3–C_4),[3] and cyclohexane[4] in molten salts and found that molten salts act not only as thermally stable reaction media, but also show catalytic activities. The present paper deals with the reaction of methylcyclohexane with chlorine in molten salts.

Since this compound has primary, secondary, and tertiary hydrogen in the molecule, useful information about their relative reactivities and about the reaction mechanism of chlorinations in molten salts can be expected to be obtained by analyzing the isomer distribution of the products.

Experimental

Materials. Commercial methylcyclohexane (I) was distilled after sulfuric acid washing. Commercially-available 4-methylcyclohexene (V) was employed without further purification. The 1-methylcyclohexene (III)[5] and 3-methylcyclohexene (IV) [contaminated with (V)] were prepared according to the reported methods.[6] The 1-chloro- (VI),[7] 3-chloro- (VIII)[8] and 4-chloro-methylcyclohexane (IX),[9] and chloromethylcyclohexane (X)[10] were synthesized by the procedures cited in the literature.

The samples prepared had the following physical constants: III, bp 110—113 °C (108—111 °C); I, bp 100—101 °C (100 °C); V, bp 56—57 °C/28.5 mmHg (50—52 °C/12 mmHg); VIII, bp 45.5 °C/18 mmHg (43.8—44.0 °C/14 mmHg); IX, bp 41—41.5 °C/12 mmHg (41 °C/10 mmHg); X, bp 66—69 °C/20 mmHg (67—68 °C/20 mmHg).

Reagent-grade zinc chloride, cuprous chloride, cupric chloride, and aluminum chloride (Wako Pure Chemical Industries, Ltd., Osaka) were used without further purification.

Apparatus. The apparatus used for the chlorination is shown schematically in Fig. 1. A vertical cylindrical Pyrex tube 30 mm in diameter, equipped with a gas inlet tube (inner diameter of the nozzle of the inlet tube: 1.0—1.5 mm) some distance from the lower end, was heated by means of a coil heater connected to an electric controller (the gas inlet tube was immersed 10 cm in the melts). The mixture of salts was melted and dried with N_2 for 60 min before carrying out the chlorination. After constant flow rates of the nitrogen (0.2 mol/hr) and chlorine (0.1 mol/hr) had been attained, the supply[11] of the reactant was started; the reaction products were collected at the exit in an acetone–Dry Ice trap and analyzed by gas chromatography after the removal of the chlorine by washing with a sodium hypochlorite solution. A blank test on the gas-phase reaction (non-catalytic) was carried out in a U-glass tube covered with aluminum foil to avoid the influence of diffused daylight and immersed 10 cm in a fused salt bath.

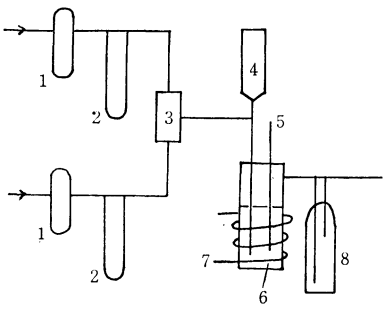

Fig. 1. Block diagram of the apparatus used.
1: $CaCl_2$ tube, 2: flow meter, 3: mixing chamber, 4: starting material, 5: thermocouple, 6: molten salt, 7: heater, 8: Dry Ice–acetone trap

Analysis of Reaction Products. The isomeric products were analyzed by means of gas chromatography [on a Shimadzu-GC-3AH gas chromatograph equipped with TCD using a combined column of Pluronic L-84 (4.5 m × 3.0 mm) and Apiezone grease (0.75 m × 3.0 mm) at 85 °C]. The oven temperature was fixed at 85 °C to avoid dehydrochlorination in the injection port of the gas chromatograph. Hydrogen was used as the carrier gas at a flow rate of about 46 ml/min.

Preparative gas chromatography and proton magnetic resonance were used when necessary for product identification.

* Present address: Department of Chemistry, Ritsumeikan University, Kita-ku, Kyoto 603.

Results and Discussion

Identification of Chlorination Products. A gas chromatogram of the GC-Mass analysis of products obtained in the $ZnCl_2$/KCl/NaCl (3: 1: 1 mole ratio)[12] melt is shown in Fig. 2.

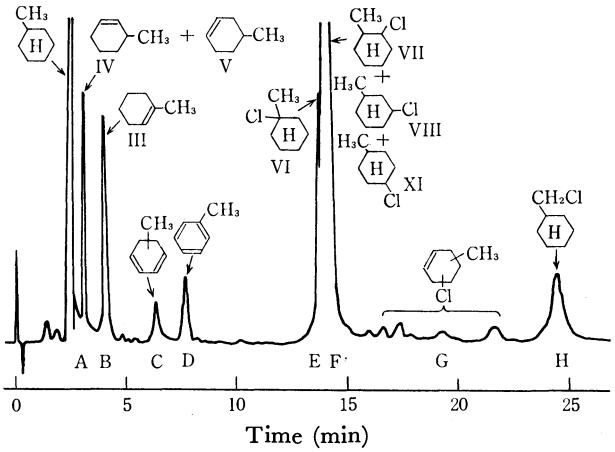

Fig. 2. Glc fractionation of chlorination products of methylcyclohexane in $ZnCl_2$/KCl/NaCl melt.
Conditions of GC-MS (Hitachi K 53 GC-Hitachi RMU-60 MS) analysis: PEG-1540 (0.02′×50 feet), 70 °C, He (0.5 kg/cm²).

The mass spectra of Peak A and Peak B (shown in Fig. 2) indicated the parent peak at *m/e*=96 [Peak A, *m/e* 96, M^+ (13), 81, M^+-CH_3 (100), 68, retro Diels Alder fraction of 3-methylcyclohexene, (39), 54, retro Diels Alder fraction of cyclohexene. Peak B, *m/e* 96, M^+ (46), 81 (100), 68 (75), 67 (43), 55 (50). The number in brackets indicates the relative intensity].[13,14] Both peaks had retention times corresponding to 3-methylcyclohexene(IV) or 4-methylcyclohexene(V) and 1-methylcyclohexene(III) respectively. Since, under these conditions, IV and V were not separated on our columns, Peak A was regarded as a mixture of V and IV. Peak D was confirmed as toluene(XIII) by mass spectral studies (*m/e* 92, M^+ (63), 91 (100), 65 (27), 63 (32)). The mass spectra of Peak C indicated the presence of methylcyclohexa-1,3-diene derivatives(XII) (*m/e* 94, M^+ (25), 91 (25), 79 (100), 77 (75)). Peak E and Peak F showed the following mass spectra [*m/e* 97, M^+-Cl, 81, $96-CH_3$ (most abundant in both peaks), 68, 67, retro Diels-Alder fraction of methylcyclohexene (secondarily abundant in Peak F), 55, retro Diels-Alder fraction of C_6H_{10} (secondarily abundant in Peak E)] and corresponded to the identical retention times of VII, VIII, and IX on the PEG 1540 column, while VI showed a bit of separation, as is shown in Fig. 2. However, using a serially-combined column of Pluronic L-84 and Apiezone glease L, VI was separated distinctly from VII, VIII, and IX (when still had identical retention times), while the fraction of VI was obtained by preparative gas chromatography and was confirmed as 1-chloro-methylcyclohexane by means of its NMR datum (τ, 8.30, CH_3, singlet in CCl_4). The small peaks between Peak F and Peak H were estimated to correspond to methylchlorocyclohexene derivatives (XI) by mass spectral studies (*m/e* 132, 134, M^+, 94 (base peak), 77, 53). Peak H was confirmed to be due to chloromethylcyclohexane by means of mass spectral studies (*m/e* 134,

Table 1. Chlorination of methylcyclohexane in the presence of various melts[a]

Exp. No.	Melts	Temp. (°C)	Recv.[b] Liq. (g)	Conv.[c] (%)	IV and/or V	% Yields III	XII	XIII	VI	VIII | IX	XI	X	Others[d]
1[e]	$ZnCl_2$+KCl +NaCl	250	10.1	11.8	t	t	—	22.4	t	60.8	t	16.8	—
2		350	10.2	45.0	23.0	8.7	3.1	9.2	43.4	3.6	3.2	4.7	0.6
3		450	10.1	52.5	25.1	7.4	2.1	16.4	44.4	3.0	t	0.4	1.2
4	CuCl+KCl +NaCl	250	9.8	4.1	t	14.9	—	—	t	71.0	t	14.1	—
5		350	9.2	48.6	10.3	6.8	—	5.9	10.8	53.2	5.5	7.4	0.5
6		450	8.1	50.6	26.1	7.8	3.3	11.6	21.6	22.7	1.0	5.5	0.4
7	$AlCl_3$[g]	250	8.1	19.8	39.7	34.7	—	7.5	11.7	—	—	—	6.9
8[f]	$CuCl_2$[h]	350	10.6	40.8	16.7	t	—	12.1	8.1	40.9	3.5	6.4	—
9[f]	$CuCl_2$[i]	350	11.1	26.7	9.6	t	—	7.4	7.2	61.0	0.9	7.2	—
10[f]		450	9.9	31.6	3.6	0.8	—	16.4	19.5	27.0	5.2	9.8	—
11	no melts[j]	350	8.9	53.8	3.8	2.3	t	1.9	7.4	75.9	1.1	7.6	—
12[f]		450	8.0	46.8	13.0	1.4	3.5	10.4	12.6	41.9	2.3	6.4	1.0

a) Duration of reaction; 1 hr, Starting material; 0.1 mol/hr, $C_6H_{11}CH_3$: Cl_2: N_2=1:1:2 (mole ratio). See Fig. 4 for structures of the products. b) Recv. Liq. implies the recovered liquid products including the reactant.
c) Conv. (%)$=\frac{\text{Recv. Liq.}-\text{Recovered methylcyclohexane}}{\text{Recv. Liq.}}\times 100$. d) Low boiling hydrocarbon. e) A large amount of polymeric products was obtained. The polymer obtained by means of the reprecipitation in methanol of their benzene solution was analyzed to give molecular weight (by Mechrolab Osmometer Model 301) 1040—1100 and C, 79.56; H, 6.45% ($C_{1.04}H_1$). f) The %yield of XIV was as follows. 11.6% (Exp. No. 8), 6.5% (No. 9), 16.7% (No. 10), and 7.5% (No. 12). The formation of dichloromethylcyclohexane was estimated by mass spectral studies of the fraction obtained by the preparative gas chromatography. g) AlCl:KCl:NaCl=3:1:1 (mole ratio). h) $CuCl_2$:KCl:NaCl=3:1:1 (mole ratio). i) In this experiment chlorine was not supplied because $CuCl_2$ acts as chlorinating reagent. j) At 250 °C, no reaction.

132, M^+, 83, M^+-CH_2Cl) and because its retention times were identical with those of the authentic compound.

Reaction of Methylcyclohexane with Chlorine in Molten Salts. The distribution of chlorination products for I is summarized in Table 1, together with the reaction conditions. With both the $ZnCl_2$ melt and the CuCl melt,[15] the conversions at 250 °C were low, but higher conversions were attained at both 350 and 450 °C. In the melt of $AlCl_3$, it was found difficult to carry out chlorination above 300 °C because of the sublimation of $AlCl_3$. A marked difference in the product distribution can be seen between a catalytic reaction in molten salts and a non-catalytic thermal reaction. In the catalytic reaction, the yield of olefin derivatives including toluene shows a high value, while the formation of these is small in the thermal reaction.

The values of f_0 (representing the sum of olefin yields) and f'_0 (f_0+toluene yields) are plotted against the reaction temperatures in Fig. 3.

In the case of the $AlCl_3$ melt, a high % yield of olefin in the recovered liquid products was observed. The small amount of recovered liquid products containing the reactant is due to the formation of a considerable amount of intractable polymeric products remaining on the surface of molten salt in the reactor.

Both the $CuCl_2$ melt and the CuCl melt showed nearly the same olefin yields, whereas, with the $CuCl_2$ melt, a higher yield of dichloro compounds was observed; this fits the finding by Kunugi[16] that the chlorine addition to olefin was predominant with the $CuCl_2$ melt. Figure 3 also indicates that the relative activities for olefin formation are $ZnCl_2$ melt>CuCl

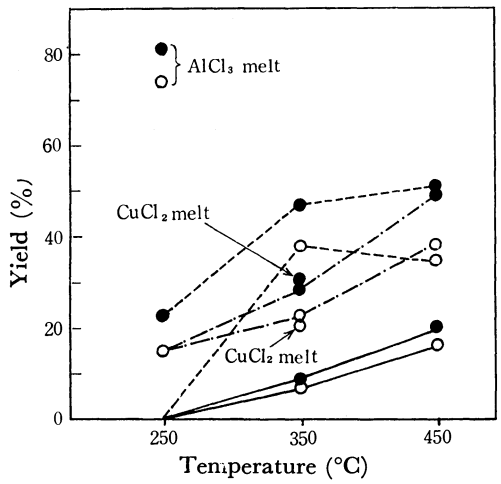

Fig. 3. Olefin yields (f_0 and f'_0) obtained from chlorination of methylcyclohexane in various fused salts at different temperatures.
—○—; f_0, —●—: f'_0, ——: non catalytic reaction, ------: $ZnCl_2$ melt. ·-·-·: CuCl melt.

melt. It is interesting to note that toluene formation was accompanied by no olefin derivatives in the $ZnCl_2$ melt at 250 °C.

As is shown in Table 1, the formation of VI was favored over that of VII, VIII, and IX in the melt of $ZnCl_2$ at both 350 and 450 °C, while the reverse was true with the CuCl melt. These observations will be discussed later.

Reaction of Methyl-Chlorocyclohexanes in Molten Salts. The results of the reaction are shown in Table 2. Three methyl-chlorocyclohexane isomers showed nearly

TABLE 2. DEHYDROCHLORINATION OF 1-CHLORO-, 3-CHLORO-, AND 4-CHLORO-METHYLCYCLOHEXANE

A) 1-CHLORO-METHYLCYCLOHEXANE[a]

Exp. No.	Melts	Temp. (°C)	Recv. Liq. (g)	Conv. (%)	% Yield II[b]	III	XIII	VI	VII—IX	f[c]
13	$ZnCl_2$+KCl+NaCl	250	1.9	84.4	6.3	75.4	1.8	15.6	0.6	0.08
14		350	2.0	99.4	10.1	89.3	t	0.6	—	0.1
15		450	2.0	98.8	9.3	89.5	t	1.2	—	0.1
16	CuCl+KCl+NaCl	250	2.1	46.5	0.5	42.1	3.9	53.5	—	0.01
17		350	2.1	53.4	1.0	50.3	2.1	46.6	—	0.02
18		450	2.0	52.3	1.3	46.2	4.8	47.7	—	0.03

a) Duration of reaction; 20 min, 1-Chloro-methylcyclohexane; 3.0 g, Gas N_2; 0.1 mol/hr, Depth of melts; 5 cm.
b) NMR spectra of products (Exp. No. 14) in CCl_4 showed the presence of III (=CH 4.7 ppm, lit,[17] 4.72 ppm) and II (=CH_2 5.5 ppm, lit,[17] 5.45 ppm). c) f=II/III.

B) 3-CHLORO-METHYLCYCLOHEXANE[a]

Exp. No.	Melts	Temp. (°C)	Recv. Liq. (g)	Conv. (%)	% Yield IV and/or V	III	VI	VII—IX	Others	f_{iso}[b]
19	$ZnCl_2$+KCl+NaC	250	1.8	89.1	47.9	22.7	17.1	10.9	1.4	0.7
20		350	1.9	100	53.0	44.6	1.6	t	1.0	0.8
21		450	1.7	100	64.3	33.6	1.0	—	1.1	0.5
22	CuCl+KCl+NaCl	250	2.1	8.9	4.4	3.2	0.3	92.1	—	0.03
23		350	2.2	31.3	23.0	6.5	1.0	69.5	—	0.08
24		450	2.0	78.8	60.9	7.9	7.7	22.1	2.3[c]	0.2

a) Duration of reaction; 18 min, 3-Chloro-methylcyclohexane; 2.0 g, Flow rate of N_2; 0.1 mol/hr, Depth of melts; 5.0 cm. b) f_{iso}=(III+VI)/(IV+V+VIII) c) All toluene, in this case.

C) 4-Chloro-methylcyclohexane[a]

Exp. No.	Melts	Temp. (°C)	Recv. Liq. (g)	Conv. (%)	% Yield IV and/or V	III	XIII	VI	VII—IX	Others[b]	f_{iso}[c]
25	$ZnCl_2$+KCl+NaCl	250	1.5	72.5	23.8	29.3	2.0	12.9	27.5	2.4	0.9
26		350	1.3	93.5	55.3	33.9	1.0	6.5	1.6	1.7	0.7
27		450	1.3	100	75.4	25.3	1.2	t	t	1.1	0.3
28	CuCl+KCl+NaCl	250	1.8	5.9	3.1	1.1	0.7	t	95.1	t	0.01
29		350	1.7	16.8	12.9	2.5	1.4	t	83.2	t	0.09
30		450	1.5	66.2	54.8	1.3	3.0	7.1	33.8	—	0.09

a) Reaction condition was the same as described in B). b) Low boiling compounds containing cyclohexane.
c) f_{iso}=(III+VI)/(V+IX).

a 100% conversion at 350 and 450 °C in the $ZnCl_2$ melts, while they indicated a lower conversion in the CuCl melt. The catalytic activity difference between these melts is particularly pronounced at 250 °C with VIII and IX as reactants.[18] In the reaction of VI, the primary elimination products were confirmed to be methylene-cyclohexane (II) and 1-methylcyclohexene (III) [see Footnote b) in Table 2A)]. The ratio of II/III, which represents the preference between the "Hofmann" and "Saytzeff" orientations, was 0.1 in the melt of $ZnCl_2$, but 0.01—0.03 in the melt of CuCl. The higher ratio of the $ZnCl_2$ melt compared with that of the CuCl melt may be explained as follows. Since the $ZnCl_2$ melt is known to have a more molecular character[19] than the CuCl melt, the presence of the $\left(\text{C}_6\text{H}_5^{\pm}\text{–CH}_3\ ZnCl_3^-\right)$ complex is seemingly possible in the melt of $ZnCl_2$, where $ZnCl_3^-$ (base) may be well situated to abstract more acidic CH_3 protons, thus leading to the formation of the thermally-unstable olefin II in the higher ratio of II/III compared with the case of the CuCl melt,[21] though 1-methylcyclohexene remains as the primary product.

In the reaction of VIII and IX, considerable amounts of VI and III were formed, together with direct dehydrochlorination products (particularly in the melt of $ZnCl_2$). Table 4 indicates that the direct dehydrochlorination products of VIII and IX, *i.e.*, IV and V, hardly isomerize even in the presence of HCl to III,

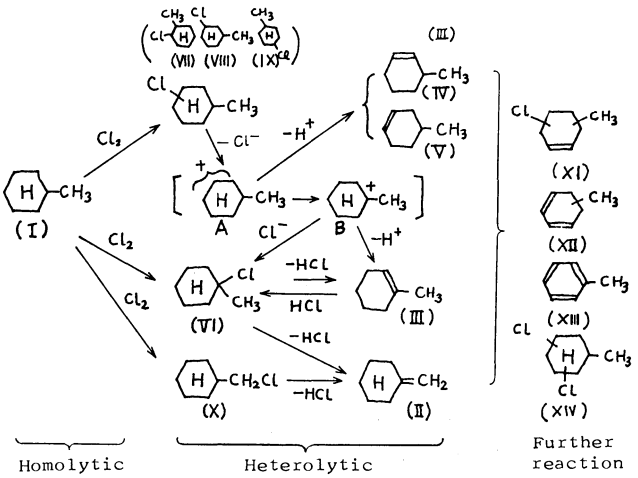

Fig. 4. Reaction scheme.

which is expected to react with HCl to give VI. Therefore, these findings can be explained in terms of rearrangements of the secondary carbonium ion[22] produced by chloride-ion abstraction from VIII or IX to the most stable tertiary carbonium ion (see Fig. 4 for the structures of probable intermediates). The value of f_{iso}(=rearranged products/direct dehydrochlorination products) was used here as a measure of the extent of isomerization. The melts of $ZnCl_2$ showed a higher f_{iso} value than that of CuCl; this can also be explained by the molecular character[19] of the $ZnCl_2$ melt.

Table 3. Dehydrochlorination of methyl-chlorocyclohexane derivatives in the presence of HCl gas through fused salts[a]

Reactant	Exp.[b] No.	Temp. (°C)	Recv. (g)	Conv. (%)	% Yield VI and/or V	III	XIII	VI	VII—IX	f_{iso}
VI	31*	350	1.7	19.5	3.7[c]	13.6	2.2	80.5	—	0.2
	32	350	1.8	—	—	t	—	100	—	—
VIII	33*	350	1.8	95.2	43.4	3.8	5.4	42.6	4.8	1.0
	34	350	1.7	26.2	18.5	—	1.8	5.9	3.8	0.06
IX	35*	350	1.9	95.2	48.6	2.3	7.1	37.2	4.8	0.7
	36	350	1.7	19.8	15.5	—	1.7	2.6	80.2	0.03
VIII	37*	450	1.7	92.6	46.2	2.8	6.9	36.6	7.4	0.7
	38	450	1.7	58.4	44.3	t	3.0	11.1	41.6	0.1

a) Starting material; 2.0 g, Duration of reaction; 17—18 min, Flow rate of N_2; 0.1 mol/hr, HCl: $\text{Cl}\text{C}_6\text{H}_4\text{CH}_3$=1:0.5 (mole ratio). b) Remark of * indicates use of $ZnCl_2$/KCl/NaCl. Another used a melt of CuCl/KCl/NaCl.
c) Methylene cyclohexane in this case.

TABLE 4. REACTION OF METHYLCYCLOHEXENE WITH HCl GAS IN THE PRESENCE OF MELTS[a)]

Reactant	Exp.[b)] No.	Temp. (°C)	Recv. Liq. (g)	Conv. (%)	% Yields						Others
					IV and/ or V	III	XIII	XII	VI	VII—IX	
III	39*	350	1.7	94.2	3.0	5.8	7.0	7.3	75.4	—	1.5
	40	350	1.8	64.5	—	35.5	4.3	7.9	50.8	—	1.5
IV+V	41*	350	1.6	11.1	88.9	1.2	3.3	—	3.6	3.0	—
	42	350	1.7	0.5	99.5	—	—	—	—	—	0.5

a) Starting material; 2.0 g. Duration of reaction; 20 min, Flow rate of HCl; 0.1 mol/hr, HCl: olefin=1:0.7, Depth of salts; 5.0 cm. b) Remarks are the same as described in Table 3.

Reaction of Methyl-Chlorocyclohexane and Methylcyclohexene with HCl in Molten Salts. In the reaction of methylcyclohexane with chlorine in molten salts, chlorine substitution and the subsequent elimination of HCl occurred; both reactions produced corresponding amount of HCl, whose effects on the reaction in molten salts should be noted. Therefore, the following experiments in the presence of added HCl were carried out; the results are listed in Tables 3 and 4. As is shown in Table 3, the reaction of VI shows a substantial recovery of the reactant in the presence of HCl, even in the $ZnCl_2$ melt, which can be expected to assist the dehydrochlorination reaction. This indicates that the olefins formed readily reacted with HCl to give the starting material. This is also confirmed by the experimental results cited in Table 4. That is, the addition of HCl to III took place preferentially with $ZnCl_2$ melts.

However, with VIII and IX as the reactants, a large amount of VI was obtained, along with direct dehydrochlorination products (IV and V), especially in the melt of $ZnCl_2$. In the $ZnCl_2$ melt, the reaction of VIII and IX afforded VI in a yield of about 40%, while the yield of VI reached only a small percentage in the CuCl melt. The preferred formation of these rearranged products with the $ZnCl_2$ melt may be considered to be due to the rearrangement of the Intermediate A to the Intermediate B (in Fig. 4), which is favored in the molecular $ZnCl_2$ melt.

Accordingly, the finding that, in the chlorination of I in molten salts, VI was a main product in the $ZnCl_2$ melt, while a mixture of VII, VIII, and IX was the primary product in the CuCl melt, could be explained by such experimental results. That is, in the $ZnCl_2$ melt, which favors carbonium-ion formation, most of the products, VII—IX, formed by the chlorination of I are converted to III *via* the carbonium-ion mechanism; they then reacts extensively with HCl to afford VI. On the other hand, these rearrangements were not assisted to such an extent by the CuCl melt. In addition, the reaction of IV and V with HCl in the $ZnCl_2$ melt gave slight addition products (3% yield), while the addition of HCl to III took place extensively with the $ZnCl_2$ melt. This is explained by the known stabilities of the carbonium ions (formed by the addition of protons to olefins), which are tertiary (from III)> secondary (from IV—V).

Reaction Process of Methylcyclohexane with Chlorine in the Presence of Molten Salts. In a previous paper[2,4] (the chlorination of cyclohexane in molten salts), the chlorination (substitution reaction) was assumed to proceed by means of a homolytic mechanism, and the subsequent elimination, by means of a heterolytic mechanism. The experimental evidence in favor of this assumption is the observation that the overall reaction was remarkably retarded by the addition of a radical inhibitor (cyclohexene), but the product distribution showed much the same distribution as that in the absence of cyclohexene. Similar observations were made in the reaction of I with chlorine in molten salts; therefore, in these studies, we also considered chlorination to follow a homolytic mechanism and the subsequent elimination and isomerization to follow a heterolytic mechanism.

The most important results obtained here (especially at 350 and 450 °C) may be summarized as follows: 1) The chlorination of I in both the $ZnCl_2$ melt and the CuCl melt affords mono-chlorinated products, VI—IX, along with olefin products, III—V. 2) The reactions of VIII and IX in both melts also give dehydrochlorination products (IV and V), along with III. The relative activities for dehydrochlorination are $ZnCl_2$ melt>CuCl melt. 3) The addition of HCl to III (to form VI) occurs more extensively in the $ZnCl_2$ melt than in the CuCl melt. The addition of HCl to IV and V hardly occurs over either melt. 4) The $ZnCl_2$ melt assists the abstraction of a chloride ion from the organic molecule to a greater extent than the CuCl melt; *i.e.*, the $ZnCl_2$ melt favors carbonium-ion formation from chloro compounds. 5) III and VI are formed from VIII—IX, especially in the $ZnCl_2$ melt, *via* a carbonium-ion mechanism involving the rearrangement of Intermediate A (from VIII—IX) to Intermediate B and the subsequent substitution by chloride ions or the removal of the protons. These results lead us to the reaction scheme shown in Fig. 4, where the inferred intermediates are also given.

References

1) W. Sundermeyer, *Angew. Chem. Int. Ed. Engl.*, **10**, 172 (1971).
2) S. Kikkawa, T. Hayashi, T. Tani, and H. Oshima, *Kogyo Kagaku Zasshi*, **73**, 964 (1970).
3) Unpublished.
4) S. Kikkawa, T. Hayashi, and T. Yamada, *Kogyo Kagaku Zasshi*, **74**, 1818 (1971).
5) P. D. Bartlett and R. H. Rosewood, *J. Amer. Chem. Soc.*, **56**, 1993 (1934).
6) H. Adkins and A. K. Roebuck, *ibid.*, **70**, 4041 (1948).
7) G. Rusen, *ibid.*, **74**, 3882 (1952).

8) H. L. Goering and I. H. McCarron, *ibid.*, **78**, 2270 (1956).
9) S. I. Goldberg and M. S. Sattli, *J. Org. Chem.*, **32**, 2059 (1967).
10) H. Gilman and W. E. Catlin, "Organic Syntheses," Coll. Vol. I, 2nd. ed., p. 188 (1941).
11) The reactant was supplied to the gas inlet tube through capillary of the resevoir and instantly evaporated. The contact time of a bubble of flow gas with the melt may be estimated less than 1 s.
12) Hereafter denoted $ZnCl_2$ melt. CuCl melt also denoted CuCl/KCl/NaCl (3: 1: 1 mole ratio) eutectic.
13) American Petroleum Institute Res. Project. 44, "Catalog of Mass Spectra Data," Carnegie Institute of Technology, Pittsburgh Pa. No. 1174 (1955) and No. 1491 (1958).
14) A. Cornu and R. Massort, "Compilation of Mass Spectral Data," Heyden & Son Ltd. (1966), 41-C.
15) The alkali metals serve to form eutectic solutions with the active constituents and thus lower the melting point, and reduce the vapor pressure.
16) T. Kunugi, H. Tominaga, A. Sawanobori, and M. Nushi, *Kogyo Kagaku Zasshi*, **72**, 2385 (1969); *ibid.*, **73**, 170 (1970).
17) F. A. Bovey "NMR Data Tables for Organic Compounds Vol. 1," Interscience Publishers, New York (1967), p. 183.
18) A possible explanation for this is as follows. As the thermal contribution becomes more significant in the elimination reaction in CuCl melt (owing to its low catalytic activity), the reaction is reluctant to proceed at such a low temperature as 250 °C even in the presence of CuCl melt, whereas the reaction shows a considerable high conversion in the presence of $ZnCl_2$ melt due to its strong catalytic activity. This probably caused the considerable difference between both conversions, being also affected by the fact that lower reactive secondary chloride (VII, VIII, and IX) may be more sensible to the change of reaction condition than the reactive tertiary chloride (VI).
19) N. E. Norman[20] divided inorganic salts roughly into two groups, molecular melts and ionic melts. This simple classification may be considered useful in analyzing the catalytic activities of different molten salts.
20) N. E. Norman and H. F. Johnstone, *Ind. Eng. Chem.*, **43**, 1553 (1951).
21) In the melt of CuCl, both the cuprous and chloride ion believed to exist, as well as undissociated cuprous chloride.
22) R. A. Railey and S. F Prest, *Can. J. Chem.*, **49**, 1 (1971).

The Acid-Catalyzed Cyclization of 2,3-Dimethyl-2-phenethyl-3-cyclohexen-1-one

Takenori KUSUMI, Nobuo OHNO, and Hiroshi KAKISAWA
Department of Chemistry, Tokyo Kyoiku University, Otsuka, Bunkyo-ku, Tokyo 112
(Received July 17, 1974)

The cyclization of 2,3-dimethyl-2-phenethyl-3-cyclohexen-1-one **6a** with aluminum chloride gave 4a,*cis*-10a-dimethyl-3,4,4a,9,10,10a-hexahydro-1(2*H*)-phenanthrone **8a**. The stereochemistry of the latter was established by synthesizing 4a,*cis*-10a-dimethyl-1,2,3,4,4a,9,10,10a-octahydrophenanthrene **10** through Diels-Alder reaction of 3-formyl-4a,*cis*-8a-dimethyl-4a,5,6,7,8,8a-hexahydro-2(1*H*)-naphthalenone **20** with butadiene.

The acid-catalyzed cyclization of aryl-olefin systems is widely used in the synthesis of steroids and polycyclic terpenes. Two asymmetric centers are produced at the ring junctions of the newly constructed ring. Recently the stereochemical investigation of this 'cyclialkylation' is reported by Ireland *et al.*[1] In their and hitherto reported cyclialkylation reactions, two newly formed angular substituents are restricted mostly to hydrogen and methyl groups, and there has been no report upon such cyclialkylation that gives rise to two angular methyl groups, which should be of importance especially in the synthetic study of triterpenes.

This report deals with the cyclialkylation of 2,3-dimethyl-2-phenethyl-3-cyclohexen-1-one **6a**, which affords the octahydrophenanthrene **8b** carrying two methyl groups at the angular positions.

The synthesis of 4a,*cis*-10a-dimethyl-1,2,3,4,4a,9,10,10a-octahydrophenanthrene **10** which serves as a standard for establishing the stereochemistry of 4a,10a-dimethyl-1,2,3,4,4a,9,10,10a-octahydrophenanthrenes is also described.

Results and Discussion

Synthesis and Cyclization of the Phenethylcyclohexenone 6a. Hageman's ester **1** readily availabe by condensation of ethyl acetoacetate and paraformaldehyde[2] was treated with phenethyl bromide and sodium hydride in benzene-dimethylformamide (DMF) to give the phenethyl derivative **2**, which was boiled with potassium hydroxide in ethanol affording the cyclohexenone **3**.[3] Methylation of **3** with methyl iodide and sodium hydride (one equivalent) in benzene-DMF gave a mixture of mono, di, and trimethylated products (**4a—c**) accompanied by unchanged **3**. The formation of the exocyclic double bond by the methylation was revealed by the NMR spectrum (4.83 and 4.90 ppm, each br. s, 2H) of the product. The yield of the methylated product was estimated as 30% by vpc. However, it was practically difficult to separate the desired monomethylated derivative **4a** from the reaction mixture.

The yield of the methylation was raised as high as 50% when the ketoester **2**, in which the carbethoxy group at C-4 activates the enone system, was treated with methyl iodide and sodium hydride in toluene. The crude product was directly hydrolyzed with potassium hydroxide in ethanol to afford a mixture of the ketoacids **5a—c** easily separable from the cyclohexenone **3** which was produced from the unreacted ester **2** through the hydrolysis and decarboxylation. The mixture of the acids **5a—c** was treated with copper chromite catalyst in quinoline[4] to yield the decarboxylated products **6a**, **b**, and **c**. From the vapor phase chromatogram the ratio of **6a**, **b**, and **c** was estimated as 62: 28: 10.

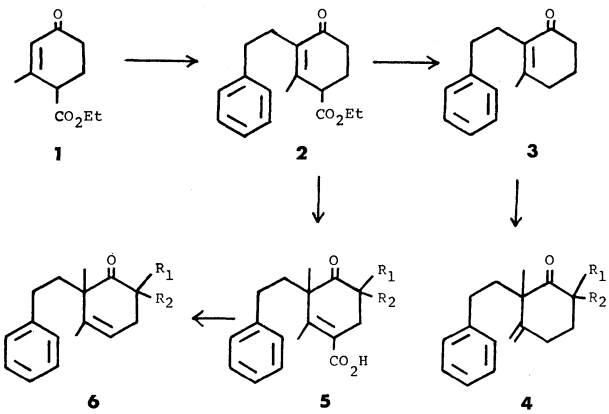

a: $R_1=R_2=H$, b: $R_1=CH_3$, $R_2=H$, c: $R_1=R_2=CH_3$

Isolation of the desired monomethylated derivative **6a** was achieved as follows; formylation of the mixture of **6a—c** followed by alkaline extraction gave a solution of the enolate **7** which was hydrolyzed to produce **6a**. Di and trimethylated derivatives, **6b** and **c**, could be removed in the course of the alkaline extraction.

Treatment of **6a** with aluminum chloride in carbon disulfide at 0 °C gave a crystalline substance (mp 64—65 °C) as a single product in 73% yield. Treatment of **6a** with 85% phosphoric acid at 120 °C afforded the same product.

The IR spectrum of the product represents a carbonyl absorption at 1702 cm^{-1} and the NMR spectrum shows two sharp singlets at 1.10 and 1.27 ppm ascribable to tertiary methyls beside a 4H-multiplet at the aromatic region. From these spectral properties the structure **8** was assigned for the crystalline product.

The NMR and the vpc showed that the only one of the two possible stereoisomers, **8a** and **b**, was afforded by the cyclization reaction. Whitlock and Overman have obtained *trans* **8a** and *cis* **8b** through Simmons-Smith reaction of the enolate **9**,[5] and our product **8** is revealed to accord with *cis* **8b** by comparison with its mp and the NMR spectrum. However, no basis to determine the stereochemical relationship of the two angular methyl groups is appeared in their report. Therefore we focussed our attention upon synthesizing the *cis*-dimethylhydrophenanthrene **10** by the stereochemically unambiguous method.

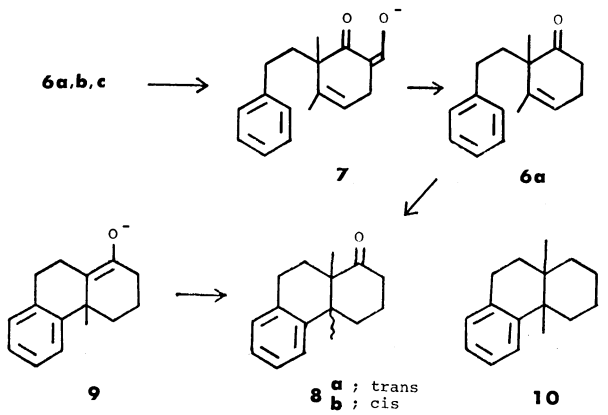

Synthesis of the cis-*Dimethylhydrophenanthrene* **10**. The anhydride **12**, prepared by Diels-Alder reaction[6] of **11** and butadiene, was hydrogenated on palladium–charcoal in ethanol affording **13**. This was treated with lithium aluminum hydride in ether to produce the diol **14**. It is obvious from surveying the series of the reaction employed that the two hydroxymethyl groups of **14** should be situated in a *cis* sence. The diol **14** was treated with methanesulfonyl chloride in pyridine at 0 °C to give the dimesylate **15**. Reduction of **15** with lithium aluminum hydride in ether or tetrahydrofuran, however, produced an intractable mixture of rearranged hydrocarbons, ethers and alcohols, and the desired *cis*-dimethyl compound **10** could not be obtained from the mixture.

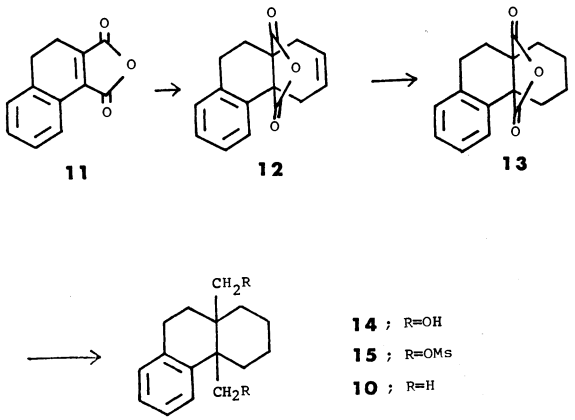

We, therefore, turned our effort to another approach to **10**. The *cis*-dimethyldecalone **17** was prepared by treatment of the octalone **16** with methylmagnesium iodide–cuprous salt[7] or dimethylcopperlithium,[8] the latter giving the higher yield. The *cis*-relationship of the two methyl groups in **17** has been already established.[7] The decalone **17** was formylated with ethyl formate and sodium methoxide to give **18** in good yield. The NMR spectrum of **18** exhibits two pairs of AB quartet centered at 2.28 (2H, J=15 Hz) and 2.29 (2H, J=19 Hz) ppm attributable to the methylene groups at C-1 and C-4, which excludes the another possible isomer **19**. The regiospecific formylation at C-3 is ascribed to severe steric hindrance around C-1 of the decalone **17**. The formylketone **18** was converted into **20** by oxidation with 2,3-dichloro-5,6-dicyano-1,4-benzoquinone (DDQ) in dioxane.[9] The NMR spectrum of the ketoaldehyde **20** shows five sharp singlets at 10.06 (1H, –CHO), 7.40 (1H, olefinic proton at C-1), 2.43 (2H, $-CH_2-$ at C-4), 1.16 (3H, $-CH_3$), and 1.05 (3H, $-CH_3$) ppm. The ketoaldehyde **20** was heated with butadiene at 200 °C, and the product was chromatographed to give rise to a ketonic substance in 7% yield. The IR spectrum of this ketone shows a strong absorption at 1710 (C=O) and a weak one at 1665 cm^{-1} (C=C). Its NMR spectrum exhibits two sharp singlets at 1.04 (3H) and 1.06 (3H) assignable to two quarternary methyls and a broad singlet at 5.60 (2H) ppm due to two olefinic protons. No signal showing the presence of an aldehyde proton was observed. From these spectral properties the structure **22** could be assigned for the ketone, and this was further justified by its mass spectrum. The molecular peak appears at *m/e* 232.184 accordant with the molecular weight of **22** (232.183 Calcd for $C_{16}H_{24}O$). Carbon monoxide was apparently removed from the initial Diels-Alder adduct **21** in the course of the reaction.

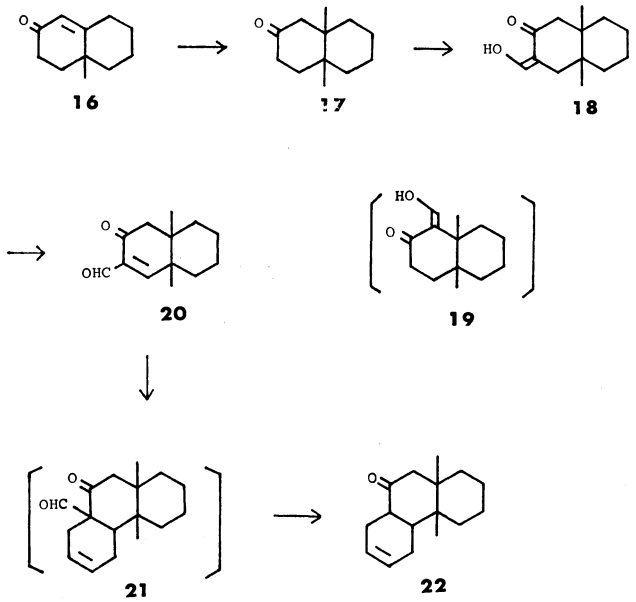

The tricyclic ketone **22** was converted into the dibromide **23** through the agency of bromine in chloroform. Dehydrobromination of **23** with quinoline[10] and subsequent dehydrogenation with DDQ gave a mixture of **24a** and **b**. The mixture was treated with lithium aluminum hydride affording **25a** and **b**. Reduction of the mixture with sodium in liquid ammonia in the presence of ethanol[11] and purification with column chromatography gave rise to the *cis*-dimethylhydrophenanthrene **10** as an oil. Its NMR spectrum exhibits two sharp singlets at 0.95 and 1.19 due to the angular methyl groups, a broad triplet at 2.84 (2H, J=7 Hz) ppm corresponding to the benzylic protons and a complex multiplet in the aromatic region (4H, 7—7.7 ppm). The IR and the mass spectra are also consistent with the structure **10**.

Finally the tricyclic ketone **8**, which had been obtained by the cyclization of **6a**, was reduced by hydrazine and sodium hydroxide to produce a hydrocarbon. The IR spectrum and the behavior on tlc and vpc of the hydrocarbon were identical with those of **10**. These facts show that the two angular methyl groups of **8**

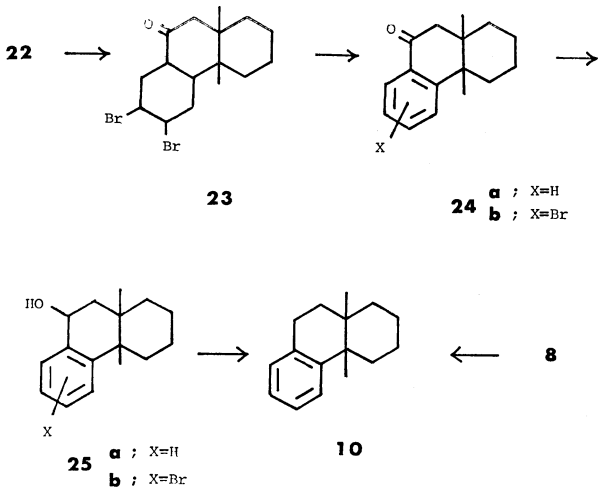

are in a *cis*-relationship.

The acid-catalyzed cyclization of **6a** proceeds in such a manner as to yield *cis* **8b** exclusively.

Experimental

NMR spectra were obtained with a Hitachi EPI-S2 spectrophotometer. Ultraviolet spectra were taken on a Hitachi EPS-3T. Melting points and boiling points are uncorrected.

3-Methyl-2-phenethyl-2-cyclohexen-1-one **3** was prepared according to the method described in Ref. 3.

Methylation of 3-Methyl-2-phenethyl-2-cyclohexen-1-one **3**. Into a suspension of sodium hydride (270 mg as a 50% dispersion in mineral oil) in dry benzene (30 ml) and DMF (10 ml) was added a solution of **3** (1.0 g) in benzene (5 ml) during 1 hr in an atmosphere of nitrogen. After the mixture was stirred at room temperature for 20 hr, a solution of methyl iodide (730 mg) in benzene (5 ml) was added during 1.5 hr. After being stirre at 40—45 °C for 18 hr, the mixture was washed with dilute hydrochloric acid, sodium bicarbonate solution and dried over sodium sulfate. Evaporation of the solvent gave an oil (1.1 g), which consisted of the starting ketone **3** and the methylated products **4a—c**. The ketone **3** could be removed by preparative thin layer chromatography, but the methylated products showed the single spot on tlc and approximate retention times on vpc, and the further attempt to isolate **4a** was discontinued. The mixture of **4a—c** has the following spectral properties; ν(film) 1705, 1630, 1600, 895, 750, 700 cm^{-1}; δ ($CDCl_3$) 4.83 (br.s, 1H), 4.90 (br.s, 1H) ppm; *m/e* 256 (M^+ of **4c**), 242 (M^+ of **4b**), 228 (M^+ of **4a**).

Methylation of **2**.[3] A solution of **2** (28.7 g) in dry toluene (170 ml) containing sodium hydride (5.90 g) was stirred at 110 °C until no more hydrogen was evolved (1.5 hr). The cooled reaction mixture was treated with methyl iodide (71.0 g) and the mixture was stirred at refluxing temperature for 70 hr. Ethanol was added to the cooled mixture and the mixture was poured into water. The toluene layer was separated, and the aqueous layer was extracted with ether. The combined organic layer was washed with sodium bicarbonate solution and dried. The solvent was removed to afford a yellow oil (29.6 g). This was dissolved into 15% ethanolic sodium hydroxide (120 ml) and the solution was heated under reflux for 23 hr. Water was added and the mixture was further refluxed for 1 hr. The ethanol was removed and the residue was treated with water and extracted with ether. The ethereal layer was washed with sodium bicarbonate solution. The aqueous layers were combined and acidified with 1.4 M hydrochloric acid to pH 1.0. Extraction with ether and removal of the ether gave a mixture of the acids **5a—c** (15.3 g). From the ethereal layer was obtained the ketone **3** (8.9 g).

Decarboxylation of the Acids **5a—c**. A mixture of the acids **5a—c** (15.3 g), copper chromite catalyst[4] (1.5 g), and freshly distilled quinoline (60 ml) was heated to reflux in a metal-bath for 10 min. The cooled reaction mixture was poured into ether and the catalyst was filtered away. The filtrate was washed with dilute hydrochloric acid, sodium bicarbonate solution and brine, and dried over sodium sulfate. The crude deep brown oil obtained after removal of the ether was fractionated under reduced pressure to afford a light yellow oil (6.9 g; bp 108—123 °C/0.2 mmHg). The oil was found to consist of **6a** (62%), **6b** (28%), and **6c** (10%) by vpc (PEGS-10% on chromosorb W; 228°C).

Isolation of **6a** *from the Mixture* **6a—c** *by Formylation*. Into an ice-cooled suspension of powdered sodium methoxide (1.35 g) in dry benzene (30 ml) was added with stirring a solution of the above mixture **6a—c** (3.07 g) in ethyl formate (2.0 g) under a nitrogen atmosphere. The mixture was allowed to stand at room temperature overnight. Ice-water was added, and the alkaline-insoluble materials (**6b** and **c**) were taken up into ether. The aqueous alkaline solution was kept at 90 °C for 4 hr. The cooled solution was extracted with ether, dried over sodium sulfate. Removal of the ether afforded the cyclohexenone **6a** (1.18 g), ν (film): 3020, 1705, 1620, 1600, 750, 695 cm^{-1}; δ (CCl_4): 1.18 (s, 3H), 1.79 (br.d, 3H), 2.0—2.7 (m, 8H), 5.73 (m, 1H), 7.2 (br.s, 5H) ppm; *m/e* 228.150; Calcd for $C_{16}H_{20}O$: 228.150; bp 110 °C/0.1 mmHg.

Cyclization of 2,3-Dimethyl-2-phenethyl-3-cyclohexen-1-one **6a**. *(A) With Aluminum Chloride*: The cyclohexenone **6a** (96 mg) was stirred with anhydrous aluminum chloride (143 mg) in dry carbon disulfide (5 ml) at 0 °C for 3 hr. The mixture was filtered and the filtrate was washed with dilute hydrochloric acid. Evaporation of the solvent gave a colorless solid (70 mg; 74%). Recrystallization from benzene–hexane gave pure **8b**, mp 64—65 °C; ν (KBr): 1702, 1498, 755 cm^{-1}; ν ($CHCl_3$): 1700, 1603, 1498 cm^{-1}; δ ($CDCl_3$): 1.10 (3H, s), 1.27 (3H, s), 1.5—3.0 (m, 10H), 7.0—7.3 (4H, m) ppm; δ (C_6H_6): 1.00 (3H, s), 1.06 (3H, s) ppm. Found: C, 84.03; H, 8.80%. Calcd for $C_{16}H_{20}O$: C, 84.16; H, 8.83%.

(B) With Phosphoric Acid: The cyclohexenone **6a** (593 mg) was heated at 120—125 °C with 85% phosphoric acid (50 ml) for 12 hr. The cooled mixture was poured into ice-water, and extracted twice with ether. The ether was evaporated to give 650 mg of oil which was chromatographed on alumina (50 g). Elution with benzene gave **8b** (443 mg; 75%), which was identical with the ketone obtained by the method (A).

4b,5,8,8a,9,10-Hexahydrophenanthrene-4b,8a-dicarboxylic Anhydride was prepared according to the Ref. 6; mp 84 °C.

4b,5,6,7,8,8a,9,10-Octahydrophenanthrene-4b,8a-dicarboxylic Anhydride **13**. The anhydride **12** (1.7 g) was dissolved in ethyl acetate (100 ml) and platinum oxide (400 mg) was added. The mixture was stirred under hydrogen. The hydrogen absorption ceased after the uptake of 267 ml of hydrogen and the catalyst was filtered away. The filtrate was concentrated to give an oil (1.71 g) which solidified on standing. Recrystallization from benzene–ligroin gave colorless needles; mp 97—98 °C; ν (KBr): 1850, 1775 cm^{-1}.

4b,8a-Bis(hydroxymethyl)-4b,5,6,7,8,8a,9,10-octahydrophenanthrene **14**. Into a stirred suspension of lithium aluminum hydride (2.1 g) in tetrahydrofuran (250 ml) was added a solution of the anhydride **13** (1.35 g) in tetrahydrofuran

(10 ml). The reaction mixture was heated under reflux for 17 hr. The complex was decomposed with water and the white precipitates were filtered away. The filtrate was concentrated to give a colorless solid (1.31 g). Recrystallization from ethanol afforded colorless needles (1.1 g); mp 130—132 °C; ν (KBr): 3300—3200 cm^{-1}.

4b,8a-Bis(methanesulfoxymethyl)-4b,5,6,7,8,8a,9,10-octahydrophenanthrene ***15***. The diol **14** (200 mg) was dissolved in pyridine (40 ml) and the solution was cooled at 0 °C in an ice-bath. Methanesulfonyl chloride (2.8 ml) was added in a portion, and the reaction mixture was stirred at 0 °C for 1 hr. This was poured onto ice, and the aqueous solution was extracted with ether. The ethereal solution was washed successively with 2 M hydrochloric acid, sodium bicarbonate solution, water and brine. After the ethereal solution was dried over sodium sulfate, the solvent was evaporated to yield a colorless solid (354 mg), which was washed with small portions of ether. The dimesylate has the following spectral properties; ν (KBr): 1335, 1170, 980 cm^{-1}; δ ($CDCl_3$): 2.85 (3H, s), 3.05 (3H, s), 4.30 (2H, s), 4.41 (2H, ABq, J=9 Hz), 7.2 (4H, m) ppm.

Reduction of 15 with Lithium Aluminum Hydride. A mixture of the dimesylate (285 mg) and lithium aluminum hydride (600 mg) in ether (100 ml) was heated under reflux with stirring overnight. After the usual treatment a colorless oil was obtained. The IR spectrum of the crude product showed strong absorption at 1170 cm^{-1} suggesting the presence of ethers in the product. The oil was chromatographed on silicic acid. Elution with hexane gave a mixture of hydrocarbons (90 mg) whose NMR spectrum showed no distinct methyl signals.

*3,4,4a,5,6,7,8,8a-Octahydro-4a,*cis*-8a-dimethyl-2(1H)-naphthalenone* ***17***. Into a suspension of cuprous iodide (34.8 g) in ether (400 ml) was added methyllithium (2 eq) in ether at −20 °C under a slow stream of nitrogen. Into the dark brown solution was added a solution of **16** (20 g) in ether (50 ml) at 0 °C during 25 min. After the reaction mixture was stirred at 0 °C for 2.5 hr, aqueous ammonium chloride solution was added cautiously. After violent evolution of gas ceased, the mixture was transferred into a separatory funnel. The ethereal layer was separated and washed with brine and dried over sodium sulfate. Evaporation of the ether afforded a crystalline solid (20.4 g) which was purified by chromatography (1 kg of alumina). Elution with hexane–benzene (8:2) yielded **17** (17.7 g; 80%). Further purification by sublimation (50 °C/1 mmHg) gave colorless crystals; mp 119—127 °C (lit, 109—116 °C). The IR and NMR spectra were identical with those of **17** prepared by Marshall's method.[7]

*3-Formyl-4a,*cis*-8a-dimethyl-3,4,4a,5,6,7,8,8a-octahydro-2(1H)-naphthalenone* ***18***. Sodium methoxide prepared by dissolving sodium (186 mg) in dry methanol (3 ml) was heated at 160 °C at 1 mmHg for several minutes to remove the trace of methanol. The solid was dispersed into dry benzene (20 ml) and a solution of the decalone **17** (300 mg) in freshly distilled dry ethyl formate (670 mg) was added at 0 °C during 15 min. After the temperature was maintained at 0 °C for 1 hr, the mixture was stirred at room temperature overnight. The yellow slurry was treated with ice-water and the aqueous layer was separated and washed with ether. The alkaline solution was acidified with hydrochloric acid, and the acidic material was extracted with ether. The usual treatment of the ether extract gave a slightly red oil (349 mg) which was used in the next reaction without further purification; ν (film): 1645, 1595 cm^{-1}; δ ($CDCl_3$): 0.98 (s, 6H), 2.28 (ABq, J=15 Hz, 2H), 2.29 (ABq, J=19 Hz, 2H) ppm.

*3-Formyl-4a,*cis*-8a-dimethyl-4a,5,6,7,8,8a-hexahydro-2(1H)-naphthalenone* ***20***. A solution of the formylketone **18** (5.6 g) and DDQ (6.2 g) in dry dioxane (60 ml) was allowed to stand at room temperature for 30 min. Fine precipitates separated out rapidly. The precipitates were filtered off, and the filtrate was diluted with methylene chloride. The solution was washed with 2% aqueous sodium hydroxide solution until the aqueous layer showed no coloration. The organic layer was washed with water and brine, and dried over sodium sulfate. Evaporation of the solvent gave a red oil (3.2 g) which was purified by distillation at reduced pressure, bp 109 °C/0.2 mmHg (2.6 g). The oil solidified on cooling and recrystallization from hexane afforded light yellow crystals; mp 35—36 °C; ν (CCl_4): 1705, 1690, 1615 cm^{-1}; δ (CCl_4): 1.05, 1.16 (each 3H, s), 2.43 (2H, s), 7.40 (1H, s), 10.06 (1H, s) ppm. Found: C, 75.65; H, 8.77%. Calcd for $C_{13}H_{18}O_2$: C, 75.69; H, 8.80%.

*4b,*cis*-8a-Dimethyl-1,4,4a,5,6,6a,7,8,9,10,10a-dodecahydro-10-oxophenanthrene* ***22***. The ketoaldehyde **20** (1.6 g) and butadiene (1.26 g; 3 eq) in dry dioxane (5 ml) was heated at 200—210 °C for 24 hr in a sealed tube. The resulting oil was chromatographed on silicic acid (100 g), and elution with hexane–benzene (3:7) yielded the ketone **22** (107 mg). The analytical sample was obtained by micro distillation of a small portion of this material at 120—140 °C bath temperature (0.4 mmHg). Found: *m/e* 232.184. Calcd for $C_{16}H_{24}O$: 232.183.

*2,3-Dibromo-4b,*cis*-8a-dimethyl-1,2,3,4,4a,4b,5,6,7,8,8a,9,10,10a-tetradecahydro-10-oxophenathrene* ***23***. Into a stirred solution of the tricyclic ketone **22** (111 mg) in freshly distilled chloroform was added a solution of bromine (92 mg) in dry carbon tetrachloride (4 ml) at −60 °C during 40 min. The mixture was stirred at −60 °C for 10 min, and the solvent was evaporated under reduced pressure to yield a yellow oil (211 mg) which crystallized on cooling.

Dehydrobromination of the Dibromide 23. A solution of the dibromide **23** (211 mg) in freshly distilled quinoline (2 ml) was heated at 160—170 °C for 4 hr. The reaction mixture became dark brown. This was cooled and poured into water, and the product was extracted with ether. The ethereal layer was washed several times with 1 M hydrochloric acid, sodium bicarbonate solution, and dried over sodium sulfate. Removal of the solvent gave a brown oil (123 mg); ν (film): 1705, 1668, 1615, 1600 cm^{-1}. The crude product was treated with DDQ (192 mg) in dry benzene (10 ml) at 80 °C for 1 hr. The dark brown mixture was filtered through alumina (15 g). The alumina was further eluted with benzene (200 ml). Evaporation of the benzene gave a yellow oil (106 mg). The oil was adsorbed on silicic acid (20 g) and eluted with hexane–benzene to afford mainly three fractions (a), (b), and (c). Fraction (a) (31 mg); the starting dibromide **23**: fraction (b) (22 mg); the bromoketone **24b**, ν (film): 1705 cm^{-1}: fraction (c) (38 mg): a mixture of **24a** and **b**, *m/e* 306 and 308 (M^+ of **24b**), 228 (M^+ of **24a**).

*4b,*cis*-8a-Dimethyl-4b,5,6,7,8,8a,9,10-octahydrophenanthrene* ***10***. A mixture of the ketones (fraction (c); 34 mg) was dissolved in ether (5 ml) and lithium aluminum hydride (359 mg) was added. The mixture was stirred at room temperature overnight. After decomposition of the excess hydride a colorless oil was obtained (32 mg); ν (film): 3400 cm^{-1}. Into liquid ammonia (10 ml) was added a solution of the above oil in dry ethanol (0.5 ml). Sodium (80 mg) was added in small portions. The ammonia was evaporated and the residue was treated with water. The product was extracted with ether and purified by column chromatography to give a colorless oil (20 mg); ν (film): 2900, 1480, 1460, 1438, 1375, 1034, 751, 737, 718 cm^{-1}; δ (CCl_4): 0.95 (3H, s), 1.19 (3H, s),

2.84 (2H, t, J=7 Hz), 7—7.7 (4H, m) ppm; *m/e* 214.169; Calcd for $C_{16}H_{22}$: 214.172.

By Wolff-Kishner Reduction of 8b. A mixture of **8b** (46 mg), 80% hydrazine hydrate (0.5 ml) and potassium hydroxide (680 mg) in diethylene glycol (5 ml) was refluxed for 1 hr. Water was then distilled until the temperature of the reaction mixture reached 200 °C, and the distillate was collected. The reaction mixture was kept at 200 °C for 3 hr. Water was added and the mixture was acidified with conc. hydrochloric acid. The mixture and the distillate were combined and extracted with benzene. After drying over sodium sulfate, the benzene was removed on a rotary evaporator to give a colorless oil (30 mg) which was purified with chromatography (silicic acid; 2 g). Elution with hexane afforded a colorless oil (20 mg). The IR spectrum, R_f value on tlc, and retention time on vpc were identical with those of **10** obtained in the above procedure.

The authors wish to thank Mr. T. Kinoshita (Sankyo Co., Ltd.) for the mass spectrum measurement.

References

1) R. E. Ireland, S. W. Baldwin, and W. C. Welch, *J. Amer. Chem. Soc.*, **94**, 2056 (1972).
2) L. I. Smith and G. F. Rouault, *ibid.*, **65**, 631 (1943).
3) G. Stork and A. Burgstahler, *ibid.*, **73**, 3544 (1951).
4) H. Adkins, R. Connor, and K. Folkers, *ibid.*, **54**, 1138 (1932).
5) H. W. Whitlock, Jr. and L. E. Overman, *J. Org. Chem.*, **34**, 1962 (1969).
6) L. Fieser and E. B. Hershberg, *J. Amer. Chem. Soc.*, **57**, 1851 (1935).
7) J. A. Marshall and A. R. Hochstetler, *J. Org. Chem.*, **31**, 1020 (1966).
8) H. O. House, W. L. Respress, and G. W. Whitesides, *ibid.*, **31**, 3128 (1966).
9) a) J. A. Edwards, M. C. Calzada, L. C. Ibanez, M. E. C. Rivera, R. Urquiza, L. Cardona, J. C. Orr, and A. Bowers, *ibid.*, **29**, 3481 (1964); b) P. Morand, S. Stavic, and D. Godin, *Tetrahedron Lett.*, **1966**, 49.
10) C. Harris and H. von Splawa-Neyman, *Ber.*, **42**, 693 (1909).
11) a) A. J. Birch, *J. Chem. Soc.*, **1945**, 809; b) A. J. Birch and S. M. Mukkerji, *ibid.*, **1949**, 2531.

Polymerizationn of Vinyl Compounds by Dihydridotetrakis-(triphenylphosphine)ruthenium(II)

Sanshiro KOMIYA, Akio YAMAMOTO, and Sakuji IKEDA

Research Laboratory of Resources Utilization, Tokyo Institute of Technology, Ookayama, Meguro, Tokyo 152

(Received July 18, 1974)

Dihydridotetrakis(triphenylphosphine)ruthenium(II) **1** initiates the polymerization of α-substituted olefins of high *e*-values such as acrylonitrile and forms unstable complexes with olefins of low *e*-values. Molecular weight of the polymer obtained by the polymerization of acrylonitrile with **1** was independent of polymerization time and increased linearly with the monomer concentration. The rate of polymerization was measured by a dilatometry and compared with the rate of decomposition of **1** in the presence of acrylonitrile followed by a spectroscopic method. The rate of decomposition of **1** was found to be equivalent to the rate of initiation of polymerization and can be expressed by the following equations:

$$-\frac{d}{dt}[Ru] = k[Ru], \quad \frac{1}{k} = A + \{B + C[PPh_3]\}/[monomer]$$

On the basis of the kinetic results and the independence of molecular weight of the polymer on time, a mechanism involving a slow initiation step followed by rapid propagation and termination steps is proposed.

Recent developments in the study of olefin polymerization by isolated transition metal allyl,[1] benzyl,[2] and alkyl[3] complexes have shed some light on the mechanism of coordination polymerization by Ziegler type catalysts. The polymerization mechanism with these isolated monometallic complexes has been accounted for as combination of elementary steps comprising the coordination of a monomer to the transition metal complex with a metal-carbon bond, the succeeding monomer insertion into the metal-carbon bond activated by coordination of the monomer and the spontaneous termination. A similar polymerization activity is expected for a transition metal hydride complex, and in fact some transition metal hydrides[4] are known to initiate the vinyl polymerization.

No detailed study, however, has been made to our knowledge on the vinyl polymerization by an isolated transition metal hydride except for the study by cobalt hydride.[5] Dihydridotetrakis(triphenylphosphine)ruthenium **1**,[6] which is a stable hydride complex easy to handle, catalyzes a variety of reactions of olefins, such as hydrogenation, H–D exchange, isomerization and polymerization, and serves as an appropriate model compound for studying the mechanisms of the olefin catalysis. This paper is mainly concerned with the kinetics of polymerization of acrylonitrile (AN) by **1**. Other ruthenium dihydride complexes with different substituted phosphine ligands have been examined as catalysts for vinyl polymerization and compared with **1**.

Results and Discussion

Polymerization of Vinyl Compounds by Ruthenium Hydride Complexes. The ruthenium hydride complex **1** reacts with a variety of olefins, substituted and unsubstituted. Table 1 summarizes the results of the reactions of **1**. The olefins in Table 1 are arranged in the decreasing order of Alfley Price's *e*-value[7] which parallels the electronegativity of the olefin. The most electronegative α,β-substituted olefins such as tetracyanoethylene and maleic anhydride give stable olefin-coordinated π-complexes and the α-substituted oefins of medium *e*-values are polymerized by **1**, whereas less electronegative olefins such as styrene and ethylene form unstable olefin-coordinated π-complexes. We have

TABLE 1. REACTIONS OF $RuH_2(PPh_3)_4$ WITH OLEFINS

Monomer	*e*-Value[a]	Time	Temp.	Polymer yield (MW)	Complex isolated
Tetracyanoethylene (TCNE)			r. t.	—	$Ru(TCNE)_3(PPh_3)_2$
Maleic anhydride (MAnh)	2.25	6 days	r. t.	—	$Ru(MAnh)_n(PPh_3)_{5-n}$
Acrylonitrile (AN)	1.20	5 min	r. t.	57% (8.1×10^4)	
Methacrylonitrile (MAN)	0.81	3 days	r. t.	23% (1.71×10^4)	
Acrolein (AC)	0.73	1 hr	r. t.	32%	
Methyl vinyl ketone (MVK)	0.69	5–6 days	r. t.	(low MW)	
Methyl acrylate (MA)	0.60	5–6 days	r. t.	90%	
Methyl methacrylate (MMA)	0.40	9 days	0 °C	0.1%	$Ru(MMA)(PPh_3)_3$[b]
Ethyl methacrylate (EMA)	0.17	1 day	r. t.	—	$Ru(EMA)(PPh_3)_3$[b]
Vinyl acetate (VAc)	−0.22	1 day	r. t.	—	$RuH(OAc)(PPh_3)_3$[c]
Styrene (St)	−0.80	1 day	0 °C	—	$Ru(St)(PPh_3)_3$
α-Methyl styrene (α-MeSt)		1 day	r. t.	—	Complex
Ethylene (E)		1 day	r. t.	—	$Ru(E)(PPh_3)_3$

a) *e*-Values were taken from Ref. 7. b) The structures of these complexes will be reported separately.
c) See Ref. 18.

TABLLE 2. POLYMERIZATION OF VINYL COMPOUNDS BY RUTHENIUM-HYDRIDE COMPLEXES COORDINATED WITH VARIOUS PHOSPHINE LIGANDS

Monomer	e-Value	$RuH_2(PPh_3)_4$	$RuH_2(PPh_2H)_4$	$RuH_2(PPh_2Me)_4$	$RuH_2(PPhMe_2)_4$
AN[a]	1.20	(57%)	(10%)	(19%)	(100%)
MAN[a]	0.81	(23%)	(94%)	X	X
MMA[b]	0.40	(0.1%)+C	X	X	X
St[b]	−0.80	C	X	X	X

The numbers in the parentheses show the polymer yields. X: No reaction was observed. C: Complex was formed. a) Room temperature. b) 0 °C.

briefly reported on the formation of the ruthenium complexes with ethylene and styrene.[8]

Kinetics of Polymerization by 1. Complex **1** is suitable for studying the kinetics of the vinyl polymerization as well as other isolated iron alkyl[3] and cobalt hydride[5] complexes, because the change of the complex can be conveniently followed by a spectroscopic method and compared with the kinetics of polymerization followed by a dilatometry.

When **1** is dissolved in dimethylformamide (DMF) and acrylonitrile is added to the solution, the visible spectrum of **1** changes with time showing an isosbestic point at 455 nm. By observing the decrease of the absorbance at 470 nm, the rate of decomposition of **1** in the presence of acrylonitrile can be followed. The decomposition rate can be expressed by the following equation, where [Ru] represents the total concentration of the dihydridoruthenium complex in solution and k_s denotes the pseudo-first-order rate constant observed by the spectroscopic method:

$$-\mathrm{d[Ru]}/\mathrm{d}t = k_s[\mathrm{Ru}] \qquad (1)$$

The rate of polymerization of acrylonitrile by **1** in DMF was followed by dilatometry and Fig. 1 demonstrates a typical time-yield curve. The polymerization is initiated without induction period and the yield levels off with time and approaches a constant value depending on the concentration of the catalyst. The dilatometric and spectroscopic experiments were carried out under the conditions that the change of the monomer concentration is negligible.

The plot of the logarithms of $(Y_\infty - Y_t)$ where Y_∞ is the yield at infinite polymerization time and Y_t is the yield at time t in Fig. 2 *versus* time gives a straight line (Fig. 2) indicating the following relationship:

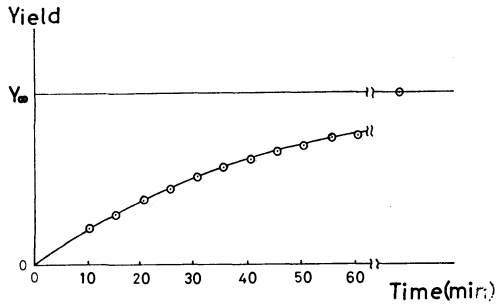

Fig. 1. Time-conversion curve of the polymeriuation of acrylonitrile by $RuH_2(PPh_3)_4$ in dimethylformamide 25 °C. [AN]=2.69 mol/l; [PPh_3]=0.109 mol/l.

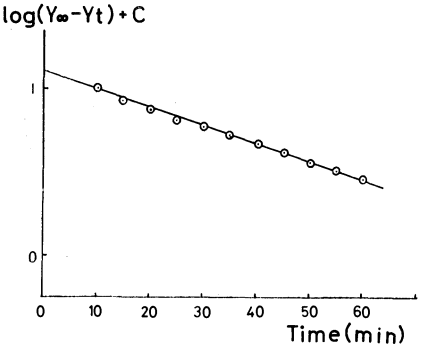

Fig. 2. The plot of logarithms of $(Y_\infty - Y_t)$ in Fig. 1 against time.

$$\log (Y_\infty - Y_t) = -kt + \text{const} \qquad (2)$$

Examination of the molecular weights of the polymers obtained after different intervals revealed that the molecular weight of the polymer was independent of the polymerization time. Since the concentration of the catalyst changes with time as expressed by Eq. (1), it can be concluded that the molecular weight is independent of the catalyst concentration.

Since the molecular weights of the polymers obtained at different conversions are almost constant, the yield of the polymer can be regarded as proportional to the number of the polymer chains produced. This suggests that the polymerization process of the vinyl monomer by **1** consists of a slow initiation step followed by rapid propagation and termination steps as in the polymerization by dialkylbis(dipyridyl)iron.[3] If we assume that the ruthenium complex initiates the polymerization with an initiator efficiency f by insertion of one monomer into the Ru–H bond followed by insertion of monomers into the Ru–C bonds, and that the growth of the polymers is terminated spontaneously after reaching a certain degree of polymerization $\overline{DP}$, which is constant, the polymerization rate can be expressed as follows:

$$R_p = \frac{\mathrm{d[Y]}}{\mathrm{d}t} = f \times \overline{DP} \times \left(-\frac{\mathrm{d[cat]}}{\mathrm{d}t}\right) \qquad (3)$$

where [Y] is the yield expressed in mol of the monomer unit polymerized and [cat] is the molar concentration of the catalyst.

From Eqs. (1) and (3) the following equation can be derived:

$$\log (Y_\infty - Y_t) = -k_s t + \log (f \times \overline{DP} \times [\mathrm{cat}]_0) \qquad (4)$$

where $[\mathrm{cat}]_0$ represents the initial concentration of the catalyst. Equation (4) is equivalent to Eq. (2). Thus if our assumptions are valid, it can be expected that the rate constant k measured from the dilatometry is equal to k_s, the rate constant obtained spectroscopically for the decomposition of the ruthenium complex **1**. Figure 3 demonstates the dependences of k and k_s on the monomer concentration. Both rate constants increase and level off with increasing monomer concentration and a satisfactory agreement is observed between k and k_s.

The plot of the reciprocal values of k in Fig. 3 against the reciprocal of the olefin concentration gives straight

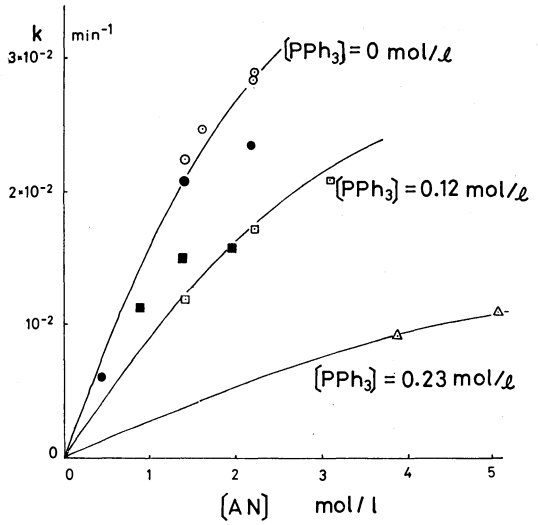

Fig. 3. Plot of the pseudo-first-order rate constants, k (observed by dilatometry ⊙, ⊡, △) and k_s (determined by spectrophotometry ●, ■).

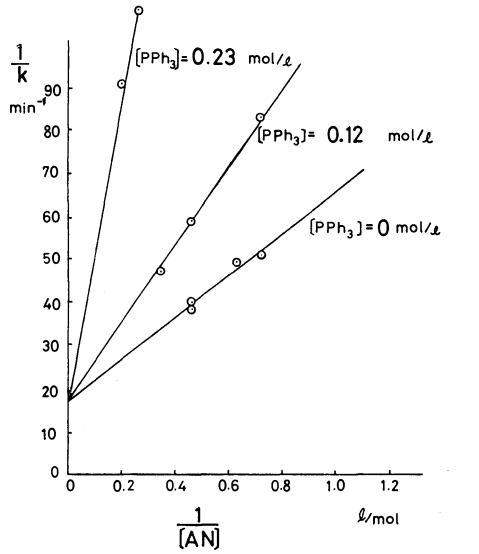

Fig. 4. Plot of the reciprocal of k *vs.* the reciprocal of [AN] at 37.1 °C.

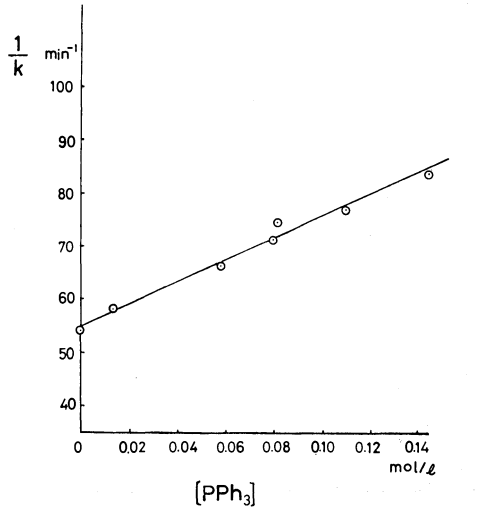

Fig. 5. Plot of the reciprocal of k *vs.* [PPh_3] at 31.7 °C.
AN=5 ml DMF=30 ml

lines converging to a constant (Fig. 4).

The addition of triphenylphosphine to the system has an inhibition effect on the polymerization and the linear dependence of the reciprocal of k on the concentration of the added triphenylphosphine is shown in Fig. 5.

These kinetic results are summarized by Eq. (5):

$$\frac{1}{k} = A + \{B + C[PPh_3]\}/[\text{monomer}] \tag{5}$$

These results are consistent with the mechanism shown below:

$$RuH_2(PPh_3)_4 + DMF \underset{k_{-1}}{\overset{k_1}{\rightleftharpoons}} RuH_2(PPh_3)_3(DMF) + PPh_3 \tag{6}$$

$$RuH_2(PPh_3)_3(DMF) + AN \underset{k_{-2}}{\overset{k_2}{\rightleftharpoons}} RuH_2(AN)(PPh_3)_3 + DMF \tag{7}$$

$$RuH_2(AN)(PPh_3)_3 \xrightarrow{k_3} \text{insertion} \tag{8}$$

$$\downarrow nAN$$

propagation

$$\downarrow$$

termination
(catalyst inactivation)

In the mechanism proposed here, we assume the predissociation of a triphenylphosphine ligand from $RuH_2(PPh_3)_4$ in solution (DMF) to give a solvent-coordinated species, $RuH_2(PPh_3)_3(DMF)$. Coordination of a monomer molecule (AN) displacing the coordinated solvent to give the monomer-coordinated species leads to activation of the Ru–H bonds and to insertion of the coordinated monomer into one of the Ru–H bonds. The first insertion is reagrded as the rate-determining step which is followed by rapid monomer insertions (propagation step). When the polymer reaches a certain length the polymer bonded with the complex may be spontaneously split from the complex which becomes thus inactive (termination step).

The kinetic result is in agreement with the scheme shown in Eqs. (6)—(8). By assuming the equilibrium for Eqs. (6) and (7) and the rate-determining step for Eq. (8), the following equations may be derived.

$$-\frac{d}{dt}[Ru] = k[Ru] = \frac{k_1k_2k_3[AN][Ru]}{k_1k_{-2}[DMF] + k_1k_2[AN] + k_{-1}k_{-2}[PPh_3]} \tag{9}$$

$$\frac{1}{k} = \frac{1}{k_3} + \frac{1}{K_1K_2k_3}\cdot\frac{[PPh_3]}{[AN]} + \frac{1}{K_2k_3}\cdot\frac{[DMF]}{[AN]} \tag{10}$$

where $K_1 = \frac{k_1}{k_{-1}}$, $K_2 = \frac{k_1}{k_{-2}}$

Equation (10) is in agreement with the experimental result shown by Eq. (5). The intercept to which the straight lines in Fig. 4 converge corresponds to $1/k_3$, the reciprocal of the rate constant for the insertion of acrylonitrile into the ruthenium-hydrogen bond. In the previous studies using $R_2Fe(dipy)_2$ and $CoH(N_2)$-

$(PPh_3)_3$ the dissociation of the ligand was rate-determining at high concentration of the monomer and the similar intercept as shown in Fig. 4 corresponded to the reciprocal of the dissociation rate of the ligand from the complex. On the other hand the kinetic decomposition behavior of $RuH_2(PPh_3)_4$ differs from those of $R_2Fe(dipy)_2$ and $CoH(N_2)(PPh_3)_3$ in that the dissociation of **1** in solution is extensive and the rate of insertion into the Ru–H bond constitutes the rate-determining step over the whole olefin concentration range. Estimation of the activation energy for the insertion of acrylonitrile into Ru–H bond based on the temperature dependence of k_3 at 25.0, 31.5, and 37.1 °C gave the value of *ca.* 20 kcal/mol.

Analysis of Fig. 4 allows the estimation of K_1 and K_2 for the equilibria of Eqs. (6) and (7). In the absence of added triphenylphosphine $1/k$ can be expressed as follows:

$$\frac{1}{k} = \frac{1}{k_3} + \frac{[DMF]}{k_3K_2}\frac{1}{[AN]}$$

Using the value of k_3, estimated from the intercept of Fig. 4 as 1/18 min^{-1}, and the concentration of DMF computed as 12 mol/l, K_2 at 37.1 °C was estimated as 4.5 from the slope of Fig. 4 where $[PPh_3]=0$. The value of K_1 at 37.1 °C was evaluated as 0.011 from the slope of Fig. 4 at PPh_3 concentration of 0.12 mol/l and using Eq. (10) with k_3 and K_2 values. Estimation of the degree of dissociation at [Ru]=1.33 mol/l using the values of 0.011 and 12 mol/l for K_1 and [DMF] indicates that over 98% of $RuH_2(PPh_3)_4$ is dissociated in DMF liberating triphenylphosphine.

The validity of this mechanism is supported by the following evidence.

(1) ^1H NMR spectrum of **1** in DMF shows two sets of hydridic protons at τ 18.2 (triplets of a doublet) and τ 16.3 (quartet) indicating the *cis* dihydride configuration[9] as shown below.

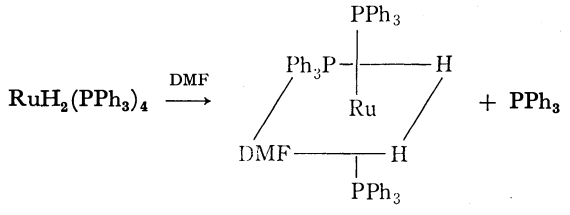

^{31}P NMR spectrum of **1** also supports the above configuration in which a triphenylphosphine ligand is completely dissociated in solution. The olefin will most probably displace the solvent molecule and coordinate to ruthenium occupying the site where the solvent was previously coordinated.

(2) The formation of such an intermediate monomer-coordinated hydride complex at 0 °C[10] was confirmed in the case of methacrylonitrile, although in the case of acrylonitrile the direct evidence for the formation of the acrylonitrile-coordinated complex could not be obtained because of the high polymerization activity of **1** toward acrylonitrile. Under the conditions that the polymerization of methacrylonitrile with **1** does not take place, the methacrylonitrile-coordinated complex was separated as a yellow solid which showed a ν(Ru–H) band at 1900 cm^{-1} and ν(C≡N) band at 2182 cm^{-1} which is shifted to lower frequency from the frequency of the uncoordinated methacrylonitrile by 40 cm^{-1}, the fact indicating the coordination of methacrylonitrile to ruthenium probably through the double bond.[11]

Copolymerization of Vinyl Monomers with 1. For obtaining further information concerning the mechanism of vinyl polymerization by **1**, copolymerizations of some sets of monomer combinations have been examined. Copolymerization of acrylonitrile with methyl methacrylate in a 1 : 1 monomer ratio by **1** gave only an acrylonitrile homopolymer and the copolymerization of methacrylonitrile with methyl acrylate in the same ratio gave a methacrylonitrile homopolymer, whereas acrylonitrile and methyl acrylate gave a copolymer.

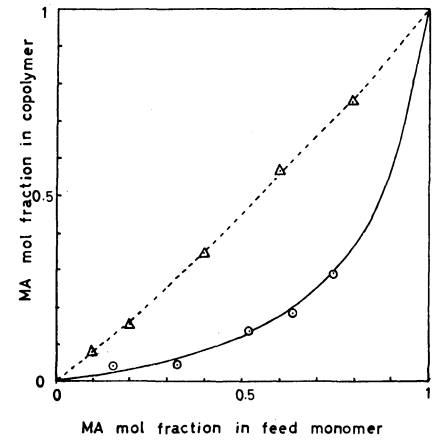

Fig. 6. Copolymerization of acrylonitrile with methyl acrylate by $RuH_2(PPh_3)_4$ catalyst. $[RuH_2(PPh_3)_4]$, 2.07 mol/l.
Solvent: toluene; solvent/monomer=1; temperature: 25 °C
—— experimental points; ------ radical polymerization.[17]

Figure 6 shows the copolymerization curve of acrylonitrile with methyl acrylate by **1**. The copolymerization curve is obviously different from that by a free-radical initiator. The monomer reactivity ratios estimated by a Fineman-Ross method[12] were as follows:

$$r_{AN} = 4.8 \pm 0.1, \quad r_{MA} = 0.1 \pm 0.05$$

Our previous study[3] on the copolymerization of vinyl monomers with an alkyl iron complex coordinated with dipyridyl ligands has shown the tendency that an electronegative monomer can be introduced in preference to the less-electronegative monomer into the copolymer, in such a way that acrylonitrile had a higher monomer reactivity ratio than methacrylonitrile and methyl acrylate higher than methacrylonitrile. The present result with **1** is somewhat different from the result with the alkyliron complex in that **1** showed a higher polymerization activity toward methacrylonitrile rather than acrylonitrile.

Termination. In order to obtain further insight into the mechanism of propagation and termination the dependences of the molecular weights of polymers on various factors were examined. As mentioned earlier, the molecular weight of the polymer was found

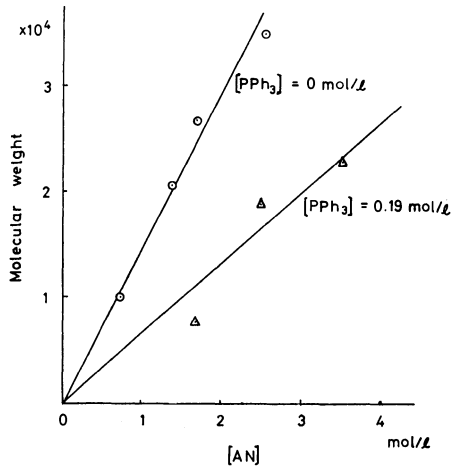

Fig. 7. The effect of the concentration of acrylonitrile on the molecular weight of polyacrylonitrile at 25 °C in DMF.

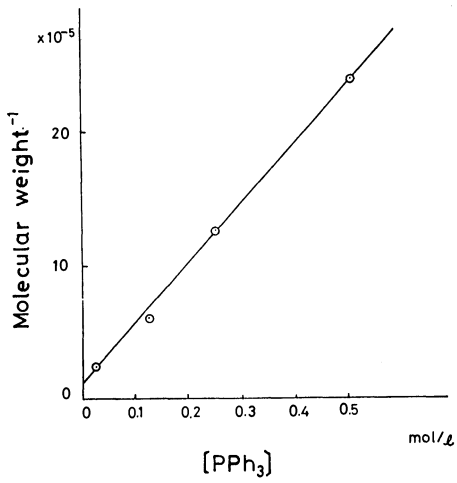

Fig. 8. The effect of the concentration of the added triphenylphosphine on the molecular weight of polyacrylonitrile at 25 °C in benzene.

to be independent of the polymerization time, the conversion, and the initiator concentration. Figure 7 demonstrates that the molecular weight of the polymer is proportional to the monomer concentration. Examination of the effect of the added triphenylphosphine concentration on the polymer weight revealed the relationship as shown in Fig. 8. The result indicates that triphenylphosphine competes with the monomer in the propagation and the coordination of triphenylphosphine to the complex having growing polymer chain leads to termination.

As we have noted in our previous paper concerning the vinyl polymerization with the alkyliron complex, the solvent may also compete with the monomer in the propagation step leading to the termination of the growing polymer chain. Thus the degree of polymerization ($\overline{DP}$) may be expressed by the following equations:

$$\overline{DP} = \frac{R_p}{R_t} = \frac{k_p[\text{Cat*}][\text{M}]}{k_t[\text{Cat*}][\text{PPh}_3] + k_t'[\text{Cat*}][\text{solv}]} \quad (11)$$

$$= \frac{k_p[\text{solv}]}{k_t[\text{PPh}_3] + k_t'[\text{solv}]} \quad (12)$$

$$\frac{1}{\overline{DP}} = \frac{1}{[\text{M}]}\left\{\frac{k_t}{k_p}[\text{PPh}_3] + \frac{k_t'}{k_p}[\text{solv}]\right\} \quad (13)$$

where [M], [PPh_3], [solv], and [Cat*] denote the concentrations of the monomer, added triphenylphosphine, the solvent and propagating polymer chain attached to the catalyst, and k_p, k_t, and k_t' the rate constants for propagation, terminations caused by coordination of triphenylphosphine and the solvents, respectively. The results demonstrated in Figs. 7 and 8 are in agreement with Eqs. (12) and (13).

The fact that the straight lines in Fig. 7 pass through the origin indicates that the chain transfer reaction with monomer can be neglected.

From the slopes [PPh_3]=0 and 0.19 in Fig. 7 and utilizing Eq. (12) an approximate value of k_t/k_t' was computed as 90, indicating that the termination process involving the participation of triphenylphosphine is the predominant reaction and the contribution of the solvent to the termination is small.

Two possibilities are considered as the mechanism of termination. One is the β-hydrogen elemination from the growing polymer chain by ruthenium regenerating the ruthenium dihydride and the other is the hydrogen migration from the ruthenium hydride to the growing polymer chain as shown below:

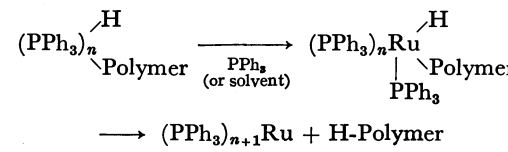

The β-hydrogen elimination mechanism does not appear reasonable, because the ruthenium hydride thus reproduced should be still active for initiating the polymerization. On the other hand the hydrogen migration mechanism as shown above seems more probable since the zero-valent ruthenium complex thus produced may not be active any more. The hydrogen migration mechanism is further supported by the result that $RuH_2(PPh_3)_4$ reacts with ethylene and styrene giving Ru(ethylene)(PPh_3)$_3$ and Ru(styrene)(PPh_3)$_3$ accompanied by the formation of 1 mol each of ethane and ethylbenzene per complex **1**.[8] Ethane and ethylbenzene were probably formed by the insertion of ethylene and styrene into a Ru–H bond giving hydrido-alkyl ruthenium complexes, resembling the propagating species, from which the alkanes are reductively eliminated by the migration of hydrogen from the remaining Ru-H to the alkyl group.

Polymerization of Vinyl Monomers by Dihydrido-ruthenium-(II) Complexes Having Various Phosphine Ligands. Some dihydrido-ruthenium complexes other than triphenylphosphine initiate the polymerization of a few vinyl monomers. Table 2 shows the polymerization activities of the dihydrido-tuthenium complexes of the type RuH_2L_4 where L=PPh_2H,[13] PPh_2Me,[9] $PPhMe_2$.[14] The results summarized in Tables 1 and 2 indicate that the triphenylphosphine-coordinated complex is most reactive toward the vinyl compounds examined and initiate the vinyl polymerization or forms π-complexes with a wide range of vinyl compounds whereas the other phosphine-coordinated complexes

reacted only with acrylonitrile and methacrylonitrile.

Two factors may be involved in determining the reactivity of the ruthenium complex toward the olefins. One is the dissociation of the phosphine ligand from the coordinatively saturated complex RuH_2L_4 for accomodating the incoming olefin to coordinate, and the other is the intrinsic reactivity of the coordinatively unsaturated RuH_2L_3 toward olefins. The fact that the triphenylphosphine-coordinated complex was most reactive may be largely due to the reason that the bulky triphenylphosphine ligand is extensively dissociated in solution as demonstrated by the NMR spectrum of **1** in DMF whereas the other phosphine-coordinated complexes are dissociated only to a minor extent as revealed by their NMR spectra.[9,13,14] The polymerization of acrylonitrile by phenyldimethylphosphine-coordinated complex might be caused, at least partially, by the free ligand itself which may be formed by dissociation from RuH_2L_4. The free tertiary phosphines are known to initiate the vinyl polymerization[15] and the polymerization activity of the phosphine ligand itself decreased in the order of $PPhMe_2 > PPh_2Me \sim PPh_2H > PPh_3$; free phenyldimethylphosphine initiated a quite rapid polymerization of acrylonitrile whereas the polymerization by free triphenylphosphine was quite sluggish and can be neglected in comparison with the rapid polymerization by the triphenylphosphine-coordinated complex. Methacrylonitrile was not polymerized by none of the free phosphines and the polymerization activities of $RuH_2(PPh_3)_4$ and $RuH_2(PPh_2H)_4$ must be associated with the intrinsic reactivities of the complexes. The most important factors in determining the intrinsic reactivity of the complex concerned may be the interaction of the complex with the olefin and the insertion of the olefin into the metal-hydrogen bond. Electronic as well as steric factors must be operative there and it is often difficult to predict the reactivity of the particular complex on the basis of our present knowledge. That the diphenylphosphine-coordinated complex was very reactive as the initiator for methacrylonitrile, moderately reactive for more electronegative acrylonitrile and inactive for methyl methacrylate and styrene suggests that an optimum activity may be developed by appropriate choice of the ligand which modifies the electron density of the dihydrido-ruthenium complex to interact with the particular olefin.

Experimental

Preparation of Materials. Dihydridotetrakis(triphenylphosphine)ruthenium(II) $RuH_2(PPh_3)_4$ was prepared as previously described.[6] It was found later that by the reflux of the system containing $RuCl_3$, PPh_3, and $AlEt_3$ in THF, the yield of the hydrido complex was increased. The addition of excess triphenylphosphine to the toluene solution of **1** caused easier recrystallization because of the prevention of the dissociation of triphenylphosphine. Dihydrido complexes containing various phosphine ligands were prepared by the method reported previously.[9,13,14] Monomers and solvents were purified by usual method and kept under nitrogen at −20 °C before use.

Chemical Reactions. The reactions were usually carried out in an ampoule in which **1**, an olefin and a solvent were transferred in a nitrogen atmosphere or by trap-to-trap distillation in a vacuum. After the set time of polymerization, the ampoule was opened and the content was poured into acidic methanol. The precipitate was filtered, washed with methanol and dried in a vacuum. Yields and molecular weights are listed in Table 1. In some cases complex formations were observed which will be reported separately.

Copolymerization by Complex 1. Copolymerization of vinyl monomers by **1** was performed in a sealed amoule in which **1** (2.07 mol/l), toluene and olefin were transferred under nitrogen or by a trap to trap distillation in a vacuum. The ampoule was kept in a thermostatted bath at 25 °C for a few hours. The content was poured into a large excess of methanol. The copolymer formed was filtered and washed with methanol a few times and dried in a vacuum. Composition of each monomer component in the copolymer was analyzed by elemental analysis performed by Mr. T. Saito of our laboratory with a Yanagimoto CHN Autocorder Type MT-2. The results are as follows.

MA mole fraction in monomers	N% in copolymer	yield	MA mole fraction in copolymer
0.745	16.00	0.2%	0.288
0.631	19.54	0.3	0.186
0.523	20.96	0.4	0.137
0.328	23.85	1.0	0.042
0.155	24.88	2.0	0.034

Dilatometry. Kinetic study of polymerization was carried out by dilatometry under nitrogen. Acrylonitrile was added into a DMF solution containing the catalystat. a constant temperature under vigorous stirring of the solution The solution was immediately transferred into a dilatometer in a thermostatted bath under nitrogen and the decrease of the volume of the solution was followed.

Molecular Weight. The molecular weight of the polymer was determined by a viscometry using an Ubbelode viscometer. Molecular weight-viscosity equation of $[\eta] = 39.2 \times 10^{-5} \times MW^{0.75}$ (25 °C in DMF) was employed for determining the molecular weight of polyacrylonitrile.[16]

Estimation of Decomposition Rate Constants k_s of 1 in the Presence of Acrylonitrile. Decomposition rate of **1** was followed by observing the decrease of absorbance in the visible spectra at a constant temperature. The pseudo-first-order rate constant k_s was estimated from the slope of $\log(A_\infty - A_t)$ *vs* time, where A_∞ and A_t represent the absorbances at infinite time and at time t.

The authors thank Dr. T. Yamamoto for his helpful discussions and for the support of the work by Ministry of Education.

References

1) D. G. H. Ballard, W. H. Janes, and T. Medinger, *J. Chem. Soc., B*, **1968**, 1168, 1176.

2) D. G. H. Ballard and P. W. van Lienden, *Chem. Commun.*, **1971**, 564.

3) T. Yamamoto, A. Yamamoto, and S. Ikeda, This Bulletin, **45**, 1104, 1111 (1972).

4) M. Takahashi, K. Iimura, M. Takeda, and A. Ohno, *Kogyo Kagaku Zasshi*, **71**, 132 (1968).

5) Y. Kubo, A. Yamamoto, and S. Ikeda, This Bulletin, **47**, 393 (1974).

6) T. Ito, S. Kitazume, A. Yamamoto, and S. Ikeda, *J. Amer. Chem. Soc.*, **92**, 3011 (1971).
7) J. Brandrup and E. H. Immergut, "Polymer Handbook," Interscience Publishers, New York. London, Sydney (1966), II-341.
8) S. Komiya, A. Yamamoto, and S. Ikeda, *J. Organometal. Chem.*, **42**, C65 (1972).
9) K. C. Dewhirst, W. Keim, and C. A. Reilly, *Inorg. Chem.*, **7**, 546 (1968).
10) S. Komiya, and A. Yamamoto, unpublished.
11) T. Yamamoto, A. Yamamoto, and S. Ikeda, *J. Amer. Chem. Soc.*, **93**, 3350 (1971).
12) M. Fineman and S. Ross, *J. Polym. Sci.*, **5**, 259 (1950).
13) J. R. Sanders, *J. Chem. Soc., A*, **1972**, 1333.
14) D. G. Gerlach, W. G. Peet, and E. L. Muetterties, *J. Amer. Chem. Soc.*, **94**, 4545 (1972).
15) L. Horner, W. Jurgeleit, and K. Klupfel, *Ann. Chem.*, **591**, 108 (1955).
16) P. F. Onyon, *J. Polym. Sci.*, **37**, 315 (1959).
17) T. Tamikado and Y. Iwakura, *ibid.*, **36**, 529 (1959).
18) S. Komiya and A. Yamamoto, *Chem. Commun.*, **1974**, 523.

Selenium Catalyzed Synthesis of of Carbonates. The Reaction of Alkoxide with Carbon Monoxide and Oxygen in the Presence of Selenium

Kiyoshi KONDO, Noboru SONODA,* and Hiroshi SAKURAI

The Institute of Scientific and Industrial Research, Osaka University, Suita, Osaka 565

**Department of Petroleum Chemistry, Faculty of Engineering, Osaka University, Suita, Osaka 565*

(Received July 22, 1974)

A novel selenium catalyzed synthetic reaction of carbonates was investigated. The reaction of alkoxides with carbon monoxide in the presence of stoichiometric amount of selenium gave carbonates in high yields under atmospheric pressure at 20 °C in THF. When the resultant reaction solution was made to react continuously with the mixture gas of carbon monoxide and oxygen, catalytic formation of carbonates was achieved. Isolation of Se-alkyl monoselenocarbonate from the reaction mixture by addition of alkyl halide indicated that carboalkoxy sodium selenide might be formed as an intermediate in the course of present reaction. In connection with these reactions, the reaction of carbonyl selenide with sodium alkoxide in alcohol was also studied.

There are many reports on the synthesis of carbonates,[1] and a very common synthesis is one by the reaction of phosgene with alcohol. Synthesis of carbonates by the reaction of cupric alkoxide and carbon monoxide was reported[2,3] by Saegusa *et al.*, and it was described[4] that carbonylation of ethanol by palladium chloride in the presence of sodium carbonate proceeded under mild conditions to give diethyl carbonate. Recently we reported[5–7] a novel synthesis of urea derivatives by the reaction of amine with carbon monoxide in the presence of selenium under mild conditions with simple operations. From further investigations on the reaction between carbon monoxide and selenium in the presence of a base, it has been noticed[8] that stoichiometric amount of carbonates based on used selenium was found to be formed by the reaction of carbon monoxide with aliphatic alkoxides under mild conditions.

Now we wish to report full results of the reaction of alkoxides with mixture gas of carbon monoxide and oxygen in the presence of selenium, which provides a new, convenient method for catalytic synthesis of carbonates [reaction (1)].

$$\mathrm{RONa} + \mathrm{CO} + \frac{1}{2}\mathrm{O_2} \xrightarrow[\substack{20^\circ\mathrm{C},\ 1\ \mathrm{atm.}\\ \mathrm{ROH,\ THF}}]{\mathrm{Se}} (\mathrm{RO})_2\mathrm{CO} + \mathrm{NaOH} \qquad (1)$$

Thus various carbonates were prepared under mild conditions with simple operations. From the investigation of the reaction path, a key intermediate was successfully trapped in the form of Se-alkyl monoselenocarbonate by alkylation with alkyl halide, and sodium hydrogen selenide was found to play an important role for the circulation of selenium. It was also confirmed that reaction of carbonyl selenide, prepared from direct reaction between carbon monoxide and selenium at elevated temperature, with sodium alkoxides was closely resembled to the present synthetic reaction.

Results and Discussion

It was confirmed that sodium alkoxide reacted easily with metallic selenium and carbon monoxide to form dialkyl carbonate [reaction (2)]. For instance, sodium ethylate and ethyl alcohol were dissolved in tetrahydrofuran (THF), to which was added metallic selenium at 20 °C, and carbon monoxide was blown into the solution for 2 hr with vigorous stirring. At this stage of the reaction, quantitative formation of diethyl carbonate based on selenium used in the reaction mixture was confirmed from glpc analyses. It is notable that the procedure is very simple. The results are shown in Table 1.

$$\mathrm{Se} + \mathrm{CO} + \mathrm{NaOR} \xrightarrow[20^\circ\mathrm{C},\ 1\ \mathrm{atm.}]{\mathrm{ROH,\ THF}} (\mathrm{RO})_2\mathrm{CO} + \mathrm{NaSeH\ and/or\ Na_2Se} \qquad (2)$$

Table 1. Stoichiometric synthesis[a] of carbonates

Run No.	RONa R	ROH mol	$(RO)_2CO$ Yield %[b]
1	Me	0.04	99
2	Et	0.04	99
3	Et	0.04	99[c]
4	Et	0.10	95
5	*n*-Pr	0.10	99
6	*n*-Bu	0.10	80
7	Benzyl	0.10	76
8	*i*-Pr	0.10	16
9	Cyclohexyl	0.10	6
10	*t*-Bu	0.10	14
11	Ph	0.10	—[d]

a) Metallic selenium (0.001 g atom), sodium alkoxide (0.04 mol), and alcohol were made to react with carbon monoxide (60 ml/min) at 20 °C in 50 ml THF for 2 hr with vigorous stirring. b) Yield % based on selenium used. c) Amorphous selenium was used. d) No reaction took place.

The yield of carbonates from primary alcohols was higher than that from secondary or tertiary alcohols, and in the case of phenol no reaction took place. These results clearly showed the excellent and novel oxidizing ability of selenium[9] in the presence of a strong base. Then, catalytic reaction [reaction (1)] could be successfully performed by passing mixture gas of carbon monoxide and oxygen continuously into the resultant reaction mixture given by the reaction (2). The

Table 2. Catalytic synthesis[a] of carbonates

Run No.	RONa R	Catalytic reaction time[b] (hr)	Oxidizing efficiency %[c]
1	Me	0	99
2	Me	1	225
3	Et	0	99
4	Et	1	240
5	Et	2	310
6	Et	4	520
7	*n*-Bu	2	292
8	*t*-Bu	2	113
9	$-CH_2CH_2OH$	2	270[d]
10	$-CH_2CHMeOH$[e]	2	220[d]

a) RONa (0.05 mol), ROH (0.05 mol), and metallic selenium (0.001 g atom) were made to react with carbon monoxide for 30 min, and then with mixture gas of carbon monoxide and oxygen (60 ml/min and 1 mmol/hr respectively) in 50 ml THF at 20 °C for catalytic reaction time. b) The time (hr) for which mixture gas of carbon monoxide and oxygen was bubbled, and the results at catalytic reaction time 0 hr corresponded to those in Table 1. c) See to Ref. 10. d) DMF (50 ml) was used for the solvent in the case of glycols. e) $-CHMe-CH_2OH$ may be contained.

results obtained by the present catalytic reaction were shown in Table 2. The circulation of selenium in the reaction system was shown in terms of oxidizing efficiency[10] of selenium, and the efficiency decreased as catalytic reaction time prolonged. This tendency might be explained by the facts that sodium hydroxide formed in the reaction system interferred the formation of carbonate and prolonged contact of carbonate with sodium hydroxide in alcohol decreased the amount of formed carbonate. Cyclic aliphatic carbonates such as ethylene carbonate, propylene carbonate were similarly synthesized when dimethylformamide[11] (DMF) was used.

The circulation of selenium in the catalytic system may be explained by the following Eqs. (3) and (4), which exhibit the regeneration[12] of selenium by the facile oxidation of hydrogen selenide with oxygen.

$$Na_2Se \underset{RONa}{\overset{ROH}{\rightleftharpoons}} NaSeH \underset{RONa}{\overset{ROH}{\rightleftharpoons}} H_2Se \quad (3)$$

$$H_2Se + \frac{1}{2}O_2 \longrightarrow H_2O + Se \quad (4)$$

In order to examine if the sodium hydrogen selenide played a significant role in the catalytic reaction, the reaction of alcoholic sodium alkoxide with the mixture gas of carbon monoxide and oxygen in the presence of sodium hydrogen selenide[13] in THF was carried out and was found to proceed successfully, clarifying that the catalytic reaction (1) might be rewritten as following equation.

$$RONa + CO + \frac{1}{2}O_2 \xrightarrow[ROH,\ THF]{NaSeH} (RO)_2CO + NaOH \quad (5)$$

The catalytic reaction was found to stop if oxygen-rich mixture gas was treated, and the ratio of carbon monoxide to oxygen was found to be such that sodium hydrogen selenide could be present in the catalytic reaction system.

In order to attain the knowledge of the reaction path, we have tried to trap an intermediate by addition of excess amount of alkyl halide into the reaction mixture. Gas-Mass spectroscopic analyses of the reaction mixture of sodium ethylate, carbon monoxide, selenium and *n*-butyl iodide at 0 °C showed the formation of di-*n*-butyl selenide and di-*n*-butyl diselenide together with the trace amount of formation of Se-*n*-butyl ethyl monoselenocarbonate, which might be formed by the reaction (6). The authentic sample of monoselenocarbonate[14] was prepared by the following unambiguous route [reaction (7)].

$$Se + CO + NaOEt \longrightarrow Na^+[EtO\text{-}\overset{\overset{O}{\|}}{C}\text{-}Se]^-$$

$$\xrightarrow[-NaI]{+n\text{-BuI}} EtO\text{-}\overset{\overset{O}{\|}}{C}\text{-}Se\text{-}Bu\text{-}n \quad (6)$$

$$n\text{-BuLi} + Se \xrightarrow[0°C]{THF} n\text{-BuSeLi} \xrightarrow[0°C,\ -LiCl]{+Cl\text{-}CO\text{-}OEt} n\text{-BuSe-}\overset{\overset{O}{\|}}{C}\text{-OEt} \quad (7)$$

ca. 15%

The retention time of the gas chromatography and the fragmentation pattern in the mass spectra of the trapped selenocarbonate were identical with those of the authentic sample. Very fast alcoholysis of the intermediate, ethoxycarbonyl sodium selenide[15] would yield the carbonate and sodium hydrogen selenide, and the driving force of the alcoholysis reaction would be attributed to the precipitation of the sodium hydrogen selenide in THF.

It was suggested[5] that carbon monoxide was readily oxidized with selenium in the presence of a strong base under mild conditions to give carbonyl selenide (SeCO).[17] Then we performed the reaction of isolated carbonyl selenide prepared by the reaction[18] of carbon monoxide with selenium at elevated temperature (550—600 °C) trapped at −120 °C, into which was added an alcoholic solution of sodium alkoxide at −80 °C. Gas chromatographic analyses revealed the quantitative formation of carbonates (dimethyl, diethyl, and di-*n*-butyl carbonate) [reaction (8)].

$$SeCO + RONa \xrightarrow[-80°C]{ROH} (RO)_2CO + NaSeH \text{ and/or } Na_2Se \quad (8)$$

The reaction of carbonyl selenide with sodium alkoxide was so fast and almost quantitative even at low temperature that it might be impossible to detect the formation of free SeCO, even if it were generated, from the reaction mixture under any reaction condition at room temperature.

These experimental findings suggested that present selenium catalyzed synthesis of carbonates might well be described by the reaction Scheme 1, in which the intervention of carbonyl selenide as an intermediate in the catalytic cycle would offer a reasonable interpretation (path a), though there should be another path, in which intermediacy of carbonyl selenide might not necessarily be required (path b).

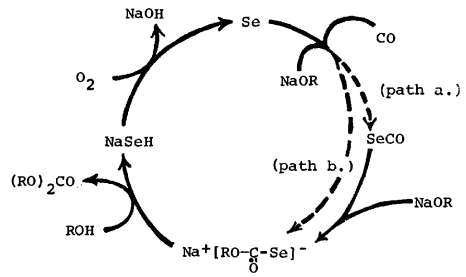

Scheme 1. Reaction path for the formation of carbonates.

In every synthesis of carbonates, however, small amounts of formates[19] were detected as the by-products, which have long been known to be produced by a base catalyzed reaction of carbon monoxide.[20]

Experimental

Materials. Alcohols (methyl, ethyl, *n*-propyl, *i*-propyl, *n*-butyl, *t*-butyl, cyclohexyl, benzyl alcohol, ethylene glycol, propylene glycol, and phenol) were all purchased from commercial sources, and purification was carried out by distillation over corresponding sodium alkoxide under nitrogen and each purity was qualified by glpc. Metallic selenium (99.99%) of Nakarai Chem. Co. and amorphous selenium prepared by reduction of selenium dioxide with sulfur dioxide were used. Carbon monoxide (99.999%) of Seitetsu Chem. Co. and oxygen (99.999%) of Osaka Sanso Co. were applied. The chemical grade of metallic sodium, sodium hydride, and sodium borohydride were used for the sodium-metallation of alcohols or preparation of sodium hydrogen selenide. The chemical grade of *n*-butyl lithium (Merck Co.), *n*-butyl iodide, ethyl chloroformate were also commercially available. Tetrahydrofuran (THF) stored with KOH were dried over sodium wire and lithium aluminum hydride, and freshly distilled under nitrogen just before use. Dimethylformamide (DMF) was distilled under vacuum just before use. Authentic samples of the carbonates and formates were purchased or synthesized by the use of phosgene or formic acid with sodium alkoxide in alcohol.

Apparatus. The product analyses were generally carried out by gas chromatography with use of PEG-20M and SE-30 in 1 or 3 meter stainless steel column. They were performed by means of Shimadzu Model GC-3BF with ion flame detector, Varian Aerograph Model 90-P, Hitachi Model K-53 with thermal conductivity detector for separation, and Hitachi Model O63 with ion collector detector for Gas-Mass. IR spectra (Shimadzu IR-27C, and Hitachi EPI-S2) and NMR spectra (Hitachi Perkin-Elmer R-20) were also used for the analyses. Mass spectra were obtained on a Hitachi Perkin-Elmer RMU-60 or on a Hitachi Model RMS-4 Mass Spectrometer for Gas-Mass.

Procedures. Reactions were generally carried out in a three necked 100 ml flask fitted with a thermometer, a cooler at whose top the gas outlet was equipped, and a gas inlet tube. Gas flow meter and nujol-sealed gas bubbler were attached between the gas inlet tube and gas supply. Gas outlet tube was also connected to the nujol-sealed gas bubbler. In catalytic synthesis of carbonates oxygen was supplied by use of 20 ml syringe. A magnetic stirrer was used for effective vigorous stirring of the reaction mixture.

The Stoichiometric Synthesis of Carbonates. A preparative example of the stoichiometric synthesis of diethyl carbonate was as follows; 0.05 mol of sodium ethylate and 0.05 mol of ethyl alcohol were dissolved in 50 ml THF to which was added 0.01 g atom sample of metallic selenium at 20 °C, and carbon monoxide was blown into the resultant solution at a rate of 60 ml/min for 2 hr with vigorous stirring. At this stage of the reaction glpc analyses revealed the quantitative formation of diethyl carbonate based on selenium in the reaction mixture. Thereafter oxygen was added into the solution at a rate of 10 ml/min without the addition of carbon monoxide. Filtration followed by distillation gave diethyl carbonate (1.086 g, 92% based on selenium used). In order to see the relative reactivity of alcohols, we showed the results of controlled experiments with the use of mole ratio of reactants as shown in Table 1, taking identical procedures as described in this section.

The Catalytic Synthesis of Carbonates. As already described in the section of Results and Discussion, the procedure of the catalytic synthesis only differed from the stoichiometric synthesis in the way that the catalytic reaction was successfully performed by passing continuously the mixture gas of carbon monoxide and oxygen into the resultant solution afforded by the stoichiometric reaction. The ratio of the reaction mixture was as shown in Table 2. In this experimental section was shown the typical example of catalytic synthesis of diethyl carbonate by the reaction of sodium ethylate (0.05 mol) and ethyl alcohol (0.05 mol) with carbon monoxide (60 ml/min) in the presence of metallic selenium (0.001 g atom) dissolved in 50 ml THF for 30 min with vigorous stirring. Catalytic reaction was then performed by adding the mixture gas of carbon monoxide and oxygen for the time given in Table 2. The flow rate of carbon monoxide was 60 ml/min and oxygen was added 1 mmol/hr. At the end of the catalytic reaction, the feed of carbon monoxide was stopped, and only oxygen gas was added (10 ml/min) for 30 min. Isolation of carbonate was identical with example in the case of stoichiometric synthesis.

The Catalytic Synthesis of Diethyl Carbonate in the Presence of Sodium Hydrogen Selenide. Sodium hydrogen selenide (0.005 mol) was prepared according to the method,[13] to which were added THF (50 ml) solution of sodium ethylate (0.05 mol) and ethanol (0.05 mol), and then the mixture gas of carbon monoxide (60 ml/min) and oxygen (0.005 mmol/hr) for 2 hr. About 0.012 mol of diethyl carbonate was found to be formed from glpc.

An Attempted Experiment for the Trapping of the Intermediate. Sodium ethylate (0.05 mol) and ethyl alcohol (0.05 mol) were dissolved in 50 ml THF to which was added 0.01 g atom sample of metallic selenium at 0 °C, and carbon monoxide was added at a rate of 60 ml/min for 30 min with vigorous stirring. Then cold (0 °C) THF solution (25 ml) of *n*-butyl iodide (0.1 mol) was added dropwise in 20 min; during the addition, a gentle flow of carbon monoxide (10 ml/min) was continued. The product analyses were performed by use of Gas-Mass Spectrometer (Hitachi Model O63 Gas Chromatograph and Hitachi Model RMS-4 Mass Spectrometer) with 3 meter PEG-20M column. The chromatogram with its retention time between those of di-*n*-butyl selenide and di-*n*-butyl diselenide was attributed to Se-*n*-butyl ethyl selenocarbonate (*ca.* 0.5%) from the mass spectrum.

The Synthesis of Authentic Sample of Se-n-Butyl Ethyl Mono selenocarbonate. Metallic selenium (0.05 g atom) was stirred vigorously under nitrogen at 0 °C in 50 ml THF well dried over $LiAlH_4$ and freshly distilled under nitrogen, to which was added 0.052 mol of *n*-butyl lithium in hexane dropwise. THF (25 ml) solution of ethyl chloroformate (0.06 mol) at 0 °C was added dropwise and the resultant solution was kept stirring for 15 hr at 0 °C. Filtration of the lithium chloride followed by distillation under vacuum gave Se-*n*-butyl ethyl monoselenocarbonate (*n*-Bu–Se–CO–

OEt) (1.58 g, 15%) with very unpleasant odor: bp 85 °C/5 mmHg IR (direct) 1717 cm^{-1} (ν_{CO}). Mass (70 eV) *m/e* 210 (M^+), 165 (*n*-Bu-Se-CO^+), 137 (*n*-Bu-Se^+), 108 ($SeCO^+$), 73 (EtO-CO^+). Found: C, 40.04; H, 6.83%. Calcd for $C_7H_{14}O_2Se$: C, 40.20; H, 6.75%.

The Reaction of Carbonyl Selenide with Sodium Alkoxide. The preparation of carbonyl selenide was carried out as described in the literature.[18] For the trapping of generated carbonyl selenide gas, we used EtBr-cold bath (−120 °C) with liq. N_2. Carbonyl selenide was then treated with excess sodium alkoxide in alcohol at −80 °C. Addition of oxygen at room temperature to the reaction mixture followed by filtration was found to contain stoichiometric amount of corresponding carbonate from glpc.

References

1) R. B. Wagner and H. D. Zook, "Synthetic Organic Chemistry," John Wiley & Sons, New York, N.Y. (1961), p. 483.

2) T. Saegusa, T. Tsuda, K. Isayama, and K. Nishijima, *Tetrahedron Lett.*, **1968**, 831.

3) T. Saegusa, T. Tsuda, and K. Isayama, *J. Org. Chem.*, **35**, 2976 (1970).

4) M. Graziani, P. Uguagliati, and G. Carturan, *J. Organometal. Chem.*, **27**, 275 (1971).

5) N. Sonoda, T. Yasuhara, K. Kondo, T. Ikeda, and S. Tsutsumi, *J. Amer. Chem. Soc.*, **93**, 6344 (1971).

6) K. Kondo, N. Sonoda, and S. Tsutsumi, *Chem. Commun.*, **1972**, 307.

7) K. Kondo, N. Sonoda, K. Yoshida, M. Koishi, and S. Tsutsumi, *Chem. Lett.*, **1972**, 401.

8) K. Kondo, N. Sonoda, and S. Tsutsumi, *Tetrahedron Lett.*, **1971**, 4885.

9) Selenium with its oxidation number 0 was found to be formally reduced to selenide anion, Se^{2-} with its oxidation number -II.

$$\underset{(0)}{Se} + \text{Substrate} \longrightarrow \underset{(-II)}{Se^{2-}} + \text{Product}$$

10) (Oxidizing Efficiency) %=[(mmol of formed $(RO)_2CO$)/(mg atom of Se used)]×100

11) The reaction in DMF gave somewhat better yield of carbonates than that in THF.

12) Equation (1) was thus derived by the combination of Eqs. (2), (3), and (4).

13) D. L. Klayman and J. S. Griffin, *J. Amer. Chem. Soc.*, **95**, 197 (1973).

14) To the best of our knowledge, reaction (7) provides the first synthesis of monoselenocarbonate.

15) The reaction of carbonyl sulfide with sodium alkoxide in alcohol was reported[16] to give sodium alkoxy carbonyl sulfide, which was called Bender's salt, and not to give carbonates.

$$SCO + RONa \xrightarrow{ROH} Na^+[RO\text{-}\underset{\underset{O}{\|}}{C}\text{-}S]^- \xrightarrow{ROH} (RO)_2CO$$

16) J. G. Weeldenberg, *Rec. Trav. Chim.*, **47**, 496 (1928); R. J. Ferm, *Chem. Revs.*, **57**, 621 (1957).

17) Some inorganic reactions of carbonyl selenide were known. For instance,

$$SeCO + 4NaOH \longrightarrow Na_2CO_3 + Na_2Se_2 + 2H_2O;$$

See to O. Glemser and T. Risler, *Z. Naturforsch*, **3B**, 1 (1948). Present reaction showed a novel utilization of carbonyl selenide in organic synthetic reaction, which would be highly reactive because of small overlap of Se–C 4pπ–2pπ bond in comparison with C–O 2pπ–2pπ bond.

18) T. G. Pearson and P. L. Robinson, *J. Chem. Soc.*, **1932**, 652.

19) The trace experiment in the presence and in the absence of selenium under the identical reaction conditions revealed that the formate generation was neither enhanced nor retarded by selenium, and that the rate of its formation was found to be much slower by 100 times than that of the formation of carbonate in the present reaction conditions.

20) M. Orchin and I. Wender, "Catalysis", Vol. 5, ed. by P. H. Emmett, Reinhold Pub. Co., New York, N.Y. (1957) p. 1.

New Furanosesquiterpenes from *Ligularia Fischeri* Turcz.[1] 1β, 10β-Epoxyfuranoeremophilan-6β-ol and Its Derivative

Toshichika Sato, Yoshihiko Moriyama, Hajime Nagano,
Yoshiaki Tanahashi, and Takeyoshi Takahashi
Department of Chemistry, Faculty of Science, The University of Tokyo, Bunkyo-ku, Tokyo 113
(Received September 17, 1974)

Two new furanosesquiterpenes, isolated from *Ligularia Fischeri* Turcz. (collected at Shiramine), were shown to be 1β,10β-epoxyfuranoeremophilan-6β-ol (**1**) and 1β,10β-epoxyfuranoeremophilan-6β-yl 2-hydroxymethylprop-2-enoate (**2**).

It has been reported by Ishii *et al.* that *Ligularia Fischeri* Turcz. (collected at Kurama) contained several sesquiterpenes, namely, ligularol,[2] ligularone,[2] furanoeremophilane,[3] eremoligenol,[3] 6β-hydroxyeremophilenolide,[3] liguloxide,[4] liguloxidol,[4] and liguloxidol acetate.[4] During chemical investigation on the genus *Ligularia* (Compositae) and related plants,[5] two new furanosesquiterpenes were isolated from *Ligularia Fischeri* Turcz. (collected at Shiramine).[6] We wish to describe the structure determination leading to 1β, 10β-epoxyfuranoeremophilan-6β-ol (**1**) and 1β,10β-epoxyfuranoeremophilan-6β-yl 2-hydroxymethylprop-2-enoate (**2**) for these sesquiterpenes.

An ether extract of the roots of the plant was subjected to separation by column and preparative thin layer chromatography to give **1** and **2**. Compound **1**, a colorless oil, was positive to the Ehrlich test. A molecular ion peak at *m/e* 248 ($C_{15}H_{20}O_3$) was observed in the mass spectrum. The IR, UV, and PMR spectra showed the presence of a secondary methyl, a tertiary methyl, a β-methyl substituted furan moiety with an α-proton,[5] a proton on an oxygen-bearing carbon, an allylic methylene linked to a carbon with no proton, an allylic proton on a hydroxyl-bearing carbon, and a hydroxyl group (*cf.* Table and Experimental).

These spectral data observed for **1** are closely related to those of furanoeremophilane-6β,10β-diol (**3**),[7,8] recently isolated from *L. japonica* Less. Treatment of **1** in tetrahydrofuran with lithium aluminium hydride under reflux yielded a diol, which was found to be identical with **3**. This showed the presence in **1** of a furanoeremophilane skeleton (**4**); a hydroxyl group of **1** must be placed on C-6β. The presence of homoallylic coupling (J=2 Hz) between a proton at C-6α and one of the allylic methylene protons (proton at C-9α) was shown by PMDR experiments. Therefore the proton at C-6α was inferred to be in a quasi-axial conformation.

A nature of two of the three oxygen atoms involved in **1** was thus characterized. The IR spectrum of **1** showed no carbonyl absorption. In the PMR spectrum of **1**, the signal due to a proton on an oxygen-bearing carbon (C-1) appeared at δ 3.06, while the corresponding signal was absent in the spectrum of **3**. The conversion of **1** to **3**, as well as the spectral data of **1** mentioned above, suggested that the third oxygen of **1** was involved as an epoxy ring and located on C-1β and C-10β as shown in **1**.

These observations received support from induced paramagnetic shift experiments[9] on **1** (Table), coupled with PMDR technique. The shift reagent, Eu(dpm)$_3$, associated more strongly with a hydroxyl rather than an ether group.[10] Signals due to protons at C-4 and C-15 shifted very largely. A small shift was observed for signals due to protons at C-14. Therefore, the epoxy ring was shown to be in a β-configuration; an 1α,10α-epoxide structure must cause a large shift for signals due to C-14 protons. As the absolute stereochemistry of the diol was determined as shown in **3**,[8] the structure including absolute configuration of **1** should be represented by 1β,10β-epoxyfuranoeremophilan-6β-ol (**1**). The results summarized in Table are best interpreted on the basis of a stereostructure (**1'**), in which rings A and B adopt a half-chair and a half-boat conformation respectively.

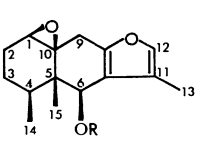

1 R = H
2 R = -CO-C(=CH$_2$)-CH$_2$OH
5 R = -CO-CH(-CH$_3$)-CH$_2$OH

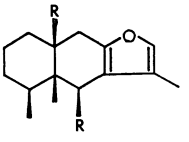

3 R = OH
4 R = H

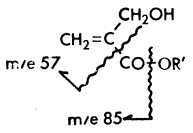

2'

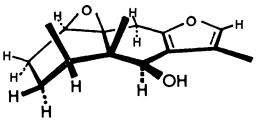

1'

The IR and UV spectra of **2** showed the presence of α,β-unsaturated ester group (*cf.* Experimental). A molecular ion peak at *m/e* 332 ($C_{19}H_{24}O_5$) was observed in the mass spectrum of **2**. The ester (**2**) was reduced with lithium aluminium hydride in ether to give **1**. Treatment of **2** with methanolic potassium hydroxide at room temperature afforded **1**. An acyl residue present in **2** was therefore inferred to be [C_3H_5O]–CO–. In the PMR spectrum of **2**, there appeared signals due to protons of a terminal methylene and a hydroxymethyl group (*cf.* Experimental), other than those due to the structure moiety of **1**. Hydrogenation of **2** in ethanol in the presence of palladium-charcoal yielded a dihydro derivative (**5**). In the PMR spectrum of **5**, a methyl signal at δ 1.26 and a methine proton signal at δ 2.77 newly appeared, while

TABLE. PMR SPECTRAL DATA OF **1**

	1α-H	2α-H	2β-H	3α-H	3β-H	4α-H	6α-H	9α-H	9β-H	12-H	13-H	14-H	15-H	OH
δ_{CDCl_3}[a]	3.06 (br. s)	—[b]	—[b]	—[b]	—[b]	1.5 (m)	4.86 (br. s)	3.22[c] (d)	2.11 (d)	7.07 (q)	2.09 (d)	1.11 (d)	1.14 (s)	1.9[d] (s)
$\delta_{Eu(dpm)_3}$[e]	11.45 (ABX)	5.0 (m)	6.8 (m)	5.9 (m)	2.6 (m)	16.3 (m)	—[f]	10.73 (d)	9.08 (d)	10.17 (br. s)	7.62 (d)	5.55 (d)	12.88 (s)	
δ[g]	−8.4					−14.8		−7.5	−7.0	−3.1	−5.5	−4.4	−11.7	

Coupling constants[a]: $J_{1\alpha,2\alpha}$= 5, $J_{1\alpha,2\beta}$=<1, $J_{2\alpha,2\beta}$=15, $J_{2\alpha,3\alpha}$=7, $J_{2\alpha,3\beta}$=1.5, $J_{2\beta,3\alpha}$=15, $J_{2\beta,3\beta}$= 5, $J_{3\alpha,3\beta}$=15, $J_{3\alpha,4\alpha}$=5, $J_{3\beta,4\alpha}$=1.5, $J_{4\alpha,14}$= 7, $J_{9\alpha,9\beta}$= 16, $J_{12,13}$= 1.5, $J_{6\alpha,9\alpha}$=2

a) Chemical shifts are expressed in downfield from TMS and coupling constants in Hz. b) Unresolved signals. c) With further splitting due to homoallylic coupling $J_{6\alpha,9\alpha}$. d) Disappeared on addition of D_2O. e) 0.97 M equivalent of $Eu(dpm)_3$ was added to the 2% (w/w) solution of **1**. f) Not measured. g) $\delta=\delta_{CDCl_3}-\delta_{Eu(dpm)_3}$.

signals due to a terminal methylene group were absent.

These observations led to a structure **2'** for the ester (**2**). This received support from an appearance of intense peaks at *m/e* 85 and *m/e* 57[11] due to fissions as shown in **2'**; these peaks were absent in the mass spectrum of **1**. The structure including absolute stereochemistry of the ester must be 1β,10β-epoxyfuranoeremophilan-6β-yl 2-hydroxymethylprop-2-enoate (**2**). The same acyl group as that of **2** has been described to be present as a part of the structures of vernodalin[11] and cynaropicrin.[12]

Experimental

IR spectra were measured using a Hitachi EPI-G2 spectrometer. UV spectra were determined on a Hitachi EPS-3 spectrometer. Measurements of optical rotation were carried out using a JASCO DIP-SL polarimeter. Mass spectra were taken on a Hitachi RMU-6-Tokugata mass spectrometer with a direct inlet system operating at 70 eV. PMR spectra were measured using a JEOL 4H-100 (100 MHz), a JEOL 3H-60 (60 MHz), a Hitachi R-20 (60 MHz) or a Hitachi R-24 (60 MHz) spectrometer. Chemical shifts were expressed in δ downfield from TMS as an internal standard, and coupling constants in Hz. Thin layer chromatography (tlc) was carried out on Kieselgel G nach Stahl, Kieselgel GF_{254} nach Stahl, and Kieselgel 60 PF_{254} (E. Merck, Darmstadt). For column chromatography Wakogel C-200 (Wako Pure Chem. Ind.) was used. All mps were determined on a hot block and reported uncorrected.

Isolation. Dried and sliced roots (226 g) of *Ligularia Fischeri* TURCZ. (collected at Shiramine, Ishikawa Prefecture) were extracted thrice with ether (total 4.5 l) at room temperature. Evaporation of the solvent gave a residue (7 g) which was chromatographed on a column of silica gel (100 g). The eluted fractions were examined by tlc (silica gel). After elution with light petroleum–ether (100: 1; 1.9 l) and then light petroleum–ether (50: 1; 750 ml), fractions eluted with light petroleum–ether (9: 1; 600 ml) were combined. Evaporation of the solvents gave a residue, which was purified by silica gel column chromatography and preparative tlc to afford 1β,10β-epoxyfuranoeremophilan-6β-ol (**1**; 50 mg), an oil, $[\alpha]_D$ −45° (*c* 0.11, EtOH); UV (EtOH) λ_{max} 215.5 nm (ε 7000); IR (liquid) 3450, 1645, and 1570 cm^{-1}; PMR data are described in Table; mass spectrum *m/e* 248 [relative intensity 7%, M^+ ($C_{15}H_{20}O_3$)] and 123 (100%).

Subsequent elution with light petroleum–ether (4: 1; 1 l) gave, on removal of the solvents, a residue, which was purified by silica gel column chromatography to yield 1β,10β-epoxyfuranoeremophilan-6β-yl 2-hydroxymethylprop-2-enoate (**2**; 2.6 g), an oil, $[\alpha]_D$ −9° (*c* 0.84, EtOH); UV (EtOH) λ_{max} 215 nm (ε 15000); IR (liquid) 3460, 1718, 1645, 1570, and 1160 cm^{-1}; PMR ($CDCl_3$) δ 1.05 (3H, d, J=7 Hz; protons at C-14), 1.22 (3H, s; protons at C-15), 1.79 (3H, d, J= 1.5 Hz; protons at C-13), 2.15 (1H, d, J=16 Hz; proton at C-9β), 3.10 (1H, br.s; proton at C-1α), 3.23 (1H, dd, J=16 and J=2 Hz; proton at C-9α), 6.46 (1H, m; proton at C-6α), 7.09 (1H, q, J=1.5 Hz; proton at C-12), 4.38 (2H, br.s; CH_2=C(–CH_2OH)–), 5.92 (1H, dt, J=1.6 and J=1.2 Hz; CH_2=C(–CH_2–)–), 6.32 (1H, dt, J=1.6 and J=1 Hz; CH_2=C(–CH_2–)–), and 2.92 (1H, br.s; OH; disappeared on addition of D_2O); mass spectrum *m/e* 332 (6%, M^+), *m/e* 109 (100%), *m/e* 85 (94%), and *m/e* 57 (50%). Found: C, 68.62; H, 7.43%. Calcd for $C_{19}H_{24}O_5$: C, 68.65; H, 7.28%. The ester (**2**) was unstable on exposure to the air, and could be stored under a nitrogen atmosphere in an icebox.

Reduction of 2 in Ether with Lithium Aluminium Hydride. To a solution of **2** (143 mg) in dry ether (10 ml) was added lithium aluminium hydride (50 mg) and the mixture was stirred at room temperature under a nitrogen atmosphere. After completion of the reaction, the excess reagent was decomposed with water. Extraction with ether and evaporation of the solvent gave a residue, which was chromatographed on a column of silica gel to afford an oil (15 mg). This oil was found to be identical with **1** in all respects.

Hydrolysis of 2. To a solution of potassium hydroxide (0.2 g) in methanol (4 ml) was added **2** (141 mg) and the mixture was stirred for 12 hr under a nitrogen atmosphere at room temperature. After removal of the solvent, the residue was extracted with ether to give **1** (86 mg).

Reduction of 1 in Tetrahydrofuran with Lithium Aluminium Hydride. Compound **1** (132 mg) in dry tetrahydrofuran (6 ml) was refluxed with lithium aluminium hydride (50 mg) for 2.5 hr under a nitrogen atmosphere. The mixture was treated as usual and the resulting residue was chromatographed on a column of silica gel (12 g) using light petroleum–ether (7: 1) as eluent to give a crystalline product (45 mg), mp 123 °C; $[\alpha]_D$ +37° (*c* 0.23, EtOH); Found: C, 72.23; H, 9.07%. Calcd for $C_{15}H_{22}O_3$: C, 71.97; H, 8.86%. This compound was found to be identical with an authentic sample of furanoeremophilane-6β,10β-diol (**3**)[7,8] in respects of mp, mixed mp, $[\alpha]_D$, IR, PMR, mass spectrum, and tlc.

Hydrogenation of 2 Over Palladium-charcoal. A solution of **2** (42 mg) in ethanol (10 ml) was hydrogenated in the presence of 10% palladium-charcoal (8 mg) at room temperature. Filtration of the catalyst and evaporation of the solvent gave a residue, which was purified by preparative tlc to afford 1β,10β-epoxyfuranoeremophilan-6β-yl 2-hydroxymethylpropanoate (**5**; 8 mg), an oil, IR (liquid) 3440, 1730, 1640, and 1565 cm^{-1}; PMR ($CDCl_3$) δ 1.09 (3H, d, J=7 Hz;

protons at C-14), 1.22 (3H, s; protons at C-15), 1.87 (3H, d, J=1.5 Hz; protons at C-13), 2.16 (1H, d, J=16 Hz; proton at C-9β), 3.10 (1H, br.s; proton at C-1α), 3.27 (1H, d, J=16 Hz; proton at C-9α), 6.43 (1H, m; proton at C-6α), 7.08 (1H, q, J=1.5 Hz; proton at C-12), 1.26 (3H, d, J=7 Hz; -CO-CH(-CH_3)-), 2.77 (1H, m; -CO-CH(-CH_2OH)-), 3.78 (2H, m; -CO-CH(-CH_2OH)), and 1.6 (1H, br.s; OH; disappeared on addition of D_2O); mass spectrum *m/e* 334 [1%, M^+ ($C_{19}H_{26}O_5$)], *m/e* 87 (20%, [CO-CH(CH_2OH)-CH_3]$^+$), *m/e* 59 (25%, [$HOCH_2$-CH-CH_3]$^+$), and *m/e* 55 (100%).

References

1) A preliminary account of this paper: Y. Moriyama, T. Sato, H. Nagano, Y. Tanahashi, and T. Takahashi, *Chem. Lett.*, **1972**, 637.

2) H. Ishii, T. Tozyo, and H. Minato, *Tetrahedron*, **21**, 2605 (1965).

3) H. Ishii, T. Tozyo, and H. Minato, *J. Chem. Soc., C*, **1966**, 1545.

4) H. Ishii, T. Tozyo, and H. Minato, *Chem. Commun.*, **1968**, 1534; H. Ishii, T. Tozyo, M. Nakamura, and H. Minato, *Tetrahedron*, **26**, 2911 (1970), and references therein.

5) F. Patil, G. Ourisson, Y. Tanahashi, M. Wada, and T. Takahashi, *Bull. Soc. Chim. France*, **1968**, 1047; T. Murae, Y. Tanahashi, and T. Takahashi, *Tetrahedron*, **24**, 2177 (1968); Y. Ishizaki, Y. Tanahashi, T. Takahashi, and K. Tori, *Chem. Commun.*, **1969**, 551; Y. Tanahashi, T. Takahashi, and H. Koyama, *Bull. Nat. Sci. Mus. Tokyo*, **12**, 633 (1969); Y. Ishizaki, Y. Tanahashi, T. Takahashi, and K. Tori, *Tetrahedron*, **26**, 5387 (1970); M. Tada, Y. Moriyama, Y. Tanahashi, T. Takahashi, M. Fukuyama, and K. Sato, *Tetrahedron Lett.*, **1971**, 4007; H. Nagano, Y. Moriyama, Y. Tanahashi, T. Takahashi, M. Fukuyama, and K. Sato, *Chem. Lett.*, **1972**, 13; H. Nagano and T. Takahashi, This Bulletin, **45**, 1935 (1972); H. Nagano, Y. Tanahashi, Y. Moriyama, and T. Takahashi, *ibid.*, **46**, 2840 (1973); Y. Moriyama, T. Tsuyuki, T. Takahashi, and H. Koyama, *Phytochemistry*, **13**, 288 (1974).

6) Koyama has described the presence of two types of *Ligularia Fischeri* Turcz. in Japan [H. Koyama, *Acta Phytotax. Geobot.*, **22**, 75 (1966)]. The tlc and glc data for constituents of our plant were very similar to those of *L. sibirica* Cass., collected at Prague by one of the authors, but different from those of *L. Fischeri* Turcz., collected at Karuizawa (late-flowering species), which contained ligularone *etc.* We are thankful to Dr. H. Koyama, National Science Museum, Tokyo, for recognition of our plant as *L. Fischeri* Turcz. (collected at Shiramine) from plant taxonomical point of view.

7) M. Tada, Y. Moriyama, Y. Tanahashi, T. Takahashi, M. Fukuyama, and K. Sato, *Tetrahedron Lett.*, **1971**, 4007.

8) M. Tada, Y. Tanahashi, Y. Moriyama, and T. Takahashi, *ibid.*, **1972**, 5255.

9) C. C. Hinckley, *J. Amer. Chem. Soc.*, **91**, 5160 (1969).

10) J. K. M. Sanders and D. H. Williams, *ibid.*, **93**, 641 (1971).

11) S. M. Kupchan, R. J. Hemingway, A. Karim, and D. Werner, *J. Org. Chem.*, **34**, 3908 (1969).

12) Z. Samek, M. Holub, B. Drozdz, G. Iommi, A. Corbella, and P. Gariboldi, *Tetrahedron Lett.*, **1971**, 4775.

Reaction of 2-Halo-1-Olefin-1-Carboxylic Acid with Cu_2O and Isonitrile

Yoshihiko Ito, Toshiro Konoike, Syotaro Fujii, Junichiro, Setsune, and Takeo Saegusa*

Department of Synthetic Chemistry, Faculty of Engineering, Kyoto University, Kyoto 606

(Received October 26, 1974)

A reaction of 2-halo-1-olefin-1-carboxylic acids with isonitrile and Cu_2O is described. *o*-Chlorobenzoic acid is treated with *tert*-butyl isocyanide and Cu_2O at 80 °C to produce benzoic acid (**1a**), phthalic anhydride (**2a**), *N-tert*-butylphthalisoimide (**3a**) and *N-tert*-butylphthalimide (**4a**) in 5, 14, 18, and 32% yields, respectively. With 2-chloro-1-cyclohexene-1-carboxylic acid, a similar result is observed. However, the reaction of acyclic 2-chloro-1-olefin-1-carboxylic acid such as β-chlorocrotonic acid with isonitrile and Cu_2O does not give any products corresponding to **1**—**4**. These reactions are interestingly compared with the reaction of *o*-iodobenzoic acid and copper(I) acetylide producing 3-alkylidenephthalide. A reaction mechanism involving a transient intermediate of α,β-unsaturated β-lactone (**11**) is proposed for the present reaction.

In the preceeding papers, we have reported that carboxylic acid[1] and carboxylic acid anhydride[2] are readily esterified with alkyl halides in the presence of Cu_2O/Isonitrile complex. For this esterification, a reaction mechanism has been established in which Cu(I) carboxylate isonitrile complex (**1**) was initially generated by the reaction of Cu_2O/Isonitrile complex with carboxylic acid or with carboxylic acid anhydride, and then **1** reacted with alkyl halides to produce the corresponding carboxylic esters. Aromatic halides could not react with **1**.

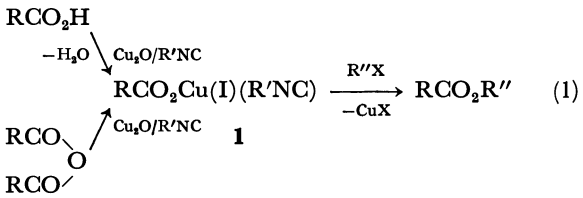

(1)

Now, we found that *o*-chlorobenzoic acid reacted with Cu_2O/*tert*-butyl isocyanide complex to give the following products, **1a**, **2a**, **3a**, and **4a**.

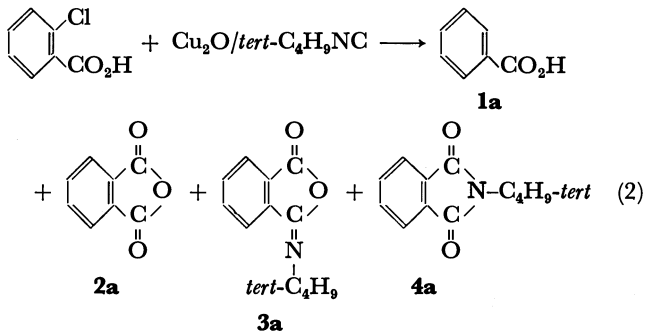

(2)

Similar reactions were observed with 2-chloro-1-cyclohexene-1-carboxylic acid and 2-chloro-1-cyclopentene-1-carboxylic acid. These reactions are interestingly compared with the following reaction reported by Castro *et al.*, *i.e.*, the reaction of *o*-iodobenzoic acid and copper(I) acetylide producing 3-alkylidenephthalide.[3]

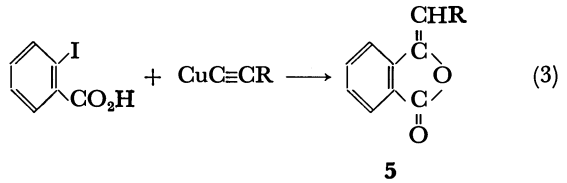

(3)

Results and Discussion

On heating a mixture of *p*-chlorobenzoic acid, Cu_2O and *tert*-butyl isocyanide in benzene at 80 °C for 12 hr under nitrogen, Cu(I) *p*-chlorobenzoate (*tert*-butyl isocyanide) complex (**6**) was only produced in an almost quantitative yield.[1]

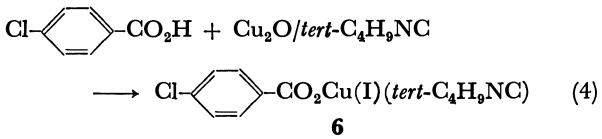

(4)

However, the reaction of *o*-chlorobenzoic acid with Cu_2O/*tert*-butyl isocyanide was quite different from that of *p*-chlorobenzoic acid. Four products **1a**, **2a**, **3a**, and **4a** were isolated by glpc in 5, 14, 18, and 32% yields, respectively. Products **2a** and **4a** appear to have been derived by the hydrolysis and rearrangement of **3a**, respectively. The rearrangement of isoimide **3** to imide **4** has been documented in a literature.[4] The remarkable difference of reactivity between the *ortho*- and the *para*-isomers strongly suggests that Cu(I) *o*-chlorobenzoate (*tert*-butyl isocyanide) complex (**7**) is

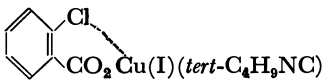

stabilized by chelation with chlorine in the *ortho* position to the carboxyl group. With 2-chloro-1-cyclohexene-1-carboxylic acid, which is considered to have an analogous geometrical circumstance, a similar result was observed. Four products, **1b**, **2b**, **3b**, and **4b** were isolated in 5, 13, 20, and 41% yields, respectively.

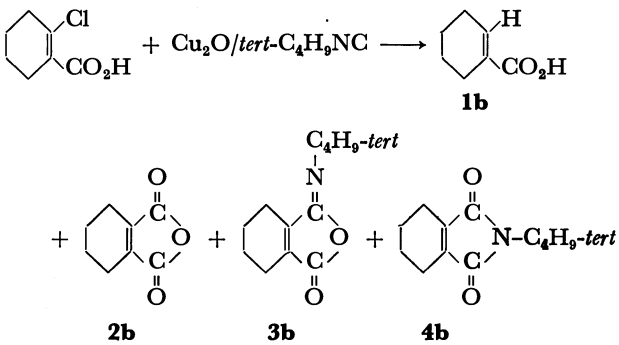

These reactions occurred slowly even at room tem-

perature. For instance, in the reaction of 2-chloro-1-cyclohexene-1-carboxylic acid with Cu_2O/*tert*-butyl isocyanide at 20 °C for 70 hr, **1b**, **2b**, **3b**, and **4b** were produced in 1, 2, 32, and 5% yields, respectively. Also, the reaction of 2-chloro-1-cyclopentene-1-carboxylic acid with Cu_2O/*tert*-butyl isocyanide at 80 °C produced **1c** and **4c** but in low yields.

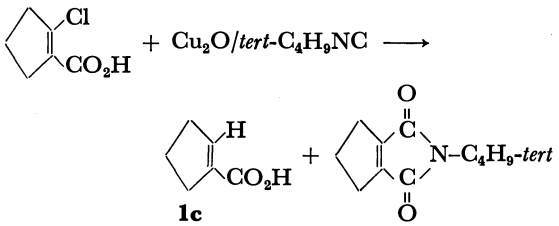

1c **4c**

However, the reaction of acyclic 2-chloro-1-olefin-1-carboxylic acid such as β-chlorocrotonic acid with Cu_2O/isonitrile did not give any product corresponding to **1**—**4**.

The treatment of *o*-bromobenzoic acid with a mixture of *tert*-butyl isocyanide and phenylacetylene in the presence of Cu_2O in pyridine solvent afforded a major product of 3-benzylidenephthalide (**8**, 53%) as reported by Castro *et al.*,[3] and by-products of **1a**, **3a**, and **4a**.

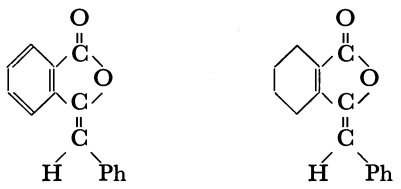

8 **9**

Similarly, 2-chloro-1-cyclohexene-1-carboxylic acid reacted with a mixture of *tert*-butyl isocyanide and phenylacetylene to produce **9** (70%) with **2b**, **3b**, and **4b**. The following scheme may possibly proposed for the reaction of Cu_2O/isonitrile with 2-halo-1-cyclic olefin-1-carboxylic acid, which involves a transient intermediate of **11**.

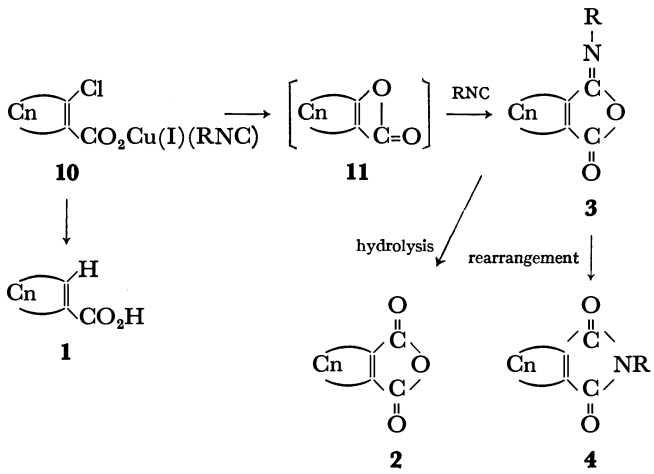

Intramolecular elimination of CuCl from **10** leading to lactone **11** is followed by the reaction with isonitrile. It is also conceibable that the elimination of CuCl from **10** and the reaction of **11** with isonitrile occur synchronously. The formation of **1** is understandable from the fact that aromatic halide is readily reduced by a system of Cu_2O–pyridine–acetic acid.[5] Concerning the intermediate of **11**, it may be pertinent to mention the following reaction. A reaction of dichloromaleic anhydride with Cu_2O/*tert*-butyl isocyanide in the presence of ethyl iodide afforded **12** in 42% yield along with **13** (5%) and **14** (10%).

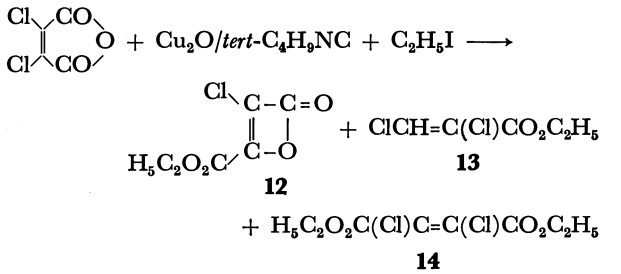

12 **13** **14**

The structure of **12** was established by IR, elemental analysis and its chemical reaction (see Experimental Section). The formation of **12** will be reasonably explained by a scheme shown below.

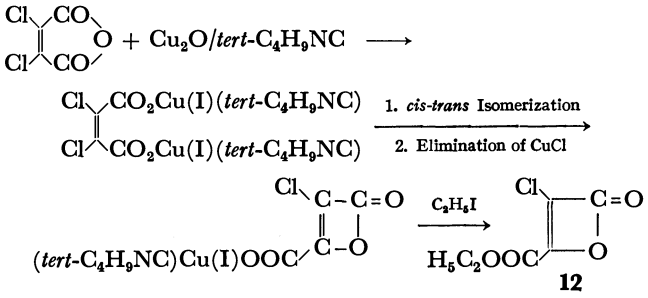

Experimental

Reaction of o*-Chlorobenzoic Acid with* Cu_2O/tert*-Butyl Isocyanide.* A mixture of 3.4 g (20 mmol) of *o*-chlorobenzoic acid, 1.43 g (10 mmol) of Cu_2O and 1.66 g (20 mmol) of *tert*-butyl isocyanide in 10 ml of benzene was heated at 80 °C for 20 hr with stirring under nitrogen. The reaction mixture was treated with 10 ml of petroleum ether to remove Cu(I)Cl-(*tert*-butyl isocyanide) complex, and filtered. The filtrate was concentrated *in vacuo*, and subjected to glpc analysis. Four products **1a**, **2a**, **3a**, and **4a** were isolated. The structures of **1a** and of **2a** were established by comparison of IR spectra with the respective authentic samples. Structures of **3a** and **4a** were determined by IR, NMR, and elemental analysis. **3a**: Found: C, 69.93; H, 6.36; N, 6.94%. Calcd for $C_{12}H_{13}NO_2$: C, 70.91; H, 6.45; N, 6.89%. IR (cm^{-1}): 1850, 1820, 1780, 1710. NMR ($CDCl_3$ with TMS): 1.48 (s, 9H), 7.70 (s, 4H). **4a**: Found: C, 70.69; H, 6.28; N, 6.91%. Calcd for $C_{12}H_{13}NO_2$: C, 70.91; H, 6.45; N, 6.89%. Mass M^+=203. IR (cm^{-1}): 1778, 1712. NMR ($CDCl_3$ with TMS): 1.68 (s, 9H), 7.71 (s, 4H).

Reaction of 2-Chloro-1-cyclohexene-1-carboxylic Acid with Cu_2O/tert*-Butyl Isocyanide.* According to the procedure described above, a mixture of 1.60 g (10 mmol) of 2-chloro-1-cyclohexene-1-carboxylic acid, 0.72 (5 mmol) of Cu_2O and 0.83 (10 mmol) of *tert*-butyl isocyanide in 5 ml of benzene was reacted at 80 °C for 30 hr. Products **1b**, **2b**, **3b**, and **4b** were isolated by glpc. The structures of **1b** and **2b** were confirmed by comparison of their IR spectra with those of the authentic samples. Structures of **3b** and **4b** were determined by IR, NMR, and elemental analysis. **3b** (mp 75—77 °C): Found: C, 69.26; H, 8.29; N, 6.62%. Calcd for

$C_{12}H_{17}NO_2$: C, 69.54; H, 8.27; N, 6.76%. IR (cm^{-1}): 1810, 1775, 1690. NMR ($CDCl_3$ with TMS): 1.34 (s, 9H), 1.72 (m, 4H), 2.32 (m, 4H). **4b** (mp 66 °C): Found: C, 69.40; H, 8.22; N, 6.84%. Calcd for $C_{12}H_{17}NO_2$: C, 69.54; H, 8.27; N, 6.76%. IR (cm^{-1}): 1770, 1710. NMR ($CDCl_3$ with TMS): 1.53 (s, 9H), 1.69 (m, 4H), 2.22 (m, 4H). Similarly, the reaction of 2-chloro-1-cyclopentene-1-carboxylic acid with Cu_2O/*tert*-butyl isocyanide was carried out. Among several products, **1c** (5%) and **4c** (2%) were identified. **1c** was identified by comparison with the authentic sample. **4c**: Found: C, 68.52; H, 7.61; N, 7.58%. Calcd. for $C_{11}H_{15}NO_2$: C, 68.37; H, 7.82; N, 7.25%. IR (cm^{-1}): 1770, 1710. NMR ($CDCl_3$ with TMS): 1.54 (s, 9H), 2.50 (m, 6H). Mass $M^+=193$.

Competitive Reaction of 2-Chloro-1-cyclohexene-1-carboxylic Acid with tert-*Butyl Isocyanide and Phenylacetylene in the Presence of Cu_2O in Pyridine.* A mixture of 2.00 g (13 mmol) of 2-chloro-1-cyclohexene-1-carboxylic acid, 1.01 g (7 mmol) of Cu_2O, 1.33 g (13 mmol) of phenylacetylene, and 1.58 g (19 mmol) of *tert*-butyl isocyanide in pyridine (25 ml) was heated at reflux under nitrogen gas for 14 hr. After the reaction mixture was filtered, the filtrate was subjected to fractional distillation *in vacuo*. Products **9**, **2b**, **3b**, and **4b** was isolated by glpc in 4, 23, and 2% yields, respectively. Product **9** (70%) was crystallized from ligroin (mp 118—120 °C); Found: C, 79.26; H, 6.61%. Calcd for $C_{15}H_{14}O_2$: C, 79.62; H, 6.24%. NMR ($CDCl_3$ with TMS): 1.75 (broad, 4H), 2.40 (broad, 4H), 5.85 (s, 1H), 7.2, 7.8 (m, 5H).

*Reaction of Dichloromaleic Anhydride with Cu_2O/*tert*-Butyl Isocyanide in the Presence of Ethyl Iodide.* A mixture of 1.67 g (10 mmol) of dichloromaleic anhydride, 1.43 g (10 mmol) of Cu_2O, 1.66 g (20 mmol) of *tert*-butyl isocyanide and 3.12 g (20 mmol) of ethyl iodide was stirred at 80 °C for 10 hr under nitrogen. After the reaction mixture was treated with petroleum ether, and filtered, the filtrate was evaporated. Products **12**, **13**, and **14** was isolated by glpc. Identity of **13** and of **14** was established by comparison of their IR spectra with those of the authentic samples. Structure determination of **12** was performed by IR, NMR, elemental analysis and its chemical reaction. **12**: Found: C, 40.84; H, 2.82; Cl, 20.37%. Calcd for $C_6H_5O_3Cl$: C, 40.81; H, 2.85; Cl, 20.82%. IR (cm^{-1}) 1875—1830, 1790, 1750, 1655. Treatment of **12** with HCl saturated ethanol at 80 °C for 2 hr gave two products **15** and **16** in the ratio of 4 to 1.

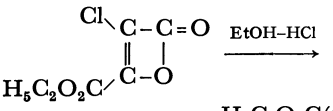

12

$H_5C_3O_2C(Cl)C{=}C(OC_2H_5)CO_2C_2H_5$

15

$H_5C_2O_2C(Cl)CH{-}C(OC_2H_5)_2CO_2C_2H_5$

16

15: Found: C, 48.12; H, 6.09; Cl, 14.05%. Calcd for $C_{10}H_{15}O_5Cl$: C, 47.91; H, 6.03; Cl, 14.14%. IR (cm^{-1}): 1741, 1710, 1610. NMR ($CDCl_3$ with TMS): 1.28 (t, 3H), 1.36 (t, 3H), 1.37 (t, 3H), 4.06 (q, 2H), 4.37 (two q, 4H). **16**: Found: C, 48.45; H, 7.20; Cl, 12.02%. Calcd for $C_{12}H_{21}O_6Cl$: C, 48.57; H, 7.13; Cl, 11.95%. IR (cm^{-1}): 1760. NMR ($CDCl_3$ with TMS): 1.29 (two t, 6H), 1.33 (t, 3H), 1.39 (t, 3H), 3.75 (two q, 4H), 4.36 (two q, 4H), 4.84 (s, 1H).

References

1) a) T. Saegusa and I. Murase, *Syn. Commun.*, **2**, 1 (1972); b) T. Saegusa, I. Murase, and Y. Ito, *J. Org. Chem.*, **38**, 1753 (1973).

2) I. Murase, Thesis, Kyoto University, 1972.

3) C. E. Castro, E. J. Gaughan, and D. C. Owsley, *J. Org. Chem.*, **31**, 4710 (1966).

4) C. K. Sauers and H. M. Relles, *J. Amer. Chem. Soc.*, **95**, 7731 (1973).

5) a) R. G. R. Bacon and H. A. O. Hill, *Proc. Chem. Soc.*, **1962**, 113; b) M. Anbar and S. Guttman, *Proc. Chem. Soc. Commun.*, **1962**, 10.

A Semi-empirical Calculation of the Substituent Effects on ^{1}H Chemical Shifts in Aromatic Side-chains

Jun NIWA

College of General Education, Nagoya University, Chikusa, Nagoya 464

(Received June 14, 1974)

The diamagnetic contribution of the hydrogen atom in the C–H bond and that from its bonded carbon have been semi-empirically expressed. By considering the "ring-current" effect in addition to such contributions, a semi-empirical expression has been obtained for ^{1}H chemical shifts relative to the unsubstituted compound in substituted aromatic side-chains. The applicability of the expression has been examined for *m*- and *p*-substituted phenylacetylenes, styrenes, toluenes, and benzaldehydes.

The well-known expression for obtaining a simple relationship for the magnetic shielding constant of the hydrogen atom, σ^A, in an aromatic side-chain can be described as a sum of the following contributions:[1]

$$\sigma^A = \sigma^{AA}_{dia} + \sum_{B\neq A}(\sigma^{AB}_{dia}+\sigma^{AB}_{para}) + \sigma^{A,ring} \quad (1)$$

where σ^{AA}_{dia} is the local diamagnetic term of the hydrogen atom, A; where σ^{AB} is the contribution from currents on the B atom to the shielding of A, and where $\sigma^{A,ring}$ is the contribution to the shielding of A from the "ring current".

Recently, Kajimoto and Fueno[2] have presented an improved LCAO MO expression for the shielding of a hydrogen atom, A (σ^A), in aliphatic compounds; their expression is derived on the basis of Ramsey's equation,[3] containing two of Pople's three assumptions,[4] (1) a zero-differential atomic integral and (2) an average excitation energy approximation, but without invoking (3) the magnetic dipole approximation. They have concluded that the diamagnetic shielding from the neighboring carbon (σ^{AB}_{dia}) constitutes an important contribution, together with the σ^{AA}_{dia} term to the chemical shifts, whereas the paramagnetic term (σ^{AB}_{para}) remains almost constant for various substituted olefinic compounds.

It is well established that the contribution from the "ring current" should be taken into consideration for the ^{1}H chemical shifts in aromatic side-chains.[5] Figeys and Flammang have indicated that the introduction of a substituent into a benzene ring decreases the effect of the "ring current" and that this effect can be interpreted as arising from the fact that an additional contribution due to the "quinonoid" structure in the resonance hybrid leads to some degree of decrease in the ring current.[6] Yamada, Yukawa, and Tsuno have shown that the extent of the contribution of the "quinonoid" structure depends on the resonance ability of the substituent introduced,[7] and they have presented an equation ($\Delta\sigma^{A,ring}$) to describe the contribution relative to the unsubstituted compound to the ^{1}H chemical shifts in *m*-substituted aromatic side-chains, utilizing Johnson and Bovey ring-current shifts:[5b]

$$\Delta\sigma^{A,ring} = -0.4f(\rho, z)|\sigma_\pi| \quad (2)$$

where $f(\rho, z)$ is the Johnson and Bovey ring-current shift in ppm, which is expressed as a function of the geometric factors for the proton located at the cylindrical co-ordinates, ρ and z, and where σ_π is Yukawa-Tsuno's parameter for measuring the resonance ability of the substituent.[8]

In the present paper, we will first attempt to evaluate the diamagnetic term, σ^{AB}_{dia}, semi-empirically. Second, we will reveal that Eq. (2) can also be applied to the case of *p*-substituted compounds. By taking the "ring-current" effect into account in addition to the diamagnetic terms, σ^{AA}_{dia} and σ^{AB}_{dia}, we have obtained a semi-empirical expression for the ^{1}H chemical shifts relative to the unsubstituted compound in substituted aromatic side-chains. We will report to what degree of accuracy the expression reproduces the chemical shifts observed for protons in side-chain of *m*- and *p*-substituted phenylacetylenes, styrenes, toluenes, and benzaldehydes.

Results and Discussion

Kajimoto *et al.*[2] have shown that the local diamagnetic term of the hydrogen atom, A (σ^{AA}_{dia}), is given by Eq. (3), using Slater's effective nuclear charge modified to $z_{eff}=1.2-0.3(q_H-1)$ for the 1s orbital of hydrogen:

$$\sigma^{AA}_{dia} = (e^2/3mc^2)p^A_{1s,1s}\langle\phi^A_{1s}|1/r_A|\phi^A_{1s}\rangle = 17.75\times10^{-6}(-0.3q^2_H+1.5q_H) \quad (3)$$

where q is the electron density on the 1s orbital of hydrogen. The value of σ^{AA}_{dia} relative to the unsubstituted compound is linearly correlated with the increment in the electron density on the hydrogen atom:

$$\Delta\sigma^{AA}_{dia} = a\times10^{-6}\Delta q^A \quad (4)$$

where the value of a has been obtained as 16.0 by Kajimoto *et al.*[2] for the case of substituted olefinic compounds.

They have also derived an LCAO MO expression for the σ^{AB}_{dia} term in the case of olefinic compounds:

$$\sigma^{AB}_{dia} = (e^2/3mc^2)\sum_I p^B_{II}\langle\phi^B_I|1/r_{AB}|\phi^B_I\rangle \quad (5)$$

$$= 10^{-6}\{8.362q^B_{2s}+10.073q^B_{2pz}+7.564(q^B_{2px}+q^B_{2py})\} \quad (6)$$

where q's are the electron densities on specified atomic orbitals and where the C–H bond length is taken to be 1.08 Å.[2] The value of σ^{AB}_{dia} relative to the unsubstituted compound can be correlated with the increment in the total (2s and 2p) electron density on the B atom:

$$\Delta\sigma^{AB}_{dia} = 8.39\times10^{-6}\Delta q^B \quad (7)$$

In order to empirically evaluate the σ^{AB}_{dia} term we will replace the quantum mechanical average of r^{-1} from each atomic orbital on the B atom with the inverse

Table 1. Comparison of values (in ppm) of σ_{dia}^{AB} calculated by Eq. (7) with those calculated by Eq. (10) in monosubstituted ethylenes

$XCH{=}CH_2$ (B)(A)

Substituent	q^B	$8.70\Delta q^B$	$8.39\Delta q^B$
H[a]	3.9945	0.00	0.00
H[b]	4.0312	0.00	0.00
OCH_3[a]	4.1058	0.97	0.93
CN[a]	3.9748	−0.17	−0.17
NO_2[a]	3.9483	−0.40	−0.39
CH_3[a]	4.0253	0.27	0.26
Cl[b]	4.0667	0.31	0.30

a) All electron densities were calculated by the INDO method. b) The electron density was calculated by the CNDO/2 method. The values of the third and fourth columns for chloroderivatives are relative to the unsubstituted compound, the electron density of which was calculated by the CNDO/2 method.

distance of A from the point charge on B. Then Eq. (5) becomes:

$$\sigma_{dia}^{AB} = (e^2/3mc^2)r_{AB}^{-1}q^B \quad (8)$$

$$= b \times 10^{-6} q^B \quad (9)$$

The expression of Eq. (9), relative to the unsubstituted compound, is given as:

$$\Delta\sigma_{dia}^{AB} = b \times 10^{-6}\Delta q^B \quad (10)$$

When Eq. (8) is applied to substituted ethylenes, where the C–H bond length is taken to be 1.08 Å, the value of b is 8.70. Table 1 shows that the respective values of $\Delta\sigma_{dia}^{AB}$, as calculated by Eqs. (7) and (10) for substituted ethylenes, agree within errors of only a few percent. Moreover, when the C–H bond length is taken to be 1.064 Å in the ethynyl bond, $\sigma_{dia}^{AB}=8.83\times 10^{-6} q^B$ using Eq. (8). In acetylene, the value of σ_{dia}^{AB} is 35.82 ppm, while the strict MO calculation by Katô has given 35.71 ppm for it, taking the 2s and 2p orbitals on carbon into account.[9] These results mean that Eq. (8) is applicable to the calculation of the substituent effect on the σ_{dia}^{AB} term in the cases of olefinic and ethynyl protons.

The paramagnetic term, σ_{para}^{AB}, calculated according to Pople's expression[4] remains almost constant for the series of compounds examined, so long as we assume the same average excitation energy and the same value of the integral $\langle r_{AB}^{-3}\rangle$ for the same series of compounds.

With regard to the "ring-current" effect on the ^1H chemical shifts in aromatic side-chains, Eq. (2) can not axiomatically hold in the case of the proton at the position *para* to substituent, where a conjugative interaction through the benzene ring between the substituent and the side-chain group might result in the difference in the "ring-current" effect compared with the case of *m*-substituted compounds.

The "ring-current" effect on the ^1H chemical shift in monosubstituted benzene may consist of two factors: the ring-current intensity due to the total π-electron density on the benzene ring and the decrease in the ring current arising from the contribution of the "quinonoid" structure due to an introduced substituent. The degree of the contribution of the "quinonoid" structure to the benzene ring due to an introduced substituent may be reflected in changes in the absolute values of the π-electron densities on carbon atoms at the C_1 and C_4 positions.

If it is assumed that the contributions of the "quinonoid" structure arising from the introduction of the X and Y substituents (Y: the side-chain group) are put one upon another in either *m*- or *p*-substituted compounds, as is shown in Fig. 1, the relative contribution of the

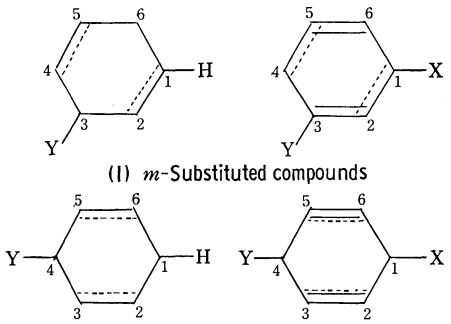

Fig. 1. Offset of quinonoid structure due to the side-chain group Y in *m*- and *p*-substituted aromatic compounds.

"quinonoid" structure between the substituted and the unsubstituted compounds can be determined only by the contribution of the X substituent, because the contributions of the side-chain group, Y, cancel each other out in the same series of compounds. Accordingly, if the total π-electron density (q_{ring}^{π}) of the aromatic ring of the *m*-substituted compound is equal to that of the *p*-substituted one, bearing the same substituent, and if the absolute values of the relative π-electron densities on C_1 (and C_4) between the substituted and the unsubstituted compounds ($|\Delta q_\pi(C_1)|$ and $|\Delta q_\pi(C_4)|$) are equal in the two compounds, the contributions by the X substituent may be regarded as equal in the two compounds. The results summarized in Table 2 show that the q_{ring}^{π} value of the *m*-substituted compound scarcely differs from that of the *p*-sbustituted one, and that the values of $|\Delta q_\pi(C_3)|$ (and $|\Delta q_\pi(C_4)|$) are almost equal in *m*- and *p*-substituted compounds. Therefore, it may be concluded that the relative contributions of the "ring current" to the unsubstituted compound are equal in *m*- and *p*-substituted compounds.

By combining Eqs. (2), (4), and (10), we obtain the following equation for the ^1H chemical shifts, $\delta(\equiv\Delta\sigma^A)$, in ppm, relative to the unsubstituted compound in *m*- and *p*-substituted aromatic side-chains:

$$\delta_{calc} = a\Delta q^A + b\Delta q^B - 0.4f(\rho, z)|\sigma_\pi| \quad (11)$$

Since the electron density on an aromatic side-chain can be altered by the substituent polar effect (the mesomeric and inductive (through bond) effects), its contribution to the ^1H chemical shift in the side-chain may be included in the first and second terms of Eq.

TABLE 2. π-ELECTRON DENSITIES ON AROMATIC RINGS

(i) *m*- and *p*-Substituted phenylacetylenes.[a]

Substituent	q^{π}_{ring}[b]	$\lvert\Delta q^{\pi}(C_1)\rvert$[c]	$\lvert\Delta q^{\pi}(C_4)\rvert$[c]
H	5.996	0.000	0.000
H[d]	6.007	0.000	0.000
m-CH_3	6.007	0.018	0.009
p-CH_3	6.004	0.019	0.009
m-CH_3O	6.074	0.042	0.037
p-CH_3O	6.066	0.043	0.036
m-NO_2	5.981	0.065	0.030
p-NO_2	5.983	0.069	0.025
m-Cl[d]	6.029	0.012	0.006
p-Cl[d]	6.026	0.009	0.005

(ii) *m*- and *p*-Substituted styrenes.[d]

Substituent	q^{π}_{ring}[b]	$\lvert\Delta q^{\pi}(C_1)\rvert$[c]	$\lvert\Delta q^{\pi}(C_4)\rvert$[c]
H	5.988	0.000	0.000
m-CH_3	6.012	0.028	0.015
p-CH_3	6.008	0.029	0.015
m-Cl	6.031	0.005	0.012
p-Cl	6.027	0.004	0.009
m-NO_2	5.984	0.064	0.030
p-NO_2	5.987	0.070	0.038
m-CN	5.984	0.000	0.006
p-CN	5.983	0.001	0.009
m-NH_2[e]	6.096	0.072	0.059
p-NH_2[e]	6.083	0.077	0.060

(iii) *m*- and *p*-Substituted toluenes.[d]

Substituent	q^{π}_{ring}[b]	$\lvert\Delta q^{\pi}(C_1)\rvert$[c]	$\lvert\Delta q^{\pi}(C_4)\rvert$[c]
H	6.013	0.000	0.000
m-CH_3	6.027	0.027	0.015
p-CH_3	6.023	0.028	0.015
m-CH_3O	6.083	0.049	0.041
p-CH_3O	6.075	0.048	0.039
m-F	6.069	0.036	0.031
p-F	6.063	0.037	0.029
m-CN	5.998	0.000	0.007
p-CN	5.994	0.001	0.009
m-NO_2	5.996	0.065	0.032
p-NO_2	5.997	0.068	0.038

(iv) *m*- and *p*-Substituted benzaldehydes.[a]

Substituent	q^{π}_{ring}[b]	$\lvert\Delta q^{\pi}(C_1)\rvert$[c]	$\lvert\Delta q^{\pi}(C_4)\rvert$[c]
H	5.952	0.000	0.000
H[d]	5.957	0.000	0.000
m-CH_3	5.959	0.019	0.010
p-CH_3	5.961	0.020	0.010
m-CH_3O	6.030	0.043	0.037
p-CH_3O	6.025	0.042	0.037
m-NO_2	5.938	0.064	0.029
p-NO_2	5.944	0.069	0.033
m-Cl[d]	5.990	0.006	0.007
p-Cl[d]	5.988	0.005	0.010

a) Electron densities were calculated by the INDO method. Values of bond lengths and bond angles of compounds examined were chosen from Ref. 10. b) The total π-electron density on the aromatic ring. c) Absolute values of relative π-electron densities on C_1 and C_4 between the substituted and the unsubstituted compounds. Numbering of atoms C_1 and C_4 correspond to that in Fig. 1. d) Electron densities were calculated by the CNDO/2 method. e) A planar model was used for amino groups.

TABLE 3. VALUES OF *a*, *b*, AND $f(\rho, z)$ IN Eq. (9) in ppm

Side-chain system		*a*	*r*[a]	*s*[a]	*b*	$f(\rho, z)$
$XC_6H_4C{\equiv}CH$		16.7	0.9998	0.0009	8.83	−0.21[b]
XC_6H_4	α	16.1	0.9999	0.0070	8.70	−0.25[c]
$C{=}C$	β	16.2	0.9999	0.0006	8.70	−0.54[c]
H_γ H_α	γ	16.1	1.0000	0.0004	8.70	−0.58[c]
$XC_6H_4CH_3$		16.0	0.9999	0.0008	8.52	−0.57[b]
XC_6H_4CHO		15.2	0.9999	0.0010	8.43	−0.61[b]

a) *r*: correlation coefficient, *s*: standard deviation. b) Cited from Ref. 7. c) Calculated from the table of the Johnson and Bovey's ring current shifts (Ref. 11). The basis of this calculation consists in that the total π-electron density on aromatic ring scarcely differs from that of benzene (see Table 2) and that the contribution due to the "quinonoid" structure of the side-chain group cancels each other out in the same seires of compounds.

(11) to a first approximation. In order to examine the applicability of Eq. (11), we have chosen ethynyl, olefinic, saturated aliphatic, and formyl groups as model

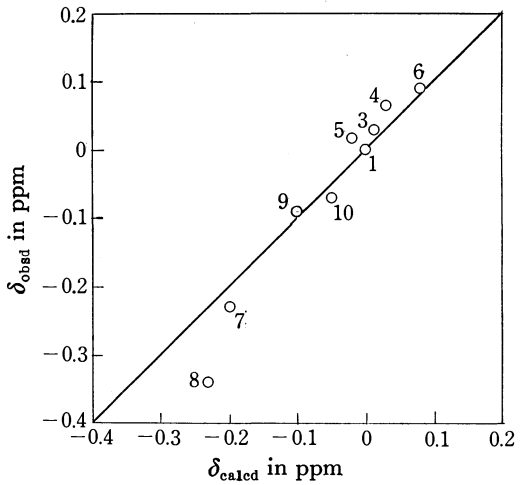

Fig. 2. Plots of δ_{calcd} against δ_{obsd} in *m*- and *p*-substituted phenylacetylenes. Numbered points correspond to entries in Table 4-(i).

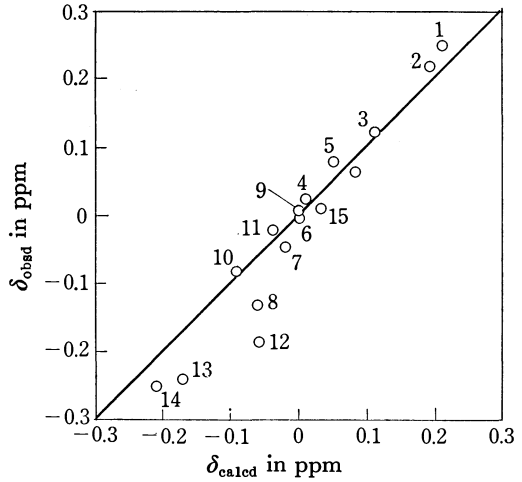

Fig. 3(a). Plots of δ_{calcd} against δ_{obsd} for protons, Hα, in *m*- and *p*-substituted styrenes. Numbered points correspond to entries in Table 4-(ii), (a).

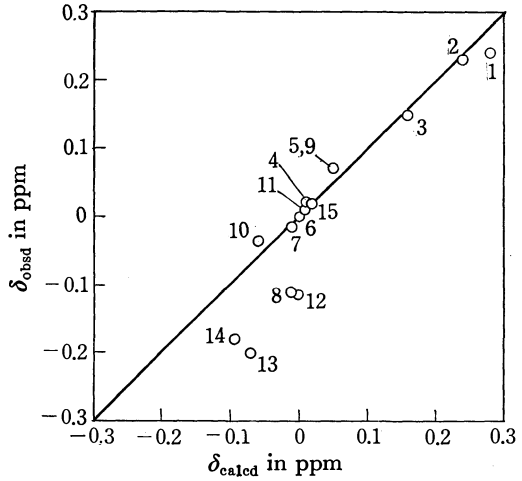

Fig. 3(b). Plots of δ_{calcd} against δ_{obsd} for protons, Hβ, in *m*- and *p*-substituted styrenes. Numbered points correspond to entries in Table 4-(ii), (b).

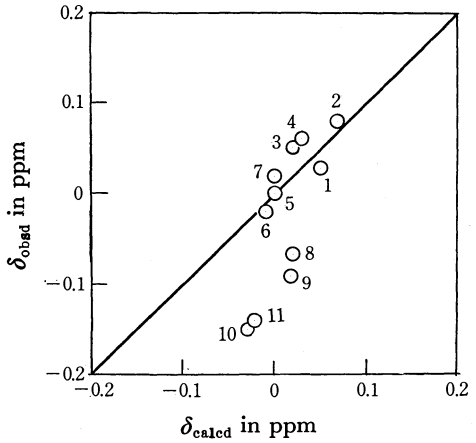

Fig. 4. Plots of δ_{calcd} against δ_{obsd} in *m*- and *p*-substituted toluenes. Numbered points correspond to entries in Table 4-(iii).

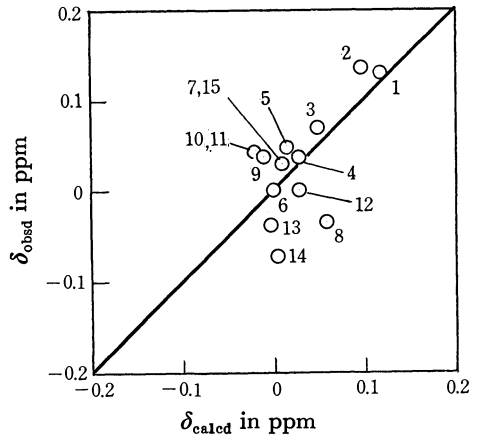

Fig. 3(c). Plots of δ_{calcd} against δ_{obsd} for protons, Hγ, in *m*- and *p*-substituted styrenes. Numbered points correspond to entries in Table 4-(ii), (c).

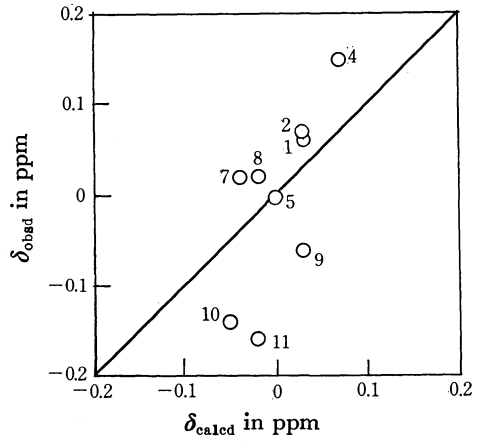

Fig. 5. Plots of δ_{calcd} against δ_{obsd} in *m*- and *p*-substituted benzaldehydes. Numbered points correspond to entries in Table 4-(iv).

systems of aromatic side-chains. Above all, the advantage of styrenes in examining the success of Eq. (11) is that they have three hydrogen atoms situated in different magnetic environments in the side-chain.

The values of a, b, and $f(\rho, z)$ obtained for the compounds examined are listed in Table 3. In Table 4, the chemical shifts calculated by Eq. (11) are compared with those observed for *m*- and *p*-substituted phenylacetylenes, styrenes, toluenes, and benzaldehydes. Even though it is a rather optional expansion to apply Eq. (8) to calculation of the σ_{dia}^{AB} term in the cases of toluenes and benzaldehydes, the results of the calcula-

Table 4. Chemical shifts of protons in side-chains of *m*- and *p*-substituted aromatic compounds[a]

(i) *m*- and *p*-Substituted phenylacetylenes.[b]

	Substituent	q^A	q^B	$\Delta\sigma_{dia}^{AA}$	$\Delta\sigma_{dia}^{AB}$	$\Delta\sigma^{A,ring}$	δ_{calcd}	δ_{obsd}[c]
1	H	0.9484	4.0991	0.000	0.000	0.000	0.00	0.000
2	H[d]	0.9378	4.1110	0.000	0.000	0.000	0.00	0.000
3	*m*-CH_3	0.9487	4.0992	0.005	0.001	0.007	0.01	0.030
4	*p*-CH_3	0.9488	4.1012	0.007	0.019	0.007	0.03	0.065
5	*m*-CH_3O	0.9479	4.0949	−0.008	−0.037	0.024	−0.02	0.020
6	*p*-CH_3O	0.9488	4.1050	0.007	0.052	0.024	0.08	0.090
7	*m*-NO_2	0.9430	4.0833	−0.090	−0.140	0.029	−0.20	−0.233
8	*p*-NO_2	0.9430	4.0801	−0.090	−0.168	0.029	−0.23	−0.340
9	*m*-Cl[d]	0.9353	4.1034	−0.042	−0.067	0.006	−0.10	−0.085
10	*p*-Cl[d]	0.9361	4.1077	−0.028	−0.029	0.006	−0.05	−0.068

(ii) *m*- and *p*-Substituted styrenes.[d]

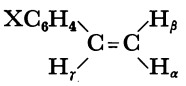

(a) H_α

	Substituent	q^A	q^B	$\Delta\sigma_{dia}^{AA}$	$\Delta\sigma_{dia}^{AB}$	$\Delta\sigma^{A,ring}$	δ_{calcd}	δ_{obsd}[e]	δ_{obsd}[h]
1	*p*-$N(CH_3)_2$[f]	0.9966	4.0569	0.050	0.109	0.054	0.21	0.250	—
2	*p*-NH_2	0.9967	4.0558	0.052	0.099	0.042	0.19	0.223	—
3	*p*-CH_3O[f]	0.9946	4.0520	0.018	0.066	0.028	0.11	0.127	0.124
4	*m*-CH_3	0.9939	4.0436	0.006	−0.007	0.008	0.01	—	0.026
5	*p*-CH_3	0.9944	4.0473	0.014	0.025	0.008	0.05	0.078	0.063
6	H	0.9935	4.0444	0.000	0.000	0.000	0.00	0.000	0.000
7	*p*-C≡CH[f,g]	0.9928	4.0438	−0.011	−0.005	0.001	−0.02	−0.047	—
8	*p*-$COCH_3$[f]	0.9912	4.0383	−0.037	−0.053	0.029	−0.06	−0.129	—
9	*p*-F[f]	0.9918	4.0462	−0.027	0.016	0.012	0.00	0.012	—
10	*m*-Cl	0.9904	4.0392	−0.050	−0.045	0.007	−0.09	—	−0.078
11	*p*-Cl	0.9913	4.0433	−0.035	−0.009	0.007	−0.04	−0.021	−0.036
12	*p*-CN	0.9907	4.0402	−0.045	−0.036	0.025	−0.06	−0.186	—
13	*m*-NO_2	0.9858	4.0356	−0.124	−0.076	0.034	−0.17	—	−0.240
14	*p*-NO_2	0.9858	4.0313	−0.124	−0.114	0.034	−0.21	−0.249	—
15	*p*-CH=CH_2[f]	0.9937	4.0455	0.003	0.010	0.011	0.03	0.012	—

(b) H_β

	Substituent	q^A	q^B	$\Delta\sigma_{dia}^{AA}$	$\Delta\sigma_{dia}^{AB}$	$\Delta\sigma^{A,ring}$	δ_{calcd}	δ_{obsd}[e]	δ_{obsd}[h]
1	*p*-$N(CH_3)_2$[f]	0.9868	4.0569	0.049	0.109	0.117	0.28	0.237	—
2	*p*-NH_2	0.9868	4.0558	0.049	0.099	0.091	0.24	0.227	—
3	*p*-CH_3O[f]	0.9857	4.0520	0.031	0.066	0.061	0.16	0.148	0.149
4	*m*-CH_3	0.9839	4.0436	0.002	−0.007	0.017	0.01	—	0.021
5	*p*-CH_3	0.9845	4.0472	0.011	0.025	0.017	0.05	0.073	0.060
6	H	0.9838	4.0444	0.000	0.000	0.000	0.00	0.000	0.000
7	*p*-C≡CH[f,g]	0.9837	4.0438	−0.002	−0.005	0.001	−0.01	−0.013	—
8	*p*-$COCH_3$[f]	0.9824	4.0383	−0.023	−0.053	0.063	−0.01	−0.109	—
9	*p*-F[f]	0.9845	4.0462	0.011	0.016	0.025	0.05	0.078	—
10	*m*-Cl	0.9821	4.0392	−0.028	−0.045	0.016	−0.06	—	−0.036
11	*p*-Cl	0.9837	4.0433	−0.002	−0.009	0.016	0.01	0.018	0.011
12	*p*-CN	0.9829	4.0400	−0.015	−0.036	0.054	0.00	−0.114	—
13	*m*-NO_2	0.9799	4.0356	−0.063	−0.076	0.073	−0.07	—	−0.200
14	*p*-NO_2	0.9808	4.0313	−0.049	−0.114	0.073	−0.09	−0.177	—
15	*p*-CH=CH_2[f,g]	0.9841	4.0455	0.005	0.010	0.005	0.02	0.020	—

(c) H_γ

	Substituent	q^A	q^B	$\Delta\sigma_{dia}^{AA}$	$\Delta\sigma_{dia}^{AB}$	$\Delta\sigma^{A,ring}$	δ_{calcd}	δ_{obsd}[e]	δ_{obsd}[h]
1	*p*-$N(CH_3)_2$[f]	1.0010	3.9907	0.060	−0.063	0.125	0.12	0.126	—
2	*p*-NH_2	1.0011	3.9912	0.061	−0.059	0.097	0.10	0.135	—
3	*p*-CH_3O[f]	0.9991	3.9930	0.029	−0.043	0.065	0.05	0.068	0.072
4	*m*-CH_3	0.9976	3.9986	0.005	0.006	0.017	0.03	—	0.042
5	*p*-CH_3	0.9983	3.9963	0.016	−0.014	0.017	0.02	0.055	0.048
6	H	0.9973	3.9979	0.000	0.000	0.000	0.00	0.000	0.000
7	*p*-C≡CH[f,g]	0.9974	3.9981	0.002	0.002	0.001	0.01	0.032	—
8	*p*-$COCH_3$[f]	0.9950	4.0001	−0.037	0.027	0.067	0.06	−0.035	—
9	*p*-F[f]	0.9964	3.9956	−0.014	−0.020	0.027	−0.01	0.039	—
10	*m*-Cl	0.9941	3.9997	−0.052	0.016	0.015	−0.02	—	0.045
11	*p*-Cl	0.9957	3.9970	−0.026	−0.008	0.015	−0.02	0.047	0.043
12	*p*-CN	0.9948	3.9993	−0.040	0.012	0.058	0.03	−0.001	—
13	*m*-NO_2	0.9910	4.0003	−0.101	0.021	0.079	0.00	—	−0.034
14	*p*-NO_2	0.9902	4.0029	−0.114	0.043	0.079	0.01	−0.073	—
15	*p*-CH=CH_2[f,g]	0.9976	3.9972	0.005	−0.006	0.012	0.01	0.029	—

(iii) *m*- and *p*-Substituted toluenes.[d]

	Substituent	q^A	q^B	$\Delta\sigma_{dia}^{AA}$	$\Delta\sigma_{dia}^{AB}$	$\Delta\sigma^{A,ring}$	δ_{calcd}	δ_{obsd}[c]
1	*m*-CH_3O	0.9933	4.0206	−0.034	0.017	0.064	0.05	0.030
2	*p*-CH_3O	0.9978	4.0146	0.038	−0.034	0.064	0.07	0.078
3	*m*-CH_3	0.9954	4.0191	0.001	0.005	0.018	0.02	0.053
4	*p*-CH_3	0.9967	4.0169	0.021	−0.014	0.018	0.03	0.057
5	H	0.9954	4.0185	0.000	0.000	0.000	0.00	0.000
6	*m*-F	0.9916	4.0209	−0.061	0.020	0.027	−0.01	−0.022
7	*p*-F	0.9955	4.0156	0.002	−0.025	0.027	0.00	0.022
8	*m*-CN	0.9926	4.0193	−0.045	0.006	0.057	0.02	−0.067
9	*p*-CN	0.9924	4.0199	−0.048	0.011	0.057	0.02	−0.090
10	*m*-NO_2	0.9881	4.0201	−0.117	0.013	0.077	−0.03	−0.150
11	*p*-NO_2	0.9868	4.0233	−0.138	0.040	0.077	−0.02	−0.140

(iv) *m*- and *p*-Substituted benzaldehydes.[b]

	Substituent	q^A	q^B	$\Delta\sigma_{dia}^{AA}$	$\Delta\sigma_{dia}^{AB}$	$\Delta\sigma^{A,ring}$	δ_{calcd}	δ_{obsd}[i]
1	*m*-CH_3	1.0869	3.6735	0.005	0.006	0.019	0.03	0.06
2	*p*-CH_3	1.0879	3.6719	0.020	−0.008	0.019	0.03	0.07
3	*m*-CH_3O	1.0853	3.6756	−0.020	0.023	0.069	0.02	—
4	*p*-CH_3O	1.0893	3.6683	0.041	−0.038	0.069	0.07	0.15
5	H	1.0866	3.6729	0.000	0.000	0.000	0.00	0.00
6	H[d]	1.0495	3.7660	0.000	0.000	0.000	0.00	0.00
7	*m*-Cl[d]	1.0455	3.7668	−0.061	0.007	0.017	−0.04	0.02
8	*p*-Cl[d]	1.0479	3.7467	−0.024	−0.011	0.017	−0.02	0.02
9	*p*-CN[d]	1.0836	3.6744	−0.046	0.014	0.061	0.03	−0.06
10	*m*-NO_2	1.0775	3.6735	−0.138	0.006	0.083	−0.05	−0.14
11	*p*-NO_2	1.0777	3.6771	−0.135	0.036	0.083	−0.02	−0.16

a) All values are relative to the unsubstituted compound. b) All electron densities in substituted phenylacetylenes and benzaldehydes were calculated by the INDO method except for chloroderivatives, for which was used the CNDO/2 method. c) The chemical shifts were measured in carbon tetrachloride. Cited from Ref. 7. d) All electron densities were calculated by the CNDO/2 method. e) The chemical shifts were measured in cyclohexane. Cited from Ref. 12. f) The electron densities in these compounds were cited from the data, calculated by the CNDO/2 method in Ref. 12. g) The σ_π-values necessary to calculate the $\Delta\sigma^{A,ring}$, which have not been established, were obtained from the correlation between π-electron densities on the carbon at *para*-position to substituent in monosubstituted benzenes and the known σ_π-values of the other substituents: σ_π(*p*-C≡CH), −0.005 and σ_π(*p*-CH=CH_2), −0.05. h) The chemical shifts were measured in CCl_4. Cited from Ref. 13. i) The chemical shifts were measured in carbon tetrachloride except for nitro- and cyano-derivatives, those of which are relative to the unsubstituted compound measured in $CDCl_3$. (Ref. 14)

tion show that the application of Eq. (11) is not unreasonable.* In Figs. 2—5, plots of the calculated chemical shifts are shown against the observed shifts. As may clearly be seen in Figs. 2, 3(a), and 3(b), the calculated chemical shifts correctly reproduce the observed shifts in the case of terminal protons, which are three bond lengths removed from the ring carbon, to which the side-chain group is bonded. On the other hand, in protons directly bonded to the carbon atom adjoining the aromatic ring (Figs. 3(c), 4 and 5), the correlation between the calculated and the observed shifts collapses to some degree. This result may be mainly attributed to the inadequacy introduced by ignoring magnetic contributions from atoms other than the bonded carbon. Even in this case, the accuracy of the chemical shifts calculated by Eq. (11) is not inferior to those which have been calculated strictly theoretically.[2,4] Therefore, Eq. (11) provides us with a brief method for predicting the substituent effect on ^1H chemical shifts in *m*- and *p*-substituted aromatic side-chains.

The INDO and CNDO/2 calculations were carried out on FACOM-230 computers at the Computation Centers of Kyoto University and Nagoya University. We wish to express our gratitude to Professor Hiroshi Kato of our college and to Dr. Naoya Nakagawa of the University of Electro-Communications for their helpful instructions and encouragements.

* When Eq. (8) is applied to calculation of the relative chemical shifts (in ppm) for methyl protons in ethyl derivatives CH_3CH_2X, the chemical shifts calculated and observed give respectively the values of 0.01 and −0.28 for X=OCH_3, −0.16 and −0.05 for X=CH_3, −0.29 and −0.70 for X=NO_2. The accuracy of the chemical shifts calculated for ethyl derivatives is not inferior to that of the chemical shifts calculated for monosubstituted ethylenes by Kajimoto *et al.*[2] This result implies the propriety of the application of Eq. (8).

References

1) A. Saika and C. P. Slichter, *J. Chem. Phys.*, **22**, 26, (1954).
2) O. Kajimoto and T. Fueno, *Chem. Lett.*, **1972**, 103.
3) N. F. Ramsey, *Phys. Rev.*, **78**, 699 (1950).
4) J. A. Pople, *J. Chem. Phys.*, **37**, 53 (1962).
5) a) J. S. Waugh and R. W. Fessenden, *J. Amer. Chem. Soc.*, **79**, 846 (1957); b) G. E. Johnson and F. A. Bovey, *J. Chem. Phys.*, **29**, 1012 (1958).
6) H. P. Figeys and R. Flammang, *Mol. Phys.*, **12**, 581 (1967).
7) H. Yamada, Y. Tsuno, and Y. Yukawa, This Bulletin **43**, 1459 (1970).
8) Y. Yukawa, Y. Tsuno, and M. Sawada, *ibid.*, **39**, 2274 (1966).
9) H. Kato, *J. Chem. Phys.*, **52**, 3723 (1960).
10) "Tables of Interatomic Distance and Configuration in Molecules and Ions," Chem. Soc., London, Spec. Publ., No. 11 (1958).
11) J. W. Emsley, J. Feeney, and L. H. Sutcliffe, "High Resolution Nuclear Magnetic Resonance Spectroscopy," Pergamon Press, Oxford, London, Edinburgh, New York, Paris and Frankfurt (1965), p. 595.
12) G. K. Hamer, I. R. Peat, and W. F. Reynolds, *Can. J. Chem.*, **51**, 897 (1972).
13) T. Fueno, O. Kajimoto, K. Izawa, and M. Masago, This Bulletin, **46**, 1418 (1973).
14) R. E. Klinck and J. B. Stothers, *Can. J. Chem.*, **51**, 897 (1972).

Pyridoxal Catalysis in the α,β-Elimination of S-(p-Substituted phenyl)cysteines[1]

Yukito MURAKAMI and Hiroki KONDO

Department of Organic Synthesis, Faculty of Engineering, Kyushu University, Hakozaki, Higashi-ku, Fukuoka 812

(Received February 6, 1974)

The pyridoxal-catalyzed α,β-elimination of S-(p-substituted phenyl)cysteines was studied at 50 °C and μ= 0.10 (KNO_3) in 79% (v/v) aqueous acetonitrile in the presence of organic bases of different strength. The rate increased with an increase in basicity. The kinetic solvent isotope effect (k_{H_2O}/k_{D_2O}) of 1.15 is consistent with the reaction mechanism in which the α-proton abstraction occurs by the direct attack of a base on the proton. The elimination rate was insensitive to a change in the electronic nature of a leaving thiophenol, indicating that the α-proton abstraction can be referred to the rate-determining step. The rate showed a considerable dependence on the water content, as reflected on the activation parameters for reactions in 79% (v/v) aqueous acetonitrile as well as in water. The larger destabilization due to water-solvation at the transition state in the aqueous reaction system seems to cause a lower reactivity relative to the organic solvent system. The catalysis of benzene analogs demonstrated that the hydroxyl group adjacent to the aldehyde in pyridoxal plays a major role in the nonenzymatic α,β-elimination reactions.

Pyridoxal-dependent enzymes catalyze various metabolic reactions of amino acids such as transamination, decarboxylation, and elimination reactions. Pyridoxal alone can go through some of these reactions in cooperation with metal ions.[2] The reaction mechanism for the pyridoxal-metal ion catalysis of the α,β-elimination reaction of O-phosphothreonine was elucidated in a previous paper.[3] Nonenzymatic pyridoxal-catalyzed reactions in the absence of metal ions, on the other hand, have been studied only to a limited extent partly because of the poor reactivity of amino acids in such systems.

Recently, De Marco and Rinaldi reported that pyridoxal phosphate catalyzes the α,β-elimination reactions of some cysteine derivatives, cystathionine and lanthionine, at 38 °C in weakly alkaline media.[4] S-Phenylcysteine itself was deaminated only at high temperature (100 °C) in an alkaline solution in the absence of both pyridoxal and metal ions.[5] However, no mechanistic elucidation was attempted in those studies. We have found that S-(p-substituted phenyl)-cysteines decompose by pyridoxal catalysis under comparatively mild conditions. Since S-substituted cysteines can be the substrates for the tryptophanase catalysis,[6] this work may provide a valuable information for elucidation of the enzymatic mechanism and for devising effective apoenzyme models.

Experimental

Materials. S-(p-Substituted phenyl)cysteines were prepared by the reactions of the corresponding thiophenols with α-acetoamidoacrylic acid and the subsequent acid hydrolysis.[7] 4-Nitrosalicylaldehyde was synthesized according to the procedure given in the literature.[8] Pyridoxal hydrochloride was obtained from Mann Research Laboratories, Inc., New York, U.S.A. and deuterium oxide (>99.7%) was from Carl Roth OHG, Karlsruhe, West Germany. The other commercial reagents were purified before use when necessary.

Kinetic Measurements. The reaction rate was followed by determining pyruvate as the 2,4-dinitrophenylhydrazone. The analytical method was essentially based on that of Metzler and Snell.[9] A solution containing 0.44×10^{-3} M substrate, 1.00×10^{-3} M pyridoxal, 0.10 M potassium nitrate, and a specified amount of a base was placed in stoppered test tubes which were then immersed in a constant temperature bath at 50.0±0.1 °C. The test tubes were taken out one by one at appropriate time intervals. A 5-ml sample from each test tube was transferred to a 25-ml volumetric flask containing 2 ml of 0.1% 2,4-dinitrophenylhydrazine in 2 M hydrochloric acid, and then allowed to stand at room temperature for 30 min. To this mixture was added 10 ml (or less for high concentrations of piperazine and piperidine) of the potassium phosphate–sodium hydroxide buffer, which was prepared by dissolving potassium dihydrogen phosphate (5.4 g), disodium hydrogen phosphate dodecahydrate (21.4 g), and sodium hydroxide (8.0 g) in 500 ml of water. The whole volume was diluted with water to 25 ml. The precipitated pyridoxal hydrazone was filtered off with fluted filter paper. The filtrate was treated with 10 ml of toluene to remove excess 2,4-dinitrophenylhydrazine. A 15-ml sample solution was taken out from the lower aqueous layer and diluted to 25 ml with 2.5 M sodium hydroxide. The absorbance at 530 nm was measured within 30 min on a Hitachi EPS-2 recording spectrophotometer.

Product Analysis. A reaction mixture (*ca.* 100 ml) containing 1.00×10^{-3} M pyridoxal, 0.44×10^{-3} M S-(p-nitrophenyl)cysteine, and 0.05 M morpholine in 79% (v/v) aqueous acetonitrile was warmed at 50 °C for 3 hr. A portion of the mixture was taken out for the analysis of p-nitrothiophenol and its oxidized product, bis(p-nitrophenyl) disulfide. When assayed by the conventional Folin method,[10] the sample solution developed a blue color characteristic of the reduced phosphotungstate complex. The nitrogen gas was bubbled through the rest of the reaction mixture for 30 min after addition of 10% sodium hydroxide (*ca.* 10 ml). Ammonia collected in 0.05 M hydrochloric acid was assayed by standard Nesslerization. Formation of pyruvic acid was detected by means of visible spectroscopy upon converting it into the corresponding 2,4-dinitrophenylhydrazone. In reference to the above survey, the decomposition of S-(p-nitrophenyl)-cysteine yielded three products, p-nitrothiophenol, pyruvic acid, and ammonia.

Results

The α,β-elimination reactions of S-(p-substituted phenyl)cysteines were carried out with an initial sub-

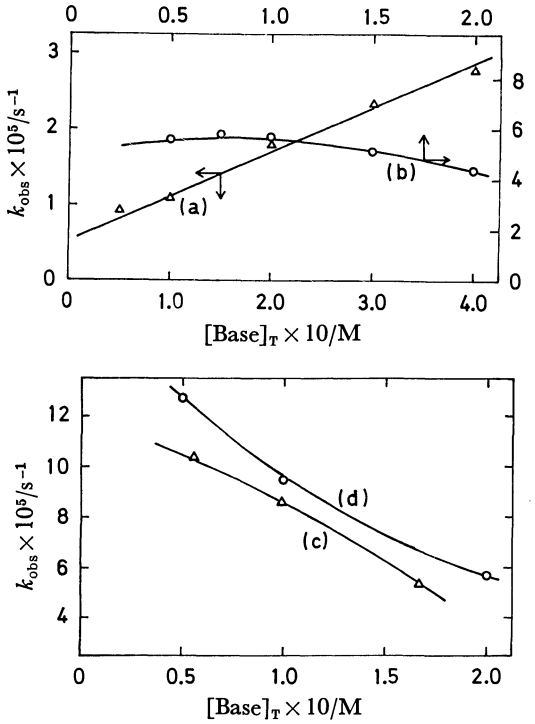

Fig. 1. Correlations between base concentration and apparent first-order rate constant for the pyridoxal-catalyzed α,β-elimination of *S*-(*p*-nitrophenyl)cysteine at 50 °C and $\mu=0.10$ (KNO_3) in 79% (v/v) acetonitrile with the following organic bases: (a), imidazole; (b), morpholine; (c), piperazine; (d), piperidine. Total initial concentrations: substrate, 0.44×10^{-3} M; pyridoxal, 1.00×10^{-3} M.

strate concentration of 0.44×10^{-3} M along with the presence of 1.00×10^{-3} M pyridoxal and a specified amount of organic bases in aqueous acetonitrile. Each reaction rate followed first-order kinetics with respect to the total concentration of unreacted substrate. The correlations between the apparent first-order rate constant and the total base concentration are shown in Fig. 1, *S*-(*p*-nitrophenyl)cysteine being adopted as a substrate. The rate increases as the imidazole concentration increases, but is insensitive to the change of morpholine concentration in the concentration range examined. Increase in either piperazine or piperidine concentration results in the rate decrease. Since the substrates underwent no decomposition in the absence of pyridoxal, the reaction was truly pyridoxal-catalyzed. The product analysis (see Experimental) provides an evidence for the α,β-elimination process.

Rate constants for the pyridoxal-catalyzed elimination of *S*-(*p*-substituted phenyl)cysteines in 79% (v/v) acetonitrile in the presence of 0.10 M morpholine were plotted against Hammett σ-values for the *p*-substituents of the leaving thiophenols (Fig. 2); the slope being 0.17. This small value of the reaction constant implies that the β-elimination is hardly affected by the electronic nature of the leaving group.

The apparent first-order rate constant for the pyridoxal-catalyzed elimination of *S*-(*p*-nitrophenyl)cysteine in the presence of 0.10 M morpholine in 79% (v/v) aqueous acetonitrile was 5.67×10^{-5} s^{-1} and the corresponding value in acetonitrile–deuterium oxide (79:21 by volume) was 4.93×10^{-5} s^{-1}; the solvent isotope effect (k_{H_2O}/k_{D_2O}) is 1.15.

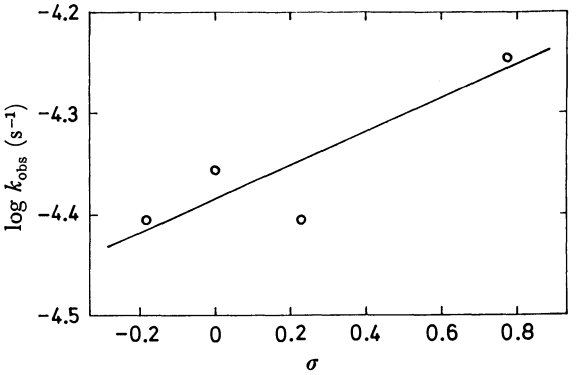

Fig. 2. Hammett plot for the pyridoxal-catalyzed α,β-elimination of *S*-(*p*-substituted phenyl)cysteines at 50 °C and $\mu=0.10$ (KNO_3) in 79% (v/v) acetonitrile with the total initial concentrations: substrate, 0.44×10^{-3} M; pyridoxal, 1.00×10^{-3} M; morpholine, 0.10 M.

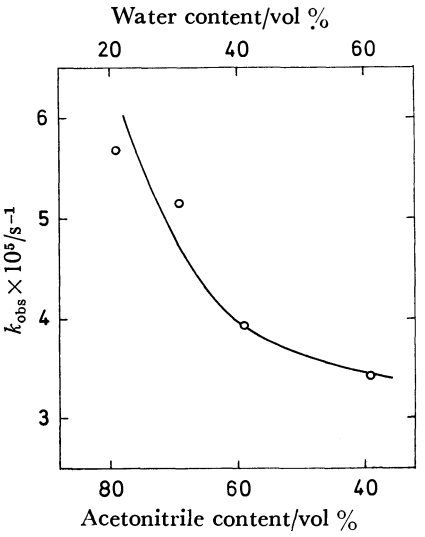

Fig. 3. Correlation between water content and reaction rate for the pyridoxal-catalyzed α,β-elimination of *S*-(*p*-nitrophenyl)cysteine at 50 °C and $\mu=0.10$ (KNO_3) with the total initial concentrations: substrate, 0.44×10^{-3} M; pyridoxal, 1.00×10^{-3} M; morpholine, 0.10 M.

The correlation between elimination rate of *S*-(*p*-nitrophenyl)cysteine and solvent composition was also examined (Fig. 3). The rate decreased considerably with the increase in water content. Activation parameters for the pyridoxal-catalyzed elimination of *S*-(*p*-nitrophenyl)cysteine and *S*-phenylcysteine in 79% (v/v) aqueous acetonitrile as well as in water are listed in Table 1. The activation entropy of large negative value is in line with the bimolecular nature of the reactions.

Catalytic activities of the benzene analogs of pyridoxal were investigated in order to clarify the catalytic roles of the ring-substituents of pyridoxal (Table 2). 4-Nitrosalicylaldehyde showed a catalytic activity to a similar extent. While 4-nitrobenzaldehyde, bearing no *o*-hydroxyl group, was practically inactive, salicylalde-

Table 1. Activation parameters for the pyridoxal-catalyzed α,β-elimination reactions of S-phenyl- and S-(p-nitrophenyl)cysteine in 79% (v/v) acetonitrile and in water[a)]

Substrate	Solvent	E_a kcal mol^{-1}	$\Delta H^{\ddagger}$[b)] kcal mol^{-1}	$\Delta S^{\ddagger}$[b)] e.u.
S-Phenylcysteine	79% (v/v) Acetonitrile	10.2	9.5	−50
S-(p-Nitrophenyl)-cysteine	79% (v/v) Acetonitrile	9.9	9.3	−49
S-(p-Nitrophenyl)-cysteine	Water	13.2	12.5	−41

a) Reactions were carried out at 40, 50, and 60 °C, and μ=0.10 (KNO_3) in the presence of 0.10 M morpholine. b) Values at 50 °C.

Table 2. Catalytic activities of pyridoxal and its benzene analogs in α,β-elimination of S-(p-nitrophenyl)cysteine at 50 °C and μ=0.10 (KNO_3) in 79% (v/v) aqueous acetonitrile[a)]

Catalyst	Pyridoxal	4-Nitro-salicyl-aldehyde	4-Nitrobenz-aldehyde	Salicyl-aldehyde
$k_{obs}\times10^5$/s^{-1}	5.67	5.92	~0	~0.8[b)]

a) Initial total concentrations: substrate, 0.44×10^{-3} M; catalyst, 1.00×10^{-3} M; morpholine, 0.10 M. b) Since the rate showed positive deviation from the first-order plot, the rate constant was estimated from the initial portion of the reaction.

hyde, lacking an electron-withdrawing nitro group, showed some catalytic effect.

Discussion

Reaction Mechanism. The pyridoxal-dependent enzymes may involve various functional groups of nucleophilic and base character in their apoenzyme moieties in a manner as approved for proteinases. The catalytic activity of the latter is provided by the concerted actions of those functional groups at their active sites. In the present study, the catalytic effect of some organic bases of different base-strength was examined in the pyridoxal-catalyzed elimination reaction in connection with the catalytic nature of base moieties which are planted in an apoenzyme skeleton. The rate constants are plotted against the pK_a of the conjugate acids of organic bases obtained in water (Fig. 4), the base concentration for the reaction being maintained at 0.10 M. The rate increases as the basicity of the organic bases rises from imidazole to morpholine, but a leveling-off trend is observed beyond p$K_a\cong9$, *i.e.*, for piperazine and piperidine. The Schiff base formed between pyridoxal and an amino acid can be present in two forms in an alkaline solution, the protonated species (**1**) and the deprotonated one (**2**)

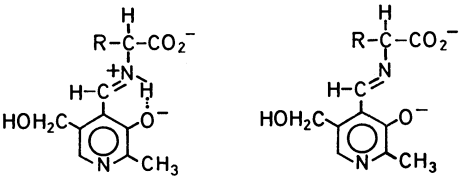

1 2

at the azomethine nitrogen. The former species pyridoxylidenevaline absorbs at 414 nm and the latter at 367 nm in aqueous media.[11)] The corresponding absorption maxima for the same Schiff base in methanol are 418 and 373 nm, respectively.[12)] The pK_a for these protonated aldimines is *ca.* 10 in aqueous phase.[3)] The visible spectra for solutions containing 1.00×10^{-3} M pyridoxal, 1.00×10^{-3} M phenylalanine (pseudo-substrate), and 0.10 M organic base showed λ_{max} (in 79% (v/v) CH_3CN) at 423 nm with imidazole and morpholine, at 382 nm with piperidine, and at the intermediate region with piperazine. This blue shift on going from weak to strong in basicity can be attributed to the deprotonation from the azomethine nitrogen. The deprotonated form can give out a weaker electron-withdrawing effect at the α-carbon, which results in the reduction of reactivity of the amino acids. Thus, the nonlinear Brønsted correlation (Fig. 4) can be interpreted in terms of these protonation-deprotonation equilibria.

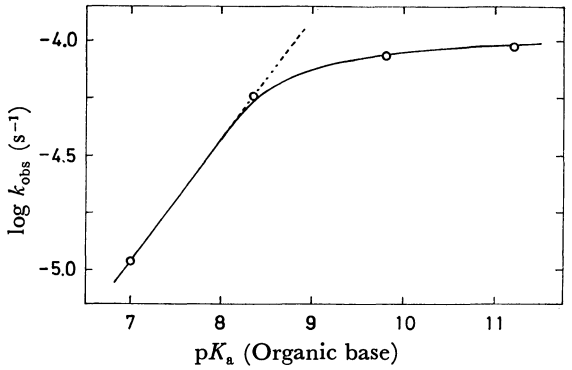

Fig. 4. Brønsted plot for the pyridoxal-catalyzed α,β-elimination of S-(p-nitrophenyl)cysteine at 50 °C and μ=0.10 (KNO_3) in 79% (v/v) acetonitrile with the initial total concentrations: substrate, 0.44×10^{-3} M; pyridoxal, 1.00×10^{-3} M; organic base, 0.10 M. pK_a-Values in aqueous phase have been adopted for organic bases.

The bimolecular attack by an organic base, which can be referred to the α-proton abstraction in the rate-determining step, is reflected on the activation entropy by a large negative value. The problem remains as to whether the α-proton abstraction occurs by the direct attack of a base on the proton or in the presence of a water molecule between them. The small solvent isotope effect (k_{H_2O}/k_{D_2O}) seems to support the former mechanism.

The reaction rate is insensitive to the electronic nature of a leaving thiophenol as can be seen from the Hammett plot (Fig. 2). If the C–S bond fission were to occur in the rate-determining step through either E1 or E1CB mechanism, a larger dependence on the substituent constant would be expected. A comparatively small activation enthalpy also suggests the C–H bond cleavage in the rate-determining step.

On the basis of all the evidences given above, the

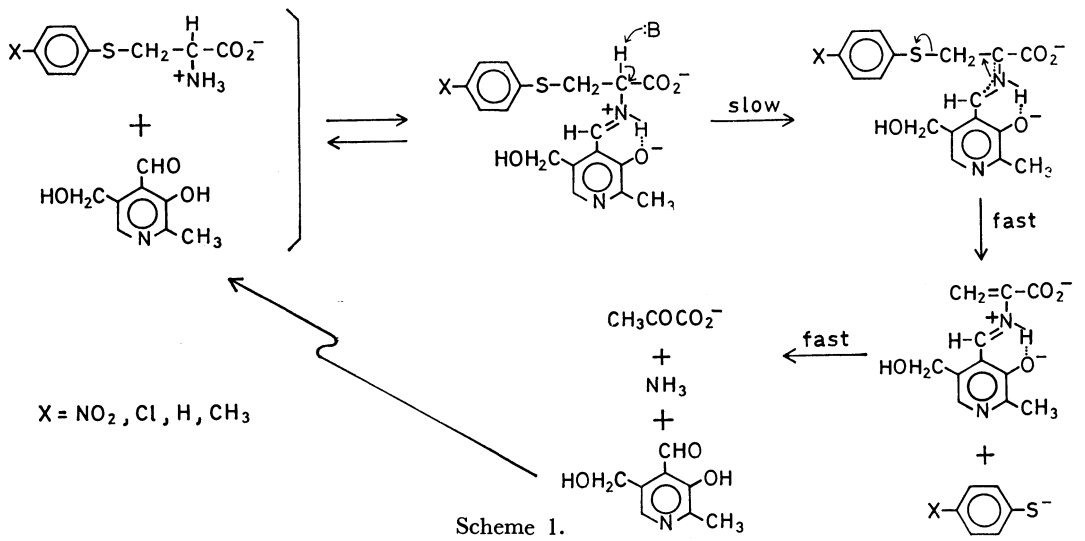

Scheme 1.

most plausible mechanism for the present reaction is as shown in Scheme 1. The Schiff base formation between substrate and pyridoxal occurs in the initial stage as the pre-equilibrium step[3,11] prior to the rate-determining α-proton liberation.

Solvent Effect. In order to observe various reactions of amino acids proceeding to a detectable extent in the absence of any apoenzyme moiety, pyridoxal catalysis requires either an elevated temperature or the presence of metal ions. In organic solvent system, however, these reactions often proceed readily at room temperature even in the absence of metal ions; the transamination from pyridoxamine to α-keto acids and the reverse reaction occurs readily in absolute ethanol without any metal ion.[13] The nonenzymatic reaction between pyridoxamine and α-ketoisovalerate was found to proceed quite smoothly at room temperature in methanol through the cooperation of zinc(II) ion.[14] Our results (Fig. 3) indicate that the α,β-elimination rate depends on the water content of the solvent system in accord with the related reactions of amino acids. The Schiff base formation is generally much favored in organic solvents. However, the rate enhancement due to the solvents cannot be explained in terms of this effect alone, since the Schiff base formation has nothing to do with the rate-determining step.

Alternatively, solvation effects seem to be responsible for the rate acceleration in organic solvents, as evident from the activation parameters listed in Table 1. Since the reaction seems to proceed through the less polar transition state (Scheme 1) relative to the initial one due to the delocalization of a positive charge as represented by Eq. (1), the reaction center may be solvated by organic solvent molecules more effectively and water molecules would be less tightly bound to the center.

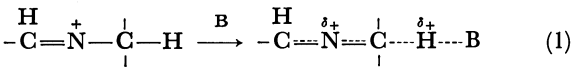

(1)

Stabilization of the transition state becomes much greater in 79% (v/v) acetonitrile than in the aqueous system. Contrarily, the polar initial state, due to a positive charge located at the Schiff base nitrogen, can be solvated by water molecules more tightly than by organic solvent molecules. Thus, the initial state would be more stabilized in water than in 79% (v/v) acetonitrile. These effects give rise to a larger activation enthalpy for the aqueous reaction system. This solvation effect is also reflected on the activation entropy values. These features would be more drastic in a higher acetonitrile content, but the lower solubility of the substrates kept us from carrying out the experiments.

Catalysis by Pyridoxal Analogs. In order to clarify the catalytic roles of various functional groups placed in pyridoxal, the catalytic activities of its benzene analogs were examined as listed in Table 2. As a result, the presence of the hydroxyl group *ortho* to the aldehyde is of primary importance for yielding catalytic activity, even though an additional electron-withdrawing group, the nitro group or the pyridyl nitrogen, accelerated the reaction rate to a greater extent. For the noenzymatic transamination reaction between glutamic acid and 3-hydroxypyridine-4-carbaldehyde, Thanassi *et al.* proposed that the general acid catalysis of the hydroxyl group acting on the azomethine bond facilitated the isomerization of this bond.[15] For the present elimination reaction, however, there is no need for such isomerization to be involved and another explanation must be invoked for the role of the hydroxyl group.

The Schiff base formed between pyridoxal and amino acid is known to possess a six-membered ring structure by a strong intramolecular hydrogen bonding (Scheme 1). Thus, the stability of the Schiff base may be greatly reduced by the deprotonation from the azomethine nitrogen or the absence of a hydroxyl group. The deprotonation at the azomethine nitrogen gives out a reduced electron-withdrawing effect on the α-carbon. In conclusion, the hydroxyl group adjacent to the aldehyde in pyridoxal plays an indispensable role in the nonenzymatic α,β-elimination of amino acids.

References

1) Contribution No. 321 from this Department.

2) a) D. E. Metzler, M. Ikawa, and E. E. Snell, *J. Amer. Chem. Soc.*, **76**, 648 (1954); b) T. C. Bruice and S. J. Benkovic,

"Bioorganic Mechanisms," Vol. II, W. A. Benjamin, Inc., New York (1966), Chap. 8.
3) Y. Murakami, H. Kondo, and A. E. Martell, *J. Amer. Chem. Soc.*, **95**, 7138 (1973).
4) C. De Marco and A. Rinaldi, *Arch. Biochem. Biophys.*, **140**, 19 (1970).
5) H. T. Clarke and J. M. Inouye, *J. Biol. Chem.*, **94**, 541 (1931).
6) Y. Morino and E. E. Snell, *ibid.*, **242**, 2800 (1967).
7) a) H. Behringer and E. Fackler, *Ann. Chem.*, **564**, 73 (1949); b) L. Goodman, L. O. Ross, and B. R. Baker, *J. Org. Chem.*, **23**, 1251 (1958).
8) T. Tsumaki, H. Ohta, and T. Tsutsumi, *Nippon Kagaku Zasshi*, **74**, 859 (1953).
9) D. E. Metzler and E. E. Snell, *J. Amer. Chem. Soc.*, **74**, 979 (1952).
10) H. Hirai, "Colorimetric Methods for Biochemical Experiments," Vol. 3 (in Japanese), ed. by T. Sekine *et al.*, Nankodo, Ltd., Tokyo (1961), p. 40; the analytical method by Folin and Marenzi (*J. Biol. Chem.*, **83**, 109 (1929)) has been somewhat modified in this literature.
11) D. E. Metzler, *J. Amer. Chem. Soc.*, **79**, 485 (1957).
12) Y. Matsushima and A. E. Martell, *ibid.*, **89**, 1322 (1967).
13) Y. Matsuo, *ibid.*, **79**, 2016 (1957).
14) Y. Matsushima and A. E. Martell, *ibid.*, **89**, 1331 (1967).
15) J. W. Thanassi, A. R. Butler, and T. C. Bruice, *Biochemistry*, **4**, 1463 (1965).

The Cd 5 $^3P_0$ State in the Cadmium-photosensitized Reaction and the Quenching of the Resonance Radiation at 326.1 nm by Nitrogen, Carbon Monoxide, and Carbon Dioxide

Shunzo YAMAMOTO, Motoaki TAKAOKA, Shigeru TSUNASHIMA, and Shin SATO

Department of Applied Physics, Tokyo Institute of Technology, Ookayama, Meguro-ku, Tokyo 152

(Received July 8, 1974)

The emission of the resonance line at 326.1 nm (5 $^3P_1 \rightarrow 5\ ^1S_0$) and the absorptions of Cd($^3P_0$) at 340.4 nm (5 $^3D_1 \leftarrow 5\ ^3P_0$) and of Cd($^3P_1$) at 346.6 nm (5 $^3D_2 \leftarrow 5\ ^3P_1$) have been measured as functions of the pressure of foreign gases at 250 °C. At the pressures higher than 1 Torr of any rare gas, an equilibrium was established between 5 $^3P_1$ and 5 $^3P_0$ states. The efficiency of nitrogen in producing the 5 $^3P_0$ state from the 5 $^3P_1$ state was found to be more than 10^3 times those of rare gases. The quenching efficiencies of nitrogen, carbon monoxide, and carbon dioxide for the resonance radiation at 326.1 nm were also measured by using argon as the diluent gas. The half-quenching pressures obtained were 73 ± 3, 0.47 ± 0.01, and 0.096 ± 0.003 Torr for nitrogen, carbon monoxide, and carbon dioxide respectively.

The energy state, 5 $^3P_0$, of cadmium is 86.1 kcal mol^{-1} above the ground state, Cd 5 $^1S_0$, and 1.6 kcal mol^{-1} below the Cd 5 $^3P_1$ state. Recently, Breckenridge and Callear observed the formation of the Cd($^3P_0$) state in the system of cadmium vapor and methane illuminated by the resonance line at 228.8 nm (5 $^1P_1 \rightarrow 5\ ^1S_0$).[1] In the 326.1 nm cadmium-photosensitized reactions, however, the participation of the 5 $^3P_0$ state has not yet been ascertained, although, by analogy with the Hg–NH_3 system, Morten *et al.* assumed the 5 $^3P_0$ state as the precursor of the emitting species in the cadmium-photosensitized emission of ammonia.[2] On the other hand, the 6 $^3P_0$ state of mercury atoms was studied by several groups,[3–7] and now it is well established that the Hg 6 $^3P_0$ state plays an important role in the mercury photosensitization.

In a previous short communication,[8] we reported that the 5 $^3P_0$ state of cadmium atoms produced in the cadmium-photosensitized reactions in argon, nitrogen, and ammonia can be observed by the absorptions at the wavelengths of 340.4 nm (5 $^3D_1 \leftarrow 5\ ^3P_0$) and 467.8 nm (6 $^3S_1 \leftarrow 5\ ^3P_0$).

The present paper will report the details of the absorption measurement of Cd($^3P_0$) and Cd($^3P_1$) as well as the quenching of the resonance radiation at 326.1 nm (5 $^3P_1 \rightarrow 5\ ^1S_0$) by nitrogen, carbon monoxide, and carbon dioxide.

Experimental

The apparatus used in the present experiment was previously outlined.[8] The reaction cell was a quartz tube, 2 cm in diameter and 30 cm long, with two flat planes. The exciting resonance lamp was a home-made, U-shaped cadmium lamp made of Pyrex, while the light source for the measurement of the absorption was made of quartz. Both lamps were kept in electric furnaces at 250 ± 1 °C and operated by an alternating current (50 Hz). The intensity from the lamp, therefore, changes with the frequency of 100 Hz. However, since the lifetimes of Cd($^3P_1$) and Cd($^3P_0$) are known to be very short compared with the period of the change in the light intensity,[9] the light intensities observed in the present experiment are regarded as the averages over the period. The vapor pressure of cadmium in the cell was kept constant (3.2×10^{-3} Torr) by maintaining the temperature of the cadmium storage at 240 ± 1 °C in all the photosensitized reactions. The light intensity from the cell was measured by means of a combination of a monochromator (Shimadzu photoelectric spectrophotometer, model QV-50), a 1P28 photomultiplier, and a Ritsu photometer, type 101A, and was recorded by means of a Yokogawa Laboratory recorder, type 3043. The slit of the monochromator was properly opened, so that the observed intensity was one integrated over the spectral line profiles at 326.1, 340.4, and 346.6 nm. The pressure of the gases was measured by a W & T model 62–075 pressure gauge supplied by the Nagano Keiki Co.

The cadmium metal used was high-purity cadmium (99.9999%) manufactured by the Osaka Asahi Metal Co. Pure-grade rare gases (He, Ne, Ar, Kr, and Xe) purchased from the Takachiho Shoji Co. were used after repeated adsorption and desorption on a molecular sieve at the temperature of liquid nitrogen. Pure-grade N_2, CO, and CO_2 were used after they had been treated as previously described.[10]

Since the absorption of the 326.1 nm resonance line with the cadmium vapor at 3.2×10^{-3} Torr is small (the *f*-value of the Cd 326.1 nm line is 0.002,[9] nearly 1/20 of that of the Hg 253.7 nm line), 30% of the absorption occurs in a path length of 1 cm. Therefore, the formation of the Cd($^3P_1$) state in the cell is almost uniform.

Results

Pressure Dependence of the Emission Intensity at 326.1 nm. When the cell containing cadmium vapor was illuminated by means of the exciting lamp, the emission was observed at 326.1 nm. Upon the addition of rare gases, the intensity of the emission increased with the increase in the pressure, as is shown in Fig. 1. Rare gases other than Ne showed almost the same pressure dependence of the intensity. The deviation observed in the case of Ne is probably due to the impurity, which could not be removed by the method described above. When N_2 was added, the intensity increased slightly up to a few Torr and then gradually decreased with the increase in pressure. In the case of CO and CO_2, the intensity decreased rapidly, even in the low-pressure region. The efficiencies of CO and CO_2 in quenching the resonance radiation must be considerably larger than that of N_2.

The Absorption of the 346.6 nm Spectral Line by Cd($^3P_1$).

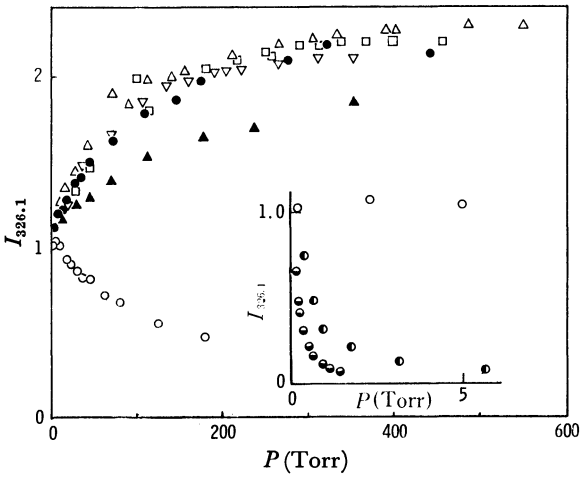

Fig. 1. The intensity of the resonance radiation at 326.1 nm as a function of the pressure of the foreign gas. △: He, ▲: Ne, ●: Ar, □: Kr, ▽: Xe, ○: N_2, ◐: CO, ◒: CO_2.

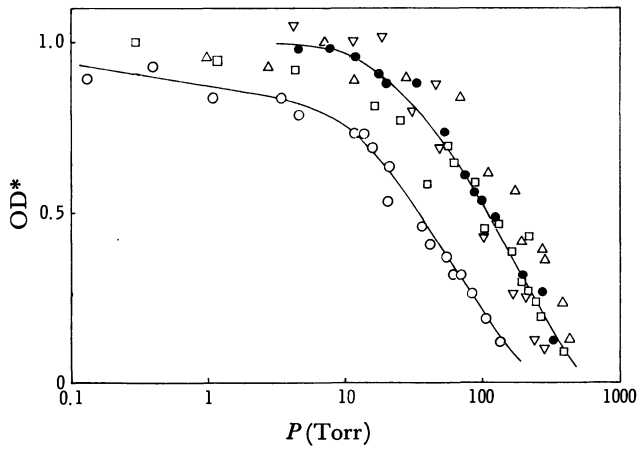

Fig. 2. The relative optical density of Cd($^3P_1$) atoms at 346.6 nm as a function of the pressure of the foreign gas. △: He, ●: Ar, □: Kr, ▽: Xe, ○: N_2.

Figure 2 shows the pressure dependence of the relative optical density at 346.6 nm. For all the gases used, the optical density was constant in the low-pressure region and decreased gradually with the increase in the pressure. The curves for rare gases are in agreement with each other within the limits of experimental error. In the case of N_2, the optical density began to decrease at lower pressures.

The Absorption of the 340.4 nm Spectral Line by Cd($^3P_0$). Figure 3 shows the relative optical density at 340.4 nm as a function of the pressure. All the curves have maxima. Obviously, the efficiency in producing the Cd($^3P_0$) state increases in the order: He<Ar~Kr<Xe<N_2. The pressure dependences of the decrease in optical density in the high-pressure region agree approximately with each other for all the rare gases. In nitrogen, the optical density began to decrease at a pressure lower than that in rare gases. This is similar to the tendency observed in the absorption of the 346.6 nm spectral line by Cd($^3P_1$).

The absorption of the 467.8 nm spectral line by Cd($^3P_0$) was also measured, although the data are not

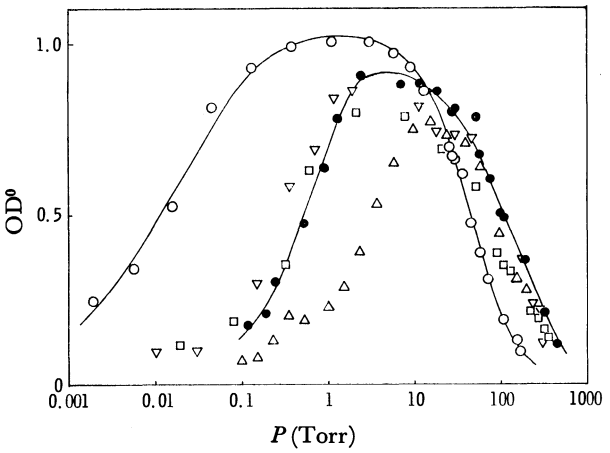

Fig. 3. The relative optical density of Cd($^3P_0$) atoms at 340.4 nm as a function of the pressure of the foreign gas. △: He, ●: Ar, □: Kr, ▽: Xe, ○: N_2.

shown here. The pressure dependence of the relative optical density was almost the same as that obtained with the absorption of the 340.4 nm line.[8] The optical density at 467.8 nm was much smaller than that at 340.4 nm.

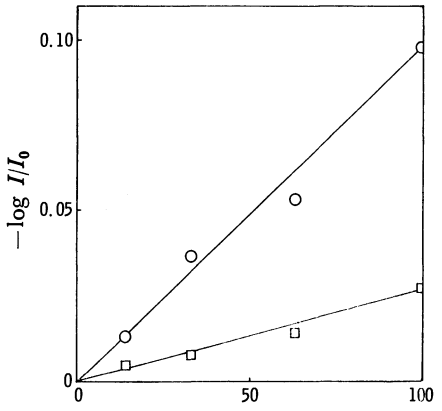

Fig. 4. The optical densities at 340.4 nm (P_{Ar}=18 Torr) (○) and at 346.6 nm (P_{Ar}=25 Torr) (□) as functions of the intensity of the exciting light.

The Lambert-Beer Law. In atomic absorption spectroscopy, it should be checked whether the Lambert-Beer law can be applied or not. In order to investigate this point in the present experiment, we measured the absorptions at 340.4 and 346.6 nm as functions of the intensity of the exciting lamp. The intensity was changed by inserting a screen between the cell and the exciting lamp. The results are shown in Fig. 4. Plots of the optical densities *vs.* the light intensity, to which the concentration of excited atoms should be proportional, give straight lines which pass through the point of origin. These results show that the Lambert-Beer law holds in the present measurements.

$$-\log (I/I_0)_{346.6} = OD^* = \varepsilon^* l[Cd^*] \quad (I)$$

$$-\log (I/I_0)_{340.4} = OD^0 = \varepsilon^0 l[Cd^0] \quad (II)$$

where, ε^* and ε^0 are the apparent extinction coefficients of the Cd($^3P_1$) and Cd($^3P_0$) atoms for the absorption of the spectral lines at 346.6 and 340.4 nm from the light

source for the absorption measurement and where l is the length of the cell.

Pressure Dependence of the Apparent Extinction Coefficient. Both the emission intensity at 326.1 nm and the optical density of the absorption at 346.6 nm are measures of the concentration of $Cd(^3P_1)$ atoms. As was shown above, the optical density at 346.6 nm can be correlated to the concentration of $Cd(^3P_1)$ atoms by Eq. (I). On the other hand, this concentration should be correlated to the emission intensity at 326.1 nm by the following equation:

$$I_{326.1} = \tau^{-1}[Cd^*] \qquad \text{(III)}$$

where τ is the effective lifetime of the $Cd(^3P_1)$ atoms. As is shown in Fig. 2, the optical density of the $Cd(^3P_1)$ atoms decreases at pressures higher than 10 Torr, while, as is shown in Fig. 1, the emission intensity at 326.1 nm does not decrease in this pressure region. This apparent discrepancy must be due to the different pressure dependences of ε^* and τ^{-1}.

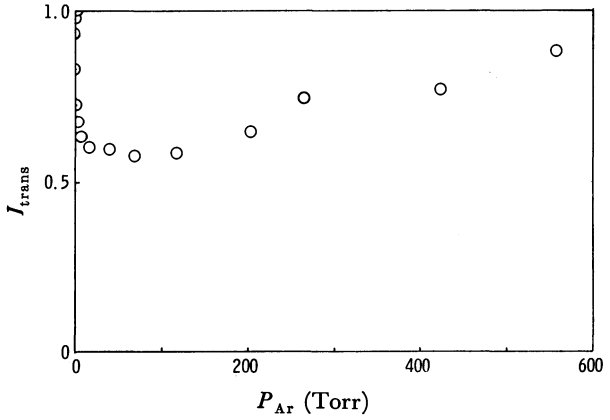

Fig. 5. The intensity of the transmitted light at 326.1 nm as a function of the pressure of argon. The vapor pressure of cadmium is 1.0×10^{-4} Torr (180 °C).

In order to examine the pressure dependence of the apparent extinction coefficient, we measured the intensity of the transmitted light at 326.1 nm from the light source for the absorption measurements at various pressures of argon, while keeping the cadmium vapor pressure constant, 10^{-4} Torr. The results are shown in Fig. 5. Obviously, the intensity of the transmitted light at 326.1 nm decreased initially with the increase in the argon pressure and then gradually increased with the further increase in pressure. The significance of this experiment will be discussed later.

In practice, we wanted to measure the pressure dependence of ε^* and ε^0. However, we could not do so because we have no proper method of producing constant concentrations of Cd* and Cd^0 by changing the argon pressure.

As will be shown later on the basis of the kinetic analysis, τ is estimated to be independent of the examined pressures of rare gases. Consequently, it may be concluded that the apparent discrepancy described above is due to the pressure dependence of the apparent extinction coefficient, ε^*.

Quenching of the Resonance Radiation at 326.1 nm by N_2, CO, and CO_2. As was mentioned above, the absorption intensity at 326.1 nm is dependent upon the pressure of foreign gases. Therefore, the curves obtained with N_2, CO, and CO_2 in Fig. 1 cannot be pure quenching curves for the $Cd(^3P_1)$ atoms. In order to minimize the effect of the pressure broadening, quenching gases were diluted with argon and the total pressure was kept constant. The experimental data thus obtained are listed in Table 1, from which we can estimate the quenching efficiencies of N_2, CO, and CO_2 quantitatively.

TABLE 1. THE INTENSITY OF THE RESONANCE RADIATION AS A FUNCTION OF THE PRESSURE OF N_2, CO OR CO_2. THE TOTAL PRESSURE IS CONTROLLED BY ADDING ARGON

Nitrogen

Total pressure (Torr)							
210		140		94		63	
N_2	I	N_2	I	N_2	I	N_2	I
0	2.05	0	1.88	0	1.73	0	1.58
2.7	1.99	3.5	1.76	2.3	1.71	1.5	1.53
5.2	1.92	6.9	1.65	4.6	1.62	3.1	1.45
10.4	1.92	10.4	1.61	6.9	1.61	4.6	1.45
15.6	1.69	17.4	1.46	11.6	1.53	7.7	1.39
26.0	1.50	26.1	1.38	17.4	1.43	15.6	1.30
39.2	1.35	34.9	1.24	23.4	1.32	23.1	1.27
52.5	1.19	51.7	1.10	34.7	1.21	32.0	1.15
77.8	1.09	71.4	1.01	48.0	1.16	39.5	1.10
106.9	0.87	88.3	0.90	59.2	1.06	46.9	1.00
131.9	0.80	104.8	0.81	70.4	0.97		
156.4	0.70						

Carbon monoxide

Total pressure (Torr)					
80		48		28.5	
CO	I	CO	I	CO	I
0	1.67	0	1.50	0	1.37
0.10	1.29	0.062	1.26	0.073	1.15
0.20	1.20	0.12	1.15	0.10	1.04
0.29	1.07	0.17	1.08	0.20	0.90
0.55	0.82	0.33	0.90	0.39	0.75
1.10	0.53	0.66	0.67	0.55	0.63
1.54	0.46	0.91	0.50	0.94	0.45
2.66	0.26	1.58	0.35		

Carbon dioxide

Total pressure (Torr)					
80		48		28.5	
CO_2	I	CO_2	I	CO_2	I
0	1.67	0	1.50	0	1.37
0.008	1.47	0.005	1.44	0.012	1.18
0.033	1.16	0.020	1.24	0.049	0.91
0.14	0.71	0.083	0.84	0.082	0.68
0.23	0.44	0.14	0.50	0.21	0.48
0.59	0.27	0.35	0.37	0.35	0.30
0.98	0.15	0.58	0.22		

Discussion

The Pressure Broadening of the Absorption Line. As Fig. 5 shows, the intensity of the transmitted light at 326.1 nm decreased with the increase in argon pressure up to 100 Torr. This is probably due to the pressure broadening of the absorption line of the cadmium atoms in the ground state. This reasoning is also applicable to the increase in the emission at 326.1 nm with the increase in the pressure of rare gases, which is shown in Fig. 1. However, the increase in the emission intensity with the increase in the pressure is much slower than the decrease in the transmitted light shown in Fig. 5. This is probably because the spectral line from the exciting lamp is much broader than that from the light source for the absorption measurement.

Upon the further increase in argon pressure over 100 Torr, the absorption line of the cadmium atoms in the ground state will be broadened more than the spectral line from the light source. Consequently, the apparent extinction coefficient will be reduced. This explanation matches the observed increase in the intensity of the transmitted light at 326.1 nm shown in Fig. 5. On the other hand, the emission intensity, which is shown in Fig. 1, does not suffer from such an effect at the pressures examined, because the spectral line from the exciting lamp is much broader than that from the light source for the absorption measurements.

In Figs. 2 and 3, we show the pressure dependences of the absorption of Cd($^3P_1$) and Cd($^3P_0$) atoms. The decrease in the optical densities at the higher pressures of rare gases may be explained by the reasoning presented above. That is, the quenching efficiency of rare gases is negligibly small and the decrease in the optical densities over 10 Torr of rare gases is due to the decrease in the apparent extinction coefficients, ε^* and ε^0. In the case of N_2, however, both the pressure broadening of the absorption line and the quenching of the excited atoms have to be considered.

Formation and Quenching of Cd($^3P_0$) Atoms. In order to make a kinetic analysis of the steady-state processes occurring in a cell under a constant illumination, the following reactions are considered:

(1)	$Cd(^1S_0) + h\nu(326.1) \longrightarrow Cd^*(^3P_1)$	I_a
(2)	$Cd^* \longrightarrow Cd + h\nu$	k_0
(3)	$Cd^* + M \longrightarrow Cd + M$	k_1
(4)	$Cd^* + M \longrightarrow Cd^0(^3P_0) + M$	k_2
(5)	$Cd^0 \longrightarrow Cd$ (on wall)	k_3
(6)	$Cd^0 + M \longrightarrow Cd + M$	k_4
(7)	$Cd^0 + M \longrightarrow Cd^* + M$	k_5

where M stands for rare gases, N_2, CO, or CO_2. If Cd is replaced by Hg, this reaction mechanism is the same as that proposed by Kimbell and LeRoy[3] for the case of the Hg–N_2 system except for the emission from the $^3P_0$ state. Such an emission could not be observed in the present system. Reaction (5) is a diffusion-controlled reaction, and its rate may be expressed as $k_3[Cd^0]/[M]$. Therefore, the steady-state-treatment of Reactions (1)—(7) gives the following relation:

$$\frac{I_a}{[Cd^0]} = \frac{A}{[M]^2} + \frac{B}{[M]} + C + D[M] \qquad \text{(IV)}$$

where A, B, C, and D are constants depending on the foreign gas. For rare gases, we can ignore Reactions (3) and (6), as has been discussed in the previous section. Therefore,

$$A = k_0k_3/k_2,\ B = k_3,\ C = k_0k_5/k_2 \text{ and } D = 0,$$

while, for nitrogen,

$$A = k_0k_3'/k_2',\ B = k_3'(k_1'+k_2')/k_2',$$
$$C = k_0(k_4'+k_5')/k_2' \text{ and } D = (k_1'k_4'+k_2'k_4'+k_1'k_5')/k_2'.$$

where the prime indicates the value in nitrogen. By using Eq. (II), the left-hand side of Eq. (IV) can be expressed as follows:

$$\frac{I_a}{[Cd^0]} = \frac{I_a}{OD^0}\varepsilon^0 l \qquad \text{(V)}$$

Since the pressure dependence of the apparent value of ε^0 can be estimated from Fig. 3, as has been discussed in the previous section, we can calculate the relative values of A, B, C, and D by the method given in the Appendix. The results are tabulated in Table 2. This procedure is the same as that used by Kimbell and LeRoy for the analysis of the Hg($^3P_0$) atoms.[3] The solid lines in Fig. 6 were drawn by substituting the values in Table 2 into Eq. (IV).

Table 2. The constants involved in Eq. (IV)

Gas	A (Torr^2 s^{-1})	B (Torr s^{-1})	C (s^{-1})	D (Torr^{-1} s^{-1})
He	0.030	4.00	0.98	0
Ar	0.015	0.58	0.98	0
Kr	0.015	0.58	0.98	0
Xe	0.005	0.33	0.98	0
N_2	8×10^{-6}	0.008	1.03	0.033

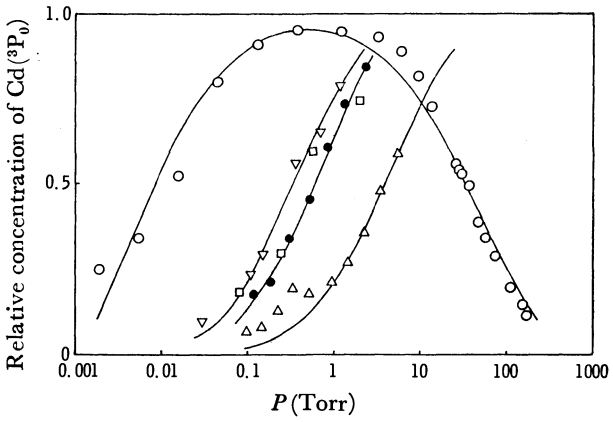

Fig. 6. The relative concentration of Cd($^3P_0$) atoms as a function of the pressure of the foreign gas. —: He, ●: Ar, □: Kr, ▽: Xe, ○: N_2. Solid lines were obtained by substituting the values in Table 2 into Eq. (IV).

From the values of A, it is found that the values of k_2 (or k_2') increase in the order: He<Ar~Kr<Xe≪N_2. This order corresponds to the efficiency of the formation of Cd($^3P_0$) atoms. A comparison suggests that the efficiency of N_2 in producing Cd($^3P_0$) is more than 10^3 times those of rare gases. The value of B for rare

gases is equal to k_3, which is directly proportional to the diffusion coefficient of $Cd(^3P_0)$ atoms in rare gases. The order of the k_3 values with respect to the kind of rare gases seems to be reasonable, because the diffusion coefficient in a lighter gas may be larger than that in a heavier gas. The values of C for all the gases examined are approximately equal. This constancy should hold for rare gases, because $C=k_0k_5/k_2$ and the ratio of k_5/k_2 should be equal to the equilibrium constant between [Cd⁰] and [Cd*]. In the case of nitrogen, this equilibrium constant should be expressed by k_5'/k_2'. The constancy of C, therefore, suggests that k_4' is much smaller than k_5'.

The equilibrium between [Cd⁰] and [Cd*] at 250 °C can be calculated as follows:

$$[Cd^0]/[Cd^*] = \frac{1}{3}\exp(1.6/RT) = 1.54$$

The ratio of the optical densities of Cd⁰ and Cd* atoms is 2.5±0.4 at pressures higher than 10 Torr. The difference in number is due to the difference in extinction coefficient. Below 10 Torr, Reaction (5) seems to play a part in the reaction mechanism.

Quenching of the Resonance Radiation by N_2, CO, and CO_2. When only argon is present in the cell, Reactions (3) and (6) may be ignored; if the pressure is higher than 10 Torr, Reaction (5) may also be ignored. Therefore, the following equation should hold in the steady state:

$$I^{Ar}_{326.1} = k_0[Cd^*] = I_a \qquad (V)$$

Here, $I^{Ar}_{326.1}$ is the intensity of the emission at 326.1 nm. When nitrogen is a substrate, the steady-state-treatment gives the following relation:

$$I^{N_2}_{326.1} = \frac{I_a}{1+\left\{\frac{k_1'}{k_0}+\frac{k_2'k_4'}{k_0(k_4'+k_5')}\right\}[N_2]} \qquad (VI)$$

By substituting Eq. (V) into Eq. (VI) and by using the $k_5' \gg k_4'$ relation, we can obtain the following equation:

$$\frac{I^{Ar}_{326.1}}{I^{N_2}_{326.1}} = 1 + \frac{1}{k_0}\left(k_1'+\frac{k_2'k_4'}{k_5'}\right)[N_2] \qquad (VII)$$

This equation can be used to compare the emission intensity at the same pressures of Ar and N_2.

Similarly, the following equations can be obtained for the absorptions at 346.6 and 340.4 nm:

$$\frac{OD^{*Ar}}{OD^{*N_2}} = 1 + \frac{1}{k_0}\left(k_1'+\frac{k_2'k_4'}{k_5'}\right)[N_2] \qquad (VIII)$$

$$\frac{OD^{0Ar}}{OD^{0N_2}} = 1 + \frac{1}{k_0}\left(k_1'+\frac{k_2'k_4'}{k_5'}\right)[N_2] \qquad (IX)$$

Here, the superscripts Ar and N_2 designate that these values were obtained in Ar and N_2 respectively.

Figure 7 shows the experimental plots for Eqs. (VII), (VIII), and (IX). The straight line obtained shows the validity of the three equations. The half-quenching pressure, which corresponds to the reciprocal of the slope, was calculated to be about 60 Torr.

When a quenching gas is diluted with argon and the total pressure is kept constant, the following Stern-Volmer expression can be obtained:

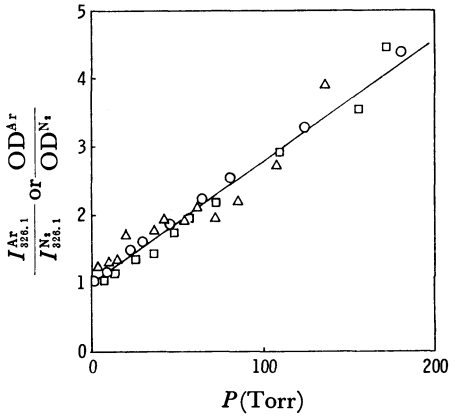

Fig. 7. Experimental plots for Eq. (VII) (○), Eq. (VIII) (△) and Eq. (IX) (□).

$$\frac{I^0_{326.1}}{I_{326.1}} = 1 + \frac{k_1'}{k_0}[N_2] + \frac{k_4'[N_2]}{k_0}\,\frac{k_2[Ar]+k_2'[N_2]}{k_4'[N_2]+k_5[Ar]+k_5'[N_2]} \qquad (X)$$

Here, $I^0_{326.1}$ and $I_{326.1}$ are the emission intensities at 326.1 nm in the absence and in the presence of a quencher, N_2. Since $k_5' \gg k_4'$ and $k_2'/k_5' = k_2/k_5$, Eq. (X) can be reduced to the form:

$$\frac{I^0_{326.1}}{I_{326.1}} = 1 + \frac{1}{k_0}\left(k_1'+\frac{k_2'k_4'}{k_5'}\right)[N_2] \qquad (XI)$$

The right-hand side of this equation is exactly the same as those of Eqs. (VII), (VIII), and (IX). The experimental plots obtained with N_2 at various total pressures are shown in Fig. 8, together with the plots obtained by using CO and CO_2 as the quencher. All the plots for each quencher lie on each straight line, and no dependence on the total pressure can be seen. This result strongly suggests that k_0 is independent of the pressure in the range examined. In other words, the lifetime of the $Cd(^3P_1)$ atoms, τ, is independent of the pressure of the foreign gas in the pressure range examined.

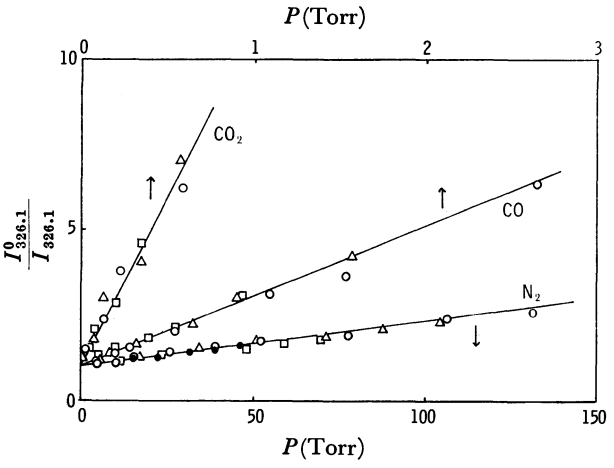

Fig. 8. Stern-Volmer plots for the quenching of the resonance radiation at 326.1 nm by N_2, CO and CO_2. The quenching gas is diluted with argon. For N_2, the total pressures are 210 (○), 140 (△), 94 (□), and 63 (●) in Torr. For CO and CO_2, the total pressures are 80 (○), 48 (△), and 28.5 (□) in Torr.

Table 3. Half-quenching pressures for the resonance radiation at 326.1 nm (Torr)

Quencher	This work	Ref. 10
N_2	73±3	220±3
CO	0.47±0.01	0.34±0.09
CO_2	0.096±0.003	0.06±0.03

Table 3 summarizes the half-quenching pressures calculated from the linear plots in Fig. 8. The value obtained for nitrogen is in fair agreement with that obtained from the plots in Fig. 7. The small discrepancy may be due to the complete neglect of k_4' in relation to k_5' in Eqs. (VII), (VIII), and (IX). The third column in Table 3 shows the half-quenching pressures reported in the previous paper.[10] These values were obtained by paying no attention to the pressure broadening of the absorption lines. Therefore, the values obtained in the present paper should be more reliable.

The authors are indebted to Dr. Soji Tsuchiya of the University of Tokyo for his valuable discussions.

Appendix

By substituting Eq. (V) into Eq. (IV), we can obtain the following equation:

$$\frac{I_a}{OD^0}\varepsilon^0 l = \frac{A}{[M]^2} + \frac{B}{[M]} + C + D[M] \qquad \text{(XII)}$$

The A, B, C, and D constants can be obtained by examining the relationship between $I_a\varepsilon^0/OD^0$ and [M] in the low-, medium-, and high pressure regions. When the pressure of the foreign gas is low, the last term on the right-hand side of Eq. (XII) can be ignored. For this pressure region, the following equation can be obtained:

$$\frac{I_a}{OD^0}\varepsilon^0 l[M]^2 = A + B[M] + C[M]^2 \qquad \text{(XIII)}$$

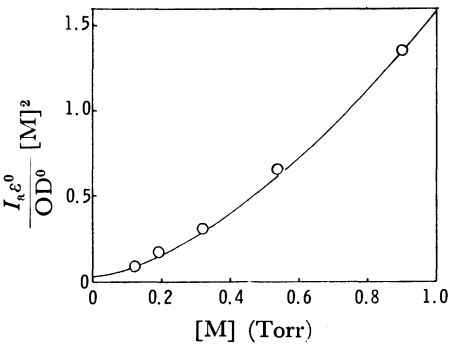

Fig. 9. $I_a\varepsilon^0[M]^2/OD^0$ in arbitrary unit as a function of argon pressure in the low pressure range.

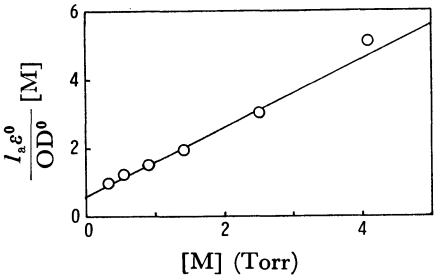

Fig. 10. $I_a\varepsilon^0[M]/OD^0$ in arbitrary unit as a function of argon pressure in the medium pressure range.

In Fig. 9, the relative value of $I_a\varepsilon^0[M]^2/OD^0$ for argon is plotted against [M] for the pressures below 1 Torr. From the curve, the relative values of A, B, and C were obtained. In Fig. 10 the relative value of $I_a\varepsilon^0[M]/OD^0$ for argon is plotted against [M] for the pressure region from 0.4 to 5.0 Torr. A linear relationship was thus obtained. This shows that the first and last terms on the right-hand side of Eq. (XII) can be ignored in this pressure region. From the intercept and the slope of the straight line in Fig. 10, the relative values of B and C can be obtained. These values were found to agree with the values obtained above. Similar treatments were carried out in order to determine the constants, A, B, and C for other foreign gases. The D constant for N_2 was obtained by taking the simple average of the quantity:

$$\{(I_a\varepsilon^0)/OD^0 - (A/[N_2]^2 + B/[N_2] + C)\}/[N_2]$$

in the pressure region from 5 to 200 Torr.

References

1) W. H. Breckenridge and A. B. Callear, *Trans. Faraday Soc.*, **67**, 2009 (1971).
2) P. D. Morten, C. G. Freeman, M. J. McEvan, R. F. C. Claridge, and L. F. Phillips, *Chem. Phys. Lett.*, **16**, 148 (1972).
3) G. H. Kimbell and D. J. LeRoy, *Can. J. Chem.*, **38**, 1714 (1960).
4) R. J. Cvetanović, *Progr. Reaction Kinet.*, **2**, 40 (1964).
5) H. Horiguchi and S. Tsuchiya, This Bulletin, **44**, 1213 (1971).
6) J. M. Cambell, S. Penzes, H. S. Sandhu, and O. P. Strausz, *Int. J. Chem. Kinet.*, **3**, 175 (1971).
7) A. B. Callear and J. C. McGurk, *J. Chem. Soc., Faraday II*, **69**, 97 (1973).
8) M. Takaoka, S. Yamamoto, S. Tsunashima, and S. Sato, *Chem. Lett.*, **1974**, 343.
9) F. W. Byron, Jr., M. N. McDermott, and R. Novick, *Phys. Rev.*, **134**, A615 (1964).
10) S. Tsunashima, T. Toyono, and S. Sato, This Bulletin, **46**, 2654 (1973).

The T←S_0 Absorption of the Acetophenone Crystal

Yoshifumi TANIMOTO, Tohru AZUMI,* and Saburo NAGAKURA

The Institute for Solid State Physics, The University of Tokyo, Roppongi, Minato-ku, Tokyo 106
**Department of Chemistry, Faculty of Science, Tohoku University, Aramaki, Sendai 980*

(Received August 30, 1974)

The polarization and Zeeman splitting of the T←S_0 absorption were measured with the acetophenone single crystal at 4.2 K. From the analyses of the polarization behavior and the Zeeman splitting pattern, it is concluded that the 26110 cm^{-1} band is in-plane polarized and has the character of the n,π^* type transition.

Aromatic carbonyls show interesting properties from both spectroscopic[1-14] and photochemical[15,16] points of view since their lowest π,π^* and n,π^* triplet states are close to each other. Acetophenone is one of the most typical aromatic carbonyls and the nature of its lowest triplet state has been studied by several authors.[2,7,8,10-14] Though there have been a number of studies for this molecule in rigid glass solutions and in mixed crystals, only a couple of papers have been published concerning the crystalline acetophenone.[13,14] From the consideration of absorption intensity, Dym and Hochstrasser[13] asserted that the longest wavelength T←S_0 absorption band at 26108 cm^{-1} is due to the n,π^* type transition. On the other hand, Case and Kearns[14] obtained the T←S_0 absorption spectra of the acetophenone single crystal at 4.2 K by the phosphorescence excitation (PE) method and concluded that its lowest triplet state is of π,π^* type. To clarify this discrepancy, we measured the polarization and Zeeman splitting of the T←S_0 absorption band of the acetophenone single crystal. In our preliminary report[17] on this subject, we indicated that the 26108 cm^{-1} band was due to the π,π^* type transition. Thereafter, we have accurately determined the crystal structure of acetophenone by the X-ray crystal analysis technique.[18] In the present paper, we report the analysis of the polarization and Zeeman splitting data made on the basis of the newly determined crystal structure.

Experimental

Acetophenone single crystals were grown from ethanol solutions. The crystal axes were determined with the aid of the X-ray diffraction technique. Since only thin crystals were obtained, three or four pieces of the crystals were piled up for the measurement of the T←S_0 absorption.

Polarization of the T←S_0 absorption was measured in a usual way. Light from a 500 W xenon lamp was passed through a home-made polyvinyl alcohol-iodine polarizer[19] which was set in front of a sample in liquid helium, and focussed on the sample. Transmitted light was detected by a Spex 1700-II grating monochromator equipped with an EMI 6256S photomultiplier tube.

To obtain a strong magnetic field enough for the measurement of the Zeeman splitting in the T←S_0 absorption bands, a solenoid type superconducting magnet was prepared. A superconducting wire (Supercon T48B, National Research Co.) was coiled on a brass bobbin (20ϕ×80 mm) 15400 turns. Its main properties are as follows: the coil impedance is 90 Ω, the inductance is 7.4 mH at room temperature, the critical field is 50000 Oe, and the critical current is 24 A at 4.2 K.

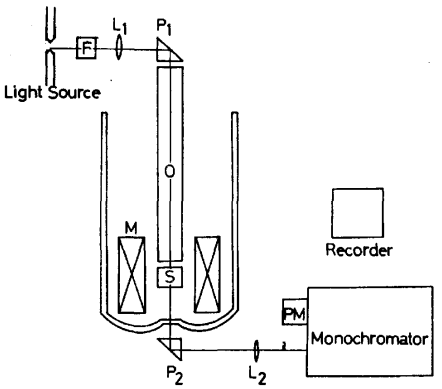

Fig. 1. Experimental setup for the Zeeman splitting measurement.
F, filter; L_1, L_2, lenses; P_1, P_2, prisms; O, optical pipe; S, sample holder; M, superconducting magnet; PM, photomultiplier tube.

Experimental arrangement for measuring the Zeeman splitting in the T←S_0 absorption is schematically shown in Fig. 1. Light from a 1 kW xenon lamp was focussed on a prism and led into a sample surrounded by the superconducting magnet. Transmitted light passing through a window at the bottom of a cryostat was led into a Spex 1700-II monochromator. Magnetic field strength was monitored by a field plate (FP15V1, Siemens A. G.) inserted in the sample holder.

Results and Discussion

Polarization of the T←S_0 Absorption. Figure 2 shows a polarized T←S_0 absorption spectrum observed with the (110) plane of the acetophenone crystal. The

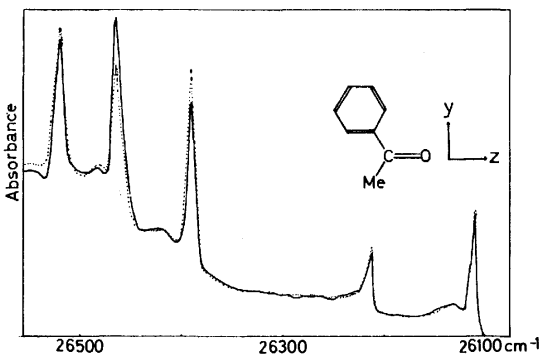

Fig. 2. Polarized T←S_0 absorption spectrum.
Light propagation is perpendicular to (110). The solid and broken lines indicate the absorbances polarized parallel and perpendicular to [1$\bar{1}$1], respectively.

solid and broken lines in the figure show the absorption spectra polarized, respectively, parallel and perpendicular to [1$\bar{1}$1]. As has been reported earlier,[13,14] strong bands appear at 26110, 26389, 26455, and 26520 cm^{-1}.

The observed longest wavelength band at 26110 cm^{-1} has been assigned to the 0–0 band of the transition to the lowest triplet state,[13,14] and we will mainly focus our attention to this band. Polarization ratio ($P=D_{//}/D_{\perp}$) is 1.0±0.3 for this band. Here $D_{//}$ and $D_{\perp}$ are the absorbances for linearly polarized light whose electric vectors are, respectively, parallel and perpendicular to [1$\bar{1}$1]. Molecular axes, x, y, and z are taken to be perpendicular to the molecular plane and perpendicular and parallel to C=O in the plane, respectively (see Fig. 2).

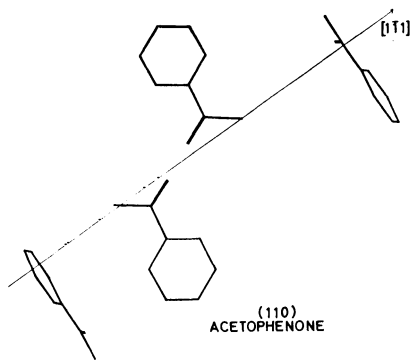

Fig. 3. (110) Projection of the structure of the acetophenone crystal.

The molecular orientation in the acetophenone crystal was determined by the X-ray crystal analysis technique.[18] The projection of the molecules in a unit cell on the (110) plane is shown in Fig. 3. From the crystal analysis data and the observed polarized spectrum shown in Fig. 2, it is concluded that the transition under consideration is polarized within the molecular plane. In order to determine the direction of the polarization within the plane, the polarization values (P) for various directions of the polarization in the plane are calculated and are shown in Fig. 4. From the figure the direction of the polarization under consideration is concluded to be inclined by ~40° or ~110° from y axis. The former and the latter directions of the polarization will be denoted by Polarizations I and II, respectively.

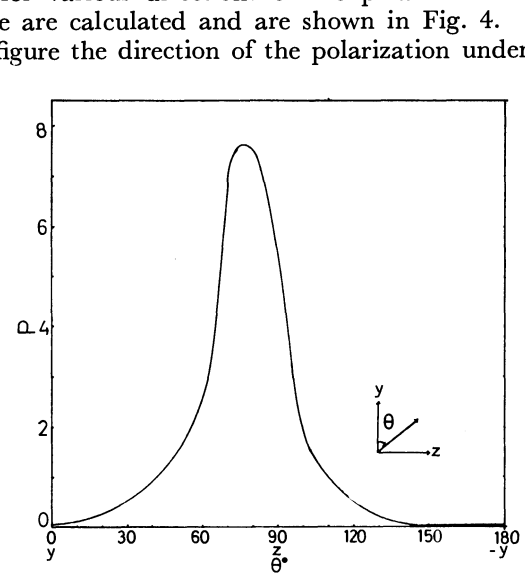

Fig. 4. Polarization ratio (P) calculated in the molecular plane.

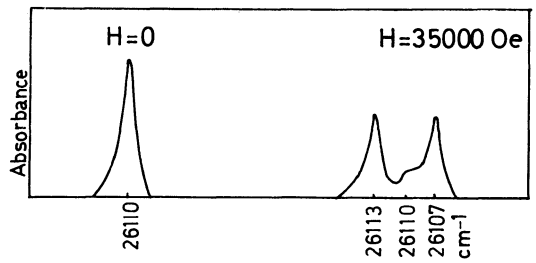

Fig. 5. Absorption profiles of the 26110 cm^{-1} band measured under the magnetic field of zero and of 35000 Oe. The field is perpendicular to (110).

The Zeeman Effect upon the T←S_0 Absorption. In Fig. 5, the Zeeman splitting pattern for the 26110 cm^{-1} band of the T←S_0 absorption at 4.2 K is shown. The directions of magnetic field and light propagation are perpendicular to the (110) plane. Magnetic field strength is 35000 Oe.

To obtain the relative intensities among the Zeeman levels quantitatively, we analyzed the spectrum by the computer simulation method. The band shape is assumed to be of the Gaussian type. Then, absorbance $D°(a)$ at a cm^{-1} at zero field, is written as follows:

$$D°(a) = D_{max} \exp\left(-(a-m)^2/2\sigma^2\right)$$

At high field, the pattern of the splitting may reasonably be calculated by neglecting the contribution from the zero-field splitting parameters. Assuming that for each split component σ is invariant with magnetic field, absorbances of the split sublevels, $D_1(a)$, $D_0(a)$, and $D_{-1}(a)$, are expressed as follows:

$$D_0(a) = \alpha\beta \exp\left(-(a-m)^2/2\sigma^2\right)$$

$$D_{\pm1}(a) = \beta \exp\left(-(a-m\mp\Delta E)^2/2\sigma^2\right)$$

where, $\alpha=D_0(m)/D_{\pm1}(m\pm\Delta E)$, ΔE is Zeeman energy (cm^{-1}), and β is the normalization term which keeps the total integrated intensity invariant with magnetic field. By comparing the observed and calculated band shapes, the value of α was determined to be 0.22 for the 26110 cm^{-1} band.

Characteristics of the 26110 cm^{-1} Band. Let us consider the character of the 26110 cm^{-1} band in detail. First, we examine the polarization of the absorption. Assuming that the acetophenone molecule is planar, the expected polarizations of the T←S_0 absorptions are shown in Table 1. The experimental result that the observed absorption is polarized in-plane indicates that the relevant triplet state is one of either T_y and/or T_z of the n,π^* state or T_x of the π,π^* state. Usually, the former possibility is assumed on the basis of the estimated magnitude of the matrix elements. However, we shall try to give the assignments from the experimental view points.

To make the assignment more concrete, let us consider the α value of the Zeeman splitting of the transition obtained above. Let absorbances for the transitions

TABLE 1. POSSIBLE POLARIZATION OF THE $T \leftarrow S_0$ TRANSITION

Triplet state	Active sublevel	Polarization
n, π^*	T_x	out-of-plane
	T_y, T_z	in-plane
π, π^*	T_x	in-plane
	T_y, T_z	out-of-plane

Here we assumed only that the acetophenone molecule is planar. The contribution of the three-center integrals is considered in the spin-orbit coupling calculation.

of the Zeeman levels, T_1^i, T_0^i, and T_{-1}^i of the i'th molecule in the crystal be denoted by D_1^i, D_0^i, and D_{-1}^i.[20] (We hereafter use the superscript and subscript, i, to denote the position of the molecule in the crystal.) We obtain the following equation:

$$\begin{bmatrix} D_1^i \\ D_0^i \\ D_{-1}^i \end{bmatrix} = c \begin{bmatrix} \frac{1-l_i^2}{2} & \frac{1-m_i^2}{2} & \frac{1-n_i^2}{2} \\ l_i^2 & m_i^2 & n_i^2 \\ \frac{1-l_i^2}{2} & \frac{1-m_i^2}{2} & \frac{1-n_i^2}{2} \end{bmatrix} \begin{bmatrix} U_x^i \\ U_y^i \\ U_z^i \end{bmatrix} \quad (1)$$

where, c is a proportionality constant, l_i, m_i, and n_i are direction cosines of the molecular axes, x, y, and z, respectively, with regard to the field direction, and U_x^i, U_y^i, and U_z^i represent the contribution to the transition intensity from the respective sublevels at zero field.

Since, in a crystal, α is represented by the equation,

$$\alpha = \sum_i D_0^i / \sum_i D_{\pm 1}^i \quad (2)$$

α can be calculated with the aid of crystallographic and polarization data. Assuming that only one sublevel is the active one,[21] α's were calculated as shown in Table 2. From the table, it is clear that there are

TABLE 2. THE VALUES OF α CALCULATED FOR THE ACETOPHENONE CRYSTAL

Active sublevel	Polarization I	Polarization II
T_x	2.17	10.7
T_y	0.18	0.18
T_z	1.47	0.16

three cases in which the calculated α-values are reasonably close to the observed value for the 26110 cm^{-1} band (α=0.22), *i.e.*, the active sublevel, T_y, with Polarizations I and II (calculated α's are both 0.18), and the active sublevel, T_z, with Polarization II (calculated α is 0.16). Thus, we may conclude that the active sublevel is not T_x. Then, in conjunction with the polarization data discussed above, the possibility of π,π^* state is discarded. It is therefore concluded that the observed transition at 26110 cm^{-1} has the character of the n,π^* type, and the active sublevel is either T_y or T_z. Unfortunately, from the experiments discussed in this paper, we are unable to determine which of the sublevels T_y or T_z is the active state.

Our conclusion on the 26110 cm^{-1} band agrees with the assertion made by Dym and Hochstrasser,[13] but disagrees with the conclusion of Case and Kearns.[14] The result of the latter authors seems to be ambiguous since they did not use the accurate crystal structure of acetophenone for the analysis of the polarized PE spectra.

We also analyzed the 26389 cm^{-1} band which was assigned to the n,π^* triplet state by Case and Kearns. From $P=0.8\pm0.3$ and $\alpha=0.27$, this band has also the character of the n,π^* type transition.

In the preliminary paper,[17] we calculated α with the aid of Eq. (1) on an inadequate assumption,[22]

$$U_j^i = U_j \quad (j=x, y, z)$$

and were led to the misinterpretation that the 26110 cm^{-1} band had the character of the π,π^* type transition.

It may be emphasized that our result is concerned only with the transition character of the longest wavelength band at 26110 cm^{-1} and cannot give any conclusion about the nature of the upper state of this band itself. In this connection, it may be necessary to mention the result obtained by Cheng and Hirota[12e] who studied the dynamic properties of the lowest triplet state of the acetophenone trap in its crystal with the aid of the microwave phosphorescence double resonance technique. From the analysis of the results, they concluded that the lowest triplet state is the π,π^* state mixed with the nearby n,π^* triplet state and that the main emissive spin sublevel is T_z. As they discussed, however, the radiative character of the lowest triplet state is mainly controlled by the n,π^* component which contributes to the state only by a few per cent. Therefore, our result on the transition character of the 26110 cm^{-1} band is not inconsistent with their result.

We thank Professor Noboru Hirota, State University of New York at Stony Brook, and Dr. Hisaharu Hayashi, The Institute of Physical and Chemical Research, for their helpful advice.

References and Notes

1) Y. Kanda, H. Kaseda, and T. Matsumura, *Spectrochim. Acta*, **20**, 1387 (1964).
2) R. Shimada and L. Goodman, *J. Chem. Phys.*, **43**, 2027 (1965).
3) D. R. Kearns and W. A. Case, *J. Amer. Chem. Soc.*, **88**, 5087 (1966).
4) G. Yamaguchi, Y. Kakinoki, and H. Tsubomura, This Bulletin, **40**, 526 (1967).
5) D. A. Warwick and C. H. J. Wells, *Spectrochim. Acta*, **24A**, 589 (1968).
6) N. Hirota, *Chem. Phys. Lett.*, **4**, 305 (1969).
7) T. Takemura and H. Baba, This Bulletin, **42**, 2756 (1969).
8) Y. H. Li and E. C. Lim, *Chem. Phys. Lett.*, **7**, 15 (1970).
9) J. C. Miller and R. F. Bookman, *J. Chem. Phys.*, **56**, 3727 (1972).
10) a) M. Koyanagi, R. J. Zwarich, and L. Goodman, *J. Chem. Phys.*, **56**, 3044 (1972); b) L. Goodman and M. Koyanagi, *Mol. Photochem.*, **4**, 369 (1972).
11) a) H. Hayashi and S. Nagakura, *Mol. Phys.*, **24**, 801 (1972); b) H. Hayashi and S. Nagakura, *Chem. Phys. Lett.*, **18**, 63 (1973); c) H. Hayashi and S. Nagakura, *Mol. Phys.*, **27**, 969 (1974).
12) a) T. H. Cheng and N. Hirota, *Chem. Phys. Lett.*, **13**, 194 (1972); b) S. W. Mao, T. C. Wong, and N. Hirota,

An Electron Spin Resonance Study of the Anion Radicals of Some Nitrotropolonates and 2-Methoxy-5-nitrotropone

Yusaku IKEGAMI and Shuichi SETO

Chemical Research Institute of Non-Aqueous Solutions, Tohoku University, Katahira 2-1-1, Sendai 980

(Received September 2, 1974)

The anion radicals of 5-nitro-, 3-nitro-, and 3,5-dinitro-tropolonates and of 2-methoxy-5-nitrotropone were generated electrolytically in *N,N*-dimethylformamide. Hyperfine structures of these ESR spectra were reasonably interpreted with the spin density calculations. The results for the 3-nitro- and 3,5-dinitro-tropolonates suggested that the 3-nitro groups were twisted about 40 and 55°, respectively, from the ring plane.

Studies on the anion radicals of tropone[1] and its some derivatives[2] revealed that the anion radicals of tropone derivatives are usually unstable and could only be generated by the electrolytic reductions for some tropones under the presence of a large amount of supporting electrolyte. Since nitro-substituted aromatic compounds are easily reduced to form the stable anion radicals, the generation of the anion radicals of nitro-substituted tropone derivatives will be expected. As a part of the electron spin resonance (ESR) study on the nonbenzenoid aromatic radicals, the electrolytic generations of the anion radicals from 5-nitro-, 3-nitro-, and 3,5-dinitro-tropolones and 2-methoxy-5-nitrotropone have been successfully examined. This paper reports the ESR spectra and the structures of these radicals. The McLachlan calculation[3] was adopted to the spin density estimation in order to interpret the ESR hyperfine structures.

Results and Discussion

5-Nitrotropolonate Anion Radical. Figure 1 shows the ESR spectrum of the radical generated by the electrolysis of a 0.007 M solution of 5-nitrotropolone in degassed *N,N*-dimethylformamide (DMF) at *ca.* 2.0 V, using tetra-*n*-propylammonium perchlorate as the supporting electrolyte. Hyperfine structure of the spectrum is readily interpreted in terms of splitting from one nitrogen nucleus and two sets of pairs of equivalent protons. The observed splitting constants are given in Table 1. Since tropolones are usually strong acid like phenols, the formation of radicals would be understood in a similar manner to the formation of phenolate and benzoate anion radicals, such as nitrophenolate and 4-cyanobenzoate anion radicals,[4-6] which were produced by the electrolyses of the corresponding phenols and benzoic acids in the presence of a large amount of supporting electrolyte. Accordingly, the equivalence of two sets of protons in the radical produced should be explained with the assumption that the radical has a symmetrical structure arising from a resonance form I, rather than a structure of tropolone anion radical in which a highly mobile tautomerism with the jump of the hydroxylic proton would be required.

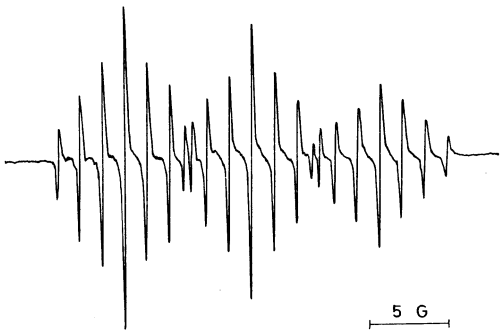

Fig. 1. ESR spectrum of the 5-nitrotropolonate anion radical generated by the electrolytic reduction in DMF (g=2.0046).

TABLE 1. SPLITTING CONSTANTS (a_i) AND SPIN DENSITIES (ρ_i) FOR THE 5-NITROTROPOLONATE ANION RADICAL

Position	a_i G	ρ_i Exptl[a]	ρ_i Calcd[b]
1, 2			0.1092
3, 7	1.42	0.060	−0.0472
4, 6	2.84	0.120	0.1178
5			−0.0093
8, 9 (CO)			0.0477
10 ($\underline{N}O_2$)	8.04		0.2110
11, 12 ($N\underline{O}_2$)			0.1716

a) With the relation $a_i=Q^H_{CH}\rho_i$, in which $|Q^H_{CH}|$=23.7 G was adopted. b) Calculated by the McLachlan procedure. The following parameters were adopted: $\alpha_8=\alpha_9=\alpha+2.0\beta$, $\beta_{1,8}=\beta_{2,9}=1.8\beta$, $\beta_{C-N}=1.2\beta$, $\alpha_N=\alpha+2.2\beta$, $\alpha_{NO}=\alpha+1.4\beta$, $\beta_{N-O}=1.67\beta$, and $\lambda=1.2$.

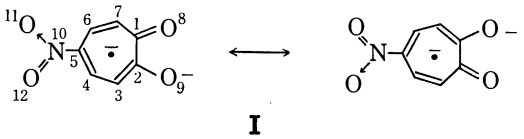

I

The Hückel MO calculations with the approximate configuration interaction treatment of McLachlan were carried out for the 5-nitrotropolonate anion radical in order to estimate the spin density distribution and to assist in assigning the splitting constants. The values of parameters used here for the nitro group were taken from the work by Rieger and Fraenkel.[5] Because of the lack of reliable MO parameters for the C⋯O group in the tropolonate ion, the parameters for this group in formula I were varied over the following ranges: $\alpha+1.0\beta\leqq\alpha_8=\alpha_9\leqq\alpha+2.2\beta$ and $1.0\beta\leqq\beta_{1,8}=\beta_{2,9}\leqq2.0\beta$, where α and β are the Coulomb and resonance integrals, respectively, for benzene. All other bond length variations were neglected, since the bond alternation in the seven-membered anion ring was not worthy of consideration even for the tropone anion radical.[1] To find out the parameters appropriate to

the C⋯⋯O group, the calculations were compared with the experimental splitting constants for the protons, adopting the relation $a_i=Q^H_{CH}\rho_i$, where $|Q^H_{CH}|=23.7$ G. A good agreement with the experimental values was obtained by using the parameters $\alpha_8=\alpha_9=\alpha+2.0\beta$ and $\beta_{1,8}=\beta_{2,9}=1.8\beta$.[7] The spin densities are given in Table 1. The calculation of $a^{NO_2}_N$ with a relation $a^{NO_2}_N\approx Q_N\rho_N+2Q_{ON}\rho_{O'}$,[5] where Q_N and Q_{ON} have the values of 99 ± 10 and 36 ± 6 G, respectively, was also in satisfactory agreement with the experimental value (calcd 8.53 and exptl 8.04 G).

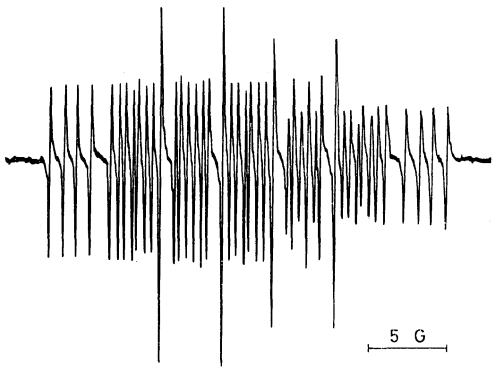

Fig. 2. ESR spectrum of the 3-nitrotropolonate anion radical generated by the electrolytic reduction in DMF (g=2.0039).

Table 2. Splitting constants (a_i) and spin densities (ρ_i) for the 3-nitrotropolonate anion radical

Position	a_i G	ρ_i Exptl[a]	ρ_i Calcd[b]
1			0.1077
2			0.0114
3			0.0048
4	3.98	0.168	0.1749
5	1.76	0.074	−0.0546
6	4.51	0.190	0.1856
7	0.95	0.040	−0.0297
8			0.0447
9			0.0022
10 ($\underline{N}O_2$)	7.19		0.2140
11, 12 ($N\underline{O}_2$)			0.1695

a) See the footnote a) in Table 1. b) Calculated by the McLachlan procedure. The values of parameters are the same as those used for the 5-nitro isomer except $\beta_{C-N}=1.2\beta\cos 40°$.

3-Nitrotropolonate Anion Radical. Electrolytic reduction of 3-nitrotropolone in DMF generated the stable anion radical which exhibited the ESR spectrum shown in Fig. 2. Hyperfine structure of this spectrum is analyzed with five splitting constants given in Table 2 and is interpreted as arising from the structure IIa. The McLachlan calculation was then applied to this structure. Using the same parameters with those for the 5-nitro isomer, however, the spin density calculations did not show a good agreement with the experimental values. It was then assumed that the disagreement is caused by the twisting of the nitro group from the seven-membered ring plane, as depicted by IIb.

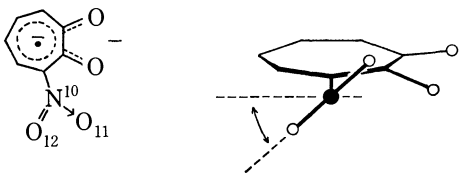

IIa IIb

In order to confirm the effect of steric hindrance between the nitro group and the CO oxygen on the ring proton splittings, the spin densities were calculated with the modification that the resonance integral of the C–N bond was estimated to be $1.2\beta\cos\theta$, where θ is a twisting angle between the nitro group and the ring. The dependence of the spin densities at the ring positions 4, 5, 6, and 7 on the angle θ is shown in Fig. 3. As seen from the figure, the theoretical spin densities at the positions 4 and 6 approach each of the corresponding experimental spin densities around 37 and 43°, respectively. The calculated values for the positions 5 and 7 with $\theta=40°$ were not far from the corresponding experimental values though some deviations are recognized. Allowing some deviations in the calculations from the experimental values, the McLachlan calculation led to the conclusion that the nitro group was twisted about 40° from the ring plane. The spin densities calculated by using $\beta_{3,10}=0.92\beta$ corresponding to this twisting angle are given in Table 2.

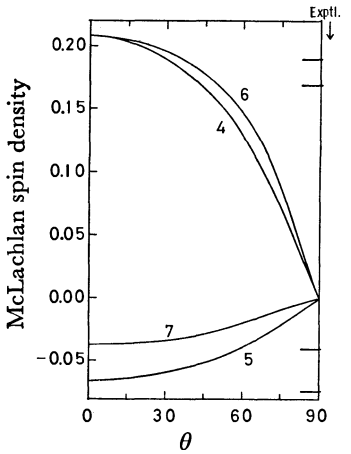

Fig. 3. Spin densities ρ calculated for the 3-nitrotropolonate anion radical by the McLachlan procedure as a function of the twisting angle θ between the ring and the nitro group. The numbers on the curves indicate the positions in the radical. See the footnote in Table 2 for the parameters in the calculation.

3,5-Dinitrotropolonate Anion Radical. The 3,5-dinitrotropolonate anion radical was produced by the electrolysis of the corresponding tropolone in DMF, similarly to the above 5- and 3-nitrotropolonates. The ESR spectrum of the radical shown in Fig. 4 is analyzed with five splitting constants, two of which represent the couplings with two different nitrogen atoms and the others the couplings with three different hydrogen atoms.

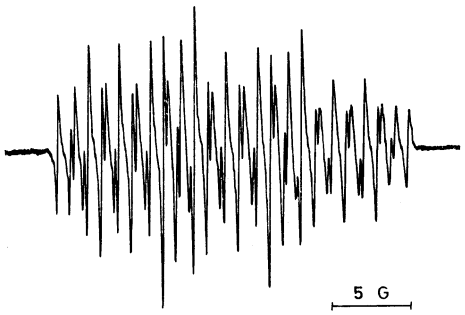

Fig. 4. ESR spectrum of the 3,5-dinitrotropolonate anion radical generated by the electrolytic reduction in DMF (g=2.0043).

With reference to the structures of the 5- and 3-nitrotropolonate anion radicals, it is readily assumed that the nitro group at 3-position is twisted considerably from the ring plane while the nitro group at 5-position is co-planar with the ring, as depicted by III. In order to confirm the twisting of the nitro group and to assist in assigning the splitting constants, the spin density calculations were carried out with the modification in which the resonance integral of the C–N bond at 3-position was estimated to be $1.2\beta \cos\theta$. The nitro

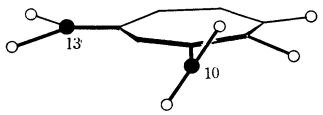

III

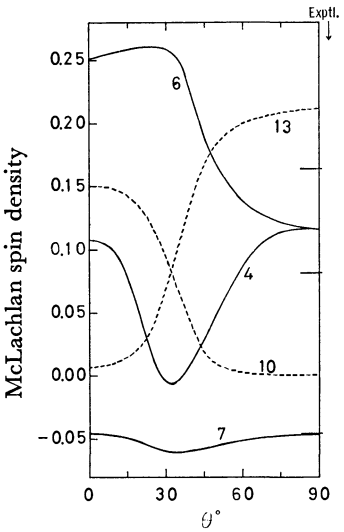

Fig. 5. Spin densities ρ calculated for the 3,5-dinitrotropolonate anion radical by the McLachlan procedure as a function of the twisting angle θ between the ring and the nitro group at 3-position.

group at the position 5 was treated to be co-planar with the ring. Figure 5 shows the dependence of the spin densities at ring positions 4, 6, and 7 and at the nitrogen atoms. As seen from the figure, the theoretical spin densities at the positions 4 and 6 approach each of the corresponding experimental values around 58 and 50°, respectively. Allowing some deviations in the MO calculation for such a complex molecule, it may

TABLE 3. SPLITTING CONSTANTS (a_1) AND SPIN DENSITIES (ρ_1) FOR THE 3,5-DINITROTROPOLONATE ANION RADICAL

Position	a_1 G	ρ_1 Exptl[a)]	ρ_1 Calcd[b)]
1			0.1311
2			0.1160
3			−0.0347
4	1.94	0.082	0.0727
5			−0.0089
6	3.92	0.165	0.1500
7	1.08	0.046	−0.0527
8			0.0582
9			0.0529
10 (3-NO_2)	0.78		0.0046
11, 12			0.0008
13 (5-NO_2)	6.78		0.1940
14, 15			0.1576

a) See the footnote a) in Table 1. b) McLachlan spin density. The values of parameters are the same as those used for the 5-nitrotropolonate anion radical except β_{C-N} (for 3-NO_2) = $1.2\beta \cos 55°$.

be concluded that the nitro group at 3-position is twisted about 55° from the ring plane. The spin densities calculated with $\beta_{3,10}=0.69\beta$ corresponding to this angle are given in Table 3. A remarkable difference of the splitting constants at 3- and 5-nitrogen atoms is reasonably understood from the contrast between the calculated spin densities at 3- and 5-nitro groups.

2-Methoxy-5-nitrotropone Anion Radical. Treatment of 2-methoxy-5-nitrotropone (IV) with lithium or sodium metal in degassed 1,2-dimethoxyethane showed neither change in its color nor the appearance of ESR signal. On the other hand, the electrolytic reduction

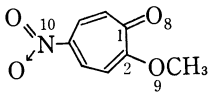

IV

of IV in DMF showed a strong ESR signal, while the yellow color of the solution turned dark brown gradually during the electrolysis. The ESR spectrum is shown in Fig. 6 and the hyperfine structure was analyzed with six splitting constants listed in Table 4. The analysis was confirmed by the spectral simulation assuming a half-width of 100 milligauss for the lines.

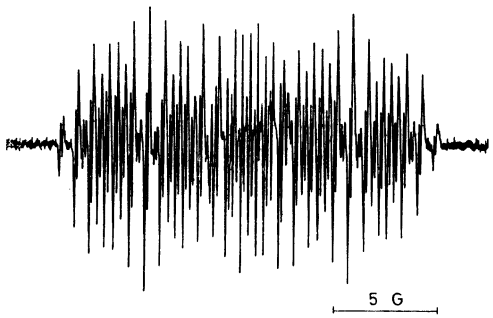

Fig. 6. ESR spectrum of the 2-methoxy-5-nitrotropone anion radical generated electrolytically in DMF (g= 2.0035).

Table 4. Splitting constants (a_i) and spin densities (ρ_i) for the 2-methoxy-5-nitrotropone anion radical

Position	a_i G	ρ_i Exptl[a]	ρ_i Calcd[b]
1			0.0050
2			0.3255
3	1.46	0.062	−0.0595
4	6.42	0.271	0.2655
5			0.0220
6	0.12	0.005	−0.0188
7	1.10	0.046	0.0354
8 (C=O)			0.0249
9 (O–CH_3)	0.75		0.0258
10 (NO_2)	3.36		0.1293
11, 12 (NO_2)			0.1225

a) See the footnote a) in Table 1. b) McLachlan spin densities calculated with the following parameters: $\alpha_8=\alpha+1.2\beta$, $\beta_{1,8}=1.8\beta$, $\alpha_9=\alpha+2.0\beta$, $\beta_{2,9}=0.8\beta$, $\alpha_N=\alpha+2.2\beta$, $\alpha_{NO}=\alpha+1.4\beta$, $\beta_{C-N}=1.2\beta$, $\beta_{N-O}=1.67\beta$, and $\lambda=1.2$.

The nitrogen splitting constants (4.88 G) was readily assigned according to the type of splitting. Other assignments were given on the basis of the spin density calculation.

On account of the complexity of the molecule IV, choice of the parameters for the calculation affects very much on the spin density distribution. But, the treatments for the nitrotropolonates above-mentioned, 2-methoxytropone,[2] and 2-methoxyazulene[8] anion radicals may be helpful to the selection of the parameters, except those for the carbonyl group which could not be evaluated appropriately in the study on the tropone anion radical.[1] Therefore, the parameters for the carbonyl group in IV were varied over the following ranges: $\alpha+1.0\beta \leqq \alpha_8 \leqq \alpha+2.0\beta$ and $1.0\beta \leqq \beta_{1,8} \leqq 2.0\beta$. The values $\alpha_9=\alpha+2.0\beta$ and $\beta_{2,9}=0.8\beta$ were chosen for the methoxy group. Assuming the co-planarity of the nitro group with the ring plane, a satisfactory agreement between the calculated and experimental spin densities was finally obtained when the parameters, $\alpha_8=\alpha+1.2\beta$ and $\beta_{1,8}=1.8\beta$, were adopted. The values are given in Table 4. Thus, the ESR hyperfine structure of the 2-methoxy-5-nitrotropone anion radical was reasonably interpreted.

During the course of the electrolytic generation of the anion radical of IV in DMF, the gradual transformation of the radical into a second paramagnetic species was observed in the ESR spectrum. The ESR spectrum of the second species fits in well with that shown in Fig. 1. This indicates that the electrolysis of IV for a long period led to the demethylation forming the 5-nitrotropolonate anion radical. The reaction may be interpreted on the analogy of the demethylation of 2,4,6-trinitroanisole in the presence of triethylamine and an aprotic solvent.[9]

Experimental

The materials, 5-nitrotropolone, mp 154 °C, 3-nitrotropolone, mp 197 °C, 3,5-dinitrotropolone, mp 174 °C, and 2-methoxy-5-nitrotropone, mp 232 °C, were prepared by the method of Nozoe *et al.*[10] and each recrystallized from methanol. *N,N*-Dimethylformamide (DMF) was degassed by at least five freezing-pumping cycles after being purified and distilled on to a molecular sieve which had been flame-dried in a vacuum.

Electrolytic generation of each free radical was performed by using a cell with platinum electrodes at room temperature. Tetra-*n*-propylammonium perchlorate was used as the supporting electrolyte.

The ESR spectra were measured with a Hitachi X-band ESR spectrometer, model 771, using a field modulation of 100 MHz. Analyses of the ESR hyperfine structures were confirmed by spectral simulation, for which a JEOL spectrum computer, JEC-5, was used. Numerical calculations were carried out at the Computer Center of Tohoku University.

The authors are grateful to Professor Takehiro Abe for his helpful discussion and to Dr. Hidetoshi Watanabe for his cooperation throughout the study.

References

1) Y. Ikegami and S. Seto, This Bulletin, **41**, 2225 (1968); Y. Ikegami, H. Watanabe, and S. Seto, *ibid.*, **45**, 1976 (1972).
2) Y. Ikegami, H. Watanabe, and S. Seto, *Chem. Lett.*, **1972**, 877.
3) A. D. McLachlan, *Mol. Phys.*, **3**, 233 (1960).
4) L. H. Piette, P. Ludwig, and R. N. Adams, *J. Amer. Chem. Soc.*, **84**, 4212 (1962).
5) P. H. Rieger and G. K. Fraenkel, *J. Chem. Phys.*, **39**, 609 (1963).
6) P. H. Rieger, I. Bernal, W. H. Reinmuth, and G. K. Fraenkel, *J. Amer. Chem. Soc.*, **85**, 683 (1963).
7) Other choice of the MO parameters such as $h_8=1.5$ and $k_{1,8}=1.7$ or $h_8=1.8$ and $k_{1,8}=1.8$ are also permitted to the calculation for the 5-nitrotropolonate anion radical. However, the values chosen in the text are applicable more satisfactorily to the calculations for the 3-nitro- and 3,5-dinitro-tropolonate anion radicals.
8) Y. Ikegami and S. Seto, This Bulletin, **44**, 1905 (1971).
9) K. L. Servis, cited in M. J. Strauss, *Chem. Revs.*, **70**, 667 (1970).
10) T. Nozoe, Y. Kitahara, K. Doi, and T. Arai, *Bull. Chem. Research Inst. Non-Aqueous Solutions, Tohoku Univ.*, **7**, 13 (1957).

Electrical Properties of TeO_2.[1] I.

Kazuo Doi, Tomoaki Sasaki, and Kenzo Hijikata

Institute of Inorganic Chemistry, Department of Chemistry, Nihon University, 3-25-40 Sakurajosui, Setagaya-ku Tokyo 156

(Received December 15, 1973)

The electrical conductivity σ of polycrystalline tellurium dioxide (paratellurite; purity: 6-nine) was measured as a function of the oxygen partial pressure (1—760 mmHg) at temperatures between 475 and 550 °C. The relations between the experimental values of $\log \sigma$ and $1/T$ were well represented by straight lines, giving the apparent activation energy of about 1.36 eV. The oxygen-pressure dependence of the isothermal conductivity was well expressed by the $\sigma \propto P_{O_2}^{1/6}$ relation; this may be interpreted by assuming that electron holes with fully-ionized oxygen interstitials predominantly act as charge carriers. The p-type behavior in the conduction process was also confirmed by thermal emf measurements.

There have been a few papers on the piezoelectric,[2] elastic and photoelastic[3] characteristics of tellurium dioxide. There have not, however, been any reports on the electrical conductivity as a function of the oxygen partial pressure or on whether the predominant semiconductivity is of the p- or n-type in tellurium dioxide. Therefore, the aim of this investigation was to observe the temperature and oxygen-pressure dependences of the electrical conductivity for highly pure polycrystalline paratellurite, and, on the basis of these, to obtain some information on the defect type of paratellurite, which had not yet been elucidated.

Experimental

Specimens. Highly pure powders of paratellurite were prepared from 6-nine tellurium metal (Osaka Asahi Metal Co., Ltd.). The white precipitate which was obtained by dissolving the tellurium metal into dilute pure nitric acid (Super Special Grade: Wako Pure Chemical Industries, Ltd.), was filtered, washed fully with distilled water, and dried in a vacuum at 80 °C. The dried powders were heated to 400 °C for 1 hr in a Pt-crucible to drive off the residual nitric acid. The X-ray diffraction patterns of the resulting powders indicated a well-crystallized structure of paratellurite. Pellets (10 mm in diameter and 3 mm thick) were made by compacting the powders at 2 ton/cm^2 and by then sintering the compacts for 150 hr at 630 °C in the Pt-crucible in air. The densities of the sintered disks were approximately 64% of the theoretical yield.

The impurities of the specimens before and after the conductivity measurements were found to be Mg and Cu by means of emission spectrographic analysis,[4] and no other elements were detected. Chemical analysis indicated Mg: 0.5 ppm and Cu: 0.0 ppm. The specimens before and after the measurements were both estimated to be 6-nine purity.

Measurements. The electrical conductivity was measured by a two-terminal method in a comparatively low temperature range so as to be able to neglect the influence of the evaporation of tellurium dioxide on the measurements.

A detailed schematic diagram of the apparatus for electrical conductivity measurements has been presented elsewhere.[5] Two thermocouples (0.3 mmϕ Pt–Pt13%Rh) were welded to each electrode of a platinum plate. The platinum arms of the thermocouples were used to measure the AC and DC conductivities and the Seebeck effect.

The various partial pressures of oxygen were provided by oxygen-nitrogen tank mixtures (dew points: −50 °C).

The specimen temperature was controlled within ±0.15 °C by regulating the SCR power supply. The AC conductivity was taken by means of a bridge (Type TR-1C: Ando Electric Co., Ltd.), applying selected frequencies in the range of 0.03—3 kHz to the specimens in all runs, while the DC conductivity was determined on an electrometer (Type TR-8651: Takeda Electric Co., Ltd.). The equilibrium value between the specimen conductivity and the oxygen partial pressure in the surrounding atmosphere was determined after the specimen resistance had been stabilized for 2 hr; this value remained constant for 30 hr or more.

The conductivity values were obtained with a good reproducibility in all the cases tried.

Results

The DC conductivity data nearly coincided with those at 30 Hz, as is shown in Fig. 1. The measured conductivity value was reproducible for both increasing and decreasing temperatures and for the ambient oxygen partial pressures.

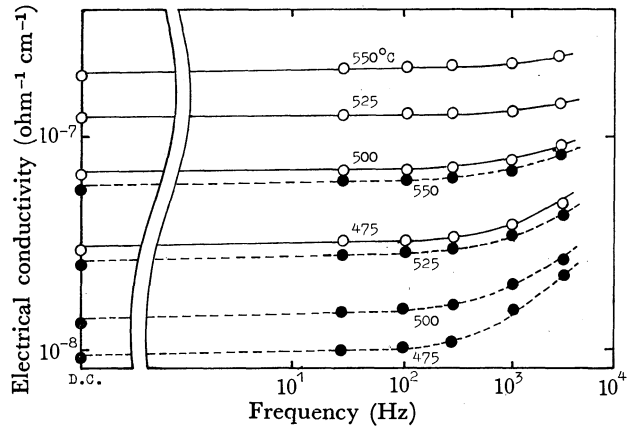

Fig. 1. Frequency dependence of the electrical conductivity TeO_2.
—○—○—: the values measured under oxygen gas (760 mmHg)
—●—●—: the values under nitrogen gas (760 mmHg)

Plots of $\log \sigma$ *vs.* $1/T$ at various oxygen partial pressures are shown in Fig. 2. In the temperature range examined, the plots were well represented by a straight line at each oxygen pressure. From these results, the apparent activation energy for the electrical conductivity of the paratellurite was calculated as about 1.36 eV in all the atmospheres tested. The oxygen

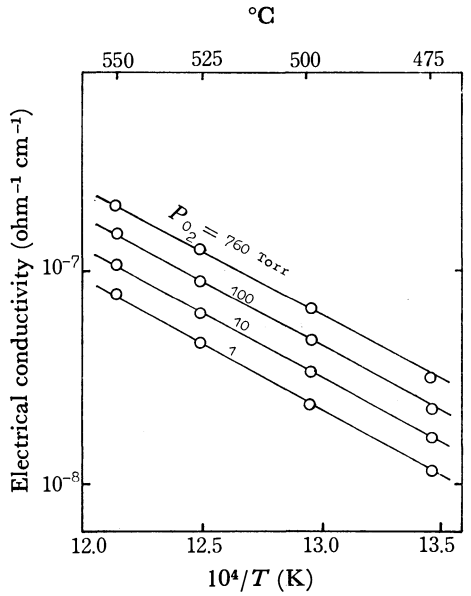

Fig. 2. The electrical conductivity of TeO_2 (at 30 Hz) *vs.* the reciprocal of absolute temperature. $P_{O_2}+P_{N_2}=760$ mmHg

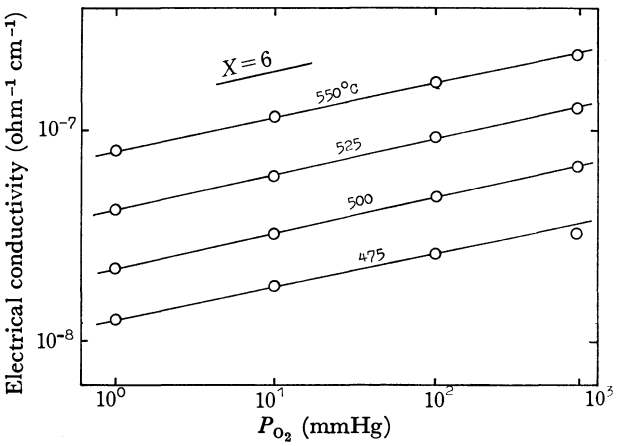

Fig. 3. The relation between the electrical conductivity of TeO_2 (at 30 Hz) and the oxygen partial pressure. X is defined in the conductivity expression $\sigma \propto P_{O_2}^{1/X}$.

partial pressure dependence of the electrical conductivity for the polycrystalline paratellurite is indicated in Fig. 3.

As may be seen, the electrical conductivity increased with an increase in the oxygen partial pressure in the surrounding atmosphere; therefore, it seems that the semiconductive nature of paratellurite is the p-type under the present experimental conditions. The p-type character of paratellurite was also confirmed from the sign of the Seebeck voltages under the temperatures examined.

The linear relationship of the conductivity isotherm can be written as $\sigma=K\cdot P_{O_2}^{1/X}$, with $X=6$.

Discussion

It could be assumed that the contamination of the specimen by its surroundings and the evaporation of the specimen were negligible in the present investigation, because a linear relationship between $\log\sigma$ and $1/T$ was obtained with a good reproducibility for both increasing and decreasing temperatures under ambient oxygen partial pressures, as may be seen in Fig. 2.

The coincidence of the DC conductivity data with those of AC (at 30 Hz) indicated that the predominant semiconduction for the paratellurite is electronic rather than ionic for the oxygen partial pressure and temperature range examined.

Considering the purity of the specimen used in this study, it may be assumed that the influence of the impurities on the pressure dependence of the conductivity is negligible.

The electrical conductivity increased with an increase in the oxygen partial pressure at each temperature, and the electrical conductivity was expressed as a function of the oxygen partial pressure by the relation: $\sigma=K\cdot P_{O_2}^{1/6}$.

If this character were intrinsic behavior, it could be determined by applying the Baumbach-Wagner law[6] whether the predominant defect is cation vacancies or anion interstitials resulting from the deviation of stoichiometry.

1) Cation-vacancy Model.

$$O_2(\text{gas}) \rightleftarrows 2O(\text{lattice}) + Te_v^{+m} + m\oplus \qquad (1)$$

where Te_v^{+m} is the cation vacancy and $\oplus$, the electron hole, and where the degree of ionization, m, takes integral values up to 4.

$$\text{Then,} \quad K'\cdot P_{O_2} = [Te_v^{+m}][\oplus]^m \quad m = 1, 2, 3, 4. \qquad (2)$$

Here, K' is an equilibrium constant and the square brackets indicate the concentration. If the electroneutrality condition can be simplified as $m[Te_v^{+m}]=[\oplus]$,

$$\text{then,} \quad \sigma = [\oplus] \propto P_{O_2}^{1/m+1}. \qquad (3)$$

Therefore, the cation-vacancy models have oxygen-pressure dependences of 1/2, 1/3, 1/4, and 1/5 ($m=$ 1, 2, 3, 4).

2) Anion-interstitial Model.

$$1/2O_2(\text{gas}) \rightleftarrows O_{\text{int}}^{-n} + n\oplus \qquad (4)$$

where O_{int}^{-n} is the oxygen interstitials; the degree of ionization, n, may be 1 or 2. Applying the mass action law,

$$K''\cdot P_{O_2}^{1/2} = [O_{\text{int}}^{-n}][\oplus]^n \qquad (5)$$

If the electroneutrality condition is now shown as:

$$n[O_{\text{int}}^{-n}][\oplus], \text{ then } [\oplus] \propto P_{O_2}^{1/2(n+1)} \qquad (6)$$

Thus, the oxygen-interstitial model has a pressure dependence of 1/4 or 1/6 ($n=1, 2$).

The slope, 1/6 ($X=6$), corresponded to the predominance of doubly-ionized oxygen interstitials, with electron holes as the charge carriers, as has been described above.

This suggests that oxygen atoms (ions) from oxygen gas in the surrounding atmosphere dissolve into the crystal of paratellurite. The crystal structure of paratellurite has been studied by several authors.[7,8] Lindqvist[9] suggested that paratellurite is four-fold coordinated by a polyhedron, being a somewhat distorted trigonal bipyramid with bond distances of

$Te-O_{eq}=1.90\pm0.02$ Å and $Te-O_{ax}=2.08\pm0.02$ Å, and lacking one atom in the equatorial position.

Therefore, it can be inferred that the oxygen atoms (ions) predominantly penetrate into these lacking sites in the crystal of paratellurite.

The authors wish to thank Dr. Hajime Kishi, Mr. Ko Yokomizo, and Mr. Takeo Hirasawa, Mitsubishi Central Research Institute, Mitsubishi Metal Corp., Oomiya, Japan, for their spectrographic and chemical analyses.

References

1) Reported at the Fall Meeting of the Japan Society of Powder Metallurgy, Osaka, Japan. Nov. 17 (1972).
2) G. Arlt and H. Schweppe, *Solid State Comm.*, **6**, 783 (1968).
3) N. Uchida and Y. Ohmachi, *J. Appl. Phys.*, **40**, 4692 (1969).
4) Jarrell-Ash Co., emission spectrograph with a diffraction grating, Ebert-mount 3.4 m.
5) J. Hattori, T. Sasaki, and K. Hijikata, *Jap. Soc. Powder Metall.*, **19**, 90 (1972).
6) H. H. Baumbach and C. Wagner, *Z. Phys. Chem.*, **B22**, 199 (1933).
7) J. Zemann, *Z. Krist.*, **127**, 319 (1968).
8) J. Leciejewicz, *ibid.*, **116**, 345 (1961).
9) O. Lindqvist, *Acta Chem. Scand.*, **22**, 977 (1968).

Nuclear Magnetic Resonance Studies of Bicyclic Thiophene Derivatives. I. Ring Current Effects of the Benzene Ring on the H_α and H_β Signals of the Thiophene Ring in Benzoylthiophene, Thienopyrimidine and Thienodiazepine Derivatives

Toshiyuki HIROHASHI, Shigeho INABA, and Hisao YAMAMOTO

Takarazuka Research Laboratories, Sumitomo Chemical Co., Takatsukasa, Takarazuka, Hyogo 665

(Received March 14, 1974)

Various thiophene derivatives such as 4-phenylthienopyrimidines (**1**), 2-acetylamino-3-benzoylthiophenes (**2**), 5-phenyl-1,4-thienodiazepines (**3**) and 5-phenyl-1,4-thienodiazepine-4-oxides (**4**) have been prepared. Their proton magnetic resonance spectra show that H_α and H_β of the thiophene ring become more shielded with an increase in bulk of *ortho* substituent of the benzene ring. This is attributed to the shielding effect of the benzene ring; a steric repulsion between *ortho* substituent of the benzene ring and some atoms on another moiety of each molecule. Such a repulsion should bring the benzene ring out of the plane of the thiophene ring. The degree of shielding on H_β by the benzene ring is found to increase in the order **1**<**2**<**3**<**4**. This can be taken to indicate that the amount of steric repulsion depends not only on the bulk of *ortho* substituent of the benzene ring but also on the geometry of each ring system of **1**—**4**.

From pharmaceutical interest, we have prepared a number of thiophene derivatives including 4-phenylthienopyrimidines (**1**), 2-acetylamino-3-benzoylthiophenes (**2**), 5-phenyl-1,4-thienodiazepines (**3**), and 5-phenyl-1,4-thienodiazepine-4-oxides (**4**). In order to

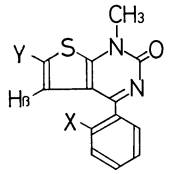

(1)

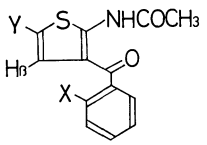

(2)

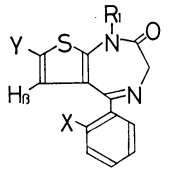

(3)

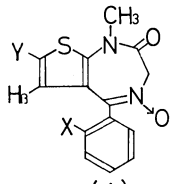

(4)

study the correlation between the biological activity and conformation of the molecules, we made studies by means of NMR spectroscopy. It was reported by Martin *et al.*[1-3] that H_3 in 2-benzoylthiophenes (**5**)

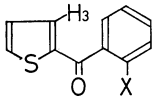

(5)

becomes more shielded with an increase in bulk of the *ortho* substituent (X) of the benzene ring. They found that, when a bulky substituent (X) is introduced, the dihedral angle between the thenoyl plane and benzene plane (*i.e.* θ_2 in formula [II]) is increased, and as a result, the shielding effect on H_3 by the benzene ring becomes more pronounced. H_β of **1**—**4** corresponds to H_3 of 2-benzoylthiophene **5**, since both protons are in close proximity with the benzene ring. However, compounds **1**—**4**, in which C=O or C=N moiety is fixed nearly co-planar with the thiophene plane by a ring formation as shown by formula [I], have a freedom of internal rotation (*i.e.* torsional angle between the

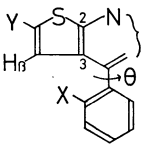

[I]

benzene and thiophene planes; θ in formula [I]). In **5**, there are two internal rotation axes (see θ_1 and θ_2 in formula [II]). Thus, there are two possible limiting

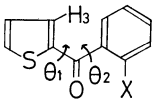

[II]

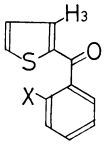

[III]

conformations of [II] and [III] for this type of compound.[2] In [III], it is apparent that the ring current effect of the benzene ring on H_3 should not be great. The chemical shifts of H_β in compounds **1**—**4** can therefore be correlated with the torsional angle θ more simply than the correlation between the chemical shifts of H_3 in compound **5** and the torsional angle θ_2. In this paper, the results of our proton-magnetic resonance measurement of compounds **1**—**4** are reported with interpretation in terms of the conformation of the compounds.

Results

NMR data for the thiophene derivatives are given in Tables 6—9. The signals of H_α and H_β of the thiophene ring show a simple AB type coupling. By substituting H_α with chlorine, we can easily tell which chemical shift is caused by H_β. High field shift of H_β by the chlorination is found to amount to 0.15 ppm. This assignment is supported by the fact that the H_α signal of the thiophene ring in compound **2** shows an extra doublet due to coupling with an amide proton (Table 7). The carbonyl oxygen of **2** is considered to form an intramolecular hydrogen bonding with an amide proton to form a six membered ring as represented by formula [IV]. This is judged from our

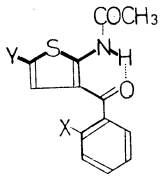
[IV]

finding the amide proton signal at an extraordinarily low field (11.9±0.1 ppm). Gribble and Bousquet found the amide proton signal at about the same position in 2-acetylamino-benzophenone.[4] When Y is a hydrogen, H_α couples with the amide proton (J=0.8 Hz) through five zig-zag bonds (thick lines, [IV]). This supports the postulation of the intramolecular hydrogen bonding.[5,6] From Tables 6—9 it is evident that H_α and H_β are shielded increasingly by the benzene ring in the order X: H<F<Cl<Br<I for **1**—**4**. The amount of increase is greater for H_β than for H_α. However, the amount of increase in the series **1**—**4** seems to differ from one another.

Discussion

Shielding Effect of the Benzene Ring on H_α and H_β. Let us define the degree ($\Delta\delta$) of shielding on H_α and H_β caused by the benzene ring in compound **1**—**4** as

$$\Delta\delta = \delta_s - \delta$$

where δ is the chemical shift of H_α or H_β in each compound with the benzene ring, and δ_s is that in the corresponding compound in which the benzene ring is substituted by an ethyl group: Degrees of shielding

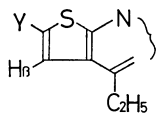
[V]

($\Delta\delta$) are listed in Tables 1—4. The $\Delta\delta$ value should include not only the ring current effect of the benzene ring, but also a through-space effect of C–X bond anisotropy and a through-bond effect of the halogen atom X. The benzene ring current itself is lowered by the inductive or mesomeric effect of the substituent X.[7] The amount of chemical shift caused by such effects, however, is considered to be sufficiently small in comparison with that caused by the benzene ring current on the basis of the following examinations.

TABLE 1. SHIELDING EFFECT ($\Delta\delta$) OF THE BENZENE RING ON H_α AND H_β OF COMPOUND **1**

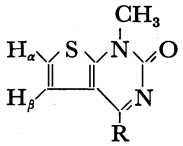
(**1a**)

	R	$\Delta\delta(H_\alpha)$ (ppm)[a]	$\Delta\delta(H_\beta)$ (ppm)[b]
A	Phenyl	−0.01	−0.13
B	*o*-Fluorophenyl	0.03	0.15
C	*o*-Chlorophenyl	0.05	0.30

a) $\Delta\delta(H_\alpha)=\delta_s(H_\alpha)-\delta(H_\alpha)$ b) $\Delta\delta(H_\beta)=\delta_s(H_\beta)-\delta(H_\beta)$

Bond Anisotropy Effect of C–X (Halogen) Bond. We prepared compounds **1**—**4** where the *ortho* substituent of benzene ring is a methyl group. The chemical shift of H_β was determined for each compound: $\delta H_\beta(X=CH_3)$, which was compared with the chemical shift of H_β of the corresponding compound, where X is chlorine: $\delta H_\beta(X=Cl)$ (Tables 6—9). The difference $[\delta H_\beta(X=CH_3)-\delta H_\beta(X=Cl)]$ was found to

TABLE 2. SHIELDING EFFECT ($\Delta\delta$)[a] OF THE BENZENE RING ON H_α AND H_β OF COMPOUND **2**

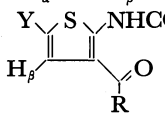
(**2**)

	R	**2a**[b] $\Delta\delta(H_\alpha)$	**2a**[b] $\Delta\delta(H_\beta)$	**2b**[c] $\Delta\delta(H_\beta)$	av.[e] $\Delta\delta(H_\beta)$
A	Phenyl	−0.01	0.07	0.07	0.07
B	*o*-Fluorophenyl	0.05	0.31	0.28	0.30
C	*o*-Chlorophenyl	0.08	0.49	0.47	0.48
D	*o*-Bromophenyl	0.09	0.51	0.50	0.51
E	*o*-Iodophenyl	0.06	0.54	0.52	0.53

a) See Table 1. b) Y=H_α. c) Y=Cl. d) Average of **2a** and **2b**.

TABLE 3. SHIELDING EFFECT ($\Delta\delta$)[a] OF THE BENZENE RING ON H_α AND H_β OF COMPOUND **3**

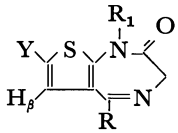
(**3**)

	R	**3a**[b] $\Delta\delta$ (H_α)	**3a**[b] $\Delta\delta$ (H_β)	**3b**[c] $\Delta\delta(H_\beta)$	**3c**[d] $\Delta\delta$ (H_α)	**3c**[d] $\Delta\delta$ (H_β)	av.[e] $\Delta\delta$ (H_β)
A	Phenyl	0.01	0.17	0.17	0.05	0.20	0.18
B	*o*-Fluorophenyl	0.06	0.32	0.31	0.08	0.34	0.32
C	*o*-Chlorophenyl	0.09	0.46	0.46	0.10	0.47	0.46
D	*o*-Bromophenyl	0.09	0.49	0.49	—	—	0.49
E	*o*-Iodophenyl	0.09	0.53	0.51	—	—	0.52

a) See Table 1. b) R_1=CH_3, Y=H_α. c) R_1=CH_3, Y=Cl. d) R_1=H, Y=H_α. e) Average of **3a**, **3b**, and **3c**.

TABLE 4. SHIELDING EFFECT ($\Delta\delta$)[a] OF THE BENZENE RING ON H_α AND H_β OF COMPOUND **4**

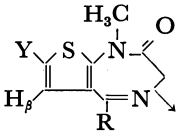
(**4**)

	R	**4a**[b] $\Delta\delta(H_\alpha)$	**4a**[b] $\Delta\delta(H_\beta)$	**4b**[c] $\Delta\delta(H_\beta)$	av.[d] $\Delta\delta(H_\beta)$
A	Phenyl	0.08	0.34	0.33	0.34
B	*o*-Fluorophenyl	0.13	0.45	0.43	0.44
C	*o*-Chlorophenyl	0.13	0.51	0.50	0.51
D	*o*-Bromophenyl	0.13	0.51	—	0.51
E	*o*-Iodophenyl	0.14	0.51	—	0.51

a) See Table 1. b) Y=H_α. c) Y=Cl. d) Average of **4a** and **4b**.

be −0.05 ppm for **1a**, −0.02 ppm for **1b**, 0.06 ppm for **2a**, −0.01 ppm for **3a** and −0.04 ppm for **4a**. Although the size of a methyl group is reported to be a little larger than that of the chlorine atom,[1,17] it is reasonable to consider that the torsional angle θ of the benzene ring with respect to the thiophene ring is nearly equal in the methyl-compound to that in the chloro-compound. The difference $[\delta H_\beta(X=CH_3)-\delta H_\beta(X=Cl)]$ might be attributed to the bond anisotropy effect of C–X (X=halogen) bond on H_β. Since the difference was found to be small, the bond anisotropy effect is considered to be very small. Nomura and Takeuchi[8] also provided an evidence that the bond anisotropy effect of C–X (halogen) must be small or nonexistent in aromatic systems.

Mesomeric and/or Inductive Effect of the ortho *Substituent X on the Benzene Ring Current.* We prepared compounds **2aF**, **2bF**, **3aF**, and **3bF**, where the *para* substituent of the benzene ring is chlorine. The chemical shift of H_β determined for each compound was $\delta H_\beta(Z=Cl)$, which was compared with the chemical shift of H_β of the corresponding compound where Z is a hydrogen: $\delta H_\beta(Z=H)$ (see Tables 7 and 8). The difference $[\delta H_\beta(Z=H)-\delta H_\beta(Z=Cl)]$ was found to be 0.07 ppm for **2a**, 0.03 ppm for **2b**, 0.02 ppm for **3a**, and 0.00 ppm for **3b**. The torsional angle of the benzene ring with respect to the thiophene ring should be nearly equal in the compound with Z=Cl to the corresponding compound with Z=H. The mesomeric and/or inductive effect of the *ortho* substituent (X=Cl) to the benzene ring current should be nearly equal to that of the *para* substituent (Z=Cl). The difference $[\delta H_\beta(Z=H)-\delta H_\beta(Z=Cl)]$ might be attributed to the mesomeric and/or inductive effect of the *ortho* substituent (X=Cl) on the benzene ring current. This effect was found to be very small. The above data seem to indicate that the through-bond effect of substituent X on the chemical shift of H_β is also very small. Martin *et al.* also examined the effect of *para* substituent Z(=H, F, Cl, Br, I, OCH_3, CH_3) in the benzene ring upon the chemical shift of H_3 in compound **5** (see formula [VI]).[1] They reported that the *para* substituent Z does not affect the chemical shift of H_3.

2aF(Y=H, Z=Cl) 3aF(Y=H, Z=Cl)
2bF(Y=Cl, Z=Cl) 3bF(Y=Cl, Z=Cl)

[VI]

Relative Amount of $\Delta\delta$ of H_α with Respect to That of H_β. We would like to show, by use of the Johnson and Bovey diagram (a figure of the isoshielding lines of benzene nucleus given by Johnson and Bovey[9]), that our observed relative amounts of $\Delta\delta$ of H_α with respect to that of H_β are explained by taking only the effect of benzene ring current into account. Let us take 2-acetamido-3-benzoylthiophene (**2a**) as an example. If we assume that the thiophene ring is in the same plane as the C–CO–C plane, the Dreiding models of this compound indicate that the center of the benzene ring and H_β and H_α come nearly on a straight line (formula [VII]). Here, the distance from the center of the benzene ring to H_β is 3.3 Å and to H_α 5.9 Å. The straight line and the distances are maintained even if the benzene ring rotates around the C–C bond by θ. In the Johnson and Bovey diagram, the position of H_β is expressed by a circle ($\mathbf{P}_\beta$) with its center at the origin and its radius of a length corresponding to 3.3 Å. The position of H_α is likewise expressed by a similar circle ($\mathbf{P}_\alpha$) whose radius has a length corresponding to 5.9 Å (Fig. 1). Here, the isoshielding lines of benzene nucleus are a modification of the figure given by Johnson and Bovey.[9] The observed shielding effect ($\Delta\delta$) of H_β of compound **2aA** is 0.07 ppm (Table 2). Therefore, the position of H_β should

[VII]

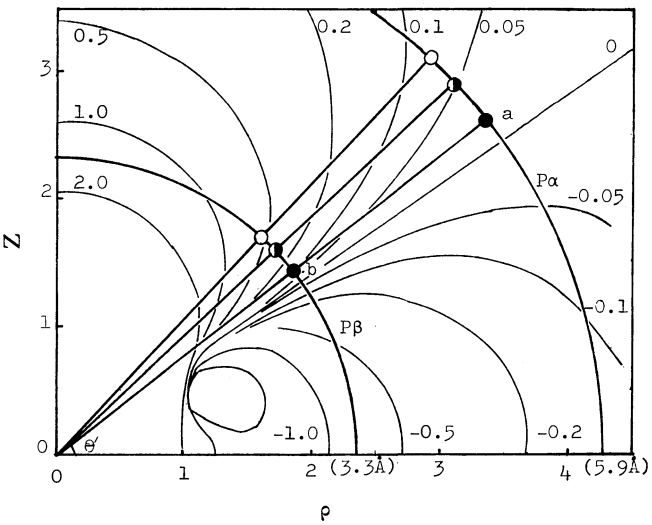

Fig. 1. Positions of H_α and H_β of compounds **2aA**—**2aC** as function of the isoshielding lines (expressed in ppm) of benzene nucleus; Z and ρ are expressed in ring radii (1.39 Å) according to Johnson and Bovey.[9] (●) Hα or H_β position of compound **2aA**, (◑) **2aB**, and (○) **2aC**. θ' is an angle between the benzene ring plane and the line which connect H_α, H_β, and center of the benzene ring. This is not the torsional angle (θ) between benzene ring plane and thiophene ring plane. When θ' is 60°, the torsional angle θ is nearly 90°.

be fixed at a point **b**. Connect point **b** with the origin. Since H_α is on the straight line connecting the center of the benzene ring and H_β in the molecule, the point representing H_α in the Johnson and Bovey diagram should also be on the straight line connecting the origin and point **b**. Let us denote the intersection of straight line **O–b** and circle $\mathbf{P}_\alpha$ by **a**. This corresponds to 0.01 ppm, which is almost equal to the observed value (−0.01 ppm) of $\Delta\delta$ for H_α (Table 2). In a similar way, the theoretical $\Delta\delta$ value for H_α derived from the observed $\Delta\delta$ value for H_β is nearly equal to the actually observed value for H_α in each compound **1a**, **2a**, **3a**, **3c**, and **4a** (Table 5).

TABLE 5. DIFFERENCE BETWEEN THE THEORETICAL AND OBSERVED VALUES FOR H_α

	R	Observed (ppm) $\Delta\delta(H_\beta)$	Observed (ppm) $\Delta\delta(H_\alpha)$	Theoretical (ppm) $\Delta\delta(H_\alpha)$	Difference[a] (ppm)
	Compound **1a**				
A	Phenyl	−0.13	−0.01	−0.02	0.01
B	*o*-Fluorophenyl	0.15	0.03	0.02	0.01
C	*o*-Chlorophenyl	0.30	0.05	0.05	0.00
	Compound **2a**				
A	Phenyl	0.07	−0.01	0.01	−0.02
B	*o*-Fluorophenyl	0.31	0.05	0.05	0.00
C	*o*-Chlorophenyl	0.49	0.08	0.08	0.00
D	*o*-Bromophenyl	0.51	0.09	0.08	0.01
E	*o*-Iodophenyl	0.54	0.06	0.08	−0.02
	Compound **3a**				
A	Phenyl	0.17	0.01	0.03	−0.02
B	*o*-Fluorophenyl	0.32	0.06	0.05	0.01
C	*o*-Chlorophenyl	0.46	0.09	0.07	0.02
D	*o*-Bromophenyl	0.49	0.09	0.08	0.01
E	*o*-Iodophenyl	0.53	0.09	0.08	0.01
	Compound **3c**				
A	Phenyl	0.20	0.05	0.03	0.02
B	*o*-Fluorophenyl	0.34	0.08	0.06	0.02
C	*o*-Chlorophenyl	0.47	0.10	0.08	0.02
	Compound **4a**				
A	Phenyl	0.34	0.08	0.06	0.02
B	*o*-Fluorophenyl	0.45	0.13	0.07	0.06
C	*o*-Chlorophenyl	0.51	0.13	0.08	0.05
D	*o*-Bromophenyl	0.51	0.13	0.08	0.05
E	*o*-Iodophenyl	0.51	0.14	0.08	0.06

a) Difference = $\Delta\delta(H_\alpha)$(observed) − $\Delta\delta(H_\alpha)$(theoretical).

Steric Effects. The correlation between the $\Delta\delta$ value (chemical shift caused by the ring current of the phenyl group) of H_β and the bulk of the *ortho* substituent X of phenyl group is shown in Fig. 2. We see that $\Delta\delta$ value increases with an increase of the bulk of X. This might be attributed to the steric repulsion between X of the phenyl ring and some atoms on another moiety of the molecule. Such a repulsion should bring the benzene ring out of the plane of thiophene ring. The $\Delta\delta$ value increases in going from compound **1** to compound **4** throgh compounds

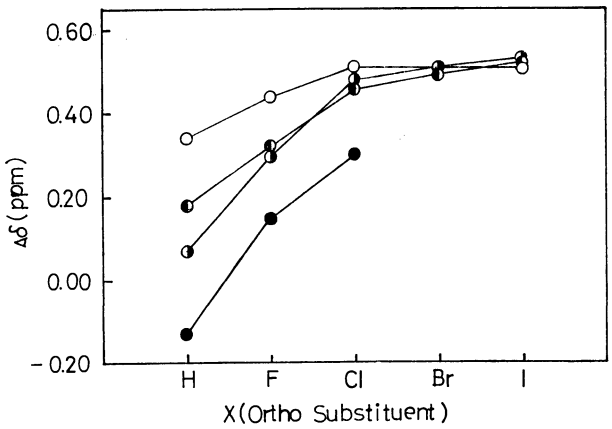

Fig. 2. Shielding effect ($\Delta\delta$) of benzene ring on H_β. (●) Compound **1**, (◑) compound 2, (◐) compound 3, and (○) compound **4**.

2 and **3**; *i.e.* **1**<**2**<**3**<**4**. This seems to indicate that the amount of steric repulsion depends not only on the bulk of X but also on the geometry and/or flexibility of the ring system condensed at 2-C and 3-C of the thiophene ring in each molecule (formula [I]). Such a steric repulsion is considered to be great even when X=H. Thus, the $\Delta\delta$ value markedly increases from compound **1** to compound **4** when X=H. This must mean that θ' greatly increases from compound **1**(X=H)→**2**(X=H)→**3**(X=H)→**4**(X=H). When X=F, on the other hand, the increase in the $\Delta\delta$ value (or the θ' value) in going from compound **1**(X=F)→**2**(X=F)→**3**(X=F)→**4**(X=F) is much smaller. When X=Cl, the corresponding increase in the $\Delta\delta$ value is even smaller. When X=Br or I, the $\Delta\delta$ value does not depend on the ring structure condensed at 2-C and 3-C of the thiophene ring. This might be explained by considering that the plane of the benzene ring is nearly perpendicular to the plane of the thiophene ring in compounds **2**—**4**, when X=Br or I.

TABLE 6. NMR DATA[a] FOR 1-METHYL-4-PHENYL (OR ETHYL)-1,2-DIHYDROTHIENO[2,3-*d*]-PYRIMIDIN-2-ONES (**1**)

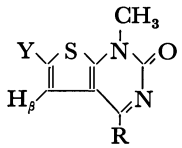

(**1**)

	R	Y	δ (ppm) H_α[b]	δ (ppm) H_β[b]
1aA	C_6H_5	H_α	6.98	7.35
1aB	*o*-F-C_6H_4	H_α	6.94	7.07
1aC	*o*-Cl-C_6H_4	H_α	6.92	6.92
1aG	*o*-Me-C_6H_4	H_α	6.93	6.87
1aH	C_2H_5	H_α	6.97	7.22
1bA	C_6H_5	Cl	—	7.19
1bB	*o*-F-C_6H_4	Cl	—	6.93
1bC	*o*-Cl-C_6H_4	Cl	—	6.77
1bG	*o*-Me-C_6H_4	Cl	—	6.75

a) See Experimental for other protons not given here.
b) $J(H_\alpha, H_\beta)$ = 5.8 Hz.

Table 7.[a] NMR data for 2-acetamido-3-benzoyl (or propionyl) thiophenes (**2**)

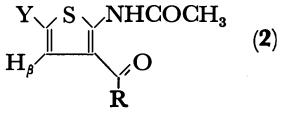

(**2**)

	R	Y	δ H_α[b]	δ H_β[b]	δ NH	(Hz) J_{NH,H_α}
2aA	C_6H_5	H_α	6.72	7.12	11.96	0.7
2aB	o-F-C_6H_4	H_α	6.66	6.88	11.94	0.8
2aC	o-Cl-C_6H_4	H_α	6.63	6.70	11.88	0.7
2aD	o-Br-C_6H_4	H_α	6.63	6.68	11.86	0.7
2aE	o-I-C_6H_4	H_α	6.65	6.65	11.85	nv[c]
2aF	p-Cl-C_6H_4	H_α	6.71	7.05	11.87	0.8
2aG	o-Me-C_6H_4	H_α	6.63	6.76	12.00	0.8
2aH	C_2H_5	H_α	6.71	7.19	11.90	0.8
2bA	C_6H_5	Cl	—	6.95	11.97	—
2bB	o-F-C_6H_4	Cl	—	6.74	11.92	—
2bC	o-Cl-C_6H_4	Cl	—	6.55	11.90	—
2bD	o-Br-C_6H_4	Cl	—	6.52	11.88	—
2bE	o-I-C_6H_4	Cl	—	6.50	11.85	—
2bF	p-Cl-C_6H_4	Cl	—	6.92	11.92	—
2bH	C_2H_5	Cl	—	7.02	11.87	—

a) Remarks and abbreviations as in Table 6. b) $J(H_\alpha,H_\beta)=5.8$ Hz. c) Not visible due to the overlapping of H_α and H_β signals.

Table 8.[a] NMR data for 5-phenyl (or ethyl)-1,3-dihydro-2*H*-thieno[2,3-*e*]-1,4-diazepin-2-ones (**3**)

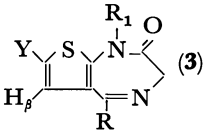

(**3**)

	R	R_1	Y	δ H_α[b]	δ H_β[b]
3aA	C_6H_5	CH_3	H_α	6.99	6.83
3aB	o-F-C_6H_4	CH_3	H_α	6.94	6.68
3aC	o-Cl-C_6H_4	CH_3	H_α	6.91	6.54
3aD	o-Br-C_6H_4	CH_3	H_α	6.91	6.51
3aE	o-I-C_6H_4	CH_3	H_α	6.91	6.47
3aF	p-Cl-C_6H_4	CH_3	H_α	7.01	6.81
3aG	o-Me-C_6H_4	CH_3	H_α	6.90	6.53
3aH	C_2H_5	CH_3	H_α	7.00	7.00
3bA	C_6H_5	CH_3	Cl	—	6.68
3bB	o-F-C_6H_4	CH_3	Cl	—	6.54
3bC	o-Cl-C_6H_4	CH_3	Cl	—	6.39
3bD	o-Br-C_6H_4	CH_3	Cl	—	6.36
3bE	o-I-C_6H_4	CH_3	Cl	—	6.34
3bF	p-Cl-C_6H_4	CH_3	Cl	—	6.68
3bH	C_2H_5	CH_3	Cl	—	6.85
3cA	C_6H_5	H	H_α	6.86	6.80
3cB	o-F-C_6H_4	H	H_α	6.83	6.66
3cC	o-Cl-C_6H_4	H	H_α	6.81	6.53
3cH	C_2H_5	H	H_α	6.91	7.00

a) Remarks and abbreviations as in Table 6. b) $J(H_\alpha,H_\beta)=5.8$ Hz.

Table 9.[a] NMR data for 1-methyl-5-phenyl (or ethyl)-1,3-dihydro-2*H*-thieno[2,3-*e*]-1,4-diazepin-2-one-4-oxides (**4**)

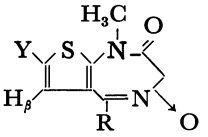

(**4**)

	R	Y	δ H_α[b]	δ H_β[b]
4aA	C_6H_5	H_α	7.06	6.63
4aB	o-F-C_6H_4	H_α	7.01	6.52
4aC	o-Cl-C_6H_4	H_α	7.01	6.46
4aD	o-Br-C_6H_4	H_α	7.01	6.46
4aE	o-I-C_6H_4	H_α	7.00	6.46
4aG	o-Me-C_6H_4	H_α	6.98	6.42
4aH	C_2H_5	H_α	7.14	6.97
4bA	C_6H_5	Cl	—	6.48
4bB	o-F-C_6H_4	Cl	—	6.38
4bC	o-Cl-C_6H_4	Cl	—	6.31
4bH	C_2H_5	Cl	—	6.82

a) Remarks and abbreviations as in Table 6. b) $J(H_\alpha,H_\beta)=5.8$ Hz.

Experimental

^1H NMR spectra were recorded at 60 MHz on a Hitachi NMR spectrometer R-20-B in dilute deuteriochloroform solution (about 10% w/v). The probe temperature was 35 °C. TMS was used as an internal reference standard. The chemical shifts expressed in δ-values (ppm) downfield from TMS were measured directly from the spectra or from a frequency counter with a precision of ±0.01 ppm. The coupling constants, measured by repeated sweeping at an expanded width (60 or 120 Hz), are expressed numerically in Hz with an accuracy of ±0.1 Hz. IR spectra were recorded as nujol mulls on a Hitachi Infrared Spectrophotometer, EPI-G-3, being expressed in terms of wave numbers. UV spectra were determined in 95% ethanol with an ultraviolet spectrophotometer, Hitachi-323 or Shimadzu D-40-R, being expressed as λ_{max} nm(ε). Melting points were determined with a Thomas-Hoover melting point apparatus and are uncorrected. Solvents for recrystallization are abbreviated as follows; ethanol (EtOH), 2-propanol (IPA), and dimethylformamide (DMF).

1) 2-Amino-3-benzoyl(or propionyl)-thiophenes.

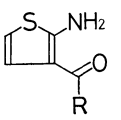

Method A: ***A–G.*** The compounds were prepared by the method of Gewald[10] from appropriate ω-cyanoacetophenones and mercaptoacetaldehyde.

A *(R: phenyl).* Yield 32.9%: mp 152—153 °C (from EtOH) (lit,[11] 147 °C).

B *(R: o-fluorophenyl).* Yield 60.0%: mp 145—146.5 °C (from IPA). IR: 3350, 3230, 3130, 1610.

C *(R: o-chlorophenyl).* Yield 47.0%: mp 137—139 °C (from IPA). IR: 3380, 3275, 1597, 1522.

D *(R: o-bromophenyl).* Yield 34.0%: mp 152—152.5 °C (from IPA). IR: 3350, 3230, 3100, 1590.

E *(R: o-iodophenyl).* Yield 27.6%: mp 162—165 °C

(from IPA). IR: 3350, 3230, 3100, 1590.

F *(R: p-chlorophenyl).* Yield 27.6%: mp 180—181.5 °C (from EtOH). IR: 3320, 3200, 3100, 1595.

G *(R: o-methylphenyl).* Yield 63.8%: mp 158—159 °C (from EtOH). IR: 3320, 3200, 3100, 1590.

*Method B: 2-Amino-3-proprionylthiophene (**H**).* This was prepared by the hydrolysis of 2-acetamido-3-propionylthiophene (**2aH**) with potassium hydroxide in aqueous ethanol at 95 °C for 10 min.

H *(R: ethyl).* Yield 87.7%: mp 140—142 °C (from Ether). IR: 3370, 3250, 3130, 1600, 1570.

*2) 2-Acetamido-3-benzoyl(or propionyl)-thiophenes (**2a**).*

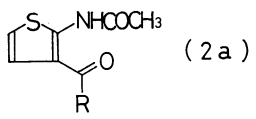

(2a)

Method A: ***2aA—2aG.*** The compounds were prepared by the method of Gewald[10] from 2-amino-3-benzoylthiophenes with acetylchloride.

2aA *(R: phenyl).* Yield 67.6%: mp 115.5—116.5 °C (from Ether). IR: 3200, 3100, 3085, 1687, 1610. NMR: 2.31 (3H, s, $COCH_3$). UV: 248.5 (14400), 270 (12700), 343 (9200). Found: C, 63.54; H, 4.58; N, 5.70%. Calcd for $C_{13}H_{11}NO_2S$: C, 63.65; H, 4.52; N, 5.71%.

2aB *(R: o-fluorophenyl).* Yield 83.5%: mp 143.5—144.5 °C (from Ether). IR: 3235, 3100, 1698, 1622, 1618. NMR: 2.34 (3H, s, $COCH_3$). UV: 239 (13700), 276 (11900), 345 (9600). Found: C, 59.04; H, 4.01; N, 5.26%. Calcd for $C_{13}H_{10}NO_2SF$: C, 59.30; H, 3.83; N, 5.32%.

2aC *(R: o-chlorophenyl).* Yield 68.9%: mp 132—132.5 °C (from Ether). IR: 3225, 3075, 1682, 1618. NMR: 2.34 (3H, s, $COCH_3$). UV: 236 (14300), 275 (10800), 343 (9600). Found: C, 55.90; H, 3.80; N, 5.00%. Calcd for $C_{13}H_{10}NO_2SCl$: C, 55.82; H, 3.60; N, 5.01%.

2aD *(R: o-bromophenyl).* Yield 76.2%: mp 122.5—123.5 °C (from Ether). IR: 3215, 3075, 3055, 1691, 1618. NMR: 2.34 (3H, s, $COCH_3$). UV: 236 (14800), 276 (10600), 343 (9500). Found: C, 48.22; H, 3.04; N, 4.24%. Calcd for $C_{13}H_{10}NO_2SBr$: C, 48.16; H, 3.11; N, 4.32%.

2aE *(R: o-iodophenyl).* Yield 26.1%: mp 125.5—127 °C (from Ether). IR: 3225, 3100, 3070, 1697, 1622. NMR: 2.33 (3H, s, $COCH_3$). UV: 232 (21800), 276 (10900), 344 (10100). Found: C, 42.37; H, 2.64; N, 3.77%. Calcd for $C_{13}H_{10}NO_2SI$: C, 42.07; H, 2.72; N, 3.77%.

2aF *(R: p-chlorophenyl).* Yield 23.6%: mp 107—108.5 °C (from Ether). IR: 3220, 3100, 1706, 1611. NMR: 2.32 (3H, s, $COCH_3$). UV: 268 (16100), 348 (9400). Found: C, 56.01; H, 3.62; N, 5.04%. Calcd for $C_{13}H_{10}NO_2SCl$: C, 55.82; H, 3.60; N, 5.01%.

2aG *(R: o-methylphenyl).* Yield 41.9%: mp 90—91.5 °C (from Ether). IR: 3235, 3105, 3087, 1695, 1623. NMR: 2.34 (3H, s, ϕ-CH_3), 2.35 (3H, s, $COCH_3$). UV: 237 (14200), 271 (10900), 338 (9700). Found: C, 64.86; H, 5.07; N, 5.34%. Calcd for $C_{14}H_{13}NO_2S$: C, 64.84; H, 5.05; N, 5.40%.

*Method B: 2-Acetamido-3-propionylthiophene (R: ethyl) (**2aH**).* To a suspension of 2-methyl-4*H*-thieno[2,3-*d*]-[1,3]oxazin-4-one (21.9 g) in dry ether (500 ml) was added dropwise a Grignard solution prepared from ethyl bromide (24.3 g), metallic magnesium (4.77 g) and ether (110 ml) at 15—20 °C. The mixture was stirred at room temperature overnight. First, water (500 ml), then conc, hydrochloric acid (120 ml) were added dropwise thereto under ice-cooling. The organic layer was separated and washed with 28% ammonia water, then condensed *in vacuo* and the residue crystallized to give 2-acetamido-α,α-diethyl-3-thiophenemethanol (8.6 g) as a by-product, mp 138—140 °C. The condensed filtrate was purified over a column of silica gel (240 g) and eluted with chloroform. Concentration of the chloroform elution gave the product (**2aH**) (3.13 g) as crystals. Recrystallization from ether gave colorless prisms, mp 73.5—74.0 °C. IR: 3220, 3100, 1665, 1640. NMR: 1.20 (3H, t, $CH_2\underline{CH_3}$), 2.26 (3H, s, $COCH_3$), 2.86 (2H, q, CH_2). UV: 236 (16600), 260 (7500), 267 (7100), 323 (8600). Found: C, 54.81; H, 5.52; N, 7.13%. Calcd for $C_9H_{11}NO_2S$: C, 54.80; H, 5.62; N. 7.10%.

*3) 2-Acetamido-3-benzoyl(or propionyl)-5-chlorothiophenes (**2b**)*

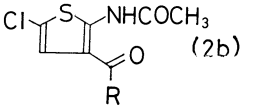

(2b)

These were prepared by the method of Hromatka *et al.*[12] from 2-acetamido-3-benzoyl (or propionyl)-thiophene (**2a**) with sulfurylchloride.

2bA *(R: phenyl).* Yield 66.6%: mp 102.5—103.5 °C (from Ether). IR: 3220, 1698, 1610, 1600. NMR: 2.28 (3H, s, $COCH_3$). UV: 253 (18300), 353 (9200). Found: C, 55.69; H, 3.52; N, 4.94%. Calcd for $C_{13}H_{10}NO_2SCl$: C, 55.82; H, 3.60; N, 5.01%.

2bB *(R: o-fluorophenyl).* Yield 62%: mp 159—160.5 °C (from EtOH). IR: 3220, 3080, 1682, 1608. NMR: 2.31 (3H, s, $COCH_3$). UV: 256 (17400), 354 (9200). Found: C, 52.28; H, 3.09; N, 4.57%. Calcd for $C_{13}H_9NO_2SClF$: C, 52.45; H, 3.05; N, 4.71%.

2bC *(R: o-chlorophenyl).* Yield 77.3%: mp 180—181 °C (from EtOH). IR: 3230, 3075, 1682, 1613. NMR: 2.32 (3H, s, $COCH_3$). UV: 242 (19600), 350 (9500). Found: C, 49.93; H, 2.85; N, 4.45%. Calcd for $C_{13}H_9NO_2SCl_2$: C, 49.70; H, 2.89; N, 4.46%.

2bD *(R: o-bromophenyl).* Yield 75.9%: mp 162—163 °C (from EtOH). IR: 3225, 3065, 1688, 1612. NMR: 2.33 (3H, s, $COCH_3$). UV: 244 (19400), 350 (9400). Found: C, 43.56; H, 2.51; N, 3.87%. Calcd for $C_{13}H_9NO_2SBrCl$: C, 43.54; H, 2.53; N, 3.91%.

2bE *(R: o-iodophenyl).* Yield 48.5%: mp 124—126 °C (from Ether). IR: 3220, 3070, 1681, 1610. NMR: 2.35 (3H, s, $COCH_3$). UV: 232 (22200), 349 (9500). Found: C, 38.47; H, 2.26; N, 3.46%. Calcd for $C_{13}H_9NO_2SClI$: C, 38.50; H, 2.24; N, 3.45%.

2bF *(R: p-chlorophenyl).* Yield 40.9%: mp 119—121 °C (from Ether). IR: 3250, 1705, 1605. NMR: 2.31 (3H, s, $COCH_3$). UV: 263 (20300), 355 (9400). Found: C, 49.71; H, 2.87; N, 4.42%. Calcd for $C_{13}H_9NO_2SCl_2$: C, 49.70; H, 2.89; N, 4.46%.

2bH *(R: ethyl).* Yield 17.2%: mp 156.5—157.5 °C (from Ether). IR: 3215, 3075, 1684, 1642. NMR: 1.19 (3H, t, J=7.1, $CH_2\underline{CH_3}$), 2.27 (3H, s, $COCH_3$), 2.78 (2H, q, J=7.1, CH_2). UV: 240 (19200), 331 (8000). Found: C, 46.70; H, 4.40; N, 5.97%. Calcd for $C_9H_{10}NO_2SCl$: C, 46.66; H, 4.35; N, 6.05%.

*4) 1-Methyl-4-phenyl(or ethyl)-1,2-dihydrothieno[2,3-d]-pyrimidin-2-ones (**1a**).*

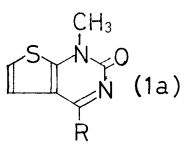

(1a)

Method A: ***1aA—1aC.***

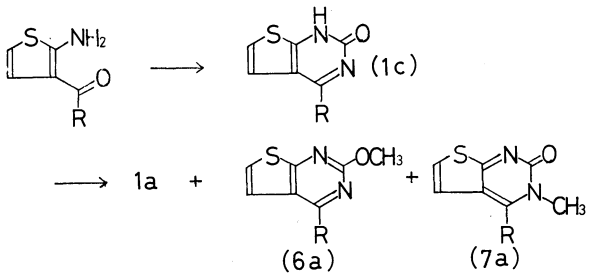

A mixture of 2-amino-3-benzoyl-thiophene and ethyl carbamate was heated at 200 °C for one hour in the presence of zinc chloride to give 4-phenyl-1,2-dihydrothieno[2,3-*d*]-pyrimidin-2-one (**1c**), which was methylated with methyl-iodide in the presence of sodium hydride to afford **1a**, 2-methoxy-4-phenylthieno[2,3-*d*]-pyrimidine (**6a**) and 3-methyl-4-phenyl-2,3-dihydrothieno[2,3-*d*]-pyrimidin-2-one (**7a**). The procedure was applied to the synthesis of 1-alkyl-4-phenyl-1,2-dihydroquinazolin-2-one.[13]

1cA *(R: phenyl).* Yield 100%: mp 247—249 °C (from EtOH–DMF). IR: 3050, 1630 (broad).

1aA *(R: phenyl).* Yield 27.6%: mp 256—257.5 °C (from EtOH). IR: 3040, 1642, 1630. NMR: 3.78 (3H, s, N-CH_3). UV: 248.5 (29800), 349 (6000). Found: C, 64.44; H, 4.15; N, 11.48%. Calcd for $C_{13}H_{10}N_2OS$: C, 64.44; H, 4.16; N, 11.56%.

6aA *(R: phenyl).* Yield 5.8%: mp 160—161.5 °C (from EtOH). IR: 3050, 1580.

7aA *(R: phenyl).* Yield 1.5%: mp 175—181 °C (from EtOH). IR: 3065, 3050, 1660. UV: 251 (26900), 276 (6400), 366 (5500). Found: C, 63.27; H, 4.34; N, 10.81%. Calcd for $C_{13}H_{10}N_2OS$: C, 64.44; H, 4.16; N, 11.56%.

1cB *(R: o-fluorophenyl).* Yield 30.5%: mp 278—279 °C (from Acetone). IR: 3100, 3050, 1600 (broad).

1aB *(R: o-fluorophenyl).* Yield 13.2%: mp 222—223 °C (from EtOH). IR: 3055, 1660, 1618. NMR: 3.75 (3H, s, N-CH_3). UV: 247 (31000), 348.5 (6200). Found: C, 60.36; H, 3.42; N, 10.76%. Calcd for $C_{13}H_9N_2OSF$: C, 59.99; H, 3.49; N, 10.76%.

6aB *(R: o-fluorophenyl).* Yield 1.7%: mp 175—176.5 °C (from EtOH). IR: 3040, 1610.

7aB *(R: o-fluorophenyl).* Yield 3.6%: mp 191—192.5 °C (from EtOH–$CHCl_3$). IR: 3090, 3050, 1660, 1650, 1615. UV: 252 (26600), 276 (5600), 370 (5500). Found: C, 59.75; H, 3.46; N, 10.77%. Calcd for $C_{13}H_9N_2OSF$: C, 59.99; H, 3.49; N, 10.76%.

1cC *(R: o-chlorophenyl).* Yield 36%: This was used in the next step without further purification.

1aC *(R: o-chlorophenyl).* Yield 13.7%: mp 225—226 °C (from EtOH–$CHCl_3$). IR: 3080, 1660, 1645. NMR: 3.78 (3H, s, N-CH_3). UV: 245 (28000), 343 (6000). Found: C, 56.56; H, 3.14; N, 9.93%. Calcd for $C_{13}H_9N_2OSCl$: C, 56.42; H, 3.28; N, 10.12%.

6aC *(R: o-chlorophenyl).* Yield 3.6%: mp 172.5—174.5 °C (from Ether). IR: 3050, 1590, 1570, 1540.

7aC *(R: o-chlorophenyl).* Yield 8.3%: mp 190—192 °C (from EtOH–Ether). IR: 3075, 3060, 1660. UV: 252 (24900), 277 (5300), 366 (5200). Found: C, 56.61; H, 3.35; N, 9.82%. Calcd for $C_{13}H_9N_2OSCl$: C, 56.42; H, 3.28; N, 10.12%.

Method B: ***1aG, 1aH.***

2a was treated with sodium hydride and methyl iodide in the usual manner[13] to afford *N*-methyl-2-acetamido-3-benzoyl (or propionyl)-thiophene (**2c**), which was hydrolyzed with potassium hydroxide by the same method as for 2-amino-3-propionylthiophene (1, method B) to give 2-methylamino-3-benzoyl(or propionyl)thiophene (**2d**). **2d** was then treated with ethyl carbamate by the same method as for **1aA—1aC** (4, method A) to afford **1a**.

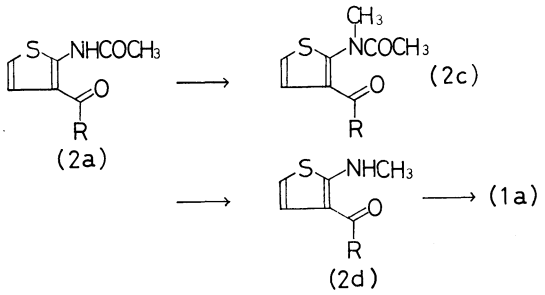

2cG *(R: o-methylphenyl).* Yield 100% (oil). This was used in the next step without further purification.

2dG *(R: o-methylphenyl).* Yield 52.2%: mp 78—79.5 °C (from isopropyl ether). IR: 3250, 1610.

1aG *(R: o-methylphenyl).* Yield 31.7%: mp 193—199 °C (from EtOH). IR: 3040, 1638. NMR: 2.33 (3H, s, ϕ-CH_3), 3.77 (3H, s, N-CH_3). UV: 244.5 (26900), 340 (6000). Found: C, 65.55; H, 4.71; N, 11.05%. Calcd for $C_{14}H_{12}N_2OS$: C, 65.60; H, 4.72; N, 10.93%.

2cH *(R: ethyl).* Yield 65.4%: mp 78.5—79.5 °C (from Ether). IR: 3100, 1670.

2dH *(R: ethyl).* Yield 55.9% (oil). IR: 3300, 1615.

1aH *(R: ethyl).* Yield 10.9%: mp 155.5—157 °C (from EtOH). IR: 3055, 1640. NMR: 1.37 (3H, t, J=7.4, $CH_2\underline{CH_3}$), 2.91 (2H, q, J=7.4, CH_2), 3.70 (3H, s, N-CH_3). UV: 241 (28900), 327 (4900). Found: C, 55.45; H, 5.23; N, 14.34%. Calcd for $C_9H_{10}N_2OS$: C, 55.65; H, 5.19; N, 14.42%.

*5) 6-Chloro-1-methyl-4-phenyl-1,2-dihydrothieno[2,3-*d*]-pyrimidin-2-ones (**1b**).* ***1bA—1bC, 1bG.***

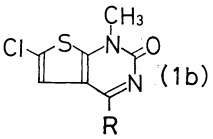

These were prepared by the method of Hromatka *et al.*[12] from 1-methyl-4-phenyl(or ethyl)-1,2-dihydrothieno[2,3-*d*] pyrimidin-2-one (**1a**) with sulfuryl chloride.

1bA *(R: phenyl).* Yield 64.8%: mp 136—140 °C (from EtOH). IR: 1673. NMR: 3.69 (3H, s, N-CH_3). UV: 252.5 (27100), 356 (6200). Found: C, 56.28; H, 3.72; N, 10.03%. Calcd for $C_{13}H_9N_2OSCl$: C, 56.42; H, 3.28; N, 10.12%.

1bB *(R: o-fluorophenyl).* Yield 24.0%: mp 192.5—194 °C (from EtOH). IR: 1677, 1622. NMR: 3.68 (3H, s, N-CH_3). UV: 251.5 (28300), 356 (6400). Found: C, 52.81; H, 2.65; N, 9.49%. Calcd for $C_{13}H_8N_2OSClF$: C, 52.98; H, 2.74; N, 9.50%.

1bC *(R: o-chlorophenyl).* Yield 52.4%: mp 164—166 °C (from EtOH–Ether). IR: 1677, 1600. NMR: 3.73 (3H, s, N-CH_3). UV: 250 (25400), 352 (6300). Found: C, 50.13; H, 2.50; N, 9.00%. Calcd for $C_{13}H_8N_2OSCl_2$: C, 50.18; H, 2.59; N, 9.00%.

1bG *(R: o-methylphenyl).* Yield 14.4%: mp 139—140 °C (from EtOH). IR: 1661, 1601. NMR: 2.34 (3H, s, ϕ-CH_3), 3.72 (3H, s, N-CH_3). UV: 249 (26800), 347 (6700). Found: C, 57.91; H, 3.85; N, 9.65%. Calcd for $C_{14}H_{11}N_2OSCl$: C, 57.83; H, 3.81; N, 9.63%.

*6) 5-Phenyl(or ethyl)-1,3-dihydro-2H-thieno[2,3-*e*]-1,4-diazepin-2-ones (**3c**).* ***3cA—3cC, 3cH.***

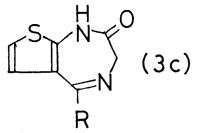

(3c)

Method:

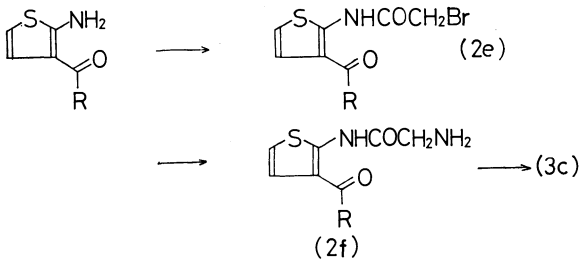

(2e)

(2f)

(3c)

3-Benzoyl(or propionyl)-2-bromoacetamido-thiophene (**2e**) was prepared from 2-amino-3-benzoyl(or propionyl)-thiophene with bromoacetylbromide. Ammonolysis of **2e** in chloroform saturated with gaseous ammonia afforded 2-aminoacetamido-3-benzoyl(or propionyl)-thiophene (**2f**), which was cyclized in dimethylsulfoxide at 100 °C to afford **3c**. The procedure was applied to the synthesis of benzodiazepine by Sternbach *et al.*[14]

2eA *(R: phenyl).* Yield 77.3%: mp 142—144 °C (from EtOH). IR: 3090, 3070, 1670, 1620.

2fA *(R: phenyl).* Yield 49.0%: mp 137.5—139 °C (lit[15], 145—147 °C).

3cA *(R: phenyl).* Yield 53.2%: mp 200.5—201.5 °C (lit[15], 203 °C).

2eB *(R: o-fluorophenyl).* Yield 77.1%: mp 101—102 °C (from Ether). IR: 3200, 1680, 1620.

2fB *(R: o-fluorophenyl).* Yield 79.1%: mp 127.5—129 °C (from CH_2Cl_2). IR: 3380, 3320, 3170, 3060, 1665, 1600.

3cB *(R: o-fluorophenyl).* Yield 75.4%: mp 201—201.5 °C from (EtOH). IR: 3060, 1685, 1615. NMR: 4.45 (2H, s, CH_2). UV: 242 (26600), 313 (2800). Found: C, 60.08; H, 3.43; N, 10.67%. Calcd for $C_{13}H_9N_2OSF$: C, 59.99; H, 3.49; N, 10.76%.

2eC *(R: o-chlorophenyl).* Yield 80.1%: mp 109—110 °C (from Ether). IR: 3060, 1670, 1600.

2fC *(R: o-chlorophenyl).* Yield 78.3%: mp 154—156 °C (from CH_2Cl_2). IR: 3390, 3320, 3220, 3050, 1685, 1635.

3cC *(R: o-chlorophenyl).* Yield 32.0%: mp 225—226 °C (from EtOH). IR: 3060, 1695, 1607. NMR: 4.47 (2H, s, CH_2). UV: 241 (22900), 311 (2900). Found: C, 56.68; H, 3.23; N, 10.04%. Calcd for $C_{13}H_9N_2OSCl$: C, 56.42; H, 3.28; N, 10.12%.

2eH *(R: ethyl).* Yield 68.7%: mp 107.5—108.5 °C (from Ether). IR: 3150, 3100, 1660, 1640.

2fH *(R: ethyl).* Yield 90.7%: mp 114—116 °C (from CH_2Cl_2). IR: 3400, 3340, 3150, 3080, 1640.

3cH *(R: ethyl).* Yield 17.0%: mp 137—140 °C (from Ether). IR: 3165, 3070, 1698, 1694, 1620. NMR: 1.16 (3H, t, $CH_2\underline{CH_3}$), 2.69 (2H, q, $CH_2\underline{CH_3}$), 4.19 (2H, s, $COCH_2N$)). UV: 233 (24200), 294 (3300). Found: C, 55.46; H, 5.08; N, 14.25%. Calcd for $C_9H_{10}N_2OS$: C, 55.65; H, 5.19; N, 14.42%.

7) 1-Methyl-5-phenyl(or ethyl)-1,3-dihydro-2H-thieno[2,3-e]-1,4-diazepin-2-ones (3a).

Method A: ***3aA—3aC, 3aH.*** These were prepared from 5-phenyl(or ethyl)-1,3-dihydro-2*H*-thieno[2,3-*e*]-1,4-diazepin-2-one (**3c**) with sodium hydride and methyliodide in the usual manner.[14]

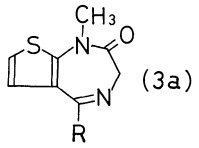

(3a)

3aA *(R: phenyl).* Yield 86%: mp 134—135 °C (from (EtOH). (lit, 136—137.5 °C).[15]

3aB *(R: o-fluorophenyl).* Yield 84.3%: mp 115.5—117 °C (from EtOH). IR: 3040, 1680, 1600. NMR: 3.50 (3H, s, N-CH_3), 4.44 (2H, s, CH_2). UV: 243 (25300), 315 (2800). Found: C, 61.37; H, 4.12; N, 10.20%. Calcd for $C_{14}H_{11}N_2OSF$: C, 61.29; H, 4.04; N, 10.21%.

3aC *(R: o-chlorophenyl).* Yield 56.0%: mp 109.5—111.0 °C (from Ether). IR: 3080, 3070, 1682. NMR: 3.52 (3H, s, N-CH_3), 4.47 (2H, s, CH_2). UV: 212.5 (27700), 240.5 (21600), 311 (2800). Found: C, 57.68; H, 3.66; N, 9.46%. Calcd for $C_{14}H_{11}N_2OSCl$: C, 57.83; H, 3.81; N, 9.64%.

3aH *(R: ethyl).* Yield 18.1%: mp 82—83 °C (from Ether). IR: 3040, 1682, 1627. NMR: 1.17 (3H, t, J=7.4, $CH_2\underline{CH_3}$), 2.68 (2H, q, J=7.4, $\underline{CH_2}CH_3$), 3.44 (3H, s, N-CH_3), 4.21 (2H, s, $COCH_2N$). UV: 235 (22000), 295 (3200). Found: C, 57.64; H, 5.75; N, 13.30%. Calcd for $C_{10}H_{12}N_2OS$: C, 57.67; H, 5.81; N, 13.45%.

Method B: ***3aD—3aG.***

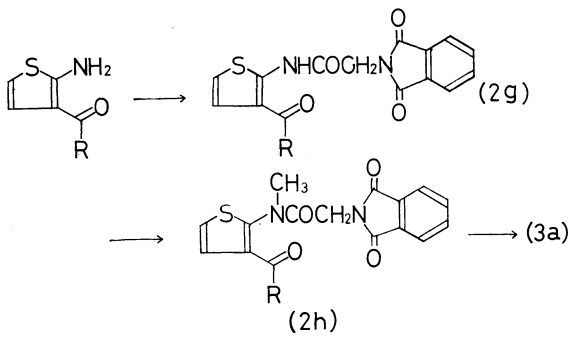

(2g)

(2h)

(3a)

3-Benzoyl-2-(*N*-phthalimidoacetyl)amino-thiophene (**2g**) was prepared from 2-amino-3-benzoylthiophene with phthaloylimidoacetylchloride. Methylation of **2g** with sodium hydride and methyliodide in the usual manner afforded 3-benzoyl-2-(*N*-methyl-*N*-phthalimidoacetyl)amino-thiophene (**2h**), which was treated with hydrazine hydrate to afford **3a**.[16]

2gD *(R: o-bromophenyl).* Yield 69.3%: mp 205—208 °C (from Acetone). IR: 3200, 3100, 1780, 1720, 1705, 1615.

2hD *(R: o-bromophenyl).* Yield 58.4%: mp 170—172 °C (from Acetone). IR: 1765, 1725, 1690, 1650.

3aD *(R: o-bromophenyl).* Yield 31.7%: mp 109—113 °C (from EtOH). IR: 3080, 3060, 1677. NMR: 3.51 (3H, s, N-CH_3), 4.46 (2H, s, CH_2). UV: 215 (26200), 240 (20500), 312 (2700). Found: C, 49.85; H, 3.46; N, 8.51%. Calcd for $C_{14}H_{11}N_2OSBr$: C, 50.16; H, 3.31; N, 8.36%.

2gE *(R: o-iodophenyl).* Yield 50.2%: mp 206—208 °C (from Acetone). IR: 3230, 1775, 1720, 1690, 1610.

2hE *(R: o-iodophenyl).* Yield 71.1%: mp 167—175 °C (from Acetone). IR: 3110, 1770, 1725, 1695, 1650, 1620.

3aE *(R: o-iodophenyl).* Yield 45.4%: mp 136—137.5 °C (from EtOH). IR: 3045, 1679, 1669. NMR: 3.53 (3H, s, N-CH_3), 4.46 (2H, s, CH_2). UV: 220 (28000), 313 (2700). Found: C, 43.91; H, 2.84; N, 7.22%. Calcd for $C_{14}H_{11}N_2OSI$: C, 43.99; H, 2.90; N, 7.33%.

2gF *(R: p-chlorophenyl).* Yield 78.4%: mp 215—216 °C (from Acetone). IR: 3220, 1765, 1710, 1605.

2hF *(R: p-chlorophenyl).* Yield 78.5%: mp 211—212 °C (from Acetone). IR: 3080, 1765, 1720, 1680, 1660.

3aF *(R: p-chlorophenyl).* Yield 76.5%: mp 139.5—141 °C (from EtOH). IR: 3040, 1678. NMR: 3.49 (3H, s, N-CH_3), 4.40 (2H, s, CH_2). UV: 251 (30100), 317 (2900). Found: C, 57.77; H, 3.71; N, 9.60%. Calcd for $C_{14}H_{11}N_2OSCl$: C, 57.83; H, 3.81; N, 9.64%.

2gG *(R: o-methylphenyl).* Yield 42.6%: mp 211—213 °C (from Acetone). IR: 3250, 3050, 1775, 1720, 1690.

2hG *(R: o-methylphenyl).* Yield 78.0%: mp 153.5—155 °C (from Acetone). IR: 3100, 1765, 1720, 1690, 1640.

3aG *(R: o-methylphenyl).* Yield 74.0%: mp 125—127 °C (from EtOH). IR: 3075, 1675, 1612, 1605. NMR: 2.08 (3H, s, ϕ-CH_3), 3.53 (3H, s, N-CH_3), 4.45 (2H, s, CH_2). UV: 240 (24700), 307 (2900). Found: C, 66.64; H, 5.21; N, 10.28%. Calcd for $C_{15}H_{14}N_2OS$: C, 66.64; H, 5.22; N, 10.36%.

*8) 7-Chloro-1-methyl-5-phenyl(or ethyl)-1,3-dihydro-2H-thieno[2,3-e]-1,4-diazepin-2-ones (**3b**), **3bA—3bF**, **3bH**.*

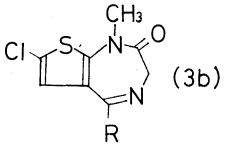

(3b)

These were prepared by the method of Hromatka *et al.*[12] from 1-methyl-5-phenyl(or ethyl)-1,3-dihydro-2*H*-thieno[2,3-*e*]-1,4-diazepin-2-one (**3a**) with sulfuryl chloride.

3bA *(R: phenyl).* Yield 80.0%: mp 117.5—119.0 °C (from EtOH), (lit[12], 120—122 °C).

3bB *(R: o-fluorophenyl).* Yield 73.5%: mp 101.5—103 °C (from IPA). IR: 1693, 1681, 1613. NMR: 3.43 (3H, s, N-CH_3), 4.44 (2H, s, CH_2). UV: 244 (24200), 320 (2900). Found: C, 54.25; H, 3.17; N, 8.81%. Calcd for $C_{14}H_{10}N_2OSClF$: C, 54.45; H, 3.26; N, 9.07%.

3bC *(R: o-chlorophenyl).* Yield 28.0%: mp 82.5—84 °C (from Ether). IR: 1692. NMR: 3.47 (3H, s, N-CH_3), 4.47 (2H, s, CH_2). UV: 243 (20800), 319 (2900). Found: C, 51.62; H, 3.22; N, 8.47%. Calcd for $C_{14}H_{10}N_2OSCl$: C, 51.70; H, 3.10; N, 8.62%.

3bD *(R: o-bromophenyl).* Yield 49.2%: mp 86—89 °C (from Ether). IR: 1690. NMR: 3.46 (3H, s, N-CH_3), 4.46 (2H, s, CH_2). UV: 242 (20200), 319 (3000). Found: C, 45.95; H, 2.75; N, 7.60%. Calcd for $C_{14}H_{10}N_2OSBrCl$: C, 45.49; H, 2.73; N, 7.58%.

3bE *(R: o-iodophenyl).* Yield 32%: mp 217—221 °C (hydrochloride), (from EtOH). IR: 3110, 3035, 2350 (broad), 1905, 1720, 1633. NMR (Measured as a free base): 3.48 (3H, s, N-CH_3), 4.46 (2H, s, CH_2). Found: C, 36.98; H, 2.41; N, 6.10%. Calcd for $C_{14}H_{10}N_2OSClI \cdot HCl$: C, 37.11; H, 2.45; N, 6.18%.

3bF *(R: p-chlorophenyl).* Yield 83.5%: mp 212—213.5 °C (from $CHCl_3$-EtOH). IR: 1693, 1678. NMR: 3.44 (3H, s, N-CH_3), 4.42 (2H, s, CH_2). UV: 251 (27200), 323 (2900). Found: C, 51.58; H, 3.09; N, 8.43%. Calcd for $C_{14}H_{10}N_2OSCl_2$: C, 51.71; H, 3.10; N, 8.61%.

3bH *(R: ethyl).* Yield 16.0%: mp 76.5—77.5 °C (from Ether). IR: 1680, 1620. NMR: 1.18 (3H, t, J=7.3, $CH_2\underline{CH}_3$), 2.65 (2H, q, J=7.3, $\underline{CH}_2CH_3$), 3.40 (3H, s, N-CH_3), 4.24 (2H, s, CH_2). Found: C, 49.45; H, 4.45; N, 11.29%. Calcd for $C_{10}H_{11}N_2OSCl$: C, 49.49; H, 4.57; N, 11.54%.

*9) 1-Methyl-5-phenyl(or ethyl)-1,3-dihydro-2H-thieno[2,3-e]-1,4-diazepin-2-one-4-oxides (**4a**), **4aA—4aE**, **4aG**, **4aH**.*

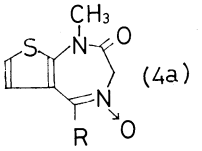

(4a)

Method: These were prepared by the method of Hromatka *et al.*[15] from 1-methyl-5-phenyl(or ethyl)-1,3-dihydro-2*H*-thieno[2,3-*e*]-1,4-diazepin-2-one (**3a**) with *m*-chloroperbenzoic acid.

4aA *(R: phenyl).* Yield 67.0%: mp 158—159 °C (from EtOH-CCl_4). IR: 3070, 1688. NMR: 3.53 (3H, s, N-CH_3), 4.73 (2H, s, CH_2). UV: 245 (20500), 313 (7700). Found: C, 61.26; H, 4.46; N, 9.96%. Calcd for $C_{14}H_{12}N_2O_2S$: C, 61.70; H, 4.40; N, 10.30%.

4aB *(R: o-fluorophenyl).* Yield 83.0%: mp 80.5—85 °C (from EtOH). IR: 3400, 3070, 3020, 1688, 1679, 1609. NMR (Measured after removal of crystalline ethanol): 3.57 (3H, s, N-CH_3), 4.78 (2H, s, CH_2). UV: 246 (20600), 267 (17200), 310 (6900). Found: C, 57.08; H, 5.19; N, 8.20%. Calcd for $C_{14}H_{11}N_2O_2SF \cdot C_2H_5OH$: C, 57.13; H, 5.10; N, 8.33%.

4aC *(R: o-chlorophenyl).* Yield 73.5%: mp 163—163.5 °C (from EtOH-CCl_4). IR: 3050, 1696. NMR: 3.57 (3H, s, N-CH_3), 4.77 (2H, s, CH_2). UV: 249 (19700), 310 (6400). Found: C, 54.77; H, 3.55; N, 8.93%. Calcd for $C_{14}H_{11}N_2O_2SCl$: C, 54.82; H, 3.62; N, 9.13%.

4aD *(R: o-bromophenyl).* Yield 61.0%: mp 162—163.5 °C (from EtOH-CCl_4). IR: 3100, 1685. NMR: 3.59 (3H, s, N-CH_3), 4.77 (2H, s, CH_2). UV: 254 (19400), 310 (5800). Found: C, 47.52; H, 3.03; N, 7.70%. Calcd for $C_{14}H_{11}N_2O_2SBr$: C, 47.88; H, 3.16; N, 7.98%.

4aE *(R: o-iodophenyl).* Yield 18.2%: mp 161 °C (decomp.) (from EtOH-CCl_4). IR: 3100, 3080, 1671. NMR: 3.60 (3H, s, N-CH_3), 4.78 (2H, s, CH_2). UV: 229.5 (24400), 252 (19800), 305 (sh) (6700). Found: C, 42.35; H, 2.66; N, 7.00%. Calcd for $C_{14}H_{11}N_2O_2SI$: C, 42.23; H, 2.78; N, 7.03%.

4aG *(R: o-methylphenyl).* Yield 54.7%: mp 149.5—150.5 °C (from EtOH). IR: 3115, 1687. NMR: 2.24 (3H, s, ϕ-CH_3), 3.61 (3H, s, N-CH_3), 4.78 (2H, s, CH_2). UV: 242.5 (21100), 275 (20400), 305 (7100). Found: C, 62.76; H, 5.14; N, 9.70%. Calcd for $C_{15}H_{14}N_2O_2S$: C, 62.92; H, 4.93; N, 9.78%.

4aH *(R: ethyl).* Yield 46.8%: mp 169—171.5 °C (from EtOH-Ether). IR: 3075, 3050, 1690. NMR: 1.20 (3H, t, $CH_2\underline{CH}_3$), 2.85 (2H, q, $\underline{CH}_2CH_3$), 3.54 (3H, s, N-CH_3), 4.62 (2H, s, CH_2). UV: 254.5 (22500), 298 (5800). Found: C, 53.61; H, 5.40; N, 12.52%. Calcd for $C_{10}H_{12}N_2O_2S$: C, 53.55; H, 5.40; N, 12.49%.

*10) 7-Chloro-1-methyl-5-phenyl(or ethyl)-1,3-dihydro-2H-thieno[2,3-e]-1,4-diazepin-2-one-4-oxides (**4b**).*

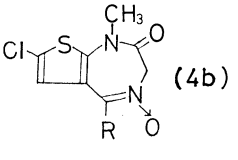

(4b)

Method A: ***4bA***, ***4bB***. These were prepared by the method of Hromatka *et al.*[12] from 1-methyl-5-phenyl-1,3-dihydro-2*H*-thieno-[2,3-*e*]-1,4-diazepin-2-one-4-oxide(**4a**) with sulfurylchloride.

4bA *(R: phenyl).* Yield 40.1%: mp 194—195 °C (from EtOH-CCl_4). IR: 3075, 1691. NMR: 3.48 (3H, s, N-CH_3), 4.74 (2H, s, CH_2). UV: 243 (23600), 275 (18100), 315 (sh) (6900). Found: C, 54.96; H, 3.64; N, 9.11%. Calcd for

$C_{14}H_{11}N_2O_2SCl$: C, 54.81; H, 3.61; N, 9.13%.

4bB *(R: o-fluorophenyl).* Yield 83.2%: mp 153—154 °C (from *n*-Hexane–Ether). IR: 1693, 1680. NMR: 3.50 (3H, s, N-CH_3), 4.78 (2H, s, CH_2). UV: 242.5 (23900), 269.5 (21800), 315 (sh) (6200). Found: C, 52.08; H, 3.08; N, 8.41%. Calcd for $C_{14}H_{10}N_2O_2SClF$: C, 51.78; H, 3.10; N, 8.62%.

Method B: ***4bC***, ***4bH***. These were prepared by the method of Hromatka *et al.*[15] from 7-chloro-1-methyl-5-phenyl-(or ethyl)-1,3-dihydro-2*H*-thieno[2,3-*e*]-1,4-diazepin-2-ones (**3b**) with *m*-chloroperbenzoic acid.

4bC *(R: o-chlorophenyl).* Yield 54.3%: mp 95—97 °C (from CCl_4). IR: 1710, 1678. NMR: 3.51 (3H, s, N-CH_3), 4.79 (2H, s, CH_2). UV: 250 (21700), 265 (22000), 315 (sh) (5500). Found: C, 36.47; H, 2.09; N, 5.57%. Calcd for $C_{14}H_{10}N_2O_2SCl_2 \cdot CCl_4$: C, 36.39; H, 2.04; N, 5.66%.

4bH *(R: ethyl).* Yield 25.2%: mp 171—172 °C (from Ether). IR: 1689. NMR: 1.19 (3H, t, J=7.4, $CH_2\underline{CH_3}$), 2.78 (2H, q, J=7.4, $\underline{CH_2}CH_3$), 3.48 (3H, s, N-CH_3), 4.63 (2H, s, CH_2). Found: C, 46.52; H, 4.63; N, 10.88%. Calcd for $C_{10}H_{11}N_2O_2SCl$: C, 46.42; H, 4.29; N, 10.83%.

The authors express their deep gratitude to Prof. Masamichi Tsuboi, the University of Tokyo, and Dr. Makoto Sunagawa in this laboratory for their guidance and encouragement throughout this work. They are also indebted to Mr. Tadashi Doi and Miss Keiko Kawazoe for measurement of the UV spectra, and to Mr. Hiromi Sato for his co-operation in the synthetic experiments.

References

1) M. L. Martin, C. Andrieu, and G. J. Martin, *Tetrahedron Lett.*, **1966**, 921.
2) M. L. Martin, C. Andrieu, and G. J. Martin, *Bull. Soc. Chim. Fr.*, **1968**, 698.
3) C. Andrieu, M. L. Martin, and G. J. Martin, *ibid.*, **1968**, 703.
4) G. W. Gribble and F. P. Bousquet, *Tetrahedron*, **27**, 3785 (1971).
5) B. Roques, S. Combrisson, C. Riche, and C. Pascard-Billy, *ibid.*, **26**, 3555 (1970).
6) J. A. Weil, A. Blum, A. H. Heiss, and J. K. Kinnaird, *J. Chem. Phys.*, **46**, 3132 (1967).
7) H. P. Figeys and R. Flammang, *Mol. Phys.*, **12**, 581 (1967).
8) Y. Nomura and Y. Takeuchi, *Tetrahedron Lett.*, **1968**, 5585; *ibid.*, **1968**, 5665.
9) C. E. Johnson, Jr. and F. A. Bovey, *J. Chem. Phys.*, **29**, 1012 (1958).
10) K. Gewald, *Chem. Ber.*, **98**, 3571 (1965).
11) M. Robba, Jeanne-Merie Lecomte, and M. C. Sevricourt, *C. R. Acad. Sci. Paris*, **267**, 697 (1968).
12) O. Hromatka, D. Binder, C. R. Noe, P. Stanetty, and W. Veit, *Monats. Chem.*, **104**, 715 (1973).
13) H. Ott and M. Denzer, *J. Org. Chem.*, **33**, 4263 (1968).
14) L. H. Sternbach, R. I. Fryer, W. Metlesics, E. Reeder, G. Sach, G. Saucy, and A. Stempel, *J. Org. Chem.*, **27**, 3788 (1962).
15) O. Hromatka and D. Binder, *Monatsh. Chem.*, **104**, 704 (1973).
16) *Chem. Abstr.*, **64**, 5120h (1966).
17) L. Pauling, "The Nature of the Chemical Bond," Cornell University Press, New York (1960), p. 260.

Studies of the Crystallization Processes of *N*-Methylquinolinium TCNQ Ion-radical Salts

Mutsuaki MURAKAMI and Susumu YOSHIMURA

Matsushita Research Institute Tokyo, Inc., Ikuta, Tama-ku, Kawasaki 214

(Received March 22, 1974)

We studied the crystallization processes of the complex ion-radical salt of 7,7,8,8-tetracyanoquinodimethan (TCNQ) and the *N*-methylquinolinium cation. A variety of solvents, rates of crystallization, and concentrations of the solution gave three groups of crystals. The crystals in the first group, which were crystallized as black rods, occluded the solvent molecules in the crystals, and their resistivities were in the range of 2.8—26 Ω cm. Those in the second group were crystallized into the form of fine needles or fine powders. Although the TCNQ-to-cation ratios in the salts varied from 1.6 to 2.2, their electrical resistivities were almost all the same (about 1.0 Ω cm), and these crystals were thought to have a metastable crystal structure. The crystals in the third group were crystallized in the form of triclinic prisms, which belonged to a stable crystal of a high resistivity (1100 Ωcm). The appearance of multiple forms is interpreted on the basis of Ostwald's "Law of Stages" of crystallization and also on the basis of information on the structures of the one-dimensional TCNQ columns of the other complex ion-radical salts of TCNQ.

Molecular compounds based on 7,7,8,8-tetracyanoquinodimethane (TCNQ) have attracted much attention in studying the behavior of electrons in the molecular crystals, because they exhibit a wide range of resistivity, 10^{-3}—10^{11} Ω cm, and also because their physical properties can, in some cases, be regarded as attributes of a one-dimensional conductor.[1] A great effort to synthesize new materials of TCNQ has led to discoveries of various kinds of phase transitions[2-7] and also of the possibility of high-temperature superconductivity.[8] The wide range of the physical properties of the TCNQ compounds is due to their possibility of being crystallized in a variety of forms. There are two limits of crystal structure, between which many variations exist, depending upon the kind and nature of the second component. One structure, which is generally found in compounds called "non-ionic charge-transfer complexes" is characterized by alternating stacks of TCNQ and the second molecule (donor), the mode of the overlap of the two neighboring molecules being nearly direct. The other is a structure in which the TCNQ molecules are stacked plane-to-plane with each other. The latter type of crystal is usually found in the ion-radical salts formed between TCNQ and organic or metallic cations and is believed to contribute to the high conductivity. It has been suggested by various works on the crystallization of the TCNQ molecular compounds that the crystal structure and the physical properties of the compounds are determined not only by the nature of the second component, but also notably by the crystallization processes. This statement may be illustrated by the following four phenomena: (1) The appearance of polymorphic modifications in simple salts of 3,3'-diethylthiacarbocyanium,[9] Rb[10,11] and *N*-methylphenazinium cations.[12] (2) Compounds of different stoichiometries, such as 1:2 salts of various onium cations, 2:3 salts of Cs,[13] morpholinium,[5] trimethylammonium,[14] and *N*-methylquinolinium cations.[15] (3) Unstable crystals, such as morpholinium$_3$(TCNQ)$_4$,[5] *N*-ethylquinolinium(TCNQ)$_2$[15] and methyldiethylcyclohexylammonium(TCNQ)$_2$.[15] (4) The formation of solvent-inclusion compounds such as benzidine·TCNQ(BD·TCNQ).[16,17]

In this paper we wish to report our experimental results on the crystallization of an ion-radical salt formed from the *N*-methylquinolinium (MeQ) cation and TCNQ and show that the MeQ·TCNQ salt can be crystallized either of the above four types of crystals. We will also discuss the effect of the crystallization process on the resulting forms of crystals, considering the unstable nature of the one-dimensional TCNQ columns, and will report that the appearance of multiple forms can be commonly observed in the TCNQ ion-radical salts.

Experimental

Materials. Crude TCNQ was refluxed for several hours with active carbon in acetonitrile; the filtered solution had then been allowed to stand overnight, orange crystals of TCNQ were collected. This procedure was repeated several times.

For the preparation of MeQ(TCNQ)$_x$ salts, *N*-methylquinolinium iodide and a two-molar excess of TCNQ were dissolved and mixed in a boiling solvent. After a suitable period, the crystals were collected, washed with the solvent, and finally washed with ether.

Determination of the Molecular Ratio of TCNQ to the Cation. The accuracy of the elemental analysis of TCNQ was too poor for us to assess the amount of the excess neutral TCNQ molecules in the salt, because the complete combustion of the salt was difficult to achieve. The electronic absorption spectrum was adopted instead. The electronic spectra of TCNQ salts in acetonitrile of high purity were measured with a Cary 14R spectrometer. Acetonitrile was purified by repeated distillations over a small amount of Li(TCNQ). The spectrum was considered to be the overlap of the absorptions of both $TCNQ^0$ and $TCNQ^-$. The value of the molar extinction coefficient for $TCNQ^0$ was 68000 $l \cdot mol^{-1} \cdot cm^{-1}$ at the wavelength of 395 nm. The coefficient of $TCNQ^-$ was obtained from the simple salt of MeQ(TCNQ), which exhibited two major maxima, at 420 and 842 nm, with coefficients of 26800 and 51600 $l \cdot mol^{-1} \cdot cm^{-1}$ respectively; the coefficient at 395 nm was 21800 $l \cdot mol^{-1} \cdot cm^{-1}$. We obtained the molar ratios of TCNQ to the MeQ cation from the following equation, assuming that the $TCNQ^0$-to-cation ratio is the same as the $TCNQ^0$-to-$TCNQ^-$ ratio:

$$TCNQ/MeQ = 1 + (\varepsilon^{-}_{842}/\varepsilon^{0}_{395})(r_2 - r_1)$$

where r_1 and r_2 are the ratios of the optical density at 395 nm to that at 842 nm in the absorption spectra of the simple and complex salts respectively (r_1=0.422) and where ε^{-}_{842} and ε^{0}_{395} are the molar extinction coefficients of $TCNQ^-$ at 842 nm (51600) and of $TCNQ^0$ at 395 nm (68000) respectively. In a conventional calculation,[18] a value of r_1 obtained from Li(TCNQ) has been used instead of that from the corresponding simple salt, but there may be no reason for believing that the absorption coefficient of $TCNQ^-$ is always the same, regardless of the kind of cation component.[19]

Measurements of Electrical Resistivity and Activation Energy. The resistivity data at room temperature were obtained on pressed pellets 13 mm in diameter, and about 5 mm thick, with four-probe electrodes pressed on the pellets with a resistivity-measuring apparatus, Model VR 4 (Kokusai Electric Co., Ltd.). For the activation-energy measurements (from −50 to 50 °C), samples in the form of pressed rods 3 mm in diameter and about 10 mm in length were prepared; on them four-point contacts were made with silver paint.

Measurement of Infrared Absorption Spectra. The infrared absorption spectra were measured using the method of Nujol mull with a Hitachi grating infrared spectrometer, Model 215, in the wave number range between 4000 and 650 cm^{-1}. In case of highly-conducting salts, special care was required in the preparation of a uniform film in order to avoid the scattering of light.

Other Measurements. The measurements of differential scanning calorimetry (DSC) and thermogravimetric analysis (TGA) were made with Shimadzu thermoflex apparatuses, SC-20 and TG-20, in a nitrogen gas atmosphere and at a heating rate of 5 °C/min.

The X-ray diffraction patterns of powder samples were obtained at room temperature with a Philips PW 1051 X-ray diffractometer by the use of a copper-Kα line.

Results and Discussion

Multiple Forms of MeQ·TCNQ Salts and Their Classification. The experimental results of the crystallization of the salts formed from the MeQ cation with TCNQ are shown in Table 1, which also summarizes the relative intensities of the electronic absorptions at 395 and 842 nm of acetonitrile solutions, the cation-to-TCNQ ratio, the crystal forms and the electrical properties at room temperature. The first typical feature of the results is that the molar ratio of the MeQ cation to TCNQ could not be assigned to an integer ratio of 1:2 or 2:3, but varied from 1.6 to 2.2 with the kind of solvent. When acetone was used as the solvent, fine needle crystals ($MeQ(TCNQ)_{1.6}$) appeared first, and then triclinic prism crystals ($MeQ(TCNQ)_{2.1}$) were obtained after a day. The second feature is that the apparent form of the crystal varied with the method of preparation; three different forms were recognized, apart from the crystal in the form of fine powders reprecipitated in cold water from a hot dimethylformamide solution (IIc). They were a rod, a fine needle, and a triclinic prism. The electrical resistivity corresponded to the crystal form and not to the content of neutral TCNQ molecules. The crystals in the form of black rods exhibited relatively low resistivities (from 2.8 to 26 Ω cm). The lowest resistivity was found in the fine needle crystal, while the highest was found in the triclinic prism crystal. The reprecipitated fine powders have almost the same resistivity as that of fine needle crystals, so they can be classified into the same group.

At this stage we can classify these crystals into three groups on the basis of both their crystal forms and their resistivities. The first group, I, consists of two compounds with relatively low resistivities which were crystallized in the form of black rods from acetonitrile and nitromethane solutions. The II group includes three types of highly-conducting crystals. The first of them, IIa, was crystallized from dichloromethane, and the second, IIb, from an acetone solution. Both of them were in the form of fine, black needles; they could be formulated as $MeQ(TCNQ)_{2.2}$ and $MeQ(TCNQ)_{1.6}$, respectively The last sample of this group, IIc, is $MeQ(TCNQ)_{2.2}$, which was obtained in the form of a fine powder. We single out as a III group the salt of the highest resistivity, $MeQ(TCNQ)_{2.1}$, which was crystallized in the form of a triclinic prism. In works by Melby *et al.*[13] and Siemons, Bierstedt, and Kepler,[20] the $MeQ(TCNQ)_x$ salt synthesized in an acetonitrile solution was regarded as a stoichiometric 1:2 complex. However, it is one of the multiple forms of $MeQ(TCNQ)_x$ salts, because Frandois *et al.*[15] have reported a crystal of 2:3 stoichiometry from an acetonitrile solution.

Figure 1 shows the infrared spectra of the six crystals obtained. The IR spectra are also divided into three groups which strictly correspond to the above classification based on the crystal forms and resistivities. The optical absorption spectra of the TCNQ ion-radical salts in both infrared and visible regions reflect the structure of the TCNQ columns. Broadenings of the vibrational bands in the infrared range from 2500 to 700 cm^{-1} are generally observed and may reasonably be related to the electron delocali-

TABLE 1. CHARACTERISTIC PROPERTIES OF $MeQ(TCNQ)_x$ COMPLEX SALTS

Solvent	Electronic spectra r_2 ($\varepsilon_{395}/\varepsilon_{842}$)	Composition (Cation: TCNQ)	Crystal form	Resistivity ρ_{20} (Ω cm)	Activation energy E (eV)	Classification
CH_3CN	1.16	1: 1.6	Rod	2.8	0.07	Ia
CH_3NO_2	1.58	1: 1.9	Fine rod	26	0.13	Ib
CH_2Cl_2	1.95	1: 2.2	Fine needle	1.0	0.05	IIa
$(CH_3)_2CO$	1.17	1: 1.6	Needle	0.8	0.06	IIb
H_2O[a]	2.04	1: 2.2	Powder	1.0	0.05	IIc
$(CH_3)_2CO$[b]	1.85	1: 2.1	Triclinic prism	1100	0.20	III

a) Reprecipitated in H_2O. b) See text.

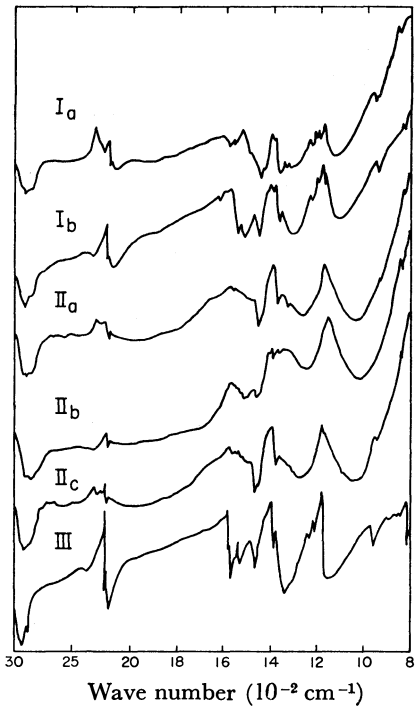

Fig. 1. Infrared absorption spectra of MeQ(TCNQ)$_x$ salts.

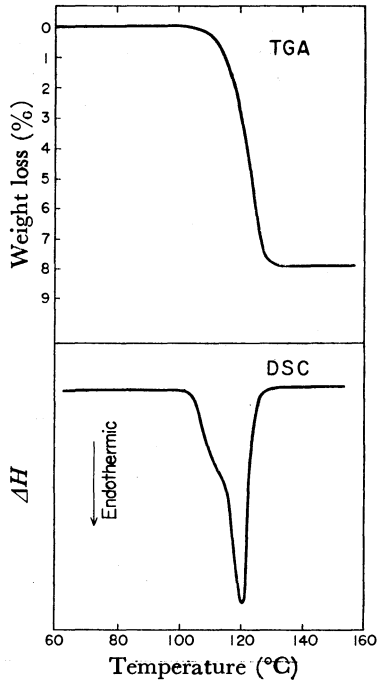

Fig. 2. Thermogravimetric analysis (TGA) and differential scanning calorimetry (DSC) curves of IIa MeQ(TCNQ)$_{1.6}$(CH_3CN).

zation and then to the orderliness of the TCNQ columns. Especially, the bands from 1100 to 1300 cm^{-1} in the spectra of highly-conducting TCNQ complexes are not due to pure intramolecular vibrations, but to some kind of vibronic interaction of conduction electrons with intramolecular TCNQ vibrations.[21]

At first, the spectra will be compared with the spectrum of a thin film of quinolinium(TCNQ)$_2$, Q(TCNQ)$_2$,[22] which exhibits a considerably broader CN stretching band at 2210—2000 cm^{-1}, with sharp lines at 2206 and 2199 cm^{-1}, and strong bands at 1270 and 1050 cm^{-1}, corresponding to, respectively, the CH bending and C–CN stretching modes of the TCNQ molecules.[23,24] The low-resistivity crystal, II, had the pattern most similar to that of Q(TCNQ)$_2$, and the coincidence of the positions and width of the CH bending and C–CN stretching bands was fairly good. The bands of the III crystal were less broad and appeared at a higher-energy side than in the case of either II or Q(TCNQ)$_2$. For example, peaks were found at 1300 cm^{-1} for the CH bending band and at 1130 cm^{-1} for the C–CN stretching band. The IR spectrum of the III-type crystal suggests that there is a different TCNQ column structure, probably with considerable distortions, which will give rise to electron localization and then to an increase in the values of both the resistivity and the activation energy. The I-type crystals, although they had as low resistivity as II, exhibited different patterns. The poor resolution and large broadening of the CN stretching band at about 2210 to 2000 cm^{-1} are similar to those of the low-resistivity crystal, II, but the positions of both the CH bending band (about 1320 cm^{-1}) and the C–CN stretching band (about 1120 cm^{-1}) are more similar to those of the intermediate resistivity compound, III.

The I-Type Crystals, Inclusion Compounds. The thermogravimetric analysis of the MeQ(TCNQ)$_x$ salts revealed that only the crystals classified as I suffered a weight loss. The TGA curves for Ia are shown in Fig. 2. For single crystals of Ia and Ib, the magnitudes of the losses were 8 and 10% in weight respectively, while the temperatures at which the weight started to decrease were 110 and 90 °C respectively. The loss component was trapped in a cell cooled with dry ice and was confirmed by means of the infrared absorption spectrum to be due to the escape of included solvent molecules, namely, acetonitrile for Ia and nitromethane for Ib. The amount of the included solvent was estimated from the magnitude of the loss; it was found that one mole of the solvent molecules was included per mole of the MeQ cation.

Measurements of differential scanning calorimetry (DSC) were made on Ia and Ib; endothermic peaks which exactly corresponded to the TGA curves were thus observed. The result for Ia is also shown in Fig. 2. The magnitudes of the heat associated with the transformation were ΔH=19.1 kcal/mol for Ia and 18.1 kcal/mol for Ib.

It is concluded that the MeQ(TCNQ)$_x$ salts classified as I in the previous section included solvent molecules in the crystal, while the crystals in the other groups did not. The factor determining the type of salt was the kind of solvent used in the preparation, and the included solvents were weakly bound in the host lattice and could leave it easily.

In the case of a BD·TCNQ system,[16,17] which is another example of the formation of inclusion compounds, the main factor determining the type of complex is the solvent used in the preparation. When the

molecular volume of the solvent is smaller than 75 cm^3/mol, the BD·TCNQ crystal includes the solvent, while the crystal does not include solvent molecules larger in volume than 80 cm^3/mol. The situation seems to be the same in the case of the MeQ(TCNQ)$_x$ salts. For example, the molecular volumes of the included acetonitrile and nitromethane are 52.2 and 53.7 cm^3/mol respectively, while the solvents not included were dichloromethane and acetone, their molecular volumes being 64.0 and 73.6 cm^3/mol respectively. The heat associated with the evaporation of the solvent molecules from the MeQ·TCNQ system is comparable with that of the solvents from the BD·TCNQ system, which has been reported to be 11.1 kcal/mol. It is striking that the two systems, which differ so sharply in crystal structure, exhibited similar behavior of solvent evaporation. These results suggest that the state of the solvent molecules is essentially the same for both the systems and that the solvent molecules may be situated in a site very weakly affected by the kind of donor or cation molecules.

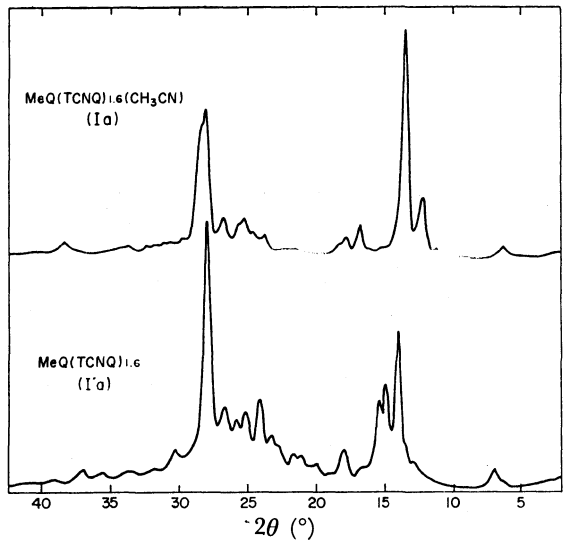

Fig. 3. X-ray diffraction patterns of MeQ(TCNQ)$_x$ salts. Ia: MeQ(TCNQ)$_{1.6}$(CH_3CN) and Ia': MeQ(TCNQ)$_{1.6}$.

The X-ray powder diffraction patterns of the Ia crystal and those treated at 120 °C for 30 min, Ia', are shown in Fig. 3. The pattern of Ia' was quite different from that of Ia; that is, the peaks of Ia at $2\theta=11.95$, 12.87, 12.96, and 27.51° disappeared after heat treatment, resulting in new peaks of Ia' at 13.50, 14.96, and 27.34°. The resistivities of these salts also changed from 2.8 Ω cm to about 3000 Ω cm. On the other hand, when Ia' was exposed to the vapor of acetonitrile in a low vacuum (about 100 mmHg) overnight at room temperature, the X-ray pattern became identical with that of Ia and the resistivity was restored to 4.0 Ω cm. Therefore, it is likely that when the solvent molecules leave the crystal, the crystal structure is greatly changed and that, when exposed to the vapor of a suitable solvent, the solvent molecules can easily be included in the crystal, thus restoring the initial structure. These properties are again in accord with the case of the BD·TCNQ system.

When IIa and III were exposed to the vapor of acetonitrile using the same method, the resistivity changed from 1.0 to 2.8 Ω cm for IIa and from 1100 to 5.0 Ω cm for III. From TGA measurements, the contents of acetonitrile molecules of the transformed crystals of IIa and III were determined to be 0.86 mol for the former and 0.90 mol for the latter per mole of the MeQ cation. This fact shows that the formation of the solvent-including salts does not depend on the initial crystal structure; all the crystals can include solvent molecules of a suitable size.

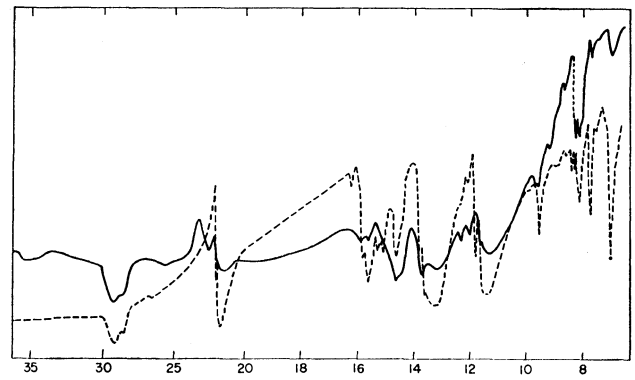

Fig. 4. Infrared absorption spectra of Ia: MeQ(TCNQ)$_{1.6}$(CH_3CN) (——) and Ia': MeQ(TCNQ)$_{1.6}$ (------).

The infrared spectrum of Ia' is shown in Fig. 4. As with the results of solvent evaporation, the resolution of the spectrum became relatively good and the width of the CN stretching band of TCNQ at 2200 cm^{-1} became narrower than that of Ia. On the contrary, the position of the characteristic bands, the CN stretching, CH bending, and C–CN stretching bands, remained unchanged. From these results, we will make some speculations on the mode of change in the TCNQ column structure, referring to the case of the BD·TCNQ system.[25,26] In a BD·TCNQ(S) crystal (where S stands for a solvent molecule), the BD and TCNQ molecules completely overlap each other to make columns as well as ordinary charge-transfer complexes, while the solvent molecules are situated in the channels between the BD·TCNQ columns and also form parallel columns. It has also been reported that the structure of the BD·TCNQ columns of the inclusion compound is almost the same as that of the solvent-free compound and that the spacings between the column axes of the latter compound are smaller than those of the former. The small change in the IR structure of the MeQ(TCNQ)$_x$(S) crystal suggests little change in the TCNQ column structure, thus excluding the possibility that the solvent molecules are located in the TCNQ columns. They may, thereby, be bound in the channels between the columns, as in the case of the BD·TCNQ system. Crystallographical studies of low-conductive TCNQ ion radical salts with 1:2[24] and 2:3 stoichiometries[27] show that there are relatively large hollows in the columns of the cation, hollows which correspond to the periodic distortions between two $TCNQ^-$'s of the

TCNQ columns. These hollows are thought to be the most probable sites for the solvent molecules. The solvent molecules have only the $TCNQ^-$ in their nearest neighbors; this is in contrast with the cations, which have both $TCNQ^0$ and $TCNQ^-$. This structure explains the low resistivity of the solvent-including crystals because the higher resistivity of the crystals with a distorted TCNQ column structure is caused by the intermolecular repulsion between the neighboring $TCNQ^-$ molecules. The X-ray powder patterns of Ia and Ia′ also support the above structure. A detailed discussion of the patterns and the mechanism of the transformation will be presented elsewhere.[28]

The resistivity, the infrared spectrum, and the X-ray powder pattern of the transformed crystal, Ia′, were very similar to those of the III-type crystal, irrespective of the content of the excess neutral TCNQ molecule. These facts suggest that the latter crystal has a stable structure of its TCNQ column, the stability being determined by the crystallization process. This will be discussed in the next section.

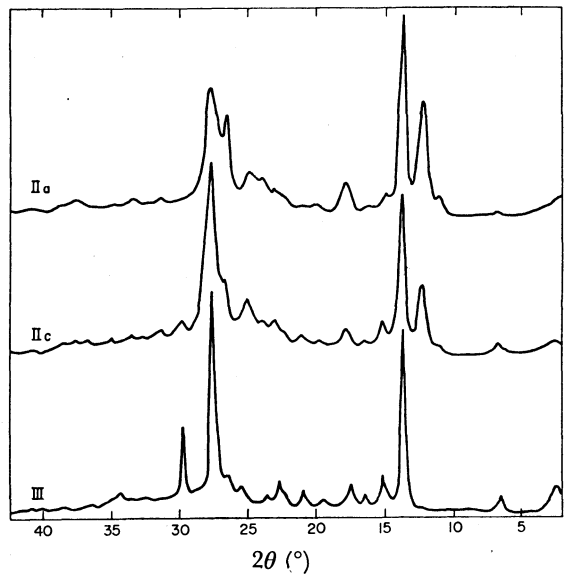

Fig. 5. X-ray diffraction patterns of $MeQ(TCNQ)_x$ salts. IIa: $MeQ(TCNQ)_{2.2}$, IIc: $MeQ(TCNQ)_{2.2}$ and III: $MeQ(TCNQ)_{2.1}$.

The II- and III-Type Crystals, Metastable and Stable Crystals. The X-ray powder patterns of the salts in Groups II and III are shown in Fig. 5. We can distinguish between the patterns of II and III. The IIa and IIc crystals had almost the same patterns, with little difference in the positions of the intense peaks. The pattern for IIa exhibited peaks at 11.8, 13.4, 26.5, and 27.5 degrees, and that for IIc, at 11.8, 13.4, 26.4, and 27.5 degrees. The main peak of III was found at 29.8°, and the peak at 11.8° was absent. Since the stability of the IIb crystal was poor, it was difficult to obtain its X-ray pattern as crystallized, but evidence was found that it may have a structure similar to that of IIa. The three compounds in Group II have, therefore, the same crystal structure, although they differ in both the TCNQ-to-cation ratio and the stability of the resistivity value.[28]

The difference in the crystallization process between II and III was the concentration of the solution. From a concentrated acetone solution (30 mmol/l), the III crystal was obtained one day after the first precipitate, IIb, had been removed by filtration. A dilute solution (13 mmol/l), however, gave only the III crystal in about a day. The IIb crystal was unstable, as has been mentioned above, and it exhibited changes in both resistivity and X-ray pattern at room temperature. For example, the resistivity of IIb was 0.8 Ω cm as crystallized but it increased to about 60 Ωcm after a week. The other crystals in Group II were also unstable or metastable crystals, because they exhibited a significant increase in resistivity at relatively lower temperatures (50—80 °C). The III crystal was thought to be a stable one, although in some cases it displayed a very small change in resistivity at elevated temperatures.

The appearance of the stable and unstable (or metastable) crystals from the same solution has been generalized thermodynamically by Ostwald in his "Law of Stages."[29] According to the law, multiple phases of different stabilities can appear in the order of their relative stabilities from a solution or melt left in a metastable state, because the crystallization takes place with the smallest loss of the free-energy content of the system. For the crystallization of the $MeQ(TCNQ)_x$ salts from a solution, the condition of a higher free-energy content may be established both in the earlier stage of crystallization from an acetone solution (high temperature and high concentration) and when the solubility of the salt is low (when dichloromethane or water was used as the solvent). Therefore, the lower resistivity of the II-type crystals can be explained quite reasonably if we assume them to be crystallized in a metastable state following the Ostwald law. The fact that the infrared spectra of II and III were almost the same as those of $Q(TCNQ)_2$ and *N-n*-propylquinolinium$(TCNQ)_2$, $NPQ(TCNQ)_2$, respectively is very helpful in understanding the structure of the TCNQ columns of the metastable and stable crystals.

In $Q(TCNQ)_2$,[30] the TCNQ molecules are stacked with an equal interplanar spacing and with an overlap mode so that one molecule is shifted longitudinally with respect to another by one-fourth the molecular length. A typical example of a distorted TCNQ column structure is $NPQ(TCNQ)_2$,[24] where the interplanar conformations of TCNQ in the column are not identical, but an extended interplanar spacing and a transversally shifted mode of overlap are found periodically.[31] Since we could not obtain any multiple phases or unstable crystals of either $Q(TCNQ)_2$ or $NPQ(TCNQ)_2$, the two structures seem to be representative of the stable TCNQ column structure of *N*-alkyl·$Q(TCNQ)_2$ salts at room temperature. Considering the size of the MeQ cation, it is not impossible that the $MeQ(TCNQ)_x$ salt assumes both types of crystal structures, the $Q(TCNQ)_2$ and $NPQ(TCNQ)_2$ types. The same discussion can apply to the case of the *N*-ethylquinolinium cation; in fact a similar phenomenon has been observed for the*N*-ethyl·$Q(TCNQ)_x$

salt,[15] a study of which is currently being made in our laboratory.

The crystallization rate was a controling factor in the difference between IIb and IIa or IIc. When an acetone solution of $MeQ(TCNQ)_x$ (20 mmol/l) was cooled from 60 to 5 °C at a rate of 0.8 or 0.2 °C/min, the IIb crystal (with a TCNQ-to-cation ratio of 1.6) was obtained. On the other hand, crystals which were obtained from an acetone solution of the same concentration cooled at a rate of 4 °C/min had a TCNQ-to-cation ratio of 2.2 and a low resistivity (about 1 Ω cm), so that they may be thought to be the same as IIa.

A calculation[30] of the stabilization energy of the $(TCNQ)_2^-$ system revealed that the most stable overlap configuration is that found in the $Q(TCNQ)_2$ crystal. The stability of the crystal as a whole is determined not only by the configuration energy of the TCNQ column, but also by the steric factor of the cations.[32] It is likely that a higher rate of crystallization gives rise to a stable configuration of TCNQ, resulting in an unstable structure as a whole. This seems to be the case in the crystallization of IIa or IIc, where the unstable structure may have been frozen with the aid of the steric hindrance of the cation molecules, probably by the rapid quenching of the crystal. This mechanism is supported by the dependence of the content of the neutral TCNQ in the II-type crystals on the crystallization rate. The higher rate prefers the stacking of the TCNQ molecules, defects being left in the column of the cation.

The authors offer their thanks to Dr. Katsue Hasegawa for his stimulating discussions. They are also indebted to Prof. Hiroo Inokuchi of the University of Tokyo for his valuable suggestions and to Dr. Hayao Kobayashi of Toho University and Prof. S. C. Wallwork of the University of Groningen for providing them with the details of crystal structures of $Q(TCNQ)_2$ and $NPQ(TCNQ)_2$ respectively and with unpublished structural data.

References

1) I. F. Shchegolev, *Phys. Stat. Sol.*, **12a**, 9 (1972).
2) J. G. Vegter, T. Hibma, and J. Kommandeur, *Chem. Phys. Lett.*, **3**, 427 (1969).
3) Y. Iida, *J. Chem. Phys.*, **59**, 1607 (1973).
4) D. B. Chesnut, *ibid.*, **40**, 405 (1964).
5) J. C. Bailey and D. B. Chesnut, *ibid.*, **51**, 5118 (1969).
6) A. J. Epstein, S. Etemad, A. F. Garito, and A. J. Heeger, *Phys. Rev.*, B **5**, 952 (1972).
7) A. N. Bloch, R. B. Weisman, and C. M. Varma, *Phys. Rev. Lett.*, **28**, 753 (1972).
8) L. B. Coleman, M. J. Cohen, D. J. Sandman, F. G. Yamagishi, A. F. Garito, and A. J. Heeger, *Solid State Commun.*, **12**, 1125 (1973).
9) M. G. Kaplunov, D. N. Fedutin, M. L. Khidekel, I. F. Shchegolev, E. B. Yagubsukii, and R. B. Lyubovskii, *Zh. Obshch. Khim.*, **42**, 2295 (1972).
10) A. Hoekstra, T. Spoelder, and A. Vos, *Acta Crystallogr.*, **B28**, 14 (1972).
11) I. Shirotani and H. Kobayashi, This Bulletin, **46**, 2595 (1973).
12) L. B. Coleman, S. K. Khanna, A. F. Garito, A. J. Heeger, and B. Morosin, *Phys. Lett.*, **42a**, 15 (1972).
13) L. B. Melby, R. J. Harder, W. R. Hertler, W. Mahler, R. E. Benson, and W. E. Mochel, *J. Amer. Chem. Soc.*, **84**, 3374 (1962).
14) H. Kobayashi, T. Danno, and Y. Saito, *Acta Crystallogr.*, **B29**, 2693 (1973).
15) S. Frandois, P. Dupis, P. Delhaes, J. Amieli, and J. Neel, *J. Chim. Phys.*, **9**, 1305 (1972).
16) M. Ohmasa, M. Kinoshita, and H. Akamatu, This Bulletin, **44**, 391 (1971).
17) M. Ohmasa, M. Kinoshita, and H. Akamatu, *ibid.*, **44**, 395 (1971).
18) R. Rembaum, V. Hadek, and S. P. S. Yen, *J. Amer. Chem. Soc.*, **93**, 2532 (1971).
19) A. R. Blythe, M. R. Boon, and P. G. Wright, *Disc. Faraday Soc.*, **51**, 110 (1971).
20) W. J. Siemons, P. E. Bierstedt, and R. G. Kepler, *J. Chem. Phys.*, **39**, 3524 (1963).
21) M. G. Kaplunov, T. P. Panova, and Yu. G. Borodko, *Phys. Stat. Sol.*, **13a**, K67 (1972).
22) S. Yoshimura, M. Murakami, Y. Itoh, and K. Hasegawa, *Chem. Lett.*, **1972**, 835.
23) B. Lunelli and C. Pecile, *J. Chem. Phys.*, **52**, 2375 (1970).
24) T. Sundaresan and S. C. Wallwork, *Acta Crystallogr.*, **B28**, 1163 (1972).
25) I. Ikemoto, K. Chikaishi, K. Yakushi, and H. Kuroda, *ibid.*, **B28**, 3502 (1972).
26) Y. Yakushi, I. Ikemoto, and H. Kuroda, "Proc. Annual Meeting of Chem. Soc. Japan," (1972), p. 250.
27) C. J. Fritchie, Jr. and P. Arthur, Jr., *Acta Crystallogr.*, **B21**, 139 (1966).
28) M. Murakami and S. Yoshimura, to be published in *J. Phys. Soc. Japan*, February, 1975.
29) W. Ostwald, *Z. Phys. Chem.*, **22**, 289 (1937).
30) H. Kobayashi, F. Marumo, and Y. Saito, *Acta Crystallogr.*, **B27**, 373 (1971).
31) S. C. Wallwork, private communication.
32) A. R. Verma and P. Krishna, "Polymorphism and Polytypism in Crystals," John Wiley and Sons, New York (1966.)

Group Interactions in Polyelectrolytes. IX. The Amination Kinetics of Chloromethylated Polystyrene in Binary Mixed Solvents

Hiroshi KAWABE

The Institute of Physical and Chemical Research, Wako-shi, Saitama 351

(Received May 18, 1974)

All the aminations of chloromethylated polystyrene (CMPS) and benzyl chloride with *i*- and *s*-butylamine in *N*,*N*-dimethylformamide (DMF), in dioxane, and in DMF–dioxane mixtures conformed to the ordinary second-order kinetics. The activation parameters in the pure solvents revealed that the much higher amination rate in DMF than in dioxane was due to both the lower value of ΔH^* and the higher value of ΔS^* in DMF. The rate of amination in DMF–dioxane was investigated as a function of the composition of the mixed solvent. The observed rate constants in DMF–dioxane mixtures fell substantially on the curves calculated on the basis of Kondo and Tokura's theory concerning reaction rates in binary mixed solvents. It is suggested in this paper that the higher rate of amination in DMF is due to the strong solvation of the activation complex in DMF to form an addition product, and that it is also due to the relative increase in the configurational entropy of the reaction system at the transition state from dioxane to DMF.

The amination of chloromethylated polystyrene (CMPS) with primary and secondary amines in several solvents was studied kinetically by the present author. All the aminations of benzyl chloride, a low-molecular model of CMPS, and most of the aminations of CMPS with primary amines such as butylamines obeyed the ordinary second-order kinetics. The amination rate of CMPS was almost the same as that of benzyl chloride, and there was not much difference in the activation parameters between them.[1] On the other hand, the rate constants were greatly affected by the species of solvent. Although there was very little difference between the rates in dioxane and in methyl ethyl ketone, the rate was markedly enhanced in dipolar aprotic solvents such as *N*,*N*-dimethylformamide (DMF) and dimethyl sulfoxide (DMSO). It was observed that, in the aminations with 2-aminobutanol and *n*-butylamine, the enthalpy of activation (ΔH^*) decreased and the entropy of activation (ΔS^*) increased in DMF or DMSO as compared with those in dioxane.[2] This is probably because of the strong solvation of the polar activated complex in such dipolar solvents.

In the present study, in order to ascertain such a solvent effect, first, CMPS and benzyl chloride were aminated with *i*- and *s*-butylamine in dioxane and their activation parameters were compared with those in DMF. Second, the rate of the aminations were measured in DMF–dioxane mixed solvents. The selective solvent effect of DMF on the rate has been revealed by the fact that the rate increases greatly upon the addition of a small amount of DMF to the dioxane. A theory with regard to the dependence of the reaction rate on the composition of a binary solvent system was proposed by Kondo and Tokura[3] on the basis of the theory of the non-electrolyte solution, and it has been applied to the Menschutkin reaction of alkyl halide with tertiary amine and the benzoylation of amine in a mixed solvent such as benzene–nitrobenzene.[3,4] In the present study, the dependence of the amination rate on the composition of DMF–dioxane has been investigated on the basis of Kondo and Tokura's equation in order to elucidate the effects of solvents on the amination of CMPS.

Experimental

Materials. As the chloromethylated polystyrene (CMPS) we used the samples described in a previous paper (CMPS-9 and CMPS-10).[1] The amines, benzyl chloride, and the solvents, all of a reagent grade, were distilled before use; they were proved to be pure by their refractive indices. All the other chemicals were of a reagent grade.

Kinetic Measurements. The procedures of the kinetic measurements in the amination of CMPS and benzyl chloride were almost the same as those described in a previous paper.[2] The initial concentrations of the chloromethyl group (of CMPS and benzyl chloride) and amine were about 0.040 and 0.400 mol/l respectively. The temperature of the reaction mixture was kept constant (within ± 0.1 °C) by means of a thermostat.

Results and Discussion

Amination in Dioxane. The aminations of CMPS and benzyl chloride with *i*- and *s*-butylamine in dioxane conformed to the ordinary second-order kinetics, and the rate constant was computed on the basis of the following equation:

$$kt = \frac{1}{(a-b)} \ln \frac{b(a-x)}{a(b-x)} \quad (1)$$

where a and b are the initial concentrations of the amines and the chloromethyl group respectively, and where x is the concentration of hydrochloride formed after a certain time, t. The rate constants measured at different temperatures are listed in Table 1, where k_P and k_B are the rate constants of CMPS and benzyl chloride respectively. The table also lists the activation energy, E_a, and the frequency factor, A, as computed by means of the least-squares method. The activation parameters, ΔH^*, ΔS^*, and ΔG^*, which were computed on the basis of the equations described in a previous paper,[2] are tabulated in Table 2. (Since the errors in ΔG^* are much smaller than those in ΔH^* and ΔS^*, they are omitted from the table.)

As has been described in a previous paper,[1] the amination rates with butylamines are $k_P > k_B$ in dioxane, and $k_P < k_B$ in DMF. All the values of ΔH^* decreases from benzyl chloride to CMPS; however, ΔS^* decreases

TABLE 1. AMINATION OF CMPS AND BENZYL CHLORIDE WITH *i*- AND *s*-BUTYLAMINE IN DIOXANE

Amine	Temp °C	Rate constants $\times 10^3$, l/mol·min k_P[a]	k_B[b]		E_a kcal/mol	log A[c]
i-Butyl	50	2.06	1.24			
	60	3.90	2.30	(k_P)	13.0±0.2	6.08±0.10
	70	7.13	4.15			
	80	11.6	7.37[d]	(k_B)	13.2±0.1	6.00±0.05
	90	19.1	11.8			
s-Butyl	60	2.04	1.04			
	70	3.65	1.93	(k_P)	13.2±0.1	5.98±0.07
	80	6.46	3.35	(k_B)	13.4±0.1	5.82±0.10
	90	10.6	5.56			

a) Rate constant of CMPS. b) Rate constant of benzyl chloride. c) A is expressed by l/mol min. d) The value at 80.3 °C.

TABLE 2. THERMODYNAMIC QUANTITIES FOR 25 °C IN THE AMINATION OF CMPS AND BENZYL CHLORIDE IN DIOXANE

Amine	Chloride	$\Delta H^{\ddagger}$ kcal/mol	$\Delta S^{\ddagger}$ e.u.	$\Delta G^{\ddagger}$ kcal/mol
i-Butyl	CMPS	12.3±0.2	−40.8±0.5	24.5
	Benzyl	12.5±0.1	−41.2±0.2	24.7
s-Butyl	CMPS	12.6±0.1	−41.3±0.3	24.9
	Benzyl	12.8±0.1	−42.0±0.3	25.4

slightly from benzyl chloride to CMPS in dioxane, and it increases a little in DMF. This difference in $\Delta S^{\ddagger}$ between CMPS and benzyl chloride is general for DMF and DMSO,[1,2] and it is considered to be characteristic of dipolar aprotic solvents.

On the other hand, the rates in DMF are much larger than those in dioxane; $\Delta H^{\ddagger}$ decreases and $\Delta S^{\ddagger}$ increases from dioxane to DMF. Similar changes in the activation parameters were also found in the amination with *n*-butylamine and 2-aminobutanol when the solvent was changed from dioxane to DMF or DMSO.[2] The decrease in $\Delta H^{\ddagger}$ is considered to be due to the strong solvation of the activation complex in a dipolar aprotic solvent; that is, it corresponds to the enthalpy of the formation of an addition product as a result of the interaction of the activation complex with the solvent. The increase in $\Delta S^{\ddagger}$ may be ascribed to the relative increase in the configurational entropy of the reaction system at the transition state from dioxane to a dipolar aprotic solvent.

Amination in DMF–Dioxane Mixtures. The amination of CMPS and benzyl chloride in DMF–dioxane conformed to the second-order rate equation. Figure

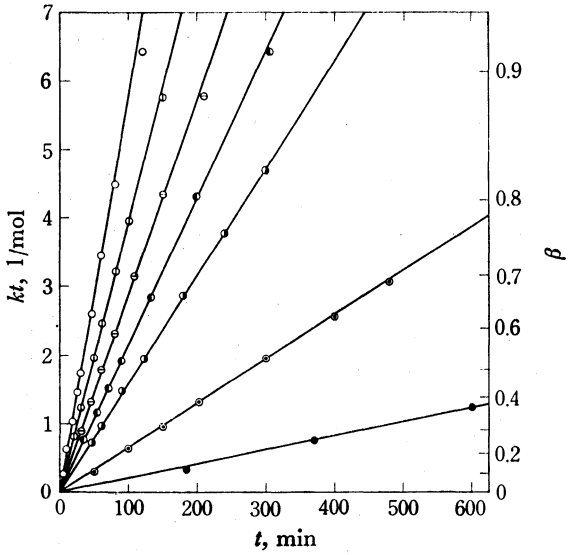

Fig. 1. The amination of CMPS with *s*-butylamine at 60 °C in DMF–dioxane systems of different DMF mole fractions (x_1).
○: $x_1=1$, ◑: $x_1=0.8$, ⊖: $x_1=0.65$, ◐: $x_1=0.50$, ◑: $x_1=0.35$, ⊙: $x_1=0.15$, ●: $x_1=0$.

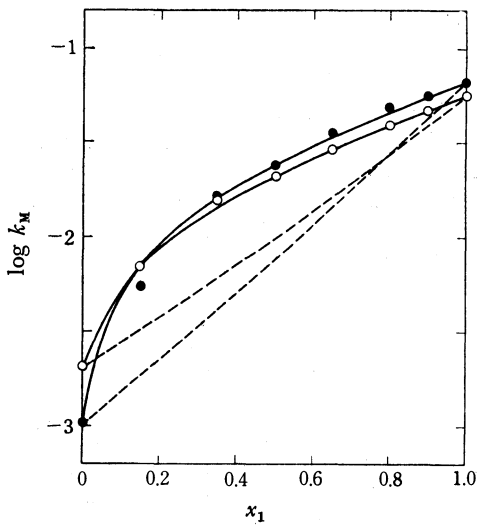

Fig. 2. Plot of log k_M *vs.* mole fraction of DMF, x_1, for the amination of CMPS (○) and benzyl chloride (●) with *i*-butylamine in DMF–dioxane mixture at 50 °C.
——: Calculated on the basis of Eq. (4)
·····: Calculated on the basis of Eq. (3)

TABLE 3. AMINATION RATE CONSTANTS OF CMPS AND BENZYL CHLORIDE IN DMF-DIOXANE MIXTURE, $10^2 k$ (l/mol min)

Amine	Chloride	Temp °C	Mole fraction of DMF (x_1) 0	0.15	0.35	0.50	0.65	0.80	0.90	1
i-Butyl	CMPS	50	0.206	0.871	1.76	2.80	4.01	5.46	6.42	7.72
	Benzyl	50	0.124	0.758	2.11	3.44	5.05	6.93	8.43	9.97
s-Butyl	CMPS	60	0.204	0.641	1.58	2.11	2.91	4.01	4.72	5.72
	Benzyl	60	0.104	0.545	1.60	2.44	3.57	4.95	5.72	6.67

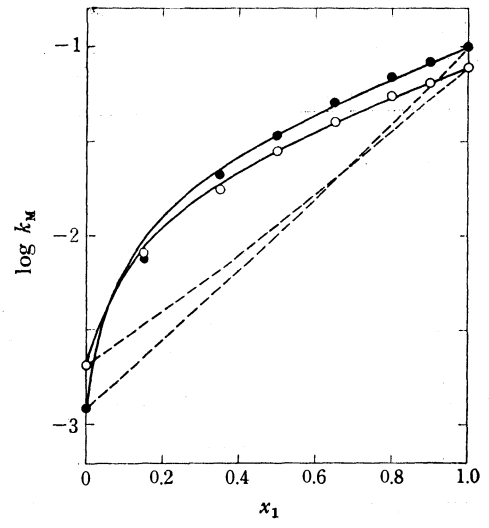

Fig. 3. Plot of log k_M *vs.* mole fraction of DMF, x_1, for the amination of CMPS (○) and benzyl chloride (●) with s-butylamine in DMF-dioxane mixture at 60 °C.
——: Calculated on the basis of Eq. (4)
·····: Calculated on the basis of Eq. (3)

1, as an example, shows the plots of kt against t for the amination of CMPS with *s*-butylamine at 60 °C, where kt represents the right-hand term in Eq. (1) and where $\beta=x/b$. Table 3 lists the rate constants, computed on the basis of Eq. (1), of the amination with *i*-butylamine at 50 °C and those with *s*-butylamine at 60 °C.

The logarithms of the rate constant in DMF–dioxane, denoted here as log k_M, are plotted against the mole fraction of DMF in the mixed solvent, denoted as x_1, in Figs. 2 and 3. In the figures, the observed values (expressed by the circles) are on the straight lines represented by Eq. (2), which are omitted in the figures;

$$\log k_M = x_1 \log k_1 + x_4 \log k_4 \qquad (2)$$

where x_1 and x_4 $(=1-x_1)$ are the mole fractions of DMF and dioxane respectively in the DMF–dioxane system and where k_1 and k_4 are the rate constants in pure DMF and pure dioxane respectively. It is shown in the figures that the addition of a small amount of DMF to dioxane increases the rate constant markedly. This result, along with that described in the preceding section, suggests that the activated complex in the mixed solvent interacts selectively with DMF to form the solvated activated complex.

With regard to a reaction in a binary mixed solvent, Kondo and Tokura[3] calculated thermodynamically the Henry constant of each species in the reaction system; they derived theoretically the relation between the rate constant and the composition of the solvent mixture on the basis of molecular models. In the first model, where two reactants, A and B, and the activation complex, M*, yield regular solutions with Solvent 1 (S_1) and Solvent 4 (S_4), the rate constant in the mixed solvent, k_M, is expressed by:

$$\log k_M = x_1 \log k_1 + x_4 \log k_4 - x_1 x_4 \alpha_{14}/2.303 \qquad (3)$$

where α_{14} is an empirical coefficient which is related to the interaction between S_1 and S_4.

In the second model, where A and B yield regular solutions with both the solvents, but where M* reacts selectively with S_1 to form an addition product, denoted here as MS_1^*, k_M is given by:

$$\log k_M = x_1 \log k_1 + x_4 \log k_4 - [x_1 \log (K+1) - \log (x_1 K+1) + x_1 x_4 \alpha_{14}/2.303] \qquad (4)$$

where K is the equilibrium constant, expressed on the basis of the mole fractions of the species, in the formation of MS_1^* from M* and S_1.

In the present study, x_1 and x_4 are the mole fractions of DMF and dioxane respectively, and k_1 and k_4, the rate constants in pure DMF and pure dioxane respectively. The coefficient, α_{14}, is related to the molar excess free energy of mixing in the binary system, ΔG_M^E, by means of the following equation:

$$\Delta G_M^E RT = \alpha_{14} x_1 x_4 \qquad (5)$$

while ΔG_M^E can be obtained from the equilibrium vapor-pressure data in the system. The data in the DMF–dioxane system were presented by Quitzch;[5] the values of ΔG_M^E and α_{14} calculated from the data are shown in Fig. 4. At $x_1=0.5$, $\alpha_{14}(50\,°C)=0.403$ and α_{14}-

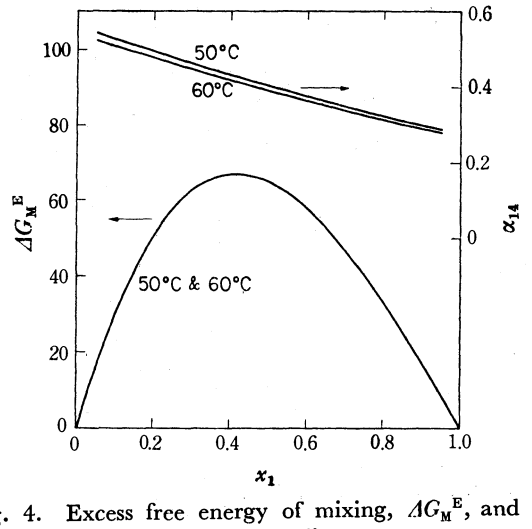

Fig. 4. Excess free energy of mixing, ΔG_M^E, and the coefficient, α_{14}, for the DMF-dioxane system.

$(60\,°C)=0.390$. The values of α_{14} and k_M at $x_1=0.5$ were introduced into Eq. (4) in order to obtain the K values, which are shown in Table 4. Then, the values of α_{14} and K were introduced into Eqs. (3) or (4) in order to calculate log k_M as a function of x_1. In Figs. 2 and 3, the broken lines and solid lines are those calculated on the basis of Eqs. (3) and (4) respectively. The observed values, expressed by the circles, are substantially on the lines calculated on the basis of Eq. (4). This agreement suggests that the activated complex is solvated selectively with DMF in DMF–dioxane.

Enhancement of the Amination Rate in a Dipolar Aprotic Solvent and Comparison of the Rate between CMPS and Benzyl Chloride. In Table 4, K is an equilibrium constant of the $M^*+S_1 \rightleftarrows MS_1^*$ reaction, which is expressed on the basis of mole fraction; this was then transformed to an equilibrium constant expressed

TABLE 4. EQUILIBRIUM CONSTANT IN THE SOLVATION OF THE ACTIVATED COMPLEX AND THERMODYNAMIC QUANTITIES

Amine	Chloride	Temp °C	K	K_c l/mol	ΔG^{*solv} kcal/mol	ΔH^{*solv} kcal/mol	$T\Delta S^{*solv}$ kcal/mol	$T\delta\Delta S^{*conf}$ a) kcal/mol
i-Butyl	CMPS	50	21.2	1.73	−0.4	−1.4	−1.0	1.9
	Benzyl	50	43.8	3.57	−0.8	−1.4	−0.6	2.0
s-Butyl	CMPS	60	15.7	1.28	−0.2	−1.1	−0.9	2.0
	Benzyl	60	38.5	3.14	−0.8	−1.2	−0.4	2.0

a) $T\delta\Delta S_i^{*conf}$ represents $T(\Delta S_1^{*conf}-\Delta S_4^{*conf})$.

on the basis of the molar concentration, $K_c=[MS_1^*]/[M^*][S_1]$, by means of the following equation:

$$K = K_c/V_{soln} \quad (6)$$

where V_{soln} is the molar volume of the solution defined as:[3]

$$V_{soln} = (\sum_i m_i V_i)/\sum_i m_i \quad (7)$$

where m_i is the moles of a component, i, of the solution and where V_i is partial molar volume of the component. Provided that the solute components are negligible, V_{soln} (DMF–dioxane)=0.0816 l/mol at x_1=0.5 (at 25 °C). The values of K_c calculated on the basis of Eq. (6) are shown in Table 4. The free energy of solvation of the activated complex with DMF (S_1), ΔG^{*solv}, in Table 4 is calculated from the K_c values.

If the activated complex is solvated merely with DMF in DMF–dioxane, the enthalpy of the solvation of the activated complex, ΔH^{*solv}, will be the difference between the enthalpy of activation in DMF, ΔH_1^*, and that in dioxane, ΔH_4^*. The $T\Delta S^{*solv}$ values in Table 4 were thus calculated. Although there is very little difference in ΔH^{*solv} values between CMPS and benzyl chloride, the $T\Delta S^{*solv}$ of CMPS is a little lower than that of benzyl chloride. This difference may be attributed to the steric hindrance to the solvation in CMPS; that is, the formation of the addition product from the activation complex and the solvent molecules is obstructed by the neighboring groups of the polymer.

Although the values of ΔS^{*solv} are negative, the values of $(\Delta S_1^*-\Delta S_4^*)$ can be seen to be positive by comparing Table 7 in Ref. 1 with Table 2 in the present paper. Since the activated complex in the amination is ionic or rather polar, there must be a large difference in the configurational entropy of the reaction system at the transition state between the system containing such a polar solvent as DMF (the solubility parameter, δ=12.11) and the system containing dioxane (δ=9.88). Accordingly, $(\Delta S_1^*-\Delta S_4^*)$ is assumed to be composed of those two terms:

$$\Delta S_1^* - \Delta S_4^* = \Delta S^{*solv} + (\Delta S_1^{*conf} - \Delta S_4^{*conf}) \quad (8)$$

where ΔS_i^{*conf} is the change in the configurational entropy of the reaction system containing a solvent, i (i is 1 or 4), from its initial state to its transition state.

Thus, we obtain the following relation:

$$(\Delta G_1^* - \Delta G_4^*) - \Delta G^{*solv} = T(\Delta S_1^{*conf} - \Delta S_4^{*conf}) \quad (9)$$

The difference between $(\Delta G_1^*-\Delta G_4^*)$ and ΔG^{*solv}, therefore, corresponds to the difference in the configurational entropy changes of the reaction systems. Since the ΔS_i^{*conf} term is not directly related to the solvation of the activated complex, the values of $(\Delta S_1^{*conf}-\Delta S_4^{*conf})$, unlike those of ΔS^{*solv}, will be almost the same for DMPS and benzyl chloride. The numerical values of $T(\Delta S_1^{*conf}-\Delta S_4^{*conf})$ calculated on the basis of Eq. (9) are shown in Table 4; they are the same for all the cases shown in the table, as had been expected.

The results of the present study suggest that the remarkable increase in the amination rate from dioxane to DMF is caused not only by the decrease in the activation energy, which is equal to the solvation energy of the activated complex with DMF, but also by the large relative increase in the configurational entropy of the reaction system at the transition state from the reaction in dioxane to that in DMF.

The author wishes to express his thanks to Dr. Masaya Yanagita for his valuable discussions. He is also grateful to Mr. Yasunori Uchiyama for his helpful assistance in preparing the polymer and in carrying out the measurements.

References

1) H. Kawabe and M. Yanagita, This Bulletin, **46**, 3627 (1973).
2) H. Kawabe and M. Yanagita, *ibid.*, **46**, 38 (1973).
3) Y. Kondo and N. Tokura, *ibid.*, **40**, 1433, 1438 (1967).
4) S. Hasegawa, S. Kashino, and Y. Mukai, *ibid.*, **44**, 69 (1971).
5) V. K. Quitzsch, *J. Prakt. Chem.*, **28**, 59 (1965).

Electrical Behavior of Alkali Metal Cation-TCNQ Anion Radical Simple Salts under Very High Pressures.

Ichimin SHIROTANI, Akifumi ONODERA,* and Nobuko SAKAI

The Institute for Solid State Physics, The University of Tokyo, Roppongi, Minato-ku, Tokyo 106
**Department of Material Physics, Faculty of Engineering Science, Osaka University, Toyonaka, Osaka 560*

(Received May 27, 1974)

The electrical resistance of alkali metal cation–TCNQ anion radical simple salts was measured over the wide pressure range from 0 to 500 kbar at room temperature. The least resistivities for Group A (Li–, Na–, K–, and Rb(I)–TCNQ) are about 0.2—3 Ω cm, while those for Group B (Rb(II)– and Cs–TCNQ) are about 0.06—0.1 Ω cm. The possibility of insulator-metal transition at high pressures is discussed. Above 140—175 kbar the electrical resistance of simple TCNQ salts increases with an increase in the pressure and drifts upward with the time. The solid-phase reaction is observed under very high pressures.

The electrical,[1,2] optical,[3–5] and magnetic properties[6,7] and the crystal structures[8,9] in simple alkali metal cation–TCNQ anion radical salts (M–TCNQ) have been studied. Phase transitions have been observed in the temperature range from −150 °C to +230 °C;[10,11] further, new, pressure-induced phase transitions have been investigated at room temperature.[11] According to the differences in the physical properties and crystal structures, alkali metal–TCNQ salts may be classified into two groups. Li–, Na–, K–, and Rb(I)–TCNQ salts are contained in Group A. These salts have exhibited typical semiconductive behavior. The dimerized structure in the $TCNQ^-$ columns appears to be typical.[8] Rb(II)– and Cs–TCNQ, on the other hand, belong to Group B. The X-ray study of Rb(II)–TCNQ shows a triclinic structure consisting of linear chains of identical TCNQ molecules stacked face-to-face and equally separated from one another.[9] This columnar structure resembles that found in the crystals of such metallic TCNQ salts as *N*-methylphenazinium–TCNQ (NMP–TCNQ).[12,13] However, no insulator-metal transition has been observed in the wide temperature range from 170 to 570 K[2] and up to 14 kbar at room temperature.[11] The interplanar spacing between the $TCNQ^-$ anion in Rb(II) salt, 3.43 Å, is much longer than that, 3.26 Å, in NMP–TCNQ. If this distance, 3.43 Å, can be contracted to about 3.2 Å by compression, it seems that it would be possible to observe a pressure-induced phase transition to the conducting state at high pressures.

In this paper, we will present our findings on the pressure dependence of the electrical resistance of M–TCNQ salts and will discuss the possibility of insulator-metal transition at high pressures. Further, we will present some results on the solid phase reactions that were found under very high pressures.

Experimental

Conductivity measurements were performed using a split-sphere apparatus[14] constructed at Osaka University. A schematic diagram is shown in Fig. 1. A sphere made of hardened steel was split into six wedge-shaped segments, the centers of which were all truncated so that a central hollow space could be made. Into this space we placed eight cubic anvils made of tungsten carbide. A corner of each cubic anvil was cut off to form a triangular face. When these eight cubic anvils were put together, the eight triangular faces formed an octahedral hollow space in the center of the whole sphere. The specimen to be compressed was embedded in the pyrophyllite octahedron, which served as a pressure-transmitting medium.

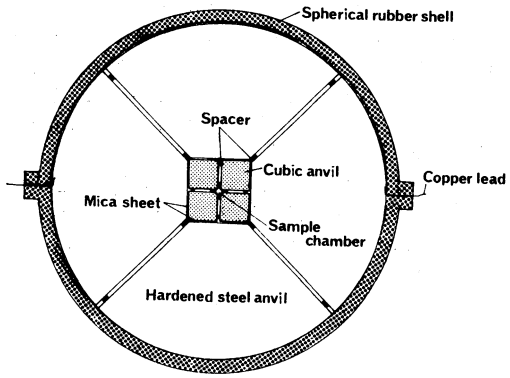

Fig. 1. Cross-section of the split-sphere apparatus showing the arrangement of inner cubes, outer segments, and spacers.

Since these inner and outer anvils were equally separated and put together with soft cardboard spacers sandwiched between them, it was possible to construct a sphere with a diameter slightly larger than before the splitting. When the anvil assemblage covered with a pair of semispherical rubber shells was compressed with a fluid, the sphere shrunk uniformly, reducing its diameter toward that of the original sphere. Quasi-hydrostatic high pressures could, as a result, be generated in the octahedral specimen chamber. The details of the sample arrangement and pressure calibration have been described elsewhere.[15]

The samples used in the experiment were Li–, Na–, K–, Rb(I)–, Rb(II)–, and Cs–TCNQ. The preparation of these compounds has been reported in detail previously.[2,11] The samples were studied in the form of powder pressure-fused into flat platelets.

Results and Discussion

According to the differences in their physical properties and crystal structures, simple TCNQ salts may be classified into two groups. As is shown in Table 1, Li–, Na–, K–, and Rb(I)–TCNQ salts are contained in Group A, while Rb(II)– and Cs–TCNQ belong to Group B. It is known that crystals of Rb(I)–TCNQ

TABLE 1. PHYSICAL PROPERTIES OF SIMPLE M–TCNQ SALTS

	Resistivity (Ω cm)		Transition temperature (K)		Location of charge transfer band[a,d] (10^3 cm^{-1})
	Single crystal[a] along the needle axis	Microcrystal[b]			
Li–TCNQ		5×10^5	No phase transition observed		8.0
Na–TCNQ	$\sim1\times10^3$	1×10^5	338[a]	348[c]	8.3
K–TCNQ	$\sim5\times10^3$	1×10^4	391	394	8.3
Rb(I)–TCNQ	$\sim3\times10^5$		374	381	8.6
Rb(II)–TCNQ	$\sim1\times10^2$		231	223	6.5
Cs–TCNQ	$\sim6\times10^2$	3×10^3	254	210	6.5

a) Ref. 2, 9 b) Ref. 1 c) Ref. 8 d) Ref. 5

in Group A have a monoclinic symmetry and that the $TCNQ^-$ ions are stacked face-to-face to form columns of diadic units of $TCNQ^-$. Within a column, two different intermolecular spacings, 3.159 and 3.480 Å, appear alternately.[8] On the contrary, the TCNQ radical ions in Rb(II) salt form columns constructed from monadic units of $TCNQ^-$. The spacing between $TCNQ^-$ is 3.43 Å.[9] Figure 2 exhibits the mode of overlapping between the nearest $TCNQ^-$ ions in both Rb salts.

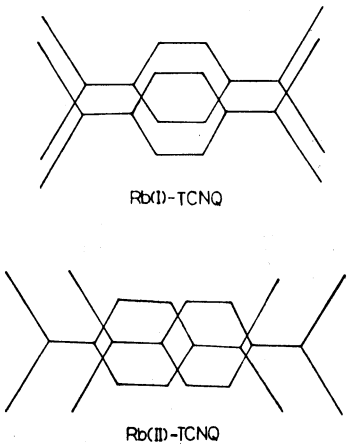

Fig. 2. The mode of overlapping between nearest $TCNQ^-$ in both Rb–TCNQ salts.

The columnar structures of TCNQ salts seem to be closely related to the electrical conductivity.[12] The TCNQ salts with diadic, triadic, and tetradic are low or intermediately conductive. The mode of overlapping between the nearest TCNQ ions in these salts is similar to that found in the Rb(I) salt. The highly-conductive salts, such as NMP–TCNQ, are constructed of monadic units of TCNQ. The mode of overlapping between the nearest TCNQ ions in these salts resembles that found in the Rb(II) salts.

The effect of the pressure on the electrical resistances of TCNQ salts in Group A is shown in Figs. 3a and 3b. Their electrical resistances decreased rapidly with an increase in the pressure and reached their minimum in the pressure range of 145—175 kbar. The behavior of the curve was reproducible below this pressure region. The least resistivities of the TCNQ salts are given in Table 2. The least resistivity of Li–TCNQ is much smaller than that of the other salts in Group A.

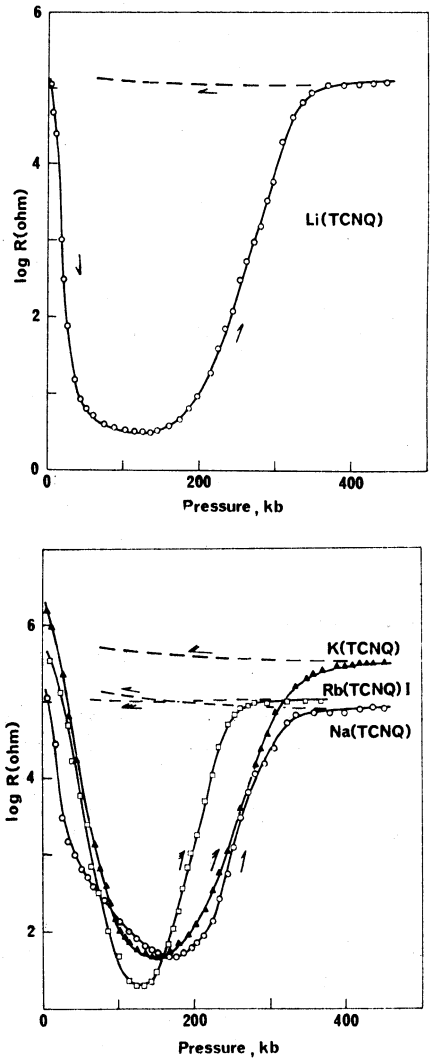

Fig. 3a and 3b. Pressure dependence of the electrical resistance of TCNQ salts in Group A.

In a previous paper,[11] we have reported that the electrical behavior of their single crystals is very complex under pure hydrostatic pressure. Several pressure-induced phase transitions are observed in the pressure range of 0—15 kbar at room temperature. However, the crystal structures do not change drastically.[16]

If the dimerized structure found in the columns of

Table 2. Minimum resistivity and minimum pressure

Compound	P_{min} a) ($\pm$5 kbar)	ρ_{min} b) (Ω cm)
Li-TCNQ	135	$\sim 2\times10^{-1}$
Na-TCNQ	174	$\sim 3\times10^{0}$
K-TCNQ	148	$\sim 3\times10^{0}$
Rb(I)-TCNQ	135	$\sim 1\times10^{0}$
Rb(II)-TCNQ	170	$\sim 6\times10^{-2}$
Cs-TCNQ	152	$\sim 1\times10^{-1}$

a) Ref. 24. b) The resistivity was calculated from the resistance data by measuring the dimensions of the retrieved specimen after the compression.

typical alkali metal-TCNQ salts is converted into the monomeric structure by the compression, and if the mode of overlapping between nearest $TCNQ^-$ ions in the column is then changed that of the Rb(II)-salt type, TCNQ salts may behave like metal at high pressures. However, the electrical resistances of Group A decreased monotonously with the pressure up to the pressure of minimum resistance. The least resistivities

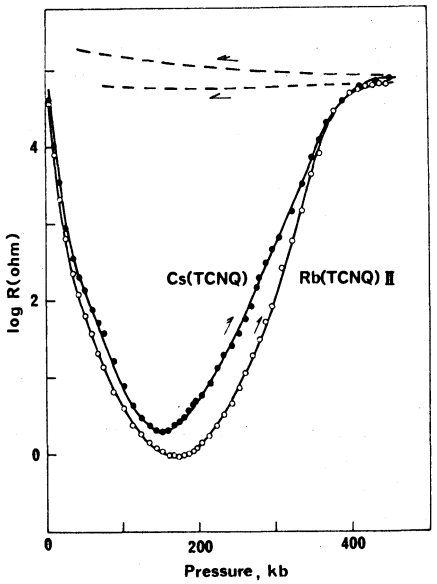

Fig. 4. Pressure dependence of the electrical resistance of TCNQ salts in Group B.

of all the TCNQ salts but Li-TCNQ were about 1—3 Ω cm at room temperature. No anomalous behavior arising from the phase transition to the metallic state was observed.

Figure 4 shows the effect of the pressure on the electrical resistances of TCNQ salts in Group B. The resistances decreased by a factor of approximately 10^4 in the first 150 kbar at room temperature. The least resistances are about one-tenth of those of Group A. The least resistivity in Rb(II)-TCNQ was about 6×10^{-2} Ω cm at 170 kbar. As is shown in Table 3, this value is less than the resistivities of a compacted specimen of the metallic TCNQ salts at atmospheric pressure.

The compressibility of Rb(II)-TCNQ has not been measured, but it is probably comparable to that of aromatic crystals.[16] From the relation between the pressure and the volume for molecular solids given by Samara and Drickamer, the average intermolecular distance at 170 kbar was estimated to be about 88% of that at atmospheric pressure.[17] Therefore, we can expect the interplanar spacing in Rb(II) salts around 170 kbar to be much shorter than 3.26 Å in NMP-TCNQ at 1 bar.

The magnetic-susceptibility and conductivity measurements for NMP-TCNQ indicate a metallic state above 200 K, with a continuous transition to an insulator below 200 K.[18] Similar behavior has also been observed in quinolinium-$TCNQ_2$ (Q-$TCNQ_2$),[19,20] acridinium-$TCNQ_2$ (Ac-$TCNQ_2$),[20] and tetrathiofulvalenium-TCNQ (TTF-TCNQ).[21,22] X-Ray studies of these metallic TCNQ salts show monoclinic or triclinic structures consisting of linear chains of identical TCNQ molecules stacked face-to-face and equally separated from one another.[12] This structure resembles that of Rb(II)-TCNQ. The electrical resistivities, the transition points, and the interplanar spacings between TCNQ molecules for metallic TCNQ salts are given in Table 3. These physical properties are also compared with those of Rb(II)-TCNQ near 170 kbar in this table.

On the basis of these data, we suggest that Rb(II)-TCNQ may show metallic behavior near 170 kbar.

The metal-insulator transitions in one-dimensional

Table 3. Comparison of physical properties between Rb(II)-TCNQ around 170 kbar and metallic TCNQ salts

	Rb(II)-TCNQ	NMP-TCNQ	Q-$TCNQ_2$	Ac-$TCNQ_2$	TTF-TCNQ
Resistivity at room temperature microcrystal (Ω cm)	6×10^{-2} a) (170 kbar)	0.5[b]	0.25[c]	0.3[d]	
Single crystal along the needle axis (Ω cm)	10^2 (1 bar)[e] 8[a] (14 kbar)	7×10^{-3} [b]	10^{-2} [f]	10^{-2} [f]	10^{-3} [g]
Interplanar spacing (Å)	below 3.2[h] (170 kbar)	3.26[i]	3.22[j]	3.25[j]	3.17[k]
Metal-insulator transition temperature (K)		200[l]	240[f]	140[f]	60[g]

a) Present work. b) L. R. Melby, *Can. J. Chem.*, **43**, 1448 (1965). c) Ref. 1. d) P. Dupuis and J. Neel, *C. R. Acad. Sci. Paris, Ser. C*, **265**, 688 (1967). e) Ref. 2, 9. f) Ref. 20. g) Ref. 21, 22. h) The predicted value from the compressibility of organic solids. i) Ref. 13. j) Ref. 12. k) T. E. Phillips, T. J. Kistenmacher, J. P. Ferrais, and D. O. Cowan, *Chem. Commun.*, **1973**, 471. l) Ref. 18.

crystals such as TCNQ salts have been observed only along the conductive axis in the single crystals. The electrical resistivity along the needle axis in Rb(II) salt has been measured at hydrostatic pressures up to 14 kbar. The resistivity at this pressure is about 8 Ω cm at room temperature.[11] If the resistivity along the conductive axis were to be studied at higher pressures, an insulator-metal transition would probably be observed.

The compaction conductivity of microcrystals of metallic TCNQ salts indicates an exponentially-activated behavior because of inter-particle contact resistance. Their activation energy does not become zero even at very high pressures.[23] Recently, Heeger *et al.*[22] have reported a new experimental technique, a voltage-shorted compaction (VSC) device, for obtaining information on the bulk electrical properties from the compaction of samples. When this technique is used, the electrical behavior of microcrystalline sample does not show the thermally-activated process. For the study of the insulator-metal transition of compacted samples at high pressures, this technique may be very useful.

Solid-Phase Reaction. As is shown in Figs. 3 and 4, above 140—175 kbar the electrical resistances of the TCNQ salts increased rapidly with the increase in the pressure and drifted upward with the time. As is shown by the broken curve, this electrical behavior is irreversible. These phenomena arise from the solid-phase reaction. The minimum pressure[24] at which the reaction was induced is given in Table 2. It should be noted that for Group B this pressure is larger than for Group A except in the case of Na–TCNQ.

The pressure-induced solid-phase reactions for TCNQ and TCNQ salts have already been investigated under very high pressures by Drickamer *et al.*[25] The electronic absorption peaks at 300—900 nm and the infrared spectra on the basis of the C≡N stretching vibration disappear under very high pressures. This seems to indicate a reaction between C≡N bonds in adjacent TCNQ molecules. Considering the similar reaction for simple alkali metal–TCNQ salts, the difference in crystal structures may be very important. The interplanar distance and the magnitude of overlapping between C≡N bonds in TCNQ salts seem to be closely correlated with the pressure-induced solid-phase reaction. As has been mentioned above, Rb(I)–TCNQ has a short interplanar distance, 3.159 Å, and the overlapping between the C≡N bonds in Rb(I) salt is larger than that in Rb(II) salt. Therefore, we can expect that the reactivity of Group A is more sensitive to the pressure than that of Group B. The differences in minimum pressure shown in Table 2 may show the strength of the reactivity at high pressures.

The authors wish to acknowledge the excellent work of Mr. Ken-ichi Tanaka in the construction of the pressure vessel. We wish to thank Professor Hiroo Inokuchi and Dr. Hayao Kobayashi for their helpful discussions.

References

1) W. J. Simons, P. E. Bierstedt, and R. G. Kepler, *J. Chem. Phys.*, **39**, 3523 (1963).
2) N. Sakai, I. Shirotani, and S. Minomura, This Bulletin, **45**, 3314 (1972).
3) I. Shirotani, N. Sakai, H. Inokuchi, and S. Minomura, *ibid.*, **42**, 2087 (1969); N. Sakai, I. Shirotani, and S. Minomura, *ibid.*, **43**, 57 (1970).
4) Y. Iida, *ibid.*, **42**, 71 (1969).
5) Y. Oohashi and T. Sakata, *ibid.*, **46**, 3330 (1973).
6) R. G. Kepler, *J. Chem. Phys.*, **39**, 3528 (1963).
7) J. G. Vegter and J. Kommandeur, *Phys. Rev.*, **B7**, 2929 (1973).
8) A. Hoekstra, T. Spoelder, and A. Vos, *Acta Crystallogr.*, **B28**, 14 (1972).
9) I. Shirotani and H. Kobayashi, This Bulletin, **46**, 2595 (1973).
10) J. G. Vegter, T. Hibma, and J. Kommandeur, *Chem. Phys. Lett.*, **3**, 427 (1969).
11) N. Sakai, I. Shirotani, and S. Minomura, This Bulletin, **45**, 3321 (1972).
12) H. Kobayashi, *ibid.*, **47**, 1346 (1974).
13) C. J. Fritchie, Jr. and P. Arthur, Jr., *Acta Crystallogr.*, **21**, 139 (1966).
14) N. Kawai and S. Endo, *Rev. Sci. Instrum.*, **41**, 1178 (1970).
15) A. Onodera, N. Kawai, K. Ishizaki, and I. L. Spain, *Solid State Commun.*, **14**, 803 (1974).
16) Yokota has studied preliminary X-ray diffraction for K–TCNQ powder under hydrostatic pressure up to 5 kbar. The volume change with pressure is comparable to that of ordinary aromatic crystals.
17) G. A. Samara and H. G. Drickamer, *J. Chem. Phys.*, **37**, 474 (1962).
18) A. J. Epstein, S. Etemad, A. F. Garito, and A. J. Heeger, *Phys. Rev.*, **B5**, 952 (1972).
19) V. Walatka, Jr. and J. H. Perlstein, *Mol. Cryst. Liq. Cryst.*, **15**, 269 (1971).
20) L. I. Buravov, D. N. Fedutin, and I. F. Shchegolev, *Soviet Physics JETP*, **32**, 612 (1971).
21) J. P. Ferraris, D. O. Cowan, V. Walatka, and J. H. Perlstein, *J. Amer. Chem. Soc.*, **95**, 948 (1973).
22) L. B. Coleman, M. J. Cohen, D. J. Sandman, F. G. Yamagishi, A. F. Garito, and A. J. Heeger, *Solid State Commun.*, **12**, 1125 (1973).
23) I. Shirotani, T. Kajiwara, H. Inokuchi, and S. Akimoto, This Bulletin, **42**, 366 (1969).
24) The value is expected to be dependent on the conditions of experimental procedures such as the velocity of pressure generation, temperature, *etc.* as well as the physical and chemical properties of samples such as particle size, defects and impurities, *etc.* In the present work care was taken so that the pressure in the sample chamber be increased with a constant rate by the use of automatically driven pumping system, and the temperature was conditioned to 20±5 °C. The minimum pressure then obtained was reproducible within ±5 kbar.
25) R. B. Aust, G. A. Samara, and H. G. Drickamer, *J. Chem. Phys.*, **41**, 2003 (1964).

Isotropic Rayleigh Light Scattering in Two-component Systems. The Interdependence of the Concentration and the Density Scattering

Yoshinobu SHIOKAWA and Shin SUZUKI

The Research Institute for Iron, Steel and Other Metals, Tohoku University, Katahira 2-chome, Sendai 980

(Received June 19, 1974)

The isotropic Rayleigh ratios in two-component systems are discussed in terms of the fluctuation of the thermodynamic quantities. It is found that the isotropic Rayleigh ratio, R_{is}, is the sum of the concentration scattering, R_c, due to fluctuation of the concentration and the so-called density scattering, R_d:

$$R_{is} = R_c + R_d$$

Thus, the cross-term of the concentration scattering and the density scattering, suggested by Bullough, is not included in the above expression. Our conclusion is confirmed by the determination of the molecular weight of sucrose.

The light-scattering measurements have been mainly applied to macromolecules. In the last decade, however, several papers have appeared with relation to small molecules, *e.g.*, the determination of the activity coefficient in a binary solution[1,2] and of the degree of polymerization for the hydrolysis product of metal ions.[3,4]

According to Einstein,[5] the isotropic Rayleigh ratio of liquid in the direction perpendicular to the incident light beam is given by:

$$R_{is} = \left(\frac{\pi^2}{2\lambda^4}\right) V\overline{(\Delta\varepsilon)^2} \tag{1}$$

where λ is the incident wavelength and $\overline{(\Delta\varepsilon)^2}$ is the mean square fluctuation in the dielectric constant in the region of a certain volume, V.

In a pure liquid the scattering of light is called the density scattering because the density fluctuation makes predominant contributions to the dielectric-constant fluctuation.[6]

The scattering of light in a solution is attributed not only to the density scattering, R_d, but also to the concentration scattering, R_c, arising from the concentration fluctuation:[7]

$$R_{is} = R_d + R_c \tag{2}$$

Thus, the isotropic Rayleigh ratio in a solution has been considered as the sum of these two contributions.

On the other hand, Bullough,[7-9] and Sicotte and Rinfret[10] have suggested such an expression for the isotropic Rayleigh ratio in two-component systems; their expression contains a cross-term, R'', besides those two contributions:

$$R_{is} = R_d + R'' + R_c \tag{3}$$

The cross-term makes a significant contribution to the isotropic Rayleigh ratio when both components of a solution have a low molecular weight.

Most of the published papers on the determination of the activity coefficient have taken the cross-term, R'', into account. Later, Sicotte,[11] and Segudovic and Deželić[12] have made theoretical considerations of this cross-term.

The purpose of the present work is to reexamine Bullough's theory. Therefore, we will discuss the isotropic Rayleigh ratio in two-component systems in terms of the statistical fluctuation concept and will determine the molecular weight of sucrose on the basis of our consideration.

The scattering of light in an aqueous sucrose solution has been studied by Debye,[13] by Halwer,[14] and by Maron and Lou.[15] Debye and Halwer made an inadequate calibration of the instrument, however, nor did they make any correction for the depolarization. Moreover, Maron and Lou made mistakes in their correction for the depolarization.

Theoretical

It is necessary to estimate the fluctuations of the thermodynamic quantities so as to ascertain the fluctuation of the dielectric constant in a solution.

Consider a small part of a two-component system containing a given number, N_0, of moles of a solvent. The probability function for the thermodynamic quantities is given by:[16]

$$\omega = C\exp\left[-\frac{1}{2kT}(\Delta S\Delta T - \Delta V\Delta P + \Delta N\Delta\mu)\right] \tag{4}$$

where ΔS, ΔT, ΔV, ΔP, ΔN, and $\Delta\mu$ are the fluctuations of the entropy, the temperature, the volume, the pressure, the number of moles of the solute, and the chemical potential of the solute respectively, and where C is a normalization constant.

Now, choose P, T, and N as independent variables. By expanding ΔS, ΔV, and $\Delta\mu$ near the equilibrium state as a series, we obtain:

$$\omega = C\exp\left[-\frac{1}{2kT}\left\{-\left(\frac{\partial^2 G}{\partial P^2}\right)(\Delta P)^2 - 2\left(\frac{\partial^2 G}{\partial P\partial T}\right)(\Delta P\Delta T) - \left(\frac{\partial^2 G}{\partial T^2}\right)(\Delta T)^2 + \left(\frac{\partial^2 G}{\partial N^2}\right)(\Delta N)^2\right\}\right] \tag{5}$$

where G is Gibbs' free energy. This relation means that the fluctuation of number of moles of the solute and the pressure or the temperature are statistically independent:

$$\overline{(\Delta N\Delta P)} = \overline{(\Delta N\Delta T)} = 0 \tag{6}$$

We thus have:

$$\overline{(\Delta P)^2} = -kT(\partial^2 G/\partial T^2)/D$$

$$\overline{(\Delta P\Delta T)} = kT(\partial^2 G/\partial T\partial P)/D$$

$$\overline{(\Delta T)^2} = -kT(\partial^2 G/\partial P^2)/D$$
$$\overline{(\Delta N)^2} = kT/(\partial^2 G/\partial N^2)$$

where:

$$D = (\partial^2 G/\partial T^2)(\partial^2 G/\partial P^2) - (\partial^2 G/\partial P \partial T)^2$$

Using the well-known thermodynamic transformations, we obtain:

$$\overline{(\Delta P)^2} = -kT(\partial P/\partial V)_{S,N} \quad (7)$$
$$\overline{(\Delta P \Delta T)} = kT^2(\partial P/\partial T)_{V,N}/C_V \quad (8)$$
$$\overline{(\Delta T)^2} = kT^2/C_V \quad (9)$$
$$\overline{(\Delta N)^2} = kT/(\partial \mu/\partial N)_{T,P} \quad (10)$$

where C_V is the specific heat at a constant volume. Equations (7), (8), and (9) are quite similar to those for one-component systems.[16]

By expanding the dielectric constant as a series, we obtain:

$$\Delta\varepsilon = (\partial\varepsilon/\partial P)_{T,N}\Delta P + (\partial\varepsilon/\partial T)_{P,N}\Delta T + (\partial\varepsilon/\partial N)_{T,P}\Delta N$$

Considering Eq. (6), we find the mean squares of the fluctuation of the dielectric constant:

$$\overline{(\Delta\varepsilon)^2} = \left[\left(\frac{\partial\varepsilon}{\partial P}\right)^2_{T,N}\overline{(\Delta P)^2} + 2\left(\frac{\partial\varepsilon}{\partial P}\right)_{T,N}\left(\frac{\partial\varepsilon}{\partial T}\right)_{P,N}\overline{(\Delta T \Delta P)} + \left(\frac{\partial\varepsilon}{\partial T}\right)^2_{P,N}\overline{(\Delta T)^2}\right] + \left(\frac{\partial\varepsilon}{\partial N}\right)^2_{T,N}\overline{(\Delta N)^2} \quad (11)$$

By substituting $\overline{(\Delta P)^2}$, $\overline{(\Delta P \Delta T)}$, $\overline{(\Delta T)^2}$, and $\overline{(\Delta N)^2}$ into the above equation, we obtain:

$$\overline{(\Delta\varepsilon)^2} = \frac{kT}{V\beta_T}\left(\frac{\partial\varepsilon}{\partial P}\right)^2_{T,N}\left[1 + \left(\frac{\beta_T}{\beta_S} - 1\right)\chi^2\right] + \frac{kT}{(\partial\mu/\partial N)_{T,P}}\left(\frac{\partial\varepsilon}{\partial N}\right)^2_{T,P} \quad (12)$$

$$\chi = 1 + \frac{\beta_T(\partial\varepsilon/\partial T)_{P,N}}{\alpha_P(\partial\varepsilon/\partial P)_{T,N}}$$

where β_T is the isothermal compressibility, β_S is the adiabatic compressibility, and α_P is the isobaric expansivity.

Since we consider only a small part of the solution containing a given number, N_0, of moles of the solvent, we can regard the fluctuation of the number of moles of the solute as that of the concentration. From Eqs. (1) and (11), the expression for the isotropic Rayleigh ratio of the solution is the sum of the concentration scattering, R_c, due to the fluctuation of the concentration and the so-called density scattering, R_d, which is independent of the fluctuation of the concentration:

$$R_{is} = R_c + R_d \quad (13)$$

By using the $\varepsilon = n^2$ relationship, where n is the refractive index, we obtain:

$$R_c = \left(\frac{2\pi^2 kT}{\lambda^4}\right)Vn^2\left(\frac{\partial n}{\partial N}\right)^2_{P,T}\Big/\left(\frac{\partial\mu}{\partial N}\right)_{P,T} \quad (14)$$

$$R_d = \left(\frac{2\pi^2 kT}{\lambda^4\beta_T}\right)n^2\left(\frac{\partial n}{\partial P}\right)^2_{T,N}\left[1 + \left(\frac{\beta_T}{\beta_S} - 1\right)\chi^2\right] \quad (15)$$

Equation (15) is the same one as that shown by Coumou *et al.* for a pure liquid.[6] Consequently, we can regard the isotropic Rayleigh ratio in a solution as being additively composed of concentration scattering and the so-called density scattering.

Experimental and Results

Experimental. The light-scattering measurements were made with light with a wavelength of 436 nm using a Shimadzu electrophotometric light-scattering photometer, PG-21. The photometer was calibrated using benzene, so as to obtain 47.5×10^{-6} cm^{-1} for the total Rayleigh ratio.[17] This benzene was washed with concentrated sulfuric acid, passed through an activated aluminum oxide column, and carefully distilled prior to use. Measurements of the redistilled water used gave values for the Rayleigh ratio of 2.70×10^{-6} cm^{-1} and for the depolarization of 0.10. The aqueous sucrose solutions were purified by passing them through an activated carbon column[15] and were then tested for dissymmetry. The total Rayleigh ratio, R_t, and the depolarization, ρ, were determined for the sucrose solution thus obtained. Each sample was filtered directly into the cell through a Millipore filter 220 or 100 nm in pore diameter under the pressure of nitrogen.

The refractive index increments were determined at 25 °C using a Shimadzu photoelectric differential refractometer, DR-3, calibrated with aqueous solution of sodium chloride.[18]

The sucrose concentration was determined with both the density and the refractive index.[18]

Results. The isotropic Rayleigh ratio was found by[19]

$$R_{is} = \frac{6-7\rho}{6+6\rho}R_t \quad (16)$$

The so-called density scattering, R_d, of the sucrose solution was assumed to be equal to the isotropic Rayleigh ratio of water. The concentration scattering, R_c, was obtained by subtracting the isotropic Rayleigh ratio of water from the isotropic Rayleigh ratio, R_{is}, obtained by Eq. (16). The Rayleigh ratios, R_t, R_{is}, and R_c, for sucrose solutions which were obtained in this way are shown in Fig. 1. The variation in Δn for sucrose solutions is shown in Fig. 2, where Δn is the difference between the refractive index of a sucrose solution and that of water.

We can obtain the molecular weight of a solute by means of the following equations:

$$Hc/R_c = 1/M + 2Bc$$
$$H = (2\pi^2 n^2/\lambda^4 N_A)(\partial n/\partial c)^2_{P,T}$$

where c is the weight of a solute per ml of solution and B is the virial coefficient.

Figure 3 shows the plot of Hc/R_c for the sucrose concen-

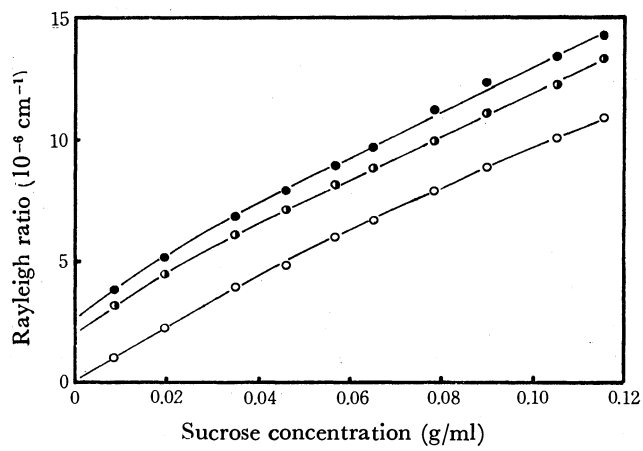

Fig. 1. Rayleigh ratio for aqueous sucrose solutions. ●: R_t, ◑: R_{is}, ○: R_c.

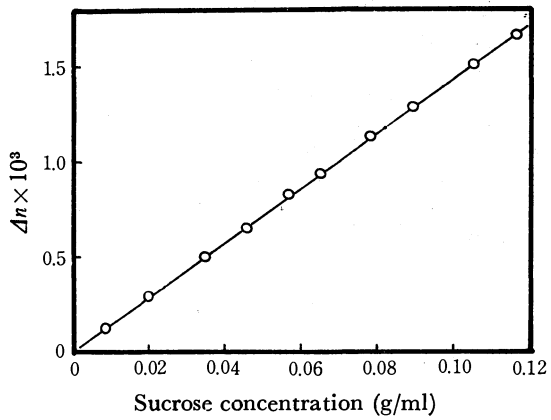

Fig. 2. Refractive index increment of aqueous sucrose solution.

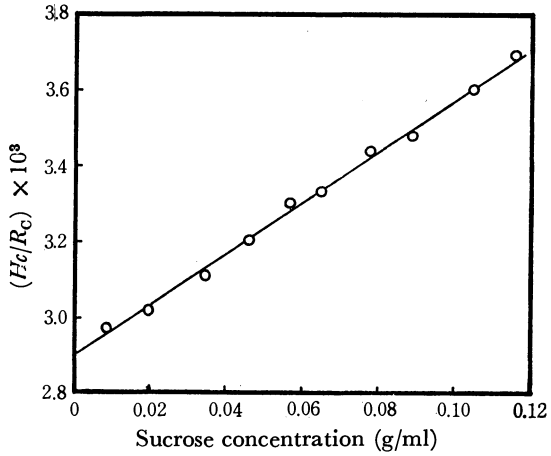

Fig. 3. Molecular weight determination of sucrose.

tration. This curve yields 344±6 as the molecular weight for sucrose, against a calculated value of 342.3.

Discussion

The good agreement of our experimental result with the calculated value confirms that the isotropic scattering is additively composed of the concentration scattering, R_c, and the so-called density scattering, R_d. This confirmation is also supported by the experimental results of Coumou and Mackor[1] and of Pethica and Smart.[20]

To elucidate the relationship between Eq. (3), which has been suggested by Bullough *et al.*, and our Eq. (13), we will express the fluctuation of the dielectric constant in terms of the density, the temperature, and the concentration thus:

$$\Delta\varepsilon = (\partial\varepsilon/\partial d)_{T,N}\Delta d + (\partial\varepsilon/\partial T)_{d,N}\Delta T + (\partial\varepsilon/\partial N)_{d,T}\Delta N \quad (17)$$

The density is given by $d=(N+N_0)/V$. We thus obtain:

$$\Delta d = -\frac{d}{V}\left(\frac{\partial V}{\partial P}\right)_{T,N}\Delta P - \frac{d}{V}\left(\frac{\partial V}{\partial T}\right)_{P,N}\Delta T + \left(\frac{\partial d}{\partial N}\right)_{P,T}\Delta N \quad (18)$$

Using Eqs. (6), (7), (8), (9), and (10), we obtain:

$$\overline{(\Delta d)^2} = -kT\left(\frac{d}{V}\right)^2\left(\frac{\partial V}{\partial P}\right)_{T,N} + kT\left(\frac{\partial d}{\partial N}\right)^2_{P,T}\Big/\left(\frac{\partial \mu}{\partial N}\right)_{P,T} \quad (19)$$

$$\overline{(\Delta d\Delta T)} = 0 \quad (20)$$

$$\overline{(\Delta N\Delta d)} = kT\left(\frac{\partial d}{\partial N}\right)_{P,T}\Big/\left(\frac{\partial \mu}{\partial N}\right)_{P,T} \quad (21)$$

Equations (10), (19), and (21) are equivalent to Eqs. (2.10), (2.12), and (2.9) in Ref. 21 respectively. Relation (20) shows that the fluctuations in the temperature and the density are statistically independent. However the fluctuations in the concentration and the density are not independent.

From Eq. (17), we obtain:

$$\overline{(\Delta\varepsilon)^2} = \left(\frac{\partial\varepsilon}{\partial T}\right)^2_{d,N}\overline{(\Delta T)^2} + \left(\frac{\partial\varepsilon}{\partial d}\right)^2_{T,N}\overline{(\Delta d)^2} + 2\left(\frac{\partial\varepsilon}{\partial d}\right)_{T,N}\left(\frac{\partial\varepsilon}{\partial N}\right)_{T,d}\overline{(\Delta d\Delta N)} + \left(\frac{\partial\varepsilon}{\partial N}\right)^2_{d,T}\overline{(\Delta N)^2} \quad (22)$$

It is easily shown that this relation is equivalent to Eq. (11). This relation means that the isotropic Rayleigh ratio is represented by Eq. (3) under the assumption that $(\partial\varepsilon/\partial T)_{d,N}=0$, an assumption which Bullough *et al.*[7-9,11,12] implicitly made use of. In this case, the concentration scattering is given by:

$$R_c = \left(\frac{2\pi^2kT}{\lambda^4}\right)Vn^2\left(\frac{\partial n}{\partial N}\right)^2_{d,T}\Big/\left(\frac{\partial \mu}{\partial N}\right)_{P,T} \quad (23)$$

However, the refractive index increment, $(\partial n/\partial N)$, is measured the pressure and the temperature being kept constant, while the density and the temperature are not. Unfortunately, attention has not been paid to this in several published papers.

It is clear from the above discussion that the isotropic Rayleigh ratio must be expressed by Eq. (13).

The authors wish to express their thanks to Professor C. Horie, Dr. A. Sato, and Mr. M. Hara for their valuable advice and encouragement throughout this work.

References

1) D. J. Coumou and E. L. Mackor, *Trans. Faraday Soc.*, **60**, 1726 (1964).
2) L. L. Haynes, R. L. Schmidt, and H. L. Clever, *J. Chem. Eng. Data*, **15**, 534 (1970).
3) F. C. Hentz, Jr. and S. Y. Tyree, Jr., *Inorg. Chem.*, **3**, 844 (1964).
4) B. H. Massey and F. G. R. Gimblett, *ibid.*, **9**, 2043 (1970).
5) A. Einstein, *Ann. Phys.*, **33**, 1275 (1910).
6) D. J. Coumou, E. L. Mackor, and J. Hijmans, *Trans. Faraday Soc.*, **60**, 1539 (1964).
7) M. Kerker, "The Scattering of Light and Other Electromagnetic Radiation," Academic Press, New York (1969).
8) R. K. Bullough, *J. Polymer Sci.*, **46**, 517 (1960).
9) R. K. Bullough, *Proc. Roy. Soc., Ser. A*, **275**, 271 (1963).
10) Y. Sicotte and M. Rinfret, *Trans. Faraday Soc.*, **58**, 1090 (1962).

11) Y. Sicotte, *J. Chim. Phys.*, **61**, 1086 (1964).
12) N. Segudovic and Gj. Deželić, *Croat. Chem. Acta*, **45**, 385 (1973).
13) P. Debye, *J. Phys. Colloid Chem.*, **51**, 18 (1947).
14) M. Halwer, *J. Amer. Chem. Soc.*, **70**, 3985 (1948).
15) S. H. Maron and R. L. H. Lou, *J. Phys. Chem.*, **59**, 231 (1955).
16) L. D. Landau and E. M. Lifschitz, "Statistical Physics," Pergamon Press, Oxford (1959).
17) J. P. Kratohvil, Gj. Deželić, M. Kerker, and E. Matijevic, *J. Polymer Sci.*, **57**, 59 (1962).
18) M. B. Hugin, "Light Scattering from Polymer Solutions," Academic Press, New York (1972).
19) D. J. Coumou, J. Hijmans, and E. L. Mackor, *Trans. Faraday Soc.*, **60**, 2244 (1964).
20) B. A. Pethica and C. Smart, *ibid.*, **62**, 1890 (1966).
21) F. J. Pearson and G. S. Rushbrooke, *Proc. Roy. Soc.*, (Edinburgh), **A64**, 305 (1957).

Combustion of Polymer Fuel-Spheres at Elevated Pressures

Takeo SAITO and Akira IWAMA

Institute of Space and Aeronautical Science, The University of Tokyo, Komaba, Meguro-ku, Tokyo 153

(Received December 7, 1973)

Two kinds of polymer spheres polyurethane (PU) and carboxyl-terminated polybutadiene (CTPB), *ca.* 3 and 5 mm, respectively, in diameter and used currently as fuel and/or binder constituents in solid and hybrid rocket propellants, were ignited electrically with a nichrome fiber in several oxidizing gases over the range 5—30 kg/cm^2. Their combustion phenomena were studied photographically with a 16 mm movie camera. The combustion flame was observed by means of direct photographs, both the variation of diameter with time and the location of contact surface being measured with shadow photographs. It was shown that PU spheres are entirely liquefied, involving slight swelling just after ignition, and then burn in a similar manner to that of distilled hydrocarbon droplets. CTPB spheres were found to expand remarkably after ignition. At the first stage the surrounding product gases formed a diffusion flame, their apparent diameters remaining nearly constant for a short time. At the second stage the remainder of the carbonaceous substance continued to burn, turning to surface combustion. It can be predicted that in an actual rocket combustion chamber the surface of the fuel-binder for PU propellants is wet and that of CTPB propellants is covered with carbonaceous layer during the course of steady state burning. The overall mass burning rate is proportional to a half and 0.3 power of total pressure for PU and CTPB, respectively, depending slightly on the kind of inert gas for dilution of the oxidizing atmosphere in both cases. A combustion model for CTPB is presented and compared with experimental results.

PU and CTPB are important fuel and/or binder constituents in current hybrid and solid composite propellants. Saito[1] and Varney and Strahle[2] demonstrated that the two polymers are contrary to each other in pyrolysis behavior. This study was undertaken to clarify the burning aspects of these polymers having different pyrolysis properties in various oxidizing gases at elevated pressures.

Most experiments on polymeric materials for propellants have placed emphasis on combustion in midget hybrid motors. In such cases, the flow pattern of oxidizer exerts strong influence and the regressing surface of the polymer displays singular geometrical configuration by gas dynamic effects. Structure of the combustion zone is more complicated with the oxidizer flow line crossing boundary layer, transition from laminar flow to turbulent on the half way in the free channel, two phase flow including carbonaceous substance and piece of polymer torn off,[3] and solid-liquid-gas reaction. Study of the combustion of polymer at simplified condition is therefore necessary for explaining this complexity of hybrid and composite propellant combustion phenomena.

The combustion of plastic materials is drawing attention from the standpoint of pollution control and fire prevention but only few reports have appeared on the combustion of polymers. Essenhigh,[4] who studied some thermoplastic polymers burning in quiescent atmosphere, concluded that a burning constant of the Nusselt d^2 law is smaller than that of hydrocarbon oil droplet, *viz.*, the burning rate is larger because of the much closer approach of the surrounding flame to the droplet surface. We have examined whether the higher burning rate of the polymer, compared to hydrocarbon oils, is valid at elevated pressures and to predict the role of the elastomeric fuel-binder in hybrid and composite propellant combustion.

Equipment and Experimental Method

The experiments were performed with the apparatus and optical system shown in Fig. 1. The equipment consists of a high-pressure vessel with a window, 30 mm in width and 350 mm in length, mounted vertically at each side for observation purpose, a mixing chamber for producing a variety of ambient gases and a photographic system.

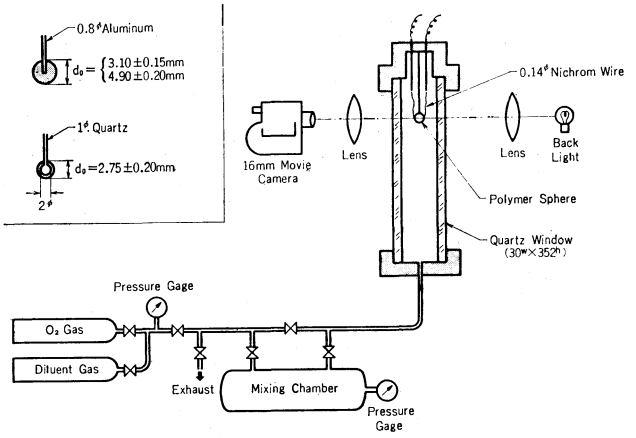

Fig. 1. Schematic diagram of the experimental apparatus.

The polymer spheres were suspended stationarily in the high-pressure vessel. PU spheres, *ca.* 3 mm in diameter, were cured at the tip of a quartz fiber; CTPB spheres, *ca.* 3 and 5 mm in diameter, were hardened and suspended at the tip of alumina fiber 0.8 mm in diameter. The spheres were ignited at the base by means of an electrically heated nichrome fiber 0.14 mm in diameter. A similar suspension method to that for CTPB was applied to PU, but the sphere could not be held stationary during the course of burning. The PU dribbled, rapidly fissuring urethane bonds and liquefying entirely to low viscosity fluid immediately after ignition. The urethane ingredient mixture was therefore cured by means of a one-shot process after being stuck to the spherical tip of a quartz fiber.

The combustion was studied with a 16 mm movie camera at the rate 49.1 frames/s. The optical system is composed of two close-up lenses and an enlargement lens set in front of a camera. Neutral density (ND) filters were used to reduce the intensity of the flame radiation on the films. While the burning spheres are shadow-photographed, the intense backward beam illuminating the sphere through the vessel is provided to drown out the surrounding flame. Variation of diameter and thickness of the boundary layers against time were measured with a film analyzer for the shadow photographs. The ambient pressure was in the range 5—30 kg/cm² (abs.). The pressurized gases, pure oxygen, oxygen diluted with nitrogen, argon and helium were used to study effects of dilution on thermal conductivity and diffusivity.

Results

Figures 2 and 3 show direct and shadow photographs of the burning PU and CTPB spheres, respectively. It is possible to distinguish two combustion phenomena for PU and CTPB. The flame of PU apparently corresponds to diffusional combustion which is similar to oil droplet combustion. On the other hand, CTPB demonstrates singularities outside the burning phenomena that were already observed on oil droplets.

Overall Mass Burning Rate. Total burning time is obtained from 16 mm movie shadow photograph records. For the *ca.* 2.7 mm diameter PU spheres in which a spherical quartz tip 2.0 mm in diameter is embraced, the total burning time t_b is obtained from the intersection of the extrapolation of variation curve of the square of diameter with the time axis. The average mass burning rate ($\dot{m}$) is calculated from initial mass of sample and total burning time.

PU: The average mass burning rate has a slight dependency upon the inert gases but an obvious dependency upon the total pressure in spite of large

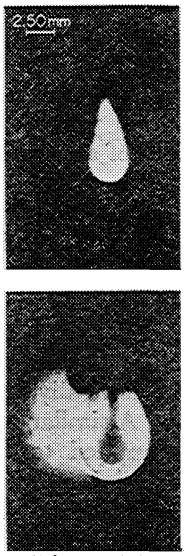

Fig. 2. Direct and shadow photographs for PU.
Upper photograph is direct one. Lower photograph is shadow one. Initial diameter: 2.65 mm. Ambient pressure: 20 kg/cm² at pure oxygen gas.

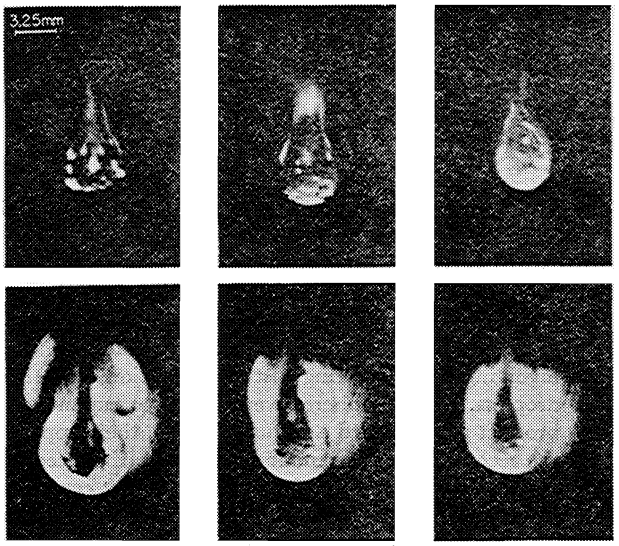

Fig. 3. Direct and shadow photographs for CTPB.
Upper photographs are direct ones. Lower photographs are shadow ones. Initial diameter: 3.25 mm. Ambient pressure: 20 kg/cm² at pure oxygen gas. Frame velocity: 49.1 frames/s.
a. 33th frame. b. 75th frame. c. 106th frame.

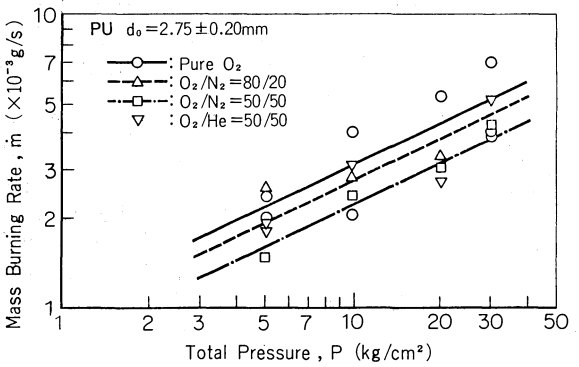

Fig. 4. Dependence of mass burning rate for PU on total pressure.

scattering of the data. The relation between mass burning rate and total pressure is given by $\dot{m}=\alpha P^{1/2}$ (Fig. 4). The effect of oxygen concentration in ambient gas on mass burning rate is included in factor α. Use of the diluent gases which differ in transport properties exerted a little influence on the mass burning rate, in particular He gas as a diluent indicates the tendency to increase $\dot{m}$ as compared with N_2 gas at the same oxygen concentration.

CTPB: The average mass burning rate for CTPB increases with an increase in the initial diameter of the sphere. Substitution of one diluent by another resulted in a somewhat different mass burning rate. For the sphere with initial diameter 4.9 mm, He and Ar included in oxygen gas lead to 10% higher mass burning rate than nitrogen gas dilution in the same fractions. However, such a difference due to the kind of diluent gas disappeared in the sphere of smaller initial diameter and lower oxygen fractions. This might be due to the coupling effect of thermal conductivity and diffusivity for inert gases. Figure 5 shows

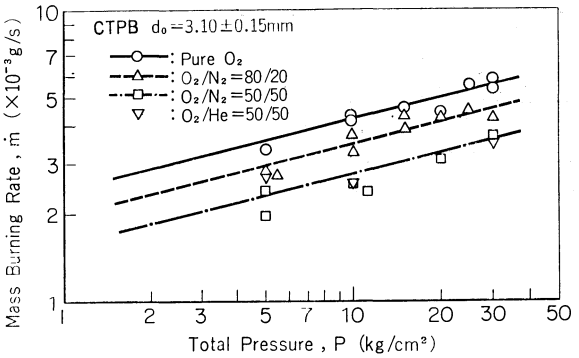

Fig. 5. Dependence of mass burning rate for CTPB on total pressure.

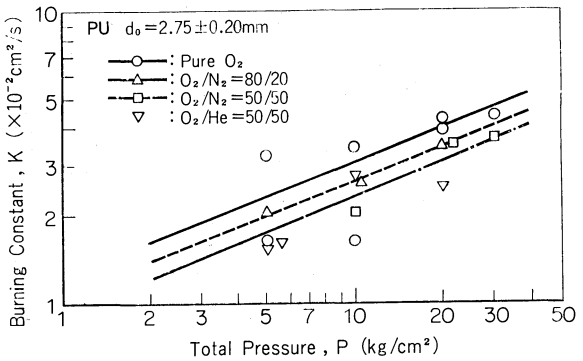

Fig. 7. Dependence of burning constant for PU on total pressure.

the dependency of the mass burning rate on total pressure given by $\dot{m}=\alpha' P^{0.3}$, where α' is a factor giving a measure of the dependency of oxygen fraction.

Square-of-Diameter Law. PU spheres swell a little just after ignition and liquefy quickly, their shape becoming ellipsoidal. According to Kobayashi's method,[5] the equivalent diameter is defined as

$$d = \sqrt[3]{a^2 b}$$

where a is a minor axis and b a major axis.

On the other hand, CTPB remains in the solid state in the core during most of the burning period and exhibits complex aspects at the surface. Closer examination revealed that the evolution of the shape of the burning drop is irregular and at lower pressures, in particular, the shape is apt to be far from spherical. The top of the drop shows a rough surface. The maximum horizontal diameter of the drop is therefore assumed to be an equivalent diameter for CTPB.

PU: After passing through a short expanding process, PU spheres decrease according to the d^2 law. Figure 6 shows plots of the variation of a PU drop diameter emerging on each frame of the 16 mm movie film. At a higher mass fraction of oxygen, discrete changes of apparent diameters exist which result from liquid-phase bubbling based on thermal cracking beneath the surface and which in turn bring about

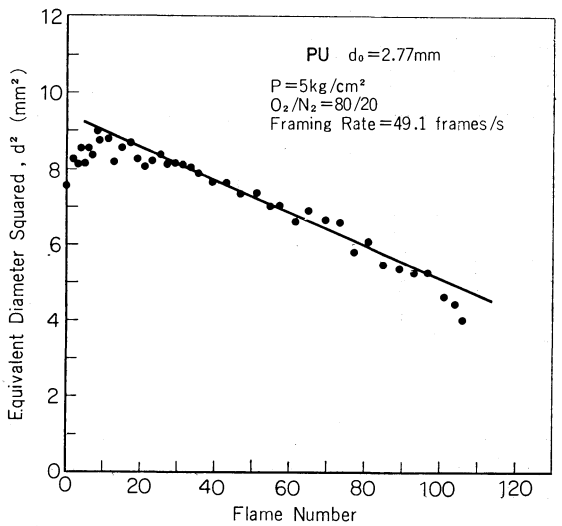

Fig. 6. Variation of equivalent diameter squared for PU with time.

flickering at the flame front.

The burning constant defined by $d_0^2-d^2=K(t-t_0)$ was derived by the method of least squares for diameter regressing drop during a limited period of steady state burning. In Fig. 7 the burning constant K is plotted *versus* P, the following relation being found.

$$K = \beta P^{0.4}$$

where β is a factor including dependence of oxygen fraction. Conventional oil droplets have 0.25[6] for this pressure index of the burning constant, the pressure index of PU being nearly equal to that for benzene.[7]

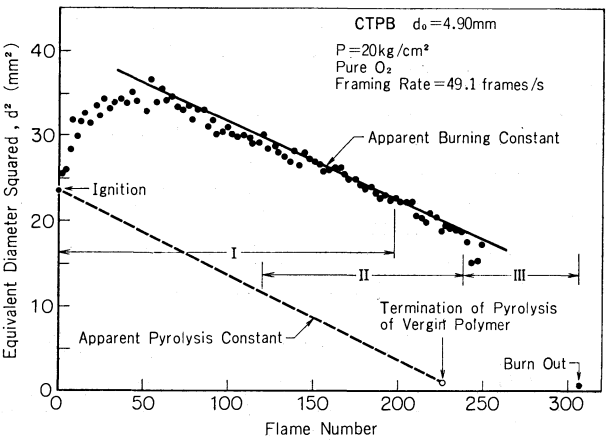

Fig. 8. Variation of equivalent diameter squared for CTPB with time.

CTPB: Figure 8 gives the change of the square of diameter during the life of a CTPB sphere in three stages:

(1) period between ignition and termination of gas emission from all burning surfaces except the top.

(2) period during surface combustion, *i.e.*, the period in which d^2 law holds. At this stage a superposition of the first stage exists.

(3) period during which the shapes change at random, the remaining cenosphere being extinguished.

At the first stage, the sphere of CTPB repeated swelling and contraction in low frequency in the order of 7—10 Hz for some time after ignition. However, the average diameter tends to be nearly constant, though for only a short time, after the initial transient period. Large scale heterogeneity of the evolving gases from surface resulted in formation of a lace pattern, producing a collection of numerous flamelets. The

porous carbonaceous substance which had become spherical was presumed to include virgin plastic. This was confirmed by interruption of burning half way, based on free falling of burning polymer spheres into a water pool.[8] From this time (second stage), the sphere began to regress along the curve of d^2 law. The coexistence of a diffusion flame formed by ambient oxygen and pyrolyzing gases with a surface combustion was observed. The linear relation between square diameter and time is valid even while virgin polymer remains, being covered with a carbonaceous layer. At the third stage, the cenosphere produced by an internal reaction occurring with the invasion of oxidizing gases into the porous layer, *i.e.*, produced by further cracking of the non-volatile carbonaceous residue, was swept out rapidly by the flame or flown away by natural convection. Apparent pyrolysis constant K_d (Fig. 8) is defined as the slope of the broken line d_0^2/t_d, linked between equivalent diameter squared at ignition d_0^2 and termination time of pyrolysis gas emission from all surfaces of burning polymer spheres. Here, the termination time of pyrolysis of virgin polymer, *i.e.*, termination of pyrolysis gas emission from all surfaces, which is defined much better than that from all surfaces except the top, was taken as t_d. Though the apparent burning constant K_r' for carbonaceous residue at the second stage, *i.e.*, the slope of the solid line, has very large scattering and even a tendency to decrease as ambient pressure increases, the corrected burning constant K_r divided by the squared swelling factor showed smaller scattering. At the third stage the shape of the porous carbonaceous residue, *i.e.*, cenosphere, changed entirely at random, and the horizontal diameter was therefore not measured. The scattering of the data prevented us from discriminating the effect of different diluent gas on the burning constant. However, it is evident that the burning constant may have weak dependency on P as shown in Fig. 9.

Extrapolation of the K–P curve at $O_2/N_2=50/50$ for PU (Fig. 7) gives *ca.* $K=0.9$ mm²/s for one atmosphere. K is assumed to be *ca.* 0.8 mm²/s at $O_2/N_2=20/80$ (in air). This corresponds to 50—80% less than constants

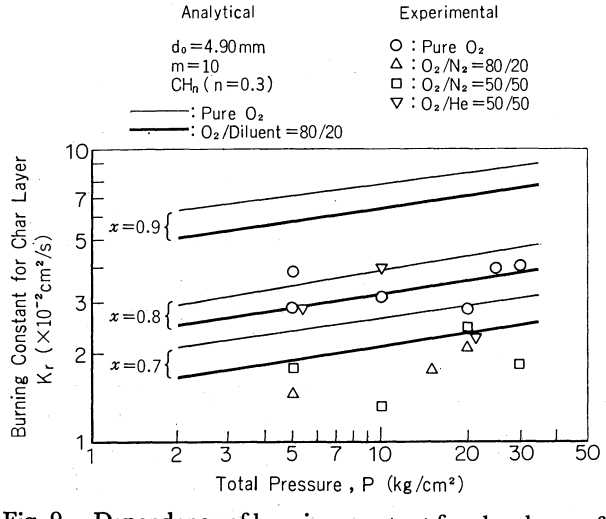

Fig. 9. Dependence of burning constant for char layer of CTPB on total pressure.

for various plastics reported by Essenhigh,[4] and suggests that PU would demonstrate substantially similar burning characteristics to those of the oil droplets.

Thickness of Contact Surface. The location of contact surface, *i.e.*, the boundary surface between surrounding ambient gas and ascending current due to natural convection, was determined by means of shadow photographs.

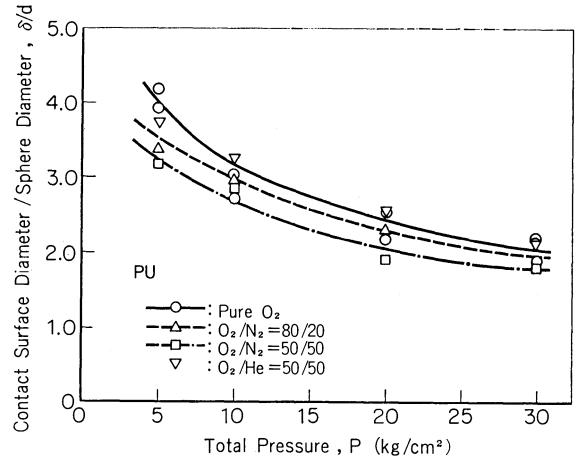

Fig. 10. δ/d for PU as a function of total pressure.

The ratio of apparent diameter of contact surface to diameter of PU sphere, δ/d, is given in Fig. 10, where δ is the maximum diameter of the contact surface envelope measured on the horizontal axis crossing at the center of the sphere. The contact surface measured in a vertical direction is five sixths of that in a horizontal direction at higher pressure and five sevenths at lower pressure. As ambient pressure decreases, δ/d increases and the contour of the contact surface expands a little in helium atmosphere because of its higher thermal conductivity.

The relationship[9] between contact surface diameter and volumetric flow rate of ascending current S is expressed by

$$\frac{\delta}{2}=\sqrt{\frac{S}{4\pi U}} \tag{1}$$

where U is the upward linear flow rate due to natural convection. Substituting $\dot{m}=\rho_g S$ into the equation and making use of the relation $\dot{m}=(\pi/4)\sigma dK$, we have

$$\frac{\delta}{d}=\sqrt{\frac{\sigma K}{8\rho_g r U}} \tag{2}$$

This equation implies that high temperature combustion of these polymers and higher density of environmental gas give a lower value of δ/d. Figure 10 shows agreement of experimental results with the trend indicated by Eq. (2). At the first stage of CTPB burning, the contact surface gives rise to oscillation in turn with the fluctuation of the burning surface. Figure 11 shows δ/d in the second stage where d^2 law holds. The contact surface becomes undulatory as oxygen fraction increases.

Swelling Factor. The swelling factor is defined as the ratio of the average maximum diameter at the first burning stage of CTPB to the initial diameter

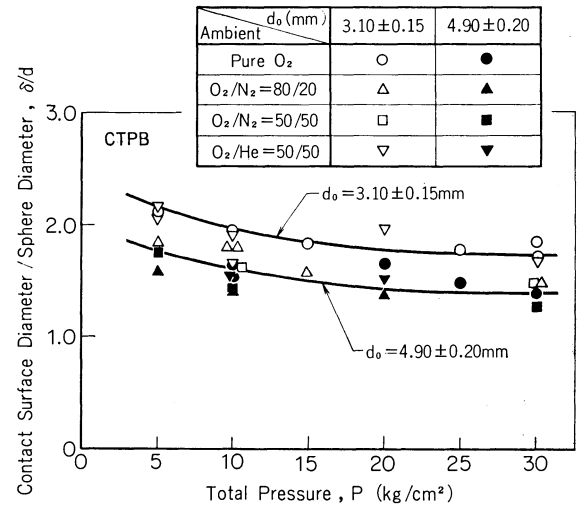

Fig. 11. δ/d for CTPB as a function of total pressure.

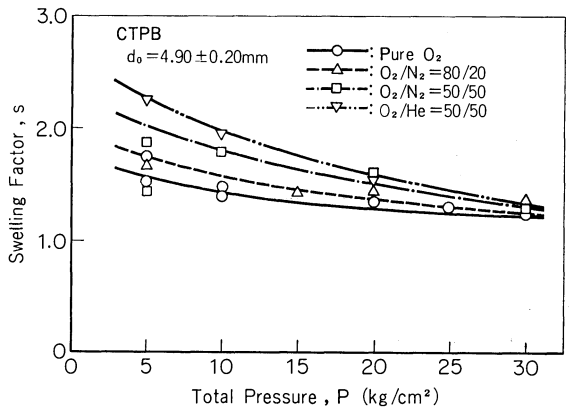

Fig. 12. Swelling factor for CTPB as a function of total pressure.

(Fig. 12). Variation of the swelling factor is affected by ambient pressure and oxygen fraction, although it is independent of the initial diameter. The use of helium gas as a diluent gave rise to an increase in the swelling factor as compared with that of N_2 diluent gas at the same oxygen fraction. Swelling for PU was negligible.

Analysis

A new combustion model for CTPB is proposed (Fig. 13). A number of semiempirical approximation apply to the region from the pyrolysis surface to the flame front:

(1) The surface of virgin polymer is maintained at constant temperature T_p with a carbonaceous layer remaining on the surface. ($\dot{m}_p=\dot{m}_g+\dot{m}_c$)

(2) The carbonaceous layer yields no dynamic interactions with the pyrolyzing gas flow (*e.g.*, its capillary flow resistance is negligible; pressure of the pyrolyzing gases passing through carbonaceous layer is constant).

(3) Quasi-steadily burning takes place.

(4) Conductive heat flux from the flame front controls the pyrolysis rate of polymer.

(5) The system is spherically symmetric.

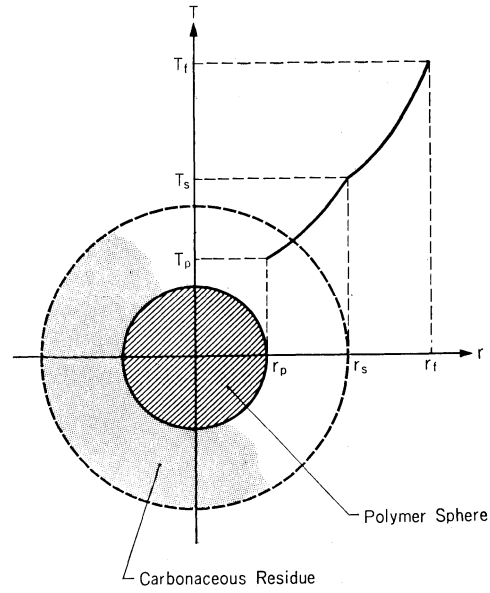

Fig. 13. A new combustion model for the sphere of CTPB.

(6) The heat released as a result of chemical reaction is removed by heat conduction and mass transport, *i.e.*, radiation and thermal convection are negligible.

(7) Temperature inclination inside virgin polymer is negligible.

The heat flow to the virgin polymer surface should balance only the heat needed for pyrolysis reaction, since the heat flow into the interior of the virgin polymer can be neglected on account of (7).

$$Q_v = h_v\dot{m}_p \doteq -4\pi r_p^2 q_v|_{r=r_p} \tag{3}$$

In addition, the heat flux to the virgin polymer surface is

$$q_v = -\bar{k}\frac{dT}{dr}\bigg|_{r=r_p} \tag{4}$$

where h_v is the pyrolysis heat per unit mass of polymer, $\dot{m}_p$ the mass pyrolysis rate and $\bar{k}$ the effective thermal conductivity of carbonaceous layer impregnated with pyrolyzing gases. The heat transport equation in terms of spherical coordinates would be written as

$$\rho_g c_p v_r \frac{dT}{dr} = \frac{\bar{k}}{r^2}\frac{d}{dr}\left(r^2\frac{dT}{dr}\right) \tag{5}$$

if the heat transfer between carbonaceous substance and gas flow is accomplished very quickly because of high porosity. Here, c_p is specific heat at constant pressure for gas and v_r the radial velocity. Equation (5) should be supplemented with boundary conditions:

$$T = T_s \text{ at } r = r_s$$
$$T = T_p \text{ at } r = r_p$$

The solution of Eq. (5) is given by

$$\frac{T-T_s}{T_p-T_s} = \frac{e^{-1/Ar}-e^{-1/Ar_s}}{e^{-1/Ar_p}-e^{-1/Ar_s}} \tag{6}$$

where $A=4\pi\bar{k}/c_p\dot{m}_g$ and $\dot{m}_g=4\pi r^2\rho_g v_r$. Substituting Eq. (6) into Eq. (4), we obtain

$$q_v|_{r=r_p} = -\bar{k}\frac{T_p-T_s}{Ar_p^2}\frac{e^{-1/Ar_p}}{e^{-1/Ar_p}-e^{-1/Ar_s}} \tag{7}$$

Substituting Eq. (7) into Eq. (3), we get

$$h_v\dot{m}_p = \frac{\dot{m}_g c_p(T_p - T_S)}{1-e^{-1/4(1/r_S-1/r_p)}} \tag{8}$$

The fraction of the polymer converted into gases on account of pyrolysis is defined as

$$\dot{m}_g = x\dot{m}_p, \qquad 0<x<1$$

Rewriting Eq. (8) with use of this definition, we have

$$\dot{m}_g = \frac{4\pi\bar{k}}{\left(\frac{1}{r_p}-\frac{1}{r_S}\right)c_p} \ln\left\{1+\frac{xc_p(T_S-T_p)}{h_v}\right\} \tag{9}$$

If polymer density σ is constant, the pyrolysis rate of the polymer can be expressed by

$$\dot{m}_p = -4\pi r_p^2\sigma\frac{dr_p}{dt} \tag{10}$$

Combination of Eqs. (9) and (10) gives

$$-xr_p^2\sigma\frac{dr_p}{dt} = \frac{\bar{k}}{c_p\left(\frac{1}{r_p}-\frac{1}{r_S}\right)} \ln\left\{1+\frac{xc_p(T_S-T_p)}{h_v}\right\} \tag{11}$$

On integration, we obtain

$$xr_0^2\left\{\frac{1}{2}-\frac{r_0}{3r_S}\right\} = t_d\frac{\bar{k}}{c_p\sigma} \ln\left\{1+\frac{xc_p(T_S-T_p)}{h_v}\right\} \tag{12}$$

where r_0/r_S is a factor combined with a swelling factor, s, as follows:

$$d_S^0 = d_0^2 + 0.8\{(sd_0)^2-d_0^2\} \tag{13}$$

The diameter of the carbonaceous layer is assumed to maintain a constant diameter squared which is averaged over the entire burning time at the first stage. Estimation of $\bar{k}$ in Eq. (12) is made by the equation

$$\bar{k} \approx \varepsilon k_g + (1-\varepsilon)k_s$$

where k_g and k_s are the thermal conductivity of pyrolyzing gases and carbonaceous substance, respectively, and ε the volumetric fraction of pyrolysis gases contained in char layer. We adopted the heat capacity of propane at $(T_S+T_p)/2$ for the approximation of heat capacity of the pyrolysis gases. From Eq. (12), we obtain the following relation for initial diameter:

$$d_0^2 = K_d t_d$$

where apparent pyrolysis constant K_d is:

$$K_d = \frac{4\bar{k}}{\left\{\frac{1}{2}-\frac{r_0}{3r_S}\right\}xc_p\sigma} \ln\left\{1+\frac{xc_p(T_S-T_p)}{h_v}\right\} \tag{14}$$

The equation indicates no explicit dependence of K_d on ambient pressure. It is apparent, however, that this expression becomes determinate when T_S or x is given as a function of total pressure and oxygen fraction by experiment.

The burning stage of CTPB transfers from gas-phase combustion of pyrolysis gas surrounding the surface of the carbonaceous layer to surface combustion similar to simple carbon. If the rate-determining process of regression for the carbonaceous layer is the diffusion of oxygen onto the surface, the specific reaction rate would be given by

$$R_S = -k_0(p_{ox}-p_S)$$

where k_0 is the velocity constant for mass transfer, p_{ox} the oxygen pressure in ambient gas and p_S the oxygen pressure on the surface of the carbonaceous layer. From the diffusion equation k_0 is given by

$$k_0 = \frac{DM_o}{RT_c\left(\frac{2r_c}{\delta}-1\right)} \tag{15}$$

where r_C is the carbonaceous layer radius, D the diffusivity for oxygen gas through combustion products, R the gas constant, δ the contact surface diameter and M_O the oxygen molecular weight. Since generally $p_{ox} \gg p_S$, the specific reaction constant can be given by

$$R_S = \frac{DM_o}{RT_c\left(1-\frac{2r_c}{\delta}\right)}p_{ox} \tag{16}$$

We shall now consider the stoichiometric reaction concerning the surface burning process which is given as follows.

$$CH_n + \left(1+\frac{1}{4}n\right)O_2 \longrightarrow CO_2 + \frac{n}{2}H_2O$$

On the other hand, the specific consumption rate for the carbonaceous sphere is given by

$$\frac{\dot{m}_c}{4\pi r_c^2} = -\rho_c\frac{dr_c}{dt} \tag{17}$$

From Eqs. (16) and (17), we get

$$-\frac{\rho_c}{M_c}\frac{dr_c}{dt} = \frac{1}{M_o\left(1+\frac{1}{4}n\right)}\frac{DM_o}{RT_c\left(1-\frac{2r_c}{\delta}\right)}p_{ox} \tag{18}$$

where ρ_C and M_C are apparent density for char layer and molecular weight for carbonaceous substance, respectively. We have herewith

$$\rho_c = \left(\frac{d_0}{d_S}\right)^3\sigma(1-x)$$

where d_S is as assumed in Eq. (13). Thus on integration of Eq. (18), we get

$$d_S^2-d_0^2 = \frac{8M_cDp_{ox}}{\left(1+\frac{1}{4}n\right)\rho_cRT\left(1-\frac{2r_c}{\delta}\right)}(t-t_0) \tag{19}$$

Since diffusion coefficient is proportional to ambient temperature and inverse to total pressure, apparent burning constant K_r' for carbonaceous layer is given by

$$K_r' = 8\frac{M_c}{1+\frac{1}{4}n}\frac{D^0p_{ox}}{\rho_cRT^0\left(1-\frac{d_c}{\delta}\right)}\frac{1}{P}\frac{T}{T^0} \tag{20}$$

where D^0 is diffusion coefficient at 273 K and one atmospheric pressure, the relation $T=(T_C+T_\infty)/2$ being adopted. Surface combustion temperature T_C at carbonaceous layer surface is then assumed to be proportional to total pressure; we can put $T_C=T_{C_0}P^{1/m}$. Here, T_{C_0} is the surface combustion temperature at atmospheric pressure dependent on oxygen fraction. $T_{C_0}=1500$ K is assumed for pure oxygen. The burning constant K_r, *i.e.*, K_r'/s'^2, is calculated by means of the above expression, where $s'^2=1+0.8(s^2-1)$ from Eq. (13).

Discussion

The process of combustion of CTPB sphere in a quiescent oxidizing gas is characterized by the develop-

ment of gaseous diffusion flame and subsequent surface combustion of char layer. High permeability for gases and high effective thermal conductivity of such a carbonaceous layer seem to introduce a mass burning rate about one and a quarter times as large as that of PU sphere. The comparatively greater apparent pyrolysis constant K_d for CTPB virgin polymer is also deduced to be mainly due to the thermal factor of the char layer.

The mass burning rates for PU and CTPB presumed at one atmosphere by the extrapolation method are given in Tables 1 and 2, respectively.

Table 1. Mass burning rate for PU at one atmosphere (mg/s)

Ambient	$d_0=2.75\pm 0.20$ mm
Pure O_2	1.1
$O_2/N_2=80/20$	0.9
$O_2/N_2=50/50$	0.75

Table 2. Mass burning rate for CTPB at one atmosphere (mg/s)

Ambient	d_0	
	4.90 ± 0.20 mm	3.10 ± 0.15 mm
Pure O_2	4.4	2.4
$O_2/N_2=80/20$	3.1	2.0
$O_2/N_2=50/50$	2.5	1.5

The first two stages are mostly the time denoted by t_d required for the burning of gases emitted from virgin polymer and a latter part of the second and the third stages are the time (t_s) of surface combustion including internal oxidation reaction. The partial superposition of the process of gas phase and surface combustion becomes considerably greater as the ambient pressure increases. For instance, t_d/t_b equals 0.75 and occurrence of the incipient surface combustion is observed when 35% of the total time of combustion has elapsed at 30 kg/cm² of pure O_2. This is shown in Fig. 14, where the broken line denotes the time when the emission of pyrolysis gases terminates from all burning surfaces except the top at the base of a supporting fiber. However, plotting for each emission is ommitted in order to avoid complexity of the figure. In this case the time of substantial superposition of both processes is approximately 20% of the total time of combustion. Afterwards, pyrolyzing gases are emitted only from the top of the sphere. At lower pressures such as 5 kg/cm² the total time of combustion can be written as

$$t_d + t_s = t_b$$

The region of gas-phase diffusional combustion, in turn, can be divided into a process in which vigorous emission of pyrolysis gases and periodically repeated swelling and contraction of sphere are observed and a process of d^2 law combustion in which a number of flamelets are established and a part of oxygen passing through undulatory flame front contributes to the process of the surface combustion. The value of t_d/t_b photographically obtained is sensitive not to the total pressure but to oxygen fraction under high pressure. However, the ratio of surface burning to the total burning time is a little stronger function of total pressure at the lower pressure below 10 kg/cm². At more elevated pressure, CTPB burning characteristics are substantially controlled by the physical nature of the carbonaceous layer.

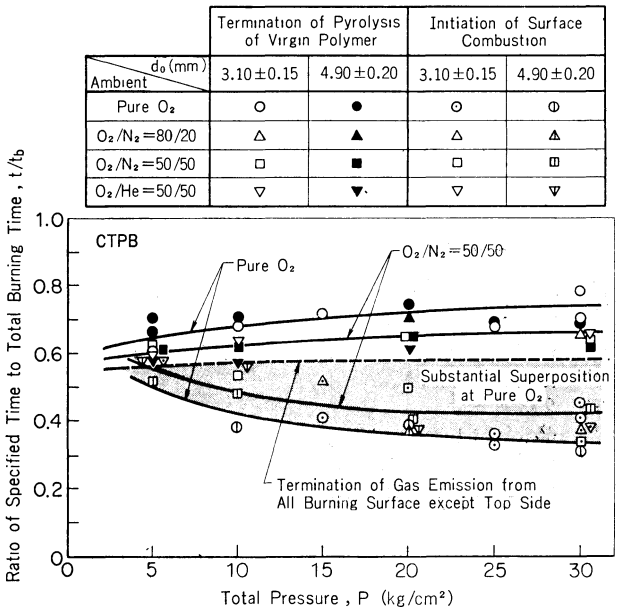

Fig. 14. Variation of ratio of specified time to total burning time with total pressure for CTPB.

The results are compared with analytical calculations for the CTPB combustion model for the case in which T_s is assumed to be a function of the total pressure of ambient gas for the gas-phase combustion at the first stage:

$$T_s = T_{s_0} P^{1/m'}$$

where T_{s_0} is the surface temperature of char layer during the first stage burning at one atmospheric pressure which is dependent upon oxygen fraction. T_{s_0} for pure oxygen gas as ambient gas is assumed to be 1000 K. According to the T_s-P diagram, a reasonable value for m' is 8—12. If the fraction of CTPB polymer converted into gases on account of pyrolysis reaction is presumed to be 0.7—0.9, the calculated results would be in good agreement with experimental data (Fig. 15). The parameters used in this calculation are $m'=10$, $\bar{k}=0.001$ cal/cm·s·deg. Similarly, the value x derived from the combustion constant for carbonaceous residue in Fig. 9 also is 0.7—0.8. In order to examine the validity of x, deduced from this analysis, a rough estimation of the apparent density of the carbonaceous layer was made by the interruption of burning at half way, yielding 0.11—0.32. The prediction based on the analytical results of the burning constant K_r for char layer of CTPB at one atmosphere including 20% oxygen by volume yielded $K_r=1$ mm²/s, which is nearly twice as large as the data of some plastics forming a carbonaceous layer at the second burning stage defined here such as cellulose acetate, phenolic resin and polycarbonate.[4]

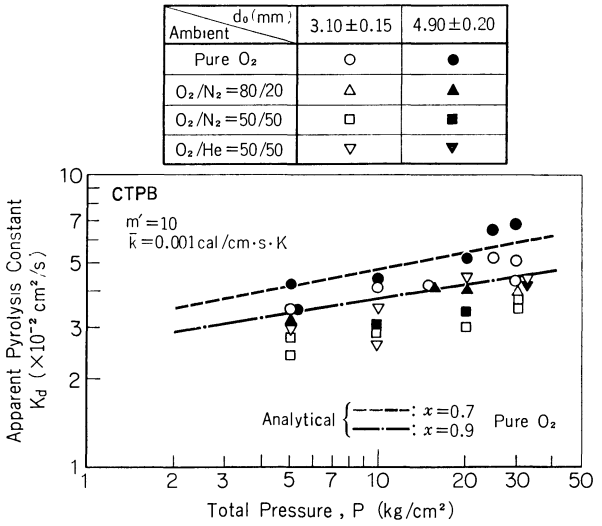

Fig. 15. Comparison of analytical results with experimental data for apparent pyrolysis constant for virgin polymer of CTPB.

Our emphasis on the CTPB burning aspects introduced by the existence of a freely-gas-permeable carbonaceous layer is to a certain extent justified by these experimental observations differing from the PU sphere burning such as common hydrocarbon droplets.

Conclusion

(1) The burning surface of PU spheres is always covered with a liquefied layer, while that of CTPB spheres remains a highly porous char layer under steady state combustion.

(2) The pressure index of the overall mass burning rates for PU and CTPB spheres are 0.5 and 0.3, respectively. Dependence of the burning constants upon the total pressure is given as follows:

$K=\beta P^{0.4}$ for PU. (experimental)

$K_d=\gamma P^{1/6}$ for virgin polymer of CTPB. (analytical)

$K_r=\gamma' P^{1/6}$ for char layer of CTPB. (analytical)

PU spheres which burn in a similar mechanism to that oil droplets regress with a rate having pressure index close to that of the burning constant for oil droplets.

(3) 70—90% of CTPB by weight is emitted as pyrolysis gases from virgin polymer on account of pyrolysis reaction and consumed in a gaseous diffusion flame with oxidizing gases, and the remainder proceeds to burn subsequently in a surface combustion mechanism.

(4) Analytical results based on a new combustion model for CTPB, which has a char layer structure formed by pyrolysis reaction, agreed with experimental observations, particularly in connection with the life of virgin polymer spheres and the fraction of the char layer.

Nomenclature

a minor axis for ellipsoid, cm
A $4\pi\bar{k}/c_p\dot{m}_g$, 1/cm
b major axis for ellipsoid, cm
c_p specific heat at constant pressure for pyrolysis gas, cal/g·K
d diameter, cm
d_0 initial diameter, cm
d_c diameter for char layer at surface combustion period, cm
d_S diameter for char layer assumed constant during gas-phase combustion, cm
D diffusion coefficient, cm²/s
D^0 diffusion coefficient at 273 K and one atmospheric pressure, cm²/s
h_v pyrolysis heat per unit mass, cal/g
$\bar{k}$ effective thermal conductivity for char layer impregnated with pyrolysis gas, cal/s·cm·K
k_0 velocity constant for mass transfer, g/s·cm²·atm
k_g thermal conductivity for pyrolysis gas, cal/s·cm·K
k_s thermal conductivity for carbonaceous substance, cal/s·cm·K
K burning constant, cm²/s
K_d apparent pyrolysis constant for virgin polymer of CTPB, cm²/s
K_r (corrected) burning constant for char layer of CTPB, cm²/s
K'_r apparent burning constant for char layer of CTPB, cm²/s
m reciprocal of pressure index
m' reciprocal of pressure index
$\dot{m}$ average mass burning rate, g/s
$\dot{m}_c$ formation rate for carbonaceous substance, g/s
$\dot{m}_g$ evolution rate for pyrolysis gas, g/s
$\dot{m}_p$ pyrolysis rate for polymer, g/s
M_c molecular weight for carbonaceous substance, g/mol
M_o oxygen molecular weight, g/mol
p_{ox} oxygen pressure in ambient gas, kg/cm²
p_S oxygen pressure on the surface of char layer, kg/cm²
P total pressure, kg/cm²
q_v heat flux, cal/s·cm²
Q_v total rate of heat flow to virgin polymer sphere, cal/s
r radius, cm
r_0 initial radius, cm
r_c radius for char layer at surface combustion period, cm
r_p radius for virgin polymer sphere, cm
r_S radius for char layer assumed constant during gas-phase combustion, cm
R gas constant, cm³·atm/K·mol
R_S specific reaction rate, g/cm²·s
s swelling factor
s'^2 $1+0.8(s^2-1)$ from Eq. (13)
S volumetric flow rate for ascending current, cm/s
t time, s
t_0 initial time, s
t_b total burning time, s
t_d termination time of pyrolysis gas emission from all burning surfaces, s
t_S surface combustion time for char layer, s
T temperature, K
T^0 273 K
T_∞ ambient temperature, K
T_C surface combustion temperature for char layer, K
T_{C_0} surface combustion temperature for char layer at one atmospheric pressure, K
T_p surface temperature for virgin polymer, K
T_S surface temperature for char layer during gas-phase combustion, K
T_{S_0} surface temperature for char layer during gas-phase combustion at one atmospheric pressure, K

U rate for natural convection, cm/s
v_r radial velocity for pyrolysis gas, cm/s
x fraction of polymer converted into gas
α factor involving the effect of oxygen fraction in mass burning rate for PU
α' factor involving the effect of oxygen fraction on mass burning rate for CTPB
β factor involving the effect of oxygen fraction on burning constant for PU
γ factor involving the effect of oxygen fraction on apparent pyrolysis constant for CTPB
γ' factor involving the effect of oxygen fraction on burning constant for CTPB
δ contact surface diameter, cm
ε volumetric fraction of pyrolysis gas contained in char layer
ρ_c apparent density for char layer, g/cm^3
ρ_g density for pyrolysis gas, g/cm^3
σ density for polymer, g/cm^3

References

1) T. Saito, Thesis, the University of Tokyo (1974).
2) A. M. Varney and W. C. Strahle, *Comb. Flame*, **16**, 1 (1967).
3) L. Nadaud and J. Biasini, *Rech. Aer.*, No. 117, 3 (1967).
4) R. H. Essenhigh, *Fuel*, **48**, 330 (1969).
5) K. Kobayashi, "5th Symposium (International) on Combustion," Reinhold, New York (1955), p. 141.
6) A. R. Hall and J. Diederichsen, "4th Symposium (International) on Combustion," Williams and Wilkins Co., Baltimore (1954), p. 837.
7) M. Goldsmith, *Jet Propulsion*, **26**, 172 (1956).
8) T. Saito and A. Iwama, *Chem. Lett.*, **1974**, 389.
9) W. A. Rosser, *Comb. Flame*, **11**, 442 (1967).

On the Selectivity in the Catalytic Hydrogenation of Methylacetylene on Group VIII Metals

Noritetsu YOSHIDA* and Kozo HIROTA**

Department of Chemistry, Faculty of Science, Osaka University, Toyonaka, Osaka 560

(Received March 30, 1974)

The reaction of methylacetylene with hydrogen and deuterium was studied over five Group VIII metals (Pd, Pt, Rh, Ir, and Ru) at 25 °C. Among these metals, palladium was the most selective for the propylene formation; the selectivity varied from metal to metal (Pd>Pt>Rh>(Ni)>Ru>Ir). A new result was obtained over ruthenium; the isomerization of methylacetylene to allene occurred simultaneously with the hydrogenation over only this metal. In the reaction with deuterium, the stereoselectivity of the metals was investigated on the products by analyzing them by the microwave spectroscopic and mass spectrometric methods. Only three hydrogen atoms were deuterated in the propylene produced over Ni, Pd, and Pt; in conformity with the above, the deuterated positions of propylene-d_1 and -d_2 were limited to three in the methylene and methylidyne groups. No such tendency was observed for Ir, Rh, and Ru, where the methyl hydrogens were also deuterated. The relative yield of the *cis*-1,2-d_2 species, always the most abundant product, decreased in this order: Pd>Pt>Ir>Ru>(Ni)>Rh at 70% conversion. A reaction mechanism which explains the relative yields of isotopic isomers of deuteropropylenes except for the methyl-deuterated species was proposed, assuming an adsorbed radical as an intermediate. The calculated isomer distributions based on the scheme coincided well with those observed in the cases of Pd, Pt, and Ni, but not in those of Ir, Rh, and Ru.

For the catalytic hydrogenation of acetylenic compounds, there have been many investigations of the kinetics, but few about reactions with deuterium. Detailed results on the reaction of dimethylacetylene with deuterium were reported by Meyer and Burwell[1] using palladium–alumina, and by Webb *et al.*[2] using other noble Group VIII metals supported on alumina. Recently, Bond *et al.*[3,4] studied the reaction of acetylene with deuterium using noble Group VIII metals supported on alumina, and determined the relative yields of the isomeric ethylene-d_2 species by infrared spectroscopy.

From these studies, it is now definitely accepted[5] that the major process involved in producing an olefin from its corresponding acetylenic compound over metal catalysts is the successive addition of two hydrogen atoms, not the direct addition of a hydrogen molecule, as has usually been presumed before. However, the previously-proposed scheme cannot explain the observed results quantitatively; for instance, *trans*-olefin is always produced to some extent as the primary product, though in a much smaller quantity than *cis*-olefin.

In order to clarify this point, in the present research the stereoselectivity in the reaction of methylacetylene with deuterium was investigated over five Group VIII metals (Pd, Pt, Rh, Ir, and Ru) by measuring with a microwave spectrometer the relative yields of the isotopic isomers of the propylene-d_1 and -d_2 produced. The mechanism of stereoselectivity is discussed on the basis of the results for the five metals and those for Ni previously reported.[6]

Experimental

Materials. The purifications of methylacetylene, deuterium (Takachiho Chem. Ind. Co.) and electrolytic hydrogen were described in a previous report.[6] The rhodium-black was prepared by the reduction of the rhodium hydroxide produced by the reaction of rhodium trichloride with sodium hydroxide. The iridium-black was prepared by adding a 0.01 mol solution of iridium tetrachloride to an excess amount of a hot solution of sodium borotetrahydride. The palladium-black, platinum-black (Nakarai Chem. Co.) and ruhtenium-black (Mitsuwa Chem. Co.) used were commercial reagents. All the metals mentioned above were, before use, reduced with hydrogen at 230—240 °C for two days in the reaction vessel. The amount of each metal used and the BET areas (mesured with N_2 at −198 °C) are as follows:

Pd 2 mg (7.7 m²/g), Pt 40 mg (2.4 m²/g),
Rh 30 mg (10.9 m²/g), Ir 20 mg (14.2 m²/g),
Ru 150 mg (33.2 m²/g).

Procedure. The reaction of methylacetylene with hydrogen or deuterium was carried out under the same conditions and by the same procedure over all the five metals, as has previously been done over nickel.[6]

The standard mixture, which consisted of P_{D_2} (or P_{H_2})= 60 mmHg and $P_{C_3H_4}$=30 mmHg, was introduced into a reaction vessel (about 300 ml) containing the catalysts; this vessel was connected to a conventional vacuum apparatus. The reactions were carried out in a simple static system at 25 °C and followed from manometric measurements. When the desired degree of hydrogenation has been reached, the reaction mixture was taken out by expanding it into a reservoir (3 l) preliminarily evacuated. The composition of hydrocarbons in the mixture was analyzed by gas chromatography, using a 4 m column of 20 wt% of dimethylsulfolane on Neopak-1B at room temperature. The samples for the isotopic analysis were prepared by the gas-chromatographic separation of the mixture into components (propane, propylene, and methylacetylene) using the column described above.

The deuterium distributions in the propylene and methylacetylene produced were determined with a mass spectrometer (Hitachi RMU-5B) in the Institute for Protein Research,

* Sagami Chemical Research Center, Nishi-Ohnuma, Sagamihara Kanagawa 229, (Present address, 3-59-1-510 Yamatedai, Ohkubo, Akashi, Hyogo 674.)

** Present address, Chiba Institute of Technology, Yatsu, Narashino, Chiba 275.

Osaka University. In the analysis, the energy of the ionizing electrons was lowered sufficiently so that only the parent ion could be produced in the mass spectrum.

Propylene-d_1 (C_3H_5D) and -d_2 ($C_3H_4D_2$) have four and seven species of isotopic isomers respectively, as is shown in Fig. 1. The relative abundances of these species in the propylene produced were determined with a microwave spectrometer, installed at the Sagami Chemical Research Center, by measuring the relative intensities of the rotational 1_{01}—0_{00} transitions of the species. A detailed description of the analysis has previously been reported.[7] The distributions of the isotopic isomers thus determined are called the hyperfine distributions of propylene-d_1 and -d_2 respectively in order to discriminate them from the usual deuterium distribution, called the fine distribution, which is determined with a mass spectrometer.

Propylene-d_1

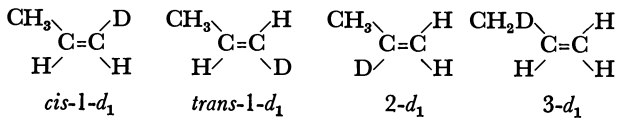

Propylene-d_2

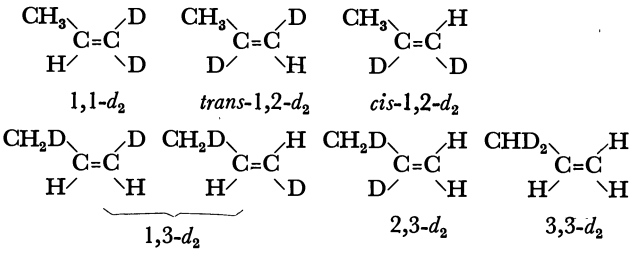

Fig. 1. Isotopic isomers of propylene-d_1 and -d_2

Results

Reaction Curves. Some typical reaction curves with the standard mixture of hydrogen (or deuterium) and methylacetylene over six metals are shown against the time in Fig. 2, taking the pressure fall ($-\Delta P$) as the ordinate. As is shown in this figure, all the curves consist of two parts with different rates, producing a point called the acceleration point ($-\Delta P_a$). The reaction rates are accelerated abruptly at this point, except in the case of palladium, where negative acceleration is observed. Each part can be regarded as corresponding to a reaction stage, as has been confirmed by another finding. The possibility of polymerization during the reaction may be ruled out over the six metals, because the total pressure decreases asymptotically to the value expected from the stoichiometric equation; $C_3H_4+2H_2=C_3H_8$. This situation is supported by the fact that no polymers were detected in the gas phase.

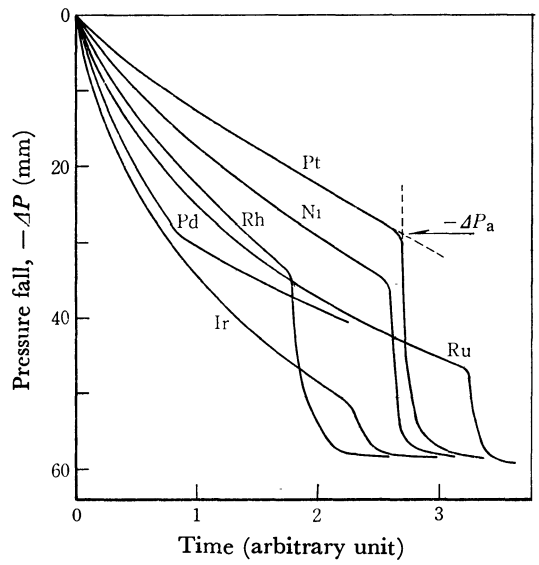

Fig. 2. Typical pressure-fall against time curves for the hydrogenation of 30 mm of methylacetylene at 25 °C. Ni, Pt, Ir $P^{\circ}_{H_2}=60$ mmHg; Pd, Rh, Ru $P^{\circ}_{D_2}=60$ mmHg.

The rates of the pressure fall during the course of the former stage was approximately proportional to the remaining hydrogen pressure. Furthermore, the initially-added propylene (26 mm) did not affect the hydrogenation rate over Ir, in accord with the results for 2-butyne with 1-pentene added[8] and that of acetylene with ethylene added.[9,10] The catalytic activities of the six metals were compared with one another by calculating the initial rate of methylacetylene removal per unit of area. The results in the reaction with deuterium were as follows:

A: Pd > Rh > Pt > Ni > Ir > Ru

A similar sequence has previously been reported in the hydrogenation of acetylene over evaporated metal films,[11] *i.e.*, Pd>Rh>Pt>Ni≫Fe>W. However, the A sequence does not coincide very well with that over supported metals.[12]

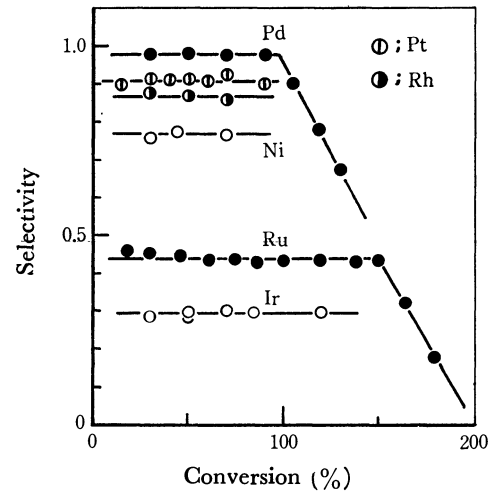

Fig. 3. Selectivity against conversion curves for the hydrogenation of methylacetylene at 25 °C. $P^{\circ}_{C_3H_4}=30$ mmHg, $P^{\circ}_{D_2}=60$ mmHg.

Selectivity. The selectivity, defined by $S=P_{C_3H_6}/(P_{C_3H_6}+P_{C_3H_8})$, was determined at various conversions of the reaction between methylacetylene and deuterium. It is shown in Fig. 3 against conversion which is defined by the percentage of the total pressure fall to the initial pressure of methylacetylene. The mean values of the selectivity, which is very different from metal to metal, are the following sequence:

B: Pd(0.98) > Pt(0.92) > Rh(0.87) > Ni(0.76) > Ru(0.44) > Ir(0.29).

This sequence is the same as that reported in the case of acetylene.[13]

The selectivity in the former stage is constant within the limits of experimental error, but it decreases rapidly in the latter stage, as is shown by the right halves of the corresponding curves of Pd and Ru in the figure. This finding indicates that methylacetylene is hydrogenated in the former stage to both propylene and propane in a certain ratio, while further hydrogenation of propylene to propane becomes dominant in the latter stage.

Formation of Allene. In the course of hydrogenation over ruthenium, a new finding was obtained; a trace of allene (CH_2=C=CH_2), which is an isomer of methylacetylene, appeared in the reaction mixture, together with the hydrogenation products. At a 70% conversion, the allene amounted to 4.3% of the initial methylacetylene. Allene was formed also in the absence of hydrogen over ruthenium; the initial rate of its formation was 1.8×10^{-6} mol/m^2·hr. This value was close to the rate of the hydrogenation, 6.8×10^{-5} mol/m^2·hr, represented by the rate of methylacetylene removal in the gas phase; therefore, allene could be detected during the hydrogenation. Over the other metals, however, allene could not be detected at all either during the hydrogenation or in the absence of hydrogen at 25 °C.

The high activity of ruthenium for the isomerization (CH_3–C≡CH⇄CH_2=C=CH_2) might be accounted for by its crystal structure, because ruthenium has the closed-packed hexagonal structure, whereas the other metals have the face-centered cubic structures. Further experiments will be required to confirm this supposition. The detailed results of the isomerization will be reported in the next paper.

Deuterium Distribution. The fine and hyperfine distributions of the propylene produced over palladium are shown in Table 1, where $\phi/100$ denotes the mean number of deuterium atoms in a propylene molecule; *i.e.*, $\sum i.d_i/100$ (i=1, 2, ----, 6). The measurement errors in the hyperfine distributions are indicated by 2.5 σ (σ: the standard deviation). Table 1 shows that neither the fine nor the hyperfine distribution changes substantially until the acceleration point or 97% conversion of the hydrogenation. Such constancy of the distribution was also observed in the case of nickel, as has previously been reported.[6] After the acceleration point, however, both distributions of propylene become dispersed, producing various kinds of species.

The fine and hyperfine distributions over six metal catalysts at a 70% conversion are compared in Tables 2 and 3 respectively. In Table 2, the fine distribution of methylacetylene is also listed. Table 2 shows that the most abundant deuteropropylene is the d_2 species,

Table 1. Palladium-catalyzed reaction

Fine distributions (%)

No.	Conv. (%)	Propylene							$\phi/100$
		d_0	d_1	d_2	d_3	d_4	d_5	d_6	
16	50	$1._1$	$11._1$	$79._2$	$8._6$	—	—	—	1.95
15	70	$0._9$	$11._6$	$78._5$	$9._0$	—	—	—	1.96
44	90	$0._8$	$9._1$	$79._2$	$10._9$	—	—	—	2.00
43	105	$0._7$	$9._1$	$72._9$	$15._3$	$0._9$	$0._6$	$0._5$	2.10
42	118	$0._8$	$9._0$	$63._9$	$21._7$	$2._2$	$1._4$	$1._1$	2.24
41	130	$0._9$	$8._3$	$50._1$	$29._2$	$5._4$	$3._6$	$2._6$	2.51

Hyperfine distributions (%)

No.	Propylene-d_1[a]			Propylene-d_2[a]			
	c-1-d_1	*t*-1-d_1	2-d_1	*c*-1,2-d_2	*t*-1,2-d_2	1,1-d_2	2,3-d_2
17[b]	5.7±0.4	51.6±8.2	42.7±4.9	88.9±0.6	10.4±0.5	0.7±0.3	—
16	5.5±0.3	49.7±6.2	44.8±4.7	88.5±0.6	10.6±0.7	0.9±0.1	—
15	5.7±0.5	49.8±7.8	44.6±8.2	87.7±0.5	11.3±0.5	1.0±0.1	—
42	8.3±0.5	38.9±3.4	52.8±7.1	79.9±0.5	16.3±0.5	2.3±0.1	1.4±0.2

$P^0_{C_3H_4}$=30 mmHg, $P^0_{D_2}$=60 mmHg, a) 3-d_1, 1,3-d_2, and 3,3-d_2 species were not detected, b) 30% conversion.

Table 2. Fine distributions (%) of methylacetylene and propylene at 70% conversion

	Methylacetylene			Propylene							$\phi/100$
	d_0	d_1	d_2	d_0	d_1	d_2	d_3	d_4	d_5	d_6	
Pd	(98.1	1.9	—)*	0.9	11.6	78.5	9.0	—	—	—	1.96
Pt	96.8	3.2	—	1.0	13.4	75.2	9.8	0.5	—	—	1.95
Rh	57.3	42.4	0.3	3.1	19.6	47.7	25.7	2.1	1.1	0.7	2.10
Ir	98.3	1.7	—	1.3	16.0	55.0	20.4	2.8	2.4	1.6	2.20
Ru	(85.1	14.9	—)*	1.7	12.8	45.4	32.8	3.2	2.2	1.9	2.37
Ni	98.6	1.4	—	1.8	18.8	49.6	29.1	0.7	—	—	2.08

$P^0_{C_3H_4}$=30 mmHg, $P^0_{D_2}$=60 mmHg *( ); Distribution at 50% conversion.

Table 3. Hyperfine distributions of propylene-d_1 and -d_2 at 70% conversion

	Propylene-d_1 (%)				Propylene-d_2 (%)					
	c-1-d_1	*t*-1-d_1	2-d_1	3-d_1	1,1-d_2	*t*-1,2-d_2	*c*-1,2-d_2	1,3-d_2	2,3-d_2	3,3-d_2
Pd	5.7±0.5	49.8±7.8	44.6±8.2	—	1.0±0.1	11.3±0.5	87.7±0.5	—	—	—
Pt	8.6±0.5	43.3±5.6	48.1±6.2	—	2.8±0.2	16.0±0.8	81.2±0.6	—	—	—
Rh	17.4±0.5	37.0±2.0	42.8±2.7	2.8±0.5	20.8±1.2	21.2±3.0	53.3±1.8	1.4±0.3	1.5±0.2	1.8±0.3
Ir	9.4±0.3	45.8±2.0	43.7±3.8	1.1±0.3	9.1±0.6	10.4±0.4	78.0±0.9	0.6±0.2	1.0±0.2	0.9±0.1
Ru	16.2±0.9	42.8±6.0	37.7±3.6	3.3±0.6	19.8±1.3	17.4±1.6	58.2±1.7	1.3±0.6	2.7±0.5	0.6±0.1
Ni	16.7±0.9	37.1±3.0	45.3±6.7	0.9±0.3	15.9±2.4	25.5±1.9	57.7±1.9	—	0.9±0.2	—

$P^0_{C_3H_4}$=30 mmHg, $P^0_{D_2}$=60 mmHg, 25 °C.

but it is not the unique product, over every metal. Propylenes more highly deuterated than d_1 are not produced over Pd; similarly, their amounts are not significant over Pt and Ni. This finding is in accord with the results shown in Table 3; *i.e.*, the deuterium atom is not substituted for the hydrogen atoms in the methyl group of a propylene molecule. The constancy of the distributions until the acceleration point was observed over Pt as well as over Pd and Ni. Over the other metals, however, the yield of the propylene-d_2 species decreased slightly as the reaction proceeded. Simultaneously, the relative yield of the *cis*-1,2-d_2 species decreased; for example, the yields over Rh and Ru at a 30% conversion were 58.6 and 63.4% respectively, while that over Ir at a 50% conversion was 82.7%.[14]

It is interesting that methylacetylene-d_1 was formed markedly in the cases of Rh and Ru. According to the microwave spectroscopic analysis of methylacetylene at a 50% conversion over Rh, methylacetylene-d_1 consisted of 99.8% CH_3-C≡CD and 0.2% CH_2D-C≡CH. The methylacetylene-d_1 produced over the other metals is estimated to be almost CH_3-C≡CD, just as over Rh, because methylacetylenes more highly deuterated than d_2 could not be detected practically, as is shown in Table 2.

The dependence of the fine and hyperfine distributions on the experimental conditions was studied over Ni, following the previous report.[6] The results are shown in Table 4. When the initial partial pressure of deuterium was increased from 60 to 150 mm, neither of the distributions changes very much. An increase in the temperature, however, reduces the yield of *cis*-1,2-d_2 species slightly. The former result is in accordance with the constancy of the distributions until the acceleration point, as described above; a very similar tendency is estimated in the hyperfine distributions over Pd and Pt as well as over Ni.

Discussion

General. The finding that the selectivity remained constant up to the acceleration point can be explained by the stronger adsorption of methylacetylene than that of propylene or propane. This is supported by the fact that the initial rate was not affected by the initially-added propylene over Ir. Therefore, methylacetylene is considered to act as poison in the hydrogenation of propylene. However, it is noteworthy that differences in selectivity are found among the metals. This may be ascribed to the degree of the adsorbability of methylacetylene to each metal, which determines the ratio of the probability of producing propylene (Path A) to that of producing propane *via* the half-hydrogenated species (Path B).

$$C_3H_6 \xrightarrow{A} C_3H_6(g)$$
$$C_3H_6 \xrightarrow{B} C_3H_7 \xrightarrow{+H} C_3H_8(g)$$

Table 4. Nickel-catalyzed reaction

Fine distributions (%) at 70% conversion

No.	P^0_{MA} (mm)	$P^0_{D_2}$ (mm)	Temp. (°C)	MA		Propylene							ϕ/100
				d_0	d_1	d_0	d_1	d_2	d_3	d_4	d_5	d_6	
5	30	60	25	98.4	1.6	2.0	18.4	49.6	29.7	0.3	—	—	2.08
7	30	150	25	98.8	1.2	1.8	17.5	53.9	26.7	0.1	—	—	2.06
13	30	60	0	99.6	0.4	1.8	18.6	52.6	26.7	0.3	—	—	2.05
14	30	60	50	98.2	1.8	2.3	16.4	46.8	32.6	0.9	0.5	0.5	2.17

Hyperfine distributions (%) at 70% conversion

No.	Propylene-d_1				Propylene-d_2[a]			
	c-1-d_1	*t*-1-d_1	2-d_1	3-d_1	*c*-1,2-d_2	*t*-1,2-d_2	1,1-d_2	2,3-d_2
7	14.6±1.1	38.7±7.4	46.7±4.0	<0.2	65.5±1.5	20.4±1.2	13.1±1.2	1.0±0.3
13	19.3±1.1	33.5±4.5	46.6±4.7	0.6±0.2	57.2±0.9	28.5±0.9	14.3±1.5	<0.2
14	19.7±0.9	32.9±4.5	46.6±3.0	0.8±0.2	48.9±1.0	29.8±2.6	21.3±0.6	<0.2

a) 1,3-d_2 and 3,3-d_2 were not detected.

After the acceleration point in the reaction curve, the metallic surface is practically covered with olefin as a result of the rapid decrease in methylacetylene, so the selectivity in the former stage decreases gradually. As can be understood easily by the material balance, the higher the selectivity in the former stage, the later the acceleration point has to be for each metal.

The poisoning effect of strongly-adsorbed methylacetylene can also explain the findings that the fine and hyperfine distributions remained constant up to the acceleration point over Pd, Pt, and Ni. In the first stage of the reaction, deuterium exchange through the readsorption of the produced propylene cannot proceed because of this effect. After the acceleration point, however, propylene can readsorb with less of the poisoning effect of the methylacetylene than before that point. Consequently, the redistribution of hydrogen atoms among propylenes can proceed easily before propane is formed, various kinds of isomeric species being thus formed. This tendency is the same as that observed in the case of 2-butyne hydrogenation over palladium supported on alumina;[8] *i.e.*, *cis*-2-butene, the main product of the reaction, began to isomerize to *trans*-2- and 1-butene after the 2-butyne has almost disappeared from the gas phase. The small variation in the deuterium distributions with the time over Rh, Ir, and Ru cannot be explained only by this effect. An explanation of the finding requires the contribution of some surface processes which are of no importance in the cases of Pd, Pt, and Ni—for example, the processes leading to the formation of highly-deuterated propylenes, as will be discussed below.

Stereoselectivity. Table 3 shows that propylene-*cis*-1,2-d_2 is always the most abundant, indicating the *cis*-type addition of two hydrogen atoms to the triple bond to be very easy. Though this tendency has already been reported for several acetylenic compounds,[5] it must be noted that the reason for the favorable production of the *cis*-1,2-d_2 species over the *trans* isomer is due not to the thermodynamic but to the kinetic nature, because the two species are different only in the substituted position of deuterium, so their stabilities must be nearly the same.

The relative yield of the *cis*-1,2-d_2 species over the six metals at 70% conversion decreased in this order;

C: Pd > Pt > Ir > Ru > (Ni) > Rh.

Palladium is also superior in stereoselectivity to produce the *cis*-1,2-d_2 species. The C sequence is practically the same as the sequence of the selectivity for producing propylene-d_2 formation—*i.e.*, Pd>Pt>Ir>Ni>Rh>Ru, as is shown in Table 2. The different positions of Ru in the two sequences might be related to the formation of allene during the reaction, which occurred only over ruthenium.

The especially high stereoselectivity of palladium has already been established. According to Burwell's research into the hydrogenation of gaseous dimethylacetylene (2-butyne),[8] *cis*-2-butene was produced exclusively over alumina-supported palladium as long as any unreacted dimethylacetylene remained. Such a surprisingly high stereoselectivity was not observed, however, in the case of methylacetylene in the present research. In the hydrogenation of acetylene with deuterium by Bond and Wells, the high stereoselectivity could not be obtained, either.[3] In this study, they determined the relative yields of three kinds of isomeric ethylene-d_2, such as *cis*-d_2, *trans*-d_2, and *asymmetric*-d_2, by means of infrared spectrometry; they reported that the yield of the *cis*-d_2 species was about 80% over Pd. These results may be due to the steric hindrance of methyl groups bonded to the C≡C group rather than to such an experimental difference as that a flow method was adopted in the case of dimethylacetylene. The above findings may be useful in discussing the mechanism of the hydrogenation process of methylacetylene, $CH_3–C{\equiv}CH + H_2 \longrightarrow CH_3–CH{=}CH_2$.

Mechanism. From the finding that the majority of the produced propylene consisted of the *cis*-1,2-d_2 species, Scheme (3) may be drawn for the mechanism of methylacetylene hydrogenation. It is based on the "associative mechanism," which is similar to that proposed for the catalytic hydrogenation of olefins.

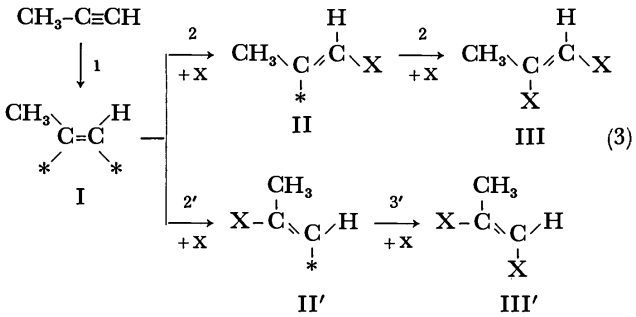

(3)

In this scheme, X denotes the adsorbed H or D atom, and the adsorbed species, I, is supported by the IR spectroscopic studies of adsorbed acetylene over silica-supported palladium[15] and alumina-supported platinum.[16] Propylene-*trans*-1-d_1 and 2-d_1 can also be produced through these processes by the addition of one protium and one deuterium atom to I species, but the propylene-*trans*-1,2-d_2, 1,1-d_2 and *cis*-1-d_1 species can not be produced thus. For the formation of the latter three isomers, some possible processes in addition to Scheme (3) might be added; they will be discussed below.

Firstly, the process concerned with producing associatively-adsorbed deuteromethylacetylene ($CH_3–C{\equiv}CD$, I′), as is shown by Process (4), is possible:

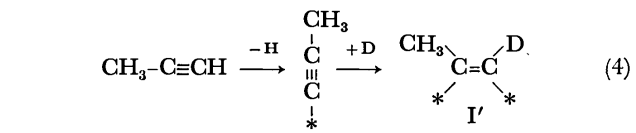

(4)

Methylacetylene is assumed in this process to be adsorbed by dissociating the acetylenic hydrogen and to pass into an associative adsorption by the addition of surface hydrogen without desorption from the surface. This process corresponds to that already proposed in the case of 1-butyne.[1] The extended scheme, (3) and (4), can explain the formation not only of propylene-*trans*-1,2-d_2, 1,1-d_2 and *cis*-1-d_1, but also of propylene-d_3, depending on whether I′ is attacked by H or D. However, the extended scheme is not yet sufficient to explain their yields quantitatively, since the *trans*-1,2-d_2 and 1,1-d_2 species can be expected to be produced in equal

amounts from I′, as is shown by Process (5), contrary to the experimental results obtained over Pd, Ni, and Pt.

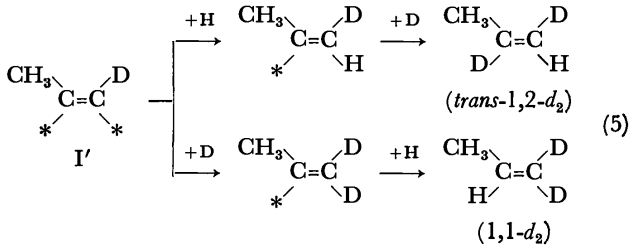

Over Pd particularly, the observed yield of propylene-*trans*-1,2-d_2 was ten or more times that of propylene-1,1-d_2. Now, even if the isotope effect is considered, it will be nearly compensated for by the first and second steps in Process (5), so that the large difference observed can not be expected on the basis of the extended scheme, (3) and (4), alone. Therefore, the contribution of another process, which will be discussed in the next paragraph, must be considered in addition to the contribution of Processes (3) and (4).

Secondly, the processes including an adsorbed propyl radical might be added to Scheme (3) as competitive, as is shown in Process (6). The IV and IV′ species are assumed to be formed by hydrogen additions to the II and II′ species respectively, and an unpaired electron is denoted by ·. Since the single C–C bond in the IV and IV′ species can rotate during adsorption, the *trans*-1,2-d_2 species can be produced from the I′ species.

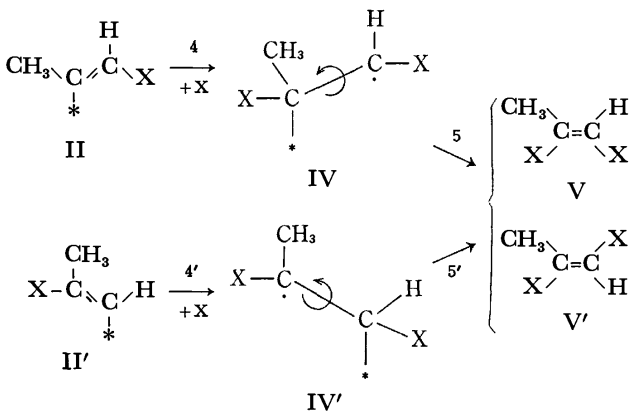

The observed difference between the yield of the *trans*-1,2-d_2 and that of the 1,1-d_2 species can now be interpreted by the following reasoning: the former species may be produced from both the adsorbed species, I and I′, but the latter, from only I′.

Quantitative Treatment of the Deuterium Distributions. The proposition presented above may be checked quantitatively, because the relative abundancies of the eight isomeric species of propylene produced are derivable by the use of the following parameters:

$$\left[\overset{H}{*}\right]\Big/\left[\overset{D}{*}\right] = x, \quad \left[CH_3\text{–}\overset{*}{C}\text{=}\overset{*}{C}D\right]\Big/\left[CH_3\text{–}\overset{*}{C}\text{=}\overset{*}{C}H\right] = y,$$

and;

$$\frac{\text{specific rate of Process (6)}}{\text{specific rate of Process (3)}} = \alpha.$$

Detailed formulae of the relative values for producing each species are shown in Table 5. The relative abundances of the isomeric species of propylene were thus calculated for suitable choices of the values for the parameters (x, y, α). They can be compared with the observed values derived from the fine and hyperfine distributions; those over Pd, Pt, and Ni are shown in Table 6. Over these metals, the methyl group of propylene was not substituted practically by deuterium, as is shown in Table 3. This is the reason why the calculation was carried out in only three metals at first. The degree of agreement between the calculated

Table 5. Relative probability of producing isomeric species of propylene

Species	From $CH_3\text{–}\overset{*}{C}\text{=}\overset{*}{C}H$	From $CH_3\text{–}\overset{*}{C}\text{=}\overset{*}{C}D$	Total probability
d_3	—	$y\cdot(1+\alpha)$	$y\cdot(1+\alpha)$
c-1,2-d_2	$1+\alpha/2$	$xy\cdot\alpha/2$	$1+(1+xy)\cdot\alpha/2$
t-1,2-d_2	$\alpha/2$	$xy\cdot(1+\alpha/2)$	$xy+(1+xy)\cdot\alpha/2$
1,1-d_2	—	$xy\cdot(1+\alpha)$	$x[y(1+\alpha)]$
2-d_1	$x\cdot(1+\alpha)$	—	$x\cdot(1+\alpha)$
t-1-d_1	$x\cdot(1+\alpha/2)$	$x^2y\cdot\alpha/2$	$x[1+(1+xy)\cdot\alpha/2]$
c-1-d_1	$x\cdot\alpha/2$	$x^2y\cdot(1+\alpha/2)$	$x[xy+(1+xy)\cdot\alpha/2]$
d_0	$x^2\cdot(1+\alpha)$	—	$x[x(1+\alpha)]$

$[\overset{H}{*}]/[\overset{D}{*}]=x$, $[CH_3\text{–}\overset{*}{C}\text{=}\overset{*}{C}D]/[CH_3\text{–}\overset{*}{C}\text{=}\overset{*}{C}H]=y$, Process (6)/ Process (3)$=\alpha$.

Table 6. Comparison of calculated relative abundance of deuteropropylene species with the observed (70% conv.)

Species	Pd		Pt		Ni		Rh	
	Obsd	Calcd	Obsd	Calcd	Obsd	Calcd	Obsd	Calcd
d_3	0.13	0.13	0.16	0.17	1.02	1.02	1.01	1.35
c-1,2-d_2	1.00	1.00	1.00	1.00	1.00	1.00	1.00	1.00
t-1,2-d_2	0.13	0.13	0.20	0.20	0.44	0.44	0.40	0.40
1,1-d_2	0.01	0.01	0.03	0.02	0.28	0.26	0.39	0.39
2-d_1	0.08	0.09	0.11	0.12	0.30	0.30	0.33	0.29
t-1-d_1	0.08	0.08	0.10	0.10	0.24	0.25	0.29	0.29
c-1-d_1	0.01	0.01	0.02	0.02	0.11	0.11	0.13	0.12
d_0	0.01	0.01	0.02	0.01	0.06	0.07	0.12	0.08
x		0.08		0.10		0.25		0.29
y		0.12		0.14		0.86		1.34
α		0.28		0.46		0.67		0.02

and observed values may be satisfactory, especially so in the case of palladium. If the observed ratios of geseous methylacetylene-d_1 to methylacetylene-d_0 are adopted for y, agreement is impossible, suggesting that the rate of the desorption process is very small; therefore, a large difference in the deuterium distributions of methylacetylene may exist between the gas phase and the adsorbed phase over these three metals. On the contrary, the difference is estimated to be small in the cases of Rh and Ru from the fact that CH_3–C≡CD was produced in a large amount.

Consequently, the hydrogenation scheme may be expressed well by (3), (4), and (6), especially over nickel, palladium, and platinum. Over iridium, rhodium, and ruthenium, however, the scheme seems somewhat more complicated, because the attempt to obtain a good agreement between theory and experiment failed, in spite of the large variation in x, y, and α parameters. In Table 6, the results for Rh are listed together with those for Ni, Pd, and Pt. This disagreement is probably ascribable to the addition of some other processes, leading to the appearance of highly-deuterated propylenes, which are remarkable over Ir, Rh, and Ru.

The authors wish to express their gratitude to Professor Yonezo Morino and Dr. Shuji Saito, Sagami Chemical Research Center, for their considerable assistance with the microwave spectroscopic measurements.

References

1) E. F. Meyer and R. L. Burwell, Jr., *J. Amer. Chem. Soc.*, **85**, 2881 (1963).
2) G. Webb and P. B. Wells, *Trans. Faraday Soc.*, **61**, 1232 (1965); J. J. Phillipson, P. B. Wells, and D. W. Gray, *Proc. 3rd Intern. Congr. Catalysis*, Amsterdam, **2**, 1250 (1964).
3) G. C. Bond and P. B. Wells, *J. Catal.*, **6**, 397 (1966).
4) G. C. Bond, G. Webb, and P. B. Wells, *ibid.*, **12**, 157 (1968).
5) For instance, G. C. Bond, "Catalysis by Metals," Chap. 12, Academic Press, New York (1962).
6) K. Hirota, N. Yoshida, S. Teratani, and S. Saito, *J. Catal.*, **15**, 425 (1969).
7) Y. Morino and E. Hirota, *Nippon Kagaku Zasshi*, **85**, 535 (1964); K. Horita and Y. Hironaka, *J. Catal.*, **4**, 602 (1965).
8) W. M. Hamilton and R. L. Burwell, Jr., *Proc. 2nd Intern. Congr. Catalysis*, **1**, 987, Editions Technip, Paris (1961).
9) G. C. Bond and P. B. Wells, *ibid.*, **1**, 1135 (1961).
10) G. C. Bond, D. A. Dawden, and N. Mochenzier, *Trans. Faraday Soc.*, **54**, 1537 (1958).
11) O. Beeck, *Discuss. Faraday Soc.*, **8**, 118 (1950).
12) J. Sheridan and W. D. Reid, *J. Chem. Soc.*, **1952**, 2962; G. C. Bond and R. S. Mann, *ibid.*, **1960**, 3560.
13) J. Sheridan, *ibid.*, **1944**, 470.
14) For the detailed results of different conversions, see N. Yoshida, Doctoral Thesis, Osaka University, Osaka (1971).
15) L. H. Little, N. Sheppard, and D. J. C. Yates, *Proc. Roy. Soc., Ser. A*, **259**, 242 (1960).
16) S. S. Randhava and A. Rehmat, *Trans. Faraday Soc.*, **66**, 235 (1970).

Electric Properties of 1-Tetradecanol-Tetradecanoic Acid (Myristyl Alcohol-Myristic Acid) Mixed Bimolecular Films

Masataka OKUYAMA, Tadayoshi YOSHIDA, Tadaaki TANII, Masahito KUNUGI, and Isao ISHIZAKI

Department of Engineering Chemistry, Nagoya Institute of Technology, Showa-ku, Nagoya 466

(Received April 19, 1974)

Stable bimolecular films (bilayers) were found to be formed in aqueous solutions from myristyl alcohol or from mixtures of myristyl alcohol and myristic acid. The electric capacitance and resistance of these bilayers were measured in solutions of pH 3—8. The capacitance of mixed bilayers was larger than that of myristyl alcohol bilayers (0.58 μF/cm^2). When the bilayers were formed from sample solutions having mole ratios 1/1 and 2.3/1 (myristic acid to myristyl alcohol), the capacitance had minima at *ca.* pH 7. The resistance of mixed bilayers at *ca.* pH 5 was smaller than one tenth of that of the myristyl alcohol bilayer (*ca.* $7\times10^8\,\Omega\cdot$cm^2). The results are explained in terms of (i) van der Waals attraction between hydrocarbon chains, (ii) the tendency for myristic acid to form expanded layers, (iii) the head group attraction between the myristic acid ion and myristyl alcohol, and (iv) the tendency for myristic acid ions to dissolve in the aqueous phase.

Bimolecular films (bilayers) have been studied as a model of biological membranes.[1-5] Substances with simple structure were chosen for a systematic study on the relation between the properties and components of bilayers.

We were able to form stable bilayers of myristyl alcohol in water. At the air/water interface under normal conditions myristyl alcohol forms a condensed monolayer[6] while myristic acid forms an expanded monolayer.[7,8] Since mixed monolayers at water surface differ from those of the individual components, mixed bilayers in water are expected to differ in character from single component bilayers. In the present work the electric properties of single component bilayers (myristyl alcohol) have been compared with those of mixed bilayers (myristyl alcohol and myristic acid).

Experimental

Materials. Guaranteed Reagents (Nakarai Chemicals Ltd.) were used. Myristyl alcohol and myristic acid (purity >99%) were recrystallized. No impurities were detectable gas-chromatographically. Cyclohexane and *n*-decane were used as solvents without purification. The aqueous solution surrounding the bilayer was controlled by several buffer solutions, *i.e.* those of Sørensen (sodium chloride, sodium hydroxide, aminoacetic acid and hydrochloric acid), McIlvaine (sodium phosphate and citric acid), and Gomori (2,4,6-trimethylpyridine and hydrochloric acid). Chemicals of reagent grade (Wako Pure Chemical Industries Ltd.) were used for the buffer solutions.

Methods. The apparatus and procedures for bilayer-formation were similar to those employed by Hanai *et al.*[9] Sample mixtures of myristyl alcohol and myristic acid (total *ca.* 0.3 g) were dissolved in a *n*-decane–cyclohexane mixed solvent [(total 2 cm^3), 1/1 (v/v)]. This sample solution was spread over a hole (diameter: 0.7 mm) of a Teflon beaker in a buffer solution through a Teflon tube (diameter: 1 mm) attached to a syringe. In order to hasten the bilayer-formation, small bubbles were ejected successively from the end of another tube to the front of the hole. When a black film was observed through a microscope, the electric capacitance (C_m) of the film was measured with an AC bridge (Ando Electric Co. Ltd., Model TR-1c). Measurements were carried out in the frequency range 1—3 MHz.

Resistances (R_m) of the bilayers were also obtained by the DC transient method. The applied polarizing potential was 25 mV. The potential across the bilayer was measured with an electrometer of high input impedance (Takeda Riken Industry Co. Ltd., Model TR-8651) through a pair of reversible Ag/AgCl electrodes. The area of the bilayer was measured by a photographic method. The temperature of the bilayer and its surrounding solution was controlled with an accuracy of $\pm$0.2 °C by circulation of thermostated water.

Results

Over the pH range 1—12, bilayers of myristyl alcohol are stable with a lifetime of over one hour. However, with an increase in myristic acid content in mixed bilayers, the pH range for stability is greatly reduced. Only at pH—7, a stable bilayer can be obtained from a sample solution with a 4/1 myristic acid to myristyl alcohol mole ratio. Hereafter the various mixed bilayers will be referred to in terms of the molar ratios in the sample solutions from which the bilayers are formed. The mole ratio in bilayers is not always equal to that in the sample solution.

Conductance G_t and capacitance C_t of the whole system (*i.e.* of the bilayer and its surrounding aqueous solution) are dependent on frequency f. A plot of $G_t/2\pi f$ against capacitance gives a semicircle (Fig. 1). The capacitance at 1 kHz agrees with that obtained by the DC transient method (0.58 μF/cm^2).

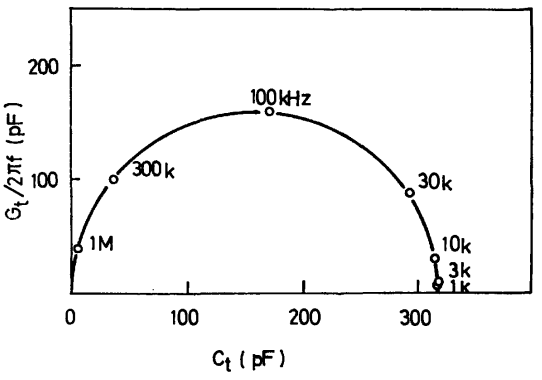

Fig. 1. Complex capacitance diagram of a whole system (a bilayer and its surrounding solution).
C_t, capacitance of a whole system; G_t, condnctance of a whole system; f, frequency; pH 5; The mole ratio of myristic acid to myristyl alcohol in sample solution is 1/1.

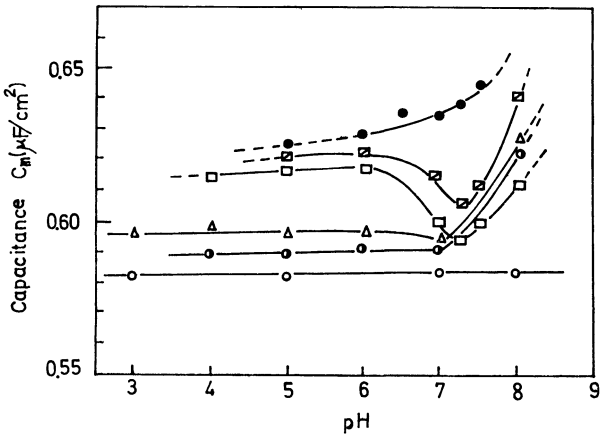

Fig. 2. The specific capacitances of bilayers as a function of pH (at 25 °C and 1 KHz). The mole ratio of myristic acid to myristyl alcohol in sample solution, ○, 0/1; ◑, 0.042/1; △, 0.25/1; □, 1/1; ⊠, 2.3/1 and ●, 4/1. ——, unstable bilayer.

The influence of pH on the capacitance C_m of bilayers (equal to C_t) is shown in Fig. 2. The capacitance is independent of the nature of the buffer solution. The capacitance of the myristyl alcohol bilayer remains constant (0.58 μF/cm²) regardless of pH, while that of all mixed bilayers increases with an increase in pH from 7 to 8. The capacitance of 1/1 and 2.3/1 mixed bilayers shows minima at pH 7 while that of the 4/1 bilayer shows no minimum over the pH range 4—8. The capacitance of mixed bilayers increases rapidly up to a mole ratio of 1/1 (Fig. 3).

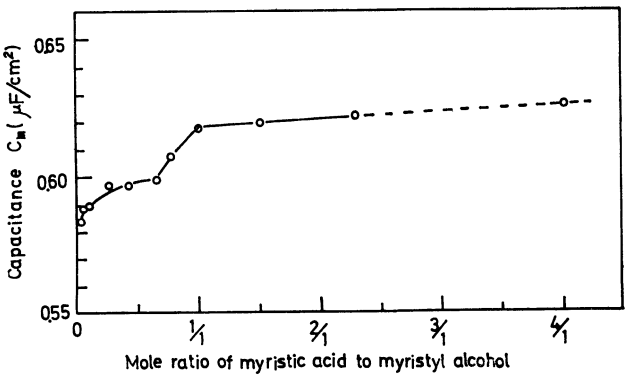

Fig. 3. Relation between the capacitance of mixed bilayer and the composition of sample solution from which the bilayer was formed (at 25 °C, 1 kHz, and pH 5). ——, unstable bilayer.

With temperature rise from 15 to 30 °C the capacitance of mixed bilayers increases gradually (Fig. 4). With increasing myristic acid content the temperature dependence of capacitance becomes more marked.

The DC resistance R_m of the myristyl alcohol bilayer has a constant value (7×10^8 Ω·cm²) regardless of pH (Fig. 5). The resistance R_m increases with pH for a 1/1 mixed bilayer. At pH 5 it is 4×10^7 Ω·cm², about one tenth of R_m for the myristyl alcohol bilayer.

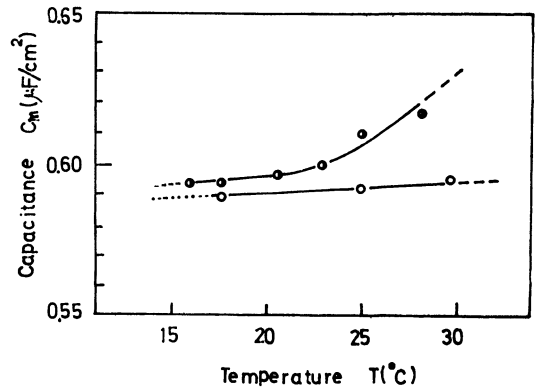

Fig. 4. The specific capacitance of bilayers as a function of temperature (at pH 5 and 1 kHz). The mole ratio of myristic acid, ○, 0.25/1; ◑, 1/1. ——, unstable bilayer, ····, stable black film, at the periphery of which some crystal parts are observed.

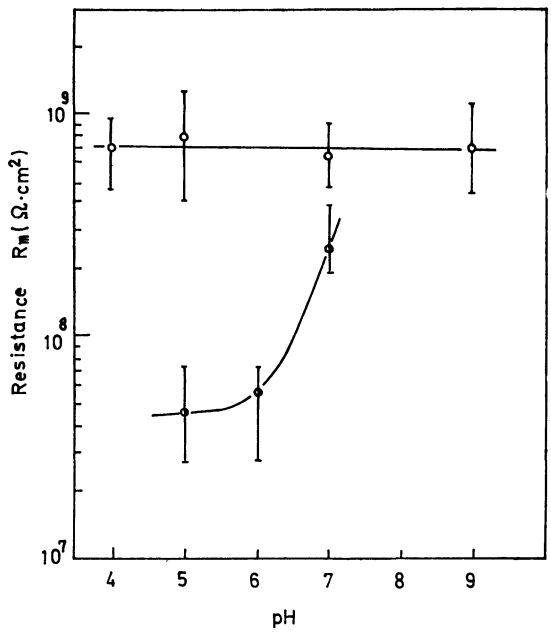

Fig. 5. The DC specific resistance of bilayers as a function of pH at 25 °C. The mole ratio of myristic acid to myristyl alcohol in sample solution. ○, 0/1; ◑, 1/1. Both ends of vertical line indicate maximum and minimum of the observed values, respectively. The mark ○ or ◑ shows the mean value.

Discussion

The semi-circular relationship between the capacitance of the whole system and its conductance divided by 2π times the frequency (Fig. 1) is similar to that obtained by Hanai *et al.*[9] for egg lecithin bilayers. They concluded from the shape of the complex plane plots that the static capacitance of the whole system was equal to the capacitance of the bilayer itself, $C_t(0\text{ Hz})=C_m(0\text{ Hz})$. For several systems we studied the static capacitance and the capacitance at 1 kHz agree with each other regradless of temperature and pH, $C_t(0\text{ Hz})=C_t(1\text{ kHz})$. Thus the static capacitance of the bilayer itself in various environments can be approximated by the observed capacitance of the whole

system at 1 kHz, $C_m = C_m(0\ \text{Hz}) = C_t(1\ \text{kHz})$.

Assuming the myristyl aclohol film to be a parallel plate condenser whose dielectric constant is 2.0, we find from the observed value of the static capacitance (0.58 μF/cm^2) that film thickenss is 31 Å, approximately twice the myristyl alcohol chain length. It seems reasonable to conclude that the film is bimolecular.

At pH 5, the capacitance of mixed bilayers increases with increasing myristic acid content (Figs. 2 and 3), *i.e.* the thickness of bilayers decreases. This is considered to be due to an increased expansion of the myristic acid parts in the mixed bilayers. The monolayer of myristic acid on water at pH 5 is not condensed, but expanded.[7,8] This property of myristic acid may appear in its mixed bilayers.

The occurrence of change of slope at a mole ratio 1/1 is noteworthy (Fig. 3), since peculiar phenomena at a mole ratio of 1/1 have been frequently reported in mixed monolayer of ionic and non-ionic surface active substances (though not as yet in mixed bilayers) *e.g.* Bernard and Dervichian.[10]

It is suggested that in mixed bilayers the myristic acid molecules oscillate chaotically and intertwine randomly although not to the degree pictured by Gaines.[11] The molecular motion, which we shall call "vermiculation", may be regarded as a type of micro Brownian motion which does not include the motion of the center of mass of the long chain molecule. Besides the myristic acid chains, even some chains of myristyl alcohol situated between myristic acid chains can vermiculate. Moreover, hydrocarbon chains in the bilayer may be more mobile than those in the monolayer, since a small amount of solvent (decane and cyclohexane) still remains among the chains in the bilayer (which will then comprise long chain molecules, solvent molecules and voids). Owing to vermiculation, the effective chain lengh (end-to-end distance) becomes shorter than the chain length of their fully extended forms. Consequently, the mixed bilayer is thinner than the single component bilayer of myristyl alcohol, the capacitance decreasing thereby.

With temperature rise the capacitance of the mixed bilayer increases, while that of the bilayer of myristyl alcohol does not change (Fig. 4). This could be also explained by the increasing tendency to the expanded state caused by temperature rise.

On the other hand some myristic acid ions in a one component monolayer dissolve in water at pH$>$5.[7] It is possible that myristic acid ions in the mixed bilayer may also dissolve at pH$>$5. Since the dissolution decreases the number density of the long chain compounds remaining in the bilayer, it should decrease the degree of molecular orientation in the bilayer, and decrease the thickness. This should give rise to an increase in capacitance. In fact, for the 4/1 bilayer the capacitance increases with increasing pH (Fig. 2). At pH$>$7.5, the bilayer is unstable, since too many long chain ions escape from bilayer into the aqueous phase. But for the 0.042/1 and 0.25/1 mixed bilayers, the increase of capacitance begins from pH 7. At pH$<$7, capacitance of these mixed bilayers is constant, regardless of pH values. Therefore, no myristic acid molecule in the two mixed bilayers seems to dissolve in the aqueous phase at pH$<$7. This might be explained in terms of the "ion-dipole attraction" discussed by Goodrich[12] and Spink.[7]

"Ion-dipole attraction" does not mean an attraction between the myristic acid ion and the dipole of water molecule, but the head group attraction between myristic acid ion and myristyl alcohol. The former attraction pulls the long chain ion into the aqueous phase out of the bilayer, while the latter induces the long ion to remain within the bilayer, the dissociation of myristic acid thus bringing about two opposing effects.

The van der Waals' attraction between the long chains and the ion-dipole head attraction causes the long chain molecules and ions to approach each other as closely as possible and to be fully extended normal to the bilayer surface. Under such conditions it is difficult for the myristic acid ions to escape from the mixed bilayer into the aqueous phase.

The results of our monolayer experiments might support the above conclusions. At pH 2—7 and 24 °C the surface pressure-molecular area (π-A) curve of 0.25/1 mixed monolayers was found to be independent of pH. Thus no myristic acid in the mixed monolayer is dissolved in the aqueous phase at pH$<$7.

With regard to interfacial forces, the bilayer/water interface more closely resembles the oil/water interface than the air/water interface. In general it is more difficult for long chain molecules to escape from an oil/water interface into water than from an air/water interface.[13] Therefore our monolayer experiments suggest that the dissolution of myristic acid in water from mixed bilayers is reduced by ion-dipole attraction with adjacent myristyl alcohol molecules.

Although the 1/1 mixed bilayer is rich in myristic acid content, it is difficult for such an intertwined structure as pictured by Gaines[11] to exist between pH 6 and 7. Since some myristic acid molecules ionize within the bilayer, ion-dipole attraction is added to the van der Waals attraction between the long chains so that some molecules and ions may be fully extended. Such an increase in bilayer thickness leads to a decrease in its capacitance. At pH 7—8, however, there is an increase in capacitance (Fig. 2) because of dissolution of myristic acid ions. Since myristic acid makes up a considerable proportion of the bilayer, the marked effect of its dissociation and hence dissolution more than compensates the effects due to ion-dipole interaction, such as a decrease in vermiculation.

In the 2.3/1 mixed bilayer, there are insufficient myristyl alcohol molecules for ion-dipole attraction to play a significant role. Thus the effect is much weaker than in the 1/1 bilayer. As a consequence dissolution of myristic acid in the aqueous phase is more pronounced and the minimum in capacitance at pH 7 is shallower (Fig. 2).

No minimum in the pH-capacitance curve is observed for the 4/1 bilayer. Since myristic acid makes up a very large proportion of the bilayer the marked effect of its dissociation and dissolution outweighs com-

peting effects. Figures 2 and 3 show that the 4/1 bilayer is the only, unstable one at pH 5. This may be attributed not only to a strong tendency towards expanded layers (because of the high myristic acid content) but also to the absence of ion-dipole attraction at pH 5.

The DC resistance of a 1/1 mixed bilayer is lower than that of a myristyl alcohol bilayer (Fig. 5). However, the former increases and approaches the latter when the pH increases from 6 to 7. The resultant increase in ion-dipole attraction together with the van der Waals attraction between the long chains causes the long chain molecules and ions in the bilayer to pack together as closely as in the crystalline state. Therefore it becomes more difficult for small ions (*e.g.* H_3O^+, OH^-, *etc.*) to cross the bilayer, or to pass between the long molecules along the direction of their orientation.

The results show that bilayers having a very low resistance typical of biological membranes may be produced by incorporating into the sample solutions substances which can form expanded monolayers. The structures of such mixed bilayers may be loosened by increases in temperature or changes in pH.

We wish to thank Dr. Hirofumi Okabayashi, this laboratory, Prof. Ryohei Matsuura, Kyushu University, Dr. Chiaki Muramatsu, Takemoto Yushi Co., Dr. Mitsuo Kimoto, Chukyo Yushi Co., and Dr. Yoichi Kato, Industrial Research Institute, Aichi Prefecture, for valuble discussions.

A part of this research was supported by a Scientific Research Grant from the Ministry of Education.

References

1) J. L. Taylor and A. D. Haydon, *Discuss. Faraday Soc.*, **42**, 51 (1966).
2) R. Fettiplace, D. M. Andrews, and D. A. Haydon, *J. Membrane Biol.*, **5**, 277 (1971).
3) M. W. Cook, W. R. Redwood, A. R. Taylor, and D. A. Haydon, *Kolloid Z. Z. Polym.*, **227**, 28 (1968).
4) J. L. Taylor and D. A. Haydon, *Nature*, **217**, 739 (1968).
5) S. Ohki, *Biophys. J.*, **9**, 1195 (1969).
6) N. K. Adam and J. W. W. Dyer, *Proc. Roy. Soc., Ser. A*, **106**, 694 (1924).
7) J. A. Spink, *J. Colloid Sci.*, **18**, 512 (1963).
8) G. A. Wolstenholme and J. H. Schulman, *Trans. Faraday Soc.*, **46**, 475 (1950).
9) T. Hanai, D. A. Haydon, and J. L. Taylor, *Proc. Roy. Soc., Ser. A*, **281**, 377 (1964).
10) L. de Bernard and D. G. Dervichian, *Bull. Soc. Chim. Biol.*, **37**, 943 (1955).
11) G. L. Gaines, "Insoluble Monolayers at Liquid-Gas Interfaces," Interscience Publishers, New York, N.Y. (1966), p. 170.
12) F. C. Goodrich, Proc. 2nd Internat. Congr. of Surface Activity, Vol. 1, Butterworths, London (1957).
13) D. A. Haydon and F. H. Taylor, *Phil. Trans.*, **252**, 225 (1960).

Semi-empirical SCF-MO Studies of Electronic Structures of Pt-Ethylene and Pt-Acetylene Complexes

Shigeyoshi SAKAKI, Hiroshi KATO,* and Takashi KAWAMURA

Department of Hydrocarbon Chemistry, Faculty of Engineering, Kyoto University, Sakyo-ku, Kyoto 606
**Department of General Education, Nagoya University, Chikusa-ku, Nagoya 464*

(Received July 18, 1974)

A parametrization in a CNDO-type MO method is presented for Pt compounds. By the use of this parametrization, the electronic spectra of $PtCl_4^{2-}$ are calculated; they agree well with the experimental spectra in transition energies and assignments. MO calculations with this parametrization are carried out on Pt(II)–ethylene, Pt(II)–acetylene, Pt(0)–ethylene, and Pt(0)–acetylene complexes. The calculated transition energies of Zeise's salt also agree well with the experimental values. In Pt(II) complexes, electrons are donated from ethylene and acetylene to the Pt atom, while they are little donated in Pt(0) complexes. The π-bonds of ethylene and acetylene are weaker in Pt(0) complexes than those in Pt(II) complexes. These results are the consequence of the stronger π-acceptor coordination bond in Pt(0) complexes than in Pt(II) complexes. Acetylene coordinates to the Pt atom more strongly than does ethylene. The coordination bonds of ethylene and acetylene are stronger in Pt(0) complexes than in Pt(II) complexes.

The organo-transition metal complexes are very attractive in view of the metal-carbon bonding character and of the models for intermediates which exist in an organic reaction catalyzed by transition metals.[1–4] Zeise's salt[5] is one of the well-known and most investigated organo-transition metal complexes.[2,6–17] Besides Zeise's salt, its bromo analogue,[2,12–14,17,18] Pt(II)–acetylene,[19,20] Pt(0)–olefin,[17,19,21–23] and Pt(0)–acetylene[17,19,24] complexes are also known. Some theoretical studies[8,25–29] have been carried out of these complexes. However, no SCF-MO calculation which explicitly includes electron-repulsion integrals has been carried out on Pt(II)–acetylene, Pt(0)–ethylene, and Pt(0)–acetylene complexes, while extended Hückel (EH) MO (noniterative) calculations have been done on them.[25,26,28,29] From the EH MO calculations, it has been proposed that the 6s orbital of the Pt atom scarcely contributes to the coordination bond of ethylene in both Pt(0) and Pt(II) complexes.[25] However, CNDO-type MO calculations reveal that the 5s orbital of the Ag atom mainly contributes to the coordination bond of olefin in $Ag(olefin)^+$ complexes.[30a] Thus, it is necessary to re-investigate the electronic structures of Pt(II)–acetylene, Pt(0)–ethylene, and Pt(0)–acetylene complexes. Also, it is of interest to compare the coordination bonds of these complexes with each other.

In this work, parametrizations are investigated in CNDO-type MO calculations on $PtCl_4^{2-}$. By the use of the established parameters, CNDO-type MO calculations are carried out on $PtX_3(C_2H_4)^-$, $PtX_3(C_2H_2)^-$ (X=Cl, Br), $Pt(PH_3)_2(C_2H_4)$, and $Pt(PH_3)_2(C_2H_2)$. Discussions are presented of the electronic structures of these compounds, and also of the coordination bonding characters of ethylene and acetylene in these complexes.

Calculation and Geometries

Calculation. A semi-empirical SCF-MO method with CNDO-type approximations is used in this work. While the method is almost the same as in our previous works,[30] some parameters are improved: (1) In our method, the resonance integrals are evaluated by means of the Wolfsberg-Helmholz equation.[31] The value of its parameter, K, is differently adopted between the AO pair including *d*-orbitals and those including only s and p orbitals; the notation K_1 is used in the former case, and the notation K_2 in the latter. While the value of K_2 is taken to be 0.80, as in our previous report,[30c] that of K_1 is determined to be 0.90 in this work, as will be described below. (2) While Ohno equation[32] was used in our previous works,[30] a modification of it which is newly presented in this work is introduced for the calculations of two-center Coulomb repulsion integrals including 6s and 6p orbitals of the Pt atom. The modification of Ohno equation is carried out for the following reason: The one-center Coulomb repulsion integrals, γ_{rt}, are calculated by the following Eq. (1) in Ohno method;

$$r_{rt} = 0.5(\gamma_{rr}+\gamma_{tt}). \quad (1)$$

This equation can be a good approximation when the AO·r and AO·t are alike.[33] In transition metals, however, this Eq. (1) can not be successfully applied to the calculation of one-center values of $\gamma_{nd(n+1)s}$ and $\gamma_{nd(n+1)p}$, since outer s and p orbitals are very different from valence-shell d-orbitals in their expansion. As examples, Table 1 presents a comparison between those values obtained by Eq. (1) and those obtained from the atomic spectra in Ni and Pd atoms; apparently, Eq. (1) gives too large values of $\gamma_{nd(n+1)s}$ and $\gamma_{nd(n+1)p}$

TABLE 1. VALUES OF $\gamma_{nd(n+1)s}$ AND $\gamma_{nd(n+1)p}$[a] OF THE Ni AND Pd ATOMS

	γ_{ds}[b]	$0.5(\gamma_{dd}+\gamma_{ss})$	Δ_{ds}[c]	γ_{dp}[b,d]	$0.5(\gamma_{dd}+\gamma_{pp})$	Δ_{dp}[c]
Ni	10.09_{eV}	12.34	−2.25	8.46	11.56	−3.10
Pd	9.14_{eV}	10.67	−1.53	7.71	10.05	−2.34

a) $n=3$ for the Ni atom and $n=4$ for the Pd atom. b) These values are obtained from Ref. 34. c) $\Delta_{ds}=-0.5(\gamma_{dd}+\gamma_{ss})$, $\Delta_{dq}=\gamma_{dp}-0.5(\gamma_{dd}+\gamma_{pp})$, d) The averaged value of various types of γ_{dp}.

as compared with the corresponding values obtained from the atomic spectra. In order to improve this defect, the following modification is carried out, only when either AO·r or AO·t is an outer orbital;

$$\gamma_{rt} = 14.3986/(d^2+R_{rt}^2)^{1/2}, \quad (2)$$

$$14.3986/d = 0.5(\gamma_{rr}+\gamma_{tt}) - a_r, \quad (3)$$

where AO·r is assumed to be an outer orbital and where R_{rt} is the distance (in Å unit) between the centers of AO·r and AO·t. The value of a_r depends on the outer AO·r, which is so determined that Eqs. (2) and (3) reproduce the experimental values of the one-center Coulomb repulsion integrals, such as $\gamma_{nd(n+1)s}$ and $\gamma_{nd(n+1)p}$, at $R_{rt}=0.0$; for example, the values of a_{4s} and a_{4p} of the Ni atom are taken as 2.25 and 3.10 eV respectively (see Table 1). The original Ohno equation is used in the other AO pairs, in which both AO's are outer orbitals or valence ones.

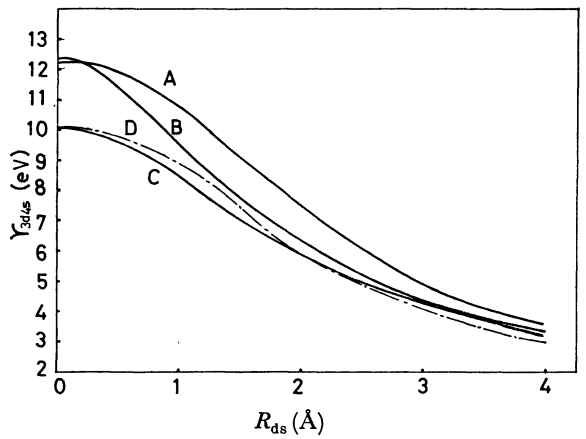

Fig. 1. Two-center Coulomb repulsion intergrals γ_{3d4s}[a] at various inter-atomic distances.
a) 3d; the 3d orbital of the Ni atom. 4s; the 4s orbital of the Ni atom.
A; The nonempirical value: the 3d orbital; the double-ζ type AO by Richardson *et al.* [36], the 4s orbital; the single Slater type AO by Clementi *et al.* [35].
B; Ohno's approximation.
C; The modified Ohno's approximation, Eqs (2) and (3).
D; These values are obtained by multiplying a correction factor to the nonempirical values so as to coincide the one-center value of γ_{3d4s} with that obtained from atomic spectra.

Figure 1 gives the values of the $\gamma_{3d\,4s}$ of the Ni atom obtained by various methods. The theoretically-calculated values (Line A) seem too large. Line D is obtained by multiplying the theoretically-calculated values by a correction factor so that the theoretical one-center value of $\gamma_{3d\,4s}$ may coincide with that obtained from the atomic spectra. Line C obtained by using the modified Ohno equation seems to be most agreeable with Line D throughout the R_{ds} range, while Line B obtained by the original Ohno equation is too large in the range of small R_{ds} values. Thus, the modified Ohno equation gives a more reasonable value of $\gamma_{3d\,4s}$ than does the original one.

In the case of the Pt atom, unfortunately, the experimental values of $\gamma_{5d\,6s}$ and $\gamma_{5d\,6p}$ can not be obtained because of the lack of atomic spectra. In the Pd atom, which forms compounds similar to those of the Pt's, a_{5s} should be taken as 1.53 eV and a_{5p} as 2.34 eV (see Table 1). By considering these values of the Pd atom, the authors examine various values of a_r within the following regions: 1.2—1.8 eV for a_{6s} and 2.2—2.8 eV for a_{6p}. From those examinations, $a_{6s}=1.5$ eV and $a_{6p}=2.5$ eV are chosen as the best values; they give good results on the electronic spectra of tetrachloroplatinate and Zeise's salt, as will be described in the following section.

For the Pt atom, the valence-state ionization potentials, I_r, are evaluated from the atomic spectra.[37] One-center Coulomb repulsion integrals, γ_{rr}, are estimated by the use of Eq. (2) in Ref. 30c. For the atoms of ligands, the values of I_r are taken from Hinze-Jaffé's work,[38] and those of γ_{rr} are evaluated from the same work[38] by the use of Pariser's approximation.[33] A double-ζ type d-function[39] is used for the 5d orbital of the Pt atom, while single Slater-type orbitals[35,40] are used for all the s and p orbitals. These data for the Pt atom are given in Table 2.

TABLE 2. IONIZATION POTENTIAL, I_r, ORBITAL EXPONENT, ζ_r, AND ONE-CENTER COULOMB REPULSION INTEGRAL, γ_{rr} OF THE PLATINUM ATOM

	ζ_r[a]	C[b]	I_r[c]	γ_{rr}[d]
5d	6.013 2.696	0.6331 0.5516	8.24 eV	12.42 eV
6s	2.554		9.00	7.17
6p	2.554		4.20	6.04

a) Ref. 39. b) The coefficients of the double-ζ form of the d-orbital after re-normalization, because the 3d and 4d terms of the platinum's 5d orbital are neglected in this work. c) The calculated values from Ref. 37. d) The estimated values obtained by using Eq. (2) in Ref. 30-c.

Geometries. The structures of Zeise's salt[15] and its bomo analogue[18] are taken from the X-ray studies. Since the accurate structures of $PtX_3(C_2H_2)^-$, (X=Cl, Br), have not been known, the bond length of the Pt–X bond is taken as equal to the corresponding one of $PtX_3(C_2H_4)^-$ and the distance between the Pt atom and the center of the triple bond of acetylene is taken as equal to that of $Pt(PPh_3)_2(PhC{\equiv}CPh)$.[24] The bond length of the C≡C triple bond is taken as equal to that of *trans*-$PtCl_2$(*p*-toluidine)[(*t*-Bu)C≡C(*t*-Bu)].[20] The ethylene and acetylene moieties are considered to be dis-

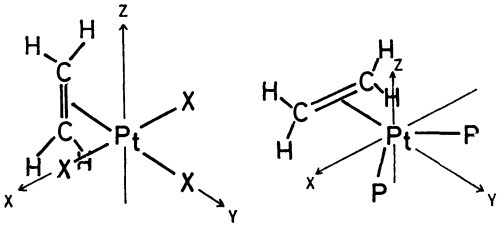

Fig. 2. Coordinate systems of Pt(II) and Pt(0) ethylene complexes.
The acetylene complexes are also the same as the above ones. X=Cl or Br, P=PH_3.

torted by their coordinations to the Pt atom.[2,16,20,21,24] Nevertheless, the ethylene and acetylene moieties are assumed not to be distorted because of the shortage of structural studies of these complexes. The structures of the Pt(0)–ethylene and Pt(0)–acetylene complexes are taken from the X-ray studies,[22,24] while the *cis*-bending of the CH_2 and CH groups and the small dihedral angle are neglected and PR_3 group is replaced by the PH_3 one for the sake of simplicity. These coordinate systems are shown in Fig. 2.

Results and Discussion

Parametrization. In order to investigate the parametrizations, MO calculations are carried out on $PtCl_4^{2-}$, since its electronic spectra have been well studied.[41,42] In these calculations, various values of K_1, a_{6s}, and a_{6p} are examined. Only some typical results are given in Tables 3 and 4. (Of course, various sets of values of K_1, a_{6s}, and a_{6p} are also examined besides the three given in Table 3.)

As is shown in Table 3, the A parametrization gives remarkably large electron densities on the 6s and 6p orbitals of the Pt atom. Furthermore, this parametrization gives too small transition energies for the intra-atomic 5d→6p transition, while these are really considered to have remarkably high transition energies.[41] Thus, this parametrization is abandoned.

By the use of the modified Ohno equation, the electron densities on 6s and 6p orbitals are extensively reduced from their values obtained by the A parametrization (see the B—D parametrizations in Table 3). Electron distributions do not depend very largely on the values of a_{6s} and a_{6p}, while the electron densities on 6s and 6p orbitals slightly decrease with an increase in the values of a_{6s} and a_{6p}. It should be noted that the use of the modified Ohno equation gives remarkably high transition energies for the intra-atomic 5d→6p transitions; thus, the defect in the A parametrization is overcome by the introduction of the modified Ohno equation.

The results on the electronic spectra are given in Table 4. The charge-transfer (C–T) bands (^1E_u and $^1A_{2u}$) are obtained at higher transition energies in all the calculations than the experimental ones, and the smaller values of a_{6s} and a_{6p} give relatively higher energies than do the larger values. Thus, the small values of a_{6s} and a_{6p} are abandoned. However, too large values of a_{6s} and a_{6p} result in too low transition energies (3.31 eV) of ^1E_g in the D parametrization, while it is experimentally obtained at 3.76 eV. The C parametrization seems to be the best one. The electronic spectra obtained by this parametrization agree well with the experimental spectra in transition energies and assignments, although the calculated C–T bands have considerably higher transition energies and the calculated d-d band, $^1B_{1g}$, has a considerably smaller transition energy than the corresponding experimental ones.[41,42] The values of a_{6s} and a_{6p} used in the C parametrization seem reasonable in view of the a_{5s} and a_{5p} values of the Pd atom.

When the value of K_1 is taken as 1.0, the C–T bands have too high transition energies; the first C–T bands is obtained at 6.06 eV, and the second one at 7.28 eV, where values of 1.5 and 2.5 eV are used for a_{6s} and a_{6p}. On the other hand, in the case of K_1=0.80, the assignments of d-d bands can not agree with the experimental ones. Thus, the value of K_1 is taken as 0.90 and the following parametrizations are adopted; a_{6s}=1.5 eV, a_{6p}=2.5 eV, and K_1=0.90 (the C para-

Table 3. Electron densities and intra-atomic 5d→6p transition energies of $PtCl_4^{2-}$

Parametrization[a]		A	B	C	D
a_{6s}[b]		0.0 eV	1.2	1.5	1.8
a_{6p}[b]		0.0 eV	2.2	2.5	2.8
Electron densities	Pt 5d	7.68	8.37	8.41	8.44
	Pt 6s	1.28	0.69	0.65	0.61
	Pt 6p	1.20	0.63	0.60	0.57
	Cl	7.46	7.58	7.59	7.59
5d→6p transition energies					
$d_{xz},d_{yz}\rightarrow p_z$		0.47 eV	9.14	9.66	10.18
$d_{z^2}\rightarrow p_z$		0.47 eV	7.58	8.29	8.94
$d_{xy}\rightarrow p_z$		0.20 eV	11.34	10.52	10.98

a) K_1=0.90. b) Constants in Eq. (3).

Table 4. Electronic spectra of $PtCl_4^{2-}$

Obsd[a]			Parametrization B			Parametrization C			Parametrization D		
δE[b]	ε_{max}		δE[b]	f_s		δE[b]	f_s		δE[b]	f_s	
2.62	16.3	$^1B_{1g}$[c]	1.75	0.0	$^1B_{1g}$	1.99	0.0	$^1B_{1g}$	2.27	0.0	$^1B_{1g}$
3.16	52.6	$^1A_{2g}$	3.08	0.0	$^1A_{2g}$	3.20	0.0	$^1A_{2g}$	3.29	0.0	$^1A_{2g}$
3.76	62.4	^1E_g	3.80	0.0	^1E_g	3.51	0.0	^1E_g	3.31	0.0	^1E_g
4.66	400	non-degenerate	3.95	0.0	^1E_g	4.04	0.0	^1E_g	4.07	0.0	^1E_g
			5.20	0.0	$^1A_{2g}$	4.88	0.0	$^1A_{2g}$	4.63	0.0	$^1A_{2g}$
			5.76	0.0	$^1A_{1g}+^1B_{2g}$	5.50	0.0	$^1B_{2g}$	5.28	0.0	$^1B_{2g}$
			5.81	0.0	$^1B_{2g}$						
5.38	8500	$^1E_u+^1A_{2u}$	5.95	0.248	^1E_u	5.73	0.284	^1E_u	5.55	0.280	^1E_u
			6.14	0.0	$^1A_{2u}$	5.88	0.0	$^1A_{2u}$	5.66	0.0	$^1A_{2u}$
			6.23	0.0	^1E_g						
			6.60	0.0	$^1B_{2u}$	6.34	0.0	$^1B_{2u}$	6.12	0.0	$^1B_{2u}$
5.72	10900	^1E_u	7.21	0.236	^1E_u	6.97	0.258	^1E_u	6.67	0.246	^1E_u

a) Ref. 41. b) in eV unit. c) Ref. 42.

metrization).

These parametrizations are also examined in Zeise's salt. The MO calculation in which $K_1=1.0$ and the original Ohno equation are used gives too large electron densities on the outer orbitals (1.17 e on the 6s and 1.85 e on the 6p orbitals) and too small transition energies of the intra-atomic 5d→6p transitions (about 0.3—0.9 eV). The use of the modified Ohno equation improves these defects in this case also; intra-atomic 5d→6p transitions are obtained at *ca.* 10 eV, and the electron densities on 6s and 6p orbitals are reduced (Table 6).

Thus, by using the C parametrization, we can carry out MO calculations on Pt(II)–ethylene, Pt(II)–acetylene, Pt(0)–ethylene, and Pt(0)–acetylene complexes, as will be described in the following sections.

TABLE 5. CALCULATED TRANSITION ENERGIES OF ZEISE'S SALT

∂E[b]	Parametrization C f_s		Obsd[a] ∂E[b]	Obsd[a] f_s
2.39	1×10^{-4}	$^1B_1$		
3.46	4×10^{-4}	$^1B_2$		
3.71	0.023	$^1A_1$	3.72	
4.37	0.024	$^1B_2$	4.26	0.01
4.50	0.089	$^1B_2$	4.67	0.019
4.94	0.082	$^1A_1$	5.16	0.066
4.95	0.025	$^1A_1$		

a) Ref. 10. b) in eV unit.

Electronic Spectra of Zeise's Salt. The C parametrization gives good results for transition energies as is shown in Table 5. The transition at 3.72 eV is assigned to the d-d band. The transitions at 4.26, 4.67, and 5.16 eV are assigned to the C–T bands from the Cl^- ligand to the d-orbital of the Pt atom. Moore assigned the weak transitions at 2.71 and 2.96 eV to the spin-forbidden ones on the basis of his EH(ω) MO calculation.[8] Our calculation gives the spin-allowed d-d bands, $^1B_1$ ($d_{yz}\rightarrow d_{x^2-y^2}$), at 2.39 eV and ^1B_i ($d_{xy}\rightarrow d_{x^2-y^2}$) at 3.46 eV, which have very small oscillator strengths, $f_s=1\times10^{-4}$ and $f_s=4\times10^{-4}$ respectively. These results suggest that the observed weak absorptions at 2.71 and 2.96 eV can not be necessarily assigned to the spin-forbidden transitions on the basis of their small absorption coefficients. Thus, there also remains the possibility that these absorptions are spin-allowed d-d transitions.

Electron Densities of Pt–ethylene and Pt–acetylene Complexes. The results for electron densities are given in Table 6, together with the quantities of ΔQ, ΔP_π, and P_π^*, which are defined in the footnote of the table. In the Pt(II) complexes, the electron density of the C atom is decreased from the value of the free ethylene by *ca.* 0.01 e, and that of the free acetylene, by *ca.* 0.1 e. In the Pt(0)–ethylene and Pt(0)–acetylene complexes, the electron densities are increased by *ca.* 0.05 e and *ca.* 0.02 e respectively. The values of ΔQ are *ca.* 0.3 e in the Pt(II) complexes, while they are nearly equal to zero in the Pt(0) complexes. This different behavior in the electron transfer between the Pt(II) and Pt(0) complexes is due to the different character of the coordination bonds of ethylene and acetylene between these complexes; the σ-donor bond contributes mainly to the coordination bonds of ethylene and acetylene in the Pt(II) complexes, while the π-acceptor bond contributes largely to the coordination bonds in the Pt(0) complexes, as will be described below.

TABLE 6. ELECTRON DENSITIES, ΔQ[a], ΔP_π[b], AND P_π^*[c] OF Pt(II) AND Pt(0) COMPLEXES WITH ETHYLENE AND ACETYLENE

(A) Ethylene complexes.

Compounds		$PtCl_3(C_2H_4)^-$	$PtBr_3(C_2H_4)^-$	$Pt(PH_3)_2(C_2H_4)$
Electron density	Pt 5d	8.490	8.530	9.341
	Pt 6s	0.618	0.646	0.579
	Pt 6p	0.588	0.586	0.559
	C	4.125	4.125	4.181
ΔQ[a]		0.287	0.295	−0.039
ΔP_π[b]		−0.166	−0.171	−0.379
P_π^*[c]		−0.033	−0.034	−0.230

(B) Acetylene complexes.

Compounds		$PtCl_3(C_2H_2)^-$	$PtBr_3(C_2H_2)^-$	$Pt(PH_3)_2(C_2H_2)$
Electron density	Pt 5d	8.495	8.541	9.362
	Pt 6s	0.610	0.635	0.574
	Pt 6p	0.603	0.590	0.571
	C	4.028	4.024	4.125
ΔQ[a]		0.289	0.302	0.004
ΔP_π[b]		−0.155	−0.160	−0.343
P_π^*[c]		−0.036	−0.036	−0.206

a) The quantity of transfered electrons from ethylene or acetylene to PtX_3^- or $Pt(PH_3)_2$ part. b) $\Delta P_\pi=(P_\pi$ of complexes ethylene$)-(P_\pi$ of free ethylene). ΔP_π of acetylene complexes is defined as the same as that of ethylene ones, while only one π-bond (Y-axis) is considered because the other π-bond scarcely interacts with the Pt atom. c) The quantity of P_π is defined as the partial bond order in which π^*-type interactions of ethylene or acetylene are only considered.

The absolute value of ΔP_π of $PtBr_3(C_2H_4)^-$ is larger than that of $PtCl_3(C_2H_4)^-$, suggesting that the C=C double bond of $PtBr_3(C_2H_4)^-$ is weaker than that of $PtCl_3(C_2H_4)^-$. This result agrees with the experimental finding that the ethylene part in $PtBr_3(C_2H_4)^-$ has a lower stretching vibration of the C=C double bond than that in $PtCl_3(C_2H_4)^-$.[12–14] Since the absolute value of P_π^* is remarkably small in the Pt(II) complexes, the decrease in the π-bond order of the ethylene part is not due to the increase in its π^*-anti-bonding character, but to the decrease in its π-bonding nature.

The absolute values of ΔP_π in the Pt(0) complexes are larger than those in the Pt(II) complexes by *ca.* 0.17—0.2 e, suggesting that the C=C double and C≡C triple bonds in the Pt(0) complexes are weaker than those in the Pt(II) complexes. Between the Pt(0) and Pt(II) complexes, the difference in the values of ΔP_π coincides well with the difference in the value of P_π^*. Therefore, roughly speaking, it can be said that the stronger π-acceptor bond results in the larger increase in the π^*-nature and the weaker C=C and C≡C bonds in the Pt(0) complexes than in Pt(II) complexes.

TABLE 7. COORDINATION BONDING CHARACTER OF Pt(II) AND Pt(0) COMPLEXES WITH ETHYLENE AND ACETYLENE

Compounds	$PtCl_3(C_2H_4)^-$	$PtBr_3(C_2H_4)^-$	$Pt(PH_3)_2(C_2H_4)$	$PtCl_3(C_2H_2)^-$	$PtBr_3(C_2H_2)^-$	$Pt(PH_3)_2(C_2H_2)$
$E_{d_\sigma-\pi}$	−0.557 eV	−0.530 eV	−0.240 eV	−0.585 eV	−0.579 eV	−0.257 eV
$E_{d_\pi-\pi^*}$	−0.545	−0.546	−1.844	−0.627	−0.624	−1.753
$E_{s-\pi}$	−1.368	−1.394	−1.853	−1.427	−1.461	−1.861
$E_{p_\sigma-\pi}$	−1.067	−1.127	−1.239	−1.074	−1.102	−1.221
E_{s-s}	−0.673	−0.663	−0.876	−1.078	−1.069	−1.225
$E_{p_\sigma-s}$	−1.015	−1.035	−1.184	−1.468	−1.490	−1.549
E_{Pt-C}	−6.547	−6.591	−8.380	−7.360	−7.698	−9.502

Interaction between Pt and C Atoms. In this section, the quantity of E_{AB} is used as the bond index, which means the energy contribution of the AB bond to the total energy of the molecule;[43,44] it is written as below under approximations used in this MO method.[30]

$$E_{AB} = E_{AB}^{(1)} + E_{AB}^{(2)} + E_{AB}^{(3)} \quad (4)$$

$$E_{AB}^{(1)} = 2\sum_r^A \sum_t^B P_{rt} H_{rt} \quad (5)$$

$$E_{AB}^{(2)} = -0.5 \sum_r^A \sum_t^B P_{rt}^2 \gamma_{rt} \quad (6)$$

$$E_{AB}^{(3)} = \sum_r^A \sum_t^B (N_r - P_{rr})(N_t - P_{tt})\gamma_{rt} \quad (7)$$

The negative value of E_{AB} represents the bonding interaction between A and B atoms, and the larger absolute value reveals the stronger interaction.

In order to investigate the bonding character, $E_{AB}^{(1)}$ and $E_{AB}^{(2)}$ are divided into AO pair terms, $E_{ArBt}^{(1)}$ and $E_{ArBt}^{(2)}$, *etc.*, where Ar represents the AO·r on the A atom. $E_{AB}^{(3)}$ is not divided into AO pair terms, however, because this term represents approximately an electrostatic energy and its meaning is lost by the division into AO pair terms.

The absolute value of E_{Pt-C} decreases in the following order: Pt(0) complexes>Pt(II) complexes, and acetylene complexes>ethylene complexes. This result shows that acetylene coordinates to the Pt atom more strongly than does ethylene, and that the coordination bonds of ethylene and acetylene in Pt(0) complexes are stronger than those in Pt(II) complexes.

As is shown in Table 7, E_{Pt-C} is contributed to largely by the $E_{s-\pi}$ and $E_{p\sigma-\pi}$ in the Pt(II) complexes, where the former subscript, such as s and p_σ, indicates the AO of the Pt atom, and the latter one the AO of the C atom. The contributions of $E_{d\pi-\pi^*}$ and $E_{p\pi-\pi^*}$ are small. These results suggest that the coordination bonds of ethylene and acetylene are mainly contributed to by the σ-donor bond in the Pt(II) complexes, through which ethylene and acetylene donate their π-electrons to the 5d, 6s, and 6p orbitals of the Pt atom. This bonding nature agrees with the proposals by Behnke *et al.*,[45] Braterman,[46] and Cooper *et al.*[47] with regard to the coordination bond of olefin in Pt(II) complexes.

In the Pt(0) complexes, the absolute values of P_π^* and $E_{d\pi-\pi^*}$ are much larger than those of Pt(II) complexes, while the $E_{d\sigma-\pi}$ value in the Pt(0) complexes is smaller than that of the Pt(II) complexes. These results suggest that the π-acceptor bond contributes more to the coordination bond in the Pt(0) complexes than to that in the Pt(II) complexes. The d_σ-π interaction seems to be reduced by the formal d^{10} configuration of the Pt(0) atom, while this interaction is considerably large in the Pt(II) complexes because of the formal d^8 configuration of the Pt(II) ion. The large absolute values of $E_{S-\pi}$ and $E_{P\sigma-\pi}$ reveal that the σ-donor bond contributes remarkably to the coordination bond in the Pt(0) complexes.

In both the Pt(II) and Pt(0) complexes, the absolute values of E_{S-S} and $E_{P\sigma-S}$ are remarkably large, suggesting that a large σ-bonding interaction exists between the 2s orbital of the C atom and the 6s and $6p_\sigma$ orbitals of the Pt atom. Thus, the hybridization of the C atom of ethylene approaches from sp^2 to sp^3 and that of acetylene from sp to sp^2, not only because of the σ-donor and π-acceptor bond but also because of these s-s and p_σ-s interactions. This result also suggests that the *cis*-bendings of the CH_2 group of ethylene and the CH group of acetylene are brought about by the σ-donor bond, the π-acceptor bond, and these s-s and p_σ-s interactions.

The relative contribution of valence orbitals of the Pt atom should be discussed not in terms of the bond order but in terms of E_{ArBs}, since the bond order is not appropriate for the bond index because of its rotational variable character. As is shown in Table 7, the 6s orbital contributes to the coordination bond as much as the 6p orbital does, and the contribution of the 5d orbital is one-half or one-third of those of the 6s and 6p orbitals. Our results do not agree with the proposal of Nelson *et al.*[25] that the hybridization of the Pt atom is dp^2 or d^2p^2 in these complexes.

In conclusion, the 6s and 6p orbitals of the Pt atom contribute greatly to the coordination bonds of ethylene and acetylene, while the 5d orbital also considerably contributes to the Pt(II) complexes. The π-acceptor bond (d_π-π^*) contributes much to the Pt(0) complexes, while its contribution in the Pt(II) complexes is about one-third of that in the Pt(0) complexes. This stronger π-acceptor bond in Pt(0) complexes results in the larger electron density on the C atom, the smaller value of ΔQ, the weaker C=C and C≡C bonds, and the larger value of E_{Pt-C}, relative to those of the Pt(II) complexes. It should be noted that strong s-s and p_σ-s interactions exist between the Pt and C atoms besides the σ-donor and π-acceptor bonds.

These calculations were carried out by the Facom 230-60 and 230-75 computers of The Data Processing Center of Kyoto University.

The authors are grateful to Professor Kimio Tarama for his generous support of this work. They also wish to thank Dr. Hideyuki Konishi for his help with the

calculations of overlap integrals and Mr. Kazuhiro Ishida for his help with the nonempirical calculations of the Coulomb respulsion integrals.

References

1) M. Herberhold, "Metal π-complexes," Vol. II, Elsevier Publishing Co., Amsterdam, 1972.
2) F. R. Hartly, *Chem. Rev.*, **69**, 799 (1969); "The Chemistry of Platinum and Palladium," Applied Science Publ. LTD., London, 1973.
3) J. Tsuji, *Ad. Org. Chem.*, **6**, 109 (1969).
4) M. L. H. Green, "Organometallic Compounds," Vol. 2, Methuene & Co. Ltd., New York (1968).
5) W. C. Zeise, *Mag. Pharm.*, **35**, 105 (1830).
6) S. Maričić, C. R. Redpath, and J. A. S. Smith, *J. Chem. Soc.*, **1963**, 4905.
7) P. D. Kaplan and M. Orchin, *Inorg. Chem.*, **4**, 1393 (1965).
8) J. W. Moore, *Acta Chem. Scand.*, **20**, 1154 (1966).
9) R. G. Denning, F. R. Hartly, and L. M. Venanzi, *J. Chem. Soc., A*, **1967**, 324.
10) R. G. Denning, F. R. Hartly, and L. M. Venanzi, *ibid.*, **1967**, 1322.
11) R. J. Goodfellow, P. L. Goggin, and D. A. Duddell, *ibid.*, **1968**, 504.
12) M. J. Grogan and K. Nakamoto, *J. Amer. Chem. Soc.*, **88**, 5454 (1966); **90**, 918 (1968).
13) J. Hiraishi, *Spectrochim. Acta*, **25A**, 749 (1969).
14) J. Hubert, P. C. Kong, F. D. Rochon, and T. Theophanides, *Can. J. Chem.*, **50**, 1595 (1972).
15) M. Black, R. H. B. Mais, and P. G. Owston, *Acta Crystallogr.*, **B25**, 1753 (1969).
16) W. C. Hamilton, K. A. Klanderman, and R. Spartly, *ibid.*, **A25**, s172 (1969).
17) See Ref. 4. (p. 7).
18) G. B. Bokii and G. A. Kukina, *Kristallografiya*, **2**, 400, (1957).
19) J. H. Nelson and H. B. Jonassen, *Coord. Chem. Rev.*, **6**, 27 (1971).
20) G. R. Davies, W. Hewerston, R. H. B. Mais, and P. G. Owston, *Chem. Commun.*, **1967**, 423.
21) C. Panattoni, G. Bombieri, U. Belluco, and W. H. Baddley, *J. Amer. Chem. Soc.*, **90**, 798 (1968).
22) P.-T. Cheng, C. D. Cook, S. C. Nyburg, and K. Y. Wan, *Inorg. Chem.*, **10**, 2210 (1971).
23) C. A. Tolman, W. C. Seidel, and D. H. Gerlach, *J. Amer. Chem. Soc.*, **94**, 2669 (1972).
24) J. O. Glanville, J. M. Stewart, and S. O. Grim, *J. Organometal. Chem.*, **7**, p 9 (1967).
25) J. H. Nelson, K. S. Wheelock, L. C. Cusachs, and H. B. Jonassen, *J. Amer. Chem. Soc.*, **91**, 7005 (1969).
26) K. S. Wheelock, J. H. Nelson, L. C. Cusachs, and H. B. Jonassen, *ibid.*, **92**, 5111 (1970).
27) H. Kato, This Bulletin, **44**, 348 (1971).
28) J. H. Nelson, K. S. Wheelock, L. C. Cusachs, and H. B. Jonassen, *Inorg. Chem.*, **11**, 422 (1972).
29) K. S. Wheelock, J. H. Nelson, J. D. Kelly, H. B. Jonassen, L. Chopin, and L. C. Cusachs, *J. Chem. Soc. Dalton*, **1973**, 1457.
30) a) S. Sakaki, *Theor. Chim. Acta*, **30**, 159 (1973); b) S. Sakaki and H. Kato, This Bulletin, **46**, 2227 (1973); c) S. Sakaki, H. Kato, H. Kanai, and K. Tarama, *ibid.*, **47**, 377 (1974).
31) M. Wolfsberg and L. Helmholz, *J. Chem. Phys.*, **20**, 837 (1952).
32) K. Ohno, *Theor. Chim. Acta*, **2**, 219 (1964).
33) R. Pariser and R. G. Parr, *J. Chem. Phys.*, **21**, 767 (1953).
34) a) L. Di Sipio, E. Tondello, G. De Michelis, and L. Oleari, *Chem. Phys. Lett.*, **11**, 287 (1971). b) E. Tondello, G. De Michelis, L. Oleari, and L. Di Sipio, *Coord. Chem. Rev.*, **2**, 65 (1967); c) L. Di Sipio, E. Tondello, G. De Michelis, and L. Oleari, *Inorg. Chem.*, **9**, 927 (1970).
35) E. Clementi, D. L. Raimondi, and W. P. Reinhart, *J. Chem. Phys.*, **47**, 1300 (1967).
36) J. W. Richardson, W. C. Nieuwpoort, R. R. Powell, and W. F. Edgell, *ibid.*, **36**, 1057 (1962).
37) C. E. Moore, "Atomic Energy Levels," Natl. Bur. Std. Circ., No. 467 (1958).
38) J. Hinze, and H. H. Jaffé, *J. Amer. Chem. Soc.*, **84**, 540 (1962).
39) H. Basch and H. B. Gray, *Theor. Chim. Acta*, **4**, 367 (1966).
40) E. Clementi and D. L. Raimondi, *J. Chem. Phys.*, **38**, 2686 (1963).
41) A. J. MacCaffery, P. N. Schatz, and P. J. Stephens, *J. Amer. Chem. Soc.*, **90**, 5730 (1968).
42) P. Day, A. F. Orchard, A. J. Thomson, and R. J. P. Williams, *J. Chem. Phys.*, **42**, 1973 (1965).
43) M. S. Gordon, *J. Amer. Chem. Soc.*, **91**, 3122 (1969).
44) S. E. Ehrenson and S. Seltzer, *Theor. Chim. Acta*, **20**, 17 (1971).
45) G. T. Behnke and K. Nakamoto, *Inorg. Chem.*, **7**, 2030 (1968).
46) P. S. Braterman, *ibid.*, **5**, 1085 (1966).
47) D. G. Cooper, G. K. Hamer, J. Powell, and W. F. Reynolds, *Chem. Commun.*, **1973**, 449.

The Thermodynamic Properties of C_9H_{18} Naphthenes. I. The Determination of the Equilibrium Constants for the Hydrogenation of Propyl- and Isopropylbenzene and Ethyltoluenes

Yasuo MIKI

National Chemical Laboratory for Industry, Mita, Meguro-ku, Tokyo 153

(Received July 30, 1974)

The equilibria for the hydrogenation of *n*-propylbenzene, isopropylbenzene, 1-methyl-2-ethylbenzene, 1-methyl-3-ethylbenzene, and 1-methyl-4-ethylbenzene were determined experimentally over the temperature range of 250 to 450 °C and under hydrogen pressures ranging from 5 to 50 atm. The data were then used to calculate the values of the free energy and the equilibrium constant of the above reactions and the values of standard free energy of formation from the elements for *n*-propylcyclohexane, isopropylcyclohexane, 1-methyl-*cis*-2-ethylcyclohexane, 1-methyl-*trans*-2-ethylcyclohexane, 1-methyl-*cis*-3-ethylcyclohexane, 1-methyl-*trans*-3-ethylcyclohexane, 1-methyl-*cis*-4-ethylcyclohexane, and 1-methyl-*trans*-4-ethylcyclohexane.

This paper will present the results of a study of the thermodynamic properties of C_9H_{18} naphthenes. Alkylbenzenes are known to react with hydrogen to form alkylcyclohexanes, and the equilibrium constant for the hydrogenation of *n*-propylbenzene(NPB) to *n*-propylcyclohexane (NPCH) can be calculated from the thermodynamic data.[1-3] Such free energy data are available for other C_9H_{12} alkylbenzenes, but not for other C_9H_{18} alkylcyclohexanes. The hydrogenation equilibrium constants have also been determined experimentally over the temperature range from 200 to 300 °C for NPB,[4] isopropylbenzene (IPB),[5] and 1,3,5-trimethylbenzene.[6]

The equilibrium constants for the hydrogenation of NPB, IPB, 1-methyl-2-ethylbenzene (1,2-MEB), 1-methyl-3-ethylbenzene (1,3-MEB), and 1-methyl-4-ethylbenzene (1,4-MEB) were determined over the temperature range from 250 to 450 °C.

From these data, the values of the free energy of formation from the elements were calculated for NPCH, isopropylcyclohexane (IPCH), 1-methyl-*cis*-2-ethylcyclohexane (*cis*-1,2-MECH), 1-methyl-*trans*-2-ethylcyclohexane (*trans*-1,2-MECH), 1-methyl-*cis*-3-ethylcyclohexane (*cis*-1,3-MECH), 1-methyl-*trans*-3-ethylcyclohexane (*trans*-1,3-MECH), 1-methyl-*cis*-4-ethylcyclohexane (*cis*-1,4-MECH), and 1-methyl-*trans*-4-ethylcyclohexane (*trans*-1,4-MECH).

These compounds are important as constituents of petroleum; hence, their properties should have considerable practical interest.

Experimental

Materials. The NPB and IPB used in these experiments were commercial, extra-pure-grade reagents and were purified by distillation in a vacuum in a helium atmosphere to give a product found by gas chromatography to be 100.0% pure. The NPCH (100.0% purity)and IPCH (99.9% purity) were obtained by the hydrogenation of NPB and IPB respectively. The *n*-octane (98% purity), 1,2-MEB (100.0% purity), 1,3-MEB (100.0% purity), and 1,4-MEB (100.0% purity) were commercial, extra-pure-grade reagents and were used without further purification. The *cis*-1,2-MECH, *trans*-1,2-MECH, *cis*-1,3-MECH, *trans*-1,3-MECH, *cis*-1,4-MECH, and *trans*-1,4-MECH were obtained from the *cis-trans* mixtures of 1,2-MECH's 1,3-MECH's and 1,4-MECH's produced by the hydrogenation of 1,2-MEB, 1,3-MEB, and 1,4-MEB respectively, using a Perkin-Elmer F21 Preparative Gas Chromatograph. Hydrogen gas was passed through a palladium catalyst column to remove the oxygen, and the resulting gas was dried with an ice bath as well as with a molecular sieve and silica gel.

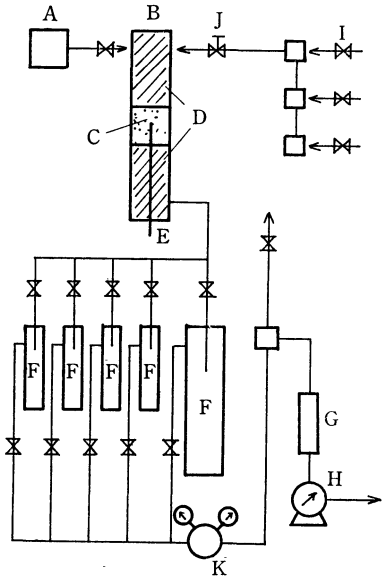

Fig. 1. Schematic diagram of reaction apparatus.
A: feed pump B: reactor C: catalyst bed
D: stainless steel bead E: thermocouple F: separator
G: flowmeter H: gasmeter I: stop valve
J: needle valve K: pressure controller

Apparatus. A flow diagram is shown in Fig. 1. The catalyst was supported inside a 14-mm-i.d. by 600-mm-long stainless steel tube. The dead space above and below the catalyst bed was packed with stainless steel beads. The catalyst temperature was measured by means of a chromel-alumel thermocouple located in a thermowell in the catalyst bed. The hydrocarbon feed rates were measured by means of a microfeed pump (Tamaseiki Co.).

The catalyst used in the present experiments was a 5 ml portion of Ketzenfine's 3% platinum on alumina (20—50 mesh). Each feed was a mixture of alkylbenzene and *n*-octane, or of alkylcyclohexane and *n*-octane. The hydrocarbon mixture feed was 1.2 ml per hr, and the mole ratio of hydrogen to the hydrocarbon mixture at the start was 17.8 ± 0.3.

The temperature variation through the catalyst bed was less than 0.5 °C when no reaction was taking place. During a run, the temperature rise due to the heat of reaction was less than 1 °C, depending on the extent of the reaction. The maximum variation in temperature through the catalyst bed during a run was usually of the order of 0.5 °C. The temperature used in the calculations was the average temperature of the last half of the catalyst bed.

A strain gauge (Kyowa Dengyo Co.) was used to measure the pressure at the inlet and outlet of the reactor. The pressure drop across the bed was negligible in the present experiments.

The reactions were carried out at temperatures ranging from 250 to 450 °C and under pressures ranging from 5 to 50 atm. In order to allow time for representative samples to be taken, the first hour was discarded.

Analysis. The products were analyzed by gas chromatography using a Hitachi Model K–53 with flame-ionization detectors and with a squalane capillary column (90 m × 0.25 mm) at 80 °C. The peak areas were measured with a Takeda Model TR-2215 electronic integrator.

Procedure

The hydrogenations of NPB, IPB, 1,2-MEB, 1,3-MEB, and 1,4-MEB are given by the following equations:

	Designation of Equilibrium Constant	
$3H_2(g)+NPB(g)=NPCH(g)$	K(n)	(1)
$3H_2(g)+IPB(g)=IPCH(g)$	K(i)	(2)
$3H_2(g)+1,2\text{-MEB}(g)=cis\text{-}1,2\text{-MECH}(g)$	K(*cis*-1,2-MECH)	(3)
$3H_2(g)+1,2\text{-MEB}(g)=trans\text{-}1,2\text{-MECH}(g)$	K(*trans*-1,2-MECH)	(4)
$3H_2(g)+1,2\text{-MEB}(g)=$equilibrium mixture of *cis*- and *trans*-1,2-MECH(g)	K(1,2-MECH)	(5)
$3H_2(g)+1,3\text{-MEB}(g)=cis\text{-}1,3\text{-MECH}(g)$	K(*cis*-1,3-MECH)	(6)
$3H_2(g)+1,3\text{-MEB}(g)=trans\text{-}1,3\text{-MECH}(g)$	K(*trans*-1,3-MECH)	(7)
$3H_2(g)+1,3\text{-MEB}(g)=$equilibrium mixture of *cis*- and *trans*-1,3-MECH(g)	K(1,3-MECH)	(8)
$3H_2(g)+1,4\text{-MEB}(g)=cis\text{-}1,4\text{-MECH}(g)$	K(*cis*-1,4-MECH)	(9)
$3H_2(g)+1,4\text{-MEB}(g)=trans\text{-}1,4\text{-MECH}(g)$	K(*trans*-1,4-MECH)	(10)
$3H_2(g)+1,4\text{-MEB}(g)=$equilibrium mixture of *cis*- and *trans*-1,4-MECH(g)	K(1,4-MECH)	(11)

The equilibrium constant, K, is given by this equation:

$$K = f_A/f_H^3 f_B = [(X_A+X)(1-3X)^3/(X_B-X)(X_H-3X)^3]K_\gamma P^{-3} \quad (12)$$

where

f_H, f_A, f_B = the fugacities of hydrogen, alkylcyclohexane, and alkylbenzene respectively

X_H, X_A, X_B = the mole fractions of the hydrogen, alkyl cyclohexane, and alkylbenzene respectively of the charge

X = the number of moles of alkylcyclohexane formed from 1 mol of the charge. In runs wherein the equilibrium is approached from the alkylcyclohexane side, $-X$ is the number of moles of alkylbenzene formed from 1 mol of the charge

P = the absolute total pressure of the equilibrium mixture at the end of the catalyst bed, atm

$K_\gamma = \gamma_A/\gamma_H^3\gamma_B$

$\gamma_H, \gamma_A, \gamma_B$ = the fugacity coefficients of hydrogen, alkylcyclohexane, and alkylbenzene respectively.

The fugacity coefficient, γ, was calculated with the aid of the concept of corresponding states, using generalized charts. The following equation, developed by Joffe,[7] was used to predict the fugacity coefficients of individual components in a gas mixture:

$$\log \gamma_i = \log \gamma_m + (H^\circ - H)(T_{cm} - T_{ci})/2.303RT \cdot T_{cm} + (Z_m - 1)(P_{cm} - P_{ci})/2.303P_{cm} \quad (13)$$

where

γ_i = the fugacity coefficient of the component, i, in the mixture

γ_m = the fugacity coefficient of the mixture

H = the molal enthalpy of the mixture at the given temperature and pressure

H° = the molal enthalpy of the mixture at a low pressure at which the gas is ideal

Z_m = the compressibility factor ($Z_m = PV/RT$) for the mixture

T_{ci} = the critical temperature of the pure component, i

P_{ci} = the critical pressure of the pure component, i

T_{cm} = the pseudocritical temperature of the mixture

P_{cm} = the pseudocritical pressure of the mixture

T = absolute temperature

R = gas constant.

The pseudocritical temperature and pressure of a mixture are sums of the products of the mole fraction of each pure component in terms of its critical temperature and pressure in accordance with the suggestion made by Kay;[8]

$$T_{cm} = \sum_i X_i T_{ci} \quad (14)$$

$$P_{cm} = \sum_i X_i P_{ci} \quad (15)$$

where X_i is the mole fraction of the component, i.

In the case of hydrogen, the pseudocritical constants recommended by Newton[9] were used in place of the experimental critical constants. The values of the critical constants of pure components were taken from the A.P.I. tables.[10] The derivatives of the fugacity coefficients of the mixture with respect to the composition variables may be evaluated by considering the fugacity coefficient of the pseudoreduced temperature, $T_{rm}(=T/T_{cm})$, and the pressure, $P_{rm}(=P/P_{cm})$, of the mixture. By using the pseudoreduced temperature and pressure instead of the true reduced temperature and pressure, γ_m was obtained from a generalized fugacity coefficient chart,[9] Z_m was read from a generalized compressibility factor chart,[11] and $(H^\circ - H)/T_{cm}$ for the mixture was obtained from a generalized enthalpy-pressure chart.[11] In the temperature range above $T_{rm}=1$, the enthalpy correction values read from the chart were multiplied by a correction factor recommended by York and Weber.[12]

Results

Tables 1—5 summarize the experimental results and gives the values of the equilibrium constants, K, calculated from the data. Figure 2 shows, for the equilibrium between NPB and NPCH, a comparison of the values derived from this report with values reported experimentally by Vvedenskii, Vinnikova, *et al.*[4] over

the temperature range of 200—300 °C, and with the values calculated from the thermodynamic data of NPB[3] and NPCH[2] using the following equation:

$$\Delta G_f^\circ(\text{NPCH}) - \Delta G_f^\circ(\text{NPB}) = \Delta G_h^\circ(\text{n}) = -2.303RT\log K(\text{n}) \quad (16)$$

where ΔG_f°(NPCH) and ΔG_f°(NPB) are the standard Gibbs energies of the formation of NPCH and NPB respectively, and where ΔG_h°(n) is the standard Gibbs energy of the hydrogenation of NPB to NPCH. Most of the runs were made with a NPB feed, the equilibrium being approached from the NPB side. In Runs A-2 and A-9, the equilibrium was approached from the NPCH side. The same results were obtained

Table 1. Experimental data and equilibrium constants for NPCH

Run No.	Compn. of hydrocarbon feed, mol%	Temp., °C	Pressure, atm	Initial mole ratio H_2/feed	Product mol/mol NPCH/NPB	Side reaction mol%	K_γ	K(n)
A- 1	9.5% NPB 90.5% Octane	245.2	4.70	18.13	344	0.0	1.01	3.88
A- 2	8.4% NPCH	272.5	4.59	17.64	27.9	0.7	1.01	3.38×10^{-1}
A- 3	9.5% NPB	320.3	4.70	18.02	0.917	1.4	1.01	1.04×10^{-2}
A- 4	9.5% NPB	298.4	10.31	17.78	25.9	0.6	1.02	2.75×10^{-2}
A- 5	9.5% NPB	329.7	10.11	17.78	5.32	1.0	1.02	5.98×10^{-3}
A- 6	9.5% NPB	366.4	10.08	17.54	0.340	1.5	1.02	3.86×10^{-4}
A- 7	9.5% NPB	348.3	50.4	18.02	114	1.0	0.929	9.77×10^{-4}
A- 8	9.5% NPB	364.7	48.4	17.98	31.7	1.2	0.930	3.08×10^{-4}
A- 9	8.4% NPCH	408.6	48.4	17.62	3.35	2.9	0.934	3.27×10^{-5}
A-10	9.5% NPB	443.8	48.4	17.82	0.641	12.2	0.937	6.28×10^{-6}

Table 2. Experimental data and equilibrium constants for IPCH

Run No.	Compn. of hydrocarbon feed, mol%	Temp., °C	Pressure, atm	Initial mole ratio H_2/feed	Product mol/mol IPCH/IPB	Side reaction mol%	K_γ	K(i)
B- 1	9.5% IPB 90.5% Octane	245.2	4.70	18.13	237	0.0	1.01	2.68
B- 2	8.4% IPCH	272.6	4.59	17.64	19.6	0.6	1.01	2.37×10^{-1}
B- 3	9.5% IPB	320.3	4.70	18.02	0.689	1.1	1.01	7.32×10^{-3}
B- 4	9.5% IPB	298.4	10.31	17.78	18.2	0.5	1.02	1.98×10^{-2}
B- 5	9.5% IPB	329.7	10.11	17.78	3.83	1.0	1.02	4.37×10^{-3}
B- 6	9.5% IPB	366.4	10.08	17.54	0.245	1.7	1.02	2.78×10^{-4}
B- 7	9.5% IPB	351.0	48.4	17.87	66.7	1.2	0.929	6.48×10^{-4}
B- 8	9.5% IPB	385.6	48.4	17.91	7.34	1.8	0.931	7.14×10^{-5}
B- 9	8.4% IPCH	406.9	48.4	17.85	2.55	3.2	0.934	2.48×10^{-5}
B-10	9.5% IPB	399.8	48.4	17.74	3.56	2.1	0.933	3.47×10^{-5}
B-11	9.5% IPB	423.1	50.4	17.82	1.26	8.3	0.935	1.09×10^{-5}

Table 3. Experimental data and equilibrium constants for 1,2-MECH's

Run No.	Compn. of hydrocarbon feed, mol%	Temp., °C	Pressure, atm	Product 1,2-MECH/1,2-MEB mol/mol		K		
				cis	*trans*	*cis*	*trans*	Total
C- 1	9.5% 1,2-MEB 90.5% Octane	262.1	5.53	8.35	25.7	6.96×10^{-2}	2.14×10^{-1}	2.84×10^{-1}
C- 2	8.4% *cis*-1,2	284.2	5.43	1.78	5.39	1.49×10^{-2}	4.49×10^{-2}	5.98×10^{-2}
C- 3	9.5% 1,2-MEB	304.1	5.44	0.396	1.17	3.30×10^{-3}	9.78×10^{-3}	1.31×10^{-2}
C- 4	8.4% *trans*-1,2	327.9	9.61	0.461	1.26	7.13×10^{-4}	1.94×10^{-3}	2.65×10^{-3}
C- 5	9.5% 1,2-MEB	288.7	10.17	8.32	24.5	1.08×10^{-2}	3.20×10^{-2}	4.28×10^{-2}
C- 6	9.5% 1,2-MEB	327.2	10.13	0.608	1.65	8.01×10^{-4}	2.17×10^{-3}	2.97×10^{-3}
C- 7	9.5% 1,2-MEB	349.5	10.17	0.191	0.507	2.49×10^{-4}	6.61×10^{-4}	9.10×10^{-4}
C- 8	9.5% 1,2-MEB	379.1	10.17	0.0350	0.0882	4.61×10^{-5}	1.16×10^{-4}	1.62×10^{-4}
C- 9	9.5% 1,2-MEB	324.3	50.4	91.9	251	1.04×10^{-3}	2.83×10^{-3}	3.87×10^{-3}
C-10	9.5% 1,2-MEB	388.6	51.3	2.63	6.72	2.96×10^{-5}	7.57×10^{-5}	1.05×10^{-4}
C-11	9.5% 1,2-MEB	423.2	50.4	0.588	1.29	6.63×10^{-6}	1.45×10^{-5}	2.11×10^{-5}

Table 4. Experimental data and equilibrium constants for 1,3-MECH's

Run No.	Compn. of hydrocarbon feed, mol%	Temp., °C	Pressure, atm	Product 1,3-MECH/1,3-MEB mol/mol		K		
				cis	*trans*	*cis*	*trans*	Total
D-1	9.5% 1,3-MEB 90.5% Octane	265.2	4.32	13.8	3.77	2.34×10^{-1}	6.41×10^{-2}	2.95×10^{-1}
D-2	8.4% *cis*-1,3	285.9	4.32	2.76	0.809	4.69×10^{-2}	1.37×10^{-2}	6.06×10^{-2}
D-3	9.5% 1,3-MEB	310.6	10.26	4.92	1.53	6.26×10^{-3}	1.95×10^{-3}	8.21×10^{-3}
D-4	8.4% *trans*-1,3	332.7	10.26	1.19	0.390	1.52×10^{-3}	4.97×10^{-4}	2.02×10^{-3}
D-5	9.5% 1,3-MEB	340.4	10.72	0.803	0.273	8.92×10^{-4}	3.03×10^{-4}	1.20×10^{-3}
D-6	9.5% 1,3-MEB	358.9	10.69	0.223	0.0784	2.51×10^{-4}	8.83×10^{-5}	3.39×10^{-4}
D-7	9.5% 1,3-MEB	348.3	49.4	49.4	17.0	5.62×10^{-4}	1.93×10^{-4}	7.55×10^{-4}
D-8	9.5% 1,3-MEB	408.6	49.4	1.20	0.486	1.37×10^{-5}	5.33×10^{-6}	1.90×10^{-5}
D-9	9.5% 1,3-MEB	443.8	49.4	0.193	0.0854	2.19×10^{-6}	9.72×10^{-7}	3.16×10^{-6}

Table 5. Experimental data and equilibrium constants for 1,4-MECH's

Run No.	Compn. of hydrocarbon feed, mol%	Temp., °C	Pressure, atm	Product 1,4-MECH/1,4-MEB mol/mol		K		
				cis	*trans*	*cis*	*trans*	Total
E-1	9.5% 1,4-MEB 90.5% Octane	267.4	5.81	8.33	24.2	5.83×10^{-2}	1.69×10^{-1}	2.27×10^{-1}
E-2	8.4% *cis*-1,2	278.4	5.81	3.24	9.07	2.26×10^{-2}	6.34×10^{-2}	8.60×10^{-2}
E-3	9.5% 1,4-MEB	293.3	10.49	6.35	17.6	7.55×10^{-3}	2.09×10^{-2}	2.85×10^{-2}
E-4	8.4% *trans*-1,4	322.6	10.47	0.838	2.07	1.00×10^{-3}	2.47×10^{-3}	3.47×10^{-3}
E-5	9.5% 1,4-MEB	346.9	10.69	0.228	0.537	2.56×10^{-4}	6.03×10^{-4}	6.59×10^{-4}
E-6	9.5% 1,4-MEB	382.2	10.59	0.0281	0.0564	3.24×10^{-5}	6.52×10^{-5}	9.75×10^{-5}
E-7	9.5% 1,4-MEB	314.7	50.4	160	407	1.72×10^{-3}	4.38×10^{-3}	6.10×10^{-3}
E-8	9.5% 1,4-MEB	364.7	50.4	7.65	16.8	8.22×10^{-5}	1.80×10^{-4}	2.62×10^{-4}
E-9	9.5% 1,4-MEB	389.5	51.3	2.04	4.03	2.07×10^{-5}	4.09×10^{-5}	6.16×10^{-5}
E-10	9.5% 1,4-MEB	443.3	50.4	0.190	0.293	2.05×10^{-6}	3.15×10^{-6}	5.20×10^{-6}

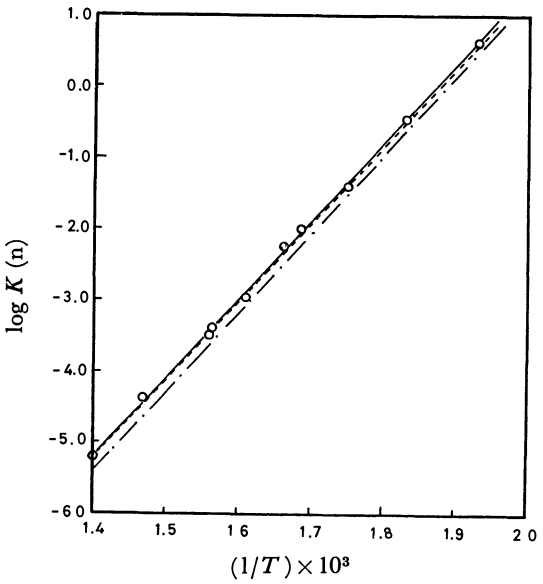

Fig. 2. Logarithn of equilibrium constants for hydrogenation of NPB to NPCH.
○: experimental plot, -·-·-: calculated from thermodynamic data of NPB and NPCH, ----: reported experimentally by Vvedenskii, Vinikova, *et al.*[4]

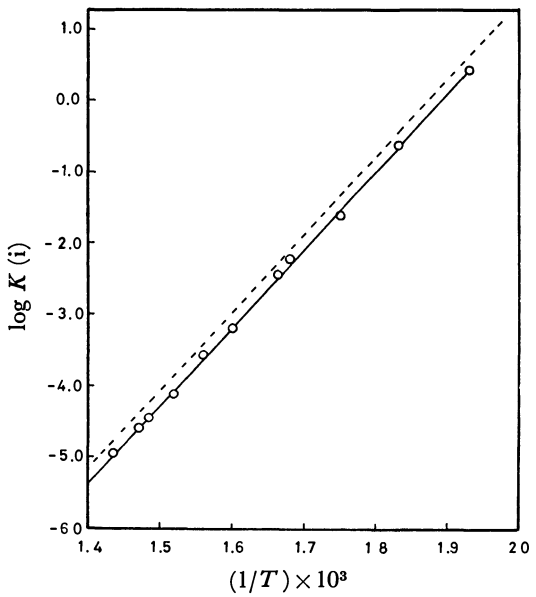

Fig. 3. Logarithm of equilibrium constants for hydrogenation of IPB to IPCH.
○: experimental plot, ----: reported experimentally by Vvedenskii and Takhtareva.[5]

regardless of the side from which equilibrium was approached, thus proving that a true equilibrium was established. Figure 3 shows, for the equilibrium between IPB and IPCH, a comparison of the values derived from this report with those reported experimentally by Vvedenskii and Takhtareva[5] over the temperature range of 204—237 °C.

In Figs. 4, 5, and 6, the values of K for 1,2-MECH's, 1,3-MECH's, and 1,4-MECH's respectively are plotted against $1/T$. Run C-2 was made using a feed containing *cis*-1,2-MECH, but no *trans*-1,2-MECH, while Run C-4 was made using a feed containing *trans*-1,2-MECH, but no *cis*-1,2-MECH. The *cis*-to-*trans* ratio obtained in those experiments is in good

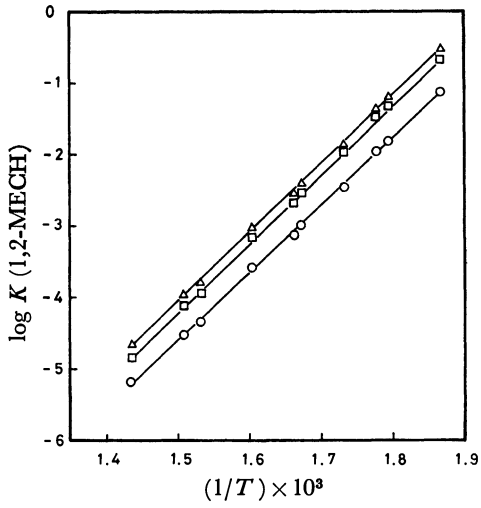

Fig. 4. Logarithm of equilibrium constants for hydrogenation of 1,2-MEB to an equilibrium mixture of *cis*- and *trans*-1-methyl-2-ethylcyclohexanes
○: *cis*-1,2-MECH, □: *trans*-1,2-MECH, △: mixture of *cis*- and *trans*-1,2-MECH's.

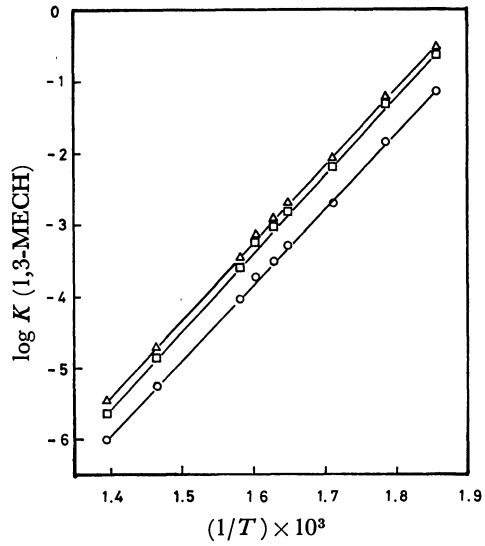

Fig. 5. Logarithm of equilibrium constants for hydrogenation of 1,3-MEB to an equilibrium mixture of *cis*- and *trans*-1-methyl-3-ethylcyclohexanes.
□: *cis*-1,3-MECH, ○: *trans*-1,3-MECH, △: mixture of *cis*- and *trans*-1,3-MECH's.

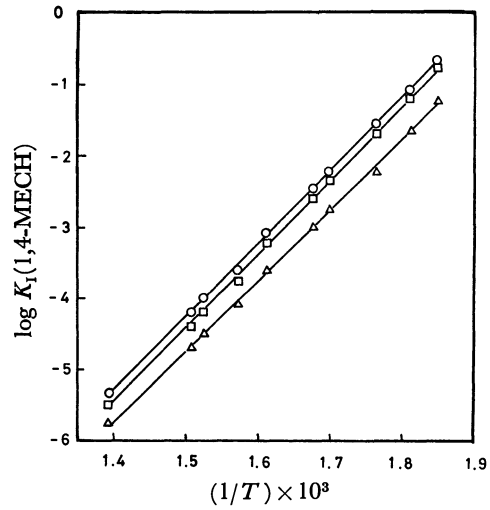

Fig. 6. Logarithm of equilibrium constants for hydrogenation of 1,4-MEB to an equilibrium mixture of *cis*- and *trans*-1-methyl-4-ethylcyclohexanes.
△: *cis*-1,4-MECH, □: *trans*-1,4-MECH, ○: mixture of *cis*- and *trans*-1,4-MECH's.

agreement with the other results, proving that the hydrogenation product is an equilibrium mixture of the *cis* and *trans* isomers.

The following equations for the best straight lines of $\log K$ against $1/T$ were obtained by the least-squares method;

$\log K(\mathrm{n}) = 10975/T - 20.58 \pm 0.03$ (518 to 717 K)
$\log K(\mathrm{i}) = 10887/T - 20.60 \pm 0.04$ (518 to 696 K)
$\log K$(1,2-MECH) $= 9536/T - 18.36 \pm 0.04$ (535 to 696 K)
$\log K$(*cis*-1,2-MECH) $= 9453/T - 18.82 \pm 0.04$
$\log K$(*trans*-1,2-MECH) $= 9651/T - 18.70 \pm 0.04$
$\log K$(1,3-MECH) $= 10758/T - 20.51 \pm 0.03$ (538 to 720 K)
$\log K$(*cis*-1,3-MECH) $= 10885/T - 20.84 \pm 0.03$
$\log K$(*trans*-1,3-MECH) $= 10431/T - 20.56 \pm 0.03$
$\log K$(1,4-MECH) $= 10342/T - 19.81 \pm 0.04$ (540 to 716 K)
$\log K$(*cis*-1,4-MECH) $= 9993/T - 19.75 \pm 0.04$
$\log K$(*trans*-1,4-MECH) $= 10493/T - 20.21 \pm 0.04$

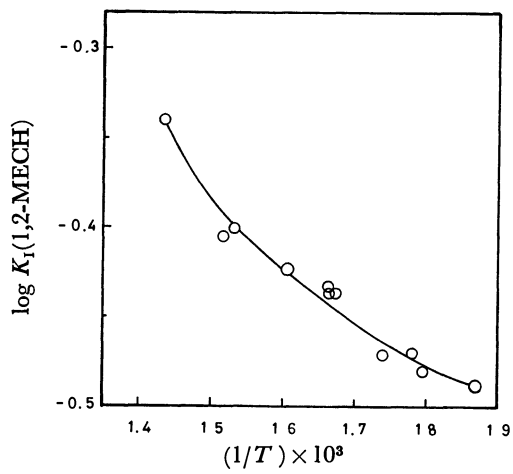

Fig. 7. Logarithm of equilibrium constants of *cis* to *trans* isomerization for 1-methyl-2-ethylcyclohexanes.

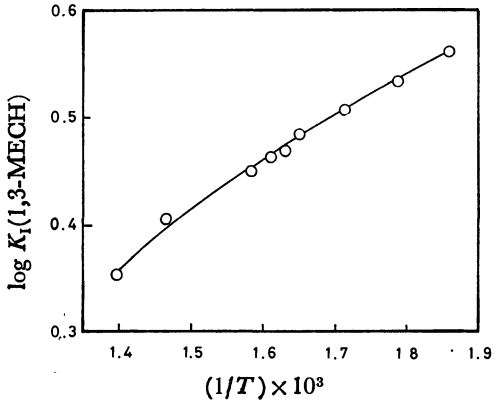

Fig. 8. Logarithm of equilibrium constants of *cis* to *trans* isomerization for 1-methyl-3-ethylcyclohexanes.

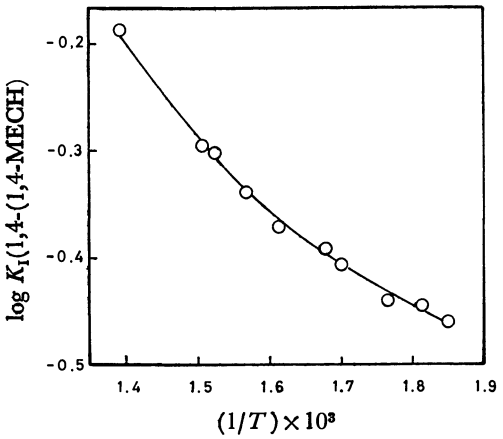

Fig. 9. Logarithm of equilibrium constants of *cis* to *trans* isomerization for 1-methyl-4-ethylcyclohexanes.

From these equations, the standard enthalpy of hydrogenation, $\Delta H_h°$, over the above temperature range for Reactions 1—11 were calculated.

In Figs. 7, 8, and 9 the logarithm of the equilibrium constants of the *cis*-to-*trans* isomerization, K_I, for 1,2-, 1,3-, and 1,4-MECH respectively are plotted against $1/T$.

Table 6 summarizes the values of $\Delta H_h°$ and of $\Delta G_h°$ calculated by Figs. 2—6 and of $\Delta G_I°$ calculated by Figs. 7—9 over the temperature range from 250 to 450 °C in the ideal gas state.

Table 7 summarizes, for the NPCH, IPCH, and six methylethylcyclohexanes, the values of the standard Gibbs energy of formation, $\Delta G_f°$, calculated from the values of $\Delta G_h°$ and of $\Delta G_f°$ of the corresponding alkylbenzenes,[3] over the temperature range from 250 to 450 °C in the ideal gas state.

Table 6. Standard enthalpies and Gibbs energies for reactions 1—11 and for the three *cis* to *trans* isomerization reactions

Compound	$\Delta G°_h$ (kcal/mol)					$\Delta H°_h$ (kcal/mol)
	250 °C	300 °C	350 °C	400 °C	450 °C	
NPCH	−0.96	3.75	8.47	13.18	17.86	−50.2
IPCH	−0.50	4.19	8.92	13.64	18.32	−49.8
1,2-MECH's	0.31	4.51	8.69	12.90	17.10	−43.6
cis-1,2-MECH	1.79	6.08	10.40	14.68	19.02	−43.3
trans-1,2-MECH	0.60	4.88	9.15	13.42	17.72	−44.2
1,3-MECH's	−0.01	4.56	9.23	13.91	18.62	−49.2
cis-1,3-MECH	0.07	4.82	9.61	14.37	19.11	−49.8
trans-1,3-MECH	1.48	6.19	10.89	15.58	20.27	−47.7
1,4-MECH's	0.10	4.64	9.15	13.67	18.22	−47.3
cis-1,4-MECH	1.53	6.06	10.57	15.08	19.61	−45.7
trans-1,4-MECH	0.36	4.98	9.61	14.22	18.85	−46.8
				$\Delta G°_I$ (kcal/mol)		
1,2-MECH	−1.18	−1.22	−1.21	−1.15	(−0.97)[a]	
1,3-MECH	1.38	1.37	1.32	1.26	1.15	
1,4-MECH	−1.13	−1.13	−1.03	−0.84	−0.60	

a) Estimated by extraporated line in Fig. 7.

Table 7. Standard Gibbs energies of formation for NPCH, IPCH, and six methylethylcyclohexanes

Compound	$\Delta G°_f$ (kcal/mol)				
	250 °C	300 °C	350 °C	400 °C	450 °C
NPCH	56.71	67.28	77.87	88.43	98.99
IPCH	57.74	68.43	79.17	89.89	100.57
cis-1,2-MECH	57.90	67.95	78.10	88.27	98.52
trans-1,2-MECH	56.71	66.75	76.85	87.01	97.19
cis-1,3-MECH	54.88	65.38	75.97	86.59	97.25
trans-1,3-MECH	56.29	66.75	77.25	87.80	98.38
cis-1,4-MECH	56.70	67.04	77.42	87.87	98.36
trans-1,4-MECH	55.53	65.96	76.46	87.01	97.60

Discussion

The structural analysis of dimethylcyclohexanes given by Beckett, Pitzer, and Spitzer[13] can be extended to the methylethylcyclohexanes. The stable form of cyclohexane is the chair form. NPCH and IPCH have their propyl groups only in the equatorial position because of the large strain energy in the axial position. A value of 0.8 kcal/mol has been given by Pitzer[14] for the strain energy, *a*, in *n*-butane twisted 120° about the central carbon-carbon bond (*gauche* conformation) as compared to the stable, planar conformation (*trans* conformation) of that molecule; the value of 0.61 kcal/mol is given by Bartell and Kohl.[15] Axial methylcyclohexane has two similar interactions and has been assigned a value of 1.8 kcal/mol, or $a=0.9$ kcal/mol, for the strain energy by Beckett, Pitzer, and Spitzer.[13]

The methylethylcyclohexanes have two isomers: (*cis*-1,2), (*trans*-1,3), and (*cis*-1,4) have one with an axial methyl and an equatorial ethyl group and one with an equatorial methyl and an axial ethyl group, while (*trans*-1,2), (*cis*-1,3), and (*trans*-1,4) have one with both alkyl groups axial and one with both alkyl groups equatorial. These isomers have more three rotational isomers for the ethyl group.

Table 8 summarizes various parameters arising from the isomerism of the methylethyl derivatives. Since *gauche* twists may be either right-handed (G) or left-handed (G'), there are more ways of realizing *gauche* than *trans* conformations. This is reflected in the multiplicity, *m*, listed in Table 8 for each type of isomer. The chair-boat isomerism has been ignored because of the latter's high strain energy.

For *cis*-1,3 derivatives, the axial form encounters much worse steric interference because both alkyl groups are on the same side of the plane. These steric interactions are similar to those of *n*-pentane with the adjacent G and G' conformations. This type of interference also exsists in rotational isomers with an axial ethyl group. The value of $2a$ given by Beckett, Pitzer, and Spitzer[13] has been assigned to this type of interference.

The calculated values of free energy are found by taking the mixture of isomers denoted in Table 8 and by giving *a* the value of 0.9 kcal/mol. They are in excellent agreement with the values of this report observed at 250 °C.

The author gratefully acknowledges helpful discussions with Dr. Toshiaki Kabe, Mrs. Shoko Yamadaya, and Mr. Masaaki Oba during this work.

Table 8. Isomerizm in methylethylcyclohexanes

Compound	Methyl group	Ethyl group	Conform. of ethyl group	m[a]	Energy	*trans*/*cis*	ΔG°_{I},[b] kcal/mol	
							Calcd	Obsd
cis-1,2	**ax**	e	TTG–TG[d]	2	4*a*			
	ax	e	TTG–GG'	1	6*a*			
	e	**ax**	GGG–TG	1	4*a*			
	e	ax	GGG–TG'	1	6*a*			
	e	ax	GGG–G'G'	1	9*a*			
trans-1,2	e	e	TTG–GG	1	3*a*			
	e	e	TTG–TG	1	2*a*			
	e	e	TTG–TG'	1	4*a*			
	ax	ax	TGG–TG	2	5*a*			
	ax	ax	TGG–G'G'	1	10*a*	2.94	−1.12	−1.18
cis-1,3	e	e	TT–TG	2	*a*			
	e	e	TT–GG	1	2*a*			
	ax	ax	G(GG')–TG	2	7*a*			
	ax	**ax**	G(GG')–G'G'	1	—[c]			
trans-1,3	ax	**e**	TT–TG	2	3*a*			
	ax	e	TT–GG	1	4*a*			
	e	ax	GG–TG	2	3*a*			
	e	ax	GG–G'G'	1	8*a*	0.322	1.18	1.38
cis-1,4	**e**	ax	GG–TG	2	3*a*			
	e	ax	GG–G'G'	1	8*a*			
	ax	e	TT–TG	2	3*a*			
	ax	e	TT–GG	1	4*a*			
trans-1,4	e	e	TT–TG	2	*a*			
	e	e	TT–GG	1	2*a*			
	ax	**ax**	GG–TG	2	5*a*			
	ax	ax	GG–G'G'	1	10*a*	3.17	−1.20	−1.13

a) Multiplicity takes into account right- and left-handed *gauche* twists. b) Values at 250 °C. c) This conformation is considered to be sterically unreasonable and is given zero weight.

d) 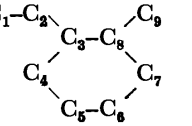

C_2 — C^1
T C_2–C_5 T C_1–C_8
T C_2–C_7—G C_1–C_4
G C_2–C_9

References

1) D.R. Stull, E. Westrum, Jr. and G.C. Sinke, "The Chemical Thermodynamics of Organic Compounds," John Wiley & Sons, New York·London·Sydney·Toronto (1967). F.D. Rossini, K.S. Pitzer, R.L. Arnett, R.M. Braun, and G.C. Pimentel, "Selected Values of Physical and Thermodynamic Properties of Hydrocarbons and Related Compounds," Carnegie Press, Pittsburgh (1953).
2) J.E. Kilpatrick, H.G. Werner, C.W. Beckett, K.S. Pitzer, and F.D. Rossini, *J. Res. Natl. Bur. Standards*, **39**, 523 (1947).
3) W.J. Taylor, D.D. Wagman, M.G. Williams, K.S. Pitzer, and F.D. Rossini, *ibid.*, **37**, 95 (1946).
4) A.A. Vvedenskii, S.G. Vinnikova, V.R. Zharkova, and B.M. Funduiler, *Zh. Obshch. Khim.*, **3**, 718 (1933).
5) A.A. Vvedenskii and N.K. Takhtareva, *ibid.*, **19**, 1083 (1949).
6) C.J. Egan and W.C. Buss, *J. Phys. Chem.*, **63**, 1887 (1959).
7) J. Joffe, *Ind. Eng. Chem.*, **40**, 1738 (1948).
8) W.B. Kay, *ibid.*, **28**, 1014 (1936).
9) R.H. Newton, *ibid.*, **27**, 302 (1935).
10) "Technical Data Book-Petroleum Refining," American Petroleum Institute, Boltimore. Md. Port City Press, (1970).
11) O.A. Hougen and K.M. Watson, "Chemical Process Principles," pt. II-Thermodynamics, John Wiley & Sons, New York (1947).
12) R. York, Jr., and H.C. Weber, *Ind. Eng. Chem.*, **32**, 388 (1940).
13) C.W. Beckett, K.S. Pitzer, and R. Spitzer, *J. Amer. Chem. Soc.*, **69**, 2488 (1947).
14) K.S. Pitzer, *J. Chem. Phys.*, **8**, 711 (1940); *Ind. Eng. Chem.*, **36**, 829 (1944).
15) L.S. Bartell and A. Kohl, *J. Chem. Phys.*, **39**, 3097 (1963).

Proton Magnetic Resonance of Metal Ammine Complexes. IV. Paramagnetic Anisotropy of Cobalt(III) Ions as Exemplified in Proton Chemical Shifts

Hayami YONEDA, Ushio SAKAGUCHI, and Yoshiaki NAKASHIMA*

Department of Chemistry, Faculty of Science, Hiroshima University, Higashisenda-machi, Hiroshima 730
**Department of Physics, Faculty of Education, Wakayama University, Masago-cho, Wakayama 640*

(Received August 6, 1974)

A theory is presented which couples the proton chemical shift induced by the paramagnetic anisotropy with the chemical shift of the central cobalt-59 nucleus. The theory has been successfully applied to twenty cobalt-(III) α-aminocarboxylate complexes. It is shown that it can be used not only to assign proton NMR signals but also to determine the structure of the complex and, in certain cases, the conformation of ligand molecules.

Recently, Watabe *et al.*[1] have given a method for assigning proton magnetic resonance spectra of diamagnetic cobalt compounds. They have noted a general trend, with a few exceptions, for the chemical shift of a proton in a H–C–N–Co(III)–X fragment where X is a nitrogen or oxygen atom and occupies the *trans* (to N) position. The proton resonates at higher or lower field according to whether X is oxygen or nitrogen. This "through-cobalt" effect has been attributed tentatively to the polarizing power of the X atom.

During the course of an investigation on the proton chemical shifts in cobalt(III) ammine complexes, we found[2] that the shifts are primarily determined by the anisotropy in the second order paramagnetism of the central cobalt ion. A theoretical relation between the proton and the cobalt-59 shielding constants was derived and used successfully to reproduce the observed ammine proton chemical shifts. In connection with this work, a recent report given by Yajima *et al.*[3] gave us an impetus to study theoretically the cobalt-59 chemical shifts. We have shown that the additivity in cobalt-59 chemical shifts observed in solution[3] originates from the additivity in each (xx, yy, and zz) component of the shielding tensor.[4] The result, coupled with the relation between ^{1}H and ^{59}Co chemical shifts, enables us to predict the shift of protons under the influence of the paramagnetic anisotropy of the central cobalt(III) ion. Thus, the anisotropy in the second order paramagnetism of diamagnetic cobalt ions will be shown to manifest itself in proton chemical shift variations. Several cobalt(III) complexes exemplifying this situation are treated in this paper. The purpose of the present study is to substantiate the empirical rule of Watabe *et al.* in the light of magnetic anisotropies. The study has been limited to cobalt(III) α-aminocarboxylate complexes. The theoretical results derived here can be utilized not only for the assignment of proton NMR signals but also, in certain cases, for the determination of the geometrical structure of complexes.

Theory

Details of the theory were given in previous papers.[2,4] It is well established that proton chemical shielding under the influence of the anisotropic magnetic susceptibility is given by[5]

$$\sigma_{xx}(^{1}H) = (1-3\sin^2\theta\cos^2\phi)\chi^{p}_{xx}/R^3 \quad (1)$$

$$\sigma_{yy}(^{1}H) = (1-3\sin^2\theta\sin^2\phi)\chi^{p}_{yy}/R^3 \quad (2)$$

$$\sigma_{zz}(^{1}H) = (1-3\cos^2\theta)\chi^{p}_{zz}/R^3 \quad (3)$$

where χ^{p}_{ii} (i=x, y, z) is the principal value of the magnetic susceptibility tensor of cobalt(III) ion, the superscript p refers to the paramagnetic part (*vide infra*), R is the distance between the metal ion and the proton in question, and θ and ϕ are the polar coordinates of the proton in a frame of reference which diagonalizes the susceptibility tensor. In general, magnetic susceptibility and shielding tensors are given, respectively, by

$$\chi = -(1/2)(e^2/2mc^2)\langle 0|\sum_i\{\boldsymbol{l}(r_i^2)-\boldsymbol{r}_i\boldsymbol{r}_i\}|0\rangle + \sum_n \Delta E_n^{-1}\{\langle 0|\sum_i \boldsymbol{m}_i|n\rangle\langle n|\sum_i \boldsymbol{m}_i|0\rangle + \text{c.c.}\} \quad (4)$$

and

$$\sigma = (e^2/2mc^2)\langle 0|\sum_i\{\boldsymbol{l}(r_i^2)-\boldsymbol{r}_i\boldsymbol{r}_i\}/r_i^3|0\rangle - 2\sum_n \Delta E_n^{-1}\{\langle 0|\sum_i \boldsymbol{m}_i/r_i^3|n\rangle\langle n|\sum_i \boldsymbol{m}_i|0\rangle + \text{c.c.}\} \quad (5)$$

The latter is based on Ramsey's formulation.[6] All the notations have their usual meaning[2,4] and c.c. is to take the complex conjugate. From Eqs. (4) and (5), it has been shown,[2] after some mathematical manipulation, that the following relation holds for a cobalt(III) ion.

$$\chi^{p}_{ii} = -\sigma^{p}_{ii}/2\langle r^{-3}\rangle \quad (i=x, y, z) \quad (6)$$

Substitution of Eq. (6) into Eqs. (1)—(3) gives

$$\sigma_{xx}(^{1}H) = -(1-3\sin^2\theta\cos^2\phi)\sigma^{p}_{xx}(^{59}Co)/2R^3\langle r^{-3}\rangle \quad (7)$$

$$\sigma_{yy}(^{1}H) = -(1-3\sin^2\theta\sin^2\phi)\sigma^{p}_{yy}(^{59}Co)/2R^3\langle r^{-3}\rangle \quad (8)$$

$$\sigma_{zz}(^{1}H) = -(1-3\cos^2\theta)\sigma^{p}_{zz}(^{59}Co)/2R^3\langle r^{-3}\rangle \quad (9)$$

Covalency effects have been taken into account through Eq. (6). Thus, proton chemical shifts are directly related to cobalt-59 chemical shifts. The additivity in cobalt-59 chemical shifts gives the relations

$$\sigma^{p}_{xx}(^{59}Co) = \sigma^{p}(C) + \sigma^{p}(D) + \sigma^{p}(E) + \sigma^{p}(F) \quad (10)$$

$$\sigma^{p}_{yy}(^{59}Co) = \sigma^{p}(A) + \sigma^{p}(B) + \sigma^{p}(E) + \sigma^{p}(F) \quad (11)$$

$$\sigma^{p}_{zz}(^{59}Co) = \sigma^{p}(A) + \sigma^{p}(B) + \sigma^{p}(C) + \sigma^{p}(D) \quad (12)$$

These relations have been derived in the O_h-approximation for a complex (Fig. 1). Thus, we obtain the following results for the chemical shift of a proton in a ligand coordinated to cobalt(III) ion.

$$\sigma_{xx}(^{1}H) = -(1-3\sin^2\theta\cos^2\phi) \times (\sigma^{p}(C)+\sigma^{p}(D)+\sigma^{p}(E)+\sigma^{p}(F))/2R^3\langle r^{-3}\rangle \quad (13)$$

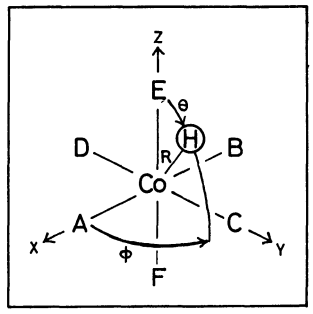

Fig. 1. The coordinate system for a complex [Co(ABCDEF)]. A, B, ……, F stand for ligand molecules or ions.

$$\sigma_{yy}(^1H) = -(1-3\sin^2\theta\sin^2\phi) \times(\sigma^p(A)+\sigma^p(B)+\sigma^p(E)+\sigma^p(F))/2R^3\langle r^{-3}\rangle \quad (14)$$

$$\sigma_{zz}(^1H) = -(1-3\cos^2\theta) \times(\sigma^p(A)+\sigma^p(B)+\sigma^p(C)+\sigma^p(D))/2R^3\langle r^{-3}\rangle \quad (15)$$

Analysis of cobalt-59 chemical shift data indicates that the magnitude of $\sigma^p(X)$ for various ligands is in the order

$$\sigma^p(N) > \sigma^p(O) > \sigma^p(Cl) \simeq \sigma^p(Br)$$

Typical values of $\sigma^p(X)$ for several ligands are given in Table 1.[4] The proton chemical shift to be observed in solution is given by

$$\sigma_{iso}(^1H) = (\sigma_{xx}(^1H)+\sigma_{yy}(^1H)+\sigma_{zz}(^1H))/3 \quad (16)$$

TABLE 1. σ^p (X) VALUES FOR SEVERAL LIGANDS[4]

X	σ^p (X) ppm	X	σ^p (X) ppm
NH_3	−4860	N_3^-	−5655
en	−9205	OH^-	−6345
Cl^-	−5910	H_2O	−6255
Br^-	−5865	CO_3^{2-}	−12090
NO_2^-	−4073	ox^{2-}	−11440
CN^-	−2760	Phen	−9135

Application to Cobalt(III) α-Aminocarboxylates Geometry. Quantities necessary for the calculation of Eqs. (13)—(15) can be estimated in the following way. An average of r^{-3} over a metal 3d orbital is transferred from that of $[Co(NH_3)_6]^{3+}$; $\langle r^{-3}\rangle = 5.77$ a.u.[2] Chemical shift values of cobalt-59 nuclei do not seem to have been reported for aminoacidato complexes. The best values might be the data for simple cobalt compounds for which shift data are available. Setting $\sigma^p(O)$ and $\sigma^p(N)$ at around −6000 and −4600 ppm, respectively, we obtain the result $\sigma^p(N)-\sigma^p(O)\simeq 1400$ ppm. This value was used for all the complexes we examined. Although this is a drastic approximation, the final results were not seriously affected (*vide infra*).

Geometrical factors R, θ, and ϕ were taken from data on α-aminocarboxylate backbones of $NH_4[Co(EDTA)]\cdot 2H_2O$[7] and $(+)_{495}$-$[Co(L\text{-glu})(en)_2]ClO_4$.[8] In the former complex, two structurally different glycine residues are present, the in-plane and out-of-plane groups. It has been reported that the out-of-plane ring is almost flat. The five-membered chelate ring in the latter complex formed by cobalt ion and L-glutamate ion is also nearly flat. This is in line with the observation that chelated α-aminoacidato rings are planar.[9-11] Thus, we assume the planar conformation for α-aminocarboxylate residues in the following. The cobalt-proton distance, R, is calculated for these complexes at about 3.47 A (6.56 a.u.). The relevant quantities are illustrated in Fig. 2. Under these conditions, we obtain

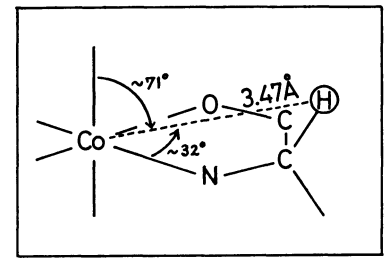

Fig. 2. The geometry of the α-aminocarboxylate residue.

$$(\sigma^p(N)-\sigma^p(O))/R^3\langle r^{-3}\rangle \simeq 0.859 \text{ ppm} \quad (17)$$

Unless otherwise stated, this value will be used for all complexes.

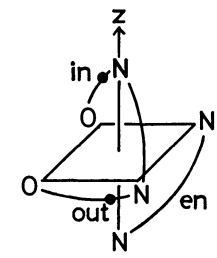

Fig. 3. Schematic presentation of *β-cis*-[Co(EDDA)(en)]$^+$ molecule. Closed circles refer to glycine methylene protons in question.

Illustrative Examples. [*Case I*] cis-O_2N_4 *Type*; *β*-cis-[*Co(EDDA)(en)*]$^+$: This complex contains two equivalent glycine methylene groups, in-plane and out-of-plane methylenes, designated as in-CH_2 and out-CH_2, respectively (Fig. 3). The ligand EDDA conformation in this inert chelate was reported to be fixed.[12] From Eqs. (13)—(16), the chemical shift of the methylene protons is given by

$$\sigma_{iso}(^1H) = (1-3\cos^2\theta)(\sigma^p(N)-\sigma^p(O))/6R^3\langle r^{-3}\rangle \quad (18)$$

The geometrical factors, coupled with Eq. (17), give

$$\sigma_{iso}(\text{in-CH}_2) \simeq -0.168 \text{ ppm} \quad (19)$$

$$\sigma_{iso}(\text{out-CH}_2) \simeq +0.099 \text{ ppm} \quad (20)$$

Thus, our estimation indicates that the out-CH_2 resonates at higher field and the in-CH_2 at lower field, the separation being about 0.26 ppm. Not much significance can be attached to this figure. Coleman *et al.*[13] observed a singlet at 3.71 ppm (from NaTMS) and an AB quartet at 3.59 ppm. Assignment was made based on a comparison with the spectra of *β-cis*-[Co(EDDA)(ox)]$^-$ and *β-cis*-[Co(EDDA)(mal)]$^-$, on the signal intensities, and the well established fact that, in coordinated EDDA, in- and out-CH_2 appear as a singlet and an AB quartet, respectively.[14,15] The assignment was further substantiated by the isotopic

deuterium exchange experiment. It was thus concluded that the singlet at higher field is the in-CH_2, which is in line with our prediction. The observed chemical shift difference between the in- and out-CH_2 is about 0.14 ppm smaller than that expected from the theory. This seems to be due to the valence angle distortion.

β-*cis*-$[Co(EDDA)(NH_3)_2]^+$ can be treated similarly. It suffices to say that the theory leads to a correct assignment.[16]

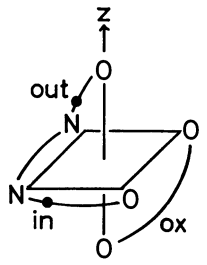

Fig. 4. β-*cis*-[Co(EDDA) (ox)]$^-$ molecule. Closed circles stand for the in- and out-methylenes.

[*Case II*] cis-N_2O_4 *Type*; β-cis-[*Co(EDDA)(ox)*]$^-$: The coordinate system is shown in Fig. 4. The two glycine methylene protons, in- and out-CH_2, can be treated in a similar manner to that for Case I if we replace $(\sigma^p(N)-\sigma^p(O))$ in Eq. (18) by $(\sigma^p(O)-\sigma^p(N))$. This leads to the conclusion that the out-CH_2 should appear at a higher field, which is also in line with the observation by Coleman *et al.*[13]

[*Case III*] mer-N_3O_3 *Type*; [*Co(ED3A)(NO₂)*]$^-$: It can easily be shown that the proton chemical shift is given by

$$\sigma_{iso}(^1H) = \sin^2\theta\cos 2\phi(\sigma^p(N)-\sigma^p(O))/2R^3\langle r^{-3}\rangle \quad (21)$$

Note that we have placed three oxygen atoms in the xz plane. We see at once that the resonance field of B methylene protons is higher than that of groups A and C (Fig. 5). A subtlety is involved in positioning A and C methylenes. There is clearly a minor difference in the chemical shift of these protons. All these predictions have been confirmed by observation.[13]

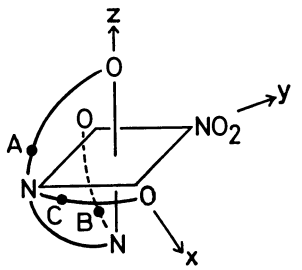

Fig. 5. [Co(ED3A)(NO₂)] ion. A, B, and C differentiate three methylene groups.

Assignments. c_1-cis-[*Co(gly)₂(en)*]$^+$: This molecule is of the *cis*-O_2N_4 type and can be treated as in Case I. The two acetate methylene groups are designated as A and B (Fig. 6). It is predicted by theory that group A should resonate at a higher field than B by about 0.2 ppm. Matsuoka *et al.*[17] observed two singlets at 3.60 and 3.44 ppm corresponding to two acetate methylenes. In this case, the valence angle

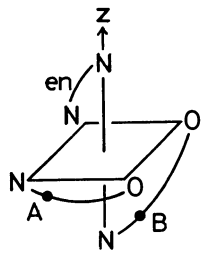

Fig. 6. c_1-*cis*-[Co(gly)₂(en)]$^+$ ion. A and B are the methylenes under consideration.

distortion is irrelevant and we may safely assign the former singlet to the B protons.

c_1-cis-[*Co(gly)₂(ox)*]$^-$: The difference between the two glycine methylene groups is shown in Fig. 7. According to our prediction B is situated in a higher field than A. It was reported[17] that two singlets at 3.58 and 3.43 ppm can be assigned to two glycine methylenes. Although the predicted separation around 0.05 ppm is rather small as compared with the observed value (0.15 ppm), it is highly probable that group B resonates at a higher field.

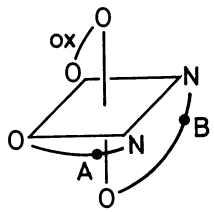

Fig. 7. c_1-*cis*-[Co(gly)₂(ox)]$^-$ ion. A and B stand for the two acetate groups in question.

cis*(O)*,cis*(N)*-[*Co(gly)₂(l-pn)*]$^+$: Two geometrical isomers exist in this *cis*-O_2N_4 type compound (Fig. 8). The complexes were obtained by the reaction of *trans*-$[CoCl_2(l\text{-}pn)_2]^+$ with glycine in an alkaline medium. Kojima and Shibata[18] obtained complexes 8a and 8b as more soluble and less soluble isomers, respectively. The glycine methylene chemical shifts are reported at 3.62 and 3.46 ppm for 8a and 3.59 and 3.46 ppm for 8b. The proton chemical shifts in these complexes can be treated in the same way as for c_1-*cis*-[Co(gly)₂(en)]$^+$. Thus, protons resonating at a higher field can be assigned to methylene group *trans* to the oxygen atom in both isomers.

cis-[*Co(IDA)₂*]$^-$: Cooke[19] measured the proton NMR spectrum and observed two signals at 3.75 and 3.635 ppm corresponding to two methylene groups.

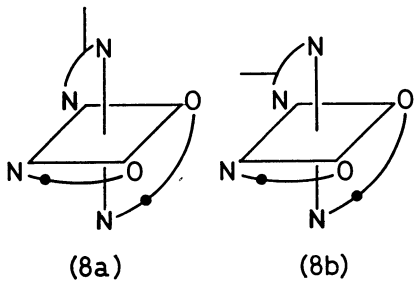

Fig. 8. Two possible isomers of *cis(O)*, *cis(N)*-[Co(gly)₂-(l-pn)]$^+$ molecule. Closed circles refer to protons in question.

This complex is of the *cis*-N_2O_4 type and can be treated as in Case II. We assign the high field signal to the out-of-plane methylenes.

mer-[*Co(gly)*$_2$(L-*glu)*]: Kawasaki and Shibata[20] prepared this complex by the reaction of $[Co(gly)_2(CO_3)]^-$ with glutamate ion in the presence of activated charcoal. They did not succeed in determining the structure. There are two possibilities; *cis(O),trans(N)*- and *cis(N)*, *trans(O)*-isomers. The chemical shift values have not been given but can be estimated from the spectrum. Two singlets at about 3.4 and 3.65 ppm can be observed. Thus, the shift difference is close to that found between groups B and C in $[Co(ED3A)(NO_2)]^-$. For the *cis(O),trans(N)*-structure, the shift difference should be much smaller, which follows from the analogy of the difference between groups A and C in $[Co(ED3A)(NO_2)]^-$. We are thus inclined to presume that the complex assumes the *cis(N),trans(O)*-structure (see Fig. 9). If this is the case, the glycine protons designated as B should appear at a higher field.

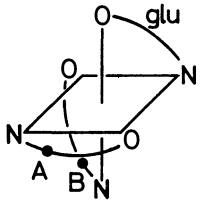

Fig. 9. *mer*-[$Co(gly)_2$(L-glu)] molecule. A and B are methylene groups.

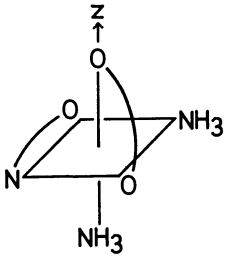

Fig. 10. *mer(cis)*-[$Co(CO_3)(gly)(NH_3)_2$] ion.

mer(cis)-[*Co(CO*$_3$*)(gly)(NH*$_3$*)*$_2$]: Let us examine the chemical shift of ammine protons of coordinated ammonia molecules (see Fig. 10). Kanazawa and Shibata[21] measured the NMR spectrum in trifluoroacetic acid. They observed the chemical shifts of ammonia protons at 5.1 and 5.8 ppm. The separation is larger as compared with separations found for glycine methylene protons discussed above. This is caused by the decrease in Co–H distance R. For the ammonia protons situated on the z-axis, the NH_3-rotation about its C_3-axis renders the factors $(1-3\sin^2\theta\cos^2\phi)$ and $(1-3\sin^2\theta\sin^2\phi)$ both averaged to $(2-3\sin^2\theta)/2$. It follows that protons of this ammonia molecule do not experience the magnetic anisotropy of the cobalt(III) ion. For the other ammonia protons, the following relation can be derived by taking the NH_3-rotation into account.

$$\sigma_{iso}(^1H) = -(3\cos^2\theta'-1)(\sigma^p(N)-\sigma^p(O))/4R^3\langle r^{-3}\rangle \quad (22)$$

Note here that θ' represents the angle between the Co–H vector and the x-axis. The geometrical factors are R=2.52 A (4.77 a.u.) and θ'=22.0.[2] These values, coupled with $(\sigma^p(N)-\sigma^p(O))\simeq 1400$ ppm, give $\sigma_{iso}(^1H)$ value of about −0.883 ppm. Thus, it can be concluded that this ammonia is shifted to low field.

mer(cis)-[*Co(CO*$_3$*)(β-ala)(NH*$_3$*)*$_2$], mer(cis)-[*Co(ox)-(gly)(NH*$_3$*)*$_2$], mer(cis)-[*Co(ox)(β-ala)(NH*$_3$*)*$_2$]: These three complexes can be treated in the same way as above. The protons of the ammonia molecule *trans* to the nitrogen should appear at a lower field and those *trans* to the oxygen at a higher field.

α-cis-[*Co(EDDA)(NH*$_3$*)H*$_2$*O*]$^+$: As expected, the glycine methylene protons exhibit two AB quartets. From a comparison of the spectrum with that of *β-cis*-$[Co(EDDA)(NH_3)_2]^+$ and *β-cis*-$[Co(EDDA)(H_2O)]^+$, the quartet at a lower field has been assigned[23] to glycine protons near the coordinated ammonia molecule. However, this assignment seems to be open to question. There are two possible ways of coordination for ammonia molecule, 11a and 11b. In either case, the theory based on the magnetic anisotropy of cobalt ion leads to an assignment just the opposite; the high field quartet should be due to the methylene near the coordinated ammonia.

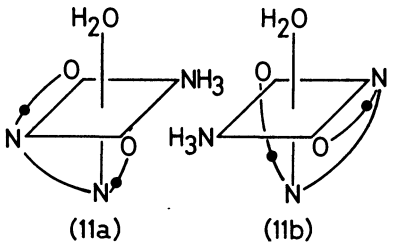

Fig. 11. Two possible ways of coordination of ammonia molecule in α-*cis*-$[Co(EDDA)(NH_3)H_2O]^+$. Closed circles stand for two glycine methylene groups.

Discussion

Several criteria have been proposed for the assignment of proton NMR spectra. They include valence angle distortions (and the consequential elongation of Co–O bonds),[25] bond anisotropies,[13–15,19] steric compressions,[24] selective labilization of α-hydrogen atoms,[26] and the paramagnetic anisotropy in the central metal ion.[1,2,4,27] The first effect, which is the most relevant to our problem, tends to vitiate a prediction based only on the paramagnetic anisotropy of metal ions. $[Co(EDTA)]^-$ and its derivatives offer such examples.

The molecular structure of $[Co(EDTA)]^-$ was determined by Weakliem and Hoard.[7] Their X-ray analysis revealed that while the out-of-plane rings are nearly flat, the in-plane rings suffer severe valence angle distortions, leading to a substantial elongation of the Co–O bonds. In accordance with this fact, the in-plane protons have been shown[14,25,28] to be more shielded than the out-of-plane ones. Similar situations have been noted for $[Co(PDTA)]^-$ and $[Co(CyDTA)]^-$.[26] These molecules belong to *cis*-N_2O_4 symmetry. From the result on *cis*-$[Co(IDA)_2]^-$, it is readily seen that the prediction based only on the paramagnetic anisotropy of the cobalt ion is contrary to observation. Thus, the valence angle distortion acts in these cases to offset paramagnetic anisotropy.

Another example of similar situation is provided by β-*cis*-[Co(EDDA)(mal)]$^-$. Coleman *et al.*[13] measured a spectrum consisting of a singlet and an AB quartet for glycine methylenes. The former resonates at a higher field, the separation being *ca.* 0.06 ppm. The assignment was based on the argument for β-*cis*-[Co(EDDA)(ox)]$^-$. The selective HD exchange experiment provided further support to this assignment. The out-of-plane methylene was shown to be more labilized and amenable to the isotopic exchange reaction. Thus, their assignment can be considered to be sound. Consideration of only the paramagnetic anisotropy leads to an erroneous conclusion, though the predicted separation between the in- and out-of-plane protons is rather small (0.05 ppm). All these examples indicate that we should be careful in applying the theory to ligands with valence angle distortions.

Watabe *et al.*[1] observed that in a number of cobalt(III) α-aminocarboxylate complexes, α protons adjacent to the amino group which is *trans* to N atom are shifted to low field and those *trans* to O atom to high field. This seems to be an over simplification. As Eqs. (13)—(15) indicate, the proton chemical shift is dependent on all the six coordinating atoms and on the position of the proton in question.

The authors wish to express sincere thanks to Dr. M. Watabe and Prof. S. Yoshikawa, Tokyo University, for permission to see their papers prior to publication, and for helpful discussions.

Appendix. Abbreviations

EDTA = ethylenediaminetetraacetato ion.
glu = glutamato ion.
en = ethylenediamine.
EDDA = ethylenediaminediacetato ion.
ox = oxalato ion.
mal = malonato ion.
ED3A = ethylenediaminetriacetato ion.
gly = glycinato ion.
pn = propylenediamine.
IDA = iminodiacetato ion.
ala = alaninato ion.
PDTA = propylenediaminetetraacetato ion.
CyDTA = cyclohexanediaminetetraacetato ion.
phen = phenanthroline.

References

1) M. Watabe, K. Onuki, and S. Yoshikawa, to be published.
2) (a) H. Yoneda and Y. Nakashima, This Bulletin, **47**, 669 (1974). (b) Y. Nakashima, U. Sakaguchi, and H. Yoneda, *Chem. Lett.*, **1974**, 503.
3) F. Yajima, Y. Koike, A. Yamasaki, and S. Fujiwara, This Bulletin, **47**, 1442 (1974).
4) Y. Nakashima, U. Sakaguchi, and H. Yoneda, to be published.
5) H. M. McConnell, *J. Chem. Phys.*, **27**, 226 (1957).
6) N. F. Ramsey, *Phys. Rev.*, **78**, 699 (1950).
7) H. A. Weakliem and J.L. Hoard, *J. Amer. Chem. Soc.*, **81**, 549 (1959).
8) R. D. Gillard, N. C. Payne, and G. B. Robertson, *J. Chem. Soc., A*, **1970**, 2579.
9) H.C. Freeman, M.R. Snow, I. Nitta, and K. Tomita, *Acta Crystallogr.*, **21**, 1463 (1964).
10) G. M. Gramaccioli, *ibid.*, **21**, 600 (1966).
11) G. M. Gramaccioli and R. E. March, *ibid.*, **21**, 594 (1966).
12) G. L. Blackmer, R. E. Hamm, and J. I. Legg, *J. Amer. Chem. Soc.*, **91**, 6632 (1969).
13) P. F. Coleman, J. I. Legg, and J. Steele, *Inorg. Chem.*, **9**, 937 (1970).
14) J.I. Legg and D.W. Cooke, *Inorg. Chem.*, **4**, 1576 (1965).
15) J.I. Legg and D.W. Cooke, *ibid.*, **5**, 594 (1966).
16) K. Kuroda, *Chem. Lett.*, **1972**, 197.
17) N. Matsuoka, J. Hidaka, and Y. Shimura, This Bulletin, **40**, 1868 (1967).
18) Y. Kojima and M. Shibata, *Inorg. Chem.*, **9**, 238 (1970).
19) D. W. Cooke, *ibid.*, **5**, 1141 (1966).
20) K. Kawasaki and M. Shibata, This Bulletin, **45**, 3100 (1972).
21) S. Kanazawa and M. Shibata, *ibid.*, **44**, 2424 (1971).
22) K. Nakai, S. Kanazawa, and M. Shibata, *ibid.*, **45**, 3544 (1972).
23) K. Kuroda, *ibid.*, **45**, 2176 (1972).
24) J. C. Dabrowiak and D. W. Cooke, *J. Amer. Chem. Soc.*, **92**, 1097 (1970).
25) D. H. Williams and D. H. Busch, *ibid.*, **87**, 4644 (1965).
26) J. B. Terrill and C. N. Reilly, *Inorg. Chem.*, **5**, 1988 (1966).
27) (a) R. V. Emanuel and E. W. Randall, *J. Chem. Soc., A*, **1969**, 3002. (b) A. D. Buckingham, *Can. J. Chem.*, **38**, 300 (1960). (c) A. D. Buckingham and P. J. Stephens, *J. Chem. Soc.*, **1964**, 2747.
28) R. J. Day and C. N. Reilly, *Anal. Chem.*, **36**, 1073 (1964).

The Effect of the pH on the Adsorption of an Ampholytic Surfactant, *N*-Dodecyl-β-alanine, at the Aqueous Surface

Akio NAKAMURA, Kazuo TAJIMA, and Tsunetaka SASAKI

Department of Chemistry, Faculty of Science, Tokyo Metropolitan University, Tokyo 158

(Received August 7, 1974)

The effect of the pH on the adsorption of an ampholytic surfactant, *N*-dodecyl-β-alanine (NDA), at the nitrogen/solution interface was studied by the radiotracer method, using a tritiated compound. The saturated amount of NDA adsorption was found to depend on the pH of the bulk solution; it shows a flat maximum in the isoelectric region from pH 4 to 10, and decreases distinctly on the both acid and alkaline sides. The Gibbs adsorption isotherm for an aqueous solution of the ampholytic surfactant was derived. Using this relation, the amount of adsorption in the pH range from 2 to 6 was calculated from the surface tension *vs.* concentration and the surface tension *vs.* pH relations observed for the NDA solution. The calculated values were in good agreement with those obtained by the radiotracer method. The degree of dissociation of the adsorbed monolayer was estimated from the pH dependence of NDA and the chloride ion adsorption.

The present authors and their collaborator have previously reported radiotracer studies on the adsorption of an ampholytic surfactant, *N*-dodecyl-β-alanine (NDA),[1] at type of surfactant upon which the adsorption had not been studied precisely;[2] they found that, in the isoelectric pH region, the Gibbs adsorption isotherm can be applied in the same form as for an aqueous nonionic surfactant[3] and that the NDA molecules in the solution were mainly in the state of the simple zwitterion.[4]

It is evident that, for such an ampholytic surfactant, a change in the pH markedly influences the state of the solute species of NDA; this further affects the adsorption and the surface tension of the solution. However, the studies of the pH effects have been mainly restricted to properties of bulk solution.[4,5]

In the present report, the pH dependence of the adsorption of NDA is studied in the pH region from 1 to 13. A Gibbs adsorption isotherm applicable to such a system is derived and experimentally confirmed. The ionic states of the adsorbed molecules are discussed, taking account of the pH dependence of NDA and the chloride ion adsorption.

Experimental

Materials and Procedures. All of the reagents used, including tritiated NDA(TNDA), and the methods of the radioactivity and surface tension measurements are the same as have been described in the previous paper.[1]

Theoretical

Gibbs Adsorption Isotherm. The Gibbs adsorption isotherm is written, in its general form, as:[6]

$$-\mathrm{d}\gamma/RT = \sum_i \Gamma_i \mathrm{d}\ln a_i \qquad (1)$$

where γ denotes the surface tension, and Γ_i and a_i, the surface excess and activity of the i'th solute in the solution respectively. Equation (1) is rewritten for the ampholytic surfactant solution containing hydrochloric acid as:

$$\begin{aligned}-\mathrm{d}\gamma/RT = {} & \Gamma_{\mathrm{A}^\pm}\mathrm{d}\ln C_{\mathrm{A}^\pm} + \Gamma_{\mathrm{A}^+}\mathrm{d}\ln C_{\mathrm{A}^+} \\ & + \Gamma_{\mathrm{A}^-}\mathrm{d}\ln C_{\mathrm{A}^-} + \Gamma_{\mathrm{H}^+}\mathrm{d}\ln C_{\mathrm{H}^+} \\ & + \Gamma_{\mathrm{OH}^-}\mathrm{d}\ln C_{\mathrm{OH}^-} + \Gamma_{\mathrm{Cl}}\mathrm{d}\ln C_{\mathrm{Cl}} \qquad (2)\end{aligned}$$

where the $\mathrm{A}^\pm$, A^+, A^-, H^+, OH^-, and Cl subscripts refer to the zwitterion, the cation, the anion of NDA, the hydrogen ion, the hydroxide ion, and the chloride ion respectively. In Eq. (2) the activities can be replaced by the concentrations, since the surfactant concentrations are dilute, and the activity coefficients can be taken as unity. The concentration of HCl is not dilute in some cases, but this does not cause much error, as may be seen from the results.

Further, we have the following relations:

$$K_1 = C_{\mathrm{A}^\pm}C_{\mathrm{H}^+}/C_{\mathrm{A}^+} \qquad (3)$$

$$K_2 = C_{\mathrm{A}^-}C_{\mathrm{H}^+}/C_{\mathrm{A}^\pm} \qquad (4)$$

$$K_{\mathrm{w}} = C_{\mathrm{H}^+}C_{\mathrm{OH}^-} \qquad (5)$$

$$\Gamma_{\mathrm{A}^+} + \Gamma_{\mathrm{H}^+} = \Gamma_{\mathrm{OH}^-} + \Gamma_{\mathrm{A}^-} + \Gamma_{\mathrm{Cl}} \qquad (6)$$

where K_1 and K_2 express the first and second dissociation constants of NDA, considered as a dibasic acid, and K_{w}, the dissociation constant of water. Equation (6) represents the electrical neutrality of the adsorbed ionic species.

By substituting the logarithmic forms of Eqs. (3) and (4) into Eq. (2), we obtain:

$$\begin{aligned}-\mathrm{d}\gamma/RT = {} & (\Gamma_{\mathrm{A}^\pm}+\Gamma_{\mathrm{A}^+}+\Gamma_{\mathrm{A}^-})\mathrm{d}\ln C_{\mathrm{A}^\pm} \\ & + (\Gamma_{\mathrm{A}^+}-\Gamma_{\mathrm{A}^-}+\Gamma_{\mathrm{H}^+})\mathrm{d}\ln C_{\mathrm{H}^+} \\ & + \Gamma_{\mathrm{OH}^-}\mathrm{d}\ln C_{\mathrm{OH}^-} + \Gamma_{\mathrm{Cl}}\mathrm{d}\ln C_{\mathrm{Cl}} \qquad (7)\end{aligned}$$

Using

$$\Gamma^{\mathrm{A}} = \Gamma_{\mathrm{A}^\pm} + \Gamma_{\mathrm{A}^+} + \Gamma_{\mathrm{A}^-} \qquad (8)$$

as the total adsorption amount of NDA, and

$$C^{\mathrm{A}} = C_{\mathrm{A}^\pm} + C_{\mathrm{A}^+} + C_{\mathrm{A}^-} \qquad (9)$$

as the bulk concentration of NDA, we obtain, from Eqs. (5), (6), (7), and (8):

$$-\mathrm{d}\gamma/RT = \Gamma^{\mathrm{A}}\mathrm{d}\ln C_{\mathrm{A}^\pm} + \Gamma_{\mathrm{Cl}}\mathrm{d}\ln C_{\mathrm{H}^+}C_{\mathrm{Cl}} \qquad (10)$$

Equation (10), together with Eqs. (3), (4), and (9), then gives:

$$\begin{aligned}-\mathrm{d}\gamma/RT = {} & \Gamma^{\mathrm{A}}\mathrm{d}\ln C^{\mathrm{A}} + K\Gamma^{\mathrm{A}}\mathrm{d}\ln C_{\mathrm{H}^+} \\ & + \Gamma_{\mathrm{Cl}}\mathrm{d}\ln C_{\mathrm{H}^+}C_{\mathrm{Cl}} \qquad (11)\end{aligned}$$

where:

$$K = (C_{\mathrm{A}^-} - C_{\mathrm{A}^+})/C^{\mathrm{A}}$$

or, using Eqs. (3), (4), and (9),

$$K = (K_1K_2 - C_{\mathrm{H}^+}{}^2)/(C_{\mathrm{H}^+}{}^2 + K_1C_{\mathrm{H}^+} + K_1K_2) \qquad (12)$$

By differentiating Eq. (11) with respect to $\ln C^{\mathrm{A}}$,

keeping C_{Cl} constant, and with respect to ln C_{Cl}, keeping C^A constant, we obtain:

$$I_{Cl} = \Gamma^A + (K\Gamma^A + \Gamma_{Cl})\alpha \quad (13)$$

$$I_A = \Gamma_{Cl} + (K\Gamma^A + \Gamma_{Cl})\beta \quad (14)$$

where:

$$I_{Cl} = -(d\gamma/RTd \ln C^A)_{C_{Cl}} \quad (15)$$

$$I_A = -(d\gamma/RTd \ln C_{Cl})_{C^A} \quad (16)$$

$$\alpha = (d \ln C_{H^+}/d \ln C^A)_{C_{Cl}} \quad (17)$$

$$\beta = (d \ln C_{H^+}/d \ln C_{Cl})_{C^A} \quad (18)$$

Equations (13) and (14) finally give:

$$\Gamma^A = [(1+\beta)I_{Cl} - \alpha I_A]/[1+\beta+\alpha K] \quad (19)$$

$$\Gamma_{Cl} = -[\beta K I_{Cl} - (1+\alpha K)I_A]/[1+\beta+\alpha K] \quad (20)$$

From Eqs. (19) and (20), Γ^A and Γ_{Cl} can be calculated from the measurements of I_A, I_{Cl}, α, and β according to Eqs. (15) to (18).

The validity of Eq. (19) can be checked by comparing the Γ^A calculated from this equation with those measured directly by the radiotracer method. Equation (20) enables us to calculate Γ_{Cl}, the direct measurement of which is impossible due to the lack of a soft radioactive nuclide.

Adsorption equations for alkaline NDA solution containing sodium hydroxide can be derived by a similar calculation. The final expressions for Γ^A and Γ_{Na^+} are the same as in Eqs. (19) and (20) except for the sign of β being the opposite and the subscript Cl being replaced by Na^+.

Results and Discussion

Effect of the pH on the Saturated Amount of Adsorption. Figure 1 shows the adsorption isotherm obtained by the radiotracer method for TNDA solutions kept at a constant pH by the addition of HCl. The amount of adsorption increases with the NDA concentration for each pH and attains a saturation values at a bulk TNDA concentration above *ca.* 2.5×10^{-4} mol/l for the pH region from 3.5 to 6 and above *ca.* 6×10^{-4} mol/l for the more acid region. Also, it can be seen that the amount of NDA adsorption is independent of the pH in the range from 4 to 6 and that it decreases

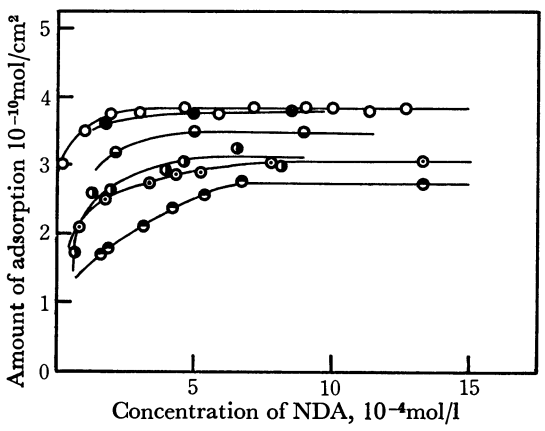

Fig. 1. Adsorption isotherm of NDA.
pH of solutions
○: 6.0 ●: 3.5 ◒: 3.0 ◑: 2.5 ◓: 2.0 ⊙: 1.0

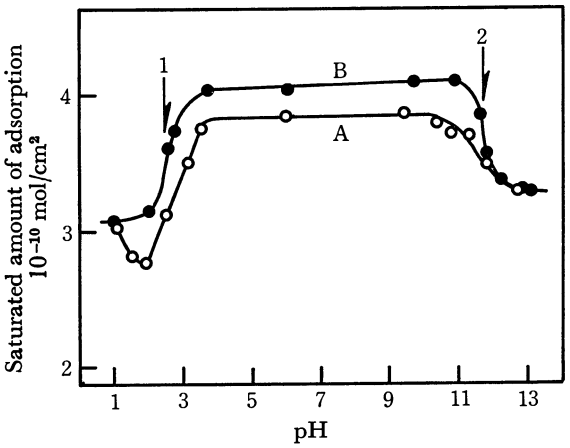

Fig. 2. Saturated amount of adsorption *vs.* pH.
○: in the absence of added NaCl
●: at constant ionic strength (μ=0.1) adjusted by NaCl

below this region, with a minimum at pH 2. The measurements of the saturated amount of adsorption were further extended over the alkaline region, and the values plotted against the pH. The results are shown by Curve A in Fig. 2. In these measurements, the concentration of NDA was maintained at 6.0×10^{-4} mol/l, which was high enough to secure the saturated adsorption. Curve A shows that the saturated amount of adsorption is nearly constant in the pH region from 4 up to 10, including the isoelectric point of pH 7, and decreases on the acid and alkaline sides, with a minimum located near pH 2.

The slight increase observed below pH 2 is considered to be due to the salting out effect on the adsorption of HCl added in a relatively large amount. To confirm this effect, another measurement was made under a constant ionic strength adjusted by the addition of NaCl. The results are shown by Curve B in the same figure. The amount of NDA adsorption in this case is also seen to be nearly constant in the pH region from 4 up to 11, while it decreases rather sharply below and above this region, tending to constant values. The minimum values increases, and the minimum disappears.

In order to elucidate the pH dependence of ampholyte adsorption, it is necessary to know the dissociation equilibrium of ampholyte in the substrate solution with which the adsorbed monolayer is in equilibrium. For this purpose, the molar fractions of NDA cations, anions, and zwitterions are calculated using two dissociation constants, $K_1=3.2\times10^{-4}$, $K_2=1.3\times10^{-11}$ mol/l[4] of the NDA as a dibasic acid; they are plotted against the pH in Fig. 3. As is shown by the curves in the figure, the two dissociations occur step-by-step, and Curve (2) indicates that, in the pH region from 5.5 up to 9, most NDA molecules exist as zwitterions in a bulk solution. Thus, the agreement, as a whole, of the plateau region of adsorption at the surface (shown by Curve B in Fig. 2) with the zwitterionic region of the bulk solution (Curve (2) in Fig. 3) might be taken as the indication that the adsorbed NDA in this pH region consists mainly of zwitterions, considering the similarity of the ionic states between the surface and

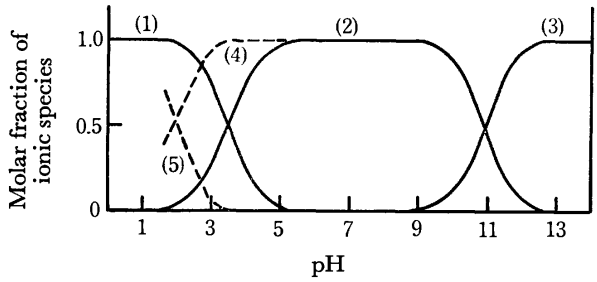

Fig. 3. Molar fractions of ionic species in the bulk solution and at the surface.
(1) —— cationic species
(2) —— zwitterionic species
(3) —— anionic species
in the bulk solution
(4) ---- zwitterionic species
(5) ---- cationic species
at the surface

the bulk. The agreement of the pH regions of relatively weak adsorptions on the acid and alkaline sides of Curve B in Fig. 2 with those of Curves (1) and (3) in Fig. 3 also indicates that cations (anions) are the main adsorbed species in the low (high) pH region.

According to these considerations, the adsorbed layer is cationic at pH 1, zwitterionic at pH values from 4 to 11, and anionic at pH 13 in Curve B of Fig. 2. Then, at the pH corresponding to the middle point between the adsorption amounts of cationic and zwitterionic molecules (Arrow 1), half of the molecules adsorbed at the surface are considered to exist as cations and half as zwitterions, while at a similar pH on the alkaline side (Arrow 2), half of the molecules adsorbed may exist as zwitterions and half as anions. These two pH values of the half-ionization of the adsorbed NDA are read as 2.5 and 11.7 respectively from Curve B. It is noticeable that the pH value of 2.5, *i.e.* the point of the half-ionization of carboxyl groups, is by 1.0 pH unit to the acid side of the point at which carboxyl groups half-ionize in the bulk solution, and that the pH value of 11.7, the point of the half-ionization of imino groups, is by 0.8 unit to the alkaline side of the point at which imino groups half-ionize in the bulk solution.

In the case of soluble and insoluble monolayers, such a shift of the half-ionization in the surface phase has been reported by many investigators on the basis of measurements of the surface potential,[7] the calcium ion adsorption,[8] *etc.*[9] These results have been explained in terms of the existence of a large potential difference, ψ, across the surface characteristic of the charged monolayer.[10] The electric charge attracts or repels hydrogen ions to or from the surface according to the Boltzmann equation:

$$[H^+]_s = [H^+]_b \exp(-\varepsilon\psi/kT)$$

or:

$$pH_s = pH_b + \varepsilon\psi/2.3kT \qquad (21)$$

where the s and b subscripts denote the surface and the bulk respectively, and ε, the protonic charge. It follows from Eq. (21) that:

$\psi > 0$ $pH_s > pH_b$ for a cationic monolayer

$\psi < 0$ $pH_s < pH_b$ for an anionic monolayer

This may explain the observed phenomena. In the case of the cationic monolayer formed in acid region, $pH_s > pH_b$ and the degree of ionization of carboxyl groups is larger at the surface than in the bulk solution. Accordingly, half-ionization at the surface occurs at a lower pH than the pH of half-ionization in the bulk solution. A similar consideration leads to the conclusion that the half-ionization of imino groups at the surface occurs at a higher pH than the pH of half-ionization in the bulk solution. Thus, we have a system of pH shifts occurring in two opposite directions each other as compared with the shift in one direction usually observed for insoluble monolayers which contain only one kind of dissociation group. The ψ values tentatively calculated according to Eq. (21) are 60 mV for the cationic monolayer and −50 mV for the anionic monolayer; these values are, however, roughly half of the values calculated according to the Gouy theory.[11] This discrepancy will be explained below.

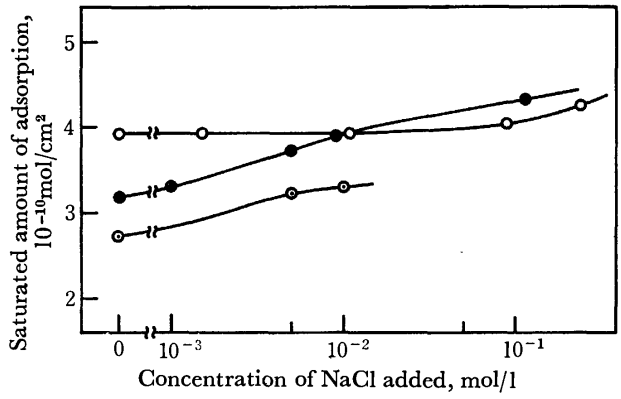

Fig. 4. Effect of polar head group and added NaCl on the saturated amount of adsorption.
Surfactants (Concentration)
○: NDA (5×10^{-4}mol/l) ●: SDS (4×10^{-3}mol/l)[12]
⊙: $D(EO)_6$ (4×10^{-5}mol/l)[13]

Effect of the Polar Head Structure and Added Salt on the Saturated Amount of Adsorption. The effect of salt on the saturated amount of adsorption of a few surfactants with equal hydrocarbon chain lengths hitherto measured directly by the radiotracer method using tritium labeled compounds are shown in Fig. 4, together with the present data. It is evident that the nature of the polar head and NaCl added affect the amount of adsorption. In the absence of added salt, the adsorption of NDA is relatively large compared with those of the sodium dodecylsulfate (SDS)[12] and hexaoxyethylenedodecylmonoether ($D(EO)_6$).[13] This may be due to the electrical repulsion between negatively charged groups in the case of SDS and due to bulky head groups in the case of $D(EO)_6$. The relatively large amount of adsorption for NDA is due to the zwitterionic and relatively compact head groups forming intra- and intermolecular salts, as has been reported for, for instance, the phospholipid monolayers.[8,14] It may be seen in Fig. 4 that the addition of a small amount of NaCl distinctly increases the adsorption of SDS and $D(EO)_6$, while it has no effect on NDA. In the case

of SDS, the increase in adsorption is mainly caused by the decrease in electrical repulsion between adsorbed molecules due to the increase in the ionic strength. In the case of $D(EO)_6$, the dehydration of weakly hydrated nonionic molecules may result in an increase in the adsorption.[15] The absence of these effects in the case of NDA in the neutral region in Fig. 4 and perhaps in the whole plateau region may explain the absence of any effect of NaCl addition. Figure 4 further shows the increase in the adsorption of NDA in the concentrated solution of NaCl, much as in the cases of SDS and $D(EO)_6$. This may be interpreted as a salting out effect of NaCl. A similar effect is also seen near pH 1 in Fig. 2, where HCl is added in a large amount.

Calculation of the Amount of Adsorption. Figures 5 to 8 show the plots of γ *vs.* $\log C^A$ (C_{Cl}=constant), of γ *vs.* pCl (C^A=constant), of pH *vs.* pCl (C^A=constant), and of pH *vs.* $\log C^A$ (C_{Cl}=constant) respectively, from which I_{Cl}, I_A, α, and β values required in Eqs. (19) and (20) may be calculated from the slopes of these

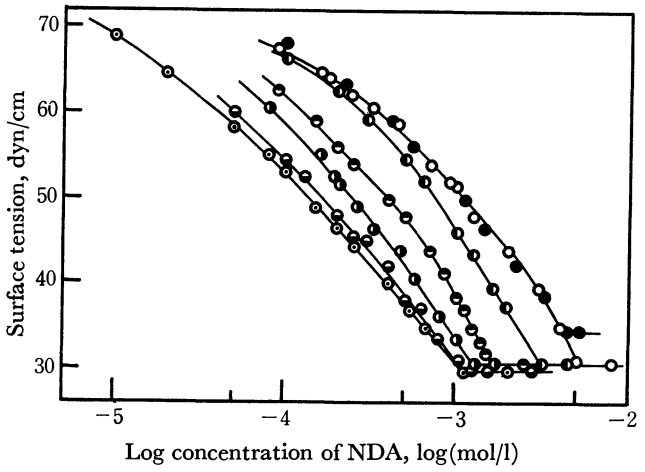

Fig. 5. Surface tension vs. concentration of NDA.
Initial concentration of HCl(pCl)
◉: 6.0 ◒: 4.0 ◑: 3.5 ◓: 3.0 ◐: 2.5 ○: 2.0
●: 1.5

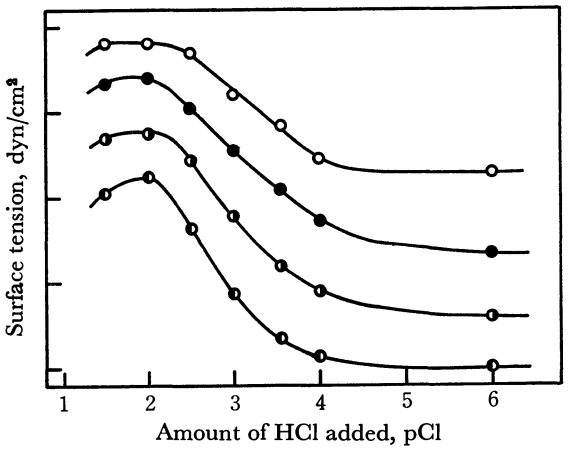

Fig. 6. Surface tension of NDA solution *vs.* amount of HCl added.
Concentration of NDA (10^{-4} mol/l)
○: 1.0 ●: 2.25 ◑: 5.0 ◐: 10.0

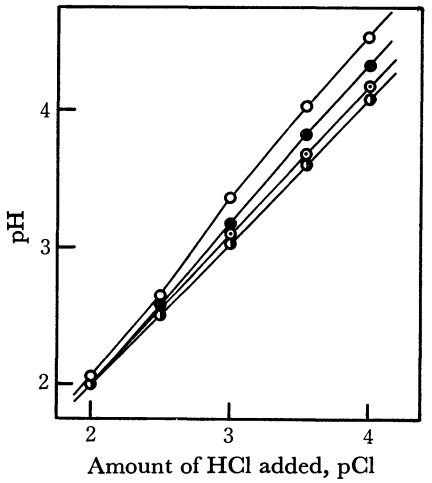

Fig. 7. pH of NDA solution *vs.* amount of HCl added.
Concentration of NDA (10^{-4} mol/l)
○: 10.0 ●: 5.0 ◉: 2.25 ◑: 1.0

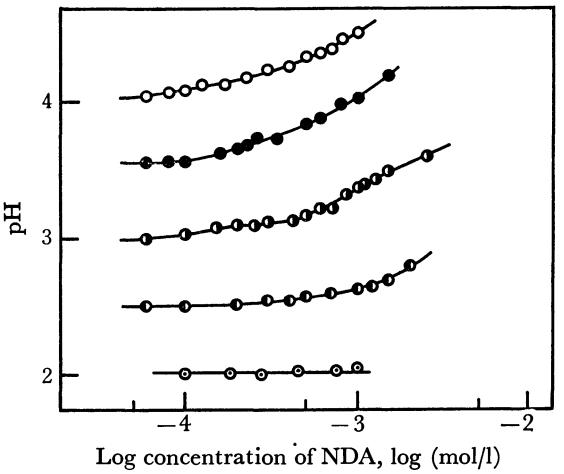

Fig. 8. pH of HCl solution *vs.* concentration of NDA.
Initial concentration of HCl(pCl)
○: 4.0 ●: 3.5 ◑: 3.0 ◐: 2.5 ◉: 2.0

curves. Γ^A and Γ_{Cl} were calculated at the NDA concentrations of 2.25×10^{-4} mol/l and 5.0×10^{-4} mol/l. Similar results were thus obtained. Figure 9 shows the plot of Γ against pH for the latter case, together with the observed values obtained by the interpolation of the curves in Fig. 1. A good agreement is seen between the calculated and observed amounts of adsorption; this shows the validity of the Gibbs adsorption isotherm derived.

It is worth noting that, in the limiting cases of $\alpha=0$, which is actually the case near pH 2 and in the neutral pH region, Eq. (19) is reduced to a simple form:

$$\Gamma^A = I_{Cl} \qquad (22)$$

As was mentioned, in the neutral region NDA exclusively exists as one zwitterionic species, regardless of the pH, while near pH 2 NDA exist mainly as cations with excess of HCl. Therefore, Eq. (22) for NDA, in the neutral pH region and near pH 2, is valid much as in the cases of the adsorption of a nonionic surfactant ($D(EO)_6$)[3] and an anionic surfactant (SDS) with excess salt[16] respectively. In the intermediate

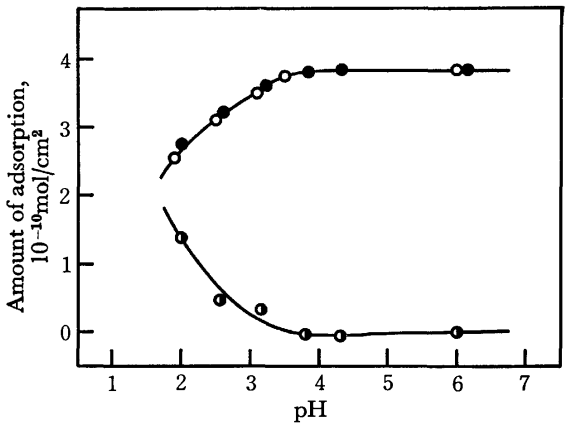

Fig. 9. Amount of adsorption of NDA and chloride ion *vs.* pH at NDA concentration of 5.0×10^{-4}mol/l.
○: observed values for NDA
●: calculated value for NDA
◑: calculated value for chloride ion

pH region from 2 to 5, the general form of Eq. (19) should be used.

As regards the adsorption of the chloride ion, calculated values are nearly zero in the pH region from 4 to 6, as may be seen in Fig. 9. This may imply the zwitterionic structure of NDA, which requires no counter ions. In a more acid region, the values increase with a decrease in the pH. Since the zwitterions change into cations at the surface in this region (Curves A and B in Fig. 2), the positive adsorption of chloride ion as counter ions can reasonably be expected. This enables another calculation of the degree of the ionization of zwitterions into cations at the surface, expressed as Γ_{Cl}/Γ^{A} at each pH, independently of the former estimation made from the curve of Fig. 2. The degrees of ionization, Γ_{Cl}/Γ^{A}, namely, the molar fraction of A^+ and the molar fraction of $A^{\pm}$ given as $1-\Gamma_{Cl}/\Gamma^{A}$, are shown in Fig. 3 as two broken (4) and (5) respectively. The point of the half-ionization pH at the surface estimated from Curve (5) is read as 2, which is 1.5 pH unit to the acid side of the point at which carboxyl groups half-ionize in the bulk solution, and is lower than the value obtained by the former method from the Curve B shown in Fig. 2. The discrepancy is probably due to the adsorbed film at the lowest pH in Fig. 2 not being in a pure cationic form, but containing some zwitterions. The ψ value in Eq. (21), calculated assuming a half-ionization at pH 2, was found to be 90 mV, roughly which is two-thirds of the values obtained according to the Gouy theory. The discrepancy might come from taking only the net charge density into account and neglecting the ampholytic nature of the adsorbed NDA in the estimation of ψ. At any rate, it may be noted that not only the total amount of adsorption, but also the composition of each ionic species or the state of the ionization of the adsorbed surface phase, can be determined for the ampholyte NDA. It is also shown that the composition is different between the surface and the bulk of the aqueous NDA solution.

References

1) T. Okumura, A. Nakamura, K. Tajima, and T. Sasaki, This Bulletin, **47**, 2986 (1974).
2) K. Durham, "3rd Inst. Congr. Surface Active Substances," Vol. 2, (1960), p. 130.
3) K. Tajima, M. Iwahashi, and T. Sasaki, This Bulletin, **44**, 3251 (1971).
4) T. Okumura, K. Tajima, and T. Sasaki, *ibid.*, **47**, 1067 (1974).
5) M. Corkill, K. Gemmel, J. Goodman, and T. Walker, *Trans. Faraday Soc.*, **66**, 1817 (1970); F. Tokiwa, and K. Ohki, *J. Phys. Chem.*, **71**, 1824 (1967); S. H. Yalkowsky, and G. Zografi, *J. Colloid Sci.*, **34**, 525 (1970); K. Tori, and T. Nakagawa, *Kolloid-Z.*, **187**, 44 (1963).
6) E. A. Guggenheim, "Thermodynamics," North Holland Publishing Co., Amsterdam (1957), p. 50.
7) J. J. Betts, and B. A. Pethica, *Trans. Faraday Soc.*, **52**, 1581 (1956); J. A. Spink, *J. Colloid Sci.*, **18**, 512 (1963); H. C. Parreira, *ibid.*, **20**, 742 (1965); E. D. Goddard, and H. C. Kung, *ibid.*, **37**, 585 (1971).
8) T. Seimiya, and S. Ohki, *Biochim. Biophys. Acta*, **298**, 546 (1973).
9) D. Deutsch, *Z. Phys. Chem.*, **60**, 353 (1928); J. F. Danielli, *Proc. Roy. Soc., Ser. B*, **122**, 155 (1937); *Biochem. J.*, **35**, 470 (1941).
10) J. T. Davies, and E. K. Rideal, "Interfacial Phenomena," Academic Press, New York and London (1963), p. 94.
11) *ibid.*, p. 75.
12) K. Tajima, This Bulletin, **44**, 1767 (1971).
13) K. Tajima, and M. Iwahashi, *ibid.*, **46**, 3370 (1973).
14) B. A. Pethica, Surface Activity and Microbial Cell Soc. Chem., Int London, Monograph, **19**, 85 (1965).
15) K. Shinoda, and H. Takeda, *J. Colloid Sci.*, **32**, 642 (1970); H. Schott, *ibid.*, **43**, 150 (1973).
16) K. Tajima, This Bulletin, **43**, 3063 (1970).

An Analysis of the Surface Composition of Passive Film on Cu-Ni Alloys by means of Auger Electron Spectroscopy and X-Ray Photoelectron Specroscopy

Yoshio TAKASU, Shun-ichi MARU, Yoshiharu MATSUDA, and Hazime SHIMIZU*

Department of Industrial Chemistry, Faculty of Engineering, Yamaguchi University, Tokiwadai, Ube, Yamaguchi 755

**Electrotechnical Laboratory, Tanashi, Tokyo 188*

(Received August 20, 1974)

A potentiostatic polarization method, Auger electron spectroscopy (AES), and photoelectron spectroscopy (XPS) were used to examine the composition of the passive films formed on Cu–Ni alloys anodized in an acid. The Flade potential of pure nickel in 0.5 M $HClO_4$ at 25 °C was −0.085 V (*vs.* SCE), while those of the alloys varied linearly from 0.180 V at 95%Ni to 0.310 V at 47%Ni. Analysis by AES and XPS revealed that (a) the passive region contained nickel and copper in the same ratio as the alloy, and (b) the chemical species of the film were made of NiO and copper oxide (Cu_2O and/or CuO). The Flade potential was assumed to be governed by the mixed potential of the formation of such oxides.

Copper–nickel alloys find extensive use in saline water environments or in chemical instruments. Nickel-rich alloys in Cu–Ni are acid-resisting materials. Experimental studies have indicated that the presence of thin films on the surface of the alloys is primarily responsible for the excellent corrosion resistance of the nickel alloys,[1] but the composition of the initial films that form on the alloys on exposure to acid has not been experimentally determined. Coulometry should be applicable to an analysis of the composition of the passive films on Cu–Ni alloys, as attempted by Okuyama,[2] however, it has been difficult to obtain a clear E–Q curve.

Recently, Auger electron spectroscopy (AES) and photoelectron spectroscopy (XPS) techniques have become available for the investigation of very thin films on surfaces. Hulett and his co-workers[3] have studied the passive film on a Cu–Ni alloy which was formed in a NaCl solution by means of XPS; they found the passive film to be enriched with nickel.

On the other hand, one of the present authors has previously established a quantitative analysis of the surface alloy composition of the Cu–Ni alloy system by using AES.[4,5]

In this paper, an electrochemical observation of the passive films on Cu–Ni alloys in an acid and the direct analysis of the surface composition of the passive films by means of AES and XPS will be described.

Experimental

Polarization Measurements. An electronic potentiostat (Hokuto Denko Corp. HA-101) and a function generator (Kowa Electronics Ltd. FG-102) were used for polarization measurements. The corresponding current flow was drawn on a X-Y recorder.

Pure nickel and seven Cu-Ni alloys, 95, 86, 76, 67, 57, 47, and 42 at% nickel, were adopted in this study. The alloys were cast from 99.99% copper and 99.9% nickel, hot rolled, scalped, cold rolled to a thickness 0.01—0.005 cm, and annealed. The apparent surface area of each test electrode was 2.0 cm^2. It was abraded with emery paper (1500#) and then rinsed in water and acetone.

The reference electrode was a saturated calomel electrode. The electrolyte was composed of 0.5 M $HClO_4$, through which purified nitrogen could be bubbled in order to remove any dissolved oxygen. The cell was located in a thermostat maintained at 25±0.1 °C.

Surface Analysis. Specimens were anodized potentiostatically in their passive region between 450—850 mV *versus* SCE for one hour. After anodization, the specimens were rinsed with distilled water and dried while being stored until examination. Auger analysis was carried out by using a CMA-type Auger spectrometer (NEVA AES-200). The X-ray photoelectron spectra were measured by the use of a Hitachi XPS E-507 analyzer.

Results

Anodic Polarization Behavior of Cu–Ni Alloys. Figure 1 shows a typical polarization curve for 86%Ni alloy in 0.5 M $HClO_4$ at 25 °C; the potential sweep rate was automatically set at 1 mV/s. The potential was moved anodically from the active region to the passive region. Potentials corresponding to P_1 were found to be affected only a little by the potential sweep rate. A slower potential sweep rate resulted in a higher corrosion rate of the electrode in the active region. In consideration of this high corrosion rate, the potential sweep rate was set at 1 mV/s. It might be previsionally possible to consider the P_1 potential as the Flade potential.

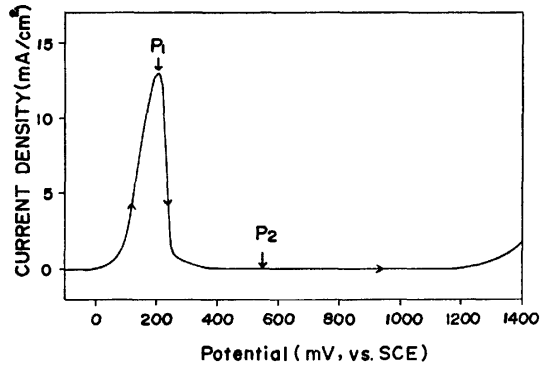

Fig. 1. Polarization curve for 86% Ni in dearated 0.5 M $HClO_4$ at 25 °C, 1 mV/s.

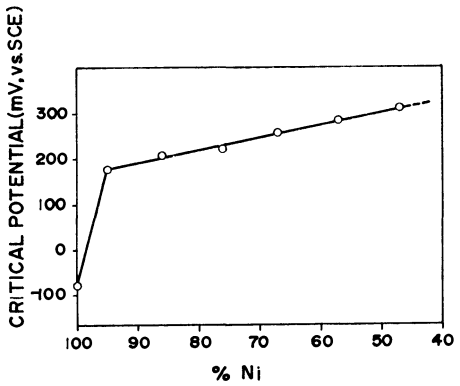

Fig. 2. Critical passivating potential (Flade potential) *versus* alloy composition.

The current density shows its minimum in the passive region at the P_2 potential. This was termed the passive current density. The Flade potential of Cu–Ni alloys in this experimental condition is shown in Fig. 2. Cu-rich alloys more than 42%Ni showed neither critical current at P_1 nor any minimum current at P_2. It is of interest that the Flade potential was changed almost linearly depending on the alloy composition.

TABLE 1. SURFACE CONTENT OF NICKEL TO COPPER IN PASSIVE FILM BY AES

Bulk content (at%Ni)	Surface content (at%Ni)
95	95—97
86	84—89
76	76—79
67	64—66
57	44—55

Surface–Alloy Composition of the Passive Films. The surface content of nickel in relation to copper in the passive films on Cu–Ni alloys, as measured by AES, are summarized in Table 1. It was reported that the surface alloy composition of the Cu–Ni system could be quantitatively analyzed by using a calibration curve.[4] As is shown in the table, the passive films contain nickel and copper in the same ratio as the alloys.

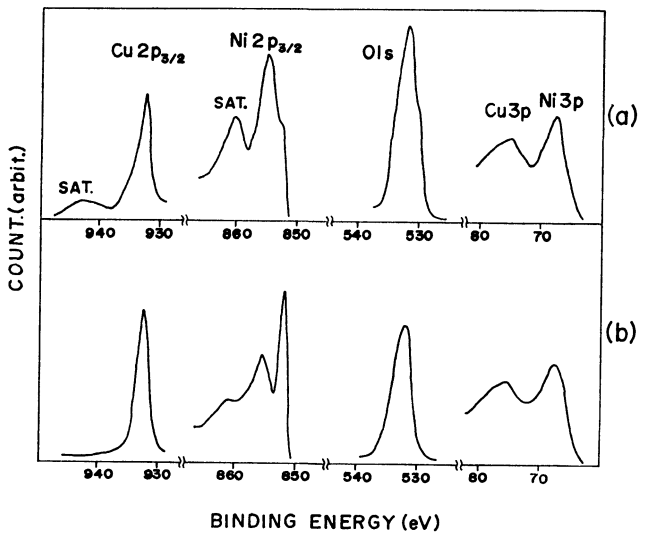

Fig. 3. Photoelectron spectra of (a) passive film and (b) abraded surface (76% Ni alloy).

Figure 3 compares the XPS spectrum from a surface of a 76%Ni specimen anodized at 500 mV *versus* SCE with that of an abraded specimen. The assignments of the peaks are marked in the figure. The intensity and the shape of the Cu3p peak and the peaks of the anodized surface and those of the abraded surface are almost identical. The O1s peak of the former is larger than that of the latter. It is noted that the peak with the binding energy of 852 eV almost disappears upon the anodization, while the peak with a binding energy about 3 eV higher grows stronger. This finding gives evidence of the formation of NiO in the passive film. The $Cu2p_{3/2}$ peak of the passive film is almost unchanged by the anodic polarization, but a weak peak at 943 eV was produced. This peak corresponds to the satellite peak from Cu_2O or CuO.[6] The XPS spectra from the $Cu2p_{3/2}$ and $Ni2p_{3/2}$ peaks for the other specimens are shown in Figs. 4 and 5 respectively. These spectra also show that NiO and copper oxide (Cu_2O and/or CuO) were formed on the surface by the anodic polarization.

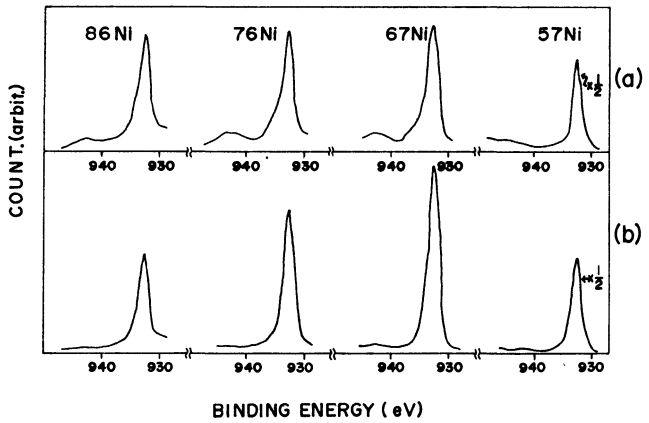

Fig. 4. Photoelectron spectra of (a) passive film and (b) abraded surface ($Cu2p_{3/2}$).

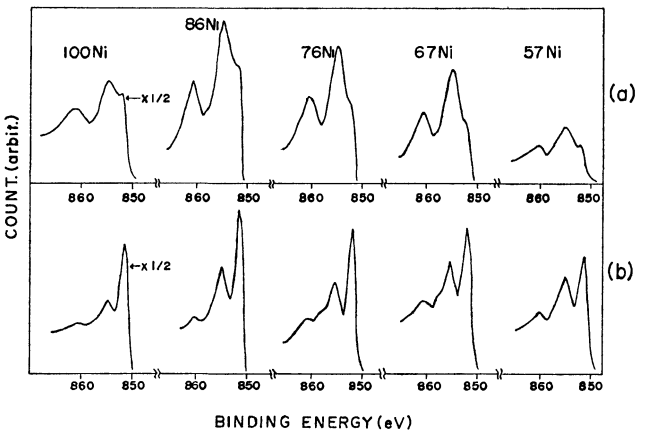

Fig. 5. Photoelectron spectra of (a) passive film and (b) abraded surface ($Ni2p_{3/2}$).

Discussion

Osterwald and Uhlig[1] insisted that a passive film of Cu–Ni alloy in 0.5 M H_2SO_4 at 25 °C was almost

identical with that on pure nickel; this phenomenon was observed on the alloy whose nickel content was over 30%Ni. However, they did not discuss copper oxide, although their data showed that the values of the Flade potential changed from 0.13 V (*vs.* SHE) at pure nickel to 0.38 V (*vs.* SHE) at 30.4%Ni.

As has been described above, Hulett and his coworkers[3] reported that the X-ray photoelectron spectrum of the passive films on 70%Ni alloy in a NaCl solution at 100 °C indicated primarily nickel oxide and was very similar to the spectrum obtained from pure nickel made passive in the same environment.

On the other hand, Okuyama[2] examined the composition of the passive film on the Cu–Ni alloy which was formed in a boric acid–sodium borate buffer solution (pH=8.39) by means of coulometry; he found that NiO, Ni_3O_4, and Cu_2O were formed in the film on the alloy whose nickel content was over 50%Ni.

These discrepancies among the data obtained by different investigators seem to be caused not only by the difference in the experimental conditions (the composition, the pH, and the temperature of the electrolyte), but also by the differing accuracies of the methods of surface analysis.

Therefore, this study makes it clear that (a) passive films formed in 0.5 M $HClO_4$ contain nickel and copper in the same ratio as the alloy, (b) and the chemical species of the film are composed of NiO and copper oxide (Cu_2O and/or CuO).

If one assumes NiO formation during the passivation of nickel at P_1, the reaction is as follows:[7]

$$Ni + H_2O = NiO + 2H^+ + 2e^- \quad (1)$$

$$E_{NiO} = -0.131\ V\ (vs.\ SCE, 25°C)$$

Moreover, the formation of Cu_2O or CuO during the passivation of copper at P_1 is shown by the following reactions:[7]

$$2Cu + H_2O = Cu_2O + 2H^+ + 2e^- \quad (2)$$

$$E_{Cu_2O} = 0.230\ V\ (vs.\ SCE, 25°C)$$

$$Cu + H_2O = CuO + 2H^+ + 2e^- \quad (3)$$

$$E_{CuO} = 0.329\ V\ (vs.\ SCE, 25°C)$$

As is shown in Fig. 2, the experimental datum on the pure nickel was −0.085 V, while those on the alloys varied linearly from 0.180 V at 95%Ni to 0.310 V at 47%Ni. The experimental data were somewhat different from the thermodynamical data shown in Eqs. (1), (2), and (3). However, some differences are usually observed between the results of thermodynamical calculation and the experimental data, depending on the variation in the activities of the species on the electrode and the measuring conditions, whether at equilibrium or at non-equilibrium. Therefore, it can be assumed that NiO and Cu_2O and/or CuO were formed in the passive film of the alloy, and that their Flade potential was governed by the mixed potential by the upper reactions. This estimation corresponds also to the findings obtained by AES and XPS. However, more precise data for the potentials at P_1 for several temperatures and pH would be needed for a more fruitful correlation.

Uhlig explained a critical composition for passivity in Cu–Ni alloys at about 30%Ni with a critical electronic configuration which is based on the "rigid band model."[8] However, recent experimental results on the electronic structure of the Cu–Ni alloy system support a "coherent potential approximation model,"[9,10] not such a "rigid band model"; that is, Cu-rich alloys in the Cu–Ni alloy system should also have holes in the 3d band. Accordingly, the reason why the Cu-rich alloy in Cu–Ni does not form passive films in acid must not include the idea of the "filled d-band."

The authors are grateful to professor Toshiro Yamashina of the Faculty of Engineering, Hokkaido University, for giving them the alloy samples; they also wish to thank Professor Shiichiro Teranishi, Assistant Professor Toshinobu Imanaka, and Dr. Yasuyuki Okamoto of the Faculty of Engineering Science, Osaka University, for their kindness and advice in using the photoelectron spectrometer.

References

1) J. Osterwald and H. H. Uhlig, *J. Electrochem. Soc.*, **108**, 515, (1961).
2) S. Okuyama, The 41st Conference of the Electrochem. Soc. of Japan, Chiba, 1974.
3) L. D. Hulett, A. L. Bacarella, L. Lidonnici, and J. C. Griess, *J. Electron Spectrosc.*, **1**, 169, (1972/73).
4) K. Nakayama, M. Ono, and H. Shimizu, *J. Vacuum Sci. Technol.*, **9**, 749, (1972).
5) Y. Takasu and H. Shimizu, *J. Catal.*, **29**, (1973), 473.
6) G. Schön, *Surface Sci.*, **35**, 96, (1973).
7) M. Pourbaix, "Atras of Electrochemical equilibria in Aqueous Solutions," Gauthier-Villars (1963); trans. by J. A. Franklin.
8) N. F. Mott and H. Jones, "Theory of the Properties of Metals and Alloys," Dover Publications Inc., New York (1958).
9) P. Soven, *Phys. Rev.*, **156**, 809, (1967) and **178**, 1136, (1969).
10) Y. Takasu and T. Yamashina, *Japan. J. Appl. Phys.*, (in press).

Kinetics and Mechanisms of Hydrothermal Reaction of Granulated Blast Furnace Slag

Renichi KONDO, Salah A. ABO-EL-ENEIN,* and Masaki DAIMON

Inorganic Materials Department, Tokyo Institute of Technology, Ookayama, Meguro-ku, Tokyo 152

(Received August 17, 1973)

Kinetics and mechanisms of hydrothermal reactions of the systems slag-lime-water (I) and slag-quartz-lime-water (II) have been studied. In the initial stage of reaction in system (I), nearly amorphous calcium silicate hydrate with low lime content was formed and continued to grow in strength. Formation of hydrogarnet ($3CaO \cdot Al_2O_3 \cdot SiO_2 \cdot 4H_2O$) accompanied by the crystallization of calcium silicate hydrate caused a reduction in strength. In the reaction in system (II), a product with high lime content was formed which was then changed into a low lime product after complete consumption of free lime. Slag was highly reactive but inhibited reaction of quartz, especially during the initial stage of the hydrothermal solidification process. The rate of hydrothermal reaction as well as the characteristics of the products change considerably with temperature.

The reactivity of granulated blast furnace slag subjected to hydrothermal reaction for a long time was compared with that of quartz, silica glass[1] and other silicates.[2] However, the composition and physical state of the compounds obtained by the hydration of slag has not been clarified. Blast furnace slag, especially granulated one, has been used as a raw material for cement.[3] Advantages attained by the use of slags are: (1) omission of the process of combining CaO and SiO_2, and (2) economization of limestone and fuel. The hydraulic properties of slag are dependent on composition included in the quaturnary system SiO_2–Al_2O_3–CaO–MgO, the presence of constituents other than those main components and the amount of crystalline material in the quenched slag.

Kondo and Ohsawa[4] reported a method to determine the amount of granulated blast furnace slag as well as the rate of hydration of slag in cements. However, the kinetics and mechanisms of the hydrothermal reaction have not yet been studied.

Kondo and Daimon[5] analyzed the hydration of tricalcium silicate as an example of solid reactions having induction and acceleration periods. The first product, which may have a structure similar to the reactant, forms on the surfaces of reactant grains. The nuclei of the stable product are produced in the first product layer and act as reaction centers; the main reaction to form a stable product occurs rapidly in the acceleration period. In the hydration of calcium silicates, hydrates produced in this stage are poorly crystalline and metastable, turning gradually to more stable form.

In the present paper, we give the kinetics and mechanisms of two hydrothermal reactions: (I) slag-lime reaction; and (II) slag-quartz-lime reaction. Slag and quartz having narrow particle size distribution were used in order to obtain better results.

Experimental

Starting Materials. Granulated blast furnace slag consisting of calcium oxide, 44.0%; silica, 34.3%; alumina, 15.5%; and magnesia, 3.4% was used. These contents are approximately the average of compositions of slags produced in Japan. Slag was first ground and particles of radii 5—10 μ were then isolated by methanol elutriation. Quartz with particle radii 3.5—5 μ and very fine powder of highly purified, special grade calcium hydroxide were used.

Autoclaving. Two mixtures were prepared. (1) Slag (80 wt.%) and calcium hydroxide (20 wt.%) were mixed for 1 hr with use of ethanol to attain homogeneity. Ethanol was evaporated and 20 wt.% of water was then added to the dry mixture which was stirred for 3 min. From the paste produced, cylindrical specimens of 3.14 cm^2 in cross-sectional area and 1 cm in height were moulded at a pressure of 50 kg/cm^2 (157 kg/3.14 cm^2). (2) Slag (50 wt.%), quartz (30 wt.%) and calcium hydroxide (20 wt.%) were mixed and moulded according to the same procedure. The moulds were placed in containers at 100% humidity for 4 hr in order to attain initial setting, then D-dried for 24 hr and kept in vacuum desiccators.

The specimens were autoclaved; temperature was raised at a rate of 2 °C/min and then kept at 180.5±0.8 or 213.1±0.4 °C, each for 0.5, 2, 6, 12 and 24 hr. Steam was then released for cooling. Specimens were transferred to a desiccator, and then dried in CO_2 free nitrogen atmosphere at 105 °C for 24 hr in order to remove free water (saturated steam pressure, 10.0 and 20.0 atm at 180.5 and 213.1 °C, respectively).

Examination of Specimens. After being dried, the specimens were tested for compressive strength. Free CaO, uncombined slag, free silica and combined (non-evaporable) water contents were determined with crushed samples. A mineralogical examination was also made by means of X-ray diffraction, the hydrates formed being identified.

The free CaO content was determined as follows. The sample (0.5 g) was dispersed in a glycerol/ethanol mixture (1 : 5 v/v, 40 cm^3), together with a small amount of barium chloride (0.5 g) as a catalyst, and phenolphthalein as an indicator. This mixture was kept boiling while being titrated with a standard ammonium acetate solution. Boiling and titration were continued until pink coloring no longer appeared.

The amount of free silica was estimated from the amount of insoluble residue. The sample (0.5 g) was treated first with 2 M-hydrochloric acid (30 cm^3) at 60 °C. The residue was treated with 5% sodium carbonate solution (50 cm^3) at 100 °C for 15 min, ignited and weighed.

Combined water was regarded as being equal to the ignition loss with correction as regards the free lime, taking into consideration the fact that each one mole of free CaO is accompanied by one mole of non-evaporable water.

* Faculty of Science, Ain Shams University, Cairo, Egypt.

The uncombined (free) slag was determined by means of X-ray diffraction with calcium fluoride as an internal standard. Conversion of amorphous granulated slag into the crystalline form was carried out by heating at 900 °C for 5 min. The calibration curve was obtained with binary mixtures of crystalline slag and quartz with various weight ratios. The diffraction lines were selected to be those at 2.85 A (31.4° 2θ) and 3.153 A (18.3° 2θ) for crystalline slag (melilite) and CaF_2, respectively. Each sample was ground, heated at 900 °C on a platinum sheet for 5 min and then mixed with CaF_2 (10 wt.%) with the use of ethanol to ensure the homogeneous mixing. After being dried, diffraction pattern was obtained between 35° and 25° in 2θ, using Cu Kα. The percentage of uncombined slag was regarded as the average of the closest four determinations.

For the determination of free slag, the method by Kondo and Ohsawa[4] is applicable only to reactions at lower temperature provided that the hydration products are nearly amorphous. The method cannot be applied under hydrothermal conditions due to the fact that the crystalline hydration products remain insoluble.

Results and Discussion

(1) Slag–Lime–Water System. The free CaO, combined water and uncombined slag contents together with the compressive strength of the specimens autoclaved at 181 and 213 °C are shown in Figs. 1 and 2, respectively. These values were calculated on the basis of the ignited weights of specimens. The molar compositions of the formed hydrates as well as some other data are given in Tables 1 and 2. The reaction ratio of CaO was defined as the ratio of combined CaO to the total CaO concerned with added $Ca(OH)_2$. The thickness of the reacted layer on surfaces as a function of the reaction ratio (reacted slag/total slag) is shown in Fig. 3. The experimental values of α' were used to calculate q, the depth of the reacted layer. It was assumed that $\alpha'=1-(r_0-q)^3/r_0^3$, where r_0 is the radius of a particle before the reaction takes place. If we assume that the proportion of the particles having a radius r is constant, and the minimum and maximum sizes are a and b respectively, the relationship between

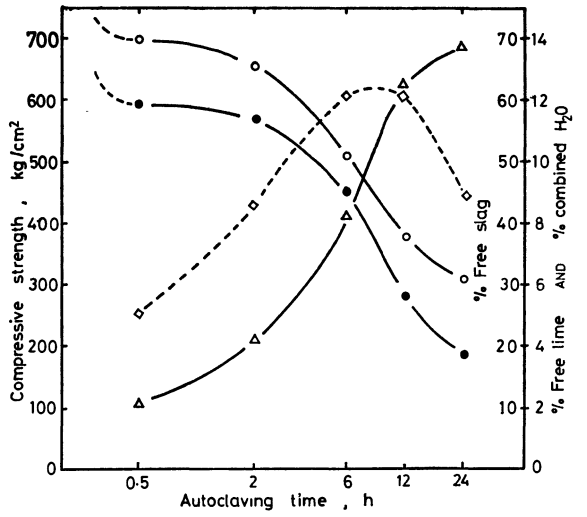

Fig. 1. Slag–lime–water system at 181 °C.
◇: strength, ○: free lime, ●: free slag, △: combined H_2O.

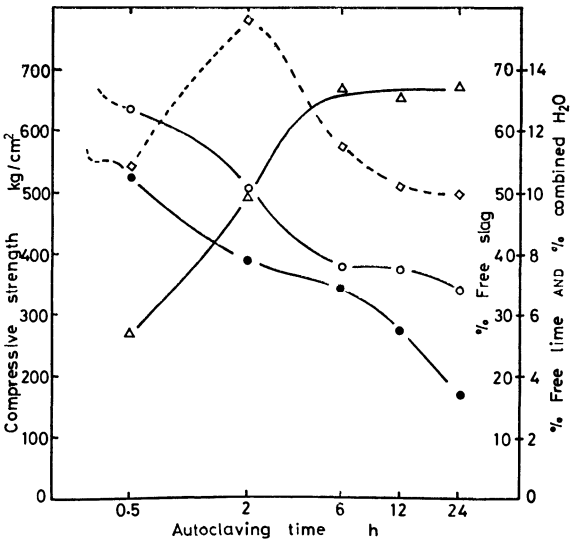

Fig. 2. Slag–lime–water system at 213 °C.
◇: strength, ○: free lime, ●: free slag, △: combined H_2O.

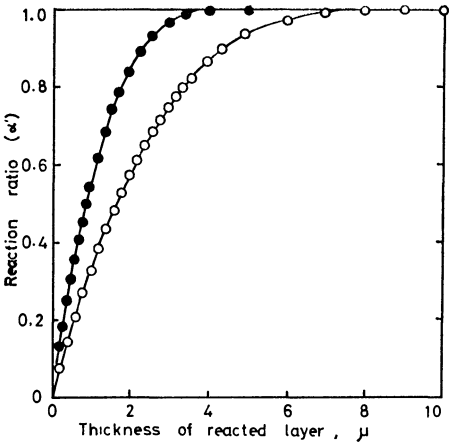

Fig. 3. Relation between reaction ratio and thickness of the reacted layer.
○: particle size 5—10 μ radius
●: particle size 3.5—5 μ radius

α' and q can be calculated by

$$1-\alpha'=\frac{\int_a^b(r-q)^3dr}{\int_a^b r^3dr}=\frac{1}{(b^4-a^4)}[(b-q)^4-(a-q)^4]$$

for $q<a$, and

$$1-\alpha'=\frac{\int_a^b(r-q)^3dr}{\int_a^b r^3dr}=\frac{1}{(b^4-a^4)}(b-q)^4$$

for $q\geq a$. For slag with particle radii 5—10 μ, the values of a and b are 5 and 10 μ, respectively. The depth of the reacted layer on the particles for all the specimens can be estimated from Fig. 3.

Reaction at 181 °C (10 atm): Nearly amorphous calcium silicate hydrates were formed as the initial product. X-ray diffraction study showed that during the first 6 hr the only phase identified was calcium silicate hydrates. Subsequent crystallization of calcium hydrosilicate led to the continuous growth of strength.

TABLE 1. CHARACTERISTICS OF SLAG–LIME–WATER SYSTEM AT 181 °C

Autoclaving time	0.5h	2h	6h	12h	24h
% Ingited hydration products	26.7	30.2	44.8	64.5	75.6
Reaction ratio of CaO	12.3	17.8	36.1	52.8	61.4
Reaction ratio of slag	29.9	32.5	46.5	66.7	78.4
Depth of reacted layer on slag particles	0.90μ	0.99μ	1.55μ	2.50μ	3.30μ
Molar compositions of the formed hydrates referred to one mole of (SiO_2+Al_2O_3):					
CaO	1.28	1.34	1.45	1.46	1.45
SiO_2	0.79	0.79	0.79	0.79	0.79
Al_2O_3	0.21	0.21	0.21	0.21	0.21
H_2O	0.66	1.18	1.63	1.71	1.60

TABLE 2. CHARACTERISTICS OF SLAG–LIME–WATER SYSTEM AT 213 °C

Autoclaving time	0.5h	2h	6h	12h	24h
% Ignited hydration products	34.9	50.9	58.1	65.3	76.3
Reaction ratio of CaO	20.8	36.5	52.8	53.0	57.5
Reaction ratio of slag	37.5	53.6	59.1	67.6	79.9
Depth of reacted layer on slag particles	1.18μ	1.83μ	2.10μ	2.55μ	3.41μ
Molar compositions of the formed hydrates referred to one mole of (SiO_2+Al_2O_3):					
CaO	1.34	1.40	1.50	1.45	1.42
SiO_2	0.79	0.79	0.79	0.79	0.79
Al_2O_3	0.21	0.21	0.21	0.21	0.21
H_2O	1.30	1.69	2.07	1.76	1.53

Hydrogarnet ($3CaO \cdot Al_2O_3 \cdot SiO_2 \cdot 4H_2O$) was also formed after 6 hr. Accumulation of hydrogarnet besides the crystallization of calcium silicate hydrate might reduce the strength.

Reaction at 213 °C (20 atm): By autoclaving for 30 min, nearly crystalline calcium silicate hydrates were formed as confirmed by X-ray diffraction. After 2 hr (Fig. 4) cubic crystals of hydrogarnet were formed, calcium silicate hydrate being crystallized in the form of interlocking fibres and rods. Continuous decrease in strength took place during the first 2 hr of autoclaving. This is also attributed to the accumulation of hydrogarnet and crystallization of calcium silicate hydrate.

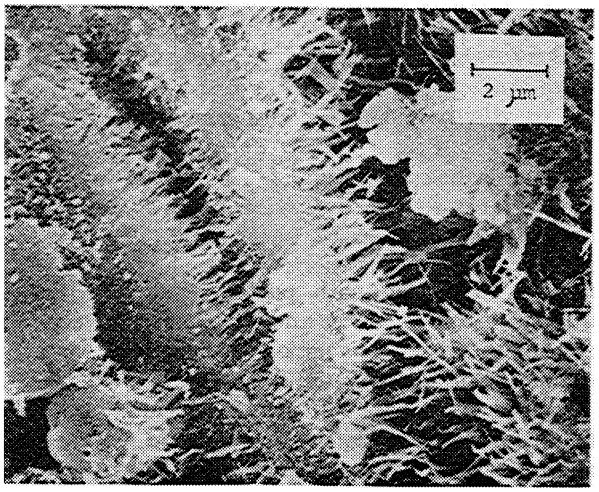

Fig. 4. The microstructure of slag-lime paste at 20 atm, 2 h autoclaving, interlocking fibres and rods of calcium silicate hydrates, beside cubic hydrogarnet.

Reaction Mechanism: It is suggested that a rapid hydrothermal change takes place until 20—25% of slag is hydrated. This stage corresponds to stage I in the induction period.[5]

A very slow hydrothermal reaction follows as a result of the formation of an almost impervious coating on the slag particles during the first stage; a dormant period which corresponds to stage II in the induction period.[5] The dormant period starts when about 25% of reactant is hydrated and lasts until about 30% is hydrated. The beginning and duration of the dormant period change with autoclaving temperature. At 181 °C, the percentage of ignited hydration product formed is 26.7% in 0.5 hr and 30.2% in 2 hr, so that the initial fast reaction is almost completed after 0.5 hr and the dormant period after about 2 hr. At 213 °C, the percentage of ignited hydration product is 34.9% in 0.5 hr, which is after the dormant period.

In the third stage crystallization of the initial products occurs. Diffusion through the crystallized product becomes free and a very fast interaction of water with the unhydrated part starts, lasting until about 80% of slag is hydrated. This leads to the formation of an "inner" product.

Hydration is retarded by accumulation of products. The diffusion through the pores of products becomes the rate determining factor. The mechanism is in line with that obtained by Brunauer and his co-workers[7] on low porosity cement pastes at 5—50 °C.

(II) Slag–Quartz–Lime–Water System. The experimental results are shown in Figs. 5 and 6 and Tables 3 and 4. Thickness of the reacted layer on the surfaces of the slag and quartz particles can be estimated by means of the relation given in Fig. 4.

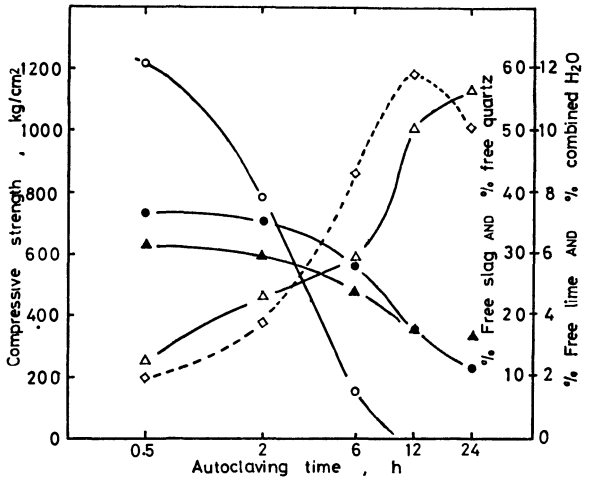

Fig. 5. Slag–quartz–lime–water system at 181 °C.
◇: strength, ○: free lime, ●: free slag,
△: combined H_2O, ▲: free quartz.

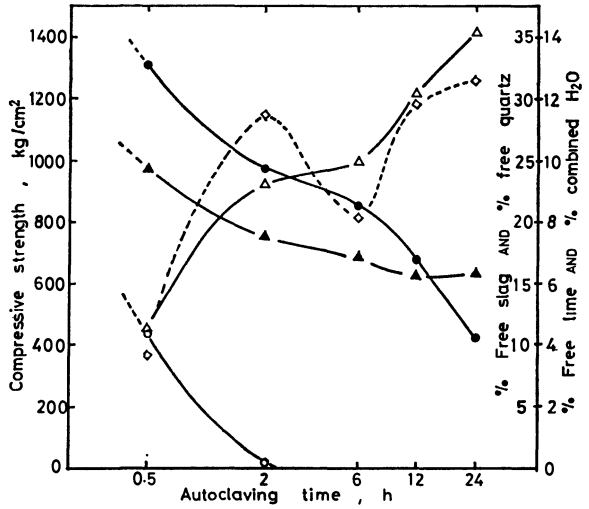

Fig. 6. Slag–quartz–lime–water system at 213 °C.
◇: strength, ○: free lime, ●: free slag,
△: combined H_2O, ▲: free quartz.

It was found that determination of uncombined slag by means of X-ray becomes difficult since the reaction products can also be converted into melilite when heated at 900 °C. The reaction ratio of slag obtained in system (I) are used.

Interaction of Slag and Quartz: The reaction ratios of both slag and quartz (Tables 3 and 4) indicate that the hydrothermal reactivity of granulated slag is greater than that of quartz, particularly in the initial stage of the reaction. The high reactivity of slag inhibits the reaction of quartz in the early stage of hydrothermal solidification. The reactivity of quartz in lime-quartz hydrothermal reaction given by Kondo[1] was higher than that we obtained. Evidence for the high reactivity of slag was obtained by comparison of the

Table 3. Characteristics of slag–quartz–lime–water system at 181 °C

Autoclaving time	0.5h	2h	6h	12h	24h
% Ignited hydration products	19.8	27.1	46.5	65.3	72.3
Reaction ratio of CaO	23.5	50.9	90.4	100.0	100.0
Reaction ratio of slag	29.9	32.5	46.5	66.7	78.4
Reaction ratio of quartz	0.9	6.0	24.3	45.5	48.1
Depth of reacted layer on slag particles	0.90μ	0.99μ	1.55μ	2.50μ	3.30μ
Depth of reacted layer on quartz particles	0.01μ	0.08μ	0.39μ	0.79μ	0.85μ
Molar compositions of the formed hydrates referred to one mole of $(SiO_2+Al_2O_3)$:					
CaO	1.61	1.80	1.48	1.14	1.10
SiO_2	0.80	0.83	0.88	0.89	0.89
Al_2O_3	0.20	0.17	0.12	0.11	0.11
H_2O	1.16	1.64	1.07	1.13	1.13

Table 4. Characteristics of slag–quartz–lime–water system at 213 °C

Autoclaving time	0.5h	2h	6h	12h	24h
% Ignited hydration products	38.4	56.9	61.3	67.3	73.6
Reaction ratio of CaO	72.6	98.9	100.0	100.0	100.0
Reaction ratio of slag	37.5	53.6	59.1	67.6	79.9
Reaction ratio of quartz	22.5	41.0	45.5	50.2	49.8
Depth of reacted layer on slag particles	1.18μ	1.83μ	2.10μ	2.55μ	3.41μ
Depth of reacted layer on quartz particles	0.35μ	0.70μ	0.79μ	0.90μ	0.89μ
Molar compositions of the formed hydrates referred to one mole of $(SiO_2+Al_2O_3)$:					
CaO	1.39	1.20	1.14	1.08	1.09
SiO_2	0.89	0.90	0.90	0.90	0.89
Al_2O_3	0.11	0.10	0.10	0.10	0.11
H_2O	0.95	1.22	1.19	1.30	1.39

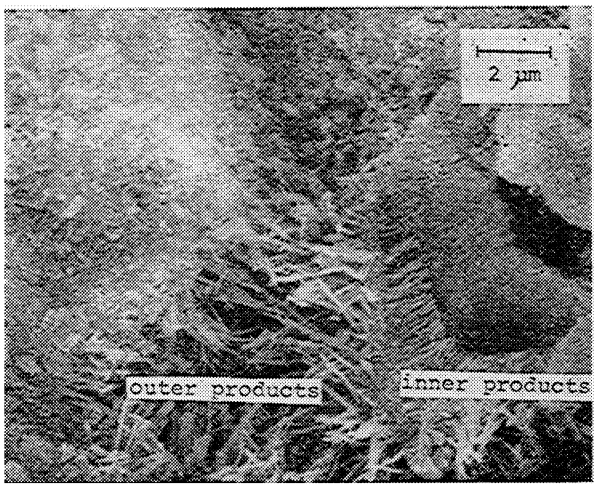

Fig. 7. The microstructure of slag–quartz–lime paste at 10 atm, 6 h autoclaving.

compressive strengths obtained in the two systems in the present study. The strength attained in the early stage was greater in system (I) than in system (II) (Figs. 1, 2, 5, and 6). However, in the latter system, growth of strength reaching a maximum of about 1200 kg/cm^2 was obtained due to the formation of much calcium silicate hydrate and lesser hydrogarnet.

Reaction at 181 °C: Nearly amorphous high lime calcium silicate hydrates were formed during the first 2 hr of hydration (Table 3). X-ray diffraction revealed only the formation of ill-crystallized calcium silicate hydrate. The accumulation and later crystallization of the high lime product account for the continuous development of strength during the first 12 hr. Scanning electron microscope observation (Fig. 7) obtained after autoclaving for 6 hr indicates the unhydrated part of the grain was directly attached to an "inner product" 1.5 μ in depth, the "outer product" with loose structure and about 2 μ in thickness being observed outside the original grains as acicular and interlocking fibres. After consumption of all free CaO during a period of 12 hr, the maximum strength of the specimens was attained. The high lime product then started to transform into a low lime product in the form of fibres and rod like crystals. Crystallization results in a reduction of strength because of its low surface area.

Reaction at 213 °C: A high lime product was formed and crystallized during the first 2 hr of autoclaving. At that time all the free CaO was consumed, high lime product changed into low lime product, and a part of the previously bound CaO was released and then bound to a new part of the unhydrated reactants. This resulted in an increases of the total contents of binding centers in the specimens. The creation of new binding centers caused an increase of strength after 6 hr autoclaving.

References

1) R. Kondo, *International Symposium on Autoclaved Calcium Silicate Building Products*, London (1965), 92—100, *Soc. of Chem. Ind.* (1967).

2) R. Kondo, S. Ohsawa, H. Matsumaru, M. Kitamura, and T. Kato, The Hydrothermal Reactions Between Lime and Siliceous Materials, *Semento Gijutsu Nenpo*, **21**, 92 (1976).

3) F. Keil, *Proceedings of the Third International Symposium on the Chemistry of Cement*, London, 530 (1952).

4) R. Kondo and S. Ohsawa, *Proceedings of the Fifth International Symposium on the Chemistry of Cement*, Tokyo, Vol. IV, 255—262 (1968).

5) R. Kondo and M. Daimon, *J. Amer. Ceram. Soc.*, **52**, 503 (1969).

6) S. Miyagi, *J. Ceram. Assoc. Japan*, **59**, 132 (1951).

7) S. Brunauer, M. Yudenfreund, I. Adler, and J. Skalny, *Cement and Concrete Research*, **3**, (2), 129 (1973).

Complex Formation between the Uranyl Ion and Citric Acid

Emiko OHYOSHI,† Junko ODA,* and Akira OHYOSHI*

Kurokami Radioisotope Laboratory, Kumamoto University, Kumamoto 860

**Department of Industrial Chemistry, Faculty of Engineering, Kumamoto University, Kumamoto 860*

(Received December 3, 1973)

A method to facilitate the analysis of the complex formation by a polybasic acid has been applied to the study of uranyl citrate complexes. The amount of the uranyl ion in equilibrium with the complexing agent was determined by the cation-exchange method. In this experiment, the uranyl-ion concentration was kept within a 10^{-5}—10^{-6} M range in order to eliminate polymeric species. By using a series of solutions prepared so as to keep $[H_3Cit^-]$ nearly constant and to vary $[H_2Cit^{2-}]$ and $[HCit^{3-}]$ in the 2.2—2.9 pH range, it has been found that three kinds of complexes, $UO_2H_3Cit^+$, UO_2H_2Cit, and UO_2HCit^-, were present in the solution. Approximate values of their formation constants were obtained.

In an investigation[1] of the photochemical reduction of U(VI) to U(IV) observed in citrate solutions, knowledge of the nature of uranyl citrate complexes and of their formation constants was required for the interpretation of the reduction mechanism. On the basis of potentiometric measurements, Rajan and Martell[2] reported that, in the 2—4 pH range, the uranyl ion combined through the dissociation of the three hydrogens from the carboxyl groups of citric acid, and also that the dimerization of this complex occurred with an increase in the uranyl-ion concentration. In this pH range, more protonated species, H_3Cit^- and H_2Cit^{2-}, are present in large proportions, and they possibly form complexes with the uranyl ion.

Matsushima[3] has studied the citrate complexes of some divalent metals by an extension of Schubert's method to a lower pH region. He found the complex of the MH_2Cit type as well as that of the $MHCit^-$ type and determined the stability constants of both. In this method, however, it is necessary to perform similar experiments at several different pH's, each of which is kept constant for the analysis of the different types of complexes.

In the present work, we have studied the complex formation between uranyl and various protonated citrate ions in a region of low concentrations of the uranyl ion by using a method devised to facilitate the analysis of the complexes with a polybasic acid.[4] The method used is based on the general principles of dissociation equilibria established in the presence of a weak acid and its salt.

Analysis of Metal (M^{2+}) Complexes Formed with Various Protonated Species. In our earlier papers[4,5] we assumed that only two species, H_3Cit^- and H_2Cit^{2-}, are advantageous for the formation of complexes in a low-pH region. However, as has been shown by the potentiometric study,[2] the complex of the UO_2-$HCit^-$ type cannot be excluded even at pH 2. Therefore, we have derived equations assuming three types of complexes, $M(H_3Cit)_i^{2-i}$, $M(H_2Cit)_j^{2-2j}$, and $M(HCit)_k^{2-3k}$, equilibrated in solution. When we use the cation-exchange method and can assume that the adsorption of the MH_3Cit^+ complex is negligible compared with that of the M^{2+} ion at a low ionic strength of 0.1 or 0.2,[6] the following equation can be derived:

$$\frac{K_d^\circ}{K_d} = 1 + \sum\beta_i[H_3Cit^-]^i + \sum\beta_j'[H_2Cit^{2-}]^j + \sum\beta_k''[HCit^{3-}]^k \quad (1)$$

where K_d° and K_d denote the distribution coefficients of uranyl species in the absence and in the presence of the complexing agent respectively, and where β_i, β_j', and β_k'' express the formation constants of the $M(H_3Cit)_i^{2-i}$, $M(H_2Cit)_j^{2-2j}$, and $M(HCit)_k^{2-3k}$ complexes respectively. When experiments were carried out by using a series of solutions in which the amount of the H_3Cit^- species remains nearly constant, while those of the H_2Cit^{2-} and $HCit^{3-}$ species vary, Eq. (1) can be given as a function of $[H_2Cit^{2-}]$ or $[HCit^{3-}]$:

$$\frac{K_d^\circ}{K_d} - 1 = \text{const.} + (\beta_1' + \beta_1''k_3/[H^+])[H_2Cit^{2-}] + (\beta_2' + \beta_2''k_3^2/[H^+]^2)[H_2Cit^{2-}]^2 + \cdots \quad (2)$$

or;

$$\frac{K_d^\circ}{K_d} - 1 = \text{const.} + (\beta_1'' + \beta_1'[H^+]/k_3)[HCit^{3-}] + (\beta_2'' + \beta_2'[H^+]^2/k_3^2)[HCit^{3-}]^2 + \cdots \quad (3)$$

where $k_3 = [H^+][HCit^{3-}]/[H_2Cit^{2-}]$. When we assume that all the complexes have a 1:1 molar ratio, Eqs. (2) and (3) are simplified as follows:

$$\frac{K_d^\circ}{K_d} - 1 = \text{const.} + (\beta_1' + \beta_1''k_3/[H^+])[H_2Cit^{2-}] \quad (4)$$

$$\frac{K_d^\circ}{K_d} - 1 = \text{const.} + (\beta_1'' + \beta_1'[H^+]/k_3)[HCit^{3-}] \quad (5)$$

From Eqs. (4) and (5), it can be seen that when we plot $K_d^\circ/K_d - 1$ *vs.* $[H_2Cit^{2-}]$ (A) or *vs.* $[HCit^{3-}]$ (B), two different types of curves should be obtained. The slope of the (A) plot increases with a decrease in $[H^+]$, while that of the (B) plot decreases with a decrease in $[H^+]$. The intercepts of both plots should be the same value. From this value and the $[H_3Cit^-]$ used, β_1 can be evaluated. Approximate values of β_1' and β_1'' can also be estimated from the slope of (A) at $[H_2Cit^{2-}]=0$ and from the slope of (B) at the relatively high value of $[HCit^{3-}]$, sufficient to show a straight line, respectively. In cases where successive complex formation takes place, we can obtain a similar curve, (A) or (B), by plotting the $(K_d^\circ/K_d - 1 - \text{const.})/[H_2Cit^{2-}]$ term *vs.* $[H_2Cit^{2-}]$ or the $(K_d^\circ/K_d - 1 - \text{const.})/$

† Present address: Yatsushiro Technical Colledge, Yatsushiro-shi, Kumamoto 866

[$HCit^{3-}$] term *vs.* [$HCit^{2-}$]; β_2' and β_2'' can also be estimated in a similar manner. A separate experiment will be necessary to obtain β_1 and β_2. The solutions used for this experiment can be prepare by varying the total citrate concentration at a constant pH, since we have already established the complexing ability of both ligands, H_2Cit^{2-} and $HCit^{3-}$.

Experimental

Materials. The stock solution of UO_2^{2+} was prepared by dissolving $UO_2(NO_3)_2 \cdot 6H_2O$ in 0.005 M HCl to give the concentration of 2.0×10^{-4} M, which was determined by EDTA titration. Citric acid (H_4Cit) in varying amounts was added to 0.2 M NaH_3Cit. A series of such solutions was diluted twice with distilled water and the uranyl stock solution. In these solutions, H_2Cit^{2-} and $HCit^{3-}$ decrease with an increase in the H_4Cit, while H_3Cit^- is maintained nearly constant (0.1 M). The ionic strength, governed by the amount of the salt, NaH_3Cit, was also maintained at 0.1. The compositions of the solutions used are given in Table 1. For the calculation of the respective ion concentrations, the dissociation constants of citric acid reported by Okac and Kolarik,[7] which were measured at $\mu=0.1$ (0.1 M KCl) and 8—20 °C, were used. The pH values calculated using this k_1 value and the amounts of acid H_4Cit and salt NaH_3Cit dissolved were in fair agreement with the measured pH values. Various concentrations of citrate at a constant pH of 3.91 were prepared by dissolving a mixture of H_4Cit and Na_3HCit (1.5: 1) in 0.1 M $NaClO_4$ to produce concentrations of $HCit^{3-}$, 10^{-5}—10^{-6} M. All the chemicals used were of a G. R. grade. The pH measurements were made with a Beckman Model SS-2 pH meter. A cation exchanger, Dowex 50 W-X8 (100—200 mesh), in sodium form was used.

Table 1. The composition of citrate solutions prepared to maintain [H_3Cit^-] nearly constant (0.1M)

[H_4Cit] (M)	[H_3Cit^-] (M)	[H_2Cit^{2-}] (10^{-3} M)	[$HCit^{3-}$] (10^{-6} M)	pH
0.600	0.103	0.65	0.22	2.19
0.484	0.102	0.79	0.32	2.28
0.360	0.102	1.07	0.58	2.41
0.237	0.101	1.58	1.30	2.59
0.202	0.101	1.85	1.75	2.65
0.166	0.100	2.23	2.64	2.74
0.143	0.99	2.55	3.47	2.80
0.118	0.99	3.06	5.02	2.88

Procedure. The cation-exchange experiments were carried out in a manner similar to that described previously.[4] The amount of U(VI) was determined as the uranyl-Arsenazo-(III) complex by spectrophotometry using a Shimadzu UV-200 spectrophotometer. This complex was stable even at pH 1, and its characteristic color (absorbance at 665 nm) could be used to determine the U(VI) in the presence of citric acid. Since the slope of the calibration curve slightly varied with the pH value, it was necessary to measure the absorbance of aliquots of slutions before the addition of the cation exchanger and after equilibrium had been reached at a constant pH. All the experiments were carried out in the dark to avoid any photochemical reduction of the uranyl ion.[1] The distribution coefficient, K_d, was calculated as follows:

$$K_d = \frac{\text{mmol of U(VI) in the resin/mass of dry resin (g)}}{\text{mmol of U(VI) in the soln./vol. of soln. (ml)}}$$

Results and Discussion

The hydrolyses of the uranyl ion in the pH range studied (pH 2—4) were checked by measuring $K_d°$ in 0.1 M $NaClO_4$, while adjusting pH's from 2.07 to 4.35. To maintain the pH at 4.35, the acetate buffer in varying concentrations ($\sim 10^{-3}$ M) was used. $K_d°$ was obtained by plotting $1/K_d$ *vs.* [acetate] and by extrapolating $1/K_d$ to a zero concentration of acetate. $K_d°$ values so obtained were practically constant ($2.3 \pm 0.1 \times 10^3$), indicating that hydrolysis does not occur in this pH range.

To check whether polymeric species were being formed or not, the K_d values were determined as a function of [U(VI)] at constant citrate concentrations. The results showed that, at pH 3.91, K_d gradually decreased at concentrations above 1×10^{-5} M, though it remained practically constant at lower pH's (2.2—2.9), indicating that polymeric species tend to be formed as the pH increases. The uranyl concentrations used in this experiment were in the 4×10^{-6}—6×10^{-6} M range at pH 3.91 and in the 6×10^{-6}—1×10^{-5} M range at pH's 2.2—2.9. The constancy of K_d was also obtained with a variation in the ratio of the volume of the solution to the mass of resin from 50—200 ml/g.

Using a series of solutions in a region of low pH's (2.2—2.9) where [H_3Cit^-] is kept approximately constant ([H_3Cit^-]$\simeq$0.1), and where [H_2Cit^{2-}] and [$HCit^{3-}$] both vary, uranyl citrate complexes have been studied by the cation-exchange method.

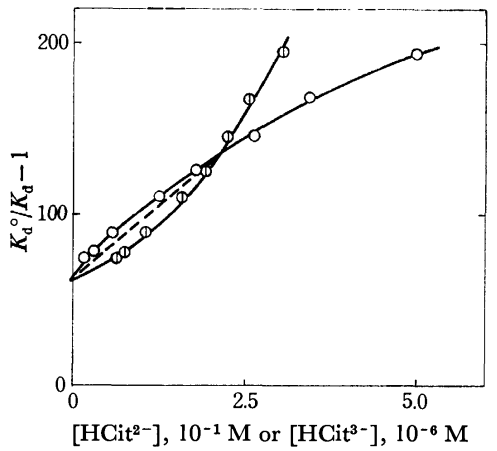

Fig. 1. Plots of $K_d°/K_d - 1$ *vs.* [H_2Cit^{2-}] and [$HCit^{3-}$] at [H_3Cit^-]=0.1 M and various pH values.

As is shown in Fig. 1, where we tried to plot $K_d°/K_d - 1$ as a function of [H_2Cit^{2-}] (Plot A) or [$HCit^{3-}$] (Plot B), the slope of Plot A increases with a decrease in [H^+] while that of Plot B decreases with a decrease in [H^+], and both plots have the same intercept. To examine the type of complex predominantly formed, a separate experiment was carried out using solutions in varying total citrate concentrations in the same range and at a constant pH of 2.88. From the fact that a linear relationship was obtained between $K_d°/K_d - 1$

and $[Citrate]_{total}$, it can be concluded that 1:1 complexes are the only predominantly-formed species.[3] Hence, the former type of curve (Plot A) corresponds to Eq. (4), while the latter (Plot B) corresponds to Eq. (5). From this it is evident that the $UO_2H_3Cit^+$, UO_2H_2Cit, and UO_2HCit^- complexes are all present in this pH range (2.2—2.9). At pH 2.28, where a major part of the complexes are assumed to be $UO_2H_3Cit^+$ from the curves in Fig. 1, the extent of adsorption of this species on the cation exchanger was studied at different ionic strengths of 0.1 and 0.2.[6] The results showed that the adsorption of $UO_2H_3Cit^+$ on the cation exchanger was negligible compared with that of UO_2^{2+} at these low ionic strengths. The formation constant of $UO_2H_3Cit^+$, β, can readily be obtained from the intercept of the two curves in Fig. 1, which equals 0.1β. The approximate values of β' and β'', the formation constants of UO_2H_2Cit and UO_2HCit^-, can be obtained, respectively, from the slope of Plot (A) at $[H_2Cit^{2-}]=0$ and from that of Plot (B) at relatively large values of $[HCit^{3-}]$, where Plot (B) approaches a straight line. The values of β, β', and β'' thus obtained are listed in Table 2.

At higher pHs, where almost all the uranyl complexes can be assumed to be of the UO_2HCit^- type we can estimate β'' with considerable accuracy. Figure 2 shows a plot of (K_d°/K_d-1) *versus* $[HCit^{3-}]$ at a constant pH of 3.91. The value of β'' calculated from the slope is also listed in Table 2. From the fact that the two values of β'' obtained by the different methods are in fair agreement, the method used in this study can be said to be applicable to the analysis of complexes formed with various protonated ligands present in a solution. The reliability of the β' thus obtained can be checked by the slope of the broken line in Fig. 1. Judging from Eqs. (4) and (5), when we plot the relations (A and B) taking a scale of $[H_2Cit^{2-}]$ equal to $10^3[HCit^{3-}]$, the two curves, A and B, should cross at $[H^+]=10^3k_3$, where $[H_2Cit^{2-}]=10^3[HCit^{3-}]$, and the slope of the broken line can be said to correspond to $\beta'+10^{-3}\beta''$ or $\beta''+10^3\beta'$ on the scale of $[H_2Cit^{2-}]$ or of $[Cit^{3-}]$ respectively. From these values and the β'' value obtained at pH 3.91, a more accurate value of β' can be calculated; it is also presented in Table 2. The two values of β' in Table 2 are in fair agreement.

Table 2. Formation constants of UO_2–citrate complexes ($\mu=0.1$, 25 °C)

	$UO_2H_3Cit^+$ $\log\beta$	UO_2H_2Cit $\log\beta'$	UO_2HCit^- $\log\beta''$
Present work	2.79	4.26[a]	7.28[a]
		4.23[b]	7.22[c]
Reference values	—	—	7.40[2]
	—	—	8.6[8]
	—	—	3.16[9]

a) The approximate values estimated from the slope of the curve A or B. b) The calculated value from the slope of the dotted line and β''. c) The value obtained at pH 3.91.

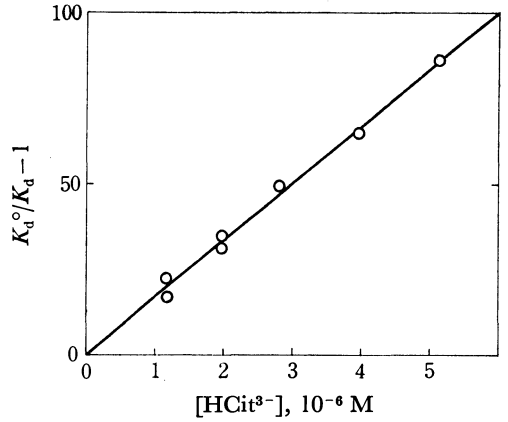

Fig. 2. A plot of K_d°/K_d-1 *vs.* $[HCit^{3-}]$ at pH 3.91.

For the formation constant of UO_2HCit^-, various values[2,8,9] have been reported. As is shown in Table 2, the logarithmic value of the formation constant contained in this study is in fair agreement with that determined potentiometrically by Rajan and Martell.[2] There are no published data for the formation constants of $UO_2H_3Cit^+$ and UO_2H_2Cit because three different complexes, $UO_2H_3Cit^+$, UO_2H_2Cit, and UO_2HCit^-, coexisting at low pH's could not be analyzed.

In conclusion, by controlling the concentration of H_3Cit^- in the solution, various species of uranyl citrate could easily be analyzed, and each formation constant could also be determined. The fraction of the species varying with the pH could be evaluated by considering these constants. The predominant species at pH's lower than 2 was $UO_2H_3Cit^+$. There was a mixture of $UO_2H_3Cit^+$, UO_2H_2Cit, and UO_2HCit^- in the pH range of 2—3, and at pH's higher than 3 almost all of the species were UO_2HCit^-.

The authors wish to thank the Ministry of Education for the financial support (No. 847009) granted to this research.

References

1) A. Ohyoshi and K. Ueno, *J. Inorg. Nucl. Chem.*, **36**, 379 (1974).
2) K. S. Rajan and A. E. Martell, *Inorg. Chem.*, **4**, 462 (1965).
3) Y. Matsushima, *Chem. Pharm. Bull.*, **11**, 566 (1963).
4) E. Ohyoshi and A. Ohyoshi, *J. Inorg. Nucl. Chem.*, **33**, 4265 (1971).
5) A. Ohyoshi, E. Ohyoshi, H. Ono, and S. Yamakawa, *ibid.*, **34**, 1955 (1972).
6) E. Ohyoshi, This Bulletin, **46**, 2758 (1973).
7) A. Okac and Z. Kolarik, *Coll. Czech. Chem. Commun.*, **24**, 1 (1959).
8) N. C. Li, A. Lindenbaum and J. M. White, *J. Inorg. Nucl. Chem.*, **12**, 122 (1959).
9) C. Heitner and M. Bobtelsky, *Bull. Soc. Chim. Fr.*, **1954**, 356.

Studies of Ruthenium Complexes. VIII.[1] Kinetic Studies of the Thermal Substitution Reaction of Hexaammine and *cis*-Dihalogenotetraammineruthenium(III) Complexes in the Solid State

Akira OHYOSHI, Shunichi HIRAKI, Tomio ODATE, Susumu KOHATA, and Junko ODA

Department of Industrial Chemistry, Faculty of Engineering, Kumamoto University, Kumamoto 860

(Received March 30, 1974)

The Kinetics of the thermal substitution reaction of hexaammineruthenium(III) halides and *cis*-dihalogenotetraammineruthenium(III) halides have been studied in the solid state. The reaction rates and kinetic parameters were determined for these two reactions; $[Ru(NH_3)_6]X_3 \rightarrow [RuX(NH_3)_5]X_2 + NH_3$, (X=Br, I) and *cis*-$[RuX_2(NH_3)_4]X \rightarrow [RuX_3(NH_3)_3] + NH_3$, (X=Cl, Br). The values of the rate constant, the activation energy, and the activation entropy were 2.10×10^{-5} s^{-1} (at 161 °C), 23.3 kcal mol^{-1}, and −29.3 e.u. for the hexaammine bromide, and 2.92×10^{-5} s^{-1} (at 162 °C), 31.3 kcal mol^{-1}, and −10.1 e.u. for the *cis*-dibromotetraammine bromide. The S_N2 mechanism is more probable for the former reaction, while the S_N1 mechanism is more probable for the latter reaction.

It has previously been reported that the thermal-decomposition reaction of a chromium(III) complex having volatile ligands such as ammonia, water, and ethylenediammine is initiated by the replacement of a ligand by an outersphere anion.[2] On the other hand, the same reaction of a cobalt(III) ammine complex is initiated by an electron transfer from the ligand or an outersphere anion to the central cobalt(III) ion.[3] In our previous paper,[4] it was shown that the thermal reactions of halogenopentaammine and *cis*-dihalogenotetraammineruthenium(III) were initiated by the repalcement of coordinated ammonia by the outersphere halide ion in the cases of chloride and bromide, while the reaction was initiated by the ammonia release, without the substitution reaction, for iodoammine iodide compounds. Trehoux and his co-workers[5] estimated the product, $[RuCl(NH_3)_5]Cl_2$, in the course of the thermal decomposition of $[Ru(NH_3)_6]Cl_3$; however, there is no information on any kinetic studies of the reactions.

In the present paper, kinetic studies of the thermal substitution reactions of $[Ru(NH_3)_6]X_3$ and *cis*-$[RuX_2(NH_3)_4]X$ will be demonstrated and the reaction mechanisms will be discussed in comparison with those of analogous chromium(III) ammine complexes.

Experimental

Preparation of Complexes. The complexes, $[Ru(NH_3)_6]X_3$, (X=Br, I) and $[RuX_2(NH_3)_4]X$, (X=Cl, Br, I), were prepared by the methods described in the literature.[6,7] The complexes were confirmed by elemental analyses and by the visible and UV spectra. Found: H, 4.26; N, 19.25%. Calcd for $[Ru(NH_3)_6]Br_3$: H, 4.05; N, 18.92%. Found: H, 3.27; N, 14.54%. Calcd for $[Ru(NH_3)_6]I_3$: H, 3.08; N, 14.39%. Found: H, 4.67; N, 18.97%. Calcd for $[RuCl_2(NH_3)_4]Cl \cdot 2/5\ H_2O$: H, 4.53; N, 19.80%. Found: H, 2.91; N, 13.82%. Calcd for $[RuBr_2(NH_3)_4]Br$: H, 2.94; N, 13.70%. Found: H, 2.09; N, 10.23%. Calcd for $[RuI_2(NH_3)_4]I$: H, 2.18; N, 10.18%.

Derivatographic and Isothermal Kinetic Study. The differential thermal analysis (DTA) curves of the complexes were obtained by means of a Shimadzu D. T. 20B micro-differential thermal analyzer, while the thermogravimetric measurement was carried out using a Shimadzu T.G.C.20-type micro-thermobalance. All the experiments were made in a helium atmosphere at the heating rate of 5 °C/min, using 3—5 mg of the sample for each run.

From the results of isothermal thermogravimetry, the kinetic plot—the time conversion curves of the mass-loss were plotted at several constant temperatures. In this experiment, the temperature was rapidly elevated so as to pyrolyze the sample in a platinum cell placed in a furnace, the temperature was kept constant within ±0.5 °C.

A Hitachi 323 recording spectrophotometer was used for the measurement of the absorption spectra of the initial compounds and of the reaction products.

Results and Discussion

DTA and TG Studies. The DTA and TG curves of the hexaammineruthenium(III) trihalides are given in Fig. 1. Those of the *cis*-dihalogenotetraammine

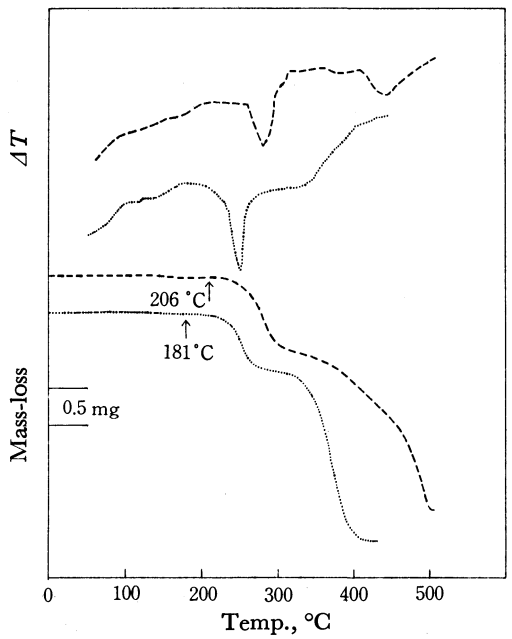

Fig. 1. DTA and TG curves of $[Ru(NH_3)_6]X_3$ in a helium atmosphere.
——: $[Ru(NH_3)_6]Br_3$, ····: $[Ru(NH_3)_6]I_3$

complexes have already been exhibited in a previous paper.[4] The DTA curves are characterized by endothermic peaks — at 280 °C (tribromide) and 251 °C (triiodide); these peaks correspond well to the first mass-loss on the TG curves. Similar results have been obtained for the cases of the *cis*-dihalogenocomplexes. The ranges of the reaction temperature were selected by reference to the results of DTA and TG studies.

Stoichiometry and Kinetic Study. The thermal decomposition products were one mole of ammonia and halogenopentaammine halide per mole of hexaammine halides in the region of the selected temperature. Thus, the thermal decomposition reaction can be expressed by Eq. (1):

$$[Ru(NH_3)_6]X_3 \longrightarrow NH_3 + [RuX(NH_3)_5]X_2, \quad (X=Br,\ I) \quad (1)$$

On the other hand, one mole of *cis*-dihalogenotetraammine halides was decomposed to form one mole of ammonia and trihalogenotriammines. The latter product was identified as the *trans*-isomer from the results of the UV and IR spectra measurements.[8,9]

$$cis\text{-}[RuX_2(NH_3)_4]X \longrightarrow NH_3 + trans\text{-}[RuX_3(NH_3)_3], \quad (X=Cl,\ Br) \quad (2)$$

In the thermal decomposition of *cis*-diiodotetraammine iodide, Reaction 3 has already been reported:[4]

$$cis\text{-}[RuI_2(NH_3)_4]I \longrightarrow 4NH_3 + RuI_3 \quad (3)$$

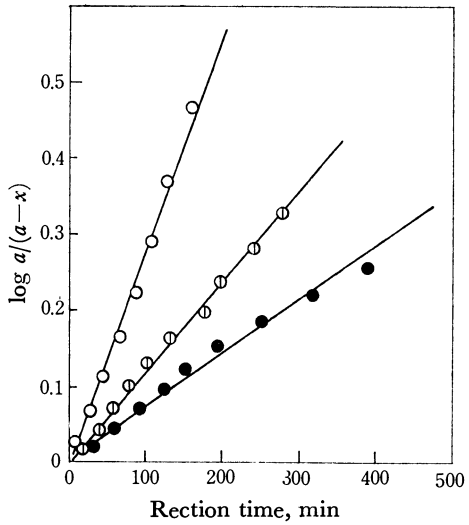

Fig. 2. Plots of a first-order rate equation for the deammonation-anation reaction of *cis*-$[RuBr_2(NH_3)_4]$-Br.
—○—: 179°C, —◑—: 166°C, —●—: 162°C

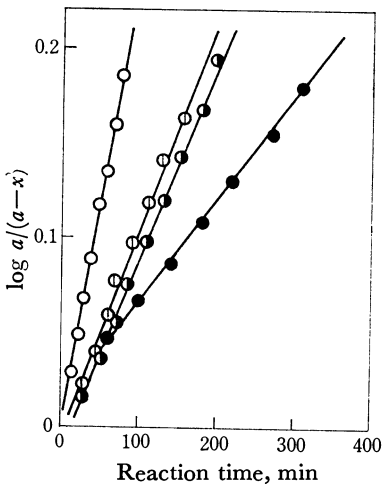

Fig. 3. Plots of a first-order rate equation for the deammonation-anation reactions of $[Ru(NH_3)_6]Br_3$.
—○—: 185°C, —◑—: 177°C, —◑—: 172°C, —●—: 161°C

Table 1. Rate constants and kinetic parameters of the deammonation-anation reactions for Ru(III) and Cr(III)[2] ammine complexes

Reaction	$k\times10^5$ s^{-1} (Temp., °C)	E_a (kcal/mol)	$\Delta S^{\neq}$ (e.u.)	Frequency factor A, s^{-1}
$[Cr(NH_3)_6]Cl_3 \rightarrow [CrCl(NH_3)_5]Cl_2 + NH_3$	2.97 (170)	30	−12	
$[Ru(NH_3)_6]Br_3 \rightarrow [RuBr(NH_3)_5]Br_2 + NH_3$	2.10 (161)			
	3.92 (172)			
	4.17 (177)			
	9.21 (185)	23.3	−29.3	9.97×10^6
$[Cr(NH_3)_6]Br_3 \rightarrow [CrBr(NH_3)_5]Br_2 + NH_3$	2.16 (192)	43	12	
$[Ru(NH_3)_6]I_3 \rightarrow [RuI(NH_3)]_5I_2 + NH_3$	4.52 (144)			
	6.02 (151)			
	11.25 (158)			
	13.07 (164)	20.7	−31.6	3.06×10^6
$[Cr(NH_3)_6]I_3 \rightarrow CrN + 3NH_4I + 2NH_3$	3.0 (204)	49	18	
cis-$[RuCl_2(NH_3)_4]Cl \rightarrow [RuCl_3(NH_3)_3] + NH_3$	2.04 (163)			
	2.72 (166)			
	4.98 (172)			
	7.78 (179)	33.1	−6.9	8.01×10^{11}
cis-$[RuBr_2(NH_3)_4]Br \rightarrow [RuBr_3(NH_3)_3] + NH_3$	2.92 (162)			
	4.48 (166)			
	5.16 (168)			
	11.73 (179)	31.3	−10.1	1.55×10^{11}
cis-$[RuI_2(NH_3)_4]I \rightarrow RuI_3 + 4NH_3$		28		
cis-$[CrCl_2(NH_3)_4]Cl \rightarrow [CrCl_3(NH_3)_3] + NH_3$	11.0 (136)	31	−2	

All the reaction products were identified by elemental analysis and/or absorption spectrophotometry. A detailed report on the stereoisomers of trihalogenotriammine will be published elsewhere.

Plots of $\log a/(a-x)$ *vs.* the reaction time for Reactions 1 and 2 are exemplified by those of *cis*-$[RuBr_2(NH_3)_4]Br$ and $[Ru(NH_3)_6]Br_3$ in Figs. 2 and 3, where "a" is the initial mass of the sample and where "$a-x$" is the mass at the reaction time, t. The plot gives a straight line with a good reproducibility for each kinetic measurement. Similar relationships were obtained for the other complexes. As a result, the thermal decomposition reaction can be regarded as a first-order reaction with respect to the reactant. The rate constant obtained from the slope of the straight line is listed in Table 1.

Arrhenius plots for the reactions are given in Fig. 4, while the kinetic parameters are listed in Table 1. The activation energy for the *cis*-diiodotetraammine iodide

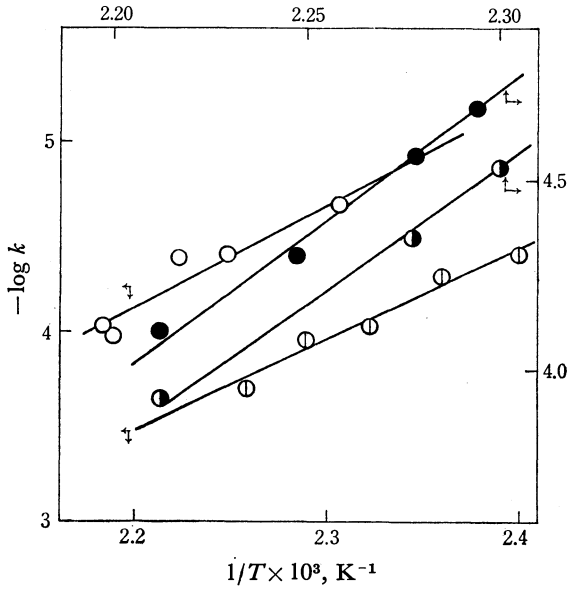

Fig. 4. Arrhenius plots of the substitution reactions for *cis*-$[RuX_2(NH_3)_4]X$, and $[Ru(NH_3)_6]X_3$.
cis-$[RuX_2(NH_3)_4]X$·····●: Cl, ◑: Br
$[Ru(NH_3)_6]X_3$·····○: Br, ⓘ: I

was determined by a graphic analysis of the Freeman-Carroll equation.

It can be seen that the rate constant for the deammonation reaction of hexaammine bromide is smaller than that of the hexaammine iodide. On the other hand, the rate constant for the *cis*-dichlorotetraammine chloride is smaller than that of the dibromotetraammine bromide. The influence of outersphere anion species is to enhance the reaction rate in the following order: Cl<Br<I.

By a comparison of the two series of complexes, it was found that the rate constant for the hexaammine halide is smaller than that of dihalogenotetraammine; however, the relation between the activation energies for the two series of complexes is inconsistent with that of the rate constants. Furthermore, the values of the activation entropy for the former series are smaller than those for the latter series. These facts suggest that there are some differences in the reaction mechanisms for the deammonation and the anation of the outersphere anion. The entering of an outersphere halide anion into the coordination-sphere is more difficult for the dihalogeno-complex halide because of the repulsion by the already-coordinated halide ligands.

Reaction Mechanism of the Deammonation-anation. For the sake of comparison, the kinetic data for the substitution reaction of the ruthenium(III) ammines are listed again, along with those for the chromium(III) ammines, in Table 1. Nagase and Tanaka[2] have demonstrated that the substitution reaction of the $[Cr(NH_3)_6]Cl_3$ complex proceeds according to the S_N2-type mechanism, while the same reaction of the bromide and iodide takes place *via* the S_N1-type mechanism. The appearances of the reactions of ruthenium(III) ammine halides are entirely different from those for the chromium(III) ammine complexes. The rate of the substitution reaction for ruthenium hexaammine iodide is about five times faster than that for the bromide. For the chromium hexaammine halide, the largest rate is found in the case of hexaammine chloride. The reaction of hexaammine iodide is different from those of chloride and bromide, and the rate is the smallest of the three compounds.

For the tetraammine series of complexes, the rate for

Table 2. The initiation temperature of deammonation and the wave number of Ru–N stretching vibration,[6] ν_{Ru-N} (cm^{-1}) for ruthenium(III) ammine complexes

Complex	X					
	Cl		Br		I	
	Temp., °C	ν	Temp., °C	ν	Temp., °C	ν
$[Ru(NH_3)_6]X_3$	200[a]	474	206	472	181	468
		464		461		457
		452		450		448
$[RuX(NH_3)_5]X_2$[b]	246	485	244	479	174	468
		463		459		450
		451		448		442
						424
cis-$[RuX_2(NH_3)_4]X$	200	—	210	—	114	—

a) Unpublished work. b) Ref. 4.

the chromium(III) complex is much larger than that of the ruthenium(III) complex. Considering the small values of the activation energy and the negative values of the activation entropy, the mechanism for the reaction of hexaammineruthenium(III) halides seems to belong to the S_N2 category. On the other hand, for the dihalogeno complex halide the S_N1-like mechanism may be most probable. This is the most important difference in comparison with the chromium(III) complexes.[2)]

The contribution of the π-bonding nature between the metal and the ligand may be considered to account for the mechanisms of the hexaammine and dihalogenotetraammine complexes. Basolo and Pearson[10)] have described how the halide ion is a stronger electron-donor rather than an ammonia molecule through the π bond from ligand to metal. The electron-donating ligand makes it possible to dissociate other ligands at the *cis* or *trans* position and to increase the reaction rate by putting more negative charge on the metal. Thus, the halide ligands in the tetraammine halide are more effective in facilitating a S_N1 mechanism for the deammonation-anation reaction than the ammine ligand in the hexaammine halide.

The initiation temperatures of the deammonation reactions for the three series of ruthenium(III) ammine complexes are listed in Table 2, along with the data of the infrared spectra. If the thermal stability of a complex is reflected in the initiation temperature, the compounds containing the iodide ion are generally less stable. When the number of iodide ions in the innersphere increases, the thermal stability of the complex decreases. One of the reasons for this may be a weakening of the strength of the ruthenium-ammine bond by the increase in the covalency of the ruthenium-halide bond. This consideration is supported by the fact that the wave number of the Ru–N stretching vibration decreases upon the replacement of the ammine ligand by the iodide ion.

The authors wish to thank the Ministry of Education for the financial support granted to this research.

References

1) Part VII of this series; A. Ohyoshi, N. Takebayashi, Y. Hiroshima, K. Yoshikuni, and K. Tsuji, This Bulletin, **47**, 1414 (1974).
2) K. Nagase and N. Tanaka, *ibid.*, **46**, 2435 (1973).
3) N. Tanaka and K. Nagase, *ibid.*, **41**, 1143 (1968).
4) A. Ohyoshi, S. Hiraki, and H. Kawasaki, *ibid.*, **47**, 841 (1974).
5) J. Trehoux, G. Nowogrocki, D. Thomas, and G. Tridot. *J. Thermal Anal.*, **1**, 171 (1969).
6) A. D. Allen and C. V. Senoff, *Can. J. Chem.*, **45**, 1337 (1967).
7) K. Gleu and W. Breuel, *Z. Anorg. Allg. Chem.*, **237**, 335 (1938).
8) R. E. Connick and D. A. Fine, *J. Amer. Chem. Soc.*, **83**, 3414 (1961).
9) J. R. During, W. A. McAllister and E. E. Mercer, *J. Inorg. Nucl. Chem.*, **29**, 1441 (1967).
10) F. Basolo and R.G. Pearson, "Mechanism of Inorganic Reactions," John Willey & Sons, New York (1967), p. 173.

Studies of 4-Diethylenetriaminemonoacetatocobalt(III) Complexes. I. The Preparation and Identification of 4-Diethylenetriaminemonoacetatocobalt(III) Complexes with Ethylenediamine, Oxalate Ion, or Acetylacetonate Ion as the Additional Ligand

Kashiro KURODA, Yoshio MORI, Hitoshi MATSUNAGA, Kazufumi KUNIGITA, and Kiyokatsu WATANABE

Department of Chemistry, Faculty of Science, Ehime University, Matsuyama, Ehime 790

(Received April 30, 1974)

The *fac(N)*- and *mer(N)*-isomers of 4-diethylenetriaminemonoacetatocobalt(III) complexes with ethylenediamine, the oxalate ion, or the acetylacetonate ion as the additional ligand have been obtained by means of reactions between chloro(4-diethylenetriaminemonoacetato)aquocobalt(III) chloride and the bidentates under different conditions. The geometrical configuration of each isomer has been identified by means of the PMR spectra and the electronic absorption spectra. The methine hydrogen in the acetylacetonato complexes has been replaced with bromine, and the resulting complexes have also been characterized.

4-Diethylenetriaminemonoacetate (NH_2–CH_2–CH_2–CH_2–COO^- / $\overset{|}{N}$–CH_2–CH_2–NH_2, abbreviated as *i*-DTMA* in this article) is a tetradentate of the $A\overset{B}{\underset{B}{<}}C$ type. It is capable of coordinating to the cobalt(III) ion in two different modes, as is shown in Fig. 1. As a result, a di(unidentate)-(*i*-DTMA)-Co(III) aggregate and a (*s*-bidentate)-(*i*-DTMA)-Co(III) aggregate may exist in two stereoisomers, and a (*uns*-bidentate)-(*i*-DTMA)-Co(III) aggregate, in four. Schneider and Collman[1] first dealt with the cobalt(III) complexes with the tetradentate. They prepared one isomer in the dinitro, the dichloro, or the carbonato complex, and two isomers in the glycinato complex. They tentatively identified the coordination mode as *fac(N)* in all of their complexes; their assignment is considered to be correct. No cobalt(III) complex having the tetradentate with the *mer(N)*-mode has been isolated so far.

In the course of our previous studies of cobalt(III) complexes containing triethylenetetramine (trien),[2] ethylenediamine-*N*,*N'*-diacetate (EDDA),[3] and 1-diethylenetriaminemonoacetate (DTMA),[4] ** we observed that the coordination mode of the ligands depends largely upon the reaction temperature of the preparations and also, to some extent, upon the kind of ligand occupying the residual coordination sites. Therefore, it was supposed that the *mer(N)*-mode of the tetradentate, which was probably the more unstable and difficult mode, would occur as a result of a reaction at high temperatures. Thus, two isomers were obtained in the ethylenediamine, the oxalato, and the acetylacetonato complexes. This report will deal with their preparation and characterization.

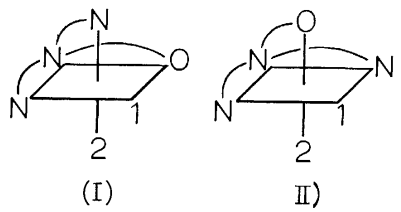

(I) (II)

Fig. 1. Coordination modes of *i*-DTMA in octahedral complexes.
(I) *fac(N)*-configuration, (II) *mer(N)*-configuration.

* This abbreviation follows that of Schneider and Collman.[1]

** The following abbreviations are used in this article besides these ligands: en, ethylenediamine; acac, acetylacetonate; Bracac, 3-bromo-2,4-pentanedionate (bromoacetylacetonate); ox, oxalate; gly, glycinate.

Experimental

Materials, Analysis, Apparatus, and Measurements. All the chemicals were of a reagent grade and were used without further purification. The carbon, hydrogen, and nitrogen in the synthesized complexes were analysed by the Analyses Center of the Institute for Chemical Research, Kyoto University. The visible and ultraviolet absorption spectra were measured in aqueous solutions with a Hitachi EPS-3 Recording Spectrophotometer. The PMR spectra were recorded with a Japan Electron Optics JNM-100 Spectrometer (100 MHz), using deuterium oxide as the solvent and *tert*-butyl alcohol as the internal reference. The temperature of the probe was maintained at 22±1 °C.

Preparation. *(1)* fac(N)-*Chloro(4-diethylenetriaminemonoacetato)aquocobalt(III) Chloride Monohydrate*, fac(N)-[*Co(i-DTMA)Cl(H_2O)]Cl·H_2O*: Dinitro(4-diethylenetriaminemonoacetato)cobalt(III) monohydrate, [Co(*i*-DTMA)-(NO_2)$_2$]·H_2O, was prepared by the method of Schneider and Collman.[1] One gram of the dinitro complex was dissolved in 10 ml of hydrochloric acid (6 M) by heating, and the resulting solution was evaporated to dryness with the aid of an air stream blown onto the surface. During the dissolution, nitric oxides were evolved, and finally a greenish blue residue was obtained. (This is probably the dichloro complex.) A small amount (~3 ml) of water was then mixed with the residue, which dissolved at once, forming a violet solution. A bright violet precipitate soon appeared. The precipitate was transferred onto a filter with a methanol (80%)–water mixture and then washed with methanol and ether. Yield, 0.8 g. By treating the filtrates of the above procedure in the same way, an additional product was obtained. The total yield was 0.95 g.

Found: C, 21.80; H, 5.86; N, 12.58%. Calcd for [Co(*i*-DTMA)Cl(H_2O)]Cl·H_2O=$CoC_6H_{18}O_4N_3Cl_2$(326.07): C, 22.10; H, 5.56; N, 12.89%.

(2) mer(N)-*Chloro(4-diethylenetriaminemonoacetato)aquocobalt(III) Perchlorate*, mer(N)-[*Co(i-DTMA)Cl(H_2O)]ClO_4*:

Into 5 ml of 2 M $HClO_4$ 0.5 g of the *fac(N)*-chloroaquo complex (1) was added, after which the mixture was heated on a boiling water bath. The starting complex dissolved at once; dark violet crystals then appeared. After heating for 15 min, the crystals were collected and washed with a small amount of cold water, methanol, and ether. Yield, 0.5 g. By the evapoartion of the filtrate, an additional product was obtained. The total yield was 0.55 g.

Found: C, 19.20; H, 4.53; N, 11.18%. Calcd for [Co(*i*-DTMA) Cl (H_2O)] ClO_4 = $CoC_6H_{16}O_7N_3Cl_2$ (372.05): C, 19.37; H, 4.33; N, 11.29%.

(3) fac (N)-*4-Diethylenetriaminemonoacetato(ethylenediamine)-cobalt(III) Perchlorate*, fac(N)-[*Co*(i-*DTMA*)(*en*)](ClO_4)$_2$: After a solution which contained 0.6 g of the *fac(N)*-chloroaquo complex in 10 ml of water had been heated for 15 min on a boiling-water bath, 0.6 ml of aqueous ethylenediamine (20%) and 0.1 g of active charcoal were added to the solution, in this order. Upon the addition of the charcoal, the color rapidly changed to a brownish orange. The mixture was then heated for 5 min, the charcoal was removed by filtration, and 1 ml of 6 M $HClO_4$ was added; a large amount of deep orange precipitate appeared upon cooling. After the product had been allowed to stand for 1 hr in a refrigerator, the precipitate was separated and recrystallized from 25 ml of warm (~60 °C) water with the addition of a few drops of 6 M $HClO_4$. Yield, 0.6 g.

Found: C, 19.97; H, 4.77; N, 14.67%. Calcd for [Co(*i*-DTMA) (en)] (ClO_4)$_2$ = $CoC_8H_{22}O_{10}N_5Cl_2$ (476.13): C, 20.10; H, 4.64; N, 14.65%.

(4) mer (N)-*4-Diethylenetriaminemonoacetato(ethylenediamine)-cobalt(III) Perchlorate*, mer(N)-[*Co*(i-*DTMA*)(*en*)](ClO_4)$_2$: The filtrate obtained in the preparation of the *fac(N)*-isomer was concentrated to ~2 ml and then cooled; a pale yellowish orange precipitate thus appeared. It was recrystallized from 2 ml of warm water with the addition of a few drops of 6 M $HClO_4$. Yield, 0.1 g.

Found: C, 19.84; H, 4.70; N, 14.45%. Calcd for [Co(*i*-DTMA) (en)] (ClO_4)$_2$ = $CoC_8H_{22}O_{10}N_5Cl_2$ (476.13): C, 20.10; H, 4.64; N, 14.65%.

(5) fac (N)-*Oxalato(4-diethylenetriaminemonoacetato)cobalt-(III)*, fac(N)-[*Co*(i-*DTMA*)(*ox*)]: A mixture of 0.3 g of the *fac(N)*-chloroaquo complex (1) and 0.13 g of oxalic acid dihydrate in 5 ml of water was heated at ~65 °C for 30 min with stirring. Reddish violet crystals came out during the reaction. After the product had been cooled in an ice-water bath for 3 hr, the crystals were collected and recrystallized from 30 ml of hot (~80 °C) water. Yield, 0.2 g.

Found: C, 30.93; H, 4.54; N, 13.81%. Calcd for [Co(*i*-DTMA)(ox)] = $CoC_8H_{14}O_6N_3$ (307.15): C, 31.28; H, 4.59; N, 13.68%.

(6) mer(N)-*Oxalato(4-diethylenetriaminemonoacetato)cobalt-(III) Dihydrate*, mer(N)-[*Co*(i-*DTMA*)(*ox*)]·$2H_2O$: A solution of 0.3 g of the *fac(N)*-chloroaquo complex (1) in 5 ml of water was heated in a boiling-water bath for 15 min. Another solution, which contained 0.13 g of sodium oxalate in 5 ml of water, was also heated to 100 °C. Then the solutions were combined, and the mixture was kept at 100 °C for 10 min; a deep red solution was thus obtained. After the solution had been cooled in an ice-water bath for 1 hr, the red precipitate formed was collected on a filter and then fractionally extracted with 10 ml portions of warm (~60 °C) water four times. In the first extract (red-colored), an orange-red precipitate amounting 0.15 g was deposited by adequate cooling. The precipitate from the second extract contained the red-violet *fac(N)*-isomer to some extent. The deposits in the third and the fourth extracts consisted entirely of the *fac(N)*-isomer. The product from the first extract was recrystallized with 5 ml of warm water. Yield, 0.1 g.

Found: C, 27.88; H, 5.41; N, 12.35%. Calcd for [Co(*i*-DTMA)(ox)]·$2H_2O$ = $CoC_8H_{18}O_8N_3$ (343.18): C, 28.00; H, 5.29; N, 12.24%.

(7) fac (N)-*Acetylacetonato(4-diethylenetriaminemonoacetato)-cobalt(III) Perchlorate*, fac (N)-[*Co*(i-*DTMA*)(*acac*)]ClO_4: A solution of the *fac(N)*-chloroaquo complex (0.5 g) in 10 ml of water was heated in a boiling-water bath for 15 min. Another solution, which contained acetylacetone (0.2 g) and sodium hydroxide (0.08 g) in 10 ml of water, was also heated to 100 °C and was then mixed with the former by stirring. The color of the mixture soon changed from blue to dark red. After the addition of 1 ml of 6 M $HClO_4$, the solution was concentrated to ~5 ml. Upon cooling, red-violet crystals came out. After the product had been placed in a refrigerator overnight, the crystals were collected and then recrystallized from 15 ml of warm water with the addition of a few drops of 6 M $HClO_4$. Yield, 0.4 g.

Found: C, 31.95; H, 5.34; N, 10.37%. Calcd for [Co(*i*-DTMA)(acac)]ClO_4 = $CoC_{11}H_{21}O_8N_3Cl$ (417.69): C, 31.63; H, 5.07; N, 10.06%.

(8) mer (N)-*Acetylacetonato(4-diethylenetriaminemonoacetato)-cobalt(III) Perchlorate*, mer(N)-[*Co*(i-*DTMA*)(*acac*)]ClO_4: The filtrate separated from the crude *fac(N)*-isomer in the above preparation (~4 ml) was concentrated to ~2 ml and then placed in a refrigerator overnight. A red precipitate, which was clearly different from the red-violet product (7), thus appeared. The precipitate was recrystallized from 5 ml of warm water with the addition of a few drops of 6 M $HClO_4$. Yield, 0.1 g.

Found: C, 31.62; H, 5.19; N, 10.16%. Calcd for [Co(*i*-DTMA)(acac)]ClO_4 = $CoC_{11}H_{21}O_8N_3Cl$ (417.69): C, 31.63; H, 5.07; N, 10.06%.

(9) Bromination of the Acetylacetonato Complexes: The *fac(N)*-isomer of the acetylacetonato complex (0.3 g) was dissolved in 50 ml of an ethanol(50%)–water mixture, and then 0.15 g of *N*-bromosuccinimide was stirred in. The mixture was concentrated to 10 ml at ~50 °C with the aid of an air stream blown onto the surface. A brownish red precipitate came out as the evaporation proceeded. After the product had been cooled at 0 °C for 1 hr, the precipitate was collected and recrystallized from 10 ml of warm water with the addition of a few drops of 6 M $HClO_4$. Yield, 0.1 g.

The *mer(N)*-isomer of the acetylacetonato complex was treated similarly. The yield of the bright red product was also 0.1 g.

Found: C, 26.34; H, 4.19; N, 8.41% for the brownish red isomer. C, 26.50; H, 4.18; N, 8.41% for the bright red isomer. Calcd for [Co(*i*-DTMA)(Bracac)]ClO_4 = $CoC_{11}H_{20}O_8N_3ClBr$ (496.59): C, 26.60; H, 4.06; N, 8.46%.

Results and Discussion

Preparation. The preparation routes in this study are shown schematically in Table 1. Schneider and Collman[1] obtained the dichloro complex, [Co(*i*-DTMA)Cl_2], by the evaporation of a suspension of the dinitro complex in concentrated hydrochloric acid, followed by the addition of ethanol. The evaporation product of the dinitro complex in our procedure probably consisted of the same dichloro complex as that of the pioneers. According to our experiment, however, the composition of the material is indefinite to some extent, since it changes quickly in the presence of moisture. The addition of a small amount of water

TABLE 1. PREPARATION SCHEME OF Co(III)-*i*-DTMA COMPLEXES

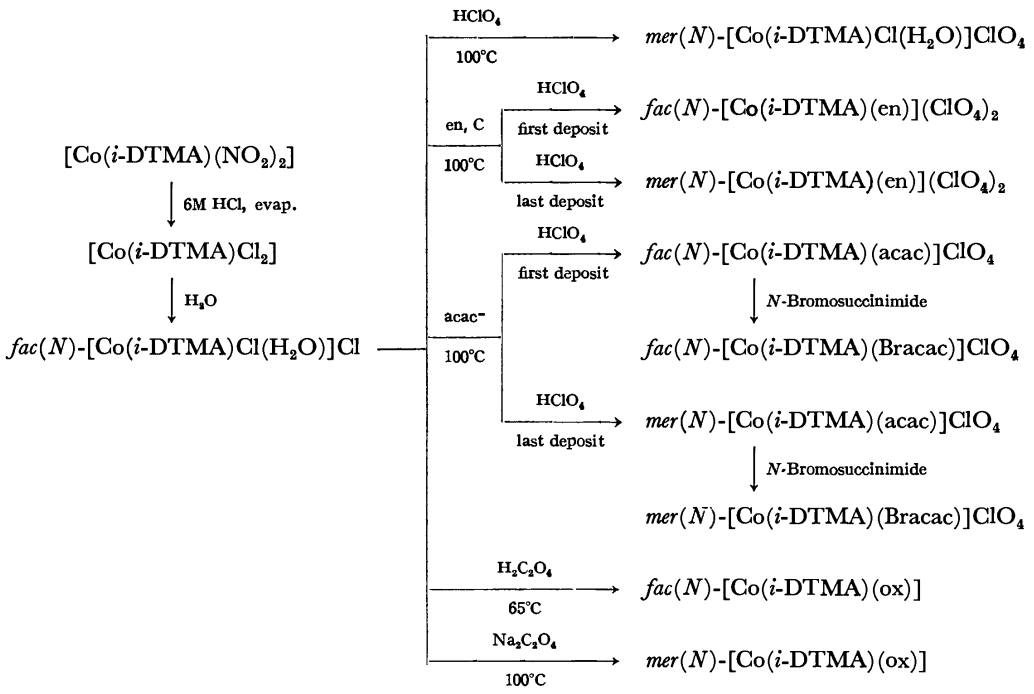

to the product, as has been described above, gives a satisfactory precipitate of the first aquation product from the dichloro complex, $[Co(i\text{-}DTMA)Cl(H_2O)]Cl \cdot H_2O$. The isolated solid is not hygroscopic at all, since it came out of the aqueous medium. The yield is nearly quantitative. It reacts with various anions and molecules to form substitution products. Therefore, it is a suitable starting substance for the preparation of the complexes of the series.

As has been described in the introduction, *i*-DTMA may coordinate with two different modes in octahedral complexes; judging from the results of Schneider and Collman,[1] the *fac*(*N*)-mode is considered to be more stable and/or to be easier to arise. Therefore, it was presumed that a high temperature was necessary for a *fac*(N)-isomer to isomerize to a *mer*(N)-isomer. It was also presumed that basic media were preferable for the isomerization, since the substitution and isomerization reactions of cobalt(III) complexes proceed faster in basic solutions than in acidic solutions.[5] Preparations were attempted on these assumptions; they were confirmed, at least qualitatively, as will be shown below.

In the preparation of the oxalato complexes, the red *mer*(*N*)-isomer, which will be identified in the following sections, occurred predominantly by means of the reaction between the starting complex and sodium oxalate at ~100 °C. On the other hand, the reaction with oxalic acid at ~65 °C produced the red-violet *fac*(*N*)-isomer. The use of sodium oxalate at ~65 °C also produced the red-violet isomer at first, but it turned to red after having been long kept at that temperature. These facts are consistent with the above assumptions. In the preparation of the ethylenediamine and the acetylacetonato complexes, two isomers of each complex were separated from the products obtained by the reactions at ~100 °C. It was observed that the yields of the *mer*(*N*)-isomers were extremely low when the reactions were performed at ~65 °C. These facts also confirm the assumptions.

The bromination of the acetylacetonato complexes at the central methine of the ligand was easily accomplished by the action of *N*-bromosuccinimide. This is in contrast with the fact that the acetylacetonatobis(ethylenediamine)cobalt(III) ion, $[Co(acac)(en)_2]^{2+}$, is not brominated even under forcing conditions.[6] On the other hand, there is much information indicating that tris(acetylacetonato)cobalt(III) and many analogues of the other metal ions, such as Cr(III), undergo bromination at the site.[7] Thus, the results indicate that the electrophilic substitution suffers an influence by the kinds of ligands which coordinate to the metal together with the reacting acetylacetonate.

Proton NMR Spectra. In the case of the coordination with the *mer*(*N*)-mode of the tetradentate, one ethylene bridge is forced to the δ and the other, to the λ conformation, and the out-of-plane glycinate ring skeleton must be planar. The oxalate and the acetylacetonate rings are considered to be planar, since these rings in many metal complexes have been confirmed to be planar by X-ray crystallographic analysis.[8] Therefore, the *mer*(*N*)-isomers of the oxalato and the acetylacetonato complexes possess a plane of symmetry; they belong to the C_s point group. On the other hand, the *fac*(*N*)-isomers have no element of symmetry; they belong to the C_1 point group. In the case of the ethylenediamine complex, neither isomer has an element of symmetry; since the conformation of the bidentate is not planar but *gauche*. However, the δ and the λ conformations of the bidentate give rise to no intrinsic difference in the *mer*(*N*)-isomer; the plane coplanar with the glycinate ring in the isomer may thus be taken as approximately a plane of symmetry.

Table 2. Resonances in the PMR spectra indicating the structure of some Co(III)-*i*-DTMA complexes (ppm downfield referred to *tert*-butyl alcohol as zero)

	CH (in acac)	CH_2 (in glycinate ring)	CH_3 (in acac)
fac(*N*)-[Co(*i*-DTMA)Cl(H_2O)]Cl	—	3.08, 2.91, 2.46, 2.29	—
mer(*N*)-[Co(*i*-DTMA)Cl(H_2O)]ClO_4	—	2.57	—
fac(*N*)-[Co(*i*-DTMA)(en)]$(ClO_4)_2$	—	3.19, 3.02, 2.78, 2.61	—
mer(*N*)-[Co(*i*-DTMA)(en)]$(ClO_4)_2$	—	2.79	—
mer(*N*)-[Co(*i*-DTMA)(ox)]	—	2.66	—
fac(*N*)-[Co(*i*-DTMA)(acac)]ClO_4	4.55	3.29, 3.12, 2.45, 2.28	1.00, 0.98
fac(*N*)-[Co(*i*-DTMA)(Barcac)]ClO_4	—	(3.29, 3.12, 2.45, 2.28)[a]	1.33, 1.31
mer(*N*)-[Co(*i*-DTMA)(acac)]ClO_4	4.50	2.70	0.99, 0.87
mer(*N*)-[Co(*i*-DTMA)(Bracac)]ClO_4	—	2.70	1.35, 1.22

a) The resonances of the glycinate ring protons of *fac*(*N*)-[Co(*i*-DTMA)(Bracac)]ClO_4 were not so clear because of the solubility limitation, but they were detectable by the comparison with the spectrum of the unbrominated complex. The spectrum of *fac*(*N*)-[Co(*i*-DTMA)(ox)] was not obtained owing to its low solubility.

Because of the symmetry described above, the glycinate ring protons in the *mer*(*N*)-isomers are exactly or approximately equivalent; hence, a singlet absorption due to the protons can be expected for the isomers. On the other hand, an AB quartet absorption is expected for the protons of the *fac*(*N*)-isomers. Thus, the PMR spectra make possible a decisive conclusion as to the structure of the complexes. Table 2 shows the observed resonances, which indicate the structure and composition. As may be seen there, one of the isomers of each complex exhibits a sharp singlet, and the other, a quartet, in the region of the glycinate absorption (around 3 ppm). The coupling constants, J_{AB}, of the latter are 17 Hz, in agreement with those obtained for other cobalt(III) complexes with a similar ring arrangement.[3] The coordination modes of the tetradentate in the isomers were, thus, assigned as has been indicated in the preceding section on preparation. It was observed that the absorption due to the methine proton of the acetylacetonato complexes (~4.5 ppm) disappeared completely in the spectra of the brominated products. This fact supports the actual bromination at the site of the ligand.

Electronic Absorption Spectra. Figures 2—5 show the visible and ultraviolet absorption spectra of the complexes studied, while the numerical values of the absorption maxima are summarized in Table 3.

As may be seen in Fig. 2, one of the chloroaquo complexes shows an intense first band with no distinct split, whereas the other shows a large split in the band. Such a large difference between their spectra cannot be expected if the tetradentate coordinates with the

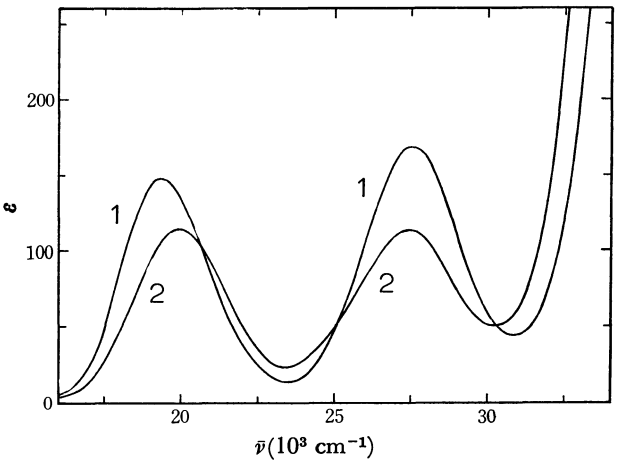

Fig. 3. Absorption spectra of *fac*(*N*)- and *mer*(*N*)-[Co(*i*-DTMA)(ox)].
1: the *fac*(*N*)-isomer; 2: the *mer*(*N*)-isomer

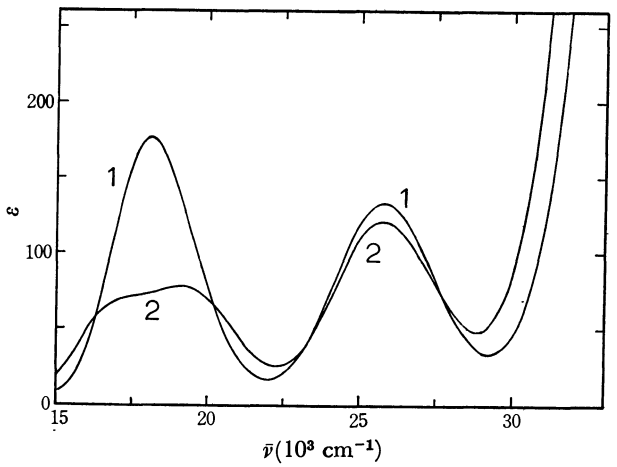

Fig. 2. Absorption spectra of *fac*(*N*)-[Co(*i*-DTMA)-Cl(H_2O)]Cl (1) and *mer*(*N*)-[Co(*i*-DTMA)Cl(H_2O)]-ClO_4 (2).

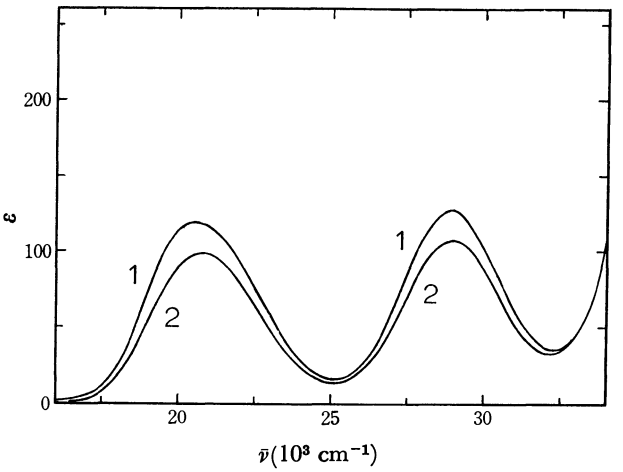

Fig. 4. Absorption spectra of *fac*(*N*)- and *mer*(*N*)-[Co(*i*-DTMA)(en)]$(ClO_4)_2$.
1: the *fac*(*N*)-isomer; 2: the *mer*(*N*)-isomer

TABLE 3. ABSORPTION MAXIMA OF THE ELECTRONIC SPECTRA OF SOME Co(III)-*i*-DTMA COMPLEXES

	I $\bar{\nu}$ (10^3 cm^{-1}) (ε) Ia	Ib	II or Sp $\bar{\nu}$ (10^3 cm^{-1}) (ε)
fac(*N*)-[Co(*i*-DTMA)Cl(H_2O)]Cl		18.08 (176.6)	25.77 (134.0)
mer(*N*)-[Co(*i*-DTMA)Cl(H_2O)]ClO_4	17 (sh)	19.08 (78.0)	25.71 (121.3)
fac(*N*)-[Co(*i*-DTMA)(en)]$(ClO_4)_2$		20.53 (119.8)	28.99 (127.8)
mer(*N*)-[Co(*i*-DTMA)(en)]$(ClO_4)_2$		20.75 (98.6)	28.99 (108.0)
fac(*N*)-[Co(*i*-DTMA)(ox)]		19.31 (148.0)	27.55 (168.4)
mer(*N*)-[Co(*i*-DTMA)(ox)]		19.92 (114.2)	27.40 (113.8)
fac(*N*)-[Co(*i*-DTMA)(acac)]ClO_4		18.98 (167.6)	30.77[a] (3880)
mer(*N*)-[Co(*i*-DTMA)(acac)]ClO_4		19.84 (156.6)	30.49[a] (4100)
fac(*N*)-[Co(*i*-DTMA)(Bracac)]ClO_4		19.01 (181.0)	29.20[a] (3760)
mer(*N*)-[Co(*i*-DTMA)(Bracac)]ClO_4		19.84 (178.0)	28.90[a] (3900)

a) Ligand specific band.

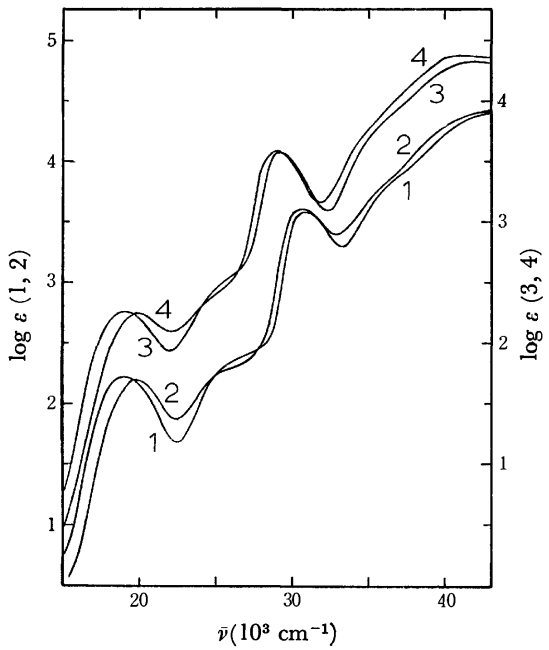

Fig. 5. Absorption spectra of [Co(*i*-DTMA)(acac)]ClO_4 and [Co(*i*-DTMA)(Bracac)]ClO_4.
1: the *fac*(*N*)-isomer of the acetylacetonato complex
2: the *mer*(*N*)-isomer of the acetylacetonato complex
3: the *fac*(*N*)-isomer of the bromoacetylacetonato complex
4: the *mer*(*N*)-isomer of the bromoacetylacetonato complex

same mode in both isomers. Therefore, it can reasonably be inferred from the spectra and the possible four configurations that the former is the *fac*(*N*)-isomer, while the latter is the *mer*(*N*)-isomer, which is in agreement with the assignment from the PMR spectra. It is not known, however, which of the residual coordination sites (1 and 2 in Fig. 1) the chlorine atom occupies in each isomer.

The oxalato and the acetylacetonato complexes are of the [CoN_3O_3] type, and there is much information about the spectra of this type of complex, *e.g.* [Co(gly)$_3$].[9] There is a general trend for the *fac*-isomer to exhibit a more intense first band with no distinct split, whereas the *mer*-isomer exhibits a less intense first band with a wider band width or a deformation from the symmetrical shape. The configurations of the isomers were assigned on the basis of this trend, as has been indicated in the Preparation section, in agreement with the assignment based on the PMR spectra. These assignments are also consistent with the observation of the preparations, in which the *mer*(*N*)-isomers, the species considered to be difficult to produce, occurred at high temperatures.

It can be found that some regularities are present among the spectra of the acetylacetonato and the bromoacetylacetonato complexes. First, the bromination hardly affects the wave number of the first band, but slightly increases the intensity of the band. Second, the ligand specific band shifts to a lower wave number with the slight decrease in intensity by the bromination. It can be concluded from the spectral observations that the *fac*(*N*)- and *mer*(*N*)-configurations of each isomer of the acetylacetonato complex are mostly retained during the brominating reaction under the conditions used in the experiments.

References

1) P. W. Schneider and J. P. Collman, *Inorg. Chem.*, **7**, 2010 (1968).
2) K. Kuroda and P. S. Gentile, *J. Inorg. Nucl. Chem.*, **29**, 1963 (1967).
3) K. Kuroda and K. Watanabe, This Bulletin, **44**, 1034 (1971); K. Kuroda, *ibid.*, **45**, 2176 (1972).
4) K. Watanabe and K. Kuroda, *Nippon Kagaku Kaishi*, **1972**, 1409.
5) D. R. Stranks, "Modern Coordination Chemistry," ed. by J. Lewis and R. G. Wilkins, Interscience Publishers I, New York, N. Y. (1960), pp. 129—130, and references cited therein; K. Kuroda and F. Mohri, *Chem. Lett.*, **1972**, 719; K. Kuroda, *ibid.*, **1974**, 17.
6) J. P. Collman, "Transition Metal Chemistry," Vol. 2, ed. by R. L. Carlin, Marcel Dekker, New York, N. Y. (1966), p. 44.
7) J. P. Collman, *ibid.*, pp. 35—45, and references cited therein.
8) For example, J. N. van Niekerk and F. R. L. Schoening, *Acta Crystallogr.*, **5**, 185 (1952); R. B. Roof, *ibid.*, **9**, 781 (1956); T. Aoki, K. Matsumoto, S. Ooi, and H. Kuroya, This Bulletin, **46**, 159 (1973); K. Matsumoto, H. Kawaguchi, H. Kuroya, and S. Kawaguchi, *ibid.*, **46**, 2424 (1973).
9) H. Kuroya and R. Tsuchida, This Bulletin, **15**, 429 (1940); F. Basolo, C. J. Ballhausen, and J. Bjerrum, *Acta Chem. Scand.*, **9**, 810 (1955).

Studies of Bivalent Metal Complexes of 2-Acetylpyridine[1)]

Yoshinori KIDANI, Masahide NOJI, and Hisashi KOIKE*

Faculty of Pharmaceutical Sciences, Nagoya City University, 3-1 Tanabe-dori, Mizuho-ku, Nagoya 467

(Received June 3, 1974)

Bivalent metal complexes of 2-acetylpyridine (abbreviated as 2AP), $M(2AP)_2X_2$, M being copper, nickel, cobalt, and zinc ions and X being chloride, bromide, and iodide ions, were synthesized in ethanol solutions. The far-infrared analyses were discussed with reference to their structures, which were determined by means of the magnetic moments and the diffuse reflectance spectra. Except for $Co(2AP)_2Cl_2$ and $Co(2AP)_2I_2$, an octahedral structure was suggested for the $M(2AP)_2X_2$ complexes. A tetrahedral structure was assigned to $Co(2AP)_2Cl_2$ and $Co(2AP)_2I_2$ on the basis of their magnetic moments of 4.55 and 4.25 B.M. respectively and the diffuse reflectance spectra. The stretching vibrations of metal-nitrogen, metal-oxygen, and metal-halogen have been discussed.

Only a few spectrochemical studies have been reported on the metal complexes of 2-acetylpyridine, Karson,[2,3)] however, studied the neutral metal complexes of $[C_5H_4NC\langle^{CH_2}_{O^-}]_2M$ being formed in aqueous solutions, where the metals were bivalent ions of copper, nickel, and cobalt. He also reported the cationic-metal-complex formation of 2-acetylpyridine in ethanol solutions, *i.e.*, $[C_5H_4NC\langle^{CH_3}_{O}]_2MX_2$, where the metals were the same as those of the neutral complexes and where X were chloride, bromide, and iodide ions, but he gave no detailed discussion.

For a better understanding of the biologically-important amide group, the present authors attempted studies of the cationic-metal complexes with 2-acetylpyridine (abbreviated as 2AP in this paper) in a series of 2-substituted pyridine-metal complexes. In analysing the data for 2AP-metal complexes, reference was made to the metal complexes of pyridine-2-carboxamide, since their structures and coordination sites have been determined by Yamasaki and Sekizaki,[4–8)] the conclusion was confirmed by Masuko *et al.*[9)]

This paper will deal with the magnetic moments and diffuse reflectance spectra for the determination of the structures of the complexes obtained, together with the band assignments in the far-infrared region for those containing different halide ions.

Experimental

Materials. The 2-acetylpyridine was purchased from the Tokyo Kogyo Co., Ltd., and was used without further purification. The bivalent metal halides (Cu, Ni, Co, and Zn) were special-grade products of Wako Pure Chemical Industries, Ltd.

Preparation of Complexes. 1) Dihalogenobis(2-acetylpyridine)copper(II): To 10 ml of an ethanolic solution containing 0.48 g (4 mmol) of the ligand, we added 0.34 g (2 mmol) of copper(II) chloride dihydrate dissolved in 10 ml of ethanol. Immediately a dark green powder was precipitated, it was then washed with ethanol. The same procedure was used to obtain the bromo complex by the addition of the ligand, together with copper bromide in ethanol. A yellowish-green powder was precipitated.

Found: C, 44.06; H, 3.77; N, 7.28; Cu, 16.7%. Calcd for $Cu(C_7H_7ON)_2Cl_2\cdot 1/4H_2O$: C, 44.12; H, 3.84; N, 7.35; Cu, 16.3%.

Found: C, 35.32; H, 3.12; N, 5.84; Cu, 12.7%. Calcd for $Cu(C_7H_7ON)_2Br_2\cdot H_2O$: C, 35.10; H, 3.36; N, 5.84; Cu, 13.0%.

2) Dihalogenobis(2-acetylpyridine)nickel(II): To 2 mmol of the ligand we added 4 mmol of nickel(II) chloride hexahydrate in 10 ml of ethanol, and the resultant solution was warmed gently on a water bath. A greenish-yellow powder was gradually precipitated. Bromo and iodo complexes were obtained as brown and reddish-brown precipitates by means of a procedure similar to that used for the chloro complex.

Found: C, 45.10; H, 3.85; N, 7.50; Ni, 15.8%. Calcd for $Ni(C_7H_7ON)_2Cl_2$: C, 45.21; H, 3.80; N, 7.53; Ni, 15.5%.

Found: C, 36.59; H, 3.18; N, 6.09; Ni, 12.7%. Calcd for $Ni(C_7H_7ON)_2Br_2$: C, 36.49; H, 3.06; N, 6.08; Ni, 12.8%.

Found: C, 30.35; H, 2.53; N, 4.86; Ni, 10.6%. Calcd for $Ni(C_7H_7ON)_2I_2$: C, 30.31; H, 2.53; N, 5.05; Ni, 10.6%.

3a) Bis(2-acetylpyridine)cobalt(II) Halides: To 2 mmol of the ligand in 10 ml of ethanol, we added 4 mmol of cobalt(II) chloride hexahydrate in 10 ml of ethanol, after which the solution was kept standing overnight at room temperature. A brown powder was thus precipitated. An iodide complex was obtained as a reddish-brown precipitate by means of the same procedure as was used for the chloride complex.

Found: C, 44.89; H, 3.69; N, 7.61; Co, 15.8%. Calcd for $Co(C_7H_7ON)_2Cl_2$: C, 45.19; H, 3.79; N, 7.35; Co, 15.5%.

Found: C, 30.35; H, 2.69; N, 5.11; Co, 10.4%. Calcd for $Co(C_7H_7ON)_2I_2$: C, 30.31; H, 2.55; N, 5.05; Co, 10.7%.

3b) Dibromobis(2-acetylpyridine)cobalt(II): A bromo complex was obtained as a dark brown precipitate by means of the same procedure as was used for the chloride complex.

Found: C, 36.58; H, 3.22; N, 6.03; Co, 12.8%. Calcd for $Co(C_7H_7ON)_2Br_2$: C, 36.47; H, 3.06; N, 6.07; Co, 12.5%.

4) Dihalogenobis(2-acetylpyridine)zinc(II): Two mmol of the ligand and 4 mmol of zinc chloride were dissolved in 10 ml of ethanol. After mixing the two solutions, the resultant solution was concentrated to half volume on a water bath and then kept standing overnight at room temperature. A yellowish-brown powder was thus precipitated. A bromo complex was obtained by mixing 2 mmol of zinc bromide and 4 mmol of the ligand in 30 ml of acetone. After the solution has been kept standing overnight at room temperature, a white crystalline precipitate was deposited out. An iodo complex was obtained as reddish-brown precipitate by means of the same procedure as was used for the chloro complex.

Found: C, 44.81; H, 3.74; N, 7.17; Zn, 16.9%. Calcd

* Present address: School of Medical Technology and Nursing, Fujita Gakuen University, Kutsukake, Toyoake, Aichi 470-11.

for $Zn(C_7H_7ON)_2Cl_2$: C, 44.42; H, 3.73; N, 7.40; Zn, 17.3%. Found: C, 35.89; H, 2.97; N, 5.86; Zn, 14.0%. Calcd for $Zn(C_7H_7ON)_2Br_2$: C, 35.97; H, 3.02; N, 5.99; Zn, 14.3%. Found: C, 29.58; H, 2.85; N, 4.99; Zn, 11.6%. Calcd for $Zn(C_7H_7ON)_2I_2$: C, 29.95; H, 2.51; N, 4.75; Zn, 11.4%.

Magnetic and Spectroscopic Measurements. The magnetic moments were determined by the Curie method with a Shimadzu MB-2-type magnetic balance at room temperature (18—21 °C). The diffuse reflectance spectra were measured with a Hitachi EPS-3T spectrophotometer equipped with an integrating sphere accessory. For the measurements, the complexes were diluted to 0.25 molality with magnesium oxide, and from 150 mg of the mixture pellets were prepared under a 600 kg/cm² pressure after evacuation. A Nihon Bunko IRA-2 spectrophotometer was used to record the infrared spectra in the region from 4000 to 400 cm^{-1}. The infrared spectra were measured with KBr discs, Nujol, and HCB mulls. For the measurements of the far-infrared spectra from 600 to 200 cm^{-1}, a Nihon Bunko DS-701G spectrophotometer was used. Solid samples were measured as mulls in Nujol; they were placed between two polyethylene films and inserted into a holder. The spectrum of the ligand was measured as a thin liquid layer placed between two polyethylene films.

Results and Discussion

Magnetic Moments. The magnetic moments observed for the 2AP-metal complexes are listed in

TABLE 1. MAGNETIC MOMENTS OF 2-ACETYLPYRIDINE–METAL COMPLEXES

Complexes	Found	Calcd for the spin-only formula
$Cu(2AP)_2Cl_2 \cdot 1/4H_2O$	1.69 B.M.	1.73 B.M.
$Cu(2AP)_2Br_2 \cdot H_2O$	1.66	1.73
$Ni(2AP)_2Cl_2$	3.02	2.82
$Ni(2AP)_2Br_2$	3.00	2.82
$Ni(2AP)_2I_2$	2.97	2.82
$Co(2AP)_2CoCl_2$	4.55	3.88
$Co(2AP)_2CoBr_2$	5.40	3.88
$Co(2AP)_2CoI_2$	4.25	3.88
$Zn(2AP)_2Cl_2$	Diamagnetic	
$Zn(2AP)_2Br_2$	Diamagnetic	
$Zn(2AP)_2I_2$	Diamagnetic	

Table 1. The magnetic moments of the copper complexes are a little lower than that of the spin-only formula, but the presence of copper–copper interaction usually produces a much larger decrease in the magnetic moment. Therefore, they may exist as mononuclear complexes. The magnetic-moment values of the nickel complexes are around 3.0 B.M., corresponding to the reported values of 2.9—3.4 B.M. for octahedral nickel complexes. As for the cobalt complexes, the bromo complex has a higher magnetic moment (5.40 B.M.) than those of the chloride and the iodide (4.55 and 4.25 B.M. respectively). These values indicate an octahedral structure for the bromo complex and a tetrahedral structure for the other two complexes.

Diffuse Reflectance Spectra. The diffuse reflectance spectra of the complexes prepared are shown in Figs. 1—3. Both $Cu(2AP)_2Cl_2$ and $Cu(2AP)_2Br_2$ show d-d

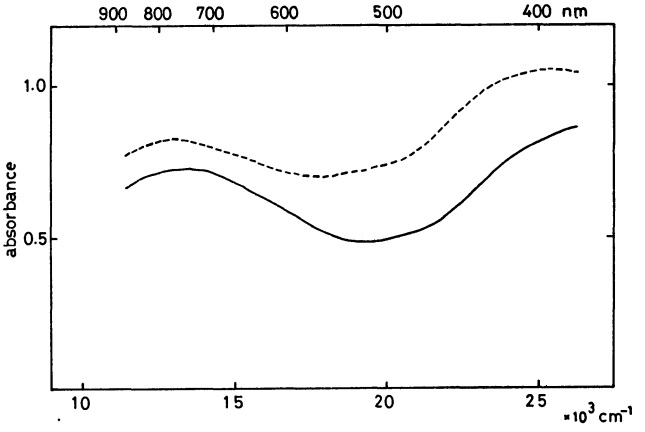

Fig. 1. Absorption spectra of $Cu(2AP)_2X_2$ measured by the diffuse reflectance method.
Solid line: X=Cl, Broken line: X=Br.

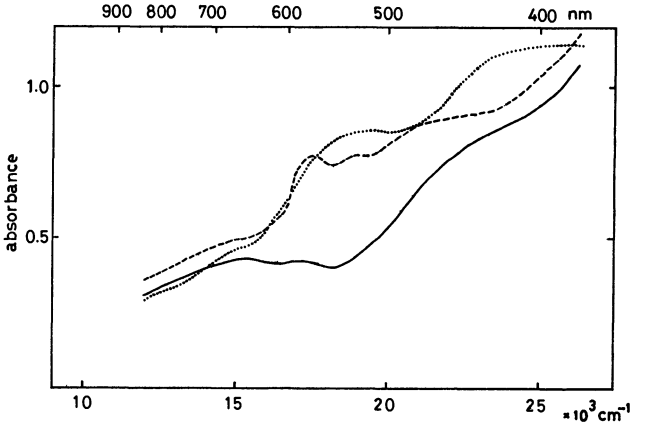

Fig. 2. Absorption spectra of $Ni(2AP)_2X_2$ measured by the diffuse reflectance method.
Solid line: X=Cl, Broken line: X=Br,
Dotted line: X=I.

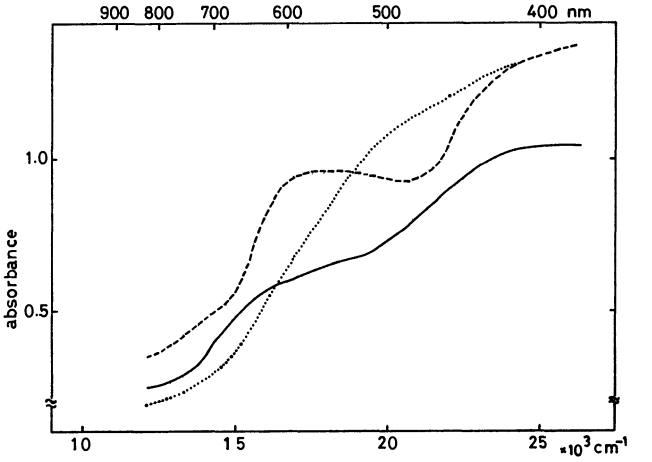

Fig. 3. Absorption spectra of $Co(2AP)_2X_2$ measured by the diffuse reflectance method.
Solid line: X=Cl, Broken line: X=Br,
Dotted line: X=I.

transition bands at 750 nm, the band at 390 nm for the bromo complex can be assigned to a charge-transfer band, whereas the corresponding band is not observed

for the chloro complex, since the band is expected to appear there at a wavelength shorter than that of the bromo complex. The spectra of 2AP-copper complexes resemble that of the copper complex of pyridine-2-carboxamide,[5-7] the shift to the longer wavelength may be due to the difference in the coordinated aquo molecule and halide ions, so the same distorted octahedral structure is conceivable.

Figure 2 shows that $Ni(2AP)_2Cl_2$ gives d-d transition bands at 580 and 660 nm, while for $Ni(2AP)_2Br_2$ only one band, at 530 nm and with a shoulder at 760 nm, is observed. $Ni(2AP)_2I_2$ shows d-d transition bands at 510 and 670 nm, the latter being observed only as a shoulder. The additional band at 390 nm, characteristic of the iodo complex, may be due to the charge transfer. Moreover, the fact that the absorbance of the nickel complexes is nearly the same as those of the copper and cobalt complexes may indicate an octahedral structure for $Ni(2AP)_2X_2$, because one of the characteristic features of tetrahedral nickel complexes is that the molar absorption coefficient is relatively higher than those of the corresponding first-transition-metal complexes. Therefore, the d-d bands observed may be assignable to the $^3A_{2g}\rightarrow{}^3T_{1g}$ transition and the splitting may be due to the mixing of the spin orbital of $^3T_{1g}(F)$ and ^1E_g, as has been reported for the hexaaquonickel(II) complex.[10]

Figure 3 shows that, among the $Co(2AP)_2X_2$ complexes only $Co(2AP)_2Br_2$ indicates a d-d transition band at 560 nm, while for $Co(2AP)_2Cl_2$ and $Co(2AP)_2I_2$ only shoulders around 650 and 500 nm respectively are observed. The band of the bromo complex is characteristic of an octahedral cobalt complex and may be assigned to the $^4T_{1g}(F)\rightarrow{}^4T_{1g}(P)$ transition.[11] However, for the other two complexes no conclusion has yet been deduced for their structures, because they show no absorption maxima.

Infrared Spectra. In the region of 1700—1500 cm^{-1} some characteristic bands due to the carbonyl group and pyridine-ring vibrations are observed in the metal complexes. These bands are shown in Figs. 4 and 5, together with that of the ligand. The stretching vibration of the carbonyl group of the ligand appears at 1700 cm^{-1}, while those of C=N and C=C in the pyridine ring appear at 1582 and 1565 cm^{-1}. Upon complex formation the stretching vibration of the carbonyl group shifts to lower frequencies, while the peak at 1582 cm^{-1} shifts to frequencies a little higher. However, the peak at 1565 cm^{-1} does not shift at all. The lower-frequency shifts of the carbonyl group indicate an interaction between the metals and the oxygen atom, while the higher-frequency shifts of the peak at 1582 cm^{-1} may suggest a bond formation of the metals and the ring nitrogen, for the dipolar contribution of $C=N^+$ in the pyridine ring increases, as has been observed in pyridine hydrogen chloride.[12,13] These stretching vibrations of C=N are not metal-sensitive and appear at a constant frequency of 1595 cm^{-1}; however, the order of shifts to lower frequencies of the carbonyl-stretching vibrations is Ni>Co>Cu>Zn in the bromo complexes. The copper complexes give peaks at 1685 and 1683 cm^{-1} for the chloro and the bromo complexes; those frequencies are higher than those of the other metal complexes examined, indicating a weaker interaction of copper with the oxygen atom. For the nickel complexes, the lower-frequency shifts of the carbonyl group depend on the halide ions; the shifts are observed in the following order of Cl>Br>I: 1665, 1653, and 1650 cm^{-1}.

The chloro complex of zinc, whose peak due to the carbonyl group appears at 1675 cm^{-1}, giving a somewhat different spectrum from those of the other two metal complexes, perhaps suggesting its structural difference. A remarkable difference in the far-infrared spectrum is alo observed; the question will be discussed more detail below. The bromo and iodo complexes give peaks at 1688 and 1675 cm^{-1}; it may be con-

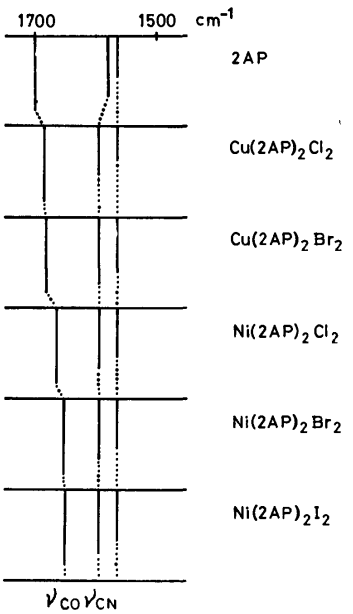

Fig. 4. Infrared spectra of the ligand, $Cu(2AP)_2X_2$, and $Ni(2AP)_2X_2$.

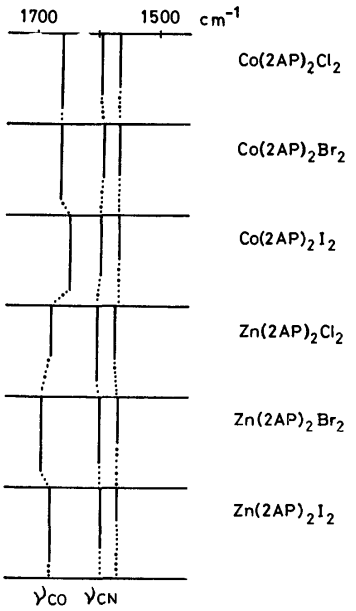

Fig. 5. Infrared spectra of $Co(2AP)_2X_2$ and $Zn(2AP)_2X_2$.

sidered from these shifts that zinc forms a weaker bond than those of the cobalt and nickel complexes.

These frequency shifts of the carbonyl group and the pyridine ring may lead to the conclusion of the chelate ring formation, which can easily be understood in view of the ligand structure and confirmed by the far-infrared data.

TABLE 2. FAR-INFRAREDRAL DATA FOR BIVALENT METAL COMPLEXES OF PYRIDINE AND α-PICOLINE (in cm^{-1})

Complexes	ν_{M-N}	ν_{M-X}	Structure
$CuCl_2 \cdot 2py$[a]	268	235(b)[b], 294(t)	Distorted polymeric octahedral
$CuBr_2 \cdot 2py$	269	202(b), 255(t)	Distorted polymeric octahedral
trans-$NiCl_2 \cdot 4py$	236	246	Monomeric octahedral
trans-$NiBr_2 \cdot 4py$	235	200	Monomeric octahedral
trans-$NiI_2 \cdot 4py$	240, 228	200	Monomeric octahedral
$NiCl_2 \cdot 2(\alpha\text{-pic})$[a]	239, 227	327, 297	Tetrahedral
$NiBr_2 \cdot 2(\alpha\text{-pic})$	239	256	Tetrahedral
trans-$CoCl_2 \cdot 4py$	217	230	Monomeric octahedral
trans-$CoBr_2 \cdot 4py$	200	214	Monomeric octahedral
$CoCl_2 \cdot 2py$	252	340, 304	Tetrahedral
$CoBr_2 \cdot 2py$	250	274, 242	Tetrahedral
$CoI_2 \cdot 2py$	237	246	Tetrahedral
$ZnCl_2 \cdot 2py$	220	329, 296	Tetrahedral
$ZnBr_2 \cdot 2py$	220	254	Tetrahedral

a) In this table py and α-pic denote pyridine and α-picoline, respectively. b) Small letters in parentheses, *i.e.*, t and b, denotes terminal and bridging halides, respectively.

Far-infrared Spectra. There have been accumulated very many data, especially concerning metal-halide complexes of pyridine and its derivatives, indicating that a change in halide ions does not affect the stretching vibrations of the metal-ligand; therefore, the absorption peaks which do remain at a fairly constant frequency upon the variation in the halide ions are attributable to the metal-ligand vibrations in $M(2AP)_2X_2$. Some far-infrared data of pyridine-metal complexes are shown in Table 2; they were utilized for the analyses of the spectra of $M(2AP)_2X_2$. The structural change has been proved to have remarkable effects on the stretching vibrations of the metal-halide and the metal-ligand. Moreover, for the $M(2AP)_2X_2$ complexes the far-infrared data present valuable information for the determination of their structures. In assigning the stretching vibrations of metal-ligand and metal-halide in $M(2AP)_2X_2$, the chelate ring formation is taken into account to produce the objective stretching vibrations at higher frequencies than those of the corresponding metal-pyridine complexes.

The far-infrared spectra of $M(2AP)_2X_2$ in the region of 600—200 cm^{-1} are shown in Figs. 6—9.

As is shown in Fig. 6, 2AP gives peaks at 593 and 412 cm^{-1} assignable to the in-plane and out-of-plane ring bending. The peak at 485 cm^{-1} may be assignable to the in-plane deformation mode of the acetyl group, while the peaks at 360 and 213 cm^{-1} are attributable to the pyridine-ring vibration and the acetyl torsion respectively.

$Cu(2AP)_2X_2$. Figure 6 shows the far-infrared spectra of $Cu(2AP)_2X_2$. The chloro complex has a strong but broad band at 275 cm^{-1}, with shoulders at 290 and 250 cm^{-1}. The bromo complex shows three bands, at 290, 250, and 225 cm^{-1}. Therefore, the common bands at 290 and 250 cm^{-1} are assignable to the chelate-ring vibrations, the former being mainly due to the stretching vibration of copper-nitrogen, and the latter, to that of copper-oxygen. The stretching vibration of copper-chloride may be assignable to the band at 275 cm^{-1}, and that of copper-bromide, to the band at 225 cm^{-1}, which is shifted 20—30 cm^{-1} toward the lower-frequency side than those of the terminal halide-copper in $CuX_2 \cdot 2py$ (py=pyridine). The theoretical prediction for infrared-active bands in octa-

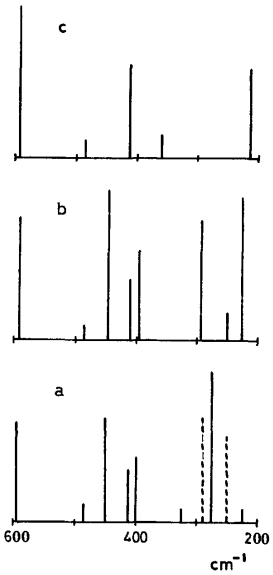

Fig. 6. Far-infrared spectra of the ligand and $Cu(2AP)_2X_2$.
a: X=Cl, b: X=Br, c: Ligand
broken line: Shoulder

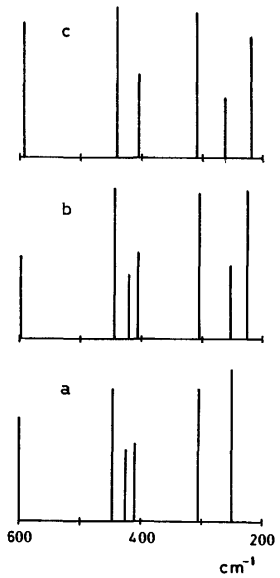

Fig. 7. Far-infrared spectra of $Ni(2AP)_2X_2$.
a: X=Cl, b: X=Br, c: X=I.

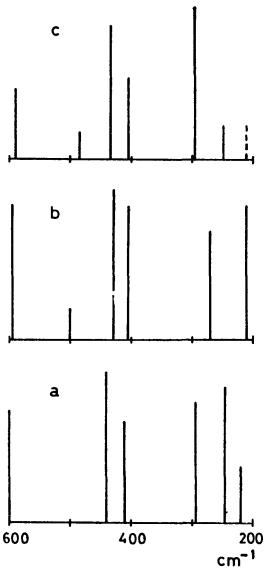

Fig. 8. Far-infrared spectra of $Co(2AP)_2X_2$.
a: X=Cl, b: X=Br, c: X=I,
broken line: shoulder

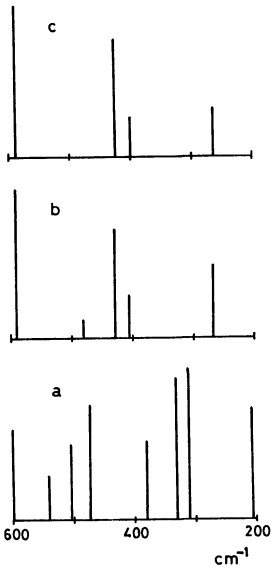

Fig. 9. Far-infrared spectra of $Zn(2AP)_2X_2$.
a: X=Cl, b: X=Br, c: X=I

hedral $Cu(2AP)_2X_2$ coincides with the number of bands observed; therefore, an octahedral structure with a *trans*-planar coordination of 2AP with halide ions bonded to the copper ion perpendicular to the chelate ring may be proposed.

Ni(2AP)$_2$X$_2$. Because of the chelate-ring formation in nickel complexes of 2AP, the bond distances between the nickel ion and the nitrogen atom will be shortened and the stretching vibrations may be expected to appear at higher frequencies than those of NiX_2–4py (py=pyridine). As is shown in Fig. 7, among the halogeno complexes examined only the chloro complex gives a band at 250 cm^{-1} assignable to the stretching vibration of nickel-chloride. The common bands are observed around 310—305 cm^{-1} and 260—250 cm^{-1}. These spectra of $Ni(2AP)_2X_2$, resembling those of octahedral $NiX_2 \cdot 4py$ (py=pyridine) rather than those of tetrahedral $NiCl_2(\alpha\text{-picoline})_2$, suggest a *trans*-planar octahedral structure.

Co(2AP)$_2$X$_2$. Since $Co(2AP)_2Cl_2$ and $Co(2AP)_2I_2$ are considered to have a tetrahedral structure belonging to the C_{2v} point group, four infrared-active cobalt-2AP stretching bands are expected to appear. However, only three bands are observed for these complexes, as is shown in Fig. 8, the missing band, due to the symmetric cobalt-oxygen stretching vibration, may appear below 200 cm^{-1}. The magnetic moment indicates an octahedral structure for $Co(2AP)_2Br_2$, where if 2AP coordinates in a *trans*-planar configuration two cobalt-2AP stretching vibrations should appear. This is the case in the bromo complex, for only two bands attributable to the stretching vibrations of cobalt-nitrogen and cobalt-oxygen are observed.

Zn(2AP)$_2$X$_2$. Among the $Zn(2AP)_2X_2$ complexes the bands about 265 cm^{-1} are consistent except for the chloro complex and may be assigned to the stretching bands of zinc-nitrogen. The chloro complex gives two bands, at 330 and 310 cm^{-1}, which are close to the asymmetric and symmetric stretching bands of zinc-chloride in tetrahedral $ZnCl_2 \cdot 2py$ (py=pyridine).[14] Therefore, they can be assigned to the asymmetric and symmetric stretching bands of zinc-chloride, indicating a *cis*-conformation of the chloride ions in $Zn(2AP)_2Cl_2$. It is sure that the chloro complex has structure different from that of the other two complexes, but the unavailability of magnetic moments and diffuse reflectance spectra makes it difficult to draw any definite conclusions.

Table 3. Experimental assignments of 2-acetylpyridine–metal complexes in the far-infrared region

Complexes	ν_{M-X}	ν_{M-N}	ν_{M-O}	Unassigned
$Cu(2AP)_2Cl_2$	275	(290) a)	(250)	
$Cu(2AP)_2Br_2$	225	293	250	
$Ni(2AP)_2Cl_2$	250	305	(250)	
$Ni(2AP)_2Br_2$		305	253	226
$Ni(2AP)_2I_2$		310	263	218
$Co(2AP)_2Cl_2$		296	218	
		245		
$Co(2AP)_2Br_2$		270	210	
$Co(2AP)_2I_2$		293	(215)	
		247		
$Zn(2AP)_2Cl_2$	330	205		
	310			
$Zn(2AP)_2Br_2$		267		
$Zn(2AP)_2I_2$		263		

a) Parenthesis denotes a shoulder.

Our experimental assignments of the far-infrared spectra are listed in Table 3. When the $M(2AP)_2X_2$ complexes are compared with $[M(piaH)_2(H_2O)_2]Cl_2$ (piaH=pyridine-2-carboxamide) from the standpoint of the far-infrared spectra, the former complexes have the following characteristics:

1) The existence of the chelate-ring vibrations of $M(2AP)_2X_2$ at frequencies lower than those of the corresponding $[M(piaH)_2(H_2O)_2]Cl_2$ may suggest lower

stability constants in the former than in the latter.
2) $Cu(2AP)_2X_2$ gives the copper-2AP stretching vibrations at frequencies rather lower than the other $M(2AP)_2X_2$ complexes.
3) $Co(2AP)_2Cl_2$ and $Co(2AP)_2I_2$ have a tendency to take a tetrahedral structure.
4) In $Zn(2AP)_2Cl_2$ the coordination of the chloride ion to zinc is in the *cis*-configuration.

Conclusion

Through the analyses of the magnetic moments, the diffuse reflectance spectra, and the infrared spectra, the following structures can be tentatively proposed for $M(2AP)_2X_2$. $Cu(2AP)_2X_2$ ($X=Cl^-$ and Br^-) are considered to have a mononuclear distorted octahedral structure, with a *trans*-planar conformation of the 2AP molecules to copper. For $Ni(2AP)_2X_2$ ($X=Cl^-$, Br^-, and I^-), an octahedral structure with a *trans*-planar coordination of 2AP is proposed. A tetrahedral structure may be assigned to $Co(2AP)_2Cl_2$ and $Co(2AP)_2I_2$, while for $Co(2AP)_2Br_2$ an octahedral structure with a *trans*-planar coordination of 2AP is supported.

The authors wish to thank Dr. N. Yamanaka of the Government Industrial Institute, Nagoya, for permitting them to use a Shimadzu MB-2 magnetic balance. Thanks are also due to Misses M. Ishiguro and S. Iwauchi of the Analytical Center of their university for the elemental analyses.

References

1) A part of this paper was presented at the 30th Annual Meeting of the Chemical Society of Japan, Osaka, April 1974.
2) B. Karson, *Isr. J. Chem.*, **6**, 1 (1968).
3) B. Karson, *ibid.*, **8**, 709 (1970).
4) K. Yamasaki and M. Sekizaki, This Bulletin, **38**, 2206 (1965).
5) M. Sekizaki, M. Tanase, and K. Yamasaki, *ibid.*, **42**, 399 (1969).
6) M. Sekizaki and K. Yamasaki, *Nippon Kagaku Zasshi*, **87**, 1053 (1966).
7) M. Sekizaki and K. Yamasaki, *Spectrochim. Acta*, **25A**, 475 (1969).
8) M. Nonoyama and K. Yamasaki, *Inorg. Chim. Acta*, **3**, 585 (1969).
9) A. Masuko, T. Nomura, and Y. Saito, This Bulletin, **40**, 511 (1967).
10) F. A. Cotton and G. Wilkinson, The Japanese Translation of "Advaced Inorganic Chemistry," 2nd Ed., Baifukan Ltd., Tokyo (1973), pp. 608—613.
11) F. A. Cotton and G. Wilkinson, The Japanese Translation of "Advanced Inorganic Chemistry," 2nd Ed., Baifukan Ltd., Tokyo (1973), pp. 778—790.
12) B. Witkop, *Experimentia*, **10**, 420 (1954).
13) B. Witkop, *J. Amer. Chem. Soc.*, **76**, 5597 (1954).
14) R. J. H. Clark and C. S. Williams, *Inorg. Chem.*, **4**, 350 (1965).
15) M. Goldstein, E. F. Mooney, A. Anderson, and H. A. Gebbie, *Spectrochim. Acta*, **21**, 105 (1965).
16) M. P. Springer and C. Curran, *Inorg. Chem.*, **2**, 1270 (1963).
17) C. W. Frank and L. B. Rogers, *ibid.*, **5**, 615 (1966).
18) P. T. T. Wong and D. G. Brewer, *Can. J. Chem.*, **46**, 139 (1968).
19) J. R. Allan, D. H. Brown, R. H. Nuttall, and D. W. A. Sharp, *J. Inorg. Nucl. Chem.*, **27**, 1305 (1965).

Studies of Bivalent Metal Chelates of 2-Aminomethylpyridine

Masahide Noji, Yoshinori Kidani, and Hisashi Koike*

Faculty of Pharmaceutical Sciences, Nagoya City University, 3-1 Tanabe-dori, Mizuho-ku, Nagoya 467

(Received June 11, 1974)

Bivalent metal chelates of 2-aminomethylpyridine (abbreviated as 2AMP), $M(2AMP)_2X_2$ (M=Cu, Ni, Co, and Zn ion; X=Cl^-, Br^-, I^-), were synthesized in ethanol. The magnetic moments and the diffuse reflectance spectra were measured. The $Cu(2AMP)_2X_2$ complexes (X=Cl^- and Br^-) were considered to have a monomeric distorted octahedral structure. The $Ni(2AMP)_2X_2$ complexes (X=Cl^-, Br^-, I^-) were also suggested to have an octahedral structure. However, for $Co(2AMP)_2Br_2$ and $Co(2AMP)_2I_2$ a tetrahedral and a square planar structure were proposed on the basis of their magnetic moments of 4.20 and 2.78 B.M. respectively. The infrared spectra of the chelates were analysed in relation to their structures; a good relationship was found between the structures and the far-infrared spectra.

Various metal chelates of 2-aminomethylpyridine have been studied by Sutton[1-3] and Michelsen[4] with regard to their electronic absorption spectra and magnetic moments. The stability constants were reported by Walter *et al.*[5] and Goldberg.[6] However, no infrared spectroscopic investigation of these chelates has ever been made. The present authors have now synthesized bivalent metal chelates of 2-aminomethylpyridine (abbreviated as 2AMP in this paper) in ethanol, that is, $M(2AMP)_2X_2$ complexes, M being copper(II), nickel(II), cobalt(II), and zinc(II) ions and X being chloride, bromide, and iodide ions. Among these complexes, two cobalt chelates, $Co(2AMP)_2Br_2$ and $Co(2AMP)_2I_2$ were newly prepared, but the chloro chelate was not obtained in spite of several trials.

In order to study their structures, the magnetic moments and the diffuse reflectance spectra were measured. By referring these data, the far-infrared spectra were then analysed in relation to the structures of the chelates obtained.

Experimental

Materials. The 2-aminomethylpyridine, a product of the Aldrich Chemical Co., Ltd., was used without further purification. The metal halides used were analytical-grade products of Wako Pure Chemical Industries, Ltd.

Preparation of Chelates. *Bis(2-aminomethylpyridine)cobalt(II) Halides*: To a solution containing 0.43 g (4 mmol) of the ligand in 10 ml of ethanol, we added 0.44 g (2 mmol) of cobalt bromide dissolved in 20 ml of ethanol; a dark brown powder was thus precipitated. The precipitate was collected by filtration and washed with ethanol.

The corresponding iodide was synthesized by a procedure similar to that used for the bromide chelate, which was obtained as a reddish-brown powder.

Found: C, 31.77; H, 3.95; N, 12.43; Co, 13.2%. Calcd for $Co(C_6H_8N_2)_2Br_2 \cdot H_2O$: C, 31.81; H, 4.01; N, 12.36; Co, 13.0%.

Found: C, 27.55; H, 3.05; N, 10.71; Co, 11.2%. Calcd for $Co(C_6H_8N_2)_2I_2$: C, 27.24; H, 3.05; N, 10.59; Co, 11.1%.

The other metal chelates were synthesized in ethanol by treating 2 mmol of the metal halides with 4 mmol of the ligand. The results of the elemental analyses of the metal chelates obtained are shown in Table 1.

Magnetic and Spectroscopic Measurements. The magnetic moments were measured by the Curie method with a Shimadzu MB-2 magnetic balance at room temperature. The diffuse reflectance spectra were measured with a Hitachi EPS-3T spectrophotometer equipped with an integrating-sphere accessory. For the measurements the chelates were diluted to a 0.25 molality with magnesium oxide, and pellets containing 150 mg of the mixtures were prepared under a 600 kg/cm^2 pressure after evacuation. A Nihon Bunko IRA-2 spectrophotometer was used to record the infrared spectra in the region from 4000 to 400 cm^{-1} using the KBr disc method and the Nujol and HCB mull method. The far-infrared spectra in the region of 600—200 cm^{-1} were measured with a Nihon Bunko DS-701G spectrophotometer using the Nujol mull method.

Table 1. Elemental analysis of $M(2AMP)_2X_2$

Chelates	Found (%)				Calcd (%)			
	C	H	N	M	C	H	N	M
$Cu(C_6H_8N_2)_2Cl_2$	40.95	4.68	15.90	17.7	41.09	4.60	15.97	18.1
$Cu(C_6H_8N_2)_2Br_2 \cdot 1/2H_2O$	32.09	3.57	12.57	14.4	32.13	3.82	12.49	14.2
$Ni(C_6H_8N_2)_2Cl_2 \cdot 3/4H_2O$	40.35	4.82	15.63	16.6	40.13	4.90	15.60	16.3
$Ni(C_6H_8N_2)_2Br_2$	32.87	3.56	12.83	13.6	33.15	3.71	12.88	13.5
$Ni(C_6H_8N_2)_2I_2$	27.10	3.02	10.59	11.2	27.25	3.05	10.59	11.1
$Zn(C_6H_8N_2)_2Cl_2 \cdot 1/4H_2O$	40.22	4.45	15.52	18.1	40.39	4.66	15.70	18.3
$Zn(C_6H_8N_2)_2Br_2$	32.72	3.45	12.73	14.5	32.65	3.65	12.69	14.9
$Zn(C_6H_8N_2)_2I_2$	26.87	3.00	10.45	12.4	26.91	3.01	10.46	12.2

* Present address: School of Medical Technology and Nursing, Fujita Gakuen University, Kutsukake, Toyoake City, Aichi Prefecture 470-11.

Results and Discussion

Magnetic Moments. The magnetic moments observed for $M(2AMP)_2X_2$ are listed in Table 2. The copper chelates give magnetic moments a little lower than that of the spin-only formula, indicating a negligible spin interaction among adjacent copper ions.

Table 2. Magnetic moments of $M(2AMP)_2X_2$ (19—21 °C)

Chelates	Observed	Calcd for spin-only formula
$Cu(2AMP)_2Cl_2$	1.64 B.M.	1.73 B.M.
$Cu(2AMP)_2Br_2$	1.71	1.73
$Ni(2AMP)_2Cl_2$	2.94	2.82
$Ni(2AMP)_2Br_2$	2.96	2.82
$Ni(2AMP)_2I_2$	2.94	2.82
$Co(2AMP)_2Br_2$	4.20	3.88
$Co(2AMP)_2I_2$	2.79	1.73
$Zn(2AMP)_2Cl_2$	Diamagnetic	
$Zn(2AMP)_2Br_2$	Diamagnetic	
$Zn(2AMP)_2I_2$	Diamagnetic	

The nickel chelates give values of the magnetic moments of 2.94—2.96 B.M., which are comparable to those reported for octahedral nickel complexes, *i.e.*, 2.9—3.4 B.M.

The magnetic moment of $Co(2AMP)_2Br_2$ is found to be 4.20 B.M., which is nearer to the values of 4.4—4.8 B.M. reported for tetrahedral cobalt complexes than to those of 4.7—5.2 B.M. for octahedral complexes.[7] On the other hand, $Co(2AMP)_2I_2$ gives a very low magnetic moment of 2.79 B.M., which can be related to the values of 2.4—2.8 B.M. reported for square planar cobalt complexes.[7]

All the zinc chelates show a diamagnetic character, as had been expected.

Diffuse Reflectance Spectra. The d-d transition bands appear at 610 nm, with a shoulder at 750 nm, for $Cu(2AMP)_2Cl_2$ and at 630 and 730 nm for $Cu(2AMP)_2Br_2$, as is shown in Fig. 1. The bands in the shorter-wavelength region are observed at a position similar to that of $Cu(2AMP)_2I_2$ in an aqueous solution,

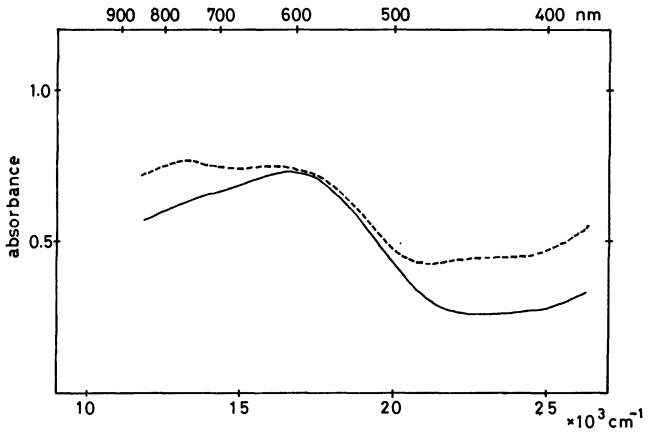

Fig. 1. Absorption spectra of $Cu(2AMP)_2X_2$ measured by the diffuse reflectance method.
—— $X=Cl^-$, ---- $X=Br^-$

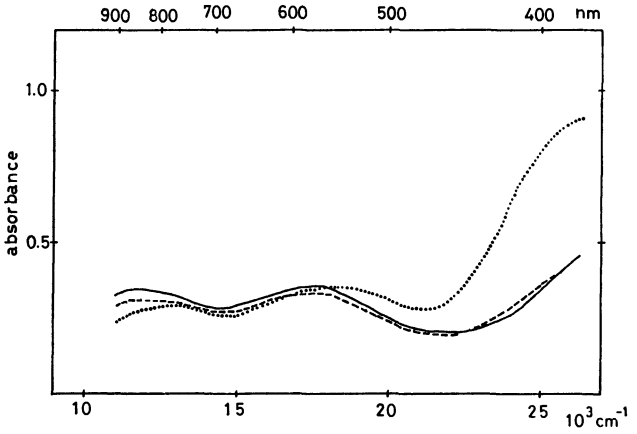

Fig. 2. Absorption spectra of $Ni(2AMP)_2X_2$ measured by the diffuse reflectance method.
—— $X=Cl^-$, ---- $X=Br^-$, ····· $X=I^-$

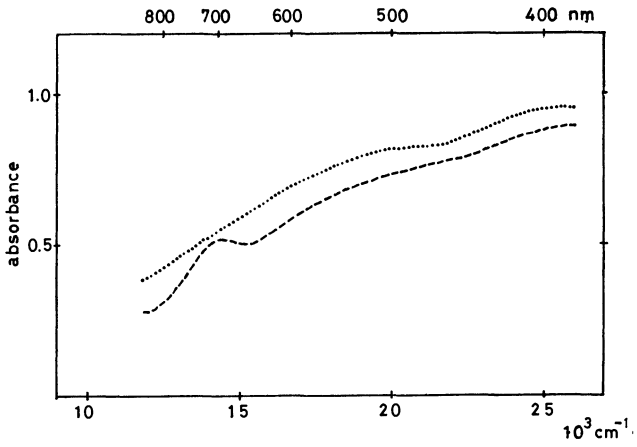

Fig. 3. Absorption spectra of $Co(2AMP)_2X_2$ measured by the diffuse reflectance method.
---- X=Br, ····· X=I

for which an octahedral structure has been proposed by Sutton.[8] Therefore, the same octahedral arrangement may be proposed for $Cu(2AMP)_2Cl_2$ and $Cu(2AMP)_2Br_2$, and the bands in the longer-wavelength region may arise from the orbital splitting due to a distortion from the octahedral configuration.

As is shown in Fig. 2, the three nickel chelates, $Ni(2AMP)_2X_2$, show spectra similar to one another, all with the d-d bands around 560—570 nm. The strong band at 380 nm of the iodo chelate may be assignable to the CT band, and a band is also observed at 770 nm. The corresponding bands for the chloro and bromo chelates appear around 850 nm. These d-d bands, all with low intensities, are characteristic of octahedral nickel complexes, which usually have molar absorption coefficients of 1—10. These diffuse reflectance spectra resemble the electronic absorption spectra of $[Nien_2(H_2O)_2]$ and $[Nibip_2(H_2O)_2]$; therefore, an octahedral structure can be assigned to $Ni(2AMP)_2X_2$, as has been postulated by Sutton.[1] The d-d bands in the shorter-wavelength region can be assigned to the $^3A_{2g}\rightarrow{}^3T_{1g}(F)$ and those in the longer-wavelength region, to the $^3A_{2g}\rightarrow{}^3T_{1g}(P)$ transition.[9]

The absorption spectra of $Co(2AMP)_2X_2$ are shown in Fig. 3. $Co(2AMP)_2Br_2$ shows the d-d band at 710 nm, as is characteristic of tetrahedral cobalt complexes, and in the shoter-wavelength region no distinct absorption maximum is observed. $Co(2AMP)_2I_2$ gives a very broad band around 500 nm, which is overlapped by the CT band at 380 nm. However, there has been reported little information as to the electronic absorption spectra of planar cobalt complexes; therefore, no difinite conclusion can be drawn from the diffuse reflectance spectrum for the structure of the iodide chelate.

Infrared Spectra. The chelate ring formation between 2AMP and the metal ions would bring about a lower-frequency shift of the stretching vibration of the amino group. The ligand shows both the asymmetric and symmetric stretching vibrations due to the amino group at 3370 and 3300 cm^{-1} respectively. These bands shift to a frequency side lower by 100—200 cm^{-1} upon the chelate formation, as is shown in Fig. 4.

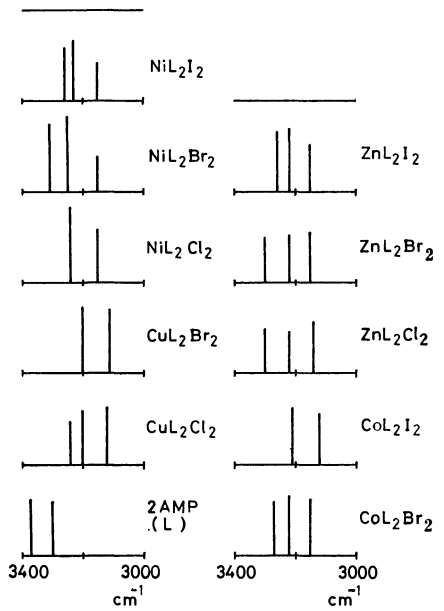

Fig. 4. Infrared spectra of 2AMP and $M(2AMP)_2X_2$ in the region of 3400—3000 cm^{-1}

The degree of the frequency shift is the largest for the copper chelates; among the other metal chelates, as is exemplified in the bromo system, the order of Cu(3200 cm^{-1})<Zn(3266 cm^{-1})<Co(3272 cm^{-1})<Ni(3305 cm^{-1}) is found for the asymmetric stretching vibrations. No regularity can be found in the effects of the halide ions on the stretching frequencies of the amino group.

The deformation frequency of the amino group in the ligand is observed at 1591 cm^{-1}; it shifts by about 10 cm^{-1} toward higher frequencies upon the chelate formation, contrary to the observation of the lower-frequency-side shifts of ammine complexes reported by Sacconi *et al.*[10]

Far Infrared Spectra. Figure 5 shows the far-infrared spectra of the ligand. It is very convenient to know that no peaks are observed below 400 cm^{-1}, since the metal complexes of pyridine derivatives usually

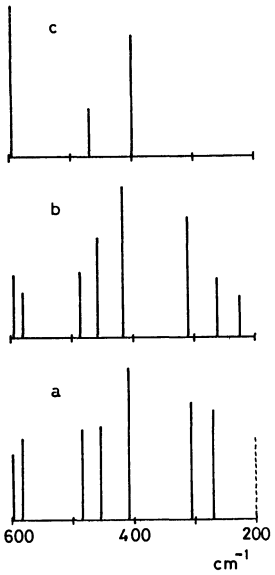

Fig. 5. Far-infrared spectra of 2AMP and $Cu(2AMP)_2X_2$
a: X=Cl, b: X=Br, broken line: shoulder
c: 2AMP

bring about absorption peaks due to the metal-pyridine nitrogen stretching vibrations below 400 cm^{-1}.

$Cu(2AMP)_2X_2$. The stretching vibration of copper-chloride is observed around 200 cm^{-1} as a broad peak; however, that of the copper-bromide is not observed above 200 cm^{-1}, as is shown in Fig. 5. The vibrations due to the chelate ring are found at 310—306 cm^{-1} and 270—263 cm^{-1}. The former may be assigned to the copper-amino nitrogen stretching, and the latter, to the copper-pyridine nitrogen stretching.

Clark and Williams[13] reported that the stretching vibration of copper-chloride in distorted octahedral pyridine complexes, $CuCl_2 \cdot 2py$ (py=pyridine), appeared at 294 and 235 cm^{-1} for the bridging-chloride and the terminal-chloride respectively. In this pyridine complex, the distance between the bridging-chloride and the copper ion was determined to be 3.05 Å by Dunitz,[14] but the peak at 200 cm^{-1} in $Cu(2AMP)_2Cl_2$ seems to indicate a longer bond distance between the chloride and the copper ion, with a stronger distortion from the octahedral structure than that of the pyridine complex. Therefore, a distorted octahedral structure is supported by the infrared spectra, coincinding with the result deduced from the magnetic moments and the diffuse reflectance spectra.

$Ni(2AMP)_2X_2$. As is shown in Fig. 6, the common peaks observed among the three nickel chelates are in two regions, 296—290 cm^{-1} and 255—250 cm^{-1}, which can be assigned to the nickel-amino nitrogen and the nickel-pyridine nitrogen stretching vibrations respectively. The nickel-chloride stretching is found at 205 cm^{-1}, and the corresponding peaks of the bromo and iodo chelates are not observed above 200 cm^{-1}. The additional peaks at 234 and 235 cm^{-1} of the bromo and iodo chelates are left unassigned. Since the octahedral nickel chelates with a *trans*-planar coordination of 2AMP molecules belong to the C_{2h} point group, two peaks due to the Ni-2AMP stretching and one

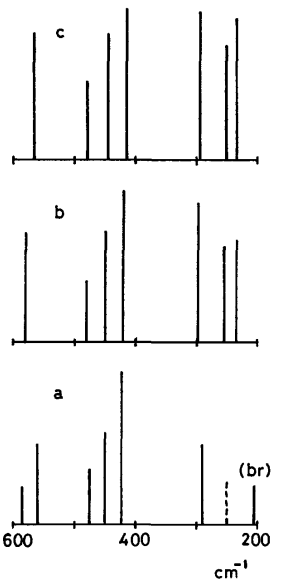

Fig. 6. Far-infrared spectra of $Ni(2AMP)_2X_2$
a: X=Cl, b: X=Br, c: X=I,
broken line: shoulder

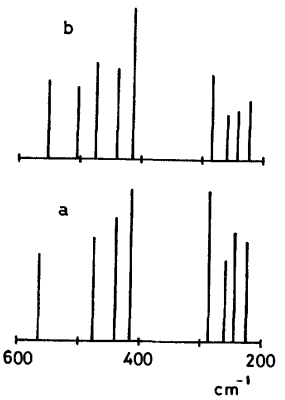

Fig. 7. Far-infrared spectra of $Co(2AMP)_2X_2$
a: X=Br, b: X=I

peak due to the nickel-halide stretching can be expected. Therefore, the far infrared spectra of $Ni(2AMP)_2X_2$ support an octahedral structure.

$Co(2AMP)_2X_2$. Figure 7 shows the far-infrared spectra of $Co(2AMP)_2X_2$. As it has been proposed from the magnetic moment that the bromide chelate is in a tetrahedral configuration which belongs to the C_{2v} point group, four Co-2AMP stretching bands can be expected. The measured spectrum of $Co(2AMP)_2Br_2$ shows four peaks assignable to Co-2AMP stretching vibrations and supports the tetrahedral structure.

The iodide chelate, which may be supposed from the magnetic moment to have a square planar configuration, also shows four peaks attributable to Co-2AMP stretching vibrations. If 2AMP molecules coordinate to cobalt ions in a *trans*-planar form belonging to the C_{2h} point group, two Co-2AMP stretching vibrations should appear. On the other hand, a *cis*-planar configuration, belonging to the C_{2v} point group, should bring about four Co-2AMP stretching vibrations; this is what is found for the iodide chelate.

$Zn(2AMP)_2X_2$. For the three zinc chelates, consistent peaks are observed in the regions of 243—240 cm^{-1} and 210—205 cm^{-1}. The peak at 270 cm^{-1} is characteristic of the chloro chelate and is assigned to the zinc-chloride stretching. These data seem to indicate an octahedral structure for the zinc chelates, with a *trans*-planar coordination of the 2AMP molecules to the zinc ion. The far-infrared assignments are listed in Table 3.

Table 3. The assignments of metal–nitrogen stretching frequencies of $M(2AMP)_2X_2$ (cm^{-1})

Chelates	ν_{M-X}	$\nu_{M-N\,(amino)}$	$\nu_{M-N\,(pyridine)}$	Unassigned
$Cu(2AMP)_2Cl_2$	200	306	270	
$Cu(2AMP)_2Br_2$		310	263	225
$Ni(2AMP)_2Cl_2$	205	290	250	
$Ni(2AMP)_2Br_2$		296	255	235
$Ni(2AMP)_2I_2$		296	252	234
$Co(2AMP)_2Br_2$		287(asym.)	245(asym.)	
		260(sym.)	224(sym.)	
$Co(2AMP)_2I_2$		287(asym.)	243(asym.)	
		260(sym.)	223(sym.)	
$Zn(2AMP)_2Cl_2$	270	240	210	
$Zn(2AMP)_2Br_2$		243	210	
$Zn(2AMP)_2I_2$		240	205	

The assignment of the metal-amino nitrogen to the higher-frequency region of the metal-2AMP stretching vibrations is made on the basis of the basicities of the objective nitrogen atoms. The dissociation constants of 2AMP have been reported to be $10^{-2.14}$ and $10^{-8.57}$ for the pyridine ring nitrogen and the amino nitrogen[11] respectively. The correlation between the pK values of the ligands and stability constants in heterocyclic ammine complexes with the silver ion has been reported to show a trend for the ligand with a higher pK value to have a larger stability constant.[12] This relationship can also be applied to other metal complexes. In the chelate ring of 2AMP with the bivalent metal ions, the linkage between the amino nitrogen and the metal ions may be much stronger than that of the pyridine nitrogen with the same metal ions, so that the former stretching vibration can be expected to appear at a higher frequency than that of the latter.

In order to ascertain the validity of the assignments

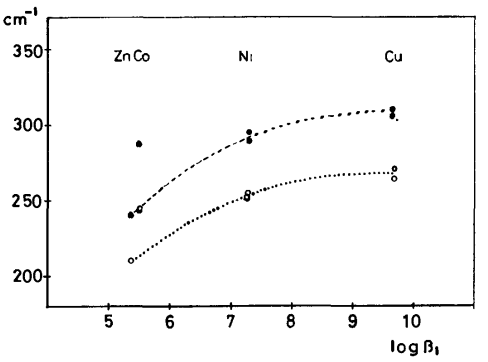

Fig. 8. Plots of M-N(amino) and M-N(pyridine) stretching frequencies *vs.* log β_1 for $M(2AMP)_2X_2$.
—●—●—●— M-N(amino)
···○···○···○··· M-N(pyridine)

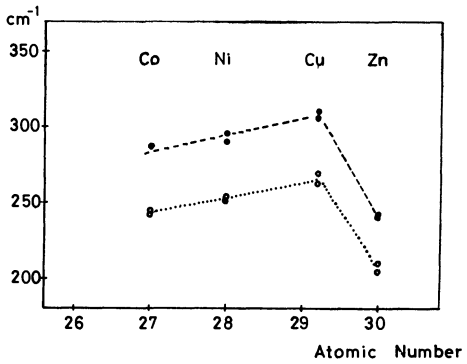

Fig. 9. Plots of M-N(amino) and M-N(pyridine) stretching frequencies *vs.* atomic number for $M(2AMP)_2X_2$.
—●—●—●— M-N(amino)
···○···○···○··· M-N(pyridine)

in the far-infrared spectra, plots were made of the metal-nitrogen stretching vibrations against the stability constants (log β_1) of $M(2AMP)_2X_2$ in aqueous solutions, as is shown in Fig. 8. The deviation of the cobalt chelates from the tendency shown by the other metal chelates may be attributed to their structural differences. However, the general trend for the metal-amino nitrogen stretching frequencies of the bromo chelates is in the following order; Zn(243 cm^{-1})<Cu(310 cm^{-1})> Ni(296 cm^{-1})>Co(287 cm^{-1}), coinciding with the Irving-Williams stability order. A further correlation, as is shown in Fig. 9, exists between the metal-2AMP stretching frequencies and the atomic numbers of the metal ions. The order found is the same as in the case of the stability constants; the Irving-Williams order also holds in spite of their structural differences.

Conclusion

The structures of the $M(2AMP)_2X_2$ complexes were studied by means of the magnetic moments, the diffuse reflectance spectra, and the far-infrared spectra. The $Cu(2AMP)_2X_2$ complexes are considered to have a monomeric distorted octahedral structure, while for $Ni(2AMP)_2X_2$ an octahedral configuration is proposed. The $Co(2AMP)_2Br_2$ complex has the magnetic moment of 4.20 B.M., and electronic absorption maximum at 710 nm, and four Co-2AMP stretching bands; therefore, an tetrahedral structure is proposed. A *trans*-planar configuration may be suitable for $Co(2AMP)_2I_2$, which has a very low magnetic moment of 2.79 B.M. and four Co-2AMP stretching vibrations in the far-infrared region. Only far-infrared spectra are available for $Zn(2AMP)_2X_2$, but the similarity of the spectra and the existence of the zinc-chloride stretching vibration seems to indicate an octahedral structure for the zinc chelates. The order of Zn<Cu>Ni>Co is found in the tentatively-assigned metal-2AMP stretching vibrations, coinciding with the Irving-Williams stability order.

The authors wish to thank Dr. N. Yamanaka of the Government Industrial Institute, Nagoya, for permitting them to use a Shimadzu MB-2 magnetic balance. Thanks are also due to Misses M. Ishiguro and S. Iwauchi of the Analytical Center of their university for the elemental analyses.

References

1) G. J. Sutton, *Aust. J. Chem.*, **13**, 74, 471 (1960).
2) G. J. Sutton, *ibid.*, **14**, 37, 545, 551 (1961).
3) G. J. Sutton, *ibid.*, **15**, 232 (1962).
4) K. Michelsen, *Acta Chem. Scand.*, **24**, 2003 (1970).
5) J. L. Walter, C. S. C. and S. M. Rosalie, O. S. F. *J. Inorg. Nucl. Chem.*, **28**, 2969 (1959).
6) D. E. Goldberg and W. C. W. Fernelis, *J. Phys. Chem.*, **63**, 1246 (1959).
7) F. A. Cotton and G. Wilkinson, The Japanese Translation of "Advanced Inorganic Chemistry," 2nd Ed., Baifukan, Tokyo (1973), pp. 784—786.
8) G. J. Sutton, *Aust. J. Chem.*, **13**, 222 (1960).
9) F. A. Cotton and G. Wilkinson, The Japanese Translation of "Advanced Inorganic Chemistry," 2nd Ed., Baifukan, Tokyo (1973), p. 793.
10) L. Sacconi, A. Sabatini, and P. Gans, *Inorg. Chem.*, **3**, 1772 (1964).
11) A. E. Martell and L. G. Sillen, "Stability Constants of Metal-Ion Complexes," The Chemical Society, Burlington House, London (1964), p. 482.
12) A. E. Martell and M. G. Calvin, "Chemistry of the Metal Chelates Compounds," Prentice-Hall Inc., Englewood Cliff, N. J. (1962), p. 158.
13) R. J. H. Clark and C. S. Williams, *Inorg. Chem.*, **4**, 350 (1965).
14) J. D. Dunitz, *Acta Crystallogr.*, **10**, 307 (1957).

gen chloride was added drop by drop to this solution. The initially dark brown solution turned greenish gradually up to moss green at the end. Petroleum ether (200 ml) was added slowly to the solution to separate out a moss green precipitate, of which filtration and vacuum-drying resulted in a very dark green powder. Yield: 0.4 g, 48%. Found: Mn, 23.14; Cl, 30.20; C, 24.06; H, 3.55%. Calcd for $MnCl_2(acac)H_2O$= $C_5H_9O_3Cl_2Mn$: Mn, 22.61; Cl, 29.18; C, 24.72; H, 3.73%. After standing at room temperature the color changed to dark brown.

Preparation of Dichloro(acetylacetonato)bis(pyridine oxide)manganese(III): Pyridine oxide, O-py (2.3 g, 23.9 mmol) was added to a solution of $Mn(acac)_3$ (2.1 g, 6.0 mmol) in methylene chloride (40 ml), and the solution was kept at −78 °C. A methylene chloride solution of hydrogen chloride (12.0 mmol) was added dropwise to this solution. After the reaction an ochreous powder was isolated by the addition of 200 ml of petroleum ether. Yield: 2.0 g, 81%. Found: Mn, 14.06; Cl, 17.69; C, 44.40; H, 4.47; N, 6.24%. Calcd for $MnCl_2(acac)(O\text{-}py)_2$=$C_{15}H_{17}O_4N_2Cl_2Mn$: Mn, 13.23; Cl, 17.08; C, 43.40; H, 4.13; N, 6.75%.

The Reactions of $MnBr(acac)_2$ and $MnI(acac)_2$ with Hydrogen Bromide or Iodide: When a solution of hydrogen bromide (6.8 mmol) in methylene chloride was added at room temperature to a solution of $MnBr(acac)_2$ (1.1 g, 3.4 mmol) in the same solvent, a white precipitate of manganese(II) bromide was produced in a 100% yield, leaving a colorless supernatant solution. Found: Mn, 24.26; Br, 72.69%. The equimolar reaction of $MnBr(acac)_2$ with hydrogen bromide at −78 °C was also examined, but a product of the composition $MnBr_2(acac)\cdot nH_2O$ was not obtained. The reaction of excess hydrogen iodide with $MnI(acac)_2$ in methylene chloride afforded bis(acetylacetonato)manganese(II). Found: C, 45.10; H, 5.26%.

Preparation of Dibromobis(acetylacetone)manganese(II): Tris(acetylacetonato)manganese(III) (1.4 g, 3.8 mmol) was dissolved in a mixture (20 ml) of methylene chloride and acetylacetone (1: 1 by volume). A methylene chloride solution of hydrogen bromide (11.4 mmol) was added dropwise to this solution with vigorous stirring. White tiny crystals were carefully filtered, quickly washed with petroleum ether, and dried under vacuum. Yield 1.2 g, 77%. Found: Mn, 13.10; Br, 38.97; C, 28.20; H, 3.74%. Calcd for $MnBr_2(acacH)_2$= $C_{10}H_{16}O_4Br_2Mn$: Mn, 13.24; Br, 38.51; C, 28.93; H, 3.89%.

Preparation of the Base Adducts of Halogenobis(acetylacetonato)-manganese(III). $Mn(acac)_3$ was allowed to react with an equimolar amount of hydrogen halide in a mixture of diethyl ether, benzene and a base in a similar fashion as described above. Alternatively, $MnX(acac)_2$ was dissolved in acetylacetone containing excess base and heated to 60—70 °C. After filtration of the undissolved residue, the filtrate was kept in a desiccator for a long time to separate out the product.

Chlorobis(acetylacetonato)(pyridine oxide)manganese(III): Pyridine oxide (2.7 g, 28.5 mmol) was added to a solution of $Mn(acac)_3$ (2.5 g, 7.1 mmol) in a mixture of diethyl ether and benzene (4: 1 by volume). A solution of hydrogen chloride (7.1 mmol) in methylene chloride was added drop by drop to this solution. Ochreous crystals (1.8 g) were obtained in a 65% yield. Found: Mn, 14.51; Cl, 8.82; C, 46.21; H, 4.94; N, 4.29%. Calcd for $MnCl(acac)_2$-$(O\text{-}py)$=$C_{15}H_{19}O_5NClMn$: Mn, 14.32; Cl, 9.24; C, 46.95; H, 4.99; N, 3.65%.

Bromobis(acetylacetonato)dioxanemanganese(III) Monohydrate: $Mn(acac)_3$ (2.1 g, 6.0 mmol) was dissolved in a mixture of diethyl ether and benzene (130 ml, 3: 1 by volume) containing dioxane (40 ml). A solution of hydrogen bromide (6.0 mmol) in methylene chloride was added to this solution and allowed to react for 6—7 hr. Black-brown crystals of product (1.0 g) were obtained in a 38% yield. Found: Mn, 12.65; Br, 18.33; C, 38.33; H, 5.56%. Calcd for $MnBr(acac)_2(C_4H_8O_2)\cdot H_2O$=$C_{14}H_{24}O_7BrMn$: Mn, 12.51; Br, 18.19; C, 38.29; H, 5.51%.

Bromobis(acetylacetonato)(4-methylpyridine)manganese(III): $MnBr(acac)_2$ (1.1 g, 3.4 mmol) was dissolved in 50 ml of acetylacetone containing 4-methylpyridine, 4-Me-py (1.2 g, 12.9 mmol), and the mixture was warmed to 60 °C for a while and filtered. The filtrate was kept standing in a desiccator for two days to afford light red crystals. Yield: 0.3 g, 22%. Found: Mn, 13.14; Br, 17.67; C, 45.15; H, 5.02; N, 3.37%. Calcd for $MnBr(acac)_2(4\text{-}Me\text{-}py)$=$C_{16}H_{21}$-$O_4NBrMn$: Mn, 12.89; Br, 18.75; C, 45.09; H, 4.97; N, 3.29%.

Bis(acetylacetonato)diaquomanganese(III) Bromide Dihydrate: $MnBr(acac)_2$ (1.0 g, 3.0 mmol) was dissolved in 40 ml of acetylacetone saturated with water on a hot water-bath. The solution was then kept standing at room temperature to deposit olive-green needles, which were washed with diethyl ether. Yield 0.36 g, 30%. Found: Mn, 13.63; Br, 19.95; C, 30.28; H, 5.46%. Calcd for $[Mn(acac)_2(H_2O)_2]Br\cdot 2H_2O$=$C_{10}H_{22}O_8BrMn$: Mn, 13.56; Br, 19.72; C, 29.65; H, 5.47%. The corresponding chloride $[Mn(acac)_2(H_2O)_2]Cl\cdot 2H_2O$ was also derived in a similar way from $MnCl(acac)_2$ in a 32% yield, and identified by the IR spectra.

The Ligand Substitution of Chlorobis(acetylacetonato)manganese-(III) with Dibenzoylmethane. A solution of dibenzoylmethane, dbmH (1.7 g, 7.5 mmol) in methylene chloride (10 ml) was added slowly to a solution of $MnCl(acac)_2$ (1.0 g, 3.7 mmol) in the same solvent (20 ml), and the mixture was kept standing for 1 hr at room temperature to separate out light red crystals of $MnCl(dbm)_2$. Yield: 0.55 g, 30%. Found: Mn, 10.11; Cl, 6.33; C, 66.05; H, 4.22%. Calcd for $MnCl(dbm)_2$=$C_{30}H_{22}O_4ClMn$: Mn, 10.23; Cl, 6.60; C, 67.11; H, 4.13%.

Analysis. Each specimen of compounds was dried *in vacuo* at room temperature before subjecting to elemental analysis. The content of manganese was determined gravimetrically as manganese(II) sulfate, and those of chlorine and bromine as the silver salts. The concentration of hydrogen chloride and bromide in methylene chloride was measured by the method reported previously.[1]

Measurements. The visible and ultraviolet absorption spectra were measured by means of a Hitachi EPS-3T autorecording spectrophotometer. The infrared spectra were taken in Nujol on JASCO IR-E (4000—700 cm^{-1}), Hitachi EPI-L (700—200 cm^{-1}) and FIS-3 (400—30 cm^{-1}) infrared spectrophotometers.

The magnetic susceptibility was measured at various temperatures down to 77 K by the Gouy method with an automatically recording magnetic balance MB-2 of Shimadzu Seisakusho Co., Ltd. Hexaamminechromium(III) chloride was prepared and used as a reference. Found: H, 6.97; N, 32.50%. Calcd for $[Cr(NH_3)_6]Cl_3$=$H_{18}N_6Cl_3Cr$: H, 6.96; N, 32.26%.

The molecular weight was determined by the vapor-pressure osmometry with an apparatus manufactured by Knauer, Germany. Methanol and methylene chloride were used as the solvent, and benzil as a reference. The electric conductivity was measured in methanol or nitromethane by means of an MY-SERIAL 814007 apparatus of Yanagimoto Seisakusho, Ltd. The thermogravimetric measurement was performed with a thermo-spring-balance C-282 of Hamada Denki Seisakusho, Ltd.

Table 1. Molecular weight, conductance and magnetic moment data of halogenobis(acetylacetonato)manganese(III)[a]

Complex	Molecular weight			Molar conductance at 25 °C/ohm^{-1}·cm^2·mol^{-1}		Magnetic moment at (temp.)/B.M.
	in CH_2Cl_2 at 37 °C	in CH_3OH at 45 °C	Calcd	in CH_3NO_2	in CH_3OH	
$MnCl(acac)_2$	283	154	289	16	102	4.88 (20 °C)
$MnBr(acac)_2$	312[b]	157	333	18	88	4.93 (21 °C)
$MnI(acac)_2$	346	198	380	28	85	4.72 (22 °C)

a) The molecular weight was measured at 1.5—4.5 × 10^{-2} M, and the molar conductance at 5 × 10^{-4} M.
b) Measured at 25 °C.

Results

Tris(acetylacetonato)manganese(III) readily reacts with excess hydrogen chloride, bromide or iodide in organic solvents to produce manganese(II) chloride, bromide or bis(acetylacetonato)manganese(II), respectively. These redox reactions seem to proceed successively *via* a few intermediates. In fact several halogenobis(acetylacetonato)- and dichloroacetylacetonato-manganese(III) complexes have been isolated as intermediary products under the controlled reaction conditions.

Characterization of Halogenobis(acetylacetonato)manganese(III). The primary intermediate was afforded by the equimolar reaction between $Mn(acac)_3$ and hydrogen halide. The composition was established by the elemental analysis to be $MnX(acac)_2$, where X is Cl, Br, or I. As shown in Table 1 the magnetic moment at room temperature lies in the range of 4.72—4.93 B.M., indicating that they are all high-spin Mn(III) complexes.

The molecular weight determined in methylene chloride is near to the calculated value, indicating that each of the $MnX(acac)_2$ complexes exists essentially as a discrete molecule in the non-coordinating solvent. The measurement was performed at several concentrations in the range of (1.5—4.5) × 10^{-2} M, and no appreciable dependence of the molecular weight on concentration was noticed. However, close examination of the figures in Table 1 discloses that the discrepancy between the observed and the calculated values becomes larger in the order of X=Cl<Br<I. The molar conductance in nitromethane at 25 °C also indicates that they are essentially nonelectrolytes in this solvent, but the observed values show a slight increase in the same order. These results might indicate that the $MnX(acac)_2$ complexes have some tendencies to ionize even in the non-coordinating solvent increasing in the order of X=Cl<Br<I.

In methanol they dissociate almost completely and the observed molecular weight nearly coincides with half of the formular weight. The molar conductance in the same solvent reveals that the halide ion is extensively dissociated although the value is smaller in comparison with 118 ohm^{-1}·cm^2·mol^{-1} of tetraethylammonium iodide in methanol (113 ohm^{-1}·cm^2·mol^{-1} in nitromethane). It may be presumed that the complex is solvolyzed in methanol and the manganese(III) atom is six-coordinated:

$$MnX(acac)_2 + 2CH_3OH \longrightarrow Mn(acac)_2(CH_3OH)_2^+ + X^-$$

The assumed compound $[Mn(acac)_2(CH_3OH)_2]X$ could not be isolated, but recrystallization of $MnCl(acac)_2$ from acetylacetone saturated with water afforded $[Mn(acac)_2(H_2O)_2]Cl\cdot 2H_2O$. The corresponding bromide $[Mn(acac)_2(H_2O)_2]Br\cdot 2H_2O$ was also obtained from $MnBr(acac)_2$ in a similar way. Bis(acetylacetonato)-diaquomanganese(III) chloride had previously been prepared by Cartledge[7] by the trituration of $Mn(acac)_3$ with 1F hydrochloric acid or by the following reaction.

$$4MnCl_2 + KMnO_4 + 10acacH + 6H_2O = 5[Mn(acac)_2(H_2O)_2]Cl + KCl + 2HCl$$

Funk and Kreis prepared $MnCl(acac)_2$ and $MnCl_2(acac)$ by the reaction of manganese(III) chloride with acetylacetone in diethyl ether at −40 °C, but reported nothing about their properties.[8] The complexes $MnBr(acac)_2$ and $MnI(acac)_2$ are new compounds. On the other hand, the Mn(III) Schiff base (SBH_2) complexes of the type MnX(SB) have been studied rather extensively[9,10] in connection with the biological interest,[11] and their behaviors in solution were investigated. Van den Bergen, *et al.*[12] recorded the molar conductance of $MnBr(sal\text{-}N\text{-}Pr^n)_2$ and $MnOCOCH_3(sal\text{-}N\text{-}Pr^n)_2$ in nitromethane to be 4.96 and 0.192 ohm^{-1}·cm^2·mol^{-1}, respectively, and that of MnBr(salen) and MnI(salen) in methanol to be 69 and 71 ohm^{-1}·cm^2·mol^{-1}, respectively. Here sal-N-Pr^n denotes salicylaldehyde-*n*-propylimine, and salen*N,N'*-bis(salicylidene)ethylenediamine. The conductance data reported by Prabhakaram and Patel also reveal that the MnX(salen) complexes (X=Cl, Br, or I) dissociate very little in acetonitrile, while to a considerable extent in methanol and water.[13]

Infrared Spectra: In order to obtain informations concerning the structure of the $MnX(acac)_2$ complexes, their infrared spectra were measured in Nujol mull. In Fig. 1 the spectrum of $MnCl(acac)_2$ is compared with that of $FeCl(acac)_2$ which was prepared by the reaction of $Fe(acac)_3$ with hydrogen chloride in methylene chloride.[5] The parent complex $Mn(acac)_3$ shows the ν_s(C=O) and ν_{as}(C=C=C) bands at 1585 and 1520 cm^{-1}, and $Fe(acac)_3$ at 1565 and 1525 cm^{-1}, respectively. The higher frequency bands are lost in both $MnCl(acac)_2$ and $FeCl(acac)_2$, and shoulders are observed at 1546 and 1549 cm^{-1}, respectively. The δ(C–H) band around 1200 cm^{-1} is very much weaker

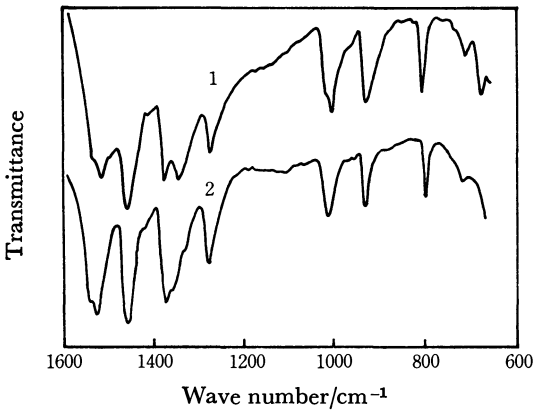

Fig. 1. Infrared spectra of $MnCl(acac)_2$ (curve 1) and $FeCl(acac)_2$ (curve 2).

in $MCl(acac)_2$ than in $M(acac)_3$, and the absorption assigned to $\nu_s(C{=}C{-}C)$ is shifted to the higher frequency 1280—1290 cm^{-1} region in the former mixed-ligand complex. Such a close resemblance in the IR spectra of $MnCl(acac)_2$ and $FeCl(acac)_2$ strongly suggests that both complexes have the same structure.

The molecular structure of $FeCl(acac)_2$ was determined by the X-ray analysis to be square-pyramidal with the chlorine atom located at the apical position,[14] and hence $MnCl(acac)_2$ can also be assumed to have the square-pyramidal structure, and not the trigonal-bipyramidal geometry. The IR spectra of $MnBr(acac)_2$ and $MnI(acac)_2$ are quite similar to that of the chloro complex, implying the structural analogy.

The infrared spectra in the 400—150 cm^{-1} region are shown in Fig. 2. The peak around 343 cm^{-1} is observed for each of the three $MnX(acac)_2$ complexes in common, and thus assigned to the ν(Mn–O) vibration. The corresponding absorption appears at 335 cm^{-1} in the parent complex $Mn(acac)_3$, and at 375 and 348 cm^{-1} in tris(salicylaldehydato)manganese(III).[12]

The stretching vibration of the terminal Mn(III)–Cl bond is observed in the 270—340 cm^{-1} region for the $MnCl_3L_3$ complexes where L is the oxide of pyridine, triphenylphosphine, or triphenylarsine,[15] and at 310 cm^{-1} for $MnCl(sal\text{-}N\text{-}Pr^n)_2$.[12] Thus the strong peak observed at 290 cm^{-1} for the present chloro complex $MnCl(acac)_2$ (Fig. 2) can reasonably be assigned to the ν(Mn–Cl) vibration. The corresponding strong absorption of $MnBr(acac)_2$ at 262 cm^{-1} is attributed to the ν(Mn–Br) vibration. Boucher[16] ascribed the most prominent absorption of the supposedly octahedral Mn(III) complex $MnX(H_2O)$ (protoporphyrin IX dimethyl ester) in the 650—160 cm^{-1} region to the manganese-halogen stretching vibration: 462 cm^{-1} for F^-, 262 cm^{-1} for Cl^-, 211 cm^{-1} for Br^-, and 190 cm^{-1} for I^-. These frequencies are rather low in comparison with the above-mentioned data, but show the expected decrease with the increasing mass of the halogen.

As is indicated in Fig. 2, $MnI(acac)_2$ exhibits two peaks in the ν(Mn–X) region. It can not be unequivocally concluded at the present stage of investigation which of the two bands at 254 and 219 cm^{-1} is related to the ν(Mn–I) vibration. Here we tentatively assign the 219 cm^{-1} peak to the ν(Mn–I) on a consideration of the mass effect. At any rate the fact that the frequencies of the ν(M–X) vibrations in the $MnX(acac)_2$ complexes lie in the region acceptable for the terminal Mn–X bonds is also compatible with the proposed five-coordinate structure.

Electronic Spectra: The $MnCl_5^{2-}$ ion was found to have a slightly elongated square-pyramidal structure in the bipyridinium[17] and phenanthrolinium[18] salts. Crystal polarized spectra of these Mn(III) compounds were recorded by Bellitto, *et al.*,[19] and it was concluded that three d-d transitions occur at $<20\times10^3$ cm^{-1}, and that the absorption present at *ca.* 24×10^3 cm^{-1} is due to

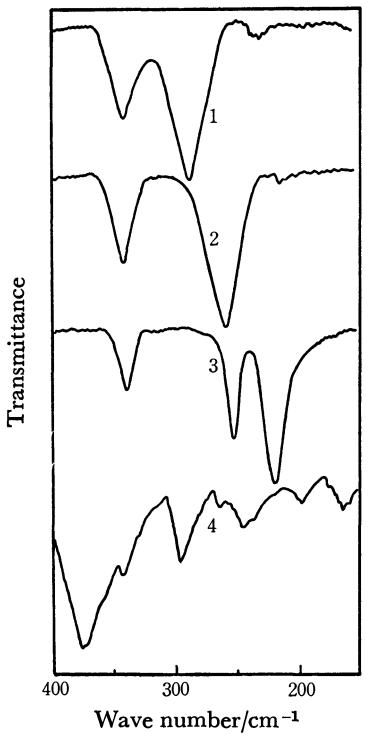

Fig. 2. Infrared spectra in the low-frequency region of $MnX(acac)_2$, where X=Cl (curve 1), Br (curve 2), or I (curve 3), and $MnCl_2(acac)\cdot H_2O$ (curve 4).

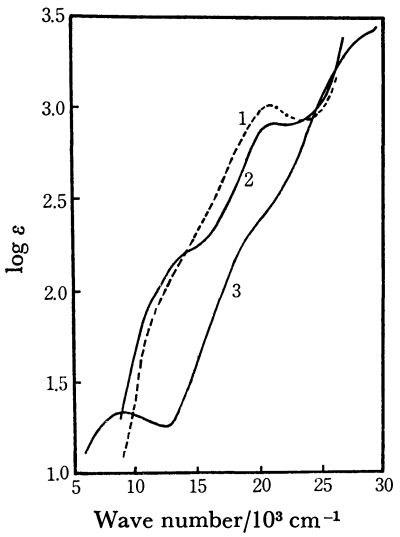

Fig. 3. Absorption spectra of $MnX(acac)_2$ in CH_2Cl_2, where X=Cl (curve 1), Br (curve 2), or I (curve 3).

a charge transfer transition. Boucher[20] also measured absorption spectra of several Schiff base complexes MnCl(SB), and assigned weak absorptions in the 12—21 $\times 10^3\,cm^{-1}$ region to the d-d transitions.

The observed visible absorption spectra of the present $MnX(acac)_2$ complexes in methylene chloride are reproduced in Fig. 3. The bromo complex shows a maximum at $20.8\times10^3\,cm^{-1}$ ($\varepsilon=850$) and two discernible shoulders at 14.3 and $11.8\times10^3\,cm^{-1}$. The chloro complex also exhibits a more intense maximum at $20.8\times10^3\,cm^{-1}$ ($\varepsilon=1070$) and very broad indistinct shoulders in the 14.3—$10\times10^3\,cm^{-1}$ region. On the other hand $MnI(acac)_2$ has shoulders at *ca.* 27.8 and $20\times10^3\,cm^{-1}$, and a broad maximum at $9.1\times10^3\,cm^{-1}$ ($\varepsilon=23$). Low energy absorptions below $20\times10^3\,cm^{-1}$ may be assigned to the d-d transitions. The reason is not clear why only the iodo complex shows a distinct maximum in the $9\times10^3\,cm^{-1}$ region, while its spectrum in methanol (Fig. 4) is quite similar to those of chloro and bromo complexes.

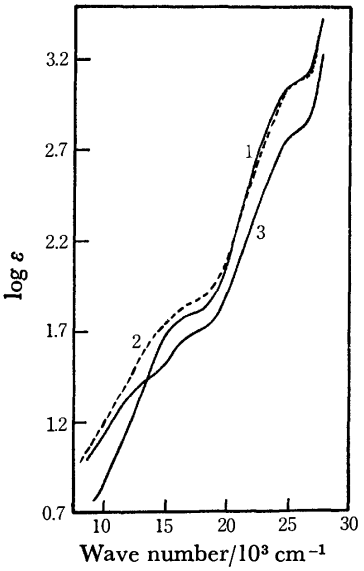

Fig. 4. Absorption spectra of $MnX(acac)_2$ in methanol, where X=Cl (curve 1), Br (curve 2), or I (curve 3).

The absorption bands at $20.8\times10^3\,cm^{-1}$ observed for methylene chloride solutions of both the chloro and bromo complexes and a shoulder at $27.8\times10^3\,cm^{-1}$ of the iodo complex seem to be ascribed to the same transition. In methanol all these absorptions appear equally as a shoulder at $25\times10^3\,cm^{-1}$. It is difficult to conclude that they are assigned to the charge transfers, since they are supported by the general (background) absorption though their extinction coefficients are apparently high.

Magnetic Properties: The magnetic susceptibility of the $MnX(acac)_2$ complexes was determined at lower temperatures down to 77 K. The reciprocal of the molar susceptibility corrected for diamagnetism was plotted in Fig. 5 against the absolute temperature. All of these three compounds gave good straight lines, indicating to obey the Curie-Weiss law $\chi_M'=C/(T+\theta)$. The θ values were obtained from an extrapolation of the straight line to be 13, 11, and 68 K for the chloro, bromo, and iodo complexes, respectively.

Preparation of Dibromobis(acetylacetone)manganese (II).

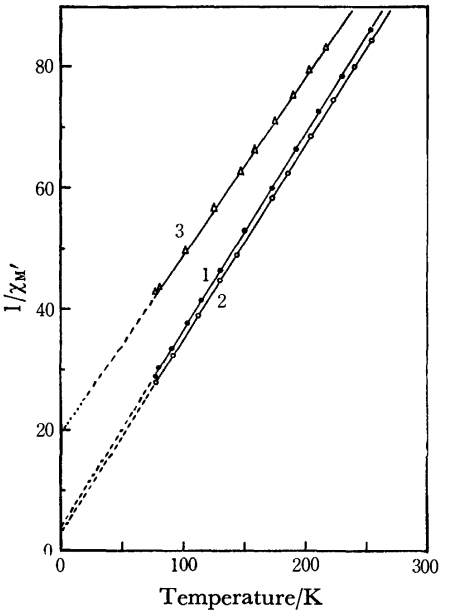

Fig. 5. Curie-Weiss plots for $MnCl(acac)_2$ (1), $MnBr(acac)_2$ (2) and $MnI(acac)_2$ (3).

As described already the reaction of excess hydrogen bromide with $Mn(acac)_3$ in methylene chloride afforded $MnBr_2$ quantitatively, but if acetylacetone had been added in advance to the solution, $MnBr_2(acacH)_2$ was produced in a good yield. This compound was previously prepared by the reaction of anhydrous $MnBr_2$ with acetylacetone,[21] but the present method offers a much more convenient route. Preparation of the corresponding chloro complex in a similar way was unsuccessful presumably because of instability of $MnCl_2(acacH)_2$.

The Six-coordinate Mixed Ligand Mn(III) Complexes. The five-coordinate complex $MnX(acac)_2$ is readily solvolyzed in methanol, producing the presumably six-coordinate cation $Mn(acac)_2(CH_3OH)_2^+$. Similarly the formula $[Mn(acac)_2(H_2O)_2]X\cdot2H_2O$ (X=Cl, Br) was assigned to the tetra-hydrate obtained by the recrystallization of $MnX(acac)_2$ from acetylacetone containing water. Non-existence of the ν(Mn–X) vibration in the IR spectrum of these salts indicates that the halide ion does not exist in the coordination sphere. As illustrated in Fig. 6 the thermogravimetric analysis of the bromide

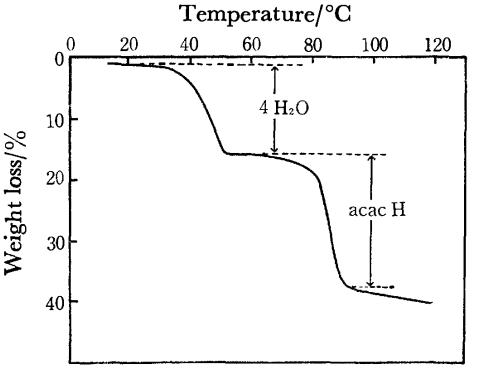

Fig. 6. Thermogravimetric analysis of $[Mn(acac)_2(H_2O)_2]Br\cdot2H_2O$ under vacuum at the heating rate of 10 °C/hr.

Fig. 7. The IR spectrum in the 1700—1500 cm^{-1} region of $[Mn(acac)_2(H_2O)_2]Cl \cdot 2H_2O$ (curve 1) and that after heating for a while at 50 °C (curve 2).

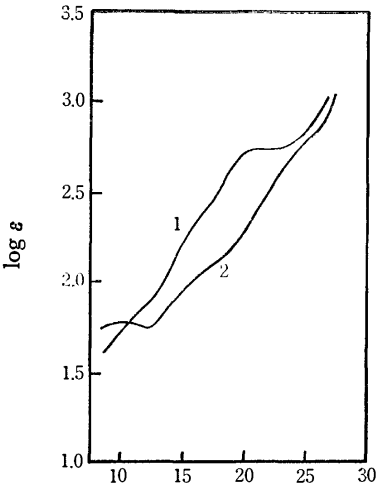

Fig. 8. Absorption spectra of $MnCl(acac)_2(O\text{-}py)$ in CH_2Cl_2 in the absence (curve 1) and the presence (curve 2) of added pyridine oxide.

in vacuo could not discriminate the two types of water involved in this compound. Water begins to vaporize gradually at around 35 °C and is lost completely at 50 °C leaving $MnBr(acac)_2$, which was recovered and identified on interuption of thermolysis.

As shown in Fig. 7 the IR spectrum of $[Mn(acac)_2(H_2O)_2]Cl \cdot 2H_2O$ exhibits two bands in the region of HOH bending vibration, and the band at 1650 cm^{-1} disappears in preference to that at 1620 cm^{-1} on heating for a while at 50 °C. The higher frequency vibration may be ascribable to the lattice water.

After the loss of water, weight of the specimen still continued to decrease with temperature and became nearly constant at 90 °C (Fig. 6). The weight loss in the 75—90 °C region corresponds to one mole of acetylacetone, and in fact the volatile material trapped at −78 °C was identified to be acetylacetone by the IR and UV assays. Composition of the residue (Mn: 21.89, Br: 31.01, C: 27.90, H: 3.21%) is close to MnBr(acac), and its IR spectrum indicates the remaining of the acetylacetonate group. Very dark color might suggest the contamination with some Mn(III) species, but the detailed course of the thermal decomposition and the exact nature of the residue are not certain.

Several neutral six-coordinate complexes of the type $MnX(acac)_2B$ were prepared, where X is Cl or Br and B is dioxane, 4-methylpyridine or pyridine oxide. Figure 8 reveals that the absorption spectrum of $MnCl(acac)_2(O\text{-}py)$ in methylene chloride resembles that of $MnCl(acac)_2$, but a spectrum in the presence of added pyridine oxide is quite similar to that of $Mn(acac)_3$. These results suggest that the base adduct is not so stable, but dissociates extensively in solution.

It is worth noting that 2,2′-bipyridine and 1,10-phenanthroline both react with MnBr(acac), reducing Mn(III) and resulting $MnBr_2(bipy)_2$ and $MnBr_2(phen)_2$, respectively. Another important finding is the lability of $MnX(acac)_2$. Although $Mn(acac)_3$ is substitution-inert and converted to $Mn(dbm)_3$ only under severe reaction conditions, the reaction of $MnX(acac)_2$ with dibenzoylmethane (dbmH) proceeds readily at room temperature, affording $MnX(dbm)_2$. The more detailed kinetic study of this interesting reaction is desirable.

Dichloro(acetylacetonato)manganese(III) Complexes. When $MnX(acac)_2$ (X=Cl or Br) was allowed to react with equimolar amount of HX in methylene chloride at room temperature, a precipitate of $MnCl_2$ or $MnBr_2$ was produced, but the solution still contained remaining $MnX(acac)_2$. Twice as many moles of hydrogen halide were necessary to complete the reaction resulting in a colorless solution. Then the manganese was quantitatively converted to MnX_2, and the freed acetylacetone in solution was determined spectrophotometrically to correspond to *ca.* 50% of acetylacetone contained in $MnX(acac)_2$. Thus the overall reaction is represented by the following reaction:

$MnX(acac)_2 + 2HX = MnX_2 + acacH +$ decomposition products. Here X is Cl or Br. In the case of $MnI(acac)_2$, a similar reaction did not produce MnI_2, but afforded $Mn(acac)_2$.

In contrast to $MnX(acac)_2$, the dihalogeno complex $MnX_2(acac)$ is not stable enough to allow isolation in the reaction at room temperature, but induces the reduction of Mn(III) to Mn(II). However, $MnCl_2(acac)H_2O$ and $MnCl_2(acac)(O\text{-}py)_2$ could be obtained by reactions at −78 °C. The IR spectrum of $MnCl_2(acac)H_2O$ in the 4000—700 cm^{-1} region is quite similar to that of $MnCl(acac)_2$ except that the former has bands related to the coorinated water at 3440 and 1605 cm^{-1}, and that the band assignable to the ν_s(C=C=C) vibrations are split into two bands at 1280 and 1310 cm^{-1}.

On the other hand the spectrum in the lower frequency region is remarkably different from that of $MnCl(acac)_2$ (Fig. 2). The strong absorption at 377 cm^{-1} may be assigned to the ν(Mn–O) vibration, and the 294 cm^{-1} peak to ν(Mn–Cl). It is not certain at the present stage of investigation whether the 235 cm^{-1} or other minor bands could be ascribed to the bridging Mn–Cl stretch. It seems worth noting that frequency

of the ν(Mn–O) vibration increases in the order of $Mn(acac)_3$ (335 cm^{-1})<$MnCl(acac)_2$ (343 cm^{-1})<$MnCl_2(acac)H_2O$ (377 cm^{-1}), and that of the ν(C=O) vibration decreases in the same sequence from 1585 to 1520 and 1510 cm^{-1}, reflecting the strengthening of the Mn–O(acac) bond by the chloride substitution.

Discussion

Except the most stable divalent state manganese can exist in several higher oxidation states[9] and even the Mn(III) species functions as an oxidant for various substrates.[22] Tris(acetylacetonato)manganese(III) is especially useful for organic substrates because of its solubility in organic solvents, and has been shown, for example, to effect the oxidative coupling of phenols[23] and oxidative intramolecular cyclization of *p*-hydroxybenzyl ketoximes.[24]

Even by the reaction with hydrogen halide in non-coordinating solvent, $Mn(acac)_3$ is reduced to the Mn(II) species. The detailed mechanism of this redox reaction could not be established by the present investigation, but the preceding reaction steps seem to proceed in the following sequence (Eq. (i)).

$$Mn(acac)_3 \xrightarrow{+HX} \left[(acac)_2Mn\begin{matrix}X\\ \diagdown acacH\end{matrix}\right] \xrightarrow{-acacH}$$

Intermediate **1**

$$(acac)\overset{X}{\underset{|}{M}}n(acac) \xrightarrow{+HX} \left[(acac)\overset{X}{\underset{|}{M}}n\begin{matrix}X\\ \diagdown acacH\end{matrix}\right] \quad (i)$$

Intermediate **2**

The intermediates **1** and **2** have not been identified, but are just presumed here. In the reaction of $MnCl(acac)_2$ with hydrogen chloride at −78 °C, addition of petroleum ether to the methylene chloride solution precipitated $MnCl_2(acac)H_2O$, but warming of the reaction mixture to room temperature instead of adding petroleum ether resulted in a precipitate of $MnCl_2$, and the filtrate contained $MnCl(acac)_2$. Thus, such a reaction as represented by Eq. (ii) might have occurred in methylene chloride at room temperature.

$$2[MnCl_2(acac)(acacH)] \longrightarrow MnCl_2 + MnCl(acac)_2 + acacH + \text{decomposition products} \quad (ii)$$

Intermediate **2**

The decomposition products are not identified, but are assumed to be resulted by reactions involving acetylacetone radicals. Equation (ii) can explain why twice as many moles of hydrogen chloride were necessary to convert $MnCl(acac)_2$ to $MnCl_2$ completely.

Electron transfer in the reaction between $Mn(acac)_3$ and a primary amine such as ethylenediamine was concluded in a previous paper[4] to occur in the following step (iii).

$$(acac)_2Mn\begin{matrix}acac\\ \diagdown en\end{matrix} \longrightarrow (acac)_2Mnen + acac\cdot \quad (iii)$$

Similarly in the reaction (ii), an electron might be transferred from the acetylacetonate ligand to Mn(III):

$$MnCl_2(acac)(acacH) \longrightarrow MnCl_2 + acacH + acac\cdot \quad (iv)$$

followed by the attack of an acetylacetone radical on a chloride ligand in another molecule of $MnCl_2(acac)(acacH)$:

$$acac\cdot + MnCl_2(acac)(acacH) \longrightarrow MnCl(acac)_2 + (acac\cdot)HCl \longrightarrow \text{decomposition} \quad (v)$$

The reaction of $MnBr(acac)_2$ with HBr seems to follow a similar sequence, while $MnI(acac)_2$ reacts with HI affording $Mn(acac)_2$ instead of MnI_2. Although $MnI(acac)_2$ is stable at room temperature, it readily liberates iodine molecules on heating or by the reaction with acids. Thus an electron must be transfered from an iodide ligand to the manganese atom in the presumable intermediate $MnI_2(acac)(acacH)$.

$$MnI(acac)_2 + HI \longrightarrow [MnI_2(acac)(acacH)] \longrightarrow Mn(acac)_2 + HI + I\cdot \quad (vi)$$

These considerations lead to the conclusion that the tendency of a ligand to deliver an electron to manganese(III) increases in the following sequence: Cl^-<Br^-<$acac^-$<I^-. In order to clarify the detailed mechanism of these redox reactions, further kinetic studies are desired.

The magnetic susceptibility of apparently five-coordinate manganese(III) complexes has been studied hitherto in connection with their structures. Goodwin and Sylva[25] determined the magnetic susceptibilities of $(bipyH_2)[MnCl_5]$, $(phenH_2)[MnCl_5]$, $MnCl_3(H_2O)$(bipy), $MnCl_3(H_2O)$(phen), $MnF_3(H_2O)$(phen), $MnCl_3$(terpy), $MnCl_3$(bipy), and $MnCl_3$(phen) over the temperature range 100—300 K. All compounds obey the Curie-Weiss law, and the first six have small θ values (7 to 25 K), indicating that they are simple paramagnetics. On the other hand the last two compounds have very large θ values (154 and 183 K, respectively), and the antiferromagnetic behavior was presumed to be due to their chloro-bridged dimeric structures.

The Curie-Weiss behavior of MnBr(salen) and MnI(salen) was reported by van den Bergen, *et al.*[12] (θ=22 and 20 K, respectively), and explained in terms of very weak antiferromagnetic interactions. Earnshaw, *et al.*[26] also measured the magnetic susceptibility of MnOAc(salen) over the temperature range 85—300 K. This compound obeys the Curie-Weiss law with θ=22 K, and was considered to have the antiferromagnetic interactions possibly due to the polymeric structure. Recent X-ray study[27] of this compound really confirmed the linear polymeric chains of Mn(salen) moieties bridged by acetate groups.

The present complexes $MnCl(acac)_2$ and $MnBr(acac)_2$ have magnetic moments of 4.88 and 4.93 B.M. at 20 and 21 °C, respectively, which are close to the calculated spin-only value of 4.90 B.M. These complexes obey the Curie-Weiss law, but their θ values (13 and 11 K, respectively) are not so large as the indicate the intermolecular linkage in the solid state. On the other hand $MnI(acac)_2$ has a lower μ_{eff} value of 4.72 B.M. at 22 °C, and a rather large θ value of 68 K.

It may be appropriate to presume that the iodo complex has a strong intermolecular interaction, the iodide ligand bridging two manganese atoms just as the azide group in $MnN_3(acac)_2$.[28] Such a structural feature might be responsible for the IR pattern in the ν(Mn–I) region which is different from those of the chloro and bromo complexes. The exact structure must be determined by the X-ray analysis in future.

The authors are grateful to Dr. Y. Nakamura for his helpful discussion and Mr. J. Gohda for the elemental analysis. The financial aid by the Ministry of Education and the kind supply of acetylacetone by the Daicel Co., Ltd. are also acknowledged.

References

1) K. Isobe, K. Noda, Y. Nakamura, and S. Kawaguchi, This Bulletin, **46**, 1699 (1973), and references cited therein.
2) Y. Nakamura, M. Gotani, and S. Kawaguchi, *ibid.*, **45**, 457 (1972).
3) C. H. Bamford and A. N. Ferrar, *Proc. Roy. Soc. Ser. A*, **321**, 425 (1971).
4) Y. Nishikawa, Y. Nakamura, and S. Kawaguchi, This Bulletin, **45**, 155 (1972).
5) A short communication appeared in K. Isobe, K. Takeda, Y. Nakamura, and S. Kawaguchi, *Inorg. Nucl. Chem. Lett.*, **9**, 1283 (1973).
6) R. G. Charles, "Inorganic Syntheses," Vol. 7, p. 183 (1963).
7) G. H. Cartledge, *J. Amer. Chem. Soc.*, **74**, 6015 (1952).
8) H. Funk and H. Kreis, *Z. Anorg. Allgem. Chem.*, **349**, 45 (1967).
9) W. Levason and C. A. McAuliffe, *Coord. Chem. Rev.*, **7**, 372 (1972).
10) M. D. Hobday and T. D. Smith, *ibid.*, **9**, 315 (1973).
11) L. J. Boucher and M. O. Farrell, *J. Inorg. Nucl. Chem.*, **35**, 3731 (1973).
12) A. van den Bergen, K. S. Murray, M. J. O'Connor, and B. O. West, *Aust. J. Chem.*, **22**, 39 (1969).
13) C. P. Prabhakaran and C. C. Patel, *J. Inorg. Nucl. Chem.*, **31**, 3316 (1969).
14) P. F. Lindley and A. W. Smith, *Chem. Commun.*, **1970**, 1355.
15) E. Contreras, V. Riera, and R. Uson, *Inorg. Nucl. Chem. Lett.*, **8**, 287 (1972).
16) L. J. Boucher, *J. Amer. Chem. Soc.*, **90**, 6640 (1968).
17) I. Bernal, N. Elliott, and R. Lalancette, *Chem. Commun.*, **1971**, 803.
18) M. Matsui, S. Koda, S. Ooi, H. Kuroya, and I. Bernal, *Chem. Lett.*, **1972**, 51.
19) C. Bellitto, A. A. G. Tomlinson, and C. Furlani, *J. Chem. Soc., A*, **1971**, 3267.
20) L. J. Boucher, *J. Inorg. Nucl. Chem.*, **36**, 531 (1974).
21) Y. Nakamura, K. Isobe, H. Morita, S. Yamazaki, and S. Kawaguchi, *Inorg. Chem.*, **11**, 1573 (1972).
22) J. Burgess, *et al.*, "Inorganic Reaction Mechanisms," Vol. 1, The Chemical Society, London (1971), pp. 31—34.
23) M. J. S. Dewar and T. Nakaya, *J. Amer. Chem. Soc.*, **90**, 7134 (1968).
24) A. R. Forrestor, R. H. Thomson, and S. O. Woo, *Chem. Commun.*, **1973**, 604.
25) H. A. Goodwin and R. N. Sylva, *Aust. J. Chem.*, **20**, 629 (1967).
26) A. Earnshaw, E. A. King, and L. F. Larkworthy, *J. Chem. Soc., A*, **1968**, 1048.
27) J. E. Davies, B. M. Gatehouse, and K. S. Murray, *J. Chem. Soc. Dalton*, **1973**, 2523.
28) B. R. Stults, V. W. Day, E. L. Tasset, and R. S. Marianelli, *Inorg. Nucl. Chem. Lett.*, **9**, 1259 (1973).

The Syntheses of R_3Sn-$Mn(CO)_{5-n}L_n$(n=0 or 1) Compounds and Their ^{119}Sn-Mössbauer and ^{1}H-NMR Studies

Satoru ONAKA and Hirotoshi SANO*,**

Department of Chemistry, Nagoya Institute of Technology, Showa-ku, Nagoya 466
**Department of Chemistry, Faculty of Science, Tokyo Metropolitan University, Fukazawa, Setagaya-ku, Tokyo 158*

(Received June 27, 1974)

Seven new compounds with the Sn–Mn bond have been prepared by carbonyl displacement with a weaker π-accepting ligand, L (L=$P(C_6H_5)_3$, $As(C_6H_5)_3$, $Sb(C_6H_5)_3$ for R_3Sn–$Mn(CO)_5$) or by reaction of the anion $[Mn(CO)_5]^-$ or $[Mn(CO)_4P(C_6H_5)_3]^-$ with R_3SnX (R=C_2H_5, n-C_3H_7, n-C_4H_9). A *trans* configuration is deduced for the mono-substituted compounds, R_3Sn–$Mn(CO)_4L$, on the basis of the infrared spectra in the ν(CO) region. The ^{119}Sn–Mössbauer and IR spectra are measured for sixteen compounds of the R_3Sn–$Mn(CO)_{5-n}L_n$ type (R=CH_3, C_2H_5, n-C_3H_7, n-C_4H_9, Cl, Br, I; L=$P(C_6H_5)_3$, $As(C_6H_5)_3$, $Sb(C_6H_5)_3$; n=0 or 1). Both the Mössbauer-isomer shift and the quadrupole splitting increase with an increase in the length of the alkyl chain attached to the tin atom. The replacement of CO on the manganese atom with the weaker π-accepting ligand, L, has a significant effect on the isomer shift and quadrupole splitting of the tin atom through the σ- and π-interaction between the tin and manganese atoms. An interpretation of the change in the chemical shift of the terminal methyl protons is also given for alkyl derivatives.

The natue of the Sn–Mn bonding and the effect of substituents on the nature of the Sn–Mn bonding have been studied by various kinds of spectroscopic means for a series of compounds, $R_{3-x}X_xSn$–$Mn(CO)_{5-n}L_n$.[1-8] It has been reported that not only the substituents attached to the Sn atom but also those attached to the Mn atom can exert significant effects on the Sn–Mn bonding nature. The present study was undertaken in order to provide further evidence for the effect of the substituent attached to the metal atoms on the nature of the Sn–Mn bonding by using ^{119}Sn–Mössbauer and proton NMR spectroscopic techniques. For this purpose, some new compounds with a Sn–Mn bond were synthesized; the effects of weak π-accepting ligands, such as $M(C_6H_5)_3$ (M=P, As, and Sb), on the Sn–Mn bonding in a series of R_3Sn–$Mn(CO)_4M(C_6H_5)_3$ compounds were also described.

Experimental

Preparation of Compounds. All the reactions were carried out under a nitrogen atmosphere.

Preparation of R_3Sn–$Mn(CO)_5$ ($R=C_2H_5$, n-C_3H_7, and n-C_4H_9). These compounds were synthesized by a procedure similar to Gorsich's method.[9] A solution containing 20 mmol of R_3SnCl in 50 ml of THF was stirred into a solution of THF containing 20 mmol of $NaMn(CO)_5$. After stirring at room temperature for 3 hr, the precipitates of sodium chloride were separated from the organic phase by centrifuging. The solution was then evaporated under reduced pressure, and traces of the solvent and unreacted trialkyltin chloride were distilled off through a fractionating column. A pale yellow liquid was obtained from the residual yellow oil by fractional distillation under reduced pressure. The boiling points of the products are presented in Table 1, along with the results of carbon and hydrogen analyses.

Preparation of $(C_2H_5)_3Sn$–$Mn(CO)_4P(C_6H_5)_3$. 0.86 g (2 mmol) of $Mn(CO)_4P(C_6H_5)_3$ was reduced to $NaMn(CO)_4P(C_6H_5)_3$ in 50 ml of THF by stirring with a 1% sodium amalgam at room temperature.[10] After stirring for 1 hr, the THF solution was decanted into another flask; 0.48 g (2 mmol) of triethyltin chloride in 50 ml of THF was then stirred in. The mixture was stirred at room temperature for 3 hr. The organic phase was separated from fine precipitates of sodium chloride by centrifugation. The orange solution was concentrated under reduced pressure, and some unreacted triethyltin chloride was distilled off at 60 °C (5×10^{-2} mmHg). The residual yellow powder was dissolved into 50 ml of n-hexane with refluxing. The hexane solution was then filtered, and the filtrate was concentrated to about 20 ml *in vacuo* to give yellow, needle-like crystals of $(C_2H_5)_3Sn$–$Mn(CO)_4P(C_6H_5)_3$ (0.8 g, yield 63%). Recrystallization was effected from the same solvent.

Preparation of $(CH_3)_3Sn$–$Mn(CO)_4P(C_6H_5)_3$ and $(CH_3)_3Sn$–$Mn(CO)_4As(C_6H_5)_3$. A mixture of 3.6 g (0.01 mol) of $(CH_3)_3Sn$–$Mn(CO)_5$ and 2.6 g (0.01 mol) of $P(C_6H_5)_3$ or 3.06 g (0.01 mol) of $As(C_6H_5)_3$ was heated at about 120 °C for 2 hr. The resulting yellow material was recrystallized from hexane several times to give pale yellow crystals. All the spectral data support the idea that both the products are mono-substituted, although the elemental analysis of the compound prepared from $P(C_6H_5)_3$ gives a little higher carbon content than the value calculated for $(CH_3)_3Sn$–$Mn(CO)_4P(C_6H_5)_3$.

Preparation of $(C_6H_5)_3Sn$–$Mn(CO)_4Sb(C_6H_5)_3$. A mixture of 1.6 g (3 mmol) of $(C_6H_5)_3Sn$–$Mn(CO)_5$ and 1.1 g (3 mmol) of $Sb(C_6H_5)_3$ was heated at about 190 °C for 2 hr. The reaction products were each extracted three times with 25 ml portions of a 2:1 mixture of ethanol and benzene. The extracts were then concentrated to about half the original volume *in vacuo*. Yellow crystals were precipitated on cooling. Recrystallization was effected from the same mixture of solvents.

The analytical data of these new compounds are shown in Table 1, along with some of their physical properties. All the other compounds were prepared by the methods described in Refs. 7 and 9.

Mössbauer Spectra. The ^{119}Sn-Mössbauer spectra were obtained against a $Ba^{119m}SnO_3$ source moving in a constant acceleration mode at room temperature. The sample was used as an absorber and was kept at 79 K in a cryostat. The calibration of the velocity was made as has previously been reported.[1]

NMR Spectra. The NMR data were obtained on dichloromethane solutions of the samples by means of a

** To whom all correspondence should be addressed.

Table 1. Analytical data

Compound	Color	Bp or mp, °C	Found % C	Found % H	Calcd % C	Calcd % H	Yield, %
$(C_2H_5)_3Sn–Mn(CO)_5$	Pale yellow[a]	62 °C at 0.07 mmHg	32.84	3.72	32.96	3.77	68
$(n\text{-}C_3H_7)_3Sn–Mn(CO)_5$	Pale yellow[a]	87 °C at 0.1 mmHg	37.96	4.94	37.96	4.94	36
$(n\text{-}C_4H_9)_3Sn–Mn(CO)_5$	Yellow[a]	99 °C at 0.06 mmHg	42.16	5.66	42.10	5.61	52
$(C_2H_5)_3Sn–Mn(CO)_4P(C_6H_5)_3$	Pale yellow	113.5 °C	54.09	4.79	52.94	4.79	63
$(CH_3)_3Sn–Mn(CO)_4As(C_6H_5)_3$	Pale yellow	164—165 °C	47.29	3.66	47.14	3.80	29
$(C_6H_5)_5Sn–Mn(CO)_4Sb(C_6H_5)_3$	Pale yellow	168—170 °C	55.36	3.34	55.22	3.48	44

a) Liquid at room temperature.

Table 2. Spectral data

Compound	^{119}Sn-Mössbauer data I.S. (mm/s)	^{119}Sn-Mössbauer data Q.S. (mm/s)	IR, ν(CO), cm^{-1} A_1(eq)	IR, ν(CO), cm^{-1} E	IR, ν(CO), cm^{-1} A_1(ax)	H-HMR data, τ(CH) (ppm)[a]	H-HMR data, J(^{119}SnCH) Hz
$(CH_3)_3Sn–Mn(CO)_5$	1.33	0.61	2091w	1995vs	2001s[b]	9.50[d]	48.9
$(CH_3)_3Sn–Mn(CO)_4P(C_6H_5)_3$	1.27	0	2035w	1940vs[c]		9.55[d]	~47
$(CH_3)_3Sn–Mn(CO)_4As(C_6H_5)_3$	1.28	0	2034w	1939vs[c]			
$(C_2H_5)_3Sn–Mn(CO)_5$	1.58	0.78	2086w	1989vs	1993s[b]	8.68	~41
$(C_2H_5)_3Sn–Mn(CO)_4P(C_6H_5)_3$	1.44	0.43	2033w	1941vs[c]		8.67	~41
$(n\text{-}C_3H_7)_3Sn–Mn(CO)_5$	1.57	0.85	2086w	1990vs	1994s[b]	8.98	
$(n\text{-}C_4H_9)_3Sn–Mn(CO)_5$	1.51	0.88	2085w	1989vs	1994s[b]	9.05	
$(C_6H_5)_3Sn–Mn(CO)_5$	1.41	0	2095w	2004vs	2004vs[b]		
$(C_6H^5)_3Sn–Mn(CO)_4P(C_6H_5)_3$	1.43	0	2044w	1951vs[c]			
$(C_6H_5)_3Sn–Mn(CO)_4As(C_6H_5)_3$	1.38	0	2045w	1951vs[c]			
$(C_6H_6)_3Sn–Mn(CO)_4Sb(C_6H_5)_3$	1.40	0	2043w	1954vs[c]			
$Cl_3Sn–Mn(CO)_5$	1.68	1.57	2126w	2046vs	2040s[b]		
$Cl_3Sn–Mn(CO)_4P(C_6H_5)_3$	1.72	1.61	2083w	1996vs[c]			
$Cl_3Sn–Mn(CO)_4As(C_6H_5)_3$	1.66	1.74	2081w	1995vs[c]			
$Br_3Sn–Mn(CO)_5$	1.79	1.41[1]	2124w	2045vs	2038s[b]		
$I_3Sn–Mn(CO)_5$	1.92	1.32	2117w	2042vs	2035s[b]		

a) Relative to $Si(CH_3)_4$. b) n-hexane solution. c) $CHCl_3$ solution. d) 0.3 mol solution.

Hitachi-Perkin-Elmer R-20B Spectrometer (60 MHz) at room temperature; the solvent was used as the internal standard. The chemical shift values listed in Table 2 were recalculated with respect to tetramethylsilane (TMS) at an infinite dilution.

IR Spectra. The IR spectra of the CO stretching region were recorded on a JASCO IR-G spectrometer in hexane or chloroform solutions by use of a 0.1 mm KBr liquid cell. The spectra were calibrated by making use of gaseous DCl by means of a superposition method.

All the spectral results are given in Table 2.

Results and Discussion

In a previous paper, it was reported that $(CH_3)_3Sn–Mn(CO)_5$ shows a quadrupole splitting, while $(C_6H_5)_3Sn–Mn(CO)_5$ shows a non-resolved quadrupole splitting.[1] A clearly-resolved quadrupole splitting is observed for the present series of trialkyltin-pentacarbonylmanganese as well. It seems reasonable, therefore, to conclude that a clearly-resolved quadrupole splitting is generally observed for trialkyltin-pentacarbonylmanganese. It was also found that the magnitude of the quadrupole splitting increases in accordance with the length of the alkyl chain and that the isomer shift value of trimethyltin-pentacarbonylmanganese is the lowest among the alkyltin-pentacarbonylmanganese compounds. As the quadrupole splitting of the Mössbauer spectra reflects mainly the p-electron imbalance in the 5p-orbitals of the tin atom, the increase in quadrupole splitting means an increased 5p-electron imbalance around the tin atom in accord with the increase of the length of the alkyl chain. The lowest isomer shift, found in $(CH_3)_3Sn–Mn(CO)_5$, indicates that the compound has the lowest s-electron density around the tin atom among the trialkyltin-pentacarbonylmanganese compounds. The NMR measurements showed that the coupling constant, J(^{119}Sn–C–H) observed for $(C_2H_5)_3Sn–Mn(CO)_5$ is lower than that of $(CH_3)_3Sn–Mn(CO)_5$ (48.9 Hz), indicating a lower s-character of the $Sn–CH_2$ bond in $(C_2H_5)_3Sn–Mn(CO)_5$. It can be concluded on the basis of the results obtained by the rehybridization theory[11,12] that the p-character of the Sn–C bond and the s-character of the Sn–Mn bond for $(C_2H_5)_3Sn–Mn(CO)_5$ are larger than those for $(CH_3)_3Sn–Mn(CO)_5$.

The proton NMR measurements showed that the τ-values of the terminal methyl proton increase in the order of $(C_2H_5)_3Sn–Mn(CO)_5 < (n\text{-}C_3H_7)_3Sn–Mn(CO)_5 < (n\text{-}C_4H_9)_3Sn–Mn(CO)_5 < (CH_3)_3Sn–Mn(CO)_5$, indicating that the methyl protons in $(CH_3)_3Sn–Mn(CO)_5$ are most highly-shielded. Many factors which affect the proton chemical shift have been discussed for some Group IV B alkyl derivatives,[13-16] and it has been

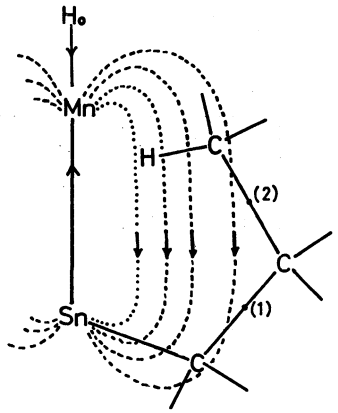

Fig. 1. The magnetic field induced by the applied field H_0 and the closest approach of methyl protons to Sn–Mn bond in $(n\text{-}C_3H_7)_3Sn\text{–}Mn(CO)_5$. (1) and (2) indicate the positions of methyl protons in ethyl and *n*-propyl derivatives, respectively. The terminal methyl protons can contact to Sn–Mn bond by rotating C–C bonds around their axis in the case of *n*-butyl derivative.

concluded that the predominant factor causing a shift to a lower field is the magnetic anisotropy effect for Group 4B ethyl derivatives.[13] As for the present series of alkyltin compounds, the magnetic anisotropy effect can account for the lower-field shift of the methyl protons in $(C_2H_5)_3Sn\text{–}Mn(CO)_5$, $(n\text{-}C_3H_7)_3Sn\text{–}Mn(CO)_5$, and $(n\text{-}C_4H_9)_3Sn\text{–}Mn(CO)_5$ as compared to $(CH_3)_3Sn\text{–}Mn(CO)_5$, as is shown in Fig. 1. However, a shift to a higher field in the order of $(C_2H_5)_3Sn\text{–}Mn(CO)_5 < (n\text{-}C_3H_7)_3Sn\text{–}Mn(CO)_5 < (n\text{-}C_4H_9)_3Sn\text{–}Mn(CO)_5$ can be explained neither in terms of the magnetic anisotropy effect nor in terms of the intramolecular van der Waals dispersion forces, since the magnetic anisotropy effect and the intramolecular van der Waals forces cause a lower-field shift. It is possible to consider that the small changes in the s-character of the Sn–Mn bond are the origin of the differences in the $\tau(CH_3)$ values of $(C_2H_5)_3Sn\text{–}Mn(CO)_5$, $(n\text{-}C_3H_7)_3Sn\text{–}Mn(CO)_5$, and $(n\text{-}C_4H_9)_3Sn\text{–}Mn(CO)_5$, since the isomer shift of ^{119}Sn changes in the same order, although such an inductive effect may be estimated to be very small.[13] One plausible explanation of this phenomenon is that the high-field shift of the methyl proton resonances going from ethyl to *n*-butyl compounds is due to the direct contact of the terminal methyl protons in $(n\text{-}C_3H_7)_3Sn\text{–}Mn(CO)_5$ and $(n\text{-}C_4H_9)_3Sn\text{–}Mn(CO)_5$ with electrons of the Sn–Mn bonding.[13]

In the effect of the replacement of CO on the manganese atom with weaker π-accepting ligands, the most striking feature is shown for $(CH_3)_3Sn\text{–}Mn(CO)_5$ and $(CH_3)_3Sn\text{–}Mn(CO)_4L$ or $(C_2H_5)_3Sn\text{–}Mn(CO)_5$ and $(C_2H_5)_3Sn\text{–}Mn(CO)_4L$ ($L=P(C_6H_5)_3$ and/or $As(C_6H_5)_3$). A well-resolved quadrupole splitting is observed for $(CH_3)_3Sn\text{–}Mn(CO)_5$ and $(C_2H_5)_3Sn\text{–}Mn(CO)_5$, whereas a non-resolved spectrum or a slightly-resolved spectrum is observed for the mono-substituted compounds, as is illustrated in Fig. 2. On the other hand, the replacement of CO with L causes a slight change in the isomer shift.

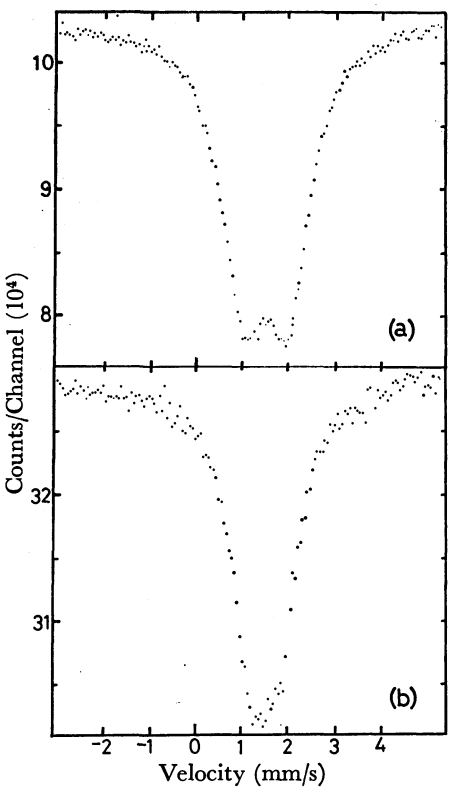

Fig. 2. ^{119}Sn-Mössbauer spectra of (a) $(C_2H_5)_3Sn\text{–}Mn(CO)_5$ and (b) $(C_2H_5)_3Sn\text{–}Mn(CO)_4P(C_6H_5)_3$ both at 78 K.

According to the X-ray analysis of $(C_6H_5)_3Sn\text{–}Mn(CO)_4P(C_6H_5)_3$, triphenylphosphine is coordinated to the manganese atom at the *trans* position with regard to the tin atom. The IR spectrum of this compound was checked, and two peaks were found in the CO stretching region (a very weak peak in the higher-energy region and a very strong one in the lower-energy region), as had been expected from its structural symmetry. All the mono-substituted compounds studied here show the same IR pattern in the CO stretching region as that of $(C_6H_5)_3Sn\text{–}Mn(CO)_4P(C_6H_5)_3$. The *trans* configuration may, therefore, be safely concluded to be found in all the substituted compounds. In the *trans* configuration, the tin atom is considered to compete with the ligand, L, to form a π-bonding with d_π-electrons of the manganese atom. Since the π-accepting ability of the ligand, L, is weaker than that of the substituted CO,[17] the d_π-electrons of the manganese atom are forced to enter both the vacant 5d orbitals of the tin atom and the remaining CO π-antibonding orbitals, thus influencing the efg around the tin nucleus. The NMR chemical-shift measurements provide other evidence of this interpretation; the methyl proton resonance is observed in a higher magnetic field for $(CH_3)_3Sn\text{–}Mn(CO)_4P(C_6H_5)_3$ than for $(CH_3)_3Sn\text{–}Mn(CO)_5$; *i.e.*, the shielding effect due to electrons around the proton nucleus is greater for $(CH_3)_3Sn\text{–}Mn(CO)_4P(C_6H_5)_3$ than for $(CH_3)_3Sn\text{–}Mn(CO)_5$. It seems reasonable to ascribe this result to the increase in the electron population around the proton nucleus stemming from the increase in the d_π-interaction between

the tin and manganese atoms. In contrast to the case of the alkyl drivatives, the quadrupole splitting of Cl_3Sn–$Mn(CO)_4L$ ($L=P(C_6H_5)_3$ and $As(C_6H_5)_3$) is slightly higher than that of the parent compound, Cl_3Sn–$Mn(CO)_5$. A similar contrast is observed in the values of the isomer shift on the comparison of Cl_3Sn–$Mn(CO)_4L$ with $(CH_3)_3Sn$–$Mn(CO)_4L$ or $(C_2H_5)_3Sn$–$Mn(CO)_4L$ ($L=P(C_6H_5)_3$, $As(C_6H_5)_3$, and CO). The reversed effect of the substitution of CO with weaker π-accepting ligands on the quadrupole splitting and isomer shift may also be ascribed to the increase of the σ- and π-interaction between the tin and manganese atoms through the substitution. The substitution of X in X_3Sn–$Mn(CO)_5$ increases the isomer shift with a decrease in the quadrupole splitting, whereas the substitution of R in R_3Sn–$Mn(CO)_5$ increases the isomer shift with an increase in quadrupole splitting, as may be seen in Table 2. Recently, Goodman *et al.* and Bancroft *et al.* have determined the sign of the quadrupole coupling constant, e^2qQ, of the tin atom in Cl_3Sn–$Mn(CO)_5$, $(CH_3)_2ClSn$–$Mn(CO)_5$, and $(CH_3)_3Sn$–$Mn(CO)_5$ by means of Mössbauer spectroscopy.[18,19] In the case of Cl_3Sn–$Mn(CO)_5$, there was concluded to be an excess of electron density in the p_z, d_{z^2}, d_{xz}, or d_{yz} orbitals because of the positive value of e^2qQ,[18] while an excess of electron density in the p_x, p_y, $d_{x^2-y^2}$, or d_{xy} orbitals was concluded for $(CH_3)_2ClSn$–$Mn(CO)_5$ and $(CH_3)_3Sn$–$Mn(CO)_5$ because of the negative value of e^2qQ.[19] As was mentioned above, the replacement of CO with weaker π-accepting ligands will increase the electron density in p_z, d_{xz}, and d_{yz} orbitals of the tin atom in $(CH_3)_3Sn$–$Mn(CO)_4L$ compared to the parent compound, thus reducing the electron imbalance around the tin atom, whereas the substitution will produce a positive contribution, thus increasing the electron density along the z axis in Cl_3Sn–$Mn(CO)_4L$ and augmenting the electron imbalance around the tin atom.

The fact that the zero quadrupole splitting in $(C_6H_5)_3Sn$–$Mn(CO)_5$ is not affected by the replacement of CO with L may well be explained in terms of the predominant π-delocalizing effect of the phenyl groups attached to the tin atom, as was described in a previous short communication.[4]

References

1) S. Onaka, Y. Sasaki, and H. Sano, This Bulletin, **44**, 726 (1971).
2) S. Onaka, T. Miyamoto, and Y. Sasaki, *ibid.*, **44**, 1851 (1971).
3) S. Onaka, *ibid.*, **44**, 2135 (1971).
4) S. Onaka and H. Sano, *ibid.*, **45**, 1271 (1972).
5) Y. Kume, D. Nakamura, M. Kubo, and S. Onaka, *J. Mag. Resonance*, **10**, 58 (1973).
6) S. Onaka, *J. Inorg. Nucl. Chem.*, in press.
7) S. Onaka, *Nippon Kagaku Kaishi*, **1972**, 1978.
8) S. Onaka, *ibid.*, **1974**, 255.
9) R. D. Gorsich, *J. Amer. Chem. Soc.*, **84**, 2468 (1962).
10) W. Hieber, G. Faulhaber, and F. Theubert, *Z. Anorg. Allgem. Chem.*, **314**, 125 (1962).
11) H. A. Bent, *Can. J. Chem.*, **38**, 1235 (1960).
12) J. R. Holmes and H. D. Kaesz, *J. Amer. Chem. Soc.*, **83**, 3903 (1961).
13) K. M. Mackay and R. Watt, *J. Organometal. Chem.*, **6**, 336 (1966).
14) K. M. Mackay, A. E. Watt, and R. Watt, *ibid.*, **12**, 49 (1968).
15) J. Lorberth and H. Vahrenkamp, *ibid.*, **11**, 111 (1968).
16) O. Yamamoto and K. Hayamizu, This Bulletin, **38**, 537 (1965).
17) F. Basolo and R. G. Pearson, "Mechanisms of Inorganic Reactions," J. Wiley & Sons, New York (1967), Chapter 7.
18) B. A. Goodman, R. Greatrex, and N. N. Greenwood, *J. Chem. Soc. A*, **1971**, 1868.
19) M. Bancroft, K. D. Butler, and A. T. Rake, *ibid.*, **1972**, 2025.

Studies on the Ruthenium Complexes. IX.[1] Kinetic Studies on the Deaquation-anation Reaction of Aquapentaammineruthenium(III) Complexes[2]

Akira OHYOSHI, Shun-ichi HIRAKI, Tomio ODATE, Susumu KOHATA, and Junko ODA

Department of Industrial Chemistry, Faculty of Engineering, University of Kumamoto, Kumamoto 860

(Received July 12, 1974)

The deaquation-anation reaction of $[Ru(OH_2)(NH_3)_5]X_3$-type complexes in the solid state, as shown by the $[Ru(OH_2)(NH_3)_5]X_3(s) \rightarrow [RuX(NH_3)_5]X_2(s) + H_2O(g)$ equation, where X is Cl, Br, I, and NO_3 respectively, was kinetically studied by means of thermogravimetry (TG) along with differential thermal analysis (DTA). The activation energy and entropy in the reaction process (E_a kcal/mol, ΔS^* e.u.) are, respectively, found by isothermal kinetic study to be (22.7, −7.1) for the chloride, (23.4, −5.2) for the bromide, (26.7, 5.8) for the iodide, and (19.3, −15.9) for the nitrate. The reaction seems to proceed through the following two steps, except in the case of the iodide: $[Ru(OH_2)(NH_3)_5]X_3 \rightarrow [RuX(OH_2)(NH_3)_5]X_2 \rightarrow [RuX(NH_3)_5]X_2 + H_2O$. The first step is regarded as the rate-determining one.

Several kinetic studies on the deaquation-anation of cobalt(III)[3-6] and chromium(III)[7-9] pentaammine complexes in the solid state have been made, and the reaction heats have been reported. These metal ions have six and three 3d-electrons respectively, while ruthenium(III) has five 4d-electrons. This difference in the electronic structure of the central metal ion may be reflected in the behavior of the deaquation-anation reaction. In the present paper, the results of the deaquation-anation study of several aquapentaammineruthenium(III) complexes in the solid state will be compared with those of the corresponding cobalt(III) and chromium(III) complexes and the reaction mechanisms will be discussed.

Experimental

Materials. The aquapentaammineruthenium(III) complexes were prepared from the chloropentaammineruthenium(III) chloride by the method of Endicott and Taube.[10] The complexes were studied immediately after identification because they were unstable with respect to deaquation, even at room temperature. The water contents of the complexes were determined by studying the mass-loss on a thermobalance. Found for the chloride: H_2O, 5.55%. Calcd for $[Ru(OH)_2(NH_3)_5]Cl_3$: H_2O, 5.79%. Found for the bromide: H_2O, 3.37%. Calcd for $[Ru(OH_2)(NH_3)_5]Br_3$: H_2O, 3.37%. Found for the iodide: H_2O, 2.84%. Calcd for $[Ru(OH_2)(NH_3)_5]I_3$: H_2O, 3.08%. Found for the nitrate: H_2O, 4.22%. Calcd for $[Ru(OH_2)(NH_3)_5](NO_3)_3$: H_2O, 4.11%. Since there were some differences between the observed and theoretical values, and since this measurement was difficult to do for the perchlorate, the absorption spectrophotometry was also carried out in order to identify these complexes and to confirm their chemical purity.

Procedures. A Shimadzu-TGC 20 micro-thermobalance and DT 20B micro differential thermal analyzer were used for the thermal analysis. A Hitachi 323 recording spectrophotometer was used for the spectrum measurements.

About a 8—10 mg sample was heated in a dynamic helium atmosphere in a furnace at a heating rate of 5 °C per min. The isothermal rate measurement was carried out by using a thermobalance at several constant temperatures, and the conversion ratios were determined by mass-loss measurements. The reaction products were spectrophotometrically analyzed for their aqueous solution.

Results and Discussion

Differential Thermal Analysis and Thermogravimetry. The DTA and TG curves recorded for the aquapentaammine halides, nitrate, and perchlorate are shown in Fig. 1. For each complex, the mass-loss step, as shown by the TG curve, corresponds to the endothermic or exothermic peak in the temperature range of 62→81(max)→92 °C for the chloride, in that of 67→78(max)→91 °C for the bromide, in that of 58→76(max)→96 °C for the iodide, in that of 56→73(max)→83 °C for the nitrate, and in that of 127→156(max)→170 °C for the perchlorate. The DTA curve of perchlorate shows an exothermic peak different from those of the other complexes. This suggests that the ligand water-molecule is maintained even at a comparatively high temperature, since the bulky perchlorate ion can not easily migrate toward the inner sphere. This fact seems to account for the mechanism by which the

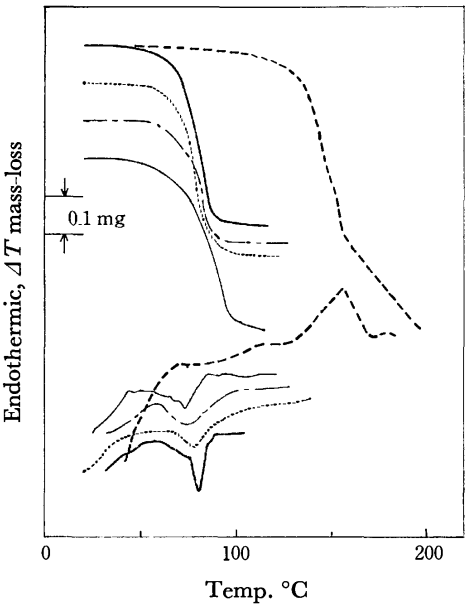

Fig. 1. TG and DTA curves of $[Ru(OH_2)(NH_3)_5]X_3$ complexes.
—— Chloride, ····· Bromide, —·— Iodide,
—— Nitrate, —— Perchlorate.

Table 1. Analysis of the reaction product of aquapentaammineruthenium(III)

Initial complex		Chloride	Bromide	Iodide	Nitrate
Sampling temp. °C		92	91	96	83
Sample color		Yellow	Orange	Black	Gray
Chemical formula assigned		$[RuCl(NH_3)_5]Cl_2$	$[RuBr(NH_3)_5]Br_2$	$[RuI(NH_3)_5]I_2$	$[Ru(NO_3)(NH_3)_5](NO_3)_2$
Elemental analysis (H%, N%)	Found	(5.24, 23.65)	(3.90, 16.80)	(2.69, 12.03)	(3.96, 29.05)
	Calcd	(5.18, 23.93)	(3.56, 16.44)	(2.67, 12.35)	(4.06, 30.24)
Electronic spectrum (ν_{max}, kK, ε, 10^3 M^{-1}, cm^{-1})	Found	(31, 1.95)	(25, 1.52)	(18, 2.15)	(34, —)[b]
	Ref.[c]	(30, 1.94)	(25, 1.95)	(18, 2.10)	(—, —)

a) Electronic spectrum was measured as a dilute nitric acid solution. b) Unstable in aqueous solution. c) From Ref. 11.

deaquation reaction is initiated by the migration of the outersphere anion.

The results of the elemental analysis and the spectral data of the reaction products are shown in Table 1. These data indicate that the reaction products accord with those of complexes resulting from the ligand-exchange reactions between the ligand water-molecule and the outersphere anions. Thus, all the peaks on the DTA curves and the mass-loss are attributable to the deaquation-anation reactions;

$$[Ru(OH_2)(NH_3)_5]X_3(s) \longrightarrow [RuX(NH_3)_5]X_2(s) + H_2O(g). \quad (1)$$

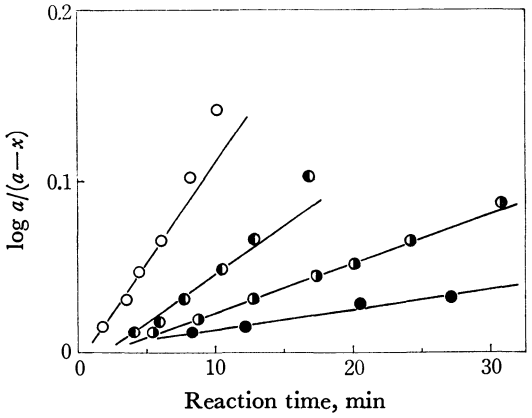

Fig. 2. Plots of log $a/(a-x)$ *vs.* reaction time for the deaquation-anation reaction of $[Ru(OH_2)(NH_3)_5]Cl_3$. —●— 41 °C, —◑— 49 °C, —◐— 55 °C, —○— 63 °C.

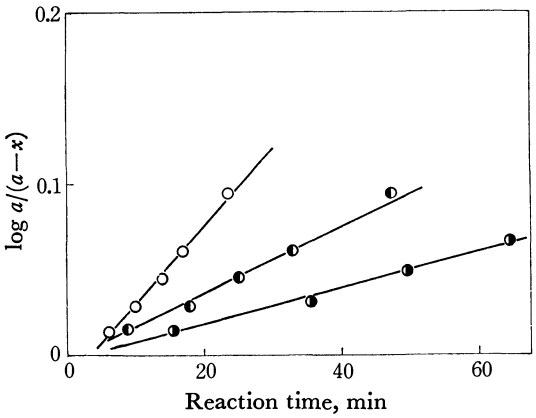

Fig. 3. Plots of log $a/(a-x)$ *vs.* reaction time for the deaquation-anation reaction of $[Ru(OH_2)(NH_3)_5]I_3$. —◑— 35 °C, —◐— 40 °C, —○— 46 °C.

Isothermal Kinetic Study. Since the thermochemical reactions of all complexes except for the perchlorate were observed to consist of the deaquation and anation of the outersphere anion, the isothermal kinetic measurements were made using a thermobalance. The changes in the conversion ratios were determined from the mass-loss data at several temperatures. The plots of log $a/(a-x)$ *vs.* the reaction time, t, are exemplified for the chloride and the iodide in Figs. 2 and 3 respectively, where "a" is the initial mass of the sample and "$a-x$" is the mass at time t. The rate was considerably accelerated as the reaction proceeded, and the plots showed a tendency to deviate from the straight lines at higher reaction temperatures. Similar trends have previously been reported for the cases of the bromide and the nitrate.[2] The rate constants and the activation energies (E_a-I), which are obtained from the Arrhenius plots (Fig. 4), are given in Table 2, along with the activation entropy calculated from the E_a—I value and along with the reference values. Kinetic plots calculated by the method of Freeman and Carroll[12] are shown in Fig. 5, while the activation energies (E_a-II) are also listed in Table 2.

It can be seen that the rate constants for the ruthenium(III) complexes are larger than those of the cobalt(III) and chromium(III) complexes, and that the activation energies for the reactions of the ruthenium(III) complexes are generally smaller than those

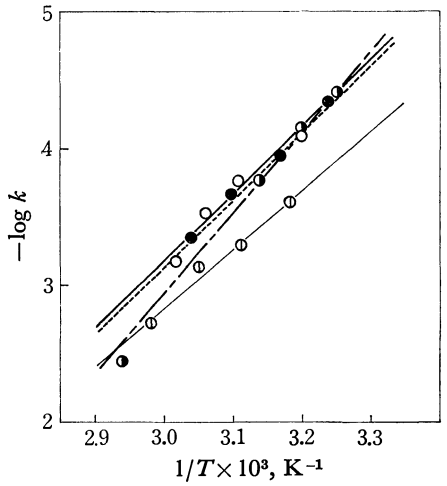

Fig. 4. Arrhenius plots for the deaquation-anation reaction of $[Ru(OH_2)(NH_3)_5]X_3$ complexes. —●— Chloride, —○— Bromide, —◑— Iodide, —⊖— Nitrate.

Table 2. Kinetic parameters for the deaquation-anation reaction of $[M(OH_2)(NH_3)_5]X_3$ type complexes

Complexes	k, 10^4 s^{-1} (Temp., °C)	E_a-I (kcal/mol)	E_a-II (kcal/mol)	ΔS^* (e.u.)	Temp.[a] (°C)	Anionic radii[b] and proton affinities[c] (Å)	(kcal/mol)
$[Ru(OH_2)(NH_3)_5]Cl_3$	1.12 (43)	22.7	24.6	−7.1	31	1.81	331
$[Ru(OH_2)(NH_3)_5]Br_3$	0.77 (40)	23.4	26.8	−5.2	40	1.96	321
$[Ru(OH_2)(NH_3)_5]I_3$	0.71 (40)	26.7	32.6	5.8	38	2.20	312
$[Ru(OH_2)(NH_3)_5](NO_3)_3$	2.38 (41)	19.3	19.0	−15.9	30	1.89	—
$[Ru(OH_2)(NH_3)_5](ClO_4)_3$	—	—	—	—	48	2.36	—
$[Co(OH_2)(NH_3)_5]Cl_3$	4.27 (86)[d]	19[d]	—	—	40[d]		
$[Co(OH_2)(NH_3)_5]Br_3$	4.79 (85)	25	—	—	80		
$[Co(OH_2)(NH_3)_5]I_3$	—	—	—	—	70		
$[Co(OH_2)(NH_3)_5](NO_3)_3$	2.51 (85)	31	—	—	50		
$[Cr(OH_2)(NH_3)_5]Cl_3$	2.41 (65)[e]	25,[f] 26.4[g]	28[h]	−2.53[e]	60[h]		
$[Cr(OH_2)(NH_3)_5]Br_3$	2.43 (76)	36, 29.7	38	9.2	68		
$[Cr(OH_2)(NH_3)_5]I_3$	1.61 (82)	19, 32.7	—	15.4	70		
$[Cr(OH_2)(NH_3)_5](NO_3)_3$	1.38 (55)	14, 24.3	18	−2.49	40		

a) Temp. of mass-loss initiation. b) From Ref. 13. c) From Ref. 14 for X^-. d) From Ref. 5. e) From Ref. 9. f) Obtained by DTA in Ref. 8. g) ΔH^* in Ref. 9. h) From Ref. 8.

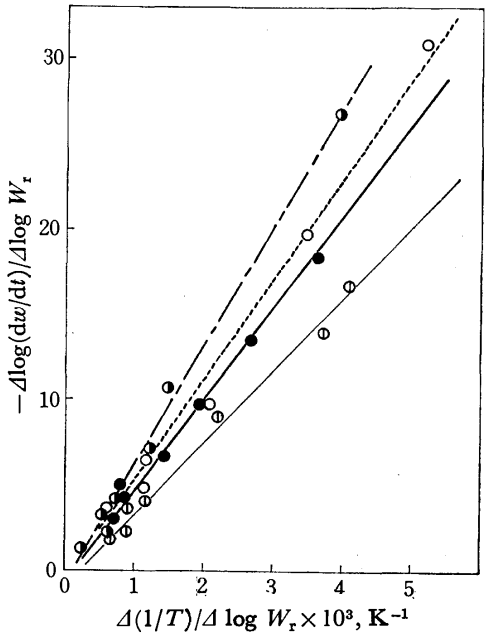

Fig. 5. The application of Freeman-Carroll Equation to the deaquation-anation reaction of $[Ru(OH_2)(NH_3)_5]X_3$ complexes.
—●— Chloride, —○— Bromide, —◑— Iodide, —ⓘ— Nitrate.

for the corresponding cobalt(III) complexes. This is attributable to the presence of a lower unoccupied t^5_{2g} d-orbital for the ruthenium(III) ion and to the great softness of the 4d transition metal. The effects of the outer sphere anion on the thermal stability of the aquapentaammine complex are somewhat complicates. If the temperature of the mass-loss initiation indicates the thermal stability of a complex, this order is in agreement with that of the increase in the ionic radius and that of the decrease in the nucleophilic affinity, which is conveniently shown by the proton affinity in Table 2. The nitrate gives the largest value of the rate constant for the deaquation-anation reaction of the aquapentaammineruthenium(III), while it gives the smallest value for the cobalt(III) aquapentaammine complex. For the ruthenium complexes, the relation between the rate constant and the activation energy is generally consistent; that is, the larger rate constant corresponds to the smaller activation energy value. The activation entropy values are generally small and negative, except for the iodide. This means that the aquapentaammine complex has less randomness in the activated state and that, therefore, the deaquation-anation probably takes the S_N2 mechanism. On the other hand, the reaction may have a S_N1-like mechanism for the iodide.

Reaction Mechanism of the Deaquation-anation. Considering the reaction mechanism, it is convenient to divide Reaction (1) into two kinds of reaction schemes, 2—3 or 4—5:

$$[Ru(OH_2)(NH_3)_5]X_3 \longrightarrow [Ru(NH_3)_5]X_3 + H_2O \quad (2)$$

$$[Ru(NH_3)_5]X_3 \longrightarrow [RuX(NH_3)_5]X_2 \quad (3)$$

and

$$[Ru(OH)_2(NH_3)_5]X_3 \longrightarrow [RuX(OH_2)(NH_3)_5]X_2, \quad (4)$$

$$[RuX(OH_2)(NH_3)_5]X_2 \longrightarrow [RuX(NH_3)_5]X_2 + H_2O. \quad (5)$$

If Reaction Path 2 is the rate-determining step, the activation energies in all the cases of deaquation-anation reactions should be approximately close to each other. When the rate of the anation process (4) is smaller than that of the deaquation process (5), the deaquation-anation reaction is a S_N2-type mechanism. The experimental results shown in Table 2 support this reaction mechanism. As is also shown in Table 2, the rate constant for the nitrate is nearly two or three times larger than those for the other complexes and the activation energies for the latter are about 1.3—1.7 times that for the nitrate. This suggests that the deaquation-anation reaction takes place through

Reactions 4 and 5, that is the S_N2 mechanism. These relations are in agreement with that predicted from the crystal-field activation energy,[15] assuming a seven-coordinated intermediate in the reaction corresponding to Reaction 4. Moreover, the reaction in the solid state will be more likely to take the S_N2 mechanism than that in the aqueous phase, because the outersphere anion may be fixed by the lattice energy at the position neighboring the innersphere ligand in the solid state.

The authors wish to thank the Ministry of Education for the financial support (No. 847009) granted to this research.

References

1) Part VIII of this series; A. Ohyoshi, S. Hiraki, T. Odate, S. Kohata, and J. Oda, This Bulletin, to be published,
2) A part of this paper was briefly reported, A. Ohyoshi. S. Hiraki, T. Odata, and S. Kohata, *Chem. Lett.*, **1973**, 1265.
3) M. Mori, R. Tsuchiya, and Y. Okano, This Bulletin, **32**, 1029 (1959).
4) M. Mori and R. Tsuchiya, *ibid.*, **33**, 841 (1960).
5) W. W. Wendlandt and J. R. Bear, *J. Phys. Chem.*, **65**, 1516 (1961).
6) W. W. Wendlandt, G. D. Ascenzo, and R. H. Gore, *J. Inorg. Nucl. Chem.*, **32**, 3404 (1970).
7) W. W. Wendlandt and J. L. Bear, *ibid.*, **22**, 77 (1961).
8) R. Tsuchiya, Y. Kaji, A. Uehara, and E. Kyuno, This Bulletin, **42**, 1881 (1969).
9) K. Nagase and H. Yokobayashi, *ibid.*, **47**, 2036 (1974).
10) J. F. Endicott and H. Taube, *J. Amer. Chem. Soc.*, **84**, 4984 (1962).
11) H. Hartmann and C. Buschbeck, *Z. Phys. Chem.*, **11**, 120 (1957).
12) E. S. Freeman and B. Carroll, *J. Phys. Chem.*, **62**, 394 (1958).
13) L. Pauling, "The Nature of the Chemical Bond," 3rd Ed., Cornell Univ. Press, Ithaca (1960).
14) G. R. Freeman, *Radiation Res. Rev.*, **1**, 1 (1968).
15) J. A. Broomhead, F. Basolo, and R. G. Pearson, *Inorg. Chem.*, **3**, 826 (1964).

Mössbauer Spectroscopic Studies of the Effect of Anions in the Second Coordination Sphere in the EC-decay

Hirotoshi SANO and Toshiaki OHNUMA

Department of Chemistry, Faculty of Science, Tokyo Metropolitan University, Fukazawa, Setagaya, Tokyo 158

(Received July 16, 1974)

The ^{57}Fe–Mössbauer emission spectra of ^{57}Co-labelled $[Co(NH_3)_6](NO_3)_3$, $[Co(en)_3](NO_3)_3$, $K_3[Co(CN)_6]$, $K_3[Co(NO_2)_6]$, $[Co(NH_3)_6]_2(C_2O_4)_3 4H_2O$, $[Co(en)_3]_2(C_2O_4)_3 \cdot 9H_2O$, $[Co(NH_3)_6][Fe(CN)_6]$, $[Co(NH_3)_6][Cr(C_2O_4)_3] \cdot 3H_2O$, and $[Co(NH_3)_6][Fe(C_2O_4)_3] \cdot 3H_2O$ sources have been determined. It has been demonstrated that oxalate anions and trisoxalatochromate and trisoxalatoferrate complex anions located outside the first coordination sphere of the decayed atom are still involved in the local radiolytic processes initiated by the EC-decay. The yields of ^{57}Fe species found in the ferrous-charge state were interpreted by using the data of γ-radiolysis and hot-atom chemistry of the $^{59}Co(n,\gamma)^{60}Co$ reaction.

A number of Mössbauer spectroscopic studies have been made of the oxidation state of ^{57}Fe after the EC-decay of ^{57}Co as well as of that of ^{119}Sn after the IT(IC)-decay of ^{119m}Sn. The ^{57}Fe atom produced in the decay suffers a modest recoil, *ca.* 6 eV, and it acquires an average positive charge of 4 or 5 units within 10^{-14} s of its formation becaues of the Auger cascade.[1] The Auger cascade can be invoked as giving rise to charge states more positive than that of the parent ^{57}Co atom, but the factors for the stabilization of the less positive charge state have not been fully understood. One of the explanations of the after-effects of the ^{57}Co EC-decay has been worked out from the difference between the ionic radii of Co^{3+} and Fe^{3+}, which could manifest itself as an internal pressure acting on the decayed atom.[2] We have previously pointed out that a plausible mechanism is the radiolytic process initiated by the Auger process.[3–6] Nath *et al.* have recently suggested the possibility of the fragmentation and the reentry of the degraded ^{57}Fe ion, undergoing excited exchange with a host cobalt molecule.[7] Friedt *et al.* have suggested a similar radiolytic self-decomposition of the molecular environment of the decaying atoms, although they have concluded that the auto-radiolysis is limited to the nearest neighbors of the decayed atom because the electrons emitted during the Auger cascade have a low energy and a short mean path.[8] In the present work, we investigated the effect of anions in the second coordination sphere by comparing the Mössbauer spectra of the ^{57}Co-labelled complex compounds.

Experimental

^{57}Co-labelled Compounds. ^{57}Co-labelled $[Co(NH_3)_6](NO_3)_3$, $[Co(en)_3](NO_3)_3$, $K_3[Co(CN)_6]$, and $K_3[Co(NO_2)_6]$ were prepared from solutions each containing 50 mg of cobalt(II) and about 1 mCi of carrier-free ^{57}Co by following the methods described in Refs. 9, 10, 11, and 12 respectively. ^{57}Co-labelled $[Co(NH_3)_6]_2(C_2O_4)_3 \cdot 4H_2O$, $[Co(NH_3)_6][Fe(CN)_6]$, $[Co(NH_3)_6][Cr(C_2O_4)_3] \cdot 3H_2O$, $[Co(NH_3)_6][Fe(C_2O_4)_3] \cdot 3H_2O$, and $[Co(en)_3]_2(C_2O_4)_3 \cdot 9H_2O$ were made from solutions of ^{57}Co-labelled $[Co(NH_3)_6](NO_3)_3$ and $[Co(en)_3](NO_3)_3$ by adding solutions of $K_2C_2O_4 \cdot 2H_2O$, $K_3[Fe(CN)_6]$, $K_3[Cr(C_2O_4)_3] \cdot 3H_2O$, and $K_3[Fe(C_2O_4)_3] \cdot 3H_2O$ respectively, purchased or prepared by the methods described in Refs. 13 and 14. The purity was checked by elemental analysis and by X-ray diffraction. All the compounds were found to be at least 98% pure.

Mössbauer Spectroscopic Measurements. The source compounds were kept in a cryostat, and the Mössbauer spectra were measured against an ^{57}Fe-enriched stainless steel absorber moving in a constant acceleration mode at room temperature. Velocity calibrations were carried out by using an ^{57}Fe-enriched iron foil absorber moving against a stationary ^{57}Co(Pt) source at room temperature.

Results and Discussion

Figures 1 to 4 show the Mössbauer spectra of the source compounds measured at 78 K. The spectrum of the ^{57}Co-labelled $K_3[Co(C_2O_4)_3] \cdot 3.5H_2O$ source at

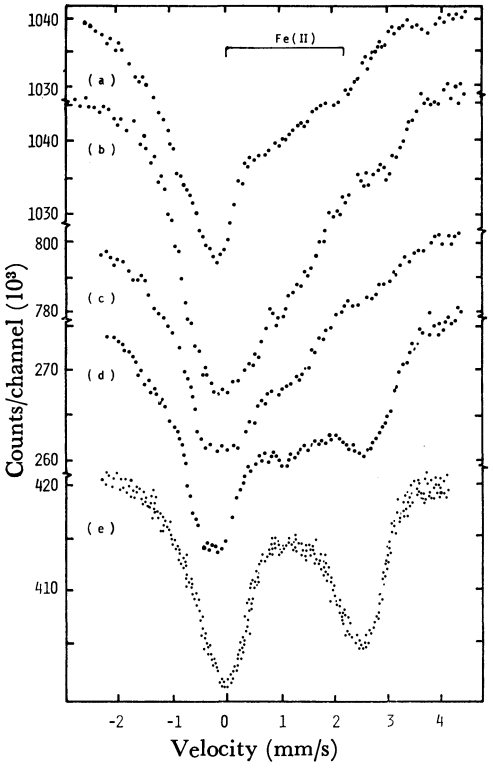

Fig. 1. Mössbauer spectra at 78 K of ^{57}Co-labelled (a) $K_3[Co(CN)_6]$, (b) $K_3[Co(NO_2)_6]$, (c) $[Co(NH_3)_6](NO_3)_3$, and (d) $[Co(en)_3](NO_3)_3$ sources. (e) Spectrum of ^{57}Co-labelled $K_3[Co(C_2O_4)_3] \cdot 3.5H_2O$ source at 93 K reproduced from ref. 15.

93 K is also reproduced in Fig. 1 from Ref. 15 for the sake of comparison. All the velocity scales were normalized with respect to metallic iron. The comparison of the spectra of the $[Co(NH_3)_6](NO_3)_3$, $[Co(en)_3](NO_3)_3$, $K_3[Co(CN)_6]$, and $K_3[Co(NO_2)_6]$ sources with the spectrum of the $K_3[Co(C_2O_4)_3]3.5H_2O$ source clearly shows that the oxalate ligand in the first coordination sphere has the largest effect in reducing the decayed atom, probably because of the decomposition of the oxalate ions to carbon dioxide.

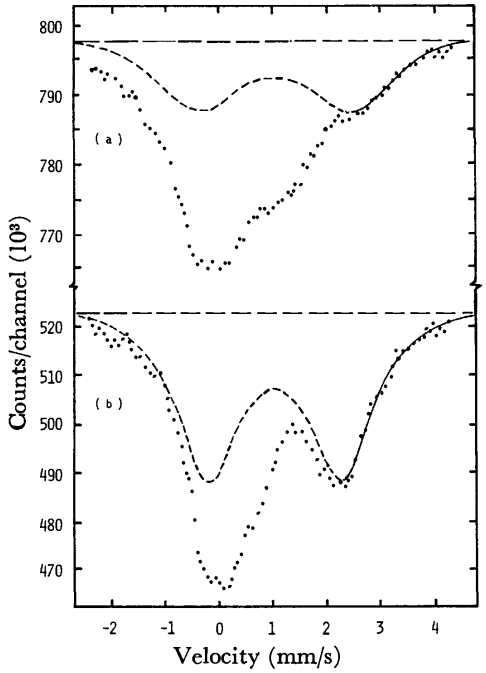

Fig. 2. Mössbauer spectra at 78 K of ^{57}Co-labelled (a) $[Co(NH_3)_6](NO_3)_3$ and (b) $[Co(NH_3)_6]_2(C_2O_4)_3\cdot 4H_2O$ sources. The peak component of ferrous ^{57}Fe species was estimated as indicated in a broken line by using the line shape in the high velocity region ($\gtrsim$2.5 mm/s, indicated in a solid line) where the contribution of ferric species is assumed to be negligible. The yield of ferrous ^{57}Fe species was evaluated from the area under the component and the total area of the spectrum.

As may be seen in Figs. 2 to 4, an increased yield of the ferrous ^{57}Fe species is unambiguously observed in the spectra of $[Co(NH_3)_6]_2(C_2O_4)_3\cdot 4H_2O$, $[Co(en)_3]_2(C_2O_4)_3\cdot 9H_2O$, and $[Co(NH_3)_6][Cr(C_2O_4)_3]\cdot 3H_2O$ and $[Co(NH_3)_6][Fe(C_2O_4)_3]\cdot 3H_2O$ sources compared with the spectra of the $[Co(NH_3)_6](NO_3)_3$, $[Co(en)_3](NO_3)_3$, and $[Co(NH_3)_6][Fe(CN)_6]$ sources respectively, although the yield of the ferrous ^{57}Fe species is lower in those compounds than in $K_3[Co(C_2O_4)_3]\cdot 3.5H_2O$. Since it is known that the water of crystallization has no reducing effect on the oxidation state of ^{57}Fe produced in the after-effect of the EC-decay in a number of ^{57}Co-labelled cobalt compounds,[15-19] it may be concluded that the increased yield of the ferrous ^{57}Fe species is due to the effect of oxalate ions. The higher yield of the ferrous ^{57}Fe species found in $[Co(en)_3](NO_3)_3$ than in $[Co(NH_3)_6](NO_3)_3$ may be explained by assuming a higher probability of bond rupture in the ethylenediamine ligand, thus producing nitrenium

Table 1. Summary of the yield of ferrous ^{57}Fe species produced after EC-decay, the $G(Co^{2+})$ value in γ-radiolysis,[20] and the radiochemical yield of cobaltous ^{60}Co species in the hot-atom chemistry of ^{59}Co(n, γ) ^{60}Co reaction[21]

Compound	Yield of $^{57}Fe^{2+}$ in EC-decay (%)	$G(Co^{2+})$	Yield of $^{60}Co^{2+}$ in ^{59}Co(n, γ) ^{60}Co (%)
$[Co(NH_3)_6](NO_3)_3$	40±1	1.1±0.2	66.7±0.2
$[Co(en)_3](NO_3)_3$	53±1	0.4±0.1	69.4±0.2
$[Co(NH_3)_6]_2(C_2O_4)_3\cdot 4H_2O$	72±1	2.9±0.2	91.0±0.2
$K_3[Co(C_2O_4)_3]\cdot 3H_2O$	85[15]	11.6±0.2	98.6±0.4

cations (H_2N^+ and $H_2NCH_2CH_2N^+H$), carbonium cations ($H_2NCH_2C^+H_2$, $H_2NCH_2C^+HNH_2$, and $H_2NC^+H_2$), cationic radicals, hydrogen molecules and cations, and electrons which may reduce the decayed atom.

We have reported previously that oxalate anions in the first or second coordination sphere exert some reducing effect both in the radiolysis and in the hot-atom chemistry in the ^{59}Co(n,γ)^{60}Co reaction of cobalt(III) complexes.[20,21] Table 1 summarizes the yields of ferrous ^{57}Fe as evaluated from the spectral area, the $G(Co^{2+})$ value in γ-radiolysis,[20] and the radiochemical yield of ^{60}Co in the hot-atom chemistry.[21] The effect of the oxalate ion on the reduction of the central cation observed in the EC-decay of ^{57}Co qualitatively parallels those data found for the $G(Co^{2+})$ values of γ-ray-irradiated cobalt(III) oxalate complexes and for the radiochemical yields of the divalent ^{60}Co species produced in the (n,γ) reaction. The low $G(Co^{2+})$

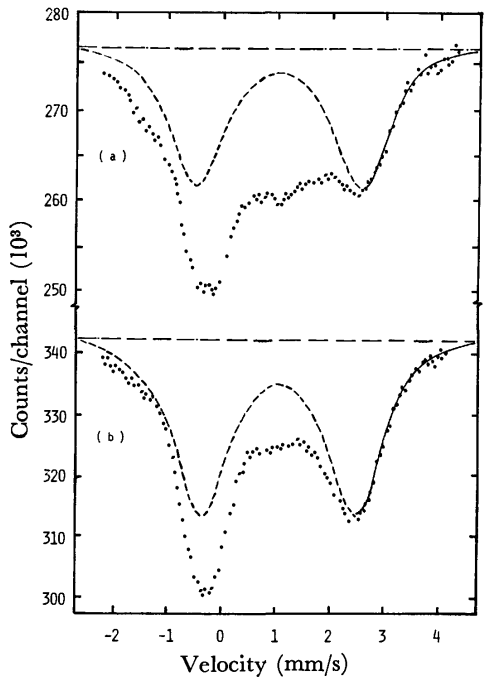

Fig. 3. Mössbauer spectra at 78 K of ^{57}Co-labelled (a) $[Co(en)_3](NO_3)_3$ and (b) $[Co(en)_3]_2(C_2O_4)_3\cdot 9H_2O$ sources. See the figure caption in Fig. 2 for the evaluation of the yield of ferrous ^{57}Fe species.

value found in the γ-radiolysis of $[Co(en)_3](NO_3)_3$ may be ascribed to the low yields of fragmentations, producing nitrenium cations, carbonium cations, cationic radicals, *etc.*, because of the lower LET value of γ-rays compared to those of Auger electrons and recoil ^{60}Co atoms.

Another interesting point concerns the comparison of the spectra of the $[Co(NH_3)_6][Cr(C_2O_4)_3]3H_2O$ and $[Co(NH_3)_6][Fe(C_2O_4)_3]\cdot 3H_2O$ sources. The larger yield of the ^{57}Fe species in the ferrous oxidation state observed in the trisoxalatoferrate(III) source compared to that observed in trisoxalatochromate(III) source may be explained by assuming a higher probability of the decomposition of oxalate ligands into carbon dioxide and electrons induced by the local radiolysis in trisoxalatoferrate. Sugimori and Tsuchihashi have reported that $K_3[Cr(C_2O_3)_3]\cdot 3H_2O$ shows a higher stability against external γ-ray irradiation than does $K_3[Fe(C_2O_4)_3]\cdot 3H_2O$, since the chromous state is much more unstable than is the ferrous state.[22] The $G(CO_2)$ values are evaluated to be 0.9 in the γ-ray irradiation of the trisoxalatochromate(III) and 7.5 in the trisoxalatoferrate(III).

The results indicate that not only the nearest neighbors of the decayed atom (the ligands in the first coordination sphere), but also the next nearest neighbors (the anions or ligands in the second coordination sphere), are involved in determining the oxidation state of the decayed atom in the local radiolytic process initiated by the EC-decay and the Auger effect. The $G(CO_2)$ value reported by Sugimori and Tsuchihashi (9.8) is approximately equal to our previous results of the $G(CO^{2+})$ values evaluated for $K_3[Co(C_2O_4)_3]\cdot 3H_2O$ (11.6). This suggests the following process:

$$C_2O_4^{2-} \longrightarrow 2CO_2 + 2e^-;$$

$$2Co(III) + 2e^- \longrightarrow 2Co(II).$$

It is obvious that the decomposition of each oxalate anion can reduce two metal cations from the trivalent to the divalent state. In the ^{57}Co-labelled compounds, however, the concentration of the decaying atom in the host matrix is so small that the electrons produced by each decomposition of oxalate ligands or anions located near the decaying atom may be used to reduce at most only one ^{57}Fe atom to the ferrous state.

As we have previously mentioned, the higher yield of ferrous ^{57}Fe in the EC-decay of $K_3[Co(C_2O_4)_3]\cdot 3H_2O$ compared to the yield of stannous ^{119}Sn in the IT(IC)-decay of $K_6Sn_2(C_2O_4)\cdot 4H_2O$ may be ascribed to the difference in the fluorescence yields of iron and tin atom.[4] The fluorescence yield of iron is known to be about 32%. The yield of ferrous ^{57}Fe reported in $K_3[Co(C_2O_4)_3]\cdot 3.5H_2O$ exceeds the value of the Auger yield of iron (68%) by 17%. As long as it is assumed that the yield of ferrous ^{57}Fe depends only upon the nearest neighbors of the decayed atom, the results can be explained in terms of two processes: (1) a direct X-ray radiolysis of oxalate ligands in the trisoxalato ^{57}Fe complex anions which escaped the Auger-electron radiolysis, and (2) an indirect electron transfer through the X-ray radiolysis of the adjacent host trisoxalatocobaltate(III) anions.

The yields of ferrous ^{57}Fe in $[Co(NH_3)_6]_2(C_2O_4)_3\cdot 4H_2O$, $[Co(en)_3]_2(C_2O_4)_3\cdot 9H_2O$, $[Co(NH_3)_6][Cr-$

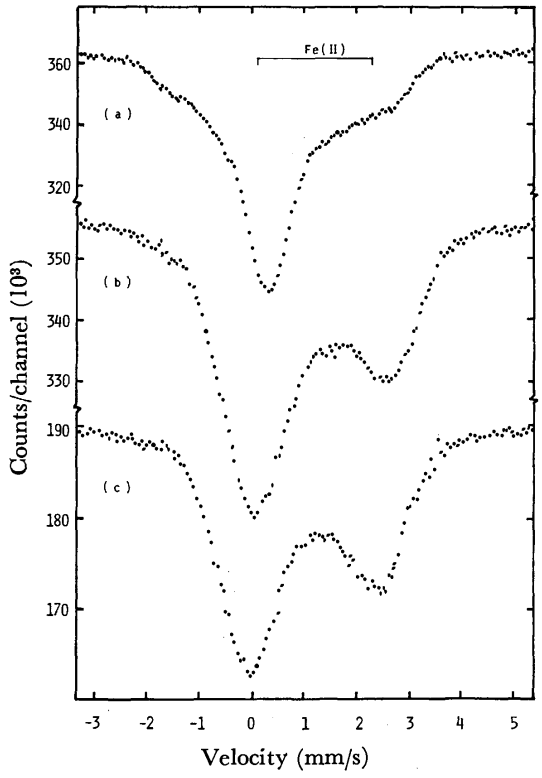

Fig. 4. Mössbauer spectra at 78 K of ^{57}Co-labelled (a) $[Co(NH_3)_6][Fe(CN)_6]$, (b) $[Co(NH_3)_6][Cr(C_2O_4)_3\cdot 3H_2O$, and (c) $[Co(NH_3)_6][Fe(C_2O_4)_3]3H_2O$ sources.

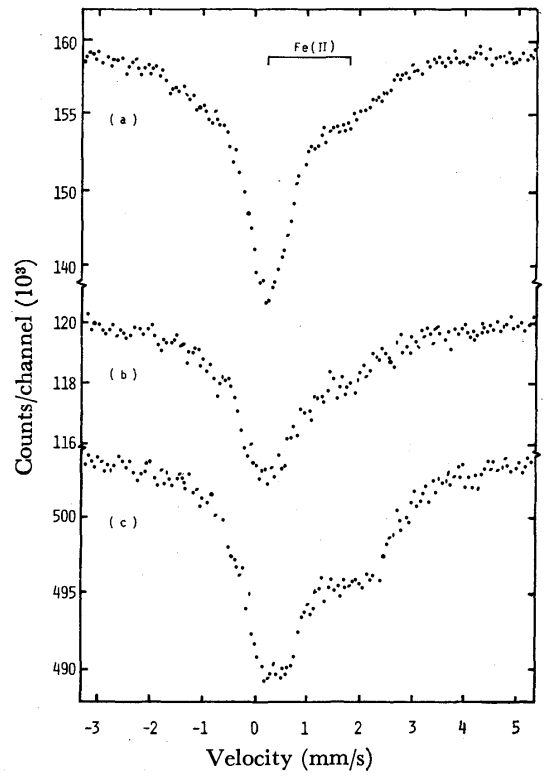

Fig. 5. Mössbauer spectra at 295 K of ^{57}Co-labelled (a) $[Co(NH_3)_6][Fe(CN)_6]$, (b) $[Co(NH_3)_6][Cr(C_2O_4)_3]\cdot 3H_2O$, and (c) $[Co(NH_3)_6][Fe(C_2O_4)_3]3H_2O$ sources.

$(C_2O_4)_3]\cdot 3H_2O$, and $[Co(NH_3)_6][Fe(C_2O_4)_3]3H_2O$ are, however, too high to be explained by the indirect electron transfer through the X-ray radiolysis. The exceptional dissimilarity found in the yield of ferrous ^{57}Fe compared to the $G(Co^{2+})$ value in $[Co(en)_3](NO_3)_3$ may also disprove the X-ray radiolysis mechanism for the interpretation of the main process initiated by the EC- or IT(IC)-decay. It may, therefore, be concluded that Auger electrons emitted from the decayed atom decompose oxalate ions outside the first coordination sphere or that the Auger process gives rise to an excitation-induced decomposition of the oxalate ions and that electrons thus produced are then transfered to the decayed atom, thus stabilizing a reduced oxidation state during the nuclear life-time of the first excited level of the Mössbauer nucleus.

These conclusions are consistent with our previous interpretation derived from the studies of $^{57}Co(acac)_3$ doped into a number of trisacetylacetonato complexes, where a remarkable dependence of the yield of ferrous ^{57}Fe is found on the kind of surrounding host matrix. A comparison of the spectrum of ^{57}Co-labelled $K_3[Co(CN)_6]$ with that of $[Co(NH_3)_6][Fe(CN)_6]$ does not show any positive evidence for the excited exchange of ^{57}Fe produced from the EC-decay of ^{57}Co with iron(III) atoms of hexacyanato complex anions, although a minor possibility of this can not be denied. The peak component assigned to the ferrous ^{57}Fe species decreases relative to that of the ferric species at room temperature, especially in the cases of the $[Co(NH_3)_6]_2(C_2O_4)_3\cdot 4H_2O$, $[Co(en)_3]_2(C_2O_4)_3\cdot 9H_2O$, $[Co(NH_3)_6][Cr(C_2O_4)_3]\cdot 3H_2O$, and $[Co(NH_3)_6][Fe(C_2O_4)_3]\cdot 3H_2O$ sources. Some typical spectra observed at 295 K are shown in Fig. 5. This suggests that the ferrous species have lower recoil-free fractions, since they are located in disturbed or thermally excited environments.

References

1) H. Pollak, *Phys. Status Solidi*, **2**, 720 (1962).
2) Y. Hazony and R. H. Herber, *J. Inorg. Nucl. Chem.*, **31**, 321 (1969).
3) H. Sano and F. Hashimoto, This Bulletin, **38**, 1565 (1965).
4) H. Sano and M. Kanno, *Chem. Commun.*, **1969**, 601.
5) H. Sano, K. Sato, and H. Iwagami, This Bulletin, **44**, 2570 (1971); H. Sano and H. Iwagami, *Chem. Commun.*, **1971**, 1637.
6) H. Sano and T. Ohnuma, *Chem. Lett.*, **1974**, 589; *Chem. Phys. Lett.*, **26**, 348 (1974).
7) A. Nath, M. D. Klein, W. Kündig, and D. Lichtenstein, *Radiation Effects*, **2**, 211 (1970); "Mössbauer Effect Methodology," Vol. 5, ed. by I. J. Gruverman, Plenum Press, New York, N. Y. (1970), p. 163.
8) J. M. Friedt, E. Baggio-Saitovitch, and J. Danon, *Chem. Phys. Lett.*, **7**, 603 (1970); E. Baggio-Saitovitch, J. M. Friedt, and J. Danon, *J. Chem. Phys.*, **56**, 1269 (1972); J. P. Sanchez, Y. Llabador, and J. M. Friedt, *J. Inorg. Nucl. Chem.*, **35**, 3557 (1973).
9) S. M. Jörgensen, *Z. Anorg. Chem.*, **17**, 457 (1898).
10) *Idem*, *J. Prakt. Chem.*, **39**, 8 (1889).
11) A. Benedetti-Pichler, *Z. Anal. Chem.*, **70**, 258 (1927).
12) S. M. Jörgensen, *Z. Anorg. Chem.*, **39**, 284 (1900).
13) A. Rosenheim, *ibid.*, **11**, 196, 225 (1892).
14) F. M. Jaeger, *Rec. Trav. Chim.*, **38**, 242 (1919); W. Thomas, *J. Chem. Soc.*, **1921**, 119, 1140.
15) J. M. Friedt and L. Asch, *Radiochim. Acta*, **12**, 208 (1969). Potassium trisoxalatocobaltate(III) reported in Ref. 15 is denoted as $K_3[Co(C_2O_4)_3]\cdot 3.5H_2O$, although the compound is known as $K_3[Co(C_2O_4)_3]\cdot 3H_2O$. It may be supposed that the small difference in the content of water of crystallization has no significant effect on the yield of ^{57}Fe(II).[15-19] Similar results have been reported by Fenger *et al.* for ^{57}Co-labelled $K_3[Co(C_2O_4)_3]3H_2O$ and ^{57}Co-doped $K_3[Fe(C_2O_4)_3]3H_2O$.[19]
16) R. Ingalls, C. J. Coston, G. Depasquali, H. G. Drickermer, and J. J. Pinajian, *J. Chem. Phys.*, **45**, 1057 (1966).
17) J. M. Friedt and J. P. Adloff, *C. R. Acad. Sci. Paris, Ser. C*, **264**, 1356 (1967).
18) A. A. Temperley, *Bull. Amer. Phys. Soc.*, **12**, 924 (1967).
19) J. Fenger, K. E. Siekierska, and A. G. Maddock, *J. Chem. Soc., A*, **1970**, 1456. A number of studies indicate that the water of hydration does not play an important role in the primary radiolysis of the hydrated salts and very slight oxidizing effect seems to be observed in several ^{57}Co-labelled compounds with various number of the water of hydration due to radicals such as OH produced in the Auger after-processes.[15,17]
20) H. Sano, N. Matsubara, and N. Saito, This Bulletin, **38**, 333 (1965).
21) N. Saito, H. Sano, and T. Tominaga, *Chem. Ind.* (London), **1964**, 1622; N, Saito, T. Tominaga, and H. Sano, This Bulletin, **33**, 1621 (1960).
22) A. Sugimori and G. Tsuchihashi, *ibid.*, **34**, 449 (1961).

The Gas Chromatographic Determination of Carbonyl Compounds as Their Thiosemicarbazone

Yoshio BABA

National Research Institute for Pollution & Resources, Kawaguchi, Saitama 332

(Received August 12, 1974)

The gas chromatographic determination of carbonyl compounds in a contaminated air sample *via* their thiosemicarbazone was studied. As the method utilizes the selective detectability of the flame photometric detector for the sulfur compound, the isolation of the sulfur-containing derivatives of the carbonyl compounds is not required; this eliminates the inaccuracy stemming from the isolation of the derivatives from the sample solution. The isolation and subsequent regeneration of the carbonyl compound was carried out *via* the thiosemicarbazone metal complex; this affords a practical method of preparing the sample required for the identification of the individual carbonyl compound.

The identification and quantitative determination of carbonyl compounds is a commonly encountered problem in air-quality analysis—for example, the analysis of the carbonyl compounds in automobile exhausts and in concentrated air samples.

Derivatization *via* 2,4-dinitrophenylhydrazine (DNPH) followed by subsequent gas chromatographic analysis, has been widely used for carbonyl analysis. The carbonyl DNPH derivatives have been analyzed directly by gas chromatography,[1-6] or, after the hydrolysis of the carbonyl DNPH derivatives by heating them with mineral or organic acid, the regenerated carbonyl compounds have been analyzed.[7-8] The gas chromatographic analysis of the carboxylic acids produced by the ozonization of the carbonyl DNPH has also been reported.[9]

In this study, the carbonyl compound was converted into its thiosemicarbazone, and the latter sulfur-containing derivative was detected by means of a flame photometric detector (FPD). As the selective detectability of FPD for the sulfur compounds permits the selective determination of the carbonyl thiosemicarbazone in a contaminated sample—for example, in auto exhaust or in concentrated air sample which contains foreign compounds other than the carbonyl compounds, the isolation of the carbonyl compound derivative from the foreign compounds is not required. This fact, in conjunction with the specific and quantitative thiosemicarbazone formation reaction, could eliminate the inaccuracy stemming from the separation or extraction of the carbonyl compound derivative which is encountered in the direct carbonyl DNPH method.

Further, the unique property of thiosemicarbazone to form an insoluble metal complex with heavy metal salts can be utilized for the isolation, followed by regeneration, in the identification of the individual carbonyl compound by GLC-Mass analysis, which requires the isolation of the carbonyl compounds from other impurities, *e.g.*, hydrocarbons.

Experimental

Thiosemicarbazones. The general procedure for the preparation of all the thiosemicarbazones listed in Table 2 was as follows. The carbonyl compound (0.01 mol) was dissolved in 10 ml of 95% ethanol, and then approximately 0.2 ml of glacial acetic acid and 0.9 g (0.01 mol) of thiosemicarbazide were added. The reaction mixture was stirred at room temperature until the thiosemicarbazide dissolved (it usually took 0.5—1 hr) and was then refluxed for 0.5 hr. The solvent was evaporated under reduced pressure, and the crude product was recrystallized from 50% ethanol or methanol.

Determination of the Response Factors and the Relative Retention Values of Thiosemicarbazones. Gas chromatography was done by means of a Micro Tek Instruments Corp. Model 160 gas chromatograph equipped with a flame photometric detector and a 4 mm i.d. × 1 m glass column packed with Diasolid ZT (Silicone). The other analytical conditions are described in Tables 1 and 2.

In the determination of the response factors of the thiosemicarbazones listed in Table 1, the sample solution was prepared by mixing 1 ml of the solution of thiosemicarbazone (1×10^{-4} mol) in 10 ml of ethanol, with 10 μl of the internal standard solution (di-*n*-amyl sulfide 1×10^{-4} mol in 3 ml ethanol). The peak areas of each thiosemicarbazone and internal standard sulfide were determined by means of a digital integrator, while the response factor (F_i) was calculated by the use of the following equation:

$$F_i = A_s/W_s \times W_i/A_i$$

where: A_s and W_s=peak area (log) and the weight of the internal standard respectively, and A_i and W_i=peak area (log) and the weight of thiosemicarbazone respectively.

The relative retention values (α) of the thiosemicarbazones listed in Table 2 were calculated by means of the following equation:

$$\alpha = (X_1 - X_0)/(X_s - X_0)$$

where X_0, X_s, and X_1 are the distances (in time) from the point of injection to the maximum of the chromatographic peaks of the solvent (ethanol, detected by means of a FID monitor coequipped with FPD), the internal standard (di-*n*-amyl sulfide), and thiosemicarbazone respectively.

Separation and Regeneration of the Carbonyl Compounds via the Thiosemicarbazone/$AgNO_3$ Complex. A solution of silver nitrate (0.01 mol) in 5 ml of distilled water was added to a thiosemicarbazone (0.01 mol)/EtOH solution. After 30 min's stirring at room temperature, the reaction mixture was evaporated to dryness under reduced pressure. The residual, black-colored solid was washed with a hydrocarbon solvent (*e.g.*, *n*-hexane) and then dissolved in 20 ml of ethanol; 5 ml of 6 M-HCl was added, and the reaction mixture was stirred for 1 hr under refluxing, cooled, and filtered. The content of the carbonyl compound in the filtrate was determined by the gravimetric 2,4-dinitrophenylhydrazine method.

Results and Discussion

The thiosemicarbazones listed in Table 2 were prepared by Campaigne's method.[11] Unlike semicarbazide, the thiosemicarbazide is stable in its free form, and in the presence of a small amount of glacial acetic acid, the reaction proceeds readily at room temperature and the thiosemicarbazone formation reaction has the minor possibility of a side reaction. The thiosemicarbazone-formation reaction with the 15 carbonyl compounds listed in Table 2 proceeded readily at room temperature: an initially insoluble crystal of thiosemicarbazide dissolved in 0.5—1 hr, and either a clear solution or a crystal of newly-formed thiosemicarbazone was obtained. The small deviations in the melting points between the crude and the purified product indicated the absence of any side reaction or isomer formation.

It has been reported that, in the direct gas-chromatographic analysis of the carbonyl DNPH, the reproducibilities were poor, the response factors varied with the concentration, spurious decomposition peaks or double peaks hampered the analysis, and a homologous series of carbonyl DNPH derivatives had widely varying responses per mole when detected by FID.[1,2] All of these results indicated that the higher-molecular-weight carbonyl DNPH derivative resulted in a varying loss of the derivatives through thermal decomposition in the gas-chromatographic system.

However, the carbonyl thiosemicarbazone, which has a smaller molecular weight than the carbonyl DNPH, makes possible milder analytical conditions, which minimize the thermal decomposition of the derivatives. In this study, column temperatures of 125—200 °C, inlet temperatures of 150—200 °C, and a detector temperature of 170 °C were used, because the melting points and the decomposing points of the 15 thiosemicarbazones were in the ranges of 70—240 °C and 165—240 °C respectively.

Table 1. Response factors (F_1) and average deviations of thiosemicarbazones

Thiosemicarbazone of	Mp (°C)	Dp (°C)	Analytical condition	F_1 value and average deviation
Acetaldehyde	139—140	180—185	a	13.86±0.04
Acetone	185—186	190—195	a	13.73±0.09
Propionic aldehyde	144—146	196—200	d	13.90±0.00
Methyl ethyl ketone	103—104	201—205	d	13.26±0.04
Diethyl ketone	85— 86	185—190	d	12.83±0.04
Methyl *n*-propyl ketone	75— 76	200—204	d	13.70±0.00
Crotonic aldehyde	159—161	200—205	d	13.90±0.00
Methyl *sec*-butyl ketone	71— 72	200—205	d	13.90±0.00
Methyl *n*-amyl ketone	78— 79	200—205	d	13.40±0.00
Acetophenone	119—120	220—227	a	13.53±0.04
Benzaldehyde	151—152	237—240	b	14.06±0.04
p-Tolualdehyde	172—173	237—240	c	14.66±0.04
p-Hydroxybenzaldehyde	238—240	238—240	c	15.06±0.47

a) N_2 20 ml/min, 150 °C isothermal. b) N_2 30 ml/min, 200 °C isothermal. c) N_2 30 ml/min, 150—200 °C (20 °C/min). d) N_2 30 ml/min, 150 °C isothermal.

The reproducibility and the uniformity of the response for various carbonyl compounds were evaluated with the thiosemicarbazones of 3 aliphatic aldehydes, 6 aliphatic ketones, 3 aromatic aldehydes, and one aromatic ketone. As is shown in Table 1, the response factors of these thiosemicarbazones, except in formaldehyde and *p*-hydroxybenzaldehyde, had a great uniformity and a high reproducibility over a wide range of homologous series.

The poor uniformity in the responses for the thiosemicarbazones of formaldehyde and *p*-hydroxybenzaldehyde is associated with a thermal decomposition of the derivatives in the gas-chromatographic system, because these two thiosemicarbazones have the same melting points as decomposition points.

Table 2. Relative retention values of thiosemicarbazones

Thiosemicarbazone of	Relative retention values		
	A	B	C
Formaldehyde	—	4.88	—
Acetaldehyde	2.96	—	—
Acetone	3.46	—	—
Propionic aldehyde	4.37	—	—
Methyl ethyl ketone	4.86	—	—
Acrolein	4.95	—	—
Diethyl ketone	7.16	—	—
Methyl *n*-propyl ketone	7.98	—	—
Crotonic aldehyde	9.84	—	—
Methyl *sec*-butyl ketone	10.14	6.19	—
Methyl *n*-amyl ketone	19.44	9.99	—
Acetophenone	—	12.21	2.50
Benzaldehyde	—	—	6.17
p-Tolualdehyde	—	—	7.50
p-Hydroxybenzaldehyde	—	—	22.00

A: N_2 30 ml/min, 125 °C isothermal, inlet temp. 150 °C.
B: N_2 30 ml/min, 160 °C isothermal, inlet temp. 160 °C.
C: N_2 30 ml/min, 200 °C isothermal, inlet temp. 200 °C.

The determination of the relative retention values of 15 thiosemicarbazones under the analytical conditions listed in Table 2 indicated that, using a 4 mm i.d. × 1 m glass column packed with Diasolid ZT, the direct gas-chromatographic analysis of the carbonyl thiosemicarbazone offers the best potential for the clear separation of the individual carbonyl compound commonly encountered in auto mobile exhausts[10] or in concentrated air samples.

In the gas-chromatographic analysis of the carbonyl compounds *via* their thiosemicarbazones, utilizing the selective response of the detector (FPD) for the sulfur compounds, purification is not required and a crude sample containing impurities can be used directly as the analytical sample. However, in the case of the identification of the individual carbonyl compounds by GLC-Mass analysis, the carbonyl compound to be iden-

Table 3. Separation and regeneration of the carbonyl compounds *via* thiosemicarbazone/$AgNO_3$ complex

Carbonyl compounds	Recovery (%)
Acetaldehyde	65.2
Diethyl ketone	51.0
Acetophenone	48.8
Crotonic aldehyde	65.3
Benzaldehyde	44.8

tified must be isolated from any foreign compounds.

The method of the regeneration of the parent carbonyl compound by treating carbonyl DNPH with mineral or organic acid cannot be applied to the unsaturated carbonyl compound and aromatic aldehydes. Similarly, method of producing the corresponding carboxylic acid by ozonization of the carbonyl DNPH cannot be applied to the unsaturated compound.

In this study, the isolation and subsequent regeneration of the parent carbonyl compounds was carried out through a heavy metal complex of thiosemicarbazone. Thiosemicarbazone is known to form an insoluble metal complex with heavy metal salts, *e.g.*, silver nitrate, cupric acetate, mercuric acetate, and mercuric cyanide. The metal complex can be decomposed to regenerate the thiosemicarbazone by a reaction with hydrochloric acid or hydrogen sulfide, and the thiosemicarbazone can be hydrolyzed to regenerate the parent carbonyl compound by heating it with mineral acid. In this work, the regeneration of the carbonyl compound *via* the thiosemicarbazone silver nitrate complex was studied in an attempt to isolate the carbonyl compound from the contaminated air sample. Table 3 indicates that the regeneration of the parent carbonyl compound, even with unsaturated or aromatic aldehyde, can be done with a 45—65% recovery.

In the analysis of the carbonyl compound in automobile exhaust by the carbonyl DNPH method, the presence of NO_x in the sample gas has been reported to interfere with the formation of the 2,4-DNPH derivative and the subsequent gas chromatographic analysis.[3)]

In this study, the effect of NO_2 on the preparation of thiosemicarbazone and the subsequent gas chromatographic analysis were examined with crotonic aldehyde, methyl ethyl ketone, and propionic aldehyde. In the presence of a 1/10 molar equivalent of NO_2, no evidence was found for the interference of NO_2 in the formation of thiosemicarbazones, which can be deduced by a comparison of the melting points of the crude and the purified products and by an examination of the gas chromatograms of the crude products.

In the presence of an equimolar amount of NO_2, although the saturated aldehyde and ketone were subject to no practical interaction with NO_2, an apparent interaction of NO_2 with the unsaturated aldehyde, crotonic aldehyde, was observed. The lower melting point of thiosemicarbazone and the appearance of foreign peaks in the gas chromatogram of the crude product indicated the occurrence of this side reaction.

References

1) L. J. Papa and L. P. Turner, *J. Chromatogr. Sci.*, **10**, 744 (1972).
2) H. Kallio, R. Linko, and J. Kaitaranta, *J. Chromatogr.*, **65**, 355 (1972).
3) M. Fracchia, F. Schuette, and P. Mueller, *Environ. Sci. Tech.*, **1**, 915 (1967).
4) E. Fedeli and M. Cirimele, *J. Chromatogr.*, **15**, 435 (1964).
5) R. Soukup, R. Scarpellino, and E. Danielczik, *Anal. Chem.*, **36**, 2255 (1964).
6) M. W. Scoggins, *ibid.*, **45**, 2204 (1973).
7) J. W. Ralls, *ibid.*, **32**, 332 (1960).
8) M. Keeney, *ibid.*, **29**, 1489 (1957).
9) P. Ronkaiene and S. Brummer, *J. Chromatogr.*, **28**, 253 (1967).
10) D. Seizinger and B. Dimitriades, *J. Air Pollution Control Assoc.*, **22**, 47 (1972).
11) E. Campaigne, P. Monroe, B. Arnwine, and W. Archer, *J. Amer. Chem. Soc.*, **75**, 988 (1953).

Anodic Wave Polarography of *N*-2-Aminoethyl-*N*-2-hydroxyethylcarbodithioic Acid

Masao SUGAWARA and Tomihito KAMBARA

Department of Chemistry, Faculty of Science, Hokkaido University, Sapporo 060

(Received August 21, 1974)

N-2-Aminoethyl-*N*-2-hydroxyethylcarbodithioic acid (Hahdtc) in an alkaline medium gives at the dropping mercury electrode an adsorption prewave due to the two-electron oxidation of mercury. The electrode reaction at pH=13.1—10.1 was inferred to proceed according to

$$Hg + 2ahdtc^- \rightleftarrows Hg(ahdtc)_2 + 2e \quad (1)$$

The surface excess of the mercury(II) chelate was estimated to be 3.0×10^{-10} mol cm^{-2}.

The polarographic behavior of compounds containing carbodithioate group have been studied by many authors.[1-7] These compounds give anodic waves corresponding to the mercury compound formation, in most cases, accompanied by adsorption phenomena. For sodium diethylcarbodithioate (Naddtc), the one-electron oxidation process was attributed to the formation of mercury complex Hg(ddtc), in which mercurous ion is present in the monomeric form, followed by rapid disproportionation to $Hg(ddtc)_2$ and Hg.[1,4] In the case of the anodic wave of ammonium 1-pyrrolidinecarbodithioate (NH_4pcd), the electrode process was ascribed to the formation of the complex $Hg(pcd)_2$.[7]

In the present work, the polarographic behavior of *N*-2-aminoethyl-*N*-2-hydroxyethylcarbodithioic acid (Hahdtc) was investigated at the dropping mercury electrode.

Experimental

N-2-Aminoethyl-*N*-2-hydroxyethylcarbodithioic acid was synthesized as follows. To 80 g of carbon disulfide in 100 ml of ethanol, 24 g of 2-aminoethylaminoethanol dissolved in 100 ml of ethanol were added dropwise under cooling in a cold water bath. The product was filtered, washed with ethanol and recrystallized from water at 65 °C. After drying in air, the Hahdtc was stored in a desiccator containing silica gel as a desiccant. Found: C, 33.09; H, 6.74; N, 15.62; S, 35.58%. Calcd for $C_5H_{12}ON_2S_2$: C, 33.31; H, 6.71; N, 15.54; S, 35.57%.

The Hahdtc in an aqueous solution was unstable and its limiting current decreased by 15% after 4 hr. Therefore, the Hahdtc solution was freshly prepared before each experiment. All other reagents used were of A. R. grade.

Direct current polarogram was recorded by means of a Shimadzu polarograph, type RP-2, and AC polarogram was recorded by using a Shimadzu AC attachment, type BF-1. The dropping mercury electrode used had the following characteristics; mercury flow-rate $m=1.50$ mg s^{-1} in deionized water, drop time $t=4.91$ s in 0.1 mol dm^{-3} sodium hydroxide solution at open circuit and at a height of the mercury reservoir $h=58.0$ cm. The potential values presented here refer to the saturated calomel electrode, which was connected to the electrolysis solution through an agar bridge (3% agar, satd. potassium nitrate). The mercury of SCE was connected to a mercury pool counterelectrode *via* a 2200 μF capacitor.

The pH measurements were carried out with a Hitachi-Horiba glass electrode pH meter, type F-5.

A portion of the freshly prepared electrolysis solution containing Hahdtc and 0.1 mol dm^{-3} sodium hydroxide as the supporting electrolyte was taken into a polarographic cell, and the polarogram was recorded at (25±0.1) °C after deaeration by bubbling nitrogen gas.

Results and Discussion

Direct Current Polarography. The DC and AC polarograms of 4.0×10^{-4} mol dm^{-3} Hahdtc in 0.1 mol dm^{-3} sodium hydroxide solution are shown in Fig. 1. At concentrations of the Hahdtc lower than 1.0×10^{-4} mol dm^{-3}, one DC prewave, A, at −0.65 V is observed. At concentrations higher than 1.0×10^{-4} mol dm^{-3}, the DC main wave B at −0.32 V appears, while the limiting current of the prewave remained constant. The sum of the limiting currents of the prewave and main wave is proportional to the concentration of Hahdtc between 1.0×10^{-4} and 8.0×10^{-4} mol dm^{-3} as shown in Fig. 2. The height of the prewave is approximately proportional to $h_{corr.}$ and that of the total wave (A+B) is to $h_{corr.}^{1/2}$ (Table 1). The limiting current

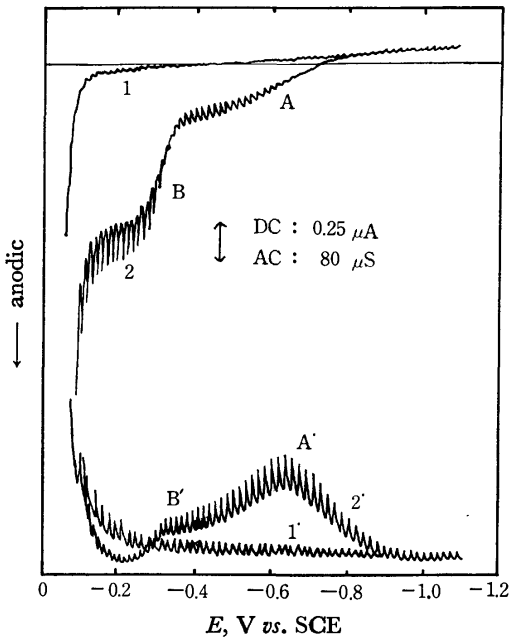

Fig. 1. Polarograms of Hahdtc in 0.1 mol dm^{-3} NaOH at 25 °C.
Concentration of Hahdtc 1, 1′: 0 mol dm^{-3}, 2, 2′: 4×10^{-4} mol dm^{-3}, 1, 2: DC polarogram, 1′, 2′: AC polarogram.

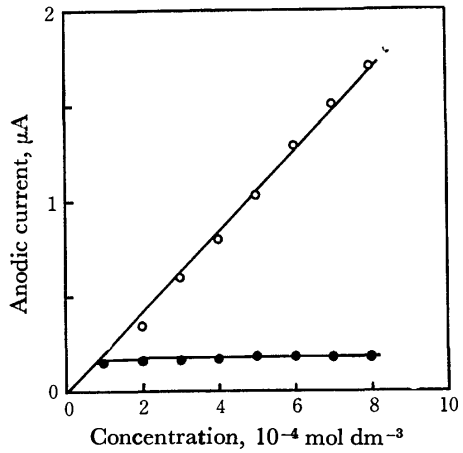

Fig. 2. Concentration dependence of the limiting currents of Hahdtc in 0.1 mol dm^{-3} NaOH at 25 °C.
●: prewave A, ○: total wave (A+B).

TABLE 1. THE EFFECT OF THE HEIGHT OF THE MERCURY RESERVOIR ON THE PREWAVE A AND THE TOTAL WAVE (A+B) OF 6×10^{-4} mol dm^{-3} Hahdtc IN 0.1 mol dm^{-3} NaOH

h (cm)	i_A (nA)	i_A+i_B (nA)	i_A/h_{corr} (nA cm^{-1})	$(i_A+i_B)/h_{corr}^{1/2}$ (nA cm$^{-1/2}$)
44.0	120	1150	2.8	180
49.0	130	1210	2.7	180
54.0	140	1310	2.7	180
59.0	150	1320	2.6	170
64.0	170	1340	2.7	170
69.0	180	1400	2.7	170
73.0	210	1510	2.9	180
78.0	230	1580	2.9	180

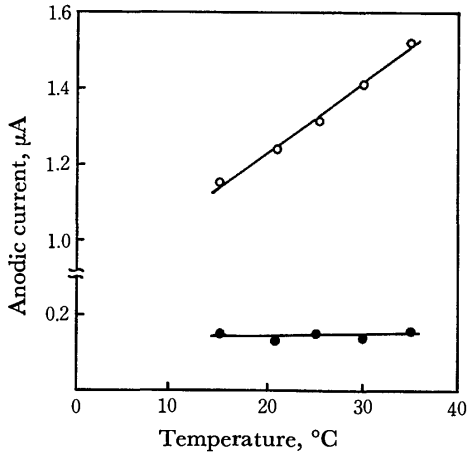

Fig. 3. The effect of temperature on the height of DC waves of 6×10^{-4} mol dm^{-3} Hahdtc in 0.1 mol dm^{-3} NaOH.
●: prewave A, ○: total wave (A+B).

of the total wave had the relative temperature coefficient of 1.60% K^{-1} in the temperature range from 15 to 35 °C; but the limiting current of the prewave was almost independent of temperature as shown in Fig. 3. These results indicate that the wave A is a typical adsorption prewave and the total wave is diffusion-controlled.

Logarithmic Analysis of DC Polarogram. If the electrode reaction in an alkaline medium is reversible and proceeds according to the following equation,

$$Hg + 2ahdtc^- \rightleftarrows Hg(ahdtc)_2 + 2e \quad (1)$$

the potential E of the electrode is given by

$$E = E_0 + \frac{RT}{2F}\ln\frac{1}{K} + \frac{RT}{2F}\ln\frac{[Hg(ahdtc)_2]_o}{[ahdtc^-]_o^2} \quad (2)$$

where K is the formation constant of $Hg^{II}(ahdtc)_2$, and subscript o denotes the concentration at the surface of the electrode. If the concentration of the Hahdtc is large enough, the average current i of the main wave B is expressed as[5]

$$i = i_t - i_A \quad (3)$$

$$i = k_1([ahdtc^-]^* - [ahdtc^-]_o) - i_A \quad (4)$$

where i_t is the theoretical current which would flow if the adsorption did not occur, i_A the limiting current corresponding to the adsorption prewave, k_1 the proportionality factor, and asterisk means the concentration in the bulk of solution. The total limiting current (i_A+i_B) of the prewave A and main wave B is proportional to the concentration of the Hahdtc in the bulk of the solution. Therefore,

$$i_A + i_B = k_1[ahdtc^-]^* \quad (5)$$

Since the complex $Hg(ahdtc)_2$ is absent in the bulk of the solution, the current i is given by

$$i = k_2[Hg(ahdtc)_2]_o \quad (6)$$

where k_2 is the proportionality factor. By combination of Eqs. (2), (4), (5), and (6), the following equation is obtained (at 25 °C).

$$E = E_0' - 0.030\log\frac{(i_B-i)^2}{i} \quad (7)$$

$$E_0' = E_0 + 0.030\log\frac{1}{K} + 0.030\log\frac{k_1^2}{k_2} \quad (8)$$

Thus, the plot of E *vs.* $\log\{(i_B-i)^2/i\}$ should give a straight line with a slope of 30 mV. As shown in Fig. 4, the experimental result agreed well with the theoretical prediction. Moreover, the half-wave potential $E_{1/2}$ of the main wave is given by

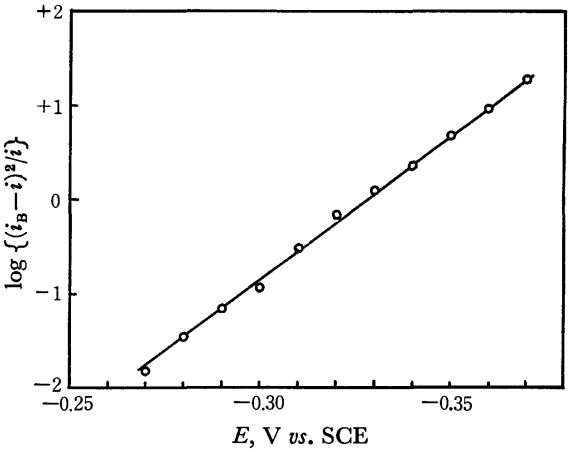

Fig. 4. Relationship between E and $\log\{(i_B-i)^2/i\}$ in 0.1 mol dm^{-3} NaOH at 25 °C.
Concentration of Hahdtc: 6×10^{-4} mol dm^{-3},
The plot has a slope of 33 mV.

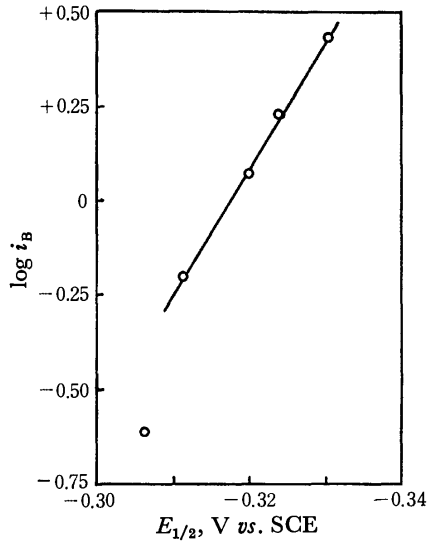

Fig. 5. Relationship between the half-wave potential $E_{1/2}$ of the main wave and log i_B in 0.1 mol dm^{-3} NaOH at 25 °C.
Concentration range of Hahdtc: (2.0—12)×10^{-4} mol dm^{-3},
The plot has a slope of 29 mV.

$$E_{1/2} = E_0' - 0.030 \log \frac{i_B}{2} \quad (9)$$

A plot of $E_{1/2}$ *vs.* log i_B is given in Fig. 5. The plot has a slope of 29 mV, in accordance with the theoretical prediction. These results indicate that the electrode reaction is a reversible oxidation process corresponding to the formation of the mercury(II) complex, Hg(ahdtc)$_2$. The same equation as that given by Eq. (7) would be obtained if the electrode process corresponded to the formation of the mercurous complex, Hg_2^I(ahdtc)$_2$. However, it was found that a gray or black precipitation was formed instantaneously when mercurous nitrate was added to the solution of Hahdtc and the UV spectrum of the filtrate was in agreement with that of the mercuric complex. The result indicates that mercurous ion is rapidly disproportionates to mercuric ion and mercury in the presence of Hahdtc.

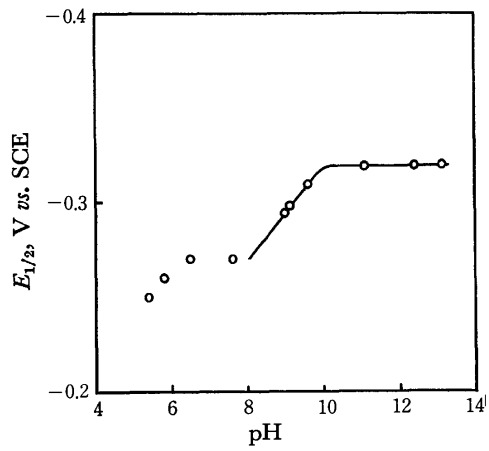

Fig. 6. Effect of pH on the half-wave potential $E_{1/2}$ of the main wave of the Hahdtc (Britton-Robinson buffer). In the pH range from 8.0 to 10.1, the plot has a slope of 25 mV.

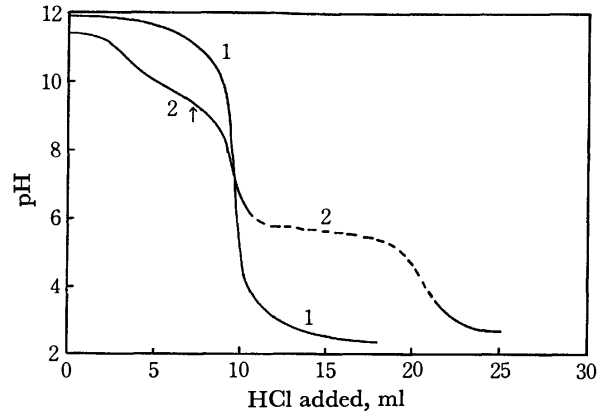

Fig. 7. Titration curve of the Hahdtc in sodium hydroxide solution with 0.104 mol dm^{-3} HCl.
Curve 1: 1 mmol NaOH; 2: 1 mmol NaOH+0.5 mmol Hahdtc, [KCl]=0.1 mol dm^{-3}.
The negative logarithm of the acid dissociation constant of amino group in the Hahdtc is estimated as 9.3, as indicated by arrow. The dashed line is the unstable region where the decomposition of Hahdtc into CS_2 and 2-aminoethylaminoethanol occurs.

Hence, it is safe to assume that the mercurous complex cannot give rise to the adsorption prewave.

Effect of pH. Effect of pH on the half-wave potential of the main wave is shown in Fig. 6. The half-wave potential is independent of pH between 10.1 and 13.1. However, at pH's lower than 10.1, the half-wave potential is shifted to more negative values with increasing pH. The pH value of the intersection of the extrapolated straight sections of the plot coincides approximately with 9.3, the value of the negative logarithm of acid dissociation constant of amino group in the Hahdtc obtained from the pH titration curve, shown in Fig. 7, which is very similar to those of other *N*-substituted carbodithioates.[8] The logarithmic analysis of DC polarogram obtained in a medium buffered at pH 9.1 indicated that a plot of E *vs.* $\log\{(i_B-i)^2/i\}$ gave a straight line with a slope of 35 mV. The result indicates that the electrode reaction is a reversible two-electron process also at the pH value. Moreover, the plot of $E_{1/2}$ *vs.* pH given in Fig. 6 had a slope of 25 mV in the pH range from 8.0 to 10.1. Therefore, the electrode reaction in the pH range from 8.0 to 10.1 may proceed according to the scheme

$$Hg + 2H^+ahdtc^- \rightleftharpoons HHg(ahdtc)_2^+ + H^+ + 2e \quad (1')$$

Further investigation in an acidic medium was impossible because Hahdtc decomposed rapidly.

Alternating Current Polarography. The Hahdtc gave two peaks on AC waves at potentials corresponding to the two DC waves (Fig. 1). The AC peak height of the prewave is considerably high in comparison with that corresponding to the main wave.

Electrocapillary Curves. The electrocapillary curves obtained in the presence and the absence of the Hahdtc are shown in Fig. 8. A marked decrease in drop time of the dropping mercury electrode is observed in the potential region between −0.2 and −0.7 V. At the potentials more negative than −0.7 V, the drop time

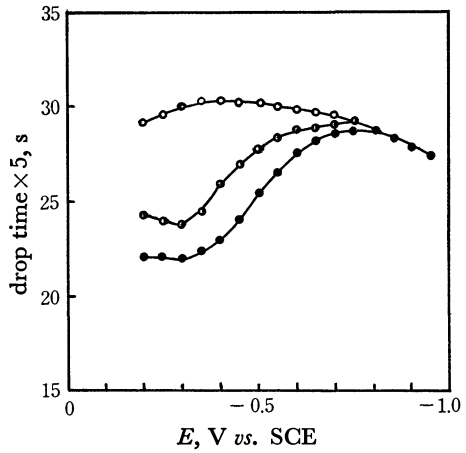

Fig. 8. Electrocapillary curves of Hahdtc in 0.1 mol dm^{-3} NaOH at 25 °C.
Concentration of Hahdtc ○: 0 ml dm^{-3}, ◑: 1×10^{-4} mol dm^{-3}, ●: 8×10^{-4} mol dm^{-3}, h=58.0 cm.

is almost equal to that in the supporting electrolyte. The results indicate that the electrode reaction product is adsorbed on the surface of mercury.

Surface Excess. The amount of substance of the adsorbed chelate molecules per unit area of the electrode surface was estimated to be 3.0×10^{-10} mol cm^{-2} by using the equation based upon the mean adsorption current of the DC polarogram.[9] From the above value, the area occupied by one molecule is calculated as 55×10^{-16} cm^2 under the assumption that a monolayer is formed.

References

1) D. J. Halls, A. Townshend, and P. Zuman, *Anal. Chim. Acta*, **41**, 51 (1968).
2) D. J. Halls, A. Townshend, and P. Zuman, *ibid.*, **41**, 63 (1968).
3) E. C. Gregg and W. P. Tyler, *J. Amer. Chem. Soc.*, **72**, 4561 (1950).
4) W. Stricks and S. K. Chakravarti, *Anal. Chem.*, **34**, 508 (1962).
5) T. Fujinaga and K. Yamashita, This Bulletin, **37**, 989 (1964).
6) T. Kambara, S. Tanaka, and K. Hasebe, *Nippon Kagaku Kaishi*, **88**, 644 (1967).
7) T. Kitagawa and K. Taku, This Bulletin, **46**, 2151 (1973).
8) A. Hulanicki and L. Shishkova, *Talanta*, **12**, 485 (1965).
9) K. Hasebe and T. Kambara, *Rev. Polarogr.* (Kyoto), **15**, 37 (1968).

Benzoyl Peroxide- and Photo-induced Reactions of Diethyl Mesoxalate in Cyclohexane and Toluene

Chyongjin PAC, Hiroshi SAKURAI, Kensuke SHIMA,* and Youichi OGATA*

Institute of Scientific and Industrial Research, Osaka University, Yamadakami, Suita, Osaka 565

**Department of Industrial Chemistry, Faculty of Engineering, Miyazaki University, Miyazaki 880*

(Received May 29, 1974)

Benzoyl peroxide-catalyzed reactions of diethyl mesoxalate in cyclohexane gave ethyl cyclohexylglyoxylate (I) as the main product, accompanied by smaller amounts of diethyl cyclohexylhydroxymalonate (II), ethyl 2-oxobutyrate (III), and diethyl ethylhydroxymalonate (IV), while similar reactions in toluene gave no ethyl phenyl-2-oxopropionate. The α-ketoesters (I) and (III) and the hydroxymalonates (II) and (IV) were considered to arise from β-cleavage and hydrogen atom-abstraction, respectively, of alkoxy radicals A, which take place with addition of cyclohexyl and ethyl radicals to ketonic carbon of diethyl mesoxalate. Irradiation of cyclohexane and toluene solutions of diethyl mesoxalate gave II and diethyl benzylhydroxymalonate (V), respectively, as main products.

A number of reports have appeared on various free radical reactions which afford derivatives of carboxylic acids by direct introduction of such radicals as chloroformyl,[1,2] ethoxycarbonyl[3,4] and carbamoyl[5] radicals into hydrocarbons. However, α-ketocarboxylation and α-hydroxycarboxylation of hydrocarbons by free radical reactions have seldom been reported.[6] In a previous paper,[1] one of us (C.P.) reported on benzoyl peroxide-catalyzed reactions of ethyl chloroglyoxylate in cyclohexane which gave cyclohexanecarbonyl chloride as a main product, accompanied by a small amount of ethyl cyclohexylglyoxylate (I). The mechanism was interpreted in terms of a radical chain mechanism in which cyclohexyl radicals attack the carbon atom of the acid chloride function of ethyl chloroglyoxylate to cleave the carbonyl-carbonyl or carbon-chlorine bond. The mechanism would imply the addition of cyclohexyl radicals to carbonyl carbon of the acid chloride function and the subsequent β-cleavage of the radical A (Scheme 1).

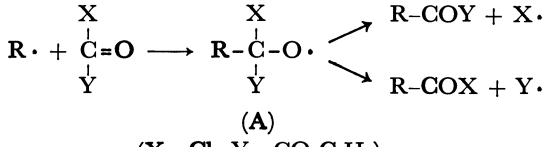

(A)

(X=Cl, Y=$CO_2C_2H_5$)

Scheme 1.

If this is the case, a benzoyl peroxide-induced reaction of diethyl mesoxalate (DEM, X=Y=$CO_2C_2H_5$) in cyclohexane is expected to give ethyl cyclohexylglyoxylate (I) as a main product. Moreover, if DEM in an electronically excited state behaves in a similar way to that of excited aliphatic ketones such as acetone,[7] photoreactions of DEM in hydrocarbons will serve as a convenient method for the preparation of α-hydroxyesters as shown in Scheme 2. Thus, DEM is expected to be available for preparation of some α-keto- and α-hydroxy-esters.

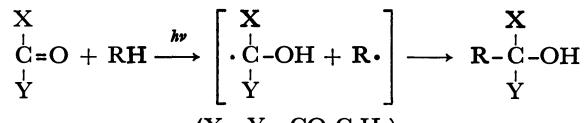

(X=Y=$CO_2C_2H_5$)

Scheme 2.

Results and Discussion

Benzoyl Peroxide-induced Reaction. When a cyclohexane solution of DEM (2.5 mol/l) containing a catalytic amount of benzoyl peroxide (BPO) (0.2 mol/l) was refluxed, ethyl cyclohexylglyoxylate (I), diethyl cyclohexylhydroxymalonate (II), ethyl 2-oxobutyrate (III) and diethyl ethylhydroxymalonate (IV) were obtained in 70—80% combined yields. The results are summarized in Table 1. Spectral data of the products (I)—(IV) are in line with the structures assigned (Table 2). The structures of (I) and (III) were unambiguously determined by direct compaison of their physical properties with those of the authentic samples and mixed melting point tests of their 2,4-dinitrophenylhydrazones with the authentic specimens.

The results support our prediction (Scheme 1), suggesting that ethyl and cyclohexyl radicals can add to ketonic carbon of DEM to generate alkoxy radicals A, which subsequently either abstract hydrogen atom from hydrogen donors to afford II and IV or undergo β-cleavage to give I and III. The mechanism is shown in Scheme 3.

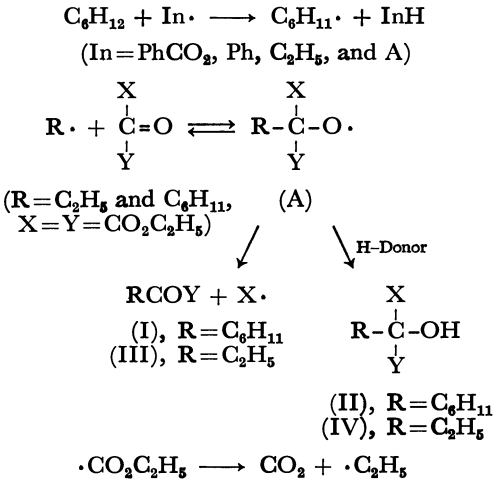

Scheme 3.

This type of addition of alkyl radicals to the carbon-oxygen double bond has not been fully investigated. Free radical addition to carbon-carbon multiple bonds

Table 1. BPO- and photo-induced reaction of diethyl mesoxalate in cyclohexane and toluene

RH (g or ml)		DEM (g)	Initiator	Yield (%)[a]	Product ratio (%)[b]				
					(I)	(II)	(II)	(IV)	Others
C_6H_{12}	(20 ml)	8.7	BPO (1 g)	70—80	50	15	15	16	4
	(150 ml)	8.7	Photo	50	2	90	2	2	4
$PhCH_3$	(9.2 g)	8.7	BPO (1 g)		$PhCOCO_2C_2H_5$ (20), $PhCH_2CH_2Ph$ (30) Others (50)				
	(23 g)	8.7	Photo	20	(V) (60), Others (40)				

a) Isolated yield of α-keto- and α-hydroxy-esters based on unrecovered DEM. b) Determined by gas chromatographic analyses of reaction mixtures. The amount of others was estimated from the area-ratio in gas chromatogram.

Table 2. Spectral properties of α-keto- and α-hydroxy-esters

Compound	IR (cm^{-1})[a]	*m/e* (M^+)	NMR (δ in CCl_4)
$C_6H_{11}COCO_2C_2H_5$ (I)	1750 (C=O) 1250 (C–O–C)	184	1.37 (3H, t), 1.18—2.05 (10H, m), 2.94 (1H, m), 4.26 (2H, q)
$C_6H_{11}C(CO_2C_2H_5)_2$ (II) OH	3500 (–OH) 1740, 1230	b	1.30 (6H, t), 0.88—1.85 (10H, m), 2.10 (1H, m), 3.32[c] (1H, s), 4.21 (4H, q)
$C_2H_5COCO_2C_2H_5$ (III)	1720, 1230	130	1.1 (3H, t), 1.4 (3H, t), 2.8 (2H, q), 4.2 (2H, q)
$C_2H_5C(CO_2C_2H_5)_2$ (IV) OH	3500, 1730 1240	b	0.87 (3H, t), 1.29 (6H, t), 1.96 (2H, q), 3.50[c] (1H, s), 4.21 (4H, q)
$PhCH_2C(CO_2C_2H_5)_2$ (V) OH	3440, 1745 1230, 750 700	b	1.28 (6H, t), 3.24 (2H, s), 3.48[c] (1H, s), 4.19(4H, q), 7.18 (5H, m)

a) Liquid film. b) No parent peak. c) Disappeared in the presence of deuterium oxide.

has been widely studied, several examples being reported on the addition of alkyl radicals to aldehydes,[8] biacetyl,[9] and hexafluoroacetone.[10] Reactions of cyclohexyl radicals with ethyl chloroglyoxylate[1] and oxalyl chloride[2] appear to fit the case. The reactions of alkyl radicals with some XCOY compounds are summarized in Table 3. There is a tendency of reactivities of XCOY toward alkyl radicals in relation to structures of XCOY; the formation of products by addition of alkyl radicals to carbonyl carbon of XCOY requires strong electron-withdrawing nature of X and/or Y and, moreover, the presence of a methoxyl group, a strong electron-donating group, in XCOY leads to lack of such addition reactions. Compare oxalyl chloride with phosgene and ethyl chloroglyoxylate with ethyl chloroformate and diethyl oxalate. This tendency of reactivities of XCOY toward alkyl radicals would be attributed to polar contributions to the transition state of additions of alkyl radicals to XCOY (Scheme 4). This transition state appears to be in line with that of β-cleavage of alkoxy radicals,[11] the reverse reaction of the addition of alkyl radicals to carbonyl compounds.

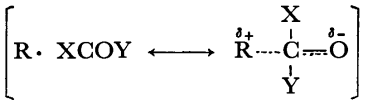

Scheme 4.

On the other hand, BPO-induced reactions of DEM in toluene gave no ethyl phenyl-2-oxopropionate. Volatile products were obtained in low yields and found to consist of various compounds, in which ethyl phenylglyoxylate and bibenzyl were detected as the main products. Since yields of the other products were very low, no structural determination was carried out. The result appears to be in line with the mechanism discussed above, since β-cleavage of the radical A (R=

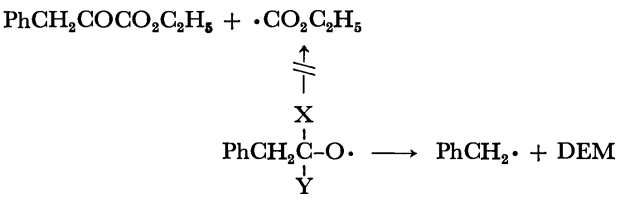

(A)

Table 3. Addition reaction of alkyl radicals to XCOY

Radical (R·)	X	Y	Product	Ref.
C_6H_{11} and C_2H_5	$CO_2C_2H_5$	$CO_2C_2H_5$	RC(OH)XY, RCOX	This work
C_6H_{11} and others	CH_3	$COCH_3$	RCOX	9a
C_3H_7 and C_6H_{13}	CF_3	CF_3	RC(OH)XY	10a
C_6H_{11}	Cl	$CO_2C_2H_5$	RCOX, RCOY	1
C_6H_{11}	Cl	COCl	RCOX	2
C_6H_{11}	Cl	Cl	No adduct[a]	2a
C_6H_{11}	Cl	OC_2H_5	No adduct[a]	3
C_6H_{11}	OC_2H_5	$CO_2C_2H_5$	No adduct[a]	1

a) No significant formation of adducts from peroxide-induced reactions in cyclohexane.

$PhCH_2$) is expected to occur exclusively in regenerating benzyl radicals and DEM, as is clarified in β-cleavage of alkoxy radicals containing a benzyl group.[12]

Photo-induced Reaction. Irradiation of a cyclohexane solution of DEM (0.33 mol/l) with light longer than 320 nm at ambient temperature gave II as a main product, accompanied by small amounts of I, III, and IV (Table 1). The product distribution differes a great deal from that of the BPO-induced reaction, suggesting a different mechanism for the formation of II from the radical chain mechanism (Scheme 3). Dominant formation of II in the photoreaction might be interpreted by assuming that an excited DEM abstracts hydrogen atom from cyclohexane to afford a radical pair (B) in a solvent cage which predominantly undergoes the radical coupling to give II (Scheme 5).

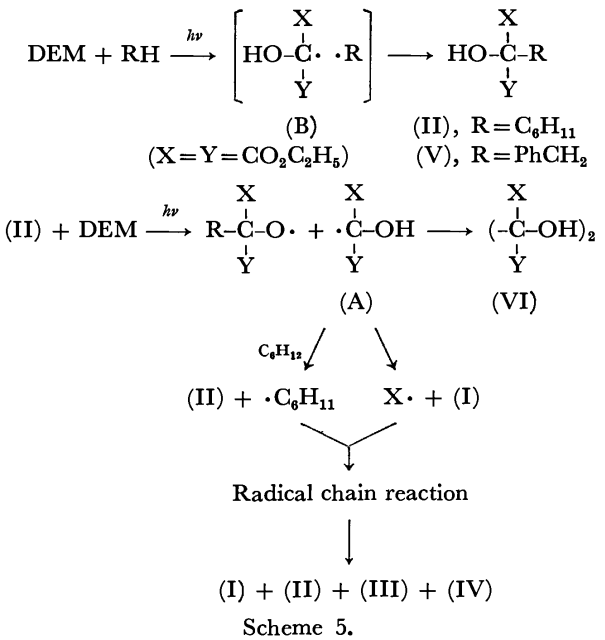

Scheme 5.

However, the product distribution in the photoreaction was found to depend on the concentration of DEM in cyclohexane; as the concentration of DEM increases, yields of II begin to decrease at the concentration of *ca.* 0.5 mol/l, while the formation of I sharply increases (Fig. 1). Such a concentration effect could not be observed in BPO-induced reactions (Fig. 2). These results suggest an oxidation of II by excited DEM, giving radical (A). In a dilute solution, however, excited DEM has less chance to encounter II in its life. In the case of a concentrated solution, II is readily accumulated to a sufficient concentration for oxidation. If radical (A) is once generated by oxidation, then the radical chain reaction described in Scheme 3 can intervene. Thus, the higher the concentration of DEM, greater the tendency for radical chain reaction to occur. It is of interest to note that irradiation of a concentrated solution of DEM gave a mixture in low yields which revealed only the NMR signals of ethoxyl protons at δ 1.35 and 4.3 and an alcoholic proton at δ 3.9[13] in an area-ratio of 7.5: 5: 1. The NMR spectra suggest that the mixture contains diethyl 1,2-diethoxycarbonyl-1,2-dihydroxysuccinate (VI). VI could not be obtained in pure form by preparative gas chromatography under any condition. Further investigation for VI was, therefore, not carried out. The reaction mechanism is shown in Scheme 5.

In a similar way, irradiation of a toluene solution of DEM gave diethyl benzylhydroxymalonate (V) in a moderate yield, accompanied by minor amounts of other volatile compounds and some polymeric materials.

Experimental

Melting and boiling points are uncorrected. IR spectra were measured with a Hitachi EPI-S2 spectrophotometer, NMR spectra with a JEOL JNM-MH-100 apparatus for solutions in carbon tetrachloride containing tetramethylsilane as an internal standard, and mass spectra with a Hitachi RMU-6E apparatus. Analytical gas chromatography was carried out with a Shimadzu GC-3BF apparatus using a column of Silicone DC 550 (20% on Shimalite W, 2 m) at 200 °C, and preparative gas chromatography with a Shimadzu GC-2C apparatus using a column of Silicone DC 550 (20% on Shimalite W, 2.3 m) at 200 °C.

Toluene and spectrograde cyclohexane (Nakarai Chemicals) were distilled over metallic sodium wire. Benzoyl peroxide was recrystallized from chloroform-methanol. DEM was prepared from diethyl malonate according to the method in literature[14] and distilled from phosphorus pentoxide *in vacuo* prior to use.

BPO-Induced Reaction of DEM in Cyclohexane. A solution of DEM (8.7 g, 0.05 mol) and BPO (1 g, 0.004 mol) in cyclohexane (20 ml) was refluxed for 8 hr. After removal of cyclohexane, fractional distillation of the residue under reduced pressure gave two fractions, bp 60—100 °C/14 mmHg (2.5 g) and bp 110—135 °C/14 mmHg (4.5 g), and a residue (1 g). Gas chromatographic analyses showed that the former fraction contained predominantly DEM along with minor

Table 4. Analhytical data of α-keto- and α-hydroxy-esters and 2,4-dinitrophenylhydrazones of α-ketoesters

Compd.	Bp (°C/mmHg) or Mp (°C)	Found (%)			Formula	Calcd (%)		
		C	H	N		C	H	N
I	(125/22)	65.10	8.75		$C_{10}H_{16}O_3$	64.76	8.73	
I-DNP[a]	[161—161.5]	52.59	5.63	15.61	$C_{16}H_{20}N_4O_6$	52.74	5.53	15.38
II	(111.5/2)	60.44	8.59		$C_{13}H_{22}O_5$	60.64	8.67	
III	(72/32)	54.88	7.70		$C_6H_{10}O_3$	55.37	7.75	
III-DNP[a]	[140—141.5]	46.43	4.32	18.07	$C_{12}H_{14}N_4O_6$	46.45	4.55	18.06
IV	(120/21)	52.73	7.90		$C_9H_{16}O_5$	52.42	7.86	
V	(131/3.5)	63.14	6.81		$C_{14}H_{18}O_5$	63.15	6.95	

a) 2,4-Dinitrophenylhydrazone.

amounts of III, whereas the latter consisted of I, II, and IV over 90% in a *ca.* 8:1:4 ratio. From the former fraction, *ca.* 0.5 g of III was isolated by preparative gas chromatography. In a similar way, products I, II, and IV were also isolated by preparative gas chromatography. Analytical data of I—IV and 2,4-dinitrophenylhydrazones of (I) and (III) are listed in Table 4.

BPO-induced Reaction of DEM in Toluene. A mixture of DEM (8.7 g, 0.05 mol), BPO (1 g, 0.004 mol) and toluene (9.2 g, 0.1 mol) was heated at 114—115 °C for 8 hr. Fractional distillation under reduced pressure gave 6 g of DEM, 1.5 g of an oil (bp 70—146 °C/3 mmHg) and 1.5 g of a residue. Analytical gas chromatography showed that the oil consists of at least seven components. Two main components were isolated by preparative gas chromatography, identified as ethyl phenylglyoxylate and bibenzyl by driect comparison of their sepectral properties with those of authentic samples.

Photo-induced Reaction of DEM in Cyclohexane. A solution of DEM (8.7 g, 0.05 mol) in cyclohexane (150 ml) was irradiated by light filtered through a hexane solution of naphthalene (0.1 mol/l, 1 cm path length) from an Eikosha PIH 300 W high-pressure mercury arc at ambient temperature for 10 hr. After removal of cyclohexane, fractional distillation gave 2.2 g of DEM, 5 g of an oil (bp 130—137 °C/13 mmHg) and 1 g of a residue. Analytical gas chromatography of the oil showed that II was contaminated over 80%. Product (II) was purified by preparative gas chromatography and vacuum distillation.

Photo-induced Reaction of DEM in Toluene. A mixture of DEM (8.7 g, 0.05 mol) and toluene (23 g, 0.25 mol) placed in a test tube was irradiated by filtered light for 100 hr. Fractional distillation of the reaction mixture under reduced pressure gave 3.5 g of DEM, 3.5 g of an oil (bp 100—160 °C/6 mmHg) and 2 g of a residue. Analytical gas chromatography showed that the oil contains five products. From the oil, 1.8 g of the main product (V) was isolated by preparative gas chromatography and V was purified by vacuum distillation.

Concentration Effect to Product Distribution. In both BPO- and photo-induced reactions, 0.8 g (0.0046 mol) of DEM was used, the amounts of cyclohexane being varied. Conversion of DEM was set in 10—30%. In the case of BPO-induced runs, 0.1 g (0.4 mmol) of BPO was used. The reaction mixtures were directly subjected to gas chromatographic analyses, and the product distribution was determined. The results are shown in Figs. 1 and 2.

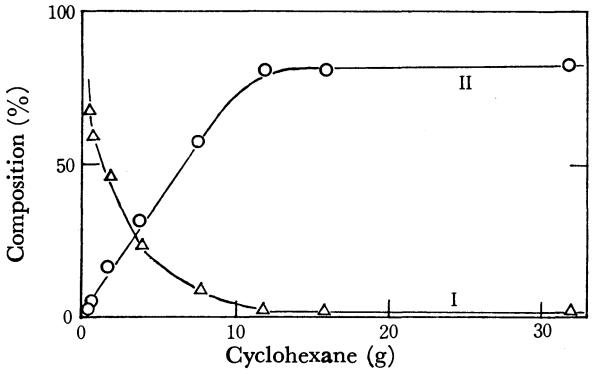

Fig. 1. Concentration effect on product distribution in photo-induced reaction of DEM in cyclohexane: DEM, 0.8 g; conversion, 10—30%.

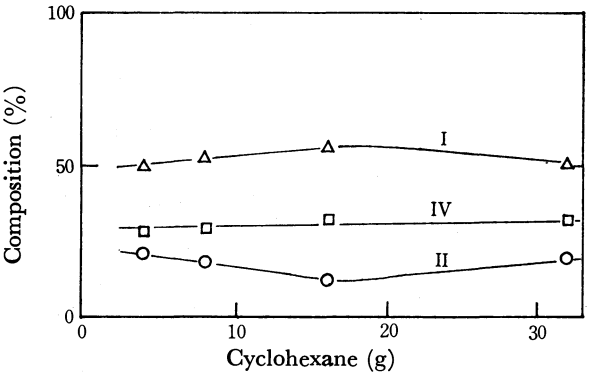

Fig. 2. Concentration effect on product distribution in BPO-induced reaction of DEM in cyclohexane: DEM, 0.8 g; BPO, 0.1 g; conversion, 10—30%.

References

1) C. Pac and S. Tsutsumi, This Bulletin, **39**, 1926 (1966).
2) a) M. S. Kharasch, S. S. Kane, and H. C. Brown, *J. Amer. Chem. Soc.*, **62**, 454 (1940); **64**, 329 (1942); b) F. Runge, *Z. Elektrochem.*, **56**, 779 (1952); **60**, 956 (1956).
3) C. Pac and S. Tsutsumi, This Bulletin, **38**, 1916 (1965); **36**, 234 (1963).
4) C. Walling and E. S. Huyser, "Organic Reactions," Vol. 13, ed. by R. Adams, John Wiley & Sons, London (1963), p. 111.
5) D. Elad, "Organic Photochemistry," Vol. 2, ed. by O. L. Chapman, Marcel Dekker, New York (1969), p. 196.
6) Y. Odaira, T. Tominaga, T. Sugihara, and S. Tsutsumi, *Tetrahedron Lett.*, **1964**, 2527.
7) K. Shima and S. Tsutsumi, This Bulletin, **36**, 121 (1963).
8) F. F. Rust, F. H. Seubold, Jr., and W. E. Vaughan, *J. Amer. Chem. Soc.*, **70**, 4253 (1948); G. Fuller and F. F. Rust, *ibid.*, **80**, 6148 (1958).
9) a) W. G. Bentrude and K. B. Darnell, *ibid.*, **90**, 3588; b) K. J. Hole and M. F. R. Mulcahy, *J. Phys. Chem.*, **73**, 177 (1969).
10) a) W. H. Urry, N. Nishihara, and J. H. Y. Niu, *J. Org. Chem.*, **32**, 347 (1967); b) W. G. Alcock and E. Whittle, *Trans. Faraday Soc.*, **61**, 244 (1965).
11) J. K. Kochi, "Free Radicals," Vol. 2, ed. by J. K. Kochi, John Wiley & Sons, New York (1973), p. 685.
12) C. Walling and A. Padwa, *J. Amer. Chem. Soc.*, **85**, 1593 (1963).
13) This signal disappeared when the solution was shaken in the presence of deuterium oxide.
14) A. W. Dox, "Organic Syntheses," Coll. Vol. 1, p. 266 (1956).

Total Synthesis of (±)-Tetrahydroligularenolide[1]

Tochiro TATEE and Takeyoshi TAKAHASHI

Department of Chemistry, Faculty of Science, The University of Tokyo, Bunkyo-ku, Tokyo 113

(Received May 29, 1974)

A total synthesis of (±)-tetrahydroligularenolide [(±)-**2**] is described. 10β-Methyl-5β-tetrahydropyranyloxy-*trans*-2-decalone (**6**) was converted in seven steps into 3-methoxycarbonyl-5,10-dimethyl-*trans*-2-decalone (**15**), which on alkylation with ethyl α-iodopropionate gave 3-(1-ethoxycarbonylethyl)-3-methoxycarbonyl-5,10-dimethyl-*trans*-2-decalone (**19**) and 6-(1-ethoxycarbonylethoxy)-7-methoxycarbonyl-1β,8aβ-dimethyl-1,2,3,4,4a,5,8,8a-*trans*-octahydronaphthalene (**20**). Hydrolysis of **19** proceeded with a loss of carbon dioxide to afford (±)-tetrahydroligularenolide [(±)-**2**].

It has been reported that a sesquiterpene lactone, ligularenolide, was isolated from "San-shion" [2] (the roots of *Ligularia* species), and its structure including an absolute stereochemistry was shown to be **1**,[3] which on hydrogenation over palladium-charcoal in ethanol gave tetrahydroligularenolide (**2**).[3] We wish to describe a total synthesis of (±)-tetrahydroligularenolide [(±)-**2**] with a 10-epi-eremophilane skeleton.[1] Some α,β-unsaturated γ-lactones of eremophilane type, (±)-eremophilenolide [(±)-**3**],[4,5] (±)-3α-hydroxyeremophilenolide [(±)-**4**][6] and (±)-3β-hydroxyeremophilenolide [(±)-**5**][6] have been synthesized. A conversion of (−)-5α,6α-epoxydihydroalantolactone into (−)-**2** has been described.[7] Recently, a total synthesis of (±)-**2** was reported;[4b] this synthesis includes a final introduction of a methyl group to C-11, while the present communication contains an alkylation by three carbon units and the subsequent lactonization.

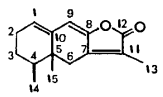

1

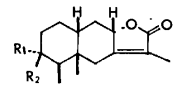

3 R_1= H, R_2= H
4 R_1= OH, R_2= H
5 R_1= H, R_2= OH

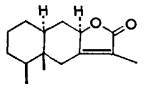

2

Acetalization of a tetrahydropyranyloxy-*trans*-decalone (**6**)[8,9] with ethylene glycol in the presence of *p*-toluenesulfonic acid gave a cyclic acetal (**7**) with concomitant hydrolysis of a tetrahydropyranyl group. The alcohol (**7**) was oxidized with chromium trioxide in pyridine to afford the known ketone (**8**),[10] which was then treated with methyl magnesium iodide in ether to give a crude alcohol (**9**). Dehydration of **9** with phosphorus oxychloride and phosphoric acid in pyridine yielded a mixture of olefins, **10**[11] and **11** (in a ratio of 2: 1). Deacetalization of the olefin mixture to yield a mixture of **12** and **13**, and the subsequent hydrogenation in acetic acid in the presence of palladium-charcoal gave a dimethyldecalone (**14**)[12] (yield from **6**: 16%). Only one stereoisomer (**14**) was obtained; a *cis* relationship of the two methyl groups could be derived after completion of the synthesis of (±)-**2**.

Pinder and Torrence[12c] described a methoxycarbonylation of **14** with dimethyl carbonate and sodium hydride in dry benzene under a nitrogen atmosphere to yield **15** as the sole product. A similar treatment of **14** in dioxane gave a mixture of β-keto-esters, which was subjected to separation by silica gel chromatography to afford **15**[12c] (y: 75%) and **16** (y: 12%). The PMR spectrum of **16** showed a doublet (J= 12 Hz) at δ 3.27 due to an axial (β)-proton coupled with a ring juncture proton; the structure **16** was therefore shown for the latter ester.

As a model experiment of alkylation of **15**, α-methoxycarbonylcyclohexanone was alkylated[13] with ethyl α-halogenopropionate in the presence of sodium hydride (or potassium hydride) under a nitrogen atmosphere. *C*-alkylated (**17**) and *O*-alkylated (**18**) products were

Table 1. Alkylation of α-methoxycarbonylcyclohexanone

Halides	Hydrides	Solvents	Products in ratio[a] 17	18	Yield (%) (17+18)
$CH_3CHBrCOOC_2H_5$	NaH	PhH[b]	70	30	73
$CH_3CHBrCOOC_2H_5$	KH	PhH	50	50	64
$CH_3CHICOOC_2H_5$	NaH	PhH	85	15	66
$CH_3CHICOOC_2H_5$	KH	PhH	74	26	57
$CH_3CHBrCOOC_2H_5$	NaH	DMSO[c]	68	32	77
$CH_3CHBrCOOC_2H_5$	KH	DMSO	29	71	82
$CH_3CHICOOC_2H_5$	NaH	DMSO	76	24	64
$CH_3CHICOOC_2H_5$	KH	DMSO	73	27	42

a) Determined by glc. b) Under reflux for 18—29 hr.
c) At room temperature for 17—24 hr.

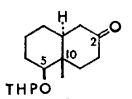

6

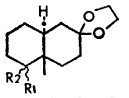

7 R_1 = β-OH, R_2 = α-H
8 R_1, R_2 = O
9 R_1 = CH_3, R_2 = OH

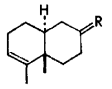

10 R= $-OCH_2CH_2O-$
12 R= O

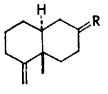

11 R = $-OCH_2CH_2O-$
13 R = O

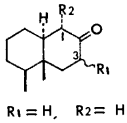

14 R_1 = H, R_2 = H
15 R_1 = CO_2CH_3, R_2 = H
16 R_1 = H, R_2 = CO_2CH_3

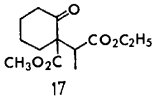

17

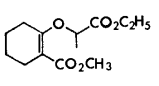

18

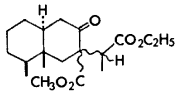

19

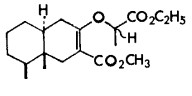

20a and 20b

obtained in the ratio listed in Table 1. When the reaction was carried out with ethyl α-iodopropionate, sodium hydride and benzene, the best yield of **17** was obtained.

The keto-ester (**15**) in benzene was alkylated with ethyl α-iodopropionate in the presence of sodium hydride under a nitrogen atmosphere. The resulting product showed three spots on tlc, and was subjected to separation by silica gel chromatography to give the *C*-alkylated (**19**; y: 30%) and the *O*-alkylated (**20a** and **20b**; y: 26%) products. The former substance (**19**) corresponding to the least polar spot was found to be a diastereomeric mixture by its PMR spectrum. The latter products (**20a** and **20b**) proved to be a diastereomeric mixture corresponding to the other two spots, and was subjected to further separation on a column of silica gel to give each diastereomer. Alkylation of **15** in benzene with ethyl α-bromopropionate and sodium hydride resulted in formation of a small amount of **19**, the *O*-alkylated products (**20a** and **20b**) were obtained as predominant products.

Hydrolysis of **19** with hydrochloric acid in acetic acid under reflux was effected with a loss of carbon dioxide to afford (±)-**2** (y: 57%), which was found to be the same (except optical rotational data) as (−)-tetrahydroligularenolide (**2**)[3] derived from natural (−)-ligularenolide (**1**).

Experimental

IR spectra were measured with a Hitachi EPI-G2 spectrometer, UV spectra with a Hitachi EPS-3 spectrometer, and mass spectra with a Hitachi RMU-6-Tokugata mass spectrometer with use of an indirect system operating at 70 eV. PMR spectra were measured with a JEOL JNM PS-100 (100 MHz), a JEOL JNM 3H-60 (60 MHz), a Hitachi R-20 (60 MHz) or a Hitachi R-24 (60 MHz) spectrometer. Chemical shifts were expressed in terms of δ downfield from TMS as an internal standard, and coupling constants in Hz. Gas chromatographic (glc) analyses were carried out on a Shimadzu gas chromatograph model GC-4APF. Thin layer chromatography (tlc) was carried out on Kieselgel G (E. Merck). Wakogel C-200 (Wako Pure Chemical Co.) was used for column chromatography. Melting points were determined on a hot block and are uncorrected.

2,2-Ethylenedioxy-5β-hydroxy-10β-methyl-trans-*decalin (7).* 10β-Methyl-5β-tetrahydropyranyloxy-*trans*-2-decalone (**6**; 5.6 g)[8,9] was dissolved in a mixture of benzene (200 ml) containing *p*-toluenesulfonic acid (120 mg) and ethylene glycol (3 ml), and the mixture was refluxed under a Dean-Stark water separator for 16 hr. The cooled solution was poured into a 5% aqueous potassium hydrogen carbonate solution, and then extracted with ether. The organic layer was washed with brine and dried over magnesium sulfate. The solvent was removed and the residue was chromatographed on a column of silica gel (300 g). Elution with a mixture of benzene and ether (9: 1) and removal of the solvents afforded an oil (**7**[10]; 3.6 g; y: 76%), IR (liquid) 3430 cm^{-1}; PMR ($CDCl_3$) δ 0.86 (3H, s; *t*-CH_3) and 3.96 (4H, s; $-OCH_2CH_2O-$); MS *m/e* 226 [M^+ ($C_{13}H_{22}O_3$); relative intensity, 4%] and *m/e* 99 (100%).

6,6-Ethylenedioxy-9-methyl-trans-*1-decalone (8).* A solution of chromium trioxide (9 g) in pyridine (90 ml) was added to a solution of **7** (3.6 g) in pyridine (90 ml), and the resulting solution was allowed to stand at room temperature overnight. Extraction with ether and the usual treatment gave an oil which was chromatographed on a column of silica gel. Elution with a mixture of benzene and ether (5: 1) gave an oil (2.7 g), which on solidification gave **8**, mp 44—47 °C (lit,[10a] mp 41—45 °C; lit,[10b] mp 45—47 °C), IR (Nujol) 1715 cm^{-1}; PMR ($CDCl_3$) δ 1.13 (3H, s; *t*-CH_3) and 3.92 (4H, s; $-OCH_2CH_2O-$); MS *m/e* 224 [M^+($C_{13}H_{20}O_3$); 4%] and *m/e* 99 (100%).

2,2-Ethylenedioxy-5-hydroxy-5,10-dimethyl-trans-*decalin (9).* To the Grignard reagent prepared from methyl iodide (25 g) and magnesium (2.5 g) in ether (30 ml) at 0 °C was added a solution of **8** (2.7 g) in ether (40 ml). The reaction mixture was stirred for 2 hr at room temperature, and then decomposed with aqueous ammonium chloride solution. Extraction with ether and the usual work-up gave a residue which was chromatographed on a column of silica gel (160 g). Elution with a mixture of benzene and ether (8: 1) gave a crude alcohol (**9**; 2 g), an oil (one spot on tlc), on removal of the solvents; IR (liquid) 3450 cm^{-1}; PMR ($CDCl_3$) δ 0.91 (3H, s; *t*-CH_3), 1.12 (3H, s; $CH_3-\overset{|}{\underset{|}{C}}-OH$), and 3.93 (4H, s; $-OCH_2CH_2O-$).

Dehydration of the Alcohol (9) and Subsequent Deacetalization. Crude alcohol (**9**; 2 g) in pyridine (100 ml) was added dropwise to a solution of phosphorus oxychloride (30 ml) and phosphoric acid (1 ml) in pyridine (60 ml) at 0 °C with stirring, and the mixture was warmed at 55 °C for 20 hr. The cooled mixture was poured into ice water, and the product was extracted with ether. After the usual treatment, a mixture of **10**[10b] and **11** (2: 1) was obtained as an oil (1.2 g); IR (liquid) 3090, 1640, 1375, 1360, 1140, and 1085 cm^{-1}; PMR ($CDCl_3$) δ 0.96 (s; *t*-CH_3 of **10**), 1.02 (s; *t*-CH_3 of **11**), 1.65 (d; J=2 Hz; CH_3–C=C), 3.94 (s; $-OCH_2CH_2O-$), 4.64 (m; C=CH_2), and 5.24 (m; C=CH); MS *m/e* 222 [M^+ ($C_{14}H_{22}O_2$); 2%] and *m/e* 99 (100%) [*cf.* lit,[10b,11] spectral data for pure **10**: bp 90—95 °C/0.04 mmHg, IR ($CHCl_3$) 1375 and 1130—1050 cm^{-1}; PMR ($CDCl_3$) δ 1.02 (s; *t*-CH_3), 1.65 (d, J=2 Hz; CH_3–C=C), 3.94 (s; $-OCH_2CH_2O-$), and 8.59 (m; C=CH)]. The signals at δ 0.96 and 1.02 appeared in an integrated intensity ratio of 2: 1.

A mixture of unsaturated cyclic ketals (1.2 g; **10** and **11**) was treated with acetic acid (48 ml) and water (12 ml) at 80 °C for 8 hr. The solvent was removed and the residue was passed through a column of silica gel (70 g) using benzene as an eluent. On removal of the solvent, a mixture of unsaturated ketones (**12** and **13**; 2: 1) was obtained as an oil (677 mg; yield from **7**: 24%); IR (liquid) 1715 and 1640 cm^{-1}; PMR ($CDCl_3$) δ 1.14 (s; *t*-CH_3 of **12**), 1.18 (s; *t*-CH_3 of **13**), 1.66 (d, J=2 Hz; CH_3–C=C), 4.59 and 4.65 (each m; C=CH_2), and 5.25 (m; C=CH); MS *m/e* 178 [M^+ ($C_{12}H_{18}O$); 55%] and *m/e* 93 (100%). The signals at δ 1.14 and 1.18 appeared in an integrated intensity ratio of 2: 1.

5β,10β-Dimethyl-trans-*2-decalone (14).* An olefin mixture (630 mg; **12** and **13**) in acetic acid (20 ml) was hydrogenated in the presence of 10% palladium–charcoal (155 mg) at room temperature for 2 hr. After filtration of the catalyst, the solvent was evaporated to give a residue which was chromatographed on a column of silica gel (30 g). Elution with a mixture of light petroleum and ether (8: 1) and removal of the solvents afforded a dimethyldecalone (**14**; 563 mg; y: 88%) (yield from **6**: 16%) as a sole product, an oil, bp 104—106 °C/2 mmHg, IR (liquid) 1715 cm^{-1}; PMR ($CDCl_3$) δ 0.86 (3H, m; *s*-CH_3) and 0.92 (3H, s; *t*-CH_3); MS *m/e* 180 [M^+($C_{12}H_{20}O$); 27%] and *m/e* 109 (100%) [lit,[12b] bp 83—86 °C/1 mmHg, IR (liquid) 1712 cm^{-1}; PMR ($CDCl_3$) δ 0.87 (m; *s*-CH_3) and 0.92 (s; *t*-CH_3)]. 2,4-Dinitrophenyl-

hydrazone (crystallized from ethanol): mp 157—158 °C. Found: C, 60.04; H, 6.53; N, 15.49%. Calcd for $C_{18}H_{24}N_4O_4$: C, 59.98; H, 6.71; N, 15.55% [*cf.* lit,[12a] 2,4-dinitrophenylhydrazone of (+)-**14**: mp 172.5—173.5 °C].

Methoxycarbonylation of the Dimethyldecalone (14). A mixture of the dimethyldecalone (**14**; 137 mg), dimethyl carbonate (1.08 g) and sodium hydride (120 mg of a 50% dispersion in mineral oil) in dioxane (3 ml) was stirred under a nitrogen atmosphere at 80—85 °C for 4 hr. The cooled mixture was treated with acetic acid (1 ml) and then extracted with ether. The extract was washed with water and dried over magnesium sulfate. The solvent was removed and the residue (239 mg) was chromatographed on a column of silica gel (20 g) using the following solvents as eluent: light petroleum (fr 1, 100 ml; frs 2—3, each 30 ml), light petroleum and ether (20: 1) (frs 4—12, each 30 ml), light petroleum and ether (10: 1) (frs 13—18, each 30 ml), and light petroleum and ether (5: 1) (frs 19—21, each 60 ml). Fraction 5 gave a keto-ester (**15**; 136 mg; y: 75%), an oil, bp 149—155 °C/2 mmHg (lit,[12c] bp 122—125 °C/0.25 mmHg), IR (liquid) 3200—2600, 1750, 1720, 1660, and 1620 cm^{-1}; UV (EtOH) λ_{max} 257 nm (ε 11000); PMR ($CDCl_3$) δ 0.68 (3H, s; *t*-CH_3), 0.89 (3H, m; *s*-CH_3), 3.76 (3H, s; $-CO_2CH_3$), and 12.19 (s; enolic proton); MS *m/e* 238 [$M^+(C_{14}H_{22}O_3$); 11%] and *m/e* 109 (100%). Fractions 13—14 afforded an isomeric keto-ester (**16**; 21 mg; y: 12%), mp 87—88 °C, IR (Nujol) 1740 and 1715 cm^{-1}; UV (EtOH) λ_{max} 258 nm (ε 130); PMR ($CDCl_3$) δ 0.89 (3H, m; *s*-CH_3), 0.97 (3H, s; *t*-CH_3), 3.27 (1H, d, J=12 Hz; $-\dot{C}H\underline{C}H(CO_2CH_3)CO-$), and 3.74 (3H, s; $-CO_2\underline{C}H_3$); MS *m/e* 238 [$M^+(C_{14}H_{22}O_3$); 4%] and *m/e* 109 (100%). Found: C, 70.26; H, 9.40%. Calcd for $C_{14}H_{22}O_3$: C, 70.55; H, 9.31%.

Alkylation of α-Methoxycarbonylcyclohexanone. To sodium hydride (910 mg of a 50% dispersion in mineral oil; washed thrice by decantation with dry light petroleum) was added α-methoxycarbonylcyclohexanone (3 g) in dry ether (50 ml) with stirring to give the enolate, which was filtered and washed with ether. Dry dimethyl sulfoxide (50 ml) and then ethyl α-bromopropionate (8 g) were added dropwise to the enolate, and the whole was stirred at room temperature for 19 hr under a nitrogen atmosphere. After addition of water (150 ml), the reaction mixture was extracted with light petroleum. The extract was washed with water, dried over magnesium sulfate and the solvent was removed to give an oil (7.6 g). Gas chromatographic analysis showed that the ratio of the *C*-alkylated (**17**) and the *O*-alkylated (**18**) products was *ca.* 2: 1. A part (326 mg) of the oil was subjected to separation by silica gel (20 g) column chromatography using the following solvents as eluent: light petroleum and ether (20: 1) (frs 1—2, each 50 ml; frs 3—9, each 30 ml), light petroleum and ether (10: 1) (frs 10—12, each 30 ml; frs 13—18, each 20 ml), and light petroleum and ether (5: 1) (frs 19—22, each 85 ml). Fractions 2 and 3 gave ethyl α-bromopropionate and a small amount of the starting material, respectively. From fractions 11—12, the *C*-alkylated product (**17**; 63 mg) was obtained as an oil, IR (liquid) 1750—1715 cm^{-1}; PMR ($CDCl_3$) δ 1.14 (3H, d, J=7 Hz; $C\underline{H}_3\dot{C}H-$), 1.26 (3H, t, J=7 Hz; $C\underline{H}_3CH_2-$), 3.18 (1H, q, J=7 Hz; $CH_3\dot{C}\underline{H}CO_2C_2H_5$), 3.75 (3H, s; $-CO_2CH_3$) and 4.13 (2H, q, J=7 Hz; $-CO_2C\underline{H}_2CH_3$); MS *m/e* 256 [$M^+(C_{13}H_{20}O_5$); 4%] and *m/e* 123 (100%). This material (50 mg) was further chromatographed on a column of silica gel (5 g). Elution with a mixture of light petroleum and ether (5: 1) gave the analytical sample. Found: C, 60.76; H, 7.83%. Calcd for $C_{13}H_{20}O_5$: C, 60.92; H, 7.87%. Glc retention time 10.0 min (column: neopentylglycol succinate, 160 °C, N_2, 85 ml/min) and 9.7 min (column: Diasolid H-523, 160 °C, N_2, 85 ml/min). Fractions 13—15 gave a mixture of **17** and **18** (53 mg). Fractions 16—22 afforded the O-alkylated product (**18**; 47 mg), an oil, IR (liquid) 1760—1720 and 1630 cm^{-1}; PMR ($CDCl_3$) δ 1.28 (3H, t, J=7 Hz; $C\underline{H}_3CH_2-$), 1.51 (3H, d, J=7 Hz; $C\underline{H}_3\dot{C}H-$), 3.70 (3H, s; $-CO_2CH_3$), 4.18 (2H, q, J=7 Hz; $-CO_2C\underline{H}_2CH_3$) and 4.56 (1H, q, J=7 Hz; $CH_3\dot{C}\underline{H}CO_2C_2H_5$); MS *m/e* 256 [$M^+(C_{13}H_{20}O_5$); 7%] and *m/e* 124 (100%). The product (49 mg) was further chromatographed on a column of silica gel (5 g). Elution with a mixture of light petroleum and ether (5: 1) gave an analytical sample. Found: C, 60.73; H, 8.05%. Calcd for $C_{13}H_{20}O_5$: C, 60.92; H, 7.87%. Glc retention time 14.2 min (column: neopentylglycol succinate, 160 °C, N_2, 85 ml/min) and 14.0 min (column: Diasolid H-523, 160 °C, N_2, 85 ml/min). The combined yield of the two alkylated products (**17** and **18**) was 77%.

Other experiments under various conditions were performed by similar procedures to those described above. The resulting mixture of products was subjected to analysis by glc; the results are summarized in Table 1.

Alkylation of the Keto-ester (15). (a) Sodium hydride (180 mg of a 50% dispersion in mineral oil), washed by decantation with dry benzene, was suspended in the same solvent (3 ml). The keto-ester (**15**; 190 mg) in dry benzene (6 ml) was added and the mixture was stirred at room temperature for 40 min. Ethyl α-iodopropionate (990 mg) was then added and the resulting mixture was refluxed under a nitrogen atmosphere for 17 hr. The cooled reaction mixture was treated with 1 M hydrochloric acid (2 ml), and extracted with ether after addition of water. The organic layer was washed with an aqueous sodium bicarbonate solution and water, and dried over magnesium sulfate. Evaporation of the solvents afforded an oil (1.04 g), which showed three spots due to alkylated products on tlc besides those due to ethyl α-iodopropionate and the starting material. The oil was subjected to separation by a column of silica gel (20 g) to give the following fractions: fr 1 [eluted with light petroleum and ether (30: 1); 50 ml], frs 2—4 [light petroleum and ether (20: 1); each 50 ml], frs 5—19 [light petroleum and ether (10: 1); each 15 ml], and frs 20—24 [light petroleum and ether (4: 1); each 30 ml].

Fractions 2—4 gave ethyl α-iodopropionate and a small amount of the starting material (580 mg in total). Fractions 10—16 afforded the *C*-alkylated product (**19**; 80 mg; y: 30%), an oil, IR (liquid) 1740 and 1720 cm^{-1}; PMR ($CDCl_3$) δ 0.81 (3H, s; *t*-CH_3), 0.88 (3H, m; *s*-CH_3), 1.24 (3H, d; J=7 Hz; $C\underline{H}_3\dot{C}H-$ in the side chain), 1.27 (3H, t; J=7 Hz; $C\underline{H}_3CH_2-$), 3.04 (1H, q; J=7 Hz; $CH_3\dot{C}\underline{H}CO_2C_2H_5$), 3.71 (3H, s; $-CO_2CH_3$) and 4.10 (2H, q; J=7 Hz; $-CO_2C\underline{H}_2-CH_3$); PMR ($C_6D_6$) δ 0.78 (3H, s; *t*-CH_3), 0.86 (3H, m; *s*-CH_3), 1.03 (3H, t; J=7 Hz; $C\underline{H}_3CH_2-$), 1.33 (3H, d; J=7 Hz; $C\underline{H}_3\dot{C}H-$ in the side chain), 3.29 (3H, s; $-CO_2-CH_3$), 3.32 (1H, q; J=7 Hz; $CH_3C\underline{H}\dot{C}O_2C_2H_5$), 4.02 (q, J=7 Hz; $-CO_2C\underline{H}_2CH_3$) and 4.04 (q, J=7 Hz; $-CO_2C\underline{H}_2-CH_3$ of the other diastereomer); MS *m/e* 338 [$M^+(C_{19}H_{30}O_5$); 1%] and *m/e* 205 (100%). The substance (11 mg) was further chromatographed on a column of silica gel (5 g). Elution with a mixture of light petroleum and ether (5: 1) gave an analytical sample. Found: C, 67.63; H, 9.06%. Calcd for $C_{19}H_{30}O_5$: C, 67.43; H, 8.94%. The product (**19**) corresponding to the least polar spot on tlc was a diastereomeric mixture as shown by the PMR spectral data mentioned above.

Fractions 17—23 gave the *O*-alkylated products (**20a** and **20b**; 69 mg in total; y: 26%), which corresponded to the other two spots. From fractions 20 and 21, more polar diastereomer (**20a**; 22 mg; one spot on tlc) was obtained

as an oil, IR (liquid) 1755, 1730, 1700, and 1640 cm^{-1}; UV (EtOH) λ_{max} 247 nm(ε 12000); PMR ($CDCl_3$) δ 0.68 (3H, s; *t*-CH_3), 0.87 (3H, m; *s*-CH_3), 1.28 (3H, t; J=7 Hz; CH_3CH_2–), 1.53 (3H, d; J=7 Hz; CH_3CH– in the side chain), 3.72 (3H, s; $-CO_2CH_3$), 4.19 (2H, q; J=7 Hz; $-CO_2CH_2CH_3$) and 4.59 (1H, q; J=7 Hz; $CH_3CHCO_2C_2H_5$); PMR (C_6D_6) δ 0.63 (3H, s; *t*-CH_3), 0.77 (3H, m; *s*-CH_3), 0.97 (3H, t; J=7 Hz; CH_3CH_2–), 1.47 (3H, d; J=7 Hz; CH_3CH– in the side chain), 3.51 (3H, s; $-CO_2CH_3$), 3.94 (2H, q; J=7 Hz; $-CO_2CH_2CH_3$) and 4.46 (1H, q; J=7 Hz; $CH_3CHCO_2C_2H_5$); MS *m/e* 338 [$M^+(C_{19}H_{30}O_5)$; 3%] and *m/e* 205 (100%). The product (15 mg) was further chromatographed on a column of silica gel (3 g). Elution with a mixture of light petroleum and ether (4: 1) gave an analytical sample. Found: C, 67.17; H, 8.97%. Calcd for $C_{19}H_{30}O_5$: C, 67.43; H, 8.94%. From fractions 17 and 18, a small quantity of crude less polar diastereomer (**20b**) was obtained. Characterization of the latter diastereomer is described below.

(b) Alkylation of the keto-ester (**15**; 71 mg) in dry benzene (10 ml) with ethyl α-bromopropionate (385 mg) and sodium hydride (71 mg of a 50% dispersion in mineral oil) was carried out as described in (a) to give a residue (270 mg), which was chromatographed on a column of silica gel (20 g) using the following solvents as eluent: light petroleum and ether (20: 1) (frs 1—3, each 50 ml), light petroleum and ether (10: 1) (fr 4, 50 ml; frs 5—24, each 15 ml), and light petroleum and ether (5: 1) (frs 25—33, each 15 ml). Fractions 12—15 gave the C-alkylated product (**19**; 4 mg). The O-alkylated products (**20a** and **20b**; 40 mg in total) were obtained from fractions 16—33. Fractions 16—22 showing a single spot on tlc afforded less polar diastereomer (**20b**; 15 mg), an oil, IR (liquid) 1750—1730, 1715, and 1640 cm^{-1}; UV (EtOH) λ_{max} 245 nm (ε 4800); PMR ($CDCl_3$) δ 0.65 (3H, s; *t*-CH_3), 0.84 (3H, m; *s*-CH_3), 1.27 (3H, t; J=7 Hz; CH_3CH_2–), 1.50 (3H, d; J=7 Hz; CH_3CH– in the side chain), 3.69 (3H, s; $-CO_2CH_3$), 4.17 (2H, q; J=7 Hz; $-CO_2CH_2CH_3$) and 4.55 (1H, q; J=7 Hz; $CH_3CHCO_2C_2H_5$); PMR (C_6D_6) δ 0.64 (3H, s; *t*-CH_3), 0.77 (3H, m; *s*-CH_3), 0.94 (3H, t; J=7 Hz; CH_3CH_2–), 1.53 (3H, d; J=7 Hz; CH_3CH– in the side chain), 3.50 (3H, s; $-CO_2CH_3$), 3.93 (2H, q; J=7 Hz; $-CO_2CH_2CH_3$) and 4.66 (1H, q; J=7 Hz; $CH_3CHCO_2C_2H_5$); MS *m/e* 338 [$M^+(C_{19}H_{30}O_5)$; 2%] and *m/e* 205 (100%). The material (10 mg) was further chromatographed on a column of silica gel (3 g). Elution with a mixture of light petroleum and ether (10: 1) gave an analytical sample. Found: C, 67.09; H, 8.98%. Calcd for $C_{19}H_{30}O_5$: C, 67.43; H, 8.94%. Fractions 25—33 gave more polar diastereomer (**20a**; 20 mg), whose spectral data were mentioned above.

(±)-Tetrahydroligularenolide [(±)-2]. A mixture of the *C*-alkylated product **19**; 65 mg), acetic acid (1 ml), water (0.3 ml), and 12 M hydrochloric acid (1.3 ml) was heated under reflux for 9 hr. Extraction with ether and the usual work-up gave an oil (49 mg), which was chromatographed on a column of silica gel (5 g). Elution with a mixture of light petroleum and ether (9: 1) and removal of the solvents afforded (±)-tetrahydroligularenolide [(±)-**2**; 24 mg; y: 57%], mp 83—84 °C, IR (CCl_4) 1770—1750 and 1690 cm^{-1}; UV (MeOH) λ_{max} 221 nm (ε 17000); PMR ($CDCl_3$) δ 0.58 (3H, s; *t*-CH_3), 0.91 (3H, d; J=6 Hz; *s*-CH_3), 1.80 (3H, t; J=1.5 Hz; CH_3–C=C), 2.77 (1H, d; J=14 Hz; proton at C-6β) and 4.58 (1H, m; proton at C-8); MS *m/e* 234 [$M^+(C_{15}H_{22}O_2)$; 21%] and *m/e* 123 (100%). Found: C, 76.79; H, 9.64%. Calcd for $C_{15}H_{22}O_2$: C, 76.88; H, 9.46%. IR (in CCl_4), PMR and mass spectra of this substance were found to be identical with those of the authentic tetrahydroligularenolide [(−)-**2**][3] obtained from natural ligularenolide [(−)-**1**].[3]

References

1) Presented at the 28th Annual Meeting of the Chemical Society of Japan, Tokyo, April 2, 1973 (Proceedings, Vol. III, p. 1792); T. Tatee and T. Takahashi, *Chem. Lett.*, **1973**, 929.

2) F. Patil, G. Ourisson, Y. Tanahashi, M. Wada, and T. Takahashi, *Bull. Soc. Chim. Fr.*, **1968**, 1047.

3) Y. Tanahashi, Y. Ishizaki, T. Takahashi, and K. Tori, *Tetrahedron Lett.*, **1968**, 3739; Y. Ishizaki, Y. Tanahashi, T. Takahashi, and K. Tori, *Tetrahedron*, **26**, 5387 (1970).

4) a) E. Piers, M. B. Geraghty, and R. D. Smillie, *Chem. Commun.*, **1971**, 614; b) E. Piers and M. B. Geraghty, *Can. J. Chem.*, **51**, 2166 (1973).

5) I. Nagakura, H. Ogata, S. Yokomori, S. Maeda, and Y. Kitahara, the 15th Symposium on the Chemistry of Natural Products, Nagoya, October, 1971 (Symposium papers, p. 239). *cf.* C. Kabuto, N. Takada, S. Maeda, and Y. Kitahara, *Chem. Lett.*, **1973**, 371.

6) S. Maeda, I. Nagakura, M. Funamizu, and Y. Kitahara, the 28th Annual Meeting of the Chemical Society of Japan, Tokyo, April, 1973 (Proceedings, Vol. III, p. 1793).

7) I. Kitagawa, H. Shibuya, Y. Yamazoe, H. Takeno, and I. Yosioka, *Tetrahedron Lett.*, **1974**, 111.

8) R. H. Jaeger, *Tetrahedron*, **2**, 326 (1958).

9) Compounds (**6**—**20**) utilized for the synthesis are racemic modifications.

10) a) For the synthesis of **8** from a mixture of 5-hydroxy-10-methyl-*trans*-2-decalone and 5-hydroxy-10-methyl-*cis*-2-decalone *via* a mixture (not isolated) of **7** and its *cis*-decalol derivative, *cf.* R. F. Church, R. E. Ireland, and D. R. Shrindhar, *J. Org. Chem.*, **27**, 707 (1962); b) A similar synthesis of **8** from pure 5-hydroxy-10-methyl-*trans*-2-decalone *via* **7** was reported, but without isolation of **7**: R. E. Ireland, S. W. Baldwin, and S. C. Welch, *J. Amer. Chem. Soc.*, **94**, 2056 (1972).

11) The olefin ketal (**10**) has been obtained on treatment of **8** with methyllithium and subsequent dehydration with iodine at 140 °C.[10b]

12) The decalone (**14**) has been synthesized *via* other routes: a) L. H. Zalkow, F. X. Markley, and C. Djerassi, *J. Amer. Chem. Soc.*, **82**, 6354 (1960); b) E. Piers, R. W. Britton, and W. de Waal, *Can. J. Chem.*, **47**, 4307 (1969); c) A. R. Pinder and A. K. Torrence, *J. Chem. Soc., Ser. C*, **1971**, 3410; See also, d) C. Berger, M. Franck-Neumann, and G. Ourisson, *Tetrahedron Lett.*, **1968**, 3451.

13) *cf.* a) S. J. Rhoads and R. W. Hasbrouck, *Tetrahedron*, **22**, 3557 (1966); b) D. M. Pond and R. L. Cargill, *J. Org. Chem.*, **32**, 4064 (1967); c) A. Chatterjee, D. Banerjee, and S. Banerjee, *Tetrahedron Lett.*, **1965**, 3851. See also Ref. 4.

The Finkelstein Reaction in Acetonitrile - Alcohol Mixtures. An Approach to an Anion Solvation by Means of a Multi-step Solvation Model*

Yasuhiko KONDO, Toshio KATO, and Niichiro TOKURA

Department of Applied Chemistry, Faculty of Engineering, Osaka University, Suita, Osaka 565

(Received June 12, 1974)

The rate constants were determined for both processes of the Finkelstein reaction in acetonitrile–alcohol mixtures at 30 °C:

$$CH_3Br + I^- \underset{k_r}{\overset{k_f}{\rightleftharpoons}} CH_3I + Br^-$$

Theoretical equations were derived describing the dependence of the rate constant on the composition changes in the solvent mixtures. These equations describe the change in the rate constant in terms of changes in the activity coefficient. The results were analyzed by means of the equations; they lead to the conclusion that anions have multiple solvation equilibria with alcohols. The relative magnitudes of the step-by-step association constants and of the solvation numbers thus determined agreed with the results determined spectrophotometrically.

In various fields of solution chemistry, quantitative discussions of solvation phenomena are often based on the concept of multi-step solvation processes. The present authors developed a theoretical expression in terms of multi-step solvation for the activity coefficient when a solute is dissolved in a binary mixed solvent. The solvation behavior of a proton in methanol–water mixtures[1] was discussed in terms of such processes. Even though it is intuitively reasonable, however, the weakness of the concept lies in the lack of experimental evidence directly pertaining to the phenomenon.

According to Parker,[2] protic and dipolar aprotic solvents most clearly manifest their characteristics on anion solvation. Recent spectroscopic investigations of the anion-protic solvent interactions successfully support the idea, and quantitative data have been accummulated.[3,4] The Finkelstein reaction, for which reaction rates have been extensively reviewed,[5,6] can be expected to be a good probe for searching into the relation between solute-solvent interactions and reaction rates in solution.

In the present work, the authors have measured the reaction rates in alcohol–acetonitrile mixtures. After analyzing the results on the basis of theoretical expressions derived by the authors, the anion-alcohol interactions and reaction rates in solvent mixtures are discussed.

Experimental

Materials: The tetra-*n*-butylammonium bromide and iodide were prepared by refluxing tri-*n*-butylamine and the corresponding halide in methyl ethyl ketone. The crude products were recrystallized three times from an acetone–ether mixture and dried *in vacuo* at 65 °C for a few days before use.

The methyl iodide was shaken with a dilute potassium carbonate solution, washed with water, dried over anhydrous calcium chloride for one day, and distilled.

The methyl bromide was washed with concentrated sulfuric acid in a pressure vessel, distilled twice, and kept over phosphorus pentoxide in a pressure vessel.

The acetonitrile was refluxed over calcium hydride and distilled, and then distilled two times from phosphorus pentoxide and calcium hydride.

The methanol, ethanol, 2-propanol, and *t*-amyl alcohol were treated as has been described elsewhere.[7]

Kinetic Procedure: The solutions of alkyl halide and tetraalkylammonium salt were prepared by weight. 5 ml aliquots from each stock solution were mixed in a glass test tube, a capacity of 20 ml: and with a ground glass stopper; the reaction was then carried out in a thermostated bath held at 30.0±0.05 °C. After a given period of time, the reaction mixture was poured into a mixture of petroleum ether and water. The electrolytes were extracted from the organic layer, and the concentrations were determined by potentiometric titration using a silver nitrate solution.

Calculation of Rate Constants: The reaction scheme is as follows:

$$\underset{a-x}{MeBr} + \underset{b-x}{I^-} \underset{k_r}{\overset{k_f}{\rightleftharpoons}} \underset{x}{MeI} + \underset{x}{Br^-} \qquad (1)$$

$$K = \frac{x^2}{(a-x)(b-x)}$$

where a and b are the initial concentrations of the reactants.

The rate law and the forward rate constant, k_f, are given by these equations:

$$(dx/dt) = k_f(a-x)(b-x) - k_r x^2 \qquad (2)$$

$$k_f = \frac{1}{2(K^{-1}-1)Bt} \ln\left\{\frac{1+x/(A+B)}{1+x/(A-B)}\right\} \qquad (3)$$

$$K = (k_f/k_r) \qquad (4)$$

$$A = \frac{(a+b)}{2(K^{-1}-1)} \qquad (5)$$

$$B = \frac{\{(a-b)^2+4K^{-1}ab\}^{1/2}}{2(K^{-1}-1)} \qquad (6)$$

When the contribution from the reverse reaction is negligibly small, the rate constant is given by this equation:

$$K_f = \frac{1}{(a-b)t} \ln\left\{\frac{b(a-x)}{a(b-x)}\right\} \qquad (7)$$

The reaction rates were followed starting from the appropriate direction; *i.e.*, for the measurement of k_f we started

* This should be referred to as "Reaction Rates in Binary Mixed Solvents, VII," part VI; Y. Kondo, K. Uosaki, and N. Tokura, This Bulletin, **44**, 2548 (1971).

TABLE 1. DENSITIES OF SOLVENT MIXTURES (30 °C)

Mole fraction of MeCN	MeCN–MeOH	MeCN–EtOH	MeCN–2-PrOH	MeCN–*t*-AmOH
0.0	0.782	0.781	0.777	0.800
0.2	0.782	0.780	0.775	0.797
0.4	0.779	0.778	0.773	0.792
0.6	0.777	0.775	0.771	0.785
0.8	0.774	0.773	0.770	0.778
0.9	0.772	0.772	0.770	0.775
1.0	0.771	0.771	0.771	0.771

from methyl bromide and tetra-*n*-butylammonium iodide, and *vice versa*.

All the calculations were performed on the basis of Eqs. (3) and (7) with a NEAC 2200-700 computer.

Measurements of Density: The densities of the solvent mixtures, *i.e.*, acetonitrile–methanol, –ethanol, –2-propanol, and –*t*-amyl alcohol, were measured with a single-stem pycnometer with a capacity of *ca.* 30 ml. The interpolated values are summarized in Table 1.

Results

Rate measurements were carried out for both forward and reverse processes; the results are summarized in Table 2. They are the average values for duplicate or triplicate runs; the experimental uncertainty was estimated to be less than ±2%.

In 2-propanol and its mixtures with acetonitrile, the rate constants showed a slight dependence on the initial concentration of the tetra-*n*-butylammonium salts used as a nucleophile. This might be partly due to the partial dissociation of the electrolytes. For such a case, the data were determined over a four-fold change of the initial concentration of the salt at *ca.* 0.001—0.01 M; the listed average values differed by *ca.* 4—5% from the extrapolation to a zero concentration of the salt, but not more. Usually rate measurements were carried out at concentrations of 0.001—0.01 M for both reactants.

TABLE 2. RATE CONSTANTS IN PURE AND MIXED SOLVENTS (30 °C)

Mole fraction of MeCN	$k_f \times 10^4$ (l·mol^{-1}·s^{-1}) MeCN–MeOH	MeCN–EtOH	MeCN–2-PrOH	MeCN–*t*-AmOH
0.0	17.3	48.8	144	445
0.2	25.4	63.0	168	600
0.4	38.2	80.5	194	692
0.6	58.6	112	225	627
0.8	120	187	292	593
0.9	209	281	374	604
1.0	705	705	705	705

Mole fraction of MeCN	$k_r \times 10^4$ (l·mol^{-1}·s^{-1}) MeCN–MeOH	MeCN–EtOH	MeCN–2-PrOH	MeCN–*t*-AmOH
0.0	1.36	4.80	20.8	112
0.2	2.86	9.51	37.9	286
0.4	5.85	17.4	59.9	422
0.6	13.6	34.2	99.2	514
0.8	47.9	93.7	216	727
0.9	150	259	485	1100
1.0	2580	2580	2580	2580

Solvent	$k_f \times 10^4$	$k_r \times 10^4$
n-PrOH	—	6.0
i-BuOH	79.4	8.33
t-BuOH	—	127
n-AmOH	—	9.3

Discussion

Equilibrium Constants and Rate Constants in Single Solvents. It is important to determine whether or not the Finkelstein reaction proceeds exactly as indicated by this equation:

$$MeBr + I^- \underset{k_r}{\overset{k_f}{\rightleftharpoons}} MeI + Br^-$$

That is, it is important to determine whether or not the reaction has only one transition state.

The equilibrium constants as determined from the rate constants presented in Table 2 ($K=k_f/k_r=0.273$ in acetonitrile) and by approaching equilibrium from both directions ($K=\{(MeI)_e\,(Br^-)_e\}/\{(MeBr)_e\,(I^-)_e\}=0.274$ in acetonitrile, where the equilibrium concentrations were determined after letting the reaction mixture stand over four half lives) were in excellent agreement. The present result is a necessary corollary of the postulated mechanism.

The rate constants in methanol are much smaller than in acetonitrile, as was pointed out by Parker *et al.*[2] Even in the series of protic solvents, the rate constant shows a marked dependence on the solvent characteristics.

In the classical treatment of the solvent effect on the reaction rate,[8] the logarithmic rate constants are plotted against the reciprocal dielectric constants of the solvents. Such a plot is presented for our data in

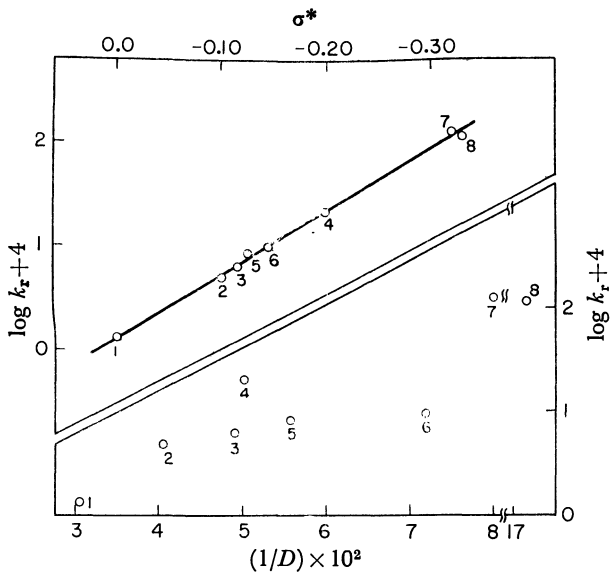

Fig. 1. Plots of log k_r *vs.* $(1/D)$ and of log k_r *vs.* σ*
1: MeOH, 2: EtOH, 3: *n*-PrOH, 4: 2-PrOH
5: *i*-BuOH, 6: *n*-AmOH, 7: *t*-BuOH, 8: *t*-AmOH

Fig. 1. Also, the same data are plotted against the Taft σ^* values.[9]

For the Finkelstein reaction, even for a homologous series of solvents, the dielectric constant does not seem to be an adequate solvent parameter. The Taft σ^* values correlate much better with the rate data. Further, it should be noted that the Taft σ^* values are fairly well correlated to the E_t values[10] for the present series of alcohols.

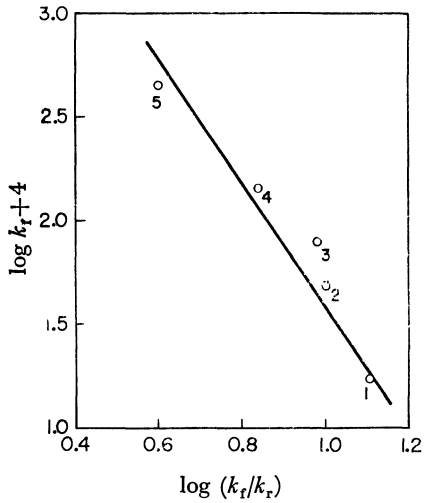

Fig. 2. Plots of log k_f *vs.* log (k_f/k_r)
1: MeOH, 2: EtOH, 3: *i*-BuOH, 4: 2-PrOH, 5: *t*-AmOH.

The logarithmic forward-rate constants, which reveal a marked solvent dependence, are plotted against the logarithmic equilibrium constants in Fig. 2. The slope is *ca.* −3.0. Since the solvent effect on the equilibrium constant is suspected to come mainly from the perturbation in the solvation free energies of the reactants and products due to the change in solvent, the abscissa may be taken as reflecting the sensitivity to the environmental change of the differential solvation energy between the two anions. In a similar way, the ordinate would serve as a measure of the solvent effect on the differential solvation energy between the reactant, the iodide ion, and an activated complex. Thus, the slope of −3.0 corresponds to an indication that the charge density difference between the iodide and the activated complex is considerably larger than the difference between bromide and iodide ions. In addition, the negative sign of the slope indicates that the charge density is more less in the transition state than in the initial state.

Generally speaking, the rate constants of the reaction in alcohol–acetonitrile mixtures show a marked negative deviation from the line connecting the values in pure solvents, *i.e.*, $x_1 \ln k_1 + x_4 \ln k_4$. According to a previous publication by the present authors,[11] this type of behavior can be expected where a solvent effect on the reaction rate mainly originates from the specific solvation of the reactant by the solvent slowing the reaction.

The above features appear to substantiate the position that, for the present system, the specific solvation of halide ions by alcohols is the major factor in producing such a big solvent influence on the reaction rate.

Reaction Rates in Binary Mixed Solvents: For the quantitative treatment of the solvent effects on the rate constants, the activity coefficient of a solute, *M*, in a solvent, s, was defined by Eq. (8):[12]

$$\beta_{M,s} = (m_{gM}/m_{lM})_s \tag{8}$$

where m_{gM} and m_{lM} stand for the molar concentration of a solute, *M*, in a gas phase over the solution and that of the solute, *M*, in solution.

Let us consider a case where a solute, *M*, exists in equilibrium with such a cluster as $M\cdot(S_4)_{Z^\circ-n}\cdot(S_1)_n$, where Z° is the true solvation number, where S_4 and S_1 stand for the 4 and 1 solvents, where these clusters are related to each other by the equations, and where the unsolvated solute, M, is in a vapor-liquid equilibrium:

$$M + Z^\circ S_4 = M\cdot(S_4)_{Z^\circ} \quad ; K_0$$

$$M\cdot(S_4)_{Z^\circ-j+1}\cdot(S_1)_{j-1} + S_1 = M\cdot(S_4)_{Z^\circ-j}\cdot(S_1)_j + S_4 \; ; K_j$$

When the mixture forms an ideal associated solution, the activity coefficient of a solute, M, in a solvent mixture composed of the 1 and 4 solvents, $\beta_{M,mix}$, is given by this equation:[1]

$$\lim_{x_M\to 0}\beta_{M,mix} = [f_M^\circ/\{1+\sum_{i=0}^{Z^\circ}(\prod_{j=0}^{i}K_j)x_4^{Z^\circ-i}x_1^i\}](V_{mix}/RT) \tag{9}$$

where x_1 and x_4 stand for the mole fraction of the 1 and 4 solvents respectively; f_M° is the fugacity of a pure solute, *M*, and V_{mix} is the molar volume of the mixed solvent.

Strictly speaking, all the solvation sites might not necessarily be equivalent to each other. In other words, the equilibrium constant on one solvation site might not be equal to that on the other site. We denote by $K_{se,m}$ the equilibrium constant for the solvent-exchange process on the *m*th solvation site. The $\sum_{i=0}^{Z^\circ}(\prod_{j=0}^{i}K_j)x_4^{Z^\circ-i}x_1^i$ term in Eq. (9) expresses the distribution of the clusters as a function of the solvent composition. In the solvent mixture each solvation site is occupied either by 1 or 4 solvents and, with respect to the *m*th solvation site, the ratio of the frequency of the occupation by the 4 solvent to that by the 1 solvent is x_4 to $K_{se,m}x_1$. Since there are Z° solvation sites around the solute, the distribution of such clusters as is specified by the occupation of the respective site either by the 1 solvent or the 4 solvent is given by the $K_0\prod_{m=1}^{Z^\circ}(x_4+K_{se,m}x_1)$ term. The activity coefficient of a solute, *M*, in the solvent mixture is given by this equation:

$$\lim_{x_M\to 0}\beta_{M,mix} = [f_M^\circ/\{1+K_0\prod_{m=1}^{Z^\circ}(x_4+K_{se,m}x_1)\}](V_{mix}/RT) \tag{10}$$

For a given solvent pair, there would exist a critical value, *z*, within the range, $1\leqq z\leqq Z^\circ$, beyond which the equilibrium constant, $K_{se,m}$, could approximately be equal to unity; that is to say, $K_{se,m}\fallingdotseq 1$ for $z+1\leqq m\leqq Z^\circ$, when the solvation sites are arranged and numbered in decreasing order of the equilibrium constant, for example, from the inner site to the outer site. Under

these conditions, the $\prod_{m=1}^{z}(x_4+K_{se,m}x_1)$ term can be approximated by $\prod_{m=1}^{z}(x_4+K_{se,m}x_1)$. When the term is expanded in series, Eq. (10) reduces to Eq. (11) and the K_j's are related to $K_{se,m}$'s by the following equations:

$$\lim_{x_M\to 0}\beta_{M,mix} = [f_M^\circ/\{1+\sum_{i=0}^{z}(\prod_{j=0}^{i}K_j)x_4^{z-i}x_1^i\}](V_{mix}/RT) \quad (11)$$

$$K_1 = \sum_{m=1}^{z}K_{se,m},\ K_1K_2 = \sum_{m>n}^{z}K_{se,m}K_{se,n},\ \cdots \prod_{j=1}^{z}K_j = \prod_{m=1}^{z}K_{se,m}$$

The z value means the "experimentally detectable" solvation number for the solvent pair or, in other words, the number of solvent molecules responsible for bringing about the observed difference in the solvation energy; it will be referred to as "specific solvation number", in contrast to the true solvation number.

For the following bimolecular reaction, the rate constant in a mixed solvent is given by this equation:[12]

$$X^- + RY \longrightarrow M^* \longrightarrow RX + Y^-$$

$$k_{mix} = k_g(\beta_{X^-,mix}\beta_{RY,mix}/\beta_{*,mix}) \quad (12)$$

where $\beta_{X,mix}$, $\beta_{RY,mix}$, and $\beta_{*,mix}$ stand for the activity coefficients of X^-, of RY, and of the activated complex in the mixed solvent respectively, and where k_g is the rate constant in an ideal gas.

As was described above, and as will be discussed below, there are indications that the rate of the Finkelstein reaction is mainly controlled by the specific solvation of the anion by a protic solvent and the concept of multi-step solvation should be taken into account in the quantitative treatment of the anion solvation in protic solvents.

In the following treatment, we assume that Eq. (11) applies only to the anion and that the other systems, *i.e.*, alkyl halide-solvent mixtures, and activated complex-solvent mixtures, are to be considered ideal mixtures; that is, $\beta_{RY,mix}=\beta_{*,mix}=1$.

For electrolytes, the $K_0 \gg 1$ condition will be satisfied; as a result, K_0 drops out of the equations, giving these approximate formulas, *i.e.*, Eqs. (13) and (14):

$$\ln k_{mix} = \ln k_1 + \ln(\prod_{j=1}^{z}K_j) - \ln\{\sum_{i=1}^{z}(\prod_{j=1}^{i}K_j)x_4^{z-i}x_1^i + x_4^z\} + \ln(V_{mix}/V_1) \quad (13)$$

$$(k_4/k_1) = (\prod_{j=1}^{z}K_j)(V_4/V_1) \quad (14)$$

The ratio of rate constants in pure solvents, Eq. (14), is mainly controlled by the $\prod_{j=1}^{z}K_j$ term, since the values of (k_4/k_1) lie *ca.* 10—10^3, whereas the values of (V_4/V_1) are *ca.* 1—2. The rate constant in acetonitrile is usually larger than in alcohols. We identify acetonitrile as the 4 solvent and alcohol as the 1 solvent.

Equation (14) gives the boundary conditions for $\prod_{j=1}^{z}K_j$. Under these conditions, the theoretical values of the rate constants were obtained as a function of the solvent compositions on the basis of Eq. (13) for a definite set of z and K_j's. The calculations were repeated by a trial and error-method, systematically changing the equilibrium constants for the respective solvation number and afterwards for the different values of z. These calculations were performed by hand.

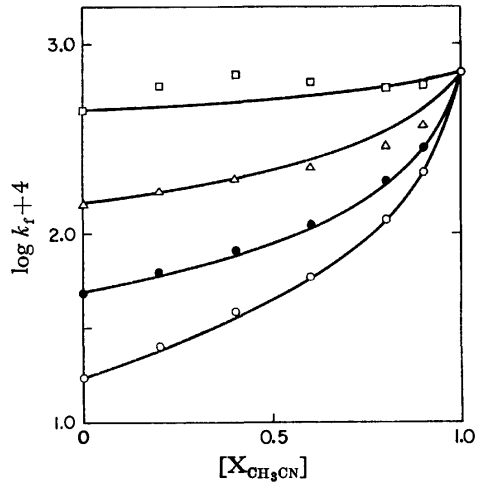

Fig. 3. Comparisons of the experimental results with the calculated values.
——: calculated.
○: MeCN–MeOH, ●: MeCN–EtOH
△: MeCN–2-PrOH, □: MeCN–*t*-AmOH.

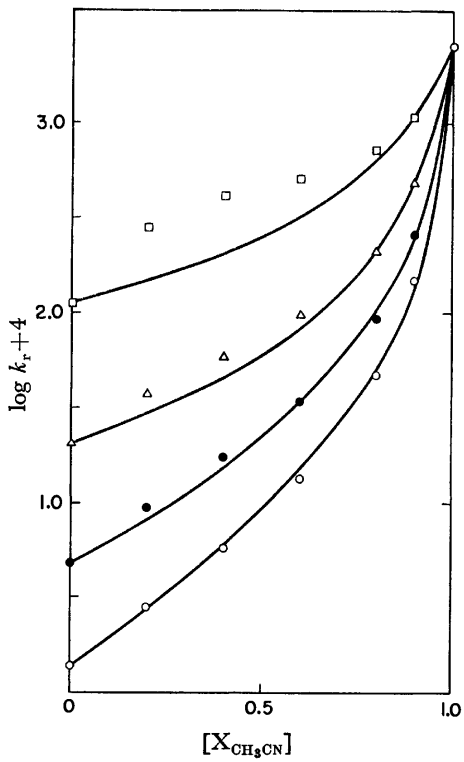

Fig. 4. Comparisons of the experimental results with the calculated values.
——: calculated.
○: MeCN–MeOH, ●: MeCN–EtOH,
△: MeCN–2-PrOH, □: MeCN–*t*-AmOH.

The calculated results are compared with the experimental data in Figs. 3 and 4. The parameters used in the calculations are summarized in Table 3.

The results in Table 3 indicate that the specific solvation number decreases with an increase in the size of the hydrocarbon moieties and of the anion. For the present systems, the specific solvation number, z, obtained above would correspond to the number of alcohol molecules interacting with the anion in a

Table 3. Experimentally determined parameters

Alcohols	I^-				Br^-					
	Z	$\prod_{j=1}^{z} K_j$	K_1	K_2	Z	$\prod_{j=1}^{z} K_j$	K_1	K_2	K_3	K_4
MeOH	2	31.36	24.1	1.30	4	1460	133	6.97	1.50	1.05
EtOH	1	16.00	16.0	—	3	595.4	75.5	4.23	1.86	—
2-PrOH	1	7.11	7.11	—	2	180.2	33.0	5.46	—	—
t-AmOH	1	3.28	3.28	—	2	47.67	14.0	3.40	—	—

different way from acetonitrile. As the protic solvent becomes more bulky, fewer protic solvent molecules can be in close proximity to the anion. This will lead to a decrease in the specific solvation number, z, that is, to a decrease in the number of protic solvent molecules interacting in a "protic" way.

This trend is observed in the equilibrium constants: $K_1>K_2>K_3>K_4\cdots$. This same trend was observed in proton solvation in methanol–water mixtures.[1]

A final point to be noticed is that, in the respective K_j values, the general trend in the interaction energy with a halide ion, *i.e.*, MeOH>EtOH>2-PrOH>*t*-AmOH, is retained.

According to the features summarized in Table 3, the solvation energy of a halide ion in a pure alcohol seems to be a composite quantity determined by two factors, a specific solvation number and the acidity of the alcohol.

Conclusions Reached by a Kinetic Procedure and by Spectroscopic Measurements. One conclusion about anion solvation has been drawn from the association equilibrium studies between phenol and halide ions by Taylor and Kuntz.[4] Both the static and dynamic procedures substantiate the concept of a multi-step solvation of anions due to protic solvents. The generalization about the interaction coefficient, *i.e.*, $K_1>K_2>K_3$, and the specific solvation number, *i.e.*, $z(Br^-)>z(I^-)$, are also supported by the two procedures. In addition, three independent studies, *i.e.*, the present work, IR studies,[4] and NMR studies,[3] give coincident results concerning the order of the interaction coefficients between the alcohol and the anion: $K_j(Br^-)>K_j(I^-)$.

From these results, a smaller anion seems to be better solvated in a less bulky solvent. The specific solvation number is larger as well. Among the multiple steps, the first solvent-exchange process makes an extraordinarily large contribution to the overall difference in the solvation energy.

Recently NMR studies of halide-alcohol association have been performed under conditions where one-to-one complex formation is favored (K_{eq}).[3] These results are shown in Fig. 5 as a function of the Taft σ^* values. The similarity in the slopes of the plots, *i.e.*, 2.8 and 2.5 for $\log K_1$ *vs.* σ^* and $\log K_{eq}$ *vs.* σ^*, lends support to the internal consistency of the assumptions involved in the above procedure.

As may be inferred from Figs. 3 and 4, with an increase in the size of the alcohols the plot of $\log k_{mix}$ *vs.* x tends to reveal an **S**-shape character. This type of behavior can not be simulated by the equations shown above. In such low dielectric solvents as *t*-amyl alcohol or its mixture with acetonitrile, electrolytes are only slightly dissociated; this might have some influence on the observed reaction rates. The possibility of the exchange of solvents in the transition state has been ignored in this treatment. The present work is incapable of confirming these possibilities.

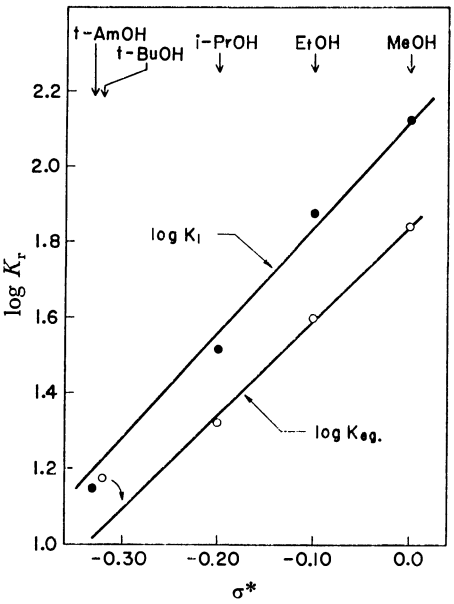

Fig. 5. Correlations of log K_1 and log K_{eq} values with Taft σ^*

From the results of our studies, it seems safe to regard the anion-alcohol interaction as taking place by means of a multi-step process; in a qualitative sense, the results obtained by several procedures are consistent.

We are grateful to Professor Donald Rosenthal, Clarkson College of Technology, for his comments on this manuscript.

References

1) Y. Kondo and N. Tokura, This Bulletin, **45**, 818 (1972).

2) A. J. Parker, *Chem. Rev.*, **69**, 1 (1969) and the references cited therein.

3) R. D. Green, J. S. Martin, W. B. McG. Cassie, and J. B. Hyne, *Can. J. Chem.*, **47**, 1639 (1969).

4) R. P. Taylor and I. D. Kuntz, Jr., *J. Phys. Chem.*, **74**, 4573 (1970).

5) C. K. Ingold, "Structure and Mechanism in Organic Chemistry," 2nd ed., Cornell University Press, Ithaca and London (1969).

6) E. A. Moelwyn-Hughes, "Chemical Statics and Kinet-

ics of Solutions," Academic Press, London and New York (1971).
7) "Technique of Organic Chemistry II, Organic Solvents," 3rd ed. by A. Weissberger, Wiley-Interscience, New York (1970).
8) A. A. Frost and R. G. Pearson, "Kinetics and Mechanism," 2nd ed., John Wiley & Sons, New York (1953).
9) R. W. Taft, Jr., *J. Amer. Chem. Soc.*, **75**, 4231 (1953).
10) Ch. Reichardt, "Lösungsmittel-Effekte in der Organischen Chemie," Springer-Verlag, Heidelberg (1969).
11) Y. Kondo, Y. Honjo, and N. Tokura, This Bulletin, **41**, 987 (1968).
12) S. Glasstone, H. Eyring, and K. J. Laidler, "The Theory of Rate Processes," McGraw-Hill, New York (1941).

The Photochemical Decomposition of Benzenediazonium *o*-Carboxylate in Several Solvents

Masahiko KATO, Taizo TAMANO, and Toshio MIWA

Faculty of Science, Osaka City University, Sugimoto-cho, Sumiyoshi-ku, Osaka 558

(Received June 17, 1974)

The photochemical decompositions of benzenediazonium *o*-carboxylate (**1**) in water, ethanol, acetone, and dichloromethane were studied. In every case, the initial loss of molecular nitrogen to give a zwitterion (**3**) and/or a diradical (**4**) was the primary process. In the solvents which are susceptible to hydrogen abstraction by a radical (ethanol and acetone), reduction takes place to give benzoic acid, through **4**, in a good yield. In water, from which a hydrogen atom is less easily abstracted homolytically, salicylic acid was the main product (24%), while benzoic acid was the minor one (9%). In CH_2Cl_2, the reduction product (benzoic acid, 20%) and biphenylene (10%) were formed. The formation of the latter compound prompted us to study the photochemical decomposition of **1** in CH_2Cl_2 in the presence of tropone. This reaction gave cycloaddition products, (**11**) and (**12**), in 3.2 and 0.7% yields respectively.

Aromatic diazonium compounds readily lose molecular nitrogen, leaving a positive charge or an odd electron on the carbon atom which have been originally bonded to the diazonium group, when irradiated in solution.[1]

It is well known that benzenediazonium *o*-carboxylate (**1**) decomposes to 1,2-dehydrobenzene (**2**), with the simultaneous loss of N_2 and CO_2, when flash-photolyzed in a solid state.[2] Although the production of **2** in solution by the photolysis of *o*-iodophenylmercuric iodide,[3] phthaloyl peroxide,[3,4] and benzothiadiazole 1,1-dioxide[5] had been confirmed, the photochemical behavior of **1** in solution has not yet been described.

The present authors were interested in comparing the fate of **1** and the reactivities of **2** under photolysis with those under thermolysis.[6] In this article, we wish to report on the photochemical reaction of **1** in several solvents. The results are summarized in Table 1, accompanied by some data of the thermal decomposition.

The table shows that the reaction proceeds with an initial loss of molecular nitrogen, followed either by a reaction with the solvent used or by a loss of carbon dioxide.[7]

The second stage of the reaction is observed to be as follows: (i) In the solvents which are susceptible to hydrogen abstraction by radicals (No. 4 and 5), the abstraction by the diradical (**4**) occurs as the main course of the decomposition to give benzoic acid, especially in the case of ethanol as a solvent in a high yield (92%). (ii) Irradiation in water, from which the hydrogen atom is less easily abstracted homolytically, gave salicylic acid as the main product (24%), along with some benzoic acid (9%). The formation of benzoic acid in water is remarkable, since the photochemical decomposition of *p*-nitrobenzenediazonium chloride in an aqueous solution proceeds heterolytically and gives no reduction product.[1c] The formation of benzoic acid was somewhat suppressed when **1** was irradiated either in dilute sulfuric acid or in aqueous sodium chloride; instead a nucleophilic attack by water on either (**1**–H^+)* or (**3**–H^+), or by the chloride ion on either (**1***) or (**3**), may occur. (iii) Dehydrobenzene is formed in only a trace amount in the solvents other

TABLE 1. PHOTOCHEMICAL AND THERMAL DECOMPOSITIONS OF BENZENEDIAZONIUM *o*-CARBOXYLATE IN SOME SOLVENTS

No.	Photochemical decomposition			Yields of the products			
	A[a] (g)	Solvents (340 ml)	Decomposition Time (hr)	Salicylic acid (%)	Benzoic acid (%)	Phenol (%)	Biphenylene (%)[14]
1	1.40	H_2O	2.0	24.4	9.2	2.6	—
2	1.40	H_2O (NaCl 40 g)	2.8	24.2 3.5[d]	2.4	—	—
3	1.40	0.1M H_2SO_4	2.0	37.0	3.5	1.9	—
4	1.40	EtOH	0.5	2.1[e]	92.5	—	—
5	1.90	Acetone	1.5	0.7	45.0	—	1
6	2.74	Acetone (LiCl 4.2 g)	4.0	3.4 2.1[d]	27.0	—	1
7	2.74	CH_2Cl_2	0.83	—	20.0	—	9.9
Thermal decomposition							
8	1.4	H_2O	1.0	88.6	—	—	—
9	1.4	EtOH	1.0	36.1[e]	18.5	2.0[f]	Trace
10	5.0	Acetone	1.0	—	15.0	—	7.0

a) The amount of anthranilic acid used for preparation of **1**. b) The yields were calculated based on the amount of **1** used. c) A similar result was reported by Stiles *et al.*[13] d) *o*-Chlorobenzoic acid. e) Salicylic acid ethyl ether. f) Phenetole.

than dichloromethane, in which the photochemical decomposition proceeds to give an appreciable amount (10%) of biphenylene (**8**) through **2**. Since a nucleophilic attack by solvent is prohibited in this case, the rate of the loss of carbon dioxide from **4** is competitive with that of H-abstraction by **4**. In the photochemical decomposition of **1** in acetone, we could not detect the dehydrobenzene-adducts of **1**, **9** and **10**, reported earlier in the thermal decomposition of **1** in acetone,[8] because **4** does not lose CO_2 to give dehydrobenzene, but instead readily abstracts hydrogen from acetone to give benzoic acid under such a comparatively low temperature.

In contrast to the photochemical decomposition, the thermal decomposition of **1** proceeds in preference to the nucleophilic substitution on **1** in protic solvents upon the radical reaction through **4**, but in the aprotic solvents the intermediate, **4**, readily loses CO_2 thermally to give **2**.[9]

As it was found that the photochemical decomposition of **1** in CH_2Cl_2 gave **2** as the reactive intermediate, we tried the reaction with tropone. After the irradiation of **1** and tropone (1.5 equivalent mole) in CH_2Cl_2 for 3 hr, the 1,4-adduct (**11**) and the 1,6-adduct (**12**) were obtained in 3.2 and 0.7% yields respectively. The ratios of the amounts of **12** to **11** in several runs varies from 0.1—0.3, but the value was clearly larger than that of the thermal reactions, **12**: **11**=0.06—0.08. Although **11** and **12**, the adducts, were known to be sensitive to the irradiation conditions used to produce rearranged products, (**13**)—(**18**),[10,11] we could not detect such products in the present photolysis experiments.*

Experimental

Benzenediazonium o-Carboxylate (1). The starting material (**1**) was prepared as has been described before[12] and was used directly after having been washed successively with cold CH_2Cl_2 and cold ether. The purity of **1** was checked by means of its UV and IR spectra.[13] The wave lengths of the UV maxima of **1** in CH_2Cl_2 (257, 303 ^{infl} nm) were similar to those taken in water, but new maxima at 244 and 253 nm, due to biphenylene, appeared within a few minutes at room temperature.

Irradiation Apparatus. Irradiation was carried out internally in an immersion-type quartz vessel using an Ushio high-pressure mercury lamp (UM-452) through a Pyrex filter. During the irradiation, the vessel was cooled externally with ice–water.

General Procedure. A solution or suspension of **1** in an appropriate solvent was deoxygenated by bubbling in nitrogen gas for five minutes and then irradiated under nitrogen until the gas evolution had ceased. In the case of irradiation in an aqueous solution, the mixture was extracted with ether. In other cases, the solvents were evaporated *in vacuo* and the residues were taken up in ether or in CH_2Cl_2. These extracts were then washed with water and extracted successively with 5% aqueous $NaHCO_3$ and aqueous NaOH; finally, they were washed with water and dried (anhyd. Na_2SO_4). From this organic layer, the neutral part was obtained and separated by column chromatography (silicic acid/$CHCl_3$). From the extracts obtained with 5% aqueous $NaHCO_3$ and 1 M NaOH mentioned above, the acidic and the phenolic products were isolated respectively after acidification with 1 M HCl and extraction with ether. The acid mixture was further characterized by glc after transformation to its esters with diazomethane in ether. The identification of the products was carried out by a direct comparison of their IR, UV, and NMR data with those of authentic samples.

* In the present stage, the reason why the ratios of **12** to **11** are different to each other between thermal and photochemical reactions is not clear.

The glc Retention Times of the Individual Compounds. The identification by glc was carried out by means of a Shimadzu GC-1A instrument using a column, 2.1 m×ϕ8 mm, packed with 20% Apiezon L on Chromosorb E at 183 °C and a H_2 flow rate of 80 ml/min; retention times (min), methyl benzoate, 3.3; methyl salicylate, 5.4; methyl o-chlorobenzoate, 6.9; methyl o-ethoxybenzoate, 10.7.

Irradiation of 1 in CH_2Cl_2 in the Presence of Tropone. **1**, prepared from anthranilic acid (3.0 g, 22 mM) and suspended in CH_2Cl_2 (340 ml) containing tropone (4.5 g, 42 mM), was irradiated at 15 °C for 3 hr using the above-mentioned apparatus. After washing with 1 M NaOH and drying (anhyd. Na_2SO_4), the CH_2Cl_2-solution was concentrated to dryness to give a brown liquid, which was then chromatographed (benzene) on silicic acid (100 g). Fractions were collected every 100 ml; Fractions 3—4 gave a 1,6-cycloaddition product (**12**) (97 mg), and Fractions 5—6, a 1,4-cycloaddition product (**11**) (151 mg). The repeated chromatography and sublimation of each product gave: **11**, 91 °C/4 mmHg, 138 mg (3.2%), mp 84—84.5 °C, tlc (silica gel/benzene) R_f-value 0.29; **12**, 80 °C/4 mmHg, 28 mg (0.7%), mp 79.5—80 °C, R_f-value 0.38. These substances were identified by direct comparison with an authentic sample reported earlier.[10]

Similar results were obtained in acetonitrile as the solvent; **11**, 3.5% yield; **12**, 0.3% yield.

References

1) a) T. Kunitake and C. C. Price, *J. Amer. Chem. Soc.*, **85**, 761 (1963); b) J. K. Stille, P. Cassidy, and L. Plummer, *ibid.*, **85**, 1318 (1963); c) W. E. Lee, J. G. Calvert, and E. W. Malmberg, *ibid.*, **83**, 1928 (1961); d) C. F. Sellers and H. Suschitzky, *J. Chem. Soc., C*, **1969**, 2139.

2) a) R. S. Berry, G. N. Spokes, and M. Stiles, *J. Amer. Chem. Soc.*, **84**, 3570 (1962); b) R. S. Berry, J. Clardy, and M. E. Schafer, *ibid.*, **86**, 2738 (1964).

3) G. Wittig and H. F. Ebel, *Ann. Chem.*, **650**, 20 (1961).

4) M. Jones, Jr. and M. R. DeCamp, *J. Org. Chem.*, **36**, 1536 (1971).

5) R. W. Hoffmann, W. Sieber, and G. Guhn, *Chem. Ber.*, **98**, 3470 (1965).

6) R. Huisgen and R. Knorr, *Tetrahedron Lett.*, **1963**, 1017.

7) R. Gompper, G. Seybold, and B. Schmolke, *Angew Chem.*, **80**, 404 (1968).

8) T. Miwa, M. Kato, and T. Tamano, *Tetrahedron Lett.*, **1968**, 2743.

9) L. Friedman and F. M. Logullo, *J. Org. Chem.*, **34**, 3089 (1969).

10) a) T. Miwa, M. Kato, and T. Tamano, *Tetrahedron Lett.*, **1969**, 1761; b) K. Kurabayashi and T. Mukai, *ibid.*, **1972**, 1049.

11) a) O. L. Chapman, M. Kane, J. D. Lassila, R. L. Loeschen, and H. E. Wright, *J. Amer. Chem. Soc.*, **91**, 6856 (1969); b) A. S. Kende, Z. Goldschmidt, and P. T. Izzo, *ibid.*, **91**, 6858 (1969); c) A. S. Kende and Z. Goldschmidt, *Tetrahedron Lett.*, **1970**, 783.

12) M. Kato, Y. Okamoto, and T. Miwa, *Tetrahedron*, **27**, 4013 (1971).

13) M. Stiles, R. G. Miller, and U. Burckhardt, *J. Amer. Chem. Soc.*, **85**, 1792 (1963).

14) H. Heaney, F. G. Mann, and I. T. Millar, *J. Chem. Soc.*, **1957**, 3930.

Structure of a Main Metabolite of Piroheptine Excreted in Urine of Rabbits; X-Ray Analysis of Its Hydrobromide

Yoji TOKUMA, Shigetaka KODA, Shinji TSUBOUCHI, and Yukiyoshi MORIMOTO
Research Laboratories, Fujisawa Pharmaceutical Co., Ltd., Yodogawa-ku, Osaka 532
(Received June 28, 1974)

The structure of a main metabolite of piroheptine excreted in urine after administered to rabbits has been determined by X-ray analysis of its hydrobromide, $C_{22}H_{26}NOBr$. The crystals are monoclinic with space group $P2_1/n$, the unit-cell dimensions are: $a=14.28$, $b=12.50$, $c=10.97$ Å, $\beta=96.06°$. The intensities were estimated visually from multiple-film equi-inclination Weissenberg photographs. The structure was solved by the heavy atom method. The atomic parameters were refined by the block-diagonal least-squares method, and the final R index was 0.11. The established structure is shown by the following formula (hereafter, named as piroheptine metabolite HBr)

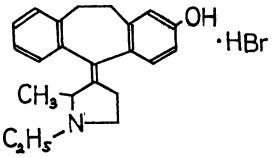

It has been cleared that the hydroxylation in the metabolic process takes place at the 2-position in the benzene ring located far from the N-ethyl group on pyrrolidine ring, and piroheptine metabolite HBr and piroheptine HBr differ considerably in their conformations in the crystalline state.

Piroheptine[1] has been found to show potent antagonism against tremorine-induced tremor in mice.[2] Nojima *et al.*[3] have suggested that 3-(10,11-dihydro-5*H*-dibenzo[*a*,*d*]cycloheptene-5-ylidene)-1,2-dialkylpyrrolidines and their salts seemed to have more than two conformations in solution on the basis of interpretation of PMR spectra. The conformation of piroheptine hydrobromide in the crystal has been found to correspond to the most stable one suggested by PMR study in solution.[4]

In the research of piroheptine metabolism, the main metabolite in urine of rabbits administered piroheptine was isolated by thin layer and gas liquid chromatography. High resolution mass spectrographical study revealed the mono-hydroxylation on benzene ring in the metabolic process, but not the position of hydroxylation. The X-ray analysis of the crystal of piroheptine metabolite hydrobromide was undertaken to elucidate the precise molecular structure and to compare it with piroheptine hydrobromide in the crystal.

Experimental

Piroheptine hydrochloride suspended in deionized water was orally given to rabbits in dose of 200 mg/kg. The urine collected for 24 hr was refluxed for 1 hr in 2 M HCl in order to hydrolyze the conjugated compounds. The main metabolite extracted from $CHCl_3$ was isolated by thin layer and gas liquid chromatography. After the main metabolite was dissolved in a slight excess of 50% HBr, it was heated in a water bath at 50 °C for 45 min and then was evaporated *in vacuo*. The residual oil was recrystallized twice in ethanol. The suitable crystals for X-ray work were obtained from the ethanol in the form of colorless prisms elongated along the *b* axis.

Unit-cell dimensions were determined by the least-squares calculation using the high angle spots of $CuK\alpha_1$ and $CuK\alpha_2$ on zero-layer Weissenberg photographs superimposed by the Al wire patterns for calibration. The density was measured by floatation in a benzene–carbon tetrachloride mixture. Crystal data are summarized in Table 1. The three dimensional intensity data were collected from multiple-film equi-inclination Weissenberg photographs for the layer lines 0 to 9 on the b axis and 0 on the a axis using nickel-filtered $CuK\alpha$ radiation. The intensities of reflection were visually estimated by comparison with a standard scale. The values of intensity ranged from 1 to 8600. Corrections were made for Lorentz, polarization factors and variation in spot size on higher layer photographs.[5] The intensity data from the a axis photograph were used only for layer scale adjustment of b axis photographs. Thus 2413 intensity data were obtained of which 379 were too weak to be observed.

TABLE 1. CRYSTAL DATA

$C_{22}H_{26}NOBr$; F.W.=400.4, mp=258 °C.
Monoclinic; $a=14.28\pm0.01$, $b=12.50\pm0.01$, $c=10.97\pm0.01$ Å, $\beta=96.06\pm0.06°$, $V=1948$ Å^3.
$D_m=1.36$, $Z=4$, $D_x=1.365$ g/cm^3.
$F(000)=832$.
Absent spectra; $h0l$ when $h+l$ is odd, $0k0$ when k is odd.
Space group; $P2_1/n$.

Structure Determination

The coordinates of a bromide ion were deduced from the Patterson function. Fourier synthesis based on the coordinates of the bromide ion clearly revealed all the 24 light atoms. The positional and thermal parameters of the atoms were refined by the block-diagonal least-squares method which minimized $\sum w(|F_o|-|F_c|)^2$. Two cycles of the least-squares refinement were carried out, using isotropic temperature factors to all the atoms and ion. Four more cycles of the refinement were performed, assigning anisotropic temperature factors to only bromide ion. The R index was reduced to 0.11, excluding non-observed reflections ($R=0.13$ for all 2413 reflections). The weighting scheme adopted in the

Table 2. The fractional atomic coordinates, isotropic temperature factors (Å²) and their standard deviations in parentheses

Atom	x	y	z	B
Br	0.2053(1)	0.1952(1)	−0.1549(1)	
N(1)	0.2476(5)	−0.0313(7)	−0.0340(7)	2.4(1)
C(2)	0.2927(6)	0.0017(8)	0.0943(8)	2.1(2)
C(3)	0.2059(6)	0.0374(8)	0.1557(8)	2.1(2)
C(4)	0.1169(7)	−0.0029(9)	0.0814(9)	2.7(2)
C(5)	0.1527(7)	−0.0800(10)	−0.0133(10)	3.4(2)
C(6)	0.3026(8)	−0.1030(10)	−0.1098(10)	4.0(2)
C(7)	0.3925(9)	−0.0476(12)	−0.1418(12)	4.8(3)
C(8)	0.3452(8)	−0.0910(10)	0.1608(10)	3.9(2)
C(9)	0.4262(7)	0.1092(10)	0.4939(10)	3.4(2)
C(10)	0.4803(8)	0.1820(10)	0.4381(10)	4.0(2)
C(11)	0.4479(7)	0.2273(9)	0.3260(9)	3.3(2)
C(12)	0.3600(6)	0.1997(9)	0.2703(9)	2.7(2)
C(13)	0.3048(6)	0.1229(8)	0.3243(7)	1.9(2)
C(14)	0.2114(6)	0.0897(8)	0.2622(8)	2.3(2)
C(15)	0.1265(6)	0.1193(8)	0.3238(8)	2.3(2)
C(16)	0.0518(6)	0.1707(8)	0.2569(8)	2.3(2)
C(17)	−0.0267(7)	0.2107(9)	0.3098(9)	3.0(2)
C(18)	−0.0303(7)	0.1902(10)	0.4351(10)	3.4(2)
C(19)	0.0411(8)	0.1394(10)	0.5012(10)	3.9(2)
C(20)	0.1201(6)	0.1014(9)	0.4509(8)	2.8(2)
C(21)	0.1918(8)	0.0433(10)	0.5403(10)	4.0(2)
C(22)	0.2781(8)	−0.0064(10)	0.4910(10)	3.9(2)
C(23)	0.3386(7)	0.0790(9)	0.4386(9)	3.0(2)
O(24)	−0.1044(6)	0.2291(8)	0.4929(8)	5.4(2)

Table 3. Anisotropic temperature factors for bromide ion (their standard deviations)

The anisotropic temperature factors are expressed in the form of $\exp[-(\beta_{11}h^2+\beta_{22}k^2+\beta_{33}l^2+\beta_{12}hk+\beta_{13}hl+\beta_{23}kl)]$

Atom	β_{11}	β_{22}	β_{33}
Br	0.00561 (0.00007)	0.00721 (0.00013)	0.00933 (0.00011)

Atom	β_{12}	β_{13}	β_{23}
Br	0.00144 (0.00013)	0.00352 (0.00014)	0.00447 (0.00017)

final least-squares calculation was; $w=0.5$ when $|F_o|=0$, $w=1.0$ when $|F_o|<24.0$ and $w=24.0/|F_o|$ when $|F_o|\geq 24.0$. The scattering factors for C, N, O, and Br^- were taken from International Tables for X-ray Crystallography.[6]

The final atomic coordinates and isotropic temperature factors are given in Table 2, and the anisotropic temperature factors for the bromide ion in Table 3. The complete F_o-F_c table are kept at the office of the Bulletin of the Chemical Society of Japan. (Document No. 7501).

Most of the computer programs used were in the UNICS.[7] All the programs were modified by the authors to allow calculations on middle size of computer, HITAC 8400 at Nippon Business Consultant and Fujisawa Pharmaceutical Co., Ltds.

Results and Discussion

Piroheptine metabolite hydrobromide viewed along the c axis is shown in Fig. 1. The bond lengths and angles are shown in Fig. 2. The averaged estimated

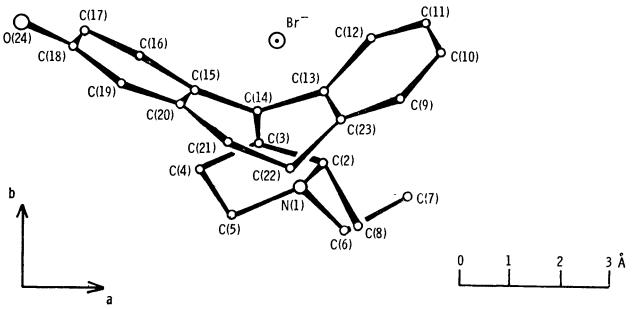

Fig. 1. Piroheptine metabolite hydrobromide viewed along the c axis.

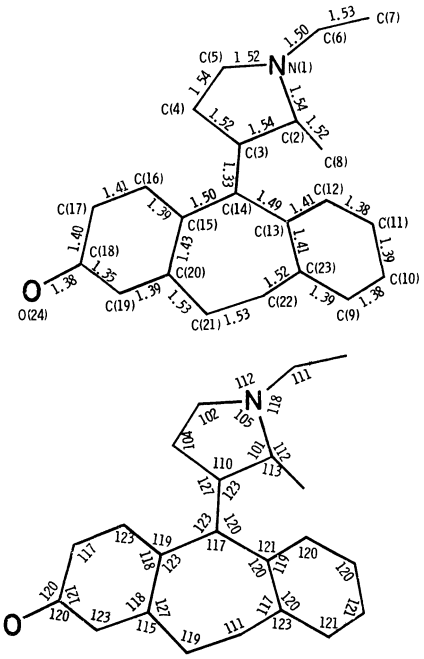

Fig. 2. Bond lengths and angles.

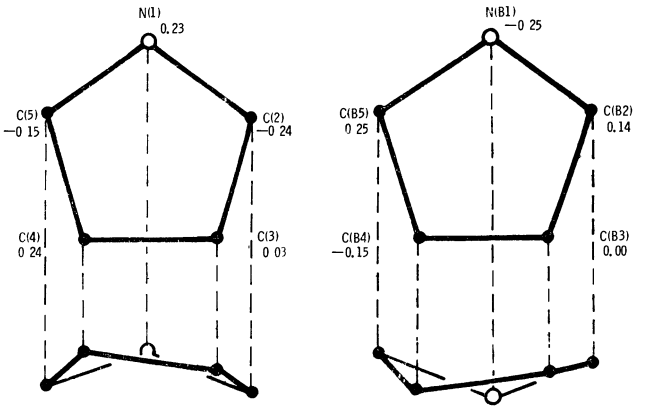

piroheptime metabolite·HBr piroheotine·HBr

Fig. 3. Conformation of the pyrrolidine ring. Arabic numerals show the displacements (in Å) of the atoms from the best plane of the pyrrolidine ring. For comparison, that of piroheptine hydrobromide B[4] is shown on the right.

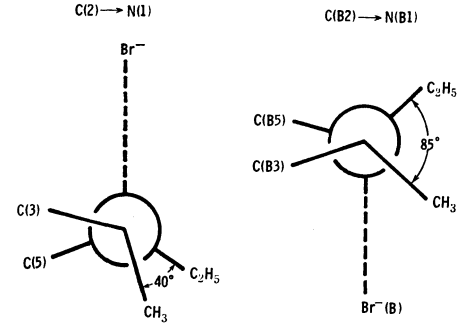

piroheptine metabolite·HBr piroheptine·HBr

Fig. 4. Stereographic projection of the conformation about C(2)–N(1) bond. For comparison, one of piroheptine hydrobromide B[4] is shown on the right.

standard deviations in the bond lengths and angles are about 0.016 Å and 1.0°, respectively. Carbon atoms C(22) and C(21) are located on 0.96 and 0.28 Å respectively out of the best plane through the four carbon atoms, C(13), C(15), C(20), and C(23), of the seven-membered ring which are jointed in the benzene rings connected in both sides. The C(20)–C(21)–C(22) angle, 119°, in the seven-membered ring has a large deviation from the tetrahedral angle. The similar angular deviation in seven-membered ring was also found in the crystal structure of piroheptine hydrobromide[4] and 5-(bromomethylene)-10,11-dihydro-5*H*-dibenzo[*a*,*d*]cycloheptene.[8]

Table 4. Best planes

(1) Equations[a]

Benezne plane I

$$0.474X - 0.742Y - 0.474Z = -0.945$$

Benzene plane II

$$0.441X + 0.873Y + 0.208Z = 2.658$$

Ylidene plane

$$-0.004X + 0.862Y - 0.507Z = -0.497$$

a) X, Y, and Z are the rectangular coordinates in Å unit.

(2) Displacements of atoms from the planes

Benzene plane I		Benzene plane II		Ylidene plane	
C(9)	−0.01 Å	C(15)	−0.01 Å	C(2)	−0.02 Å
C(10)	0.01	C(16)	0.02	C(3)	0.03
C(11)	0.01	C(17)	−0.02	C(4)	0.01
C(12)	−0.02	C(18)	0.01	C(14)	0.00
C(13)	−0.02	C(19)	0.00	C(13)	0.01
C(23)	0.00	C(20)	0.00	C(15)	−0.02
C(14)*	0.05	C(14)*	−0.11		
C(22)*	0.08	C(21)*	0.03		
		O(24)*	−0.05		

The atoms with asterisk were not included in the least-squares calculations.

(3) Dihedral angles between the planes

	Piroheptine metabolite HBr	Piroheptine[4] HBr
Benzene plane I and Benzene plane II	58°	63°
Benzene plane I and Ylidene plane	66	59
Benzene plane II and Ylidene plane	50	76

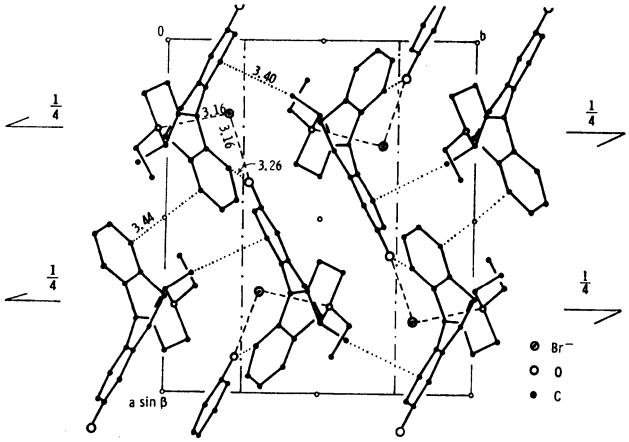

Fig. 5. A drawing of the structure viewed along the c axis. Hydrogen bonds and van der Waals contacts are indicated by broken and dotted lines, respectively.

The conformation of the pyrrolidine ring is shown in Fig. 3 with one of piroheptine hydrobromide.[4] Arabic numerals denote the displacements (in Å) of the atoms from the best plane of the pyrrolidine ring.

The conformation about the C(2)–N(1) bond is compared with one of piroheptine hydrobromide[4] in Fig. 4. The relation between the ethyl and methyl group is *cis*-position in contrast with the case of piroheptine hydrobromide that corresponds to the most stable one suggested by PMR study in solution.[4]

The 2-hydroxy-10,11-dihydro-5*H*-dibenzo[*a*,*d*]cyclohepten-5-ylidene part consists of the three planes. The equations for these planes, displacements of the individual atoms from the planes and dihedral angles between the planes are given in Table 4. The oxygen atom O(24) of hydroxyl group is situated on benzene plane II within the limits of error.

The drawing of the structure viewed along the c axis is shown in Fig. 5. It seems that two hydrogen bondings (N(1)–H···Br⁻ and O(24)–H···Br⁻) are formed in this crystal structure, and the N(1) is protonated. These hydrogen bondings are:

N(1)–H···Br⁻		O(24)–H···Br⁻	
N(1)···Br⁻	3.16 Å	Br⁻···O(24)*	3.16 Å
Br⁻···N(1)–C(2)	101°	Br⁻···O(24)*–C(18)*	122°
Br⁻···N(1)–C(5)	107		
Br⁻···N(1)–C(6)	113,		

asterisks denote the (1/2+x, 1/2−y, −1/2+z) transformation relative to the reference molecule at (x,y,z). These hydrogen bonds are indicated by the broken lines in Fig. 5. Some shorter intermolecular distances are indicated by dotted lines in Fig. 5. No unusually short contact is found in this structure.

The authors are indebted to Professor Masao Kakudo and Dr. Tamaichi Ashida, Institute for Protein Research, Osaka University, for many helpful discussions and suggestions during this analysis.

References

1) Piroheptine: 3-(10,11-dihydro-5*H*-dibenzo[*a*,*d*]cyclohepten-5-ylidene)-1-ethyl-2-methylpyrrolidine.

2) S. Umio, M. Hitomi, H. Nojima, N. Kumadaki, I. Ueda, T. Kanaya, and Y. Deguchi, *J. Med. Chem.*, **15**, 891 (1972).
3) H. Nojima, S. Umio, Y. Morimoto, and H. Tamura, private communication.
4) Y. Tokuma, H. Nojima, and Y. Morimoto, This Bulletin, **44**, 2665 (1971).
5) D. C. Phillips, *Acta Crystallogr.*, **7**, 746 (1954).
6) "International Tables for X-ray Crystallography," Vol. III, Kynoch Press, Birmingham (1962), p. 202.
7) "Universal Crystallographic Computation Program System (UNICS)," ed. by T. Sakurai, The Crystallographic Society of Japan, Tokyo (1967).
8) K. Larsson, *Acta Chem. Scand.*, **24**, 1503 (1970).

The Total Synthesis of (±)-Royleanone[1,2]

Yakudo TACHIBANA

Department of Chemistry, Faculty of Science, Hiroshima University, Higashisenda-machi, Hiroshima 730

(Received July 6, 1974)

The total synthesis of (±)-royleanone (I) has been achieved. 5,7,8-Trimethoxy-1-tetralone (III) was converted into (±)-5,7,8-trimethoxy-1-methyl-2-tetralone (VII) *via* a dihydronaphthalene derivative (IV). The annelation of VII with methyl vinyl ketone gave a (±)-hexahydro-2-oxophenanthrene derivative (VIII), which was then further converted into (±)-11,12,14-trimethoxy-3-oxopodocarpa-5,8,11,13-tetraene (IX). The hydrogenation of IX over platinum oxide gave two dihydro derivatives, (X) and (XI), in a ratio of *ca.* 1: 7, these configurations in the A/B ring juncture were identified as *trans* and *cis* respectively. Therefore, IX was subjected to thioketalization, followed by desulfurization, to give (±)-11,12,14-trimethoxypodocarpa-5,8,11,13-tetraene (XV). The hydrogenation of XV over 10% palladium on carbon gave (±)-11,12,14-trimethoxypodocarpa-8,11,13-triene (XII), along with a small amount of its *cis* isomer (XIII). Finally, XII was converted into a hydroxy-1,4-quinone derivative (XIX), which was then treated with isobutyryl peroxide to give (±)-I, whose IR, UV, and NMR spectra were identical in every respect with those of natural royleanone.

Royleanone (I), a diterpenoid quinone, was isolated from the roots of *Inula royleana* D.C. by Edwards *et al.*[3] On the basis of chemical and spectral studies, they deduced its structure to be I. Kupchan *et al.*[4] also isolated royleanone from *Taxodium distichum* Rich (Taxodiaceae) and reported on its cytotoxity against Eagle's KB strain of human carcinoma of the nasopharynx. Although royleanone has been derived[3] from ferruginol (II)[5] in a 7% yield by oxidation with hydrogen peroxide, as a part of his own synthetic studies of quinone diterpenoids the present author attempted the total synthesis of (±)-royleanone (I) by the route of CB→A ring construction. The introduction of the isopropyl group at the C-13 position by using isobutyryl peroxide[6] was successfully carried out in the final step in the synthesis.

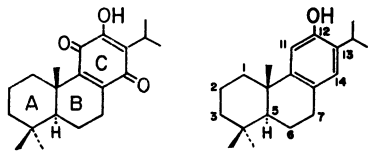

I II

5,7,8-Trimethoxy-1-tetralone (III),[7] which corresponds to the B and C rings in I, was chosen as the starting material. The Grignard reaction of III with methylmagnesium iodide and the subsequent dehydration of the resulting alcohol with dilute sulfuric acid gave 3,4-dihydro-5,7,8-trimethoxy-1-methylnaphthalene (IV), along with a small amount of a hydroxylic compound (IR 3530 cm^{-1}) (V). V showed a positive ferric chloride test, and the NMR spectrum in $CDCl_3$ showed a signal due to an aromatic proton at 6.45 ppm, while in Py-d_5 it shifted downfield to 6.68 ppm. Taking into account this pyridine-induced solvent shift and the ease of the cleavage of ether bonding *ortho* to a carbonyl group,[8] we tentatively identified V as 3,4-dihydro-8-hydroxy-5,7-dimethoxy-1-methylnaphthalene. With an intent to obtain (±)-5,7,8-trimethoxy-1-methyl-2-tetralone (VII), IV was treated with lead tetraacetate in acetic acid to give yellow crystals, whose structure was identified, on the basis of its spectral data (see Experimental section), as 2-methoxy-8-methyl-1,4-naphthoquinone (VI). Therefore, IV was oxidized with perbenzoic acid and then treated with dilute sulfuric acid to give VII. The construction of the A ring could be achieved by the annelation of VII with methyl vinyl ketone in the presence of sodium ethoxide in ethanol; after chromatographic purification, (±)-2,3,4,8,10,12-hexahydro-12-methyl-5,6,8-trimethoxy-2-oxophenanthrene (VIII) was obtained. This was further converted into (±)-11,12,14-trimethoxy-3-oxopodocarpa-5,8,11,13-tetraene (IX) with methyl iodide in the presence of potassium *t*-butoxide in *t*-butanol. Since the hydrogenation of IX over 10% palladium on carbon in acetic acid had not proceeded either at room temperature or at 50 °C, the catalyst was replaced by platinum oxide. After a smooth absorption of hydrogen, the crude product was separated by means of column chromatography on silica gel to give two corresponding dihydro derivatives, (X) and (XI), in a ratio of *ca.* 1: 7. In order to determine the configurations of the A/B ring juncture in X and XI, each of them was subjected to thioketalization with ethanedithiol in the presence of boron trifluoride etherate, followed by desulfurization with Raney nickel in boiling ethanol; after chromatographic purification (±)-11,12,14-trimethoxypodocarpa-8,11,13-triene (XII) and its *cis* isomer (XIII) were obtained respectively. The NMR spectrum of XII in CCl_4 showed signals due to three methyl groups at 0.89, 0.93, and 1.23 ppm,[9] while that of XIII showed corresponding signals at 0.51, 0.92, and 1.24 ppm. These NMR spectra, especially the signals of a significantly higher field at 0.51 ppm, strongly suggest the *cis* nature of the A/B ring juncture in XIII.[10] Therefore, the configurations of the A/B ring juncture in XII and XIII, also including those of X and XI, were identified as *trans* and *cis* respectively. Since natural royleanone possesses a *trans* A/B ring juncture, the above procedure was not effective for the preparation of the intermediate (X) because of its low yield. The desired *trans* compound (XII) could be effectively obtained by the following procedure. The ketone (IX) was first converted into its thioketal (XIV), which was then desulfurized with Raney nickel to give (±)-11,12,14-trimethoxypodocarpa-5,8,11,13-tetraene (XV). The hydrogenation of XV over 10% palladium on carbon in acetic acid afforded the requisite XII, along with a small amount of its *cis* isomer (XIII).

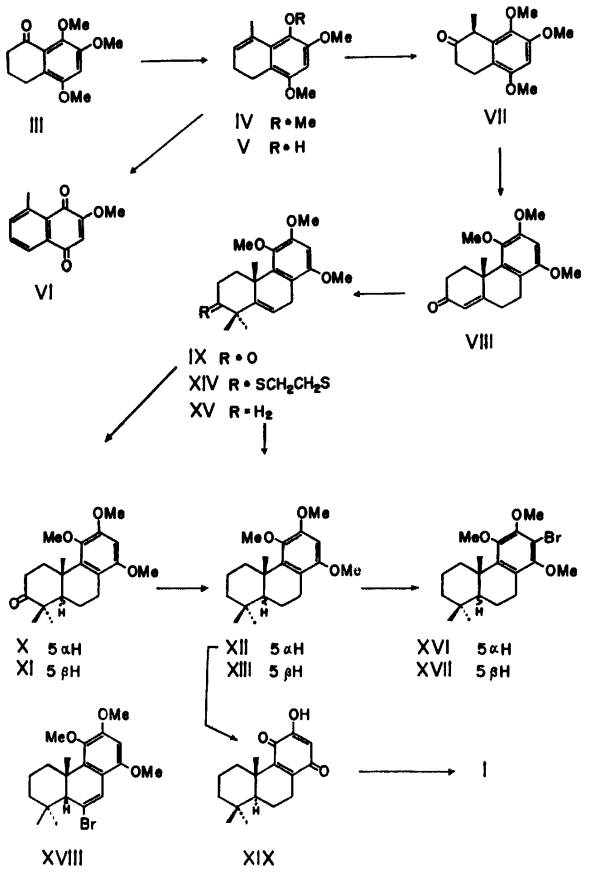

At this stage, some experiments regarding the introduction of isopropyl group at the C-13 position in XII and XIII were carried out.[11] The bromination of XII gave a bromide (XVI), while that of XIII under the same conditions gave two bromides, (XVII) and (XVIII). By the disappearance of the aromatic proton in the NMR spectrum the structure of XVI and XVII was determined to be nuclear-brominated (±)-13-bromo-11,12,14-trimethoxypodocarpa-8,11,13-triene and its *cis* isomer respectively. On the other hand, the NMR spectrum of XVIII showed three methyl signals, at 0.42, 1.06, and 1.21 ppm, together with three one-proton singlets attributable to the protons at the C-5, C-13, and C-7 positions at 1.89, 6.22, and 7.06 ppm respectively. Therefore, XVIII was identified as (±)-6-bromo-11,12,14-trimethoxy-5βH-podocarpa-6,8,11,13-tetra-ene. The treatment of XVI and XVII with sodium or phenylsodium in dry toluene, followed by the addition of either acetone or Dry Ice, resulted only in debromination giving XII and XIII respectively.

The final step of the present synthesis was carried out as follows; XII was demethylated with boron tribromide in methylene chloride, and the resulting hydroxylic product was oxidized in refluxing benzene with bubbling oxygen gas to give (±)-12-hydroxy-11,14-dioxopodocarpa-8,12-diene (XIX). This was then alkylated[6] with isobutyryl peroxide[12,13] in acetic acid at 100—105 °C to yield (±)-I as yellow crystals, whose IR, UV, and NMR spectra were found by a direct comparison to be identical in every respect with those of natural royleanone.

Experimental

The melting points are uncorrected. The NMR spectra were taken on a Hitachi Model R-20 spectrometer (60 MHz), with tetramethylsilane as the internal standard. The UV spectra were measured in ethanol, the IR spectra, in chloroform, and the NMR spectra, in carbon tetrachloride, unless otherwise stated. The chemical shifts are represented in terms of the δ values: s: singlet; bs: broad singlet; d: doublet; t: triplet; q: quartet; m: multiplet. Column chromatography was performed on Merck silica gel (0.08 mm).

3,4-Dihydro-5,7,8-trimethoxy-1-methylnaphthalene (IV). A solution of III (25 g) in dry benzene (250 ml) was dropped, over a period of 30 min, into a Grignard reagent (prepared from magnesium (3.1 g), methyl iodide (20 g) and dry ether (50 ml)) at room temperature. Stirring was continued at this temperature for 30 min, and then at 65 °C for 4 hr. The cooled mixture was poured into dilute hydrochloric acid (10%: 250 ml) and extracted with ether. The extract was washed with aqueous sodium thiosulfate and water and dried over sodium sulfate. After the removal of the solvent, the residue was refluxed for 4 hr in methanol containing dilute sulfuric acid (20%: 38 ml), cooled, and then extracted with ether. The extract was washed with saturated brine and dried over sodium sulfate. After the evaporation of the solvent, the crude product was chromatographed on silica gel (700 g), using benzene–hexane (7: 3) as the eluent, to give IV (19.1 g: 76%) as an oil and V (2.1 g: 11%) as a solid, which was then recrystallized from petroleum ether–ether; mp 51.5—52.5 °C. IV; NMR 2.13 (d, J=1.5 Hz, =CCH$_3$), 3.61, 3.70, 3.76 (each s, -OCH$_3$), 5.77 (m, =CH–), 6.30 (s, aromatic proton). Found: C, 71.92; H, 7.85%. Calcd for $C_{14}H_{18}O_3$: C, 71.77; H, 7.74%.

V; IR 3530 cm^{-1} (OH); NMR ($CDCl_3$) 2.28 (d, J=1.5 Hz, =CCH$_3$), 3.76, 3.86 (each s, 2-OCH$_3$), 5.56 (s, OH), 5.84 (m, =CH–), 6.45 (s, aromatic proton). NMR (Py-d_5) 2.59 (d, J=1.5 Hz, =CCH$_3$), 3.71 (6H, s, 2-OCH$_3$), 5.87 (m, =CH–), 6.68 (s, aromatic proton). Found: C, 70.97; H, 7.39%. Calcd for $C_{13}H_{16}O_3$: C, 70.89; H, 7.32%.

In another experiment, an azeotropic distillation of benzene solution of the crude Grignard reaction product containing two or three drops of concentrated hydrochloric acid, similar results were obtained.

2-Methoxy-8-methyl-1,4-naphthoquinone (VI). A mixture of IV (3.70 g), acetic acid (10 ml), and lead tetraacetate (freshly prepared from red lead oxide (11 g) and acetic acid (35 ml)) was stirred at room temperature for 2 hr; then ethylene glycol (4 ml) was added, and the mixture was stirred for an additional 30 min. The mixture was diluted with water and extracted with ether. The ether was washed with aqueous sodium hydrogen carbonate and water, dried over sodium sulfate, and then evaporated. The column chromatography and crystallization of the residue from methanol afforded VI (1.13 g: 35%); mp 151.5—152.5 °C; IR 1676, 1645, 1618 cm^{-1} (C=O); UV nm (ε): 243 (15700), 248.5 (15900), 276 (14700), 345 (3700); NMR ($CDCl_3$) 2.73 (s, =CCH$_3$), 3.87 (s, -OCH$_3$), 6.10 (s, =CH–), 7.4—8.1 (3H, m, aromatic protons) and an unreacted starting material (1.16 g). Found: C, 71.28; H, 4.84%. Calcd for $C_{12}H_{10}O_3$: C, 71.28; H, 4.99%.

(±)-5,7,8-Trimethoxy-1-methyl-2-tetralone (VII). A solution of perbenzoic acid (19 g) in chloroform (450 ml) was added to a cooled solution of IV (20 g) in chloroform (600 ml) at below 10 °C. After storage overnight in a refrigerator, the red solution was washed with a sodium hydroxide solution and water, and evaporated. The residue was refluxed

for 1.5 hr in methanol (110 ml) containing sulfuric acid (17 ml) and water (90 ml), and the product was extracted with ether. After a usual work-up, the crude product was purified by column chromatography on silica gel (400 g), using benzene–ether (95: 5) as the eluent, to give VII (10.32 g: 48%), which was subsequently recrystallized from petroleum ether–ether; mp 90—91 °C; IR 1707 cm^{-1} (C=O); NMR ($CDCl_3$) 1.36 (d, J=7 Hz, $-\dot{C}H\underline{C}H_3$), 3.77, 3.78, 3.87 (each s, 3-$OC\underline{H}_3$), 6.44 (s, aromatic proton). Found: C, 67.31; H, 7.36%. Calcd for $C_{14}H_{18}O_4$: C, 67.18; H, 7.25%.

(±)-2,3,4,9,10,12-Hexahydro-5,6,8-trimethoxy-12-methyl-2-oxophenanthrene (VIII). Under a stream of nitrogen, a solution of VII (6.9 g) in ethanol (150 ml) was added, by drop, to a solution of sodium ethoxide (prepared from sodium (1.32 g) and absolute ethanol (70 ml)) at room temperature. After stirring for 1 hr at room temperature, the mixture was cooled to −20——30 °C, and then freshly-distilled methyl vinyl ketone (2.95 g) in absolute ethanol (5 ml) was added. Stirring was continued for 7 hr at this temperature, for 1.5 hr at room temperature and at reflux for 30 min. After cooling, the mixture was poured into dilute hydrochloric acid (10%: 200 ml) and extracted with ether. The extract was washed with saturated brine, dried, and evaporated. The residue was purified by column chromatography on silica gel (350 g), using benzene–ether (97: 3) as the eluent, to give VIII (5.34 g), which was then recrystallized from petroleum benzin–methylene chloride; mp 134.5—135.5 °C; IR 1660 cm^{-1} (C=O); NMR ($CDCl_3$) 1.69 (s, $-\dot{C}\underline{C}H_3$), 3.80, 3.85, 3.87 (each s, 3-$OC\underline{H}_3$), 5.84 (s, $=C\underline{H}-$), 6.46 (s, aromatic proton). UV nm (ε): 236 (24200), 290.5 (4500). Found: C, 71.75; H, 7.34%. Calcd for $C_{18}H_{22}O_4$: C, 71.50; H, 7.33%.

(±)-11,12,14-Trimethoxy-3-oxopodocarpa-5,8,11,13-tetraene (IX). Under a stream of nitrogen, a solution of VIII (4.15 g) in *t*-butanol (50 ml) was added, by drop, to a solution of potassium *t*-butoxide (5.6 g) in *t*-butanol (60 ml) at 10—15 °C. After stirring for 1.5 hr at this temperature, freshly-distilled methyl iodide (8.5 g) was added in one portion. The mixture was further stirred for 3.5 hr at room temperature and refluxed for 30 min. After cooling, the mixture was poured into dilute hydrochloric acid (10%: 160 ml) and extracted with ether. After a usual work-up, the crude product was purified by column chromatography on silica gel, using benzene–ether (97 :3) as the eluent; on recrystallization from petroleum ether–methylene chloride it gave IX (3.51 g: 77%) as colorless needles; mp 153—154 °C; IR 1700 cm^{-1} (C=O); NMR ($CDCl_3$) 1.32 (6H, s, 2-$\dot{C}\underline{C}H_3$), 1.35 (s, $-\dot{C}\underline{C}H_3$), 3.27 (m, $-C\underline{H}_2-$), 3.81, 3.83, 3.87 (each s, 3-$OC\underline{H}_3$), 5.83 (t, J=4 Hz, $=C\underline{H}-$), 6.47 (s, aromatic proton). Found: C, 72.90; H, 7.97%. Calcd for $C_{20}H_{26}O_4$: C, 72.70; H, 7.93%.

Hydrogenation of IX over Platinum Oxide. A solution of IX (3.3 g) in acetic acid (180 ml) was hydrogenated in the presence of platinum oxide (490 mg) at room temperature. After the absorption of hydrogen had ceased (after *ca.* 480 ml), the mixture was filtered, the filtrate was then evaporated under reduced pressure. The crude solid was separated (2.4 g) and chromatographed on silica gel (170 g), using benzene–ether (98: 2) as the eluent. The remaining oil was also chromatographed on silica gel (70 g) with the same eluent. X (0.225 g) (recrystallized from petroleum benzin–acetone; mp 156—158 °C; IR 1700 cm^{-1} (C=O); NMR 1.08 (9H, s, 3-$\dot{C}\underline{C}H_3$), 3.74 (6H, s, 2-$OC\underline{H}_3$), 3.78 (s, $-OC\underline{H}_3$), 6.28 (s, aromatic proton); Found: C, 72.50; H, 8.97%. Calcd for $C_{20}H_{28}O_4$: C, 72.26; H, 8.49%) and XI (1.64 g) (recrystallized from petroleum benzin–acetone; mp 141.5—142.5 °C; IR 1700 cm^{-1} (C=O); NMR 0.95, 1.08, 1.31 (each s, 3-$\dot{C}\underline{C}H_3$), 3.74 (6H, s, 2-$OC\underline{H}_3$), 3.79 (s, $-OC\underline{H}_3$), 6.28 (s, aromatic proton); Found: C, 72.27; H, 8.53%. Calcd for $C_{20}H_{28}O_4$: C, 72.26; H, 8.49%) were thus obtained.

(±)-11,12,14-Trimethoxypodocarpa-8,11,13-triene (XII) and Its cis Isomer (XIII). A mixture of X (100 mg), ethanedithiol (0.3 ml), freshly-distilled boron trifluoride etherate (1.0 ml), and benzene (5 ml) was allowed to stand 1 day at room temperature. The mixture was washed with a sodium hydroxide solution and water and then dried over sodium sulfate. After the removal of the solvent, the crude product was refluxed for 3 hr with Raney nickel (W-7, prepared from Raney alloy (5 g) in ethanol (50 ml)) and allowed to stand overnight at room temperature. The subsequent filtration and evaporation of the solvent gave an oil, which was chromatographed on silica gel (10 g), using benzene–petroleum ether (70: 30) as the eluent, to give XII (62 mg: 65%) as an oil. NMR 0.89, 0.93, 1.23 (each s, 3-$\dot{C}\underline{C}H_3$), 3.67 (6H, s, 2-$OC\underline{H}_3$), 3.73 (s, $-OC\underline{H}_3$), 6.31 (s, aromatic proton). Found: C, 75.59; H, 9.50%. Calcd for $C_{20}H_{30}O_3$: C, 75.43; H, 9.50%.

A similar treatment of XI (1.5 g) with ethanedithiol (1 ml), freshly-distilled boron trifluoride etherate (5 ml), and dry benzene (150 ml), followed by desulfurization with Raney nickel (W-7, prepared from Raney alloy (50 g)), gave XIII (1.09 g: 76%) after chromatographic purification on silica gel (150 g), using benzene–petroleum ether as the eluent. This was subsequently crystallized from petroleum ether; mp 69—72 °C; NMR 0.51, 0.92, 1.24 (each s, 3-$\dot{C}\underline{C}H_3$), 3.65, 3.68, 3.75 (each s, 3-$OC\underline{H}_3$), 6.24 (s, aromatic proton). Found: C, 75.22; H, 9.48%. Calcd for $C_{20}H_{30}O_3$: C, 75.43; H, 9.50%.

(±)-11,12,14-Trimethoxypodocarpa-5,8,11,13-tetraene (XV). A solution of IX (3.9 g), ethanedithiol (1.9 ml), freshly-distilled boron trifluoride etherate (11 ml), and dry benzene (60 ml) was allowed to stand 2 days at room temperature. After a usual work-up, the crude product was recrystallized from acetone to give a thioketal (XIV: 3.3 g 70%) as cubic crystals (mp 143—144 °C), which showed no carbonyl band in its IR spectrum. NMR ($CDCl_3$) 1.45, 1.46, 1.48 (each s, $-\dot{C}\underline{C}H_3$), 3.0—3.3 (6H, m, $-C\underline{H}_2-$), 3.75, 3.78, 3.83 (each s, 3-$OC\underline{H}_3$), 5.92 (m, $=C\underline{H}-$), 6.40 (s, aromatic proton). Found: C, 64.90; H, 7.54%. Calcd for $C_{22}H_{30}O_3S_2$: C, 65.01; H, 7.44%.

The above thioketal (3.2 g) was desulfurized with Raney nickel (W-7, prepared from Raney alloy (50 g)) in refluxing ethanol for 3 hr. After a usual work-up, the crude oil was purified by column chromatography on silica gel (150 g), using benzene–hexane (80: 20) as the eluent, to give XV (1.9 g: 76% from XIV) as an oil; NMR 1.17, 1.25, 1.45 (each s, 3-$\dot{C}\underline{C}H_3$), 3.72, 3.73, 3.78 (each s, 3-$OC\underline{H}_3$) 5.76 (m, $=C\underline{H}-$), 6.30 (s, aromatic proton). Found: C, 76.20; H, 8.76%. Calcd for $C_{20}H_{28}O_3$: C, 75.91; H, 8.92%.

Hydrogenation of XV. A solution of XV (2.1 g) in acetic acid (50 ml) was hydrogenated in the presence of 10% palladium on carbon (550 mg) at room temperature, and then the mixture was filtered and evaporated. The crude oil was purified by means of column chromatography on silica gel (100 g), using benzene–petroleum ether (70: 30) as the eluent, to give XII (1.7 g: 81%). The NMR spectrum

of XII showed a small peak at 0.51 ppm, corresponding to the inseparable *cis* isomer (XIII). Its integration areas indicated the amount of XIII to be, at most, less than 15%.

Bromination of XII and XIII. A solution of bromine (290 mg) in carbon tetrachloride (5.8 ml) was stirred, drop by drop into a solution of XII (508 mg) in carbon tetrachloride (10 ml) over a period of 2.5 hr at 15—20 °C. After a usual work-up, the crude oil was chromatographed on silica gel, using benzene–petroleum ether as the eluent, to give XVI (533 mg: 84% as an oil; NMR 0.92, 0.95, 1.25 (each s, 3-$\overset{|}{\underset{|}{C}}C\underline{H}_3$), 3.70, 3.73, 3.81 (each s, 3-OC$\underline{H}_3$). Found: C, 60.75; H, 7.24%. Calcd for $C_{20}H_{29}O_3Br$: C, 60.45; H, 7.63%.

A similar treatment of XIII (420 mg) with bromine (230 mg) afforded XVII (293 mg: 53%) as an oil (NMR 0.56, 0.98, 1.25 (each s, 3-$\overset{|}{\underset{|}{C}}C\underline{H}_3$), 3.70, 3.76, 3.80 (each s, 3-OC$\underline{H}_3$); Found: C, 60.32; H, 7.48%. Calcd for $C_{20}H_{29}O_3Br$: C, 60.45; H, 7.36%) and XVIII (117 mg: 22%) as a solid, which was then recrystallized from petroleum benzin–methylene chloride (mp 142—143 °C; NMR 0.42, 1.06, 1.21 (each s, 3-$\overset{|}{\underset{|}{C}}C\underline{H}_3$), 1.89 (s, -$\overset{|}{\underset{|}{C}}$H), 3.64, 3.73, 3.79 (each s, 3-OC$\underline{H}_3$), 6.22 (s, aromatic proton), 7.06 (s, =C$\underline{H}$–). Found: C, 60.77; H, 6.76%. Calcd for $C_{20}H_{27}O_3Br$: C, 60.76; H, 6.88%).

After a suspension of XVI (186 mg) and sodium (50 mg) in dry toluene (3.5 ml) had been stirred at room temperature for 4.5 hr, acetone (5 ml) was added. Stirring was continued for an additional hr; the mixture was then poured into dilute hydrochloric acid (10%: 5 ml) and extracted with ether. The chromatography of the crude product on silica gel gave an oil whose IR and NMR spectra were identical with those of XII. A similar treatment of XVII gave XIII. Such debromination phenomena were also observed on the treatment of XVI and XVII with either *n*-butyllithium or phenylsodium in dry toluene.

(±)-12-Hydroxy-11,14-dioxopodocarpa-8,12-diene (XIX). A solution of boron tribromide (1.6 ml) in methylene chloride (10 ml) was stirred at −60 °C into a solution of XII (279 mg) in methylene chloride (5 ml) over a period of 5 min. Stirring was continued at −30 °C for 1 hr, and then at room temperature for 30 min. After the excess reagent and the solvent had been removed under reduced pressure, ice was added and the mixture was extracted with ethyl acetate. The extract was washed with a sodium thiosulfate solution and saturated brine, and then dried over sodium sulfate. After the removal of the solvent, the crude solid was chromatographed on silica gel (20 g), using benzene–ethyl acetate (50: 50) as the eluent, to give a trihydroxy derivative. Without further purification, a part of this colorless solid (142 mg) was oxidized in refluxing benzene (10 ml) with bubbling oxygen gas for 4 hr. On recrystallization from acetone–benzene, XIX (60 mg: 31%) was obtained as yellow crystals; mp 195.5—197 °C decomp.; IR (KBr) 3235, 1655, 1625, 1595 cm^{-1}; NMR ($CDCl_3$) 0.89, 0.92, 1.24 (each s, 3-$\overset{|}{\underset{|}{C}}C\underline{H}_3$), 5.95 (s, =C$\underline{H}$–), 7.19 (s, O$\underline{H}$); UV nm (ε): 276.5 (15400), 418 (600). Found: C, 74.53; H, 8.33%. Calcd for $C_{17}H_{22}O_3$: C, 74.42; H, 8.08%.

(±)-Royleanone (I). A solution of isobutyryl peroxide[13] (196 mg) in ether (2 ml) was added to a vigrously stirred solution of XIX (180 mg) in acetic acid (10 ml) at 110 °C, after which the mixture was stirred at 105 °C for 1 hr. After cooling, the mixture was diluted with water and extracted with ether. The ether was washed with a sodium hydrogen carbonate solution and saturated brine, and then dried over sodium sulfate. After the removal of the solvent, the crude solid (recovered starting material, XIX: 58 mg) was removed and the residual oil was chromatographed on silica gel (10 g), using benzene–chloroform (60: 40) as the eluent, to give (±)-I (107 mg: 76% based on the sample consumed) as yellow crystals, which were subsequently recrystallized from hexane; mp 153—154 °C; IR 3355, 1672, 1632, 1600 cm^{-1}, UV $\lambda_{max}^{CCl_4}$ nm(ε): 277(13800), 283(13400), 403(430); NMR ($CDCl_3$) 0.91, 0.94, 1.27 (each s, 3-$\overset{|}{\underset{|}{C}}C\underline{H}_3$), 1.16, 1.27 (each s, -CH(C$\underline{H}_3$)$_2$), 7.28 (s, OH); Mass *m/e* 316 (M^+). Found: C, 76.09; H, 8.97%. Calcd for $C_{20}H_{28}O_3$: C, 75.91; H, 8.92%.

The identity of the synthetic I with natural royleanone was confirmed by direct comparisons of their IR and NMR spectra. The following spectral data have been reported for natural royleanone;[3] IR ($CHCl_3$) 3350, 1672, 1632, 1602 cm^{-1}; UV $\lambda_{max}^{CCl_4}$ nm(ε): 277(15900), 283(15200), 403 (510).

Thanks are due to Professor O. E. Edwards, National Research Council, Ottawa, and to Professor S. Morris Kupchan, University of Virginia, for their kind supply of the spectral copies of natural royleanone. The author also wishes to express his warm thanks to Professor Kenji Fukui and Dr. Takashi Matsumoto, Hiroshima University, for their useful suggestions and con tinual encouragement.

References

1) Most of these works have been reported in preliminary form; T. Matsumoto, Y. Tachibana, and K. Fukui, *Chem. Lett.*, **1972**, 321.

2) Although the formulas depicted represent only one enantiomer, they are taken to indicate a racemate.

3) a) O. E. Edwards, G. Feniak, and M. Los, *Can. J. Chem.*, **40**, 1540 (1962); b) J. H. Gough and M. D. Sutherland, *Aust. J. Chem.*, **19**, 329 (1966).

4) S. M. Kupchan, A. Karim, and C. Marcks, *J. Amer. Chem. Soc.*, **90**, 5923 (1968); *J. Org. Chem.*, **34**, 3912 (1969).

5) C. Brandt and L. G. Neubauer, *J. Chem. Soc.*, **1939**, 1031.

6) a) L. F. Fieser and A. E. Oxford, *J. Amer. Chem. Soc.*, **64**, 2060 (1942); L. F. Fieser and Coworkers, *ibid.*, **70**, 3174 (1948); b) A. C. Baillie and R. H. Thomson, *J. Chem. Soc., C*, **1968**, 48.

7) H. Kakisawa, M. Tateishi, and T. Kusumi, *Tetrahedron Lett.*, **1968**, 3787; *Tetrahedron*, **27**, 237 (1971).

8) a) V. Arkley, J. Attenburrow, G. I. Gregory, and T. Walker, *J. Chem. Soc.*, **1962**, 1260; b) Grignard, *C. R. Acad. Sci. Paris*, **151**, 322 (1910). c) A. Schönberg and R. Moubasher, *J. Chem. Soc.*, **1944**, 462.

9) M. Ribi, A. Chang Sin-Ren, H. P. Kung, C. H. Eugster, *Helv. Chim. Acta*, **52**, 1685 (1969); They reported that dihydroroyleanone trimethyl ether showed three methyl signals at 0.92, 0.95, and 1.26 ppm in its NMR spectrum (CCl_4).

10) a) M. Fetizon and G. Moreau, *Bull. Soc. Chim. Fr.*, **1965**, 3479; b) Y. Kondo and T. Ikenoue, *Chem. Pharm. Bull.* (Tokyo), **11**, 678 (1963).

11) Some of these results will be reported elsewhere.

12) M. S. Khrash, S. S. Kane, and H. C. Brown, *J. Amer. Chem. Soc.*, **63**, 526 (1941).

13) Isobutyryl peroxide was titrated before use according to the method cited in; V. R. Kokatanur and M. Jelling, *ibid.*, **63**, 1432 (1941).

Pyrimidine-Fused 1,4-Benzodiazepines. Reaction of 1,4-Benzodiazepines with Formamide-$POCl_3$

Shigeru KOBAYASHI

Medicinal Research Laboratories, Central Research Division, Takeda Chemical Industries, Ltd., Jusohonmachi, Yodogawa-ku, Osaka 532

(Received July 6, 1974)

Synthesis of new pyrimidine-fused 1,4-benzodiazepines was achieved practically in a single step by heating 1,4-benzodiazepines with formamide and $POCl_3$ in a sealed tube. A plausible mechanism of the reaction is proposed.

Various 1,4-benzodiazepines (**1**) with an additional ring attached to the parent ring system have been synthesized,[1] their interesting psychopharmacological properties being expected. Thus, 10-chloro-2,3,7,11b-tetrahydro-oxazolo[3,2-*d*][1,4]benzodiazepin-6(5*H*)-ones (**2a**: oxazolam, **2b**: cloxazolam) having an oxazole ring fused to the *d* face of the benzodiazepine system are now being clinically used as antianxiety agents.[2] 8-Chloro-6-phenyl-4*H*-*s*-triazolo[4,3-*a*][1,4]benzodiazepines (**3a**: estazolam, **3b**: alprazolam) having a triazole ring fused to the *a* face have also been reported to be pharmacologically active and are under extensive clinical evaluation.[3] However, the derivatives having a third ring fused to the *b* face are only scarcely reported.[4] This prompted us to synthesize 1,4-benzodiazepines having a pyrimidine ring fused to the *b* face described in this paper.

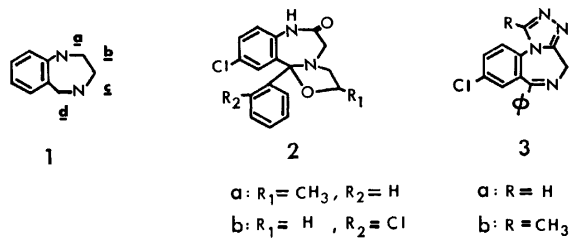

Previously, we reported a new synthetic route of pyrimidines from carboxamides containing a methylene group alpha to the carbonyl group. The reaction involves heating of the amides with formamide (FA) and phosphoryl chloride ($POCl_3$) in a sealed tube.[5] Since some pharmacologically important 1,4-benzodiazepin-2-ones (**4** and **7**)[6] possess the carboxamide group adjacent to a methylene group, we envisaged that similar treatment of these 1,4-benzodiazepin-2-ones might lead to the synthesis of new 1,4-benzodiazepines with a pyrimidine ring fused to the *b* face of the benzodiazepine system (Schemes 1 and 3).

Results and Discussion

Attempts to obtain 8-nitro-6-phenyl-11*H*-pyrimido[4,5-*b*][1,4]benzodiazepine (**6a**) in a single step by heating 1,3-dihydro-7-nitro-5-phenyl-2*H*-1,4-benzodiazepin-2-one[7] (**4a**) with FA and $POCl_3$ at 110 °C for 10 hr in a sealed tube were unsuccessful. The main product separated from the reaction mixture was a yellow crystalline compound which was proved to be 5-amino-4-(2-benzoyl-4-nitroanilino)pyrimidine (**5a**, a hydrolysis product of the C=N double bond of **6a**; yield, 25%). Evidences for the structure (**5a**) are mainly based on its mass spectrum, which shows intense peaks at *m/e* 335 (M^+, 100), 317 (62), 270 (38), 258 (43), 230 (83), 184 (41), 105 (33), and 77 (49%). Peaks at *m/e* 258, 230, 184, 105, and 77 are rationalized as shown in Scheme 2. Appearance of peaks at *m/e* 317 and 270 indicates the occurrence of cyclodehydration of **5a** to **6a** upon preheating (200 °C) or under electron impact in a vaporizing vessel of a mass spectrometer, and the concomitant loss of HNO_2 from **6a** (Scheme 2).[8]

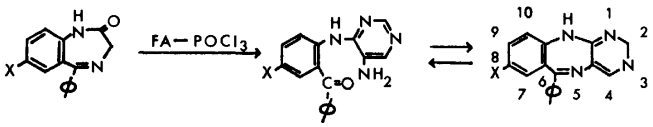

4a: X = NO_2
4b: X = Cl

5a: X = NO_2
5b: X = Cl

6a: X = NO_2
6b: X = Cl

Scheme 1.

This assignment was corroborated by its NMR spectrum ($CDCl_3$), which displays a broad singlet at δ 3.60 (2H, NH_2), a multiplet at 7.44—7.80 (5H, Hc), a singlet at 8.07 (1H, Hb), a double doublet at 8.40 (1H, J=3 and 9 Hz, He), a singlet at 8.50 (1H, Ha), a doublet at 8.54 (1H, J=3 Hz, Hd), a doublet at 9.18 (1H, J=9 Hz, Hf), and a broad singlet at 11.42 (1H, NH).

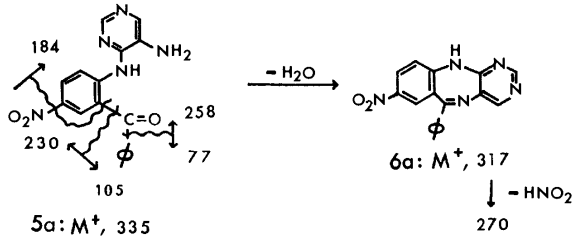

Scheme 2.

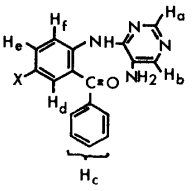

5a: X = NO_2
5b: X = Cl

The NMR spectrum of **5a** measured in DMSO-d_6 at room temperature gives a broad signal not clearly resolved in the aromatic region (δ 7.0—8.5). However, the NMR spectrum determined in DMSO-d_6 at about 100 °C shows a doublet at δ 7.21 (1H, J=9 Hz, C_{10}–H), a multiplet at 7.3—7.7 (6H, C_7–H and phenyl moiety), a double doublet at 8.10 (1H, J=2.5 and 9 Hz, C_9–H), a singlet at 8.29 (1H, C_4–H), a singlet at 8.37 (1H, C_2–H), and a broad singlet at 9.01 (1H, NH). These are rationalized by the structure **6a** (a cyclodehydration product of **5a**). Indeed, the NMR spectrum of **6a** is identical with that of **5a** when determined in DMSO-d_6 at about 100 °C. This result, together with the mass spectral observation, indicates that **5a** would cyclize to **6a** upon heating. In fact, cyclization of **5a** to **6a** easily proceeded when it was heated in DMSO at 100 °C for 10 min.[9] Cyclization of **5a** to **6a** also occurs when a solution of **5a** in a mixture of ethyl acetate and ethyl alcohol (2: 1, v/v) is heated at 70 °C for 1 hr in the presence of *p*-toluenesulfonic acid. The structure of **6a** is further supported by its mass spectrum which displays intense peaks at *m/e* 317 (M^+, 100%) and 270 (M^+-HNO_2, 52%) as indicated in Scheme 2.

The compound **6a** was found to be readily hydrolyzed to the pyrimidine **5a** when an ethyl acetate solution of **6a** was treated with 1 M HCl for a few minutes (Scheme 1).

When 1,3-dihydro-1-methyl-7-nitro-5-phenyl-2*H*-1,4-benzodiazepin-2-one (**7a**)[7] was treated with FA–$POCl_3$, 11-methyl-8-nitro-6-phenyl-11*H*-pyrimido[4,5-*b*][1,4]-benzodiazepine (**8a**) was obtained in a single step in a yield of 20% (Scheme 3); the reaction, though somewhat sluggishly (120 °C, 24 hr in a sealed tube), was not accompanied with hydrolysis. The mass spectrum of **8a** has a strong molecular ion at *m/e* 331 (100%) and the phenyl radical ion at *m/e* 77 (11%). Other important fragmentations are loss of HNO_2[8] (*m/e* 284, 26%), and losses of a phenyl group (*m/e* 254, 16%), and then HCN (*m/e* 227, 11%). The NMR spectrum shows a singlet at δ 3.36 (3H, N–CH_3), a multiplet at 7.35—7.87 (7H, phenyl protons, C_7–H, and C_{10}–H), a double doublet at 8.37 (1H, J=3 and 9 Hz, C_9–H), a broad singlet at 8.56 (1H, C_4–H), and a singlet at 8.72 (1H, C_2–H).

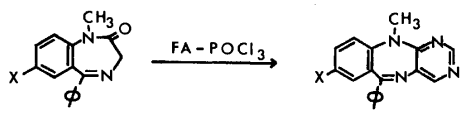

7a: X = NO_2
7b: X = Cl

8a: X = NO_2
8b: X = Cl

Scheme 3.

Similar reactions of the chloro derivatives (**4b** and **7b**) proceed along the same pathway. Thus, 7-chloro-1,3-dihydro-5-phenyl-2*H*-1,4-benzodiazepin-2-one (**4b**)[10] reacts with FA–$POCl_3$ to give 5-amino-4-(2-benzoyl-4-chloroanilino)pyrimidine (**5b**; yield, 23%), which cyclized to 8-chloro-6-phenyl-11*H*-pyrimido[4,5-*b*][1,4]benzodiazepine (**6b**) when heated with *p*-toluenesulfonic acid in a mixture of ethyl acetate and ethyl alcohol (1: 1, v/v) at 70 °C for 30 min. Cyclization of **5b** to **6b** was also accomplished when a solution of **5b** in DMSO was heated at 100 °C for 10 min. The NMR spectrum of **5b** ($CDCl_3$) showed a broad singlet at δ 3.49 (2H, NH_2), a multiplet at 7.46—7.68 (7H, Hc, Hd, and He), a singlet at 8.01 (1H, Hb), a singlet at 8.41 (1H, Ha), a doublet at 8.77 (1H, J=10 Hz, Hf), and a broad singlet at 10.80 (1H, NH), supporting the structure **5b**. In contrast, the *N*-methyl derivative[11] (**7b**) produced **8b** in a single step when treated with FA–$POCl_3$ at 110 °C for 40 hr in a sealed tube; yield, 18% (Scheme 3). Compound **6b** was also hydrolyzed easily to **5b** by treatment with 1 M HCl.

Compound **5b** was also obtained when 7-chloro-1,3-dihydro-5-phenyl-2*H*-1,4-benzodiazepine-2-thione (**9**),[12] and 2-amino-7-chloro-5-phenyl-3*H*-1,4-benzodiazepine (**10**)[13] were treated with FA–$POCl_3$ in yields of 10 and 25%, respectively (Scheme 4).

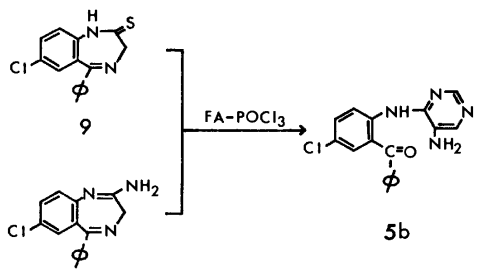

Scheme 4.

Recently, an introduction method of an α,β-unsaturated β-chloroaldehyde moiety to five,[14] six,[15] and seven-membered lactams[15a] has been reported, and α,β-unsaturated β-chloroaldehydes have been reported to provide pyrimidines when treated with FA at above 150 °C.[16] However, attempts to obtain the corresponding α,β-unsaturated β-chloroaldehyde (**11**) from 7-chloro-1,3-dihydro-1-methyl-5-phenyl-2*H*-1,4-benzodiazepin-2-one (**7b**) by treating with Vilsmeier reagent (DMF–$POCl_3$), have thus far met with failure[17] (Scheme 5).

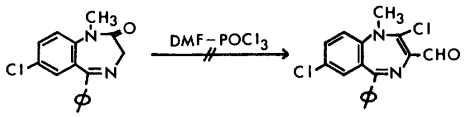

7b 11

Scheme 5.

When FA was treated with $POCl_3$ at 120 °C for 1 hr in a sealed tube and the resulting complex was washed with $CHCl_3$, there were obtained hygroscopic pale yellow powders, which were treated with an excess amount of cyclohexylamine to give *N,N'*-dicyclohexylformamidine hydrochloride (**16**) and phosphoric dicyclohexylamidate cyclohexylammonium salt (**17**) (Scheme 6; for details, see Experimental section).

From the above-mentioned experimental results, a possible mechanistic interpretation of the present one-step synthesis can be advanced. The reaction of FA with $POCl_3$ gives a Vilsmeier compound **12**.[18] Its further reaction with FA produces **13**[19] which upon reaction with $POCl_3$ yields **14**. In the absence of **7b**,

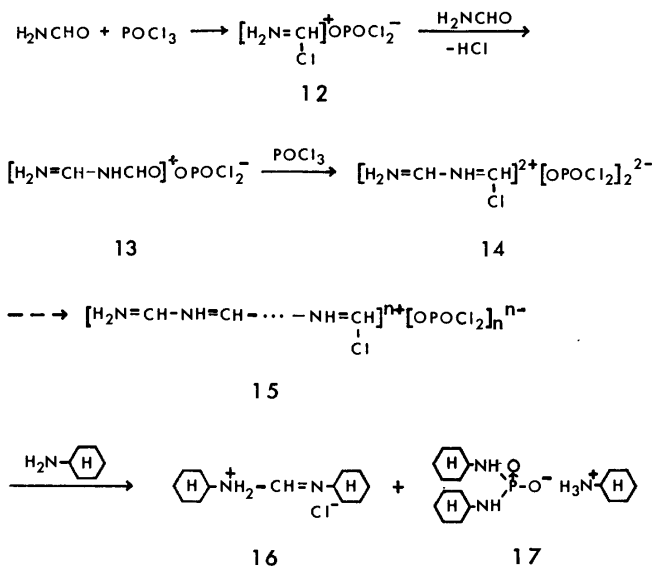

Scheme 6.

the polymerization of the Vilsmeier compound would proceed until it reaches a possible intermediate of adenine (**15**, $n=5$) which cyclizes to yield adenine as reported previously.[20] However, when **7b** is present, it would react with **14** to give **18**, which cyclizes to give **8b** as shown in Scheme 7.

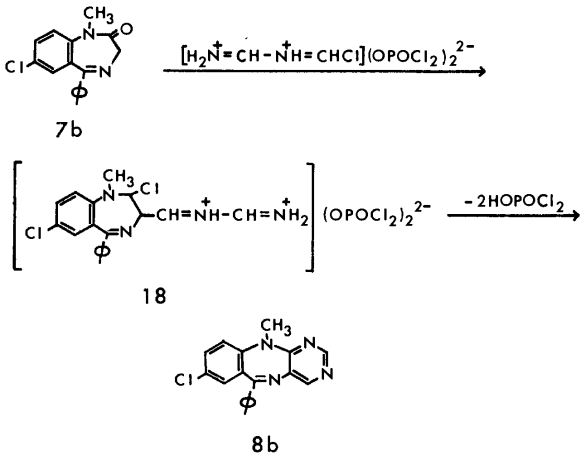

Scheme 7.

Another route which involves the reaction of **7b** with **12**, appears less plausible because, as previously mentioned, all attempts to isolate **11** were unsuccessful. Interesting enough, despite the similarity of the present reaction conditions to those of adenine synthesis, formation of adenine was greatly suppressed if **7b** is present in the reaction mixture. For instance, adenine is obtained in 40% yield if **7b** is absent, whereas its yield is quite poor (3%) in the presence of 0.5 mol equivalents of **7b**. These observations could be reasonably accounted for by the assumption that the dimeric Vilsmeier reagent (**14**) is more reactive than the monomer (**12**) for the reaction with carboxamides or formamides. If so, one could ingeniously explain the reason that addition of any alkyl amide or *N*-alkyl formamide to the reaction mixture of FA–$POCl_3$ leads to poor yields of adenine[21] and also that **11** is not produced from the reaction of **7b** with DMF–$POCl_3$ whereas the reaction leads to the formation of **8b** *via* its precursor **18**.

Experimental

Melting points were measured in open capillaries and are uncorrected. NMR spectra were recorded in $CDCl_3$ or in DMSO-d_6 (internal TMS standard) on a Varian T-60, A-60, or HA 100 spectrophotometer. Mass spectra were recorded on a Hitachi RMU-6D double focusing spectrometer with an ionizing voltage of 70 eV at a temperature of 200 °C. IR and UV spectra were recorded on a Hitachi EPI-S_2 recording spectrophotometer and a Hitachi EPS-2 recording spectrophotometer, respectively.

General Procedure. 1,4-Benzodiazepines (0.02 mol) and FA (0.05 mol) were charged in a stainless steel vessel (100 ml). $POCl_3$ (0.07 mol) was added into this mixture with cooling and the vessel was sealed. After being left standing for 10 min at room temperature, the vessel was heated at 110 °C for 10 hr with stirring. The reaction mixture was then cooled and dissolved in EtOAc. The EtOAc extract was carefully washed with 4M NaOH under cooling until the aqueous layer remained basic, and then with water until neutral. The organic layer was dried over Na_2SO_4 and evaporated. The residue was chromatographed on a silica gel column (Kieselgel 60, Merck) using $CHCl_3$–acetone (4: 1, v/v) as a solvent. Recrystallization from $CHCl_3$–EtOH gave a pure product.

The following compounds (**5** and **8**) were prepared by the general procedure.

5-Amino-4-(2-benzoyl-4-nitroanilino)pyrimidine (5a). 1,3-Dihydro-7-nitro-5-phenyl-2*H*-benzodiazepin-2-one (**4a**, 5.6 g, 0.02 mol) yielded 1.68 g of **5a**; mp 198—199 °C; MS (*i*): *m/e* 335 (M^+, 100), 317 (62), 270 (38), 258 (43), 230 (83), 184 (41), 105 (33), 77 (49); NMR (δ) $CDCl_3$: 3.60 (2H, bs), 7.44—7.80 (5H, m), 8.07 (1H, s), 8.40 (1H, dd, $J=3$ and 9 Hz), 8.50 (1H, s), 8.54 (1H, d, $J=3$ Hz), 9.18 (1H, d, $J=9$ Hz), 11.42 (1H, bs); IR ν_{max}^{KBr} (cm^{-1}): 1630 (C=O); UV (mμ) λ_{max} (ε) EtOH: 248 (16900), 398 (14000). Found: C, 60.90; H, 3.85; N, 20.83%. Calcd for $C_{17}H_{13}O_3N_5$: C, 60.89; H, 3.91; N, 20.89%.

5-Amino-4-(2-benzoyl-4-chloroanilino)pyrimidine (5b). (i) 7-Chloro-1,3-dihydro-5-phenyl-2*H*-1,4-bnezodiazepin-2-one (**4b**, 2.70 g, 0.01 mol) yielded 0.75 g of **5b**; mp 201—202 °C; MS (*i*): *m/e* 324 (M^+, 23), 306 (9), 271 (9), 247 (11), 219 (43), 105 (63), 77 (100); NMR (δ) $CDCl_3$: 3.49 (2H, bs), 7.46—7.68 (7H, m), 8.01 (1H, s), 8.41 (1H, s), 8.77 (1H, d, $J=10$ Hz), 10.80 (1H, bs); IR ν_{max}^{KBr} (cm^{-1}): 1630 (C=O); UV (mμ) λ_{max} (ε) EtOH: 253 (20300), 308 (10400). Found: C, 62.58; H, 3.88; N, 17.20%. Calcd for $C_{17}H_{13}ON_4Cl$: C, 62.87; H, 4.03; N, 17.25%.

(ii) 7-Chloro-1,3-dihydro-5-phenyl-2*H*-1,4-benzodiazepine-2-thione (**9**, 572 mg, 2 mmol) yielded 69 mg of **5b**.

(iii) 2-Amino-7-chloro-5-phenyl-3*H*-1,4-benzodiazepine (**10**, 540 mg, 2 mmol) yielded 165 mg of **5b**

11-Methyl-8-nitro-6-phenyl-11H-pyrimido[4,5-b][1,4]benzodiazepine (8a). 1,3-Dihydro-1-methyl-7-nitro-5-phenyl-2*H*-1,4-benzodiazepin-2-one (**7a**, 738 mg, 2.5 mmol) was heated at 120 °C for 24 hr under the same conditions, yielding 167 mg of **8a**; mp 163—164 °C; MS (*i*): *m/e* 331 (M^+, 100), 284 (26), 254 (16), 227 (11), 77 (11); NMR (δ) DMSO-d_6: 3.36 (3H, s, N–CH_3), 7.35—7.87 (7H, m, phenyl protons, C_7–H, and C_{10}–H), 8.39 (1H, dd, $J=3$ and 9 Hz, C_9–H), 8.56 (1H, bs, C_4–H), 8.72 (1H, s, C_2–H); UV (mμ) λ_{max} (ε) EtOH: 228 (24700), 267 (19600), 303 (21900). Found: C, 64.89; H, 3.84; N, 21.15%. Calcd for $C_{18}H_{13}O_2N_5$: C, 65.25;

H, 3.96; N, 21.14%.

8-Chloro-11-methyl-6-phenyl-11H-pyrimido[4,5-b][1,4]benzodiazepine (8b). 7-Chloro-1,3-dihydro-1-methyl-5-phenyl-2*H*-1,4-benzodiazepin-2-one (**7b**, 284 mg, 1 mmol) was heated at 110 °C for 40 hr under the same conditions, yielding 59 mg of **8b**; mp 208—209 °C; MS (*i*): *m/e* 320 (M^+, 100), 285 (24), 243 (36), 216 (44), 77 (56); NMR (δ) $CDCl_3$: 3.31 (3H, s, N-CH_3), 6.93—7.87 (8H, m), 8.53 (1H, bs, C_4-H), 8.66 (1H, s, C_2-H); UV (mμ) λ_{max} (ε) EtOH: 244 (23600), 280 (12800), 303 (12100). Found: C, 67.64; H, 4.11; N, 17.54%. Calcd for $C_{18}H_{13}N_4Cl$: C, 67.40; H, 4.08; N, 17.47%.

8-Nitro-6-phenyl-11H-pyrimido[4,5-b][1,4]benzodiazepine (6a). 5-Amino-4-(2-benzoyl-4-nitroanilino)pyrimidine (**5a**, 1.0 g) and *p*-TsOH·H_2O (50 mg) were dissolved in a mixture of EtOH–EtOAc (100 ml, 2: 1, v/v). The solution was refluxed for 1 hr. The solvent was removed under reduced pressure and the residue was dissolved in $CHCl_3$ (100 ml). The solution was washed with water and dried over Na_2SO_4, and the solvent was evaporated. Crystallization of the residue from MeOH–$CHCl_3$ gave 0.9 g of **6a**; mp 261—262 °C; MS (*i*): *m/e* 317 (M^+, 100), 270 (52); NMR (δ) DMSO-d_6: 7.21 (1H, d, J=9 Hz, C_{10}-H), 7.3—7.7 (6H, m, C_7-H and phenyl protons), 8.10 (1H, dd, J=2.5 and 9 Hz, C_9-H), 8.29 (1H, s, C_4-H), 8.37 (1H, s, C_2-H), 9.01 (1H, bs, NH); UV (mμ) λ_{max} (ε) EtOH: 227 (25000), 262 (13700), 303 (22000). Found: C, 63.52; H, 3.28; N, 21.97%. Calcd for $C_{17}H_{11}O_2N_5 \cdot 1/4H_2O$: C, 63.45; H, 3.52; N, 21.76%.

8-Chloro-6-phenyl-11H-pyrimido[4,5-b][1,4]benzodiazepine (6b). 5-Amino-4-(2-benzoyl-4-chloroanilino)pyrimidine (**5b**, 250 mg) and *p*-TsOH·H_2O (25 mg) were dissolved in a mixture of EtOH–EtOAc (10 ml, 1: 1, v/v). The solution was heated at 70 °C for 3 hr, then concentrated to about 4 ml and set aside in a refrigerator overnight. The resulting fluffy crystals were collected (226 mg); mp 240—241 °C; MS (*i*): *m/e* 306 (M^+, 100), 271 (76), 77 (6); NMR (δ) DMSO-d_6: 6.80 (1H, d, J=2.5 Hz, C_7-H), 7.21 (1H, d, J=8.5 Hz, C_{10}-H), 7.45 (1H, dd, J=2.5 and 8.5 Hz, C_9-H), 7.55 (5H, s, phenyl protons), 8.36 (1H, s, C_4-H), 8.46 (1H, s, C_2-H), 8.70 (1H, bs, NH); UV (mμ) λ_{max} (ε) EtOH: 244 (27500), 280 (15000), 303 (12800). Found: C, 66.16; H, 3.49; N, 18.33; Cl, 11.60%. Calcd for $C_{17}H_{11}N_4Cl$: C, 66.56; H, 3.62; N, 18.27; Cl, 11.56%.

Hydrolysis of 8-Chloro-6-phenyl-11H-pyrimido[4,5-b][1,4]benzodiazepine (6b). A solution of compound **6b** (122 mg, 0.4 mmol) in EtOAc (40 ml) was shaken with 1 M HCl (10 ml) for 1 min. The organic layer was washed with 5% $NaHCO_3$, then with water, dried over Na_2SO_4, and evaporated. Recrystallization of the residue from EtOH–$CHCl_3$ gave 122 mg of 5-amino-4-(2-benzoyl-4-chloroanilino)pyrimidine (**5b**).

8-Nitro-6-phenyl-11*H*-pyrimido[4,5-*b*][1,4]benzodiazepine (**6a**) was hydrolyzed under the same conditions to give 5-amino-4-(2-benzoyl-4-nitroanilino)pyrimidine (**5a**,80.3%).

N,N'-Dicyclohexylformamidine Hydrochloride (16) and Phosphoric Dicyclohexylamidate Cyclohexylammonium Salt (17). FA (1.35 g, 30 mmol) was charged in a stainless steel vessel (30 ml), which was cooled with dry ice–acetone. $POCl_3$ (10 g, 66 mmol) was added into a solidified mass of FA and the vessel was sealed tightly. After being left standing for 30 min at room temperature, the vessel was heated at 120 °C for 1 hr in an oil bath. The reaction mixture was cooled and washed with $CHCl_3$ to remove an excess of $POCl_3$. An excess of cyclohexylamine was added into the resulting pale yellow hygroscopic powders. Evaporation of cyclohexylamine under reduced pressure left a residue, which was treated with $CHCl_3$ and then with ethyl ether. The crude **16** (3.0 g) obtained was twice recrystallized from $CHCl_3$–EtOAc(1:1, v/v) to give 1.9 g of pure **16**; mp 230 °C decomp. (lit, mp 229—230 °C decomp.,[22] 228—230 °C decomp.[23]); MS (*i*): *m/e* 208 (M^+, 55), 110 (HC^+=NC_6H_{11}, 100), 98 (C_6H_{11}–NH^+, 50), and 83 (H_2C=$CHCH_2CH_2CH_2CH_2^+$, 52); IR ν_{max}^{Nujol} (cm^{-1}): 3100 (-C=N), 1680 (-C=NH^+-).

The sulfate was prepared by passing the hydrochloride through a column of Amberlite IRA-400 (SO_4^{2-}) and crystallized from EtOAc–EtOH (3: 1, v/v); mp 240 °C decomp. Found: C, 58.53; H, 9.56; N, 10.41; S, 6.00%. Calcd for $C_{13}H_{24}N_2 \cdot 1/2H_2O \cdot 1/2H_2SO_4$: C, 58.64; H, 9.77; N, 10.53; S, 6.02%.

From the recrystallization mother liquor for **16**, 100 mg of fine needles (**17**) was obtained; mp 173—174 °C decomp.; white precipitates were obtained by treatment with $AgNO_3$; positive for $(NH_4)_6Mo_7O_{24}$ reagent;[24] IR ν_{max}^{Nujol} (cm^{-1}): 1120 (monobasic phosphoramidate). Found: C, 60.32; H, 11.04; N, 11.78; P, 8.62%. Calcd for $C_{18}H_{38}O_2N_3P$: C, 60.17; H, 10.59; N, 11.70; P, 8.64%.

The author is grateful to Prof. K. Maruyama of Kyoto University for his valuable suggestions in this study. Thanks are also due to Drs. K. Morita, Y. Kuwada, and M. Ochiai of the same division for their discussions and encouragement throughout this work.

References

1) For example, D. L. Coffen, J. D. DeNoble, E. L. Evans, G. F. Field, R. Ian Fryer, D. A. Katonak, B. J. Mandel, L. H. Sternbach, and W. J. Zally, *J. Org. Chem.*, **39**, 167 (1974).

2) T. Miyadera, A. Terada, M. Fukunaga, Y. Kawano, T. Kamioka, C. Tamura, H. Takagi, and R. Tachikawa, *J. Med. Chem.*, **14**, 520 (1971).

3) K. Meguro and Y. Kuwada, *Tetrahedron Lett.*, **1970**, 4039; J. B. Hester, Jr., D. J. Duchamp, and C. G. Chidester, *ibid.*, **1971**, 1609; J. B. Hester, Jr., A. D. Rudzik, and B. V. Kamdar, *J. Med. Chem.*, **14**, 1078 (1971).

4) S. C. Bell, C. Gochman, and S. J. Childress, *J. Org. Chem.*, **28**, 3011 (1963); E. C. Taylor and F. Yoneda, *Angew. Chem. Int. Ed. Engl.*, **6**, 878 (1967).

5) K. Morita, S. Kobayashi, H. Shimadzu, and M. Ochiai, *Tetrahedron Lett.*, **1970**, 861; S. Kobayashi, This Bulletin, **46**, 2835 (1973).

6) For a recent review, see L. H. Sternbach, *Angew. Chem. Int. Ed. Engl.*, **10**, 34 (1971).

7) L. H. Sternbach, R. Ian Fryer, O. Keller, W. Metlesics, G. Sach, and N. Steiger, *J. Med. Chem.*, **6**, 261 (1963).

8) From the mass spectral studies on a series of 5-phenyl-1,3-dihydro-2*H*-1,4-benzodiazepin-2-ones by high resolution mass measurement of the major peaks and by metastable scanning, W. Sadée, (*J. Med. Chem.*, **13**, 475 (1970)) claims that the species **a** degraded to **b** by loss of HNO_2. In this study, loss of HNO_2 from the parent ion is likely to occur in a similar way.

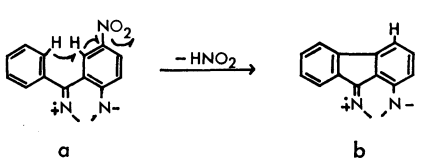

a b

9) When **5a** was heated at 100 °C for 7 hr in various high boiling solvents such as dimethylformamide, nitrobenzene, benzonitrile, and quinoline, no conversion to **6a** was

observed as revealed from tlc [Kieselgel 60 F_{254} pre-coated, Merck: solvent system, chloroform–acetone–ethanol (80:20:1)]. Therefore, DMSO appears to serve as a solvent for promoting dehydration of **5a** and a simple thermal elimination of water must be excluded; *cf.* V. J. Traynelis, W. L. Hergenrother, H. A. Hanson, and J. A. Valicenti, *J. Org. Chem.*, **29**, 123 (1964).

10) S. C. Bell, T. S. Sulkowski, C. Gochman, and S. J. Childress, *ibid.*, **27**, 562 (1962); L. H. Sternbach, R. Ian Fryer, W. Metlesics, E. Reeder, G. Sach, G. Saucy, A. Stempel, *ibid.*, **27**, 3788 (1962); A. Stempel and W. Landgraf, *ibid.*, **27**, 4675 (1962).

11) L. H. Sternbach and E. Reeder, *ibid.*, **26**, 4936 (1961).

12) G. A. Archer and L. H. Sternbach, *ibid.*, **29**, 231 (1964).

13) L. H. Sternabch, E. Reeder, O. Keller, and W. Metlesics, *ibid.*, **26**, 4488 (1961); K. Meguro, H. Tawada, and Y. Kuwada, *J. Pharm. Soc. Japan*, **93**, 1253 (1973).

14) K. E. Schulte, J. Reisch, and U. Stoess, *Angew. Chem. Int. Ed. Engl.*, **4**, 1081 (1965); *Idem*, *Arch. Pharmaz.*, **305**, 523 (1972).

15) a) M. Mazharuddin and G. Thyagarajan, *Tetrahedron Lett.*, **1971**, 307; b) O. Aki and Y. Nakagawa, *Chem. Pharm. Bull.* (Tokyo), **20**, 1325 (1972).

16) H. Bredereck, R. Gompper, H. G. v. Schuh, and G. Theilig, "Newer Methods of Preparative Organic Chemistry," Vol. III, ed. by W. Foerst, translated by H. Birnbaum, Academic Press, New York and London (1964), p. 270.

17) Reaction conditions described in Ref. 15b were employed.

18) C. E. Loader and C. J. Timmons, *J. Chem. Soc., C*, **1967**, 1343.

19) *N*-Monosubstituted formamide chloride is prone to dimerization; *cf.* W. Jentzsch, *Chem. Ber.*, **97**, 1361 (1964).

20) M. Ochiai, R. Marumoto, S. Kobayashi, H. Shimadzu, and K. Morita, *Tetrahedron*, **24**, 5731 (1968).

21) The yields of adenine were less than 5% in all cases reported in Ref. 5 (unpublished).

22) M. T. Leplawy, D. S. Jones, G. W. Kenner, and R. C. Sheppard, *Tetrahedron*, **11**, 39 (1960).

23) T. G. Miller, *J. Org. Chem.*, **31**, 3178 (1966).

24) C. S. Hanes and F. A. Isherwood, *Nature*, **164**, 1107 (1949).

Synthetic Photochemistry. VI.[1] The Cycloaddition of Methyl Acetopyruvate with Cyclopentadiene: A Concomitant Formation of $(4+2)\pi$ and $(2+2)\pi$ Adducts

Hitoshi TAKESHITA, Akira MORI, and Yoshinori TOYONAGA

Research Institute of Industrial Science, Kyushu University, Hakozaki, Fukuoka 812

(Received July 12, 1974)

The irradiation of methyl acetopyruvate in cyclopentadiene using a high-pressure mercury lamp yielded two $(4+2)\pi$ and two $(2+2)\pi$ adducts. These products were inert under the photochemical conditions.

Since the observation of stereospecific $(6+2)\pi$ and $(4+2)\pi$ cycloadditions together with an ene reaction in the UV-light induced reaction of methyl acetopyruvate (I) with tropylidene (II),[2] we have been interested in reaction of I with cyclic diene systems in order to examine the general reactions of I with conjugated olefins. The results obtained with cyclopentadiene (III) are herein described.

When I and III were irradiated in the usual manner, cycloadditions proceeded rapidly to give four products, IV (25.0), V (30.0), VI (8.9), and VII (13.7%) together with some amounts of a cyclopentadiene-dimer. Isolation of the products was achieved by fractional recrystallization and by means of preparative chromatographic techniques. One of the photo-products, IV easily crystallized out from the reaction mixture and its IR (ν: 3380, 1738, and 1695 cm^{-1}) and NMR [δ: 1.69 (H_{7a}, dq, J=9.0, 1.7 Hz), 2.15 (H_{7a}, br, d, J=9.0 Hz), 2.19 (3H, s), 2.85 (H_1, br), 3.10 (H_4 and H_6, overlapping, br. d, J=1.7 Hz), 3.79 (3H, s), 3.84 (OH, s), 5.99 (H_2, ddd, J=5.5, 3.0, 0.8 Hz) and 6.32 (H_3, ddd, J=5.5, 2.8, 0.8 Hz)] spectra suggested that it was a norbornene derivative, a $(4+2)\pi$ adduct, since the splitting patterns of the olefinic protons were symmetrical, and since the presence of an aldol group was certain. In addition, the following observations provided further evidence for its structure: An irradiation of IV under the formation conditions caused no change, resulting in its complete recovery, but when IV was heated at 160 °C for 30 min, I was regenerated by a *retro*-Diels-Alder reaction. The catalytic reduction of IV gave a dihydro-derivative (VIII), in whose NMR spectrum the H_6-signal had $J_{6,7}$=2 Hz. Therefore, VIII and IV have an *endo*-H_6. When VIII was reduced by sodium borohydride at room temperature, an epimeric mixture of 1,3-glycols (IX and X) was produced. However the same reduction at 0 °C afforded only IX. An oily formal (XI) was obtained from IX by the reaction of dimethyl formal in the presence of a trace amount of *p*-toluenesulfonic acid and subsequent silica-gel column chromatography. In the NMR spectrum, the *gem*-protons of the formal group of XI appeared as a pair of AB-type doublets, and the magnitude of *gem*-coupling constant coincided well with that of a strain-free 1,3-dioxane system.[3] Therefore, the *cis*-relationship for the hydroxyl group and 1′-hydroxyethyl group of IX was verified, and the whole stereochemistry of IV was established as depicted.

The product VII also exhibited symmetrical olefinic proton signals in its NMR spectrum [δ: 1.5—1.8 (2H, m), 2.10 (3H, s), 2.50 (1H, m), 3.10 (1H, m), 3.61 (1H, d, J=3 Hz), 3.81 (3H, s), 4.32 (1H, s, OH), 6.14 (1H, dd, J=6, 3 Hz), 6.46 (1H, dd, J=6, 3 Hz)]. In VII and its dihydro-derivative (XII), NMR splittings indicated that H_6 had an *exo*-orientation. The rest of the sterochemistry was deduced by a similar sequence to that for IV, *i.e.*, the formation of the strain-free formal (XIV) from XIII, a stereoselective sodium borohydride reduction product of XII.[4] The structure of VII is therefore as shown.

It is interesting to note that the structures of IV and VII suggest that the $(2+4)\pi$ photocycloaddition is non-stereo-selective, and the configurations of IV and VII are determined by the original geometry of I in the ground state.[5]

In this respect, there have been a couple of examples of the photo-cycloaddition of III and butadiene with α-acetoxyacrylonitrile;[6] the photochemical step of this reaction was however non-stereoselective and interpreted in terms of stepwise cyclization *via* a stable 1,4-biradical intermediate. The present results show some contrasts with this, and furthermore contrasts with the results of our previous study on the cycloaddition of I and II. Since the $(4+2)\pi$ addition in this case was stereospecific (expressed as $({}_s4+{}_s2)\pi$), but non-stereoselective, forming the *exo*- and *endo*-adducts, while the $(4+2)\pi$ addition in the case of I and II was also stereospecific (as $({}_s4+{}_s2)\pi$), but stereoselective with regard to the *exo-endo*-relationship, and non-regiospecific, giving a pair of double-bond isomers.[2]

V and VI were both shown to be $(2+2)\pi$ adducts; they gave the same dihydro-derivative (XV) which was identical with the adduct of cyclopentene and I. XV was dehydrated to an α,β-unsaturated keto-ester (XVI),[7] which was characterized by formation of a crystalline DNP. V and VI were separated by silica-gel column chromatography, but V was isomerized under mild conditions to VI. The NMR spectrum of VI revealed a characteristically broadened signal at δ: 7.08 (1H, m) which was ascribable to an α,β-unsaturated glyoxaloyl group (ν: 1680, 1700, 1740, and 1620 (strong) cm^{-1}). Thus, the structures of VI, an artifact formed during the work up, and V were deduced as follows.

Obviously, a merit of the photochemical addition reaction for synthetic purposes is an easy C–C bond formation at an unactivated C=C group, but an oridnary cycloaddition affords a cyclobutane derivative which sometimes reduces the usefulness of the process unless the transformation of the ring system can be achieved.

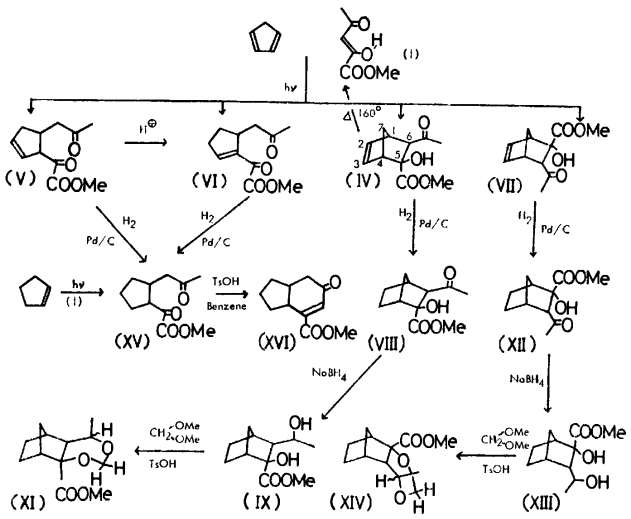

In this regard, the present results show that the utility of the photocycloaddition reaction may be extended to systems that are usually obtained by Diels-Alder-type reactions, and that the skeletal transformation of the adducts can be performed as having suitable functional groups.

In the present experiment, we could not detect an ene product, whose formation was a predominant process in the case of I and II.[2] This sharp contrast could be a reflection of a difference in chemical properties of the allylic methylenes, *i.e.*, the methylene hydrogens of III, being more acidic than that of II, would be unfavorable for abstraction by an electron-deficient n,π^*-excited carbonyl of I. Finally, a facile reaction with a cyclic diene such as those frequently used as triplet quenchers,[6] would be of theoretical interest in connection with the stereoelectronic factor of product formation.

Experimental

The NMR spectra were measured in deuteriochloroform solutions with either a Hitachi R-20 Model (60 MHz) or a JEOL PS-100 Model (100 MHz) spectrometer. Some of the NMDR experiments were carried out on a Varian HA-100 Model spectrometer owned by the Department of Chemistry, Tohoku University. The IR spectra were measured as a liquid film or in a KBr disk. Elemental analyses were performed by Mr. A. Abe, Division of Elemental Analyses, Kyushu University, stationed in the Department of Chemistry.

Photochemical Reaction of Methyl Acetopyruwate (I) with Cyclopentadiene (III). Isolation of the endo-*(4+2)π Adduct(IV) from the Product Mixture*: I (3.0 g) was dissolved in III (50 ml) and internally irradiated by a 450 W high-pressure mercury lamp for 4 hr. Then, the excess III was evaporated *in vacuo*, and the residue (16.7 g) was briefly passed through a silica-gel column to separate a hydrocarbon fraction, mainly a photodimer of III (13.7 g), and the product mixture, from which a crystalline mass, IV (680 mg), was separated out by refrigeration. Specimen of IV for analysis, colorless needles, mp 95—96 °C, was obtained by recrystallization from benzene–*n*-hexane. (Found: C, 62.80; H, 6.70%. Calcd for $C_{11}H_{14}O_4$: C, 62.84; H, 6.71%. *m/e*: 210 (M^+)).

Chromatographic Separation of the Mixture. Isolation of the (2+2)π Adducts, V and VI, and Enrichment of the exo-*(4+2)π Adduct (VII)*: The combined filtrate of IV was then fractionated by a silica-gel column chromatography to give V (a colorless liquid, 1.31 g), VI (a colorless liquid, 390 mg), an additional amount of IV (214 mg) and VII (a colorless liquid, 800 mg, a mixture with 25% of IV). V and VI were extremely sensitive to air, and easily polymerized.[8]

Catalytic Hydrogenation of IV. Formation of VIII: A methanol solution of IV (100 mg) was reduced in the presence of 5% palladium charcoal (200 mg) to give a colorless crystals (VIII), mp 98—99.5 °C (from benzene-*n*-hexane). (Found: C, 62.04; H, 7.55%. Calcd for $C_{11}H_{16}O_4$: C, 62.25; H, 7.60%. δ: 1.0—1.7 (6H, m), 2.10 (3H, s), 2.0—2.3 (1H, m), 3.20 (1H, d, J=2 Hz), 3.2—3.8 (1H, br., OH), and 3.80 (3H, s). ν: 3380, 1735, and 1708 cm^{-1}).

The DNP of VIII was obtained as yellow needles. Mp 195—198 °C (Found: C, 52.17; H, 5.10; N, 14.22%. Calcd for $C_{17}H_{20}O_7N_4$: C, 52.04; H, 5.14; N, 14.28%. δ: 1.97 (3H, s), 3.83 (3H, s), 7.80 (1H, d, J=9.5 Hz), 8.17 (1H, dd, J=9.5, 2.5 Hz), 8.95 (1H, d, J=2.5 Hz), and 10.85 (1H, br.s, NH). λ_{max}^{MeOH}: 363 nm(ε: 20800). ν: 3450, 3320, 1720, 1620, and 1598 cm^{-1}).

Sodium Borohydride Reduction of VIII. Isolation of a Dihydroxy-Ester (IX): a) VIII (48.3 mg) was dissolved in methanol (2 ml) and reduced with sodium borohydride (7.2 mg) for 3 hr at room temperature. The mixture was then acidified with hydrochloric acid and extracted by ether. A colorless oil (38 mg), initially obtained by cold-finger distillation, was gradually crystallized to give colorless needles (IX), mp 98—99 °C (from *n*-hexane). (Found: C, 61.48; H, 8.45%. Calcd for $C_{11}H_{18}O_4$: C, 61.66; H, 8.47%. δ: 1.23 (3H, d, J=6.5 Hz), 1.0—1.6 (6H, m), 2.0—2.5 (3H, m), 3.40 (2H, s, OH), 3.78 (3H, s), and 4.12 (1H, qd, J= 6.5, 3.3 Hz). ν: 3370 and 1745 cm^{-1}). The filtrate showed the presence of an epimeric glycol, X (δ: 1.26 (3H, d, J=6.5 Hz) and 3.78 (3H, s)), but no further characterization was attempted.

b) VIII (343 mg) was dissolved in cold methanol (4 ml) and reduced by sodium borohydride (22.1 mg) overnight at 0 °C. Then, the mixture was washed with dilute hydrochloric acid and extracted with benzene. Crystalline IX (128 mg) was obtained by silica-gel column chromatography in order to remove the recovered VIII. An absence of X in the mixture was assured by NMR spectral analysis.

Formation of a Formal-Derivative (XI) from IX: IX (28 mg) was dissolved in dimethyl formal (0.5 ml) and benzene (0.5 ml) in the presence of a catalytic amount of *p*-toluenesulfonic acid and refluxed for 3 hr. The mixture was then washed with water and extracted with benzene. A colorless liquid (23 mg) was obtained by cold-finger distillation of the extract. (Found: C, 63.77; H, 8.13%. Calcd for $C_{12}H_{18}O_4$: C, 63.70; H, 8.02%. δ: 1.28 (3H, d, J=7 Hz), 1.0—1.7 (5H, m), 1.9—2.5 (4H, m), 3.80 (3H, s), 3.7—4.1 (1H, m), 4.58 (1H, d, J=6 Hz), and 4.95 (1H, d, J=6 Hz). ν: 1732 cm^{-1}).

Catalytic Reduction of VII. Formation of a Dihydro-Derivative (XII): VII (170 mg, containing *ca.* 25% of IV) was dissolved in methanol (5 ml) and reduced by 5% palladium charcoal (300 mg) for 50 min, then the usual work up of the mixture afforded a colorless oil (124 mg) which appeared as a single peak on a gas-liquid chromatogram, but the NMR analysis indicated the presence of the dihydro-derivative (XII) and the previously characterized VIII in the same ratio as IV to VII in the starting material. (δ: 1.0—1.8 (6H, m), 2.15 (3H, s), 2.4—2.8 (2H, m), 3.25 (1H, br.d, J=3 Hz), 3.77 (3H, s), and 5.65 (1H, br., OH)).

Sodium Borohydride Reduction of XII: XII (125 mg, contaminated by *ca.* 25% VIII) was dissolved in methanol

(5 ml) and reduced with sodium borohydride (26.8 mg) for 5 hr. Then the mixture was acidified by dilute hydrochloric acid and extracted with benzene. The extract was subsequently passed through a silica-gel column to separate the desired glycol (XIII) from the less polar fraction as a colorless liquid (51 mg). (Found: C, 61.94; H, 8.45%. Calcd for $C_{11}H_{18}O_4$: C, 61.66; H, 8.47%. δ: 1.17 (3H, d, J=6.2 Hz), 1.0—2.6 (9H, m), 2.87 (2H, br. s, OH), 3.83 (3H, s), and 4.03 (1H, dq, J=7.5, 6.2 Hz). ν: 3525 and 1730 cm^{-1}).

Formation of a Formal-Derivative (XIV) from XIII: XIII (35 mg) was dissolved in dimethyl formal (0.5 ml) and benzene (0.5 ml) with a small amount of *p*-toluenesulfonic acid and heated under reflux for 2 hr. The mixture was then washed with water and extracted with ether to give a colorless liquid (30 mg) which showed a single peak on a gas-liquid chromatogram (Found: C, 63.57; H, 8.05%. Calcd for $C_{12}H_{18}O_4$: C, 63.70; H, 8.02%. δ: 1.33 (3H, d, J=7 Hz), 1.2—4.0 (10H, m), 3.79 (3H, s), 4.75 (1H, d, J=6.2 Hz), and 5.03 (1H, d, J=6.2 Hz). ν: 1740 cm^{-1}).

Isomerization of V into VI: A benzene solution of V (30 mg) was held on a silica-gel column for 48 hr, and subsequently eluted with benzene–ether (10: 1) mixture. The NMR spectrum showed that consisted solely of VI.

Catalytic Hydrogenation of V. Formation of a Dihydro-Derivative (XV): V (37.6 mg) was dissolved in methanol (2 ml) and reduced by 5% palladium charcoal (75 mg) to give XV as a faint yellow liquid (21.1 mg) (Found: C, 62.20; H, 7.63%. Calcd for $C_{11}H_{16}O_4$: C, 62.25; H, 7.60%. δ: 1.0—3.0 (10H, m), 2.02 (3H, s), and 3.80 (3H, s). ν: 1735 cm^{-1} (very strong)).

Catalytic Hydrogenation of VI. Formation of XV: VI (37.4 mg) was similarly hydrogenated to give XV (23 mg) which had an NMR spectrum identical with the previous sample of XV.

Photochemical Reaction of Cyclopentene with I. Formation of XV: I (503 mg) was dissolved in cyclopentene (5 ml) and externally irradiated by means of a high-pressure mercury lamp through a Pyrex glass filter for 8 hr. The excess olefin was then evaporated and the residue separated by silica-gel column chromatography. After elution of a hydrocarbon fraction (a cyclopentene-dimer), a pale yellow fraction (330 mg) was collected and purified by cold-finger distillation to give a faint yellow liquid which was identical with authentic XV obtained from V.

Acid-Induced Dehydration of XV. Formation of the α,β-Unsaturated Keto-Ester (XVI): XV (34 mg) was dissolved in benzene (5 ml) containing a small amount of *p*-toluenesulfonic acid and refluxed for 3 hr. The solution was washed with water and extracted with benzene. Removal of the solvent afforded a pale yellow residue which was further purified by cold-finger distillation to give a pale yellow liquid (27 mg). (*m/e*: 194 (M^+), 166, 163, 162, 152, 135 (base), 134, 107, 93, 91, 80, 79, 78, 67, 65, and 59. λ_{max}^{MeOH}: 209 nm(ε: 3640), 241 (5460). δ: 1.0—3.0 (10H, m), 3.76 (3H, s), and 6.50 (1H, br. s). ν: 1730 and 1680 cm^{-1}).

The DNP of XVI was obtained as bright-yellow needles. Mp 173—174 °C (Found: C, 54.16; H, 4.90; N, 14.83%. Calcd for $C_{17}H_{18}O_6N_4$: C, 54.54; H, 4.85; N, 14.97%. $\lambda_{max}^{CHCl_3}$: 380 nm(ε: 28800).

Further Irradiation of IV: IV (30 mg) was dissolved in deuteriochloroform and externally irradiated under its formation conditions. After 8 hr, no reaction has been detected by NMR spectral analysis.

Attempted Thermal Reaction of I and III: I (32.7 mg) and III (2 ml) were kept at room temperature for 4 hr, but no detectable reaction occurred other than slight dimerization of III. Then, the same mixture was heated on a steam bath for 1 hr, but evaporation of the olefin left unreacted I and the dimer of III.

Pyrolysis of IV: a) IV (31.3 mg) was dissolved in benzene (0.5 ml) and heated for 1 hr at 80 °C. IV was recovered quantitatively.

b) IV (33.4 mg) was dissolved in dichlorobenzene (0.4 ml) and heated for an hour at 160 °C. Silica-gel column chromatography of the mixture afforded a hydrocarbon fraction (oligomeric mixture of III) and colorless needles (15 mg) which were found to be I by mixed-mp, NMR, and IR comparisons.

Further Irradiation of V: V (35 mg) was dissolved in deuteriochloroform and externally irradiated under its formation conditions for 5 hr. NMR spectral analysis revealed no reaction.

Further Irradiation of VII. VII (60 mg, containing *ca.* 25% of IV) was dissolved in deuteriochloroform and irradiated under the formation conditions. No detectable reaction was observed after 4 hr.

The authors wish to thank Prof. S. Itô, Dr. Y. Fujise and Mr. K. Sasaki of Tohoku University, for help in carrying out laborious NMDR experiments on IV. H. T. and A. M. are also grateful for financial support from the Ministry of Education.

References

1) Part V: H. Takeshita and A. Mori, This Bulletin, **47**, 2901 (1974).

2) H. Takeshita, A. Mori, and S. Itô, *ibid.*, **47**, 1767 (1974).

3) M. Anteunis, G. Swaelens, F. Anteunis-de Ketelaere, and P. Dirinck, *Bull. Soc. Chim. Belg.*, **80**, 409 (1971).

4) According to the NMR analysis, the diastereomeric carbinol of XIII was not formed. This might be a reflection of the *endo*-configuration for the acetyl-group of XII.

5) We thank a referee for his comment on the possible isomerization of an aldol to another aldol *via* ring-opened diketo-ester derivative under our reaction conditions resulting in the exclusive formation of the thermodynamically stable product, IV or VII. However, we think that this possibility can be eliminated since (a) IV and other (4+2)π and (6+2)π adducts of I have showed no tendency to cleave their aldol linkage by treatment with toluenesulfonic acid,[2] (b) the recyclization of such a diketo-ester to a strained norbornene frame-work with adjacent bulky substituents under our conditions seems improbable, and (c) no isomeric aldol has been detected during the pyrolysis of IV (NMR and glc analyses).

6) *e.g.*, W. L. Dilling and R. D. Kroening, *Tetrahedron Lett.*, **1968**, 5601; **1968**, 5101.

7) XVI was free from the stereoisomers judging from its NMR spectrum (see Experimental). The configuration of XVI was ascribed as *cis*-fused.

8) Correct figures for elemental analyses were not obtained despite an intensive effort.

N-Halogen Compounds of Cyanamide Derivatives. V.[1] The Preparation and Reaction of Δ^4-1,2,4-Thiadiazolines

Toshio FUCHIGAMI and Keijiro ODO

Faculty of Engineering, Tokyo Institute of Technology, Meguro-ku, Tokyo 152

(Received August 15, 1974)

Five new Δ^4-1,2,4-thiadiazolines (TDZ), IIa,b, IIIa,b, and IV, were easily prepared by the reaction of potassium methyl cyanoiminodithiocarbonate (I) with *N*-chloro compounds of *O*-alkylisoureas, guanidines, and guanylurethane. 2-Methoxyimidoyl-3-imino-5-methylthio-TDZ (IIa), with a reactive imidoether group, was converted into the 2-carbamoyl-TDZ derivative (V) by treatment with excess dry hydrogen chloride. The reaction of IIa with aliphatic amines gave 2-amidino-TDZ derivatives (IIIc—e) in good yields in the presence of both free amines and amine hydrochlorides (molar ratio, 2: 1). The mechanism of this amidination was discussed.

In our previous work,[2] it was found that 2-imidoyl-3-imino-5-methylthio-Δ^4-1,2,4-thiadiazolines (VI) could easily be prepared by the reaction of *N*-chloroamidines with I and that VI was readily cleft by reduction at the N–S link and recyclized to two kinds of *s*-triazines.

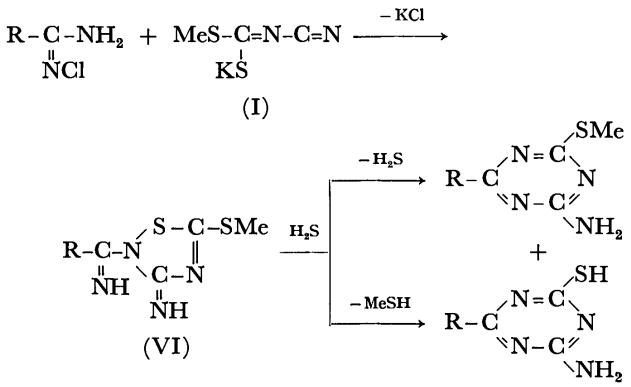

Scheme 1.

In this paper, we wish to report on the synthesis of new TDZ (IIa,b, IIIa,b, and IV) using *N*-chloro compounds of cyanamide derivatives (*O*-alkylisoureas, guanidines, and guanylurethane) and their properties, together with the reaction between IIa and amines to give 2-amidino-TDZ (IIIc—e).

Results and Discussion

Preparation and Reaction of 2-Alkoxyimidoyl-3-imino-5-methylthio-TDZ (IIa,b). *N*-Chloro-*O*-alkylisoureas readily reacted with I in methylene chloride to form IIa and b. The yield of IIa increased considerably when the solvent was acetonitrile, which is more polar than methylene chloride, while that of IIb did not. The same effect was also observed in the case of *N*-chloroguanidine (Table 3).

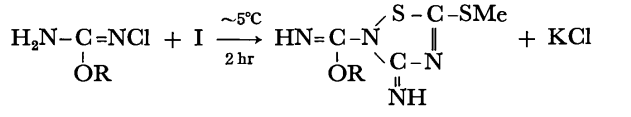

(II)

Table 1. Preparation of TDZ

R	Solvent	Product	Yield (%)
Me	CH_2Cl_2	IIa	63
	MeCN		79
Et	MeCN	IIb	41

The structures of IIa and b were confirmed by means of elemental analysis and by a study of the IR spectrum. Compounds IIa and b can both be regarded as *N*,*N*-disubstituted-*O*-alkylisourea with a reactive imidoether group. By the treatment of IIa with excess dry hydrogen chloride in methanol, IIa was further converted into the 2-carbamoyl-TDZ derivative (V).

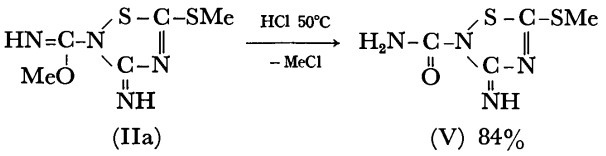

Scheme 2.

The reaction of IIa with amines was likewise examined. The reaction of IIa with amines in ethanol under reflux gave 2-amidino-3-imino-5-methylthio-TDZ (IIIc—e). It was found that IIIc—e were obtained as free bases in good yields in the presence of both free amines and amine hydrochlorides (molar ratio,

Table 2. Reaction of IIa with amines

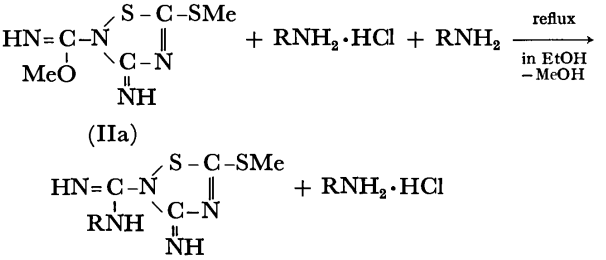

(IIIc—e)

R	Free amine[a]	Amine salt[a]	R. Time (hr)	Product (Yield %)
Me	2	1	4.0	IIIc (80)
Et	1	0	4.0	(0)
	0	1	4.0	IIId (0)
	2	1	4.0	(97)
Bzl	1	0	2.5	IIIe (0)
	2	1	3.0	(75)
Ph	2	1	3.0	V (80)

a) Molar ratio.

2: 1). It is notable that no substitution reaction occurred in the absence of either free amine or amine hydrochloride. In the case of such a weak base as aniline, no substitution reaction occurred and V was obtained. The basicity of IIa seems to be stronger than that of aniline, so IIa may take hydrogen chloride from aniline hydrochloride to form V, thus evolving methyl chloride.

As is shown in Table 2, the methylthio group of IIa was found not to be reactive.

The mechanism of this amidination, judging from the above results, is as follows. Free amine attacks the protonated imidoether group of IIa to form a tetrahedral addition intermediate (**A**)—Step (**a**). Then, the elimination of methanol and a proton from A gives IIIc—e as a free base—Step (**b**). The first step and the second step seem to be subjected to acid catalysis (HCl) and base catalysis (free amine) respectively

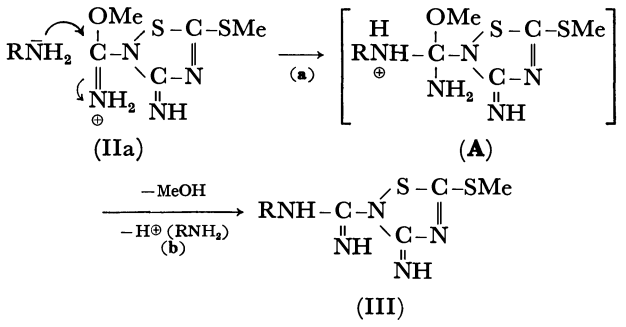

Scheme 3.

Table 3. Preparation of TDZ

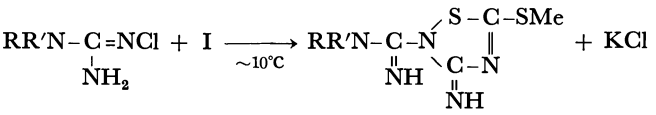

(III)

R	R′	Solvent	R. Time (hr)	Product	Yield (%)
H	H	CH_2Cl_2	2	IIIa	55
		MeCN	1		91
⬡		MeCN	1	IIIb	44

(Scheme 3).

Preparation of Other TDZ. 2-Amidino-TDZ (IIIa,b). In a manner similar to that described above, *N*-chloroguanidines and I gave IIIa, and b. The yield of IIIa in acetonitrile increased considerably, as had been observed in the case of IIa. The low yield of IIIb may be attributable to the steric hyndrance of the piperidyl group. Since IIIa is too weak a base, IIIa could not be subjected to benzoylation by benzoyl chloride.

2-N-Carbethoxyamidino-TDZ (IV). In a similar manner, *N*-chloroguanylurethane and I gave IV in a good yield (85%). Its NMR spectrum showed three singlet signals, at δ 2.70 (SMe), 3.67 (OMe), and 8.50 (NH, broad). In the mass spectrum, the parent peak, *m/e* 247, and other fragment peaks appeared appropriately. It would be expected that the elimination of

Table 4. Physical properties and analytical data of Δ^4-1,2,4-thiadiazolines

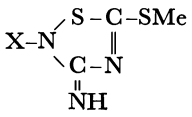

Compoud No.	X	Free base Mp (°C)	Anal (Calcd %) C	H	N	IR (KBr) (cm^{-1}) C=N	C=O	Picrate Mp (°C)	Anal (Calcd %) C	H	N
IIa	MeO–C(=NH)–	112—115	29.43	3.96	27.55	1650	—	143—145	29.78	2.74	22.96
			(29.40)	(3.95)	(27.43)	1610	—		(30.49)	(2.56)	(22.62)
IIb	EtO–C(=NH)–	108—109	33.11	4.56	25.70	1640	—	184	32.20	2.74	21.92
			(33.01)	(4.62)	(25.66)	1610			(32.22)	(2.93)	(21.91)
IIIa	H_2N–C(=NH)–	225—228	25.55	3.72	37.08	1660	—	230	28.78	2.41	27.14
			(25.39)	(3.73)	(37.00)	1620		(Dp)	(28.71)	(2.41)	(26.78)
IIIb	N–C(=NH)–	139	42.37	5.98	27.13	1630	—	179—180	37.02	3.78	32.94
			(42.00)	(5.89)	(27.21)				(37.03)	(3.73)	(23.03)
IIIc	MeHN–N(=NH)–	183—184	29.10	4.65	34.40	1620	—	196—197	30.18	2.81	25.90
			(29.54)	(4.46)	(34.45)				(30.56)	(2.80)	(25.91)
IIId	EtHN–C(=NH)–	165—166	33.36	5.11	31.89	1620	—	170—172	32.53	3.07	24.91
			(33.16)	(5.10)	(32.23)				(32.29)	(3.16)	(25.10)
IIIe	BzlNH–C(=NH)–	167—169	47.10	4.71	25.06	1620	—	148—153	40.10	3.03	22.04
			(47.29)	(4.69)	(25.07)			(Dp)	(40.16)	(3.17)	(22.06)
IV	MeCNH–C(=O)–NH–	190	28.80	3.63	28.57	1640	1720	—	—	—	—
		(Dp)	(29.10)	(3.67)	(28.32)	1620					
V	NH_2–C(=O)–	237—238	25.60	3.15	29.34	1670		—	—	—	—
			(25.25)	(3.18)	(29.45)						

methanol from IV would give rise to the formation of a condensed ring. However, no product due to such a condensation was formed, and decomposition only took place when IV was heated gradually at 190 °C.

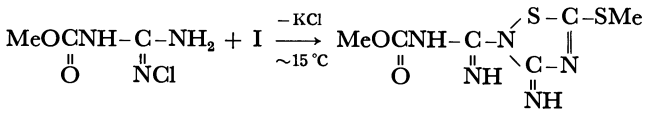

(IV) 80%

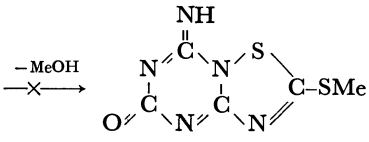

Scheme 4.

The physical properties and analytical data of the products are summarized in Table 4.

Compounds IIa, IIIa, and IV display approximately similar UV spectra (Fig. 1), perhaps because of their structural resemblance.[3]

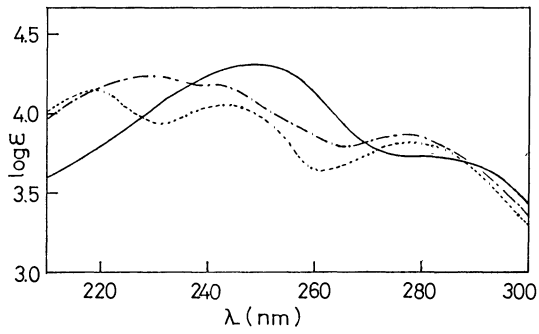

Fig. 1. Ultraviolet absorption of TDZ in water.
——: IIa, ——: IIIa, ----: V.

Experimental

The melting points are uncorrected. The IR spectra were taken with a Hitachi EPI-S 2 spectrophotometer. The NMR spectrum was recorded at 90 MHz in DMSO-d_6, with TMS as the internal standard, using a Hitachi R-22 spectrometer. The mass spectrum was taken with a JEOL JMS-D100 mass spectrometer. The UV spectra were taken with a Hitachi 624 spectrophotometer.

N-Chloro Compounds. *N*-Chloro-*O*-methylisourea,[4] *N*-chloro-*O*-ethylisourea,[4] *N*-chloroguanidine,[5] *N*-chloro-*N'*, *N'*-pentamethyleneguanidine,[6] and *N*-chloroguanylurethane were prepared by a previously described method.[7] *N*-chloroguanylurethane; yield, 80%; dp 124—125 °C; active chlorine 22.40% (calcd for $C_3H_6N_3O_2Cl$ 23.40%).

Potassium methyl cyanoiminodithiocarbonate (I) was prepared according to the method of Timmons *et al.*[8]

2-Methoxyimidoyl-3-imino-5-methylthio-Δ⁴-1,2,4-thiadiazoline (IIa). To a stirred mixture of I (10.20 g, 60 mmol) and methylene chloride (55 ml), we added a solution of *N*-chloro-*O*-methylisourea (5.97 g, 55 mmol) in methylene chloride (45 ml). The temperature was maintained below 5 °C during the reaction. After about 2 hr of continued stirring, the mixture was refluxed for 0.3 hr. After the precipitated salt had been removed by filtration, the filtrate was concentrated. Washing the residue with ether afforded IIa (7.10 g, 63%, mp 110—112 °C). Recrystallization from methanol gave a pure product; mp 112—115 °C. The above reaction, when carried out in acetonitrile by a similar method, gave IIa in a 79% yield.

2-Ethoxyimidoyl-3-imino-5-methylthio-Δ⁴-1,2,4-thiadiazoline (IIb). Using the same procedure, the crude product of IIb was obtained as an oily material from *N*-chloro-*O*-ethylisourea. The oily material was crystallized from aqueous methanol, and the yield was 41% (mp 99—100 °C). Recrystallization from aqueous methanol yielded an analytical sample; mp 108—109 °C.

2-Carbamoyl-3-imino-5-methylthio-Δ⁴-1,2,4-thiadiazoline (V). A slow stream of dry hydrogen chloride was passed through a solution of IIa (2.04 g, 10 mmol) in methanol at 50 °C for 2 hr. The white crystalline precipitate (V, 1.34 g) was collected by filtration, and the filtrate was concentrated. Washing the residue with a small amount of methanol or acetone gave V (0.25 g). The total yield was 84%; dp 237 °C. Recrystallization from DMF–methanol gave pure V; dp 237—238 °C.

Reaction of IIa with Amines. *2-N-Methylamidino-3-imino-5-methylthio-Δ⁴-1,2,4-thiadiazoline (IIIc)*: A solution of IIa (2.04 g, 10 mmol), 40% aqueous methylamine (20 mmol) and methylamine hydrochloride (0.68 g, 10 mmol) in ethanol (25 ml) was refluxed for 4 hr. After cooling, a crystalline precipitate was collected by filtration (IIIc, 1.45 g; mp 170—174 °C). After the concentration of the filtrate, the washing of the residue with water afforded IIIc (0.20 g, mp 170—174 °C). The total yield was 81%. Recrystallization from methanol gave pure IIIc; mp 183—184 °C.

Similarly, reactions with other amines were carried out. The products and reaction conditions are given in Table 2.

2-Amidino-3-imino-5-methylthio-Δ⁴-1,2,4-thiadiazoline (IIIa). To a stirred suspension of I (2.38 g, 14 mmol) in acetonitrile (30 ml), we gradually added *N*-chloroguanidine (1.31 g, 14 mmol). The temperature was maintained below 10 °C during the reaction. After about 1 hr of continued stirring, an insoluble matter (IIIa and KCl) was separated by filtration. Washing the solid with water (to remove KCl) and acetone afforded IIIa (2.41 g; 91%; dp 214—215 °C). Recrystallization from DMF gave pure IIIa; dp 225—228 °C. The above reaction, undertaken in methylene chloride in a similar manner, gave IIIa in a 55% yield.

2,N,N-Pentamethyleneamidino-3-imino-4-methylthio-Δ⁴-1,2,4-thiadiazoline (IIIb). To a stirred solution of I (1.19 g, 7 mmol) in acetonitrile (8 ml), we added a solution of *N*-chloro-*N'*,*N'*-pentamethyleneguanidine (1.13 g, 7 mmol) in acetonitrile (10 ml). After 1 hr of continued stirring below 10 °C, an insoluble matter was separated by filtration. The oily material obtained by concentrating the filtrate was dissolved in 2 M hydrochloric acid and (5 ml) and methanol (5 ml). After stirring the solution for 0.5 hr at room temperature, IIIb was precipitated by making the solution neutral (0.80 g; 44%; mp 130—132 °C). Recrystallization from methanol gave pure IIIb; mp 139 °C.

2-N-Carbethoxyamidino-3-imino-5-methylthio-Δ⁴-1,2,4-thiadiazoline (IV). To a stirred suspension of I (2.72 g, 16 mmol) in acetonitrile we gradually added *N*-chloroguanylurethane (2.42 g, 16 mmol), the temperature being kept below 15 °C. After about 1 hr of continued stirring, the mixture was refluxed for 0.1 hr. After the insoluble matter had then been separated by filtration, washing with water and ether afforded IV (3.30 g; 85%; dp 190 °C). Recrystallization from ethyl acetate–DMF (2: 1) gave pure IV; dp 190 °C.

We wish to thank Dr. Ichikawa of our laboratory for his invaluable discussions.

References

1) Part 96 of "Studies of Cyanamide Derivatives."
2) T. Fuchigami and K. Odo, *Chem. Lett.*, **1973**, 917.
3) M. Takimoto, *Nippon Kagaku Zasshi*, **85**, 159 (1964).
4) J. Goerdeler and F. Bechlars, *Chem. Ber.*, **88**, 848 (1955).
5) A. Heesing, G. Imsieke, G. Maleck, R. Reppmoller, and H. Schulze, *ibid.*, **103**, 547 (1970).
6) J. Goerdeler and M. Willig, *ibid.*, **88**, 1071 (1955).
7) T. Fuchigami, E. Ichikawa, and K. Odo, This Bulletin, **46**, 1765 (1973).
8) R. J. Timmons and L. S. Wittenbrook, *J. Org. Chem.*, **32**, 1566 (1967).

Syntheses of Indolo[2,3-*b*]tropones and Benzo[*b*]-1-azaazulenes from 2-Hydrazinotropones[1)]

Tetsuo NOZOE,† Je-Kyun SIN,†† Kameji YAMANE,* and Kunihide FUJIMORI*

Department of Chemistry, Faculty of Science, Tohoku University, Sendai 980

**Department of Chemistry, Faculty of Science, Shinshu University, Matsumoto 390*

(Received August 26, 1974)

The application of Fischer's indole synthesis to cyclohexanone 2-troponylhydrazone gave 1,2,3,4-tetrahydroindolo[2,3-*b*]tropone (II), which was then dehydrogenated to indolo[2,3-*b*]tropone (III). 8-, 10-Isopropyl-, and 7-bromoindolo[2,3-*b*]tropone (XIIa—c) were also obtained by a similar method. The treatment of 2-troponylhydrazones of cycloheptanone and *N*-benzylpiperidone with dilute sulfuric acid or PPA gave 2,3-pentamethylenepyrrolo[2,3-*b*]tropone (XIII) and 2-benzyl-1,2,3,4-tetrahydrocyclohept[*b*]pyrido[3,4-*d*]pyrrol-6(5H)-one (XIV) respectively. The reaction of III with phosphoryl chloride or thionyl chloride yielded 8-chlorobenzo[*b*]-1-azaazulene (XV), which was subsequently converted into a hydrazino derivative (XVI). The oxidative decomposition of XVI with copper sulfate in acetic acid afforded benzo[*b*]-1-azaazulene (XVII).

Several methods have been reported for the preparation of various indolotropones(cycloheptindolones). 1,2,3,4-Tetrahydroindolo[2,3-*b*]tropone (II) obtained by the application of Fischer's indole synthesis to cyclohexanone 2-troponylhydrazone (I) was dehydrogenated to indolo[2,3-*b*]tropone (III) and then derived to benzo[*b*]-1-azaazulene (XVII).[1)] On the other hand, indolo[3,2-*f*]tropolone (VI) was obtained by the SeO_2 oxidation of the compound V produced by the same indole synthesis from cycloheptanedione monophenylhydrazone (IV),[2)] and more recently benzoindolotropone (VII) was synthesized by similar methods.[3)]

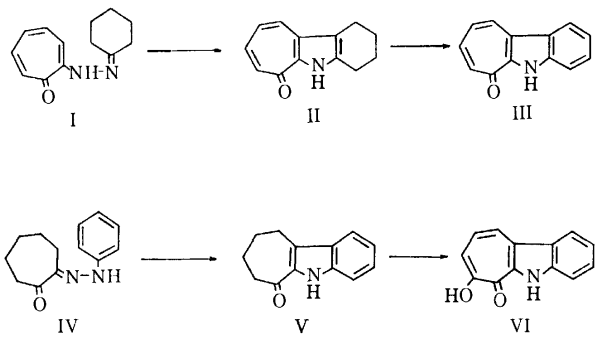

I II III

IV V VI

Furthermore, indolo[3,2-*d*]tropolone (VIII) was obtained by the thermolysis of 5-azido-4-phenyltropolone,[4)] and compound III and its isomer (IX) were isolated from the photochemical products of acridine-10-oxide.[5)]

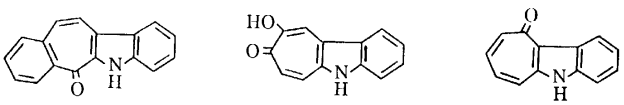

VII VIII IX

In this paper we wish to describe in full the experimental details of our earlier report,[1)] along with the results of a reexamination carried out recently.

† Present address: No. 811, 2-5-1, Kamiyoga, Setagaya-ku, Tokyo 158.

†† Present address: Faculty of Science, Korean University, 1-700, Ogawa-cho, Kodaira-shi, Tokyo 187.

Results and Discussion

The heating of cyclohexanone 2-troponylhydrazone (I) with dilute sulfuric acid afforded the ring-closure product (II), which was then converted to indolo-[2,3-*b*]tropone (III) by dehydrogenation with chloranil or DDQ.

The application of the same treatment to 4-, 6-isopropyl-, and 7-bromo-2-troponylhydrazone (Xa—c) of cyclohexanone gave compounds XIa—c, the dehydrogenation of which subsequently afforded 8-, 10-isopropyl, and 7-bromo derivatives (XIIa—c) respectively.

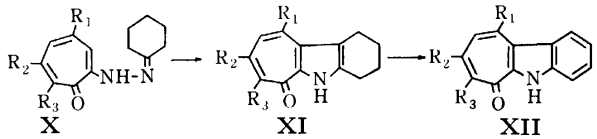

X XI XII

a: R_1=i-Pr, R_2=R_3=H
b: R_2=i-Pr, R_1=R_3=H
c: R_3=Br, R_1=R_2=H

The structures of these new compounds were discussed on the basis of the spectral data. The IR spectrum of II exhibited characteristic absorption bands at 3140 cm^{-1} (NH st.), 2920 cm^{-1} (CH_2 st.), and 1620 cm^{-1} (C=O or C=C conjugated). Compound III showed IR-absorption bands at 3195 cm^{-1} (NH st.) and 1614 cm^{-1} (C=O or C=C conjugated), but no paraffinic C–H streching absorption bands (Table 1).

The NMR spectrum of II exhibited signals corresponding to two methylene groups at δ 2.5—2.9 ppm (4H, m, $-CH_2-$) and δ 1.7—1.9 ppm (4H, m, $-CH_2-$), besides signals of tropone-ring protons at δ 6.76 ppm (1H, t, d, J=7.0, 2.0 Hz, H_9), δ 7.1—7.4 ppm (2H, m, $H_{7,8}$), and δ 7.49 ppm (1H, d,d, J=9.0, 1.0 Hz, H_{10}). In the NMR spectrum of III, the signals due to the methylene groups disappeared and those of aromatic protons were observed as a complex multiplet at δ 7.0—8.3 ppm. The IR and NMR spectra of XIa—c and XIIa—c supported the structure described above (Tables 1 and 2).

The bromo compound, XIIc, was obtained by treating III with NBS. It was quite stable even when

Table 1. IR spectra of II, III, XIa—c, and XIIa—c

Compound	NH cm^{-1}	CH cm^{-1}	C=O conjugated and others cm^{-1} (KBr)
II	3140	2920, 2860	1620, 1591, 1545, 1520, 1495
XIa	3180	2950, 2860	1613, 1582, 1549, 1515, 1490
XIb	3140	2935, 2860	1621, 1554, 1514, 1495
XIc	3200	2940, 2850	1605, 1586, 1548, 1501, 1486
III	3195		1614, 1589, 1555, 1531, 1491
XIIa	3208		1606, 1521, 1479
XIIb	3150		1608, 1555, 1525, 1485
XIIc	3215		1600, 1552, 1482

Table 2. NMR spectra of XI and XII

Compound	δ ppm in $CDCl_3$ (100 MHz)
XIa	1.30 (6H, d, J=7.0 Hz, $-CH_3$), 1.7—1.9 (4H, m, $-CH_2-$), 2.7—3.1 (4H, m, $=-CH_2-$), 3.76 (1H, sept., J=7.0, $-CH-$), 6.80 (1H, d,d, J=7.0, 2.0, H_9), 7.05 (1H, d,d, J=9.0, 2.0, H_7), 7.27 (1H, d,d, J=9.0, 7.0, H_8)
XIb	1.25 (6H, d, J=7.0, $-CH_3$), 1.7—1.9 (4H, m, $-CH_2-$), 2.6—3.0 (5H, m, $=-CH_2-$, $-CH-$), 6.73 (1H, d,d, J=7.0, 2.0, H_9), 7.12 (1H, d, J=2.0, H_7), 7.46 (1H, d,d, J=8.0, 1.0, H_{10})
XIIa	1.49 (6H, d, J=7.0, $-CH_3$), 4.18 (1H, sept., J=7.0, $-CH-$), 7.00 (1H, d,d, J=7.0, 2.0, H_9), 7.18—7.55 (4H, m, $H_{2,3,7,8}$), 7.76 (1H, d, J=6.0, H_4), 8.23 (1H, d, J=6.0, H_1)
XIIb	1.35 (6H, d, J=7.0, $-CH_3$), 2.98 (1H, sept., J=7.0, $-CH-$), 6.98 (1H, d,d, J=9.0, 2.0, H_9), 7.20—7.55 (4H, m, $H_{2,3,7,8}$), 7.73 (1H, d, J=7.0, H_4), 8.03 (1H, d, J=7.0, H_1), 8.05 (1H, d,d, J=9.0, 1.0, H_{10})

heated with conc. sulfuric acid, 85% phosphoric acid and when refluxed in methanol with sodium methylate. Thus, we were unable to derive indolo[3,2-*f*]tropolone (VI).

The 2-troponylhydrazones of cycloheptanone and *N*-benzylpiperidone were also easily converted to XIII and XIV respectively by heating with dilute sulfuric acid or PPA, but the ring closure of cyclopentanone 2-troponylhydrazone did not take place under the same conditions.

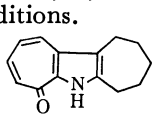

XIII

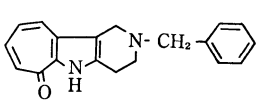

XIV

When compound III was heated with phosphoryl chloride or thionyl chloride, 8-chlorobenzo[*b*]-1-azaazulene (XV) was obtained; the original compound III had been obtained by the hydrolysis with aqueous sodium hydroxide. The reaction of XV with hydrazine hydrate gave the hydrazino derivative (XVI). The UV and visible absorption spectra suggested that XVI is probably indolo[2,3-*b*]troponehydrazone (Table 3).

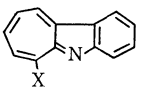

XV: X=Cl
XVII: X=H

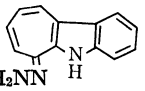

XVI

Table 3. Ultraviolet and visible absorption maxima

Compound	λ_{max} nm (log ε)
III	225 (4.40), 277 (4.40), 383 (3.81), 404 (3.89)
XVI	243 (4.39), 307 (4.06), 317 (4.06), 350 (4.17), 365 (4.08) (in CH_3OH)
XV	245 (4.41), 301 (4.51), 314 (4.62), 326 (4.55), 365 (3.78), 385 (3.79), 400 (3.38), 500 (2.74), 532 (2.74)
XVII	228 (4.34), 264 (4.14), 289 (4.54), 299 (4.56), 311 (4.62), 323 (3.50), 347 (3.66), 359 (3.70), 379 (3.68), 394 (3.22), 500 (2.58), 538 (2.57) (in cyclohexane)

By oxidative decomposition with copper sulfate in aqueous acetic acid, XVI was converted into benzo-[*b*]-1-azaazulene (XVII) as reddish-purple needles; mp 140—141 °C.

The structure was identified by a spectral comparison with an authentic sample.[2] The visible absorption spectra of XV and XVII are quite different from those of III and XVI, as is shown in Table 3.

Experimental**

All the melting points are uncorrected. The NMR spectra were obtained on a JEOL Model JMN-4H-100 spectrometer in $CDCl_3$ solution, with TMS as the internal standard.

Cyclohexanone 2-Troponylhydrazone (I). To a solution of 2-hydrazinotropone (21 g) in ethanol (210 ml), we added cyclohexanone (15 g), and the mixture was refluxed for 30 min. After cooling, the reaction mixture was diluted with water (210 ml). The separated material was collected and dried. Recrystallization from petroleum ether gave yellow needles (32 g, 96%); mp 75—76 °C. IR (KBr): 3220 (NH), 1625, and 1585 cm^{-1} (C=O or C=C conjugated). UV: $\lambda_{max}^{CH_3OH}$ 264 (log ε=4.31), 353 (4.24), and 415 (4.27) nm. Found: C, 71.92; H, 7.50; N, 13.08%. Calcd for $C_{13}H_{16}ON_2$: C, 72.19; H, 7.46; N, 12.95%.

1,2,3,4-Tetrahydroindolo[2,3-b]tropone (II). A mixture of I (30 g), water (500 ml), and conc. sulfuric acid (30 ml) was refluxed at 120 °C for 2 hr. After cooling, 30% aqueous sodium carbonate was added to adjust the pH value to 6 and then extracted with chloroform. The extract was dried over anhydrous sodium sulfate and condensed to dryness to give light yellow needles, which were subsequently recrystallized from benzene (15.8 g, 57%); mp 212—215 °C. UV: $\lambda_{max}^{CH_3OH}$ 237 (log ε=4.43), 293 (4.50), 360 (3.63), and 382 (3.65) nm. Found: C, 78.25; H, 6.40; N, 6.83%. Calcd for $C_{13}H_{13}ON$: C, 78.36; H, 6.58; N, 7.03%.

N-Benzyl Compound: Light yellow needles (from *n*-hexane); mp 136.5—137.5 °C. IR (KBr): 1628, 1558, and 1518 cm^{-1} (C=O or C=C conjugated). UV: $\lambda_{max}^{CH_3OH}$ 237 (log ε=4.39), 296 (4.47), 369 (3.50), and 387 (3.48) nm. Found: C, 82.86; H, 6.58; N, 4.65%. Calcd for $C_{20}H_{19}ON$: C, 83.00; H, 6.63; N, 4.84%.

** The authors are grateful to the Sankyo Co., Ltd., for doing a part of the elemental analyses.

N-Benzoyl Compound: Colorless micro prisms (from benzene–cyclohexane); mp 167—168 °C. IR (KBr): 3050, 2940 (CH), 1716, and 1620 cm^{-1} (C=O). UV: $\lambda_{max}^{CH_3OH}$ 237 ($\log \varepsilon$=4.47), 290 (4.29), 360 (3.54), and 378 (3.44) nm. Found: C, 79.25; H, 5.69; N, 4.76%. Calcd for $C_{20}H_{17}O_2N$: C, 79.18; H, 5.65; N, 4.62%.

Indolo[2,3-b]tropone (III). *Method A*: Dehydrogenation with chloranil. A mixture of II (7.0 g) and chloranil (18.0 g) in xylene (115 ml) was refluxed at 160—165 °C for 24 hr. After cooling, the reaction mixture was made alkaline by adding 2 M sodium hydroxide, and the insoluble material was filtered off. After the organic layer had been dried over anhydrous sodium sulfate, the solvent was removed to give a residue. The water layer and the insoluble material were then extracted with chloroform. The extract was dried and condensed to give the residue. The combined residue was recrystallized from benzene to give III as yellow needles (3.6 g, 52%); mp 245—246 °C.

Method B: Dehydrogenation with DDQ. DDQ (2.1 g) was added to a solution of II (1.0 g) in benzene (60 ml), and the mixture was refluxed for 5 hr. After cooling, the reaction mixture was poured into 10% sodium hydroxide, and the benzene layer was isolated. The water layer was extracted with chloroform. The organic layers were dried over anhydrous sodium sulfate and condensed, and the residues were recrystallized from benzene to give III as yellow plates (0.43 g, 45%); mp 245—246 °C. The IR spectrum was identical with that of a sample prepared by Method A and the mixed melting point was not depressed. Found: C, 80.02; H, 4.65; N, 7.14%. Calcd for $C_{13}H_9ON$: C, 79.97; H, 4.67; N, 7.18%.

N-Benzoyl Compound: Yellow needles (from cyclohexane–benzene); mp 196—196.5 °C. IR (KBr): 1706 cm^{-1} (C=O). UV: $\lambda_{max}^{CH_3OH}$ 222 ($\log \varepsilon$=4.48), 275 (4.46), 310 (4.17), 382 (3.71), and 400 (3.71) nm. Found: C, 80.42; H, 4.36; N, 4.44%. Calcd for $C_{20}H_{13}O_2N$: C, 80.23; H, 4.39; N, 4.68%.

Cyclohexanone 4-Isopropyltroponyl-2-hydrazone (Xa). A mixture of 2-hydrazino-4-isopropyltropone (0.2 g) and cyclohexanone (0.1 g) in ethanol (2 ml) was refluxed for 15 min on a water bath. The solvent was then removed, and a saturated solution of picric acid in ethanol was added to the residual oil. The picrate was treated with aqueous sodium bicarbonate and the separated oil was extracted with benzene. The extract was dried and condensed to leave a residual oil. The oil solidified under reduced pressure in a vacuum desiccator. The solid was purified from ethyl ether to give a yellow powder (0.18 g, 62%); mp 104—106 °C. IR (KBr): 3255 (NH), 1592, and 1542 cm^{-1} (C=O or C=C conjugated). UV: $\lambda_{max}^{CH_3OH}$ 270 ($\log \varepsilon$=4.40), 353 (4.23), 412 (4.27) nm. Found: C, 74.40; H, 8.57; N, 10.91%. Calcd for $C_{16}H_{22}ON_2$: C, 74.38; H, 8.58; N, 10.85%.

Picrate: Yellow needles; mp 127—128 °C. Found: C, 54.12; H, 5.18; N, 14.35%. Calcd for $C_{22}H_{25}O_8N_5$: C, 54.20; H, 5.17; N, 14.38%.

Cyclohexanone 6-Isopropyltroponyl-2-hydrazone (Xb). A mixture of 2-hydrazino-6-isopropyltropone (0.3 g) and cyclohexanone (0.16 g) in ethanol (2 ml) was treated by a method similar to that used for the preparation of Xa. Yellow rhombic crystals (0.2 g, 47%); mp 76—78 °C. IR (KBr): 3276 (NH), 1590, and 1541 cm^{-1} (C=O or C=C conjugated). UV: $\lambda_{max}^{CH_3OH}$ 265 ($\log \varepsilon$=4.40), 353 (4.21), and 4.08 (4.27) nm. Found: C, 74.15; H, 8.51; N, 10.79%. Calcd for $C_{16}H_{22}ON_2$: C, 74.38; H, 8.58; N, 10.85%.

Picrate: Orange yellow needles; mp 146—147 °C. Found: C, 54.51; H, 4.79; N, 14.22%. Calcd for $C_{22}H_{25}O_8N_5$: C, 54.20; H, 5.17; N, 14.37%.

Alternate Method for Preparation of Xa and Xb. A mixture (3.6 g) of two isomers of hinokitiol methyl ether from the methylation of hinokitiol with diazomethane were directly treated with 85% hydrazine hydrate to give a mixture of 4- and 6-isopropyl-2-hydrazinotropones, which were then converted into the hydrazones of cyclohexanone. The resulting hydrazones (Xa and Xb) were separated in the form of picrates by fractional crystallization.

The picrates were treated with a sodium bicarbonate solution to give Xa (1.0 g) and Xb (1.6 g).

10-Isopropyl-1,2,3,4-tetrahydroindolo[2,3-b]tropone (XIa). A solution of Xa (7.2 g) in 3 M sulfuric acid (90 ml) was refluxed at 110—120 °C for 2 hr. After cooling, the reaction mixture was made slightly alkaline by adding aqueous sodium hydroxide and extracted with benzene. The extract was dried and condensed, and the residue was recrystallized from benzene to give slightly red needles (3.0 g, 45%); mp 221—222 °C. Found: C, 79.32; H, 7.77; N, 5.96%. Calcd for $C_{16}H_{19}ON$: C, 79.63; H, 7.94; N, 5.80%. UV: $\lambda_{max}^{CH_3OH}$ 243 ($\log \varepsilon$=4.51), 294 (4.47), 365 (3.77), and 383 (3.82) nm.

8-Isopropyl-1,2,3,4-tetrahydroindolo[2,3-b]tropone (XIb). A solution of X (11.9 g) in 3 M sulfuric acid (150 ml) was treated by a method to that used for the preparation of XIa. Light yellow needles (5.9 g, 53%); mp 205—206 °C. UV: $\lambda_{max}^{CH_3OH}$ 242 ($\log \varepsilon$=4.48), 292 (4.46), and 373 (3.59) nm. Found: C, 79.48; H, 7.69; N, 5.85%. Calcd for $C_{16}H_{19}ON$: 79.63; H, 7.94; N, 5.80%.

10-Isopropylindolo[2,3-b]tropone (XIIa). A mixture of XIa (1.0 g) and DDQ (2.0 g) in dry benzene (60 ml) was refluxed for 4.5 hr. The reaction mixture was then poured onto 10% sodium hydroxide and the benzene layer was isolated. The water layer was subsequently extracted with chloroform. The organic layers were washed with water, dried over anhydrous sodium sulfate, and condensed to give yellow micro prisms (0.63 g, 64%), which were then recrystallized from benzene; mp 199—201 °C. Found: C, 80.81; H, 6.44; N, 5.82%. Calcd for $C_{16}H_{15}ON$: C, 80.98; H, 6.37; N, 5.90%.

8-Isopropylindolo[2,3-b]tropone (XIIb). *Method A*: Dehydrogenation with DDQ. A mixture of XIb (1.0 g) and DDQ (2.0 g) in dry benzene (60 ml) was treated by a method similar to that used for the preparation of XIIa. Light yellow micro prisms (0.69 g, 70%); mp 222—224 °C. UV: $\lambda_{max}^{CH_3OH}$ 226 ($\log \varepsilon$=4.46), 277 (4.48), 306 (4.28), and 394 (3.87) nm. Found: C, 81.25; H, 6.30; N, 5.96%. Calcd for $C_{16}H_{15}ON$: C, 80.98; H, 6.37; N, 5.90%.

Method B: Dehydrogenation with Pd–C. A mixture of XIb (0.5 g) and 5% Pd–C (0.2 g) in *p*-cymene (5 ml) was refluxed at 198—200 °C for 48 hr. The catalyst was then removed, and the filtrate was cooled to give light yellow micro needles (0.16 g, 32%), which were then recrystallized from benzene; mp 222—224 °C.

The IR spectrum was identical with that of the sample prepared by Method A, and the mixed melting point with the sample was not depressed.

Cyclohexanone Bromotroponylhydrazone (Xc). Cyclohexanone (2.5 g) was added to a solution of 2-bromo-7-hydrazinotropone (5.0 g) in ethanol (250 ml), and the mixture was refluxed for 20 min. The solvent was then removed, and the residue was recrystallized from ethanol to give yellow prisms (6.24 g, 91%); mp 134.5—135 °C. IR (KBr): 3270 (NH), 1620, 1597 cm^{-1} (C=O or C=C conjugated). UV: $\lambda_{max}^{CH_3OH}$ 275 ($\log \varepsilon$=4.33), 358 (4.20), and 430 (4.28) nm. Found: C, 52.76; H, 5.14; N, 9.47%. Calcd for $C_{13}H_{15}ON_2Br$: C, 52.98; H, 5.13; N, 9.49%.

7-Bromo-1,2,3,4-tetrahydroindolo[2,3-b]tropone (XIc). *Method A*: A solution of Xc (1.0 g) in water (10 ml) and conc. sulfuric acid (0.6 ml) was refluxed at 130—140 °C for

2 hr. After cooling, 4 M sodium hydroxide was added to adjust the pH values to 5—6 and the solution was extracted with chloroform. The extract was dried and condensed to give a residue. The residue was dissolved in ethanol and treated with activated charcoal to crystallize it as yellow needles (0.44 g, 41%); mp 274—275 °C (decomp.). IR (KBr): 3200 (NH), 1605, and 1545 cm^{-1} (C=O or C=C conjugated). UV: $\lambda_{max}^{CH_3OH}$ 250 (log ε=4.38), 300 (4.53), 375 (3.68), and 393 (3.76) nm. Found: C, 56.27; H, 4.40; N, 4.72%. Calcd for $C_{13}H_{12}ONBr$: C, 56.13; H, 4.36; N,5.04%.

Method B: To a solution of II (0.6 g) in benzene (50 ml), *N*-bromosuccinimide (0.58 g) and benzoyl peroxide (0.06 g) were added; the mixture was then refluxed with stirring for 1 hr.

The solvent was removed, and then the residue was made alkaline by adding aqueous sodium hydroxide and extracted with benzene. The extract was dried and condensed to leave a residue. This residue was dissolved in benzene–chloroform and passed through a silica-gel column. The product obtained from the yellowish effluent was recrystallized from ethanol to give yellow needles (0.12 g, 14%); mp 274—275 °C (decomp.). The IR spectrum was identical with that of the sample obtained by means of Method A.

7-Bromoindolo[2,3-b]tropone (XIIc). *Method A*: A mixture of XIc (0.2 g) and DDQ (0.35 g) in dry benzene (20 ml) was refluxed for 5 hr. The reaction mixture was then treated by a method similar to that used for the preparation of III. Orange micro needles (0.08 g, 41%); mp 291—292 °C. IR (KBr): 3215 (NH), 1600, and 1552 cm^{-1} (C=O or C=C conjugated). UV: $\lambda_{max}^{CH_3OH}$ 235 (log ε=4.25), 282 (4.47), 325 (4.10), 342 (4.04), 395 (3.82), and 416 (3.87) nm. Found: C, 56.59; H, 3.04; N, 5.19%. Calcd for $C_{13}H_8ONBr$: C, 56.75; H, 2.93; N, 5.09%.

Method B: *N*-Bromosuccinimide (0.07 g) and benzoyl peroxide (0.02 g) were added to a solution of III (0.07 g) in dry benzene (15 ml), after which the mixture was refluxed for 3 hr. The solvent was then removed, and the residue was treated with boiling water to leave an insoluble solid. The solid was collected and dried.

Recrystallization from benzene gave yellow needles (0.07 g, 92%); mp 291—292 °C. The IR spectrum was identical with that of the sample obtained by means of Method A.

Attempt at the Ring Closure of Cyclopentanone 2-Troponylhydrazone. Cyclopentanone 2-Troponylhydrazone: A mixture of 2-hydrazinotropone (0.3 g) and cyclopentanone (0.22 g) in acetic acid (6 ml) was refluxed for 1 hr. The reaction mixture was then treated by a method similar to that used for the preparation of I.

Orange yellow prisms (0.27 g, 61%); mp 78—79 °C. IR (KBr): 3230 (NH), 1637, and 1592 cm^{-1} (C=O or C=C conjugated). UV: $\lambda_{max}^{CH_3OH}$ 265 (log ε=4.34), 354 (4.26), and 418 (4.26) nm. Found: C, 70.94; H, 6.94; N, 14.02%. Calcd for $C_{12}H_{14}ON_2$: C, 71.26; H, 6.98; N, 13.85%.

When this hydrazone was heated with dilute sulfuric acid or 85% phosphoric acid, the starting material was recovered.

2,3-Pentamethylenepyrrolo[2,3-b]tropone (XIII). Cycloheptanone 2-Troponylhydrazone: A mixture of 2-hydrazinotropone (0.3 g) and cycloheptanone (0.3 g) in ethanol (5 ml) was refluxed for 30 min. The reaction mixture was then treated by a method similar to that used for the preparation of I.

Yellow needles (0.4 g, 79%); mp 91—92 °C. IR (KBr): 3255 (NH), 1595, and 1550 cm^{-1} (C=O or C=C conjugated). UV: $\lambda_{max}^{CH_3OH}$ 264 (log ε=4.35), 353 (4.25), and 415 (4.28) nm. Found: C, 73.15; H, 7.84; N, 12.21%. Calcd for $C_{14}H_{18}ON_2$: C, 73.01; H, 7.88; N, 12.17%.

Method A: Ring-closure with PPA. A solution of the hydrazone (2.0 g) described above in 105% PPA (30 ml) was heated at 150 °C for 2 hr. After cooling, the reaction mixture was diluted with water and neutralized by adding aqueous sodium bicarbonate.

The resulting precipitate was collected, dried, and recrystallized from benzene to give light yellow plates (1.1 g, 58%); mp 185—186 °C. IR (KBr): 3160 (NH), 1621, 1545, and 1525 cm^{-1} (C=O or C=C conjugated). UV: $\lambda_{max}^{CH_3OH}$ 235 (log ε=4.41), 295 (4.53), and 363 (3.63) nm. Found: C, 78.46; H, 7.02; N, 6.71%. Calcd for $C_{14}H_{15}ON_2$: C, 78.84; H, 7.09; N, 6.57%.

Method B: Ring-closure with dilute sulfuric acid. A solution of the hydrazone described above (0.5 g) in water (12 ml) and conc. sulfuric acid (0.8 ml) was refluxed for 1 hr. The reaction mixture was treated by a method similar to that used for the preparation of II. Light yellow plates (0.03 g, 7%); mp 185—186 °C.

The IR spectrum was identical with that of the sample prepared by means of Method A, and the mixed melting point with the sample was not depressed.

N-Benzoyl Compound: Colorless micro prisms (from cyclohexane); mp 157—158 °C. IR (KBr): 1720 cm^{-1} (C=O). UV: $\lambda_{max}^{CH_3OH}$ 237 (log ε=4.48), 288 (4.33), 360 (3.57), and 380 (3.50) nm. Found: C, 79.17; H, 5.53; N, 4.91%. Calcd for $C_{21}H_{19}O_2N$: C, 79.47; H, 6.03; N, 4.41%.

2-Benzyl-1,2,3,4-tetrahydrocyclohept[b]pyrido[3,4-d]pyrrol-6(5H)-one (XIV). 1-Benzyl-4-piperidone 2-Troponylhydrazone: A mixture of 2-hydrazinotropone (1.5 g) and 1-benzyl-4-piperidone (2.0 g) in ethanol (5 ml) was refluxed for 2 hr. The solvent was then removed, and the residue was recrystallized from ethanol to give yellow needles (2.6 g, 77%); mp 97—98 °C. IR (KBr): 3266 (NH), 1601, and 1590 cm^{-1} (C=O or C=C conjugated). UV: $\lambda_{max}^{CH_3OH}$ 263 (log ε= 4.34), 354 (4.28), and 418 (4.29) nm. Found: C, 74.29; H, 6.88; N, 13.81%. Calcd for $C_{19}H_{21}ON_3$: C, 74.24; H, 6.89; N, 13.67%.

A solution of the hydrazone described above (0.3 g) in PPA (4 ml) was heated at 150 °C for 30 min. After cooling, the reaction mixture was diluted with water; aqueous potassium carbonate was then added to adjust the pH value to 8. The solution was then extracted with chloroform. The extract was dried and condensed, and the residue was recrystallized from benzene or methanol to give colorless plates (0.04 g, 14%); mp 219—220 °C. IR (KBr): 3115 (NH), 1620, 1551, and 1501 cm^{-1} (C=O or C=C conjugated). UV: $\lambda_{max}^{CH_3OH}$ 236 (log ε=4.42), 291 (4.46), 366 (3.66), and 383 (3.66) nm. Found: C, 78.77; H, 6.33; N, 9.62%. Calcd for $C_{19}H_{18}ON_2$: C, 78.59; H, 6.25; N, 9.62%.

8-Chlorobenzo[b]-1-azaazulene (XV). *Method A*: Reaction of III with thionyl chloride. To a solution of III (0.6 g) in dry benzene (20 ml), we added thionyl chloride (1.9 g); the mixture was then refluxed at 90—100 °C for 20 hr. After cooling, the reaction mixture was poured into a saturated sodium bicarbonate solution and extracted with benzene. The extract was dried and condensed to leave a residue. It was recrystallized from benzene–cyclohexane to give violet needles (0.14 g, 21%); mp 144—146 °C. IR (KBr): 3040 (CH), 1602, and 1580 cm^{-1} (conjugated C=C or C=N). NMR (in $CDCl_3$): δ 7.3—8.7 ppm (m). Found: C, 73.51; H, 3.87; N, 6.98%. Calcd for $C_{13}H_8NCl$: C, 73.10; H, 3.77; N, 6.56%.

Picrate: Orange micro prisms; mp 204 °C (decomp.). Found: C, 51.56; H, 2.50; N, 12.44%. Calcd for $C_{19}H_{11}O_7N_4Cl$: C, 51.52; H, 2.48; N, 12.66%.

Method B: Reaction of III with phosphoryl chloride. A mixture of III (1.37 g) and phosphoryl chloride (6.23 g) was heated at 105—110 °C for 1 hr. After cooling, the

reaction mixture was poured onto ice water; the solution was then made slightly alkaline by adding aqueous sodium bicarbonate.

The solution was extracted with benzene. The extract was dried over anhydrous sodium sulfate and condensed to leave a residue. The recrystallization of this residue from cyclohexane–benzene gave violet needles (1.11 g, 67%); mp 144—145 °C.

The IR spectrum was identical with that of the sample prepared by means of Method A, and the mixed melting point with the sample was not depressed.

Hydrolysis of XV. To a solution of XV (0.1 g) in ethanol (4 ml), we added 2 M sodium hydroxide (4 ml), and the mixture was refluxed for 1 hr. The ethanol was then removed, water was added, the solution was acidified with 2 M hydrochloric acid, and the separated material was collected. It was subsequently recrystallized from ethanol to give yellow needles (mp 245—246 °C). The mixed melting point with III was not depressed.

8-Hydrazinobenzo[b]*-1-azaazulene (XVI).* A solution of XV (0.1 g) in methanol (10 ml) was added, drop by drop, to a solution of 80% hydrazine hydrate (0.2 g) in methanol (10 ml), and the solution was stirred at room temperature for 3 hr. The insoluble material was removed by filtration. The filtrate was evaporated; then water was added and extracted with benzene. The extract was dried and condensed to leave a residue. It was recrystallized from benzene–cyclohexane to give reddish-violet needles (0.04 g, 43%); mp 158—159 °C. IR (KBr): 3348, 3140 (NH), 1616, 1538, and 1486 cm^{-1} (conjugated C=C or C=N). Found: C, 74.53; H, 4.97; N, 19.68%. Calcd for $C_{13}H_{11}N_3$: C, 74.62; H, 5.30; N, 20.08%.

Benzo[b]*-1-azaazulene (XVII).* A mixture of XVI (0.34 g), acetic acid (20 ml), water (20 ml), and 2M copper sulfate (34 ml) was heated for 15 min on a water bath. After cooling, the reaction mixture was made slightly alkaline by adding 2 M sodium hydroxide and the solution was extracted with chloroform. The extract was dried and condensed to leave a residue. The residue was dissolved in benzene and passed through an alumina column. The product obtained from the reddish effluent was recrystallized from cyclohexane to give reddish-violet needles (0.07 g, 24%); mp 140—141 °C.

The IR and UV spectra were identical with those of the sample prepared by Treibs' method,[2a] and the mixed melting point with the sample was not depressed.

This work was financially supported by grants from the Ministry of Education of Japan and the Sankyo Co., Ltd., to which the authors' thanks are due.

One of the authors (Je-Kyun Sin) especially wishes to express his deep gratitude to Professor Yoshio Kitahara of Tohoku University for his kind guidance. We all also wish to thank Dr. Masafumi Yasunami of Tohoku University for his helpful suggestions regarding the spectra.

References

1) a) Presented at the 10th Annual Meeting of the Chemical Society of Japan, Tokyo, April, 1957; J.-K. Sin, Doctoral Thesis, Tohoku University, Sendai, March, 1958; b) Outline of this work was mentioned in the following reviews: T. Nozoe, *Croat. Chim. Acta*, **29**, 207 (1957); T. Nozoe and K. Kikuchi, in "Dai-Yukikagaku (Comprehensive Organic Chemistry)," ed. by M. Kotake, Asakura Shoten, Tokyo (1959), p. 573; T. Nozoe in "Non-benzenoid Aromatic Compound," ed. by D. Ginsburg, Interscience, New York, N. Y. (1959), p. 442.

2) a) M. Mühlstädt and W. Treibs, *Liebigs Ann. Chem.*, **608**, 38 (1957); b) M. Mühlstädt and H. Lichtmann, *J. Prakt. Chem.*, **312**, 466 (1970).

3) K. Yamane and K. Fujimori, This Bulletin, **45**, 269 (1972).

4) T. Nozoe, H. Horino, and T. Toda, *Tetrahedron Lett.*, **1967**, 5349.

5) S. Yamada, M. Ishikawa, and C. Kaneko, *ibid.*, **1972**, 971, 977.

The Crystal Structure of Trichloroti-npentacarbonylmanganese, Cl_3Sn–$Mn(CO)_5$

Satoru ONAKA

Department of Chemistry, Nagoya Institute of Technology, Showa-ku, Nagoya 466

(Received March 8, 1974)

The crystal structure of trichlorotin–pentacarbonylmanganese, Cl_3Sn–$Mn(CO)_5$, has been determined by means of X-ray diffraction. The crystal is monoclinic; $a=14.10(1)$, $b=13.38(5)$, $c=13.27(2)$ Å, and $\beta=97.39(21)°$ with the $P2_1/c$ space group and with $Z=8$. The structure, established by the heavy-atom method, has been refined by a least-squares method based on 2581 reflections collected by diffractometry to give an R value of 10%. The asymmetric unit contains two quite similar molecules. The geometry around the tin atom is distorted tetrahedrally, while the manganese atom exhibits a distorted octahedral coordination. The four equatorial carbonyl groups are displaced from the equatorial plane toward the tin atom. There is an approximate mirror plane through the Sn–Mn–CO(axial) axis. The Sn–Mn bond distance, 2.590(5) Å, is shorter by about 0.08 Å than that of the triphenyl and trimethyl analogues. The mean Mn–C distance of 1.87 Å is longer than that of the trimethyl analogue. These changes in bond distances may be interpreted in terms of the π-interaction between the two metal atoms, which is more pronounced in the chloro-derivative than in the methyl derivative.

In a series of papers concerning the X_3M–$Mn(CO)_{5-n}L_n$ compounds (X stands for CH_3, C_6H_5, Cl, Br, and I; M for Si, Ge, and Sn; L for $P(C_6H_5)_3$, $As(C_6H_5)_3$, and $Sb(C_6H_5)_3$, and n=0 or 1), the effect of IV b metal atoms or the effect of the substituents of the component-metal atoms on the nature of the strength of the M–Mn bonds has been studied by means of IR,[1-4] NMR,[5] NQR,[6] and the ^{119}Sn–Mössbauer effect.[7,8] It has been concluded that the π-interaction between manganese and IV b metal atoms is influenced by the substituent, X or L. In order to provide further evidence of the effect of the substituents on the M–Mn bond nature and in order to confirm other results or estimations previously obtained,[4,6] it is desirable to obtain information regarding the details of the molecular structure in this series of compounds by the X-ray diffraction method. However, no trihalogeno compound, X_3Sn–$Mn(CO)_5$, has yet been subjected to X-ray crystal structure analysis,[9] though the crystal structures of $(C_6H_5)_3Sn$–$Mn(CO)_5$,[10] $(CH_3)_3Sn$–$Mn(CO)_5$,[11] and $(C_6H_5)_3Sn$–$Mn(CO)_4P(C_6H_5)_3$[12] have been determined by Bryan *et al.* This may be partly because of the instability of these trihalogeno compounds toward X-rays.[13] We succeeded in the preparation of stable and suitable crystals of Cl_3Sn–$Mn(CO)_5$ for X-ray analysis from a dichloromethane solution. In this paper, we wish to report on the crystal structure of Cl_3Sn–$Mn(CO)_5$ and to discuss the effect of the Cl atom as a substituent on the molecular geometry.

Experimental

Trichlorotin–pentacarbonylmanganese was synthesized by the method of Gorsich,[14] and the crystals of this compound were grown from various solutions in a form of pale yellow needles. Suitable crystals for X-ray analysis were obtained from crops from a dichloromethane solution.

Single-crystal X-ray Data. The space group and the lattice constants were determined from Weissenberg photographs; the latter were then refined by the least-squares method. The crystal data are given in Table 1. The intensity measurements were made by using two crystals, with dimensions of 0.29×0.35×0.37 mm and 0.29×0.35×0.41 mm, on a Rigaku four-circle automatic diffractometer. Mo $K\alpha_1$ radiation (λ=0.7107 Å) monochromated by graphite was used with a scintillation counter, an ω-2θ scan technique being employed. The scan speed was 4°/min in 2θ. Background measurements were made on both sides of every peak. 3585 reciprocal lattice points were surveyed in the $2\theta<45°$ range; a significant intensity was observed at 2581 points. Three standard reflections were measured every 50 measurements. The intensities for the second crystal were adjusted to those of the first crystal based on the three standard reflections. The intensities were corrected for the Lorents and polarization effects. No corrections were applied for absorption and extinction.

Table 1. Crystal data of Cl_3Sn–$Mn(CO)_5$

Chemical formula	$C_5O_5Cl_3MnSn$
Crystal system	monoclinic
Space group	$P2_1/c$
Cell dimensions; a	14.10±0.01Å
b	13.38±0.05
c	13.27±0.02
β	97.39±0.21°
V	2483Å^3
Z	8
D_x	2.25 g·cm^{-3}
D_m	2.30 g·cm^{-3}

Determination of the Structure. All the calculations were carried out on a FACOM 230-60 computer at the Computation Center of Nagoya University, using the RSSFR-5 and HBLS-IV programs, which are included in the UNICS program system.[15] The positions of the tin atoms were deduced from the three-dimensional sharpened Patterson maps. The Fourier synthesis based on the positions of the tin atoms easily located the manganese atoms. The positions of the other atoms were readily determined from successive three-dimensional Fourier syntheses. A refinement of the structure was carried out by the block-diagonal least-squares method for thirty atoms in the asymmetric unit with isotropic thermal parameters. The unit weight was given for each reflection. The discrepancy index, R, was 11.7%. The difference Fourier synthesis at this stage left no appreciable peaks. A further refinement by the use of anisotropic thermal parameters reduced the R value to 9.98%. At the final stage, several strong reflections were excluded from the least-squares refinement, since they were considered to be

TABLE 3. FINAL POSITIONAL AND THERMAL PARAMETERS OF Cl_3Sn-$Mn(CO)_5$ WITH THEIR ESTIMATED STANDARD DEVIATIONS (in parantheses).

All values have been multiplied by 10^4. The anisotropic thermal parameters are of the form: $\exp[-(B_{11}h^2+B_{22}k^2+B_{33}l^2+B_{12}hk+B_{13}hl+B_{23}kl)]$.

Atom	x	y	z	B_{11}	B_{22}	B_{33}	B_{12}	B_{13}	B_{23}
Molecule 1.									
Sn	9034(1)	1297(2)	1530(2)	40(1)	42(1)	42(1)	−3(2)	10(2)	10(2)
Mn	8928(3)	3112(4)	880(3)	31(3)	38(3)	35(3)	2(5)	9(4)	21(5)
Cl(1)	8011(7)	908(8)	2759(7)	70(6)	92(8)	64(7)	−41(12)	68(11)	−4(12)
Cl(2)	10474(7)	731(8)	2343(9)	56(6)	79(8)	93(8)	20(11)	−11(11)	26(14)
Cl(3)	8666(8)	−17(8)	359(9)	81(7)	64(7)	78(8)	−43(12)	5(12)	−54(12)
C(1)	8852(22)	4406(32)	442(23)	30(18)	117(35)	32(20)	21(41)	−5(31)	−38(45)
C(2)	10137(27)	3340(35)	1607(29)	60(24)	122(39)	69(29)	37(50)	102(45)	58(55)
C(3)	8318(30)	3496(21)	2080(24)	126(33)	12(18)	39(21)	1(37)	−132(45)	4(32)
C(4)	7760(19)	2859(38)	200(22)	7(14)	215(54)	15(17)	83(46)	−30(26)	2(49)
C(5)	9497(20)	2651(26)	−258(26)	26(16)	61(24)	74(26)	−8(33)	63(35)	70(43)
O(1)	8883(17)	5233(14)	133(18)	83(17)	9(11)	74(17)	48(23)	−8(28)	12(24)
O(2)	10839(18)	3437(21)	2074(22)	59(17)	84(22)	109(25)	−63(31)	−40(33)	18(38)
O(3)	7991(17)	3644(19)	2742(15)	85(17)	77(18)	24(13)	28(30)	72(24)	−11(26)
O(4)	7024(18)	2605(21)	−185(22)	69(18)	76(21)	98(23)	2(31)	17(33)	20(37)
O(5)	9828(19)	2417(17)	−949(18)	106(20)	38(15)	66(18)	13(29)	91(32)	10(27)
Molecule 2.									
Sn′	4016(1)	1296(2)	3219(2)	42(1)	42(1)	40(1)	−2(2)	23(2)	−4(2)
Mn′	3918(3)	3141(4)	3819(3)	31(3)	41(3)	35(3)	0(5)	16(4)	1(5)
Cl(1′)	5512(6)	704(8)	2919(8)	47(5)	66(7)	100(8)	33(10)	42(11)	−11(13)
Cl(2′)	3098(7)	874(7)	1673(7)	81(7)	66(7)	46(6)	−38(11)	−15(10)	−11(10)
Cl(3′)	3542(8)	43(8)	4303(8)	103(8)	68(7)	62(7)	−26(13)	61(12)	28(11)
C(1′)	3862(21)	4494(26)	4273(8)	36(18)	69(26)	51(22)	45(35)	64(34)	5(39)
C(2′)	3284(19)	3466(22)	2555(24)	20(16)	37(20)	59(22)	7(27)	−53(31)	11(34)
C(3′)	5109(20)	3355(19)	3367(22)	35(16)	12(15)	47(20)	4(25)	−7(30)	60(29)
C(4′)	4522(25)	2715(24)	5049(21)	86(25)	39(21)	19(18)	−44(38)	−22(35)	37(31)
C(5′)	2735(21)	2762(23)	4224(24)	34(17)	38(20)	58(23)	−62(31)	−22(32)	−46(35)
O(1′)	3860(21)	5263(20)	4572(21)	115(24)	73(20)	86(22)	99(36)	106(38)	−32(35)
O(2′)	2983(21)	3670(24)	1736(19)	107(23)	109(25)	51(17)	26(41)	39(32)	7(37)
O(3′)	5833(14)	3500(19)	3058(18)	32(12)	87(20)	71(18)	2(25)	20(24)	29(31)
O(4′)	4927(19)	2428(28)	5822(19)	72(18)	160(32)	56(18)	37(41)	36(30)	13(42)
O(5′)	2072(15)	2552(19)	4491(20)	34(13)	65(18)	104(22)	−27(25)	−1(27)	20(34)

seriously affected by the extinction effect. The neutral atomic scattering factors used were those listed in International Tables.[16] Table 2* lists the observed and calculated structure factors.

Results and Discussion

Table 3 gives the final positional and thermal parameters of atoms, along with their standard deviations. The molecular structure is shown in Fig. 1, along with the numbering scheme. The intramolecular atomic distances and bond angles are presented in Table 4. A projection of the molecule 1 down the Sn–Mn axis is drawn in Fig. 2. In Table 5, the torsional angles are listed. The molecular geometry of this compound is quite similar to those observed for triphenyltin-pentacarbonylmanganese and trimethyltin-pentacarbonylmanganese.[10,11] The geometry around the tin atom is distorted tetrahedrally, while that of the manganese atom is approximately octahedral.

As is shown in Table 4, the covalent Sn–Mn bond distances in Cl_3Sn–$Mn(CO)_5$ are 2.575(5) Å and 2.604(5) Å (average 2.59 Å), which are considerably shorter than those of $(CH_3)_3Sn$–$Mn(CO)_5$ (2.674 Å)

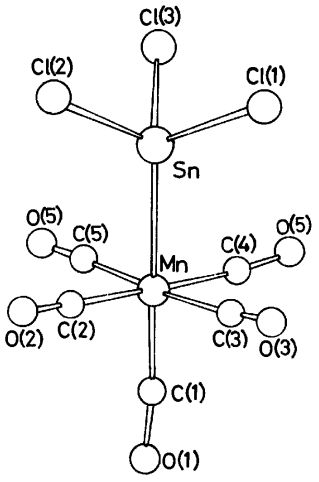

Fig. 1. The molecular structure of trichlorotin-pentacarbonylmanganese, Cl_3Sn–$Mn(CO)_5$.

* Table 2 is kept as Document No. 7426 at the Chemical Society of Japan.

TABLE 4. INTRAMOLECULAR DISTANCES (Å) AND BOND ANGLES (°)

Bonds	Bond distances		Bonds	Bond angles		Bonds	Non-bonded distances (less than 4.0 Å)	
	Molecule 1	Molecule 2		Molecule 1	Molecule 2		Molecule 1	Molecule 2
Sn–Mn	2.575(5)	2.604(5)	Cl(1)–Sn–Mn	115.0(3)	117.6(3)	Sn·····C(2)	3.14(5)	3.17(3)
Sn–Cl(1)	2.369(11)	2.334(11)	Cl(2)–Sn–Mn	118.5(3)	116.8(3)	Sn·····C(3)	3.23(4)	3.15(3)
Sn–Cl(2)	2.302(12)	2.349(11)	Cl(3)–Sn–Mn	118.9(3)	117.3(3)	Sn·····C(4)	3.15(5)	3.09(4)
Sn–Cl(3)	2.360(11)	2.362(12)	Cl(1)–Sn–Cl(2)	100.6(4)	100.3(4)	Sn·····C(5)	3.12(4)	3.08(3)
Mn–C(1)	1.826(43)	1.913(35)	Cl(2)–Sn–Cl(3)	99.7(4)	101.2(4)	Cl(1)···Cl(2)	3.60(2)	3.59(2)
Mn–C(2)	1.873(47)	1.849(32)	Cl(3)–Sn–Cl(1)	100.8(4)	101.3(4)	Cl(2)···Cl(3)	3.56(2)	3.64(2)
Mn–C(3)	1.973(42)	1.877(29)	Sn–Mn–C(1)	179.0(14)	178.2(12)	Cl(3)···Cl(1)	3.65(2)	3.63(2)
Mn–C(4)	1.805(52)	1.832(36)	Sn–Mn–C(2)	88.4(14)	88.6(10)	C(1)···C(2)	2.64(6)	2.70(5)
Mn–C(5)	1.901(35)	1.885(32)	Sn–Mn–C(3)	89.3(12)	87.3(10)	C(1)···C(3)	2.68(6)	2.72(5)
C(1)–O(1)	1.183(49)	1.103(46)	Sn–Mn–C(4)	90.1(16)	86.7(12)	C(1)···C(4)	2.58(7)	2.71(6)
C(2)–O(2)	1.106(55)	1.148(45)	Sn–Mn–C(5)	87.0(11)	84.6(11)	C(1)···C(5)	2.72(6)	2.81(5)
C(3)–O(3)	1.061(49)	1.164(39)	C(1)–Mn–C(2)	91.2(20)	91.6(15)	C(2)···C(3)	2.73(6)	2.66(4)
C(4)–O(4)	1.147(59)	1.173(51)	C(1)–Mn–C(3)	89.8(18)	91.8(14)	C(3)···C(4)	2.66(7)	2.62(5)
C(5)–O(5)	1.126(44)	1.080(42)	C(1)–Mn–C(4)	90.4(21)	92.7(16)	C(4)···C(5)	2.61(6)	2.62(5)
			C(1)–Mn–C(5)	93.9(17)	95.2(15)	C(5)···C(2)	2.69(6)	2.61(5)
			C(2)–Mn–C(3)	90.2(19)	91.3(13)			
			C(2)–Mn–C(4)	178.4(22)	175.5(15)			
			C(2)–Mn–C(5)	90.7(18)	88.8(14)			
			C(3)–Mn–C(4)	89.3(20)	90.0(14)			
			C(3)–Mn–C(5)	176.2(16)	173.0(14)			
			C(4)–Mn–C(5)	89.7(20)	89.4(15)			
			Mn–C(1)–O(1)	174.1(36)	176.7(33)			
			Mn–C(2)–O(2)	176.2(41)	172.8(30)			
			Mn–C(3)–O(3)	175.6(37)	177.9(26)			
			Mn–C(4)–O(4)	173.0(44)	178.1(34)			
			Mn–C(5)–O(5)	177.2(31)	177.3(30)			

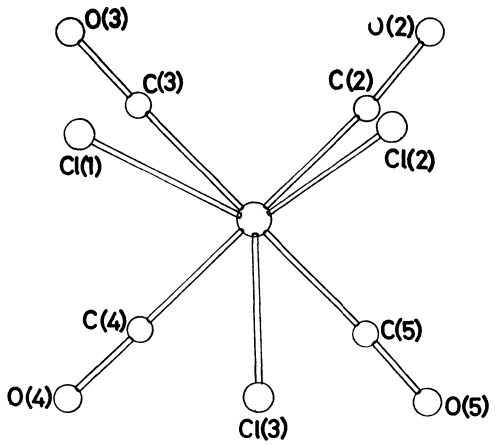

Fig. 2. A molecular view of Cl_3Sn-$Mn(CO)_5$ down the Sn–Mn axis from the Cl_3Sn moiety.

TABLE 5. TORSIONAL ANGLES

	Molecule 1	Molecule 2
Cl(1)–Sn–Mn–C(2)	108.7°	107.3°
Cl(1)–Sn–Mn–C(3)	18.8	16.8
Cl(1)–Sn–Mn–C(4)	71.3	72.7
Cl(1)–Sn–Mn–C(5)	161.2	163.2
Cl(2)–Sn–Mn–C(2)	10.3	11.7
Cl(2)–Sn–Mn–C(3)	100.2	102.2
Cl(2)–Sn–Mn–C(4)	169.7	168.3
Cl(2)–Sn–Mn–C(5)	79.8	77.8
Cl(3)–Sn–Mn–C(2)	131.6	131.8
Cl(3)–Sn–Mn–C(3)	138.5	137.6
Cl(3)–Sn–Mn–C(4)	48.4	48.2
Cl(3)–Sn–Mn–C(5)	41.5	42.4

and $(C_6H_5)_3Sn$-$Mn(CO)_5$ (2.674 Å).[10,11] This fact accords with our previous finding[1] that the Sn–Mn bond strength in Cl_3Sn-$Mn(CO)_5$ is greater than that of $(CH_3)_3Sn$-$Mn(CO)_5$. In order to correlate the Sn–Mn bonding-distance with the bonding nature, especially with the degree of the d_π-interaction between the tin and manganese atoms, let us examine the formula proposed by Pauling:[17]

$$R(\delta, Z) = 1.825 - 0.043Z - (1.600 - 0.100Z)\delta \quad (1)$$

where $R(\delta, Z)$ is the bonding radii of the metal atom concerned, Z is the effective nuclear charge (the number of electrons outside the rare-gas shell), and δ is the amount of the d-character in the bonding orbitals. The bonding radius of the manganese atom can be calculated as follows: if the single-bond radius of the chlorine atom in the Sn–Cl bond is assumed to be 0.99 Å,[18] the covalent radius of the tin atom is calculated to be 1.36 Å from the Sn–Cl bond distance in the present compound (mean, 2.35 Å). The subtraction of this value from the Sn–Mn bond distance leaves the value of 1.23 Å for the covalent radius of the manganese atom. In the same manner, we obtain 1.31 Å for the covalent radius of the manganese atom in $(CH_3)_3Sn$-$Mn(CO)_5$,[11] the single-bond radius of the methyl carbon being assumed to be 0.77 Å.[18] The application of these manganese radii to Pauling's equa-

tion yields δ values of 32.2 and 23.3% for Cl_3Sn–$Mn(CO)_5$ and $(CH_3)_3Sn$–$Mn(CO)_5$ respectively. The absolute magnitude of these values seems suspicious, because we used the value of 1.36 Å as the covalent-bond radius of the tin atom despite the usually-accepted covalent radius of the Sn(IV) of 1.399 Å. However, the most important feature is that the increased trend of the d_π-interaction going from $(CH_3)_3Sn$–$Mn(CO)_5$ to Cl_3Sn–$Mn(CO)_5$ predicted by normal coordinate analysis is clearly exhibited in the present results.

The results of normal coordinate analysis suggested also elongated Mn–C and shortened C–O bond distances in Cl_3Sn–$Mn(CO)_5$ compared with those in $(CH_3)_3Sn$–$Mn(CO)_5$. The finding that the mean Mn–C distance of the present molecule, 1.87 Å, is longer than that of $(CH_3)_3Sn$–$Mn(CO)_5$, 1.81 Å, is parallel to this prediction. However, the latter prediction is not clear, since the mean C–O distance, 1.13 Å, is close to the value, 1.15 Å, for $(CH_3)_3Sn$–$Mn(CO)_5$.

The mean Sn–Cl bond distance (2.35 Å) is equal to that of Cl_3Sn–$Fe(CO)_2(\pi\text{-}C_5H_5)$ (2.36 Å)[13] and slightly shorter than that of $Cl_2(C_6H_5)Sn$–$Fe(CO)_2(\pi\text{-}C_5H_5)$ (2.39 Å).[19] The observed Sn–Cl(2) bond distance in the molecule 1 is considerably shorter than the other Sn–Cl bond distances. It is not clear at present why this bond distance is shorter than the others.

Each molecule has an approximate mirror plane through the Cl(3)–Sn–Mn–C(1)–O(1) atoms. A slight rotation of the $SnCl_3$ moiety along the Sn–Mn bond about 3.9 ° for the molecule 1 and 2.8° for the molecule 2 leads to an exact mirror symmetry, and the rotational angles may be compared with those of 1° and 3.5° in $(CH_3)_3Sn$–$Mn(CO)_5$ and $(C_6H_5)_3Sn$–$Mn(CO)_5$ respectively.[10,11] Similar distortions are also observed in $(C_6H_5)_3Sn$–$Mn(CO)_4P(C_6H_5)_3$[12] and $(\pi\text{-}C_5H_5)Fe(CO)_2$–$Mn(CO)_5$.[20] There is a possibility that these distortions around the Sn–Mn axis are due to the Jahn-Teller effect, arising from the nonequivalence of ligands around the manganese atom.

Another interesting feature is that all the equatorial carbonyl groups are bent toward the tin atom with respect to the plane perpendicular to the Sn–Mn axis, the mean Sn–Mn–C (equatorial) bond angle being 87.8°. The diviations of the manganese atoms from the planes defined by four equatorial carbon atoms are 0.05 Å for the molecule 1 and 0.09 Å for the molecule 2. The equation of the least-squares plane is given by: $0.007X+0.940Y-0.341Z-3.464=0$ for the molecule 1 and $-0.106X+0.938Y+0.341Z-6.491=0$ for the molecule 2, where the coordinates X, Y, and Z, are in Å referred to the orthogonal axes, a, b, and c*. The same kind of distortion is observed in a number of molecules with direct metal-metal bonds: $(C_6H_5)_3Sn$–$Mn(CO)_5$,[10] $(CH_3)_3Sn$–$Mn(CO)_5$,[11] $(C_6H_5)_3Sn$–$Mn(CO)_4P(C_6H_5)_3$,[12] $(\pi\text{-}C_5H_5)Fe(CO)_2$–$Mn(CO)_5$,[20] $(C_6H_5)_2Sn[Mn(CO)_5]_2$,[21] $Hg[Mn(CO)_5]_2$,[22] $C_{15}H_{11}N_3$–$Cd[Mn(CO)_5]_2$,[23] and Br_3Ge–$Mn(CO)_5$.[9] The mean M–Mn–C (equatorial) bond angles in these compounds range from 87 to 83°. It seems that the steric effect of the substituents or the counter metal atom on M–Mn–C (equatorial) angles is unimportant. In earlier studies,[10,11] these distortions have been ascribed to the effect of molecular packing in crystals. Gapotchenko *et al.*, however, recently observed similar distortions even in an isolated molecule of Br_3Ge–$Mn(CO)_5$ by the electron-diffraction method.[9] The present author previously reported[4] that such distortion could also be expected in the case of Cl_3Sn–$Mn(CO)_5$ on the basis of the study of the dependence of the CO (equatorial) stretching IR intensity on the force constant, K(M–Mn), for a series of X_3M–$Mn(CO)_5$ molecules; he interpreted this relationship in terms of the interaction between the π^* orbitals of the four equatorial carbonyl groups and the M–Mn σ bond under the condition of the distorted M–Mn–C (equatorial) bond angle from 90°.

A distortion from the tetrahedral symmetry around the tin atom is usually observed in those compounds in which the tin atom is bonded to transition elements.[10–13]

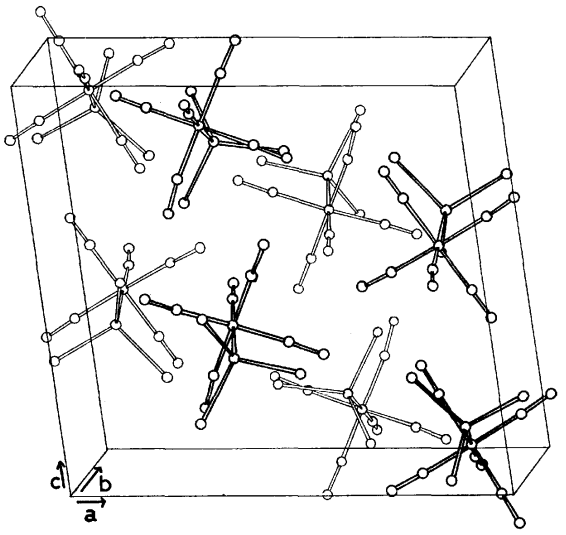

Fig. 3. Molecular packing in the unit cell.
Those molecules drawn by bold lines are located between 0 and 0.5b concerning the tin atom.

TABLE 6. SELECTED INTERMOLECULAR DISTANCES (Å) LESS THAN 4 Å BETWEEN THE BASIC MOLECULE AND ITS NEIGHBOURS.

The symmetry codes, I—XI, refer to the positions: I=(x,y,z), II=$(1+x,y,z)$, III=$(-1+x,y,z)$, IV=$(1-x, 1-y, -z)$, V=$(1-x, -y, 1-z)$, VI=$(1-x, 1-y, 1-z)$, VII=$(1-x, 1/2+y, 1/2-z)$, VIII=$(1-x, -1/2+y, 1/2-z)$, IX=$(x, 1/2-y, 1/2+z)$, X=$(x, 1/2-y, -1/2+z)$, and XI=$(1+x, 1/2-y, -1/2+z)$

Sn···O(5)(IX)	3.80(3)	Cl(3′)···C(3)(VIII)	3.64(4)
Sn′···O(4′)(X)	3.97(4)	Cl(1)···O(2′)(VII)	3.41(3)
Cl(1)···Cl(1′)(I)	3.57(2)	Cl(2)···O(5)(IX)	3.56(3)
Cl(1′)···Cl(3′)(V)	3.89(2)	O(4)···O(3′)(X)	3.07(4)
Cl(2)···Cl(2′)(II)	3.92(2)	O(2)···O(2′)(II)	3.13(5)
C(1)···Cl(2)(VII)	3.46(5)	O(3)···O(3′)(I)	3.13(4)
Cl(1)···C(1)(IX)	3.63(4)	O(5)···O(5′)(XI)	3.14(4)
Cl(1)···C(4)(IX)	3.69(5)	C(1′)···C(1′)(VI)	3.78(5)
Cl(1)···C(5)(IX)	3.69(4)	C(3′)···O(4)(IX)	3.36(4)
Cl(1′)···C(1′)(VIII)	3.54(4)	C(3)···O(5)(IX)	3.38(5)
Cl(1′)···C(2′)(VIII)	**3.54**(4)	C(1′)···O(1′)(VI)	3.39(5)
Cl(1′)···C(3′)(VIII)	3.63(3)	C(1)···O(1)(IV)	3.41(5)
Cl(3′)···C(1)(VIII)	3.54(4)	C(2′)···O(2)(III)	3.42(4)
Cl(3′)···C(4)(VIII)	3.56(4)	C(3)···O(3′)(I)	3.89(5)

Figure 3 shows the molecular packing in a unit cell.[24] Table 6 lists intermolecular atomic contacts less than 4 Å. The shortest one is 3.07 Å, between two oxygen atoms. This distance and the other minimum non-bonded intermolecular distances given in Table 6 correspond to normal van der Waals interactions. All these distances in Cl_3Sn–$Mn(CO)_5$ are rather shorter than those in the trimethyl analogue,[11] and the molecular packing of the present compound is more compact than that of the trimethyl compound. In those regions where chlorine and carbonyl groups come into contact, the chlorine atom tends to be located equidistant from the carbon atoms of the carbonyl groups, as may be seen in Table 6.

The author is deeply indebted to Dr. Kyōyū Sasaki of Nagoya University for his helpful advice and his kind permission to use some programs. Thanks are also due to Professor Yukiyoshi Sasaki of the University of Tokyo for his preliminary experiments and permission to use the diffractometer and to Professor Yoshihiko Saito and Dr. Fumiyuki Marumo of the University of Tokyo for their valuable discussions.

References

1) S. Onaka, This Bulletin, **44**, 2135 (1971).
2) S. Onaka, *Nippon Kagaku Kaishi*, **10**, 1978 (1972).
3) S. Onaka, This Bulletin, **46**, 2444 (1973).
4) S. Onaka, *J. Inorg. Nucl. Chem.*, **36**, 1721 (1974).
5) S. Onaka, Y. Miyamoto, and Y. Sasaki, This Bulletin, **44**, 1851 (1971).
6) Y. Kume, D. Nakamura, M. Kubo, and S. Onaka, *J. Magn. Resonance*, **10**, 58 (1973).
7) S. Onaka, Y. Sasaki, and H. Sano, This Bulletin, **44**, 726 (1971).
8) a) S. Onaka and H. Sano, *ibid.*, **45**, 1271 (1972). b) S. Onaka and H. Sano, *ibid.*, in press.
9) The molecular structure of Br_3Ge–$Mn(CO)_5$ was determined by electron diffraction method; N. I. Gapotchenko, N. V. Alekseev, A. B. Antonova, K. N. Anisimov, N. E. Kolobova, I. A. Ronova, and Yu. T. Struchkov, *J. Organometal. Chem.*, **23**, 525 (1970).
10) H. P. Weber and R. F. Bryan, *Acta Crystallogr.*, **22**, 822 (1967).
11) R. F. Bryan, *J. Chem. Soc., A*, **1968**, 696.
12) R. F. Bryan, *ibid.*, **1967**, 172.
13) P. T. Greene and R. F. Bryan, *ibid.*, **1970**, 1696.
14) R. D. Gorsich, *J. Amer. Chem. Soc.*, **84**, 2486 (1962).
15) "Universal Crystallographic Computation Program System (UNICS)," ed. by T. Sakurai, The Crystallographic Society of Japan, Tokyo (1967).
16) "International Tables for X-ray Crystallography," Vol. III, Kynoch Press, Birmingham (1962).
17) L. Pauling, "The Nature of the Chemical Bond," Cornell University Press, Ithaca, New York (1960), Chapter 11. Equation (1) is valid for iron group transition elements.
18) L. Pauling, *ibid.*, Chapter 7.
19) P. T. Greene and R. F. Bryan, *J. Chem. Soc., A*, **1970**, 2261.
20) P. J. Hansen and R. A. Jacobson, *J. Organometal. Chem.*, **6**, 389 (1966).
21) B. T. Kilbourn and H. M. Powell, *Chem. Ind.*, **1964**, 1578.
22) M. L. Katcher and G. L. Simon, *Inorg. Chem.*, **11**, 1651 (1972).
23) W. Clegg and P. J. Wheatley, *J. Chem. Soc. Chem. Commun.*, **1972**, 760.
24) According to the previous NQR study,[6] the presence of six nonequivalent chlorine atoms in crystal was concluded. It is reasonable to consider that the six chlorine atoms in an asymmetric unit correspond to the six nonequivalent chlorine atoms observed in the NQR spectrum.

The Interpretation of Surface Tension Data for Solutions of Ionic Surfactants in the Presence of Electrolyte

Denver G. HALL, Brian A. PETHICA, and Kozo SHINODA*

Unilever Research, Port Sunlight Laboratory, Port Sunlight, Wirral, Merseyside, England L62 4XN

**Department of Chemistry, Faculty of Engineering, Yokohama National University, Minami-ku, Yokohama 233*

(Received April 18, 1974)

An improved method is presented for interpreting surface tension data on solutions of an ionic surfactant to which has been added an electrolyte whose co-ion has the same valence as the surfactant ion. Adequate account is taken of co-ion adsorption and of deviations from ideality of the solution. When a monolayer of surfactant ions is formed and the distributions of free surfactant ions and co-ions in the region adjacent to it are determined predominantly by electrostatic repulsion, it is shown that the separate contributions to the total Gibbs excess of surfactant ions from the monolayer and the adjacent region can be obtained. Finally some experimental data are re-examined and a simple explanation is given for the minimum reported to occur in co-ion adsorption as the surfactant ion concentration is increased at constant co-ion concentration.

In a previous paper Shinoda and Nakayama[1] described a method based on the Gibbs adsorption isotherm of interpreting surface tension data for a solution of an ionic surfactant plus electrolyte. This method was applied to suitable data then available to determine amounts adsorbed. Later, Lucassen-Reynders[2] suggested that it should be modified to include co-ion adsorption. In both papers ideal behaviour of the bulk solution was assumed. In this paper a more rigorous analysis is given in which both co-ion adsorption and solution non-ideality are allowed for. Tajima, Muramatsu and Sasaki[3-6] have also considered this problem but from a viewpoint somewhat different and, in our opinion, less illuminating than that described below.

Theory

We let subscripts 1—4 refer to water, surfactant ions, counterions and co-ions respectively and take as our starting point the Gibbs adsorption isotherm which, for the system of interest, at equilibrium at constant T and p can be written as

$$\mathrm{d}\sigma = -\Gamma_2 RT\mathrm{d}\ln m_2 f_2 - \Gamma_3 RT\mathrm{d}\ln m_3 f_3 - \Gamma_4 RT\mathrm{d}\ln m_4 f_4 \quad (1)$$

where σ is the surface tension, Γ_2—Γ_4 are the surface excesses of species 2—4 referred to the dividing surface for which $\Gamma_1=0$, m_2—m_4 are the molalities of species 2—4, f_2—f_4 are the corresponding bulk ionic activity coefficients and the ionisation of water is considered to be negligible.

In the case that the valence of 3 is z_3 whereas species 2 and 4 are both monovalent, the electrical neutrality conditions for the interface and the bulk solutions enable us to write

$$\left.\begin{aligned} z_3\Gamma_3 &= \Gamma_2 + \Gamma_4 \\ z_3 m_3 &= m_2 + m_4 \end{aligned}\right\} \quad (2a, b)$$

Eliminating Γ_3 from Eq. (1) we obtain

$$\mathrm{d}\sigma = -\Gamma_2 RT\mathrm{d}\ln m_2 - \frac{(\Gamma_2+\Gamma_4)}{z_3} RT\mathrm{d}\ln m_3 - \Gamma_4 RT\mathrm{d}\ln m_4 - \Gamma_2 RT\mathrm{d}\ln\gamma_2 - \Gamma_4 RT\mathrm{d}\ln\gamma_4 \quad (3)$$

where

$$\left.\begin{aligned} \ln\gamma_2 &= \ln f_2 + \frac{\ln f_3}{z_3} \\ \ln\gamma_4 &= \ln f_4 + \frac{\ln f_3}{z_3} \end{aligned}\right\} \quad (4a, b)$$

From Eqs. (2), (3), and (4) after elementary manipulation we obtain

$$\frac{1}{RT}\left(\frac{\partial\sigma}{\partial m_2}\right)_{m_4} = -\left[\frac{\Gamma_2}{m_2} + \frac{\Gamma_2+\Gamma_4}{z_3(m_2+m_4)} + \Gamma_2\left(\frac{\partial\ln\gamma_2}{\partial m_2}\right)_{m_4} + \Gamma_4\left(\frac{\partial\ln\gamma_4}{\partial m_2}\right)_{m_4}\right]$$

$$\frac{1}{RT}\left(\frac{\partial\sigma}{\partial m_4}\right)_{m_2} = \frac{1}{z_3 RT}\left(\frac{\partial\sigma}{\partial m_3}\right)_{m_2} = -\left[\frac{\Gamma_4}{m_4} + \frac{\Gamma_2+\Gamma_4}{z_3(m_2+m_4)} + \Gamma_2\left(\frac{\partial\ln\gamma_2}{\partial m_4}\right)_{m_2} + \Gamma_4\left(\frac{\partial\ln\gamma_4}{\partial m_4}\right)_{m_2}\right]$$

$$\frac{1}{RT}\left(\frac{\partial\sigma}{\partial m_2}\right)_{m_4} = -\frac{1}{RT}\left(\frac{\partial\sigma}{\partial m_4}\right)_{m_2} = -\left[\frac{\Gamma_2}{m_2} - \frac{\Gamma_4}{m_4} - \Gamma_2\left(\frac{\partial\ln\gamma_2}{\partial m_2}\right)_{m_4} + \Gamma_4\left(\frac{\partial\ln\gamma_4}{\partial m_2}\right)_{m_4}\right] \quad (5a, b, c)$$

A considerable simplification results when it is legitimate to write

$$\gamma_2 = \gamma_4 \quad (6)$$

As under these circumstances and at constant T and p, γ_2, and γ_4 depend only on m_3.

For the case that a monolayer of adsorbed surfactant is present we write

$$\Gamma_2 = \Gamma_2^{\mathrm{m}} + \Gamma_2^{\mathrm{s}} \quad (7)$$

where Γ_2^{m} is the amount of surfactant ion in the monolayer and Γ_2^{s} is the contribution to Γ_2 from the region adjacent to the monolayer. Also we suppose that Γ_2^{s} and Γ_4 are determined primarily by electrostatic repulsion due to the monolayer and that, as a consequence of this, the distribution of surfactant ions in the region adjacent to the monolayer is sufficiently like that of the co-ions to enable us to write

$$\frac{\Gamma_2^s}{m_2} = \frac{\Gamma_4}{m_4} \tag{8}$$

If we now define the quantity α by

$$\alpha = -2\frac{(\Gamma_2^s+\Gamma_4)}{\Gamma_2^m}, \tag{9}$$

assume that $\gamma_2=\gamma_4$ and put $\beta=(\partial\ln\gamma_2/\partial m_3)$ Eqs. (5a, b, and c) become respectively

$$\frac{1}{RT}\left(\frac{\partial\sigma}{\partial \ln m_2}\right)_{m_4} = -\Gamma_2^m\left[1-\frac{\alpha m_2}{2(m_2+m_4)} + (1-\alpha/2)\left(\frac{m_2}{z_3(m_2+m_4)}+m_2\beta\right)\right] \tag{10a}$$

$$\frac{1}{RT}\left(\frac{\partial\sigma}{\partial \ln m_3}\right)_{m_4} = -\Gamma_2^m\left[(1-\alpha/2)\left(\frac{1}{z_3}+m_3z_3\beta\right)-\frac{\alpha}{2}\right] \tag{10b}$$

$$\frac{1}{RT}\left(\frac{\partial\sigma}{\partial \ln m_2}\right)_{m_4} = -\Gamma_2^m \tag{10c}$$

Discussion

Equation (10c) is the main result of this paper. It shows that even for non ideal solutions Γ_2^m, the amount of adsorbed surfactant present in the monolayer, can be obtained directly from measurements of the variation of surface tension with surfactant concentration at constant counterion concentration provided that Eqs. (7) and (8) are valid. These two equations are closely related. When species 2 and 4 distribute similarly with respect to each other and with respect to species 3,[7] (γ_2 is equal to γ_4), whereas Eq. (8) holds when species 2 and 4 distribute similarly with respect to the monolayer and is unlikely to be valid when Eq. (7) is invalid. According to Debye-Hückel theory, Eq. (7) must hold when m_3 is small and there is no significant ion association.

The concentration at which equating γ_2 and γ_4 leads to significant errors cannot be estimated from experimental data on surfactant solutions because insufficient data are available. However, freezing-point depression measurements[8] and EMF measurements[9-11] indicate that, below their critical micelle concentrations, most 1:1 ionic surfactants do not associate significantly and are reasonably well-behaved 1:1 electrolytes. If this is so, the value of m_3 at which Eq. (6) ceases to be a good approximation may be similar to corresponding values for mixtures of simple 1:1 electrolytes. The activity coefficients of such mixtures can be described quite well by the expression[12]

$$\ln\gamma_2 = \frac{-A\sqrt{m_3}}{1+\sqrt{m_3}} + B_{22}m_2 + B_{24}m_4 \tag{11}$$

where A, given by the Debye-Hückel limiting law, is the same for all 1:1 electrolytes, the Bs are empirical constants and $B_{24}=B_{42}$. At constant m_3 the sum of the last two terms of Eq. (5c) is given by $\Gamma_2(B_{22}-B_{24})-\Gamma_4(B_{44}-B_{42})$. Typical values of $(B_{22}-B_{24})$ are of the order 0.3 kg mol^{-1}.[13] Such values lead to errors in Γ_2 and Γ_2^m which are proportional to m_2 and which can be expected to be of the order 3% when $m_2=0.1$ mol kg^{-1}. When $\gamma_2=\gamma_4$, Eq. (11) becomes

$$\ln\gamma_2 = \ln\gamma_4 = \frac{-A\sqrt{m_3}}{1+\sqrt{m_3}} + Bm_3 \tag{12}$$

where $B=B_{22}=B_{24}=B_{44}$. From Eq. (12) we find that

$$\beta = \frac{-A}{2(1+\sqrt{m_3})}\left(\frac{1}{\sqrt{m_3}}-\frac{1}{1+\sqrt{m_3}}\right)+B \tag{13}$$

Since $A=2.342$ kg$^{1/2}$ mol$^{-1/2}$ at 298 K, whereas B is typically of order 0.4 kg mol^{-1}, it is evident that the final term of Eq. (13) can be ignored when m_3 is small. Also the term $m_2\beta$, which is always $\leqslant m_3\beta$, decreases with increasing m_3 at constant m_2. When $m_3=0.1$ mol kg^{-1}, $m_3\beta\simeq0.21$; whereas when $m_3=0.01$ mol kg^{-1}, $m_3\beta\simeq0.10$. Consequently, the activity terms in Eqs. (10) and (5) are not negligible when $m_3>0.01$ mol kg^{-1}, although that in Eq. (10a) is negligible when $m_3\gg m_2$.

Less information is available for mixtures of 2:1 eelctrolytes with a common divalent ion than for mixtures of 1:1 electrolytes. The errors which arise through equating γ_2 and γ_4 can be expected to be somewhat greater in this case than in that above.

No direct experimental evidence for the conditions under which Eq. (8) ceases to be a good approximation appears to be available and it is not obvious how such evidence can be obtained. However when Eq. (8) is valid, the dependence of σ on m_2 and m_3 should be independent of the nature of the co-ion, provided that it has the same valence as the surfactant ion and does not form part of the monolayer. The experimental data of Matuura *et al.*[14] suggest that this may be so. Whether or not it is provides an indirect test of Eq. (8).

When $m_4\gg m_2$ and Eq. (8) is valid, $\Gamma_2\simeq\Gamma_2^m$. This result can be expected to hold when $m_4\gg m_2$ even if Eq. (8) is not valid, provided that Γ_2^s is determined primarily by electrostatic effects. Hence experimental values of Γ_2 in the presence of excess salt are essentially values of Γ_2^m. The results of Brooks and Pethica[15] reinforce this conclusion. They found that the π *vs.* A curves obtained directly for insoluble monolayers of long chain surfactants at the *n*-heptane/aqueous NaCl interface are independent of chain length for a given head group. Also the curves are the same as the π *vs.* A curves for the shorter chain length homologues obtained from application of the Gibbs adsorption isotherm to the appropriate interfacial tension data. Such agreement can be regarded as confirming the Gibbs equation. Alternatively it is strong evidence that $\Gamma_2=\Gamma_2^m$ under the conditions concerned.*

Equations (10b and c) show that the surface tensions of the solutions of interest behave as if the solutions were ideal and as if the surface phase were a charged phase[1,16] consisting of Γ_2^m mol per unit area of surfactant ion and $\Gamma_2^m[(1-\alpha/2)[1/z_3+m_3z_3\beta]-\alpha/2]$ mol per unit area of counterion. Hence the above theory enables the data for the air-solution interface considered previously[1] to be reinterpreted as in Table 1.

The values of α for the hydrocarbon surfactants are considerably smaller when deviations from solution

* Although the equation used by Brooks and Pethica to obtain Γ_2 contains the approximation $\Gamma_4=0$, the errors attributable to this approximation are less than the experimental errors in this particular case.

Table 1.

Compound	$\Gamma_2^m \times 10^6$ mol m^{-2}	$-\frac{1}{RT}\left(\frac{d\sigma}{d \ln m_3}\right)_{m_2} \times 10^6$ mol m^{-2}	$z_3 m_3 \beta$	α	Ref
$C_7F_{15}CO_2H$	4.0	1.8	−0.10	0.47	1
$C_7F_{15}CO_2K$	3.9	2.0	−0.15	0.37	1
$(C_7F_{15}CO_2)_2Ba$	3.3	1.0	−0.13	0.10	1
$C_{11}H_{23}CO_2K$	4.2	2.9	−0.21	0.11	17
$C_{12}H_{25}NH_3Cl$	5.2	3.5	−0.21	0.13	17
$C_{12}H_{25}SO_4Na$	4.4	3.2	−0.21	0.07	17

ideality are taken into account than they are when such deviations are ignored. These values show that the negative adsorptions of co-ions, although small, are not negligible and should be allowed for when interpreting accurate data rigorously. Somewhat surprisingly, the values of α for the two monovalent fluorocarbon surfactants are considerably bigger than those of the hydrocarbon surfactants despite the similar values of Γ_2^m.

Subsequent to the work of Shinoda and Nakayama, Tajima *et al.*[3-6] have examined the adsorption of sodium dodecyl sulphate (SDS) at the air/solution interface in the presence of NaCl, both by measuring surface tension and by direct measurement of adsorption using radiotracers. An interesting feature of this work is the observed minimum in Γ_4 as m_2 is increased at constant m_4. This is precisely what one expects from the above theory as Eqs. (8) and (9) enable us to write

$$\Gamma_4 = \frac{-\Gamma_2^m \alpha m_4}{2(m_2+m_4)} \qquad (14)$$

which shows that Γ_4 can be expected to decrease initially as Γ_2^m increases; when Γ_2^m and α are both close enough to their limiting values to be essentially independent of m_2 the rate of increase of Γ_4 becomes smaller as m_4 becomes larger. An equally simple alternative explanation of this behaviour is difficult to envisage.

Also of interest is the increase in saturation adsorption of surfactant as m_4 is increased. We have from Eq. (9)

$$\Gamma_2 = \Gamma_2^m\left[1-\frac{\alpha}{2}\frac{m_2}{m_2+m_4}\right] \qquad (15)$$

which shows that Γ_2 increases with increasing m_2 more slowly than does Γ_2^m and that when Γ_2^m is constant, Γ_2 should decrease with increasing m_2. If we assume that Γ_2^m and α have attained their limiting values at the surfactant critical micelle concentration (CMC) and are both independent of m_4, we can use Eq. (15) to calculate the change in Γ_2 at the CMC as m_4 is increased. The results of such a calculation agree well with experiment when Γ_2^m is taken as 4.33×10^{-6} mol m^{-2} and α is taken as 0.56. However, this value of α is much larger than that shown in Table 1. Consequently we conclude that only a small proportion of the increase in saturation adsorption of surfactant with increasing m_4 is due to the effect described by Eq. (15).

References

1) K. Shinoda and H. Nakayama, *J. Colloid Sci.*, **18**, 705 (1963).
2) E. H. Lucassen-Reynders, *ibid.*, **19**, 584 (1964).
3) K. Tajima, M. Muramatsu, and T. Sasaki, This Bulletin, **43**, 1991 (1970).
4) K. Tajima, *ibid.*, **43**, 3063 (1970).
5) K. Tajima, *ibid.*, **44**, 1767 (1971).
6) K. Tajima and T. Sasaki, *ibid.*, **45**, 348 (1972).
7) D. G. Hall, *J. Chem. Soc. Faraday II*, **68**, 1439 (1972).
8) A. L. Smith, personal communication.
9) F. van Voorst Vader, *Trans. Faraday Soc.*, **57**, 110 (1961).
10) B. J. Birch and D. E. Clarke, *Anal. Chim. Acta*, **61**, 159 (1972).
11) C. Botre, D. G. Hall, and R. V. Scowen, *Kolloid. Z.*, **250**, 900 (1972).
12) E. A. Guggenheim, *Phil. Mag.*, **19**, 588 (1935).
13) E. A. Guggenheim, "Applications of Statistical Mechanics," Clarendon press, Oxford (1966).
14) R. Matuura, H. Kimizuka, A. Matsubara, K. Matsunobu, and T. Matsuda, This Bulletin, **35**, 552 (1962).
15) J. H. Brooks and B. A. Pethica, *Trans. Faraday Soc.*, **61**, 571 (1965).
16) K. Shinoda, "Chemistry, Physics and Application of Surface Active Substances," Vol. 2, ed. by J. Th. G. Overbeek, Gordon and Breach (1967), p. 527.
17) C. P. Roe and P. D. Brass, *J. Amer. Chem. Soc.*, **76**, 4703 (1954).

Dielectric Dispersion and Relaxation Mechanism in Some Trifluoro Compounds at Microwave Frequencies

H. D. PUROHIT, H. S. SHARMA, and A. D. VYAS
Microwave Laboratory, University of Jodhpur, Jodhpur, India
(Received June 21, 1974)

The permittivity and dielectric loss of 2,2,2-trifluoroethanol and trifluoroacetic acid have been measured in benzene solutions at three microwave frequencies, 24.01, 9.83, and 6.01 GHz and also at 1 MHz and optical frequency at 35 °C. The permittivity and dielectric loss at different frequencies have been plotted against concentration (wt. fraction). The slopes of these straight lines have been used for the complex plane plots (a' *vs.* a''). The complex plane plots for 2,2,2-trifluoroethanol and trifluoroacetic acid are of the Cole-Cole type. The relaxation time (τ_0) and distribution parameter (α) have been calculated. The values of dipole moments (μ) of these compounds have also been calculated and reported. The relaxation mechanism in these two compounds has been explained.

Fluoro compounds have been of great interest because of their high value of permittivity in liquid state.[1] Ethanol and acetic acid are associated liquids and have a tendency to dimerize even at a very low dilution in benzene solution by intermolecular hydrogen bonding. The present investigations on 2,2,2-trifluoroethanol and trifluoroacetic acid have been made to study the effect of the replacement of CH_3 group by CF_3 group in ethanol and acetic acid on intermolecular hydrogen bonding. The dielectric dispersion and relaxation mechanism studies in these compounds have been carried out in dilute solutions of benzene[2] for the first time, to study their dielectric behaviour in explaining their molecular structure. The studies have been carried out in dilute solutions because this enables us to reduce to a considerable extent the dipole-dipole interaction and solute-solute co-operative phenomenon and also to avoid the ambiguity[3–5] concerning the internal field.

Method of Measurement and Analysis of Data.
The static permittivity was measured at a frequency 1 MHz by means of a Toshniwal dipolemeter type CL01 (INDIA) based on the principle of heterodyne beat method. The cell used for the purpose was calibrated with standard liquids. Refractive indices of all the solutions were measured for sodium D-line by the help of an Abbe's refractometer and the square of the refractive index gave the values of optical permittivity ($\varepsilon_\infty = n_D^2$).

The permittivity (ε') and dielectric loss (ε'') at microwave frequencies 24.01, 9.83, and 6.01 GHz were determined by the measurement of wavelength in the dielectric and standing wave ratio using a short circuited movable plunger by the method suggested by Heston *et al.*[6] adapted for short circuited termination. All measurements were carried out at 35 °C. The values of ε_0, ε_∞, ε', and ε'' thus obtained are recorded in Table 1.

The compounds used were obtained from Messrs Fluka, A. G. (Switzerland). They were of puriss grade having 99% purity. Their constants were checked with the literature values before use. Benzene, Analar grade (B.D.H., India) was used for making solutions and was distilled twice before use.

It has been observed that the permittivity and dielectric loss in solutions are linear functions of concentration.[7] Thus one can represent the permittivity and dielectric loss by the following equations:

TABLE 1. VALUES OF ε_0, ε', ε'', AND ε_∞ AT DIFFERENT FREQUENCIES FOR 2,2,2-TRIFLUROETHANOL AND TRIFLUOROACETIC ACID IN BENZENE SOLUTION AT CONSTANT TEMPERATURE OF 35 °C

Frequency / Concentration (wt. fraction)	1 MHz ε_0	Optical ε_∞	9.83 GHz ε'	9.83 GHz ε''	Frequency / Concentration (wt. fraction)	24.01 GHz ε'	24.01 GHz ε''	6.01 GHz ε'	6.01 GHz ε''
2,2,2-Trifluoroethanol									
0.0000	2.260	2.229	2.259	—	0.0000	2.256	—	2.260	—
0.0111	2.328	2.226	2.309	0.021	0.0112	2.304	0.027	2.332	0.031
0.0218	2.396	2.220	2.378	0.036	0.0218	2.339	0.055	2.391	0.037
0.0323	2.460	2.217	2.439	0.056	0.0318	2.405	0.076	2.458	0.046
0.0416	2.518	2.211	2.491	0.072	0.0439	2.433	0.101	2.522	0.056
0.0519	2.584	2.208	2.543	0.089	0.0515	2.472	0.121	2.569	0.062
Trifluoroacetic acid									
0.0000	2.255	2.229	2.259	—	0.0000	2.260	—	2.262	—
0.0123	2.318	2.223	2.308	0.046	0.0121	2.279	0.038	2.330	0.032
0.0251	2.370	2.217	2.338	0.068	0.0292	2.299	0.065	2.382	0.055
0.0378	2.428	2.211	2.381	0.083	0.0400	2.313	0.083	2.420	0.071
0.0486	2.470	2.208	2.395	0.100	0.0523	2.328	0.100	2.460	0.088
0.0646	2.534	2.202	2.446	0.120	0.0665	2.348	0.123	2.500	0.107

$$\left.\begin{aligned}\varepsilon_0 &= \varepsilon_{10} + a_0 W_2 \\ \varepsilon' &= \varepsilon_1 + a' W_2 \\ \varepsilon'' &= a'' W_2 \\ \varepsilon_\infty &= \varepsilon_{1\infty} + a_\infty W_2\end{aligned}\right\} \quad (1)$$

where ε_0 and ε_∞ are the static and the optical permittivity respectively. The subscript 1 refers to the pure solvent, W_2 is the concentration of the polar solute in weight fraction and a's are the slopes of the st. lines obtained by plotting the dielectric quantity against concentration. The slopes thus obtained are recorded in Table 2.

Table 2. Values of the slopes of plots of ε' and ε'' *versus* concentration for 2,2,2-trifluoroethanol and trifluoroacetic acid

Frequency	a'	a''
2,2,2-Trifluoroethanol		
1 MHz	$a_0=6.20$	...
6.01 GHz	5.90	0.85
9.83 GHz	5.40	1.65
24.01 GHz	4.28	2.30
Optical	$a_\infty=-0.40$	—
Trifluoroacetic acid		
1 MHz	$a_0=4.20$	...
6.01 GHz	3.22	1.40
9.83 GHz	2.72	1.48
24.01 GHz	1.50	1.60
Optical	$a_\infty=-0.38$	—

The values of τ_0 and α for 2,2,2-trifluoroethanol and trifluoroacetic acid have been calculated from the Cole-Cole[8] arc plots using the slopes (a', a''). These plots are shown in the Figs. 1 and 2.

Higasi[9] has also proposed that the values of relaxation time and the distribution parameter may be determined from the measurement of a' and a'' at a single frequency

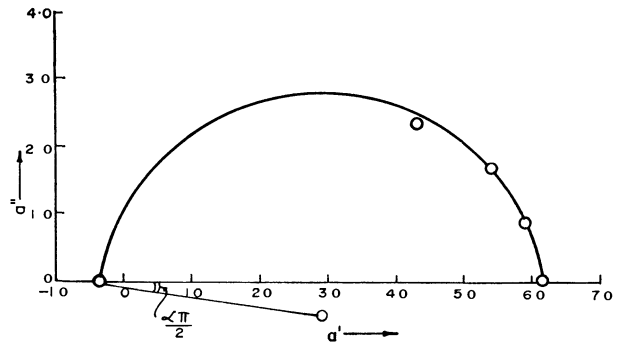

Fig. 1. The a', a'' plot of trifluoroethanol.

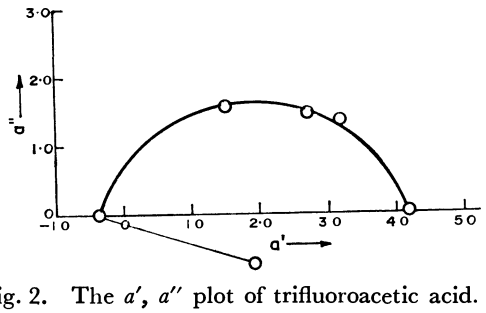

Fig. 2. The a', a'' plot of trifluoroacetic acid.

in the dispersion region. The equations for τ_0 and α are as follows:

$$\tau_0 = \frac{1}{\omega}\left(\frac{A^2+B^2}{C^2}\right)^{1/2(1-\alpha)} \quad (2)$$

$$1-\alpha = \left(\frac{2}{\pi}\right)\tan^{-1}\left(\frac{A}{B}\right) \quad (3)$$

$$\left.\begin{aligned}A &= a''(a_0-a_\infty) \\ B &= (a_0-a')(a'-a_\infty) - a''^2 \\ C &= (a'-a_\infty)^2 + a''^2\end{aligned}\right\} \quad (4)$$

For trifluoroethanol and trifluoroacetic acid, we have calculated τ_0 and α from Eqs. (2) and (3) using the data at 9.83 GHz. The values of τ_0 and α determined by these two methods have been compared in Table 3.

Table 3. Values of τ_0, α and μ for trifluoroethanol and trifluoroacetic acid

Compound	τ_0 (ps)		α		μ (D)
	Cole-Cole	Higasi	Cole-Cole	Higasi	
Trifluoroethanol	3.63	3.39	0.10	0.11	2.52[a]
Trifluoroacetic acid	8.91	8.58	0.21	0.22	2.26[b]

a) Present work, literature value not available. b) Literature value 2.28 D[20] (gas).

The dipole moments of these solute molecules have been calculated by the Eq. (5) proposed by Higasi[10]

$$\mu = A(a_0-a_D)^{1/2} \quad (5)$$

where A is a constant and is given by

$$A = \left[\frac{27kT}{4\pi N}\frac{M_2}{(\varepsilon_1+2)^2 d_1}\right]^{1/2} \quad (6)$$

Here d_1 is the density of the solvent and M_2 is the molecular weight of the solute. The values of dipole moments (μ) are also recorded in Table 3.

Results and Discussion

The complex plane plot a' *vs.* a'' in case of 2,2,2-trifluoroethanol is a Cole-Cole plot. The low value of relaxation time $\tau_0=3.63$ ps corresponds to the relaxation time of the hydroxyl group. Further the small value of distribution parameter ($\alpha=0.10$) points to the fact that the predominant mode of relaxation is the rotation of the hydroxyl group and not the rotation of the molecule as a whole. The tan δ-concentration curve is a straight line and does not show anomalous absorption so that there is no possibility of association as in the case of ethanol and other alcohols in benzene solution[11] which have a tendency for dimerization even at very low concentration. Krishnamurthy and Sundarajan[12] have examined the possibility of two extreme conformations, the *cis* and *trans* forms which refer to hydroxyl hydrogen being near or away from halogens. They have computed the equilibrium constant and corresponding free energies for isomerization of *cis*⇌*trans*, from the knowledge of the experimental and theoretical moments for the two conformers. Their results indicate that for trichloro and tribromo ethanols the equilibrium lies to the left (Structure I). This

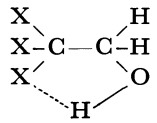

I *cis*

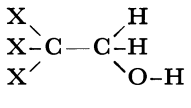

II *trans*

implies a stabilization of the *cis*-structure by intramolecular hydrogen bonding X—H–O. In tribromoethanol, the hydrogen-bonded form predominates to greater extent than in trichloroethanol. From spectroscopic studies Krueger and Mettee[13] have found that the intramolecular hydrogen bonding in trihaloethanols increases in the order $F_3C<Cl_3C<Br_3C$, a trend which is reverse of the normal accepted order of propensity of hydrogen bonding by halogens. The measurements of relaxation time and distribution parameter confirm the *trans*-structure (Structure II) of 2,2,2-trifluoroethanol. The dipole moment increases from tribromoethanol to trifluoroethanol *i.e.*

$Br_3C\cdot CH_2OH$	1.73 D[12]
$Cl_3C\cdot CH_2OH$	2.04 D[12]
$F_3C\cdot CH_2OH$	2.52 D*

(* present work.)

The dielectric studies of trifluoroacetic acid show that the molecule of trifluoroacetic acid remains in monomeric form in benzene solution as distinct from acetic acid and trichloroacetic acid[14] ($\mu=1.1$ D) which exist in the dimeric form even in dilute solutions. Tan δ-concentration curve is a straight line and shows no anomalous absorption. The complex plane plot a' *vs.* a'' is a Cole-Cole arc which shows that there is a symmetrical distribution of relaxation times. The relaxation time measurements ($\tau_0=8.91$ ps) show that the molecule relaxes predominantly by overall rotation, the other possibilities being rotation of carboxyl group about C–C axis and that of the hydroxyl group undergoing a torsional or restricted rotation, since the hydroxyl hydrogen does not lie in the plane of the rest of the carboxyl group. The large value of the distribution parameter ($\alpha=0.21$) points towards these possibilities.

The electron diffraction[15] and spectroscopic measurements[16,17] indicate the presence of a single bond between the hydroxyl oxygen and carboxyl carbon, with the hydroxyl group turned so that its hydrogen is well out of the OCO plane. By combining vectorially the group moment 1.73 D for the carboxyl group acting at the calculated angle 74° with the C–C bond, with the moment 2.35 D of 1,1,1-trifluoroethane[18,19] the value of 2.50 D is obtained which is in reasonable agreement with the observed value of 2.28 D[20] (gas). Thus the presence of the three atoms of fluorine which greatly increase the acidity of the molecule, does not greatly alter the moment of the carboxyl group. The hydroxyl hydrogen does not lie in the plane of the rest of the carboxyl group and is undergoing a torsional or restricted rotation with the hydrogen on an average well outside this plane.[20] The possibility of the existence of the molecule in isomeric planar form is not completely excluded.

The authors are indebted to Professor Krishnaji, University of Allahabad, Allahabad, for his helpful advice and discussions. Their thanks are also due to Professor A. N. Nigam, Head of Physics Department of this University for providing facilities for the study and to Professor G. P. Srivastava, University of Delhi, Delhi, for the facilities provided in connection with some measurements.

References

1) J. H. Simson and K. E. Lorentzen, *J. Amer. Chem. Soc.*, **72**, 1426 (1950).
2) H. S. Sharma, Dielectric dispersion and relaxation mechanism, D. Phil. Thesis, Jodhpur University, Jodhpur (1971).
3) C. P. Smyth, "Dielectric Behaviour and Structure," McGraw Hill Co., New York (1955), Chapter 2.
4) C. J. F. Böttcher, "Theory of Electric Polarisation," Elsevier Publishing Co., Amersterdam (1952), Chapter 6.
5) R. H. Cole, *J. Chem. Phys.*, **43**, 637 (1965).
6) W. M. Heston, Jr., A. D. Franklin, E. J. Hennelly, and C. P. Smyth, *J. Amer. Chem. Soc.*, **72**, 3443 (1950).
7) A. D. Franklin, W. M. Heston, Jr., E. J. Hennelly, and C. P. Smyth, *ibid.*, **72**, 3447 (1950).
8) K. S. Cole and R. H. Cole, *J. Chem. Phys.*, **9**, 341 (1941).
9) K. Higasi, This Bulletin, **39**, 2157 (1966).
10) K. Higasi, *Bull. Inst. Phys. Chem. Research*, **22**, 865 (1943).
11) H. D. Purohit and H. S. Sharma, *Indian J. Pure Appl. Phys.*, **9**, 450 (1971).
12) S. S. Krishnamurthy and S. Sundarajan, *J. Phys. Chem.*, **73**, 4036 (1969).
13) P. J. Krueger and H. D. Mettee, *Can. J. Chem.*, **42**, 340 (1964).
14) R. J. W. LeFevre and H. Vine, *J. Chem. Soc., Part 2*, **1938**, 1795.
15) J. Karle and L. O. Brockway, *J. Amer. Chem. Soc.*, **66**, 574 (1944).
16) G. Connet and R. Hofstadter, *J. Chem. Phys.*, **6**, 531 (1938).
17) M. M. Davies and L. B. Sutherland, *ibid.*, **6**, 755 (1938).
18) C. H. Townes, R. G. Shulman, and B. P. Dailly, *Phys. Rev.*, **76**, 472 (1949).
19) R. M. Fuoss, *J. Amer. Chem. Soc.*, **60**, 1633 (1938).
20) J. H. Gibbs and C. P. Smyth, *ibid.*, **73**, 5115 (1951).

Kinetics and Mechanism of Oxidation of D(+)-Sorbose by Chloramine-T

R. SANEHI, K. C. GUPTA, R. M. MEHROTRA, and S. P. MUSHRAN*
Chemical Laboratories, University of Allahabad, Allahabad, India
(Received July 2, 1974)

The kinetics of oxidation of D(+)-sorbose by chloramine-T has been investigated in high alkaline media. The reaction shows a brief induction period after which a first order dependence in both chloramine-T and substrate is followed. The order in hydroxide ion is observed as fractional being 1.3 under the experimental conditions. The values of energy of activation, frequency factor and entropy of activation have been computed as 28.2 kcal mol^{-1}, 2.90×10^{19} l mol^{-1} s^{-1} and +29.8 e.u. respectively. A plausible mechanism consistent to the experimental result is proposed.

Reducing sugars have been oxidised using several oxidants. The most common oxidants used have been halogens and mainly bromine water. The earlier work on these investigations has been reviewed by Green[1] and Shafizadeh.[2] Isbell and co-workers[3,4] have investigated the oxidation of several reducing sugars by bromine and concluded that β-form of the sugar was more reactive than α-form. The kinetics of oxidation of several sugars (aldoses and ketoses) by chromium (VI),[5] peroxydisulphate[6] were investigated. Ghosh and co-workers[7] studied the kinetics and mechanism of oxidation of various reducing sugars by ammoniacal silver nitrate. The reactions were found to be first order dependent on silver nitrate and independent to the reducing substrate and a suitable mechanism was suggested. Recently Mushran and co-workers[8,9] have investigated the kinetics and mechanism of oxidation of various aldoses (*viz.* xylose, arabinose, ribose, mannose, and galactose) by chloramine-T in high alkaline media.

It was observed that the oxidation of ketose *viz.* D(+)-sorbose by chloramine-T takes place only in highly alkaline media. In this communication, the study of the kinetics of oxidation of D(+)-sorbose by chloramine-T is made and a suitable mechanism is suggested.

Experimental

Aqueous solution of D(+)-sorbose (AR, B.D.H. sample) was always freshly prepared. Stock solutions of chloramine-T, osmium (VIII) and sodium hydroxide were prepared as mentioned earlier.[10] All other chemicals used were of analytical grade. Double-distilled water was always used for preparation and dilution of the solutions. The reactions were carried out in outside blackened Jena glass bottles to avoid any photochemical influences.

The alkali sugar mixture was allowed to equilibrate for exactly 45 min after which chloramine-T was added to start the reaction. The kinetics was followed by estimating chloramine-T iodometrically in aliquot portion of the reaction mixture withdrawn in different interval of time.

Stoichiometry. Reaction mixture containing excess of chloramine-T over sorbose were allowed to equilibrate at 50 °C in respective sodium hydroxide concentration. The results showed that 1 mol of sorbose was oxidised by 1 mol of chloramine-T to the aldonic acid of lesser one carbon atom than the parent ketose and thus the stoichiometric equation may be represented as follows:

$$\underset{\text{Chloramine-T}}{CH_3C_6H_4SO_2N\cdot NaCl} + \underset{\text{D(+)-sorbose}}{CH_2OH\cdot C(-O-)(OH)\,(CHOH)_3\text{-}CH_2} + OH^- = CH_3C_6H_4SO_2NH_2 + \underset{\text{Xylonic acid anion}}{^-OOC(CHOH)_3\cdot CH_2OH} + HCHO + NaCl \quad (1)$$

The product formaldehyde was confirmed by spot test.[11]

Results

The kinetics of oxidation of D(+)-sorbose by chloramine-T in alkaline media was investigated and it was observed that the reaction shows a marked induction period. The influence of the change of equilibrating time of sugar-alkali mixture on induction period was studied. The results show that induction period diminishes as the time of equilibrating increases and after 45 min of equilibrating time, the induction period almost disappears (Fig. 1).

The kinetics of oxidation of D(+)-sorbose by chloramine-T was followed at several initial concentrations of reactants. It was observed that the reaction follows a first order dependence in chloramine-T. Pseudo first order rate constants (k_1) in chloramine-T, calculated from the slope of the linear log-time plots, increase linearly with the increase of sugar concentration. The second order rate constants $k_2=k_1/[\text{Sorbose}]$ were calculated and the average value of k_2 was ob-

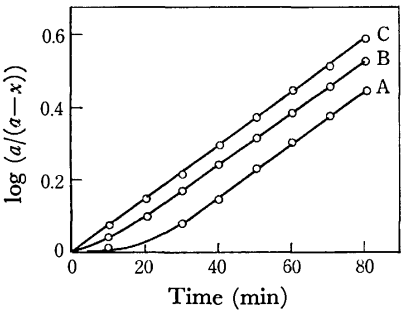

Fig. 1. First order plots at 32.5 °C.
[D(+)-sorbose]=2.0×10^{-2} M, [Chloramine-T]=2.0×10^{-3} M, [NaOH]=0.05 M, [KCl]=0.1 M and equilibrating time=0, 30, and 45 min for A, B, and C respectively.

* To whom correspondence should be made.

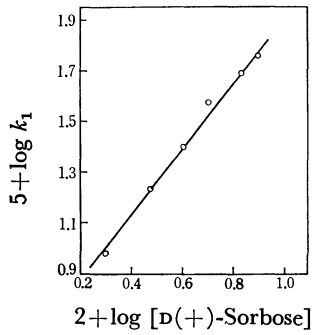

Fig. 2. Plot of log k_1 *vs.* log [D(+)-sorbose]. Conditions same as in Table 1 at [Chloramine-T]= 2.0×10^{-3} M.

tained as 13.3 l mol^{-1} s^{-1} (Table 1). The slope of the linear plot of log k_1 *vs.* log [D(+)-sorbose] (Fig. 2) was found to be unity which establishes a first order dependence in sugar concentration.

Table 1. Effect of reactants' concentration on rate constants[a)]

10^3[Chloramine-T] M	10^2[D(+)-sorbose] M	$k_1\times10^5$ s^{-1}	$k_2\times10^3$ l mol^{-1} s^{-1}
2.0	2.0	28.0	—
2.4	2.0	27.8	—
2.8	2.0	26.9	—
3.2	2.0	26.0	—
2.0	1.0	13.2	13.2
2.0	1.3	17.8	12.9
2.0	1.6	22.5	14.1
2.0	2.5	33.8	13.5
2.0	3.0	39.1	13.0

a) In presence of 0.05 M NaOH, equilibrating time=45 min and temp.=32.5 °C.

The kinetic investigations were carried out at several initial concentrations of hydroxide ions at constant ionic strength (μ=0.1 M). It was observed that the rate of oxidation of D(+)-sorbose is highly susceptible to change in alkali concentration. The order of the reaction in hydroxide ion was calculated from the slope of the plot of log k_1 *vs.* log [OH$^-$] (Fig. 3) as 1.3 for the oxidation of sorbose by chloramine-T.

The influence of neutral salts *viz.* $NaClO_4$ and KCl was investigated (Table 2). The results show that this reaction exhibits a positive salt effect.

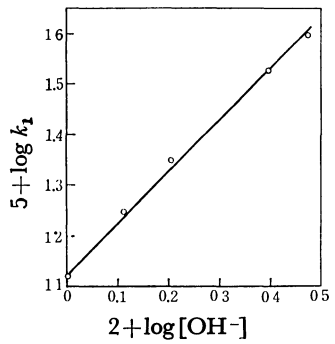

Fig. 3. Plot of log k_1 *vs.* log [OH$^-$] at 32.5 °C. [D(+)-sorbose]=2.0×10^{-2} M, [Chloramine-T]=2.0×10^{-3} M, equilibrating time 45 min and μ=0.1 M.

Table 2. Effect of neutral salts on the reaction rates[a)]

μ M	$k_1\times10^5$ s^{-1}	
	$NaClO_4$	KCl
0.05	30.9	30.0
0.10	38.1	37.3
0.20	46.1	44.1
0.35	52.6	56.4
0.50	66.8	—

a) [Chloramine-T]=2.0×10^{-3} M, [D(+)-sorbose]= 2.0×10^{-2} M, [NaOH]=0.05 M, equilibrating time =45 min and temp.=32.5 °C.

A negligible effect of dielectric constant of the media on the reaction rate was observed. Like the oxidation of aldoses,[8,9)] osmium (VIII) ions were found to be inactive as a catalyst on the rate of oxidation of ketose by chloramine-T.

The effect of temperature was quite marked on the rate constants. The values of energy of activation, frequency factor and entropy of activation were obtained as 28.2 kcal mol^{-1}, 2.90×10^{19} l mol^{-1} s^{-1} and +29.8 e.u. respectively.

Discussion

Extensive investigations of Howorth and co-workers[12)] have shown that sugars exist as ring structures and not as open chain compounds. The most generally referred structure of sorbose is pyranose structure. It is well known that ketoses in alkaline solutions exist as anion derived from β-anomers.[13,14)] Thus the following steps are involved:

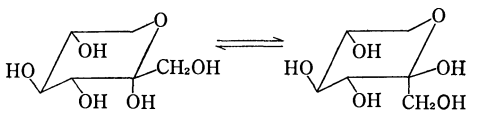

(2a)

α-D(+)-sorbopyranose β-D(+)-sorbopyranose

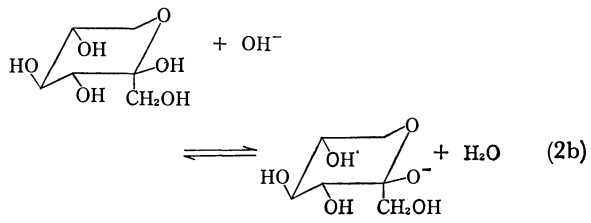

(2b)

anion of β-D(+)-sorbopyranose

It has been now generally accepted that β-form of the sugar is more reactive as compared to α-form. Furthermore, Hayman and Persky[14)] suggested that the anion of β-anomers is more reactive as compared to its unionised molecule.

Chloramine-T (CAT) in alkaline solutions[15)] hydrolyses to *p*-chlorotoluene sulphonamide (CAT'), *p*-toluene sulphonamide (TSA) and hypochlorite ion (ClO^-) and the steps are given as follows:

$$CH_3C_6H_4SO_2N\cdot NaCl + H_2O \underset{\text{CAT}}{} \rightleftharpoons CH_3C_6H_4SO_2NHCl + NaOH \quad (3a)$$
CAT'

$$CH_3C_6H_4SO_2NHCl + NaOH \rightleftharpoons \underset{TSA}{CH_3C_6H_4SO_2NH_2} + Na^+ + ClO^- \quad (3b)$$

From close examinations of steps (3a) and (3b) and the catalysing nature of alkali reveal the fact that any one of the hydrolysis product *viz.* CAT itself, or ClO^- would be the oxidising species. Further, a positive effect of salt clearly points out to the fact that ClO^- ion would occur in the slowest and rate determining step.

Thus, first order dependence of the reaction rate in each chloramine-T and sorbose and fractional order (1.3) dependence in hydroxide ion leads to the contention that the rate determining step involves the anion of β-D(+)-sorbopyranose, hypochlorite ion and hydroxide ion. The oxidation products were found as formaldehyde and xylonic acid and a mechanism is suggested as follows:

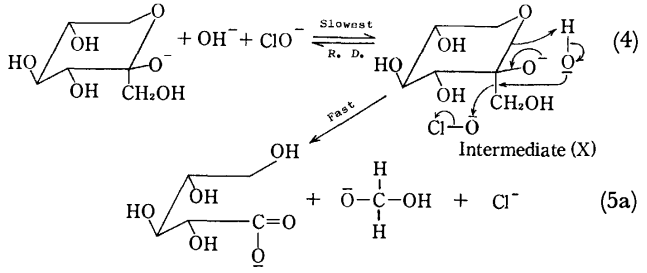

$$\bar{O}\text{-}\underset{H}{\overset{H}{C}}\text{-}OH \xrightarrow{\text{fast}} HCHO + OH^- \quad (5b)$$

The mechanism of oxidation of D(+)-sorbopyranose (S) by chloramine-T may, therefore, be summarised as follows:

$$S + OH^- \underset{k_{-2}}{\overset{k_2}{\rightleftharpoons}} S^- + H_2O \quad \text{slow} \quad (2)$$

$$CAT + H_2O \underset{k_{-4}}{\overset{k_4}{\rightleftharpoons}} TSA + Na^+ + ClO^- \quad \text{fast} \quad (3)$$

$$S^- + ClO^- + OH^- \xrightarrow{k_5} \text{Intermediate (X) slowest and R.D.} \quad (4)$$

$$X \xrightarrow{k_6} \text{Products fast} \quad (5)$$

In the above scheme the step (2) is also slow but not so slow as the rate determining step (4). On adding sugar to the alkali solution, the concentration of sugar anion (S^-) increases with time. After some time when S^- becomes sufficiently high, the consumption of S^- in step (4) becomes regular and steady state is achieved. The steady state in oxidation of ketose is thus not achieved instantaneously as has also been observed in the first order rate plots (Fig. 1) where there are induction period effects. As the alkali sugar mixture has been equilibrated for 45 min for these investigations, the induction period has completely vanished. It has also been experimentally observed that the induction period minimises on increasing the temperature of the reaction mixture.

Applying steady state condition to (S^-), the rate of disappearance of ClO^- is given as:

$$-\frac{d}{dt}[ClO^-] = \frac{k_2k_5[S][ClO^-][OH^-]^2}{k_{-2}[H_2O] + k_5[ClO^-][OH^-]} \quad (6)$$

In highly alkaline solution, ClO^- may be taken as CAT and thus Eq. (6) becomes

$$-\frac{d}{dt}[CAT] = \frac{k_2k_5[S][CAT][OH^-]^2}{k_{-2}[H_2O] + k_5[CAT][OH^-]} \quad (7)$$

The derived Eq. (7) predicts first order dependence in both chloramine-T and sugar and a fractional order in hydroxide ion concentration. At very low concentration of alkali *i.e.* $k_{-2}[H_2O] \gg k_5[CAT][OH^-]$, the order in OH^- would be 2 and at very high concentration of alkali when $k_{-2}[H_2O] \ll k_5[CAT][OH^-]$, the dependence of the reaction rate on alkali would be unity. At the experimental conditions, however, both the extreme conditions are not achieved and thus the reaction shows a fractional order dependence in $[OH^-]$ ion being 1.3. Further from Eq. (7), the rate constant should decrease on increasing the chloramine-T concentration which has also been observed experimentally (Table 1).

A positive salt effect also confirms the rate controlling step (4). Since the rate determining step involves three similarly charged ions and, therefore, a high energy of activation value is expected and this is in agreement with the high experimental value observed *viz.* 28.2 kcal mol^{-1}.

R. S. and R. M. M. are thankful to CSIR and UGC, New Delhi for the award of Senior Research Fellowships.

References

1) J. W. Green, *Advan. Carbohydrate Chem.*, **3**, 129 (1948).
2) F. Shafizadeh, *ibid.*, **13**, 9 (1958).
3) H. S. Isbell, *J. Amer. Chem. Soc.*, **54**, 1692 (1932).
4) H. S. Isbell and W. W. Pigman, *J. Res. NBS*, **18**, 141 (1937).
5) M. D. Bon, *Nauk. Zapiski Krivonz'k Derzhav. Pedagog. Inst.*, No. 2, 107 (1957).
6) S. P. Srivastava and G. B. Purohit, *Vijnana Parishad Anusandhan Patrika*, **4**, 199, 303 (1961).
7) A. P. Modi and S. Ghosh, *J. Indian Chem. Soc.*, **46**, 687, 807 (1969).
8) M. C. Agrawal and S. P. Mushran, *J. Chem. Soc. Perkin II*, 762 (1973).
9) S. P. Mushran, K. C. Gupta, and R. Sanehi, *J. Indian Chem. Soc.*, **51**, 145 (1974).
10) S. P. Mushran, R. Sanehi, and M. C. Agrawal, *Z. Naturforsch*, **27b**, 1161 (1972).
11) Fritz Feigl, "Qualitative Analysis by Spot Tests," Elsevier Publishing Company, Inc., New York (1946), p. 395.
12) W. N. Haworth, "The Constitution of Sugars," Edward Arnold and Co., London (1929).
13) I. R. L. Barker, W. G. Overend, and C. W. Rees, *Chem. Ind.*, **1960**, 1298.
14) B. Perlmutter-Hayman and A. Persky, *J. Amer. Chem. Soc.*, **82**, 276 (1960).
15) A. Berka, J. Zyka, and J. Vulterin, "Newer Redox Titrants," Pergamon Press, New York (1965).

NOTES

BULLETIN OF THE CHEMICAL SOCIETY OF JAPAN, VOL. 48 (1), 333—334 (1975)

X-Ray Photoelectron Spectroscopy of EDTA-Metal Chelates

Tooru YOSHIDA and Shigemasa SAWADA

Osaka Prefectural Industrial Research Institute, Enokojima, Nishi-ku, Osaka 550

(Received March 4, 1974)

Synopsis. Photoelectron spectra of metal chelates of ethylenediaminetetraacetic acid (EDTA) were measured. A nearly linear relationship holds between the chemical shifts of the N(1s) electron binding energies and the charge on the nitrogen atoms of the chelates, calculated by means of Pauling's electronegativity concept.

A technique for studying X-ray photoelectron spectroscopy (ESCA) and the results for EDTA were previously reported.[1] The use of ESCA to determine the effect of coordination on the electron density of a ligand is based on the fact that changes in the electron density about an atom are reflected on changes in the binding energies of the core electrons. It is the aim of this study to determine whether it will be possible to correlate the electronegativity of the metal or the calculated charge on the nitrogen atom with the chemical shift of N(1s) binding energy in the EDTA-metal chelates. The chelate compounds studied (commercial products, analytical grade) are given in Table 1. Al$K\alpha$ X-ray was used as an excitation source.

The C(1s), N(1s), and O(1s) electron spectra of the EDTA-Zn chelate are shown in Fig. 1. The spectra of all the other compounds show profiles similar to those of the EDTA-Zn chelate. Two peaks in the C(1s) electron spectrum correspond to the carbon atoms of a methylene group and a carbonyl group, respectively. The peak with the lower binding energy (the carbon of the methylene group) was used as an energy standard, its binding energy being taken to be 285.0 eV throughout this experiment. The N(1s) and O(1s) electron spectra of all compounds were single peaks with full-width at half-height (FWHH) of 2.0—2.2 eV and 2.1—2.3 eV, respectively. The measured

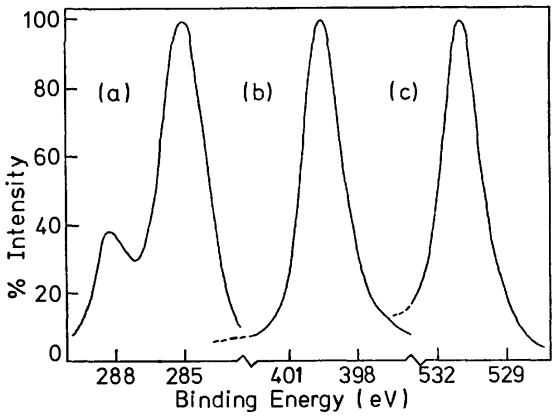

Fig. 1. (a) C(1s), (b) N(1s) and (c) O(1s) photoelectron spectra of the EDTA-Zn chelate.

N(1s) electron binding energies are given in Table 1. The chemical shifts ΔE are the differences between the N(1s) electron binding energies of free EDTA (the type of $(-CH_2)_3N$) and the chelates. The value of free EDTA was 399.1 eV.[1] The chemical shifts in all chelates are considered to be due to the decrease in the electron density on the nitrogen atoms caused by the coordination of lone-pair electrons of the nitrogen atoms to the metal.

In the charge-potential model[2] the chemical shift can be expressed in terms of the charge on the atom Q and the Coulomb potential energy V of an electron due to the other atoms of the molecule:

$$\Delta E = k_1 Q + V + k_2 \quad (k_1, k_2; \text{ constants})$$

In an ionic compound, V includes the contribution

Table 1. N(1s) binding energy values

Compounds	M	B.E. of N(1s)[a] (eV)	ΔE[b] (eV)	χ[c]	Q[d]	pK[e]
EDTA,NaM(II)	Ba	399.1	0	0.9	−0.21	7.7
	Ca	399.2	+0.1	1.0	−0.18	10.7
	Mg	399.3	+0.2	1.2	−0.12	8.6
	Mn	399.3	+0.2	1.5	−0.01	13.9
	Zn	399.5	+0.4	1.6	+0.04	16.5
	Pb	399.6	+0.5	1.8	+0.12	18.0
	Ni	399.6	+0.5	1.8	+0.12	18.5
	Co	399.6	+0.5	1.8	+0.12	16.2
	Cu	399.5	+0.4	1.9	+0.16	18.8
EDTA, NaM(III)	Fe	399.2	+0.1	1.8	+0.12	25.1
	Bi	399.2	+0.1	1.9	+0.16	—

a) Uncertainties are less than or equal to ±0.1 eV. b) Chemical shift of the N(1s) electron binding energy. c) Pauling's electronegativity of the metal. d) Calculated charge on the nitrogen atom. e) The common logarithm of the stability constant of a chelate.

from other ions and is thus a Madelung term. V may play a very important role in ionic compounds. However, for the covalent species the chemical shift should be dominated by the charge Q on the atom concerned.

The charge Q was calculated by means of the correlation $Q=q+\sum I$, proposed by Nordberg *et al.*,[3] where Q is the charge on an atom, q the formal charge of a concerned atom and $\sum I$ the summation of partial ionic characters of various bonds in which the atom is involved. The partial ionic character I was estimated by the relationship $I=1-\exp\{-0.25(\chi_A-\chi_B)^2\}$ derived by Pauling,[4a] in which χ_A and χ_B are the electronegativities of A and B atoms, respectively, in the A–B bond concerned.

In the case of EDTA chelates, the relation $Q=1+3I_{N^+-C}+I_{N^+-M}$ was obtained for the charge on the nitrogen atom since q is $+1$. I_{N^+-C} and I_{N^+-M} are the partial ionic characters in the nitrogen-carbon and nitrogen-metal bonds, respectively. The calculated charges using the value 3.3 as the electronegativity of N^+ [4b] are listed in Table 1.

On the other hand, the charge calculated in this way on the nitrogen atom of the type of $(-CH_2)_3N$ in free EDTA was -0.18. This value corresponds to the charge (-0.20) on the nitrogen atom in $(CH_3)_3N$ calculated by del Re,[5] by a semiempirical LCAO-MO method.

A nearly linear relation holds between the chemical shift of the N(1s) electron binding energy (ΔE) and the charge Q on the nitrogen atom in the bivalent metal chelates (Fig. 2). The chemical shifts of the N(1s) in Ba and Ca chelates are very small as expected from their calculated charges.

There are certain trends in the bivalent metal chelates between the chemical shift and the electronegativity of the metal, and between the chemical shift and the common logarithm of the stability constant[6] of the chelate. The chemical shift becomes larger as the electronegativity becomes larger, and the stability of chelates

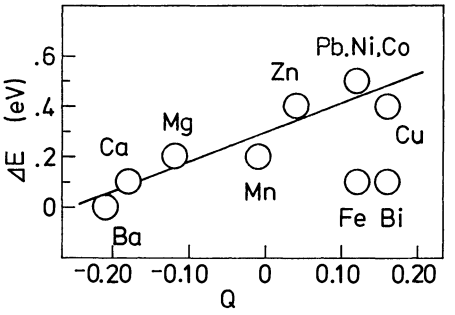

Fig. 2. Relationship between the chemical shift of N(1s) electron binding energy (ΔE) and the charge(Q) on the nitrogen atom.

becomes greater.

In the case of Fe(III) and Bi(III), their chemical shifts are small as compared to those expected from their calculated charges.

There is no appreciable difference in the O(1s) electron binding energy over all the chelates, values being 531.0—531.2 eV.

References

1) T. Yoshida and S. Sawada, This Bulletin, **47**, 50 (1974).

2) K. Siegbahn, C. Nordling, A. Fahlman, K. Nordberg, K. Hamrin, J. Hedman, J. Johansson, T. Bergmark, S. E. Karlson, I. Lindgren, and B. Lindberg, "ESCA Applied to Free Molecule," North Holland, Amsterdam (1969).

3) R. Nordberg, R. G. Albridge, T. Bergmark, U. Ericson, J. Hedman, C. Nordling, K. Siegbahn, and B. J. Lindberg, *Ark. Kemi*, **28**, 257 (1967).

4) a) L. Pauling, "The Nature of the Chemical Bond," 3rd Ed., New York (1960), p. 98; b) L. Pauling, "The Nature of the Chemical Bond," 2nd Ed., New York (1945), p. 65.

5) Giuseppe del Re, *J. Chem. Soc.*, **1958**, 4031.

6) K. Ueno and T. Sakaguchi, "Kinzoku Kireito," Vol. 3, Nankodo Co., Tokyo (1967), p. 65.

BULLETIN OF THE CHEMICAL SOCIETY OF JAPAN, VOL. 48 (1), 335—336 (1975)

The Chlorine Nuclear Quadrupole Resonance in an Organic Free Radical, *p*-Cl-BDPA

Toshio YOSHIOKA, Jun YAMAUCHI,* Hiroaki OHYA-NISHIGUCHI, and Yasuo DEGUCHI**

Department of Chemistry, Faculty of Science, Kyoto University, Sakyo-ku, Kyoto 606

**The Institute for Chemical Research, Kyoto University, Uji 611*

***College of Liberal Arts and Science, Kyoto University, Kyoto 606*

(Received March 29, 1974)

Synopsis. The ^{35}Cl nuclear quadrupole resonance in a stable organic free radical, 1,3-bisdiphenylene-2-*p*-chlorophenyl-allyl, has been measured from 4.2 to 1.6 K. On lowering the temperature, the resonance line became weaker and broader, and it disappeared near the Néel temperature. This behavior has been interpreted in terms of the presence of a hyperfine interaction.

The magnetic property of a stable organic free radical, *p*-Cl-BDPA (1,3-bisdiphenylene-2-*p*-chlorophenyl-allyl), has been investigated by examining the magnetic susceptibility and by ESR, PMR, and heat capacity measurements.[1-3] The *p*-Cl-BDPA radical has the molecular structure shown in Fig. 1. The

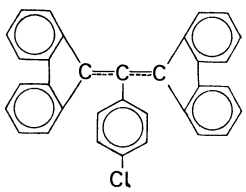

Fig. 1. Molecular structure of *p*-Cl-BDPA

unpaired electron is delocalized over the whole molecular framework. In the paramagnetic region, *p*-Cl-BDPA exhibits a one-dimensional antiferromagnetism, with a Heisenberg-type isotropic exchange interaction ($J/k=-4.4$ K), and undergoes a magnetic-phase transition to the antiferromagnetic state ($T_N=3.25$ K). In this note, we would like to report on our results on the ^{35}Cl nuclear quadrupole resonance (NQR) in a polycrystalline sample of *p*-Cl-BDPA. One of the objects of this study is to investigate the effects on the NQR of the electron-spin fluctuation near the magnetic-phase transition.

There have been few works so far concerned with the ^{35}Cl NQR measurements of paramagnetic organic substances, except for the charge-transfer complexes which exhibit a weak paramagnetism.[4] At room and liquid nitrogen temperatures, we could not find any ^{35}Cl resonance line in *p*-Cl-BDPA, probably because of the line broadening. In order to improve the signal-to-noise ratio, therefore, we carried out NQR measurements in the liquid-helium-temperature region, as a saturation effect at low temperatures usually encountered in diamagnetic substances could be excluded in our paramagnetic sample.

A sample of about 1.5 g of *p*-Cl-BDPA was prepared according to the procedure of Kuhn and Neugebauer,[5] as introduced in a previous paper.[1] The ^{35}Cl NQR line was searched for in the frequency range of 30—40 MHz at the temperature of liquid helium with a Dean-type super-regenerative detector,[6] equipped with the frequency modulation of 40 Hz. We could find one broad line on an oscilloscope; its signal-to-noise ratio was about three. The resonance frequency was determined to be 35.117 ± 0.005 MHz on the oscilloscope by use of a VHF signal generator (Meguro-Denpa-Sokki MSG-235) and a frequency counter (Takeda Riken TR-5667). The resonance was also studied by means of a recording technique employing a narrow-band amplifier and a phase-sensitive detection. A typical tracing is shown in Fig. 2(a). On lowering the temperature from 4.2 K by pumping of liquid helium, the resonance line became broader and weaker; it was not detected at 3.0 K, not even by the recording procedure, as is shown in Figs. 2(b) and (c). The resonance frequency did not appreciably change in the 4.2—3.5 K temperature range. Unsuccessful attempts were made to find new ^{35}Cl resonance lines at 1.6 K. When the temperature returned to 4.2 K, the resonance line was reproduced at the same frequency.

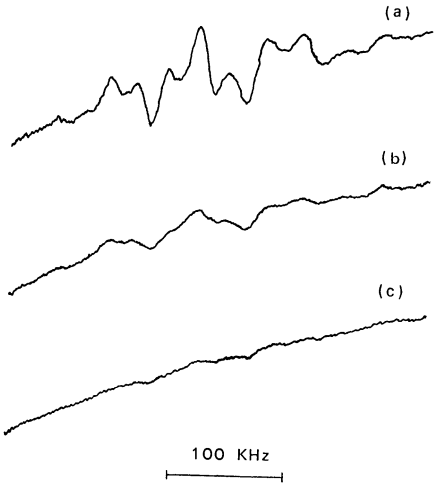

Fig. 2. Tracings of ^{35}Cl nuclear quadrupole resonance in a polycrystalline sample of *p*-Cl-BDPA.
(a) $T=4.2$ K, (b) $T=3.4$ K, (c) $T=3.2$ K
In each case the quenching frequency was about 40 kHz.

We have already investigated the mechanisms of the electron-proton hyperfine interaction in an organic free radical by PMR in single crystals of the DPPH–benzene complex.[7] Taking these results into account, the Hamiltonian for a free radical in which one chlorine nucleus interacts with the electric-field gradient at the chlorine site and one unpaired electron can be described by the following equation:

$$\mathcal{H} = \mathcal{H}_Q + a\boldsymbol{S}\cdot\boldsymbol{I} + \boldsymbol{S}\cdot\boldsymbol{D}\cdot\boldsymbol{I} \quad (1)$$

where $\mathcal{H}_Q$, a, and $\boldsymbol{D}$ are the quadrupolar Hamiltonian, the isotropic hyperfine coupling constant, and the traceless dipolar tensor respectively. The second term is an isotropic-hyperfine part arising from Fermi contact interaction, and the third term is an anisotropic part due to the electron-nuclear dipolar interaction. These terms depend upon the spin densities on the chlorine atom and the carbon atom adjacent to the chlorine. In our concentrated paramagnetic system, the correlation time is short in comparison with the nuclear precessional frequency because of the strong electron-exchange interaction; therefore, the resonance line is subjected to the so-called exchange narrowing, and then the electron spin, $\boldsymbol{S}$, of Eq. (1) is replaced by $\langle\boldsymbol{S}\rangle+\delta\boldsymbol{S}$. Here, $\langle\boldsymbol{S}\rangle$ is the time average of $\boldsymbol{S}$, and $\delta\boldsymbol{S}$ is the electron-spin fluctuation, which may provide a mechanism for nuclear-spin relaxation at low temperatures through the hyperfine interaction.[8] In the paramagnetic region, $\langle\boldsymbol{S}\rangle$ vanishes when there is no external field. Hence, the pure NQR eigenvalues are unaffected by the presence of the hyperfine interaction. The ^{35}Cl resonance frequency of *p*-Cl-BDPA is near that of chlorobenzene, which has been determined to be 34.6216 MHz at the temperature of liquid nitrogen.[9] This fact indicates that the electric-field gradient at the chlorine site is not intensively affected by the unpaired electron; that is, the unpaired electron is not delocalized very much on the *p*-chlorophenyl ring. From the electron-nuclear double resonance (ENDOR) results for *p*-Cl-BDPA,[10] the unpaired electron-spin density on the carbon atom adjacent to the chlorine can be estimated to be about 0.01 at most. The unpaired electron could also be distributed slightly on the chlorine atom.

The broadening of the resonance line may be interpreted as indicating that the correlation time becomes longer because of the short-range magnetic ordering below the temperature of the susceptibility maximum (T_m=5.6 K). This result corresponds to the line broadening of the ESR and PMR in this temperature region.[1,2] The disappearance of the ^{35}Cl resonance line near the temperature of 3.2 K is attributable to a magnetic-phase transition to the antiferromagnetic state at T_N=3.25 K.[3] This fact is consistent with the disappearance of the ESR and PMR lines near the Néel temperature.[1,2] In the antiferromagnetic state, the time-averaged spin, $\langle\boldsymbol{S}\rangle$, does not vanish even in the absence of an external magnetic field and is proportional to the sublattice magnetization, $M(T)$. Therefore, the pure NQR eigen values are affected by the internal field created by electron-spin through the hyperfine interaction of Eq. (1). Below the Néel temperature, a hyperfine splitting is expected in the ^{35}Cl NQR as a result of the weak hyperfine interaction between the chlorine nucleus and the unpaired electron, although the crystal structure of *p*-Cl-BDPA and the spin structure in the antiferromagnetic state are not determined. Unfortunately, however, new ^{35}Cl resonance lines could not be detected at 1.6 K in the 30—40 MHz frequency range. This result is probably due to the lack of spectrometer sensitivity, a line broadening in the antiferromagnetic state which has not been investigated in such a delocalized spin system, or some other effect. We hope to determine the crystal structure and the spin structure in the antiferromagnetic state in the future.

The authors would like to express their thanks to Dr. Nobuo Nakamura, Osaka University, for his helpful advice regarding the Dean-type spectrometer operation.

References

1) J. Yamauchi, This Bulletin, **44**, 2301 (1971).
2) K. Uchino, J. Yamauchi, H. Ohya-Nishiguchi, and Y. Deguchi, *ibid.*, **47**, 285 (1974).
3) J. Yamauchi, K. Adachi, and Y. Deguchi, *Chem. Lett.*, **1972**, 733; *J. Phys. Soc. Japan*, **35**, 443 (1973).
4) H. Chihara and N. Nakamura, This Bulletin, **44**, 2676 (1971).
5) R. Kuhn and F. A. Neugebauer, *Monatsh.*, **95**, 3 (1964).
6) C. Dean, *Rev. Sci. Instr.*, **31**, 934 (1960).
7) T. Yoshioka, H. Ohya-Nishiguchi, and Y. Deguchi, This Bulletin, **47**, 430 (1974).
8) K. R. Jeffrey, B. L. Armstrong, and K. E. Kisman, *Phys. Rev.*, **B1**, 3770 (1970).
9) R. Livingston, *ibid.*, **82**, 289 (1951).
10) K. Watanabe, J. Yamauchi, H. Ohya-Nishiguchi, Y. Deguchi, and K. Ishizu, *Chem. Lett.*, **1974**, 489.

BULLETIN OF THE CHEMICAL SOCIETY OF JAPAN, VOL. 48 (1), 337—338 (1975)

The Catalytic Reduction of Nitric Oxide by Carbon Monoxide over a Fe_2O_3 Catalyst

Yoshihiro SUGI, Naoyuki TODO, and Toshio SATO
National Chemical Laboratory for Industry, 2-19-19, Mita, Meguro-ku, Tokyo 153
(Received March 29, 1974)

Synopsis. When nitric oxide was admitted during the course of the reduction of N_2O by CO, a discontinuous increase in the N_2O pressure and a decrease in the NO pressure were observed. The reduction of N_2O stopped completely, and only the reduction of NO to N_2O proceeded.

Earlier papers[1-5] have noted the appearance of N_2O as an intermediate in the catalytic reduction of NO by CO. High activity at low temperatures and low N_2O formation are desirable properties of the catalyst for the removal of NO from stack gas. However, the fundamental aspects of the N_2O formation still remain ambiguous. Fe_2O_3 is one of the catalysts over which the N_2O formation is most prominent.[2] We wish to investigate the catalytic reduction of NO by CO over a Fe_2O_3 catalyst in a closed circulating system, in order to obtain more detailed information relating to the appearance of N_2O in the gas phase.

Experimental

The apparatus employed is a closed circulating system, the total volume of which is 861 ml.

The Fe_2O_3 catalyst was prepared by impregnating silicon carbide, pulverized into 14—30 mesh, with a $Fe(NO_3)_3$ solution. The catalyst thus obtained was dried at 110 °C and then calcined at 500 °C for 5 hr. The metal content was 10 wt% as Fe_2O_3, and its total surface area was 2.40 m^2/g.

Before initiating the experimental runs, the catalyst was degassed at 350 °C for 1 hr and was then treated with a mixture of NO and CO in the same composition, or with the same combination of N_2O and CO as that used for the reaction runs, and at the same temperatures. This procedure allowed us to obtain a good reproducibility in a series of experiments. The experimental runs were carried out at such circulating velocities of gasses that the reaction rate was not affected.

The analyses of the reactant and the product were conducted using a series of two gas-chromatographic apparatuses equipped with thermoconductivity detectors. The first apparatus was operated at 80 °C, using a stainless steel column (3 mm × 1 m) packed with Unipack 1A (60—80 mesh) obtained from Gasukuro Kogyo, Tokyo, for the N_2O and CO_2 separations. The second apparatus was operated at 60 °C, using a stainless steel Column (3 mm × 2 m) packed with Molecular Sieve 13X (60—80 mesh), for the N_2, NO, and CO separations. Helium was used as a carrier gas. The reproducibility of each component was within 0.3 Torr.

Results and Discussion

Figure 1 shows a typical result of the reduction o NO by CO over a Fe_2O_3 catalyst at 200 °C. Only the partial reduction of NO to N_2O took place at an early stage, and the reduction of N_2O to N_2 occurred after most of the NO had been consumed. At such a high temperature as 300 °C, a small amount of N_2 was produced even at an early stage, but the reduction of NO to N_2O was still dominant.† The initial rates of the reduction of N_2O to N_2 by CO in the absence of NO were comparable with those of NO to N_2O. We are, therefore, interested in the selective formation of N_2O in the reduction of NO by CO. Previous workers[1-4] using the flow system also observed N_2O formation in the reduction of NO by CO at low temperatures or at high space velocities, but little attention has been paid to the reasons why NO reduces to N_2O selectively and why scarcely reduction of the N_2O formed on the catalyst proceeds. Therefore, it is of interest to investigate the perturbation effect of NO on the reduction of N_2O by CO; NO was admitted during the course of the reduction of N_2O, as is shown in Fig. 2. A discontinuous increase in the N_2O pressure and a decrease in the NO pressure were observed upon the introduction of NO at a certain time, *A*. However, the CO and CO_2 pressures were changed continuously. Moreover, the reduction of N_2O and the N_2 formation stopped completely, and the reduction of NO to N_2O occurred. A similar effect of NO was also observed at 250 °C, although a slight formation of N_2 was found.

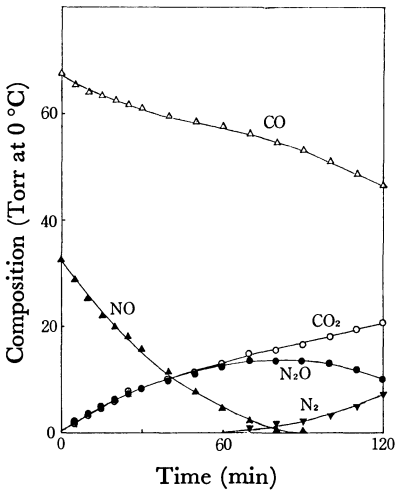

Fig. 1. The reduction of NO over 5 g of 10 wt% Fe_2O_3 on silicon carbide at 200 °C.

The following reaction schemes are generally accepted for the reduction of NO by CO:[1-4]

$$CO + cat \xrightarrow{k_1} CO_2 + cat^* \quad (1)$$

† No decomposition of NO to N_2O and O_2, or of N_2O to N_2 and O_2, in the absence of CO was observed under our conditions.

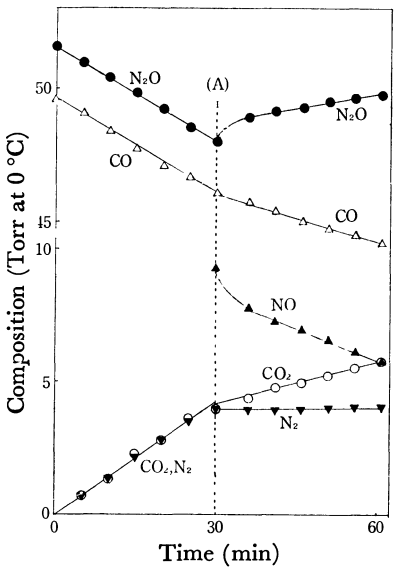

Fig. 2. The effect of NO on the reduction of N_2O by CO over 2 g of 10 wt% Fe_2O_3 on silicon carbide at 200 °C. NO (9.2 Torr) was introduced at a time *A*.

$$2NO + cat^* \xrightarrow{k_2} N_2O + cat \quad (2)$$

$$N_2O + cat^* \xrightarrow{k_3} N_2 + cat \quad (3)$$

where cat and cat* are an active site on the catalyst and its reduced site by CO respectively, and where k_1, k_2, and k_3 are the rate constants for each reaction. If the selective formation of N_2O is due to $k_2 \gg k_3$ (the last step may be rate-limiting), the introduction of NO during the course of the reduction of N_2O should result in the enhancement of the N_2 formation, because the concentration of N_2O on the catalyst should increase. Therefore, our results cannot be explained by the difference in rate constants, but must be related to the strong adsorption of NO on the catalyst.

Our results do not permit any definitive descriptions of the selective formation of N_2O in the reduction of NO by CO, but we have adopted the one presented below as a tentative postulate. The selective formation of N_2O observed at an early stage of the reduction of NO reflects the difference in adsorptivity between NO and N_2O: the adsorption of NO is stronger than that of N_2O. The NO and N_2O formed on the catalyst will establish an adsorption equilibrium, and the N_2O is displaced by NO before it is converted to N_2. As the temperature is raised, a part of the N_2O formed on the catalyst will be reduced to N_2 before the displacement by NO. The effect of NO on the reduction of N_2O shown in Fig. 2 also supports the above postulate: the discontinuous increase in N_2O pressure and the stopping of the N_2 formation may be ascribed to the displacement of N_2O by NO.

References

1) R. A. Baker and R. C. Doerr, *Ind. Eng. Chem., Process Des. Develop.*, **4**, 188 (1965).
2) M. Shelef and K. Otto, *J. Catal.*, **10**, 408 (1968).
3) M. Shelef, K. Otto, and H. Gandhi, *ibid.*, **12**, 361 (1968).
4) G. L. Bauerle, G. R. Service, and K. Nobe, *Ind. Eng. Chem., Prod. Research Develop.*, **11**, 54 (1972).
5) J. W. London and T. Bell, *J. Catal.*, **31**, 96 (1973).

BULLETIN OF THE CHEMICAL SOCIETY OF JAPAN, VOL. 48 (1), 339—340 (1975)

Extinction Coefficients of Maleate and Fumarate Radical Anions and Relative Yield of *cis-trans* Isomerization in Methanol Glass at 77 K

Ayako TORIKAI, Fumio NAKANO, Kenji FUEKI, and Zen-ichiro KURI

Department of Synthetic Chemistry, Faculty of Engineering, Nagoya University, Chikusa-ku, Nagoya 464

(Received April 3, 1974)

Synopsis. The photoisomerization of the γ-ray-induced maleate radical anion (DEM^-) to the fumarate radical anion (DEF^-) has been studied. The molar extinction coefficients of DEM^- and DEF^- have been determined to be $2.4_3\times10^4$ l mol^{-1} cm^{-1} and $3.4_0\times10^4$ l mol^{-1} cm^{-1} respectively. The yield of the isomerization from DEM^- to DEF^- is found to be 0.95.

In a previous paper,[1] we reported the photoisomerization of the maleate radical anion produced in 2-methyltetrahydrofuran (MTHF) glasses by γ-irradiation. The reaction intermediates observed were identified as radical anions. However, some problems remained to be resolved in the previous study. Because of the poor solubility of the *trans* isomer (dimethyl fumarate) to MTHF, for instance, the experiment changing the concentration of the *trans* isomer was not possible, so that the extinction coefficient could not be estimated accurately in that case.

We have now made an attempt to determine the molar extinction coefficients of the radical anions and to estimate the yield of the isomerization in rigid media. We have chosen diethyl maleate or diethyl fumarate–methanol systems in order to have a good solubility of the esters to methanol and for the convenience for optical studies.

Experimental

Spectro-grade methanol containing 5.7 mol% of triply distilled water was used as the solvent. The diethyl maleate (*cis*, DEM) and diethyl fumarate (*trans*, DEF) were purified by passage through an activated aluminum column. The samples were degassed by the freeze-pump-thaw technique. The samples were irradiated with Co-60 γ-rays at 77 K and, in most cases, at a dose rate of 2.0×10^{18} eV/g hr and a dose to 1.0×10^{18} eV/g. The photobleaching of γ-irradiated samples was carried out with visible light from a slide projector. The optical absorption spectra of γ-irradiated samples were measured at 77 K on a Hitachi EPU 2A spectrophotometer.

Results and Discussion

γ-Irradiated pure methanol glass gives an optical spectrum with an absorption maximum at 530 nm; this maximum has been assigned to the trapped electron (e_t) in methanol.[2]

When solutions containing DEM at low concentrations are irradiated, the spectrum shows absorption maxima at 530 and 345 nm(Fig. 1a). Upon an illumination with visible light (λ>490 nm), the 530 nm band diminishes in intensity, while the 345 nm band increases (Fig. 1b). The 345 nm band first shifts to 335 nm upon an illumination with visible light(no filter),

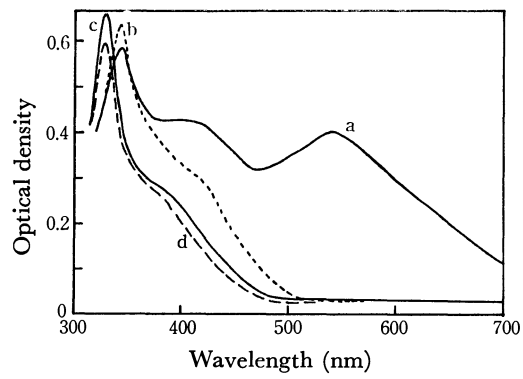

Fig. 1. Absorption spectra of γ-irradiated 0.08 mol% DEM in methanol at 77 K. a: sample γ-irradiated to a dose of 1.0×10^{18} eV/g, b: after 2 min illumination of sample a with visible light (λ—490 nm), c: after 2 min illumination of sample a with a visible light (no filter), d: after 60 min illumination of sample a with visible light.

while it is bleached by prolonged illumination (Fig. 1c, d). It is obvious from these experimental results that the *cis*→*trans* isomerization can occur by means of the illumination of visible light at wavelength shorter than 490 nm. The 345 and 335 nm bands are attributable to the DEM and DEF anion radicals respectively, judging from similar results in the previous work.[1] The reaction mechanism is proposed to be:

$$CH_3OH \rightsquigarrow CH_3OH^+ + e_t$$
$$DEM + e \longrightarrow DEM^-$$
$$DEM + e_t \xrightarrow{\lambda>490\,nm} DEM^-$$
$$DEM^- \xrightarrow{\lambda<490\,nm} DEF^-$$
$$DEF^- \xrightarrow{h\nu} DEF + e_m$$

The molar extinction coefficients (ε) of the radical anions were determined from the competitive reaction

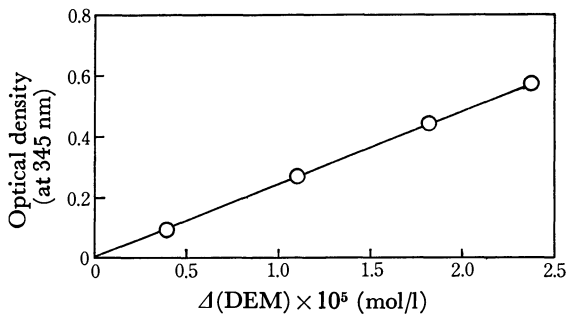

Fig. 2. Plot of optical density at 345 nm *vs.* Δ (DME) for γ-irradiated DEM in methanol at 77 K.

of mobile electrons between the esters and methanol (Fig. 2). Since the extinction coefficient of e_t has been known, the extinction coefficient of DEM^- can be determined by the following method, assuming that the decrease in e_t contributes to the increase in DEM^-. In Fig. 2, Δ(DEM) indicates $OD-OD'/\varepsilon(e_t)d$, where OD: optical density at 530 nm in pure methanol glass; OD': optical density at 530 nm in a DEM-methanol glass; $\varepsilon(e_t)$: molar extinction coefficient of e_t at 530 nm, and d: thickness of the cell. The value of $\varepsilon(e_t)$ has been reported to be 1.38×10^4 l mol^{-1} cm^{-1}.[3] The molar extinction coefficient (ε) of the DEM anion radical can be obtained from the slope of the straight line in Fig. 2. The ε of the DEF anion radical can also be obtained by the same method. The molar extinction coefficients of the DEM and DEF radical anions have been estimated to be $2.4_3\times10^4$ l mol^{-1} cm^{-1} at 345 nm and $3.4_0\times10^4$ l mol^{-1} cm^{-1} at 335 nm respectively.

The concentrations of DEM^- and DEF^- can be estimated by using these extinction coefficients. The DEM-methanol solutions were illuminated with visible light ($\lambda>490$ nm) after γ-irradiation at 77 K; the concentrations of DEM^- were estimated at this stage of the experiment. Subsequent illumination of the sample with visible light (2 min) produced DEF^-, and the concentrations of DEF^- were estimated. The concentrations of DEM^- and DEF^- obtained in this manner are shown in Fig. 3.

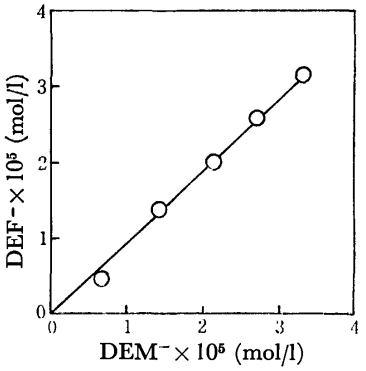

Fig. 3. Plot of the concentration of DEF^- *vs.* the concentration of DEM^- for photoisomerization of γ-irradiated DEM in methanol at 77 K.

The yield of the *cis*→*trans* isomerization is found to be 0.95 from the slope of the straight line in Fig. 3. This means that 95% of the DEM^- produced undergoes the *cis*→*trans* isomerization.

References

1) A. Torikai, T. Suzuki, T. Miyazaki, K. Fueki, and Z. Kuri, *J. Phys. Chem.*, **75**, 482 (1971).

2) F. S. Dainton, G. A. Salmon, and J. Teplý, *Proc. Roy. Soc., Ser. A*, **286**, 27 (1965).

3) A. Habersbergerova, Lj Josimovic, and J. Teplý, *Trans. Faraday Soc.*, **66**, 669 (1970).

BULLETIN OF THE CHEMICAL SOCIETY OF JAPAN, VOL. 48 (1), 341—342 (1975)

The ESR Spectra of the Anthanthrene and Binaphthylene Dioxide Cation-radicals

Kôichi IKEGAMI, Yoshio MATSUNAGA,* Kazuteru OSAFUNE, and Eiji OSAWA
Department of Chemistry, Faculty of Science, Hokkaido University, Sapporo 060
(Received June 7, 1974)

Synopsis. The ESR spectra of the anthanthrene and binaphthylene dioxide cation-radicals were recorded and analysed.

Some aromatic hydrocarbons have been known to form stable cation-radicals when dissolved in concentrated sulfuric acid and to exhibit ESR spectra with well-resolved hyperfine structures. Perylene and tetracene are notable examples.[1,2] During the course of our work on photoemission from solid aromatic compounds, we noted that anthanthrene and a compound with the same framework, binaphthylene dioxide, have ionization potentials close to those of the above-mentioned hydrocarbons. Therefore, an examination of the ESR spectra of their cation-radicals was undertaken.

When 98% sulfuric acid solutions are diluted enough to resolve the hyperfine structure, the anthanthrene cation-radical gives sixty-one lines, with a total span of 27.6 G. The left-hand half of the spectrum is shown in Fig. 1. All the intervals except those in the terminal quintet are equal to d, while those in the quintet are 2d. The separation between the terminal quintet and the neighboring one, 9d, gives the second smallest coupling constant. As the total span is equal to 68d, the only possible constants for the remaining protons are 10d and 11d.[3] Therefore, a pair of the protons does not contribute to the hyperfine structure. The stick diagram reconstructed with these constants reproduces well the relative intensities of the experimental lines. McConnell has derived the $a_i=Q\rho_i$ relationship, which shows that the proton-coupling constant, a_i, of the aromatic free radical is proportional to the spin density, ρ_i, at the attached carbon atom, i.[4] As the HMO spin densities at the carbon atoms

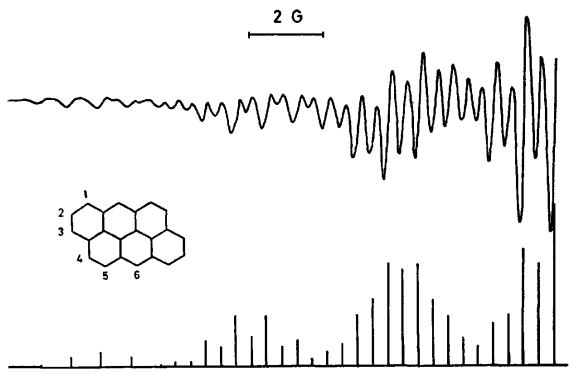

Fig. 1. First derivative of ESR spectrum of the anthanthrene cation-radical and the reconstructed stick diagram.

* To whom inquiries may be addressed.

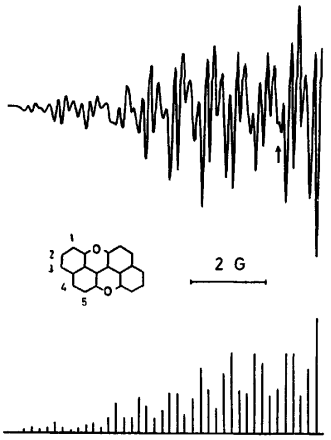

Fig. 2. First derivative of ESR spectrum of the binaphthylene dioxide cation-radical and the reconstructed stick diagram.

are 0.1074, 0.0003, 0.0969, 0.0436, 0.0431, and 0.1414 in the order of numbering given in Fig. 1, the large constants, 4.46, 4.06, and 3.65 G, may be assigned to the protons attached to the carbon atoms, 6, 1, and 3, and their equivalents respectively. The quintet with the spacing of 0.81 G arises from the coupling with the protons on the 4 and 5 carbon atoms and their equivalents.

The spectrum of the binaphthylene dioxide cation consists of seventy-seven lines, with an approximately equal spacing, d, if we ignore the partial resolution indicated by an arrow (see Fig. 2). The total span decreases to 15.7 G upon the introduction of two oxygen atoms into the framework. As the assignment of coupling constants did not seem easy, we employed the computing program proposed by Pomponiu and Balaban.[5] The summation of all the line intensities indicates that all the protons in this radical contribute to the hyperfine structure. The most probable partition of the thirty-eight intervals into five non-zero integers is d, 3d, 8d, 11d, and 15d. The stick diagram computed with these values appears to be consistent with the experimental spectrum. On the basis of the total span, the coupling constants can be approximated as 0.21, 0.62, 1.65, 2.27, and 3.10 G. The HMO spin densities on the carbon atoms calculated with the parameters of $\alpha_O=\alpha_C+2.0\beta_{CC}$ and $\beta_{CO}=0.8\beta_{CC}$[6] are 0.0591, 0.0175, 0.0754, 0.0947, and 0.0001, in the order of numbering in Fig. 2. The order of spin densities is different from that in the hydrocarbon cation-radical, but it is not affected by α_O even if this value is varied by $\pm 0.5\beta_{CC}$. Therefore, the largest constant may safely be assigned to the protons on the 4 carbon atom and the equivalent, and the second

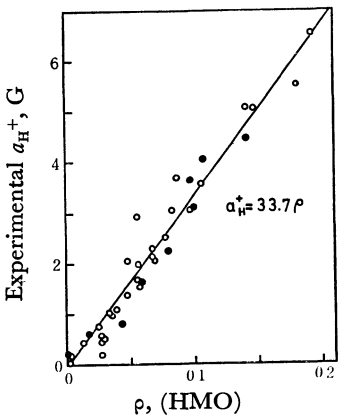

Fig. 3. Relation between experimental coupling constants, a_H^+, and HMO spin densities, ρ, for the anthanthrene and binaphthylene dioxide cations (●) and for other aromatic hydrocarbon cations (○).

largest, to those on the 3 carbon atom and the equivalent. On the other hand, the protons with the smallest constant are undoubletly attached to the 5 carbon atom and its equivalent, and those with the second smallest, to the 2 carbon atom and its equivalent. This cation-radical was found to be not quite stable; that is, a modification of the central part of the spectrum could be noted three days after the dissolution.

In order to verify the above choice of coupling constants, the constants for the present cation-radicals are plotted in Fig. 3 by shaded circles against the spin densities determined by the simple HMO theory. The plots show a linear relationship as good as those indicated by open circles for the eleven aromatic hydrocarbon cations compiled by Lewis and Singer.[7] We employed Q=33.7 G in this figure, following Griffith and Poole.[8]

The authors wish to express their thanks to Dr. Jun-ichi Aihara for his help in the calculation of the HMO spin densities.

References

1) E. de Boer and S. I. Weissman, *J. Amer. Chem. Soc.*, **80**, 5342 (1958).
2) A. Carrington, F. Dravnieks, and M. C. R. Symons, *J. Chem. Soc.*, **1959**, 947.
3) A. T. Balaban, *Rev. Roum. Chim.*, **17**, 9 (1972).
4) H. M. McConnell, *J. Chem. Phys.*, **24**, 764 (1956).
5) C. Pomponiu and A. T. Balaban, *Rev. Roum. Chim.*, **18**, 1173 (1973).
6) A. Streitwieser, Jr., "Molecular Orbital Theory for Organic Chemists," John Wiley & Sons, New York, London (1961), p. 135.
7) I. C. Lewis and L. S. Singer, *J. Chem. Phys.*, **43**, 2712 (1965).
8) O. F. Griffith, III, and C. P. Poole, Jr., *ibid.*, **47**, 4528 (1967).

BULLETIN OF THE CHEMICAL SOCIETY OF JAPAN, VOL. 48 (1), 343—344 (1975)

Thermally Stimulated Current in Perylene Crystals

Mizuka SANO
Department of Materials Science, The University of Electro-Communications, Chofu, Tokyo 182
Fukuji EGUSA* and Hideo AKAMATU**
Department of Chemistry, Faculty of Science, The University of Tokyo, Hongo, Tokyo 113

(Received June 25, 1974)

Synopsis. A single current peak characteristic of thermally detrapped holes was observed at 220 K, the depth of the traps being determined to be 0.50±0.02 eV. This value showed no apparent correlation with the activation energy for photoconduction, 0.18±0.01 eV.

In many high-resistivity semiconductors, localized states in the forbidden energy gap play a dominant role in the mechanism of transport of charge carriers. Perylene crystals show a photocurrent under illumination of light in the visible and ultraviolet spectral regions.[1] A photocurrent signal induced by a light pulse, however, shows a diffused shape with a long tail of decay, indicating the presence of charge carrier traps. The low mobility of charge carriers in perylene crystals has been attributed to the trapping of carriers in an excess-electron-dimeric state.[2] In this note we would like to report a trap level of perylene crystals studied by means of thermally stimulated currents.

Single crystal platelets of chromatographically purified perylene, thickness *ca.* 100 μ, were obtained by sublimation. A crystal platelet, *ca.* 8×5 mm², was sandwiched between two electrodes, one with semi-transparent gold coating and the other lead foil covered with a 6 μ Mylar film. The crystal was mounted on the top of a copper block which could be cooled by a stream of cold nitrogen gas. The whole assembly surrounded by an electric heater was accommodated in a glass chamber (Fig. 1).

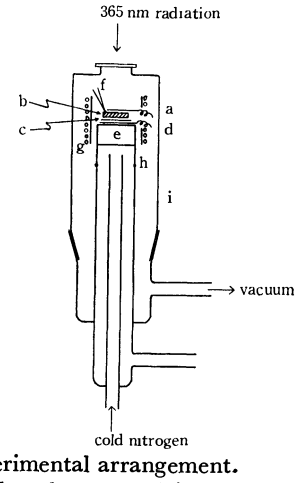

Fig. 1. Experimental arrangement.
(a) gold film electrode, (b) crystal, (c) Mylar film, (d) lead foil electrode, (e) copper block, (f) thermocouple, (g) electric heater, (h) Kovar seal, (i) glass chamber.

The gold electrode was connected to the positive side of a 90 V battery. The crystal was cooled to about 170 K and then illuminated through the electrode with 365 nm mercury radiation. After illumination for ten minutes, the polarity of the applied voltage was reversed, and thermally stimulated currents at a predetermined uniform heating rate were subsequently measured in the dark. The heating rate was controlled with an electric heater, an appropriate amount of helium gas being introduced into the chamber. The current through a 10^{10} ohm input resistor was recorded by a Takedariken vibrating reed electrometer, the temperature of the crystal being recorded simultaneously with a copper-constantan thermocouple junction pasted to the crystal surface with silicone rubber.

In the range 170—245 K, a single current peak characteristic of thermally detrapped holes was observed, indicating that there is one kind of trapping center observable in this temperature range. At a heating rate of 0.38 K/s, the peak appeared at 220 K. As the heating rate was increased to 0.45 K/s, the peak shifted to a higher temperature and became narrower (Fig. 2). Garlick and Gibson's method[3] was adopted for evaluation of the trap depth, on the assumption that the trapping centerslie with a uniform depth E. The thermally stimulated current i is expressed by the equation

$$i = n_t \nu \exp\left(-\frac{E}{kT}\right), \qquad (1)$$

where n_t is the number of carriers in the traps and ν is the effective attempt-to-escape frequency.

Plots of the logarithm of current against the reciprocal of the temperature gave a straight line in the initial current rising region. From the slope of the line, the depth of traps for holes was evaluated to be 0.50± 0.02 eV. When the crystal was illuminated through a

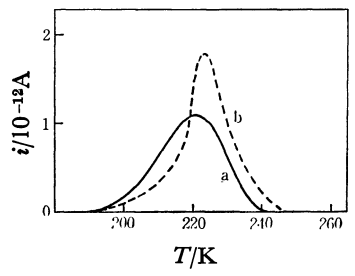

Fig. 2. Thermally stimulated currents.
Heating rate: (a) 0.38 K/s, (b) 0.45 K/s.

* Present address: The Mainichi Newspapers, Chiyoda-ku, Tokyo 101.

** Present address: Department of Applied Chemistry, Faculty of Engineering, Yokohama National University, Minami-ku, Yokohama 233.

negatively biased gold film electrode, no thermally stimulated current could be observed. This means that electrons could not be injected from the electrode or the injected electrons were trapped too deeply to be released thermally. The nature of trapping centers could not be determined from the present experiment. The depth of hole traps for melt-grown anthracene crystals was determined to be 0.76 eV with the same experimental arrangement. This is in good agreement with the value obtained previously.[4] Similarity in the trap depths for organic crystals; 0.50 eV for perylene, 0.53—0.76 eV for anthracene,[4,5] and 0.36 eV for metal-free- and lead-phthalocyanine crystals[6] suggests that a physical cause of the same kind might be responsible for trapping of holes.

Variation of a photocurrent with temperature has been considered to be an evidence for the existence of trapping centers.[7] We measured the temperature dependence of a photocurrent for perylene single crystals by the method given in the leterature.[8] The photocurrent was found to increase with an increase in temperature in the range 200—330 K. Plots of the logarithm of photocurrent against the reciprocal of the temperature gave a straight line, the activation energy for photoconduction being evaluated to be 0.18 ± 0.01 eV. The value of the activation energy was found to be independent of the exciting wavelength in the visible spectral region. The activation energy for photoconduction, however, showed no apparent correlation with the trap depth. It might be associated with the process of carrier generation rather than the process of carrier transport.

References

1) M. Sano and H. Akamatu, This Bulletin, **35**, 587 (1962).

2) Y. Maruyama, T. Kobayashi, H. Inokuchi, and S. Iwashima, *Mol. Cryst. and Liq. Cryst.*, **20**, 373 (1973).

3) G. F. J. Garlick and A. F. Gibson, *Proc. Phys. Soc. Ser. A*, **60**, 574 (1948).

4) H. Kokado and W. G. Schneider, *J. Chem. Phys.*, **40**, 2937 (1964).

5) T. Garofano and S. Morelli, *Il. Nuovo Chim.*, **B13**, 173 (1973).

6) C. R. Westgate and G. Warfield, *J. Chem. Phys.*, **46**, 537 (1967).

7) J. Kommandeur, G. J. Korineck, and W. G. Schneider, *Can. J. Chem.*, **35**, 998 (1957); J. W. Weigl, *J. Mol. Spectrosc.*, **1**, 216 (1957).

8) M. Sano, This Bulletin, **34**, 1668 (1961).

BULLETIN OF THE CHEMICAL SOCIETY OF JAPAN, VOL. 48 (1), 345—346 (1975)

The X-Ray Photoelectron Spectroscopy of *o*-Hydroxy Aromatic Azo Metal Complexes

Tooru YOSHIDA and Shigemasa SAWADA

Osaka Prefectural Industrial Research Institute, Enokojima, Nishi-ku, Osaka 550

(Received July 26, 1974)

Synopsis. The photoelectron spectra of azo metal complexes were measured. There was no significant change in the profile or the binding energy of the N(1s) peak upon coordination. It was deduced that, in the bond between the azo-group and the metal, there is a contribution of a π-bonding.

o-Hydroxy aromatic azo compounds, which are bidentate complexing agents containing an azo-group and a hydroxy group *ortho* to the azo-group, are of considerable practical and theoretical interest because of their ability to form stable chelate complexes with some metal ions. There have been many studies of them by means of physico-chemical methods. Ueno[1] has reported an IR study of *o*-hydroxy azobenzene and its metal chelates, while Jarvis[2] and Alcock *et al.*[3] studied the structures of Cu(II)bis(1-phenylazo-2-naphthol) and Ni(II)bis(1-*m*-tolylazo-2-naphthol) by X-ray analysis.

In recent years a method of X-ray photoelectron spectroscopy (ESCA) has been developed; it is capable of yielding information pertinent to the study of chemical bonds in that the binding energy of an inner-shell electron is characteristic in both its elemental identity and the chemical environment of the atom. The differences in binding energies between coordinated and uncoordinated ligand atoms have been used to support arguments concerning π back-bonding in some coordination compounds.[4] The purpose of this paper is to report the results of a study by this method of some *o*-hydroxy aromatic azo metal complexes.

The X-ray photoelectron spectra were measured on an AEI ES100 spectrometer under the control of a DS100/32 computer data-processing system. An AlKα (1486.6 eV) X-ray line was used as the excitation source. All the samples measured are given in Table 1. The 2-arylazophenol and 1-arylazo-2-naphthol derivatives were prepared by coupling diazotized amines with *p*-tolylphenol and β-naphthol respectively. Chelate compounds with a ligand-metal ratio of 2:1 were synthesized according to the procedures of Elkins and Hunter.[5] The samples were ground to powder, dusted onto a double-backed adhesive tape, and set inside the measuring chamber. The measurements were run at room temperature under a vacuum of about 10^{-6} Torr. A few volatile samples were introduced *via* a heatable reservoir shaft and condensed on a cooled copper holder.

The binding energy of the C(1s) peak was used as the energy standard throughout the present experiments; it was taken to be 285.0 eV, the C(1s) binding energies for all the samples being assumed to be constant.

The N(1s) spectra of all the compounds were composed of single peaks with full-width half-heights of 1.6—1.8 eV in all the free azo compounds and Cu chelates, and 1.5—1.7 eV in all the Ni chelates. In view of these results, the difference between the charge densities on the two nitrogen atoms of an azo-group is considered to be so small that they can not be distinguished by ESCA in all these compounds.

The measured values for the N(1s) binding energies are listed in Table 1. There were no remarkable changes in the N(1s) binding energy upon the coordination of all azo compounds to metals, although barely appreciable minus changes appear to be observed in 1-arylazo-2-naphthol derivatives. Therefore, it seems reasonable to assume that there is no significant change in the electron density around the azo-group on the complex formation.

There are chiefly two known modes of the formation of a bond between an azo-group and a metal atom. The one is Type (1), in which one lone-pair electron of a component nitrogen atom is coordinated to the

TABLE 1. N(1s) BINDING ENERGY VALUES

Sample	R	B.E. of N(1s) (eV)[a]			E (eV)[b]	
		Free	Cu-Chelate	Ni-Chelate	Cu-Chelate	Ni-Chelate
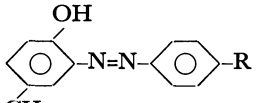	$-OCH_3$	399.8	400.0	—	+0.2	—
	$-H$	400.0	400.1	400.2	+0.1	+0.2
	$-NO_2$	400.2	400.1	400.2	−0.1	±0.0
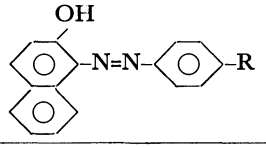	$-OCH_3$	400.3	400.0	400.2	−0.3	−0.1
	$-H$	400.6	400.1	400.3	−0.5	−0.3
	$-NO_2$	400.5	400.0	400.2	−0.5	−0.3

a) Uncertainties are equal to ±0.1 eV. b) The differences between the N(1s) binding energies of the chelate and the free azo compounds.

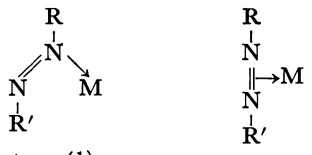

metal, while the other is Type (2),[6] in which the whole of the N=N bond itself is coordinated to the metal, just as in metal-olefin complexes, in which the π-electrons of the carbon-carbon double bond are capable of coordination with a metal.

The results of the X-ray analysis[2,3] suggest that the bonds between the azo-group and the metals in the Cu and Ni chelates of 1-phenylazo-2-naphthol are of Type (1).

Aromatic compounds containing an N=N bond generally exhibit absorption bands at approximately 320—315 nm; these bands are attributed to the conjugation of the unsaturated nitrogen with the phenyl rings. Kleiman and Dubeck[7] have suggested that, on complex formation, the disappearance and the retaining of such absorption bands indicate that the nitrogen system in the complex is bonded to the metal as is shown in Type (2) and in Type (1) respectively.

The UV measurements in the above region for all the chelates listed in Table 1 indicate absorption peaks with almost the same intensities as those of free azo compounds.

Accordingly, it may be concluded that all the chelates used in this study belong to Type (1). In the case of Type (1), it appears that the charge densities on the nitrogen atoms of the azo-group are not equal. If this is really true, the ESCA spectrum of the N(1s) of the chelate should give a different profile from that of the free one, for instance, with two well-resolved peaks or a single broad peak. As has been stated previously, however, scarcely no such phenomena were observed in this study.

From these experimental facts, the data obtained in this experiment may be explained as follows.

In all the chelates in Table 1, there are two effects of opposing factors. One is the σ-bonding by the coordination of a lone-pair electron of a nitrogen atom to the bonding orbital of Cu or Ni; the other is the π-bonding by the coordination (back-donation) of the *d*-electrons of Cu or Ni to the vacant anti-bonding orbital of the azo-group. These effects result in a neat cancellation of the total electron drift and a small change in the total electron density in the neighborhood of the nitrogen atom. This is the explanation for the facts that the difference between the N(1s) binding energies of the free ligand and the chelate is too small in view of the stability of the chelates, and that the profile of the N(1s) of the chelate is almost the same as that of the free ligand.

Though the problem remains unsolved, it is noteworthy that the change in the N(1s) binding energies is very small throughout all the chelates.

The authors wish to thank Mr. Taichiro Hirohara for his elemental analysis of all the samples.

References

1) K. Ueno, *J. Amer. Chem. Soc.*, **79**, 3066 (1957).
2) J. A. J. Jarvis, *Acta Crystallogr.*, **14**, 961 (1961).
3) N. W. Alcock, R. C. Spencer, R. H. Prince, and O. Kennard, *J. Chem. Soc., A*, **1968**, 2383.
4) a) D. N. Hendrickson, J. M. Hollander, and W. L. Jolly, *Inorg. Chem.*, **8**, 2642 (1969); b) G. Kumar, J. R. Blackburn, R. G. Albridge, W. E. Moddeman, and M. M. Jones, *ibid.*, **11**, 296 (1972).
5) M. Elkins and L. Hunter, *J. Chem. Soc.*, **1935**, 1598.
6) a) S. Otsuka, T. Yoshida, and Y. Tatsuno, *Chem. Commun.*, **1971**, 67 b) H.F. Klein and J.F. Nixon, *ibid.*, **1971**, 42; c) R. S. Dickson and J. A. Ibers, *J. Amer. Chem. Soc.*, **94**, 2988 (1972).
7) J. Kleiman and M .Dubeck, *ibid.*, **85**, 1544 (1963).

BULLETIN OF THE CHEMICAL SOCIETY OF JAPAN, VOL. 48 (1), 347—348 (1975)

Photochemical Reduction of Vanadium(V) in Aqueous Perchloric Acid Solutions

Bojana G. JELIAZKOWA,* Shigeru NAKAMURA, and Hiroshi FUKUTOMI

Research Laboratory for Nuclear Reactors, Tokyo Institute of Technology, Meguro-ku, Tokyo 152

(Received December 19, 1973)

Synopsis. It was found that irradiation of V(V) solution gives V(IV) and an equivalent amount of oxygen. The dependence of the quantum yield on light intensity, acid concentration, wave number and the concentration of V(IV) was investigated.

It was found that reduction of vanadium(V) proceeds during irradiation of its aqueous perchloric acid solution with argon laser at 488 nm. The photochemical reduction of metal ions of a high valence state such as cerium(IV)[1-6] and iron(III)[7-11] has been studied and probable mechanisms have been discussed. However, no data have been given of vanadium(V).

Experimental

Irradiation of vanadium(V) solution was carried out with an ultra high pressure mercury lamp with solution- and glass-filters.[12] A qualtz cell for spectrophotometry (1 cm light-path length) with a suitable modification was used as a reaction vessel. The cell was thermostated at 20.0±0.1 °C in an optical bench. Stirring of the solution was carried out magnetically with a small glass-coated bar. The reactant solution was deaerated in the reaction vessel with pure nitrogen gas.

The concentration of vanadium(V) was determined photometrically at 270 nm. The value 863 $M^{-1}\cdot cm^{-1}$ was used as a molar extinction coefficient for V(V), and 143 $M^{-1}\cdot cm^{-1}$ for V(IV). The incident light intensity before and after the irradiation, and the transmitted light intensity during the irradiation were measured in an arbitrary unit with a photomultiplier. These relative intensities were converted into absolute values by means of a ferrioxalate actinometer. Inner filter effect of V(IV) is found to be negligible.

Oxygen gas generated by photolysis was identified and determined by gas-chromatography using an active carbon column and helium as a carrier gas. The equipment is shown in Fig. 1. After prolonged irradiation, the resulting gas was expelled and collected in the syringe (2 in Fig. 1) by bubbling with helium, and the gas sample was injected into a gas-chromatograph. The reaction vessel was replaced by an electrolytic cell, and the gas-chromatograph was calibrated by measuring the amount of oxygen produced by the electrolysis of 0.1 M sulfuric acid.

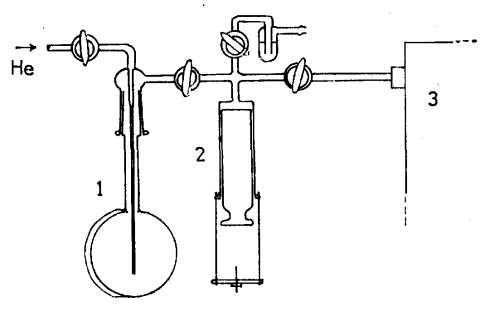

Fig. 1. Equipment used for the determination of oxygen
1: Cylindrical irradiation vessel, 2: syringe
3: gas-chromatograph.

All the solutions were prepared from analytical grade reagents. Triply distilled water obtained from an alkaline permanganate solution was used.

Results and Discussion

Stoichiometry. The EPR spectrum of the irradiated sample showed the octet signal of vanadium(IV). It was found that V(IV) is the final reduction product since no change was observed after prolonged irradiation of V(IV) solution. Under the conditions employed $VO_2(H_2O)_4^+$ was found to be the main species present in V(V) solutions and $VO(H_2O)_5^{2+}$ the main species of V(IV).[13-14]

The amount of oxygen evolved is equivalent to the amount of V(V) reduced by photolysis (Table 1). The overall reaction is thus given by the following scheme.

$$VO_2(H_2O)_4^+ + 1/2H_2O + H^+ \xrightarrow{h\nu} VO(H_2O)_5^{2+} + 1/4O_2 \quad (1)$$

Effect of Light Intensity on the Quantum Yield of V(IV). The results show that the quantum yield of V(IV) does not depend upon the intensity of the absorbed light (Table 2). This suggests that V(IV) is formed

Table 1. Yields of V(IV) and oxygen

$HClO_4$	Yield of V(IV)	Yield of O_2
1.0 M	2.3×10^{-6} mol	5.5×10^{-7}mol
	2.2×10^{-6}	5.5×10^{-7}
	1.6×10^{-6}	4.5×10^{-7}

Table 2. Dependence of the quantum yield of V(IV) on absorbed light intensity

Absorbed light intensity	Quantum yield of V(IV)
1.15×10^{-4} Einstein$\cdot l^{-1}\cdot min^{-1}$	0.0037
1.20×10^{-4}	0.0033
1.40×10^{-4}	0.0036
2.51×10^{-4}	0.0036
3.34×10^{-4}	0.0036
3.40×10^{-4}	0.0035
3.90×10^{-4}	0.0037
4.31×10^{-4}	0.0033
4.90×10^{-4}	0.0037

$[V(V)]=1.0\times10^{-3}$ M, $[HClO_4]=1.0$ M, at 313 nm.

* Present address: Department of Chemistry, Sofia University, Sofia, Bulgaria.

by reaction of the first order with respect to the concentration of some intermediate. A similar result was obtained in the photochemical reduction of cerium(IV).

Effect of the Wave Number of Absorbed Light on the Quantum Yield of V(IV). The wave number effect was studied without any particular attention to light intensity, since the quantum yields of V(IV) and O_2 were independent of light intensity. Figure 2 shows the dependence of the quantum yield of V(IV) on the wave number and the absorption spectrum of reactant $VO_2(H_2O)_4^+$. The value 3.4 eV corresponding to the wave number 27 kK (Fig. 2) is reasonable for the formation of ·OH radical by the reaction

$$V(V) + H_2O \xrightarrow{h\nu} V(IV) + \cdot OH + H^+ \qquad (2)$$

since it is assumed in similar reactions of cerium(IV)[3-5] and iron(III).[7-11] The standard oxidation potential of the thermal reaction corresponding to the reaction (2) is $E^0 = -1.82$ V, calculated from the standard oxidation potentials $E^0(V(V) \rightarrow V(IV)) = 1.00$ V and $E^0(H_2O \rightarrow \cdot OH) = -2.82$ V. The quantum yield of V(IV) increases gradually with wave number. This might indicate that the probability of the ·OH radical escaping from the solvent cage of V(IV) increases with the photon energy.

Effect of Perchloric Acid and Vanadium(V). We see from Table 3 that the quantum yield of V(IV) does not depend upon the concentration of perchloric acid in the region 0.01—1.0 M. The quantum yields of V(IV), determined at two vanadium(V) concentrations 5×10^{-4} M and 1×10^{-3} M, were found to be $(3.5 \pm 0.3) \times 10^{-3}$ and $(3.4 \pm 0.2) \times 10^{-3}$ respectively in 0.1 M $HClO_4$ at unit ionic strength ($NaClO_4$).

The fact that neither perchloric acid nor vanadium(V) affects the quantum yield of V(IV) is in line with the fact that neither hydrolysis nor polymerization of vanadium(V) occurs under the conditions employed.

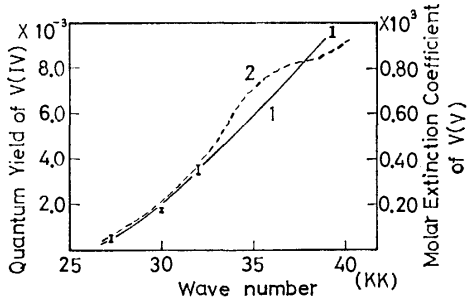

Fig. 2. The dependence of the quantum yield of V (IV) on wave number at 1.0 M $HClO_4$ and the absorption spectrum of $VO_2(H_2O)_4^+$.
1: Quantum yield of V (IV),
2: absorption spectrum of $VO_2(H_2O)_4^+$.

Table 3. Dependence of the quantum yield of V(IV) on the concentration of perchloric acid

($HClO_4$)	Quantum yield of V(IV)
0.01 M	$(3.3 \pm 0.2) \times 10^{-3}$
0.05	$(3.2 \pm 0.1) \times 10^{-3}$
0.10	$(3.4 \pm 0.2) \times 10^{-3}$
0.50	$(3.6 \pm 0.3) \times 10^{-3}$
1.00	$(3.5 \pm 0.2) \times 10^{-3}$

[V(V)] = 1×10^{-3} M, (ionic strength) = 1.0 M and at 313 nm.

Retardation Effect of Vanadium(IV). It was found that the quantum yield of V(IV) decreased with an increase in the concentration of V(IV) produced by photolysis. Since the inner filter effect of V(IV) was negligible and no change was observed after prolonged irradiation of V(IV), the effect of V(IV) is attributed to the back reaction

$$\cdot OH + V(IV) \longrightarrow OH^- + V(V) \qquad (3)$$

Expenses for this work were defrayed in part by the Ministry of Education and in part by a grant from the Japan Society for the Promotion of Science under the Japan-U.S. Cooperative Science Program. One of the authors (B. Jeliazkowa) wishes to express her appreciation to the International Post-graduate University Course sponsored by UNESCO.

References

1) J. J. Weiss and D. Porret, *Nature*, **139**, 1019 (1937).
2) L. J. Heidt and M. E. Smith, *J. Amer. Chem. Soc.*, **70**, 2476 (1948).
3) M. G. Evans and N. Uri, *Nature*, **166**, 602 (1950).
4) T. J. Sworski, *J. Amer. Chem. Soc.*, **77**, 1074 (1955); **79**, 3655 (1957), *J. Phys. Chem.*, **67**, 2858 (1963).
5) L. Dogliotti and E. Hayon, *J. Phys. Chem.*, **71**, 3802 (1967).
6) A. A. Kachan and P. P. Makhovka, *J. Phys. Chem. (Russ)*, **36**, 526 (1962).
7) J. H. Baxendale and J. Magee, *Trans. Faraday Soc.*, **51**, 205 (1955).
8) F. S. Dainton and M. Tordoff, *ibid.*, **53**, 666 (1957).
9) M. G. Adamson, D. L. Baulch, and F. S. Dainton, *ibid.*, **58**, 1388 (1962).
10) G. V. Buxton, S. P. Wilford, and R. J. Williams, *J. Chem. Soc.*, **1962**, 4957.
11) B. Y. Dain and A. A. Kachan, *Dokl. Acad. Nauk SSSR*, **61**, 471 (1948).
12) J. G. Calvert and J. N. Pitts, "Photochemistry," John Wiley & Sons, New York (1967), pp. 728—747.
13) M. T. Pope and B. W. Dale, *Quart. Rev.*, **22**, 527 (1968).
14) F. J. C. Rossotti and H. Rossotti, *Acta Chem. Scand.*, **9**, 1177 (1955).

BULLETIN OF THE CHEMICAL SOCIETY OF JAPAN, VOL. 48 (1), 349—350 (1975)

Stability Constants of Several Aliphatic Uranyl Carboxylates

Bong-il KIM, Chie MIYAKE, and Shosuke IMOTO

Department of Nuclear Engineering, Faculty of Engineering, Osaka University, Suita, Osaka 565

(Received July 8, 1974)

Synopsis. The stability constants of uranyl carboxylates were determined spectrophotometrically; for butyrate, they were log K_1=2.96, log K_2=2.66, log K_3=2.43, and log K_4=2.23; for isobutyrate, log K_1=2.74, log K_2=2.20, and log K_3=1.66; for valerate, log K_1=2.91 and log K_2=2.52, and for isovalerate, log K_1=2.90 and log K_2=1.91.

The consecutive and gross stability constants of a number of mononuclear uranyl complexes with anions of common carboxylic acids, such as formic, acetic, propionic, lactic, oxalic, and succinic acids, were determined spectrophotometrically at an ionic strength of 1.0 in an aqueous solution.[1] As part of a series of studies we hereby report the stability constants of aliphatic uranyl carboxylates with the anions of butyric, isobutyric, valeric, and isovaleric acid obtained by the same method.

Experimental

Materials. All the chemicals were of an analytical grade, made by Nakarai Chemicals, Ltd., and were used without further purification. The solutions were prepared with double-distilled water. The uranyl perchlorate was recrystallized from water, and its constitution ($UO_2(ClO_4)_2$–$6H_2O$) was confirmed by the gravimetric determination of uranium as U_3O_8.

Measurements. Hitachi Perkin-Elmer 139 UV–VIS spectrometer was used to record the absorption spectra with cells 0.2, 0.5, and 1.0 cm thick, according to the respective concentration. The pH determinations were performed with a Hitachi pH meter, M-5. The temperature was controlled to 20+0.2 °C for the spectrophotometric and pH measurements. The systems studied are listed in Table 1. The ionic strength was maintained at 1.0 by adding an appropriate amount of $NaClO_4$ solution to the buffer solution. The procedure of the measurement was as has been described in a previous publication.[1]

Results and Discussion

The data obtained spectrophotometrically and potentiometrically were analysed by Fronaeus' method.[2,3] The linear relationship obtained between the total effective ligand concentration and total uranyl ion concentration for various extinctions suggests the existence of only mononuclear complexes under these conditions. The consecutive stability constants thus obtained are given in Table 2. As is to be expected, the stability of the complexes decreases with an increase in the coordinated ligand number for a given anion. The maximum ligand number attained (Table 3) increases steadily with the length of the carbon chain, reaching 4 for propionate and butyrate, but the steric requirement may prevent the fatty acid with a carbon chain of a sufficient length to occupy more than four of the coordination sites.

Figure 1 shows the relationship between the stability constant, K_1, for the first uranyl complex (UO_2A^+) and the value of K_{1HA} for the corresponding carboxylic acid. As may be seen from the figure, the four carboxylate anions studied here may fall in the group that is classified as showing "normal" behavior, as defined by a previous paper.[1] It is interesting that water lies on this linear line extrapolated to log K_{1HA} of 16. According to Schwarzenbach's classification of cations into the A-character cations and B-character cations, on the basis of complex-formation behavior,[4] both the uranyl ion and the proton may be said to have the A-character, in which the formation reaction entropy term mainly contributes to the association with the ligand and in which the heat of reaction is positive or slightly negative. On the other hand, the B-character association is dominantly controlled by the negative heat of formation.

The relationship between the number of the carbon of monocarboxylic acid and the first stability constant, K_{1MA}, of the respective various metal complexes shown in Fig. 2. The iron(III) ion and the indium(III) ion

TABLE 2.

Complex	log K_1	log K_2	log K_3	log K_4
UO_2-*n*-butyrate	2.96	2.66	2.43	2.23
	2.91[a)]	1.62[a)]		
UO_2-isobutyrate	2.74	2.20	1.66	
	3.40[a)]	2.43[a)]		
UO_2-*n*-valerate	2.91	2.52		
UO_2-isovelerate	2.90	1.91		

(at 20±0.2 °C)

a) 31±0.1 °C and =0.1 ($NaClO_4$); S. Ramamoorthy, A. Raghavan, and M. Santappa, *J. Inorg. Nucl. Chem.*, **31**, 1765 (1969).

TABLE 1.

System	Concentration of uranyl ion (mmol/l)	Concentration of organic Na salt (mmol/l)	Buffer solution (acid: salt)	pH range
UO_2-*n*-butyrate	0.2, 0.5, 1.5	1, 2, 4, 6, 8, 10, 12	2:1, 5:1, 20:1	2.7 to 4.2
UO_2-isobutyrate	0.2, 0.5, 1.5	0.5, 1, 2, 4, 6, 8, 10	2:1, 5:1, 20:1	2.9 to 4.2
UO_2-*n*-valerate	0.1, 0.3, 1.0	0.1, 0.2, 0.4, 0.8, 1.2, 1.4, 1.8	5:1, 10:1, 20:1	3.0 to 4.4
UO_2-isovalerate	0.1, 0.3, 1.0	0.1, 0.2, 0.4, 0.8, 1.2, 1.6, 2.0	2:1, 5:1, 20:1	3.0 to 4.4

Table 3.

Complex	Maximum ligand number attained n_{max}
UO_2-formate	2
UO_2-acetate	3
UO-propionate	4
UO_2-*n*-butyrate	4
UO_2-isobutyrate	3
UO_2-*n*-valerate	2
UO-isovalerate	2

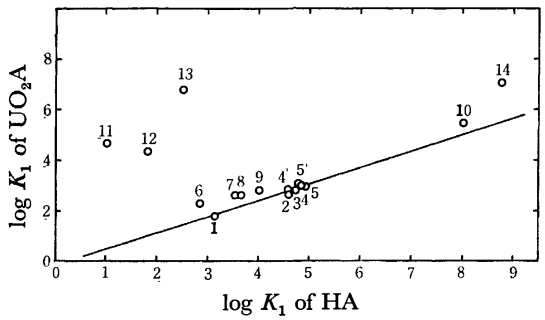

Fig. 1. Relationship between the stability constant K_1 of MA-type uranyl complexes and the first stability constant K_1 of the corresponding carboxylic acid, HA.
1: formate, 5′: isovalerate, 11: oxalate,
2: acetate, 6: salicylate, 12: maleate,
3: propionate, 7: glycollate, 13: citrate,
4: *n*-butyrate, 8: lactate, 14: acetylacetonate,
5: *n*-valerate, 9: succinate,
4′: isobutyrate, 10: glycineamide,

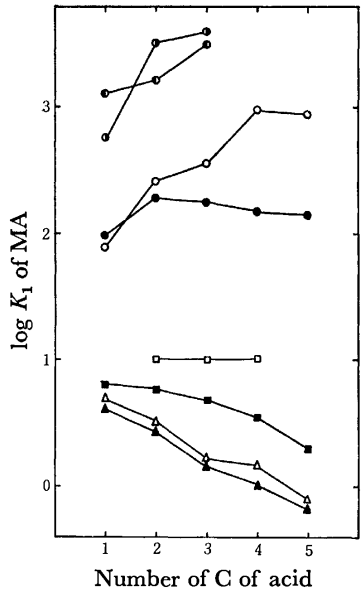

Fig. 2. Relationship between the number of carbon of monocarboxylic acid and the first stability constant of various metal complexes.
◑: In^{3+} at 20 °C and μ=2. N. Sunden, *Svensk. Kem. Tidskr.*, **65**, 257 (1953).
◐: Fe^{3+} at 20 °C and μ=1. D. D. Perrin, *J. Chem. Soc.*, **1959**, 1710.
●: Cu^{2+} at 25 °C and $\mu\rightarrow 0$. M. Llovd, V. Wycherley, and C. B. Monk, *J. Chem. Soc.*, **1951**, 1786.
□: Zn^{2+} at 25 °C and μ=0.2. P. K. Cannon and A. Kibrick, *J. Amer. Chem. Soc.*, **60**, 2314 (1938).
■: Ca^{2+}, △: Sr^{2+} and ▲: Ba^{2+} at 25 °C and $\mu\rightarrow 0$. C. A. Coleman-Porter and C. B. Monk, *J. Chem. Soc.*, **1952**, 4363.
○: UO^{2+} at 20 °C and μ=1.

behave much like the uranyl ion does, corresponding to the fact that these ions are classified as having the A-character. The copper(II) ion and the zinc(II) ion, belonging to the B-character group, remain nearly constant, independently on the temperature. Apart from Schwarzenbach's consideration, there is a possibility of interpreting these tendencies on the basis of the electronic energy level scheme of the metal ion. Alkali earth metal ions, Ca(II), Sr(II), and Ba(II), have stable configurations, with completely-filled $3s^2$-$3p^6$, $4s^24p^6$, and $5s^25p^6$ shells respectively. Since the levels of the 3d, 4d, and 5d orbitals, which accept the electrons of the approaching ligands, lie considerably higher than the filled 3p, 4p, and 5p levels respectively, the stability of the complex may not be affected by the dissociation behavior of carboxylic acid, log K_{1HA}, thus, they are decreased with the length of the carbon chain, which generally causes an increase in the stability of the acid. In the copper(II) ion, however, the unfilled 3d shell with 9 electrons has some capacity to accept electrons from ligands, so the tendency of the stability of the complex to decrease with the length of the carbon chain is compensated for by the increased donating properties of the corresponding acid. The zinc(II) ion seems also to fall in this category, because superposed 3d—4s levels may have the capacity to accept some electrons.

On the other hand, the iron(III) ion with a half-filled 3d shell can accept more electrons within the same 3d shell than can the copper(II) ion or the zinc(II) ion, even if some energy levels are more or less raised by the ligand-field effect. In the uranyl ion, 5f, 6d, and 7s orbitals are distributed in nearly equal energy levels, so there is much capacity to accept the electrons of ligands, though some of the orbitals are used to construct strong bonds of the uranyl ion by hybridization. In the indium(III) ion, which is completely filled up to the 4d shell, the 5s shell is more easily occupied by electrons from ligands than the 4s shell of the zinc(II) ion which is adopted by ligand electrons.

References

1) C. Miyake and H. W. Nurnberg, *J. Inorg. Nucl. Chem.*, **29**, 2411 (1967).
2) S. Fronaeus, Dissertation, Univ. Lund (1944).
3) S. Ahrland, *Acta Chem. Scand.*, **7**, 485 (1953).
4) G. Schwarzenbach, Plenary Lecture at XII International Conference on Coordination Chemistry, Sydney, Australia (1969).

BULLETIN OF THE CHEMICAL SOCIETY OF JAPAN, VOL. 48 (1), 351—352 (1975)

Tantalum Carbide Formed by the Carbonization of Ta_2O_5 in an Argon Plasma Arc

Osamu MATSUMOTO and Michio SAITO

Department of Chemistry, College of Science and Engineering, Aoyama Gakuin University, Chitosedai, Setagaya-ku, Tokyo 157

(Received August 3, 1974)

Synopsis. The formation of tantalum carbide by the carbonization of Ta_2O_5 with graphite by heating in an argon plasma arc was studied. Chemical and X-ray analyses showed that the product obtained was either stoichiometric or a defect carbide with the formula of TaC_{1-x}. The products were found to be superconductors.

Tantalum carbide is known to exist as from $TaC_{0.99}$ to $TaC_{0.85}$.[1] Giorgi *et al.*[2] found that the superconducting transition temperature decreased from 9.7 K to below 2.04 K as the carbon content decreased from 49.5 to 46.5 at%. In this case, tantalum carbide samples were prepared by heating mixtures of the elemental powders in a graphite crucible at 1850 °C under a vacuum of 10^{-5} Torr, with reaction times varying from 2 to 24 hr.

The present authors[3] previously formed niobium carbide by the carbonization of Nb_2O_5 with graphite by heating in an argon plasma arc and found that the product was a superconductor. Tantalum carbide was obtained by the carbonization of Ta_2O_5 with graphite in the same way. The products were confirmed, their properties, such as the density and the superconducting transition temperature, will be described in this note.

Ta_2O_5 (purity above 99.9%; H. C. Stark, Berlin) and graphite (spectroscopic grade; Tokai Electrode Mfg. Co.) were mixed in the desired molar ratio (C/Ta_2O_5). About one gram of the mixture was pressed into the tablet. Purified argon was used as the plasma gas. The plasma arc furnace and heating procedure were the same as have been described previously.[3,4] The temperature of the sample in the plasma arc was about 2900 °C. Heating was continued for 3 min. The products were investigated by X-ray diffraction and chemical analysis. The density of the products was measured picnometrically. The superconducting transition temperatures of some products were measured by means of 21 Hz mutual-inductance bridge and a Ge thermometer.

The chemical analysis data of the products with various C/Ta_2O_5 values are given in Table 1, while the X-ray analysis data of the products given in Table 2. The product obtained by $6.5 \leq C/Ta_2O_5 \leq 7.0$ was either stoichiometric TaC or a defect carbide with the formula TaC_{1-x}. Tantalum carbide, which has an fcc crystal structure, had a homogeneity range from 50.0 at% C to 43.5 at% C. The sum of the Ta and C contents of the products reached 100 wt%. It seems that only a little oxygen is present in the products in each case.* The lattice parameter of tantalum carbide, a, gradually increased with an increace in the carbon content. The product containing 50 at% C had a lattice parameter of 4.455 Å, which was comparable to that of the $TaC_{1.0}$ formed by the carbonization of metallic tantalum.[5]

TABLE 2. X-RAY ANALYSIS DATA OF PRODUCTS LISTED IN TABLE 1

Sample No.	Identified compounds	a of TaC (Å)
1	TaC, Ta_2C	4.419
2	TaC	4.421
3	TaC	4.435
4	TaC	4.441
5	TaC	4.448
6	TaC	4.450
7	TaC	4.455
8	TaC, C	4.456

TABLE 1. CHEMICAL ANALYSIS DATA OF PRODUCTS BY THE CARBONIZATION OF VARIOUS C/TaO IN AN ARGON PLASMA ARC

Sample No.	C/Ta_2O_5	Ta content		Combined C content		Free C content		$\sum$ (Ta, C) (wt %)
		(wt %)	(at %)	(wt %)	(at %)	(wt %)	(at %)	
1	6.4	96.5	58.5	4.46	41.5	—	—	100.1
2	6.5	95.2	56.5	4.48	43.5	—	—	100.1
3	6.6	94.4	53.0	5.56	47.0	—	—	100.1
4	6.7	94.2	52.0	5.77	48.0	—	—	100.0
5	6.8	94.1	51.1	5.95	48.9	—	—	100.1
6	6.9	94.0	50.5	6.04	49.5	—	—	100.0
7	7.0	93.8	50.0	6.22	50.0	—	—	100.0
8	7.1	93.0	46.6	6.18	46.7	0.89	6.70	100.1

* In the NbC formed by the carbonization of Nb_2O_5, the oxygen content in the product was found to be 0.008 wt% by radioactivation analysis.[3]

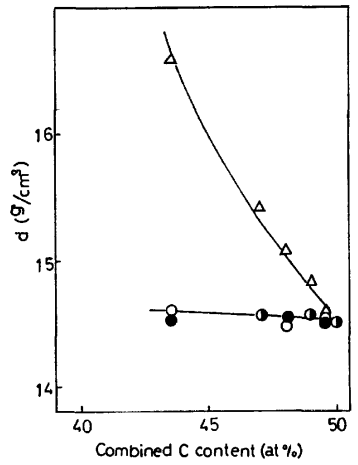

Fig. 1. Density *vs.* combined carbon content.
○: measured value, ●: calculated value assuming that the carbon position was vacant, △: calculated value assuming that the carbon position was substituted by Nb.

The relation between the density of the product at 25 °C and the combined carbon content is shown in Fig. 1. The density was about 14.5 g/cm³ for the product containing 50 at% C. This value agreed with the value calculated for stoichiometric TaC from the X-ray diffraction data. The density for TaC_{1-x} also agreed with that determined by means of X-ray diffraction, if we assumed that some carbon positions in the TaC lattice were vacant.

The relation between the superconducting transition temperature, T_c, of the product and the combined carbon content is shown in Fig. 2. The highest transition temperature was reached for the stoichiometric composition; it was 10.1 K. T_c decreased from 10.1 K to less than 4.2 K as the carbon content decreased from 50 to 47 at% C. This is similar to the decrease observed for tantalum carbide made by the carbonization

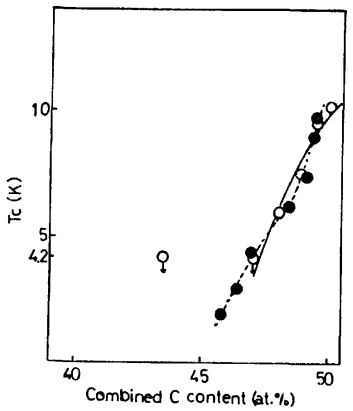

Fig. 2. T_c *vs.* combined carbon content.
○: this experiment, ●: Giorge *et al.*[2]

of metallic tantalum.[2]

The small amount of oxygen contained in the carbide remarkably decreases the T_c.[6] The oxygen content of the product formed in this work seems to be small. Therefore, it may be concluded that increasing the number of vacant carbon sites in the TaC lattice decreases the T_c. This conclusion is also supported by the results of the density measurement.

References

1) R. Lesser and C. Brauer, *Z. Metalk.*, **49**, 622 (1958).
2) A. L. Giorgi, E. G. Szkrarz, E. K. Storms, A. L. Bowman, and B. T. Matthias, *Phys. Rev.*, **125**, 837 (1962).
3) O. Matsumoto and M. Saito, *High Temp. Sci.*, **6**, 135 (1974).
4) O. Matsumoto and T. Miyazaki, *ibid.*, **5**, 40 (1973).
5) A. L. Bowman, *J. Phys. Chem.*, **65**, 1596 (1961).
6) V. H. Zackay, M. F. Merrian, and K. M. Ralls, "Superconductivity and Phase Diagram" in "Phase Diagram", ed. by A. M. Alper, Vol. III, Academic Press, New York (1970), p. 87.

BULLETIN OF THE CHEMICAL SOCIETY OF JAPAN, VOL. 48 (1), 353—354 (1975)

The Formation of the Rhodium Carbonyl Complexes from Chlorotris-[triphenylphosphine]rhodium with Alcohols in the Presence of Diene and Olefin

Akira YAMADA, Takashi FUKUDA, and Masaya YANAGITA
The Institute of Physical and Chemical Research, Wako-shi, Saitama 351

(Received February 8, 1974)

Synopsis. The decarbonylation of alcohols using chlorotris[triphenylphosphine]rhodium in the presence of diene or olefin occurs with the formation of the rhodium carbonyl complex and a hydrocarbon originating from the alcohol. The most suitable reaction system is rhodium compound/methanol/butadiene. The results suggest catalysis by a rhodium species.

It is well known that the decarbonylation of acyl halides and aldehydes by chlorotris[triphenylphosphine]rhodium ($RhCl(PPh_3)_3$: W-complex) yields chlorocarbonylbis[triphenylphosphine]rhodium ($RhCl(CO)(PPh_3)_2$: CO-complex) *via* an acyl complex as an intermediate.[1-3] A similar reaction of allylic alcohols by means of the W-complex occurs easily,[4-6] while the reaction of the common alcohols does not thus occur, though it does occur by means of another complex, $RhCl_3(PPh_3)_3$, with an alkaline base.[7] This note will briefly describe the successful abstraction of carbon monoxide from an alcohol molecule by means of the W-complex in the presence of diene or olefin.

When an alcoholic solution of the W-complex and diene or olefin was heated, the crystalline CO-complex[8] was formed quantitatively with the saturated hydrocarbon originating from the alcohol used. Only hydrogen gas instead of the hydrocarbon evolves from methanol. The reactions with other alcohols proceed at very low rates. These results are summarized in Table 1.

The title reaction requires a satisfactory dissolution of the W-complex into the reaction mixture at 80 °C. If one uses less of either alcohol or diene, the completion of the reaction requires a very long time. The reaction is insensitive to air and humidity. Olefin is also effective for the reaction, but shows a lower rate than diene. The presence of diene or olefin is essential to achieve the reaction, as is supported by Experiment No. 13 in Table 1. The reaction of allyl alcohol proceeds even in the absence of diene, as has previously been reported.[4-6]

The clarification of the reaction mechanism can be

TABLE 1. FORMATION OF $RhCl(CO)(PPh_3)_2$ BY REACTION OF $RhCl(PPh_3)_3$ (100 mg) WITH ALCOHOLS IN THE PRESENCE OF DIENE OR OLEFIN AT 80 °C

No.	Alcohol	ml	Diene or Olefin	ml	Reaction Time hr	Yield %	Observed by-products
1	Methyl	3.3	1,3-Butadiene	3.3	12	96	C_4H_8, hydrogen[a]
2	Methyl	5	Isoprene	1	24	83	2-Methyl-1-butene 2-Methyl-2-butene
3[b]	Methyl	5	Isoprene	1	60	89	3-Methyl-1-butene Hydrogen[a]
4[c]	Methyl	5	Isoprene	5	30	92	
5	Methyl	1	Isoprene	1.3	48	17	
6	Methyl	3.3	1,3-Pentadiene[d]	2	11	63	
7[e]	Methyl	2	Styrene	1.3	72	61	Ethylbenzene
8	Methyl	3	2-Methyl-2-butene	1	76	73	Isopentane
9[e]	Methyl	3	2-Methyl-2-butene	1	15	53	
10	Ethyl	5	Isoprene	1	72	5	Methane[a]
11	*n*-Propyl	5	Isoprene	1	115	20	Ethane[a]
12	Isopropyl	5	Isoprene	1	115	5	
13	Methyl	5	None	—	24	trace	
14[f]	Allyl	4	None	—	0.5	91	

a) Originated from alcohol. b) At 60 °C. c) Air and humidity were removed by a high vacuum line technique. d) Purity: 38.6%. e) Used 3 ml of methylene chloride as a solvent. f) *cf.* Ref. 4.

TABLE 2. COMPOSITION (%) OF HYDROGENATED PRODUCTS OF ISOPRENE

Reactions	2-Methyl-2-butene	3-Methyl-1-butene	2-Methyl-1-butene	Isopentane
$RhCl(PPh_3)_3$/methanol/isoprene[a]	42	12	46	(0)
$RhCl(CO)(PPh_3)_2$/methanol/isoprene[b]	55	2.2	43	(0)
$RhCl(PPh_3)_3$/hydrogen/isoprene[c]	63	6	13	17

a) Experimental No. 2 in Table 1. b) Same conditions as a). c) Atm. Press., at 25 °C.

made by an analysis of the by-products. When the W-complex/methanol/isoprene system was used, the hydrogenated products of isoprene could be observed as the main products, the total amount was found by gas chromatography to be 10 times as much as the yield of the CO-complex. Their compositions, shown on Table 2, resemble those of the reaction products from CO-complex/methanol/isoprene, but not those from W-complex/hydrogen/isoprene. It is noticeable that the products lack isopentane.

The above results indicate the following two conclusions: [1] on an identical rhodium atom, two hydrogen atoms of the methanol molecule migrate to isoprene and two others evolve as hydrogen gas, and [2] the CO-complex also induces the decarbonylation of the alcohol, suggesting a ligand-exchange reaction between carbonyl and isoprene. Consequently, the title reaction involves a catalytic scheme.

Experimental

In a glass autoclave, 100 mg of $RhCl(PPh_3)_3$ prepared according to the literature,[9] 5 ml of purified methanol, and 1 ml of distilled isoprene were placed. After evacuation, the reaction was carried out for 24 hr at 80 °C. The resultant yellow prism crystalline was isolated and washed with dry diethyl ether. The elemental-analytical results and IR spectrum of the product were identical with those of *trans*-$RhCl(CO)(PPh_3)_2$[8] prepared from $RhCl(PPh_3)_3$ and carbon monoxide. The crude product obtained in a lower yield was purified by recrystallization from methylene chloride–methanol. The hydrogenated products of diene and olefin and the evolved gas were analyzed by gas chromatography, using "benzyl cyanide–$AgNO_3$" and "Carbocieve" columns.

We wish to thank Dr. Jiro Tsuji of the Toray Co., Ltd., for his fruitful discussions and the Takeda Chem. Ind. Co., Ltd., and the Riken Vitamin Oil Co., Ltd., for their financial support.

References

1) J. Tsuji and K. Ohno, *Tetrahedron Lett.*, **1965**, 3969; **1966**, 4713; I. Tsuji and K. Ohno, *J. Amer. Chem. Soc.*, **90**, 99 (1968); I. Tsuji and K. Ohno, *Synthesis*, **1969**, 157.

2) J. Blum, *Tetrahedron Lett.*, **1966**, 1605; J. Blum, E. Oppenheimer, and E. D. Bergmann, *J. Amer. Chem. Soc.*, **89**, 2338 (1967).

3) M. C. Baird, C. J. Nyman, and G. Wilkinson, *J. Chem. Soc., A*, **1968**, 348.

4) M. A. Bennett and P. A. Longstaff, *Chem. and Ind.*, (London), **1965**, 846.

5) A. J. Birch and K. A. M. Walker, *J. Chem. Soc., C*, **1966**, 1894.

6) A. Emery, A. C. Oehlschlager, and A. M. Unrau, *Tetrahedron Lett.*, **1970**, 4401.

7) J. Chatt and B. L. Shaw, *Chem. and Ind.*, (London), **1960**, 931; J. Chatt and B. L. Shaw, *J. Chem. Soc., A*, **1966**, 1437.

8) L. Vallarino, *J. Chem. Soc.*, **1957**, 2287; J. Chatt and B. L. Shaw, *Chem. and Ind.*, (London), **1961**, 290.

9) J. A. Osborn, G. Wilkinson, and J. F. Young, *Chem. Commun.*, **1965**, 17; J. A. Osborn, F. H. Jardine, J. F. Young, and G. Wilkinson, *J. Chem. Soc., A*, **1966**, 1711.

BULLETIN OF THE CHEMICAL SOCIETY OF JAPAN, VOL. 48 (1), 355—356 (1975)

The Reaction of 3*H*-1,2-Benzodithiole-3-thione with Diphenyldiazomethane[1)]

Seizo TAMAGAKI, Ryoichi ICHIHARA, and Shigeru OAE*

Department of Applied Chemistry, Faculty of Engineering, Osaka City University, Sugimoto-cho, Sumiyoshi-ku, Osaka 558

**Department of Chemistry, University of Tsukuba, Sakura-mura, Niihari-gun, Ibaraki 300-31*

(Received April 13, 1974)

Synopsis. 3*H*-1,2-Benzodithiole-3-thione (^{35}S=C<) reacted with diphenyldiazomethane in the presence of copper-(II) acetylacetonate to afford the corresponding 4,5-benzo-3-diphenylmethylene-1,2-dithiole with a predominant extrusion of the exocyclic sulfur atom, while with its selenium analog the exclusive loss of in-ring sulfur was observed, resulting in the formation of the selenium-migrated 4,5-benzo-3-diphenylmethylene-1,2-thiaselenole.

Recently, it has been extensively investigated by Schoenberg[2)] and other workers[3-7)] that thiocarbonyl compounds react with diphenyldiazomethane to afford, eventually olefinic compounds presumably *via* a transient ylide[8)] which would cyclize,[9)] and then eliminate sulfur, as is shown below:

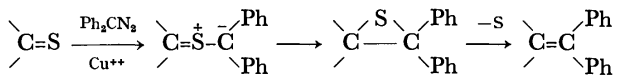

Under similar conditions, however, 1,2-dithiole-3-thione (trithione), bearing a relatively stable thiocarbonyl moiety, has been reported to fail to give the anticipated olefin.[2)] In this report, we would like to present the results on one detailed mechanistic examination of the reaction between benzotrithione (I) and diphenyldiazomethane in the presence of a catalytic amount of copper salt. For the sake of comparison, ^{35}S-labeled 3*H*-1,2-benzodithiole-3-thione (^{35}S=C<) (II) and selenium-substituted 4,5-benzo-1,2-dithiole-3-selone (III) were synthesized and treated with diphenyldiazomethane.

Results and Discussion

When 3*H*-1,2-benzodithiole-3-thione (I) was treated with three equivalents of diphenyldiazomethane in refluxing benzene in the presence of a catalytic amount of copper acetylacetonate, a product (IV) was obtained in a moderate yield. Similarly, the benzotrithione labeled with ^{35}S, both at the thione sulfur and the thiol sulfur by the ratio of 60: 40, was subjected to the same reaction. The ^{35}S-containing values are shown below:

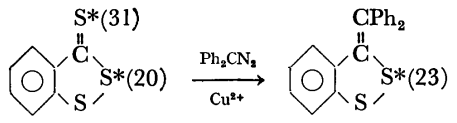

(I) or (II) (IV) (10^4 cpm/mol)

An inspection of the ^{35}S-labeling experiment suggests that the major part (72.7%) of the reaction apparently proceeds through the incipient formation of the thiirane ring, which is subsequently converted to the corresponding olefin, with the extrusion of the sulfur atom of the three-membered ring itself, as observed in usual cases (as is shown below (Path A)), while the remaining minor portion (27.3%) of the reaction is considered to take an alternative migration, Path B:

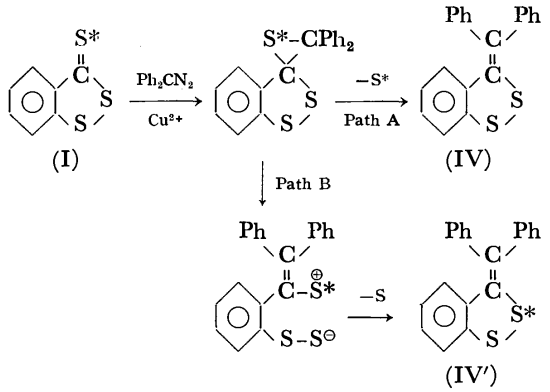

Scheme 1.

Meanwhile, sulfur migration proceeding along Path B was observed to take place exclusively when the corresponding selenium-substituted trithione (III) was allowed to react, but at the somewhat lower temperature of 60 °C. The selenium-migrated olefin, *i.e.*, 4,5-benzo-3-diphenylmethylene-1,2-thiaselenole (V), was found to be formed as a sole product in a 43% yield, apparently resulting from the extrusion of thiol sulfur rather than from that of exocyclic selenium. In this case, no formation of the corresponding olefinic sulfur product (IV) is noticiably not even by a careful gas-chromatographic analysis of the reaction mixture.

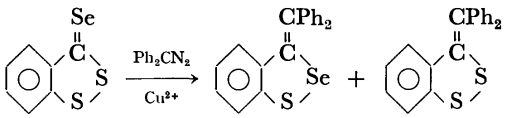

(III) (V) (IV not detected)

The marked difference in reaction modes between the sulfur (II) and selenium (III) compounds can not be explained with our present knowledge. Several lines of experiments to clarify this point are now under way here.

Experimental

Reaction of I with Diphenyldiazomethane. Treating 0.3 g (1.6 mmol) of I with 1.0 g (5.1 mmol) of diphenyldiazomethane in 30 ml of refluxing benzene containing copper acetylacetonate as the catalyst for 6 hr afforded a viscous liquid, which was then subjected to column chromatography through silica gel, using *n*-hexane as the solvent. The major, orange-colored portion (IV) eluted second was collected and recrystallized from *n*-hexane. The yield was 0.2 g (40%); mp 162—163 °C; IR (KBr) 1610, 1585, 1500, 1450, 1170,

970, 750, 700 cm^{-1}; UV λ_{max} ($CHCl_3$) 385 nm (ε: 7300). Found: C, 75.11; H, 4.39%. Calcd for $C_{20}H_{14}S_2$: C, 75.48; H, 4.43%. Mass spectrum *m/e*: 318 (M^+), 286 (M^+-S), 257 (metastable).

Reaction of III with Diphenyldiazomethane. A mixture of 0.2 g (0.7 mmol) of III, 0.3 g (1.5 mmol) of diphenyldiazomethane, and a small amount of the catalyst was treated at 60 °C for 3 hr. A procedure similar to that employed above gave 0.1 g of V; mp 175—176 °C. IR (KBr) 1580, 1490, 1060, 750, 695 cm^{-1}; UV λ_{max} ($CHCl_3$) 391 nm (ε: 6400). Found: C, 65.29; H, 3.75%. Calcd for $C_{20}H_{14}SSe$: C, 65.74; H, 3.86%. Mass spectrum *m/e*: 366 (M^+), 286 (M^+-Se), 223.5 (metastable).

We wish to thank Professor Takayuki Otsu for his helpful discussions and Dr. Reiko Kiritani of the Radiation Center of Osaka Prefecture for performing the ^{35}S-activity determination.

References

1) Derivatives of 1,2-dithiole-3-thiones. VI. Part V, *Tetrahedron Lett.*, **1974**, 1659.
2) A. Schoenberg and Renata von Ardenne, *Chem. Ber.*, **101**, 346 (1968).
3) H. Staudinger and J. Siegwart, *Helv. Chim. Acta*, **3**, 833, 840 (1920).
4) N. Latif and I. Fathy, *J. Org. Chem.*, **27**, 1633 (1962).
5) A. Schoenberg and E. Freese, *Chem. Ber.*, **95**, 2810 (1962).
6) W. J. Middleton, E. G. Haward, and W. H. Sharky, *J. Org. Chem.*, **30**, 1375 (1965).
7) D. Seyferth and W. Tronich, *J. Amer. Chem. Soc.*, **91**, 2138 (1969).
8) E. B. Knott, *J. Chem. Soc.*, **1955**, 916.
9) J. Buter, S. Wassenaar, and R. M. Kellogg, *J. Org. Chem.*, **37**, 4045 (1972).

BULLETIN OF THE CHEMICAL SOCIETY OF JAPAN, VOL. 48 (1), 357—358 (1975)

The Syntheses of Several *N,N'*-Bis(hydroxymethyl)parabanic Acid Derivatives

Shigeo TANIMOTO,* Ryozo TANIYASU, and Masaya OKANO
Institute for Chemical Research, Kyoto University, Uji, Kyoto 611

(Received July 17, 1974)

Synopsis. Starting from *N,N'*-bis(hydroxymethyl)-parabanic acid, the following new compounds have been synthesized: *N,N'*-bis(arylaminomethyl)parabanic acids, *N,N'*-bis(bromomethyl)parabanic acid, and *N,N'*-bis(alkoxymethyl)parabanic acids.

Though *N,N'*-bis(hydroxymethyl)parabanic acid (**1**) may serve as a reactive bifunctional heterocycle, little is known about its reactions or about its derivatives. The present communication will be concerned with the syntheses some of its derivatives.

The preparation of **1** from parabanic acid and two moles of formaldehyde was first reported by Oda and Baba:[1]

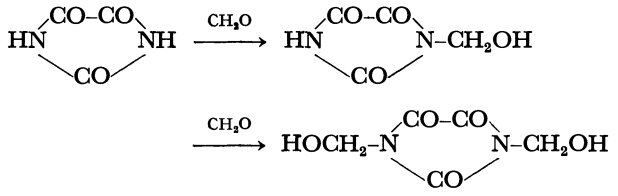

1

When **1** was mixed with aromatic primary or secondary amines in 50% ethanol at room temperature, the corresponding bisarylaminomethyl compounds (**2**) were readily formed. They separated out from the reaction medium in good yields and were easily purified by recrystallization. Several bisarylaminomethyl compounds are listed in Table 1.

A similar transformation, proposed by Winstead and Heine[2] as a method for the identification of aromatic amines, involves the condensation of phthalimide with formaldehyde and aromatic amines in boiling 80% ethanol. Since our reaction proceeds smoothly without heating, it may also offer advantages in the identification of primary or secondary aromatic amines as well as in their removal from the mixture with tertiary amines.

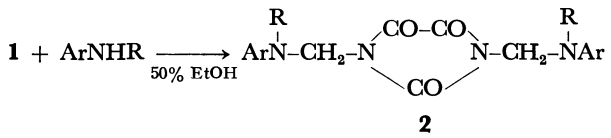

2

The conversion of **1** into *N,N'*-bis(bromomethyl)-parabanic acid (**3**) was achieved by treatment with excess phosphorus tribromide in refluxing benzene. The bisbromomethyl compound thus obtained was considerably reactive toward nucleophiles. For example, when the reaction of **3** with primary or secondary aliphatic alcohols was carried out in the presence of potassium iodide, the expected *N,N'*-bis(alkoxymethyl)-

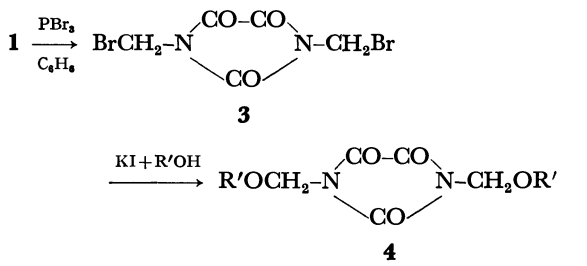

4

R'=Et, *n*-Pr, *iso*-Pr, *n*-Bu, *iso*-Bu

Table 1. Preparation of *N,N'*-bis(arylaminomethyl)parabanic acids

Ar	R	Method[a,b]	Yield[c] (%)	Mp (°C)	Found (%)			Calcd (%)		
					C	H	N	C	H	N
	H	A	73	71—74[d]	62.65	5.15	17.07	62.95	4.97	17.28
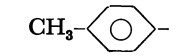	H	B	99	134—137[d]	64.47	5.71	15.95	64.76	5.72	15.90
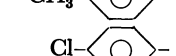	H	B	93	68—72[e]	51.76	3.70	14.35	51.92	3.59	14.52
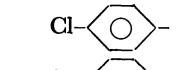	H	B	76	231—234[d]	49.62	3.47	20.32	49.28	3.41	20.29
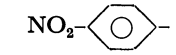	H	A	70	60—64[d]	66.59	6.37	14.74	66.30	6.36	14.73
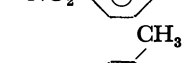	H	B	89	69—73[d]	59.63	5.34	14.58	59.37	5.24	14.58
	CH_3	A	46	54—56[d]	64.72	5.82	15.87	64.76	5.72	15.90

a) Method A, amine dissolved in the same amount of 50% ethanol was added. b) Method B, amine dissolved in a minimum amount of 50% ethanol was added. c) Yields were based upon **1**, and referred to isolated ones. d) Recrystallized from ethanol. e) Recrystallized from benzene–*n*-hexane.

Table 2. Preparation of *N,N'*-bis(alkoxymethyl)parabanic acids

R'	Reaction temperature (time)	Yield (%)	Mp (°C)	Found (%)[a]			Calcd (%)		
				C	H	N	C	H	N
Me	Room temperature (2 hr)	Unidentified product of mp 195—198 °C							
Et	Room temperature (4 hr)	70	103—105[b]	46.82	6.19	12.17	46.95	6.13	12.17
n-Pr	Reflux (4—5 hr)	72	92—93[b]	51.00	6.99	10.82	51.15	7.03	10.85
iso-Pr	Reflux (5—6 hr)	45	86—88[b]	50.91	7.05	10.61	51.15	7.03	10.85
n-Bu	Reflux (4—5 hr)	78	75—77[b]	54.43	7.63	9.97	54.53	7.75	9.78
iso-Bu	Reflux (5—6 hr)	61	89—90.5[b]	54.66	8.01	9.64	54.53	7.75	9.78

a) Besides elemental analyses, the structure of the products was confirmed by NMR. b) Recrystallized from ligroin.

parabanic acids (**4**) were obtained in yields of 45—78%. However, the reaction with methanol failed to give the desired product. The results are shown in Table 2.

Experimental

N,N'-*Bis(hydroxymethyl)parabanic Acid (1).* A mixture of 5.7 g (0.05 mol) of parabanic acid and 8.0 g (0.10 mol) of 37% formalin was refluxed for 3—4 hr. The reaction mixture soon became a clear solution. When the solution was then allowed to cool, a crystalline solid separated. This was collected and dried to give 6.4 g (74%) of a white powder. Recrystallization from ethanol gave the pure compound; mp 127—131 °C (lit,[1] mp 130 °C).

N,N'-*Bis(arylaminomethyl)parabanic Acids (2).* A typical procedure will be described; all the other products were obtained in an analogous manner. A mixture of 1.4 g (0.015 mol) of aniline and the same amount of 50% ethanol was added, drop by drop, to a solution of 1.1 g (0.0063 mol) of **1** in 30 ml of 50% ethanol at room temperature. The solution immediately turned yellow, and a crystalline solid soon began to precipitate. After standing for 3—4 hr, the precipitate was collected and recrystallized from ethanol. Yield, 1.5 g (73%); mp 71—74 °C.

N,N'-*Bis(bromomethyl)parabanic Acid (3).* To a stirred suspension of 5.0 g (0.029 mol) of **1** and 200 ml of dry benzene, we added 30 g (0.11 mol) of phosphorus tribromide; the reaction mixture was then refluxed for 3 hr, during which time a vigorous reaction occurred. The filtration of the concomitant resinous product from the reaction mixture, followed by the removal of the solvent *in vacuo*, provided 3.9 g (45%) of a crude light-yellow solid. Recrystallization from benzene gave light-yellow crystals of **3**; mp 159—162 °C. Found: C, 20.35; H, 1.36; N, 9.36%. Calcd for $C_5H_4Br_2N_2O_3$: C, 20.02; H, 1.34; N, 9.34%. When stored in a moist atmosphere, **3** showed signs of decomposition, as evidenced by brown-coloring and a lowered melting point.

N,N'-*Bis(alkoxymethyl)parabanic Acids (4).* A typical example will be given. A solution of 1.5 g (0.005 mol) of **3** in 50 ml of ethanol containing 1.7 g (0.01 mol) of potassium iodide was stirred for 4 hr at room temperature. The subsequent evaporation of the ethanol gave white crystals of *N,N'*-bis(ethoxymethyl)parabanic acid (**4**, R'=Et); yield, 0.8 g (70%); mp 103—105 °C.

References

1) R. Oda and R. Baba, *Kogyo Kagaku Zasshi*, **64**, 741 (1961).

2) M. B. Winstead and H. W. Heine, *J. Amer. Chem. Soc.*, **77**, 1913 (1955).

BULLETIN OF THE CHEMICAL SOCIETY OF JAPAN, VOL. 48 (1), 359—360 (1975)

The Preparation of 3- and 4-Fluorophthalic Anhydrides by Fluorodenitration

Nobuo ISHIKAWA, Toshio TANABE, and Dan HAYASHI
Tokyo Institute of Technology, Department of Chemical Engineering, Meguro-ku, Tokyo 152

(Received July 22, 1974)

Synopsis. 3- And 4-fluorophthalic anhydrides were prepared by heating the respective nitrophthalic anhydrides with potassium fluoride with or without an aprotic polar solvent.

Mono and difluorophthalic anhydrides have been synthesized mainly by the oxidation of fluorinated *o*-xylenes.[1,2] However, these preparative routes involve a tedious Balz-Schiemann reaction in order to introduce the fluorine atom into an aromatic ring. A simple preparative method for 3-fluorophthalic anhydride has, however, been reported by Heller, who used a halogen exchange process which involves merely baking 3-chlorophthalic anhydride with potassium fluoride.[3] 3-Chlorophthalic anhydride, on the other hand, is most conveniently prepared by the chlorination of 3-nitrophthalic anhydride,[4] which is obtained by the nitration of phthalic anhydride together with the 4-nitro isomer.[5] In this connection, we examined the fluorination of 3- and 4-nitrophthalic anhydrides directly with potassium fluoride, since fluorodenitration on aromatic nitro compounds is not unusual in the literature.[6,7]

When 3-nitrophthalic anhydride was heated with about three moles of potassium fluoride at 180—190 °C, a temperature which is a little higher than the melting point of the nitro compound, the reaction proceeded smoothly, with the evolution of a brown gas of nitrogen oxide. The reaction was completed within a rather short period, 30—60 min, judging from the gas chromatographic observation. The yield of almost pure 3-fluorophthalic anhydride was about 65%. A higher temperature or a longer reaction time had unfavorable results; for instance, an explosive reaction occurred above 210 °C.

4-Nitrophthalic anhydride was also subjected to a similar process. The nitro group of this compound was less reactive for the fluorination, and the reaction required a higher temperature (190—195 °C) and a longer reaction time (—75 min). This is probably due to the weaker inductive effect of the electron-withdrawing dicarboxyl anhydride group, which is located farther from the nitro group than in the case of the 3-nitro isomer.

Since such polar aprotic solvents as dimethylformamide, dimethylsulfoxide, sulfolane, and hexamethyl phosphortriamide are well known to accelerate nucleophilic aromatic substitutions, including fluorination, we also used these solvents. In these aprotic solvents, the reactions seemed to proceed more easily and a lower temperature (80—90 °C) was enough for them to take place. However, the separation of the products from the reaction mixture was difficult because of their high solubility in these solvents as well as in water. We had to extract them with diethyl ether several times from the reaction mixture after dilution with water. This process made the yield of the fluorophthalic anhydride unreproducible. Further, a part of the fluorophthalic anhydride seemed to be attacked nucleophilically with these solvents.

The results of several runs carried out are shown in Table 1.

TABLE 1. FLUORODENITRATION OF NITROPHTHALIC ANHYDRIDES

[NPA] [FPA]

	Start materials		Reaction conditions			Yield of FPA (%)
	NPA	KF/NPA (molar ratio)	Solvent	Temp. (°C)	Time (min)	
1	3-NO_2	3	—	160—165	60	62
2	3-NO_2	3	—	180	30	66
3	3-NO_2	3	—	190	45	49
4	3-NO_2	3	—	200	30	39
5	3-NO_2	2.5	—	190	30	42
6	3-NO_2	2	—	190	30	16
7	4-NO_2	3	—	190—195	75	56
8	4-NO_2	3	—	200—205	70	52
9	3-NO_2	3	DMF	95	60	42
10	3-NO_2	3	DMSO	80	60	61

Experimental

Nitrophthalic Acids and Their Anhydrides. The nitration of phthalic anhydride was carried out according to the procedure described in Org. Syn.;[5] it gave pure 3-nitrophthalic acid (mp 214—216 °C (lit,[5] 215—218 °C)) in a 30% yield after recrystallization from water. This acid was then converted into the anhydride (mp 163—165 °C (lit,[8] 163—164 °C)) by treating it with acetic anhydride.[8]

From the mixture of isomers of nitro compounds which was obtained from the mother liquors of the recrystallizations, 4-nitrophthalic acid (mp 159—160 °C (lit,[9] 164—164.5 °C)) was separated *via* esterification.[10] A subsequent treatment with acetic anhydride gave 4-nitrophthalic anhydride (mp 118—119 °C (lit,[9] 120—120.5 °C)).

Fluorophthalic Anhydrides. Without Any Solvent: A typical procedure was as follows. A mixture of 3-nitrophthalic anhydride (4.85 g, 0.026 mol) and potassium fluoride dehydrated by baking (4.35 g, 0.075 mol) was heated in an oil-bath and vigorously stirred for 30 min, keeping the temperature at 180—185 °C. During the reaction, nitrogen oxide gas evolved; it was led into a hood. After cooling, the reaction mixture was treated with benzene, and the fluorinated product was extracted by filtration. The solvent was then evaporated from the filtrate, giving 3-fluorophthalic anhydride (2.72 g, 66%, mp 159—160 °C). Recrystallization from benzene gave pure crystals (mp 161.5—162.5 °C (lit,[3] 160 °C)). IR (KBr): 1870, 1855, 1780 (C=O), 1265 (C–F) cm^{-1}. ^{19}F NMR (from int. C_6H_5F in C_6H_6): δ −3.4 ppm.

The reaction between 4-nitrophthalic anhydride and potassium fluoride was run in a similar manner, giving 4-fluorophthalic anhydride (mp 79—80 °C (lit,[2] 76—78 °C) (Table 1)). IR: 1855, 1830, 1780 (C=O), 1280 (C–F) cm^{-1}. ^{19}F NMR: δ −13.0 ppm.

With A Solvent: Nitrophthalic anhydride (5 g) and baked potassium fluoride (4.5 g) were heated in a solvent while being mechanically stirred. On cooling, the mixture was diluted with water, made acidic with hydrochloric acid, and extracted with diethyl ether several times. The ethereal extract was dried over magnesium sulfate and evaporated to give fluorophthalic anhydride (Table 1).

References

1) M. S. Newman and E. H. Wiseman, *J. Org. Chem.*, **26**, 3208 (1961).
2) G. Valkanas and H. Hopff, *J. Chem. Soc.*, **1963**, 3475.
3) A. Heller, *J. Org. Chem.*, **25**, 834 (1960).
4) M. S. Newman and P. G. Scheurer, *J. Amer. Chem. Soc.*, **78**, 5004 (1956).
5) P. J. Culhane and G. E. Woodward, "Org. Syntheses", Coll. Vol. I, p. 408 (1941).
6) G. C. Finger and C. W. Kruse, *J. Amer. Chem. Soc.*, **78**, 6034 (1956).
7) G. Bartoli, A. Latrofa, F. Naso, and P. E. Todesco, *J. Chem. Soc. Perkin Trans. I.*, **1972**, 2671.
8) B. H. Nicolet and J. A. Bender, "Organic Syntheses," Coll. Vol. I, p. 410 (1941).
9) M. Hayashi and K. Kawasaki, *Kogyo Kagaku Zasshi*, **36**, 391 (1933).
10) F. F. Blicke and F. D. Smith, *J. Amer. Chem. Soc.*, **51**, 1865 (1929).

BULLETIN OF THE CHEMICAL SOCIETY OF JAPAN, VOL. 48 (1), 361—362 (1975)

The Preparation of Several Copper(I) and Silver Polyfluoroalkanethiolates and of Polyfluoroalkyl Aryl (or Alkyl) Sulfides

Tomoya KITAZUME and Nobuo ISHIKAWA

Department of Chemical Engineering, Tokyo Institute of Technology, Meguro-ku, Tokyo 152

(Received July 29, 1974)

Synopsis. 2,2,4,4-Tetrakis(trifluoromethyl)-1,3-dithietane (**1**) in the KF-DMF system was treated with hexafluoropropene in the presence of CuBr to give copper(I) 1,1,2-tris(trifluoromethyl)tetrafluoropropanethiolate (**4**). A similar reaction of **1** with alcohols in the presence of CuBr or $AgNO_3$ gave copper(I) (**6**) and silver 1-alkoxy-1-trifluoromethyl-2,2,2-trifluoroethanethiolate (**7**) respectively. These copper(I) and silver polyfluoroalkanethiolates condensed with aryl or alkyl iodides to afford 1,1,2-tris(trifluoromethyl)-tetrafluoropropyl (**8**) and 1-alkoxy-1-trifluoromethyl-2,2,2-trifluoroethyl aryl(or alkyl) sulfides (**9**).

In our previous paper[1] on the nucleophilic reactions of 2,2,4,4-tetrakis(trifluoromethyl)-1,3-dithietane (**1**) in the presence of potassium fluoride in dimethylformamide, we reported that hexafluorothioacetone (**2**) seems to be released during the reaction by the action of the fluoride ion on **1**, and that reaction products between **2** and nucleophiles were obtained. That study has now been continued, examining a similar reaction in which the heptafluoroisopropyl anion was used as the nucleophile. The expected product, 1,1,2-tris(trifluoromethyl)tetrafluoropropanethiol (**3**) was isolated in the form of copper(I) salt (**4**), and it was found that this copper thiolate was a useful reagent for the preparation of branched perfluorohexyl aryl or alkyl sulfides (**8**).

Copper and silver 1-alkoxy-1-trifluoromethyl-2,2,2-trifluoroethanethiolates, **6** and **7**, were also obtained by the reaction of **1** with alcohols in the presence of metal ion, and these thiolates condensed easily with aryl iodides to give 1-alkoxy-1-trifluoromethyl-2,2,2-trifluoroethyl aryl sulfides, **9**.

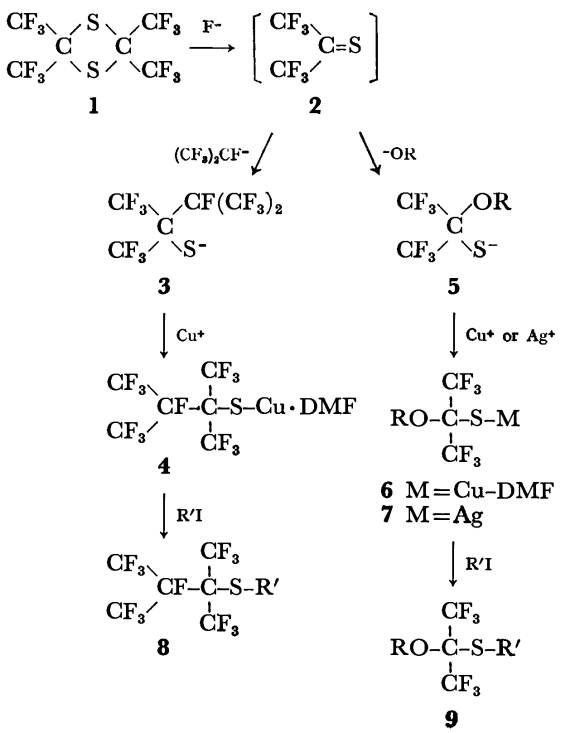

The Preparation of Copper(I) 1,1,2-Tris(trifluoromethyl)-tetrafluoropropanethiolate. The heptafluoroisopropyl anion, which is formed readily by the action of the fluoride ion on hexafluoropropene, is known to be an effective nucleophile.[2] The reaction between 2,2,4,4-tetrakis(trifluoromethyl)-1,3-dithietane (**1**) and hexafluoropropene was examined in the presence of potassium fluoride in dimethylformamide. Since the resulting perfluoroalkanethiol was presumed to be readily oxidized, we carried out the reaction in the presence of copper(I) bromide in order to trap the thiol in the form of copper(I) thiolate. The reaction proceeded smoothly at 50 °C, and the expected copper thiolate was isolated from the reaction products in a yield of 52% by acetone extraction. This compound was a fairly stable solid, with a melting point of 78—80 °C; it was an adduct with one mole of dimethylformamide. The structure was evident from its IR, NMR, and mass spectra. In the IR spectrum, the presence of an amide group was revealed by the strong band at 1650 cm^{-1}. In the ^{19}F NMR spectrum, three signals appeared, at −18.8 (doublet), −17.0 (singlet), and 124.7 (multiplet) ppm;* they are probably due to $CF(CF_3)_2$, $C(CF_3)_2$, and $CF(CF_3)_2$, respectively. In the mass spectrum, two important fragment peaks, *m/e* 415 ($C_6F_{13}SCu^+$) and *m/e* 73 ($C_3H_7NO^+$), appeared, in addition to the molecular ion, M^+ 488. The other fragment peaks at *m/e* 351 and *m/e* 344 can be explained by the elimination of Cu and CF_3 respectively from *m/e* 415. The ions of *m/e* 182 (C_3F_6S), 132 (C_2F_4S), and 113 (C_2F_3S), which are characteristic of hexafluorothioacetone derivatives, also appeared.

The Preparation of Copper(I) and Silver 1-Alkoxy-1-trifluoromethyl-2,2,2-trifluoroethanethiolates. In our investigation of the reactions between 2,2,4,4-tetrakis(trifluoromethyl)-1,3-dithietane (**1**) and alcohols in the potassium fluoride–dimethylformamide system, 1-alkoxy-1-trifluoromethyl-2,2,2-trifluoroethanethiols (**5**) seemed to be formed; however, they were finally oxidized and isolated as disulfides.[1]

As we desired to capture the thiol, **5**, in the form of metal thiolates as evidence of the reaction pass, these reactions were carried out in the presence of silver or copper salt. When silver nitrate was used, silver thiolates were obtained as stable white crystals, which were isolated from the reaction products by extraction with acetone.

* All the ^{19}F NMR chemical shifts throughout this article are given in ppm from external trifluoroacetic acid.

Table 1. Preparation of **8**

R′	Yield (%)	Bp (°C/mmHg) (mp °C)	^{19}F NMR[a]			F-Anal (%)	
			$(CF_3)_2CF$	$-(CF_3)_2$	>CF	Found	(Calcd)
C_6H_5	69	58—60/26	−12.6	−10.7	108.5	57.4	(57.7)
m-Me·C_6H_4	50	96—99/24	−12.0	−10.7	110.0	55.6	(55.9)
p-Me·C_6H_4	42	86—89/25	−11.8	−10.3	110.2	55.3	(55.9)
o-O_2N·C_6H_4	45	(63—65)	−13.0	−11.0	105.5	51.9	(52.2)

a) δ ppm from ext. CF_3CO_2H in CCl_4.

Table 2. Preparation of **9** (R=OMe)

R′	Yield (%)	Bp (°C/mmHg) (mp °C)	^{19}F NMR[a] CF_3	F-Anal(%)	
				Found	(Calcd)
C_6H_5	57	73—75/32	−8.70	39.6	(39.3)
o-MeC_6H_4	60	107—108/27	−8.70	37.8	(37.3)
p-MeC_6H_4	64	98—99/19	−8.75	36.8	(37.3)
p-FC_6H_4	70	108—110/71	−8.70	43.0	(43.2)
o-$O_2NC_6H_4$	75	(69—70)	−8.84	33.4	(34.0)
m-$O_2NC_6H_4$	51	114—115/4	−8.70	33.7	(34.0)
p-$O_2NC_6H_4$	56	(41—43)	−8.76	33.0	(34.0)
o-$HO_2CC_6H_4$	59	(105—106)	−8.75	34.4	(34.1)
o-$MeO_2CC_6H_4$	55	107—108/4	−8.70	32.5	(32.7)
p-$MeOC_6H_4$	67	86—89/3	−8.65	35.2	(35.6)

a) ^{19}F Chemcal shifts are given in δ ppm from ext. CF_3CO_2H in CCl_4.

Copper thiolates were also obtained by using copper(I) bromide instead of silver nitrate in the above reaction. The product isolated from the acetone extract was an adduct with one mole of dimethylformamide, as in the case of **4**. The IR spectrum revealed a strong band at 1640 cm^{-1} due to the amide group; the other major bands were similar to those of **7**.

The Condensation of Silver and Copper(I) Thiolates with Aryl(or Alkyl) Iodides. The condensation of silver and copper alkanethiolates with aryl or alkyl iodides is well known.[3-5] The silver and copper thiolates mentioned above also underwent condensation with aryl and alkyl iodides to give polyfluoroalkyl aryl or alkyl sulfides (Tables 1 and 2). The reactions proceeded in dimethylformamide at 80—100 °C under a nitrogen atmosphere. Especially, the condensation of various substituted aryl iodides and the copper perfluorohexanethiolate (**4**) seems to be a useful synthetic method for higher perfluoroalkyl thiobenzenes, which are valuable intermediates for surface-active compounds.

Experimental

Copper(I) 1,1,2-Tris(trifluoromethyl)tetrafluoropropanethiolate-DMF Adduct (4). Hexafluoropropene was bubbled into a mixture of the dimer of hexafluorothioacetone, **1** (7.3 g, 0.02 mol), copper(I) bromide (5.7 g, 0.04 mol), potassium fluoride (4.5 g, 0.077 mol), and dimethylformamide (50 ml) at 50 °C until no more absorption of the gas took place. The reaction mixture was then poured into water, and the precipitates were separated by filtration and washed with water. This black solid was subjected to extraction with hot acetone, and the solvent was removed by evaporation to give an orange product; mp 78—80 °C (10 g, 52%). This was a 1:1 adduct of **4** with dimethylformamide. Found: C, 21.5; H, 1.71; N, 2.48; F, 50.5%. Calcd for $C_9H_7F_{13}NOSCu$: C, 22.2; H, 1.44; N, 2.87; F, 50.7%.

Copper(I) 1-Methoxy-1-trifluoromethyl-2,2,2-trifluoroethanethiolate (6). A mixture of **1** (3.64 g, 0.01 mol), methyl alcohol (0.64 g, 0.02 mol), copper(I) bromide (2.86 g, 0.02 mol), and potassium fluoride (1.71 g, 0.029 mol) in dimethylformamide (30 ml) was stirred for 24 hr at room temperature. The resulting mixture was worked up as above to give **6** (yield, 63%); mp 68—70 °C. Found: C, 24.3; H, 2.95; N, 4.21; F, 32.4%. Calcd for $C_7H_{10}F_6NO_2SCu$: C, 24.1; H, 2.88; N, 4.01; F, 32.6%. IR: 1640 cm^{-1} (-CO-N-).

Silver 1-Methoxy-1-trifluoromethyl-2,2,2-trifluoroethanethiolate (7) (R=Me). A mixture of **1** (3.64 g, 0.01 mol), methyl alcohol (0.64 g, 0.02 mol), silver nitrate (3.4 g, 0.02 mol), potassium fluoride (1.30 g, 0.022 mol), and dimethylformamide (30 ml) was worked up as above, giving a white product; mp 132—133 °C (4.04 g, 57%). Found: C, 15.2; H, 0.76; F, 35.2%. Calcd for $C_4H_3F_6OSAg$: C, 15.0; H, 0.94; F, 35.5%. NMR (in DMSO-d_6): ^{1}H, 5.76 (OMe, s); ^{19}F, −6.00 (CF_3, s).

The reaction with ethanol was run similarly; here the product (mp 150—151 °C) was obtained in a yield of 34%.

Condensation Reactions. A): A mixture of **4** (5.32 g, 0.011 mol), *o*-iodonitrobenzene (2.50 g, 0.01 mol), and DMF (50 ml) was stirred under an atmosphere of nitrogen at 80—90 °C for 24 hr. After the copper iodide had been removed by filtration, the filtrate was poured into water, and the precipitates were collected and recrystallized from *n*-hexane to give **8** (R′=*o*-$NO_2C_6H_5$) (mp 63—65 °C) in a yield of 45%. Found: C, 30.7; H, 0.96; N, 2.73; F, 51.9%. Calcd for $C_{12}H_4F_{13}NO_2S$: C, 30.5; H, 0.85; N, 2.96; F, 52.2%. IR: 1510, 1358 (NO_2) cm^{-1}.

B): A mixture of **6** (R=Me, 7.0 g, 0.025 mol), *o*-iodonitrobenzene (5.0 g, 0.02 mol) and DMF (50 ml) was worked up such as has been described above at 90—100 °C for 24 hr. The product was recrystallized from *n*-hexane to give **9** (R′=*o*-$NO_2C_6H_5$, 75%); mp 69—70 °C. Found: C, 36.0; H, 2.31; N, 4.25; F, 33.9%. Calcd for $C_{10}H_7F_6NO_3S$: C, 35.8; H, 2.10; N, 4.18 F, 34.0%. IR: 1525, 1358 (NO_2) cm^{-1}.

References

1) T. Kitazume and N. Ishikawa, This Bulletin, **46**, 3285 (1973).
2) J. A. Young, "Fluorine Chemistry Reviews," Vol. 1, Marcel Dekker, New York (1967), p. 359.
3) R. Adams, W. Reifschneider, and M. D. Nair, *Croatica Chem. Acta*, 29 (1959).
4) R. Adams and A. Ferretti, *J. Amer. Chem. Soc.*, **81**, 4927 (1959).
5) L. M. Yagupol'skii and N. V. Kondratenko, *Zh. Obshch. Khim.*, **39**, 1755 (1969).

BULLETIN OF THE CHEMICAL SOCIETY OF JAPAN, VOL. 48 (1), 363—364 (1975)

The Bromination of 1- and 2-Methylthiophenazine Derivatives

Masao TADA

The Research Institute for Tuberculosis, Leprosy and Cancer, Tohoku University, Hirosemachi, Sendai 980

(Received August 7, 1974)

Synopsis. The bromination of 1-methylthiophenazine has been investigated and found to occur in Position 4. 2-Methylthiophenazine and its 5-oxide have been found to be brominated in Position 1. The bromination of these compounds in acetic acid gave both a ring-substituted product and its oxidised product.

In a previous paper,[1] it was reported that the methylthio- and bis(methylthio)phenazine derivatives were readily synthesized by the reactions of halogenophenazine derivatives with methyl mercaptan. In connection with the synthetic study of methylthiophenazine derivatives with potential biological activities, this paper will describe the brominations of 1- and 2-methylthiophenazine derivatives, by which it becomes feasible to prepare bis(methylthio)phenazines as a second route of synthesizing them.

The bromination of 1- (**1**) and 2-methylthiophenazine (**2**) was carried out using bromine in chloroform, to give two bromo compounds, **3** and **4** respectively. When the bromination of **1** was carried out using bromine in acetic acid, both the ring-substituted product, **3**, and its oxidised product, **5**, were produced. Compound **2** was treated with bromine under similar conditions to form **4** and its oxidised product, **6**, in good yields. Compounds **5** and **6** were also obtained by the controlled oxidation of **3** and **4** respectively with potassium bromate. It has been reported that the bromination of alkyl aryl sulfides in acetic acid gives ring-substituted products,[2] while the chlorination in acetic acid gives oxidised products.[3] It may be anticipated that **1** and **2** will prove susceptible to electrophilic attack in the 4- and 1-positions respectively. This results from the localizing of a negative charge at C_4 in **1** and at C_1 in **2**.[2,4] The positions of the bromine atoms in **3** and **4** were confirmed by the substitution reactions of **3** and **4** with methyl mercaptan.

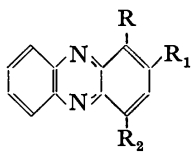

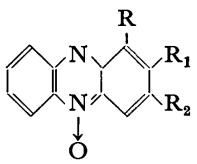

1: R=SCH_3; R_1=R_2=H
2: R=R_2=H; R_1=SCH_3
3: R=SCH_3; R_1=H; R_2=Br
4: R=Br; R_1=SCH_3; R_2=H
5: R=$SOCH_3$; R_1=H; R_2=Br
6: R=Br; R_1=$SOCH_3$; R_2=H
7: R=R_2=SCH_3; R_1=H
8: R=R_1=SCH_3; R_2=H
9: R=SCH_3; R_1=R_2=H
10: R=R_1=H; R_2=SCH_3
11: R=$SOCH_3$; R_1=R_2=H
12: R=R_1=H; R_2=$SOCH_3$
13: R=R_2=H; R_1=SCH_3
14: R=Br; R_1=SCH_3; R_2=H
15: R=SO_2CH_3; R_1=H; R_2=Br
16: R=Br; R_1=SO_2CH_3; R_2=H
17: R=Br; R_1=SO_2CH_3; R_2=H

The reactions of **3** and **4** with the reagent afforded 1,4- (**7**) and 1,2-bis(methylthio)phenazine (**8**) respectively, which had both been derived from 1,4- and 1,2-dichlorophenazine.[1] It was thus confirmed that the oxidised products, **5** and **6**, are 1-bromo-4-methylsulfinyl- and 1-bromo-2-methylsulfinylphenazine respectively.

The bromination of 1- (**9**) and 3-methylthiophenazine-5-oxide (**10**) gave 1- (**11**) and 3-methylsulfinylphenazine-5-oxide (**12**) respectively, and no ring-substituted product was obtained in either case. 2-Methylthiophenazine-5-oxide (**13**) was treated with bromine under similar conditions to yield 1-bromo-2-methylthiophenazine-5-oxide (**14**), which was then converted into **4** by the reduction. The replacement reaction of **14** with an excess of methyl mercaptan afforded **8**, accompanied by the removal of the oxide group in *N*-oxide.

The oxidation of the methylthio compound (**3**) and its sulfoxide (**5**) with an excess of hydrogen peroxide in acetic acid gave sulfone (**15**). The treatment of **4** with a limited amount of hydrogen peroxide in acetic acid produced 1-bromo-2-methylsulfonylphenazine (**16**), which was also obtained from sulfoxide **6**. The oxidations of **4**, **6**, **14**, and **16** all afforded the same compound, 1-bromo-2-methylsulfonylphenazine-5-oxide (**17**).

Experimental

The melting points, the appearances, the solvents of recrystallization, and the results of elemental analyses are all listed in Table 1.

The Bromination of 1. *In Chloroform*: Into a solution of **1** (2.26 g, 10 mmol) in chloroform (30 ml), a solution of bromine (1.9 g, 12 mmol) in chloroform (10 ml) was stirred, drop by drop. The solution was stirred for a further 6 hr and then allowed to stand overnight at room temperature. The reaction mixture was evaporated under reduced pressure to dryness. The residue was suspended in diluted ammonia water, washed with water, dried, and chromatographed over alumina, using benzene as the solvent. From the effluent, **3** (1.12 g, 37%) was obtained.

In Acetic Acid: Into a solution of **1** (2.26 g, 10 mmol) in acetic acid (200 ml), a solution of bromine (1.9 g, 12 mmol) in acetic acid (10 ml) was stirred, drop by drop. The solution was then stirred for a further 3 hr and allowed to stand overnight. The mixture was then poured into water to yield crystals, which were subsequently dissolved in benzene. The benzene solution was then passed through a column of alumina and eluted with benzene. From the first effluent, **3** (0.87 g, 29%) was obtained. When the column was then further eluted with chloroform, **5** (0.84 g, 26%) was obtained.

The Bromination of 2. *In Chloroform*: **2** (2.26 g, 10 mmol) and bromine (1.9 g, 1.2 mmol) were treated as in the Procedure used in the preparation of **3** to afford **4** (2.36 g, 77%).

Table 1. Properties of phenazine derivatives

Compound	Mp (°C)[a]	Appearance[b]	Recrystal. from	Molecular formula	Analytical data: Found C	Found H	Found N	Calcd C	Calcd H	Calcd N (%)
3	197—198	Orange g	C_6H_6	$C_{13}H_9BrN_2S$	50.91	2.77	9.27	51.16	2.97	9.18
4	170—171	Bright yellow n	C_6H_6	$C_{13}H_9BrN_2S$	51.29	2.84	9.16	51.16	2.97	9.18
5	279—280	Yellow g	$CHCl_3$	$C_{13}H_9BrN_2OS$	48.75	2.69	8.86	48.61	2.82	8.72
6	225—226	Pale yellow g	C_6H_6	$C_{13}H_9BrN_2OS$	48.55	2.70	8.77	48.61	2.82	8.72
11	212—214[c]	Red-orange g	$CHCl_3$–EtOH	$C_{13}H_{10}N_2O_2S$	60.43	3.71	10.62	60.45	3.90	10.85
12	193—194	Yellow n	C_6H_6–EtOH	$C_{13}H_{10}N_2O_2S$	60.51	3.76	10.69	60.45	3.90	10.85
14	229—230[c]	Orange n	$CHCl_3$	$C_{13}H_9BrN_2OS$	48.89	2.72	8.94	48.62	2.82	8.72
15	297—298	Yellow p	$CHCl_3$–C_6H_6	$C_{13}H_9BrN_2O_2S$	46.46	2.65	8.46	46.31	2.69	8.31
16	226—227	Pale yellow n	$CHCl_3$	$C_{13}H_9BrN_2O_2S$	46.56	2.75	8.49	46.31	2.69	8.31
17	232—233[c]	Yellow n	$CHCl_3$	$C_{13}H_9BrN_2O_3S$	44.34	2.56	8.15	44.21	2.57	7.93

a) All the melting points are uncorrected. b) Granules, needles, and prisms are abbreviated as g, n, and p, respectively.
c) Decomposition point.

In Acetic Acid: **2** (2.26 g) was treated in the way described in the bromination of **1** to give both **4** (1.52 g, 50%) and **6** (1.02 g, 32%).

1-Bromo-4-methylsulfinylphenazine (5). Into a solution of **3** (305 mg) in acetic acid (50 ml), potassium bromate (56 mg) was stirred in small portions. The mixture was then warmed at 40 °C for 4 hr and allowed to stand overnight at room temperature. After the dilution of the water, sodium bicarbonate (10 g) was added to the reaction mixture. The crystals which separated were collected and washed with water to give **5** (310 mg, 97%).

1-Bromo-2-methylsulfinylphenazine (6). **4** (305 mg) was treated as in the above experiment to afford **6** (290 mg, 90%).

1,4-Bis(methylthio)phenazine (7). A mixture of **3** (305 mg) and a 20% aqueous solution (1.5 ml) of sodium methyl mercaptide in ethanol (150 ml) was refluxed for 6 hr and then diluted with water (100 ml). The crystals therby formed were collected and washed with water to yield **7** (230 mg, 85%), which showed no depression of melting point on admixture with an authentic specimen[1] of **7**.

1,2-Bis(methylthio)phenazine (8). *From 4*: **4** (915 mg) was treated as in the case of **7** to afford **8** (730 mg, 89%).

From 14: **14** (320 mg) was treated as in the case of **7** to give **8** (216 mg, 80%).

1-Methylsulfinylphenazine-5-oxide (11). Into a solution of **9** (1.41 g) in chloroform (50 ml), a solution of bromine (0.8 g) in chloroform (10 ml) was stirred, drop by drop. The mixture was then treated as in the Procedure used in the preparation of **3** to give **11** (530 mg, 41%). **9** (550 mg, 39%) was also recovered.

3-Methylsulfinylphenazine-5-oxide (12). **10** (1.41 g) was treated as in the above experiment to yield **12** (800 mg, 62%). **10** (260 mg, 18%) was also recovered.

1-Bromo-2-methylthiophenazine-5-oxide (14). **13** (1.41 g) was treated as in the case of **11** to give **14** (1.15 g, 72%).

A solution of **14** (160 mg) in dimethylaniline (4 ml) and acetic anhydride (10 ml) was refluxed for 4 hr and then evaporated to dryness under reduced pressure. The residue was chromatographed over alumina, using benzene as the solvent. From the effluent, **4** (110 mg, 72%) was obtained.

1-Bromo-4-methylsulfonylphenazine (15). *From 3*: To a solution of **3** (100 mg) in acetic acid (50 ml), a 30% aqueous solution (2 ml) of hydrogen peroxide was added. The mixture was warmed at 55 °C for 2 hr and then poured into water to give **15** (105 mg, 95%).

From 5: **5** (100 mg) was treated as in the case described above to afford **15** (85 mg, 81%).

1-Bromo-2-methylsulfonylphenazine (16). *From 4*: To a solution of **4** (610 mg) in acetic acid (35 ml), a 30% aqueous solution (3 ml) of hydrogen peroxide was added. The mixture was treated as in the procedure used in the preparation of **15** to give **16** (640 mg, 95%).

From 6: **6** (100 mg) and a 30% hydrogen peroxide aqueous solution (0.5 ml) were treated in the way described above to yield **16** (80 mg, 86%).

1-Bromo-2-methylsulfonylphenazine-5-oxide (17). *From 4*: To a solution of **4** (610 mg) in acetic acid (80 ml) and acetic anhydride (2 ml), a 30% aqueous solution (5 ml) of hydrogen peroxide was added. The mixture was warmed at 55 °C for 20 hr and then treated as in the above experiment to give **17** (630 mg, 89%).

From 6: **6** (320 mg) was treated as in the case described above to give **17** (317 mg, 90%).

From 14: *14* (100 mg) was treated as in the procedure in the preparation of **15** to yield **18** (95 mg, 86%).

From 16: *16* (220 mg) was treated as in the case of the From **4** above to give **17** (200 mg, 86%).

The author is grateful to Professor Yusaku Ikegami of Tohoku University for his encouragement and to Miss Mieko Sasaki to her experimental cooperation.

References

1) M. Tada, This Bulletin, **47**, 1803 (1974).
2) S. Clemanti and P. Linda, *Tetrahedron*, **26**, 2869 (1970).
3) H. M. Gilow, R. B. Camp, and E. C. Clifton, *J. Org. Chem.*, **33**, 230 (1968).
4) A. R. Forrester and J. L. Wardell, "Rodd's Chemistry of Carbon Compounds," 2nd ed., Vol. III, Part A, ed. by S. Coffey, Elsevier Publishing Co., Amsterdam (1971), p. 431.

BULLETIN OF THE CHEMICAL SOCIETY OF JAPAN, VOL. 48 (1), 365—366 (1975)

Synthesis and Rearrangement of Ethyl Aryloxyglyoxalate Arylhydrazones

A. Sami SHAWALI[1] and N. F. EWEISS
Department of Chemistry, Faculty of Science, University of Kuwait, Kuwait
H. M. HASSANEEN and M. SAMI
Department of Chemistry, Faculty of Science, University of Cairo, Giza, Egypt

(Received July 18, 1974)

Synopsis. Ethyl chloroglyoxalate arylhydrazones (III) react with sodium phenolates in ethanol and give ethyl aryloxyglyoxalate arylhydrazones (IV). The latter ester hydrazones rearrange at high temperatures to the hydrazides (V). Structural assignments have been made on the basis of elemental and spectral analyses and independent chemical evidence whenever possible.

Arylhydrazones of aryl carboxylates (I)[2-5] have been recently found to undergo a Chapman-like rearrangement[6] on heating and give the hydrazides (II). In previous communications, the synthesis and thermal rearrangement of two types of these esters were discussed.[2-5] In view of our continuing interest in this reaction, we have extended it to arylhydrazones of dicarboxylic acid esters. In this communication we wish to report on the synthesis and thermolysis of a series of ethyl aryloxyglyoxalate arylhydrazones (IV).

$RC(OAr'):NNHAr$ (I) $\quad RCONHN(Ar')Ar$ (II)

$EtOOCC(Cl):NNHAr$ (III) $\quad EtOOCC(OAr')=NNHAr$ (IV)

$EtOOCCONHN(Ar')Ar$ (V) $\quad EtOOCCON(Ar')NHAr$ (VI)

Treatment of ethyl chloroglyoxalate arylhydrazones (III)[7] with ethanolic sodium phenolate at room temperature gave the corresponding esters (IV) in 60—80% yields. The structure assignments of the latter esters were derived from their elemental analyses and the following spectral data. Thus, the IR spectra of all products (IV) obtained exhibit two characteristic strong absorption bands near 1245 and 1720 cm^{-1}. The former band was assigned to the asymmetric stretch of the aryl ether linkage[3,8] whereas the latter to the α,β-unsaturated ester carbonyl group.[9] The absorption in the UV region was in each case characterized by the presence of three bands in the 340—320; 290—270; and 240—225 nm regions. Such spectral characteristics are similar to those of typical hydrazones.[3,9,10] The physical constants of the esters (IV) prepared are shown in Table 1.

Next we have found that heating IVa ($Ar=Ar'=C_6H_5$) in xylene for 4 hr under reflux afforded a colorless product that was analyzed correctly to be $C_{16}H_{16}N_2O_3$. It was distinguished from the starting material (IVa) by the lack of the C–OAr band and the presence of two CO bands at 1740 and 1710 cm^{-1} in its IR spectrum. On the basis of these data, the product thus obtained was assigned the structure of the hydrazide (Va, $Ar=Ar'=C_6H_5$). That the product obtained was the hydrazide Va and not the isomeric hydrazide (VIa, $Ar=Ar'=C_6H_5$) was supported by the fact that it gives upon hydrolysis an asymmetric diphenylhydrazine identified as its benzoyl derivative.[11]

The foregoing results indicate that the thermolysis of IV results in a 1,4-shift of an aryl group from oxygen to nitrogen probably *via* a five-membered cyclic transition state of type VII.[3]

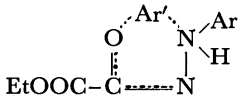

VII

Chemical evidence for the structure V was further provided by the thermal rearrangement of the two isomeric esters IVb ($Ar=C_6H_5$; $Ar'=4\text{-}CH_3C_6H_4$) and

TABLE 1. ETHYL ARYLOXYGLYOXALATE ARYLHYDRAZONES $C_2H_5OOCC(OC_6H_4X)=NNHC_6H_4Y$

Compound No.	Substituents X	Substituents Y	Mp °C	Yield %	Molecular Formula	C % Calcd	C % Found	H % Calcd	H % Found	N % Calcd	N % Found
IVa	H	H	82—83	68	$C_{16}H_{16}N_2O_3$	67.59	67.50	5.67	5.70	9.85	10.00
IVb	H	4-CH_3	89—90	65	$C_{17}H_{18}N_2O_3$	68.43	67.93	6.08	6.10	9.39	9.37
IVc	4-CH_3	H	115—117	81	$C_{17}H_{18}N_2O_3$	68.43	68.26	6.08	6.04	9.39	9.33
IVd	4-Br	H	109	65	$C_{16}H_{15}BrN_2O_3$	52.90	52.84	4.16	4.18	7.71	7.67
IVe	4-Cl	H	107	72	$C_{16}H_{15}ClN_2O_3$	60.09	59.89	5.04	4.80	8.76	8.58
IVf	4-NO_2	H	129—130	78	$C_{16}H_{15}N_3O_5$	58.35	58.41	4.60	4.64	12.76	12.90
IVg	4-Br	4-CH_3	92—93	83	$C_{17}H_{17}BrN_2O_3$	54.12	54.08	4.54	4.47	7.42	7.60
IVh	4-NO_2	4-CH_3	167—168	80	$C_{17}H_{17}N_3O_5$	59.46	59.62	4.99	5.02	12.23	12.04
IVi	4-Br	3-CH_3	107—108	64	$C_{17}H_{17}BrN_2O_3$[a]	54.12	53.93	4.54	4.47	7.42	7.38
IVj	4-NO_2	3-CH_3	120—121	70	$C_{17}H_{17}N_3O_5$	59.46	59.01	4.99	4.85	12.23	12.15
IVk	3-CH_3	H	119	65	$C_{17}H_{18}N_2O_3$	68.43	68.50	6.08	5.98	9.39	9.30

a) Br, %: Calcd, 21.18; Found, 21.19%.

Table 2. Hydrazides (V), $C_2H_5OOCCONHN<^{C_6H_4X}_{C_6H_4Y}$

Compound No.	Substituents X	Substituents Y	Mp °C	Yield %	Molecular Formula	Nitrogen % Calcd	Nitrogen % Found
Va	H	H	128—129	80	$C_{16}H_{16}N_2O_3$[a]	9.85	9.80
Vb	H	4-CH_3	104—105	85	$C_{17}H_{18}N_2O_3$[b]	9.39	9.50
Vd	4-Br	H	126	81	$C_{16}H_{15}BrN_2O_3$[c]	7.71	7.66
Ve	4-Cl	H	136—137	79	$C_{16}H_{15}ClN_2O_3$[d]	8.76	8.59
Vf	4-NO_2	H	184—185	82	$C_{16}H_{15}N_3O_5$	12.76	12.69
Vg	4-Br	4-CH_3	95—96	80	$C_{17}H_{17}BrN_2O_3$	7.42	7.39
Vk	3-CH_3	H	86—87	80	$C_{17}H_{18}N_2O_3$	9.39	9.18

a) Anal. Found: C, 67.43; H, 5.50%. Calcd: C, 67.59; H, 5.67%. b) Anal. Found: C, 68.27; H, 6.01%. Calcd: C, 68.43; H, 6.08%. c) Anal. Found: Br, 21.65%. Calcd: Br, 22.00%. d) Anal. Found: Cl, 11.04%. Calcd: Cl, 11.08%.

IVc (Ar=4-$CH_3C_6H_4$; Ar′=C_6H_5). The products obtained from the thermolysis of these two esters were identical in all respects. Other ester hydrazones in series IV, when subjected to the same treatment gave the corresponding hydrazides (V) in 80—88% yields. Table 2 lists the rearrangement products obtained together with their properties.

Experimental

Mp's were determined on a Meltemp apparatus and are uncorrected. IR spectra were obtained on a Beckman IR 12 spectrophotometer in KBr. UV spectra were measured on a Unicam SP1000 spectrophotometer in 95% EtOH. Microanalyses were performed by Alfred Bernhardt, Microanalytisches Laboratorium, West Germany.

Ethyl chloroglyoxalate arylhydrazones (IIIa—c) used in the synthesis of IV were prepared from the corresponding substituted anilines by diazotization and coupling with ethyl α-chloroacetoacetate in NaOAc-buffered solution of EtOH as previously described.[7] The compounds prepared gave the following values on analysis: (Compound No., Ar, mp, N% found, N% calcd): IIIa, C_6H_5, 79—80 °C (lit,[7b] mp 77—79 °C); IIIb, 4-$CH_3C_6H_4$, 96—97 °C, 11.62, 11.65; and IIIc, 3-$CH_3C_6H_4$, 74—75 °C, 11.59, 11.65.

Ethyl Aryloxyglyoxalate Arylhydrazones (IVa—k). To an ethanolic solution of sodium ethoxide [prepared from sodium metal (0.11 g, 0.005 g·atom) and 20 ml of absolute ethanol] was added 0.005 mol of the appropriate phenol. After being stirred for 10 min, III (0.005 mol) was added and the mixture was stirred for further 60 min, then left overnight at room temperature. The crude product precipitated was collected, washed with water and finally recrystallized from ethanol. The compounds prepared and their physical constants are given in Table 1.

Thermolysis of IV. Ethyl phenoxylglyoxalate *p*-tolylhydrazone (IVb) (0.8 g) in xylene (25 ml) was refluxed for 4 hr, then cooled. The white solid precipitated was collected and recrystallized from ethanol. A yield of 0.65 g (80%) of the hydrazide (Vb) melting at 104—105 °C was obtained.

When the isomeric ester (IVc) was similarly treated, the same hydrazide (Vb) was obtained in 85% yield, mp 104 °C, not depressed when mixed with the product formed above by thermolysis of IVb.

The thermolysis of other ester hydrazones in series IV was performed by the same method described above and afforded the hydrazides listed in Table 2.

Hydrolysis of Va. Va (1 g) was refluxed in 95% ethanol (20 ml) and concd hydrochloric acid (20 ml) for 6 hr. The reaction mixture was concentrated to 1/4 volume, cooled, made alkaline and finally was extracted with ether. Treatment of the ether extract, after being dried, with benzoyl chloride while cooling and work up yielded white solid (0.5 g), which, on recrystallization from ethanol, gave *N′*-benzoyl-*N,N*-diphenylhydrazine, mp 189—190 °C. The mixture mp of the latter with an authentic sample[11] showed no depression.

References

1) To whom all inquiries should be addressed.
2) A. S. Shawali and H. M. Hassaneen, *Tetrahedron Lett.*, **1972**, 1299.
3) A. S. Shawali and H. M. Hassaneen, *Tetrahedron*, **28**, 5903 (1972).
4) A. S. Shawali and M. K. Ibrahim, This Bulletin, **46**, 1798 (1973).
5) A. F. Hegarty, J. A. Kearney, and F. L. Scott, *Tetrahedron Lett.*, **1972**, 3211.
6) J. W. Schulenberg and S. Archer, "Organic Reactions," Chap. 1, John Wiley & Sons, Inc., New York (1965).
7) a) D. A. Bowack and A. Lapworth, *J. Chem. Soc.*, **87**, 1859 (1905); b) R. Huisgen and H. J. Koch, *Ann. Chem.*, **591**, 200 (1955).
8) R. M. Silverstein and G. C. Bassler, "Spectroscopic Identification of Organic Compounds," John Wiley & Sons, Inc., New York (1967), pp. 91—93.
9) A. S. Shawali and A. Osman, *Tetrahedron*, **27**, 2517 (1971).
10) A. S. Shawali, M. I. Ali, M. M. Naoum, and A. L. Elansari, *ibid.*, **28**, 3805 (1972).
11) D. B. Sharp and C. S. Hamilton, *J. Amer. Chem. Soc.*, **68**, 588 (1946).

BULLETIN OF THE CHEMICAL SOCIETY OF JAPAN, VOL. 48 (1), 367 (1975)

Synthesis of *o*-Ethynylcinnamaldehyde

Jūro Ojima, Akihiko Kimura, Yōji Yokoyama, and Tai Yokoyama
Faculty of Literature and Science, Toyama University, Gofuku, Toyama 930

(Received July 1, 1974)

Synopsis. A synthesis of *o*-ethynylcinnamaldehyde-(IV) starting from *o*-ethynylbenzaldehyde(I) by the Wittig reaction is described.

In a previous paper, we reported a synthesis of *o*-ethynylbenzaldehyde(I) and an attempt to synthesize dibenzo[18]annulene.[1] As an extension of our work on benz-fused annulenes, we found it necessary to synthesize *o*-ethynylcinnamaldehyde(IV). Howes *et al.* recently described syntheses and properties of [13],[15], [17]-membered annulenones and heteroannulenes.[2] For realizing the effect of annelation of benzene nuclei on the conjugated systems, the title compound is considered to be a key intermediate for syntheses of these benz-fused compounds.

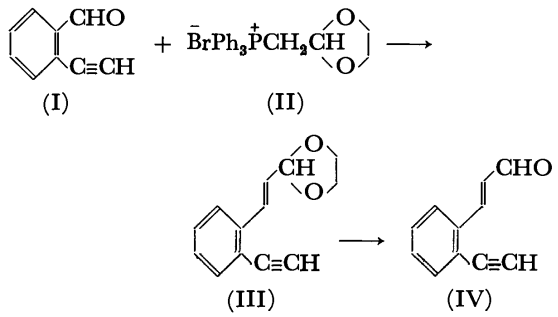

The synthesis of *o*-ethynylcinnamaldehyde(IV) was carried out as follows.

The method of Müller-Cunradi and Pieroh[3] has been used extensively in the synthesis of $\alpha\beta$-unsaturated aldehyde. We used this method to prepare the title compound, the starting *o*-ethynylbenzaldehyde being recovered. Cresp, Sargent, and Vogel[4] have reported the use of 1,3-dioxolan-2-yl-methyltriphenylphosphonium bromide(II) in the syntheses of some $\alpha\beta$-unsaturated aldehydes. We applied their method to *o*-ethnylbenzaldehyde(I). The desired *o*-ethynylcinnamaldehyde-(IV) was obtained with a satisfactory yield.

Experimental

The melting point is uncorrected. The electronic spectrum and infrared spectrum were taken on Hitachi-124 and Hitachi-EPI-S2 spectrophotometers, respectively, and the NMR spectrum and mass spectrum on JEOL-JNM-MH-60 and JEOL-JMS'-OI-SG'-2 spectrometers, respectively.

o-Ethynylcinnamaldehyde(IV): Lithium methoxide prepared from lithium (327 mg, 0.047 gatm) in dry methanol (150 ml) was added dropwise with stirring under nitrogen at 80—90 °C for 3 hr to *o*-ethynylbenzaldehyde(I) (4.0 g, 0.031 mol) and 1,3-dioxolan-2-yl-methyltriphenylphosphonium bromide (II) (20 g, 0.047 mol) in dry *N,N*-dimethylformamide (150 ml). After addition of the base, the reaction mixture was stirred under nitrogen at 82—85 °C for further 5 hr.

The reaction mixture was then poured into water (1800 ml) and extracted thoroughly with ether. The ether extract was washed with saturated brine, dried over sodium sulfate and evaporated.

The residue thus obtained was stirred at room temperature with tetrahydrofuran (150 ml) and 10% aqueous hydrochloric acid (150 ml) for 3 hr. After addition of water (150 ml), the reaction mixture was extracted with ether and the extract was washed with water, saturated aqueous sodium bicarbonate and water successively. After being evaporated, the residue was chromatographed on alumina (200 g) and the column was eluted with a mixture of light petroleum ether–ether (9: 1). Solids obtained after evaporating were collected (3.12 g, 67%) and recrystallized from *n*-hexane affording yellow needles. Mp, 89—90 °C. Found: C, 84.33; H, 4.95%; mol wt (mass spectroscopy) 156 (M^+, 65%), 128 (base). Calcd for $C_{11}H_8O$: C, 84.59; H, 5.16%; mol wt 156.17: IR (KBr disc); 3250(s), 2060(w), 1685(s), 1620(m), 960(s): UV (in EtOH); λ_{max} (ε), 242 (24100), 247 (23100), 292 nm (21700): NMR (τ in $CDCl_3$) 0.14 (d, 1H, -CHO, J=8 Hz), 1.90 (d, 1H, vinyl H, J=16 Hz), 2.16—2.66 (m, 4H, aromatic), 3.20 (dd, 1H, vinyl H, J=8, 16 Hz), 6.53 (s, 1H, -C≡CH).

The authors are grateful to Prof. F. Sondheimer, University College London, for kindly providing unpublished results.

This research was financially supported by the grants from the Ministry of Education.

References

1) J. Ojima, T. Yokomachi, and T. Yokoyama, *Chem. Lett.*, **1972**, 633.

2) P. D. Howes, E. LeGoff, and F. Sondheimer, *Tetrahedron Lett.*, **1972**, 3691, 3695; P. J. Beeby and F. Sondheimer, *Angew. Chem. Intern. Ed. Engl.*, **11**, 833 (1972).

3) M. Müller-Cunradi and K. Pieroh, U.S.P. 2165962 (*Chem. Abstr.*, **33**, 8210 (1939); M. Iyoda, H. Miyazaki, and M. Nakagawa, *Chem. Commun.*, **1972**, 431.

4) T. M. Cresp, M. V. Sargent, and P. Vogel, *J. Chem. Soc. Perkin I*, **1974**, 37.

BULLETIN OF THE CHEMICAL SOCIETY OF JAPAN, VOL. 48 (1), 368 (1975)

Some Considerations on the Electronic Spectra of Cyclic Polyenes

Sadhan BASU

Department of Pure Chemistry, University College of Science, Calcutta-9, India

(Received July 30, 1974)

Synopsis. The theoretical prediction of a convergence limit in the electronic spectra of cyclic polyenes is nicely borne out by exerimental findings.

In a recent communication hole particle formalism[1] has been used to explain the convergence limit in the π-electronic spectra of linear polyenes. The hole-particle pair creation operator expressed in terms of particle creation and destruction operators was written as

$$b_i = u_i c_i + v_i c_i^+ \qquad (1)$$

in order to diagonalize the Hamiltonian. For Boglyubov-Valentin[2,3] transformation this should be written as

$$b_i = u_i^* c_i + v_i^* c_i^+ \qquad (2)$$

where $-i$ is the time reversed partner of the state i. Since n is the only good quantum number in the FE function of linear polyenes there is no genuine time reversed partner for the states described by n. The transformation (1) was therefore an *ad-hoc* assumption. The FE function for cyclic polyenes in cylindrical coordinate may be written as[4]

$$\Psi n_z n_\rho m(Z, \rho, \Phi) = N e^{-Kz^2/2} H_{n_z}(\sqrt{K}z) e^{-C\rho^2/2} F_{n_\rho}^m(\sqrt{C}\rho) e^{im\Phi}$$

where $C^2 = 1/R^{2\alpha}$ and $K^2 = 4\pi^2 mk/h^2$, where R is the radius of the ring and k and α are two parameters determined from experimental data. For these functions state m has a time reversed partner $-m$ and the transformation (2) may be written as

$$b_m = u_m^* C_m + v_m^* C_m^+$$

which will be truely cannonical. Rest of the deductions will be the same as given in a previous paper and we will get for hole-particle energy as

$$E = \sqrt{\varepsilon_a - \varepsilon_f + \Delta^2}$$

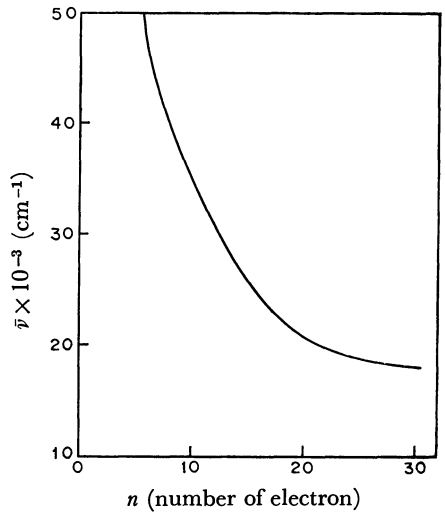

Fig. 1. $\bar{\nu}$ *vs.* n.

This means that even for cyclic polyenes there should exist a convergence limit. In Fig. 1 is given the plot of longest wave length transition *versus* the ring size for a number of conjugated cyclic systems known as Sondheimer hydrocarbon.[5] It is evident that the convergence do exist.

References

1) S. Basu, This Bulletin, **47**, 735 (1974).
2) N. N. Boglyubov, *Doklady. Akad. Nauk. SSSR*, **119**, 244 (1958).
3) J. G. Valantin, *Phys. Rev.*, **122**, 1012 (1961).
4) P. N. Sen, and S. Basu, *Int. J. Quant. Chem.*, **3**, 611 (1969).
5) F. Sondheimer and R. Wolovsky, *J. Amer. Chem. Soc.*, **81**, 4755 (1959); F. Sondheimer, R. Wolovsky, and Y. Gaoni, *ibid.*, **82**, 755, (1960); F. Sondheimer and Y. Gaoni, *ibid*, **82**, 5765 (1960).

Solvent Effects under High Pressure. II.[1] Determination and Applications to Kinetic Studies of the E_T-Value at High Pressures

Katsuhiro TAMURA and Tatsuya IMOTO

Department of Applied Chemistry, Faculty of Engineering, Osaka City University, Sumiyoshi-ku, Osaka 558

(Received February 5, 1974)

The E_T-value was determined for eight solvents at 25 °C over the pressure range 1—1,960 kg/cm². They increase with pressure; the pressure dependence is affected by the nature of the solvents. It was also found that there is a linear relationship between the pressure coefficient of E_T and that of the logarithm of the rate constant of a Menschutkin reaction: $\ln k = a + bE_T$. On the basis of this relationship, an equation was derived in which the volume of activation $\Delta V^{\neq}$ is represented by the pressure coefficient of E_T; the effect of solvents on $\Delta V^{\neq}$ is discussed by making use of this equation.

One of the most important factors in determining the rate of a chemical reaction is the choice of solvent. This becomes more important and complex for reactions under high pressure.

Frequently, solvent polarity is represented by its dielectric constant. However, this is a macroscopic measure of a solvent response to an electric field. For the analysis of chemical reactions it is necessary to know the microscopic situation, the solute-solvent interaction, at the active point in which reaction occurs. It seems impossible to express adequately all the interactions between solute and solvent molecules by using a single physical parameter of a solvent. The problem of the correlation has therefore been tackled empirically. A standard reaction or dye is chosen, and the significant parameters of the reaction or the dye are observed as the solvent is changed. These parameters may be rate constants for the reaction or spectral shifts of the dye, and they have been used as measures of solvent polarity and have been correlated with reaction rate. Various empirical measures of solvent polarity have been proposed in order to rank the ionizing power of solvents more accurately;[2,3] these avoid the need to understand fully the complexities of molecular interactions in solution.

Most polarity parameters useful at atmospheric pressure are not available at high pressure, because there are generally extraneous factors which completely shield the effects of the changes of solvent polarity with increasing pressure in either the standard reaction or the spectral shifts of the standard dye being investigated. The determination of the parameters would then be meaningless. Therefore, the effects of the change of solvent polarity with pressure on reaction rate must be studied by using an adequate polarity parameter. The so-called E_T-value proposed by Dimroth *et al.*[4] is defined as the transition energy of the solvatochromic absorption band of *N*-(4-hydroxy-3,5-diphenyl-phenyl)-2,4,6-triphenylpyridiniumbetaine (Scheme 1). This can be determined for many solvents, and one can get a direct insight into solute-solvent interactions, since the microscopic transition energy of an electron is measured. In addition, the E_T-value bears a good linear relationship to many other solvent polarity parameters. For these reasons, we adopted the E_T-value as a parameter to study the pressure dependence of the solvent polarity, and evaluated it for the kinetic studies at high pressure. It was consequently concluded that at least for Menschutkin reactions the E_T-value can be used as a convenient solvent polarity parameter under high pressure.

The pressure coefficients of the E_T-value were applied to the investigation of the solvent effects on the volumes of activation $\Delta V^{\neq}$. For Menschutkin reactions, an extensive study of the influence of the solvent on the $\Delta V^{\neq}$ has been made by Gonikberg and his collaborators.[5] As a general tendency concerning these reactions, the solvation term of $\Delta V^{\neq}$ is large and negative for solvents whose compressibilities are high and whose dielectric constants increase greatly with pressure. The reason for this is as follows. Since the transition state is partially ionic, the volume of the solvation shell will be decreased due to the electrostriction of the surrounding solvent molecules. The contraction becomes larger if the solvent used has a higher compressibility. However, there are numerous exceptions to this analysis based on the changes in compressibility or dielectric constant with pressure, especially, since the relationship between $\Delta V^{\neq}$ and the pressure-dependence of the dielectric constant is extremely complex.[6,7] So we attempted to analyze the solvent effects on $\Delta V^{\neq}$ by using the E_T-value, and $\Delta V^{\neq}$ was correlated with the pressure dependence of the E_T-value.

Experimental

Materials. Commercial nitrobenzene of special grade was purified as noted in the literature.[8] The other solvents used, commercial spectro grade, were used withot purification.

The standard indicator, *N*-(4-hydroxy-3,5-diphenyl-phenyl)-2,4,6-triphenylpyridiniumbetaine, used for the determination of the E_T-value, was synthesized according to the method described in the previous paper.[1] The betaine was recrystallized from a methanol–water mixture (1 : 1); mp 207—280 °C.[4,9] (Found: C, 83.58; H, 5.26; N, 2.61%).

Apparatus. Figure 1 illustrates a part of the Drickamer-type high pressure equipment used, with optical windows, for the determination of the E_T-value. This is modified to circulate water through the jacket around the equipment from a thermostat in order to keep the temperature constant (25 °C); the E_T-value is very sensitive to temperature. A sample solution in a cylindrical quartz cell with path length of 10 mm is separated with mercury from the *n*-hexane used as a pressure transmitting medium. When the absorption spectra are measured at high pressures, attention must be paid to the mercury pushed into the cell with pressure so as not block the light.

The pressure was measured with a Bourdon gauge con-

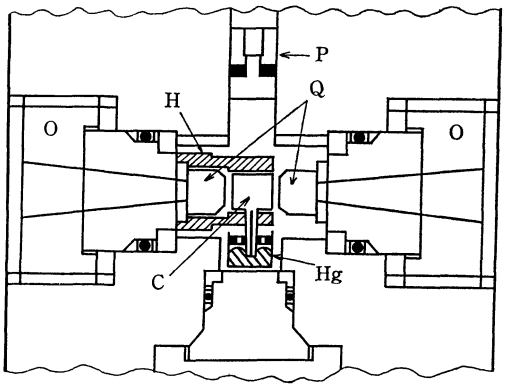

Fig. 1. Equipment for high pressure spectroscopic studies.
O: window plug Q: quartz window C: cell
H: cell holder P: high pressure piston

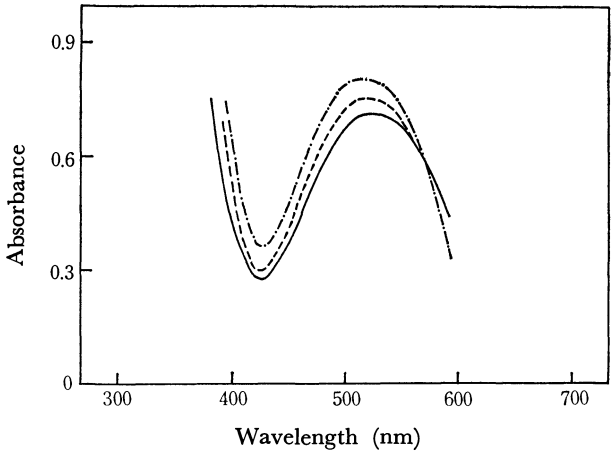

Fig. 2. Absorption spectra of the betaine in methanol at 25 °C and various pressures.
——: 1 kg/cm², — — —: 820 kg/cm², —·—·—: 1960 kg/cm²
The absorbance at high pressures is not corrected for the contraction of the solvent.

nected to the manual pump; it was calibrated by a manganin resistance gauge.

The area ratio of the pistons of the intensifier is 1 : 25. This indicates that the pressure ratio of the low pressure section to that of the high pressure must theoretically be equal to the reciprocal of the ratio of the pistons. However, the actual pressure measured in the high pressure section was lower than the theoretical value by about 20% due to friction between the packing and the piston cylinder.

The spectra were measured by means of Hitachi Model-139 Spectrophotometer. The details of the arrangement were described in the previous paper.[10]

Procedure. The quartz cell containing a sample solution of adequate concentration was set on a holder in the equipment, and then *n*-hexane was poured into it. This was allowed to stand for a few hours until the temperature of the system became 25 °C; it was then attached to the spectrophotometer. First the wavelength of the absorption maximum was measured at atmospheric pressure employing sensitivity values which had been determined relative to blank (100% transmittance) at each wavelength and at each pressure prior to the measurement of the absorption band. The described pressure was applied for about one hour, and then the measurement was carried out. The procedure for the measurement under high pressure is similar to that under atmospheric pressure.

Results

The betaine is a chemically stable indicator. It was confirmed that the betaine does not react with the mercury used to separate the sample solution from the pressure transmitting *n*-hexane, and its absorbance did not change with time. Also, the wavelength of absorption maximum (λ_{max}) was the same as before compression.

The position of λ_{max} at atmospheric pressure is very sensitive to the nature of the solvents, for example, the difference between the λ_{max} of methanol (516 nm) and that of acetone (675 nm) was about 160 nm. Pressure effects on the spectra were also observed, as shown for a methanol solution in Fig. 2. The absorption peak for this solution shifted to the shorter wavelength region (blue shift) with increasing pressure. The wavelengths of the absorption maximum at 1, 820, and 1,960 kg/cm² pressure were observed at 516, 512, and 508 nm, respectively. Similarly, such a blue shift with pressure was found in all other solvents used. The E_T-value can be calculated from the values of λ_{max} (in nm) with the following equation.

$$E_T = h\nu = 2.859\times10^4/\lambda_{max} \quad \text{kcal/mol}$$

The E_T-values and the λ_{max} for each solvent at various pressures are summarized in Tables 1 and 2. The error range in λ_{max} is $\pm1\sim\pm2$ nm, depending on the solvent. The E_T-values for benzene, nitrobenzene, and a benzene-nitrobenzene mixture (0.6 mole fraction of nitrobenzene) at 25 °C cannot be determined at or above 1,000 kg/cm² pressure since these solvents freeze under these conditions. Although the betaine was only slightly soluble in benzene, the measurement of the λ_{max} was possible. The E_T-value for benzene determined at atmospheric pressure was larger than the value in the literature,[4] while that for nitrobenzene was smaller, and those for the other solvents were in agreement. As a general tendency, the rate of increase of the E_T-value with respect to pressure decreases with increasing pressure. In order to compare the relative changes of the E_T-values with pressure, $(E_T)_p/(E_T)_1$ was plotted against pressure for each solvent as shown in Figs. 3 and 4. The curves are evidently dependent on the nature of the solvents; however, the differences between the solvents are small in our pressure range. This behavior is distinct from that of the *Z*-value, another solvent polarity parameter proposed by Kosower.[11,12]

For each solvent one can culculate the slope $(\partial E_T/\partial P)_T$. This term has the dimension of volume; in the case of iodide ion, it has in fact been considered the volume change upon excitation.[13]

TABLE 1. E_T-VALUE AND λ_{max} FOR A SERIES OF ALCOHOLS AND ACETONE AT 25 °C AND VARIOUS PRESSURES

Pressure (kg/cm²)		1	430	820	1170	1520	1960
MeOH	λ_{max}	516	513	512	510	509	508
	E_T	55.41	55.69	55.84	56.06	56.17	56.28
EtOH	λ_{max}	551	549	547	545	544	542
	E_T	51.89	52.11	52.32	52.49	52.59	52.72
iso-PrOH	λ_{max}	591	588	586	584	583	581
	E_T	48.38	48.61	48.81	48.94	49.06	49.19
iso-BuOH	λ_{max}	583	581	579	578	577	576
	E_T	49.04	49.21	49.38	49.46	49.55	49.64
Acetone	λ_{max}	675	672	670	668	666	665
	E_T	42.39	42.54	42.67	42.82	42.91	42.99

These are the average values of three to five measurements. The values of λ_{max} are rounded to the nearest whole numbers. λ_{max} (in nm), E_T (in kcal/mol).

TABLE 2. E_T-VALUE AND λ_{max} FOR NITROBENZENE, 0.6 MOLE FRACTION OF NITROBENZENE MIXTURE, AND BENZENE AT 25 °C AND VARIOUS PRESSURES

Pressure (kg/cm²)		1	200	400	610	780
Nitrobenzene	λ_{max}	690	689	688	687	686
	E_T	41.45	41.51	41.56	41.62	41.68
0.6 mole fraction of	λ_{max}	699	698	697	696	695
nitrobenzene mixture	E_T	40.90	40.96	41.02	41.08	41.14
Benzene	λ_{max}	815	813	812	811	810
	E_T	35.10	35.17	35.21	35.28	35.32

These are the average values of three to five measurements. The values of λ_{max} are rounded to the nearest whole numbers. λ_{max} (in nm), E_T (in kcal/mol).

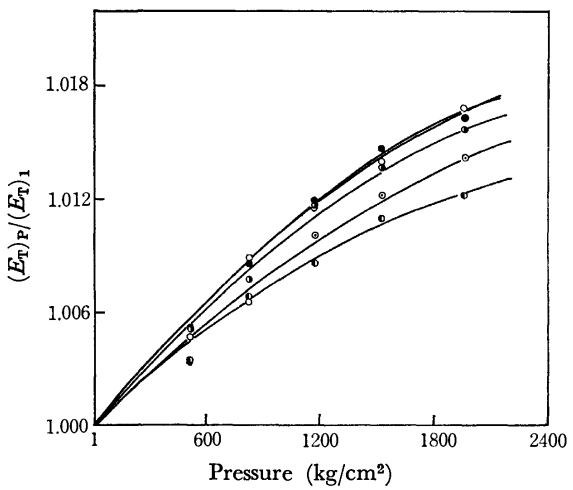

Fig. 3. Pressure dependence of the relative E_T-values for a series of alcohols and acetone at 25 °C.
○: *iso*-PrOH ●: EtOH ◑: MeOH ⊙: Acetone
◐: *iso*-BuOH

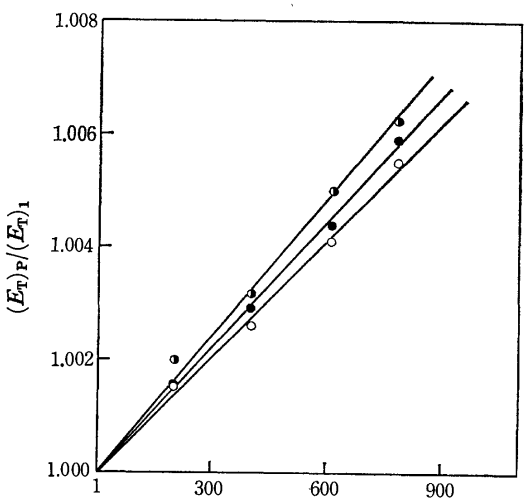

Fig. 4. Pressure dependence of the relative E_T-values for benzene, 0.6 mole fraction of nitrobenzene mixture, and nitrobenezne at 25 °C.
◐: Benzene ●: 0.6 mole fraction mixture ○: Nitrobenzene

Before the evaluation of $(\partial E_T/\partial P)_T$ from a set of E_T-values, the functional dependence of E_T-value on pressure must be established. The following two functions were checked by the least mean squares method.

$$E_T = A + BP \quad (1)$$

$$E_T = A + BP + CP^2 \quad (2)$$

It was concluded that the linear Eq. (1) was well suited for benzene, nitrobenzene and the benzene-nitrobenzene mixture which were measured over a small pressure range; the second-order polynomial (2) gives an adequate description for the other solvents. The constants A, B, and C in the above two equations were evaluated by using a computer programmed least mean squares technique; they are listed in Table 3. One can evaluate $(\partial E_T/\partial P)_T$ by differentiating the linear and quadratic expressions with respect to pressure:

TABLE 3. THE CONSTANTS A, B, AND C IN Eqs. (1) AND (2), STANDARD DEVIATION, AND THE PRESSURE COEFFICIENT OF E_T

	$A\times10^{-1}$ (kcal/mol)	$B\times10^{4}$ (kcal/mol)/(kg/cm²)	$C\times10^{7}$ (kcal/mol)/(kg/cm²)²	$S.D.\times10^{2}$	$(\partial E_T/\partial P)_T$ (cm³/mol)
MeOH	5.542	6.662	−1.113	2.2	28.4
EtOH	5.188	6.139	−0.9515	1.2	26.2
iso-PrOH	4.838	5.865	−0.8907	0.5	25.0
iso-BuOH	4.904	4.595	−0.7782	1.0	19.6
Acetone	4.238	4.209	−0.5502	1.5	17.9
Nitrobenzene	4.145	2.891		0.4	12.3
0.6 mole fraction mix.	4.090	3.045		0.3	13.0
Benzene	3.510	2.795		0.6	11.9

$$(\partial E_T/\partial P)_T = B \text{ or } (B + 2CP) \quad (3)$$

The values of $(\partial E_T/\partial P)_T$, together with standard deviations, are summarized for each solvent at atmospheric pressure in Table 3. The order of the quantity of $(\partial E_T/\partial P)_T$ for each solvent almost corresponds to that of E_T. As there is some scatter in the data shown in Figs. 3 and 4, the values $(\partial E_T/\partial P)_T$ as estimated from the slopes in the figures are not necessarily consistent with those calculated from Eq. (3).

Although the physical meaning of the $(\partial E_T/\partial P)_T$ cannot be interpreted strictly, owing to insufficient information about the excited state, the experimental results suggest that the ground state interaction between the ionic solute and the surrounding solvent molecules is stronger in a more polar solvent, and consequently that the overall volume contraction of the solvation shell becomes greater.

Discussion

Pressure Dependence of E_T-value. In the visible region, the betaine shows a large hypsochromic effect with an increase in solvent polarity; *i.e.*, the wavelength of the absorption maxima shifts toward the blue with increasing solvent polarity. This is apparently due to the disappearance of the electric charges of the betaine when it is excited, together with intramolecular charge transfer as shown in Scheme 1.[14] These phenomena have been often observed in n→π^* transitions.[15]

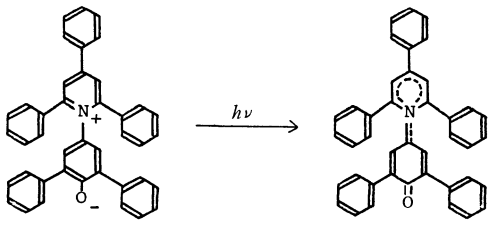

Scheme 1

The changes of E_T with pressure are due to the shifts of the energy levels in ground and excited states; however, precise information about the pressure dependence of the shifts of these levels cannot be obtained. A solute molecule, which in its ground state is in equilibrium with the surrounding solvent molecules that form its solvation shell, should be stabilized in the solution with increasing solvent polarity. According to the Franck-Condon principle an optical transition occurs within a time far shorter than the period of nuclear motions, and hence the molecule in the excited state (Franck-Condon state) is momentarily surrounded by a solvent shell whose size and orientation are those appropriate to the ground state. In the Franck-Condon state the solvation shell is unstable, because the dipole moment of the solute becomes small compared with that in the ground state, and the solute-solvent interactions become likewise smaller. Therefore, the more stable the ground state is, the more unstable is the excited state, owing to the increase in solvent polarity with pressure. The matter described above may be expressed qualitatively by Fig. 5. The energy level of the excited state rises with pressure, and on the contrary, that of the ground state falls. The slope of the curve may be dependent on the nature of the solvent. In the figure, the slopes have been selected arbitrarily for illustrative purposes.

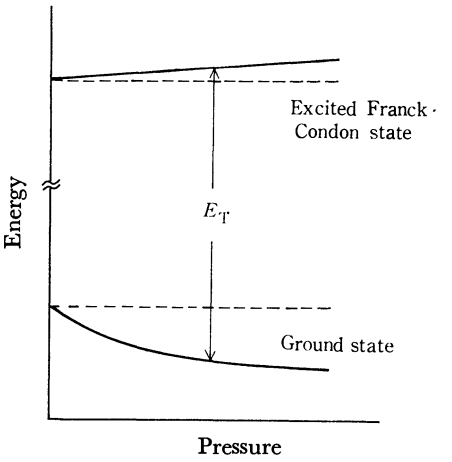

Fig. 5. Diagramatic representation of changes in ground and excited state energies for the betaine in a solvent as a function of pressure.

Correlation of Rate Constants with E_T-values. There are some examples of good linear relationship between E_T-values and logarithms of rate constants at atmospheric pressure. For example, as described in the previous paper,[1] the Menschutkin reaction of 3,5-lutidine with ethyl iodide in benzene-nitrobenzene mixtures shows good linearity. These relationships provide a valuable means of estimating the effect of solvents on the rate of chemical reactions, and of confirming abnormal solvent effects on reaction rates

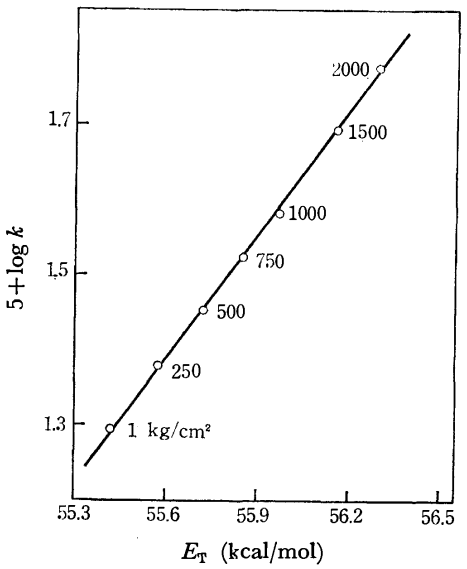

Fig. 6. A plot of $\log k$ *vs.* E_T for the Menschutkin reaction of pyridine with methyl iodide in methanol at various pressures.

or electronic transition. The reaction between pyridine and methyl iodide in six solvents (carbon tetrachloride, benzene, methanol, chlorobenzene, acetone, and nitrobenzene)[6] has a linear relationship, except for methanol, which is the only protic solvent. This means that the degree of solute-solvent interaction for methanol is different from that of the aprotic solvents.

We now discuss whether the E_T-value can also be employed for kinetic studies at high pressures. In order to investigate the linear relationship at high pressures, the logarithms of rate constants[6] of the reaction between pyridine and methyl iodide were plotted against the E_T-values with respect to four kinds of solvents (benzene, nitrobenzene, methanol, and acetone), up to 2,000 kg/cm². Figure 6 shows a plot of $\log k$ *vs.* E_T-value for methanol at various pressures. It is obvious that there is a good, linear relationship between them. Similar good linearity was observed in the plots for the other three solvents.[16] This relationship can be expressed in terms of the following linear equation.

$$\ln k = a + bE_T \tag{4}$$

The constants a and b were determined by means of the least mean squares method for each solvent; they are summarized in Table 4. The value of a becomes progressively larger as the E_T-value of the solvent increases, whereas the value of b becomes smaller.

Table 4. The constants a and b in Eq. (4) for various solvents

	Methanol	Acetone	Nitrobenzene	Benzene
a	−74.06	−99.69	−107.5	−144.3
b (mol/kcal)	1.186	2.192	2.439	3.824
E_T at 1 kg/cm²	55.41	42.39	41.45	35.10

By the use of the empirical equation (4), the volume of activation $(\partial E_T/\partial P)_T$. $\Delta V^{\ddagger}$ can be correlated with $(\partial E_T/\partial P)$.

According to the transition state theory[17] the volume of activation $\Delta V^{\ddagger}$ for a reaction is related to the pressure dependence of the rate constant by Eq. (5).

$$\left(\frac{\partial \ln k}{\partial P}\right)_T = -\frac{\Delta V^{\ddagger}}{RT} \tag{5}$$

If one differentiates Eq (4) with respect to pressure, one obtains

$$\left(\frac{\partial \ln k}{\partial P}\right)_T = b\left(\frac{\partial E_T}{\partial P}\right)_T + E_T\left(\frac{\partial b}{\partial P}\right)_T \tag{6}$$

The following equation can be obtained from the Eqs. (5) and (6) by assuming $(\partial b/\partial P)_T=0$ in our pressure range.

$$\Delta V^{\ddagger} = -bRT(\partial E_T/\partial P)_T \tag{7}$$

In order to discuss Eq. (7), the Menschutkin reaction of pyridine with methyl iodide has been chosen as an example; it has been cited in the case of discussing the linear relationship between ln k and E_T-value at high pressures. Table 5 lists both of the volumes of activation $\Delta V^{\ddagger}$, one calculated from the pressure dependence of k (Eq. (5)), and one evaluated using the values of $(\partial E_T/\partial P)_T$ and the constant b in Eq. (4) (summarized in Tables 3 and 4, respectively). By comparing these volumes of activation, it can be found that they appear to be in fairly good agreement. This means that the assumption, $(\partial b/\partial P)_T=0$, is valid and further the experimental equations (1), (2), and (4) are also adequate expressions. Eq. (7) shows that $\Delta V^{\ddagger}$ can be correlated with two components, b and $(\partial E_T/\partial P)_T$ representing the polarity effects of solvents. The b defined by Eq. (4) represents the sensitivity of rate constants to changes of solvent polarity.

Table 5. Comparison of the volumes of activation calculated from Eq. (7) with those obtained by Hartmann *et al.*[6]

	Methanol	Acetone	Nitrobenzene	Benzene
$\Delta V^{\ddagger}$ a) (cm³/mol)	−22.6	−28.8	−19.7	−31.9
$\Delta V^{\ddagger}$ b) (cm³/mol)	−21.6	−25.2	−19.3	−29.2

a) Hartmann's data. b) The values calculated from Eq. (7).

In order to discuss the solvent effects on the $\Delta V^{\ddagger}$ by means of Eq. (7), the solvent dependence of $\Delta V^{\ddagger}$, $(\partial E_T/\partial P)_T$ and b was compared with respect to the four solvents shown in Table 4, and it was found that there is a correlation between these values and the nature of the solvent, except for the case of nitrobenzene. The absolute values of $\Delta V^{\ddagger}$ and b become large in the order of methanol, acetone, and benzene, whereas that of $(\partial E_T/\partial P)_T$ becomes smaller in the same order. So far as these solvents are concerned, it seems that the contribution of b to the changes of $\Delta V^{\ddagger}$ with the nature of the solvent is greater than that of $(\partial E_T/\partial P)_T$.

As described above, the solvent effect on $\Delta V^{\neq}$ was discussed on the basis of the values of $(\partial E_T/\partial P)_T$ and b; however, at the present stage a more detailed discussion about the correlation between the $\Delta V^{\neq}$ and the corresponding $(\partial E_T/\partial P)_T$ cannot be given due to the unavailability of suitable kinetic data. The problem of solvation at high pressures is very complex, and mechanisms depend on reaction and solvent used. Therefore, the procedures mentioned here are severely limited; however, they may furnish a guide to studies of solvent effects on the volume of activation.

The authors are indebted to Prof. W. J. le Noble for his valuable comments.

References

1) Part I: K. Tamura, Y. Ogo, and T. Imoto, This Bulletin, **46**, 2988 (1973).
2) C. Reichardt, *Angew. Chem.*, **77**, 30 (1965).
3) M. R. J. Dack, *Chem. Brit.*, **1970**, 347.
4) K. Dimroth, C. Reichardt, T. Siepmann, and F. Bohlmann, *Ann. Chem.*, **661**, 1 (1963).
5) M. G. Gonikberg and B. S. El'yanov, *Dokl. Akad. Nauk SSSR*, **130**, 545 (1960); **138**, 1103 (1961): *idem*, *Izv. Akad. Nauk SSSR, Otd. Khim. Nauk*, **1959**, 413; **1960**, 629.
6) H. Hartmann, H. Kelm, and G. Rinck, *Z. Phys. Chem.*, **44**, 335 (1965).
7) H. Hartmann, A. Heumann, and G. Rinck, *ibid.*, **44**, 204 (1965).
8) J. A. Riddick and W. B. Bunger, "Organic Solvents", John Wiley and Sons, Inc., New York (1970), p. 796.
9) This compound is a dihydrate and the broad melting point seems due to the water being given off.
10) Y. Ogo, K. Tamura, M. Yokawa, and T. Imoto, *Memoirs of the Faculty of Engineering, Osaka City University*, **13**, 109 (1972).
11) E. M. Kosower, *J. Amer. Chem. Soc.*, **80**, 3253, 3261, 3267 (1958).
12) K. Tamura and T. Imoto, *Chem. Lett.*, **1973**, 1251.
13) M. J. Blandamer and T. R. Burdett, *J. Chem. Soc., Faraday Trans.*, 2, **1972**, 577.
14) N. Tokura, "Yobaiwa", Kagakudojin, Kyoto (1972), p. 142.
15) H. H. Jaffe and M. Orchin, "Theory and Applications of Ultraviolet Spectroscopy", John Wiley and Sons, Inc., New York (1962), p. 186.
16) The plots for acetone is shown in the following reference: K. Tamura, Y. Ogo, and T. Imoto, *Chem. Lett.*, **1973**, 625.
17) M. G. Evans and M. Polanyi, *Trans. Faraday Soc.*, **31**, 875 (1935).

The Circular Dichroism Spectra of the β-Cyclodextrin Complex with Naphthalene Derivatives

Kazuaki HARATA and Hisashi UEDAIRA

Research Institute for Polymers and Textiles, Sawatari, Kanagawa-ku, Yokohama 221

(Received May 13, 1974)

The circular dichroism spectra of β-cyclodextrin complexes with naphthalene derivatives were investigated. A remarkable difference in the spectra was observed between the 1-substituted naphthalene complex and the 2-substituted naphthalene complex, indicating that the steric effect of substituents on the formation of the complex is so strong that the structures may be different for these complexes. The calculation of the rotational strength by the method of Kirkwood-Tinoco revealed that the structure of the 2-substituted naphthalene complex is an axial inclusion.

Cyclodextrins, which are produced by the action of *Bacillus macerans* amylase on starch, are cyclic α-1,4-linked D-glucose oligomers. The rings with six, seven, and eight glucose residues in the molecule have different internal diameters ranging from 6 Å to 10 Å.

Cyclodextrins form a number of crystalline adducts with aromatic compounds, paraffins, alkyl halides, *etc.* Of those crystalline adducts, the α-cyclodextrin-iodine complex[1] and the α-cyclodextrin-potassium acetate complex[2] were found by X-ray structure analysis to be inclusion compounds, and the other crystalline adducts have been also regarded as inclusion compounds.

The evidence for the formation of inclusion compounds in a solution have been derived from the kinetic data[3] and the NMR spectra.[4] The interior cavity of the cyclodextrin ring is hydrophobic in nature and binds a hydrophobic portion of the guest molecule, usually forming a 1 : 1 complex. Moreover, cyclodextrins catalyze a number of chemical reactions, such as hydrolysis,[5] oxidation,[6] and decarboxylation,[7] and have been shown to be a good model for enzyme-catalyzed reactions. Tutt and Schwartz[8] showed, in their work on the β-cyclodextrin-catalyzed hydrolysis of penicillin derivatives, that the reaction rate of 2-naphthylpenicilin is four times as fast as that of 1-naphthylpenicillin, although the dissociation constant of the 2-naphthylpenicillin complex is five times as large as that of 1-naphthylpenicillin complex.

Our aim of the present paper is to reveal the structure of the β-cyclodextrin complex with naphthalene derivatives in an aqueous solution by means of the circular dichroism (CD) spectra. When optically-inactive compounds form complexes with cyclodextrins, these compounds exhibit optical activity.[9,10] The circular dichroism spectra of these complexes will give information about their structures, since the optical activity will be induced by the interaction between the cyclodextrin and the guest molecule.

Experimental

The β-cyclodextrin(β-CDx) and naphthalene derivatives were commercial products. β-CDx was recrystallized three times from an aqueous solution. Potassium salts of 1-naphthylacetic acid(1-NAT), 2-naphthylacetic acid(2-NAT), 1-naphthoic acid(1-NA) and 2-naphthoic acid(2-NA) were prepared because these acids are insoluble in water, and were recrystallized from ethanol. 1-Naphthylamine (1-NAM), 2-naphthylamine(2-NAM), 1,8-diaminonaphthalene(1,8-DAN) and 2,3-diaminonaphthalene (2,3-DAN) were recrystallized from a dilute HCl solution as hydrochlorides.

The circular dichroism and absorption spectra were measured using a JASCO J-10 Spectropolarimeter at room temperature. The concentration of β-CDx was adjusted to 0.01 M throughout the measurements. The CD spectra of the 1-substituted naphthalene derivatives were not measurable in the wavelength region longer than 250 nm because of the low intensity. In the region of high absorbancy, the intensity of the CD spectra has a large experimental error, about $\pm 1 \times 10^{-5}$ in $\Delta\varepsilon/\varepsilon$.

In the solution, the following equilibrium is established:

β-CDx + naphthalene derivatives ⇌ complex.

The intensity of the CD spectra depends on the concentration of the complex. In the present work, $\Delta\varepsilon$ was estimated by assuming that all the molecules of the naphthalene derivatives in the solution form the complex.*

Calculation

The coupled oscillator model of Kirkwood[11] may account for most of the rotational strength of a strong electric-dipole transition interacting with far-ultraviolet transitions of the vicinal groups. In the Kirkwood model as developed by Tinoco[12] the contributions of individual groups of perturbers were emphasized. According to the Kirkwood-Tinoco expression, the rotational strength is given as follows:

$$R_{0aj} = \frac{\pi \nu_a \nu_0^2 \mu_{0a}^2 (\alpha_{33} - \alpha_{11})_j (\mathrm{GF})_j}{c(\nu_0^2 - \nu_a^2)} \tag{1}$$

$$(\mathrm{GF})_j = \frac{1}{r_j^3}\left[\vec{e}_{0a}\cdot\vec{e}_j - \frac{3(\vec{e}_{0a}\cdot\vec{r}_j)(\vec{e}_j\cdot\vec{r}_j)}{r_j^2}\right]\vec{e}_{0a}\times\vec{e}_j\cdot\vec{r}_j$$

where $\vec{e}_{0a}$ is the unit vector in the direction of the electric dipole moment; $\vec{\mu}_{0a}$, that of the transition from 0 to a, and ν_a, its frequency; $\vec{e}_j$ is the unit vector in the direction of the symmetry axis of the j group, and $\vec{r}_j$ is the distance from the chromophor to the j group with the frequency ν_0 of the exited state; α_{33} and α_{11} are the electric polarizabilities parallel and perpendicular respectively to the symmetry axis of the j group. The values of α_{33}, α_{11},[13] and ν_0 are listed in Table 1. The ν_0 value of the C–C bonds

* Our discussion is not affected by this assumption.

TABLE 1. THE VALUES OF α_{33}, α_{11} AND ν_0.

Bond	$\nu_0 \times 10^{-15}$(1/s)	α_{33}(Å^3)	α_{11}(Å^3)
C-O	1.67	0.089	0.046
C-C	2.00	0.098	0.027

was estimated from the absorption spectra of cyclohexane.[14] The midway value of the first absorption bands of ethylether and ethanol[15] was used as the ν_0 value of the C–O bonds. The transition frequency, ν_a, and the dipole strength, μ_{0a}^2, were estimated from the absorption spectra. The coordinates of β-CDx, which was assumed to have a seven-fold symmetry axis, were estimated on the basis of the coordinates of a glucose residue taken from the X-ray data of the α-cyclodextrin-potassium acetate complex. The origin of the coordinate was fixed on the plane determined by the seven O_4 atoms as is shown in Fig. 6. In the calculation, the effects of all the C_6–O_5 and O–H bonds were neglected because of the flexibility; the effects of all the C–H bonds were also neglected since these bonds may be isotropic and may contribute little to the rotational strength.

Results and Discussion

Figures 1—4 show the absorption and CD spectra of β-CDx complexes with naphthalene derivatives. The CD curves of 1- and 2-substituted naphthalene complexes are remarkably different from each other. For example, in the 2-NAT complex, the ^1L_b and ^1L_a transitions both give negative CD curves, while the ^1B_b transition gives a positive CD curve. On the other hand, the 1-NAT complex shows two weak CD bands with positive and negative signs in the 200—250 nm region. The difference in spectral shape between the 1- and 2-substituted naphthalene com-

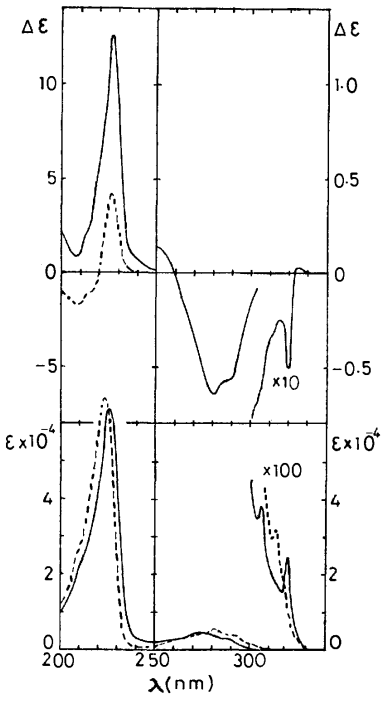

Fig. 1. Absorption and CD spectra of potassium 1-naphthylacetate (----) and potassium 2-naphthylacetate (——) at 0.002 M (250—350 nm) and 0.0002 M (200—250 nm), in 0.01 M β-cyclodextrin solution.

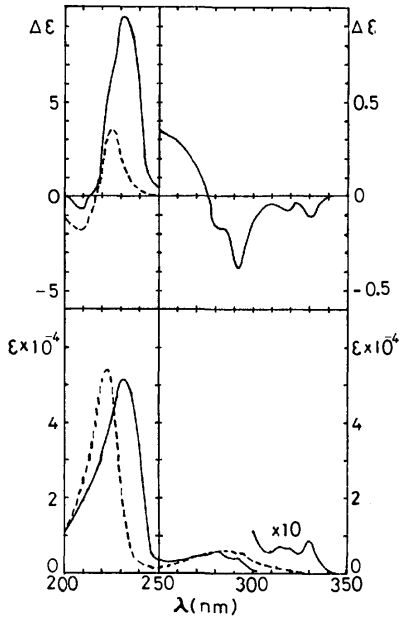

Fig. 2. Absorption and CD spectra of potassium 1-naphthoate (----) and potassium 2-naphthoate (——) at 0.002 M (250—350 nm) and 0.0002 M (200—250 nm), in 0.01 M β-cyclodextrin solution.

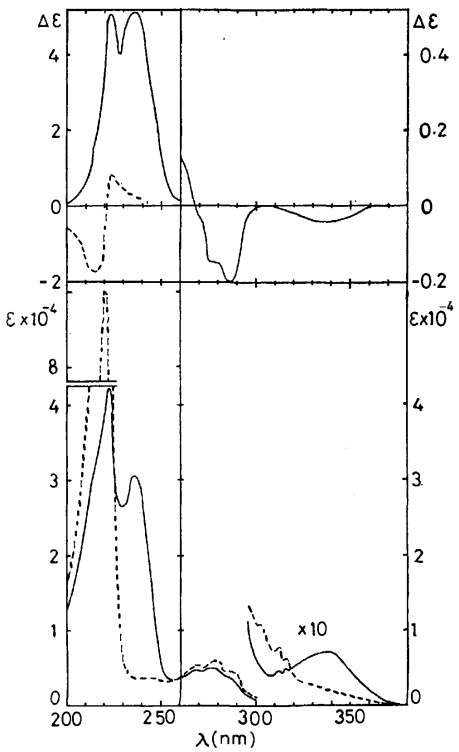

Fig. 3. Absorption and CD spectra of 1-naphthylamine (----) and 2-naphthylamine (——) at 0.002 M (260—380 nm) and 0.0002 M (200—260 nm), in 0.01 M β-cyclodextrin solution.

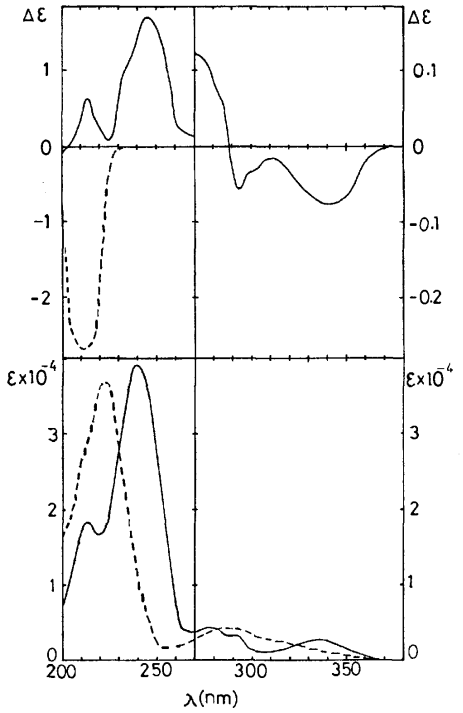

Fig. 4. Absorption and CD spectra of 1,8-diaminonaphthalene (----) and 2,3-diaminonaphthalene (——) at 0.002 M (270—380 nm) and 0.0002 M (200—270 nm), in 0.01 M β-cyclodextrin solution.

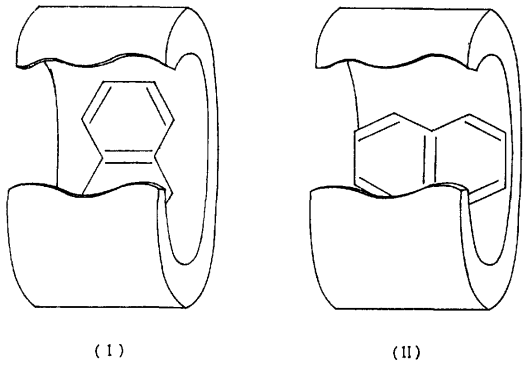

Fig. 5. The two models of the complex; equatorial inclusion (I) and axial inclusion (II).

plexes is considered to be due to the fact that the structure of the 1-substituted naphthalene complex is different from that of the 2-substituted naphthalene complex. As may be seen in Fig. 5, it is impossible for 2-substituted naphthalene, especially 2,3-DAN, to form an equatorial inclusion complex. Therefore, the CD spectra of the 2-substituted naphthalene complex will be atributed to the structure of the axial inclusion. In the case of the 1-substituted naphthalene complex, both types of inclusion are possible, and from a study of the molecular models it is not found which structure is more reasonable.

The two models of the inclusion compounds of β-CDx with naphthalene derivatives, shown in Fig. 5, were examined by comparing the calculated rotational strength with the observed one. The calculation of the rotational strength of the 2-NAT complex was

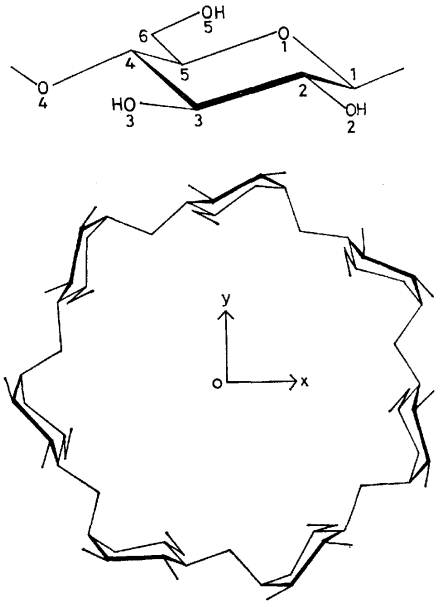

Fig. 6. The assumed structure of β-cyclodextrin.

Table 2. Calculated and observed rotational strength of β-cyclodextrin complex with potassium 2-naphthylacetate.

	$R\times10^{40}$(cgs)	
	^1L_a	^1B_b
Calculation		
(I) Equatorial	1.52	−30.4
(II) Axial	−0.76	60.7
Experimental	−2.65	22.9

carried out by putting the center of the electric dipole moment on the point of origin and by assuming its direction to be the same as that of naphthalene.[16] In the cases of the ^1L_a and ^1B_b transitions, the results are listed in Table 2, along with the observed values. The signs of the calculated rotational strengths based on the axial inclusion complex are in agreement with the observed ones, whereas the signs based on the equatorial inclusion complex are opposite to those observed; thus, the structure of the 2-NAT complex is estimated to be an axial inclusion and the other 2-substituted naphthalene complexes are thought to have similar structures.

The naphthalene ring which is included in the cavity of β-CDx has two degrees of freedom along the symmetry axis of β-CDx, the translation and the rotation. If an electric dipole moment makes the θ angle with the z-axis, as is shown in Fig. 7, its position and direction are determined by θ, φ, and z. In the cases of the ^1L_a and ^1B_b transitions, the rotational strength was shown to be independent of φ. The z-dependence of the rotational strength is shown in Fig. 8. It is found that the complex gives a large CD value when the naphthalene group is situated in the cavity; the rotational strength of the ^1B_b transition takes its maximum value when the electric dipole moment is almost at the center of the cavity, while that

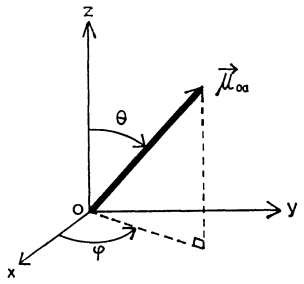

Fig. 7. The coordinate system of the electric dipole moment.

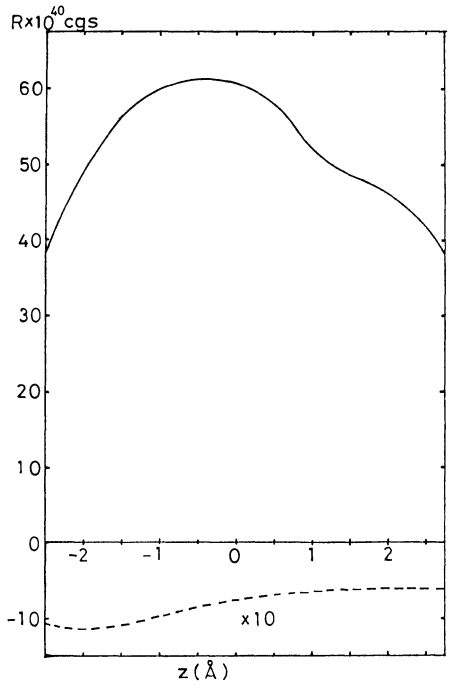

Fig. 8. The z-dependence of rotational strengths of ^1L_a (----) and ^1B_b (——) transition.

of the ^1L_a transition takes its minimum value at −2.0 Å.

It is interesting to calculate the dependence of the rotational strength of θ. If $\vec{e}_{0a}=(\sin\theta, 0, \cos\theta)$, Eq. (1) is expressed as follows:

$$R_{0a} = [A_{0a} + B_{0a}\cos 2\theta + C_{0a}\sin 2\theta]\mu_{0a}^2$$

where A_{0a}, B_{0a}, and C_{0a} are shown in Fig. 9. R_{0a} takes its maximum value at $\theta=0°$ and its minimum value at $\theta=90°$, since C_{0a} is negligible, so the transition with an electric dipole moment parallel to the z-axis gives a positive CD value and the transition with an electric dipole moment perpendicular to the z-axis gives a negative CD value. Thus, it is possible to estimate the orientation of the chromophor in the cavity of β-CDx if the direction of the electric dipole moment in the chromophor is known.

Conclusion

Both experiments and calculations proved that the structure of β-CDx complexes with 2-substituted naphthalene is an axial inclusion and that the assumed

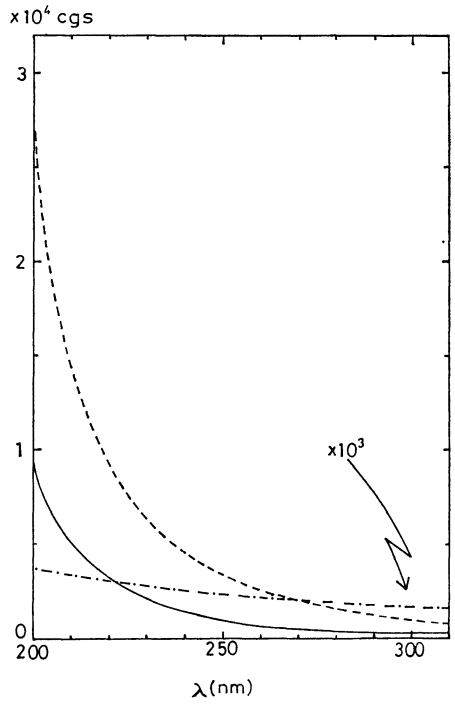

Fig. 9. The wavelength-dependence of A_{0a} (——), B_{0a} (----) and C_{0a} (-·-·-).

conformation of β-CDx is reasonable. The calculated rotational strength is in fairly good agreement with the observed value in spite of the use of a crude approximation. The calculated rotational strengths do not explain the CD spectra of the 1-substituted naphthalene complexes; the positive CD band in the 200—250 nm region suggests an axial inclusion, while the nagative CD band suggests the equatorial inclusion. It is possible that the two species exist in equilibrium.

References

1) W. J. James, D. French, and R. E. Rundle, *Acta Crystallogr.*, **12**, 385 (1959).
2) A. Hybl, R. E. Rundle, and D. E. Williams, *J. Amer. Chem. Soc.*, **87**, 2779 (1956).
3) F. Cramer, W. Seanger, and H. -Ch. Spatz, *ibid.*, **89**, 14 (1967).
4) P. V. Demarco and A. L. Thakker, *Chem. Commun.*, **1970**, 2.
5) F. Cramer and W. Dietsche, *Chem. Ber.*, **92**, 1739 (1959).
6) F. Cramer, *Angew. Chem.*, **68**, 115 (1956).
7) F. Cramer and W. Kampe, *J. Amer. Chem. Soc.*, **87**, 1115 (1965).
8) D. E. Tutt and M. A. Schwartz, *ibid.*, **93**, 767 (1971).
9) K. Sensse and F. Cramer, *Chem. Ber.*, **102**, 509 (1969).
10) K. Takeo and T. Kuge, *Stärke*, **24**, 281 (1972).
11) J. P. Kirkwood, *J. Chem. Phys.*, **5**, 479 (1937).
12) I. Tinoco, Jr., "Advan. Chem. Phys.," **4**, 113 (1962).
13) G. C. Le Fevre and R. J. W. Le Fevre, *J. Chem. Soc.*, **1956**, 3549.
14) L. W. Picket, M. Muntz, and E. M. McPherson, *J. Amer. Chem. Soc.*, **73**, 4862 (1951).
15) H. Tsubomura, K. Kimura, K. Kaya, J. Tanaka, and S. Nagakura, This Bulletin, **37**, 417 (1964).
16) J. R. Platt, *J. Chem. Phys.*, **17**, 484 (1949).

Physico-chemical Studies of the Reversible and Irreversible Phase Transitions in Potassium Ferrocyanide Trihydrate and Its Deuterate Analogue*

Masaharu OGUNI, Takasuke MATSUO, Hiroshi SUGA, and Syûzô SEKI
Department of Chemistry, Faculty of Science, Osaka University, Toyonaka, Osaka 560
(Received June 1, 1974)

Phase transitions of $K_4Fe(CN)_6 \cdot 3H_2O$ and its deuterate were studied through the measurements of differential thermal analysis curves, heat capacity, volume expansion and Raman spectra. Samples prepared by recrystallization from the aqueous solution were found to be in the metastable phase. The ferroelectric transition temperature between two stable monoclinic phases was determined to be 247.8 K and 252.7 K for the hydrate and deuterate, respectively. The enthalpy and entropy changes of the transition were estimated to be 2592 J mol^{-1} and 12.41 JK^{-1} mol^{-1}, respectively, for the hydrate, and 3017 J mol^{-1} and 14.36 JK^{-1} mol^{-1}, respectively, for the deuterate. The molecular mechanism of the transition was discussed in terms of entropy change. The transition was also concluded to be of the second order according to Ehrenfest's criterion. Irreversible transformation of tetragonal to monoclinic phase was observed for the first time for the deuterate as a new type of phase change having a Martensitic nature. These irreversible transformations took place in the temperature region covering 20 K below *ca.* 232 K and *ca.* 237 K for the hydrate and deuterate, respectively. The anhydrous salt showed no transformation in the temperature region between 13 K and room temperature.

A number of studies have been carried out on potassium ferrocyanide trihydrate and its deuterate as ferroelectrics having hydrogen-bond networks. Posperov and Zhdanov[1] (1947) disclosed the existence of both monoclinic and tetragonal crystal structures by X-ray diffraction at room temperature. Dielectric, optical and X-ray studies by Waku *et al.*,[2] Toyoda *et al.*[3] and Kiriyama *et al.*[4] also contributed to the elucidation of the structure, various types of twinning being found in particular by Toyoda *et al.* Proton and deuteron magnetic resonance methods were applied to the determination of the hydrogen position by Blinc *et al.*,[5] Tsang and O'Reilly,[6] Kiriyama *et al.*[4] and Habuda *et al.*[7] Neutron diffraction method was also applied by Taylor *et al.*[8] for the same purpose. Both the hydrate and deuterate crystals have layer structures which consist of hydrogen (or deuterium)-bonded water layers sandwiched between two double layers containing ferrocyanide octahedra and potassium ions. The monoclinic and tetragonal forms of both crystals which exist as stable and metastable modifications at room temperature, respectively, differ in the pattern of stacking of the layers, *viz.*, the layer structure can be constructed by rotating each successive layer 90° around the b-axis.[3] The monoclinic crystal has the space group C^6_{2h}–$A_{2/a}$ with four molecules in the unit cell and the tetragonal one the space group C^6_{4h}–$I_{4_1/a}$ with eight molecules in it. On being cooled, the monoclinic crystal undergoes a ferroelectric phase transition at 248.6 K and 255.1 K for the hydrate and the deuterate, respectively. The low-temperature space group is C^4_s–A_a, lacking the center of symmetry. On the other hand, the metastable tetragonal modification undergoes an irreversible phase transition to the twinned monoclinic one on being cooled below 218 K. The twinned crystal thus obtained shows only the reversible transition at 248.6 K for the hydrate on heating. The results of dielectric and optical investigations were reported for this irreversible transition by Krasnikova *et al.*[9]

The ferroelectric behavior was discovered by dielectric measurement by Waku *et al.*[10,11] in 1959. The origin of ferroelectricity can be classified into two types, the order-disorder mechanism and the displacive one. The former model involves alignment of the water molecules in the hydrogen-bonded layers, although there are two alternative models for the orientation of the water molecules as well as for the direction of spontaneous polarization.[4,6–8] Both models indicate that the compound has two different states per three water molecules at the disordered state. The latter, *viz.* the displacive mechanism, was derived from Moessbauer studies by Hazony *et al.*[12] and by Montano *et al.*[13] It involves a relative shift of the potassium ions, ferrocyanide ions and the water molecules within the crystal lattice. High pressure dielectric study was also reported by Krasnikova and Polandov[14] who constructed a phase diagram of the hydrate around the ferroelectric transition.

In spite of these studies, the thermal properties of the compound have remained relatively unexplored. The heat capacity on the monoclinic hydrate given by Nakagawa *et al.*[15] seems to be the only available datum. However, accuracy and precision of measurement were not specified and important characteristics of phase transition such as the entropy and enthalpy changes remained unclarified. We have thus investigated the properties of reversible phase transition based on the data of heat capacity and dilatometric measurements, in order to clarify the thermodynamic properties of the compounds. We have tried to elucidate the nature of the irreversible phase transition which was first discovered for the deuterate in the present investigation. The heat capacity of the anhydrous salt was also measured for the sake of comparison.

After the publication of our paper on heat capacity and dilatometric studies,[16] Malcolm *et al.*[17] reported the results of heat capacity and heat of solution on the monoclinic hydrate and anhydrous salt, and of the dissociation pressure of the monoclinic hydrate-anhydrous salt system. Compared with our results, their heat-capacity data are larger by nearly 0.5% for the hydrate except in the transition region, and smaller by about 0.6% for the anhydrous salt.

* A part of this paper has been published.[16]

Experimental

Material. The hydrate sample (special grade from Wako Pure Chemical Co., Ltd.) was recrystallized twice from its aqueous solution. The deuterate sample was prepared by recrystallization from the saturated solution in 99.75% heavy water (E. Merck) at a slow rate after dehydration of the purified hydrate *in vacuo* at 70 °C. Special care was taken to avoid photochemical decomposition. Crystals obtained were kept in a desiccator together with the anhydrous salt for over one month in order to remove excess water. The purity of the samples was determined from the weight loss caused by complete dehydration *in vacuo* at 70 °C. The water contents thus determined are given in Table 1.

Differential Thermal Analysis. Preliminary DTA studies were carried out in the transition regions for confirmation of results obtained by other workers. Details of the apparatus were already reported.[18] Granular (*ca.* 2 mm in size) and fine samples, both powdered in an agate mortar for a few minutes, were used.

Heat Capacity. The heat capacity of monoclinic modification in the range 15—300 K and that of tetragonal modification in the range 210—290 K were measured with an adiabatic calorimeter.[19] Accuracy of the measurement was better than 1% at liquid hydrogen temperature and 0.3% at room temperature. The amounts of each sample are given in Table 1. Helium gas and nitrogen gas at 100 kPa were used for the monoclinic and tetragonal samples, respectively, to facilitate heat transfer inside the calorimeter.

Monoclinic Hydrate: The sample was cooled twice down to liquid-nitrogen temperature for complete transformation to the monoclinic phase from the tetragonal modification. Samples were prepared by different methods for comparison, one being obtained by cracking a large single crystal into appropriate pieces in an agate mortar, and the other by cutting a large crystal with a razor blade. The former contained a small amount of powder in addition to the relatively large crystallites (3—5 mm), and the latter consisted of almost uniform size pieces (3—5 mm). The heat capacity curve of the crushed hydrate sample first measured showed a gentle hump in the temperature region slightly lower than the melting point of ice besides a ferroelectric phase transition. Re-examination was carried out with the same sample (see hydrate(a), Table 1) after removal of 35 mg of water from the loaded cell. The amount of water corresponds to the excess calculated from the heat-capacity hump on the assumption that it melted with the same heat of fusion as pure ice.

Monoclinic Deuterate: The same two kinds of deuterate samples as for (a) were used (see Table 1). Measurement (220—270 K) on the sample subjected to cutting treatment was carried out after the measurement of the irreversible transition region had been carried out.

Tetragonal Modification: The hydrate sample was crushed in an agate mortar, and the deuterate sample was cut with a razor blade. Measurements were carried out for samples pretreated under different pre-cooling conditions.

Dilatometric Study. The temperature dependence of the molar volume of the monoclinic hydrate was determined in the range 235—280 K in both cooling and heating with a glass-dilatometer containing degassed mercury as a confining liquid. The temperature of the methanol dry-ice bath surrounding the dilatometer was measured with a chromel-p-to-constantan thermopile. The height of the mercury column was measured with a cathetometer to the reading of 0.01 mm. The amount of the sample was determined to be 19.896 cm^3 at 26.2 °C in terms of density from X-ray data.[4]

Raman Spectroscopy. The Raman spectra of the monoclinic and tetragonal hydrates were obtained at room temperature with a Japan Spectroscopic Co., Ltd. model 750 Laser-Raman spectrometer. The incident beam was introduced parallel to the a-axis of the crystal and the scattered beam was taken out along the b-axis.

Results and Discussion

Differential Thermal Analysis (DTA). Results on the granular hydrate and deuterate recrystallized from their water and heavy water solutions, respectively, are shown in Figs. 1 and 2, respectively. In both figures Run 1 shows the cooling curves at the rate of *ca.* 1 K/min to 228 K for the hydrate and 234 K for the deuterate. These values are lower than the respective ferroelectric to paraelectric transition temperatures between their two monoclinic forms. The samples were kept for one and a half hours at the lowest respective temperatures for the purpose of testing the metastability of the tetragonal phase, and then heated up to room temperature. No change appeared throughout Runs 1 and 2, indicating that the crystals obtained were of the metastable tetragonal system, remaining metastable for a long enough time to allow calorimetric measurement in that modification. Runs 3 and 4 show the cooling curves down to 200 K and the subsequent heating ones up to room temperature, respec-

Table 1. Weights and water contents of samples

	(A)	(B)	(C)
	monoclinic modification		
hydrate(a)	61.371 g (=0.145 29 mol)	12.77%	12.794%
hydrate(b)	56.213 g (=0.133 08 mol)	12.75%	12.794%
deuterate(a)	67.302 g (=0.157 08 mol)	13.96%	14.020%
deuterate(b)	54.165 g (=0.126 42 mol)	13.97%	14.020%
	tetragonal modification		
hydrate	50.621 g (=0.119 84 mol)	12.75%	12.794%
deuterate	54.165 g (=0.126 42 mol)	13.97%	14.020%
	anhydrous salt		
	56.989 g (=0.154 71 mol)		

(A) sample weight *in vacuo*, (B) observed water content, (C) calculated water content, (a) granular crystals crushed into pieces in an agate mortar, (b) granular crystals cleaved into pieces with a razor blade.

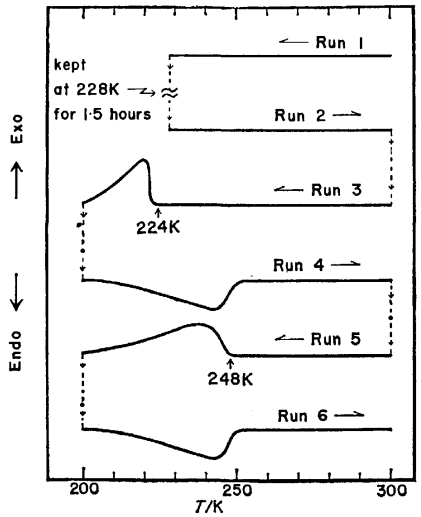

Fig. 1. DTA curves of stable and metastable $K_4Fe(CN)_6 \cdot 3H_2O$.

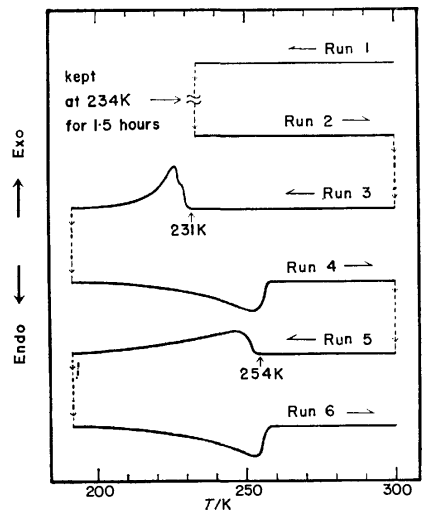

Fig. 2. DTA curves of stable and metastable $K_4Fe(CN)_6 \cdot 3D_2O$.

tively. Run 3 of the hydrate showed an exothermic effect at 234 K, whereas Run 4 no longer showed the corresponding endothermic peak but a new anomaly at 248 K. The same anomalies as found for the hydrate were observed at 231 K and 253 K for the deuterate, respectively. These results show that the metastable tetragonal crystals undergo irreversible transformation into the stable monoclinic modification when they are cooled below each transformation temperature, and that anomalies in Run 4 correspond to the reversible ferroelectric transition.

The appearance or disappearance of a shoulder in the exothermic peak in Run 3 for the deuterate changes with the sample. Runs 5 and 6 confirmed good reproducibility of the anomalies in Run 4. This indicates that the pre-cooling of the sample to a sufficiently low temperature is indispensable to studies on monoclinic modification although the sample thus obtained is heavily twinned. On the other hand, DTA curves of the powder samples did not give rise to any well-defined anomaly over the entire temperature range. The reason for this seems to be as follows. The sample might not only be partially dehydrated during the course of grinding but the surface of the crystal might also be perturbed so that complexity in the electric boundary conditions causes a broad distribution of the Curie temperatures. In fact, handling of the sample has a serious effect on experimental results, particularly with respect to the critical phenomenon.

Ferroelectric Reversible Phase Transition. Heat Capacity: The heat capacity of the crushed hydrate in the monoclinic form was measured twice. The heat capacity in the second run had no anomaly due to the loss of excess water and coincided with the first one in the temperature region below 240 K and above 273 K. A broadening at the transition point was found in the second measurement. This is attributed to partial dehydration of the sample, since the slight deficiency of water content might have a drastic effect on the shape of heat capacity curve in the transition region. Heat capacity values (13—300 K) from the first measurement (with correction for excess water) and the second measurements were adopted as the final data.

Heat capacity results are schematically shown in Fig. 3. The data of the sample obtained by cutting the crystal are adopted for respective transition regions. Selected values** for the hydrate and deuterate are given in Tables 2 and 3, respectively. Values for the sample subjected to cutting are given in series 9—11 in Table 10. Graphically smoothed heat capacities and derived thermodynamic functions for the hydrate and the deuterate are given in Tables 4 and 5, respectively. The heat capacity values of the hydrate obtained by Malcolm *et al.*[17] are larger by nearly 0.5% than the present values except in the transition region, while those obtained by Nakagawa *et al.*[15] are larger by about 50% at room temperature. We found that the anomaly due to the transition extends over a

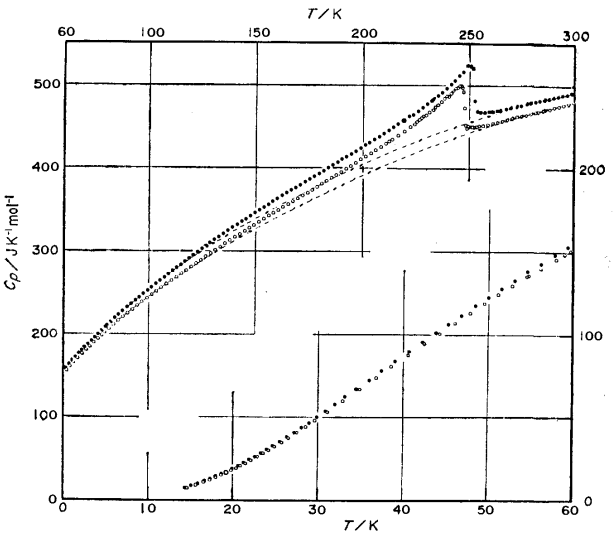

Fig. 3. Heat capacity of the monoclinic modification. ○: $K_4Fe(CN)_6 \cdot 3H_2O$, ●: $K_4Fe(CN)_6 \cdot 3D_2O$.

** The complete data of Tables 2,3,6,9 and 10 are kept as Document No. 7502 at the Chemical Society of Japan.

Table 2. Selected heat capacity data of monoclinic $K_4Fe(CN)_6 \cdot 3H_2O$

T_{av}/K	C_p/J K^{-1} mol^{-1}	T_{av}/K	C_p/J K^{-1} mol^{-1}	T_{av}/K	C_p/J K^{-1} mol^{-1}	T_{av}/K	C_p/JK^{-1} mol^{-1}	T_{av}/K	C_p/JK^{-1} mol^{-1}
		62.87	160.3	164.99	356.3	248.29	447.6	229.70	463.8
Series 1		66.54	170.4	169.52	363.3	249.58	448.0	231.87	469.4
hydrate(a)		70.55	180.5	174.01	370.5	252.17	449.0	234.00	472.8
		74.27	189.7	178.55	377.4	256.20	451.0	236.12	478.4
14.59	7.01	78.00	198.4	183.04	384.5	260.20	453.3	238.22	484.0
16.57	10.45	81.25	206.1	187.58	391.7	264.30	456.1	240.35	486.7
18.04	13.44	83.46	211.3	192.10	398.8	268.44	459.0	242.37	494.1
19.23	16.11	87.85	221.0	196.65	406.1	272.55	461.9	244.41	497.4
20.41	18.97	92.30	229.9	201.29	413.8	276.64	464.5	246.19	499.8
21.50	21.87	96.76	238.9	206.02	421.6	280.71	467.1	247.21	492.5
22.88	25.89	101.41	247.4	210.72	429.5	284.82	470.5	248.27	452.0
24.22	30.04	105.94	255.9	214.43	435.9	289.78	475.0	249.36	450.9
25.74	34.72	110.66	264.7	218.84	443.1	294.98	477.6	251.27	450.0
27.54	40.77	115.29	273.1	223.20	451.2	300.14	480.6	253.45	450.1
29.65	47.96	119.80	281.2	227.48	459.9			255.63	450.9
32.96	59.97	124.35	289.0	231.71	467.2	Series 2		261.11	454.4
36.81	74.00	128.87	297.1	235.88	476.2	hydrate(b)		265.67	457.4
40.53	87.56	133.37	304.7	239.99	483.6			270.19	460.8
44.23	100.8	137.90	312.5	243.26	490.2	205.85	421.1	274.69	463.5
47.83	113.4	142.43	320.0	244.12	491.2	210.81	429.5	279.17	466.7
51.17	124.6	146.92	327.4	245.41	491.3	216.61	439.5	285.92	471.6
54.57	135.5	151.45	334.8	246·22	492.7	222.38	449.9	290.32	474.5
56.18	140.4	155.90	342.1	246.89	488.7	255.35	455.6	294.71	477.1
59.73	151.0	160·44	349.0	247.43	480.3	227.54	460.4	299.41	481.1

Table 3. Selected heat capacity data of monoclinic $K_4Fe(CN)_6 \cdot 3D_2O$

T_{av}/K	C_p/J K^{-1} mol^{-1}	T_{av}/K	C_p/J K^{-1} mol^{-1}	T_{av}/K	C_p/J K^{-1} mol^{-1}	T_{av}/K	C_p/J K^{-1} mol^{-1}	T_{av}/K	C_p/J K^{-1} mol^{-1}
14.41	6.95	51.57	128.2	115.05	283.6	190.26	410.4	252.19	493.6
15.90	9.59	54.67	138.3	118.91	291.3	194.60	417.0	252.92	477.7
17.37	12.46	57·89	148.5	122.88	298.9	198.96	424.0	253.51	468.4
18.65	15.42	61.01	158.2	126.83	306.2	203.26	430.8	254.31	468.4
19.97	18.67	64.01	167.2	130.75	313.2	207.69	438.0	255.10	465.6
21.33	22.32	67.18	175.0	134.91	320.9	212.10	445.5	256.19	466.1
22.66	26.16	69.94	183.3	139.09	328.2	216.50	453.2	258.27	466.4
24.05	30.41	73.11	191.5	143.40	335.4	220.85	460.5	261.07	468.4
25.51	35.04	76.28	199.6	147.60	342.4	225.12	467.2	267.42	471.9
27.24	40.77	79.72	208.8	151.73	349.4	229.36	474.5	270.17	473.5
28.98	46.74	84.14	219.2	155.96	356.3	233.73	483.6	274.57	476.5
30.92	53.74	87.95	228.2	160.19	363.2	238.11	488.8	279.13	479.4
33.19	62.33	91.81	236.6	164.49	370.1	242.43	496.2	283.47	482.2
36.00	72.54	95.69	244.7	168.74	376.8	246.68	502.1	287.77	484.7
39.07	84.02	99.50	252.6	173.02	383.2	248.23	503.1	289.92	486.5
42.24	95.55	103.35	260.3	177.43	390.2	249.68	503.8	294.20	489.1
45.36	106.9	107.23	268.4	181.77	397.0	250.68	502.3	298.45	492.0
48.49	117.9	111.11	276.0	186.04	403.7	251.62	497.4	300.56	493.3

wide region of temperature, having the transition point at 247.8 K and 252.7 K*** for the hydrate and deuterate, respectively. The anomalous part was estimated by separating the normal part from the total heat capacity. The normal part, determined from the smooth extrapolation of the higher and lower temperature sides of the transition region, is thus given by the equation

$$C_p(T) = A(\ln T)^3 + B(\ln T)^2 + C(\ln T) + D + E(\ln T)^{-1} + F(\ln T)^{-2}, \quad (1)$$

where $A = -0.101196 \times 10^4$, $B = 0.240747 \times 10^5$, C=

*** The revised data of transition point, which is 0.2 K higher than the old value,[16] were taken as the more accurate temperature of the steepest drop.

Table 4. Thermodynamic functions of monoclinic $K_4Fe(CN)_6 \cdot 3H_2O$

T / K	$C_p°$ / J K^{-1} mol^{-1}	$S°-S_0°$ / J K^{-1} mol^{-1}	$[H°-H_0°]/T$ / J K^{-1} mol^{-1}	$[G°-H_0°]/T$ / J K^{-1} mol^{-1}
10	(2.25)	(0.81)	(0.60)	(0.21)
20	18.0	6.10	4.61	1.49
30	49.2	19.00	12.00	7.00
40	85.3	38.13	27.38	10.75
50	120.6	61.05	42.59	18.46
60	152.2	85.88	58.27	27.61
70	179.1	111.4	73.65	37.75
80	203.3	136.9	88.35	48.35
90	225.4	162.2	102.4	59.77
100	244.8	186.9	115.7	71.27
110	263.4	211.1	128.2	82.86
120	281.5	234.8	140.3	93.54
130	299.1	258.0	151.8	106.2
140	315.9	280.8	162.9	117.9
150	332.4	303.2	173.7	129.5
160	384.4	325.2	184.2	141.0
170	364.1	346.8	191.5	155.2
180	379.6	368.0	204.1	163.9
190	395.3	389.0	213.7	175.2
200	411.8	409.6	223.2	186.4
210	428.2	430.1	232.6	197.5
220	445.4	450.4	241.9	208.5
230	465.0	470.6	251.1	219.5
240	488.0	490.9	260.5	230.4
250	450.4	510.6	269.5	241.2
260	453.6	528.3	276.5	251.8
270	460.1	545.5	283.1	252.4
280	467.0	562.4	289.6	272.8
290	473.8	578.9	295.8	283.1
300	480.5	595.1	301.9	293.2
273.15	462.2	550.9	285.2	265.7
298.15	479.2	592.1	300.7	291.3

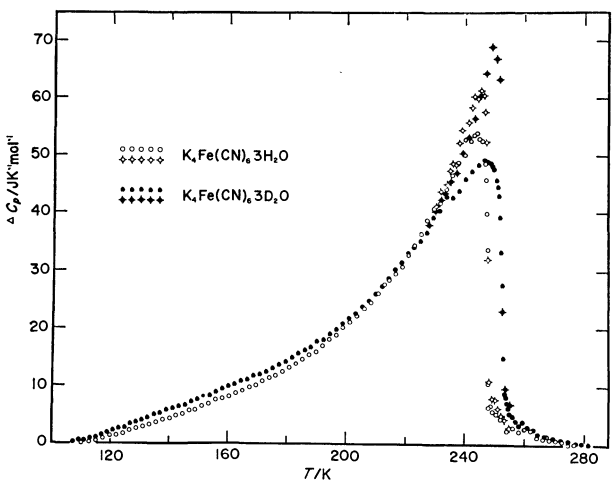

Fig. 4. Anomalous part of heat capacity of the monoclinic modification.
○ and ●: subjected to cracking treatment,
-○- and -●-: subjected to cleaving treatment.

-0.227928×10^6, $D=0.107619\times10^7$, $E=-0.253369\times10^7$ and $F=0.237844\times10^7$ for the hydrate, and $A=-0.140903\times10^4$, $B=0.340826\times10^5$, $C=-0.328633\times10^6$, $D=0.158175\times10^7$, $E=-0.379924\times10^7$ and $F=0.364163\times10^7$ for the deuterate. Figure 4 shows the anomalous part of heat capacity thus derived which does not diverge at the transition temperature. Discrepancies between the samples subjected to different treatment are of significance; the sample obtained by cutting with a razor blade has a high, sharp peak at the transition temperature as compared with that of the sample obtained by crushing into pieces. Since there is no difference in the preparation of the two samples, the discrepancy in the heat capacity is considered to be due to this difference in handling. Partial dehydration from the crystal surface and/or stacking faults including other physical impurities, both of which are possibly caused by crushing, might be responsible for the local disappearance of clearly defined critical temperature. The discrepancy between the present data and those by Malcolm *et al.* (Fig. 5) arises from a similar cause.

No anomaly was observed in the heat capacity of anhydrous salt (Fig. 6). This confirms the view that the water molecules play an essential role in the transition phenomenon. The selected data and the derived

Table 5. Thermodynamic functions of monoclinic $K_4Fe(CN)_6 \cdot 3D_2O$

T / K	$C_p°$ / J K^{-1} mol^{-1}	$[S°-S_0°]/T$ / J K^{-1} mol^{-1}	$[H°-H_0°]/T$ / J K^{-1} mol^{-1}	$-[G°-H_0°]/T$ / J K^{-1} mol^{-1}
10	(2.25)	(0.81)	(0.60)	(0.21)
20	18.6	6.210	4.705	1.51
30	50.6	19.46	14.41	5.05
40	87.5	39.05	28.06	10.99
50	122.9	62.43	43.53	18.90
60	155.1	87.68	59.48	28.20
70	183.7	113.8	75.23	38.57
80	208.9	140.0	90.36	49.62
90	232.7	160.6	104.9	61.10
100	253.7	191.6	118.7	72.90
110	273.6	216.7	131.9	84.82
120	293.4	241.4	144.5	96.89
130	311.9	265.6	156.7	108.9
140	329.6	289.4	168.4	121.0
150	346.4	312.7	179.7	133.0
160	362.8	335.6	190.7	144.9
170	378.6	358.1	201.3	156.8
180	394.4	380.2	211.6	168.6
190	409.9	402.0	221.6	180.4
200	425.4	423.4	231.4	192.0
210	442.0	444.6	241.0	203.6
220	458.5	465.5	250.5	215.0
230	476.5	486.2	260.0	226.2
240	498.2	507.0	269.4	237.6
250	524.5	527.8	279.1	248.7
260	468.7	546.8	286.9	259.9
270	474.0	564.6	293.7	270.9
280	480.0	581.9	300.3	281.6
290	486.4	598.8	306.6	292.2
300	493.0	615.4	312.7	302.7
273.15	476.0	570.1	295.8	274.3
298.15	491.7	612.4	311.6	300.8

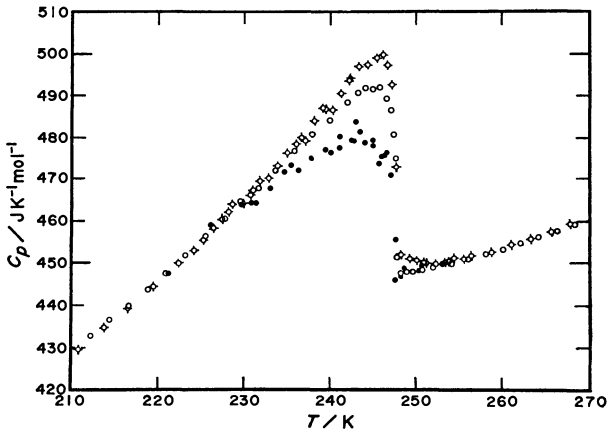

Fig. 5. Heat capacity of $K_4Fe(CN)_6 \cdot 3H_2O$ for the monoclinic modification near the transition region.
-⊙-: subjected to cleaving treatment,
○: subjected to cracking treatment,
●: from Ref. 17.

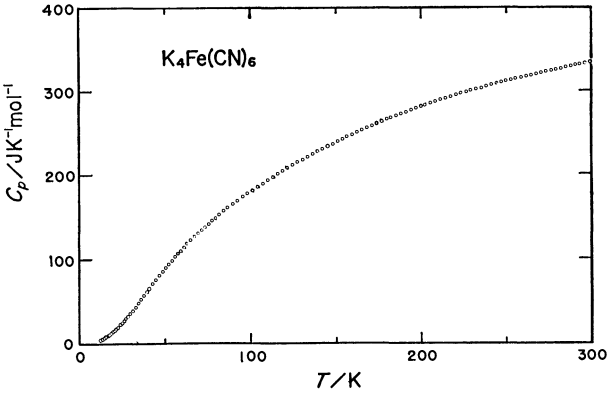

Fig. 6. Heat capacity of $K_4Fe(CN)_6$.

thermodynamic functions are given in Tables 6 and 7, respectively. The smoothed heat capacity values by Malcolm *et al.* are smaller by *ca.* 0.6% below 200 K, by *ca.* 0.8% near 250 K and by *ca.* 0.4% at 300 K than ours.

Enthalpy and Entropy Changes and the Mechanism of Phase Transition: The enthalpy and entropy changes at the transition point were estimated from the anomalous part of the heat capacities obtained. The numerical

Table 6. Selected heat capacity values of $K_4Fe(CN)_6$

T_{av}/K	C_p/J K^{-1} mol^{-1}	T_{av}/K	C_p/J K^{-1} mol^{-1}	T_{av}/K	C_p/J K^{-1} mol^{-1}	T_{av}/K	C_p/J K^{-1} mol^{-1}	T_{av}/K	C_p/J K^{-1} mol^{-1}
12.28	4.51	42.75	70.33	95.57	174.1	171.57	259.3	247.08	310.3
14.60	7.05	46.74	80.58	101.27	182.0	177.30	264.4	253.05	313.4
16.49	9.55	50.44	89.72	107.38	190.2	182.98	269.0	255.95	314.8
17.31	10.18	54.08	98.36	113.26	197.7	188.82	273.6	261.98	317.8
18.63	12.75	57.80	106.8	119.01	205.0	194.58	278.1	267.77	320.4
20.47	15.93	61.06	114.2	124.76	211.9	200.15	282.2	270.66	321.7
22.30	19.41	65.06	122.5	130.60	218.8	205.70	285.9	276.47	324.4
24.82	24.61	69.28	130.7	136.34	225.3	211.78	289.8	282.25	327.0
26.95	29.76	73.36	138.1	142.18	231.6	217.69	293.4	285.11	328.3
29.46	35.85	77.48	145.5	148.16	237.7	223.65	297.2	290.82	330.7
32.58	43.87	81.76	152.9	154.00	243.5	229.60	300.6	296.53	332.9
35.91	52.66	84.44	157.5	159.80	249.0	235.48	303.8	299.51	334.2
39.35	61.38	89.67	165.8	165.70	254.6	241.31	307.2	302.47	335.3

Table 7. Thermodynamic functions of $K_4Fe(CN)_6$

T/K	$C_p°$/J K^{-1} mol^{-1}	$[S°-S_0°]/T$/J K^{-1} mol^{-1}	$[H°-H_0°]/T$/J K^{-1} mol^{-1}	$-[G°-H_0°]/T$/J K^{-1} mol^{-1}
10	(2.19)	(0.75)	(0.58)	(0.17)
20	15.1	5.58	4.17	1.41
30	37.3	15.57	11.27	4.30
40	63.2	29.79	20.97	8.82
50	88.6	46.64	31.98	14.66
60	111.7	64.84	43.37	21.47
70	132.1	83.67	54.36	29.04
80	149.8	102.49	65.44	37.05
90	166.3	121.1	75.76	45.37
100	180.3	139.4	85.52	53.86
110	193.6	157.2	94.74	62.44
120	206.1	174.6	103.5	71.04
130	218.0	191.5	111.9	79.67
140	229.2	208.1	119.8	88.25
150	239.5	224.3	127.5	96.79
160	249.2	240.1	134.8	105.3
170	258.5	253.6	141.8	111.8
180	266.8	270.5	148.5	122.0
190	274.5	285.1	154.1	130.2
200	281.9	299.4	161.1	138.3
210	288.5	313.3	167.0	146.3
220	294.9	326.8	172.7	154.1
230	300.9	340.1	178.1	162.0
240	306.3	353.0	183.4	169.6
250	311.8	364.0	188.4	175.6
260	316.7	377.9	193.2	184.7
270	321.5	390.0	197.9	192.1
280	326.1	401.7	202.4	199.3
290	330.3	413.3	206.9	206.4
300	334.3	424.5	210.9	213.6
273.15	323.0	393.7	199.3	194.4
298.15	333.5	422.5	210.1	212.4

data are given in Table 8 together with the jump of heat capacity at the transition temperature, $\Delta C_p(T_{tr})$, where data for the sample subjected to cutting are adopted. The heat capacity jump at the transition point was estimated by the extrapolation of low and high temperature sides of C_p-values to the transition temperature by taking the rounding effect into consideration. A slight difference between the present value, 55.3 J K^{-1} mol^{-1}, and the old value,[16] 53.7 J K^{-1} mol^{-1}, for the hydrate comes from the difference in

Table 8. Thermodynamic quantities of ferroelectric reversible transition

	T_{tr} / K	ΔH_{tr} / J mol^{-1}	ΔS_{tr} / J K^{-1} mol^{-1}	ΔC_p / J K^{-1} mol^{-1}	$\Delta\alpha$ / K^{-1}
$K_4Fe(CN)_6\cdot 3H_2O$	247.8	2592 491[a]	12.41 1.93[a] 8.75[b]	55.3	3.32×10^{-5}
$K_4Fe(CN)\cdot 3D_2O$	252.7	3017	14.36	68.7	

a) from Ref. 15, b) from Ref. 17.

heat capacity data; the present datum was determined from data of the cut sample and the previous one from those of the crushed sample. The entropy change of the transition thus estimated is 12.41 and 14.36 JK^{-1} mol^{-1} for the hydrate and deuterate, respectively. In the empirical classification of ferroelectric transitions, the present values of the entropy change definitely favor the order-disorder mechanism rather than the displacive one. In contrast, if we adopt the previous value 1.93 JK^{-1} mol^{-1} by Nakagawa *et al.* it may be explained also by the displacive mechanism. However, their data are not accurate enough to draw this conclusion. The entropy change expected from the structural data is $R\ln 2$ per mole of the substance, which is significantly smaller than the present values corresponding to $R\ln 4.45$ and $R\ln 5.62$ for the hydrate and deuterate, respectively.

Order of Transition: The heat capacity exhibits its jump without divergence at the transition temperature. This suggests that the transition would be of a second or higher order nature. If the phase transition is of the second order, the following Ehrenfest relation holds:

$$\left(\frac{dp}{dT}\right)_{tr} = \frac{\Delta C_p(T_{tr})}{T_{tr}V\Delta\alpha}, \tag{2}$$

where the left-hand side is the slope of the transition line, $\Delta C_p(T_{tr})$ and $\Delta\alpha$ are the jumps of heat capacity and thermal expansion coefficient, respectively, at the transition point, and T_{tr} and V the transition temperature and volume of the crystal, respectively. The volume *vs.* temperature curve for the hydrate shows no jump at the transition point. No hysteresis effect was found in the heating and cooling. This is also a characteristic of the second-order phase transitions. The best fit to the measured values is given by the following equation.

$$V_m = 0.03530\,T + 215.9170 \quad (T<248.5\text{ K}), \text{ and}$$
$$V_m = 0.02818\,T + 217.6863 \quad (T>248.5\text{ K})$$

where V_m is the molar volume in cm^3 and T in K. The change of thermal volume expansion coefficients, $\Delta\alpha$, at the transition point is 3.32×10^{-5} K^{-1}. Substitution of the measured $\Delta C_p(T_{tr})$ and $\Delta\alpha$ into the Ehrenfest relation gives 3.22×10^{7} Nm^{-2} K^{-1} for $(dp/dT)_{tr}$. This is to be compared with 3.77×10^{7} Nm^{-2} K^{-1}, the direct data of Krasnikova and others. The two values differ from each other by 17%, but the discrepancy is not significant in view of the difficulty of assessing the accuracy. The phase transition in the hydrate is of the second order or very close to it.

Energy to Reorient a Unit Dipole in the Completely Ordered State: The alignment of the water molecules is responsible for the ferroelectric transition. In the ferroelectric state, provided that the number of dipoles in the wrong orientation n is small compared with that of total dipoles N, the following approximate equation is valid;

$$\frac{n}{N} = \exp\left(\frac{\Delta s}{k}\right)\exp\left(-\frac{\Delta h}{kT}\right), \tag{3}$$

where Δh is the enthalpy required to orient a unit dipole in the environment of the almost ordered neighbors and Δs the entropy term associated with the free energy change. The anomalous heat capacity is given by

$$\Delta C_p = \frac{d(n\Delta h)}{dT} = \frac{N}{T^2}\frac{(\Delta h)^2}{k}\exp\left(\frac{\Delta s}{k}\right)\exp\left(-\frac{\Delta h}{kT}\right). \tag{4}$$

The value of $(-\Delta h/k)$ is evaluated from the slope of $\ln(\Delta C_p T^2)$ plotted against $1/T$ (Fig. 7). Linear fit to the plot between 130 and 190 K gives $n/N = 13.1\times\exp(-1006/T)$ for the hydrate, and $n/N = 10.4\exp(-905/T)$ for the deuterate. Thus, n/N values calculated at 190 K are 0.066 and 0.088 for the hydrate and deuterate, respectively. The reorientation enthalpies Δh are also estimated to be 8.36 and 7.52 kJ mol^{-1}, and the reorientation entropies 21.4 and 19.5 J K^{-1} mol^{-1} for the hydrate and deuterate, respectively.

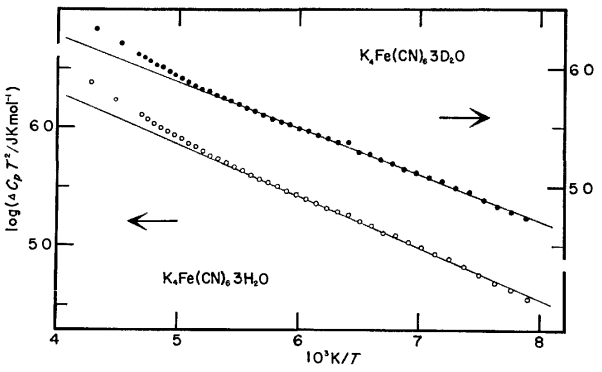

Fig. 7. Reorientation energy of a unit dipole in the completely ordered state.

The Metastable Phase and Its Irreversible Phase Transition. Heat Capacities Obtained under Different Pre-cooling Conditions: The heat capacities measured under different pre-cooling conditions are given in Tables 9 and 10 for the hydrate and deuterate, respectively. The process of measurement and results are as follows.

TABLE 9. CHRONOLOGICAL ORDER OF MEASUREMENT AND SELECTED HEAT CAPACITY VALUES FOR $K_4Fe(CN)_6 \cdot 3H_2O$ UNDER DIFFERENT PRE-COOLING CONDITIONS

room temperature —cooling→ 232.8 K —measurement (1st series)→ 288.1 K —cooling→ 226.0 K —measurement (2nd series)→ 236.1 K —cooling→ 229.8 K
—measurement (3rd series)→ 251.0 K —cooling→ 212.9 K —measurement (4th series)→ 249.6 K —cooling→ 221.2 K —measurement (5th series)→ 255.2 K —cooling→ 220.9 K
—measurement (6th series)→ 228.7 K —cooling→ 80 K —heating→ 226.4 K —measurement (7th series)→ 257.5 K —cooling→ 239.7 K —measurement (8th series)→ 254.5 K
—cooling→ 232.8 K —measurement (9th series)→ 257.2 —measurement (10th series)→ 269.0 K

T_{av}/K	C_p/J K^{-1} mol^{-1}	T_{av}/K	C_p/J K^{-1} mol^{-1}	T_{av}/K	C_p/J K^{-1} mol^{-1}	T_{av}/K	C_p/J K^{-1} mol^{-1}	T_{av}/K	C_p/J K^{-1} mol^{-1}
				245.41	472.6				
1-st series		3-rd series		246.60	460.9	7-th series		9-th series	
				250.16	446.1				
233.21	433.1	230.82	432.3			227.46	460.6	233.80	472.6
236.53	434.9	235.02	435.0	5-th series		231.50	466.9	237.66	480.5
240.93	437.5	239.19	438.1			235.48	474.6	241.58	489.5
245.52	440.3	243.34	440.3	221.81	441.5	239.41	483.8	243.52	494.2
250.14	443.6	247.46	442.1	225.93	448.0	243.27	492.0	245.45	495.4
254.73	446.8			230.56	455.0	246.75	484.5	246.91	487.2
259.29	450.1	4-th series		234.58	460.5	247.95	452.8	247.91	453.7
263.36	453.3			238.35	467.0	248.90	448.1	248.94	448.5
267.55	456.0	213.29	431.0	242.28	473.1	250.40	448.6	250.22	448.4
272.30	459.7	215.30	434.2	245.80	469.2	254.46	449.9	254.08	449.3
277.08	461.6	217.42	436.2	248.09	446.3				
282.00	466.0	219.58	439.4	251.70	447.5	8-th series		10-th series	
286.91	469.5	221.84	443.5						
		224.86	448.2	6-th series		240.63	484.1	257.80	450.9
2-nd series		229.48	455.8			242.55	487.6	259.84	452.3
		234.04	461.3	221.85	441.8	244.44	487.7	261.88	453.9
228.34	431.9	238.37	470.1	223.82	444.5	247.67	459.1	263.91	455.3
231.32	432.9	240.41	473.6	225.80	447.9	251.14	448.1	265.94	456.2
234.81	435.2	244.30	475.4	227.74	451.6	255.59	448.4	267.96	458.1

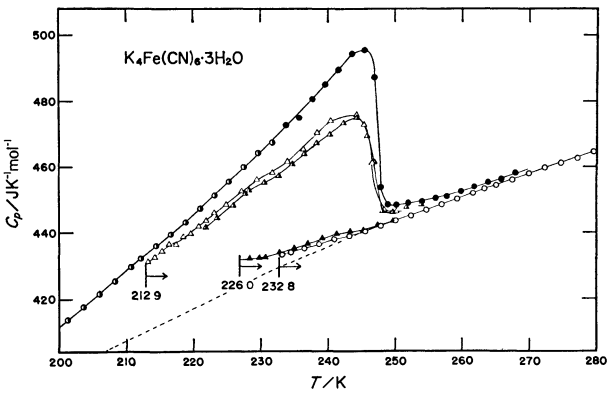

Fig. 8. Heat capacity of $K_4Fe(CN)_6 \cdot 3H_2O$ under different pre-cooling condition.
○: 1-st series, ▲: 2-nd and 3-rd series,
△: 4-th series, ◭: 5-th and 6-th series,
◑: 8-th, 9-th and 10-th series in Table 9,
●: cited from Table 2.

Measurements were carried out first in the temperature range 232.8—228.1 K with a specimen containing no monoclinic form (open circle, Fig. 8). The specimen was then cooled down to 226 K, where a slight exothermic phenomenon was observed corresponding to partial transformation of tetragonal into stable monoclinic phase. The heat capacity subsequently measured with increasing temperature (2nd and 3rd series) had a small hump in the vicinity of 240 K (symbol: ▲). This is due to the contribution of the reversible transition between the low and high temperature monoclinic phases. The 4th series (△) which started after cooling this specimen down to 212.9 K gave a much higher peak at 244 K. The measurements of the 5th and 6th (◭) series were carried out in order to confirm the reproducibility of the results under the same pre-cooling conditions. Spontaneous heat evolution was observed when the adiabatic condition was established after rapid cooling prior to measurement of the 4th series, but not of 5th and 6th series. The heat capacities of the 7th and subsequent three series coincided with those of the twinned monoclinic samples (Table 2). The heat capacity of the deuterate was measured under five different pre-cooling conditions. Reproducibility of heat capacity was checked at each stage by repeating the measurement, except for the last one in which the entire specimen was transformed into the monoclinic form. Measurement of the first series was commenced at 241.3 K

Table 10. Chronological order of measurement and selected heat capacity values for $K_4Fe(CN)_6 \cdot 3D_2O$ under different conditions

room temperature —cooling→ 241.3 K —measurement (1st series)→ 290.4 K —cooling→ 238.1 K —measurement (2nd series)→ 241.7 K —cooling→ 231.5 K —measurement (3rd series)→ 257.7 K —cooling→ 232.0 K —measurement (4th series)→ 255.4 K —cooling→ 227.3 K —measurement (5th series)→ 256.7 —cooling→ 227.8 K —measurement (6th series)→ 258.0 K —cooling→ 221.3 K —measurement (7th series)→ 256.1 K —cooling→ 222.5 K —measurement (8th series)→ 256.9 K —cooling→ 80 K —heating→ 263 K —cooling→ 232.3 K —measurement (9th series)→ 288.9 K —cooling→ 210.1 K —measurement (10th series)→ 233.2 —cooling→ 180.2 —measurement (11th series)→ 211.6 K

T_{av}/K	C_p/J K^{-1} mol^{-1}	T_{av}/K	C_p/J K^{-1} mol^{-1}	T_{av}/K	C_p/J K^{-1} mol^{-1}	T_{av}/K	C_p/J K^{-1} mol^{-1}	T_{av}/K	C_p/J K^{-1} mol^{-1}
1-st series				235.75	469.7	253.97	467.7		
		4-th series		239.78	477.8			10-th series	
				243.94	481.6	9-th series			
241.81	456.2	232.50	454.0	245.92	485.9			211.07	443.5
245.15	457.8	234.65	461.5	247.88	488.4	233.23	483.7	215.33	450.3
248.94	459.9	236.80	459.6	249.74	489.0	237.26	491.2	219.64	457.6
252.75	461.5	238.93	462.5	251.53	482.9	241.27	501.4	223.91	464.2
256.46	463.9	241.07	464.2	253.35	465.9	245.23	512.0	228.10	473.0
260.40	466.9	243.18	467.2	255.19	465.7	249.12	524.1	232.16	481.6
264.16	469.7	245.29	468.2			250.62	523.3		
268.06	472.1	246.35	469.1	8-th series		251.67	520.6	11-th series	
272.36	475.0	247.40	471.3			252.75	481.4		
276.64	478.0	248.45	472.1	223.07	459.6	255.39	467.6	181.29	395.9
280.93	480.0	249.50	473.3	226.52	464.6	259.38	468.8	183.47	400.4
285.17	482.5	250.54	473.6	230.31	471.7	263.43	471.7	185.64	402.7
287.28	484.2	251.71	469.2	234.15	478.4	267.55	472.9	187.79	406.2
289.39	486.1	252.77	464.7	238.23	484.3	271.65	475.0	189.93	409.9
				242.07	492.5	275.72	477.9	194.16	416.3
2-nd series		6-th series		246.05	501.4	279.78	480.4	198.35	423.0
				248.01	505.3	283.85	482.5	202.47	429.0
238.99	454.6	228.41	460.2	249.97	507.6	287.87	485.3	206.56	434.5
240.78	455.7	231.77	464.9	251.94	492.1	289.87	487.0	210.59	441.6

after the calorimeter had been cooled from room temperature and ended at 290.4 K. The specimen did not contain the monoclinic form at all, as evidenced by the fact that no heat capacity anomaly was observed in the 1st and 2nd series (open circle, Fig. 9). The 3rd series measured after cooling down to 231.5 K gave scattered data which coincided neither with the heat capacities of the monoclinic form nor with those of the 1st and 2nd series. The 4th series repeated under the same precooling conditions as for the 3rd one (▲) yielded a smooth curve in contrast. The heat capacity was significantly larger than that of the tetragonal form. The 5th and 6th series (◑) give heat capacities for the specimen pre-cooled to 227.3 K, which were larger than those of the previous series, the difference between heat capacities in these series being small as compared with that between the 3rd and 4th series. The difference was still less and hardly occurred between those of the 7th and 8th series (△) in which the specimen was pre-cooled to 221.3 K. The heat capacities in the 9th, 10th and 11th series (●) correspond to those of the twinned monoclinic phase. Spontaneous heat evolution was observed prior to the measurements of

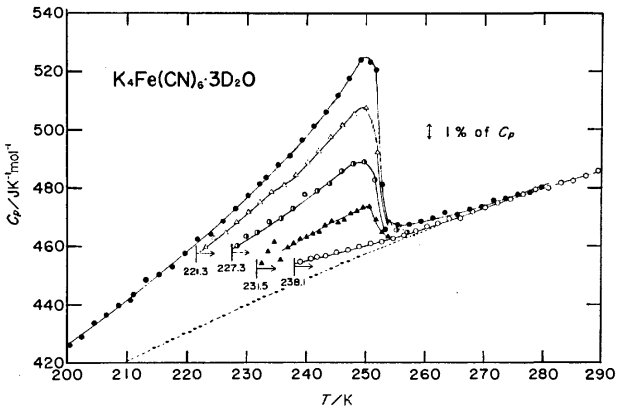

Fig. 9. Heat capacity of $K_4Fe(CN)_6 \cdot 3D_2O$ under different pre-cooling conditions.
The data of the 1-st, 2-nd (these two series: ○), 4-th (▲), 6-th (◑), 8-th (△), 9-th, 10-th and 11-th (these three series: ●) are selected by considering that these series would offer the reproducible data, while the 3-rd, 5-th and 7-th series were liable to yield scattered values.

the 3rd, 5th and 7th series as in the case of the hydrate.

From the results the following conclusions are reached. (1) The heat capacities obtained immediately after the establishment of the pre-cooling condition differ from the data of subsequent measurements performed under the same pre-cooling conditions. (2) All the data after the second agree with each other. (3) The mode of difference of heat capacity between the first and the following series depends upon the lowest temperature as well as the rate of the pre-cooling procedure, *etc.*

Similarity of the Monoclinic and Tetragonal Phases: The molecular arrangement of stable monoclinic and metastable tetragonal modifications at room temperature is quite the same in each layer and the modifications differ only in the mode of stacking. This suggests a slight difference in their lattice energies. Similarity of the two phases was also found in the Raman spectra and heat capacity values. The Raman spectra of each phase at room temperature were found to be in complete agreement except for a slight difference in intensity. Good coincidence in heat capacity and its dependence is shown in the case of the deuterate in Fig. 9. For the hydrate this cannot be definitely concluded for lack of data on the same sample in the temperature range where the short range ordering of the water molecules in the monoclinic phase is expected to vanish. However, between these two phases a distinct similarity in the thermal motion, and also in total enthalpy and entropy at room temperature is expected.

Properties of the Metastable Tetragonal Phase: The hydrate crystal in the tetragonal modification does not transform into the monoclinic phase in the temperature range between 232.8 K and room temperature. The tetragonal modification for the deuterate remains metastable at temperatures above 238 K. This is evident from the absence of heat capacity anomaly which should appear in the monoclinic modification (open circle, Figs. 8 and 9). It should be added that the hydrate sample crystals could be kept in a desiccator for six months without transformation. The heat capacity curve of the tetragonal modification (Figs. 8 and 9) deviates anomalously around 240 K. This is also the case for the tetragonal deuterate. The anomalous shape of the heat capacity curve suggests further contribution of a configurational one due to the development of the short range order of water molecule. In view of the structural similarity of the monoclinic and tetragonal phases within the hydrogen-bonded layer, the water molecules would be ordered in each layer around the same temperature where the stable monoclinic-monoclinic transition takes place.

Nature of the Phase Transition: The irreversible exothermic transformation of the tetragonal phase into the *twinned* monoclinic phase takes place below 232 K for the hydrate and below 237 K for the deuterate. This phase transformation develops in a strange way and is to some extent characteristic of the lowest temperature to which the specimen has been chilled down. Thus, the heat capacity curves measured exhibit different behaviors in accordance with the pre-cooled lowest temperatures (Tables 9 and 10, Figs. 8 and 9). In the

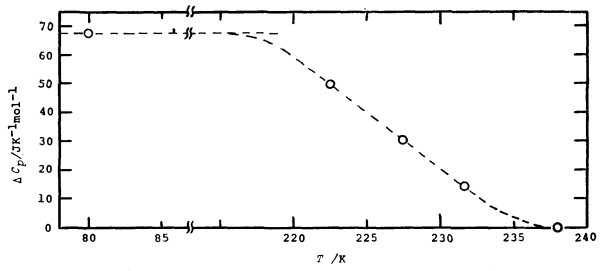

Fig. 10. The dependence of the peak heights of heat capacity on pre-cooling temperatures in $K_4Fe(CN)_6 \cdot 3D_2O$.

case of the deuterate the heat capacity peaks for the samples pretreated under different pre-cooling conditions appear at *the same temperature* 250 K, at which the pure monoclinic-monoclinic phase transition takes place. This indicates that the original tetragonal and the partially grown monoclinic phases coexist independently so that the peak height of the heat capacity has a linear relation to the ratio of amounts of the monoclinic to the tetragonal phases. The relation between the peak height and the precooled temperature is given in Fig. 10. This peculiar behavior suggests that the metastability of the tetragonal phase is due not to the absence of the nucleation by which the tetragonal phase is transformed into the complete monoclinic phase, but to the nature of the transformation: *viz.* in spite of enough macroscopic amount of stable monoclinic phase, the transformation in this crystal stops at any intermediate stage. This was evidenced by cessation of spontaneous heat evolution and also by the reproducibility of heat capacity data as long as the sample was not cooled below the lowest temperature to which the specimen had been brought. This new type of phase transformation with the characteristics of the Martensitic one[20] rarely observed in non-metals might occur from the following viewpoint based on the free energy difference between the monoclinic and tetragonal phases. The transformation does not seem to occur until the driving force attains a characteristic threshold value as in the case of Martensitic transition. This driving force will be given by the free energy difference between the two phases. On the other hand, the threshold value may arise from the sum of the interface and/or strain free energies, *etc.* associated with the creation of *twinned* monoclinic phase and it becomes larger with the increased amount of this monoclinic phase. As long as there is no reversible transformation in the tetragonal phase, the free energy diagram is such as depicted schematically in Fig. 11 for the deuterate, where the dotted area stands for the transformation region experimentally confirmed. The free energy difference at room temperature is imagined to be fairly small from similarity in structure as well as in thermal motion between the two modifications. This difference will increase with a fall in temperature through the reversible ferroelectric transition, since the heat capacity is larger for the monoclinic form than that for the tetragonal. The actual transformation will be initiated when the threshold value is reached with

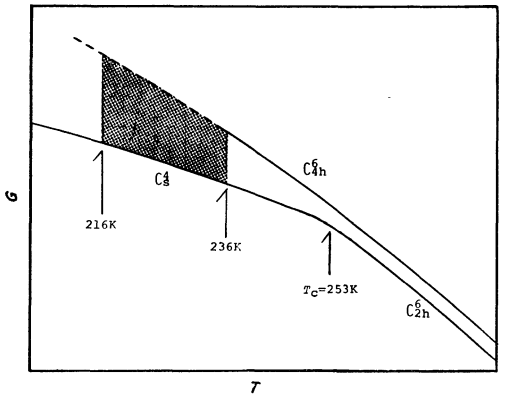

Fig. 11. Schematical free energy diagram of $K_4Fe(CN)_6 \cdot 3D_2O$. The upper curve, C^6_{4h}, corresponds to the tetragonal modification. The portion, C^6_{2h}, of the lower curve stands for the paraelectric monoclinic phase, and the portion, C^4_s, for the ferroelectric monoclinic phase. Dotted area is of the irreversible transition region to the monoclinic form.

decreasing temperature. If production of the *twinned* monoclinic phase were to lead to an increase of the threshold value preventing further transformation, the process would be stopped at the intermediate stage which is constrained by the balance between the temperature dependent-free-energy difference of two phases and the threshold value determined by the amount of the coexisting monoclinic phase. This view will also explain why the difference between the Curie temperature and the irreversible transition temperature is almost the same for the hydrate and deuterate, since the anomalous heat capacities behave analogously for these two compounds.

The created monoclinic crystal in the tetragonal phase has a *twinned* structure. In parallel with this it is interesting that the Martensitic materials are often composed of an assembly of thin plates.

According to the report of Krasnikova *et al.* in which irreversible transition was studied through the measurement of double refraction, the irreversible transition temperature becomes higher with the increase in the monoclinic fraction of a macroscopic sample. Our results indicate the opposite tendency as regards the transition point. This apparent contradiction will necessitate further elucidation of the intrinsic properties or textures of starting materials they used.

The Rate of Phase Transformation: A spontaneous temperature rise accompanied with irreversible transformation was observed immediately after rapid precooling. This phenomenon was carefully followed at five different temperatures in the transition region for the deuterate, an example being in Fig. 12. The procedure taken for every measurement of the spontaneous temperature rise was always the same. After the calorimeter was first cooled to a temperature 2 K above that at which the measurement was started, adiabatic conditions were established, and then the calorimeter was cooled again by introducing the exchange gas into the cryostat. When the desired temperature was reached, the cryostat was evacuated and the adiabatic control system was started to function. This round-about pro-

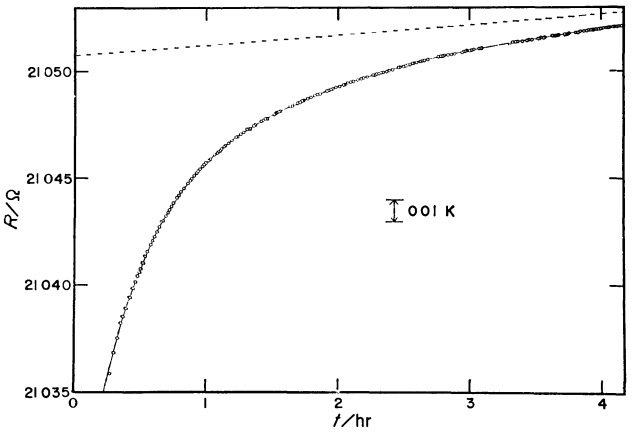

Fig. 12. A spontaneous heat evolution after rapid pre-cooling.

cedure was designed to realize as similar a cooling rate and temperature distribution in the cryostat as possible for each measurement. A control run performed after the entire specimen was transformed into the monoclinic form showed that the heat leak effect was small enough to be neglected as compared with the observed temperature rise. The broken line in Fig. 12 shows the natural drift observed in the control run. We tried to fit the time dependence of temperature into an exponential law with single time constant τ, on the assumption that the molar enthalpies of the monoclinic and tetragonal phases and the heat capacity of the calorimeter cell containing the sample were constant during the course of measurement. The time constant was evaluated with an estimated error of 20%, the observed temperature rise being fitted to the following equation.

$$T(t) - T(\infty) = A \exp(-t/\tau), \qquad (5)$$

where T and t are temperature and time, respectively, and A is a numerical constant. Fig. 13 shows the temperature dependence of the time constant which corresponds to the half-life. The value of τ decreases with decreasing temperature, except at the lowest

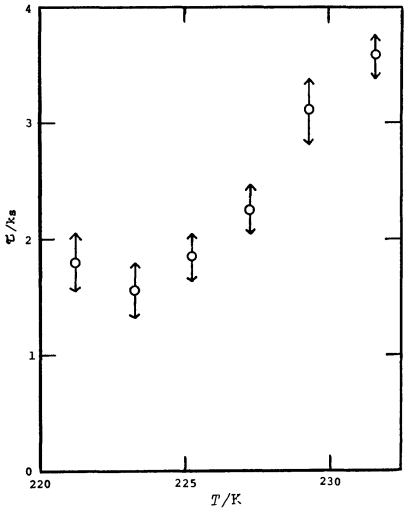

Fig. 13. Temperature dependence of time constant of spontaneous heat evolution in $K_4Fe(CN)_6 \cdot 3D_2O$.

temperature, in contrast to a thermal activation process. Explanation should be given taking into account the free energy difference between the tetragonal and monoclinic phases as the driving force of the transformation. The simplest expression will be

$$\frac{dX_m}{dt} = -B\{X_m(t)-X_m(\infty)\}\Delta G \qquad (6)$$

where X_m, B and ΔG stand for the molar fraction of the monoclinic phase, some positive constant dependent on temperature, and the free energy difference between the two phases, respectively. The time constant in Eq. (5) is identified with $1/(B\Delta G)$. As ΔG increases with decreasing temperature (Fig. 11), the initial decrease of τ on cooling can be attributed to the increase in the driving force of the transformation. The increase in the time constant by further decreasing temperature can be ascribed to the temperature factor through constant B.

Conclusion

Thermal properties we obtained give important information on the stability and phase transitions of $K_4Fe(CN)_6 \cdot 3H_2O$ and its deuterate. The amount of entropy change at the ferroelectric transition between two stable monoclinic phases strongly suggests the molecular mechanism of an order-disorder type. Behavior of heat capacity and molar volume changes at the transition point indicates that this phase change is very close to the second-order type, the Ehrenfest relation for the second-order phase transitions being found to hold. This is a rare example of the second-order transition tested by Ehrenfest's relation.

The metastable tetragonal crystals underwent an irreversible transition to the stable monoclinic phase. The transition was found to be a new type with some characteristics of the Martensitic transition which is rarely found in non-metallic compounds.

We wish to thank Professors Ryoichi Kiriyama and Hideko Kiriyama for fruitful discussions. We are grateful to Mr. Mitsuo Ôhama for the measurements of Raman spectra.

References

1) V. A. Pospelov and G. S. Zhdanov, *Zh. Fiz. Khim. SSSR*, **21**, 405, 521, 879 (1947).
2) S. Waku, K. Masuno, T. Tanaka, and H. Iwasaki, *J. Phys. Soc. Japan*, **15**, 1185 (1960).
3) H. Toyoda, N. Niizeki, and S. Waku, *J. Phys. Soc. Japan*, **15**, 1831 (1960).
4) R. Kiriyama, H. Kiriyama, T. Wada, N. Niizeki, and H. Hirabayashi, *ibid.*, **19**, 540 (1964).
5) R. Blinc, M. Brenman, and J. S. Waugh, *J. Chem. Phys.*, **35**, 1770 (1961).
6) T. Tsang and D. E. O'Reilly, *ibid.*, **43**, 4234 (1955).
7) S. P. Habuda, A. G. Lundin, and E. P. Zeer, *Ferroelectrics*, **1**, 71 (1970).
8) J. C. Taylor, M. H. Mueller, and R. H. Hitterman, *Acta Crystallogr*, **A26**, 559 (1970).
9) A. Ya. Krasnikova, V. A. Koptsik, B. A. Strukov, and Wang Ming, *Sov. Phys. Solid State*, **9**, 85 (1967).
10) S. Waku, H. Hirabayashi, H. Iwasaki, and R. Kiriyama, *J. Phys. Soc. Japan*, **14**, 973 (1959).
11) S. Waku, K. Masuno, and Y. Tanaka, *ibid.*, **15**, 1698 (1959).
12) Y. Hazony, D. E. Earls, and I. Lefkowitz, *Phys. Rev.*, **166**, 507 (1968).
13) P. A. Montano, H. Shecter, and U. Shimony, *ibid.*, **B3**, 858 (1971).
14) A. Ya. Krasnikova and I. N. Polandov, *Sov. Phys. Solid State*, **11**, 1421 (1970).
15) T. Nakagawa, S. Sawada, T. Kawakubo, and S. Nomura, *J. Phys. Soc. Japan*, **18**, 1227 (1963).
16) T. Matsuo, M. Oguni, H. Suga, and S. Seki, *Proc. Japan Acad.*, **48**, 237 (1972).
17) I. R. Malcolm, L. A. K. Staveley, and R. D. Worswick, *Trans. Faraday Soc.*, **A69**, 1532 (1973).
18) H. Suga, H. Chihara, and S. Seki, *Nippon Kagaku Zasshi* **82**, 24 (1961).
19) H. Suga and S. Seki, This Bulletin, **38**, 1000 (1965).
20) L. Kaufman and M. Cohen, *Prog. Met. Phys.*, *Pergamon Press*, **7**, 165.

Nuclear Quadrupole Resonances of Tellurium Tetrachloride and Tellurium Tetrabromide

Tsutomu OKUDA, Koji YAMADA, Yoshihiro FURUKAWA, and Hisao NEGITA
Department of Chemistry, Faculty of Science, Hiroshima University, Hiroshima 730

(Received June 3, 1974)

The nuclear quadrupole resonances (NQR) due to ^{35}Cl and ^{81}Br in $TeCl_4$ and $TeBr_4$ have been observed and their Zeeman effects have been examined. Each spectrum consists of six resonance lines with equal intensities, which are assigned to the two species of $TeCl_3^+$ ions or $TeBr_3^+$ ions. The asymmetry parameter of the electric-field gradient is, at most, 5% in each case. The relative orientation among the zero-splitting patterns of six resonance lines is consistent with the crystal structure of $TeCl_4$, which consists of the tetramers of $(TeCl_3^+Cl^-)_4$, as was recently determined by X-ray diffraction analysis. The zero-splitting patterns of the $TeBr_4$ crystal are so similar to those of $TeCl_4$ that the former crystal seems likely to consist of tetramers of $(TeBr_3^+Br^-)_4$ as well. The average $\angle$X-Te-X bond angles in TeX_3^+ ions were found to be 95.9° for the chloride and 96.7° for the bromide. The values for the chloride are in good agreement with those obtained by the X-ray analysis. On the other hand, the bond character of the TeX_3^+ ions in TeX_4AlX_3 (X=Cl, Br) was compared with that of TeX_4 from NQR.

It has been described that the molecular shape of $TeCl_4$[1] in the gaseous state is a trigonal bipyramid with lone-pair electrons on one of its equatorial orbitals. From the nuclear quadrupole resonance study,[2] the molecular shape in the solid state has been presumed to be a trigonal bipyramid, as in the gaseous state, though six resonance lines were observed at the temperature of liquid nitrogen.

On the other hand, the structural study of solid TeX_4 (X=Cl, Br) by means of infrared spectroscopy[3-6] has suggested that the crystal consists essentially of the ionic structure $TeX_3^+X^-$ because of the existence of four infrared-active vibrations similar to those of $SbCl_3$ and $SbBr_3$.

Recently, from a three dimensional X-ray analysis of $TeCl_4$[7] it has been concluded that this compound crystallizes in the space group C2/c of the monoclinic system with $a=17.076$ Å, $b=10.404$ Å, $c=15.252$ Å, and $\beta=116.28$ °. As is show in Fig. 1, the crystal consists of tetramers formed with an arrangement of alternate $TeCl_3^+$ and Cl^- ions at the apexes of the distorted cube. The unit cell contains four tetramers, all of which are equivalent and have two-fold axes. Every Te atom has three terminal Cl atoms and three bridging Cl atoms at average distances of 2.31 Å and 2.93 Å respectively. The X-ray diffraction studies of $SeCl_4$ and $TeBr_4$[8,9] have shown that these compounds are isomorphous with $TeCl_4$.

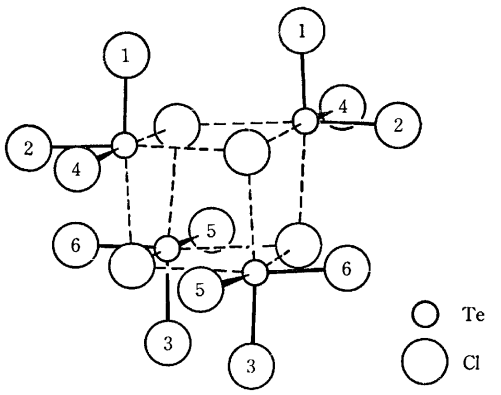

Fig. 1. Te_4Cl_{16} molecular unit in the $TeCl_4$ crystal. The number in the circle represents the order of the resonance lines from the lowest. The two-fold crystallographic axis passes vertically.

In the present experiment, the NQR spectra of $TeCl_4$ and $TeBr_4$ were observed in the temperature range from 77 K to 339 K, and the Zeeman effects on the spectra of the single crystals were examined at room temperature in order to clarify the bond character and molecular shape in the crystals. Furthermore, the bond characters were compared with those of TeX_3^+ ions in the TeX_4AlX_3 crystal.

Experimental

The single crystals of $TeCl_4$ and $TeBr_4$ were grown by the Bridgman-Stockbarger method. The NQR spectrometer used in this experiment was a super-regenerative oscillator with frequency modulation, and the absorption lines were observed on an oscilloscope. An LC-type super-regenerative oscillator was made to seach for the resonance lines of bromine isotopes in the region about 200 MHz. This oscillator was used only at room temperature and was put in the magnetic field for the study of the Zeeman effect. The resonance frequencies of the ^{81}Br nuclei were observed by the use of a super-regenerative oscillator consisting of Lecher-lines at various temperatures. The resonance frequencies were determined with a VHF signal generator and frequency counter of the Takeda Riken Co., TR-5578.

The Zeeman effect was examined by means of the zero-splitting cone method.[10] The orientation of the magnetic field for the zero-splitting was determined by means of polar coordinates (Φ, Θ), where Φ and Θ were the azimuthal and polar angles respectively, in the coordinate fixed to the sample. About forty experimental points were observed for each zero-splitting pattern. From these values, the best quadratic cone was obtained by the use of the least squares method, then the center of each zero-splitting pattern and the value of η were determined precisely.

Results and Discussion

The resonance frequencies of $TeCl_4$ and $TeBr_4$ are listed in Table 1. Powder samples of both $TeCl_4$ and $TeBr_4$ give rise to six resonance lines with equal intensities, although the ν_2' and ν_3' lines of $TeBr_4$ coincide at the temperature of liquid nitrogen. All the reso-

Table 1. ^{35}Cl and ^{81}Br NQR frequencies in TeX_4 (X=Cl, Br)

Compounds		Resonance frequencies (MHz) 26 °C	−196 °C
$TeCl_4$	ν_1	26.782	27.304
	ν_2	26.947	27.370
	ν_3	27.024	27.471
	ν_4	27.471	27.926
	ν_5	27.685	28.110
	ν_6	27.968	28.461
$TeBr_4$	ν_1'	185.18	188.13
	ν_2'	187.68	190.42
	ν_3'	187.81	190.42
	ν_4'	190.91	193.56
	ν_5'	195.36	197.88
	ν_6'	197.34	200.06

nance frequencies decrease continuously with an increase in the temperature, and the temperature coefficients are nearly equal in each compound. This must result from the fact that the crystal consists of tetramers which have an approximately Td symmetry and that the terminal halogens therefore undergo nearly equal thermal vibrations.

The zero-splitting patterns of $TeCl_4$ are shown in Fig. 2, where Cl_1, Cl_2,$\cdots$, Cl_6 indicate the direction of the z-axes of the field gradients at the chlorine atoms showing ν_1, ν_2,$\cdots$, ν_6 resonance lines respectively. Two zero-splitting patterns were observed for each resonance line, and a two-fold axis was determined, as is shown in Fig. 2. The two zero-splitting patterns of all the resonance lines except ν_2 were well separated from one another. However, the ν_2 line gave partly overlapping zero-splitting patterns. Therefore, the evaluation of the asymmetry parameter for this line was less accurate. As the asymmetry parameters of field gradients are small, it can be assumed that the z-axis coincides with the bond direction. Therefore, the assignment of the z-axes to chlorine atoms in the tetramer is based on the two-fold symmetry axis determined from Zeeman experiments and on the various angles determined from X-ray analysis. In

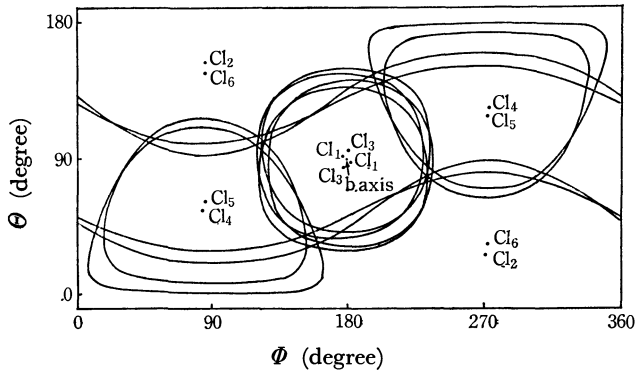

Fig. 2. Zero-splitting patterns of Zeeman lines of $TeCl_4$. The axis of $\Theta=0$ is taken as the rotation axis of the sample tube. The plane of $\Phi=0$ is arbitrarily chosen.

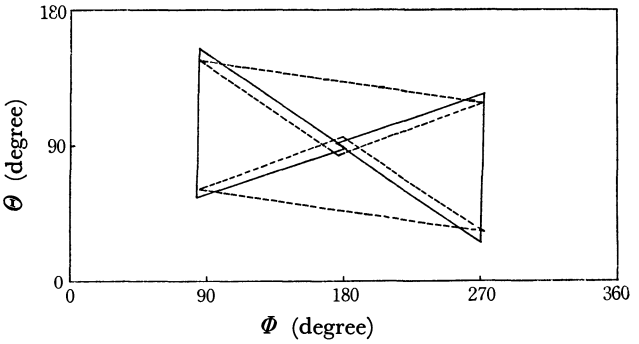

Fig. 3. Principal z-axes and its relationship in $TeCl_4$ crystal.

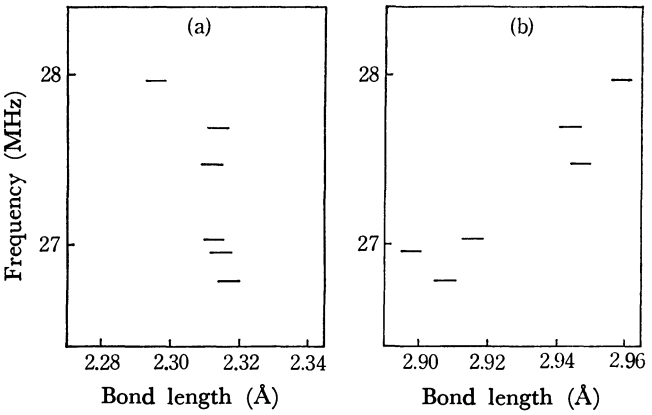

Fig. 4. The relationship between resonance frequencies and bond length in $TeCl_4$. a) resonance frequencies are plotted against their terminal bond length, b) resonance frequencies are plotted against the bond length of the bridging bond being located at the *trans* position to the terminal Cl atoms.

Fig. 3, the principal z-axes which are considered to arise from the same $TeCl_3^+$ ions are connected with solid or broken lines; triangles are thus formed. The triangles represented by solid or broken lines correspond to nonequivalent $TeCl_3^+$ ions in the crystal. Figure 3 supports the existence of the tetramers of $(TeCl_3^+Cl^-)_4$ for the $TeCl_4$ crystal, although these results are derived on the basis of the crystal structure from the X-ray analysis. The numbers in the circles in Fig. 1 show the chlorine species determined by the present experiment. In Fig. 4, the resonance frequencies of the terminal Cl atoms are plotted against the terminal bond length and the bond length of the bridging bonds which are located at the *trans* position to the terminal Cl atoms. This figure shows that each resonance frequency is affected by the bridging Cl atom which is located at the *trans* position to the terminal Cl atom. Therefore, the large spread in the resonance frequencies may be considered mainly due to the difference in the strength of the bonds between the bridging Cl atom and the Te atom.

The zero-splitting patterns of $TeBr_4$ are quite similar to those of $TeCl_4$. From the similarity of the zero-splitting patterns of $TeBr_4$ to those of $TeCl_4$, and from the fact that they are isomorphous with each other,[8,9] it is evident that the former crystal consists of tetramers of $(TeBr_3^+Br^-)_4$. It may be considered on the basis

Table 2. The bond angles $\angle XTeX$ in TeX_3^+ ions (X=Cl, Br)

Compounds		$\angle X_1Te_1X_2$	$\angle X_2Te_1X_4$	$\angle X_1Te_1Y_4$	$\angle X_3Te_2X_5$	$\angle X_5Te_2X_6$	$\angle X_6Te_2X_3$
$TeCl_4$	NQR	94.4°	98.2°	95.1°	96.2°	95.5°	96.3°
	X-ray	93.7°	95.7°	94.2°	94.9°	95.0°	95.1°
$TeBr_4$	NQR	94.6°	98.5°	95.6°	97.4°	96.8°	97.5°

Table 3. ^{35}Cl and ^{81}Br NQR parameters in TeX_4 (X=Cl, Br) (26 °C)

Compounds	η(%)	e^2Qq/h(MHz)	U_p	i(%)
$TeCl_4$	2.4±0.2	53.559	48.8	42.6
	up to 5.0	53.867	49.1	42.2
	3.0±0.2	54.040	49.2	42.1
	2.8±1.0	54.932	50.1	41.1
	1.9±0.2	55.362	50.4	40.7
	2.5±0.5	55.926	51.0	40.0
$TeBr_4$	4.5±0.3	370.22	57.6	32.2
	up to 5.0	375.34	58.4	31.3
	4.4±0.2	375.50	58.4	31.3
	3.6±0.3	381.74	59.4	30.1
	1.5±0.5	390.71	60.8	28 3
	2.7±0.2	394.63	61.4	27.8

of the orientation of the z-axes that this tetramer has a two-fold axis and contains two nonequivalent $TeBr_3^+$ ions. As the NQR spectra and their Zeeman patterns in $TeBr_4$ are similar to those in $TeCl_4$, one $TeBr_3^+$ ions contributes to the ν_1', ν_2', and ν_4' lines, and the other, to the ν_3', ν_5', and ν_6' lines. Table 2 shows the bond angles of the TeX_3^+ ions obtained from NQR, together with those obtained by X-ray analysis. The former values are slightly larger than the latter.

In the $TeCl_4$ crystal, π-bond character of the terminal Te-Cl bond may be neglected for three reasons: a) the terminal Te-Cl bond length is nearly equal to the corrected sum of the single covalent bond radii of 2.34 Å,[11] b) the resonance frequencies show negative temperature coefficients, and c) the asymmetry parameters are small. Table 3 lists the asymmetry parameter of the electric-field gradient (η), the quadrupole coupling constant (e^2Qq), the number of unbalanced p electrons (U_p), and ionic character (i) for the Te-X bond. These parameters are related by the following equations:

$$h\nu = (e^2Qq_{obs}/2)(1+\eta^2/3)^{1/2}, \quad (1)$$

$$U_p = e^2Qq_{obs}/e^2Qq_{atom} = (1-s)(1-i), \quad (2)$$

where e^2Qq_{obs}/h is the observed quadrupole coupling constant and e^2Qq_{atom}/h is 109.74 MHz for ^{35}Cl and 643.03 MHz for ^{81}Br.[12] s is the s-electron character in the bonding orbital of the halogen, which is assumed to be 0.15.[13] The ionic character of the terminal Te-X bond in $TeBr_4$ is smaller than that of $TeCl_4$, as is shown in Table 2. The same tendency is seen between chloride and bromide, which have the same structure, and may be attributed to the differences in the electronegativities of the relevant halogen atoms.

As is obvious from the crystal structure, $TeCl_4$ acts as a Cl^- donor and forms a compound with the Cl^- acceptor. An example is $TeCl_4AlCl_3$,[14] the crystal structure of which has recently been determined to be as is shown in Fig. 5. The $TeCl_3^+$ ion has a shape similar to that in $TeCl_4$, but the Te–Cl bonds in $TeCl_4$-$AlCl_3$ are shorter than those in $TeCl_4$. Table 4 shows the NQR parameters of $TeCl_4AlCl_3$ and $TeBr_4AlBr_3$. The resonance frequencies are assigned to those of halogens in TeX_3^+ ions, because those in AlX_4^- ions are expected to be much lower. The quadrupole coupling constants in the TeX_4AlX_3 crystal are larger than those in $TeCl_4$ and $TeBr_4$ by about 9.3% and 10.0% respectively. According to the X-ray analysis of the crystals of $TeCl_4AlCl_3$,[14] $TeCl_4$,[7] and $(NH_4)_2$-$TeCl_6$[15,16] all the tellurium atoms are octahedrally coordinated by six chlorine atoms. Although the $TeCl_6^{2-}$ ion in $(NH_4)_2TeCl_6$ is a regular octahedron, the $TeCl_3^+$ ion in $TeCl_4AlCl_3$ forms a distorted octahedron, as is shown in Fig. 5. There is a linear relationship between the quadrupole coupling constants and the bond lengths of the terminal Te–Cl bonds. From this relationship, it is obvious that the bond character of Te–Cl in the $TeCl_4$ crystal is intermediate

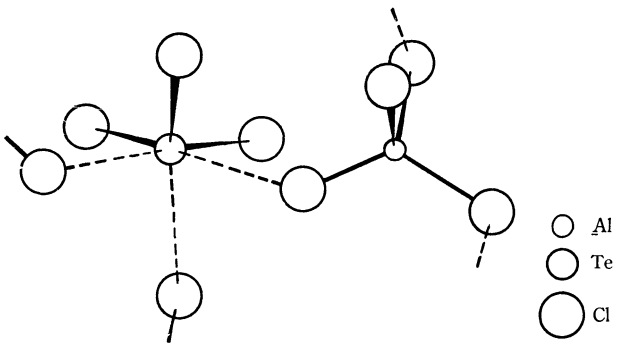

Fig. 5. The crystal structure of $TeCl_4AlCl_3$.

Table 4. NQR parameters of TeX_3^+ ions in TeX_4AlX_3 (X=Cl, Br) (25 °C)

Compounds	ν(MHz)	e^2Qq/h(MHz)[a]	Up(%)
$TeCl_4AlCl_3$	29.420	58.840	53.6
	29.574	59.149	53.9
	30.570	61.140	55.7
$TeBr_4AlBr_3$	207.33	414.66	64.5
	207.67	414.34	64.6
	208.12	416.24	64.7
	208.90	417.80	65.0
	212.45	424.90	66.1
	214.37	428.74	66.7

a) η is assumed to be zero, referring to the recent X-ray analysis.

between $TeCl_4AlCl_3$ and $(NH_4)_2TeCl_6$. The same tendency is seen in the bromine compounds.

References

1) D. P. Stevenson and V. Schomaker, *J. Amer. Chem. Soc.*, **62**, 1267 (1940).
2) A. Schmitt and W. Zeil, *Z. Naturforsch., A*, **18**, 428 (1963).
3) N. N. Greenwood, B. P. Straughan, and A. E. Wilson, *J. Chem. Soc., A*, **1966**, 1479.
4) J. W. George, N. Katsaros, and K. J. Wynne, *Inorg. Chem.*, **6**, 903 (1967).
5) I. R. Beattie and H. Chudzynska, *J. Chem. Soc., A*, **1967**, 984.
6) I. Lindqvist and A. Niggli, *J. Inorg. Nucl. Chem.*, **2**, 345 (1956).
7) B. Buss and B. Krebs, *Inorg. Chem.*, **10**, 2795 (1971).
8) C. B. Shoemaker and S. C. Abrahams, *Acta Crystallogr.*, **18**, 296 (1965).
9) A. W. Cordes, R. F. Kruh, E. K. Gordon, and M. K. Kemp, *ibid.*, **17**, 756 (1964).
10) T. P. Das and E. L. Hahn, "Nuclear Quadrupole Resonance Spectroscopy," Solid State Physics, Supple. 1, Academic Press, New York (1957).
11) L. Pauling, "The Nature of the Chemical Bond," 3rd Ed., Cornell University Press, Ithaca, New York (1960).
12) V. Jaccarino and J. G. King, *Phys. Rev.*, **83**, 471 (1951); V. Jaccarino and J. G. King, *ibid.*, **94**, 1610 (1954).
13) C. H. Townes and B. P. Dailey, *J. Chem. Phys.*, **17**, 782 (1949).
14) B. Krebs, B. Buss and D. Altena, *Z. Anorg. Allg. Chem.*, **386**, 257 (1971).
15) D. Nakamura, K. Ito, and M. Kubo, *J. Amer. Chem. Soc.*, **84**, 163 (1962).
16) A. C. Hazell, *Acta Chem. Scand.*, **20**, 165 (1966).

A Torsional Braid Analysis of Polymethacrylates, Polyacrylate, Poly(vinyl alcohol), and Their Related Polymers during the Thermal Degradation

Noboru FURUSHO, Tsuyoshi KOMATSU, and Tsurutaro NAKAGAWA

Department of Polymer Science, Faculty of Science, Hokkaido University, Sapporo 060

(Received June 15, 1974)

The torsional braid analysis (TBA), thermogravimetry, and IR spectroscopy of polymethacrylates, polyacrylate, poly(vinyl alcohol), and their related polymers were carried out in air. The chemorheological properties of these polymers are markedly dependent on their chemical structures. First, the α-hydrogen atom plays an important role. In poly(methyl acrylate), the chemorheological behavior is similar to that of the polymers which have tendency to crosslink, whereas poly(methyl methacrylate) does not show any such behavior. A similar situation was found when comparing poly(acrylic acid) with poly(methacrylic acid). At the same time, the influence of the functional groups was examined. Second, the change in the mechanical properties due to crosslinking becomes more noticeable with an increase in the side-chain length of the methacrylate polymers. Furthermore, in addition to procedures used in the previous work, a new method of kinetic analysis of the heating-rate dependence was carried out in the case of poly(acrylic acid). The apparent activation energies estimated by this treatment are in good agreement with those estimated by other procedures.

Studies of the thermal degradation of polymers have been carried out by various methods—for example, pyrolysis gas chromatography, and thermogravimetry. Among those studies, relatively few studies have been done on the basis of the measurements of mechanical properties. Previously, we have reported some results of a thermal-degradation study of polymers by the measurement of their dynamic mechanical properties using the TBA method.[1,3] We found some interesting features not observable by other methods and proposed to use this method as a convenient tool for kinetic studies.

In the present paper, we wish to report some results of the TBA of polymethacrylates, polyacrylate, poly (vinyl alcohol) and their related polymers. Moreover, with the aid of the results of the thermogravimetry and IR spectroscopy, we will discuss the correlation between the chemorheological behavior and the chemical processes.

The purpose of this work is to elucidate the effects of the α-hydrogen atom, the side-chain length of the alkyl methacrylate polymers, and the character of the functional group on the chemorheological properties during the thermal degradation. We also intended to examine the applicability of the kinetic treatment usually used in thermogravimetry to the TBA studies.

Experimental

The poly(methyl acrylate)(PMA), poly(methyl methacrylate)(PMMA), poly(vinyl alcohol)(PVA), poly(acrylamide)(PAAm), poly(methyl vinyl ether)(PVME), and poly(vinyl acetate)(PVAc) were all commercial materials. The poly(acrylic acid)(PAA), poly(methacrylic acid)(PMAA), poly(ethyl methacrylate)(PEMA), poly(butyl methacrylate)(PBMA), poly(hexyl methacrylate)(PHMA), and poly(2-ethyl hexyl methacrylate)(PEHMA) were synthesized in the ordinary way.

The procedures of the torsional braid analysis(TBA) have been described in a previous paper.[1] The relative shear modulus ($G_r=(P_0/P)^2$) is calculated from the periods of oscillations, P, where the values of P_0 are the period of oscillation 10 min after the setting of the specimen under isothermal conditions or that at room temperature under the conditions of a constant heating rate (and where the values of P are the period at the time t or that at the temperature T). The logarithmic decrement ($\lambda=(1/n)\ln(A_{2n+1}/A_1)$) is calculated from the amplitudes of the damped oscillations, where n is the number of oscillations and where A_1 and A_{2n+1} are the amplitudes of the first and nth oscillations. The studies of the heating-rate dependence of the mechanical properties were carried out using an automatic TBA apparatus made by Takahashi *et al.*[2]

The IR measurements and the thermogravimetry(TG) were carried out in the same way as in a previous work.[3]

Results and Discussion

Chemorheological Behavior and Its Relation to the Chemical Process. The mechanical properties of these polymers are shown in the following figures. Each curve consists of several regions. The lower-temperature regions correspond to the physical process (glass transition, fusion, *etc.*). Their details will not be discussed here.

PMA and PMMA: In order to clarify the effect of the α-hydrogen atom on the chemorheological behavior, TBA measurements of PMA and PMMA, which both have ester groups and which differ each other in the point of whether the α-hydrogen atom exists or not, were carried out. As is shown in Fig. 1, the chemorheological properties of PMA and PMAA are very different from each other. In PMA, the gradual increase in G_r, its abrupt increase and the corresponding maximum of λ are observed above 150 °C. This situation resembles that in systems in which crosslinking occurs.[4]. However, for PMMA, no significant change is observed other than the glass transition at about 120 °C and the fusion at about 240 °C, in spite of the occurrence of a considerable weight loss above 200 °C; this weight loss is the result of the depolymerization. This mechanical behavior will be discussed below.

The IR spectra of these two heat-treated polymers remained essentially unchanged. The TG curve (Fig. 2) and the TBA curve (Fig. 1) show that, in PMA, the increase in G_r above 150 °C is not accompanied by any weight loss and that the decrease in G_r near 400 °C is closely connected with the large weight loss. Those observations are quite different from those of

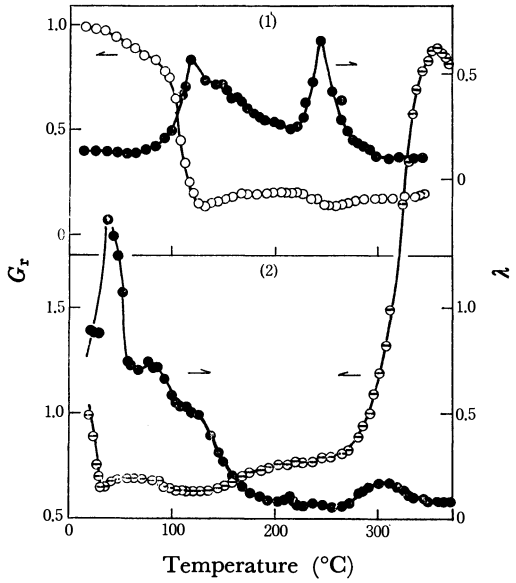

Fig. 1. G_r, λ *vs.* T plots of PMA and PMMA heated in air.
Heating rate: 1 °C/min. (1): PMMA, (2): PMA, G_r: ○⊖, λ: ●.

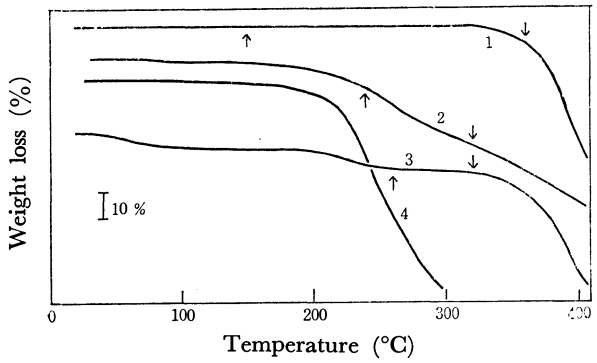

Fig. 2. TG curves of PMA, PMAA, PAA and PMMA in air.
Heating rate: 10 °C/min(1), 3 °C/min(2, 3 and 4). (1): PMA, (2): PAA, (3): PMAA, (4): PMMA. The arrows indicate the point at which G_r begins to increase (↑) and to decrease (↓).

the halogen-containing polymers, in which the chemorheological behavior is closely related to the weight loss resulting from the dehydrohalogenation.[3]

From the above discussion it may be concluded that, in PMA, the increase in G_r is attributable to the cross-linking caused by the α-hydrogen atom removal, while the decrease in G_r is due to the destruction of the network structure by the chain scission of the polymers, as is suggested by the large weight loss at higher temperatures. However, the nature of the slowing down of the rate of the increase in G_r just above 200 °C is not clear at present.

PAA and PMAA: From the study of PMA and PMMA, it has been made clear that the ester group does not affect the chemorheological behavior. Therefore, TBA measurements of PAA and PMAA were made. The PAA and PMAA are different from PMA and PMMA in only the point that PAA and PMAA have carboxyl groups instead of methyl ester groups.

In the cases of PAA and PMAA (Fig. 3), in contrast to the cases of their ester analogues, the chemorheological properties resemble each other. The IR spectra shown in Fig. 4 give important information on the mechanism of the mechanical change. In PAA, the peaks were observed at about 1050 and 1150 cm^{-1}, and a small shoulder, at about 1800 cm^{-1}. The former is probably due to the oxidative cross-linking, as has been suggested by Otani,[5] and the latter, to the formation of the anhydride structure.[6]

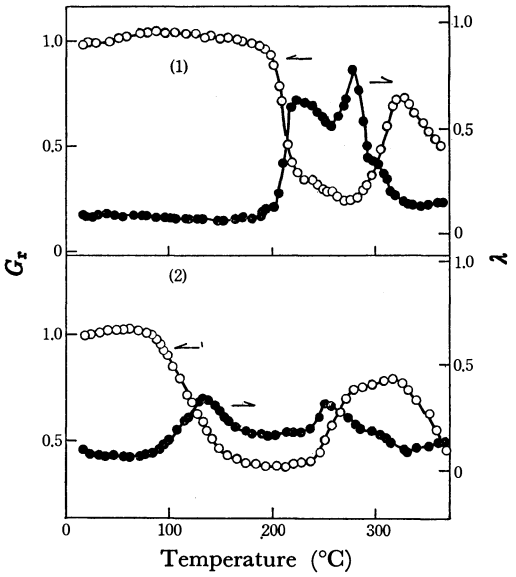

Fig. 3. G_r, λ *vs.* T plots of PMAA and PAA heated in air.
Heating rate: 1 °C/min. (1): PMAA, (2): PAA, G_r: ○, λ: ●.

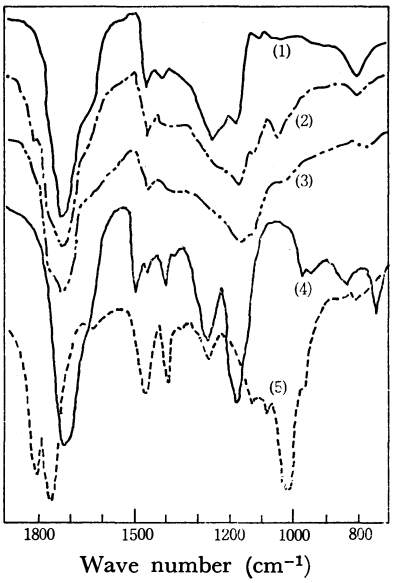

Fig. 4. IR spectra of PAA and PMAA heated in air.
(1): original PAA, (2): PAA heated at 210 °C for 165 min, (3): PAA heated at 246 °C for 70 min, (4): original PMAA, (5): PMAA heated at 246 °C for 40 min.

On the other hand, the formation of the anhydride structure is slight. In PMAA, on the other hand, very intense peaks were found at about 1760 and 1810 cm^{-1}, shifted from 1720 cm^{-1}; these peaks can be assigned to the vibrations of the carbonyl group in the acid anhydride and the acid form. This finding suggests the formation of a typical acid-anhydride structure. Grant and Grassie have pointed out that this occurs both intramolecularly and intermolecularly.[7] Moreover, quite different behavior was found in the change in mechanical properties due to the chemical process by means of isothermal TBA measurements of the two polymers, as will be discussed below.

These results indicate that, in PAA, the α-hydrogen atom, not the carboxyl group, is the principal factor in determining the chemorheological behavior in air. On the other hand, in PMAA, the formation of both intermolecular and intramolecular anhydride structures is the predominant factor. From the viewpoint of weight loss, in both PAA and PMAA the weight loss occurs with the chemorheological change; this weight loss is presumably related to the formation of the anhydride structure. This situation is different from that in the case of PMA, in which only the α-hydrogen atom plays an important role in the chemorheological behavior.

PVA, PVME, PVAc, and PAAm: From a comparison of the results on PMA and PAA, it can be expected that the chemorheological properties of the polymers with the α-hydrogen atom will be greatly influenced by the functional group in the side chain. Therefore, TBA studies of PVA, PVME, PVAc and PAAm, which all have the α-hydrogen atom, just as PAA and PMA have, were carried out. The results for these polymers are shown in Figs. 5 and 6. It should be pointed out here that the increase in G_r at lower temperatures in PVME is due to the evaporation of

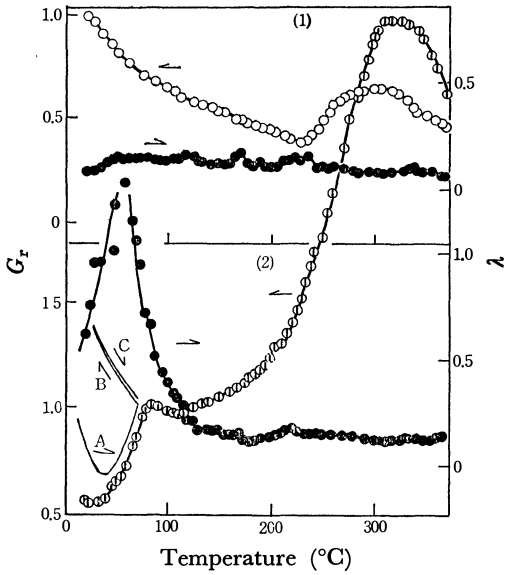

Fig. 5. G_r, λ *vs.* T plots of PVA and PVME heated in air.
The solid line shows the change in G_r of PVME during the repeated run (A-B-C). Heating rate: 1 °C/min. (1): PVA, (2): PVME, G_r: ○①, λ: ●.

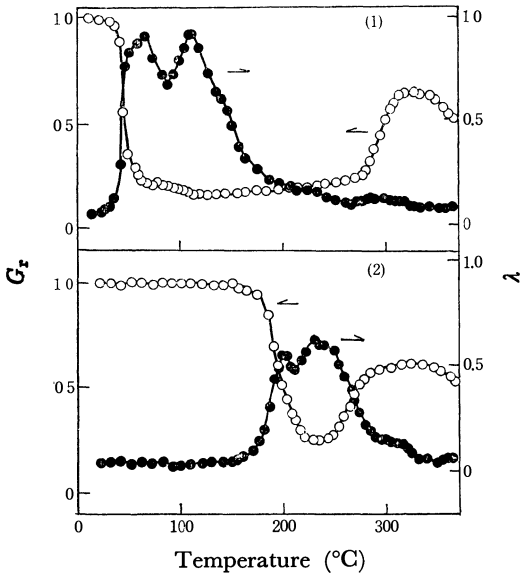

Fig. 6. G_r, λ *vs.* T plots of PVAc and PAAm heated in air.
Heating rate: 1 °C/min. (1): PVAc, (2): PAAm, G_r: ○, λ: ●.

the residual solvent used for the specimen preparation. The fact that an ordinary decrease in G_r is observed by heating it up to 100 °C supports this consideration (see Curves A—B—C in Fig. 5).

In these four polymers, as in PMA and PAA, a considerable increase in G_r is observed at higher temperatures. In the IR measurements and thermogravimetry, we found the formation of the carbon-carbon double bond and the imide group, and also a close relation between the increase in G_r and the weight loss. Moreover, in these polymers, it is known that such reactions as the dehydration in PVA,[8] the deacetylation in PVAc,[9] and the imidization in PAAm[10] occur at higher temperatures. Considering this, it may be concluded that the increase in G_r in these four polymers is closely connected to such reactions as dehydration, which involve the functional group in the side chain.

This situation resembles to some extent that in the halogen-containing polymers, in which the dehydrohalogenation is a dominant factor in their chemorheological properties. However, the findings that the IR absorptions of the double bond and of the imide group are not very intense and that the G_r increases without any weight loss from 120 to 180 °C in PVME suggest an undeniable role of α-hydrogen atom.

The order of the temperatures at which G_r begins to increase is; PVME<PVAc<PVA<PAAm. However, it is not clear that this order of temperatures corresponds to the order of the reactivities of the methoxyl, acetyl, hydroxyl, and amide groups because of the difference in the glass-transition temperatures and the undeniable effect of the α-hydrogen atom.

Polymethacrylates: The role of the α-hydrogen atom has been demonstrated in the above discussions. Furthermore, we compared poly(alkyl methacrylate)s, with a large number of hydrogen atoms in the side chain, with poly(methyl methacrylate), in which no

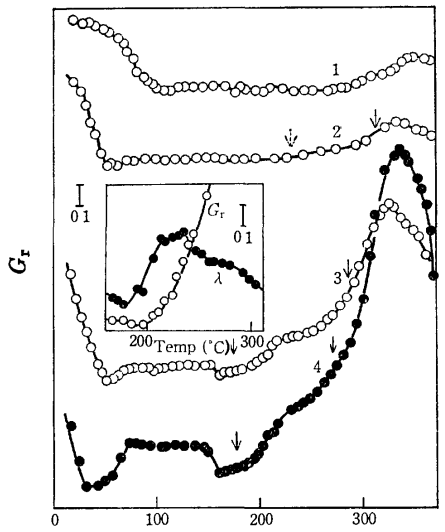

Fig. 7. G_r *vs.* T plots of the alkyl methacrylate polymers heated in air.
Inside figure: G_r, λ *vs.* T plots of polyethylene. Heating rate: 1 °C/min. (1): PEMA, (2): PBMA, (3): PEHMA, (4): PHMA. The arrows indicate the direction of the increase in G_r.

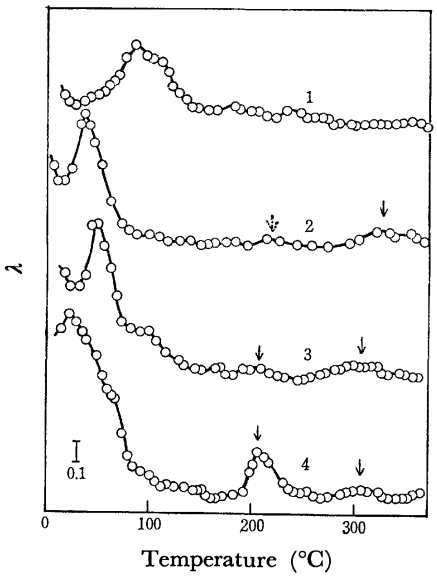

Fig. 8. λ *vs.* T plots of the alkyl methacrylate polymers heated in air. Heating rate: 1 °C/min. (1): PEMA, (2): PBMA, (3): PEHMA, (4): PHMA. The arrows indicate the maxima of λ which correspond to the increase in G_r.

significant mechanical change other than the glass transition and fusion is observed. In the alkyl methacrylate series, as is shown in Figs. 7 and 8,* the chemorheological properties approach those in polyethylene, which has a tendency to crosslink, with an increase in the alkyl side-chain length. The feature that λ shows a maximum corresponding to the increase in G_r becomes perceptible from PBMA. Considering the absence of the significant mechanical change due to the chemical process in PMMA, the resemblance between the TBA curves of polyethylene and polyalkyl methacrylates, and the results of other workers, which will be discussed later, this increase in G_r and the corresponding maximum of λ can be explained by assuming that the crosslinking occurs between the hydrocarbon parts of the side chains.** However, the details of the relation of the mechanical change to the chemical process and the nature of the fact that the change in λ in polyalkyl methacrylates is smaller than that in polyethylene are not clear at present.

Graham found that gelation occurs in poly(heptyl methacrylate) and higher alkyl methacrylate polymers, and not in the polymers with a branched alkyl side-chain including longer ones. He pointed out that the length of the alkyl side chain is important and that the crosslinking probably occurs between side chains, but that the apparent relationship between the glass transition temperature and the behavior on γ-irradiation *in vacuo* is absent.[11] Burlant *et al.* have also found a similar role of hydrocarbon parts in the side chain during the γ-irradiation of polyalkyl acrylates.[12] On the other hand, in their study by UV irradiation in air, Morimoto and Suzuki observed gelation in PBMA and crosslinking without gelation in poly(lauryl methacrylate); they concluded that the degree of the crosslinking, estimated from the distribution of the molecular weight, increases with the increase in the glass transition temperature.[13] The results in the present study agree partially with those of the above two investigations. That is, they agree with Graham's suggestion of the importance of the side chain length, on the one hand, and with Morimoto's finding of the crosslinking in PBMA and higher alkyl methacrylate polymers, on the other hand. A systematic investigation is a subject in the future.

Relation of the Shapes of TBA Curves to the Degradation Mechanism. From the above discussions, the relation of the chemorheological behavior to the chemical process and the effect of the difference in chemical structure on the mechanical properties have been elucidated. Here, turning to the viewpoint of the relation of the shapes of the TBA curves to the degradation mechanism, it is possible to classify the curves into several types.

The first type is found in the case of PMMA, in which no significant mechanical change due to the chemical process is observed. Considering the PMMA and poly(α-methyl styrene), which are known to depolymerize mostly to monomers, behave chemorheologically in the same way,[14] it may be suggested that the flatness in the TBA curve can be explained by assuming that the modulus of the unchanged glass braid was observed as a result of the formation of substances with a lower mechanical reactance and/or the evaporation of such substances from the braid.

* In these figures, the ordinates are arbitrarily shifted in order to avoid the overlapping of the curves.

** It should be pointed out here that the scission of the main chain and other reactions occur simultaneously with the crosslinking.

In the second type, G_r increases considerably at higher temperatures, but the change in λ is slight; especially the change in λ due to the chemical process in the isothermal measurements was negligibly small. The PVA, PVME, PVAc, PAAm, and PMAA belong to this type. Halogen-containing polymers, reported in the previous paper,[3] also belong to this type. In these polymers, reactions which involve the functional group in the side chain, such as dehydration, deacetylation, and dehydrohalogenation, are closely connected with the chemorheological behavior.

The third type is characterized by a maximum of λ which corresponds to the considerable increase in G_r on the curves of the temperature dependence and by one of λ found at the transition between the two stages of increase in G_r in the isothermal measurements (Fig. 10). The PMA, PAA, and other samples, which have a tendency to crosslink, belong to this type. Probably, higher alkyl methacrylate polymers can also be classified into this type. On the relation of the shapes of the TBA curves to the degradation mechanism, further extensive work is necessary.

Kinetic Studies. In the previous work,[3] a kinetic approach was carried out, in which the measurements of the relative shear modulus due to the chemical process under isothermal conditions and the superposition of G_r *vs.* time curves were tested. In addition to these procedures, two new approaches were undertaken in this study. One was the superposition of the λ *vs.* time curves, while the other was the application of the kinetic treatment used in such thermal analysis as thermogravimetry.

The curves of the changes in the mechanical properties due to the chemical process under isothermal conditions are classified into two categories in Figs. 9 and 10. No kinetic studies of the polyalkyl methacrylates were made. The PMAA, PVA, PVME,

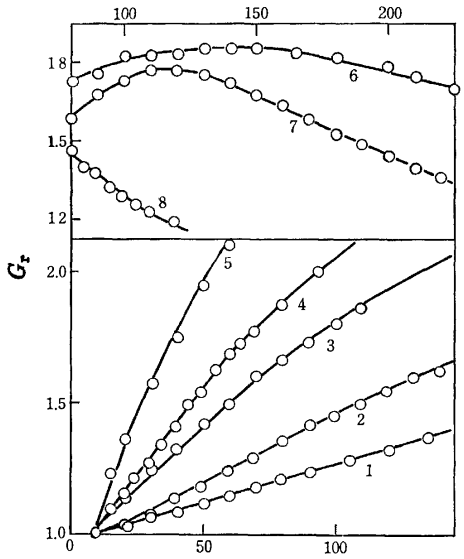

Fig. 9. G_r *vs.* t plots of PVME during degradation in air at various temperatures.
(1): 172 °C, (2): 196 °C, (3): 221 °C, (4): 246 °C, (5): 270 °C, (6): 343 °C, (7): 356 °C, (8): 370 °C.

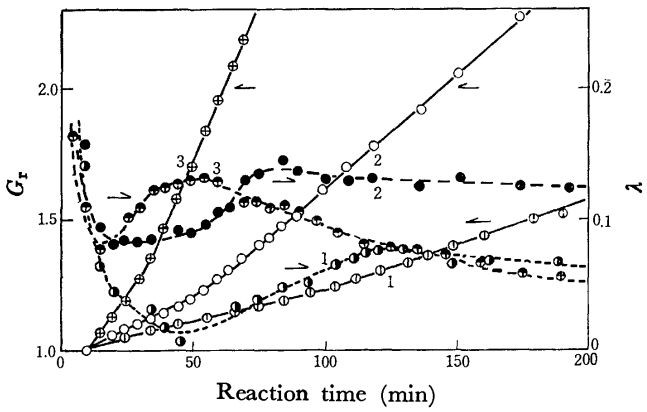

Fig. 10. G_r, λ *vs.* t plots of PMA during degradation in air at various temperatures.
(1): 246 °C, (2): 270 °C, (3): 294 °C. G_r: ⊕○⊕, λ: ◑●◒.

PVAc, and PAAm, in which the role of the functional group is important, as has been stated above, belong to the type shown in Fig. 9 (the case of PVME), where λ is omitted because of its slight change with the reaction time. On the other hand, the PMA and PAA belong to the other type, shown in Fig. 10 (PMA). A situation similar to that in the latter case, in which λ shows a maximum corresponding to the transition between the two stages of the increase in G_r, has been found in the samples in which crosslinking mainly occurs.[15] In all cases, the linearity of the curves was observed at the initial stage. As in a previous work,[3] the logarithms of the initial slopes and the time of the maximum, λ, were each plotted against the reciprocal temperature (K^{-1}). The apparent activation energies estimated from this analysis are listed in Table 1.

A typical superposed curve is shown in Fig. 11, where the relative shear moduli were plotted on the scale of $(1/P)^2$ instead of G_r ($(P_0/P)^2$), because P_0 varies considerably as a result of the progress of the reaction after the setting of the specimen at higher temperatures. The superposition procedure for the shear moduli was satisfactorily used except for the temperature region of about 200 °C in PAAm. Superposition was done in the following manner; first plot the values of $(1/P)^2$ and λ as a function of log t, and then shift their isothermal curves along with the axis of log t until they overlap the superposed curve. The quantities of the shift in relation to the reference curve are the shift factor, a. For the logarithmic decrements, only in the cases of PMA and PAA, which belong to the type shown in Fig. 10, was the superposition successful. In other polymers, the superposition was difficult because of the absence of any significant mark in the change in λ due to the chemical process in the isothermal curve. The apparent activation energies were estimated from the Arrhenius plot of the shift factor. Table 1 shows that the values obtained from the superpositions of λ's agree well with those from the moduli.

In PMAA, the activation energy estimated from the increase in G_r agrees well with that obtained by Grant

TABLE 1. THE APPARENT ACTIVATION ENERGIES ESTIMATED FROM THE VARIOUS PROCEDURES OF ANALYSIS

Sample	Temp. range (°C)	Mech.[a] process	The apparent activation energy (kJ/mol)[b] From intial slope[c] G_r *vs.* t	From intial slope[c] log G_r *vs.* t	shift factor $(1/P)^2$	shift factor λ	time of max. λ	log(h) *vs.* $(1/T_m)$
PMA	190—320	in.	92	90	77	64	67	
	290—360	de.	143	167	99	101		
PAA	170—270	in.	92	107	110	97	102	99[d]
	270—360	de.	119	135	78	69	—	126[e]
PMAA	250—320	in.	142	142	126			
	270—340	de.	97	134	126			
PVA	170—240	in.	92	105	105			
	240—340	de.	71	115	67			
PVME	170—270	in.	39	42	44			
	315—370	de.	172	260	96			
PVAc	190—280	in.	118	99	103			
	290—360	de.	109	146	70			
PAAm	210—270	in.	110	110	92			
	270—350	de.	64	69	59			

a) G_r increases or decreases. b) 1J=1/4.184 cal. c) Assuming $dG_r/dt=k_0$ and $d(\log G_r)/dt=k_{1st}$, where k_0 and k_{1st} are the apparent rate constants of the zero-order and first-order reactions, respectively. d), e) The ranges of T_m are 250—290 °C and 380—420 °C, respectively.

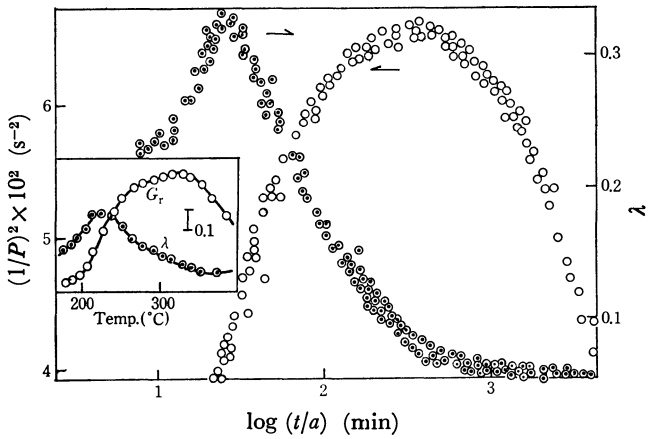

Fig. 11. Superposed curves for shear moduli, $(1/P)^2$, and λ of PAA. (T_0=246 °C) Inside figure: G_r, λ *vs.* T plots of PAA. G_r: ○, λ: ⊙.

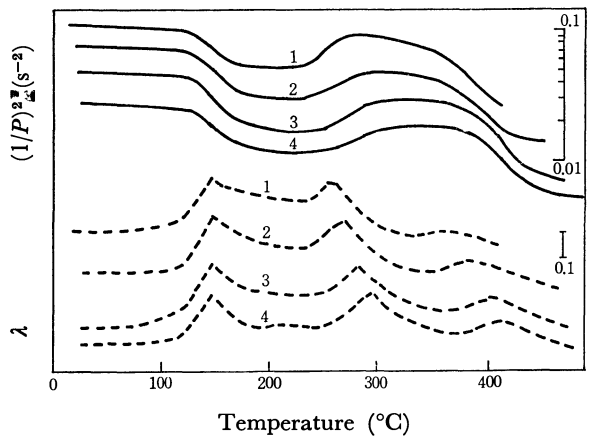

Fig. 12. The heating rate dependence of the chemorheological properties of PAA.
Heating rate, (1): 1.04 °C/min, (2): 2.04 °C/min, (3): 3.13 °C/min, (4): 4.24 °C/min. Solid line: relative shear moduli, dotted line: λ.

and Grassie, 37±3 kcal/mol (155±13 kJ/mol),[7] but the value in PVA is lower than that determined by Yamaguchi *et al.* by thermogravimetry, 35—55 kcal/mol (146—230 kJ/mol).[8] Popa *et al.* have pointed out that the apparent activation energies in PVA change greatly with the degree of conversion on the basis of the heating-rate dependence of the weight loss.[16] The values calculated by them become analogous to that estimated from the decrease in G_r as the conversion grows higher. Perhaps, this situation can be explained by considering that, at relatively lower conversions, in addition to the dehydration, the α-hydrogen atom affects the mechanical properties through crosslinking, which does not bring about any significant weight loss, whereas at higher conversions, the decrease in G_r is due to the chain scission, which leads to a weight loss.

The heating-rate dependence of the chemorheological behavior of PAA is shown in Fig. 12, where the shear moduli are plotted on the scale of $(1/P)^2$ and where the ordinates are shifted arbitrarily in order to avoid the overlapping of the curves. The glass transition temperature at about 140 °C remained unchanged. However, in the higher temperature region, the curves are displaced to higher temperatures as the rate becomes faster. These findings suggest that the inspection of the heating-rate dependence aids in the identification of the physical processes and the chemorheological processes.

It is known that the kinetic parameters can be determined by a study of the heating-rate dependence of the TG curve. Ozawa pointed out that the apparent activation energy can be obtained from the slope in the plot of the logarithm of the heating rate (log h)

against the reciprocal of temperature, T_m(K), at which certain reactions with various heating rates reach the same extent.[17] In the present study, the temperature at which λ shows a maximum corresponding to the increase or decrease in G_r was taken as T_m, assuming that the reactions reached the same extent at this point. From the linear plot of log h *vs.* $(1/T_m)$, the activation energies were estimated. As is shown in Table 1, the two values are both in excellent agreement with those from initial slopes. The nature of the discrepancy between the values (78 and 69 kJ/mol) from the shift factor and those from other means (119 and 135 kJ/mol from the slopes and 126 kJ/mol from log h *vs.* $(1/T_m)$) in the range from 270 to 360 °C in PAA is not clear at present.

It is noteworthy that the kinetic method used in the thermal analysis can be successfully applied for the chemorheological measurements, in which chemical processes are investigated through the change in structure that controls the mechanical properties. The examination of the application of this procedure to the other polymers, especially to the polymers grouped in Fig. 9 or to the halogen-containing polymers, is a subject for future study.

The authors wish to thank Mr. Yoshio Takahashi and Mr. Takeo Ozawa (Electrotechnical Laboratory) for their helpful advice and for affording the facilities for the use of the TG and the automatic TBA apparatus.

References

1) N. Furusho, T. Komatsu, and T. Nakagawa, *Nippon Kagaku Kaishi*, **1973**, 1166.
2) Y. Takahashi, K. Nozaki, and T. Ozawa, *Oyo Butsuri*, **42**, 48 (1973).
3) N. Furusho, T. Komatsu, and T. Nakagawa, This Bulletin, **47**, 1573 (1974).
4) J. K. Gillham, *Appl. Polym. Symposia*, **2**, 45 (1966).
5) S. Otani, *Kogyo Kagaku Zasshi*, **61**, 447 (1958).
6) J. Mercier and G. Smets, *J. Polym. Sci., Part A*, **1**, 1491 (1963).
7) D. H. Grant and N. Grassie, *Polymer.* **1**, 125 (1960).
8) T. Yamaguchi, M. Amagasa, and S. Uchiyama, *Kobunshi Kagaku*, **18**, 406 (1961).
9) N. Grassie, *Trans. Faraday Soc.*, **48**, 379 (1952).
10) H. C. Haas and R. L. Macdonald, *J. Polym. Sci., Part A*, **9**, 3583 (1971).
11) R. K. Graham, *ibid.*, **38**, 209 (1959).
12) W. Burlant, J. Hinsch, and C. Taylor, *ibid., Part A*, **2**, 57 (1964).
13) K. Moriomto and S. Suzuki, *J. Appl. Polym. Sci.*, **16**, 2947 (1972).
14) N. Furusho, T. Komatsu, and T. Nakagawa, *Repts. Progr. Polym. Phys. Japan*, **17**, 337 (1974).
15) A. F. Lewis, *SPE Trans.*, **3**, 201 (1963).
16) M. Popa, C. Vasile, and I. A. Schneider, *J. Polym. Sci., Polym. Chem. Ed.*, **10**, 3679 (1972).
17) T. Ozawa, This Bulletin, **38**, 1881 (1965).

Pressure Effect on the Optical Spectra of Some One-Dimensional Pt-Complexes

Yoji HARA, Ichimin SHIROTANI, Yukako OHASHI, Katsuyuki ASAUMI, and Shigeru MINOMURA

The Institute for Solid State Physics, The University of Tokyo, Roppongi, Minato-ku, Tokyo 106

(Received July 15, 1974)

The absorption and luminescence spectra of the polycrystalline magnesium, barium, and potassium salts of tetracyano platinate (II) were measured at hydrostatic pressures up to 5.4 kbar. These three salts showed an anomalously large red shift with pressure in both the absorption and luminescence spectra. The X-ray powder diffraction measurement was carried out for the magnesium salt up to 70 kbar. At 70 kbar the Pt–Pt distance decreased from 3.16 Å to 2.93 Å, 7.3% in linear compressibility. In the low pressure region up to ~20 kbar, the Pt–Pt distance was observed to decrease greatly. The intramolecular transition $5dz^2 \rightarrow 6pz$ energy was calculated as a function of the Pt–Pt distance. By comparing the calculated and observed values, such a large red shift in the absorption spectra was tentatively explained in terms of electrostatic stabilization of the intramolecular transition $5dz^2 \rightarrow 6pz$ due to the decrease of the intermolecular distance and due to the consequent increase of the $5dz^2 \rightarrow 6pz$ intermolecular CT character.

In a previous paper,[1] we partly reported the optical behavior of quasi-one-dimensional solids under high pressure, such as potassium tetracyano platinate (II); $K_2Pt(CN)_4 \cdot 3H_2O$, magnesium tetracyano platinate (II); $MgPt(CN)_4 \cdot 7H_2O$, barium tetracyano platinate (II); $BaPt(CN)_4 \cdot 4H_2O$. When pressure was applied up to 5.4 kbar, the Mg-salt showed the largest red shift of the absorption peak that we had ever known, including organic compounds.

The optical properties of square planar complexes of platinum (II), which are composed of quasi-one-dimensional Pt-chains, at high pressures have long been a subject of interest. Through X-ray diffraction studies,[2] it has been shown that $MgPt(CN)_4 \cdot 7H_2O$, $BaPt(CN)_4 \cdot 4H_2O$, and many of their related compounds have the one-dimensional columnar stacking structure of $Pt(CN)_4^{2-}$.

Interrante and Bundy have investigated the X-ray diffraction patterns for $K_2Pt(CN)_4Br_{0.3} \cdot 2.3H_2O$,[3a] $Pt(NH_3)_4 \cdot PtCl_4$ (Magnus' green salt, MGS) and $Ir(CO)_2(acac)$[3b] at high pressures and found that the lattice constant and the metal-metal distance in d^8 metal complexes decrease with increasing pressure.

Yamada studied the polarized absorption spectra of $K_2Pt(CN)_4 \cdot 3H_2O$, $MgPt(CN)_4 \cdot 7H_2O$, $BaPt(CN)_4 \cdot 4H_2O$, and related compounds and found the existence of weak bonding between adjacent Pt ions.[4] Polarization spectral measurements for the Mg-, Ca-, Sr-, and Ba-salts led Moncuit and Poulet to assign the absorption band in the visible region to the intramolecular transition $5dz^2 \rightarrow 6pz$, polarized along the Pt-chain (c axis).[5]

Krogmann assigned the band to the transition from the $5zd^2$ band to the 6pz band formed by adjacent Pt ions.[6] Zahner *et al.*[7] considered the visible absorption band in nickel dimethylglyoxime ($Ni(DMG)_2$) and its related compounds to be the intramolecular transition $3dz^2 \rightarrow 4pz$. They also suggested that the electrostatic interaction between the adjacent metal ions was responsible for the red shift which they had observed for such compounds.

Ohashi *et al.* quantitatively explained the polarized spectra of $Ni(DMG)_2$ and its related compounds.[8]

In this paper, the optical properties of the tetracyano platinate (II) solids at high pressures will be shown. The Pt–Pt distance of the Mg-salt as a function of pressure was investigated by the X-ray diffraction study, and the result will also be shown. A calculation was tried to know the nature of the large red shift with pressure, since neither a qualitative nor semi-quantitative investigation has been carried out for the $MPt(CN)_4 \cdot nH_2O$ type solids. We show the results of the calculation for the absorption energy ($5dz^2 \rightarrow 6pz$ in the central Pt ion) as a function of Pt–Pt distance. These results will be compared with the experimental one.

Experimental

X-Ray Measurement. For high pressure X-ray powder diffraction studies, the Bridgman type apparatus with moving tungsten carbide anvils was used, where pressure was cramped. The samples were put in a hole of 0.3 mm diameter in the center of a boron disk of 3 mm diameter and 0.3 mm thickness. The radiation used was Mo$K\alpha$ with 0.7107 Å wavelength. A Zr filter was used. Camera diameter was 75.74 mm. The pressure was determined from measurements of the (200), (220), (222), (400), (420), and (422) reflections caused by the NaCl, using the pressure *vs.* compression values calculated by Decker.[9] As the Mg-salt was reactive with NaCl, it was measured solely without mixing with NaCl. It follows that no absolute determination of pressure values could be obtained.

The Mg-salt has the tetragonal structure.[10] The lattice constants "c" and "a" at each pressure were determined from measurements of the (022) and (232) reflections.

Spectral Measurement. The absorption spectra were measured as a function of pressure. The pressure was generated by an intensifier using white gasoline medium up to 5.4 kbar. The absorption and emission spectra were measured with nujol mulls and in the polycrystalline state held tightly between glasses, respectively. The optical measurements were performed with a Shimadzu double beam spectrophotometer.

Preparation of Samples. The K-, Mg-, and Ba-salts[11] were prepared as described in the literature. Attention was paid to the preservation of the Mg-salt so as to keep it in an atmosphere with a high vapor pressure of water.

Results and Discussion

Absorption and Luminescence Spectra. *$MgPt(CN)_4 \cdot 7H_2O$*: The Mg-salt is composed of one-dimensional Pt-chains with tetragonal crystal structure and has a

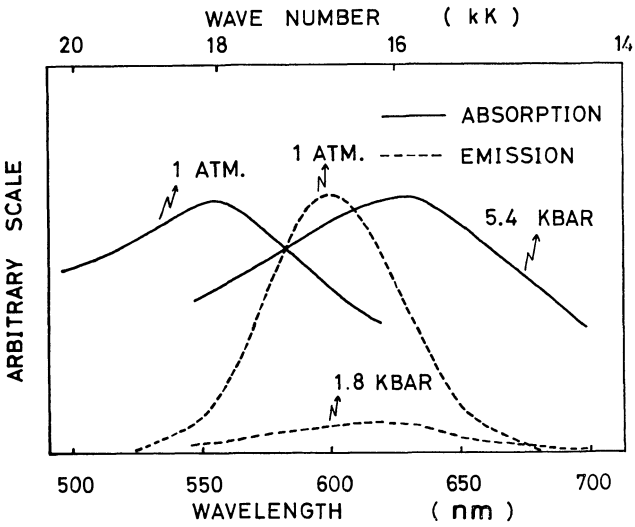

Fig. 1. Pressure effect on the absorption and luminescence spectra of polycrystalline $MgPt(CN)_4 \cdot 7H_2O$.

crimson color. The Pt–Pt distance was reported to be 3.16 Å.[2a] The effect of pressure on the absorption and on the luminescence spectra of the polycrystalline Mg-salt is shown in Fig. 1. The absorption peak of 555 nm (18.0 kK) showed an anomalously large red shift up to 629 nm (15.9 kK) at 5.4 kbar with increasing pressure, in a rate of -389 cm^{-1}/kbar.

The emission band of 600 nm (16.7 kK) at atmospheric pressure shifted to 620 nm (16.1 kK) at 1.8 kbar, in a rate of -320 cm^{-1}/kbar. The red shift observed both in the absorption and in the luminescence spectra was the largest so far detected by the present authors. The emission intensity decreased sharply with increasing pressure and was almost completely extinguished at pressures over 5 kbar.

$K_2Pt(CN)_4 \cdot 3H_2O$: In Fig. 2 the pressure effect on the absorption and luminescence spectra of the polycrystalline K-salt is displayed. The absorption peak of 382 nm (26.2 kK) showed a large red shift up to 402.5 nm (24.85 kK) at 5.4 kbar with increasing pressure, in a rate of -250 cm^{-1}/kbar.

The emission band of 437.5 nm (22.9 kK) at atmoshperic pressure shifted to 450 nm (22.2 kK) at 5.4 kbar, in a rate of -130 cm^{-1}/kbar.

$BaPt(CN)_4 \cdot 4H_2O$: The Ba-salt has the monoclinic crystal structure and a yellow-green color.[2b] The Pt–Pt distance is predicted to be 3.32 Å. Figure 3 shows the pressure effect on the absorption and

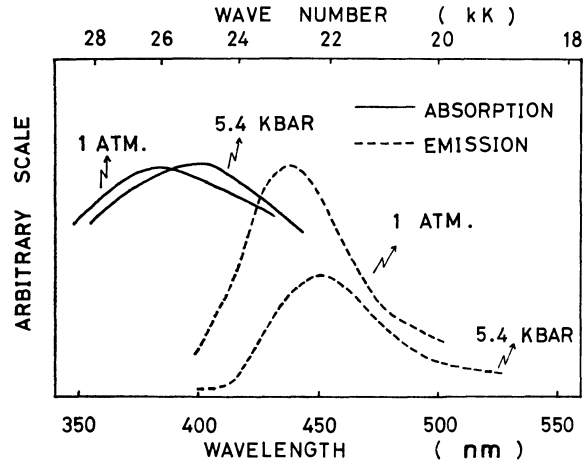

Fig. 2. Pressure effect on the absorption and luminescence spectra of polycrystalline $K_2Pt(CN)_4 \cdot 3H_2O$.

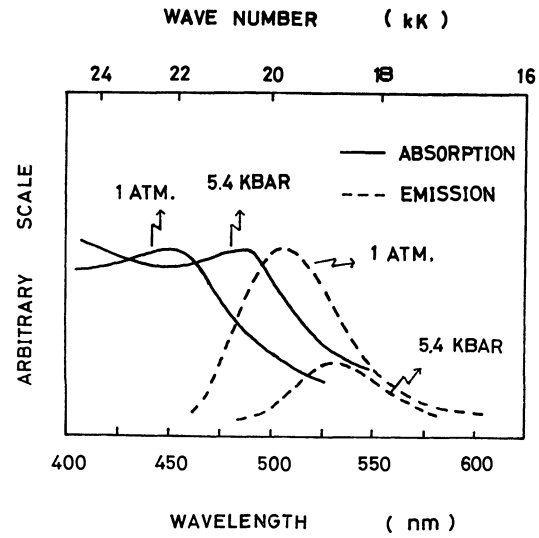

Fig. 3. Pressure effect on the absorption and luminescence spectra of polycrystalline $BaPt(CN)_4 \cdot 4H_2O$.

luminescence spectra of the polycrystalline Ba-salt. The absorption peak of 450 nm (22.2 kK) showed a large red shift up to 488 nm (20.5 kK) at 5.4 kbar with increasing pressure, in a rate of -315 cm^{-1}/kbar. The emission band of 505 nm (19.8 kK) at atmospheric pressure shifted to 530 nm (18.9 kK) at 5.4 kbar, in a rate of -167 cm^{-1}/kbar. These results are summarized with those for the Mg- and K-salts in Table 1.

Table 1. Absorption and emission maxima in the visible region, red shift, and Pt–Pt distance

Material	Absorption maximum nm (kK)	Red shift (cm^{-1}/kbar)	Emission maximum nm (kK)	Red shift (cm^{-1}/kbar)	Pt–Pt distance (Å)
$K_2Pt(CN)_4 \cdot 3H_2O$	382 (26.2)	-250	437.5 (22.9)	-130	>3.35[a]
$BaPt(CN)_4 \cdot 4H_2O$	450 (22.2)	-315	505 (19.8)	-167	3.32[b]
$MgPt(CN)_4 \cdot 7H_2O$	555 (18.0)	-389	600 (16.7)	-320	3.16[b]

a) S. Yamada, *Kagaku*, **41**, 651 (1971). b) Ref. 6.

The fact that the ratio of the quantum yield at each pressure to that of 1 atmosphere increased in the order K>Ba≫Mg might be explained in terms of the difference of the mixing of the intermolecular charge transfer $5dz^2 \rightarrow 6pz$ into both excited and ground state,[4] which will be discussed in more detail in a later part of the paper.

Moncuit *et al.* tentatively assigned the emission band to vibronically induced d–d transitions.[5] However, it is doubtful that such d–d transition may show such large red shift with pressure. It might be possible to assign it to the allowed 6pz (a_{2u})→$5dz^2$(a_{1g}) intramolecular transition.

X-Ray Diffraction. $MgPt(CN)_4 \cdot 7H_2O$ has a tetragonal unit cell with the metal chain axis aligned along the "c" unit cell direction with the "a" perpendicular to it. The lattice constants for the "c" and "a" unit cell dimensions are 6.32 and 14.54 Å, respectively.[2a] Figure 4 illustrates the pressure effect on the X-ray powder diffraction of the Mg-salt up to 70 kbar. Both the "c" and "a" unit cell dimensions decrease continuously over the pressure range. In the low pressure region up to ~20 kbar, the Pt–Pt distance, which is the half of the "c" unit cell dimension, was observed to decrease greatly. At 20 and 70 kbar the Pt–Pt distance decreased by 4.7% (3.01 Å) and 7.3% (2.93 Å) in linear compressibility, respectively. At 70 kbar the "a" unit cell dimension decreased to 14.11 Å, 2.9% in linear compressibility. These results are compared with those given by Interrante *et al.* in Table 2.

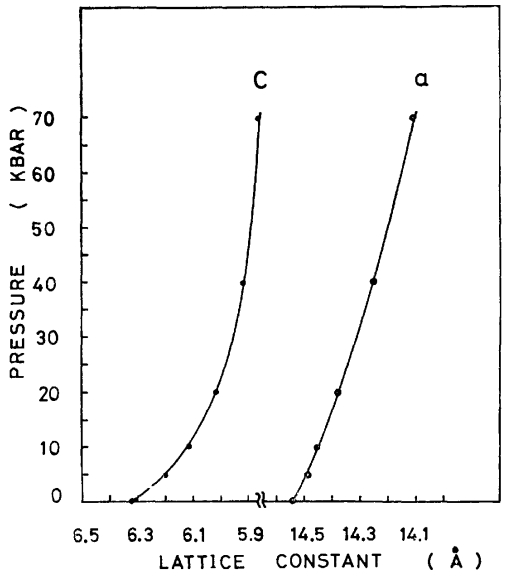

Fig. 4. Change in the "c" and "a" unit cell dimensions of $MgPt(CN)_4 \cdot 7H_2O$ with pressure.

TABLE 2. COMPARISON OF THE Pt–Pt DISTANCE OF SOME ONE-DIMENSIONAL Pt-COMPLEXES AT 1 atm. AND 70 kbar

Compound	Pt–Pt	Overall change in "a" dimension (Å)[d]
$MgPt(CN)_4 \cdot 7H_2O$	3.16 2.93[d] (7.3)[e]	0.43
$Pt(NH_3)_4 \cdot PtCl_4$[a] (MGS)	3.25 3.00 (7.7)[e]	~0.47
$Ir(CO)_2 \cdot (acac)$[a]	3.23 2.89 (10.5)[e]	
$K_2Pt(CN)_4 \cdot Br_{0.3} \cdot 2.3H_2O$[b]	2.89 2.78 (3.8)[f]	~0.47

a) Ref. 3b. b) Ref. 3a. c) Data at 1 atm. d) Data at 70 kbar. e) Linear compressibility at 70 kbar. f) Linear compressibility at 50 kbar.

As is seen from Table 2, firstly the linear compressibility along the c axis at 70 kbar increases in the order, $Ir(CO)_2 \cdot (acac) > Pt(NH_3)_4 \cdot PtCl_4 \simeq MgPt(CN)_4 7H_2O > K_2Pt(CN)_4 \cdot Br_{0.3} \cdot 2.3H_2O$. Here, the charges on each metal are Ir(+1), Pt(+2) in the Mg-salt and MGS, and Pt(+2.3) in $K_2Pt(CN)_4 \cdot Br_{0.3} \cdot 2.3H_2O$. The Coulombic repulsion due to the plus charges on the central metal ion presumably reflects the relative tendency for the extent of the linear compressibility along the "c" axis. Secondly, the overall change in the "a" dimension up to 70 kbar seems to be independent of the kinds of ligands.

Calculation. Ohashi *et al.* calculated the intramolecular transition ($3dz^2 \rightarrow 4pz$) energy of Ni $(DMG)_2$.[8] Here, we apply again the same method to the calculation of intramolecular transition($5dz^2$—6pz) energy of solid platinocyanide complexes and compare the calculated value with the observed one.

It was assumed,

(i) minus charge is located on the carbon atom and (ii) the Pt–C distance in the coordination plane was unchanged under pressure. The Pt–C distance was taken to be 2.06 Å, the same value as that of $K_2Pt(CN)_4 \cdot Br_{0.3} \cdot 2.3H_2O$.

We consider only the electrostatic effect on the 6pz and $5dz^2$ orbitals of the Pt^+ ion in the complex plane 1, due to Pt^+ ion in 2 and 3, and due to −3/4 charged CN ion in 1, 2, and 3, as is shown in Fig. 5. But we are compelled to neglect, for example, the CT effect and the electrostatic influence of the surrounding alkaline or alkaline earths cation, due to the lack of the corresponding data.

For each of the wave function ϕ_{5d} and ϕ_{6p}, the Slater-type AOs' were used. The orbital exponent values necessary for the calculation were taken as $\xi_{5d}=3.8815$, given by Clementi *et al.*,[12] and $\xi_{6p}=1.9820$, extrapolated from the data of the former authors.

We introduced next equation, the same as that given by Ohashi *et al.*,[8]

$$E_1 = E_1^{\nu} + \Delta_0 + \Delta(R)$$

Here, we put $\Delta(R)=\Delta(R_1)+\Delta(R_2)$, E_1 is the energy necessary for the local excitation of intramolecular transition $5dz^2 \rightarrow 6pz$. E_1^{ν} is the energy necessary for the transition from the $(5dz^2)^2$ valence state to the ($5dz^2$, 6pz) one. These quantities were obtained from the analysis of the observed atomic spectra.[13] Δ_0 is an electrostatic energy difference between 6pz and $5dz^2$ orbitals due to the formal charges on the atoms of the ligands in the complex plane 1, as is shown in Fig. 5. $\Delta(R_1)$ is the electrostatic energy difference between 6pz and $5dz^2$ orbitals of the Pt atom in the complex plane 1, due to the negative charges on the

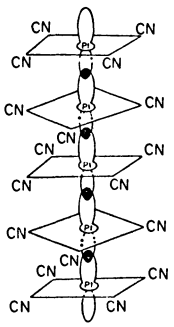

Fig. 5. The coordinate system used in the calculation on $[Pt(CN)_4^{2-}]_5$. Z axis is perpendicular to the complex plane. The complex plane numbers are also given.

TABLE 3. INTRAMOLECULAR TRANSITION $5dz^2 \rightarrow 6pz$ ENERGY CALCULATION FOR (A) Pt^+ AND (B) Pt^0

Pt-Pt distance	E_1 case (A) (kK)[a]	case (A) (kK) $\Delta(R_1)$	case (A) (kK) $\Delta(R_2)$	E_1 case (B) (kK)
3.50	26.04	−11.12	− 6.70	
3.32	23.64	−12.40	− 7.82	
3.16	21.18	−13.68	− 9.01	8.91
3.13	20.58	−14.00	− 9.28	8.69
3.09	19.90	−14.40	− 9.57	8.39
3.00	18.20	−15.28	−10.38	7.85
2.89	16.06	−16.32	−11.49	7.09

a) calculated values are recorded in kilokaysers.

ligand carbon atoms in the complex plane 2 and 3, and $\Delta(R_2)$ is the electrostatic energy difference between 6pz and $5dz^2$ orbitals of the Pt atom in the complex plane 1, due to the positive charges on the Pt atoms in the complex plane 2 and 3. Furthermore, the calculation was carried out for the case of (A) Pt^+ and (B) Pt^0. The results are summarized in Table 3.

As is indicated in Table 3, (i) case (A) reproduces the observed value well, (see the symbol X in Fig. 7), (ii) though $|\Delta(R_1)|$ is larger than $|\Delta(R_2)|$ for case (A), the contribution to the red shift is almost the same between them. In other words, the 6pz orbital is almost equally stabilized relative to the $5dz^2$ orbital by the −3/4 charged carbon and +1 charged Pt in the complex plane 2 and 3 with decreasing Pt–Pt distance.

Figure 6 illustrates the electrostatic energy of the 6pz and $5dz^2$ orbitals as a function of the Pt–Pt distance. Within the limit of the calculation, it is clear that the relative stabilization of the 6pz orbital to the $5dz^2$ one causes the red shift.

These calculated values are compared with the observed values in Fig. 7. The results of spectral measurements on the Mg-salt at pressures up to 5.4 kbar evidence a direct relationship between the magnitude of these spectral shifts and the interionic distance in the solid. The calculated values will represent the observed values including the K-, Ca-, and Ba-salts. But when the Pt–Pt distance becomes less than that of the Ba-salt, 3.32 Å, the discrepancy between the calculated and observed values becomes larger. This discrepancy can be explained in terms of (i) the mixing

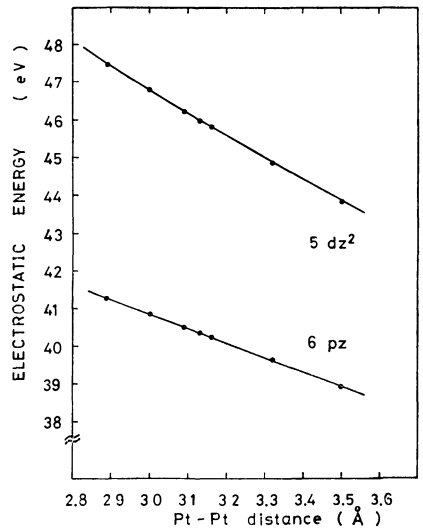

Fig. 6. The electrostatic energy dependence of the $5dz^2$ and 6pz orbitals of the central Pt ion on the Pt–Pt distance.

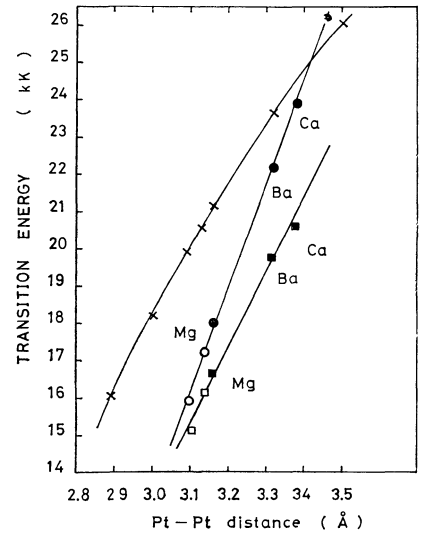

Fig. 7. The observed transition energy between $5dz^2$ and 6pz orbitals as a function of the Pt–Pt distance in various $Pt(CN)_4^{2-}$ derivatives:
Ca, $CaPt(CN)_4 \cdot 5H_2O$; Ba, $BaPt(CN)_4 \cdot 4H_2O$;
Mg, $MgPt(CN)_4 \cdot 7H_2O$;
The symbols ●, ○ and ■, □ refer to data obtained from absorption and luminescence experiments respectively, where the symbols ○ and □ refer to the one obtained for the Mg-salt at high pressures. The Pt–Pt distance is 3.13 Å at 2.5 kbar, 3.1 Å at 5 kbar and 3.09_5 Å at 5.4 kbar for the Mg-salt. The symbol X represents the calculated values of the intramolecular transition $5dz^2 \rightarrow$ 6pz energy for case (A) in Table 3.

effect of the $5dz^2 \rightarrow$6pz intermolecular charge transfer configuration between adjacent Pt ions into both of ground and excited state, (ii) the electrostatic effect of the surrounding alkaline or alkaline earths cations and (iii) the effect of a bond formation. According to our calculation, (ii) should decrease the intramolecular $5dz^2 \rightarrow$6pz energy by ~1.5 kK at most. Referring to the band calculation on MGS by Inter-

rante *et al.*,[3c] we tentatively evaluate (iii) to be ~2 kK at 3.0 Å in the Pt–Pt distance. Ohashi *et al.*[8] calculated the ground state stabilization energy due to (i) at 3.0 Å in the Ni–Ni distance of $Ni(DMG)_2$ to be ~2 kK. At 3.0 Å the calculated value is more than the observed value by 4.7 kK. So on a rough estimation, the excited state stabilization energy at 3.0 Å of platinocyanide complexes should be ~3.2 kK. Apart from this value, such mixing of CT character into the excited state should be closely related to the decrease of the emission intensity at high pressures (see the section for the Mg salt).

For the case of a single configuration coordinate Drickamer *et al.* obtained:[15]

$$\frac{(h\nu_{1max}-h\nu_{2max})_{abs.}}{(h\nu_{1max}-h\nu_{2max})_{emiss.}}=\left(\frac{\omega'}{\omega}\right)^4$$

Here, the 1 and 2 refer to two different pressures. They assumed harmonic potential wells with different force constants ω and ω' for the ground state and excited state respectively.

In our study, the ω'/ω values for the K-, Ba-salts at 5.4 kbar were found to be 1.178 and 1.172 respectively and 1.050 at 5.0 kbar for the Mg-salt. The smaller value for the Mg-salt is reasonable when one considers that the ground state mixes with the excited state through CT character much more in the Mg-salt than in the K- and Ba-salts. This is supported by the fact that the Mg-salt has a higher absorption intensity in the visible region than the other salts,[5] which should be due to the larger transition moment between the CT^- and CT^+ configuration than that between the ground and local excitation configurations for the intermolecular distance of ~3 Å[8].

References

1) Y. Hara, I. Shirotani, and S. Minomura, *Chem. Lett.*, **1973**, 579.

2) (a) R. M. Bozorth and L. Pauling, *Phys. Rev.*, **39**, 538 (1932). (b) K. Krogmann and D. Stephan, *Z. Anorg. Allg. Chem.* **362**, 290 (1968), and so forth, see ref. 6.

3) (a) L. V. Interrante and F. P. Bundy, *Solid State Commun.*, **11**, 1641 (1972). (b) L. V. Interrante and F. P. Bundy, *Inorg. Chem.*, **10**, 1169 (1971). (c) L. V. Interrante and R. P. Messmer, *ibid.*, **10**, 1174 (1971).

4) S. Yamada, This Bulletin, **24**, 125 (1951).

5) C. Moncuit and H. Poulet, *J. Phys. Radium.*, **23**, 353 (1962).

6) K. Krogmann, *Angew. Chem.*, **81**, 10 (1969).

7) J. C. Zahner and H. G. Drickamer, *J. Chem. Phys.*, **33**, 1625 (1960).

8) Y. Ohashi, I. Hanazaki, and S. Nagakura, *Inorg. Chem.*, **9**, 2551 (1970).

9) D. L. Decker, *J. Appl. Phys.*, **37**, 5012 (1966).

10) K. Krogmann and H. D. Hausen, *Z. Anorg. Allg. Chem.*, **358**, 67 (1968).

11) (a) S. Yamada, This Bulletin, **24**, 125 (1951). (b) "Handbuch der präparaitven anorganischen Chemie.", P. Haas and G. Brauer, (1954), p. 1179.

12) E. Clementi, D. L. Raimondi, and W. P. Reinhardt, *J. Chem. Phys.*, **47**, 1300 (1967).

13) C. E. Moore, "Atomic Energy Levels", National Bureau of Standards Circular 467, U. S. Government Printing Office, Washington D. C., (1958).

14) Since the present theoretical results on the polycrystal spectra depend to some extent on the adopted parameters, ξ_{6p} for example, too much importance should not be attached to them from the quantitative point of view. Qualitatively, however, the present treatment gives a reasonable interpretation of the observed polycrystal spectra at high pressure.

15) "Electronic transitions and the high pressure chemistry and physics of solid". H. G. Drickamer and C. W. Frank, Chapman and Hall, London, (1973).

Detection of Hydrophobic Stain on Cotton Surface by Fluorescent Probe*

Toshiko SEIMIYA** and Mary E. PURCHASE

Department of Design and Environmental Analysis, College of Human Ecology, Cornell University, Ithaca, New York, 14850

(Received August 6, 1974)

The minute amount of hydrophobic substances $10^{-8}\sim10^{-7}$ mol/cm^2 (geometric area) on cotton fabric surface can effectively be detected by fluorescent probe using magnesium-8-anilino-1-naphthalenesulfonate (ANS). The cotton fabrics were dyed in aqueous ANS solution (1×10^{-4} mol/l), before and after the staining with stearic acid, palmitic acid, tristearin, oleic acid, and squalene, and the intensities of fluorescence from the cotton surface was measured by reflectance spectrophotometer under the varying wavelength of ultra-violet (200—300 mμ). The intensity of fluorescence increased with the increase of fatty stain on the surface, but showed the tendency of saturation by exceeding the closest packing of the fatty acid monolayers. Correlation was also found between the fluorescent intensity and the yellowness (*b*-value) of naturally soiled cotton fabrics. The bleaching of the yellowed fabrics by sodium hypochlorite effectively reduced the *b*-value but did not change the fluorescence appreciably, and suggested that the hydrophobic substances still remained on the fabric surfaces in spite of their white appearance.

The surface reflectance of the whiteness of the cloths might be the most practical and fundamental standard of the cleanliness of the fabrics which agrees most with the human sense. Thus, the surface reflectometry is now the widely accepted method to detect the soils on fabric in the study of detergency. The reflectometry is versatile for its easy measurement in the practical systems, but its application is limited to the case where the amount of the soil adhering to the fabric is enough to change the reflectance of incident light by absorption. Generally speaking, the monomolecular layer of fatty acid adsorbed on soiled surface is too little in amount to change the intensity of light by a single reflection at solid/air interface.

A number of studies have been reported to estimate the trace amount of fatty substances on fabric surfaces, by extracting them with solvent followed by equilibrium lens[1] or gravimetric method[2,3] of analyses, as well as gas, liquid, thin layer or gel-filtration chromatography followed by spectroscopic analyses.[4–6] The radiotracer technique is also useful especially in detecting minute amounts of multi-component soils, without extraction procedure, by dual-lebelling and measuring the residual soil with a liquid scintillation counter,[7–11] or useful in the kinetic studies of detergency using an end-windowed dip-counter.[12] All these methods are excellent and have offered much useful information on the molecular mechanism of detergency, however, they always accompany some limitations in their application. For chromatographic analysis, all the soils should have such nature that is extractable by the certain solvent, which is not necessarily the case. And the latter radiotracer method, which utilizes artificial soils labelled with radioisotope, is only significant in the model system. Any physicochemical method which detects minute stains and gives a strict measure of cleanliness or dirtiness of the fabrics without an extraction procedure, should be helpful at present in the study of detergency as a measure of cleansing efficiency.

Some derivatives of naphthalenesulfonate are practically non-fluorescent when dissolved in water but fluorescent strongly when dissolved in organic solvent,[13] or one bound to the hydrophobic part of molecules.[14] These fluorescent dyes are utilized by a number of investigations in the determination of hyper-structure of proteins[15–17] or detergent micelles,[18] and in the analysis of various biological phenomena,[19] and are called as "fluorescent probe", or "hydrophobic probe."

The present paper deals with some experimental trials, using magnesium-8-anilino-1-naphthalenesulfonate as an adsorption indicator,[20] to detect minute fatty stain on cotton fabric stains, which are too small in amount to be detected by ordinary reflectance spectroscopy, or to be extracted for successive physicochemical analyses.

The results suggest that the fluorescent probe might offer a new measure of cleanliness of fabrics useful for the study of detergency.

Experimental

Materials. *Probe*: The fluorescent probe grade magnesium-8-anilino-1-naphthalenesulfonate (ANS) obtained from Eastman-Kodak Co., N. Y. was dissolved in distilled water to make a stock solution of 1×10^{-3} mol/l. The stock solution was kept in a dark and cool place until needed. The concentration of the dyeing solution about 1×10^{-4} mol/l was found optimal from the preliminary experiment to visualize the stain by naked eye under the ultraviolet light.

Hydrophobic Stains: Stearic acid, palmitic acid, oleic acid, tristearin, and squalene, all analytical grade (Fischer Scientific Co., N. J.) were dissolved in benzene to make the staining solution. The concentration ranged between $2\times10^{-4}\sim1\times10^{-2}$ mol/l.

Cotton: The cotton cloth for the specimen was obtained from the Test Fabric Inc., N. Y. in the form of plain-woven fabric without an optical brightner (20×20 threads/cm, 17.7 mg/cm^2 at the standard condition of the present experiment). In order to eliminate any residual greasy substance originally contaminating the fabrics, the specimens were purified by the following procedure.[11] The cotton cloth, cut into 45×45 cm, was washed in a Terg-O-Tometer in 0.25% Calgon solution for 10 min at 50 °C, rinsed twice for 5 min in distilled water, and air dried. The samples were further cut into a smaller 6×6 cm size and extracted with ethyl ether for

* The paper presented at the 28th Annual Meeting of Japan Chemical Society (Tokyo 1973)

** Present address: Faculty of Home Economics, Kyoritsu Women's University, Kanda, Tokyo, Japan.

24 hr by Soxhlet extracting apparatus, and stored in a greasless glass container after being dried in clean air.

Procedure. After the prolonged exposure of cotton sample to a standard condition (20±2 °C, 65±2% R.H.) to equilibrate it, 0.2 ml of the staining benzene solution was applied to the center of cotton cloth from a micro-syringe. The cloth stained was conditioned again after the evaporation of benzene, then dyed in 100 ml of ANS dyeing solution for 20 min, rinsed in 250 ml of 1/100 M NaCl aqueous solution, and damp dried between absorbing filter papers. The aqueous NaCl solution helped to wash off any extra ANS in the cloth without losing a large portion of the ANS bound to the hydrophobic stain.

The fluorescence from the cloth dyed with ANS was measured by a Bausch & Lomb 505 spectrophotometer equipped with reflectance attachment under varying wavelength of incident ultraviolet light (280~300 mμ). The intensity of fluorescence of the test specimen is expressed in percent to that of control cloth, which is the sample with a known amount of fatty stain dyed with ANS. All these procedures were carried out at room temperature (24—28 °C), and precautions were taken to avoid unnecessary exposure of the specimen to the light which might accelerate the decomposition of ANS.

Results and Discussion

Figures 1a and b demonstrate the hydrophobic stain of stearic acid on cotton fabrics visualized by fluorescent probe. Under an ultra-violet light the hydrophobic stain shows as a white circular area (Fig. 1a), which can not be observed under the ordinary white light from an incandescent source (Fig. 1b). The cotton cloth in Fig. 1 was stained with stearic acid by dropping an aliquot of benzene solution of stearic acid to the center of the cloth to make a circular stain, and dyed with ANS by the procedures mentioned above. The pictures were taken, one (Fig. 1a) under the ultra-violet light with a yellow filter on the lens, and the other (Fig. 1b) under the ordinary white light without a filter using panchromatic B & W film (Tri-X, Kodak). These experiments show the fluorescent probe being as effective as to detect minute 8.61×10^{-8} mol/cm² amount of stearic acid, by leaving it on the fabric surface without applying any extraction processes.

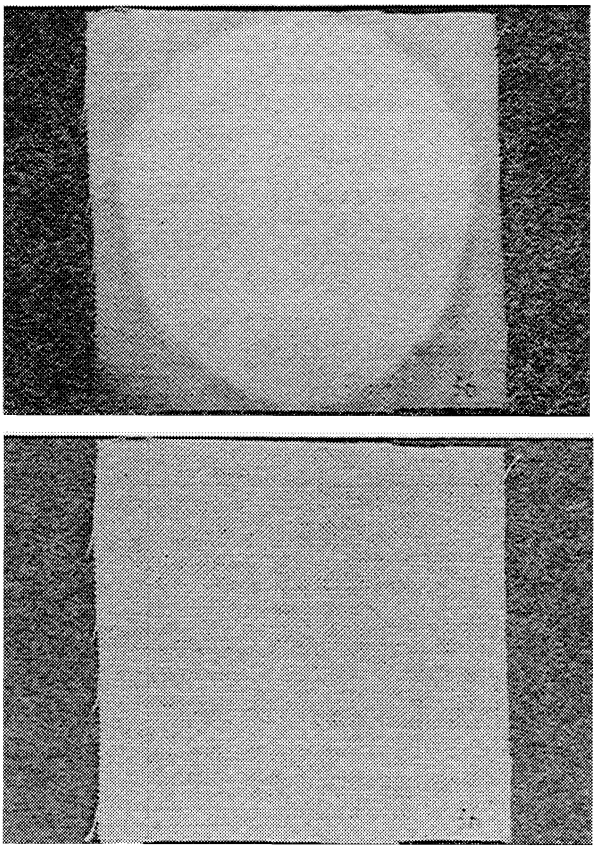

Fig. 1. Stearic acid stain on cotton fabrics visualized by fluorescent probe.
(a): Picture taken under the ultra-violet light using yellow filter.
(b): Picture of the same sample (a) taken under the white light.

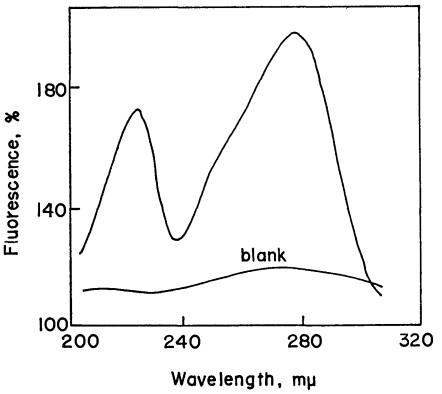

Fig. 2. Fluorescence of cloths with and without stearic acid stain against the wavelength of incident light.

Figure 2 shows the typical fluorescence intensity *vs.* wavelength of incident light curves of cotton dyed by ANS with and without the stearic acid stain. The amount of stearic acid put on cloth is 8.61×10^{-8} mol/cm². The intensity of fluorescence increased with stearic acid stain, and the two characteristic maxima were observed at 225 and 275 mμ of ultra-violet irradiation compared with the blank cotton surface which showed very weak fluorescence. Any appreciable differences in the fluorescence spectra have never been observed also for the other fatty acids as well as tristearin and squalene. The intensity of fluorescence increased with the amount of fatty stains, and the two characteristic maxima appeared around 225 and 275 mμ respectively.

The fluorescence intensities at these maxima were plotted against the amount of fatty stain on the cloth surface, and are shown in Figs. 3~6. The increase of fluorescence in these figures indicates the net increase of intensity from the blank cotton surface which is the clean specimen dyed with ANS without the oily stains. The saturation of fluorescence is observed for stains applied in excess of certain levels which seemed to be specific to the kind of stain. The amount of stain in these figures is expressed in moles per apparent (geometric) unit area of the fabrics (mol/cm²). The true surface area of the cloth, however, should be far larger than the geometric one,

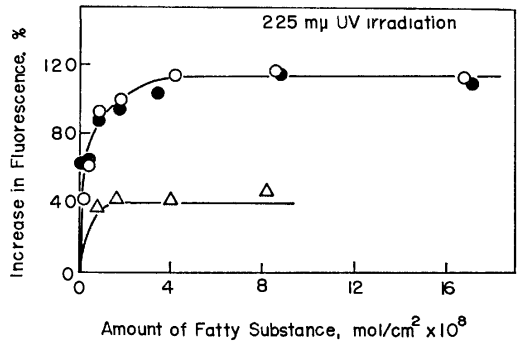

Fig. 3. Relation between fluorescence and amount of fatty substances on cotton fabrics.
○: Palmitic acid, ●: Stearic acid, △: Tristearin.

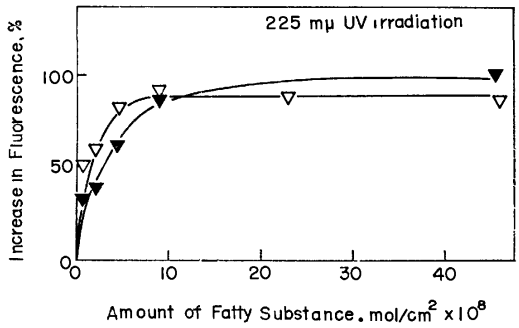

Fig. 4. Relation between fluorescence and amount of fatty substances on cotton fabrics.
▽: Oleic acid, ▼: Squalene

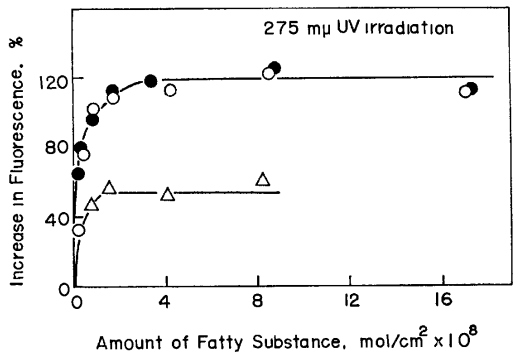

Fig. 5. Relation between fluorescence and amount of fatty substances on cotton fabrics.
○: Palmitic acid, ●: Stearic acid, △: Tristearin.

if we take into account the true surface area of each cotton fibers which compose the fabrics. The specific surface area of cotton fibers has been determined by several workers to be around $2.37\sim2.75\times10^3$ cm²/g.[21,22] Using these values, we can estimate the actual amount of the stains on cotton fiber in moles per true unit area. The closest monolayer coverage of cotton fibers in the cloth by fatty acid molecules should be attained at $3.00\sim3.98\times10^{-8}$ mol/cm² (geometric), assuming the molecular area of fatty acids to be 20.5 Å²/molecule.[23] The saturation of fluorescence in Figs. 3 and 5 occurred for the stain of both stearic and palmitic acids around at 4×10^{-8} mol/cm² which agreed with the monolayer value given above. The similar agreement between

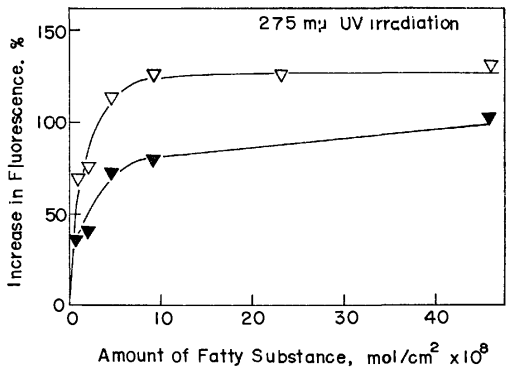

Fig. 6. Relation between fluorescence and amount of fatty substances on cotton fabrics.
▽: Oleic acid, ▼: Squalene

observed and calculated monolayer values is also observed for tristearin which has a molecular area[12] nearly three times larger than that of fatty acid. The saturation of fluorescence is observed for tristearin at smaller amount of stains (about 1/3 of fatty acid) as expected.

The fluorescent probe was also applied to naturally soiled cotton cloths (pillow cases) of different degree of yellowness, which were obtained by the repeated soiling and washing procedures. In Fig. 7, the intensity of fluorescence at 275 mμ ultra-violet irradiation from yellowed fabrics are plotted against the degree of yellowness (*b*-value) of the fabrics. Here, the *b*-values are estimated by using a Hunter D25 Color and Color-Difference Meter with the ultra-violet filter in place to eliminate any fluorescent effects of the cloths.[11] Stronger fluorescence was observed for more yellowed fabrics. The intensity of fluorescence

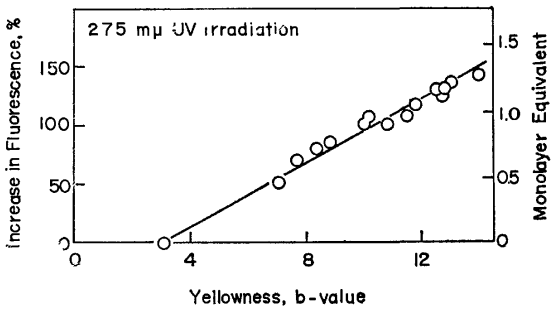

Fig. 7. Relation between *b*-value and fluorescence.

Table 1. Effects of bleaching on both *b*-value and fluorescence at 275 mμ ultra-violet irradiation

b-Value		Fluorescence	
Before bleaching	After bleaching	Before bleaching	After bleaching
9.47	3.54	85%	74%
10.44	3.74	100	80
11.84	3.87	120	100
12.89	4.01	125	81
12.99	3.65	130	110
13.58	4.47	140	112

is also expressed conveniently in monolayer equivalent of fatty acid as seen in the right hand ordinate.

The bleaching of yellowed fabrics by 0.5% aqueous sodium hypochlorite effectively reduced the *b*-value, but fluorescent probe still showed for these bleached white fabrics a fluorescence nearly as strong as that of unbleached cloths, as shown in Table 1. This might mean that any hydrophobic substances are still remaining on the fabrics in spite of their whiteness. It may be generally recognized that the yellowing of the cotton fabrics during the recycling process of soiling and washing in everyday life, is probably caused by the oxidation or polymerization of fatty substances which have not been removed by laundering.[3,24] The residual fatty substances after washing might be a so small amount as that of monomolecular layer, and might not be detected until accumulated and yellowed by usual reflectance measurements hitherto been utilized.

The fluorescent probe should offer an useful measure of cleanliness in the study of detergency not only for its simple and inexpensive background.

The authors wish to thank all the supporting staffs of Department of Design and Environmental Analysis of Cornell University, for their kind take-care in every stage of this research.

References

1) T. Tachibana, A. Yabe, and M. Tsubomura, *J. Colloid Sci.*, **15**, 278 (1960).
2) W. C. Powe, *J. Amer. Oil Chem. Soc.*, **40**, 290 (1963).
3) V. Mclendon and F. Richardson, *Amer. Dyestuff Rept.*, **52**, 27 (1963).
4) A. T. James and V. R. Wheatly, *Biochem. J.*, **63**, 269 (1956).
5) W. C. Powe, 14th Ann. Mtg. of ACS, Chicago (1964).
6) T. Tsunoda, *Bull. Chem. Soc. Japan*, **41**, 475 (1968).
7) B. E. Gordon, J. Roddewig, and W. T. Shebs, *J. Amer. Oil Chem. Soc.*, **44**, 289 (1967).
8) B. E. Gordon, W. T. Shebs, and R. U. Bonnar, *ibid.*, **44**, 711 (1967).
9) B. E. Gordon, *ibid.*, **45**, 367 (1968).
10) B. E. Gordon and W. T. Shebs, *ibid.*, **46**, 537 (1969).
11) M. S. Sontag, M. E. Purchase, and B. F. Smith, *Textile Res. J.*, **40**, 529 (1970).
12) T. Fort Jr., H. R. Billica, and T. H. Grindstaff, *ibid.*, **36**, 99 (1966); *J. Amer. Oil Chem. Soc.*, **45**, 354 (1968).
13) W. O. McClure and G. M. Edelman, *Biochemistry*, **5**, 1908 (1966).
14) G. Weber and D. J. R. Laurence, *Biochem. J.*, **56**, xxxi (1954).
15) G. Weber and L. B. Young, *J. Biol. Chem.*, **239**, 1415 (1964).
16) L. Stryer, *J. Mol. Biol.*, **13**, 482 (1965).
17) J. A. Gally and G. M. Edelman, *Biolchim. Biophys. Acta*, **94**, 175 (1965).
18) C. E. Williamson and A. H. Corwin, *J. Colloid Interface Sci.*, **38**, 577 (1972).
19) S. Udenfriend, "Fluorescence Assay in Biology and Medicine," Academic Press, New York and London (1962) (Fifth Printing, 1969).
20) G. M. Edelman and W. O. McClure, *Accounts Chem. Res.*, **1**, 65 (1968).
21) A. J. Stamm and M. A. Millett, *J. Phys. Chem.*, **45**, 43 (1941).
22) C. H. Giles and A. H. Tolia, *J. Appl. Chem.*, **14**, 186 (1964).
23) N. K. Adam, *Proc. Roy. Soc., Ser. A*, **99**, 336 (1921); **101**, 452 (1922).
24) R. E. Wagg, D. M. Meek, and A. L. Willian, Chem. Phys. Appl. Surface Active Subst., Proc. Int. Congr., 4th, **3**, 269 (1964).

Photoelectron Spectra of the *cis*- and *trans*-Isomers of Some Ethylene Derivatives

Tsunetoshi KOBAYASHI, Katsuyuki YOKOTA, and Saburo NAGAKURA

The Institute for Solid State Physics, The University of Tokyo, Roppongi, Minato, Tokyo 106

(Received August 20, 1974)

The photoelectron spectra of *cis*- and *trans*-stilbenes, fumaric acid, dimethyl maleate, and dimethyl fumarate were measured and interpreted, special attention being paid upon their difference between the corresponding *trans*- and *cis*-isomers. The two characteristics were found for the photoelectron spectra of *cis*- and *trans*-stilbenes: (1) the splitting between the first and fifth bands is smaller for the *cis*-isomer (steric-hindrance effect); (2) the splitting between the second and third bands is larger for the *cis*-isomer (through-space interaction). The difference in the carbonyl n orbital ionization potentials between dimethyl maleate and fumarate was interpreted in terms of through-bond interaction.

The effect of steric configuration upon photoelectron spectra (PES) of organic molecules is an interesting research subject not only from the study of their electronic structures but also from the application of the spectra to the structural determination. So far several studies have been carried out for the PES of *cis*- and *trans*-isomers of some ethylene derivatives. The PES of dichloroethylenes were studied by Jonathan and coworkers[1] and also by Lake and Thompson.[2] Chadwick and coworkers[3] studied the PES of dibromoethylenes. Bock and coworkers studied the PES of dicyanoethylenes,[4] dibromo- and dichloroethylenes,[5] and dithiomethoxyethylenes.[6] In a series of compounds mentioned above, the out-of-plane π orbital vertical ionization potentials, I_v's, of a *cis*-isomer are rather similar to those of the corresponding *trans*-isomer. In *cis*-dihalogenoethylenes or *cis*-dicyanoethylene in-plane orbitals often show I_v's different from those of the corresponding *trans*-isomer because of the difference in the through-bond and through-space interactions[7] between these isomers. Wittel and coworkers[8] have demonstrated the importance of spin-orbit coupling in the case of iodoethylenes.

We have studied the PES of *cis*- and *trans*-stilbenes, dimethyl maleate, and dimethyl fumarate for the purpose of clarifying experimentally and explaining theoretically the difference in PES between the corresponding *cis*- and *trans*-isomers. The PES of fumaric acid has also been studied for the sake of comparison. Concerning the PES of *cis*- and *trans*-stilbenes, a brief report was published by Maier and Turner[9] after our work had been completed. In this paper, we report the more details of the PES of *cis*- and *trans*-stilbenes.

Experimental and Theoretical

cis-Stilbene was purified with the alumina column chromatography, *trans*-stilbene and fumaric acid by recrystallization from ethanol and aqueous ethanol, respectively. Dimethyl maleate was purified by distillation and dimethyl fumarate by sublimation.

The PES of these compounds were measured with the photoelectron spectrometer described previously,[10] 584 Å He resonance line being used as the excitation source. The sample inlet and target chamber system was heated to 97 °C for *trans*-stilbene, 46 °C for *cis*-stilbene, 124 °C for fumaric acid and 38 °C for dimethyl fumarate and 47 °C for dimethyl maleate.

The CNDO/2[11] calculations of the compounds under consideration were carried out with a FACOM 230—60 computer at the Institute of Physical and Chemical Research. Their structures were properly assumed on the basis of the appropriate structural data given in Refs. 12, 13, and 14.

Results and Discussion

cis- and trans-Stilbenes. The observed PES of *cis*- and *trans*-stilbenes are shown in Fig. 1 and those

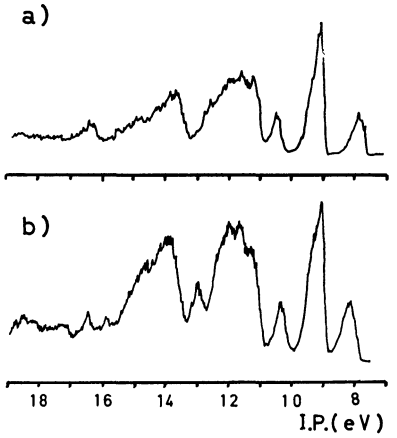

Fig. 1. Photoelectron spectra of (a) *trans*-stilbene and (b) *cis*-stilbene.

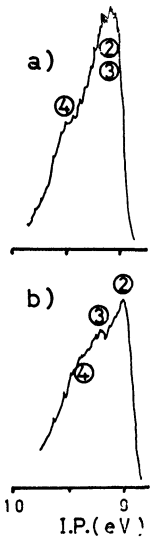

Fig. 2. Expanded photoelectron spectra in the 8.5~10 eV region: (a) *trans*-stilbene; (b) *cis*-stilbene.

Table 1. Vertical ionization potentials of stilbenes and related compounds in eV

PES band	1	2	3	4	5	6
cis-Stilbene	8.17	8.99	9.22	9.36	10.27	11.3
trans-Stilbene	7.87	9.08	9.08	9.50	10.51	11.3
Benzene[a)]	9.23	11.67	12.32	13.97		
Ethylene[b)]	10.51	12.85	14.66	15.87		

a) T. Kobayashi and S. Nagakura, *Chem. Lett.*, **1972**, 903. b) Ref. 16.

measured on the expanded energy scale around 9~10 eV are shown in Fig. 2, and the I_v's of these compounds and related ones obtained from the PES are summarized in Table 1.

The stilbenes commonly show three groups of bands in the region of 7.5~11 eV. This is also the region for the benzene $e_{1g}\pi$[15] (9.23 eV) and ethylene $b_{3u}\pi$ (10.51 eV[16]) bands. The stilbenes contain two benzene rings and one ethylene group. So it is quite reasonable to consider that the observed three groups of bands correspond to the five occupied π orbitals constructed mainly from the four benzene $e_{1g}\pi$ orbitals and one ethylenic π orbital.

The experimental orbital energy diagram obtained on the assumption $\varepsilon=-I_v$ (Koopmans' theorem[17]) is shown in Fig. 3.

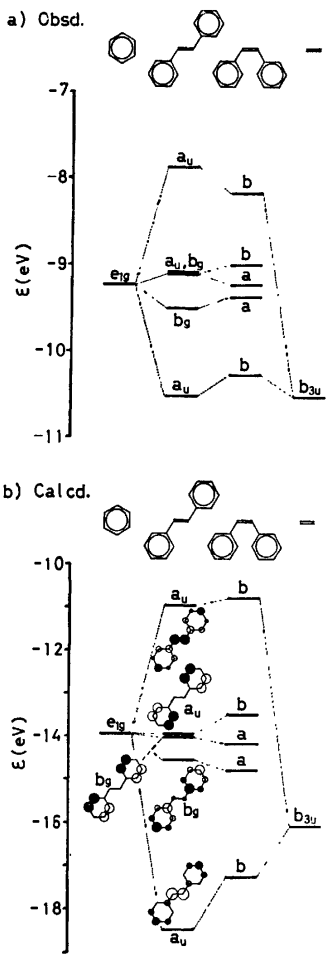

Fig. 3. Observed and calculated π orbital energy diagrams for stilbenes.

The CNDO/2 calculations and also qualitative consideration show that the first and fifth bands of each isomer should be assigned to the ionizations from two π orbitals in which the two benzene rings and the ethylene group interact strongly and, therefore, π electrons delocalize over the entire molecular carbon framework; the higher one corresponding to the highest occupied π orbital of each isomer is antibonding in the nature of the C–C bonds connecting the benzene rings with the ethylene group and the lower one corresponding to the fifth highest occupied π orbital of each isomer is bonding.

According to the CNDO/2 calculations the second and third bands of each isomer should be assigned to the two occupied π orbitals completely localized on the two benzene rings. This is consistent with the fact that the I_v's of both bands are close to that of the first band of benzene corresponding to the ionization from the $e_{1g}\pi$ orbitals.

According to the CNDO/2 calculations the fourth band of each isomer should be assigned to the π orbital almost completely localized on the benzene rings but slightly mixed with the antibonding π orbital of the ethylene group. The fact that the I_v of the band is only slightly greater than that of the first band of benzene, supports this assignment. The slight mixing of the vacant antibonding π orbital of the ethylene group shifts the fourth band to the slightly higher ionization energy side than the second and third bands.

The PES of *cis*- and *trans*-stilbenes are different from each other in the following points:

i) The splitting between the first and fifth bands of *cis*-stilbene (2.10 eV) is smaller than that of *trans*-stilbene (2.64 eV). This can be explained in terms of the fact that in the *cis*-isomer the conjugation between the ethylenic group π orbital and the benzene ring π orbitals decreases because of the twisting of the two benzene rings from the molecular plane caused by the steric hindrance effect between them.[13] This was pointed out also by Maier and Turner.[9]

ii) The second and third bands of *cis*-stilbene split by 0.2 eV but those of *trans*-stilbene are almost degenerate. This fact can be explained as follows. The corresponding π orbitals of *trans*-stilbene are completely localized on the two benzene rings and the I_v's of these orbitals should be equal to each other. On the other hand, in the case of *cis*-stilbene the two benzene rings approach each other so closely that the $p\pi$ atomic orbitals at the *ortho* positions can overlap with each other, though slightly. This is a reason why the second and third bands split from each other for the *cis*-isomer. This tendency was qualitatively reproduced by the CNDO/2 calculation (see Fig. 3). Therefore this difference between the *trans*- and *cis*-isomers is due to the so-called through-space interaction[7] at the classically non-bonded position.

Fumaric Acid, Dimethyl Fumarate, and Dimethyl Maleate. The PES of fumaric acid, dimethyl fumarate, and dimethyl maleate are shown in Fig. 4. The PES of dimethyl fumarate and dimethyl maleate measured on the expanded energy scale around 10~12 eV are shown in Fig. 5.

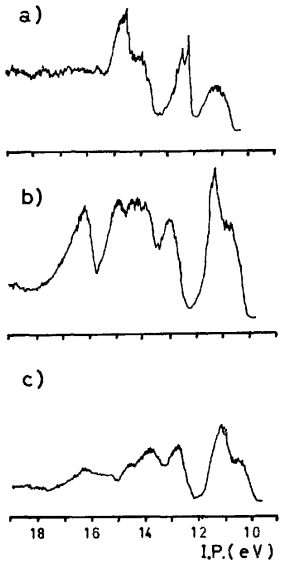

Fig. 4. Photoelectron spectra of (a) fumaric acid, (b) dimethyl fumarate, and (c) dimethyl maleate.

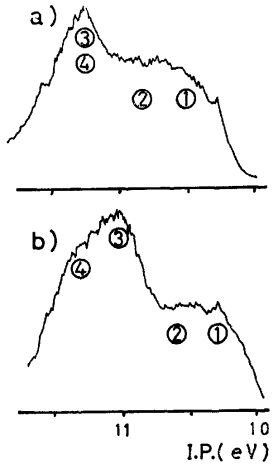

Fig. 5. Expanded photoelectron spectra around 11 eV: (a) dimethyl fumarate; (b) dimethyl maleate.

TABLE 2. VERTICAL IONIZATION POTENTIALS OF FUMARIC ACID, DIMETHYL FUMARATE, DIMETHYL MALEATE, AND RELATED COMPOUNDS IN eV

PES band	1	2	3	4	5
Fumaric acid	10.9	11.1	12.15	12.41	13.9
Dimethyl fumarate	10.5	10.8	11.27	11.27	12.91
Dimethyl maleate	10.3	10.6	11.04	11.3	12.77
Acetic acid[a)]	10.87	12.05			
Methyl acetate[a)]	10.48	11.16			

a) Ref. 18.

The vertical ionization potentials of these compounds and related ones obtained from their PES are summarized in Table 2.

The correlation diagram for the higher occupied orbitals of these compounds obtained on the assumption $\varepsilon = -I_v$ (Koopmans' theorem[17]) is shown in Fig. 6. The calculated orbital energy diagram given by the CNDO/2 method is also shown in Fig. 6 for the sake of comparison.

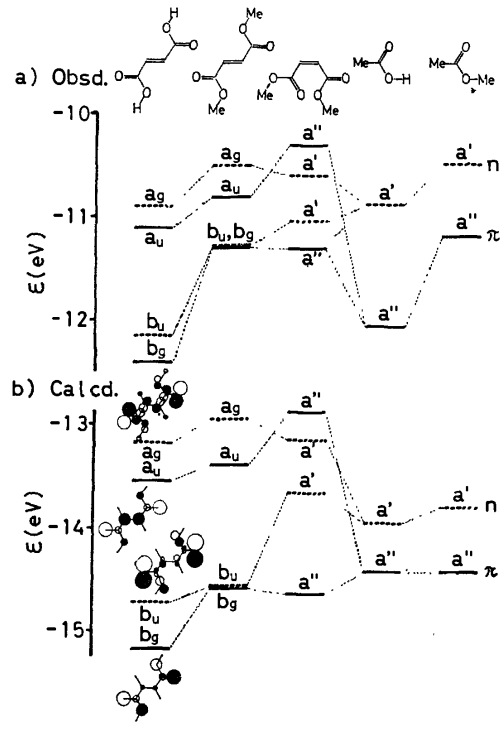

Fig. 6. Observed and calculated orbital energy diagrams for fumaric acid, dimethyl fumarate, and dimethyl maleate.

The PES of fumaric acid has two groups of bands in the region of 10.5~13 eV. This is also the region for the bands of the acetic acid carbonyl n (10.87 eV[18]) and carboxyl π (12.05 eV[18]) orbitals and also for the band of the ethylenic π orbital (10.51 eV[16]). So the observed bands under consideration may correspond to the molecular orbitals constructed by the interaction among the two n orbitals and two π orbitals of the two carboxyl groups and the ethylenic π orbital.

The calculated orbital energy diagram for fumaric acid can explain satisfactorily from the qualitative point of view the observed relative pattern of the first two groups of bands. The calculation suggests that the first group of bands may correspond to $a_g n$ and $a_u \pi$ orbitals and the second group of bands to $b_u n$ and $b_g \pi$ orbitals from the top, respectively.

Sweigart and Turner[18] studied the assignment of the PES of acetic acid and showed that the n band of the acid is quite sharp and the π band is rather broad. According to our CNDO/2 calculation of fumaric acid the fourth highest occupied molecular orbital, $b_g \pi$ orbital, is quite similar to the corresponding π orbital of acetic acid, and the third highest occupied molecular orbital, $b_u n$ orbital, is of the nonbonding nature and is almost completely localized on the two carbonyl groups. So it is reasonable to assign the sharp band at 12.15 eV to the ionization from the third highest occupied $b_u n$ orbital. Accordingly, the remaining fourth band at 12.41 eV may be assigned to the fourth highest occupied $b_g \pi$ orbital.

The first and second bands highly overlap with each other. The CNDO/2 calculation indicates that they are assigned to $a_g n$ and $a_u \pi$ orbitals, respectively.

Here let us turn to dimethyl fumarate and dimethyl maleate. The CNDO/2 calculations predict that the third and fourth highest occupied orbitals are nearly accidentally degenerate for dimethyl fumarate and split from each other for dimethyl maleate. The experimental result shown in Fig. 5 satisfies this prediction. Furthermore, according to the CNDO/2 calculations, the fourth highest occupied orbitals of both compounds are almost completely composed of the carbomethoxyl π orbitals and have almost the same energy. In agreement with this prediction, the observed fourth bands of both compounds show almost the same I_v's; 11.27 eV for dimethyl fumarate and 11.3 eV for dimethyl maleate. Therefore, the fourth bands of both compounds may reasonably be assigned to the fourth highest occupied π orbitals obtained by the CNDO/2 calculations. The fact that the I_v's of these bands are close to the carbomethoxyl π I_v of methyl acetate, 11.16 eV,[18] also supports this assignment.

The third band of dicarbomethoxyethylenes may be assigned to the n orbitals, b_un in dimethyl fumarate and a'n in dimethyl maleate. The b_un I_v of the former is larger than the corresponding a'n I_v of the latter. This difference between both isomers is brought about by through-bond interaction. According to the CNDO/2 calculations, the through-bond interaction between the carbonyl n orbitals is greater for the *cis*-isomer than for the *trans*-isomer.

According to the CNDO/2 calculations the first and second bands of dimethyl fumarate may be assigned to the a_gn and $a_u\pi$ orbitals, respectively, and those of dimethyl maleate to the a''π and a'n orbitals, respectively. The overall qualitative agreement between the pattern of the calculated orbital energy diagram and the observed spectral pattern may support the assignment predicted by the CNDO/2 method for fumaric acid, dimethyl fumarate, and dimethyl maleate.

The authors wish to express their sincere gratitude to Prof. H. Bock of the University of Frankfurt for his kindness to allow us to read his manuscripts before publication.

References

1) N. Jonathan, K. Ross, and V. Tomlinson, *Int. J. Mass Spectrom. Ion Phys.*, **4**, 51 (1970).
2) R. F. Lake and H. Thompson, *Proc. Roy. Soc. Ser. A.*, **315**, 323 (1970).
3) D. Chadwick, D. C. Frost, A. Katrib, C. A. McDowell, and R. A. N. McLean, *Can. J. Chem.*, **50**, 2642 (1972).
4) H. Bock and H. Stafast, *Chem. Ber.*, **105**, 1158 (1972).
5) K. Wittel and H. Bock, *ibid.*, **107**, 317 (1974).
6) H. Bock, G. Wagner, K. Wittel, J. Sauer, and D. Seebach, to be published.
7) R. Hoffmann, A. Imamura, and W. J. Hehre, *J. Amer. Chem. Soc.*, **90**, 1499 (1968).
8) K. Wittel, H. Bock, and R. Manne, *Tetrahedron*, **30**, 651 (1974).
9) J. P. Maier and D. W. Turner, *J. Chem. Soc. Faraday II*, **69**, 196 (1973).
10) T. Kobayashi, K. Yokota, and S. Nagakura, *J. Electron Spectrosc.*, **3**, 449 (1973).
11) J. A. Pople and G. A. Segal, *J. Chem. Phys.*, **44**, 3289 (1966).
12) "Interatomic Distances", Sp. Pub. No. 11, ed. by L. E. Sutton, The Chem. Soc., London (1958); "Interatomic Distances", Sp. Pub. No. 18, ed. by L. E. Sutton, The Chem. Soc., London (1965).
13) G. Rasch, *Z. Phys. Chem.* (Leipzig), **219**, 180 (1962).
14) C. J. Brown, *Acta Crystallogr.*, **21**, 1 (1966).
15) D. W. Turner, C. Baker, A. D. Baker, and C. R. Brundle, "Molecular Photoelectron Spectroscopy", John Wiley & Sons, London (1970).
16) C. R. Brundle, M. B. Robin, N. A. Kuebler, and H. Basch, *J. Amer. Chem. Soc.*, **94**, 1451 (1972).
17) T. Koopmans, *Physica*, **1**, 104 (1934).
18) D. A. Sweigart and D. W. Turner, *J. Amer. Chem. Soc.*, **94**, 5592 (1972).

ESR Studies on the Anion Radicals of Some Triptycene and [2.2]Paracyclophane Derivatives

Toyoharu HAYASHI, Noboru MATAGA, Yoshiteru SAKATA,* and Soichi MISUMI*

Department of Chemistry, Faculty of Engineering Science, Osaka University, Toyonaka, Osaka 560

**Institute of Sciencific and Industrial Research, Osaka University, Suita, Osaka* 565

(Received September 14, 1974)

ESR spectra of anion radicals of some triptycene and [2.2]paracyclophane derivatives were observed and analyzed in order to study the delocalization interactions between composite aromatic rings.

It is important to study the delocalization interactions between the groups when a molecule contains two or more π-electronic groups separated by saturated chemical bonds. The mechanisms of charge transfer complex formation and of electron transfer reaction are closely connected with this problem. One can investigate electron transfer between the composite aromatic rings in anion radicals of [2.2]paracyclophane and triptycene derivatives by means of ESR measurements.

Weissman[1] reported the fast exchange or delocalization of the unpaired electron between the two benzene rings of the [2.2]paracyclophane anion. Furthermore, Gerson and Martin[2] observed that the unpaired electron in the anion radical of [2.2]paracyclophane in DME(dimethoxyethane) is completely delocalized between the two benzene rings, while it is only partially delocalized in the case of the THF (tetrahydrofuran) solution. In the latter solution, the interaction of the unpaired electron with the counter ion seems to suppress the complete delocalization.

Recently, Williams *et al.*[3] made ESR studies on anion radicals of some paracyclophane derivatives, [2.2](9,10)anthracenophane and [2.2](1,4)naphthalenophane. On the basis of their experimental results, they indicated that the unpaired electron is completely delocalized in the case of [2.2](1,4)naphthalenophane. However, they failed to determine its constants. On the other hand, Dessau[4] reported the complete delocalization of aromatic cationic site in the study of triptycene cation radical.

We have made also some ESR and optical studies on triptycene 1,4-quinone anion and 1,4-dimethoxytriptycene cation radicals, and have found out that there are no significant intramolecular delocalizations of the excess electron or the positive hole in the case of these ion radicals.[5] These results may be of some interest from the viewpoint of the electronic structures of ions and molecular complexes in solution. In the present paper, we discuss the results of ESR studies on anion radicals of related compounds, including benzotriptycene (abbreviated as I–1), dibenzotriptycene (I–2), naphthobenzotriptycene (I–3), [2.2](9,10)anthracenophane (II–1), and others.

Experimental

Triptycene and paracyclophane derivatives were synthesized and purified as reported elsewhere.[6] Commercially available THF and DME were dried over sodium sulphate, refluxed over metallic sodium wire for a day, and fractionally distilled. These solvents were degassed completely in the presence of metallic sodium flakes, distilled several times, and finally stored over the sodium-potassium alloy in a vacuum.

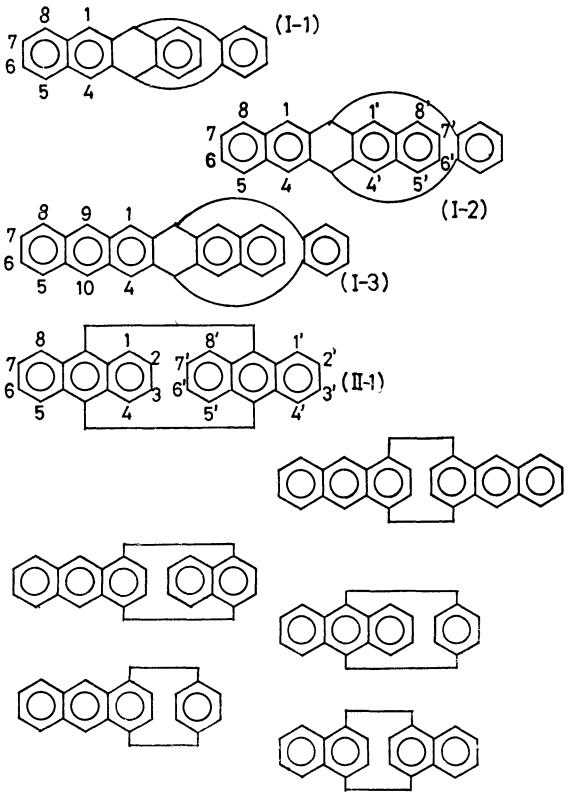

Fig. 1.

The purified solvent was distilled into the sample tube containing the compound. The solution was stirred with a magnetic stirrer and deaerated completely. Alkali metal mirror was formed inside the glass tube after distilling the alkali metal several times. The sample tube containing the alkali metal mirror and the sample solution (separated by a breakable seal from the mirror) was sealed off the evacuating system and immersed in a dry ice–ethanol bath. Then, the solution was put in contact with the metal mirror.

A tube containing anion radical solution prepared by the method as described above was placed in the microwave cavity cooled below −80 °C by the cold nitrogen gas flow. Temperature was then raised near to −50 °C carefully in order to attain the best condition for detecting the ESR signal. When the temperature was raised further, the anion radical was converted to some diamagnetic species and the ESR signal intensity was not recovered when the temperature was lowered again.

Some compounds were examined also by the method of electrochemical reduction in order to exclude the effect of the counter ion. These studies were conducted at room

temperature with dimethylformamide(DMF) solutions, and halfwave potentials were also determined. The electrochemical measurements were kindly performed by Drs. T. Kubota and H. Miyazaki of Shionogi Research Laboratory.

The ESR spectra were recorded with a JES-ME-2X or 3BX spectrometer using X-band. The simulation of the spectra, assuming the Lorentzian line shape and appropriate line widths, were made by using the HITAC-700.

Results and Discussion

Benzotriptycene Anion Radical. The anion radical was prepared by the electrochemical reduction in DMF at room temperature. The halfwave potential, $E_{1/2}=-2.58$ V *vs.* SCE, is nearly the same as that of naphthalene. The spectrum in Fig. 2 shows a hfs due to a set of four equivalent protons and a set of two equivalent protons. Their hfs constants are $A_1=3.43$ gauss(G) and $A_2=1.24$ G, respectively. In conformity with the case of 2,3-dimethylnaphthalene anion radical, we assume that the constant A_1 is due to the protons in positions 5, 6, 7, 8, namely H_5, H_6, H_7, H_8, and A_2 to protons H_1, H_4. The contribution from the two bridgehead protons are not very clear being masked by the relatively large line widths (about 0.5 G). It is suggested that four equivalent protons are further separated to two sets of two equivalent protons because of the fact that the line widths of outer lines are a little larger than those of inner ones. In any way, since we cannot observe any hfs due to the delocalization of the unpaired electron on two benzene rings, the odd electron seems to be well localized on the naphthalene ring.

Dibenzotriptycene Anion Radical. The spectrum obtained by either electrochemical reduction in DMF at the first reduction potential or reduction with sodium metal in DME at -78 °C is exactly the same. Therefore, the spectrum obtained by reduction with sodium metal does not seem to be affected significantly by the counter ion. The first and second half-wave

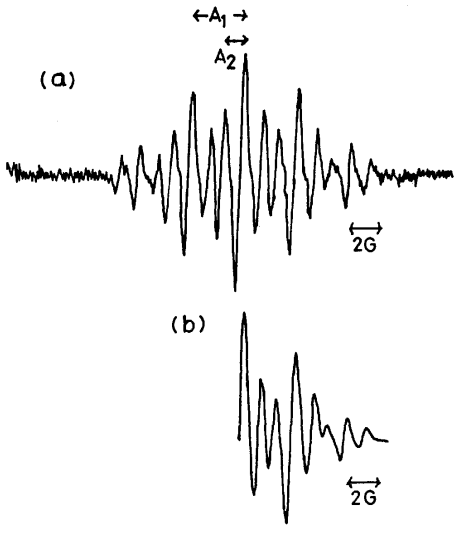

Fig. 2. (a) ESR spectrum of benzotriptycene (I-1) anion radical generated by electrolytic reduction; solvent DMF room temperature, (b) Computer simulated spectrum.

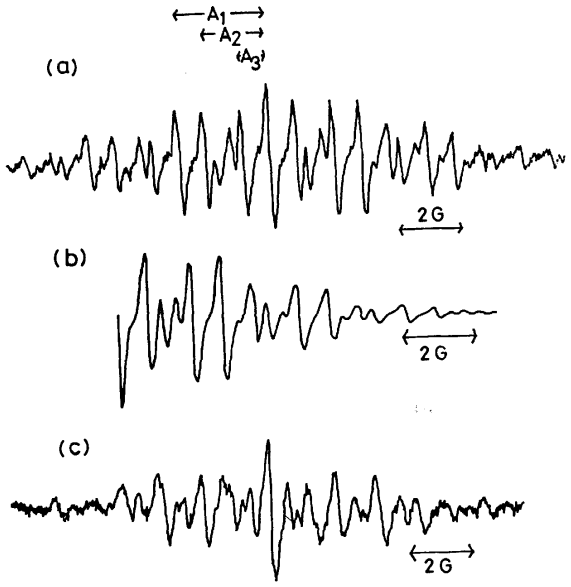

Fig. 3. (a) ESR spectrum of dibenzotriptycene (I-2) anion radical generated by sodium metal reduction; solvent dimethoxyethane (DME), temperature -50 °C. (b) Computer simulated spectrum. (c) Generated by electrolytic reduction at second reduction potential, solvent DMF, room temperature.

Table 1. Assignment of the hfs constants of dibenzotriptycene anion radical (I-2) in comparison with those of 2,3-dimethylnaphthalene anion radical (DMN) (in units of G)

	DMN	I-2
a_1, a_4 (a_1', a_4')	4.09	2.02
a_5, a_8 (a_5', a_8')	5.20	2.83
a_6, a_7 (a_6', a_7')	1.73	0.81
a (CH_3)	1.73	

reduction potentials were $E_{1/2}=-2.65$ V and -2.85 V *vs.*, SCE respectively. We have not yet completed the analysis of the spectrum at the second reduction potential. The spectrum obtained by the reduction with sodium metal in DME is shown in Fig. 3. Its hfs seems to be ascribed to three sets of four equivalent protons, their hfs constants being $A_1=2.93$ G, $A_2=2.09$ G, and $A_3=0.89$ G, respectively. The assignment of hfs constants was made as indicated in Table 1. One can see from the table that the hfs constants of (I-2) are about one-half of the corresponding ones of the 2,3-dimethylnaphthalene anion radical. Thus, it may be concluded that the unpaired electron is completely delocalized over the two naphthalene rings. However, it is not delocalized on the benzene ring.

Naphthobenzotriptycene Anion Radical. The ESR spectrum of (I-3) obtained by reduction of the neutral molecule with sodium metal in DME is shown in Fig. 4a. Its hfs can be ascribed to a set of two equivalent protons ($A_1=5.44$ G), a set of four equivalent protons ($A_2=2.88$ G), a set of two equivalent protons ($A_3=1.52$ G), and a set of two equivalent protons ($A_4=0.25$ G). The assignment of these hfs constants was made as indicated in Table 2, where they are

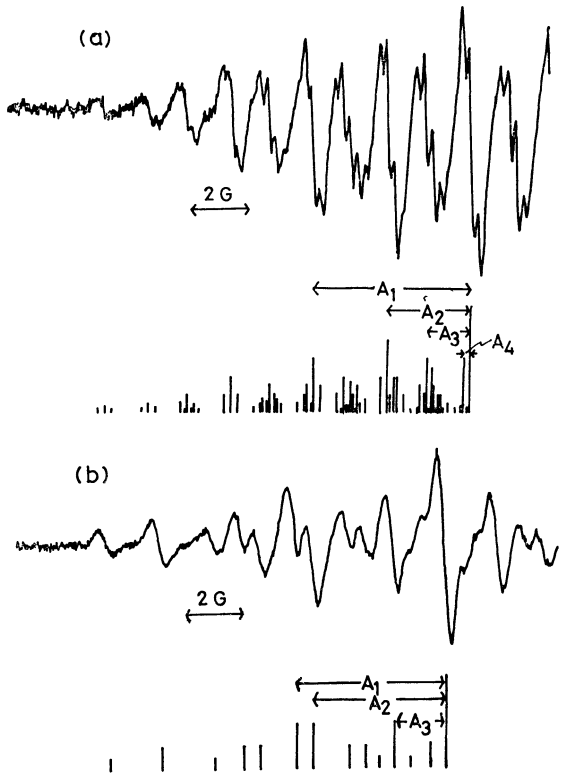

Fig. 4. ESR spectrum of naphthobenzotriptycene (I-3) anion radical; (a) solvent DME, temperature −50 °C, sodium metal reduction, (b) solvent THF, temperature −50 °C, sodium metal reduction.

TABLE 2. ASSIGNMENT OF THE hfs CONSTANTS OF NAPHTHOBENZOTRIPTYCENE ANION RADICAL (I-3) IN COMPARISON WITH THOSE OF ANTHRACENE ANION RADICAL (A).
(in units of G)

	A	I-3
a_1, a_4, a_5, a_8	2.66	2.88
a_6, a_7	1.53	1.52
a_9, a_{10}	5.28	5.44

compared with those of anthracene anion radical. The assignment of A_4 to the bridgehead protons seems to be quite reasonable. As far as we know, there has been no clear-cut observation of hfs due to the bridgehead protons of triptycene. For example, Stock and Suzuki[7] investigated the semiquinone anion radicals of 1,4-dihydroxytriptycene and 9-methyl-1,4-dihydroxytriptycene, and Dessau[4] studied the cation radical of triptycene. However, the hfs due to the bridgehead protons was not observed clearly in both cases being covered with rather large line widths. In any way, the present result clearly show that the unpaired electron in (I-3) is well localized on anthracene ring.

In contrast to other compounds investigated here, (I-3) gave a quite different spectrum when the reduction was conducted in THF as indicated in Fig. 4b. Its hfs can be analyzed, but its origin is not yet elucidated. The hfs of the spectrum can be ascribed to three sets of two equivalent protons, their hfs constants being A_1=5.4 G, A_2=4.8 G, and A_3=1.8 G, respectively. It appears that we can ascribe formally this ESR spectrum to an unpaired electron being on the naphthalene composite ring. However, that the unpaired electron is on the naphthalene ring in (I-3) is highly improbable.

On reduction in THF, the solution becomes purple at first, which is also the characteristic color of the anion formed in DME solution, and then the color of solution changes drastically to blue on further reduction by sodium or potassium metal in Dry Ice-ethanol bath. We have confirmed that this phenomenon does not occur even in mixed solvents of DME and THF, the volume ratio of DME to THF being changed from 1 to 0.1.

This remarkable solvent effect might be explained as follows. It seems to be more easy to make anion-metal cation ion-pair in THF than in DME, since the solvation of ions is stronger in DME than in THF, leading to dissociation of the pairs in DME. Therefore, the ion-pair is formed in THF, and two anion radicals may be linked together, assisted by the positive counter ions, at the position of anthracene composite ring to become diamagnetic, since the unpaired electron is located on this ring. On further reduction, the naphthalene ring may react with alkali metal, and the ESR spectrum of naphthalene anion radical may be obtained. Some other explanations than this might be possible including the mechanism assuming the decomposition of the compound on reduction. Further studies on the problem is now going on in our laboratory.

[2.2](9,10)Anthracenophane Anion Radical. The anion radical prepared in DME at −78 °C gave too complicated ESR spectra to be analyzed completely. However, when the temperature was carefully raised near to but a little below 0 °C and again lowered to −50 °C, quite neat spectrum was obtained. The spectrum indicated in Fig. 5 shows hfs due to three sets of eight equivalent protons, and their hfs con-

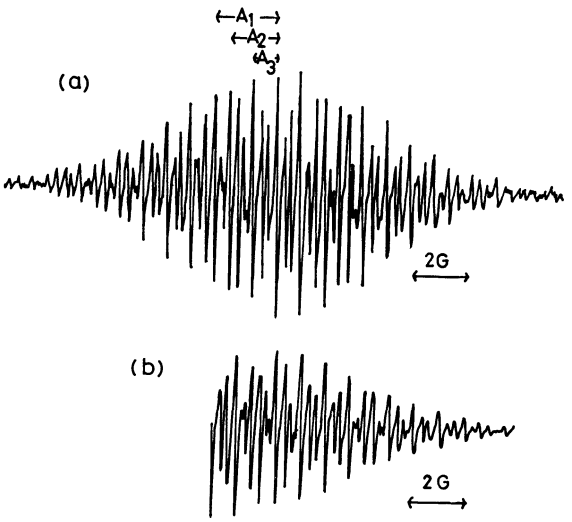

Fig. 5. (a) ESR specturm of [2.2](9,10)anthracenophane anion radical; solvent THF, temperature −50 °C, sodium metal reduction, (b) Computer simulated spectrum.

stants are $A_1=2.14$ G, $A_2=1.63$ G, and $A_3=0.82$ G, respectively. Computer simulated spectrum is in a good agreement with the observed.

Williams *et al.*[3] also reported the ESR spectra of (II-1). However, they failed to analyze the complicated spectra. Their spectra were similar to those we have obtained just after the preparation of the anion radicals at −78 °C in DME. Only the hfs constant of the methylene protons was determined by them to be 1.63 G, using the deuteration technique. This value of the hfs constant is exactly the same as our A_2 value. The complicated spectrum obtained immediately after the preparation of radicals at −78° C seems to be a superposition of the spectra of several species probably including some paramagnetic decomposition products. When the temperature was raised up to near 0 °C the decomposition products were presumably converted to some diamagnetic species, and finally some portion of (II-1) remained. Our assignment was performed by taking into consideration the ESR spectra of 9,10-dimethylanthracene and also the results of Williams *et al.* The hfs constants of (II-1) are compared with those of 9,10-dimethylanthracene in Table 3. These results seem to indicate that the unpaired electron is completely delocalized over the two anthracene rings.

We have measured also ESR spectra of anion radicals of other paracyclophane derivatives. Among them are [2.2]paracycloanthracenophanes, [2.2](1,4)-naphthaleno(1,4)anthracenophane, and anti-[2.2](1,4)-anthracenophane.[6] Their ESR spectra are very complicated, and we have not yet attained to any complete agreement between the experimental and computer simulated spectra. Only can it be said that the unpaired electron is fairly well delocalized over the different composite aromatic rings in the case of these paracyclophane derivatives in contrast to the case of triptycene derivatives where the localization of the unpaired electron on the aromatic ring with the largest electron affinity prevails. This result seems to be reasonable in view of the stronger interaction between the composite aromatic rings in the paracyclophane derivatives than in the triptycene derivatives.

From the results of the present investigation, one may conclude that, in the case of the triptycene derivatives, the unpaired electron is localized on a aromatic ring of the largest electron affinity, and when the triptycene derivative contains the same two aromatic rings, it is completely delocalized over them. In the case of paracyclophane derivatives, the unpaired electron is delocalized over two groups even if they are different from each other.

Table 3. Assignment of the hfs constants of [2.2]-(9,10)anthracenophane anion radical (II-1) in comparison with those of 9,10-dimethylanthracene anion radical (DMA) (in units of G)

	DMA	II-1
a_1, a_4, a_5, a_8 (a_1', a_4', a_5', a_8')	2.90	2.14
a_2, a_3, a_6, a_7 (a_2', a_3', a_6', a_7')	1.52	0.82
$a(CH_3)$ or $a(CH_2)$	3.88	1.63

The authors are grateful to Drs. T. Kubota and H. Miyazaki of Shionogi Research Laboratory for the electrochemical measurements.

References

1) S. I. Weissman, *J. Amer. Chem. Soc.*, **80**, 6462 (1958).
2) F. Greson and W. B. Martin, Jr., *ibid.*, **91**, 1883 (1969).
3) D. J. Williams, J. M. Pearson, and M. Levy, *ibid.*, **93**, 5483 (1971).
4) R. M. Dessau, *J. Chem. Phys.*, **54**, 5430 (1971).
5) F. Tanaka and N. Mataga, This Bulletin, **46**, 2591 (1973).
6) a) M. Sugihashi, R. Kawagita, T. Otsubo, Y. Sakata, and S. Misumi, This Bulletin, **45**, 2836 (1972). b) T. Toyoda, I. Otsubo, T. Otsubo, Y. Sakata, and S. Misumi, *Tetrahedron Lett.*, **1972**, 1731; A. Iwama, T. Toyoda, T. Otsubo, and S. Misumi, *ibid.*, **1973**, 1725; *Chem. Lett.*, **1973**, 587.
7) L. M. Stock and J. Suzuki, *J. Amer. Chem. Soc.*, **87**, 3909 (1965).

The Triplet-Triplet Absorption Spectra and Electronic Structures of Some Cyano-Substituted Benzenes

Hiroshi MORITA, Satoru MATSUMOTO,* and Saburo NAGAKURA

The Institute for Solid State Physics, The University of Tokyo, Roppongi, Minato-ku, Tokyo 106

(Received October 7, 1974)

Triplet-triplet (T–T) absorption bands were observed at 300, 297, and 320 nm for *m*- and *p*-dicyanobenzenes, and 1,3,5-tricyanobenzene, respectively. The nature of the observed spectra was investigated by calculating the wave functions of the triplet states and by analyzing them by the configuration analysis method. It was concluded that the T–T absorption bands of *m*- and *p*-dicyanobenzenes, and 1,3,5-tricyanobenzene correspond essentially to the transition from the locally (within the benzene ring) excited state to the intramolecular charge-transfer state.

Intramolecular charge-transfer (CT) interaction between the benzene ring and substituent groups is important to understand the electronic structures of some substituted benzene molecules. A large number of studies has hitherto been made on the effect of the interaction upon the singlet-singlet transition spectra of substituted benzenes and the intramolecular CT absorption characteristic of the interaction has been observed for various substituted benzene molecules.[1–10] Only a few studies, however, have been done on triplet-triplet transition spectra of substituted benzenes. Kimura and Tsubomura[11] studied theoretically the nature of the lowest triplet state for such substituted benzenes as phenol, anisole, aniline, *p*-phenylenediamine, and *N,N,N',N'*-tetramethyl-*p*-phenylenediamine (TMPD), paying special attention to the intramolecular CT character. Experimental studies have been made on the triplet-triplet absorption spectrum of the TMPD molecule.[12,13]

In the present study, in order to elucidate the electronic structures of the excited triplet states of benzonitrile (BN), *o*-, *m*-, and *p*-dicyanobenzenes (*o*-, *m*-, and *p*-DCNB), 1,3,5-tricyanobenzene (TRCNB), and 1,2,4,5-tetracyanobenzene (TCNB), we have measured their triplet-triplet (T–T) absorption spectra at 77 K and interpreted them with the aid of the configuration analysis[14] of the wave functions obtained by the Pariser-Parr-Pople SCF MO method[15,16] combined with the configuration interaction (CI) treatment.

Experimental

Commercially available *o*-, *m*-, and *p*-DCNB's of G.R. grade were purified by recrystallization from water, ethyl acetate, and methanol, respectively. TRCNB was prepared by the method described in the literature[17,18] and purified by recrystallization from methanol and thereafter from ethyl acetate. TCNB was purified by vacuum sublimation. Commercially available BN of G.R. grade was used without further purification.

The T–T absorption spectra were measured at 77 K in ethyl ether–isopentane (1 : 1) mixed solvent (EP). The samples were excited by a 500 W super-high-pressure mercury lamp. The details of the measurement were described in a previous paper.[19]

* Present address: Pioneering Research and Development Laboratories, Toray Industries, Inc., Sonoyama, Otsu, Shiga 520.

Theoretical

The π-electron structures of the ground and triplet excited states were calculated for all the molecules under consideration by taking the configuration interaction among all the singly excited configurations constructed from the Pariser-Parr-Pople SCF MO's.[15,16] The semi-empirical parameters chosen by Iwata *et al.*[20] for TCNB complexes were used for the present calculation. Electron paramagnetic resonance[21] and optical[22] studies of the lowest triplet states of benzene and methyl-substituted benzenes like toluene and mesitylene show that the geometrical structure of the benzene ring deviates from the hexagonal symmetry in the lowest triplet state. Slight distortion of the benzene ring from the hexagonal symmetry is also expected for the triplet states of the cyano-substituted benzene molecules under consideration. Because of the lack of the quantitative knowledge on the geometrical structures of their lowest triplet states, however, we assume in the present calculations that the molecules are planar and their benzene rings are of the hexagonal symmetry. The bond lengths are taken as follows; 1.39 Å for the C–C bond in the benzene ring, 1.46 Å for the C–C bond between the benzene ring and the substituent group, and 1.16 Å for the C≡N bond in the cyano group.

The wave functions obtained for some triplet states and the ground states of *m*- and *p*-DCNB's and TRCNB were analyzed with the aid of the configuration analysis method.[14] In the analysis, MO's of the benzene ring and those of the substituent groups were taken as the reference MO's. This choice of the reference MO's is appropriate to elucidate the intramolecular CT and locally excited (LE) characters for the triplet states of *m*- and *p*-DCNB's and TRCNB. In order to obtain the satisfactory convergence in the configuration analysis, it is necessary to take doubly excited configurations in addition to the singly excited ones.

Results and Discussion

As is shown in Fig. 1, the T–T absorption bands were observed at 300, 297, and 320 nm for *m*-DCNB, *p*-DCNB, and TRCNB, respectively. We measured the T–T absorption in the region 290~700 nm. But we

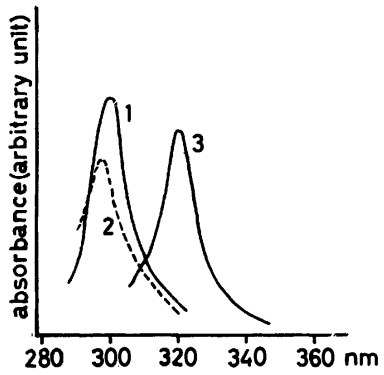

Fig. 1. T-T absorption spectra observed with (1) *m*-DCNB, (2) *p*-DCNB, and (3) TRCNB in EP solutions at 77 K.

could observe no band in the longer wavelength region for the respective molecules. Therefore, the observed bands are the longest wavelength band for the respective molecules. The observed T-T transition energies are listed in Table 1. We could observe no T-T absorption band for BN and *o*-DCNB in the wavelength region available in the present experiment. Concerning TCNB, we could not obtain any conclusive result on the T-T absorption.[23]

Table 1. The T-T transition energies (ΔE) and oscillator strengths (f) obtained experimentally and theoretically for benzene, BN, *o*-, *m*-, and *p*-DCNB's, TRCNB, and TCNB

	Obsd	Calcd		
	ΔE(eV)	ΔE(eV)	f	Upper state
Benzene	2.88[a]	2.91	0.000	T_4[d]
	5.36[b] (~5.17)[c]	5.49	0.180×2	T_5[d]
BN		4.52	0.498	T_8
o-DCNB		4.56	0.494	T_9
		4.59	0.138	T_{10}
m-DCNB	4.13	4.38	0.425	T_9
p-DCNB	4.17	4.22	0.783	T_9
TRCNB	3.87	4.27	0.228×2	T_7[d]
TCNB	(3.87)[e]	4.01	0.625	T_{11}

a) See Ref. 26. b) See Ref. 27. c) See Ref. 28. d) Degenerate upper state. e) See Ref. 23.

In Table 2, the calculated T-T transition energies and oscillator strengths of *m*-DCNB, *p*-DCNB, and TRCNB are tabulated. From the comparison between the observed and calculated transition energies and absorption intensities, the observed T-T absorption bands of *m*-DCNB, *p*-DCNB, and TRCNB are safely assigned to the transitions to the T_9, T_9, and degenerate T_7 states, respectively.

The triplet states of benzene, BN, *o*-DCNB, and TCNB were also calculated. The calculated transition energies of the T-T absorption bands that are expected to appear with considerable intensities in the longest wavelength region are tabulated in Table 1, together with the results of *m*- and *p*-DCNB's and TRCNB. The transition energies of benzene were calculated to be 2.91 and 5.49 eV for the transitions to the $^3E^+_{2g}$ and $^3E^-_{2g}$ states, respectively. These calculated values agree well with the observed values, 2.88 and 5.36 (or ~5.17) eV.[26-28] This agreement seems to show the validity of the present calculation and to support the assignment of the T-T absorption bands observed with *m*- and *p*-DCNB's and TRCNB. The transitions to the T_8 state of BN and the T_9 and T_{10} states of *o*-DCNB are theoretically expected to be observed with considerable intensity near 4.5 eV (~270 nm): this is consistent with the experimental fact that no corresponding bands were observed at wavelengths greater than 290 nm.

As shown in Table 1, the T-T transition energies of the substituted benzenes under consideration are calculated to be at least 1 eV smaller than that of benzene. This is due to the interaction between the locally excited and intramolecular CT (between the substituent group and the benzene ring) configurations. In order to clarify the situation in more detail, the results of the configuration analysis for the T_1 and T_9 states of *m*- and *p*-DCNB's are tabulated in Table 3 and those for the T_1 and T_7 states of TRCNB are tabulated in Table 4. In these tables, the results of the ground states of the respective compounds are

Table 2. The T-T transition energies (ΔE) and oscillator strengths (f) calculated for *m*-DCNB, *p*-DCNB, and TRCNB

Transition	*m*-DCNB		*p*-DCNB		TRCNB	
	ΔE(eV)	f	ΔE(eV)	f	ΔE(eV)	f
$T_2 \leftarrow T_1$	0.66	0.000	0.86	0.000	0.76[a]	0.000
$T_3 \leftarrow T_1$	1.13	0.000	1.07	0	1.44	0
$T_4 \leftarrow T_1$	1.37	0	1.29	0	1.46[a]	0.000
$T_5 \leftarrow T_1$	1.53	0.000	1.74	0	1.86	0
$T_6 \leftarrow T_1$	1.94	0.000	2.06	0	3.06[a]	0.003×2
$T_7 \leftarrow T_1$	2.97	0.001	2.86	0.000	4.27[a]	0.228×2
$T_8 \leftarrow T_1$	3.14	0.002	3.27	0.004	5.07	0
$T_9 \leftarrow T_1$	4.38	0.425	4.22	0.783	5.25[a]	0.104×2
$T_{10} \leftarrow T_1$	4.63	0.104	4.81	0.004	5.42	0
$T_{11} \leftarrow T_1$	5.07	0.038	5.00	0	5.68[a]	0.015×2

a) Degenerate upper state.

Table 3. The results of the configuration analysis (weights) obtained for the ground, T_1, and T_9 states of *m*- and *p*-DCNB's

Group	*m*-DCNB			*p*-DCNB		
	G	T_1	T_9	G	T_1	T_9
G^0	0.6945			0.6934		
A	0.0006	0.4688	0.2166	0.0005	0.4412	0.1762
A'		0.0001			0.0002	0.0001
A + B		0.1120	0.0846		0.1067	0.0778
B	0.1502	0.1564	0.0498	0.1508	0.1724	0.0774
B'		0.0169	0.0053		0.0187	0.0080
(Total from G^0 and LE configurations)	(0.8453)	(0.7542)	(0.3563)	(0.8447)	(0.7392)	(0.3395)
C	0.0716	0.0624	0.3276	0.0708	0.0710	0.3488
C + A		0.0368	0.0184		0.0324	0.0136
C + B		0.0298	0.0626		0.0332	0.0752
C'		0.0030	0.0170		0.0036	0.0082
(Total from CT_1 configurations)[a]	(0.0716)	(0.1320)	(0.4256)	(0.0708)	(0.1402)	(0.4458)
D	0.0418	0.0506	0.1516	0.0430	0.0588	0.1600
D + A		0.0231	0.0108		0.0202	0.0080
D + B		0.0102	0.0228		0.0116	0.0214
D'		0.0015	0.0044		0.0017	0.0022
(Total from CT_2 configurations)[b]	(0.0418)	(0.0854)	(0.1896)	(0.0430)	(0.0923)	(0.1916)
Total	0.9587	0.9716	0.9715	0.9585	0.9717	0.9769

a) CT configurations from the benzene ring to the cyano groups. b) CT configurations from the cyano groups to the benzene ring.

Table 4. The results of the configuration analysis (weights) obtained for the ground, T_1, and T_7 states of TRCNB

Group	G	T_1	T_7
G°	0.5781		
A	0.0009	0.3784	0.1801
A'		0.0002	0.0001
A + B	0.0066	0.1389	0.1059
B	0.1890	0.1338	0.0526
B'	0.0258	0.0291	0.0113
(Total from G^0 and LE configurations)	(0.8004)	(0.6804)	(0.3500)
C	0.0879	0.0586	0.2359
C + A		0.0458	0.0234
C + B	0.0240	0.0393	0.0778
C'	0.0052	0.0057	0.0249
(Total from CT_1 configurations)[a]	(0.1171)	(0.1494)	(0.3620)
D	0.0530	0.0487	0.1517
D + A		0.0289	0.0139
D + B	0.0143	0.0186	0.0409
D'	0.0016	0.0022	0.0095
(Total from CT_2 configurations)[b]	(0.0689)	(0.0984)	(0.2160)
Total	0.9864	0.9282	0.9280

a) CT configurations from the benzene ring to the cyano groups. b) CT configurations from the cyano groups to the benzene ring.

also given for the purpose of comparison. In these tables, G^0 denotes the ground configuration, and Groups A and A' represent the singly and doubly excited LE configurations in the benzene ring, respectively; Groups B and B', the singly and doubly excited LE configurations in the substituent groups, respectively; Groups C and C', the singly and doubly excited CT configurations from the benzene ring to the substituent groups, respectively; Groups D and D', the singly and doubly excited CT configurations from the substituent groups to the benzene ring, respectively, and Group C+A, *etc.*, the doubly excited configurations composed of configurations in Groups C and A, *etc.*

As is clearly seen in Table 3, the results of the configuration analysis for *m*- and *p*-DCNB's are similar to each other; the ground singlet state (G) and the lowest triplet state (T_1) are mainly composed of the ground and LE configurations, while in the T_9 states, the contribution of the CT configurations is more predominant than that of the LE configurations. This shows that the observed T-T absorption bands of *m*- and *p*-DCNB's correspond to the transition from the LE state to the intramolecular CT state.

Concerning *p*-DCNB, the contribution of the CT configurations in Group C may increase the double bond character of the C-C bonds between the benzene ring and the cyano groups. Hence, the molecular geometry may tend towards a quinoid structure. In actuality, this tendency was observed by Hirota[29] from the measurement of the spin densities in the T_1

state of *p*-DCNB.

As is seen in Table 4, the nature of the T-T absorption band of TRCNB is analogous to that of *m*- and *p*-DCNB's. The T-T absorption bands of BN, *o*-DCNB, and TCNB listed in Table 1 also correspond to the transition from the LE state to the intramolecular CT state.

References

1) S. Nagakura and J. Tanaka, *J. Chem. Phys.*, **22**, 236 (1954); S. Nagakura, *ibid.*, **23**, 1441 (1955).

2) H. C. Longuet-Higgins and J. N. Murrell, *Proc. Phys. Soc.* (London), **A68**, 601 (1955); J. N. Murrell, *ibid.*, **A68**, 969 (1955); *Tetrahedron, Suppl.* **2**, **19**, 277 (1963).

3) T. E. Peacock, *Mol. Phys.*, **3**, 453 (1960).

4) J. E. Bloor, *Canad. J. Chem.*, **39**, 2256 (1961); J. E. Bloor and F. Peradejordi, *Theor. Chim. Acta*, **1**, 83 (1962).

5) I. Fischer-Hjalmars, *Ark. Fys.*, **21**, 123 (1962).

6) S. Nagakura, *Pure* and *Appl. Chem.*, **7**, 79 (1963).

7) J. Tanaka, This Bulletin, **36**, 833 (1963).

8) S. Nagakura, M. Kojima, and Y. Maruyama, *J. Mol. Spectrosc.*, **13**, 174 (1964); K. Tabei and S. Nagakura, This Bulletin, **38**, 965 (1965).

9) K. Kimura, H. Tsubomura, and S. Nagakura, *ibid.*, **37**, 1336 (1964).

10) K. Kimura and S. Nagakura, *Mol. Phys.*, **9**, 117 (1965).

11) K. Kimura and H. Tsubomura, *ibid.*, **11**, 349 (1966).

12) H. Tsubomura, N. Yamamoto, and Y. Nakato, This Bulletin, **39**, 1092 (1966); N. Yamamoto, Y. Nakato, and H. Tsubomura, *ibid.*, **39**, 2603 (1966).

13) K. D. Cadogan and A. C. Albrecht, *J. Phys. Chem.*, **73**, 1868 (1969).

14) H. Baba, S. Suzuki, and T. Takemura, *J. Chem. Phys.*, **50**, 2078 (1969).

15) R. Pariser and R. G. Parr, *ibid.*, **21**, 466, 767 (1953).

16) J. A. Pople, *Proc. Roy. Soc.* (London), **A68**, 81 (1955).

17) G. M. Bennet and R. L. Wain, *J. Chem. Soc.*, **1936**, 1108.

18) A. S. Bailey, B. R. Henn, and J. M. Langdon, *Tetrahedron*, **19**, 161 (1963).

19) S. Matsumoto, S. Nagakura, S. Iwata, and J. Nakamura, *Mol. Phys.*, **26**, 1465 (1973).

20) S. Iwata, J. Tanaka, and S. Nagakura, *J. Amer. Chem. Soc.*, **88**, 894 (1966).

21) M. S. de Groot and J. H. van der Waals, *Mol. Phys.*, **6**, 545 (1963); M. S. de Groot, I. A. M. Hesselmann, and J. H. van der Waals, *ibid.*, **10**, 91 (1965); *ibid.*, **13**, 583 (1967).

22) G. C. Nieman and D. S. Tinti, *J. Chem. Phys.*, **46**, 1432 (1967); G. C. Nieman, *ibid.*, **50**, 1674 (1969).

23) A weak band was observed for TCNB around 320 nm. Since the TCNB molecule ionizes fast in the excited state,[24,25] it is not sure whether or not this band corresponds to the T–T absorption.

24) M. Sofue and S. Nagakura, This Bulletin, **38**, 1048 (1965).

25) H. Masuhara, M. Shimada, N. Tsujino, and N. Mataga *ibid.*, **44**, 3310 (1971).

26) R. Astier and Y. H. Meyer, *Chem. Phys. Lett.*, **3**, 399 (1969).

27) C. S. Burton and H. E. Hunziker, *ibid.*, **6**, 352 (1970).

28) T. S. Godfrey and G. Porter, *Trans. Faraday Soc.*, **62**, 7 (1966).

29) Private communication from Professor Noboru Hirota, State University of New York at Stony Brook.

Use of the Copper(II)-Selective Electrode for the Determination of the Stability Constants of Copper(II) Complexes

Genkichi NAKAGAWA, Hiroko WADA, and Tomohiko HAYAKAWA

Nagoya Institute of Technology, Showa-ku, Nagoya 466

(Received March 12, 1974)

In the determination of stability constants of metal complexes, usually the measurements of the activities of free metal ions at very low levels are required. The electrode response of an Orion Model 94—29 copper(II) ion selective electrode at very low activity levels was studied in the various metal buffers composed of copper(II) ions and an excess of ligand. Usually the linear calibration range of the copper(II) ion selective electrode was extended to very low activity levels in the presence of a strong complexing agent. The stability constants of copper(II) complexes with acetate, ammonia, ethylenediamine, glycine, iminodiacetic acid, 1,10-phenanthroline, *etc.* were determined successfully. In the cases of EDTA and NTA, however, the lower limit of the linear calibration range was abnormally high and the stability constant of copper-EDTA or -NTA chelate could not be obtained. Some experimental results on the potentiometric titration of copper(II) ion with EDTA were also presented.

In recent years many types of ion-selective electrodes have been developed which are very useful for direct determination of various ions in solutions.[1-6] These electrodes have been also used in the study of solution equilibria[7,8] as well as for the detection of the end-point in titrations.[9-11] In these cases the measurements of activities of free ions at very low levels are usually required. However, less attention has been paid on the detection limit of the electrode.

In the present paper the potential response of an Orion solid-state copper(II) ion selective electrode Model 94—29 at very low activity levels of copper(II) ions is studied by the use of various metal buffers, and the stability constants of some copper(II) complexes are determined successfully.

Experimental

Reagents. *Stock solution of copper*: A 10^{-1} M copper(II) nitrate solution was prepared from metallic copper (99.99%). A series of standard solutions of copper(II) from 10^{-2} to 10^{-6} M was prepared by dilution of the stock solution immediately before measurements.

Complexing Agents: Reagent grade EDTA·2Na and NTA were recrystallized from water. Ammonia and ethylenediamine were purified by distillation. Other chemicals were of reagent grade and used without further purification. Deionized and redistilled water was used.

Apparatus. For the measurements of copper(II) ion activities, an Orion copper(II) ion selective electrode Model 94-29 and a Horiba SCE reference electrode were used with a Hitachi-Horiba F-5 expanded scale pH meter. The pH measurements were made with a Hitachi-Horiba M-5 pH meter equipped with Horiba glass and calomel electrodes.

Three Orion copper(II) ion selective electrodes were examined, and these showed the same characteristics of potential response.

The surface of a sulfide membrane of the electrodes was occasionally polished lightly with tooth paste to keep the electrodes at the best condition. During the potential measurement magnetic stirring with a Teflon bar was applied.

All experiments were carried out in air thermostated at 25±1 °C.

Results and Discussion

The potential response of the electrode. The experimental cell can be represented as follows.

copper(II) ion selective electrode | test solution μ=0.1(KNO_3) | 0.1 M KNO_3 | SCE

The measurements being carried out at a constant ionic strength of 0.1, the junction potential was kept constant and the cell emf is given:

$$E = \text{const.} + 2.303\frac{RT}{2F}\log a_{Cu^{2+}} \qquad (1)$$

The potential response of the copper(II) ion selective electrode at various copper(II) ion activity levels was examined in a pH range between 2 and 10. As shown in Fig. 1 the Nernstian response held down to 10^{-6} M of copper(II) ions in a pH range of 4—6. Below 10^{-6} M the calibration curve reached to a pla-

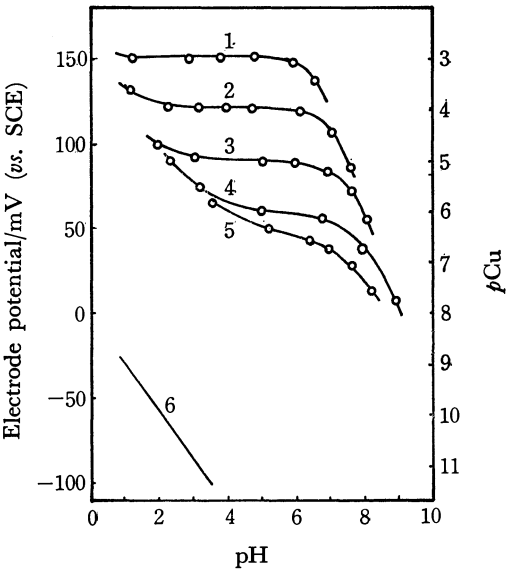

Fig. 1. Potential response of an Orion 94-29 copper(II) ion-selective.
$Cu(NO_3)_2$ 1: 10^{-3} M, 2: 10^{-4} M, 3: 10^{-5} M, 4: 10^{-6} M, 5: 0 (lower detection limit in 0.1 M MES buffer), 6: theoretical solubility of CuS.

teau, and the electrode no longer responded to change in copper(II) ion activity. This detection limit rose markedly in highly acidic solutions. At pH higher than 6 copper precipitates as a hydroxide.

The potential response of the copper(II) ion selective electrode was fast and the electrode attained a constant value within a few seconds at 10^{-2}—10^{-3} M and within a few minutes at 10^{-6} M copper(II) ion. In spite of very low activities of copper(II) ion, usually 2—5 minutes were sufficient in metal buffer solutions. The reproducibility of the electrode potential was within ±0.5 mV for 24 hours. However, since the drift of the potential during several months ranged to a few tens mV, it is advisable to calibrate the electrode with the standard copper(II) solution of 10^{-3} M before the measurements.

The Detection Limit of the Electrode. The membrane of the Orion copper(II) ion selective electrode consisting of mixed sulfides of copper(II) and silver is a source of copper(II) ions in test solutions, the lower activity limit of detection is governed by the solubility of the sulfide membrane. As seen from curves 5 and 6 in Fig. 1, however, the actual limit of detection was much higher than that calculated from the solubility of copper(II) sulfide. This disagreement may be partly attributed to copper(II) ion contamination of the test solution and partly to high activity of copper(II) ion at the surface of the sulfide membrane caused by the

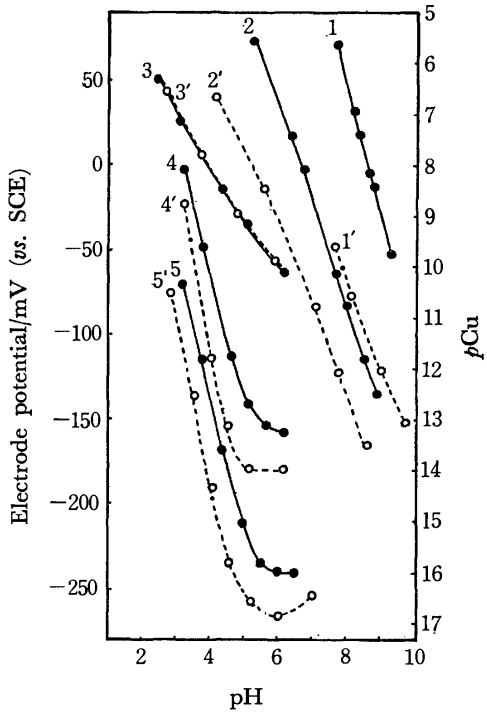

Fig. 2. The potentials of the copper(II) ion selective electrode in various copper(II) ion buffers.
Broken line shows the detection limit of the electrode in the solution containing the same ligand only.

system	C_{Cu} (M)	C_L (M)
1: NH_3	1.22×10^{-3}	0.99×10^{-1}
2: Glycine	1.99×10^{-3}	2.01×10^{-2}
3: EDTA	4.98×10^{-4}	1.02×10^{-3}
4: 1,10-Phenanthroline	0.99×10^{-4}	1.00×10^{-3}
5: 1,10-Phenanthroline	0.99×10^{-4}	5.01×10^{-3}

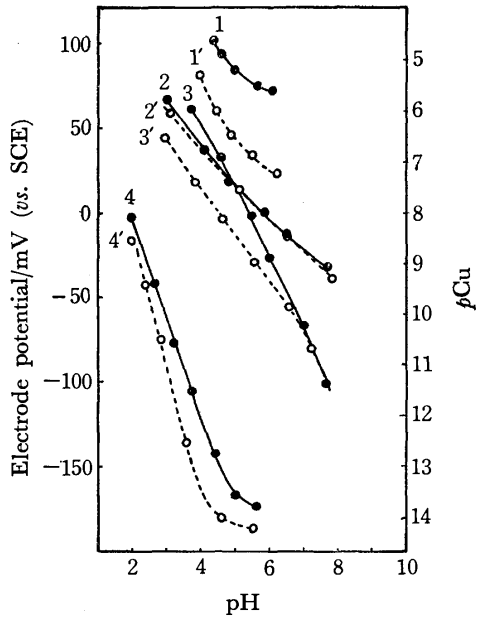

Fig. 3. The potentials of the copper(II) ion selective electrode in various copper(II) ion buffers.
Broken line shows the detection limit of the electrode in the solution containing the same ligand only.

System	C_{Cu} (M)	C_L (M)
1: OAc⁻	0.99×10^{-3}	1.03
2: NTA	4.95×10^{-3}	0.95×10^{-3}
3: IDA	2.43×10^{-3}	4.01×10^{-2}
4: Bipyridine	0.99×10^{-4}	4.98×10^{-3}

adsorption.

Many complexing agents forming stable complexes with copper(II) ions may reduce the activity of copper(II) ion in solutions or at the electrode surface. The detection limit of the electrode was measured in various ligand solutions containing no copper ion. As shown in Figs. 2 and 3, the detection limit was affected markedly by the type of complexing agent in the test solutions, its concentration and pH. Strong complexing agents lowered the detection limit to a large extent. For example, the lower activity limit of detection was around 10^{-6} M at pH 4 in the buffer solution composed of MES[12] which forms copper complex only negligibly, while in the presence of 0.001 M 1,10-phenanthroline the detection limit became to the order of 10^{-14} M at a pH higher than 5.

However, in spite of a high stability of copper(II)-EDTA chelate the detection limit in EDTA solutions was abnormally high. Since the stability of silver-EDTA chelate is relatively small, the activity of silver ion at the electrode surface may be much higher than that of copper. The Orion copper(II) ion selective electrode also responds to silver ion, thus the detection limit in this case may be determined by the activity of silver ion at the electrode surface. On the other hand, ligands which form fairly stable complexes with both silver and copper(II) ions, *i.e.* NH_3, ethylenediamine, 1,10-phenanthroline *etc.*, may shift the detection limit of the electrode to very low copper(II) ion levels.

Determination of the Stability Constants of Copper(II) Complexes. The stability constants of various cop-

per(II) complexes were determined by measuring the activities of free copper(II) ion in the metal buffer solutions which consist of copper complex CuL_n and the excess of the ligand L.

From the over-all stability constant of the complex CuL_n, the activities of free copper(II) ion in a metal buffer solution are given:

$$pCu = \log \beta_n + n \log[L] - \log[CuL_n] \quad (2)$$

When the solution contains a large excess of ligand and the formation of CuL_n is practically complete, $[CuL_n]=C_{Cu}$, and [L] can be represented by Eq. (3).

$$[L] = \frac{C_L}{\alpha_{L(H)}} \quad (3)$$

where C_L is the total concentration of the ligand, and $\alpha_{L(H)}$ is the side reaction coefficient taking into account the protonation of ligand and calculated from the concentration of hydrogen ion in the solution and the acid dissociation constants of the ligand. As pCu is obtained from the measured cell potential, β_n can be calculated by Eq. (2).

Figures 2 and 3 show the cell potential measured in various copper(II) buffer solutions. The relation between pCu and pL are plotted in Fig. 4. These plots yielded the straight lines of slope n. In the case of bipyridine the slope was 2 at pL>5 and 3 at pL<4, and β_2 and β_3 could be evaluated.

The stability constants determined are summarized in Table 1. Those values are in good agreement with the values reported in the literature.[13]

For the EDTA or NTA chelate, however, good results could not be obtained, because in these cases the activities of copper(II) ion in the solutions were much lower than the detection limit of the electrode, so the true activities of copper(II) ion were not obtained. Also this was the case for IDA at pH>7.

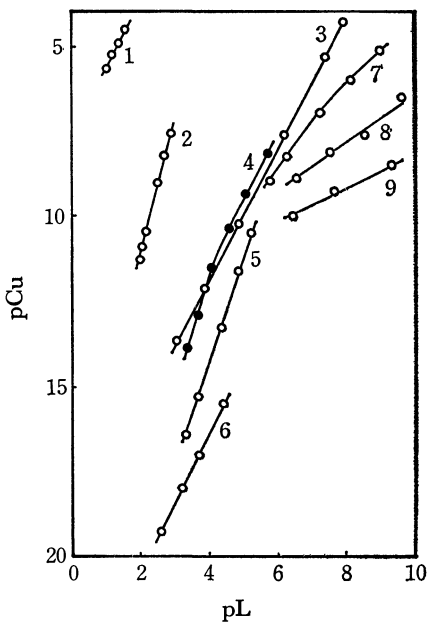

Fig. 4. Relations between pCu and pL.
1: OAc^-, 2: NH_3, 3: glycine, 4: bipyridine, 5: 1,10-phenanthroline, 6: ethylenediamine, 7: iminodiacetic acid, 8: NTA, 9: EDTA.

Table 1. Stability constants of copper(II) complexes (μ=0.1, 25 °C)

Ligand		Logarithmic values of β_n (measured)	(literature)
OAc^-	β_2	2.58 (μ=1.0)	2.7
NH_3	β_4	12.49	12.59
Ethylenediamine	β_2	19.40	19.60
Glycine	β_2	15.28	15.1
Iminodiacetic acid	β_1	10.54	10.5
Bipyridine	β_2	13.65	13.57
	β_3	16.75	17.0
1,10-Phenanthroline	β_3	19.10	21.0

These values were omitted for the calculation of the stability constant.

The use of the ion selective electrode provides the simple and reliable method for studying the stability of metal complexes. However, the lower limits of detection of the ion selective electrode should be checked under the same experimental conditions.

Application to EDTA Titration. The potentiometric titration curves of copper(II) ion with EDTA using the copper(II) ion selective electrode are shown in Fig. 5A. The titration curves after the equivalence point were leveled at the detection limit of the electrode and deviated from the typical sigmoid shape. Addition of a small amount of 1,10-phenanthroline *i.e.* 10^{-5} M improved titration curves markedly. As seen from Fig. 5B this is of special advantage when the metals stabilities of EDTA chelates of which are lower than that of copper, are to be determined by back titration of the

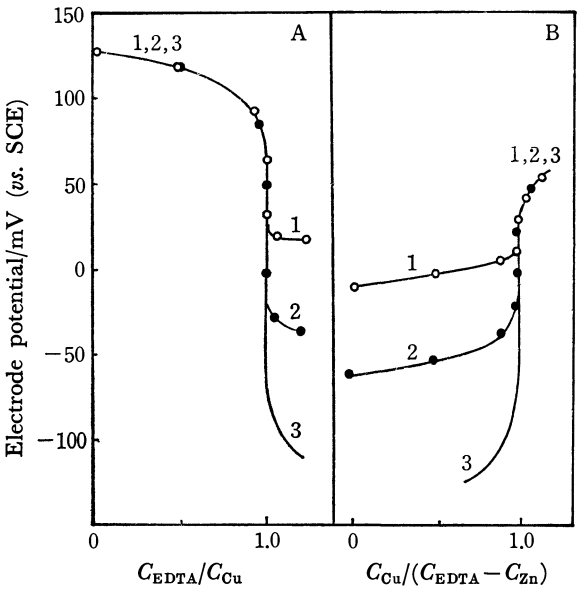

Fig. 5. Titration of copper with EDTA (A) and determination of zinc by back titration of excess EDTA with copper (B).
(A) 1: Cu 2×10^{-3}M, pH 5.8 (0.1M HOAc-OAc^-), 2: the same as 1 but 10^{-5} M 1,10-phenanthroline added, 3: theoretical curve.
(B) 1: Zn 2×10^{-3} M, EDTA 4×10^{-3} M, 2: the same as 1 but 10^{-5} M 1,10-phenanthroline added, 3: theoretical curve.

excess of EDTA with copper(II) ion standard solution. In these cases the potential jump at the equivalence point is depressed by the following exchange reaction:

$$ZnY^{2-} + Cu^{2+} \rightleftharpoons CuY^{2-} + Zn^{2+}$$

Thus the electrode response in the low copper(II) ion levels becomes increasingly important to obtain a sharp end point.

Reference

1) M. S. Frant and J. W. Ross, *Science*, **154**, 1553 (1966).
2) R. A. Durst, "Ion-Selective Electrodes," Special Publication No. 314, NBS, Washington, D. C. (1969).
3) E. Pungor and K. Tóth, *Analyst*, **95**, 625 (1970).
4) H. Hirata, K. Higashiyama, and K. Date, *Anal. Chim. Acta*, **51**, 209 (1970).
5) G. J. Moody and J. D. R. Thomas, *Talanta*, **19**, 623 (1972).
6) E. H. Hansen, C. G. Lamm, and J. Růžička, *Anal. Chim. Acta*, **59**, 403 (1972).
7) G. A. Rechinitz and Z. F. Lin, *Anal. Lett.*, **1**, 23 (1967).
8) H. Wada and Q. Fernando, *Anal. Chem.*, **43**, 751 (1971).
9) J. W. Ross and M. S. Frant, *ibid.*, **41**, 1900 (1969).
10) E. W. Baumann and R. M. Wallace, *ibid.*, **41**, 2072 (1969).
11) L. Šůcha and M. Suchánek, *Anal. Lett.*, **3**, 613 (1970).
12) 2-(*N*-morpholino)ethanesulfonic acid.
13) L. G. Sillén and A. E. Martell, "Stability Constants of Metal-Ion Complexes," The Chemical Society, London (1964).

An Investigation of the Hebb-Wagner's d-c Polarization Technique I. Steady-state Chemical Potential Profiles in Solid Electrolytes

Jun-ichiro MIZUSAKI, Kazuo FUEKI, and Takashi MUKAIBO

Department of Industrial Chemistry, Faculty of Engineering, The University of Tokyo, Hongo, Bunkyo-ku, Tokyo 113

(Received September 24, 1974)

Using an electrochemical cell, Ag/AgX (X=Br or I)/C, the steady-state chemical potential profiles of silver in AgX were determined under d-c polarization conditions. Several Pt probes were attached to the AgX specimens, and the potential differences between the Ag electrode and the Pt probes were measured. It was found that, in order to obtain the correct chemical potential profiles, the Pt probes must be embedded in the specimen to avoid influences of the degradation of AgX at the surface of the specimen. The results obtained by the cell with carefully assembled probes revealed that Wagner's theory holds for AgX.

Hebb-Wagner's d-c polarization technique[1,2] is generally used for the determination of electronic transport numbers of mixed conductors. The cell arrangements employed in this technique are as follows:

⊖ cation reversible electrode/mixed conductor/ion-blocking electrode ⊕ (I)

or;

⊖ ion-blocking electrode/mixed conductor/anion reversible electrode ⊕ (II)

The theory of this technique, originated by Wagner,[2] is based on the assumption that there is no gradient of the electrochemical potential of blocked ions in the steady state; in other words, the driving force due to the electrical potential gradient is cancelled by that due to the chemical potential gradient. The chemical potential profiles in the steady state were calculated theoretically and illustrated graphically by Choudhury and Patterson.[3,4]

Direct measurements of the chemical potential profile in mixed conductors of predominantly electronic conduction were carried out by Hebb (Ag_2S[1]), Miyatani (Ag_2S,[5] Ag_2Te[6]), and Yokota (Cu_2S[7]). The observed results agreed well with those calculated in a similar manner.

As to the mixed conductors of a predominantly ionic conduction, the electrical potential profile of $PbBr_2$[8] has previously been measured. However, no explanation has been given to correlate the observed potential profiles with Wagner's theory.

The purpose of the present study is to measure the chemical potential profiles in ionic conductors, such as AgBr and AgI, using a cell of the (I) type to reveal whether or not Wagner's theory holds in these systems.

Experimental

Circut and Experimental Procedures. The circuit employed for the measurement is shown in Fig. 1. AgX (X=Br or I) was placed between Ag and graphite electrodes to construct a Hebb-Wagner's d-c polarization cell. Several Pt wires were attached to AgX as probes. This cell was placed in an electric furnace, the temperature of which was controlled by means of an electronic controller to within ±1 °C. The potential difference between the Ag and graphite electrodes was kept constant by means of a potentiostat. When the current flowing through the circuit reached a stationary value, the chemical potential profile in a steady-state was determined by measuring the potential differences between the Ag electrode and the Pt probes by means of a high impedance d-c digital voltmeter.

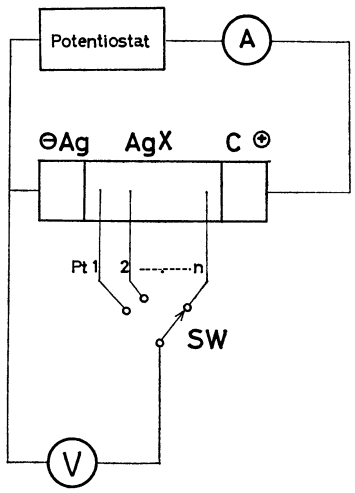

Fig. 1. Circuit diagram for the measurement.

The measurement was performed in a purified nitrogen flow of 2 cm s^{-1} at 350 and 400 °C for AgBr, and 500 °C for AgI.

Cells. Three types of cell arrangements were employed. In the first and second types, Pt probes were embedded in the specimen, while in the third type, Pt probes were in contact with the surface of the specimen.

The first type, Cell (i), is illustrated in Fig. 2. Reagent-grade AgBr was purified 50 times by zone refining and then solidified in a rod-shaped single crystal, 15 mm in length and 10 mm in diameter, by the Bridgeman method. Holes 0.8 mm in diameter were drilled from the side surface to the axis of the AgBr rod. In these holes, Pt wires (0.2 mm in diameter) protected by an alumina tube (0.8 mm in outer diameter and 0.4 mm in inner diameter) were buried as probes so that only the tips of the wires were in contact

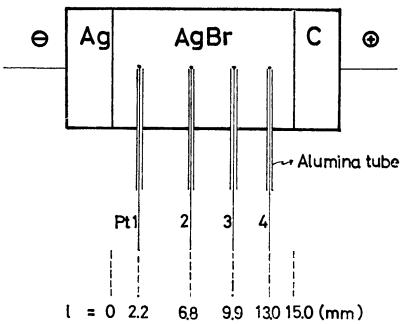

Fig. 2. Arrangement of Cell (i).

with the AgBr rod. The AgBr rod was then sandwiched by Ag and graphite electrodes and pressed by means of a spring to ensure contact.

As AgI experiences a phase transformation at 146 °C, the rod-shaped specimen prepared from the solidification of the molten AgI is quite brittle at room temperature and can not endure mechanical treatment such as the drilling of holes from the side surface. Therefore, instead of the first type, the second type, Cell (ii), was employed for the measurement of AgI. Figure 3 shows the arrangement of Cell (ii). Three pellets, 10 mm in diameter and a, b, and c mm thick respectively, were prepared by pressing reagent-grade AgI in a die. An Ag electrode, three AgI pellets, and a graphite electrode were assembled in series. The Ag and graphite electrodes and two of the AgI pellets, a and c mm thick, have holes, 0.8 mm in diameter, along the axis. Pt wires protected by an alumina tube were inserted in the holes from both ends, so that their tips were in contact with the end surfaces of the middle AgI pellet, b mm thick. In Cell (ii-A), the thicknesses of the AgI pellets employed were $a=3.0$ mm, $b=5.7$ mm and $c=1.1$ mm, and in Cell (ii-B), $a=1.1$ mm, $b=6.0$ mm, and $c=3.0$ mm.

The third type, Cell (iii-A) or Cell (iii-B), consists of an AgBr or AgI rod, 10 mm in diameter, solidified from the melt. Pt probes were wound around the rod at appropriate intervals. The rod was then sandwiched between Ag and graphite electrodes. The arrangement of Cell (iii-B) is shown in Fig. 4.

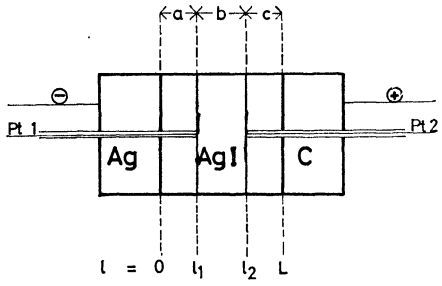

Fig. 3. Arrangement of Cell (ii).

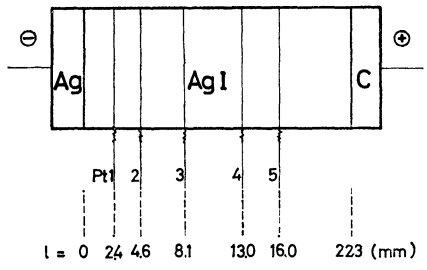

Fig. 4. Arrangement of Cell (iii-B).

Results and Discussion

The experimental results obtained by the use of Cell(i) and Cell(iii-A) are shown in Fig. 5. Those obtained by the use of Cell (ii) and Cell(iii-B) are shown in Fig. 6. The steady-state was attained within 48 hours.

Chemical Potential Profiles in the Steady-state. When AgX shows an n-type electronic conduction, μ_{Ag}, the chemical potential of silver in AgX in a steady-state,

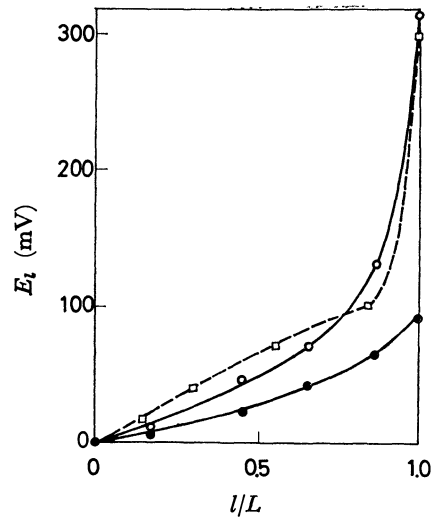

Fig. 5. Steady-state potential profiles of AgBr at 400 °C.
●; Cell (i), $E_L=93$ mV, $i=1.0$ μA cm^{-2}, $L=15.0$ mm.
○; Cell (i), $E_L=318$ mV, $i=1.4$ μA cm^{-2}.
□; Cell (iii-A), $E_L=300$ mV, $i=2.3$ μA cm^{-2}, $L=10.8$ mm.

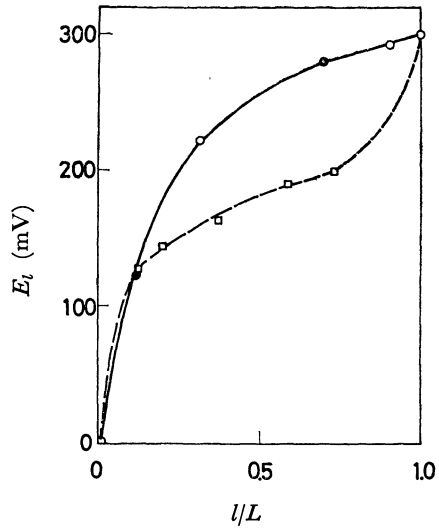

Fig. 6. Steady-state potential profiles of AgI at 500 °C.
○; Cell (ii-A), $E_L=300$ mV, $i=57$ μA cm^{-2}, $L=9.8$ mm. ●; Cell (ii-B), $E_L=300$ mV, $i=38$ μA cm^{-2}, $L=10.3$ mm. □; Cell (iii-B), $E_L=300$ mV, $i=45$ μA cm^{-2}, $L=22.3$ mm.

is represented in the same manner as is used in Wagner's theory, by this equation;

$$il = \frac{\sigma_e^0 RT}{F}\left\{1-\exp\left(\frac{\mu_{Ag}(l)-\mu_{Ag}^0}{RT}\right)\right\} \quad (1)$$

where μ_{Ag}^0 is the μ_{Ag} of metallic silver, $\mu_{Ag}(l)$ is μ_{Ag} distance of l from the Ag/AgX interface, and σ_e^0 is the electronic conductivity of AgX at the Ag/AgX interface. At the AgX/C interface, $l=L$; therefore,

$$iL = \frac{\sigma_e^0 RT}{F}\left\{1-\exp\left(\frac{\mu_{Ag}(L)-\mu_{Ag}^0}{RT}\right)\right\} \quad (2)$$

From Eqs. (1) and (2), we obtained:

$$\frac{l}{L}=\frac{1-\exp\left(\frac{\mu_{Ag}(l)-\mu_{Ag}{}^{0}}{RT}\right)}{1-\exp\left(\frac{\mu_{Ag}(L)-\mu_{Ag}{}^{0}}{RT}\right)} \quad (3)$$

In the case of p-type AgX

$$il=\frac{\sigma_h{}^{0}RT}{F}\left\{\exp\left(\frac{\mu_{Ag}{}^{0}-\mu_{Ag}(l)}{RT}\right)-1\right\} \quad (4)$$

where $\sigma_h{}^{0}$ is the conductivity due to hole conduction at the Ag/AgX interface. Therefore,

$$\frac{l}{L}=\frac{\exp\left(\frac{\mu_{Ag}{}^{0}-\mu_{Ag}(l)}{RT}\right)-1}{\exp\left(\frac{\mu_{Ag}{}^{0}-\mu_{Ag}(L)}{RT}\right)-1} \quad (5)$$

Eqs. (3) and (5) represent the relationship between $(\mu_{Ag}(l)-\mu_{Ag}{}^{0})$ and l/L for n-type and p-type AgX respectively.

Comparison of the Experimental Results with the Theoretical Results. Under the present experimental conditions, the Ag electrode at the Ag/AgX interface acts as a reversible electrode for both silver ions and electrons, while at the Pt/AgX or C/AgX interface, the Pt or graphite electrode is chemically inert in effect and reversible only for electrons. Therefore, the electrical potential difference, E_l, between the Pt electrode at l and the Ag electrode is written as:

$$E_lF=\eta_e{}^{0}-\eta_e(l) \quad (6)$$

where $\eta_e{}^{0}$ and $\eta_e(l)$ are the electrochemical potentials of electrons in AgX at the Ag/AgX interface and that at l respectively. Under the ion-blocking conditions, the electrochemical potential of silver ions is constant throughout the cell; therefore,

$$\eta_{Ag^+}{}^{0}=\eta_{Ag^+}(l) \quad (7)$$

Therefore, we can obtain from Eqs. (6) and (7):

$$E_lF=\mu_{Ag}{}^{0}-\mu_{Ag}(l) \quad (8)$$

In the same manner, the potential difference, E_L, between the Ag electrode and the graphite electrode located at L is:

$$E_LF=\mu_{Ag}{}^{0}-\mu_{Ag}(L) \quad (9)$$

The insertion of Eqs. (8) and (9) into (3) and (5) yields:

$$\frac{l}{L}=\frac{1-\exp\left(-\frac{E_lF}{RT}\right)}{1-\exp\left(-\frac{E_LF}{RT}\right)} \quad (10)$$

and:

$$\frac{l}{L}=\frac{\exp\left(\frac{E_lF}{RT}\right)-1}{\exp\left(\frac{E_LF}{RT}\right)-1} \quad (11)$$

The experimntal results for AgBr are represented in Fig. 7 as a plot of l/L *vs.* $\dfrac{1-\exp\left(-\frac{E_lF}{RT}\right)}{1-\exp\left(-\frac{E_LF}{RT}\right)}$, while those for AgI are given in Fig. 8 as a plot of l/L *vs.* $\dfrac{\exp\left(\frac{E_lF}{RT}\right)-1}{\exp\left(\frac{E_LF}{RT}\right)-1}$. In the Figure, the results obtained by the use of Cells(i) and (ii), in which the Pt probes embedded in the specimens show a good linearity. This indicates that Eq. (10) holds in Cell(i) and Eq. (11) in Cell(ii). Therefore, it may be concluded that AgBr and AgI are n-type and p-type conductors respectively under the present experimental conditions, as was found by Ilschner[9] and Raleigh,[10] and that Wagner's theory holds for the mixed conductors of a predominantly ionic conduction.

However, the results obtained by using Cell(iii),

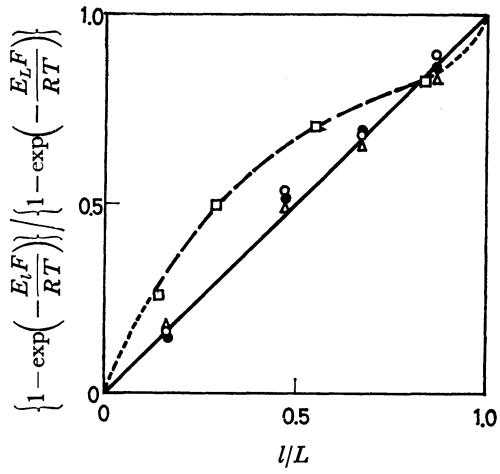

Fig. 7. Comparison of experimental results with theoretical one about AgBr.
Solid line; theoretical result
○; Cell(i), E_L=318 mV, 400 °C.
●; Cell(i), E_L=93 mV, 400 °C.
△; Cell(i), E_L=300 mV, 350 °C, i=0.1 μA cm^{-2}.
□; Cell(iii-A), E_L=300 mV, 400 °C.

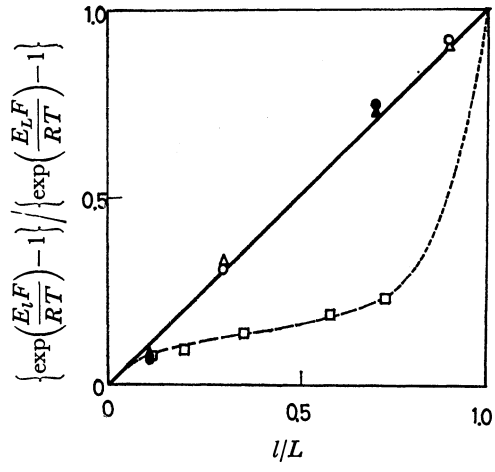

Fig. 8. Comparison of experimental results with theoretical one about AgI, 500 °C.
Soild line; theoretical result
○; E_L=300 mV, Cell(ii-A).
△; E_L=350 mV, Cell(ii-A).
●; E_L=300 mV, Cell(ii-B).
▲; E^7=350 mV, Cell(ii-B).
□; E_L=300 mV, Cell(iii-B).

in whish Pt probes are placed in contact with the surface of a specimen, do not agree with Wagner's theory.

Electronical Conductivity of AgBr. Inserting the values of a steady-state current, the applied potential difference, E_L, and the sample length, L, of Cell(i) into Eqs. (2) and (8), one obtains 3.0×10^{-6} ℧ cm^{-1} (350 °C) and 4.0×10^{-5} ℧ cm^{-1} (400 °C) as the σ_e^0 of AgBr. These values are in good agreement with the results obtained by Ilschner.

The Effect of the Degradation of AgI at the AgI/C Interface on the Potential Profiles. Using Eqs. (3) and (8), the σ_h^0 of AgI at 500 °C was calculated. The result obtained from Cell(ii–A) was 9.5×10^{-6} ℧ cm^{-1}. However, this value is about one order of magnitude larger than the value obtained by the extrapolation of Ilschner's data.[9] This fact suggests that the current passed through AgI might be an ionic current due to the degradation of AgI at the AgI/C interface.

When the ionic current is predominant in AgI, the ionic current, i_{ion}, correlates with the electrochemical potential difference of Ag^+ between Ag and graphite electrodes as follows:

$$\eta_{Ag^+}(L) - \eta_{Ag^+}{}^0 = \frac{i_{ion}LF}{\sigma_i} \qquad (12)$$

where σ_i represents the ionic conductivity of AgI. The length of the AgI specimen used in this work is less than 2.23 cm, the current density is less than 180 μA/cm^2, and the σ_i of AgI at 500 °C is 2.5 ℧ cm^{-1}.[11] Therefore, $i_{ion}L/\sigma_i<0.16$ mV. It is evident that the drop of the electrochemical potential of silver ions in the AgI specimen is negligibly small compared to the observed potential differences. Therefore, Eq. (7) holds in the present system and the observed potential profiles coincide with those under the complete ion-blocking conditions.

The Effect of the Degradation of AgX at the Side Surface of the Specimen on the Potential Profile. The equilibrium halogen vapor pressure with regard to each observed silver chemical potential can be calculated from the standard free energy of the formation of AgX and the equilibrium constant of the $X_2=2X$ reaction. As for AgBr in Fig. 5, the chemical potential near the AgBr/C interface corresponds to the bromine vapor pressure of the order of 10^{-8} atm, whereas those of the other part of the AgBr rod corresponds to the order of 10^{-10}—10^{-11} atm; as for AgI in Fig. 6, most of the AgI rod corresponds to the iodine vapor pressure of the order of 10^{-4}—10^{-5} atm. Therefore, a large difference in equilibrium halogen-vapor pressure exists between the nitrogen atmosphere and the AgX rod, resulting in the degradation of AgX at the surface of the rod.

As in Cells(i) and (ii), Pt probes were embedded in the specimen, whereas in Cell(iii) Pt probes were attached to the surface of the specimen; the disagreement of the results obtained by the use of Cell(iii) with the theoretical values may be due to this degradation of the AgX surface.

In conclusion, we must embed the Pt probes in the specimen in order to observe the correct chemical potential profiles in a solid electrolyte.

Summary

(i) Using an electrochemical cell, Ag/AgBr (or AgI)/C, the steady-state chemical potential profiles in AgBr and AgI were measured under the d-c polarization conditions.

(ii) It was found that Wagner's theory holds for mixed conductors of a predominantly ionic conduction.

(iii) It was concluded that Pt probes must be embedded in AgX in order to obtain the correct chemical potential profile.

References

1) M. Hebb, *J. Chem. Phys.*, **20**, 185 (1952).
2) C. Wagner, *Proc. C.I.T.C.E.*, **7**, 361 (1955).
3) N. S. Choudhury and J. W. Patterson, *J. Electrochem. Soc.*, **117**, 1384 (1970).
4) N. S. Choudhury and J. W. Patterson, *ibid.*, **118**, 1398 (1971).
5) S. Miyatani, *J. Phys. Soc. Japan*, **10**, 786 (1955).
6) S. Miyatani, *ibid.*, **13**, 341 (1958).
7) I. Yokota, *ibid.*, **8**, 595 (1953).
8) J. Schoonmann and F. G. Dijkman, *J. Solid State Chem.*, **5**, 111 (1972).
9) B. Ilschner, *J. Chem. Phys.*, **28**, 1109 (1958).
10) D. O. Raleigh, *J. Phys. Chem. Solids*, **26**, 329 (1965).
11) W. Biermann and W. Jost, *Z. Phys. Chem., N.F.*, **25**, 139 (1960).

The Effect of the Pressure on the Micellization of the Surfactant in Aqueous Urea Solutions

Mitsuru TANAKA, Shoji KANESHINA,* Seiji KURAMOTO,** and Ryohei MATUURA***

Department of Chemistry, Faculty of Science, Fukuoka University, Nanakuma, Nishi-ku, Fukuoka 814

**College of General Education, Kyushu University, Ropponmatsu, Chūō-ku, Fukuoka 810*

***Department of Chemistry, Faculty of Science, Kyushu University, Hakozaki, Higashi-ku, Fukuoka 812*

(Received October 19, 1974)

The critical micelle concentrations (CMC) of dodecyltrimethylammonium bromide (DTAB) in aqueous urea solutions have been determined over a range of pressures up to 2500 atm at 25 and 35 °C. The partial molal volumes of DTAB in micellar ($\overline{V}_m$) and singly-dispersed states ($\overline{V}_s$) have also been determined in aqueous urea solutions at 25 °C. $\overline{V}_s$ increases with the addition of urea, while $\overline{V}_m$ remains approximately constant. The partial molal entropy change of micellization ($\Delta\overline{S}_m$) in water increases with an increase in the pressure up to about 1500 atm, while $\Delta\overline{S}_m$ in 3-m urea solution remains virtually unaltered in the low-pressure region. The results suggest that the "iceberg" structure of water around the hydrocarbon chain of the monomeric surfactant is effectively broken down by urea.

The effect of urea on the micelle formation has already been studied by many workers,[1-9] and it is well known that the addition of urea raises the critical micelle concentration (CMC) of surfactant solutions. A smaller negative free energy change and a smaller positive entropy change on micellization have been interpreted in terms of the breakdown of the water structure by urea.

The study of the pressure effect as well as the temperature effect on the CMC of a surfactant in aqueous solutions has given very important thermodynamic information on micelle-forming properties.[10-15] Therefore, the effects of the pressure and temperature on the CMC of a surfactant in aqueous urea solutions are expected to give a deeper insight into the surfactant solution than has hitherto been reported. A knowledge of the thermodynamic properties of model compounds such as surfactants in aqueous urea solutions helps to understand the urea denaturation of proteins and the effect of urea on the water structure.

In this study the CMC of dodecyltrimethylammonium bromide (DTAB) in aqueous urea solutions of various concentrations was determined over a range of pressures up to 2500 atm at 25 and 35 °C. Then the partial molal volumes of DTAB in aqueous urea solutions were determined above and below the CMC. The effect of urea on the thermodynamic parameters for micellization was also examined.

Experimental

The DTAB used was synthesized and purified by the method described previously.[16] The CMC of the DTAB solution determined by the conductivity method was 0.01554 in molality (m) at 25 °C. This value is in good agreement with that in the literature. All the solutions were prepared on a molal basis. Urea was recrystallized from an ethanol-water (95 : 5) mixture. The urea concentrations of 3.0 and 6.0 in molality correspond to the values in 2.64 and 4.75 in molarity (M) at 25 °C respectively.

The high-pressure apparatus used is the same as has been described previously.[17] The CMC of DTAB in aqueous urea solutions under high pressures was determined by the conductivity method in a way similar to that used under atmospheric pressures.

The densities of a series of solutions were simultaneously measured by using ten pycnometers with a capacity of about 20 ml; the error of measurements was within $\pm 5 \times 10^{-5}$ g/cm^3. The thermostated bath was controlled to 25 ($\pm$0.005) °C. The volume of solution per 1000 g of solvent (water+urea) was plotted against the molality of DTAB, resulting in a straight line below and above the CMC. The partial molal volume of DTAB in aqueous urea solutions was taken as the slope of the line; it was determined by the least-squares method. Since the partial molal volume is almost independent of the surfactant concentration over the concentration ranges studied here,[18,19] the experimental values thus obtained have been assumed to be identical with those corresponding to an infinite dilution.

Results and Discussion

The CMC of DTAB in several urea solutions is shown in Fig. 1 as a function of the pressure. The

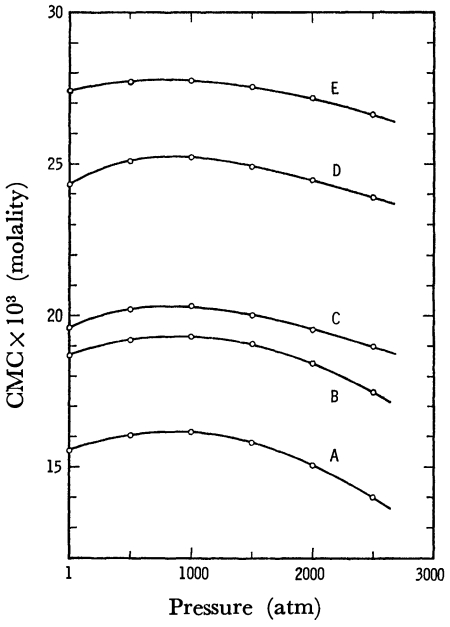

Fig. 1. Effect of pressure on the CMC in some urea solutions at 25 °C. Urea concentration; A: 0, B: 1.99, C: 2.94, D: 4.49, and E: 6.08 (mole/kg-H_2O).

** Present address: Sekisui Kasehin Kogyo Co., Ltd., Nara 630

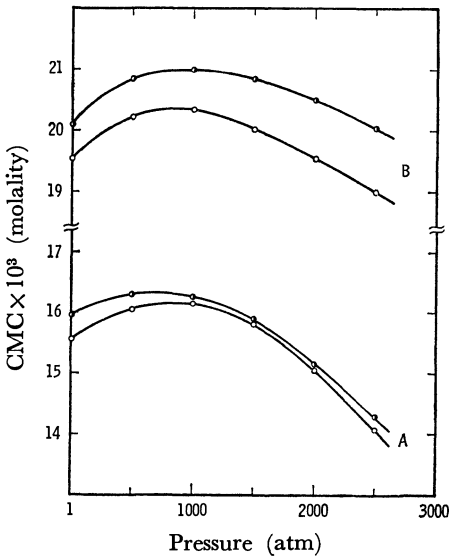

Fig. 2. Effect of pressure on the CMC in water and 3 m (2.94 molality) urea solution at two temperatures, 25 °C (○) and 35 °C (◑). A: in water, B: in 3 m urea solution.

CMC *vs.* pressure curve in water is in fair agreement with that of Tuddenham and Alexander.[11] At about 800 atm, the CMC *vs.* pressure curve has a maximum which remains even in a 6-m urea solution. The CMC of DTAB increases with the addition of urea in the whole pressure region studied. This increase in the CMC by urea at 1 atm is comparable with the results reported by other workers.[2,5,9] In Fig. 2, the effects of the temperature and pressure on the CMC of DTAB in water and a 3-m urea solution are compared. It is known that the CMC *vs.* temperature curve for DTAB reaches a minimum at about 25 °C in water[5,17] and at 15—20 °C in the 3-M urea solution.[5,9] As may be seen from Fig. 2, in water the increase in the CMC by the elevation of the temperature is reduced upon the application of pressure, while in the 3-m urea solution it becomes progressively greater as the pressure increases.

There remain some factors to be considered in the interpretation of the effect of urea on the micelle formation; the change in the dielectric constant of the solution, the solubilization of urea into the micelle, the change in the structured water around the hydrocarbon chain of the monomeric surfactant, and so on. It is known that the dielectric constant of a solution increases with the urea concentration up at least to 3 M;[20] this increase of the dielectric constant of urea solution is most likely responsible for the dissociation of the ionic micelle.[9] In the methanol–water mixture, however, the effective micellar charge increases with the methanol content to a 0.3 mole fraction of methanol[21] in spite of the decrease in the dielectric constant with the increase in the methanol content.[20] The CMC increases in both solutions. The micellar weight decreases not only in a methanol solution,[21,22] but also in an urea solution.[23] Thus, the change in the dielectric constant which is due to the change in the composition of solvent seems not to affect the micelle formation very much. Secondly, it is known that in general the addition of solubilizates lowers the CMC.[24] The solubilization effect of urea on the micellization is very little, if any, because the CMC increases with the addition of urea.

The change in the partial molal volume on micellization, $\Delta\overline{V}_m$, was calculated from the pressure dependence of the CMC through the following equation which has previously been discussed:[14,15]

$$\Delta\overline{V}_m = (1+\beta)RT\left(\frac{\partial \ln \mathrm{CMC}}{\partial P}\right)_{T,\,\Delta\overline{G}_m} \qquad (1)$$

where β is a constant which indicates the ratio of the number of the gegenion to that of the surfactant ion in a micelle. The values of $\Delta\overline{V}_m$ in water and aqueous urea solutions are calculated from Eq. (1) using the results shown in Fig. 1; they are given in Table 1. The value of β used was taken from the literature[9,25] except for that in a 6-m urea solution, which was assumed to be 0.76 by an extrapolation of the available data.

Table 1. Partial molal volumes of micellar and singly dispersed surfactant, and the changes of partial molal volume on micellization

Urea concn. (mol/kg)	β	From CMC $\Delta\overline{V}_m$	From density measurement $\overline{V}_m$	$\overline{V}_s$	$\overline{V}_m-\overline{V}_s$
0	0.744	4.1	295.5	287.0	8.5
2.94	0.756	4.2	295.4	290.2	5.2
6.08	(0.76)	1.5	294.7	291.0	3.7

The values of the partial molal volumes in the micellar ($\overline{V}_m$) and singly dispersed ($\overline{V}_s$) states and their difference ($\overline{V}_m$—$\overline{V}_s$) are also shown in Table 1. The values of $\Delta\overline{V}_m$ calculated from the pressure dependence of the CMC are somewhat smaller not only in water, as has been described previously,[14] but also in urea solutions than the $\overline{V}_m$—$\overline{V}_s$ determined from the density measurement. It is obvious from Table 1 that the partial molal volume change on micellization is reduced by the addition of urea. This reduction may be attributed to the increase in $\overline{V}_s$ with the addition of urea, as $\overline{V}_m$ is kept approximately constant.

The change in the partial molal volume for the transfer of the solute molecule, which has a hydrophobic tail, from water to urea solutions has been studied by several authors.[26,27] This volume change is positive, and it tends to increase as the length of the hydrocarbon chain increases. It is known that the transfer of hydrocarbons from a nonpolar environment to water results in a negative volume change;[28] this is considered to reflect the ordering of water molecules around the hydrocarbon chains, or the "iceberg" formation.[29] Therefore, the positive volume changes for the transfer of a monomeric surfactant from water to urea solutions are consistent with a structure-breaking role of urea in aqueous solutions. On the other hand, $\overline{V}_m$ is quite insensitive to the presence of urea. This constancy of $\overline{V}_m$ can be attributed to the loss of hydrocarbon-water contact due to the formation of micelles.

The change in the partial molal entropy on micelliza-

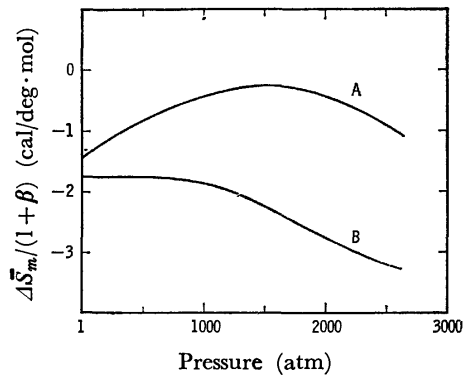

Fig. 3. Partial molal entropy change of micelle formation in the range of temperature, 25—35 °C, as a function of pressure. A: in water, B: in 3 m urea solution.

tion is given by the following equation, as has been described previously:[15]

$$\Delta\bar{S}_m = -(1+\beta)RT\left(\frac{\partial \ln CMC}{\partial T}\right)_{P,\,\Delta\bar{G}_m} \quad (2)$$

On the basis of the data shown in Fig. 2, the partial molal entropy change on micellization was calculated at the mean temperature, 30 °C. Of course, the value of the CMC has no minimum or maximum in the range of temperature of 25—35 °C.[5,9,17] Values of β under high pressures are not available at present. Thus, the $\Delta\bar{S}_m/(1+\beta)$ value calculated from the CMC's at two temperatures is shown in Fig. 3 as a function of the pressure. As β probably changes with the pressure,[15] the form of the pressure dependence of $\Delta\bar{S}_m$ may be slightly transformed from that shown in Fig. 3. It may be noted from Fig. 3, however, that the $\Delta\bar{S}_m$ in water increases initially with an increase in the pressure and then decreases with the pressure via a maximum at about 1500 atm, while the $\Delta\bar{S}_m$ in the 3-m urea solution remains virtually unaltered at low pressures and then decreases gradually with the pressure.

The pressure dependence of $\Delta\bar{S}_m$ is related to the temperature dependence of $\Delta\bar{V}_m$ as follows:

$$\left(\frac{\partial\Delta\bar{S}_m}{\partial P}\right)_T = -\left(\frac{\partial\Delta\bar{V}_m}{\partial T}\right)_P \quad (3)$$

Regarding micellization in water, it is known that $(\partial\Delta\bar{S}_m/\partial P)_T>0$ in the region of lower pressures; *i.e.*, $(\partial\Delta\bar{V}_m/\partial T)_P<0$.[15,18] The effect of the temperature on the partial molal volume for singly dispersed and micellar states leads to $(\partial\bar{V}_s/\partial T)_P>(\partial\bar{V}_m/\partial T)_P>0$.[18] The positive larger value for $(\partial\bar{V}_s/\partial T)_P$ than for $(\partial\bar{V}_m/\partial T)_P$ is attributable to the thermal expansion as well as to the breakdown of the "iceberg" structure around the hydrocarbon chain as a results of thermal motion. Thus, we can regard $(\partial\bar{S}_s/\partial P)_T<(\partial\bar{S}_m/\partial P)_T<0$ as true at low pressures. That is, the entropy decrease with the compression for the singly dispersed state outweighs that for the micellar state. According to Le Chatelier's principle, the compression leads to a decrease in volume and is more favorable to a structure-making of water around hydrocarbon. Therefore, it may be concluded that the compression causes the promotion of the "iceberg" formation around the hydrocarbon chain. In the micelle formation in the 3-m urea solution, on the other hand, $(\partial\Delta\bar{S}_m/\partial P)_T\simeq 0$ at lower pressures, judging from Fig. 3. Consequently, $(\partial\bar{S}_s/\partial P)_T\simeq(\partial\bar{S}_m/\partial P)_T<0$ and/or $(\partial\bar{V}_s/\partial T)_P\simeq(\partial\bar{V}_m/\partial T)_P>0$, which means that the "iceberg" structure of water around the hydrocarbon chain is effectively broken down by the urea added.

References

1) M. L. Corrin and W. D. Harkins, *J. Amer. Chem. Soc.*, **69**, 683 (1947).
2) W. Brunning and A. Holtzer, *ibid.*, **83**, 4865 (1961).
3) P. Mukerjee and A. Ray, *J. Phys. Chem.*, **67**, 190 (1963).
4) M. J. Schick, *ibid.*, **68**, 3585 (1964).
5) M. F. Emerson and A. Holtzer, *ibid.*, **71**, 3320 (1967).
6) J. M. Corkill, J. F. Goodman, S. P. Harrold, and J. R. Tate, *Trans. Faraday Soc.*, **63**, 240 (1967).
7) M. J. Schwuger, *Kolloid-Z. Z. Polym.*, **232**, 775 (1969).
8) M. N. Johes, G. Pilcher, and L. Espada, *J. Chem. Thermodynamics*, **2**, 233 (1970).
9) J. Piercy, M. N. Jones, and G. Ibbotson, *J. Colloid Interfac. Sci.*, **37**, 165 (1971).
10) S. D. Hamann, *J. Phys. Chem.*, **66**, 1359 (1962).
11) R. F. Tuddenham and A. E. Alexander, *ibid.*, **66**, 1839 (1962).
12) J. Osugi, M. Sato, and N. Ifuku, *Nippon Kagaku Zasshi*, **87**, 329 (1966); *Rev. Phys. Chem. Japan*, **35**, 32 (1965); **38**, 58 (1968).
13) M. Tanaka, S. Kaneshina, T. Tomida, K. Noda, and K. Aoki, *J. Colloid Interfac. Sci.*, **44**, 525 (1973).
14) M. Tanaka, S. Kaneshina, K. Shinno, T. Okajima, and T. Tomida, *ibid.*, **46**, 132 (1974).
15) S. Kaneshina, M. Tanaka, T. Tomida, and R. Matuura, *ibid.*, **48**, 450 (1974).
16) M. Tanaka, S. Kaneshina, W. Nishimoto, and H. Takabatake, This Bulletin, **46**, 364 (1973).
17) S. Kaneshina, M. Tanaka, and R. Matuura, *Mem. Fac. Sci., Kyushu Univ., C*, **9**, 71 (1974).
18) K. Shinoda and T. Soda, *J. Phys. Chem*, **67**, 2072 (1963).
19) J. M. Corkill, J. F. Goodman, and T. Walker, *Trans. Faraday Soc.*, **63**, 768 (1967).
20) "International Critical Tables" Vol. 6, McGraw-Hill Book Co., Inc., New York (1921), p. 101.
21) G. D. Parfitt and J. A. Wood, *Kolloid-Z. Z. Polym.*, **229**, 55 (1969).
22) H. Uehara, M. Manabe, and R. Matuura, *Mem. Fac. Sci. Kyushu Univ., C*, **8**, 55 (1972).
23) H. Amano and T. Sasaki, presented at the 26th Symposium on Colloid and Surface Chemistry, Chemical Society of Japan, Fukui, 1973.
24) P. H. Elworthy, A. T. Florence, and C. B. MacFarlene, "Solubilization by Surface-Active Agents," Chapman and Hall Ltd., London (1968), p. 61.
25) T. Ingram and M. N. Jones, *Trans. Faraday Soc.*, **65**, 297 (1969).
26) W. A. Hargraves and G. C. Kresheck, *J. Phys. Chem.*, **73**, 3249 (1969).
27) P. R. Philip, J. E. Desnoyers, and A. Hade, *Can. J. Chem.*, **51**, 187 (1973).
28) W. L. Masterton, *J. Chem. Phys.*, **22**, 1830 (1954).
29) G. Nemethy and H. A. Scheraga, *ibid.*, **36**, 3401 (1962).

The Polarographic Behavior and Determination of Orotic Acid (Vitamin B_{13}) in Milk

Toshio YAO and Sōichirō MUSHA

Department of Applied Chemistry, College of Engineering, University of Osaka Prefecture, Mozuumemachi, Sakai 591

(Received April 30, 1974)

The polarographic behavior of orotic acid at the dropping mercury electrode was studied in the Britton-Robinson buffer solution; it was found to be a complex function of the pH. Three polarographic waves were observed over the pH range from 2 to 12. In the 1M $HClO_4$ electrolyte, orotic acid showed a very well-defined, diffusion-controlled, two-electron polarographic reduction wave which enabled us to determine orotic acid polarographically. A polarographic method for the determination of orotic acid in milk was proposed, and the effect of the presence of surface-active substances like proteins was investigated. The proposed method is very simple and rapid, and permits the accurate determination of 4—1000 μg/g of orotic acid in milk.

In recent years, the electrochemical reduction and oxidation of biologically-important compounds have been investigated with much interest. An examination of the oxidation-reduction behavior of compounds of biological significance is often of considerable value. Although actual biological redox systems may be of extreme complexity as a result of enzyme interactions, much information can be obtained from the study of these compounds in aqueous solutions with regard to factors affecting the electron-transfer processes, such as the pH.

Orotic acid (2,6-dihydroxypyrimidine-4-carboxylic acid), one of the uracil derivatives, is also known as vitamin B_{13}. Icha[1] has described orotic acid as polarographically-active. However, no detailed study of the electrode process and no application of polarography to the analysis of orotic acid in biological materials have been carried out. Recently, Archer[2] determined the orotic acid content in milk bread by the colorimetric method[3] as modified by Brieskorn and Wallrauch.[4] This method, however, is time-consuming and complicated.

The present work was carried out in order to study the polarographic behavior of orotic acid in detail and to investigate the applicability of polarography to the rapid analysis of orotic acid in cow's milk.

Experimental

Chemicals. The orotic acid (reagent of the Wako Pure Chemical Co.) was recrystallized three times from distilled water before drying at 60 °C *in vacuo*. A 5 mM stock solution was prepared by dissolving an appropriate amount of orotic acid in distilled water. The solutions used for the analysis were prepared by the dilution of the stock solution with aqueous buffer solutions and acid solutions to give the desired concentrations. The other chemicals were of a reagent grade and were used without further purification.

Apparatus. The polarograms were recorded using a Yanagimoto P-8 type Polarograph. Cyclic voltammetry was performed with a versatile solid-state instrument constructed in this laboratory following the design of Goolsby and Sawyer,[5] while the voltammograms were recorded using a Hewlett Packard Model 7045A X-Y recorder.

The dropping mercury electrode had the following characteristics: mercury flow rate, $m=2.25$ mg/s and drop time, $t=3.38$ s at open circuit and at a height of the mercury reservoir of 70 cm in 1 M $HClO_4$. A hanging mercury-drop electrode was used as a working electrode for the cyclic voltammetric experiments, while a mercury pool was employed for the controlled potential coulometric measurements. The reference electrode was SCE, and a platinum coil was used as an auxiliary electrode. All the experiments were carried out at 25.0±0.1 °C.

Results and Discussion

Polarographic Behavior of Orotic Acid. Effect of the pH: The effect of the pH on the polarographic curves was investigated by recording the polarograms of 0.5 mM orotic acid in the Britton-Robinson buffer solution. The half-wave potential and the reduction current of orotic acid with respect to the pH values are shown in Fig. 1.

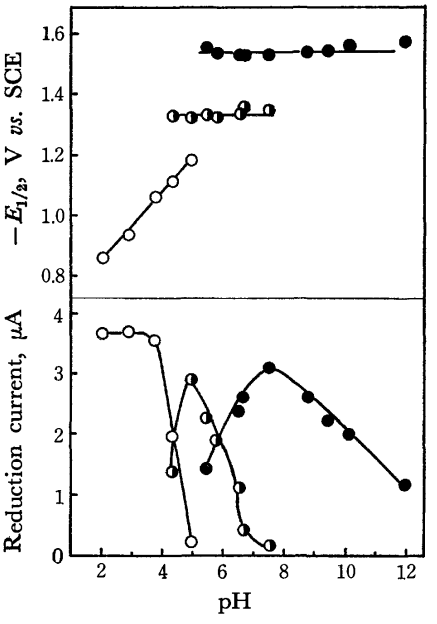

Fig. 1. The effect of pH on the reduction current and the half-wave potential of 0.5 mM orotic acid (Britton-Robinson buffer).
○: 1st wave, ◑: 2nd wave, ●: 3rd wave

Between pH 2 and 12, three polarographic reduction waves were observed. The first wave appeared in the pH range of 2—5. The half-wave potential shifted linearly towards a negative potential with an increase in the pH; this implies that hydrogen ions are consumed in the first reduction step. At pH values below 5, the half-wave potential of the first wave is given by the equation:

$$E_{1/2} = -0.635 - 0.108\ \mathrm{pH} \quad (1)$$

The height of the wave remained almost constant up to about pH 3.8. Above pH 3.8 it decreased sharply, and it vanished at about pH 5.1. The diffusion-current constant ($I=i_d/Cm^{2/3}t^{1/6}$) of the first wave at pH 3.1 was 3.92, corresponding to a two-electron Faradaic process.

The half-wave potentials of the second wave and the third wave were independent of the pH of the electrolyte. The second wave appeared in the pH range of 4—8, and the third wave, above pH 5. The reduction current of both waves was dependent on the pH. The sum of the heights of these three waves was almost constant up to about pH 7.5.

Calculation of αn_a *and* P: The values of αn_a and of P(the number of hydrogen ions involved per molecule of the reactant in the rate-controlling step) were calculated on the basis of Eqs. (2) and (3);[6,7] they are summarized in Table 1.

$$E_{1/4} - E_{3/4} = 0.0517/\alpha n_a \quad (2)$$

$$\mathrm{d}(E_{1/2})/\mathrm{d}(\mathrm{pH}) = -0.05915\,P/\alpha n_a \quad (3)$$

For the first wave, an average αn_a value of 1.32 and an average P value of 2.41 were determined. The average αn_a values of the second and third waves were 1.48 and 0.99 respectively.

Effects of the Drop-Time and the Temperature: The effect of the drop-time on the limiting current was investigated by recording the polarograms of 0.5 mM orotic acid at various heights of the mercury column. The $I/\sqrt{h}$ values, where h is the height of the column after correction for the back pressure, for all three polarographic waves were constant. The temperature coefficient of the limiting current of the three polarographic waves of orotic acid was 0.6—1.4% per degree in the temperature range from 15 to 45 °C. These results indicate that each of the three polarographic waves is diffusion-controlled.

Controlled Potential Coulometry. Coulometric reductions at the controlled potential of orotic acid in the Britton-Robinson buffer were performed in an attempt to determine the number of electrons involved in the overall electron transfer reactions. At pH 2.57 the potential of the mercury pool was first controlled at −1.15 V *vs.* SCE In this experiment, 5.23 coulombs were consumed in the reduction of 2.5×10^{-5} mol of orotic acid, which yielded n=2.17 for the first reduction wave. The experiments were repeated at pH 5.00 and 7.90 with new solutions containing the same amount of orotic acid and with the potentials of the working electrde controlled at −1.45 and −1.75 V respectively. The n values of the second and third reduction waves were 1.83 and 1.86 respectively. These experiments imply that two electrons are involved in each of the three polarographic steps.

Cyclic Voltammetry. Cyclic voltammetric experiments were performed at a hanging mercury drop electrode. The mercury drop was renewed each time. If the potential sweep was repeated at the same mercury drop, the peak height decreased and the peak potential shifted towards a more negative value, indicating the adsorption of a reduction product at the electrode. Orotic acid gave a cathodic peak corresponding to each of the three polarographic waves observed at various pH values, the heights of which were proportional to the square root of the scan rate in the range from 1.0 to 15 V/min. However, no anodic peak resulting from the reoxidation of the reduction product was observed at any scan rate or any switching potential.

Analytical Application. Effect of Buffer and Acid Components: Polarographic experiments revealed that a well-defined wave appeared at low pH values; the height of this wave was almost constant up to about pH 3.8. Therefore, the polarographic behavior of the first wave at low pH values was investigated by using other buffers (acetate and chloride buffer) and acids (HCl, H_2SO_4, and $HClO_4$) as electrolytes. In these electrolytes, the half-wave potential of orotic acid shifted towards a positive potential with a decrease in the pH. The $E_{1/4}$–$E_{3/4}$ value decreased with a decrease in the pH of the electrolytes. The buffer and acid components, however, had no influence on the wave-height.

When HCl and H_2SO_4 were used as supporting electrolytes, a large maximum appeared in any acid concentration. However, in the case of a $HClO_4$ background, no maximum appeared and the polarographic

Table 1. Effect of pH on the polarographic reduction waves of 0.5 mM orotic acid in the Britton-Robinson buffer

pH	1st wave			2nd wave		3rd wave	
	$E_{1/4}-E_{3/4}$ (mV)	αn_a	P	$E_{1/4}-E_{3/4}$ (mV)	αn_a	$E_{1/4}-E_{3/4}$ (mV)	αn_a
2.93	40	1.29	2.36				
3.86	39	1.33	2.43	39	1.32		
4.36	39	1.33	2.43	38	1.36		
5.02				34	1.52		
5.54				33	1.57	68	0.76
5.83				32	1.61	50	1.03
6.60				35	1.47	51	1.01
6.72						54	0.95
7.56						57	0.90
8.80						54	0.95
9.53						49	1.05
10.20						51	1.01

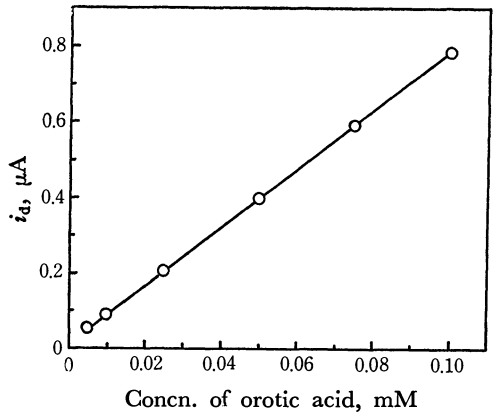

Fig. 2. Calibration curve for orotic acid in 1 M $HClO_4$.

wave was well-defined. The effect of the drop-time was investigated by recording polarograms of 0.1 mM orotic acid in 1 M $HClO_4$ at various heights of the mercury column. The limiting current of orotic acid was approximately proportional to $h^{1/2}$, indicating that the reduction current is controlled by diffusion. The diffusion current of orotic acid in 1M $HClO_4$ was proportional to the concentration in the $5\times10^{-6}-10^{-4}$ M range as is shown in Fig. 2.

Consequently, 1M $HClO_4$ was used as the supporting electrolyte in the following experiments for the determination of orotic acid.

Effect of Protein Addition: A polarographic wave of orotic acid was observed even in the presence of 50% milk. However, the proteins present in milk are surface-active, and so the polarographic wave of orotic acid was partly distorted by the adsorbed layer of proteins on the electrode. The limiting current was depressed, and the half-wave potential shifted towards a more negative potential.

The effect of proteins on polarograms of 0.1 mM orotic acid in 1M $HClO_4$ was investigated by adding proteins refined by centrifuging milk several times. The results are shown in Table 2. On the addition of more than 0.3% of proteins, the half-wave potential became more negative and the $E_{1/4}$—$E_{3/4}$ value increased. However, the wave height of orotic acid was not affected by the presence of less than 0.5% of proteins. These results indicate that the presence of a large amount of proteins produces a drawn-out wave at a more negative potential with an increase in the protein concentration, and that the removal of most proteins is necessary for the determination of orotic acid in milk.

Table 2. Effect of protein on the polarograms of 0.1 mM orotic acid in 1 M $HClO_4$

Protein, wt%	$-E_{1/2}$, V *vs.* SCE	$E_{1/4}-E_{3/4}$, mV	i_d, μA
0	0.678	30	0.771
0.02	0.675	30	0.780
0.05	0.680	30	0.759
0.08	0.680	30	0.783
0.15	0.680	30	0.790
0.30	0.693	38	0.776
0.45	0.710	50	0.773
0.60	0.732	72	0.742
0.90	0.750	85	0.720
1.2	0.770	80	0.721
1.5	0.780	135	0.674

Determination of Orotic Acid in Milk: The method for the determination of orotic acid in milk is as follows: Weigh accurately a quantity of a sample expected to contain from 0.1 to 0.6 mg of orotic acid into a 100-ml beaker. Add 10—20 ml of 1M $HClO_4$, mix, and place the mixture in a water-bath at 65 °C for 30 min. Then remove the beaker from the water-bath, cool to room temperature, and filter the coagulated proteins through fluted filter-paper. Wash the precipitate with 20 ml of 1M $HClO_4$, transfer the solution into a 50-ml calibrated flask, and dilute to the mark with 1M $HClO_4$. Transfer this solution into a polarographic cell. Remove the dissolved air with nitrogen and record a polarogram.

Various types of artificial milk containing known amounts of orotic acid and known amounts of refined proteins were prepared, and the proteins present in these milk were removed by the proposed procedure. The recovery experiments were carried out by analyz-

Table 3. Recovery of orotic acid

Taken orotic acid (μg)	Added protein (wt%)	Found (μg)	Recovery (%)
99.8	1.02	98.2	98.4
99.8	1.57	97.5	97.7
171.6	0.44	170.0	99.1
171.6	0.63	170.0	99.1
171.6	1.04	161.5	94.1
240.2	0.59	234.0	97.4
255.1	0.35	243.7	95.5

Table 4. Determination of orotic acid in cow's milk

Taken cow's milk (g)		Found (μg/g) This work (A)[a]	This work (B)[b]	Colorimery
A	1.001	109	102	106
	2.205	118	115	
	3.197	113	117	108
	4.763	105	117	
	Average	111	113	
Deviation coefficient (%)		4.7	6.1	
B	1.129	82	78	74
	2.100	78	80	
	3.331	79	72	71
	4.605	75	78	
	Average	79	77	
Deviation coefficient (%)		3.7	4.5	
C	1.022	118	122	120
	2.536	126	126	
	3.198	115	116	102
	4.501	122	117	
	Average	120	120	
Deviation coefficient (%)		4.0	3.9	

a) Determined by using the calibration graph.
b) Determined by the standard addition method.

ing orotic acid in these filtrates. The $E_{1/4}$—$E_{3/4}$ values of the polarograms recorded were about 30 mV, indicating that most proteins were removed by this procedure(see Table 2). The results, shown in Table 3, indicate that a tolerable agreement between the amounts of orotic acid added and the amounts recovered is obtained by this procedure.

The precision of this analytical method for orotic acid was determined by analyzing three samples(A, B, and C) of cow's milk four times each. The determination was carried out by both the calibration graph method and the standard addition method. The results, shown in Table 4, were compared with those obtained by the colorimetric method.[2)]

Compared with the colorimetric method, which involves very time-consuming and complicated procedures, the proposed polarographic method is very simple and rapid and permits the accurate determination of 4—1000 μg/g of orotic acid in milk.

References

1) F. Icha, *Pharmazie*, **14**, 684 (1959).
2) A. W. Archer, *Analyst*, **98**, 755 (1973).
3) T. Adachi, A. Tanimura, and M. Asahina, *J. Vitam.*, **9**, 217 (1963).
4) C. H. Brieskorn and S. Wallrauch, *Z. Lebensmittelunters. u.-Forsch.*, **138**, 154 (1968).
5) A. D. Goolsby and D. T. Sawyer, *Anal. Chem.*, **39**, 411 (1967).
6) G. Dryhurst and P. J. Elving, *ibid.*, **40**, 492 (1968).
7) K. B. Oldham and E. P. Parry, *ibid.*, **40**, 65 (1968).

Thermal Dehydration and Decomposition Reactions of Bivalent Metal Oxalates in the Solid State

Kenzo NAGASE, Katsuya SATO,* and Nobuyuki TANAKA*

College of General Education, Tohoku University, Kawauchi, Sendai 980

**Department of Chemistry, Faculty of Science, Tohoku University, Aoba, Aramaki, Sendai 980*

(Received May 13, 1974)

The thermal dehydration and decomposition of the oxalates of Mg(II), Ca(II), Sr(II), Ba(II), Mn(II), Fe(II), Co(II), Ni(II), Cu(II) and Zn(II) were investigated by means of TG, DTA, DSC, EGA, X-ray powder diffraction analysis, and reflectance and infrared spectroscopies. In general, the temperature at which the oxalates were dehydrated increased with $1/r$, where r denotes the radius of metal ion. The heats of dehydration (ΔH_{H_2O}) of the alkaline earth metal oxalates increased with $1/r$, but those of transition metal oxalates decreased as $1/r$ increased. By considering the decomposition products, the reactions of anhydrous oxalates were classified into three groups and the relations between the decomposition temperatures and $1/r$ were discussed for each group.

The thermal decomposition reactions of metal oxalates have been extensively investigated. The thermographic curves of a number of metal oxalates have been described by Ugai[1] and many other researchers. Dollimore and his co-workers[2-4] measured changes in length or volume of samples subjected to heat treatment, or surface-area changes occurring on dehydration, and discussed the effect of dehydration on the subsequent decompositions. Lagier and his co-workers[5-7] found that, for the oxalates of Mg, Mn, Fe, Co and Zn, at least two phases of the compounds exist and that the phases observed depended on the method of preparation. They studied the dependence of dehydration of $CoC_2O_4 \cdot 2H_2O$ on the differences of the two phases. Kinetic studies on the dehydration and decomposition of a number of oxalates were carried out by isothermal and temperature elevation methods. In many cases, however, the parameters reported by each researcher for a given oxalate were different.

In the present paper, the thermal dehydration and decomposition reactions of bivalent metal oxalates were systematically discussed on the basis of the relations between the nature of the metal ions and the initial weight-loss temperatures or enthalpy changes.

Experimental

Materials. The oxalates of alkaline earth metals and transition metals investigated were precipitated with alkali oxalates (or oxalic acid) from solutions of soluble salts of the corresponding metals, washed thoroughly with water and dried in air. The elemental analyses for C and H agreed with the calculated values within $\pm 0.3\%$.

Measurements. Thermogravimetric (TG) and differential thermal analytic (DTA) curves were obtained with a Shinku Riko TGD-3000 at a heating rate of 5 °C/min in an atmosphere of nitrogen flowing at 50 ml/min. About twenty milligrams of powdered sample in a platinum crucible were used for each measurement. Differential scanning calorimetric (DSC) curves were recorded with a Rigaku Denki 8002 CS at a heating rate of 5 °C/min in an atmosphere of nitrogen flowing at 30 ml/min. About twenty milligrams of powdered sample were placed in a crucible made from 0.1 mm thick aluminum sheet. A lid of the same material was placed inside the crucible. The reference material was α-Al_2O_3. The instrument was calibrated against the heat of the transition of KNO_3 which appears at 128 °C with ΔH equal to 12.28 kcal/mol.

High temperature X-ray diffractions were measured in an atmosphere of nitrogen flowing at 30 ml/min with a Toshiba ADG-101 diffractometer equipped with a standard high temperature sample holder. Cu$K\alpha$ radiation and a nickel filter were used in all measurements. Infrared absorption spectra were measured from 2500 to 400 cm^{-1} in KBr disks with a Hitachi EPI-3G spectrophotometer. The sample was heated under conditions identical to those for the TG measurements. When the temperature of the sample reached the desired value, heating was stopped, the sample was cooled to room temperature and its infrared absorption spectrum was recorded. Diffuse reflectance spectra were measured with a Hitachi EPS-3T spectrophotometer equipped with a standard integrating sphere attachment. MgO was used as the reference material. The heated sample was treated in the same way as for the measurement of the infrared spectra.

Evolved gas (EG) curves were obtained using a conductometric technique. The evolved gas analyses (EGA) were carried out using an activated charcoal column (2 meters long) and a helium carrier gas (50 ml/min). In both cases the procedures described in a previous paper[8] were employed.

Results

TG and DTA curves in the temperature range from room temperature to 1000 °C in a flowing nitrogen atmosphere are given in Figs. 1 and 2. The thermal data obtained are summarized in Table 1 together with the radii of the metal ions (Goldschmidt's crystallographic radii). The TG curve of $CaC_2O_4 \cdot H_2O$ shows that the decomposition took place at three stages, as indicated in previous paper.[1] On the DTA curve, a small exothermic peak, which has not been previously reported, was observed at 290 °C without any weight-loss. $SrC_2O_4 \cdot 2H_2O$ decomposed to $SrCO_3$ after dehydration; $SrCO_3$ did not decompose further, but the γ-$SrCO_3$ to β-$SrCO_3$ phase transition was observed at 875 °C. The DTA curve for $SrC_2O_4 \cdot 2H_2O$ also had an exothermic peak at 259 °C which was more prominent than that of $CaC_2O_4 \cdot H_2O$. This change without weight-loss was not reversible (*i.e.* not reflected on the cooling curve), indicating that the lower-temperature form is metastable with respect to the higher-temperature one. The X-ray powder diffraction patterns showed that this change corresponds to recrystallization of poorly crystalline SrC_2O_4 formed

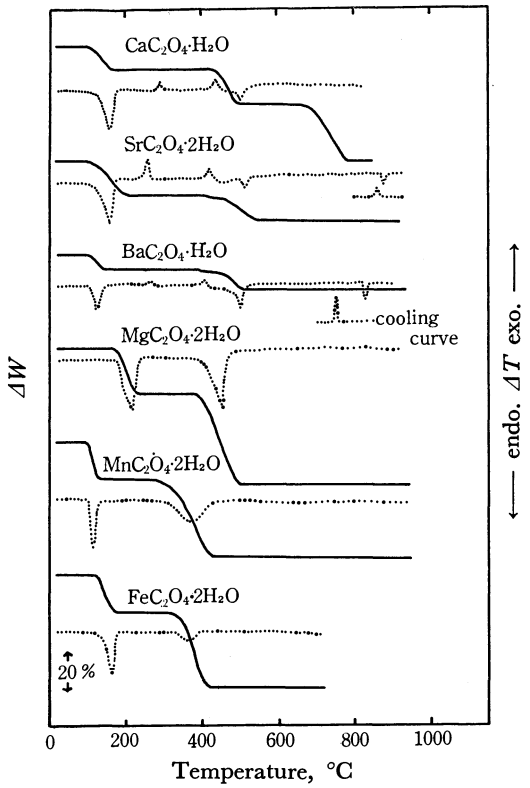

Fig. 1. TG (solid line) and DTA (dotted line) curves of metal oxalates in a flowing nitrogen atmosphere.

on dehydration. The heat of this process was found to be 3.2 kcal/mol by DSC. The TG and DTA curves of $BaC_2O_4 \cdot H_2O$ were very similar to those of $SrC_2O_4 \cdot 2H_2O$.

The oxalates containing metal ions with radii smaller than that of calcium ion decomposed to metal oxides or metals. The oxalates of Mg, Mn, Fe and Zn decomposed at lower temperatures as the radius of the metal ion increased and formed the metal oxides and an equimolar mixture of CO and CO_2, whereas the oxalates of Co, Ni and Cu decomposed at higher temperatures as the metal ion radius increased, and gave the metals and CO_2.

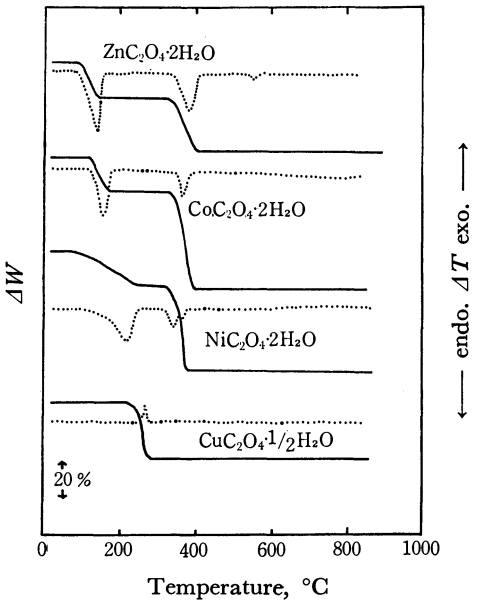

Fig. 2. TG (solid line) and DTA (dotted line) curves of metal oxalates in a flowing nitrogen atmosphere.

The reactions of the oxalates investigated may be expressed as,

$$MC_2O_4 \rightarrow MCO_3 + CO,$$
where M = Ca(II), Sr(II) and Ba(II) (1)

$$MC_2O_4 \rightarrow MO + CO + CO_2,$$
where M = Mg(II), Mn(II), Fe(II) and Zn(II) (2)

$$MC_2O_4 \rightarrow M + 2CO_2,$$
where M = Co(II), Ni(II) and Cu(II) (3)

These stoichiometries were confirmed by analyses of gaseous products, *cf.* Table 2.

The heats of dehydration (ΔH_{H_2O}) and of decomposition (ΔH_d) were measured by DSC. The results are given in Table 3. The values of ΔH_{H_2O} of alkaline earth metal oxalates increased almost parallel to the increase of the initial weight-loss temperatures(t_{H_2O}), while ΔH_{H_2O} of transition metal oxalates decreased with increasing t_{H_2O}. For decomposition of the an-

Table 1. Thermal analyses and radii of metal ions

Compound	Dehydration			Decomposition of anhydrous oxalate				Radius of metal ion/Å
	$t^{a}_{H_2O}$/°C	Weight-loss/%		t_d [b]/°C	Product	Weight-loss/%		
		obsd	calcd			obsd	calcd	
$MgC_2O_4 \cdot 2H_2O$	157	23.6	24.3	380	MgO	46.4	48.5	0.78
$CaC_2O_4 \cdot H_2O$	100	12.5	12.3	418	$CaCO_3$	19.1	19.2	0.99
$SrC_2O_4 \cdot 2H_2O$	93	16.8	17.0	403	$SrCO_3$	14.0	13.2	1.27
$BaC_2O_4 \cdot H_2O$	97	6.2	7.4	395	$BaCO_3$	10.3	11.5	1.43
$MnC_2O_4 \cdot 2H_2O$	95	20.5	20.1	290	MnO	41.6	40.2	0.91
$FeC_2O_4 \cdot 2H_2O$	116	20.2	20.0	310	FeO	39.9	40.0	0.83
$CoC_2O_4 \cdot 2H_2O$	118	21.0	19.7	338	Co	47.0	48.1	0.82
$NiC_2O_4 \cdot 2H_2O$	137	18.6	19.7	310	Ni	46.7	48.2	0.78
$CuC_2O_4 \cdot 1/2H_2O$	—	—	—	235	Cu	59.8	60.2	0.72
$ZnC_2O_4 \cdot 2H_2O$	92	18.7	19.0	329	ZnO	39.3	38.0	0.83

a) Initial weight-loss temperature of dehydration. b) Initial weight-loss temperature of decomposition.

Table 2. Analyses of gaseous products of the anhydrous oxalates by EGA

Compound	Analysis temp./°C	Evolved gas (mol%)
MnC_2O_4	360	CO(48), CO_2(52)
FeC_2O_4	355	CO(44), CO_2(56)
CoC_2O_4	350	CO(17), CO_2(83)
NiC_2O_4	310	CO(0), CO_2(100)
CuC_2O_4	240	CO(0), CO_2(100)
ZnC_2O_4	350	CO(46), CO_2(54)

Table 3. Heat of the dehydration(ΔH_{H_2O}) and heat of decomposition(ΔH_d) of the metal oxalates determined by DSC

Compound	ΔH_{H_2O}/kcal per 1 mol of H_2O	ΔH_d/kcal per 1 mol of oxalate
$MgC_2O_4\cdot 2H_2O$	15.4	24.7
$CaC_2O_4\cdot H_2O$	15.1	—
$SrC_2O_4\cdot 2H_2O$	10.9	—
$BaC_2O_4\cdot H_2O$	11.2	—
$MnC_2O_4\cdot 2H_2O$	16.1	16.4
$FeC_2O_4\cdot 2H_2O$	14.9	7.3
$CoC_2O_4\cdot 2H_2O$	13.7	8.6
$NiC_2O_4\cdot 2H_2O$	13.2	9.3
$CuC_2O_4\cdot 1/2H_2O$	—	—
$ZnC_2O_4\cdot 2H_2O$	15.1	19.6

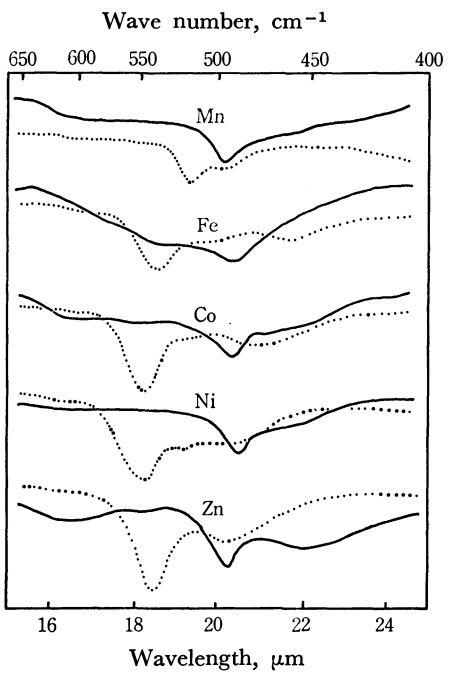

Fig. 3. Infrared absorption spectra of metal oxalates before and after dehydration.
——: $MC_2O_4\cdot 2H_2O$, ····: MC_2O_4.

hydrous oxalates, the values of ΔH_d of the oxalates which gave metal oxides or metals as decomposition products had no particular relation to the initial weight-loss temperatures (t_d). The values of ΔH_d of oxalates which gave the corresponding metal carbonates could not be measured accurately.

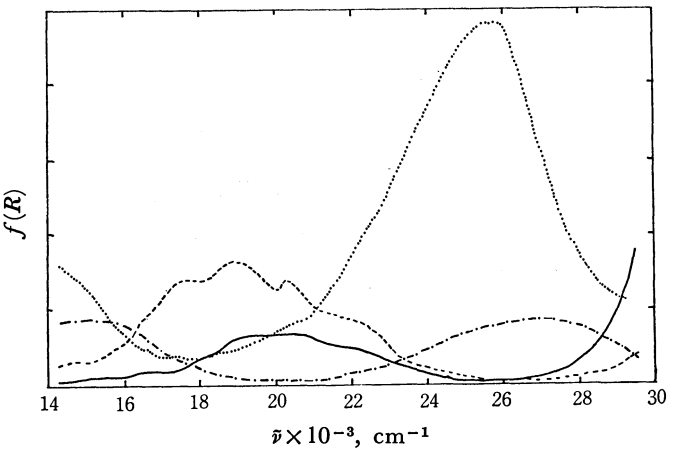

Fig. 4. Reflectance spectra of $CoC_2O_4\cdot 2H_2O$, $NiC_2O_4\cdot 2H_2O$ and their anhydrous compounds.
——: $CoC_2O_4\cdot 2H_2O$, ----: CoC_2O_4, -·-: NiC_2O_4, ····: NiC_2O_4.

The infrared absorption spectra were measured before and after the dehydration. In the region from 2500 to 650 cm^{-1}, the spectra of the anhydrous oxalates were almost the same as those of the hydrated oxalates, whereas in the region of 650 to 400 cm^{-1}, considerable differences were observed between MC_2O_4 and $MC_2O_4\cdot 2H_2O$ as shown in Fig. 3. The peaks near 500 cm^{-1} which were attributed mainly to ν(M–O (ox)) were shifted to higher frequencies by the removal of water molecules, where O(ox) represents an oxygen atom of oxalate ion. On dehydration, the color of $CoC_2O_4\cdot 2H_2O$ changed from pink to purple and that of $NiC_2O_4\cdot 2H_2O$ from bluish green to yellowish green. The reflectance spectra in the visible region of both the oxalates which were measured before and after the dehydration are given in Fig. 4. The d–d transition bands shifted slightly to lower frequencies and the value of $f(R)$ increased on dehydration, where R denotes the reflectance and $f(R)$ the Kubelka-Munk function, $f(R)=(1-R)^2/(2R)$.

Discussion

From X-ray analysis, structure of $MC_2O_4\cdot 2H_2O$ has been reported to be as shown in Fig. 5, where the oxalate ions act as a quadridentate ligand and the water molecules coordinate directly to the metal ions.[5] Therefore, t_{H_2O} and ΔH_{H_2O} are considered to reflect the nature of the metal ions.

The values of t_{H_2O} in Table 1 give information about the dissociation energy of M–OH_2. On the other hand, it is supposed that, since the water molecules are bonded to the metal ions by electrostatic forces, the

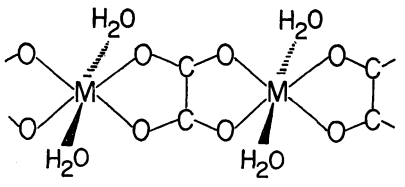

Fig. 5. Bonding structure of $MC_2O_4\cdot 2H_2O$.[5]

bond energy is a function of the size of metal ion. Therefore, the observation that t_{H_2O} increases with $1/r$, as seen in Table 1, seems to be reasonable. The bond energy of M–OH_2 may be estimated from the value of ν(M–O(ox)), since it seems that the more strongly the water molecules are bonded to the metal ion, the weaker the M–O(ox) bond is. On this basis, the experimental results, which are given in Fig. 3, suggest that the bond energies of M–OH_2 increase in the order: Mn<Zn<Fe<Co<Ni. Therefore, the results obtained from the thermal studies are consistent with those from infrared absorption spectra.

The heat of dehydration (ΔH_{H_2O}) gives the difference in potential energy between the hydrated and anhydrous oxalates. In the transition metal group the values of ΔH_{H_2O} decreased almost parallel with the increase in $1/r$. This indicates that the increase of the potential energy on the dissociation of M–OH_2 is somewhat cancelled by an increase in the bond energy of M–O(ox). In fact, the increase of the bond energies of M–O(ox) on removing the coordinated water molecules increased in the order: Mn<Zn<Fe<Co<Ni (*cf.* Fig. 3). The frequency shifts for ν(M–O(ox)) were as follows: Mn, 23; Zn, 45; Fe, 48; Co, 55; Ni, 63 cm^{-1}. In the case of the alkaline earth metal oxalates, the oxalates of Mg(II) and Sr(II) each contain two water molecules, while those of Ca(II) and Ba(II) each contain one water molecule. Therefore, a systematic interpretation similar to that made the transition metal oxalates may not be possible.

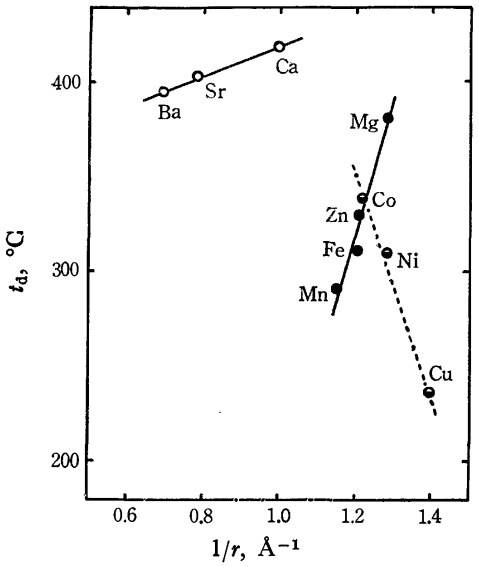

Fig. 6. Relation of initial weight-loss temperatures of the decomposition (t_d) with $1/r$.
○: $MC_2O_4 \rightarrow MCO_3+CO$, ●: $MC_2O_4 \rightarrow MO+CO+CO_2$, ◒: $MC_2O_4 \rightarrow M+2CO_2$.

The relation of the initial weight-loss temperature of for the decomposition (t_d) to $1/r$ depends on the decomposition mechanism as seen in Fig. 6. The M–O (ox) bond energies in the anhydrous oxalates are considered to be the larger, the smaller the complexed metal ions are. Therefore, decomposition of the oxalates to the metal oxides may be initiated by M–O (ox) bond breaking, since these oxalates decomposed at higher temperatures as $1/r$ increased. On the other hand, the oxalates of Co, Ni and Cu, which decompose at lower temperatures as $1/r$ increases, may decompose by electron transfer from the oxalate ion to the metal ions. This is supported by the fact that the electron affinities of metal ions, in general, increase with increasing effective ionic charge.

The authors are grateful to Prof. Yoshito Amako for his comments during the course of this study, and to Mr. Mitsuo Sato for the measurements of the infrared absorption spectra. They also wish to thank the Ministry of Education for financial support for this research.

References

1) Y. A. Ugai, *Zhur. Obshchei Khim.*, **24**, 1315 (1954).
2) D. Dollimore and D. Nicholson, *J. Chem. Soc.*, **1962**, 960.
3) D. Dollimore and D. Nicholson, *J. Chem. Soc., Ser. A*, **1966**, 281.
4) D. Broadbent, D. Dollimore, and J. Dollimore, *ibid.*, **1966**, 1491.
5) J. P. Lagier, H. Pezernat, and J. Dubernat, *Rev. Chem. Miner.*, **6**, 1081 (1969).
6) G. Abond, H. Pezernat, J. P. Lagier, and J. Dubernat, *ibid.*, **6**, 1095 (1969).
7) F. Fievet, J. P. Lagier, H. Pezernat, and J. Dubernat, *C. R. Acad. Sci., Ser. C*, **271** 549 (1970).
8) K. Nagase, This Bulletin, **46**, 144 (1973).

Several Novel Ru(II) and Ru(III) Complexes Formed by Reduction of [RuO_4bipy] and [RuO_3phen]$_2O$ with Hydroquinone and Methanol

Toshio Ishiyama

Radiation Center of Osaka Prefecture, Shinke-cho, Sakai, Osaka 593

(Received June 14, 1974)

The geometrical isomers, *cis*-dichloro-*trans*-(methanol)(hydroquinone)(2,2′-bipyridine)ruthenium(II) and *cis*-dichloro-*cis*-(methanol)(hydroquinone)(2,2′-bipyridine)ruthenium(II), [$RuCl_2$(MeOH)(QH_2)bipy] (complex I and II), were synthesized by reduction and substitution reactions of [RuO_4bipy] and [$RuO_2(OH)_2$bipy] with hydroquinone in hydrochloric acid solution, and methanol. *cis*-Chloro(hydroquinonato)bis(2,2′-bipyridine)-ruthenium(II), *cis*-[RuCl(QH)$(bipy)_2$], was obtained from the substitution reaction of complex I or II with 2,2′-bipyridine in methanol, and *cis*-chloro(hydroquinone)bis(2,2′-bipyridine)ruthenium(II) chloride, *cis*-[RuCl(QH_2)-$(bipy)_2$]Cl, was also obtained from the substitution of *cis-trans*-[$RuCl_2$(MeOH)(QH_2)bipy] in methanol containing hydrochloric acid. *cis*-Dihydroxobis(2,2′-bipyridine)ruthenium(II), *cis*-[$Ru(OH)_2(bipy)_2$], was obtained by heating an aqueous solution of *cis*-[RuCl(QH)$(bipy)_2$]. Trihydroxoaquo(1,10-phenanthroline)ruthenium(III), [$Ru(OH)_3(H_2O)$phen] was also synthesized from [RuO_3phen]$_2O$ and [$Ru(OH)_3$phen]$_2O$ by reduction reactions similar to those used for [$RuCl_2$(MeOH)(QH_2)bipy]. These complexes were characterized by the infrared, visible and ultraviolet absorption spectra, and also by polarographic and magnetic measurements. The structures are discussed.

The isolation and identification of metal complexes of hydroquinone has not yet been carried out. Wells and Kuritsyn[1] investigated the kinetics of the reduction of aquomanganase(III) ions with hydroquinone in aqueous perchlorate media using the stopped-flow technique. They suggested the presence of an intermediate Mn^{III}–hydroquinone complex, $Mn\cdot QH_2^{3+}{}_{aq}$, on the basis of the oscilloscope trace, and the higher value of the extinction coefficient of the intermediate complex than the extinction coefficients of Mn^{3+} and $MnOH^{2+}{}_{aq}$ at 470 nm.

In previous work,[2–5] [RuO_4bipy] and [RuO_3phen]$_2O$ were obtained by the reactions of ruthenium tetraoxide with 2,2′-bipyridine and 1,10-phenanthroline in carbon tetrachloride, and [$RuO_2(bipy)_2$], [RuO_2(bipy)-(phen)], [$RuO_2(phen)_2$], [$Ru(OH)_2(py)_2$bipy] and [$Ru(OH)_2(py)_2$phen] were obtained by the reduction and substitution reactions of [RuO_4bipy], [RuO_3-phen]$_2O$ and [$RuO_4(py)_2$] with 2,2′-bipyridine and 1,10-phenanthroline in methanol. In the present paper, six new complexes, *cis*-dichloro-*trans*-(methanol)-(hydroquinone)(2,2′-bipyridine)ruthenium(II), *cis*-dichloro-*cis*-(methanol)(hydroquinone)(2,2′-bipyridine)-ruthenium(II), [$RuCl_2$(MeOH)(QH_2)bipy] (complex I and II), [RuCl(QH)$(bipy)_2$], [$Ru(OH)_2(bipy)_2$], [RuCl(QH_2)$(bipy)_2$]Cl and [$Ru(OH)_3(H_2O)$phen], are reported, and their structures are discussed.

Experimental

Materials. Ruthenium(III) chloride monohydrate (extra pure grade) supplied by Mitsuwa Chemicals was used without further purification. Oxalic acid (extra pure grade), hydroquinone, 2,2′-bipyridine and 1,10-phenanthroline were supplied by Wako Pure Chemicals. The first three were purified by recrystallization from water, and phenanthroline by recrystallization from ethanol after drying at 110 °C for 3 hr. Commercial methanol was dried by treatment with magnesium ribbon and iodine and distilled. Lithium perchlorate (Mitsuwa chemicals extra pure grade) was purified by recrystallization from methanol after heating at 110 °C for 3 hr. Wako Pure Chemicals dimethyl sulfoxide was used without further treatment. Monodeuteriomethanol made by E. Merck, Germany, was used for deuteration without further purification.

Syntheses. Tetraoxo(2,2′-bipyridine)ruthenium(VIII), [RuO_4bipy]$\cdot 3H_2O$, dioxodihydroxo(2,2′-bipyridine)ruthenium(VI), [$RuO_2(OH)_2$bipy]$\cdot 3H_2O$, μ-oxobis[trioxo(1,10-phenanthroline)ruthenium(VII)], [RuO_3phen]$_2O$ and μ-oxobis[trihydroxo(1,10-phenanthroline)ruthenium(IV)], [Ru-$(OH)_3$phen]$_2O$: These complexes were synthesized as before,[2–4] and gave satisfactory elemental analyses.

(1) Dichloro(methanol)(hydroquinone)(2,2′-bipyridine)ruthenium(II), [$RuCl_2$(MeOH)(QH_2)bipy]: To a solution of 1 g of [RuO_4bipy]$\cdot 3H_2O$ or [$RuO_2(OH)_2$bipy]$\cdot 3H_2O$ in 150 ml of 0.1 M hydrochloric acid, 2 g of hydroquinone was added. The mixture was refluxed with occasional shaking on a water bath for about 2 hr until the solution turned orange-brown. The solution was then evaporated to dryness, and the residue was washed repeatedly with diethyl ether and then dissolved in methanol. An insoluble material was filtered off. The solution was concentrated, and the crystals which formed were recrystallized from methanol and dried *in vacuo*. Complex I which was derived from [RuO_4bipy] was stable in air, but complex II which was derived from [$RuO_2(OH)_2$-bipy] was slightly hygroscopic.

Found for complex I: Ru, 20.85; C, 43.55; H, 3.89; N, 5.36; Cl, 16.48; CH_3OH, 7.24%; mol wt, 510; yield 72.5%.

Found for complex II: Ru, 20.63; C, 43.00; H, 4.02; N, 5.22; Cl, 15.58; CH_3OH 7.49%; mol wt, 520; yield 90.1%. Calcd for [$RuCl_2(CH_3OH)(C_6H_6O_2)(C_{10}H_8N_2)$]: Ru, 21.49; C, 43.40; H, 3.83; N, 5.96; Cl, 15.10; CH_3OH, 6.80%; mol wt, 470.

Both complexes were insoluble in carbon tetrachloride, benzene, diethyl ether, ethyl acetate, chloroform and dioxane, but were slightly soluble in methanol, acetone, DMSO and DMF, and very slightly soluble in water. These complexes were green in methanol, but dark-brown in acetone, black in DMSO or DMF and pink in water, probably due to the replacement of coordinated methanol by the solvent molecules.

(2) Chloro(hydroquinonato)bis(2,2′-bipyridine)ruthenium(II), [RuCl(QH)$(bipy)_2$]: To a solution of 0.5 g of [$RuCl_2$(MeOH)-(QH_2)bipy] (complex I or II) in 250 ml methanol, 2 g of 2,2′-bipyridine was added. The mixture was refluxed with occasional shaking on a water bath for about 3 hr until the solution turned reddish-brown. The solution was then evaporated to dryness, and the residue was repeatedly washed with diethyl ether. The product was dissolved in methanol.

An insoluble material was filtered off. The solution was concentrated, and the crystals which formed were recrystallized from methanol and dried *in vacuo*. Yield: 89.5%. The complex was insoluble in carbon tetrachloride, benzene, diethyl ether, ethyl acetate, dioxane and chloroform, but soluble in water, methanol, ethanol, acetic acid, DMSO and DMF, and slightly soluble in acetone.

Found: Ru, 17.35; C, 57.89; H, 4.11; N, 10.39; Cl, 5.85%; mol wt, 585. Calcd for $[RuCl(C_6H_5O_2)(C_{10}H_8N_2)_2]$: Ru, 18.11; C, 55.96; H, 3.79; N, 10.04; Cl, 6.36%; mol wt, 558.

(3) Dihydroxobis(2,2'-bipyridine)ruthenium(II), $[Ru(OH)_2(bipy)_2]\cdot 1.5H_2O$: A solution of 0.5 g of $[RuCl(QH)(bipy)_2]$ in 150 ml of distilled water was refluxed with occasional shaking on a water bath for 3 hr. An insoluble material was filtered off. The solution was then evaporated to dryness, and the residue was repeatedly washed with diethyl ether. The product was recrystallized twice from water and dried *in vacuo*. Yield: 79.8%. The water content of the complex was determined by measuring the weight loss in the temperature range 100~130 °C with a thermobalance. The complex was insoluble in carbon tetrachloride, benzene, diethyl ether, ethyl acetate, dioxane and chloroform, but soluble in water, methanol, ethanol, acetic acid, acetone, DMSO and DMF.

Found: Ru, 20.15; C, 49.09; H, 4.39; N, 10.87; H_2O, 5.39%. Calcd for $[Ru(OH)_2(C_{10}H_8N_2)_2]\cdot 1.5H_2O$: Ru, 21.32; C, 50.62; H, 4.42; N, 11.81; H_2O, 5.69%.

(4) Chloro(hydroquinone)bis(2,2'-bipyridine)ruthenium(II) chloride, $[RuCl(QH_2)(bipy)_2]Cl$: To a solution of 0.2 g of $[RuCl_2(MeOH)(QH_2)bipy]$ (complex I) in 100 ml methanol containing 0.05 ml of conc. hydrochloric acid, 0.8 g of 2,2'-bipyridine was added. The mixture was refluxed with occasional shaking on a water bath for about 3 hr until the solution turned reddish-brown. Then we followed the procedure described in section (2). Yield: 94.3%. The solubility of the complex in the several solvents was similar to $[RuCl(QH)(bipy)_2]$, but the complex was slightly hygroscopic.

Found: Ru, 16.35; C, 53.78; H, 4.36; N, 10.41; Cl, 13.50%. Calcd for $[RuCl(C_6H_6O_2)(C_{10}H_8N_2)_2]Cl$: Ru, 17.00; C, 52.53; H, 3.73; N, 9.42; Cl, 11.93%.

(5) cis-*Dichlorobis(2,2'-bipyridine)ruthenium(II)*, cis-$[RuCl_2(bipy)_2]\cdot 0.5H_2O$: To a solution of 0.2 g of $[RuCl_2(MeOH)(QH_2)bipy]$ (complex II) in 100 ml methanol containing 0.05 ml of conc. hydrochloric acid, 0.8 g of 2,2'-bipyridine was added. The mixture was refluxed with occasional shaking on a water bath for 3 hr until the solution turned reddish-brown. The solution was slowly evaporated to dryness and the residue was repeatedly washed with diethyl ether. Then I followed the procedure in section (2). Yield: 75.6%. (Found: C, 50.49; H, 4.02; N, 11.11; Cl, 15.15%. Calcd for $[RuCl_2(C_{10}H_8N_2)_2]\cdot 0.5H_2O$: C, 48.72; H, 3.46; N, 11.36; Cl, 14.38%).

cis-$[RuCl_2(bipy)_2]$ was also obtained by heating $[RuCl(QH)(bipy)_2]$ and $[RuCl(QH_2)(bipy)_2]Cl$ in methanol containing hydrochloric acid. Then we followed the procedure in section (2). The product which was synthesized from $[RuCl(QH)(bipy)_2]$ was further recrystallized from chloroform according to the method reported by Liu *et al.*[6]

(6) Oxalatobis(2,2'-bipyridine)ruthenium(II), $[Ru(ox)(bipy)_2]\cdot 4H_2O$: To a solution of 0.5 g of $[Ru(OH)_2(bipy)_2]\cdot 1.5H_2O$ in 75 ml of methanol, 0.5 g of oxalic acid was added. The reaction mixture was refluxed with occasional shaking on a water bath for about 2 hr. The solution was then slowly evaporated to dryness and the residue was repeatedly washed with diethyl ether. The crystals were recrystallized from methanol and dried *in vacuo*. Yield: 86.7%. (Found: Ru, 18.26; C, 46.01; H, 3.89; N, 8.96%. Calcd for $[Ru(C_2O_4)(C_{10}H_8N_2)_2]\cdot 4H_2O$: Ru, 17.62; C, 46.07; H, 4.12; N, 9.76%).

(7) Trihydroxoaquo(1,10-phenanthroline)ruthenium(III), $[Ru(OH)_3(H_2O)phen]$: To a solution of 1 g of $[RuO_3phen]_2O$ or $[Ru(OH)_3phen]_2O$ in 150 ml of 0.1 M hydrochloric acid, 2 g of hydroquinone was added. Then we followed the procedure described in section (1). Yield: 79.3% and 83.5%, on the basis of $[RuO_3phen]_2O$ and $[Ru(OH)_3phen]_2O$, respectively. The complex was insoluble in carbon tetrachloride, benzene, chloroform, diethyl ether, ethyl acetate and dioxane, but soluble in methanol, acetone, DMSO, and DMF, and slightly soluble in water.

Found: Ru, 28.36; C, 40.47; H, 3.42; N, 8.07%; mol wt, 350. Calcd for $[Ru(OH)_3(H_2O)(C_{12}H_8N_2)]$: Ru, 28.94; C, 41.41; H, 3.71; N, 8.00%; mol wt, 350.

Measurements. Ruthenium in these complexes was determined spectrophotometrically by measuring the absorbance at 465 nm after thermal decomposition of the complexes at 350 °C followed by alkali fusion.[7] Chlorine was determined by use of micro-determing apparatus for halogens. The molecular weights of $[RuCl_2(MeOH)(QH_2)bipy]$ (complex I and II) and $[RuCl(QH)(bipy)_2]$, $[RuCl(QH_2)(bipy)_2]Cl$, $[Ru(OH)_3(H_2O)phen]$ were measured in DMSO at 40 °C and in CH_3OH at 45 °C, respectively, with a Shibayama Model S-601 Vapor Pressure Osmometer. NMR spectra could not be measured owing to the poor solubilities of the complexes I and II in DMSO-d_6 and CD_3OD. Methanol in the complexes was determined by measuring the β-activity of $[RuCl_2(^{14}CH_3OH)(QH_2)bipy]$ which was prepared using $^{14}CH_3OH$ (supplied by Daiichi Pure Chemical) with a liquid scintilator. Hydroquinone in the complexes was detected with a Shimadzu LKB-9000 GC-Mass spectrometor, but the amount could not be measured. The infrared absorption spectra were measured in KBr disks on a JASCO Model IR-S infrared spectrophotometer. In order to confirm the presence of coordinated water the complex was deuterated by standing at room temperature for two days in monodeuteriomethanol. Far infrared absorption spectra of the geometrical isomers (complex I and II) could not be obtained, because the two complexes did not mix well with Nujol. Visible and ultraviolet absorption spectra were measured with a Beckmann Model DU spectrophotometer. The magnetic susceptibility was measured by the Faraday method[8] at 25 °C with a Cahn R. G. electrobalance. Polarographic measurements were carried out at 25 °C with a Yanagimoto automatic recording polarograph (Type PA 101). A conventional H-type electrolytic cell was used with a saturated mercury(II) sulfate reference electrode, and an agar plug saturated with potassium sulfate was used for the junction. Lithium perchlorate was used as the supporting electrolyte. The measurements were performed in methanol as described previously.[4] The molar conductivity was measured at 25 °C with a Yanagimoto Model MY-7 conductivity outfit.

Results and Discussion

The ruthenium(II) and Ru(III) compounds obtained and the preparative pathways are summarized in Fig. 1. Two kinds of complex, I and II, of the same composition were formed by the reaction of $[RuO_4bipy]$ and $[RuO_2(OH)_2bipy]$, respectively, with hydroquinone in methanol. The compounds $[RuCl(QH)(bipy)_2]$ and $[RuCl(QH_2)(bipy)_2]Cl$ were derived

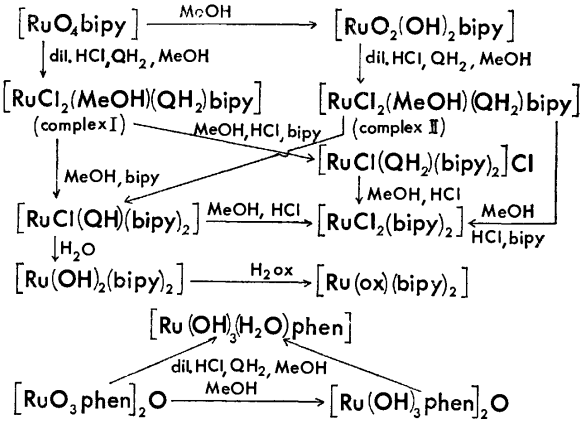

Fig. 1. Reduction and substitution reactions of [RuO_4-bipy] and [RuO_3phen]$_2$O.

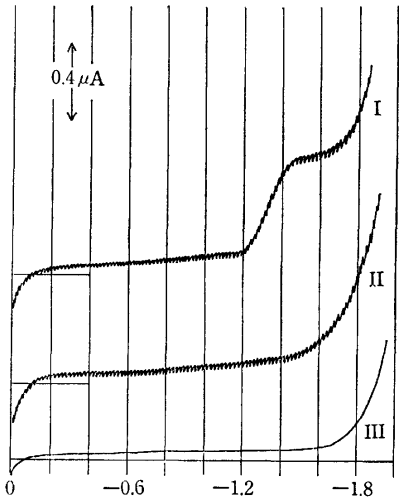

E, V *vs.* Hg, Hg_2SO_4(satd.) elec.

Fig. 2. Polarograms of the complexes.
I: 5×10^{-4} mol/l [$Ru(OH)_3(H_2O)$phen], II: 5×10^{-4} mol/l [$RuCl_2(MeOH)(QH_2)$bipy](complex I), III: 0.5 mol/l $LiClO_4$ in CH_3OH.

from the complex I and II, and the complex I, respectively. [$RuCl_2$(bipy)$_2$] could not be directly derived from complex I without passing [RuCl(QH)-(bipy)$_2$] or [RuCl(QH_2)(bipy)$_2$]Cl. This indicates that the methanol and hydroquinone ligands of the complex I are coordinated at the *trans* positions, assuming that the positions of the other ligands were not changed by the ligand substitution reactions. On the other hand, [$RuCl_2$(bipy)$_2$] was derived directly from complex II by a ligand substitution reaction. This indicates that the methanol and hydroquinone ligands of the complex II are coordinated at the *cis* positions. It was confirmed that three complexes with the same compostion, [$RuCl_2$(bipy)$_2$], which were derived from [$RuCl_2$(MeOH)(QH_2)bipy] (complex II), [RuCl(QH)(bipy)$_2$] and [RuCl(QH_2)(bipy)$_2$]Cl, all had *cis* configurations by comparing their spectra with the spectrum of *cis*-[$RuCl_2$(bipy)$_2$] which was reported by Bryant *et al.*[9] and Fergusson and Harris.[10] Since *cis*-[$RuCl_2$(bipy)$_2$] could be directly derived from the monochlororuthenium(II) complexes, [RuCl(QH)-(bipy)$_2$] and [RuCl(QH_2)(bipy)$_2$]Cl, the two complexes were both *cis* configurations. This difference in reactivity of the geometrical isomers indicates that complex I was *cis-trans*- and complex II was *cis-cis*-[$RuCl_2$(MeOH)(QH_2)bipy].

It was confirmed by elemental analyses by comparison of spectra that the same compound, [$Ru(OH)_3(H_2O)$-phen], was formed by the reaction of [RuO_3phen]$_2$O and [$Ru(OH)_3$phen]$_2$O.

Polarograms of [$RuCl_2$(MeOH)(QH_2)bipy] (complex I) and [$Ru(OH)_3(H_2O)$phen] are shown in Fig. 2. In the case of [$RuCl_2$(MeOH)(QH_2)bipy], no reduction wave was observed in 0.5 mol/l $LiClO_4$ methanol solution. The complex, [$Ru(OH)_3(H_2O)$phen], was reduced polarographically in one step. The half-wave potential of the reduction wave of [$Ru(OH)_3(H_2O)$-phen] was −1.33 V *vs.* Hg, Hg_2SO_4 (satd.) elec. in 0.5 mol/l $LiClO_4$ methanol solution. The height of the reduction wave corresponded to a gain of one electron, indicating a reduction from Ru(III) to Ru(II). It has been reported by Niedrach and Tevebaugh[11] that ruthenium(IV) undergoes a stepwise reduction through Ru(III) to Ru(II) in perchloric acid solution. It was therefore concluded that the oxidation number of ruthenium in [$Ru(OH)_3(H_2O)$phen] was 3. Since no reduction wave was obtained under the same experimental conditions as that of [$Ru(OH)_3(H_2O)$-phen], the oxidation number of ruthenium in [$RuCl_2$(MeOH)(QH_2)bipy] must be 2, indicating that

Table 1. The characteristic infrared absorption bands of the present Ru(II) complexes (cm^{-1})

Assignment	QH_2	bipy	[$RuCl_2$(MeOH)-(QH_2)bipy] (complex I)	[$RuCl_2$(MeOH)-(QH_2)bipy] (complex II)	[RuCl(QH)-(bipy)$_2$]	[$Ru(OH)_2$-(bipy)$_2$]	[RuCl(QH_2)-(bipy)$_2$]Cl
ν(O-H)	3300 s		3350 s, br	3340 s, br	3400 s	3400 s, br	3340 s
ν(C-H)	3080 s		3100 sh	3080 sh	3060 m	3060 w	3050 m
δ(C-H)	1845 s		1880 m	1875 m	1870 m		1868 m
ν(C=N)		1582 s	1605 s	1605 s	1603 s	1602 s	1602 s
ν(C=C)		1560 m	1580 sh	1585 sh	1590 m	1585 m	1586 s
ν(C-O)	1250 s		1260 sh	1260 sh	1265 w		1273 m
	1235 w		1235 m	1235 m	1240 w		1240 m
	1180 s		1197 s	1202 m	1210 m		1210 m
δ(C-H)	825 s		833 s	830 s	837 w		835 w
δ(C-H)		739 s	733 s	730 s	737 s	735 s	731 s

s=strong, m=medium, w=weak, br=broad, sh=shoulder

tetraoxo(2,2′-bipyridine)ruthenium(VIII) was reduced to Ru(II) complex in hydroquinone in hydrochloric acid solution.

Infrared Spectra. The characteristic infrared absorption bands of the present Ru(II) complexes with hydroquinone and 2,2′-bipyridine are shown in Table 1 together with those of free QH_2 and bipy ligands. In the two geometrical isomers of $[RuCl_2(MeOH)(QH_2)bipy]$, ν(O–H), ν(C–H), ν(C–O) and δ(C–H) vibrations of coordinated hydroquinone closely resembled those of the free ligand, and the bands due to the benzoquinone were not observed. This shows that the hydroquinone which was added in excess to the hydrochloric acid solution of $[RuO_4bipy]$ or $[RuO_2(OH)_2bipy]$ as a reducing agent was coordinated to the metal atom, and that benzoquinone which was formed by oxidation of hydroquinone with $[RuO_4bipy]$ or $[RuO_2(OH)_2bipy]$ was not coordinated. In the present complexes, $[RuCl_2(MeOH)(QH_2)bipy]$ (complexes I and II), $[RuCl(QH)(bipy)_2]$ and $[RuCl(QH_2)(bipy)_2]Cl$, characteristic absorption bands of the coordinated hydroquinone were clearly observed in the regions from 837 to 830 and from 1880 to 1868 cm^{-1}, probably due to the C–H bending vibrations and their overtones. These were all shifted to higher frequency by coordination. The absorption bands observed in the regions from 3400 to 3340 and from 1273 to 1197 cm^{-1} were assigned to the phenolic O–H and C–O stretching vibrations, respectively.[12,13]

In five present ruthenium-2,2′-bipyridine complexes, characteristic absorption bands of coordinated 2,2′-bipyridine were observed in the regions from 1605 to 1602, from 1590 to 1580 and from 737 to 730, probably due to the C=N, C=C stretching and C–H bending vibrations, respectively. The ν(C=N) and ν(C=C) vibrations were shifted to higher frequency on coordination, indicating that the bond orders of the carbon-nitrogen and carbon-carbon links were increased.[14,15]

The absorption band at 3420 cm^{-1} of $[Ru(OH)_3(H_2O)phen]$ was assigned to the coordinated OH and H_2O stretching vibrations, and the absorption band at 1635 cm^{-1} was assigned to the H_2O bending vibration. These two bands were shifted to 2460 and 1200 cm^{-1} by deuteration.

Electronic Absorption Spectra. The visible and ultraviolet absorption spectra of $[RuCl_2(MeOH)(QH_2)bipy]$, $[RuCl(QH)(bipy)_2]$, $[Ru(OH)_2(bipy)_2]$, $[RuCl(QH_2)(bipy)_2]Cl$ and $[Ru(OH)_3(H_2O)phen]$ were measured in methanol, and are shown in Figs. 3, 4 and 5. The absorption spectra of the complexes are summarized in Table 2.

The spectrum of complex II (Fig. 3, curve II) resembles that of complex I, but the CT bands of complex II are stronger than those of the complex I, while the order of the π–π^* bands is reversed. The spectrum of $[RuCl(QH_2)(bipy)_2]Cl$ resembles that of $[RuCl(QH)(bipy)_2]$ except in the vicinity of 520 nm.

The spectrum of $[Ru(OH)_3(H_2O)phen]$ resembles that of $[Ru(phen)_3]^{3+}$[16], but $[Ru(OH)_3(H_2O)phen]$ had the lower intensity in the vicinity of 450 nm than that $[Ru(phen)_3]^{3+}$. Fergusson and his co-workers[10,17] of attributed the absorption bands observed in the visible region for tervalent ruthenium-2,2′-bipyridine complexes to the charge-transfer transitions from ligand to metal.

Conductivity. The molar conductivity of

TABLE 2. ELECTRONIC ABSORPTION DATA OF THE COMPLEXES

Complexes	Charge-transfer transitions: Metal-to-ligand ($t_{2g}\rightarrow\pi^*$) λ_{max}, nm	(log ε)	Charge-transfer transitions: Ligand-to-metal λ_{max}, nm	(log ε)	Intraligand transitions ($\pi\rightarrow\pi^*$) λ_{max}, nm	(log ε)
$[RuCl_2(MeOH)(QH_2)bipy]$ (complex I)	640	(2.66)			295	(4.22)
	440 sh	(3.18)			245 sh	(4.10)
	375	(3.50)			224	(4.46)
$[RuCl_2(MeOH)(QH_2)bipy]$ (complex II)	640	(3.14)			295	(4.04)
	460 sh	(3.36)			245 sh	(3.94)
	382	(3.56)			224	(4.26)
$[RuCl(QH)(bipy)_2]$	580 sh	(2.75)			287	(4.78)
	455	(3.93)			256 sh	(4.30)
	420 sh	(3.82)			244	(4.50)
	350 sh	(3.74)				
$[Ru(OH)_2(bipy)_2]$	640	(3.04)			290	(4.56)
	460	(3.84)			255 sh	(4.08)
	425 sh	(3.77)			244	(4.17)
	360 sh	(3.74)				
$[RuCl(QH_2)(bipy)_2]Cl$	600 sh	(2.65)			288	(4.68)
	520 sh	(3.30)			257	(4.26)
	460	(3.58)			237	(4.45)
	425 sh	(3.50)				
	350 sh	(3.50)				
$[Ru(OH)_3(H_2O)phen]$			450	(3.67)	290 sh	(3.87)
			383	(3.72)	265	(4.20)
					224 sh	(4.27)

sh=shoulder

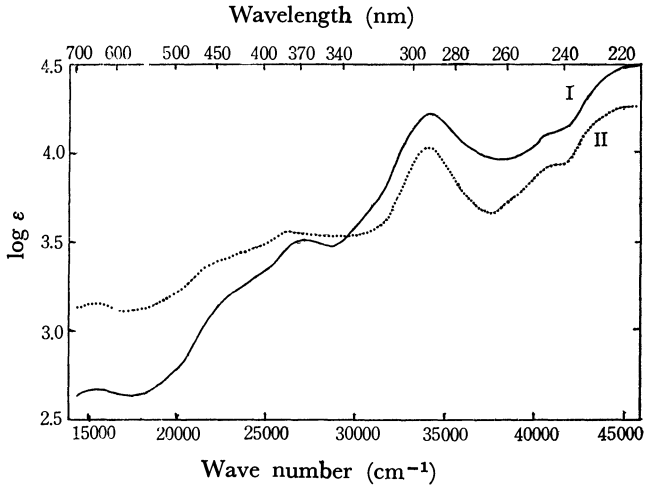

Fig. 3. Electronic spectra of the geometrical isomers of [$RuCl_2(MeOH)(QH_2)bipy$].
I: complex I (*cis-trans* form), II: complex II (*cis-cis* form).

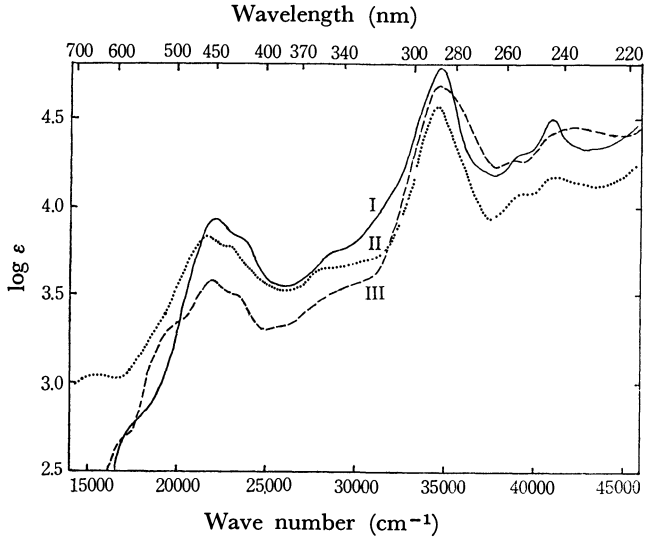

Fig. 4. Electronic spectra of the bis(2,2′-bipyridine)-ruthenium(II) complexes.
I: [$RuCl(QH)(bipy)_2$], II: [$Ru(OH)_2(bipy)_2$], III: [$RuCl(QH_2)(bipy)_2$]Cl.

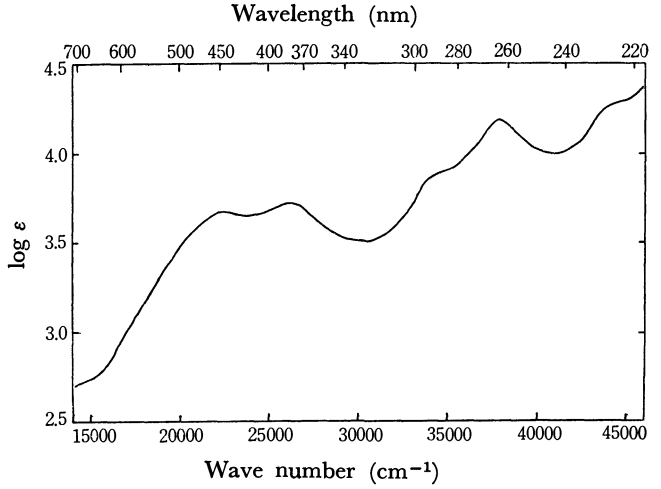

Fig. 5. Electronic spectrum of [$Ru(OH)_3(H_2O)phen$].

chloro(hydroquinone)bis(2,2′-bipyridine)ruthenium(II) chloride in methanol solution was 111.4 $ohm^{-1}\cdot cm^2\cdot mol^{-1}$ at 25 °C, showing that the complex was a 1 : 1 type electrolyte.

Magnetic Properties. The observed diamagnetism of the geometrical isomers of [$RuCl_2(MeOH)(QH_2)bipy$] indicated that the ruthenium atom has a spin-paired d^6 configuration.

[$Ru(OH)_3(H_2O)phen$] had a magnetic moment of 1.81 B.M., indicating that the ruthenium atom has a spin-paired d^5 configuration. The stereochemical configuration of [$Ru(OH)_3(H_2O)phen$] is not clear.

The structures thus proposed for the geometrical isomers of [$RuCl_2(MeOH)(QH_2)bipy$] are shown in Fig. 6.

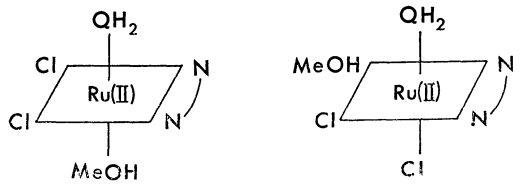

cis-trans form Complex I — *cis-cis* form complex II

Fig. 6. The proposed structures of the geometrical isomers, [$RuCl_2(MeOH)(QH_2)bipy$].

The author wishes to express his thanks to Professor Shinichi Kawaguchi of Osaka City University for his kind guidance and encouragement throughout this work, and to Dr. Masayuki Hamada, the chairman of the Department of Chemistry of the Radiation Center of Osaka Prefecture, for his guidance in the measurements of GC-Mass spectra and methanol analysis. His thanks are also due to Dr. Toyokichi Kitagawa of Osaka City University for his guidance in the measurement of polarograms, and to Dr. Shichio Kawai, Osaka University, for his guidance in the measurement of magnetic susceptibilities.

References

1) C. F. Wells and L. V. Kuritsyn, *J. Chem. Soc., A*, **1970**, 676.
2) T. Ishiyama, *Ann. Rep. Rad. Center Osaka*, **8**, 40 (1967).
3) T. Ishiyama, This Bulletin, **42**, 2071 (1969).
4) T. Ishiyama, *ibid.*, **44**, 1571 (1971).
5) T. Ishiyama and Y. Koda, *Inorg. Chem.*, **11**, 2837 (1972).
6) C. F. Liu, N. C. Liu, and J. C. Bailar, Jr., *ibid.*, **3**, 1197 (1964).
7) E. D. Marshall and R. R. Rickard, *Anal. Chem.*, **22**, 795 (1950).
8) L. N. Mulay, "Magnetic Susceptibility", Wiley, New York, London, Sydney (1963), p. 1836.
9) G. M. Bryant, J. E. Fergusson, and H. K. J. Powell, *Aust. J. Chem.*, **24**, 257 (1971).
10) J. E. Fergusson and G. M. Harris, *J. Chem. Soc., A*, **1966**, 1293.
11) L. W. Niedrach and A. D. Tevebaugh, *J. Amer. Chem. Soc.*, **73**, 2835 (1951).
12) D. H. Anderson and N. B. Woodall, *Anal. Chem.*, **25**, 1906 (1953).
13) R. T. O'Connor, P. V. Haar, E. F. DuPre, L. E. Brown, and C. H. Pominski, *J. Amer. Chem. Soc.*, **76**, 2368 (1954).
14) D. H. Busch and J. C. Bailor, Jr., *ibid.*, **78**, 1147 (1956).
15) R. G. Inskeep, *J. Inorg. Nucl. Chem.*, **24**, 763 (1962).
16) A. J. McCaffery, S. F. Mason, and B. J. Norman, *J. Chem. Soc., A*, **1969**, 1428.
17) J. E. Fergusson, *Aust. J. Chem.*, **24**, 275 (1971).

Magnetic Circular Dichroism of $[Cr(CN)_5NO]^{3-}$

Hiroshi KOBAYASHI, Ken EGUCHI, and Youkoh KAIZU

Department of Chemistry, Tokyo Institute of Technology, Ookayama, Meguro-ku, Tokyo 152

(Received July 27, 1974)

Magnetic circular dichroism (MCD) was observed in the region of the 22000 cm^{-1} band of $[Cr(CN)_5NO]^{3-}$. The absorption band was assigned to a charge-transfer transition linearly polarized in the direction of Cr–NO, while the MCD observed in the same region was assigned to B term extrema of the (d, d*) transitions hidden beneath the charge-transfer band. The charge-transfer transition gives rise to an absorption peak but no MCD, since the transition is polarized in the direction of the orbital angular momentum, even in the case where a degenerate excited state is involved.

The electronic structure of $[M(CN)_5NO]^{n-}$ complexes has been established on the basis of magnetic, spectroscopic and theoretical studies.[1-15] The weight of evidence shows a strong M–NO π-bonding.[16-21] However the important role of the π^*_{NO} orbital in the low-energy excitations had not been considered until Manoharan and Gray interpreted the electronic excitations of $[M(CN)_5NO]^{n-}$ in terms of self-consistent charge and configuration-molecular orbital (SCCC MO) calculations.[20]

According to the most recent suggestion,[22] the order of the orbitals responsible for the outer electronic configuration is: $1e < xy < 2e < x^2-y^2 < z^2$, where xy, x^2-y^2, and z^2 denote the molecular orbitals predominantly distributed on the metal d_{xy}, $d_{x^2-y^2}$, and d_{z^2} orbitals, and 1e and 2e are the highest occupied and the lowest vacant degenerate orbital pairs, which are mainly composed of metal d_{zx} and d_{yz} orbitals and the lowest nitric oxide antibonding π orbitals $\pi_x^*{}_{NO}$ and $\pi_y^*{}_{NO}$.

The ESR data for $[CrL_5NO]$ (L: CN^-, NH_3, OH_2) have been interpreted for the ground electronic configuration $(1e)^4(xy)$.[20,23,24] The unpaired electron relevant to an almost isotropic ESR signal is localized predominantly in the d_{xy} orbital. A characteristic absorption band observed around 22000 cm^{-1} is fairly constant both in position and intensity for L=CN^-, NH_3, H_2O and C_2H_5OH in $[CrL_5NO]$,[25] and has been assigned to the transition $^2B_2 \rightarrow {}^2B_2$ $((1e)^4(xy) \rightarrow (1e)^3(2e)(xy))$ which is linearly polarized in the direction of the Cr–NO bond.[20] In the present work, however, magnetic circular dichroism (MCD) was observed in the region of the 22000 cm^{-1} band of $[CrL_5NO]$.

Experimental

$K_3[Cr(CN)_5NO]\cdot H_2O$ was prepared by the method described in the literature.[26] The sample was recrystallized twice from water. The bright green crystals thus obtained were identified by elemental analysis.

Found: C, 17.2; H, 0.4; N, 24.5; Cr, 15.0%. Calcd for $K_3[Cr(CN)_5NO]\cdot H_2O$: C, 16.7; H, 0.6; N, 24.2; Cr, 15.0%.

$[Cr(NH_3)_5NO]Cl_2$ was prepared and purified by the method of Mori, Ueshiba and Kawaguchi.[27] The brown crystals thus obtained were identified by analysis for chromium.

Found: Cr, 22.1%. Calcd for $[Cr(NH_3)_5NO]Cl_2$: Cr, 21.8%.

A perchloric acid solution of $[Cr(OH_2)_5NO](ClO_4)_2$ was prepared by the method described in the literature.[25]

Our MCD measurement technique has been described elsewhere,[28] All the measurements were carried out on a JASCO Model ORD/UV-5 instrument with its electromagnet. The magnetic field was set at 10000 G The electronic absorption spectra of solutions and films were taken on a Shimadzu automatic recording spectrophotometer Model MPS-50. The instruments were furnished with a Dewar for low-temperature measurement. The polarizing microscope absorption spectrum of a single crystal was taken by courtesy of Professors Kondo and Nakahara, St. Paul's University, on a Hitachi automatic recording spectrophotometer Model EPS-3T equipped with a special microscope. A single crystal suitable for the measurement was selected on a polarizing microscope from crystals deposited on a clean glass plate by the spontaneous evaporation of an aqueous solution of $K_3[Cr(CN)_5NO]$. The extinction axis of the crystal was coincident with the direction of growth of the crystal needles (c axis).

The magnitude of MCD is reported here in terms of molar circular dichroism per unit external magnetic field, $(\varepsilon_l - \varepsilon_r)/H_z$, where ε_l and ε_r represent the molar absorption coefficients for left and right circularly polarized light, respectively, and H_z is the strength of external magnetic field.

The magnitude of molar circular dichroism per unit external magnetic field observed at a transition a→j is given by

$$(\varepsilon_l - \varepsilon_r)/H_z = -\left(\frac{16\pi}{3hc}\right)\frac{N}{10^3 \ln 10}\{f_1 A + f_2(B + C/kT)\},$$

where the function f_1 is a shape function of the sigmoidal dispersion at the position of the absorption maximum ν_{Ja}, the function f_2 is a shape function as approximated by a Gaussian with an extremum at the absorption maximum.[29-21]

The MCD and absorption spectra were measured with $[Cr(OH_2)_5NO]^{2+}$ in concd $HClO_4$ solution, $[Cr(NH_3)_5NO]^{2+}$ in 0.1 M HCl solution, and $[Cr(CN)_5NO]^{3-}$ in aqueous solution, in 2 : 1 mixture of propyleneglycol and water, and in a polyvinyl alcohol (PVA) film. The 2 : 1 mixture of propyleneglycol and water gave a transparent rigid glass dispersing an electrolyte such as $K_3[Cr(CN)_5NO]$ down to dry ice-methanol temperature (195 K). However the transparence of the rigid glass in the near-ultraviolet region became poor at dry ice-methanol temperature. The MCD spectrum of $[Cr(CN)_5NO]^{3-}$ in a PVA film was obtained at various temperatures down to liquid nitrogen temperature. A PVA film was made by spontaneous evaporation of an aqueous solution of PVA on a glass plate and then the film was heated up to 90 °C for 1 hr in order to increase its transparence. A transparent PVA film thus obtained was swelled a little in water and then dyed in an aqueous solution of $K_3[Cr(CN)_5NO]$. The dyed film was dried at room temperature for 24 hr over phosphorous pentoxide under reduced pressure. The spectrum of this yellow ochreous transparent film was in good agreement with the solution spectrum.

Results and Discussion

The visible and near-ultraviolet MCD and absorption spectra of $[Cr(CN)_5NO]^{3-}$ in aqueous solution and in a 2 : 1 mixture of propyleneglycol and water are shown in Fig. 1. The MCD and absorption spectra around 22000 cm^{-1} of $[Cr(CN)_5NO]^{3-}$ in PVA film were also measured at various temperatures down to liquid nitrogen temperature. The result is shown in Fig. 2.

An apparent dispersion of MCD was observed at 23700 cm^{-1}. An MCD maximum corresponds to the absorption peak at 22100 cm^{-1}, whereas no absorption maximum was observed corresponding to the MCD minimum at 25400 cm^{-1}. $[Cr(NH_3)_5NO]^{2+}$ and $[Cr(OH_2)_5NO]^{2+}$ also show a similar absorption band

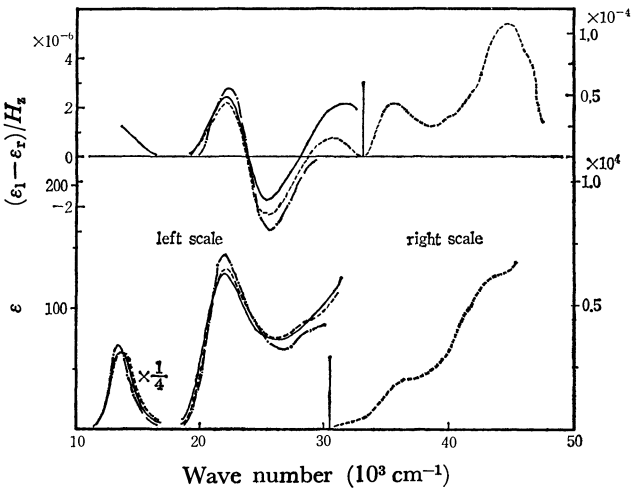

Fig. 1. Magnetic circular dichroism and absorption spectra of $[Cr(CN)_5NO]^{3-}$.
----: in 2 : 1 mixture of propyleneglycol and water (at 300 K), -·-·-: in 2 : 1 mixture of propyleneglycol and water (at 195 K), ——: in aqueous solution.

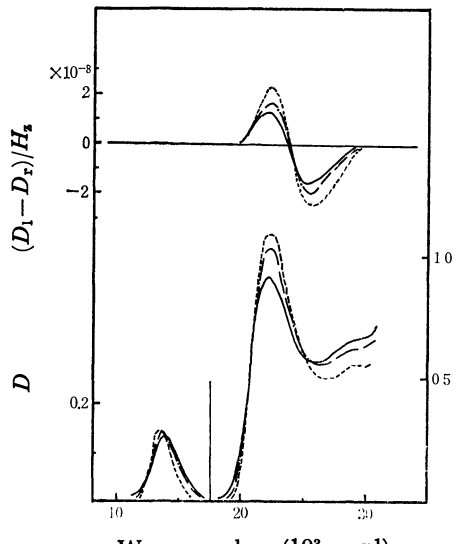

Fig. 2. Magnetic circular dichroism and absorption spectra of $[Cr(CN)_5NO]^{3-}$ on polyvinyl alcohol film. ——: at 300 K, -·-·-: at 195 K, ----: at 77 K.

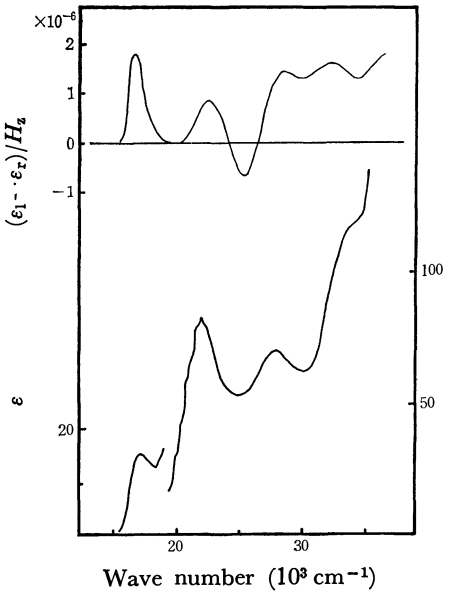

Fig. 3. Magnetic circular dichroism and absorption spectra of $[Cr(NH_3)_5NO]^{2+}$ in 0.1 M HCl solution.

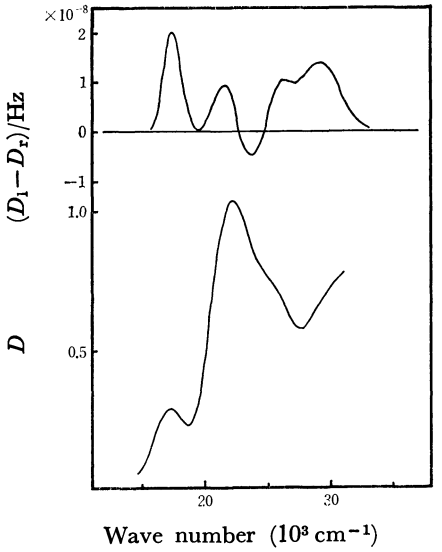

Fig. 4. Magnetic circular dichroism and absorption spectra of $[Cr(OH_2)_5NO]^{2+}$ in concd $HClO_4$ solution.

around 22000 cm^{-1}, and their MCD extrema are also not coincident with their absorption maxima. The substitution of L in $[CrL_5NO]$ gives rise to a small but detectable shift of the 22000 cm^{-1} absorption maximum in the opposite direction to the shift of the MCD maximum. The MCD and absorption spectra of $[Cr(NH_3)_5NO]^{2+}$ in 0.1 M HCl solution and of $[Cr(OH_2)_5NO]^{2+}$ in concd $HClO_4$ solution are shown in Figs. 3 and 4 although the spectra of the latter are rather qualitative. The whole profile of the MCD spectra of $[Cr(NH_3)_5NO]^{2+}$ and $[Cr(OH_2)_5NO]^{2+}$ is similar to that of $[Cr(CN)_5NO]^{3-}$. It should be noted that the lowest energy MCD peak and its corresponding absorption maximum (at about 22000 cm^{-1}) show a shift opposite to the spectrochemical series upon substitution of L in $[CrL_5NO]$ whereas the other MCD extrema show a shift coincident with the spectrochem-

TABLE 1. THE MAGNETIC CIRCULAR DICHROISM EXTREMA AND ABSORPTION MAXIMA OF THE CHROMIUM NITROSYL COMPLEXES

Complex	Absorption maxima (10^3 cm^{-1})					MCD extrema (10^3 cm^{-1})				
	I	II	III	IV	V	I	II	III	IV	V
$[Cr(CN)_5NO]^{3-}$	13.7	22.2		28.6			22.1	25.6	30.4	
$[Cr(NH_3)_5NO]^{2+}$	17.1	21.9		27.8	33.4	16.6	22.4	25.2	28.4	32.2
$[Cr(OH_2)_5NO]^{2+}$	17.4	22.2		25.8		17.4	21.6	23.7	25.2	29.0

ical series. The observed MCD extrema are summarized in Table 1. The 22000 cm^{-1} band of $[Cr(CN)_5NO]^{3-}$ in PVA does not show ripple structure even at 77 K, although the single crystal absorption spectrum at room temperature shows a trace of ripple structure. The corresponding band of $[Cr(NH_3)_5NO]^{2+}$, however, displays a remarkable ripple structure in 0.1 M HCl solution even at room temperature. On the other hand, the MCD spectrum of $[Cr(NH_3)_5NO]^{2+}$ around 22000 cm^{-1} does not show any indication of vibrational fine structure. The differences observed in the behavior of the MCD and absorption spectra around 22000 cm^{-1} indicate that MCD measurements can detect a ligand-field (d, d*) transition hidden in a characteristic absorption band arising from the charge-transfer transition 1e→2e in Cr–NO. This charge-transfer band is rather independent of the other ligands present in the complexes.

Since the molecular orbital pairs, both 1e and 2e, have a z component of orbital angular momentum $\Lambda_z=\pm1$, the charge-transfer excitation 1e→2e gives rise to $^2\Delta$ ($\Lambda_z=\pm2$) and $^2\Sigma$ ($\Lambda_z=0$) states. A transition from the ground $^2\Sigma$ state to the excited $^2\Sigma$ state is allowed, whereas the one to the excited $^2\Delta$ state is forbidden. The molar absorption coefficient of the band around 22000 cm^{-1} is about 130 in $[Cr(CN)_5NO]^{3-}$. If this band arises from a charge-transfer transition in Cr–NO, it should be assigned to a forbidden transition, $^2\Sigma\rightarrow{}^2\Delta$. The forbidden transition can borrow spectral intensity from the allowed transition $^2\Sigma\rightarrow{}^2\Sigma$ by a degenerate vibration which removes the degeneracy of the molecular orbital pairs and gives rise to a mixing between allowed and forbidden transitions. The participating vibration is either a degenerate bending vibration of the Cr–NO skeleton or, less possibly, a degenerate stretching vibration of the Cr–$(CN)_4$ skeleton in a plane perpendicular to the Cr–NO axis. In fact, a vibrational progression has been found on the low-energy side of the 22000 cm^{-1} band of $[(n\text{-}C_4H_9)_4N]_3[Cr(CN)_5NO]$ in EPA solution at 100 K.[20] The band around 22000 cm^{-1} in $[Cr(NH_3)_5NO]^{2+}$ is also accompanied by ripples spaced at about 480—490 cm^{-1} intervals. Bernal assumed a contribution of the Cr–$(NH_3)_4$ stretching vibration in a place perpendicular to the Cr–NO bond.[20] Kobayashi, Tsujikawa, Mori, and Yamamoto, suggested participation of the degenerate bending vibration of the Cr–NO skeleton which is observed at 531—535 cm^{-1} in the vibration spectrum.[24] However they assigned the 22000 cm^{-1} band to the ligand-field transition $^2B_2(xy)\rightarrow{}^2B_1(x^2-y^2)$ which should be coupled with a vibration of E symmetry in order to be allowed. Since no similar ripple structure had been found in the (d, d*) transitions of other chromium ammine complexes, a possibility of participation of the degenerate Cr–$(NH_3)_4$ stretching mode was eliminated. If the 22000 cm^{-1} band arises from a forbidden charge-transfer transition $^2\Sigma\rightarrow{}^2\Delta$ in Cr–NO, the transition can borrow intensity from the allowed $^2\Sigma\rightarrow{}^2\Sigma$ transition, coupled either with a degenerate bending vibration of the Cr–NO skeleton or much less possibly, with a degenerate stretching vibration in the Cr–$(NH_3)_4$ skeleton. In the case of $[Cr(NH_3)_5NO]^{2+}$ the bond between chromium and coordinated NH_3 has the nature of a σ coordination bond, whereas in the case of $[Cr(CN)_5NO]^{3-}$ the back-bonding character of the chromium–CN^- bond is appreciable. Thus, in $[Cr(CN)_5NO]^{3-}$, a small participation of the stretching vibration cannot always be eliminated.

The fact that the position of the 22000 cm^{-1} band is rather independent of other ligands present in the complex and the band has a ripple structure indicates a transition mainly localized in the Cr–NO bond. The charge-transfer excitations in Cr–NO, both allowed and forbidden, are polarized in the direction of the Cr–NO bond and do not have any appreciable transition dipole in the plane perpendicular to the bond axis. It was experimentally proved that a similar forbidden charge-transfer transition in $Na_2[Fe(CN)_5NO]$ is polarized in the direction of the Fe–NO bond.[20] Since a linear oscillator collinear with the orbital angular momentum shows no Zeeman splitting, a charge-transfer transition linearly polarized in the direction of the Cr–NO bond does not display any MCD.

A schematic energy diagram of the orbitals responsible for the outer electronic configuration is shown in Fig. 5. The order of orbitals $a_1(z^2)$ and $b_1(x^2-y^2)$ depends upon σ donations from coordinated NO^+ and CN^-, NH_3 or OH_2. The bonding molecular orbital pair 1e is appreciably lower than orbital $b_2(xy)$ for a π-bonding interaction between metal $d\pi$ orbitals

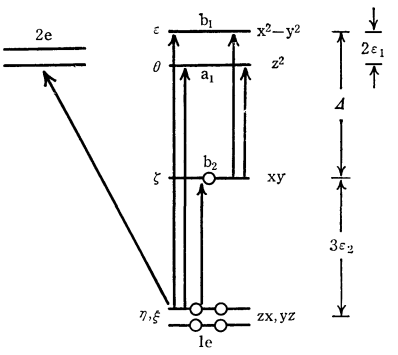

Fig. 5. The energy diagram of the outer shell electrons (schematic).

TABLE 2. THE LOWEST LIGAND-FIELD (d, d*) EXCITED DOUBLETS

Excited doublets	Diagonal energy
$^2B_1(1e^4b_1)$ $\|\varepsilon\bar{\xi}\eta\bar{\eta}\|$	Δ
$^2A_1(1e^4a_1)$ $\|\theta\bar{\xi}\eta\bar{\eta}\|$	$\Delta - 2\varepsilon_1 + 20kB$
$1^2E_0(1e^3b_2^2)$[a] $\|\bar{\xi}\zeta\eta\bar{\eta}\|$	$3\varepsilon_2 + (16-3k+13k^2)B$
$2^2E_0(1e^3b_2a_1)$[a] $[\|\theta\zeta\bar{\xi}\eta\bar{\eta}\| - \|\theta\zeta\bar{\xi}\eta\bar{\eta}\|]/\sqrt{2}$	$\Delta + 3\varepsilon_2 - 2\varepsilon_1 + (-8+45k-26k^2)B/2$
$3^2E_0(1e^3b_2b_1)$[a] $[2\|\bar{\varepsilon}\zeta\bar{\xi}\eta\bar{\eta}\| - \|\varepsilon\bar{\zeta}\bar{\xi}\eta\bar{\eta}\| - \|\varepsilon\zeta\bar{\xi}\eta\bar{\eta}\|]/\sqrt{6}$	$\Delta + 3\varepsilon_2 + (20+k-26k^2)B/2$
$4^2E_0(1e^3b_2b_1)$[a] $[\|\varepsilon\bar{\zeta}\bar{\xi}\eta\bar{\eta}\| - \|\varepsilon\zeta\bar{\xi}\eta\bar{\eta}\|]/\sqrt{2}$	$\Delta + 3\varepsilon_2 + (12+15k-26k^2)B/2$
$5^2E_0(1e^3b_2a_1)$[a] $[2\|\bar{\theta}\zeta\bar{\xi}\eta\bar{\eta}\| - \|\theta\bar{\zeta}\bar{\xi}\eta\bar{\eta}\| - \|\theta\zeta\bar{\xi}\bar{\eta}\bar{\eta}\|]/\sqrt{6}$	$\Delta + 3\varepsilon_2 - 2\varepsilon_1 + (8+27k-26k^2)B/2$
Non-zero mixing term	**energy**
$<2^2E_0\|\hat{H}\|3^2E_0>$	$-1.5\,kB$
$<2^2E_0\|\hat{H}\|4^2E_0>$	$-2.5\sqrt{3}\,kB$
$<2^2E_0\|\hat{H}\|5^2E_0>$	$\frac{1}{\sqrt{12}}(15k-24)B$
$<3^2E_0\|\hat{H}\|4^2E_0>$	$\frac{1}{\sqrt{12}}(21k-12)B$
$<3^2E_0\|\hat{H}\|5^2E_0>$	$-3.5\sqrt{3}\,kB$
$<4^2E_0\|\hat{H}\|5^2E_0>$	$-1.5\,kB$

a) For the degenarate states, only one component of the wave functions is given.

zx and yz and NO antibonding orbitals π^*_{NO}. As ESR studies show, the ground state should be a ^2B state with electronic configuration $(1e)^4(b_2)$. The energy of the lowest one-electron excited doublets is obtained in terms of orbital energy parameters Δ, ε_1, and ε_2 and Racah's electrostatic parameter B as in Table 2. An empirical relationship $C=4.0B$ was assumed and the value of B was reduced for the delocalization in molecular orbital 1e following Koide and Pryce:[32] $B(e,e)=k^2B$, $B(e,b_2)=kB$, and $B(b_2,b_1)=B$.

The empirical values of Δ are 13900 cm^{-1} in $[Cr(OH_2)_6]^{2+}$ and 17400 cm^{-1} in $[Cr(OH_2)_6]^{3+}$.[33] Since the formal oxidation state of chromium in $[Cr(OH_2)_5NO]^{2+}$ is 1+, the value of Δ should be less than 13900 cm^{-1}. Furthermore an almost isotropic ESR signal indicates a large energy gap between 1e and b_2. The energies of ligand-field excited doublets were calculated for a variety of parameters Δ, ε_1, ε_2 in units of B. The lowest observed ligand-field bands in $[Cr(OH_2)_5NO]^{2+}$ and $[Cr(NH_3)_5NO]^{2+}$ are assigned to transitions to excited states $^2A_1$ ($b_2\rightarrow a_1$) and 1^2E ($1e\rightarrow b_2$). The next four ligand-field transitions above 20000 cm^{-1} are assigned to four ^2E states arising from excitations $1e\rightarrow b_1$ and $1e\rightarrow a_1$. In the case of $[Cr(CN)_5NO]^{3-}$, an increase in Δ gives rise to a blue-shift of the transitions to $^2B_1(b_2\rightarrow b_1)$ and to $^2A_1(b_2\rightarrow a_1)$. The back-bonding interactions of coordinated CN^- push down orbital b_2. This reduces the value of ε_2 and gives rise to a red-shift of the transition to $1^2E(1e\rightarrow b_2)$. As shown in Figs. 3 and 4, a red absorption band and its closely corresponding MCD maximum are observed in $[Cr(NH_3)_5NO]^{2+}$ and $[Cr(OH_2)_5NO]^{2+}$. Because insufficient sensitivity of our instrument, the MCD maximum of $[Cr(CN)_5NO]^{3-}$ in near-infrared region could not be detected. An MCD maximum, however, is expected at 13700 cm^{-1} corresponding to the absorption peak (Fig. 1). The lowest wave number band is red-shifted in the order

$$[Cr(CN)_5NO]^{3-} > [Cr(NH_3)_5NO]^{2+} > [Cr(OH_2)_5NO]^{2+}.$$
(13700 cm^{-1}) (17100 cm^{-1}) (17400 cm^{-1})

The absorption intensity of the lowest wave number band of $[Cr(NH_3)_5NO]X_2$ depends upon the outer sphere anions in the complex salts: the color of the complex salts varies from brown to green. Thus Kobayashi, Tsujikawa, Mori and Yamamoto have assigned the lowest wave number band to a charge-transfer excitation in the Cr–NO bond.[24] The observations in the present work, however, indicate that the red absorption band should be assigned to a (d, d*) transition rather than a charge-transfer transition. The red absorption band, however, should have two components corresponding to $^2B_1(b_2\rightarrow b_1)$ and $1^2E(1e\rightarrow b_2)$. In fact, the single crystal absorption spectrum of $K_3[Cr(CN)_5NO]\cdot H_2O$ exhibits two different peaks in the red band for polarized light $\parallel$ and $\perp$ to the c axis as shown in Fig. 6. The spectra polarized $\parallel$ and $\perp$ to the optically equivalent Cr–NO axis could not be obtained because of the crystal disorder, which had been revealed by X-ray crystallography.[34] Since the 22000 cm^{-1} absorption is linearly polarized along the Cr–NO axis, the fact that the absorption for the light polarized $\parallel$ to the c axis is a little more intense than that for the light polarized $\perp$ to the c axis indicates that a slightly higher number of complexes have their Cr–NO bonds $\parallel$ to the c axis. Thus the lower wavenumber component of the red absorption band (680 nm, 14700 cm^{-1}) is polarized more $\parallel$ to the Cr–NO axis and the higher wave number component (670 nm, 14900 cm^{-1}) is polarized more $\perp$ to the Cr–NO axis.

The excited states n^2E arising from the excitations $1e\rightarrow b_1$ and $1e\rightarrow a_1$ in $[Cr(CN)_5NO]^{3-}$ correspond well to

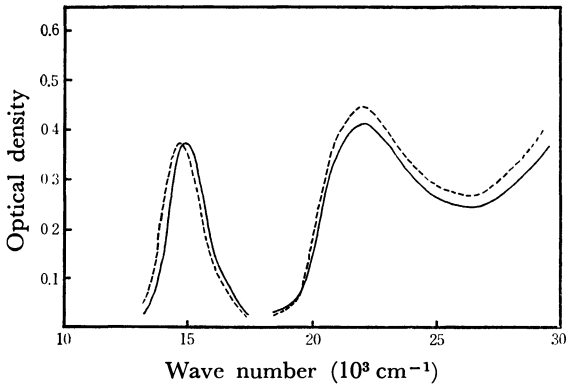

Fig. 6. The polarized single crystal absorption spectrum of $K_3[Cr(CN)_5NO]\cdot H_2O$.
——: polarized $\perp$ to c axis
----: polarized $\parallel$ to c axis

those in $[Cr(NH_3)_5NO]^{2+}$ and $[Cr(H_2O)_5NO]^{2+}$. The calculated energy of the lowest excited doublets is shown in Fig. 7. For a reasonable choice of parameters, theory can reproduce the ligand-field (d, d*) excited states which were detected by MCD spectra as in Fig. 8. The same parameters also predict that the ground state of $[CrL_5NO]$ is ^2B rather than ^6A, and that 1^4E arising from configurations $(1e)^3b_2b_1$ in $[Cr(CN)_5NO]^{3-}$ is higher than 1^2E, which arises from configuration $(1e)^3b_2^2$, whereas 1^4E is lower than 1^2E in $Cr(NH_3)_5NO]^{2+}$ and $[Cr(OH_2)_5NO]^{2+}$. In fact, the anisotropy of the g value for $[Cr(CN)_5NO]^{3-}$ is different from that of $[Cr(NH_3)_5NO]^{2+}$ and $[Cr(OH_2)_5NO]^{2+}$, *i.e.* the sign of $\Delta g_\perp$ ($\equiv g_\perp - 2.0023$) is reversed. The g values observed and calculated for $[CrL_5NO]$ are summarized in Table 3. The g values are given within

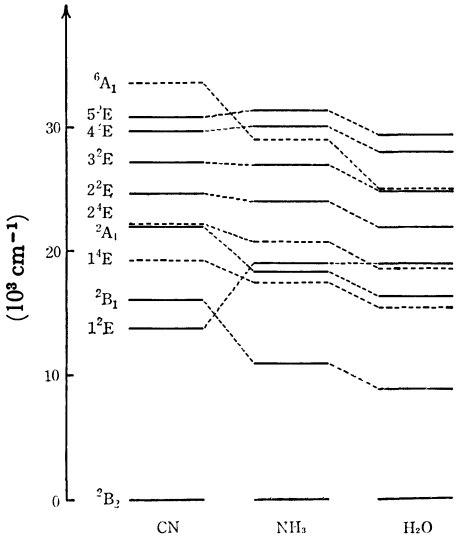

Fig. 7. The lowest ligand-field excited doublets in $[CrL_5NO]$ (L=CN$^-$, NH_3, OH_2).
L=CN$^-$ Δ=16,000 cm^{-1}, ε_1=500 cm^{-1} ε_2=10000/3 cm^{-1}, B=500 cm^{-1}, k=0.7
L=NH_3 Δ=11,000 cm^{-1}, ε_1=500 cm^{-1} ε_2=14500/3 cm^{-1}, B=600 cm^{-1}, k=0.7
L=OH_2 Δ=9,000 cm^{-1}, ε_1=500 cm^{-1} ε_2=14500/3 cm^{-1}, B=600 cm^{-1}, k=0.7

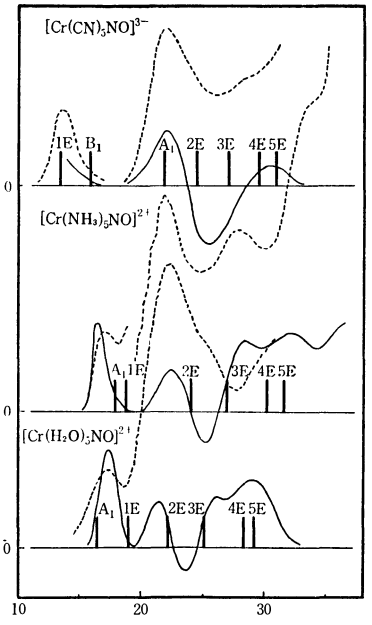

Fig. 8. Assignments of the ligand-field excited states of $[CrL_5NO]$ (L=CN$^-$, NH_3, OH_2).
——: MCD spectrum, ----: absorption spectrum
Vertical lines indicate the calculated energies of the ligand-field excited states.

TABLE 3. THE g VALUES OF $[CrL_5NO]$ (L=CN$^-$, NH_3, OH_2)

L	g obsd			g calcd		
	$g_\parallel$	$g_\perp$	g_{iso}	$g_\parallel$	$g_\perp$	g_{iso}
CN$^-$	1.975	2.005	1.995[a]	1.952	2.004	1.987
NH_3	1.947	1.993	1.980[b]	1.930	1.996	1.974
H_2O	1.916	1.991	1.966[c]	1.913	1.995	1.968

a) Ref 19. b) Estimated from the values for $[Cr(H_2O)_5NO]^{2+}$ (Ref. 35.) c) Ref. 10.

the first-order term of spin-orbit coupling parameter λ as follows:

$$g_\parallel = 2.0023 - 8\lambda/E(^2B_1),$$

$$g_\perp = 2.0023 + 2\lambda/E(1^2E) - \sum_m 2\lambda/E(m^4E_{1/2})\{(1/3)(c_1^m)^2+(c_2^m)^2\} + \sum_n 2\lambda/E(n^2E)\{-(3/2)(c_1^n)^2+(1/3)(c_2^n)^2 - (1/2)(c_3^n)^2 + (c_4^n)^2\},$$

where $E(\Gamma)$ denotes the energy of excitation to state Γ, c_i^m and c_j^n denote the coefficients in the state wave functions

$$\phi(m^4E_{1/2}) = \sum_i c_i^m \phi_i',$$

$$\phi(n^2E) = \sum_j c_j^n \phi_j,$$

$$\phi_1' = \{|\bar{\varepsilon}\zeta\xi\eta\bar{\eta}| + |\varepsilon\bar{\zeta}\xi\eta\bar{\eta}| + |\varepsilon\zeta\bar{\xi}\eta\bar{\eta}|\}/\sqrt{3},$$

$$\phi_2' = \{|\bar{\theta}\zeta\xi\eta\bar{\eta}| + |\theta\bar{\zeta}\xi\eta\bar{\eta}| + |\theta\zeta\bar{\xi}\eta\bar{\eta}|\}/\sqrt{3},$$

$$\phi_1 = \{|\theta\bar{\zeta}\xi\eta\bar{\eta}| - |\theta\zeta\bar{\xi}\eta\bar{\eta}|\}/\sqrt{2},$$

$$\phi_2 = \{2|\bar{\varepsilon}\zeta\xi\eta\bar{\eta}| - \varepsilon\bar{\zeta}\xi\eta\bar{\eta}| - |\varepsilon\zeta\bar{\xi}\eta\bar{\eta}|\}/\sqrt{6}\ ,$$

$$\phi_3 = \{|\varepsilon\bar{\zeta}\xi\eta\bar{\eta}| - |\varepsilon\zeta\bar{\xi}\eta\bar{\eta}|\}/\sqrt{2}\ ,$$

$$\phi_4 = \{2|\bar{\theta}\zeta\xi\eta\bar{\eta}| - |\theta\bar{\zeta}\xi\eta\bar{\eta}| - |\theta\zeta\bar{\xi}\eta\bar{\eta}|\}/\sqrt{6}\ ,$$

and ε, θ, ζ, ξ, and η denote x^2-y^2, z^2, xy, yz, and zx orbitals, respectively. This indicates that $\Delta g_\perp > 0$ when ^1E is higher than $^1A_2$ as in $[Cr(CN)_5NO]^{2-}$, whereas $\Delta g_\perp < 0$ when it is lower as in $[Cr(NH_3)_5NO]^{2+}$ and $[Cr(OH_2)_5NO]^{2+}$. The $g_\perp$ value was evaluated assuming $\lambda = 100\ cm^{-1}$ which correctly predicts the value of $g_\parallel$. The delocalization in molecular orbitals reduces the spin-orbit coupling effect in Cr and thus the value of λ in the complex should be smaller than that observed in the atomic spectrum. The calculated values are in good agreement with the observed values. This confirms the assignment of MCD extrema to the ligand-field excitations.

Plots of the ratio of $\int\left(\frac{\varepsilon_l-\varepsilon_r}{H_z}\right)\Big/\bar{\nu}\ d\bar{\nu}$ to $\int \varepsilon/\bar{\nu}\ d\bar{\nu}$ against $1/kT$ give a straight line. If an MCD maximum is assumed at 22000 cm^{-1}, apparent values of B/D and C/D in units of transition dipole strength D are obtained as $-0.11\times10^{-3}\beta/cm^{-1}$ and $-0.0059\,\beta$, respectively. Such a relatively temperature-independent MCD is seemingly consistent with the non-degenerate ground state $^2B_2$. These values, however, are less significant in this particular case, where the transition detected by MCD is not the transition detected by absorption in the same wave number region.

The authors would like to thank Dr. Hanako Kobayashi, Kyoto University, and Professor Masayasu Mori, Osaka City University, for more than useful comments. The authors wish to express their appreciation to Professors Yukio Kondo and Masayoshi Nakahara, St. Paul's University, for the measurements of polarizing microscope absorption spectrum. This work was supported by a grant from the Ministry of Education.

References

1) F. A. Cotton, R. R. Monchamp, R. J. M. Henry, and R. C. Young, *J. Inorg. Nucl. Chem.*, **10**, 28 (1959).
2) I. Bernal and S. E. Harrison, *J. Chem. Phys.*, **34**, 102 (1961).
3) C. S. Naiman, *ibid.*, **35**, 1503 (1961).
4) H. B. Gray and C. J. Ballhausen, *ibid.*, **36**, 1151 (1962).
5) I. Bernal and S. E. Harrison, *ibid.*, **38**, 2581 (1963).
6) Y. J. Israeli, *Bull. Soc. Chim. Fr.*, **1964**, 1145.
7) P. T. Manoharan and H. B. Gray, *J. Amer. Chem. Soc.*, **87**, 3340 (1965).
8) H. B. Gray, P. T. Manoharan, J. Pearlman, and R. F. Riley, *Chem. Commun.*, **1965**, 62.
9) H. A. Kuska and M. T. Rogers, *J. Chem. Phys.*, **42**, 3034 (1965).
10) I. Bernal, S. D. Robinson, L. S. Meriwether, and G. Wilkinson, *Chem. Commun.*, **1965**, 571.
11) B. A. Goodman, J. B. Raynor, and M. C. R. Symons, *J. Chem. Soc., A*, **1966**, 994.
12) J. Danon, R. P. A. Muniz, and A. O. Caride, *J. Chem. Phys.*, **46**, 1210 (1967).
13) D. B. Brown, *Inorg. Chim. Acta*, **5**, 314 (1971).
14) P. T. Manobaran, and P. Ganguli, *Chem. Phys. Lett.*, **11**, 281 (1971).
15) L. Tosi, *J. Chim. Phys.*, **69**, 1052 (1972).
16) J. Lewis, R. J. Irving, and G. Wilkinson, *J. Inorg. Nucl. Chem.*, **7**, 32 (1958).
17) P. T. Manoharan and W. C. Hamilton, *Inorg. Chem.*, **2**, 1043 (1963).
18) J. Danon, *J. Chem. Phys.*, **41**, 3378 (1964).
19) J. J. Fortaman and R. G. Hayes, *ibid.*, **43**, 15 (1965).
20) P. T. Manoharan and H. B. Gray, *Inorg. Chem.*, **5**, 823 (1966).
21) G. Paliani and A. Polette., *Spectrosc. Lett.*, **5**, 105 (1972).
22) R. F. Fenske and R. L. DeKock, *Inorg. Chem.*, **11**, 437 (1972).
23) J. Danon, H. Panepucci, and A. A. Misetich, *J. Chem. Phys.*, **44**, 4154 (1966).
24) H. Kobayashi, I. Tsujikawa, M. Mori, and Y. Yamamoto, This Bulletin, **42**, 709 (1969).
25) W. P. Griffith, *J. Chem. Soc.*, **1963**, 3286.
26) W. P. Griffith, J. Lewis, and G. Wilkinson, *ibid.*, **1959**, 872.
27) M. Mori, S. Ueshiba, and S. Kawaguchi, This Bulletin, **36**, 796 (1963).
28) H. Kobayashi, M. Shimizu, and I. Fujita, *ibid.*, **43**, 2335 (1970).
29) A. D. Buckingham and P. J. Stephens, *Ann. Rev. Phys. Chem.*, **7**, 399 (1966).
30) P. J. Stephens, *J. Chem. Phys.*, **52**, 3489 (1970).
31) The conventional molar ellipticity per unit external magnetic field $[\theta]_M$ is obtained by 3300 $(\varepsilon_l-\varepsilon_r)/H_z$.
32) S. Koide and M. H. L. Pyrce, *Phil. Mag.*, **3**, 607 (1958).
33) J. S. Griffith, "The Theory of Transition-Metal Ions," Cambridge University Press (1961), p. 302.
34) N. G. Vannerberg, *Acta Chem. Scand.*, **20**, 1571 (1966).
35) W. B. Lewis and L. O. Morgan, "Transition Metal Chemistry" Vol. IV, ed. by R. L. Carlin, M. Dekker New York (1968), p. 67.

Metal Complexes of Amino Acids. VII.[1] The *trans*(*N*) and *cis*(*O*)*cis*(*N*) Isomers of the Type [Co(aa)$_2$phen]X and [Co(aa)$_2$dipy]X

Takaji YASUI

Faculty of Arts and Sciences, Kochi University, Asakura, Kochi 780

(Received September 9, 1974)

Fourteen complexes of the type [Co(aa)$_2$phen]X and [Co(aa)$_2$dipy]X (where aa is the anion of glycine, β-alanine, L-serine, or L-proline) were newly prepared. Two geometrical isomers (*trans*(*N*) and *cis*(*O*)*cis*(*N*)) for the glycinato and β-alaninato complexes, four geometrical and/or diastereomeric isomers ((+)$_D$- and (−)$_D$-*trans*(*N*) and -*cis*(*O*)*cis*(*N*)) for the L-serinato complexes, and two diastereomers ((+)$_D$- and (−)$_D$-*trans*(*N*)) for the L-prolinato complex were separated. These complexes were characterized by absorption, circular dichroism spectra, and ^{1}H and ^{13}C NMR spectra. The absolute configurations of the L-serinato and L-prolinato complexes were assigned as *Λ* and *Δ* for the (+)$_D$- and (−)$_D$-isomers, respectively.

In our previous study[2] one of the three possible geometrical isomers for the type [Co(aa)$_2$(diimine)]X (where aa is the anion of amino acid and diimine is 1,10-phenanthroline or dipyridyl) was separated. It was concluded that this isomer has the *trans*(*N*) (C_2 symmetry) structure with respect to the amino groups. Matsuoka and coworkers succeeded in separating the three geometrical isomers for [Co(gly)$_2$en]$^+$ and for [Co ox(gly)$_2$]$^-$ complex ions,[3] and the six geometrical and/or diastereomeric isomers for [Co ox(L-ser)$_2$]$^-$ complex ion[4] by a column chromatographic method. Analogous separations of the six geometrical and/or diastereomeric isomers for the [Co(L-aspH)$_2$en]$^+$ complex ion have been performed by Kojima and Shibata.[5]

In the present paper two geometrical isomers of the type [Co(aa)$_2$(diimine)]X which were newly separated are characterized on the basis of the absorption, ^{1}H and ^{13}C NMR, and circular dichroism (CD) spectra.

Experimental

Preparation and Separation of Four Isomers of the [Co(L-ser)$_2$phen]Br Complex. Four isomers were obtained by modifying the method reported in the previous paper.[2]

To an aqueous solution containing $CoCl_2 \cdot 6H_2O$ (4.8 g, 0.02 mol) and L-serine (4.2 g, 0.04 mol) in 50 ml of water was added PbO_2 (10 g, excess), and the mixture was stirred for about 15 min. To the mixture was added gradually 1,10-phenanthroline (3.9 g, 0.02 mol) with stirring, and the solution was heated at 65 °C for 15 min. The resulting purple solution was allowed to stand at room temperature overnight and filtered. The filtrate was diluted with 100 ml of water and poured into a column containing cation-exchange resin (Dowex 50W×8, 200—400 mesh, K-form, φ3.5 cm×60 cm). Purple and pink solutions (neutral complexes) were swept out with water in that order and then the purple solution of the bis(L-serinato)diaquo complex ions was swept out with a 0.025 M aqueous solution of KBr. The brownish-orange ((+)$_D$-*trans*(*N*)), the scarlet ((−)$_D$-*cis*(*O*)*cis*(*N*)), the brownish-orange ((−)$_D$-*trans*(*N*)), and the scarlet ((+)$_D$-*cis*(*O*)-*cis*(*N*)) bands were eluted with a 0.1—0.5 M aqueous solution of KBr in that order. Each eluate was concentrated at below 35 °C under reduced pressure, and a large amount of methanol was added to the concentrated solution. Each crude complex was recrystallized by dissolving it in a small amount of warm water, by adding methanol–acetone (1 : 2) mixture to the concentrated solution, and by keeping in a refrigerator overnight.

Four isomers ((+)$_D$- and (−)$_D$-*trans*(*N*) and -*cis*(*O*)*cis*(*N*)) of [Co(L-ser)$_2$dipy]Br and two geometrical isomers (*trans*(*N*) and *cis*(*O*)*cis*(*N*)) of [Co(gly)$_2$phen]Br, [Co(β-ala)$_2$phen]Br and [Co(gly)$_2$dipy]Br were obtained as described above for the [Co(L-ser)$_2$phen]Br. The *cis*(*O*)*cis*(*N*) isomers have lower solubility in water than the *trans*(*N*) isomers. Only two diastereomers ((+)$_D$- and (−)$_D$-*trans*(*N*)) were separated for the [Co(L-pro)$_2$phen]Br.

The elemental analyses for the newly prepared complexes are shown in Table 1.

Measurements. The absorption spectra were measured with a Hitachi Model EDS-3T spectrophotometer. The CD data were obtained by using a JASCO Model ORD/UV-5 spectrophotometer. The measurements of the ^{1}H and ^{13}C NMR spectra were made by a JEOL MH-100 spectrometer (with pulsed Fourier transform/proton noise decoupled mode for the ^{13}C NMR measurements) in D_2O solutions. DSS and cyclohexane were used as an internal standard for ^{1}H NMR and as an external standard for ^{13}C NMR, respectively. The chemical shifts of the carbon resonances are shown relative to TMS using the relation $\delta_{TMS} = \delta_{cyclohexane} - 27.5$.

Results and Discussion

For either [Co(L-aa)$_2$phen]X or [Co(L-aa)$_2$dipy]X, six geometrical and/or diastereomeric isomers (*Λ*- and *Δ*-*trans*(*O*) (C_2 symmetry), *Λ*- and *Δ*-*trans*(*N*) (C_2 symmetry), and *Λ*- and *Δ*-*cis*(*O*)*cis*(*N*) (C_1 symmetry)) are possible, as shown in Fig. 1. In our previous study[2] the *trans*(*N*) isomers for the [Co(aa)$_2$-(diimine)]X (where aa is the anion of glycine, L-alanine, L-hydroxyproline, or *allo*-L-hydroxyproline, and diimine is phen or dipy) complexes were separated and characterized. In this study the separations of the three geometrical isomers (six isomers for the L-amino acid) were tried repeatedly by the column chromatographic method, but unfortunately only two geometrical isomers were obtained. This result suggestes that the stereoselectivity of the two amino acidato

trans(*O*) (C_2) *trans*(*N*) (C_2) *cis*(*O*)*cis*(*N*) (C_1)

Fig. 1. Three possible isomers (all *Λ*) for the [Co(aa)$_2$(diimine)]$^+$ ion.

ligands for the complexes containing phen or dipy is different from that for the corresponding ethylenediamine and oxalato complexes.[3,4]

Absorption Spectra. The absorption curves of the two geometrical isomers of the $[Co(gly)_2phen]^+$ and $[Co(\beta\text{-ala})_2phen]^+$ ions are shown in Fig. 2. The new geometrical isomer (isomer eluted late) of the glycinato complex does not show any splitting in the first band as was also found[2] for the *trans(N)* isomer (complex eluted early). The *trans(O)* isomer is expected to show large splitting of the bands, as observed for other $trans(O)_2(N)_4$ type complexes.[3,5] The first band maximum ($\nu=19610\ cm^{-1}$, $\log\varepsilon=2.10$) of the new isomer has higher intensity and occurs at lower energy, as compared with that ($\nu=20660\ cm^{-1}$, $\log\varepsilon=2.02$) of the *trans(N)* isomer. The greater dipole strength and greater band width of the first band of the isomer eluted late are consistent with the lower symmetry (C_1) of the *cis(O)cis(N)* isomer in comparison to the *trans(N)* isomer. The sharpest bands are expected for the *trans(N)* isomer for which the effective field along each axial direction (amine *N*–amine *N* and two imine *N*–*O*) should be most nearly the same. For geometrical isomers one might expect a lower crystal filed strength, indicated by lower energy of the first band, and one might also expect a lower stability. In fact, the new isomer is easily decomposed in the aqueous solution on heating, as compared with the *trans(N)* isomer. Therefore, the geometrical structure of the new isomer is concluded to be *cis(O)cis(N)* (C_1 symmetry). This assignment agrees with the results of ^1H NMR (*vide infra*).

The geometrical structures of the isomers for the $[Co(\beta\text{-ala})_2phen]X$ (Fig. 2), $[Co(gly)_2dipy]X$ (not shown), $[Co(L\text{-ser})_2phen]X$ (Fig. 3), and $[Co(L\text{-ser})_2dipy]X$ (Fig. 4) are assigned by comparing their first bands with those of the *trans(N)* and *cis(O)cis(N)* isomers for the $[Co(gly)_2phen]X$ complex. The structural assignments of these complexes are indicated in Table 1. The absorption spectra of the diastereomeric L-prolinato complexes correspond to that of *trans(N)*-$[Co(gly)_2phen]X$ (Fig. 5).

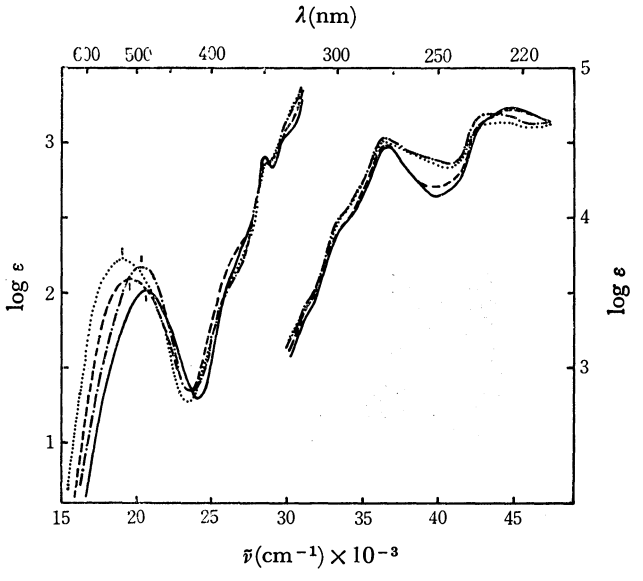

Fig. 2. Absorption curves of (——) *trans(N)*- and (----) *cis(O)cis(N)*-$[Co(gly)_2phen]^+$, and (-·-·-) *trans(N)* and (·····) *cis(O)cis(N)*-$[Co(\beta\text{-ala})_2phen]^+$ ions.

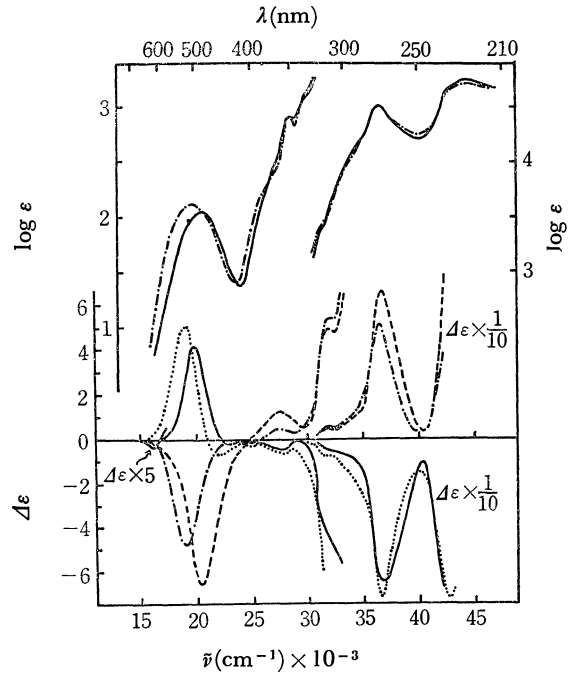

Fig. 3. Absorption and CD curves of (——) $(+)_D$-*trans(N)*-, (----) $(-)_D$-*trans(N)*-, (·····) $(+)_D$-*cis(O)*-*cis(N)*- and (-·-·-) $(-)_D$-*cis(O)cis(N)*-$[Co(L\text{-ser})_2phen]^+$ ions.

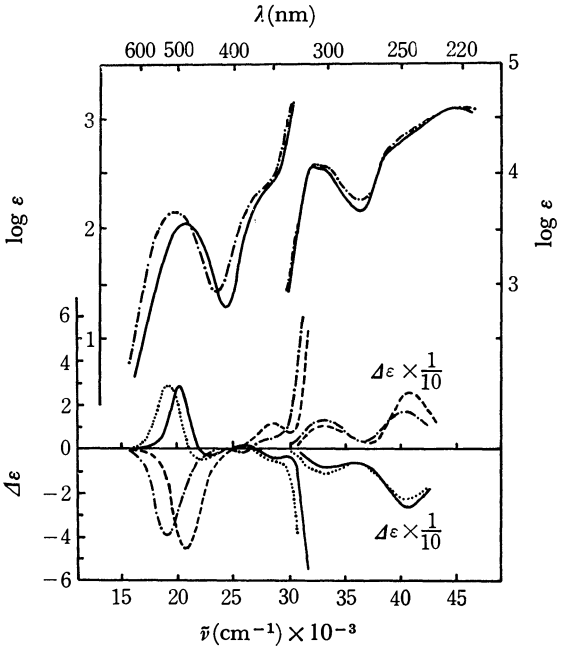

Fig. 4. Absorption and CD curves of (——) $(+)_D$-*trans(N)*-, (----) $(-)_D$-*trans(N)*-, (·····) $(+)_D$-*cis(O)*-*cis(N)*- and (-·-·-) $(-)_D$-*cis(O)cis(N)*-$[Co(L\text{-ser})_2dipy]^+$ ions.

Circular Dichroism (CD). The CD spectra of the $[Co(L\text{-ser})_2phen]^+$, $[Co(L\text{-ser})_2dipy]^+$ and $[Co(L\text{-pro})_2phen]^+$ ions are shown in Figs. 3—5. The CD spectra of the $(+)_D$- and $(-)_D$-*trans(N)*-$[Co(L\text{-ser})_2$-

Table 1. Analytical data of $[Co(aa)_2(diimine)]X$ type complexes

Complex	$[M]_D$ (°)	C, % Found(Calcd)	H, % Found(Calcd)	N, % Found(Calcd)
cis(*O*)*cis*(*N*)-C_1-$[Co(gly)_2phen]Br\cdot 2H_2O$		38.24(38.18)	4.12(4.01)	11.12(11.14)
trans(*N*)-C_2-$[Co(\beta\text{-ala})_2phen]Br\cdot 4H_2O$		38.33(38.10)	5.03(4.98)	9.64 (9.88)
cis(*O*)*cis*(*N*)-C_1-$[Co(\beta\text{-ala})_2phen]Br\cdot 2H_2O$		40.54(40.68)	4.67(4.56)	10.20(10.55)
$(-)_D$-*trans*(*N*)-C_2-$[Co(L\text{-pro})_2phen]Br\cdot 3.5H_2O$	−2110	43.38(43.28)	4.97(5.13)	9.12 (9.18)
$(+)_D$-*trans*(*N*)-C_2-$[Co(L\text{-pro})_2phen]Br\cdot 1.5H_2O$	+1930	46.03(46.00)	4.64(4.75)	9.80 (9.76)
$(+)_D$-*trans*(*N*)-C_2-$[Co(L\text{-ser})_2phen]Br\cdot H_2O$	+773	39.81(39.64)	4.22(4.07)	10.17(10.28)
$(-)_D$-*cis*(*O*)*cis*(*N*)-C_1-$[Co(L\text{-ser})_2phen]Br\cdot H_2O$	−5732	39.97(39.64)	4.30(4.07)	10.16(10.28)
$(-)_D$-*trans*(*N*)-C_2-$[Co(L\text{-ser})_2phen]Br\cdot H_2O$	−3370	39.81(39.64)	4.11(4.07)	10.24(10·28)
$(+)_D$-*cis*(*O*)*cis*(*N*)-C_1-$[Co(L\text{-ser})_2phen]Br\cdot 2H_2O$	+3300	38.45(38.37)	4.30(4.30)	9.84 (9.94)
cis(*O*)*cis*(*N*)-C_1-$[Co(gly)_2bipy]Cl$		41.97(42.17)	4.11(4.05)	14.02(14.05)
$(+)_D$-*trans*(*N*)-C_2-$[Co(L\text{-ser})_2bipy]Br\cdot 3H_2O$	+245	34.52(34.47)	4.71(4.71)	10.05(10.05)
$(-)_D$-*cis*(*O*)*cis*(*N*)-C_1-$[Co(L\text{-ser})_2bipy]Br\cdot 1.5H_2O$	−4950	36.19(36.23)	4.57(4.38)	10.63(10.57)
$(-)_D$-*trans*(*N*)-C_2-$[Co(L\text{-ser})_2dipy]Br\cdot 1.5H_2O$	−2470	36.33(36.23)	4.49(4.38)	10.21(10.57)
$(+)_D$-*cis*(*O*)*cis*(*N*)-C_1-$[Co(L\text{-ser})_2bipy]Br\cdot H_2O$	+2220	36.69(36.86)	4.18(4.27)	10.66(10.75)

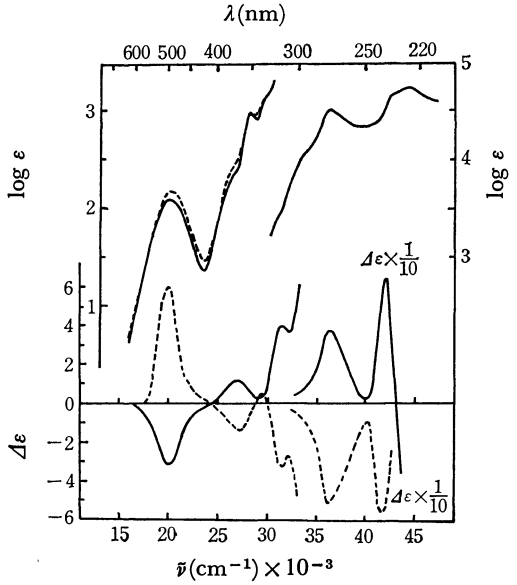

Fig. 5. Absorption and CD curves of (----) $(+)_D$- and (——) $(-)_D$-*trans*(*N*)-$[Co(L\text{-pro})_2phen]^+$ ions.

phen]$^+$ ions are quite similar to those of the corresponding $[Co(L\text{-ala})_2phen]^+$ ions reported in our previous paper.[2] The $(+)_D$- and $(-)_D$-*cis*(*O*)*cis*(*N*) isomers show also CD spectra of the same form as those of the corresponding *trans*(*N*) isomers, although the main CD peaks in the first band region shift to lower energy (Figs. 3 and 4). Therefore, the absolute configurations of these complexes can be assigned as *Λ* and *Δ* for the $(+)_D$- and $(-)_D$-*trans*(*N*) and -*cis*(*O*)*cis*(*N*) isomers, from the sign of the main CD band in the first band region.[6] The same comparisons can be made for the *trans*(*N*)- and *cis*(*O*)*cis*(*N*)-$[Co(L\text{-ser})_2dipy]^+$ ions (Fig. 4). The diastereomers of the *trans*(*N*)-$[Co(L\text{-pro})_2$-phen]$^+$ ion show also CD curves quite similar to those of the corresponding L-hydroxyprolinato complex previously reported.[2] The absolute configurations of these isomers can also be assigned as *Λ* and *Δ* to the $(+)_D$- and $(-)_D$-isomers, respectively. The same assignments of the absolute configuration can also be made from CD spectra in the region of the phen or bipy ligand π-π^* transition (ultraviolet).[2,7] In this case the *Λ*-configuration is assigned to the isomer having an intense negative CD peak in this region (*ca.* 37000 and 33000 cm^{-1} for the phen and bipy complexes, respectively).

^1H and ^{13}C NMR Spectra. The ^1H NMR spectra of two isomers for the $[Co(gly)_2phen]^+$ ion are shown in Fig. 6. The methylene proton resonance of the chelated glycinate ion for the isomer eluted early (*trans*(*N*)) shows a typical single AB pattern expected for the C_2 symmetry. On the other hand, the isomer eluted late shows the methylene resonances of two AB patterns in 3.2—4.2 ppm region. This split pattern is attributed to the low symmetry (C_1) and supports the conclusion that this isomer takes the *cis*(*O*)*cis*(*N*) structure, in agreement with the interpretation of the absorption spectra.

The ^{13}C NMR spectroscopy has been applied to

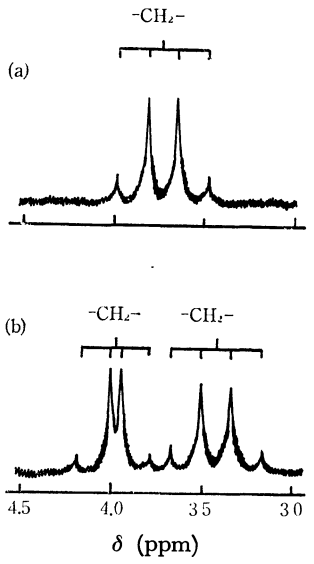

Fig. 6. ^1H NMR spectra of (a) *trans*(*N*)- and (b) *cis*(*O*)*cis*(*N*)-$[Co(gly)_2phen]^+$ ions in D_2O solutions.

the determination of the structure for a large number of organic compounds.[8,9] Recently, Fuhr and Rabenstein pointed out that ^{13}C NMR study is more useful than ^{1}H NMR for elucidating the binding of metal ions by peptides and proteins.[10]

The ^{13}C NMR spectra of two isomers of the $[Co(\beta\text{-ala})_2phen]^+$ ion are shown in Fig. 7. The sharp carbon resonances of ethylene and carboxyl groups of the chelated β-alaninate ions, and phenanthroline are observed in the ranges of 33—41, 128—155 and 182—185 ppm, respectively. The resonances of the *cis(O)-cis(N)* isomer show complicated patterns as compared with those of the *trans(N)* isomer, as expected from the symmetry. In particular, each signal for a single carbon resonance of the latter isomer (C_2 symmetry) appears as a doublet for the former isomer of lower (C_1) symmetry. This ascertainment of the geometrical structure of two isomers of $[Co(\beta\text{-ala})_2phen]^+$ ion from ^{13}C NMR spectra supports the conclusion which was obtained from their absorption spectra.

Formation Ratios of Isomers. Kojima and Shibata[5] separated six isomers for $[Co(L\text{-aspH})_2en]^+$ and $[Co(L\text{-aspH})_2(l\text{-pn})]^+$ using activated carbon in the preparation. They showed that the yields decrease in the order of *Λ-trans(O)>Λ-cis(O)cis(N)>Δ-trans(O)≃Λ-trans(N)>Λ-cis(O)cis(N)≫Δ-trans(N)* for the former complex and *Λ-trans(O)>Λ-cis(O)cis(N)>Δ-trans(O)>Λ-trans(N)=Λ-cis(O)cis(N)≫Δ-trans(N)* for the latter complex. These results suggest that the *trans(N)* isomer is less favored in this type of complex and for these preparative conditions. Similar results were obtained by Matsuoka *et al.* for the type $[Co(aa)_2en]^+$.[3,4]

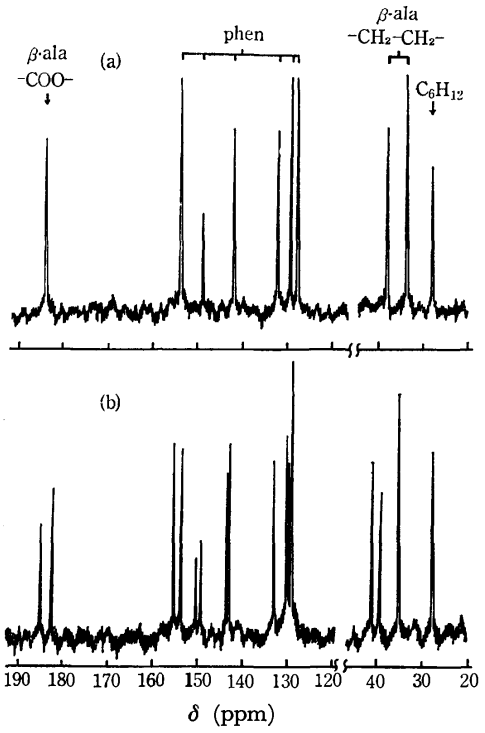

Fig. 7. ^{13}C NMR spectra of (a) *trans(N)*- and (b) *cis(O)cis(N)*-$[Co(\beta\text{-ala})_2phen]^+$ ions in D_2O solutions.

For the complexes reported here the formation ratios of *Λ-*, *Δ-trans(N)*, *Δ-* and *Λ-cis(O)cis(N)* isomers were 5.1 : 2.3 : 1.6 : 1.0 for $[Co(L\text{-ser})_2phen]^+$ ion, and 9.4 : 4.1 : 2.1 : 1.0 for $[Co(L\text{-ser})_2bipy]^+$ ion. On the other hand, the formation ratios of *trans(N)* and *cis(O)cis(N)* isomers were 2.6 : 1.0 for $[Co(gly)_2phen]^+$ and 4.4 : 1.0 for $[Co(gly)_2bipy]^+$, and these ratios also agree with those of the L-serinato complexes (2.8 : 1.0 for phen and 4.3 : 1.0 for bipy). From the preparation using activated carbon, however, only one geometrical isomer, *trans(N)* was identified. These results suggest that the *trans(N)* isomer in the phen and bipy complexes is more easily formed and more stable in aqueous solution than the *cis(O)cis(N)* and *trans(O)* isomers.

The author is grateful to Professor Bodie E. Douglas and Professor Y. Shimura for their valuable discussions and suggestions.

References

1) Part VI of this series: T. Yasui, H. Kawaguchi, Z. Kanda, and T. Ama, This Bulletin, **47**, 2393 (1974).
2) T. Yasui and B. E. Douglas, *Inorg. Chem.*, **10**, 97 (1971).
3) N. Matsuoka, J. Hidaka, and Y. Shimura, This Bulletin, **40**, 1868 (1967).
4) N. Matsuoka, J. Hidaka, and Y. Shimura, *Inorg. Chem.*, **9**, 719 (1970).
5) Y. Kojima and M. Shibata, *ibid.*, **12**, 1009 (1973).
6) A. J. McCaffery and S. F. Mason, *Mol. Phys.*, **6**, 359 (1963); *J. Chem. Soc.*, **1965**, 5094.
7) J. Hidaka and B. E. Douglas, *Inorg. Chem.*, **3**, 1180 (1964).
8) G. C. Levy and G. L. Nelson, "Carbon-13 Nuclear Magnetic Resonance for Organic Chemists," Wiley-Interscience, New York (1972).
9) L-R. F. Johnson and W. C. Jankowski, "Carbon-13 NMR Spectra," Wiley-Interscience, New York (1972).
10) B. J. Fuhr and D. L. Rabenstein, *J. Amer. Chem. Soc.*, **95**, 6944 (1973).

Studies of the Mixed Amino Acid Complexes of Cobalt(III). III.[1] Absorption and Circular Dichroism Spectra of Bis(amino acidato)ethylenediaminecobalt(III) and Bis(amino acidato)oxalatocobaltate(III) Complexes

Nobuko MATSUOKA, Jinsai HIDAKA, and Yoichi SHIMURA

Department of Chemistry, Faculty of Science, Osaka University, Toyonaka, Osaka 560

(Received October 7, 1974)

Three isomers of *cis(O)*-bis(L-alaninato)ethylenediaminecobalt(III) perchlorate, four isomers of potassium *cis(N)*-bis(L-alaninato)oxalatocobaltate(III) and two isomers of potassium *trans(N)*-bis(L-prolinato)oxalatocobaltate(III) have been prepared, and their configurations have been assigned by absorption and circular dichroism spectra. From analysis of the circular dichroism spectra of about 25 complexes of these types (the aminoacidato ligands are glycinato, L-alaninato, L-serinato and L-prolinato), the configurational and the vicinal circular dichroism curves have been separated and discussed. The vicinal circular dichroism curve shows a pattern characteristic of the absolute configuration of α-aminoacidato ligand and of the geometrical structure of the complex.

Three geometrical isomers, *trans*, C_2-*cis* and C_1-*cis*, exist for $[Co(amac)_2en]^+$ or $[Co(amac)_2ox]^-$ type complexes[1] (amac=aminoacidato, en=ethylenediamine, and ox=oxalato ligand). In earlier works, we reported the circular dichroism (CD) spectra of all the geometrical isomers of the glycinato and L-serinato complexes and of the *trans* isomers of the L-alaninato complexes.[2,3] Because more data are required to investigate the so-called vicinal effect displayed by the coordinated optically active α-aminoacidato ligand, we have prepared three *cis(O)* isomers of $[Co(L\text{-}ala)_2en]^+$ and four *cis(N)* isomers of $[Co(L\text{-}ala)_2ox]^-$ and two *trans(N)* isomers of $[Co(L\text{-}prol)_2ox]^-$. In the present paper, details are given for the preparation and separation of the isomers, the assignments of their geometrical structures and absolute configurations. The CD spectra of several complexes of the general types, $[Co(amac)_2en]^+$ and $[Co(amac)_2ox]^-$, are discussed and summarized.

Experimental

Preparation and Separation of Complexes. 1) Isomers of Bis(L-alaninato)ethylenediaminecobalt(III) Perchlorate. A solution of $[Co(L\text{-}ala)_2en]^+$ was prepared from cobalt(II) chloride hexahydrate, L-alanine and ethylenediamine by the method described in the previous paper,[3] and it was poured into a column (3 cm×90 cm) of cation-exchange resin (Dowex 50W-X8, 200—400 mesh, H^+ form). The neutral species, *mer*- and *fac*-$[Co(L\text{-}ala)_3]$, were swept out with water, and the two dark red species, *Δ*- and *Λ-trans(O)*-$[Co(L\text{-}ala)_2en]^+$, were eluted out with 0.02 M $NaClO_4$ solution. The separation and optical properties of these two *trans(O)* isomers have already been reported.[3] With further elution, three red bands appeared in the middle region of the column. The first red band was composed of $(-)_{546}$-isomers, which showed absorption maxima at 502 and 360 nm in the earlier eluted part and at 500 and 356 nm in the later eluted part. The second and the third red bands contained $(+)_{546}$-isomers. The species in the second band had absorption maxima at 503 and 360 nm, and that in the third band at 500 and 356 nm. By comparing the above experimental data with those of the corresponding glycinato and L-serinato complexes,[3] it was confirmed that the first band consisted of the two isomers, $(-)_{546}$-(*Δ*)-C_1-*cis(O)* and $(-)_{546}$-(*Δ*)-C_2-*cis(O)*, and that the second band contained $(+)_{546}$-(*Λ*)-C_1-*cis(O)* and the third band $(+)_{546}$-(*Λ*)-C_2-*cis(O)*.

$(-)_{546}$-C_1-cis(O)-$[Co(L\text{-}ala)_2en]ClO_4$: The earlier eluate of first red band was concentrated with a vacuum evaporator, and ethanol and ether were added to it. A large amount of white precipitate of sodium perchlorate deposited and it was filtered off. If an oily substance was formed, the supernatant was removed by decantation. The oil was treated with a little amount of water, and ethanol and ether were again added to it. After repeated precipitation and removal of sodium perchlorate by the same procedure, red crystals were deposited. They were isolated by using a centrifuge and recrystallized from water by adding ethanol and ether. Pure crystals (E–C–1) were filtered, washed with water–ethanol mixture and ethanol, and dried in air.

From the later eluate of the first red band, no pure complex could be obtained.

$(+)_{546}$-C_1-cis(O)-$[Co(L\text{-}ala)_2en]ClO_4$: This isomer (E–C–2) was obtained from the eluate of second red band by the same method used for the $(-)_{546}$-C_1-*cis(O)* isomer.

$(+)_{546}$-C_2-cis(O)-$[Co(L\text{-}ala)_2en]ClO_4$: The eluate of third red band was evaporated to dryness with a vacuum evaporator, and the red substance was extracted with methanol. When ether was added to the methanol solution a large amount of white sodium perchlorate precipitate was formed, which was filtered off. After repeated precipitation and removal of sodium perchlorate, red crystals began to deposit. They were isolated by using a centrifuge. The crude complex was dissolved in water, and a small amount of insoluble material was filtered off. The pure complex (E–C–3) was obtained by evaporating the mother liquor in a vacuum desiccator.

2) Isomers of Potassium Bis(L-alaninato)oxalatocobaltate(III). A solution of $[Co(L\text{-}ala)_2ox]^-$ was prepared from cobalt(II) chloride hexahydrate, L-alanine and potassium oxalate by the method described in the previous paper.[4] From a column (3 cm×90 cm) of anion-exchange resin (Dowex 1–X8, 200—400 mesh, Cl^- form) the upper layer (about 4 cm) of resin was sucked out by a syringe, and stirred in a separate beaker with a saturated potassium acetate solution. It was again stirred with the solution of $[Co(L\text{-}ala)_2ox]^-$ and the resulting resin which adsorbed several isomers of the complex ion returned to the top of the column. By elution with 0.02—0.01 M KCl solution, a colored band was progressively separated into the three bands which were, in order of elution, blue-violet, red-violet and blue-violet. From their visible and ultraviolet absorption spectra, CD and ORD curves, these bands were assigned as follows. The first blue-violet band consisted of two species, $(-)_{546}$-(*Δ*)-*trans(N)*- and $(+)_{546}$-(*Δ*)-*trans(N)*-$[Co(L\text{-}ala)_2ox]^-$, which were eluted in this order. In the second red-violet band there were also two species, $(-)_{546}$-(*Λ*)-C_1-*cis(N)*- (eluted earlier) and $(+)_{546}$-(*Δ*)-C_1-*cis(N)*-$[Co(L\text{-}ala)_2ox]^-$ (eluted later), both of which showed absorption maxima at 542 and 386 nm. The last

blue-violet band was further separated into two bands. The species in the earlier eluted band was $(+)_{546}$-(*Δ*)-C_2-*cis*(*N*)-[Co(L-ala)$_2$ox]$^-$ which had absorption maxima at 548 and 381 nm, and the species in the later eluted band was $(-)_{546}$-(*Λ*)-C_2-*cis*(*N*)-[Co(L-ala)$_2$ox]$^-$ which had absorption maxima at 551 and 381 nm.

$(-)_{546}$-(*Λ*)- and $(+)_{546}$-(*Δ*)-trans(N)-*K*[*Co(L-ala)$_2$ox*]: The $(-)_{546}$- and $(+)_{546}$-isomers in the first blue-violet band were identical to the less soluble and the more soluble isomers, respectively, in the earlier paper.[4] Therefore the isolation and purification were carried out as before.

$(-)_{546}$-(*Λ*)- and $(+)_{546}$-(*Δ*)-C_1-cis(N)-*K*[*Co(L-ala)$_2$ox*]: The eluate of the second red-violet band was concentrated with a vacuum evaporator. By adding a limited amount of ethanol in portions to the concentrated solution, several fractions of the complex were obtained, after the white precipitates of potassium chloride formed at first had been removed. By measurement of their ORD, these fractions were divided into two groups, $(-)_{546}$- and $(+)_{546}$-fractions. It was found that the isomer in the $(-)_{546}$-fraction (O-C-1) was less soluble and the one in $(+)_{546}$-fraction (O-C-2) more soluble. Both isomers were independently recrystallized from water by adding ethanol (and ether too for the $(+)_{546}$-isomer), and they were filtered, washed with ethanol and dried in a desiccator. The $(-)_{546}$-isomer was also isolated by adding ethanol to the earlier eluted part of the second band.

$(+)_{546}$-(*Δ*)-C_2-cis(N)-*K*[*Co(L-ala)$_2$ox*]: The earlier eluted part of the third blue-violet band was evaporated to dryness with a vacuum evaporator. The complex was extracted with methanol, and then ether was added to this methanol solution. The crude complex deposited was recrystallized from water by adding ether. Pure violet crystals (O-C-3) were filtered, washed with ether and dried in a vacuum desiccator.

$(-)_{546}$-(*Δ*)-C_2-cis(N)-*K*[*Co(L-ala)$_2$ox*]: This isomer (O-C-4) was obtained from the later eluted part of the third band by the same method used for the $(+)_{546}$-isomer.

3) Trans(N) *Isomers of Potassium Bis(L-prolinato)oxalatocobaltate(III).* A solution of 4.7 g (0.02 mol) of cobalt (II) chloride hexahydrate in 20 ml of water was mixed with a solution of 4 g (0.02 mol) of potassium oxalate and 5 g (0.04 mol) of L-proline in 40 ml of water. The resulting solution was mechanically stirred with 5 g of lead dioxide and a small amount of active charcoal at 60 °C for about 40 min, and cooled to room temperature. After standing overnight, insoluble material was removed. The resin which adsorbed the resulting complex ion was prepared by the method described for [Co(L-ala)$_2$ox]$^-$, and it was transferred into the top of a 3 cm×90 cm column packed with anion-exchange resin (Dowex 1-X8, 200—400 mesh, Cl^- form). The adsorbed complexes were progressively separated into two bands colored blue-violet and violet, by elution with about 0.05 M KCl solution. From the absorption and CD spectra, it was shown that the blue-violet band contained two isomers of *trans(N)*-[Co(L-prol)$_2$ox]$^-$, which was the *Δ*-isomer in the earlier eluted fraction and the *Λ*-isomer in the later eluted fraction. Similarly, the violet band was shown to contain *cis(N)*-[Co(L-prol)$_2$ox]$^-$ isomer.

Only two *trans* isomers have been successfully isolated as follows.

$(+)_{546}$-(*Δ*)-trans(N)-*K*[*Co(L-prol)$_2$ox*]: The earlier eluted fraction of the blue-violet band was evaporated to dryness with a vacuum evaporator, and then the violet substance was extracted with methanol. An insoluble mixture of white precipitate (potassium chloride) and reddish violet solid (*Λ-trans* isomer) was filtered off, and then ether was added to the mother liquor. Violet crystals were deposited. They were recrystallized from methanol by adding ether. After repeated recrystallizations, pure crystals (P-T-1) were filtered, washed with ether and dried in a desiccator.

$(+)_{546}$-(*Λ*)trans(N)-*K*[*Co(L-prol)$_2$ox*]: The later eluted fraction of the blue-violet band was concentrated with a vacuum evaporator. By adding ethanol to the concentrate, a large amount of pinkish violet crystals was deposited. If a precipitate of potassium chloride was formed prior to precipitating the complex, it was removed, and ethanol was again added to the mother liquor. The crude complex was recrystallized from water by adding ethanol. The pure crystals (P-T-2) were filtered, washed with ethanol-water mixture and then with ethanol and dried in air.

Measurements. The electronic absorption spectra were measured with a Shimadzu UV-200 spectrophotometer. The CD spectra were recorded with a JASCO Model MOE-1 spectropolarimeter or with a Roussel-Jouan Dichrograph. The ORD curves were recorded with a Yanagimoto Model-185 spectropolarimeter. All measurements were made in aqueous solutions at room temperature.

Results and Discussion

The three newly obtained isomers of *cis(O)*-[Co(L-ala)$_2$en]$^+$ were labeled as E-C-1, E-C-2 and E-C-3, the four isomers of *cis(N)*-[Co(L-ala)$_2$ox]$^-$ as O-C-1, O-C-2, O-C-3 and O-C-4, and the two isomers of *trans(N)*-[Co(L-prol)$_2$ox]$^-$ as P-T-1 and P-T-2, in the order of elution. The analytical data for these complexes are presented in Table 1, together with

Table 1. Analytical data of [Co(L-ala)$_2$en]ClO_4, K[Co(L-ala)$_2$ox] and K[Co(L-prol)$_2$ox]

Label	Complex	Found			Calcd		
		C	H	N	C	H	N
E-C-1	$(-)_{546}$-*Λ*-C_1-*cis(O)*-[Co(L-ala)$_2$en]$ClO_4\cdot 2H_2O$	22.61	5.72	13.10	23.31	5.62	13.01
E-C-2	$(+)_{546}$-*Λ*-C_1-*cis(O)*-[Co(L-ala)$_2$en]ClO_4	24.11	5.11	14.21	24.35	5.11	14.20
E-C-3	$(+)_{546}$-*Λ*-C_2-*cis(O)*-[Co(L-ala)$_2$en]$ClO_4\cdot 2H_2O\cdot 0.5NaClO_4$	20.17	4.77	10.84	19.53	4.92	11.39
O-T-1	$(-)_{546}$-*Λ-trans(N)*-K[Co(L-ala)$_2$ox]	26.26	3.53	7.76	26.53	3.33	7.74
O-T-2	$(+)_{546}$-*Λ-trans(N)*-K[Co(L-ala)$_2$ox]$\cdot 2.5H_2O$	23.47	4.19	6.87	23.59	4.21	6.88
O-C-1	$(-)_{546}$-*Λ*-C_1-*cis(N)*-K[Co(L-ala)$_2$ox]$\cdot 3H_2O$	22.94	4·30	6.69	23.08	4.36	6.73
O-C-2	$(+)_{546}$-*Λ*-C_1-*cis(N)*-K[Co(L-ala)$_2$ox]$\cdot 3.5H_2O$	22.35	4.34	6.44	22.59	4.50	6.59
O-C-3	$(+)_{546}$-*Λ*-C_2-*cis(N)*-K[Co(L-ala)$_2$ox]$\cdot 3H_2O\cdot 2.4KCl$	16.48	2.96	4.59	16.14	3.05	4.71
O-C-4	$(-)_{546}$-*Λ*-C_2-*cis(N)*-K[Co(L-ala)$_2$ox]$\cdot 3H_2O\cdot 2.3KCl$	16.56	2.95	4.85	16.35	3.09	4.77
P-T-1	$(+)_{546}$-*Λ-trans(N)*-K[Co(L-prol)$_2$ox]$\cdot 2.5H_2O$	30.68	4.66	6.12	31.38	4.61	6.10
P-T-2	$(+)_{546}$-*Λ-trans(N)*-K[Co(L-prol)$_2$ox]$\cdot 2.5H_2O$	31.36	4.55	6.15	31.38	4.61	6.10

those of the two isomers of *trans*(*N*)-[Co(L-ala)$_2$ox]$^-$ (O-T-1 and O-T-2).

The sample of *Δ-trans*(*N*)-K[Co(L-ala)$_2$ox] prepared in the present work (O-T-2) had 2.5 mol of water of crystallization (*cf.* Table 1), although the sample prepared in the earlier paper[4] was anhydrous. The optical purity of the present sample is greater than that of the previous one. It seems that the sample in the earlier work was partly racemic, *i.e.* it was mixed with a little of the *Λ-trans*(*N*) isomer. The E-C-3 isomer of [Co(L-ala)$_2$en]$^+$ and O-C-3 and O-C-4 isomers of [Co(L-ala)$_2$ox]$^-$ are contaminated with small amounts of sodium perchlorate or potassium chloride. However, further purifications have not been carried out, because of the low yields of the complexes.

Structural Assignments of Isomers. The geometrical structures of [Co(amac)$_2$en]$^+$ or [Co(amac)$_2$ox]$^-$ complexes can be determined from their absorption spectra in the d-d transition region. Thus the O-T-1, O-T-2, P-T-1 and P-T-2 isomers are easily identified as *trans*-(*N*) structures from the large splitting of their first absorption bands[1] (*cf.* Fig. 1).

The absorption spectra of the C_2-*cis* and C_1-*cis* isomers of the present complexes are similar in appearance in the d-d transition region, as seen in Figs. 2 and 3. However, we have found previously some regular differences in the absorption maxima between the C_2-*cis* and the C_1-*cis* isomers in both series of [Co(gly)$_2$en]$^+$ and [Co(gly)$_2$ox]$^-$. The geometrical structures of these bis(glycinato) isomers were determined unambiguously from their NMR spectra.[1] For instance, the C_2-*cis*(*O*) isomer of [Co(gly)$_2$en]$^+$ shows a second absorption maxima at a higher energy than that of the corresponding C_1-*cis*(*O*) isomer. The same behavior has also been observed for the [Co(L-ser)$_2$en]$^+$ isomers. The data are presented in Table 2 together with those of the [Co(L-ala)$_2$en]$^+$ isomers,

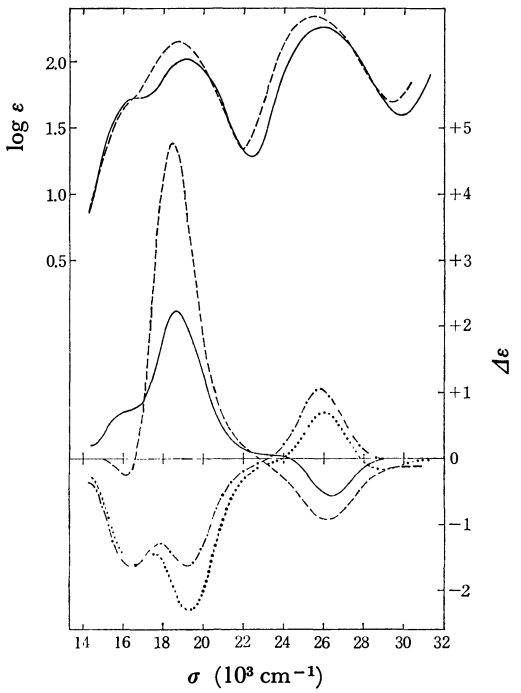

Fig. 1. Absorption and CD spectra of *trans*(*N*)-[Co(L-amac)$_2$ox]$^-$.
——: *Λ*-L-alaninato complex (O-T-1), ----: *Δ*-L-alaninato complex (O-T-2), ——: *Δ*-L-prolinato complex (P-T-1), ——: *Λ*-L-prolinato complex (P-T-2).

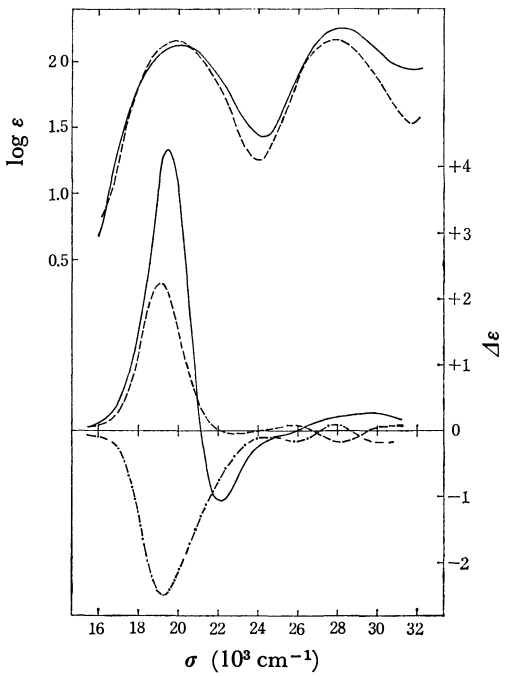

Fig. 2. Absorption and CD spectra of *cis*(*O*)-[Co(L-ala)$_2$en]$^+$.
——: *Δ*-C$_1$-*cis*(*O*) isomer (E-C-1), ——: *Λ*-C$_1$-*cis*(*O*) isomer (E-C-2), ——: *Λ*-C$_2$-*cis*(*O*) isomer (E-C-3).

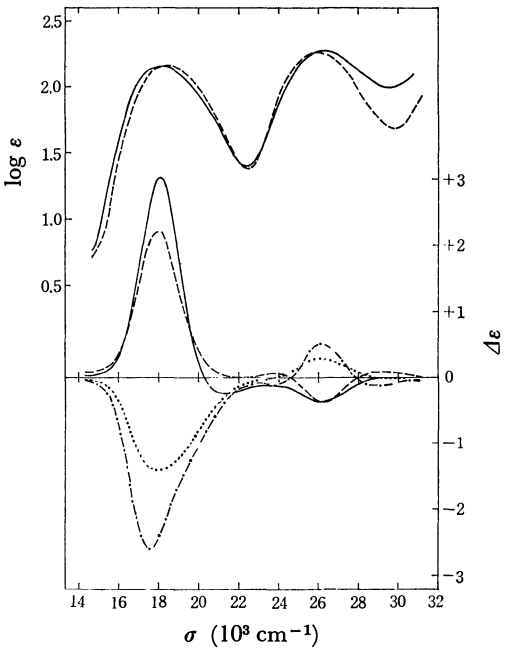

Fig. 3. Absorption and CD spectra of *cis*(*N*)-[Co(L-ala)$_2$ox]$^-$.
——: *Λ*-C$_1$-*cis*(*N*) isomer (O-C-1); ——: *Δ*-C$_1$-*cis*(*N*) isomer (O-C-2); ----: *Δ*-C$_2$-*cis*(*N*) isomer (O-C-3); ——: *Λ*-C$_2$-*cis*(*N*) isomer (O-C-4).

E–C–1, E–C–2, and E–C–3. By comparing these values, the geometrical structures of E–C–1 and E–C–2, both of which have their second absorption maxima at 27800 cm^{-1}, are assigned to C_1-*cis*(*O*), and E–C–3, which has a second absorption maximum at 28200 cm^{-1}, to C_2-*cis*(*O*). In the oxalato complexes such as $[Co(gly)_2ox]^-$ and $[Co(L\text{-}ser)_2ox]^-$, the C_2-*cis*(*N*) isomer has its first absorption maximum at a lower energy and the second absorption maximum at a higher energy than the C_1-*cis*(*N*) isomer, as seen in Table 2. Therefore, the geometrical structures of O–C–1 isomer (absorption maxima at 18500 and 25900 cm^{-1}) and the O–C–2 isomer (maxima at 18400 and 25900 cm^{-1}) are assigned as C_1-*cis*(*N*), while the structures of O–C–3 (maxima at 18200 and 26200 cm^{-1}) and O–C–4 isomers (maxima at 18200 and 26300 cm^{-1}) are assigned as C_2-*cis*(*N*).

The absolute configurations of all the isomers were assigned from the sign of major CD band in the region of the first absorption band.[5] It has been confirmed that the absolute configurations derived from this CD method agree with conclusions from PMR studies, which were reported for several mixed aminoacidatocobalt(III) complexes including *trans*(*O*)-$[Co(L\text{-}ala)_2en]^+$ and *trans*(*N*)-$[Co(L\text{-}ala)_2ox]^-$.[6,7] Since the E–C–2, E–C–3, O–C–1, O–C–4, and P–T–2 isomers have a positive major CD band in the region of the first absorption band (Figs. 2 and 3), these isomers are assigned to the *Λ*-configuration. The other four complexes have a negative major CD band, and they are assigned to the *Δ*-configuration. Consequently, the nine newly obtained complexes are characterized as follows: in the $[Co(L\text{-}ala)_2en]^+$ series, E–C–1 is *Δ*-C_1-*cis*(*O*), E–C–2 *Λ*-C_1-*cis*(*O*), and E–C–3 *Λ*-C_2-*cis*(*O*); in the $[Co(L\text{-}ala)_2ox]^-$ series, O–C–1 is *Λ*-C_1-*cis*(*N*), O–C–2 *Δ*-C_1-*cis*(*N*), O–C–3 *Δ*-C_2-*cis*(*N*), and O–C–4 *Λ*-C_2-*cis*(*N*); in the $[Co(L\text{-}prol)_2ox]^-$ series, P–T–1 is *Δ*-*trans*(*N*), and P–T–2 *Λ*-*trans*(*N*). We have failed in isolation of the *Δ*-C_2-*cis*(*O*) isomer in the $[Co(L\text{-}ala)_2en]^+$ series, though it has been confirmed that this isomer certainly exists in a fraction eluted from the column after the E–C–1 fraction.

Absorption Spectra. The absorption spectra of the complexes in the $[Co(amac)_2en]^+$ and $[Co(amac)_2ox]^-$ series are summarized in Table 2. As mentioned above, the second absorption band maximum of

Table 2. d-d Absorption data of $[Co(amac)_2en]^+$ and $[Co(amac)_2ox]^-$ complexes

Complex	I-Band		II-Band		Ref.
	σ_{max}[a]	($\log \varepsilon_{max}$)	σ_{max}[a]	($\log \varepsilon_{max}$)	
trans(*O*)-$[Co(gly)_2en]I\cdot H_2O$	18.9	(1.94)	27.8	(2.12)	1
Δ-*trans*(*O*)-$[Co(L\text{-}ala)_2en]ClO_4$	18.9	(1.98)	27.6	(2.13)	3
Λ-*trans*(*O*)-$[Co(L\text{-}ala)_2en)ClO_4$	18.8	(1.97)	27.7	(2.17)	3
Δ-*trans*(*O*)-$[Co[L\text{-}ser)_2en]I$	18.9	(1.95)	27.8	(2.13)	3
Λ-*trans*(*O*)-$[Co(L\text{-}ser)_2en]ClO_4$	18.9	(1.95)	27.7	(2.13)	3
C_2-*cis*(*O*)-$[Co(gly)_2en]Br\cdot H_2O$	19.9	(2.04)	28.0	(2.11)	1
Λ-C_2-*cis*(*O*)-$[Co(L\text{-}ala)_2en]ClO_4\cdot 2H_2O\cdot 0.5NaClO_4$	20.1	(2.12)	28.2	(2.25)	
Δ-C_2-*cis*(*O*)-$[Co(L\text{-}ser)_2en]I\cdot 2H_2O\cdot 0.5serH$	20.0	(2.10)	28.3	(2.29)	3
Λ-C_2-*cis*(*O*)-$[Co(L\text{-}ser)_2en]I$	20.0	(2.05)	28.1	(2.14)	3
C_1-*cis*(*O*)-$[Co(gly)_2en]Br\cdot 3H_2O$	20.0	(2.09)	27.7	(2.13)	1
Δ-C_1-*cis*(*O*)-$[Co(L\text{-}ala)_2en]ClO_4\cdot 2H_2O$	19.9	(2.16)	27.8	(2.17)	
Λ-C_1-*cis*(*O*)-$[Co(L\text{-}ala)_2en]ClO_4$	19.8	(2.15)	27.8	(2.15)	
Δ-C_1-*cis*(*O*)-$[Co(L\text{-}ser)_2en]I$	20.0	(2.12)	27.8	(2.14)	3
Λ-C_1-*cis*(*O*)-$[Co(L\text{-}ser)_2en]ClO_4$	20.0	(2.12)	27.9	(2.15)	3
trans(*N*)-$K[Co(gly)_2ox]$	18.9	(2.00)	25.8	(2.23)	1
Δ-*trans*(*N*)-$K[Co(L\text{-}ala)_2ox]\cdot 2.5H_2O$	19.0	(2.02)	25.9	(2.25)	
Λ-*trans*(*N*)-$K[Co(L\text{-}ala)_2ox]$	19.1	(2.02)	25.9	(2.26)	
Δ-*trans*(*N*)-$K[Co(L\text{-}ser)_2ox]\cdot 3.5H_2O$	19.0	(1.96)	26.0	(2.21)	2
Λ-*trans*(*N*)-$K[Co(L\text{-}ser)_2ox]\cdot 3H_2O$	19.0	(1.97)	26.0	(2.20)	2
Δ-*trans*(*N*)-$K[Co(L\text{-}prol)_2ox]\cdot 2.5H_2O$	18.9	(2.08)	25.5	(2.29)	
Λ-*trans*(*N*)-$K[Co(L\text{-}prol)_2ox]\cdot 2.5H_2O$	18.7	(2.15)	25.5	(2.34)	
C_2-*cis*(*N*)-$Na[Co(gly)_2ox]$	17.8	(2.08)	25.9	(2.20)	1
Δ-C_2-*cis*(*N*)-$K[Co(L\text{-}ala)_2ox]\cdot 3H_2O\cdot 2.4KCl$	18.2	(2.17)	26.2	(2.26)	
Λ-C_2-*cis*(*N*)-$K[Co(L\text{-}ala)_2ox]\cdot 3H_2O\cdot 2.3KCl$	18.2	(2.15)	26.3	(2.27)	
Δ-C_2-*cis*(*N*)-$K[Co(L\text{-}ser)_2ox]\cdot 2.5H_2O$	18.0	(2.07)	26.0	(2.17)	2
Λ-C_2-*cis*(*N*)-$K[Co(L\text{-}ser)_2ox]\cdot 2.5H_2O$	18.0	(2.14)	26.1	(2.25)	2
C_1-*cis*(*N*)-$Na[Co(gly)_2ox]$	18.3	(2.15)	25.8	(2.24)	1
Δ-C_1-*cis*(*N*)-$K[Co(L\text{-}ala)_2ox]\cdot 3.5H_2O$	18.4	(2.16)	25.9	(2.26)	
Λ-C_1-*cis*(*N*)-$K[Co(L\text{-}ala)_2ox]\cdot 3H_2O$	18.5	(2.16)	25.9	(2.26)	
Δ-C_1-*cis*-(*N*)-$K[Co(L\text{-}ser)_2ox]\cdot 2H_2O$	18.5	(2.16)	25.9	(2.29)	2
Λ-C_1-*cis*(*N*)-$K[Co(L\text{-}ser)_2ox]\cdot 1.5H_2O$	18.5	(2.09)	25.9	(2.20)	2

a) In the unit of 10^3 cm^{-1}.

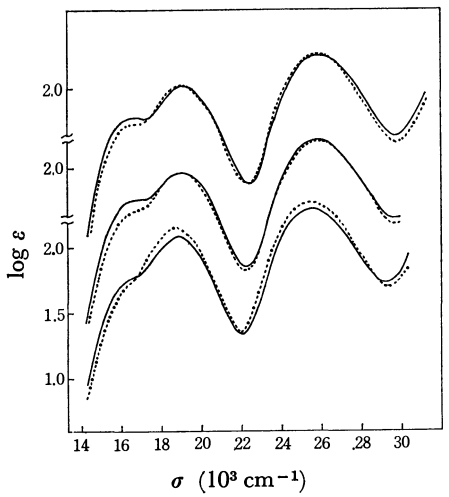

Fig. 4. Absorption spectra of *trans*(*N*)-[Co(L-amac)$_2$ox]$^-$. {L-amac=L-ala (upper); L-ser (middle); L-prol (lower)}: ——: *Δ*-isomer, ----: *Λ*-isomer

C_2-*cis* isomer is generally at a higher energy than that of the corresponding C_1-*cis* isomer.

For the *trans*(*N*)-[Co(amac)$_2$ox]$^-$ complexes, the position of the first absorption band maximum shifts to higher energies in the order of aminoacidato ligands: L-prolinato, glycinato, L-serinato and L-alaninato. The same order is also observed for the C_2-*cis*(*O*)-[Co(amac)$_2$en]$^+$ and C_2-*cis*(*N*)-[Co(amac)$_2$ox]$^-$ complexes. This spectrochemical series for aminoacids agrees with that observed for the [Co(amac) $(NH_3)_4]^{2+}$ complexes.[8] In Fig. 4, it is interesting to note that the intensity of the longer wavelength component of the first absorption band is always stronger in the *Δ* diastereomer of the *trans*(*N*)-[Co(L-amac)$_2$ox]$^-$ complex than in the corresponding *Λ* one.

Configurational Circular Dichroism. The observed CD data for the [Co(L-amac)$_2$en]$^+$ and [Co(L-amac)$_2$ox]$^-$ complexes are summarized in Table 3. By applying the following relations,[2,3] the configurational (Figs. 5 and 6) and the vicinal (Fig. 7) curves have been derived from the observed curves.

$$\Delta\varepsilon(2L) = 1/2\{\Delta\varepsilon(\Lambda_{2L}) + \Delta\varepsilon(\Delta_{2L})\}$$
$$\Delta\varepsilon(\Delta) = 1/2\{\Delta\varepsilon(\Delta_{2L}) - \Delta\varepsilon(\Lambda_{2L})\}$$
$$\Delta\varepsilon(\Lambda) = 1/2\{\Delta\varepsilon(\Lambda_{2L}) - \Delta\varepsilon(\Delta_{2L})\}$$

where $\Delta\varepsilon(\Delta_{2L})$ and $\Delta\varepsilon(\Lambda_{2L})$ are the observed CD for the *Δ* and *Λ* diastereomers, respectively, of the [Co(L-amac)$_2$en]$^+$ or [Co(L-amac)$_2$ox]$^-$ complex, and $\Delta\varepsilon(\Delta)$ and $\Delta\varepsilon(\Lambda)$ the configurational CD, and $\Delta\varepsilon(2L)$ the vicinal CD of the two mol of L-aminoacidato ligands.

The configurational CD curves agree well with the observed ones of the corresponding glycinato isomers, as seen in Figs. 5 and 6. Each configurational curve is quite characteristic of its geometrical structure irrespective of the kind of aminoacidato ligand. This means that the configurational chiralities of these complexes are almost identical regardless of the sub-

Table 3. Observed CD data of [Co(L-amac)$_2$en]$^+$ and [Co(L-amac)$_2$ox]$^-$ complexes

Complex	First band region		Second band region			Ref.
	σ_{ext}[a] ($\Delta\varepsilon_{ext}$)	σ_{ext}[a] ($\Delta\varepsilon_{ext}$)	σ_{ext}[a] ($\Delta\varepsilon_{ext}$)	σ_{ext}[a] ($\Delta\varepsilon_{ext}$)	σ_{ext}[a] ($\Delta\varepsilon_{ext}$)	
Δ-*trans*(*O*)-[Co(L-ala)$_2$en]$^+$	18.3(−2.63)	21.9(−1.40)		27.8(+0.36)		3
Λ-*trans*(*O*)-[Co(L-ala)$_2$en]$^+$	19.2(+2.88)			28.2(−0.74)		3
Δ-*trans*(*O*)-[Co(L-ser)$_2$en]$^+$	18.6(−2.81)	21.3(−1.26)		28.1(+0.51)		3
Λ-*trans*(*O*)-[Co(L-ser)$_2$en]$^+$	18.4(+2.13)	21.9(+0.75)		28.1(−0.30)		3
Λ-C_2-*cis*(*O*)-[Co(L-ala)$_2$en]$^+$	19.5(+4.26)	22.1(−1.07)		29.5(+0.25)		
Δ-C_2-*cis*(*O*)-[Co(L-ser)$_2$en]$^+$	19.7(−3.67)			27.8(+0.33)		3
Λ-C_2-*cis*(*O*)-[Co(L-ser)$_2$en]$^+$	19.5(+3.38)	22.1(−0.83)		29.9(+0.18)		3
Δ-C_1-*cis*-(*O*)-[Co(L-ala)$_2$en]$^+$	19.3(−2.48)		25.9(−0.15)	27.9(+0.09)	30.3(−0.18)	
Λ-C_1-*cis*(*O*)-[Co(L-ala)$_2$en]$^+$	19.1(+2.24)	22.8(−0.04)	25.8(+0.07)	28.2(−0.18)	30.8(+0.06)	
Δ-C_1-*cis*(*O*)-[Co(L-ser)$_2$en]$^+$	19.3(−2.84)		25.8(−0.08)	28.0(+0.24)	30.5(−0.11)	3
Λ-C_1-*cis*(*O*)-[Co(L-ser)$_2$en]$^+$	19.3(+1.64)		26.0(+0.09)	28.1(−0.18)	30.8(+0.08)	3
Δ-*trans*(*N*)-[Co(L-ala)$_2$ox]$^-$	16.6(−1.60)	19.3(−2.30)		26.0(+0.69)	28.9(−0.16)	
Λ-*trans*(*N*)-[Co(L-ala)$_2$ox]$^-$	15.9(+0.68)	18.6(+2.23)		26.4(−0.55)		
Δ-*trans*(*N*)-[Co(L-ser)$_2$ox]$^-$	16.7(−1.79)	19.4(−2.06)		26.0(+0.39)	28.8(−0.19)	2
Λ-*trans*(*N*)-[Co(L-ser)$_2$ox]$^-$	16.7(+0.45)	18.7(+2.08)		26.5(−0.41)		2
Δ-*trans*(*N*)-[Co(L-prol)$_2$ox]$^-$	16.5(−1.64)	19.2(−1.64)		25.8(+1.05)		
Λ-*trans*(*N*)-[Co(L-prol)$_2$ox]$^-$	16.1(−0.23)	18.5(+4.77)		26.2(−0.91)		
Δ-C_2-*cis*(*N*)-[Co(L-ala)$_2$ox]$^-$	18.0(−1.41)			26.1(+0.27)		
Λ-C_2-*cis*(*N*)-[Co(L-ala)$_2$ox]$^-$	18.0(+3.02)	21.3(−0.23)		26.2(−0.35)		
Δ-C_2-*cis*(*N*)-[Co(L-ser)$_2$ox]$^-$	18.2(−2.76)			26.2(+0.42)		2
Λ-C_2-*cis*(*N*)-[Co(L-ser)$_2$ox]$^-$	18.0(+3.24)	22.4(−0.05)		26.1(−0.41)		2
Δ-C_1-*cis*(*N*)-[Co(L-ala)$_2$ox]$^-$	17.6(−2.60)		23.8(−0.11)	26.2(+0.51)	29.2(−0.12)	
Λ-C_1-*cis*(*N*)-[Co(L-ala)$_2$ox]$^-$	18.0(+2.24)		23.9(+0.05)	26.3(−0.36)	29.2(+0.07)	
Δ-C_1-*cis*(*N*)-[Co(L-ser)$_2$ox]$^-$	18.0(−2.91)		24.1(−0.09)	26.3(+0.38)	29.2(−0.08)	2
Λ-C_1-*cis*(*N*)-[Co(L-ser)$_2$ox]$^-$	18.0(+2.46)	21.6(−0.06)	24.2(+0.05)	26.2(−0.33)	29.1(+0.09)	2

a) In the unit of 10^3 cm^{-1}.

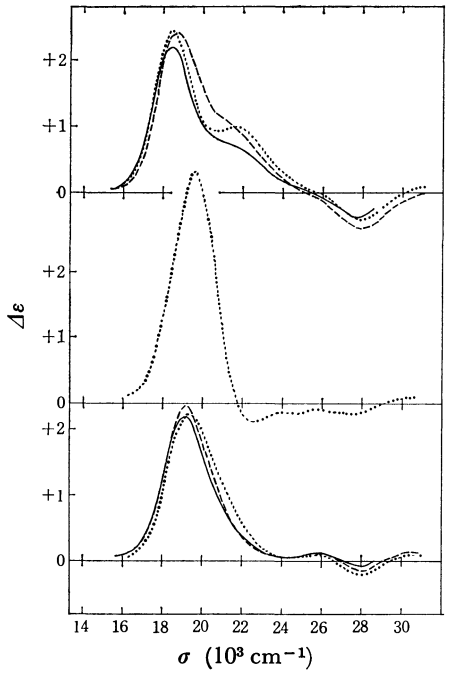

Fig. 5. Configurational CD curves of Λ-[Co(amac)$_2$en]$^+$ for *trans*(*O*) (upper), C_2-*cis*(*O*) (middle) and C_1-*cis*(*O*) (lower) isomers.
——: glycinato complexes (observed curves); ———: L-alaninato complexes (calculated curves); ----: L-serinato complexes (calculated curves).

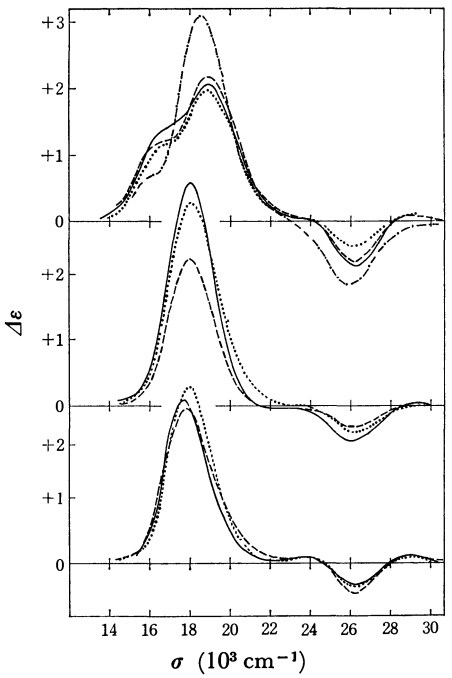

Fig. 6. Configurational CD curves of Λ-[Co(amac)$_2$ox]$^-$ for *trans*(*N*) (upper), C_2-*cis*(*N*) (middle) and C_1-*cis*(*N*) (lower) isomers.
——: glycinato complexes (observed curves); ———: L-alaninato complexes (calculated curves); ----: L-serinato complexes (calculated curves); ————: L-prolinato complex (calculated curves).

stituent on the α carbon atom of the aminoacidato chelate ring. The configurational CD of the *trans* isomers show two bands of the same sign in the first absorption band region. On the other hand, those of the C_2-*cis* and C_1-*cis* isomers show a single main band in this region. A clear difference between the C_2-*cis* and C_1-*cis* isomers appears in the second absorption band region. The C_1-*cis* isomer shows three bands whose signs are positive, negative and positive (for the Λ isomer) from lower energy side, while the C_2-*cis* isomer shows one (or two) negative band (for the Λ isomer), in the second absorption band region. This behavior of the C_1-*cis* and C_2-*cis* isomers is common to both the [Co(amac)$_2$en]$^+$ and [Co(amac)$_2$ox]$^-$ complexes.

Table 4. CD extrema in configurational CD curves of Λ-[Co(amac)$_2$en]$^+$ and Λ-[Co(amac)$_2$ox]$^-$

Complex	First band region		Second band region		
	σ_{ext}[a)]($\Delta\varepsilon_{ext}$)	σ_{ext}[a)]($\Delta\varepsilon_{ext}$)	σ_{ext}[a)]($\Delta\varepsilon_{ext}$)	σ_{ext}[a)]($\Delta\varepsilon_{ext}$)	σ_{ext}[a)]($\Delta\varepsilon_{ext}$)
trans(*O*)-[Co(gly)$_2$en]$^+$	18.4(+2.19)	21.6(+0.64)		27.7(−0.32)	
trans(*O*)-[Co(L-ala)$_2$en]$^+$	18.8(+2.40)	21.2(+1.12)		28.0(−0.54)	
trans(*O*)-[Co(L-ser)$_2$en]$^+$	18.5(+2.44)	21.6(+0.98)		27·9(−0.22)	
C_2-*cis*(*O*)-[Co(L-ser)$_2$en]$^+$	19.6(+3.51)	22.5(−0.30)		27.5(−0.17)	
C_1-*cis*(*O*)-[Co(gly)$_2$en]$^+$	19.0(+2.21)		25.8(+0.11)	27.9(−0.08)	
C_1-*cis*(*O*)-[Co(L-ala)$_2$en]$^+$	19.2(+2.36)		25.6(+0.11)	27.9(−0.13)	30.8(+0.12)
C_1-*cis*(*O*)-[Co(L-ser)$_2$en]$^+$	19.4(+2.24)		25.8(+0.09)	27.9(−0.10)	30.7(+0.09)
trans(*N*)-[Co(gly)$_2$ox]$^-$	16.7(+1.37)	18.8(+2.07)		26.2(−0.69)	
trans(*N*)-[Co(L-ala)$_2$ox]$^-$	16.7(+1.19)	18.9(+2.20)		26.2(−0.61)	29.0(+2.07)
trans(*N*)-[Co(L-ser)$_2$ox]$^-$	16.7(+1.16)	18.9(+1.94)		26.2(−0.40)	
trans(*N*)-[Co(L-prol)$_2$ox]$^-$	16.0(+0.66)	18.5(+3.13)		25.8(−1.98)	
C_2-*cis*(*N*)-[Co(gly)$_2$ox]$^-$	18.0(+3.39)	22.5(−0.04)		26.0(−0.52)	
C_2-*cis*(*N*)-[Co(L-ala)$_2$ox]$^-$	18.0(+2.22)	22.2(−0.03)		26.0(−0.31)	
C_2-*cis*(*N*)-[Co(L-ser)$_2$ox]$^-$	18.0(+3.08)			26.3(−0.42)	
C_1-*cis*(*N*)-[Co(gly)$_2$ox]$^-$	17.7(+2.48)	22.3(+0.04)	23.9(+0.09)	26.3(−0.32)	29.0(+0.10)
C_1-*cis*(*N*)-[Co(L-ala)$_2$ox]$^-$	17.8(+2.36)		23.8(+0.08)	26.3(−0.44)	29.2(+0.09)
C_1-*cis*(*N*)-[Co(L-ser)$_2$ox]$^-$	18.0(+2.68)		23.9(+0.08)	26.3(−0.35)	29.0(+0.09)

a) In the unit of 10^3 cm^{-1}.

The extrema in the calculated configurational CD curves are listed in Table 4. In general, the positions of the CD extrema in the calculated configurational CD curves coincide closely with those of the absorption maxima in the first absorption band region. However, in C_1-*cis* isomers of both types, $[Co(amac)_2en]^+$ and $[Co(amac)_2ox]^-$, the configurational CD extrema are 500—1000 cm^{-1} lower in energy than the absorption maxima.

Vicinal Circular Dichroism. The calculated vicinal CD curves also show systematic patterns characteristic of the geometrical structures, as seen in Fig. 7. The vicinal CD curve of C_2-*cis*(*O*)-$[Co(L\text{-}ala)_2en]^+$ has been drawn by subtracting the configurational curve of Λ-C_2-*cis*(*O*)-$[Co(L\text{-}ser)_2en]^+$ from the observed curve of Λ-C_2-*cis*(*O*)-$[Co(L\text{-}ala)_2en]^+$, because neither Δ-C_2-*cis*(*O*)-$[Co(L\text{-}ala)_2en]^+$ nor optically active C_2-*cis*(*O*)-$[Co(gly)_2en]^+$ has been isolated. The three bands whose signs are negative, positive and negative from lower energy side are observed for the *trans* isomers of $[Co(L\text{-}ala)_2en]^+$, $[Co(L\text{-}ala)_2ox]^-$ and $[Co(L\text{-}ser)_2ox]^-$ complexes. In these three bands, the highest energy band of $[Co(L\text{-}amac)_2en]^+$ and the lowest energy band of $[Co(L\text{-}amac)_2ox]^-$ appeared in the region of the shoulder of the first absorption band. Thus the vicinal CD in these *trans* type complexes, which contain L-aminoacidato ligands, may be summarized as follows: the $A_{2g}(D_{4h})$ transition has a negative CD component and the $E_g(D_{4h})$ splits into two CD components with opposite signs, by lowering the molecular symmetry. Hawkins has proposed an empirical rule for the vicinal effects of aminoacidato ligands: "In tetragonal or rhombic complexes, amino acids with the L configuration impose a negative Cotton effect on the transition with $A_{2g}(D_{4h})$ parentage and give rise to two nondegenerate transitions of opposite sign corresponding to the $E_g(D_{4h})$ band".[9] This is just the case for the present *trans* type complexes. The $E_g(D_{4h})$ component of $[Co(L\text{-}prol)_2ox]^-$ does not appear split. The strong positive intensity of this component may be related to the existence of asymmetric (S) nitrogen atoms of the coordinated L-prolinate ligands.

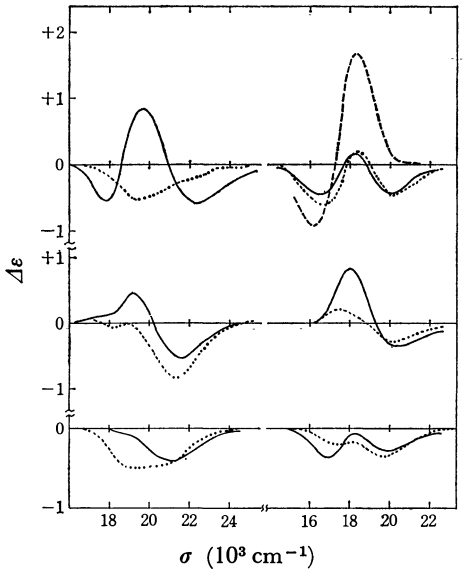

Fig. 7. Vicinal CD curves of $[Co(L\text{-}amac)_2en]^+$ (left) and $[Co(L\text{-}amac)_2ox]^-$ (right), for *trans* (upper), C_2-*cis* (middle) and C_1-*cis* (lower) isomers.
——: L-alaninato complexes; ----: L-serinato complexes; ———: L-prolinato complex.

The vicinal CD curves of the C_2-*cis*(*O*) isomers of $[Co(L\text{-}ala)_2en]^+$, $[Co(L\text{-}ala)_2ox]^-$ and $[Co(L\text{-}ser)_2ox]^-$ have two bands, whose signs are positive and negative from lower energy side, while those of all the C_1-*cis* isomers have two (or one in appearance) negative bands. It is interesting that the same pattern is observed in both types of complex, C_2-*cis*(*O*)-$[Co(L\text{-}amac)_2en]^+$ and C_2-*cis*(*N*)-$[Co(L\text{-}amac)_2ox]^-$, because the order of the energies of their $A_{2g}(D_{4h})$ and $E_g(D_{4h})$ transitions are reversed.

The vicinal CD curves of *trans*(*O*)- and C_2-*cis*(*O*)-$[Co(L\text{-}ser)_2en]^+$ deviate from the ordinary patterns. A molecular model examination indicates that an intramolecular hydrogen-bond is possible for the Λ-isomers of these two complexes: a hydrogen-bond is possible between two L-serinato ligands for the Λ-*trans*(*O*) isomer, and two hydrogen-bonds between an L-serinato and an ethylenediamine ligand for the Λ-C_2-*cis*(*O*) isomer. Such hydrogen-bond interactions may more or less fix the conformation of chelate ring or restrict the internal rotation of the substituent group on the α-carbon atom, and thus be responsible for the anomalous vicinal CD.

References

1) Part II of this series: N. Matsuoka, J. Hidaka, and Y. Shimura, This Bulletin, **40**, 1868 (1967).
2) N. Matsuoka, J. Hidaka, and Y. Shimura, *Inorg. Chem.*, **9**, 719 (1970).
3) N. Matsuoka, J. Hidaka, and Y. Shimura, This Bulletin, **45**, 2491 (1972).
4) J. Hidaka and Y. Shimura, *ibid.*, **40**, 2312 (1967).
5) A. J. McCaffery, S. F. Mason, and B. J. Norman, *J. Chem. Soc.*, **1965**, 5094.
6) J. C. Dabrowiak and D. W. Cooke, *J. Amer. Chem. Soc.*, **92**, 1097 (1970).
7) E. A. Berends and J. G. Brushmiller, *Inorg. Nucl. Chem. Lett.*, **6**, 847 (1970).
8) T. Yasui, J. Hidaka, and Y. Shimura, This Bulletin, **39**, 2417 (1966).
9) C. J. Hawkins, "Absolute Configuration of Metal Complexes," Wiley-Interscience, New York, N. Y. (1971), p. 187.

Magnetic Circular Dichroism of Dicyanobis(2,2′-bipyridine)iron(II)

Hiroshi KOBAYASHI, Badri Vishal AGARWALA,* and Youkoh KAIZU

Department of Chemistry, Tokyo Institute of Technology, Ookayama, Meguro-ku, Tokyo 152

(Received October 19, 1974)

Magnetic circular dichroism (MCD) of *cis*-dicyanobis(2,2′-bipyridine) iron(II) was measured for a variety of solvents. The visible absorption band is assigned to the lowest "iron(II) to bipyridine" charge-transfer transition. The complex exhibits a significant MCD in its lowest charge-transfer absorption band. The transition shows a shift to higher wave number with an increase in the proton-donating power of solvent. This spectral shift is attributed to hydrogen-bonding interactions of protolytic solvent molecules. In H_2SO_4 this dibasic complex is subjected to stepwise protonations. The complex is diamagnetic in protolytic solvents, and even in conc H_2SO_4 the diprotonated complex formed is mostly present in the diamagnetic state.

Schilt has described the mixed-ligand complex of iron(II) with cyanide and 2,2′-bipyridine.[1] The neutral complex $[Fe(CN)_2(2,2'\text{-bipyridine})_2]$ was found to be especially interesting because of its unique property. It gives violet, blue, red, orange and yellow colors depending upon the nature of the solvent. Concentrated sulfuric acid dissolves large amounts without decomposition. The compound shows dibasic character and reacts reversibly with acids to form stable protonated species.[2] $[Fe(2,2'\text{-bipyridine})_3]^{2+}$ is stable against oxidation, but $[Fe(CN)_2(2,2'\text{-bipyridine})_2]$ is rather readily oxidized. It has been employed as nonaqueous acid-base and aqueous oxidation-reduction indicators.[3]

A change between high-spin $^5T_2$ and low-spin $^1A_1$ ground states has been established within the series of *cis*-$[FeX_2(2,2'\text{-bipyridine})_2]$ complexes. Considerable efforts have been achieved in the synthesis and physical measurements of the complexes with ligands X covering a wide range of ligand field strengths.[4] Only when X=CN, a stable diamagnetic complex is obtained. In the present work, the magnetic circular dichroism (MCD) spectra of *cis*-$[Fe(CN)_2(2,2'\text{-bipyridine})_2]$ (abbreviated to $[Fe(CN)_2(bipy)_2]$) in a variety of solvents were measured for understanding of the lowest electronic excitations.

Experimental

Materials. *cis*-Dicyanobis(2,2′-bipyridine)iron(II) trihydrate was prepared by the method of Schilt[1] and identified by elemental analysis.

Found: C, 55.66; H, 4.44; N, 17.37%. Calcd for $C_{22}H_{16}N_6Fe\cdot 3H_2O$: C, 55.70; H, 4.68; N, 17.72%. By means of Sasse's method, 4,4′-dimethyl- and 5,5′-dimethyl-2,2′-bipyridine (abbreviated to 4 dmbip and 5 dmbip, respectively) were prepared.[5,6] The dimethyl bipyridine analogs of dicyanobis(2,2′-bipyridine)iron(II) were also prepared by the method of Schilt:[1]

Found: C, 63.30, H, 5.24, N, 16.96%. Calcd for $C_{26}H_{24}N_6$ (4 dmbip) $Fe\cdot H_2O$: C, 63.17; H, 5.30; N, 17.00%.

Found: C, 59.12; H, 5.28; N, 15.93%. Calcd for $C_{26}H_{24}N_6$ (5 dmbip) $Fe\cdot 3H_2O$: C, 58.88; H, 5.70; N, 15.85%. The 4 dmbip complex was dried over silicagel prior to the elemental analysis.

All solvents including C_2H_5OH and $CHCl_3$ were commercially available and purified by distillation except H_2SO_4.

Measurements. MCD spectra were recorded on a JASCO ORD/UV-5 spectropolarimeter with its CD attachment and electromagnet. The measurement technique had been described earlier.[7] The magnetic field was set at 10,000 G. The visible and ultraviolet absorption spectra were taken on a Shimadzu automatic recording spectrophotometer Model MPS-50. The NMR spectra were taken on a 60 MHz Varian T-60 NMR spectrometer using sodium 2,2-dimethyl-2-silapentane-5-sulfonate (DSS) as an internal standard.

Results and Discussion

The MCD and absorption spectra of $[Fe(CN)_2(bipy)_2]$ in $CHCl_3$, C_2H_5OH, H_2O and H_2SO_4 are shown in Figs. 1 and 2. The prominent maxima are summarized in Table 1. The electronic transitions which give rise to the MCD extrema and absorption maxima in 15000—30000 cm^{-1} are assigned to the lowest "iron to bipyridine" charge-transfer excitations. The lowest wave number absorption peak exhibits a blue shift in the order bipy<4 dmbip<5 dmbip and the second peak shows a blue shift in the order 4 dmbip<5 dmbip≤bipy. Such spectral shifts for the dimethyl substitutions in coordinated bipyridine have been observed in the lowest and the second "metal to

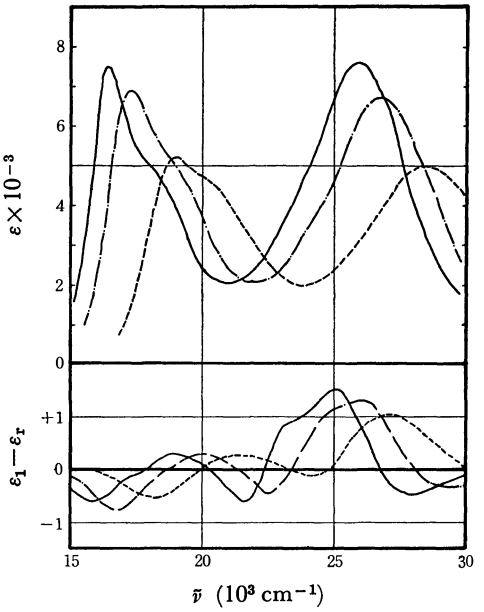

Fig. 1. The MCD and absoption spectra of $[Fe(CN)_2(bipy)_2]$.
——; in $CHCl_3$, —·—·; in C_2H_5OH, ----; in H_2O.

* A UNESCO fellow from the Department of Chemistry, University of Allahabad, Allahabad, India.

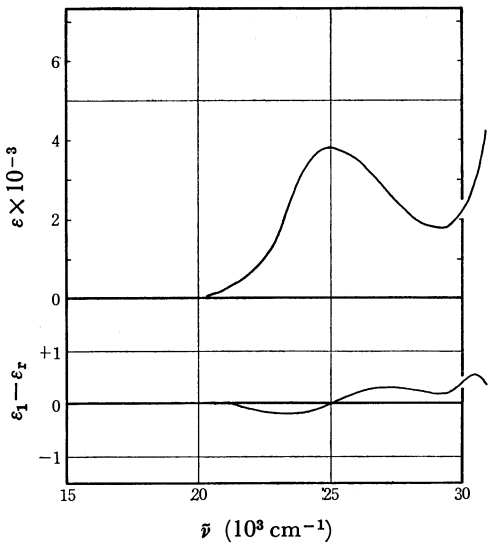

Fig. 2. The MCD and absorption spectra of $[Fe(CN)_2(bipy)_2]$ in 18 M H_2SO_4.

bipyridine" charge-transfer excitations in 2,2'-bipyridine tetracarbonylchromium, -molybdenum, and -wolfram.[8] The ultraviolet peak shows a shift for dimethyl substitutions in the order 5 dmbip<bipy≤4 dmbip. This indicates that the ultraviolet peak arises from the lowest (π, π^*) excitation in coordinated bipyridine.[8]

The nature of MCD and absorption spectra does not change in different solvents. However a shift observed in different solvents should be noted. With an increase in the proton-donating power of solvent, the absorption band shifts to higher wave number : chloroform<ethanol<water. Figure 3 shows a linear relationship obtained between the first and second absorption peaks for a variety of proton-donating power

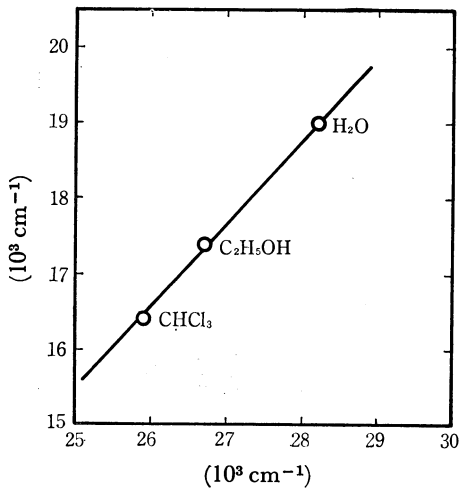

Fig. 3. A linear relationship between the first and second charge-transfer bands.

of solvents. In a protolytic solvent, a hydrogen-bonding interaction of the solvent molecules arises on coordinated cyano groups. The coordinated cyano group is a σ-donor but a π-acceptor. The iron dπ electrons even in the ground state migrate into the lowest vacant π^* molecular orbitals which delocalize not only over coordinated bipyridines but also over coordinated cyano groups. Thus the hydrogen-bonding interaction of protolytic solvent molecules with coordinated cyano groups encourages the migration of iron dπ electrons into the coordinated cyano groups. This gives rise to a blue-shift of the "iron to bipyridine" charge-transfer excitations in protolytic solvents. In conc H_2SO_4, the lowest wave number absorption peak appears at 25000 cm^{-1}. This blue-shift, however, should be attributed to the protonations in conc H_2SO_4 since the effect is greater than expected for the hy-

Table 1. The MCD and absorption data

Solvent		Absorption peaks (10^3 cm^{-1})		MCD extrema (10^3 cm^{-1})
	I	16.5	Ia	15.8
$CHCl_3$	II	25.9	Ib	19.0
	III	33.0	IIa	21.5
	IV	40.0	IIb	25.0
			IIIa	28.0
	I	17.4		16.9
C_2H_5OH	II	26.7		20.0
	III	33.2		22.5
	IV	40.2		26.0
				30.0
	I	19.1		18.3
H_2O	II	28.4		21.5
	III	33.5		24.3
	IV	40.6		27.2
				31.5
	I	25.1		23.3
18 M H_2SO_4	II	35.0		27.2
	IV	41.0		30.4

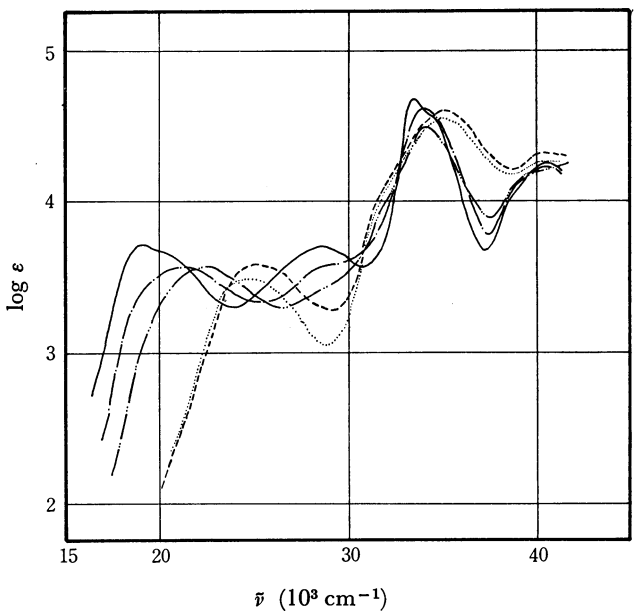

Fig. 4. The absorption spectra of $[Fe(CN)_2(bipy)_2]$ as a function of the concentration of H_2SO_4.
——: H_2O, —·—·: 1.8 M H_2SO_4, —··—··: 3.6 M H_2SO_4, ·····: 9 M H_2SO_4, ----: 18 M H_2SO_4.

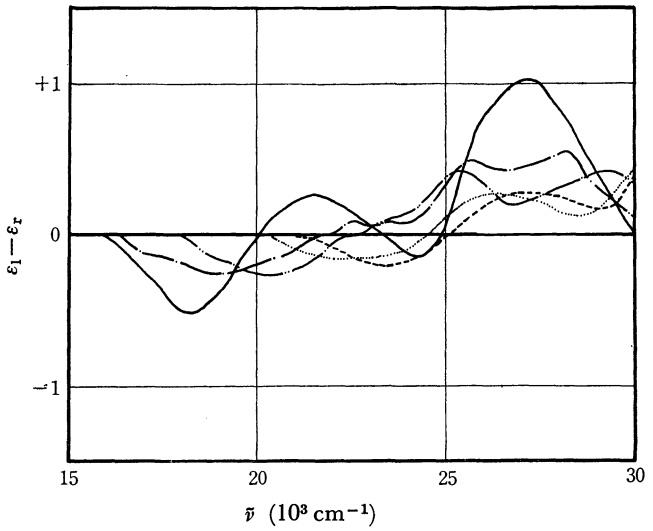

Fig. 5. The MCD spectra of $[Fe(CN)_2(bipy)_2]$ as a function of the concentration of H_2SO_4.
——: H_2O, —·—·: 1.8 M H_2SO_4, —··—··: 3.6 M H_2SO_4, ·····: 9 M H_2SO_4, ----: 18 M H_2SO_4.

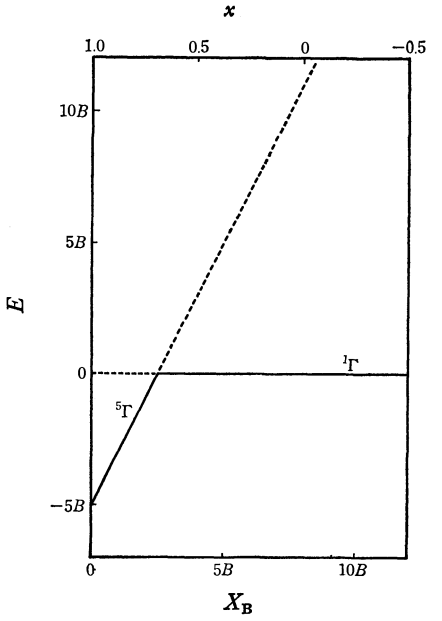

Fig. 6. The energy diagram of the ground state of $[FeX_2(bipy)_2]$.
$X_B=X_A-x\Delta/3=(1-x)X_A$ $\quad X_A=8B$

drogen-bonding interactions in protolytic solvents. Hamer and Orgel have suggested the protonation of the complex in conc H_2SO_4.[9] The MCD and absorption spectra measured for a variety of concentrations of H_2SO_4 in solution are presented in Figs. 4 and 5. These stepwise spectral changes for an increase in the concentration of H_2SO_4 indicate the stepwise protonation toward two coordinated cyano groups. The straight line with a slope of 1.00 in Fig. 3 predicts the second peak in conc H_2SO_4 at 34200 cm^{-1} for the first peak at 25000 cm^{-1}. Since the second band as well as the first band is not so intense as the bipyridine (π, π^*) band, the second band of the complex in conc H_2SO_4 must be present beneath the ligand (π,π^*) band.

The energy of the ground state of *cis*-$[FeA_4B_2]$ complex is given as follows:

$^5\Gamma(^5T_2$ in Oh symmetry: $(xy)^2(yz)(zx)(z^2)(x^2-y^2))$
$2\{\Delta-(X_A-X_B)\}+15A-35B+7C$
$^1\Gamma_1(^1A_1$ in Oh symmetry: $(xy)^2(yz)^2(zx)^2)$
$15A-30B+15C$,

where Δ is the cubic ligand field parameter of $[FeA_6]$, (X_A-X_B) is a correction for the ligand field of ligand B at *cis*-positions (X_B is defined as a one third of the cubic ligand field parameter of $[FeB_6]$ as well as $X_A=\Delta/3$), and A, B, and C are Racah's interelectronic electrostatic energy parameters. Provided that $3(X_A-X_B)=x\Delta$ and $4B=C$, an energy difference between the quintet and singlet ground states is given by $2(1-x/3)\Delta-37B$. Since the ground state of $[Fe(bipy)_3]^{2+}$ ($x=0$) is singlet, $\Delta>(37/2)B$. In fact, the d-d transition $^3T_1\leftarrow{}^1A_1(\Delta-12B)$ in $[Fe(bipy)_3]^{2+}$ is observed at 12000 cm^{-1},[10] which indicates that $\Delta=24B$ if $B=1000$ cm^{-1}. The energy diagram of the ground state of $[FeA_4B_2]$ is shown in Fig. 6. When the value of x increases, the ligand field of B decreases. For high values of x, the ground state of $[FeA_4B_2]$ should be quintet even for a fairly high value of Δ which gives the singlet ground state for $[FeA_6]$. In fact, the ground states of $[FeX_2(bipy)_2]$ are mostly quintet, whereas the ground

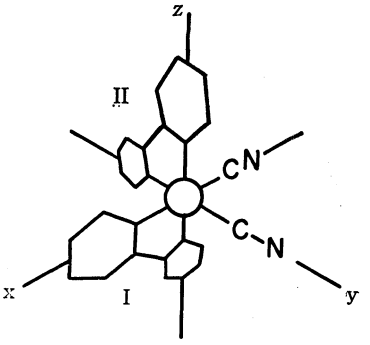

Fig. 7. Molecular coordinate.

state of $[Fe(bipy)_3]^{2+}$ is singlet.[4] A decrease in x, which is revealed by a greater value of Δ in $[Fe(CN)_6]^{4-}$, gives rise to diamagnetic $[Fe(CN)_2(bipy)_2]$. The vacant antibonding π^* orbitals of coordinated bipyridines and cyano groups accept iron $d\pi$ electrons, and thus an enhancement of the ligand field splitting in diamagnetic $[Fe(CN)_2(bipy)_2]$ should be attributed partly to the back-donation effect. The back donation also gives rise to a splitting in $d\pi$ orbitals: d_{xy} is a little more stabilized than d_{yz} and d_{zx} orbitals in $[Fe(CN)_2(bipy)_2]$ (Fig. 7).

The lowest "metal to bipyridine" charge-transfer transitions borrow their intensity from the allowed (π, π^*) transitions localized in coordinated bipyridines I and II, $1/\sqrt{2}\{(j\rightarrow k)_I\pm(j\rightarrow k)_{II}\}$.[11] Among possible six charge-transfer excitations $d\pi\rightarrow k_I$, k_{II}, $1/\sqrt{2}\{(xy\rightarrow k_I)\pm(xy\rightarrow k_{II})\}$ and $1/\sqrt{2}\{(yz\rightarrow k_I)\pm(zx\rightarrow k_{II})\}$ can borrow the intensity. Since d_{xy} orbital is lower than d_{yz} and d_{zx} orbitals, the charge-transfer transitions arising from the d_{xy} orbital must be in a wave number higher than those from the d_{yz} and d_{zx} orbitals. The MCD spectra indicate separate four B peaks with alternating sign corresponding to two components of the charge-

transfer transitions to the lowest and the second lowest vacant π^* orbitals. Since the plus and minus combinations in $1/\sqrt{2}\{(xy\rightarrow k_I)\pm(xy\rightarrow k_{II})\}$ and $1/\sqrt{2}\{(yz\rightarrow k_I)\pm(zx\rightarrow k_{II})\}$ form a degenerate pair, an *A*-term dispersion is expected in the corresponding absorption peak. However the expectation value of angular momentum between the wave functions within the degenerate pair is vanished and thus the *A*-term dispersion does not appear. On the other hand, a non-zero value of angular momentum comes out between the wave functions of different degenerate pairs and gives rise to a magnetic-field induced mixing between different degenerate excited states.[12,13] The MCD spectra thus exhibit *B*-term extrema with alternating sign.

The blue shift of the lowest charge-transfer transitions in conc H_2SO_4 is as great as 5000 cm^{-1}. This spectral blue shift is attributed to protonation rather than hydrogen-bonding. Since the character of the lowest charge-transfer transition is still conserved even in conc H_2SO_4, the complex is mostly in the diamagnetic state. The ionization potential of $d\pi$ orbitals is dependent upon the spin state of iron(II) in complex. The values given in Table 2 were obtained by the procedure described in Griffith's book.[14] In the high spin state, only an electron pair in d_{xy} orbital shows a higher tendency of back donation. In the diamagnetic state, all $d\pi$ electrons equally show an enhanced tendency of back donation. If a change of the spin state of the complex comes out upon protonation, the charge-transfer transition should exhibit a more drastic red shift or blue shift since the ionization potential of $d\pi$ electrons in the high spin state is very different (more than 10000 cm^{-1}) from the corresponding ionization potential of diamagnetic iron(II) as shown in Table 2. The spectral intensity of the complex in conc H_2SO_4 is almost reproducible within experimental error, however, the spectral intensity depends on somewhat how to prepare the solution. The high spin complex must be labile, and thus the high spin species, if it is formed upon protonation, suddenly dissociates ligands and/or is oxidized. The NMR spectrum of the complex in conc H_2SO_4 shows, in fact, a significant line broadening which indicates the presence of some high spin species. One of the authors (B.V.A.) wishes to express his gratitude to the Japanese Government for a UNESCO fellowship.

TABLE 2. THE $d\pi$ IONIZATION POTENTIALS

$^1A_1$	
$(xy)^2(yz)^2(zx)^2 \rightarrow (xy)(yz)^2(zx)^2$	$\Phi - 10B$
$^5T_2$	
$(xy)^2(yz)(zx)(z^2)(x^2-y^2)$	
$\rightarrow (xy)(yz)(zx)(z^2)(x^2-y^2)$	$\Phi - 28B$
$(xy)^2(yz)(zx)(z^2)(x^2-y^2)$	
$\rightarrow (xy)^2(yz)(z^2)(x^2-y^2)$	$\Phi + 12B$

References

1) A. A. Schilt, *J. Amer. Chem. Soc.*, **82**, 3000 (1960).
2) A. A. Schilt, *ibid.*, **82**, 5779 (1960); *ibid.*, **85**, 904 (1963).
3) A. A. Schilt, *Anal. Chim. Acta*, **26**, 134 (1962).
4) E. König, *Coord. Chem. Rev.*, **3**, 471 (1968).
5) G. M. Badger and W. H. F. Sasse, *J. Chem. Soc.*, **1956**, 616.
6) W. H. F. Sasse and C. P. Whittle, *ibid*, **1961**, 1847.
7) H. Kobayashi, M. Shimizu, and I. Fujita, This Bulletin, **43**, 2335 (1970).
8) Y. Kaizu, I. Fujita, and H. Kobayashi, *Z. Phys. Chem. (N. F.)*, **77**, 298 (1972).
9) N. K. Hamer and L. E. Orgel, *Nature*, **190**, 439 (1961).
10) R. A. Palmer and T. S. Piper, *Inorg. Chem.*, **5**, 864 (1966).
11) I. Hanazaki and S. Nagakura, *ibid.*, **8**, 648 (1969).
12) A. D. Buckingham and P. J. Stephens, *Ann. Rev. Phys. Chem.*, **17**, 399 (1966).
13) P. J. Stephens, *J. Chem. Phys.*, **52**, 3489 (1970).
14) J. S. Griffith, "The Theory of Transition-Metal Ions," Cambridge University Press (1961), p. 100.

Reaction of Cupric Ion Fixed on the Ion Exchange Resin with Acetylacetone

Takashi Okamura, Kunio Ohzeki, and Tomihito Kambara
Department of Chemistry, Faculty of Science, Hokkaido University, Sapporo 060
(Received November 19, 1974)

It was found that the cupric ions fixed on the resin are removed by acetylacetone(Hacac) to form bisacetylacetonatocopper(II), $Cu(acac)_2$. By the addition of a small amount of pyridine-water mixture to the copper(II) form resin in acetylacetone milieu, the cupric ions are quantitatively removed from the resin in the form of pyridine adduct, and the pyridinium ions are adsorbed on to the resin in place of the cupric ions. The reaction was successfully applied to the synthesis of $Cu(acac)_2$.

Recently, the conversion of a metal ion fixed on the ion exchanger to a chelate compound based on the ion exchange reaction in organic medium[1,2] has been studied. Higgins[1] developed the new preparation method of cesium lanthanoids hexafluoroacetylacetonates by treating the rare earth ion fixed on Dowex 50 with 0.4 mol/l of cesium hexafluoroacetylacetonate in 50% ethanol.

The authors[2] have reported the quantitative removal of iron(III) ions fixed on Amberlyst 15 by Hacac with the aid of the addition of a small amount of pyridine-water mixture. In this work, the reaction of the cupric ions fixed on Amberlyst 15 resin with Hacac is investigated and the conditions of the quantitative removal of the cupric ions are discussed. The reaction of Cu(II)-form resin with Hacac is shown by

$$(RSO_3)_2Cu + 2\,Hacac = 2\,RSO_3H + Cu(acac)_2 \qquad (1)$$

where R denotes the resin matrix.

Experimental

Apparatus and Reagents. A Hitachi 356 two-wavelength double beam spectrophotometer with 10-mm cells was used for the absorption measurement. A Hitachi 508 atomic absorption spectrophotometer was used for the copper absorption measurement at 324.8 nm in air-acetylene flame. Acetylacetone and pyridine, both of analytical grade (Wako Pure Chemical Inc.), were used without further purification.

Preparation of Copper(II)-Form Resin. The resin used is the sulfonic acid cation exchanger, Amberlyst 15, with a macroreticular structure. The commercially available Amberlyst 15 is crushed and sieved to a fraction of 60—80 mesh. The resin was converted to Cu(II)-form by treatment with 0.1 mol/l solution of cupric nitrate. The Cu(II)-form resin was washed with water, dried at 110 °C and then stored in a desiccator over phosphorus pentoxide.

Determination of Cupric Ions on the Resin. The cupric ions on the dried Cu(II)-form resin were eluted by 2 mol/l hydrochloric acid solution and determined by EDTA titration. It was found that 3.90 ± 0.13 meq of cupric ions were adsorbed onto 1 g of the dried Cu(II)-form resin.

Water Associated with Cu(II)-form Amberlyst Resin. It was pointed out that the water plays an important role in the reaction of β-diketone with metal ion fixed on the resin,[2] and so it is necessary to determine the water content in the oven-dried cupric form resin. The air-dried H-form resin is weighed in a glass filter and dried at 110 °C in oven until a constant weight, and then the resin is converted into cupric form and washed with deionized water, and the resulting resin is dried at 110 °C until a constant weight. Cupric ions fixed on the resin are eluted by 2 mol/l hydrochloric acid and determined by EDTA titration. The data obtained are summarized in Table 1. The ratio of exchange capacity of cupric ion to proton was 1.03. When the H-form resin is converted to Cu(II)-form, the increase in weight is expected, but as is shown in Table 1, the weight increase is larger than that of copper determined by titration. It may be safe to say that the difference is caused by water coordinated to the copper ion on the resin. Consequently, it is supposed that one molecule of water is coordinated to a copper(II) ion on the resin, such as $(RSO_3)_2Cu\cdot H_2O$.

Reaction of Cu(II)-Form Resin with Hacac. A portion of 3 ml of Hacac was poured onto the 40 mg of dried Cu(II)-form resin in a test tube and shaked by hand for 10 min. at room temperature (around 22 °C). After the filtration, the resin was washed with ethyl alcohol and water. The cupric ions remaining on the resin were eluted by 2 mol/l hydrochloric acid solution, and determined by atomic absorption spectrophotometry.

Results and Discussion

Effect of Pyridine. The reaction of $Cu(acac)_2$ with pyridine(py) has been investigated and the adduct formation of $Cu(acac)_2\cdot py$ has been reported.[3] Upon addition of pyridine to Hacac in contact with Cu(II)-form resins, the color of the solution turned from pale blue to green, indicating the formation of $Cu(acac)_2\cdot py$.

Table 1. Water associated with Cu(II)-form resin

Weight of H-form resin, taken (g)	Weight of resin converted into Cu-form, found (g)	Increase in weight (g)	Cu on resin, found by titration (mmol)	Weight increase calculated[a] (g)	Coordinated water estimated[b] (mmol)	Mole ratio H_2O/Cu
0.8146	0.9667	0.1521	1.83	0.1145	2.09	1.14
0.7366	0.8740	0.1374	1.71	0.1066	1.71	1.00
0.7273	0.8634	0.1361	1.74	0.1089	1.51	0.87

a) Provided that the non-hydrated cupric ion is adsorbed on the resin. b) If two mmol hydrogen ions on the resin are replaced by one mmol copper(II) ion, the increase in resin weight should be $(63.54-1.008\times2)$ mg, provided that no water molecule is coordinated to the cupric ion on the resin.

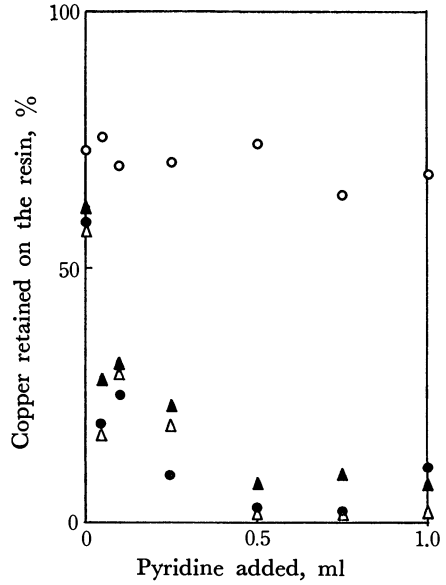

Fig. 1. Effect of pyridine and water.
The pyridine and water were added to 3 ml of Hacac in contact with 40 mg of Cu(II)-form resin. Water added, μl, 0(○), 10(▲), 25(●), 50(△).

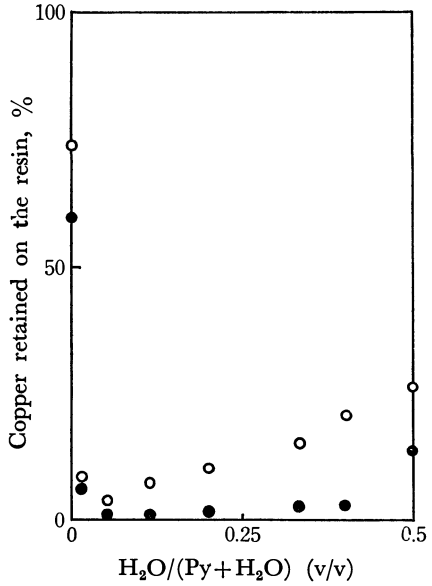

Fig. 2. Effect of the pyridine-water mixture with various ratios on the removal of the copper(II) from 40 mg of the Cu(II)-form resin with 3 ml of Hacac. The pyridine-water mixture added, 0.5 ml (○), 1 ml (●).

Nevertheless, the amount of the copper removed from the resin is hardly affected by the addition of pyridine to Hacac as shown in Fig. 1.

Effect of Pyridine and Water. The separate addition of pyridine or water does not effect remarkably, but the coexistence of them in Hacac is found highly effective for adduct formation, as shown in Fig. 2. More than 99% of copper ions are removed from the resin by addition of *ca.* 30 : 1 pyridine–water mixture to the extent of one-third of the volume of Hacac employed.

The dissociation of the Hacac is accelerated in the presence of pyridine–water mixture as shown by equations (2) and (3).

$$py + H_2O = pyH^+ + OH^- \quad (2)$$

$$Hacac + OH^- = acac^- + H_2O \quad (3)$$

Acetylacetonate anion withdraws the copper ion from the resin and pyridinium ion is adsorbed on the resin instead of monoaqua cupric ion and the resulting $Cu(acac)_2$ coordinates the excess pyridine to form $Cu(acac)_2 \cdot py$. The total reaction can be written as follows.

$$(RSO_3)_2Cu + 2\,Hacac + 3\,py \xrightarrow{H_2O} Cu(acac)_2 \cdot py + 2\,RSO_3Hpy \quad (4)$$

The air-dried Cu(II)-form resin, one gram of which contains 3.64±0.16 meq copper, has an appropriate amount of water, namely, around 10% by weight. Thus, there may occur the reaction shown by equation (4) even without addition of water. The various amounts of pyridine are added to 10 ml of Hacac containing 40 mg of air-dried Cu(II)-form resin. After the reaction, the resin is separated by filtration. The absorbance measurement of the filtrate at 655 nm *vs.* Hacac clearly reveals that the amount of copper liberated from the resin increases with increasing amount of pyridine added, as shown in Fig. 3.

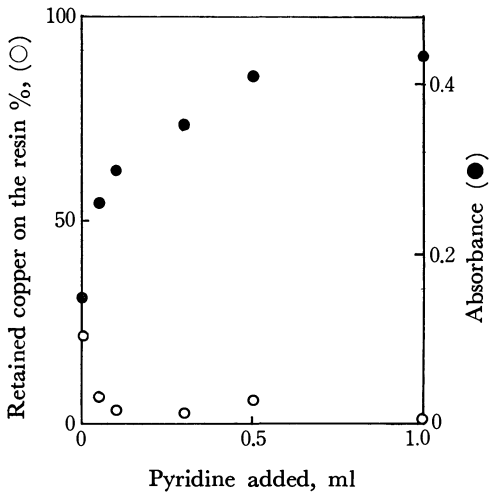

Fig. 3. Effect of pyridine on the air-dried resin.
The absorbance mesurement of the filtrate (●), and copper retained on the resin (○).

Application to the Synthesis of Chelate Compound. Treat 500 mg of air-dried Cu(II)-form resin with 10 ml of Hacac and add 3 ml of pyridine. After the reaction, separate the resin by filtration and wash it with Hacac containing appropriate amount of pyridine until the filtrate shows no color of $Cu(acac)_2 \cdot py$. Boil off the excess Hacac and pyridine by bubbling the nitrogen gas into the filtrate at 130 °C. In the course of this procedure, the adduct $Cu(acac)_2 \cdot py$ is decomposed to $Cu(acac)_2$, which is confirmed by color change of the chelate compound. The crude $Cu(acac)_2$ is purified

by sublimation at 175 °C under 1 mmHg. One obtains 0.209 g of $Cu(acac)_2$ in 85% yield. The result of elementary analysis was: Found: C, 45.84; H, 5.35%. Calcd for $Cu(acac)_2$: C, 45.89; H, 5.39%.

We wish to thank the Ministry of Education for financial support granted to this research.

References

1) C. E. Higgins, *J. Inorg. Nucl. Chem.*, **35**, 1941 (1973).
2) K. Ohzeki, M. Ikeuchi, and T. Kambara, This Bulletin, **48**, 67 (1975).
3) W. R. May and M. M. Jones, *J. Inorg. Nucl. Chem.*, **25**, 507 (1963).

Metal Complexes Containing Six-membered Chelate Rings V. Preparation and Structure of Oxalato Complexes of Cobalt(III) with Substituted 3,7-Diaza-1,9-nonanediamine Derived from 2,4-Pentanediamine[1]

Fujio MIZUKAMI*

Department of Chemistry, Faculty of Science, Tohoku University, Aoba, Aramaki, Sendai 980

(Received July 10, 1974)

The syntheses, resolution and structure of three oxalato complexes of cobalt (III) with tetramine ligand, *R*(4), *R*(6)- and *R*(4), *S*(6)-4,6-dimethyl-1,9-nonanediamine (*RR*- and *RS*-2,3'', 2-tet), and *R*(6), *S*(8)-6,8-dimethyl-2,5,9,12-tetraazatridecane (*N,N'*-Me_2-*RS*-2,3'',2-tet) are reported. Only one geometrical isomer (*cis* β) was isolated for each complex, [Co(ox)(*N,N'*-Me_2-*RS*-2,3,'',2-tet)]$^+$, [Co(ox)(*RS*-2,3'',2-tet)]$^+$ and [Co(ox)(*RR*-2,3'',2-tet)]$^+$. The central six-membered chelate rings of $(-)_{546}$-*cis* β-[Co(ox)(*N,N'*-Me_2-*RS*-2,3'',2-tet]$^+$ and $(-)_{546}$-*cis* β-[Co-(ox)(*RS*-2,3'',2-tet)]$^+$ take a chair conformation with two equatorial methyl groups, and that of $(-)_{546}$-*cis* β-[Co-(ox)(*RR*-2,3'',2-tet)]$^+$ a chair conformation with an axial and equatorial methyl group.

Studies have been carried out on cobalt(III) complexes of 2,4-pentanediamine, a β-diamine with a methyl group on each α-carbon atom of trimethylenediamine.[2-5] Transition metal complexes containing 3,7-diaza-1,9-nonanediamine (2,3,2-tet) were investigated by Hamilton and Alexander and others.[6-14] However, few stereochemical studies have been carried out on the cobalt(III) complexes of tetramine involving a substituted trimethylenediamine part.[15] Complexes of cobalt(III) with 2,3,2-tet derivatives containing 2,4-pentanediamine part were prepared in order to elucidate the correlations between the configuration of asymmetric carbon and nitrogen atom, the conformation of the chelate ring, and the configuration about metal ion.

Only one isomer (*trans*) was isolated for each dichloro complex of cobalt(III) with tetramine ligand, *R*(4), *R*(6)- and *R*(4), *S*(6)-4,6-dimethyl-3,7-diaza-1,9-nonanediamine (*RR*- znd *RS*- 2,3'',2-tet) and *R*(6), *S*(8)-6,8-dimethyl-2,5,9,12-tetraazatridecane (*N,N'*-Me_2-*RS*-2,3'',2-tet).[1] This paper deals with the preparation of *cis* oxalato complexes of cobalt(III) each with tetramine, *N,N'*-Me_2-*RS*-2,3'',2-tet, *RS*-2,3'',2-tet and *RR*-2,3'',2-tet, and their stereochemistry on the basis of CD and PMR spectra.

Experimental

R(4),R(6)-, and *R(4),S(6)-4,6-dimethyl-3,7-diaza-1,9-nonanediamine* (RR-*2,3'',2-tet and* RS-*2,3'',2-tet)* and *R(6),S(8)-6,8-dimethyl-2,5,9,12-tetraazatridecane* (N,N'-*Me_2*-RS-*2,3'',2-tet)*: Prepared according to the method described previously.[1]

trans-[*$CoCl_2$*(RR-*2,3'',2-tet)*]*ClO_4*, trans-[*$CoCl_2$*(RS-*2,3'',2-tet)*]*ClO_4* *and* trans-[*$CoCl_2$*(N,N'-*Me_2*-RS-*2,3'',2-tet)*]*ClO_4*: Prepared according to the reported method.[1]

$(-)_{546}$-cisβ-[*Co(ox)*(RR-*2,3'',2-tet)*]*ClO_4*: A solution containing 0.7 g of *trans*-[$CoCl_2$(*RR*-2,3'',2-tet)]ClO_4 and 0.4 g of sodium oxalate in 40 ml of water was warmed at 65—70 °C for 2 hr. After being cooled to room temperature, the red crystals (I) were filtered off and washed with a small amount of cold water. The filtrate and washing were combined and concentrated to 10 ml in a vacuum desiccator over phosphorus pentoxide. A second crop of red crystals (II) was filtered off and washed with a small amount of cold water. Crystal II was found to be the same as crystal I on the basis of absorption, CD and PMR spectra. The crystals were recrystallized by evaporating the aqueous solution in a vacuum desiccator over phosphorus pentoxide. Yield: 0.6 g. Found: C, 30.44; H, 5.82; N, 12.91%. Calcd for $C_{11}H_{24}N_4ClO_8Co$: C, 30.39; H, 5.56; N, 12.89%.

Racemic-cisβ-[*Co(ox)*(RS-*2,3'',2-tet)*]*$ClO_4 \cdot H_2O$*: This was prepared from *trans*-[$CoCl_2$(*RS*-2,3''-2-tet)]ClO_4 (1.5 g) and sodium oxalate (0.5 g) by a similar method to that for corresponding *RR*-2,3,2-tet complex described above. Yield: 1.15 g. Found: C, 29.17; H, 6.24; N, 12.82%. Calcd for $C_{11}H_{26}N_4ClO_9Co$: C, 29.18; H, 5.79; N, 12.38%.

$(-)_{546}$-cisβ-[*Co(ox)*(RS-*2,3'',2-tet)*]$^+$ *Complex*: To a stirred solution of racemic-*cis*β-[Co(ox)(*RS*-2,3'',2-tet)]$ClO_4 \cdot H_2O$ (1 g) in 100 ml of water at 70 °C was added slowly 0.9 g of sodium hydrogen dibenzoyltartrate in 50 ml of hot water. After *ca.* two hr, the solution was evaporated to 50 ml at 70 °C under reduced pressure and cooled to room temperature. A deposited pink powder was filtered off. The powder was suspended in 50 ml of water at 60 °C, stirred for 30 min, and then filtered off. The insoluble material was treated further twice with warm water in the same way. The residue was dissolved in an appropriate amount of 10% perchloric acid, and gradually evaporated to remove less soluble dibenzoyltartaric acid and racemic-*cis*β-[Co(ox)(*RS*-2,3'',2-tet)]$ClO_4 \cdot H_2O$ which were filtered off occasionally. Evaporation was continued until the ratio of $\Delta\varepsilon$ and ε values of the filtrate became constant. More soluble, optically active, crystalline perchlorate was obtained from the final filtrate. However, it was contaminated with dibenzoyltartaric acid which could not be removed completely. Thus, the quantitative CD curve of $(-)_{546}$-*cis*β-[Co(ox)(*RS*-2,3'',2-tet)]$^+$ was determined by the aid of the ε values of racemate.

Racemic-cisβ-[*Co(ox)*(N,N'-*Me_2*-RS-*2,3'',2-tet)*]*$ClO_4 \cdot H_2O$*: A solution containing 1.2 g of *trans*-[$CoCl_2$(*N,N'*-Me_2-*RS*-2,3'', 2-tet)]ClO_4 and 0.36 g of sodium oxalate was warmed at 70 °C for 6 hr, and filtered while hot. The filtrate was cooled to room temperature and evaporated to 4 ml under reduced pressure in a vacuum desiccator over phosphorus pentoxide. The deposited crystals were filtered off, washed with a small amount of cold water and ethanol, and air-dried. The crystals were recrystallized from a small amount of hot water. Yield: 1.1 g. Found: C, 32.79; H, 6.56; N, 11.41%. Calcd for $C_{13}H_{30}N_4ClO_9Co$: C, 32.48; H, 6.29; N, 11.65%.

$(-)_{546}$- *and* $(+)_{546}$-cisβ-[*Co(ox)*(N,N'-*Me_2*-*RS-2,3'',2-tet)*]-*ClO_4*: Half a gram of racemic-*cis*β-[Co(ox)(*N,N'*-Me_2-2,3'', 2-tet)]$ClO_4 \cdot H_2O$ was dissolved in 70 ml of water at 70 °C. To the solution was added slowly 1 g of sodium hydrogen

* Present Address, National Chemical Laboratory for Industry (Tokyo Kogyo Shikensho), 1-1-5, Honmachi, Shibuya-ku, Tokyo 151.

dibenzoyltartrate in 50 ml of hot water and stirred for 1 hr. After being cooled to room temperature, a pink powder was filtered off to give crude dibenzoyltartrate salt of $(-)_{546}$-isomer. The filtrate was stored to obtain $(+)_{546}$-isomer. The powder dissolved in an appropriate amount of 10% perchloric acid at 65 °C and cooled to room temperature. The deposited crystals of dibenzoyltartaric acid were filtered off and the filtrate was allowed to stand for a while. The crude perchlorate of $(-)_{546}$-isomer was filtered off and recrystallized from water fractionally until the CD showed a constant curve. The filtrate free of pink powder was evaporated to 50 ml at 60 °C. To the solution was added slowly an appropriate amount of 60% perchloric acid and cooled to room temperature. The deposited crystals of dibenzoyltartaric acid were filtered off and the filtrate was allowed to stand for a while. The crude perchlorate of $(+)_{546}$-isomer was filtered off and recrystallized from water fractionally until the CD of $(+)_{546}$-isomer became constant. The pure optically active perchlorate is less soluble in water than the racemate. Found: C, 33.56; H, 6.59; N, 11.78%. Calcd for $C_{11}H_{24}N_4ClO_8Co$: C, 33.74; H, 6.10; N, 12.11%.

Measurements. Visible and ultraviolet absorption spectra were obtained with a Hitachi 124 recording spectrophotometer. The CD curves were recorded with a Model ORD/UV-5 JASCO spectrophtometer with a CD attachment. PMR spectra in D_2O were obtained with a Varian T-60 spectrometer using Na–TMS as an internal standard. The perchlorate salts of $(-)_{546}$-*cisβ*-[Co(ox)(*RR*-2,3″,2-tet)]$^+$ and $(-)_{546}$-*cisβ*-[Co(ox)(*N,N'*-Me_2-*RS*-2,3″,2-tet)]$^+$ were converted into chloride salts by use of the anion exchanger Dowex 1-X4 in chloride form. $(-)_{546}$-*cisβ*-[Co(ox)(*RS*-2,3″,2-tet)]$ClO_4 \cdot H_2O$ was converted into sulphate by treating with potassium sulphate, because of poor solubility of these complexes in D_2O. All the measurements were carried out at room temperature.

Results and Discussion

Structures of Complexes. Two geometrical isomers are possible for the oxalatotetramine complexes of cobalt(III). In the present study, however, only one could be isolated for [Co(ox)(*N,N'*-Me_2-*RS*-2,3″,2-tet)]$^+$, [Co(ox)(*RS*-2,3″,2-tet)]$^+$, and [Co(ox)(*RR*-2,3″,2-tet)]$^+$. Each complex was fractionally crystallized as a perchlorate salt, all the fractions being spectrophotometrically identical and giving the same pattern in the PMR spectra. Accordingly, the geometrical configuration for [Co(ox)(*N,N'*-Me_2-*RS*-2,3″,2-tet)]$^+$, [Co(ox)(*RS*-2,3″,2-tet)]$^+$ and [Co(ox)(*RR*-2,3″,2-tet)]$^+$ should be assigned to *cisα* or *cisβ*.

For [Co(ox)(*N,N'*-Me_2-*RS*-2,3″,2-tet)]$^+$, molecular models indicate that *cisα* isomer is a less stable form than *cisβ* in which the two *C*-methyl groups locate in the equatorial orientation and the central chelate ring takes a chair conformation (Table 1). For the *cisβ* form, four isomers can exist with respect to the orientation of the two *N*-methyl groups. Of the isomers, the form in which one methyl group on the in-plane nitrogen atom takes an axial orientation to the terminal five-membered chelate ring and the other on the out-plane nitrogen atom exists in an equatorial position to another terminal five-membered chelate ring, seems to involve smaller steric interaction than the other forms. Accordingly, [Co(ox)(*N,N'*-Me_2-*RS*-2,3″,2-tet)]$^+$ seems to be assigned to an enantiomeric pair of the structure (Fig. 1-a). The PMR spectrum of $(-)_{546}$-[Co(ox)(*N,N'*-Me_2-*RS*-2,3″,2-tet)]$^+$ is consistent with this assignment since two doublets at 1.2—2.2 ppm and two singlets at 2.2 ppm and 3.2 ppm are assigned to two kinds of *C*-methyl group and two kinds of *N*-methyl group, respectively (Fig. 3-b).

Table 1. Conformations of 2,4-pentanediamine part in tetramines

Ligand	Conformation		
	Chair	δ-skew-boat	λ-skew-boat
RR-2,3″,2-tet	a, e	a, a	e, e
RS-2,3″,2-tet	a, a e, e	a, e	a, e
N,N'-Me_2-*RS*-2,3″,2-tet	a, a e, e	a, e	a, e

a: methyl axial e: methyl equatorial.

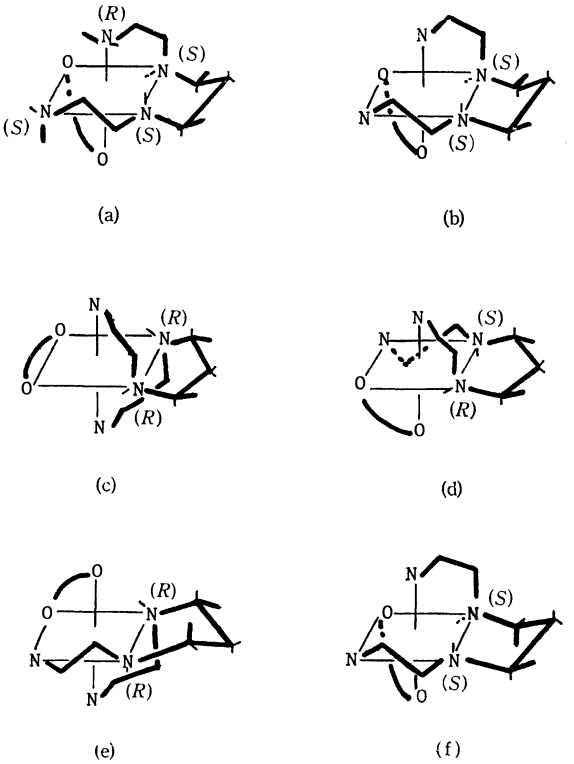

Fig. 1. Schematic structures of *cis*-[Co(ox)(2,3″,2-tet)]$^+$
(a) *Λ-cisβ-N(S),N(S),N(S),N(R)*-[Co(ox)(*N,N'*-Me_2-*RS*-2,3″,2-tet)]$^+$
(b) *Λ-cisβ-N(S),N(S)*-[Co(ox)(*RS*-2,3″,2-tet)]$^+$
(c) *Λ-cisα-N(R),N(R)*-[Co(ox)(*RR*-2,3″,2-tet)]$^+$
(d) *Λ-cisβ-N(R),N(S)*-[Co(ox)(*RR*-2,3″,2-tet)]$^+$
(e) *Λ-cisβ-N(R),N(R)*-[Co(ox)(*RR*-2,3″,2-tet)]$^+$
(f) *Λ-cisβ-N(S),N(S)*-[Co(ox)(*RR*-2,3″,2-tet)]$^+$

The CD spectra of the complexes prepared here are similar to the spectrum of $(+)_{546}$-*cisβ*-[Co(ox)(2,3,2-tet)]$^+$ which is assiged *Λ* configuration and in which the central six-membered chelate ring takes a chair conformation[9–11] (Fig. 2, Table 2). Similarity between the CD spectra of the four complexes strongly suggests that these complexes belong to the same chilarity. Thus, $(-)_{546}$-[Co(ox)(*N,N'*-Me_2-*RS*-2,3″,2-tet)]$^+$ should be assigned to the structure, *Λ-cisβ-N(S), N(S), N(S), N(R)*-[(*δ-gauche*)(chair)(*δ-gauche*)] (Fig.

Table 2. Numerical data of absorption (AB) and circular dichroism (CD) $\tilde{\nu}$ in $10^3\,cm^{-1}$, (log ε) and ($\varepsilon_l-\varepsilon_r$)

Complex	AB	CD
$(-)_{546}$-*cisβ*-[Co(ox)(*RR*-2,3″,2-tet)]ClO_4	19.80(2.16)	18.42 (+2.34)
		20.62 (−1.27)
	27.55(2.24)	*ca.* 25.97 (+0.27)
		28.41 (+0.43)
		32.26 (−0.03)
	43.10(4.39)	39.06 (+3.44)
		46.08(−22.39)
$(-)_{546}$-*cisβ*-[Co(ox)(*RS*-2,3″,2-tet)]$ClO_4\cdot H_2O$	10.92(2.12)	18.48 (+1.68)
		20.75 (−0.90)
		25.64 (+0.04)
	28.09(2.27)	28.99 (+0.23)
	42.55(4.34)	
$(-)_{546}$-*cisβ*-[Co(ox)(*N,N′*-Me_2-*RS*-2,3″,2-tet)]ClO_4	19.23(2.08)	18.18 (+1.56)
		20.20 (−0.84)
	26.95(2.22)	25.00 (+0.10)
		28.17 (+0.07)
		32.79 (−0.19)
		36.50 (+0.83)
	41.15(4.38)	45.05(−19.33)

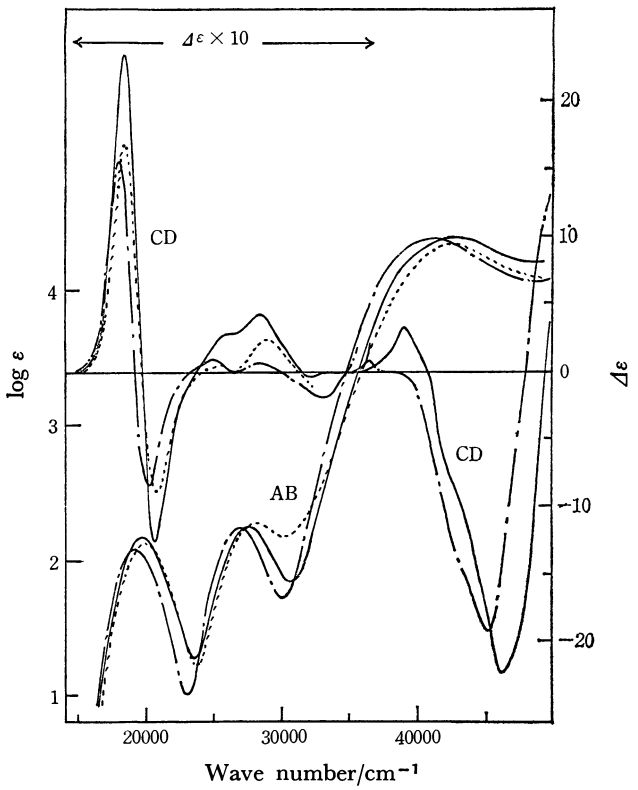

Fig. 2. Absorption (AB) and CD spectra of
(——) $(-)_{546}$-*cisβ*-[Co(ox)(*RR*-2,3″,2-tet)]ClO_4
(----) $(-)_{546}$-*cisβ*-[Co(ox)(*RS*-2,3″,2-tet)]$ClO_4\cdot H_2O$
(—·—) $(-)_{546}$-*cisβ*-[Co(ox)(*N,N′*-Me_2-*RS*-2,3″,2-tet)]-ClO_4 in H_2O.

l-a). This was substantiated by X-ray analysis of the crystalline $(-)_{546}$-[Co(ox)(*N,N′*-Me_2-*RS*-2,3″,2-tet)]ClO_4.[16]

$(-)_{546}$-[Co(ox)(*RS*-2,3″,2-tet)]$^+$ gives a CD curve similar to that of *Λ*-$(-)_{546}$-*cisβ*-[Co(ox)(*N,N′*-Me_2-*RS*-2,3″,2-tet)]$^+$ (Fig. 2). The *RS*-2,4-pentadiamine part of *RS*-2,3″,2-tet tends to take a chair conformation in the complex of cobalt(III) because of the steric regulation coming from the methyl groups in the six-membered chelate ring (Table 1).[1-5] The PMR spectrum of $(-)_{546}$-[Co(ox)(*RS*-2,3″,2-tet)]$^+$ is shown in Fig. 3-a. Two doublets at 1.4 ppm are assigned to two kinds of methyl signal. This seems to support the view that [Co(ox)(*RS*-2,3″,2-tet)]$^+$ takes *cisβ* configuration. Thus, $(-)_{546}$-[Co(ox)(*RS*-2,3″,2-tet)]$^+$ is assigned to the structure, *Λ-cisβ-N(S)*, *N(S)*-[(*δ-gauche*)(chair)-(*δ-gauche*)] (Fig. 1-b).

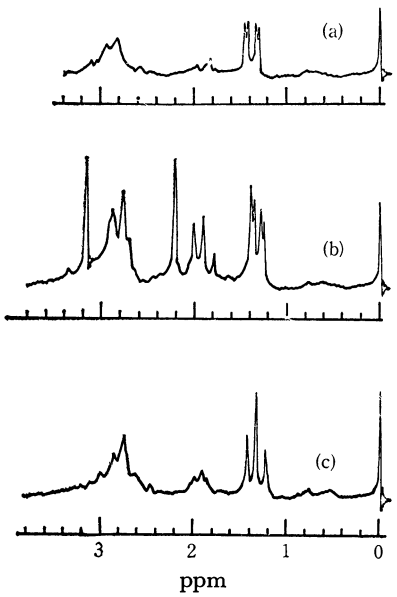

Fig. 3. PMR spectra of
(a) $(-)_{546}$-*cisβ*-[Co(ox)(*RS*-2,3″,2-tet)]$_2SO_4$
(b) $(-)_{546}$-*cisβ*-[Co(ox)(*N,N′*-Me_2-*RS*-2,3″,2-tet)]Cl
(c) $(-)_{546}$-*cisβ*-[Co(ox)(*RR*-2,3″,2-tet)]Cl in D_2O.

For the complex of $(-)_{546}$-[Co(ox)(*RR*-2,3″,2-tet)]$^+$, the central six-membered chelate ring adopts *λ* skew-boat conformation (Table 1) as long as the two methyl groups locate in the equatorial orientation. In this case, the probable structure of $(-)_{546}$-[Co(ox)(*RR*-2,3″,2-tet)]$^+$ are *Λ-cisβ-N(R)*, *N(S)* and *Λ-cis α-N(R)*, *N(R)* form (Figs. 1-c and 1-d). In the former structure, the two methyl groups are non-equivalent to each other, whereas, in the latter structure, they are equivalent to each other. If the central six-membered chelate ring forms a chair conformation, one methyl group locates in the equatorial orientation and the other takes axial position (Table 1). In this case, both structures *Λ-cisβ-N(R)*, *N(R)* and *Λ-cisβ-N(S)*, *N(S)* are possible for [Co(ox)(*RR*-2,3″,2-tet)]$^+$ (Figs. 1-e and 1-f). In these structure, the two methyl groups are non-equivalent to each other.

The CD spectrum of $(-)_{546}$-[Co(ox)(*RR*-2,3″,2-tet)]$^+$ is similar to that of *Λ*-$(-)_{546}$-*cisβ*-[Co(ox)(*N,N′*-Me_2-

RS-2,3″,2-tet)]$^+$ whose absolute configuration was determined by the X-ray method (Fig. 2).[16] Thus, [Co(ox)(*RR*-2,3″,2-tet)]$^+$ should be assigned to *Λ-cisα-N(R)*, *N(R)* or *Λ-cisβ-N(S)*, *N(S)* structure. The PMR spectrum of $(-)_{546}$-[Co(ox)(*RR*-2,3″,2-tet)]$^+$ gives a triplet signal which seems to be an accidental overlapping of two doublet signals due to the two methyl groups (Fig. 3-c). Thus, $(-)_{546}$-[Co(ox)(*RR*-2,3″,2-tet)]$^+$ is assigned to the structure, *Λ-cisβ-N(S)*, *N(S)*-[(*δ-gauche*)(chair)(*δ-gauche*)] (Fig. 1-f). The validity of this assignment was established by the X-ray method.[17]

The [Co(ox)(*RR*-2,3″,2-tet)]$^+$ was prepared by the reaction of $[Co(ox)_3]^{3-}$ and *RR*-2,3″,2-tet. The obtained crystals also have *Λ*-$(-)_{546}$-*cisβ-N(S)*, *N(S)* form as assigned above. These results lead to the conclusion that the *Λ*-$(-)_{546}$-*cisβ-N(S),N(S)* -[Co(ox)(*RR*-2,3″,2-tet)]$^+$ could be prepared stereospecifically.

Absorption Spectra. The absorption spectra of three oxalatotetramine cobalt(III) complexes are compared in Table 2 and Fig. 2. The absorption bands including the first and second band are shifted from longer to shorter wavelength, *i.e.* in the order $(-)_{546}$-*cisβ*-[Co(ox)(*N,N′*-Me_2-*RS*-2,3″,2-tet)]$^+$ $(-)_{546}$-*cisβ*-[Co(ox)(*RR*-2,3″,2-tet)]$^+$ and $(-)_{546}$-*cisβ*-[Co(ox)(*RS*-2,3″,2-tet)]$^+$. This is in line with the fact that the absorption bands of *trans*-[$CoCl_2$(*N,N′*-Me_2-*RS*-2,3″,2-tet)]$^+$ are shifted to longer wavelength compared with those *trans*-[$CoCl_2$(*RR*-2,3″,2-tet)]$^+$ and *trans*-[$CoCl_2$(*RS*-2,3″,2-tet)]$^+$.[1] At present, it is difficult to explain why the absorption bands of $(-)_{546}$-*cisβ*-[Co(ox)(*RR*-2,3″,2-tet)]$^+$ are shifted to longer wavelength than those of $(-)_{546}$-*cisβ*-[Co(ox)(*RS*-2,3″,2-tet)]$^+$. However, this result seems to be related to the structural stabilities of these complexes, since *Λ*-$(-)_{546}$-*cisβ-N(S)*, *N(S)*-[Co(ox)(*RR*-2,3″,2-tet)]$^+$ with an axial and equatorial methyl group is less stable than *Λ*-$(-)_{546}$-*cisβ-N(S)*, *N(S)*-[Co(ox)-(*RS*-2,3″,2-tet)]$^+$ with two equatorial methyl groups.

The author thanks Drs. S. Yano and M. Saburi for their valuable suggestions. Expenses for the work were defrayed by a grant-in-aid from the Ministry of Education.

References

1) Part IV of this series, F. Mizukami, This Bulletin, in press.
2) F. Mizukami, H. Ito, J. Fujita, and K. Saito, This Bulletin, **44**, 3051 (1971).
3) F. Mizukami, H. Ito, J. Fujita, and K. Saito, *ibid.*, **45**, 2129 (1972).
4) F. Mizukami, H. Ito, J. Fujita, and K. Saito, *ibid.*, **46**, 2410 (1973).
5) A. Kobayashi, F. Marumo, Y. Saito, J. Fujita, and F. Mizukami, *Inorg. Nucl. Chem. Lett.*, **7**, 777 (1971).
6) H. G. Hamilton, Jr. and M. D. Alexander, *Inorg. Chem.*, **5**, 2060 (1966).
7) H. G. Hamilton, Jr. and M. D. Alexander, *J. Amer. Chem. Soc.*, **89**, 5066 (1967).
8) P. C. Harrington, S. Linke, and M. D. Alexander, *Inorg. Chem.*, **12**, 168 (1973).
9) G. R. Brubaker and D. P. Schaefer, *ibid.*, **9**, 2372 (1970).
10) G. R. Brubaker and D. P. Schaefer, *ibid.*, **10**, 811 (1971).
11) G. R. Brubaker and D. P. Schaefer, *ibid.*, **10**, 968 (1971).
12) G. R. Brubaker and D. P. Schaefer, *ibid.*, **10**, 2170 (1971).
13) B. Bosnich, R. D. Gillard, E. D. McKenzie, and G. A. Webb, *J. Chem. Soc. A*, **1966**, 1331.
14) R. Niththyananthan and M. L. Tobe, *Inorg. Chem.*, **8**, 1589 (1969).
15) L. J. DeHayes, M. Parris, and D. H. Busch, *Chem. Commun.*, **1971**, 1398.
16) S. Yano, K. Furuhashi, and S. Yoshikawa, presented at the 23rd Symposium on Coordination Chemistry, Fukuoka, Japan, October 16—18 (1973).
17) S. Yano, A. Fujioka and S. Yoshikawa, presented at the 24th Symposium on Coordination Chemistry, Kanazawa, Japan, October 7—9 (1974).

Photochemical Deuteration of *ortho*-Substituted *N*-(Diphenylmethylene)acetamides[1]

Masaru SAEKI, Naoki TOSHIMA, and Hidefumi HIRAI
Department of Industrial Chemistry, Faculty of Engineering
The University of Tokyo, Hongo, Bunkyo-ku, Tokyo 113
(Received April 15, 1974)

The alkyl hydrogens of *N*-(2-alkyldiphenylmethylene)acetamides were found to be readily replaced with deuterium on irradiation in deuteriomethanol (CH_3OD). It is proposed that the deuteration proceeds *via* an enamide isomer produced by intramolecular hydrogen transfer from the *o*-alkyl group to the excited C=N double bond. An intermolecular hydrogen atom abstraction pathway was excluded because neither *N*-(4-methyldiphenylmethylene)acetamide in deuteriomethanol(CH_3OD) nor diphenylmethane in deuteriomethanol(CH_3OD) in the presence of *N*-(diphenylmethylene)acetamide was deuterated. Intramolecular hydrogen abstraction is essential for the deuteration, because no deuteration occurs on irradiation of 2-methylbenzophenone semicarbazone which undergoes no photoreduction. The difference in reactivities of the *ortho*-substituted imines between in solution and in a rigid matrix is discussed from the viewpoint of *syn-anti* isomerization.

In previous papers we have reported that the imine **1** which has a C=N double bond conjugated with a carbonyl group undergoes photochemical reduction in hydrogen-donating solvents such as alcohol or ether,[2] and reduction and reductive addition in alkyl benzenes or aliphatic olefins.[3] In spite of the recent accumulation of reports of the photoreduction of simple imines,[2-5] its reduction pathway has not yet been unambiguously characterized. Fischer[4] and Padwa and others[6,7] have proposed that the reactive intermediates in these reactions are exclusively the excited states of the carbonyl compounds contained as impurities in the reaction mixtures. The lack of reactivity of the excited states of imines was explained by a feasible deactivation *via* *syn-anti* isomerization.[7] Nevertheless, it is still open to question whether this interpretation is applicable to different kinds of imine, *e.g.*, **1**.

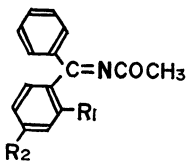

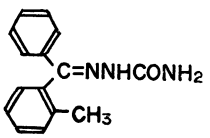

1; R_1=H, R_2=H **4**
2a; R_1=CH_3, R_2=H
2b; R_1=$CH_2C_6H_5$, R_2=H
3; R_1=H, R_2=CH_3

We expected that participation of an impurity in the hydrogen abstraction reaction could be prevented by setting the hydrogen-accepting imino group and the hydrogen-donating alkyl group in one molecule. *N*-(2-Methyldiphenylmethylene)acetamide (**2a**), *N*-(2-benzyldiphenylmethylene)acetamide (**2b**), and *N*-(4-methyldiphenylmethylene)acetamide (**3**) were prepared and the photogenerated intermediates were detected by the exchange of hydrogen in the alkyl group with deuterium in deuteriomethanol (CH_3OD). Changes in the absorption spectra during irradiation and the photochemical behavior of 2-alkylbenzophenone semicarbazone (**4**) were investigated as well.

Results and Discussion

Deuteration. The 2- (**2a**) and 4-methyl (**3**) substituted *N*-(diphenylmethylene)acetamides were prepared and photochemically deuterated at the 2- and 4-methyl positions. A solution of each compound in a deuteriomethanol(CH_3OD)–benzene mixed solvent was irradiated with light of wavelength longer than 320 nm at room temperature for 8 hr. After irradiation, the solvent was removed and the NMR spectrum of the recovered imine was measured. The spectrum of the recovered **2a** revealed that 0.30±0.09 atoms of deuterium per molecule were incorporated in the 2-methyl group of **2a**, while no deuteration was observed in **3**. This striking contrast is apparently due to the difference between the geometrical positions of the hydrogen-donating methyl groups. In other words, this is an example of the *ortho*-effect. It is also noteworthy that the acetyl hydrogens in **2a** or **3** remained undeuterated throughout the above irradiations.

Mechanism of Deuteration. The lack of deuteration of **3** indicates that some intramolecular interaction between the *N*-acetylimino group and the 2-methyl group of **2a**, possibly intramolecular hydrogen atom abstraction *via* a six-membered cyclic transition state formation, is involved in the photodeuteration of **2a**.

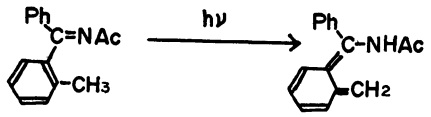

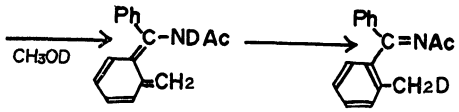

The following experiment showed that the deuteration of **2a** does not proceed *via* an intermolecular hydrogen atom abstraction. Thus diphenylmethane and imine **1** were used as a hydrogen donor and an acceptor, respectively, for a typical intermolecular reaction. When a solution of diphenylmethane and **1** in deuteriomethamol(CH_3OD)–benzene was irradiated at room temperature, even after irradiation for 86 hr NMR and mass spectra showed no evidence of deuteration. This shows that the deuteration of **2a** must proceed *via* an intramolecular hydrogen abstraction pathway.

Furthermore, the participation of the hydrogen abstraction in the deuteration was confirmed by studying the photochemical behavior of 2-methylbenzophenone semicarbazone (**4**). Generally, it is known that irradiation of *N*-acylimines in hydrogen donors results in reduction of the C=N double bond, but no photoreductions of semicarbazones have been reported yet. In fact, semicarbazone **4** gave no photoreduction product. As might have been expected from the inability of semicarbazones to abstract a hydrogen atom photochemically, no deuteration of **4** was observed after irradiation for 20 hr in deuteriomethanol(CH_3OD). This result indicates that the deuteration of **2a** results from hydrogen abstraction in its excited state.

Attempts of Spectrophotometrical Detection of Intermediate. 2-Methylbenzophenone (**5a**) isoelectronic with the imine **2a**, is known to undergo photochemical deuteration, which has been interpreted as the consequence of the hydrogen-deuterium exchange between deuteriomethanol(CH_3OD) and the enol isomer of **5a** generated by the intramolecular hydrogen atom transfer.[8,9] This photoenol was detected spectrophotometrically as a colored species which was stable only at low temperature. It was, therefore, expected that upon irradiation at 77 K the imine **2a** would also produce the corresponding enamide which might be detected as a colored species in a rigid matrix. Since it was not possible to eliminate the impurity **5a** completely from the liquid **2a**, the crystalline 2-benzyl derivative **2b** was used for measuring the absorption spectra of the reaction system. The imine **2b** was carefully recrystallized several times from dry cyclohexane. 2-Benzylbenzophenone (**5b**), as well as **5a**, has also been reported to generate a colored species at low temperature and to undergo deuteration upon irradiation.[9]

A solution of **2b** in an alcoholic solvent was irradiated and the change in the absorption spectrum of the reaction mixture was followed. At room temperature no color change was observed. At 77 K in the matrix, the colored enol of the impurity **5b** was often observed (λ_{max} 430—480 nm) when insufficiently purified **2b** was used. However more careful purification removed the coloration completely. When a small amount of water was added to the purified sample which was subsequently allowed to stand at room temperature for 48 hr, coloration due to **5b** produced by the hydrolysis of **2b** was again observed at 77 K. Furthermore, a solution of unpurified **2a** in an alcoholic solvent gave a colored species (λ_{max} 405 nm and 430 nm) on irradiation at 77 K, but the coloration was removed by addition of phenylhydrazine to the system. Phenylhydrazine would react with the impurity **5a** to give a less reactive species, phenylhydrazone. As described above, it was concluded that the observed colorations were due to the photoenols of impurities.[10] An attempt to detect the intermediate enamide spectroscopically was unfortunately unsuccessful. This observation, however, is not in conflict with the contention that the enamides are involved in deuteration, as discussed in the next section.

In order to examine the influence of impurities, the deuteration of the impurity-free **2b** was rigorously checked. A solution of impurity-free **2b** in a deuteriomethanol(CH_3OD)–toluene solvent was first irradiated at 77 K to check the absence of the coloration due to the impurity. Then the irradiation was continued at room temperature for 20 hr. The amount of deuterium contained in the recovered **2b** was found by NMR spectroscopy to be 0.3 atom per molecule in good agreement with the figure determined by mass spectroscopy. The deuterium atom was found to be located at the benzylic position. It was, therefore, concluded that the deuteration of the *ortho*-substituted imines **2** proceeded indeed *via* the excited states of **2** and that the impurity, a ketone, did not participate in the deuteration *via* a chemical sensitization mechanism.

Intramolecular Hydrogen Atom Abstraction and Molecular Geometry of 2. Padwa and Dharan[6] claimed that irradiation of simple imines resulted in isomerization about the C=N double bond which dissipated the excitation energy and resulted in inhibition of hydrogen abstraction by the excited imine. The results of the present study, however, showed that hydrogen abstraction is indeed able to proceed when the hydrogen-donating alkyl group is located at a geometrically and consequently kinetically preferable position within the molecule. Moreover it has been found in our laboratory and will be reported in a separate paper[11] that the excited state of imine **1** also underwent hydrogen abstraction to a considerable extent even without any chemical sensitizers. The deuteration of the *ortho*-alkyl groups in **2** provided strong evidence for the participation of the excited states of these imines (**1** and **2**) in the hydrogen abstraction.

It was necessary to consider the molecular geometry of **2** to discuss the geometrical features of the hydrogen abstraction. Several reports on the *syn-anti* isomerization of asymmetric benzophenone imines in solution showed that the *para*-substituted derivatives[12] mostly undergo rapid isomerization at room temperature whereas the *ortho*-substituted ones[13] exist exclusively in the *syn*(*Z*)-form. This would be the case in *ortho*-substituted **2a** and **2b**, shifting the equilibrium to the *syn(Z)*-form. The fact that the intermediate enamide was not detected even at low temperature can be reasonably explained as follows. Because the lone pair of the nitrogen atom in *syn(Z)*-**2** is in position opposite to the *ortho*-alkyl group and also the isomerization of *syn(Z)*-**2** to the *anti(E)*-isomer is prevented at

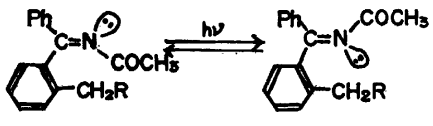

syn(*Z*)-**2** *anti*(*E*)-**2**

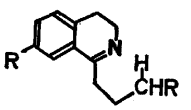

6

77 K in a rigid matrix, the excitation energy is dissipated by radiative or radiationless processes without hydrogen abstraction.[14] In fact, no deuteration could be detected on irradiation of **2a** at 77 K, which is consistent with the absence of coloration of the pure imine.[15] On the contrary, irradiation of **2** at room temperature in solution results in the formation of the *anti(E)*-isomer by rotation about the C=N double bond.[16] The excited state of the *anti(E)*-isomer is supposed to be the active species in the hydrogen abstraction and the photochemical deuteration. In fact, Ogata[17] and Stermitz[18] reported that azomethine **6** undergoes photochemical intramolecular hydrogen abstraction.

Experimental

General. Ultraviolet spectra were recorded on a Shimadzu MPS-50L spectrophotometer. Infrared spectra were taken as liquid film or in Nujol mulls on a Jasco IR-E spectrophotometer. Nuclear magnetic resonance spectra were taken on a Japan Electron Optics Laboratory Model PS-100 spectrometer using tetramethylsilane as the internal standard. The mass spectra were recorded on a Hitachi RMS-4 mass spectrometer, in which the ionization energy was 80 eV. The samples were injected directly at 120 °C or injected through a Hitachi 063 gas chromatograph (SE30, 3 mmϕ × 2 m, 225 °C). Melting points were determined with a Yanagimoto micro melting point apparatus. All irradiations were carried out in a quartz reactor equipped with a Ushio type 501C 500W ultrahigh pressure mercury lamp through a glass filter transparent to wavelengths longer than 320 nm.

Materials. Monodeuteriomethanol(CH_3OD) was obtained from Merck. Benzene, toluene, and cyclohexane were dried over metallic sodium, methanol over magnesium, and 2-propanol over barium oxide, and distilled. Diphenylmethane was recrystallized from petroleum ether.

N-(Diphenylmethylene)acetamide (***1***) was prepared in the usual way.[19] *N*-Acetylation was carried out with acetic anhydride.

N-(2- or 4-Methyldiphenylmethylene)acetamide (***2a*** *or* ***3***) was prepared by the coupling of benzonitrile with the Grignard reagent of the corresponding bromotoluene,[19] followed by *N*-acetylation with acetic anhydride. **2a**: bp, 152 °C (1 mmHg); IR (liquid film): 1690(C=O), 1640(C=N) cm^{-1}; NMR(CCl_4): δ 1.9(acetyl CH_3), 2.2(CH_3), 7.1—7.8 (9H, aromatic ring protons). **3**: IR(liquid film): 1690(C=O), 1640(C=N) cm^{-1}; NMR(CCl_4): δ 1.9 (acetyl CH_3), 2.3(CH_3), 7.0—7.6(9H, aromatic).

*N-(2-Benzyldiphenylmethylene)acetamide(**2b**).* The Grignard coupling of bromobenzene and 2-chlorobenzyl chloride gave 2-chlorodiphenylmethane.[20] 2-Chlorodiphenylmethane was refluxed in pyridine in the presence of cuprous cyanide to give 2-benzylbenzonitrile.[21] A solution of 20 g of 2-benzylbenzonitrile in 50 ml of dry diethyl ether was added to the Grignard reagent prepared from 15.7 g of bromobenzene and 2.5 g of magnesium in 100 ml of diethyl ether. The reaction mixture was refluxed for 6 hr, cooled, decomposed with 100 ml of methanol, and filtered. The solvent was evaporated and the residue was distilled under reduced pressure to give 2-benzyldiphenylmethyleneimine; 22% yield; bp, 200 °C(1 mmHg); IR(liquid film): 3240(NH), 1605(C=N) cm^{-1}; NMR(CCl_4): δ 3.8(CH_2), 6.9—7.7(14H, aromatic), 8.6(NH); Anal.: Found: C, 86.65; H, 6.00; N, 4.94%. Calcd for $C_{20}H_{17}N$: C, 88.52; H, 6.32; N, 5.16%.[22] This imine was easily acetylated with acetic anhydride to give *N*-(2-benzyldiphenylmethylene)acetamide. Careful recrystallization from cyclohexane was repeated several times until impurity-free white crystals were obtained: bp, 205 °C (1 mmHg); mp, 100—101 °C; Mass: m/e=313; IR(Nujol mull): 1690(C=O), 1640(C=N) cm^{-1}; λ_{max}^{MeOH} (log ε_{max}):

Table 1. Results of the photodeuteration in deuteriomethanol(CH_3OD)

Compound	Irr. time (hr)	Analysis: Method	Analysis: Observed value (Calcd value)	Deuterium content (%)
1 200 mg + **Dm** 200 mg[b]	20	NMR	$\frac{\text{methylene}}{\text{phenyl}} = 0.20\pm0.01$	0
1 350 mg + **Dm** 200 mg[b]	86	mass	$\frac{M+1}{M} = 0.14\pm0.02$ (0.15)[c]	0
2a 230 mg	8	NMR	$\frac{\text{2-methyl}}{\text{acetyl}} = 0.90\pm0.03$	10±3
2a 230 mg (at 77 K)[d]	8	mass	$\frac{M+1}{M} = 0.19\pm0.02$ (0.19)[c]	0
2b 150 mg[e]	20	NMR	$\frac{\text{2-methylene}}{\text{acetyl}} = 0.59\pm0.03$	12±4
		mass	$\frac{M+1}{M} = 0.51\pm0.02$ (0.25)[c]	15±2
		mass	$\frac{M+2}{M} = 0.13\pm0.02$ (0.03)[c]	14±2
3 500 mg	8	NMR	$\frac{\text{4-methyl}}{\text{acetyl}} = 1.00\pm0.03$	0
4 100 mg	20	mass	$\frac{M+1}{M} = 0.20\pm0.02$ (0.18)[c]	0

a) The NMR spectra were taken in CCl_4 at room temperature. b) Recovered diphenylmethane (**Dm**) was analyzed in this run. c) The figure in the parentheses is the ratio calculated from the natural isotope abundance. d) Toluene was used in this run instead of benzene as a solvent. e) The corresponding ketone was completely eliminated from the starting material and dry toluene was used instead of benzene in this case.

215(4.54), 234(4.40), 253(4.40), 372(sh)(0.97), 382(0.66), 392(0.66)nm; NMR(CCl_4): δ 1.8(acetyl CH_3), 3.8(CH_2), 6.9—7.6(14H, aromatic). Anal.: Found: C, 84.48; H, 6.09; N, 4.44%. Calcd for $C_{22}H_{19}NO$: C, 84.31; H, 6.11; N, 4.47%.

2-Methylbenzophenone Semicarbazone(4) To a solution of 1 g of semicarbazide hydrochloride and 1.5 g of sodium acetate in 10 ml of water was added 10 ml of ethanol containing 1 g of 2-methylbenzophenone. Ethanol was added until the mixture became transparent. The solution was heated for half an hour and allowed to stand at room temperature over a period of several days. A new crystalline compound **4** was separated from the reaction mixture and recrystallized from ethanol: mp, 156—157 °C; Mass: *m/e*= 253; IR(Nujol mull): 3300(NH), 1680(C=O)cm^{-1}; NMR (CCl_4): δ 2.2(CH_3), 6.0(NH, NH_2), 7.5(9H, aromatic). Anal.: Found: C, 71.19; H, 5.92%. Calcd for $C_{15}H_{15}N_3O$: C, 71.11; H, 5.98%.

Deuterium Exchange. Usually 2 ml of a deuteriomethanol (CH_3OD)-benzene solvent containing 100—500 mg of an imine was degassed and pure nitrogen was introduced until the system reached atmospheric pressure for experimental convenience. After being irradiated at room temperature in a quartz tube, the starting material was recovered and analyzed by NMR and mass spectroscopy. The results are summarized in Table 1.

Irradiation at Low Temperature. Unless otherwise mentioned, an oxygen-free 10^{-1} mol/l solution of the substrate in 4 ml of a methanol-2-propanol (1 : 1) solvent was irradiated at 77 K in a quartz cell with light of wavelengths longer than 320 nm. Changes in the absorption spectra were measured at 77 K in a quartz Dewar filled with liquid nitrogen.

References and Notes

1) N. Toshima, M. Saeki, and H. Hirai, *Chem. Commun.*, **1971**, 1424.

2) T. Okada, M. Kawanisi, H. Nozaki, N. Toshima, and H. Hirai, *Tetrahedron Lett.*, **1969**, 927.

3) S. Asao, N. Toshima, and H. Hirai, unpublished results. N. Toshima, S. Asao, K. Takada, and H. Hirai, *Tetrahedron Lett.* **1970**, 5123.,

4) M. Fischer, *ibid.*, **1966**, 5273; *Chem. Ber.*, **100**, 3599 (1967).

5) H. Göth, P. Cerutti, and H. Schmid, *Helv. Chem. Acta*, **48**, 1395 (1965). E. S. Huyser, R. H. S. Wang, and W. T. Short, *J. Org. Chem.*, **33**, 4323 (1968). R. O. Kan and R. L. Furey, *J. Amer. Chem. Soc.*, **90**, 1666 (1968). A. Padwa, W. Bergmark, and D. Pashayan, *ibid.*, **90**, 4458 (1968); **91**, 2653 (1969). G. Balogh and F. C. De Shryver, *Tetrahedron Lett.*, **1969**, 1371. N. Toshima, H. Hirai, and S. Makishima, *Kogyo Kagaku Zasshi*, **72**, 184 (1969). B. Fraser-Reid, A. McLean, and E. W. Usherwood, *Can. J. Chem.*, **47**, 4511 (1969). P. Beak and C. R. Payet, *J. Org. Chem.*, **35**, 3281 (1970). T. Okada, K. Saeki, M. Kawanisi, and H. Nozaki, *Tetrahedron*, **26**, 3661 (1970).

6) A. Padwa and M. Dharan, *Tetrahedron Lett.*, **1972**, 1053.

7) A. Padwa and F. Albrecht, *J. Amer. Chem. Soc.*, **94**, 1000 (1972).

8) N. C. Yang and C. Rivas, *ibid*, **83**, 2213 (1961).

9) E. F. Zwicker, L. I. Grossweiner, and N. C Yang, *ibid*, **85**, 2671 (1963). E. F. Ullman and K. R. Huffman, *Tetrahedron Lett.*, **1965**, 1863. G. Porter and M. F. Tchir, *Chem. Commun.*, **1970**, 1372. K. R. Huffman, M. Loy, and E. F. Ullman, *J. Amer. Chem. Soc.*, **87**, 5417 (1965).

10) In the preliminary communication,[1] these colored species were incorrectly attributed to the enamide isomers of the corresponding imines.

11) S. Asao, N. Toshima, and H. Hirai, in preparation.

12) D. Y. Curtin and J. W. Hausser, *J. Amer. Chem. Soc.*, **83**, 3474 (1961). D. Y. Curtin, E. J. Grubbs, and C. G. McCarty, *ibid*, **88**, 2773 (1966). M. Tabata, K. Yokota, Y. Takada, and A. Suzuki, *Chem. Lett.*, **1972**, 659. H. A. Stabb, F. Vögtle, and A. Mannschreck, *Tetrahedron Lett.*, **1965**, 697.

13) R. Van der Linde, J. W. Dornseiffen, J. U. Veenland, and Th. J. de Boer, *Spectrochim. Acta*, **25A**, 375 (1969).

14) N. J. Turro and D. S. Weiss, *J. Amer. Chem. Soc.*, **90**, 2187 (1968).

15) We acknowledge the suggestion of a referee to carry out this experiment.

16) The preceding discussion was developed on the assumption that the n-orbital on the nitrogen atom is operative in the hydrogen abstraction. The participation of the n-orbital on the oxygen atom could not be eliminated by the present study. In this case, hydrogen abstraction must proceed *via* an eight-membered cyclic transition state and the lack of coloration in the matrix must be interpreted as due to the loss of flexibility of the C=N-C=O chromophore to form an eight-membered cyclic transition state.

17) Y. Ogata and K. Takagi, *Tetrahedron*, **27**, 2785 (1971).

18) F. R. Stermitz, C. C. Wei, and C. M. O'Donnel, *J. Amer. Chem. Soc.*, **92**, 2745 (1970).

19) P. L. Pickard and T. L. Tolbert, "Organic Synthesis," Coll. Vol. V, p. 520 (1973).

20) F. A. Vingiello, S. Que, and J. Sheridan, *J. Org. Chem.*, **26**, 3202 (1961).

21) C. K. Bradsher, *J. Amer. Chem. Soc.*, **62**, 486 (1940).

22) Since this imine is easily hydrolyzed, it contains 2-methylbenzophenone inevitably. This causes the discrepancy of the elemental analysis.

Reactions of Sulfenes with Schiff Bases. The Stereochemistry and Thermal Fragmentation of Thiazetidine 1,1-Dioxide

Tetsuo HIRAOKA and Takeo KOBAYASHI

Central Research Laboratories, Sankyo Co., Ltd. Hiromachi, Shinagawa-ku, Tokyo 140

(Received April 17, 1974)

Phenylsulfene (II) generated from benzylsulfonyl chloride (I) and triethylamine, reacted with *N*-(*p*-substituted)-benzylidene-methylamine to give 2-methyl-4-phenyl-3-(*p*-substituted-phenyl)-1,2-thiazetidine 1,1-dioxide whose *cis* and *trans* isomers were separated. Both *cis* and *trans* 3,4-diphenyl-2-methyl-1,2-thiazetidine 1,1-dioxide (IV and V) afforded *trans* stilbene and benzaldehyde on pyrolysis. This new fragmentation reaction could be explained by a stepwise decomposition because of its non-stereospecificity.

Although heterocyclic four-membered ring compounds have been well investigated,[1] little is known about 1,2-thiazetidine 1,1-dioxide due to the scarcity of synthetic examples. Whereas thermal [2+2] cycloaddition reactions for the synthesis of this four-membered saltam have been reported,[2] no stereochemical aspects are known. This report deals with reactions of sulfenes with Schiff bases and the synthesis of 1,2-thiazetidine 1,1-dioxide derivatives which sheds light on the stereochemistry and a thermal fragmentation.

Phenylsulfene (II) generated from benzylsulfonyl chloride (I) and triethylamine in tetrahydrofuran was treated with *N*-benzylidene-methylamine (III) to give 3,4-diphenyl-2-methyl-1,2-thiazetidine 1,1-dioxide whose *cis* (IV) and *trans* (V) isomers were separated by silica gel chromatography. This is the first instance of isolation of the both stereoisomers in thiazetidine 1,1-dioxide system. The other components of the reaction mixture were the starting Schiff base and stilbene which has been known to be derived from phenylsulfene.[3] Similarly substituted *N*-benzylidene-methylamine afforded the desired four-membered saltams, whose physical data are summarized in Table 1. The determination of the structures was made on the basis of NMR data which showed a typical AB type quartet due to hydrogens at 3 and 4 positions. The assignment of *cis* and *trans* isomers was also based on the coupling constants between C^3-H and C^4-H. The difference between J_{cis} and J_{trans} is relatively small (1.5—2.0 Hz), leaving the possibility of a misassignment which was pointed out by Fleming and Williams[4] in four-membered carbocyclic ring systems. The validity of these *cis* and *trans* assignments is supported by the following chemical interconversions. Heating the *cis*

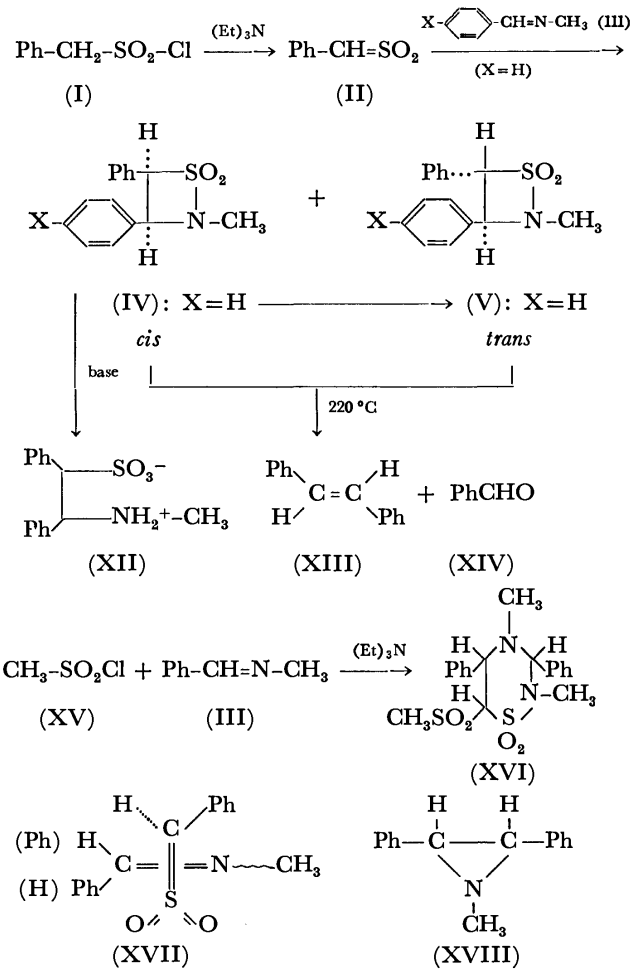

Chart 1.

TABLE 1. 1,2-THIAZETIDINE 1,1-DIOXIDE

Compound X			NMR spectra[a]					
			Mp (°C)	N-CH_3	C_3-H	C_4-H	$J_{3,4}$(Hz)	aromatic H
H	IV	*cis*	147—148	2.89	4.75(d)	5.74(d)	8.5	6.98—7.28(m)
	V	*trans*	81— 82	2.80	4.28(d)	5.22(d)	7.0	7.12—7.60(m)
Cl	VI	*cis*	154—155	2.88	4.72(d)	5.73(d)	8.8	7.10—7.32(m)
	VII	*trans*	89— 90	2.78	4.24(d)	5.16(d)	7.5	7.33—7.52(m)
OCH_3	VIII	*cis*	132—133	2.88[b]	4.73(d)	5.68(d)	8.5	6.62—7.32(m)
	IX	*trans*	oil	2.74[c]	4.22(d)	5.18(d)	7.0	6.78—7.58(m)
NO_2	X	*cis*	179—180	2.94	4.81(d)	5.82(d)	9.0	7.10—8.18(m)
	XI	*trans*	170—171	2.85	4.37(d)	5.18(d)	7.0	7.43—8.39(m)

a) ppm in $CDCl_3$. b) OCH_3 3.70. c) OCH_3 3.78.

isomer(IV) in tetrahydrofuran in the presence of triethylamine for 15 hr gave a mixture of the *cis* (IV) and *trans* isomer (V) in a ratio of 4 : 1, whereas the same treatment of the *trans* compound (V) afforded the unchanged starting material together with a trace amount of the *cis* isomer (IV).

The yields of these 1,2-thiazetidine 1,1-dioxides changed significantly depending on the reaction conditions. The best result was obtained when two equivalents of Schiff base and one equivalent of benzylsulfonyl chloride were used without triethylamine or another base (Table 2).

Table 2. Formation of 1,2-thiazetidine 1,1-dioxides from benzylsulfonyl chloride and Schiff bases in THF

Schiff base	Reaction conditions	Yield[c]	Ratio[d] *cis* : *trans*
Ph-CH=N-CH_3	A[a]	17.5%	64 : 36
	B[b]	80.0%	61 : 39
p-Cl-Ph-CH=N-CH_3	A	14.6%	62 : 38
	B	88.3%	58 : 42
p-CH_3O-Ph-CH=N-CH_3	A	16.7%	68 : 32
	B	79.7%	64 : 36
p-NO_2-Ph-CH=N-CH_3	A	12.3%	60 : 40
	B	51.7%	52 : 48

a) Molar ratio of benzylsulfonyl chloride-Schiff base-triethylamine=1 : 1 : 1, −78 °C, 5 hr, then, allowed to warm slowly to room temperature and kept at this temperature overnight. b) Molar ratio of benzylsulfonyl chloride-Schiff base=1 : 2, room temperature, 42 hr. When the reaction was stopped after 18 hr, 10—30% decrease of yields was observed. c) Otained from NMR data. The reactions were carried out using 0.05 equivalents of hexamethylbenzene as an internal standard for NMR analysis. The isolated yields were given in experimental part. d) Calculated from NMR data.

The preferred formation of the *cis* isomer over the *trans* isomer in the reaction of the sulfene with the Schiff base suggests that the reaction would be a concerted [$_\pi 2_s + _\pi 2_a$] cycloaddition (depicted as XVII) with some secondary effects.[5]

Treatment of the saltam (IV) with sodium methoxide in methanol and subsequent work-up with hydrochloric acid gave 1,2-diphenyl-2-methylamine-ethanesulfonic acid (XII). This ring cleavage presents a striking contrast with a base-catalyzed ring opening of four-membered saltam, in which 2—3 bond fission took place.[2b,2c]

According to the literature[3] the structures of the products obtained by the reactions of sulfene with Schiff bases have not been established. In our experiments only phenylsulfene afforded a four-membered sulfonamide, and alkyl sulfenes gave many products whose structures could not be clarified at this time. In the case of unsubstituted sulfene the reaction proceeded in a different way. Methanesulfonyl chloride was treated with *N*-benzylidene-methylamine in tetrahydrofuran in the presence of triethylamine to yield a crystalline substance, mp 181—182 °C. The NMR spectrum of this compound exhibited peaks at 1.87 (3H, singlet), 2.84 (3H, singlet), 2.85 (3H, singlet), 4.39 (1H, doublet, J=9.0Hz), 4.83 (1H, doublet, J=9.0Hz), and 5.30ppm (1H, singlet), in addition to aromatic hydrogen peaks (10H, multiplet). This fact suggests that 2 mol of sulfene and 2 mol of Schiff base were incorporated into the product. The molecular ion peak at *m/e* 394 in the mass spectrum supported this inference. When this reaction was carried out in acetonitrile instead of tetrahydrofuran the yield of the product increased appreciably, suggesting the involvement of a dimeric sulfene: similarly Optiz[6] observed O_2S=CH-SO_2-CH_3 was formed from methanesulfonyl chloride and triethylamine in acetonitrile. Degradation of this product with hydrochloric acid gave methylamine hydrochloride, and treatment with sodium hydroxide afforded benzylalcohol, which was not helpful in the elucidation of the structure. From these facts we propose the structure (XVI) *i.e.* 2,4-dimethyl-3,5-diphenyl-6-methylsulfonyl-tetrahydro-1,2,4-thiadiazine 1,1-dioxide for the reaction product from methanesulfonyl chloride and *N*-benzylidene-methylamine. The measurement of nuclear Overhauser effect of XVI in NMR also suported this structure. This NOE results are shown in Fig. 1, together with the stereochemistry.

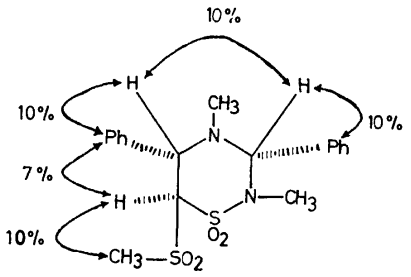

Fig. 1. Nuclear Overhauser effect of XVI.

Next our attention was directed towards thermal fragmentation reaction of such four-membered saltams. Pyrolysis of the *cis* saltam (IV) at 220 °C in nitrogen atmosphere yielded *trans*-stilbene (XIII) (37% yield) and benzaldehyde (XIV) (5% yield) together with the unchanged starting material (*ca* 10%). Analogously heating the *trans* isomer (V) at the same temperature afforded also *trans*-stilbene (XIII) and benzaldehyde (XIV) in 7% and 8% yield, respectively, in addition to the starting *trans* compound (V) (*ca* 7%) and polymeric substance. Recovery of a part of the unchanged *cis* (IV) and the *trans* saltam (V) indicates no interconversions between the two isomers during pyrolysis. Under these reaction conditions (220 °C, 2 hr) *cis*-stilbene gave a mixture of *cis* and *trans* stilbene (3 : 2), whereas *trans*-stilbene isomerized to a negligible amount of *cis*-stilbene (vpc analysis). Thus the formation of *trans*-stilbene from both *cis*-and *trans*-thiazetidine dioxide took place non-stereospecifically. This thermal fragmentation exhibits a striking contrast to that of β-lactams wherein cleavage leading to an olefinic compound proceeded with total retention of stereochemistry.[7] The concerted fragmentation of a four membered ring is only symmetry allowed in the case of [$_\sigma 2_s + _\sigma 2_a$] pathway,[5] which is not apparently applicable to the present cleav-

age reaction. A mechanistic possibility might be the extrusion of sulfur dioxide from the four-membered saltam to give an aziridine derivatives, which will subsequently afforded stilbene by a cheletropic reaction.[5] This route seems reasonable since thietane has been known to lose sulfur dioxide to give a cyclopropane derivatives.[8] However, to our knowledge, no aziridine derivative produces an olefinic compound without its conversion to the corresponding *N*-oxide.[9] In order to clarify this point *cis*-2,3-diphenyl-1-methylaziridine (XVIII) was prepared according to the literature.[10] The compound (XVIII) was pyrolyzed under the same conditions as in the case of IV and V to afford an unidentified mixture with a trace amount of *trans*-stilbene (XIII), thus excluding the intermediacy of XVIII. At present, the fragmentation of IV and V could be explained by a stepwise decomposition as in the case of cyclobutane derivatives.[11] An intermediate leading to benzaldehyde is not clear at present time.

The mass spectra of IV and V are interesting in connection with their thermal reactions. The peak due to (M^+–SO_2) appeared in medium intensity, and (M^+–SO_2–H) peak constituted a base peak. A fragment corresponding to stilbene was not observed, whereas a peak assignable to Ph–C≡N^+–CH_3 was very strong.

Experimental

All melting points were determined in open capillaries and are uncorrected. IR spectra were measured with a Hitachi IRA-2 spectrophotometer. NMR spectra were recorded on a Varian D-60 spectrometer.

General Procedure for Reactions of Sulfonyl Chlorides with N-p-*substituted-Benzylidene-methylamine.* A stirred solution of 0.01 mol of the *N-p*-substituted-benzylidene-methylamine and 0.01 mol of triethylamine in 25 ml of a dry solvent, under slight pressure of dry nitrogen, was maintained at −78 °C while a solution of 0.01 mol of a sulfonyl chloride in 5 ml of a dry solvent was slowly added over a period of 30 min. Usually triethylamine hydrochloride separated immediately. The resulting suspension was allowed to warm slowly to room temperature and was then stirred overnight. The solid (triethylamine hydrochloride) was removed by filtration and washed with a small amount of a solvent. The filtrate and washings were combined and concentrated under reduced pressure. The residue, oil or crystals, was purified by column chromatography using silica gel or alumina. Recrystallization from a suitable solvent gave a desired compound.

*2-Methyl-3,4-diphenyl-1,2-thiazetidine 1,1-Dioxide (*cis *IV and* trans *V).* Under the general procedure with THF as solvent, *N*-benzylidene-methylamine (1.19 g) and benzylsulfonyl chloride (1.91 g) in the presence of triethylamine (1.01 g) gave a mixture of IV and V. The mixture was purified by column chromatography using silica gel (solvent: benzene) to give 222 mg (after recrystallization from isopropyl ether) of *cis*-isomer IV and 70 mg (after recrystallization from ethanol) of *trans*-isomer V; 10.7% yield, *cis*-isomer (IV): mp 147—148 °C; IR (Nujol) 1142 and 1303 (SO_2) cm^{-1}; NMR see Table 1. (Found: C, 65.78; H, 5.59; N, 5.21; S, 11.67%. Calcd for $C_{15}H_{15}NO_2S$: C, 65.91; H, 5.53; N, 5.12; S, 11.73%), *trans*-isomer (V): mp 81—82 °C; IR (Nujol) 1160 and 1303 (SO_2) cm^{-1}; NMR see Table 1. (Found: C, 66.11; H, 5.52; N, 5.29; S, 11.76%. Calcd for $C_{15}H_{15}NO_2S$: C, 65.91; H, 5.53; N, 5.12; S, 11.73%).

*3-*p*-Chlorophenyl-2-methyl-4-phenyl-1,2-thiazetidine 1,1-Dioxide (*cis *VI and* trans *VII).* Analogously *N-p*-chlorobenzylidene-methylamine (1.54 g) and benzylsulfonyl chloride (1.91 g) in THF with triethylamine (1.01 g) gave a mixture of VI and VII. The mixture was purified by column chromatography using silica gel (solvent: benzene) to give 199 mg (after recrystallization from isopropyl ether) of *cis*-isomer VI and 117 mg (after recrystallization from ethanol) of *trans*-isomer VII; 10.2% yield, *cis*-isomer (VI): mp 154—155 °C; IR (Nujol) 1120 and 1308 (SO_2) cm^{-1}; NMR see Table 1. (Found: C, 58.77; H, 4.54; N, 4.67; S, 10.51; Cl, 11.58%. Calcd for $C_{15}H_{14}NO_2SCl$: C, 58.53; H, 4.58; N, 4.55; S, 10.42; Cl, 11.52%), *trans*-isomer (VII): mp 89—90 °C; IR (Nujol) 1092 and 1298 (SO_2) cm^{-1}; NMR see Table 1. (Found: C, 58.73; H, 4.58; N, 4.78; S, 10.56; Cl, 11.64%. Calcd for $C_{15}H_{14}NO_2SCl$: C, 58.53; H, 4.58 N, 4.55; S, 10.56; Cl, 11.64%).

*3-*p*-Methoxyphenyl-2-methyl-4-phenyl-1,2-thiazetidine 1,1-Dioxide (*cis *VIII and* trans *IX).* According to the general procedure, *N-p*-methoxybenzylidene-methylamine (1.49 g) and benzylsulfonyl chloride (1.91 g) with triethylamine (1.01 g) afforded a mixture of VIII and IX. The mixture was purified by column chromatography using silica gel (solvent: benzene) to give 204 mg (after recrystallization from isopropyl ether) of *cis*-isomer VIII and 115 mg (oil) of *trans*-isomer IX; 10.5% yield, *cis*-isomer (VIII): mp 132—133 °C; IR (Nujol) 1142 and 1320 (SO_2) cm^{-1}; NMR see Table 1. (Found: C, 63.85; H, 5.60; N, 4.69; S, 10.74%. Calcd for $C_{16}H_{17}NO_3S$: C, 63.34; H, 5.65; N, 4.62; S, 10.57%), *trans*-isomer (IX): oil; IR (Nujol) 1160 and 1302 (SO_2) cm^{-1}; NMR see Table 1. (Found: C, 63.72; H, 5.82; N, 4.55; S, 9.94%. Calcd for $C_{16}H_{17}NO_3S$: C, 63.34; H, 5.65; N, 4.62; S, 10.57%).

*2-Methyl-3-*p*-nitrophenyl-4-phenyl-1,2-thiazetidine 1,1-Dioxide (*cis *X and* trans *XI).* As described in the general procedure, *N-p*-nitrobenzylidene-methylamine (1.64 g) and benzylsulfonyl chloride (1.91 g) in the presence of triethylamine (1.01 g) in THF gave a mixture of X and XI. The mixture was purified by column chromatography using silica gel (solvent: benzene) to give 114 mg (after recrystallization from ethanol-ethyl acetate) of *cis*-isomer X and 73 mg (after recrystallization from ethanol) of *trans*-isomer XI; 5.9% yield, *cis*-isomer (X): mp 179—180 °C; IR (Nujol) 1142 and 1309 (SO_2), 1346 and 1520 (NO_2) cm^{-1}; NMR see Table 1. (Found: C, 56.53; H, 4.36; N, 8.86; S, 10.27%. Calcd for $C_{15}H_{14}N_2O_4S$: C, 56.59; H, 4.43; N, 8.80; S, 10.07%), *trans*-isomer (XI): mp 170—171 °C; IR (Nujol) 1162 and 1315 (SO_2), 1350 and 1512 (NO_2) cm^{-1}; NMR see Table 1. (Found: C, 56.68; H, 4.40; N, 8.81; S, 10.27%. Calcd for $C_{15}H_{14}N_2O_4S$: C, 56.59; H, 4.43; N, 8.80; S, 10.07%).

2,4-Dimethyl-3,5-diphenyl-6-methylsulfonyl-tetrahydro-1,2,4-thiadiazine 1,1-Dioxide (XVI). Under the general procedure with THF as solvent, *N*-benzylidene-methylamine (1.19 g) and methanesulfonyl chloride (1.15 g) in the presence of triethylamine (1.01 g) gave a solid. The solid was purified by column chromatography using alumina (solvent: benzene-ethyl acetate 7 : 1) to give 378 mg (after recrystallization from ethyl acetate-ethanol) of XV; 19.3% yield. When the reaction was carried out in acetonitrile 28.0% yield of XV was obtained: mp 181—182 °C; IR (Nujol) 1140 and 1300 (SO_2) cm^{-1}; NMR ($CDCl_3$) δ 1.87 (3H, s, N-C**H**$_3$), 2.84 (3H, s, SO_2-C**H**$_3$), 2.85 (3H, s, SO_2-N-C**H**$_3$), 4.39 (1H, d, Ph-C**H**-N, J=9.0 Hz), 4.83 (1H, d, SO_2-C**H**-SO_2, J=9.0 Hz), 5.30 (1H, s, Ph-C**H**(N)-N), 7.21-7.83 (10H, m, aromatic H). (Found: C, 54.88; H, 5.51; N, 7.17; S, 16.32%. Calcd for $C_{18}H_{22}N_2O_4S_2$: C, 54.80;

H, 5.62; N, 7.10; S, 16.26%).

1,2-Diphenyl-2-methylamino-ethanesulfonic Acid (XII). A stirred suspension of compound IV (136 mg, 0.0005 mol) in 5 ml of 1 M-sodium methoxide-methanol was heated under reflux in an atomosphere of nitrogen. The solution was allowed to cool to room temperature and then treated with 1M-aqueous hydrochloric acid solution until the pH reached 1.0. The separated white solid was collected by filtration and recrystallized from acetone-water to give 104 mg (yield 60.9%) of 1,2-diphenyl-2-methyl-amino-ethanesulfonic acid (XII).: mp >300 °C: IR (Nujol) 2750 and 2520 (N^+H_2), 1618 (benzene), 1249 and 1050 (SO_3^-) cm^{-1}; NMR (DMSO-d_6) δ 2.46 (3H, s, N-C**H**$_3$), 4.56 (1H, d, C**H**-SO_3^- or C**H**-NH_2^+, J=11.0 Hz), 4.98 (1H, d C**H**-SO_3^- or C**H**-NH_2^+, J=11.0 Hz), 6.99—7.54 (10H, m, aromatic H). (Found: C, 61.92; H, 5.65; N, 5.06; S, 11.06%. Calcd for $C_{15}H_{17}NO_3S$: C, 61.83; H, 5.88; N, 4.81; S, 11.00%).

Isomerization of cis- *and* trans-*2-Methyl-3,4-diphenyl-1,2-thiazetidine 1,1-Dioxide (IV and V).* *cis-* or *trans*-2-Methyl-3,4-diphenyl-1,2-thiazetidine 1,1-dioxide (IV or V, 91.0 mg, 0.3 m mol) was dissolved in 10 ml of dry THF, followed by the addition of 10 ml (0.14 mol) of triethylamine. The solution was heated on an oil bath (80 °C) for 3 hr under dry nitrogen. Thin layer chromatography indicated no interconversion between *cis*-isomer IV and *trans*-isomer V. Then the solution was further refluxed for 15 hr. The resulting solution was evaporated under reduced pressure. The residue was dissolved in deuteriochloroform and examined by NMR. In the case of the *cis* compound IV, 80% *cis*-20% *trans* mixture was established, whereas *trans*-isomer V was unchanged under these reaction conditions.

Thermal Fragmentation of cis- *and* trans-*2-Methyl-3,4-diphenyl-1,2-thiazetidine 1,1-Dioxide (IV and V).* *cis-* or *trans*-2-Methyl-3,4-diphenyl-1,2-thiazetidine 1,1-dioxide (IV and V, 100 mg) was placed in a 30 ml flask equipped with a Dimroth-type condenser. A stirred sample was then heated at 220 °C under slight pressure of dry nitrogen for 3 hr. The cooled sample was dissolved in 10 ml of chloroform which was washed with 5 ml of water. The organic layer was evaporated under reduced pressure and the residue was checked by VPC and NMR.

Similarly *cis-* and *trans*-stilbene were heated at 220 °C for 3 hr and analysis of the products was carried out using VPC.

The compound IV was completely recovered on heating at 200 °C for 2 hr.

We wish to thank Mr. H. Kuwano for NOE measurement.

Starting compound	Products distribution (%)				
	(IV)[a]	(V)[a]	*cis*-stilbene[b]	*trans*-stilbene[b]	benzaldehyde[c]
(IV)	10	0	0	37	5
(V)	0	7	0	7	8

a) Determined by NMR. b) Determined by vpc, column SE-30, 140 °C. c) Determined by vpc, column SE-30, 60 °C.

Starting compound	Products distribution (%)[a]	
	cis-stilbene	*trans*-stilbene
cis-Stilbene	30	19
trans-Stilbene	2	51

a) Determined by vpc, column SE-30, 140 °C.

References

1) For example, L. L. Muller and J. Hamer, "1,2-Cycloaddition Reactions," Interscience Publishers, New York (1967).

2) a) H. Staudinger and E. Pfenninger, *Chem. Ber.*, **49**, 1941 (1916); (b G. M. Atkins, Jr. and E. M. Burgess, *J. Amer. Chem. Soc.*, **89**, 2502 (1967); c) O. Tsuge and S. Iwamami, This Bulletin, **43**, 3543 (1970); d) E. M. Burgess and W. M. Williams, *J. Amer. Chem. Soc.*, **94**, 4386 (1972).

3) G. Opitz, *Angew. Chem. Int. Edit. Engl.*, **6**, 107 (1967), see especially p. 122.

4) I. Fleming and D. H. Williams, *Tetrahedron*, **23**, 2747 (1967).

5) R. B. Woodward and R. Hoffman, *Angew. Chem. Int. Edit. Engl.*, **8**, 781 (1969).

6) G. Opitz, M. Kleeman, D. Bucher, G. Walz, and K. Rieth, *ibid.*, **5**, 594 (1966).

7) L. A. Paquette, M. J. Wyvratt, and G. R. Allen, Jr., *J. Amer. Chem. Soc.*, **92**, 1763 (1970).

8) R. M. Dodson and G. Klose, *Chem. Ind.* (London), **1963**, 450.

9) H. W. Heine, J. D. Myers, and E. T. Peltzer, *Angew. Chem. Int. Edit. Engl.*, **9**, 374 (1970).

10) K. Tanaka and T. Sugawa, *Yakugaku Zasshi*, **72**, 1551 (1952).

11) J. F. King, P. DE Mayo, C. L. McIntosh, K. Piers, and D.J.H. Smith, *Can. J. Chem.*, **48**, 3704 (1970).

Formation of Phosphate Derivatives by the Reaction of Propyl and Allyl Halides with Phosphorus Trichloride and Oxygen

Yoshiki Okamoto, Toshihiro Okada, and Hiroshi Sakurai

The Institute of Scientific and Industrial Research, Osaka University, Yamada-kami, Suita-shi, Osaka 565

(Received April 22, 1974)

In addition to phosphonyl dichlorides, a significant amount of phosphoryl dichlorides was obtained by the reaction of propyl and allyl halides with phosphorus trichloride in oxygen atmosphere. Formation of the P–O–C bond can be explained by a scheme involving a preferential reaction of the bridged intermediate radical with oxygen.

The reaction of hydrocarbons with phosphorus trichloride and oxygen provides a convenient route to alkylphosphonyl dichloride derivatives (P–C bond formation). Phosphoryl compounds occur only as minor products under high pressure of oxygen.[1] Boyce and Webb found that the reaction of 1,2-dichloroethylene with phosphorus trichloride–oxygen gives 1,2,2-trichloroethyl phosphate as the major product (*ca.* 40% yield) despite the fact that oxygen was used at atmospheric pressure.[2] No further investigations were made.

We have found that phosphoryl dichlorides are obtained from propyl and allyl halides in various yields under atmospheric pressure conditions of oxygen. The formation of phosphoryl dichloride was more remarkable in bromine-substituted hydrocarbon. The mechanism of the formation of phosphoryl dichloride will be discussed.

Results and Discussion

In a typical run, 0.1 mol of alkyl halide and 0.5 mol of phosphorus trichloride were placed in a 200 ml-cylindrical flask, fitted to a drying tube. Dried oxygen gas was bubbled into the mixture at a 50 ml/min rate for 3 hr. After the removal of phosphorus oxychloride and unreacted material at reduced pressure, the residue was distilled. The products were esterified with excess absolute ethanol, and analyzed by glc.

Chlorophosphonation of n-, *Isopropyl Chlorides, and the Same Bromides.* The yields and compositions of the products from these halides are given in Tables 1 and 3, respectively.

Table 1. Products from *n*- and isopropyl chlorides and the same bromides

Alkyl halide	Component (relative ratio %)	
n-Propyl chloride	$CH_3CH_2CHClPO(OC_2H_5)_2$	(14)
	$CH_3CH[PO(OC_2H_5)_2]CH_2Cl$	(44)
	$CH_2[PO(OC_2H_5)_2]CH_2CH_2Cl$	(32)
	$CH_3CH[OPO(OC_2H_5)_2]CH_2Cl$	(10)
Isopropyl chloride	$CH_3CHClCH_2PO(OC_2H_5)_2$	
n-Propyl bromide	$CH_3CH_2CHBrPO(OC_2H_5)_2$	(23)
	$CH_3CH[PO(OC_2H_5)_2]CH_2Br$	(34)
	$CH_3CH[OPO(OC_2H_5)_2]CH_2Br$	(7)
	$CH_3CHBrCH_2OPO(OC_2H_5)_2$	(7)
	$CH_2[PO(OC_2H_5)_2]CH_2CH_2Br$	(29)
Isopropyl bromide	$CH_3CH[PO(OC_2H_5)_2]CH_2Br$	(47)
	$CH_3CH[OPO(OC_2H_5)_2]CH_2Br$	(33)
	$CH_3CHBrCH_2OPO(OC_2H_5)_2$	(20)

n-Propyl chloride and bromide gave 10% and 14% of phosphate in composition, respectively. In the case of isopropyl bromide, the content of phosphate increased up to 53%.

The following facts suggest that the formation of a phosphoryl structure proceeds *via* a bridged intermediate radical. 1) In all the phosphoryl products, the P–O–C bonds are only at the β-position of halogen atom. 2) 1,2-Rearrangment of bromine atom occurs at the same time. 3) Phosphoryl dichloride production from the bromide is much greater than that from the chloride. It is well-known that bromine atom is more favorable in the formation of a symmetrical and stabilized bridged radical than chlorine atom.[3] 4) The phosphoryl dichloride production from the alkanes with other substituents (CN, COCl, Ph, and $OCOCH_3$) could not be observed under the same conditions.[4]

The bridged radical seems to be the more resonance-stabilized radical by means of delocalization of unpaired electron than the unbridged β-haloalkyl radical. The great reactivity of stable radical $Ph_3C\cdot$ with oxygen is well-known.[5] However, the stable radicals $(CH_3)_2\dot{C}CN$ and $Ph_3C\cdot$ were found to be unreactive toward phosphorus trichloride.[6] The bridged radical is therefore preferentially scavenged with oxygen to form the alkyl peroxide radical.

The subsequent process of the phosphoryl dichloride production can be explained by the mechanism represented by reactions (1)—(5).

$$R\cdot + O_2 \longrightarrow ROO\cdot \quad (1)$$

$$ROO\cdot + PCl_3 \longrightarrow RO\cdot + OPCl_3 \quad (2)^{6}$$

$$RO\cdot + PCl_3 \longrightarrow RO\dot{P}Cl_3 \quad (3)$$

$$RO\dot{P}Cl_3 + O_2 \longrightarrow ROPCl_3OO\cdot \quad (4)$$

$$ROPCl_3OO\cdot + PCl_3 \rightarrow ROPOCl_2 + OPCl_3 + Cl\cdot \quad (5)$$

In order to explain phosphate production from alkanes, Mayo, Durham, and Griggs suggested a heterolytic reaction (7) between phosphorus oxychloride and the alcohol produced by reaction (6).[1]

$$RO\cdot + RH \longrightarrow ROH + R\cdot \quad (6)$$

$$ROH + POCl_3 \longrightarrow ROPOCl_2 + HCl \quad (7)$$

The alkoxy radical appears to be the hydrogen-abstracting species. However, the isomer distributions of these reaction products differ from those of the reaction in which hydrogen abstraction by the alkoxy radical is operative, eliminating the possibility of mechanisms (6) and (7).[8]

Chlorophosphonation of Allyl Chloride and Bromide. Olefin also reacts with phosphorus trichloride–oxygen to give β-chloroalkylphosphonyl dichloride. The formation is explained by the following sequences of reactions.[9]

$$RCH{=}CHR' + Cl\cdot \rightarrow R\dot{C}HCHClR' \quad (I) \qquad (8)$$

$$R\dot{C}H\text{-}CHClR' + PCl_3 \rightarrow RCH(PCl_3\cdot)\text{-}CHClR' \qquad (9)$$

$$RCH(PCl_3\cdot)\text{-}CHClR' + O_2 \rightarrow RCH(PCl_3OO\cdot)\text{-}CHClR' \qquad (10)$$

$$RCH(PCl_3OO\cdot)\text{-}CHClR' + PCl_3 \rightarrow RCH(POCl_2)CHClR' + POCl_3 + Cl\cdot \qquad (11)$$

In the case of allyl halide, the intermediate radical (I, R=CH_2X, R'=H) has two halogen atoms on both sides and the bridging effect thus seems to be more enhanced. The results obtained from allyl chloride and bromide are given in Table 2.

Table 2. Products from allyl chloride and allyl bromide

Allyl halide	Component (relative ratio mol %)	
Allyl chloride	$CH_2ClCH[PO(OC_2H_5)_2]CH_2Cl$	(19)
	$CH_2ClCH[OPO(OC_2H_5)_2]CH_2Cl$	(79)
	$CH_2ClCHClCH_2OPO(OC_2H_5)_2$	(2)
Allyl bromide	$CH_2ClCH[PO(OC_2H_5)_2]CH_2Cl$	(3)
	$CH_2ClCH[OPO(OC_2H_5)_2]CH_2Cl$	(22)
	$CH_2ClCHClCH_2OPO(OC_2H_5)_2$	(1)
	$CH_2ClCH[OPO(OC_2H_5)_2]CH_2Br$	(25)
	$CH_2BrCH[OPO(OC_2H_5)_2]CH_2Br$	(49)
	$CH_2BrCHBrCH_2OPO(OC_2H_5)_2$	(trace)
	$CH_2ClCHBrCH_2OPO(OC_2H_5)_2$	(trace)
(and/or	$CH_2BrCHClCH_2OPO(OC_2H_5)_2$)	

In the case of allyl bromide, the content of phosphate in the product exceeds 97%, halogen exchange occurring at the same time. The formations are illustrated by Scheme 1.

The addition of chlorine atom to the double bond of allyl bromide gives 1-chloromethyl-2-bromoethyl radical (II), which reacts only with oxygen to give phosphate. On the other hand, elimination of bromine atom from II gives allyl chloride. The resulting bromine atom reacts with allyl bromide to give 1-bromomethyl-2-bromoethyl radical (III), which is the most resonance-stabilized radical by bridging with either of bromine atom in both sides. III also reacts with oxygen to give the phosphate. Addition of chlorine atom to allyl chloride gives 1-chloromethyl-2-chloroethyl radical (IV), which is best described as an unsymmetrically bridged radical.[4] IV seems to be less resonance-stabilized than radicals II or III. It therefore reacts not only with oxygen but also phosphorus trichloride to give both phosphoryl and phosphonyl dichlorides.

Experimental

All the boiling points are uncorrected. NMR spectra were obtained at 100 MHz on a JNM-100 spectrometer with TMS as an internal reference in CCl_4 solution. The mass spectra were obtained on a Hitachi RMU-6 or RMU-7 spectrometer with a direct inlet. GC-MS were obtained on a Hitachi RMS-4 spectrometer.

Glc analyses were carried out with a Shimadzu GC-3AF on a 3 m×3 mmφ column packed with 5% Ucon LB 550X on Shimalite W. Preparative work was carried out with a

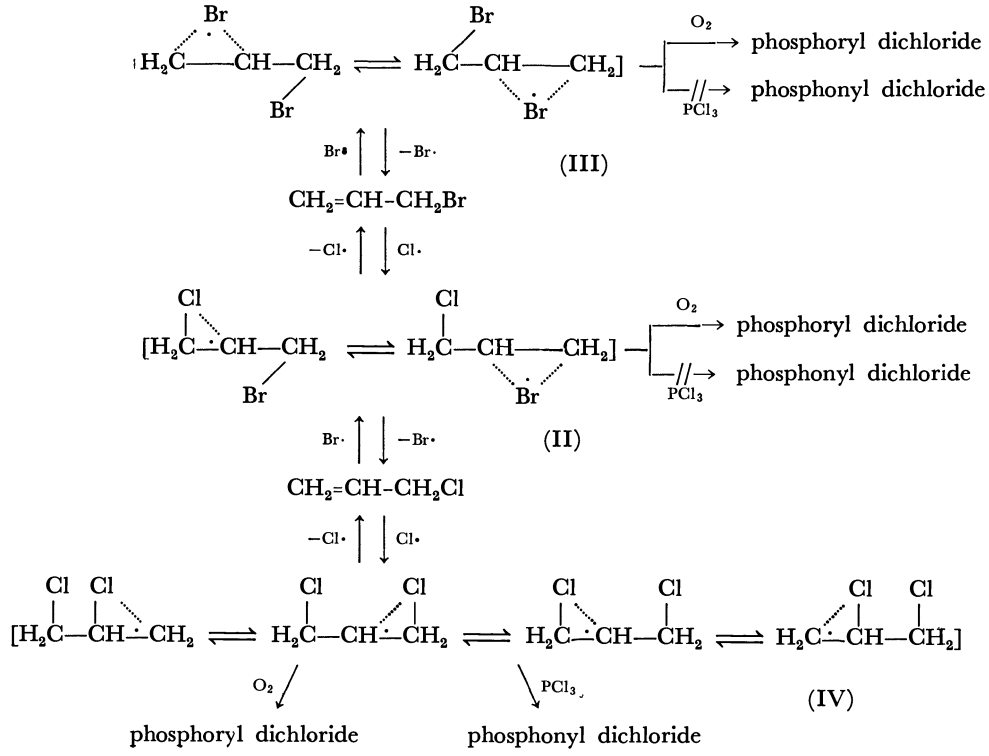

Scheme 1.

Hitachi 023 on a 1 m×12 mmϕ column with the same packing.

All the reagents were prepared by purifying commercial products. Vacuum distillation was carried out under nitrogen.

General Procedure of Chlorophosphonation. Oxygen was bubbled for 3 hr into a mixture of phosphorus trichloride (1.0 mol) and halide (0.2 mol) cooled in a bath at −15—0 °C at such a rate (50 ml/min) that the temperature of the mixture did not rise above 0 °C. After removal of a large portion of unreacted material and phosphorus oxychloride, the residue was vacuum-distilled yielding a colorless liquid. The yields and boiling points of the products from *n*-, isopropyl chlorides, *n*-, isopropyl bromides, allyl chloride, and allyl bromide are given in Table 3.

Table 3. Yields in the chlorophosphonation of the halides

Halide	Yield (g)	Bp °C/mmHg
n-Propyl chloride	7.5	55—83 /1
Isopropyl chloride	5.7	58—78 /1
n-Propyl bromide	4.0	85—123/7
Isopropyl bromide	2.1	65—75 /1
Allyl chloride	35.0	68—84 /0.5
Allyl bromide	34.8	70—95 /0.5

Ethanolysis of the Reaction Products. The above reaction product (2.0 g) was stirred and cooled at −5 °C and a stream of dry nitrogen was passed through it. Absolute ethanol (20 ml) was then added dropwise for 2 hr. The mixture was stirred at 0—5 °C for 3 hr and then at room temperature overnight. Glc analysis of residue after removal of ethanol *in vacuo* was carried out.

Analysis. The products were identified by comparison of their retention times with those of authentic samples prepared by the methods described below. The other products were identified by elemental analysis, NMR, and mass spectra after being fractionated by preparative glc.

Authentic Sample. Diethyl 3-chloropropylphosphonate (bp 78—80 °C/1 mmHg)[10] and diethyl 3-bromopropylphosphonate (bp 94—95 °C/2 mmHg)[10] were prepared by Arbuzov reactions of 3-chloropropyl bromide and trimethylene dibromide with triethyl phosphite respectively. Diethyl 1-chloropropylphosphonate (bp 53—54 °C/0.1 mmHg)[4] was prepared by chlorination of diethyl 1-hydroxypropylphosphonate with thionyl chloride. Diethyl 2-chloropropylphosphonate(bp 77—79 °C/1 mmHg)[10] was prepared by the ethanolysis of 2-chloropropylphosphonyl dichloride, obtained by the reaction of propylene with phosphorus pentachloride.[10] Diethyl 2-bromopropyl phosphate (bp 95—97 °C/2 mmHg, Found: C, 30.41; H, 5.88%. Calcd for $C_7H_{16}O_4PBr$: C, 30.56; H, 5.86%), diethyl 2,3-dichloropropyl phosphate (bp 123—125 °C/4 mmHg).[10] Diethyl 1-chloromethyl-2-chloroethyl phosphate (bp 112—114 °C/2 mmHg)[10] were prepared from the corresponding alcohols and diethyl phosphorochloridate.[10] Diethyl 2,3-dibromopropyl phosphate (bp 122—123 °C/10^{-3} mmHg, Found: C, 23.61; H, 4.30%. Calcd for $C_7H_{15}O_4PBr_2$:C, 23.75; H, 4.27%.) were prepared by the addition of bromine to diethyl allyl phosphate.[11]

The following products were identified by means of the data of NMR, mass spectra and elementary analysis. Diethyl 1-methyl-2-chloroethylphosphonate; NMR: δ 1.05 (d, 3H, J_{HH} 7.0 Hz, CH-C$\underline{H}_3$), 1.35(t, 6H, J_{HH} 7.5 Hz, CH_2-C$\underline{H}_3$), 1.5—2.0(m, 1H, -C$\underline{H}$-CH_3), 3.65(d, 2H, J_{HH} 5.0 Hz, -C$\underline{H}_2$Cl), and 4.10(q-d, 4H, J_{POCH} 7.4 Hz, -OC$\underline{H}_2$-). Found: C, 39.08; H, 7.48%. Calcd for $C_7H_{16}O_3PCl$: C, 39.17; H, 7.51%. Diethyl 1-methyl-2-chloroethyl phosphate;[11] NMR: δ 1.40(d, 3H, J_{HH} 7.2 Hz, -CH-C$\underline{H}_3$), 1.44(t, 6H, J_{HH} 7.5 Hz, CH_2C$\underline{H}_3$), 3.54(d, 2H, J_{HH} 7.2, CH_2Cl), 4.05(q-d, 4H, J_{POCH} 7.5 Hz, -OC$\underline{H}_2$-), and 4.3—4.6 (m, 1H, OCH-CH_3). Diethyl 1-bromopropylphosphonate; NMR δ 1.12(t, 3H, J_{HH} 7.0 Hz, CH-C$\underline{H}_3$) 1.34(t, 6H, J_{HH} 7.0 Hz, OCH_2-C$\underline{H}_3$), 2.00(m, 2H, C$\underline{H}_2$-CH), 3.62(d-t, 1H, J_{HH} 10 Hz, J_{PCH} 5.0 Hz, C$\underline{H}$Br-P), and 4.12(qui, 4H, J_{POCH} 7.0 Hz, -C$\underline{H}_2$-CH_3). Found: C, 32.64; H, 6.18%. Calcd for $C_7H_{16}O_3PBr$: C; 32.45; H, 6.23%. Diethyl 1-methyl-2-bromoethylphosphonate; NMR δ 1.30(d-d, 3H, J_{HH} 7.0 Hz, J_{PCCH} 15 Hz, CH-C$\underline{H}_3$), 1.33(t, 6H, J_{HH} 7.0 Hz, -CH_2C$\underline{H}_3$), 2.04(m, 1H, P-C$\underline{H}$-), 3.20(t-d, 1H, J_{HH} 5.0 Hz, $J_{H_aH_b}$ 11.0 Hz, J_{PCCH} 11.0 Hz, -C$\underline{H}_a$$H_b$Br), 3.76(t-d, 1H, J_{HH} 5.0 Hz, J_{PCCH} 11.0 Hz, -$CH_a$$\underline{H}_b$Br), and 4.06 (qui, 4H, J_{POCH} 0.7 Hz, -OC$\underline{H}_2$-). Found: C, 32.40; H, 6.33%. Calcd for $C_7H_{16}O_3PBr$: C, 32.45; H, 6.23%. Diethyl 1-methyl-2-bromoethyl phosphate; NMR δ 1.41(t, 6H, J_{HH} 7.0 Hz, -CH_2C$\underline{H}_3$) 1.44(d, 3H, J_{HH} 7.0 Hz, -CH-C$\underline{H}_3$), 3.46 (d, 2H, J_{HH} 5.0 Hz, C$\underline{H}_2$Br), and 4.06(q-d, 4H, J_{POCH} 7.4 Hz, -OC$\underline{H}_2$-), Found: C, 29.87; H, 5.80%. Calcd for $C_7H_{16}O_4PBr$: C, 30.56; H, 5.86%. Diethyl 1-chloromethyl-2-chloroethylphosphonate; NMR δ 1.36(t, 6H, J_{HH} 7.0 Hz, CH_2C$\underline{H}_3$), 2.48(m, 1H, P-C$\underline{H}$-), 3.90(d-d, 4H, J_{HH} 5.0 Hz, J_{PCCH} 14.5 Hz, -C$\underline{H}_2$Cl), and 4.08(qui, 4H, J_{POCH} 7.0 Hz, -C$\underline{H}_2$-). Found: C, 34.21; H, 6.12%. Calcd for $C_7H_{15}O_3PCl_2$: C, 33.75: H, 6.07%. Diethyl 1-chloromethyl-2-chloroethyl phosphate;[10] NMR δ 1.36(t, 6H, J_{HH} 7.0 Hz, -CH_2C$\underline{H}_3$), 3.78(d, 4H, J_{HH} 4.0 Hz, -C$\underline{H}_2$Cl), 4.08(qui, 4H, J_{POCH} 7.0 Hz, -OC$\underline{H}_2$-), and 4.60(m, 1H, P-OC$\underline{H}$-). Diethyl 1-chloromethyl-2-bromoethyl phosphate; NMR δ 1.36(t, 6H, J_{HH} 7.0 Hz, CH_2C$\underline{H}_3$), 3.62(d, 2H, J_{HH} 5.0 Hz, -C$\underline{H}_2$Br), 3.78(d, 2H, J_{HH} 5.0 Hz, -C$\underline{H}_2$Cl), 4.08 (qui, 4H, J_{POCH} 7.0 Hz, -OC$\underline{H}_2$-), and 4.20(m, 1H, -OC$\underline{H}$-). Found: C, 27.04; H, 4.90%. Calcd for $C_7H_{15}O_4PBrCl$: C, 27.16; H, 4.88%. Diethyl 1-bromomethyl-2-bromoethyl phosphate; NMR δ 1.36(t, 6H, J_{HH} 7.0 Hz, CH_2C$\underline{H}_3$), 3.63(d, 4H, J_{HH} 5.0 Hz, -C$\underline{H}_2$Br), 4.08(qui, 4H, J_{POCH} 7.0 Hz, -OC$\underline{H}_2$-), and 4.48(m, 1H, OC$\underline{H}$-). Found: C, 23.65; H, 4.21%. Calcd for $C_7H_{15}O_4PBr_2$: C, 23.75; H, 4.27%.

A strong ion peak of *m/e* 99($P(OH)_4^+$) was observed in the mass spectra of all the phosphate components, not of the phosphonate components. Diethyl 1(2)-bromo-2(1)-chloropropyl phosphate was identified by comparison of its relative retention time in glc. The mass spectrum of this fraction showed no molecular ion peak but strong peaks at *m/e* 229 and 231 (M^+–Br) and at *m/e* 81 and 79 ($^{81}Br^+$ and $^{79}Br^+$). A significant amount of allyl chloride was detected in the chlorophosphonation of allyl bromide.

References

1) F. R. Mayo, L. J. Durham, and K. S. Griggs, *J. Amer. Chem. Soc.*, **85**, 3156 (1963).

2) C. B. C. Boyce and S. B. Webb, *J. Chem. Soc.*, (*C*), **1971**, 1613.

3) P. S. Skell, R. R. Pavlis, D. C. Lewis, and K. J. Shea, *J. Amer. Chem. Soc.*, **95**, 6735 (1973).

4) Y. Okamoto and H. Sakurai, *J. Japan Oil Chemists' Soc.*, **20**, 246, 310, 573, 821, 868 (1971); **21**, 62, 893 (1972); **22**, 18, 81 (1973).

5) J. P. Lorand and P. D. Bartlett, *J. Amer. Chem. Soc.*, **88**, 3294 (1972).

6) L. Dulog, F. Nierlich, and A. Verhelst, *Chem. Ber.*, **105**, 874 (1972).
7) S. W. Benson and R. Shaw, "Organic Peroxides 1" Chapter 2, ed by D. Swern, Wiley, New York (1970).
8) C. Walling and B. B. Jacknow, *J. Amer. Chem. Soc.*, **82**, 6108 (1960).
9) K. Chikamine, Y. Okamoto, and H. Sakurai, *Kogyo Kagaku Zasshi*, **74**, 132 (1971).
10) K. Sasse, "Methoden der Organischen Chemie, XII/1, Organische Phosphor Verbindungen," ed. by E. Müller, Georg Thieme Verlag, Stuttgart (1963).
11) E. Cherbuliez, "Organic Phosphorus Compounds" Vol 6, Chapter 15, ed. by G. M. Kosolapoff and L. Maier, John Wiley & Sons, Inc., (1973).

A Synthesis of 3-Hydroxy-5-methoxyphenanthro[4,5-*bcd*]furan

Takaaki HORAGUCHI and Takahachi SHIMIZU

Department of Chemistry, Faculty of Science, Niigata University, Igarashi, Niigata 950–21

(Received May 1, 1974)

3-Hydroxy-5-methoxyphenanthro[4,5-*bcd*]furan (Ia) was synthesized by the dehydrogenation of 5-methoxy-3-oxo-1,2,3,8,9,9a-hexahydrophenanthro(4,5-*bcd*)furan (IVa), starting from 8-hydroxy-7-methoxy-1-tetralone (IIb).

In previous papers,[1,2] the first synthetic route to phenanthro[4,5-*bcd*]furans which contain a ring strain[3] has been reported; by this method Ib and Ic (morphenol) were prepared starting from 8-hydroxy-1-tetralones (IIe and IIf respectively). In the syntheses, however, the yields were not satisfactory in two kinds of cyclization reactions, the formation of naphtho[1,8-*bc*]furans (IIIb and IIIc) from 8-hydroxy-1-tetralones (IIe and IIf) and ethyl bromoacetate, and the intramolecular cyclization of naphtho[1,8-*bc*]furans (IIIb and IIIc) to the corresponding phenanthro[4,5-*bcd*]-furans (IVb and IVc); on the other hand, a methoxyl group on the benzene ring in IIe and IIf served to increase the yield in the latter cyclizations (IIe,f→IIIe,f) and did not have any effect on the yield in the other cyclizations (IIIe,f→IVb,c). These results have required us to make a further attempt to prepare 3-hydroxy-5-methoxyphenanthro[4,5-*bcd*]furan (Ia), an isomer of Ib, starting from a 8-hydroxy-1-tetralone derivative (IId), which has a substituent at the *ortho*-position to the hydroxyl group.

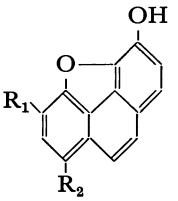

Ia: R_1=OMe, R_2=H
Ib: R_1=H, R_2=OMe
Ic: R_1=H, R_2=H

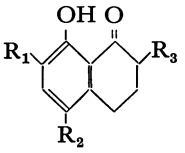

IIa: R_1=OMe, R_2=Cl, R_3=H
IIb: R_1=OMe, R_2=H, R_3=H
IIc: R_1=OMe, R_2=H, R_3=CHO
IId: R_1=OMe, R_2=H, R_3=CH_2CH_2COOH
IIe: R_1=H, R_2=OMe, R_3=CH_2CH_2COOMe
IIf: R_1=H, R_2=H, R_3=CH_2CH_2COOH

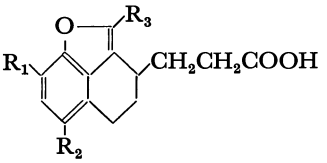

IIIa: R_1=OMe, R_2=H, R_3=COOH
IIIb: R_1=H, R_2=OMe, R_3=COOH
IIIc: R_1=H, R_2=H, R_3=COOH
IIId: R_1=OMe, R_2=H, R_3=H
IIIe: R_1=H, R_2=OMe, R_3=H
IIIf: R_1=H, R_2=H, R_3=H

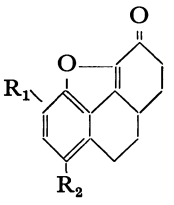

IVa: R_1=OMe, R_2=H
IVb: R_1=H, R_2=OMe
IVc: R_1=H, R_2=H

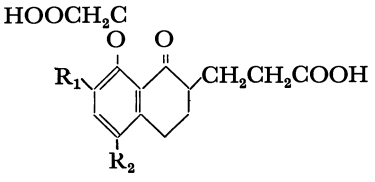

V: R_1=OMe, R_2=H

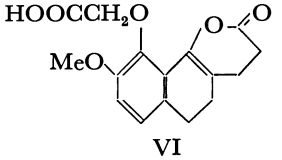

VI

Fig. 1.

Results and Discussion

The tetralone (IId) was prepared from 3-(3,4-dimethoxybenzoyl)propionic acid through a series of intermediates (IIa), (IIb), and (IIc), as will be described in the Experimental section.

When IId was treated with ethyl bromoacetate at 170 °C, followed by hydrolysis, the expected di- and monocarboxylic acids, 3-(2-carboxy-8-methoxy-4,5-dihydro-3*H*-naphtho[1,8-*bc*]furan-3-yl)propionic acid (IIIa) and 3-(8-methoxy-4,5-dihydro-3*H*-naphtho[1,8-*bc*]furan-3-yl)propionic acid (IIId), were obtained in 39 and 1.5% yields respectively. An attempt to prepare IIId from V by treating it with a mixture of acetic anhydride and sodium acetate was unsuccessful; the reaction mixture gave a crystalline product. The infrared absorption spectrum of the product, unlike that of V, shows no bands corresponding to the conjugated-carbonyl group near 1660 cm^{-1} and to the carboxyl group of the propionic acid near 1700 cm^{-1}; instead, it has a new band at 1756 cm^{-1} which is characteristic of a γ,δ-unsaturated δ-lactone ring. Therefore, the compound is believed to have the lactone structure (VI).

The monocarboxylic acid (IIId), which was also obtained from the dicarboxylic acid (IIIa) by decarboxylation (58%), was subjected to a polyphosphoric acid-catalyzed intramolecular cyclization to give 5-methoxy-3-oxo-1,2,3,8,9,9a-hexahydrophenanthro[4,5-*bcd*]furan (IVa) in a 59% yield. For the aromatization of IVa to the phenol (Ia), palladium on charcoal was used as the catalyst; the yield was 10%.

The yields of the di- and monocarboxylic acids

(IIIa and IIId) were comparable to those of the corresponding carboxylic acids (IIIc and IIIf) from IIf in the synthesis of Ic (34 and 2%).[2] The results, combined with previously reported,[1,2] seem to indicate that the methoxyl groups of IId and IIe have no effect on the yields of the cyclizations. The yield of the ketone (IVa) was almost the same as that of IVb (67%)[1] and better than that of IVc (45%).[2] The results indicate that the methoxy groups of IIId and IIIe serve to increase the yields in the cyclizations. As the IVa–c are obtained in fairly good yields from IId–f under mild conditions, no large strain is introduced into the reactions. If the strain is present in phenanthro[4,5-*bcd*]furan derivatives (IV),[3] it is mainly present in the naphtho[1,8-*bc*]furan ring. The problem of the strain in naphtho[1,8-*bc*]furan derivatives will be further investigated later.

Experimental

All the melting points are uncorrected. The column chromatography was performed on silica gel (WAKOGEL C-200). The polyphosphoric acid was prepared from 85% phosphoric acid (100 ml) and phosphorus pentoxide (123 g) by heating them at 160—165 °C for 5 hr. Unless otherwise stated, anhydrous sodium sulfate was employed as the drying agent. The infrared absorption spectra were determined with a JASCO Model DS 402 G infrared spectrophothometer. The ultraviolet absorption spectra were determined with a Shimadzu Model UV-200 spectrophothometer. The nuclear magnetic resonance spectra were determined at 100 MHz with a JEOL Model 4H-100 NMR spectrometer, using tetramethylsilane as the internal standard.

4-(3,4-Dimethoxyphenyl)butyric Acid. A mixture of 3-(3,4-dimethoxybenzoyl)propionic acid (40 g) in acetic acid (150 ml), palladium chloride (520 mg) in 0.1M hydrochloric acid (30 ml), and charcoal (10 g) was shaken under a hydrogen atmosphere at room temperature.[4] After the usual treatment, the recrystallization of the resulting solid from chloroform-petroleum ether gave 30.3 g (85%) of 4-(3,4-dimethoxyphenyl)butyric acid as colorless plates; mp 60—61 °C (lit,[5] 58—59 °C).

4-(2-Chloro-4,5-dimethoxyphenyl)butyric Acid. This acid was prepared according to the method of Brown *et al.*[6] Colorless prisms; mp 106—108 °C (lit,[5] 112 °C).

5-Chloro-8-hydroxy-7-methoxy-1-tetralone (IIa). A mixture of 4-(chloro-4,5-dimethoxyphenyl)butyric acid (30.0 g) and polyphosphoric acid (390 g) was heated with stirring at 90 °C for 7 hr. The deep red mixture was decomposed with ice water, and the resulting precipitates were extracted with ether. The ethereal layer was washed with 1M potassium carbonate and then water, dried, and evaporated. The recrystallization of the residue from ethanol gave 22.7 g (86%) of IIa as yellow needles; mp 102—103 °C (lit,[5] 104—105 °C).

8-Hydroxy-7-methoxy-1-tetralone (IIb). A mixture of charcoal (4.0 g), palladium chloride (500 mg) in 0.1 M hydrochloric acid (20 ml), and ethanol (50 ml) was shaken under a hydrogen atmosphere at room temperature until no hydrogen was consumed. After adding of IIa (30 g) in ethanol (200 ml), the mixture was then shaken at 40 °C until 2.3 l of hydrogen had been consumed.[6,7] After the usual subsequent treatment, the recrystallization of the resulting solid from hexane gave 15.2 g (60%) of IIb as yellow plates; mp 76—77 °C. IR(KBr): 1625 (C=O), 829 (OH), and 811 cm^{-1} (two adjacent aromatic hydrogen atoms). NMR(CD_3COCD_3): δ 12.67 (s, OH), 3.82 (s, OCH_3), 7.15 (d, 1H, J=8 Hz, Ar–H), and 6.70 (d, 1H, J=8 Hz, Ar–H).

Found: C, 68.81; H, 6.28%. Calcd for $C_{11}H_{12}O_3$: C, 68.74; H, 6.29%.

8-Hydroxy-2-hydroxymethylidene-7-methoxy-1-tetralone (IIc). To a mixture of sodium methoxide (8.0 g, from 4.3 g of sodium and absolute methanol) and benzene (50 ml), we added ethyl formate (14.5 ml) under a nitrogen atmosphere at room temperature, after which the mixture was stirred for 30 min. To the mixture we then added IIb (8 g) in benzene (50 ml), drop by drop, over a 30min period under cooling with ice water, after which the mixture was stirred for an additional 4 hr at room temperature. The resulting green-yellow mixture was decomposed with 1 M sulfuric acid (120 ml) and extracted with benzene. The benzene layer was extracted with a 1 M potassium carbonate solution. The alkaline solution thus obtained was acidified with 6 M hydrochloric acid, and the resulting precipitates were recrystallized from 60% aqueous ethanol to give 7.7 g (84%) of IIc as yellow plates; mp 110—111 °C. IR(KBr): 1625 (C=O), 832 (OH), and 800 cm^{-1} (two adjacent aromatic hydrogen atoms). NMR(CD_3COCD_3): δ 13.36 (broad s, Ar–OH+ =C–OH), 11.98 (s, –C–OH), 2.00 (broad s, =CH–O–), 2.43 (broad s, =CH–O–), 7.10 (d, 1H, J=8 Hz, Ar–H), 6.68 (d, 1H, J=8 Hz, Ar–H), and 3.84 (s, OCH_3). UV(EtOH): λ_{max} 225 (ε 14500) and 315—356 nm, (10500).

Found: C, 65.33; H, 5.54%. Calcd for $C_{12}H_{12}O_4$: C, 65.45; H, 5.49%.

3-(Hydroxy-7-methoxy-1-oxo-1,2,3,4-tetrahydro-2-naphthyl)-propionic Acid (IId). A mixture of IIc (15.0 g), methyl acrylate (75.0 g), triethylamine (7.5 g), and 80% aqueous methanol (120 ml) was refluxed at 115 °C for 1 hr. The reaction mixture was then concentrated under reduced pressure, and the resulting oil was extracted with ether. The ethereal layer was washed with 2 M hydrochloric acid, a 1 M potassium carbonate solution, and then water, and dried, after which the ether was evaporated. The residue was heated in a water-bath under reduced pressure to remove any unreacted methyl acrylate. The residue was then dissolved in a small amount of ethanol and hydrolyzed with a 3 M potassium hydroxide solution. The alkaline solution was acidified with 6M hydrochloric acid. The resulting precipitates were collected and recrystallized from 70% aqueous ethanol to give 15.2 g (85%) of IId as orange yellow needles; mp 157—158.5 °C. IR(KBr): 1708 (COOH), 1625 (C=O), and 812 cm^{-1}, (two adjacent aromatic hydrogen atoms). NMR(CD_3COCD_3): δ 12.67 (s, OH), 7.14 (d, 1H, J=8 Hz, Ar–H), and 6.70 (d, 1H, J=8 Hz, Ar–H). UV (EtOH): λ_{max} 227 (ε 16300), 267 (10200), and 353 nm (3100).

Found: C, 63.66; H, 6.13%. Calcd for $C_{14}H_{16}O_5$: C, 63.63; H, 6.10%.

3-(2-Carboxy-8-methoxy-4,5-dihydro-3H-naphtho[1,8-bc]furan-3-yl)propionic Acid (IIIa) and 3-(8-Methoxy-4,5-dihydro-3H-naphtho-[1,8-bc]furan-3-yl)propionic Acid (IIId). A mixture of IId (2.0 g), ethyl bromoacetate (18.6 g), and potassium carbonate (12.8 g) was gradually heated to 170 °C and then refluxed for an additional 6 hr at this temperature. The dark brown mixture was extracted with hot acetone, and then the acetone was evaporated. The residue was dissolved in a small amount of ethanol and hydrolyzed with a 3 M potassium hydroxide solution. The alkaline solution was acidified with 6M hydrochloric acid, and the resulting precipitates were extracted with ether. The ethereal solution was washed with water and dried, and then the solvent was evaporated. The residue was divided into soluble and insoluble portions with benzene. The benzene-insoluble portion (0.9 g, 39%) was recrystallized from 60% aqueous

ethanol to give IIIa as colorless needles; mp 213—214 °C. IR(KBr): 1705 and 1690 cm^{-1} (COOH). UV(EtOH): λ_{max} 234 (ε 22500) and 277 nm (14500).

Found: C, 63.20; H, 5.37%. Calcd for $C_{16}H_{16}O_6$: C, 63.15; H, 5.30%.

The benzene-soluble portion was chromatographed on silica gel and eluted with benzene–ether (9 : 1). A yellow fraction was collected to give crystals. Recrystallization from benzene–*n*-hexane gave 30 mg (1.5%) of IIId as colorless plates; mp 136—138 °C. IR(KBr): 1705 cm^{-1} (COOH). NMR(CD_3COCD_3): δ 7.60 (d, 1H, J=1 Hz, furan H), 6.91 (d, 1H, J=8 Hz, Ar–H), 6.76 (d, 1H, J=8 Hz, Ar–H), and 5.97 (s, OCH_3). UV(EtOH): λ_{max} 216 (ε 30700), 247 (10000), 255 (9200), 280 (1900), and 290 nm (1700).

Found: C, 69.22; H, 6.22%. Calcd for $C_{15}H_{16}O_4$: C, 69.92; H, 6.20%.

Decarboxylation of IIIa. A mixture of IIIa (1.0 g), copper powder (1.0 g), and quinoline (10 g) was heated at 160 °C for 1 hr. The reaction mixture was extracted with ether and acidified with 2M hydrochloric acid. The ethereal layer was washed with 2M hydrochloric acid and then water, dried, and then evaporated. The residue was chromatographed on silica gel and eluted with benzene–ether (9 : 1). A yellow fraction was collected, and after the removal of the solvent the residue was recrystallized from benzene–*n*-hexane to give 500 mg (58%) of IIId as colorless plates; mp 137—138 °C.

5-Methoxy-3-oxo-1,2,3,8,9,9a-hexahydrophenanthro[4,5-bcd]-furan (IVa). A mixture of IIId (2.0 g) and polyphosphoric acid (260 g) was heated while being stirred at 80 °C for 4 hr. The green reaction mixture was then decomposed with ice water, and the resulting precipitates were extracted with ether. The ethereal layer was washed with a 1M potassium carbonate solution and then water, and dried. The ether was evaporated, and the residue was recrystallized from ethanol to give 1.1 g (59%) of IVa as colorless needles; mp 161—162 °C. IR(KBr): 1659 cm^{-1} (C=O). NMR ($CDCl_3$): δ 6.97 (d, 1H, J=8 Hz, Ar–H), 6.86 (d, 1H, J=8 Hz, Ar–H), and 4.06 (s, OCH_3). UV(EtOH): λ_{max} 240 (ε 16500) and 294 nm (20200).

Found: C, 74.06; H, 5.85%. Calcd for $C_{15}H_{14}O_3$: C, 74.36; H, 5.82%.

3-Hydroxy-5-methoxyphenanthro[4,5-bcd]furan (Ia). A mixture of IVa (200 mg), 20% palladium on charcoal (400 mg), and α-methylnaphthalene (3.5 g) was heated under a nitrogen atmosphere at 240 °C for 30 hr.[8,9] The reaction mixture was then filtered, and the filtrate was extracted with ether. The ethereal layer was extracted with a 1 M potassium hydroxide solution. The alkaline solution thus obtained was washed with carbon tetrachloride and then acidified with 6M hydrochloric acid. The resulting precipitates were extracted with ether. The ethereal layer was washed with water, dried, and then evaporated. The residue was chromatographed on silica gel and eluted with benzene–ether (9 : 1). A yellow fraction was collected, and after the removal of the solvent the residue was recrystallized from benzene to give 40 mg (10%) of Ia as colorless needles; mp 127—128 °C. IR(KBr): 3250 (Ar–OH) and 816 cm^{-1} (two adjacent aromatic hydrogen atoms). NMR(CD_3COCD_3): δ 9.61 (s, OH), 7.75 (s, 2H, Ar–H), 2.25—2.60 (m, 6H, Ar–H), and 5.65 (s, OCH_3). UV(EtOH):[10] λ_{max} 232 (ε 38200), 245 (48300), 258 (25300), 268 (24600), 315 (14000), 327 (14100), and 356 nm (23000).

Found: C, 75.76; H, 4.25%. Calcd for $C_{15}H_{10}O_3$: C, 75.62; H, 4.23%.

3-(8-Carboxymethoxy-7-methoxy-1-oxo-1,2,3,4-tetrahydro-2-naphthyl)propionic Acid (V). A mixture of IId (1.0 g), ethyl bromoacetate (3.7 g), potassium carbonate (6.0 g), and dioxane (15 ml) was refluxed for 6.5 hr at 115 °C. The reaction mixture was then extracted with acetone, and the acetone was evaporated. The residue was dissolved in ethanol and hydrolyzed with a 3M potassium hydroxide solution. The alkaline solution was acidified with 6M hydrochloric acid, and the resulting precipitates were extracted with ether. The ethereal layer was washed with water, dried, and then evaporated. The residue was washed with benzene to give 650 mg (53%) of V; mp 183—185 °C. Recrystallization from acetone–tetrahydrofuran gave colorless prisms; mp 185—187 °C. IR(KBr): 1750 (COOH), 1698 (CO-OH), 1658 (C–O), and 815 cm^{-1} (two adjacent aromatic hydrogen atoms). UV(EtOH): λ_{max} 219 (ε 18700), 253 (6000), and 320 nm (2300).

Found: C, 59.62; H, 5.63%. Calcd for $C_{16}H_{18}O_7$: C, 59.53; H, 5.82%.

Lactone (VI). A mixture of V (1.0 g), sodium acetate (4.6 g), and acetic anhydride (15 ml) was heated for 1 hr at 145 °C and then for 5 min at 150 °C. The reaction mixture was poured into water to decompose the acetic anhydride and then extracted with ether. The ethereal layer was washed with water, dried, and then evaporated. The residue was washed with benzene to give 500 mg (53%) of VI; mp 168—169 °C. Recrystallization from acetone gave colorless needles; mp 169—170 °C. IR(KBr): 1756 (lactone), 1736 (COOH), and 816 cm^{-1} (two adjacent aromatic hydrogen atoms).

Found: C, 62.97; H, 5.34%. Calcd for $C_{16}H_{16}O_6$: C, 63.15; H, 5.30%.

The authors wish to thank Mr. Hideo Saisu for the infrared analyses and Mr. Hideo Ōno for the nuclear magnetic resonance analyses.

References

1) T. Shimizu, T. Horaguchi, and A. Watanabe, This Bulletin, **46**, 1772 (1973).
2) T. Horaguchi and T. Shimizu, *ibid.*, **47**, 485 (1974).
3) A. V. Dendy, J. H. P. Tyman, and W. B. Whalley, *J. Chem. Soc.*, **1963**, 4040.
4) M. Seki, H. Saito, and H. Mamuro, *Nippon Kagaku Zasshi*, **81**, 292 (1960).
5) R. Ghosh and Sir Robert Robinson, *J. Chem. Soc.*, **1944**, 508; R. D. Haworth and C. R. Mavin, *ibid.*, **1932**, 1486.
6) A. G. Brown, J. C. Lovie, and R. H. Thomson, *ibid.*, **1965**, 2348.
7) D. B. Bruce and R. H. Thomson, *ibid.*, **1955**, 1089.
8) R. B. Turner, D. E. Nettleton, J. R., and R. F. Ferebee, *J. Amer. Chem. Soc.*, **76**, 5923 (1956); W. S. Johnson and H. Posvic, *ibid.*, **69**, 1361 (1947).
9) E. Mosettig and H. M. Duvoll, *ibid.*, **59**, 367 (1939).
10) H. Rapoport, A. D. Batchs, and J. E. Gordon, *ibid.*, **80**, 5767 (1958).

A Convenient Synthesis of 5-Substituted-2,5-dihydro-2-furoic Acids

Tadashi MASAMUNE, Mitsunori ONO, and Hajime MATSUE
Department of Chemistry, Faculty of Science, Hokkaido University, Sapporo 060
(Received May 17, 1974)

Nine 5-alkyl- and 5-aryl-2-furoic acids were reduced under controlled Birch conditions and then esterified with acidic methanol. 2-Furoic acids with 5-alkyl groups gave good yields of methyl 5-alkyl-2,5-dihydro-2-furoates, which were obtained as mixtures of *cis*- and *trans*-diastereoisomers. These 2,5-dihydrofuroates revealed interesting spectroscopic properties; (1) large long-range coupling constants, 5—7 and 3—4 Hz, between protons at C_2 and C_5 were observed in the NMR spectra of *cis*- and *trans*-diastereoisomers, respectively, and (2) two high absorption maxima due to the ester carbonyl group of each furoate appeared near 1750 and 1730 cm^{-1} in the IR spectrum. On the other hand, the furoic acids with 5-aryl substituents afforded 5-arylpentanoate or 5-arylpent-3-enoate as main products. These esters would be produced as a result of reductive cleavage at C_5 of 5-aryl-2,5-dihydrofuroates formed as intermediates.

In connection with a study aimed at the total synthesis of laurencin[1] with a tetrahydrooxocin skeleton, we have been in search of a facile method for preparation of the titled furoic acids, because an elegant synthesis[2] of the skeleton involved a 3-oxagranatanine derivative[3] as a key intermediate, which had been prepared by the Robinson-Schöpf condensation starting from 3-oxaglutaraldehyde. Only a few papers have been reported of syntheses of 2,5-dihydrofurans.[4] The reduction of furans with dissolving metals seems to be highly dependent on the reaction conditions and gives many products.[5] However, it has been reported recently that 2-furoic acid is reduced efficiently to the 2,5-dihydro derivative under the controlled Birch conditions.[6] We have developed the method for 5-alkyl- and 5-aryl-furoic acids. The present paper describes the reduction result and the spectroscopic properties of resulting 5-alkyl-2,5-dihydro-2-furoic acids. In view of the occurrence of natural products containing this moiety, such as carotenoids,[7] sesquiterpenoids[8] and antibiotics,[9] this result would be useful for synthesis of some of these compounds.

Nine 5-substituted furoic acids (**1a**—**1i**) were used as starting materials. All these compounds are known but were not always obtained under the reported processes or conditions. The first three acids **1a**, **1b** and **1c** (R=CH_3, C_2H_5 and n-C_3H_7) were prepared more readily and/or in better yields according to a modified process (Scheme 1). This method, however, was not available for preparation of two other alkyl acids **1d** and **1e** (R=i-C_3H_7 and t-C_4H_9) with 5-branched alkyl substituents. These two acids and two 5-benzylfuroic acids **1f** and **1g** (R=$C_6H_5CH_2$ and p-$CH_3OC_6H_4CH_2$) were synthesized by Friedel-Crafts alkylation of methyl furoate followed by hydrolysis. Two 5-phenylfuroic acids **1h** and **1i** (R=C_6H_5 and p-$CH_3OC_6H_4$) were not prepared by the reported methods;[10,11] after careful examination of the reaction process and conditions, the latter **1i**, mp 186—187 °C, was obtained by the Meerwein reaction of p-anisidine and 2-furoic acid under the limited conditions, and the former **1h**, mp 150—150.5 °C, by the Vilsmeyer reaction of 2-phenyl-

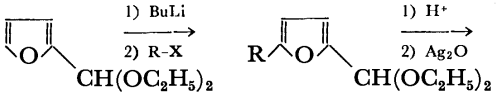

1

Scheme 1.

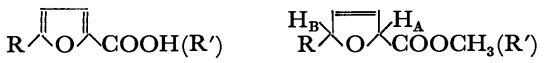

1 2

furan followed by oxidation

The reductions of 2-furoic acids (**1**) to the 2,5-dihydro derivatives (**2**) were searched under various Birch reductions, using 5-ethyl-2-furoic acid (**1b**). (1) Reduction of **1b** in liquid ammonia with sodium (3 mol) and subsequent addition of methanol afforded, as a main product, a nicely crystalline acid (**3**, R=H) mp 229—230 °C, which was converted into the methyl ester (**3**, R=CH_3), mp 88—89 °C, having a molecular formula of $C_{16}H_{22}O_6$ corresponding to a dihydro dimeric compound; Mass, m/e 310 (M^+) and IR, ν_{max} 1760 and 1740 cm^{-1}. The (planar) formula was assigned on the basis of the NMR spectrum; each of two protons (H_A), on the carbon flanked by a double bond, an oxygen atom and a carbomethoxy group, appeared at low field, δ 5.20, as a double doublet with coupling constants of 2.6 (J_{AB}) and 1.5 Hz (J_{AC}) with olefinic protons (H_B and H_C). On the other hand, (2) treatment of **1b** in both liquid ammonia and methanol with sodium or lithium (3 mol) followed by esterification produced good yields of a 1 : 1 mixture of diastereoisomeric methyl 5-ethyl-2,5-dihydro-2-furoates (**2b**), bp 88—89 °C/13 mmHg. Thus, the reductions of all other furoic acids (**1**) were carried out under these conditions. The products were separated and purified by distillation, gas (glc), thin layer (tlc) and/or column chromatographies, and identified on the spectral data. The results are summarized in Table 1.

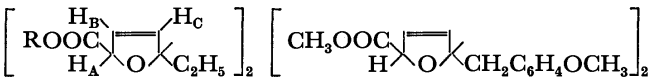

3 4

One example of the structure elucidations of the 2,5-dihydro products (**2**) will be illustrated by the 5-ethyl derivative (**2b**). This compound **2b** proved to be obtained as a 1 : 1 mixture of diastereoisomers by glc, though isolation of each isomer (*cis* and *trans*) was not attempted. The elemental analysis and the Mass [m/e 156 (M^+), 127 (M^+–C_2H_5) and 97 (M^+–$COOCH_3$)] and IR spectra (ν_{max} 1768 and 1743 cm^{-1}) confirmed the molecular formula $C_8H_{12}O_3$, and indicated **2b** to be a dihydro methyl ester of **1b**. In accordance

Table 1. The Birch reduction of 5-substituted 2-furoic acids

Compound (R′=H)	Substituent	Metal	Yield[a] Product[b]	1 (R′=CH_3)[c]
1a	CH_3	Na	**2a** (1:1); 70 (80)	(10)
		Li	83 (90)	(5)
1b	C_2H_5	Na	**2b** (1:1); 65 (85)	(5)
		Li	85 (93)	(3)
1c	C_3H_7	Na	**2c** (1:1); 64 (80)	(13)
		Li	75 (93)	(5)
1d	*i*-C_3H_7	Na	**2d** (1:1); 69 (81)	(10)
		Li	70 (85)	(8)
1e	*t*-C_4H_9	Na	**2e** (1:1); 70 (80)	(13)
		Li	71 (87)	(10)
1f	$C_6H_5CH_2$	Na	**2f** (3:2); 40 (55)	(20)
		Li	40 (55)	(20)
1g	*p*-$CH_3OC_6H_4CH_2$	Na	**2g** (3:2); 40 (50) **4**; (8)	(35)
1h	C_6H_5	Na	**5h**; (40) : **6h**; (5)	(40)
1i	*p*-$CH_3OC_6H_4$	Na	**5i**; (9) : **6i**; (40)	(40)

a) The figures in parentheses denote yields estimated by glc. b) The figures in parentheses following **2a** to **2g** denote ratios of *cis*- and *trans*-diastereoisomers estimated by glc. c) Recovered acid methyl esters.

with this assigned structure, the NMR spectrum exhibited two triplets (total 3H, J=7 Hz) at δ 0.88 and 0.91, a multiplet (2H) centered at 1.57, two singlets (3H) at 3.64 and 3.66, a multiplet (2H) centered at 4.90, and a double quartet (2H) centered at 5.88, which were attributed to ethyl CH_3, ethyl CH_2, and $COOCH_3$ protons, two protons at C_2 and C_5 (H_A and H_B), and two olefinic protons at C_3 and C_4. Irradiation at both δ 1.57 and 5.88 collapsed a H_A and H_B multiplet into two simple AB-type quartets, indicating that H_A and H_B protons in one of the diastereoisomers absorbed at δ 4.91 and 4.62, respectively, with coupling constant of 3—4 Hz, and these protons in the other at δ 4.96 and 4.77 with coupling constant of 5—6 Hz. The latter isomer would be oriented *cis* and the former *trans*, as discussed later. These large, long-range coupling constants and also the two absorption maxima due to a carbomethoxy group in each of compounds **2** are listed in Table 2.

As shown in Table 1, all alkylfuroic acids (**1a**—**1e**) produced the corresponding dihydro methyl esters

Table 2. The IR and NMR spectra of methyl 5-alkyl-2,5-dihydro-2-furoates

Compound	Absorption maximum[a] (cm^{-1})	Coupling constant[b] (Hz) *cis*	*trans*
2a	1768, 1743	5—6	3—4
2b	1768, 1743	5—6	3—4
2c	1755, 1725	5—6	3
2d	1755, 1725	6	3—4
2e	1755, 1725	7	4
2f	1756, 1735	5—6	3—4
2g	1745, 1735	5—6	3—4

a) Absorption due to the ester carbonyl group in chloroform. b) Coupling constant between protons at C_2 and C_5 in deuterochloroform.

(**2a**—**2e**) in good yields, only about 10% of the starting acid methyl esters being identified by glc. However, two benzylfuroic acids (**1f** and **1g**) gave only moderate yields (ca. 50%) of the expected dihydro esters (**2f** and **2g**) and most of the remaining esters consisted of the unreacted acid esters and, in case of **1g**, a small amount of the dimer (**4**), mp 210—211 °C. The structure of **4** was determined in the same manner as that of **3**. The lower yields of **2f** and **2g** would be explained well if some sodium metal would be consumed for partial reduction of the phenyl ring followed by dehydrogenation during work-up.

The reductions of 5-phenylfuroic acids (**1h** and **1i**) proceeded in different way. Two products, methyl 2-hydroxy-5-phenylpentanoate (**5**) and the corresponding *cis*-pent-3-enoate (**6**), were identified along with the unreduced methyl esters, the main product from **1h** being pentanoate **5h** and that from **1i** pentenoate **6i**. These compounds would be resulted from facile reductive cleavage at C_5, the carbon atom adjacent to both phenyl and vinyl groups, of the 2,5-dihydro derivative, which would be formed in the same manner as other alkyl- and benzyl-furoic acids. The structure determination of **6i** will be discussed as a representative of these esters. Compound **6i**, oil, was hydrolyzed to give the acid (**6i**, R′=H), mp 101—102 °C, in good yield. The Mass [m/e 222 (M^+) and 121 (base peak, $M^+-C_6H_5CH_2$)] and IR spectra (ν_{max} 3648 and 1738 cm^{-1}) suggested this formula, which was confirmed by the NMR spectrum; a doublet (2H) at δ 3.52, a doublet (1H) at 5.12, a triplet (1H) at 5.52 and a double triplet (1H) at 5.92 were assigned to protons at C_5, C_2, C_3, and C_4, respectively. A broad peak centered at δ 6.42 disappeared on addition of D_2O. The signal at δ 5.92 was simplified to a doublet (J=11 Hz) by irradiation at δ 3.52, and that at 5.52 to a doublet (J=11 Hz) by irradiation at δ 5.12. These double resonance experiments were consistent with the assigned

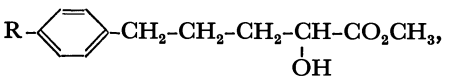

5h R=H
5i R=OCH_3

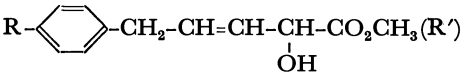

6h R=H
6i R=OCH_3

structure.

In summary, the present result indicates that the relevant Birch reductions under controlled conditions are generally available for the synthesis of methyl 5-alkyl-2,5-dihydro-2-furoates, which will be derived into 2,5-unsymmetrically substituted 2,5-dihydrofurans not readily accessible. The spectroscopic properties of these 2,5-dihydrofuroates deserve some comments. (1) Extremely large long-range coupling constants were demonstrated between two protons (H_A and H_B) at C_2 and C_5 of the dihydrofurans, irrespective of their configurations, *cis* and *trans*. Usually, homoallylic coupling constants fall in a range of 1—3 Hz.[12] On the other hand, large coupling constants as shown by these compounds have also been observed between protons across five single bonds.[13] In general, these large values have been interpreted as a result of the transmission through the double "zig-zag" paths of the bonds between the two protons.[14] 2,5-Dihydrofuroates with *cis*-configuration would readily take this "zig-zag" type of conformation,[9] whereas those with *trans*-configuration would not be able to adopt such conformations. However, in view of the variety of the coupling constants in question in other 2,5-dihydrofurans,[15] no definite configurational assignment could not be made to each of the diastereoisomers **2**. Now we only tentatively assign the larger constants (5—7 Hz) to the *cis*-isomers and the smaller (3—4 Hz) to the *trans*-isomers, and point out that both the intervending double bond and oxygen atom would probably play a significant role for this noteworthy finding. (2) Two high absorption maxima due to the ester carbonyl groups were observed near 1750 and 1730 cm^{-1} in the IR spectra. It would not be reasonable to ascribe these two absorptions to the existence of two diastereoisomers, because such two bands have appeared in the spectra of methyl 2,5-dihydro-2-furoate[6] and ethyl tetrahydro-2-furoate and 2,3-dimethyl-2,3-epoxybutanoate.[16] This would result from the presence of two conformers caused by rotation of the carbomethoxy group around the bond between the epoxy carbon and carbonyl carbon. Further investigations concerning these bands by the CMR are now in progress.

Experimental

All the mps and bps were uncorrected. The homogenity of each compound was always checked by tlc over silica gel (Wakogel B-5) and/or by glc (Hitachi K-53) over 10% SE-30. Column chromatographies were carried out over silicic acid (Merck, Kieselgel 60 or Mallinckrodt, silicic acid 100 mesh). The IR spectra were taken in chloroform, unless otherwise stated. The NMR spectra were obtained in deuterochloroform, unless otherwise stated, at 100 MHz, and the chemical shifts were given in δ-values, TMS being used as an internal reference. The abbreviations "s, d, t, q, m, and br" in the NMR spectra denote "singlet, doublet, triplet, quartet, multiplet, and broad", respectively.

*5-Methyl-2-furoic Acid (**1a**).* 2-Furfural diethyl acetal was prepared by a modified method;[17] a solution of furfural (96 g) and triethyl orthoformate (165 ml) in ethanol (150 ml) containing ammonium chloride (1.5 g) was refluxed for 3 hr and then distilled fractionally to give the acetal (134 g), bp 77—79 °C/20 mmHg.

To a suspended mixture of lithium (3.0 g), finely cut, in dry tetrahydrofuran (THF, 90 ml) cooled at −25 °C with Dry Ice-ethanol, was added dropwise *n*-butyl chloride (18.5 g) in THF (90 ml) under stirring and under a stream of nitrogen. When the reaction had started as indicated by the appearance of cloudiness after addition of a small volume of the chloride solution, the remaining solution was further added at −30 °C to −35 °C during 45 min to the mixture, which was then stirred at −25 °C (bath temp) for 4 hr. To this mixture was added dropwise the afore-mentioned acetal (18 g) at this temperature, and the whole mixture was again stirred at −15 °C (bath temp) for 4 hr, forming the 5-furyllithium derivative.[18] A solution of methyl iodide (28.4 g) in THF (equal weight, 28.4 g) was added to the mixture, which was further stirred at −15 °C (bath temp) for 1 hr and allowed to stand overnight at room temperature. The reaction mixture was poured into cracked ice and water, forming two layers. After separation of the THF layer, the aqueous solution was extracted with ether (3×150 ml). The THF and ether solutions were combined, dried over sodium sulfate and evaporated to leave resinous oil, which was distilled fractionally under reduced pressure to give 5-methyl-2-furfural diethyl acetal (10.3 g), bp 84—85 °C/9 mmHg; NMR (CCl_4), δ 1.15 (6H, t, J=7 Hz, acetal CH_3), 2.23 (3H, s, 5-CH_3), (4H, q, J=7 Hz, acetal CH_2), 5.34 (1H, s, acetal CH), 5.80 and 6.12 (each 1H, ABq, J=3.5 Hz, 3- and 4-H).

To the acetal (10.25 g) was added 2 M hydrochloric acid (6 ml), and the mixture was stirred at room temperature for 25 min. After addition of water (10 ml) the mixture was extracted with ether (5×10 ml), and the ether solution was washed with 5% sodium hydrogen carbonate solution (2× 10 ml) and water (2×10 ml), dried and distilled to give 5-methyl-2-furfural[19] (3.1 g), bp 75—76 °C/15 mmHg (lit,[19] 72—73 °C/11 mmHg).

To a semisolid mixture prepared from silver nitrate (12.75 g) in water (30 ml) and sodium hydroxide (5.0 g) in water (30 ml), was added dropwise 5-methyl-2-furfural (3.1 g) under cooling with ice. The mixture was stirred at room temperature for 12 hr and then filtered to remove silver oxide. The separated precipitate was washed with hot water repeatedly, and these washings and the filtrate were combined, acidified to pH 3 with concd hydrochloric acid, and extracted with ethyl acetate (3×20 ml). The acetate solution afforded crude acid (3.0 g), which was recrystallized from ethyl acetate to give **1a**[19] (2.14 g), mp 107—108 °C (lit,[19] 107—108 °C); NMR, δ 2.42 (3H, s, 5-CH_3), 6.21 and 7.28 (each 1H, ABq, J=3 Hz, 3- and 4-H), and 12.68 (1H, s, COOH).

*5-Ethyl-2-furoic Acid (**1b**).* A mixture of 2-diethoxylmethyl-5-furyllithium, prepared from 2-furfural diethyl acetal (13.6 g), lithium (3.0 g), and *n*-butyl chloride (18.5 g) in THF (180 ml), was treated with ethyl bromide (21.8 g) in THF (21.8 g) in the same manner as with methyl iodide and gave 5-ethyl-2-furfural diethyl acetal (9.7 g), bp 103—106 °C/15 mmHg. The acetal (9.5 g) was hydrolyzed with acid (2M HCl, 4 ml) for 30 min and gave the aldehyde[19] (4.32 g),

bp 88—89 °C/14 mmHg (lit,[19] 82—83 °C/11 mmHg); NMR (CCl_4), δ 1.24 (3H, t, J=7.5 Hz, ethyl $C\underline{H}_3$), 2.68 (2H, q, J=7.5 Hz, ethyl $C\underline{H}_2$), 6.14 and 7.06 (each 1H, ABq, J=3.5 Hz, 3- and 4-H), and 9.42 (1H, s, C$\underline{H}$O). This aldehyde (7.15 g), when oxidized with silver oxide, prepared from silver nitrate (24.3 g) and sodium hydroxide (11.4 g) in water (86 ml), afforded crude acid (6.3 g), mp 89—90 °C, which was recrystallized from ethyl acetate to give **1b**[19] (5.1 g), mp 91—92 °C (lit,[19] 93.5—94.5 °C).

*5-Propyl-2-furoic Acid (**1c**).* A mixture of 2-diethoxymethyl-5-furyllithium, prepared from 2-furfural diethyl acetal (13.6 g), lithium (3.0 g), and *n*-butyl chloride (18.5 g) in THF (180 ml), was treated with propyl bromide (24.4 g) in THF (24.4 g) in the same manner as with methyl iodide and gave 5-propyl-2-furfural diethyl acetal (4.76 g), bp 104—106 °C/15 mmHg. Found: C, 67.63; H, 9.70%. Calcd for $C_{12}H_{20}O_3$: C, 67.89; H, 9.50%.

The acetal (4.65 g) was hydrolyzed with acid (2M HCl, 4 ml) for 15 min to the aldehyde[20] (3.0 g), which was oxidized immediately with silver oxide, prepared from silver nitrate (9.35 g) and sodium hydroxide (4.4 g) in water (22 ml), and gave crude acid (2.97 g), mp 57—58 °C, which was recrystallized from ethyl acetate to give **1c**[20] (2.3 g), mp 63—64 °C (lit.,[20] 63—63.5 °C).

*5-Isopropyl-2-furoic Acid (**1d**), 5-tert-Butyl-2-furoic Acid (**1e**), and 5-Benzyl-2-furoic Acid (**1f**).* These acids were prepared according to the reported procedures.[21,22] Methyl 2-furoate was converted by the Friedel-Crafts reactions into methyl 5-isopropyl-2-furoate, bp 103—106 °C/14 mmHg (lit.,[21] 110—112 °C/20 mmHg), and methyl 5-*tert*-butyl-2-furoate, bp 95—97 °C/14 mmHg (lit,[21] 110—114 °C/15 mmHg), and methyl 5-benzyl-2-furoate, mp 41—41.5 °C and bp 187—189 °C/7 mmHg (lit,[22] 41—42 °C and 157—160 °C/3 mmHg). These esters were hydrolyzed to the corresponding acids **1d**, mp 65—65.5 °C (lit,[21] 65—66 °C), and **1e**, mp 104—105 °C (lit,[21] 104—105 °C), and **1f**, mp 106—107 °C (lit,[22] 105—105.5 °C).

*5-p-Methoxybenzyl-2-furoic Acid (**1g**).* To a mixture of methyl 2-furoate (17 g) in carbon disulfide (26 ml) containing anhydrous zinc chloride (1.45 g) was added dropwise *p*-methoxybenzyl chloride[23] in carbon disulfide (26 ml) under stirring at 0 °C. The mixture was kept for 30 min at 0 °C and further for 45 min at room temperature. It was poured onto crushed ice and the resulting two layers were separated. The aqueous phase was extracted with ether (50 ml). The carbon disulfide and ether layers were combined, washed with 5% sodium carbonate solution (2×50 ml) and water (50 ml), dried and distilled to give methyl *p*-methoxybenzyl-2-furoate (4.0 g), bp 166—167 °C/5 mmHg; IR, ν_{max} 1720, 1595, and 1030 cm^{-1}; NMR, δ 3.76 (3H, s, OCH_3), 3.84 (3H, s, $COOC\underline{H}_3$), 3.96 (2H, s, $C\underline{H}_2$), 6.08 and 7.14 (each 1H, ABq, J=3 Hz, 3- and 4-H), 6.88 and 7.22 (each 2H, ABq, J=7.5 Hz, $CH_3OC_6\underline{H}_4CH_2$).

A mixture of the ester (4.0 g) and 10% sodium hydroxide solution (40 ml) was boiled under reflux for 1 hr, when it became homogeneous. The solution was poured onto ice and water, acidified to pH 1 with concd hydrochloric acid, and extracted with ethyl acetate (3×50 ml). The acetate solution, after being washed with water, dried and evaporated, gave crude acid (3.1 g), mp 116—120 °C, which on recrystallization afforded **1g**[22] (2.6 g), mp 124—124.5 °C (lit,[22] 123—124 °C). Found: C, 66.82; H, 5.25%. Calcd for $C_{13}H_{12}O_4$: C, 67.23; H, 5.21%.

*5-Phenyl-2-furoic Acid (**1h**).* 2-Phenylfuran was prepared according to the procedure by Johnson;[24] a fraction boiling at 107—109 °C/15 mmHg (lit.,[24] 92—95 °C/10 mmHg) was further separated by column chromatography (Merck, benzene) into 3-phenylfuran,[25] mp 53—54 °C, and 2-phenylfuran, bp 107—109 °C/15 mmHg; NMR, δ 6.38 (1H, double d, J=3.5 and 1.7 Hz, 4-H), 6.60 (1H, d, J=3.5 Hz, 3-H), 7.36 (5H, m, $C_6\underline{H}_5$), and 7.61 (1H, d, J=1.7 Hz, 5-H).

To a mixture of dry dimethylformamide (1.9 g) and phosphorus oxychloride (3.96 g), which had been kept at 0 °C for 20 min, was added freshly distilled 2-phenylfuran (2.4 g) under stirring below 20 °C.[19] The whole mixture was kept at 0—5 °C for 1 hr and then at room temperature for 1.5 hr, and poured into ice water. The resulting mixture was neutralized with 5% sodium carbonate solution and allowed to stand for 16 hr, forming two layers. The organic layer was separated and the aqueous was extracted with ether (3× 60 ml). The organic and the ether solutions were combined, dried and evaporated to leave crude 5-phenyl-2-furfural, (2.86 g), ν_{max} 1660 and 1593 cm^{-1}, which was used for the next oxidation without further purification.

The aldehyde (2.56 g) was added into a semisolid mixture, prepared from silver nitrate (5.03 g) and sodium hydroxide (2.37 g) in water (20 ml) cooled with a ice bath, under vigorous stirring. The whole mixture was stirred at room temperature overnight and worked up as usual to give crude acid (2.20 g), mp 126—130 °C, which was recrystallized from chloroform to give **1h** (1.6 g), mp 150—150.5 °C (lit,[10] no mp, bp 120—122 °C/30 mmHg); IR, ν_{max} 3400, 1695, and 1195 cm^{-1}; NMR, δ 6.76 and 7.80 (each 1H, ABq, J=3.5 Hz, 3- and 4-H), 7.40 (5H, m, $C_6\underline{H}_5$), and 10.20 (1H, br s, COO$\underline{H}$). Found: C, 70.00; H, 4.16%. Calcd for $C_{11}H_8O_3$: C, 70.21; H, 4.29%.

*5-p-Methoxyphenyl-2-furoic Acid (**1i**).* This compound was not prepared by the reported method.[10] *p*-Anisidine (12.0 g) was dissolved in boiling 25% hydrochloric acid (40 ml) and cooled, when the hydrochloric acid salt precipitated. To the mixture were added crushed ice (30 g) and then rapidly sodium nitrite (8.0 g) in water (30 ml) under stirring, when the mixture became homogeneous. A saturated sodium acetate solution was added to the solution, until the pH value became 1.0, during which the temperature was kept at 0—10 °C. The solution was added dropwise under cooling to a mixture of 2-furoic acid (11.2 g) in water (100 ml) containing sodium acetate (32.0 g), which had been homogeneous on warming. The resulting mixture was mixed with an aqueous solution (10 ml) containing cupric chloride (4.0 g as $CuCl_2 \cdot 2H_2O$), and the whole mixture was stirred below 15 °C for 5 hr and then at room temperature for 60 hr. After removal of resinous material by filtration and evaporation of volatile substance by steam distillation, the solution became heterogeneous and, after being cooled, was filtered. The precipitate was treated with saturated sodium hydrogen carbonate solutions (3×100 ml). The carbonate extracts and the filtrate were combined, acidified with concd hydrochloric acid, and extracted with ethyl acetate (3× 100 ml). The acetate solution was washed with water (100 ml) and a saturated sodium chloride solution (100 ml), dried and evaporated to leave crude acid (4.5 g), mp 166—167 °C. This was recrystallized from 20% ethanol to give **1i** (2.9 g), mp 187—188 °C; IR (Nujol), ν_{max} 1670, 1265, and 1028 cm^{-1}; NMR, δ 3.80 (3 H, s, $OC\underline{H}_3$), 6.62 and 7.38 (each 1 H, ABq, J=3.5 Hz, 3- and 4-H), 6.94 and 7.74 (each 2 H, ABq, J=8 Hz, $CH_3OC_6\underline{H}_4$), and 8.84 (1 H, br s, COO$\underline{H}$). Found: C, 66.03; H, 4.64%. Calcd for $C_{12}H_{10}O_4$: C, 66.05; H, 4.62%.

*2,2'-Diethyl-2,2',5,5'-tetrahydro[2,2'-bifuran]-5,5'-dicarboxylic Acid (**3**).* To a mixture of 5-ethyl-2-furoic acid (**1b**) (0.3 g, 0.045 mol) in refluxing ammonia (300 ml) was added sodium (3.1 g, 0.145 mol), when the blue color appeared.

The mixture was stirred for 20 min and, when methanol (4.64 g, 0.145 mol) was added, became colorless and was further stirred for 3 hr. After removal of ammonia, the residue was diluted with water (20 ml), acidified with 2M hydrochloric acid, and extracted with ether (3×20 ml). The ether solution, on being dried and evaporated, gave crude acid (2.85 g), mp 210—215 °C, which was recrystallized from benzene to yield **3** (2.1 g), mp 229—230 °C; IR (Nujol), ν_{max} 1728, 1708, 1108, and 1060 cm^{-1}; NMR (C_6D_5N), δ 0.92 (6 H, t, J=6.5 Hz, $2C\underline{H}_3$), 2.20 (4 H, m, $2C\underline{H}_2$), 5.54 (2 H, double d, J=2.6 and 1.5 Hz, 5- and 5′-H), 6.03 (2H, double d, J=4.6 and 1.5 Hz, 3- and 3′-H), 6.60 (2H, double d, J=4.6 and 2.6 Hz, 4- and 4′-H), and 13.62 (2H, s, COO$\underline{H}$).

Compound **3** (243 mg) in ether was converted with diazomethane to the methyl ester (268 mg), which was recrystallized from ethanol to give **3** (R=CH_3) (215 mg), mp 88—89 °C; Mass, *m/e* 310 (M^+) and 155 (base); IR, ν_{max} 1760, 1740, 1278, and 1105 cm^{-1}; NMR (the text). Found: C, 62.22; H, 7.12%. Calcd for $C_{16}H_{22}O_6$: C, 61.92; H, 7.15%.

*Methyl 5-Ethyl-2,5-dihydro-2-furoates (**2b**).* To a refluxing ammonia (49 ml) containing 5-ethyl-2-furoic acid (**1b**, 3.5 g, 0.025 mol) dissolved in dry methanol (12 ml, 0.38 mole) was added lithium (0.53 g, 0.075 mol) during 15 min. The mixture was stirred under reflux for 30 min and, after removal of the ammonia, was mixed with dry methanol (35 ml). Into the solution was passed hydrogen chloride gas, until the pH value became 1 (universal test paper), when salts precipitated and were removed off by filtration. The mother liquors were refluxed for 4 hr, evaporated to remove methanol, diluted with water (30 ml), and then extracted with ether (3×20 ml). The ether solution was dried and evaporated to leave oily substance, which proved to contain a small amount of the unreacted acid methyl ester (**1b**, R′=CH_3) by glc, as shown in Table 1. The oil was distilled fractionally and a fraction (3.3 g), boiling 88—89 °C/13 mmHg, was collected. This was identified as a 1 : 1 mixture of diastereoisomers **2b**; Mass (the text); IR, ν_{max} 1768, 1743, 1270, and 1125 cm^{-1}; NMR (the text). Found: C, 61.47; H, 7.97%. Calcd for $C_8H_{12}O_3$: C, 61.52; H, 7.75%.

*Methyl 5-Methyl-, 5-Propyl-, 5-Isopropyl-, 5-*tert*-Butyl-, and 5-Benzyl-2,5-dihydro-2-furoates (**2a**, **2c**, **2d**, **2e**, and **2f**).* These compounds were produced from the corresponding furoic acids essentially in the same manner as the 5-ethyl derivatives (**2b**) and their physical constants are described in the following.

Compounds **2a**, bp 74—75 °C/15 mmHg; Mass, *m/e* 142 (M^+) and 83 (base, $M^+-COOCH_3$); NMR, δ 1.28 and 1.32 (total 3H, two d J=6 Hz, $C\underline{H}_3$), 3.68 (3H, s, $COOC\underline{H}_3$), 5.16 (2H, br m, 2- and 5-H), and 5.90 (2H, m, 3- and 4-H). Found: C, 58.81; H, 7.36%. Calcd for $C_7H_{10}O_3$: C, 59.14; H, 7.09%.

Compounds **2c**, bp 80—82 °C/13 mmHg; Mass, *m/e* 170 (M^+), 127 ($M^+-C_3H_7$) and 111 (base, $M^+-COOCH_3$); NMR, δ 0.90 (3H, br t, $CH_2CH_2C\underline{H}_3$), 1.48 (4H, br m, $C\underline{H}_2C\underline{H}_2CH_3$), 3.64 (3H, s, $COOC\underline{H}_3$), 5.15 (2H, m, 2- and 5-H), and 5.89 (2H, m, 3- and 4-H). Found: C, 63.19; H, 8.11%. Calcd for $C_9H_{14}O_3$: C, 63.51; H, 8.29%.

Compounds **2d**, bp 90—91 °C/15 mmHg; Mass, *m/e* 170 (M^+), 127 ($M^+-C_3H_7$) and 111 ($M^+-COOCH_3$); NMR, δ 0.90 (6H, m, isopropyl $C\underline{H}_3$), 1.74 (1H, septet, J=7.5 Hz, isopropyl C$\underline{H}$), 3.63 (3H, s, $COOC\underline{H}_3$), 4.60 (0.5 H, m, 5-H of *trans*-**2d**), 4.84 (0.5H, s, 5-H of *cis*-**2d**), 5.16 (1H, m, 2-H), and 5.88 (2H, br s, 3- and 4-H). Found: C, 63.35; H, 8.48%. Calcd for $C_9H_{14}O_3$: C, 63.51; H, 8.29%.

Compounds **2e**, bp 102—103 °C/15 mmHg; Mass, *m/e* 184 (M^+), 127 ($M^+-C_4H_9$), 125 ($M^+-COOCH_3$), and 57 (base, $C_4H_9^+$); NMR, δ 0.84 and 0.86 (total 9H, each s, $3C\underline{H}_3$), 3.65 (3H, s, $COOC\underline{H}_3$), 4.54 (0.5H, br d, J=4 Hz, 5-H of *trans*-**2e**), 4.72 (0.5H, br d, J=7 Hz, 5-H of *cis*-**2e**), 5.22 (1H, m, 2-H), and 5.92 (2H, br s, 3- and 4-H). Found: C, 65.02; H, 8.71%. Calcd for $C_{10}H_{16}O_3$: C, 65.19; H, 8.75%.

Compounds **2f**, oil, were separated from the unreacted acid methyl ester (**1f**, R=CH_3) and purified by repeated column chromatographies (Merck, benzene); Mass, *m/e* 218 (M^+) and 91 ($C_7H_7^+$); NMR, δ 2.86 and 3.04 (1.2 and 0.8H, each d, J=7 Hz, $C_6H_5C\underline{H}_2$), 3.64 and 3.66 (total 3H, each s, $COOC\underline{H}_3$), 5.12 (2H, m, 2- and 5-H), 5.90 (2H, br s, 3- and 4-H), and 7.25 (5H, m, $C_6\underline{H}_5CH_2$). Found: C, 71.50; H, 6.59%. Calcd for $C_{13}H_{14}O_3$: C, 71.54; H, 6.47%.

*Methyl 5-*p*-Methoxybenzyl-2,5-dihydro-2-furoates (**2g**) and Dimethyl 2,2′-*p*-Methoxybenzyl-2,2′,5,5′-tetrahydro[2,2′-bifuran]-5,5′-dicarboxylate (**4**).* 5-*p*-Methoxybenzyl-2-furoic acid (**1g**, 1.1 g) in ammonia (15 ml) and methanol (6 ml) was treated with sodium (0.33 g) in the same manner as **1b** and worked up as usual to give oily product (1.05 g), which on standing crystallized partially. The whole components were checked by glc (Table 1) and separated by column chromatography (Merck a 2 : 1 mixture of benzene and chloroform). Fractions with high R_f afforded oil (0.4 g), which was identified as the unreacted acid methyl ester (**1g**, R′=CH_3). Middle fractions gave **2g** (0.45 g), oil, Mass, *m/e* 248 (M^+) and 121 ($CH_3OC_7H_6^+$); NMR, δ 2.88 (2H, m, $CH_3OC_6H_4C\underline{H}_2$), 3.70 (3H, s, $C\underline{H}_3OC_6H_4CH_2$), 3.76 (3H, s, $COOC\underline{H}_3$), 5.12 (2H, m, 2- and 5-H), 5.84 (2H, m, 3- and 4-H), 6.81 and 7.10 (4H, br d, J=8 Hz, $CH_3OC_6\underline{H}_4CH_2$). Found: C, 66.75; H, 6.79%. Calcd for $C_{14}H_{16}O_4$: C, 66.73; H, 6.50%.

Fractions with low R_f gave crystalline material **4** (50 mg), mp 120—121 °C, which was recrystallized from chloroform for analysis; Mass, *m/e* 494 (M^+) and 247 (base); IR ν_{max} 1748, 1738, 1280, and 1215 cm^{-1}; NMR, δ 3.26 (4H, m, $2C\underline{H}_2$), 3.68 (6H, s, $2C\underline{H}_3O$), 3.76 (6H, s, $2COOC\underline{H}_3$), 4.56 (2H, m, 2×5-H), 5.40 and 5.56 (each 1H, m, 2×4-H), 5.96 and 6.04 (each 1H, m, 2×3-H), 6.74 and 7.12 (each 4H, ABq, J=8 Hz, 2×$C_6\underline{H}_4$). Found: C, 68.21; H, 6.08%. Calcd for $C_{28}H_{30}O_8$: C, 68.00; H, 6.12%.

*Methyl 2-Hydroxy-5-phenylpentanoate (**5h**).* 5-Phenyl-2-furoic acid (**1h**, 1.08 g) in ammonia (15 ml) and methanol (3 ml) was treated with sodium (0.41 g) in the same manner as **1b** and worked up as usual to give oily product (0.99 g), which consisted of two main components (by glc) and was separated by column chromatography (Merck, a 7 : 2 mixture of benzene and chloroform). Fractions eluted early afforded crystalline material (270 mg), which was recrystallized from ethanol to yield an unreacted acid methyl ester (**1h**, R′=CH_3) (245 mg), mp 90—91 °C; IR, ν_{max} 1730 (shoulder), 1715, 1591 (shoulder), 1575, 1273, and 1075 cm^{-1}. The remaining fractions (580 mg) were combined and separated by chromatography under the same conditions, giving small amounts of crude **1h** (R′=CH_3) (50 mg) and an unidentified oil (60 mg). After removal of these materials, the residual fraction (390 mg) was again submitted to column chromatography (a 3:1 mixture of benzene and hexane) to yield a colorless main product (200 mg), showing a single spot on tlc, along with an oily mixture (75 mg). The latter was presumed to consist mainly of methyl 2-hydroxy-5-phenylpent-3-enoate (**6h**) on the NMR spectrum but was not further purified. A part of the main product was purified by preparative tlc (benzene) for analysis to give **5h** in pure state; Mass, *m/e* 208 (M^+), 131 ($M^+-C_6H_5$), 117 ($M^+-C_6H_5CH_2$), 91 (base, $C_6H_5CH_2^+$), 77 ($C_6H_5^+$), and 59 ($COOCH_3^+$); IR, ν_{max} 3600, 1743, 1608, 1258, 1093, and 1070 cm^{-1} (shoulder); NMR δ 1.74 (4H, m,

3- and 4-H), 2.68 (3H, m, OH and 5-H), 3.76 (3H, s, CO-OCH$_3$), 4.20 (1H, t J=7 Hz, 2-H), and 7.16 (5H, s, C$_6$H$_5$). Found: C, 68.96; H, 7.68%. Calcd for $C_{12}H_{16}O_3$: C, 69.21; H, 7.74%.

*Methyl 2-hydroxy-5-p-methoxyphenylpent-3-enoate (**6i**).* 5-*p*-Methoxyphenyl-2-furoic acid (**1i**, 2.50 g) in ammonia (20 ml) and methanol (6 ml) was treated with sodium (0.80 g) in the same manner as **1b** and gave an oily product (2.56 g), which proved to consist of two main components by glc and tlc. This reaction product was separated by column chromatography (Merck, a 1 : 1 mixture of chloroform and hexane) into 3 parts. The most mobile fractions gave colorless oil (870 mg), which was further purified by column chromatography (a 2 : 1 mixture of benzene and ethyl acetate) to yield crystalline substance (560 mg), which on recrystallization from ethanol afforded the unreacted acid methyl ester (**1i**, R'=CH$_3$) (500 mg), mp 83—83.5 °C; Mass, *m/e* 232 (M$^+$), 201 (M$^+$—CH$_3$O) and 145 (base); IR, ν_{max} 1738 (shoulder), 1723, 1610, 1253, and 1073 cm^{-1}.

The middle fractions consisted mainly of the main product (**6i**), but resisted further purification. A part (100 mg) of these fractions was hydrolyzed with 5% potassium hydroxide in boiling methanol for 30 min to give crystalline acid (70 mg), mp 90—94 °C, which was recrystallized from chloroform to yield **6i** (R'=H), mp 101—102 °C; Mass (the text); IR (Nujol), ν_{max} 3468, 3030, 1738, 1611, and 1098 cm^{-1}; NMR (the text). Found: C, 64.57; H, 6.28%. Calcd for $C_{12}H_{14}O_4$: C, 64.85; H, 6.35%.

The least mobile fractions gave oily substance (206 mg), which was further purified by chromatography (a 10 : 1 mixture of benzene and ethyl acetate) to give colorless oil (110 mg), identified as methyl 2-hydroxy-5-*p*-methoxypentanoate (**5i**); Mass, *m/e* 238 (M$^+$) and 121 (base, CH$_3$OC$_6$H$_4$-CH$_2^+$); IR, ν_{max} 3368, 1743, 1723 (shoulder), 1608, and 1248 cm^{-1}; NMR, δ 1.73 (4H, m, 3- and 4-H), 2.57 (2H, m, 5-H), 2.84 (1H, br, s, OH), 3.75 (3H, s, CH$_3$O), 3.77 (3H, s, CO-OCH$_3$), 4.17 (1H, br t, J=6 Hz, 2-H), 6.80 and 7.08 (each 2H, ABq, J=8.5 Hz, C$_6$H$_4$). Found: C, 65.70; H, 7.79%. Calcd for $C_{13}H_{18}O_4$: C, 65.53; H, 7.61%.

References

1) T. Irie, M. Suzuki, and T. Masamune, *Tetrahedron Lett.*, **1967**, 3187; *Tetrahedron*, **24**, 4193 (1968).

2) L. A. Paquette and R. W. Begland, *J. Org. Chem.*, **32**, 2723 (1967); L. A. Paquette, R. W. Begland, and P. C. Storm, *J. Amer. Chem. Soc.*, **90**, 6148 (1968).

3) C. L. Zirkle, F. R. Gerns, A. M. Pavloff, and A. Burger, *J. Org. Chem.*, **26**, 395 (1961).

4) a) G. Leandri, H. Monti, and M. Bertrand, *Tetrahedron*, **30**, 289 (1974). b) E. E. Schweizer and J. G. Liehr, *J. Org. Chem.*, **33**, 583 (1968). c) J. Cleophax, J. Hildesheim, and S. D. Gero, *Bull. Soc. Chim. France*, **1967**, 4111. Also see; S. Arita, T. Takahashi, and K. Takeshita, *Kogyo Kagaku Zasshi*, **72**, 2289 (1969); D. M. Burness, "Organic Syntheses", **40**, p. 29 (1960).

5) A. D. Bedenbaugh, J. H. Bedenbaugh, J. D. Adkins, and W. A. Bergin, *J. Org. Chem.*, **35**, 543 (1970), and refs cited therein.

6) L. Rosenblum, Ph. D. Thesis, Ohio State University, 1952. We are also indebted to Professor T. Miwa, Osaka City University, for helpful suggestions on the Birch reduction conditions. Cf., T. Kinoshita, K. Miyano, and T. Miwa, Abstracts of the Annual Meeting of the Chemical Society of Japan, Vol. 3, Osaka, 1971, p. 1463.

7) *e. g.*, Mutatochrome, P. Larrer and E. Jucker, *Helv. Chim. Acta*, **28**, 300 (1945); Auroxanthin, P. Karrer, and J. Rutschmann, *ibid.*, **29**, 1624 (1942); Flavoxanthin, P. Karrer, H. Wehrli, and A. Helfenstein, *ibid.*, **13**, 268, 1084 (1930).

8) *e. g.*, Elephantin, S. M. Kupchan, A. Aynehchi, J. M. Cassady, A. T. McPhail, G. A. Sim, H. K. Schnoes, and A. L. Burlingame, *J. Amer. Chem. Soc.*, **88**, 3679 (1966).

9) *e. g.*, Furanomycin, K. Katagiri, K. Tori, Y. Kimura, T. Yoshida, T. Nagasaki, and H. Minato, *J. Med. Chem.*, **10**, 1149 (1967).

10) H. Akashi and K. Oda, *Kogyo Kagaku Zasshi*, **55**, 271 (1952); *ibid.*, **53**, 81 (1950).

11) Cf., S. Yoshina, A. Tanaka, Gang-Nan Yang, and Hsing-Chien Hsiu, *Yakugaku Zasshi*, **90**, 1150 (1970), and refs cited therein; K. B. L. Mathur and H. S. Mehra, *J. Chem. Soc.*, **1961**, 2576; C. S. Rondestvedt, Jr., "Orgnic Reactions," **11**, p. 189 (1960).

12) For a review, see; S. Sternhell, *Rev. Pure Appl. Chem.*, **14**, 15 (1964).

13) K. Tori and M. Ohtsuru, *Chem. Commun.*, **1966**, 886; W. G. Woods and P. L. Strong, *J. Amer. Chem. Soc.*, **88**, 4667 (1966); D. J. Atkinson and M. J. Perkins, *Tetrahedron Lett.*, **1969**, 2335.

14) Cf., M. Barfield, *J. Chem. Phys.*, **41**, 3825 (1964); L. J. Durham, J. Studebaker, and M. J. Perkins, *Chem. Commun.*, **1965**, 456.

15) L. Benati, M. Tiecco, A. Tundo, and F. Taddei, *J. Chem. Soc., B*, **1970**, 1443; C. Barbier, D. Gagnaire, and P. Vottero, *Bull. Soc. Chim. France*, **1968**, 2330. We are indebted to a referee for these suggestions.

16) H. O. House and J. W. Blaker, *J. Amer. Chem. Soc.*, **80**, 6389 (1958).

17) Cf., Ja L. Goldfarb, Ju. B. Volkenstein, and L. L. Belenkij, *Angew. Chem.*, **80**, 547 (1968); C. F. H. Allen and C. O. Edens, Jr., "Organic Syntheses", Coll. Vol. III, p. 731 (1955).

18) Cf., V. Ramanathan and R. Levine, *J. Org. Chem.*, **27**, 1216 (1962).

19) V. J. Traynelis, J. J. Miskel, Jr., and J. R. Sowa, *ibid.*, **22**, 1269 (1957).

20) K. Yu. Novitskii, Kh. Gresl, and Yu. K. Yur'ev, *Khim. Geterotsikl. Soedim*, **6**, 832 (1966); *Chem. Abstr.*, **67**, 32530x (1967).

21) H. Gilman and N. O. Calloway, *J. Amer. Chem. Soc.*, **55**, 4197 (1933).

22) I. P. Tsukernanik and G. G. Gelust'yen, *Dokl. Akad. Nauk Uz. SSR*, **20**, 26 (1963); *Chem. Abstr.*, **59**, 6341a (1963).

23) R. Grice and L. N. Owen, *J. Chem. Soc.*, **1963**, 1947.

24) A. W. Johnson, *J. Chem. Soc.*, **1946**, 895.

25) M. Matsumoto, M. Hatsutani, and K. Kondo, Abstracts of the Annual Meeting of the Chemical Society of Japan, Vol. 3, Tokyo, 1973, p. 1711.

Hetera-*p*-carbophanes. III. Conformation of Amide Groups in and Internal Rotation of Diaza[*n*]paracyclophanes with Two Alkoxy Groups at the Benzene Ring[1]

Kazuhiko SAKAMOTO and Michinori ŌKI*

Department of Chemistry, Faculty of Science, The University of Tokyo, Tokyo 113

(Received May 27, 1974)

A series of diazadioxo[*n*]paracyclophane derivatives with two alkoxy groups at the benzene ring were prepared. The conformation of amide groups in these compounds were studied by infrared, PMR, and ^{13}C NMR spectra to draw a conclusion that both amide groups are *s-trans*. Thus the infrared absorptions at 3430 and 3405 cm^{-1} are attributed to N—H···π interacting and N—H···O bonded *trans* forms, respectively. NCH_2 protons, which are separated by 5 bonds from the asymmetric center, as well as benzylic protons, were found to be non-equivalent when the rotation of the aromatic ring was slow. PMR spectra of the compounds studied at various temperatures indicate that introducing alkoxy groups in place of methyls at the benzene ring increases the barrier to rotation of the aromatic ring to a great extent.

In a recent paper, preparation and internal rotation of diaza[*n*]paracyclophane derivatives ($\mathbf{1}_n$ and $\mathbf{2}_n$, n=12—16) were reported.[2] Two amide groups in these compounds were suggested to take single conformation. From the infrared N—H stretching (ν_{NH}) absorptions, there were two possibilities: *s-cis* or *s-trans* with N—H···π interaction. From the scale model of the molecule, single absorption due to N—H stretching at the lower region, and PMR results which showed a single signal for NCH_2 protons, *s-cis* conformation was considered favorable.

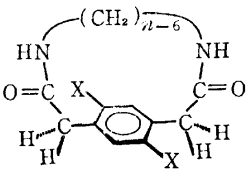

$\mathbf{1}_n$: X=H, n=12—16
$\mathbf{2}_n$: X=CH_3, n=11—16
$\mathbf{3}_n$: X=OCH_3, n=11—16 and 18
$\mathbf{4}_{18}$: X=OC_2H_5, n=18

Further evidence will be needed to confirm the conformation of the amide group, because formation of N—H···π bond will lower the ν_{NH} frequency to the region of ν_{NH} absorption due to *s-cis* conformation and PMR data themselves can not rule out the *s-trans* conformation. Furthermore, the scale model of a molecule may not be taken as decisive evidence. Introduction of methoxy groups to the benzene ring will increase electron density on the benzene ring to favor the N—H···π bond.[3] Thus investigation on diaza[*n*]paracyclophane with methoxy groups will lend help in interpretation of the conformation of the amide groups.

The purpose of this paper is four fold. The first is to report results of preparation and characterization of $\mathbf{3}_n$ and $\mathbf{4}_{18}$ which carry alkoxy groups at the benzene ring, the second is finding of N—H···π and N—H···O bondings in these compounds, the third is establishment of *s-trans* conformation of the amide group by various means, and the fourth is barriers to rotation of the dialkoxybenzene rings. A part of the results on the last item was reported briefly in a short communication.[1]

Experimental

The syntheses of $\mathbf{3}_n$ and $\mathbf{4}_{18}$ were accomplished by condensation of α,ω-diamines with 2,5-dialkoxy-1,4-phenylenediacetyl dichloride under high dilution conditions. The latter compounds were prepared from 1,4-dialkoxybenzene according to the previously reported scheme.[2]

2,5-Dimethoxy-1,4-bis(chloromethyl)benzene. A mixture of 46 g(0.33 mol) of 1,4-dimethoxybenzene, 70 g(0.87 mol) of 37% formalin, 350 ml of concd. hydrochloric acid, and 300 ml of glacial acetic acid was warmed at 50—60 °C for 7 hr with stirring and introducing dry hydrogen chloride. The resulting solid was collected by filtration and was washed with water. Recrystallization from chloroform gave 58 g (yield, 74%) of pure compound, mp 163—164 °C (lit,[4] mp 165 °C).

2,5-Diethoxy-1,4-bis(chloromethyl)benzene was obtained similarly in a 60% yield, mp 148—151 °C (from chloroform). IR: 1225 and 1055 (ν_{C-OEt}), 700(ν_{C-Cl}) cm^{-1}. NMR ($CDCl_3$,δ): 1.42(6H, t, J=8 Hz), 4.04(4H, q, J=8 Hz), 4.62(4H, s), 6.92(2H, s). This compound was directly used for the next reaction.

2,5-Dimethoxy-1,4-bis(cyanomethyl)benzene. A suspension of 35 g(0.15 mol) of the above dichloride in 400 ml of dimethyl sulfoxide was slowly added to a stirred solution of 26 g(0.53 mol) of sodium cyanide in 300 ml of dimethyl sulfoxide at room temperature during a period of 1.5 hr. After the addition, the reaction mixture was warmed at 50—60 °C for 2 hr with stirring. The reaction mixture was poured into ice-water (*ca.* 3 l) and the resulting solid was collected by filtration. Recrystallization from chloroform gave 28 g(85%) of pure compound, mp 191—192 °C. IR: 2250($\nu_{C\equiv N}$), 1225 and 1045(ν_{C-OMe}) cm^{-1}. NMR($CDCl_3$, δ): 3.70(4H, s), 3.85(6H, s), 6.93(2H, s).

Found: C, 66.41; H, 5.36; N, 13.05%. Calcd for $C_{12}H_{12}N_2O_2$: C, 66.65; H, 5.39; N, 12.96%.

2,5-Diethoxy-1,4-bis(cyanomethyl)benzene was prepared similarly in a 90% yield, mp 177.5—178.5 °C (from hexane-ether). IR: 2250($\nu_{C\equiv N}$), 1230 and 1050(ν_{C-OEt}) cm^{-1}. NMR ($CDCl_3$, δ): 1.42(6H, t, J=8 Hz), 3.50(4H, s), 4.05(4H, q, J=8 Hz), 6.91(2H, s). This compound was directly used for the next reaction.

2,5-Dimethylphenylacetonitrile was obtained similarly from 2,5-dimethylbenzyl chloride[5] in an 86% yield, mp 29.5—31.0 °C (from hexane) (bp 126—128 °C/11—12 mmHg). IR (neat): 2250($\nu_{C\equiv N}$) cm^{-1}. NMR($CDCl_3$, δ): 2.28(3H, s), 2.32(3H, s), 3.60(2H, s), 7.07(2H, s), 7.16(1H, s).

Found: C, 82.88; H, 7.64; N, 9.65%. Calcd for $C_{10}H_{11}N$: C, 82.72; H, 7.64; N, 9.65%.

2,5-Dimethoxy-1,4-phenylenediacetic acid, mp 232—235 °C (decompn.), was prepared from the corresponding dicyanide by the previously reported method[2] in a 77% yield. IR: 1710($\nu_{C=O}$), 1230 and 1045(ν_{C-OMe}) cm^{-1},

Table 1. Diaza[*n*]paracyclophanes

Compound	Molecular formula	Mp (°C)	Analytical data C(%)	H(%)	N(%)	Mol wt (M^+)	Recrystallization solvent	Yield (%)	IR (KBr disk) (cm^{-1}) ν_{NH}	Amide I	Amide II	ν_{C-OR}
$\mathbf{2}_{11}$	$C_{17}H_{24}N_2O_2$	199.5—200.5	70.82	8.12	9.62[a]	288[a]	CH_2Cl_2—CCl_4	25	3340	1650	1545	
			70.80	8.39	9.71[a]	288.4[a]						
$\mathbf{3}_{11}$	$C_{17}H_{24}N_2O_4$	183.5—184.5	63.81	7.68	8.85	320	$CHCl_3$—CCl_4	11	3320	1665, 1640	1540	1220, 1045
			63.73	7.55	8.74	320.4						
$\mathbf{3}_{12}$	$C_{18}H_{26}N_2O_4$	183.5—184.0	64.36	7.86	8.23	334	$CHCl_3$—CCl_4	56	3320	1665	1520	1220, 1050
			64.65	7.84	8.38	334.4						
$\mathbf{3}_{13}$	$C_{19}H_{28}N_2O_4$	190.5—192.0	64.87	8.64	7.79	348	CH_3OH	46	3250	1640	1540	1215, 1040
			65.49	8.10	8.04	348.4						
$\mathbf{3}_{14}$	$C_{20}H_{30}N_2O_4$	156.5—157.5	66.02	8.63	7.54	362	CH_2Cl_2—CCl_4	71	3300	1650	1530	1215, 1040
			66.27	8.34	7.73	362.5						
$\mathbf{3}_{15}$	$C_{21}H_{32}N_2O_4$	180.0—181.5	66.77	8.79	7.37	376	$CHCl_3$	66	3280	1660, 1630	1545	1220, 1050
			66.99	8.57	7.44	376.5						
$\mathbf{3}_{16}$	$C_{22}H_{34}N_2O_4$	198.0—199.5	67.62	8.55	6.90	390	$CHCl_3$—CCl_4	18	3300	1645	1545	1220, 1050
			67.66	8.78	7.17	390.5						
$\mathbf{3}_{18}$	$C_{24}H_{38}N_2O_4$	234.0—235.0	68.70	9.11	6.88	418	$CHCl_3$—CCl_4	—	3300	1640	1545	1220, 1050
			68.87	9.15	6.69	418.6						
$\mathbf{4}_{18}$	$C_{26}H_{42}N_2O_4$	198.5—199.5	69.91	9.76	6.15	446	$CHCl_3$	—	3350, 3300	1645	1545	1200, 1060
			69.92	9.48	6.27	446.4						

a) The numerical data in the upper column are those found and those in the lower column are the calculated.

2,5-Diethoxy-1,4-phenylenediacetic acid, mp 218—221 °C (decompn.), was prepared similarly in a 70% yield. IR: 1710($\nu_{C=O}$), 1220 and 1045(ν_{C-OEt}) cm^{-1}.

2,5-Dimethylphenylacetic acid, mp 124.5—126.0 °C (from chloroform), was prepared similarly in a 74% yield. IR: 1700($\nu_{C=O}$) cm^{-1}.

Found: C, 73.07; H, 7.07%. Calcd for $C_{10}H_{12}O_2$: C, 73.20; H, 7.37%.

2,5-Dimethoxy-1,4-phenylenediacetyl dichloride was obtained by the action of thionyl chloride in absolute ether in an 81% yield, mp 141.0—143.0 °C (from ether). IR: 1800($\nu_{C=O}$), 1220 and 1040(ν_{C-OMe}) cm^{-1}. NMR($CDCl_3$, δ): 3.78(6H, s), 4.11(4H, s), 6.71(2H, s).

2,5-Diethoxy-1,4-phenylenediacetyl dichloride, mp 110—112 °C (from ether), was prepared similarly in an 82% yield. IR: 1800($\nu_{C=O}$), 1225 and 1045(ν_{C-OEt}) cm^{-1}. NMR($CDCl_3$, δ): 1.39(6H, t, J=8 Hz), 4.00(4H, q, J=8 Hz), 4.10(4H, s), 6.73(2H, s).

2,5-Dimethylphenylacetyl chloride, yellowish oil, was prepared similarly in an almost quantitative yield. IR(neat): 1800 ($\nu_{C=O}$) cm^{-1}. NMR(CCl_4, δ): 2.26(3H, s), 2.31(3H, s), 4.02(2H, s), 7.00(3H, s).

Syntheses of Diaza[n]*paracyclophanes.*

Synthetic method will be described by taking the case of 13,16-dimethyl-3,9-diaza-2,10-dioxo[11]paracyclophane ($\mathbf{2}_{11}$) as an example.

A solution of 1.3 g(*ca.* 5 mmol) of 2,5-dimethyl-1,4-phenylenediacetyl dichloride in 100—150 ml of tetrahydrofuran was slowly added to a vigorously stirred and refluxing mixture of 2.0—3.0 g of potassium carbonate and 0.5 g (*ca.* 5 mmol) of pentamethylenediamine in 800 ml of tetrahydrofuran over a period of 26 hr, employing a high-dilution appratus. After filtration, the solvent was evaporated *in vacuo* to give a yellow solid. This solid was chromatographed on silica-gel (25 g). The fraction eluted with dichloromethane gave 370 mg(25%) of $\mathbf{2}_{11}$, mp 199.5—200 °C on recrystallization from carbon tetrachloride—dichloromethane. The melting points, the analytical data, and the solvent of recrystallization for each compound are summarized in Table 1.

N,N'-*Dipropyl-2,5-dimethoxy-1,4-phenylenediacetamide*(**5**) was prepared by the previously reported method[2] in an 86% yield, mp 197.0—197.5 °C (from carbon tetrachloride—chloroform). IR: 3290(ν_{NH}), 1645(amide I), 1550(amide II), 1220 and 1050(ν_{C-OMe}) cm^{-1}. NMR($CDCl_3$, δ): 0.85 (6H, m), 1.45(4H, m), 3.15(4H, q), 3.51(4H, s), 3.81(6H, s), 5.95(2H, b), 6.82(2H s).

Found: C, 64.30; H, 8.37; N, 8.16%. Calcd for $C_{18}H_{28}N_2O_4$: C, 64.62; H, 8.39; N, 8.33%.

N,N'-*Hexamethylenebis(2,5-dimethylphenylacetamide)*. A stirred mixture of 0.5 g(43 mmol) of hexamethylenediamine, 1.5 g(0.83 mmol) of the 2,5-dimethylphenylacetyl chloride, 3 g of potassium carbonate, and 100 ml of tetrahydrofuran was refluxed for 2 hr. The resulting solid was collected by filtration and washed with water. After recrystallization from carbon tetrachloride—chloroform, it was obtained in an almost quantitative yield, mp 176.5—177.0 °C. IR: 3300(ν_{NH}), 1640(amide I), 1540(amide II) cm^{-1}. NMR ($CDCl_3$, δ): 1.0—1.6(8H, b), 2.22(6H, s), 2.30(6H, s), 3.13 (4H, q), 3.51(4H, s), 5.15—5.60(2H, b), 6.9—7.1(6H, m).

Found: C, 76.26; H, 9.06; N, 6.62%. Calcd for $C_{26}H_{36}N_2O_2$: C, 76.43; H, 8.88; N, 6.86%.

Measurement of the Spectra. The infrared spectra were recorded on either a Hitachi EPI-G2 grating infra-red spectrometer (4000—400 cm^{-1}) with KBr disk or a Perkin-Elmer 112G single beam grating spectrophotometer (3500—3000 cm^{-1}) with dilute chloroform solution. The PMR spectra were measured on a Hitachi R-20B spectrometer operating at 60 MHz at 34 °C. Samples were dissolved in deuteriochloroform, using TMS as an internal reference. Chemical shifts are recorded as ppm down field from TMS. Lanthanide induced shift measurements were performed by the stepwise addition of lanthanide shift reagents (either Eu(fod)$_3$-d_{27} or Eu(dpm)$_3$) to the deuteriochloroform solution of substrate. The molar ratios of the shift reagent to the substrate were from 0 through 0.6. ^{13}C FT NMR spectra were taken with a JEOL PFT-100 spectrometer in the deuteriochloroform-locked mode at 15.358808 MHz. Samples were dissolved in deuteriochloroform and TMS was used an internal reference. The mass spectra were observed on a Hitachi RMU-6L spectrometer.

Results and Discussion

Infrared Spectra. The ν_{NH} absorptions of these compounds are summarized in Table 2 together with those of compounds $\mathbf{1}_n$, $\mathbf{2}_n$, and open-chain models of **5**, **6**, and **7**.

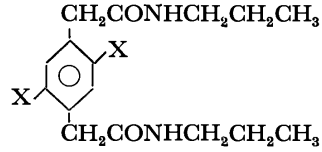

5: X=OCH_3
6: X=H
7: X=CH_3

Table 2. Absorption maxima due to N—H stretching vibration of diaza[n]paracyclophanes and related compounds in $CHCl_3$ (cm^{-1})[a]

	s-trans	*s-cis* or N—H···π interacting	*s-trans*	*s-cis* or N—H···π interacting	*s-cis* or N—H···π interacting	N—H···O interacting
		$\mathbf{1}_n$		$\mathbf{2}_n$		$\mathbf{3}_n$
n=11				3428(272)	3432(200)	3408(70)
12		3436(277)		3433(423)	3433(176)	3404(91)
13		3436(171)		3431(259)	3431(130)	3407(108)
14		3437(251)		3433(244)	3436(141)	3404(105)
15		3440(267)		3432(188)	3434(117)	3406(75)
16		3439(181)		3431(161)	3435(107)	3403(71)
						$\mathbf{4}_{18}$
					3432(148)	3390(80)
		6		**7**		**5**
	3453(133)	3437(223)	3449(64)	3427(192)	3433(185)	3400(78)

a) The numerical data in parentheses are ε_{max}.

As are seen from Table 2, hetera-*p*-carbophanes which carry alkoxy groups at the benzene ring show two ν_{NH} absorptions in contrast to the presence of only one ν_{NH} absorption in $\mathbf{1}_n$ and $\mathbf{2}_n$. These absorptions occur at *ca.* 3430—3440 cm^{-1} region for compounds $\mathbf{1}_n$ and $\mathbf{2}_n$, whereas $\mathbf{3}_n$ and $\mathbf{4}_{18}$ show absorption at *ca.* 3405 cm^{-1} in addition to an absorption corresponding to those of $\mathbf{1}_n$ and $\mathbf{2}_n$. As a clue to solve the assignment problem, the model compounds (**5**, **6**, and **7**) may be examined. The amide groups in these open-chain compounds may be assumed to take *s-trans* conformation.[2] Interestingly, those which do not possess alkoxy group showed only one absorption due to N—H stretching, whereas **5** showed two ν_{NH} absorptions which correspond to those of $\mathbf{3}_n$ and $\mathbf{4}_{18}$. The absorption at the higher frequency which is common for both types of compounds may be assigned to the *s-trans* amide which is interacting with the π-electrons of the benzene ring.[3] Since the extra band existing in the alkoxy compounds is located at lower frequency than that of N—H···π interacting form, it can not be attributed to a free form. The most probable candidate for the absorption is the N—H···O hydrogen bonded form (**8**), because it is improbable to assume that *s-cis* conformation is possible for compound **5** and the N—H···O bond will lower ν_{NH} frequency to a considerable extent.[6]

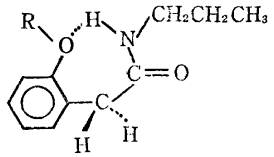

8

The same discussion will apply to the assignment of the N—H stretching absorption of $\mathbf{3}_n$ and $\mathbf{4}_{18}$. Thus the ν_{NH} absorption at *ca.* 3405 cm^{-1} is attributed to intramolecular N—H···O bond. However the origin of the absorption at higher frequency is not yet established because none of the possibilities of *s-cis* conformation and N—H···π interaction has yet been ruled out. Thus evidence from other sources is needed for assignment of the IR absorption.

PMR Spectra. PMR spectral data of $\mathbf{3}_n$ and $\mathbf{4}_{18}$ are summarized in Table 3 as well as those of $\mathbf{2}_{11}$ and open-chain compound for comparison. Change in signal shapes of the bridge methylene protons, except the NCH_2 in $\mathbf{3}_n$, according to the bridge length resembles the case of $\mathbf{2}_n$ and reflects rigidity and mobility of the molecules. However the chemical shifts of the bridge methylenes of $\mathbf{3}_n$ with small ring size are located at the higher field, relative to the corresponding methylenes of $\mathbf{2}_n$, by *ca.* 0.1 ppm, suggesting the larger anisotropy effect of the dimethoxybenzene ring. Benzylic protons of $\mathbf{2}_{11}$ and $\mathbf{3}_{11}$—$\mathbf{3}_{16}$ gave signals of the AB type, whereas those of $\mathbf{3}_{18}$, $\mathbf{4}_{18}$, and the open-chain amide (**5**) gave singlet signals. These changes must be interpreted by assuming the fast internal rotation of the benzene ring for the compounds showing the A_2 type signals and the slow rotation for the compounds showing the AB type, because these compounds are expected to give rise to nonequivalent benzylic protons when the internal rotation is frozen on the NMR time scale.

The spectral feature of $\mathbf{3}_{11}$—$\mathbf{3}_{16}$ is that they show two signals at *ca.* 2.8 and *ca.* 3.5 ppm due to NCH_2 protons. In sharp contrast, $\mathbf{2}_n$ was reported to show only one signal for the NCH_2 groups. $\mathbf{3}_{18}$, $\mathbf{4}_{18}$, and **5** also show one signal for the NCH_2. The internal

TABLE 3. NMR DATA OF DIAZA[*n*]PARACYCLOPHANES AND RELATED COMPOUND IN $CDCl_3$ AT 34 °C (δ from internal TMS)[a]

Compound	Ar-H	NH	OCH_3	CH_2CO	NCH_2	NCH_2'	β-CH_2[b]	γ—δ-CH_2[b]
$\mathbf{2}_{11}$	7.08	4.85	2.32[c]	3.56 (q, J=15.0,	3.15		1.25	0.3—0.9
	(s, 2H)	(b, 2H)	(s, 6H)	$\Delta\delta$=17.3 Hz, 4H)	(m, 4H)		(m, 4H)	(m, 2H)
$\mathbf{3}_{11}$	6.88	5.32	3.84	3.56 (q, J=14.7,	3.40	2.85	1.15	0.2—0.8
	(s, 2H)	(b, 2H)	(s, 6H)	$\Delta\delta$=49.3 Hz, 4H)	(m, 4H)		(b, 4H)	(m, 2H)
$\mathbf{3}_{12}$	6.87	5.57	3.85	3.56 (q, J=14.7,	3.40	2.85	1.23	0.80
	(s, 2H)	(b, 2H)	(s, 6H)	$\Delta\delta$=46.5 Hz, 4H)	(m, 4H)		(b, 4H)	(b, 4H)
$\mathbf{3}_{13}$	6.91	5.82	3.84	3.57 (q, J=13.8,	3.55	2.80	1.25	0.88
	(s, 2H)	(b, 2H)	(s, 6H)	$\Delta\delta$=47.1 Hz, 4H)	(m, 4H)		(b, 4H)	(b, 6H)
$\mathbf{3}_{14}$	6.88	5.85	3.84	3.57 (q, J=14.6,	3.50	2.80		1.60—0.60
	(s, 2H)	(b, 2H)	(s, 6H)	$\Delta\delta$=44.3 Hz, 4H)	(m, 4H)			(b, 12H)
$\mathbf{3}_{15}$	6.87	5.88	3.84	3.52 (q, J=14.7,	3.50	2.85		1.60—0.85
	(s, 2H)	(b, 2H)	(s, 6H)	$\Delta\delta$=43.0 Hz, 4H)	(m, 4H)			(b, 14H)
$\mathbf{3}_{16}$	6.87	5.95	3.83	3.50 (q, J=14.4,	3.50	2.85		1.60—0.85
	(s, 2H)	(b, 2H)	(s, 6H)	$\Delta\delta$=39.8 Hz, 4H)	(m, 4H)			(b, 16H)
$\mathbf{3}_{18}$	6.82	5.85	3.81	3.52	3.22			1.70—1.00
	(s, 2H)	(b, 2H)	(s, 6H)	(s, 4H)	(q, 4H)			(b, 20H)
$\mathbf{4}_{18}$	6.83	5.93		3.52	3.21			1.70—1.05
	(s, 2H)	(b, 2H)		(s, 4H)	(q, 4H)			(b, 20H)
5	6.82	5.95	3.81	3.51	3.15		1.45	0.85[d]
	(s, 2H)	(b, 2H)	(s, 6H)	(s, 4H)	(q, 4H)		(m, 4H)	(m, 6H)

a) s=singlet, q=quartet, m=multiplet, b=broad signal b) relative to N-atom c) aromatic methyl
d) propyl methyl

rotation in compounds $\mathbf{3}_{11}$—$\mathbf{3}_{16}$ is slow, as will be discussed later, whereas that in $\mathbf{3}_{18}$ and $\mathbf{4}_{18}$ is fast. Bifurcation of the NCH_2 signals of $\mathbf{3}_{11}$—$\mathbf{3}_{16}$ may arise from such a steric environment. Namely, because of severe steric conditions in these compounds, one of the amide groups may take *s-cis* conformation, while the other takes *s-trans* conformation. Even in $\mathbf{3}_{18}$ and $\mathbf{4}_{18}$, the amide groups may be *s-cis* and *s-trans*, although they may exchange rapidly at the temperature in question. There is another possibility, however, for the apparent two signals for the NCH_2 group. That is although both amide groups take *s-trans* conformations, the NCH_2 protons are stereoheterotopic due to the slow internal rotation in $\mathbf{3}_{11}$—$\mathbf{3}_{16}$, whereas they become homotopic due to the fast rotation in $\mathbf{3}_{18}$ and $\mathbf{4}_{18}$. In the former case, the NCH_2 protons become nonequivalent and give different chemical shifts, though they both belong to the *s-trans* conformation of amides.

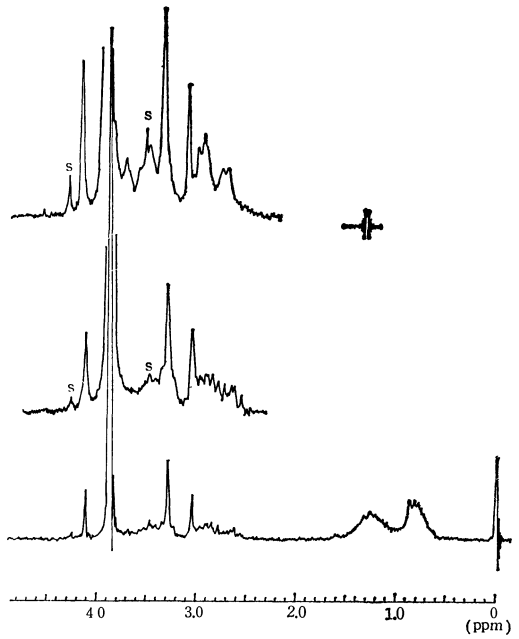

Fig. 1. Normal and decoupled (irradiated at *ca.* 1.3 ppm) PMR spectra of $\mathbf{3}_{12}$.
s: side band of OCH_3 at 3.85 ppm.

Double resonance technique would lend help in determining which of the two is the real reason for the bifurcation. Thus β-methylene protons to the nitrogen were irradiated and signals due to α-methylenes were observed. As are seen in Fig. 1, which shows the spectrum of $\mathbf{3}_{12}$ as a typical example, the α-methylenes seem to give a broad AB type signal which is coupled with a proton on nitrogen, although the signals at the lower field are obscured by other strong signals. The broadness of the signals owes to the presence of nitrogen. Thus double resonance experiment is in favor of the postulation that the bifurcation is caused because of the heterotopic nature of the NCH_2 protons. If the bifurcation were to be attributed to the presence of *s-cis* and *s-trans* conformations, the methylene signals would have appeared as a pair of doublets at two magnetic fields. The fact that the mean chemical shift of two signals due to NCH_2's of $\mathbf{3}_{11}$—$\mathbf{3}_{16}$ is very close to the chemical shift of those of diaza[18]paracyclophanes ($\mathbf{3}_{18}$ and $\mathbf{4}_{18}$) in which the dialkoxybenzene ring is rotating rapidly, may be taken as another piece of supporting evidence for the sole presence of *s-trans* conformation.

If the change from heterotopic to homotopic protons *vice versa* could be detected by the temperature dependence study of the PMR spectra, it would be almost a decisive support for the cause that the bifurcation is due to the heterotopy. Thus PMR spectra of $\mathbf{3}_{16}$ in tetrachloroethane were observed at elevated temperatures. The temperature-raise caused coalescence of the two signals in question at 2.9 and 3.5 ppm and a new signal was observed at 3.2 ppm which is very close to the chemical shift of NCH_2's of $\mathbf{3}_{18}$. On the contrary, lowering the temperature of $\mathbf{4}_{18}$ in deuteriochloroform caused the separation of NCH_2 signal at 3.2 ppm into two, at 2.9 and 3.5 ppm. These results suggest that the cause of bifurcation of the NCH_2 signal in these compounds is really the heterotopic nature of the protons of the *s-trans* conformation.

^{13}C NMR Spectra. It was recently reported that the conformation of *N*-monosubstituted amides had a significant effect upon the chemical shifts of carbonyl carbons and those of carbons adjacent to the nitrogen. The difference in chemical shifts due to *s-cis* and *s-trans* conformations amounts to 3.4 ppm in *N*-methylformamide and differences between the two methylene (or methyl) carbons attached to nitrogen in *N,N'*-dimethylformamide, *N,N'*-dibutylformamide, and *N,N'*-dibutylacetamide are found to be 5.1, 5.2, and 3.3 ppm, respectively.[7] Therefore, it is expected that, if the amide groups in diaza[*n*]paracyclophanes in question took *s-cis* and *s-trans* conformation, ^{13}C NMR spectra of these compounds would show a pair of carbonyl carbon signals and pairs of other carbons which are α, β, *etc.* to the nitrogens. Contrary to the expectation, however, ^1H-noise-decoupled ^{13}C FT NMR spectra of $\mathbf{3}_{12}$ and $\mathbf{3}_{13}$ in deuteriochloroform gave rise to nine and ten signals, respectively, as are listed in Table 4 which includes data of $\mathbf{2}_{12}$ and **5** also. The signals are tentatively assigned by use of the single frequency off-resonance ^1H-decoupling technique, known chemical shift rules for various kinds of carbons,[8] and signal intensities. The number of different carbon signals of diaza[*n*]paracyclophanes points out that these should exist as a single conformer which has C_2 symmetry element.

Lanthanide Induced Shift. Lanthanide shift reagent would provide further information about the conformations of amides. In the absence of the steric hindrance, protons in a methyl group *cis* to the carbonyl oxygen in amide moiety are known to experience a larger shift than their counterparts at *trans* position.[9] Thus in *N,N'*-dimethylacetamide, the following data are known.[10]

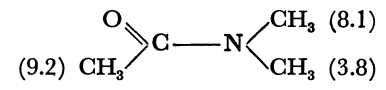

Since lanthanide shift reagents are known to cause appearence of unexpected peaks and this effect depends

TABLE 4. ^{13}C NMR DATA OF DIAZA[n]PARACYCLOPHANES ($\mathbf{2}_{12}$, $\mathbf{3}_{12}$, AND $\mathbf{3}_{13}$) AND RELATED COMPOUND (**5**) IN $CDCl_3$[a)]

Compound	$\mathbf{2}_{12}$ (50 °C)	$\mathbf{3}_{12}$ (28 °C)	$\mathbf{3}_{13}$ (28 °C)	**5** (50 °C)
C=O	170.4	171.5 (s)	171.6	170.9
Aromatic C—OMe	135.6 (C-Me)	150.9 (s)	150.7	151.3
Aromatic C—CH_2	134.1	124.8 (s)	124.6	123.9
Aromatic C—H	132.8	113.8 (d)	113.7	114.3
O—CH_3	18.8 (C-Me)	56.4 (q)	56.3	56.2
Ar-CH_2—CO	41.7	39.3 (t)	38.4	41.3
$NHCH_2$	39.3	38.3 (t)	38.1	38.8
β-CH_2	28.5	29.6 (t)	27.6	22.9
γ-CH_2	27.7	27.8 (t)	26.3	11.2 (CH_3)
δ-CH_2			26.5	

a) Chemical shifts are written as ppm down field from internal TMS on the δ scale.

TABLE 5. RELATIVE SLOPES OF LIS *vs.* [L]/[S][a)]

Compound $\mathbf{3}_n$	n=11	12	13	14	15	16	18
CH_2CO	1	1	1 (1)	1	1	1	1
NCH_2[b)]	1.06	0.93	1.05 (1.07)	0.97	0.95	1.02	0.81
NCH_2'[c)]	0.67	0.73	0.62 (0.62)	0.69	0.72	0.81	
OCH_3	0.22	0.19	0.21 (0.18)	0.20	0.20	0.20	0.18
Ar-H	0.66	0.54	0.61 (0.65)	0.54	0.53	0.52	0.47
$\frac{R_{CH_2N} + R_{CH_2N'}}{2}$	0.87	0.83	0.84 (0.84)	0.83	0.84	0.87	(0.81)[d)]

Compound	**4**	**5**	$\mathbf{2}_{12}$	$\mathbf{2}_{13}$	$C_{26}H_{36}N_2O_2$[e)]
CH_2CO	1	1 (1)	1 (1)	1	1 (1)
NCH_2	0.85	0.77 (0.80)	0.96 (0.98)	0.90	0.91 (1.00)
OCH_3 or OCH_2	0.18	0.19 (0.12)			
Ar-CH_3			0.41 (0.40)	0.42	0.30 (0.36)
Ar-H	0.47	0.45 (0.47)	0.45 (0.44)	0.47	0.30 (0.36) 0.10 (0.08)

a) The numerical data in parentheses are obtained by using $Eu(dpm)_3$ and the others by using $Eu(fod)_3$-d_{27}. b) NCH_2 signal at the lower magnetic field. c) NCH_2 signal at the higher magnetic field. d) This signal appeared as a quartet. e) *N,N'*-Hexamethylenebis(2,5-dimethylphenylacetamide).

on the nature of the shift reagents used,[11)] careful examination of the spectra will be necessary. However, under the conditions examined, none of the anomalous peaks appeared, the lanthanide shift reagent causing no trouble in obtaining the relative lanthanide induced shift (LIS).

LIS was plotted against [L]/[S] where [L] and [S] are the molar concentrations of a lanthanide shift reagent and a substrate, respectively. These plots yielded good linear relationships and relative slopes of various protons, taking the slope of CH_2CO as a reference, were calculated. The results are listed in Table 5. $Eu(fod)_3$-d_{27} was mainly used but $Eu(dpm)_3$ gave very close values.

The results may be interpreted that the predominant interaction between amides under investigation and the lanthanide reagent is of pseudo-contact nature.[12)] The lower field multiplets for NCH_2' proton suffered a larger induced shift than the NCH_2 proton at a higher magnetic field. The first look of these data would lead to an assignment of the higher and the lower signals to *s-cis* and *s-trans* conformations, respectively, because the signal of NCH_2 protons *trans* to carbonyl is known to appear at the higher magnetic field than that of the *cis*.[13)] Looking carefully at the relative ratios, however, a rather large relative slope for the signals at the lower magnetic field is noticed. The relative slope for the methyl which is *cis* to the acetyl methyl group in *N,N'*-dimethylacetamide is 0.41 (*loc. cit.*) and NCH_2 protons of *N*-methyl-γ-butyrolactam gives the relative slope of 0.41.[14)] Our results on ε-caprolactam indicate that the relative slope for NCH_2 is 0.4, using $Eu(fod)_3$-d_{27}. Although the complexing site of europium may vary from compound to compound to some extent, the relative slope seems to be fairly small in these compounds. On the other hand, the relative ratios of the signals at the lower magnetic field are 0.6—0.8. In addition, average slopes of the two NCH_2 signals are close to the relative slope of NCH_2 in $\mathbf{3}_{18}$ and to those of open-chain amides examined. These results favor that the both amide groups take *s-trans* conformation.

All the above discussions support that the amide groups in $\mathbf{3}_n$ are the *s-trans* form. This necessarily leads to a conclusion that the ν_{NH} absorption of $\mathbf{3}_n$ at *ca.* 3430 cm^{-1} is due to the N—H···π interacting *s-trans* form.

Amide Conformations as Reinvestigated with the Aid of Lathanide Shift Reagent. Since all the evidence presented above indicate that the amide groups in

$\mathbf{3}_n$ take *s-trans* conformation, reinvestigation of the conformations of amides in $\mathbf{1}_n$ and $\mathbf{2}_n$ becomes necessary. Thus $\mathbf{2}_{12}$ and $\mathbf{2}_{13}$ were submitted to the study with the aid of lanthanide shift reagent. The results are shown in Table 5. The PMR spectral data suggest that these compounds take also *s-trans* form only, because the ratios of the chemical shifts of NCH_2 protons referred to that of CH_2CO protons are characteristic of the *s-trans* form. Thus we wish to correct our earlier suggestion that $\mathbf{1}_n$ and $\mathbf{2}_n$ take *s-cis* conformations as regard the amide groups. The ring strain associated with the formation of this kind of cyclophanes does not seem to be large enough to cause preference of the *s-cis* form over the *s-trans*. Thus the ν_{NH} absorption at *ca.* 3430 cm^{-1} of $\mathbf{1}_n$ and $\mathbf{2}_n$ should now be attributed to the N—H$\cdots\pi$ interacting form rather than the *s-cis* conformation.

Internal Rotation of the Dialkoxybenzene Ring. Temperature dependence of the PMR spectra was studied to obtain the free energies of activation for the internal rotation of the aromatic ring. Those of which ansa chain members are 15 or less do not show any temperature dependency on raising the temperature. The barrier to rotation seems very high for these compounds. The AB quartet of $\mathbf{3}_{16}$ in tetrachloroethane gradually broadened on raising the temperature but coalescence was not observed up to 174 °C, though the NCH_2 signals coalesced into a broad singlet at about 160 °C. On changing the solvent to hexadeuteriodimethyl sulfoxide, however, the signals coalesced at 141 °C. On the other hand, the signal of benzylic protons of $\mathbf{4}_{18}$ in deuteriochloroform broadened considerably at low temperatures: the coalescence temperature was found to be −30 °C. Attempts at observing exact chemical shifts and coupling constant of the AB type protons of $\mathbf{4}_{18}$ were unsuccessful because of broadening of signals, and poor solubility in solvents at low temperatures.

The free energies of activation were obtained by putting the NMR parameters into the following equation:[15]

$$\Delta G_c^{\ddagger} = 4.57\, T_c\{9.97+\log_{10}(T_c/\sqrt{\Delta\delta_{AB}^2+6J_{AB}^2})\}$$

The parameters of $\mathbf{3}_{16}$ obtained at 34 °C were used. On the other hand it was not possible to obtain $\Delta\delta_{AB}$ and J_{AB} for $\mathbf{3}_{18}$ and $\mathbf{4}_{18}$. Thus those parameters for compound $\mathbf{3}_{16}$ were used to obtain approximate barriers to rotation of $\mathbf{3}_{18}$ and $\mathbf{4}_{18}$. It will not be too unreasonable to use these parameters because the structures of these compounds are alike. The results are shown in Table 6.

$\mathbf{3}_{16}$ which has two methoxy groups at the aromatic ring shows higher free energy of activation for rotation of the aromatic ring than that of $\mathbf{2}_{16}$ with two methyl groups by about 10 kcal/mol. This large difference in activation energies must be caused by replacement of the methyl groups by the methoxy because the other part of the molecules is the same. Since much difference in energies of the ground states of these molecules is not expected, the results may be attributed to the difference in energies at the transition states. Then the methoxy group must give more steric hindrance at the transition state than the methyl group.

The apparent bulkiness of the methoxy and the methyl groups in these compounds is just the opposite of the generally accepted. Methyl group is known to retard racemization of biphenyls more effectively than methoxy group,[16] even though the latter group contains more atoms than the former. This apparent reversal in giving the steric effect is understood by assuming that, by taking a conformation in which methoxy methyl is far from the site of interaction, oxygen only becomes the part giving steric hindrance. This deduction was supported by essentially the same ultraviolet absorption spectra of 2-*n*-alkylbiphenyls.[17]

In the process of internal rotation of $\mathbf{3}_{16}$, however, the methoxy group must pass through the space provided by the ansa chain. Namely, the methoxy group gives steric effect to the transition state not by the oxygen only but by the group as a whole. The apparent bulkiness of the methoxy group may be reduced by torsion from the coplanarity with the aromatic ring. But this torsion occurs only at the expense of resonance energy.[18] Therefore, the barrier to rotation of the benzene ring is high irrespective to the steric situation of the methoxy group. This, we believe, is the first example that the methoxy group is proven to be bulkier than the methyl.[19]

The ethoxy group seems to be even bulkier than the methoxy group along the lines expected from the above discussion, because it was impossible to observe coalescence temperature for $\mathbf{3}_{18}$ under the similar conditions. Although the ethoxy group may be folded at the transition state to minimize the free energy of activation for rotation, it is still bulkier than the methoxy group. It is expected that other alkoxy groups will affect the barrier to rotation of the aromatic ring in a similar fashion.

The authors wish to express their hearty thanks to Professor T. Shimanouchi and Mr. M. Kakimoto for helpful discussions and technical assistance in using a Perkin-Elmer 112G single beam grating spectrophotometer and to Mr. K. Matsushita of JEOL Ltd. for the measurement of ^{13}C FT NMR spectra.

Table 6. Free energies of activation for internal rotation of the aromatic ring[a]

Compound	$\Delta\delta_{AB}$ (Hz)	J_{AB} (Hz)	T_c (°C)	$\Delta G_c^{\ddagger}$ (kcal/mol)	Solvent
$\mathbf{2}_{16}$[2]	(14.1)	(15.9)	< − 50	<10.8	$CDCl_3$
$\mathbf{3}_{16}$	36.8	14.4	> 174	>22.2	$CHCl_2CHCl_2$
	32.9	13.8	141	20.6	DMSO-d_6
$\mathbf{3}_{18}$	(39.8)[b]	(14.4)	< − 50	<10.9	$CDCl_3$
$\mathbf{4}_{18}$	(39.8)[b]	(14.4)	− 30	11.9	$CDCl_3$

a) The figures in parentheses are the assumed values. b) Chemical shift difference of AB protons of $\mathbf{3}_{16}$ in $CDCl_3$.

References

1) K. Sakamoto and M. Ōki, *Tetrahedron Lett.*, **1973**, 3989.
2) K. Sakamoto and M. Ōki, This Bulletin, **46**, 270 (1973).
3) I. Suzuki, M. Tsuboi, and T. Shimanouchi, *Spectrochim. Acta*, **16**, 467 (1960).
4) A. Brunner, U.S. 1887396 (1933); *Chem. Abstr.*, **27**, 1359 (1933); J. H. Wood and R. E. Gibson, *J. Amer. Chem. Soc.*, **71**, 393 (1949).
5) J. V. Braun and J. Nelles, *Ber.*, **67**, 1094 (1934).
6) V. C. Farmer and R. H. Thomposn, *Spectrochim. Acta*, **16**, 559 (1960); M. Ōki and K. Mutai, *ibid.*, **25A**, 1941 (1969).
7) G. C. Levy and G. L. Nelson, *J. Amer. Chem. Soc.*, **94**, 4897 (1972).
8) G. C. Levy and G. L. Nelson, "Carbon-13 Nuclear Magnetic Resonance for Organic Chemists," Wiley-Interscience, New York (1972).
9) A. F. Cockerill, G. L. O. Davies, R. C. Harden, and D. M. Rackham, *Chem. Rev.*, **73**, 553 (1973).
10) G. M. Montaudo and P. Finocchiaro, *J. Org. Chem*, **37**, 3434 (1972).
11) R. A. Fletton, G. F. H. Green, and J. E. Page, *Chem. Commun.*, **1972**, 1134.
12) K. Tori and Y. Yoshimura, *Tetrahedron Lett.*, **1973**, 1573.
13) A. G. Whittaker, D. W. Moore, and S. Siegel, *J. Phys. Chem.*, **68**, 3431 (1964).
14) L. R. Isbrandt and M. T. Rogers, *Chem. Commun.*, **1971**, 1378.
15) J. A. Pople, W. G. Schneider, and H. J. Bernstein, "High Resolution Nuclear Magnetic Resonance," McGraw-Hill Book Co., Inc., New York (1958), p. 218; J. W. Emsley, J. Feeney, and C. H. Sutcliffe, "High Resolution Nuclear Magnetic Resonance Spectroscopy," Pergamon Press, Oxford (1965), p. 481.
16) R. Adams and J. B. Hale, *J. Amer. Chem. Soc.*, **61**, 2825 (1939); S. L. Chien and R. Adams, *ibid.*, **56**, 1787 (1934).
17) H. Suzuki, This Bulletin, **32**, 1350 (1959).
18) T. H. Goodwin, M. Przyblska, and J. M. Robertson, *Acta Crystallogr.*, **3**, 279 (1950).
19) The bulkiness referred to here is defined by the free energy of activation. We believe, however, the methoxy group is bulkier than the methyl in the sense of enthalpy of activation also, because the largest entropy of activation known in the internal rotation of methoxy-substituted biphenyl[20] is not sufficient to reverse the difference of 10 kcal/mol in free energy of activation at ambient temperature.
20) B. M. Graybill and J. E. Leffler, *J. Phys. Chem.*, **63**, 1461 (1959).

The Convenient Synthesis of Anhydronucleosides *via* the 2′,3′-*O*-Sulfinate of Pyrimidine Nucleosides as the Active Intermediates

Tsuneo SOWA and Kozo TSUNODA

Research Section, Foodstuffs Plant, Asahi Chemical Ind. Co., Ltd. Nobeoka, Miyazaki 882

(Received June 6, 1974)

The synthesis of 2,2′-*O*-anhydro(1-β-D-arabinofuranosyl) cytosine (**3a**) and 2,2′-*O*-anhydro(1-β-D-arabinofuranosyl) uracil (**3b**) is described. The active intermediates, 2′,3′-*O*-sulfinyl cytidine (**2a**) and 2′,3′-*O*-sulfinyl uridine (**2b**), were prepared from the corresponding nucleosides (**1a** or **1b**) by successive treatment with thionyl chloride in acetonitrile and with water. The 2,2′-*O*-anhydropyrimidine nucleosides were formed quantitatively by heating the intermediates in an acidic aqueous solution or in *N*,*N*-dimethylformamide in the presence of sodium acetate. The treatment of the anhydronucleosides with alkali gave the corresponding arabinonucleosides.

Anhydronucleosides are important modifications of natural nucleosides and have been used as intermediates in the chemical synthesis of arabinonucleosides. 2,2′-*O*-Anhydro-1-β-D-arabinofuranosyl cytosine has been shown to be an useful intermediate[1–3] for the synthesis of a carsinostatic nucleoside, 1-β-D-arabinofuranosyl cytosine,[4] and by itself to be a potent carsinostatic agent.[5] Anhydronucleosides have been synthesized by several procedures from natural nucleosides *via* the corresponding activated intermediates, such as tosyl,[6,7] mesyl,[8,9] carbonyl[10,11] and thiocarbonyl[12] derivatives, but most of those procedure involve tedious steps. Recently, 2,2′-*O*-anhydro(1-β-D-arabinofuranosyl)cytosine was successfully synthesized directly from cytidine with a Vilsmeier-Haack reagent.[13] We wish to describe another simple method for the synthesis of anhydronucleosides.

Results and Discussion

The synthesis of anhydronucleosides is outlined in Scheme 1. The essential step in the scheme is the introduction of a good leaving group at the 2′ and 3′ positions in the ribose moiety of natural nucleosides. In order to establish a convenient method usable on a large scale, a cyclic sulfinyl group was used as the leaving group; it was considered to be more active than either the cyclic carbonyl group[10,11] or the cyclic thiocarbonyl group.[12]

Thionyl chloride, which is readily obtainable on a commercial scale, was reacted with cytidine (**1a**) in dry acetonitrile at room temperature for 2 hr. Paper chromatography showed a single spot with an R_f-value of 0.7, different from that of **1a** (R_f 0.33). The reaction product was isolated in an 80% yield by adding a small amount of water to the reaction mixture. The structure of the acylation product was identified as 2′,3′-*O*-sulfinyl cytidine hydrochloride (**2a**), which was negative to a periodate-benzidine test[14] and which gave an ultraviolet spectrum similar to that of **1a**. The alkali hydrolysis of **2a** eliminated the cyclic sulfinyl group and so yielded **1a**. The **2a** product had three fairly sharp bands due to S=O stretching at 1010, 1021, and 1053 cm^{-1}, and three sharp bands associated with the five-membered cyclic sulfinyl group at 1201, 1205, and 1210 cm^{-1} in the infrared spectrum.[15] The elemental analysis of **2a** agreed with the proposed structure. The structure of **2a** was further confirmed by a subsequent reaction in which it was converted into 1-β-D-arabinofuranosyl cytosine (**4a**) through 2,2′-*O*-anhydro(1-β-D-arabinofuranosyl) cytosine hydrochloride (**3a**).

In the acidic solution, **2a** was stable at room temperature but was transformed into **3a** at an elevated tem-

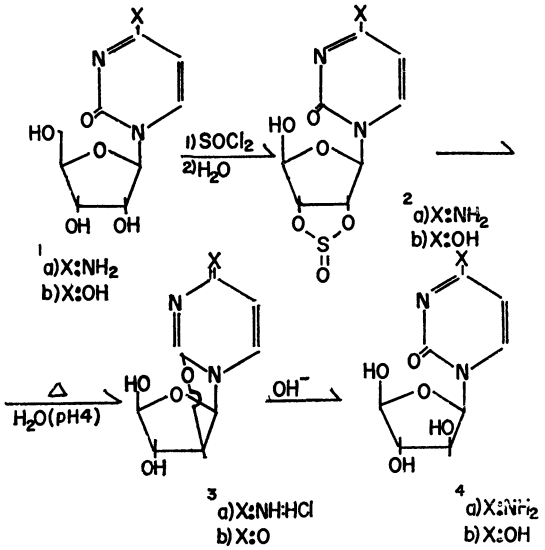

Scheme 1.

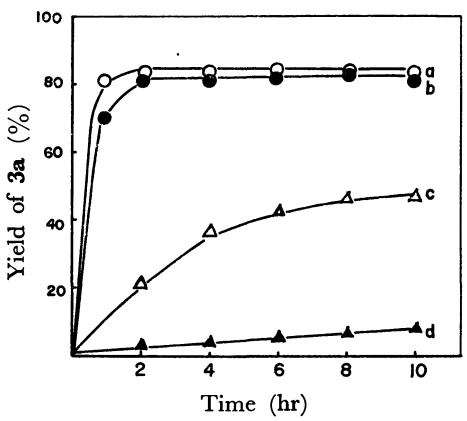

Fig. 1. Effect of reaction temperature on the preparation of 2′,3′-*O*-sulfinyl cytidine (**3a**).
Experimental conditions:
CH_3CN 10 ml, $SOCl_2$ 15 mmol, cytidine 3 mmol at pH 4.0, at the temperature of a) 100 °C, b) 80 °C, c) 60 °C, d) 40 °C.

Table 1. Properties of nucleoside derivatives

Compd.	Mp (dec.)	R_f, P. C.		$[\alpha]_D^{20}$	UV spectrum[a]	
		solv. A	solv. B		λ_{max}	λ_{min}
1a	220—230 °C	0.33	0.53	29.9	280	241
2a	253—254 °C	0.70	—	−50.4	278	240
3a	262 °C		0.81	−22.0	232, 263	243
4a	215 °C	0.33	0.65	158.0	280	241
1b	165 °C	0.51	0.54	4.0	263	230
2b	104—105 °C	0.69	—	—	260	229
3b	234—236 °C	0.48	0.67	11.0	223, 252	236
4b	215—216 °C	0.48	0.58	116.8	263	230

a) at pH 2.0

perature (Fig. 1). When **2a** was refluxed in the acidic aqueous solution at pH 4.0, the reaction went essentially to completion after 1 hr to form a 2,2′-*O*-anhydro-linkage and it could be heated at 80 °C for 2 hr without any deterioration in the reaction yield. By anion-exchange column chromatography, **3a** was isolated in a 74.7% yield and was identified as 2,2′-*O*-anhydro(1-β-D-arabinofuranosyl)cytosine hydrochloride by a comparison of its physical properties with those of an authentic sample.[13] The overall yield of **3a** from **1a** could be increased to 72.8% by omitting the isolation of the intermediate, **2a**.

Uridine (**1b**) was reacted with thionyl chloride under the same conditions as **1a** to give 2′,3′-*O*-sulfinyl uridine (**2b**) as a single product, as was shown by paper chromatography. Its chromatographic behavior and ultraviolet absorption properties are shown in Table 1. By heating **2b** in *N*,*N*-dimethylformamide (DMF) at 80 °C in the presence of sodium acetate, 2,2′-*O*-anhydro-(1-β-D-arabinofuranosyl)uracil (**3b**) was obtained from **1b** in an overall yield of 46.7%. The physical properties of **3b** were in good agreement with those of an authentic material.[11] Compounds **3a** and **3b** were easily converted to 1-β-D-arabinofuranosyl cytosine (**4a**) and 1-β-D-arabinofuranosyl uracil (**4b**) respectively by treating them with alkali. The physical properties of **4a** and **4b** are listed in Table 1; they are identical with those of authentic samples.

The method of synthesizing anhydronucleosides described above is superior to that of Kikugawa[13] or Furukawa[11] in respect to the yield and the simplicity of the procedure.

Experimental

The ultraviolet spectra were recorded on a Hitachi DPS-3T spectrophotometer, and the infrared spectra, on a Hitachi EPI-G2 apparatus. The paper chromatography of the reaction products was carried out by the ascending technique on Toyo-Roshi No. 51 paper (40×40 cm) using the following solvent systems: Solvent A; *n*-butanol–acetic acid–water (4 : 1 : 5); Solvent B; isopropanol–saturated ammonium sulfate–1M-sodium acetate (2 : 79 : 19).

2′,3′-O-Sulfinyl Cytidine Hydrochloride Obtained by the Reaction of Cytidine with Thionyl Chloride. Freshly distilled thionyl chloride (6 g, 50 mmol) was placed in 30 ml of acetonitrile, and the mixture was set aside at room temperature. To the solution was then added cytidine (2.6 g, 10 mmol), and the mixture was stirred at room temperature for 2 hr. A 15-ml portion (0.8 mol) of water was then added to the reaction mixture to destroy the reactant under vigorous stirring. Paper chromatography showed a single spot having an R_f value of 0.7, an aqueous extract of which showed the absorption maximum at 278 nm (pH 1.0). The resulting reaction mixture was kept in the refrigerator overnight, and then the white precipitate thus obtained was collected by filtration, washed with water and then twice with methanol, and dried to yield 2.63 g (81.0%) of 2′,3′-*O*-sulfinyl cytidine hydrochloride; mp 253—254 °C (dec.), $[\alpha]_D^{20}$-50.4 ° (*c*, 0.5, H_2O). The UV and chromatographic properties are shown in Table 1.

Found C; 33.30, H; 3.70, N; 11.30, S; 9.30, Cl; 11.53%. Calcd for $C_9H_{12}N_3O_6SCl$, C; 33.18, H; 3.69, N; 11.90, S; 9.83; Cl; 10.91%.

*2,2′-O-Anhydro(1-β-D-arabinofuranosyl) Cytosine Hydrochloride (**3a**). From 2′-3′-O-Sulfinyl Cytidine Hydrochloride (**2a**):* 2′,3′-*O*-Sulfinyl cytidine hydrochloride (32.5 g, 100 mmol) was dissolved into 1 l of water, and then the solution was adjusted to pH 4.0 with 6M-sodium hydroxide. After refluxing the resulting solution for 4 hr, the reaction mixture was cooled and was then applied to a Diaion W.A.-30 (acetate form) column (2.5×40 cm). The column was washed with 3 l of water, the washings were evaporated *in vacuo* to about 200 ml after the pH of the solution had been adjusted to 4.0 with 6M-hydrochloric acid. A 300-ml portion of ethanol was added to the concentrated solution, and the solid thus precipitated was collected by filtration, washed twice with ethanol, and dried to give 19.5 g (78.4% yield) of 2,2′-*O*-anhydro(1-β-D-arabinofuranosyl) cytosine hydrochloride. Mp 262 °C (dec.), $[\alpha]_D^{22}$ −22 ° (*c*, 0.5, H_2O). The UV and chromatographic properties are shown in Table 1. Found, C; 41.30, H, 4.65, N; 15.85, Cl; 13.60%. Calcd for $C_9H_{11}O_4N_3$ HCl, C; 41.32, H; 4.63; N; 16.07, Cl; 13.61%.

*From Cytidine (**1a**):* Cytidine (2.6 g, 10 mmol) and thionyl chloride (6 g, 50 mmol) were mixed in acetonitrile (30 ml) at room temperature for 2 hr, and then the reaction mixture was poured into ice water (1 l). The aqueous solution was adjusted to pH 4.0 with 6M-sodium hydroxide and then refluxed for 2 hr. The resulting solution was cooled to room temperature and treated essentially by the above method. 1.9 g of 2,2′-*O*-anhydro(1-β-D-arabinofuranosyl) cytosine hydrochloride was obtained as white needles in the yield of 72.8% from material cytidine. mp 262—263 °C (dec.), $[\alpha]_D^{20}$ −22 ° (*c*, 0.5, H_2O). Found, C; 41.28, H; 4.70, N; 16.01, Cl; 13.63%.

*1-β-D-Arabinofuranosyl Cytosine (**4a**).* 2,2′-*O*-Anhydro-(1-β-D-arabinofuranosyl) cytosine hydrochloride (52 g, 200 mmol) was dissolved in 3 l of water, after which the solution was adjusted to pH 10.0 with 2M-sodium hydroxide. The solution was allowed to stand at room temperature for

1 hr and was then applied to an Amberlite 200 (H^+ form) column (5×200 cm). The column was washed with water and eluted with 2 l of 1M-ammonium hydroxide. Fractions having an UV absorption at 260 nm (as checked on an UV spectrophotometer) were collected and concentrated to dryness. The residual crystalline product was recrystallized from ethanol to give 43.7 g of 1-β-D-arabinofuranosyl cytosine; mp 215 °C (dec.), $[\alpha]_D^{20}+158°$ (*c*, 0.5, H_2O). Found, C; 44.49, H; 5.41, N; 17.21%. Calcd for $C_9H_{12}O_5N_3$, C; 44.44, H; 5.39, N; 17.28%.

*2′,3′-O-Sulfinyl Uridine (**2b**).* Into a mixed solution of thionyl chloride (20 g, 160 mmol) and acetonitrile (100 ml) was vigorously stirred uridine (10 g, 40 mmol), and then the reaction mixture was maintained for 4 hr at 5 °C. After water (4.3 g, 240 mmol) had been added to the resulting mixture, the white precipitates were collected, washed with methanol, and then dried to yield 11.1 g (85%) of 2′,3′-*O*-sulfinyl uridine dihydrate. mp 104—105 °C (dec.), Found; C; 33.04, H; 2.98, N; 8.49, S; 9.78%. Calcd for $C_9H_{10}O_2N_7$-$S\cdot 2H_2O$ C; 33.13, H; 3.06, N; 8.58, S; 9.81%.

*2′,3′-O-Anhydro(1-β-D-arabinofuranosyl) Uracil (**3b**)* 2′,3′-*O*-Sulfinyl uridine dihydrate (6.96 g, 21 mmol) and sodium acetate (7.9 g, 96 mmol) were heated in *N,N*-dimethylformamide (400 ml) at 80 °C for 4 hr and then cooled. The solid thus precipitated was filtered off and washed with 50 ml of DMF. The filtrate and washings were combined and concentrated to dryness. The resulting syrup was crystallized from ethanol. The crystalline product (4.7 g) was recrystallized from water to give 2.7 g of 2,2′-*O*-anhydro-(1-β-D-arabinofuranosyl) uracil; mp 234—236 °C (dec.), $[\alpha]_D^{20}-11.0°$ (*c*, 0.5, H_2O). Found, C; 48.15, H; 4.41, N; 12.40%. Calcd for $C_9H_{10}N_2O_5$, C; 48.23, H; 4.45, N; 12.41%.

*1-β-D-Arabinofuranosyl Uracil (**4b**).* 2,2′-*O*-Anhydro(1-β-D-arabinofuranosyl) uracil (1.1 g, 5 mmol) was dissolved in 100 ml of water, and then the solution was adjusted to pH 10.0 with 2M-ammonium hydroxide. The mixture was allowed to stand at room temperature for 1 hr and was then applied to a column containing 20 g of active carbon, granule type. The column was subsequently washed with water and eluted with 50 ml of 0.5 M-ammonium hydroxide. The effluent was evaporated *in vacuo*. The crystallization of the residue from ethanol afforded 1.03 g of 1-β-D-arabinofuranosyl uracil, mp 215—216 °C (dec.), $[\alpha]_D^{20}+114.3°$ (*c*, 0.5, H_2O). Found, C; 44.29, H; 5.01, N; 11.40%. Calcd for $C_9H_{12}N_2O_6$, C; 44.26, H; 4.92, N; 11.48%.

References

1) E. R. Walwick, W. K. Roberts, and C. A. Dekker, *Proc. Chem. Soc.*, **1959**, 84.
2) I. L. Doerr and J. J. Fox, *J. Org. Chem*, **32**, 1465 (1967).
3) W. V. Royle and T. Y. Shen, *J. Med. Chem.*, **10**, 331 (1967).
4) S. S. Cohen, "Progress in Nucleic Acid Research and Molecular Biology," Vol. V, J. N. Dabidson and W. E. Cohen, Ed., Academic Press, New York, N. Y. (1966), p. 1.
5) A. Hashi, F. Kanazawa, K. Kuretani, M. Saneyoshi, and Y. Arai, *Gann*, **62**, 145 (1971).
6) J. F. Codington, I. L. Doerr, and J. J. Fox, *J. Org. Chem.*, **29**, 558 (1964).
7) N. C. Yung and J. J. Fox, *J. Amer. Chem. Soc.*, **83**, 3061 (1961).
8) J. F. Codington, R. Fecher, and J. J. Fox, *ibid.*, **82**, 2794 (1960).
9) J. J. Fox and N. C. Miller, *J. Org. Chem.*, **28**, 936 (1966).
10) A. Hampton and A. R. Nichol, *Biochem.*, **5**, 2076 (1966).
11) S. Furukawa, *Anual Report Takeda Research Lab.*, **30**, 371 (1971) M. Honjo, *ibid.*, **26**, 21 (1967).
12) I. Wempen and J. J. Fox, *Tetrahedron Lett.*, **1964**, 2081.
13) K. Kikukawa and M. Ichino, *J. Org. Chem.*, **37**, 284 (1972).
14) M. Viscontini, D. Hoch, and P. Karrer, *Helv. Chim. Acta*, **38**, 642 (1955).
15) L. J. Bellamy, "The Infrared-Spectra of Complex Molecules", L. J. Bellamy, Ed, Richard Clay and Company Ltd., Great Britain (1960), p. 360.

Metalation of 2-Methyl-4*H*-pyran-4-one and its Reactions

Makoto YAMAMOTO and Noboru SUGIYAMA*

Department of Chemistry, Saga University, Saga 840

**Department of Chemistry, Tokyo Kyoiku University, Otsuka, Tokyo 112*

(Received June 24, 1974)

2-Methyl-4H-pyran-4-ones formed metalated products in the presence of sodium amide in liquid ammonia, and the metalated product reacted with alkyl and aralkyl halides or carbonyl compounds to give alkylated or condensed products. Self condensation reactions of 2-methyl-4*H*-pyran-4-ones also occurred in liquid ammonia to give flavone and the γ-pyrone dimer.

Boon[1] reported that 2,6-dimethyl-4*H*-pyran-4-one (**1**) reacts with benzaldehyde in an alkaline aqueous solution to give 2,6-distyryl-4*H*-pyran-4-one. 6-Methyl 1,2-diphenyl-2,3-dihydro-4-pyridone also condensed with benzaldehyde in an alkaline methanol solution to form 6-styryldihydropyridone.[2] These results indicate that the β-methyl hydrogen of an α,β-unsaturated ketone is acidic enough to react with an electrophile in an alkaline media.

This paper describes the metalation of 2-methyl-4*H*-pyran-4-one, and its reaction with some electrophiles.

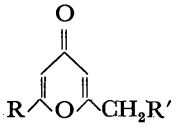

1 : R=CH_3, R′=H
1′ : R=CH_3, R′=Na
3 : R=CH_3, R′=$CH_2C_6H_5$
5 : R=$CH_2CH_2C_6H_5$, R′=$CH_2C_6H_5$
6 : R=CH_3, R′=*n*-C_4H_9
8 : R=*n*-C_5H_{11}, R′=*n*-C_4H_9
9 : R=C_6H_5, R′=H
9′ : R=C_6H_5, R′=Na
10 : R=C_6H_5, R′=$CH_2C_6H_5$
12 : R=C_6H_5, R′=$CH(OH)C_6H_5$
13 : R=C_6H_5, R′=$CH(C_6H_5)CH_2COC_6H_5$
16 : R=C_6H_4-OCH_3-*p*, R′=H

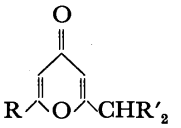

4 : R=CH_3, R′=$CH_2C_6H_5$
7 : R=CH_3, R′=*n*-C_4H_9
11 : R=C_6H_5, R′=$CH_2C_6H_5$

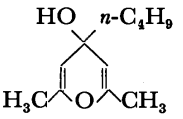

2

Fig. 1.

Results and Discussion

Compound **1** did not give the metalated product **1′** by treating **1** with (a) sodium hydride in refluxing benzene, (b) lithium dimethylamide in ether, or (c) lithium *N*-methylanilide in ether or in tetrahydrofuran at room temperature, and **1** was recovered quantitatively in each case. Compound **1** reacted with *n*-butyl lithium in ether or in tetrahydrofuran at −78 °C under a nitrogen atmosphere to give 2,6-dimethyl-4-*n*-butyl-4*H*-pyran-4-ol (**2**), but at −20 °C or at room temperature **1** merely decomposed.

However treatment of **1** with sodium amide gave the metalated product **1′**. The formation of **1′** was proved that **1** was allowed to react with an equimolar amount of sodium amide in liquid ammonia at −78 °C under a nitrogen atmosphere, and to the resulting red solution was added an equimolar amount of benzyl bromide to give 2-methyl-6-phenethyl-4*H*-pyran-4-one (**3**) in 32% yield, accompanied by 14.5% of a mixture of dialkylated products, 2-methyl-6-(α-benzylphenethyl)-4*H*-pyran-4-one (**4**) and 2,6-diphenethyl-4*H*-pyran-4-one (**5**) (**4** : **5**=73 : 27), and 38% of the starting material **1** was recovered. When the ratio of **1** sodium amide and benzyl bromide was 1 : 2 : 2, the yields of **3** and the dialkylated products (**4**+**5**) were 31.5 and 22.5% (**4** : **5**=1 : 1), and 26% of **1** was recovered.

The reaction of **1′** with *n*-butyl bromide gave 2-methyl-6-*n*-pentyl-4*H*-pyran-4-one (**6**) (14.0% yield) and the dialkylated products (**7**+**8**) (6.5%).

2-Methyl-6-phenyl-4*H*-pyran-4-one (**8**) also formed the metalated product **9′** with an equimolar amount of sodium amide in liquid ammonia. An alkylation reaction of **9**, similar to that of **1′**, was carried out with an equimolar amount of benzyl bromide to give 2-phenethyl-6-phenyl-4*H*-pyran-4-one (**10**) in 77.0% yield. When the ratio of **9**, sodium amide and benzyl bromide was 1 : 2 : 2, the products were 2-(α-benzylphenethyl)-6-phenyl-4*H*-pyran-4-one (**11**) (75% yield) and **10** (13% yield).

Compound **9′** condensed with benzaldehyde to afford 2-(β-hydroxyphenethyl)-6-phenyl-4*H*-pyran-4-one (**12**) in 65% yield. Chalcone also reacted with **9′** to give only a Michael type addition product, 2-(4-oxo-2,4-diphenylbutyl)-6-phenyl-4*H*-pyran-4-one (**13**) in 81 % yield. The structures of all compounds were determined from their spectra and elemental analyses.

On the other hand, the formation of an aldol type condensation product by the reaction of γ-pyrone with malononitrile[3] suggested that the carbonyl group of γ-pyrone is reactive to a nucleophile. Anticipating a dimerization reaction with one part of **9** behaving as an electrophile and the other part behaving as a nucleophile, **9** was treated with sodium amide in liquid ammonia. When the molar ratio of **9** and sodium amide was 2 : 1, two new compounds **14** and **15** were obtained in 49.0 and 12.1% yields. From spectral data and elemental analyses it was deduced that **14** was 5-methyl-7-phenacylflavone and that **15** was a γ-pyrone dimer. Since the treatment of the dimer **15** with concentrated sulfuric acid or sodium amide in liquid ammonia gave **14**, the dimer **15** was considered to be an intermediate in the formation of flavone **14**. Thus this reaction is a self condensation of **9**.

However when **9** was treated with sodium methoxide

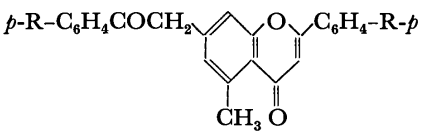

14 : R=H
17 : R=OCH_3

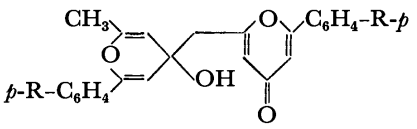

15 : R=H
18 : R=OCH_3

Fig. 2.

in methanol or with sodium in tetrahydrofuran, neither **14** nor **15** was detected. The formation of **14** and **15** was observed only in liquid ammonia.

A similar treatment of 2-(*p*-methoxyphenyl)-6-methyl-4*H*-pyran-4-one (**16**) gave 7-(*p*-methoxyphenacyl)-4'-methoxy-5-methylflavone (**17**)(38.5% yield) and the dimer (**18**) (7.0% yield). Treatment of the dimer **18** with concentrated sulfuric acid also gave the flavone **17**. The structures of **17** and **18** were supported by spectral data and elemental analyses.

The mechanism of the formation of the flavone **14** from γ-pyrone **9** was assumed to be an attack on the carbonyl group of **9** by the monoanion **9'** to give γ-pyrone dimer **15**, followed by elimination of water and isomerization to form the flavone **14**.

Experimental

*2,6-Dimethyl-4H-pyran-4-one (**1**).* Compound **1** was synthesized by reaction of dehydroacetic acid with concentrated hydrochloric acid,[4] mp 130—131 °C (lit,[4] 130 °C).

*2-Methyl-6-phenethyl-4H-pyran-4-one (**3**).* Procedure A: In a 200 ml three-necked flask, about 120 ml of liquid ammonia, containing 11 mmol of sodium amide, were placed. To this solution 1.24 g (10 mmol) of **1** and 20ml of dry ether were added. After stirring for 1 hr at −78 °C, 1.88 g (11 mmol) of benzyl bromide in 10 ml of dry ether was added and the mixture was stirred for an additional 3 hr at −78 °C under a nitrogen atmosphere. After quenching the reaction mixture with excess ammonium chloride, the liquid ammonia was evaporated rapidly on a water bath. Fifty ml of diluted hydrochloric acid and 50 g of crushed ice were added to the resulting residue. The resulting acidic aqueous solution was extracted with chloroform, washed with water, dried over anhydrous sodium sulfate and concentrated giving crude alkylated products. This residue was chromatographed on a silica gel (Merck 7734, 70—230 mesh) column with benzene-ethyl acetate (2 : 1 v/v). The fractions which showed R_f-values of 0.16 and 0.26 on silica gel (Merck 7721) thin layer chromatographs with benzene-ethyl acetate (2 : 1 v/v).

The fractions with R_f=0.16 were collected, concentrated and recrystallized from *n*-hexane-benzene (4 : 1 v/v) to give 694 mg (32.4%) of **3**, mp 75—77 °C (lit,[5] 76.5—77 °C).

IR(KBr): 1660 (νC=O), 1610 (C=C) and 695 cm^{-1} (phenyl).

UV λ_{max}^{EtOH} (ε): 250 (15700) and 261 nm (9060).

NMR(in $CDCl_3$): δ 2.16 (s, 3H), 2.51—3.02 (m, 4H), 5.96 (s, 2H) and 7.00—7.24 (m, 5H).

*The Dialkylated Products (**4**+**5**).* The fractions with R_f=0.26, were collected and concentrated to give 441 mg (14.5%) of the mixture (**4**+**5**), as a light brownish-yellow oil.

IR(liquid film): 1660 (νC=O), 1600 (C=C) and 750, 700 cm^{-1} (phenyl).

The ratio of **4** and **5** was determined from the NMR spectrum as follows: The NMR spectrum of the dialkylated mixture showed a singlet at δ 2.16 (intergration: 36), which corresponded to the 2-methyl protons of compound **4**. The multiplet signal at δ 7.08—7.56 (integration: 165) corresponded to the overlapping of the aromatic protons of the two isomers **4** and **5**. The integration of the ten aromatic protons of the two phenyl groups of **4** was calculated to 120. While the integration 45 was obtained for ten aromatic protons of two phenyl groups of **5**. Thus, 73% of **4** and 27% of **5** were contained in the mixture.

After **4** and **5** had been eluted, the column was again eluted with acetone, and the eluate was concentrated. The residue was crystallized from benzene to give 471 mg (38%, recovered) of the starting material, γ-pyrone (**1**), 128—130 °C.

Five mmol of **1**, 10.5 mmol of sodium amide and 10.5 mmol of benzyl bromide were treated according to procedure A. Three handred and thirtyseven mg of (31.5%) of **3**, 342 mg (22.5%) of the dialkylated products (**4**+**5**) (**4** : **5**=1 : 1) were obtained and 161 mg (26%) of **1** was recovered. Five mmol of **1**, 5.3 mmol of sodium amide and 5.3 mmol of benzyl bromide were treated according to procedure A. When the reaction was quenched after 30 min, 68 mg (11%) of **3** and 197 mg (13%) of the sole dialkylated product **4** were obtained.

NMR spectrum of **4** (in $CDCl_3$): δ 2.16 (s, 3H), 3.00 (broad s, 5H), 5.96 (d, 1H), 6.08 (broad s, 1H) and 7.10—7.56 (m, 10H).

*2-Methyl-6-pentyl-4H-pyran-4-one (**6**).* Using procedure A, from 10 mmol of **1**, 10.5 mmol of potassium amide and 10.5 mmol of *n*-butyl bromide, 252 mg (14.0%) of **6** and 153 mg (6.5%) of the dialkylated products (**7**+**8**) were obtained.

IR spectrum of **6** (liquid film): 1660 (νC=O) and 1610 cm^{-1} (C=C).

NMR spectrum of **6** (in $CDCl_3$): δ 0.90 (t, 3H), 1.12—1.72 (m, 6H), 2.20 (s, 3H), 2.45 (t, 2H) and 5.96 (s, 2H).

*Treatment of **1** with Different Bases*: Compound **1** (5 mmol) was treated with an equimolar amount of sodium hydride (50% in oil) in 50 ml of refluxing benzene, with 5 mmol of lithium dimethylamide in 50 ml of dry ether (distilled from $LiAlH_4$) at —20 °C, at room temperature or under refluxing, with an equimolar amount of lithium *N*-methylanilide in 30 ml of dry ether or in 50 ml of dry THF (distilled from $LiAlH_4$) at room temperature or under refluxing. But in each case, the metalated product **1'** which was tested for by adding benzyl bromide, was not formed, and **1** was recovered quantitatively. This was checked by thin layer chromatography and NMR.

*Treatment of **1** with n-Butyl Lithium*: Compound **1** (5 mmol) was treated with an equimolar amount of *n*-butyl lithium (15% in hexane) in 50 ml of dry THF (distilled from $LiAlH_4$) at −78 °C under a nitrogen atmosphere. After 1 hr an equimolar amount of benzyl bromide in 10 ml of dry THF was added to the resulting red solution, the mixture was then stirred for 2 hr at −78 °C. Thin layer chromatography of the reaction mixture revealed a component with R_f=0.19, which was isolated by silica gel (Merck 7734) column chromatography with benzene-ethyl acetate (2 : 1 v/v). From the spectral data it was speculated that this product was 2,6-dimethyl-4-*n*-butyl-4*H*-pyran-4-ol (**2**).

IR(liquid film): 3200—3450 (broad, νOH) and 1600 cm^{-1}

(C=C).

NMR(in $CDCl_3$): δ 0.90, 1.22—1.82, 2.12 and 6.42.

Compound **1** was also treated with *n*-butyl lithium, as described above, at −20 °C or at room temperature. However after working up as usual, a red oil was obtained. This red oil did not show a clear spot on a thin layer chromatograph, and also **1** could not be detected.

*2-Methyl-6-phenyl-4H-pyran-4-one (**9**)* was synthesized from 1-phenyl-1,3,5-hexanetrione and concentrated sulfuric acid, mp 86—88 °C (lit.[6] 87—88 °C).

*2-Phenethyl-6-phenyl-4H-pyran-4-one (**10**).* Using procedure A, from 10 mmol of **9** and 11 mmol of benzyl bromide, **10** was obtained. Eluting solvent: benzene-ethyl acetate (4 : 1 v/v), yield 2.12 g (77.0%), mp 84—85 °C (lit,[7] 85—86.5 °C).

IR(KBr): 1660 (νC=O) and 1595 cm^{-1} (C=C).

NMR (in $CDCl_3$): δ 3.01 (s, 4H, 6.00 (d, 1H), 6.62 (d, 1H), 7.15 (s, 5H) and 7.50 (m, 5H).

*2-(α-Benzylphenethyl)-6-phenyl-4H-pyran-4-one (**11**).* Following procedure A, 10 mmol of **9**, 20 mmol of sodium amide and 20 mmol of benzyl bromide were reacted. 2.75 g of the dialkylated product **11** was obtained (75%), mp 117—119 °C, accompanied by 380 mg (13%) of **10**. Eluting solvent: Benzene-ethyl acetate (4 : 1 v/v).

IR(KBr): 1640 (νC=O), 1620 (C=C) and 695 cm^{-1} (phenyl).

NMR(in $CDCl_3$): δ 2.98—3.15 (m, 5H), 5.91 (d, 1H), 6.60 (d, 1H), 7.05—7.24 (m, 10H) and 7.44—7.68 (m, 5H).

Found: C, 85.10; H, 6.19%. Calcd for $C_{26}H_{22}O_2$: C, 85.21; H, 6.05%.

*2-(β-Hydroxyphenethyl)-6-phenyl-4H-pyran-4-one (**12**).* Following procedure A, from 5 mmol of **9** and 5 mmol of benzaldehyde, 950 mg (65%) of **12** was obtained. Eluting solvent: Benzene-ethyl acetate (2 : 1 v/v). Crystallized from hot acetone, mp 163—164 °C.

IR(KBr): 3200(νOH), 1645 (C=O) and 700 cm^{-1} (phenyl).

UV λ_{max}^{EtOH} (ε): 228 (12300) and 273 nm (17800).

NMR(in $CDCl_3$): δ 3.00 (d, 2H), 3.60 (s, 1H), 5.14 (t, 1H), 6.22 (d, 1H), 6.59 (d, 1H) and 7.29—7.70 (m, 10H).

Found: C, 77.86; H, 5.40%. Calcd for $C_{19}H_{16}O_3$: C, 78.06; H, 5.52%.

*2-(4-Oxo-2,4-diphenylbutyl)-6-phenyl-4H-pyran-4-one (**13**).* Using procedure A, **13** was synthesized from 10 mmol of **9** and 10 mmol of chalcone. Eluting solvent: Benzene-ethyl acetate (2 : 1 v/v). The fractions which contained **13** were collected, concentrated and crystallized from benzene to give 3.20 g (81%) of **13**, mp 120—122 °C, as white leaflets.

IR(KBr): 1680, 1660 (νC=O), 1625 (C=C) and 695 cm^{-1} (phenyl).

UV λ_{max}^{EtOH} (ε): 248 (19900) and 273 nm (19100).

NMR(in $CDCl_3$): δ 3.01 (m, 2H), 3.38 (d, 2H), 3.80 (m, 1H), 6.01 (d, 1H), 6.56 (d, 1H) and 7.17—7.97 (m, 15H).

Found: C, 82.15; H, 5.62%. Calcd for $C_{27}H_{22}O_3$: C, 82.21; H, 5.62%.

*5-Methyl-7-phenacylflavone (**14**).* Procedure B: In a 300 ml three-nicked flask, 10 mmol of sodium amide, 20 mmol of **9** and 200 ml of liquid ammonia were mixed. The mixture was then refluxed for 3 hr under a nitrogen atmosphere. After quenching with excess ammonium chloride, the reaction mixture was worked up as in procedure A. Thin layer chromatography of the reaction residue with benzene-ethyl acetate (1 : 1 v/v) showed two spots, R_f=0.39 and 0.20, while that of **9** was 0.26. The residue was chromatographed on a silica gel (Merck 7729, 230 mesh) column with benzene-ethyl acetate (1 : 1 v/v). The fractions with R_f=0.39 were collected, concentrated and crystallized from benzene-acetone (4 : 1 v/v) to give 1.70 g (49.0%) of **14**, mp 208—210 °C, as yellow cubic crystals.

IR(KBr): 1640 (νC=O), 1585, 1560 (C=C) and 700, 690 cm^{-1} (phenyl).

UV λ_{max}^{EtOH} (ε): 268 nm (28500).

$\lambda_{max}^{KOH/EtOH}$ (ε): 233 (38200), 268 (33200) and 354 nm (11100).

NMR(in DMSO-d_6): δ 2.31 (s, 3H), 6.12 (d, 1H, J=2.3 Hz), 6.70 (d, 1H, J=2.3 Hz), 6.74 (s, 1H), 6.78 (s, 1H), 7.27 (m, 5H), 7.45 (m, 5H) and 10.01 (broad, disappeared in D_2O).

Mass (*m/e*): 354 (parent peak), 336 (base peak, P–18), 308, 234, 178, 102 and 77.

Found: C, 81.11; H, 5.20%. Calcd for $C_{24}H_{18}O_3$: C, 81.34; H, 5.12%.

*The γ-Pyrone Dimer (**15**).* The fractions with R_f=0.20 were collected, concentrated and crystallized from acetone-ethanol (3 : 1 v/v) to give 450 mg (12.1%) of **15**, mp 188—189 °C.

IR (KBr): 3360 (νOH), 1650 (C=O), 1620 (C=C) and 695 cm^{-1} (phenyl).

UV λ_{max}^{EtOH} (ε): 232 (21100), 273 (19400), 292 (14790) and 307 nm (6000).

NMR(in DMSO-d_6): δ 1.97 (s, 3H), 3.60 (s, 2H), 5.94 (d, 2H), 6.17 (d, 1H), 6.67 (d, 1H) and 7.10—7.47 (m, 10H).

Mass (*m/e*): 372 (parent peak), 354 (P–18), 226, 186, 105 and 77.

Found: C, 77.24; H, 5.45%. Calcd for $C_{24}H_{20}O_4$: C, 77.40; H, 5.41%.

*Conversion of **14** to **15**.* *(a) By Concentrated Sulfuric Acid*: A solution of 5 mg of **15** in 2 ml of concentrated sulfuric acid was allowed to stand at room temperature for 10 min. The reaction mixture was poured into ice-water, and the aqueous layer was extracted with ether. By treating the etheral solution as usual, compound **14** was obtained, which was compared with an authentic sample by thin layer chromatography.

(b) By Sodium Amide in Liquid Ammonia: A mixture of 50 ml of liquid ammonia, 200 mg of **15** and 60 mg of sodium amide was stirred for 3 hr. After evaporation of liquid ammonia and treatment of the residue as usual, the formation of **14** was confirmed by thin layer chromatography using an authentic sample for comparison.

*Treatment of **9** with Bases in Methanol or in Tetrahydrofuran. In Methanol*: 930 mg of **9** was added to a solution of 130 mg of sodium metal in 25 ml of absolute methanol. The mixture was stirred for 4 hr at room temperature. After concentration of the reaction mixture, the residue was added to 10 ml of chloroform and 15 ml of diluted hydrochloric acid, and extracted with chloroform. Thin layer chromatography of the chloroform layer showed neither **14** nor **15** and **9** was recovered.

In Tetrahydrofuran: A mixture of 930 mg of **9** and 130 mg of sodium metal in 80 ml of dry THF was stirred at room temperature for 2 hr. The reaction mixture was treated as described above. Neiter **14** nor **15** was detected.

*2-(p-Methoxyphenyl)-6-methyl-4H-pyran-4-one (**16**).* A solution of 50 mmol (11.7 g) of 1-(*p*-methoxyphenyl)-1,3,5-hexanetrione[6] in 40 ml of concentrated sulfuric acid was cooled to 0 °C and allowed to stand at 0 °C for 2 hr. The reaction mixture was then poured into ice-water and extracted with chloroform. The chloroform layer was washed with water and dried over anhydrous sodium sulfate. After removing chloroform, the resulting residue was crystallized from benzene to give 10.2 g (94%) of **16**, mp 144—146 °C, as colorless needles.

IR(KBr): 1670 (νC=O), 1615 (C=C) and 1510 cm^{-1} (phenyl).

UVλ_{max}^{EtOH} (ε): 224 (17600) and 304 nm (25100).

NMR(in $CDCl_3$): δ 2.33 (s, 3H), 3.84 (s, 3H), 6.11 (d, 1H), 6.57 (d, 1H), 6.95 (d, 2H) and 7.67 (d, 2H).

Found: C, 72.12; H, 5.66%. Calcd for $C_{13}H_{12}O_3$: C, 72.21; H, 5.59%.

*7-(p-Methoxyphenacyl)-4'-methoxy-5-methylflavone (**17**).* Following procedure B, from 4.32 g (20 mmol) of **16** and 10 mmol of sodium amide, **17** was prepared in 38.5% (1.6 g) yield. Compound **17** was isolated from the dimer **18** by silica gel (Merck 7729) column chromatography with benzene-ethyl acetate (2 : 1 v/v). The fractions which contained **17** were collected, concentrated and crystallized from acetone to give light yellow cubic crystals, mp 236—239 °C.

IR(KBr): 1640 (νC=O), 1610 and 1565 cm^{-1} (C=C).

UVλ_{max}^{EtOH} (ε): 225 (33100), 248 (26000), 288 (27000) and 305 nm 24500).

NMR(in DMSO-d_6): δ 2.28 (s, 3H), 3.68 (s, 3H), 3.80 (s, 3H), 6.02 (d, 1H), 6.67 (d, 1H), 6.83 (d, 2H), 6.90 (d, 2H), 6.96 (d, 2H), 7.19 (d, 2H), 7.53 (d, 2H), and 9.90 (broad, 1H).

Found: C, 75.38; H, 5.26%. Calcd for $C_{26}H_{22}O_5$: C, 75.35; H, 5.35%.

*The Dimer **18**.* The dimer eluted after the fraction **17**. Yield 300 mg (7.0%).

NMR(in $CDCl_3$): δ 1.64 (s, 3H), 2.70 (s, 2H), 3.80 (s, 3H), 3.83 (s, 3H), 6.00 (s, 1H), 6.24 (d, 1H), 6.63 (d, 2H), 6.78 (d, 2H), 6.84 (d, 2H), 7.55 (d, 2H) and 7.58 (d, 2H).

*Treatment of the Dimer **18** with Sulfuric Acid.* A mixture of 20 mg of **18** and 3 ml of concentrated sulfuric acid was allowed to stand at room temperature for 10 min. The mixture was added to 10 g of crushed ice and extracted with ether. The flavone **17** was detected by thin layer chromatography of the ether solution using an authentic sample for comparison.

This work was supported by the Scientific Research Fund of Ministry of Education, Japanese Government.

References

1) A. A. Boon, K. G. McKinzie, and J. Trotter, *Proc. Chem. Soc.*, **30**, 205 (1914).

2) N. Sugiyama, M. Yamamoto, and C. Kashima, This Bulletin, **43**, 3937 (1970).

3) L. L. Woods, *J. Amer. Chem. Soc.*, **80**, 1440 (1958).

4) M. Ohta, and H. Kato, This Bulletin, **32**, 707 (1959).

5) A. J. Birch, D. W. Cameron, and R. W. Richards, *J. Chem. Soc.*, **1960**, 4395.

6) R. J. Light, and C. R. Hauser, *J. Org. Chem.*, **25**, 538 (1960).

7) K. G. Hampton, T. M. Harris, C. M. Harris, and C. R. Hauser, *ibid.*, **30**, 4263 (1965).

Studies of Reaction Mechanisms with All-valence Electron Semi-empirical SCF MO Theories. IX.[1] The Role of Tetracyclo[4.2.0.0^{2,8}0^{5,7}]oct-3-ene on the Ground State Potential Energy Hypersurfaces of $(CH)_8$ Isomers

Hiizu IWAMURA and Hiroshi KIHARA

Department of Chemistry, Faculty of Science, The University of Tokyo, Hongo, Tokyo 113

(Received July 2, 1974)

Tetracyclo[4.2.0.0^{2,8}0^{5,7}]oct-3-ene (**1**) is estimated by a MINDO MO calculation to be moderately strained. Interaction between the ethylenic π orbital and the Walsh orbitals of the two cyclopropane rings is extensive in the ground state structure of **1**. The third highest occupied MO is an out-of-phase combination of the ethylenic 2pπ AO's on C_3 and C_4, while the corresponding in-phase combination appears in the lower unoccupied MO's. The interconversion between **1** and bicyclo[4.2.0]octa-2,4,7-triene (**2**) is a typical symmetry-allowed reaction as revealed by a smooth change in bond indices along the reaction coordinates. The isomerization of substituted cyclooctatetraenes *via* **1** and **2** (Eq. (2)) is predicted to be possible at elevated temperatures. The symmetry-allowed degenerate valence isomerization of **1** (Eq. (3)) is energetically less favorable due to skeletal constraint.

While compounds with the tetracyclo[4.2.0.0^{2,8}0^{5,7}]-oct-3-ene structure have never been prepared, the parent hydrocarbon **1** has often been quoted as a possible intermediate in many thermal as well as photochemical interconversions between other $(CH)_8$ isomers. One of the earliest suggestions was that **1** was the intermediate in the singlet excited state reaction of barrelene to give cyclooctatetraene (Eq. (1)).[2] Recently Paquette *et al.* found evidence that **1'** was an intermediate in the thermal isomerization between 1,2- and 1,4-disubstituted cyclooctatetraenes (Eq. (2)).[3]

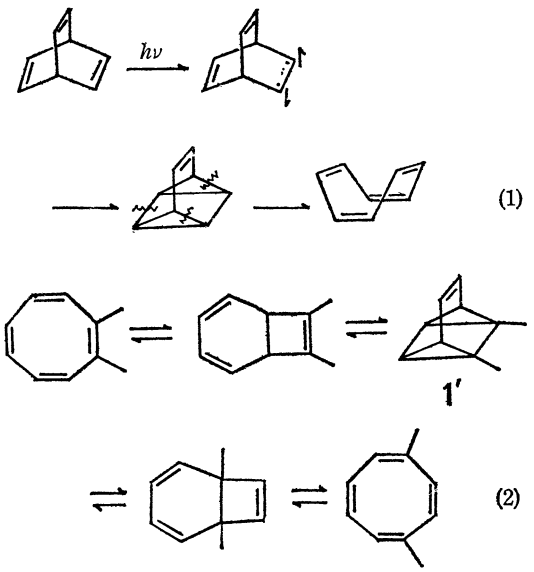

We have examined the electronic structure of **1** and the ground state potential energy hypersurfaces surrounding the minimum corresponding to structure **1** by MINDO/2 methods.[4] Specifically the reaction coordinates for the intramolecular Diels-Alder reaction of bicyclo[4.2.0]octa-2,4,7-triene (**2**) leading to **1** (see Eq. (2)) have been determined. A degenerate valence isomerization of **1** as represented by Eq. (3) has also been examined.

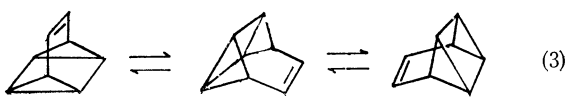

Method of Calculation

Details of the procedure are nearly the same as reported in the preceding paper.[1] Since no experimental data concerning the structure of the molecules studied here are available, the theoretical geometries of the ground states were sought by minimizing the total energies with respect to changes in all bond lengths and angles. It was only assumed that **1** and **2** have C_{2v} and C_s symmetry, respectively. Although a large number of nuclear configurations have to be considered in order to get information on the reaction paths, it would require tremendous effort to take all conceivable intermediate configurations into account. We have, therefore, made some simplifying assumptions to reduce the computational effort in finding the

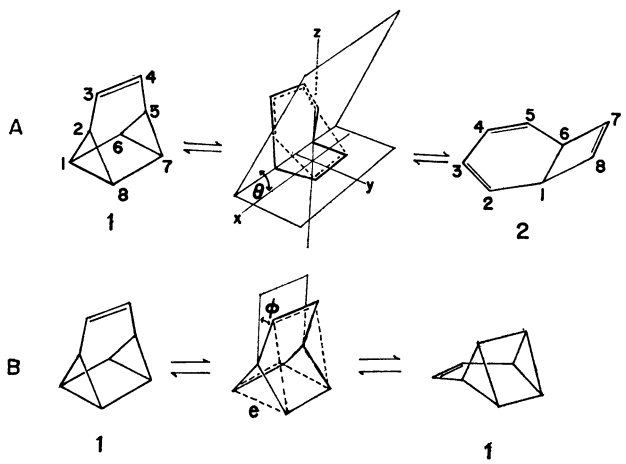

Fig. 1. Parameters used in calculating the reaction paths and numbering of atoms and bonds used in the text and in Table 1.
A: s is a smoothing parameter to describe a profile of **1** (**2**) in passing from **1** (**2**) into **2** (**1**) in the (retro) Diels-Alder reaction. All other geometrical parameters except θ are assumed to vary linearly with s from their values at the end points $s=0.0$ (=**1**) and $s=1.0$ (=**2**), respectively.
B: φ describe the inclination of C_2-C_3-C_4-C_5 plane towards C_7-C_8.

transition state geometries. A few parameters were chosen to describe the most relevant reaction coordinates. These parameters are detailed in Fig. 1. The eigenvalues and eigenfunctions were computed using a set of numerical values of these parameters, and the total energy was minimized by varying these parameters empirically to arrive at the transition state geometries.

An energy partitioning analysis was also made. The total energy (E) of a molecule can be expressed as a sum of one-center terms (E_A) and two-center terms (E_{AB}). The former sum was subdivided into one due to carbon atoms (E_A^C) and one due to hydrogen atoms (E_A^H). The two-center terms were divided into resonance (E_{AB}^R), exchange (E_{AB}^X), and electrostatic (E_{AB}^S) terms. Terms E_{AB} can also be divided into neighboring (E_{AB}^N) and non-neighboring (E_{AB}^{NN}) terms. The definition of each term and standard integrals representations in MINDO/2 formalism were given in the preceding paper.[1] A FORTRAN program was written for a HITAC 8700/8800 system at the Computer Centre of the University of Tokyo.

Results and Discussion

The Optimized Structure, Energy and Bond Parameters. Table 1 shows the equilibrium geometries, two-center energies, Wiberg bond indices, W_{AB},[5] and bond populations defined by taking into account the overlap, P_{AB}^S, defined in Eq. (5).

$$W_{AB} = \sum_{\mu}^{A} \sum_{\nu}^{B} P_{\mu\nu}^2 \tag{4}$$

$$P_{AB}^S = \sum_{\mu}^{A} \sum_{\nu}^{B} P_{\mu\nu} S_{\mu\nu} \tag{5}$$

The numerical values of W_{AB} are close to the conventional bond orders: 2 for double bonds and 1 for single bonds. The calculated geometries are generally in good agreement with those observed for many hydrocarbons possessing three or four-membered rings, except for slightly shorter C–C single bond lengths.

Energies and ionization potentials obtained by using Koopmans' theorem are listed in Table 2.

The absolute values of the heats of formation obtained for **1** and **2** by MINDO/2 might be considerably lower than the actual values, since this method is reputed to underestimate the strain energies of small rings and compounds having a compact skeleton.[4,6] The MINDO/1 method is thought to be more acceptable in calculating the heats of formation.[6] Heats of formation of 12.3 and 54.5 kcal/mol were obtained for **1** and **2** by Franklin's group-equivalent method.[7] The strain energy of **1** was therefore estimated to be 65.6 kcal/mol (the heat of formation from the MINDO/1 method minus that from Franklin's). The strain energy value so obtained is around mid-value among those estimated for all the possible $(CH)_8$ isomers.

Molecular Orbitals of ***1***. **1** may be regarded formally as being constructed of two cyclopropane rings, a cyclobutane ring and an ethylenic double bond. The ability of cyclopropanes to conjugate with an adjacent unsaturated center is well known. Structure **1** has a most desirable configuration for the cyclopropyl and vinyl moieties allowing them to interact adequately (*i.e.* bisected conformation). It is obvious from Table 1 that the C_2–C_3 (and C_4–C_5) bond has double bond character to some extent while the C_1–C_8 (and C_6–C_7) bond is slightly weakened as a result of the cyclopropyl-vinyl-cyclopropyl conjugation. A close inspection of the AO coefficients of the molecular orbitals reveals that the orbital interactions between the Walsh type orbitals of cyclopropane e′ and localized orbitals (π_{CC}, π_{CH_2}, σ_{CC}) of the ethylenic moiety and additional interactions between the orbitals resulting from the interactions described above are evident in the molecular orbital profile of **1**. This qualitative molecular orbital description can be obtained by considering in-phase and out-of-phase combinations between those localized orbitals with the same symmetry. Some higher occupied and lower unoccupied molecular orbitals are illustrated in Fig. 2. It is interesting to note that the third highest occupied

TABLE 1. GROUND STATE GEOMETRIES, TWO-CENTER ENERGY TERMS, BOND POPULATION, AND WIBERG'S BOND INDICES OF TETRACYCLO[4.2.0.$0^{2,8}0^{5,7}$]OCT-3-ENE **1** AND BICYCLO[4.2.0]OCTA-3,5,7-TRIENE **2**

		C_1-C_2	C_2-C_3	C_3-C_4	C_1-C_8	C_7-C_8	C_2-C_8
1	Bond length (Å)	1.50	1.47	1.36	1.51	1.49	1.50
	E_{AB}^R (eV)	−12.456	−15.091	−19.792	−10.794	−13.570	−12.456
	E_{AB}^N (eV)	−12.988	−15.728	−22.421	−11.572	−14.161	−12.988
	P_{AB}^s	0.6414	0.7591	1.0275	0.5833	0.6813	0.6414
	W_{AB}	0.9115	1.0066	1.8441	0.9586	0.9504	0.9115
2	Bond length (Å)	1.54	1.34	1.47	1.49	1.33	2.333
	E_{AB}^R (eV)	−14.368	−20.362	−15.135	−13.328	−20.004	−0.219
	E_{AB}^N (eV)	−14.971	−22.720	−15.841	−13.956	−22.437	−0.060
	P_{AB}^s	0.7269	1.0527	0.7650	0.6825	1.0423	0.0151
	W_{AB}	0.9752	1.8432	1.0279	0.9594	1.8949	0.0218

1: Cyclobutane-cyclopropane dihedral angle = 119.4°. **2**: Cyclohexadiene-cyclobutane dihedral angle = 103.1°.

TABLE 2. DISSECTED TOTAL ENERGIES, HEATS OF FORMATION AND IONIZATION POTENTIALS OF **1** AND **2**

	$\sum E_A$ (eV)	$\sum\sum E_{AB}$ (eV)	ΔH_f (kcal/mol)	I_p (eV)	ΔH_f (MINDO/1)
1	−904.341	−247.446	35.99	7.97	77.9
2	−905.876	−245.605	43.02	8.58	76.8

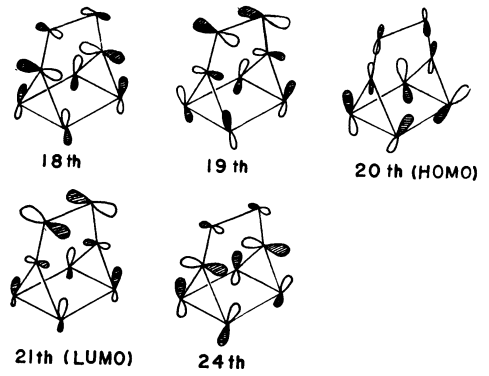

Fig. 2. Higher occupied and lower unoccupied molecular orbitals of **1**. The atomic orbital sizes present only approximately the magnitude of the relevant coefficients; their direction is similarly idealized.

molecular orbital is an out-of-phase combination of the ethylenic $2p\pi$ AO's on C_3 and C_4, while the corresponding in-phase combination appears among the lower unoccupied molecular orbitals.

Potential Energy Surfaces and Reaction Paths for ***1*** *and* ***2***. By calculating a large number of nuclear configurations, the energies of their electronic ground states along the reaction paths was obtained as a function of θ and s. A two dimensional presentation of the energy (in units of the heat of formation) as a function of θ and s is shown in Fig. 3. The most probable reaction path for the interconversion of **1** and **2** is indicated by the dotted line. A clearer picture of this cross section of the potential energy surface is given in Fig. 4 together with the change of bond indices. A smooth change of the bond indices for the bonds, which are formed or broken as the reaction proceeds along the reaction coordinates, is characteristic of symmetry-allowed reactions. Symmetry-forbidden reactions show, in contrast, abrupt changes in bond index.[1] This can be easily understood in

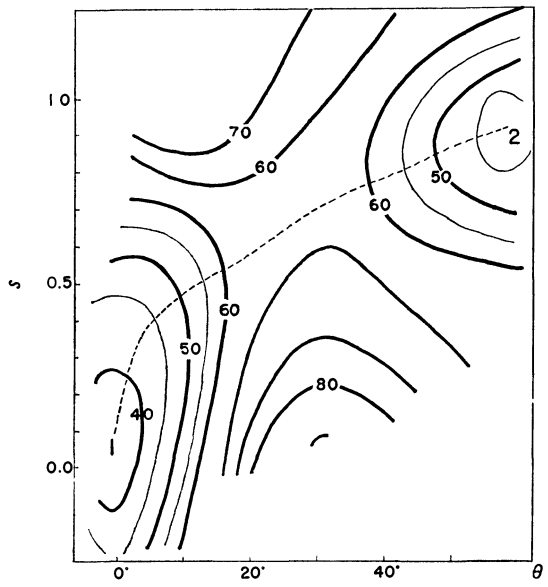

Fig. 3. The potential energy surface for the interconversion of **1** and **2**.

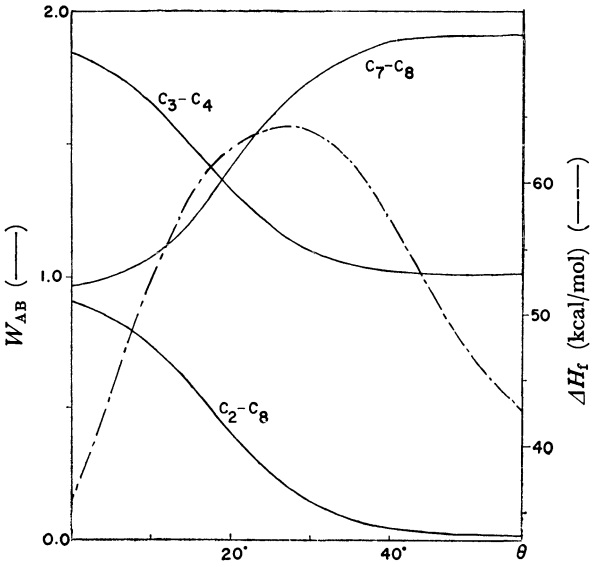

Fig. 4. The energy and the bond indices during the reaction of **1** and **2**.

terms of the well-known orbital correlation diagram.[8] In the case of allowed reactions, no alternation of occupied and unoccupied orbitals occurs anywhere along the reaction paths. In other words, all the occupied orbitals of the reactant can be transformed into the occupied orbitals of the product with continous changes in their shapes. The smooth change of bond indices results from the continuous change of the corresponding AO coefficients of the occupied molecular orbitals. An abrupt change of bond index indicates that alternation of occupied and unoccupied levels takes place somewhere in the reaction path.[9]

Figure 5 shows the calculated geometry and (in parentheses) Wiberg's bond indices for the transition state of the reaction, **2** to **1**. Note that the bond indices are about 1.6 for bonds C_2–C_3 (and C_4–C_5) and C_1–C_8, 1.17 for C_3–C_4, and 0.2 for C_2–C_8 (and C_5–C_7). As shown in Table 3, the two-center energy terms E_{AB} for the transition state geometry are more in pararell with those of **2**. The dihedral angles 83° and 200° of the transition state structure correspond to 57° and 213° in **1** and 104° and 180° in **2**. Thus the configuration of the transition state is electronically similar to **2**, while it is similar to **1** in terms of skeletal displace-

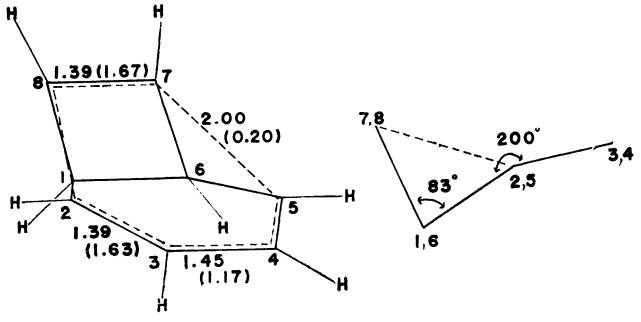

Fig. 5. The calculated geometry and the Wiberg's bond indices (in parentheses) for the transition state of the reaction of **2** to **1**.

Table 3. Neighboring two-center energies (eV) for the transition state **t**

C_1-C_2	C_2-C_3	C_3-C_4	C_1-C_8	C_7-C_8	C_2-C_8
−14.133	−20.969	−17.231	−13.453	−20.181	−2.464

Table 4. One-center and two-center terms in the activation energies (eV) for the reaction of **1** and **2**

	1	$\Delta E_{1\to t}$	**t**	$\Delta E_{2\to t}$	**2**
E_A^H	−84.1694	0.1038	−84.0656	0.2804	−84.3460
E_A^C	−820.1734	−1.9006	−822.0740	−0.5424	−821.5316
E_A	−904.3411	−1.7976	−906.1387	−0.2627	−905.8760
E_{AB}^N	−259.5897	4.4817	−255.1080	1.0959	−256.2039
E_{AB}^{NN}	12.1428	−1.4348	10.7080	0.1093	10.5987
E_{AB}	−247.4469	3.0469	−244.4000	1.2052	−245.6052
E	−1151.788	1.249	−1150.539	0.943	−1151.481

Table 5. Difference in electron populations on the carbon atoms and dissection of one-center contribution to the activation energy (eV) for rearrangement of **1** and **2**

	1		**2**	
	Δq_A	ΔE_A^C	Δq_A	ΔE_A^C
C_1 (C_6)	−0.077	0.5844	0.010	−0.0194
C_2 (C_5)	0.071	−1.0399	−0.020	0.0099
C_3 (C_4)	0.001	0.0567	0.021	−0.1449
C_8 (C_7)	0.013	−0.5515	0.009	−0.1168

ments. This is in accord with Hammond's postulate[11] and is also reasonable when the geometrical constraints imposed on the molecule in attaining the transition state are considered. It is noted that partial bonds C_2–C_8 (and C_5–C_7) are considerably weaker than those occurring in more facile reactions, *e.g.*, the Cope rearrangements of bridged homotropilidenes.[12] In the latter, the partial bonds in the transition states have a W_{AB} value of 0.4. The smaller W_{AB} value corresponds to the fact that the resonance energy of the aromatic transition state is not large in the present case.

In order to fully characterize the electronic structure of the transition state, the total contribution to the activation energy of the one-center term (ΔE_A) and of the two-center terms (ΔE_{AB}) are given in Table 4. Those were obtained by taking differences between the corresponding values for the ground state and transition state.

The stabilizing contribution to the activation energy comes from changes (ΔE_A) in the one-center terms on passing from the reactants to the transition state. Further inspection reveals that the contribution of hydrogen atoms is very small and that the ΔE_A values are governed by changes in the one-center terms for carbons. The first and third columns of Table 5 show the change (Δq_A) in the electron population of atom A in passing from the reactant to the transition state. A positive Δq_A implies an increase in electron density and also in negative charge. It is seen that the variation of ΔE_A values correlates with those of Δq_A.[13] Note that the terms leading to smaller activation energy are those for the carbon atoms in the "aromatic ring" of the transition state, *e.g.*, atoms 2,3,4,5,7 and 8. In other words, the six carbons involved become effectively more electrogative in going from the reactants to the transition state and the transition state is correspondingly stabilized by a drift of negative charge to those six carbons from the rest of the molecule. On the contrary, the net change in the two-center neighboring terms ΔE_{AB}^N is relatively large with positive sign. Thus the relief of steric strain is not contributing much to the driving force of the reaction.

The activation energy for the valence isomerization of **1** to **2** is estimated at 29 kcal/mol by taking the difference in the energies of **1** and the transition state. Thus the isomerization of substituted cyclooctatetraene *via* **1** and **2** (see Eq. (2)) is predicted theoretically to be possible at elevated temperatures. It is also concluded that **1** is reasonably stable kinetically as well as thermodynamically (see Section A). The height of the potential energy barrier is large enough to give **1** a reasonable life-time at room temperature once prepared by an authentic route.

The reaction of **2** to **1** is favored in terms of orbital interaction owing to the proper geometry in the transition state. It would lead to activation energy of the same order as a typical Diels-Alder reaction of butadienes with ethylenes.[14]

A Degenerate Valence Isomerization of ***1*** *(Eq. (3)).* The reaction represented by Eq. (3) is a symmetry-allowed process. A precedent for the analogous [$_\pi 2_s + {}_\sigma 2_s + {}_\sigma 2_s$] reactions may be found in the bimolecular reaction of quadricyclene with TCNE:[15]

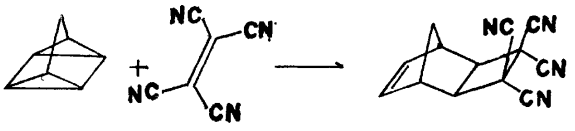

However, the ethylenic pπ orbitals are not suitably disposed for overlap with those of the cyclopropane ring in **1**. Inclination of the etheno bridge by 20° is attained only at the expense of 18 kcal/mol strain. The calculated energy values rise nearly in direct proportion to the increase in the values of φ and e. This is illustrated in Fig. 6. The ethylenic pπ orbitals cannot interact sufficiently with those of the cyclopropane

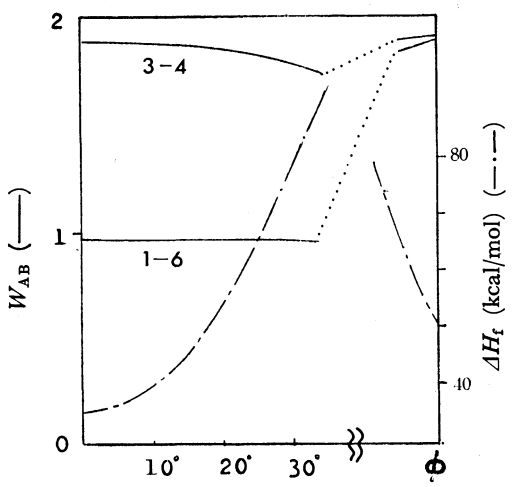

Fig. 6. The energy and the bond indices for the degenerate valence isomerization of **1**.

rings even when a large increase in energy due to strain is imposed. Therefore this formally symmetry-allowed valence isomerization will not take actually place even under severe conditions. Instead, the reaction coordinate represented by the elongation of the bond between C_1 and C_8 (C_6 and C_7), *e*, leads to an unexpected product, barrelene, across a high energy barrier demanded by symmetry considerations.[16]

References and Notes

1) Part VIII: H. Iwamura, H. Kihara, K. Morio, and T. L. Kunii, This Bulletin, **46**, 3248 (1973).

2) H. E. Zimmerman and G. L. Grunewald, *J. Amer. Chem. Soc.*, **88**, 183 (1966); H. E. Zimmerman, R. W. Binkley, R. S. Givens, G. L. Grunewald, and M. A. Sherwin, *ibid.*, **91**, 3316 (1969).

3) L. A. Paquette and R. E. Wingard, Jr., *ibid.*, **94**, 4398 (1972); L. A. Paquette, R. H. Meisinger, and R. E. Wingard, Jr., *ibid.*, **94**, 9274 (1972).

4) N. Bodor, M. J. S. Dewar, A. Harget, and E. Haselbach, *ibid.*, **92**, 3854 (1970).

5) K. B. Wiberg, *Tetrahedron*, **24**, 1083 (1968).

6) H. Iwamura, K. Morio, and T. L. Kunii, *Chem. Commun.*, **1971**, 1408.

7) J. L. Franklin, *Ind. Eng. Chem.*, **41**, 1070 (1949).

8) R. B. Woodward and R. Hoffmann, "The Conservation of Orbital Symmetry," Academic Press Inc., New York, N. Y. (1970).

9) We find it more advantageous to utilize this criterion to predict the allowedness or forbiddenness of concerted reactions of complex systems which have little or no elements of symmetry. While "snap-shot" calculations on a reaction path are often not sufficient to give acceptable activation energy values, they are adequate to show changes in bond index. The conclusion on the allowedness of the reaction under discussion must of necessity agree with the rule obtained more easily by application of the "Conservation of Orbital Symmetry."[8] We prefer the latter rule to be expressed in terms of the concept of the continuity of phase or nodal characteristic of orbitals, since the transition states of concerted reactions are not necessarily symmetric in general.[10]

10) J. W. McIver, Jr., *Accounts Chem. Res.*, **7**, 72 (1974).

11) G. S. Hammond, *J. Amer. Chem. Soc.*, **77**, 334 (1953).

12) (a) H. Iwamura, K. Morio, and T. L. Kunii, This Bulletin, **45**, 841 (1972); (b) M. J. S. Dewar and D. H. Lo, *J. Amer. Chem. Soc.*, **93**, 7201 (1971).

13) This can be readily understood as follows. When q_A increases (accumulation of electron density on atom A), the one-center core attraction energy increases, while the one-center Coulomb repulsion increases. Since both terms vary with *q* and in opposite directions, they almost cancel one another. The values ΔE_A for the individual carbon atoms pararell quite closely those for the one-center exchange term ΔE_A^x and the latter is correlated with Δq_A. Thus an increase in electron density on carbon A makes E_A^x more negative and consequently E_A more negative.[12b]

14) W. von E. Doering, M. Franck-Neumann, D. Hasselmann, and R. L. Kaye, *J. Amer. Chem. Soc.*, **94**, 3833 (1973) and references cited therein.

15) C. D. Smith, *ibid.*, **88**, 4273 (1966).

16) Lastly, [1,5]sigmatropy in **2** which might be also one of the possible paths taking part in the substituent migration of cyclooctatetraene, has been shown to be a very energetically unfavorable path because of peculiar electronic and steric factors, *i. e.*, additional $p\pi$ orbitals and the length of the migrating carbon chain. Results on energetically unfavorable sigmatropic reactions will appear in a forthcoming paper.

Resonance Energies of Annulenes and Radialenes

Jun-ichi AIHARA
Department of Chemistry, Faculty of Science, Hokkaido University, Sapporo 060
(Received July 10, 1974)

Resonance energies of annulenes and radialenes were estimated on the basis of the π-bond energies of infinitely large annulene and radialene, respectively. The widely accepted Hückel's $(4n+2)\pi$ rule was verified for annulenes, whereas radialenes were substantially nonaromatic regardless of the number of π-electrons.

Though the Hückel molecular orbital (HMO) model has shown a great degree of success in the interpretation of gross electronic structures of conjugated systems,[1] the extension of this approach has given rather limited agreement. In particular, it was recently shown that the delocalization energy is not useful in predicting the relative stability of benzenoid and nonbenzenoid hydrocarbons.[2]

In 1965, Dewar and Gleicher, using the semiempirical SCF–MO method, have found that the bond energies of acyclic polyenes are additive.[3] Adopting this principle, Hess and Schaad defined the HMO resonance energy as the difference between the total HMO π-energy and the additive contribution obtained by summing individual π-bond energies.[4] An excellent correlation between the resonance energies calculated in this manner and the observed stability and chemical behavior of many cyclic polyenes was obtained.

We also verified the additivity of π-bond energies of linear polyenes on the basis of the total HMO π-energies of infinitely large annulene and polyene.[5] The most striking advantage of our treatment was that the somewhat arbitrary assignment of values for eight types of π-bond energies made by Hess and Schaad[4] was completely avoided. In order to extend our understanding of aromatic stabilization of cyclic systems within the framework of the HMO theory and without additional assumptions, the same idea was applied to two typical cyclic systems; annulenes and radialenes.

Results and Discussion

It is generally accepted that sufficiently large annulene is considered to suffer from bond alternation, and is almost nonaromatic cyclic polyene.[6,7] It is hence assumed without difficulty that the additive contribution to the total π-energy of any annulene can be estimated from the π-energy of infinitely large annulene. When the classical resonance structure is written for annulene, it is a cyclic chain composed of unit structures, each of which involves the CH=CH bond and the adjacent CH–CH bond. The π-energy of the unit structure (E_U) is then evaluated by dividing the total HMO π-energy of [infinity]-annulene by half the number of carbon atoms. With the use of Hess and Schaad's notation,[2,4] it is expressed as follows:

$$E_U(\text{annulene}) = E_{22} + E_{12} = \frac{8}{\pi}, \quad (1)$$

where E_{22} and E_{12} signify the π-bond energies of the CH=CH and CH–CH bonds, respectively.

The ability to calculate accurately in an additive manner the total π-energy of linear polyene[5] allows us to calculate the additive contribution to the total π-energy of annulene. The additive contribution to the total π-energy of annulene as is defined as the π-energy of the localized structure of annulene is simply expressed as follows:

$$E_A([N]\text{-annulene}) = \frac{N}{2}(E_{22}+E_{12}) = \frac{4N}{\pi}, \quad (2)$$

where N is the number of carbon atoms in annulene.

The resonance energy (E_R) of annulene is hence obtained by substracting E_A from the total HMO π-energy (E_{HMO}), that is,

$$E_R([N]\text{-annulene}) = E_{HMO}([N]\text{-annulene}) - E_A([N]\text{-annulene}). \quad (3)$$

The resonance energies determined by using Eq. (3) as well as E_{HMO} and E_A are all listed in Table 1. REPE denotes resonance energy per π-electron. The geometry of the annulenes investigated is tacitly assumed to be planar with constant resonance integrals over all carbon-carbon bonds.

As is easily seen, the total resonance energy oscillates about zero-axis, approaching zero with increasing N. All [$4n$]-annulenes are correctly predicted to be

Table 1. Resonance energies of ordinary annulenes in units of β

N	E_{HMO}	E_A	E_R	REPE
4	4.0000	5.0930	−1.0930	−0.2732
6	8.0000	7.6394	0.3606	0.0601
8	9.6569	10.1859	−0.5291	−0.0661
10	12.9443	12.7324	0.2119	0.0212
12	14.9282	15.2789	−0.3507	−0.0292
14	17.9758	17.8254	0.1505	0.0107
16	20.1094	20.3718	−0.2625	−0.0164
18	23.0351	22.9183	0.1168	0.0065
20	25.2550	25.4648	−0.2098	−0.0105
22	28.1067	28.0113	0.0954	0.0043
24	30.3830	30.5577	−0.1747	−0.0073
26	33.1849	33.1042	0.0807	0.0031
28	35.5010	35.6507	−0.1497	−0.0053
30	38.2671	38.1972	0.0699	0.0023
32	40.6127	40.7437	−0.1310	−0.0041
34	43.3518	43.2901	0.0617	0.0018
36	45.7202	45.8366	−0.1164	−0.0032
38	48.4383	48.3831	0.0552	0.0015
40	50.8248	50.9296	−0.1048	−0.0026

antiaromatic with negative resonance energies. The $[4n+2]$-annulenes are predicted to be aromatic up to [infinity]-annulene. Hückel's famous $(4n+2)\pi$ rule which states that $[4n+2]$-annulenes will possess relative electronic stability[8] has been nicely verified in this manner. Above all, it must be noted that, though our present results are in fair agreement with earlier theoretical studies on annulenes,[4,9-12] our simple approach is best grounded on the additivity of π-bond energies of the nonaromatic reference structure.

Dewar and Gleicher predicted that the critical size of annulene at which the bond alternation occurs is between [22]- and [26]-annulene, which was supported by some experimental evidence.[7,13] Though we can not predict the critical size of annulene at which Hückel's $(4n+2)\pi$ rule ceases to hold, their statement seems to be quite consistent with our results as higher annulenes with an REPE less than 0.004 β are considered to be substantially nonaromatic in accordance with the interpretation of the additivity of π-bond energies of acyclic polyenes made by Hess and Schaad.[4] When Hess and Schaad's π-bond energies are employed to calculate the π-energy of the reference structure, the limiting REPE of annulene amounts to $0.0053\,\beta$.[14] This suggests that sufficiently large annulenes are still aromatic with resonance energies of about $0.0053N\beta$, which is in contradiction to the premise that higher annulenes should be nonaromatic. In our case, the resonance energy of $[4n+2]$-annulene diminishes monotonously as n increases.

Similar results can be obtained by taking linear polyene as a reference compound for annulene. According to the procedure given in the previous paper,[5] the additive contribution to the total π-energy of annulene may be rewritten as follows:

$$E_R([N]\text{-annulene}) = E_{HMO}([N]\text{-polyene}) - 2E_{23} + 2E_{22} + E_{12}$$
$$= E_{HMO}([N]\text{-polyene}) + 2 - \frac{4}{\pi} . \quad (4)$$

The list of resonance energies derived from Eq. (4) was omitted here because of their close resemblance to those in Table 1.

On the other hand, the potential utility of the Möbius conformation of annulene in ring-opening reactions has been pointed out by Zimmerman.[15] The Möbius cyclic system is a singly twisted cyclic polyene in which there is only one side of the π-surface.[16] Craig and Paddock also considered the possibility of the Möbius conformation for cyclic phosphonitrilic derivatives.[17]

The resonance energies of the Möbius systems of annulenes were calculated by assuming the same reference structures as those of ordinary annulenes, although the additive principle of π-bond energies may be somewhat obscured for these systems. The change in resonance integrals with twisting was neglected to simplify the calculation. The obtained resonance energies of the Möbius systems are shown in Table 2. They were found to have positive resonance energies when they have $4n$ π-electrons. The resonance energies were negative for the systems with $(4n+2)$ π-electrons. The aromaticity is thus determined by the converse of Hückel's $(4n+2)\pi$ rule in agreement with the conclusion lead by Heilbronner.[16]

TABLE 2. RESONANCE ENERGIES OF MÖBIUS-TYPE ANNULENES IN UNITS OF β

N	E_{HMO}	E_A	E_R	REPE
4	5.6569	5.0930	0.5639	0.1410
6	6.9282	7.6394	−0.7112	−0.1185
8	10.4525	10.1859	0.2666	0.0333
10	12.3107	12.7324	−0.4217	−0.0422
12	15.4548	15.2789	0.1759	0.0147
14	17.5251	17.8254	−0.3002	−0.0214
16	20.5033	20.3718	0.1315	0.0082
18	22.6851	22.9183	−0.2332	−0.0130
20	25.5698	25.4648	0.1050	0.0053
22	27.8206	28.0113	−0.1907	−0.0087
24	30.6452	30.5577	0.0874	0.0036
26	32.9430	33.1042	−0.1613	−0.0062
28	35.7256	35.6507	0.0749	0.0027
30	38.0575	38.1972	−0.1397	−0.0047
32	40.8092	40.7437	0.0655	0.0020
34	43.1669	43.2901	−0.1233	−0.0036
36	45.8949	45.8366	0.0582	0.0016
38	48.2728	48.3831	−0.1103	−0.0029
40	50.9820	50.9296	0.0524	0.0013

As a further application, we may compare the total HMO π-energies and the additive contributions of π-bond energies for radialenes. Radialenes form an apparently very dissimilar series of conjugated polyenes containing a ring of carbon atoms, each doubly bound to a methylene group. In other words, radialenes are all composed of the same unit structures, each involving a CH_2=C bond and an adjacent C–C bond. Therefore, the numbers of the single and double carbon-carbon bonds are the same, and are equated to M. If the π-bonds are localized as in the classical resonance structure, the total π-energy of $[M]$-radialene should be given by (in Hess and Schaad's notation[2,4]):

$$E_A([M]\text{-radialene}) = M(E_{22'} + E_{10}) , \quad (5)$$

where $E_{22'}$ and E_{10} denote the π-bond energies of the CH_2=C and C–C bonds, respectively.

In order to determine the π-energy of the radialene unit structure, we employed the same procedure as used for annulenes. Here, radialenes are assumed to be coplanar with the rings forming regular polygons and free from ring strains. The general HMO solution for radialene was presented by Hess and Schaad.[4] According to them, the m-th orbital energy of $[M]$-radialene is expressed in units of β as follows:

$$\varepsilon_m([M]\text{-radialene}) = \cos\lambda_{Mm} + (\cos^2\lambda_{Mm} + 1)^{1/2} , \quad (6)$$

where

$$\lambda_{Mm} = \frac{2m\pi}{M} \qquad m = 0, 1, 2, \cdots\cdots, (M-1) . \quad (7)$$

As in the case of annulene, if the radialene ring is large enough, it can be considered as a nonaromatic cyclic polyene. The π-energy of the unit structure of radialene is therefore estimated at the nonaromatic limit as

$$E_U(\text{radialene}) = E_{22'} + E_{10}$$
$$= \lim_{M\to\infty} \frac{2}{M} \sum_{m=0}^{M-1} [\cos\lambda_{Mm} + (\cos^2\lambda_{Mm} + 1)^{1/2}]$$
$$= 2\int_0^1 [\cos 2\pi x + (\cos^2 2\pi x + 1)^{1/2}]dx$$
$$= 2.4320134\cdots\cdots . \quad (8)$$

The numerical estimation of the unit energy was made by the double-precision computation. The π-energy of the reference structure of $[M]$-radialene is equated to $2.4320134M\beta$. Table 3 shows the resonance energies of radialenes based on this value, *i.e.*, the differences between the total HMO π-energies and the additive contributions defined by Eq. (5).

Table 3. Resonance energies of radialenes in units of β

M	E_{HMO}	E_A	E_R
3	7.3006	7.2960	0.00452
4	9.6569	9.7281	−0.07119
5	12.1602	12.1601	0.00009
6	14.6011	14.5921	0.00904
7	17.0241	17.0241	0.00000
8	19.4548	19.4561	−0.00129
9	21.8881	21.8881	0.00000
10	24.3203	24.3201	0.00019
11	26.7521	26.7521	0.00000
12	29.1841	29.1842	−0.00002
13	31.6162	31.6162	0.0
14	34.0482	34.0482	0.0
15	36.4802	36.4802	0.0
16	38.9122	38.9122	0.0
17	41.3442	41.3442	0.0
18	43.7762	43.7762	0.0
19	46.2083	46.2083	0.0
20	48.6403	48.6403	0.0
30	72.9604	72.9604	0.0
40	97.2805	97.2805	0.0
50	121.6007	121.6007	0.0

In contrast to annulenes, the agreement between the total π-energies and the additive contributions for radialenes is surprisingly excellent for all M's. All REPE's range between -0.00890β for $M=4$ and 0.00075β for $M=3$. This implies that they are to be considered nonaromatic regardless of the number of the π-electrons, and supports strongly that our way of determining the π-energy of the unit structure is quite reasonable. Radialenes can therefore be well represented in terms of localized single and double bonds in accordance with more elaborate calculations carried out by Dewar and his collaborators.[7,18]

If Table 3 is further examined in detail, it is found that the resonance energies are slightly negative for $M=4$, 8, and 12, and that they are slightly positive for $M=6$ and 10. This behavior of the resonance energies tempts us to present a new version of Hückel's $(4n+2)\pi$ rule for radialenes, in which the number of π-electrons (n) should be replaced by the number of methylene groups (M). However, the applicability of this rule fades very rapidly with increasing M. The additivity of π-bond energies are perfect for radialenes with M-values more than 12, though they are chemically of little importance. These aspects of the resonance energies of radialenes have so far been disregarded because of the tiny deviation of the total HMO π-energies from the additive contributions. The resonance energies of radialenes calculated by Hess and Schaad[4] were all negative as the sum of $E_{22'}$ and E_{10} (2.4358β) was slightly larger than the corresponding value calculated by us.

We have assumed in the present treatment that the geometries of annulenes and radialenes are all planar with constant resonance integrals. This is, however, exactly true only for the six-membered ring systems when they are substantially aromatic with little bond-order fluctuation. In most cases, ring strain and H–H nonbonded repulsions become significant; they would tend to destabilize both small and large rings relative to the six-membered rings. On the other hand, the introduction of bond alternation would often reduce the π-energy of the system. These effects were completely neglected in our simplified approach modeled after Hess and Schaad's.[4] Nevertheless, it must be noted that the resonance energies obtained here still appear to be much improved as an aromaticity index of the compound, and should be utilized, instead of the delocalization energies, to discuss the stability of these cyclic systems.

In conclusion, the well-established additivity of π-bond energies of nonaromatic polyenes allowed us to take infinitely large annulene and radialene as reference compounds in estimating the aromaticity of a given annulene and radialene. Such a procedure removed the difficulty encountered in evaluating the resonance energies of these compounds within the framework of the HMO theory. It is noticeable that the concept of aromaticity thus derived does not violate the simplicity and straightforwardness of the HMO theory, and may be considered as a practical extension of the HMO theory.

We are grateful to the Hokkaido University Computing Center for the use of their FACOM 230-60 on which all the calculations were performed.

References

1) A. Streitwieser, Jr., "Molecular Orbital Theory for Organic Chemists," John Wiley & Sons, Inc., New York, N. Y. (1961).
2) B. A. Hess, Jr. and L. J. Schaad, *J. Amer. Chem. Soc.*, **93**, 2413 (1971).
3) M. J. S. Dewar and G. J. Gleicher, *ibid.*, **87**, 692 (1965).
4) B. A. Hess, Jr. and L. J. Schaad, *ibid.*, **93**, 305 (1971).
5) J. Aihara, This Bulletin, **47**, 3169 (1974).
6) G. M. Badger, "Aromatic Character and Aromaticity," Cambridge University Press, Cambridge, England (1969).
7) M. J. S. Dewar and G. J. Gleicher, *J. Amer. Chem. Soc.*, **87**, 685 (1965).
8) E. Hückel, *Z. Phys.*, **70**, 204 (1931); **72**, 310 (1931).
9) T. M. Krygowski, *Tetrahedron Lett.*, **1970**, 1311.

10) I. Gutman, M. Milun, and N. Trinajstic, *Croat. Chem. Acta*, **44**, 207 (1972).
11) W. D. Hobey, *J. Org. Chem.*, **37**, 1137 (1972).
12) H. P. Figeys, *Tetrahedron*, **26**, 5225 (1970).
13) F. Sondheimer, *Accounts Chem. Res.*, **5**, 81 (1972).
14) B. A. Hess, Jr., L. J. Schaad, and C. W. Holyoke, Jr., *Tetrahedron*, **28**, 5299 (1972).
15) H. E. Zimmerman, *Accounts Chem. Res.*, **4**, 272 (1971).
16) E. Heilbronner, *Tetrahedron Lett.*, **1964**, 1923.
17) D. P. Craig and N. L. Paddock, "Nonbenzenoid Aromatics," Vol. 2, ed. by J. P. Synder, Academic Press, New York, N. Y. (1971), Ch. 5.
18) M. J. S. Dewar and C. De Llano, *J. Amer. Chem. Soc.*, **91**, 789 (1969).

The Reaction of Open-chain Unconjugated Dienes with Palladium Acetate. Dependence of the Products on Disposition of the Two Double Bonds

Nobuo ADACHI, Kiyoshi KIKUKAWA, Makoto TAKAGI, and Tsutomu MATSUDA

Department of Organic Synthesis, Faculty of Engineering, Kyushu University; Hakozaki, Higashi-ku, Fukuoka 812

(Received July 16, 1974)

The reaction of open-chain unconjugated dienes with palladium acetate in acetic acid was investigated with particular reference to the behavior of the two double bonds in the course of the acetoxylation. 1,5-Hexadiene produced 3-acetoxymethylenecyclopentane (64%), but 2,6-octadiene bearing two terminal methyl groups gave open-chain acetoxylated products: 3-acetoxy-1,6-octadiene (46%) and 7-acetoxy-2,5-octadiene (47%). The reactions of 1,6-heptadiene and diallyl ether are found to proceed *via* abnormal anti-Markovnikov addition to afford *cis* and *trans* 1-acetoxy-1,6-heptadienes (63%) and γ-acetoxyallyl allyl ethers (84%), respectively. No participation of the second double bond has been observed in the reaction of 1,7-octadiene. The behaviors of these dienes to palladium acetate can be reasonably explained by assuming the formation of π,σ-palladium species possessing a stable pseudo-six membered ring.

Although considerable efforts have been devoted to the reaction of conjugated dienes, especially of 1,3-butadiene, with palladium salts, studies of unconjugated dienes seem to be limited to such compounds as 1,5-cyclooctadiene, dicyclopentadiene, norbornadiene and so on, in which the two double bonds are fixed in cyclic system and favorably located so that they can interact with palladium salt to form a diene-palladium complex of considerable stability. Moreover, the resultant complexes are known to react with several nucleophiles to give π,σ-palladium species.[1]

We previously reported[2] that in the reaction with palladium acetate 1,5-hexadiene underwent cyclization to form a methylenecyclopentyl acetate. This fact strongly suggests that a cyclic intermediate similar to the π,σ-palladium species is involved in the cyclization. This paper deals with the reactions of other open-chain unconjugated dienes and diallyl compounds containing oxygen, nitrogen and sulfur with palladium acetate, and presents a relationship between the structures of the dienes and the oxidation products.

Results

The oxidation of dienes with palladium acetate (1 g) was generally carried out in acetic acid (40 ml) at 50 °C in the presence of ten-fold excess of diene until precipitation of palladium metal was completed (5—7 hr). The principal products obtained from the reactions and their yields based on palladium acetate are tabulated in Table 1. Their analytical data are shown in Table 2. The crude reaction products were usually obtained in yields over 90%, and virtually consisted of monoacetates (or monoketone). The excess dienes were recovered free from isomerization of the double bonds.

The cyclization product obtained from 1,5-hexadiene had previously been assumed to be 2-acetoxymethylenecyclopentane, mainly on the basis of considerably large chemical shift (δ 5.15) of the proton at the carbon carrying an acetoxyl group.[2] However, comparison of its NMR spectrum with that obtained in the reactions of methylenecyclopentane with palladium acetate[5] or mercuric acetate led us to conclude the product to be 3-acetoxy isomer (**1**) (see Table 2, **1** and **1'**). 1,6-Heptadiene yielded a mixture consisting

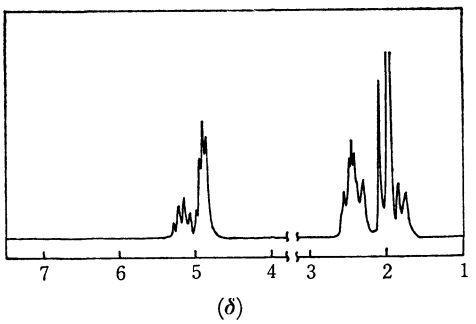

Fig. 1. NMR spectrum of **1**.

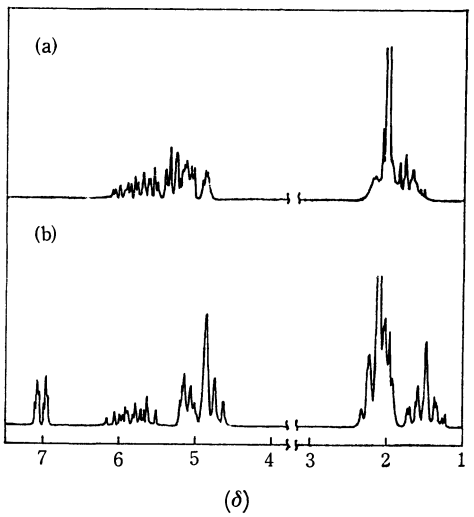

Fig. 2. NMR spectra of **2**(a) and **3**(b).

of three monoacetoxydienes bearing a terminal vinyl group (δ_{CH} 990—980 and 910 cm^{-1}, and multiplet at δ 4.8—6.2). Two of them were characterized by the presence of higher carbonyl absorption (1765—1770 cm^{-1}) and a doublet absorption at around δ 7 region (Fig. 2b) indicating the presence of CH=CH– group.
OAc

By considering coupling constants of the doublet absorptions, they were assigned to be *cis* (**3**, J=6.5 Hz) and *trans* (**4**, J=12 Hz) isomers of 1-acetoxy-1,6-heptadiene. The structure of the other one was tentatively assigned to 3-acetoxy-1,6-heptadiene (**2**) on the basis of $\nu_{C=C}$ at 1648 cm^{-1} (refer to $\nu_{C=C}$: 1653

Table 1. Acetoxylation of unconjugated dienes

Diene	Product, (%)[a]
1,5-Hexadiene	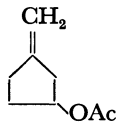 **1** (64)
1,6-Heptadiene	$CH_2=CHCH(CH_2)_2CH=CH_2$, OAc **2** (13); $CH=CH(CH_2)_3CH=CH_2$, OAc **3** (*cis*, 32), **4** (*trans*, 31)
2,6-Octadiene	$CH_2=CHCH(CH_2)_2CH=CHCH_3$, OAc **5** (46); $CH_3CHCH=CHCH_2CH=CHCH_3$, OAc **6** (47)
1,7-Octadiene	$CH_2=CH(CH_2)_4CCH_3$, O **7** (7); $CH_2=C(CH_2)_4CH=CH_2$, OAc **8** (72); $CH_2CH=CH(CH_2)_3CH=CH_2$, OAc **9** (14)
Diallyl ether	$CH=CHCH_2OCH_2CH=CH_2$, OAc **10** (*cis*, 41), **11** (*trans*, 43)

a) Yields are based on $Pd(OAc)_2$ and obtained by glc analyses.

Table 2. Spectral data of the products

Compound	NMR,[b] ppm (no. of proton)	IR, cm^{-1}
1	1.90m (2), 1.95 s (3), 2.40m (4), 4.90 bs (2), 5.15m (1)	$\nu_{C=O}$ 1730, $\nu_{C=C}$ 1655, δ_{CH} 970, 900 sh, 880
1'[a]	1.80m (4), 2.0 s (3), 2.35m (2), 5.05 b and 5.15 b (2) 5.42 bs (1)	$\nu_{C=O}$ 1730, $\nu_{C=C}$ 1655, δ_{CH} 965, 910 sh, 900
2	1.75m (2), 2.0 s and 2.0m (5), 4.8—6.1m (7)	$\nu_{C=O}$ 1740, $\nu_{C=C}$ 1648, δ_{CH} 990, 910
3	1.55m (2), 2.10 s and 2.10m (7), 4.8—6.2m (3), 4.75 t (1), 7.0 d (1, J=6.5 Hz)	$\nu_{C=O}$ 1770, $\nu_{C=C}$ 1680, 1650 δ_{CH} 980, 910, 745
4	1.55m (2), 2.05 s and 2.10m (7), 4.45 d (1), 4.8—6.1m (3), 7.05 d (1, J=12 Hz)	$\nu_{C=O}$ 1765, $\nu_{C=C}$ 1680, 1650 δ_{CH} 990, 930, 910
5	1.68m (5), 2.0 s and 2.0m (5), 5.0—5.8m (6)	$\nu_{C=O}$ 1735, $\nu_{C=C}$ 1653, δ_{CH} 995, 965, 930
6	1.26 d (3), 1.68m (3), 1.95 s (3), 2.70m (2), 5.2—5.7m (5)	$\nu_{C=O}$ 1730, $\nu_{C=C}$ 1670, δ_{CH} 965, 845
7	1.50m (4), 2.05 s (3), 2.25m (4), 4.8—6.2 (3)	$\nu_{C=O}$ 1718, $\nu_{C=C}$ 1648, δ_{CH} 995, 910
8	1.45m (4), 2.05 s and 1.85—2.3m (7), 4.65 bs (2), 4.8—6.2m (3)	$\nu_{C=O}$ 1765, $\nu_{C=C}$ 1670, 1650, δ_{CH} 995, 966, 910, 865
9	1.55m (2), 2.0 s and 1.9—2.3m (7), 4.45 d (2), 4.8—6.1m and 5.6m (5)	$\nu_{C=H}$ 1745, $\nu_{C=C}$ 1670, 1645, δ_{CH} 985, 965, 910
10	2.10 s (3), 4.0m (4), 4.8—6.1m (3), 7.1 d (1, J=7 Hz)	$\nu_{C=O}$ 1765, $\nu_{C=C}$ 1670, ν_{COC} 1090, δ_{CH} 925, 910
11	2.05 s (3), 3.90 bd (4), 4.9—5.6m (3), 7.25 d (1, J=13 Hz)	$\nu_{C=O}$ 1765, $\nu_{C=C}$ 1675, ν_{COC} 1080, δ_{CH} 935, 905

a) 2-Acetoxymethylenecyclopentane. b) Bs and bd stand for broad singlet and doublet, respectively.

Anal. **1**, Found: C, 68.33; H, 8.66%. Calcd for $C_8H_{12}O_2$: C, 68.54; H, 8.63%.
3, Found: C, 69.92; H, 9.20%.
4, Found: C, 69.93; H, 9.21%. } Calcd for $C_9H_{14}O_2$: C, 70.10; H, 9.15%.
10, Found: C, 60.94; H, 8.08%.
11, Found: C, 60.96; H, 7.95%. } Calcd for $C_8H_{12}O_3$: C, 61.52; H, 7.75%.

cm^{-1} for **5**, but 1670 cm^{-1} for **6** and **9**) and the presence of a methylene group at δ 1.75, although an ambiguity remains in excluding the another isomer, 7-acetoxy-1,5-heptadiene. Two products were obtained from *trans,trans*-2,6-octadiene in nearly equal amount. One of them contained a methyl group (δ 1.68) and a vinyl group, and the other showed the presence of two methyl groups (3H each, δ 1.26 and 1.68). Their NMR and IR spectra were most reasonably explained by assigning their structure to 3-acetoxy-1,6-octadiene (**5**) and 7-acetoxy-2,5-octadiene (**6**), respectively (Figs. 3a and 3b). 1,7-Octadiene afforded a methyl ketone and two acetoxylated dienes (Figs. 4a, 4b, and 4c). Examination of their NMR spectra showed that the structures corresponded to those which were made up by replacing the terminal ethyl group (C7 and C8) with a vinyl group from 2-octanone, 2-acetoxy-1-octene and 1-acetoxy-2-octene, respectively, which were produced in the reaction of 1-octene.[2] Thus, they were concluded to be 1-octen-7-one (**7**), 2-acetoxy-1,7-octadiene (**8**) and 1-acetoxy-2,7-octadiene (**9**), respectively.

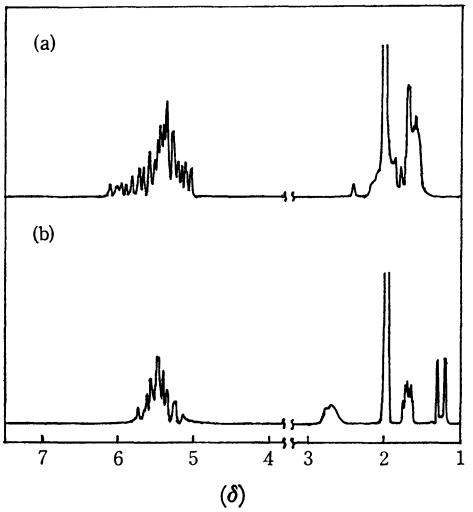

Fig. 3. NMR spectra of **5**(a) and **6**(b).

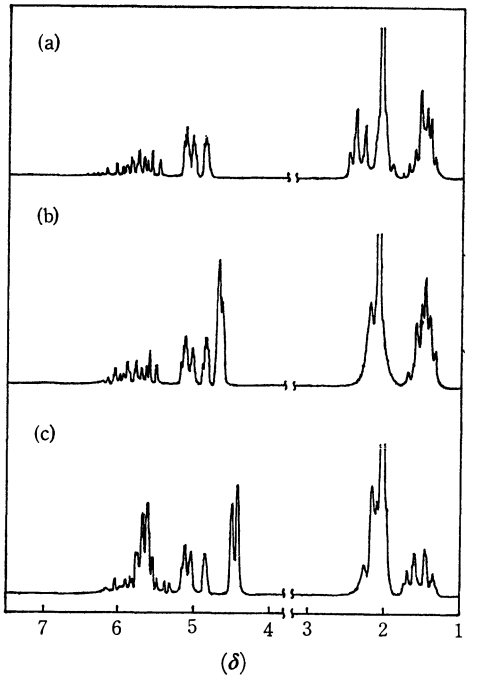

Fig. 4. NMR spectra of **7**(a), **8**(b), and **9**(c).

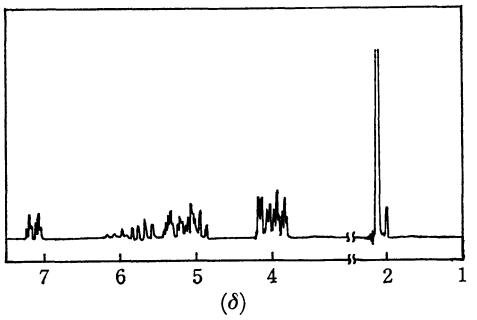

Fig. 5. NMR spectrum of **10**.

Diallyl ether reacted like other dienes to produce two acetoxylated products. They were assigned to *cis* and *trans* γ-acetoxyallyl allyl ethers (**10** and **11**) by their NMR spectra (Fig. 5) and elementary analyses.

The reactions of diallylamine and diallyl sulfide with palladium acetate proceeded in markedly different manner from the other dienes, and produced little liquid product but a considerable amount of intractable solid materials containing palladium. Since normal acetoxylation attended by precipitation of palladium metal was scarcely observed, the reactions were not examined further.

Discussion

The reaction of 1-octene with palladium acetate in acetic acid yielded 2-acetoxy-1-octene and 1-acetoxy-2-octene in a ratio of 5 : 1 along with 2-octanone and the other minor acetoxylated products.[2] This fact is understood to indicate that in the reaction of palladium acetate with a terminal olefin Markovnikov addition prefers considerably to anti-Markovnikov addition in view of the established route to the palladium acetate oxidation of olefins involving 1,2-addition of PdOAc (acetoxypalladation) and the subsequent *cis* 1,2-elimination of HPdOAc.[3] The formation of **8** and **9** from 1,7-octadiene in a ratio of nearly 5 : 1 as well as of **7** strongly suggests that one of the terminal double bonds reacts like 1-octene without being affected by the presence of the second double bond. However, other dienes utilized in this study afforded characteristic products which reflect the structures of the starting dienes. 1,5-Hexadiene gave the cyclic product **1**, while

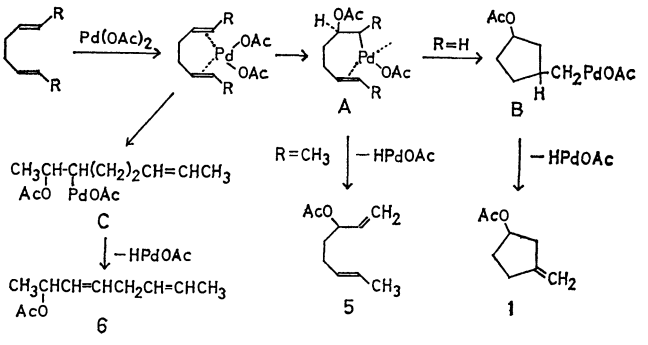

Scheme 1.

2,6-octadiene yielded two open-chain oxidation products **5** and **6**. The marked difference in the products between the two dienes could be reasonably explained in terms of the following scheme.

Addition of one mole of palladium acetate to the dienes would result in the formation of a cyclic π,σ-Pd intermediate since the coordination of the second double bond to palladium can stabilize the initial σ-bonded palladium species. It is noteworthy that in the intermediate (A, R=H) from 1,5-hexadiene β-hydrogen is forced to locate in anti or anti-periplanar position to PdOAc group and cannot enter into the usual *cis* 1,2-elimination of HPdOAc. There are several experimental facts that in the absence of β-hydrogen to be eliminated σ-Pd species enters into another slower processes, such as insertion of a double bond to σ-Pd–C bond[4,5] or formation of π-allylic palladium species.[5,6] Thus, the reaction of 1,5-hexadiene could be depicted that the second double bond in the π,σ-Pd intermediate reacts with σ-Pd–C bond intramolecularly to lead to B, which then undergoes 1,2-elimination to give **1**. On the other hand, in the intermediate (A, R=CH_3) from 2,6-octadiene, a terminal methyl group can act as a β-hydrogen source for the facile 1,2-elimination. Thus, the presence of the methyl group can be regarded as a contributing factor to the formation of **5**, in place of cyclization product. In contrast to the preference for Markovnikov addition of palladium acetate to a terminal double bond, palladium acetate can add to an internal double bond in two alternative ways with much less selectivity.[2] The anti-Markovnikov addition of palladium acetate to 2,6-octadiene is considered to give the intermediate C, which then collapses directly to **6** without forming any cyclic intermediate, since the pseudo-five membered ring species expected by π-donation to palladium must be subjected to considerable steric strain due to a methyl group at C–7 and an α-acetoxyethyl group (–$\underset{\displaystyle CH_3}{\overset{|}{C}}$HOAc) at C–3.

The rationalization of the reaction pathway based on the formation of the stable π,σ-Pd intermediate of pseudo-six membered ring is also applicable to account for the products obtained from 1,6-heptadiene or diallyl ether. Formation of **3** and **4** seems somewhat curious since in the palladium acetate oxidation of simple olefins (except for ethylene) there is no previous example describing the formation of the product bearing 1-acetoxy-1-enyl structure in a considerable yield. If palladium acetate adds to one of the double bonds of 1,6-heptadiene in Markovnikov manner, it would be expected to form either 2-acetoxy-1,6-heptadiene (and/or its isomeric allylic acetates) or a cyclic product through an intermediate of pseudo-seven membered ring. However, it is not the case with the present result except for the formation of a relatively small amount of **2**. On the other hand, a pathway through the pseudo-six membered ring intermediate (D) formed *via* anti-Markovnikov addition is consonant well with the formation of **3** and **4**, because D can not only receive the similar stabilizing effect as was discussed in the reactions of 1,5-hexadiene and 2,6-octadiene, but also possesses β-hydrogen at C–1 available for the facile 1,2-elimination (Scheme 2).

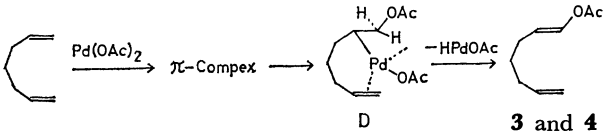

Scheme 2.

Thus, it can be concluded that the formation of a stable π,σ-Pd intermediate of pseudo-six membered ring controls not only the orientation of palladium acetate addition to double bond, but also alters the direction of 1,2-palladium hydride elimination.

The formation of **2** is unusual in view of the normal palladium acetate oxidation involving 1,2-addition and 1,2-elimination, and cannot be explained at present. Although a route involving π-allylic species in place of the σ-Pd bond in D might be an explanation, it is hardly compatible with the formation of **3** and **4**.

Cis and *trans* γ-acetoxyallyl allyl ethers are considered to be produced from diallyl ether in the same route discussed for 1,6-heptadiene, though none of α-acetoxyl isomer was observed. It is to be noted that in the absence of the second double bond the acetoxylation proceeded in a normal manner under the same reaction conditions as evidenced by the formation of β-acetoxyallyl ethyl ether[7] from allyl ethyl ether as a principal product.

It has been reported that allylamines[8] and allyl sulfides[9] gave stable complexes with palladium chloride. The strong dative power of nitrogen and sulfur to palladium could be a principal factor for the present results that diallylamine and diallyl sulfide did not undergo normal acetoxylation with palladium acetate, but afforded intractable solid materials.

Experimentals

Materials. 1,5-Hexadiene[10] and diallylamine[11] were synthesized by the standard methods. 1,7-Octadiene and diallyl sulfide were commercial grade and distilled before use. 1,6-Heptadiene was obtained by the coupling of 4-butenylmagnesium bromide with allyl chloride in the presence of a catalytic amount of ferric chloride,[12] bp 89.0—90.0 °C (lit,[13] bp 91 °C). *Trans,trans*-2,6-octadiene was prepared by the method reported by Webb and Borcherdt[14] consisting of the coupling of crotyl bromide in the presence of nickel carbonyl, bp 123.2—124.0 °C (lit,[14] bp 124.5 °C). Diallyl ether was prepared by the method reported by Skrabal.[15] Palladium acetate was prepared according to the procedure of Wilkinson.[16]

Reaction Procedure. Palladium acetate (1 g, 4.3 mmol) in 40 ml of acetic acid was placed in a 100 ml flask equipped with a reflux condenser and a magnetic stirrer. After the addition of ten-fold excess of diene (43 mmol), the mixture was stirred at 50 °C for 5—7 hr until precipitation of palladium metal was completed. The palladium metal was separated from the reaction mixture by centrifuge, and the supernatant solution was mixed with 300 ml of ether. The ethereal solution was washed successively with water, 30% sodium bicarbonate solution, and saturated sodium chloride solution and dried. Ether and the excess diene were recovered by distillation, and the residue was distilled under reduced pressure to give the following amounts of crude products from the dienes indicated (yields were calculated

as monoacetate and based on the quantity of palladium acetate utilized). 1,5-Hexadiene; 0.58 g (94%), 1,6-heptadiene; 0.68 g (103%), *trans,trans*-2,6-octadiene; 0.72 g (92%), 1,7-octadiene; 0.74 g (100%), and diallyl ether; 0.61 g (100 %).

The crude products were analyzed by glc using one of the 3 mm×2 m columns of Ucon Oil 50HB5100 (10%)-Celite or Reoplex 400 (10%)-Celite. After separation of the main components from the products by glc, their structures were determined by the measurements of IR, NMR and elementary compositions as shown in Table 2.

References

1) P. M. Maitlis, "The Organic Chemistry of Palladium," Vol. 1, Academic Press, N. Y. (1971), p. 161.
2) T. Matsuda, T. Mitsuyasu, and Y. Nakamura, *Kogyo Kagaku Zasshi*, **72**, 1751 (1969).
3) P. M. Maitlis, "The Organic Chemistry of Palladium," Vol. 2, Academic Press, N. Y. (1971), p. 77.
4) R. F. Heck, *J. Organometal. Chem.*, **37**, 389 (1972).
5) K. Kikukawa, K. Sakai, K. Asada, and T. Matsuda, *ibid.*, **77**, 131 (1974).
6) (a) R. Hüttel, J. Kratzer, and M. Becker, *Chem. Ber.*, **94**, 766 (1961), (b) H. C. Volger, *Amer. Chem. Soc., Div. Petr. Chem. Prepr.*, **14**, B72 (1969), see also P. M. Maitlis, "The Organic Chemistry of Palladium," Vol. 1, Academic Press, N. Y. (1971), p. 176.
7) The product was obtained in a yield of 16% (bp 60—63 °C/10 mmHg) on a $Pd(OAc)_2$ basis, together with the formation of a considerable amount of higher boiling complex mixture (bp 90 °C/3 mmHg—93 °C/1 mmHg). After purification by glc, it showed the following analytical data. IR: 1760, 1665, 1200, 1120, 1030, 890 cm^{-1}, NMR: 1.16 (t, 3H), 2.08(s, 3H), 3.47(q, 2H), 3.90(bs, 2H), 4.88 (bs, 2H), MW: 143 (cryoscopy in benzene).
8) A. C. Cope, J. M. Kliegman, and E. C. Friedrich, *J. Amer. Chem. Soc.*, **89**, 287 (1967).
9) Y. Takahashi, A. Tokuda, S. Sakai, and Y. Ishii, *J. Organometal. Chem.*, **35**, 415 (1972).
10) A. Turk and H. Chanan, "Organic Syntheses," Coll. Vol. III, p. 121 (1955).
11) E. B. Vliet, "Organic Syntheses," Coll. Vol. I, p. 201 (1941).
12) Y. Ohbe and T. Matsuda, *Tetrahedron*, **29**, 2989 (1973).
13) W. D. Huntsman, *J. Amer. Chem. Soc.*, **86**, 5455 (1958).
14) I. D. Webb and G. T. Borcherdt, *ibid.*, **73**, 2654 (1951).
15) R. Skrabal, *Z. Phys. Chem.*, [**A**] **185**, 92 (1939).
16) T. A. Stephenson, S. M. Morehouse, A. R. Powell, J. P. Heffer, and G. Wilkinson, *J. Chem. Soc.*, **1965**, 3632.

The Stereochemistry of Autoxidation of Methylcyclohexanes

Shingo MIYAJIMA* and Osamu SIMAMURA**

Department of Chemistry, Faculty of Science, The University of Tokyo, Hongo, Tokyo 113

(Received August 30, 1974)

Autoxidation of 1, *c*-3, *c*-5- or 1, *c*-3, *t*-5-trimethylcyclohexane with oxygen in the presence of azobisisobutyronitrile at 60 °C and subsequent reduction with lithium aluminium hydride gave 1, *t*-3, *t*-5- and 1, *c*-3, *c*-5-trimethyl-*r*-1-cyclohexanol in the same ratio of 1/0.85. Such an almost random attack of oxygen on both sides of intermediate methylcyclohexyl radicals was also observed in autoxidation of 1,2-dimethyl-, 1,4-dimethyl-, and 1,1,3,5-tetramethylcyclohexanes. Approximate relative reactivities of tertiary hydrogens in various steric environments in methylcyclohexanes towards abstraction were determined. Steric effects on the attack of oxygen and the abstraction of hydrogen are discussed.

Although the autoxidation of hydrocarbons with formation of hydroperoxides has been extensively studied, the stereochemical features of the reaction seem to deserve more detailed investigation. The present paper deals with the relative reactivity of tertiary hydrogens in various steric environments in methylcyclohexanes towards abstraction and the stereochemistry of the reaction of oxygen with intermediate methylcyclohexyl radicals.

Results and Discussion

Methylcyclohexanes were autoxidized with oxygen in the presence of azobisisobutyronitrile at 60 °C and the stereoisomeric hydroperoxides formed were reduced with lithium aluminium hydride. Since this reagent is expected to reduce stereospecifically the hydroperoxides to the corresponding alcohols,[1] the alcohol compositions reflect the hydroperoxide compositions of the oxidates. The reduced oxidates were analysed by gas-liquid partition chromatography (glpc).

1,3,5-Trimethylcyclohexanes. 1,*c*-3,*c*-5-Trimethylcyclohexane (**1**) gave two products 1,*t*-3,*t*-5- and 1, *c*-3,*c*-5-trimethyl-*r*-1-cyclohexanol (**5** and **6**), while the 1,*c*-3,*t*-5-isomer (**2**) afforded, besides these alcohols, a third one (**7**). Samples of alcohols **5** and **6** were collected and separated by glpc. The analytical and spectral data show that both of them are monohydric tertiary alcohols, which must have been derived from intermediate radical **3** (Fig. 1).

The configurations of alcohols **5** and **6** are assigned on the basis of the IR data. It has been reported that, in a considerable number of secondary and tertiary cyclohexanols, an axial hydroxyl group has a free O–H stretching absorption in the IR spectrum at a higher frequency than that of its equatorial epimer.[2] For example, *c*-4-*t*-butyl-1-methyl- (with an axial hydroxyl) and *t*-4-*t*-butyl-1-methyl-*r*-1-cyclohexanol (with an equatorial hydroxyl) absorb at 3616—7 and 3611—2 cm^{-1}, respectively.[2c,d] According to this correlation, it is concluded that alcohol **5** has an axial hydroxyl group and alcohol **6** an equatorial one, since alcohols **5** and **6** absorb at 3617 and 3611 cm^{-1}, respectively. The assignments are further supported by NMR measurements of the proton resonance due to a hydroxyl group (see Experimental Part).

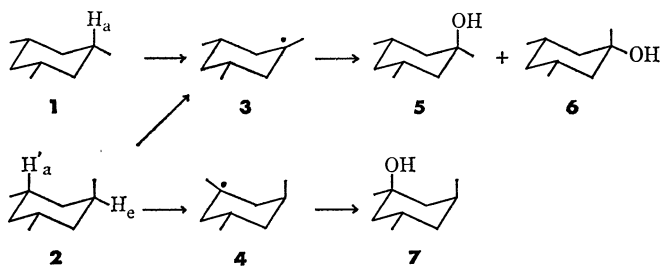

Fig. 1. Autoxidation of 1,3,5-trimethylcyclohexanes.

Isolation of alcohol **7** was not successful. Unquestionably it was derived from intermediate radical **4** generated by abstraction of H_a' in structure **2**, and two forms resulting from axial and equatorial attack of oxygen on radical **4** are of identical configuration and conformationally interconvertible. No other products were detected, indicating that the reaction took place only at tertiary hydrogen atoms.

As shown in Table 1, stereoisomeric 1,3,5-trimethylcyclohexanes **1** and **2** give epimeric alcohols **5** and **6** in the same ratio (1/0.85). Apparently, trimethylcyclohexane **1** or **2**, on abstraction of H_a or H_e, gives radical **3** as a common intermediate. Oxygen attacks this radical from the axial side a little more readily than from the equatorial side. In view of conformational energy, the intermediate peroxy radical corresponding to alcohol **5** should be favoured, at equilibrium, over that corresponding to alcohol **6** by a factor of about 4;[3] consequently, the observed ratio of 1/0.85 indicates an almost random attack of oxygen on both sides of radical **3**. The planar structure of cyclohexyl radicals at the radical centre[5] suggests that oxygen will attack radical **3** with equal probability on both sides of the ring, but the slight preference for axial attack of oxygen may be accounted for by the steric hindrance by the axial hydrogen atoms at positions 2 and 6 to oxygen approaching from the equatorial side. Such steric hindrance has also been suggested to explain the stereochemistry of several reactions including reduction of various cyclohexanones with metal hydrides.[6] It may also be possible that the torsional bond-bond interactions in the transition state suggested by Jensen and coworkers[7] may be a controlling factor in causing this preference.

The relative amounts in which trimethylcyclohexa-

* Present address: Department of Applied Chemistry, Faculty of Engineering, Toyo University, Kawagoe, Saitama 350.

** Present address: Sagami Chemical Research Center, Nishi-onuma, Sagamihara, Kanagawa 229.

Table 1. Autoxidation of 1,3,5-trimethylcyclohexanes[a]

	Trimethylcyclohexane mmol	Azobisisobutyronitrile mmol	Hydroperoxide mmol	Alcohols[b] (mmol) 5	6	7	Total
1	9.16	0.038	0.43	0.205	0.174	0	0.38
				(1	: 0.85	: 0)	
1	9.16	0.036	0.46	0.228	0.191	0	0.42
				(1	: 0.84	: 0)	
2	9.37	0.037	0.55	0.193	0.165	0.059	0.42
				(1	: 0.85	: 0.31)	
2	9.31	0.037	0.50	0.184	0.158	0.059	0.40
				(1	: 0.86	: 0.32)	

a) At 60.2 °C for 48 hr. b) After reduction with lithium aluminium hydride.

Table 2. Autoxidation of 1,4- and 1,2-dimethylcyclohexanes

	Dimethylcyclohexane mmol	Azobisisobutyronitrile mmol	Temp. °C	Reaction time hr	Hydroperoxide mmol	Mole ratio of alcohols[a] **11** : **12** or **16** : **17**
1,4-[b]	10.4	0.036	60.2	48	0.38	1 : 0.71
	10.4	0.038	100.3	5	0.46	1 : 0.75
	10.4	0.037	110.5	4	0.70	1 : 0.76
13	7.0	0.026	60.5	24	0.18	1 : 1.28
13	7.1	0.024	60.2	48	0.30	1 : 1.13
14	6.9	0.024	60.2	48	0.055	1 : 1.16
14[c]			60.2	48		1 : 1.19

a) After reduction with lithium aluminium hydride. b) A mixture of **8** and **9** (75/25). c) Competitive autoxidation with trimethylcyclohexane **1**.

nols **5**, **6**, and **7** are formed reflect approximately the relative reactivities of H_e, H_a, and H_a' towards abstraction. In the accepted scheme of autoxidation[8] involving propagation and termination steps subsequent to initiation:

$$R\cdot + O_2 \rightarrow ROO\cdot \quad \text{(addition)}$$

$$RH + ROO\cdot \rightarrow ROOH + R\cdot \quad \text{(abstraction)}$$

$$2ROO\cdot \rightarrow \text{Inert product} \quad \text{(termination)}$$

the rate constants for abstraction and termination are assumed to be independent of minor difference in structure between the isomeric methylcyclohexylperoxy radicals, and the usual steady-state approximation gives, for the autoxidation of trimethylcyclohexane **1**, the following equation:

$$d([\mathbf{5}^*]+[\mathbf{6}^*])/dt = k_a[H_a](r_i/k_t)^{1/2} \quad (1)$$

where the numerals with an asterisk denote the hydroperoxides corresponding to the alcohols shown in Fig. 1, r_i is the rate of initiation, k_t the rate constant of termination, and k_a that of abstraction of hydrogen atom H_a. Similarly, in the autoxidation of trimethylcyclohexane **2**, we obtain

$$d([\mathbf{5}^*]+[\mathbf{6}^*]+[\mathbf{7}^*])/dt = (k_e[H_e]+k_a'[H_a'])(r_i/k_t)^{1/2} \quad (2)$$

and

$$(d[\mathbf{7}^*]/dt)/\{d([\mathbf{5}^*]+[\mathbf{6}^*])/dt\} = k_a'[H_a']/k_e[H_e] \quad (3)$$

where k_e and k_a' are the rate constants of abstraction of hydrogen atoms H_e and H_a', respectively. Since the autoxidations of hydrocarbons **1** and **2** were carried out under almost the same conditions, we have

$$\frac{d([\mathbf{5}^*]+[\mathbf{6}^*] \text{ from } \mathbf{1})/dt}{d([\mathbf{5}^*]+[\mathbf{6}^*]+[\mathbf{7}^*] \text{ from } \mathbf{2})/dt} = \frac{k_a[H_a]}{k_e[H_e]+k_a'[H_a']} \quad (4)$$

By substituting for the rates of formation of hydroperoxides in Eqs. 3 and 4 the amounts of the corresponding alcohols obtained given in Table 1, since the extent of autoxidation was very limited, the relative rates of hydrogen abstraction are calculated to be $k_e/k_a=2.6$ and $k_a'/k_a=0.22$. Thus, H_e is more reactive than H_a, since it is a less hindered equatorial hydrogen; moreover, the steric strain between the axial methyl group and hydrogens at positions 3 and 5 will be relieved in the transition state of hydrogen abstraction. In contrast, H_a' is less reactive because of the steric hindrance by the axial methyl group at position 3.

1,4- and 1,2-Dimethylcyclohexanes. 1,4- and 1,2-Dimethylcyclohexanes gave corresponding stereoisomeric 1,4-dimethyl- (**11** and **12**) and 1,2-dimethylcyclohexanols (**16** and **17**) (Figs. 2 and 3). These were identified by comparing their glpc retention times with those of authentic samples. The observed ratios **11**/**12** and **16**/**17** are shown in Table 2.

Döring *et al.*[9] reported that *cis*- or *trans*-1,4-dimethylcyclohexane, on autoxidation at 95—110 °C and subsequent reduction with triphenylphosphine or sodium sulphite, afforded alcohols **11** and **12** in a ratio of 1/0.24, which is considerably different from our result (1/0.74), while the ratio of axial to equatorial attack of oxygen on 4-*t*-butyl-1-methylcyclohexyl radical was 1/0.83, in agreement with our data on 1,3,5-trimethylcyclohexanes. The value of 1/0.74 for **11**/**12** is close to that for **5**/**6** from radical **3**, and this is what is

expected, because 1,4-dimethylcyclohexyl radicals are in a rapid conformational equilibrium before reacting with oxygen (**10e** and **10a** in Fig. 2), conformer **10e** predominating over conformer **10a** approximately to the same extent that prevails in the case of methylcyclohexane. The rapid equilibration is supported by Ogawa and Fessenden's conclusion[5b] that the change of linewidth in the ESR spectrum of cyclohexyl radical with temperature (−85—0 °C) corresponds to an activation energy for the ring inversion of 4.9 kcal/mol, which corresponds to a rate of *ca.* $10^9\ s^{-1}$ at 60 °C. Thus, the rate of the inversion will be faster than that of the reaction with oxygen.[10]

With 1,2-dimethylcyclohexanes, the formation of alcohol **17** is slightly favoured over that of alcohol **16**. Conformer **15a** might play a role because of eclipsing of the two methyl groups in conformer **15e** (Fig. 3).

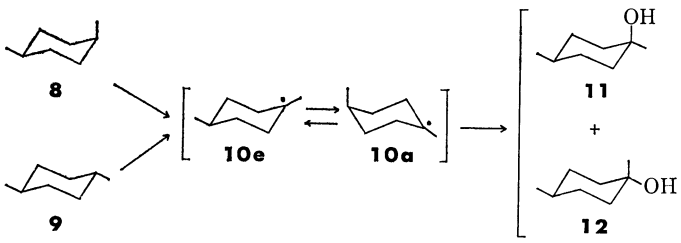

Fig. 2. Autoxidation of 1,4-dimethylcyclohexanes.

The relative reactivity of the axial tertiary hydrogen in *trans*-1,2-dimethylcyclohexane (**14**) towards abstraction was determined by competitive oxidation with trimethylcyclohexane **1**, using the same kind of equation as Eq. 3. The results are shown in Tables 4 and 5. The axial hydrogen in dimethylcyclohexane **14** is less reactive than H_a in trimethylcyclohexane **1**. This retardation is probably due to the steric hindrance by the equatorial methyl group at position 2 to approach of peroxy radicals and/or a crowded transition state with the incipient eclipsing of the two methyl groups.

1,1,3,5-Tetramethylcyclohexanes. Glpc analysis of the reduced oxidate from *cis*- (**18**) or *trans*-1,1,3,5-tetramethylcyclohexane (**19**) revealed two main product peaks. Apparently, these are due to stereoisomeric alcohols **21** and **22** derived from intermediate radical **20** (Fig. 4); the shorter retention time agrees with that of an authentic sample of 1,3,3,*t*-5-tetramethyl-*r*-1-cyclohexanol (**21**) prepared from 3,3,5-trimethylcyclohexanone and methylmagnesium iodide.[13] Although there should be a considerable energy difference (*ca.* 2.0 kcal/mol[14]) between the products from axial and equatorial attack of oxygen on radical **20**, an almost random attack of oxygen was observed also in this case (Table 3). The ratio of axial to equatorial oxygen attack on radical **20** (1/0.96) is slightly smaller than that of oxygen attack on radical **3** (1/0.85), apparently

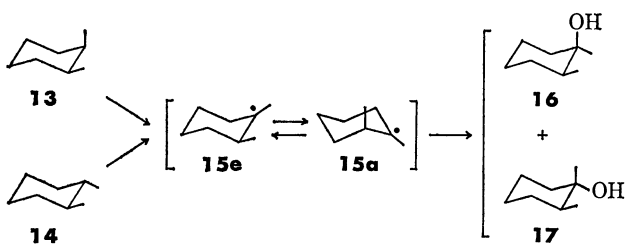

Fig. 3. Autoxidation of 1,2-dimethylcyclohexanes.

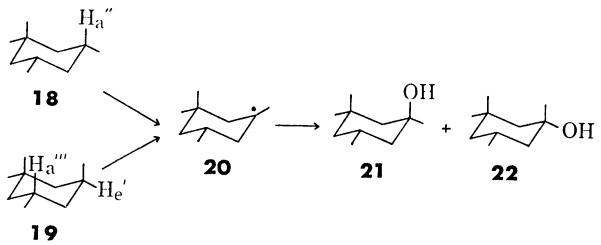

Fig. 4. Autoxidation of 1,1,3,5-tetramethylcyclohexanes.

Table 3. Autoxidation of 1,1,3,5-tetramethylcyclohexanes

Tetramethylcyclohexane mmol		Azobisisobutyronitrile mmol	Temp. °C	Reaction time hr	Hydroperoxide mmol	Mole ratio of alcohols[a] **21 : 22**
18	5.57	0.024	59.8	48	0.030	1 : 1.0
18[b]			60.0	48		1 : 1.0
19	5.68	0.024	59.8	24	0.70	1 : 0.91
19[b]			60.0	24		1 : 0.91

a) After reduction with lithium aluminium hydride. b) Competitive autoxidation with trimethylcyclohexane **1**.

Table 4. Competitive autoxidation[a]

Methylcyclohexane mmol		Azobisisobutyronitrile mmol	Reaction time hr	Hydroperoxide mmol	Mole ratio of alcohols[b] **16 : 17 : 5 : 6** or **21 : 22 : 5 : 6**
14	5.54	0.037	48	0.095	0.80 : 0.95 : 1 : 0.81
1	1.22				
18	5.58	0.061	48	0.10	0.44 : 0.44 : 1 : 0.83
1	1.53				
19	1.44	0.030	24	0.30	0.82 : 0.75 : 1 : 0.79
1	6.11				

a) At 60.0 °C. b) After reduction with lithium aluminium hydride.

Table 5. Relative rates of hydrogen abstraction from methylcyclohexanes

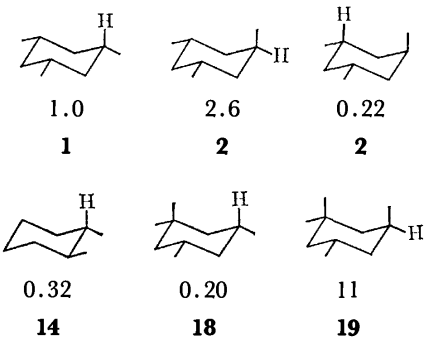

1.0	2.6	0.22
1	**2**	**2**
0.32	0.20	11
14	**18**	**19**

because of the steric effect of the axial methyl group at position 3 in radical **20**.

The relative rate of hydrogen abstraction from tetramethylcyclohexane **18** or **19** was determined by competitive autoxidation with 1,3,5-trimethylcyclohexane **1**. The results are shown in Tables 4 and 5. The relative reactivity of H_a'' in hydrocarbon **18** (0.20) agrees reasonably with that of H_a' in trimethylcyclohexane **2** (0.22). It is noteworthy that equatorial hydrogen H_e' in hydrocarbon **19** is much more reactive (relative reactivity, 11).[16] This large value is certainly due to steric acceleration caused by relief of the 1,3-diaxial strain between the two methyl groups at positions 1 and 3 in the transition state for hydrogen abstraction.

Experimental

All melting points and boiling points are uncorrected. Analytical glpc measurements were carried out with a Perkin-Elmer model 154D instrument. Preparative scale glpc was carried out with a Yanagimoto preparative gas chromatograph and an F & M Prep Master 775. NMR data were obtained with a Varian A-60 spectrometer using tetramethylsilane as an internal standard. IR spectra were recorded on a Nihon-Bunko DS-402G or a Perkin-Elmer 112G spectrometer.

1,3,5-Trimethylcyclohexanes. Mesitylene was hydrogenated in acetic acid over platinum oxide at 30—45 °C with an initial pressure of 50 atm of hydrogen to yield a mixture of 1,*c*-3,*c*-5- (**1**) and 1,*c*-3,*t*-5-trimethylcyclohexane (**2**) in a ratio of 83/17. This mixture was separated into each isomer by preparative glpc on a Silicone DC-550 column at 100 °C. Reinjection of the collected materials showed that the *cis* isomer was free of impurities and that the *trans* isomer contained 1.6% of **1**. The IR and NMR spectra were identical with those published.[17,18]

1,2- and 1,4-Dimethylcyclohexanes. Hydrogenation of *o*-xylene by the same procedure as above afforded a mixture of *cis*- (**13**) and *trans*-1,2-dimethylcyclohexane (**14**) in a ratio of 88/12. Dehydration of 1,2-dimethylcyclohexanol, prepared from methylmagnesium iodide and 2-methylcyclohexanone, followed by hydrogenation in methanol with hydrogen at 1 atm on 5% palladium-on-charcoal at room temperature gave a 22/78 mixture of *cis*- and *trans*-1,2-dimethylcyclohexane. From these mixtures each isomer was obtained by preparative glpc using a Silicone DC-550 column at 95 °C: *cis* isomer **13**, n_D^{20} 1.4349 (lit,[19] n_D^{20} 1.43596); *trans* isomer **14**, n_D^{20} 1.4259 (lit,[19] n_D^{20} 1.42695). Reinjection of the collected materials showed that the *cis* isomer contained 1.9% of **14** and that the *trans* isomer was free of impurities.

1,4-Dimethylcyclohexanes were prepared from *p*-xylene in the same manner as with 1,3,5-trimethylcyclohexanes, the *cis*/*trans* ratio being 75/25. This mixture was used without separating it into the isomeric components.

1,1,3,5-Tetramethylcyclohexanes. A procedure similar to that of Allinger and Miller[20] was used. Isophorone was hydrogenated in methanol over palladium-on-charcoal to yield 3,3,5-trimethylcyclohexanone, which was then converted with methylmagnesium iodide into 1,3,3,*t*-5-tetramethyl-*r*-1-cyclohexanol (**21**), mp 80.5—81.5 °C (lit,[13] 80—81.5 °C). Dehydration of this alcohol with formic acid followed by hydrogenation in acetic acid with hydrogen at 1 atm on platinum oxide at room temperature yielded a mixture of *cis*- (**18**) and *trans*-1,1,3,5-tetramethylcyclohexane (**19**) in a ratio of 1.34/1. The components were separated by preparative scale glpc using an SE-30 column at 128 °C: the *cis* isomer, bp 153—153.5 °C (lit,144.5—145 °C,[20] 152.4—152.5 °C[21]), n_D^{20} 1.4300 (lit, n_D^{25} 1.4288,[20] n_D^{20} 1.4319[21]); the *trans* isomer, bp 157.5—158 °C (lit, 148.5—149 °C,[20] 156.4—156.5 °C[21]), n_D^{20} 1.4357 (lit, n_D^{25} 1.4342,[20] n_D^{20} 1.4370[21]). Each of the collected materials showed no impurities on reinjection.

General Procedure of Autoxidation Experiments. Samples (1.0—1.5 ml) of methylcyclohexanes were autoxidized with oxygen at 1 atm in the presence of azobisisobutyronitrile (4—6 mg) in a small glass vessel attached to a gas burette. The reaction temperature was controlled by immersing the vessel in a constant temperature oil bath. The samples were stirred by means of a glass-encased magnetic stirring bar. At a conversion of less than 10% the reaction was stopped, and a portion (0.20—0.50 ml) of the oxidate was withdrawn to determine the hydroperoxide content by the iodometric method of Wagner *et al.*[22]

The rest of the oxidate was transferred into a dropping funnel, using 10 ml of anhydrous ether to rinse the reaction vessel, and was added to a suspension of 0.5 g of lithium aluminium hydride in 10 ml of anhydrous ether with stirring. The mixture was heated under reflux for 2 hr and then allowed to stand overnight at room temperature. Excess of lithium aluminium hydride was destroyed with dilute sulphuric acid, and the aqueous phase extracted with three 10 ml portions of ether. The combined ether solutions were washed with 5% sodium hydrogencarbonate solution and dried over anhydrous sodium sulphate, and then the ether was removed. The resulting solution was analysed for alcohols by glpc.

Product Identification. *1,3,5-Trimethylcyclohexanols*: 1,3,5-Trimethylcyclohexanols **5** and **6** were isolated by preparative glpc using a Carbowax column at 130 °C from reduced oxidate of a mixture of 1,3,5-trimethylcyclohexanes **1** and **2**.

*1,t-3,t-5-Trimethyl-r-1-cyclohexanol (**5**)*: n_D^{20} 1.4498 (Found: C, 75.95; H, 12.71%. Calcd for $C_9H_{18}O$: C, 76.00; H, 12.76%); ν_{max} (0.022 M in CCl_4) 3617 cm^{-1} (OH); δ (0.71 M in CCl_4) 0.85 (d, J 6 Hz, 6H, 3-CH_3 and 5-CH_3), 1.14 (s, 3H, 1-CH_3), 0.2—1.9 (complex, ring protons), 2.32 (s, 1H, OH).[23] The signal of OH proton was shifted to δ 1.02 upon dilution to 0.158 M.

*1,c-3,c-5-Trimethyl-r-1-cyclohexanol (**6**)*: mp 41.5—42.5 °C (Found: C, 76.26; H, 12.86%. Calcd for $C_9H_{18}O$: C, 76.00; H, 12.76%); ν_{max} (0.022 M in CCl_4) 3611 cm^{-1} (OH); δ (0.71 M in CCl_4) 0.91 (d, J 5 Hz, 6H, 3-CH_3 and 5-CH_3), 1.15 (s, 3H, 1-CH_3), 0.3—1.8 (complex, ring protons), 2.90 (s, 1H, OH).[23] The signal of OH proton was shifted to δ 1.38 upon dilution to 0.158 M.

1,4- and 1,2-Dimethylcyclohexanols: The products from 1,4- and 1,2-dimethylcyclohexanes were identified by comparison of their glpc retention times with those of authentic samples

of 1,*c*-4- (**11**) and 1,*t*-4-dimethyl-*r*-1-cyclohexanol (**12**) and those of the components of a mixture of 1,*c*-2- (**16**) and 1,*t*-2-dimethyl-*r*-1-cyclohexanol (**17**). Authentic samples of alcohols **11** and **12** were obtained by reaction of 4-methylcyclohexanone with methylmagnesium iodide, followed by separation of the resulting *cis* and *trans* mixture (**11**/**12**=1/1) by glpc using a Carbowax column at 140 °C: alcohol **11**, mp 66—68 °C (lit,[24] 72.5 °C); alcohol **12**, mp 23—24 °C (lit,[24] 24 °C). A sample of a **16** and **17** mixture was prepared from 2-methylcyclohexanone and methylmagnesium iodide, the **16**/**17** ratio being 3.8/1 in fairly good agreement with the reported value (3/1).[25]

1,3,3,5-Tetramethylcyclohexanols: The preparation of 1,3,3-*t*-5-tetramethyl-*r*-1-cyclohexanol (**21**) has been described above. Glpc analysis of the reduced oxidate from 1,1,3,5-tetramethylcyclohexane **18** or **19** revealed two main product peaks corresponding to alcohol **21** and the epimeric alcohol **22**, the shorter retention time agreeing with that of a sample of alcohol **21**.

Product Analysis. The reduced oxidate from 1,3,5-trimethylcyclohexane **1** or **2** was examined by glpc on a Carbowax column 4 m long at 165 °C; the order of elution was alcohols **5**, **7**, and **6**. Quantitative analysis for alcohol **5** or **6** was carried out using anisole as an internal standard. Since the mole ratio was found to be approximately equal to the peak area ratio with stereoisomers **5** and **6** [mol **5**/mol **6**=0.974× (area **5**/area **6**)], the amount of alcohol **7**, whose authentic specimen was not available, was estimated on the assumption that the mole ratio of **7**/**5** equals the peak area ratio. Stereoisomeric 1,2- or 1,4-dimethylcyclohexanols were analysed using a Carbowax column 2 m long at 150 °C; the order of elution was alcohols **16** and **17** or alcohols **11** and **12**. Analysis of the alcohols from competitive autoxidation of 1,2-dimethylcyclohexane **14** with trimethylcyclohexane **1** was carried out on a Carbowax column (2 m) and a Ucon Oil LB-550-X column (2 m) connected in series at 160 °C; alcohols were eluted in the order **16**, **5**, **17**, and **6**. The products from autoxidation of tetramethylcyclohexane **18** or **19** and competitive autoxidation with trimethylcyclohexane **1** were analysed with the above-mentioned series of columns at 170 °C; the elution of alcohols took place in the order **5**, **21**, **6**, and **22**.

It is apparent that in each pair of the epimeric alcohols examined the one, which has an hydroxyl group predominantly in the axial position, has a shorter retention time than the other, when chromatographed on polyethylene glycol (Carbowax) or polypropylene glycol (Ucon Oil). This observation is in accord with the results by Komer *et al.*,[26] who studied the retention times of the epimeric 2-, 3-, and 4-alkylcyclohexanols using glycerol or erythritol as a stationary phase.

References and Notes

1) a) A. G. Davies and R. Feld, *J. Chem. Soc.*, **1956**, 665. b) A. G. Davies, *ibid.*, **1958**, 3474.

2) a) A. R. H. Cole, P. R. Jefferies, and G. T. A. Müller, *ibid.*, **1959**, 1222, and preceding papers. b) G. Chiurdoglu and W. Masschelein, *Bull. Soc. Chim. Belges*, **68**, 484 (1959). c) B. Cross and G. H. Whitham, *J. Chem. Soc.*, **1960**, 3892. d) F. Dalton, G. D. Meakins, J. H. Robinson, and W. Zaharia, *ibid.*, **1962**, 1566. e) H. S. Aaron and C. P. Rader, *J. Amer. Chem. Soc.*, **85**, 3046 (1963). f) H. S. Aaron, C. P. Ferguson, and C. P. Rader, *ibid.*, **89**, 1431 (1967).

3) Assuming that the energy difference between **5** and **6** is the difference in conformational energy between methyl (1.7 kcal/mol[4]) and an oxygen function (*ca.* 0.7 kcal/mol[4]), *i.e.*, *ca.* 1.0 kcal/mol.

4) E. L. Eliel, N. L. Allinger, S. J. Angyal, and G. A. Morrison, "Conformational Analysis," Interscience Publishers, New York (1965), p. 44.

5) a) R. W. Fessenden and R. H. Schuler, *J. Chem. Phys.*, **39**, 2147 (1963). b) S. Ogawa and R. W. Fessenden, *ibid.*, **41**, 994 (1964).

6) J. C. Richer, *J. Org. Chem.*, **30**, 324 (1965).

7) F. R. Jensen, L. H. Gale, and J. E. Rodgers, *J. Amer. Chem. Soc.*, **90**, 5793 (1968).

8) See, *e.g.*, C. Walling, "Free Radicals in Solution," John Wiley, New York (1957), p. 419.

9) C. E. Döring, H. G. Hauthal, H. Noglik, and W. Pritzkow, *J. Prakt. Chem.*, **24**, 183 (1964).

10) Assuming that the rate constant (k_0) for the reaction of the radical with oxygen is 10^8 M^{-1} s^{-1} [11] and using the solubility of oxygen in cyclohexane (1×10^{-2} M at 25 °C[12]), the ratio of the rate of inversion (rate constant, k_t) to that of the reaction with oxygen becomes

$$\frac{k_t[R\cdot]}{k_0[R\cdot][O_2]} = \frac{10^9}{10^8\cdot10^{-2}} = 10^3$$

11) W. H. Starnes, Jr., *J. Org. Chem.*, **31**, 1443 (1966), and references cited therein.

12) A. B. McKeown and R. R. Hibbard, *Anal. Chem.*, **28**, 1490 (1956).

13) E. J. Corey and M. Chaykovsky, *J. Amer. Chem. Soc.*, **87**, 1353 (1965).

14) Assuming that the 1,3-diaxial interaction energies of OH–H, CH_3–H, OH–CH_3, and CH_3–CH_3 are 0.35, 0.85, 2.2, and 3.7 kcal/mol, respectively,[15] the energy difference between alcohols **21** and **22** is calculated as *ca.* 2.0 kcal/mol.

15) E. L. Eliel, N. L. Allinger, S. J. Angyal, and G. A. Morrison, "Conformational Analysis," Interscience Publishers, New York (1965), p. 44, 52.

16) In the calculation of the relative reactivity of H_e', abstraction of H_a''' was neglected, since H_a''' is screened by two *syn*-axial methyl groups and must have, therefore, a very small relative reactivity (less than that of H_a'' (0.2)).

17) A. P. I. Res. Project, **44**, No. 1950, 2056 (1958); **44**, No. 2107, 2108 (1959).

18) A. Segre and J. I. Musher, *J. Amer. Chem. Soc.*, **89**, 706 (1967).

19) F. D. Rossini, K. S. Pitzer, R. L. Aanett, R. M. Braun, and G. C. Pimentel, "Selected Values of Physical and Thermodynamic Properties of Hydrocarbons and Related Compounds," Carnegie Press, Pittsburgh (1953), p. 51.

20) N. L. Allinger and M. A. Miller, *J. Amer. Chem. Soc.*, **83**, 2145 (1961).

21) G. Chiurdoglu and A. Maquestiau, *Bull. Soc. Chim. Belges*, **63**, 357 (1954).

22) C. D. Wagner, R. H. Smith, and E. D. Peters, *Ind. Eng. Chem., Anal. Ed.*, **19**, 976 (1947).

23) *Cf.*, *e.g.*, L. M. Jackman and S. Sternhell, "Applications of Nuclear Magnetic Resonance Spectroscopy in Organic Chemistry," 2nd Ed., Pergamon Press, Oxford (1969), p. 240.

24) G. Chiurdoglu, *Bull. Soc. Chim. Belges*, **47**, 241 (1938).

25) I. N. Nazarov, A. A. Akhrem, and A. V. Kamernitskii, *Izvest Akad. Nauk SSSR, Otdel Khim. Nauk*, **1958**, 631.

26) a) R. Komers, K. Kochloefl, and V. Bazant, *Chem. Ind.* (London), **1958**, 1405. b) R. Komers and K. Kochloefl, *Collect. Czech. Chem. Commun.*, **28**, 46 (1963).

The Stereochemistry of the Reaction of Hydrogen Bromide with Cyclohexene and 1-Methylcyclohexene in the Presence of Oxygen

Shingo MIYAJIMA,* Sadao ICHIHARA,** and Osamu SIMAMURA***

Department of Chemistry, Faculty of Science, The University of Tokyo, Hongo, Tokyo 113

(Received August 30, 1974)

The reaction of hydrogen bromide with cyclohexene or 1-methylcyclohexene in the presence of oxygen, followed by reduction with lithium aluminium hydride afforded *trans*-2-bromocyclohexanol or *t*-2-bromo-1-methyl-*r*-1-cyclohexanol. These findings show that oxygen attacks intermediate bromocyclohexyl radicals formed by addition of a bromine atom to a double bond exclusively on the side opposite to the bromine substituent. Mechanistic implications are discussed.

The free radical addition of hydrogen bromide to olefins takes place preferentially in *anti* fashion.[1] If oxygen is present, it attacks an intermediate radical generated by addition of a bromine atom to an olefinic bond in competition with hydrogen bromide, giving rise to a bromine-containing hydroperoxide[2] or oxygenated bromine compounds,[3] probably through an intermediate hydroperoxide.

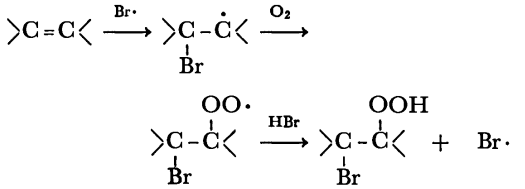

It seemed of interest to examine the stereochemistry of attack of oxygen on the cyclohexyl type of radicals generated by addition of a bromine atom to cyclohexenes, because in the autoxidation of methylcyclohexanes it has been shown that oxygen attacks intermediate radicals with nearly equal probability on both sides of the radical centre.[4] The present report deals with the stereochemistry of reaction of oxygen with the radicals generated by addition of a bromine atom to cyclohexene and 1-methylcyclohexene.

Results and Discussion

Anhydrous hydrogen bromide and oxygen were passed through cyclohexene or 1-methylcyclohexene containing a little benzoyl peroxide at about 60 °C, and reaction mixtures were treated with lithium aluminium hydride to reduce hydroperoxides produced to the corresponding alcohols. Gas-liquid partition chromatographic (glpc) analysis showed that *trans*-2-bromocyclohexanol or *t*-2-bromo-1-methyl-*r*-1-cyclohexanol was formed, but no *cis* isomers were detected. The results are summarized in Table 1.

It is evident that oxygen attacks the intermediate radicals formed by addition of a bromine atom to the cyclohexenes exclusively on the side opposite to the bromine atom, in striking contrast to the case of autoxidation of methylcyclohexanes, in which an almost random attack of oxygen occurs.[4] The completely stereoselective attack of oxygen may be explained in terms of a bromine bridged radical[5] (Fig. 1); thus, oxygen would attack intermediate radical **1** only from the opposite direction of the bromine bridge resulting in *anti* stereochemistry. An alternative explanation for the observed stereochemistry might involve intermediate radical **2**, in which the C-2 bromine occupies an axial position and would prevent an access of oxygen from the *cis* direction (Fig.

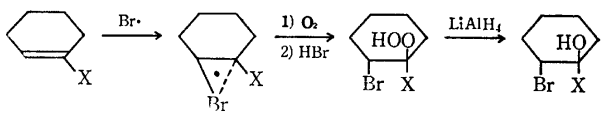

1 X=H, CH_3

Fig. 1.

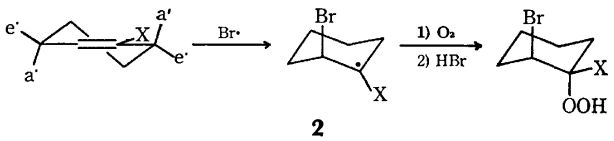

2

Fig. 2.

TABLE 1. REACTIONS OF HYDROGEN BROMIDE WITH CYCLOHEXENE AND 1-METHYLCYCLOHEXENE IN THE PRESENCE OF OXYGEN

Olefin (mol)		BPO[a] (mmol)	Temp. (°C)	Reaction time (hr)	Peroxide[b] (mmol)	Bromohydrin[c] (mmol)	
						cis	*trans*
Cyclohexene	0.34	1.09	64±3	3.0	10.2	0	1.6[d]
1-Methylcyclohexene	0.25	0.96	61±3	3.5	22.8	0	1.3[e]

a) Benzoyl peroxide. b) Titrated iodometrically by Wagner's method.[11] c) After reduction with lithium aluminium hydride. d) *trans*-2-Bromocyclohexanol. e) *t*-2-Bromo-1-methyl-*r*-1-cyclohexanol.

* Present address: Department of Applied Chemistry, Faculty of Engineering, Toyo University, Kawagoe, Saitama 350.

** Present address: Toyo Soda Manufacturing Co., Ltd., Akasaka, Minato-ku, Tokyo 107.

*** Present address: Sagami Chemical Research Center, Nishi-onuma, Sagamihara, Kanagawa 229.

2). This explanation, however, does not seem convincing, because, although the 2-bromocyclohexyl radical will be produced in the form shown in Fig. 2 with the bromine substituent in an axial conformation, it will interconvert in quick equilibrium with the form in which the bromine is equatorial before it reacts with oxygen,[6] undoubtedly resulting in almost random attack of oxygen.

Experimental[7]

Materials. Cyclohexene was prepared by dehydration of cyclohexanol with potassium hydrogensulphate,[8] followed by fractional distillation with a packed column, bp 82—82.5 °C. 1-Methylcyclohexene was prepared according to the method of Bartlett and Rosenwald[9] by the Grignard reaction of cyclohexanone to give 1-methylcyclohexanol, followed by dehydration and fractionation with a concentric column, bp 110.2—110.4 °C. Hydrogen bromide was evolved by the action of bromine on tetralin.[10] The hydrogen bromide was freed from bromine by bubbling through tetralin and dried by passing through a trap cooled at —50 °C and then a tube packed with anhydrous calcium sulphate.

Reactions of Hydrogen Bromide with Cyclohexene and 1-Methylcyclohexene in the Presence of Oxygen. Cyclohexene (0.34 mol) or 1-methylcyclohexene (0.25 mol) containing benzoyl peroxide (1 mmol) was placed in a reaction flask equipped with two bubbler tubes and a reflux condenser protected from moisture by a drying tube filled with anhydrous calcium sulphate. The reaction flask was immersed in a water bath which was kept at about 60 °C. The cyclohexene was stirred by means of a magnetic stirrer, and dry hydrogen bromide and oxygen were passed through simultaneously. The reaction was allowed to proceed for 3—3.5 hr. The reaction mixture was washed with water and dried over anhydrous magnesium sulphate. A portion of this mixture was analysed for peroxides formed by the iodometric method of Wagner *et al.*[11] The remaining portion was dissolved in anhydrous ether and added to a suspension of excess of lithium aluminium hydride in anhydrous ether. After the mixture had been stirred for 1 hr at room temperature, excess of lithium aluminium hydride was destroyed with dilute sulphuric acid. The ether layer was separated, the aqueous layer extracted with ether, and the combined ether solutions were dried over anhydrous sodium sulphate. The ether was removed by distillation and the residue subjected to glpc analysis.

Gas-Liquid Partition Chromatography. A Perkin-Elmer model 154D instrument was utilized. The product mixture from cyclohexene was examined using a Carbowax column 1 m long (steel tube) at 111 °C. The products from 1-methylcyclohexene was analysed using a diisodecyl phthalate column 0.5 m long (glass tube) at 103 °C or a Carbowax column 0.5 m long (glass tube) at 99.5 °C.

Preparation and Characterization of Authentic Samples. cis-*2-Bromocyclohexanol*: To 35 g (0.20 mol) of 2-bromocyclohexanone[12] in 50 ml of methanol was added portionwise 6 g (0.16 mol) of sodium borohydride with stirring. Stirring was continued for an additional 20 min. Dilute aqueous solution of acetic acid was added, the organic layer separated, and the aqueous layer extracted with ether. The combined organic layer and extracts were dried over anhydrous sodium sulphate, and then distilled to give 11 g of colourless liquid, bp 50 °C/1 mmHg, which crystallized in a refrigerator. Glpc analysis showed that it consisted of 90% of *cis*-2-bromocyclohexanol and 10% of the *trans* isomer. Two recrystallizations from petroleum ether gave a pure specimen of the *cis*-isomer in needles, mp 28.5—29.0 °C (lit,[13] mp 29.0—29.5 °C), ν_{max} (liquid film) 3450 cm^{-1} (OH); *p*-toluenesulphonate, mp 77—78 °C (lit,[14] mp 79—80 °C) (Found: C, 47.13; H, 5.35%. Calcd for $C_{13}H_{17}BrO_3S$: C, 46.85; H, 5.14%). The Meerwein-Ponndorff reduction of 2-bromocyclohexanone[13] afforded a mixture of *cis*- and *trans*-2-bromocyclohexanol in a ratio of about 1 : 2.

trans-*2-Bromocyclohexanol*: This compound was obtained according to the procedure of Guss and Rosenthal[15] by the reaction of cyclohexene with *N*-bromosuccinimide in water, bp 87—87.5 °C/10 mmHg, mp 26.5—27 °C (lit, bp 90—91 °C/13 mmHg,[16] mp 27.5 °C[17]), ν_{max} (liquid film) 3400 cm^{-1} (OH); *p*-toluenesulphonate, mp 42—42.5 °C (lit,[14] mp 44—45 °C).

c-*2-Bromo-1-methyl*-r-*1-cyclohexanol*: This compound was prepared according to the method of Bartlett and Rosenwald[9] by the reaction of 2-bromocyclohexanone with methylmagnesium iodide, bp 51—52.5 °C/2 mmHg, n_D^{27} 1.5057 (lit,[9] bp 83 °C/7 mmHg, n_D^{27} 1.5032), ν_{max} (liquid film) 3500 cm^{-1} (OH) (Found: Br, 40.3%. Cald for $C_7H_{13}BrO$: Br, 41.4%). Glpc analysis showed that this material contained trace amount of the *trans* isomer.

t-*2-Bromo-1-methyl*-r-*1-cyclohexanol*: This compound was synthesized according to the directions of Filler *et al.*[18] by the reaction of 1-methylcyclohexene with *N*-bromosuccinimide in water, bp 70.8—72.9 °C/3 mmHg, n_D^{25} 1.5150 (lit,[18] bp 96—98 °C/8.5 mmHg, n_D^{25} 1.5150), ν_{max} (liquid film) 3450 cm^{-1} (OH) (Found: Br, 41.4. Calcd for $C_7H_{13}BrO$: Br, 41.4%).

References

1) For reviews of the stereochemistry of free radical addition to olefins, see B. A. Bohm and P. I. Abell, *Chem. Rev.*, **62**, 599 (1962) and O. Simamura, "Topics in Stereochemistry," Vol. 4, ed. by N. L. Allinger and E. L. Eliel, Interscience Publishers, New York (1969), p. 1.

2) A. Rieche, M. Schulz, and K. Kirschke, *Chem. Ber.*, **99**, 3244 (1966).

3) O. Simamura, This Bulletin, **17**, 326 (1942); O. Simamura and M. Takahashi, *ibid.*, **22**, 60 (1949).

4) S. Miyajima and O. Simamura, This Bulletin, **48**, 526 (1975).

5) For the concept of bridged radicals, see P. S. Skell and K. J. Shea, "Free Radicals," Vol. 2, ed. by J. K. Kochi, John Wiley & Sons, New York (1973), p. 809.

6) See note 10 in reference 4.

7) All melting points and boiling points are uncorrected.

8) L. Brunel, *Bull. Soc. Chim. Fr.*, [3] **33**, 270 (1905).

9) P. D. Bartlett and R. H. Rosenwald, *J. Amer. Chem. Soc.*, **56**, 1990 (1934).

10) D. R. Duncan, "Inorganic Syntheses," Vol. 1, p. 151 (1939).

11) C. D. Wagner, R. H. Smith, and E. D. Peters, *Ind. Eng. Chem., Anal. Ed.*, **19**, 976 (1947).

12) J. Allinger and N. L. Allinger, *Tetrahedron*, **2**, 64 (1958).

13) S. J. Cristol and L. E. Rademacher, *J. Amer. Chem. Soc.*, **81**, 1600 (1959).

14) S. J. Cristol, J. Q. Weber, and M. C. Brindell, *ibid.*, **78**, 598 (1956).

15) C. O. Guss and R. Rosenthal, *ibid.*, **77**, 2549 (1955).

16) M. Tiffeneau and B. Tchoubar, *C. R. Acad. Sci. Paris*, **207**, 218 (1938).

17) F. Swarts, *Bull. Soc. Chim. Belges*, **46**, 13 (1937).

18) R. Filler, B. R. Camara, and S. M. Naqvi, *J. Amer. Chem. Soc.*, **81**, 658 (1959).

The Stereochemistry of Autoxidation of 2-Bromo-1-methylcyclohexane

Shingo MIYAJIMA* and Osamu SIMAMURA**

Department of Chemistry, Faculty of Science, The University of Tokyo, Hongo, Tokyo 113

(Received August 30, 1974)

Autoxidation of *cis*-2-bromo-1-methylcyclohexane and subsequent reduction of the resulting hydroperoxide with lithium aluminium hydride gave only *t*-2-bromo-1-methyl-*r*-1-cyclohexanol to the exclusion of the *c*-2-bromo-isomer. The reactivity ratio of the C–1 hydrogen in *cis*-2-bromo-1-methylcyclohexane to that in 1, *c*-3, *c*-5-trimethylcyclohexane towards abstraction was estimated to be about 4 by competitive oxidation experiments. An explanation for the acceleration of hydrogen abstraction and the stereospecific oxygen attack on the intermediate radical is given in terms of a bromine bridged radical. Autoxidation of a sample of 2-bromo-1-methylcyclohexane, containing about 90% of the *trans* isomer, took place very slowly as compared with the *cis* isomer.

In previous papers,[1,2] it was shown that oxygen attacks the bromocyclohexyl radicals generated by addition of a bromine atom to cyclohexene and 1-methylcyclohexene exclusively from the *trans* direction to the bromine atom, while an almost random attack of oxygen occurs on both sides of the methylcyclohexyl radicals formed by hydrogen abstraction from a variety of methylcyclohexanes. This paper is concerned with the autoxidation of 2-bromo-1-methylcyclohexane carried out in order to examine the effect of the neighbouring bromine substituent on the reactivity of the hydrogen at position 1 towards abstraction as well as the stereochemical course of oxygen attack on the intermediate radical.

Results and Discussion

cis-2-Bromo-1-methylcyclohexane (**1**) was prepared by radical addition of hydrogen bromide to 1-methylcyclohexene in heptane followed by partial hydrolysis and fractionation for separation from 1-bromo-1-methylcyclohexane, a by-product. The NMR spectrum indicated that the product obtained was free of the *trans* isomer (**2**), as evidenced by the absence of the signal (doublets of a triplet) centered at δ 3.61 due to a Br–C–H proton in the *trans* isomer.[3]

The *cis* bromide (**1**) was autoxidized with oxygen in the presence of azobisisobutyronitrile at 60 °C, and the resulting hydroperoxide was reduced with lithium aluminium hydride to the corresponding alcohol. Gas-liquid partition chromatographic analysis showed that *t*-2-bromo-1-methyl-*r*-1-cyclohexanol (**3**) was the sole detectable alcohol, the retention time agreeing with that of an authentic specimen on each of three different columns (diisodecyl phthalate, polyethylene glycol, and cyanosilicone). The *cis* isomer could not be detected. The results are summarized in Table 1.

In order to estimate the relative rate of abstraction of the C-1 hydrogen in *cis*-2-bromo-1-methylcyclohexane (**1**), competitive oxidation experiments with 1, *c*-3, *c*-5-trimethylcyclohexane (**4**) were performed. The results are shown in Table 2. Treatment of these data with the same method as described previously[1] gave a reactivity ratio of the C-1 hydrogen in bromomethyl-

Table 1. Autoxidation of 2-bromo-1-methylcyclohexane[a]

Bromide (mmol)		AIBN[b] (mmol)	Reaction time (hr)	Hydroperoxide (mmol)	Bromohydrin (mmol)	
					cis	*trans* (**3**)
cis (**1**)	7.18	0.024	22	0.21	0	Formed[c]
cis (**1**)	7.21	0.048[e]	24	0.28	0	0.22[d]
cis+*trans* (**1**+**2**)[f]	7.09	0.025	22	0.040		

a) At 60.0 °C. b) Azobisisobutyronitrile. c) After reduction with sodium borohydride. The amount was not determined. d) After reduction with lithium aluminium hydride. e) AIBN was added in two portions. f) **1** : **2**=10 : 90.

Table 2. Competitive autoxidation of *cis*-2-bromo-1-methylcyclohexane (**1**) with 1,*c*-3,*c*-5-trimethylcyclohexane (**4**)[a]

1 (mmol)	**4** (mmol)	AIBN[b] (mmol)	Hydroperoxide (mmol)	Alcohols[c] (mmol)		
				trans-Bromohydrin **3**	1,3,5-Trimethyl-cyclohexanol	Total
7.20	6.05	0.148	0.491	0.227	0.137	0.364
7.19	6.04	0.143	0.485	0.217	0.144	0.361

a) At 60.0 °C for 24 hr. b) Azobisisobutyronitrile. c) After reduction with lithium aluminium hydride.

* Present address: Department of Applied Chemistry, Faculty of Engineering, Toyo University, Kawagoe, Saitama 350.

** Present address: Sagami Chemical Research Center, Nishi-onuma, Sagamihara, Kanagawa 229.

Table 3. Relative rates of hydrogen abstraction

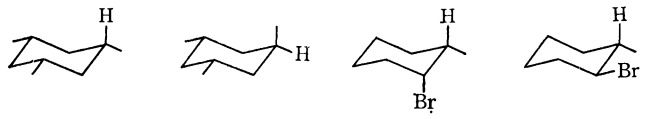

1.0	2.6[a)]	4	*ca.* 0.4
4	**5**	**1**	**2**

a) Ref. 1.

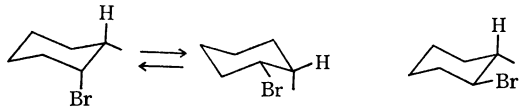

1a **1e** **2**

Fig. 1. Conformation of 2-bromo-1-methylcyclohexanes.

cyclohexane **1** to that in trimethylcyclohexane **4** towards abstraction of about 4 (Table 3), a considerably large value compared with that for an axial hydrogen atom in the ordinary situation.

Although the *cis* bromide (**1**) is not conformationally uniform, conformer **1a** should predominate largely over **1e** (Fig. 1), since the conformational equilibrium constant of **1**, the *gauche* interactions between the methyl and bromine substituent cancelling out for the pair of conformers, is considered to be almost equal to 0.1 for *cis*-4-bromo-1-methylcyclohexane.[4)] The large reactivity of the C-1 hydrogen in the *cis* bromide (**1**) may be in part due to steric acceleration caused by relief, in the transition state, of a *gauche* interaction between the C-1 methyl group and the C-2 bromine in conformer **1a**. However, the contribution of this effect would be of minor importance, since the observed reactivity ratio of 4 corresponds to a difference of 0.9 kcal/mol in free energy of activation, while the *gauche* interaction between a methyl group and a bromine atom is only 0.25 kcal/mol.[5)] The contribution of conformer **1e** would also be insignificant; the equatorial C-1 hydrogen in **1e** would be hindered by the C-2 equatorial bromine substituent, whereas there is no such hindrance suffered by the hydrogen at C-5 in 1, *c*-3,*t*-5-trimethylcyclohexane (**5**). Moreover, the abstraction of the C-1 hydrogen in **1e** would be less favoured than that at C-5 in **5** because of the incipient eclipsing of the methyl and bromine substituent, as the methyl tends to be planar with the other two bonds at carbon atom 1 in the course of abstraction. Even if the relative reactivity of the equatorial hydrogen in **1e** should be equal to 2.6 for compound **5**, the contribution of **1e** to the relative reactivity is only 0.26, since the conformational population of **1e** is estimated to be about 10%.

The relative reactivity of 4 found for *cis*-2-bromo-1-methylcyclohexane (**1**) is thus attributed mainly to the hydrogen in axial position at carbon atom 1, and apparently the value is higher than that expected for a hydrogen in similar steric environments. A special effect causing such an acceleration must be due to the bromine substituent at position 2, although the halogen substituent is known to retard the hydrogen abstraction

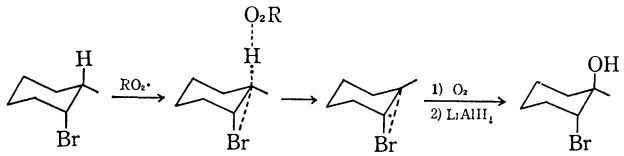

1 **3**

Fig. 2. Autoxidation of *cis*-2-bromo-1-methylcyclohexane.

reaction because of electron-attracting inductive effect.[6)] A possible explanation of both the acceleration of hydrogen abstraction and the stereospecific oxygen attack in *cis* bromo-compound **1** may be that the axial bromine substituent anchimerically delocalizes an incipient odd electron in the transition state of hydrogen abstraction and then forms a bridged intermediate radical[7)] (Fig. 2).

Although a mixture of *cis*- and *trans*-2-bromo-1-methylcyclohexane (**1** and **2**) was obtained in a ratio of about 10 : 90 by the Hunsdiecker reaction of silver 2-methylcyclohexanecarboxylate,[3)] attempts to isolate the pure *trans* isomer from this mixture were unsuccessful. Autoxidation of a sample of the mixture took place very slowly, as shown in Table 1. From comparison of the amount of hydroperoxide formed from this mixture with that from the pure *cis* isomer, the approximate reactivity ratio of the C-1 hydrogen in *trans*-2-bromo-1-methylcyclohexane (**2**) to that in trimethylcyclohexane **4** towards abstraction was estimated to be about 0.4. The observed retardation may be ascribed to inductive effect of a bromine substituent and/or a sterically unfavourable transition state with the methyl group and bromine substituent tending to eclipse each other.

Experimental

All melting points and boiling points are uncorrected. Glpc work was carried out with a Perkin-Elmer model 154 D instrument. NMR data were obtained with a Varian A-60 spectrometer using tetramethylsilane as an internal standard. IR spectra were recorded on a Nihon-Bunko DS-402 G spectrometer.

*cis-2-Bromo-1-methylcyclohexane (**1**).* Hydrogen bromide, dried by passing through a trap cooled at −50 °C and a tube packed with anhydrous calcium sulphate, was bubbled through a solution of 80 ml (64.8 g) of 1-methylcyclohexene and 8.2 g of benzoyl peroxide in 600 ml of heptane for 4 hr at 65—75 °C with stirring. After removal of excess of hydrogen bromide with solid sodium hydrogencarbonate, the solution was filtered and the solvent removed from the filtrate under reduced pressure. Distillation of the residual material in vacuum furnished 77 g of a crude addition product, bp 35—38 °C/3 mmHg. To this material was added 500 ml of water and the mixture stirred for 24 hr at room temperature. The organic layer was separated, mixed with 1 l of a 4 : 1 acetone-water mixture, and allowed to stand for 48 hr at room temperature to hydrolyse accompanying 1-bromo-1-methylcyclohexane. Hygrogen bromide liberated amounted to 8.2 mol% based on the starting addition product. After dilution with water, the organic layer was separated and dried over anhydrous magnesium sulphate. A portion (25 g) of this material (66 g) was fractionally distilled through a

spinning band column to yield 19 g of the *cis* bromide (**1**), bp 68 °C/19 mmHg, n_D^{30} 1.4888 (Found: C, 47.53; H, 7.69; Br, 45.17%. Calcd for $C_7H_{13}Br$: C, 47.48; H, 7.40; Br, 45.12%), ν_{max} 656 cm^{-1} (axial C–Br).[8] The NMR spectrum indicated three methyl protons at δ 0.99 (d; J, 5 Hz), a Br–C–H proton at 4.40 (unresolved multiplet), and ring protons at 0.8—2.3 (a complex series of peaks).

A Mixture of cis- *and* trans-*2-Bromo-1-methylcyclohexane.* Methyl *trans*-2-methyl-4-cyclohexene-1-carboxylate[9] (70 g) was hydrogenated with hydrogen at 1 atm on 9 g of 5% palladium-charcoal catalyst in 300 ml of methanol at room temperature. The resulting saturated ester was hydrolysed by boiling with 10% aqueous sodium hydroxide solution, and acidification of the reaction mixture gave 56 g of *trans*-2-methylcyclohexanecarboxylic acid, mp 53—54 °C (lit,[10] mp 51—52 °C). The acid (50 g) was dissolved in a solution of 15.5 g of sodium hydroxide in 160 ml of water. Nitric acid was added dropwise until turbidity appeared; then a solution of 59.7 g of silver nitrate in 96 ml of water was added. The precipitated silver salt was collected on a filter, washed with water and ethanol, air-dried, and then dried over phosphorus pentoxide in a vacuum desiccator. The silver salt (64 g) was treated with bromine (41 g) in carbon tetrachloride (420 ml) according to the directions of Marvel and Sexton.[3] After working up the reaction mixture, fractionation with a spinning band column gave 12.1 g of a middle fraction, bp 62.5 °C/18 mmHg −61.5 °C/15.5 mmHg, ν_{max} 681 cm^{-1} (equatorial C–Br).[8] The NMR spectrum showed an unresolved multiplet at δ 4.40 due to the presence of the *cis* isomer, a sextet (doublets of a triplet; J, 4.5 and 10 Hz) at 3.61 due to the *trans* isomer, a doublet (J, 6 Hz) at 1.11, and a complex series of peaks at 0.8—2.6. The ratio of *cis*-(**1**) to *trans*-2-bromo-1-methylcyclohexane (**2**) was estimated to be 10 : 90 by comparing the areas of the peaks at δ 4.40 and 3.61.

Autoxidation and Reduction of the Oxidates. The experimental procedures for autoxidation have been described previously.[1] After a portion of the oxidate had been titrated iodometrically for hydroperoxide,[11] the rest was dissolved in dry ether and added to a suspension of lithium aluminium hydride (2—3 times the theoretical amount) in dry ether. The mixture was stirred for 30 min at room temperature, and excess of lithium aluminium hydride destroyed with dilute sulphuric acid. The ether layer was separated, washed with water, and dried over anhydrous sodium sulphate. The ether was removed and the residue analysed by glpc.

Product Analysis. The preparations of authentic samples of *c*-2- and *t*-2-bromo-1-methyl-*r*-1-cyclohexanol have been described previously.[2] Qualitative analyses by glpc were carried out using either a diisodecyl phthalate column 0.5 m long at 100 °C, a Carbowax column 1 m long at 111.5 °C, or a cyanosilicone column 1 m long at 112.5 °C. For quantitative analyses a Carbowax column 1 m long was used at 100 °C for 1,3,5-trimethylcyclohexanols and at 112 °C for *t*-2-bromo-1-methyl-*r*-1-cyclohexanol. In gas-liquid partition chromatography of the present bromine containing compounds the use of glass columns was necessary for reliable analyses.

References

1) S. Miyajima and O. Simamura, This Bulletin, **48**, 526 (1975).
2) S. Miyajima, S. Ichihara, and O. Simamura, This Bulletin, **48**, 531 (1975).
3) E. Marvell and H. Sexton, *J. Org. Chem.*, **29**, 2919 (1964).
4) F. R. Jensen and L. H. Gale, *ibid.*, **25**, 2075 (1960).
5) E. L. Eliel, N. L. Allinger, S. J. Angyal, and G. A. Morrison, "Conformational Analysis," Interscience Publishers, New York (1965), p. 44.
6) J. M. Tedder, *Quart. Rev.* (London), **14**, 336 (1960); C. Walling, "Free Radicals in Solution," John Wiley & Sons, New York (1957), p. 347, 417.
7) For the concept of bridged radicals, see P. S. Skell and K. J. Shea, "Free Radicals," Vol. 2, ed. by J. K. Kochi, John Wiley & Sons, New York (1973), p. 809.
8) E. L. Eliel and R. G. Haber, *J. Org. Chem.*, **24**, 143, 2074 (1959).
9) The authors are indebted to Dr. Takashi Inukai, Chisso Corporation, for providing them with this material.
10) A. K. Mcbeth, J. A. Mills, and D. H. Simmonds, *J. Chem. Soc.*, **1949**, 1011.
11) C. D. Wagner, R. H. Smith, and E. D. Peters, *Ind. Eng. Chem., Anal. Ed.*, **19**, 976 (1947).

Structural Studies of Tryptophan Metabolites by X-ray Diffraction Method. III. The Crystal and Molecular Structure of 5-Methoxyindole-3-acetic Acid

Toshimasa SAKAKI, Akio WAKAHARA, Takaji FUJIWARA, and Ken-ichi TOMITA
Faculty of Pharmaceutical Sciences, Osaka University, Toneyama, Toyonaka, Osaka 560
(Received September, 7, 1974)

The crystal structure of 5-methoxyindole-3-acetic acid (5-MIAA) has been solved by application of the direct method with symbolic addition procedure. 5-MIAA, colorless transparent prism, is monoclinic, space group C2/c, with lattice parameters: $a=34.461(9)$ Å, $b=6.150(5)$ Å, $c=9.480(5)$ Å, $\beta=96.14(2)$ °, $Z=8$. The molecules are hydrogen-bonded into dimers related by the center of symmetry, which are held together in an infinite double-layered sheet structure perpendicular to the *a*-axis with N–H···O hydrogen bond between indole nitrogen and carboxyl oxygen atoms. The methyl groups of adjacent molecules contact to each other by van der Waals forces. The conformation of the side-chain is quite distinguishable from that of indole-3-acetic acid. The dihedral angle between carboxyl and indole planes is 59.5 ° in this molecule, whereas that is 90.0 ° in indole-3-acetic acid, and the carboxyl group sticks out to be perpendicular to the indole plane.

5-MIAA, one of the final products in a metabolic pathway of tryptophan, is excreted into urine, through 5-hydroxyindole-3-acetaldehyde, *etc.*[1] As a series of structural investigation of tryptophan metabolites,[2–4] the authors describe here the crystal and molecular structure of 5-MIAA in order to obtain the substantial information about the stereospecific conformation of individual metabolites suitable for performing the related enzyme action in living cells.

Experimental

The sample was purchased from the Sigma Co., and preliminary oscillation and Weissenberg photographs using the suitable crystal showed it to be monoclinic with space group as Cc or C2/c from systematic absent spectra, (hkl) with $h+k=2n+1$ and $(h0l)$ with $l=2n+1$. The space group was determined finally as C2/c from the statistical distribution of normalized structure factors (E).[5] The unit cell dimensions were determined with the Rigaku Denki automatic four circle diffractometer at room temperature. The density was measured by the floatation method in a benzene-carbon tetrachloride mixture. The crystallographic data are shown in Table 1. Intensities of 951 independent reflections having the number of counts over three times of standard deviation were measured with the diffractometer using Ni-filtered Cu–$K\alpha$ radiation, by means of $\omega/2\theta$ scan technique (crystal dimension: $0.10\times0.10\times0.35$ mm), and adjusted to the absolute scale by the program for Wilson's statistics. A $\sum_2$ list was then computed using 270 reflections with the normalized structure factors E, greater than 1.2.

Table 1. Crystal data of 5-MIAA

$C_{11}H_{11}NO_3$, MW. 205.22
Colorless and transparent prisms, Monoclinic
$a=34.461(9)$, $b=6.150(5)$, $c=9.480(5)$ Å
$\beta=96.14(2)°$
$V=1997.3$ Å^3, $Z=8$, $F(000)=864$
μ (for Cu-$K\alpha$) $=9.67$ cm^{-1}
$D_m=1.363$ g/cm^3, $D_x=1.365$ g/cm^3
Absent spectra; (hkl) : $h+k=2n+1$
$(h0l)$: $l=2n+1$
Space group; C2/c

Table 2. Starting set of 5-MIAA chosen for symbolic addition procedure

h	k	l	Phase	$\|E\|$
8	2	3	+	3.118
31	1	−1	+	3.325
3	1	2	a	4.152
6	2	5	b	3.067
22	2	−4	c	3.465

Determination and Refinement of Structure

Phases for the reflections were determined by means of the symbolic addition procedure. To specify the origin for nonprimitive space group C2/c, two reflections with large E-values were chosen to have positive sign.[6] The signs of other reflections having many $\sum_2$ interactions were specified by symbols a, b and c, respectively. This starting set is summarized in Table 2. By hand calculation, the phases of additional 219 reflections were determined in terms of the starting sign and symbols. Of the three-dimensional E maps calculated with possible two combinations (a=b=+, c=− and a=b=−, c=+), the former one revealed reasonable positive peaks which correspond to all non-hydrogen atoms. These positional parameters were refined by successive Fourier syntheses and block-diagonal least-squares method, first with the isotropic thermal parameters for all the non-hydrogen atoms, and then with the anisotropic temperature factors. At this stage, R-value was dropped to 0.120, and the difference Fourier synthesis was computed in order to find the position of eleven hydrogen atoms. (see Fig. 1). The

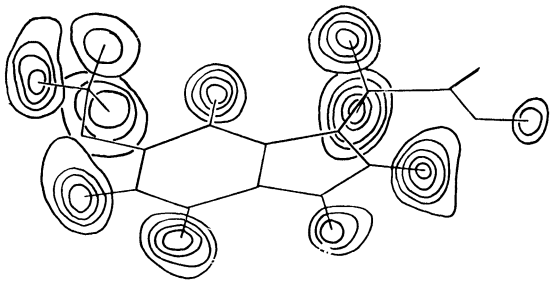

Fig. 1. The location of hydrogen atoms from a three-dimensional difference Fourier map.
Contours from 0.2 e. Å^{-3} at intervals of 0.2 e. Å^{-3}.

TABLE 3. OBSERVED AND CALCULATED STRUCTURE FACTORS FOR 5-MIAA

H	FO	FC	H	FO	FC	H	FO	FC	H	FO	FC	H	FO	FC	H	FO	FC	H	FO	FC	H	FO	FC
K,L= 0	0	0	K,L= 0		-8	19	8	6	3	36	37	22	16	-18	8	8	7	17	16	16	20	19	18	3	24	22
2	28	27	2	19	18	21	6	5	5	8	8	K,L= 2		7	12	6	-6	19	27	26	K,L= 4		4	5	26	26
4	66	-65	6	7	-8	K,L= 1		8	7	6	-3	0	8	-8	K,L= 3		0	21	15	17	0	20	-18	7	15	14
6	78	-77	10	17	18	3	7	5	9	13	14	2	10	-11	1	41	-44	23	6	-7	2	13	-11	9	18	-19
8	59	-56	12	17	19	5	8	-8	11	9	9	4	7	-6	3	22	-23	27	48	-48	4	7	9	11	22	-22
10	32	-28	16	25	-26	11	8	9	13	18	-20	10	15	17	7	34	-38	29	15	-12	6	21	21	13	21	20
12	11	-13	18	52	-53	17	7	-7	15	13	-13	12	12	13	9	12	-13	K,L= 3		-3	8	29	31	17	9	-10
14	45	-42	22	21	22	K,L= 1		9	17	9	-9	16	6	-8	11	5	5	1	30	25	14	28	-26	19	11	-11
16	99	-92	K,L= 0		-10	1	8	-10	21	9	10	K,L= 2		8	13	23	23	3	19	-16	16	12	10	21	5	-6
18	44	-39	2	6	-4	3	5	-6	23	11	-14	4	18	-19	15	39	40	7	15	12	18	7	4	K,L= 5		3
20	58	-52	6	16	19	11	9	-6	K,L= 1		-9	6	6	-5	17	45	48	9	15	16	20	10	-13	1	7	-6
22	76	71	K,L= 1		0	K,L= 1		-1	1	9	-8	10	9	10	19	28	29	11	13	-13	22	9	-10	3	23	-22
24	13	14	1	59	77	3	80	-87	3	13	13	12	8	9	21	22	-21	13	6	6	K,L= 4		5	9	17	-14
26	37	35	3	25	34	5	11	-12	7	14	-14	14	15	14	23	8	7	21	8	6	0	11	8	13	7	-8
28	39	-37	5	92	113	7	31	-33	11	7	8	K,L= 2		9	25	14	-14	25	5	2	2	13	-11	17	8	8
30	8	-7	7	62	-70	9	11	13	17	20	-22	0	12	13	29	6	-6	29	14	-15	4	13	-12	19	8	9
32	48	46	9	20	21	13	22	-25	K,L= 2		0	2	9	7	31	17	-18	31	7	7	6	16	-15	K,L= 5		4
36	13	-13	11	58	-68	15	45	51	0	77	66	K,L= 2		-1	K,L= 3		1	K,L= 3		-4	8	6	-7	3	11	9
K,L= 0		2	13	16	-20	17	38	-40	2	12	-18	4	22	-23	1	57	-55	1	14	12	12	12	-11	5	6	1
0	58	53	15	93	-98	19	25	-24	4	30	-32	6	30	32	3	23	22	3	25	-24	14	2	-10	9	10	11
2	122	-112	17	9	-7	21	8	8	6	41	-46	10	27	30	5	12	12	5	33	30	16	8	-8	11	16	14
4	233	223	19	14	12	23	15	14	8	19	-21	14	29	-29	7	12	11	7	28	-26	20	14	14	13	7	-2
6	157	152	21	14	17	25	19	18	10	13	-12	16	31	-36	9	18	21	9	15	16	K,L= 4		6	15	13	-14
8	53	51	23	23	24	31	45	43	12	41	42	20	15	15	13	8	-8	11	51	49	4	9	-8	K,L= 5		5
10	44	-41	25	6	-6	35	19	-19	14	47	50	22	8	7	15	12	-12	15	26	29	6	11	12	3	6	-4
12	26	-25	29	13	-14	K,L= 1		-2	16	51	-53	24	7	9	17	5	-2	17	9	11	8	6	6	7	16	-17
14	37	-37	31	23	24	1	32	30	18	32	33	30	12	13	19	17	-17	19	16	-17	14	11	11	9	16	-16
18	65	-60	33	19	-17	3	87	-83	20	23	24	32	9	7	21	10	10	21	44	-45	16	9	9	K,L= 5		6
20	11	8	K,L= 1		1	5	32	-31	22	16	13	K,L= 2		-2	25	5	-1	23	24	-26	K,L= 4		7	1	15	-12
22	39	35	1	156	-155	7	58	-58	24	10	11	2	7	-3	27	14	-19	25	15	-15	2	10	9	5	6	-3
24	13	-14	3	66	72	9	31	31	28	21	-22	4	44	-45	29	7	9	27	7	8	4	9	8	K,L= 5		-1
26	16	16	5	143	161	11	57	-59	30	29	-30	6	22	-23	31	7	9	K,L= 3		-5	10	11	-11	3	6	-4
30	13	-7	7	31	-35	13	82	-84	32	8	-5	8	24	24	K,L= 3		2	1	13	13	K,L= 4		-1	7	13	12
32	19	-17	9	31	34	17	11	-11	K,L= 2		1	10	9	9	1	16	14	5	11	13	4	43	42	9	7	-7
34	8	-6	11	52	-58	19	51	49	0	34	30	12	15	-13	3	18	-15	7	16	-17	6	12	-13	13	15	16
K,L= 0		4	13	10	-10	23	36	36	2	69	69	14	88	92	5	12	-12	11	15	17	10	13	-14	15	28	-30
0	30	-30	15	25	-28	25	41	-39	4	64	67	20	13	13	7	42	-43	13	11	-11	12	9	9	17	19	19
2	34	31	17	52	-53	27	15	15	6	42	-47	22	7	-8	11	13	-11	15	17	-15	16	8	8	K,L= 5		-2
4	26	26	19	17	-15	29	8	10	8	21	25	24	16	-17	15	13	-14	17	18	17	18	8	9	1	9	-7
6	45	42	21	7	8	31	18	19	10	20	-22	26	24	-24	17	27	28	19	5	-2	20	7	-5	3	9	-9
8	28	28	23	19	-20	33	7	4	12	18	-17	28	9	-9	19	27	-28	21	23	-24	22	10	-11	7	14	-12
10	33	-28	25	8	5	35	18	-18	14	12	-16	30	13	-12	21	10	7	27	12	15	24	16	-19	9	6	8
12	17	-16	27	11	13	K,L= 1		-3	16	8	-10	32	9	6	23	35	37	K,L= 3		-6	26	16	19	13	16	-18
14	8	-7	29	11	14	1	61	-55	18	15	-16	K,L= 2		-3	27	5	6	3	5	4	K,L= 4		-2	15	15	-13
18	14	9	31	10	9	3	38	32	20	40	-40	2	11	9	29	15	-17	5	16	15	2	24	-23	17	11	12
20	33	35	35	21	20	5	50	46	22	21	-24	4	23	20	K,L= 3		3	9	44	-44	6	16	-17	19	34	32
22	12	-16	K,L= 1		2	7	38	34	24	6	-6	6	12	13	1	9	-11	11	38	39	10	6	1	21	6	-8
24	22	-22	3	282	299	9	63	60	26	22	21	8	25	27	3	37	37	13	8	5	12	14	13	K,L= 5		-3
26	22	21	5	60	64	11	24	25	28	19	21	12	42	41	5	11	9	15	10	11	14	39	41	1	19	17
28	13	13	7	94	-100	13	32	-36	30	17	17	14	15	16	7	16	15	17	10	-10	16	10	8	5	14	-12
30	13	11	9	21	-23	15	10	12	32	14	-15	16	13	14	9	35	-34	19	24	-24	20	6	6	7	22	-22
K,L= 0		6	11	24	-26	17	38	37	K,L= 2		2	18	18	-17	11	7	5	K,L= 3		-7	22	18	-19	11	12	-11
0	10	-9	15	13	12	19	7	-9	0	57	50	20	9	-11	13	18	19	5	12	12	24	6	-4	13	22	21
2	25	-25	17	26	29	23	41	-43	2	20	-21	22	6	-6	17	11	-13	7	8	8	26	10	-11	15	10	-9
4	11	-10	19	37	-43	25	13	15	4	17	-13	24	23	-24	19	12	15	9	24	-25	28	8	-10	17	9	-7
6	22	22	21	13	-16	27	15	16	6	51	-55	26	12	12	23	16	-17	11	8	8	K,L= 4		-3	19	11	10
8	17	-14	25	26	26	29	28	-29	8	36	37	28	20	21	29	9	10	13	15	14	6	18	-16	21	8	-11
10	23	-20	27	19	20	33	16	13	10	21	-20	32	7	-9	K,L= 3		4	15	14	-15	8	6	4	K,L= 5		-4
12	30	26	31	18	-17	35	7	-6	12	15	-14	K,L= 2		-4	1	23	-21	17	14	-13	12	30	-30	3	8	-5
14	13	-11	33	30	-29	K,L= 1		-4	14	12	-11	2	11	9	3	17	17	19	22	23	14	15	17	5	13	-11
16	13	-12	K,L= 1		3	1	21	-20	16	12	-12	4	8	6	5	19	18	K,L= 3		-8	16	19	-19	7	14	-15
18	15	-12	1	54	48	3	15	-13	18	21	20	6	63	60	7	14	12	1	17	-17	18	14	-14	9	6	-8
24	15	14	3	141	137	5	27	-28	22	24	26	10	10	11	9	30	-27	3	20	-20	20	14	13	13	17	17
26	11	11	5	20	-23	7	21	-22	24	6	5	12	40	-40	11	7	5	5	9	-10	22	28	29	15	7	11
K,L= 0		8	7	22	19	9	33	-35	26	8	7	14	16	18	17	8	8	7	23	25	24	10	-11	17	17	-15
0	21	20	9	39	42	11	30	27	28	10	-11	16	29	29	19	35	-36	9	6	2	K,L= 4		-4	19	5	6
2	25	24	11	25	26	13	28	-30	32	5	1	18	24	26	21	11	10	11	9	9	2	25	-25	K,L= 5		-5
4	14	-13	15	16	-17	15	30	34	K,L= 2		3	20	6	-3	23	7	-10	15	7	-7	4	9	-7	1	18	-16
6	11	-10	17	24	-25	17	10	11	0	16	12	22	62	-64	K,L= 3		5	17	20	20	6	38	31	3	6	-5
8	23	-24	21	22	-23	19	11	13	2	90	82	24	16	-18	1	11	10	K,L= 4		0	8	11	10	7	8	-7
10	16	16	23	33	-31	21	22	-20	4	50	-49	28	16	18	7	16	-14	0	20	-18	10	6	-2	9	14	-13
12	10	11	27	6	-8	23	40	43	6	44	46	32	6	-2	11	33	31	4	17	-18	12	29	-30	11	10	-10
14	20	-19	29	7	6	25	12	13	8	116	115	K,L= 2		-5	13	10	-11	6	27	-28	14	23	26	13	6	-5
18	5	-4	31	12	10	27	35	-33	10	5	5	2	17	18	15	22	-20	8	7	5	16	21	21	15	8	6
K,L= 0		-2	33	14	14	29	19	20	12	14	15	4	23	23	17	10	11	10	8	11	22	21	-20	K,L= 5		-6
2	123	113	K,L= 1		4	31	8	-7	14	24	-23	6	57	57	19	12	13	12	9	10	24	20	-21	1	14	-12
4	93	-85	1	9	-8	33	7	5	16	24	-24	8	27	28	21	15	-17	14	22	20	26	6	-6	3	5	1
6	80	73	3	57	54	K,L= 1		-5	18	25	-28	10	12	13	23	6	7	16	24	-26	K,L= 4		-5	K,L= 6		0
8	165	156	5	70	-71	1	31	30	20	9	-11	12	6	8	K,L= 3		6	18	8	7	2	14	-14	0	37	32
10	38	-33	7	32	33	3	7	7	22	13	-13	16	23	-24	1	23	-22	20	16	18	4	8	-9	2	14	14
12	185	-172	9	64	66	5	54	56	24	14	14	18	7	-10	3	18	-18	22	17	19	6	22	-19	4	11	8
14	56	-50	11	8	-7	7	10	-10	26	16	-16	20	35	-38	5	6	-7	24	9	11	8	13	-12	6	17	-16
16	25	-23	13	18	-17	9	27	29	28	7	-9	22	23	26	7	12	13	26	19	-19	10	14	14	8	14	-14
18	69	67	15	25	-25	11	51	51	K,L= 2		4	24	13	-12	9	33	34	28	11	-9	12	31	-31	10	7	6
20	24	22	17	6	-7	13	23	25	0	63	-55	26	37	-40	11	49	50	K,L= 4		1	16	26	23	14	10	-9
22	12	14	21	6	6	15	21	-22	2	32	-28	30	8	9	13	21	-22	2	15	15	24	8	10	K,L= 6		1
24	12	-10	23	5	6	17	29	-30	4	36	33	K,L= 2		-6	15	10	-11	4	18	-20	K,L= 4		-6	0	19	-14
26	42	40	25	22	23	19	34	-35	6	51	53	2	7	8	17	9	-8	6	34	-35	4	31	-29	6	6	5
28	74	69	K,L= 1		5	23	8	-8	8	38	38	4	31	-31	21	9	10	8	19	18	6	9	-8	8	8	-5
30	67	-61	1	25	-22	25	24	-27	10	73	-75	6	8	10	K,L= 3		7	10	24	24	10	23	23	10	12	-10
32	27	25	5	46	44	27	12	13	18	8	-7	12	30	32	1	13	10	14	7	-6	12	9	10	12	9	8
34	15	11	7	37	39	29	7	-5	22	9	-10	14	14	15	7	5	-5	16	30	31	16	14	13	K,L= 6		2
K,L= 0		-4	9	13	17	31	6	5	24	10	-12	16	21	-21	9	7	5	18	17	-17	18	16	-16	0	9	6
2	28	-23	11	25	24	K,L= 1		-6	26	17	18	18	41	-42	11	7	-8	20	9	8	20	7	-8	2	7	8
4	71	-71	13	8	8	1	10	9	28	10	12	20	20	22	13	9	-9	22	15	13	K,L= 4		-7	4	19	16
6	51	44	15	11	11	3	36	35	K,L= 2		5	22	11	-12	15	7	6	28	8	-10	4	8	-7	6	14	12
8	123	-113	17	7	-6	5	26	-26	0	9	-9	K,L= 2		-7	K,L= 3		8	K,L= 4		2	6	8	-8	K,L= 6		3
10	74	-68	19	7	-8	11	12	14	2	16	16	2	34	35	7	7	-9	2	8	11	8	14	-14	0	8	7
12	37	35	21	16	-17	13	15	15	4	9	-9	4	30	-29	9	6	5	6	15	-12	12	5	6	2	13	10
14	6	2	29	6	-3	15	22	24	6	79	82	6	18	20	11	6	0	10	21	-21	14	9	8	4	13	-11
16	27	28	K,L= 1		6	19	14	-12	8	5	-3	8	27	27	K,L= 3		-1	12	11	11	K,L= 5		0	6	10	-10
18	17	15	1	21	-20	21	33	-35	10	15	-15	10	7	-7	1	23	-24	16	17	-20	1	26	28	K,L= 6		-1
20	30	32	3	10	-10	23	12	-13	12	16	-16	12	14	-14	3	11	-12	18	22	20	5	19	-19	4	9	-8
24	19	19	5	23	-23	25	47	51	14	18	20	16	14	-16	5	31	33	22	5	0	9	17	16	6	10	-8
26	22	-21	7	29	32	K,L= 1		-7	16	10	11	20	30	-32	9	18	-16	24	11	-9	11	23	-22	8	14	11
28	73	69	13	12	-12	1	11	12	18	6	3	22	25	-26	13	11	11	26	11	10	13	12	-13	10	15	-14
32	22	-22	15	9	-10	3	11	11	20	23	-22	24	23	26	15	16	-19	K,L= 4		3	21	6	-2	K,L= 6		-2
34	8	-8	17	6	5	5	26	28	26	21	-23	K,L= 2		-8	21	16	-15	0	19	-15	23	15	16	2	9	-6
K,L= 0		-6	23	8	8	7	31	32	K,L= 2		6	4	14	-15	25	15	18	2	9	-6	K,L= 5		1	6	14	12
4	26	-28	K,L= 1		7	11	13	-13	0	13	-12	6	7	-9	31	15	17	4	24	-25	1	11	-9	8	21	-19
6	44	42	1	5	0	13	27	-29	2	16	16	8	27	29	K,L= 3		-2	6	5	1	5	16	-18	10	10	-10
8	46	46	3	7	-2	15	7	-8	4	9	-10	18	20	-22	1	36	-32	8	9	-10	9	23	-22	12	8	-10
10	28	-30	5	6	2	17	10	-11	10	16	15	22	7	9	3	65	-65	10	17	-18	11	24	24	K,L= 6		-3
12	6	6	7	20	-20	21	20	-22	12	28	29	K,L= 2		-9	7	9	11	12	16	-15	17	20	20	6	7	-6
20	18	19	9	21	21	23	9	-10	14	11	-12	2	24	27	0	82	83	14	28	30	19	5	3	8	11	10
22	9	-8	11	11	12	K,L= 1		-8	16	14	-13	4	11	10	11	42	43	16	12	14	21	6	4			
28	8	-10	17	7	6	1	18	-19	20	7	7	6	20	-22	15	7	8	18	11	-11	K,L= 5		2			

final refinement by block-diagonal least-squares method was carried out with anisotropic temperature factors for all non-hydrogen atoms and with isotropic temperature factors for all hydrogen atoms to reduce R-value to 0.078. The electron density map is illustrated in Fig. 2. The observed and calculated structure factors obtained by the last cycle of refinement are given in Table 3, and the atomic coordinates and thermal parameters with their estimated standard deviations in Table 4. In the structure factor calculation of 5-MIAA, the atomic scattering factors cited in "*International Tables for X-ray Crystallography*" (1962)[7] were used, and all the numerical calculations were carried out on an NEAC-2200-700 computer of computation center of this University, using the UNICS programs.

TABLE 4. THE FINAL ATOMIC COORDINATES AND THERMAL PARAMETERS WITH THEIR ESTIMATED STANDARD DEVIATIONS IN PARENTHESES
($\times 10^4$ for non-hydrogen atoms, $\times 10^3$ for hydrogen atoms)

Atom	X	Y	Z	B_{11}	B_{22}	B_{33}	B_{12}	B_{13}	B_{23}
C (1)	0.4508 (2)	0.5029 (12)	0.0775 (7)	0.0009 (1)	0.0242 (23)	0.0098 (9)	0.0015 (7)	0.0010 (4)	0.0004 (24)
C (2)	0.4109 (2)	0.4994 (13)	0.1347 (8)	0.0006 (1)	0.0306 (26)	0.0131 (10)	−0.0003 (7)	0.0023 (4)	−0.0051 (27)
C (3)	0.4063 (2)	0.6864 (12)	0.2365 (7)	0.0006 (1)	0.0267 (23)	0.0095 (8)	−0.0007 (6)	0.0010 (4)	−0.0006 (25)
C (4)	0.3720 (2)	0.7048 (12)	0.3115 (6)	0.0006 (1)	0.0276 (24)	0.0080 (8)	0.0000 (6)	0.0009 (4)	−0.0013 (24)
C (5)	0.3386 (2)	0.5771 (12)	0.3149 (7)	0.0007 (1)	0.0288 (25)	0.0103 (9)	0.0003 (7)	0.0012 (4)	−0.0047 (25)
C (6)	0.3112 (2)	0.6368 (12)	0.4051 (7)	0.0006 (1)	0.0307 (25)	0.0108 (9)	−0.0008 (7)	0.0015 (4)	−0.0011 (26)
C (7)	0.3170 (2)	0.8290 (13)	0.4873 (7)	0.0007 (1)	0.0358 (28)	0.0114 (10)	0.0003 (8)	0.0022 (4)	−0.0055 (27)
C (8)	0.3493 (2)	0.9536 (13)	0.4864 (7)	0.0009 (1)	0.0325 (28)	0.0112 (10)	0.0003 (8)	0.0017 (5)	−0.0046 (27)
C (9)	0.3770 (2)	0.8946 (12)	0.3940 (7)	0.0006 (1)	0.0294 (25)	0.0101 (9)	−0.0003 (7)	0.0008 (4)	−0.0001 (25)
C (10)	0.4292 (2)	0.8582 (13)	0.2750 (7)	0.0008 (1)	0.0323 (27)	0.0113 (10)	−0.0003 (8)	0.0012 (4)	−0.0003 (28)
C (11)	0.2682 (2)	0.3487 (14)	0.3301 (8)	0.0008 (1)	0.0372 (31)	0.0171 (13)	−0.0024 (8)	0.0030 (5)	−0.0061 (33)
N	0.4125 (2)	0.9845 (11)	0.3714 (6)	0.0009 (1)	0.0324 (22)	0.0127 (9)	−0.0021 (6)	0.0014 (4)	−0.0086 (23)
O (1)	0.4713 (1)	0.3326 (9)	0.1087 (5)	0.0009 (1)	0.0413 (21)	0.0153 (8)	0.0036 (6)	0.0036 (3)	0.0167 (21)
O (2)	0.4611 (1)	0.6541 (9)	0.0072 (5)	0.0009 (1)	0.0336 (19)	0.0175 (8)	0.0026 (5)	0.0039 (3)	0.0131 (21)
O (3)	0.2770 (1)	0.5327 (9)	0.4182 (5)	0.0008 (1)	0.0418 (21)	0.0143 (7)	−0.0031 (5)	0.0033 (3)	−0.0103 (21)
				B					
H (1)	0.496 (2)	0.332 (15)	0.074 (8)	6.19					
H (2)	0.409 (2)	0.344 (11)	0.188 (6)	2.01					
H (3)	0.387 (2)	0.506 (13)	0.045 (7)	3.06					
H (4)	0.459 (2)	0.897 (12)	0.246 (7)	3.02					
H (5)	0.424 (2)	1.116 (12)	0.416 (7)	3.65					
H (6)	0.335 (2)	0.428 (11)	0.260 (6)	1.75					
H (7)	0.293 (2)	0.886 (12)	0.535 (7)	2.73					
H (8)	0.353 (2)	1.098 (11)	0.545 (7)	2.59					
H (9)	0.285 (2)	0.181 (14)	0.353 (8)	4.33					
H (10)	0.265 (2)	0.381 (13)	0.232 (8)	4.21					
H (11)	0.241 (2)	0.331 (12)	0.342 (7)	3.11					

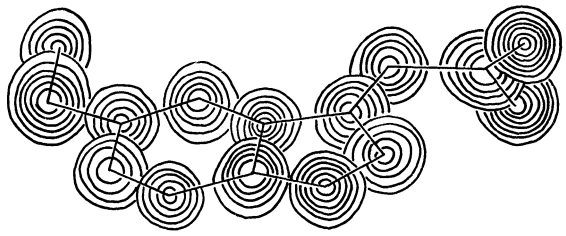

Fig. 2. Electron-density map for 5-MIAA viewed along *b*-axis.
Contours are drawn at intervals of 0.2 e. Å^{-3}.

Description and Discussion of the Structure

The final bond lengths and angles are shown in Fig. 3, where the average standard deviations for non-hydrogen atoms are about 0.009 to 0.011 Å and 0.6 to 0.7°, respectively. The deviation from a regular trigonal angle of C(2)–C(3)–C(10) is about 11°, which is also observed in serotonin creatinine sulfate (about 6°)[5] and melatonin (about 5°).[2] This may be explained by the fact that the *cis*-orientation of C(3)–C(10) bond with respect to C(1)–C(2) bond around C(2)–C(3) bond causes bond angle C(2)–C(3)–C(10) to be larger by the repulsion between C(10) and C(1). The angle of O(3)–C(6)–C(5) is also about 11° larger than that of O(3)–C(6)–C(7), as well as melatonin (9°)[2] or 5-methoxy-*N*,*N*-dimethyltryptamine HCl (10°).[8] This may be also explainable by similar reason described above, provided the special orientation of methoxy group around C(5)–C(6) bond is effective. The planarity of the two parts of the molecule, indole ring and carboxyl group, was examined by the equation of the least-squares plane.

Equation for indole ring;

$$0.39119X - 0.54044Y + 0.74491Z = 4.74731.$$

Equation for carboxyl group and α-carbon atom;

$$0.31420X + 0.44497Y + 0.83862Z = 6.83928.$$

The deviations of the individual atoms from the best planes are given in Table 5. The H(1) atom lies almost on the plane through four atoms, C(1), O(1), O(2) and α-carbon C(2), whereas C(2) and O(3) are on the plane through indole ring, except C(11) atom which is slightly deviated. It is of interest to compare the molecular conformation of this compound with that of indole-3-acetic acid (IAA).[9] Relevant torsion angles[10] of IAA and 5-MIAA are given in Table 6 in order to elucidate the difference of conformation. The torsion angle C(10)–C(3)–C(2)–C(1) is in the region of anti-clinal in IAA, but syn-periplanar in 5-MIAA. (see Figure 4). The dihedral angle between the two

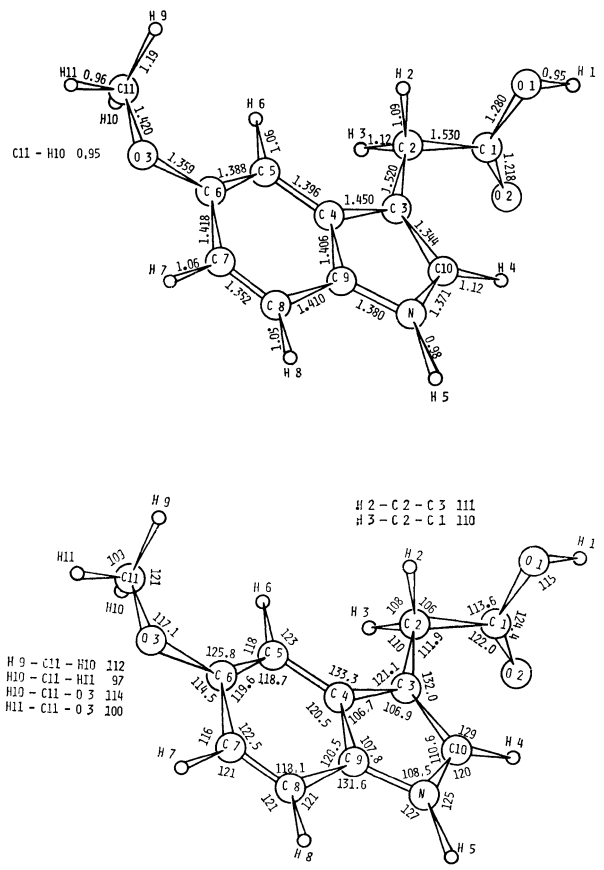

Fig. 3. The final bond lengths and angles of 5-MIAA.

Table 5. Deviations of atoms from the least-squares planes through the indole ring and carboxyl group (in Å)

Indole group		Acid group	
Atom	Distance	Atom	Distance
C (3)	−0.0157	O (1)	0.0019
C (4)	0.0117	O (2)	0.0021
C (5)	0.0146	C (1)	−0.0056
C (6)	−0.0159	C (2)	0.0016
C (7)	0.0011		
C (8)	−0.0143	*C (3)	−1.2325
C (9)	0.0278	*C (4)	−1.4799
N	−0.0017	*C (10)	−2.2417
C (10)	−0.0072	*H (1)	0.0025
*C (1)	−0.1715		
*C (2)	−0.0247		
*C (11)	0.1036		
*O (1)	−1.2203		
*O (2)	0.6575		
*O (3)	0.0126		

Atoms with asterisk were excluded from the least-squares calculations. The mean deviation from the indole ring is 0.0122 Å and from the acid group is 0.0028 Å.

Table 6. Comparison of torsion angles between 5-MIAA and IAA

Bond sequence	IAA	5-MIAA
C (10)-C (3)-C (2)-C (1)	97.7°	6.0°
C (3)-C (2)-C (1)-O (1)	173.6	119.2
C (3)-C (2)-C (1)-O (2)	−11.7	−61.9
C (2)-C (1)-O (1)-H (1)	−175.2	−179.7
O (2)-C (1)-O (1)-H (1)	−0.5	−0.8
C (5)-C (6)-O (3)-C (11)		−1.1

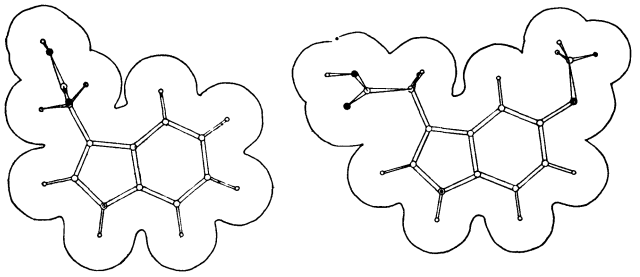

Indole-3-acetic acid 5-Methoxyindole-3-acetic acid

Fig. 4. Comparison of conformation between 5-MIAA and IAA projected to indole ring plane.

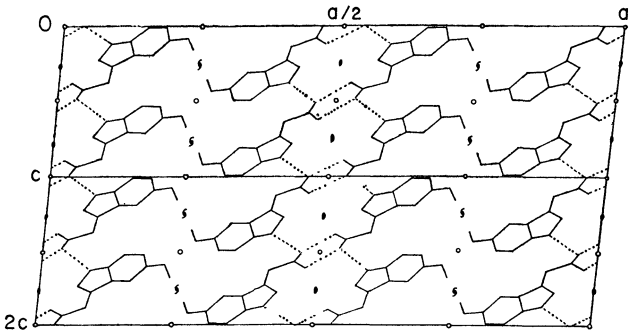

Fig. 5. The crystal structure of 5-MIAA viewed down along *b*-axis.

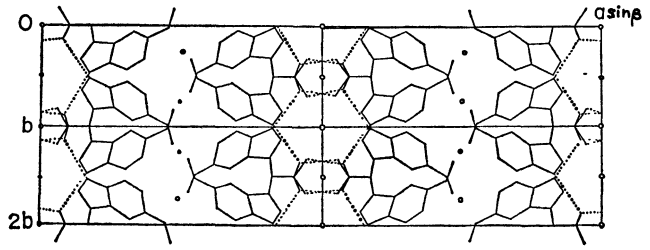

Fig. 6. The crystal structure of 5-MIAA viewed down along *c*-axis.

planes, one through carboxyl group and the other through indole ring, is 59.5° in 5-MIAA, while that is 90.0° in IAA. These facts may reflect that IAA and 5-MIAA are the final products of tryptophan metabolites in different metabolic pathways.[1,11] The molecular arrangements in crystals viewed along b- and c-axes are shown in Figs. 5 and 6. Between the two adjacent molecules related by the center of symmetry, a dimer was formed at carboxyl end with O–H···O hydrogen bond. This dimer was also connected by hydrogen bond N–H(5)··· O(2) around diad axis to make the infinite sheet elongated toward b- and c-axes. The methyl groups have very short contact to each other around the screw diad axis. (3.596 Å) In crystals, the polar part of the molecules is held together by hydrogen bond and the nonpolar part, by van der Waals forces. Therefore, it seems that the molecules are arranged into a double layered sheet structure perpendicular to a-axis with N–H···O hydrogen bonds between indole nitrogen and carboxyl oxygen atoms.

References

1) "Metabolic Maps," Third Edition, ed. by M. Ishimoto, S. Minakami, S. Mizushima, T. Oshima, and H. Wada, Kyoritsu Publishing Company, Ltd., Tokyo (1971), p. 46.
2) A. Wakahara, T. Fujiwara, and K. Tomita, *Chem. Lett.*, **1972**, 1139.
3) A. Wakahara, M. Kido, T. Fujiwara, and K. Tomita, This Bulletin, **46**, 2475 (1973).
4) A. Wakahara, T. Fujiwara, and K. Tomita, This Bulletin, **46**, 2481 (1973).
5) I. L. Jarle, K. S. Dragonette, and S. A. Brenner, *Acta Crystallogr.*, **19**, 713 (1965).
6) H. Hauptman and J. Karle, *ibid.*, **12**, 93 (1959).
7) "International Tables for X-ray Crystallography," Vol. III, p. 202.
8) G. Falkenberg and D. Carlström, *Acta Crystallogr.*, **B27**, 411 (1971).
9) I. L. Karle, K. Britts, and P. Gum, *ibid.*, **17**, 496 (1964).
10) W. Klyne and V. Prelog, *Experientia*, **16**, 521 (1960).
11) A. Wakahara, Dissertation, Faculty of Pharm. Sci., Osaka University (1974).

Micellar and Metal Ion Catalysis in the Pyridoxal-Promoted α,β-Elimination of *S*-Phenylcysteine*

Yukito MURAKAMI and Hiroki KONDO

Department of Organic Synthesis, Faculty of Engineering, Kyushu University, Hakozaki, Higashi-ku, Fukuoka 812

(Received September 26, 1974)

The effects of metal ions and detergents on the pyridoxal-catalyzed α,β-elimination reaction of *S*-phenylcysteine have been investigated in 0.01 M borate buffer at 50 °C (the copper ion catalysis at 40 °C in the presence of CTAB micelles). Both copper(II) and nickel(II) ions markedly accelerated the elimination reaction of *S*-phenylcysteine. Since the catalytic efficiency of nickel(II) seems to be obtained due to the poor coordination ability of the leaving group in the present reaction, the previous working hypothesis which was provided for the elucidation of catalytic roles of metal ions in the α,β-elimination of *O*-phosphothreonine has now been approved. Among cationic, anionic, and non-ionic detergents employed in this work as apoenzyme models, only CTAB of cationic nature showed a considerable rate acceleration even in the absence of metal ions. The micellar binding constant was evaluated from the saturation-type correlation between reaction rate and CTAB concentration. The surfactant micelles demonstrated some enzyme-like features of catalysis in the pyridoxal-promoted α,β-elimination reaction, where the reaction is controlled by the entropy term. The CTAB catalysis was greatly inhibited by organic and inorganic anions due to the electrostatic nature of the micellar surface. The catalytic mechanisms for the micellar reactions and their significance as an enzyme model system are discussed.

Although the apoenzyme moieties of pyridoxal-dependent enzymes have not been fully characterized up to the present time, their specific roles may be counted tentatively as follows: (1) they provide the hydrophobic binding site inside the enzymes where pyridoxal phosphate is buried in its vicinity as the coenzyme function, and then (2) catalyze the specified reactions by their various functional groups such as the imidazole group of histidine residue and the ε-amino group of lysine. In our previous work, the catalytic effect of some organic bases of different base-strength was examined in the pyridoxal-catalyzed α,β-elimination reaction of *S*-(*p*-substituted phenyl)cysteines in connection with the catalytic nature of base moieties which are planted in an apoenzyme skeleton.[1] Our special concern has also been placed on the correlation between hydrophobic medium effect and reaction kinetics in these reactions by adopting acetonitrile-water mixed solvent system.[1]

In spite of the substrate and reaction specificity as well as the acceleration effect due to the vitamin B_6 apoenzymes, only a limited information has been obtained on their catalytic and structural nature. Micellar surfactants have often been granted to behave as an enzyme or apoenzyme model as reviewed by several workers.[2,3] In the present study, we have investigated the effects of these detergents as an apoenzyme model for the pyridoxal-catalyzed α,β-elimination reaction of *S*-phenylcysteine. As for the catalytic roles of metal ions in the elimination, *S*-phenylcysteine would render the metal ion effects different from those for *O*-phosphothreonine.[4] A metal ion of strong hexa-coordination tendency has been suggested to bind the leaving phosphate group in the Schiff base derived from pyridoxal and the latter amino acid, thus inactivating the amino acid toward elimination reaction. On the contrary, such a metal ion would not demonstrate any significant coordination ability toward thioether-sulfur in the present amino acid. We have studied from these viewpoints the effects of copper(II) and nickel(II) ions on the pyridoxal-catalyzed α,β-elimination of *S*-phenylcysteine.

* Contribution No. 348 from the Department of Organic Synthesis, Faculty of Engineering, Kyushu University.

Experimental

Materials. *S*-Phenylcysteine was prepared by the reaction of thiophenol with α-acetoamidoacrylic acid and the subsequent acid hydrolysis.[5] Pyridoxal hydrochloride was obtained from Mann Research Laboratories, Inc., New York, U.S.A. Cetyltrimethylammonium bromide (CTAB, Katayama Chemical Co.), sodium lauryl sulfate (NaLS, Eastman Kodak Co.), and polyoxyethylene(23) dodecanol (Brij 35, Nakarai Chemical Co.) were obtained from commercial sources.

Kinetic Measurements. For the micellar catalysis, the reaction was carried out in 0.01 M borate buffer (pH 9.0) at 50.0±0.1 °C without inorganic salt as being a supporting electrolyte. Fifty ml of a reaction mixture containing specified amounts of substrate, detergent, and borate buffer was placed in a jacketed reaction vessel. When the constant temperature was attained, 5 ml of the pyridoxal solution was added. The initial concentrations of *S*-phenylcysteine and pyridoxal were 7.31×10^{-4} and 9.09×10^{-4} M, respectively and the detergent concentration was varied. Aliquot samples were withdrawn from the reaction mixture at appropriate time intervals after the thermal equilibrium was attained (5 min after the pyridoxal solution was added). The reaction rate was determined by measuring the yielded pyruvate as its 2,4-dinitrophenylhydrazone. The analytical procedures were essentially the same as those described previously,[1] but with slight modifications. In the presence of detergents the 2,4-dinitrophenylhydrazone of pyridoxal did not precipitate and the extraction of an excess hydrazine from the resulting filtrate with toluene was not possible due to foam formation. In order to overcome these difficulties 5 ml of acetonitrile was added to the sample solution before treating it with the potassium phosphate—sodium hydroxide buffer to allow the precipitation of pyridoxal hydrazone. Secondly, the extraction of an excess hydrazine with toluene was omitted since this modification did not cause any serious analytical error.

For the metal ion catalysis, the reaction was carried out in borate buffer at either 40 or 50 °C with or without 0.91×10^{-4} M CTAB. The reaction was started by the addition of 5 ml of cupric nitrate or nickel nitrate solution prewarmed to the reaction temperature to 50 ml of a metal-free reaction mixture. The initial concentrations of substrate, pyridoxal, and borate buffer were the same as those for the micellar catalysis, and the initial metal ion concentration was adjusted at either 1.81×10^{-4} or 4.54×10^{-4} M. The reaction rate was measured by the above-mentioned procedures.

Results

Effects of Micellar Surfactants. The kinetic runs for the pyridoxal-catalyzed α,β-elimination reaction were carried out at 50 °C in 0.01 M borate buffer in the presence of three kinds of detergents, cetyltrimethylammonium bromide (CTAB), sodium lauryl sulfate (NaLS), and polyoxyethylene(23) dodecanol (Brij 35). Each reaction rate followed apparent first-order kinetics with respect to the total concentration of unreacted substrate. While the anionic and non-ionic micelles showed little catalytic effect or rather retarding, the cationic micelle promoted the elimination rate (Table 1). The correlation between the apparent first-order rate constant and the CTAB concentration is illustrated in Fig. 1. The rate is markedly accelerated above 1×10^{-3} M CTAB, and tends to level off beyond approximately 3×10^{-3} M of the detergent concentration. The rate acceleration at this saturation level is about 18-fold of the rate without the cationic detergent. On the other hand, CTAB did not show any significant catalytic effect in the absence of pyridoxal under the similar conditions.

The micellar catalysis by CTAB was effectively inhibited by inorganic and organic salts as shown in Table 2. Potassium nitrate is the more effective inhibitor than potassium chloride in a manner as observed for the solvolysis reactions of carboxylic esters,[6] while both of the organic salts, sodium benzoate and sodium benzenesulfonate, demonstrated the larger inhibition effect than the inorganic salts.

Activation parameters for the micellar reaction are listed in Table 3 together with those for the reaction without detergent. The micellar reaction becomes enthalpically unfavorable, and the catalysis is apparently controlled by the entropy term.

Table 1. The effects of anionic and non-ionic surfactants on the pyridoxal-catalyzed α,β-elimination reaction of *S*-phenylcysteine in 0.01 M borate buffer (pH 9.0) at 50 °C[a]

Surfactant	concentration M	$k_{obs}\times10^5$ s^{-1}	Relative rate
—	—	1.38[b]	1[b]
NaLS	2.90×10^{-3}	1.69	1.23
Brij 35	3.10×10^{-4}	0.84	0.61

a) Initial concentrations: substrate, 7.31×10^{-4} M; pyridoxal, 9.09×10^{-4} M. b) Micellar surfactant absent.

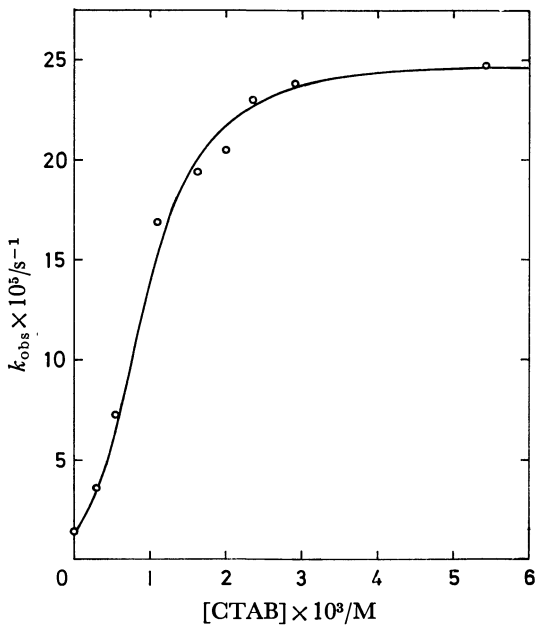

Fig. 1. Correlation between rate and CTAB concentration in the pyridoxal-catalyzed α,β-elimination reaction of *S*-phenylcysteine at 50 °C in 0.01 M aqueous borate buffer with the following initial concentrations: substrate, 7.31×10^{-4} M; pyridoxal, 9.09×10^{-4} M.

Table 2. Inhibition of CTAB catalysis in the pyridoxal-promoted α,β-elimination reaction of *S*-phenylcysteine in 0.01 M borate buffer at 50 °C[a]

Salt	Concentration M	$k_{obs}\times10^5$ s^{-1}	Relative rate
—	—	1.38[b]	1[b]
—	—	23.8	17.1
KNO_3	0.05	4.22	3.04
KNO_3	0.10	2.68	1.93
KCl	0.10	5.71	4.13
Na Benzoate	0.040	2.27	1.64
Na Benzenesulfonate	0.040	2.67	1.92

a) Initial concentrations: substrate, 7.31×10^{-4} M; pyridoxal, 9.09×10^{-4} M, CTAB, 2.91×10^{-3} M. b) Both CTAB and salt absent.

Table 3. Activation parameters for the pyridoxal-catalyzed α,β-elimination reaction of *S*-phenylcysteine in the presence and absence of CTAB at 50 °C[a]

[CTAB] M	$\Delta H^{\neq}$ kcal mol^{-1}	$\Delta S^{\neq}$ e. u.	$\Delta G^{\neq}$ kcal mol^{-1}
2.91×10^{-3}	16.4	−25	24.5
0	12.5	−41	25.7

a) Initial concentrations: substrate, 7.31×10^{-4} M; pyridoxal, 9.09×10^{-4} M.

Effects of Metal Ions. When the copper(II) and nickel(II) solutions were added to the reaction mixture containing substrate, pyridoxal, and borate buffer, precipitates were formed. The reduction of metal ion concentration and/or the increase in the acidity of the medium did not improve the situation. Thus, the reaction was carried out in a heterogeneous system.

The reaction followed a fairly good apparent first-order kinetics up to 70% conversion of the substrate in the presence of nickel(II); the initial concentration of the metal ion is 4.54×10^{-4} M. The rate constant of 2.84×10^{-4} s^{-1} corresponds to the 20.6-fold acceleration relative to the non-metallic system. On the other hand, any detectable amount of pyruvate was not liberated in about 30 min of the reaction time upon addition of copper(II); the initial concentration of the metal ion is 4.54×10^{-4} M. This apparently means that copper(II) inhibited the α,β-elimination of S-phenylcysteine completely through the complex formation. The precipitates were recovered for IR measurements (Fig. 2). The precipitates formed in the reaction of these metal ions with the substrate in the absence of pyridoxal were also subjected to IR measurements (Fig. 2). A broad band at 2800 cm^{-1} due to the ammonium group of S-phenylcysteine disappeared in the spectra of these metal complexes. The 1640 cm^{-1} band attributable to the carbonyl stretching mode shifted to the lower frequency region upon coordination. From these evidences the precipitates formed during the reaction can be identified as bis(S-phenylcysteinato)copper(II) and bis(S-phenylcysteinato)nickel(II).

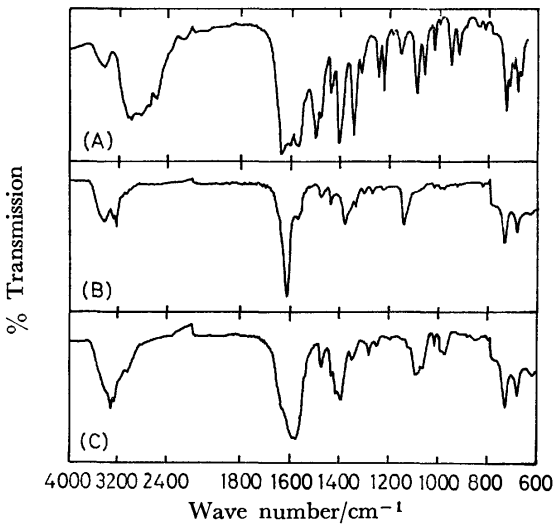

Fig. 2. Infrared spectra (KBr disc method): (A), S-phenylcysteine; (B), the copper(II) complex of S-phenylcysteine; (C), the nickel(II) complex of S-phenylcysteine. S-phenylcysteine underwent reaction with the metal ions in the absence of pyridoxal at the same respective concentrations as employed for the kinetic runs. The precipitates obtained by raising pH up to 9.0 with sodium hydroxide were used for IR measurements. The respective precipitates recovered from the reaction mixtures for kinetic runs gave the completely identical spectra.

The addition of CTAB prevented the precipitation of the metal complexes and consequently the reaction was carried out in a homogeneous system. But the situation is rather complicated in this system (0.91×10^{-3} M CTAB present) as follows. At the outset of the reaction the "burst" of pyruvate formation was detected, followed by the rate deceleration. The overall reaction, therefore, did not follow the first-order kinetics. The rate constants estimated from the initial "burst" part (~2 min period after the addition of metal ions), where the true thermal equilibrium was not still attained, are listed in Table 4. This table also gives the rate data for the reaction period following the "burst" part (a 2—10 min period after the metal addition). The reaction rate was so fast at 50 °C in the presence of copper(II) that the reaction temperature needs to be lowered to 40 °C and the metal concentration to two-fifths of the nickel(II) ion. The rate constants obtained for the "burst" part are greater by one order than those for the following period. Approximately a 60% portion of the substrate has been converted to the products in the "burst" part under these experimental conditions.

Discussion

Metal Ion Catalysis. In our previous investigations on the pyridoxal-catalyzed α,β-elimination of O-phosphothreonine,[4] the examined six metal ions were classified into two categories from the catalytic aspect: the active group includes copper(II) and vanadyl(IV) while the inactive group consists of nickel(II), iron(III), aluminum(III), and thorium(IV). We pointed out that the differences in catalytic activity of metal ions could not be explained merely in terms of the thermodynamic stability of the metal complexes. But the structural feature of these metal complexes was suggested to be responsible for the catalytic activity. The axial coordination site is available for metal ions of the latter category to bind the leaving phosphate group as shown by **1**. The lack of catalysis by these metal ions was thus attributed to this coordination effect. Taking for example nickel(II) ion of the latter category, this metal ion does not demonstrate any significant coordination ability toward the thioether group as investigated for S-methylcysteine and methionine.[7] The leaving group of S-phenylcysteine, therefore, must be free from coordination with nickel(II) ion. Consequently, nickel ion can be

Table 4. Metal ion catalysis in the pyridoxal-promoted α,β-elimination reaction of S-phenylcysteine in the presence of 0.91×10^{-3} M CTAB

Metal ion	concentration, M	Temp. °C	After "burst" part		Initial "burst" part	
			k_{obs}, s^{-1}	k_{rel}[a]	k_{obs}, s^{-1}	k_{rel}[a]
Ni^{2+}	4.54×10^{-4}	50	5.7×10^{-4}	4.1	3×10^{-3}	21
Cu^{2+}	1.82×10^{-4}	40	5.7×10^{-4}	9.5	5×10^{-3}	83

a) Relative to the corresponding rate constant in the absence of metal ions: $k_{obs}(Ni^{2+})$, 1.40×10^{-4} s^{-1}; $k_{obs}(Cu^{2+})$, 6.00×10^{-6} s^{-1}.

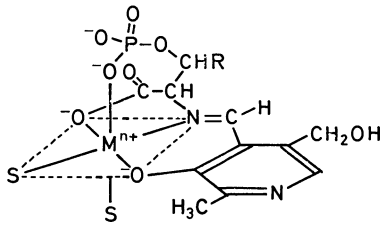

1 S : solvent

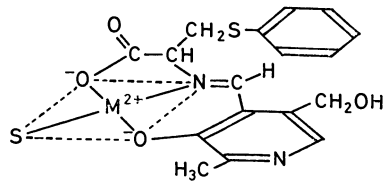

2 M^{2+} : Cu^{2+}, Ni^{2+}

expected to exert an effective catalytic activity in the present elimination reaction through formation of a metal complex as shown by **2**. In fact, a profound rate acceleration was observed in the presence of nickel(II) under the present experimental conditions, even though a minor part of the substrate and metal ion was out of the reaction mixture due to the complex formation. The apparent complete inertness of copper(II) is undoubtedly attributed to the high thermodynamic stability of bis(*S*-phenylcysteinato)copper(II) which resulted in precipitation in the aqueous system. These behaviors of metal ions are consistent with the reaction sequence given in Scheme 1.

When the reaction was carried out in a homogeneous micellar system, the rate acceleration at the "burst" part reaches nearly a hundred-fold in the copper(II) catalysis (Table 4). In our previous work,[4] the copper(II) catalysis in the α,β-elimination of *O*-phosphothreonine was so enormous that the reaction proceeded smoothly at 45 °C, although the reaction did not occur in the absence of the metal ion even at 80 °C. In conformity with the previous work, both nickel(II) and copper(II) form the corresponding metal complexes at a 1 : 1 ratio of metal to Schiff base ligand of structure **2** in the electrostatic layer of surfactant micelles as the preequilibrium stage. In addition, the metal complexes would be more favorably incorporated into the micellar phase than the metal-free Schiff base since the anionic character of the Schiff base ligand can be neutralized through metal-coordination. The rate-determining α,β-elimination then takes place by the attack of hydroxide ion which has been accumulated in the electrostatic layer due to the micellar effect. It is quite reasonable that copper(II) showed a larger catalytic activity than nickel(II) in homogeneous systems on the basis of the relative stability constants of their Schiff base complexes.[8]

In conclusion, it is interesting to note that copper and nickel did show the catalytic effect on the pyridoxal-catalyzed α,β-elimination reaction of *S*-phenylcysteine, although a part of the catalytic activity was exerted by the micellar effect.

Micellar Catalysis. Only the cationic detergent showed a considerable effect on the pyridoxal-catalyzed α,β-elimination of *S*-phenylcysteine. This micellar catalysis resulted in the 18-fold rate acceleration at the level-off region as shown in Fig. 1. Since the conventional micellar catalysis demonstrates rate enhancement in a 10- to 100-fold range, the present value can be referred to as the indication of moderate catalytic efficiency.[2,3]

One of the prominent features of the CTAB-catalyzed reaction is the saturation behavior of the reaction rate with respect to the detergent concentration as shown in Fig. 1. The rate-saturation is characteristic of the enzymic and related model reactions, and the following formula is consistent with the present scheme.

$$\begin{array}{l} S + M \overset{K}{\rightleftharpoons} SM \xrightarrow{k_m} P + M \\ \quad\downarrow k_0 \\ \quad P \end{array}$$

where S, M, and P respectively represent substrate (a Schiff base derived from *S*-phenylcysteine and pyridoxal), micelle, and product, and SM is the substrate-micelle complex. Upon defining C_D, N, and K as detergent concentration, aggregation number (assumed to be 61 in this case), and binding constant, respectively, the above scheme provides the correlation among observed (k_{obs}), spontaneous (k_0), and micellar (k_m) rate constants by Eq. (1).

$$\frac{1}{k_{obs}-k_0} = \frac{1}{k_m-k_0} - \left(\frac{1}{k_m-k_0}\right)\left(\frac{N}{K(C_D-CMC)}\right) \quad (1)$$

An analysis of th present data (Fig. 1) gave fairly good linear relationship: $K \simeq 10^5$ and $CMC \simeq 5\times10^{-4}$ M.

A question arises as to the binding and reaction sites in the micellar phase. It has been shown that charged and polar organic compounds are bound to the electrostatic layer of micelle where the charged head groups of surfactant molecules are located, while apolar

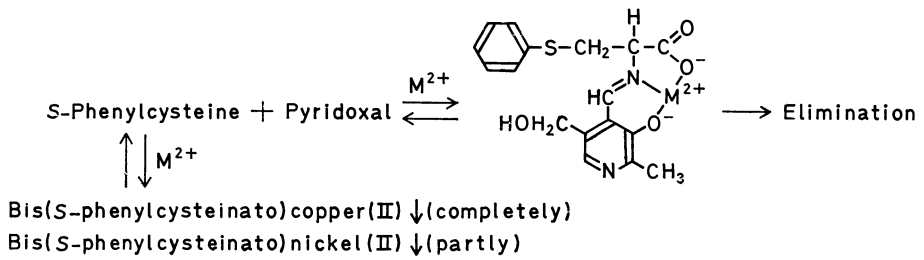

Scheme 1.

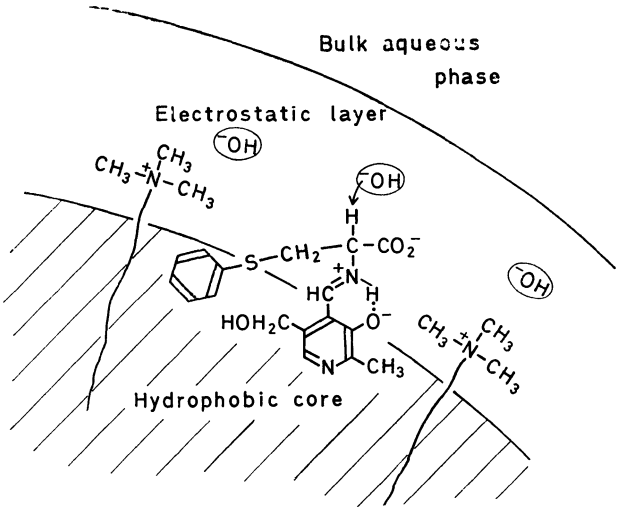

Scheme 2.

hydrocarbons are incorporated into the hydrophobic interior of the micelle.[9] Thus, a reactive Schiff base molecule of the present study is most likely incorporated into the micellar phase where the apolar pyridyl ring moiety is inserted into the hydrophobic core and the polar part composed of the Schiff base bond is located on the micellar surface (Stern and electric double layers). This state of affairs is schematically shown in Scheme 2.

Activation parameters obtained at the level of rate saturation for the micellar reaction of *S*-phenylcysteine are listed in Table 2. Although the increase in activation enthalpy has been observed by Bunton and Robinson for the micellar reaction of *p*-nitrophenyldiphenyl phosphate with hydroxide and fluoride ions,[10] it would seem rather unexpected. They ascribed the larger activation enthalpy for the micellar reaction to the high solubility of the neutral substrate in the micellar phase. In the present study, however, another explanation is needed for the high activation enthalpy since the Schiff base formed between *S*-phenylcysteine and pyridoxal possesses a much polar structure relative to the above neutral substrate. In conformity with the reaction scheme given for the non-micellar system,[1] the reaction center of the Schiff base may become less polar in the transition state **3** relative to the initial one. The electrostatic micellar surface in which the reactive center is incorporated destabilizes the transition state

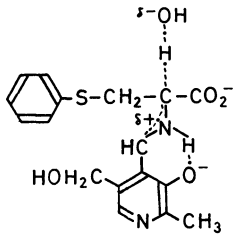

3 (transition state)

and may consequently provide a larger activation enthalpy.

The hydroxide ion is presumably more concentrated on the micellar surface than in the bulk aqueous phase, and the included Schiff base may be readily subject to the attack of hydroxide ion. This state of affairs acts in favor of the activation entropy. As a whole, the CTAB micellar catalysis is exclusively controlled by the entropy term.

When inorganic salts are added to the micellar reaction system, hydroxide ion on the micellar surface is presumably substituted with the chloride or nitrate ion to some extent depending upon the relative concentrations of these salts. Since these inorganic anions are much poorer nucleophiles than the hydroxide ion, the substitution may result in the effective inhibition of the CTAB catalysis. The organic anions may exclude not only the hydroxide ion from the micellar surface but also the Schiff base by occupying the binding site around the charged head groups of surfactant molecules. Thus, these organic salts exerted an inhibition effect much greater than the inorganic salts.

In conclusion, the surfactant micelles demonstrated some enzyme-like features of catalysis in the pyridoxal-promoted α,β-elimination reaction of *S*-phenylcysteine, where the reaction is controlled by the entropy term. This seems to be the first effective organic catalyst ever provided for the pyridoxal-concerned reactions. The catalytic effectiveness is rather small at present relative to the enzyme system, but the modification of the detergent structure by introducing various functional groups into the skeleton will lead to the development of novel and eminent enzyme models of higher activity.

References

1) Y. Murakami and H. Kondo, This Bulletin, **48**, 125 (1975).

2) E. H. Cordes and C. Gitler, "Progress in Bioorganic Chemistry," Vol. 2, ed. by E. T. Kaiser and F. J. Kezdy, John Wiley & Sons, Inc., New York, N.Y. (1973), p. 1.

3) E. J. Fendler and J. H. Fendler, "Advances in Physical Organic Chemistry," Vol. 8, ed. by V. Gold, Academic Press, New York, N.Y. (1970), p. 271.

4) Y. Murakami, H. Kondo, and A. E. Martell, *J. Amer. Chem. Soc.*, **95**, 7138 (1973).

5) a) H. Behringer and E. Fackler, *Ann. Chem.*, **564**, 73 (1949). b) L. Goodman, L. O. Ross, and B. R. Baker, *J. Org. Chem.*, **23**, 1251 (1958).

6) L. R. Romsted and E. H. Cordes, *J. Amer. Chem. Soc.*, **90**, 4404 (1968).

7) G. R. Lenz and A. E. Martell, *Biochemistry*, **3**, 745 (1964).

8) See for general reference: L. G. Sillén and A. E. Martell, "Stability Constants of Metal-Ion Complexes," Special Publication No. 17, The Chemical Society, London (1964).

9) S. Riegelman, N. A. Allawala, M. K. Hrenoff, and L. A. Strait, *J. Colloid Sci.*, **13**, 208 (1958).

10) C. A. Bunton and L. Robinson, *J. Org. Chem.*, **34**, 773 (1969).

Phosphinidenes and Related Intermediates. III.[1] Reactions of Phosphinylidenes and Phosphinothioylidenes with Conjugated Dienes

Shigenobu NAKAYAMA, Masaaki YOSHIFUJI, Renji OKAZAKI, and Naoki INAMOTO

Department of Chemistry, Faculty of Science, The University of Tokyo, Hongo, Tokyo 113

(Received September 28, 1974)

Phenylphosphonic and phenylphosphonothioic dichlorides were dechlorinated with magnesium to generate phenylphosphinylidene and phenylphosphinothioylidene, respectively, in the presence of several 1,3-dienes. Reactions of phenylphosphinothioylidene with 2,3-dimethylbutadiene and 1,3-cyclohexadiene gave Diels-Alder type reaction products, that is, 3,6-dihydro-1,2-thiaphosphorin derivatives (**5** and **6**) and 6-phenyl-5,6-thiaphosphabicyclo[2.2.2]oct-2-ene 6-sulfide (**14**), respectively. Reaction of 2,3-diphenylbutadiene with phenylphosphinothioylidene afforded 1,2,4,5-tetraphenyl-1,2,3,6-tetrahydro-1,2-diphosphorin 1,2-disulfide (**10**), whereas that with phenylphosphinylidene gave 1,3,4-triphenyl-3-phospholene 1-oxide (**12**). The differences of these reactions have been discussed.

Schmidt and Boie[2] reported that thermal decomposition or photolysis of pentaphenylcyclopentaphosphine in the presence of 1,3-dienes gave cyclic compounds such as **1** and **2**, the formation of which can be interpreted by attack of phenylphosphinidene (Ph–P) or a diradical (**3**)[3] upon the 1,3-dienes.

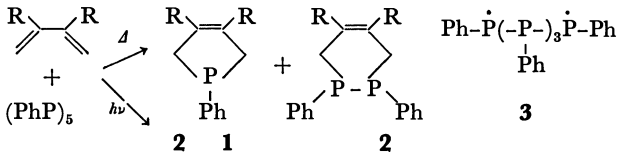

2 **1** **2** **3**

Thus, in the decomposition of the cyclopentaphosphine, phosphinidene is not necessarily the sole reactive intermediate. Furthermore, it is expected that phosphinylidenes (R–P=O) and phosphinothioylidenes (R–P=S) behave not only as analogues of nitrenes and phosphinidenes but also as those of nitroso[4] and thionitroso compounds.[5]

The present paper describes reactions of 1,3-dienes and the related compounds with phosphinylidenes or phosphinothioylidenes[6] generated from magnesium and phosphonic or phosphonothioic dichlorides, respectively.

When phenylphosphonothioic dichloride (**4**) was dechlorinated with magnesium in tetrahydrofuran (THF) in the presence of 2,3-dimethylbutadiene at 50 °C, 4,5-dimethyl-2-phenyl-3,6-dihydro-1,2-thiaphosphorin 2-sulfide (**5**) and the corresponding 2-oxide (**6**) were obtained in 44 and 21% yields, respectively,[7] but another expected product (**8**) could not be isolated.

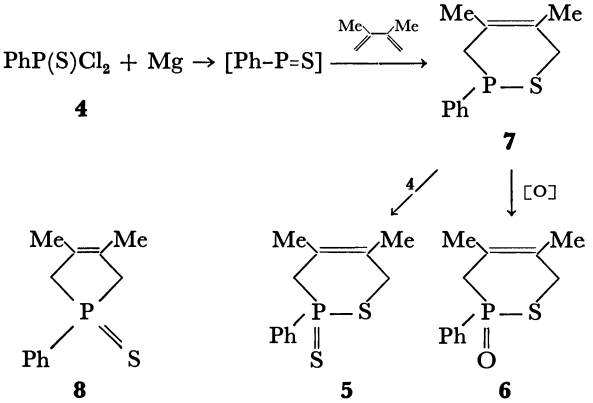

4 **7** **8** **5** **6**

The formation of **5** and **6** is attributable to sulfurization of **7** with **4** and oxidation of **7** during the isolation, respectively. Thus, it is clear that the intermediate (**7**) is formed *via* the Diels-Alder type reaction of the diene with phenylphosphinothioylidene as a 1,2-dipole like thionitroso compounds.[5] The same compound (**5**) has recently been obtained in the following reaction.[8]

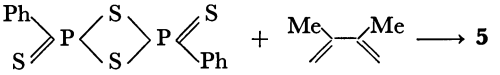

Reaction of **4** with 2,3-diphenylbutadiene and magnesium in THF gave 3-methyl-2-phenylindene (**9**) and 1,2,4,5-tetraphenyl-1,2,3,6-tetrahydro-1,2-diphosphorin 1,2-disulfide (**10**) in 52.5 and 13.5% yields, respectively, after separation by column chromatography.

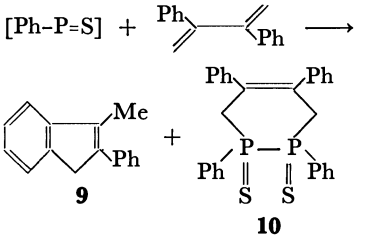

9 **10**

It was proven by a separate experiment that **9** was produced by cyclization of unchanged 2,3-diphenylbutadiene on silica gel (see Experimental).

When phenylphosphonic dichloride (**11**) was used instead of **4**, 1,3,4-triphenyl-3-phospholene 1-oxide (**12**) was obtained in 10% yield.

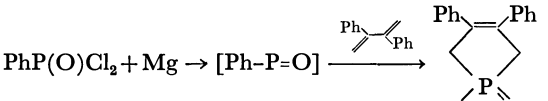

11 **12**

Dechlorination of **4** with magnesium in the presence of 1,3-cyclohexadiene in THF afforded 2-phenyl-1,3,2-oxathiaphosphepane 2-sulfide (**13**) and 6-phenyl-5,6-thiaphosphabicyclo[2.2.2]oct-2-ene 6-sulfide (**14**) in 6 and 21% yields, respectively.

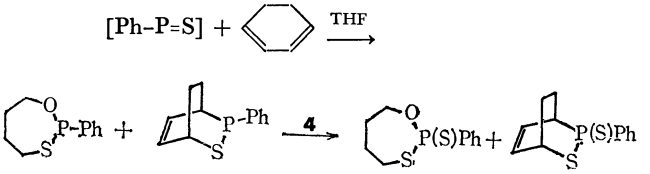

13 **14**

The compound (**13**) is an insertion product of phenylphosphinothioylidene into the C–O bond of THF. The formation mechanism will be discussed elsewhere.[9] The compound (**14**) is of the same type as **5**.

In the NMR spectrum of **14**, a decoupling experiment showed that two quartets centered at δ 5.98 and 6.58 coupled with two multiplets at δ 2.9—3.4 (–P–CH〈) and 3.8—4.4 (–S–CH〈), respectively, indicating that the two quartets are assignable to olefinic protons adjacent to the C–P and C–S bonds, respectively. From the result, the coupling constants may be evaluated as $J_{H-C=C-H}=J_{HCCH}=J_{PSCCH}=8$ Hz. However, since J_{PSCCH} values are generally very small, it would be more reasonable to consider that the quartet centered at δ 6.58 is due to overlapping of two triplets centered at δ 6.52 and 6.64 assignable to each olefinic proton adjacent to the C–S bond of the two isomers on the phosphorus atom, and that the signals of each olefinic proton adjacent to the C–P bond in the two isomers perhaps coincided with each other by chance. Thus, **14** is suggested to be an equimolar mixture of two isomers.

Detectable reaction products could not be isolated in the reactions of phenylphosphinylidene and cyclohexylphosphinothioylidene with 2,3-dimethylbutadiene, the reactions of cyclohexylphosphinylidene and -phosphinothioylidene with 2,3-diphenylbutadiene, and the reactions of phenylphosphinothioylidene with 1,3-cyclooctadiene, *trans,trans*-1,4-diphenylbutadiene, 1,1′-dicyclohexenyl, thiophene, 2,5-diphenylbenzo[*c*]furan, acetophenone azine, and 1,2-bis(*p*-tolylimino)-1,2-diphenylethane. In some reactions with phenylphosphinothioylidene in THF, **13** was also isolated in 3—11% yields.

In the reaction of phenylphosphinothioylidene with tetraphenylcyclopentadienone, 2,3,*trans*-4,5-tetraphenylcyclopent-2-en-1-one (**15**) was obtained in 21% yield as the sole product, and may be formed by an analogous mechanism to that reported by Dimroth and Laufenberg[10] or by reduction of tetraphenylcyclopentadienone with magnesium-magnesium(II) chloride system.[1]

Since usually the 1,3-dienes do not react with nucleophiles, participation of Grignard-type intermediate (R–P(X)Cl–MgCl; X=O,S) might be ruled out. Thus, the reactive intermediate is considered to be phosphinylidene and phosphinothioylidene.

As mentioned above, the types of the products depend on not only the structure of reactive intermediates but also the structure of 1,3-dienes used.

In the reactions of phenylphosphinothioylidene with 1,3-dienes such as 1,3-cyclohexadiene and 2,3-dimethylbutadiene which are fixed in cisoid form or take easily cisoid, phenylphosphinothioylidene behaves as 1,2-dipolar dienophile for 1,3-dienes.

On the contrary, 2,3-diphenylbutadiene takes cisoid form not so easily as 2,3-dimethylbutadiene. Thus the phosphorus atom of phenylphosphinylidene attacks electrophilically on transoid 2,3-diphenylbutadiene and the transoid zwitter ion thus formed converts to the cisoid to form **12**, which is more stable than the isomer (**16**) by a consideration of the bond energies. This difference between the formation of **5**, **6** and **14** and that of **12** may be attributed to the difference in the bond energies of P=O and P=S bonds and to the large nucleophilicity of the sulfur anion.

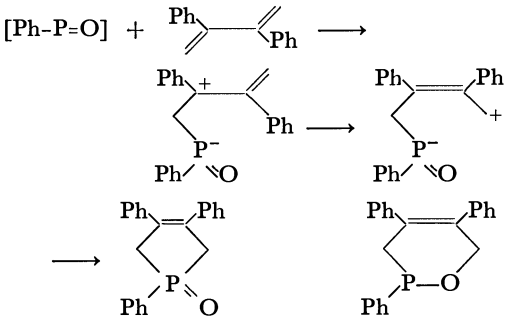

12 **16**

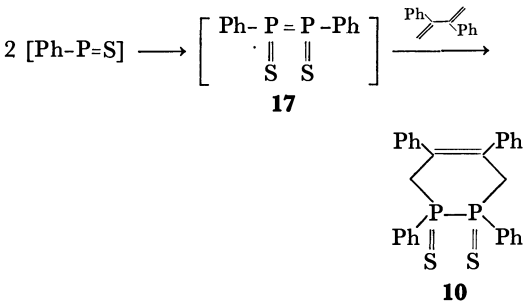

17

10

In the case of phenylphosphinothioylidene, an analogous transoid zwitter ion is probably less stable because of low electronegativity of the sulfur atom. Then phosphinothioylidene is considered to dimerize competitively to produce a reactive intermediate (**17**) which cyclizes with 2,3-diphenylbutadiene to give **10**.

It is very interesting that phenylphosphinothioylidene shows dual properties in the reactions.

Experimental

All melting and boiling points are uncorrected. IR and mass spectra were measured with Hitachi EPI-G2 and Hitachi RMU-6L spectrometers. ^{1}H-NMR spectra were recorded on Hitachi R-20B, R-24 (60 MHz), R-22 (90 M Hz), and JEOL JNM-4H-100 (100 MHz) spectrometers using TMS as an internal standard. ^{31}P-NMR spectra were taken with a Hitachi R-20B-R-204-PB spectrometer using 85% phosphoric acid as an external standard. All reactions were carried out under nitrogen atmosphere.

Materials. The following compounds were prepared by the method described in the literature: 2,3-dimethyl-[11] (mp 68—71 °C), 2,3-diphenylbutadienes[12] (mp 43—46 °C), 1,3-cyclohexadiene[13] (bp 79—82 °C), tetraphenylcyclopentadienone[14] (mp 218—220 °C), phenylphosphonic[15] (**11**) (bp 143 °C/27 mmHg), and phenylphosphonothioic dichlorides[16] (**4**) (bp 134—138 °C/14 mmHg).

Reaction of 4 and Magnesium with 2,3-Dimethylbutadiene. At room temperature, **4** (2.6 g, 12.4 mmol) was added dropwise to a mixture of 2,3-dimethylbutadiene (12 ml, 107 mmol) and magnesium (0.33 g, 13.9 mg-atom) in THF (10 ml) with stirring. A few drops of methyl iodide were added to start the reaction, and the mixture was stirred at 50 °C overnight. After removal of the solvent, the residue was extracted with chloroform. The chloroform extract was washed with water, dried with anhydrous magnesium sulfate, and chromatographed on silica gel to give **5** (0.69 g, 2.7 mmol,

44%) with benzene and **6** (0.62 g, 2.6 mmol, 21%) with dichloromethane and chloroform.

5: mp 61—62 °C (from ether) (lit,[8] 62 °C); IR (KBr): 1650 cm^{-1} (C=C); NMR (CCl_4, 100 MHz): δ 1.68 (s, 3H, 5-Me), 1.93 (d, J_{PCCCH} 5 Hz, 3H, 4-Me), 2.7—3.9 (m, 4H, $2CH_2$), and 7.2—8.0 (m, J_{PH^o} 15 Hz, 5H, Ph).

Found: C, 56.62; H, 5.86; S, 25.34%. Calcd for $C_{12}H_{15}PS_2$: C, 56.66; H, 5.96; S, 25.21%.

6: mp 85.5—86 °C (from ether); IR (KBr): 1660 (C=C) and 1205 cm^{-1} (P=O); NMR (CCl_4, 100 MHz): δ 1.77 (s, 3H, 5-Me), 1.97 (d, J_{PCCCH} 5 Hz, 3H, 4-Me), 2.4—4.0 (m, 4H, $2CH_2$), and 7.4—8.0 (m, 5H, Ph); MS: *m/e* 238 (M^+).

Found: C, 60.71; H, 6.49%. Calcd for $C_{12}H_{15}OPS$: C, 60.49; H, 6.35%.

Reaction of ***4*** *and Magnesium with 2,3-Diphenylbutadiene.* At room temperature, **4** (5.31 g, 25.2 mmol) in THF (5 ml) was added drop by drop with stirring to a mixture of 2,3-diphenylbutadiene (6.08 g, 29.5 mmol), magnesium (0.66 g, 27.5 mg-atom), and THF (20 ml). A small amount of iodine was added to activate magnesium. The mixture was stirred for 1 hr. Unchanged magnesium and produced magnesium chloride were filtered off, and THF was evaporated from the filtrate *in vacuo*. The residue was treated in a similar way. Elution with carbon tetrachloride and carbon tetrachloride-benzene (2 : 1—1 : 1) afforded unchanged **4** (0.02 g, 0.1 mmol) and **9** (3.19 g, 15.5 mmol, 52.5%), mp 76—77 °C (from *n*-hexane) (lit,[17] 76—77 °C), respectively. Elution with benzene and dichloromethane afforded **10** (0.84 g, 1.7 mmol), mp 233—234 °C (from benzene). The yield was 13.5% based on **4** consumed. IR (KBr): 1110 (P-Ph), 625, and 620 cm^{-1} (P=S); NMR ($CDCl_3$): δ 3.3—4.5 (m, 4H, $2CH_2$), and 7.0—8.2 (m, 20H, 4Ph); MS: *m/e* 486 (M^+, 21%), 346 (M^+-PhPS, 69), 314 (M^+-PhPS_2, 100), 280 (PhP(S)P(S)Ph, 14), and 205 ($CH_2CPhCPhCH_2$, 32).

Found: C, 69.02; H, 4.66%. Calcd for $C_{23}H_{24}P_2S_2$: C, 69.11; H, 4.98%.

Reaction of ***11*** *and Magnesium with 2,3-Diphenylbutadiene.* A solution of **11** (4.29 g, 22.0 mmol) in THF (5 ml) was added dropwise to a stirred suspension of magnesium (0.58 g, 24.0 mg-atom) and 2,3-diphenylbutadiene (4.54 g, 22.0 mmol) in THF (20 ml) under occasional cooling with water. The exothermal reaction ceased in about 1 hr. Then the reaction mixture was refluxed for 3 hr, and treated similarly. Elution with carbon tetrachloride and chloroform afforded unchanged diene (3.23 g, 15.7 mmol) and **12** (0.75 g, 2.3 mmol), respectively. The yield of **12** was 37% based on the diene consumed.

12: mp 162.5—163.5 °C (from carbon tetrachloride); IR (KBr): 1190 cm^{-1} (P=O); ^1H-NMR ($CDCl_3$, 90 MHz): δ 3.0—3.75 (m, 4H, $2CH_2$), 6.9—7.3 (m, 10H, 2Ph), 7.4—7.65 (m, 3H, $2H^m$ and H^p of P-Ph), and 7.65—8.1 (m, 2H, $2H^o$ of P-Ph); ^{31}P-NMR ($CHCl_3$): δ −48 ppm; MS: *m/e* 330 (M^+).

Found: C, 80.10; H, 5.64%. Calcd for $C_{22}H_{19}OP$: C, 77.98; H, 5.80%.

Conversion of 2,3-Diphenylbutadiene into ***9*** *on Silica Gel Column.* 2,3-Diphenylbutadiene (4.95 g, 23.8 mmol) was adsorbed on silica gel for 6 days. Elution with carbon tetrachloride gave 3.72 g (17.9 mmol, 75%) of **9**, mp 76—77 °C.

Reaction of ***4*** *and Magnesium with 1,3-Cyclohexadiene.* A solution of **4** (5.24 g, 24.8 mmol) in THF (7 ml) was added drop by drop to a stirred mixture of 1,3-cyclohexadiene (8.0 g, 100 mmol) and magnesium (0.67 g, 27.9 mg-atom) in THF (10 ml). A small amount of iodine was added to initiate the reaction. Exothermal reaction ended in 1 hr. Then the reaction mixture was refluxed for 3 hr and treated similarly. Elution with benzene afforded 0.20 g (0.8 mmol, 6%) of **13** and 0.66 g (2.6 mmol, 21%) of **14**.

13: mp 62—63.5 °C (from *n*-hexane); IR (KBr): 1115 (P-Ph), 1030 (P-O-C), 650, 645, and 545 cm^{-1} (P(S)-S); NMR ($CDCl_3$, 100 MHz): δ 1.7—2.4 (m, 4H, $2CH_2$), 2.72 (dt, J_{PSCH} 22.5, J_{HCCH} 9 Hz, 2H, SCH_2), 4.0—4.5 and 4.5—5.0 (m, 2H, OCH_2), 7.3—7.6 (m, 3H, $2H^m$ and H^p of P-Ph), and 7.90 (m, J_{PH^o} 15 Hz, 2H, $2H^o$ of P-Ph); MS: *m/e* 244 (M^+).

Found: C, 49.09; H, 5.45; S, 26.44%. Calcd for $C_{10}H_{13}OPS_2$: C, 49.16; H, 5.45; S, 26.25%.

14: mp 92—93.5 °C (from ether); IR (KBr): 1100 (P-Ph), 680, 578, 520, and 488 cm^{-1} (P(S)-S); NMR ($CDCl_3$): δ 1.0—2.9 (m, 4H, $2CH_2$), 2.9—3.4 (m, 1H, P-CH<), 3.8—4.4 (m, 1H, S-CH<), 5.98 (q, $J_{HC=CH}=J_{HCCH}=J_{PCCH}=8$ Hz, 1H, =CH-), 6.52 and 6.64 (2t, $J_{HC=CH}=J_{=CH-CH}=8$ Hz, 1H, =CH-), 7.2—7.6 (m, 3H, $2H^m$ and H^p), and 7.65—8.1 (m, J_{PH^o} 13.5 Hz, 2H, $2H^o$); MS: *m/e* 252 (M^+).

Found: C, 57.28; H, 5.02; S, 25.34%. Calcd for $C_{12}H_{13}PS_2$: C, 57.12; H, 5.19; S, 25.41%.

Reaction of ***4*** *and Magnesium with Tetraphenylcyclopentadienone.* At room temperature, **4** (0.59 g, 2.8 mmol) was added to a stirring suspension of magnesium (0.17 g, 6.9 mg-atom) and tetraphenylcyclopentadienone (1.16 g, 3.0 mmol) in THF (25 ml), and the mixture was heated at 80 °C for 1 day. After similar treatment, elution with dichloromethane gave 0.23 g (0.6 mmol, 21%) of **15**, mp 165—168 °C (from dichloromethane-ethanol) (lit,[10] 161—163 °C); NMR ($CDCl_3$): δ 3.76 (d, J 3 Hz, 1H, CH), 4.56 (d, J 3 Hz, 1H, CH), and 7.0—7.5 (m, 20H, 4Ph).

This work was supported by a grant from the Ministry of Education.

References

1) For Part II see: S. Nakayama, M. Yoshifuji, R. Okazaki, and N. Inamoto, *J. Chem. Soc. Perkin I*, **1973**, 2069.
2) U. Schmidt and I. Boie, *Angew. Chem.*, **78**, 1061 (1966).
3) U. Schmidt, I. Boie, C. Osterroht, R. Schröer, and H.-F. Grützmacher, *Chem. Ber.*, **101**, 1381 (1968).
4) J. Hamer and M. Ahmad, in "1,4-Cycloaddition Reactions—The Diels-Alder Reactions in Heterocyclic Systems," ed. by J. Hamer, Academic Press, New York (1967), P. 419.
5) P. Tavs, *Angew. Chem.*, **78**, 1057 (1966).
6) M. Yoshifuji, S. Nakayama, R. Okazaki, and N. Inamoto, *J. Chem. Soc. Perkin I*, **1973**, 2065.
7) Preliminary report: S. Nakayama, M. Yoshifuji, R. Okazaki, and N. Inamoto, *Chem. Commun.*, **1971**, 1186.
8) A. Ecker, I. Boie, and U. Schmidt, *Angew. Chem., Int. Ed. Engl.*, **10**, 191 (1971); *Monatsh. Chem.*, **104**, 503 (1973).
9) S. Nakayama, M. Yoshifuji, R. Okazaki, and N. Inamoto, This Bulletin, the forthcoming paper (Part IV).
10) K. Dimroth and J. von Laufenberg, *Chem. Ber.*, **105**, 1044 (1972).
11) E. -E. Blaise and A. Courtot, *C. R. Acad. Sci. Paris.*, **140**, 371 (1905).
12) K. Alder and J. Haydn, *Ann. Chem.*, **570**, 212 (1950).
13) J. Hine, J. A. Brown, L. H. Zalkow, W. E. Gardner, and M. Hine, *J. Amer. Chem. Soc.*, **77**, 594 (1955).
14) J. R. Johnson and O. Grummitt, "Organic Syntheses," Coll. Vol. 3, p. 806 (1955).
15) A. D. F. Toy, *J. Amer. Chem. Soc.*, **70**, 186 (1948).
16) W. L. Jensen, U.S. 2,662,917 (1951); *Chem. Abstr.*, **48**, 13711h (1954).
17) W. Hausmann and A. E. W. Smith, *J. Chem. Soc.*, **1949**, 1030.

Absolute Stereochemistry of Farfugin A[1]

Masahiro TADA, Yoshihiko MORIYAMA, Yoshiaki TANAHASHI, and Takeyoshi TAKAHASHI
Department of Chemistry, Faculty of Science, The University of Tokyo, Bunkyo-ku, Tokyo 113
(Received October 16, 1974)

4,6-Dimethylcoumarin (**3**) was converted to an enantiomer (**1b**) of farfugin A, *via* a levorotatory carboxylic acid (**5b**). This led to the absolute configuration (**1a**) for farfugin A.

The structure of farfugin A, a dextrorotatory benzofuranosesquiterpene isolated from *Farfugium japonicum*, was shown to be **1**.[2] A skeletal rearrangement of furanoeremophilane-6β,10β-diol [(+)-**2**][3] gave farfugin A [(+)-**1**].[4] We wish to report the determination of an absolute configuration of farfugin A (**1a**), which is indispensable for elucidation of the mechanism of this rearrangement.

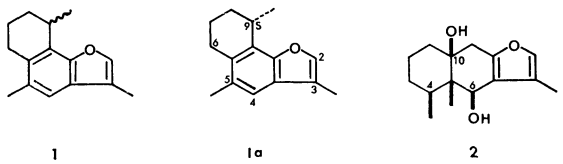

1 1a 2

4,6-Dimethylcoumarin (**3**)[5] was hydrogenated over palladium-charcoal to yield a dihydro derivative (**4**;[6] mp 35—35.5 °C; yield: 90%). Alkaline hydrolysis of **4** followed by methylation with dimethyl sulfate gave 3-(2-methoxy-5-methylphenyl)butanoic acid (**5**; mp 60.5—61.5 °C; yield: 89%). A resolution of the (+)- and (−)-acid [(+)- and (−)-**5**] was carried out *via* their strychnine salts to give a dextrorotatory acid [**5a**; mp 60—60.5 °C, $[\alpha]_D$ +19° (C_6H_6)][7] and a levorotatory acid [**5b**; mp 60 °C, $[\alpha]_D$ −27° (C_6H_6)].[7]

The dextrorotatory acid (**5a**) was converted to (+)-3,7-dimethylindan-1-one (**8**) to determine an absolute configuration of **5a**. When **5a** was treated with polyphosphoric acid, **5a** was cyclized to give (+)-4-methoxy-3,7-dimethylindan-1-one (**6**; an oil; y: 94%), which was demethylated to yield a phenol (**7**;[8] mp 203 °C; yield: 68%). The phenol (**7**) was phosphorylated according to Kenner and Williams,[9] reduced with lithium in liquid ammonia, and then oxidized with Jones' reagent to give (+)-3,7-dimethylindan-1-one (**8**; an oil; y: 50%). These indanone derivatives (**6** and **8**)[10] showed the ORD curves which were almost mirror images to that of known (−)-(3R)-3-methylindan-1-one (**9**).[11] An asymmetric center of the dextrorotatory acid (**5a**) must therefore be in the configuration (S), and that of levorotatory acid (**5b**) in the configuration (R).

The levorotatory acid (**5b**) was subjected to the Arndt-Eistert homologation to give (−)-4-(2-methoxy-5-methylphenyl)-pentanoic acid (**10**; mp 87.5 °C; y: 75%),[12] which was converted *via* **11** and **12** to (+)-8-hydroxy-1,5-dimethyl-1,2,3,4-tetrahydronaphthalene (**13**; mp 91 °C; y: 72%) according to the procedures described in the literatures.[12] By the reaction sequence already reported,[2] **13** was converted to a (−)-8-acetonyloxy-1,5-dimethyl-1,2,3,4-tetrahydronaphthalene (**14**; mp 77 °C; y: 61%), which was then cyclized to give a levorotatory benzofuran [**1b**; mp

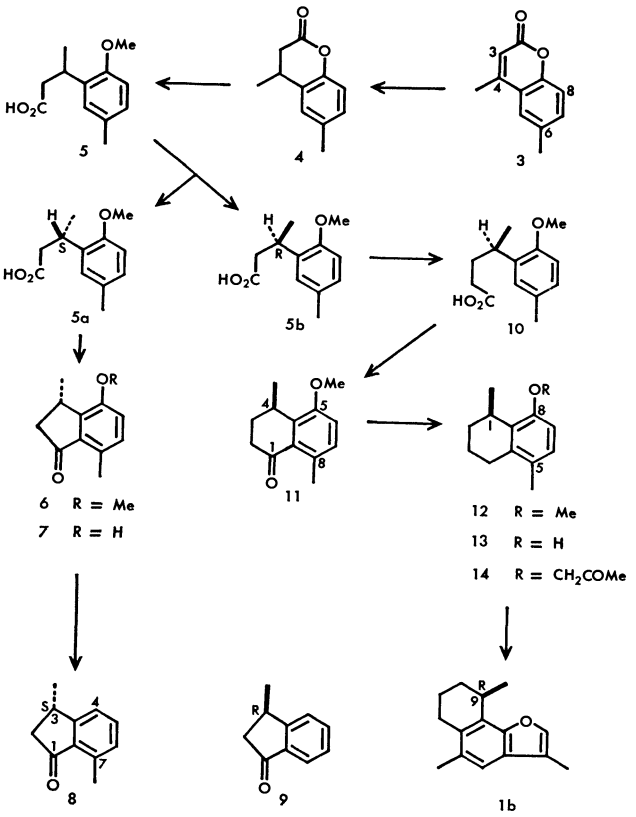

78 °C, $[\alpha]_D$−27° (EtOH); y: 55%). This compound (**1b**) was found to be an enantiomer of natural (+)-farfugin A[2] (*cf.* Experimental). Thus, the absolute stereochemistry of natural farfugin A was shown to be **1a** whose configuration at C-9 must be (S).

Experimental

IR spectra were measured using a Hitachi EPI-G2 spectrometer in Nujol mull, unless otherwise stated. UV spectra were determined on a Hitachi EPS-3 spectrophotometer. ORD measurements were carried out on a JASCO ORD/UV-5 spectrometer. Optical rotations were measured on a JASCO DIP-SL polarimeter. Mass spectra were taken on a Hitachi RMU-6-Tokugata mass spectrometer with a direct inlet system operating at 70 eV. PMR spectra were measured using a JEOL PS-100 (100 MHz) or a Hitachi R-20 (60 MHz) spectrometer. Chemical shifts were expressed in δ downfield from TMS as internal standard, and coupling constants in Hz. Thin layer chromatography (tlc) was carried out on Kieselgel PF_{254} (E. Merck, Darmstadt). For column chromatography Wakogel C-200 (Wako Pure Chemical Ind.) was used. All mps were determined on a hot block and reported uncorrected.

4,6-Dimethylcoumarin (3). According to the known procedures,[5] *p*-cresol (76 g) was condensed with ethyl aceto-

acetate (90 g) in polyphosphoric acid [prepared from phosphoric acid (85%; 300 ml) and phosphorus pentoxide (500 g)] at 80 °C for 1 hr to give 4,6-dimethylcoumarin (**3**; 55 g; y: 45%), mp 150—151.5 °C [crystallized from a mixture of light petroleum and benzene (1 : 1)] (lit,[5a] mp 148 °C; lit,[5b] mp 150 °C); IR: 1720, 1627, 1612, 1573, 1491, 1200, 938, 860, and 830 cm^{-1}; PMR ($CDCl_3$): δ 2.41 (6H, s; $C_{(4)}$-CH_3 and $C_{(6)}$-CH_3), 6.22 (1H, m; $C_{(3)}$-H), and 7.2—7.4 (3H, m; $C_{(5)}$-H, $C_{(7)}$-H, and $C_{(8)}$-H); mass spectrum: *m/e* 174 (M^+) and *m/e* 145 (base peak). Found: C, 75.87; H, 6.02%. Calcd for $C_{11}H_{10}O_2$: C, 75.84; H, 5.79%; mol wt 174.2.

*3,4-Dihydro-4,6-dimethylcoumarin (**4**).* 4,6-Dimethylcoumarin (**3**; 45 g) dissolved in a mixture of ethyl acetate (200 ml) and acetic acid (1.8 l) was hydrogenated in the presence of 10% palladium-charcoal (10 g) for 4 hr at 100 °C. The catalyst was removed by filtration and the solvents were evaporated to give a residue, which was extracted with ether. A usual treatment gave an oil which solidified to afford 3,4-dihydro-4,6-dimethylcoumarin (**4**; 41 g; y: 90%), mp 35—35.5 °C (lit,[6] bp 100—105 °C/5 mmHg); IR: 1760, 1620, 1595, 1500, 1260, 1212, 1176, and 832 cm^{-1} (lit,[6] 1770 cm^{-1}); PMR ($CDCl_3$): δ 1.30 (3H, d, J=7 Hz; $C_{(4)}$-CH_3), 2.33 (3H, s; $C_{(6)}$-CH_3), and 6.95 (3H, m; $C_{(5)}$-H, $C_{(7)}$-H, and $C_{(8)}$-H); mass spectrum: *m/e* 176 (M^+) and *m/e* 134 (base peak). Found: C, 75.07; H, 6.75%. Calcd for $C_{11}H_{12}O_2$: C, 74.97; H, 6.86%; mol wt 176.2.

*3-(2-Methoxy-5-methylphenyl)butanoic Acid (**5**).* To a solution of 3,4-dihydro-4,6-dimethylcoumarin (**4**, 90 g) in ethanol (300 ml) was added 2 M sodium hydroxide (1 l), and the mixture was heated under reflux for 2 hr. To the cooled mixture dimethyl sulfate (65 g) was added dropwise with stirring at 0 °C, and the whole was heated under reflux for 8 hr. These procedures were repeated by further addition of dimethyl sulfate (20 g) and 2 M sodium hydroxide (90 ml). The cooled reaction mixture was acidified with 2 M sulfuric acid and heated under reflux for 2 hr. The mixture was cooled, alkalized with 2 M sodium hydroxide, and extracted with chloroform. The organic layer was separated and the solvents (chloroform and ethanol) were removed to give the starting material (**4**: 17 g). The alkaline layer was acidified with 2 M sulfuric acid, and then extracted with chloroform. The chloroform layer was separated, washed with brine, and dried over anhydrous sodium sulfate. The solvent was removed and the residue was distilled at 153 °C under 1 mmHg pressure. The distillate solidified to give 3-(2-methoxy-5-methylphenyl)-butanoic acid (**5**; 95 g; y: 89%), mp 60.5—61.5 °C; IR: *ca.* 3000 (br.), 1710, 1610, 1502, 1250, and 812 cm^{-1}; PMR ($CDCl_3$): δ 1.30 (3H, d, J=7 Hz; *s*-CH_3), 2.27 (3H, s; aromatic CH_3), 3.80 (3H, s; OCH_3), and 6.65—6.95 (3H, m; aromatic protons); mass spectrum: *m/e* 208 (M^+) and *m/e* 149 (base peak). Found: C, 69.36; H, 7.53%. Calcd for $C_{12}H_{16}O_3$: C, 69.21; H, 7.74%; mol wt 208.2.

*Resolution of (+)- and (−)-3-(2-Methoxy-5-methylphenyl)butanoic Acid [**5a** and **5b**].* To a solution of the racemic acid (**5**; 20 g) and strychnine (32 g) in chloroform (25 ml), ethanol (80%; 80 ml) was added. The resulting solution was concentrated to a volume of 20 ml. Water (10 ml) was added, and the solution was kept at room temperature overnight. There appeared the strychnine salt [18 g; $[\alpha]_D$ −68 ° (*c* 2.0, H_2O)], which was separated by filtration and crystallized thrice from ethanol (50%) to give the levorotatory strychnine salt. The rotation values of the salt at different stages of crystallization were: first crystallization, $[\alpha]_D$ −78.7 °; second, $[\alpha]_D$ −81.8 °; third, $[\alpha]_D$ −82.2 ° (*c* 2.0, H_2O).

The third crop (14 g) was added to 1 M sodium hydroxide (80 ml). The resulting mixture was extracted with chloroform, and the organic layer was discarded. The aqueous layer was then acidified with 2 M sulfuric acid and extracted with chloroform. The chloroform layer was washed with brine, dried over anhydrous sodium sulfate, and evaporated to yield an oil which was distilled at 150 °C under 1 mmHg pressure. The distillate solidified to give (−)-3-(2-methoxy-5-methylphenyl)butanoic acid (**5b**; 5 g), mp 60 °C, $[\alpha]_D$ −27 ° (*c* 2.0, C_6H_6).[7]

The mother liquor after separating the levorotatory strychnine salt was concentrated to a volume of *ca.* 20 ml to give the salt of **5b** (1 g); no salt was precipitated on further concentration of the mother liquor. The mother liquor was then alkalized with 1 M sodium hydroxide. The subsequent treatments were followed as before to give an oil which was distilled at 150 °C under 1 mmHg pressure. The distillate solidified to give (+)-3-(2-methoxy-5-methylphenyl)butanoic acid (**5a**; 9 g), mp 60—60.5 °C, $[\alpha]_D$ +19 ° (*c* 2.0, C_6H_6).[7]

*(+)-4-Methoxy-3,7-dimethylindan-1-one (**6**).* The dextrorotatory acid (**5a**; 7 g) was dissolved in polyphosphoric acid [prepared from phosphoric acid (85%; 80 ml) and phosphorus pentoxide (130 g)] at 30 °C, and the resulting solution was then heated at 100 °C for 1 hr. The cooled reaction mixture was poured into a mixture of ice and water and extracted with chloroform. The organic layer was washed with brine, dried, and evaporated to give an oil (6 g; y: 94%). A part of this material was purified by preparative tlc to give (+)-4-methoxy-3,7-dimethylindan-1-one (**6**), an oil; IR (liquid): 1715, 1590, 1500, 1270, 820, and 760 cm^{-1}; UV (cyclohexane): λ_{max} 317 nm (ε 3300), 308 (3500), 252.5 (8600), 246 (8300), and 238 (8000); PMR ($CDCl_3$): δ 1.34 (3H, d, J=7 Hz; $C_{(3)}$-CH_3), 2.20 (1H, dd, J=19 and J=3 Hz; $C_{(2)}$-H), 2.53 (3H, s; $C_{(7)}$-CH_3), 2.85 (1H, dd, J=19 and J=7 Hz; $C_{(2)}$-H), 3.45 (1H, m; $C_{(3)}$-H), 3.82 (3H, s; OCH_3), 6.88 and 7.00 (each 1H, d, J=8 Hz; $C_{(5)}$-H and $C_{(6)}$-H); ORD (*c* 0.18, cyclohexane): $[\Phi]_{589}$ +40 °, $[\Phi]^{peak}_{365}$ +1100 °, $[\Phi]^{trough}_{358}$ +720 °, $[\Phi]^{peak}_{350}$ +1000 °, $[\Phi]^{trough}_{340}$ +220 °, $[\Phi]^{peak}_{335}$ +330 °, $[\Phi]_{325}$ −1200 ° (shoulder), $[\Phi]^{trough}_{313}$ −2200 °, and $[\Phi]_{297}$ 0°; mass spectrum: *m/e* 190 [$M^+(C_{12}H_{14}O_2)$] and *m/e* 175 (base peak).

*(+)-4-Hydroxy-3,7-dimethylindan-1-one (**7**).* To a solution of crude (+)-4-methoxy-3,7-dimethylindan-1-one (**6**; 6 g) in acetic acid (30 ml) was added 5.9 M hydrobromic acid (12 ml), and the mixture was heated under reflux for 8 hr. The solvent was removed under reduced pressure to give a residue. The residue was extracted with ether, washed with 1 M sodium carbonate and then brine, dried over anhydrous sodium sulfate, and evaporated to give a residue, which was crystallized from a mixture of benzene and ether (1 : 1) to yield (+)-4-hydroxy-3,7-dimethylindan-1-one (**7**; 3.8 g; y: 68%), mp 203 °C (lit,[8] racemic **7**, mp 175 °C), $[\alpha]_D$ +25 ° (*c* 0.28, EtOH); IR: *ca.* 3200, 1670, 1590, 1505, 1380, 1305, 1285, and 1250 cm^{-1}; PMR (acetone-d_6): δ 1.36 (3H, d, J=7 Hz; $C_{(3)}$-CH_3), 2.14 (1H, dd, J=19 and J=3 Hz; $C_{(2)}$-H), 2.45 (3H, s; $C_{(7)}$-CH_3), 2.82 (1H, dd, J=19 and J=7 Hz; $C_{(2)}$-H), *ca.* 3.4 (1H, m; $C_{(3)}$-H), and 6.88 (2H, s; $C_{(5)}$-H and $C_{(6)}$-H); mass spectrum: *m/e* 176 (M^+) and *m/e* 161 (base peak). Found: C, 75.29; H, 6.67%. Calcd for $C_{11}H_{12}O_2$: C, 74.97; H, 6.86%; mol wt 176.2.

*(+)-3,7-Dimethylindan-1-one (**8**).* To a solution of (+)-4-hydroxy-3,7-dimethylindan-1-one (**7**; 3.5 g) in a mixture of carbon tetrachloride (30 ml) and ether (10 ml), was added diethyl phosphite (5 ml) and triethylamine (4 ml). The mixture was kept overnight at room temperature, and

then extracted with chloroform. The organic layer was washed successively with 2 M hydrochloric acid, 1 M sodium hydroxide, and brine, dried over anhydrous sodium sulfate, and evaporated to give an oil (6 g). Lithium (4 g) was added to a solution of this oil (6 g) in liquid ammonia (120 ml), and the whole was stirred for 1 hr. Ethanol (20 ml) and then water (40 ml) were added, and the ammonia was allowed to evaporate. The resulting mixture was extracted with ether, washed successively with 1 M sodium hydroxide and brine, dried over anhydrous sodium sulfate, and evaporated to give an oil, which was oxidized with Jones' reagent at 0 °C. The product was taken up in ether and treated as usual to give a residue, which was chromatographed on a column of silica gel (320 g). Elution with a mixture of light petroleum and ether (40 : 3) gave an oil (1.6 g; y: 50%). A part of this material was purified by preparative tlc to afford (+)-3,7-dimethylindan-1-one (**8**) an oil, IR (liquid): 1715, 1600, 1480, and 795 cm^{-1}; UV (cyclohexane): λ_{max} 297.5 nm (ε 2600), 294 (shoulder), 287.5 (2500), 260 (shoulder), and 234 (12000); PMR (CCl_4): δ 1.38 (3H, d, J=7 Hz; $C_{(3)}$-CH_3), 2.26 (1H, dd, J=19 and J=4 Hz; $C_{(2)}$-H), 2.65 (3H, s; $C_{(7)}$-CH_3), 2.90 (1H, dd, J=19 and J=7 Hz; $C_{(2)}$-H), 3.40 (1H, m; $C_{(3)}$-H), and 7.0—7.6 (3H, m; $C_{(4)}$-H, $C_{(5)}$-H, and $C_{(6)}$-H); ORD (c 0.44, cyclohexane): $[\Phi]_{589}$ +8° $[\Phi]_{368}^{peak}$ +600°, $[\Phi]_{359}^{trough}$ +410°, $[\Phi]_{352}^{peak}$ +640°, $[\Phi]_{339}$ +60° (shoulder), $[\Phi]_{324}$ −1200° (shoulder), $[\Phi]_{311}$ −2000° (shoulder), $[\Phi]_{300}^{trough}$ −2700°, and $[\Phi]_{290}$ −2300°; mass spectrum: *m/e* 160 [M^+ ($C_{11}H_{12}O$)] and *m/e* 145 (base peak).

*(−)-4-(2-Methoxy-5-methylphenyl)pentanoic Acid (**10**).* Thionyl chloride (3 ml) was added with stirring to a cooled solution (at 0 °C) of the levorotatory acid (**5b**; 5 g) in a mixture of dry benzene (10 ml) and pyridine (0.5 ml). The mixture was kept at room temperature for 30 min and then warmed at 40 °C for 10 min. The precipitated solid was removed by filtration. To the filtrate was added dropwise at 0 °C with stirring a *ca.* 3% solution of diazomethane in ether (100 ml). After 40 min, the solvents were removed under reduced pressure at room temperature to give a residue. Anhydrous methanol (50 ml) and then silver oxide (0.8 g) were added to this residue. The mixture was warmed at 50 °C for 20 min (an evolution of nitrogen was observed) and then heated under reflux for 20 min. The cooled mixture was filtered, and the filtrate was evaporated to give a residue which was taken up in ether. The ethereal solution was treated with cold 1 M sodium hydroxide to give, after a work-up as usual, (i) a neutral and (ii) an acidic fraction. Ethanol (30 ml), water (20 ml), and potassium hydroxide (2 g) were added to the neutral product (i), and the whole was heated under reflux for 3 hr. The cooled reaction mixture was acidified with 2 M sulfuric acid and extracted with ether to give, after a treatment as usual, (−)-4-(2-methoxy-5-methylphenyl)pentanoic acid (**10**; 4 g; y: 75%), mp 87.5 °C (crystallized from benzene) (racemic **10** prepared by other routes: lit,[12a] mp 94 °C; lit,[12b] mp 93.5—94 °C), $[\alpha]_D$ −14° (c 2.0, EtOH), IR: 1710, 1610, 1500, 1250, 815, 805, and 750 cm^{-1}; PMR ($CDCl_3$): δ 1.20 (3H, d, J=7 Hz; s-CH_3), 2.28 (3H, s; aromatic CH_3), 3.76 (3H, s; OCH_3), and 6.5—7.0 (3H, m; aromatic protons); mass spectrum: *m/e* 222 (M^+) and *m/e* 149 (base peak). Found: C, 70.31; H, 8.31%. Calcd for $C_{13}H_{18}O_3$: C, 70.24; H, 8.16%; mol wt 222.3. The acidic fraction (ii; *ca.* 300 mg) was suggested to be a mixture (*ca.* 1 : 1) of the starting acid (**5b**) and the homoacid (**10**) by examination on tlc.

*(+)-5-Methoxy-4,8-dimethyl-1-oxo-1,2,3,4-tetrahydronaphthalene (**11**).* A cyclization of (−)-4-(2-methoxy-5-methylphenyl)pentanoic acid (**10**) to give **11** was accomplished according to the procedures described for the preparation of racemic **11**.[12b] The homoacid (**10**; 3.8 g) in polyphosphoric acid [prepared from phosphoric acid (85%; 100 ml) and phosphorus pentoxide (160 g)] was heated at 100 °C for 1 hr. After a treatment as usual, the product was purified by chromatography on a column of silica gel (60 g; elution with benzene) to give (+)-5-methoxy-4,8-dimethyl-1-oxo-1,2,3,4-tetrahydronaphthalene (**11**; 3.5 g; y: quantitative), mp 76.5—77 °C (crystallized from light petroleum) (lit, [12b] racemic **11**, mp 50—51 °C; lit, [12a] racemic **11** prepared by other route, bp 150—153 °C/7 mmHg), $[\alpha]_D$ +28° (c 2.0, EtOH); IR: 1675, 1575, 1270, 1045, and 815 cm^{-1}; PMR (CCl_4): δ 1.24 (3H, d, J=7 Hz; $C_{(4)}$-CH_3), 2.48 (3H, s; $C_{(8)}$-CH_3), 3.83 (3H, s; OCH_3), 6.75 and 6.90 (each 1 H, d, J=8 Hz; $C_{(6)}$-H and $C_{(7)}$-H); mass spectrum: *m/e* 204 (M^+) and *m/e* 189 (base peak). Found: C, 76.50; H, 7.60%. Calcd for $C_{13}H_{16}O_2$: C, 76.44; H, 7.90%, mol wt 204.3.

*(−)-8-Methoxy-1,5-dimethyl-1,2,3,4-tetrahydronaphthalene (**12**).* (+)-5-Methoxy-4,8-dimethyl-1-oxo-1,2,3,4-tetrahydronaphthalene (**11**) was converted to **12** according to the procedures described for the preparation of racemic **12**.[12a] A mixture of the tetralone (**11**; 1 g), ethanol (15 ml), and 6.5 M hydrochloric acid (30 ml) was heated under reflux, and then amalgamated zinc (*ca.* 70 g) and 10 M hydrochloric acid (25 ml) were added in portions during 12 hr (under reflux). After a work-up as usual, the product was purified by chromatography on a column of silica gel (20 g; elution with light petroleum) to give (−)-8-methoxy-1,5-dimethyl-1,2,3,4-tetrahydronephthalene (**12**: 930 mg; y: quantitative), an oil (lit,[12a] racemic **12**, bp 120—122 °C/3 mmHg), $[\alpha]_D$ −65.5° (c 0.12, EtOH), IR (liquid): 1590, 1480, 1260, 1245, 1100, and 805 cm^{-1}; PMR ($CDCl_3$): δ 1.17 (3H, d, J=7 Hz; $C_{(1)}$-CH_3), 2.13 (3H, s; $C_{(5)}$-CH_3), 3.78 (3H, s; OCH_3), 6.62 and 6.96 (each 1H, d, J=8 Hz; $C_{(6)}$-H and $C_{(7)}$-H); mass spectrum: *m/e* 190 [M^+ ($C_{13}H_{18}O$)] and *m/e* 175 (base peak).

*(+)-8-Hydroxy-1,5-dimethyl-1,2,3,4-tetrahydronaphthalene (**13**).* (−)-8-Methoxy-1,5-dimethyl-1,2,3,4-tetrahydronaphthalene (**12**) was demethylated according to the procedures described for the preparation of racemic **13**.[12b] The methyl ether (**12**; 900 mg) in acetic acid (10 ml) was demethylated under reflux (for 7 hr) by addition of 5.9 M hydrobromic acid (3.5 ml). After a treatment as usual, the product was chromatographed on a column of silica gel (20 g; elution with benzene) to give the crude tetrahydronaphthol (**13**; 600 mg; y: 72%). A part of this material was purified by preparative tlc to afford (+)-8-hydroxy-1,5-dimethyl-1,2,3,4-tetrahydronaphthalene (**13**), mp 91 °C (crystallized from ethanol) (lit, [12b] racemic **13**, mp 93—94 °C), $[\alpha]_D$ +5° (c 2.1, EtOH); IR (liquid): 3400 (br.), 1590, 1485, 1460, 1270, 1015, and 810 cm^{-1}; PMR ($CDCl_3$): δ 1.23 (3H, d, J=7 Hz; $C_{(1)}$-CH_3), 2.13 (3H, s; $C_{(5)}$-CH_3), 6.53 and 6.85 (each 1H, d, J=8 Hz; $C_{(6)}$-H and $C_{(7)}$-H); mass spectrum: *m/e* 176 [M^+ ($C_{12}H_{16}O$)] and *m/e* 161 (base peak).

*(−)-8-Acetonyloxy-1,5-dimethyl-1,2,3,4-tetrahydronaphthalene (**14**).* (+)-8-Hydroxy-1,5-dimethyl-1,2,3,4-tetrahydronaphthalene (**13**) was acetonylated to give **14** according to the procedures reported for the preparation of racemic **14**.[2] A solution of the crude tetrahydronaphthol (**13**; 400 mg) in dry acetone (20 ml) was refluxed with chloroacetone (0.4 ml), potassium iodide (150 mg), and potassium carbonate (1.5 g). After a work-up as usual, the product was purified by chromatography on a column of silica gel [25 g; elution with a mixture of light petroleum and ether (10 : 1)] to afford (−)-8-acetonyloxy-1,5-dimethyl-1,2,3,4-tetrahydronaphtha-

lene (**14**; 320 mg; y: 61%), mp 77 °C (crystallized from light petroleum) (lit,[2] racemic **14**, mp 50—51 °C), $[\alpha]_D$ −5° (*c* 1.7, EtOH), IR (liquid): 1725, 1590, 1475, and 1105 cm^{-1}; PMR ($CDCl_3$): δ 1.26 (3H, d, J=7 Hz; $C_{(1)}$-CH_3), 2.13 (3H, s; $C_{(5)}$-CH_3), 2.30 (3H, s; -$COCH_3$), 4.48 (2H, s; -OCH_2CO-), 6.46 and 6.92 (each 1H, d, J= 8 Hz; $C_{(6)}$-H and $C_{(7)}$-H); mass spectrum: *m/e* 232 [M^+ ($C_{15}H_{20}O_2$)] and *m/e* 174 (base peak).

(−)-*Farfugin A* (***1b***; *an Enantiomer of Natural Farfugin A*). (−)-8-Acetonyloxy-1,5-dimethyl-1,2,3,4-tetrahydronaphthalene (**14**) was converted to **1b** according to the procedures described for the preparation of racemic farfugin A [(±)-**1**].[2] The ether (**14**; 296 mg) was heated with polyphosphoric acid [prepared from phosphoric acid (85%; 10 g) and phosphorus pentoxide (16 g)] at 100 °C for 20 min. The cooled mixture was poured into a mixture of ice and water and extracted with ether. The organic layer was washed successively with 1% sodium hydroxide and brine, dried over anhydrous magnesium sulfate, and evaporated to give a residue, which was chromatographed on a column of silica gel. Elution with light petroleum gave (−)-farfugin A (**1b**; 150 mg; y: 55%), mp 78 °C (crystallized from ethanol) [lit.,[2] racemic farfugin A [(±)-**1**], mp 73—73.5 °C; lit,[2] natural (+)-farfugin A (**1a**), mp 80.5—82.5 °C], $[\alpha]_D$ −27° (*c* 0.7, EtOH)[7] [lit,[2] natural (+)-farfugin A, $[\alpha]_D$ +39° (*c* 0.34, EtOH)]; IR: 1590, 1540, 1525, 1430, 1325, 1100, 1018, 855, 780, and 765 cm^{-1}; UV (EtOH): λ_{max} 291 nm (ε 2500), 281 (2300), and 252 (10500); PMR ($CDCl_3$): δ 1.38 (3H, d, J=7.5 Hz; $C_{(9)}$-CH_3), 2.18 (3H, d, J=1.2 Hz; $C_{(3)}$-CH_3), 2.28 (3H, s; $C_{(5)}$-CH_3), 7.08 (1H, s; $C_{(4)}$-H), and 7.23 (1H, m; $C_{(2)}$-H); mass spectrum: *m/e* 214 (M^+) and *m/e* 199 (base peak). Found: C, 84.25; H, 8.64%. Calcd for $C_{15}H_{18}O$: C, 84.07; H, 8.47%; mol wt 214.2. The spectral data (IR, UV, PMR, and mass spectrum) of **1b** were identical with those[2] of natural (+)-farfugin A. The compound (**1b**) was thus shown to be an enantiomer of natural (+)-farfugin A.

References

1) A preliminary account of this paper: M. Tada, Y. Moriyama, Y. Tanahashi, and T. Takahashi, *Tetrahedron Lett.*, **1972**, 5251.

2) H. Nagano, Y. Moriyama, Y. Tanahashi, T. Takahashi, M. Fukuyama, and K. Sato, *Chem. Lett.*, **1972**, 13; H. Nagano, Y. Moriyama, Y. Tanahashi, and T. Takahashi, This Bulletin, **47**, 1994 (1974).

3) M. Tada, Y. Moriyama, Y. Tanahashi, T. Takahashi, M. Fukuyama, and K. Sato, *Tetrahedron Lett.*, **1971**, 4007; M. Tada, Y. Moriyama, Y. Tanahashi, and T. Takahashi, This Bulletin, **47**, 1999 (1974).

4) M. Tada, Y. Tanahashi, Y. Moriyama, and T. Takahashi, *Tetrahedron Lett.*, **1972**, 5255.

5) a) H. v. Pechmann and J. B. Cohen, *Ber.*, **17**, 2187 (1884); b) K. Fries and W. Klostermann, *Ann.*, **362**, 1 (1908).

6) K. Sato, T. Amakasu, and S. Abe, *J. Org. Chem.*, **29**, 2971 (1964); 3,4-dihydro-4,6-dimethylcoumarin (**4**) was prepared by other route.

7) Optical purities of **5a**, **5b**, and **1b** were undetermined.

8) N. F. Hayes and R. H. Thompson, *J. Chem. Soc.*, **1956**, 1585; racemic **7** was prepared by other route.

9) G. W. Kenner and N. R. Williams, *J. Chem. Soc.*, **1955**, 522.

10) Though these compounds (**6** and **8**) were prepared from optically less active dextrorotatory acid (**5a**), the ORD data showed enough that their asymmetric centers must be (S).

11) J. Almy and D. J. Cram, *J. Amer. Chem. Soc.*, **91**, 4459 (1969).

12) a) O. P. Vig, S. S. Sandhu, and S. M. Mukherji, *J. Indian Chem. Soc.*, **34**, 81 (1957); *Chem. Abstr.*, **51**, 16347f (1957); b) S. M. Bloom, *J. Amer. Chem. Soc.*, **80**, 6280 (1958).

Conformation and Circular Dichroism of Several *N*-Acyl-L-prolines

Hisao NISHIHARA, Koji NISHIHARA, Tamio UEFUJI, and Naokazu SAKOTA

Department of Industrial Chemistry, Faculty of Engineering, Ehime University, Bunkyo-cho, Matsuyama 790

(Received Mach 19, 1974)

NMR and CD studies were carried out for acetyl-L-proline, isovaleroyl-L-proline, isobutyroyl-L-proline, pivaloyl-L-proline and benzoyl-L-proline. It was found that *N*-acetyl-L-proline has two rotational isomers about the amide bond, *S-trans* and *S-cis* conformers even at room temperature, and that the population of the former is greater than that of the latter except for pivaloyl-L-proline, which consists only of the *S-trans* conformer. The two isomeric *N*-acyl-L-prolines showed different CD peaks of opposite sign associated with the n→π^* transition of the amide group.

Investigations have been reported for the hindered internal rotation about an amide bond. Phillips[1] reported that two NMR peaks assigned to the methyl groups of *N,N*-dimethyl formamide suggest the coexistence of the two rotational isomers about the amide bond even at room temperature. The alternating photocopolymerization of methacryloyl-L-valine methyl ester with maleic anhydride[2,3] also suggests that the amide compound assumes a planar *S-trans* conformation about the amide bond and the hydrogen bond between the amide proton and the ester carbonyl oxygen. In order to elucidate the participation of the amide proton in this planar conformation, the conformation of methacryloyl-L-proline (MAP)[4] was studied, one of the two rotational isomers about the amide bond, the *S-trans* isomer, being predominant at room temperature.

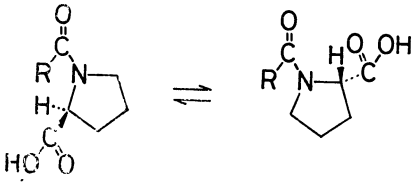

S-cis *S-trans*

On the other hand, the CD spectrum of MAP shows a negative CD maximum at 227 nm., accompanied by a shoulder at about 245 nm,[4] which would be ascribed to the *S-cis* isomer which was less stable than the other one.

We have synthesized several *N*-acyl-L-prolines, acetyl-L-proline (AP), isovaleroyl-L-proline (IVP), isobutyroyl-L-proline (IBP), pivaloyl-L-proline (PP) and benzoyl-L-proline (BP) in order to investigate their CD and NMR spectra. The NMR signals assigned to the α-methine proton of L-proline moiety are given in Fig. 1. Two quartet resonances appeared except for PP. They would be ascribed to the two rotational isomers about the amide bond as in the case of MAP. PP, however, showed only one resonance peak at 4.17 ppm even at −30 °C. The Stewart model of PP showed that the *S-cis* conformation could not possibly exist and the resonance peak of the methine proton of PP would correspond to that of the *S-trans* conformer. This suggests that a resonance peak at a higher magnetic field (Fig. 1) should be assigned to the methine proton of the *S-trans* conformer, which was the more predominant of the two conformations.

The equilibrium constant ($K=[S\text{-}trans]/[S\text{-}cis]$) (Table 1) was calculated from the area ratio of the corresponding two resonance peaks (Fig. 1), and tends to increase with the bulkiness of the R group.

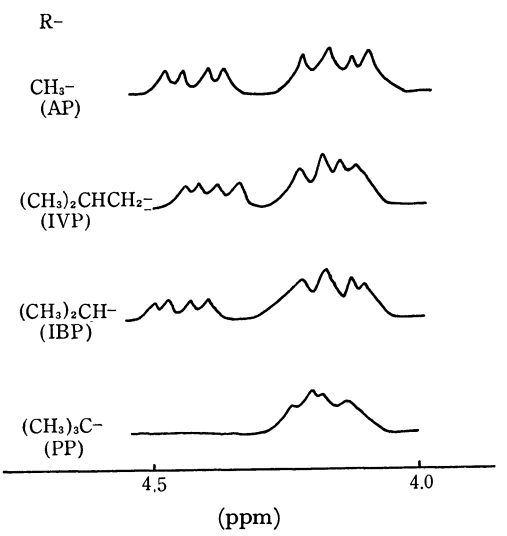

Fig. 1. NMR signal of α-methine proton of *N*-acyl-L-prolines in DMSO-d_6 at 21 °C. Lock; HMDS

TABLE 1. EQUILIBRIUM CONSTANT AND ACTIVATION FREE ENERGY FOR THE TRANSFORMATION BETWEEN *S-cis* AND *S-trans* CONFORMERS (in DMSO-d_6)

Compound	R-	$K\left(=\frac{[S\text{-}trans]}{[S\text{-}cis]}\right)$	$\Delta F^{\neq}_{Tc}$ (kcal/mol)	T_c (K)
AP	CH_3-	2.9	19.0±0.2	365
IVP	$(CH_3)_2CHCH_2$-	3.1	18.6±0.2	361
IBP	$(CH_3)_2CH$-	3.5	18.5±0.2	359
PP	$(CH_3)_3C$-	*a)	—	—

a) *S-trans* only

Temperature dependence of the NMR signals assigned to the α-methine proton of IVP (Fig. 2) shows coalescence between them as well as AP and IBP. The activation free energy for the transformation between the two isomers at the coalescence temperature ($\Delta F^{\neq}_{Tc}$) was caluclated from the NMR data in DMSO-d_6 by

$$\Delta F^{\neq}_{Tc} = 2.303\, RT_c \log \frac{\sqrt{2}\,\kappa k T_c}{\pi \Delta \nu h} \qquad (1)$$

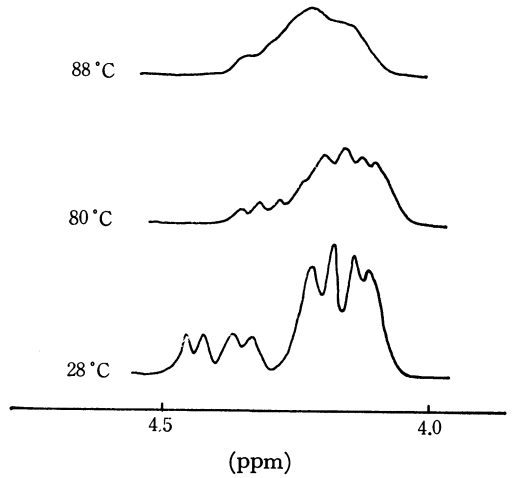

Fig. 2. NMR signal of α-methine proton of IVP in DMSO-d_6. Lock; HMDS

Table 2. Chemical shift of α-methine proton of *N*-acyl-L-prolines from HMDS at 21 °C

Compound	in $CDCl_3$		in DMSO-d_6	
	S-cis	*S-trans*	*S-cis*	*S-trans*
AP	4.37 ppm	4.50 ppm	4.43 ppm	4.15 ppm
IVP	4.42	4.53	4.40	4.17
IBP	4.44	4.51	4.47	4.17
PP	—	4.48	—	4.19
BP	4.22	4.67	4.27	4.37
MAP	4.52	4.53	4.43	4.19

where T_c is the coalescence temperature, $\Delta\nu$ the difference in chemical shift of the α-methine proton of the two isomers, the transmission coefficient κ being assumed to be unity. The $\Delta F^{\neq}_{T_c}$ values suggest that it would not be easy to separate the two isomers from each other.

The chemical shift of α-methine proton of *N*-acyl-L-proline was measured in DMSO-d_6 and $CDCl_3$ at 21 °C. The δ values are shown in Table 2. PP showed only one methine proton signal in both solvents at 21 °C and −30 °C, but the other *N*-acyl-L-prolines showed two methine proton signals in both solvents even at room temperature. The larger of the two methine proton signals was assigned to that of *S-trans* conformer. Thus a methine proton of *S-cis* conformer shows an almost equal δ value in both solvents, but the δ value of methine proton of *S-trans* conformer differed by about 0.35 ppm. It seems that the methine proton of *S-trans* conformer has a larger solvent effect than that of *S-cis* conformer, since the latter would receive a larger steric hindrance by the R group. In the case of BP, however, the methine proton signal of *S-trans* conformer appeared at a lower magnetic field than that of *S-cis* one in both solvents. This might be ascribed to the magnetic anisotropy due to the benzene ring.

The CD spectra of *N*-acyl-L-prolines and L-proline were measured in methanol at 25 °C (Fig. 3). The small CD absorption maximum of L-proline at 220 nm derived from the n–π^* transition of the carboxyl group

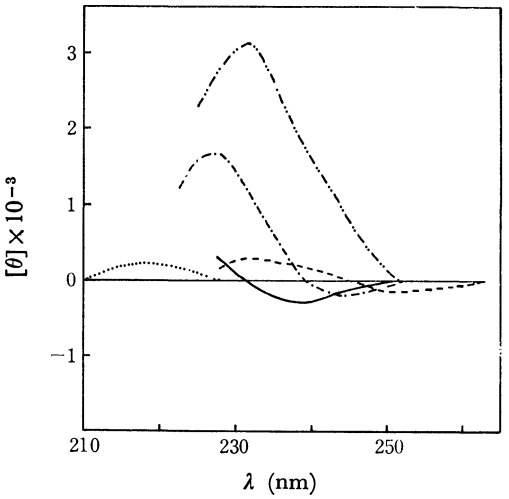

Fig. 3. The CD spectra of AP (——), IVP (----), IBP (—·—), PP (—··—) and L-proline (·····) in methanol at room temperature.

would contribute a negligible effect on the CD curves of *N*-acyl-L-prolines below 225 nm. The CD absorption of the four *N*-acyl-L-prolines over the spectral region from 225 to 255 nm. would be correlated to the n–π^* transition of the amide group. Since the only one conformation of PP was illustrated to be the *S-trans* one by NMR data, the positive CD maximum of PP at 230 nm. would be ascribed to the n–π^* transition of the amide group with *S-trans* conformation. In the case of AP, IVP and IBP which have a *S-cis* conformer together with the *S-trans* conformer, a weak negative absorption maximum appears at 235 to 250 nm. besides a positive absorption maximum around 230 nm. The negative CD maximum, therefore, would be due to the *S-cis* conformer of *N*-acyl-L-proline. The same CD phenomenon as this was found for poly-L-proline.[5,6] The maximum wavelength and sign of the CD maximum of the *trans* isomer was found to differ from those of the *cis* isomer.

The CD spectrum of MAP was measured at 25 °C in methanol.[4] MAP showed a CD curve with a different shape from those of *N*-acyl-L-prolines (Fig. 3).

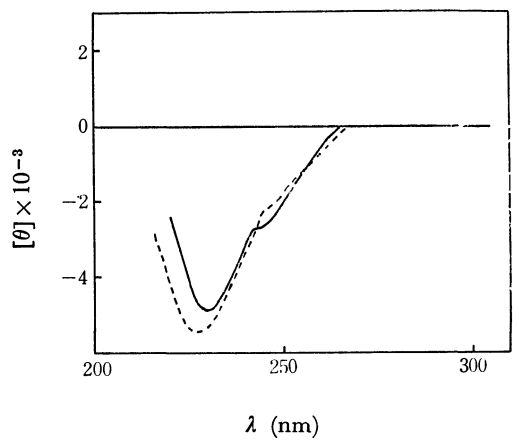

Fig. 4. The CD spectra of BP (——) and MAP (----) in methanol at room temperature.

The former showed a large negative peak centered at 228 nm with a shoulder near 245 nm, while the latter showed a positive peak with a small negative one which appeared at a higher wavelength region. The CD spectrum of BP was similar to that of MAP. Both spectra are shown in Fig. 4. The result will be explained from the fact that both BP and MAP have an α,β-unsaturated carbonyl group.[4,7] They also have two rotational isomers, *S-trans* and *S-cis* conformers as in the case of AP, IVP and IBP, all of which exhibited two CD peaks of opposite sign. Thus, it seems that the sign of the CD maximum of *S-cis* conformer of *N*-acyl-L-proline differs from that of *S-trans* conformer. A shoulder at *ca.* 245 nm appearing in the negative large CD absorption of MAP and BP, would be ascribed to the overlap of a minor positive CD absorption of the *S-cis* conformer on a major negative one of the *S-trans* conformer.

Experimental

N-Acyl-L-prolines were prepared by the reaction of the corresponding acyl chloride with L-proline according to the method of Sakota.[7] Acetyl-L-proline: mp 114.0—115.5 °C, $[\alpha]_D^{24}$ −79.1 ($c=1$, methanol). Isovaleryol-L-proline: mp 70.2—71.9 °C, $[\alpha]_D^{24}$ −81.1 ($c=1$, methanol). Isobutyrol-L-proline: mp 123.0—124.1 °C, $[\alpha]_D^{24}$ −86.7 ($c=1$, methanol). Pivaloyl-L-proline: mp 128.3—129.6 °C $[\alpha]_D^{24}$ −71.9 ($c=1$, methanol). Benzoyl-L-proline: mp 153.9—154.3 °C, $[\alpha]_D^{24}$ −90.9 ($c=1$, methanol).

NMR spectra were recorded with a JEOL Model JNM-4H-100 spectrometer operating at 100 MHz. CD spectra were measured with a JASCO Model ORD/UV5 spectropolarimeter.

References

1) W. D. Phillips, *J. Chem. Phys.* **23**, 1363 (1955).
2) K. Nishihara, A. Suzuoka, and N. Sakota, *J. Polym. Sci., Polym. Chem. Ed.*, **11**, 2315 (1973).
3) K. Nishihara and N. Sakota, *ibid.*, **11**, 3171 (1973).
4) K. Nishihara, H. Nishihara, and N. Sakota, This Bulletin **46**, 3894 (1973).
5) F. A. Bovey and F. P. Hood, *J. Amer. Chem. Soc.*, **88**, 2326 (1966).
6) M. L. Tiffany and S. Krimm, *Biopolymers*, **8**, 347 (1969).
7) N. Sakota, *Nippon Kagaku Zasshi*, **88**, 1087 (1968).

Synthesis of Dihydrostreptobiosamine[1]

Sumio UMEZAWA, Hiroshi SANO, and Tsutomu TSUCHIYA

Department of Applied Chemistry, Faculty of Engineering, Keio University, Hiyoshi, Kohoku-ku, Yokohama 223

(Received May 28, 1974)

The isopropylidene derivative (**4**) of benzyl dihydrostreptoside and 3,4,6-tri-*O*-acetyl-2-amino-*N*-anisylidene-2-deoxy-α-L-glucopyranosyl bromide (**7**) were prepared, and they were coupled by a modified Koenigs-Knorr condensation. After hydrolysis of the *N*-anisylidene group of the product, *N*-methoxycarbonylation followed by *N*-methylation was accomplished to afford the fully protected derivative (**9**) of dihydrostreptobiosamine, which was, after deblocking, led to benzyl dihydrostreptobiosaminide and dihydrostreptobiosamine.

Dihydrostreptobiosamine is the disaccharide portion of dihydrostreptomycin and obtained[2] by acid hydrolysis of dihydrostreptomycin. In our synthesis of dihydrostreptomycin,[1] the initial objective was the synthesis of dihydrostreptobiosamine, that will be described here in detail.

The syntheses of the individual components of dihydrostreptomycin have been reported by 1965. Dihydrostreptose has been synthesized by Dyer *et al.*[3] and 2-deoxy-2-methylamino-L-glucose, by Folkers and his associates.[4]

Glycosidation of dihydrostreptose[3] or transglycosidation of methyl dihydrostreptosides with benzyl alcohol and hydrogen chloride gave a syrup of benzyl α-dihydrostreptoside (**1**) respectively. Its structure was confirmed by the NMR spectral studies of its diacetyl derivative (**2**), thus excluding a potential rearrangement which may result in the formation of another furanoid compound (**1'**) having the C-3' oxygen atom as a ring oxygen.

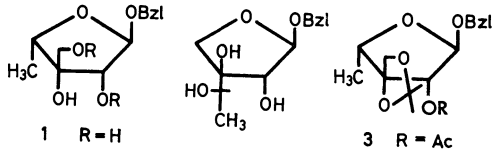

The glycosidic linkage between dihydrostreptose and 2-deoxy-2-methylamino-L-glucose is known to be resistant to acid-hydrolysis, however, we found that methanolysis of methyl *N*-methoxycarbonyldihydrostreptobiosaminide, prepared from methyl dihydrostreptobiosaminide[2,5] and methyl chloroformate, was smooth to give methyl α- and β-dihydrostreptoside together with methyl 2-deoxy-2-methoxycarbonylamino-*N*-methyl-L-glucopyranosides.

The glycoside (**1**) was treated with 2,2-dimethoxypropane in *N,N*-dimethylformamide (DMF) in the presence of *p*-toluenesulfonic acid, and the resulting isopropylidene derivative was acetylated with acetic anhydride in pyridine to give the 2-*O*-acetyl-3,3'-*O*-isopropylidene derivative (**3**) in a 50% yield. Isopropylidenation was, therefore, found to occur between hydroxyl groups at C-3 and C-3' in preference to those at C-2 and C-3. The NMR spectrum of **3** revealed the presence of an *O*-acetyl group at C-2. Deacetylation of **3** with sodium methoxide gave **4**. An alternative protection of the hydroxyl groups at C-3 and C-3' with a carbonate group was also found to be successful.[6]

Another key compound for the synthesis of dihydrostreptobiosamine was a fully blocked glycosyl halide of 2-amino-2-deoxy-L-glucose. The 2-amino-2-deoxy-L-glucose has been synthesized from L-arabinose by Kuhn and Kirschenlohr.[7] Incidentally, we have previously reported an improved synthesis[8] of paromamine which is an α-glycoside of 2-amino-2-deoxy-D-glucose. The synthesis of this structurally rather simple antibiotic is characterized by some interesting points such as the formation of α-D-glycosidic linkage and a suitable blocking method for the coupling materials. The Koenigs-Knorr condensation of 3,4,6-tri-*O*-acetyl-2-amino-*N*-anisylidene-2-deoxy-α-D-glucopyranosyl bromide[9] with a protected 2-deoxystreptamine has already been found to give an 85% yield of a mixture of two α-glycosides.

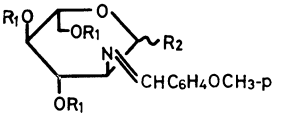

	R_1	R_2
5	H	OH
6	Ac	OAc(β-anomer)
7	Ac	Br (α-anomer)

In analogy to this synthesis, 2-amino-2-deoxy-L-glucose was converted into a Schiff base (**5**) by treatment with anisaldehyde in aqueous ethanol, and, acetylation of the anisylidene derivative with acetic anhydride in pyridine gave the 1,3,4,6-tetra-*O*-acetyl derivative (**6**), which, on treatment with hydrogen bromide–acetic acid in methylene chloride, gave the desired α-glycosyl bromide (**7**). The structure was well defined by the NMR spectrum.

Condensation of **4** with the glycosyl bromide (**7**) in benzene in the presence of mercuric cyanide and Drierite at room temperature was followed by treatment with a mixture of 50% acetic acid and methanol and the crude deanisylidenated product was treated with methyl chloroformate and sodium carbonate in aqueous acetone to give the *N*-methoxycarbonyl disaccharide (**8**) in 42% overall yield from **4**. The NMR spectrum clearly showed that the two components were successfully coupled, and the IR spectrum showed that there occurred no O→N acetyl migration which is sometimes experienced between adjacent amino and acetoxy groups.

Treatment of **8** with methyl iodide and silver oxide in DMF gave the corresponding *N*-methyl derivative (**9**) in a 72% yield. In the NMR spectrum the coupling constant (J 3.3 Hz) indicated an equatorial-axial H-1-H-2 relationship and thus the α-configuration for the 2-amino-2-deoxy-L-glucose moiety.

Deacetylation of **9** with sodium methoxide gave **10**,

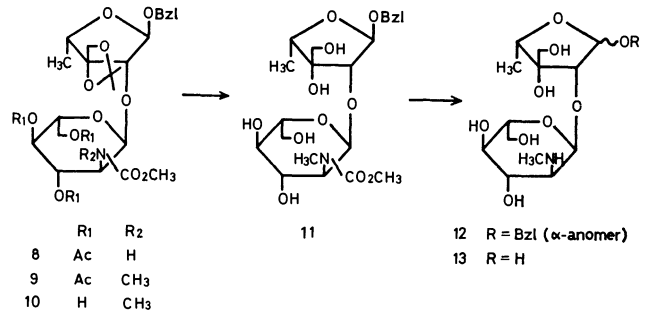

	R_1	R_2
8	Ac	H
9	Ac	CH_3
10	H	CH_3

11

12 R = Bzl (α-anomer)
13 R = H

and, deisopropylidenation with 2 M hydrochloric acid–methanol (1 : 1) at room temperature gave the benzyl *N*-methoxycarbonyl-α-dihydrostreptobiosaminide (**11**). It was identified with the authentic specimen, which was prepared from benzyl α-dihydrostreptobiosaminide.[10] Treatment of the benzyl α-dihydrostreptobiosaminide with methyl chloroformate readily gave the natural specimen.

Hydrolysis of **11** with aqueous barium hydroxide, followed by neutralization with dilute hydrochloric acid, gave the hydrochloride of benzyl α-dihydrostreptobiosaminide (**12**) in a 48% overall yield from **9**. Finally, hydrogenolysis of the benzyl glycoside (**12**) over palladium black gave dihydrostreptobiosamine (**13**). The IR and NMR spectra of these synthetic benzyl dihydrostreptobiosaminide and dihydrostreptobiosamine were identical with those of the natural specimens,[2,10] respectively, in every respect.

Experimental

Thin layer (tlc) and column chromatography were carried out on silica gel of Silica Rider 5B (Daiichi Pure Chemicals Co., Ltd., Tokyo) and Wakogel C-200 (Wako Pure Chemicals Co., Ltd., Osaka) unless otherwise stated, respectively, and the spots on tlc were visualized with sulfuric acid.

*Benzyl α-Dihydrostreptoside (**1**).* *a) From Dihydrostreptose*: A solution of well dried dihydrostreptose (78 mg) in 2 M hydrogen chloride in benzyl alcohol (4.4 ml) was heated at 50 °C for 40 hr. Basic lead carbonate (1.37 g) was then added and the mixture was stirred for 3 hr. The mixture was filtered and the solid was washed with chloroform. The filtrate and the washings were combined and evaporated to give a yellow oil, which was chromatographed on a column of the silica gel with benzene-ethanol (8 : 1). A colorless syrup (62 mg, 52%) was obtained, $[\alpha]_D^{25}$ −100° (*c* 1, $CHCl_3$).

Found: C, 61.40; H, 7.24%. Calcd for $C_{13}H_{18}O_5$: C, 61.40; H, 7.14%.

NMR (in $CDCl_3$ containing D_2O): τ 8.78 (3H d, *J* 6.6 Hz, CH_3), 6.47 (2H s, CH_2 at C-3′), 5.88 (1H d, 2 Hz, H-2), 5.40 (AB q centered at τ 5.40, *J* 12 Hz, $OCH_2C_6H_5$), 4.98 (1H d, *J* 2 Hz, H-1), 2.68 (5H s).

b) From Methyl α-Didydrostreptoside and Methyl β-Dihydrosteptoside: Methyl α- or β-dihydrostreptoside was treated with benzyl alcohol and hydrogen chloride in a similar manner as described above to give **1** in yields of 50—60%.

Methyl N-Methoxycarbonyldihydrostreptobiosaminide. A solution of methyl dihydrostreptobiosaminide hydrochloride[2,5] (5.20 g) and anhydrous sodium carbonate (1.84 g) in aqueous acetone (1 : 1, 100 ml) was treated with methyl chloroformate (2.65 ml) in a usual manner to give a syrup, 5.15 g (94%), $[\alpha]_D^{24}$ −121° (*c* 1, MeOH).

Found: C, 46.36; H, 7.42; N, 3.17%. Calcd for $C_{16}H_{29}NO_{11}$: C, 46.71; H, 7.11; N, 3.40%.

NMR (in D_2O): τ 8.80 (3H d, CCH_3), 6.98 (3H s, NCH_3), 6.58 (3H s, OCH_3), 6.49 (2H s, CH_2 at C-3′), 6.27 (3H s, CO_2CH_3), 4.95 (2H m, H-1,1′).

Methyl Dihydrostreptosides. A solution of methyl *N*-methoxycarbonyldihydrostreptobiosaminide (44.3 g) in 2 M methanolic hydrogen chloride (720 ml) was refluxed for 64 hr. Basic lead carbonate (223 g) was added and the mixture was stirred for several hours to give pH about 4. Filtration was followed by evaporation under reduced pressure to give an oil, which was chromatographed on a short column of Dowex 50W-X4 (K form) to remove the color impurities accompanied, and then again chromatographed on Dowex 50W-X4 (K form, 6000 ml) with water as eluent to give five fractions. Evaporation of the fractions in turn gave the starting material, methyl α-dihydrostreptoside, methyl 2-deoxy-2-methoxycarbonylamino-*N*-methyl-β-L-glucopyranoside, methyl β-dihydrostreptoside and methyl 2-deoxy-2-methoxycarbonylamino-*N*-methyl-α-L-glucopyranoside, respectively (cited in the order of elution).

Methyl α-Dihydrostreptoside. A syrup, 9.62 g (53%), $[\alpha]_D^{25}$ −111° (*c* 2, $CHCl_3$), R_f 0.39 (tlc with benzene-ethanol 4 : 1); NMR ($CDCl_3$): τ 8.78 (3H d, CCH_3), 6.58 (3H s, OCH_3), 6.44 (2H s, CH_2), 5.10 (1H d, *J* 4.0 Hz, H-1). Found: C, 47.14; H, 7.92%. Calcd for $C_7H_{14}O_5$: C, 47.18; H, 7.92%.

Methyl β-Dihydrostreptoside. A syrup, 1.80 g (10%), $[\alpha]_D^{20}$ +100° (*c* 2, $CHCl_3$), R_f 0.20 (tlc with benzene-ethanol 4 : 1); NMR ($CDCl_3$): τ 8.72 (3H d, CCH_3), 6.53 (3H s, OCH_3), 6.36 (2H s, CH_2), 5.14 (1H d, *J* 4.6 Hz, H-1). Found: C, 46.89; H, 7.84%.

Methyl 2- Deoxy-2- methoxycarbonylamino- N- methyl-α-L-glucopyranoside. A solid, 9.39 g (35%), $[\alpha]_D^{22}$ −143° (*c* 2, MeOH), R_f 0.30 (tlc with benzene-ethanol 4 : 1); NMR (D_2O): τ 7.02 (3H s, NCH_3), 6.58 (3H s, OCH_3), 6.23 (3H s, CO_2CH_3), 5.14 (1H d, *J* 2.1 Hz, H-1). Found: C, 45.18; H, 7.15; N, 5.24%. Calcd for $C_{10}H_{19}NO_7$: C, 45.28; H, 7.22; N, 5.28%.

Methyl 2-Deoxy-2-methoxycarbonylamino-N-methyl-β-L-glucopyranoside. A crystal (from ethanol-ether), 3.59 g (13%), mp 184—185 °C, $[\alpha]_D^{23}$ +19° (*c* 2, MeOH), R_f 0.14 (tlc with benzene-ethanol 4 : 1); NMR (D_2O): τ 7.06 (3H s, NCH_3), 6.43 (3H s, OCH_3), 6.23 (3H s, CO_2CH_3), 5.23 (1H d, *J* 8.0 Hz, H-1). Found: C, 44.90; H, 7.10; N, 5.12%.

Both of the 2-deoxy-2-methylamino-α- and β-L-glucoside derivatives obtained above could be transformed to 2-deoxy-2-methylamino-L-glucose hydrochloride[4] by refluxing them in 6 M hydrochloric acid for 2 hr, respectively, in yield of ~80%, mp 156—161 °C (decomp) (from ethanol).

*Benzyl 2,3′-Di-O-acetyl-α-dihydrostreptoside (**2**).* Compound **1** (178 mg) was treated with acetic anhydride in pyridine in a usual manner to give a syrup, 156 mg (66%), $[\alpha]_D^{21}$ −107° (*c* 2, $CHCl_3$).

Found: C, 60.39; H, 6.33%. Calcd for $C_{17}H_{22}O_7$: C, 60.35; H, 6.55%.

NMR (in $CDCl_3$): τ 8.70 (3H d, CCH_3), 7.92 and 7.87 (each 3H s, Ac), 5.75 (AB q centered at 5.75, *J* 12 Hz, CH_2 at C-3′), 4.87 and 4.78 (each 1H d, H-1 and H-2).

*Benzyl 2-O-Acetyl-3,3′-O-isopropylidene-α-dihydrostreptoside (**3**).* To a solution of **1** (1.26 g) and anhydrous *p*-toluenesulfonic acid (46 mg) in dry DMF (21 ml), 2,2-dimethoxypropane (4.2 ml) was added and the solution was heated at 60 °C for 2.5 hr. The solution was poured into a mixture of saturated sodium hydrogen carbonate solution (100 ml) and benzene (65 ml) under stirring. The aqueous layer was

separated and extracted with benzene (65 ml×2). The combined benzene layer was dried with sodium sulfate, and evaporated to give a syrup (1.4 g). To a solution of the syrup in pyridine (27 ml), acetic anhydride (1.7 ml) was added and the solution was allowed to stand overnight at room temperature. Water (0.3 ml) was added and the solution was poured into water. The mixture was extracted with benzene (70 ml×3). The combined benzene layer was dried over sodium sulfate and evaporated. Chromatography of the resulting syrup on a short column of silica gel with benzene–methyl ethyl ketone (MEK) (30 : 1) gave a syrup, 841 mg (50%), $[\alpha]_D^{25}$ −110° (*c* 2, $CHCl_3$).

Found: C, 64.28; H, 7.22%. Calcd for $C_{18}H_{24}O_6$: C, 64.27; H, 7.19%.

NMR (in $CDCl_3$): τ 8.70 (3H d, CCH_3), 8.64 and 8.59 (each 3H s, isopropylidene), 7.89 (3H s, Ac), 6.13 and 5.69 (each 1H d, J 9.2 Hz, CH_2 at C-3′), 4.93 and 4.82 (each 1H d, J 1.6 Hz, H-1 and H-2).

*Benzyl 3,3′-O-Isopropylidene-α-dihydrostreptoside (**4**).* To a solution of **3** (203 mg), sodium methoxide in methanol was added and the mixture was allowed to stand for 2 hr. After evaporation, the residue was dissolved in benzene (12 ml) and the solution was washed with water, dried over sodium sulfate, and the solvent was removed to give an oil (165 mg, 94%). Tlc with benzene–MEK (20 : 1) gave R_f 0.26, $[\alpha]_D^{18}$ −85° (*c* 1, $CHCl_3$).

Found: C, 65.24; H, 7.28%. Calcd for $C_{16}H_{22}O_5$: C, 65.29; H, 7.53%.

NMR (in $CDCl_3$): τ 8.54 (6H s, isopropylidene), 4.95 (1H d, J∼1 Hz, H-1).

*2-Amino-N-anisylidene-2-deoxy-L-glucose (**5**).* To a solution of 2-amino-2-deoxy-L-glucose hydrochloride (3.21 g) in 1 M sodium hydroxide (15 ml), a solution of anisaldehyde (1.87 ml) in ethanol (3.8 ml) was added and the mixture was stirred at room temperature for 40 min. On seeding, **5** was precipitated as crystals. After storage in a refrigerator overnight, the crystals were filtered and washed with cold water and with a mixture of ethanol–ether (1 : 2), 3.19 g (72%), mp 181—182 °C, $[\alpha]_D^{20}$ −33° (*c* 1, pyridine); IR (KBr): 1610, 1645 cm^{-1}.

Found: C, 56.85; H, 6.43; N, 4.87%. Calcd for $C_{14}H_{19}NO_6$: C, 56.56; H, 6.44; N, 4.71%.

*1,3,4,6-Tetra-O-acetyl-2-amino-N-anisylidene-2-deoxy-β-L-glucopyranose (**6**).* To a suspension of **5** (2.85 g) in ice cold pyridine (14 ml), acetic anhydride (7.46 ml) was added and the mixture was stirred for 1 hr at the temperature. The resulting clear solution was allowed to stand overnight at room temperature and poured into ice-water. Precipitates occurred were filtered and washed with cold water to give a solid of **6**, 3.85 g (86%), mp 187—189 °C, $[\alpha]_D^{24}$ −100° (*c* 1, $CHCl_3$).

Found: C, 56.56; H, 5.77; N, 3.13%. Calcd for $C_{22}H_{27}NO_{10}$: C, 56.77; H, 5.85; N, 3.01%.

NMR (in $CDCl_3$): τ 8.12, 7.98, 7.97, 7.90 (each 3H s, Ac), 6.15 (3H s, OCH_3), 4.02 (1H d, J 8.0 Hz, H-1), 1.81 (1H s, =CH–).

*3,4,6-Tri-O-acetyl-2-amino-N-anisylidene-2-deoxy-α-L-glucopyranosyl Bromide (**7**).* To a suspension of **6** (1.50 g) in dichloromethane (0.7 ml), a saturated solution (2.6 ml) of hydrogen bromide in glacial acetic acid containing 5% acetic anhydride was added and the solution was allowed to stand for 3 hr at room temperature in the dark. A mixture of dry ether (6 ml) and petroleum ether (6 ml) was added to precipitate an oil, which was triturated with the above mixture to give a solid. The solid was dissolved in dichloromethane and washed with an aqueous phosphate buffer (pH 6.8) and then with cold water. After drying over sodium sulfate and then over molecular sieves (3A, Wako Pure Chemicals Co., Ltd., Osaka), the solution was concentrated. Addition of ether deposited some amorphous impurities, which was removed by filtration. Subsequent addition of petroleum ether gave needles, 705 mg (45%), mp 110—111 °C, $[\alpha]_D^{20}$ −194° (*c* 1, $CHCl_3$).

Found: C, 49.35; H, 5.02; N, 2.79, Br, 16.42%. Calcd for $C_{20}H_{24}NO_8Br$: C, 49.40; H, 4.97; N, 2.88, Br, 16.44%.

NMR (in $CDCl_3$): τ 8.12, 7.94, 7.89 (each 3H s, Ac), 3.64 (1H d, J 3.5 Hz, H-1), 1.69 (1H s, =CH–).

*Benzyl 2-O-(3,4,6-Tri-O-acetyl-2-deoxy-2-methoxycarbonylamino-α-L-glucopyranosyl)-3,3′-O-isopropylidene-α-dihydrostreptoside (**8**).* To a solution of well dried **4** (270 mg) in dry benzene (5.1 ml), freshly prepared Drierite (730 mg) was added and the mixture was stirred for 1 hr at room temperature. The glycosyl bromide **7** (723 mg) and well dried mercuric cyanide (705 mg) were added and the mixture was stirred at room temperature for 45 hr. Chloroform (60 ml) was added and the organic layer was filtered and washed with saturated sodium hydrogen carbonate solution and then with water. After drying over sodium sulfate, evaporation of the solvents gave a syrup (826 mg). On tlc with benzene–MEK (7 : 1), the syrup gave a main spot at R_f 0.43.

The syrup was dissolved in a mixture of methanol (34 ml) and 50% acetic acid (14 ml) and the solution was allowed to stand at room temperature for 5 hr. Sodium carbonate (6.3 g) was added and the mixture was concentrated to a small volume (∼15 ml). Addition of acetone (60 ml) gave precipitates, which were filtered off. The filtrate was evaporated to give a syrup. On tlc with benzene–MEK (1 : 1), the syrup gave a main spot at R_f 0.42.

To a solution of the syrup in aqueous 60% acetone (15 ml), sodium carbonate (130 mg×3) and methyl chloroformate (0.16 ml×3) were added at 4 hr intervals with stirring at room temperature. On tlc with benzene–MEK (7 : 1), the mixture gave a main spot at R_f 0.3. The reaction mixture was evaporated, and the resulting syrup was chromatographed on a short column of silica gel with benzene–MEK (7 : 1) to give a syrup of **8**, (248 mg, 42% from **4**); $[\alpha]_D^{24}$ −133° (*c* 0.8, $CHCl_3$); IR (in CH_2Cl_2): 1750, 1725 (shoulder), 1520 cm^{-1}.

Found: C, 56.45; H, 6.21; N, 2.32%. Calcd for $C_{30}H_{41}NO_{14}$: C, 56.32; H, 6.46; N, 2.19%.

NMR (in $CDCl_3$): τ 8.67 (3H d, CCH_3), 8,59 (6H s, isopropylidene), 7.98 and 7.95 (6H s and 3H s, Ac), 6.32 (3H s, CO_2CH_3), 5.36 (AB q, $OC\underline{H}_2C_6H_5$), 2.64 (5H s, C_6H_5).

*Benzyl 2-O-(3,4,6-Tri-O-acetyl-2-deoxy-2-methoxycarbonylamino-N-methyl-α-L-glucopyranosyl)-3,3′-O-isopropylidene-α-dihydrostreptoside (**9**).* To a solution of **8** (168 mg) in dry DMF (2.3 ml), methyl iodide (0.066 ml×4) and silver oxide (80 mg×4) were added at 10 hr intervals and the mixture was stirred at room temperature. Chloroform was added to the reaction mixture and the mixture was filtered. The solution was washed with 5% aqueous sodium cyanide and then with water, and dried over sodium sulfate. Evaporation gave a syrup (167 mg), which was purified by column chromatography on silica gel with benzene–MEK (9 : 1) to give a syrup of **9** (122 mg, 72%), $[\alpha]_D^{20}$ −133° (*c* 1.2, $CHCl_3$); IR (KBr): 1760, 1710 cm^{-1}. The peak at 1520 cm^{-1} in **8** had disappeared.

Found: C, 57.06; H, 6.41; N, 2.33%. Calcd for $C_{31}H_{43}NO_{14}$: C, 56.96; H, 6.63; N, 2.14%.

NMR (in $CDCl_3$): τ 8.73 (3H d, CCH_3), 8.64 (6H s, isopropylidene); 8.01, 7.98, 7.96 (each 3H s, Ac); 7.13 (s, more intense) and 7.09 (s) (3H in total, NCH_3, rotamers;

in pyridine-d_6, the signals collapsed to a singlet at 50 °C), 6.29 (3H s, CO_2CH_3), 4.94 (1H d, J 1 Hz, H-1), 4.86 (1H d, J 3.3 Hz, H-1').

*Benzyl 2-O-(2-Deoxy-2-methoxycarbonylamino-N-methyl-α-L-glucopyranosyl)-3,3'-O-isopropylidene-α-dihydrostreptoside (**10**).* Compound **9** was treated with sodium methoxide in methanol in a similar manner as described for the preparation of **4** to give a syrup in a yield of 99%; $[\alpha]_D^{18}$ −121° (*c* 1.7, $CHCl_3$).

Found: C, 56.84; H, 7.07; N, 2.44%. Calcd for $C_{25}H_{37}NO_{11}$: C, 56.92; H, 7.07; N, 2.65%.

*Benzyl 2-O-(2-Deoxy-2-methoxycarbonylamino-N-methyl-α-L-glucopyranosyl)-α-dihydrostreptoside (**11**).* A solution of **10** (64 mg) in 2 M hydrochloric acid–methanol (1 : 1, 3 ml) was allowed to stand at room temperature for 7.5 hr. After neutralization of the solution with Amberlite IRA-900 (OH form), the solution was evaporated to give a syrup. Recrystallization from methanol-chloroform gave needles (38 mg, 67%), mp 184.5—185 °C, $[\alpha]_D^{18}$ −153° (*c* 2, MeOH); IR (KBr): 1675 cm^{-1}.

Found: C, 53.34; H, 6.81; N, 2.83%. Calcd for $C_{21}H_{33}NO_{11}$: C, 53.05; H, 6.99; N, 2.95%.

NMR (in CD_3OD): τ 8.79 (3H d, CCH_3), 6.92 (3H s, NCH_3), 6.48 (2H s, CCH_2OH), 6.24 (3H s, CO_2CH_3), 4.87 (1H broad s, H-1), 4.78 (1H d, J 3 Hz, H-1').

The melting point of this derivative (**11**) was not depressed by admixture with the specimen derived from natural benzyl dihydrostreptobiosaminide.

*Conversion of Natural Benzyl Dihydrostreptobiosaminide into **11**.* Natural benzyl dihydrostreptobiosaminide hydrochloride[10] was treated with methyl chloroformate and sodium carbonate in a similar manner as described in the preparation of **8** to give **11**; mp 184.5—186 °C, $[\alpha]_D^{22}$ −150° (*c* 1, MeOH).

*Benzyl 2-O-(2-Deoxy-2-methylamino-α-L-glucopyranosyl)-α-dihydrostreptoside Hydrochloride (Benzyl α-Dihydrostreptobiosaminide Hydrochloride) (**12**).* A mixture of **10** (90 mg) and 10% aqueous barium hydroxide (4.5 ml) was heated at 70 °C for 2 hr. Carbon dioxide was introduced and the precipitates were filtered off. The filtrate was evaporated and the residue was dissolved in methanol. After filtration, the solution was again evaporated. The procedure was repeated twice. Neutralization of the final methanol solution with hydrochloric acid followed by evaporation gave a glassy solid (62 mg, 72%), $[\alpha]_D^{20}$ −140° (*c* 1, H_2O) (lit[10], −110°).

Found: C, 51.12; H, 7.02; N, 3.08%. Calcd for $C_{20}H_{31}NO_9 \cdot HCl$: C, 51.56; H, 6.92; N, 3.00%.

NMR (in D_2O): τ 8.70 (3H d, CCH_3), 7.06 (3H s, NCH_3), 4.64 (1H d, J 3 Hz), 4.39 (1H d, J 3.5 Hz), 2.46 (5H s, C_6H_5).

*Dihydrostreptobiosamine (**13**).* To a solution of **12** (67 mg) in water (2 ml), 0.05 ml of acetic acid was added and the solution was hydrogenated with palladium black. The solution was filtered and evaporated to give a solid 41 mg (75%), $[\alpha]_D^{21}$ −104° (*c* 1, H_2O).

Found: C, 44.82; H, 7.32; N, 3.40%. Calcd for $C_{13}H_{25}NO_9 \cdot CH_3CO_2H$: C, 45.11; H, 7.32; N, 3.51%.

NMR (in D_2O): τ 8.78 (d, J 6.7 Hz, more intense than the other) and 8.73 (d, J 6.7 Hz) (3H in total, CCH_3); 8.05 (3H s, Ac), 6.88 (3H, NCH_3), 4.52 (1H d, J 3.7 Hz), 4.34 (1H d, J 3.2 Hz).

References

1) "Studies on Aminosugars, XXXVII" by S. Umezawa. (a) Announced previously in a communication to the editor by S. Umezawa, T. Tsuchiya, T. Yamasaki, H. Sano, and Y. Takahashi, *J. Amer. Chem. Soc.*, **96**, 920 (1974). (b) Presented at the 189th Meeting of Japan Antibiotics Research Association, Tokyo, Sept. 1973, at the 3rd Joint Annual Congress of the Chemical Society and the Royal Institute of Chemistry, Imperial College, London, Apr. 1974, and the 30th Annual Meeting of the Chemical Society of Japan, Apr. 1974.

2) J. Fried and O. Wintersteiner, *J. Amer. Chem. Soc.*, **69**, 79 (1947).

3) J. R. Dyer, W. E. McGonigal, and K. C. Rice, *ibid.*, **87**, 654 (1965).

4) F. A. Kuehl, Jr., E. H. Flynn, F. W. Holly, R. Mozingo, and K. Folkers, *ibid.*, **68**, 536 (1946); *ibid.*, **69**, 3032 (1947).

5) N. G. Brink, F. A. Kuehl, Jr., E. H. Flynn, and K. Folkers, *ibid.*, **68**, 2557 (1946).

6) The detail will be published elsewhere.

7) R. Kuhn and W. Kirschenlohr, *Justus Liebigs Ann.*, **600**, 115 (1956).

8) S. Umezawa, T. Miyazawa, and T. Tsuchiya, *J. Antibiot.* (Tokyo), **25**, 530 (1972).

9) L. Zervas and S. Konstas, *Chem. Ber.*, **93**, 435 (1960).

10) G. K. J. Ferguson, I. J. McGilveray, and J. B. Stenlake, *J. Pharm. Pharmacol.*, **17**, Suppl., 68S (1965).

Synthesis of Di-*N*-acetyl-di-*N*-benzyloxycarbonyl-*O*-cyclohexylidenestreptidine[1]

Sumio UMEZAWA, Yoshikazu TAKAHASHI, and Tsutomu TSUCHIYA

Department of Applied Chemistry, Faculty of Engineering, Keio University, Hiyoshi, Kohoku-ku, Yokohama 223

(Received May 28, 1974)

Reaction of streptidine with excess benzyloxycarbonyl chloride, followed by partial alkaline hydrolysis, gave di-*N*-benzyloxycarbonylstreptidine (**1**), which, by treatment with 3,4-dihydro-2*H*-pyran, gave a tetra-*O*-tetrahydropyranyl derivative (**3**). Acetylation of **3** then gave a di-*N*-acetyl derivative (**4**), which was, after removal of the tetrahydropyranyl groups, allowed to react with 1,1-dimethoxycyclohexane to furnish di-*N*-acetyl-di-*N*-benzyloxycarbonyl-*O*-cyclohexylidenestreptidine (**6**). This is the first preparation of a useful intermediate for the synthesis of streptidine glycosides

Streptidine[2] is the aglycone component of streptomycin and related antibiotics. The gross structure of this strongly basic compound was degradatively established by Carter, Folkers, Wintersteiner, and their coworkers,[3] and, its all-*trans* configuration was confirmed by the total synthesis by Wolfrom *et al.*[4]

For the total synthesis of antibiotics of streptomycin series, glycosidation of streptidine is an inevitable process, however, it has been hindered by the extremely low solubility of streptidine and its ordinary derivatives in organic solvents. Thus, a suitable derivative of streptidine for the Koenigs-Knorr condensation was investigated. In the initial stage of our studies, we prepared *O*-cyclohexylidene-di-*N*-nitro-streptidine* from streptamine by the reaction with *S*-methyl-*N*-nitroisothiourea followed by cyclohexylidenation with 1,1-dimethoxycyclohexane, however, the derivative still showed limited solubility in organic solvents, giving poor yields of glycosides when condensed with some glycosyl halides such as tetra-*O*-benzyl-glucopyranosyl chloride. After some attempts, di-*N*-acetyl-di-*N*-benzyloxycarbonyl-*O*-cyclohexylidenestreptidine (**6**) was found to be useful for the glycosylation. The present paper deals with its synthesis.

Reaction of streptidine sulfate with excess benzyloxycarbonyl chloride and 2 M sodium hydroxide in aqueous dioxane gave a mixture of per-*N*,*O*-benzyloxycarbonylated products, which however gave the di-*N*-benzyloxycarbonylstreptidine (**1**) in a 51% yield on prolonged treatment with a mixture of 2 M sodium hydroxide in dioxane at room temperature. In the formula of **1**, the positions of the benzyloxycarbonyl groups attached to nitrogens remain to be established and thus arbitrarily assigned.

Attempts to prepare tetra-*N*-benzyloxycarbonylstreptidine were unsuccessful because the benzyloxycarbonyl groups further introduced to the guanidino groups were unusually unstable to be hydrolyzed together with *O*-benzyloxycarbonyl groups by weak alkaline treatment. Acetylation of **1** with acetic anhydride and pyridine gave the hexaacetyl derivative (**2**). Its structure was confirmed by the NMR spectrum except for the positions of acetyl and benzyloxycarbonyl groups attached to the nitrogens which had been arbitrarily assigned. All attempts to convert **2** into di-*N*-acetyl-di-*N*-benzyloxycarbonylstreptidine (**5**) by alkaline treatment were unsuccessful.

* Mp 195 °C (decomp.). The details will be published elsewhere.

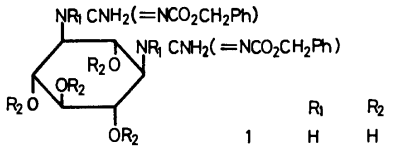

	R_1	R_2
1	H	H
2	Ac	Ac
3	H	THP
4	Ac	THP
5	Ac	H

The following route successfully led to **5**. **1** was converted into the tetra-*O*-tetrahydropyranyl derivative (**3**) in a yield of 70% by the treatment with 3,4-dihydro-2*H*-pyran and *p*-toluenesulfonic acid in DMF. Acetylation of **3** with acetic anhydride and pyridine then gave the di-*N*-acetyl derivative (**4**) quantitatively. Removal of the tetrahydropyranyl groups by the treatment with 50% acetic acid at room temperature for 2.5 hr gave **5** in a yield of 56%. This yield was variable according to the reaction conditions and prolonged reaction lowered the yield.

Finally, treatment of the *N*-protected streptidine with 1,1-dimethoxycyclohexane in the presence of *p*-toluenesulfonic acid in DMF furnished the cyclohexylidene derivative (**6**) as a racemate in a yield of 70%.

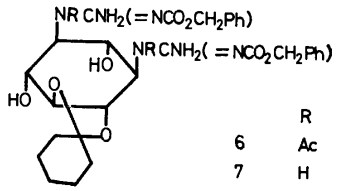

	R
6	Ac
7	H

An alternative simplified route to **6** from di-*N*-benzyloxycarbonylstreptidine (**1**) involving the reaction sequence of cyclohexylidenation, per-*N*,*O*-acetylation, and selective removal of the *O*-acetyl group was unsuccessful owing to the difficulty of the last selective hydrolysis.

Compound **6** was successfully used for the synthesis of dihydrostreptomycin as described in the successive paper. In this stage we tested for deblocking; on treatment of **6** under weakly alkaline condition, de-*N*-acetylation proceeded smoothly to give **7**, whose benzyloxycarbonyl groups remained intact. Further treatment of **7** with 50% acetic acid followed by hydrogenolysis with palladium black gave streptidine. It should be noted that the first introduced benzyloxycar-

bonyl groups at the guanidino portions are relatively stable to weak alkali, while the next introduced *N*-acetyls are easily removed by weakly alkaline hydrolysis. We were pleased with this demonstration, because, if the *N*-acetyl groups are normally resistant to weak alkali, removal of the benzyloxycarbonyl groups would simultaneously occur and the guanidino groups would be further transformed into ureido groups.

Experimental

Thin layer (TLC) and column chromatography were carried out on silica gel of Silica Rider 5B (Daiichi Pure Chemicals Co., Ltd., Tokyo) and Wakogel C-200 (Wako Pure Chemicals Co., Ltd., Osaka) unless otherwise stated, respectively, and the spots on tlc were visualized with sulfuric acid.

Di-N-*benzyloxycarbonylstreptidine (**1**).* To a suspension of streptidine sulfate (10 g) in aqueous dioxane (2 : 1, 750 ml), 2M sodium hydroxide solution (28 ml) was added under stirring. The mixture was cooled in an ice bath and 2M sodium hydroxide solution (68 ml) and benzyl chloroformate (19 ml) were added all at once under vigorous stirring, and stirring was continued for 10 min under cooling. Another aliquot of 2M sodium hydroxide solution (68 ml) and benzyl chloroformate (19 ml) were added and stirring was continued for 10 min. After neutralization with hydrochloric acid, the reaction mixture was evaporated and the residue was extracted with dimethylformamide (DMF) (100 ml×2). Evaporation of the solvent gave a syrup. On tlc with benzene–methanol (10 : 1), the syrup gave at least seven spots ranging in R_f 0.05—0.9.

To a suspension of the syrup in dioxane (200 ml), 2M sodium hydroxide (17 ml×5) was added at intervals. After 120 hr, the mixture gave, on TLC with benzene–methanol (6 : 1), two spots of R_f 0.05 (**1**) and 0.56 (benzyl-alcohol). The mixture was neutralized with hydrochloric acid and evaporated to give a residue, which was extracted with DMF. The solution was concentrated and, to the concentrate, ether was added to give a yellow solid. The solid was chromatographed on a column of Amberlite CG 50 (NH_4 form) with dioxane–water–1M ammonia (1 : 3 : 0.2) as eluent. The fraction containing **1** was evaporated to give a colorless solid (7.55 g, 51%), mp 216—217 °C (decomp.), R_f 0.46 (tlc with chloroform–ethanol–17% NH_3 (20 : 10 : 1)); IR (KBr): 1530—1680 cm^{-1} (five peaks).

Found: C, 54.00; H, 5.70; N, 15.77%. Calcd for $C_{24}H_{30}N_6O_8$: C, 54.33; H, 5.70; N, 15.84%.

NMR (in DMSO-d_6; the sample was treated three times with D_2O): τ 7—6 (6H, skeleton protons), 4.95 (4H s, $C\underline{H}_2C_6H_5$), 2.6 (10H s, C_6H_5).

Di-N-*acetyl-tetra*-O-*acetyl-di*-N-*benzyloxycarbonylstreptidine (**2**).* To a suspension of **1** (150 mg) in pyridine (1.5 ml), acetic anhydride (0.43 ml) was added and the mixture was stirred at room temperature overnight. Two drops of water were added and the solution was evaporated. Addition of water gave a solid, which was washed throughly with water, 170 mg (77%), mp 210—211 °C; IR(KBr): 1550, 1635 (s), 1710 (w), 1760 cm^{-1}.

Found: C, 55.01; H, 5.45; N, 10.74%. Calcd for $C_{36}H_{42}N_6O_{14}$: C, 55.24; H, 5.41; N, 10.74%.

NMR (in $CDCl_3$): τ 8.07, 8.03, 7.96, 7.81 (3, 6, 3, 6H s respectively, Ac), 5.5—4.9 (2H, C$\underline{H}$NAc (?)), 4.75 (4H s, $C\underline{H}_2C_6H_5$), 4.85—4.45 (4H, C$\underline{H}$OAc (?)), 2.6—2.46 (10H m, C_6H_5).

Di-N-*benzyloxycarbonyl-tetra*-O-*tetrahydropyranylstreptidine (**3**).* A solution of **1** (720 mg), 3,4-dihydro-2*H*-pyran (1.83 ml) and fuse dried *p*-toluenesulfonic acid (600 mg) in DMF (9 ml) was heated at 50 °C overnight. Triethylamine (1.5 ml) was added and the solution was evaporated. A chloroform solution of the residue was washed with sodium hydrogen carbonate solution, and then with water, dried (Na_2SO_4) and concentrated. Petroleum ether was added to give a solid (980 mg), which was chromatographed in a short column of silica gel with chloroform–ethanol–17% ammonia (400 : 32 : 3)), affording a colorless solid, 830 mg (70%), mp 118—119.5 °C, R_f 0.46 (with chloroform–ethanol–17% ammonia (100 : 8 : 1)); IR (KBr): 1540—1660 cm^{-1}.

Found: C, 60.53; H, 7.10; N, 9.31%. Calcd for $C_{44}H_{62}N_6O_{12}$: C, 60.95; H, 7.21; N, 9.69%.

NMR (in $CDCl_3$): τ 8.8—8.1 (24H, $(-CH_2-)_3$ of THP), 6.8—5.8 (14H, $-OCH_2-$ of THP and skeleton protons), 5.4—4.9 (4H, -OCHO- of THP), 4.82 (4H s, $C\underline{H}_2C_6H_5$), 3.5—2.7 (4H, disappeared on deuteration), ~2.6 (10H, C_6H_5).

Di-N-*acetyl-di*-N-*benzyloxycarbonyl-tetra*-O-*tetrahydropyranylstreptidine (**4**).* To a solution of **3** (200 mg) in pyridine (2 ml), acetic anhydride (0.086 ml) was added and the solution was allowed to stand overnight. After addition of a drop of water, the solution was evaporated and the residue was poured into water to give a solid, 214 mg (98%), mp 82—84 °C, R_f 0.41 (tlc with benzene–acetone (8 : 1)); IR (KBr): 1570, 1645 (with fine slight shoulders), 1705(w) cm^{-1}.

Found: C, 60.61; H, 7.04; N, 8.64%. Calcd for $C_{48}H_{66}N_6O_{14}$: C, 60.62; H, 7.00; N, 8.84%.

NMR (in $CDCl_3$): τ 7.80 (6H s, NAc).

Di-N-*acetyl-di*-N-*benzyloxycarbonylstreptidine (**5**).* A solution of **4** (50 mg) in 50% aqueous acetic acid (0.5 ml) was allowed to stand for 2.5 hr. Sodium hydrogen carbonate (360 mg) was added with stirring and water (20 ml) was then added to give colorless solid (27 mg). The solid was chromatographed on a column of silica gel with ethyl acetate–methyl ethyl ketone (4 : 1), affording a solid, 18 mg (56%), mp 114—116 °C, R_f 0.26 (**4** : 0.9) (tlc with chloroform–ethanol (15 : 1)); IR (KBr): 1570, 1640, 1660, 1705(w) cm^{-1}.

Found: C, 55.04; H, 5.68; N, 13.33%. Calcd for $C_{28}H_{34}N_6O_{10}$: C, 54.72; H, 5.58; N, 13.67%.

NMR (in $CDCl_3$): τ 7.84 (6H s, NAc).

Di-N-*acetyl-di*-N-*benzyloxycarbonyl-4,5 (and 5,6)*-O-*cyclohexylidenestreptidine (**6**).* To a solution of **5** (1.50 g) in DMF (30 ml), 1,1-dimethoxycyclohexane (5 ml) and fuse dried *p*-toluenesulfonic acid (230 mg) were added and the solution was heated at 50 °C under reduced pressure (~30 Torr) for 3 hr. Triethylamine (0.5 ml) was added and the solution was evaporated and the residue was dissolved in chloroform. The solution was washed with sodium hydrogen carbonate solution, dried (Na_2SO_4) and evaporated. The residue was chromatographed on a short column of silica gel with benzene–ethyl acetate (2 : 1) and the fraction containing **6** was evaporated and the solid was reprecipitated from chloroform–petroleum ether, 1.18 g (70%), mp 117—118 °C; IR (KBr): 1570, 1640, 1660, 1705 (w) cm^{-1}.

Found: C, 58.41; H, 5.98; N, 11.83%. Calcd for $C_{34}H_{42}N_6O_{10}$: C, 58.78; H, 6.09; N, 12.10%.

NMR (in $CDCl_3$): τ 8.7—8.2 (10H, cyclohexylidene), 7.79 and 7.75 (each 3H s, NAc), 4.84 (4H s, $C\underline{H}_2C_6H_5$), 2.59 (10H s, $CH_2C_6\underline{H}_5$).

Di-N-*benzyloxycarbonyl-4,5 (and 5,6)*-O-*cyclohexylidenestreptidine (**7**).* *(a) From **6**:* To a solution of **6** (45 mg) in acetone (2 ml), 15M aqueous ammonia (1 ml) was added and the solution was allowed to stand for 1 hr. Evaporation of the solution gave a residue, which was dissolved in chloroform. The solution was washed with sodium hydrogen carbonate solution, dried over sodium sulfate and the solvent

was evaporated to give a solid, 31 mg (78%), mp 147—148.5 °C, R_f 0.33 (tlc with benzene–ethanol (10 : 1)).

Found: C, 58.70; H, 6.35; N, 13.55. Calcd for $C_{30}H_{38}N_6O_8$: C, 59.01; H, 6.27; N, 13.76.

NMR (in $CDCl_3$): No peaks assignable to Ac were observed.

(b) From ***1***: Compound **1** was treated similarly as described for the preparation of **6** from **5**. Yield of **7** was 95%.

Recovery of Streptidine from ***7***. A mixture of **7** (35 mg) and 50% acetic acid (1 ml) was heated at 60 °C for 1 hr. The solution was concentrated and ether was added to give a solid, 30 mg, which was dissolved in aqueous dioxane (1 : 1, 3 ml) and, after addition of two drops of acetic acid, the solution was treated with palladium black and hydrogen in a usual manner. The mixture was filtered, concentrated, and an aqueous solution of the residue was passed through a short column of Dowex 1-X2 (Cl form) with water to afford streptidine dihydrochloride (18 mg).

References

1) "Studies on Aminosugars, XXXVIII" by S. Umezawa. (a) Announced previously in a communication to the editor by S. Umezawa, T. Tsuchiya, T. Yamasaki, H. Sano, and Y. Takahashi, *J. Amer. Chem. Soc.*, **96**, 920 (1974). (b) Presented at the 189th Meeting of Japan Antibiotics Research Association, Tokyo, Sept. 1973, at the 3rd Joint Annual Congress of the Chemical Society and the Royal Institute of Chemistry, Imperial College, London, Apr. 1974, and the 30th Annual Meeting of the Chemical Society of Japan, Apr. 1974.

2) N. G. Brink, F. A. Kuehl, Jr., and K. Folkers, *Science*, **102**, 506 (1945).

3) Review paper: R. U. Lemieux and M. L. Wolfrom, *Advan. Carbohyd. Chem.*, **3**, 337 (1948).

4) M. L. Wolfrom, S. M. Olin, and W. J. Polglase, *J. Amer. Chem. Soc.*, **72**, 1724 (1950).

Total Synthesis of Dihydrostreptomycin[1)]

Sumio UMEZAWA, Tetsuro YAMASAKI, Yutaka KUBOTA, and Tsutomu TSUCHIYA

Department of Applied Chemistry, Faculty of Engineering, Keio University, Hiyoshi, Kohoku-ku, Yokohama 223

(Received May 28, 1974)

Dihydrostreptomycin has been synthesized from dihydrostreptobiosamine and streptidine. A glycosyl chloride derivative (**10**) of the former was coupled with a protected derivative (**26**) of the latter to give a mixture of four isomeric glycosides, which were separated by chromatography. Deblocking of the desired glycoside led to dihydrostreptomycin. Several other protected derivatives of dihydrostreptobiosamine have also been described.

Streptomycin is the first useful streptomyces antibiotic discovered by Waksman[2)] in 1943. Dihydrostreptomycin[3,4)] is produced by hydrogenation of streptomycin or by fermentation.[5)] Its structure was established by 1948 except for the glycosidic linkage between streptose and streptidine, which was again revised[6,7)] to be α in 1965. We wish here to describe the total synthesis of dihydrostreptomycin in detail as the first synthesis of an antibiotic of streptomycin series.

There appeared to be two possible routes for synthetic approach to dihydrostreptomycin; one of which involves the synthesis of dihydrostreptobiosamine and subsequent coupling of its derivative with protected streptidine, and the other involves the coupling of protected derivatives of dihydrostreptose and streptidine followed by formation of second glycosidic linkage with a protected derivative of 2-deoxy-2-methylamino-L-glucose or 2-amino-2-deoxyl-L-glucose derivative. We chose the former route because the α glycosidic linkage between dihydrostreptose and streptidine is less stable for hydrolytic treatment than that between 2-deoxy-2-methylamino-L-glucose and dihydrostreptose owing to the presence of the methylamino group at C-2 of the latter glycoside moiety. Thus, we have already completed the total synthesis of dihydrostreptobiosamine[1,8)] and the preparation of an appropriate derivative of streptidine.[1,9)]

The next aspect of the synthesis of dihydrostreptomycin was concerned with the preparation of a protected glycosyl halide of dihydrostreptobiosamine. As for a per-*N*,*O*-acylated glycosyl halide of benzyl dihydrostreptobiosaminide,[8)] it was considered to be unfavorable for the deblocking of the condensation product with a streptidine derivative because the guanidino groups are susceptible to alkaline hydrolysis to give urethane. Consequently, the dihydrostreptobiosamine was protected as follows: Treatment of the benzyl α-dihydrostreptobiosaminide (**1**) with 2,2-dimethoxypropane by the usual ketal-exchange procedure[10,11)] gave the diisopropylidene derivative (**2**) in an 81% yield. **2** was further blocked by treatment with *p*-nitrophenyl chloroformate (NPCF) and 1 M sodium hydroxide to give the carbamate (**4**) in a 75% yield, which was alternatively prepared through the intermediate (**3**). We have previously reported[12)] the protecting method of *trans*-vicinal hydroxyl and amino groups. We can confirm the presence of the carbamate ring by an IR absorption band near 1770 cm^{-1}.

In the next step, we faced a problem arising from the isopropylidenated dihydrostreptose moiety, which was labile in the reaction of the anomeric hydroxyl

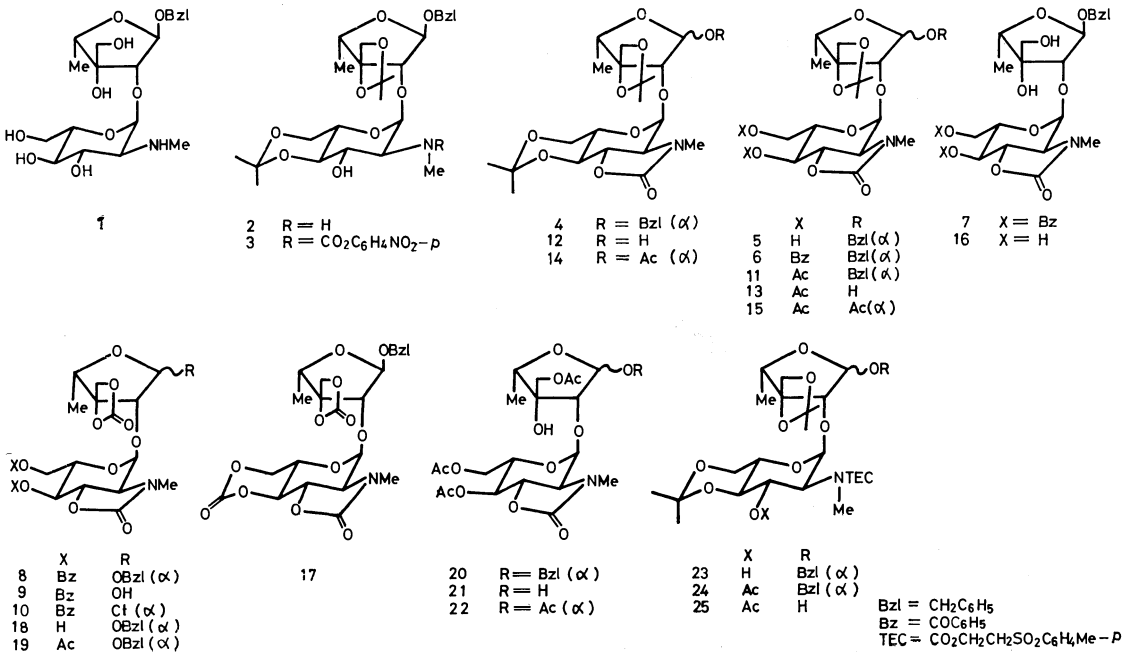

Chart 1.

group with halogenating agents. In a preliminary experiment with a dihydrostreptose derivative, we have observed that transketalization occurred in the chlorination of 2-*O*-acetyl-3,3'-*O*-isopropylidenedihydrostreptose with thionyl chloride. Therefore, we had to take a round-about way as follows: Treatment of **4** with 25% methanolic acetic acid under reflux overnight selectively removed the 4', 6'-*O*-isopropylidene group to give the monoisopropylidene derivative **5** in an 80% yield. This deisopropylidenation was found delicate; when **4** was treated with 50% acetic acid at 70 °C for 4 hr, both of the isopropylidene groups were hydrolyzed to give **16**. The free hydroxyl groups of **5** were then benzoylated to give the dibenzoyl derivative (**6**) in a 90% yield; **6** was found to have larger solubility in benzene. Treatment of **6** with aqueous 75% acetic acid at 70 °C for 6 hr removed the 3,3'-*O*-isopropylidene group to give the diol (**7**) in an 83% yield. When **7** was treated with NPCF in pyridine at room temperatures overnight, the carbonate (**8**) was obtained in a 91% yield. The infrared spectrum of **8** exhibited three distinct carbonyl absorptions for the cyclic carbonate, cyclic carbamate and benzoic esters. Direct treatment of benzyl α-dihydrostreptobiosaminide with NPCF or phosgene followed by benzoylation gave a poor yield of **8.** Hydrogenolysis of the glycosidic linkage of **8** on palladium black in dioxane gave the 1–OH-free disaccharide (**9**) quantitatively. Conversion of **9** into a glycosyl halide was achieved by the thionyl chloride procedure in a usual way. The fully protected glycosyl chloride (**10**) was obtained in a 68% yield. Glycosidation of **10** with benzyl alcohol gave **8** in yield of 59%.

Before proceeding along the main synthetic pathway, we prepared several other derivatives of dihydrostreptobiosamine which were found to be unsatisfactory for the glycoside synthesis.

Acetylation of **5** gave the di-*O*-acetyl derivative (**11**). Hydrogenolysis of **4** and **11** on palladium black gave the free disaccharides **12** and **13**, respectively, and they were respectively acetylated to give the glycosyl acetates, **14** and **15**. However, when the isopropylidene derivatives **14** and **15** were respectively treated with hydrogen bromide in acetic acid, and when **12** and **13** were respectively allowed to react with thionyl chloride, no glycosyl halide was isolated from these reaction products. It is noteworthy that an *N*-anisylidene derivative is useful for C-1 halogenation with hydrogen bromide–acetic acid as described in a preceding paper.[8]

Hydrolysis of **4** or **5** with 50% acetic acid gave the tetrol (**16**), which, on treatment with NPCF, gave the dicarbonate (**17**). When **17** was treated with silica gel in 80% aqueous acetone under reflux, the 4',6'-diol (**18**) was obtained, and this was converted into **8** by benzoylation. Thus, this constitutes an alternative route to **8** which is an intermediate in the main synthetic pathway. Acetylation of **18** gave **19**, which is the diacetyl analog of the above-mentioned useful dibenzoyl derivative (**8**). However, its solubility in organic solvents was still not satisfactory for the further coupling reaction.

Acetylation of **16** gave the triacetate (**20**), which led to the glycosyl acetate (**22**) by way of the free disaccharide (**21**). We have again here experienced that the glycosyl bromide of **21** could not be obtained from **22** by treatment with hydrogen bromide–acetic acid, and that the reaction of **21** with thionyl chloride did not give the glycosyl chloride.

Protection of the methylamino group with (β-*p*-tolylsulfonylethoxy)carbonyl group, which can easily be removed by alkaline hydrolysis,[13] was also studied. Acetylation of the derivative (**23**) gave **24**, which was led to the free disaccharide (**25**) by hydrogenolysis. After reaction with thionyl chloride in pyridine or without pyridine, the glycosyl chloride, which could not be isolated in pure form, was allowed to react with benzyl alcohol in order to test the glycoside formation. However, the benzyl glycoside (**24**) was obtained in a poor yield (13%) only in the presence of pyridine.

Returning to the final stage leading to dihydrostreptomycin, condensation of the glycosyl chloride (**10**) with the protected derivative (**26**)* of streptidine was carried out in anhydrous benzene in the presence of silver carbonate, silver perchlorate, and molecular sieves at 50 °C overnight. Examination of the products by tlc proved the formation of four products, *A*, *B*, *C*, and *D* in their order of mobility. Their separation was accomplished by repeated column chromatography on silica gel. Total yield of the condensation products was 81%. Their IR and NMR spectra respectively supported the structures of these products.

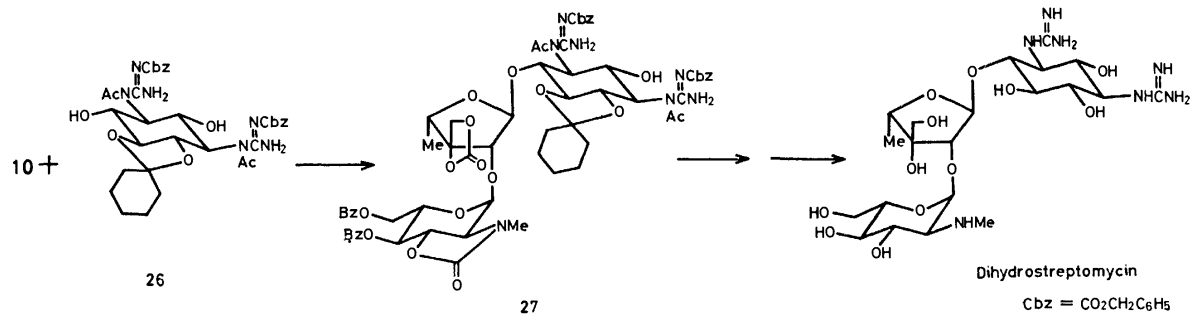

Chart 2.

* The positions of acetyl and benzyloxycarbonyl groups are arbitrarily assigned. See Ref. 9.

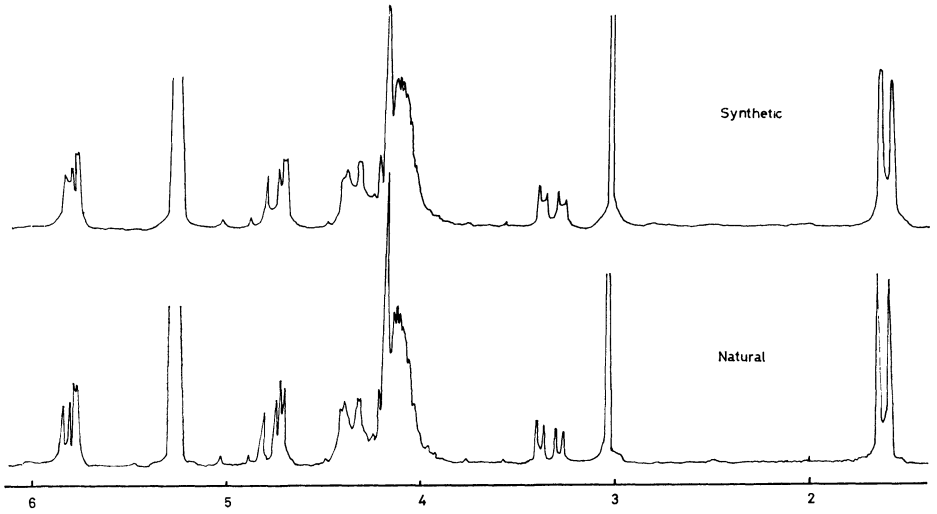

Fig. 1. NMR spectra of natural and synthetic dihydrostreptomycin sesquisulfate (in D_2O at 100 MHz).

Deblocking of the product A (**27**)* led to dihydrostreptomycin. By its treatment with a mixture of 0.025 M barium hydroxide and dioxane at 50 °C, the acetyl, benzoyl, carbonate, and carbamate groups were removed. The remaining cyclohexylidene group was removed by treatment with 50% acetic acid, and the benzyloxycarbonyl groups were removed by hydrogenolysis on palladium black in aqueous dioxane in a usual way to afford dihydrostreptomycin, which was converted into its sesquisulfate. The synthetic dihydrostreptomycin was identical in every respect with natural specimen. The identity was also established by optical rotational shift due to copper complexing ($\Delta[M]_{CuAm}$),[14] specific rotation, IR and NMR spectra (Fig. 1), thin layer and paper chromatographic behavior, paper electrophoresis mobility, and antibacterial spectra (Table 1).

Table 1. Antibacterial spectra of natural and synthetic dihydrostreptomycin

Test organisms[a]	MIC (mcg/ml)	
	Natural	Synthetic
Staphylococcus aureus FDA 209P	1.56	1.56
FDA 209P SM STf	>50	>50
Bacillus subtilis NRRL B-558	6.25	6.25
PCI 219	<0.2	0.2
Bacillus agri	>50	>50
Escherichia coli K-12	0.39	0.78
K-12 R-5	>50	>50
K-12 ML1629	>50	>50
K-12 ML1410	0.78	0.78
K-12 ML1410 R81	>50	>50
K-12 LA290 R55	1.56	1.56
K-12 W677	0.78	0.78
K-12 JR66/W677	>50	>50
NIHJ	3.12	3.12
NIHJ SMf	>50	>50
Pseudomonas aeruginosa A3	25	25
No. 12	50	50
Mycobacterium smegmatis ATCC 607[b]	0.39	0.39

a) Agar dilution streak method, nutrient agar 37 °C, 18 hr. b) 47 hr.

Similar procedures were carried out for deblocking of the other products, *B*, *C*, and *D*, respectively, giving three isomers of dihydrostreptomycin (**29**, **30**, and **31**) which showed no antibacterial activity.

Experimental

General procedure was the same as described in the foregoing paper.

Benzyl 2-O-(2-Deoxy-4,6-O-isopropylidene-2-methylamino-α-L-glucopyranosyl)-3,3'-O-isopropylidenedihydrostreptoside (2). To a solution of the hydrochloride (5.00 g) of **1** in dry DMF, 2,2-dimethoxypropane (8 ml), anhydrous *p*-toluenesulfonic acid (500 mg) and freshly dried Molecular Sieves 5A (30 g, Wako Pure Chem. Ind., Ltd., Osaka) were added, and the mixture was stirred at 60 °C overnight. To the mixture triethylamine (5 ml) was added and the mixture was evaporated. The residue was chromatographed on a short column of silica gel with chloroform–acetone (1 : 1) to give a syrup, 4.90 g (89%), $[\alpha]_D^{18}$ −121° (*c* 0.5, acetone).

Found: C, 61.03; H, 7.60; N, 2.55%. Calcd for $C_{26}H_{39}NO_9$: C, 61.28; H, 7.71; N, 2.75%.

NMR (in $CDCl_3$): δ 1.28 (3H d, $CHCH_3$), 1.42 and 1.50 (9H and 3H s, respectively, isopropylidene), 2.50 (3H s, NCH_3), 5.05 (1H d, J ~1 Hz, H-1), 5.21 (1H d, J 3.5 Hz, H-1').

Benzyl 2-O-[2-Deoxy-4,6-O-isopropylidene-2-(N-methyl-p-nitrophenoxylcarboxamido)-α-L-glucopyranosyl]-3,3'-O-isopropylidenedihydrostreptoside (3). To a solution of **2** (260 mg) in aqueous acetone (1 : 2, 3 ml), triethylamine (60 mg) was added and the solution was cooled to −10 °C. A solution of NPCF (125 mg) in acetone (2 ml) was added and the solution was stirred for 15 min under cooling and at room temperature for additional 2 hr. After addition of triethylamine (70 mg), the solution was evaporated. A solution of the residue in chloroform was washed with saturated sodium hydrogen carbonate solution and with saturated sodium chloride solution, dried over sodium sulfate, and evaporated to give a syrup, 355 mg (98%), $[\alpha]_D^{21}$ −122° (*c* 1, $CHCl_3$); IR (KBr): $\nu_{C=O}$ 1775, 1732 cm^{-1}, ν_{NO_2} 1530, 1350 cm^{-1}.

Found: C, 58.83; H, 6.23; N, 4.11%. Calcd for $C_{33}H_{42}N_2O_{13}$: C, 58.75; H, 6.27; N, 4.15%.

Benzyl 2-O-(2,3-N,O-Carbonyl-2-deoxy-4,6-O-isopropylidene-2-methylamino-α-L-glucopyranosyl)-3,3'-O-isopropylidenedihydrostreptoside (4). To a solution of **2** (1.61 g) in acetone (16 ml) maintained at −10 °C, a cold solution of NPCF (770 mg) in acetone (8 ml) and 1 M aqueous sodium hydroxide (4 ml) were simultaneously added dropwise with stirring. tlc of the reaction mixture with benzene–ether (1 : 1) showed the single spot of **3** at R_f 0.75. An aliquot (4 ml) of the sodium hydroxide solution was added and after standing at −10 °C for 15 min, another aliquot (2 ml) was added and the solution was allowed to stand for further 15 min. On tlc with the above-mentioned solvent system, the spot of R_f 0.75 disappeared and the spot of **4** (R_f 0.55) appeared. After neutralization with 10% acetic acid, the solution was extracted with ether. The ethereal solution was washed with cold 1 M sodium hydroxide until the yellow color of sodium *p*-nitrophenoxide disappeared. The solution was then washed with saturated sodium chloride solution, dried over sodium sulfate, and evaporated. The solid was recrystallized from ether–petroleum ether to give needles, 1.27 g (75%), mp 169—170 °C, $[\alpha]_D^{23}$ −152° (*c* 1, MeOH); IR (KBr): 1770 cm^{-1}.

Found: C, 60.42; H, 6.90; N, 2.60%. Calcd for $C_{27}H_{37}NO_{10}$: C, 60.55; H, 6.96; N, 2.62%.

NMR (in $CDCl_3$): δ 1.28 (3H d), 1.43 and 1.53 (9H and 3H s, respectively, isopropylidene), 2.87 (3H s, NCH_3), 3.37 (1H q, *J* 3 and 11.5 Hz, H-2'), 5.11 (1H d, *J* ~1 Hz, H-1), 5.42 (1H d, *J* 3 Hz, H-1'), 7.32 (5H s, Ph).

Benzyl 2-O-(2,3-N,O-Carbonyl-2-deoxy-2-methylamino-α-L-glycopyranosyl)-3,3'-O-isopropylidenedihydrostreptoside (5). A solution of the diisopropylidene derivative **4** (2.24 g) in 25% acetic acid and methanol (45 ml) was refluxed overnight. The solution was evaporated with toluene to give a solid, which was recrystallized from methanol, 1.75 g (80%), mp 190—190.5 °C, $[\alpha]_D^{23}$ −177° (*c* 1, MeOH); IR (KBr): 1775 cm^{-1}.

Found: C, 58.10; H, 6.78; N, 2.88%. Calcd for $C_{24}H_{33}NO_{10}$: C, 58.17; H, 6.71; N, 2.83%.

NMR (in pyridine-d_5): δ 1.40 (6H s, isopropylidene).

Benzyl 2-O-(4,6-Di-O-benzoyl-2,3-N,O-carbonyl-2-deoxy-2-methylamino-α-L-glucopyranosyl)-3,3'-O-isopropylidenedihydrostreptoside (6). A sample of **5** (1.17 g) was treated with benzoyl chloride and pyridine to give a syrup, which was chromatographed on silica gel (50 g) with chloroform to yield a solid, 1.30 mg, (90%), mp 78—81 °C, $[\alpha]_D^{18}$ −145° (*c* 1, $CHCl_3$); IR (KBr): 1775, 1725 cm^{-1}.

Found: C, 64.59; H, 5.83; N, 1.90%. Calcd for $C_{38}H_{41}NO_{12}$: C, 64.87; H, 5.87; N, 1.99%.

Benzyl 2-O-(4,6-Di-O-benzoyl-2,3-N,O-carbonyl-2-deoxy-2-methylamino-α-L-glucopyranosyl)dihydrostreptoside (7). A sample of **6** (1.20 g) was treated with 75% acetic acid at 70 °C for 6 hr, and the reaction mixture was evaporated. To the resulting syrup was added toluene and the mixture was again evaporated to remove the remaining acetic acid. The residue was chromatographed on a silica gel with benzene–ethyl acetate (1 : 1) to yield a solid, 937 mg (83%), $[\alpha]_D^{18}$ −177° (*c* 1, $CHCl_3$).

Found: C, 63.63; H, 5.67; N, 1.95%. Calcd for $C_{35}H_{37}NO_{12}$: C, 63.14; H, 5.61; N, 2.11%.

Benzyl 2-O-(4,6-Di-O-benzoyl-2,3-N,O-carbonyl-2-deoxy-2-methylamino-α-L-glucopyranosyl-3,3'-O-carbonyldihydrostreptoside (8).

a) From 7. To a solution of **7** (830 mg) in pyridine (20 ml), NPCF (800 mg) was added and the solution was stirred at room temperature overnight. The solution was filtered and, to the filtrate, methanol (1 ml) was added. After standing for 30 min, the solution was evaporated. To the residue was added toluene and the mixture was again evaporated. The residue was chromatographed on a short column of silica gel (40 g) with benzene–ethyl acetate (1 : 2) to give a solid, 798 mg (91%), $[\alpha]_D^{18}$ −145° (*c* 1, $CHCl_3$); IR (KBr): $\nu_{C=O}$ 1815 (carbonate), 1715 (cyclic carbamate), 1725 cm^{-1} (ester).

Found: C, 62.88; H, 5.30; N, 1.91%. Calcd for $C_{36}H_{35}NO_{13}$: C, 62.69; H, 5.12; N, 2.03%.

NMR (in $CDCl_3$): δ 1.40 (3H d, $CHC\underline{H}_3$), 2.91 (3H s, NCH_3), 3.57 (1H q, *J* 3 and 11.5 Hz, H-2'), 5.32 (1H d, *J* ~2 Hz, H-1), 5.33 (1H d, *J* 3 Hz, H-1'), 5.70 (1H t, *J* 10 Hz, H-4').

b) From 18. Treatment of **18** with benzoyl chloride and pyridine in a usual manner gave **8** in yield of 95%.

2-O-(4,6-Di-O-benzoyl-2,3-N,O-carbonyl-2-deoxy-2-methylamino-α-L-glucopyranosyl)-3,3'-O-carbonyldihydrostreptose (9). A solution of **8** (798 mg) in dioxane (20 ml) was hydrogenated (50 psi) with palladium black (prepared from 2 g of palladium chloride), and the product was chromatographed on a 30 g of silica gel with chloroform–acetone (4 : 1) to give a solid, 681 mg, (98%), mp 150 °C, $[\alpha]_D^{18}$ −95° (*c* 1, $CHCl_3$); IR (KBr): 1820, 1775, 1730 cm^{-1}.

Found: C, 58.38; H, 5.07; H, 2.19%. Calcd for $C_{29}H_{29}NO_{13}$: C, 58.10; H, 4.88; N, 23.3%.

2-O-(4,6-Di-O-benzoyl-2,3-N,O-carbonyl-2-deoxy-2-methylamino-α-L-glucopyranosyl)-3,3'-O-carbonyldihydrostreptosyl Chloride (10). A solution of **9** (200 mg) in thionyl chloride (2.0 ml) was allowed to stand at room temperature for 3 hr, and evaporated under reduced pressure (<1 Torr). The residue was dissolved in a mixture of benzene and ethyl acetate (1 : 1, dried over Molecular Sieves 4A). The solution was evaporated to give a syrup, which was chromatographed on 10 g of silica gel (activated at 260 °C *in vacuo* for 5 hr) by elution with dry benzene–ethyl acetate (1 : 1). The product was reprecipitated from dry benzene–*n*-hexane, 141 mg (68%), mp 114—116 °C (decomp), $[\alpha]_D^{20}$ −170° (*c* 1, $CHCl_3$); IR (KBr): 1820, 1770, 1725 cm^{-1}.

Found: C, 55.96; H, 4.59; N, 1.95; Cl, 5.89%. Calcd for $C_{29}H_{28}NO_{12}Cl$: C, 56.36; H, 4.57; N, 2.27; Cl, 5.74%.

NMR (in $CDCl_3$): δ 1.43 (3H d), 2.94 (3H s), 5.32 (1H d, *J* 3 Hz, H-1'), 5.70 (1H t, H-4'), 6.28 (1H d, *J* ~1 Hz, H-1).

Formation of 8 from 10. A mixture of **10** (48 mg), benzyl alcohol (14 mg), and Molecular Sieves 3A (200 mg) in dry benzene (1 ml) was stirred at room temperature for 3 hr. When checked by tlc, hardly any progress of reaction was observed. Freshly prepared and well dried (at 120 °C) silver carbonate (180 mg) and silver perchlorate (20 mg) were added and the mixture was vigorously stirred at room temperature for 2 hr. The reaction mixture was filtered with the aid of benzene and the filtrate was evaporated. The residue was chromatographed on a short column of silica gel with benzene–ethyl acetate (2 : 1) to give a solid, 31 mg (59 %). Its optical rotation and IR and NMR spectra were identical with those of authentic **8**.

Benzyl 2-O-(4,6-Di-O-acetyl-2,3-N,O-carbonyl-2-deoxy-2-methylamino-α-L-glucopyranosyl)-3,3'-O-isopropylidenedihydrostreptoside (11). A sample of **5** was treated with acetic anhydride and pyridine at room temperature overnight and worked up to give a solid in 98% yield, mp 53—56 °C, $[\alpha]_D^{20}$ −176° (*c* 1, MeOH); IR (KBr): 1750, 1780 cm^{-1}.

Found: C, 57.83; H, 6.53; N, 2.39%. Calcd for $C_{28}H_{37}NO_{12}$: C, 58.02; H, 6.43; N, 2.42%.

NMR (in $CDCl_3$): δ 2.05 and 2.10 (each 3H s, Ac).

2-O-(2,3-N,O-Carbonyl-2-deoxy-4,6-O-isopropylidene-2-methylamino-α-L-glucopyranosyl)-3,3'-O-isopropylidenedihydrostreptose (12). A solution of **4** (1.48 g) in dioxan–methanol (1 : 5, 12 ml) was treated with palladium black and hydrogen (50 psi) at

room temperature overnight to yield a syrup, which was reprecipitated from chloroform–*n*-hexane (1 : 3). The solid was chromatographed on silica gel with chloroform–acetone (1 : 1) to give needles, 887 mg (85%), which was recrystallized from chloroform–*n*-hexane, mp 188—190 °C, $[\alpha]_D^{20}$ −113° (*c* 1, $CHCl_3$); IR (KBr): 1765 cm^{-1}.

Found: C, 54.24; H, 6.92; N, 3.22%. Calcd for $C_{20}H_{31}NO_{10}$: C, 53.93; H, 7.02; N, 3.14%.

2-O-(4,6-Di-O-acetyl-2,3-N,O-carbonyl-2-deoxy-2-methylamino-α-L-glucopyranosyl)-3,3′-O-isopropylidenedihydrostreptose (**13**). Compound **11** was hydrogenated by a method similar to that described for the preparation of **12** from **4**. Mp 185—186 °C, $[\alpha]_D^{20}$ −108° (*c* 1, EtOAc); IR (KBr): 1750, 1780 cm^{-1}.

Found: C, 51.66; H, 6.12; N, 2.85%. Calcd for $C_{21}H_{31}NO_{12}$: C, 51.54; H, 6.38; N, 2.87%.

1-O-Acetyl-2-O-(2,3-N,O-carbonyl-2-deoxy-4,6-O-isopropylidene-2-methylamino-α-L-glucopyranosyl)-3,3′-O-isopropylidenedihydrostreptose (**14**). A sample of **12** (887 mg) was treated with acetic anhydride and pyridine and the product was recrystallized from chloroform–*n*-hexane to give crystals, 783 mg (81%), mp 247—250 °C (decomp), $[\alpha]_D^{21}$ −130° (*c* 1, $CHCl_3$).

Found: C, 54.01; H, 6.88; N, 2.80%. Calcd for $C_{22}H_{33}NO_{11}$: C, 54.20; H, 6.82; N, 2.87%.

NMR (in $CDCl_3$): δ 1.30 (3H d, *J* 6.5 Hz, $CHC\underline{H}_3$), 1.43 and 1.52 (9H and 3H s, respectively, isopropylidene), 2.07 (3H s, Ac), 2.84 (3H s, NCH_3), 5.36 (1H d, *J* 3 Hz, H-1′), 6.13 (1H d, *J* 1.5 Hz, H-1).

1-O-Acetyl-2-O-(4,6-di-O-acetyl-2,3-N,O-carbonyl-2-deoxy-2-methylamino-α-L-glucopyranosyl)-3,3′-O-isopropylidenedihydrostreptose (**15**). A sample of **13** was acetylated by a method to that similar described for the preparation of **14** from **12**. Mp 137—138 °C, $[\alpha]_D^{21}$ −142° (*c* 1, $CHCl_3$).

Found: C, 51.73; H, 6.21; N, 2.37%. Calcd for $C_{23}H_{33}NO_{13}$: C, 51.97; H, 6.26; N, 2.64%.

NMR (in $CDCl_3$): δ 2.10 and 2.13 (6H and 3H s, respectively, Ac), 6.14 (1H d, *J* ~1 Hz, H-1).

Benzyl 2-O-(2,3-N,O-carbonyl-2-deoxy-2-methylamino-α-L-glucopyranosyl)dihydrostreptoside (**16**). A solution of **4** (1.00 g) in 50% aqueous acetic acid (20 ml) was heated at 70 °C for 4 hr. Toluene was added and the solution was evaporated. The residue was recrystallized from methanol–ether, 632 mg (74%), mp 199—202 °C, $[\alpha]_D^{20}$ −186° (*c* 1, MeOH); IR (KBr): 1760 cm^{-1}.

Found: C, 55.30; H, 6.34; N, 3.12%. Calcd for $C_{21}H_{29}NO_{10}$: C, 55.38; H, 6.42; N, 3.07%.

Benzyl 3,3′-O-Carbonyl-2-O-(2,3-N,O-carbonyl-4,6-O-carbonyl-2-deoxy-2-methylamino-α-L-glucopyranosyl)dihydrostreptoside (**17**). A sample of **16** was treated with NPCF by a method similar to that described for the preparation of **8** from **7**. On monitoring with tlc with benzene–acetone (2 : 1), the spot of **16** (R_f 0.1) gradually disappeared and two spots of R_f 0.17 and 0.46 (dicabonyl derivatives) appeared. Finally there appeared only one spot of **17** (R_f 0.55). The crude product was recrystallized from acetone–benzene, yielding **17** in 40% yield, mp 269—272 °C (decomp), $[\alpha]_D^{17}$ −120° (*c* 1, acetone); IR (KBr): 1800, 1765 cm^{-1}.

Found: C, 54.39; H, 4.93; N, 2.82%. Calcd for $C_{23}H_{25}NO_{12}$: C, 54.44; H, 4.97; N, 2.76%.

Compound **17** is soluble in acetone, scarcely soluble in methanol, ethyl acetate, and chloroform and insoluble in benzene and ether.

Benzyl 3,3′-O-Carbonyl-2-O-(2,3-N,O-carbonyl-2-deoxy-2-methylamino-α-L-glucopyranosyl)dihydrostreptoside (**18**). To a solution of **17** (100 mg) in 80% aqueous acetone (2 ml), silica gel (1.0 g) was added and the mixture was refluxed for 2 hr. The mixture was filtered and the filtrate was evaporated to give a solid, which was recrystallized from acetone–*n*-hexane, 86 mg (90%), mp 196—197 °C, $[\alpha]_D^{25}$ −160° (*c* 1, MeOH), IR; 1805, 1775 cm^{-1}.

Found: C, 54.61; H, 5.62; N, 2.73%. Calcd for $C_{22}H_{27}NO_{11}$: C, 54.88; H, 5.65; N, 2.90%.

Conversion of **18** *into* **8**. A sample of **18** was treated with benzoyl chloride, pyridine, and triethylamine, and worked up in a usual way. The product was reprecipitated from benzene–*n*-hexane to give **8**, quantitatively, which was identical with the specimen prepared from **7**.

Benzyl 2-O-(4,6-Di-O-acetyl-2,3-N,O-carbonyl-2-deoxy-2-methylamino-α-L-glucopyranosyl)-3,3′-O-carbonyldihydrostreptoside (**19**). A sample of **18** was treated with acetic anhydride and pyridine in a usual manner to yield **19** (80%), $[\alpha]_D^{21}$ −150° (*c* 1, $CHCl_3$); IR (KBr): 1815, 1765, 1740 cm^{-1}.

Found: C, 55.35; H, 5.62; N, 2.42%. Calcd for $C_{26}H_{31}NO_{13}$: C, 55.21; H, 5.53; N, 2.48%.

NMR (in $CDCl_3$): δ 2.05 and 2.11 (each 3H s, Ac).

Benzyl 3′-O-Acetyl-2-O-(4,6-di-O-acetyl-2,3-N,O-carbonyl-2-deoxy-2-methylamino-α-L-glucopyranosyl)dihydrostreptoside (**20**). A sample of **16** was treated with acetic anhydride and pyridine and worked up to give a solid of **20** in 98% yield, which was reprecipitated from ethyl acetate–*n*-hexane, mp 35—36 °C, $[\alpha]_D^{18}$ −149° (*c* 1, MeOH); IR (KBr): 1750, 1775 cm^{-1}.

Found: C, 55.49; H, 6.02; N, 2.40%. Calcd for $C_{27}H_{35}NO_{13}$: C, 55.76; H, 6.07; N, 2.41%.

NMR (in $CDCl_3$): δ 2.03, 2.08, and 2.11 (each 3H s, Ac).

3′-O-Acetyl-2-O-(4,6-di-O-acetyl-2,3-N,O-carbonyl-2-deoxy-2-methylamino-α-L-glucopyranosyl)dihydrostreptose (**21**). A sample of **20** was dissolved in methanol and hydrogenated with palladium black in a usual manner to give **21**, quantitatively, mp 170—172 °C, $[\alpha]_D^{20}$ −103° (*c* 1, MeOH); IR (KBr): 1780, 1745 cm^{-1}.

Found: C, 49.07; H, 5.98; N, 2.75%. Calcd for $C_{20}H_{29}NO_{13}$: C, 48.88; H, 5.95; N, 2.85%.

1,3′-Di-O-acetyl-2-O-(4,6-di-O-acetyl-2,3-N,O-carbonyl-2-deoxy-2-methylamino-α-L-glucopyranosyl)dihydrostreptose (**22**). A sample of **21** was treated with acetic anhydride and pyridine to give **22**, quantitatively, mp 152—153 °C, $[\alpha]_D^{20}$ −128° (*c* 1, $CHCl_3$); IR (KBr): 3600 (sharp), 1780, 1740 cm^{-1}.

Found: C, 49.58; H, 5.77; N, 2.66%. Calcd for $C_{22}H_{31}NO_{14}$: C, 49.53; H, 5.86; N, 2.62%.

Benzyl 2-O-[2-Deoxy-4,6-O-isopropylidene-2-(N-methyl-β-(p-toluenesulfonyl)ethoxycarboxamido)-α-L-glucopyranosyl]-3,3′-O-isopropylidenedihydrostreptoside (**23**). To an ice-cold solution of **2** (2.00 g) in tetrahydrofuran (15 ml), ice-cold sodium hydrogen carbonate solution (600 mg in 15 ml water) and β-(*p*-toluenesulfonyl)ethyl chloroformate[13] (1.4 g) in acetone (15 ml) were added and the mixture was stirred at room temperature for 2 hr. Evaporation of the mixture gave a syrup, which was dissolved in chloroform. The solution was washed with water, dried with anhydrous sodium sulfate and evaporated to give a syrup. The syrup was chromatographed on a short column of silica gel with chloroform–ether (1 : 1) to give a solid, 2.39 g (83%); $[\alpha]_D^{13}$ −91° (*c* 0.4, $CHCl_3$); IR (KBr): 1700 cm^{-1}.

Found: C, 58.73; H, 6.54; N, 1.90%. Calcd for $C_{36}H_{49}NO_{13}S$: C, 58.76; H, 6.71; N, 1.98%.

Benzyl 2-O-[3-O-Acetyl-2-deoxy-4,6-O-isopropylidene-2-(N-methyl-β-(p-toluenesulfonyl)ethoxycarboxamido)-α-L-glucopyranosyl]-3,3′-O-isopropylidenedihydrostreptoside (**24**). A sample of **23** (2.28 g) was treated with acetic anhydride in pyridine at room temperature overnight. The reaction mixture was poured into cold water (5 ml) and then the mixture was evaporated. The residue was stirred with a mixture of water (200 ml) and chloroform (100 ml). The aqueous layer was separated and extracted with chloroform. The chloroform

layers were combined, washed with saturated aqueous solution of potassium hydrogen sulfate, dried over magnesium sulfate and evaporated to give a solid in 90% yield, $[\alpha]_D^{13}$ −74° (*c* 1, $CHCl_3$); IR (KBr): 1753, 1705 cm^{-1}.

Found: C, 58.82; H, 6.51; N, 2.11; S, 4.05%. Calcd for $C_{38}H_{51}NO_{14}S$: C, 58.67; H, 6.61; N, 1.80; S, 4.12%.

NMR (in $CDCl_3$): δ 1.26 (3H d, *J* 6.5 Hz, $CHC\underline{H}_3$), 1.31, 1.35, 1.36, and 1.45 (each 3H s, isopropylidene), 2.03 (3H s, Ac), 2.44 (3H s, $C\underline{H}_3Ph$), 2.75 (~1.8 H s) and 2.94 (~1.2H s) (both NCH_3, rotamers), 5.02 (1H d, *J* ~1 Hz, H-1), 5.09 (1H d, *J* 3.5 Hz, H-1').

*2-O-[3-O-Acetyl-2-deoxy-4,6-O-isopropylidene-2-(N-methyl-β-(p-toluenesulfonyl)ethoxycarboxamido)-α-L-glucopyranosyl]-3,3'-O-isopropylidenedihydrostreptose (**25**).* A sample of **24** (1.70 g), dissolved in dioxane (10 ml), was treated with palladium black and hydrogen in a usual manner. The product was purified by chromatography on a short column of silica gel by elution with chloroform–ether (1 : 1) to yield **25**, 827 mg (55%), $[\alpha]_D^{21}$ −57° (*c* 1, $CHCl_3$); IR (KBr): 1750, 1705 cm^{-1}.

Found: C, 54.03; H, 6.45; N, 1.72; S, 4.89%. Calcd for $C_{31}H_{45}NO_{14}S$: C, 54.13; H, 6.60; N, 2.04; S, 4.66%.

*Formation of **24** from **25**.* A sample of **25** (100 mg) was dissolved in a mixture (0.5 ml) of thionyl chloride, dry benzene, and dry pyridine (0.25 : 10 : 0.31 by volume), Molecular Sieves 3A was added and the mixture was allowed to stand at room temperature for 1 hr. A solution (0.5 ml) of benzyl alcohol in benzene (3 : 100) was added and the mixture was allowed to stand at room temperature overnight. Saturated sodium hydrogen carbonate solution and chloroform were added with stirring and the organic layer was washed with water, dried over sodium sulfate and evaporated to give a syrup, which was chromatographed on a column of silica gel by elution with benzene–MEK (10 : 1) to give **24** (15 mg, 13%). The IR and NMR spectra of the product was quite superimposable on those of authentic **24** prepared from **23**.

*Condensation of **10** with **26**.* To a solution of **26** (1.20 g) in dry benzene (30 ml; dried over $LiAlH_4$ and distilled before use) was added freshly prepared and well dried silver carbonate (3.6 g), well dried silver perchlorate (0.4 g) and Molecular Sieves 3A (dried at 250 °C) and the mixture was stirred at room temperature overnight in the dark. The glycosyl chloride **26** (1.60 g) was added and the mixture was stirred at 50 °C overnight in the dark. The mixture was filtered with the aid of chloroform and the filtrate was evaporated. On tlc with benzene–chloroform–ethanol–concentrated ammonium hydroxide (50 : 50 : 4 : 0.5) (Solvent A), the residue gave four spots other than those of starting materials **10** and **26** and **9** derived from **10**. The condensation products were designated **A**, **B**, **C**, and **D** in their order of mobility. The chromatography of the residue on a column of silica gel (100 g) with Solvent A afforded fractions containing **A**+**B** (434 mg), **C** (669 mg), and **D** (730 mg); total yield 81%. The first fraction was further chromatographed three times on a column of silica gel (20 g) with benzene–90% ethanol (25 : 1) to give **A** and **B**. The second fraction **C** was further purified by chromatography on silica gel (35 g) with Solvent A. The third fraction **D** was also further chromatographed on silica gel (40 g) with chloroform–90% ethanol (10 : 1). Each product, which is chromatographically homogeneous was reprecipitated from benzene–petroleum ether to give **A** (196 mg, 11% based on **26**), **B** (85 mg), **C** (371 mg), and **D** (416 mg; still containing a trace of impurity).

A: $[\alpha]_D^{23}$ −70° (*c* 2, $CHCl_3$); IR (KBr): 1810, 1775, 1725, 1640, 1570 cm^{-1}; NMR (in $CDCl_3$): δ 1.29 (3H d, $CHC\underline{H}_3$), 1.6 (10H broad, cyclohexylidene), 2.07 and 2.20 (each 3H s, Ac), 2.83 (3H s, NCH_3).

Found: C, 59.29; H, 5.58; N, 7.85%. Calcd for $C_{61}H_{69}N_7O_{22}$: C, 59.29; H, 5.45; N, 7.68%.

B: $[\alpha]_D^{22}$ −70° (*c* 2, $CHCl_3$); IR: Almost identical with that of **A**; NMR (in $CDCl_3$): δ 1.24 (3H d), 1.45 (10H), 2.15 (6H s), 2.87 (3H s).

Found: C, 59.13; H, 5.51; N, 7.45%.

C: $[\alpha]_D^{22}$ −8° (*c* 2, $CHCl_3$); IR: Almost identical with that of **A**; NMR (in $CDCl_3$): δ 1.27 (3H d), 1.6 (10H), 2.10 and 2.21 (each 3H s), 2.85 (3H s).

Found: C, 59.21; H, 5.45; N, 7.42%.

D: $[\alpha]_D^{22}$ −10° (*c* 2, $CHCl_3$); IR: Almost identical with that of **A**; NMR (in $CDCl_3$): δ 1.30 (3H d), 1.58 (10H), 2.15 and 2.22 (each 3H s), 2.90 (3H s).

Found: C, 58.88; H, 5.49%.

*Deblocking of the Condensation Products. a) Deblocking of **A**.* To a solution of compound **A** (120 mg) in dioxane (20 ml), 0.025 M barium hydroxide (8 ml×4) was added at 1 hr intervals and the mixture was heated at 50 °C for 3 hr. Carbon dioxide was introduced and the precipitate was filtered off. The filtrate was evaporated and the residue was chromatographed on a column of silica gel with chloroform–ethanol–17% ammonia (20 : 10 : 1) to give a solid (**28**, 38 mg, 44%). In the NMR spectrum of **28**, peaks attributable to the carbobenzoxy and cyclohexylidene groups were observed, and peaks corresponding to acetyl and benzoyl groups disappeared. Additionally, in the IR spectrum of **28**, no trace of the carbonyl absorptions of acetyl, benzoyl, carbonate, and carbamate groups was observed.

Next, a solution of **28** (38 mg) in 50% acetic acid (2 ml) was heated at 60 °C overnight and evaporated. The residue was dissolved in a mixture of water and dioxane (2 : 1) and the solution was hydrogenated (50 psi) with palladium black (about 0.3 ml) at room temperature overnight. The mixture was filtered, and the filtrate was evaporated. The residue was chromatographed on 20 ml of Amberlite CG-50 (NH_4 form) with 5% ammonium carbonate to give a solid (18 mg). An aqueous solution of the solid was passed through a column of Dowex 1×2 (OH form) with water to give the free base of dihydrostreptomycin, which was transformed into its sesquisulfate by neutralizing with sulfuric acid, 14 mg (48%), $[\alpha]_D^{17}$ −85° (*c* 0.1, H_2O); natural specimen: $[\alpha]_D^{17}$ −85° (*c* 0.1, H_2O) [lit,[15] $[\alpha]_D^{25}$ −88.5° (*c* 1, H_2O); $\Delta[M]_{436(CuAm)}^{10}$ −1200°; natural specimen: $\Delta[M]_{436(GuAm)}^{17}$ −1170° [lit,[16] dihydrostreptomycin: $\Delta[M]_{436(CupraB)}$ −1180°].

Found: C, 33.50; H, 6.52; N, 12.37%. Calcd for $C_{21}H_{41}N_7O_{12}\cdot 3/2H_2SO_4\cdot 3/2H_2O$: C, 33.29; H, 6.25; N, 12.94%.

*b) Deblocking of **B**, **C**, and **D**.* Compounds **B**, **C**, and **D** were respectively treated in the same way as described above for **A** to give sesquisulfates **29**, **30**, and **31** respectively.

29: $[\alpha]_D^{17}$ −88° (*c* 0.1, H_2O); $\Delta[M]_{436(CuAm)}^{17}$ +320°.
30: $[\alpha]_D^{17}$ −35° (*c* 0.1, H_2O); $\Delta[M]_{436(CuAm)}^{17}$ +580°.
31: $[\alpha]_D^{17}$ −35° (*c* 0.1, H_2O); $\Delta[M]_{436(CuAm)}^{17}$ −3200°.

The authors are grateful to Professor Hamao Umezawa of The University of Tokyo and of the Institute of Microbial Chemistry for his important ideas and encouragement.

References

1) "Studies on Aminosugars, XXXIX." by S. Umezawa. (a) Announced previously in a communication to the editor by S. Umezawa, T. Tsuchiya, T. Yamasaki, H. Sano, and Y.

Takahashi, *J. Amer. Chem. Soc.*, **96**, 920 (1974). (b) Presented at the 189th Meeting of Japan Antibiotics Research Association, Tokyo, Sept. 1973, at the 3rd Joint Annual Congress of the Chemical Society and the Royal Institute of Chemistry, Imperial College, London, Apr. 1974, and at the 30th Annual Meeting of the Chemical Society of Japan, Apr. 1974.

2) A. Schatz, E. Bugie, and S. A. Waksman, *Proc. Soc. Exp. Biol. Med.*, **55**, 66 (1944); Review: R. U. Lemieux and M. L. Wolfrom, *Advan. Carbohyd. Chem.*, **3**, 337 (1948).

3) Q. R. Bartz, J. Controulis, H. M. Crooks, Jr., and M. C. Rebstock, *J. Amer. Chem. Soc.*, **68**, 2163 (1946).

4) R. L. Peck, C. E. Hoffhine, and K. Folkers, *ibid.*, **68**, 1390 (1946).

5) S. Tatsuoka, T. Kusaka, A. Miyake, M. Inoue, H. Hitomi, Y. Shiraishi, H. Iwasaki, and M. Imanishi, *Chem. Pharm. Bull.* (Tokyo), **5**, 343 (1957).

6) I. J. McGilveray and K. L. Rinehart, Jr., *J. Amer. Chem. Soc.*, **87**, 4003 (1965).

7) S. Neidle, D. Rogers, and M. B. Hursthouse, *Tetrahedron Lett.*, 4725 (1968).

8) S. Umezawa, H. Sano, and T. Tsuchiya, This Bulletin, **48**, 556 (1975).

9) S. Umezawa, Y. Takahashi, and T. Tsuchiya, *ibid.*, **48**, 560 (1975).

10) M. E. Evans, F. W. Parrish, and L. Long, Jr., *Carbohyd. Res.*, **3**, 453 (1967).

11) S. Umezawa, K. Tatsuta, and S. Koto, This Bulletin, **42**, 533 (1969).

12) S. Umezawa, Y. Takagi, and T. Tsuchiya, *ibid.*, **44**, 1411 (1971).

13) A. T. Kader and C. M. J. Stirling, *Proc. Chem. Soc.*, 363 (1962); *J. Chem. Soc.*, **1964**, 258.

14) S. Umezawa, T. Tsuchiya, and K. Tatsuta, This Bulletin, **39**, 1235 (1966).

15) I. A. Solomons and P. P. Regna, *Science*, **109**, 515 (1949).

16) C. B. Barlow and L. Anderson, *J. Antibiot.* (Tokyo), **25**, 281 (1972).

Synthesis of (3*S*, 4*S*)- and (3*S*, 4*R*)-4-Amino-3-hydroxy-6-methylheptanoic Acid, and Their *N*-(Acetyl-L-valyl-L-valyl) Derivatives

Mitsuhiro KINOSHITA, Akito HAGIWARA, and Shinpei ABURAKI

Department of Applied Chemistry, Faculty of Engineering, Keio University, Hiyoshi, Kohoku-ku, Yokohama 223

(Received May 30, 1974)

Natural (−)(3*S*,4*S*)-4-amino-3-hydroxy-6-methylheptanoic acid (**10a**) present in pepstatins, specific inhibitors of acid proteases, and its (+)(3*S*,4*R*) diastereomer (**10b**) were synthesized starting from 3-deoxy-1,2-*O*-isopropylidene-α-D-*erythro*-pentodialdo-1,4-furanose (**1**) through highly stereoselective and stereospecific routes. The partial peptide of pepstatin Ac, *N*-(acetyl-L-valyl-L-valyl)-(3*S*,4*S*)-4-amino-3-hydroxy-6-methylheptanoic acid (**15a**) and its (3*S*,4*R*) diastereomer (**15b**) were synthesized *via* azide-coupling of the *t*-butyl esters of **10a** and **10b** with acetyl-L-valyl-L-valine azide, respectively. Compound **15a** inhibited proteolysis by pepsin, however, the diastereomer **15b** showed no inhibition against pepsin.

A new amino acid, (−)4-amino-3-hydroxy-6-methylheptanoic acid[1b](abbreviated (−)AHMHA) which has been isolated from the hydrolyzates of all kinds of pepstatins,[1a–1e] specific inhibitors of acid proteases, was first synthesized together with its (−)diastereomer from L-leucine by Morishima *et al.*[2] Recently, we reported in a communication[3] that the natural (−) AHMHA was identical with (3*S*,4*S*)AHMHA (**10a**), through stereospecific syntheses of all four diastereomers of AHMHA from the appropriate deoxy-sugar derivatives. The synthetically determined absolute configuration 3(*S*), 4(*S*) of natural (−)AHMHA was consistent with the result of the X-ray diffraction study on the natural amino acid which was independently performed by Nakamura *et al.*[4]

The recent studies on pepstatin by Umezawa *et al.*[5,6] have revealed the interesting relationships between the structures of pepstatins and some partial peptides containing natural (−)AHMHA and their inhibition activities against acid proteases. In connection with these studies, it was considered to be important to evaluate the stereochemical effect concerning to the 4(*S*) configuration of natural AHMHA, which may play its role in the enzyme-inhibition activity in the peptide chains of pepstatins or their partial peptides. This paper presents the details of the previously reported synthesis[3] of natural (−) (3*S*,4*S*)AHMHA(**10a**) and its diastereomer (+)(3*S*, 4*R*)AHMHA(**10b**), and the preparation of *N*-(acetyl-L-valyl-L-valyl)-(3*S*,4*S*)AHMHA(**15a**) which is a partial peptide of pepstatin Ac,[1c,1e] and its diastereomer, *N*-(acetyl-L-valyl-L-valyl)-(3*S*,4*R*)AHMHA (**15b**).

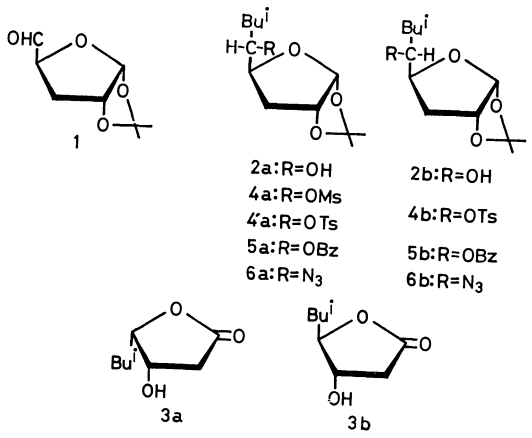

Chart 1.

For the purpose of the stereospecific synthesis of the natural (3*S*,4*S*)AHMHA(**10a**) and its diastereomer (3*S*,4*R*)AHMHA (**10b**), two kinds of diastereomeric deoxy-sugar derivatives, *i.e.*, 3-deoxy-5-*C*-isobutyl-1,2-*O*-isopropylidene-β-L-*lyxo*-pentofuranose(**2a**) and 3-deoxy-5-*C*-isobutyl-1,2-*O*-isopropylidene-α-D-*ribo*-pentofuranose(**2b**) were selected as the starting materials.

The Grignard reaction of 3-deoxy-1,2-*O*-isopropylidene-α-D-*erythro*-pentodialdo-1,4-furanose[7] (**1**) with isobutylmagnesium bromide in ether yielded a crude crystalline addition product (91% yield), which was recrystallized from petroleum ether to afford the pure isomer **2a** in a 67% yield. The 5(*S*) configuration of **2a** was confirmed by the fact that hydrolysis of **2a** followed by oxidation with periodate-hypoiodite[8] gave (3*S*,4*S*)-3,4-dihydroxy-6-methylheptanoic acid-1,4-lactone(**3a**), the 4(*S*) configuration of which was determined by application of Hudson's lactone rule[9] on the rotational change ($\Delta[\alpha]_D^{MeOH}$ (Lactone−potassium salt)=−36 °) of **3a** measured by Witkop's method.[10]

In the following fashion it was ascertained that the Grignard reaction product contained the diastereomer (**2b**) of **2a** as a minor product and that in this case the Grignad reaction was highly stereoselective (about 91%). The minor product **2b** which was concentrated in the mother liquor of the recrystallization of the Grignard reaction product could be isolated in a form of its 5-*O*-benzoyl derivative(**5b**) which was easily separable by silica gel chromatography from the isomeric 5-benzoate(**5a**).

The compound **2a** was converted with methylsulfonyl chloride in pyridine to 5-mesylate (**4a**), which was treated with sodium benzoate in dimethylformamide (DMF) at 140 to 150 °C to afford **5b** in a 52% yield. De-*O*-benzoylation of **5b** with sodium methoxide in methanol gave **2b** in an 81% yield. The 5(*R*) configuration of **2b** was confirmed by the same procedure as that in the case of **2a**; hydrolysis of **2b** followed by oxidation gave (3*S*,4*R*)-3,4-dihydroxy-6-methylheptanoic acid-1,4-lactone(**3b**) which showed a rotational change $\Delta[\alpha]_D^{MeOH}$ +24 °. Compounds **2a** and **2b** could not be separated by tlc in any of the solvent systems examined. The PMR spectra of **2a** and **2b** were apparently distinguishable in the region at δ 3.63 to 4.40, which contains the signals attributed to C–4 and C–5 protons.

Treatment of 5-tosylate (**4b**) prepared from **2b** with sodium azide in DMF at 90 to 97 °C gave 5-azido-3,5-dideoxy-5-*C*-isobutyl-1,2-*O*-isopropylidene-β-L-*lyxo*-pentofuranose (**6a**) as a sole product in an 85% yield. The configuration of C–5 in **6a** was assumed to be "S" because a facile S_N2 displacement of the 5-tosyloxy group by azide ion would proceed under the similar condition to that for the S_N2 reaction of the 5-mesyloxy group in **4a** by benzoate ion. Based on the same principle, the isomeric 5-tosylate **4'a** was treated with sodium azide in DMF at 87 to 95 °C to afford the epimeric (5*R*)-azido compound (**6b**) in an 81% yield.

Hydrolysis of **6a** with 50% aqueous acetic acid, followed by oxidation with sodium periodate gave (3*S*,4*S*)-4-azido-3-formyloxy-6-methylheptanal (**7a**) as a practically pure syrup in a 96% yield. In the same manner the compound **6b** afforded the isomeric aldehyde (**7b**) in a 98% yield.

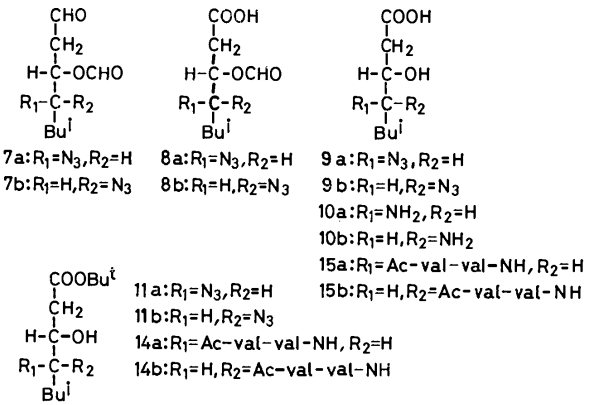

Chart 2.

Oxidations of **7a** and **7b** with a solution of chromium trioxide in acetic acid and pyridine[11] at room temperature afforded (3*S*,4*S*)-4-azido-3-formyloxy-6-methylheptanoic acid (**8a**) and its isomer **8b** as colorless syrup in 76% and 63% yields, respectively. De-*O*-formylations of **8a** and **8b** with dilute hydrogen chloride in aqueous dioxane at room temperature gave the corresponding azido hydroxy acids, **9a**(syrup) and **9b**(crystal) in 72% and 58% overall yields from **7a** and **7b**, respectively. The diastereomeric **9a** and **9b** were stable and their structures were confirmed by elemental analyses, IR, and PMR spectroscopy. By the use of the chromium trioxide solution, instead of the hypoiodite reagent which was previously used[3] the yields of the synthetic steps, **7a**→**9a** and **7b**→**9b** were remarkably improved (about twice).

Hydrogenolysis of **9a** on palladium black in methanol gave (−)(3*S*,4*S*)-4-amino-3-hydroxy-6-methylheptanoic acid (**10a**) in a 93% yield. The synthetic amino acid **10a** was proved to be identical with natural (−)AHMHA by mixture mp, optical rotation, PMR, IR, and high performance liquid chromatography. Hydrogenolysis of **9b** gave the diastereomeric (+)(3*S*,4*R*)AHMHA (**10b**, 81% yield), whose high performance liquid chromatogram showed a single peak having a longer elution time than that of **10a**.

The modified azide coupling according to Rudinger[12] between the free amino acid **10a** and *N*-acetyl-L-valyl-L-valine azide yielded only a small amount of condensation product, *N*-(acetyl-L-valyl-L-valyl)-(3*S*,4*S*)AHMHA (**15a**), probably because of poor solubility of **10a** in DMF. From this result it was decided to use *t*-butyl ester of **10a** for the azide coupling reaction.

t-Butylations of **8a** and **8b** with isobutene and a catalytic amount of sulfuric acid in dichloromethane, followed by de-*O*-formylations with sodium hydroxide in aqueous dioxane afforded the isomeric azidohydroxy acid *t*-butyl esters, **11a** and **11b** in 57% and 58% yields, respectively. Hydrogenolysis of **11a** on palladium black gave *t*-butyl ester of **10a** in quantitative yield, which was immediately coupled with the acid azide prepared from *N*-acetyl-L-valyl-L-valine hydrazide (**13**) by the Rudinger modification to afford *N*-(acetyl-L-valyl-L-valyl)-(3*S*,4*S*)AHMHA *t*-butyl ester (**14a**) in a 74% yield. Treatment of **14a** with trifluoroacetic acid yielded **15a** in a 94% yield. In the same method, the *t*-butyl ester **10b** prepared from **11b** was coupled with the acid azide. Resulting peptide ester (**14b**, 75%) was de-*t*-butylated to give the isomeric peptide (**15b**, 93%).

The synthetic partial peptide **15a**, which contains natural AHMHA, inhibited proteolysis of pepsin at the concentration of 6 μg/ml, in contrast, the diastereomeric peptide **15b** showed no inhibition against pepsin even the high concentration of 250 μg/ml. From this results it is noteworthy that the enzyme-inhibitory activities of pepstatins and their partial peptides may be reflected by the (*S*) configuration of the 4-amino group of AHMHA present in their peptide chains.

Experimental

Melting points were determined on a Mitamura Riken micro hot-stage and uncorrected. IR spectra were taken on a Hitachi IPI-2 spectrometer. PMR spectra were recorded on a Varian A-60D and HA-100D spectrometers using TMS as internal and external standards. Specific rotations were determined with a Zeiss Photoelectric Precision Polarimeter. TLC was performed on WAKOGEL B-5 and silica gel column chromatography on WAKOGEL C-200 which was activated at 110 °C for 1 hr. The following solvent systems were used: A_1 [benzene-ethyl acetate (12 : 1)], A_2[*ibid.* (50 : 1)], A_3[*ibid.* (3 : 1)], A_4[*ibid.* (1 : 1)], B_1[hexane-ethyl acetate (6 : 1)], B_2[*ibid.* (20 : 1)], B_3[*ibid.* (30 : 1)], B_4[*ibid.* (10 : 1)], C[hexane-acetone (6 : 1)], D_1 [hexane-butanone-acetic acid (10 : 1 : 0.17)], D_2[*ibid.* (20 : 2 : 1)], E_1[Chloroform-methanol (30 : 1)] E_2[*ibid.* (20 : 1)], F[chloroform-methanol-acetic acid (80 : 10 : 1)] and G [butanol-ethanol-chloroform-17% aqueous ammonia (7 : 3 : 3 : 3)]. High performance liquid chromatography (HPLC) was carried out on a Waters Associates Liquid Chromatograph ALC 201(RI-Detector) employing an Aminex A-7 (Bio-Rad) column (2.2×600 mm) with 0.1 M pyridine-acetate buffer (pH 5.00) in a flow rate of 0.1 ml/min at 95 °C. In general, all concentrations were carried out under reduced pressure below 40 °C

*1) 3-Deoxy-5-C-isobutyl-1,2-O-isopropylidene-β-L-lyxo-pentofuranose (**2a**).* A solution of 3-deoxy-1,2-*O*-isopropylidene-α-D-*erythro*-pentodialdo-1,4-furanose[7] (**1**) (5.28 g, 31 mmol) in dry ether (240 ml) was added dropwise with stirring over a period of 10 min to an ether solution of iso-

butylmagnesium bromide prepared from magnesium turnings (6.01 g, 247 mmol) and isobutyl bromide (26.6 ml, 247 mmol) in dry ether (100 ml). The mixture which was stirred for 40 min at room temperature, was decomposed with cold water (200 ml), and neutralized with ice-cooled 10% sulfuric acid. The aqueous layer was extracted with ether (200 ml×4). The combined ether layers were washed with saturated aqueous NaCl, dried (Na_2SO_4), and evaporated to afford a crystalline solid (6.40 g, 91%). Recrystallization from petroleum ether gave pure material (**2a**): yield 4.70 g (67%), mp 62.5—63.0 °C, $[\alpha]_D^{19}$ −33° (*c* 1.86, chloroform), δ ($CDCl_3$), 0.93 and 0.95 (each d, $(CH_3)_2CH$, J=6.4 Hz], 1.33 and 1.52 [each s, $(CH_3)C$], 3.63 (dq, H-5, $J_{5,6}$=9.0 Hz, $J_{5,6}$=4.0 Hz), 4.20 (quintet, H-4, $J_{4,5}$=5.2 Hz, $J_{3,4}$=10.2 Hz, $J_{3',4}$=5.2 Hz), 4.82 (dt, H-2, $J_{2,3}$=3.9 Hz, $J_{2,3'}$=~0.5 Hz), and 5.90 (d, H-1, $J_{1,2}$=3.8 Hz).

Found: C, 62.73; H, 9.45%. Calcd for $C_{12}H_{22}O_4$: C, 62.58; H, 9.63%.

*2) 5-O-Benzoyl-3-deoxy-5-C-isobutyl-1,2-O-isopropylidene-β-L-lyxo-pentofuranose (**5a**).* Benzoyl chloride (0.11 ml, 0.94 mmol) was added to a solution of **2a** (108 mg, 0.47 mmol) in pyridine (1 ml), and the mixture was kept at room temperature overnight. It was then diluted with ice-cooled water (6 ml) and extracted with chloroform (3 ml×4). The chloroform extracts were washed successively with saturated aqueous $KHSO_4$ (10 ml), saturated aqueous $NaHCO_3$ (5 ml), and saturated aqueous NaCl (10 ml), dried and evaporated. The syrupy residue (154 mg) immediately crystallized: recrystallization from ether afforded the pure benzoate **5a** (127 mg, 81%); mp 108.5—109 °C, $[\alpha]_D^{13}$ −43° (*c* 2.28, chloroform).

Found: C, 68.56; H, 7.94%. Calcd for $C_{19}H_{26}O_5$: C, 68.24; H, 7.84%.

*3) 3-Deoxy-5-C-isobutyl-1,2-O-isopropylidene-5-O-methanesulfornyl-β-L-lyxo-pentofuranose (**4a**).* To a solution of **2a** (2.64 g, 11.6 mmol) in dry pyridine (26.4 ml) was added methyl-sulfonyl chloride (1.8 ml, 23.2 mmol) and the mixture was set aside overnight at room temperature. Workup in the same manner as described in Exp. 2 afforded a practically pure sample of 5-mesylate **4a** (3.66 g, 100%) as a pale yellow syrup. Silica gel column chromatography of the sample (85 mg) with the solvent A_1 gave an analytical sample of **4a** (72 mg, 85%) as a colorless syrup: $[\alpha]_D^{13}$ −49° (*c* 2.7, chloroform).

Found: C, 50.30; H, 7.70; S, 10.56%. Calcd for $C_{13}H_{24}O_6S$: C, 50.63; H, 7.84; S, 10.40%.

*4) 3-Deoxy-5-C-isobutyl-1,2-O-isopropylidene-5-O-p-toluenesulfonyl-β-L-lyxo-pentofuranose (**4'a**).* Tosylation of **2a** was performed in a usual manner to afford **4'a** as a colorless syrup in a 80% yield: $[\alpha]_D^{13}$ −32° (*c* 2.1 chloroform).

Found: C, 59.51; H, 7.33; S, 8.17%. Calcd for $C_{19}H_{28}O_6S$: C, 59.35; H, 7.34; S; 8.34%.

*5) 5-O-Benzoyl-3-deoxy-5-C-isobutyl-1,2-O-isopropylidene-α-D-ribo-pentofuranose (**5b**).* A solution of **4a** (764 mg, 2.48 mmol) in DMF (55 ml) containing sodium benzoate (1.07 g, 7.43 mmol) was heated at 140—150 °C for 2 hr; tlc (solvent B_1) then revealed the absence of **4a**. The precipitare deposited was filtered off and washed with ethyl acetate. The filtrate and washings were diluted with cold water (100 ml) and was extracted with ethyl acetate (50 ml×3). The combined extracts were washed with saturated aqueous NaCl (30 ml×2), dried and evaporated. The syrupy residue (808 mg) was purified through a silica gel column (120 g, 3×40 cm) with the solvent B_2 to afford a pure sample of **5b** (405 mg, 52%): $[\alpha]_D^{21}$ +13° (*c* 1.31, chloroform).

Found: C, 67.99; H, 7.83%. Calcd for $C_{19}H_{26}O_5$: C, 68.24; H, 7.84%.

*6) 3-Deoxy-5-C-isobutyl-1,2-O-isopropylidene-α-D-ribo-pentofuranose (**2b**).* To a solution of **5b** (900 mg, 2.7 mmol) in dry methanol (4.5 ml) was added 1.32 M methanolic sodium methoxide (4.07 ml, 5.4 mmol) and the mixture was kept for 5 hr at room temperature. An excess of sodium methoxide was neutralized with 20% acetic acid; the solution was evaporated and the residue was extracted with chloroform (20 ml×3). The extracts were washed with saturated aqueous NaCl (20 ml×2), dried and evaporated to give a crystalline mass (620 mg) wihch was recrystallized from petroleum ether: yield of pure **2b** 500 mg (81%), mp 56—57 °C, $[\alpha]_D^{15}$ —4° (*c* 1.38, chloroform), δ ($CDCl_3$), 0.92 and 0.95 [each d, $(CH_3)_2CH$, J=6.3 Hz], 1.33 and 1.52 [each s, $(CH_3)_2C$], 3.8—4.4 (m, H-4 and H-5), 4.80 (dq, H-2, $J_{2,3}$=6.0 Hz, $J_{2,3'}$=0.7 Hz) and 5.89 (d, H-1, $J_{1,2}$=3.8 Hz).

Found: C, 62.27; H, 9.45%. Calcd for $C_{12}H_{22}O_4$: C, 62.58; H, 9.63%.

*7) 3-Deoxy-5-C-isobutyl-1,2-O-isopropylidene-5-O-p-toluenesulfonyl-α-D-ribo-pentofuranose (**4b**).* The tosylation of **2b** was performed in a usual manner to afford **4b** as a colorless syrup: $[\alpha]_D^{15}$ −1° (*c* 1.0, chloroform).

Found: C, 59.47; H, 7.28; S, 8.49%. Calcd for $C_{19}H_{28}O_6S$: C, 59.35; H, 7.34; S, 8.34%.

*8) (3S,4S)-3,4-Dihydroxy-6-methylheptanoic Acid-1,4-lactone (**3a**).* Treatment of **2a** (202 mg) with 20% acetic acid at 120 °C for 20 min gave a syrup of 3-deoxy-5-*C*-isobutyl-L-lyxo-pentose (165 mg). The free sugar was dissolved in acetone (3 ml) and to the solution was added a solution of sodium metaperiodate (645 mg) in water (6.3 ml). After standing at room temperature for 20 min, the precipitate was filtered off and acetone was removed from the filtrate by evaporation. The aqueous layer was extracted with chloroform and the extract was dried and evaporated to afford a syrup (165 mg), which was immediately subjected to the next oxidation reaction. To a solution of the product (163 mg) in dioxane (4 ml) and water (1.6 ml) was added a solution of K_2CO_3 (855 mg) and $KHCO_3$ (618 mg) in water (6 ml) and then a solution of iodine (730 mg) and KI (912 mg) in water (0.8 ml), and the mixture was stirred for 1 hr. The excess of iodine was reduced with solid sodium thiosulfate and then the solution was neutralized with 10% sulfuric acid, extracted with ether (10 ml×3), and the extracts were washed with saturated aqueous NaCl, dried and evaporated. The residual syrup (81 mg) was purified by silica gel chromatography with the solvent C to afford a pure sample of **3a** a colorless liquid: yield 31 mg (23%). Optical rotation in methanol; $[\alpha]_D$ −81°, $[\alpha]_{436}$ −167°, and $[\alpha]_{365}$ −266° (*c* 1.12, 21 °C). Optical rotation in methanol-0.1 M aqueous KOH (1 : 1 vol); $[\alpha]_D$ −45°, $[\alpha]_{436}$ −89°, and $[\alpha]_{365}$ −130° (*c* 0.56, 21 °C). IR: $\nu_{max}^{CCl_4}$ 3480 (OH) and 1775 cm^{-1} (γ-lactone).

Found: C, 60.71; H, 8.79%. Calcd for $C_8H_{14}O_3$: C, 60.74; H, 8.92%.

*9) (3S,4R)-3,4-Dihydroxy-6-methylheptanoic Acid-1,4-lactone (**3b**).* The title compound **3b** was obtained from **2b** (176 mg) in the same procedure as described in Exp. 8; colorless liquid, yield 49 mg (42%). Optical rotation in methanol; $[\alpha]_D$ +41°, $[\alpha]_{436}$ +76°, and $[\alpha]_{365}$ +105° (*c* 1.73, 18 °C). Optical rotation in methanol-0.1 M aqueous KOH (1 : 1 vol); $[\alpha]_D$ +17°, $[\alpha]_{436}$ +34°, and $[\alpha]_{365}$ +57° (*c* 0.87, 18 °C). IR; $\nu_{max}^{CCl_4}$ 3480 (OH) and 1775 cm^{-1} (γ-lactone).

Found: C, 60.57; H, 8.73%. Calcd for $C_8H_{14}O_3$: C, 60.74; H, 8.92%.

10) Isolation of the Minor Product ***2b*** *produced in the Grignard Reaction of* ***1*** *with Isobutylmagnesium Bromide.* A crude product (898 mg) of the Grignard reaction, which was obtained in the same manner as described in Exp. 1, was chromatographed through a silica gel column (100 g, 2.8× 38 cm) with the solvent A_3. The effluent containing the reaction product was collected in the fore-run, the main fraction, and the after-run, which gave crystal I (pure **2a**, 36 mg), crystal II (**2a** contaminated with a small amount of **2b**, 660 mg), and crystal III (a 4 : 3 mixture of **2a** and **2b**, 18 mg), respectively. The ratio of **2a** to **2b** in the mixture was estimated by PMR analysis. The crystals II and III were combined and recrystallized from petroleum ether to afford pure **2a** (485 mg, 72% yield). The mother liquor was evaporated and the residual solid (143 mg, *ca.* 4 : 3 mixture of **2a** and **2b**) was benzoylated with benzoyl chloride (0.15 ml) in pyridine (1.41 ml). The product was chromatographed on a silica gel column (30 g, 2.2×20 cm) with the solvent B_2 to give **5b** (76 mg, syrup) as the faster-moving component, a mixture of **5a**+**5b** (21 mg, syrup), and **5a** (95 mg, mp 107—108.5 °C) as the slower-moving component. From these results, the content of **2b** in the original Grignard reaction product may be estimated as about 9%.

*11) 5-Azido-3,5-dideoxy-5-*C*-isobutyl-1,2-*O*-isopropylidene-β-*L*-lyxo-pentofuranose (****6a****).* A solution of **4b** (1.17 g, 3.05 mmol) in dry DMF (26 ml) was heated at 90—97 °C with sodium azide (646 mg, 9.93 mmol) for 2.5 hr, and then poured into cold water (130 ml). The mixture saturated with NaCl was extracted with chloroform (50 ml×3). The extracts were washed with saturated aqueous NaCl (80 ml), dried and evaporated. The residual syrup (742 mg) was purified through a silica gel column (90 mg, 2.8×38 cm) with the solvent A_2 to afford **6a** as a colorless syrup. Yield 657 mg (85%); $[\alpha]_D^{18}$ −61° (*c* 0.35, chloroform); $\nu_{max}^{CCl_4}$ 2140 cm^{-1} (N_3); δ ($CDCl_3$), 0.94 and 0.96 [each d, $(CH_3)_2CH$ J=6.0 Hz), 1.33 and 1.51 [each s, $(CH_3)_2C$], 3.08—3.40 (m, H-5), 4.28 (quintet, H-4, $J_{4,5}$=5.0 Hz, $J_{3,4}$=5.0 Hz, $J_{3',4}$=10.0 Hz), 4.78 (t, H-2, $J_{2,3}$=5.0 Hz, $J_{2,3'}$=1.0 Hz) and 5.89 (d, H-1, $J_{1,2}$=3.8 Hz).

Found: C, 56.70; H, 8.29; N, 16.71%. Calcd for $C_{12}H_{21}O_3N_3$: C, 56.45; H, 8.29; N, 16.46%.

*12) 5-Azido-3,5-dideoxy-5-*C*-isobutyl-1,2-*O*-isopropylidene-α-*D*-ribo-pentofuranose (****6b****).* The tosylate **4'a** (2.17 g, 5.66 mmol) was treated with sodium azide (1.13 g, 17.4 mmol) in dry DMF (40 ml) at 87—95 °C for 1.7 hr. The S_N2 reaction product (1.63 g) was isolated by the procedure of Exp. 11, and purified by chromatography on silica gel (90 g) with the solvent B_3 to afford **6b** as a colorless syrup. Yield 1.17 g (81%); $[\alpha]_D^{30}$ −31° (*c* 1.88, chloroform); $\nu_{max}^{CCl_4}$ 2140 cm^{-1} (N_3); δ ($CDCl_3$), 0.97 [d, $(CH_3)_2CH$, J=6.0 Hz], 1.35 and 1.52 [each s, $(CH_3)_2C$], 3.60—3.95 (m, H-5), 4.30 (dq, H-4), 4.81 (dq, H-2, $J_{2,3}$=5.5 Hz, $J_{2,3'}$=1.0 Hz), and 5.89 (d, H-1, $J_{1,2}$=3.7 Hz).

Found: C, 56.70; H, 8.26; N, 16.48%. Calcd for $C_{12}H_{21}O_3N_3$: C, 56.45; H, 8.29; N, 16.46%.

*13) (3S,4S)-4-Azido-3-formyloxy-6-methylheptanal (****7a****).* Treatment of **6a** (589 mg) in 50% aqueous acetic acid (10 ml) at 115—125 °C for 20 min, followed by concentration afforded a pale red syrup (497 mg), which was dissolved in acetone (5.6 ml) and treated with a solution of sodium metaperiodate (1.48 g) in water (12.5 ml). After standing at room temperature for 15 min, the reaction mixture was concentrated to an aqueous residue, which was extracted with chloroform (10 ml×3). The extracts were washed with saturated aqueous NaCl, dried and evaporated to give **7a** as a pale yellow syrup; yield 470 mg (96%). This sample appeared as a practically pure material by tlc (solvent A_4) and PMR: $\nu_{max}^{CCl_4}$ 2100 (N_3) and 1730 cm^{-1} (CHO and OCHO); δ ($CDCl_3$), 8.28 (s, OC<u>H</u>O) and 10.07 (dd, $CH_2C\underline{H}O$).

*14) (3S,4R)-4-Azido-3-formyloxy-6-methylheptanal (****7b****).* By the procedure described in Exp. 13, **7b** was obtained from **6b** in a 98% yield: $\nu_{max}^{CCl_4}$ 2100 (N_3) and 1728 cm^{-1} (CHO and OCHO); δ ($CDCl_3$), 8.25 (s, OC<u>H</u>O) and 10.05 (dd, CH_2CHO).

*15) (3S,4S)-4-Azido-3-hydroxy-6-methylheptanoic Acid (****9a****).* A solution of **7a** (470 mg) in a 28.7 ml of chromium trioxide solution[11] (CrO_3 1.1 g in acetic acid 3.3 ml and pyridine 1.1 ml) was allowed to stand at room temperature for 3 hr. The reaction mixture diluted with cold water (160 ml) was extracted with ether (30 ml×4) and the extracts were washed with saturated aqueous NaCl (20 ml×2). The dried ether solution was evaporated to afford a pale green syrup (526 mg). The syrup was chromatographed on a silica gel column (63 g, 2.3×36 cm) with the solvent D_1 to give (3*S*,4*S*)-4-azido-3-formyloxy-6-methylheptanoic acid **8a** (382 mg, 76%) as a colorless syrup; δ ($CDCl_3$), 8.21 (s, OC<u>H</u>O) and 9.60 (COOH). The syrup (382 mg) was dissolved in a mixture of conc. HCl (3.3 ml) and 50% (V/V) aqueous dioxane (56 ml) and the solution was kept at room temperature for 2 hr. The reaction mixture was concentrated and extracted with ether (10 ml×3). The extracts were washed with saturated aqueous NaCl (10 ml), dried and evaporated to afford **9a** (318 mg, 72% based on **7a**). A sample (27 mg) of this product was purified by silica gel chromatography with the solvent D_2 to give the pure sample (21 mg) of **9a** as a syrup: $[\alpha]_D^{21}$ −19° (*c* 0.57, chloroform); $\nu_{max}^{CCl_4}$ 3500 (OH), 2800—2500 (COOH), 2120 (N_3), and 1720 cm^{-1} (COOH); δ ($CDCl_3$), 0.97 and 0.98 (each d, $(CH_3)_2CH$, J=6.2 Hz), 1.13—2.0 (m, H-5, H-5', H-6, and OH), 2.57 (dd, H-2, $J_{2,3}$=4.7 Hz), 2.77 (dd, H-2', $J_{2',3}$=7.9 Hz, $J_{2,2'}$=16.7 Hz), 3.29 (dq, H-4, $J_{4,5}$=8.7 Hz, $J_{4,5'}$=5.0 Hz), 4.08 (dq, H-3, $J_{3,4}$=3.5 Hz), and 6.3 (broad, COOH).

Found: C, 47.85; H, 7.47; N, 21.22%. Calcd for $C_8H_{15}O_3N_3$: C, 47.75; H, 7.51; N, 20.88%.

*16) (3S,4R)-4-Azido-3-hydroxy-6-methylheptanoic Acid (****9b****).* By the procedure described in Exp. 15, **7b** (96 mg) was treated with the chromium trioxide solution to afford (3*S*,4*R*)-4-azido-3-formyloxy-6-methylheptanoic acid (**8b**) (65.2 mg, 63%) as a colorless syrup. A sample (31 mg) of **8b** was then de-*O*-formylated with hydrogen chloride in aqueous dioxane. The product (25.5 mg, 92%, mp 50—55 °C) was purified by silica gel chromatography (solvent D_2) and thereafter was recrystallized from petroleum ether to give a pure sample (16 mg) of **9b**: mp 60.5—61 °C; $[\alpha]_D^{15}$ +1° (*c* 2.82, chloroform); ν_{max}^{KBr} 3380 (OH), 2800—2500 (COOH), 2130 (N_3), and 1725 cm^{-1} (COOH); δ ($CDCl_3$), 0.96 and 0.98 (each d, $(CH_3)_2CH$, J=6.2 Hz), 1.25—1.50 (m, H-5 and H-5'), 1.55—2.0 (m, H-6 and OH), 2.63 (d, H-2 and H-2', $J_{2,3}$=$J_{2',3}$=6.0 Hz), 3.54 (quintet, H-4, $J_{4,5}$=4.5 Hz, $J_{4,5'}$=9.1 Hz), 4.07 (dt, H-3, $J_{3,4}$= 4.5 Hz), and 6.5 (broad, COOH).

Found: C, 47.52; H, 7.37; N, 21.17%. Calcd for $C_8H_{15}O_3N_3$: C, 47.75; H, 7.51; N, 20.88%.

*17) (−)(3S,4S)AHMHA (****10a****).* A solution of **9a** (110 mg) in methanol (10 ml) and water (3 ml) was vigorously stirred for 30 min in a hydrogen atmosphere with palladium black. The crystalline product was washed with dry ether and dry ethanol to afford **10a** (97 mg, 93%) whose HPLC showed a single peak having the same elution time (137 min) as that of natural (−)AHMHA. An analytical sample was obtained by recrystallization from water-ethanol: mp 201—203 °C (decomp.) (lit,[1b] mp 199—

201 °C (decomp.)]; $[\alpha]_D$ −20°, $[\alpha]_{546}$ −28°, $[\alpha]_{436}$ −52°, $[\alpha]_{405}$ −62°, $[\alpha]_{365}$ −75° (*c* 0.64, water, 16 °C) [lit.[1b] $[\alpha]_D^{20}$ −18.9° (*c* 0.424, water), lit,[2] $[\alpha]_{541}$ −20°, $[\alpha]_{436}$ −34°, $[\alpha]_{405}$ −40°, $[\alpha]_{365}$ −49° (*c* 1, water, 21 °C)]. The IR (KBr) and PMR (D_2O) spectra were identical with those of authentic sample* of natural (−)AHMHA.

Found: C, 54.79; H, 9.78; N, 7.93%. Calcd for $C_8H_{17}O_3N$: C, 54.83; H, 9.78; N, 7.99%.

*18) (+) (3S,4R)AHMHA (**10b**).* A solution of **9b** (58 mg) in methanol (6 ml) and water (1.2 ml) was hydrogenolyzed on palladium black. The crystalline product was washed with dry ether and dry ethanol to give **10b** (41 mg, 81%) whose HPLC showed a single peak which has a longer retension time (140 min) than that of **10a**. Recrystallization from water-ethanol afforded an analytical sample: colorless prisms, mp 202.5—203.5 °C (decomp.); $[\alpha]_D$ +20°, $[\alpha]_{546}$ +23°, $[\alpha]_{436}$ +46°, $[\alpha]_{405}$ +53°, $[\alpha]_{365}$ +68° (*c* 0.66, water, 16°C).

Found: C, 54.58; H, 9.54; N, 7.76%. Calcd for $C_8H_{17}O_3N$: C, 54.83; H, 9.78; N, 7.99%.

*19) t-Butyl (3S,4S)-4-Azido-3-hydroxy-6-methylheptanoate (**11a**).* A sample (392 mg) of 4-azido-3-formyloxy-6-methylheptanoic acid (**8a**) (Exp. 15) was dissolved in dichloromethane (3.3 ml) and cooled to −40 °C. To the solution was added isobutene (2.2 ml) and conc. H_2SO_4 (0.033 ml), and the mixture was allowed to warm to room temperature. After standing for 3 hr, the reaction mixture was neutralized with triethylamine and evaporated. The residue was dissolved in ethyl acetate (15 ml) and washed with saturated aqueous NaCl, dried and evaporated to give a syrup (438 mg). To a solution of the syrup (398 mg) in dioxane (7 ml) was added 0.2 M NaOH (7 ml), and the mixture was stirred for 30 min at room temperature, evaporated, the residue was extracted with ethyl acetate (6 ml × 4). The ethyl acetate layers were washed with saturated aqueous NaCl, dried and evaporated. The oily product (358 mg) was chromatographed on silica gel (40 g) with the solvent B_4 to afford a pure sample of **11a**: colorless oil, yield 225 mg (57% based on **7a**); $[\alpha]_D^{15}$ −25° (*c* 2.62, chloroform).

Found: C, 56.09; H, 9.00; N, 16.24%. Calcd for $C_{12}H_{23}O_3N_3$: C, 56.01; H, 9.01; N, 16.33%.

*20) t-Butyl (3S,4R)-4-Azido-3-hydroxy-6-methylheptanoate (**11b**).* By the same procedure as in the preparation of **11a**, a sample (421 mg) of **8b** (Exp. 16) was *t*-butylated and the crude *t*-butyl ester (372 mg) was de-*O*-formylated. The oily product (429 mg) was purified by silica gel column (50 g) with the solvent B_4 to afford a pure sample of **11b**; yield 274 mg (58%), $[\alpha]_D^{26}$ +7° (*c* 1.72, chloroform).

Found: C, 56.19; H, 8.83; N, 16.58%. Calcd for $C_{12}H_{23}O_3N_3$: C, 56.01; H, 9.01; N, 16.33%.

*21) N-Acetyl-L-valyl-L-valine Methyl Ester (**12**).* *N*-Benzyloxycarbonyl-L-valyl-L-valine methyl ester[13] (2.3 g, 6.32 mmol) was hydrogenolyzed on palladium black in methanol (20 ml). The reduction product was acetylated in methanol (20 ml) with triethylamine (0.88 ml, 6.32 mmol) and acetic anhydride (1.18 ml, 12.64 mmol) in a usual manner to afford a crystalline solid (1.71 g). It was recrystallized from ethyl acetate; yield 1.47 g (86%), mp 147—150 °C. This sample was again recrystallized from ethyl acetate to give a pure sample of **12**, mp 155—157 °C, $[\alpha]_D^{33}$ −65° (*c* 1.07, methanol).

Found: C, 57.32; H, 8.90; N, 10 28%. Calcd for $C_{13}H_{24}O_4N_2$: C, 57,33; H, 8.88; N, 10.29%.

*22) N-Acetyl-L-valyl-L-valine Hydrazide (**13**).* A mixture of **12** (1.3 g), methanol (12 ml), and 80% hydrazine hydrate (5.9 ml) was kept overnight at room temperature. The crystalline hydrazide separated was collected by filtration and washed with methanol, chloroform, and water, successively, and dried; yield 1.14 g (88%). Analytical sample was obtained by recrystallization from DMF-water; mp 280 °C (decomp.), $[\alpha]_D^{31}$ −45° (*c* 0.5, dimethylsulfoxide).

Found: C, 53.09; H, 8.70; N, 20.71%. Calcd for $C_{12}H_{24}O_3N_4$: C, 52.92; H, 8.88; N, 20.57%.

*23) N-(Acetyl-L-valyl-L-valyl)-(3S,4S)AHMHA t-Butyl Ester (**14a**).* Isoamyl nitrite (0.056 ml, 0.015 mmol) and 3.93 M HCl in tetrahydrofuran (0.31 ml, 1.21 mmol) was added to a solution of **13** (106 mg, 0.388 mmol) in DMF (0.5 ml) cooled to −20 °C and the mixture was stirred at −20 °C for 30 min to make a clear solution. To this solution containing acetyl-L-valyl-L-valine azide was added triethylamine (0.223 ml, 1.6 mmol) and a solution of (3*S*,4*S*) AHMHA *t*-butyl ester, which was prepared from **11a** (99.6 mg, 0.388 mmol) by catalytic hydrogenolysis on palladium black, in DMF (0.6 ml). After stirring at −20 °C for 4 hr and standing overnight in a refregerator, the solvents were removed. The residue was triturated with water to give a crystalline product which was collected by filtration and washed with water; yield 183 mg (74%). Silica gel chromatography (solvent E_1) of the product (183 mg) gave a practically pure sample of **14a** (98 mg). Recrystallization from methanol-water afforded an analytical sample; mp 219—220 °C, $[\alpha]_D^{16}$ −85° (*c* 0.55, methanol).

Found: C, 60.92; H, 9.43; N, 9.04%. Calcd for $C_{24}H_{45}O_6N_3$: C, 61.12; H, 9.62; N, 8.91%.

*24) N-(Acetyl-L-valyl-L-valyl)-(3S,4R)AHMHA t-Butyl Ester (**14b**).* The *t*-butyl ester of **10b** obtained by hydrogenolysis of **11b** (103 mg) was coupled with acetyl-L-valyl-L-valine azide prepared from **13** (109 mg) by the procedure described in Exp. 23 to afford the product **14b** (141 mg, 75%) which appeared as a homogeneous material on tlc (solvent E_2). A sample (30 mg) of this product was purified by silica gel chromatography (solvent E_2) and by recrystallization from ethanol to give a pure sample (16 mg); mp 215 °C ~ (sublimated), $[\alpha]_D^{17}$ −43° (*c* 0.5, methanol).

Found: C, 61.25; H, 9.49; N, 8.90%. Calcd for $C_{24}H_{45}O_6N_3$: C, 61.12; H, 9.62; N, 8.91%.

*25) N-(Acetyl-L-valyl-L-valyl)-(3S,4S)AHMHA (**15a**).* A solution of **14a** (63 mg) in trifluoroacetic acid (1.5 ml) was allowed to stand for 25 min at room temperature and then evaporated to dryness. The syrupy residue was treated with ether to afford **15a** as a crystalline solid (52 mg, 94%). Silica gel chromatography (solvent F) of the product, followed by recrystallization from methanol-water gave an analytical sample; mp 226—227 °C, $[\alpha]_D^{13}$ −100° (*c* 0.68, methanol).

Found:. C, 57.68; H, 8.97; N, 10.28%. Calcd for $C_{20}H_{37}O_6N_3$: C, 57.81; H, 8.98; N, 10.11%.

*26) N-(Acetyl-L-valyl-L-valyl)-(3S,4R)AHMHA (**15b**).* Treatment of **14b** (144 mg) with trifluoroacetic acid (1.2 ml) for 20 min at room temperature afforded **15b** as a crystalline solid (118 mg, 93%) which appeared to be homogeneous on tlc (solvent F and G). Recrystallization from methanol-water gave a pure sample; mp 215—217 °C, $[\alpha]_D^{15}$ −40° (*c* 0.21, methanol).

Found: C, 57.57; H, 8.77; N, 10.09%. Calcd for $C_{20}H_{37}O_6N_3$: C, 57.81; H, 8.98; N, 10.11%.

The authors wish to express their sincere thanks to Dr. Hamao Umezawa, Institute of Microbial Chemistry, for his helpful advice, and to Prof. Sumio Umezawa,

* The authentic sample of (−)AHMHA was generously supplied by Dr. Tomohisa Takita, Institute of Microbial Chemistry, to whom the authors' thanks are due.

Keio University, for his interest and kind advice. Thanks are also due to Dr. Takaaki Aoyagi and Dr. Takeshi Hara, Institute of Microbial Chemistry, for the enzyme inhibition activity tests and for the measurement of high performance liquid chromatograms.

References

1) (a) H. Umezawa, T. Aoyagi, H. Morishima, M. Matuzaki, M. Hamada, and T. Takita, *J. Antibiot.* (Tokyo), **23**, 259 (1970). (b) H. Morishima, T. Takita, T. Aoyagi, T. Takeuchi, and H. Umezawa, *ibid.*, **23**, 263 (1970). (c) S. Murao and S. Satoi, *Agr. Biol. Chem*, **34**, 1265 (1970). (d) T. Miyano, M. Tomiyasu, H. Iizuka, S. Tomisaka, T. Takita, T. Aoyagi, and H. Umezawa, *J. Antibiot.* (Tokyo), **25**, 489 (1972). (e) T. Aoyagi, Y. Yagisawa, M. Kumagai, M. Hamada, H. Morishima, T. Takeuchi, and H. Umezawa, *ibid.*, **26**, 539 (1973). (f) H. Umezawa, T. Miyano, T. Murakami, T. Takita, T. Aoyagi, T. Takeuchi, H. Naganawa, and H. Morishima, *ibid.*, **26**, 615 (1973).

2) H. Morishima, T. Takita, and H. Umezawa, *ibid.*, **26**, 115 (1973).

3) M. Kinoshita, S. Aburaki, A. Hagiwara, and J. Imai, *ibid.*, **26**, 249 (1973).

4) H. Nakamura, H. Morishima, T. Takita, H. Umezawa, and Y. Iitaka, *ibid.*, **26**, 255 (1973).

5) T. Aoyagi, S. Kunimoto, H. Morishima, T. Takeuchi, and H. Umezawa, *ibid.*, **24**, 687 (1971).

6) T. Aoyagi, H. Morishima, R. Nishizawa, S. Kunimoto, T. Takeuchi, and H. Umezawa; H. Ikezawa, *ibid.*, **25**, 689 (1972).

7) D. H. Murrary and J. Prokop, *J. Pharm. Sci.*, **54**, 1468 (1965).

8) E. Zissis, R. K. Ness, and H. G. Flecher, Jr., *Carbohyd. Res.*, **20**, 9 (1971).

9) C. S. Hudson, *J. Amer. Chem. Soc.*, **61**, 1525 (1939).

10) B. Witkop, *Experientia*, **12**, 372 (1959).

11) J. C. Sheehan, H. G. Zachan, and W. B. Lawson, *J. Amer. Chem. Soc.*, **80**, 3349 (1958).

12) J. Honzl and J. Rudinger, *Collect. Czechoslov. Chem. Commun.*, **26**, 2333 (1961).

13) J. W. Hinman, E. L. Caron, and H. N. Christensen, *J. Amer. Csem. Soc.*, **72**, 1620 (1950).

Stereochemical Aspects of the Photo-Beckmann Rearrangement. Stereochemical Integrity of the Terminus of the Migrating Carbon in the Photo-Beckmann Rearrangements of 5α- and 5β-Cholestan-6-one Oximes[1]

Hiroshi SUGINOME and Hajime TAKAHASHI

Department of Chemistry, Faculty of Science, Hokkaido University, Sapporo 060

(Received July 4, 1974)

The Beckmann rearrangement of either *syn*-5β-cholestan-6-one oxime or *anti*-5β-cholestan-6-one oxime with polyphosphoric acid at 90° takes place prior to the *syn-anti* equilibration of these isomers. In the photo-Beckmann rearrangement a pair of lactams, in both of which the original configurations of C_α with respect to the oximino-group of the starting oximes were retained, was produced irrespective of the configuration of the oximino-group of the starting oxime. The difference of the amounts between two isomeric lactams formed in each photolysis is small but the lactams due to the migration of the more substituted carbon are produced always in a slightly larger amount than those due to the migration of the less substituted carbon. Oxygen does not affect the formation of lactams. All these results indicate a concerted reorganization of an excited singlet oxaziridine intermediate, hydrogen-bonded with protic solvent molecule (s), into the corresponding lactams. During these studies, the photochemical epimerization of 5β-steroid-6-one into the 5α-isomer by α-cleavage-recombination sequence was observed.

Since the first report of the photo-Beckmann rearrangement of arylaldoximes by de Mayo[2] further examples with a variety of oximes have been recorded during this decade. The types of oximes investigated include alicyclic ketone oximes,[3a,3c-3f,6,7] naphthalenone oximes,[3b] aliphatic ketone oximes,[3a] styryl ketone oximes,[3g] and α,β,γ,δ-unsaturated aldehyde oxime.[3h]

The mechanistic aspects of this intriguing and potentially useful photochemical rearrangement have been discussed for arylaldoximes,[4] naphthalenone oxime,[3b] styrylketone oximes[3g] and alicyclic ketone oximes.[3c-3e] Common mechanistic features with respect to the formation of amides from all the types of oximes cited above are as follows.

The formation of amides takes place *via* oxaziridine intermediates which are formed rapidly from the excited oximes. This excited state was proved to be a singlet for the arylaldoxime rearrangement[4] and later for the styryl ketone oxime rearrangements.[3g]

Protic solvents, without exception, considerably accerelated the formation of amides from oximes. The photolysis of some steroidal ketone oximes in an aprotic solvent such as benzene does not afford lactams but the parent ketones.[5] In some instances, even alcohol is not sufficient and an acid such as AcOH is needed to cause the rearrangement.[3c]

These observations were taken as evidence that a protonation may be involved at some stage of the rearrangement[3b,3g] or that the oxaziridine formation may proceed *via* a polarized excited state.[3b,3d,3g] Several other features of the mechanism of the amide formation, however, do not conform with hypothesis based on a single mechanism for the all types of oximes and the correct mechanism and the excited species involved for each type of oxime must await further elaboration.

We wish to report here a study of the stereochemical aspects of the over-all rearrangement which had previously been disclosed by us only as a brief communication.[6] Since our publication, similar results were reported by Just and his colleagues.[7] We believe this aspect of the rearrangement is important both from the synthetic and mechanistic point of view.

We have chosen 5α- and 5β-cholestan-6-one oximes as the substrates for this study.

Results

Preparation of Cholestan-6-one Oximes. It was found that the oximation of 5α-cholestan-6-one **1** proceeds at an undetectable rate at room temperature. On the other hand, at reflux temperature, the oximation afforded only a single known oxime **2**.[8-10]

In contrast to the 5α-cholestan-6-one, the oximation of 5β-cholestan-6-one **7** at room temperature proceeded readily and afforded a mixture of two isomeric oximes. These oximes could be separated by preparative tlc to afford the more polar amorphous oxime **5** and the less polar crystalline oxime **6**, mp 144—146 °C, approximately in the ratio of 3 : 1. The methanolic solution of the *syn* isomer or that of the *anti* isomer was set aside for 48 hr at room temperature and examination of the solution by tlc indicated that virtually no *syn* to *anti* nor any *anti* to *syn* isomerization took place under these conditions. However, it has been found that benzene solutions of neither the *syn* isomer nor the *anti* isomer are as stable as methanolic solutions and a significant amount of *syn* isomer is produced from *anti* (and *vice versa*) after 48 hr at room temperature. The observed stability of the configuration of the oximino group in MeOH would probably be associated with the hydrogen bonding between the oximino-group and the protic solvent or with the higher dielectric constant of MeOH.[11]

The Configuration of Cholestan-6-one Oximes: The configuration of the oximino-hydroxyls of the three oximes **2**, **5** and **6** were established both by the Beckmann rearrangement and ^1H NMR spectra.

5α-Cholestan-6-one Oxime 2: In view of the fact that a single oxime is formed it would be reasonable to assume[9b] that the oximino group of **2** will possess the less sterically hindered and more stable *anti* configuration with respect to the C_5–C_6 bond since the interaction between the 4-methylene group and the OH group in both the initial adduct and the oxime in oximation reaction seems considerable.[12] The treat-

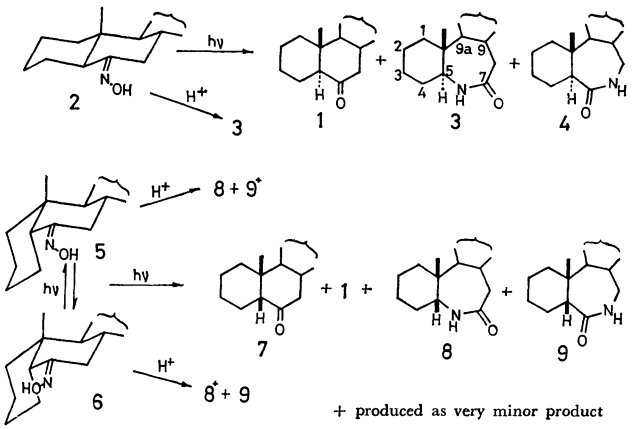

Scheme 1.

ment of **2** with PPA[13] afforded a known lactam **3**[9b] as the sole product in 65% yield. This lactam was confirmed as 6-aza-*B*-homo-5α-cholestan-7-one by ^{1}H NMR (Table 2). On this basis it was established that the configuration of the oximino group of **1** was *anti* with respect to the C_5–C_6 bond.

Hydrogens attached to a carbon α to an oximino-group are known to appear downfield,[14] in the ^{1}H NMR spectrum. The NMR spectrum of the oxime **2** exhibited a quartet centered at τ 6.69 (J=13.5 and 3.8 Hz) (Table 1) which may be assignable to a proton α to the oximino-group. This should be the 7β proton on the basis of the examination of the Dreiding model of **2** together with the coupling constants required by the model. The model of the oxime **2** reveals that the dihedral angle between the oximino π bond and the adjacent methylene group is about 74° and a π-bond contribution of approximately 0—1 Hz to the methane geminal coupling constant (12.4 Hz) is expected.[15] This affords the anticipated value of $J_{gem} \simeq 11.4$ Hz for the C-7 protons which is close to the observed geminal coupling constant. Moreover, the dihedral angle between the C_7–βH and the C_8–βH is about 55° and a small splitting of 3.8 Hz is also consistent with the above assignment.

Since the Beckmann rearrangement indicates that the configuration of the oximino-group of **2** is *anti* with respect to the C_5–C_6 bond, it is concluded that a proton H_α, *syn* to the oximino OH of saturated oximes should appear generally downfield from its *anti*-counterpart and this downfield shift of a proton is caused by the oximino OH.

*5β-Cholestan-6-one Oximes (**5** and **6**)*: The configurations of the oximino-groups of the 5β-cholestan-6-one oximes are not able to be differentiated merely from their NMR spectra. Assuming that the preferred conformations of the B-rings of **5** and **6** are chair forms, the 7β–H of the *anti* form should appear as a quartet with $J_{7\alpha,7\beta} \simeq 12$ Hz and $J_{7\beta,8\beta} \simeq 2$—3 Hz and the 5β–H of the *syn* form should also appear as a quartet with $J_{5\beta,4\beta} \simeq 2$ Hz and $J_{5\beta,4\alpha} \simeq 9$—11 Hz.

Table 1. The NMR data of oximes (τ, *J* (Hz), $CDCl_3$, TMS, 100 MHz)

Oxime	18-H	19-H	7β-H	5β-H	
2	9.34	9.25	6.69 (q) (3.8 and 13.5)	—	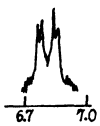
5	9.36	9.17	6.84 (d) (<1 and 10.5)	—	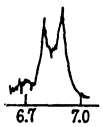
6	9.36	9.17	—	6.92 (q) (4 and 11)	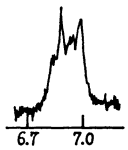

Table 2. The NMR data of lactams (τ, *J* (Hz), $CDCl_3$, TMS, 100 MHz)

Lactam	18-H	19-H	8-H	5-H	NH
3	9.35	9.17	—	6.76 (q) (4.0 and 11.0)	4.48 (d) (5.5)
4	9.33	9.11	6.90 ~7.03 (m)	7.44 (q) (5.0 and 11.5)	3.96 (broad)
8	9.34	9.03	—	7.70 (d) (8.0)	3.8 (broad)
9	9.32	8.97	7.02 (b. s) (W_H=11)	—	3.85 (broad)

The NMR spectrum of **5** revealed a one proton doublet at τ 6.84 (J=10.5 Hz, Fig. in Table 1) with a small splitting of less than 1 Hz in each signal and the NMR spectrum of the oxime **6** revealed a one-proton quartet centered at τ 6.92 (J=4 Hz and 11 Hz, Fig. in Table 1). These signals are attributable to a proton α to the oximino-groups but it is not possible to distinguish between the *syn* and *anti*-isomers from the above figures of the coupling constants. Therefore, we carried out Beckmann rearrangements of the two oximes to obtain more reliable evidence for the configurations of the oximino hydroxyls of **5** and **6**.

Treatment of **5** with PPA afforded a single crystalline lactam **8** (IR), mp 95—100 °C, in 80% yield. The NMR spectrum of **8** revealed a broad one-proton doublet at τ 7.70 (J=8.0 Hz) (Table 2). Decoupling the signals at τ 8.35 caused a collapse of the doublet at τ 7.70 into a broad singlet. These data are consistent with those required for the 5β-proton of 6-aza-*B*-homo-5β-cholestan-7-one.

Beckmann rearrangement of **6** using the same proced ure used for **5** afforded an amorphous compound **9**, $C_{27}H_{47}ON$, isomeric with **8** in 90% yield. This was a lactam (IR) and the NMR spectrum of **9** (Table 2) was in agreement with the 7-aza-*B*-homo-5β-cholestan-6-one structure.

It has frequently been pointed out that care must be exercised in relating the stereochemistry of oximes with the lactams derived from the Beckmann rearrangement since *syn anti* isomerization is catalyzed by the reagents used for the Beckmann rearrangement[16,17] and the position of and rate of attaining the *syn* to *anti* equilibrium are temperature dependent.

The distinction among three lactams **3**, **8** and **9** could be readily made with the aid of the different chemical shifts of the 10β-methyl protons in their NMR spectra. Examination of the NMR spectrum of the crude product (see Fig. 1 in Experimental) from the Beckmann rearrangement of **5** indicated the presence of a small amount of **9** (revealed by a pair of weak signals at τ 8.97 and τ 9.32) and the NMR spectrum of the crude product from **6** (see Fig. 2 in Experimental) showed the presence of a small amount of **8** (revealed by a pair of weak signals at τ 9.03 and τ 9.34). The appearance of these signals in the products indicated that the equilibration from *syn* to *anti* or from *anti* to *syn* took place to some extent prior to the Beckmann rearrangement under our experimental conditions. However, it is apparent that the rearrangement of either oxime **5** or **6** is faster than the equilibration of these isomers.

On the basis of these results we concluded that the configurations of the oximino-hydroxyl of the oxime **5** and the oxime **6** are respectively *anti* and *syn* with respect to the C_5–C_6 bond.

Photo-Beckmann Rearrangement of Cholestan-6-one Oximes: The photo-Beckmann rearrangements of all three oximes **2**, **5**, and **6** were carried out in methanolic solution under a N_2 atmosphere at room temperature using a 15-W low pressure Hg arc lamp dipped in the solution. The progress of the photolysis was traced by tlc.

*Photolysis of 5α-Cholestan-6-one Oxime **2***: The photolysis of **2** in dry methanol (3.56×10^{-3} M) for 27 hr resulted in partial transformation of the oxime. Since further irradiation was found to cause secondary photochemical decomposition of the initial products the irradiation was stopped at this stage. Examination of the product by tlc revealed that several products were produced but these were able to be divided into four fractions by preparative tlc (see Experimental). The major part of the least polar fraction was found to be 5α-cholestan-6-one (8% as a ketone) by examination of its spectra. The second least polar fraction (6% as an oxime) was found to be the crude oxime. The third least polar fraction was further separated into two fractions by preparative tlc, using a different solvent system. Of these, the less polar fraction (11% as a lactam) afforded a compound **4** which melted at 110—114 °C after recrystallization from ethanol and the more polar fraction (15% as a lactam) afforded a lactam which was identical with the lactam **3**. Product **4** was also a lactam with the molecular formula $C_{27}H_{47}ON$ but was not identical with either the lactam **8** or the lactam **9** and the NMR spectrum of **4** (Table 2) was consistent with the 7-aza-*B*-homo-5α-cholestan-6-one structure. The 10β-Me protons appeared at τ 9.11 which is 0.06 ppm downfield from those of the isomeric 6-aza-lactam **3**.

*Photolyses of 5β-Cholestan-6-one Oximes **5** and **6***: The *syn*-oxime **6** in dry methanol (5.0×10^{-3} M) was then photolyzed and examination of the progress of the photolysis by tlc indicated that a rapid photostationary state between the *syn* and *anti* forms was established. Tlc examination of the reaction mixture after 3 hr revealed the presence of nearly equal amounts of *syn* and *anti* forms in the solution. The photolysis was stopped after 12 hr irradiation. The reaction mixture was analyzed by preparative tlc as in the case of 5α-cholestan-6-one oxime to afford two gummy ketone fractions, which yielded crystalline 5α-cholestan-6-one (3%) and crystalline 5β-cholestan-6-one (7%), the recovered oxime, and a lactam fraction in order of increasing polarity.

The NMR spectrum of the lactam fraction revealed the presence of sharp peaks at τ 8.97 and τ 9.03. This immediately suggested the presence of 6-aza-*B*-homo-5β-cholestan-7-one and 7-aza-*B*-homo-5β-cholestan-6-one. Preparative tlc of this mixture afforded the lactam **8** (24%) and the lactam **9** (17%). In addition, a fraction considerably less polar than the ketones was also obtained. Judged by the spectra this gum was 5,6-seco-cholestan-6-oic acid methyl ester derived from α-cleavage of the 6-ketone.[18] Nearly the same results were obtained when the photolysis was started with the anti-oxime. The results in this case were as follows; 5α-cholestan-6-one (3%), 5β-cholestan-6-one (5%), 6-aza-*B*-homo-5β-cholestan-7-one (30%) and 7-aza-*B*-homo-cholestan-6-one (12%).

Throughout these photolyses, it was found that the disappearance of the oxime and the appearance of the lactams were faster in the 5β-series than the 5α-series and the yields of lactams were higher in the 5β-series although no quantitative studies were undertaken.

Photo-Beckmann Rearrangement of 5β-Cholestan-6-one Oxime in the Presence of Oxygen: In order to obtain some information on the properties of the excited oxaziridine

from which the observed lactams are formed, the photolysis was carried out in the presence of oxygen. Oxygen is believed to remove triplet state species by both chemical and physical quenching.[19] A mixture of *syn* and *anti* 5β-oximes was chosen as the substrate, since, when compared with the 5α-oxime, the results of the reaction with this substrate were found to contain less by-products.

The photolysis of a methanolic solution of 5β-oximes (3.7×10^{-3} M) in the presence of O_2 afforded crystalline 5α-ketone (1%), crystalline 5β-ketone (7%), 6-aza-*B*-homo-5β-cholestan-7-one (16%, amount eluted from tlc) and 7-aza-*B*-homo-5β-cholestan-6-one (14%, amount eluted from tlc) and 4% of the starting oximes were recovered.

Discussion

In the foregoing part we have shown that in the photo-Beckmann rearrangements of 5α- and 5β-cholestan-6-one oximes, when we start off from 5β-oxime, lactams retaining the 5β-configuration are produced but from 5α-epimer only those having the 5α-configuration are formed. Through these experiments, the lactam part of the products was very carefully examined but we were unable to detect any lactams in which the initial configuration at C_a to the oximino-group of the starting oximes was reversed. It should also be noted that in the present results two isomeric lactams due to the migration of the tri-substituted carbon (C_5) and the di-substituted carbon (C_7) were produced in each case and the relative amounts of two lactams were not significantly different in the photolysis of **2** and in the photolysis of **5** or **6**, although in all the photolyses some preference for the migration of tri-substituted carbon over that of disubstituted carbon was shown.

The present results suggest that the reorganization from the oxaziridine intermediate to lactams occurs in a fully concerted manner (*e.g.*, A→B→C and D). At the time of our preliminary publication, we suggested that this mechanistic pathway might operate generally for all aliphatic ketones and aldehydes. However, we subsequently found[20] an exception to that rule. We found that the photolysis of androsterone oxime afforded an epimeric pair of lactams at the 13–Me, although the yields were very poor.

In order to get a general and consistent picture of the mechanistic pathway in regard to the migration step of the saturated oximes, we considered two possibilities for the mode of formation of a lactam from oxaziridine. The first was the migration through the intervention of an ionic or radical intermediate[20] in which bond between oxaziridine ring carbon and the migrating α-carbon (*e.g.*, C_5–C_6 bond or C_6–C_7 bond in A) is cleaved. According to this mechanistic view the present results with cholestan-6-one oxime might be rationalized by considering the involvement of a similar ion pair or radical pair intermediate which is configurationally stable. However, this unifying mechanism for all the saturated ketone oximes fails to interpret the small difference in migratory aptitude between C_5 and C_7 in the present case and in several other cases, *i.e.*, 3α,5-cyclo-5α-cholestan-6-one oxime,[3f] unsymmetrically α-substituted cyclohexanone oxime[7] and norcamphor oxime.[3d] These observation would be better explained if we assumed the formation of lactams *via* a concerted breakdown of the oxaziridines (Scheme 2).

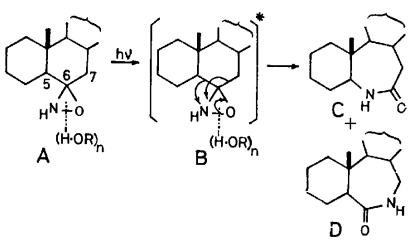

Scheme 2.

This would mean that a dual mechanism is operative in the saturated oximes, depending upon their structural features in the immediate environment of the relevant oximino group. The oxime which can afford a stable ionic or radical species by cleavage would be able to rearrange through an intermediate in which the migrating group becomes free of the migration terminus. The rearrangement of the oximes of androsterone and 13α-androsterone perhaps fall in this category. On the other hand, oximes of cholestan-6-ones, menthone, isomenthone and norcamphor bear the tri-substituted migrating carbon within the framework of the six-membered ring and oxaziridines formed from these oximes would rearrange to afford lactams *via* a concerted breakdown of the oxaziridines.

No meaningful difference between the *syn*-oxime and the *anti*-oxime of 5β-cholestan-6-one was observed with respect to the photolysis products. This shows a fast establishment of photostationary states between *syn* and *anti* prior to substantial progress of the photorearrangement. On the other hand, we could not detect even a trace of the *syn*-form of 5α-cholestan-6-one oxime during the photolysis of *anti* 5α-cholestan-6-one oxime. This difference between 5α-6-one oxime and 5β-6-one oxime is readily understandable since it is inferred that, in the 5α-steroid-6-one oximes, the energy difference between the *syn* form and the *anti* form is large and the thermal relaxation from photogenerated *syn* to *anti* should be very fast. In contrast, in the 5β-steroid-6-one oximes, the energy difference between *syn* and *anti* is not as large and both forms are isolatable species at room temperature.

With regard to the properties of the excited oxaziridine, the result of the photolysis of 5β-cholestan-6-one oxime in the presence of oxygen would imply that a) no radical intermediate would be involved in the present photo-Beckmann rearrangement and b) the formation of lactams from the oxaziridine takes place in its singlet state. The former result is contrasted with the reported case of adamantanone oxime in which the intervention of a radical intermediate at some stage was inferred.[3c] The latter results differ from the case of styrylketone oximes in which a triplet state of protonated oxaziridine rearranges to afford lactams. All the present results of the photolysis are consistent with our original proposal that lactam is formed *via* a concerted breakdown of the oxaziridine.[6]

During the photo-isomerization experiments it was observed that the rate of disappearance of the oxime **5** or **6** was considerably faster than that of the oxime **2** and the yields of lactams were much higher than those of the oxime **2**. The faster rates observed in A/B *cis* oxime **5** or **6**, when compared with A/B *trans* oxime **2**, could be mainly attributed to the relief of steric compression due to nonbonded interactions of 2α- and 4α-axial hydrogens with 7α- and 9α-axial hydrogens in going from oxaziridine intermediates formed from the oxime **5** or **6** to the lactam **8** and **9**. With regard to the role of protic solvents in the rearrangement, in all the examples of photo-Beckmann rearrangements described, protic media or organic acids as solvents are reported to be essential.

Mukai and co-workers recently proposed that the excited triplet species of a protonated oxaziridine is involved in the formation of the corresponding lactams from styryl ketone oxime.

In our case the role of methanol would be associated with influencing the rate or efficiency of an electronic energy transfer process, by making hydrogen bonds between the unshared electrons of excited oxaziridines and methanol molecule(s), in the reorganization from excited oxaziridines to lactams. When the protic solvents are absent the excited singlet oxaziridines would lose their singlet energy by various physical deactivation processes prior to their rearrangement to lactams.

The isolation of 5α-cholestan-6-one together with 5β-cholestan-6-one in the photolysis of the 5β-cholestan-6-one oximes would demand an explanation. It was rather difficult to explain the isolation of these isomeric ketones in terms of the initial isomerization of 5β-oximes into 5α-oxime through an α-cleavage-recombination process followed by the decomposition of these oximes into the 5α- and 5β-ketones. The isolation of of both 5α and 5β ketones could be better explained if we assumed an initial formation of 5β-cholestan-6-one either via collision between ground state oxazirdine molecules[3g] or via other routes, including a photochemical one followed by isomerization into the 5α-one via a photochemical α-cleavage-recombination sequence (Scheme 3). This is supported by the results of the separate irradiation of 5β-cholestan-6-one in dry methanol containing dioxane. The solution in a quarz vessel was irradiated for 3 hr with a 15-W low pressure Hg arc lamp. Separation of the product by preparative tlc afforded 5α-ketone (13%), and 5,6-seco-cholestan-6-oic acid methyl ester **10** (14%), together with the original 5β-ketone (44%).

This isomerization is the second case of a photochemical isomerization of a steroidal ketone by an α-cleavage-recombination sequence. The first case of isomerization of steroidal ketone was reported by Butenandt *et al.*,[21] who found that steroidal 17-ketones epimerize at C-13,[22] and later the reversibility of the process was clarified by Schaffner.[23]

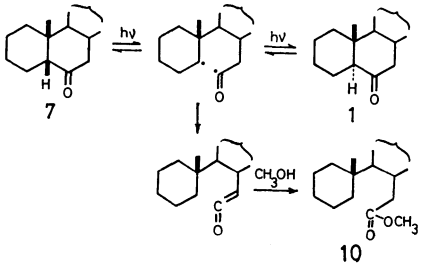

Scheme 3.

Experimental

All mps were determined with a Yanagimoto-type hot stage and are uncorrected. Unless stated otherwise, IR spectra were determined in Nujol using a JASCO model IR-E spectrophotometer. The NMR spectrum of oxime **2** was measured on a JEOLCO-JNM-PS-100 high resolution NMR spectrometer in $CDCl_3$ solution using TMS as an internal reference. Other NMR spectra were taken at Japan Electric & Varian Ltd. Wako gel B-5 was used for preparative tlc.

5α-Cholestan-6-one Oxime 2: This was prepared according to the literature procedure. mp 197—201 °C (lit, mp 204—206 °C,[10] mp 195 °C,[8] mp 196—198 °C,[9a] mp 197—198 °C[9b]); IR: 3272 cm^{-1} (OH), 1669 cm^{-1} (C=N), 896, 923, 947 cm^{-1}.

Beckmann Rearrangement of 5α-Cholestan 6-one Oxime 2: 5α-Oxime (94 mg) was added to PPA (Koso Chemical Co., Ltd. Tokyo) (1 g) kept at 100 °C. The reaction mixture was heated at 110—115 °C for 15 min. After being cooled the reaction mixture was neutralized with 10% Na_2CO_3 solution (10 ml) and extracted with ether. The ethereal solution was worked up as usual. Removal of the solvent left a residue which was recrystallized from acetone to yield 61 mg of lactam **3**. mp 173—175 °C (lit,[9b] mp 175—176 °C); IR: 1669 cm^{-1} (lactam C=O), 3230 cm^{-1}, 3090 cm^{-1} (lactam NH); Mass: *m/e* 401 (M^+).

Anti-5β-cholestan-6-one Oxime 5 and syn-5β-Cholestan-6-one Oxime 6: 5β-Cholestan-6-one (320 mg), hydroxylamine hydrochloride (450 mg) and NaOAc (320 mg) in 95% aqueous EtOH (30 ml) were stirred for 2 hr at room temperature. The solvent was removed under reduced pressure and the residue was extracted with ether. Usual work-up of the ethereal solution afforded an amorphous residue (350 mg). Preparative tlc of the residue (305 mg) using benzene as the solvent gave two fractions. The less polar fraction (120 mg) was recrystallized from acetone yielding 63 mg of *syn*-oxime **6**. mp 144—146 °C. (Found: C, 80.82; H, 11.85; N, 3.66%; Calcd for $C_{27}H_{47}ON$: C, 80.73; H, 11.80; N, 3.49%) Mass: *m/e* 401 (M^+); IR: 3276 cm^{-1} (OH), 1656 cm^{-1} (C=N), 925, 942, 954 cm^{-1}. The more polar fraction (249 mg) which was contaminated with a small amount of the less polar fraction was purified twice by preparative tlc ($CHCl_3$/ether—4/1 in vol.) to yield 68 mg of *syn*-oxime **6** and amorphous *anti*-oxime **5**. It was difficult to obtain the *anti*-oxime completely free from the *syn*-form, since during elution with acetone and $CHCl_3$ in the preparative tlc **5** seemed to undergo slight *anti-syn* isomerization. Analysis of *anti-oxime* **5**: (Found: C, 80.82; H, 11.77; N, 3.44%; calcd for $C_{27}H_{47}ON$: C, 80.73; H, 11.80; N, 3.49%).

Beckmann Rearrangement of syn-5β-Cholestan-6-one Oxime 6: Freshly prepared **6** (26 mg) was added to a small amount of PPA kept at 90 °C. The mixture was stirred for 5 min at that temperature and then cooled by ice. The reaction mixture was neutralized with 10% aqueous Na_2CO_3 solution and the solution was extracted twice with ether. Usual work-up of the ethereal solution left amorphous compound **9** (20 mg). The Me proton part of the NMR spectrum of this is shown in Fig. 2. The lactam **8** was removed by preparative tlc. (Found: C, 79.36; H, 11.57; N, 3.22%; Calcd for $C_{27}H_{47}ON$: C, 80.73; H, 11.80; N, 3.49%);

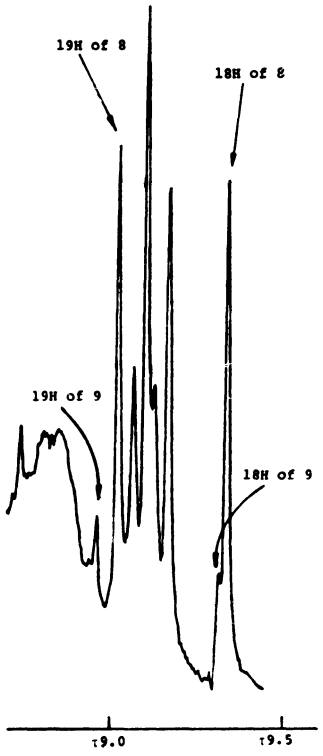

Fig. 1. NMR spectrum of crude **8**.

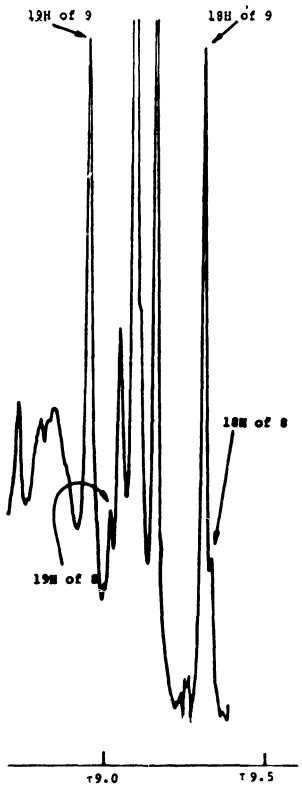

Fig. 2. NMR spectrum of crude **9**.

IR: ($CHCl_3$) 1643 cm^{-1} (lactam C=O), 3210 cm^{-1}, 3410 cm^{-1} (lactam NH).

Beckmann Rearrangement of anti-*5β-Cholestan-6-one Oxime 5*: Compound **5** (20 mg) was added to a few drops of PPA kept at 90 °C. The mixture was stirred for 5 min at that temperature. After being cooled by ice the reaction mixture was neutralized with 10% Na_2CO_3 solution and the solution was extracted twice with ether. Work up of the ethereal solution in the usual manner left 18 mg of an oily residue. The Me proton part of the NMR spectrum of this is shown in Fig. 1. This residue was purified by preparative tlc and then recrystallized from EtOH to yield lactam **8**. mp 76—80 °C.* (Found: C, 80.27; H, 11.94; N, 3.29%; Calcd for $C_{27}H_{47}ON$: C, 80.73; H, 11.80; N, 3.49%); IR: ($CHCl_3$) 1645 cm^{-1} (lactam C=O), 3390 cm^{-1} (lactam NH).

Photo-Beckmann Rearrangement of 5α-Cholestan-6-one Oxime 2: Oxime **2** (500 mg) in dry MeOH (350 ml) was irradiated for 23 hr. Examination of the reaction products by tlc revealed the presence of four major spots and these were separated by preparative tlc to afford 4 fractions A, B, C, and and D ($CHCl_3$/ether; 10/1 in vol.) in order of increasing polarities. The amount of fraction A was 40 mg and the major part of this was found to be 5α-cholestan-6-one. Recrystallization of fraction B (28 mg) from acetone afforded only 4 mg of the starting oxime. Fraction C (150 mg) was found to be a mixture of two compounds and this fraction gave two spots on a tlc with a mixed solvent of equal volumes of $CHCl_3$ and ether. Preparative tlc of the mixture with this solvent system afforded two compounds. The less polar and amorphous substance (53 mg) afforded 40 mg of crystals of 7-aza-*B*-homo-5α-cholestan-6-one. mp 110—114 °C. (Found: C, 79.12; H, 11.58; N, 3.77%; Calcd for $C_{27}H_{47}ON$: C, 80.73; H, 11.80; N, 3.49%); IR: 1656 cm^{-1} (lactam C=O), 3270 cm^{-1}, 3530 cm^{-1} (lactam NH). The more polar and crystalline compound (75 mg) melted at 174—179 °C and was identical with 6-aza-*B*-homo-5α-cholestan-7-one obtained from a Beckmann rearrangement of oxime **2**. Fraction D (80 mg) did not contain any lactam and was not examined further.

Photo-Beckmann Rearrangement of syn-*5β-Cholestan-6-one Oxime 6*: Oxime **6** (500 mg) in dry MeOH (250 ml) was irradiated for 12 hr. After removal of the solvent under reduced pressure, tlc of the residue revealed the formation of several products. However, there were two major spots. Preparative tlc ($CHCl_3$/ether; 4/1) afforded four fractions A, B, C and D in order of increasing polarity. Fraction A (198 mg) was again submitted to preparative tlc (benzene) and afforded 4 fractions. The NMR spectrum of the least polar fraction showed that this fraction was most probably 5, 6-seco ester. The polarities of the second and the third least polar fractions were close together and the second least polar fraction (30 mg) afforded 15 mg of crystals which were identical with 5α-cholestan-6-one. The third least polar fraction (100 mg) afforded 5β-cholestan-6-one (34 mg).

Fraction B was mainly crude starting material. The amorphous fraction C (229 mg) was again submitted to preparative tlc ($CHCl_3$/ether; 4/1) and afforded 120 mg of lactam **8** and 83 mg of lactam **9**. The most polar fraction D did not contain any lactams and was not examined further.

Photo-Beckmann Rearrangement of anti-*5β-cholestan-6-one Oxime 5*: Freshly prepared anti-5β-cholestan-6-one oxime (500 mg) in dry MeOH (300 ml) was photolyzed in the same manner as the *syn*-isomer. After 11 hr examination of the products by tlc revealed that nearly all the starting oxime had disappeared. After removal of the solvent the residue was extracted with ether. The ethereal solution was washed and dried as usual. The residue was separated by preparative tlc. Using the procedure employed for the *syn*-oxime, pure 5α-cholestan-6-one (13 mg) was obtained from 20 mg of crude fraction. In addition 22 mg of pure 5β-cholestan-6-one was obtained from 30 mg of crude 5β-compound. From the lactam part, 150 mg of lactam **8**

* Recorded previously as mp 95—100 °C.

and 90 mg of crude lactam **9** were obtained and the latter was recrystallized from ethanol to yield 59 mg of pure compound.

*The Photo-Beckmann Rearrangement of 5β-Cholestan-6-one Oxime, **5** and **6**, in the Presence of Oxygen*: A mixture of *syn* and *anti* isomers of 5β-cholestan-6-one oxime (420 mg) in dry methanol (280 ml) was photolyzed for 17.5 hr while dry oxygen was bubbled slowly. After removal of the solvent under reduced pressure the residue was dissolved in $CHCl_3$ and the solution was washed twice with H_2O, dried and evaporated. Another 300 mg of oxime in dry methanol (200 ml) was photolyzed under comparable condition and the solution was treated as above. The residues from these two photolyses were submitted to preparative tlc. The first preparative tlc was carried out with a mixed solvent of $CHCl_3$ and ether (4/1 in vol.). This enabled us to separate the mixture into two major fractions, a less polar fraction A (300 mg) and a more polar fraction B (300 mg). Between these two major bands on the tlc plate, several minor products were observed but these did not contain any lactams and were not examined further.

Fraction A was again submitted to preparative tlc with benzene and afforded four fractions A_1, A_2, A_3 and A_4 in order of increasing polarity. Fraction A_1 (120 mg) was amorphous and it was found to be 5, 6-seco-cholestan-6-oic acid methyl ester on the basis of its IR spectrum. The crystalline fraction A_2 (30 mg) was recrystallized from acetone to yield 5 mg of pure 5α-cholestan-6-one. The crystalline fraction A_3 (70 mg) was recrystallized from acetone to yield 30 mg of pure 5β-cholestan-6-one. The most polar fraction A_4 (30 mg) was found to be a mixture of the starting oximes.

Fraction B was also submitted to further preparative tlc with a mixed solvent of $CHCl_3$ and ether (5/1). Development was carried out twice. This afforded 70 mg of lactam **8** and 60 mg of lactam **9**.

The Photo-isomerization of 5β-Cholestan-6-one: 5β-Cholestan-6-one (80 mg) in dry methanol (25 ml) and dry dioxane (5 ml) was irradiated with a 15-W low pressure Hg arc lamp under an argon atmosphere. After 3 hr irradiation, examination of the solution revealed the formation of a fair amount of 5α-cholestan-6-one, which was less polar than 5β-cholestan-6-one, and a material considerably less polar than these ketones (R_f=0.88, benzene solvent). The solvent was then removed and the residue was submitted to preparative tlc and afforded a gum (16 mg), 5α-cholestan-6-one (10 mg) and 5β-cholestan-6-one (35 mg). The IR spectrum of the gum revealed it to be an ester (ester C=O, 1740 cm^{-1}, $CHCl_3$). The NMR spectrum showed a three-proton singlet at τ 6.34 ($COOCH_3$) two three proton singlets at τ 9.08 (19-H) and τ 9.32 (18-H) and a two-proton triplet at τ 7.44 ($-CH_2$ adjacent to $COOCH_3$). On the basis of these data, the gum should be 5,6-seco-cholestan-6-oic acid methyl ester.

The signals due to the 10β-methyls and the 13β-methyls of the 5α-isomer[24] and the 5β-isomer in the NMR spectra appeared at the following positions:

	19-H (τ)	18-H (τ)
5α-isomer ($CDCl_3$)	9.27	9.34
(CCl_4)	9.30	9.34
5β-isomer ($CDCl_3$)	9.17	9.35

We are grateful to the Ministry of Education of Japan for financial assistance. We thank Dr. T. Nishida of Japan Electric & Varian Ltd., for measuring the 100 MHz NMR spectra and Mrs. T. Okayama for carrying out the spin decoupling experiments.

References

1) Photoinduced transformations. XXVIII. Preliminary communication (Ref. 6). The previous paper in this series. H. Suginome, K. Kato, and T. Masamune, *Tetrahedron Lett.*, **1974**, 1165.

2) J. H. Amin and P. de Mayo, *ibid.*, **1963**, 1585.

3) a) R. T. Taylor, M. Douek, and G. Just, *ibid.*, **1966**, 4143. b) T. Oine and T. Mukai, *ibid.*, 157 (1969). c) T. Sasaki, S. Eguchi, and T. Toru, *Chem. Commun.*, **1970**, 1239. d) B. L. Fox and H. M. Rosenberg, *ibid.*, **1969**, 1115 e) G. Just and L. S. Ng, *Can. J. Chem.*, **46**, 3381 (1968). f) H. Suginome, H. Takahashi, and T. Masamune, This Bulletin, **45**, 1836 (1972). g) T. Oine, T. Mukai, and K. Kikuchi, *Sci. Rep. Tohoku University*, **1**, vol. 54, (1971). h) G. Just and C. Pace-Asciak, *Tetrahedron*, **22**, 1069 (1966).

4) H. Izawa, P. de Mayo, and T. Tabata, *Can. J. Chem.*, **47**, 51 (1969).

5) J. Vermes and R. Beugelmans, *Tetrahedron Lett.*, **1969**, 2091.

6) H. Suginome and H. Takahashi, *ibid.*, **1970**, 5119.

7) M. Cunningham, L. S. N. Lim, and G. Just, *Can. J. Chem.*, **49**, 2891 (1971).

8) A. Windaus and E. K. Dalmer, *Ber.*, **52**, 162 (1919).

9) a) C. W. Shoppee, D. E. Evans, and G. H. R. Summers, *J. Chem. Soc.*, **1957**, 97. b) C. W. Shoppee, R. E. Lack, and S. K. Roy, *ibid.*, **1963**, 3767.

10) J. R. Bull, Sir E. R. H. Jones, and G. D. Meakins, *ibid.*, **1965**, 2601.

11) R. J. W. Le Fevre and J. Northcott, *ibid.*, **1949**, 2235.

12) W. P. Jencks, *Prog. Phys. Org. Chem.*, **2**, 63 (1964).

13) E. C. Hornig, V. L. Stromberg, and H. A. Lloyd, *J. Amer. Chem. Soc.*, **74**, 5153 (1952).

14) W. D. Phillips, *Ann. N. Y. Acad. Sci.*, **70**, 817 (1958); H. Saito, K. Nukada, and M. Ohno, *Tetrahedron Lett.*, **1964**, 2124; W. F. Trager and A. C. Huitric, *ibid.*, **1966**, 825.

15) S. Sternhell, *Quart. Rev.*, **23**, 236 (1969).

16) R. H. Mazur, *J. Org. Chem.*, **28**, 248 (1963).

17) C. G. McCarty, in "The Chemistry of the Carbon-Nitrogen Double Bond," ed. S. Patai, Interscience Publ., p. 363 (1970), New York.

18) *c.f.* G. Quinkert, B. Wegemund, F. Homburg, and G. Cimbollek, *Chem. Ber.*, **97**, 958 (1964). G. Quinkert, *Angew. Chem.*, **77**, 229 (1965).

19) G. Porter, *Disc. Faraday Soc.*, **17**, 178 (1954). D. W. Setser, D. W. Placzek, R. J. Cvetanovic, and B. S. Ravinovitch, *Can. J. Chem.*, **40**, 2179 (1962).

20) H. Suginome and T. Uchida, *Tetrahedron Lett.*, **1973**, 2293; H. Suginome and T. Uchida, This Bulletin, **47**, 687 (1974).

21) A. Butenandt, A. Wolff and P. Karlson, *Chem. Ber.*, **74**, 1308 (1941).

22) Other examples of the photo-epimerization at C-13 of 17-ketosteroids, see J. P. L. Bots, *Rec. Trav. Chim.*, **77**, 1010 (1958); J. Iriarte, K. Schaffner, and O. Jeger, *Helv. Chim. Acta*, **47**, 1255 (1964); A. Butenandt and L. Poschmann, *Chem. Ber.*, **77**, 394 (1944); J. R. Billeter and K. Miescher, *Helv. Chim. Acta.*, **34**, 2053 (1951).

23) H. Wehrli and K. Schaffner, *ibid.*, **45**, 385 (1962).

24) The reported chemical shifts (CCl_4, 60 MHz) of the 19-H and the 18-H of 5α-cholestan-6-one are τ 9.25 and τ 9.22 and these seem erroneous. W. G. Dauben and E. J. Deviny, *J. Org. Chem.*, **31**, 3794 (1966).

The Photolysis of 3,4-Bis(hydroxydiphenylmethyl)cyclobut-3-ene-1,2-dione and Related Compounds. The Formation of a New Bislactone, 4,4,8,8-Tetraphenyl-3,7-dioxabicyclo[3.3.0]oct-1(5)-ene-2,6-dione

Fumio TODA and Eishiro TODO

Department of Industrial Chemistry, Faculty of Engineering, Ehime University, Matsuyama 790

(Received July 15, 1974)

The photolysis of 3,4-bis(hydroxydiphenylmethyl)cyclobut-3-ene-1,2-dione (**1**) in benzene afforded 4,4,8,8-tetraphenyl-3,7-dioxabicyclo[3.3.0]octane-2,6-dione (**3**) in an 80% yield. The photolysis of **1** in MeOH afforded 4,4,8,8-tetraphenyl-3,7-dioxabicyclo[3.3.0]oct-1(5)-ene-2,6-dione (**4**), 4-methoxycarbonyl-3,3-diphenyl-5-diphenylmethylene-2-oxacyclopentan-1-one (**5**), and 4-carboxy-3,3-diphenyl-5-diphenylmethyl-2-oxacyclopent-4-en-1-one (**6**), in 3, 8, and 22% yields respectively. The mechanisms of the formation of the **5** and **6** are discussed. The photolysis of 3-hydroxydiphenylmethyl-4-diphenylmethoxymethylcyclobut-3-ene-1,2-dione (**14**) and 3,4-bis(diphenylmethyl)cyclobut-3-ene-1,2-dione (**18**) was also investigated.

Since the isolation of a novel fungicidal bislactone, *avenaciolide*, which has a 2,7-dioxabicyclo[3.3.0]octane-3,8-dione system (I),[1,2] some bislactones which have 2,7-dioxabicyclo[3.3.0]octane-3,6-dione (II),[3] 4,8-dioxabicyclo[3.3.0]octa-1,5-diene-3,7-dione (III),[4] 2,8-dioxabicyclo[3.3.0]octane-3,7-dione (IV),[5] and 3,7-dioxabicyclo[3.3.0]octane-2,6-dione (V)[6] systems have been reported. This paper will deal with the formation of the title bislactone, which has a hitherto unknown 3,7-dioxabicyclo[3.3.0]oct-1(5)-ene-2,6-dione (VI) system, and a new synthetic route of the bislactone, with the system of V.

The photolysis of 3,4-bis(hydroxydiphenylmethyl)-cyclobut-3-ene-1,2-dione (**1**) in benzene under nitrogen at room temperature afforded 4,4,8,8-tetraphenyl-3,7-dioxabicyclo[3.3.0]octane-2,6-dione (**3**) in an 80% yield. Because the photochemical ring-opening of cyclobutenedione into bisketene has been established,[7] the initial product of the photolysis of **1** should be bisketene (**2**). In order to trap **2**, the photolysis of **1** was carried out in MeOH. The photolysis, however, afforded 4,4,8,8-tetraphenyl-3,7-dioxabicyclo-[3.3.0]oct-1(5)-ene-2,6-dione (**4**), 4-methoxycarbonyl-3,3-diphenyl-5-diphenylmethylene-2-oxacyclopentan-1-one (**5**), and 4-carboxy-3,3-diphenyl-5-diphenylmethyl-2-oxacyclopent-4-en-1-one (**6**) in 3, 8, and 22% yields respectively. Compound **5** was also obtained from **3**. The treatment of **3** with KOH–MeOH afforded 4-carboxy-3,3-diphenyl-5-diphenylmethylene-2-oxacyclopentan-1-one (**8**). The reaction probably proceeds *via* an anion (**7**), which is formed by the deprotonation of **3** (Scheme 1). The treatment of **8** with $SOCl_2$ and then with MeOH afforded **5**.

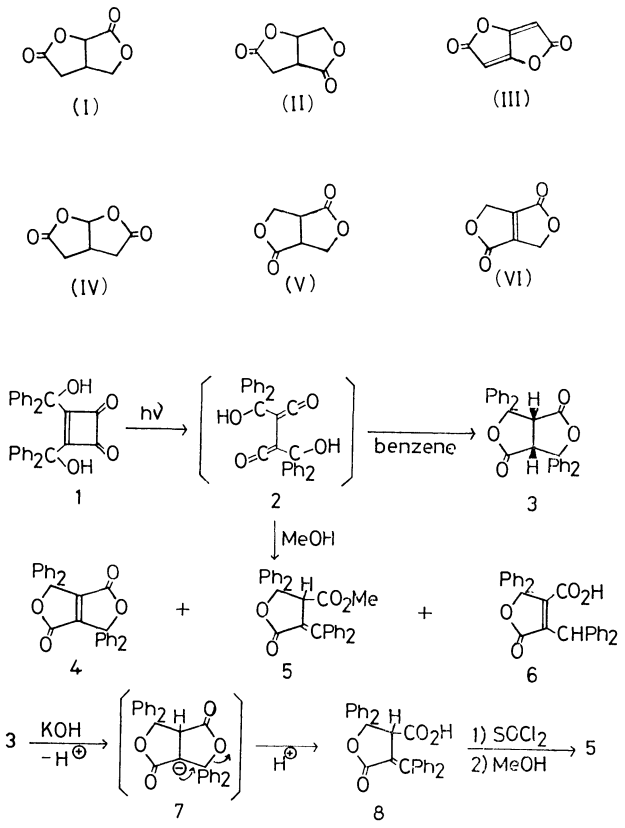

Scheme 1.

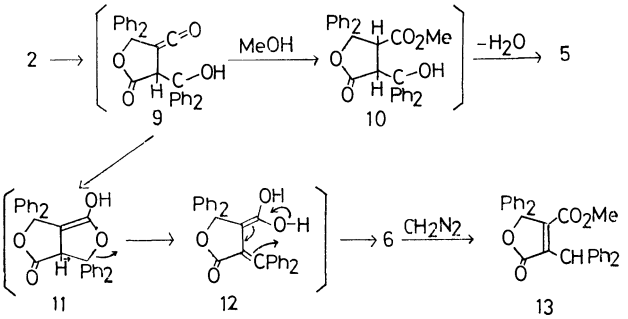

Scheme 2.

The formation of **5** and **6** in the photolysis of **1** in MeOH can be interpreted by the reaction sequence shown in Scheme 2. The reaction of **9**, the half-cyclized product of **2**, with MeOH should afford **10**. The dehydration of **10** then finally affords **5**. Because the product ratio of **3**, **4**, and **5** was not varied by a prolonged irradiation of **1** in MeOH, interconversion among the three products during the photolysis can be ruled out. The ring-cleavage of **11**, which is formed by an intramolecular cyclization of **9**, affords **6** *via* the diol (**12**). The reaction of **6** with CH_2N_2 afforded 4-methoxycarbonyl-3,3-diphenyl-5-diphenylmethyl-2-oxacyclopent-4-en-1-one (**13**). Nevertheless, the pathway of the formation of **4** is not clear.

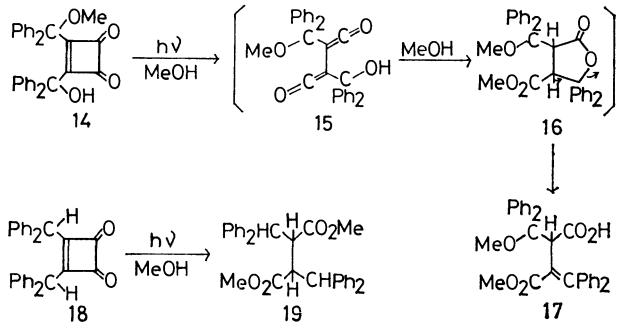

Scheme 3.

The photolysis of 3-hydroxydiphenylmethyl-4-methoxydiphenylmethylcyclobut-3-ene-1,2-dione (**14**) in MeOH afforded 3-methoxycarbonyl-3-diphenylmethylene-2-methoxydiphenylmethylpropionic acid (**17**) in a 65% yield. A possible pathway for the formation of **17** is the ring-cleavage of **16**, which is produced by an intramolecular cyclization of the initially formed bisketene intermediate (**15**) (Scheme 3). The photolysis of 3,4-bis(diphenylmethyl)cyclobut-3-ene-1,2-dione (**18**) in MeOH afforded dimethyl 2,3-bis(diphenylmethyl)succinate (**19**) in a 23% yield. However, both **14** and **18** were inert to the photolysis in benzene.

Experimental

All the melting points are uncorrected. Photolysis was carried out at room temperature under a nitrogen atmosphere, using light from a 100-W high-pressure mercury lamp (Riko Kagaku Sangyo Co.), filtered through Pyrex glass. The IR, UV, and NMR spectra were measured in Nujol mull, EtOH, and $CDCl_3$ respectively, unless otherwise stated. The mass spectra were measured with an ionization energy of 75 eV.

*Photolysis of **1** in Benzene.* A solution of **1**[8] (0.5 g) in benzene (150 ml) was irradiated under stirring for 5.5 hr. The crude crystals left after the evaporation of the solvent were recrystallized from AcOEt to afford **3** as colorless needles; 0.4 g (80%); mp 227—228 °C. IR: 1780 (C=O) and 1210 and 1180 cm^{-1} (lactone); $\lambda_{max}^{CHCl_3}$: 242 (1400), 253 (1000), 259 (1200), 262 (1000), and 269 sh nm (ε, 700); NMR: 2.6—3.2 (m, Ph, 20 H) and 5.85 τ (s, CH, 2H); MS: *m/e* (rel intensity) 446 (M^+, 100), 402 ($M^+ - CO_2$, 7), 358 ($M^+ - 2CO_2$, 15), 264 ($M^+ - Ph_2CO$, 70), and 236 ($M^+ - (Ph_2CO + CO)$, 62).

Found: C, 80.95; H, 4.75%. Calcd for $C_{30}H_{22}O_4$: C, 80.70; H, 4.97%.

*Photolysis of **1** in MeOH.* A solution of **1** (3 g) in MeOH (500 ml) was irradiated under stirring for 6 hr. The crude crystals which separated out after the concentration of the reaction mixture to *ca.* 5 ml were collected by filtration. Recrystallization from MeOH afforded **4** as colorless plates; 0.075 g (3%); mp 280—281 °C. IR: 1765 (C=O) and 1080 and 1010 cm^{-1} (lactone); $\lambda_{max}^{CHCl_3}$: 275 sh nm (ε, 2700); NMR: 2.6—3.2 τ (m, Ph); MS: *m/e* (rel intensity) 444 (M^+, 31), 400 ($M^+ - CO_2$, 23), 356 ($M^+ - 2CO_2$, 38), 278 ($M^+ - Ph_2C$, 100), and 218 ($M^+ - CO_2 - Ph_2CO$, 70).

Found: C, 81.08; H, 4.31%. Calcd for $C_{30}H_{20}O_4$: C, 81.06; H, 4.54%.

The MeOH solution left after the separation of the crude **4** was evaporated to dryness, and the residue was recrystallized from benzene–MeOH to afford **6** as colorless prisms; 0.653 g (22%); mp 204—205 °C. IR: 2800—2500 (OH), 1720 (C=O), and 1635 cm^{-1} (C=C); λ_{max}: 240 sh nm (ε, 8500); NMR: 2.2—3.0 (m, Ph, 20H) and 3.88 τ (s, CH, 1H).

Found: C, 80.84; H, 4.86%. Calcd for $C_{30}H_{22}O_4$: C, 80.70; H, 4.97%.

The benzene–MeOH solution left after the separation of **6** was evaporated to dryness, and the residue was chromatographed on Al_2O_3 with benzene to afford **5** as colorless prisms, after recrystallization from acetone–MeOH; 0.24 g, (8%); mp 189—190 °C. IR: 1775 and 1730 (C=O), 1630 (C=C), 1210 (ester), and 1120 cm^{-1} (lactone); λ_{max}: 287 nm (ε, 11600); NMR: 2.5—3.5 (m, Ph, 20H), 5.6 (s, CH, 1H), and 6.85 τ (s, CH_3, 3H).

Found: C, 80.65; H, 5.35%. Calcd for $C_{31}H_{24}O_4$: C, 80.85; H, 5.25%.

*Methyl Ester of **6**.* A solution of **6** (0.1 g) in THF (10 ml) was combined with a CH_2N_2-ether solution (10 ml), and the mixture was kept at 0 °C overnight. The crude crystals left after the evaporation of the solvent were recrystallized from acetone-MeOH to afford **13** as colorless prisms; 0.09 g (87%); 131—133 °C. IR: 1780 and 1740 (C=O), 1650 (C=C), and 1230 cm^{-1} (ester); λ_{max}: 240 sh nm (ε, 8200); NMR: 2.3—2.8 (m, Ph, 20H), 4.06 (s, CH, 1H), and 6.62 τ (s, CH_3, 3H).

Found: C, 80.63; H, 5.36%. Calcd for $C_{31}H_{24}O_4$: C, 80.85; H, 5.25%.

*Hydrolysis of **3**.* A solution of **3** (0.10 g) in 5% KOH–MeOH (10 ml) was heated under reflux for 1 hr. The crude crystals which were separated out by the acidification of the reaction mixture were recrystallized from CCl_4 to afford **8** as colorless prisms; 0.08 g (80%); mp 206—207 °C. IR: 2800—2500 (OH), 1780 and 1740 (C=O), and 1620 cm^{-1} (C=C); λ_{max}: 286 nm (ε, 10900).

Found: C, 80.54; H, 5.07%. Calcd for $C_{30}H_{22}O_4$: C, 80.70; H, 4.97%.

A mixture of **8** (0.04 g), benzene (15 ml), and $SOCl_2$ (0.05 ml) was heated under reflux for 9 hr. The crude product left after the evaporation of the solvent was dissolved in MeOH (20 ml), and the solution was heated under reflux for 6 hr. The crude crystals left after the evaporation of the solvent were recrystallized from MeOH to afford **5**; 0.02 g (48%).

*Photolysis of **14** in MeOH.* A solution of **14**[8] (0.4 g) in MeOH (150 ml) was irradiated under stirring for 3.5 hr. The crude crystals left after the evaporation of the solvent were recrystallized from AcOEt to afford **17** as colorless needles; 0.277 g (65%); mp 179—180 °C. IR: 2800—2600 (OH), 1710 (C=O), and 1230 cm^{-1} (ester); λ_{max}: 252 (8800), 263 sh (8200), and 270 sh nm (ε, 7200); NMR: 2.3—3.3 (m, Ph, 20 H), 5.31 (s, CH, 1H), 6.68 (s, CH_3,3H), and 6.87 τ (s, CH_3, 3H).

Found: C, 77.84; H, 5.95%. Calcd for $C_{32}H_{28}O_5$: C, 78.03; H, 5.73%.

*Photolysis of **18** in MeOH.* A solution of **18**[8] (0.5 g) in MeOH (150 ml) was irradiated under stirring for 4 hr. The crude crystals left after the evaporation of the solvent were recrystallized from acetone–MeOH to afford **19** as colorless needles; 0.16 g (23%); mp 166—167 °C. IR: 1740 (C=O) and 1220 cm^{-1} (ester); λ_{max}: 260 nm (ε, 1000); NMR: 2.5—3.5 (m, Ph, 20 H), 5.55 (d, J=12 Hz, CH, 2H), 6.52 (s, CH_3, 6H), and 6.60 τ (d, J=12 Hz, CH, 2H).

Found: C, 80.45; H, 6.12%. Calcd for $C_{32}H_{28}O_4$: C, 80.64; 5.92%.

The authors are grateful to the Ministry of Educa-

tion, Japanese Government, for its financial support.

References

1) D. Brookes, B. K. Tidd, and W. B. Turner, *J. Chem. Soc.*, **1963**, 5385.
2) J. J. Ellis, F. H. Stodola, R. F. Vesonder, and C. A. Glass, *Nature*, **203**, 1382 (1964).
3) A. Yoshikoshi, Japan. Pat. 7340796, 7340797 (1972).
4) H. Besl, A. Bresinsky, W. Steglich, and K. Zipfel, *Chem. Ber.*, **106**, 3223 (1973).
5) W. L. Parker and F. Johnson, *J. Org. Chem.*, **38**, 2489 (1973).
6) R. Ahmed, M. Lehrer, and R. Stevenson, *Tetrahedron*, **29**, 3753 (1973).
7) F. B. Mallory and J. D. Roberts, *J. Amer. Chem. Soc.*, **83**, 393 (1961).
8) F. Toda and N. Ooi, This Bulletin, **46**, 1733 (1973).

The Michael Reactions of Chloro-substituted-9,9′-bifluorenylidenes with Fluorenes and a Comparison with Analogous Halogen Compounds[1)]

Masahiro MINABE and Kazuo SUZUKI

Department of Industrial Chemistry, Faculty of Technology, Utsunomiya University, Ishii-cho, Utsunomiya 321-31

(Received July 19, 1974)

The Michael reactions of 2-chloro- and 2,7-dichloro-9,9′-bifluorenylidenes with fluorenes were investigated. Structures of these products were confirmed by syntheses through the well-established reactions of 9-lithiofluorenes and 9-bromo-9,9′-bifluorenyls. The formation of some abnormal compounds is explained by intermediary formation of 2,7-dichloro-9,9′-bifluorenylidene from the reaction of 9,9′-bifluorenylidene with 2,7-dichlorofluorene as with the bromo-derivatives. The corresponding fluoro- and iodo-series gave predominantly normal addition products. These differences are explained in terms of the inductive and steric effects of the halogen substituents.

The Michael reactions of chloro-substituted-9,9′-bifluorenylidenes with fluorenes, and the syntheses of some new chloro-derivatives were investigated. 2,7-Dibromo-substituted substrates afforded a large amount of abnormal 2,7,2″,7″-tetrabromo-9,9′ : 9′,9″-terfluorenyl and a small amount of bromine-free 9,9′ : 9′,9″-terfluorenyl (mp 293 °C (dec), **24**).[2)] However, the fluoro-[3)] and iodo-[4)] derivatives underwent predominantly normal additions.

In the present paper, the substituent effect of chlorine atoms in these Michael reaction is examined and compared with the effects of other halogen atoms in the crowded molecule 9,9′ : 9′,9″-terfluorenyl.

The reaction of 9,9′-bifluorenylidene (**7**) with 2,7-dichlorofluorene (**5**) gave the expected 2,7-dichloro-9,9′ : 9′,9″-terfluorenyl (**19**) and abnormal compounds 2,7,2″,7″-tetrachloro-9,9′ : 9′,9″-terfluorenyl(**22**) and **24**. The pathway of the reaction may be similar to that of the bromo-derivatives in which 2,7-dibromo-9,9′-bifluorenylidene is one of the intermediates.

TABLE 1. MICHAEL REACTION OF 2-SUBSTITUTED 9,9′-BIFLUORENYLIDENES WITH FLUORENES

Reactants g		React. conditions			Products g(%)				Recovered g	
9,9′-Bifluorenylidene	Fluorene	Solvent ml	Catalyst g	Time hr					9,9′-Bifluorenylidene	Fluorene
7	**3**				**14**	**4**	**2**		**7**	**3**
3.28	2.01	EtOH 30	NaOEt 1.5	5	4.63 (88)	0.02			0.11	0.08
3.28	2.01	Py. 30	KOH 0.3	15	3.15 (60)	0.01	0.02		0.60	0.25
3.28	2.01	Py. 30	KOH 3.0	5	4.93 (93)	0.01	trace			
3.28	3.01	Py. 30	KOH 3.0	5	5.26 (99)	0.005				0.75
4.92	2.01	Py. 30	KOH 3.0	5	5.25 (99)		0.10		0.42	
8	**1**				**16**	**4**				**1**
3.97	1.66	Py. 30	KOH 0.3	5	5.00 (79)	0.03				0.02
3.97	1.66	Py. 30	KOH 3.0	5	5.22 (93)	0.02				0.02
3.97	3.32	Py. 30	KOH 3.0	5	5.35 (95)	0.03				1.60
8	**3**				**18**	**25**	**12**	**4**		
1.99	1.01	EtOH 30	NaOEt 1.5	5	1.77 (59)	0.14	0.30	0.02		
1.99	1.01	Py. 30	KOH 3.0	5	2.68 (89)			0.05		
9	**1**				**14**	**15**	**2**			**1**
1.45	0.83	Py. 15	KOH 0.15	5	1.17 (58)	0.73 (36)	0.02			0.13
9	**3**				**16**	**17**	**4**			**3**
1.45	1.00	Py. 15	KOH 0.15	5	0.45 (22)	0.69 (34)	0.03			0.08

a) Found for **14**: C, 88.29; H, 4.63%. For **15**: C, 88.75; H, 4.66%. For **16**: C, 82.91; H, 4.21%. For **17**: C, 83.44; H, 4.19%. For **18**: C, 78.48; H, 3.91%.

Results and Discussion

Various normal and abnormal chloro-substituted-9,9′ : 9′,9″-terfluorenyls and elimination products were obtained by the reaction of 9,9′-bifluorenylidenes with fluorenes, as shown in Tables 1 and 2.

These reactions of chloro-derivatives afforded exclusively normal products in the presence of sodium carbonate or sodium ethoxide, but the yield of abnormal products in the reactions of **7** with **5** and of 2,7,2′,7′-tetrachloro-9,9′-bifluorenylidene (**10**)[5] with fluorene (**1**) increased with increasing concentration of potassium hydroxide in pyridine.

Table 2. Michael reaction of 2,7-disubstituted 9,9′-bifluorenylidenes with fluorenes

Reactants g		React. Conditions			Products g(%)						Recovered g	
9,9′-Bifluorenylidene	Fluorene	Solvent (30 ml)	Catalyst g	Time hr							9,9′-Bifluorenylidene	Fluorene
7	**5**				**19**	**22**	**24**	**1**	**2**	**6**	**7**	**5**
2.2	1.6	EtOH	NaOEt 0.3	4	2.31 (61)				trace			
2.2	1.6	Py.	KOH 0.015	40	0.27 (7)	0.17		0.09	0.05	0.03	0.97	0.16
2.2	1.6	Py.	KOH 0.3	3	0.57 (15)	1.35		0.21	0.09	0.16		
1.1	1.6	Py.	KOH 0.3	3	0.34 (18)	0.48		0.09	0.04	0.08		0.16
3.3	1.6	Py.	KOH 0.3	3	0.37 (10)	1.15	0.20	0.07	0.06	0.07	0.53	
10	**1**				**21**	**22**	**19**	**5**	**6**	**2**	**10**	**1**
2.33	2.49	Py.	Na_2CO_3 1.5	200	1.97 (62)				0.02	trace	0.32	1.85
2.33	2.49	Py.	KOH 0.15	9	1.54 (49)	0.23	0.40	0.26	0.03	0.01		1.74
2.33	2.49	Py.	KOH 0.9	7	0.19 (6)	0.67	0.55	0.39	0.01	trace		1.52
2.33	0.83	Py.	KOH 0.9	7		1.67	0.10	trace	0.07	trace	0.11	0.05
10	**5**				**23**	**26**		**6**			**10**	**5**
1.86	1.6	EtOH	NaOEt 1.5	50	2.39 (86)	0.19		0.01			0.03	0.60
1.86	1.6	Py.	KOH 1.5	3	2.64 (94)			0.12				0.49
11	**1**				**19**	**20**		**2**	**6**			**1**
2.4	1.13	Py.	KOH 0.3	1/4	2.33 (69)	0.79 (23)		0.04	0.06			0.10
11	**5**				**22**	**6**						**5**
2.4	1.6	Py.	KOH 0.3	1/4	3.56 (93)	0.03						0.08

a) Found for **19**: C, 83.34; H, 4.22%. For **20**: C, 83.14; H, 4.06%. For **21**: C, 74.22; H, 3.63%. For **22**: C, 74.21; H, 3.39%. For **23**: C, 67.10; H, 3.13%. For **26**: C, 67.95; H, 2.56%.

Table 3. Michael reaction of 9,9′-bifluorenylidene (**7**) with 2,7-dihalogenofluorene

Reactants (g)		9,9′ : 9′,9″-Terfluorenyls g(%); (mp) °C			**1**	**2**	2,7-Di-halogeno-fluorenone
7	Fluorene	2,7-Dihalogeno-	2,7,2″,7″-Tetra-halogeno	**24**	g	g	g
3.28	2,7-Difluoro- 2.02	5.01(95); 285—286 (dec)					0.07
3.28	2,7-Dichloro- 2.35	2.66(47); 285—287 (dec)	1.69; 314—315 (dec)	0.26; 292—293 (dec)	0.02	trace	
3.28	2,7-Dibromo- 3.24	2.30(35); 285—286 (dec)	2.60; 313—314 (dec)	0.77; 292—293 (dec)	0.05		0.01
3.28	2,7-Diiodo 4.18	6.40(86); 287—289 (dec)	0.10; 316—318 (dec)			0.04	0.10

a) A mixture of 0.01 mol of reactants, 28 ml of pyridine, 0.3 g of KOH in 2 ml of water was heated in a sealed tube at 99—100 °C for 3 hr.

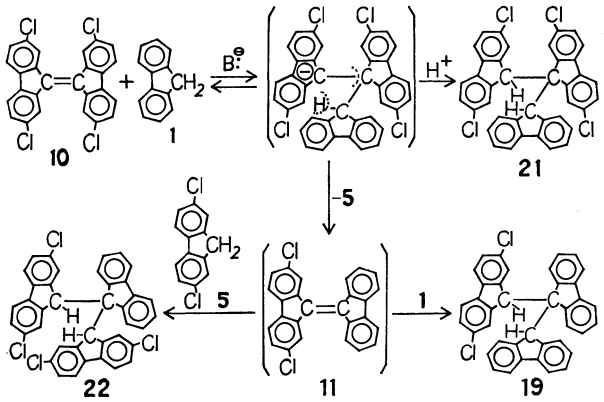

14 (X_1=Cl, X_2=X_3=H)
15 (X_2=Cl, X_1=X_3=H)
16 (X_1=X_2=Cl, X_3=H)
17 (X_1=X_3=Cl, X_2=H)
18 (X_1=X_2=X_3=Cl)

20 (X_2=Cl, X_1=X_3=H)
23 (X_1=X_2=X_3=Cl)
24 (X_1=X_2=X_3=H)

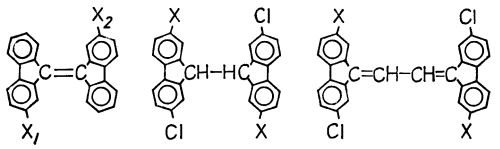

7 (X_1=X_2=H)
8 (X_1=X_2=Cl)
9 (X_1=Cl, X_2=H)

12 (X=H)
13 (X=Cl)

25 (X=H)
26 (X=Cl)

Scheme 1.

The structures of the new addition compounds were confirmed by syntheses through the interconversion reactions between 9-lithiofluorenes and 9-bromo-9,9′-bifluorenyls.

The Michael reaction of **7** with 2,7-dihalofluorene was carried out in order to examine the effects of different halogen substituents. It is noteworthy that the reaction of **7** with **5** gave significant amounts of abnormal compounds as with the corresponding bromo-derivative: however, 2,7-difluorofluorene gave only the expected compound, and the iodo-derivative afforded chiefly normal product. These irregular results are illustrated in Table 3.

In the primary addition, the overcrowded carbanion (A) (X=Cl) is formed by an attack of 2,7-dichloro-9-fluorenyl ion on the 9-position of the twisting central double bond in **7**. Carbanion (B) may be formed by intramolecular proton-transfer in (A), thus we propose the equilibrium shown in Scheme 2:

The ions (A) and/or (B) are transformed to the normal compound **19** by protonation.

The formation of the abnormal compounds can be explained by a series of reactions: elimination, re-

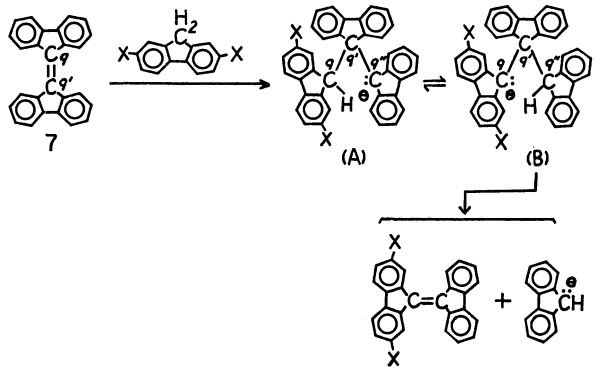

Scheme 2.

addition, and protonation. Compound 2,7-dichloro-9,9′-bifluorenylidene (**11**) and 9-fluorenyl ion are probably formed by fission of the 9′-9″ carbon-carbon bond in ion (B). Subsequently, the secondary addition product **22** may be obtained by the nucleophilic attack of the 2,7-dichloro-9-fluorenyl ion on the highly-polarized **11**, followed by protonation. The tertiary product **24** could be formed by further reaction of **7** with a fragmentary 9-fluorenyl ion.

The stable abnormal compound **22** was obtained as one of the reaction products of three reactions: **7** with **5**, **10** with **1**, and also **11** with **5**. The reactive **11** which played an important role in the formation of **22** was not isolated in these experiments.[6] In this connection, Scheme 3 shows the reactions of halogen analogues of **11** with fluorenes.

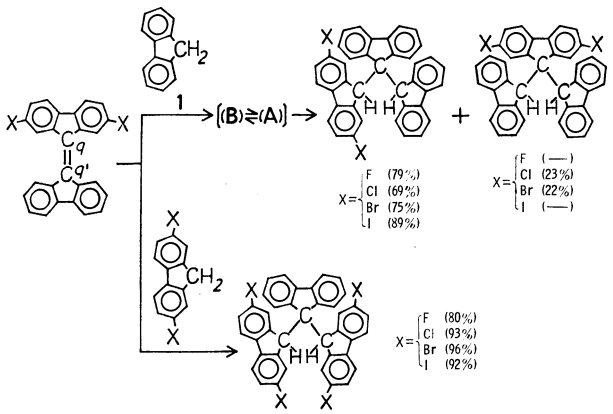

Scheme 3.

From these findings, the 9-carbon atom on **11** is apparently more electronegative than the 9′-carbon due to the inductive effect of the two substituents.[7] The reaction of **11** with **5** gave exclusively **22** instead of 2,7,2′,7′-tetrachloro-9,9′ : 9′,9″-terfluorenyl (**21**). The formation of **22** can be explained by the steric effect in addition to the inductive effect: that is, the mutually repulsive 2,7- and 2″,7″-dichlorofluorenyl groups are placed as far from one another as possible. Therefore, the most stable compound, **22** is formed so as to minimize the steric hindrance.

Isomers **19** and 2′,7′-dichloro-9,9′ : 9′,9″-terfluorenyl (**20**) were obtained by the reaction of **11** with **1**, but no **20** was isolated by the reaction of **10** with **1**. This

can be ascribed to the greater reactivity of **5** compared to **1** and to the low concentration of fragmentary **11** in the latter reaction.

The formation of the expected compound by reaction of **7** with 2,7-difluorofluorene can be explained as follows. The greater inductive effect of the two fluorine atoms will stabilize the ion (B) (X=F) (Scheme 2), and hence prevent the dissociation of the ion (B) into 2,7-difluoro-9,9′-bifluorenylidene and 9-fluorenyl ion. Consequently, protonation of ions (A) and/or (B) may occur readily (see Table 3). Actually, the expected fluoro compound was obtained by the reaction of 2,7-difluoro-9,9′-bifluorenylidene with **1** (Scheme 3).

The influence of the inductive effect of the two iodine atoms in the ion (A) (X=I) is smaller than those of other halogen atoms. Since, in addition to this effect, the 9-carbon atom of ion (A) cannot easily approach the 9″-carbanion on account of the steric repulsion of the bulky two iodine atoms attached to 9-fluorenyl group, intramolecular proton-transfer of (A) to (B) (X=I) is hindered (Scheme 2). Therefore, the normal iodo compound was formed with ease *via* the 9″-carbanion (A) (see Table 3).

The inductive influence of iodine atoms in 2,7-diiodo-9,9′-bifluorenylidene may be smaller than those of other halogen atoms. However, the reaction of 2,7-diiodo-9,9′-bifluorenylidene with **1** afforded predominantly 2,7-diiodo-9,9′ : 9′,9″-terfluorenyl. This indicates that no attack of 9-fluorenyl carbanion on the 9-position of the acceptor occurred due to the steric repulsion between the 9-fluorenyl group and the bulky 2,7-diiodo-9-fluorenylidene.

Consequently, the inductive effects and steric influences of chlorine and bromine atoms in (A) and (B) (X=Cl, Br) are intermediate between those of fluorine and iodine atoms (X=F, I). Thus, in the chloro- and bromo-substituted compounds, both normal and abnormal compounds could be formed in these crowded molecules.

Experimental[8]

*Syntheses of 9,9′-Bifluorenylidenes. 2-Chloro-9,9′-bifluorenylidene (**9**)*: **9** was produced from 2-chloro-9-bromo-9,9′-bifluorenyl or 2-chloro-9′-bromo-9,9′-bifluorenyl by the reaction with potassium hydroxide-methanol in acetone at 2—5 °C, with yields of 60% and 70%, respectively, mp 145—147 °C. Found: C, 85.79; H, 3.83%. Calcd for $C_{26}H_{15}Cl$: C, 86.06; H, 4.17%.

Complexes with 2,4,7-trinitrofluorenone, mp 219—220 °C. Found: C, 62.50; H, 2.32; N, 8.27%. Calcd for $C_{52}H_{25}N_6O_{14}Cl$: C, 62.88; H, 2.54; N, 8.46%.

Dehydration of 2-chloro-9′-hydroxy-9,9′-bifluorenyl by sulfuric acid in acetic acid afforded **9** in 25% yield, accompanied by 2-chloro-9′-acetoxy-9,9′-bifluorenyl (8%), mp 211—211.5 °C. Found: C, 79.37; H, 4.39%. Calcd for $C_{28}H_{19}O_2Cl$: C, 79.52; H, 4.53%. IR (>C=O): 1745 cm^{-1}.

*2,2′-Dichloro-9,9′-bifluorenylidene (**8**)*: 2-Chloro-9-bromofluorene was allowed to react with 1.1 mol equivalent of methanolic sodium hydroxide in acetone at 5—7 °C: red needles of **8** were formed (85%), mp 250 °C (Lit.,[9] mp 258—261 °C). Found: C, 78.64; H, 3.40%. Calcd for $C_{26}H_{14}Cl_2$: C, 78.60; H, 3.55%.

*2,7-Dichloro-9,9′-bifluorenylidene (**11**)*: A mixture of 4.1 g of 2,7-dichloro-9′-hydroxy-9,9′-bifluorenyl, 150 ml of acetic acid, and 2 ml of concentrated sulfuric acid was refluxed for 20 min. Red needles **11** were obtained in 94% yield after recrystallization from acetone, mp 227—228 °C. Found: C, 78.87; H, 3.61%.

*2,7,2′,7′-Tetrachloro-9,9′-bifluorenylidene (**10**)*: **10**, mp 426—428 °C (dec), was synthesized in 84% yield from 2,7-dichloro-9-bromofluorene in a similar manner to **8**. Found: C, 66.69; H, 2.65%. Calcd for $C_{26}H_{12}Cl_4$: C, 66.99; H, 2.59%.

In another method, the reaction mixture obtained as described above was heated for 20 min, and allowed to stand overnight. The resulting mixture was worked up to give **10** in 34% yield, mp 428 °C (dec), 3% of 2,7,2′,7′,2″,7″-hexachloro-9,9′ : 9′,9″-terfluorenyl (**23**), mp 319—320 °C (dec), and 26% of 2,7-dichlorofluorenone (**6**), mp 188—189 °C. Found for **23**: C, 66.92; H, 3.15%. Calcd for $C_{39}H_{20}Cl_6$: C, 66.79; H, 2.87%.

Synthesis of 2,7-Dichloro-9,9′-bifluorenyl. Four milliliters of concentrated hydrochloric acid was added to a boiling mixture of 0.2 g of **11**, 50 ml of acetic acid, and 1.0 g of zinc dust and the mixture was refluxed for 30 min. After filtration of the hot colorless reaction mixture, the dried precipitate was recrystallized from benzene to afford 0.19 g (95%) of colorless needles of 2,7-dichloro-9,9′-bifluorenyl, mp 263—264 °C. Found: C, 78.22; H, 4.01%. Calcd for $C_{26}H_{16}Cl_2$: C, 78.21; H, 4.04%.

*2,2′-Dichloro-9,9′-bifluorenyl (**12**)*:[10] This compound was synthesized from **8** under similar conditions to those for 2,7-dichloro-9,9′-bifluorenyl. Yield 99%, mp 275—276 °C. Found: C, 78.23; H, 3.89%.

2-Chloro-9,9′-bifluorenyl: **9** was reduced by the standard procedure. Yield 90%, mp 237—238 °C. Found: C, 85.82;, H, 4.37%. Calcd for $C_{26}H_{17}Cl$: C, 85.59; H, 4.70%.

*2,7,2′,7′-Tetrachloro-9,9′-bifluorenyl (**13**)*: The compound was obtained from **10**. Yield 90%, mp 300—301 °C. Found: C, 66.36; H, 2.92%. Calcd for $C_{26}H_{14}Cl_4$: C, 66.70; H, 3.01%.

*Syntheses of Bis(4-chloro-2,2′-biphenylylene)-1,3-butadiene (**25**) and Bis(4,4′-dichloro-2,2′-biphenylylene)-1,3-butadiene (**26**).*[11] A mixture of 1.00 g (5 mmol) of 2-chlorofluorene (**3**), 45 ml of ethanol, and 2.5 g of potassium hydroxide in 5 ml of water was refluxed under a gentle stream of air for 20 hr. The precipitate was recrystallized from pyridine to give 0.66 g (62%) of orange needles **25**, mp 386—388 °C (dec). Found: C, 79.75; H, 3.64%. Calcd for $C_{28}H_{16}Cl_2$: C, 79.44; H, 3.81%.

In addition, a small amount of 2-chlorofluorenone (**4**), mp 123—124 °C, was obtained from the ethanol mother solution.

Compound **26** was obtained from **5** in 55% yield, red needles, mp 392—393 °C (dec). Found: C, 68.23; H, 2.59%. Calcd for $C_{28}H_{14}Cl_4$: C, 68.32; H, 2.87%.

Syntheses of 9-Hydroxy-9,9′-bifluorenyls and 9-Bromo-9,9′-bifluorenyls. General procedure: 9-Hydroxy-9,9′-bifluorenyl was prepared under a slow stream of oxygen-free nitrogen in the usual way. To 9-lithiofluorene (obtained by the reaction of 0.035 mol of fluorene with *n*-butyl lithium) in xylene was added 0.03 mol of fluorenone (**2**), and the mixture was refluxed for 30 min. After cooling, the reaction mixture was hydrolyzed with aqueous ammonium chloride, washed with water, dried, and concentrated to dryness *in vacuo*. The precipitate was recrystallized from benzene, cyclohexane, or a mixture of both.

9-Bromo-9,9′-bifluorenyl was synthesized by the reaction of 9-hydroxy-9,9′-bifluorenyl with dry hydrogen bromide in acetic acid below 25 °C

1): 2-Chloro-9-hydroxy-9,9′-bifluorenyl, 97% yield, mp 184—186 °C. IR (–OH): 3540 cm^{-1} (sharp). Found: C, 81.97; H, 4.60%. Calcd for $C_{26}H_{17}OCl$: C, 81.99; H, 4.50%.

2-Chloro-9-bromo-9,9′-bifluorenyl, 86%. mp 180—182 °C (dec). Found: C, 70.57; H, 3.46%. Calcd for $C_{26}H_{16}ClBr$: C, 70.36; H, 3.64%.

2): 2-Chloro-9′-hydroxy-9,9′-bifluorenyl, 95%, mp 177—179 °C. IR (–OH): 3280 cm^{-1}. Found: C, 82.22; H, 4.49%.

2-Chloro-9′-bromo-9,9′-bifluorenyl, 94%, mp 153—155 °C (dec). Found: C, 70.51; H, 3.48%.

3): 2,2′-Dichloro-9-hydroxy-9,9′-bifluorenyl, 81%, mp 182—183 °C. IR (–OH): 3300 cm.$^{-1}$ Found: C, 75.44; H, 3.69%. Calcd for $C_{26}H_{16}OCl_2$: C, 75.19; H, 3.88%.

2,2′-Dichloro-9-bromo-9,9′-bifluorenyl, 83%, mp 184—185 °C (dec). Found: C, 65.67; H, 3.03%. Calcd for $C_{26}H_{15}Cl_2Br$: C, 65.30; H, 3.16%.

4): 2,7-Dichloro-9-hydroxy-9,9′-bifluorenyl, 59%, mp 197—198 °C. IR (–OH): 3265 cm^{-1}. Found: C, 74.85; H, 4.03%.

2,7-Dichloro-9-bromo-9,9′-bifluorenyl, 72%, mp 217—219 °C (dec). Found: C, 65.47; H, 3.32%.

5): 2,7-Dichloro-9′-hydroxy-9,9′-bifluorenyl, 44%, mp 189—191 °C. IR (–OH): 3550 cm^{-1} (sharp). Found: C, 75.39; H, 3.85%.

2,7-Dichloro-9′-bromo-9,9′-bifluorenyl, 83%, mp 201—202 °C (dec). Found: C, 65.76; H, 3.26%.

6): 2,7,2′,7′-Tetrachloro-9-hydroxy-9,9′-bifluorenyl, 51%, mp 227—229 °C. IR (–OH): 3555 cm^{-1} (sharp). Found: C, 64.37; H, 2.80%. Calcd for $C_{26}H_{14}OCl_4$: C, 64.49; H, 2.91%.

2,7,2′,7′-Tetrachloro-9-bromo-9,9′-bifluorenyl, 41%, mp 215—217 °C (dec). Found: C, 57.47; H, 2.35%. Calcd for $C_{26}H_{13}Cl_4Br$: C, 57.08; H, 2.40%.

Formation of 9,9′ : 9′,9″-Terfluorenyls by Lithium-Halogen Interconversion Reaction. General Procedure: To a 9-lithiofluorene solution (prepared from 0.014 g-atom of lithium chips, 7 mmol of *n*-butyl bromide, and 7 mmol of fluorene) was added 4 mmol of 9-bromo-9,9′-bifluorenyl in xylene at 5—10 °C over a period of about 1 hr. After refluxing for 1 hr, the reaction mixture was worked up as usual.

*2-Chloro-9,9′ : 9′,9″-terfluorenyl (**14**)*: This compound was synthesized from **3** and 9-bromo-9,9′-bifluorenyl, mp 255—257 °C (dec) (benzene-ethanol). Found: C, 88.64; H, 4.54%. Calcd for $C_{39}H_{25}Cl$: C, 88.54; H, 4.76%.

*2′-Chloro-9,9′ : 9′,9″-terfluorenyl (**15**)*: From **1** and 2-chloro-9-bromo-9,9′-bifluorenyl, mp 271—272 °C (dec) (ethyl acetate). Found: C, 88.66; H, 4.53%.

*2,2′-Dichloro-9,9′ : 9′,9″-terfluorenyl (**16**)*: From **3** and 2-chloro-9-bromo-9,9′-bifluorenyl, mp 253—254 °C (dec) (benzene-ethanol) Found: C, 83.01; H, 4.36%. Calcd for $C_{39}H_{24}Cl_2$: C, 83.13; H, 4.29%.

*2,2″-Dichloro-9,9′ : 9′,9″-terfluorenyl (**17**)*: From **3** and 2-chloro-9′-bromo-9,9′-bifluorenyl, mp 275—276 °C (dec) (ethyl acetate). Found: C, 83.43; H, 4.15%.

*2,2′,2″-Trichloro-9,9′ : 9′,9″-terfluorenyl (**18**)*: From **3** and 2,2′-dichloro-9-bromo-9,9′-bifluorenyl, mp 279—280 °C (dec) (ethyl acetate). Found: C, 78.02; H, 3.69%. Calcd for $C_{39}H_{23}Cl_3$: C, 78.34; H, 3.88%.

*2,7-Dichloro-9,9′ : 9′,9″-terfluorenyl (**19**)*: From **5** and 9-bromo-9,9′-bifluorenyl, mp 285—287 °C (dec) (ethyl acetate). Found: C, 83.10; H, 4.25%.

*2′,7′-Dichloro-9,9′ : 9′,9″-terfluorenyl (**20**)*: From **1** and 2,7-dichloro-9-bromo-9,9′-bifluorenyl, mp 305—306 °C (dec) (benzene). Found: C, 83.38; H, 4.47%.

*2,7,2′,7′-Tetrachloro-9,9′ : 9′,9″-terfluorenyl (**21**)*: From **5** and 2,7-dichloro-9-bromo-9,9′-bifluorenyl, mp 296—297 °C (dec) (ethyl acetate). Found:,C, 74.26; H, 3.46%. Calcd for $C_{39}H_{22}Cl_4$: C, 74.07; H, 3.51%.

*2,7,2″,7″-Tetrachloro-9,9′ : 9′,9″-terfluorenyl (**22**)*: From **5** and 2,7-dichloro-9′-bromo-9,9′-bifluorenyl, mp 314—315 °C (dec) (pyridine). Found: C, 74.38; H, 3.71%.

*2,7,2′,7′,2″,7″-Hexachloro-9,9′ : 9′,9″-terfluorenyl (**23**)*: From **5** and 2,7,2′,7′-tetrachloro-9-bromo-9,9′-bifluorenyl, mp 320 °C (dec) (benzene). Found: C, 66.91; H, 3.01%. Calcd for $C_{39}H_{20}Cl_6$: C, 66.79; H, 2.87%.

*Michael Reaction of 2,7-Dichloro-9,9′-bifluorenylidene (**11**) with 2,7-Dichlorofluorene (**5**). Typical Procedure*: A mixture of 2.4 g (6 mmol) of **11**, 1.6 g (6.6 mmol) of **5**, 28 ml of pyridine, and 0.3 g (1% for solvent) of potassium hydroxide in 2 ml of water was heated in a sealed tube at 98—100 °C for 15 min. During the heating, the color turned from red to dark green, and colorless crystalline was deposited. Upon cooling, the reaction mixture was added to 400 ml of water, and the deposited material was filtered and sublimed at 160 °C *in vacuo*. The residual part after sublimation was recrystallized from pyridine to afford **22** in 3.56 g (93%), mp 314—315 °C (dec).

The sublimate was chromatographed on alumina with benzene solvent. The elute was concentrated under reduced pressure, and the residue was recrystallized from ethanol to give **5** in 0.08 g yield, mp 123—124 °C: 0.03 g of **6**, mp 186—187 °C (from ethanol), was isolated from the yellow band on the column.

This work was partially supported by a Grant-in-Aid for Scientific Research from the Ministry of Education, which is gratefully acknowledged.

References

1) Studies on Fluorene Derivatives. XXX. Part XXIX of this series: M. Minabe and K. Suzuki, This Bulletin, **46**, 1573 (1973).

2) K. Suzuki, M. Minabe, M. Fujimoto, and N. Nohara, *ibid.*, **42**, 1609 (1969).

3) M. Minabe, A. Tanaka, M. Wakui and K. Suzuki, *ibid.*, **44**, 1614 (1971).

4) M. Minabe and K. Suzuki, *ibid.*, **45**, 3196 (1972).

5) J. Schmidt and H. Wagner, *Ann.*, **387**, 147 (1912).

6) The Michael reaction of **7** with 2-bromofluorene afforded a trace of 2-bromo-9,9′-bifluorenylidene. See K. Suzuki and M. Fujimoto, This Bulletin, **37**, 1833 (1964).

7) For example, the addition of hydrogen bromide to 2,7-dibromo-9,9′-bifluorenylidene gave exclusively 2,7,9′-tribromo-9,9′-bifluorenyl, but 2,7,9-tribromo- (63%) and 2,7,9′-tribromo-9,9′-bifluorenyl (14%) were obtained in the presence of peroxide.

8) All the melting points are uncorrected.

9) D. Bethell, A. F. Cockerill, and D. B. Frankham *J. Chem. Soc., B*, **1967**, 1287.

10) E. Bergmann, H. Hoffmann, and D. Winter, *Ber.*, **66B**, 46 (1933).

11) A Sieglitz and J. Schatzkes, *ibid.*, **54**, 2072 (1921).

The Reactions of β-Amino α,β-Unsaturated Esters with Amines. II. Syntheses of Some New Derivatives of Quinazolines

Yasukazu YOKOYAMA, Katsuya SHIBATA, Osamu FUJII, and Eiji IWAMOTO

Research Center of Tekkosha Co., Ltd., 2743-1 Uehara, Hayakawa, Ayase-cho, Koza-gun, Kanagawa 252

(Received July 30, 1974)

The reaction of 1,4-bis(ethoxycarbonyl)-2,5-diamino-1,4-cyclohexadiene(Ia) with aniline in aprotic solvents gave *N,N'*-diphenylurea, whereas in the presence of a proton acid this reaction gave an amine-exchanged product, 1,4-bis(ethoxycarbonyl)-2,5-dianilino-1,4-cyclohexadiene(Ib). However, when 2-aminopyridine was used in place of aniline for this reaction, 1,4-bis(ethoxycarbonyl)-2,5-bis(2-pyridylamino)-1,4-cyclohexadiene(Ic) was not isolated but its cyclyzed analogue, 6,7,14,15-tetrahydropyrido[2,1-*b*]pyrido[1',2' : 1,2]pyrimido[4,5-*g*]quinazoline-7,15-dione(IIa), was obtained. The reaction of 2-amino-6-methylpyridine with Ia also gave a quinazoline derivative without producing a 1,8-naphthyridine derivative. Since this reaction took place easily in a weak acid, AcOH, this cyclization could proceed by an intramolecular proton-transfer mechanism.

Aminopyridines have two basic nitrogen atoms in the molecule, and their reaction with β-keto esters or β-amino α,β-unsaturated esters is of interest. The condensation of 2-aminopyridine with β-keto ester followed by cyclization in Dowtherm A (a mixture of 23.5% by weight of biphenyl and 76.5% of diphenyl ether) affords the pyridopyrimidines.[1] When the 2-aminopyridine is substituted in the 6-position with an electron-releasing group, the naphthyridine is formed.[2]

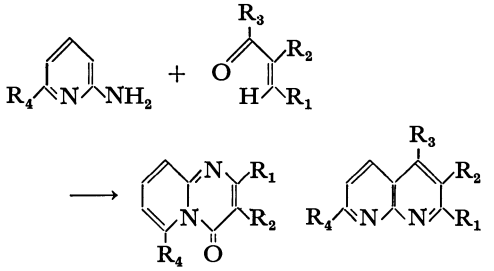

Antaki and Petrow have studied the reaction of 2-aminopyridines with ethyl β-aminocrotonate, and obtained pyridopyrimidines and *N,N'*-bis(6-methyl-2-pyridyl)urea.[3] However, this reaction has not been further investigated.

Therefore, in this work, 1,4-bis(ethoxycarbonyl)-2,5-diamino-1,4-cyclohexadiene(Ia) was used as a β-amino α,β-unsaturated ester, and its reaction with 2-aminopyridines was studied. Some new compounds were synthesized and possible reaction mechanisms were investigated by comparing the reactivity to Ia of 2-aminopyridine with that of aniline.

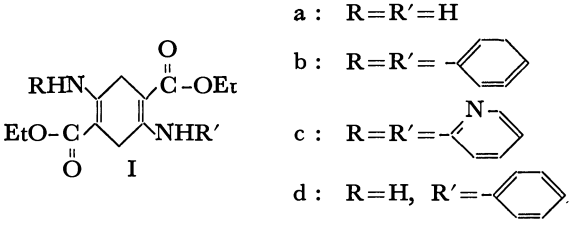

Results and Discussion

When a mixture of Ia and aniline was heated in *N*-methyl-2-pyrrolidone(NMP) or dimethyl sulfoxide (DMSO) under a nitrogen atmosphere at 200 °C for 2 hr, *N,N'*-diphenylurea was the main product.

However, when a proton acid was used as a catalyst, the amino groups of Ia were replaced by anilino groups, giving Ib and 1,4-bis(ethoxycarbonyl)-2-amino-5-anilino-1,4-cyclohexadiene(Id). When glacial acetic acid was used as the solvent, the yield of Ib was higher. On the other hand, when the reaction was carried out in aqueous acetic acid at elevated temperatures, the amino groups of Ia were replaced by hydroxyl groups, and 1,4-bis(ethoxycarbonyl)-2,5-cyclohexanedione(diethyl succinylsuccinate, DSS) was formed.

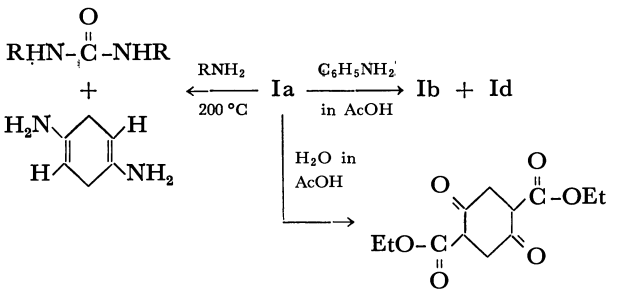

DSS

These results indicate that in the absence of a proton acid the nucleophilic attack of an amine takes place upon the carbonyl carbon atom, whereas in the presence of a proton acid this attack takes place upon the β-carbon atom. The former reaction-mechanism has been reported previously.[4] In the latter case, the protonation of β-amino α,β-unsaturated esters could take place on the nitrogen, α-carbon or carbonyl oxygen atom, giving **1**, **2**, or **3**, respectively. The iminium ions **2** and **3** are expected to react with nucleophiles easily.[5] Therefore, an amine-exchange or amine-hydrolysis reaction should proceed readily.

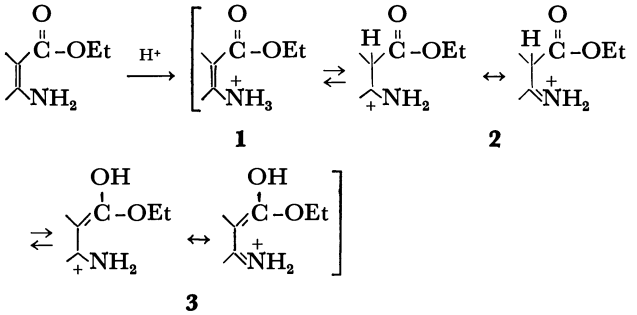

1 **2**

3

The product expected from the reaction between Ia and 2-aminopyridine in glacial acetic acid is Ic. However, its elemental analysis showed the empirical formula $C_9H_6N_2O$. Possible structures are 6,7,14,15-

tetrahydropyrido[2,1-*b*]pyrido[1′,2′ : 1,2]pyrimido[4,5-*g*]quinazoline-7,15-dione(IIa) and 5,6,7,12,13,14-hexahydropyrido[2′,3′ : 2,3]quino[6,7-*b*]-1,8-naphthyridine-7,14-dione (IIb).

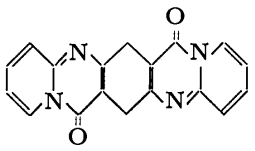

IIa

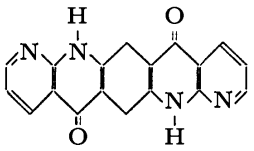

IIb

The same compound was also obtained when DSS was allowed to react with 2-aminopyridine in glacial acetic acid. This compound was determined to be IIa on the basis of its UV, IR, and NMR spectrum.

A similar reaction has been studied by Antaki and Petrow. That is, they have reported that 2-methylpyrido[1,2-*a*]pyrimidin-4-one(III) was obtained by heating ethyl β-aminocrotonate with 2-aminopyridine in the absence of a solvent at 160—180 °C for 6—8 hr, and then for a further hour at 200—220 °C.[3] Adams and Pachter confirmed the structure of III by studying its UV spectrum.[1b]

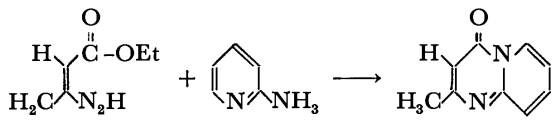

III

However, we easily obtained the same compound by heating ethyl acetoacetate and 2-aminopyridine in glacial acetic acid.

Therefore, it seems that intramolecular cyclization takes place directly in acetic acid, and the reaction between Ia and 2-aminopyridine is postulated to proceed as follows: the amino groups of Ia are replaced

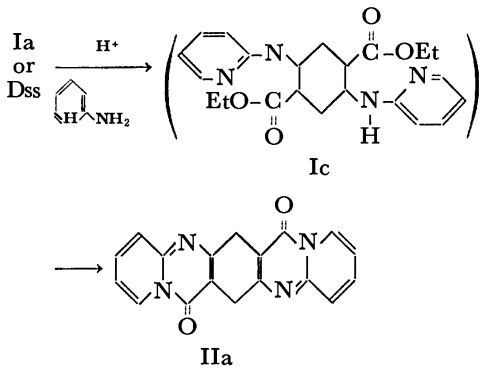

Ic

IIa

by the 2-pyridylamino groups and the Ic formed is converted to IIa by intramolecular cyclization.

Furthermore, 2-amino-3-,4-, and 5-methylpyridine also reacted with Ia or DSS in acetic acid to give 6,7,14,15-tetrahydrodimethylpyrido[2,1-*b*]pyrido[1′,2′ : 1,2]pyr-imido[4,5-*g*]quinazoline-7,15-diones(IIc–e).

On the other hand, Lappin has reported that the condensation of 2-amino-6-methylpyridine with ethyl ethoxymethylenemalonate followed by cyclization affords the 1,8-naphthyridine.[1a] Antaki and Petrow have described the reaction of ethyl β-aminocrotonate with 2-amino-6-methylpyridine and have obtained *N*,*N*′-bis(6-methyl-2-pyridyl)urea.[3] Therefore, 2-amino-6-methylpyridine was treated with Ia or DSS in acetic acid, and 6,7,14,15-tetrahydro-1,9-dimethylpyrido[2,1-*b*]pyrido[1′,2′ : 1,2]pyrimido[4,5-*g*]quinazoline-7,15-dione(IIf) was formed.

These compounds were identified on the basis of elemental analyses, IR, UV, and NMR spectra. Tables 1 and 2 show some pertinent data on II and III.

These results indicate that β-amino α,β-unsaturated esters react with 2-aminopyridine or its methyl-derivatives in acetic acid to give only pyridopyrimidines

Table 1. Physical properties of compounds II and III

Compound	Reaction[a] Time (hr)	Reaction[a] Yield (%)	Mp (°C)	Found (Calcd) % C	Found (Calcd) % H	Found (Calcd) % N	IR absorption maxima $\nu_{C=O}$	IR absorption maxima $\nu_{C=N}$	IR absorption maxima $\nu_{C=C}$	IR absorption maxima $\delta_{C=H}$ (cm^{-1})	UV absorption maxima[b] nm (ε)
IIa	2	12	>300	68.11 (68.35)	3.80 (3.83)	17.59 (17.70)	1670	1630	1570 1530 1490	770	240 (19,000) 322 (21,000)
IIc	3.5	9.7	>300	69.04 (69.77)	4.51 (4.65)	16.28 (16.28)	1680	1635	1580 1547 1485	768	244 (15,000) 324 (25,000)
IId	11	6.8	>300	69.43 (69.77)	4.51 (4.65)	16.23 (16.28)	1672	1640	1570 1520 1485	777	237 (27,000) 320 (28,000)
IIe	13	26	>300	69.26 (69.77)	4.87 (4.65)	16.16 (16.28)	1675	1640	1569 1533 1482	781	245 (12,000) 322 (9,000)
IIf	15	14	>300	67.57 (69.77)	4.91 (4.65)	16.30 (16.28)	1670	1640	1590 1550 1483	805	245 (33,000) 343 (37,000)
III	2	70	121—122	67.53 (67.50)	4.97 (5.00)	17.45 (17.50)	1710	1635	1575 1540 1473	825	240 (6,000) 249 (6,200) 311 (7,800)

a) The reactions were carried out by refluxing in AcOH. b) In 0.5 M H_2SO_4.

Table 2. NMR spectral data of compounds II and III

Compound		δR_1	δR_2	δR_3	δR_4	$\delta(6, 14)$ ppm
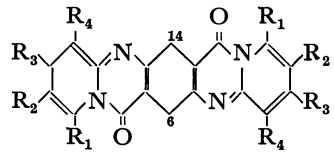	IIa	d 2H	t 2H	t 2H	d 2H	s 4H
		9.38	7.84	8.55	8.08	4.36
	IIc	d 2H	t 2H	d 2H	(CH_3) s 6H	s 4H
		9.30	7.76	8.39	2.80	4.39
	IId	d 2H	d 2H	(CH_3) s 6H	s 2H	s 4H
a : $R_1=R_2=R_3=R_4=H$		9.20	7.64	2.78	7.82	4.30
c : $R_1=R_2=R_3=H$, $R_4=CH_3$	IIe	s 2H	(CH_3) s 6H	d 2H	d 2H	s 4H
d : $R_1=R_2=R_4=H$, $R_3=CH_3$		9.18	2.67	8.41	7.98	4.32
e : $R_1=R_3=R_4=H$, $R_2=CH_3$	IIf	(CH_3) s 6H	d 2H	t 2H	d 2H	s 4H
f : $R_2=R_3=R_4=H$, $R_1=CH_3$		3.22	7.43	8.23	7.76	4.10

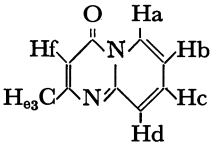

III

a	d 1H	9.40
b	t 1H	7.84
c	t 1H	8.54
d	d 1H	8.10
e	s 3H	2.70
f	s 1H	6.63

directly without producing a 1,8-naphthyridine derivative.

When Ia or DSS was allowed to react with aniline in glacial acetic acid, only Ib was formed and no further cyclization took place. The cyclization of Ib was achieved by heating in inert solvents at high temperature[6] or in polyphosphoric acid (PPA).[7]

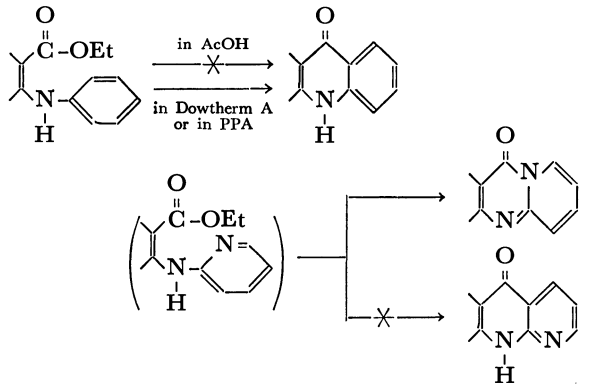

However, the cyclization of Ic occurs more easily than that of Ib in weak acid, acetic acid. This may be explained by assuming the following reaction mechanism. That is, the proton on the nitrogen atom of the

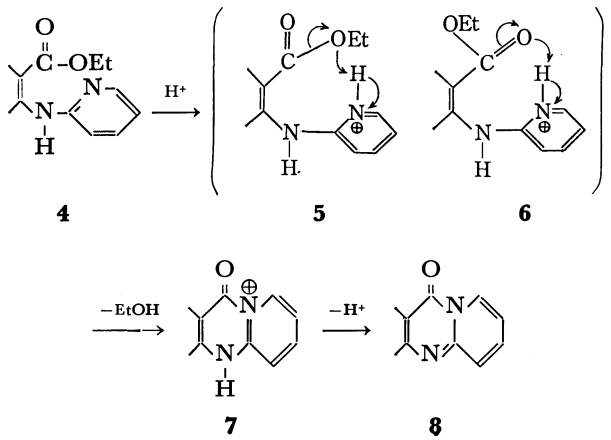

pyridinium ion, **5** and **6**, transfers to the oxygen atom of the ethoxy or the carbonyl group. Then, the carbonium ion formed attacks the nitrogen atom of the pyridine nucleus.

When the reaction of Ia or DSS with 2-aminopyridine in glacial acetic acid was carried out at lower temperatures, the products were 8-amino-7-ethoxycarbonyl-6,9-dihydro-10*H*-pyrido[2,1-*b*]quinazolin-10-one(IVa) or 7-ethoxycarbonyl-6,9-dihydro-8-hydroxy-10*H*-pyrido[2,1-*b*]quinazolin-10-one(IVb), respectively, but Ic was not isolated. The reaction of Ia with 2-aminopyridine in NMP in the presence of *p*-toluenesulfonic acid at 200 °C gave a mixture of IIa and IVa, and that with 2-amino-3-methylpyridine gave a mixture of IIc and 8-amino-7-ethoxycarbonyl-6,9-dihydro-4-methyl-10*H*-pyrido[2,1-*b*]quinazolin-10-one(IVc).

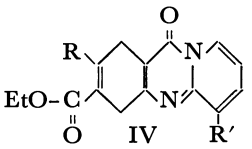

IV

a : $R=NH_2$, $R'=H$
b : $R=OH$, $R'=H$
c : $R=NH_2$, $R'=CH_3$

These observations suggest that the condensation between 2-aminopyridine and Ia or DSS is slow but that the intramolecular cyclization step is very fast.

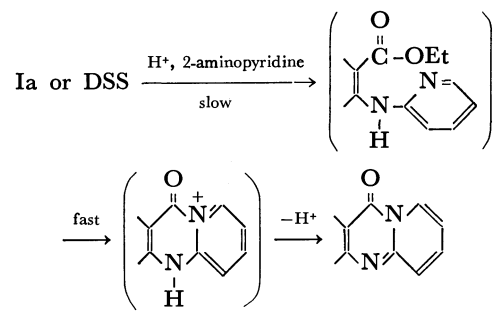

Compounds II and III are basic compounds and are soluble in acidic solutions such as sulfuric acid or trifluoroacetic acid, and they are reprecipitated upon neutralization or dilution. The UV spectra of III are greatly affected by the change of pH of the solution, as shown in Fig. 1. The absorption of III at 338 nm

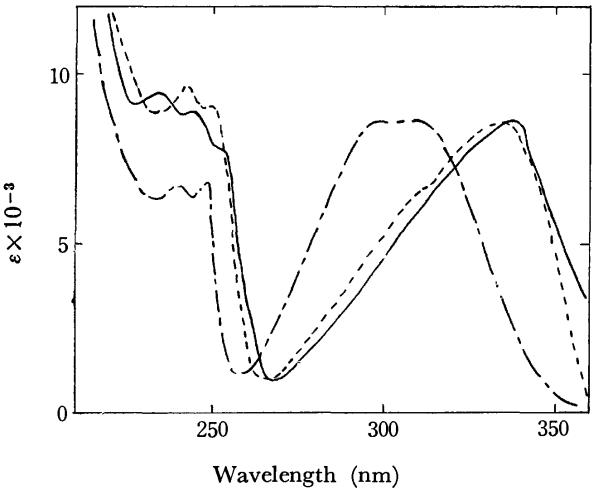

Fig. 1. Electronic absorption spectra of III.
——: in 95% ethanol; ----: in water; ——: in 0.5 M H_2SO_4.

(attributed to the carbonyl group) showed a hypsochromic shift in 0.5 M sulfuric acid solution. The acidic solutions of II showed similar absorptions. These findings suggest that II and III exist in aqueous sulfuric acid solution as tautomers.

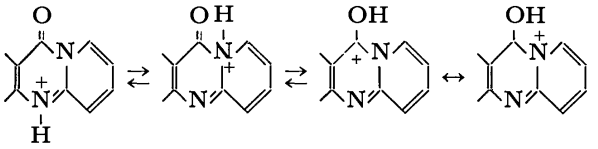

Experimental

The IR spectra were determined in KBr disks with a Hitachi EPI-G3 infrared spectrophotometer. The UV spectra were recorded with a Hitachi EPS-3T recording spectrophotometer. The NMR spectra were obtained with a Varian HA-100 high resolution NMR spectrometer, using TMS as an internal standard. For thin layer chromatography (tlc), a plate of Silica-gel HF (E. Merck) was used. Plates were developed with a mixture of benzene and tetrahydrofuran (1 : 1 v/v). Melting points were uncorrected.

Materials. All the reagents except those listed below were obtained from commercial sources and were used without further purification. DMSO and NMP were dried over aluminum oxide and distilled before use. Aniline and 2-amino-3-methylpyridine were dried over synthetic zeolite (Zeolum A-4, Tekkosha) and distilled before use. 2-Aminopyridine, 2-amino-4-, 5-, and 6-methylpyridine were purified by recrystallization. 1,4-Bis(ethoxycarbonyl)-2,5-di(amino- or anilino)-1,4-cyclohexadiene(Ia: mp 117—119 °C, Ib: mp 164—165 °C) were prepared according to the methods described in the literature.[8]

Reactions. *The Reaction of Ia with Aniline*: *a)* A mixture of Ia (9 g), aniline (8 g), and NMP (50 ml) was heated at 197—200 °C for 2 hr while being stirred under a nitrogen atmosphere. The red solution obtained was then cooled and added with stirring to ice-cold 1 M hydrochloric acid (500 ml). The product was extracted with three 200 ml portions of benzene. The combined benzene extracts were washed once with 1 M hydrochloric acid, twice with water, twice with 10% potassium carbonate, once with water, and were finally dried over anhydrous sodium sulfate. The benzene was removed by distillation at reduced pressure, and the residue was washed with methanol, and dried under vacuum. Yield 1.5 g, mp 122—123 °C, Found: C, 56.14; H, 6.13%. IR (cm^{-1}): 1672(C=O), 1640(C=C), 122 and 1070 (ester). The compound was identified as diethyl succinylsuccinate(DSS) by a comparison of its IR spectrum, mp, and tlc R_f value with those of an authentic sample.[9]

White precipitates were formed from the water layer, and were collected by filtration, washed with water, and dried at 60 °C; 2.5 g of white crystals were obtained. The product was determined to be *N,N'*-diphenylurea(DPU) on the basis of a mixed-melting-point determination and a comparison of its IR spectrum and tlc R_f value with those of an authentic sample: mp 242 °C, IR (cm^{-1}): 3325 and 3280(-NH-), 1652, 1557, and 1319 (amide), 755 and 695(phenyl).

b) A mixture of Ia (5 g), aniline (5 g), and DMSO (50 ml) was heated at 186—196 °C for 2 hr with stirring under a nitrogen atmosphere. By the procedure described in *a)*, unreacted Ia was recovered from the benzene layer, and 0.3 g of DPU was isolated from the water layer. Both compounds were confirmed by a mixed-melting-point determination and a comparison of their IR spectra and tlc R_f value with those of authentic samples.

c) A mixture of Ia (5 g), aniline (5 g), and NMP (50 ml) was stirred at room temperature for 2 hr under a nitrogen atmosphere. The orange crystals which appeared were collected by filtration, washed with methanol, and dried in a vacuum to give Ib, which was confirmed by a comparison of its IR spectrum with that of an authentic sample.

d) To a mixture of Ia (5 g), aniline (5 g), and benzene (50 ml), glacial acetic acid (3 ml) was added. The solution was refluxed for 2 hr with stirring under a nitrogen atmosphere. After it was cooled, it was washed with water (120 ml) and concentrated by distillation at reduced pressure. The residue was washed with methanol yielding 2.0 g of Ib as pale orange crystals. The melting point was not depressed when mixed with an authentic sample. The methanol washings were concentrated to give 3.8 g of orange crystals, which were recrystallized from methanol-water: its structure was determined to be 1,4-bis(ethoxycarbonyl)-2-amino-5-anilino-1,4-cyclohexadiene by IR spectroscopy and elemental analysis. Found: C, 65.37; H, 6.61; N, 8.42%. Calcd for $C_{18}H_{22}N_2O_4$: C, 65.44; H, 6.71; N, 8.48%. IR (cm^{-1}): 3460 and 3330 (-NH-), 1650—1670, 1230, and 1100(ester), 750 and 690 (phenyl).

The Hydrolysis of I: A mixture of Ia (5 g), water (5 ml), and glacial acetic acid (50 ml) was refluxed for 2 hr while being stirred under a nitrogen atmosphere. After cooling the solution, pale yellow crystals separated out, yield 70%. This compound was determined to be DSS by a comparison of its IR spectrum, mp, and tlc R_f value.

In a similar manner, the hydrolysis of Ib gave DSS, yield 52%.

The Reaction of Ia or DSS with 2-Aminopyridines: *a)* A mixture of Ia (5.0 g), 2-aminopyridine (5.0 g), and glacial acetic acid (50 ml) was refluxed with stirring under a nitrogen atmosphere for 3 hr. White solids separated, and they were collected on a filter, washed with acetic acid and methanol, and dried at 60 °C. This compound was soluble in strong acid solutions, such as aqueous sulfuric acid or trifluoroacetic acid, and it was reprecipitated upon neutralization or dilution. The UV spectrum was measured in a 0.5 M aqueous sulfuric acid solution, and the NMR spectrum was recorded in trifluoro acetic acid. Its yield and analytical data are listed in Tables 1 and 2. These results proved that the compound was 6,7,14,15-tetrahydropyrido[2,1-*b*]pyrido[1',2' : 1,2]

pyrimido[4,5-*g*]quinazoline-7,15-dione(IIa).

b) Diethyl succinylsuccinate (5.0 g) also reacted with 2-aminopyridine (5.0 g) under the same reaction conditions described above to give 1.5 g of IIa.

c) The reactions of Ia with 2-amino-3-, 4-, 5-, and 6-methylpyridine were carried out in a similar way to that described in *a*). The yields, products, and analytical data of each run are listed in Tables 1 and 2.

The Reaction of Ethyl Acetoacetate with 2-Aminopyridine: An equimolar admixture of ethyl acetoacetate (13.5 ml) and 2-aminopyridine (12 g) was refluxed in glacial acetic acid (50 ml) for 2 hr. After evaporation of the mixture to dryness under reduced pressure, the residue was recrystallized from petroleum benzine as white needles. It was dried at 60 °C, mp 121—122 °C. Its IR, NMR, and UV absorption, and analytical data are summarized in Tables 1 and 2. These results proved that this compound was 2-methylpyrido-[1,2-*a*]pyrimidin-4-one(III).

*8-Amino-7-ethoxycarbonyl-6,9-dihydro-10*H-*pyrido*[*2,1*-b]*quinazolin-10-one(IVa)*: *a)* A mixture of Ia (5.0 g) and 2-aminopyridine (11.0 g) was heated in glacial acetic acid (50 ml) at 100 °C for 30 min under a nitrogen atmosphere. After cooling, the precipitate was collected by filtration, washed with methanol, and dried under vacuum, yielding 5.0 g of white crystals. This compound was soluble in strong acid solutions from which it was reprecipitated on neutralization. The reprecipitated solid was used for analyses, and its structure was determined to be IVa on the basis of its IR spectrum and elemental analysis. Found: C, 63.07; H, 5.21; N, 14.72%. Calcd for $C_{15}H_{15}N_3O_3$: C, 63.16; H, 5.26; N, 14.74%. IR (cm^{-1}): 3425 and 3325 ($-NH_2$), 1680, 1270, and 1060 (ester).

b) A mixture of Ia (5.0 g) and 2-aminopyridine (5.0 g) was refluxed in NMP (50 ml) in the presence of small amounts of *p*-toluenesulfonic acid for 3 hr under a nitrogen atmosphere. After the reaction mixture was cooled, the precipitate was collected by filtration, washed with methanol, and extracted with hot glacial acetic acid. The residue (2.0 g) was determined to be IIa on the basis of its IR spectrum. The extract was diluted with water and neutralized with aqueous ammonia. The white crystals obtained were identified as IVa on the basis of their IR spectra, and the yield was 1.6 g.

*7-Ethoxycarbonyl-6,9-dihydro-8-hydroxy-10*H-*pyrido*[*2,1*-b]*quinazolin-10-one(IVb)*: A mixture of DSS (15 g) and 2-aminopyridine (15 g) was refluxed in glacial acetic acid (100 ml) for an hour while being stirred under a nitrogen atmosphere. The resulting solid (4.5 g) was filtered out at 60 °C, and was determined to be IIa. After cooling the filtrate to room temperature, a white solid separated out. This precipitate was collected and recrystallized from ethanol, yielding 4.7 g of pale yellow crystals. The purified precipitate showed a single spot on tlc and was identified as IVb on the basis of the IR spectrum and elemental analysis. Mp 219—220 °C, IR (cm^{-1}): 1680 (C=O), 1640 (C=C), 1270 and 1060 (ester), Found: C, 62.72; H, 4.95; N, 9.76%. Calcd for $C_{15}H_{14}N_2O_4$: C, 62.94; H, 4.90; N, 9.79%.

*8-Amino-7-ethoxycarbonyl-6,9-dihydro-4-methyl-10*H-*pyrido*[*2,1*-b]*quinazolin-10-one (IVc)*: The reaction of Ia (5.0 g) with 2-amino-3-methylpyridine (5.0 g) gave IIc (1.5 g) and IVc (1.4 g). The structure of IVc was confirmed on the basis of the IR spectrum and elemental analysis. IR (cm^{-1}): 3430 and 3325 ($-NH_2$), 1665—1680 (C=O), 1635 (C=C), 1250 and 1060 (ester), Found: C, 65.18; H, 5.97; N, 14.40 %. Calcd for $C_{16}H_{17}N_3O_3$: C, 64.21; H, 5.69; N, 14.47%.

References

1a) G. R. Lappin, *J. Amer. Chem. Soc.*, **70**, 3348 (1948). b) R. Adams and I. J. Pachter, *ibid.*, **74**, 5491 (1952).

2) J. T. Adams, C. K. Breslow, S. T. Amore, and C. R. Hauser, *ibid.*, **68**, 1317 (1946).

3) H. Anatki and V. Petrow, *J. Chem. Soc.*, **1951**, 551.

4) Y. Yokoyama and A. Tai, This Bulletin, **46**, 530 (1973).

5) A. G. Cook, "Enamines: Synthesis, Structure, and Reactions," Marcel Dekker Inc., New York, N. Y. (1969), p. 117, 169.

6a) W. S. Struve, U. S. 3009916 (1961). b) A. Tai, Y. Yokoyama, K. Shindo, and O. Fujii, *Yuki Gosei Kagaku Kyokai Shi*, **31**, 410 (1973).

7) N. S. Corby, E. D. Harvey, and D. G. Wilkinson, Brit. 894610 (1960).

8) H. Liebermann, *Ann. Chem.*, **404**, 272 (1914).

9) This compound was probably formed by the hydrolysis of Ia with moisture in the NMP or in the atmosphere. It is also possible that the oxygen atom of NMP attacked a β-carbon atom of Ia and the complex obtained was hydrolyzed during the subsequent treatment. No further treatment of the product was undertaken.

Restricted Rotation Involving the Tetrahedral Carbon. XIV. Conformational Equilibria and Attractive Interactions in Substituted 9-Benzyltriptycenes[1]

Fumio Suzuki and Michinori Ōki

Department of Chemistry, Faculty of Science, The University of Tokyo, Hongo, Tokyo 113

(Received October 2, 1974)

Several 9-benzyltriptycene derivatives were prepared by addition of benzynes to 9-benzylanthracenes. Rotation about the C_9–C_{benzyl} bond of compounds with a substituent at a *peri*-position to the benzyl group was found to be frozen at low temperatures on the NMR time scale but not at room temperature. In contrast, compounds with two substituents at two *peri*-positions to the benzyl group showed a frozen rotation about the C_9–C_{benzyl} bond at room temperature. Distribution of the conformers, as judged from the PMR intensities, showed preference to the *dl*-isomers in spite of the fact that they are the ones which are highly disfavored by steric effects. Interpretation of the phenomenon was based on the fact that attractive interactions, mainly charge-transfer type, exist between the substituted benzo group in the triptycene skeleton and the benzene ring in the benzyl group.

Many works have been carried out to elucidate the intramolecular interaction in cyclohexanes,[2] heterocyclic systems,[3] and substituted ethanes.[4] They disclosed that the steric interaction and hydrogen bonding are the important factors in determining conformational equilibria. The steric interaction may comprise van der Waals interactions including lone-pair-lone-pair interactions and dipole-dipole interactions. However, we come across examples for which the simple concept of nonbonding interelectronic repulsion does not give correct prediction.[5] In conformational equilibria, anomeric effect[6] and gauche effect[7] are notable examples. Attempts have been made to rationalize these effects on the basis of classical electrostatic interactions or the electron delocalization, but the origin of attractive interaction has remained ambiguous for a long time.

Weak attractive interactions may be present in many cases but they are usually overshadowed by strong repulsive interactions and not detectable. However, if the atoms and groups are held together at the closest proximity and other interactions are surpressed to minimum, there may be a possibility to find such interactions.[8] 9-Substituted triptycenes provide good examples since the substituents at 9- and peri-positions are held within the sum of the respective van der Waals radii.

9-Isopropyltriptycene derivatives exist as conformers of the least repulsion.[9] Thus the isopropyl group is too large to exhibit a weak attractive interaction. A group of the RCH_2 type will give less steric repulsions and there is a possibility that, if group R can possess attractive interaction with a substituent at a peri-position, such a conformation would be favored. Thus it is of interest to study the case of 9-benzyltriptycene derivatives since the phenyl group in the benzyl has relatively low-lying antibonding orbitals which may interact with bonding electrons of high levels of the substituted benzo group in triptycene.

This paper describes the conformational equilibria of 9-benzyltriptycene derivatives, giving evidence for a weak interaction between the phenyl group and the substituted benzene moiety. The phenomena are discussed in terms of orbital interactions. A preliminary report on the conformational equilibria has been published.[10]

Experimental

Syntheses. 9-Benzyltriptycenes were prepared by treating 9-benzylanthracenes with benzynes, as illustrated in the following schema. Some new 9-benzylanthracene derivatives were synthesized by the Grignard reaction of substituted benzylmagnesium chlorides with substituted anthrones, followed by dehydration of the products.

1,4-Dimethyl-9-benzylanthracene. To a solution of benzylmagnesium chloride, prepared from 3.8 g (0.03 mol) of benzyl chloride, 0.7 g (0.03 mol) of magnesium, and 100 ml of ether, was added 2.2 g (0.01 mol) of 1,4-dimethylanthrone[11] in small portions at room temperature. After 30 min, 50 ml of benzene was added and the resulting mixture was refluxed for 1 hr. The mixture was decomposed at 0 °C with dilute hydrochloric acid. The organic layer was separated, dried over sodium sulfate, and evaporated. The residue was taken up in 150 ml of carbon tetrachloride and heated on a steam bath with 30 g of phosphorus pentoxide for 2 hr. The supernatant liquid was decanted, washed with water, and dried over sodium sulfate. After removal of the solvent, the residue was chromatographed on neutral alumina. Elution with hexane gave the desired material, mp 133—134 °C, in 0.9 g (*ca.* 30%) yield. PMR (δ, $CDCl_3$): 2.78 (6H, s), 5.12 (2H, s), 6.90—8.15 (12H, m). Found: C, 93.37; H, 6.91%. Calcd for $C_{23}H_{20}$: C, 93.20; H, 6.80%.

1,2,3,4-Tetrachloro-9-benzylanthracene, mp 174—175 °C, was similarly prepared from 1,2,3,4-tetrachloroanthrone[12] and benzylmagnesium chloride. The yield was *ca.* 15%. PMR (δ, $CDCl_3$): 5.17 (2H, s), 6.80—8.10 (9H, m), 8.85 (1H, s). Found: C, 62.32; H, 2.71; Cl, 35.07%. Calcd for $C_{21}H_{12}Cl_4$: C, 62.10; H, 2.98; Cl, 34.92%.

9-(4-Chlorobenzyl)anthracene, mp 124—125 °C, was prepared from anthrone and 4-chlorobenzylmagnesium chloride[13] in *ca.* 40% yield. PMR (δ, $CDCl_3$): 4.90 (2H, s), 6.80—8.25 (12H, m), 8.38 (1H, s).

1,4-Dimethyl-9-(4-chlorobenzyl)anthracene, mp 170—172 °C, was similarly prepared from 1,4-dimethylanthrone and 4-chlorobenzylmagnesium chloride. The yield was *ca.* 25%. PMR (δ, $CDCl_3$): 2.73 (6H, s), 5.00 (2H, s), 6.80—8.00 (10H, m), 8.42 (1H, s). Found: C, 83.42; H, 5.71; Cl, 10.93%. Calcd for $C_{23}H_{19}Cl$: C, 83.50; H, 5.79; Cl, 10.71%.

9-(4-Methoxybenzyl)anthracene, mp 138—139 °C, was prepared from anthrone and 4-methoxybenzylmagnesium chlo-

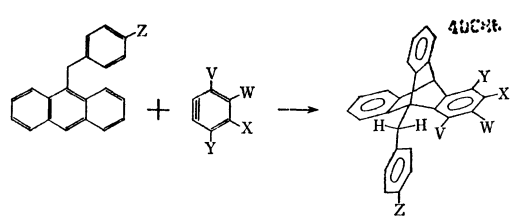

(**3**) V=W=X=Y=Cl, Z=H
(**4**) V=W=X=Y=Br, Z=H
(**5**) V=Y=OCH_3, W=X=Z=H
(**6**) V=Y=OCH_3, Z=Cl, W=X=H
(**7**) V=Y=Z=OCH_3, W=X=H
(**8**) W=Y=CH_3, V=X=Z=H

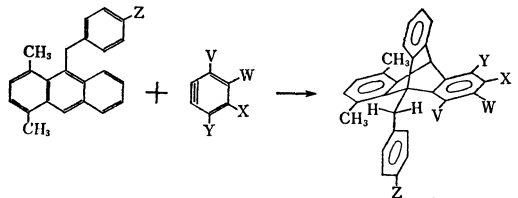

(**1**) V=W=X=Y=Z=H
(**2**) V=W=X=Y=H, Z=Cl
(**10**) V=W=X=Y=Cl, Z=H
(**11**) V=Y=OCH_3, W=X=H
(**12**) V=W=X=Y=Br, Z=H

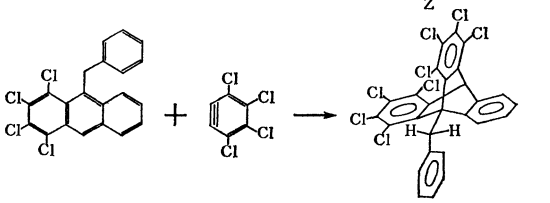

(**13**)

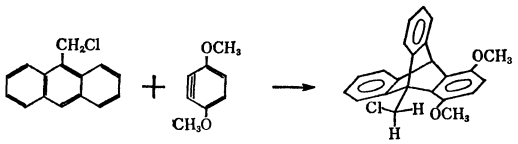

(**9**)

ride[14] in 30% yield. PMR (δ, $CDCl_3$): 3.69 (3H, s), 4.93 (2H, s), 6.64—8.45 (13H, m). This compound was directly used for the preparation of a triptycene derivative **7**.

*1,4-Dimethyl-9-benzyltriptycene (**1**).* To a refluxing solution of 0.6 g (0.005 mol) of butyl nitrite and 1.48 g (0.005 mol) of 1,4-dimethyl-9-benzylanthracene in 20 ml of dichloromethane was added 0.68 g (0.005 mol) of anthranilic acid in 20 ml of acetone with stirring. Heating and stirring were discontinued after 0.5 hr and the solvent was evaporated. The residue was taken up in benzene and chromatographed on alumina. Elution with a mixture of hexane and benzene gave 0.61 g (30% yield) of **1**, mp 172—174 °C. The compound was purified by recrystallization from chloroform–ethanol. Found: C, 93.31; H, 6.47%. Calcd for $C_{29}H_{24}$: C, 93.51; H, 6.49%.

*1,4-Dimethyl-9-(4-chlorobenzyl)triptycene (**2**)*, mp 254—256 °C, was similarly prepared by treating a solution of butyl nitrite and 9-(4-chlorobenzyl)anthracene in dichloromethane with anthranilic acid in dry acetone. The yield was 28%. Recrystallization from chloroform-ethanol afforded a pure sample. Found: C, 85.80; H, 5.95; Cl, 8.73%. Calcd for $C_{29}H_{23}Cl$: C, 85.59; H, 5.70; Cl, 8.71%.

*1,2,3,4-Tetrachloro-9-benzyltriptycene (**3**)*, mp 247—248 °C, was prepared by treating butyl nitrite and 9-benzylanthracene with tetrachloroanthranilic acid.[15] The yield was *ca.* 20%. Recrystallization from benzene-hexane afforded a pure sample. Found: C, 67.82; H, 3.08; Cl, 29.31%. Calcd for $C_{27}H_{16}Cl_4$: C, 67.88; H, 3.19; Cl, 29.41%.

*1,2,3,4-Tetrabromo-9-benzyltriptycene (**4**)*, mp 237.5—239.5 °C, was prepared by treating butyl nitrite and 9-benzylanthracene with tetrabromoanthranilic acid.[16] The yield was 20%. The compound gave no satisfactory analytical results probably because of poor combustibility. Purity was checked by PMR spectrum. Mass spectrum showed molecular ion peaks at 656 for ^{79}Br compound and at 664 for ^{81}Br compound.

*1,2,3,4,5,6,7,8-Octachloro-9-benzyltriptycene (**13**)*, mp 258—260 °C, was prepared with the use of tetrachloroanthranilic acid, butyl nitrite, and 1,2,3,4-tetrachloro-9-benzylanthracene. The yield was *ca.* 7%. The compound gave no satisfactory analytical data owing to the poor combustibility. However, no impurities were detected by spectral methods. Mass spectrum showed a molecular ion peak at 616 for a compound with ^{35}Cl.

*1,2,3,4-Tetrachloro-5,8-dimethyl-9-benzyltriptycene (**10**)*, mp 233—235 °C, was prepared from tetrachloroanthranilic acid, butyl nitrite, and 1,4-dimethyl-9-benzylanthracene in 15% yield. Found: C, 68.49; H, 4.22; Cl, 28.09%. Calcd for $C_{29}H_{20}Cl_4$: C, 68.26; H, 3.95; Cl, 27.79%.

*1,2,3,4-Tetrabromo-5,8-dimethyl-9-benzyltriptycene (**12**)*, mp 233—235 °C, was prepared similarly in 15% yield. Found: C, 50.70; H, 3.05%. Calcd for $C_{29}H_{20}Br_4$: C, 50.62; H, 2.93%.

*1,4-Dimethoxy-9-benzyltriptycene (**5**).* A suspension of phenylsodium,[17] prepared from 2.25 g (0.02 mol) of chlorobenzene, 0.92 g (0.04 mol) of sodium and 50 ml of benzene, was added to a stirred solution of 1.72 g (0.01 mol) of 2-chloro-1,4-dimethoxybenzene[18] and 2.14 g (0.008 mol) of 9-benzylanthracene in 20 ml of benzene at room temperature under a nitrogen atmosphere. Stirring was discontinued after 3 hr and the mixture was treated with water. The organic layer was separated, dried over sodium sulfate, and evaporated. The residue was taken up in benzene and chromatographed on alumina. Elution with benzene gave the desired product which was recrystallized from chloroform-ethanol to give a pure sample, mp 256.5—258.5 °C, in 0.97 g (30%) yield. Found: C, 85.81; H, 5.92%. Calcd for $C_{29}H_{24}O_2$: C, 86.11; H, 5.98%.

*1,4-Dimethoxy-5,8-dimethyl-9-benzyltriptycene (**11**)*, mp 239—240 °C, was prepared similarly by treating a mixture of 2-chloro-1,4-dimethoxybenzene and 1,4-dimethyl-9-benzylanthracene with phenylsodium. The yield was 25%. Found: C, 85.96; H, 6.22%. Calcd for $C_{31}H_{28}O_2$: C, 86.08; H, 6.52%.

*1,4-Dimethoxy-9-(4-methoxybenzyl)triptycene (**7**)*, mp 218—219 °C, was prepared from phenylsodium, 2-chloro-1,4-di-

methoxybenzene, and 9-(4-methoxybenzyl)anthracene in 20 % yield. Found: C, 83.14; H, 5.89%. Calcd for $C_{30}H_{26}O_3$: C, 82.92; H, 6.03%.

3,6-Dimethoxyanthranilic acid was prepared according to the method of Banerjee and Chaudhury.[19] Tedious separation of isomers was avoided since products other than the desired one did not form the corresponding benzyne on treatment with nitrite esters. 2,5-Dimethoxybenzoic acid[20] (5 g or 0.027 mol) was added to 20 ml of nitric acid (d=1.38) in small portions at 0—2 °C with stirring. Stirring was discontinued after 3 hr and the mixture was poured into ice-water to precipitate yellow solids in 5.6 g yield. The PMR spectrum of the product indicated that it was a 2 : 1 mixture of 2,5-dimethoxy-6-nitro- and 2,5-dimethoxy-3-nitro-benzoic acids. The mixture in 100 ml of ethanol was hydrogenated over 1 g of 5% Pd-C under atmospheric pressure to give a viscous brown oil which was a 2 : 1 mixture of 3,6-dimethoxyanthranilic acid and 3-amino-2,5-dimethoxybenzoic acid. This mixture was used for subsequent reactions.

*1,4-Dimethoxy-9-(4-chlorobenzyl)triptycene (**6**).* To a refluxing solution of 0.6 g (0.005 mol) of butyl nitrite and 0.60 g (0.002 mol) of 9-(4-chlorobenzyl)anthracene in 20 ml of dichloromethane was added 1.15 g (0.005 mol) of the mixture of aminodimethoxybenzoic acids in 30 ml of dry acetone. Heating and stirring were discontinued after 0.5 hr and the solvent was evaporated. The residue was taken up in benzene and chromatographed on alumina. Elution with hexane–benzene followed by recrystallization of the product from chloroform–ethanol gave the desired product, mp 264—265 °C, in 30% (0.26 g) yield. Found: C, 79.05; H, 5.40; Cl, 7.95%. Calcd for $C_{29}H_{23}Cl$: C, 79.35; H, 5.28; Cl, 8.08%.

*1,4-Demethoxy-9-chloromethyltriptycene (**9**)*, mp 224—225 °C, was similarly prepared from the crude 3,6-dimethoxyanthranilic acid, butyl nitrite, and 9-chloromethylanthracene[21] in 20% yield. Found: C, 76.32; H, 5.17; Cl, 9.41%. Calcd for $C_{23}H_{19}Cl$: C, 76.12; H, 5.25; Cl, 9.77%.

*2,4-Dimethyl-9-benzyltriptycene (**8**).* To a refluxing mixture of 0.36 g (0.015 mol) of magnesium, 2.68 g (0.01 mol) of 9-benzylanthracene and 70 ml of dry tetrahydrofuran was added 2.0 g (0.01 mol) of 3,5-dimethyl-2-fluoro-1-bromobenzene[22] in 20 ml of dry ether with stirring. After 5 hr, the mixture was cooled and treated with water. The organic layer was separated after addition of 100 ml of ether, dried over sodium sulfate, and evaporated. The residue was taken up in benzene and chromatographed on alumina. Elution with hexane–benzene gave pure **8**, mp 145—147 °C, in 0.56 g (*ca.* 15%) yield. Found C, 93.21; H, 6.60%. Calcd for $C_{29}H_{24}$: C, 93.51; H, 6.49%.

The original product was a mixture of **8** and 1,3-dimethyl-9-benzyltriptycene [PMR (δ, $CDCl_3$): 2.10 (3H, s), 2.26 (3H, bs), 4.52 (2H, bs), 5.07 (1H, s), 6.60—8.20 (15H, m)] in 2 : 1 ratio. Assignments of the structure were based on the observation of coalescence at a lower temperature for **8** than the isomer.

Spectral Measurement. PMR spectra were recorded on a Hitachi R-20B spectrometer operating at 60 MHz. The samples were dissolved in appropriate solvents to make up *ca.* 10% (wt/vol) solutions. The temperatures were read by the difference in chemical shifts between methyl and hydroxy protons of methanol and are believed to be accurate within the error of ±1 °C.

The populations of rotational isomers were measured by the direct integration of the signals. The values are given as the averages of 10 integrations. The maximum deviation from the average was not greater than 7%. Logarithms of the equilibrium constants at various temperatures were plotted against $1/T$. Linearity was obtained for every case and ΔH and ΔS were calculated in the usual way.

It was not possible to find a single suitable solvent for the measurements of the whole series because of the poor solubility of some compounds at low temperatures (below −55 °C). However, at relatively high temperatures, it was possible to measure the solvent effect on populations: change of the solvent from chloroform-d or carbon disulfide to acetone-d_6 did not affect the conformational equilibria within the experimental errors. The triptycenes with *p*-substituted benzyl groups or those which have two substituents at two *peri*-positions had such poor solubility that the derivation of ΔH and ΔS values was abandoned.

Results and Discussion

Peak Assignment. PMR data of the triptycene (**1**—**8**) in chloroform-*d* at 34 °C are summarized in Table 1. Compounds **1**—**7** give broadened signals for benzyl methylene groups at this temperature, indicating that the rotation about the C_9–C_{benzyl} bond is fairly slow on the NMR time scale. Lowering the temperature generally resulted in the appearance of an AB quartet and a singlet. These signals are best assigned to *dl* and *meso* forms, respectively, since the former should have two benzyl hydrogens in different magnetic environments (**14a** and **14b**) and the latter in the identical ones (**14c**). The down-

Table 1. PMR data of 9-benzyltriptycenes carrying substituents in one benzo group at 34 °C ($CDCl_3$, δ)

Compound	Methyls		Methylene	Bridge head proton	Aromatic protons
1	2.38(3H, bs)	2.48(3H, s)	4.70(2H, bs)	5.64(1H, s)	6.45—7.50(15H, m)
2	2.37(3H, bs)	2.48(3H, s)	4.65(2H, bs)	5.66(1H, s)	6.42—7.60(14H, m)
3			4.91(2H, bs)	6.08(1H, s)	6.85—7.55(13H, m)
4			4.99(2H, bs)	6.18(1H, s)	6.70—7.82(13H, m)
5	3.16(3H, s)	3.81(3H, s)	4.62(2H, bs)	5.91(1H, s)	6.38—7.46(15H, m)
6	3.19(3H, s)	3.81(3H, s)	4.60(2H, bs)	5.94(1H, s)	6.30—7.50(14H, m)
7	3.26(3H, s)	3.75(3H, s) 3.81(3H, s)	4.60(2H, bs)	5.95(1H, s)	6.32—7.62(14H, m)
8	2.11(3H, s)	2.49(3H, s)	4.43(2H, s)	5.62(1H, s)	6.62(1H, bs) 6.80—7.45(14H, m)
9	3.72(3H, s)	3.77(3H, s)	5.45(2H, bs)	5.84(1H, s)	6.47(2H, s) 6.80—7.95(8H, m)

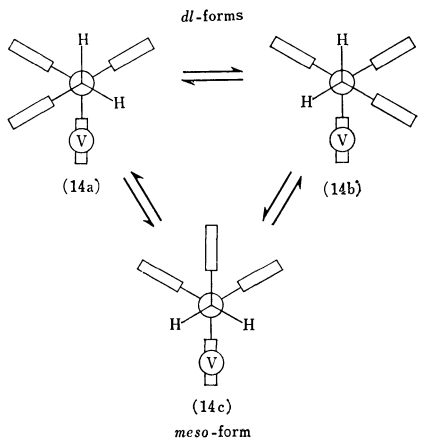

field signal of the AB quartet is reasonably assigned to the proton between the substituent at 1-position and the *peri*-hydrogen at 8-position on the basis that its chemical shift is close to that of the benzyl protons of the *meso* form, the magnetic environment of which is considered to be alike.

At −17 °C, the methyl signal of **1** comprises three signals at δ 2.03, 2.67, and 2.48. The first two are generated by the splitting of the signal at δ 2.38 at 34 °C, the last signal being split into two signals at δ 2.40 and 2.49 on further cooling. A similar phenomenon was also observed for **2** and **11**. The assignment of the signals is self-evident, if the areas of benzyl methylene protons are taken into consideration. Thus the signals at δ 2.03 and 2.49 correspond to methyls of the *dl* form and those at δ 2.40 and 2.67 to those of the *meso* form. Other factors must be taken into consideration for assignment of the signals to methyls at 1- and 4-positions.

The molecular models of these triptycenes show that the phenyl group in the benzyl (benzyl-phenyl hereafter) should take a conformation in which the phenyl group resides in the aperture made by the benzo groups in the triptycene skelton and bisects both the angles of H–C–H (benzyl methylene) and C–C–C (triptycene skelton). This type of conformation is also supported from the coupling constants (−17.4∼−18.0 Hz) of the AB protons in benzyl groups. Theoretically, the π-contribution to the geminal coupling constants is a function of the dihedral angle made by the plane of the π-system and the H–C–C plane,[23] and the π-contribution was estimated to be slightly larger than 4 Hz in a conformation in which the carbon frame of the π-system bisects the angle H–C–H. Since the coupling constant in methane is 13 Hz[24] the coupling constant should be 17 Hz or a little more, if the conformation of the benzyl group is like the one postulated from the molecular model. The observed and the calculated values agree fairly well, conformation **15** thus becoming reasonable.

In such a conformation, substituent (V) at the *peri*-position would be located in a shielding cone of the benzyl-phenyl group. Thus it is reasonable to assume that the methyl at 1-position gives the PMR signal at a higher field than the methyl at 4-position. From the foregoing discussion, the signal at δ 2.03 is assigned

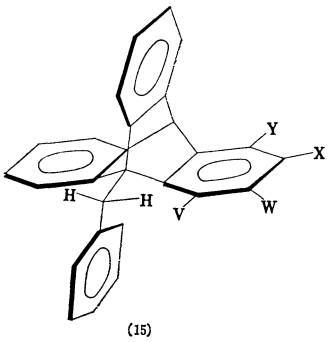

(15)

to the methyl group at 1-position of the *dl*-form and that at δ 2.49 to the methyl at 4-position. The chemical shifts of the methyl groups in the *meso* form are not self-evident, but from the coalescence-splitting behavior with the corresponding signals of the *dl*-forms the signals at δ 2.67 is assigned to the methyl groups at 1-position and that at δ 2.40 to the methyl at 4-position. Assignments along this line are carried out with other compounds and are listed in Table 2.

The situation of the methoxyl groups at *peri*-positions differs slightly from that of the methyl groups. The chemical shift difference between the methoxy-methyls at 1- and 4-positions becomes very small for the *meso* forms. This is reasonable since intervention of the oxygen between the methyl and the benzo groups makes the distance from the phenyl group larger and gives a greater freedom of rotation reducing the chemical shift difference. Nevertheless, since it is possible to assign methoxyl groups in the *dl*-forms, the methoxyl groups in the *meso* form of **6** are assigned from the coalescence-splitting behavior (Table 2).

PMR spectra of compound **9** showed a curious behavior when the temperature was varied. A signal of the chloromethyl group was a little broad at 34 °C, whereas rise and fall in temperature caused sharpening of the signal instead of further broadening or splitting at a low temperature. Sergeyev and co-workers[25] suggested that the barrier to rotation about the C_9–C_{CH_2Cl} bond in 9-chloromethyltriptycene should be higher than 15 kcal/mol. It is thus unlikely that the rotation about the C_9–C_{CH_2Cl} bond in **9** is still too fast on the NMR time scale at −30 °C. It is unrealistic to assume that the chemical shifts of the protons at three sites coincide both for methoxy and methylene protons because of the large magnetic effect of the chlorine substituent.[24,26] Solvent effect did not change the above situations. If the phenomenon is caused neither by the change in solute-solvent interaction nor by the rapid rotation about the bond in question, it is reasonable to interpret the results from the change in population of the rotamers. The internal rotation is slow enough at room temperature to be detected by the NMR technique as a broadening of the signal and the population of the *dl*-isomer is present to the extent that it can be observed. At a lower temperature, however, the less stable *dl*-isomer decreases in population and is not detected, although the rotation in question is sufficiently slow. At a higher temperature, the rotation becomes too fast for the detection of individual species, although the popula-

Table 2. PMR data of 9-benzyltriptycenes carrying substituents in one benzo group at low temperatures (δ)

Compound	Assignment	*meso*	*dl*	J_{gem} (Hz)	Temperature (°C)	Solvent
1	benzyl methylene	4.69	4.19, 4.63	−17.4	−40	$CDCl_3$-CS_2 (2 : 3)
	methyl-1	2.67	2.03			
	methyl-4	2.40	2.49			
2	benzyl methylene	4.70	4.20, 4.65	−17.5	−45	$CDCl_3$-CS_2 (2 : 3)
	methyl-1	2.71	2.06			
	methyl-4	2.41	2.50			
3	benzyl methylene	5.00	4.19, 5.07	−18.0	−50	CS_2
4	benzyl methylene	5.02	4.20, 5.10	−18.0	−23	CS_2
5	benzyl methylene	4.97	4.30, 4.94	−18.0	−56	$CDCl_3$-CS_2 (3 : 1)
	methoxy-1	3.80	2.95			
	methoxy-4	3.80	3.80			
6	benzyl methylene	4.96	4.30, 4.92	−18.0	−52	$CDCl_3$-CS_2 (3 : 1)
	methoxy-1	3.79	3.01			
	methoxy-4	3.82	3.82			
7	benzyl methylene	4.95	4.31, 4.93	−18.0	−50	$CDCl_3$-CS_2 (3 : 1)
	methoxy-1	a)	3.03			

a) Other peaks at δ 3.80 and 3.84 are not assigned because of the presence of *p*-methoxy group in the benzylbenzene.

Table 3. PMR data of 9-benzyltriptycenes carrying substituents in two benzo groups at 34 °C ($CDCl_3$, δ)

Compound	Assignment	**16a**	**16b**
10	benzyl methylene	4.82, 5.60 (1.09H, J_{gem} = −17.7 Hz)	4.57, 5.75 (0.91H, J_{gem} = −17.4 Hz)
	methyl-5	2.59(1.64H, s)	2.46(1.36H, s)
	methyl-8	2.19(1.64H, s)	2.79(1.36H, s)
	bridgehead proton	6.35(1H, s)	
	aromatic protons	6.50—7.75(11H, m)	
11	benzyl methylene	4.55, 5.37 (2H, J_{gem} = −16.8Hz)	
	methyl-5	2.46(3H, bs)	
	methyl-8	2.74(3H, bs)	
	methoxy-1	2.95(3H, bs)	
	methoxy-4	3.78(3H, bs)	
	bridgehead proton	6.20(1H, s)	
	aromatic protons	6.30—7.60(13H, m)	
11[a]	benzyl methylene	4.57, 5.39[b] (2H, J_{gem} = −16.8 Hz)	
	methyl-5	2.57(0.71H, s)	2.46(2.29H, s)
	methyl-8	2.15(0.71H, s)	2.77(2.29H, s)
	methoxy-1	3.74(0.71H, s), 3.78(0.71H, s)[c]	2.94(2.29H, s)
	methoxy-4		3.81(2.29H, s)
12	benzyl methylene	4.80, 5.76 (1.05H, J_{gem} = −18.0 Hz)	4.46, 6.00 (0.95H, J_{gem} = −18.0 Hz)
	methyl-5	2.62(1.57H, s)	2.50(1.43H, s)
	methyl-8	2.21(1.57H, s)	2.81(1.43H, s)
	bridgehead proton and aromatic protons	6.40—7.10(12H, m)	
13	benzyl methylene	4.76, 6.08 (2H, J_{gem} = −18.2Hz)	
	bridgehead proton	6.38(1H, s)	
	aromatic protons	6.85—7.70(9H, m)	

a) Data obtained at 0 °C. b) A single AB quartet is observed to indicate that the chemical shifts of a pair of quartets coincide. c) Assignment of these peaks are reserved because of a small chemical shift difference.

tion of the *dl*-isomers increases. Thus the signal observed at low temperatures should be due to the *meso* form which exists as an overwhelming species among the possible conformations.

1,8-Disubstituted 9-benzyltriptycenes (**10**—**12**) showed PMR signals corresponding to two isomers at room temperature (Table 3). The results suggest that the barrier to rotation is still higher. The absence of an isomer of **16c** type is assumed since the conformation should be of high energy. The assumption is supported by the fact that compound **13** gives only one set of AB quartet, indicating that the compound solely exists as a *dl* form which has the benzyl-phenyl group at the site of the least steric interaction. The conformation **16a** should give a methyl signal at higher magnetic field than **16b**, for the methyl group at 1-position is located within the shielding cone of the benzyl-phenyl group. From the data of compounds **1** and **2**, the methyl group in a similar situation gives the signal at the highest magnetic field among other methyls. Other methyl signals are assigned by considering the signal intensities. The benzyl methylene protons due to conformations **16a** and **16b** can be assigned by taking the intensities into consideration. The downfield signal of each pair of AB protons of the benzyl group is assigned to the proton placed between the substituents at 1- and 8-positions in the Newman projection, since the proton is likely to give a signal at a lower field due to the steric compression and/or the magnetic effects of the substituents. The assignment is in line with the chemical shifts of benzylic protons in **1**—**5** in which a proton neighboring the peri-substituent gives a signal at the lower field.

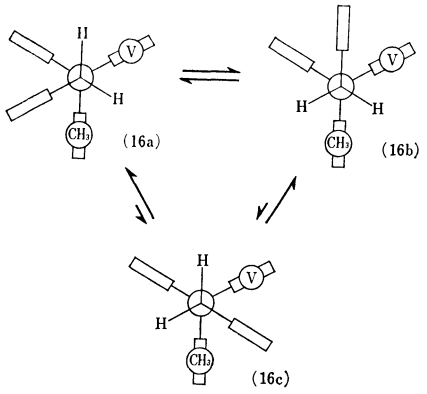

Rotamer Populations. The quilibrium constants for the equilibria *meso*⇌*dl* of compounds **1**—**8**, the thermodynamic parameters obtained by the measurement of the equilibria at various temperatures, and solvent systems are listed in Table 4. The solvent system had to be varied due to the poor solubility of the compounds. However, those compounds examined in various solvents showed no solvent dependency of the population. Thus, the following discussion seems to be valid.

The data in Table 4 indicate that the *dl*-forms of benzyltriptycenes (**1**—**7**) which carry one substituent at a *peri*-position to the benzyl group are anomalously favored, particularly for compounds **5**—**7**. The equilibrium constant is even larger than 2, which value is expected from mere statistical consideration. The anomaly is striking when we compare the data with that for compound **9** which shows the presence of *dl*-isomers only to a detectable amount at room temperature (*vide supra*), giving a signal corresponding to a *meso* isomer only at lower temperatures. We may thus conclude that the *dl*-forms of the benzyltriptycenes **1**—**7** are anomalously favored.

The relative stability of conformers can be discussed on the assumption that the potential function is approximately divided into three terms: steric repulsion, electrostatic interaction including dipole-dipole interaction and electron delocalization. Such an assumption seems to be supported in simple molecules by theoretical calculations.[27]

The overwhelming relative stability of the *meso* form of compound **9** over the *dl*-form may be explained on a basis that the steric repulsion term outweighs the electrostatic interaction and the electron delocalization. The destabilization factor of dipole-dipole interaction should operate for the *meso* form of compound **9** since the dipole of C–Cl and that of the C–O–C are arranged in the same direction. Electron delocalization by transfer of an electron from the highest occupied molecular orbital (HOMO) of the *p*-dimethoxybenzene to the lowest unoccupied molecular orbital (LUMO) σ^* of the $ClCH_2$ group may occur to a limited extent, but the σ^* orbital seems to be too high to make this contribution significant. On the

Table 4. Equilibrium constants and thermodynamic parameters for 9-benzyltriptycenes **1**—**9**

Compound	Equilibrium constant $K=\frac{dl}{meso}$ (temp. °C)	ΔH (kcal/mol)	ΔS (eu)	Solvent
1	0.85±0.10 (−50)	1.1±0.1	4.9±0.9	$CDCl_3$-CS_2 (2 : 3)
2	0.84±0.10 (−50)			$CDCl_3$-CS_2 (2 : 3)
3	0.68±0.10 (−50)	1.2±0.1	4.3±0.5	CS_2
	1.0 ±0.1 (−23)			
4	1.0 ±0.1 (−23)			CS_2
5	2.8 ±0.1 (−50)	0.0±0.1	2.1±0.3	$CDCl_3$-CS_2 (3 : 1)
6	3.5 ±0.1 (−50)			$CDCl_3$-CS_2 (3 : 1)
7	2.4 ±0.1 (−50)			$CDCl_3$-CS_2 (3 : 1)
8	1.2 ±0.1 (−83)			CS_2
9	0 (−30)			$CDCl_3$

other hand, steric repulsion is very severe since the atoms in the chloromethyl and *peri*-regions are located within the sum of their van der Waals radii, and weak interactions of electrostatic nature and electron delocalization are not strong enough to overcome it.

The steric conditions of 9-benzyltriptycenes should be more severe than those of compound **9**, since the phenyl group is larger than the chlorine. As in the case of other systems such as cyclohexanes[2] and substituted ethanes,[28] we may expect such overcrowding caused by the benzyl group and the substituent to greatly increase the free energy difference of the two forms. Preference of the *dl*-form therefore cannot be explained by the steric effect. The dipole-dipole interaction also is not favorable for these compounds, since substitution of a chlorine atom by a phenyl group should result in a decrease in bond dipoles. Consequently the preference of the *dl*-form on the electrostatic basis is reduced. Benzene might have a high microscopic dielectric constant along an axis which is perpendicular to the ring. The model is supported by the anomalous behaviors of benzene as a solvent.[29] Application of this idea leads to a conclusion that *dl* isomers are provided stabilization by the electrostatic interactions between the negative benzyl-benzene ring and the oxygen or halogen at 1-position which becomes partly positive due to the electron delocalization. If this were the case, the solvent effect on the conformational equilibria would have been large. It is also difficult to explain the effect of the substituent in the benzyl group on the conformational equilibria. The electron-donating substituent would have given more *dl*-forms contrary to the observed ratio.

Thus the electron delocalization effect becomes a likely cause of the phenomenon. From the data of compounds **5**—**7** we note that the electron-donating substituent disfavors the *dl*-form, whereas the electron-attracting substituent favors it. Since the steric effect in these compounds may be assumed to be the same, the stabilization due to delocalization or through-space interaction will be the major factor, if not the only one. When the through-space interaction[30] between the benzyl-benzene and the *p*-dimethoxybenzene moities in the triptycenes is taken into consideration, the magnitude of stabilization would depend on the difference in energy between the orbitals concerned and the extent to which they overlap, if other factors such as steric repulsion, medium effects and electrostatic interactions are the same. The lower the energy level of LUMO of the benzene ring, the greater the orbital interaction with HOMO of the other moiety, provided that the level of HOMO of the donor is the same, to increase the presence of the *dl*-forms. No such stabilization is possible in the *meso* form since the orbitals lie too far apart from each other. Since the HOMO's of *p*-dimethoxybenzenes in **5**—**7** can be considered to be of the same energy, the lowering in energy of LUMO of the benzyl-benzene should result in the more preferred interaction which leads to the preference of the *dl*-form to a greater extent. The HOMO's and LUMO's of some simple benzene derivatives are given in Table 5. Since the levels of HOMO may be regarded as equal to ionization potentials to a first approximation and we are dealing with the charge transfer type interaction, the ionization potential data have been collected from those given in the literature.[31] The levels of LUMO can be estimated from those of HOMO and the data of electronic absorption spectra.[32]

Table 5. Energy levels of HOMO and LUMO of some benzene derivatives

Compound	HOMO (eV)	LUMO (eV)
Benzene	9.40	4.52
Chlorobenzene	9.31	4.72
Anisole	8.54	3.89
p-Dimethoxybenzene	7.90	3.58
p-Dichlorobenzene	9.17	4.59
p-Xylene	8.71	4.00

The observed trend is in line with what is expected from the HOMO–LUMO interactions. It may be concluded that the preference of the *dl*-forms in compounds **5**—**7** is due to the electron delocalization approximated by donation of electrons from HOMO of *p*-dimethoxybenzene to the antibonding LUMO of the benzyl-benzene. Although the effect of the alkyl substituents on the energy level is neglected here, such approximation may be accepted in a qualitative discussion.

The relative population in these compounds results from a balance between the attractive interaction due to the delocalization and the repulsive interaction due to the steric size. In compounds **5**—**7**, the former factor exceeds the latter. This will be a consequence of the high HOMO level of *p*-dimethoxybenzene moiety. If the HOMO level of the donor is lowered and other steric and electric factors are kept constant, preference for the *dl*-form will be diminished. Comparison of the equilibrium constants of compounds **1** and **5** which possess the same acceptor group indicates that the *dl*-form of **5** is more favored than that of **1**. The result is in line with the available data of HOMO (Table 5).

Stabilization of the *dl*-forms in **1** might be attributed to the interaction between the benzene ring and the electronegative methyl group, as suggested for acetonitrile–benzene system.[33] However, if this were the case, compound **2** should have disfavored the *dl*-form relative to compound **1** because of the lower electron density (or the lower HOMO level) in the chlorophenyl group. Since the equilibrium constants for both compounds are the same within the limit of error, and the phenomenon is understood in terms of orbital interactions, we prefer to attribute the phenomenon to the HOMO–LUMO interaction where the benzene moiety acts as an electron acceptor.

The effectiveness of the overlap of orbitals concerned should be considered, the difference between *meso* and *dl*-forms being a typical example. The more bulky the substituents, the more effective the overlap of orbitals is prevented since the orbitals concerned are more separated from each other. Similarly more accurate estimation for the stabilization by the electron delocalization needs coefficients of atomic orbitals

in most interacting molecular orbitals. In the *dl*-forms of dimethyl compounds **1** and **2**, the interaction may become less favorable because electrons belonging to the methyl group are relatively localized to molecular orbitals of low energy relative to those of the methoxy group in **5**—**7**.

The larger K value for compound **8** than for compound **1** can be attributed to the decrease in steric effect for the former because it has no substituent at peri-positions to interact with the benzyl group. Preference of the *dl*-forms for compound **8** is reduced, as compared with that in 2,4-dimethyl-9-isopropyltriptycene which has been reported to give an equilibrium constant of 2, a statistical factor.[9] The phenomenon can be attributed to the fact that, being an elongated group, the benzyl-phenyl group extends deeply into the aperture of the triptycene skeleton and the repulsive force between the phenyl group and 2-methyl group may become significant in some conformations: the entropy term becomes unfavorable.

In compounds **10**—**13**, the presence of a form of **16c** type is not detected at all. This may arise either by thermodynamic control or kinetic control. Thermal equilibration at 250 °C for 12 hr was attempted. Since a pair of AB quartet signals of these compounds becomes broad at a higher temperature and then collapse into a broad singlet at 120 °C, probably because of the coincidence of the chemical shifts, 250 °C is considered to be high enough to cause a full rotation about the C_9–C_{benzyl} bond and thermal equilibration will ensue to at least some extent, if the energies are feasible. However, it was not possible to detect any of the forms of **16c** by even rapid cooling after the above operation. Although the possibility that the barrier leading to **16c** form is still too high under the conditions applied cannot be ruled out completely, the results strongly suggest that **16c** is thermodynamically unstable. From the standpoint of electron delocalization, the **16c** type conformation should be favored. The steric effect seems to outweigh the electronic effect in these cases.

The data in Table 6 suggest that the conformational preference between **16a** and **16b** can be understood also from the standpoint of HOMO–LUMO interaction. In compound **11**, the conformation of **16b** type will be favored, because the HOMO of the *p*-dimethoxybenzene is higher than that of the *p*-xylene. Compounds **10** and **12** give almost the same equilibrium constants in agreement with the fact that compounds **1**, **3** and **4** give similar equilibrium constants and that the conformational energy of the *meso* forms of these monosubstituted compounds may be assumed the same.

Table 6. Relative populations of rotamers in 9-benzyltriptycenes **10**—**13** at 0 °C ($CDCl_3$)

Compound	Equilibrium constant $K=\frac{\mathbf{16a}}{\mathbf{16b}}$
10	1.2±0.1
11	$\frac{1.0}{3.2}$=0.31±0.02
12	1.1±0.1
13	1.0

In conclusion, the electron delocalization plays a significant role in determining the conformational equilibria in 9-benzyltriptycene derivatives, although the steric effect is also very important. This is an observation rarely made on the charge transfer type interaction in which a benzene ring without any strongly electron-attracting substituent acts as an acceptor in combination with donors of medium to low ability. This kind of orbital interaction is undoubtedly caused by the extreme proximity of the orbitals concerned in the overcrowded molecules.

References

1) Preceding paper: G. Yamamoto and M. Ōki, *Chem. Commun.*, **1974**, 713.

2) E. L. Eliel, N. L. Allinger, S. J. Angyal, and G. A. Morrison, "Conformational Analysis," Interscience, New York (1965), Chap. 2 and 7: F. R. Jensen, C. H. Bushweller and B. H. Beck, *J. Amer. Chem. Soc.*, **91**, 344 (1969).

3) E. L. Eliel, *Accounts Chem. Res.*, **3**, 1 (1970): E. L. Eliel, *Angew. Chem.*, **84**, 779 (1972); *Angew. Chem., Int. Ed. Engl.*, **11**, 739 (1972).

4) F. J. Weigert, M. B. Winstead, J. I. Garrels, and J. D. Roberts, *J. Amer. Chem. Soc.*, **92**, 7359 (1970): B. L. Hawkins, W. Bremser, S. Borcic, and J. D. Roberts, *ibid.*, **93**, 4472 (1971): N. Sheppard, *Advan. Spectroscopy*, **1**, 288 (1959): J. P. Lowe, *Progr. Phys. Org. Chem.*, **6**, 1 (1968): J. E. Anderson and H. Pearson, *J. Chem. Soc. Perkin II*, **1973**, 960: R. J. Abraham and K. Parry, *J. Chem. Soc., B*, **1970**, 539.

5) N. D. Epiotis, *J. Amer. Chem. Soc.*, **95**, 3087 (1973): N. D. Epiotis, D. Bjorkquist, L. Bjorkquist, and S. Sarkanen, *ibid.*, **95**, 7558 (1973): W. J. Hehre and L. Salem, *Chem. Commun.*, **1973**, 754.

6) R. U. Lemieux, *Pure Appl. Chem.*, **25**, 527 (1971): S. Wolfe, A. Rauk, L. M. Tel, and I. G. Csizmadia, *J. Chem. Soc. B*, **1971**, 136.

7) S. Wolfe, *Accounts Chem. Res.*, **5**, 102 (1972).

8) C. Romers, C. Altona, H. R. Buys and E. Havinga, *Topics in Stereochemistry*, **4**, 39 (1969): G. Baddeley, *Tetrahedron Lett.*, **1973**, 1645: S. David, O. Eisenstein, W. J. Hehre, L. Salem, and R. Hoffmann, *J. Amer. Chem. Soc.*, **95**, 3806 (1973).

9) F. Suzuki, H. Nakanishi, and M. Ōki, This Bulletin, **47**, 3114 (1974).

10) F. Suzuki and M. Ōki, *Tetrahedron Lett.*, **1974**, 2845.

11) F. Bell and D. H. Waring, *J. Chem. Soc.*, **1949**, 267.

12) M. Goi and K. Konishi, *Osaka Furitsu Kogyo-Shoreikan Hokoku*, No. 24, 51 (1960): P. Kniel, *Helv. Chim. Acta*, **46**, 492 (1963).

13) M. S. Kharasch and H. C. Brown, *J. Amer. Chem. Soc.*, **61**, 2142 (1939).

14) G. Baddeley, N. H. P. Smith, and M. A. Vichars, *J. Chem. Soc.*, **1956**, 2455.

15) H. Heaney and J. M. Jablonski, *J. Chem. Soc., C*, **1968**, 1895.

16) H. Heaney, K. G. Mason, and J. M. Sketchley., *ibid.*, **1971**, 567.

17) G. Ehrhart, *Chem. Ber.*, **96**, 2042 (1963): G. Ehrhart and G. Seidl, *ibid.*, **97**, 1994 (1964).

18) G. Catelframchi and G. Borra, *Ann. Chim. (Roma)*,

43, 293 (1953).
19) P. K. Banerjee and D. N. Chaudhury, *J. Indian Chem. Soc.*, **36**, 257 (1959).
20) F. J. Villani and J. Lang, *J. Amer. Chem. Soc.*, **72**, 2301 (1950).
21) W. T. Hunter, J. S. Buck, F. W. Gubitz, and C. H. Bolen, *J. Org. Chem.*, **21**, 1512 (1956).
22) S. R. Sandler and W. Karo, "Organic Functional Group Preparations," Vol. 1, Academic Press, New York (1968), p. 138.
23) M. Barfield and D. M. Grant, *J. Amer. Chem. Soc.*, **85**, 1899 (1963).
24) M. Nakamura, M. Ōki, H. Nakanishi, and O. Yamamoto, This Bulletin, **47**, 2415 (1974).
25) N. M. Sergeyev, K. F. Abdulla, and V. R. Skvarchenko, *Chem. Commun.*, **1972**, 368.
26) Even methyl groups in the *t*-butyl group at 9-position of triptycene have been found to give a chemical shift difference of ca. 0.3 ppm, if a chloro group is present at 1-position: M. Ōki and T. Morinaga, unpublished work.
27) L. Radom, W. J. Hehre, and J. A. Pople, *J. Amer. Chem. Soc.*, **94**, 2371 (1973).
28) C. H. Bushweller and W. G. Anderson, *Tetrahedron Lett.*, **1972**, 1811.
29) R. J. Abraham, *Mol. Phys.*, **4**, 369 (1961): L. W. Reeves and W. G. Schneider, *Can. J. Chem.*, **35**, 251 (1957).
30) R. Hoffmann, *Accounts Chem. Res.*, **4**, 1 (1971).
31) A. D. Baker, D. P. May, and D. W. Turner, *J. Chem. Soc., B*, **1968**, 22.
32) J. Petruska, *J. Chem. Phys.*, **34**, 1120 (1961).
33) R. J. Abraham, *ibid.*, **34**, 1062 (1961).

A New Synthesis of 3,6-Dialkyl-1,4-dimethyl-3,6-epithio- and -3,6-epidithio-2,5-piperazinediones

Juji YOSHIMURA, Hiroshi NAKAMURA, and Kenji MATSUNARI*

Laboratory of Chemistry for Natural Products, Faculty of Science, Tokyo Institute of Technology, Meguro-ku, Tokyo 152

(Received October 12, 1974)

A new route for synthesis of 3,6-dialkyl-1,4-dimethyl-3,6-epithio- (**8**) and -3,6-epidithio-2,5-piperazinediones (**9**) *via* the corresponding bromo derivatives was described. Bromination of 3,6-dialkyl-1,4-dimethyl-2,5-piperazinedione with *N*-bromosuccinimide gave 3,3α,6,6α-tetrabromo (**2**) and 3,6-dibromo (**3**) derivatives, depending upon the straight chain (methyl, ethyl, propyl, butyl) or α-branched (isopropyl, *sec*-butyl) alkyl groups, respectively. After tentative substitution of 3,6-bromine atoms of **2** with methanol, 3α,6α-bromine atoms were reduced to give the corresponding 3,6-dialkyl-3,6-dimethoxy derivatives (**5**). Substitution of **3** or **5** with hydrogen sulfide in the absence or presence of zinc chloride, and successive oxidation with potassium triiodide gave **8** and **9** at the same time. Discussions were made on the structure of isomers and on the reaction mechanisms.

3,6-Epidithio-2,5-piperazinedione skeleton is the unique partial structure of a class of antibiotics such as gliotoxin,[1] sporidesmin,[2] and others.[3,4] The simplest compound has been first synthesized through substitution of 3,6-dibromo-1,4-dimethyl-2,5-piperazinedione with sodium thioacetate or sodium tetrasulfide,[5] and the method was successfully applied only for 3,6-diphenyl derivative.[6] A few derivatives were synthesized through condensation of sulfur or sulfur chloride with the corresponding 3,6-dicarbanions obtained by treatment of parent 2,5-piperazinediones with sodium hydride[7] or sodium amide.[8] Recently, Kishi *et al.* synthesized dehydrogliotoxin and sporidesmin A by alkylation of similar carbanions of 3,6-dimercapto-2,5-piperazinediones whose mercapto groups were protected as thioacetal of anisaldehyde.[9] We have tried to extend the first method to 3,6-dialkyl derivatives. However, bromination of 1,3,4,6-tetramethyl-2,5-piperazinedione gave the 3,3α,6,6α-tetrabromo derivative, and substitution of its 3,6-bromine atoms with sulfur-containing nucleophiles gave only 3,6-dimethylene derivative and sulfur, in participation with 3α,6α-bromine atoms.[10] To exclude the participation, reductive removal of the 3α,6α-bromine atoms prior to the introduction of mercapto groups gave successful results. Thus, it was communicated that substitution of 3,6-bromine atoms of the tetrabromide with methanol, reduction of 3α,6α-bromine atoms, substitution of 3,6-methoxy groups with mercapto groups in the presence of zinc chloride,[11] and oxidation gave the corresponding 3,6-epithio and 3,6-epidithio derivatives.[12]

In this paper, this new synthesis is described in detail, together with discussions on the structure of related compounds and on reaction mechanism of the final step.

Results and Discussion

3,6-Dialkyl-1,4-dimethyl-2,5-piperazinediones and their bromination with N-*bromosuccinimide.* *N*-Methylation of 3,6-dialkyl-2,5-piperazinediones obtained by thermal dehydration of α-amino acids[13] with methyl iodide and sodium hydride, instead of silver oxide as a neutralizing reagent,[14] gave a *cis* and *trans* mixture of the corresponding 1,4-dimethyl derivatives (**1**) in over 80% yields. The ratios of isomers were determined by glc, and pure isomers were isolated by fractional crystallization from ether or ether–petroleum ether. As standards, *cis* isomers of **1a**, **1e** and **1f** were synthesized by *N*-methylation of optically active 3,6-dialkyl-2,5-piperazinediones with methyl iodide and silver oxide, and the glc data of the latter one and *cis*-**1g** were supported with that of Manger.[15] For examination of the relationship between the configuration and properties of isomers, physical constants of **1** were summarized in Table 1, in which an isomer having a shorter retention time was arranged at first.

Among the above four examples, **1a** showed an exceptional relationship between the configuration and retention time. However, the chemical shift of 3,6-hydrogens in *trans* isomer showed commonly larger δ value than that of *cis* isomer, as was pointed out for several derivatives in a previous paper.[10] Thus, the common observation was applied for the deduction of the configuration of isomers of **1b–d**. It was shown by X-ray analysis that *cis* and *trans* 3,6-disubstituted-2,5-piperazinedione have a skewed boat and a planar conformation, respectively.[16] If these conformations are maintained to some extent in a solution state, 3,6-hydrogens in *trans* isomer are sterically closer to the plane of vicinal carbonyl groups than those in *cis* isomer, and consequently show a more larger δ value.

The *cis* and *trans* mixture of **1** was used for the next bromination, because the 2,5-piperazinedione ring has a strong tendency to make carbonium cations in substitutions at 3,6-positions. Treatment of **1a** in carbon tetrachloride with four equimolar amount of *N*-bromosuccinimide (NBS) in the presence of 2,2′-azobisisobutyronitrile as an initiator gave the 3,3α,6,6α-tetrabromide (**2a**) in a much better yield (80%) than that with bromine (less than 20%).[10] When two equimolar amount of NBS was used, the corresponding 3,3α-dibromo derivative was produced, which was ascertained as 3-bromomethyl-3-methoxy derivative (**2a′**) by treatment with methanol. This fact indicates that the bromination at 3,6-positions takes place stepwise, and it is followed by elimination of hydrogen bromide addition of bromine produced from hydrogen bromide and NBS to give **2a**. Such successive reactions; *i.e.*,

* Present address: Central Research Laboratory of Kumiai Chemical Industry Co. Ltd., Shibukawa, Shimizu.

Table 1. Physical properties of 3,6-dialkyl-1,4-dimethyl-2,5-piperazinediones (**1**)

Compound		Yield[a] (%)	Mp (°C)	glc[b] Ratio	glc[b] Time	IR (cm^{-1}) amide	NMR (δ) NMe	NMR (δ) $H_{3,6}$	Molecular formula	Anals. (Calcd)[c] C%	H%	N%
a	*cis*	40	122—123	1	3.15	1640	2.94	3.89	$C_8H_{14}N_2O_2$	56.47	8.24	16.03
	trans	19	135—136	0.56	3.5	1630	2.94	3.95		(56.45	8.29	16.46)
b	*trans*[d]	52	126—127	1	3.5	1640	2.94	4.03	$C_{10}H_{18}N_2O_2$	60.72	9.13	14.07
	cis	13	73—74.5	0.5	4.4	1650	2.96	3.82		(60.58	9.15	14.13)
c	*trans*	49	105—106	1	7.75	1640	2.96	3.98	$C_{12}H_{22}N_2O_2$	63.78	9.88	12.46
	cis	20	83—85	0.86	9.5	1650	2.94	3.81		(63.68	9.80	12.38)
d	*trans*	52	131—133	1	10.9	1640	2.92	4.02	$C_{14}H_{26}N_2O_2$	66.55	10.25	11.15
	cis	2	49—50	0.75	13.0	1640	2.97	3.83		(66.10	10.30	11.01)
e	*trans*	48	96—97	1	10.0	1640	2.94	4.00	$C_{14}H_{26}N_2O_2$	66.07	10.46	10.95
	cis	22	114—116	0.85	10.9	1645	2.93	3.80		(66.10	10.30	11.01)
f	*trans*	25	151—153	1	5.5	1640	2.93	3.83	$C_{12}H_{22}N_2O_2$	63.69	9.65	12.35
	cis	36	133—134	1.4	7.3	1650	3.02	3.47		(63.68	9.80	12.38)
g	*trans*	44	122—124	1	10.0	1640	2.89	3.86[e] 3.91	$C_{14}H_{26}N_2O_2$	66.37	10.26	11.04
	cis	—	—	0.54	13.3	—	—	—		(66.10	10.30	11.01)

a) Actually separated yield. b) Silicone SE-52 on Chromosorb G-AW; 200 °C; N_2 flow rate, 60 ml/min; retention time in min. c) Analytical values before the fractional crystallization. d) Configurations in parentheses were deduced from NMR data. e) The appearance of two kinds of 3,6-proton signals also indicates the trans configuration. Such a magnetic environmental difference should be caused by the asymmetric 3,6-dialkyl groups only into *trans* **1g** derived from L-isoleucine, but not into *cis* **1g**.

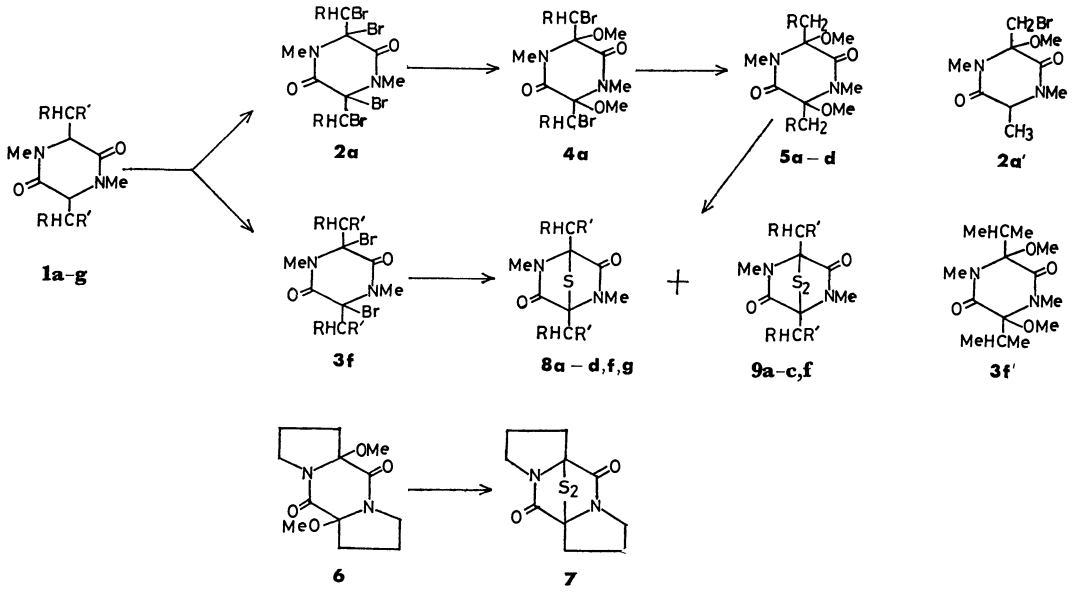

a: R=R'=H **b**: R=Me, R'=H **c**: R=Et, R'=H **d**: R=*n*-Pr, R'=H
e: R=*iso*-Pr, R'=H **f**: R=R'=Me **g**: R=Et, R'=Me

Fig. 1. The synthetic routes to **8** and **9**.

bromination, elimination and addition, were also observed in the bromination with bromine.[10]

In a similar way, **1b–d** having linear alkyl groups gave homologous 3,3α,6,6α-tetrabromides, whereas **1f** having α-branched alkyl groups gave the corresponding 3,6-dibromide (**3f**), which was proved by conversion into 3,6-diisopropyl-3,6-dimethoxy-1,4-dimethyl-2,5-piperazinedione (**3f'**) by treatment with methanol. This fact will be attributed to the steric hindrance to be arose in the corresponding elimination product.[17] Although **2b–d** and **3g** were not isolated, the above relation between the structure of 3,6-alkyl groups and the bromination product was confirmed by their conversions to be mentioned in the next item.

Conversion of Bromo Derivatives into 3,6-Epithio- and 3,6-Epidithio-2,5-Piperazinediones. To avoid the participation of 3α,6α-bromine atoms of **2** to the substitution of 3,6-bromine atoms with hydrogen sulfide,[10] the former were removed by hydrogenation after tentative conversion of the latter into methoxy groups, and then the methoxy groups were substituted with mercapto groups. Treatment of **2a** with methanol gave the 3,6-dimethoxy derivative (**4a**) in 86% yield, and hydrogenation of **4a** with tri-*n*-butyltin hydride

TABLE 2. 3,6-DIALKYL-1,4-DIMETHYL-3,6-EPITHIO- AND -3,6-EPIDITHIO-2,5-PIPERAZINEDIONES (**8** AND **9**)

Compd.	Yield[a] (%)	Mp. (°C)	Molecular formula	Anals. (Calcd) C%	H%	N%	S%	NMR (δ) NMe	IR (cm^{-1}) amide[b]
8a	72	63—65	$C_8H_{12}N_2O_2S$	47.82(47.98)	6.00(6.04)	13.91(13.99)	15.99(16.01)	2.81	1700
9a	18	145—146	$C_8H_{12}N_2O_2S_2$	41.67(41.36)	5.28(5.21)	12.45(12.06)	27.40(27.60)	3.05	1680
8b	20	76—78	$C_{10}H_{16}N_2O_2S$	52.78(52.61)	7.01(7.06)	12.02(12.27)	14.02(14.04)	2.77	1700
9b	56	110—111	$C_{10}H_{16}N_2O_2S_2$	46.25(46.13)	6.27(6.19)	10.50(10.76)	24.60(24.63)	3.05	1680
8c	27	96—98	$C_{12}H_{20}N_2O_2S$	56.48(56.22)	8.01(7.86)	10.68(10.93)	12.26(12.51)	2.76	1700
9c	17	sirup	$C_{12}H_{20}N_2O_2S_2$	50.22(49.97)	6.99(6.99)	9.72(9.71)	22.18(22.23)	3.05	1670
8d[c]	69	sirup	$C_{14}H_{24}N_2O_2S$	58.92(59.12)	8.25(8.51)	10.03(9.85)	11.10(11.27)	2.77	1710
8f	88	146—147	$C_{12}H_{20}N_2O_2S$	56.06(56.22)	7.91(7.86)	10.69(10.93)	12.41(12.51)	2.72	1700
9f	2	109—110	$C_{12}H_{20}N_2O_2S_2$	50.21(49.97)	6.84(6.99)	9.72(9.71)	22.20(22.23)	3.06	1680
8f	43	146—147	$C_{12}H_{20}N_2O_2S$	56.01(56.22)	7.93(7.86)	10.70(10.93)	12.30(12.51)	2.72	1700
9f	2.3	109—110	$C_{12}H_{20}N_2O_2S_2$	50.12(49.97)	6.90(6.99)	9.70(9.71)	22.15(22.23)	3.06	1680
8g[c]	19	89—90	$C_{14}H_{24}N_2O_2S$	59.18(59.12)	8.62(8.51)	9.87(9.85)	11.38(11.27)	2.70	1700

a) The first five runs (a—f) indicate yields from **6**, and the last two (f, g) from **1** *via* **3**. b) It is characteristic that the amide absorptions of **8** and **9** appeared broad and sharp, respectively. c) The corresponding **9** could not be obtained.

gave 1,3,4,6-tetramethyl-3,6-dimethoxy-2,5-piperazinedione (**5a**) quantitatively. In the case of **1b–d**, **5b–d** were synthesized by the successive reactions without isolation of **2b–d** and **4b–d**, because they include too many isomers and **2b–d** are unstable. The compound **5e** could not be separated in a pure state by the similar reactions of **1e**. By the same hydrogenation as above, 5a,10a-dimethoxyoctahydro-5*H*,10*H*-dipyrrolo-[1,2-*a* : 1′,2′-*d*]pyrazine-5,10-dione (**6**) was quantitatively obtained from the corresponding 1,6-dibromo-5a,10a-dimethoxy derivative.[10]

The most of **5**, **3f′** and **4a** were separated into two isomers, but, their configurations could not be determined. It seems likely that the configuration of 2,5-piperazinediones having two substituents at both 3,6-positions should be determined by X-ray analysis at the present stage.

For preparation of epidithio derivatives, **6** was treated with hydrogen sulfide in the presence of zinc chloride and then oxidized with potassium triiodide, according to the method of Schmidt *et al.*[11] which was applied to the corresponding 5a, 10a-dihydroxy derivative, to give desired epidithio derivative (**7**) in 78% yield. However, application of the same procedure to **5** gave a mixture of 3,6-epithio (**8**) and 3,6-epidithio-(**9**) derivatives. Moreover, the simple substitution of **3** with hydrogen sulfide and successive oxidation gave again a mixture of **8** and **9**. These mixtures were separated by preparative tlc, and physical constants of pure compounds were summarized in Table 2.

The remarkable difference in the reaction products from **6** and **3** or **5** will be attributed to the rigid planar conformation of **6**, which is caused by fused pyrrolidine rings. The ratios of **8** to **9** were not so much changed by the configuration of **5** (*cis* or *trans*) and also by reaction conditions (temperature and molar ratio of reagents). An attempted reaction of **3f′** with thioacetic acid in the presence of zinc chloride gave directly **8f** as a main product. Similar results were obtained in the conversion of **3f** into **8f** and **9f**. These facts indicate that the both conversions of **3** and **5** into **8** and **9** proceed by the S_N1 mechanism. The first substitution of **3** or **5** with thiol anion and the

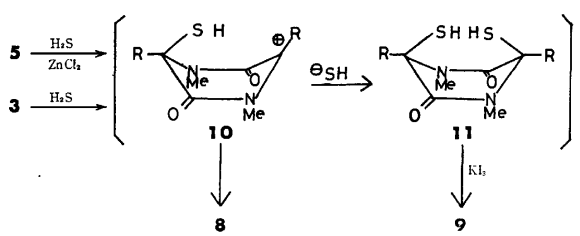

Fig. 2. The mechanism of the formation of **8** and **9**.

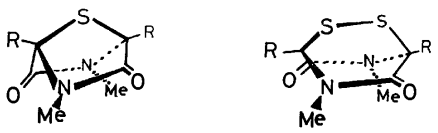

Fig. 3. The conformation of **8** and **9**.

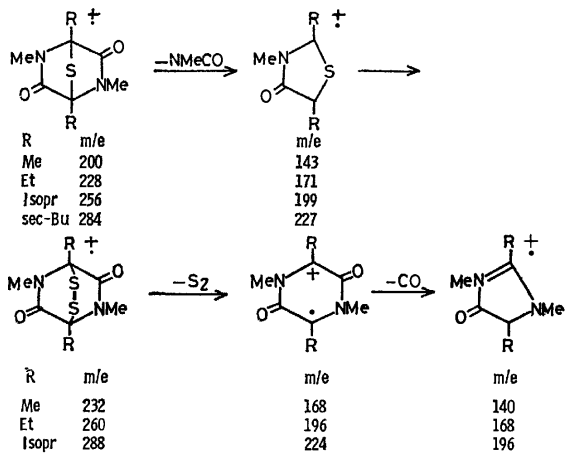

Fig. 4. The characteristic fragmentation of **8** and **9**.

formation of the second carbonium ion will give the key-intermediate (**10**), in which the intramolecular nucleophilic attack of sulfur atom to the carbonium ion affords **8**. While, an intermolecular attack of a thiol anion to **10** gives the corresponding dithiol (**11**), which is oxidized to **9** by potassium triiodide.

On the other hand, NMe proton signal of **8** in NMR spectra appeared generally in higher magnetic field than that of **9**. This fact indicates that the more strained conformation of **8** than **9** draws NMe groups into the diamagnetic field of the carbonyl group in the opposite side of the molecule sterically closer than that of **9**. The characteristic IR absorption of amido groups also clearly distinguishes **8** and **9** (Table 2). Moreover, mass fragmentations of **8** and **9** showed the most intense peaks of *m/e* (M–NMeCO) and *m/e* (M–2S), respectively, as the characteristic peaks.

Experimental

All melting points are uncorrected. The solutions were evaporated under reduced pressure at a bath temperature not exceeding 60 °C. The infrared spectra were measured in KBr discs with a Hitachi EPI-G2 spectrometer. The NMR spectra were obtained at 100 MHz with a JEOL JNM-100H spectrometer in deuteriochloroform, using TMS as an internal reference. Specific rotations were measured in a 0.5-dm tube with a Carl Zeiss LEP-Al polarimeter. The mass spectra were obtained on a JEOL JNS-OLS mass spectrometer, using a direct inlet and an ionization energy of 70 eV. Chemical shifts and coupling constants were recorded in δ and Hz units, and IR frequencies in cm^{-1}.

*3,6-Dialkyl-1,4-dimethyl-2,5-piperazinediones (**1a–g**).* To a suspension of 3,6-dialkyl-2,5-piperazinedione (0.11 mol) in dried DMF (200 ml) was added sodium hydride (10.5 g, 50% in oil, 0.22 mol) portionwise during 30 min under a violent stirring. After the evolution of hydrogen gas subsided, methyl iodide (0.25 mol) was added dropwise to the solution with stirring under ice-cooling, and the reaction mixture was kept at room temperature for 30 min, and then evaporated. The residue in water (200 ml) was extracted with carbon tetrachloride (2×100 ml), and the chloroform layer was dried over sodium sulfate, and evaporated to give **1** quantitatively, which were fractionally recrystallized from ether (**1a-b**) or ether-petroleum ether (**1c–g**) (Table 1).

*Optically Active 3,6-Dialkyl-1,4-dimethyl-2,5-piperazine-diones (**1a, 1e** and **1f**).* Optically active 3,6-dimethyl-, 3,6-diisobutyl- and 3,6-diisopropyl-2,5-piperazinediones were methylated in DMF (*ca* 100 part) with methyl iodide (60 equivalent) and silver oxide (20 part), according to the reported method,[14] to give *N*-methyl derivatives in 2%, 10% and 50% yields, respectively. The low yield of **1a** will be attributed to the insolubility of the starting material, but the reaction does not proceeded in HMPA. These compounds gave correct analytical values, and spectral (IR and NMR) and glc data were consistent with those of *cis* isomers in Table 1.

1a: mp 120 °C, $[\alpha]_D^{22}$ +56.99° (*c* 0.55, $CHCl_3$); **1e**: mp 110 °C, $[\alpha]_D^{22}$ +48.81° (*c* 1.0, $CHCl_3$): **1f**: mp 104—105 °C, $[\alpha]_D^{22}$ −33.31° (*c* 1.0, $CHCl_3$).

*3,6-Dibromo-3,6-bis(bromomethyl)-1,4-dimethyl-2,5-piperazinedione (**2a**).* A solution of **1a** (1 g, 5.9 mmol), NBS (4 g, 24 mmol) and 2,2′-azobisisobutyronitrile (10 mg) in carbon tetrachloride was refluxed until NBS has dissolved, and succinimide deposited was filtered and washed with chloroform (50 ml). The filtrate and washings were evaporated to give white powder, which was triturated with a small amount of ethanol and filtered. Yield, 2.4 g (82%), mp 186—188 °C (lit, [10] 185—188 °C, 18%).

*3-Bromomethyl-3-methoxy-1,4,6-trimethyl-2,5-piperazinedione (**2a′**).* A solution of **1a** (300 mg, 1.765 mmol), NBS (628 mg, 3.53 mmol) and 2,2′-azobisisobutyronitrile (10 mg) in carbon tetrachloride (50 ml) was refluxed for 20 min, and succinimide deposited was filtered and washed with chloroform (20 ml). The filtrate and washings were evaporated, and then a solution of the residue and sodium acetate (1 g, 12.2 mmol) in methanol (50 ml) was refluxed for 2 hr, evaporated, and the residue was extracted with chloroform. The extract was washed with water, dried, and evaporated to give a mixture of **1a**, **2a** and **2a′**, which were separated on a preparative tlc. **2a** and **2a′** were obtained in 24% (165 mg) and 22% (110 mg) yield, respectively. **2a′**: mp 88 °C, IR: 1660 (amide), NMR: 1.59 (CMe; d, J_{vic}=6.5), 2.90 and 3.04 (NMe), 4.01 and 3.53 (CH_2Br; ABq, J_{gem}=10.8).

Found: C, 38.61; H, 5.28; N, 10.01; Br, 28.90%. Calcd for $C_9H_{15}N_2O_3Br$: C, 38.72; H, 5.42; N, 10.03; Br, 28.62%.

*3,6-Diisopropyl-1,4-dimethyl-3,6-dimethoxy-2,5-piperazinedione (**3f′**).* A solution of **1f** (0.5 g, 2.2 mmol), NBS (800 mg, 4.5 mmol) in carbon tetrachloride (30 ml) was treated as above to give a sirupy **3f**, which was then treated with methanol and sodium acetate in a similar manner using benzene as extracting solvent. The sirupy product was crystallized and recrystallized from petroleum ether to give a mixture of isomers (270 mg, 43%) which was separated on a silica gel column using benzene – ethyl acetate (20 : 1) as an eluent.

A: mp 113—115 °C, IR: 1660 (amide), NMR: 0.79 and 1.14 (CMe; d, J_{vic}=7.0), 2.33 (CH; sep), 2.94 (NMe), 3.09 (OMe).

B: mp 193—194 °C, IR: 1660 (amide), NMR: 0.88 and 1.08 (CMe; d, J_{vic}=7.0), 2.27 (CH; sep), 2.87 (NMe), 3.17 (OMe).

Found (A): C, 58.47; H, 9.35; N, 9.67%. (B): C, 58.50; H, 9.31; N, 9.66%. Calcd for $C_{14}H_{26}N_2O_4$: C, 58.72; H, 9.15; N, 9.78%.

*3,6-Bis(bromomethyl)-1,4-dimethyl-3,6-dimethoxy-2,5-piperazinedione (**4a**).* A solution of **2a** (1 g, 2.1 mmol) and sodium acetate (1 g, 12 mmol) in methanol (50 ml) was stirred at room temperature for 10 hr, evaporated, and the residue was extracted with chloroform. The extract was washed with water three times, dried, and evaporated to give crystals (700 mg, 86%) which were recrystallized from chloroform-ligroin. Analytical values of the crystals were consistent with theoreticals, but which were fractionally crystallized into two isomers. A: mp 160 °C (decomp.), IR: 1670 (amide), NMR: 3.01 (OMe), 3.35 (OMe), 3.54 and 4.12 (CH_2Br; ABq, J_{gem}=11.0). B: mp 198—200 °C (sublime), IR: 1670 (amide), NMR: 308 (NMe), 3.28 (OMe), 3.60 and 4.18 (CH_2Br; ABq, J_{gem}=11.3).

Found: C, 31.30; H, 3.91; N, 7.16%. Calcd for $C_{10}H_{16}N_2O_4Br_2$: C, 30.95; H, 4.16; N, 7.22%.

*3,6-Dimethoxy-1,3,4,6-tetramethyl-2,5-piperazinedione (**5a**).* A solution of **4a** (300 mg, 0.77 mmol), tri-*n*-butyltin hydride (465 mg, 1.6 mmol) and 2,2′-azobisisobutyronitrile (5 mg) in toluene (50 ml) was heated at 70 °C for 1 hr under nitrogen atmosphere, and evaporated to give a half-crystalline mass which was triturated with ligroin and filtered. The crystals (180 mg, quantitative) obtained were recrystallized from ether. Analytical values of the crystals were consistent with theoreticals, but which were separated into two isomers by a preparative tlc. A: mp 130 °C (sublime), IR: 1670

(amide), NMR: 1.58 (CMe), 2.98 (NMe), 3.12 (OMe). B: 201—202 °C, IR: 1670 (amide), NMR: 1.69 (CMe), 2.98 (NMe), 3.07 (OMe).

Found: C, 51.70; H, 7.88; N, 12.08%. Calcd for $C_{10}H_{18}N_2O_4$: C, 52.16; H, 7.88; N, 12.17%.

*3,6-Dialkyl-1,4-dimethyl-3,6-dimethoxy-2,5-piperazinedione (**5b–d**).* The compounds **1b–d** (500 mg) were brominated with NBS (4 equivalent) and then methylated, in the same manner as **2a** and **4a**, to give sirupy products (**4b**: 850 mg, **4c**: 830 mg, **4d**: 930 mg, respectively). These sirups were reduced with tri-*n*-butyltin hydride (2.1 equivalent) in the same manner as above to give products (**5b**: 470 mg, 72%, **5c**: 210 mg, 34%, **5d**: 280 mg, 47%, respectively), which were separated into two isomers on a silicagel column using benzene-ethyl acetate (15 : 1) as an eluent.

5b: mp 165—167 °C, IR: 1660 (amide), NMR: 0.83 (CMe; t, J_{vic}=7.2), 1.82 and 2.29 (CH_2; each sex, J_{gem}= 14.5), 2.95 (NMe), 3.16 (OMe).

Found: C, 55.84; H, 8.48; N, 10.97%. Calcd for $C_{12}H_{22}N_2O_4$: C, 55.78; H, 8.58; N, 10.85%.

5c: A: mp 82—83 °C, IR: 1665 (amide), B: mp 110 °C, IR: 1660 (amide). NMR: 0.91 (CMe; t, J_{vic}= 6.5), 0.7—2.45 (CH_2: broad m), 2.94 (NMe), 3.14 (OMe).

Found (A): C, 59.02; H, 8.84; N, 10.01%. (B): C, 59.00; H, 8.90; N, 9.98%. Calcd for $C_{14}H_{26}N_2O_4$: C, 58.72; H, 9.15; N, 9.78%.

5d: A: mp 85—86 °C, IR: 1655 (amide), B: sirup, IR: 1670 (amide). NMR: 0.7–2.5 (CMe and CH_2; broad m), 2.94 (NMe), 3.16 (OMe).

Found (A): C, 60.82; H, 9.46; N, 8.84%. (B): C, 60.65; H, 9.29; H, 8.54%. Calcd for $C_{16}H_{30}N_2O_4$: C, 61.12; H, 9.62; N, 8.91%.

Isomers of **5c** and **5d** could notbe distinguished by NMR spectra.

*5a,10a-Dimethoxyoctahydro-5H,10H-dipyrrolo[1,2-a : 1′,2′-d]pyradine-5,10-dione (**6**).* 1,6-Dibromo-5a,10a-dimethoxyoctahydro-5*H*,10*H*- dipyrrolo[1,2-*a*: 1′2′-*d*]pyridine- 5,10-dione[10] (300 mg, 0.73 mmol) was hydrogenated with tri-*n*-butyltin hydride in the same manner as **5a** to give crystals (185 mg, 99%) which were recrystallized from petroleum ether. Mp 185 °C. IR: 1660 (amide).

Found: C, 56.32; H, 7.11; N, 11.00%. Calcd for $C_{12}H_{18}N_2O_4$: C, 56.68; H, 7.14; N, 11.02%.

*Tetrahydro-6H,10H-5a,10a-epidithio-1H,5H-dipyrrolo[1,2-a : 1′,2′-d]pyradine-5,10-dione (**7**).* To a suspension of **6** (100 mg, 39.3 mmol) in chloroform (30 ml, saturated with hydrogen sulfide) was added zinc chloride (10 mg) and passed dried hydrogen sulfide for 3 hr, and then evaporated. The residue was extracted with chloroform, and the extract was washed with water and shaked with potassium triiodide solution until the chloroform layer colored with iodine. The colored solution was washed successively with sodium thiosulfate and water, dried, and then evaporated to give crystals which were recrystallized from ether. Yield, 78.5 mg (78%), mp 135—136 °C (lit,[11] 135—136 °C), IR: 1680 (amide).

Found: C, 46.55; H, 4.56; N, 10.98%. Calcd for $C_{10}H_{12}N_2O_2S_2$: C, 46.88; H, 4.72; N, 10.93%.

*General Procedure for Preparation of 3,6-Dialkyl-1,4-dimethyl-3,6-epithio- (**8**) and -3,6-epidithio-2,5-piperazinedione (**9**).* i) From 3,6-dialkyl-3,6-dimethoxy derivatives (**8a–d,f** and **9a–d,f**). Compounds **5a–d** and **3f′** were treated in a similar manner as above to give crude products, which were purified and separated into **8** and **9** on a silica gel column (WAKOGEL C–200) using benzene-ethyl acetate (20 : 1) as an eluent.

ii) From **1f,g** *via* the corresponding 3,6-dialkyl-3,6-dibromide (**8f,g** and **9f,g**). Compounds **1f** and **1g** were brominated with NBS (2 equivalent) in the same manner as described in **3f′**. Hydrogen sulfide was passed into a solution of the resulting dibromide in chloroform for 3 hr in the absence of zinc chloride, and the reaction mixture was treated as above to give **8f,g** and **9f,g**.

The yields and their physical constants were summarized in Table 2.

The authors are indebted to the members of the Laboratory of Organic Analysis for microanalyses, to Mr. H. Matsumoto for NMR measurements, and to the members of Analytical center of Kitasato University for mass spectral measurements.

References

1) M. R. Bell, J. R. Johnson, B. S. Wildi, and R. B. Woodward, *J. Amer. Chem. Soc.*, **80**, 1001 (1958).
2) S. Safe and A. Taylor, *J. Chem. Soc., C*, **1970**, 432.
3) R. Nagarajan, L. L. Huckstep, D. H. Lively, D. C. Delong, M. H. Marsh, and N. Neuss, *J. Amer. Chem. Soc.*, **90**, 2980 (1968).
4) D. Hauser, H. P. Weber, and H. P. Sigg, *Helv. Chim. Acta*, **53**, 1061 (1970); F. A. Anet and J. M. Muchowski, *Chem. Ind.*, **1963**, 81.
5) P. W. Trown, *Biochem. Biophys. Res. Commun.*, **33**, 402 (1968); H. Poisel and U. Schmidt, *Chem. Ber.*, **104**, 1714 (1971).
6) S. G. Svoks and R. B. Angier, Ger., 2029305 (1971).
7) T. Hino and T. Sato, *Tetrahedron Lett.*, **1971**, 3127.
8) E. Öhler, H. Poisel, F. Tataruch, and U. Schmidt, *Chem. Ber.*, **105**, 635 (1972).
9) Y. Kishi, T. Fukuyama, and S. Nakatsuka, *J. Amer. Chem. Soc.*, **95**, 6490, 6492, 6493 (1973).
10) J. Yoshimura, Y. Sugiyama, and H. Nakamura, This Bulletin, **46**, 2850 (1972).
11) H. Poisel and U. Schmidt, *Chem. Ber.*, **106**, 165 (1973).
12) J. Yoshimura, H. Nakamura, K. Matsunari, and Y. Sugiyama, *Chem. Lett.*, **1974**, 559.
13) C. Sannie, *Bull. Soc. Chim. Fr.*, **1942**, 487.
14) B. C. Das, S. D. Gero, and E. Lederer, *Biochem. Biophys. Res. Commun.*, **29**, 211 (1967).
15) A. B. Manger, *J. Chromatogr.*, **37**, 315 (1968).
16) E. Sletten, *J. Amer. Chem. Soc.*, **92**, 172 (1970).
17) C. Shin, K. Sato, A. Ohtsuka, K. Mikami, and J. Yoshimura, This Bulletin, **46**, 3876 (1973); K. W. Blake and P. G. Sammes, *J. Chem. Soc., C*, **1970**, 980; A. E. A. Porter and P. G. Sammes, *ibid.*, **1970**, 2530.

Aminosugars. XXIII. L-Idofuranose Derivatives Containing a Heterocycle at *C*-5,6 Position[1]

Masaharu IWAKAWA and Juji YOSHIMURA

Laboratory of Chemistry for Natural Products, Faculty of Science, Tokyo Institute of Technology, Meguro-ku, Tokyo 152

(Received October 12, 1974)

2-Aryl-(5*S*)- and -(4*S*)-(3′-*O*-benzyl- and 3′-*O*-methyl-1′,2′-*O*-isopropylidene-α-D-xylo-tetrofuranos-4′-yl)-2-oxazolines (**3** and **7**) were prepared from 6-aroylamido-6-deoxy-5-*O*-tosyl-D-glucofuranose and 5,6-aroylepimino-5,6-dideoxy-L-idofuranose derivatives, respectively. The corresponding 2-thioxo-(4*R*)- and -(5*S*)-thiazolidine derivatives (**11** and **13**) were also synthesized from 5,6-dideoxy-5,6-epimino-L-idofuranose and 6-azido-6-deoxy 5-*O*-tosyl-D-glucofuranose derivatives, respectively. 2-S-Methylated derivatives of **11** and **13** were reduced with aluminum amalgam to give the corresponding (4*R*)- and (5*S*)-thiazolidine derivatives, respectively. Formation of an intramolecular hemiaminal ring in **11** gave a new type of bicyclic derivatives; (5*S*,6*R*,8*R*)-triacetoxy-(7*S*)-substituted-2-thioxo-(8a*R*)-perhydropyrido[1,2-*c*]thiazole (**16a** and **16b**). The structure of new compounds was examined by NMR spectroscopy.

Although carbohydrate derivatives having fused heterocyclic rings at *C*-1,2 or *C*-2,3 position have been extensively studied,[2] those having a heterocycle at *C*-5,6 position have been scarcely reported, excepting oxazoline,[3,4] isoxazoline,[5] aziridine,[6,7] and triazole derivatives.[8] We have recently communicated syntheses of some isomeric pairs of L-idofuranose derivatives having 2-oxazoline or 2-thioxo-thiazolidine ring at *C*-5,6 position.[9] In this paper, syntheses of these derivatives which can be considered as a kind of reversed *C*-glycoside[5] will be reported in detail.

Results and Discussion

2-Phenyl-(5*S*)-(1′,2′-*O*-isopropylidene-α-D-xylo-tetrofuranos-4′-yl)-2-oxazoline was already synthesized in 50% yield by treatment of 6-benzamido-6-deoxy-5-*O*-tosyl-1,2-*O*-isopropylidene-α-D-glucofuranose with excess sodium acetate in 96% ethanol.[3] Similar treatment of the corresponding 3-*O*-benzyl derivative (**1a**) gave the corresponding oxazoline derivative (**3a**) in 52% yield, together with the corresponding hydrolyzed product; 6-benzamido-3-*O*-benzyl-6-deoxy-1,2-*O*-isopropylidene-β-L-idofuranose (**4a**) in 19% yield. In general, **3** and **4** would be formed by deprotonation or hydrolysis of intermediate carbonium cation (**2**), respectively.[10] To avoid the hydrolysis process the above conversion was tried in an anhydrous condition. When the solution of **1a** and anhydrous sodium acetate in absolute dimethylformamide was refluxed overnight, only **3a** was obtained in 87% yield. In the same manner, the corresponding 2-anisyl derivative (**3b**), and 2-phenyl-(5*S*)-(1′,2′-*O*-isopropylidene-3′-*O*-methyl-α-D-xylo-tetrofuranos-4′-yl)-2-oxazoline (**3c**) were also prepared in good yields from the corresponding 6-aroylamido-6-deoxy derivatives, without isolation of **1b** and **1c**. The compound **1c** was prepared from 1,2-*O*-isopropylidene-3-*O*-methyl-6-*O*-tosyl-α-D-glucofuranose[11] through the corresponding 6-azido, 6-amino, and 6-benzamido derivatives successively.

Moreover, isomeric (4*S*)-2-oxazolines (**7**) were prepared by the isomerization of the corresponding 5,6-aroylepimino derivatives by treatment with sodium iodide in acetone.[12] 3-*O*-Benzyl-5,6-dideoxy-5,6-epimino-1,2-*O*-isopropylidene-β-L-idofuranose (**5**),[7] which was prepared by an improved method, was treated

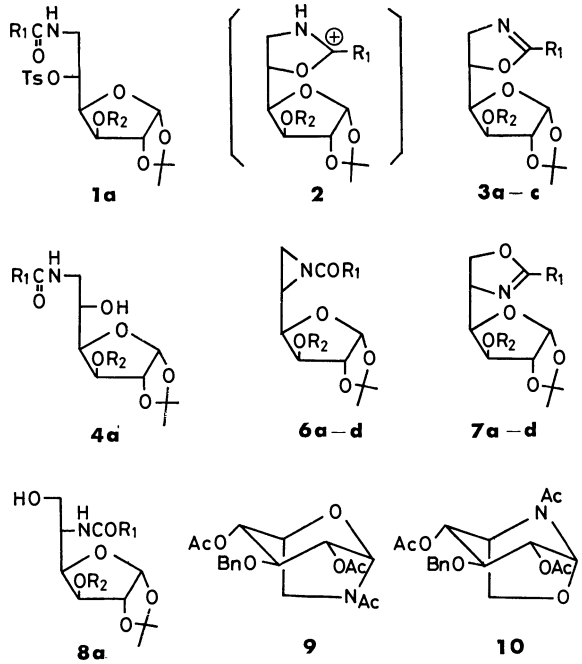

a: R_1=phenyl, R_2=benzyl
b: R_1=anisyl, R_2=benzyl
c: R_1=phenyl, R_2=methyl
d: R_1=*p*-nitrophenyl, R_2=benzyl

with equimolar amount of aroyl chloride in absolute benzene in the presence of excess triethylamine to give the 5,6-aroylepimino derivatives (**6a**,**b**,**d**) in good yields. The corresponding 3-*O*-methyl derivative (**6c**) was prepared in the same procedure, in which the 5,6-epimino derivative was obtained from the corresponding 6-azido-6-deoxy-5-*O*-tosyl or -5-*O*-mesyl derivative. Refluxing of a solution of **6** and excess amount of sodium iodide in absolute acetone overnight, followed by purification of the product by preparative tlc or by recrystallization gave the corresponding 2-aryl-(4*S*)-(3′-*O*-substituted-1′,2′-*O*-isopropylidene-α-D-xylo-tetrofuranos-4′-yl)-2-oxazolines (**7a**—**d**) in 40—96% yields. Physical constants of **6** and **7** are summarized in Table 1.

Because these oxazoline rings in **3** and **7** are labile to acid, both **3a** and **7a** were easily hydrolyzed to the corresponding benzamido derivatives (**4a** and **8a**) in

Table 1. Physical constants of compounds **6** and **7**

Compound	Mp (°C)	Yield (%)	$[\alpha]_D^{20}$ $CHCl_3$	Molecular formula	Anals. (Calcd) C%	H%	N%	IR[a] (cm^{-1})
6a	97—98	90	−67.4°	$C_{23}H_{25}NO_5$	69.94(69.85)	6.38(6.37)	3.48(3.54)	1670
6b	sirup	91	−55.3°	$C_{24}H_{27}NO_6$	67.98(67.75)	6.37(6.40)	3.20(3.29)	1660
6c	118—119	13	−90.3°	$C_{17}H_{21}NO_5$	64.26(63.93)	6.75(6.63)	4.50(4.39)	1670
6d	123—124	99	−51.8°	$C_{23}H_{24}N_2O_7$	62.89(62.72)	5.55(5.49)	6.27(6.36)	1670
7a	sirup	86	−44.3°	$C_{23}H_{25}NO_5$	69.31(69.85)	6.41(6.37)	3.38(3.54)	1640
7b	sirup	86	−51.0°	$C_{24}H_{27}NO_6$	67.85(67.75)	6.59(6.40)	3.19(3.29)	1640
7c	sirup	40	+1.3°	$C_{17}H_{21}NO_5$	64.21(63.93)	6.49(6.63)	4.15(4.39)	1640
7d	193—194	96	−50.3°	$C_{23}H_{24}N_2O_7$	62.74(62.72)	5.50(5.49)	6.41(6.36)	1640

a) The characteristic absorptions of **6** and **7** indicate that of the amide and C=N bond, respectively.

48% and 88% yields, respectively, by treatment with 80% acetic acid for two days at 30—40 °C. Conversion of **4a** into the corresponding bicyclic *N,O*-acetal (**9**)[13] was easily performed by successive de-*N*-benzoylation, de-isopropylidenation, and *N,O*-acetylation. To avoid the conversion into the corresponding pyridine derivatives,[13] *N*-benzoyl group of **8a** was previously converted into *N*-acetyl group, and successive de-isopropylidenation and *O*-acetylation gave successfully the desired *N,O*-acetal (**10**).

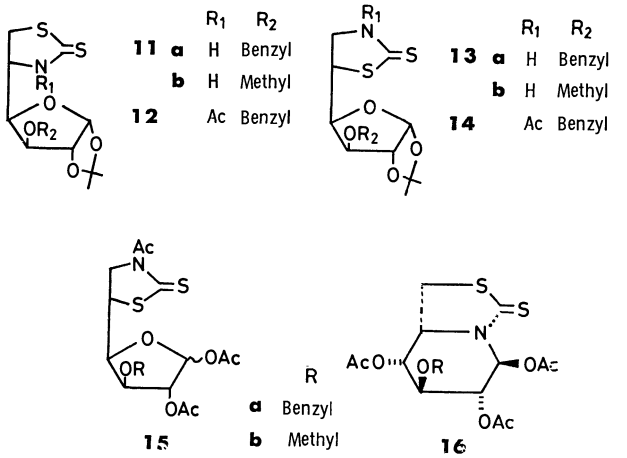

On the other hand, aziridines are known to give 2-thioxo-thiazolidines by treatment with carbon disulfide.[14] Thus, **5** was treated with carbon disulfide in a sealed tube at 98 °C for 6 hr to give crystalline 2-thioxo-(4*R*)-(3′-*O*-benzyl-1′,2′-*O*-isopropylidene-α-D-xylo-tetrofuranos-4′-yl)-thiazolidine (**11a**) in 84% yield. Crystalline 3′-*O*-methyl derivative (**11b**) was analogously obtained in 40% yield. Presence of characteristic absorptions at 3260 cm^{-1} (NH) and at 1470 cm^{-1} (NC=S) in IR spectrum supported the formation of 2-thioxo-thiazolidine ring. The structure was also confirmed by the comparison of the NMR spectrum of **11a** with that of *N*-acetylated derivative (**12**). *N*-Acetylation of **11a** caused a remarkable lower shift (1.43 ppm) of H_4 and a higher shift (0.68 ppm) of one of H_5-proton signals (*cf.* Table 2), depending on the acetylation shift[15] and the anisotropic effect of *N*-acetyl group, respectively. For the preparation of isomeric 2-thioxo-(5*S*)-thiazolidine derivatives, the synthetic procedure from a sulfate of β-aminoalcohols and carbon disulfide[16,17] was modified. Refluxing of a solution of 6-amino-3-*O*-benzyl-6-deoxy-5-*O*-tosyl-1,2-*O*-isopropylidene-α-D-glucofuranose,[7] large excess carbon disulfide, and two equimolar potassium hydroxide in ethanol for 2.5 hr gave 2-thioxo-(5*S*)-(3′-*O*-benzyl-1′,2′-*O*-isopropylidene-α-D-xylo-tetrofuranos-4′-yl)-thiazolidine (**13a**) in 98% yield. The corresponding 3′-*O*-methyl derivative (**13b**) was also obtained in 89% yield. Although the acetylation effect could not be clearly observed in the NMR spectrum of the corresponding *N*-acetate (**14**), IR spectrum and elemental analyses supported the structure of **13**. NMR parameters of typical examples of *L*-idofuranose derivatives having a heterocycle at *C*-5,6 position shown in Table 2 indicate that both the heterocyclic ring and the twist furanose ($^3T_2$) ring are generally in the *trans*-conformation with regard to the C_4–C_5 bond axis of the sugar chain, as was deduced in the isoxazoline derivatives.[5]

Hydrolysis of the isopropylidene group of **13** with 70% acetic acid at 90 °C for 5 hr and successive acetylation of the product gave a yellow sirup (**15**). Presence of one *N*-acetyl and two *O*-acetyl groups in NMR spectra, and an amide (1690 cm^{-1}) and an ester (1750 cm^{-1}) absorptions in IR spectra indicated the structure to be 3-*N*-acetyl-2-thioxo-(5*S*)-(1′,2′-di-*O*-acetyl-3′-*O*-benzyl- and -3′-*O*-methyl-α,β-D-xylo-tetrofuranos-4′-yl)-thiazolidine (**15a** and **15b**), respectively. While, analogous conversions of **11a** and **11b** gave crystalline and sirupy products (**16a** and **16b**), respectively, which showed no absorption of an amide. Chemical shifts and coupling constants in NMR spectrum of **16a** (Table 3) indicated that the conformation of the sugar moiety of these compounds is entirely different from those of ordinary D-xylofuranoses (Table 2). Since many long range couplings caused by the W-letter rule[18] were observed, ring protons; H_1, H_2, H_3, and H_4 should be in equatorial position (1*C* conformation of a pyranose ring). The values of $J_{1,4}$, $J_{1,3}$, and $J_{2,4}$ (0.5, 1.5, and 1.0 Hz) were consistent with the values of $J_{1,4}$ and $J_{1,3}$ (0.7 and 1.3 Hz) in the α-gulopyranose pentaacetate system reported by Lemieux.[19] Remarkable lower chemical shift of H_1 will be attributed to the large anisotropic effect of thiocarbonyl group of 2-thioxo-thiazolidine ring.[20] Thus **16a** and **16b** were determined to be a new class of bicyclic sugar derivatives; (5*S*,6*R*,8*R*)-triacetoxy-(7*S*)-benzyloxy- and -(7*S*)-

Table 2. NMR parameters of some L-idofuranose derivatives having a heterocycle at C-5,6 position

Compound	H_1	H_2	H_3	H_4	H_5	H_6	$H_{6'}$[a]
3a	6.06(d)	4.64(d)	4.00(d)	4.30(q)	4.90(m)	4.00(q)	3.51(q)
	$J_{1,2}=3.75$		$J_{3,4}=3.75$	$J_{4,5}=8.5$	$J_{5,6}=10.0$	$J_{5,6'}=8.75$	$J_{6,6'}=15.0$
3c	6.02(d)	4.60(d)	3.79(d)	4.32(q)	4.90(m)	4.20(q)	3.25(q)
	$J_{1,2}=3.75$		$J_{3,4}=3.75$	$J_{4,5}=8.75$	$J_{5,6}=10.0$	$J_{5,6'}=8.75$	$J_{6,6'}=15.0$
4c	6.05(d)	4.16(d)	3.95(d)	4.25(q)	4.73(q)	4.38(t)	4.15(t)
	$J_{1,2}=3.75$		$J_{3,4}=3.75$	$J_{4,5}=8.5$	$J_{5,6}=J_{5,6'}=J_{6,6'}=8.75$		
11a	5.97(d)	4.65(d)	3.96(d)	4.22(q)	4.40(m)	3.30(q)	3.18(q)
	$J_{1,2}=3.75$		$J_{3,4}=3.75$	$J_{4,5}=6.25$	$J_{5,6}=8.75$	$J_{5,6'}=7.5$	$J_{6,6'}=11.3$
12	5.95(d)	4.65(d)	3.96(d)	4.62(q)	5.83(q)	3.36(q)	2.50(d)
	$J_{1,2}=3.75$		$J_{3,4}=3.75$	$J_{4,5}=9.5$	$J_{5,6}=8.0$	$J_{5,6'}=0$	$J_{6,6'}=12.0$
17	6.01(d)	4.64(d)	3.94(d)	4.30(q)	4.73(q)	3.27(q)	3.05(q)
	$J_{1,2}=4.0$		$J_{3,4}=3.8$	$J_{4,5}=J_{5,6}=J_{5,6'}=9.5$			$J_{6,6'}=10.5$

a) The numbering of hydrogens indicates that of the carbon chain of L-idose.

Table 3. NMR parameters of compounds **16a** and **16b**

Compound	H_1	H_2	H_3	H_4	H_5	H_6	$H_{6'}$[a]
16a	7.09(m)	5.27(m)	3.90(m)	5.13(m)	4.92(sex)	3.35(q)	3.28(q)
	$J_{1,2}=2.0$	$J_{2,3}=3.0$	$J_{3,4}=3.0$	$J_{4,5}=2.5$	$J_{5,6}=9.0$	$J_{6,6'}=11.0$	
	$J_{1,3}=1.5$	$J_{2,4}=1.0$			$J_{5,6'}=9.0$		
	$J_{1,4}=0.5$						
16b	7.08(m)	5.20(m)	3.13(m)	5.18(m)	4.85(m)		ca. 3.3(m)

a) The numbering of hydrogens indicates that of the carbon chain of L-idose.

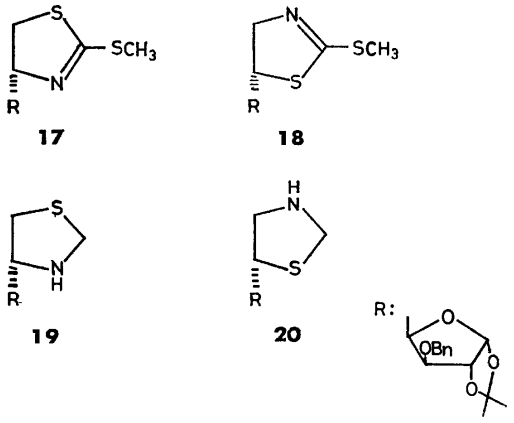

methoxy-3-thioxo-(8a*R*)-perhydropyrido[1,2-*c*]thiazole, respectively.

Conversion of **11a** and **13a** into the corresponding 2-methylthio-2-thiazoline derivatives (**17** and **18**) was easily performed by successive treatment with equimolar sodium hydride and slight excess methyl iodide under the nitrogen atmosphere. Furthermore, reduction of **17** and **18** with aluminum amalgam[21] gave the corresponding thiazolidine derivatives (**19** and **20**) in good yields.

Because of unexpectedly stable character of heterocycles in **17**—**20**, a few attempts to synthesize *S,N*-analogues of **9** and **10** gave negative results, and it is still under investigation.

Experimental

All melting points were determined with Yanaco micro melting point apparatus and not corrected. The solutions were evaporated under reduced pressure at a bath temperature not exceeding 45 °C. Optical rotations were measured in a 0.5-dm tube with a Carl Zeiss LEP-A1 Polarimeter, using chloroform as a solvent unless otherwise stated. IR spectra were recorded with a Hitachi Model EPI-GS grating spectrometer. NMR spectra were taken with JEOL 4H-100 spectrometer in deuteriochloroform containing tetramethylsilane as an internal reference. Chemical shifts and coupling constants were recorded in δ and Hz units, and IR frequencies in cm^{-1}.

*6-Benzamido-3-O-benzyl-6-deoxy-1,2-O-isopropylidene-5-O-p-toluenesulfonyl-α-D-glucofuranose (**1a**).* Benzoylation of 6-amino-3-*O*-benzyl-6-deoxy-1,2-*O*-isopropylidene-α-D-glucofuranose[7] in methanol with benzoic anhydride gave the corresponding 6-benzamide which was recrystallized from ethanol-*n*-hexane. Yield, 92%, mp 94—95.5 °C, $[\alpha]_D^{22}$ −22.5° (*c* 0.89), IR: 3400 (NH and OH), 1640 and 1520 (amide).

Found: C, 66.38; H, 6.53; N, 3.34%. Calcd for $C_{23}H_{27}NO_6$: C, 66.81; H, 6.58; N, 3.39%.

A solution of 6-benzamide (0.84 g) and *p*-toluenesulfonyl chloride (0.47 g) in pyridine(4 ml) was kept for two days at room temperature, poured into ice-water, and a sirup deposited was extracted with chloroform. Treatment of the extract in a usual manner gave a sirupy product which was purified with a silica gel column, using benzene–ethyl acetate (4 : 1) as an eluent. Yield, 0.96 g (83%), $[\alpha]_D^{22}$ −35.2° (*c* 0.95), IR: 3350 (NH), 1640 and 1520 (amide), 1360 (sulfate).

Found: C, 64.04; H, 5.97; N, 2.23%. Calcd for $C_{30}H_{33}NO_8S$: C, 63.48; H, 5.86; N, 2.47%.

*2-Aroyl-(5S)-(3'-O-benzyl-1',2'-O-isopropylidene-α-D-xylo-tetrofuranos-4'-yl)-2-oxazoline (**3**). i) 2-Phenyl Derivative (**3a**).* (a) A solution of **1a** (220 mg) and anhydrous sodium acetate (200 mg) in 96% ethanol (10 ml) was refluxed for 20 hr, and evaporated. The residue was extracted with

chloroform, after the addition of a small amount of water, and the organic layer was washed with 5% sodium chloride, dried, and evaporated to give a sirup. This sirup showed two components (R_f=0.40 and 0.11) on tlc (benzene : ethyl acetate=4 : 1 in v/v), which were separated on a preparative tlc. The both fractions gave a sirupy **3a** and crystalline **4a** in 52.5% and 19% yields, respectively.

3a: $[\alpha]_D^{22}$ −97.6° (*c* 0.68), IR: 1640 (C=N).

Found: C, 70.03; H, 6.45; N, 3.58%. Calcd for $C_{23}H_{25}NO_5$: C, 69.85; H, 6.37; N, 3.54%.

4a: mp 175 °C, $[\alpha]_D^{22}$ −62.2° (*c* 0.81), IR: 3440 and 3340 (OH and NH), 1630 and 1530 (amide).

Found: C, 66.83; H, 6.58; N, 3.28%. Calcd for $C_{23}H_{27}NO_6$: C, 66.81; H, 6.58; N, 3.39%.

(b) A suspension of **1a** (410 mg) and anhydrous sodium acetate (600 mg) in dry dimethylformamide (20 ml) was treated as above to give **3a** in 87.5% (290 mg) yield, which was identical with the authentic sirup in IR spectrum.

*ii) 2-Anisyl Derivative (**3b**)*: Acylation of 6-amino-3-*O*-benzyl-6-deoxy-1,2-*O*-isopropylidene-α-D-glucofuranose[7] with anisoyl chloride in pyridine in a usual manner gave the corresponding 6-anisamide in 77% yield. Mp 147—147.5 °C, $[\alpha]^{22}$ −24.2° (*c* 1.05), IR: 3460 and 3340 (OH and NH), 1620 and 1530 (amide).

Found: C, 64.92; H, 6.66; N, 3.27%. Calcd for $C_{24}H_{29}NO_7$: C, 65.00; H, 6.59; N, 3.16%.

A solution of the above 6-anisamide (400 mg) and *p*-toluenesulfonyl chloride (250 mg) in pyridine (2 ml) was kept at room temperature overnight, poured into ice-water, and extracted with chloroform. The extract was treated in a usual manner to give a sirupy 5-Otosylate (**1b**, 560 mg). The sirup was dried over phosphorus pentoxide, and treated with anhydrous sodium acetate (770 mg) in DMF in the same procedure as above to give sirupy **3b** in 69% (320 mg) yield. $[\alpha]_D^{22}$ −83.0° (*c* 0.90), IR: 1640 (C=N).

Found: C, 67.70; H, 6.42; N, 3.24%. Calcd for $C_{24}H_{27}NO_6$: C, 67.75; H, 6.40; N, 3.29%.

*2-Phenyl-(5S)-(1′,2′-O-isopropylidene-3′-O-methyl-α-D-xylo-tetrofuranos-4′-yl)-2-oxazoline (**3c**)*. Treatment of 1,2-*O*-isopropylidene-3-*O*-methyl-6-*O*-tosyl-α-D-glucofuranose[11] with sodium azide in a usual manner gave the corresponding azide in 71% yield as a sirup. Reduction of the azide in the presence of Raney-nickel, and acylation of the resulted amine with benzoic anhydride in a usual manner gave the corresponding 6-benzamide as a sirup, which was purified on a silica gel column using benzene–ethyl acetate (4 : 1 in v/v) as an eluent. Yield, 72%; $[\alpha]_D^{22}$ −25.2° (*c* 1.17), IR: 3350 (OH and NH), 1630 and 1530 (amide).

Found: C, 60.72; H, 6.95; N, 4.00%. Calcd for $C_{17}H_{23}NO_6$: C, 60.52; H, 6.87; N, 4.15%.

Tosylation of the above sirup (530 mg) in a usual manner gave 6-benzamido-6-deoxy-1,2-*O*-isopropylidene-3-*O*-methyl-5-*O*-tosyl-α-D-glucofuranose (**1c**, 590 mg) as a sirup. Isomerization of **1c** as before, and fractionation of the product on a silicagel column gave pure **3c** in 28% yield. $[\alpha]_D^{22}$ −75.1° (*c* 0.94). IR: 1640 (C=N).

Found: C, 63.83; H, 6.60; N, 4.26%. Calcd for $C_{17}H_{21}NO_5$: C, 63.93; H, 6.63; N, 4.39%.

*3-O-Benzyl-5,6-dideoxy-5,6-epimino-1,2-O-isopropylidene-β-L-idofuranose (**5**)*. A suspension of 3-*O*-benzyl-5,6-di-*O*-mesyl-1,2-*O*-isopropylidene-α-D-glucofuranose[22] (2.33 g) and sodium azide (1 g) in DMF (50 ml) was heated at 90—100 °C for one hr, poured into cold 5% sodium chloride after cooling, and extracted with ether. The extract was washed with 5% sodium chloride, dried, and evaporated to give a sirupy product (92%). Crystallization and recrystallization of the sirup from ethanol gave 6-azido-3-*O*-benzyl-6-deoxy-1,2-*O*-isopropylidene-5-*O*-mesyl-α-D-glucofuranose as prisms of mp 79.5—80.5 °C. $[\alpha]_D^{22}$ −39.0° (*c* 1.26), IR: 2100 (N_3), 1340 (sulfate), NMR: 1.29 and 1.48 (2x C-CH_3), 3.03 (SO_3CH_3), 3.60 ($H_{6'}$; q, $J_{6,6'}$=13.8, $J_{5,6'}$=10.5), 3.83 (H_6; q, $J_{5,6}$=3.1), 4.09 (H_3; d, $J_{3,4}$=3.7), 4.37 (H_4; q, $J_{4,5}$=7.75), 4.58 (H_2; d, $J_{1,2}$=3.75), 4.60 (CH_2; s), 5.13 (H_5; m), 5.86 (H_1; d), 7.35 (Ph; s).

Found: C, 49.66; H, 5.52; N, 10.08; S, 7.93%. Calcd for $C_{17}H_{23}N_3O_7S$: C, 49.39; H, 5.61; N, 10.17; S, 7.75%.

To an ice-coled solution of the above 6-azido-5-*O*-mesyl derivative (8.39 g) in dry ether (130 ml) was added lithium aluminum hydride (1.67 g) with stirring portionwise, and the mixture was stirred for one hr at room temperature, excess hydride was decomposed by adding a small volume of water, and filtered. The filtrate was evaporated to give a half crystalline mass (5.21 g, 84%), which melts at 93—94 °C (lit,[7] mp 91—94 °C, 69%), after recrystallization from benzene-*n*-hexane.

5,6-Dideoxy-5,5-epimino-1,2-O-isopropylidene-3-O-methyl-β-L-idofuranose. Treatment of 6-azido-6-deoxy-1,2-*O*-isopropylidene-3-*O*-methyl-α-D-glucofuranose, mentioned in the preparation of **3c**, with excess *p*-tosyl chloride or methanesulfonyl chloride in the usual manner gave crystalline 5-*O*-sulfates in 90% and 99% yields, respectively.

5-*O*-Tosylate: mp 134—135 °C, $[\alpha]_D^{23}$ −53.6° (*c* 1.01).

Found: C, 49.54; H, 5.61; N, 9.60%. Calcd for $C_{17}H_{23}N_3O_7S$: C, 49.39; H, 5.60; N, 10.16%.

5-*O*-Mesylate: mp 79—80 °C, $[\alpha]_D^{23}$ −49.8° (*c* 0.98).

Found: C, 39.62; H, 5.72; N, 11.98; S, 9.69%. Calcd for $C_{11}H_{19}N_3O_7S$: C, 39.16; H, 5.68; N, 12.46; S, 9.51%.

Treatment of the above 5-*O*-tosylate or 5-*O*-mesylate in THF with lithium aluminum hydride in the same manner as **5** gave the 5,6-epimino derivative as a sirup in *ca.* 90% yield, which showed no absorption of azide. This sirup was used for preparation of **6c** and **12b** without further identification.

*General procedure for preparation of 5,6-Aroylimino-5,6-dideoxy-1,2-O-isopropylidene-3-O-substituted-β-L-idofuranose (**6a-d**)*. To a solution of **5** or its 3-*O*-methyl derivative and excess triethylamine in dry benzene was added equimolar amount of aroyl chloride, and the precipitate was filtered off, after stirring the reaction mixture for 1—2 hr at room temperature. Evaporation of the filtrate gave the crude product, which was purified by recrystallization or by fractionation with a silica gel column chromatography.

*General procedure for preparation of 2-aroyl-(4S)-(1′,2′-O-isopropylidene-3′-O-substituted-α-D-xyol-tetrofuranos-4′-yl)-2-oxazoline (**7a-d**)*. A solution of **6a-d** (140 mg) and dried sodium iodide (1 g) in dry acetone (5 ml) was refluxed for 15—24 hr, evaporated, and the residue was extracted with chloroform. The extract was washed with 5% sodium chloride, and evaporated to give the product, which was purified by recrystallization, by a preparative tlc, or by a silica gel column chromatography.

*Ring-opening of oxazoline derivatives (**3a** and **7a**)*. A solution of **7a** (700 mg) in 80% acetic acid (40 ml) was heated at 30—36 °C for 2 days, evaporated, and the residue was trituated with ethanol to give crude crystals, which were recrystallized from ethanol to give needles of 5-benzamido-3-*O*-benzyl-5-deoxy-1,2-*O*-isopropylidene-β-L-idofuranose (**8a**) in 48% (350 mg) yield. Mp 161—162 °C, $[\alpha]_D^{22}$ −9.4° (*c* 1.0), IR: 3460 and 3330 (OH and NH), 1620 and 1530 (amide).

Found: C, 66.80; H, 6.57; N, 3.40%. Calcd for $C_{23}H_{27}NO_6$: C, 66.81; H, 6.58; N, 3.39%.

In a similar way, **3a** was converted into **4a** in 88% yield, which was identical with that mentioned before.

*1,6-Acetylimino-3-O-benzyl-6-deoxy-2,4-di-O-acetyl-β-L-idopyranose (**9**).* A suspension of **4a** (130 mg) and potassium hydroxide (800 mg) in 90% ethanol (8 ml) was refluxed for 2 days, poured into ice-water, and extracted with chloroform. The extract was washed with 5% sodium chloride, and evaporated to give de-*N*-benzoylated sirup (80 mg). A solution of the sirup in 2*N*-sulfuric acid (30 ml) was heated at 70—80 °C for 4 hr, neutralized with barium carbonate, and then filtered after the addition of methanol. The filtrate was evaporated, and the residue was dried over phosphorus pentoxide, acetylated with acetic anhydride in a usual manner to give a sirup (30 mg), which was crystallized from ethanol. Yield, 12.5% (15 mg), mp 148—149 °C, $[\alpha]_D^{22}$ −12.9° (*c* 0.52), IR: 1740 (ester), 1640 (amide).

Found: C, 60.30; H, 6.08; N, 3.57%. Calcd for $C_{19}H_{23}NO_7$: C, 60.47; H, 6.14; N, 3.71%.

*N-Acetyl-1,6-anhydro-3-O-benzyl-5-deoxy-2,4-di-O-acetyl-β-L-idopiperidinose (**10**).* A solution of **8a** (250 mg) and potassium hydroxide (2.5 g) in 80% ethanol was refluxed overnight, and then extracted with methylene chloride in a usual manner to give the corresponding 6-amino derivative (70 mg), which was acetylated with acetic anhydride (0.2 g) and triethylamine (0.3 g) in methanol (3 ml) by the procedure reported by Paulson *et al.*[21] to give a sirup. The *N*-acetyl derivative was hydrolyzed with 0.05 M-sulfuric acid (30 ml) at 70 °C for 1 hr, and the dried product obtained by evaporation of the reaction mixture was again acetylated in a usual manner to give a sirup (120 mg) which was purified by a preparative tlc. Yield, 26% (60 mg), $[\alpha]_D^{22}$ +40.8° (*c* 0.85), IR: 1740 (ester), 1660 (amide).

Found: C, 59.85; H, 6.40; N, 3.84%. Calcd for $C_{19}H_{23}NO_7$: C, 60.47; H, 6.14; N, 3.71%.

*2-Thioxo-(4R)-(1',2'-O-isopropylidene-3'-O-substituted-α-D-xylo-tetrofuranos-4'-yl)-thiazolidine (**11**).* *i) 3'-O-Benzyl derivative (**11a**).* A mixture of **5** (1.75 g) and carbon disulfide (5 ml) was sealed in a Pyrex glass at −70 °C, and kept with occasional shaking at room temperature for 1 hr and at 98 °C for 6 hr. The tube was opened at −70 °C, and the content was evaporated to give a sirup which was purified on a silica gel column, using benzene–ethyl acetate (9 : 1) as an eluent, to give crystals in 84% yield. Mp 140—141 °C, $[\alpha]_D^{22}$ −32.1° (*c* 0.87), IR: 3250 (NH), 1469 (NHCS).

Found: C, 55.52; H, 5.76; N, 3.73; S, 17.17%. Calcd for $C_{17}H_{21}NO_4S_2$: C, 55.55; H, 5.76; N, 3.81; S, 17.45%.

*ii) 3'-O-Methyl derivative (**11b**).* 5,6-Dideoxy-5,6-epimino-1,2-*O*-isopropylidene-3-*O*-methyl-β-L-idofuranose (0.52 g) described before was treated with carbon disulfide (2.5 ml) in the same manner as above to give crystals in 40% (280 mg) yield. Mp 195—196 °C, $[\alpha]_D^{22}$ −29.6° (*c* 0.75), IR: 3220 (NH), 1470 (NHCS).

Found: C, 45.44; H, 5.83; N, 4.70; S, 21.91%. Calcd for $C_{11}H_{17}NO_4S_2$: C, 45.34; H, 5.88; N, 4.81; S, 22.01%.

*3-N-Acetyl-2-thioxo-(4R)-(3'-O-benzyl-1',2'-O-isopropylidene-α-D-xylo-tetrofuranos-4'-yl)-thiazolidine (**12**).* A solution of **11a** (100 mg) and acetic anhydride (1 ml) in pyridine (1 ml) was kept at room temperature overnight, poured into ice-water, and the yellow sirup deposited was extracted with chloroform. A usual treatment of the extract gave a sirup (110 mg) which was purified on a silica gel column, using 5% ethyl acetate in benzene as an eluent, to give the pure sirup in 81% (90 mg) yield. $[\alpha]_D^{22}$ −295° (*c* 0.84), IR: 1700 (amide).

Found: C, 55.68; H, 5.73; N, 3.32; S, 15.44%. Calcd for $C_{19}H_{23}NO_5S_2$: C, 55.77; H, 5.67; N, 3.42; S, 15.67%.

When the acylation was performed with *p*-nitrobenzoyl chloride and triethylamine in benzene, the crystalline *N-p*-nitrobenzoate was obtained as yellow needles in 71% yield. Mp 154—155 °C, $[\alpha]_D^{22}$ −148° (*c* 1.18), IR: 1700 (amide).

Found: C, 55.86; H, 4.67; N, 5.49; S, 12.51%. Calcd for $C_{24}H_{24}N_2O_7S_2$: C, 55.81; H, 4.68; N, 5.42; S, 12.41%.

*2-Thioxo-(5S)-(1',2'-O-isopropylidene-3'-O-substituted-α-D-xylo-tetrofuranos-4'-yl)-thiazolidine (**13**).* *i) 3'-O-Benzyl Derivative (**13a**):* A suspension of 6-azido-3-*O*-benzyl-6-deoxy 1,2-*O*-isopropylidene-5-*O*-tosyl-α-D-glucofuranose[7] (3.8 g) in ethanol (150 ml) was reduced in the presence of 10% palladium-charcoal (1.66 g) and acetic acid (0.56 g) for 4 hr, and the catalyst was filtered off. A mixed solution of the filtrate, carbon disulfide (4 ml), and ethanolic potassium hydroxide (1.15 g) was refluxed for 2.5 hr, evaporated, and the residue was washed with water to give crude crystals (2.81 g, 98%) which was recrystallized from ethanol. Mp 120—125 °C, $[\alpha]_D^{22}$ +5.8° (*c* 1.0, acetone), IR: 3250 (NH), 1500 (NHCS).

Found: C, 55.26; H, 5.97; N, 3.66; S, 17.19%. Calcd for $C_{17}H_{21}NO_4S_2$: C, 55.55; H, 5.76; N, 3.81; S, 17.45%.

*ii) 3'-O-Methyl Derivative (**13b**).* 6-Azido-6-deoxy-1,2-*O*-isopropylidene-3-*O*-methyl-5-*O*-tosyl-α-D-glucofuranose mentioned before was treated in the same manner as above to give crystals of mp 148—150 °C in 89% yield. $[\alpha]_D^{22}$ +58.7° (*c* 1.19), IR: 3200 (NH), 1500 (NHCS).

Found: C, 45.59; H, 5.90; N, 4.60; S, 21.77%. Calcd for $C_{11}H_{17}NO_4S_2$: C, 45.34; H, 5.88; N, 4.81; S, 22.01%.

*3-N-Acetyl-2-thioxo-(5S)-(3'-O-benzyl-1',2'-O-isopropylidene-α-xylo-tetrofuranos-4'-yl)-thiazolidine (**14**).* Acetylation of **13a** in the usual manner gave crystals of mp 156—156.5 °C in 90% yield. $[\alpha]_D^{22}$ +34.5° (*c* 1.3), IR: 1690 (amide).

Found: C, 55.43; H, 5.48; N, 3.40; S, 15.72%. Calcd for $C_{19}H_{23}NO_5S_2$: C, 55.73; H, 5.66; N, 3.42; S, 15.66%.

*3-N-Acetyl-2-thioxo-(5S)-(1',2'-di-O-acetyl-3'-O-substituted-α,β-D-xylo-tetrofuranos-4'-yl)-thiazolidine (**15**).* *i) 3'-O-Benzyl Derivative (**15a**).* A solution of **13a** (420 mg) in 70% acetic acid (20 ml) was heated at 90 °C for 5 hr, evaporated, and the residue was dried over phosphorus pentoxide, acetylated in a usual manner to give a sirup which was purified on a silica gel column using 5% ethyl acetate in benzene as an eluent. Yield, 71.5% (345 mg), $[\alpha]_D^{22}$ +96.5 (*c* 1.37), IR: 1750 (ester), 1690 (amide), 1500 (NHCS), NMR: 2.05 and 2.09 (2 x OAc), 2.72 (NAc).

Found: C, 53.01; H, 5.23; N, 3.26; S, 14.32%. Calcd for $C_{20}H_{23}NO_7S_2$: C, 52.97; H, 5.11; N, 3.09; S, 14.14%.

*ii) 3'-O-Methyl Derivative (**15b**).* In the same manner as above **15b** was obtained from **13b** in 56% yield as a sirup. $[\alpha]_D^{22}$ +113.5° (*c* 1.4), IR: 1750 (ester), 1690 (amide), 1500 (NHCS).

Found: C, 45.41; H, 5.24; N, 3.55; S, 16.57%. Calcd for $C_{14}H_{19}NO_7S_2$: C, 44.54; H, 5.07; N, 3.71; S, 16.99%.

*(5S,6R,8R)-Triacetoxy-(7S)-alkoxy-3-thioxo-(8aR)-perhydropyrido[1,2-c]thiazole (**16**).* *i) (7S)-Benzyloxy Derivative (**16a**).* A suspension of **11a** (150 mg) in 70% acetic acid (40 ml) was heated at 90 °C for 4 hr, evaporated, and the residue was dried over phosphorus pentoxide, acetylated in a usual manner to give needles of mp 129—130 °C in 74% (230 mg) yield. $[\alpha]_D^{22}$ −82.0° (*c* 1.1), IR: 1740 (ester), 1380 (NHCS).

Found: C, 53.17; H, 5.10; N, 3.10; S, 13.92%. Calcd for $C_{20}H_{23}NO_7S_2$: C, 52.98; H, 5.11; N, 3.09; S, 14.14%.

*ii) (7S)-Methoxy Derivative (**16b**):* In the same manner as above, **16b** was obtained from **11b** as a sirup in 48% yield. $[\alpha]_D^{22}$ −56.6° (*c* 0.63), IR: 1740 (ester), 1370 (NHCS).

Found: C, 44.35; H, 5.07; N, 3.65; S, 16.51%. Calcd for $C_{14}H_{19}NO_7S_2$: C, 44.56; H, 5.08; N, 3.71; S, 17.00%.

*2-Methylthio-(4R)-(3'-O-benzyl-1',2'-O-isopropylidene-α-D-xylo-tetrofuranos-4'-yl)-2-thiazoline (**17**).* To a suspension

of sodium hydride (170 mg, dispersed in oil *ca.* 50%) in DMSO (4 ml) stirred for 1 hr under nitrogen atmosphere was added dropwise a solution of **11a** (1.2 g) in DMSO (5 ml) and then methyl iodide (2 ml). After keeping the reaction mixture at room temperature for 4 hr, it was poured into ice-water, and extracted with chloroform. The chloroform layer was washed with 5% sodium chloride, dried with magnesium sulfate, and evaporated to give a sirup which was purified on a silica gel column, using 10% ethyl acetate in toluene as an eluent, to give crystals of mp 113—114 °C in 66.5% (0.83 g) yield. $[\alpha]_D^{22}$ −50.0° (*c* 1.0), IR: 1560 (C=N).

Found: C, 56.94; H, 6.06; N, 3.60; S, 16.62%. Calcd for $C_{18}H_{23}NO_4S_2$: C, 56.68; H, 6.08; N, 3.67; S, 16.78%.

The corresponding (5*S*)-2-thiazoline (**18**) was analogously obtained from **13a** in 79% yield as a sirup. $[\alpha]_D^{22}$ −11.8° (*c* 1.22), IR: 1570 (C=N).

Found: C, 57.12; H, 6.06; N, 3.74; S, 16.29%. Calcd for $C_{18}H_{23}NO_4S_2$: C, 56.68; H, 6.08; N, 3.67; S, 16.78%.

*(4R)-(3'-O-Benzyl-1',2'-O-isopropylidene-α-D-xylo-tetrofuranos-4'-yl)thiazolidine (**19**).* To a solution of **17** (0.3 g) in THF (30 ml) was added aluminum amalgam prepared from aluminum turnings (1 g) and then water (5 ml) portionwise under stirring. The reaction mixture was then stirred at 50—60 °C for 24 hr, filtered through filtercell, and the filtrate was evaporated to give crystals almost quantitatively (270 mg). Recrystallization of it from ethanol gave needles of mp 149—151 °C. $[\alpha]_D^{22}$ −95.4° (*c* 0.74), IR: 3200 (NH).

Found: C, 60.58; H, 6.85; N, 4.13; S, 9.55%. Calcd for $C_{17}H_{23}NO_4S$: C, 60.52; H, 6.87; N, 4.15; S, 9.50%.

The corresponding (5*S*)-thiazolidine (**20**) was analogously obtained from **18** in 95% yield as a sirup. $[\alpha]_D^{22}$ −7.9° (*c* 0.63), IR: 3300 (NH).

Found: C, 59.63; H, 6.81; N, 4.09; S, 9.40%. Calcd for $C_{17}H_{23}NO_4S$: C, 60.52; H, 6.87; N, 4.15; S, 9.50%.

The authors are indebted to Mr. H. Matsumoto for NMR measurements, and members of the Laboratory of Organic Analysis for the microanalyses.

References

1) Part XXII: This Bulletin, **47**, 1219 (1974).
2) H. E. Khadem, *Adv. Carbohyd. Chem. Biochem.*, **25**, 351 (1970).
3) W. M. zu Reckendorf and N. Wassiliadon-Micheri, *Chem. Ber.*, **101**, 2294 (1968).
4) M. Miljkovic, T. Satoh, M. Konopka, E. A. Daridson, and D. Miljkovic, *J. Org. Chem.*, **38**, 716 (1973).
5) J. M. J. Tronchet, S. Jaccard-Thorndahl, L. Faivre, and R. Massard, *Helv. Chim. Acta*, **56**, 1303 (1973).
6) H. Paulsen and D. Stoye, *Chem. Ber.*, **102**, 820 (1969).
7) H. Saeki and E. Ohta, *Chem. Pharm. Bull.* (Tokyo), **16**, 2471 (1968).
8) G. Hanish and G. Henseke, *Chem. Ber.*, **101**, 2074 (1968).
9) M. Iwakawa and J. Yoshimura, *Chem. Lett.*, **1974**. 519,
10) S. Hannesian, *J. Org. Chem.*, **32**, 163 (1967).
11) Yu. A. Zhdanov and V. A. Polenov, *Carbohyd. Res.*, **16**, 466 (1971).
12) H. W. Heine, M. E. Fetter, and E. M. Nicholson, *J. Amer. Chem. Soc.*, **81**, 2202 (1959).
13) H. Paulsen and K. Todt, *Adv. Carbohyd. Chem.*, **23**, 116 (1968).
14) T. A. Foglia, L. M. Gregory, G. Mearker, and S. F. Osman, *J. Org. Chem.*, **36**, 1068 (1971).
15) J. Yoshimura and H. Hashimoto, This Bulletin, **41**, 261 (1968).
16) T. C. Owen, *J. Chem. Soc., C*, **1967**, 1373.
17) C. S. Dewey and R. A. Bafford, *J. Org. Chem.*, **30**, 491 (1965).
18) L. M. Jackman and S. Sternhell, "Application of Nuclear Magnetic Resonance Spectroscopy in Organic Chemistry," 2nd. Ed., Pergamon Press, (1969), p. 334.
19) R. U. Lemieux and J. D. Stevens, *Can. J. Chem.*, **43**, 2057 (1965).
20) T. S. Batterham, "NMR Spectra of Simple Heterocycles," John Wiley and Sons, (1973), p. 219.
21) L. Goodman and J. E. Christensen, *J. Org. Chem.*, **28**, 2610 (1963).
22) H. Paulsen and K. Todt, *Chem. Ber.*, **99**, 3450 (1966).
23) H. Paulsen and D. Stoye, *Angew. Chem.*, **80**, 120 (1968).

Studies of Enamines. VI.[1] The Formation of New Michael Type Adducts and Pyrrolizine Compounds in the Reaction of Enamines with Pyrrole

Masashi TASHIRO, Yoko KIRYU, and Otohiko TSUGE*

Research Institute of Industrial Science, Kyushu University, Hakozaki, Higashi-ku, Fukuoka 812

(Received October 16, 1974)

While the reaction of 1-(1-pyrrolidinyl)propene (**1a**) and -1-butene (**1b**) with pyrrole (**2**) under mild conditions afforded the Michael type N,N–1 : 1 adducts **3**, under forcing conditions enamines **1** reacted with **2** to give the Michael type C,N– 1 : 1 adducts **4**, accompanied with pyrrolizine compounds **5**. It has been shown that the pyrrolizine **5** was formed *via* the cycloaddition reaction of **1** with an azafulvene intermediate arising from **4** by the elimination of pyrrolidine.

In a previous communication,[2] we have reported that under mild conditions 1-(1-pyrrolidinyl)propene (**1a**), -1-butene (**1b**), and -cyclohexene (**1c**) reacted with pyrrole (**2**) to give the Michael type N,N-1 : 1 adducts **3a**, **3b**, and **3c**, respectively. It has been also found that the adduct **3c** decomposed at elevated temperature to regenerate **1c** and **2**, and that the reaction of **1c** with **2** under forcing conditions afforded the novel pyrrolizine compound **A**, accompanied with cyclohexenylpyrroles. The pathway depicted in Scheme 1 has been tentatively proposed for this novel reaction: under forcing conditions the reaction would proceed *via* an initial formation of Michael type C,N–1 : 1 adducts, **B** and **C**, followed by the elimination of pyrrolidine to yield cyclohexenylpyrroles and azafulvene intermediate **D**. The azafulvene **D** would undergo cycloaddition reaction with **1c** to afford the pyrrolizine **A**.[1]

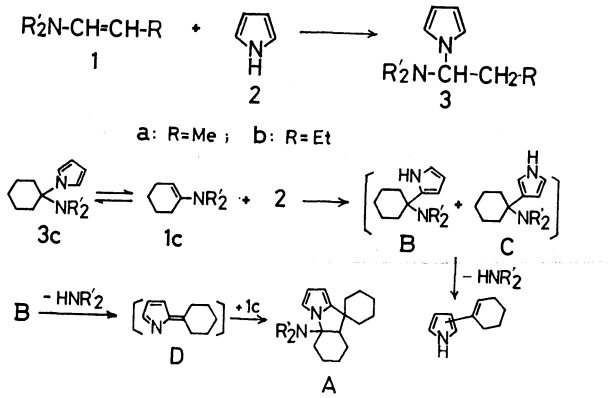

Scheme 1.

During the course of a further investigation of the reaction of enamines with pyrrole (**2**), it has been found that enamines **1a** and **1b** reacted with **2** to give the new Michael type C,N–1 : 1 adducts whose structures correspond to that of **B**. This paper deals with the reaction of **1a** and **1b** with **2**, and with the discussion of the pathway for the formation of pyrrolizine compounds.

Results and Discussion

The reaction of **1a** with **2** at 110 °C for 12 hr in a stream of nitrogen gave two new compounds **4a**, mp 93—94 °C, and **5a**, bp 124—126 °C/4 mmHg, in 20.6 and 6.1% yields respectively, and Michael type N,N–1 : 1 adduct **3a**, which is a main product in the reaction at 80 °C for 5 min,[2] was not formed.

The molecular formula of **4a** agreed with that of a 1 : 1 adduct of **1a** and **2**, that is, **4a** is an isomer of **3a**, and the IR spectrum showed the band ascribable to NH absorption at 3190 cm^{-1}. The NMR spectrum in carbon tetrachloride (CCl_4) exhibited signals at δ 3.03 (1H, q, $\rightarrow$CH), 5.89 (2H, m, β-protons of pyrrole ring (β-**H**)), and 6.52 ppm (1H, dd, α-proton of pyrrole ring (α-**H**)), besides methylene and methyl protons. On the basis of above spectral data, **4a** was clearly assigned as 1-(1-pyrrolidinyl)-1-(2-pyrrolyl)propane, whose structure corresponds to that of a compound of type **B** assumed as an initial intermediate in Scheme 1.

The minor product **5a**, whose molecular formula corresponded to that of a compound arising from a 2 : 1 adduct of **1a** and **2** by the elimination of one mole of pyrrolidine, was deduced to be 1,2-dihydro-1-ethyl-2-methyl-3-(1-pyrrolidinyl)-3H-pyrrolizine. The IR spectrum showed no NH absorptions, and the NMR spectrum in CCl_4 exhibited signals at δ 4.65 (1H, d, $\rightarrow$C**H**, J=4.5 Hz), 5.60, 5.97 (each 1H, m, β-**H**), and 6.41 ppm (1H, dd, α-**H**), besides methyl, methylene, and methine protons.

A potential structure, 1-ethyl-3-methyl-2-(1-pyrrolidinyl)pyrrolizine **5'**, might be excluded from the structure for the minor product, because the signal at δ 4.65 ppm in the NMR spectrum might be assignable to the 3-methine proton of **5a**, but not to 2- or 3-methine proton of **5'**. Furthermore, the relative arrangements of substituents of **5a** are similar to those of the pyrrolizine **A** whose structure has been clearly established.[1]

The configuration of **5a** is not clear, because of appearance of 1- and 2-methine protons in a region of methylene protons. In view of the value of coupling constant of 3-methine proton (J=4.5 Hz), however, it may be thought that the 2-methyl and 3-pyrrolidinyl groups are situated *trans*.

Similarly, the reaction of **1b** with **2** at 100 °C for 11 hr afforded the corresponding Michael type C,N–1 : 1 adduct **4b** and pyrrolizine compound **5b** in 44.1 and 7.7% yields, respectively.

When the *N,N*-adduct **3a** was heated at 120 °C for 10 hr, **4a** was obtained in 22.6% yield, along with traces of **5a**. Under similar conditions, however, **3b** gave only **4b**, and no **5b** could be isolated. These facts indicate that **3a** and **3b** as well as **3c** decomposed at elevated temperature to regenerate the correspond-

* To whom inquiries should be addressed.

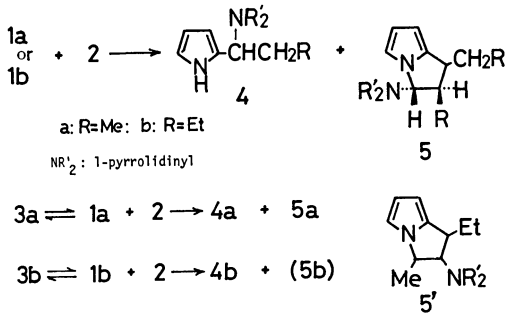

Scheme 2.

ing enamines **1** and **2** (Scheme 2).

In order to know whether the Michael type C,N-1 : 1 adduct is a real intermediate producing alkenylpyrrole and pyrrolizine compound or not, several reactions toward **4b** were investigated.

On heating of **4b** at 150 °C for 5 hr in a stream of nitrogen, the expected 2-(1-butenyl)pyrrole (**6**) and a dimer **7** of **6** were obtained in 34.6 and 39.4% yields, respectively. On the basis of the spectral data, the structure of dimer **7** has been tentatively assigned 1-(2-pyrrolyl)-1-{2-[5-(1-butenyl)]pyrrolyl}butane.

On the other hand, heating of **4b** in the presence of **1b** at 100 °C for 10 hr afforded the expected pyrrolizine compound **5b** in 31.2% yield. Furthermore, **4b** was allowed to react with 1-(1-pyrrolidinyl)cyclohexene (**1c**), -cyclopentene (**1d**), and -cycloheptene (**1e**) under similar conditions, giving the corresponding pyrrolizine compounds **5c**, **5d**, and **5e**, in 65.0, 60.0, and 98.7% yields, respectively (Scheme 3). These facts strongly indicate that an azafulvene intermediate would be initially formed by an alternative elimination mode of pyrrolidine from **4b**, followed by cycloaddition reaction of the azafulvene with enamine **1** to give pyrrolizines **5**.

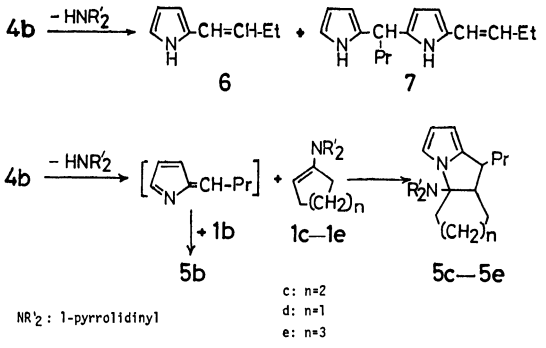

Scheme 3.

Furthermore, the following results seem to provide evidence for the formation of pyrrolizine compound *via* the cycloaddition reaction of an azafulvene with enamine.

2-(1-Pyrrolidinylmethyl)pyrrole (**8**), which would form only an azafulvene by the elimination of pyrrolidine, reacted with enamine **1c** at 120 °C to give the expected pyrrolizine compound **9** in 49.3% yield.

In both reactions of enamine **1b** with the *N,N*-adduct **3c**, and of enamine **1c** with the *N,N*-adduct **3b** at 120 °C, pyrrolizine compound **5c** as a sole isolated product was obtained in 35.3 and 33.7% yields, respectively. These facts indicate the participation of the same intermediate for the formation of **5c** in both reactions. Under the reaction contitions, both *N,N*-adducts **3b** and **3c** decompose to regenerate the respective enamines, **1b** and **1c**, and pyrrole (**2**). This is followed by the reaction of regenerated pyrrole (**2**) with more reactive enamine **1b** than **1c** to form the C,N-adduct **4b**. Then, **4b** is converted to an azafulvene, and the azafulvene undergoes cycloaddition reaction with the remaining enamine **1c** to give **5c** (Scheme 4).

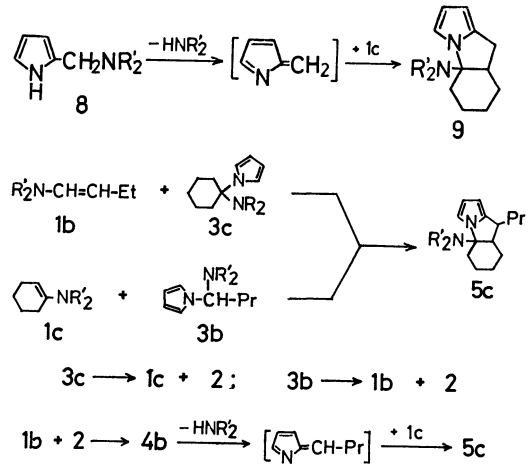

Scheme 4.

In conclusion it is now clear that the reaction of enamine **1** with pyrrole (**2**) proceeds through the pathway illustrated by the reaction of **1c** with **2** in Scheme 1.

Experimental

All melting and boiling points are uncorrected. The mass spectra were obtained on a Hitachi RMS-4 mass spectrometer with a direct inlet and an ionization energy of 70 eV. The NMR spectra were determined at 60 MHz with a Hitachi R-20 NMR spectrometer with TMS as an internal reference.

*Reaction of 1-(1-Pyrrolidinyl)propene (**1a**) with Pyrrole (**2**).* A mixture of 10.0 g (0.09 mol) of **1a** and 4.0 g (0.06 mol) of **2** was stirred at 110 °C for 12 hr in a stream of nitrogen. The reaction mixture was subjected to fractional distillation to give 2.2 g (20.6% based on **2**) of 1-(1-pyrrolidinyl)-1-(2-pyrrolyl)-propane (**4a**), bp 90—93 °C/5 mmHg, as colorless oil which solidified, and 0.8 g (6.1% based on **2**) of 1,2-dihydro-1-ethyl-2-methyl-3-(1-pyrrolidinyl)-3H-pyrrolizine (**5a**), bp 124—126 °C/4 mmHg, as pale yellow oil. Recrystallization from petroleum ether (bp 40—65 °C) afforded pure **4a**, mp 93—94 °C, as colorless prisms.

4a; IR (KBr): 3190 cm^{-1} (ν_{NH}). NMR (CCl_4): δ 0.7 (3H, t, CH_3), 1.5—2.1 (6H, m, CH_2), 2.1—2.9 (4H m, CH_2), 3.03 (1H, q, $>CH$), 5.89 (2H, m, β-**H**), 6.52 (1H, dd, α-**H**), 9.32 (1H, broad **NH**). Mass: *m/e* 178 (M^+). Found: C, 74.30; H, 10.43; N, 15.85%. Calcd for $C_{11}H_{18}N_2$: C, 74.11; H, 10.18; N, 15.71%.

5a; NMR (CCl_4): δ 1.1 (6H, m, CH_3), 1.4—1.95 (6H, m, CH_2), 2.0—3.1 (6H, m, $2\times CH_2+2\times >CH$), 4.65 (1H,

d, >CH, J=4.5 Hz), 5.60, 5.97 (each 1H, m, β-H), 6.41 (1H, dd, α-H). Mass: *m/e* 218 (M^+). Found: C, 76.85; H, 10.19; N, 12.77%. Calcd for $C_{14}H_{22}N_2$: C, 77.01; H, 10.16; N, 12.71%.

*Reaction of 1-(1-Pyrrolidinyl)-1-butene (**1b**) with **2**.* A mixture of 40.0 g (0.32 mol) of **1b** and 43.0 g (0.64 mol) of **2** was stirred at 100 °C for 11 hr in a stream of nitrogen. Excess of **2** was removed by vacuum distillation, and the residue was allowed to stand over night to give colorless crystals. Filtration and recrystallization from petroleum ether (bp 40—65 °C) afforded 26.5 g of 1-(2-pyrrolyl)-1-(1-pyrrolidinyl)butane (**4b**), mp 89 °C, as colorless prisms.

Vacuum distillation of the filtrate afforded 0.6 g of **4b** and 6.06 g (7.7%) of 1,2-dihydro-2-ethyl-1-propyl-3-(1-pyrrolidinyl)-3H-pyrrolizine (**5b**), bp 117—118 °C/2 mmHg, as pale yellow oil.

The total yield of **4b** was 27.1 g (44.1% based on **1b**). IR (KBr): 3180 cm^{-1} (ν_{NH}). NMR (CCl_4): δ 0.7—1.4 (5H, m, CH_3+CH_2), 1.5—2.0 (6H, m, CH_2), 2.1—2.9 (4H, m, CH_2), 3.15 (1H, q, >CH), 5.99 (2H, m, β-H), 6.54 (1H, dd, α-H), 9.37 (1H, broad, NH). Mass: *m/e* 192 (M^+). Found: C, 75.18; H, 10.71; N, 14.66%. Calcd for $C_{12}H_{20}N_2$: C, 74,95; H, 10.48; N, 14.57%.

5b; NMR (CCl_4): δ 1.0 (6H, m, CH_3), 1.2—3.1 (16H, m, $7\times CH_2+2\times$ >CH), 4.8 (1H, d, >CH, J=4.5 Hz), 5.54 (1H, m, β-H), 5.99 (1H, dd, β-H), 6.39 (1H, dd, α-H). Mass: *m/e* 246 (M^+). Found: C, 78.12; H, 10.60; N, 11.44%. Calcd for $C_{16}H_{26}N_2$: C, 77.99; H, 10.64; N, 11.37%.

*Thermal Decomposition of 1-(1-Pyrrolidinyl)-1-(1-pyrrolyl)propane (**3a**).* After 6.45 g of the *N,N*-adduct **3a**[2] was stirred at 120 °C for 10 hr, the reaction mixture was subjected to fractional distillation to give 1.46 g (22.6%) of **4a** and 0.16 g (2.0%) of **5a**.

Under similar conditions heating of 12.0 g of **3b**[2] afforded 2.4 g (20.2%) of **4b**.

*Thermal Decomposition of **4b**.* i) Twenty grams of the *C,N*-adduct **4b** was heated at 150 °C for 5 hr in a stream of nitrogen, and the reaction mixture was then subjected to fractional distillation to afford 4.46 g (34.6%) of 2-(1-butenyl)-pyrrole (**6**), bp 76—78 °C/3 mmHg, as colorless oil, and 4.95 g (39.4%) of 1-(2-pyrrolyl)-1-{2-[5-(1-butenyl)]pyrrolyl}butane (**7**), bp 167—170 °C/3 mmHg, as pale rose viscous oil.

6; IR (neat): 3500 cm^{-1} (ν_{NH}). NMR (CCl_4): δ 1.07 (3H, t, CH_3), 2.18 (2H, m, CH_2), 5.3—5.9 (1H, m, =CH), 6.03 (3H, m, $2\times$β-H+=CH), 6.43 (1H, m, α-H), 7.65 (1H, broad, NH). Mass: *m/e* 121 (M^+). Found: C, 79.18, H, 8.89; N, 11.23%. Calcd for $C_8H_{11}N$: C, 79.29; H, 9.15; N, 11.56%.

7; IR (neat): 3500 cm^{-1} (ν_{NH}). NMR (CCl_4): δ 0.8—1.5 (8H, m, $2\times CH_3+CH_2$), 1.5—2.4 (4H, m, CH_2), 3.7 (1H, t, >CH), 5.3—5.7 (1H, m, =CH), 5.8—6.15 (5H, m, $4\times$β-H+=CH), 6.27 (1H, dd, α-H), 7.29 (2H, broad, NH). Mass: *m/e* 242 (M^+). Found: C, 79.26; H, 9.44; N, 11.62%. Calcd for $C_{16}H_{22}N_2$: C, 79.29; H, 9.15; N, 11.56%.

ii) A mixture of 6.0 g (0.031 mol) of **4b** and 16.0 g (0.128 mol) of **1b** was heated at 100 °C for 10 hr. Fractional distillation of the reaction mixture afforded 2.4 g (31.2% based on **4b**) of **5b**.

*1,2-Dihydro-1-propyl-3-(1-pyrrolidinyl)-2,3-tetramethylene-3H-pyrrolizine (**5c**).* After a mixture of 5.0 g (0.026 mol) of **4b** and 3.9 g (0.026 mol) of 1-(1-pyrrolidinyl)cyclohexene (**1c**) was stirred at 100 °C for 5 hr in a stream of nitrogen, vacuum distillation afforded 4.6 g (65.0%) of **5c**, bp 148—149 °C/2 mmHg, as colorless oil. NMR (CCl_4): δ 1.0 (3H, broad t, CH_3), 1,2—3.2 (22H, m, $10\times CH_2+2\times$ >CH), 5.65 (1H, m, β-H), 5.95 (1H, dd, β-H), 6.38 (1H, dd, α-H). Mass: *m/e* 272 (M^+). Found: C, 79.41; H, 10.57; N, 10.31%. Calcd for $C_{18}H_{28}N_2$: C, 79.36; H, 10.36; N, 10.28%.

Similarly, the reaction of **4b** with 1-(1-pyrrolidinyl)cyclopentene (**1d**) and -cycloheptene (**1e**) afforded 1,2-dihydro-2,3-trimethylene- (**5d**) and -2,3-pentamethylene-3H-pyrrolizine (**5e**) in 60.0 and 98.7% yields, respectively.

5d; bp 163 °C/5 mmHg. NMR (CCl_4): δ 1.0 (3H, m, CH_3), 1.2—3.0 (20H, m, $9\times CH_2+2\times$ >CH), 5.45 (1H,m, β-H), 6.02 (1H, dd, β-H), 6.35 (1H, dd, α-H). Mass: *m/e* 258 (M^+). Found: C, 78.80; H, 10.31; N, 10.74%. Calcd for $C_{17}H_{26}N_2$: C, 79.02; H, 10.14; N, 10.84%.

5e; bp 177—179 °C/3.5 mmHg. NMR (CCl_4): δ 1.0 (3H, m, CH_3), 1.2—3.0 (24H, $11\times CH_2+2\times$ >CH), 5.52, 5.97 (each 1H, dd, β-H), 6.33 (1H, m, α-H). Mass: *m/e* 286 (M^+). Found: C, 79.65; H, 10.58; N, 9.90%. Calcd for $C_{19}H_{30}N_2$: C, 79.66; H, 10.56; N, 9.78%.

*2-(1-Pyrrolidinylmethyl)pyrrole (**8**).* Twenty grams (0.3 mol) of pyrrole (**2**) was added, drop by drop, to a solution prepared from 21.5 g (0.3 mol) of pyrrolidine and 24.5 ml of 37% aqueous formaldehyde with stirring at 0 °C. The reaction mixture was stirred at room temperature for 3 hr and then at 95 °C for 30 min. The mixture was extracted with diethyl ether and the extract was dried over sodium sulfate, and then evaporated *in vacuo* to leave a residue. Several fractional distillations of the residue afforded 18.5 g (41.2%) of **8**, bp 103—104 °C/5 mmHg, which solidified. Recrystallization from petroleum ether (bp 40—65 °C) gave pure **8**, mp 48 °C, as colorless needles. IR (KBr): 3190 cm^{-1} (ν_{NH}). NMR (CCl_4): δ 1.75, 2.52 (each 4H, m, CH_2), 3.56 (2H, s, CH_2), 5.90 (2H, m, β-H), 6.45 (1H, dd, α-H), 10.05 (1H, broad, NH). Mass: *m/e* 150 (M^+). Found: C, 71.68; H, 9.41; N, 18.68%. Calcd for $C_9H_{14}N_2$: C, 71.95; H, 9.39; N, 18.65%.

*1,2-Dihydro-3-(1-pyrrolidinyl)-2,3-tetramethylene-3H-pyrrolizine (**9**).* After a mixture of 4.2 g (0.028 mol) of **1c** and 3.8 g (0.028 mol) of **8** was stirred at 120 °C for 5 hr in a stream of nitrogen, distillation gave 3.0 g (49.3%) of **9**, bp 138—140 °C/3 mmHg, as pale yellow oil. NMR (CCl_4): δ 1.2—3.2 (19H, m, $9\times CH_2+$ >CH), 5.55 (1H, m, β-H), 5.97 (1H, dd, β-H), 6.50 (1H, dd, α-H). Mass: *m/e* 230 (M^+). Found: C, 78.43; H, 9.45; N, 12.05%. Calcd for $C_{15}H_{22}N_2$: C, 78.21; H, 9.63; N, 12.16%.

*Reaction of **1b** with 1-(1-Pyrrolidinyl)-1-(1-pyrrolyl)cyclohexane (**3c**).* A mixture of 2.9 g (0.023 mol) of **1b** and 5.0 g (0.023 mol) of **3c**[2] was stirred at 120 °C for 7 hr in a stream of nitrogen, and then distillation afforded 2.2 g (35.3%) of **5c**.

Similarly, 2.8 g (33.7%) of **5c** was also obtained from the reaction of 4.7 g (0.031 mol) of **1c** with 6.0 g (0.031 mol) of **3b**.

References

1) Part V of this series: M. Tashiro, Y. Kiryu, and O. Tsuge, *Heterocycles*, **2**, 575 (1974).

2) O. Tsuge, M. Tashiro, and Y. Kiryu, *Chem. Lett.*, **1974**, 795.

Aromatic Thiocyanation by a Mixture of Antimony(V) Chloride and Lead(II) Thiocyanate

Sakae UEMURA,* Akira ONOE, Hajime OKAZAKI, and Masaya OKANO
Institute for Chemical Research, Kyoto University, Uji, Kyoto 611
(Received November 5, 1974)

Alkyl- and halobenzenes give thiocyano-derivatives when treated with a mixture of $SbCl_5$ and $Pb(SCN)_2$ in CCl_4. The reaction proceeds *via in situ* formation of ClSCN from $SbCl_5$ and $Pb(SCN)_2$ followed by its attack on aromatic compounds catalyzed by $SbCl_5$, the reaction species being $SCN^+SbCl_6^-$.

Nuclear thiocyanation of aryl ethers and amines and polymethylbenzenes has been carried out with thiocyanogen[1] or thiocyanogen chloride.[2] However, thiocyanation of less reactive aromatic compounds requires a Lewis-acid catalyst such as $AlCl_3$.[3] Other methods for the preparation of aromatic thiocyano-derivatives involve the Gattermann and Sandmeyer reaction[1] and the reaction of arylthallium compounds with copper thiocyanates[4] or with KSCN under irradiation of light.[5] We report here another simple method of nuclear thiocyanation of less reactive aromatic compounds such as alkyl- and halobenzenes by a mixture of $SbCl_5$ and $Pb(SCN)_2$.

Results and Discussion

To a heterogeneous mixture of antimony (V) chloride and lead (II) thiocyanate in carbon tetrachloride was added aromatic compound, and the mixture was then heated under reflux for 3 hr to give aryl thiocyanate occasionally together with aryl chloride. Aryl thiocyanate was generally obtained predominantly and in good yield when aromatic compound was added drop by drop at 58—62 °C where the color of the mixture is yellow-orange owing to the formaion of ClSCN, and when the molar ratio of $SbCl_5$ to $Pb(SCN)_2$ is 1—1.67. No isomeric aryl isothiocyanate was found in the reaction products. When more $SbCl_5$ was used, the formation of aryl chloride became predominant as expected.[6] Only in the case of benzene, the best yield of phenyl thiocyanate was obtained when benzene was added at room temperature (20—25 °C) and the mixture was then rapidly heated to reflux. The results are summarized in the Table. Reactions in other solvents such as chloroform and 1,2-dichloroethane did not give the satisfactory results.

The reaction is clearly electrophilic, and no reaction occurred with compounds having strong deactivating substituent, such as nitrobenzene, acetophenone, and ethyl benzoate. The reaction seems to proceed by the following schemes 1 and 2.

$$2SbCl_5 + Pb(SCN)_2 \rightarrow 2SbCl_3 + PbCl_2 + 2ClSCN \quad (1)$$

$$ClSCN + R\text{-}C_6H_5 \xrightarrow{SbCl_5} R\text{-}C_6H_4\text{-}SCN + HCl \quad (2)$$

Namely, thiocyanogen chloride is formed by the interaction of antimony(V) chloride with lead (II) thiocyanate and then it attacks aromatic compound. When cyclohexene instead of aromatic compound was added as substrate in this reaction system ($SbCl_5$/$Pb(SCN)_2$=1−1.67), *trans*-1-chloro-2-thiocyanocyclohexane was formed in 60—80% yield together with *cis*- and *trans*-1,2-dichlorocyclohexanes (10—40%), showing clearly the presence of ClSCN in the reaction mixture. The addition of ClSCN to olefin has already been known.[2a] Here, any trace of 1,2-dithiocyanocyclohexane was not detected in the reaction products. Further, it is clear that $SbCl_5$ activates ClSCN in the succeeding thiocyanation as in the case of the $SbCl_5$-catalyzed halogenation,[7] since only a trace amount and 13% yield of aryl thiocyanate was obtained respectively from the reaction of benzene and toluene with ClSCN formed *in situ* from a mixture of $Pb(SCN)_2$ (10 mmol) and $PhICl_2$ (20 mmol) instead of $SbCl_5$ in CCl_4 (50 ml). The k_T/k_B value of 150—160 and *o*-/*p*- ratio of 0.40—0.46 observed in competitive reaction between toluene and benzene suggest that the attacking species is not molecular ClSCN but slightly activated species. If molecular ClSCN is the reaction species, larger k_T/k_B value should be obtained since the reactivity of ClSCN is known to be nearly the same as ICl[2a] which is less reactive than Br_2. Taking into account the Lewis-acidity of $SbCl_5$, the reaction species seems to be $SCN^+SbCl_6^-$. The above facts mean that $SbCl_5$ acts as both the source of thiocyanogen chloride and a Lewis-acid catalyst for the thiocyanation.

By use of other metal thiocyanates such as AgSCN, CuSCN or $Hg(SCN)_2$ in place of $Pb(SCN)_2$, phenyl thiocyanate was formed from benzene in 41%, 26% or 21% yield respectively under the conditions where 32% yield was obtained by use of the lead salt. Reactions with $Cu(NCS)_2$, $Zn(SCN)_2$, $Cd(SCN)_2$, and KSCN did not give the satisfactory results.

Experimental

The NMR spectra were measured with a Varian A-60 spectrometer in CCl_4, using TMS as an internal standard. The IR spectra were taken with a Perkin-Elmer Model 521 spectrometer. Glc analyses were carried out on Shimadzu 5APTF apparatus, using PEG 6000 (25%)-Chromosorb W (3m) and Apiezon L (30%)-Celite (1 m) columns (N_2 as carrier gas), phenyl isothiocyanate being used as an internal standard for the determination of aryl thiocyanate. Commercial organic materials, $SbCl_5$, and metal thiocyanates were used without purification. The identification of phenyl, tolyl and 3,4-dimethylphenyl thiocyanates[4] and *trans*-1-chloro-2-thiocyanocyclohexane[8] was reported previously. Competitive reaction was carried out by rapid addition of a mixture of benzene (0.2 mol) and toluene (0.1 mol) to a CCl_4 solution of $Pb(SCN)_2$ (10 mmol) and $SbCl_5$ (16.7 mmol)

* To whom all correspondences should be addressed.

Table. Thiocyanation of alkyl- and halobenzenes in CCl_4 (50 ml)

Aromatics (100 mmol)	$SbCl_5$ (mmol)	$Pb(SCN)_2$ (mmol)	Products		
			ArSCN(%)[a]	(*p*/*o*)	ArCl(%)[a]
Benzene	25	15	32		11
Benzene[b]	25	15	64		13
Toluene	10	10	41	(2.50)	0
Toluene	16.7	10	42	(2.50)	1
Ethylbenzene	10	10	41	(2.74)	0
Cumene	10	10	36	(5.79)	0
t-Butylbenzene	10	10	45[c]		—[d]
o-Xylene	10	10	55[e]		3
m-Xylene	10	10	69[f]		trace
p-Xylene	10	10	62[g]		trace
Mesitylene	10	10	68[h]		0
Fluorobenzene	16.7	10	25[i]		1
Chlorobenzene	16.7	10	15	(4.70)	1
Bromobenzene	10	10	14	(2.46)	3

a) Based on $SbCl_5$ charged. b) Only in this case benzene was added at 25 °C and the mixture was then rapidly heated to reflux. c) Almost *p*-isomer. d) Not determined. e) 2,3- and 3,4-Dimethylphenyl thiocyanates (1 : 9). f) 2,4-Dimethylphenyl thiocyanate. g) 1,4-Dimethylphenyl thiocyanate. h) 2,4,6-Trimethyl phenyl thiocyanate. i) Only *p*-isomer.

at 62 °C and then by stirring at reflux for 1 hr.

Preparation of 2,5-Dimethylphenyl Thiocyanate. The following is a typical procedure for the thiocyanation. *p*-Xylene (10.6 g, 0.1 mol) was added drop by drop (*ca.* in 5 min) at 58—60 °C under vigorous stirring to a yellow-orange heterogeneous solution of $SbCl_5$ (3 g, 10 mmol) and $Pb(SCN)_2$ (3.23 g, 10 mmol) in CCl_4 (50 ml). The mixture was then heated to 79 °C (reflux) and stirred for 3 hr. After being cooled down to room temperature, 300 ml of water was added to the solution and the precipitated white solid of SbOCl (1.6 g, 9.25 mmol) was filtered off. Organic layer of the filtrate was washed with water, dried over Na_2SO_4, and concentrated to *ca.* 25 ml which contained 6.2 mmol (62% yield) of 2,5-dimethylphenyl thiocyanate and a trace amount of chlorinated *p*-xylene. Distillation gave 0.82 g (5 mmol) of 2,5-dimethylphenyl thiocyanate; bp 136—138 °C/20 mmHg. IR 2162 cm^{-1} (ν_{SCN}). NMR δ 2.31 (s. 3H), 2.37 (s. 3H), 7.0—7.1 (m, 2H), 7.34 (s. 1H). Found: C, 65.68; H, 5.67; N, 8.28%. Calcd for C_9H_9NS: C, 66.22; H, 5.56; N, 8.58%.

Characterization of other aryl thiocyanate is as follows. NMR and IR spectra of all compounds were consistent with the structure. IR 2126 cm^{-1} (ν_{SCN}). Ethylphenyl(*p*/*o*=2.7), bp 137—139 °C/19 mmHg; Found: C, 66.47; H, 5.61; N, 8.58%. Calcd for C_9H_9NS: C, 66.22; H, 5.56; N, 8.58. Isopropylphenyl(*p*/*o*=5.8), bp 140—142 °C/20 mmHg; Found: C, 67.49; H, 6.27; N, 7.75%. Calcd for $C_{10}H_{11}NS$: C, 67.76; H, 6.25; N, 7.90%. 4-*t*-Butylphenyl, bp 152—154 °C/20 mmHg; Found: C, 69.21; H, 7.00; N, 7.19%. Calcd for $C_{11}H_{13}NS$: C, 69.06; H, 6.85; N, 7.32%. 2,4-Dimethylphenyl, bp 141—143 °C/26 mmHg (lit,[2c] bp 133—134 °C/12 mmHg). 2,4,6-Trimethylphenyl, bp 135—137 °C/28 mmHg, mp 70—72 °C (lit,[3] 71—72 °C). 4-Fluorophenyl, bp 89—91 °C/6 mmHg (lit,[9] bp 103—105 °C/10 mmHg). Chlorophenyl(*p*/*o*=4.7), bp 96.5—97 °C/4 mmHg (lit, *o*-isomer,[9] bp 120—123 °C/9 mmHg; *p*-isomer,[10] mp 35—36 °C. Bromophenyl(*p*/*o*=2.4), bp 130—132 °C/21 mmHg; *p*-isomer, mp 52—53.5 °C (lit,[9] *p*-isomer, mp 53—54 °C).

References

1) J. L. Wood, "Organic Reactions," Wiley and Sons, New York (1946), Vol. III, p. 240.
2) a) A. B. Angus and R. G. R. Bacon, *J. Chem. Soc*, **1958**, 774.
b) R. G. R. Bacon and R. G. Guy, *ibid.*, **1960**, 318.
c) R. G. R. Bacon and R. G. Guy, *ibid.*, **1961**, 2428.
3) E. Söderbäck, *Acta Chem. Scand.*, **8**, 1851 (1954).
4) S. Uemura, S. Uchida, M. Okano, and K. Ichikawa, This Bulletin, **46**, 3254 (1973).
5) E. C. Taylor, F. Kienzle, and A. McKillop, *Syntheses*, **1972**, 38.
6) P. Kovacic and A. K. Sparks, *J. Amer. Chem. Soc.*, **82**, 5740 (1960).
7) S. Uemura, A. Onoe, and M. Okano, This Bulletin, **47**, 147 (1974).
8) A. Onoe, S. Uemura, and M. Okano, *ibid.*, **47**, 2818 (1974).
9) K. Kottke, F. Friedrich, and R. Pohloudek-Fabini, *Arch. Pharm.*, **300**, 583 (1967).
10) A. Hantzsch and B. Hirsch, *Ber.*, **29**, 952 (1896).

Reactions of 2,4,6-Tri-*t*-butylnitrosobenzene with Grignard Reagents

Yoshio INAGAKI, Renji OKAZAKI, and Naoki INAMOTO

Department of Chemistry, Faculty of Science, The University of Tokyo, Hongo, Bunkyo-ku, Tokyo 113

(Received November 27, 1974)

Reactions of 2,4,6-tri-*t*-butylnitrosobenzene (**1**) with alkylmagnesium halides afforded 6-alkyl-1-hydroxyimino-2,4,6-tri-*t*-butyl-2,4-cyclohexadienes (**2**), 4-alkyl-1-hydroxyimino-2,4,6-tri-*t*-butyl-2,5-cyclohexadienes (**3**), and *N*-alkyl-2,4,6-tri-*t*-butylanilines (**4**) depending on the Grignard reagents used. The distribution of the reaction products indicated that the oximes were formed *via* an attack of the anionic species on the *ortho*- and the *para*-carbons, respectively, to the nitroso group, but that the *N*-alkylanilines *via* a free radical mechanism involving an electron transfer from the Grignard reagent to **1**. The free radical mechanism was confirmed in the case of *t*-butylmagnesium chloride by trapping the *t*-butyl radicals as 1-*t*-butoxyimino-2,4,4,6-tetra-*t*-butyl-2,5-cyclohexadiene (**8**). Such a mechanistic difference has been explained in terms of the difference in electron affinities of the free radicals derived from Grignard reagents.

As part of studies on the steric effects in the reactions of 2,4,6-tri-*t*-butylaniline (**6**) and 2,4,6-tri-*t*-butylnitrosobenzene (**1**),[1-4] we investigated the reaction of **1** with Grignard reagents.

In the reactions of nitrosobenzenes with Grignard reagents, the formation of *N*,*N*-disubstituted hydroxylamines, secondary amines, and azobenzenes has been demonstrated,[5-9] and the free radical mechanism has been proposed for the formation of the hydroxylamines.[10]

We have preliminarily communicated, in the reactions of **1**, Grignard reagents attack not only the nitrogen atom but also the *ortho*- and *para*-positions of the nitroso group.[11] This paper describes detailed accounts of these reactions and discuss the factors influencing the products distribution and the reaction mechanism.

Results and Discussion

Reaction Products. Reactions of 2,4,6-tri-*t*-butylnitrosobenzene (**1**) with a large excess of Grignard reagents (RMgX) in ether under nitrogen for *ca.* 1 hr at 0 °C, in which an ethereal solution of **1** was added dropwise into a solution of the Grignard reagent, gave 6-alkyl-1-hydroxyimino-2,4,6-tri-*t*-butyl-2,4-cyclohexadienes (**2**), 4-alkyl-1-hydroxyimino-2,4,6-tri-*t*-butyl-2,5-cyclohexadienes (**3**), *N*-alkyl-2,4,6-tri-*t*-butylanilines (**4**), 6-alkyl-2,4-di-*t*-butylanilines (**5**), and 2,4,6-tri-*t*-butylaniline (**6**) depending on the R group. The yields of the products are shown in Table 1.

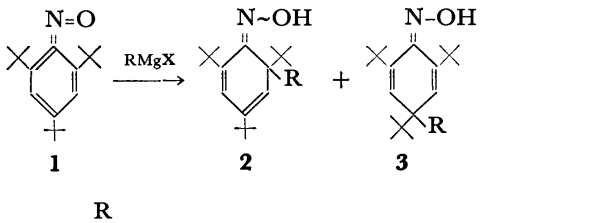

R	
a	Me
b	Et
c	*i*-Pr
d	*t*-Bu
e	$PhCH_2$
f	1-Ad*

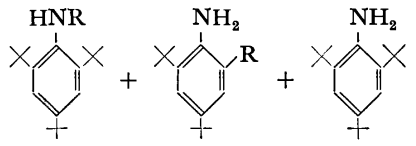

* Ad represents adamantyl group.

TABLE 1. YIELD (%) OF THE REACTION PRODUCTS

	RMgX	2	3	4	5	6
a	MeMgI	46	4	—	—	2
b	EtMgBr	26	30	—	—	8
c	*i*-PrMgBr	2	54	6	3	—
d	*t*-BuMgCl	—	trace	43	—	38
e	$PhCH_2MgCl$	29	44	—	—	6
f	1-AdMgBr	—	55	—	—	3

The structures of the products were confirmed by their analytical and spectral data. Two isomeric oximes (**2** and **3**) were distinguished each other by the UV spectra: isomers with absorption maxima at longer wave length (304—313 nm) were identified as **2**, whereas those with absorption maxima at shorter wave length (243—251 nm) as **3**. There are also some differences between the NMR spectra of the two isomers: a typical spectrum of **2** consists of three singlets due to the three *t*-butyl groups and a pair of doublets due to the two olefinic protons, but a typical spectrum of **3** consists of two singlets with intensity of 2 : 1 due to the *t*-butyl groups and an AB quartet due to the two olefinic protons. However, in the case of **3e** the three *t*-butyl groups appeared as three singlets with equal intensity and the two olefinic protons were equivalent. The abnormality may be ascribed to magnetic anisotropy of the phenyl group.

The oximes **2** and **3** correspond to the 1,4- and 1,6-conjugate addition products of the Grignard reagents to the nitrosobenzene (**1**) respectively, and this is the first example of conjugate addition to the nitrosobenzene system in marked contrast with a great many examples of conjugate addition in carbonyl compounds.[12]

The formation of **4c** and **4d** is noteworthy in view of difficult preparation of the corresponding methyl and ethyl derivatives,[13] the only known *N*-alkylated 2,4,6-tri-*t*-butylanilines; this reaction might provide a synthetic method for 2,4,6-tri-*t*-butylanilines with a bulky alkyl group on the nitrogen.

Mass Spectra of the Reaction Products. The oxime (**2**) was characterized by the four outstanding peaks at *m/e* M−56, M−73, M−87, and M−89, but the oxime (**3**) by the three peaks at *m/e* M−56, M−73, and M−89. The oximes (**2** and **3**) showed very weak molecular ion peaks, which were often obscure

in the oxime (**3**), but the metastable ion peak corresponding to loss of isobutylene (56 mass units) from the molecular ion was observed.

Two outstanding peaks M^+ (23—47%) and $(M-15)^+$ (100%) were characteristic of the anilines **4a**, **4b**, **4c**, **5c**, and **6**. Namely, loss of a methyl radical from the molecular ion was the predominant process, and the corresponding metastable ion peak was observed.

In contrast with those five anilines, the aniline **4d** showed a weak peak at *m/e* 302 (M−15) but outstanding peaks at *m/e* 317 (M^+, 11%), 261 (M−56, 33%), and 246 (M−71, 100%). A metastable ion peak corresponding to loss of 56 mass units from the molecular ion was observed. Therefore the pronounced feature of aniline **4d** is loss of isobutylene (56 mass units) from the molecular ion. Radical cation of **6** thus produced readily loses a methyl radical, as mentioned above, to exhibit the base peak.

Reaction Mechanism. The yields of the products changed systematically depending on the R group. As the bulkiness of the R group increases from methyl to 1-adamantyl (1-Ad), the yield of oxime **2** with a longer conjugate system decreased, while the yield of sterically less hindered oxime **3** increased. The yield ratios of the oximes (**2**/**3**) were alike each other in the reactions of the ethyl and the benzyl Grignard reagents with primary anionic centers, but much different in other cases. Thus the yields of **2** or **3** seem to be dependent mainly on a steric factor.

On the other hand, formation of the secondary amine **4** seems to be independent of the steric factor. Namely, the reaction with *t*-butylmagnesium chloride produced **4d** as a major product along with **3d** only a trace amount. whereas 1-adamantylmagnesium bromide which has also a tertiary anionic center afforded the oxime (**3f**) in a high yield. Moreover, the reactions with methyl, ethyl, and benzyl Grignard reagents did not afford **4**, although they should be sterically much more favorable in the attack onto the nitrogen.

These facts suggest the difference in the formation mechanisms of the oximes (**2** and **3**) and the secondary amine (**4**); the oximes were produced *via* attack of the anionic species on the *ortho*- and *para*-carbons to the nitroso group, while the secondary amine (**4**) *via* the following pathway involving an electron transfer from the Grignard reagent to the nitrosobenzene (**1**)

$$\mathrm{Ar\text{-}N{=}O + RMgX \rightarrow [Ar\text{-}\dot{N}\text{-}O\text{-}MgX + R\cdot]} \quad \mathbf{7}$$
$$\rightarrow \mathrm{ArN(R)OMgX} \xrightarrow{\mathrm{RMgX}} \mathrm{ArN(R)MgX} \xrightarrow{\mathrm{H_2O}} \mathbf{4}$$
(Ar: 2,4,6-(t-Bu)$_3$C$_6$H$_2$)

Such a mechanistic difference can be interpreted as the difference in electron affinitiy of a free radical (R·). The relation between the electron affinities of free radicals and the yields of reaction products is shown in Table 2, in which the order of electron affinities of methyl, ethyl, and isopropyl radicals suggests that the electron affinity of *t*-butyl radical is smaller than that of isopropyl radical. Since 1-adamantyl radical is not so much stabilized as *t*-butyl radical because of its rigid structure,[17] the electron affinity should be much higher than that of *t*-butyl radical. Hence the easiness of the oxidation of the alkyl anion into the corresponding free radical is in the following order:

$$\mathrm{Me} < \mathrm{Et},\ \mathrm{PhCH_2} < i\text{-Pr} < t\text{-Bu} \gg \text{1-Ad}$$

A similar order has recently been reported also for the rates of electron transfer reactions from Grignard reagents to di-*t*-butyl peroxide.[16]

In the case of isopropyl and *t*-butyl Grignard reagents, isopropyl and *t*-butyl anions are so easily oxidized into the corresponding free radicals by **1** that the free radical mechanism which produces **4** is predominant. However, in other cases the anions are not easily oxidized into the corresponding free radicals, so that the anionic mechanism which produces oximes **2** and **3** is predominant. Consequently the Grignard reagents containing an anionic center which is more easily oxidized than isopropyl anion are expected to afford the secondary amine **4** in the reaction with **1**.

If such a free radical mechanism is actually operative, the *t*-butyl radicals derived from the Grignard reagent, in the reaction system composed of *t*-butylmagnesium chloride and an excess of the nitrosobenzene **1**, are expected to attack **1** itself on the oxygen atom, because tertiary alkyl radicals are trapped by **1** on the oxygen atom.[4,18]

This possibility was examined by the following inverse Grignard reaction. To a solution of **1** in ether, an ethereal solution of *t*-butylmagnesium chloride was added dropwise, but the total amount of the Grignard reagent added was a large excess in order to attain a similar final condition. This reaction resulted in the formation of 1-*t*-butoxyimino-2,4,4,6-tetra-*t*-butyl-2,5-cyclohexadiene (**8**) at the expense of **4d**; **8** is the same type of compound as **9** produced by the reaction of **1** with 1-cyano-1-methylethyl radicals.[4]

Thus, this result shows the existence of *t*-butyl radicals in the reaction system, and therefore substantiate the free radical mechanism mentioned above.

The reaction of **1** with *t*-butylmagnesium chloride

Table 2. Relation between yields of reaction products and electron affinities of alkyl radicals

R	Me	Et	*i*-Pr	*t*-Bu	$PhCH_2$	1-Ad
4 (%)	—	—	6	43	—	—
2 + **3** (%)	50	56	56	trace	73	55
Electron affinities of R· (eV)	1.1[a]	0.9[a]	0.6[a]	—	1.8[a], 0.9[b]	—
$-\log k$[c] (l. mol^{-1} sec^{-1})	5.4	3.8	2.8	2.3	—	—

a) Data from electrode reactions.[14] b) Data in gas phase.[15] c) k denotes the rate constants of the reaction of Grignard reagents with di-*t*-butyl peroxide.[16]

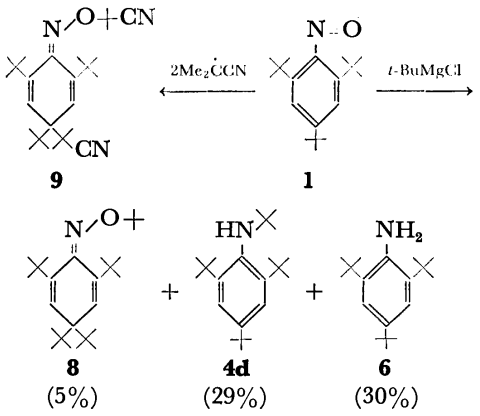

gave a considerable amount of **6** in contrast with the reactions with the other five Grignard reagents. Considering the facility of an electron transfer from *t*-butylmagnesium chloride mentioned above, the following pathway appears to be the most probable for the formation of the aniline (**6**): the radical **7** initially formed by an electron transfer from *t*-butylmagnesium chloride as in the formation of **4** is further reduced by the Grignard reagent to give **10**, hydrolysis of which afford **6**.[19]

$$\underset{\mathbf{1}}{Ar\text{-}N{=}O} \xrightarrow{RMgX} \underset{\mathbf{7}}{ArNOMgX} \xrightarrow{2RMgX} \underset{\mathbf{10}}{ArN(MgX)_2} \xrightarrow{H_2O} \underset{\mathbf{6}}{ArNH_2}$$

(Ar: 2,4,6-(*t*-Bu)$_3$C$_6$H$_2$)

The formation mechanism of **5c** is obscure. Since a nucleophilic substitution on the aromatic ring of **1** is improbable, it was presumably formed by reduction of oxime **2c** accompanied by elimination of *t*-butyl group.

Experimental

All melting points were not corrected. The IR and UV spectra were recorded with Hitachi EPI-G2 and Hitachi EPS-3 spectrophotometers respectively. The NMR spectra were measured with a Hitachi R-24 (60 MHz) spectrometer using tetramethylsilane as an internal standard. The mass spectra were recorded with a Hitachi RMU-6L mass spectrometer. All reactions were carried out under nitrogen. Chromatographic separations were performed using dry column chromatography method (Woelm silica gel for dry column chromatography) unless otherwise noted.

Materials. 2,4,6-Tri-*t*-butylnitrosobenzene (**1**),[1] (mp 166.0—166.5 °C; lit, 166—168 °C), 2,4,6-tri-*t*-butylaniline (**6**), (mp 135.5—138.6 °C; lit, 147—148 °C),[13] 2,4,6-tri-*t*-butyl-*N*-methylaniline (**4a**), (mp 109.5—111.0 °C; lit, 111—112 °C),[13] and 2,4,6-tri-*t*-butyl-*N*-ethylaniline (**4b**), (mp 79.5—81.0 °C; lit, 77.78 °C)[13] were prepared by the reported methods.

Reaction of 2,4,6- Tri- t- butylnitrosobenzene (1) with Methylmagnesium Iodide. To an ice-cold ethereal solution (25 ml) of methylmagnesium iodide (31 mmol), 2 g (7.3 mmol) of **1** in 30 ml of ether was added with stirring. After stirring at 0 °C for 3.5 hr, the reaction mixture was poured into cold aqueous ammonium chloride, extracted with ether, washed with water and dried over anhydrous magnesium sulfate. After removal of the solvent *in vacuo*, the residue (1.9 g) was chromatographed on silica gel. Elution with carbon tetrachloride gave 147 mg of white crystals, which were submitted to dry column chromatography with carbon tetrachloride to give 30 mg (2%) of 2,4,6-tri-*t*-butylaniline (**6**), the IR and NMR spectra of which were identical with those of an authentic sample, and 83 mg (4%) of 1-hydroxyimino-2,4,6-tri-*t*-butyl-4-methyl-2,5-cyclohexadiene (**3a**), which was recrystallized three times from aqueous methanol, mp 119.5—120 °C; IR (KBr): 3250 (νOH) and 960 cm^{-1} (νNO); NMR (CCl_4): δ 0.83 (s, 9H), 1.05 (s, 3H), 1.21 (s, 18H), 5.77 (ABq, $\Delta\delta$=0.11, J=2 Hz, 2H), and 7.68 (broad s, 1H); λ_{max} (*n*-hexane): 243 nm (ε 10300); MS: *m/e* 291 (M$^+$, trace), 235 (34%), 218 (43), 202 (46), and 57 (100).

Found: C, 78.29; H, 11.06; N, 5.03%. Calcd for $C_{19}H_{33}NO$: C, 78.28; H, 11.42; N, 4.80%.

Elution with benzene gave 915 mg (46%) of 1-hydroxyimino-2,4,6-tri-*t*-butyl-6-methyl-2,4-cyclohexadiene (**2a**), which was recrystallized three times from *n*-hexane, mp 160.8—161.5 °C; IR (KBr): 3250 (νOH) and 960 cm^{-1} (νNO); NMR ($CDCl_3$): δ 0.96 (s, 9H), 1.08 (s, 9H), 1.32 (s, 12H), 5.42 (d, J=2 Hz, 1H), 6.15 (d, J=2 Hz, 1H), and 9.30 (broad s, 1H); λ_{max} (*n*-hexane): 304 nm (ε 4400); MS: *m/e* 291 (M$^+$, trace), 235 (42%), 218 (60), 204 (46), 202 (41), and 57 (100).

Found: C, 78.29; H, 11.06; N, 5.03%. Calcd for $C_{19}H_{33}NO$: C, 78.28; H, 11.42; N, 4.80%.

Further elution with dichloromethane afforded only tarry mass which could not be identified.

Reaction of 1 with Ethylmagnesium Bromide. To an ice-cold ethereal solution (30 ml) of ethylmagnesium bromide (73 mmol), 2 g (7.3 mmol) of **1** in 25 ml of ether was added dropwise during 15 min with stirring. After additional stirring at 0 °C for 1 hr, the reaction mixture was worked up as usual to give 1.79 g of the residue, which was chromatographed with carbon tetrachloride. The column could be divided into six fractions, each of which was eluted with ether, and the solvent was removed. From the first fraction a trace of **1** was recovered. The second fraction gave white crystals (129 mg), which were tentatively assigned as an isomer of 1-hydroxyimino-2,4,6-tri-*t*-butyl-6-ethyl-2,4-cyclohexadiene (**2b**) from the spectral data, but not purified, IR (KBr): 3300 (νOH) and 970 cm^{-1} (νNO); NMR (CCl_4): δ 0.83 (t, J=7 Hz, 3H), 0.84 (s, 9H), 1.05 (s, 9H), 1.23 (s, 9H), 2.50 (m, 2H), 5.15 (d, J=2 Hz, 1H), and 6.13 (d, J=2 Hz, 1H, and the signal of OH proton was obscure); λ_{max} (*n*-hexane): 311 nm (ε 3400); MS: *m/e* 305 (M$^+$, 2%), 249 (46), 232 (79), 218 (41), 216 (59), and 57 (100).

The third fraction afforded 143 mg (8%) of **6**. The fourth fraction afforded 692 mg (30%) of 1-hydroxyimino-2,4,6-tri-*t*-butyl-4-ethyl-2,5-cyclohexadiene (**3b**), which was recrystallized five times from methanol, mp 120.2—121.1 °C; IR (KBr): 3300 (νOH) and 970 cm^{-1} (νNO); NMR ($CDCl_3$): δ 0.67 (t, J=7 Hz, 3H), 0.85 (s, 9H), 1.27 (s, 18H), 1.65 (q, J=7 Hz, 2H), 5.75 (ABq $\Delta\delta$=0.14, J=2 Hz, 2H), and 8.24 (broad s, 1H): λ_{max} (*n*-hexane): 246 nm (ε 8800); MS: *m/e* 305 (M$^+$, trace), 249 (49%), 232 (63), 216 (58), and 57 (100).

Found: C, 78.56; H, 11.36; N, 4.52%. Calcd for $C_{20}H_{35}NO$: C, 78.63; H, 11.55; N, 4.58%.

The fifth fraction gave 589 mg (26%) of 1-hydroxyimino-2,4,6-tri-*t*-butyl-6-ethyl-2,4-cyclohexadiene (**2b**), which was recrystallized four times from methanol, mp 123.5—124.5 °C; IR (KBr): 3400 (νOH) and 970 cm^{-1} (νNO); NMR ($CDCl_3$): δ 0.75 (t, J=7 Hz, 3H), 0.93 (s, 9H), 1.10 (s, 9H), 1.33 (s, 9H), 1.4—2.3 (m, 2H), 5.33 (d, J=1.5 Hz, 1H), 6.22 (d, J=1.5 Hz, 1H), and 9.75 (broad s, 1H); λ_{max} (*n*-hexane): 308 nm (ε 4400); MS: *m/e* 305 (M$^+$, 0.5%),

249 (37), 232 (62), 218 (37), 216 (43), and 57 (100).

Found: C, 78.69; H, 11.20; N, 4.74%. Calcd for $C_{20}H_{35}NO$: C, 78.63; H , 11.55; N, 4.58%.

Reaction of **1** *with Isopropylmagnesium Bromide.* To an ice-cold ethereal solution (30 ml) of isopropylmagnesium bromide (73 mmol), 2 g (7·3 mmol) of **1** in 23 ml of ether was added dropwise during 15 min with stirring. After additional stirring at 0 °C for 30 min, the reaction mixture was worked up as usual to give 1.95 g of a tarry material, which was chromatographed with carbon tetrachloride. The column could be divided into six fractions. The first fraction gave 129 mg (6%) of 2,4,6-tri-*t*-butyl-*N*-isopropylaniline (**4c**), which was recrystallized three times from methanol, mp 80.5—81.0 °C; IR (KBr): 3440 cm^{-1} (νNH); NMR (CCl_4): δ 0.94 (d, J=7 Hz, 6H), 1.28 (s, 9H), 1.43 (s, 18H), 3.42 (sep, J=7 Hz, 1H), 3.90 (broad s, 1H), and 7.07 (s, 2H); λ_{max} (*n*-hexane): 256.5 (ε 7500) and 292 nm (1400); MS: *m/e* 303 (M^+, 41%) and 288 (100).

Found: C, 83.04; H, 12.27; N, 4.90%. Calcd for $C_{21}H_{37}N$: C, 83.10; H, 12.29; N, 4.61%.

The second fraction afforded 308 mg of a mixture of **2c** and **3c** (by NMR). Further twice dry column chromatography with carbon tetrachloride gave 53 mg (2%) of 1-hydroxyimino-2,4,6-tri-*t*-butyl-6-isopropyl-2,4-cyclohexadiene (**2c**), which was recrystallized three times from methanol, mp 117—120 °C; IR (KBr): 3300 (νOH) and 975 cm^{-1} (νNO); NMR (CCl_4): δ 0.71 (d, J=7 Hz, 6H), 1.07 (s, 9H), 1.13 (s, 9H), 1.24 (s, 9H), 3.72 (sep, J=7 Hz, 1H), 5.62 (d, J=2 Hz, 1H), and 6.12 (d, J=2 Hz, 1H, and the signal of OH proton was obscure); λ_{max} (*n*-hexane): 311 nm (ε 4900); MS: *m/e* 319 (M^+, trace), 263 (19%), 246 (63), 232 (56), 230 (70), and 57 (100).

Found: C, 78.53; H, 11.67; N, 4.20%. Calcd for $C_{21}H_{37}NO$: C, 78.94; H, 11.67; N, 4.38%.

The third fraction gave 1.24 g (54%) of 1-hydroxyimino-2,4,6-tri-*t*-butyl-4-isopropyl-2,5-cyclohexadiene (**3c**) as a tarry material, which crystallized on cooling and was recrystallized five times from cold methanol at −78 °C, mp 73.5—74.5 °C; IR (neat): 3330 (νOH) and 975 cm^{-1} (νNO); NMR ($CDCl_3$): δ 0.96 (d, J=7 Hz, 6H), 0.93 (s, 9H), 1.27 (s, 18H), 1.95 (sep, J=7 Hz, 1H), 5.90 (ABq, $\Delta\delta$=0.16, J= 2 Hz, 2H, and the signal of OH proton was obscure, but in carbon tetrachloride solution observed at 8.60 as a broad singlet); λ_{max} (*n*-hexane): 246.5 nm (ε 8800); MS: *m/e* 319 (M^+, trace), 263 (41%), 246 (54), 230 (61), and 57 (100).

Found: C, 79.04; 11.75; N, 4.56%. Calcd for $C_{21}H_{37}NO$: C, 78.94; H, 11.67; N, 4.38%.

The fourth fraction afforded 50 mg (3%) of 2,4-di-*t*-butyl-6-isopropylaniline (**5c**), which was recrystallized twice from methanol and identical with an authentic sample obtained from the reaction of 2,4,6-tri-*t*-butylnitrobenzene with isopropylmagnesium bromide[22] with respect to the spectral data, mp 84—85 °C; IR (KBr): 3485 and 3405 cm^{-1} (νNH_2); NMR (CCl_4): δ 1.20 (d, J=7 Hz, 6H), 1.26 (s, 9 H), 1.43 (s, 9H), 2.89 (sep, J=7 Hz, 1H), 3.54 (broad s, 2H), and 7.00 (ABq, $\Delta\delta$=0.08, J=2 Hz, 2H); MS: *m/e* 247 (M^+, 23%) and 232 (100).

Reaction of **1** *with t-Butylmagnesium Chloride.* To an ice-cold ethereal solution (40 ml) of *t*-butylmagnesium chloride (73 mmol), 2 g (7.3 mmol) of **1** in 15 ml of ether was added dropwise during 10 min with stirring. After additional stirring at 0 °C for 50 min, the reaction mixture was worked up as usual to give 1.79 g of crystals, which were chromatographed with carbon tetrachloride. The column was divided into four fractions. The first fraction gave 993 mg (43%) of 2,4,6,*N*-tetra-*t*-butylaniline (**4d**), which was recrystallized four times from methanol, mp 63—64.5 °C; IR (KBr): 3045 cm^{-1} (νNH); NMR ($CDCl_3$): δ 0.93 (s, 9H), 1.28 (s, 9H), 1.42 (s, 18H), 3.00 (broad s, 1H), and 7.14 (s, 2H); λ_{max} (*n*-hexane): 223 (ε 1680) and 260 nm (4200); MS: *m/e* 317 (M^+, 11%), 302 (4), 261 (33), and 246 (100).

Found: C, 83.33; H, 12.22; N, 4.21%. Calcd for $C_{22}H_{39}N$: C, 83.21; H, 12.38; N, 4.41%.

The second fraction afforded 714 mg (38%) of **6**. The third fraction gave 84 mg of a colorless tarry substance, which was again chromatographed with carbon tetrachloride. On the basis of the spectral data (IR and NMR) the resulting material was identified as 1-hydroxyimino-2,4,4,6-tetra-*t*-butyl-2,5-cyclohexadiene (**3d**), but failed to be isolated in pure state, IR (neat): 3300 (νOH) and 955 cm^{-1} (νNO); NMR (CCl_4): δ 1.01 (s, 18H), 1.25 (s, 18H), 6.17 (ABq, $\Delta\delta$=0.12, J=2 Hz, 2H, and the signal of OH proton was obscure).

Reaction of **1** *with Benzylmagnesium Chloride.* To an ice-cold ethereal solution (30 ml) of the Grignard reagent (73 mmol), 2 g (7.3 mmol) of **1** in 15 ml of ether was added dropwise during 20 min with stirring. After additional stirring at 0 °C for 30 min, the reaction mixture was worked up as usual to give 4.2 g of partly crystalline substance, which was chromatographed with carbon tetrachloride. The column could be divided into five fractions. The first and the second fractions gave 1.4 g of bibenzyl and 150 mg (6%) of **6** respectively. The third fraction gave 1.16 g (44%) of 1-hydroxyimino-4-benzyl-2,4,6-tri-*t*-butyl-2,5-cyclohexadiene (**3e**), which was recrystallized four times from methanol, mp 169.7—170.8 °C; IR (KBr): 3280 cm^{-1} (νOH); NMR ($CDCl_3$): δ 0.98 (s, 9H), 1.09 (s, 9H), 1.21 (s, 9H), 3.04 (s, 2H), 5.95 (s, 2H), 7.12 (s, 5H), and 7.55 (broad s, 1H); λ_{max} (*n*-hexane): 247 nm (ε 9200); MS: *m/e* 367 (M^+, trace), 311 (34%), 294 (32), 278 (28), 91 (79), and 57 (100).

Found: C, 81.88; H, 10.38; N, 4.01%. Calcd for $C_{25}H_{37}NO$: C, 81.69; H, 10.15; N, 3.81%.

The fourth fraction gave 776 mg (29%) of 1-hydroxyimino-6-benzyl-2,4,6-tri-*t*-butyl-2,4-cyclohexadiene (**2e**), which was recrystallized four times from methanol, mp 158—158.5 °C; IR (KBr): 3280 cm^{-1} (νOH); NMR ($CDCl_3$): δ 0.89 (s, 9H), 0.99 (s, 9H), 1.28 (s, 9H), 2.85 (d, J=15 Hz, 1H), 3.78 (d, J=15 Hz, 1H), 5.47 (d, J=2 Hz, 1H), 6.20 (d, J=2 Hz, 1H), 7.14 (s, 5H), and 8.75 (broad s, 1H); λ_{max} (*n*-hexane): 313 nm (ε 4000); MS: *m/e* 367 (M^+, 1.5%), 311 (32), 294 (100), 276 (15), 278 (26), 91 (43), and 57 (82).

Found: C, 81.91; H, 10.33; N, 3.85%. Calcd for $C_{25}H_{37}NO$: C, 81.74; H, 10.08; N, 3.81%.

Reaction of **1** *with 1-Adamantylmagnesium Bromide.* To an ice-cold ethereal solution (31 ml) of the Grignard reagent (42 mmol), 1.76 g (6.4 mmol) of **1** in 24 ml of ether was added dropwise during 1 hr with stirring. The reaction mixture was worked up as usual to give 7.9 g of light green tar, which was chromatographed with carbon tetrachloride as eluent. The column could be divided into four fractions. The first fraction gave 5 g of a light green crystalline material, which was composed mainly of decomposition product of the Grignard reagent, but contained 300 mg of unchanged **1** according to the signal intensity on the NMR spectra. Yields were calculated on the base of **1** consumed. The second fraction, colorless tarry mass, was a mixture of **6** (36 mg, 3%) and 1-hydroxyimino-4-(1-adamantyl)-2,4,6-tri-*t*-butyl-2,5-cyclohexadiene (**3f**, 1.2 g, 55%) according to the signal intensity on the NMR spectra. By further chromatography with carbon tetrachloride, **3f** was isolated, but **6** could not be isolated in pure state. **3f**: mp 135—136 °C

(five times from methanol); IR (KBr): 3300 (νOH) and 960 cm^{-1} (νNO); NMR (CCl_4): δ 1.05 (s, 9H), 1.28 (s, 18H), 1.60 (broad s, 6H), 1.82 (broad s, 9H), 6.15 (ABq, $\Delta\delta=0.1$, $J=2$ Hz, 2H), and 7.86 (s, 1H); λ_{max} (*n*-hexane): 251 nm (ε 9300); MS: *m/e* 411 (M^+, trace), 355 (2%), 354 (3), 339 (6), 338 (3), 324 (5), 322 (3), 244 (23), 135 (100), and 57 (31).

Found: C, 81.72; H, 10.71; N, 3.36%. Calcd for $C_{28}H_{45}NO$: C, 81.69; H, 11.03; N, 3.40%.

The subsequent fractions afforded about 700 mg of unidentified materials, which could not be isolated in pure state.

Reaction of **1** *with* t-*Butylmagnesium Chloride (Inverse Addition).* To an ice-cold solution of 1.5 g (5.5 mmol) of **1** in 10 ml of ether, an ethereal solution (43 ml) of the Grignard reagent (55 mmol) was added dropwise with stirring during 30 min. After additional stirring at 0 °C for 30 min, the reaction mixture was worked up as usual to give 1.5 g of pale yellow, partly crystalline material, which was chromatographed with *n*-hexane. The column could be divided into three fractions. The first fraction gave 110 mg (5%) of 1-*t*-butoxyimino-2,4,4,6-tetra-*t*-butyl-2,5-cyclohexadiene (**8**) as colorless oil, which was purified by TLC (silica gel, *n*-hexane) and distilled once *in vacuo*, IR (neat): 960 cm^{-1} (νNO); NMR (CCl_4): δ 1.00 (s, 18H), 1.21 (s, 9H), 1.29 (s, 18H), and 6.15 (ABq, $\Delta\delta=0.1$, $J=2$ Hz, 2H); λ_{max} (*n*-hexane): 260 nm (ε 6700); MS: *m/e* 332 (38%), 276 (88), 244 (43).

Found: C, 80.26; H, 11.81; N, 3.89%. Calcd for $C_{26}H_{47}NO$: C, 80.14; H, 12.16; N, 3.59%.

The second fraction gave 477 mg (29%) of **4d**. The third fraction was again chromatographed with a mixture of *n*-hexane and dichloromethane (2 : 1) as eluent. The column could be divided into three fractions. The first fraction gave 421 mg (30%) of **6**. The second fraction afforded 49 mg (3%) of 1-hydroxyimino-2,4,4,6-tetra-*t*-butyl-2,5-cyclohexadiene (**3d**) as white crystals, which were recrystallized three times from aqueous methanol, mp 123—127 °C. Although satisfactory elemental analysis could not be obtained, the following spectral data suggested the structure **3d**; IR (KBr): 3300 (νOH) and 955 cm^{-1} (νNO); NMR (CCl_4): δ 1.02 (s, 18H), 1.26 (s, 18H), 6.17 (ABq, $\Delta\delta=0.12$, $J=2$ Hz, 2H), and 8.0 (broad s, 1H); λ_{max} (*n*-hexane): 249 nm (ε 9700); MS: *m/e* 277 (16%), 276 (14), 260 (28), 246 (30), 244 (43), and 57 (100).

The subsequent fractions gave 82 mg of partly crystalline substance, which could not be purified.

Mass Spectra of Anilines ***4a***, ***4b***, *and* ***6a***. **4a**; *m/e* 275 (M^+, 30%) and 260 (100). **4b**; *m/e* 239 (M^+, 47%) and 224 (100). **6**; *m/e* 261 (M^+, 27%) and 246 (100).

References

1) R. Okazaki, T. Hosogai, E. Iwadare, M. Hashimoto, and N. Inamoto, This Bulletin, **42**, 3611 (1969).

2) R. Okazaki, T. Hosogai, M. Hashimoto, and N. Inamoto, *ibid.*, **42**, 3559 (1969).

3) R. Okazaki and N. Inamoto, *J. Chem. Soc., B*, **1970** 1583.

4) T. Hosogai, N. Inamoto, and R. Okazaki, *J. Chem. Soc., C*, **1971**, 3399.

5) H. Wieland and A. Roseeu, *Ber.*, **45**, 494 (1912).

6) *idem*, *ibid.*, **48**, 1117 (1915).

7) H. Wieland and F. Kögl, *ibid.*, **55**, 1798 (1922).

8) H. Gilman and R. McCracken, *J. Amer. Chem. Soc.*, **49**, 1052 (1927).

9) G. A. Russell, E. G. Jantzen, and E. J. Strom, *ibid.*, **86**, 1807 (1964).

10) K. Maruyama, This Bulletin, **37**, 1013 (1964).

11) R. Okazaki, Y. Inagaki, and N. Inamoto, *Chem. Commun.*, **1974**, 414.

12) M. S. Kharasch and O. Reinmuth, "Grignard Reagents for Nonmetallic Substances," Prentice-Hall, Engelwood Cliffs, N. J., p. 196 (1954); R. C. Fuson, *Adv. Organometal. Chem.*, **1**, 221 (1964), Academic Press, New York; T. Eicher, in "The Chemistry of the Carbonyl Group," ed. by S. Patai, Interscience Publishers, New York, p. 621 (1966).

13) J. Burgers, M. A. Hoefnagel, P. E. Verkade, H. Visser, and B. M. Wepster, *Rec. Trav. Chim.*, **77**, 491 (1958).

14) H. O. Pritchard, *Chem. Rev.*, **52**, 529 (1953).

15) A. F. Gaines and F. M. Page, *Trans. Faraday Soc.*, **59**, 1266 (1963).

16) W. A. Nugent, F. Bertini, and J. K. Kochi, *J. Amer. Chem. Soc.*, **96**, 4945 (1974).

17) C. Rüchardt, *Angew. Chem., Internat. Ed. Engl.*, **9**, 830 (1970).

18) S. Terabe and R. Konaka, *J. Chem. Soc., Perkin II*, **1973**, 369.

19) The possibility of the reduction of **1** into **6** with magnesium metal, probably in combination with magnesium halides or impurities in the metal, cannot be ruled out completely.[20,21] If **6** is formed in such a way, the yield of **6** should be constant irrespective of the Grignard reagents used, but this is not the case. Therefore the reduction with magnesium metal may not be a predominant pathway leading to **6**.

20) M. S. Kharasch and S. Weinhouse, *J. Org. Chem.*, **1**, 209 (1936).

21) E. C. Ashby, J. Laemmle, and H. M. Neumann, *Accounts Chem. Res.*, **7**, 272 (1974).

22) R. Okazaki, Y. Inagaki, and N. Inamoto, *Chem. Lett.*, **1974**, 1503.

The Mass-transfer Rate through the Liquid-Liquid Interface. V. Diffusion through an Interface Considering the Variation in the Amount of Adsorption

Teruya SHIMBASHI

Department of Chemical Engineering, Tokyo Institute of Technology, Meguro-ku, Tokyo 152

(Received November 28, 1973)

The diffusion through an interface has been re-formulated considering the variation in the amount of adsorption on the interface in the case of linear diffusion in a finite composite medium.

In the treatment of the diffusion of a substance through interfaces,[1-4] it has generally been assumed that the flux from one phase to the interface is equal to the flux from the interface to the other phase; this implies that the amount of adsorption on the interface is constant during the diffusion process.

Accordingly, if the concentration in a phase immediately next to the interface, which is in an equilibrium relation with the amount of adsorption, actually varies during the diffusion process, the above treatment may give erroneous results.

In this paper, the diffusion through an interface will be theoretically treated by allowing the amount of adsorption on the interface to vary reasonably during the diffusion process in case of linear diffusion in a finite composite medium.[5]

Theory

Fick's diffusion equation is defined by:

$$\partial c_1/\partial t = D_1(\partial^2 c_1/\partial x^2),\ -a<x<0,\ t>0; \tag{1}$$

$$\partial c_2/\partial t = D_2(\partial^2 c_2/\partial x^2),\ 0<x<a,\ t>0, \tag{2}$$

where c_1 and c_2 are the local concentrations of the solute in Phases 1 and 2 respectively, where D_1 and D_2 are the diffusion coefficients, where x is the diffusion coordinate (the direction from Phase 1 to Phase 2 is selected as positive), and where t is the time.

The boundary conditions are represented by:

$$-D_1(\partial c_1/\partial x) + D_2(\partial c_2/\partial x) = \Gamma_\infty(\mathrm{d}\theta/\mathrm{d}t),\ x=0,\ t>0; \tag{3}$$

$$-D_1(\partial c_1/\partial x) = k_{a1}c_1(1-\theta) - k_{d1}\theta,\ x=0,\ t>0; \tag{4}$$

$$D_2(\partial c_2/\partial x) = k_{a2}c_2(1-\theta) - k_{d2}\theta,\ x=0,\ t>0; \tag{5}$$

$$\partial c_1/\partial x = 0,\ x=-a,\ t>0; \tag{6}$$

$$\partial c_2/\partial x = 0,\ x=a,\ t>0, \tag{7}$$

where Γ_∞ is the saturated value of the amount of adsorption per unit of area of the interface, where θ is the fraction of the total interface that is occupied by adsorbed molecules, where k_{a1} and k_{a2} are the rate constants of adsorption to the interface from Phase 1 and Phase 2 respectively, and where k_{d1} and k_{d2} are the rate constants of desorption from the interface to Phase 1 and Phase 2 respectively. Equation (3) relates the variation in the amount of adsorption to the fluxes, while Eqs. (4) and (5) give the relation between the adsorption-desorption mechanism and the fluxes. Equations (6) and (7) give the impermeable wall conditions of the solute.

The initial conditions are assumed to be:

$$c_1 = c_{10},\ -a<x<0,\ t=0; \tag{8}$$

$$c_2 = c_{20},\ 0<x<a,\ t=0; \tag{9}$$

$$\theta = \theta_0,\ x=0,\ t=0, \tag{10}$$

where c_{10}, c_{20}, and θ_0 are constants.

The Laplace transforms of these equations are represented by:

$$\mathrm{d}^2\bar{c}_1/\mathrm{d}x^2 - q_1^2\bar{c}_1 + (c_{10}/D_1) = 0,\ -a<x<0; \tag{1'}$$

$$\mathrm{d}^2\bar{c}_2/\mathrm{d}x^2 - q_2^2\bar{c}_2 + (c_{20}/D_2) = 0,\ 0<x<a; \tag{2'}$$

$$-D_1(\mathrm{d}\bar{c}_1/\mathrm{d}x) + D_2(\mathrm{d}\bar{c}_2/\mathrm{d}x) = \Gamma_\infty(p\bar{\theta}-\theta_0),\ x=0; \tag{3'}$$

$$-D_1(\mathrm{d}\bar{c}_1/\mathrm{d}x) = k_{a1}\bar{c}_1 - \frac{k_{a1}}{2\pi i}\times\int_{x_1-i\infty}^{x_1+i\infty}\bar{c}_1(\sigma)\bar{\theta}(p-\sigma)\mathrm{d}\sigma - k_{d1}\bar{\theta},\ x=0; \tag{4'}$$

$$D_2(\mathrm{d}\bar{c}_2/\mathrm{d}x) = k_{a2}\bar{c}_2 - \frac{k_{a2}}{2\pi i}\times\int_{x_2-i\infty}^{x_2+i\infty}\bar{c}_2(\sigma)\bar{\theta}(p-\sigma)\mathrm{d}\sigma - k_{d2}\bar{\theta},\ x=0; \tag{5'}$$

$$\mathrm{d}\bar{c}_1/\mathrm{d}x = 0,\ x=-a; \tag{6'}$$

$$\mathrm{d}\bar{c}_2/\mathrm{d}x = 0,\ x=a, \tag{7'}$$

where $\bar{c}_1$, $\bar{c}_2$, and $\bar{\theta}$ are the image functions corresponding to c_1, c_2, and θ respectively, where p is the conversion parameter of the Laplace transformation, and where $q_1=(p/D_1)^{1/2}$ and $q_2=(p/D_2)^{1/2}$.

The general solution of Eqs. (1') and (2') may be represented by:

$$\bar{c}_1 = (c_{10}/p) + A_1\sinh(q_1x) + B_1\cosh(q_1x); \tag{11}$$

$$\bar{c}_2 = (c_{20}/p) + A_2\sinh(q_2x) + B_2\cosh(q_2x), \tag{12}$$

where A_1, B_1, A_2, and B_2 are the intergration constants.

These four constants can be solved by virtue of the boundary conditions of Eqs. (4')—(7'). Equation (3') is considered to define the mediate variable, $\bar{\theta}$. If we set the non-linear terms in Eqs. (4') and (5') at zero for the moment, we obtain a solution for the zero perturbation; by then substituting this solution into the non-linear terms, we obtain the solution for the first perturbation, and so on. The solution for the ith perturbation may be represented as:

$$\bar{c}_{1,i}(p) = (c_{10}/p) - A_{1,i}\cosh[q_1(a+x)]; \tag{13}$$

$$\bar{c}_{2,i}(p) = (c_{20}/p) - A_{2,i}\cosh[q_2(a-x)]; \tag{14}$$

$$\bar{\theta}_i(p) = (\theta_0/p) + \Gamma_\infty^{-1}[A_{1,i}q_1^{-1}\sinh(q_1a) + A_{2,i}q_2^{-1}\sinh(q_2a)]; \tag{15}$$

$$A_{1,i} \equiv (pD)^{-1}[\alpha_{1,i}\sinh(q_2a) + \beta_{1,i}\cosh(q_2a)];$$

$$A_{2,i} \equiv (pD)^{-1}[\alpha_{2,i}\sinh(q_1a) + \beta_{2,i}\cosh(q_1a)];\ .$$

$$\alpha_{1,i} \equiv \Gamma_\infty D_1 q_1 [k_{a1}(c_{10} - pI_{1,i}) - k_{d1}\theta_0] + q_1^{-1}[k_{a1}k_{d2}(c_{10} - pI_{1,i}) - k_{a2}k_{d1}(c_{20} - pI_{2,i})];$$

$$\beta_{1,i} \equiv k\Gamma_\infty k_{a2}[k_{a1}(c_{10} - pI_{1,i}) - k_{d1}\theta_0];$$

$$\alpha_{2,i} \equiv k\{\Gamma_\infty D_1 q_1 [k_{a2}(c_{20} - pI_{2,i}) - k_{d2}\theta_0] - q_1^{-1}[k_{a1}k_{d2}(c_{10} - pI_{1,i}) - k_{a2}k_{d1}(c_{20} - pI_{2,i})]\};$$

$$\beta_{2,i} \equiv k\Gamma_\infty k_{a1}[k_{a2}(c_{20} - pI_{2,i}) - k_{d2}\theta_0];$$

$$\boldsymbol{D} \equiv [a_1 \sinh(q_1 a) + a_2 \cosh(q_1 a)] \sinh(q_2 a) + [a_3 \sinh(q_1 a) + a_1 \cosh(q_1 a)] \cosh(q_2 a);$$

$$a_1 \equiv D_1(\Gamma_\infty p + k_{d1} + k_{d2});$$

$$a_2 \equiv k_{a1}(\Gamma_\infty D_1 q_1 + k_{d2} q_1^{-1});$$

$$a_3 \equiv k k_{a2}(\Gamma_\infty D_1 q_1 + k_{d1} q_1^{-1});$$

$$a_4 \equiv k\Gamma_\infty k_{a1} k_{a2};$$

$$k \equiv (D_1/D_2)^{1/2};$$

$$I_{1,i+1} \equiv \frac{1}{2\pi i}\int_{x_1-i\infty}^{x_1+i\infty} [\bar{c}_{1,i}(\sigma)]_{x=0}\bar{\theta}_{,i}(p-\sigma)\mathrm{d}\sigma;$$

$$I_{2,i+1} \equiv \frac{1}{2\pi i}\int_{x_2-i\infty}^{x_2+i\infty} [\bar{c}_{2,i}(\sigma)]_{x=0}\bar{\theta}_{,i}(p-\sigma)\mathrm{d}\sigma,$$

where the subscript i designates the ith perturbation, provided $I_{1,0}=I_{2,0}=0$.

$\bar{c}_{1,i}$, $\bar{c}_{2,i}$, and $\bar{\theta}_{,i}$ are single-valued functions of an arbitrary complex number of p; the inversion to the original functions by the Inversion Theorem, like the integrals of non-linear terms ($I_{1,i}$, $I_{2,i}$), includes only the pole-effects, according to Cauchy's Residue Theorem.

$\bar{c}_{1,i}$, $\bar{c}_{2,i}$, and $\bar{\theta}_{,i}$ have only simple poles at $p=0$ and $p=-D_1\alpha_m^2$, where $\pm\alpha_m$ ($m=1, 2, \cdots$) are the roots (generally complex) of

$$[b_1 \sin(a\alpha) + b_2 \cos(a\alpha)] \sin(ka\alpha) + [b_3 \sin(a\alpha) + b_4 \cos(a\alpha)] \cos(ka\alpha) = 0, \quad (16)$$

where: $b_1 \equiv D_1(\Gamma_\infty D_1\alpha^2 - k_{d1} - k_{d2})$;

$b_2 \equiv -k_{a1}(\Gamma_\infty D_1\alpha - k_{d2}\alpha^{-1})$;

$b_3 \equiv -k k_{a2}(\Gamma_\infty D_1\alpha - k_{d1}\alpha^{-1})$;

$b_4 \equiv k\Gamma_\infty k_{a1}k_{a2}$.

Inversion to the original functions gives:

$$c_{1,i} = k_{a2}k_{d1}A + 2\sum_{n=1}^{\infty}[\boldsymbol{D}']^{-1}[\xi_{1,i}\sin(ka\alpha_n) + \eta_{1,i}\cos(ka\alpha_n)]\cos[(a+x)\alpha_n]\exp(-D_1\alpha_n^2 t); \quad (17)$$

$$c_{2,i} = k_{a1}k_{d2}A + 2\sum_{n=1}^{\infty}[\boldsymbol{D}']^{-1}[\xi_{2,i}\sin(a\alpha_n) + \eta_2\cos(a\alpha_n)]\cos[k(a-x)\alpha_n]\exp(-D_1\alpha_n^2 t); \quad (18)$$

$$\theta_{,i} = k_{a1}k_{a2}A - 2\Gamma_\infty^{-1}\sum_{n=1}^{\infty}[\alpha_n\boldsymbol{D}']^{-1}\{[\xi_{1,i}\sin(ka\alpha_n) + \eta_{1,i}\cos(ka\alpha_n)]\sin(a\alpha_n) + [\xi_2\sin(a\alpha_n) + \eta_{2,}\cos(a\alpha_n)]k^{-1}\sin(ka\alpha_n)\}\exp(-D_1\alpha_n^2 t); \quad (19)$$

$$A \equiv [a(k_{a1}k_{d2} + k_{a2}k_{d1}) + \Gamma_\infty k_{a1}k_{a2}]^{-1}[a(c_{10}+c_{20}) + \Gamma_\infty\theta);$$

$$\boldsymbol{D}' \equiv [\phi_1\sin(a\alpha_n) + \phi_2\cos(a\alpha_n)]\sin(ka\alpha_n) + [\phi_3\sin(a\alpha_n) + \phi_4\cos(a\alpha_n)]\cos(ka\alpha_n);$$

$$\phi_1 \equiv -\Gamma_\infty D_1[2D_1 + a(k_{a1} + k^2{}_{a2})] + a\alpha_n^{-2}(k_{a1}k_{d2} + k^2 k_{a2}k_{d1});$$

$$\phi_2 \equiv -\Gamma_\infty D_1^2 a\alpha_n + \alpha_n^{-1}\{a[k^2\Gamma_\infty k_{a1}k_{a2} + D_1(k_{d1}+k_{d2})] + \Gamma_\infty k_{a1}D_1\} + k_{a1}k_{d2}\alpha_n^{-3};$$

$$\phi_3 \equiv k(-\Gamma_\infty D_1^2 a\alpha_n + \alpha_n^{-1}a[\Gamma_\infty k_{a1}k_{a2} + D_1(k_{d1}+k_{d2})] + \Gamma_\infty k_{a2}D_1\} + k_{a2}k_{d1}\alpha_n^{-3});$$

$$\phi_4 \equiv ka[\Gamma_\infty D_1(k_{a1}+k_{a2}) - \alpha_n^{-2}(k_{a1}k_{d2} + k_{a2}k_{d1})];$$

$$\xi_{1,i} \equiv -\Gamma_\infty D_1\alpha_n^{-1}[k_{a1}(c_{10} + D_1\alpha_n^2 I_{1,i}) - k_{d1}\theta_0 + \alpha_n^{-3}[k_{a1}k_{d2}(c_{10} + D_1\alpha_n^2 I_{1,i}) - k_{a2}k_{d1}(c_{20} + D_1\alpha_n^2 I_{2,i})];$$

$$\eta_{1,i} \equiv k\Gamma_\infty k_{a2}\alpha_n^{-2}[k_{a1}(c_{10} + D_1\alpha_n^2 I_{1,i}) - k_{d1}\theta_0];$$

$$\xi_{2,i} \equiv -k\{\Gamma_\infty D_1\alpha_n^{-1}[k_{a2}(c_{20} + D_1\alpha_n^2 I_{2,i}) - k_{d2}\theta_0] + \alpha_n^{-3}[k_{a1}k_{d2}(c_{10} + D_1\alpha_n^2 I_{1,i}) - k_{a2\,d1}(c_{20} + D_1\alpha_n^2 I_{2,i})]\};$$

$$\eta_{2,i} \equiv k\Gamma_\infty k_{a1}\alpha_n^{-2}[k_{a2}(c_{20} + D_1\alpha_n^2 I_{2,i}) - k_{d2}\theta_0],$$

where $I_{1,i}$ and $I_{2,i}$ are the values[6] at $p=-D_1\alpha_n^2$.

The amounts of the solute in Phase 1 and Phase 2 per unit of area of the interface are represented as:

$$Q_1 = \int_{-a}^{0} c^*{}_1\mathrm{d}x = k_{a2}k_{d1}aA + 2\sum_{n=1}^{\infty}[\boldsymbol{D}']^{-1}[\xi^*{}_1\sin(ka\alpha_n) + \eta^*{}_1\cos(ka\alpha_n)]\alpha_n^{-1} \times \sin(a\alpha_n)\exp(-D_1\alpha_n^2 t); \quad (20)$$

$$Q_2 = \int_0^{a} c^*{}_2\mathrm{d}x = k_{a1}k_{d2}aA + 2\sum_{n=1}^{\infty}[\boldsymbol{D}']^{-1}[\xi^*{}_2\sin(a\alpha_n) + \eta^*{}_2\cos(a\alpha_n)](ka\alpha_n)^{-1} \times \sin(ka\alpha_n)\exp(-D_1\alpha_n^2 t), \quad (21)$$

where the superscript * indicates the convergence value.

Remarks on the Application

Figures 1 and 2 show the time-dependences of the transfer amount of the solute and of the coverage of the interface giving hypothetical values to the parameters in Eqs. (21) and (19). Sample 1 corresponds to the case of less interfacial resistance ($\Delta F^{\ddagger}{}_{di}\sim 4$ kcal/mol), and Samples 2 and 3, to the cases of a distinct interfacial resistance ($\Delta F^{\ddagger}{}_{di}\sim 16$ kcal/mol), where $\Delta F^{\ddagger}{}_{di}$ is the activation free energy of desorption from interface into the ith phase.[7] The dotted curve gives the relation obtained by the usual equation of the semi-infinite composite medium. The equilibrium transfer-amount is computed to be 1.5×10^{-6} mol/cm^2.

The values of the rate constants of adsorption and desorption are given by the following equations:[7]

$$k_{ai} = \lambda_i\frac{\boldsymbol{k}T}{\boldsymbol{h}}\exp(-\Delta F^{\ddagger}{}_{ai}/\boldsymbol{R}T);$$

$$k_{di} = \Gamma_\infty\frac{\boldsymbol{h}T}{\boldsymbol{h}}\exp(-\Delta F^{\ddagger}{}_{di}/\boldsymbol{R}T);$$

$i=1$ and 2, where λ_i ($\sim$10 Å) is the length of the adsorption path from the boundary site of phase i to the interface; $\Delta F^{\ddagger}{}_{ai}$ is the activation free energy of adsorption from phase i to the interface; $\boldsymbol{k}$ is the Boltzmann constant; $\boldsymbol{h}$ is the Planck constant; $\boldsymbol{R}$ is the

gas constant, and T ($\sim$300 K) is the absolute temperature.

The procedure of calculation is as follows.

Assign definite values to k, D_1, Γ_∞, a, k_{a1}, k_{a2}, k_{d1}, and k_{d2} in Eq. (16), and find the positions of the pole on the plane of the complex variable, p. Although the roots of Eq. (16), α_m ($m=1, 2, \cdots$), are generally complex, they are real in our case.

Assign the values to k, D_1, Γ_∞, a, k_{a1}, k_{a2}, k_{d1}, k_{d2}, c_{10}, c_{20}, θ_0, and α_n's ($n\leq 20$ suffices for convergence in our case if $t>1$ s) in Eqs. (21) and (19), and compute the amount of the solute in Phase 2, Q_2, and the coverage, θ, as functions of the time, t. In our case, $\theta\sim 0.005\ll 1$, and the Q_2 and the θ were computed approximately by means of the zero perturbation (see Eqs. (4) and (5)).

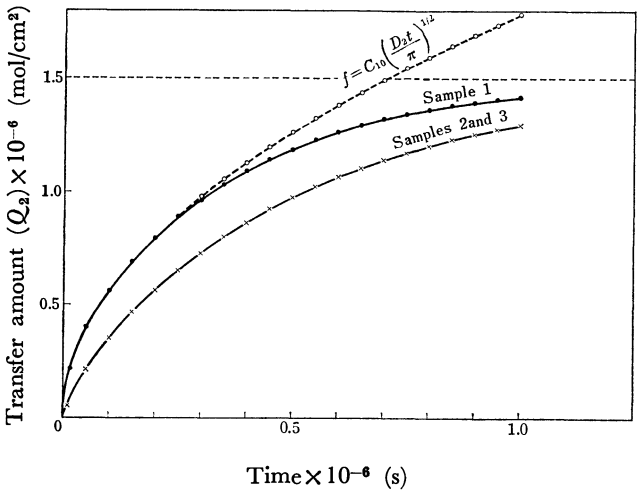

Fig. 1. Time dependences of the transfer amount.

Sample		1	2	3
k	[−]	1	1	1
D_1	[cm²/s]	10^{-5}	10^{-5}	10^{-5}
Γ_∞	[mol/cm²]	7×10^{-10}	7×10^{-10}	7×10^{-10}
a	[cm]	3	3	3
k_{d1}	[mol/(cm²) s]	1	10^{-9}	5×10^{-9}
k_{d2}	[mol/(cm²) s]	1	5×10^{-9}	10^{-9}
k_{a1}	[cm/s]	10^4	10^{-5}	5×10^{-5}
k_{a2}	[cm/s]	10^4	5×10^{-5}	10^{-5}
C_{10}	[mol/cm³]	10^{-6}	10^{-6}	10^{-6}
C_{20}	[mol/cm³]	0	0	0
θ_0	[−]	0	0	0

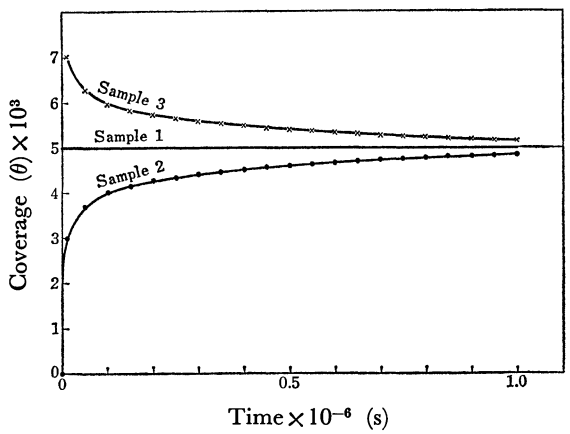

Fig. 2. Time dependences of the coverage of interface.

The curves of Samples 2 and 3 are distinctly below the curve of Sample 1 in Fig. 1, suggesting the possibility of the determination of the interfacial resistances (of this magnitude) by experimental observations of the time-dependence of the transfer amount.

The curves of Samples 2 and 3 are degenerate to a single curve in Fig. 1, indicating the impossibility of the determination of k_{d1} and k_{d2}[8] separately by the same experiment.

On the contrary, the curves of Samples 2 and 3 are greatly separated from each other, and the signs of the tangent differ in a short time in Fig. 2, suggesting the possibility of the determination of the rate-controlling step of desorption by an observation of the interfacial tensions for early stages.

On reflection, the manipulative disturbance on bringing two layers into contact for a transfer experiment may not strictly be avoidable; also, a spontaneous turbulence[9] is likely to occur near the touching time of two layers. These disturbances may generally accelerate the transfer of the solute. We must consider the effect of these disturbances on the analysis of the experimental data.

Suppose that an abnormally swift transfer ceases by $t=\Delta t$, and that the final condition of concentration is approximately given by $c_1=c'_{10}$, $-a<x<0$, $t=\Delta t$; $c_2=c'_{20}$, $0<x<a$, $t=\Delta t$; $\theta=\theta'_0$, $x=0$, $t=\Delta t$, where c'_{10}, c'_{20}, and θ'_0 are constants.

Let the origin of time be transferred to $t=\Delta t$, so that Eq. (21) is applicable.

The rate-controlling step of desorption may be conventionally set up on the side of second phase (for example), by virtue of the exchangeability of the values of k_{d1} and k_{d2}; when k_{d1} is sufficiently greater than k_{d2}, $c'_{10}=c'_{10}(c'_{20})$, and $\theta'_0=\theta'_0(c'_{20})$.

Consequently we may obtain approximate values of k_{di} ($i=1$ or 2), evaluated under the name of k_{d2} in Eq. (21), and c'_{20} by means of experimental determinations of the transfer amount through an interface at each contact time $t(\gg\Delta t)$. The following results of computation show the extent of approximation: $k_{d1}=5\times 10^{-9}$ mol/cm² s, $k_{d2}=0.999\times 10^{-9}$ mol/cm² s, $c'_{20}=1.001\times 10^{-7}$ mol/cm³; $k_{d1}=1$ mol/cm² s, $k_{d2}=0.833\times 10^{-9}$ mol/cm² s, $c'_{20}=1.001\times 10^{-7}$ mol/cm³ ($k=(D_1/D_2)^{1/2}=1$, $D_1=10^{-5}$ cm²/s, $\Gamma_\infty=7\times 10^{-10}$ mol/cm², $a=3$ cm, $K_1=k_{a1}/k_{d1}=10^4$ cm³/mol, $K_2=k_{a2}/k_{d2}=10^4$ cm³/mol, $c_{10}=10^{-6}$ mol/cm³, $c_{20}=\theta_0=0$, $t(1)=5\times 10^5$ s, $t(2)=10^5$ s, $Q_2(1)=1.080\times 10^{-6}$ mol/cm², $Q_2(2)=5.825\times 10^{-7}$ mol/cm²).

The author is indebted to Professors Hikoji Inazumi and Tadao Shiba of this Institute for their helpful discussions concerning this subject.

References

1) E. J. Scott, L. H. Tung, and H. G. Drickamer, *J. Chem. Phys.*, **19**, 1075 (1951).
2) P. L. Auer and E. W. Murbach, *ibid.*, **22**, 1054 (1954).
3) J. Crank, "The Mathematics of Diffusion", Oxford

University Press, London (1956).

4) T. Shimbashi and T. Shiba, This Bulletin, **38**, 581, 588 (1965).

5) The diffusion in the composite spherical system can also be treated in the same way.

6) The calculation of $I_{1,t}$ and $I_{2,t}$ is easy but somewhat lengthy including the double poles, and so it is omitted here.

7) T. Shimbashi and T. Shiba, This Bulletin, **38**, 572 (1965).

8) k_{a1} and k_{a2} are to be shown as functions of k_{d1} and k_{d2} respectively, provided the equilibrium constants of adsorption are known.

9) C. V. Sternling and L. E. Scriven, *A. I. Ch. E. J.*, **5**, 514 (1959).

Surface Tension of Aqueous Solutions of Disodium Monoalkyl Phosphates and Their Mixtures[1)]

Masayuki NAKAGAKI and Tetsurou HANDA

Faculty of Pharmaceutical Sciences, Kyoto University, Sakyo-ku, Kyoto 606

(Received April 9, 1974)

Disodium mono-dodecyl, mono-tetradecyl, and mono-hexadecyl phosphates were synthesized and the surface tension of aqueous solutions of each disodium monoalkyl phosphate (SAP) and of their mixtures were measured. On the basis of the surface tension values thus obtained, the influence of the hydrocarbon chain length of SAP and the effect of the mixing of SAP on the adsorption and the micelle formation were discussed. A modified Szyszkowski equation was derived from the Gibbs adsorption equation and the modified Langmuir adsorption equation by using the activity instead of the concentration. The modified Szyszkowski equation gave calculated values which were in good agreement with the experimental values of the surface tension. It was also found that the energy of adsorption per methylene group, ω, is 682 cal/mol. In mixed solutions, the modified Szyszkowski equation was used to obtain results in good agreement with the measured values of the surface tension, assuming an ideal mixing of SAP in the adsorption layer. Further, the change in the standard free energy was calculated for the micelle formation for each SAP from the hypothetical standard state of the hydrated monomer in solution; it gave the energy of micelle formation per methylene group, ω_m, is 613 cal/mol. The theoretical equation to give the cmc of SAP, was obtained also, assuming the ideal mixing of SAP in the mixed micelle phase; it was proved to be in good agreement with the experimental values of the cmc.

Disodium monoalkyl phosphates (SAP) are interesting materials because they are bi-valent anionic surfactants, in contradistinction to the anionic detergents extensively used, which are mostly uni-valent. This group of surfactants is interesting also as a model compound of phospholipid because it containes a phosphate group, which might have properties different from many other uni-valent polar groups.

Disodium mono-dodecyl and mono-hexadecyl phospates have previously been synthesized in this laboratory, and the degree of hydrolysis of the ester bond measured. As a result, it has been concluded that the aqueous solution of SAP was very stable, at least, at room temperature.[2,3)] The surface tensions of aqueous solutions of these compounds were measured at various concentrations of added salt, and the adsorption amount of SAP at the air-water interface was calculated by applying the Gibbs adsorption equation. It was shown that S-shaped adsorption isotherms were obtained when the adsorption amount was plotted against the concentration, but Langmuir adsorption isotherms of the usual shape were obtained when the same data were plotted against the activity of SAP in the solutions. Furthermore, it was concluded that the activity at the critical micelle concentration was constant, irrespective of the concentration of the added salt.[4,5)]

In the present paper, the influence of the length of the hydrocarbon chain of SAP on the adsorption and the micelle formation will be discussed on the basis of the surface-tension measurements of aqueous solutions of disodium mono-dodecyl, -tetradecyl and -hexadecyl phosphates (SDP, STP and SHP respectively). The adsorption and the micelle formation of mixtures of SAP will also be discussed on the basis of the surface-tension measurements, the latter being performed in 0.01 M sodium hydroxide in order to diminish the binding of H^+ to the long-chain anion in the solutions.[6,7)] By using the experimental values of the surface tension, the modified Szyszkowski equation which is derived from the Gibbs adsorption equation and the modified Langmuir adsorption equation, using the activity instead of the concentration, are tested. A good agreement between the theory and experiments is obtained. As a result, the saturated adsorption amount and the Langmuir coefficients for each SAP are obtained. The theory is then extended to an aqueous solution of mixed SAP.

Experimental

Synthesis of Monoalkyl Phosphoric Acid and Preparation of the Solution of Disodium Salts. Monoalkyl phosphoric acid is synthesized from pyrophosphoric acid and an alcohol of the corresponding chain length, C_{12}, C_{14} or C_{16} in benzene,

$$ROH+H_4P_2O_7=ROPO(OH)_2+H_3PO_4$$

where R is a hydrocarbon chain. Alcohol (0.5 mol) and pyrophosphoric acid (0.7 mol) are dissolved in 200 ml of benzene in an Erlenmeyer flask, after which the mixture is allowed to stand for 4 days at room temperature. The benzene is then evaporated, and the viscous liquid produced dissolved in 300 ml of ether. The ether solution is then added to 500 ml of 1.5 M NaOH solution to extract the product, after which the ethereal layer is separated from the aqueous layer. The pH of the aqueous solution, 12.5, is then changed to 0.5 by the addition of concentrated HCl. The monoalkyl phosphoric acid thus precipitated is extracted with 300 ml of ether. The ether is then evaporated, and the crude product is vacuum-desiccated. Recrystallization from hexane gives a white, crystalline product. Found: C, 54.22; H, 10.13; P, 11.59%. Calcd for $C_{12}H_{26}O_4P$: C, 54.14; H, 10.15; P, 11.70%; mol wt, 265.1. Found: C, 57.24; H, 10.50; P, 10.44%. Calcd for $C_{14}H_{30}O_4P$: C, 57.14; H, 10.54; P, 10.54%; mol wt, 293.1. Found: C, 59.73; H, 10.82; P, 9.50%. Calcd for $C_{16}H_{34}O_4P$: C, 59.62; H, 10.87; P, 9.63%; mol wt. 321.1.

The melting points are 58, 68, and 78 °C respectively in good agreement with the values reported in the litetrature.[8)] An aqueous solution is prepared by dissolving a known amount of monoalkyl phosphoric acid in an adequate amount of NaOH solution. In the final solution, an excess of NaOH (0.01 M) should be remained to prevent the hydrolysis of di-valent phosphate.

Surface-tension Measurements. The surface-tension is measured by the capillary-rise method at 25 °C in 0.01 M NaOH as the solvent. The Willhelmy method was also tested, but it gave values which were different not only from those obtained by the capillary-rise method but also from those reported in the literature. Therefore, the capillary-rise method is adopted in this work, because it gave the surface tension values which are in good agreement with the reported values.[9] The values of the surface-tension γ, can be calculated from the ratio of the heights of the meniscus above the surface for the solution (h) to that for pure water (h_0). According to the Sugden theory,[10]

$$\gamma = \gamma_0 \times \frac{h\rho}{h_0\rho_0} \times \left(\frac{b}{b_0}\right)$$

Here, γ_0 is the surface tension of pure water and is 71.96 dyn/cm at 25 °C. (b/b_0) is the ratio of the principal radii at the bottom of the meniscus of the solution to that of pure water, the value is obtained from Sugden's table.[10] In our experiments, (b/b_0) is 1.0013 for the solution which had the lowest surface tension. (ρ/ρ_0) is the ratio of the density of the solution to that of pure water; its value was, at most, 1.01. The capillary is washed in a chromic acid-sulfuric acid mixture for a day. It can thus be confirmed that solutions wet the wall of the capillary very well. The solution was once raised by an air pump and then lowered freely in the capillary; the equilibrium value of the height was then read within 15 min at most. The error in the readings for the solution of the same concentration was less than 1%.

Results

Surface Tension of SAP Solutions. The surface tensions of aqueous solutions of SAP were measured in the presence of surface-inactive electrolytes. The concentration of SAP is expressed by C (in M). In the case of a mixed solution of two kinds of SAP, C is used for the total concentration, while the concentrations of the individual SAPs are expressed by C_1 and C_2, where $C_1+C_2=C$. The sodium-ion concentration from the surface-inactive electrolytes is expressed by C'(M), so that the total sodium-ion concentration in the solution is $(2C+C')$. When the added electrolyte is NaOH only, C' is equal to its concentration, but when NaOH and Na_2SO_4 are added, C' is equal to $[NaOH]+2[Na_2SO_4]$.

The surface tension measured as a function of the logarithm of the SAP concentration, C, at the added sodium-ion concentration, $C'=0.01$ M, is given in Fig. 1 for a solution of disodium mono-dodecyl, -tetradecyl, or -hexadecyl phosphotes. When comparison is made at a constant concentration, the surface tensions of SDP, STP, and SHP are found to decrease with the increase in chain length. The kink point for each curve is considered to be the critical micelle concentration (cmc); the values of cmc thus obtained are given in Table 1.

The surface tensions measured as functions of the total concentration, C, are also given in Fig. 1. These solutions contain SDP and SHP at various mole fractions of mixing. The concentration of SDP is $C_1=CX_1$, and that of SHP, $C_2=C(1-X_1)$. X_1 is the mole fraction of mixing. When comparsion is made at a constant total concentration, C, the increase in X_1 increases the surface tension. In other words, the total concentration needed to give a constant surface tension in-

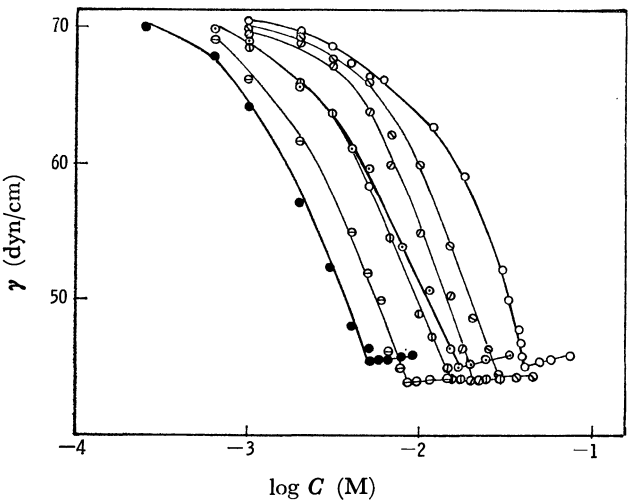

Fig. 1. Surface tension, γ *vs.* log C.
○; SDP, ⊙; STP, ●; SHP, ⓘ; $X_1=0.5$, ⊖; $X_1=0.8$, ⊘; $X_1=0.90$, ⊗; $X_1=0.95$. 25 °C, $C'=0.01$ M.

Table 1. The values of the Langmuir coefficient, k, and the critical micelle concentration (CMC)

	k	CMC (M)
SDP	4.5×10^5	4.0×10^{-2}
STP	4.8×10^6	1.7×10^{-2}
SHP	3.3×10^7	6.0×10^{-3}
$X_1=0.5$	—	1.0×10^{-2}
$X_1=0.8$	—	1.5×10^{-2}
$X_1=0.9$	—	2.0×10^{-2}
$X_1=0.95$	—	3.0×10^{-2}

creases with X_1. At $X_1=0.5$, the total concentration of a mixture is smaller than the concentration of STP for the same surface tension, as is shown in Fig. 2. The kink points are also considered as cmc.

Figure 3 shows the surface tension of an aqueous solution containing SDP and SHP as a function of the concentration of one of them, while the concentration of the other is kept constant. Moreover, both the total sodium-ion concentration, $(2C+C')$, and the ionic strength, J, are kept constant by using a mixture of NaOH and Na_2SO_4 as the added electrolyte. The

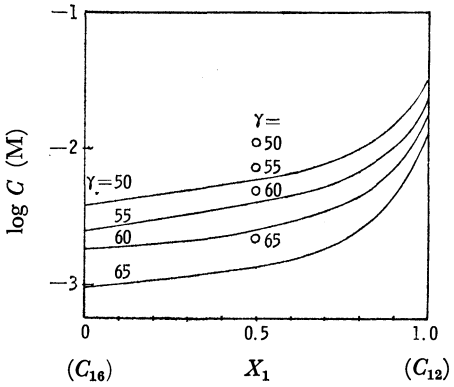

Fig. 2. logarithm of total concentration *vs.* mole fraction of mixing.
The parameter; γ (dyn/cm), ○; STP.

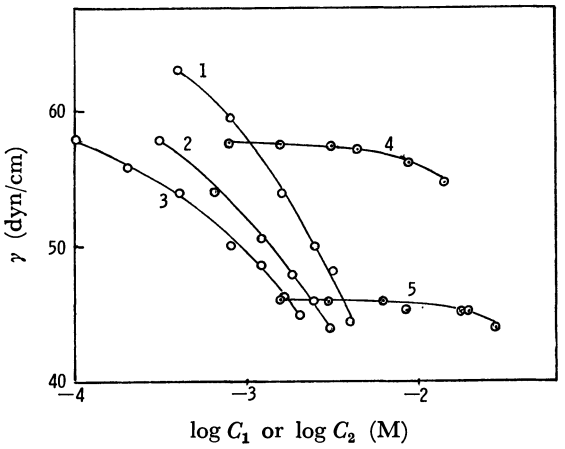

Fig. 3. Surface tension, γ, *vs.* log C_1 or log C_2.
○; γ *vs.* log C_2. Curve 1; $a_1=9.17\times10^{-7}$ ($C_1=4\times10^{-3}$, $C+[Na_2SO_4]=8\times10^{-3}$), 2; $a_1=5.07\times10^{-6}$ ($C=1.2\times10^{-2}$, $C+[Na_2SO_4]=1.5\times10^{-2}$), 3; $a=1.04\times10^{-5}$ ($C_1=1.8\times10^{-2}$, $C+[Na_2SO_4]=2\times10^{-2}$).
⊙; γ *vs.* log C_1. Curve 4; $a_2=3.17\times10^{-7}$ ($C_2=7.5\times10^{-4}$, $C+[Na_2SO_4]=1.5\times10^{-2}$), 5; $a_2=1.36\times10^{-6}$ ($C_2=1.5\times10^{-3}$, $C+[Na_2SO_4]=3\times10^{-2}$).

surface tension changes more with the concentration of SHP, C_2 (Curves 1, 2 and 3) than with that of SDP, C_1 (Curves 4 and 5).

Discussion

Effect of the Chain Length on Adsorption. As is well known,[5,11] the Gibbs adsorption equation is a general equation relating adsorption amount, Γ, surface tension, γ, and activity, a.

$$\Gamma = \frac{-1}{RT}\left(\frac{\partial\gamma}{\partial \ln a}\right)_{T,\,P} \tag{1}$$

The activity of SAP in a single solution, a, is defined as:

$$a = \gamma_{\pm}{}^3C(2C+C')^2 \tag{2}$$

where γ is the mean ionic activity coefficient and can be calculated from the Güntelberg approximation of the Deby-Hückel theory:

$$\log\gamma_{\pm} = \frac{-A\sqrt{J}}{1+\sqrt{J}} \tag{3}$$

Here, J is the ionic strength and A is a constant, whose value is 1.022 for SAP at 25 °C.[12] As has already been stated in our previous papers,[4,5] the modified Langmuir adsorption equation using activity instead of concentration is written as:

$$\Gamma = \frac{\Gamma_s ka}{1+ka} \tag{4}$$

where Γ_s is the saturated adsorption amount and where k is the Langmuir coefficient. Equation (1) is integrated with equation (4) to give the modified Szyszkowski equation:

$$F = \gamma_0 - \gamma = \Gamma_s RT\ln(1+ka) \tag{5}$$

F is the surface pressure and γ_0, the surface tension of pure water. A proper numerical value, k, could give a linear relation between F and ln $(1+ka)$.

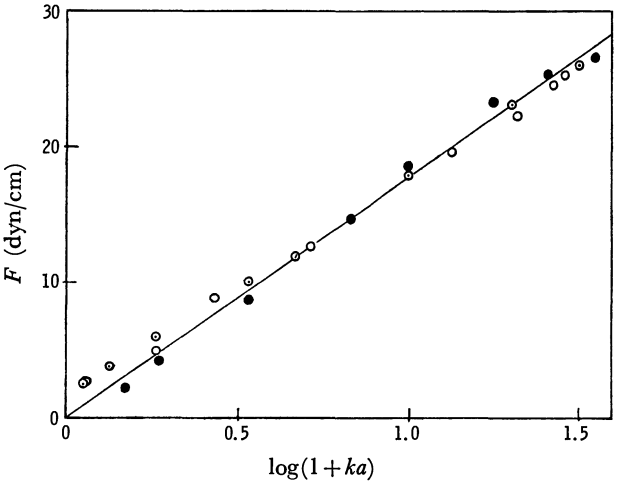

Fig. 4. Surface pressure, F, *vs.* log$(1+ka)$.
○; SDP, ⊙; STP, ●; SHP

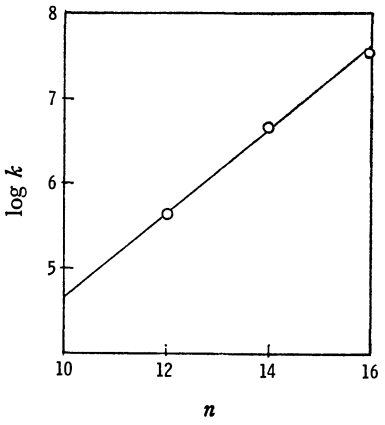

Fig. 5. Logarithm of Langmuir coefficient, log k, *vs.* hydrocarbon length, n.

In Fig. 4, F is plotted against $\ln(1+ka)$. When we used the Langmuir coefficients, the k values of 4.5×10^5, 4.8×10^6, and 3.3×10^7 for SDP, STP, and SHP respectively, the data for these three SAP solutions, plotted in this way, fell on a straight line. The value of Γ_s is 3.1×10^{-10} mol/cm^2, independent of the hydrocarbon-chain length. This corresponds to 53 Å^2 of the area occupied by one molecule. It is shown in Fig. 5 that the logarithm of the Langmuir coefficient, k, changes linearly with the number of carbon atomes in the hydrocarbon-chain, n. This means that the energy of adsorption per methylene group, ω, is constant, because the standard adsorption free energy $\Delta G°$, is given by the following equation:

$$\Delta G° = -RT\ln k \tag{6}$$

The value of ω obtained from the inclination of the straight line in Fig. 5 is 682 cal/mol. This result agrees with Traube's value (ω=650 cal/mol).[13]

Mixed Adsorption of Disodium Monoalkyl Phosphates. Not much works has been reported on the adsorption from aqueous solutions of mixed detergents because of difficulty involved in the calculation of the adsorption amount of each component. It has been shown in our previous paper, moreover that the adsorption

amount calculated directly from the Gibbs adsorption equation and from the modified Szyszkowski equation, which is based on the modified Langmuir adsorption equation, agreed well with each other for an aqueous solution of a single SAP. In this paper, the modified Langmuir adsorption equation is extended to a mixture of the disodium monoalkyl phosphates. Assuming that the mixing of these homologous surfactants in the adsorption layer is ideal, and remembering that Γ_s is independent of the number of carbon atoms, as has been stated in the previous section, the modified Langmuir adsorption equation for a mixed solution may be written as:

$$\Gamma_1 = \frac{\Gamma_s k_1 a_1}{1+k_1a_1+k_2a_2} \tag{7}$$

$$\Gamma_2 = \frac{\Gamma_s k_2 a_2}{1+k_1a_1+k_2a_2} \tag{8}$$

where a_1 and a_2 are the activities of SDP and SHP, where $a_1=\gamma_\pm^3 C_1(2C+C')^2$, and, where $a_2=\gamma_\pm^3 C_2(2C+C')^2$. On the other hand, the Gibbs adsorption equation of a mixed solution is:

$$-d\gamma = \Gamma_1 RT\, d\ln a_1 + \Gamma_2 RT\, d\ln a_2 \tag{9}$$

Equation (9) is integrated with Equation (7) and (8) to give:

$$F = \gamma_0 - \gamma = \Gamma_s RT \ln(1+k_1a_1+k_2a_2) \tag{10}$$

$\ln(1+k_1a_1+k_2a_2)$ is calculated using the values of the Langmuir coefficients, k_1 and k_2, which have previously been obtained for each single solute solution. They are given in Table 1. When F is plotted against $\ln(1+k_1a_1+k_2a_2)$, the linear relation shown in Fig. 6 is obtained. From this slope, the value of $\Gamma_s=3.1\times10^{-10}$ mol/cm^2 is obtained, exactly the same value as was obtained from Fig. 4.

In Fig. 3, the surface tension is measured by holding the activity of one component, $a_2=\gamma_\pm^3 C_2(2C+2[Na_2SO_4]+[NaOH])^2$ or $a_1=\gamma_\pm^3 C_1(2C+2[Na_2SO_4]+[NaOH])^2$, constant; then Equation (9) reduces to either

$$-d\gamma = \Gamma_1 RT\, d\ln a_1 \tag{11}$$

or

$$-d\gamma = \Gamma_2 RT\, d\ln a_2 \tag{12}$$

These equations are integrated using Eq. (7) or (8) respectively; the same equation as Eq. (10) is obtained in both cases. In Fig. 7, the surface pressure, F, is plotted against $\ln(1+k_1a_1+k_2a_2)$. In Figs. 8 and 9, the adsorption amounts, Γ_1 and Γ_2, are calculated from Eqs (11) and (12) respectively by the direct differentiation of the experimental curves and compared with the theoretical values calculated from Eqs (7) and (8). These experimental results agree well with the theoretical ones. Thus, it may be concluded that the modified Langmuir adsorption equation using the activity is valid also in an aqueous solution of mixed SAP, and that the mixing of these homologous surfactants in the adsorption layer is ideal.

Micelle Formation and Chain Length. Herraman treated micelle formation as phase separation and assumed standard states of the hydrated monomer and

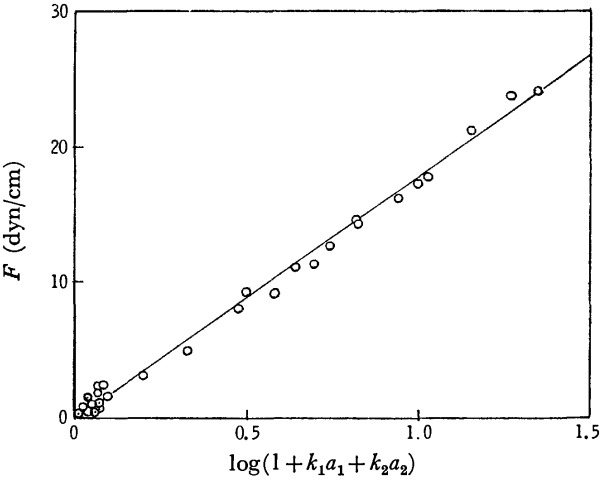

Fig. 7. Surface pressure, F, *vs.* $\log(1+k_1a_1+k_2a_2)$.
——; Theory.

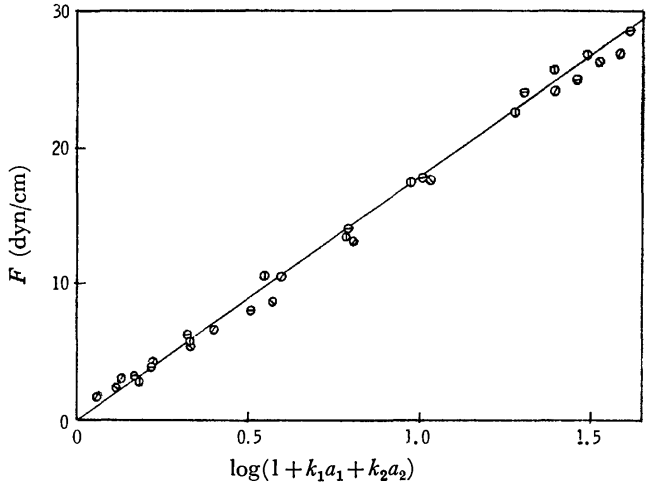

Fig. 6. Surface pressure, F, *vs.* $\log(1+k_1a_1+k_2a_2)$.
⓪; $X_1=0.5$, ⊖; $X_1=0.8$, ⊘; $X_1=0.9$, ⊗; $X_1=0.95$.
——; Theory ($\Gamma_s=3.1\times10^{-10}$ mol/cm^2).

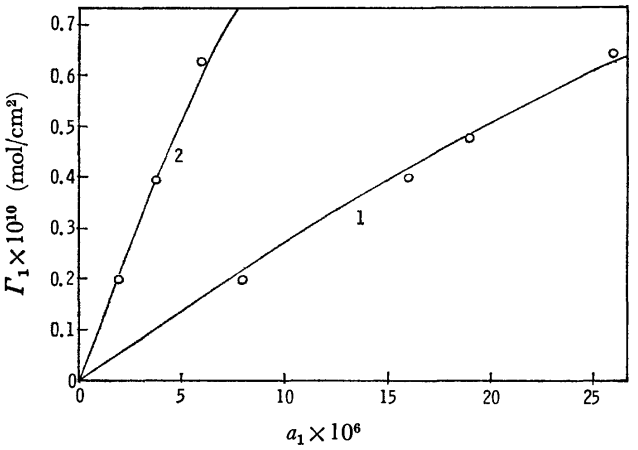

Fig. 8. Adsorption amount Γ_1 *vs.* a_1 (a_2=constant).
1; $a_2=1.37\times10^{-5}$, 2; $a_2=3.17\times10^{-7}$.
——; Calculated from equation (7).

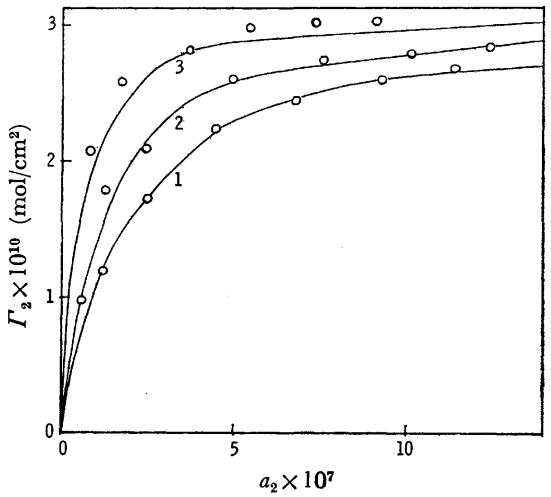

Fig. 9. Adsorption amount Γ_2 *vs.* a_2 (a_1=constant).
1; $a_1=1.05\times10^{-5}$, 2; $a_1=5.07\times10^{-6}$,
3; $a_1=9.17\times10^{-7}$.
——; Calculated from equation (8).

of hydrated micelle in an aqueous solution. Then he showed that the thermodynamic quantities calculated on this basis were in good agreement with the experimental values.[14] Applying his theory to SAP, but using the activity instead of the concentration in Herraman's equation, the standard free energy of the micelle formation, ΔG^*, is written as:

$$\Delta G^* = RT \ln a_m \tag{13}$$

where a_m is the activity at the critical micelle concentration. In the case of SAP, the activity, a_m, is given by the following equation:

$$a_m = \gamma_\pm^3 C_m (2C_m + C')^2 \tag{14}$$

where C_m is the critical micelle concentration of SAP and C' is that of the inorganic salt added to the solution. In our previous paper, it was verified that the micelle formation occurred at a constant activity, irrespective of the added amount of inorganic salt. When the logarithm of a_m is plotted against the number of carbon atoms in the hydrocarbon chain, n, for a solution of each SAP, the linear relation shown by the solid line in Fig. 10 is obtained. The energy of micelle

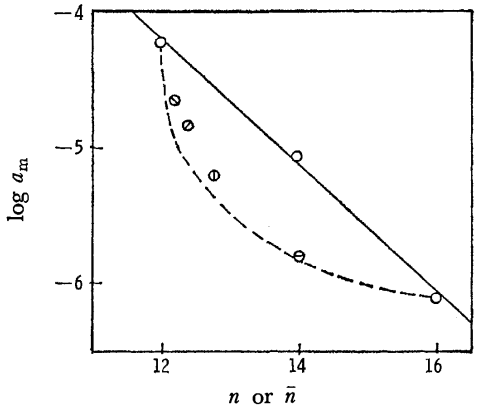

Fig. 10. log a_m *vs.* n or $\bar{n}$.
----; Theory, Eq. (18).

formation per methylene group is therefore, constant and is calculated to be ω =613 cal/mol from the slope of the straight line. On the basis of these results, ΔG^* can be expressed as:

$$\Delta G^* = -n\omega_m + h \tag{15}$$

where h is a constant. As in a previous discussion of the effect of added salt on micelle formation,[4] the critical micelle concentration, C_m, of disodium monoalkyl phosphates can be represented as a function of the counter-ion concentration [Na^+] and the number of carbon atoms in the hydrocarbon chain, n, by the following equation at 25 °C.

$$\log C_m = -31 \log \gamma_\pm - 21 \log[Na^+] - 0.471n + 1.424 \tag{16}$$

Mixed Micelle Formation. Shinoda presented a theory of micelle formation in an aqueous solution of mixed homologous detergents and represented the critical micelle concentration as a function of the hydrocarbon chain length and the mole fraction of mixing.[15] His theory was essentialy based on Hobb's theory[16] and also on the assumption that ideal mixing occurred in a mixed micelle of homologous detergents. In this paper, a theory is derived from a different basis that the activity at the critical micelle concentration is given as a function of the hydrocarbon chain length and the mixing mole fraction of each surfactant.
A mixed micelle is considered to be formed in an aqueous solution of the mixed SAP, and the mixing of the two surfactants in the mixed micelle phase is assumed to be ideal. Then the following equation is obtained:

$$RT \ln a_{m1} = \Delta G^*_1 + RT \ln Y_1 \tag{17}$$

where a_{m1} is the activity of SDP at the critical micelle concentration and where y_1 is its mole fraction in the mixed micelle phase. ΔG_1^* is equal to the ΔG^* of Eq. (15) introduced 12 into n. A similar equation can be written for the 2 component, SHP with n= 16. When y_1 and y_2 are eliminated, the following equation is readily obtained:

$$a_m = e^h (X_1 e^{n_1 \omega_m / RT} + X_2 e^{n_2 \omega_m / RT}) \tag{18}$$

where $a_m = a_{m1} + a_{m2}$, $a_{m1} = X_1 a_m$, and $a_{m2} = X_2 a_m$, because the mean ionic activity coefficients are equal for both components as long as the Güntelberg equation (13) is presumed. Numerical values are introduced into n_1, n_2 and ω_m, and the theoretical value of a_m is calculated. In Fig. 10, the experimental and theoretical values of a_m are compared for various values of the average numbers of carbon atoms:

$$\bar{n} = n_1 X_1 + n_2 X_2 \tag{19}$$

The experimental results plotted are in good agreement with the theoretical values shown by a broken curve. It is, therefore, verified that the theory of ideal mixing is valid for the mixed micelle phase in an aqueous solution of mixed SAP.

References

1) This paper was presented at the 24th Colloquy on Colloid and Interface Chemistry, Gifu, October, 1971.
2) M. Nakagaki and T. Handa, *Yakugaku Zasshi*, **92**, 614 (1972).

3) M. Nakagaki, H. Kishimoto, and K. Hirano, *ibid.*, **90**, 1118, (1970).
4) M. Nakagaki and T. Handa, *ibid.*, **92**, 1490, (1972).
5) M. Nakagaki, T. Handa, and S. Shimabayashi, *J. Colloid Interface Sci.*, **43**, 521, (1973).
6) E. G. Cockbain, *Trans. Faraday Soc.*, **50**, 876, (1954).
7) B. A. Pethica, *ibid.*, **50**, 413 (1954).
8) K. Nelson, *Inorg. Chem.*, **2**, 775, (1963).
9) S. J. Refeld, *J. Phys. Chem.*, **71**, 738, (1967).
10) S. J. Sugden, *J. Chem. Soc.*, **119**, 38, (1921).
11) M. Nakagaki, "Hyomen Jotai to Colloid Jotai," Gendai Buturikagaku Kōza, Vol. 6, Tokyo Kagaku Dōjin (1968).
12) E. Güntelberg, *Z. Phys. Chem.*, **123**, 199, (1926).
13) J. Traube, *Ann.*, **265**, 27, (1891).
14) K. W. Herraman, *J. Phys. Chem.*, **66**, 295 (1962).
15) K. Shinoda, *ibid.*, **58**, 541 (1954).
16) M. E. Hobbs, *ibid.*, **55**, 675, (1951).

ESR Spectra of Monoprotonated Semiquinone Radicals Formed during Photolysis of *p*-Benzoquinone and Its Methyl Derivatives

Tetsuo WARASHINA, Ove EDLUND,* and Hiroshi YOSHIDA*

Research Reactor Institute, Kyoto University, Kumatori-cho, Osaka 590-04

**Faculty of Engineering, Hokkaido University, Kita-ku, Sapporo 060*

(Received May 4, 1974)

Proton hyperfine coupling constants of monoprotonated *p*-benzosemiquinone, durosemiquinone, 2,6-dimethyl-*p*-benzosemiquinone, 2,5-dimethyl-*p*-benzosemiquinone and methyl-*p*-benzosemiquinone radicals were determined from ESR spectra during photolysis of the corresponding quinones under identical conditions, *i.e.*, in ethanol and at about 20 °C. By considering all these constants together, the ESR spectra were assigned and following results obtained: (1) the hydroxyl groups were at the oxygen atom further from the methyl substituents, (2) the coupling constant was generally −1.86—−1.65 G for the hydroxylic protons, (3) the absolute value of the coupling constant for both ring and methyl protons was in the range 0—0.7 G for *ortho*-positions and 4.3—5.2 G for *meta*-positions relative to the hydroxyl group, and (4) the hydroxylic proton of durosemiquinone had an exceptionally small coupling constant because of steric hindrance of the methyl groups. The temperature dependence of the coupling constants in *p*-benzosemiquinone revealed an asymmetry of the meta-ring protons at low temperature due to the hindrance of hydroxyl group rotation. The coupling constants for *p*-benzosemiquinone were calculated with the INDO method. However, the results were not satisfactory because the calculated coupling constant was too large for the ortho-protons and the asymmetry calculated for the conformation with the hydroxylic proton fixed at one of the stationary sites was too small to interpret the observations.

Ultra-violet photolysis of quinones in a hydrogen-donating solvent results in the formation of monoprotonated semiquinone radicals, which have been characterized by flash photolysis studies[1] and by electron spin resonance (ESR) studies during photolysis. ESR spectra of the semiquinone radicals have been observed under various conditions as listed below:

quinone	solvent
p-benzoquinone	alcohols,[2,3,8,9] acetone,[2] tri-*n*-butyl phosphate,[2,3] 1,2-dimethoxyethane,[2,5] tetrahydrofuran,[2,3,4] 1,4-dioxane,[2,8]
duroquinone	alcohols,[3,6,8] acetone,[4,6] tri-*n*-butyl phosphate,[3,6] sulpholane,[6] tetrahydrofuran,[3,4,6] 1,4-dioxane,[6,8] benzene,[6]
2,3-dimethyl-*p*-benzoquinone	1,2-dimethoxyethane,[4]
2,5-dimethyl-*p*-benzoquinone	1,2-dimethoxyethane,[4]
2,6-dimethyl-*p*-benzoquinone	alcohols,[7] acetone,[7] tri-*n*-butyl phosphate,[7] 1,2-dimethoxyethane,[7] tetrahydrofuran,[4,7] 1,4-dioxane,[7]
1,4-naphthoquinone	alcohols,[8,9] 1,4-dioxane,[8]
anthraquinone	2-propanol,[8] 1,4-dioxane.[8]

One of the principal aims of the present investigation is the comparison of the ESR spectra of the *p*-benzosemiquinone radical and its methyl derivatives in a particular solvent, ethanol, because hyperfine coupling constants of semiquinone radicals depend on the nature of solvent[3,6,7] and on the temperature as well.[3,5]

The ESR spectra during photolysis of *p*-benzoquinone and its derivatives in alcohols have been studied:[10,11] it was found that the spectra of both semiquinone radicals and semiquinone anions were recorded simultaneously even in neutral solution. The mechanism of formation of these radicals has also been discussed.[10,11] The present investigation is an extension of our previous ones and concerns only the semiquinone radical spectra observed during steady-state photolysis. The observed hyperfine coupling constants of the *p*-benzosemiquinone[2] and durosemiquinone radicals[6] were compared with those calculated using a valence-bond treatment with variable parameters in an attempt to understand the dependence of the hyperfine coupling constants on the nature of solvent. Later, the spectrum of *p*-benzosemiquinone was reproduced with McLachlan's simple SCF molecular orbital treatment,[5] but the agreement seems to be fortuitous because this treatment included many adjustable parameters and, in addition, it is valid only for alternant hydrocarbon radicals.[12] In the present investigation, the *p*-benzosemiquinone radical spectrum was calculated in the INDO approximation, which has been successful in reproducing ESR spectra of a fairly large number of free radicals.[13] Unfortunately, the INDO treatment did not give satisfactory results for the *p*-benzosemiquinone radical. To demonstrate the failure of the INDO method for this particular radical is another aim of this report.

Experimental

The apparatus used has been described in detail elsewhere.[14] A solution of the quinones in ethanol was first bubbled with helium and then photolyzed with unfiltered light from a super-high pressure mercury arc while flowing at a rate of about 4 ml/min. All chemicals were analytical grade and were used without further purification.

When the intense spectrum of the semiquinone anion interfered the recording of that of the semiquinone radical, the anion was suppressed by adding a small amount of acetic acid to the solution.[10]

Results and Discussion

Assignment of Hyperfine Coupling Constants. The ESR spectrum recorded during the photolysis of durosemiquinone in ethanol with a small amount of acetic acid is shown in Fig. 1A. It clearly shows a hyperfine structure attributable to two sets of six equivalent protons and a proton (as shown by the stick spectrum in the figure), though the outmost hyperfine lines were too weak to be recorded with our conditions. The spectrum is attributed to a monoprotonated durosemiquinone radical and is essentially the same as those previously reported.[3,6] Although the hyperfine coupling constants are temperature dependent, their values at 22 °C are given in Table 1 for comparison with those of other semiquinone radicals.

Figure 1B shows an ESR spectrum (indicated by the sticks) of 2,6-dimethylbenzosemiquinone radical recorded during the photolysis. Some weak lines are observed in the central part, which are thought to be due to 2,6-dimethyl-*p*-benzosemiquinone anion, because they disappeared when a small amount of acetic acid was added to the solution. A large hyper-

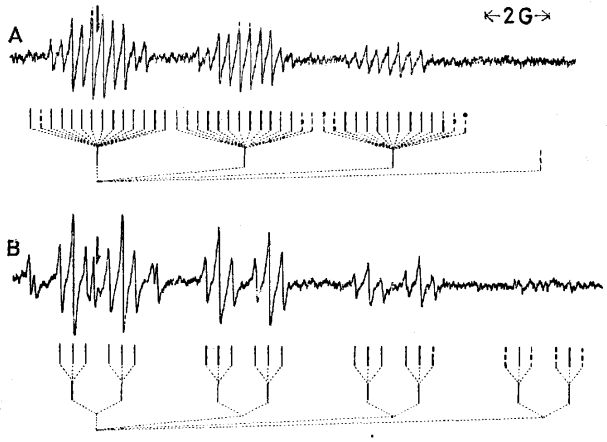

Fig. 1. ESR spectra of monoprotonated (A) durosemiquinone radical observed during photolysis of ethanol solution of duroquinone (5 mM) in the presence of a small amount of acetic acid at 31 °C and (B) 2,6-dimethylbenzosemiquinone radical observed during photolysis of ethanol solution of 2,6-dimethyl-*p*-benzoquinone (5 mM) at 32 °C. A high-field half of the spectra is shown. Arrows indicate the center of the spectra.

Table 1. Observed hyperfine coupling constants of protons in monoprotonated semiquinone radicals formed during photolysis of ethanol solutions

Parent molecule	Temperature	Radicals and hyperfine coupling constants (in G)
p-Benzoquinone	19 °C	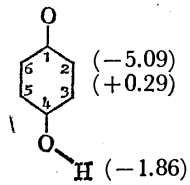 (−5.09) (+0.29) (−1.86)
Duroquinone	22 °C	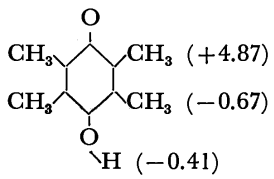 (+4.87) (−0.67) (−0.41)
2,6-Dimethyl-*p*-Benzoquinone	23 °C	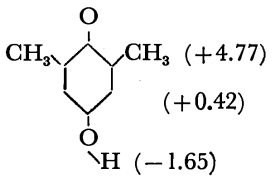 (+4.77) (+0.42) (−1.65)
2,5-Dimethyl-*p*-Benzoquinone	18 °C	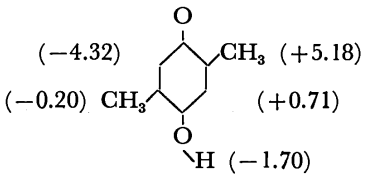 (−4.32) (+5.18) (−0.20) (+0.71) (−1.70)
Methyl-*p*-Benzoquinone	24 °C	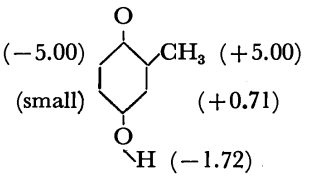 (−5.00) (+5.00) (small) (+0.71) (−1.72)

fine splitting of 4.77 G, due to six equivalent protons, indicates that hydrogen addition occurs exclusively on the oxygen atom attached to the carbon at the 4-position, remote from the two methyl groups. The observed hyperfine coupling constants are essentially the same as those reported previously[7] and are listed in Table 1.

In addition to the coupling constants of the two semiquinone radicals, hyperfine coupling constants previously determined[10] at about 20 °C for *p*-benzosemiquinone radical, 2,5-dimethylbenzosemiquinone radical and methyl-*p*-benzosemiquinone radical are shown in Table 1 for comparison. The ESR spectra of 2,5-dimethylbenzosemiquinone radical in alcohols and of methyl-*p*-benzosemiquinone radical have not been assigned before.

Based on a molecular orbital[3,4] and a valence-bond[2,6] treatment, the spin density has a large positive value on carbon atoms at the *meta*-position (relative to the hydroxyl group) and a small negative value on the carbon atom at the *ortho*-position. Therefore, if one considers the induction of a negative spin on the orbital of the ring-hydrogen and a positive spin on the orbital of the methyl-hydrogen, the observed hyperfine coupling constants as well as their sign may be assigned as shown in the third column in Table 1, except for the monoprotonated methyl-*p*-benzosemiquinone radical. The ESR spectrum observed during photolysis of the methyl-*p*-benzoquinone in acidic ethanol had a hyperfine structure due to six protons, four of which are equivalent (see Fig. 6b in Ref. 10). Although one proton is missing, the spectrum is tentatively assigned to methyl-*p*-benzosemiquinone radical as shown in Table 1 by comparing hyperfine coupling constants of other semiquinone radicals and by analogy with photochemical reactions of other quinones. The hyperfine coupling constants of the ring proton and that of the methyl protons at the *meta*-positions are probably accidentally the same, and the hyperfine coupling constant of one of the *ortho*-ring protons was too small relative to the line-width (150 mG) to be observed. The hyperfine coupling constant of the hydroxylic proton was in the range $-1.7\sim-1.9$ G for all semiquinone radicals except for durosemiquinone radical where a large steric hindrance of the methyl groups may exist (see below).

The Temperature Dependence of the Hyperfine Coupling Constants. The absolute value of the hyperfine coupling constant of the ring protons and methyl protons decreases slightly with decreasing temperature, whereas the hyperfine coupling constant of the hydroxylic proton increases rather remarkably, as shown in Fig. 2 for the *p*-benzosemiquinone radical. Although such a tendency has already been reported,[3] it should be stressed that the protons at 2- and 6-positions become inequivalent at low temperature because of hindrance to rapid rotation of the hydroxyl group.

The spectrum of *p*-benzosemiquinone radical consists of three pairs of triplets at high temperature. The third and fourth triplet patterns from the low-field end of the spectrum change of five-line patterns at low temperature. Using the modified Bloch equation,[15] the change of the patterns could be reproduced well from the hyperfine coupling constants and the linewidth estimated from the outer triplets, as shown in Fig. 3. The good agreement between observed and simulated patterns shows unambiguously that the difference in hyperfine coupling constant between protons at 2- and 6-positions is equal to 7.5%. The difference was found to be 6.3% in tetrahydrofuran[4]

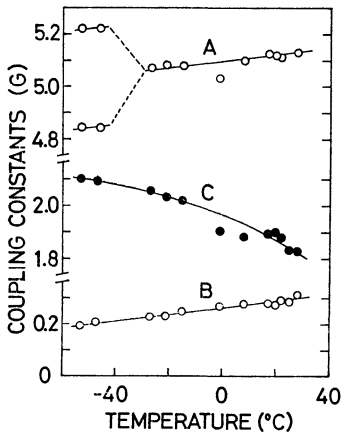

Fig. 2. Temperature dependence of the hyperfine coupling constants of the ring proton at (A) 2- and 6-positions (negative in sign) and (B) 3- and 5-positions and (C) of hydroxylic proton (negative in sign) in monoprotonated *p*-benzosemiquinone radical in ethanol.

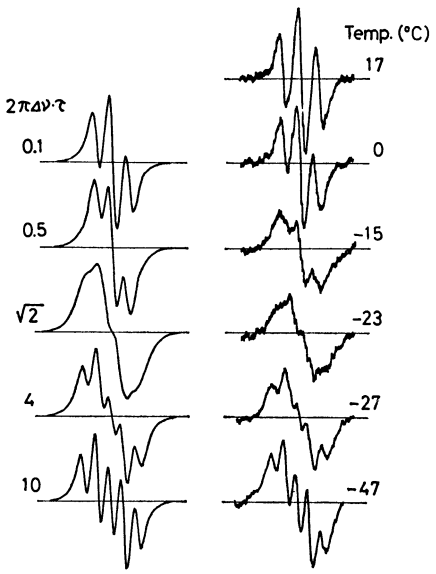

Fig. 3. Change of the ESR spectrum of *p*-benzosemiquinone radical due to the conformational exchange of the hydroxylic proton between two stationary sites in the nodal plane of ring π-system in the intermediate range of exchanging rate. Left spectra: simulated from the modified Bloch equations and the hyperfine coupling constants in Fig. 2 for each value of $2\pi\Delta\nu\cdot\tau$ shown in the figure (see also the text). Right spectra: observed at each temperature shown in the figure. Only the third triplet component (at room temperature) from the low field is shown.

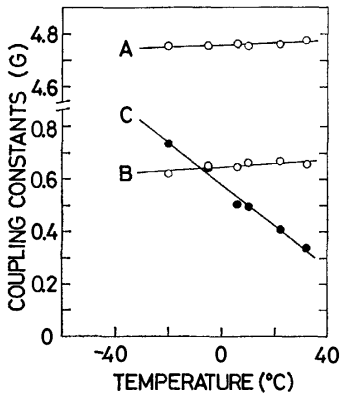

Fig. 4. Temperature dependence of hyperfine coupling constant of methyl protons at (A) 2- and 6-positions (negative in sign) and (B) 3- and 5-positions and (C) of hydroxylic proton (negative in sign) in monoprotonated durosemiquinone radical in ethanol.

and 5.4% in 1,2-dimethoxyethane.[5]

The temperature dependence of the hyperfine coupling constants in durosemiquinone radical is shown in Fig. 4. The absolute value of the hyperfine coupling constant of the hydroxylic proton increases greatly with decreasing temperature, consistent with the previous observation for durosemiquinone radical in 2-propanol, tetrahydrofuran and tri-*n*-butyl phosphate.[3] In addition, it was found in the present study that the hyperfine coupling constants of the methyl protons decrease slightly in absolute value, with decreasing temperature, as do those of the ring protons in the *p*-benzosemiquinone radical. The magnitude and sign of the hyperfine coupling constant of the hydroxylic proton is determined by two opposing contributions: one is a negative contribution from conjugation between the oxygen and the aromatic π-system and the other is a positive contribution from the direct overlap between the aromatic π-system and the proton.[3,16] If the hydroxylic proton is in the nodal plane of the π-system, its hyperfine coupling constant is determined exclusively by the former contribution and therefore has a negative sign. When rotation about the C–O bond brings the proton out of the nodal plane, the coupling constant approaches zero and then increases. The observed magnitude and temperature dependence of the hyperfine coupling constant of the hydroxylic proton indicate that it is negative in ethanol as in 2-propanol and tetrahydrofuran,[3] although the proton is located more out of the nodal plane in the durosemiquinone radical than in the other semiquinone radicals because bulky methyl groups are closer to the hydroxyl group in the durosemiquinone radical. At low temperatures, the position of the hydroxylic proton is closer to the nodal plane, giving a hyperfine coupling with a large negative value.

Molecular Orbital Calculations. Hyperfine coupling constants of semiquinone radicals were first examined theoretically with a valence-bond treatment with parameters adjusted to fit the calculated spin densities to those observed and to account for the dependence of the coupling constants upon the solvent polarity.[2,6] Later, McLachlan's approximate self-consistent treatment was used to reproduce the observed hyperfine coupling constants.[3–5] However, agreement between the observed and calculated coupling constants obtained by this molecular orbital treatment seem to be fortuitous,[5] because the calculation involved many adjustable parameters.

In the present investigation, we tried to calculate the hyperfine coupling constants of the protons in a semiquinone radical using the INDO approximation. However, though this molecular orbital treatment developed by Pople and Beveridge has been shown to be promising in predicting the value of the hyperfine coupling constants for several kinds of free radicals without any parametrization other than the conformation of the free radicals,[12] we could not get satisfactory results.

Table 2. Proton hyperfine coupling constants of monoprotonated *p*-benzosemiquinone radical calculated by the INDO method and those observed in ethanol solution

Hyperfine coupling constants (G)	
Calculated	Observed
Planar	At −53 °C
$a_2 = -6.0218$	−5.22
$a_6 = -6.0041$	−4.84
$a_3 = 3.3539$, $a_5 = 3.4095$	0.20
$a_{OH} = -0.7276$	−2.10
Non-planar	At 19 °C
$a_2 = a_6 = -6.0747$	−5.09
$a_3 = a_5 = 3.4945$	0.29
$a_{OH} = 15.7278$	−1.86

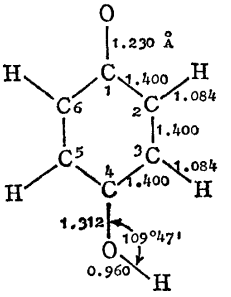

Table 2 shows representative results obtained from the INDO calculations of the proton hyperfine coupling constants in *p*-benzosemiquinone radical for the conformation with normal bond lengths and bond angles also shown in the same table. The isotropic hyperfine coupling for all the protons was derived from the 1s spin density on the corresponding hydrogen atoms obtained from the INDO approximation by using the proportionality constant relating the spin density to the coupling constant, 539.86 G.[13]

The calculated hyperfine coupling constants of the protons do not agree with the observed ones. The hyperfine coupling constants of the hydroxylic proton depend very much on the conformation of the radical, *i.e.*, whether the proton is in the nodal plane or out of it. However, the coupling constants of the ring protons are not affected by the conformation. Both of two extreme conformations (one was planar with the hydroxylic proton in the nodal plane and the other was non-planar with the hydroxylic proton in the symmetry plane perpendicular to the ring) gave hyperfine coupling constants of 3.4~3.5 G for protons at 3- and 5-positions (*ortho*-position relative to the

hydroxyl group) and about −6.0 G for 2- and 6-positions (*meta*-positions relative to the hydroxyl group). Although the values for the *meta*-positions are rather close to the observed ones, the values for the ortho-positions are ten times as large as the observed values. In addition, the calculated difference in hyperfine coupling between the two protons at the *meta*-position is 0.29% for the planar conformation, which is very much smaller than the observed difference of 7.5%.

The agreement between calculation and observation for the hydroxylic proton could be obtained by arbitrarily adjusting the angle of rotation of the hydroxyl group around the C–O bond. However, the disagreement between calculation and observation in the magnitude of the hyperfine coupling constants of the protons at *ortho*-positions and that in the difference in hyperfine coupling of the protons at *meta*-positions indicate that INDO calculations produce very poor results for the monoprotonated *p*-benzosemiquinone radical. The reason for this is not known at this moment and is left to further theoretical investigation. We made several calculations for other bond lengths and bond angles in the acceptable range, but no appreciable improvement could be attained in the calculated results. We also examined unsuccessfully the effect of a hydrogen bond between the hydroxyl group of the radical and solvent ethanol. It may be interesting to note that the INDO method did not give satisfactory results for the hyperfine coupling constants of *p*-benzosemiquinone anion either.[13]

Conclusions

The proton hyperfine coupling constants of shortlived monoprotonated semiquinone radicals (*p*-benzosemiquinone, durosemiquinone, 2,6-dimethylbenzosemiquinone, 2,5-dimethylbenzosemiquinone and methyl-*p*-benzosemiquinone radicals) have been compared with each other under identical conditions, namely, in ethanol solvent and at about 20 °C and assigned. Among them, 2,5-dimethylbenzosemiquinone and methyl-*p*-benzosemiquinone radicals, at least in ethanol, were first assigned in this investigation. The observed hyperfine coupling constants of the hydroxylic proton are all in the range −1.86∼−1.65 G except for the durosemiquinone radical, where the hyperfine coupling constant is as small as −0.41 G, indicating that the hydroxylic proton is far out of the nodal plane of the ring π-system due to the bulky methyl groups located close to the hydroxyl group. The ESR spectrum of methyl-*p*-benzoquinone shows a hyperfine structure due to six protons, but it has been tentatively assigned to methyl-*p*-benzosemiquinone radical by comparing with the coupling constants in other semiquinone radicals.

The proton hyperfine coupling constants for *p*-benzosemiquinone radical were calculated in the INDO approximation. However, the results were unsatisfactory because the calculated hyperfine coupling constant of the protons in the *ortho*-positions relative to the hydroxyl group was much smaller in magnitude than the observed one. Furthermore, the calculated difference in hyperfine coupling between two protons in the *meta*-positions was too small to account for the hyperfine structure of the spectrum observed at low temperature where the hydroxylic proton is thought to be fixed at one of the stationary positions in the nodal plane of the ring π-system.

References

1) N. K. Bridge and G. Porter, *Proc. Roy. Soc. Ser. A.*, **244**, 259 (1958), **244**, 276 (1958). D. R. Kemp and G. Porter, *Proc. Roy. Soc. Ser. A*, **326**, 131 (1972); *Chem., Commun.* **1969**, 1029.
2) T. E. Gough, *Trans. Faraday Soc.*, **62**, 2321 (1966).
3) T. E. Gough and G. A. Taylor, *Can. J. Chem.*, **47**, 3717 (1969).
4) T. E. Gough, *ibid.*, **47**, 331 (1969).
5) R. Wilson, *J. Chem. Soc., B*, **1968**, 1581.
6) T. A. Claxton, T. E. Gough, and M. C. R. Symons, *Trans. Faraday Soc.*, **62**, 279 (1967).
7) T. A. Claxton, J. Oakes, and M. C. R. Symons, *ibid.*, **63**, 2125 (1967).
8) S. K. Wong, W. Sytnyk, and J. K. S. Wan, *Can. J. Chem.*, **50**, 3052 (1972).
9) P. B. Ayscough and R. C. Sealy, *J. Chem. Soc., B*, **1973**, 543.
10) H. Yoshida, K. Hayashi, and T. Warashina, This Bulletin, **45**, 3515 (1972).
11) H. Yoshida, J. Shoma, and T. Warashina, *ibid.*, **47**, 1396 (1974).
12) A. D. McLachlan, *Mol. Phys.*, **3**, 233 (1960).
13) A. Pople and D. L. Beveridge, "Approximate Molecular Orbital Theory," McGraw-Hill, New York (1970).
14) H. Yoshida and T. Warashina, This Bulletin, **44**, 2950 (1971).
15) J. A. Pople, W. G. Schneider, H. J. Bernstein, "High Resolution Nuclear Magnetic Resonance," McGraw Hill, New York (1959).
16) A. B. Barabas, W. F. Farbes, and P. D. Sullivan, *Can. J. Chem.*, **45**, 224 (1967).

Physico-chemical Properties of Selenium-Tellurium-Sulfur Crystals

Toshio NAKAGAWA

Department of Chemistry, Faculty of General Education, Hosei University, Fujimi, Chiyoda-ku, Tokyo 102

(Received May 17, 1974)

The temperature dependence of electric conductivity and Vickers hardness of Selenium-Tellurium-Sulfur (Se-Te-S) crystals were studied. The conductivity decreased with an increase in sulfur content, remaining almost constant when the sulfur content was 40—80 atomic % at 20 and 30 atomic % of tellurium content. When tellurium content was 10%, both conductivity and hardness decreased abruptly when sulfur content exceeded 10%. It was found by means of X-ray diffraction that a hexagonal crystal structure with size twice the lattice constant of Se-Te crystals is formed when the sulfur content is 20% at 10% of tellurium content. When sulfur content exceeds 80%, the crystal structure becomes similar to that of pure sulfur (orthorhombic) at 20 and 30% of tellurium.

Hansen[1] reported that the phase diagram of Se-S system is of a complicated peritectic type, that of Se-Te system a basic solid solution type and that of Te-S system a eutectic type with a eutectic point at *ca.* 98—99 atomic % sulfur content. Many reports have appeared on the properties of Se-S, Se-Te, and Te-S systems.[2~5] The phase diagram of the Se-Te-S system has been reported,[6] but not its properties.

In this study, Se-Te-S crystals were prepared by heating amorphous Se-Te-S at 95 °C. The electric conductivity and Vickers hardness were measured. The results were discussed on the basis of X-ray diffraction data.

Experimental

Materials. Selenium (99.999%, Showa. Kagaku Co., Ltd.) and tellurium (99.999% Yokozawa Kagaku Co., Ltd.) were used. Sulfur of special grade was recrystallized twice.

Procedure. Three mixtures of powdered selenium and tellurium (Te, 10, 20 and 30 atomic %) were sealed separately in glass tubes under 10^{-3} Torr and melted at 470 °C. The glass tubes were exposed to the air for quenching. The products were powdered, and various amounts of sulfur were added. The mixtures were sealed separately in glass tubes, melted at 250—300 °C and quenched. The samples were crystallized at 95 °C for 2—24 hr. Specimens for measurement (4×4×7 mm) were cut out and left in the dark for *ca.* 24 hr. Electric conductivity was measured by the voltage drop method under 50 V. Vickers hardness was measured with a micro hardness tester of MVA type (Akashi Co.) under a load of 25~200 g for 1 min. X-ray diffraction was studied by the powder method with a Geigerflex (Rigaku Denki Co.) by means of CuKα line.

Results

Electric Conductivity (σ). The temperature dependence of electric conductivity of three Se-Te-S crystals with tellurium contents (a) 10%, (b) 20% and (c) 30% was studied in the range from room temperature to 95 °C. The relation between log σ and $1/T$ shows a nearly straight line. The relation between electric conductivity and sulfur content at 30 °C is shown in Fig. 1. The conductivity decreases with an increse in sulfur content. In (a), the conductivity decreases abruptly when the sulfur content exceeds 10%. In (b) and (c), the conductivity gradually decreases with an increase in sulfur content up to *ca.* 40%, remains almost constant, and decreases abruptly when

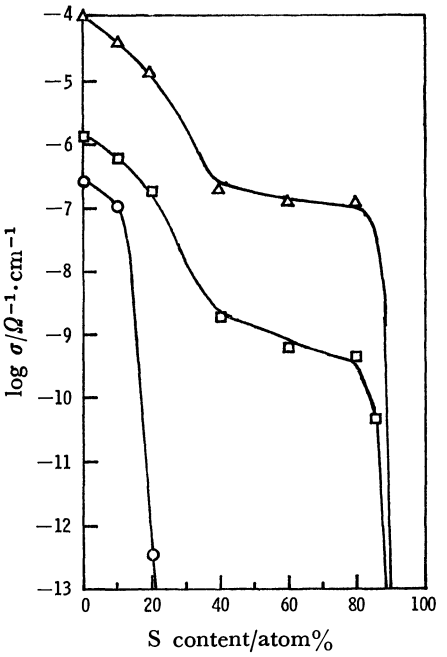

Fig. 1. Electric conductivity of Se-Te-S crystals n 30 °C.
Te content/atom% ○: 10, □: 20, △: 30.

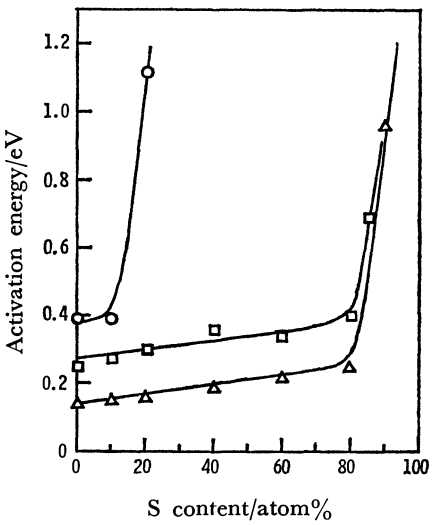

Fig. 2. Activation energy of the electric conductivity of Se-Te-S crystals.
Te content/atom% ○: 10, □: 20, △: 30.

the sulfur content exceeds 80%. The greyish black color of Se-Te crystals turned reddish brown in (a), brown in (b) and (c) at the sulfur concentration at which electric conductivity decreases abruptly.

Figure 2 shows the relation between sulfur content and activation energy. The activation energy was calculated by

$$\sigma = \sigma_0 \exp(-E/kT),$$

where σ and σ_0 are electric conductivities, E activation energy, k the Boltzmann constant, and T absolute temperature. The activation energy remains almost constant in (a) for sulfur content up to 10%, but increases abruptly when it exceeds 10%. The results seem to be the reverse of that for conductivity (Fig. 1). In (b) and (c), the activation energy increases abruptly when sulfur content exceeds *ca.* 80%. Activation energy above 80% sulfur approaches 1.52 eV,[7] the energy of pure sulfur.

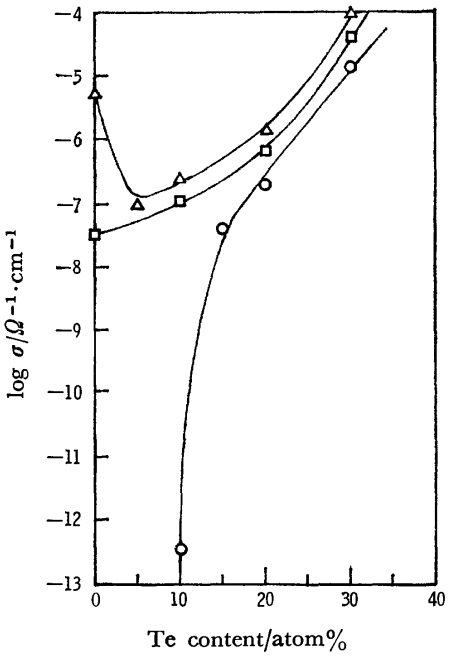

Fig. 3. Electric conductivity of Se-Te-S crystals at 30 °C.
S content/atom% △: 0, □: 10, ○: 20.

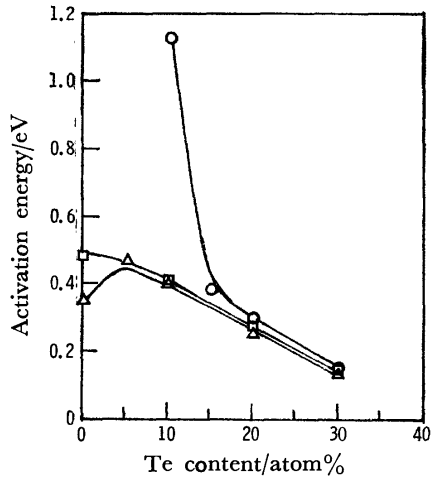

Fig. 4. Activation energy of the electric conductivity of Se-Te-S crystals.
S content/atom% △: 0, □: 10, ○: 20.

The relation between the electric conductivity of Se-Te-S crystals and tellurium content is shown in Fig. 3. When no sulfur is contained, the conductivity decreases with an increase in tellurium content up to ca. 5%, but increases above 5%. When sulfur content is 10%, the conductivity increases with an increase in tellurium content. When sulfur content is 20%, the conductivity abruptly decreases with a decrease in tellurium content below 15%. The relation between activation energy and tellurium content is shown in Fig. 4. The results seem to be the reverse of those for conductivity (Fig. 3).

Hardness. The relation between sulfur content and Vickers hardness of Se-Te-S crystals (a), (b) and (c) is shown in Fig. 5. The hardness decreases abruptly with an increase in sulfur content up to *ca.* 20% in (a) and decreases gradually above 20%. The rapid lowering of hardness corresponds to the decrease in conductivity (Fig. 1). The hardness of selenium crystallized at 95 °C is *ca.* 90 kg/mm², decreasing abruptly with an increase in tellurium content up to *ca.* 20% and decreases gradually above 20%. There is no change in hardness when sulfur content exceeds 80% in (b) and (c).

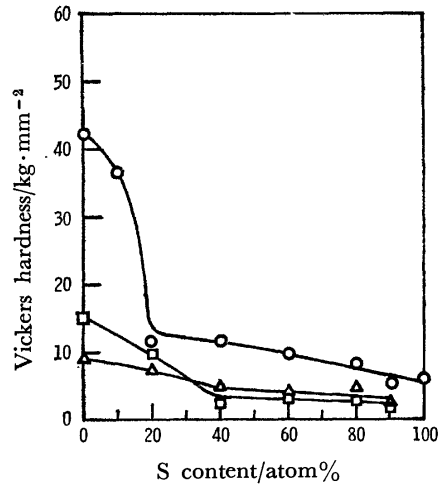

Fig. 5. Vickers hardness of Se-Te-S crystals.
Te content/atom% ○: 10, □: 20, △: 30.

X-Ray Diffraction. The X-ray diffraction patterns for (a), shown in Fig. 6, are nearly the same for the 0 and 10% sulfur contents. When sulfur content is 20%, the diffraction pattern of 0% sulfur disappears, a different pattern appearing. For the samples with sulfur contents 40 and 60%, the diffraction pattern corresponding to 20% sulfur content appears accompanied by a different pattern. The diffraction pattern for 60% sulfur is similar to that of the SeS compound.[8] For 90% sulfur, it is similar to that of pure sulfur. The diffraction patterns for (b) (Fig. 7) are sharper than those for (a). When sulfur content is 10%, the diffraction pattern of 0% sulfur appears, its peaks shifting slightly towards small angles; it partly disappears when sulfur content is 20%, a new pattern appears differing

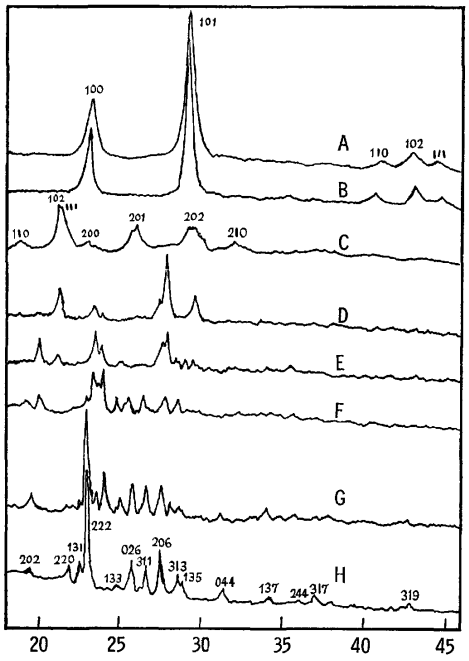

Fig. 6. X-ray diffraction patterns of Se-Te-S crystals containing 10 atom% of tellurium.
S content/atom%
A: 0, B: 10, C: 20, D: 40, E: 60, F: 80, G: 90, H: Pure sulfur (orthorhombic).

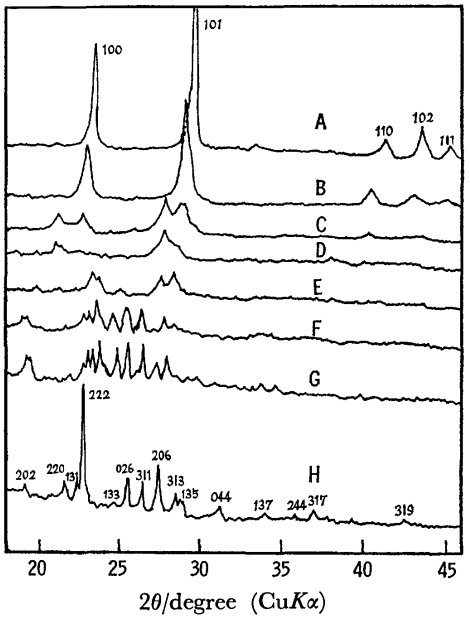

Fig. 7. X-ray diffraction patterns of Se-Te-S crystals containing 20 atom% of tellurium.
S content/atom%
A: 0, B: 10, C: 20, D: 40, E: 60, F: 80, G: 90, H: Pure sulfur (orthorhombic).

from that of (a) with 20% sulfur. The diffraction patterns for 40 and 60% sulfur differ from the pattern for 20% sulfur. The diffraction patterns for 80 and 90% sulfur differ from those for 40 and 60% sulfur, being similar to that of pure sulfur. The diffraction

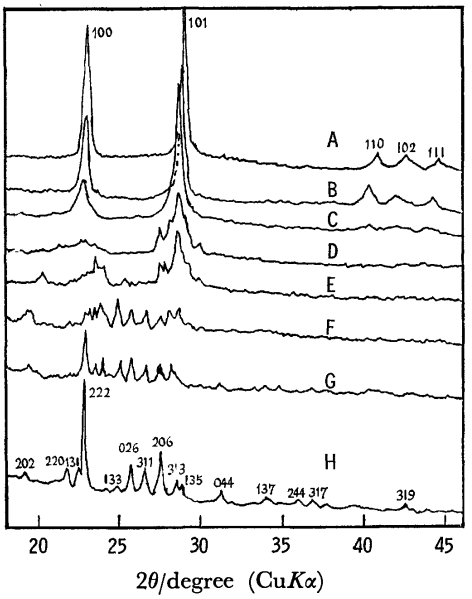

Fig. 8. X-ray diffraction patterns of Se-Te-S crystals containing 30 atom% of tellurium.
S content/atom%
A: 0, B: 10, C: 20, D: 40, E: 60, F: 80, G: 90, H: Pure sulfur (orthorhombic).

patterns for (c) are shown in Fig. 8. When sulfur content is 20%, the diffraction pattern of 0% sulfur partly remains the peaks shifting slightly towards small angles as in (b). The diffraction pattern of 0% sulfur partly remains in those of the Se–Te–S crystals with sulfur contents 40 and 60%. When sulfur content exceeds 80%, the diffraction pattern becomes similar to that of pure sulfur.

Discussion

In (a), the diffraction pattern for 20% sulfur differs entirely from that of the systems with 0 and 10% sulfur. Electric conductivity, activation energy and hardness indicate characteristic behavior when sulfur content exceeds 10%. It can be assumed that the diffraction pattern for 20% sulfur is due to the hexagonal crystal which has a unit cell with size twice Se–Te crystals lattice. Tellurium is substituted into a fixed position of the selenium crystal lattice and sulfur is substituted into a fixed position of the selenium of this lattice. The lattice constant of the new lattice is twice that of Se–Te crystal. It is possible to assign the diffraction pattern (Fig. 6, C). In Se–S crystal, the diffraction pattern differs from that of selenium when sulfur content exceeds *ca.* 7%.[2] In this Se–Te–S crystal (S= 20%), electric conductivity increases abruptly with an increase in tellurium content when tellurium content is below 15% (Fig. 3). For 10% sulfur, no rapid lowering in electric conductivity was observed in the presence of tellurium. No such phenomenon appears when tellurium content exceeds 20% (Figs. 7 and 8). This is due to the fact that sulfur and tellurium form eutectic crystals for large tellurium content. When sulfur content exceeds 80%, the diffraction patterns resemble that of pure sulfur (orthorhombic). It seems

that this causes the electric conductivity to decrease abruptly with an increase in sulfur content when the sulfur content exceeds 80% in (b) and (c).

References

1) M. Hansen, "Constitution of Binary Alloys," McGraw-Hill, New York (1958), pp. 1162, 1165, 1189.
2) T. Nakagawa, *Nippon Kagaku Kaishi*, **1973**, 1822.
3) O. Watanabe and S. Tamaki, *Electrochim. Acta*, **13**, 11 (1968).
4) E. Grison, *J. Chem. Phys.*, **19**, 1109 (1951).
5) A. Kraus and W. Johnson, *J. Phys. Chem.*, **32**, 1281 (1928).
6) L. Losana, *Gazz. Chim. Ital.*, **53**, 396 (1923).
7) B. Meyer, "Elemental Sulfur," John Wiley & Sons, New York (1965), p. 187.
8) ASTM Card (2–0320).

Emission Spectra of Dimethoxybenzenes by Controlled Electron Impact

Teiichiro OGAWA, Totaro IMASAKA, Minoru TOYODA,
Masaharu TSUJI, and Nobuhiko ISHIBASHI
Faculty of Engineering, Kyushu University, Hakozaki, Fukuoka 812

(Received June 14, 1974)

The emission spectra of *o*-, *m*-, and *p*-dimethoxybenzenes under controlled electron impact excitation (200 eV) were measured in the 220—450 nm region at very low pressures. The photoemissions of the excited parent species and such fragment species as H, CH, CO, and CO^+ were observed and assigned. The relative intensities of the photoemissions of the parent species were compared with those of the fluorescence spectra (photoexcitation) in an *n*-hexane solution. The excited parent species, H, and CH were concluded to be produced in one-electron processes; however, the CO^+ species were assumed to be produced in both one- and two-electron processes, and the relative contributions are evaluated. It was concluded that the rate of the predissociation of *o*-dimethoxybenzene was faster than those of the other two isomers, and the observed characteristics of *o*-dimethoxybenzene had something to do with this faster rate.

Research on molecular excited states has recently been carried out by many investigators, mostly by the photoexcitation method. Among various methods for excitation, the controlled electron impact method has two advantages; (1) the photoemission of excited species can be obtained at very low pressures, where the effect of molecular collision is greatly reduced, and (2) the energy of incident electrons can be controlled externally and continuously from the X-ray energy region (1000 eV) down to the ultraviolet energy region (several eV). Thus, the investigation of emission spectra by this method will be fruitful for the study of the mechanism of the excitation and fragmentation of various molecules.

The emission spectra of various aliphatic[1–3] and aromatic[4–10] molecules produced by this method have been reported, and the mechanism of excitation has been discussed in relation to the intensity measurements. However, no kinetic treatment on the species which may not be produced primarily has ever been carried out. In the present report, the emission spectra of *o*-, *m*-, and *p*-dimethoxybenzenes will be described and the mechanism of their excitation and fragmentation, including species produced secondarily, will be discussed.

Experimental

The electron-impact apparatus is essentially identical with that described in a previous paper.[8] The sample vapor was crossed so as to collide with an electron beam *in vacuo* and the photoemission was observed photoelectrically with a Jarrel-Ash JE 25 monochromator. The slit width used was 100 μ, corresponding to a bandpass of 3.3 Å. The intensity was measured by the peak height of the band at each specified wavelength, where there was negligible overlap with other features.

The dimethoxybenzenes used were obtained from Wako Pure Chemical Ind. They were degassed *in vacuo* a few times just before use.

The relative intensities of the fluorescence were measured with a Hitachi 204 fluorescence spectrophotometer. The solvent, *n*-hexane, was of a non-fluorescent grade (Luminasol) of the Dojindo Co.

Results

Typical emission spectra of *o*-xylene and *o*-dimethoxybenzene in the region of 250—450 nm under electron impact excitation are shown in Fig. 1, where the impact voltage is 300 V and the electron-beam current is 1 mA for *o*-xylene and 200 V and 0.7 mA for *o*-dimethoxybenzene. The characteristic band in the 280—340 nm region of the latter, which overlapped with several sharp bands, was assigned to the electronic transition from the lowest excited singlet state to the ground state of the parent molecule, as in the case of the emission spectra of *o*-xylene,[6] methoxybenzene,[5] and other aromatic molecules,[7–9] since the location of the band was identical to the fluorescence spectra in the n-hexane solution. Many sharp bands in these spectra were assigned to the fragment species. The lines at 434, 410, and 397 nm in both spectra were assigned to the hydrogen Balmer series, and the bands at 431 and 389 nm, to CH ($A^2\Delta$—$X^2\Pi$) and CH ($B^2\Sigma^-$—$X^2\Pi$) respectively. The other bands in the spectrum of *o*-dimethoxybenzene were assigned to the bands of CO and of CO^+, as in the case of methoxybenzene;[5] the bands in the 230—260 nm region, to the first negative system of CO^+ ($B^2\Sigma^+$—$X^2\Sigma^+$), the sharp bands in the 280—330 nm region, to the third positive system of CO ($b^3\Sigma^+$—$a^3\Pi$), and the doublet bands above 336 nm, to the comet-tail

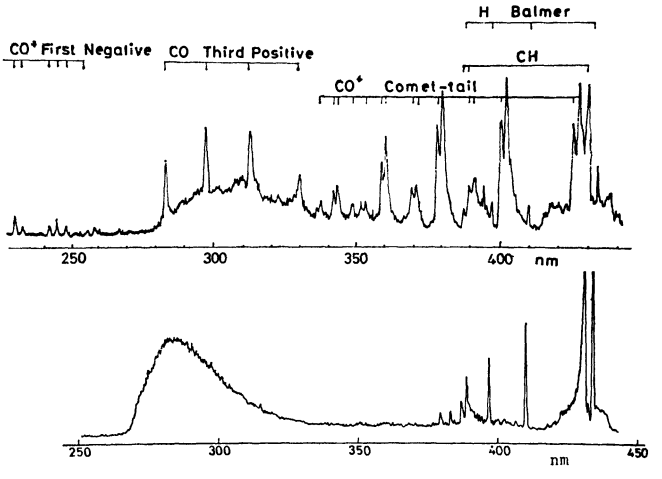

Fig. 1. Emission spectra by controlled electron impact.
Top; *o*-dimethoxybenzene, electron energy 200 eV, electron-beam current 0.7 mA.
Bottom; *o*-xylene, electron energy 300 eV, electron-beam current 1 mA.

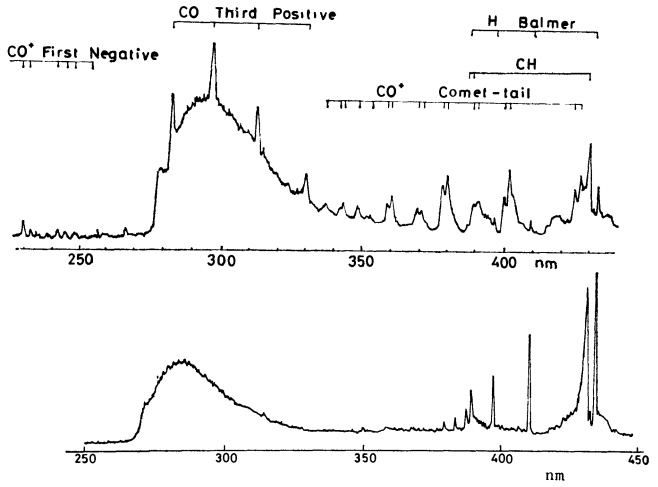

Fig. 2. Emission spectra by controlled electron impact.
Top; *m*-dimethoxybenzene, electron energy 200 eV, electron-beam current 1 mA.
Bottom; *m*-xylene, electron energy 300 eV, electron-beam current 0.5 mA.

system of CO^+ ($A^2\pi\Pi - X^2\Sigma^+$).

Typical emission spectra of *m*-xylene and *m*-dimethoxybenzene under controlled electron impact excitation are shown in Fig. 2. The band of the A—X transition of *m*-dimethoxybenzene was shifted to wavelengths shorter by several nanometers from that of *o*-dimethoxybenzene, and it is more intense than the latter. Those of *p*-xylene and *p*-dimethoxybenzene are shown in Fig. 3. The band of the A—X transition of *p*-dimethoxybenzene is shifted to wavelengths longer by about 15 nm from that of *o*-dimethoxybenzene, and it is the most intense among the three isomers.

The intensities of the photoemissions of these molecules were determined for various amounts of incident electrons. The dependence of the emission intensities

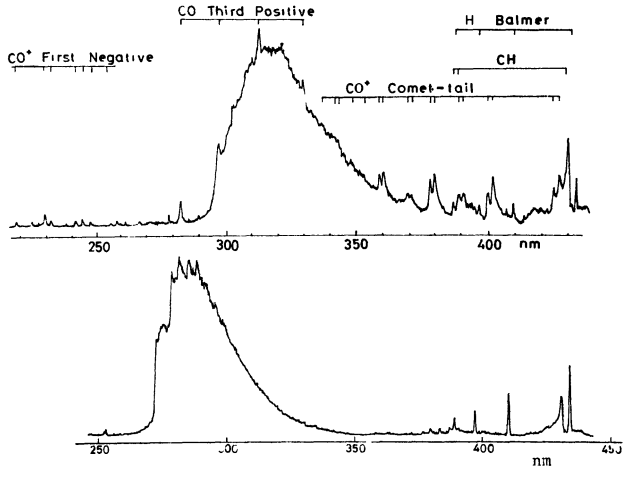

Fig. 3. Emission spectra by controlled electron impact.
Top; *p*-dimethoxybenzene, electron energy 200 eV, electron-beam current 1 mA.
Bottom; *p*-xylene, electron energy 200 eV, electron-beam current 1 mA.

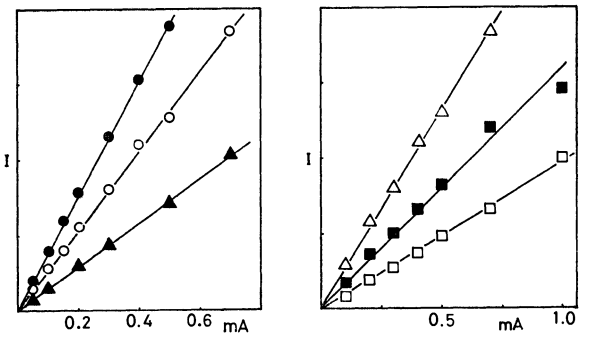

Fig. 4. Dependence of photoemission intensity (I, arbitrary units) on the electron-beam current (mA).
Left; Emission of dimethoxybenzenes at 200 eV.
▲ *ortho* (303 nm), ○ *meta* (294 nm), ● *para* (316 nm).
Right; Emission of fragment species from *m*-dimethoxybenzene at 200 eV.
△ parent (294 nm), ■ H (410 nm), □ CH (431 nm).

of the parent molecules of *o*-, *m*-, and *p*-dimethoxybenzenes, and those of H and CH from *m*-dimethoxybenzene, on the electron-beam current are shown in Fig. 4. In all cases, the relative intensity is proportional to the electron-beam current, and an identical relation was obtained for H and CH from the other isomers. The dependence of the emission intensity on the gas pressure was difficult to determine accurately because of the low vapor pressure of dimethoxybenzenes; however, the intensity of the band of *m*-dimethoxybenzene seemed to be proportional to the pressure.

Contrary to these results, the dependence of the emission intensities of the comet-tail bands of CO^+ from dimethoxybenzenes on the electron-beam current failed to show any proportionality. The results are shown in Fig. 5, together with that of CO^+ from CO. A considerable deviation from the linear relationship was observed for CO^+ ($A^2\Pi$) from *m*-dimethoxybenzene, as in the case of CO^+ ($A^2\Pi$) from nitrobenzene;[9] however, the emission of CO^+ ($A^2\Pi$) from CO showed a linear relationship as in the case of CO^+ ($A^2\Pi$) from methanol.[2] Quantitative measurements were difficult for $CO^+(B^2\Sigma^+)$ and for CO

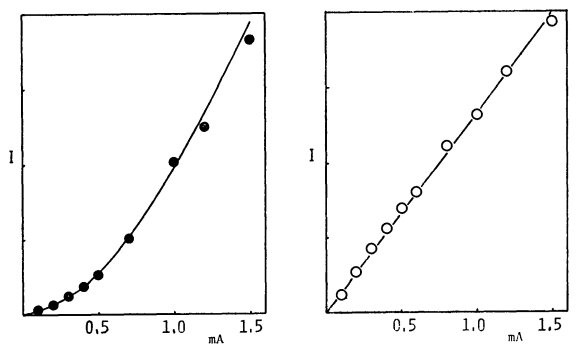

Fig. 5. Dependence of photoemission intensity (*I*, arbitrary units) on the electron-beam current (mA). 200 eV impact.
Left; CO^+ ($A^2\Pi$) from *m*-dimethoxybenzene (402 nm).
Right; CO^+ ($A^2\Pi$) from CO (402 nm).

($b^3\Sigma^+$) because of the weak intensity and the band overlap.

Discussion

The three isomers of dimethoxybenzenes give equally the emission spectra of the parent species and of such fragment species as H, CH, CO, and CO^+. While the spectrum of *p*-xylene shows some distinct vibrational structures, no clear structures are observed in the spectra of dimethoxybenzenes. Since the symmetry of the molecule is approximately D_{2h} for *p*-xylene, but lower for *p*-dimethoxybenzene because of the oxygen atoms in the methoxy groups, the spectrum of the latter becomes more diffuse as a result of the increase in the vibrational levels, which interact with the electronic level.

The relative intensities of the A—X transitions of three dimethoxybenzenes to those of the bands of CO^+ differ from each other, as are shown in Figs. 1, 2, and 3; *o*-dimethoxybenzene gives the weakest intensity for the bands of the parent species and the strongest intensity for those of CO^+, while *p*-dimethoxybenzene gives the opposite.

Table 1. Relative emission intensities of the parent species from xylenes and dimethoxybenzenes

isomers			*o*-	*m*-	*p*-
Xylene	photo-excitation	FM[a]	1.3	1.0	1.7
		B[b]	1.1	1.0	2.4
	electron impact[c]		1.2	1.0	2.6
Dimethoxy-benzene	photo-excitation[d]		1.4	1.0	2.8
	electron impact[c]		0.4	1.0	3.2

a) P. M. Froehlich and H. A. Morrison, *J. Phys. Chem.*, **76**, 3566 (1972). b) I. B. Berlman, "Handbook of Fluorescence Spectra of Aromatic Molecules" 2nd Ed. Academic Press. New York (1971). c) Measured at 200 V and 0.1 mA. d) Measured in *n*-hexane solution (7×10^{-6} mol/l).

The relative emission intensities of the parent species from the three isomers of xylenes and of dimethoxybenzenes are shown in Table 1, both for the cases of electron impact excitation (the energy of the electrons was 300 eV; however, the energy which the molecules receive is expected to be around 5—30 eV) and for those of photoexcitation (5.59 eV) in an n-hexane solution. In the case of xylenes, *p*-xylene has a stronger emission band than do *o*- and *m*-xylenes for both methods of excitation. It is noteworthy that there is no notable difference between the results of electron impact excitation and that of photoexcitation, even though the energies in the former method are considerably higher. However, in the case of dimethoxybenzenes, though the relative intensity under photoexcitation is similar to the case of xylenes, the intensity of the photoemission from *o*-dimethoxybenzene by electron impact is remarkably weaker than that of other isomers.

The weak intensity of the band of *o*-dimethoxybenzene under electron impact excitation is probably related to the faster predissociation of the parent molecule from highly excited states. The observation of a more intense photoemission of the fragments from *o*-dimethoxybenzene seems to support this conclusion. Since the sum of the bond-scission energy, the ionization energy (14 eV),[11] and the excitation energy (2.5 eV) of CO^+ ($A^2\Pi$) is larger than the ionization potential of dimethoxybenzenes (7—8 eV),[11] the processes of the production and excitation of CO^+ ($A^2\Pi$) probably involve superexcited species.[12] Identical conclusion can be drawn for H and CH on the basis of similar considerations.[7-9]

The intensities of the photoemission of the parent species, H, and CH were found to be proportional to the electron-beam current, as are shown in Fig. 4. Thus, the mechanism of the production of these excited species was concluded to be one-electron processes for all isomers. However, some secondary process should be involved in the production of CO^+ ($A^2\Pi$) from dimethoxybenzenes, since the linear relation was not established, as is shown in Fig. 5. Ajello did not observe the comet-tail bands of CO^+ in the dissociative excitation of CO_2 by electron impact.[13] In the present study, however, distinct comet-tail bands were observed, and so the mechanism of CO^+ ($A^2\Pi$) production from dimethoxybenzene should be different from that from CO_2.

In the emission spectra by controlled electron impact, the band intensities of photoemission of most of the species have been found to be proportional to the electron-beam current. Two kinds of exceptions have been found; (1) species which have at least two heavy (non-hydrogen) atoms and which are produced through the scission of at least two skeletal bonds (*e.g.*, CN from aniline[9]), (2) species which have to form a new chemical bond on formation (*e.g.*, HCl^+ from chlorobenzene[7]). CO^+ ($A^2\Pi$) from dimethoxybenzene seems to belong to the first group of exceptions; its kinetic behavior was examined in the present study.

Since the emission of CO^+ ($A^2\Pi$) from CO shows a linear relationship (Fig. 5), the non-linear relationship of the photoemission of CO^+ from dimethoxybenzenes is essential to the mechanism of its production from dimethoxybenzenes. This intensity dependence of CO^+ on the electron-beam current can be interpreted by use of the following reaction scheme:

$$M + e \xrightarrow{k_1} CO^{+*} + 2e \quad (1)$$

$$M + e \xrightarrow{k_2} X + e \quad (2)$$

$$X + e \xrightarrow{k_3} CO^{+*} + 2e \quad (3)$$

$$CO^{+*} \xrightarrow{k_4} CO^+ + h\nu \quad (4)$$

where M, e, and X stand for dimethoxybenzene, an electron, and some intermediate species respectively. X may be neutral or ionic; however, X is not such a species as CO_2, as has been mentioned before.

The rate of the appearance of X will be:

$$\frac{d(X)}{dt} = k_2(M)(e) - k_3(X)(e) \quad (5)$$

The second term is assumed to be small and is neglected, since the concentration of X is smaller than that of M

by a few orders of magnitude and since k_3 is not expected to be larger than k_2 by such a magnitude. Then, most of the X produced is removed in the process of evacuation, and the concentration of X is proportional to (M) (e):

$$(X) = k_2'(M)(e) \tag{6}$$

CO^{+*} is produced in Processes (1) and (3) and disappears in the Process (4).

$$\frac{d(CO^{+*})}{dt} = k_1(M)(e) + k_3(X)(e) - k_4(CO^{+*}) \tag{7}$$

The radiative lifetime of CO^{+*} was measured as 2.1—2.9 μs,[14] considerably smaller than the inverval in which the X species remains in the collision region. Thus, the concentration of CO^{+*} can be set as stationary and Equation (7) is equal to 0.
Then,

$$(CO^{+*}) = \frac{k_1(M)(e)}{k_4} + \frac{k_3(X)(e)}{k_4}$$
$$= \frac{k_1(M)(e)}{k_4} + \frac{k_2'k_3(M)(e)^2}{k_4} \tag{8}$$

The intensity (I) of the photoemission of CO^+ ($A^2\Pi$) is proportional to its concentration:

$$I = ak_4(CO^{+*}) \tag{9}$$

where a is a constant. From Eqs. (8) and (9) we obtain:

$$I/e = ak_1(M)(1 + (k_2'k_3/k_1)(e)) \tag{10}$$

The dependence of I/e on e for the bands of CO^+ ($A^2\Pi$) from m-dimethoxybenzene is plotted in Fig. 6. The data reasonably fit a straight line, and so it can be presumed that two-electron dissociative excitation processes, such as (2) and (3), are involved in the production of CO^+ ($A^2\Pi$). From the slopes of the lines, the ratios of CO^+ ($A^2\Pi$) production in the two-electron excitation process to that in the one-electron excitation process, $k_2'k_3/k_1$, are determined to be 1, 5, and 4 for o-, m-, and p-dimethoxybenzenes respectively. Thus, the one-electron process is the most important for o-dimethoxybenzene, which has the weakest parent band and the strongest CO^+ bands.

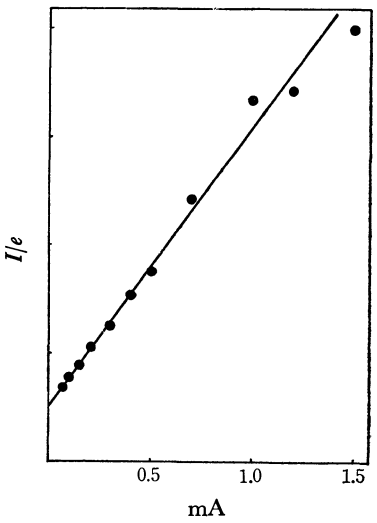

Fig. 6. Dependence of I/e (arbitrary units) on e (mA) for m-dimethoxybenzene at 200 eV.

It may be concluded that the intra-molecular interaction of two adjacent methoxy groups makes the molecule unstable in the highly excited states and that the rate of Process (1) (predissociation) for o-dimethoxybenzene becomes much faster than those of other isomers. This faster rate of Process (1) in o-dimethoxybenzene is concluded to be responsible for the smaller $k_2'k_3/k_1$ ratio; this interaction and the resulting instability of highly excited states probably have something to do with the weaker intensity of the photoemission of the parent species (Table 1). The evaluation of the contribution of the highly excited states on the photoemission by the cascading process in such large molecules has scarcely been studied; a recent investigation of naphthalene has, however, shown the importance of cascading processes.[10]

Although the investigation of CO^+ ($B^2\Sigma^+$) and CO ($b^3\Sigma^+$) as described here will be useful in clarifying the mechanism of the fragmentation of dimethoxybenzene, the research will be left for future study, because of the difficulties involved in the intensity measurements of these species.

The results presented above indicate the usefulness of the controlled electron impact method for the study of the excited states and their reactions.

References

1) T. Ogawa, I. Fujita, M. Hatada, and K. Hirota, This Bulletin, **44**, 659 (1971).
2) I. Fujita, M. Hatada, T. Ogawa, and K. Hirota, *ibid.*, **44**, 1751 (1971).
3) M. Toyoda, T. Ogawa, and N. Ishibashi, *ibid.*, **47**, 95 (1974).
4) W. H. Smith, *J. Chem. Phys.*, **54**, 4169 (1971).
5) T. Ogawa, M. Tsuji, M. Toyoda, and N. Ishibashi, *Chem. Lett.*, **1972**, 233.
6) T. Ogawa, M. Tsuji, M. Toyoda, and N. Ishibashi, *ibid.*, **1972**, 1157.
7) T. Ogawa, M. Tsuji, M. Toyoda, and N. Ishibashi, This Bulletin, **46**, 1063 (1973).
8) T. Ogawa, M. Tsuji, M. Toyoda, and N. Ishibashi, *ibid.*, **46**, 2637 (1973).
9) M. Tsuji, T. Ogawa, and N. Ishibashi, *ibid.*, **46**, 3380 (1973).
10) M. Tsuji, T. Ogawa, and N. Ishibashi, *Chem. Phys. Lett.*, **26**, 586 (1974).
11) D. W. Turner, C. Baker, A. D. Baker, and C. R. Brundle, "Molecular Photoelectron Spectroscopy", John Wiley, New York (1970).
12) R. L. Platzman, *Radiation Res.*, **17**, 419 (1962); K. Hirota, *Nippon Kagaku Zasshi*, **89**, 327 (1968); **91**, 585 (1970).
13) J. M. Ajello, *J. Chem. Phys.*, **55**, 3158, 3169 (1971).
14) G. W. Lawrence, *J. Quant. Spectrosc. Radiat. Transfer*, **5**, 359 (1965).

The Molecular Vibrations and Rotational Isomerism of Chloro(chloromethyl)silane[1]

Keiichi SERA*

Department of Chemistry, Faculty of Science, Hiroshima University, Hiroshima 730

(Received June 22, 1974)

The infrared spectra of chloro(chloromethyl)silane, $ClCH_2SiH_2Cl$, and its deuterated species, $ClCH_2SiD_2Cl$, have been measured in the gaseous, liquid, and crystalline states. The Raman spectra have also been measured in the liquid state. The vibrational spectra have shown that two rotational isomers coexist in the gaseous and liquid states, while only one isomer persists in the crystalline state. The fundamental vibrations have been assigned for each isomer. The product rule, the calculation of the skeletal frequencies, and the band contours have indicated that the isomer persisting alone in the crystalline state is the *trans* form and that the other isomer is the *gauche* form. The solvent effects of the spectra have shown that the *gauche* form is more polar than the *trans* form. The normal vibrations have been calculated in a modified Urey-Bradley force field, and the force constants have been adjusted to predict well the observed frequencies for the isomers of both the parent and its deuterated species.

Many studies have been accumulated concerning the rotational isomerism of 1,2-substituted ethanes.[2] We have taken an interest in studying organosilicon compounds of these homologous series, in which the height of the potential barrier around a C–Si bond may be lower than that around a C–C bond.[3] Investigations of such organosilicon compounds as chloroethylsilane,[4] (chloromethyl)methylsilane,[5] and ethylmethylsilane[5] have been reported previously. Chloro(chloromethyl)silane is a molecule in which both the substituents around the C–Si bond are chlorine atoms; it is a homologous molecule of 1,2-dichloroethane, which has previously been investigated in detail.[6]

Therefore, in this paper, we will deal with the molecular vibrations of chloro(chloromethyl)silane in relation to the rotational isomerism in order to compare the results with those of 1,2-dichloroethane and the analogues of alkylsilanes. By methods similar to those used for 1,2-dichloroethane; that is, the product rule and the calculation of the skeletal frequencies, the molecular forms of the isomers will be determined. The normal vibration calculation will also be carried out for each molecular form in a modified Urey-Bradley force field, and the force constants will be adjusted by a least-squares method in order to predict the observed frequencies well.

Experimental

Tetrachlorosilane was treated with diazomethane,[7] and the product ($ClCH_2SiCl_3$) was reduced with $LiAlH_4$ or $LiAlD_4$ in *n*-butyl ether.[8] Chloromethylsilane was then reacted with $HgCl_2$ in a vacuum.[9] The sample of chloro(chloromethyl)silane was purified by distillation in a dry nitrogen atmosphere; bp 75—76 °C/760 mmHg.

The infrared spectra were recorded on a Perkin-Elmer instrument (Model 621) in the 200—4000 cm^{-1} region and on a Hitachi Fis-3 far-infrared spectrophotometer in the 40—300 cm^{-1} region. The spectra in the liquid state were recorded in CsI and polyethylene cells. The spectra in the gaseous state were measured at room temperature with a 10-cm gas cell fitted with CsI windows. In the crystalline state, the vapor of the sample was condensed on a CsI window cooled with liquid nitrogen in a vacuum and was then annealed near the melting point. The solution spectra were measured using a sealed KRS-5 cell (0.2 mm thick), with *n*-hexane and acetonitrile as the solvents. The Raman spectra in the liquid state were measured with a JEOL Raman spectrometer (Model JAS-O2AS), using an argon-ion laser (488.0 nm) for excitation.

* Former name: Keiichi Ohno.

Results and Discussion

Rotational Isomerism. It has been determined by microwave studies that such molecules as chloromethylsilane[10] and dimethylsilane[11] have a staggered con-

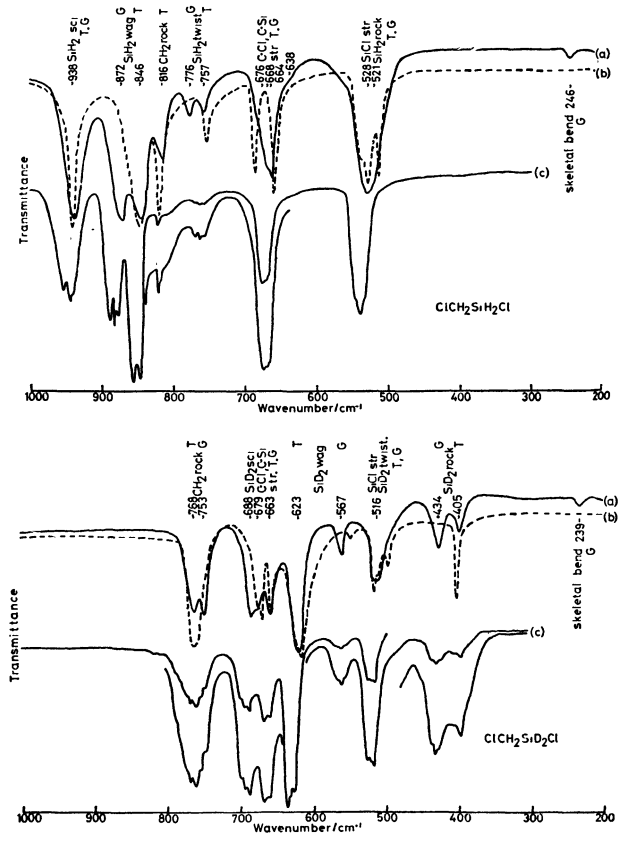

Fig. 1. Infrared spectra of chloro(chloromethyl)silane in the 200—1000 cm^{-1} region; (a): in the liquid state, (b): in the crystalline state, (c): in the gaseous state.

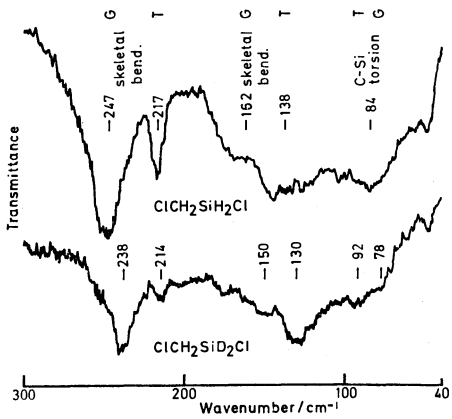

Fig. 2. Far-infrared spectra of chloro(chloromethyl)-silane in the liquid state in the 40—300 cm^{-1} region.

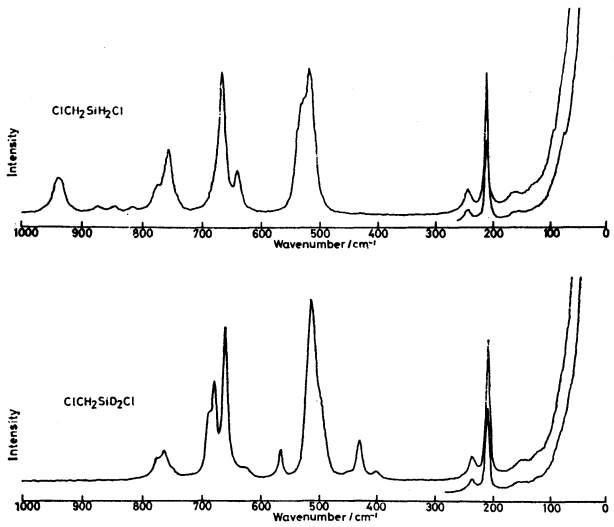

Fig. 3. Raman spectra of chloro(chloromethyl)silane in the liquid state in the region below 1000 cm^{-1}.

figuration around a C–Si bond. Therefore, in this substance, two rotational isomers of the *trans* and *gauche* forms can be expected. If this substance had a unique molecular form, it would show eighteen fundamental frequencies in both the infrared and Raman spectra.

Figures 1—2 and Fig. 3 show the infrared spectra in the 40—1000 cm^{-1} region and the Raman spectra in the region below 1000 cm^{-1} respectively. In the vibrational spectra, too many bands for one isomer are observed in the liquid state, while the absence of some of the bands in the crystalline state shows the existence of the rotational isomers in the liquid state. In the crystalline state, however, the existence of only one isomer is sufficient to account for the number of observed bands.

The vibrational assignments of this substance are made on the basis of the spectra of (chloromethyl)silane[12] and chloromethylsilane,[13] the relative intensities of both the infrared and Raman bands, and the infrared-band contours in the gaseous state. From the assignments of the observed spectra, given in Table 1, the sums of the squares of the fundamental frequencies are found to be:

$$\sum \nu_i^2 = 3.638 \times 10^7 \quad (0.1\% \text{ difference})$$
$$\sum \nu'^2_i = 3.639 \times 10^7$$

for $ClCH_2SiH_2Cl$ and:

$$\sum \nu_i^2 = 3.044 \times 10^7 \quad (0.2\% \text{ difference})$$
$$\sum \nu'^2_i = 3.038 \times 10^7$$

for $ClCH_2SiD_2Cl$, where ν_i and ν'_i indicate the frequencies of the isomers persisting and disappearing in the crystalline state respectively. From the above results, the assignments in Table 1 can be considered as acceptable.

Band Contours. The principal moments of inertia are calculated from the following parameters: C–Cl= 1.788 Å, C–Si=1.889 Å, Si–Cl=2.052 Å, C–H=1.096 Å Si–H=1.477 Å, tetrahedral bond angles, and the internal rotation angles of 180° (*trans*) and 60° (*gauche*). The bond lengths are transferred from those of (chloromethyl)silane[10] and chloromethylsilane[14] determined by microwave studies. Figure 4 shows the *trans* and *gauche* forms of chlorochloromethylsilane in the principal axis system. The *trans* form of this substance may have the C_s symmetry. The 18 normal vibrations are reduced to 11 vibrations of the A′ species and 7 of A″. The a and b internal axes are in the plane of symmetry, while the c axis is perpendicular to it. The A′ vibrations may have either a-, b-, or ab-type infrared-band contours in the case of an asymmetric top. The A″ vibrations, on the other hand, have c-type band contours. The *gauche* form may have no symmetry (point group C_1). All the 18 normal vibrations are of the same symmetry of A.

The principal moments of inertia of I_a, I_b, and I_c calculated are 31.742 (38.838), 424.52 (427.66), and 447.17 (451.55) amu·Å² for the *trans* form of $ClCH_2SiH_2(-D_2)Cl$ and 87.086 (95.978), 275.95 (281.16), and 338.37 (346.60) amu·Å² for the *gauche* form. The Ray asymmetry parameters, κ, are −0.9918 (−0.9895) and −0.8432 (−0.8218) for the *trans* and *gauche* forms of $ClCH_2SiH_2(-D_2)Cl$ respectively; these values show both the forms to be prolate asymmetric top molecules. The expected PR separations are calculated by the use of the method of Seth-Paul and Dijkstra.[15] The

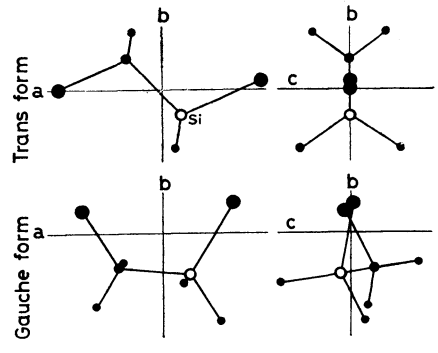

Fig. 4. Possible molecular forms of chloro(chloromethyl)-silane in the principal axis system.

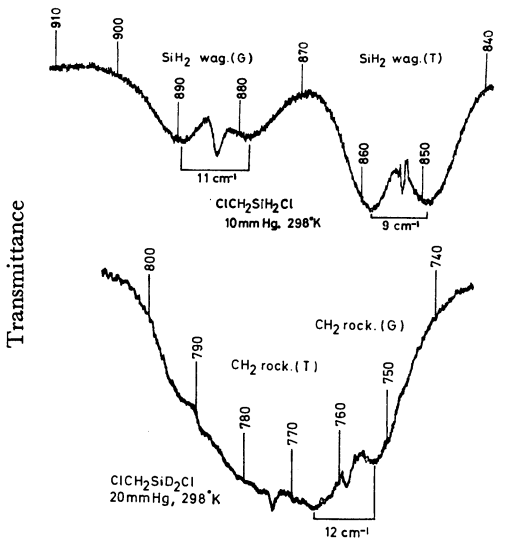

Fig. 5. Infrared band contours of the SiH_2 wagging vibration for $ClCH_2SiH_2Cl$ and the CH_2 rocking vibration for $ClCH_2SiD_2Cl$.

PR separations of the a-, b-, and c-type band contours at the temperature of 298 K are estimated to be 9.6 (9.6), 8.0 (8.0), and 14.4 (14.3) cm^{-1} for the *trans* form of $ClCH_2SiH_2(-D_2)Cl$ and 11.6 (11.6), 9.5 (9.4), and 17.5 (17.4) cm^{-1} for the *gauche* form, where the c-type band contours are expected to produce a PQR structure featuring a sharp Q branch but ill-defined P and R branches.[16]

The PR separations of $ClCH_2SiH_2(-D_2)Cl$ observed are between 8 and 12 cm^{-1}, as is shown in Fig. 5 and Table 1. Especially, for the bands assigned to the SiH_2 wagging vibration, the PR separation of the band at 883 cm^{-1} (11 cm^{-1}) is larger than that of the band at 853 cm^{-1} (9 cm^{-1}), where the former disappears in the crystalline state. The bands assigned to the CH_2 and SiD_2 rocking vibrations and persisting in the crystalline state (the band at 820 cm^{-1} for $ClCH_2SiH_2Cl$ and the bands at 774 and 403 cm^{-1} for $ClCH_2SiD_2Cl$) have c-type band contours, while the corresponding bands disappearing in the crystalline state (the bands at 759 and 436 cm^{-1} for $ClCH_2SiD_2Cl$) feature PQR structures with PR separations of 11—12 cm^{-1}. The results are consistent with the determination of the molecular forms using the product rule and the calculation of the skeletal frequencies to be described below.

Molecular Forms of Isomers. It has been mentioned by Mizushima *et al.*[6] that the product rule and the calculation of the skeletal frequencies are useful for the determination of the molecular forms of the rotational isomers.

The products of the fundamental frequencies are:

$$\pi\nu_i'/\pi\nu_i = 1.146$$

for $ClCH_2SiH_2Cl$ and:

$$\pi\nu_i'/\pi\nu_i = 1.099$$

for $ClCH_2SiD_2Cl$, where ν_i and ν_i' indicate the frequencies of the isomers persisting and disappearing in the crystalline state respectively. When it is assumed that the force field is identical for both the rotational isomers, the relationship between the frequencies of the two isomers is:

$$\pi\nu_i'/\pi\nu_i = (|G(\nu')|/|G(\nu)|)^{1/2}.$$

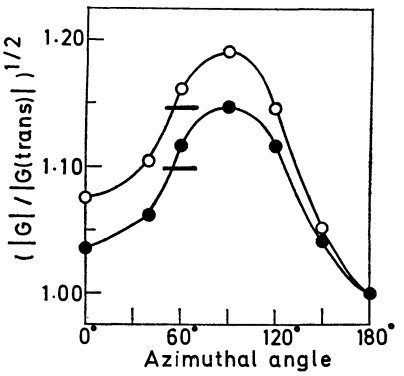

Fig. 6. The calculated values of $(|G'|/|G(trans)|)^{1/2}$ and the observed values of $\pi\nu'/\pi\nu(trans)$;
—○—: $(|G'|/|G(trans)|)^{1/2}$ for $ClCH_2SiH_2Cl$,
—●—: $(|G'|/|G(trans)|)^{1/2}$ for $ClCH_2SiD_2Cl$,
——: observed values.

Figure 6 gives the calculated values of $(|G|/|G(trans)|)^{1/2}$ of a different azimuthal angle, where it is assumed that this substance has a staggered configuration. This shows that the bands persisting in the crystalline state are attributable to the *trans* form and that the bands disappearing in the crystalline state are attributable to the *gauche* form.

In order to confirm the above results, the skeletal frequencies of the parent species are calculated on the basis of the simple Urey-Bradley force field. The force constants used are K(C–Cl)=2.90, K(C–Si)=2.80, K(Si–Cl)=2.59, H(Cl–C–Si)=0.093, H(C–Si–Cl)=0.117, F(Cl·C·Si)=0.21, and F(C·Si·Cl)=0.16 md/Å. The bending and repulsion force constants are transferred from those of (chloromethyl)silane[12] and

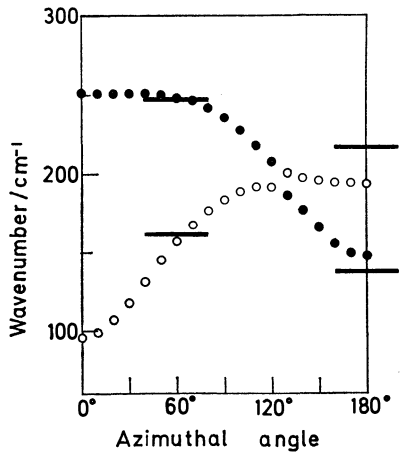

Fig. 7. Dependence of skeletal deformation frequencies of azimuthal angle;
○: calculated frequencies of the symmetric mode,
●: calculated frequencies of the antisymmetric mode, ——: observed frequencies.

TABLE 1. OBSERVED AND CALCULATED FREQUENCIES OF CHLORO(CHLOROMETHYL)SILANE[a] (cm^{-1})

Infrared			Raman liquid	Calculated		P. E. D.[b]
Gas Int.	Liquid Int.	Crystal Int.	Int.	T form	G form	
			$ClCH_2SiH_2Cl$			
	3000 vw	2999 vw	2997 mw	2998 A″	2998	ν_aCH_2 (100)
			2989 mw			
2960 w, 2950	2945 vw	2945 vw	2945 s	2945 A′		ν_sCH_2 (100)
2933 b vw	2936 vw	—	2936 s		2945	ν_sCH_2 (100)
2227 sh, 2222 s, 2217		2232 s, 2221		2222 A″	2222	ν_aSiH_2 (100)
2208, 2198 s, 2185 s	2208 b s		2200 vs	2220 A′	2220	ν_sSiH_2 (100)
1412, 1408 m, 1402	1398 m	1398 m	1398 w	1396 A′		sCH_2 (92)
	1392 sh	—	1392 sh w		1396	sCH_2 (92)
1180, 1175 vw, 1170	1180 sh w	—	1179 w		1162	wCH_2 (100)
	1174 w	1171 m	1174 w	1157 A′		wCH_2 (100)
1112, 1107 vw, 1101	1106 w	—	1105 w		1116	tCH_2 (84)
	1097 sh w	1092 m	1096 w	1116 A″		tCH_2 (85)
954 s, 945	938 s	940 s	938 m	953 A′	951	$sSiH_2$ (95)
941 sh, 933 s						
889, 883 s, 878	872 vs	—	873 vw	873 vw	902	$wSiH_2$ (85), rCH_2 (10)
858, 853 vs, 849	846 vs	846 vs	846 vw	885 A′		ωSiH_2 (99)
822 w, 817 w	816 m	818 vs	816 vw	835 A″	776	rCH_2 (51), $tSiH_2$ (30); $tSiH_2$ (37), rCH_2 (32)

Table 1. Continued

Infrared			Raman	Calculated		P. E. D.[b]
Gas Int.	Liquid Int.	Crystal Int.	Liquid Int.	T form	G form	
770	776 w	—	774 mw		708	rCH$_2$ (40), tSiH$_2$ (33)
764 w						
758	757 w	753 m	757 m	674 A″		tSiH$_2$ (51), rCH$_2$ (20), rSiH$_2$ (23)
677	676 sh m	684 s		685 A′		νC–Cl (53), νC–Si (41)
671 m	668 sh m	—			686	νC–Si (48), νC–Cl (36)
667	664 s	657 s	664 s	640 A′		νC–Si (47), νC–Cl (33)
	638 vw	—	638 w		645	νC–Si (37), rSiH$_2$ (23)
575 sh vw						
567 sh vw	567 vw					
546 sh		534 sh		536 A′		νSi–Cl (95)
539 s	528 b s	527 s	528 s		514	νSi–Cl (89)
535	521 sh s	512 s	517 s	511 A″		rSiH$_2$ (42), rCH$_2$ (32)
					500	rSiH$_2$ (50), νC–Cl (35)
	247 vw	—	245 w		253	δClCSi (55), δClSiC (28)
	217 vvw		212 s	205 A′		δClSiC (31), δClCSi (27)
	162 b vvw		160 w		161	δClSiC (43), δClCSi (20), τ (24)
	138 b vw			134 A′		δClCSi (52), δClSiC (46)
	84 b vvw		92 vw ?	92 A″		τ (87)
			78 vw		78	τ (56), δClCSi (21), δClSiC (20)
			ClCH$_2$SiD$_2$Cl			
	2998 vw	3000 vw	2997 mw	2998 A″	2998	ν_aCH$_2$ (100)
			2988 mw			
2962 m 2953	2947 m	2947 vw	2947 s	2945 A′		ν_sCH$_2$ (100)
2935 sh w	2936 m	—	2937 s		2945	ν_sCH$_2$ (100)
1627						
1623 s	1618 s	1630 s	1619 m	1604 A″	1604	ν_aSiD$_2$ (100)
1616						
1605						
1594 s	1591 s	1602 s	1591 vs	1588 A′	1587	νSiD$_2$ (100)
1584 s			1563 w			
1408						
1404 m	1394 m	1395 m	1394 w	1396 A′		sCH$_2$ (92)
1398	1391 m	—	1391 w		1396	sCH$_2$ (92)
1179						
1177 w	1178 sh m	—	1178 w		1159	wCH$_2$ (100)
1168	1172 m	1169 m	1173 w	1156 A′		ωCH$_2$ (100)
1110						
1104 vw	1103 w	—	1104 w		1114	tCH$_2$ (84)
1099	1084 b w	1089 w	1094 w	1114 A″		tCH$_2$ (85)

Table 1. Continued

Infrared			Raman	Calculated		P. E. D.[b]
Gas Int.	Liquid Int.	Crystal Iint.	Liquid Int.	T form	G form	
1059 1052 vw 1048						
	856 w	859 vw				
844 b mw	839 w					
824 mw 815	822 sh w					
			777 mw			
774 s	768 s	767 s 762	767 mw	785 A″		rCH$_2$ (79)
765 759 s 753	753 s	—	754 sh w		778	rCH$_2$ (71), wSiD$_2$ (16)
703					703	νC-Cl (48), νC-Si (21), sSiD$_2$ (28)
699 s	688 s	675 s	688 m	714 A′		νC-Si (32), νC-Cl (32), wSiD$_2$ (30)
692	679 sh	671	681 m	700 A′	681	sSiD$_2$ (67), νC-Cl (26) sSiD$_2$ (77)
					676	νC-Si (48), sSiD$_2$ (38)
672 s 663	663 s	659 s	663 s	637 A′		νC-Cl (58), wSiD$_2$ (32)
640 635 vs 630	623 vs	618 vs	629 sh w	618 A′		ωSiD$_2$ (32), νC-Si (42), sSiD$_2$ (16)
567 m	567 m	—	568 mw		596	wSiD$_2$ (48), νC-Si (18), rCH$_2$ (11)
		552 vw				
530 525 s 521	516 m	517 m 512	517 vvs	523 A′	 509	νSi-Cl (88) νSi-Cl (39), tSiD$_2$ (47)
		500 w	500 sh s	502 A″		tSiD$_2$ (74)
					504	tSiD$_2$ (30), νSi-Cl (52)
442 436 m 431	434 m	—	434 mw		412	rSiD$_2$ (66), νC-Cl (22)
403 w	405 w	405 m	405 w	407 A″		rSiD$_2$ (54), tSiD$_2$ (18)
	238 vw	—	239 mw		246	δClCSi (58), δClSiC (23)
	214 vvw		212 s	204 A′		δClSiC (28), δClCSi (28)
	150 b vvw		150 w		151	δClSiC (53), δClCSi (20), τ (32)
	130 b vw		129 vw	132 A′		δClCSi (52), δClSiC (47)
	92 b vvw ?			91 A″		τ (88)
	78 b vvw ?				78	τ (58), δClCSi (20)

a) Int.=intensity; s, m, w=strong, medium, weak; v=very; b=broad; sh=shoulder; T=the *trans* isomer; G=the *gauche* isomer; A′, A″=A′ symmetry species, A″ symmetry species; P.E.D.=potential energy distributions; and ν, s, w, t, r, δ, τ=stretching, scissoring, wagging, twisting, rocking, deformation, torsion. b) Only contributions greater than 20% are included.

chloromethylsilane.[13] Figure 7 shows the dependence of the calculated skeletal frequencies for a different azimuthal angle, where the highest-frequency band observed vanishes in the crystalline state. If this substance had a staggered configuration, the isomer disappearing in the crystalline state would be the *gauche* form, though the calculated frequencies do not satisfactorily reproduce the observed frequencies. Therefore, the previous conclusion of the molecular form determined from the product rule is confirmed.

Solvent Effects of the Spectra. The solvent effects of the infrared spectra are measured using the pair band assigned to the SiD_2 rocking vibrations at 434 and 405 cm^{-1}, where the former disappears in the crystalline state. The band at 434 cm^{-1} increases in its relative intensity when it is mixed with a polar solvent such as acetonitrile, while the band at 405 cm^{-1} increases in its relative intensity in a mixture with a non-polar solvent such as *n*-hexane, as is shown in Fig. 8. Therefore, it can be concluded that the isomer persisting in the crystalline state (the *trans* form) is less polar than the other (the *gauche* form).

On the basis of these results, if the C–Cl bond moment is assumed to have the direction of C^+–Cl^-, the group moment of the $CSiH_2(-D_2)Cl$ group should be mainly in the direction of Si^+–Cl^-, though it has been reported that, for (chloromethyl)methylsilane,[5] the group moment of the C_2SiH_2 group is $+\overset{C}{\underset{C}{>}}Si\overset{H}{\underset{H}{<}}-$ on the bisector of the C–Si–C angle. Therefore, the bond moment of SiCl may be larger than the group moment of C_2SiH_2.

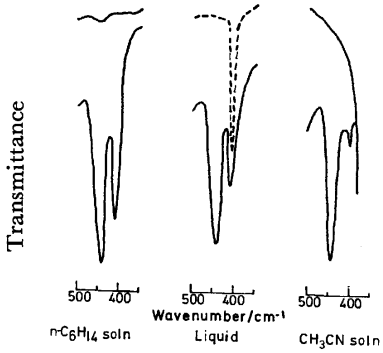

Fig. 8. Solvent effects of the infrared spectra.

Normal Vibration Calculation. The normal vibrations of chloro(chloromethyl)silane were calculated in order to get a reliable set of force constants. The bond lengths and angles used were of the same values used in the calculation of the moments of inertia.

First, we attempted to determine the force constants in the modified Urey-Bradley force field for (chloromethyl)silane[12] and chloromethylsilane[13] and their deuterated species, $ClCH_2SiD_3$ and CH_3SiD_2Cl, in order to get a set of transferable force constants. Second, we tested it for the case of this substance and found that, among the calculated frequencies, the skeletal vibrational frequencies were not in good agreement with the observed frequencies especially. Therefore, the force constants were adjusted by a least-squares method in order to predict well the observed frequencies for both the *trans* and *gauche* forms of the parent and its deuterated species as the assumption that the repulsion force constants were transferable. Modifications of the force field were also made as follows: 1) the bond interaction force constant, p(C–H), was introduced in order to reproduce the observed C–H stretching frequencies and 2) the *trans* coupling constants, $t(CH_2, SiH_2)$, $t(SiCCl, SiH_2)$, and $t(CSiCl, SiCCl)$ were introduced in order to reproduce satisfactorily the observed frequencies of the CH_2 and SiH_2 groups and the skeletal deformation frequencies, where the *gauche* couplings were assumed to be $g=-0.5t$. As a fair agreement was obtained between the observed and calculated frequencies, no further adjustments of the force constants were made.

The calculated frequencies are given in Table 1, together with the predominant internal symmetry coordinates in the potential energy distributions. The force constants obtained are given in Table 2, together

Table 2. Force constants for chloro(chloromethyl)silane[a]

Force const.	$ClCH_2SiH_2Cl$	$ClCH_2SiH_3$[b]	CH_3SiH_2Cl[c]	Force const.	$ClCH_2SiH_2Cl$	$ClCH_2SiH_3$[b]	CH_3SiH_2Cl[c]
K(C-H)	4.393	4.390	4.453	$\kappa(CH_2)$	0.024	0.027	−0.008
K(Si-H)	2.607	2.638	2.565	$\kappa(SiH_2)$	0.138	0.056	0.112
K(C-Cl)	1.510	1.697		Y(C-Si)	0.130	0.080	
K(C-Si)	1.580	1.991	2.393	$t(CH_2, SiH_2)$[d]	0.086	0.081	0.067
K(Si-Cl)	2.205		2.272	$t(SiH_2, SiCCl)$[d]	−0.107	0.032	
p(C-H)	−0.098	—	−0.082	$t(CSiCl, SiCCl)$[d]	0.178		
H(Si-C-H)	0.103	0.104	0.123	F(Si·C·H)	0.271	0.271	0.271
H(Cl-C-H)	0.147	0.147		F(Cl·C·H)	0.558	0.558	
H(H-C-H)	0.331	0.349	0.353	F(H·C·H)	0.200	0.200	0.200
H(Si-C-Cl)	0.071	0.093		F(Si·C·Cl)	0.210	0.210	
H(Cl-Si-H)	0.077		0.077	F(Cl·Si·H)	0.243		0.243
H(C-Si-H)	0.101	0.113	0.102	F(C·Si·H)	0.149	0.149	0.149
H(H-Si-H)	0.170	0.170	0.170	F(H·Si·H)	0.041	0.041	0.041
H(C-Si-Cl)	0.096		0.117	F(C·Si·Cl)	0.160		0.160

a) The units of the force constants are in md/Å for stretching, K; bending, H; repulsion, and F; bond interaction, p; and in md·Å for intramolecular tension, κ; and *trans* coupling, t. b) Ref. 12. c) Ref. 13. d) The *gauche* coupling constants are assumed to be $g=-0.5\,t$.

with those of (chloromethyl)silane and chloromethylsilane. The values of the adjusted force constants, except for these of the skeleton, are similar to those of such analogues as (chloromethyl)silane and chloromethylsilane; under the repulsion-force constants we fixed the transferred values. However, all the values of the skeletal stretching constants are considerably smaller than those of the analogues. It is interesting to note that the higher-frequency band for the SiH_2 wagging vibration and the lower-frequency band for the SiD_2 wagging vibration vanish in the crystalline state. The potential energy distributions indicate that this is mainly due to the coupling with the CH_2 rocking vibration in the 750—820 cm^{-1} region. The tendency of the $SiH_2(\text{-}D_2)$ wagging and SiD_2 rocking vibrations between the liquid and crystalline states is the same as those of (chloromethyl)methylsilane and ethylmethylsilane.[5]

The author wishes to express his gratitude to Professor Hiromu Murata and Professor Michiro Hayashi of Hiroshima University for their valuable suggestions and kind encouragement. He also wishes to express his thanks to Professor Tatsuo Miyazawa and Dr. Teizo Kitagawa for the use of the far-infrared and Raman spectrophotometers and to Mr. Tsutomu Sato for his help in the syntheses of the samples.

References

1) Presented in part at the 29th Annual Meeting of the Chemical Society of Japan, Hiroshima, October, 1973.

2) For example, S. Mizushima, "Structure of Molecules and Internal Rotation," Academic Press Inc., New York 1954; I. Nakagawa, C. Tanaka, and M. Tasumi, *Kagaku no Ryoiki*, **18**, 623 (1964).

3) R. A. Scott and H. A. Scheraga, *J. Chem. Phys.*, **42**, 2209 (1965).

4) S. E. Rudakova, T. F. Tulyakova, and Yu. A. Pentin, *Opt. Spectry.*, **20**, 353 (1966).

5) M. Hayashi, K. Ohno, and H. Murata, This Bulletin, **46**, 797, 2044 (1973).

6) S. Mizushima, T. Shimanouchi, I. Nakagawa, and A. Miyake, *J. Chem. Phys.*, **21**, 215 (1953); I. Ichishima, H. Kamiyama, T. Shimanouchi, and S. Mizushima, *ibid.*, **29**, 1190 (1958); K. Fukushima, *Kagaku to Kogyo*, **18**, 1162 (1965).

7) D. Seyferth and E. G. Rochow, *J. Amer. Chem. Soc.*, **77**, 907 (1955).

8) M. Kumada, M. Ishikawa, and S. Maeda, *J. Organometal. Chem.*, **2**, 478 (1964).

9) H. H. Anderson, *J. Amer. Chem. Soc.*, **82**, 1323 (1960); N. S. Nametkin, T. I. Chernysheva, O. V. Kuz'min, and K.I. Kobrakov, *Dokl. Akad. Nauk SSSR*, **178**, 1332 (1968).

10) R. H. Schwendeman and G. D. Jacobs, *J. Chem. Phys.*, **36**, 1251 (1962).

11) L. Pierce, *ibid.*, **34**, 498 (1961).

12) K. Ohno and H. Murata, This Bulletin, **45**, 3333 (1972); J. R. Durig and C. W. Hawley, *J. Chem. Phys.*, **59**, 1 (1973).

13) E. A. V. Ebsworth, M. Onyszchuk, and H. Sheppard, *J. Chem. Soc.*, **1958**, 1453; J. R. Durig and C. W. Hawley, *J. Chem. Phys.*, **59**, 1 (1973); K. Sera *et al.*, to be published.

14) W. Zeil, R. Gegenheimer, S. Pferrer, and M. Dakkouri, *Z. Naturforsch.*, **27A**, 1150 (1972).

15) W. A. Seth-Paul and G. Dijkstra, *Spectrochim. Acta*, **23A**, 2861 (1967); W. A. Seth-Paul and H. de Meyer, *ibid.*, **25A**, 1671 (1969).

16) R. M. Badger and L. R. Zumwalt, *J. Chem. Phys.*, **6**, 711 (1938).

Electronic Spectra and Electric Properties of Poly(1-methyl-4-vinylpyridinium)-TCNQ Salt

Kenji NAKATANI, Tadayoshi SAKATA, and Hiroshi TSUBOMURA

Department of Chemistry, Faculty of Engineering Science, Osaka University, Toyonaka, Osaka 560

(Received June 24, 1974)

Electronic spectra and conductivities of poly(1-methyl-4-vinylpyridinium)-TCNQ anion radical salts and complex salts which contain additional neutral TCNQ were studied. By addition of neutral TCNQ, a new electronic absorption band appears at 3500 cm^{-1} and the charge-transfer band between TCNQ anion radicals disappears. It was concluded that this new absorption band is the charge-resonance band between a TCNQ anion radical and neutral TCNQ molecule from the dependence of its absorption intensity on the amount of added neutral TCNQ. The conductivity of the salt changed from 7×10^{-8} to 8×10^{-3} Ω^{-1} cm^{-1} by inclusion of the neutral TCNQ. This change of conductivity was explained in relation with the change of the absorption spectra of these polymer salts.

The salts of tetracyanoquinodimethane(TCNQ) anion radical have high electrical conductivity which depends on the properties of the counter cations and the whole crystal structure.[1,2] There are many kinds of crystals of the type $M^+(TCNQ)_n^-(n>1)$.[3,4] The relation between the crystal structure[5] and anisotropy of the electrical conductivity[6] shows that the conduction arises from the transfer of unpaired electrons through the TCNQ molecules which are stacked face-to-face.[3,4] The optical properties of TCNQ salts were discussed in connection with the motion of unpaired electrons.[7] Iida obtained electronic spectra of various TCNQ salts from diffuse reflectance spectra and found that some salts have intense bands in the infrared region besides the charge-transfer bands.[8,9] Kondow and Sakata found that the infrared absorption spectra show a remarkable temperature dependence and explained it by employing a singlet-triplet model and a band model.[10]

Poly-4-vinylpyridinium TCNQ salt is a film-forming polymer salt,[11,12] suitable for the measurement of electronic spectra. Lupinski *et al.* reported that the conductivity of poly-2-vinylpyridinium TCNQ salt increases remarkably by addition of neutral TCNQ.[11] Recently, Mizoguchi *et al.* proposed the conduction mechanism of TCNQ salts of ionene polymers.[13]

In this paper we report the electronic spectra and electrical conductivity at various temperatures of poly-4-vinyl-pyridinium TCNQ salt ($P4VP^+TCNQ^-$) and complex salts ($P4VP^+TCNQ^-TCNQ_x$) ($0\leqq x<1.5$).

Experimental

Synthesis. Poly(1-methyl)-4-vinylpyridinium TCNQ salt and the complex salts including neutral TCNQ were synthesized according to the method in the literature.[11]

Electronic Spectra. The polymer salt was dissolved in dimethylformamide under nitrogen atmosphere. By evaporation on a quartz plate, a coherent film was deposited. The electronic absorption spectra of films were measured with a Shimadzu: SL-50L spectrometer.

Infrared Absorption Spectra. A coherent film was deposited on a thin aluminum mirror, which was prepared by evaporating aluminum on a glass surface. The infrared absorption spectra were measured with a Hitachi-Perkin Elmer infrared spectrometer, and a reflectrance apparatus we made, shown in Fig. 1.

Electrical Conductivity. The electrical conductivity was measured with a compaction sample prepared by pressing at 50 kg/cm^2, with a Yokogawa-Hewlett Packard Model 4305 A Volt-Ohm meter. The temperature dependence of the electrical resistance was measured *in vacuo* by use of a surface-type cell, consisting of a sample film and vacuum-evaporated Au electrodes.

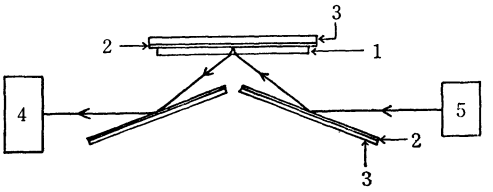

Fig. 1. Infrared reflectance apparatus.
1: Sample film, 2: Evaporated Al mirror, 3: Glass plate, 4: Detector, 5: Monochromator.

Results

Electronic Spectra. Both $P4VP^+TCNQ^-$ and $P4VP^+TCNQ^-TCNQ_x$ form homogeneous green films.[11] As Fig. 2 shows, the spectrum of $P4VP^+TCNQ^-$ changes by inclusion of neutral TCNQ so that the charge-transfer band between $TCNQ^-$s at around 9000 cm^{-1} disappears and a new band appears in the near infrared region below 7000 cm^{-1}. As shown

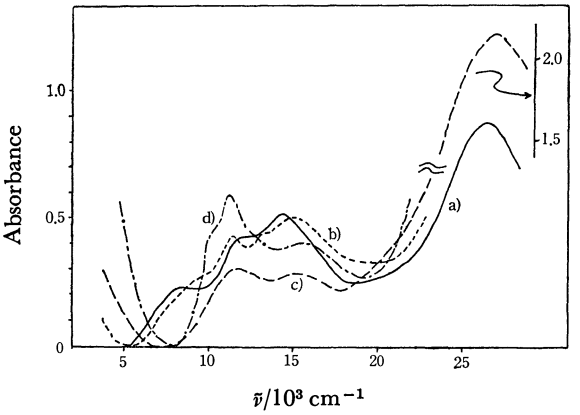

Fig. 2. Absorption spectra of $P4VP^+TCNQ^-TCNQ_x$ polymer films at various mole ratio (x) of added neutral TCNQ:
a) 0, b) 0.5, c) 1.0, d) 1.5.

in Fig. 3, by increasing the amount of neutral TCNQ, the intensity of the new infrared band increases to a mole ratio of about 1.0 and levels constantly. Figure 4 shows the infrared spectrum measured by the mirror reflection method. The new infrared absorption band

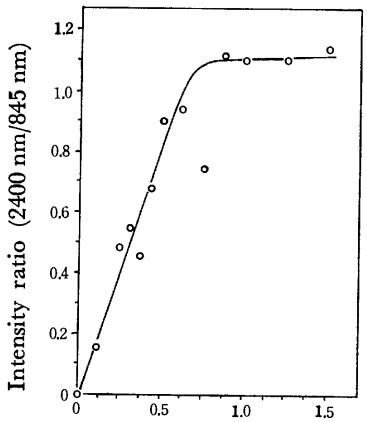

Fig. 3. The dependence of intensity of the new IR band (at 2400 nm) on the neutral TCNQ content.

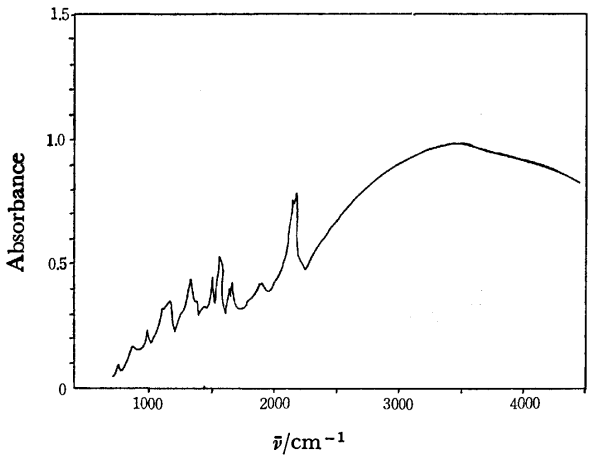

Fig. 4. Infrared spectrum of P4VP+TCNQ-TCNQ

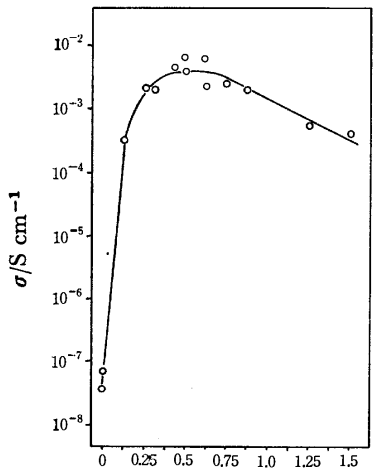

Fig. 5. The dependence of electric conductivity on the neutral TCNQ content.

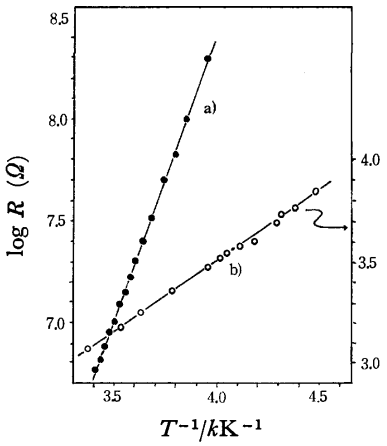

Fig. 6. The temperature dependence of electric resistance.
a) P4VP+TCNQ- b) P4VP+TCNQ-TCNQ$_{1/2}$

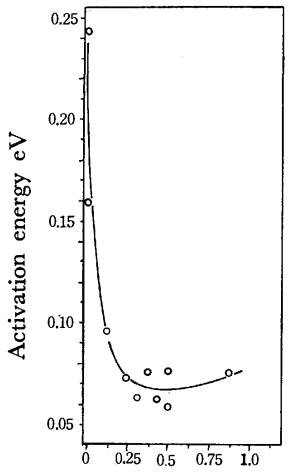

Fig. 7. The dependence of activation energy (E_a) on the neutral TCNQ content.

is seen to have a maximum near 3500 cm^{-1}.

Electrical Properties. The electrical conductivities of powdered samples are shown in Fig. 5 at various mole ratios of neutral TCNQ *vs.* polymer TCNQ salt. With increasing neutral TCNQ, the conductivity changes from 7×10^{-8} to 8×10^{-3} Ω^{-1} cm^{-1} and has a maximum at about a mole ratio of 0.5. The conductivity decreases with the addition of more neutral TCNQ. Log R(electrical resistance) *vs.* T^{-1} (Fig. 6) gives good straight lines for both P4VP+TCNQ- and P4VP+TCNQ-TCNQ$_{1/2}$.

As shown in Fig. 7, the activation energy(E_a) calculated from $R(\Omega)\propto\exp(E_a/KT)$ changed from 0.24 eV for the sample containing no neutral TCNQ to 0.07 eV for the sample containing neutral TCNQ. The variation of activation energy with the TCNQ content has a relationship similar to that of the electrical conductivities (see Figs. 5 and 7) and has a minimum near the mole ratio of 0.5.

Discussion

Absorption Spectra. Poly-4-vinylpyridine is an atactic polymer[11] but the structures of the polymer

TCNQ salts are not known. The absorption spectra of the films are similar to those of other TCNQ salts. It can therefore be presumed that in these polymer salts the TCNQ molecules are packed face-to-face forming somewhat irregular columns as in other TCNQ salts whose crystal structures[5] are known.

The band of P4VP+TCNQ$^-$ at *ca.* 9000 cm^{-1} (Fig. 2) can be assigned to a charge transfer band arising from the charge transfer between the highest half occupied orbitals of TCNQ$^-$ molecules.[8,9] The CT energy has been calculated by use of the SCF-MO method.[14] We measured the absorption spectra of films at various temperatures, from 150 K to room temperature. It was found that the intensity of the CT band increases by lowering the temperature. This suggests that an antiferromagnetic interaction arises between odd electrons of TCNQ$^-$ molecules.[15] The band at *ca.* 11000 cm^{-1} is assigned to the TCNQ$^-$ monomer since the band resembles that of TCNQ$^-$ in EtOH.[16] The band at *ca.* 15000 cm^{-1} (Fig. 2) is attributable to aggregated TCNQ$^-$s since the band resembles that of the TCNQ$^-$ dimer in an aqueous solution[16] and of solid TCNQ$^-$ salts.[8,9]

In the absorption spectra of complex salts with growing amount of neutral TCNQ, the intensity of the CT band at 9000 cm^{-1} decreases and a new absorption band in the IR region below 7000 cm^{-1} arises (Figs. 2 and 3). The intensity of the TCNQ$^-$ monomer band at 11000 cm^{-1} increases relative to that of the TCNQ$^-$ aggregation band at 15000 cm^{-1}. These results can be explained by taking into consideration the fact that added neutral TCNQ is introduced into the TCNQ column as shown by $\langle\cdots A^{\circ}A^{-}A^{\circ}A^{-}A^{\circ}\cdots\rangle$ so that the anion radicals are separated from each other by it. From the two results described above, it seems probable that the new IR absorption band is a charge-resonance band between TCNQ$^-$ and neutral TCNQ. This charge-resonance band is shown to have a peak at 3500 cm^{-1}. Figure 8 illustrates the transitions corresponding to the CT absorption between TCNQ$^-$s and the charge-resonance absorption between TCNQ$^-$ and neutral TCNQ by adopting dimer models.

We have estimated the resonance integral $\langle\phi(A^{-}A^{\circ})|H|\phi(A^{\circ}A^{-})\rangle$ to be *ca.* 0.2 eV from the maximum position of the charge resonance band at ~0.4 eV. This value agrees in the order of magnitude with values obtained by other methods.[7,17] The intensity of this charge-resonance band saturated at about the mole ratio of one neutral TCNQ molecule to one TCNQ$^-$ ion (Fig. 3). This shows that the number of neutral TCNQ molecules which can be inserted into the TCNQ$^-$ column is *ca.* one per one TCNQ$^-$. The CT absorption between TCNQ$^-$ molecules disappeared at a mole ratio of 1.0, suggesting that the neutral TCNQ molecule is evenly distributed and TCNQ$^-$ is isolated (Fig. 2).

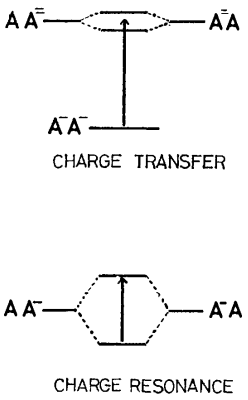

Fig. 8. Schematic illustration of the charge transfer and charge resonance absorptions.

Electrical Properties. According to Onodera's measurements of compressed powder samples, the electrical resistances of both P4VP+TCNQ$^-$ and P4VP+-TCNQ$^-$TCNQ drop rapidly by applying pressure up to *ca.* 100 kbar.[18] This shows that the conduction is due to electron motions[19,20] along the TCNQ column as seen in other TCNQ salts.[21]

The electrical conduction in the solid P4VP+TCNQ$^-$ can be attributed to an electron transfer from a TCNQ$^-$ anion to another, forming TCNQ^0···TCNQ^{2-}.[22] The charge-transfer spectrum, on the other hand, corresponds to an electron transfer from one TCNQ$^-$ to an adjacent TCNQ$^-$. For the usual solid, this corresponds to an excited state, its energy being still much lower than the conduction state. However, in the present case, the two states lie close to each other, because of the lack of coulombic attraction between the hole, TCNQ^0, and electron, TCNQ^{2-}. In the case of the complex salt containing neutral TCNQ, the conduction state corresponds to the charge resonance between TCNQ and TCNQ$^-$, and, hence, corresponds in energy to the charge-resonance band we observed. The absorption spectra of P4VP+TCNQ$^-$ polymer films show that the CT band between TCNQ ions is rather intense and the local excitation bands shift largely as compared with those of monomer ion in solution. This suggests that the interaction between TCNQ$^-$s is not weak in this polymer matrix. The mobility of a carrier is related to the resonance integral expressed as $\beta=\langle\phi_n|H|\phi_{n+1}\rangle$, where ϕ is the lowest vacant molecular orbital of TCNQ, and the suffix n represents the site number.[17] Oohashi and Sakata reported that the resonance integral between the half-occupied orbitals of TCNQ$^-$ is 0.15~0.4 eV, depending on the kind of salt investigated, from the intensity of CT band of reflection spectra.[17] From our preliminary ESR measurement for P4VP+TCNQ$^-$, exchange energy (J) was obtained to be about 0.06 eV and the resonance integral was was calculated as ~0.12 eV by means of the equation $J=4\beta^2/E_{CT}$(E_{CT}=CT energy) which holds for the linear chain radical crystal.[23] This value is slightly smaller than the resonance integral 0.2 eV for the complex salt estimated from the peak position of the charge-resonance band.

Since the difference in resonance integral is small, it can be concluded that the mobility of the simple salt does not differ so much from that of the complex salt.

The variation of conductivity with the mole ratio is parallel to that of activation energy obtained from temperature dependence of resistance (Figs. 5 and 7).

The band gap from the lowest wavelength absorp-

tion edge can be roughly estimated as $\Delta E_1=0.74$ eV for P4VP$^+$TCNQ$^-$ and $\Delta E_2=0.18$ eV for P4VP$^+$TCNQ$^-$-TCNQ, if the CT band and the charge-resonance band are assumed to correspond to transitions from the valence band to the conduction band. The number of carriers per unit cell is assumed to be N for P4VP$^+$-TCNQ$^-$ and 1/2 N for P4VP$^+$TCNQ$^-$TCNQ. Then, the ratio of conductivity σ_c(P4VP$^+$TCNQ$^-$TCNQ)/σ_s(P4VP$^+$TCNQ$^-$) can be represented by the equation

$$\sigma_c/\sigma_s=e\mu 2^{-1}N\exp(-\Delta E_1/2kT)/e\mu N\exp(-\Delta E_2/2kT),$$

which leads to 2.5×10^4 with use of the above values of of ΔE_1 and ΔE_2. This value is in good agreement with the experimental result of the variation of conductivity. Thus, contrary to the explanation given by Mizoguchi *et al.*,[13] the remarkable difference in conductivity might be attributed to the difference in the band gaps. The band gap estimated from the temperature dependence of resistance is about 0.14 eV for P4VP$^+$TCNQ$^-$TCNQ, which is also in good agreement with $\Delta E_2=0.18$ eV obtained from the absorption spectrum. For P4VP$^+$-TCNQ$^-$, the band gap estimated from the activation energy is *ca.* 0.48 eV and smaller than the value, 0.74 eV, obtained from the absorption spectrum, which can be interpreted as giving the lower limit for the band gap. The discrepancy seems to arise from the presence of a trace of neutral TCNQ in P4VP$^+$TCNQ$^-$. Most samples of P4VP$^+$TCNQ$^-$ contain neutral TCNQ. By extracting with benzene, the electrical conductivity of the sample decreases. However, it seems impossible to exclude all the neutral TCNQ which behaves as electron-accepting impurities from the polymer salt.

The intensity of charge-resonance band saturates at over 1.0 mole ratio of neutral TCNQ (Fig. 3). This suggests that the column can include neutral TCNQ molecules as long as the mole ratio becomes 1.0 with TCNQ$^-$ and TCNQ packed one by one, and the TCNQ molecules further added are present at the interstices. The present view also explained the results of conductivities (Fig. 5). The decrease in conductivity at the higher TCNQ content can be attributed to the increasing amount of neutral TCNQ present in the interstices which hinders the electron transfer. The results show that the conductivity shows a maximum at the TCNQ content much lower than unity. This might suggest that, at an increasing TCNQ content, there grows a chance for two TCNQ molecules being packed between two TCNQ$^-$ ions.

In conclusion, the polymer TCNQ salts can be classified into four types according to the neutral TCNQ content.

(1) P4VP$^+$TCNQ$^-$, which does not contain neutral TCNQ and whose conduction state arises from the charge transfer between TCNQ$^-$s.

(2) A salt containing a small amount of neutral TCNQ which acts as an electron-accepting impurity. The situation seems to be analogous to the impurity-doped semiconductor.

(3) P4VP$^+$TCNQ$^-$TCNQ ($0.25<x<1.0$). The conducting state arises from the charge-resonance interaction between TCNQ$^-$ and TCNQ, acquiring quite a different electronic structure from that of P4VP$^+$-TCNQ$^-$. (4) P4VP$^+$TCNQ$^-$TCNQ ($x>1.0$), containing a large amount of neutral TCNQ. The presence of excess neutral TCNQ diminishes the electronic conduction.

References

1) L. E. Melby, R. L. Harder, W. R. Hertler, W. Mahler, R. E. Benson, and W. E. Mochel, *J. Amer. Chem. Soc.*, **84**, 3374 (1962).
2) L. R. Melby, *Can. J. Chem.*, **43**, 1448 (1965).
3) J. C. Bailey and D. B. Chesnut, *J. Chem. Phys.*, **51**, 5118 (1969).
4) W. Siemons, P. Bierstedt, and R. G. Kepler; *ibid.*, **39**, 3523 (1963).
5) C. J. Fritchie, Jr. and P. Arthur, Jr., *Acta Crystallogr.*, **21**, 139 (1966).
6) R. G. Kepler; *J. Chem. Phys.*, **39**, 3528 (1963).
7) Z. G. Soos and D. J. Klein., *ibid.*, **55**, 3284 (1971).
8) Y. Iida, This Bulletin, **42**, 71 (1969).
9) Y. Iida, *ibid.*, **42**, 637 (1969).
10) T. Kondow and T. Sakata, *Phys. Stat. Sol.*, (a), **6**, 551 (1971).
11) J. H. Lupinski, K. D. Kopple, and L. J. Hertz, *J. Polym. Sci., Part C.*, **16**, 1561 (1967).
12) A. Mizoguchi, H. Moriga, T. Shimizu, and Y. Amano, *National Technical Report*, **9**, (5) 407.
13) K. Mizoguchi, T. Suzuki, E. Tsuchida, and I. Shinohara, *Nippon Kagaku Kaishi*, **1973**, 1751.
14) S. Hiroma, H. Kuroda, and H. Akamatu, This Bulletin, **44**, 9 (1971).
15) T. Sakata and S. Nagakura, *ibid.*, **43**, 2414 (1970).
16) R. Boyd and W. D. Phillips, *J. Chem. Phys.*, **43**, 2927 (1965).
17) Y. Oohashi and T. Sakata, This Bulletin, **46**, 3330 (1973).
18) private communication from A. Onodera in this University.
19) S. Saito, Reports on Progress in Polymer Physics in Japan, **12**, 407 (1969).
20) S. Saito, H. Sasabe, and T. Nakajima, *J. Polym. Sci., A-2* **6**, 1297 (1968).
21) D. B. Chesnut and P. Arthur, Jr., *J. Chem. Phys.*, **36**, 2969 (1962).
22) O. H. LeBlanc, Jr.; *ibid.*, **42**, 4307 (1965).
23) T. Sakata and S. Nagakura, presented at the Symposium on Molecular Structure, Tokyo, October, 1970.

Ultrasonic Absorption Mechanism in an Aqueous Solution of *n*-Propyl Alcohol

Sadakatsu NISHIKAWA, Mitsuo MASHIMA, and Tatsuya YASUNAGA*

Department of Chemistry, Faculty of Science and Engineering, Saga University, Honjo-machi, Saga 840

**Department of Chemistry, Faculty of Science, Hiroshima University, Higashisenda-machi, Hiroshima 730*

(Received July 17, 1974)

Ultrasonic absorption in aqueous solutions of *n*-propyl alcohol was measured in the frequency range of 4.5—220 MHz and in the concentration range of 2.0—13.4 M at 25 °C. Two different relaxation processes were observed; they were attributed to the perturbation of the equilibria expressed by $AB \rightleftarrows A \rightleftarrows 1/3A_3$ where A and B are a single water molecule and an alcohol molecule respectively. The forward and backward rate constants for the two processes were determined from the concentration dependences of the relaxation frequencies. Furthermore, the influence of *n*-propyl alcohol on the water structure was discussed; the addition of *n*-propyl alcohol to liquid water was concluded to promote the water structure.

Because of the predominance of water as the medium in living systems, the hydrogen-bonding properties of water have been of particular interest to chemists and biologists. The effects of electrolyted on the structure of water have attractes considerable attention in recent years, but relatively little work has been published dealing with the solution properties and hydrodynamic behavior of neutral solutes. During the course of an investigation of the properties of aqueous solutions of several amines[1-5] by means of ultrasonic absorption, it became desirable to understand the properties of alcohols in aqueous solutions. The physico-chemical properties of aqueous solutions of alcohols have been studied by many authors[6-9], and the ultrasonic techniques[10-13] have also been applied to the investigation of these solutions. However, though Blandamer and his co-workers[14] have reported on the ultrasonic absorption spectra in an aqueous solution of *n*-propyl alcohol, no quantitative analysis of the excess absorption mechanisms has been done.

The present investigation has aimed at the establishment of the excess absorption mechanisms of ultrasonic waves in an aqueous solution of *n*-propyl alcohol on the basis of the water structure. This type of information is particularly desirable for an understanding of more complex biochemical reactions.

Experimental

The chemicals used were of a guaranteed reagent grade; the purity of the *n*-propyl alcohol, which had been distilled once, was verified to be more than 99.9% by gas chromatography. Water which had been deionized and then distilled was used as the solvent. The sample solutions were made at the required concentrations by weight. The concentration range of all the measurements was 2.00—13.4 M, which corresponded to 0.0402—1.00 mole fractions of *n*-propyl alcohol. The measurements of the ultrasonic absorption were carried out at the odd harmonic frequencies of 0.5, 5, and 20 MHz X-cut transducers by means of the pulse technique.[15] The frequency range of the absorption measurement was 4.5—220 MHz. The sing-around technique operated at a fixed frequency of 1.92 MHz was used to measure the sound velocity. The densities were measured by means of a standard pycnometer, the volume of which was 3.717 cm^3. All the measurements were made at 25 °C. A thermostat was built capable to perform within ±0.03 °C.

Results

The quantity α/f^2, where α is the sound absorption coefficient, and f, the frequency, was found to be frequency dependent for an aqueous solution of *n*-propyl alcohol. The plots of α/f^2 *vs.* the concentration of *n*-propyl alcohol are shown in Fig. 1 at various frequencies. The fact that α/f^2 depends on the frequency leads us to the idea that relaxational phenomena exist in the frequency range measured. In general, the sound absorption caused by the several relaxation processes can be described by the following equation:

$$\alpha/f^2 = \sum_i A_i/[1+(f/f_{ri})^2] + B \qquad (1)$$

where f_{ri} is the relaxation frequency for the i-th process and where A_i and B are constants. Figure 2 shows some representative ultrasonic absorption spectra of aqueous solutions of *n*-propyl alcohol. The spectra in the concentrations lower than 2.75 M show the behavior characteristic of a single relaxation process, which is expressed by $i=1$ in Eq. (1). On the other hand, the experimental results in the concentrations higher than 2.95 M can be expressed by two relaxation processes. The double relaxation spectra were analyzed by a nonlinear least-squares routine, employing a Toshiba 3400 computer. In Table 1, the ultrasonic

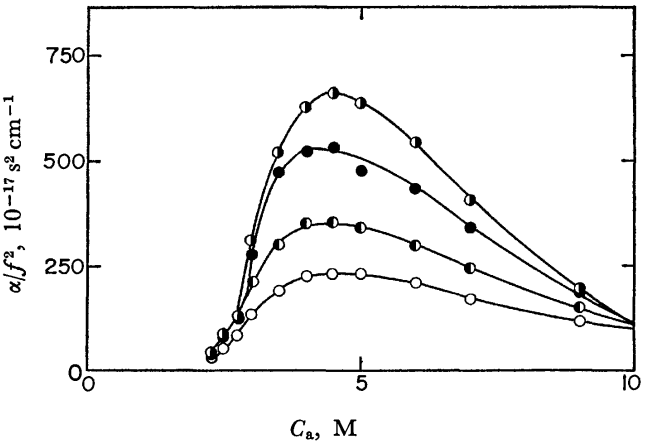

Fig. 1. The plots of α/f^2 *vs.* concentration for the aqueous solution of *n*-propyl alcohol at 25 °C.
◑: f=6.5 MHz, ●: f=15 MHz, ◐: f=45 MHz, ○: f=100 MHz.

Table 1. Relaxation parameters, sound velocity in the aqueous solution of *n*-propyl alcohol

C_a (M)	n_f[a]	ρ (g me^{-1})	c (m s^{-1})	f_{r_1} (MHz)	f_{r_2}	A_1	A_2 (10^{-17} s^2 cm^{-1})	B
2.00	0.0402	0.9797	1583.7	—	—	—	—	34.5
2.25	0.0461	0.9771	1588.1	85	—	17.3	—	55.3
2.50	0.0518	0.9752	1590.6	80	—	61.0	—	41.4
2.75	0.0579	0.9723	1589.2	78	—	145	—	54.1
2.95	0.0630	0.9699	1585.0	82	18	196	80	69.0
3.03	0.0649	0.9690	1581.8	86.5	21	220	113	37.8
3.50	0.0772	0.9647	1566.6	80	12	425	273	44.7
4.00	0.0914	0.9570	1546.8	71	11	432	387	140
4.50	0.107	0.9500	1527.3	90	14	378	463	131
5.00	0.123	0.9429	1508.3	85.5	13	355	457	143
6.02	0.161	0.9280	1471.0	81	12	287	379	151
7.00	0.204	0.9130	1436.5	84	16	193	246	144
9.00	0.322	0.8816	1371.9	110	26	71.0	83.8	116
13.4	1.00	0.8005	1207.5	—	—	—	—	69.1

a) n_f is the mole fraction of *n*-propyl alcohol.

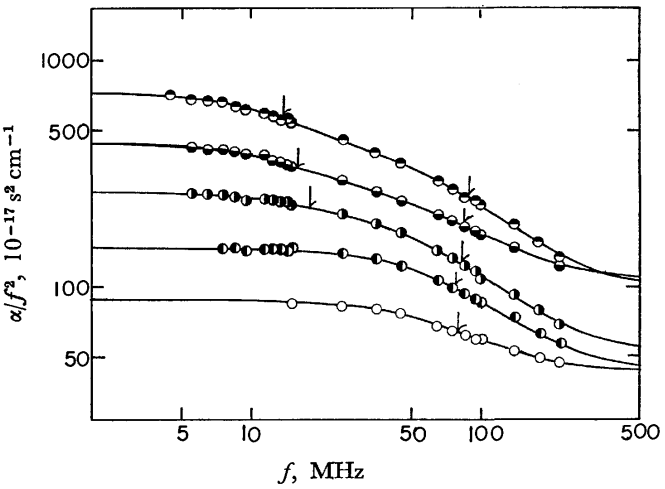

Fig. 2. Ultrasonic absorption spectra in the aqueous solution of *n*-propyl alcohol at 25 °C. The arrows show the relaxation frequencies. ○: 2.50 M, ◐: 2.75 M, ◑: 2.95 M, ◓: 4.50 M, ◒: 7.00 M.

absorption parameters and the sound velocities are listed, together with the densities. As may be seen in this table, both the excess absorption, A_4, and the sound velocity, c, exhibit a maximum.

Interpretation of Results

Both water and alcohol molecules have a tendency to form hydrogen bonding, and the latter also has a hydrophobic group. Therefore, the following reaction mechanisms for the relaxation processes will be considered:

$$AB_m \underset{k_{21}}{\overset{k_{12}}{\rightleftharpoons}} mB + A \overset{k_{23}}{\underset{k_{32}}{\rightleftharpoons}} \frac{1}{n}A_n \qquad (2)$$

where A is the molecule of alcohol; B, that of water, and k_{ij}, the rate constant. In this equation, the first equilibrium indicates the interaction between alcohol and water molecules, and the second, the self-association reaction of alcohol. The general approach of the treatment used here is similar to that of Eigen and de Maeyer[16] or that of Hammes and Knoche.[17] If one denotes the molar concentrations of the components, AB_m, B, A, and A_n by C_1, C_2, C_3, and C_4 respectively, the returning rate of the system to equilibrium is governed by the rate law:

$$\frac{dC_1}{dt} = -k_{12}C_1 + k_{21}C_2^m C_3 \qquad (3)$$

$$\frac{dC_4}{dt} = k_{22}C_3^n - k_{32}C_4 \qquad (4)$$

These equations can be linearized in the neighborhood of the equilibrium by the usual procedure:

$$\frac{d\Delta C_1}{dt} = a_{11}\Delta C_1 + a_{21}\Delta C_4 \qquad (3')$$

$$\frac{d\Delta C_4}{dt} = a_{21}\Delta C_1 + a_{22}\Delta C_4 \qquad (4')$$

with $a_{11}=-[k_{12}+k_{21}\ (m^2\bar{C}_2^{m-1}\bar{C}_3+\bar{C}_2^m)]$, $a_{12}=-k_{21}n\bar{C}_2^m$, $a_{21}=-k_{23}n\bar{C}_3^{n-1}$ and $a_{22}=-(k_{23}n^2\bar{C}_3^{n-1}+k_{32})$, where a bar over a symbol indicates the equilibrium value. In the derivation of Eqs. (3') and (4'), the relations of $\Delta C_3=-n\Delta C_4-\Delta C_1$ and $\Delta C_1=-1/m\Delta C_2$ were used. The (3') and (4') rate equations can be written as:

$$\frac{d\boldsymbol{X}}{dt} = \boldsymbol{AX} \qquad (5)$$

where $\boldsymbol{A}$ is the column matrix made up of the a_{ij}'s. Using the normal coordinate transformation, Eq. (5) can be transformed to:

$$\frac{d\boldsymbol{Y}}{dt} = \boldsymbol{BY} \qquad (6)$$

where $\boldsymbol{Y}$ is the column matrix of eigenvectors, and $\boldsymbol{B}$, a diagonal matrix of the negative reciprocal relaxation times. The transformation matrix is as follows[17]:

$$\boldsymbol{M} = \begin{bmatrix} 1 & -[(1/\tau_1+a_{11})/a_{11}] \\ a_{21}/a_{11} & -[(1/\tau_2+a_{11})/a_{11}] \end{bmatrix} \qquad (7)$$

where the relations of $\boldsymbol{Y}=\boldsymbol{MX}$ and $\boldsymbol{B}=\boldsymbol{MAM}^{-1}$ are satisfied. If the first step in Eq. (2) is assumed to

equilibriate rapidly compared to the second, one gets:

$$1/\tau_1 = 2\pi f_{r1} = -a_{11} = k_{21}(m^2\bar{C}_2^{m-1}\bar{C}_3+\bar{C}_2^m) + k_{12} \quad (8)$$

$$1/\tau_2 = 2\pi f_{r2} = \frac{a_{12}a_{21}}{a_{11}} - a_{22}$$

$$= k_{32}+k_{23}n^2\bar{C}_3^{n-1} - \frac{n^2k_{21}k_{23}\bar{C}_2^m\bar{C}_3^{n-1}}{k_{12}+k_{21}(m^2\bar{C}_2^{m-1}\bar{C}_3+\bar{C}_2^m)} \quad (9)$$

$$y_1 = \Delta C_1 + \frac{a_{12}}{a_{11}}\Delta C_4 \quad (10)$$

$$y_2 = -\Delta C_4 \quad (11)$$

For the two relaxation processes, the chemical absorption per wavelength is:

$$\mu_{ch} = 4\mu_{m_1}\pi f\tau_1/[1+(f/f_{r1})^2] + 4\mu_{m_2}\pi f\tau_2/[1+(f/f_{r2})^2] \quad (12)$$

The expression for the maximum excess absorption per wave length, μ_{mi}, for the i-th process is derived as follows:

$$\mu_{mi} = \frac{1}{2}A_i f_{ri} c = (\rho\pi c^2\Gamma_i/RT)\left(\Delta V_i - \frac{\alpha_p^\infty}{\rho C_p^\infty}\Delta H_i\right)^2 \quad (13)$$

where ρ is the density; R, the gas constant; T, the absolute temperature; α_p^∞, the high-frequency limit of the thermal expansion coefficient; C_p^∞, the high-frequency limit of the constant pressure specific heat, and ΔV_i and ΔH_i, the parameters related to the volume and enthalpy changes associated with the reactions. The Γ_i terms is the function of the reactant concentrations and is derived by means of:

$$\Gamma_i = -\frac{RT}{V}\left(\frac{\partial y_i}{\partial A'_i}\right)_{TPy_j} \qquad i \neq j \quad (14)$$

where A_i' is the affinity. In the conditions of a constant temperature and a constant pressure, the maximum excess absorption per wavelength is proportional to $\rho c^2\Gamma_i$ and the other terms are nearly constant. For the reactions expressed by Eq. (2), one can calculate the Γ_i terms using Eq. (14):

$$\Gamma_1 = \frac{1}{V}\left(\frac{1}{\bar{C}_1}+\frac{1}{\bar{C}_3}+\frac{m^2}{\bar{C}_2}-\frac{m^2}{\bar{C}_T}\right)^{-1} \quad (15)$$

$$\Gamma_2 = \frac{1}{V}\left[\frac{n}{\bar{C}_3}\left(n-\frac{a_{12}}{a_{11}}\right)+\frac{n-1}{\bar{C}_T}\left(n-1+\frac{a_{12}}{a_{11}}\right)+\frac{1}{\bar{C}_4}\right]^{-1} \quad (16)$$

where $\bar{C}_T=\bar{C}_1+\bar{C}_2+\bar{C}_3+\bar{C}_4$.

If one denotes the analytical concentration of alcohol by C_a and that of water by C_w, the next equations are set up:

$$C_a = \bar{C}_1 + \bar{C}_3 + n\bar{C}_4 \quad (17)$$

$$C_w = C_w^s + m\bar{C}_1 + \bar{C}_2 \quad (18)$$

where C_w^s is the concentration of the cluster, that is, the concentration of the hydrogen-bonded water molecules. It is well known that the physico-chemical properties of liquid water can be interpreted by a two-state model.[18,19] Therefore, we assume that, in an aqueous solution of alcohol, there exists an equilibrium between hydrogen-bonded and non-hydrogen-bonded water in addition to those equilibria expressed by Eq. (2) and that only non-hydrogen-bonded water molecules participate in the interaction with alcohol molecules. Then, if one denotes the concentration of non-hydrogen-bonded water by C_w^s, the next equations are held:

$$C_w^s/C_w^s = \exp(-\Delta F_w/RT), \quad C_w = C_w^s + C_w^s \quad (19)$$

where ΔF_w is the free energy difference between hydrogen-bonded and non-hydrogen-bonded water molecules.

At this stage, we shall first consider the reaction mechanism associated with the excess absorption observed in the higher frequency range and the case of $m=1$, namely, the case in which a single alcohol molecule interacts with a single water one. We also assume that the concentration of the aggregate of alcohol, $\bar{C}_4$, is very small as compared with those of the other components. Then, one obtains the next equation from Eqs. (8), (17), (18) and (19):

$$1/\tau_1 = 2\pi f_{r_1} = k_{21}\sqrt{(C_a-\beta C_w+K_{12})^2+4\beta C_w K_{12}} \quad (20)$$

where β is the mole fraction of non-hydrogen-bonded water and where K_{12} is defined as $K_{12}=k_{12}/k_{21}=\bar{C}_2\bar{C}_3/\bar{C}_1$. As may be seen in Table 1, the value of the relaxation frequency, f_{r1}, goes through minimum near $C_a=4.5$ M. Therefore, the next condition must be satisfied at $C_a=4.5$ M.

$$\frac{\partial(1/\tau_1)}{\partial C_a} + \frac{\partial(1/\tau_1)}{\partial\beta C_w}\cdot\frac{d\beta C_w}{dC_a} = 0 \quad (21)$$

Thus, the parameters, β and K_{12}, are not independent of each other. A trial-and-error procedure was used to obtain the values of these parameters which provided the best fit to the experimental data using Eq. (20). The best values are $K_{12}=2.6$ M, $\beta=0.15$, and $k_{21}=6.2\times10^7$ M^{-1} s^{-1}. Then, one gets also $k_{12}=1.6\times10^8$ s^{-1} from the definition of K_{12}. The relaxation frequencies calculated by Eq. (20) using the obtained parameters are shown in Fig. 3, along with the experimental values. One can evaluate the concentration dependence of the maximum chemical absorption per wavelength using Eq. (15). Figure 4 shows the calculated values of $\rho c^2\Gamma_1 V$ along with the experimental values of μ_{m1}. As may be seen in this figure, both maxima

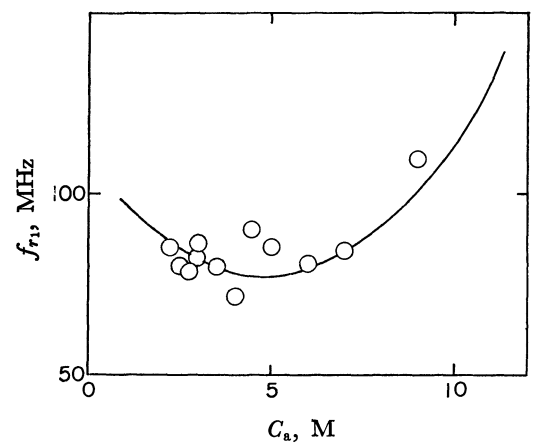

Fig. 3. Concentration dependence of the relaxation frequencies, f_{r_1}.

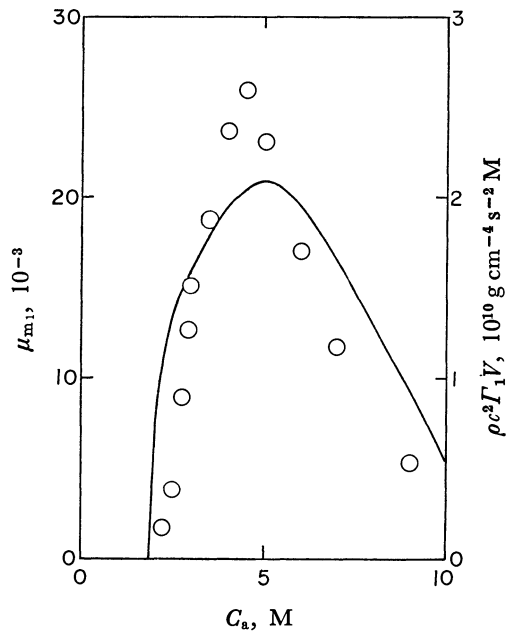

Fig. 4. The variation of μ_{m1} and $\rho c^2\Gamma_1 V$ with the concentration of *n*-propyl alcohol. The solid line represents the calculated values of $\rho c^2\Gamma_1 V$. The circles are the experimental points of μ_{m1}.

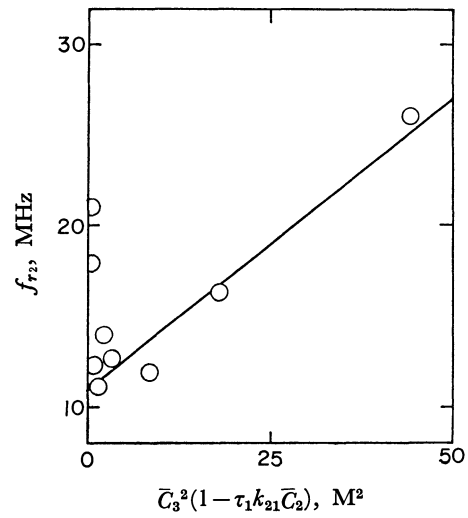

Fig. 5. The plots of f_{r2} *vs.* $\bar{C}_3^2(1-\tau_1 k_{21}\bar{C}_2)$ for the aqueous solution of *n*-propyl alcohol at 25 °C.

appear at almost the same position. This confirms that the excess absorption mechanism in the higher frequency range is due to the perturbation of the first equilibrium expressed in Eq. (2).

Second, let us consider the mechanism of the excess absorption in the lower frequency range. Equation (9) can be transformed as follows.

$$1/\tau_2 = 2\pi f_{r2} = n^2 k_{23}\bar{C}_3^{n-1}(1-\tau_1 k_{21}\bar{C}_2) + k_{32} \qquad (22)$$

Figure 5 shows the plots of f_{r2} *vs.* $\bar{C}_3^2(1-\tau_1 k_{21}\bar{C}_2)$. The parameter, n, which is the aggregation number of *n*-propyl alcohol, was determined so as to give a straight line of the plots of f_{r2} *vs* $\bar{C}_3^{n-1}$ $(1-\tau_1 k_{21}\bar{C}_2)$ and resulted in $n=3$. The rate constants were determined to be $k_{23}=2.2\times10^5$ M^{-2} s^{-1} and $k_{32}=6.9\times10^7$ s^{-1} from the slope and intercept of the straight line respectively. We also calculated the concentration dependence of the maximum chemical absorption per wavelength associated with this aggregation reaction, but the value of $\rho c^2\Gamma_2 V$ increases monotonically with the alcohol concentration.

Discussion

The most interesting and important feature in the ultrasonic absorption study of an aqueous solution of *n*-propyl alcohol is that the excess absorption is observed only in the solutions, not in pure water and pure alcohol, in the frequency range investigated. This means that the causes of the excess absorption mechanisms are closely associated with the peculiar properties of water and *n*-propyl alcohol molecules. The model which is proposed here is a general one which covers all of the equilibria considered in an aqueous solution of neutral solutes, because any molecule which consists of hydrophilic and hydrophobic groups has a tendency to interact with water molecules and to aggregate. The equilibrium between hydrogen-bonded (cluster) and non-hydrogen-bonded water molecules is also taken into accout for the elucidation of the observed excess absorption mechanisms, although the relaxation time for the perturbation of this equilibrium is too short to be observed[18] (It is of the order of 10^{-12} s). At this stage, it is very useful to consider the water structure in an aqueous solution of *n*-propyl alcohol. The parameter, β, is related to the free energy difference between the two states for hydrogen-bonded and non-hydrogen-bonded water molecules, ΔF_w, by the relation; $\beta/(1-\beta)=\exp(-\Delta F_w/RT)$ and one gets $\Delta F_w=1.0$ kcal. In pure liquid water, however, the free energy difference is of an order of less than 1 kcal.[19] The increase in the free energy difference is due to the decrease in the non-hydrogen-bonded water molecule in an aqueous solution of *n*-propyl alcohol. This means that the *n*-propyl alcohol molecule acts as water structure promoter. This conclusion is consistent with the results of other investigations.[8,20] In order to examine the influence

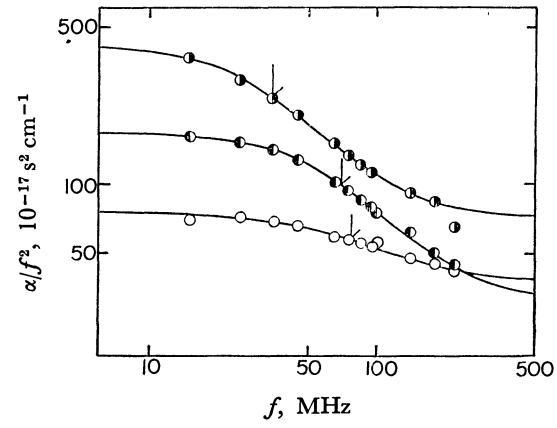

Fig. 6. Ultrasonic absorption spectra of the aqueous solution of 2.60 M *n*-propyl alcohol. The influence of NaCl to the absorption spectra. ○: no added, ◐: 0.507 M NaCl added, ◑: 1.00 M NaCl added.

of the water structure on the water and *n*-propyl alcohol interaction, we also measured the ultrasonic absorption in an aqueous solution of *n*-propyl alcohol to which NaCl was added. The measurements were performed in a solution of 2.60 M of *n*-propyl alcohol, where only a single relaxation process is observed in the higher frequency range. Figure 6 shows the absorption spectra in these solutions; the relaxation frequency decreases with increase of concentration of NaCl. Addition of NaCl to liquid water acts as water structure promoter.[21] According to Eq. (20), the decrease in the non-hydrogen-bonded water molecule must result in the decrease in the relaxation frequencies. As may be seen in Fig. 6, the experimental results are consistent with the above interpretation; this criterion is also taken as sufficient evidence for the correct assignment of the excess absorption mechanism in the higher frequency range observed.

More extensive ultrasonic absorption measurements in aqueous solutions of other alcohols may be desirable to confirm the ultrasonic absorption mechanisms of these solutions. The studies of these solutions are now in progress; the results will be reported in due course.

The authors wish to express their thanks to Dr. Keishiro Shirahama in Saga University for his helpful discussions.

References

1) S. Nishikawa, T. Nakamoto, and T. Yasunaga, This Bulletin, **46**, 324 (1973).
2) S. Nishikawa and T. Yasunaga, *ibid.*, **46**, 1098 (1973).
3) S. Nishikawa, T. Yasunaga, and N. Tatsumoto, *ibid.*, **46**, 1573 (1973).
4) S. Nishikawa, *J. Colloid Interfac. Sci.*, **45**, 259 (1973).
5) S. Nishikawa, T. Yasunaga, and K. Takahashi, This Bulletin, **46**, 2992 (1973).
6) F. Franks and D. J. G. Ives, *Quart. Rev.*, **20**, 1 (1966).
7) N. Laiken and G. Nemethy, *J. Phys. Chem.*, **74**, 3501 (1970).
8) M. M. Rousselot and M. Lucas, *ibid.*, **77**, 1056 (1973).
9) T. T. Herskovits and T. M. Kelly, *ibid.*, **77**, 38 (1973).
10) V. P. Romanov and V. A. Solovev, *Soviet Physics-Acoustics*, **11**, 219 (1965).
11) O. Nomoto, *J. Phys. Soc. Jap.*, **11**, 827 (1956).
12) O. Nomoto, *ibid.*, **12**, 300 (1957).
13) O. Nomoto, *ibid.*, **11**, 1146 (1956).
14) M. J. Blandamer, N. J. Hidden, M. C. R. Symons and N. C. Treloar, *Trans. Faraday Soc.*, **64**, 3242 (1968).
15) N. Tatsumoto, *J. Chem. Phys.*, **47**, 4561 (1967).
16) M. Eigen and L. de Maeyer, "Technique of Organic Chemistry," S. L. Friess, E. S. Lewis and A. Weissberger, Eds. (Interscience Publishers, Inc., New York, 1963) Vol. 8.
17) G. G. Hammes and W. Knoche, *J. Chem. Phys.*, **45**, 4041 (1966).
18) L. Hall, *Phys. Rev.*, **73**, 775 (1948).
19) T. A. Litovitz and E. H. Carnevale, *J. Appl. Phys.*, **26**, 816 (1955).
20) J. Oakes, *J. Chem. Soc. Faraday II*, **69**, 1311 (1973).
21) M. Gross, J. Azoulay, and D. Gerlich, *J. Chem. Phys.*, **58**, 5812 (1973).

Molecular Structure of Molybdenum Oxide Tetrachloride Studied by Gas Electron Diffraction

Kinya IIJIMA and Shuzo SHIBATA

Department of Chemistry, Faculty of Science, Shizuoka University, Oya, Shizuoka 422

(Received July 27, 1974)

The molecular structure of molybdenum oxide tetrachloride was determined to be a square pyramid by a sector-microphotometer method of gas electron diffraction. The following molecular parameters were obtained by a least-squares method: r_g(Mo–Cl)=2.279±0.003 Å, r_g(Mo–O)=1.658±0.005 Å, and r_g(Cl···Cl(s))=3.142±0.008 Å. The structure of gaseous $MoOCl_4$ is similar to that of gaseous $WOCl_4$. The infrared spectra of $MoOCl_4$ were also measured in solutions.

The molecular structure of MXY_4, where M is a central atom, can be classified into two groups: trigonal bipyramid and square pyramid. The structure of gaseous SOF_4[1,2] was reported to be a trigonal bipyramid, and the structures of $XeOF_4$[3,4] and $WOCl_4$[5,6] in the gas phase were found to be square pyramids, although the OXeF angle (92°) and the OWCl angle (102.4°) differ a great deal from each other. According to infrared spectroscopic study,[7] the $MoOCl_4$ molecule is monomeric and has a square-pyramidal structure in the gas phase as well as in inert solvents. The present study was undertaken in order to determine in more detail the structure of $MoOCl_4$ in the gas phase by the sector-microphotometer method of electron diffraction,[8] in order to see the difference between the configuration of $MoOCl_4$ and those of $WOCl_4$ and $XeOF_4$ and to compare the Mo–O and Mo–Cl bond distances of $MoOCl_4$ with those of other molybdenum compounds such as MoO_2Cl_2,[9] $MoCl_5$,[10] and $MoOCl_3$ (in solid state).[11,12]

The vibrational spectra of $MoOCl_4$ have been measured in the gas phase [7,13] and in solutions.[7,14] We have obtained the infrared spectra of $MoOCl_4$ in inert solvents in a wider range for the purpose of calculating the mean amplitudes of vibration.

Experimental

The sample prepared by refluxing molybdenum trioxide with thionyl chloride[15] was purified by repeated sublimation *in vacuo*. It was then loaded into a high-temperature nozzle in a dry box, vaporized at *ca.* 80 °C. Electron diffraction photographs were taken with an r^3-sector at a camera distance of 144.4 mm. The accelerating voltage was about 40 kV, the exposure times 30∼40 s, and the electron-beam current 0.7 μA. The electron wavelength was determined by means of gold powder patterns. The lattice constant of gold was calibrated by means of X-ray diffraction and checked by an electron diffraction study of CCl_4. Photographs were recorded on Fuji process hard plates. The photographic densities of four plates were measured with a digital microphotometer at intervals of 0.4 mm, and the intensity of each plate was used independently for the structure analysis.

The infrared spectra of $MoOCl_4$ in carbon tetrachloride and cyclohexane solutions were measured in the range 4000∼40 cm^{-1} with a Hitachi EPI-G3 spectrophotometer and a Hitachi FIS-3 far-infrared spectrometer. Carbon tetrachloride and cyclohexane were dried by use of phosphorus pentoxide and sodium metal, respectively, since $MoOCl_4$ readily decomposed with a trace of water in the solvent. Measurement of the Raman spectrum was impracticable because of the intense color of the $MoOCl_4$ solutions.

Structure Analysis

Intensities measured in the range $q=17\sim102$ $Å^{-1}$ were leveled theoretically. The elastic scattering factors of Schäfer *et al.*[16] and the inelastic scattering factors of Cromer and Mann[17,18] were used. The radial distribution is shown in Fig. 1. The N_{ij} functions which fit μ_{ij}[5,19] in a whole range of the scattering angle were as follows:

$$N_{Mo-Cl} = 1.000$$

$$N_{Mo-O} = 1.020 + 0.147\exp(-0.00040\,q^2)$$

$$N_{Cl\cdots Cl} = 1.202 + 0.076\exp(-0.00028\,q^2)$$

$$N_{Cl\cdots O} = 1.245 + 0.395\exp(-0.00060\,q^2)$$

The radial distribution curve, which is very similar to that of $WOCl_4$,[5] suggests that the molecular structure of $MoOCl_4$ is a square pyramid.

Least-squares calculations were carried out in order to refine the molecular parameters. Least-squares analyses of background[20] and molecular intensity[21] values were repeated alternately. An experimental background was approximated using a polynomial of 7th degree, and the weight function given by Konaka and Kimura[22] was assumed.

The molecule was assumed to be a trigonal bipyramid C_{2v}. The OMoCl(equatorial) angles 90°, 100°, 110°, 120°, and 130° with the OMoCl(polar) angle 90° were used as initial values for the least-squares calculations. No convergence was obtained for 90° or 130°. For the other cases, the OMoCl(polar) and OMoCl(equatorial) angles as well as the Mo–Cl(polar) and Mo–Cl(equatorial) distances converge to

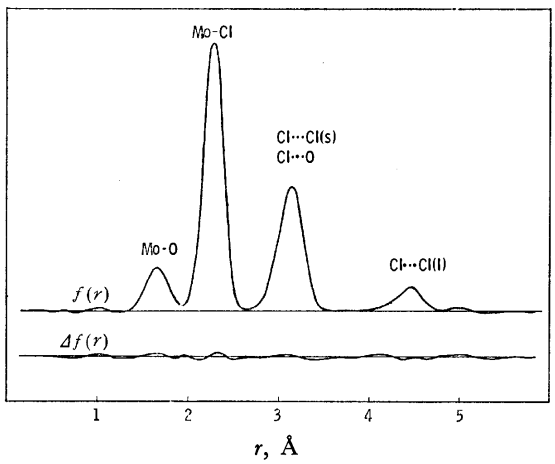

Fig. 1. Experimental radial distribution, $f(r)$, and the difference between the experimental and calculated ones, $\Delta f(r)$. A damping factor, $\exp(-0.0002\,q^2)$, was used.

the same values within the limits of error, indicating that the molecular structure of $MoOCl_4$ is a square pyramid, C_{4v}.

The index of resolution, r(Mo–Cl), r(Mo–O), r(Cl···Cl(s)), and four root-mean-square amplitudes l(Mo–Cl), l(Mo–O), l(Cl···Cl(s)), and l(Cl···Cl(l)) were determined by the least-squares analysis with C_{4v} (Table 1), where l(Cl···O) was fixed because of a large correlation between l(Cl···Cl(s)) and l(Cl···O). The value was obtained by the normal coordinate analysis. Asymmetry parameters for the Mo–Cl and Mo–O were estimated by the diatomic molecule approximation[23] to be 4.0×10^{-6} and 0.6×10^{-6} Å^3, respectively. The parameter in the Morse function, a, was assumed to be 2.0 Å^{-1}, the frequencies of Mo–Cl and Mo–O stretching vibrations 450 and 1015 cm^{-1}, respectively,[7] and the asymmetry parameters for nonbonded distances zero.

The results of the analysis are given in Table 2. r_g parameters were calculated from r_a parameters by means of $r_g=r_a+l^2/r_a$. Random errors were estimated to be 2.5 σ_1 or 2.5 σ_2.[21,24] Systematic errors were estimated from the error in the lattice constant of the reference material (0.06%) and errors in the optical measurement of the diffraction patterns of gold (0.08%) and of the camera distance (0.04%). Correlation matrices[25] are given in Table 3, and the observed and best-fit theoretical intensity curves are shown in Fig. 2.[26] The least-squares computations were carried out by the use of a FACOM 230—60 computer at Nagoya University Computing Center.

Table 1. Results of the least-squares analysis (r_a and l in Å)

Parameter		σ_1	σ_2
r_a(Mo–Cl)	2.2774	0.0003	0.0005
r_a(Mo–O)	1.6570	0.0018	0.0004
r_a(Cl···Cl(s))	3.1374	0.0028	0.0019
l(Mo–Cl)	0.0613	0.0004	0.0012
l(Mo–O)	0.0431	0.0037	0.0047
l(Cl···Cl(s))	0.1253	0.0017	0.0034
l(Cl···Cl(l))	0.1231	0.0033	0.0014
R	0.9597	0.0044	0.0143

Table 2. Distances and mean amplitudes (in Å)

	r_g	l_{obsd}	l_{calcd}
Mo–Cl	2.279±0.003	0.061±0.003	0.050
Mo–O	1.658±0.005	0.043±0.012	0.035
Cl···Cl(s)	3.142±0.008	0.125±0.009	0.104
Cl···Cl(l)	4.440±0.011	0.123±0.008	0.071
Cl···O	3.108±0.013	0.099 (assumed)	0.099
∠OMoCl	102.8±0.7°		
∠ClMoCl	87.2±0.3°		

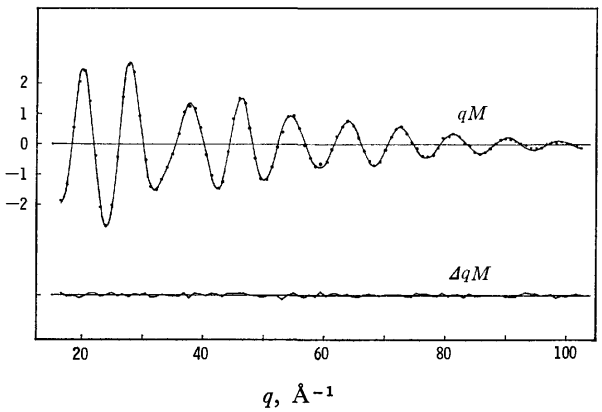

Fig. 2. Observed (dots) and calculated (curve) molecular intensities, qM, and the difference between the observed and calculated ones, ΔqM.

The infrared spectra for $MoOCl_4$ were assigned by analogy with the spectra of related molecules such as $WOCl_4$,[27,28] IF_5, BrF_5, ClF_5, and $XeOF_4$.[29] Since the vibrational frequencies of $MoOCl_4$ are similar to those of $WOCl_4$, the frequencies for the B_1 and B_2 modes, which are infrared-inactive, were assumed to be equal to the corresponding values for $WOCl_4$.[28] The fundamental frequencies are given in Table 4. The valence force constants were calculated by the GF matrix method. The mean amplitudes for the bonded and nonbonded distances were calculated by a normal coordinate analysis. The results are given in Table 2.

Discussion

The structure of $MoOCl_4$ in the gas phase is found to be a square pyramid similar to those of $WOCl_4$,[5] $XeOF_4$,[4] and IF_5.[30] The OMoCl angle (102.8±0.7°) is essentially equal to the OWCl angle (102.4±1.3°) in $WOCl_4$ but is much larger than the corresponding angles in $XeOF_4$ (92°) and in IF_5 (81°), where the small angles in the latter molecules can be explained in terms of a nonbonding valence electron pair of central atoms.[31]

The Mo–Cl bond distance in gaseous $MoOCl_4$ (2.279±0.003 Å) is equal to that in $MoCl_5$ (2.27±0.02 Å)[10] and also to that in MoO_2Cl_2 (2.28±0.03 Å).[9] The Mo–O bond distance in MoO_2Cl_2 (1.75±0.10 Å) can not be compared exactly with that in $MoOCl_4$ (1.658±0.005 Å) because of the large experimental errors. The molybdenum atom in $MoOCl_3$

Table 3. Correlation matrices for molecular parameters of $MoOCl_4$[a]

	r_{Mo-Cl}	r_{Mo-O}	$r_{Cl\cdots Cl(s)}$	l_{Mo-Cl}	l_{Mo-O}	$l_{Cl\cdots Cl(s)}$	$l_{Cl\cdots Cl(l)}$	R
r_{Mo-Cl}	1.0	−0.253	0.038	−0.030	0.007	0.034	−0.001	−0.013
r_{Mo-O}		1.0	0.114	0.139	0.004	0.117	0.020	0.195
$r_{Cl\cdots Cl(s)}$			1.0	0.014	0.001	−0.551	−0.015	0.018
l_{Mo-Cl}				1.0	0.127	0.275	0.065	0.720
l_{Mo-O}					1.0	0.076	0.020	0.199
$l_{Cl\cdots Cl(s)}$						1.0	0.052	0.388
$l_{Cl\cdots Cl(l)}$							1.0	0.091
R								1.0

a) The elements are defined as $\rho_{ij}=B_{ii}^{-1}/(B_{jj}^{-1}\times B_{ij}^{-1})^{1/2}$.

Table 4. Fundamental vibrational frequencies of $MoOCl_4$ (in cm^{-1})

		Obsd	Calcd			Obsd	Calcd
A_1	ν_1	1015[a]	1015	B_2	ν_6	220[b]	220
	ν_2	450[a]	450	E	ν_7	396	396
	ν_3	143	143		ν_8	256	257
B_1	ν_4	400[b]	400		ν_9	172	172
	ν_5	148[b]	148				

a) Ref. 7. b) Ref. 27.

has a distorted octahedral arrangement due to bridging of chlorine atoms in the crystal state.[12] The terminal Mo–Cl and Mo–O distances in $MoOCl_3$ are 2.26±0.02 Å and 1.63±0.04 Å, respectively. They agree with the corresponding distances in $MoOCl_4$ in the gas phase, although the bridging Mo–Cl is much greater than the terminal one. The OMoCl(terminal) angle in $MoOCl_3$ (103.8±1.4°) is also in good agreement with that in $MoOCl_4$ (102.8±0.7°).

By a normal coordinate analysis the force constants for the Mo–O and Mo–Cl bonds in $MoOCl_4$ were estimated to be 8.29 and 2.68 md/Å, respectively. The Mo–O force constant and the observed Mo–O distance give a good fit to the correlation curve between the distances and the force constants for the Mo–O bond.[32] Although the Mo–O bond in $MoOCl_4$ is formally a double bond, its bond order is estimated to be 3 from the correlation curve between the distance and the bond order.[32] Gray and Hare[33] gave the same bond order in their molecular orbital treatment for the Mo–O bond in the MoO^{3+} group, whose electronic structure consists of Mo^{5+} of [Krypton]$4d^1$ and oxide ion. Since the electronic structure of Mo^{6+} in $MoOCl_4$ is [Krypton]$4d^0$, the properties of the Mo–O bond would differ considerably from that of MoO^{3+}. However, the smallness of the Mo–O distance in $MoOCl_4$ might be mainly due to the double π-bonds formed between the $2p_x$ and $2p_y$ of oxygen and the $4d_{xz}$ and $4d_{yz}$ of molybdenum as in the Mo–O bond in MoO^{3+}.

The elastic scattering factor and the phase angle calculated by means of the Thomas-Fermi-Dirac (TFD) potential[34] were also used for molybdenum atom, a remarkable increment of 0.013 Å being found in the Mo–O mean amplitude but no changes in the bond distances. The case is very similar to the results of tetramethyltin given by Nagashima *et al.*[35] It seems that the phase angle for the molybdenum atom from the TFD potential is too small.

All the mean amplitudes we obtained are significantly larger than those calculated from the normal vibrations, especially with regard to Cl···Cl(1). This is probably due to the lack of accuracy in the frequencies of the B_1 and B_2 modes. A similar discrepancy between the observed mean amplitude of Cl···Cl(1) and the calculated value was reported by McAdam *et al.*[6] in their electron diffraction study of $WOCl_4$ in which they suggested the effect of an anharmonic vibration of the WCl_4 group.

A grant from the Ministry of Education is acknowledged.

References

1) K. Kimura and S. H. Bauer, *J. Chem. Phys.*, **39**, 3172 (1963).
2) J. L. Hencher, D. W. J. Cruickshank, and S. H. Bauer, *ibid.*, **48**, 518 (1968).
3) J. Martins and E. B. Wilson, Jr., *ibid.*, **41**, 570 (1964).
4) E. J. Jacob, H. B. Thompson, and L. S. Bartell, *J. Mol. Struct.*, **8**, 383 (1971).
5) K. Iijima and S. Shibata, This Bulletin, **47**, 1393 (1974).
6) A. McAdam, A. Clark, and B. Beagley, private communication, *(Chem. Commun., in press)*.
7) C. G. Barraclough and D. J. Kew, *Aust. J. Chem.*, **23**, 2387 (1970).
8) Preliminary results were reported in *Chem. Lett.*, **1972**, 1033.
9) H. A. Skinner, Thesis, Oxford, England (1941), cited in "Tables of Interatomic Distances and Configuration in Molecules and Ions," Special Publication No. 11, The Chemical Society, London, 1958, p. M80.
10) V. P. Spiridonov and G. V. Romanov, *Vestn. Mosk. Univ., Ser. II*, **22**(1), 98 (1967).
11) G. Ferguson, M. Mercer, and D. W. A. Sharp, *J. Chem. Soc. A*, **1969**, 2415.
12) N. G. B. Drew and I. B. Tomkins, *ibid.* A, **1970**, 22.
13) T. V. Iorns and F. E. Stafford, *J. Amer. Chem. Soc.*, **88**, 4819 (1966).
14) M. L. Larson and F. W. Moore, *Inorg. Chem.*, **5**, 801 (1966).
15) R. Colton, I. B. Tomkins, and P. W. Wilson, *Aust. J. Chem.*, **17**, 496 (1964).
16) L. Schäfer, A. C. Yates, and R. A. Bonham, *J. Chem. Phys.*, **55**, 3055 (1971).
17) D. T. Cromer and J. B. Mann, *ibid.*, **47**, 1892 (1967).
18) D. T. Cromer, *ibid.*, **50**, 4857 (1969).
19) R. M. Gavin and L. S. Bartell, *ibid.*, **48**, 2460 (1968).
20) S. Shibata, This Bulletin, **45**, 1631 (1972).
21) Y. Morino, K. Kuchitsu, and Y. Murata, *Acta Crystallogr.*, **18**, 549 (1965).
22) S. Konaka and M. Kimura, This Bulletin, **43**, 1693 (1970).
23) K. Kuchitsu, *ibid.*, **40**, 505 (1967).
24) S. Konaka, Y. Murata, K. Kuchitsu, and Y. Morino, *ibid.*, **39**, 1134 (1966).
25) O. Bastiansen, L. Hedberg, and K. Hedberg, *J. Chem. Phys.*, **27**, 1311 (1957).
26) Numerical experimental data of the leveled total intensity and the background have been deposited with the Chemical Society of Japan (Document No. 7508).
27) R. Beattie, K. M. S. Livingston, D. J. Reynolds, and G. A. Ozin, *J. Chem. Soc., A*, **1970**, 1210.
28) D. M. Adams and R. G. Churchill, *ibid.* A, **1968**, 2310.
29) G. M. Begun and W. H. Fletcher, *J. Chem. Phys.*, **42**, 2236 (1965).
30) G. R. Jones, R. D. Burbank, and N. Bartlett, *Inorg. Chem.*, **9**, 2264 (1970).
31) R. J. Gillespie, *J. Amer. Chem. Soc.*, **82**, 5978 (1960); *J. Chem. Educ.*, **40**. 295 (1963).
32) F. A. Cotton and R. M. Wing, *Inorg. Chem.*, **4**, 867 (1965).
33) H. B. Gray and C. R. Hare, *ibid.*, **1**, 363 (1962).
34) M. Kimura, S. Konaka, and M. Ogasawara, *J. Chem. Phys.*, **46**, 2599 (1967); M. Ogasawara, S. Konaka, and M. Kimura, *ibid.*, **50**, 1488 (1969).
35) M. Nagashima, H. Fujii, and M. Kimura, This Bulletin, **46**, 3708 (1973).

Electron Spin Resonance of Oriented Solid of Isocyanic Acid Irradiated with γ-Rays

Hidefumi HIRAI and Masato FUJIWARA

Department of Industrial Chemistry, Faculty of Engineering, University of Tokyo, Bunkyo-ku, Tokyo 113

(Received July 30, 1974)

Free radicals in the γ-irradiated solid of isocyanic acid at -196 °C have been studied by electron spin resonance (ESR) spectroscopy at -196——-100 °C. An oriented solid of isocyanic acid was prepared by solidification of isocyanic acid around an aluminum rod with cooling for the measurement. The ESR spectra consisted of a pair of triplets and a pair of sextets, when the longitudinal axes of the oriented solid were parallel and perpendicular, respectively, to the dc magnetic field. The absorptions were assigned to an anion radical ($HNCO^-$) by analysis of anisotropy of the spectrum and by deuteration of isocyanic acid. The observed constants were: $g_\perp=2.0025$, $g_{//}=1.9985$; $A_x(N)=21.2$ G, $A_y(N)=24.8$ G, $A_z(N)=21.8$ G. The anion radical was assumed to be preferentially oriented in the oriented solid, taking two orientations whose $g_{//}$ axes were perpendicular both to each other and to the longitudinal axis of the oriented solid.

On the flash photolysis of isocyanic acid vapor, NH, NH_2 and NCO radicals were detected by absorption spectroscopy.[1,2] They were also postulated to account for the result of gas chromatography on the photolysis of vapor.[3] Radicals formed on the γ-irradiation of isocyanic acid solid at low temperatures, however, have not been studied.

In the present work, ESR measurements on isocyanic acid solid irradiated with γ-rays have been carried out. An attempt was made to prepare an oriented solid of isocyanic acid which can be used instead of a single crystal of the acid, since the melting point of the acid, -86 °C,[4] is too low to prepare a single crystal without special apparatus. In addition, deuteration of isocyanic acid was performed for identification of the radicals. Changes in the ESR spectra with light irradiation and with elevation of temperature were also examined.

Experimental

Materials. Isocyanic acid was prepared by the pyrolysis of cyanuric acid vapor in a stream of dry nitrogen at 600 °C according to reported method.[1] Further purification of the resulting isocyanic acid was carried out by distillation under reduced pressure of 5 mmHg. Deuterated isocyanic acid was prepared by the pyrolysis of deuterated cyanuric acid with a 33% yield. The deuterated cyanuric acid was prepared by dissolving cyanuric acid (3.0 g, 0.07 mol) in deuterium oxide (100 g, 5.56 mol) with heating under reflux for 6 hr. The degree of deuteration determined by mass spectrometry was 88%.

Preparation of Oriented Solid of Isocyanic Acid. Oriented solid of isocyanic acid was prepared in the following way. Isocyanic acid was solidified around an aluminum rod (1 mm diameter) in a glass tube (8 mm diameter) by cooling with liquid nitrogen (Fig. 1a), and the resulting oriented solid was sealed in another sample tube (10 mm diameter) in nitrogen atmosphere, as shown in Fig. 1b. After γ-ray irradiation at -196 °C, the solidified isocyanic acid was dislodged from the surface of the aluminum rod. It was then divided radially into several wedge-formed pieces (Fig. 1c), one of which was inserted into a crack in a Teflon tube so as to have the longitudinal axis of the piece, *i.e.* the axis of the mark of aluminum rod, held horizontally (Fig. 1d). The angle between the longitudinal axis of the piece and the direction of the dc magnetic field is referred to as orientation-angle, orientation-angles 0° and 90° indicating the axes parallel and perpendicular, respectively, to the dc magnetic field. The wedge-formed piece was inserted into the Teflon tube crack in order to keep the longitudinal axis parallel to the vertical tube axis and was rotated around its longitudinal axis.

ESR Measurement. The solid of isocyanic acid was irradiated with ^{60}Co γ-rays to a dose of 8×10^5~8×10^6 rad at -196 °C. The ESR measurement was run using a Varian V-4502 X-band spectrometer with a cylindrical cavity in the TE_{110} mode and with 100 kHz field modulation at several different temperatures between -196 °C and -100 °C. The oriented solid could be rotated in the cavity so that ESR spectrum was obtained at any desired orientation-angle. The γ-irradiated solids of isocyanic acid were subsequently exposed to light from an Ushio Denki HB 500/B high pressure mercury lamp (500W; wavelengths>2800 Å) in a transparent quartz Dewar vessel at -196 °C.

Mass Spectrometry. Mass spectra of deuterated isocyanic acid vapor were analyzed with a Hitachi RMU-6 mass spectrometer.

Results

Oriented Solid of Isocyanic Acid. On cooling with liquid nitrogen, solidification of isocyanic acid proceeded from the wall of the glass sample tube to the

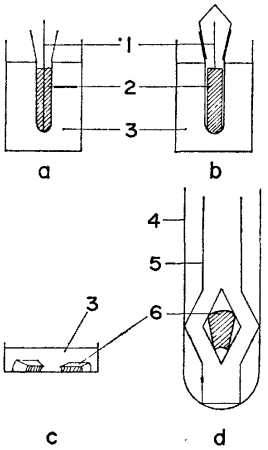

Fig. 1. Preparation of oriented solid of isocyanic acid; aluminum rod (1), isocyanic acid (2), liquid nitrogen (3), ESR sample tube (4), Teflon tube (5) and γ-irradiated isocyanic acid (6).

surface of the aluminum rod. The gradient of temperature of the isocyanic acid turned out to have a cylindrical symmetry around the axis of the aluminum rod. The resulting solid of isocyanic acid was a polycrystal made of needle-like crystallite preferentially oriented with the cylindrical symmetry, since any piece of oriented solid exhibited the same anisotropic spectrum. The narrower wedge-angle of the piece (Fig. 1d) gave a sharper and more symmetric spectrum. It was found that the use of a Teflon rod for solidification of isocyanic acid yielded a broader and less anisotropic spectrum than that obtained with an aluminum rod.

ESR Spectrum of Isocyanic Acid. The above procedure for preparing the oriented solid is hereafter referred to as the oriented solid method. The experimental rectangular coordinate system of the oriented solid, X, Y and Z, was defined as shown in Fig. 2. The Z axis corresponds to the longitudinal axis of the aluminum rod and the Y axis coincides with the bisector of the wedge-angle of the wedge-formed piece. The X axis is perpendicular to both the Y axis and Z axis.

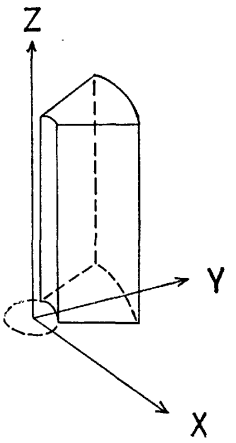

Fig. 2. Experimental rectangular coordinate system of oriented solid.

The γ-irradiated oriented solid prepared by the oriented solid method gave the spectra as shown in Fig. 3 when the solid was rotated around the Y axis keeping the Y axis perpendicular to the dc magnetic field. Remarkable changes in the pattern occurred with change in the orientation-angle from 0° to 90°. The spectrum at 0° consisted of six strong lines with equal intensity, though the lines in higher field became broader (Fig. 3a). At 90° ten lines were observed with relative intensity ratios of about 1 : 1 : 1 : 2 : 1 : 1 : 2 : 1 : 1 : 1 (Fig. 3d). A slight change in pattern can be seen on variation from 0° to 60° (Figs. 3b and 3c).

The six lines can be interpreted by a pair of triplets due to the hyperfine interaction with ^{14}N nucleus (I=1) and with ^{1}H nucleus (Fig. 3a), from a consideration of both line intensities and line spacings. The ten lines can be ascribed to the twelve lines with equal intensity, four of which coalesce forming a pair of lines with relative intensity of two (Fig. 3d). The

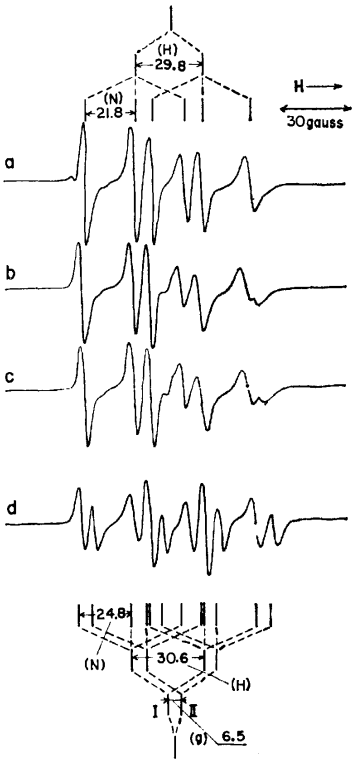

Fig. 3. ESR spectra of oriented solid of isocyanic acid irradiated with γ-rays at −196 °C with orientation-angle 0° (a), 30° (b), 60° (c) and 90° (d).

twelve lines can be divided into two groups, I and II, each of which consists of six lines similar to those observed at orientation-angle 0°. The values of nitrogen splitting change from 21.8 G to 24.8 G, while the change of proton splitting (0.8 G) is small and the proton splitting remains almost constant. The relative intensity ratios of the lines and the hyperfine structure due to N and H of Radical I are equal to those of Radical II. Consequently, Radicals I and II should have the same molecular structure and a different orientations which yield a site splitting of 6.5 G through g-anisotropy at 90°.

The angular dependence of the g-value around the Y axis is shown in Fig. 4, where two kinds of g-value are found, one (Radical I) remains constant throughout the angular change (g=2.0025), while the other (Radical II) takes the minimum value (g=1.9985) at orientation-angle 90°.

The oriented solid gave the spectra as shown in Fig. 5, when the solid was rotated around the Z axis keeping the Z axis perpendicular to the dc magnetic field. Spectrum 5a was obtained when the dc magnetic field was applied in a direction parallel to the Y axis. A rotation of the solid by 90° gave spectrum 5c which is similar both to 5a and 3d. The nitrogen splitting was observed to take a value 21.2 to 24.8 G on the rotation of the oriented solid, while the hydrogen splitting remained almost constant (*ca.* 30 G). The angular dependence of the g-value around the Z axis was also examined. The anisotropies of g-value are shown in Fig. 6. The observed g-values change between 2.0025 and 1.9985, corresponding to the

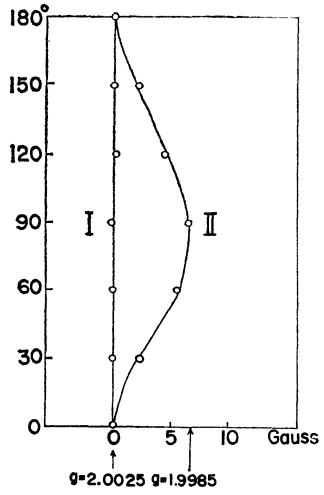

Fig. 4. Plots of the g-values of Radicals I and II for various orientations of the dc magnetic field in the XZ plane, with angles measured from the direction of the dc magnetic field in the direction of Z axis.

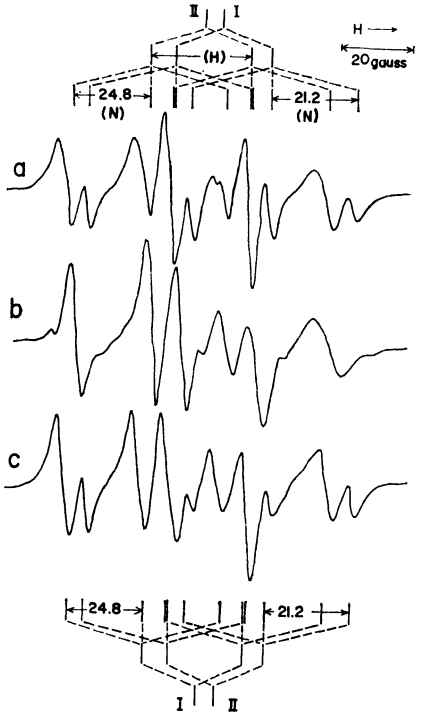

Fig. 5. ESR spectra of oriented solid of isocyanic acid irradiated with γ-rays at −196 °C. The specimen was rotated in the XY plane around the Z axis. Spectrum a was obtained, when the dc magnetic field was parallel to the Y axis. Spectra b and c correspond to a rotation of the sample tube by 45° and 90°, respectively, from the position for Spectrum a around the Z axis.

maximum g-value of Radical I and the minimum value of Radical II, respectively.

When the oriented solid is rotated about the Y axis, one of the triplet patterns (Radical I) remains fixed in position, while the others (Radical II) change (Fig. 3). The oriented solid is considered to be symmetric about the Z axis. Accordingly, the g-tensor of

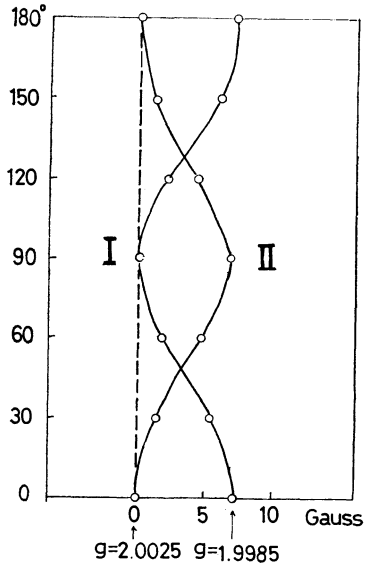

Fig. 6. Plots of the g-value of Radicals I and II for various orientations of the dc magnetic field in the XY plane, with angles measured from the direction of the dc magnetic field in the direction of the Y axis.

the radical produced in γ-irradiated oriented solid is axially symmetric. Both Radicals I and II seem to align to keep the $g_{//}$ axis in the XY plane (Fig. 7). The $g_{//}$ axis of Radical I is parallel to the Y axis, that of Radical II to the X axis. Both the $g_{//}$ axes of Radicals I and II are perpendicular to the Z axis. These orientation states of Radicals I and II can reasonably explain the results shown in Figs. 4 and 6. Both the molecular planes of Radicals I and II are expected to be perpendicular to the Z axis. The observed maximum and minimum values (24.8 and 21.2 G) of nitrogen splitting are considered to be the principal values of nitrogen hyperfine tensor, since the two principal axes of nitrogen hyperfine tensor can be expected to be in the molecular plane (XY plane) of

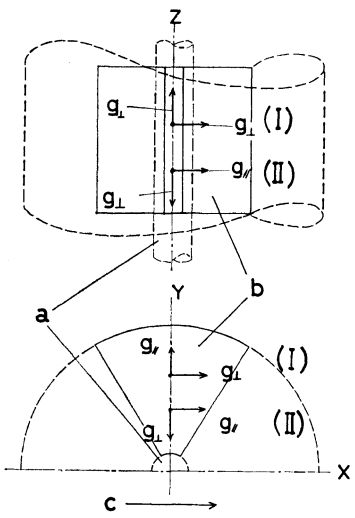

Fig. 7. The orientation state of the radicals in the oriented solid; aluminum rod (a), isocyanic acid solid (b) and the direction of the dc magnetic field at orientation-angle 90° (c).

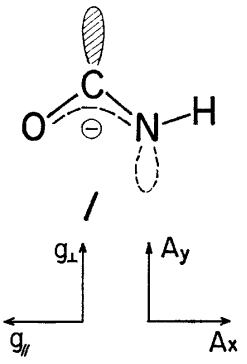

Structure 1

TABLE 1. PRINCIPAL VALUES OF THE NITROGEN HYPERFINE TENSOR (A) AND THE SPECTROSCOPIC SPLITTING FACTOR (g)

$A_x = 21.2$ G	
	$g_\perp = 2.0025$
$A_y = 24.8$ G	
	$g_{//} = 1.9985$
$A_z = 21.8$ G	

The x, y and z axes are given in Structure 1.

the radicals. The principal values 24.8 and 21.2 G were obtained when the Y axis of the oriented solid was rotated around the Z axis by 0° and 90°, respectively (Fig. 5). Another principal value, 21.8 G, was also obtained when the magnetic field was applied in a direction parallel to the Z axis (Fig. 3a). Structure 1 shows the directions of the g-tensor and the nitrogen hyperfine tensor, and also the radical structure. The experimental g-values and hyperfine splitting constants of nitrogen are given in Table 1.

For the sake of comparison, isocyanic acid in a Spectrosil tube was solidified by cooling with liquid nitrogen without aluminum rod and subsequently γ-irradiated (1×10^6 rad) at -196 °C; this procedure of preparation of specimen for ESR measurement is hereafter referred to as the usual method. The specimen made in this manner exhibits a spectrum as shown in Fig. 8. Almost no changes in the pattern occurred when the Spectrosil tube was rotated about its longitudinal tube axis. The spectrum consisted of six strong lines and additional weak three lines. The six strong lines were centered at $g=2.0025$ and separated by 22 G with equal intensity, though the lines in the higher field also became broader. The absorption lines of hydrogen atom separated by 508 G and two weak lines separated by about 170 G were also recorded.

In order to examine the orientation of the isocyanic acid molecule in the solid prepared by the usual method, the spectra were also measured with the dc magnetic field perpendicular to the longitudinal axis of the Spectrosil tube in the following manner similar to the oriented solid method; the Spectrosil tube containing the γ-irradiated isocyanic acid solid was broken in liquid nitrogen and the resulting wedge-form piece of isocyanic acid solid was inserted in a crack of Teflon tube so as to hold the longitudinal axis of the piece horizontally. The spectra obtained at orientation-angles 0° and 90° are shown in Fig. 9. The dependence of the ESR pattern on the angle was similar to that in the case of the oriented solid method, while the absorption lines in the former case were less anisotropic and broader.

A wider wedge-angle (*ca.* 150°) of the wedge-formed specimen gave a broader absorption lines where the separation of the absorption lines of Radical II from that of Radical I at 90° was not observable (Fig. 10). This suggests that the isocyanic acid molecule in the oriented solid is oriented radially.

The subsequent light irradiation (wavelengths>

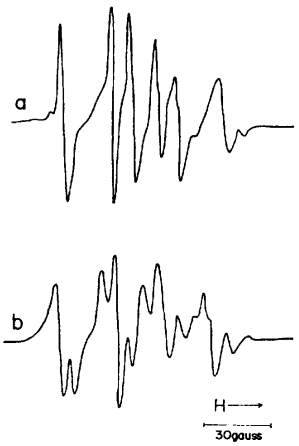

Fig. 9. ESR spectra of isocyanic acid prepared by the usual method with γ-irradiation 1×10^6 rad at -196 °C measured by keeping the longitudinal axis horizontal; orientation-angle 0° (a) and 90° (b).

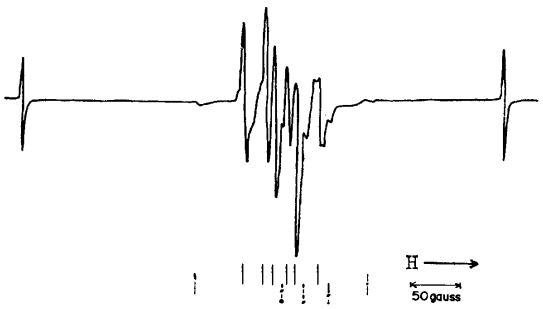

Fig. 8. ESR spectrum of isocyanic acid prepared by the usual method and three kinds of line-spectra shown at the bottom of this figure.

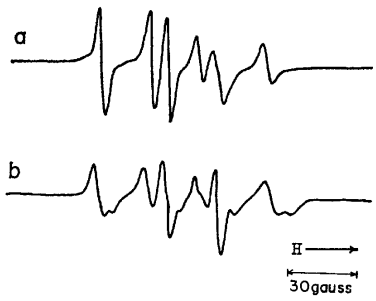

Fig. 10. ESR spectra of a piece of oriented solid of isocyanic acid with a wider wedge-angle (*ca.* 150°); orientation-angle 0° (a) and 90° (b).

2800 Å) on the specimen caused no change in those spectra obtained in the dark at −196 °C. Raising the temperature of the specimen to about −110 °C gave no change either in intensity or in shape of the spectra. The intensity, however, decreased remarkably at −90 °C with the disappearance of Q-dip on mode check.

ESR Spectrum of Deuterated Isocyanic Acid. Figure 11 shows an ESR spectrum of deuterated isocyanic acid γ-irradiated in a Spectrosil tube at −196 °C according to the usual method. The spectrum consists of nine strong lines with equal intensity due to the hyperfine splitting with ^{14}N nucleus and ^{2}H nucleus. The small line spacing is 4.6 G, corresponding to 1/6.43 of the splitting constant of ^{1}H and ascribed to the deuteron splitting. The large spacing is 22.1 G, corresponding to the coupling of N nucleus. Two weak lines on both ends of he spectrum are due to the coupling of ^{1}H nucleus of undeuterated isocyanic acid. Deuterated isocyanic acid behaves in the same manner as isocyanic acid both on cooling and on γ-irradiation according to the usual method.

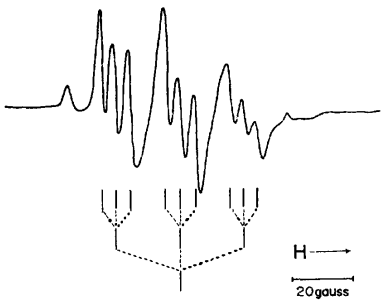

Fig. 11. ESR spectrum of deuterated isocyanic acid irradiated with γ-rays of 1×10^{6} rad at −196 °C.

Discussion

Analysis of ESR Spectrum. The structure of isocyanic acid determined by Jones *et al.*[5] using the microwave absorption spectroscopy, is represented by the following structure. The equivalent doublet pattern (Fig. 3) should arise from one β-proton coupling, since the proton splitting almost remains constant throughout the orientation-angle change. The result of deuterated isocyanic acid confirms this conclusion.

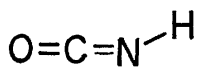

Formula 1.

From the experimental values of nitrogen hyperfine tensor, an unpaired electron spin density on nitrogen atom ($=\rho_N$) can be calculated. Isotropic Fermi contact component (A_f) and anisotropic component (A_d) arising from dipole-dipole interaction can be written, respectively, as

$$A_f = \pm 1/3(A_{//}+2A_{\perp}) \quad (1)$$

$$A_d = \pm 1/3(A_{//}-A_{\perp}) \quad (2)$$

where $A_{//}$ and $A_{\perp}$ represent the principal values of the axially symmetric hyperfine tensor. For this case, $A_{\perp}$ is the average value of A_x and A_z, since the value of A_x is nearly equal to that of A_z. In formulas (1) and (2), we can obtain A_f and A_d, using the observed values, $A_{//}=24.8$ and $A_{\perp}=21.5$ G

$$A_f = 22.6 \text{ (G) and } A_d = 1.1 \text{ (G)}$$

Although it could not be determined in this experiment, A_f and A_d may have the same sign. The dipole-dipole term for the 2p electron and Fermi term on a nitrogen atom can be estimated, respectively, by use of the data by Barns and Smith:[6] $A_{2p}=17.1$ G and $A_{2s}=550$ G. Consequently, the spin density of the $2p_z$ orbital and of the 2s orbital can be set, respectively, as

$$\rho_{2p} = A_d/A_{2p} = 0.064$$

$$\rho_{2s} = A_f/A_{2s} = 0.041$$

Thus, the spin density on nitrogen atom ($\rho_N=\rho_{2p}+\rho_{2s}$) is estimated to be 0.11. The value is similar to that on oxygen atom of CO_2^- anion radical ($\rho_0=0.11$).[7] The results indicate that the unpaired electron occupies an orbital of carbon atom and the unpaired electron spin density is produced upon the sp^2 hybrid orbital of nitrogen atom by the spin delocalization. The radical represented by Structure **1** whose structure is similar to that of CO_2^- anion radical[7] might give a large negative shift of *g*-value through the effect of spin-orbital coupling of the unpaired electron in the sp^2 hybrid orbital of carbon atom with the in-plane 2p orbitals of oxygen atom and nitrogen atom.

The direction of the largest principal value of nitrogen hyperfine tensor of Structure **1** should be expected to correspond reasonably to the direction of the lobe of the nitrogen sp^2 hybrid orbital occupied by the lone pair electrons, since the unpaired electron spin density is caused upon the sp^2 hybrid orbital by the spin polarization of the lone pair electrons. This is supported by the results for CO_2^- anion radical,[7] $\cdot NO_2$ radical[8] and the radical of γ-irradiated dimethyl glyoxime.[9] The largest principal value (A_y) and the maximum *g*-value of Radical I were obtained when the Y axis of the oriented solid was rotated around the Z axis by 90° from the position where the Y axis became parallel to the dc magnetic field (Figs. 5 and 6). The direction of A_y of Structure **1** might not coincide with that of $g_{\perp}$ axis, since the $g_{\perp}$ axis is not a symmetrical axis of Structure **1**. However, the shift between the two directions can not be distinguished from the experimental results. Therefore, the A_y axis is almost parallel to the $g_{\perp}$ axis.

In Structure **1**, the N–H bond of the radical is in the *cis*-position with respect to the carbon sp^2 hybrid orbital occupied by the unpaired electron. On the other hand, the N–H bond of Structure **1′** is in the *trans*-position. If the N–H bond is in the *trans*-position, the direction of the lobe of the nitrogen sp^2 hybrid orbital occupied by the lone pair electrons might cut the $g_{//}$ axis at an angle 30° (Structure **1′**). This is in line with the result where the A_y axis cuts the $g_{//}$ axis at an angle 90°. The N–H bond of the radical is, therefore, in the *cis*-position with respect to the carbon sp^2 hybrid orbital.

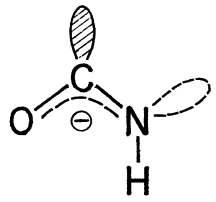

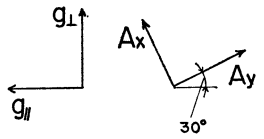

Structure **1**

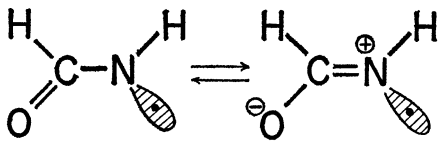

Structure **2**

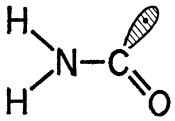

Structure **3**

Two possible structures for the radical are given in the following.

They represent the σ-type neutral radicals produced by the addition reactions of a hydrogen atom to isocyanic acid. In each structure, an unpaired electron occupies in sp^2 orbital of nitrogen atom or carbon atom. The large negative shift of g-value can not be explained by Structure **2** which has a similar structure to that of the vinyl radical. Structure **2**, thus, seems to be less acceptable. The resonance pattern arising from Structure **3** might consist of a triplet of triplets, since the unpaired electron couples with two hydrogen nuclei and nitrogen nucleus. The observed pattern, however, consists of a doublet of triplets. Consequently, Structure **3** is discarded and Structure **1** is the most preferable for the assignment of the radical.

The weak absorption separated by 170 G (Fig. 8) may be ascribed to a moiety of decomposed molecule.

Orientation of Isocyanic Acid. From the spectrum 3d, the population of Radical I in the isocyanic acid solid should be equal to that of Radical II. Thus it seems that the N=C=O axis of the isocyanic acid molecule is perpendicular to that of the adjacent acid molecule through a hydrogen bond (Fig. 12). When isocyanic acid molecule (A) traps an electron produced by γ-irradiation, the unpaired electron of the resulting radical (A) occupies the sp^2 hybrid orbital in the *cis*-position to the proton of the molecule (A). This is why the proton is in the *cis*-position of the unpaired electron.

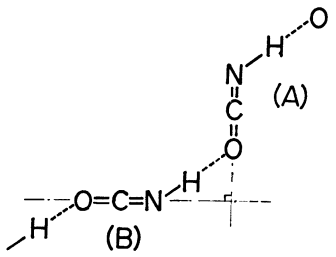

Fig. 12. Alignment of isocyanic acid molecule in the oriented solid.

Radicals which locate on both outer sides of Radicals I and II (Fig. 7), making a wider wedge-angle, should have slightly different orientations of the g-tensors, since they are oriented radically around the aluminum rod. Thus, a wider wedge-angle of the wedge-formed specimen makes the absorption lines broader resulting in a coalescence of the absorption lines of Radical II with those of Radical I (Fig. 10).

The authors wish to thank Dr. Naoyuki Tamura, Japan Atomic Energy Research Institute, for his valuable discussions. They are grateful to Dr. Tosho Sugiura of the same Institute for his kindness in measuring mass spectrum of deuterated isocyanic acid.

References

1) G. Herzberg and C. Reid, *Discuss. Faraday Soc.*, **9**, 92 (1950).
2) R. Holland, D. W. G. Style, R. N. Nixon, and D. A. Ramsay, *Nature*, **182**, 336 (1958).
3) J. Y. P. Mui and R. A. Back, *Can. J. Chem.*, **41**, 826 (1963).
4) H. Hamada, T. Iwai, K. Hayashi, and S. Okamura, *Kobunshi Kagaku*, **22**, 639 (1965).
5) L. H. Jones, J. N. Schoolery, R. G. Shulman, and D. M. Yost, *J. Chem. Phys.*, **18**, 990 (1950).
6) R. G. Barns and W. V. Smith, *Phys. Rev.*, **93**. 95 (1945).
7) D. W. Overnall and D. H. Whiffen, *Mol. Phys.*, **4**, 135 (1961).
8) H. Zeldes and R. Livingstone, *J. Chem. Phys.*, **35**, 563 (1961).
9) M. C. R. Symons, *J. Chem. Soc.*, **1963**, 1186.

^{14}N Nuclear Quadrupole Resonances of Sulfuric Diamide and Its Derivatives

Hisao NEGITA, Tsuneo KUBO, and Kaoru SHIBATA

Department of Chemistry, Faculty of Science, Hiroshima University, Hiroshima 730

(Received August 13, 1974)

The study of ^{14}N nuclear quadrupole resonance (NQR) was performed on sulfuric diamide (sulfamide) and its methyl derivatives, such as *N,N*-dimethylsulfamide and tetramethylsulfamide. The ^{14}N NQR parameters for sulfuric diamide and tetramethylsulfamide were ($|e^2Qq|=3905.3$ kHz; $\eta=0.5082$) and ($|e^2Qq|=5325.9$ kHz; $\eta=0.1768$) respectively. In the case of *N,N*-dimethylsulfamide, the parameters were ($|e^2Qq|=4022.9$ kHz; $\eta=0.4799$) for the nitrogen atoms of NH_2 groups and ($|e^2Qq|=5125.0$ kHz; $\eta=0.2024$) for the nitrogen atoms of $N(CH_3)_2$ groups. From the temperature dependence of the resonance lines due to nitrogen atoms in sulfuric diamide, tetramethylsulfamide, and the NH_2 group of *N,N*-dimethylsulfamide, it is considered that the hydrogen bonds in sulfuric diamide are stronger than those in *N,N*-dimethylsulfamide. On the other hand, the electron densities for the N–S bond in sulfuric diamide and its methyl derivatives were derived from the corresponding NQR parameters.

The structural studies of sulfuric diamide have been performed by various spectroscopic means, but not by the nuclear quadrupole resonance (NQR). The NQR method is of especial interest in clarifying the charge distribution on the nitrogen atom. Therefore, we planned to examine ^{14}N NQR in sulfuric diamide and its methyl derivatives such as *N,N*-dimethylsulfamide and tetramethylsulfamide. On the basis of the ^{14}N NQR studies, the hydrogen bond in sulfuric diamide was compared with that in *N,N*-dimethylsulfamide, and the charge distributions on the nitrogen atoms in sulfuric diamide and its derivatives were compared with those in urea and tetramethylurea.

Experimental

The ^{14}N NQR spectra of these compounds were obtained by the use of a frequency-modulated spectrometer described previously.[1] The resonance frequencies were measured by a heterodyne-type frequency meter whose frequency was checked by means of a frequency counter, TR-5578, from the Takeda Riken Co. The Zeeman field was supplied by a Helmholz coil, 40 cm in diameter and 20 cm in gap width. Measurements were carried out at several temperatures between liquid nitrogen and room temperature. The temperatures were measured by the use of a copper-constantan thermocouple.

The sulfuric diamide and tetramethylsulfamide were obtained by the reactions of sulfuryl chloride with liquid ammonia[2] and liquid dimethylamine[3] respectively. The *N,N*-dimethylsulfamide was prepared by the reaction of dimethylsulfamyl chloride with liquid ammonia.[4] These samples were purified by recrystallization from organic solvents, such as acetone, ethyl ether, and ethyl alcohol. In the cases of sulfuric diamide and tetramethylsulfamide, about a 10-g portion of each sample was melted in a tube and used for measurements. In the case of *N,N*-dimethylsulfamide, about a 6-g single crystal was prepared by the Bridgman-Stockbarger method and examined.

Results and Discussion

Generally a pair of ^{14}N NQR frequencies, ν_I and ν_{II}, are observed for a species of nitrogen atoms:

$$\nu_I = |e^2Qq|(3-\eta)/4, \qquad \nu_{II} = |e^2Qq|(3+\eta)/4, \tag{1}$$

where $|e^2Qq|$ and η are the quadrupole coupling constant and the asymmetry parameter respectively. In sulfuric diamide and tetramethylsulfamide, a pair of resonance lines was found. The quandrupole coupling constants and asymmetry parameters derived from these frequencies are listed in Table 1. In *N,N*-dimethylsulfamide, four resonance lines were paired in two groups, depending upon the frequency shifts due to the influence of the Zeeman field. The two pairs of resonance frequencies due to NH_2 and $N(CH_3)_2$ in *N,N*-dimethylsulfamide are not very different from the corresponding pairs of the related compounds, sulfuric diamide and tetramethylsulfamide. The quadrupole coupling constants and asymmetry parameters observed are also listed in Table 1.

Table 1. NQR parameters in sulfuric diamide and its methyl derivatives

Compound	ν_I (kHz)	ν_{II} (kHz)	$\lvert e^2Qq\rvert$ (kHz)	η (%)
$O_2S(NH_2)_2$	2432.8	3425.1	3905.3	50.82
$O_2S(NH_2)N(CH_3)_2$	2534.5	3499.9	4022.9	47.99[a]
	3584.4	4103.1	5125.0	20.24[b]
$O_2S(N(CH_3)_2)_2$	3759.0	4229.8	5325.9	17.68

a) NQR parameters due to NH_2. b) NQR parameters due to $N(CH_3)_2$.

In the case of *N,N*-dimethylsulfamide, the temperature dependence of the ν_I of the NH_2 group was observed only in the temperature range from 148 K to 173 K. The other three resonance lines of the same compound were too weak to be found in this temperature range. Figure 1 shows the temperature dependence of the ν_I frequencies observed in sulfuric diamide, tetramethylsulfamide, and *N,N*-dimethylsulfamide. The absolute temperature coefficient of resonance frequencies in the NH_2 group can be expected to be larger than that in the $N(CH_3)_2$ group, because a hydrogen atom is much lighter than a methyl group. However, this is not the cases in sulfuric diamide and tetramethylsulfamide, as is shown in Fig. 1. This fact can be explained by the intermolecular

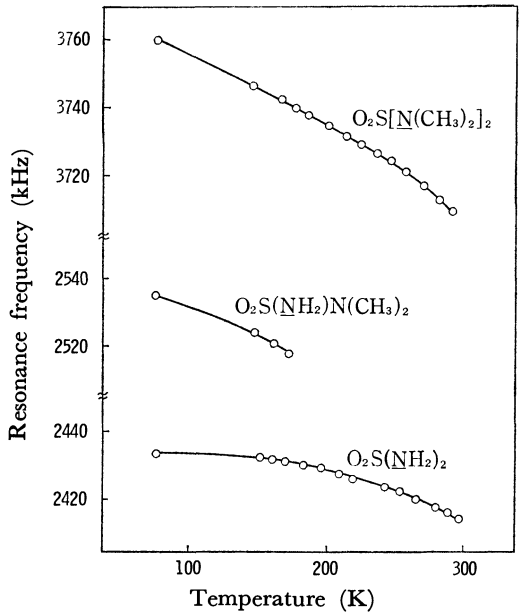

Fig. 1. Temperature dependence of resonance line, ν_I, of the nitrogen atoms (marked by underlines) in sulfuric diamide, tetramethylsulfamide and *N,N*-dimethylsulfamide.

interaction by which the nitrogen atom in sulfuric diamide is fixed by three hydrogen bonds, N–H···O (3.02 Å), N–H···N (3.18 Å) and N···H–N (3.18 Å),[5] while there are no hydrogen bonds in tetramethylsulfamide.[6] That is, the vibration of the nitrogen atom in sulfuric diamide is more suppressed than in tetramethylsulfamide. On the other hand, Fig. 1 shows that the temperature dependence in *N,N*-dimethylsulfamide is nearly equal to that in tetramethylsulfamide. This suggests that the hydrogen bonds in *N,N*-dimethylsulfamide are weaker than in sulfuric diamide.

The ∠HNH bond angle in sulfuric diamide was recently determined by Pedersen to be 110.6°,[7] which is close to the tetrahedral angle (109.5°). However, as the S–N bond length determined by Trueblood and Mayer, 1.60 Å,[5] is appreciably shorter than the single-bond length predicted from the covalent atomic radii, about 1.73 Å, the shape of the NH_2 group may be considered to be nearly planar. Therefore, we assumed sp^2-hybridization for the nitrogen σ-bond orbitals. The crystal structure of tetramethylsulfamide was determined by Jordan *et al.*[6] Despite the ∠CNC bond angle, 112.9°, which is close to the tetrahedral angle, the three bonds around the nitrogen atom in the $N(CH_3)_2$ group lie in a plane. Therefore, we assumed that the nitrogen σ-bond orbitals are sp^2-hybrids. The structure of *N,N*-dimethylsulfamide, however, is not known; therefore, we assumed that both two non-equivalent nitrogen atoms form an sp^2-hybridization and that the ∠HNH and ∠CNC bond angles are 110.6° and 112.9° respectively.

The electron densities on nitrogen atoms in sulfuric diamide and its methyl derivatives were derived from the following equations by Lucken:[8]

TABLE 2. ELECTRON DENSITIES IN SULFURIC DIAMIDE, UREA AND THEIR METHYL DERIVATIVES

Compound	Lone pair	σ_{NC} or σ_{NS}	σ_{NH} or σ_{NCH_3}
$OC(NH_2)_2$	1.68	1.21	1.33
$OC[N(CH_3)_2]_2$	1.76	1.21	1.22
$O_2S(NH_2)_2$	1.74	1.10	1.38
$O_2S(NH_2)N(CH_3)_2$	1.75	1.10	1.37[a]
	1.75	1.08	1.22[b]
$O_2S[N(CH_3)_2]_2$	1.78	1.10	1.22

a) Electron densities due to NH_2. b) Electron densities due to $N(CH_3)_2$.

$$2\eta\cdot|e^2Qq/e^2Qq_p| = 3(c-b)(1-\cot^2\gamma), \quad (2)$$

$$(1-\eta/3)\cdot|e^2Qq/e^2Qq_p| = a-c, \quad (3)$$

where a is the electron density in the lone-pair orbital; b and c, the σ-electron densities in the N–S bond and N–H or N–CH_3 bond respectively; 2γ, the ∠HNH or ∠CNC bond angle, and $|e^2Qq_p|$, the quadrupole coupling constant due to one 2p-electron of a nitrogen atom. In the cases of the $N(CH_3)_2$ groups of tetramethylsulfamide and *N,N*-dimethylsulfamide, it is assumed that $|e^2Qq_p|$ is 9 MHz and that the σ-electron density for the N–CH_3 bond is the same as that for the N–CH_3 bond in tetramethylurea (1.22);[9] therefore, the values of a and b parameters can be evaluated. In the cases of the NH_2 groups of sulfuric diamide and dimethylsulfamide, the σ-electron density in the N–S bond is assumed to be the same as in tetramethylsulfamide; therefore, the values of a and c can be evaluated. Table 2 lists the values obtained in sulfuric diamide, urea, and their methyl derivatives. It may be seen that the σ-electron densities for the N–S bonds in sulfuric diamide and its methyl derivatives are smaller than for the N–C bond in the amido group in urea and tetramethylurea. The ^{35}Cl NQR frequencies in sulfuryl chloride, O_2SCl_2, 37.822 MHz and 37.613 MHz,[10] are higher than those in phosgene, $OCCl_2$, 36.225 MHz and 35.081 MHz.[11] Accordingly, the Cl–S bond in sulfuryl chloride is more covalent than the Cl–C bond in phosgene. From these facts, it may be concluded that the electron-attracting ability of an SO_2 group is stronger than that of a CO group.

References

1) H. Negita, M. Hayashi, and T. Okada, *J. Sci. Hiroshima Univ., Ser.* **A**, **35**, 85 (1971).

2) Ed. F. Degering and G. C. Gross, *Ind. Eng. Chem.*, **35**, 751 (1943).

3) H. Nöth and G. Mikulaschek, *Chem. Ber.*, **97**(3), 709 (1964).
4) K. W. Wheeler, *J. Amer. Chem. Soc.*, **66**, 1242 (1944).
5) K. N. Trueblood and S. W. Mayer, *Acta Crystallogr.*, **9**, 628 (1956).
6) T. Jordan, H. W. Smith, L. L. Lohr, Jr., and W. N. Lipscomb, *J. Amer. Chem. Soc.*, **85**, 846 (1963).
7) B. Pedersen, *Acta Chem. Scand.*, **22**, 1813 (1968).
8) E. A. C. Lucken, "Nuclear Quadrupole Coupling Constants," Academic Press, London and New York (1969), p. 225.
9) Dinesh and M. T. Rogers, *J. Chem. Phys.*, **57**, 3726 (1972).
10) P. J. Bray, *ibid.*, **23**, 703 (1955).
11) R. Livingston, *J. Phys. Chem.*, **57**, 496 (1953).

Nuclear Quadrupole Resonances of 2,4,6-Trichlorobenzonitrile

Hisao NEGITA, Kaoru SHIBATA, and Tsuneo KUBO

Department of Chemistry, Faculty of Science, Hiroshima University, Hiroshima 730

(Received August 13, 1974)

2,4,6-Trichlorobenzonitrile was examined by means of the nuclear quadrupole resonances (NQR) resulting from ^{14}N and ^{35}Cl nuclei. One ^{14}N resonance line (the higher line of the pair) and three ^{35}Cl resonance lines were observed. The Zeeman effect on a single crystal was studied in an attempt to predict the lower ^{14}N line. Thus, $|e^2Qq|=3936.7$ kHz and $\eta=0.1298$ were calculated for the nitrogen atom; the frequency of the lower line was estimated at 2824.8 kHz. On the other hand, ($\eta=0.130$; $|e^2Qq|=71.209$ MHz), (0.128; 72.594), and (0.116; 73.720) were determined for the chlorine atoms in the order of increasing frequencies by studying the Zeeman effect of ^{35}Cl NQR on the single crystal.

Short intermolecular distances between nitrogen and halogen atoms have been known from structural studies of X-ray diffraction in the cyanogen halides and *p*-halobenzonitriles.[1,2] These results have been interpreted as indicating donor-acceptor interaction between adjacent molecules. The crystal structure of 2,4,6-trichlorobenzonitrile was recently determined to be as is shown in Fig. 1,[3] where the intramolecular bonds are represented by the solid lines, while the intermolecular bonds are represented by the broken lines. The shortest distance between the nitrogen and chlorine atoms in this crystal is 3.22 Å, which is shorter by 0.08 Å than the sum of their van der Waals radii.

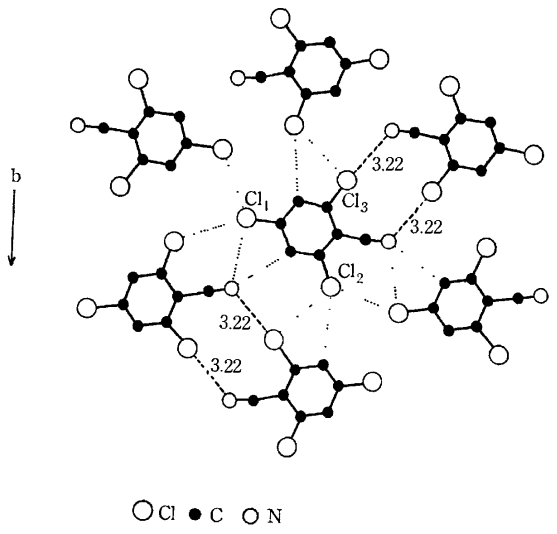

Fig. 1. The projection to the layer of 2,4,6-trichlorobenzonitrile. (Space group $P2_1/c$)

Therefore, there should be a weak interaction between the cyanide groups and *ortho* chlorine atoms, both of which serve to form the dimer. In this respect it seemed that it would be interesting to examine and discuss the chemical bonding in this crystal.

Experimental

The ^{14}N NQR spectrum of 2,4,6-trichlorobenzonitrile was obtained at 77 K by the use of a frequency-modulated spectrometer described previously,[4] whereas the ^{35}Cl NQR spectra of this compound were obtained by the use of a superregenerative spectrometer at 290 K. The resonance frequencies were measured by means of two kinds of heterodyne-type frequency meters, whose frequencies were checked by means of a frequency counter, TR-5578, of the Takeda Riken Co. The Zeeman field was supplied by a Helmholz coil described previously.[5,6]

2,4,6-Trichlorobenzonitrile was prepared from 2,4,6-trichloroaniline *via* 2,4,6-trichloroiodobenzene. This compound was identified by means of its infrared spectrum, its mass spectrum, and its melting point. About a 10-g portion of the sample was used, and a single crystal, 15 mm in diameter and 35 mm in length, was prepared by the Bridgman-Stockbarger method.

Results and Discussion

Our sample of 2,4,6-trichlorobenzonitrile revealed one weak ^{14}N resonance line and three fairly strong ^{35}Cl resonance lines.

^{14}N Resonance Line. Generally a pair of ^{14}N NQR frequencies, ν_I and ν_{II}, are observed as follows:

$$\nu_I = |e^2Qq|(3-\eta)/4, \qquad \nu_{II} = |e^2Qq|(3+\eta)/4, \tag{1}$$

where $|e^2Qq|$ and η are the quadrupole coupling constant and the asymmetry parameter respectively. However, only one resonance line was observed at 3080.2 kHz; it was assigned to the higher line by observing the Zeeman shift. The frequency of the lower line was calculated from the shift of the higher line by applying the Zeeman field, using a single crystal in the same way as before.[6] Figure 2 shows the angular dependence of the Zeeman shift of the higher line when the sample is rotated about a given axis. The Zeeman field was applied along the Y-axis of the laboratory frame, and the resonance frequencies were measured at various rotating angles (Θ) about the X-axis for a constant rotating angle ($\Phi=0°$) about the Z-axis. The maximum frequency or shift was found for $\Theta=335°$. Next, the frequencies were measured at various rotating angles (Φ) about the Z-axis for $\Theta=335°$. The shift was at its maximum at $\Phi=350°$. Therefore, the procedures were repeated until a self-consistent maximum shift was obtained; the maximum frequency was determined to be 3083.4 kHz. Under this condition, the perturbed resonance frequency is at its maximum and expressed as $3083.4=K(3+\eta)+D^2/(2\eta K)$, where K is $|e^2Qq|/4$ and D^2 is 807.8 kHz^2.[6] On the other hand, the higher line in the absence of the Zeeman field is expressed by $3080.2=K(3+\eta)$. Thus, the NQR parameters are calculated as $|e^2Qq|=3936.7\pm7.0$ kHz and $\eta=0.1298\pm0.0057$. Substituting these values into Eq. 1, the frequency of the lower line is obtained as 2824.8±

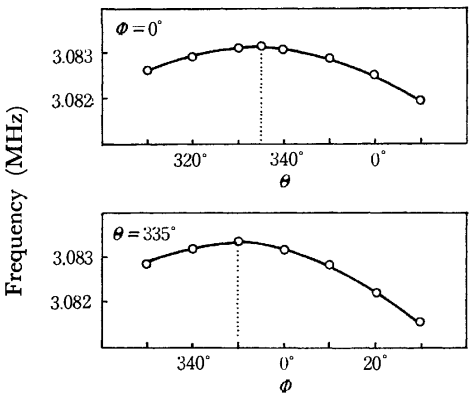

Fig. 2. The angular dependences of the Zeeman shifts.

10.6 kHz. The neighborhood of this frequency was carefully swept again, but, unfortunately, no resonance line was observed.

^{35}Cl Resonance Lines. The ^{35}Cl NQR frequency, ν, is obtained according to the following equation:

$$\nu = |e^2Qq|(1+\eta^2/3)^{1/2}/2. \quad (2)$$

The ^{35}Cl resonance lines of the sample were observed at 35.704, 36.395, and 36.941 MHz, as is shown in Table 1. These lines are labeled as ν_1, ν_2, and ν_3 respectively. Then, referring to the crystal structure of the sample, these lines can be ascribed to the three kinds of chlorine atoms, Cl_1, Cl_2, and Cl_3, in one molecule. One of the zero-splitting patterns of the Zeeman effect on the resonance lines is shown in Fig. 3. For each of the resonance lines, ν_1, ν_2, and ν_3, two loci were obtained. The direction of the principal z-axis of the field gradient on the chlorine atom can be obtained from the zero-splitting pattern; it is assumed to be parallel to the direction of the C–Cl bond. The direction of the b-axis (C_2-axis) of the crystal can be found easily from the symmetrical distributions of the z-axis. The resonance line can be assigned by means of the angle between the b-axis and the z-axis. Thus, it

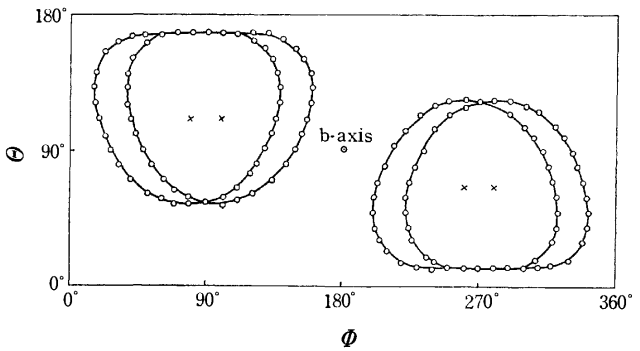

Fig. 3. Zero-splitting patterns of the Zeeman effect on the resonance line, ν_1.

is evident that ν_1, ν_2, and ν_3 originate from the *para-*, *ortho-*, and *ortho-*chlorine atoms respectively. The last interacts weakly with the cyanide group of the adjacent molecule. The condition under which the zero-splitting occurs for the ^{35}Cl nucleus is given[7] by:

$$\sin^2\theta = 2/(3-\eta\cos^2\varphi), \quad (3)$$

where θ and φ are the polar and azimuthal angles for the Zeeman magnetic field with respect to the coordinates of the principal axes of the field gradient at the resonant nucleus. The asymmetry parameters were determined from Eq. (3) by the use of the least-squares method. If the crystal field effects are negligibly small, the quadrupole coupling constant and the double-bond character, f, can be determined from the following equation:[8]

$$f = 2|e^2Qq|\eta/(3|e^2Qq_{\text{atom}}|), \quad (4)$$

where $|e^2Qq_{\text{atom}}|$ is 109.7 MHz.[9] These results are listed in Table 1. The f value of ν_3 is rather smaller. This suggests that the *ortho-*chlorine atom assigned ν_3 interacts with the cyanide group of the adjacent molecule, as is to be expected from the crystal structure of this compound.[3] The ∠CN···Cl angle is 122.4°, although generally the ∠CN···halogen angle is about 180°, as in the acetonitrile–bromine complex.[10] This seems to suggest that the σ-orbital of the nitrogen atom in this molecule has an s-character of less than 50%.

Table 1. NQR parameters in 2,4,6-trichlorobenzonitrile

		ν(MHz)	$\lvert e^2Qq\rvert$(MHz)	η(%)	f(%)
^{14}N		2.8248[a]	3.9367[a]	12.98[a]	—
		3.0802			
^{35}Cl	Cl_1	35.704	71.209	13.0	5.63
	Cl_2	36.395	72.594	12.8	5.65
	Cl_3	36.941	73.720	11.6	5.19

a) Estimated by the experiment of Zeeman effects.

References

1) R. B. Heiart and G. B. Carpenter, *Acta Crystallogr.*, **9**, 889 (1956).
2) E. O. Schlemper and D. Britton, *ibid.*, **18**, 419 (1965).
3) V. B. Carter and D. Britton, *ibid.*, **B28**, 945 (1972).
4) H. Negita, M. Hayashi, and T. Okada, *J. Sci. Hiroshima Univ., Ser. A*, **35**, 85 (1971).
5) T. Okuda, H. Terao, O. Ege, and H. Negita, This Bulletin, **43**, 2398 (1970).
6) H. Negita, K. Shibata, and T. Kubo, *ibid.*, **46**, 110 (1973).
7) C. Dean, *Phys. Rev.*, **96**, 1053 (1954).
8) R. Bersohn, *J. Chem. Phys.*, **22**, 2078 (1954).
9) V. Jaccarino and J. G. King, *Phys. Rev.*, **83**, 471 (1951).
10) K. M. Marstokk and K. O. Strømme, *Acta Crystallogr.*, **B24**, 713 (1968).

Polarographic Studies of Bis(2,2′,2″-terpyridine) Complexes of Manganese(II), Cobalt(II), Nickel(II) and Europium(III) in Acetonitrile

Makoto AIHARA,* Hirofumi KISHITA, and Seizo MISUMI**

Inorganic Chemistry Laboratory, Faculty of Science, Kyushu University, Fukuoka 812

(Received June 8, 1974)

The reduction mechanism of bis 2,2′,2″-terpyridine complexes of manganese(II), cobalt(II), nickel(II) and europium(III) were investigated in acetonitrile by means of DC and AC polarograph and Kalousek polarograph at DME and cyclic voltammetry at an HDME. It was found that univalent metal complex anions, such as $[M(terpy)_2]^-$ (M=manganese and nickel), were formed at the electrode surface in acetonitrile. For the europium(III) complex, the standard rate constant of the second reduction step was estimated.

It is well-known that ligands such as 2,2′-bipyridine and 1,10-phenanthroline which have available acceptor orbitals for π electrons stabilize low valency states of these metal complexes.[1] Acetonitrile is a more inert solvent than water in the reduction of metal complexes. Formation of univalent tris(2,2′-bipyridine)metal complex anions in acetonitrile has been reported in polarographic studies.[2-4]

In this work, the electrode processes of bis(2,2′,2″-terpyridine)metal(II, III) complexes (metal ions; manganese(II), cobalt(II), nickel(II) and europium(III)) in acetonitrile were investigated by polarography.

Experimental

Materials. Bis(2,2′,2″-terpyridine)metal(II, III) perchlorates were prepared by the methods of Morgan and Burstall,[5] Hogg and Wilkins[6] and Sinha.[7] The compositions were identified by elementary analysis. Acetonitrile (AN) was purified[8] and water content was determined to be 5 mM by Karl Fischer titration. Et_4NClO_4(TEAP) was used as a supporting electrolyte.

Apparatus. The electrolysis cell and reference electrode were the same as previously reported.[9] Cyclic voltammograms were recorded by a Rikendenshi X-Y recorder. Triangular potential signals were obtained from the Yokogawa-Hewlett-Packard 3300 A Function Generator. The DME had the following characteristics: m=0.706 mg/s, t=6.17 s in 0.1 M TEAP–AN medium at −1.4 V *vs.* SCE. The HDME(surface area of HDME; 0.031 cm^2) was used for cyclic voltammetry as a working electrode.

Procedure. A sample solution was prepared by dissolving 0.1—1.0 mM bis (terpyridine) metal(II, III) perchlorate and 0.1 M TEAP in AN. Triton X-100 was used as a maximum suppressor. The dissolved oxygen in the solution was removed by bubbling pure nitrogen presaturated with acetonitrile vapour for 20 min. All the experiments were carried out at 25.0±0.1 °C. Other procedures were the same as previously described.[9]

Results and Discussion

Bis(2,2′,2″-terpyridine)manganese(II) Complex. DC polarograms of 0.5 mM $[Mn(terpy)_2](ClO_4)_2$ complex in acetonitrile are shown in Fig. 1. The complex gave a six-step reduction wave. The maximum (2B) at the second step was not suppressed by the addition of

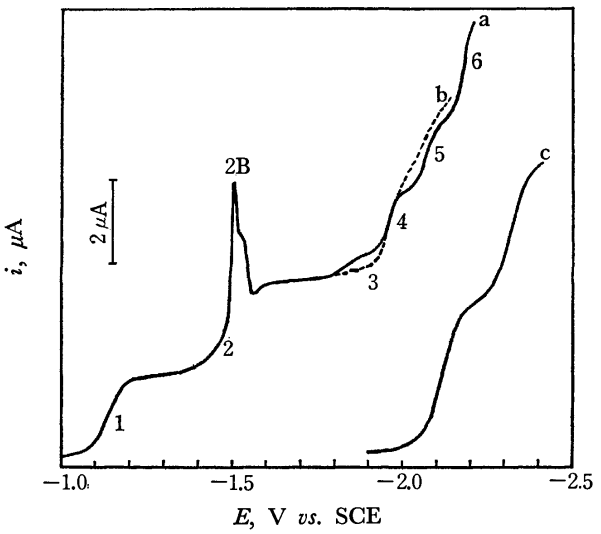

Fig. 1. DC polarograms of $[Mn(terpy)_2](ClO_4)_2$ in 0.1 M TEAP-AN.
a: 0.5 mM $[Mn(terpy)_2](ClO_4)_2$, b: a) +5 mM 2,2′, 2″-terpyridine, c: 0.5 mM 2,2′,2″-terpyridine.

TABLE 1. HALF-WAVE POTENTIALS AND RECIPROCAL SLOPES OF 0.5 mM BIS(2,2′,2″-TERPYRIDINE)METAL(II, III) PERCHLORATES IN 0.1 M TEAP-AN

	$E_{1/2}$ V *vs.* SCE	Slope mV
Mn(II) complex		
1st wave	−1.155	58
2nd wave	−1.506	80
3rd wave	*ca.* −1.85	—
4th wave	−1.962	—
Co(II) complex		
1st wave	−0.789	57
2nd wave	−1.725	56
Ni(II) complex		
1st wave	−1.246 (−1.249)[a]	60 (47)[a]
2nd wave	−1.479 (−1.485)[a]	47 (47)[a]
3rd ware	−1.919	—
Eu(III) complex		
1st wave	−0.258	88
2nd wave	−1.595	64

a) In the presence of 5.0 mM 2,2′,2″-terpyridine

* Present address: Fukuoka Women's University, Kasumigaoka, Higashi-ku, Fukuoka 813.

** Present address: Kyushu Sangyo University, Matsugadai, Higashi-ku, Fukuoka 812.

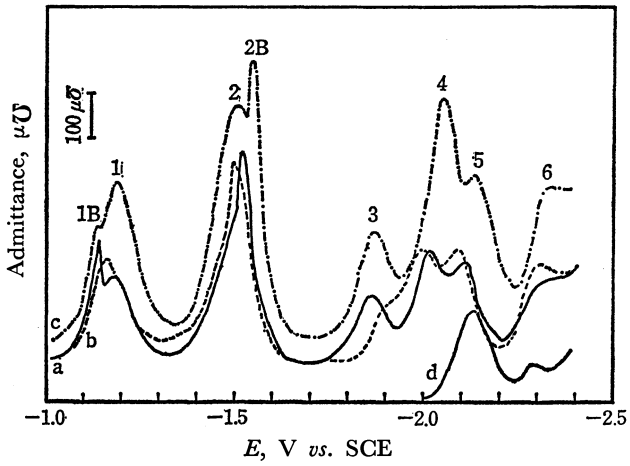

Fig. 2. AC polarograms of $[Mn(terpy)_2](ClO_4)_2$ in 0.1 M TEAP-AN.
a: 0.5 mM $[Mn(terpy)_2](ClO_4)_2$, b: a) + Triton X-100, c: 1.0 mM $[Mn(terpy)_2](ClO_4)_2$, d: 0.5 mM 2,2′,2″-terpyridine.

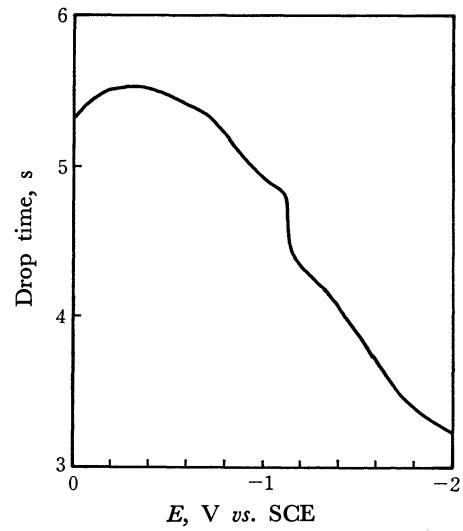

Fig. 3. The electrocapillary curve for $[Mn(terpy)_2](ClO_4)_2$ in 0.1 M TEAP-AN.

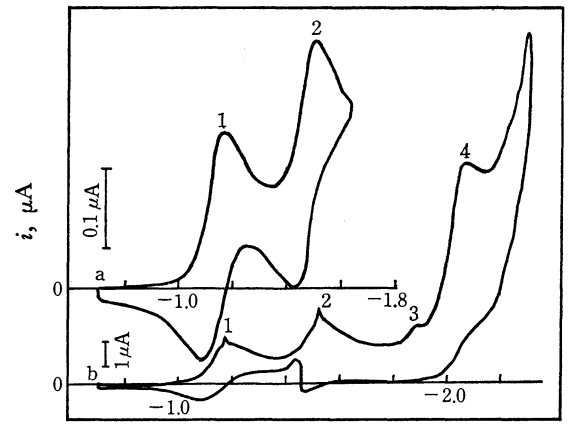

Fig. 4. Cyclic voltammograms of a) 0.1 mM $[Mn(terpy)_2](ClO_4)_2$ at 0.04 V/s, b) 0.5 mM $[Mn(terpy)_2](ClO_4)_2$ at 0.26 V/s in 0.1 M TEAP-AN.

Triton X-100. The third and fourth waves were close to each other, making it difficult to analyze them. The electrode reactions of the first and second waves were found to be diffusion-controlled. The polarographic data are given in Table 1. The ratio of wave heights for the first four waves was 1.00 : 1.07 : 0.30 : 0.71. The diffusion current constant at the first step was 2.05, which is nearly equal to the value of one-electron reduction of various metal ions[10] and tris(2,2′-bipyridine)manganese(II).[3] From log-plot analysis and Kalousek polarogram, the first and second steps were found to be due to reversible one-electron and quasi-reversible one electron reductions, respectively. The first and second waves were not affected by the addition of free 2,2′,2″-terpyridine, but the third wave was suppressed and the fourth wave showed no distinct diffusion plateau (Fig. 1). AC polarograms of the complex are shown in Fig. 2. The main peak admittance increased with the increase in concentration of the complex, sharp peaks (1B and 2B) being observed at the first and second steps. The 1B peak was suppressed by the addition of triton X-100 but the 2B peak remained unchanged. The electrocapillary curve of manganese(II) complex, shown in Fig. 3, shows a depression in the cathodic potential range. The depression was observed at the potentials whose maximum appeared in AC polarography. This shows that the adsorption of the complex occurs on the electrode surface.

Cyclic voltammograms of manganese(II) complex are shown in Fig. 4. Sharp peaks corresponding to the 1B and 2B peaks appeared at 0.5 mM $[Mn(terpy)_2](ClO_4)_2$ but not at 0.1 mM $[Mn(terpy)_2](ClO_4)_2$. The values of ΔE_{peak} (the difference in peak potentials at the anodic and cathodic sides) are 74 and 51 mV for the first and second waves, respectively. No anodic peak of the third step was observed because of irreversibility of the electrode reaction.

It was found that: 1) the reduction potentials of the third and fourth waves differ from those of 2,2′, 2″-terpyridine; 2) the total diffusion current constant (2.07) of the third and fourth waves is nearly equal to the value of one electron reduction of various metal ions; and 3) the third wave was suppressed by the addition of 2,2′,2″-terpyridine. From these results and those for the first and second waves, the electrode processes are estimated as follows:

$$[Mn(terpy)_2]^{2+}$$

1st wave e ⇓

$$[Mn(terpy)_2]^{+}$$

2nd wave e ⇓

$$[Mn(terpy)_2] \rightleftharpoons [Mn(terpy)] + terpy$$

4th wave e ↓ 3rd wave ↓ e ↓

$$[Mn(terpy)_2]^{-} \rightleftharpoons [Mn(terpy)]^{-} + terpy$$

The 5th and 6th waves correspond to the reduction of terpyridine liberated from the complex.

Thus, the formation of univalent $[Mn(terpy)_2]^{-}$ anion was found at the DME in acetonitrile. The 1B peak is considered to be caused by the weak adsorption

of product, from the fact that the maximum did not interfere with the DC polarogram of the first wave, and the peak at cyclic voltammogram was suppressed by the addition of Triton X-100. On the other hand, the second wave was affected appreciably by the maximum and was not suppressed by the addition of Triton X-100.

Bis(2,2',2"-terpyridine)cobalt(II) Complex. The DC polarogram of 0.5 mM $[Co(terpy)_2](ClO_4)_2$ in acetonitrile is shown in Fig. 5. A four-step reduction wave was observed and the electrode reactions of the first three steps found to be diffusion-controlled (Table 1). The ratio of the first and second wave heights was 1 : 1. The diffusion current constant for the first wave was 1.96, nearly equal to the value of a one-electron reduction of tris(2,2'-bipyridine)cobalt(II) complex.[2] The value of the reciprocal slope for the first and second waves was close to the theoretical value of 0.059 V, while the log-plot of the third wave gave a curve with two linear parts. The AC polarogram of the complex is also shown in Fig. 5. AC peaks corresponding to the first and second steps were observed, but the peak potential of the third did not coincide with that of the ligand.

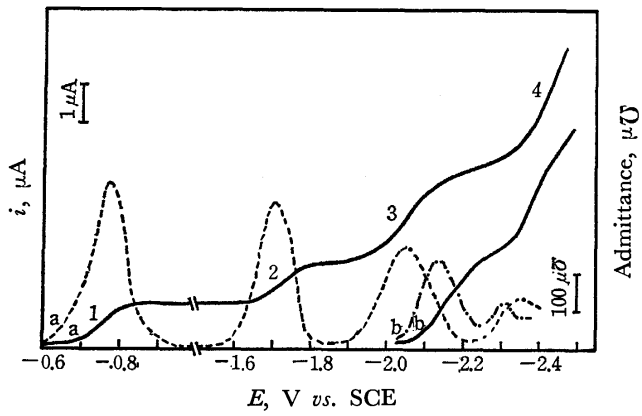

Fig. 5. DC and AC polarograms of 0.5 mM $[Co(terpy)_2](ClO_4)_2$ (curve a) and 0.5 mM 2,2',2"-terpyridine (curve b) in 0.1 M TEAP-AN.

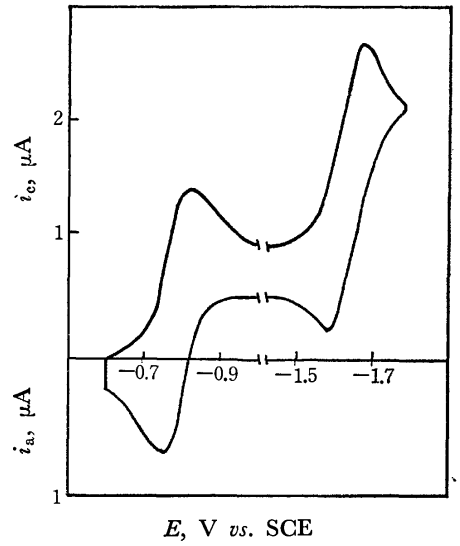

Fig. 6. Cyclic voltammograms of 0.5 mM $[Co(terpy)_2](ClO_4)_2$ in 0.1 M TEAP-AN. Scan rate: 0.03 V/s.

The effect of free 2,2',2"-terpyridine upon the reduction wave was investigated. No effect was observed upon the first and second waves, but the third and fourth waves increased in height with increase in the concentration of 2,2',2"-terpyridine.

Cyclic voltammograms of 0.5 mM cobalt(II) complex are shown in Fig. 6. The values of ΔE_{peak} for the first and second steps are close to the theoretical value of reversible one-electron reduction.

Thus, the electrode reactions are written as,

$$[Co(terpy)_2]^{2+} + e \rightleftarrows [Co(terpy)_2]^{+}$$

$$[Co(terpy)_2]^{+} + e \rightleftarrows [Co(terpy)_2]$$

The formation of $[Co(terpy)_2]^+$ and $[Co(terpy)_2]$ was found in the same way as in the case of bis(2,2',2"-terpyridine) iron(II) complex,[11] but that of $[Co(terpy)_2]^-$ could not be confirmed by DC or AC polarography.

Bis(2,2',2"-terpyridine)nickel(II) Complex. DC and AC polarograms of the nickel(II) complex are shown in Fig. 7. It gave a five-step reduction wave. A small maximum appeared at the positive side of the third wave in DC polarograms. The electrode reactions for the first three waves were found to be diffusion-controlled (Table 1). By the addition of free 2,2',2"-terpyridine to the solution of 0.5 mM complex, the first wave increased and the second wave decreased. The reciprocal slope of the first wave approached the value of a reversible two-electron reduction. The diffusion current constant for the third step is 2.23, which nearly equals the value of one-electron reduction of various metal ions.[10] The total height of the first and second waves was about twice as much as that of the third wave. The 1B peak in AC polarogram was suppressed but the 3B peak remained with the addition of Triton X-100 (Fig. 7). Cyclic voltammetry of the nickel(II) complex was investigated. The sharp peaks corresponding to the 1B and 3B waves also appaered in the cyclic voltammogram. The 1B peak was significantly large at the anodic and cathodic sides. The clear anodic and cathodic peaks of the first and the second steps were observed and the cathodic peak of the third step was observed as a shoulder at −1.9 V *vs.* SCE.

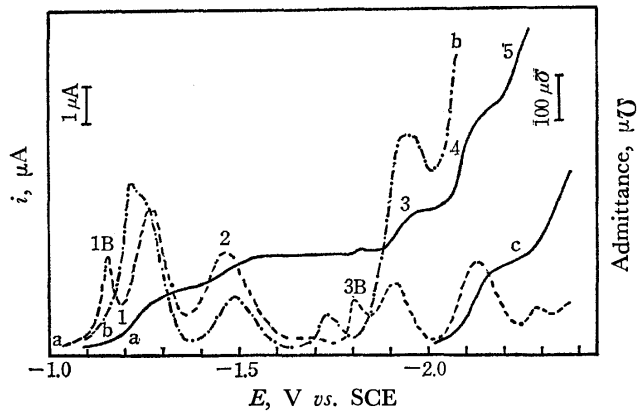

Fig. 7. DC and AC polarograms of $[Ni(terpy)_2](ClO_4)_2$ in 0.1 M TEAP-AN.
a: 0.5 mM $[Ni(terpy)_2](ClO_4)_2$, b: a) +5 mM 2,2',2"-terpyridine, c: 0.5 mM 2,2',2"-terpyridine.

The electrode reactions for the first and third waves are estimated as follows.

$$[Ni(terpy)_2]^{2+} + 2e \rightleftarrows [Ni(terpy)_2]$$

$$[Ni(terpy)_2] + e \rightleftarrows [Ni(terpy)_2]^-$$

The univalent $[Ni(terpy)_2]^-$ anions are formed at the electrode surface. From the fact that the second wave decreased with the addition of 2,2′,2″-terpyridine, the second wave might correspond to the irreversible two electron reduction of dissociated complex species, *e.g.* $[Ni(terpy)]^{2+}$.

Bis(2,2′,2″-terpyridine)europium(III) Complex. DC and AC polarograms of 0.5 mM $Eu(terpy)_2(ClO_4)_3$ are shown in Fig. 8. The europium complex gave a four-step reduction wave, the electrode reactions of the first and second waves being found to be diffusion-controlled (Table 1). The diffusion current constant of the first step was 2.05, which is nearly equal to the value of one-electron reduction. The ratio of the wave heights of the first and second steps is 1 : 1.9. It was concluded that the first and second waves were one- and two-electron reduction waves, respectively. The third and fourth waves are due to the reduction of the ligand.

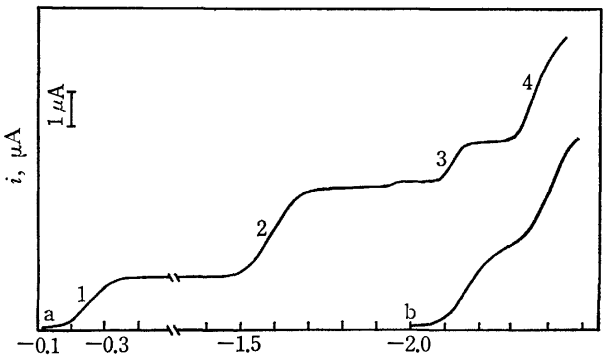

Fig. 8. DC polarograms of 0.5 mM $[Eu(terpy)_2](ClO_4)_3$ (curve a) and 0.5 mM 2,2′,2″-terpyridine (curve b) in 0.1 M TEAP-AN.

With the addition of free 2,2′,2″-terpyridine, the first wave was shifted to a more negative potential and the value of the reciprocal slope became equal to that of a reversible one-electron reduction. The reversibility of the second wave decreased with an increase in concentration of the ligand reagent.

A cyclic voltammogram of the complex is shown in Fig. 9. Peaks of the first and second steps were observed, the peak potential of the second wave shifting to a more negative potential with increasing scan rate. This indicates the irreversibility of the second step, also. The electrode reaction scheme is shown to be as follows.

$$[Eu(terpy)_2]^{3+} + e \rightleftarrows [Eu(terpy)_2]^{2+}$$

$$[Eu(terpy)_2]^{2+} + 2e \rightleftarrows Eu^0 + 2terpy$$

The standard rate constant (k_s) for the second step

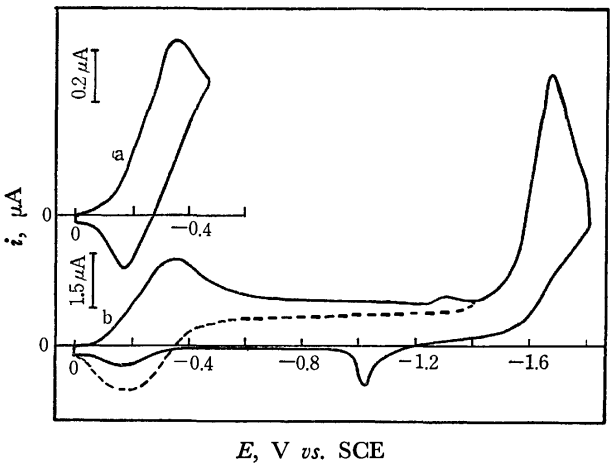

Fig. 9. Cyclic voltammograms of $[Eu(terpy)_2](ClO_4)_3$ in 0.1 M TEAP-AN.
a: 0.5 mM $[Eu(terpy)_2](ClO_4)_3$ at 0.038 V/s, b: 0.7 mM $[Eu(terpy)_2](ClO_4)_3$ at 0.285 V/s.

was determined to be 6.7×10^{-4} cm/s by the single sweep method.

The waves corresponding to the formation of $[M(terpy)_2]^-$ (M=Mn and Ni) were observed in DC polarograms. In the case of the Co(II) complex, the formation of $[Co(terpy)_2]^-$ was not confirmed since the wave overlapped with that of the free 2,2′,2″-terpyridine.

On the other hand, bis(2,2′,2″-terpyridine)europium (III) complex was not reduced to the univalent complex anion but decomposed into metal amalgam and ligands after reduction at the potential of the second wave. This indicates that there is a more stable and stronger tendency of complex formation of d-element than that of f-element in bisterpyridine complexes of metal(0).

The work was carried out with financial support from the Ministry of Education.

References

1) G. M. Waind and B. Martin, *J. Inorg. Nucl. Chem.*, **8**, 551 (1958).
2) N. Tanaka and T. Sato, This Bulletin, **41**, 2059 (1968).
3) Y. Sato and N. Tanaka, *ibid.*, **41**, 2064 (1968).
4) N. Tanaka and T. Sato, *Inorg. Nucl. Chem. Letters.*, **4**, 487 (1968).
5) G. Morgan and F. H. Burstall, *J. Chem. Soc.*, **1937**, 1649.
6) R. Hogg and R. G. Wilkins, *ibid.*, **1962**, 341.
7) S. P. Sinha, *Z. Naturforschg.* **20a**, 552 (1965).
8) J. F. Coetzee, G. P. Cunningham, D. K. McGuire, and G. R. Padmanabhan, *Anal. Chem.*, **34**, 1139 (1962).
9) S. Misumi and M. Aihara, *Talanta*, **19**, 549 (1972).
10) I. M. Kolthoff and J. F. Coetzee, *J. Amer. Chem. Soc.*, **79**, 1852 (1957).
11) S. Musumeci, E. Rizzareili, S. Sammartano, and R. P. Bonomo, *J. Inorg. Nucl. Chem.*, **36**, 853 (1974).

Polarography of Europium(III) in Acetonitrile in the Presence of Thiocyanate and Halide Ions

Makoto AIHARA* and Seizo MISUMI**

Inorganic Chemistry Laboratory, Faculty of Science, Kyushu University, Fukuoka 812

(Received August 28, 1974)

Studies were carried out on the polarographic behavior of europium in acetonitrile in the presence of SCN^-, Br^-, I^- and Cl^-. Two reduction waves were found in the Eu(III)–SCN^- system, one corresponding to the reduction of $[Eu(NCS)_6]^{3-}$ and the other to the reduction of $[Eu(NCS)_2]$. In the Eu(III)–Br^- system, the reduction potential of Eu(III)-bromide complex species was more positive than that of the $[HgBr_4]^{2-}$/Hg couple. In the Eu(III)–I^- system, iodide ions were oxidized in acetonitrile by europium(III). The formation constants of Eu(III)–SCN^- system were found to be: $\log \beta_6 = 24.4$ for $[Eu(NCS)_6]^{3-}$ and $\log \beta_2 = 6.0$ for $[Eu(NCS)_2]$. The degree of complexation of europium(III) and mercury(II) with bromide ion was also determined.

Polarographic and potentiometric studies of metal-(II, III)–halide and –thiocyanate complexes in acetonitrile have been reported.[1–3] The polarographic reduction of europium (III) in tetraethylammonium perchlorate in acetonitrile was studied by several authors,[4,5] the reduction process at DME in acetonitrile being Eu(III)→Eu(II) and Eu(II)→Eu(0). In a study on the influence of water on the reduction waves, the addition of small amounts of water was found to give a negative shift of the half-wave potential, which is caused by the rate of the electrode reaction being affected by the presence of water molecules adsorbed on the mercury electrode surface.[5]

The polarographic behavior of europium(III) in the presence of halide ions in non-aqueous solvents has not been studied. The waves of lanthanoids(III) in acetonitrile occur at considerably more negative potentials with tetraethylammonium bromide than with tetraethylammonium perchlorate as a supporting electrolyte.[4] This paper deals with the polarography of europium(III) in the presence of SCN^-, Br^-, I^- and Cl^-. The formation constants for Eu(III)–SCN^- and Eu(III)–Br^- systems were obtained and the electrode process of these systems was also determined.

Experimental

Materials. Commercial acetonitrile was purified by the method of Coetzee *et al.*[6] The water contant was found to be less than 0.01% by Karl Fischer titration. Tetraethylammonium halides and tetraethylammonium thiocyanate were prepared by the procedures reported.[2,3]

Apparatus. The electrolysis cell consists of three electrodes.[1] The reference electrode was an SCE with a salt bridge:

$$\left(\frac{0.5\ \mathrm{M}\ Et_4NClO_4}{AN}\middle|\frac{1\ \mathrm{M}\ NaClO_4}{H_2O}\middle|\frac{1\ \mathrm{M}\ NaCl}{H_2O}\middle|\frac{1\ \mathrm{M}\ KCl}{H_2O}\right)$$

Procedure. Sample solutions were prepared by dissolving 0.5 mM europium(III) perchlorate in acetonitrile with an appropriate amount each of Et_4NX(X^-: SCN^-, Cl^-, Br^- and I^-). Et_4NClO_4 was used to keep the concentration of Et_4N^+ 0.1 M. Other procedures were the same as described previously.[1]

* Present address: Fukuoka Women's University, Kasumigaoka, Higashi-ku, Fukuoka 813.

** Present address: Kyushu Sangyo University, Matsugadai, Higashi-ku, Fukuoka 812.

Results and Discussion

Europium(III) Perchlorate in Acetonitrile. Europium(III) gave a two-step reduction wave corresponding to the one- and two-electron reduction. The half-wave potentials were in line with those reported by Cokal and Wise.[5] The electrode reaction of the first and second waves was found to be reversible and diffusion-controlled.

Eu(III)–SCN^- System. Polarograms of 0.5 mM Eu(III) in the presence of thiocyanate ions are shown

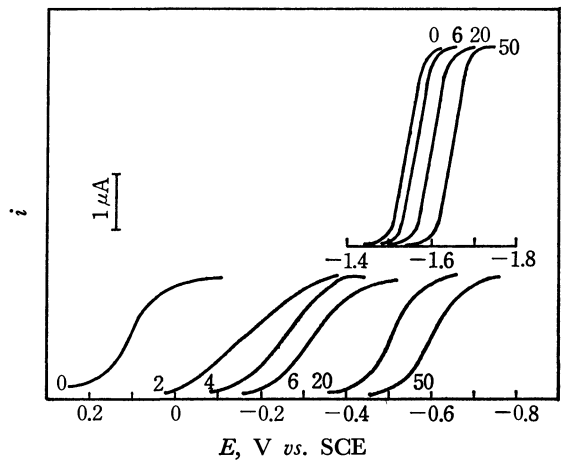

Fig. 1. DC polarograms of europium(III) in the presence of thiocyanate ion. Numbers on curves indicate mole ratio, $[SCN^-]_t/[Eu(III)]_t$.

TABLE 1. POLAROGRAPHIC DATA FOR EUROPIUM(III)–THIOCYANATE SYSTEM

$[Eu(III)] = 0.5$ mM

$[SCN]_t$ / $[Eu(III)]_t$	1st Wave			2nd Wave		
	$E_{1/2}$ V *vs.* SCE	i_d μA	Slope mV	$E_{1/2}$ V *vs.* SCE	i_d μA	Slope mV
0	0.113	1.80	58	−1.624	3.40	28
6	−0.318	1.87	—	−1.650	3.40	30
10	−0.407	1.87	61	−1.660	3.32	30
20	−0.493	1.80	60	−1.687	3.44	31
30	−0.541	1.79	58	−1.696	3.18	34
40	−0.571	1.80	60	−1.714	3.15	35
50	−0.590	1.84	58	−1.725	3.60	34

in Fig. 1. The first wave was shifted towards more negative potentials with increasing concentration of thiocyanate ions. The log-plot was found to be non-linear for $[SCN^-]_t/[Eu(III)]_t<10$. Above this ratio, the electrode reaction of the first wave was found to be a reversible, one electron reduction and diffusion-controlled. The polarographic data are shown in Table 1. The second wave was also shifted towards more negative potentials with increasing concentration of thiocyanate ions. The electrode reaction of the second wave was found to be a reversible, two-electron reduction and diffusion-controlled.

Assuming that Eu^{3+}, EuX_p^{3-p}, Eu^{2+} and EuX_q^{2-q} are reduced reversibly, the electrode reactions are given by

$$Eu^{3+} + e \rightleftharpoons Eu^{2+} \quad (1)$$

$$EuX_p^{3-p} + e \rightleftharpoons EuX_q^{2-q} + (p-q)X^- \quad (2)$$

$$Eu^{2+} + 2e \rightleftharpoons Eu(0) \quad (3)$$

$$EuX_q^{2-q} + 2e \rightleftharpoons Eu(0) + qX^- \quad (4)$$

where X^- is SCN^- or halide ion. The difference of the half-wave potentials for Eqs. (1) and (2), $(E_{1/2})_c-(E_{1/2})_s$, is given by

$$\Delta E = 0.0591 \log (\beta_{EuX_q}/\beta_{EuX_p}) - 0.0591(p-q) \log [X]_0 - 0.0591 \log (I_{EuX_p}\cdot I_{Eu^{2+}}/I_{EuX_q}\cdot I_{Eu^{3+}}) \quad (5)$$

where β is overall formation constant for the complex species, I the diffusion current constant for each species and $[X]_0$ the concentration of the ligand species $[SCN^-]$, at the electrode surface; $[X]_0=(C_x-PC_M/2)/(1+K_A[Et_4N^+])$.[1] The value of $p-q$ can be obtained by

$$p-q = \frac{d(\Delta E)}{d \log[SCN^-]_0}/0.0591 \quad (6)$$

From the plot of ΔE *vs.* $\log[SCN^-]_0$ for the first wave, $(p-q)$ and $\log(\beta_{Eu(NCS)_p}/\beta_{Eu(NCS)_q})$ were obtained to be 4.0 and 18.4, respectively. From the same plot for the second wave, q and $\log \beta_{Eu(NCS)_q}$ were found to be 1.9 and 6.0, respectively. Thus, the electrode reactions are presumed to be as follows.

$$Eu(NCS)_6^{3-} + e \rightleftharpoons Eu(NCS)_2 + 4SCN^- \quad (7)$$

$$Eu(NCS)_2 + 2e \rightleftharpoons Eu(0) + 2SCN^- \quad (8)$$

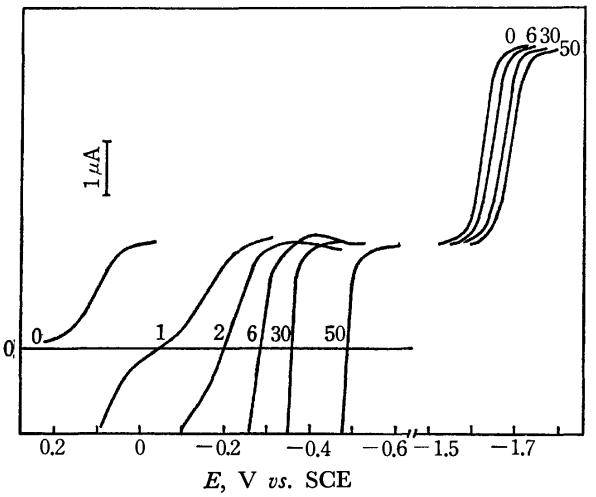

Fig. 2. DC polarograms of europium(III) in the presence of bromide ion. Numbers on curves indicate mole ratio, $[Br^-]_t/[Eu(III)]_t$.

The values of $\log \beta_{Eu(NCS)_6^{3-}}$ and $\log \beta_{Eu(NCS)_2}$ were found to be 24.4 and 6.0, respectively. Formation of $Eu(NCS)_6^{3-}$ in acetonitrile has also been confirmed by Burmeister *et al.*[7]

With increasing concentration of SCN^-, the reciprocal slope of the second wave deviated from the theoretical one. The standard rate constant of reduction ($[SCN_t/[Eu(III)]_t=50$) was determined to be 1.7×10^{-4} cm/s by cyclic voltammetry, indicating that the electrode reaction was quasi-reversible at high concentrations of SCN^-.

Eu(III)-Br^- System. Polarograms of 0.5 mM Eu (III) in the presence of bromide ion are shown in Fig. 2. The solution containing Eu(III) and bromide ions was pale yellow, the coloration disappearing on addition of water. The formation of Eu(III)-bromide complex in acetonitrile was assumed. The first wave may be a composite wave of $EuBr_p^{3-p}\rightleftharpoons EuBr_q^{2-q}$ and $Hg\rightleftharpoons HgBr_x^{2-x}$ couples. Thus, the electrode reactions are given by

$$EuBr_p^{3-p} + e \rightleftharpoons EuBr_q^{2-q} + (p-q)Br^- \quad (9)$$

$$HgBr_x^{2-x} + 2e \rightleftharpoons Hg + XBr^- \quad (10)$$

The half-wave potentials for the reduction of $EuBr_p^{3-p}$ and $HgBr_x^{2-x}$ are as follows.

$$(E_{1/2})_c^{Eu} = (E_{1/2})_s^{Eu} - 0.0591 \log K - 0.0591(p-q) \log [Br^-]_0 \quad (11)$$

$$(E_{1/2})_c^{Hg} = (E_{1/2})_s^{Hg} - 0.0295 \log \beta_{HgBr_x^{2-x}} - 0.0295 \log [Br^-]_0 \quad (12)$$

where $K=\beta_{EuBr_p^{3-p}}/\beta_{EuBr_q^{2-q}}$. In the case of Eu(III)–Br^- system, the half-wave potential of mercury(II) bromide complex is more negative than that of Eu(III) bromide complex; $(E_{1/2})_c^{Hg}<(E_{1/2})_c^{Eu}$. From Eqs. (11) and (12), the following relationship can be obtained at $[Br^-]_0=1$ M.

$$(E_{1/2})_s^{Hg} - 0.0295 \log \beta_{HgBr_x^{2-x}} < (E_{1/2})_s^{Eu} - 0.0591 \log K \quad (13)$$

Since $(E_{1/2})_s^{Hg}=0.557$ and $(E_{1/2})_s^{Eu}=0.113$ V *vs.* SCE in acetonitrile, Eq. (13) is reduced to

$$\log \beta_{HgBr_x^{2-x}} > 2 \log K + 15 \quad (14)$$

The value of $\log \beta_{HgBr_4^{2-}}$ was calculated to be *ca.* 38 by the plot of $\Delta E_{1/2}$ *vs.* $\log [Br^-]_0$. From Eq. (14), we obtain $\log K<$ *ca.* 12. On the other hand, the value of $2 \log K+15$ for Eu(III)–SCE^- system is 52. Thus $2 \log K+15 \gg \log \beta_{Hg(SCN)_4^{2-}}$ ($\approx$38). This indicates that the wave of Eu(III)–SCN^- complex was completely separated from the wave of Hg(II)–SCN^- complex (Fig. 1).

The second wave was found to be a reversible, two-electron reduction and diffusion-controlled. The values of q and $\log \beta_{EuBr_2}$ were calculated to be 1.8 and 5.31, respectively.

Eu (III)–I^- System. Figure 3 shows the polarograms of 0.5 mM Eu (III) in the presence of iodide ions. By addition of iodide ions, the first wave was shifted towards more negative potentials, the height of the second wave becoming smaller. Limiting currents *vs.* $[I]_t/[Eu(III)]_t$ ($=x$) are shown in Fig. 4. The height of the first wave in the presence of iodide ions was nearly equal to that in the absence of iodide ions until $x=2$ and the height of the first wave started

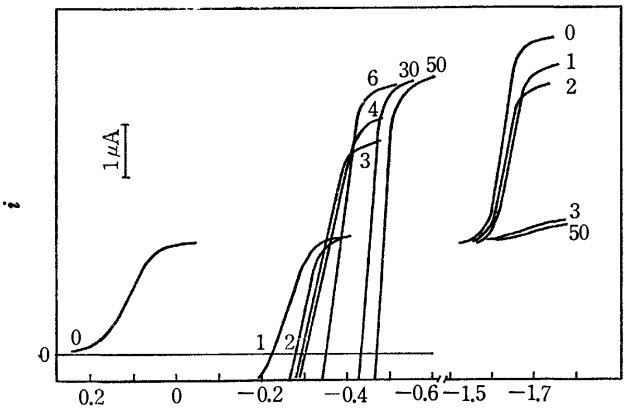

Fig. 3. DC polarograms of acetonitrile solutions containing europium(III) and iodide ion. Number on curves indicates mole ratio, $[I^-]_t/[Eu(III)]_t$.

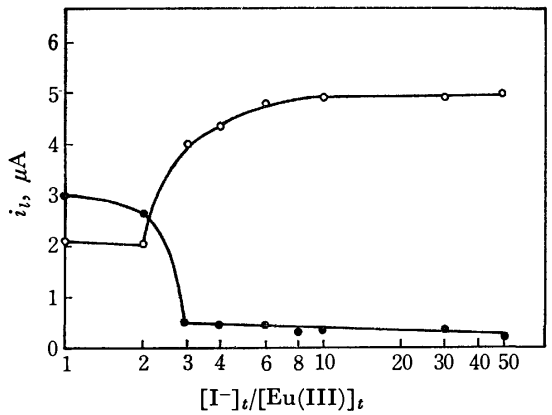

Fig. 4. Limiting currents *vs.* $[I^-]_t/[Eu(III)]_t$ for europium(III)-iodide system.
○: 1st wave, ●: 2nd wave.

to increase at *ca.* $x=2$. The solution containing Eu (III) and iodide ions was yellowish brown, the coloration became stronger with increasing concentration of iodide ions, finally becoming the same as that of iodine in acetonitrile. A polarogram of the solution containing I_2 and Et_4NI was similar to that of the first wave in the presence of excess of iodide ions. This indicates that Et_4NI is oxidized in acetonitrile by europium(III). The reaction product, I_2, is known to form triiodide ion (I_3^-) in the presence of iodide ions.

Since iodine and triiodide ions react rapidly with mercury of the electrode,[8] the mechanisms of chemical and electrochemical processes are given as follows.

chemical processes

$$Eu^{3+} + I^- \longrightarrow Eu^{2+} + \frac{1}{2}I_2 \quad (15)$$

$$I_2 + I^- \rightleftharpoons I_3^- \quad (16)$$

$$I_2 + Hg \rightleftharpoons HgI_2 \quad (17)$$

$$I_3^- + Hg \rightleftharpoons HgI_3^- \quad (18)$$

electrode processes

1st wave

$$Eu^{3+} + e \rightleftharpoons Eu^{2+} \quad (19)$$

$$3HgI_2 + 2e \rightleftharpoons Hg + 2HgI_3^- \quad (20)$$

$$2HgI_3^- + 4e \rightleftharpoons 2Hg + 6I^- \quad (21)$$

2nd wave

$$Eu^{2+} + 2e \rightleftharpoons Eu(0) \quad (22)$$

At $x \leq 2$, the oxidation of iodide ion by europium(III) is not complete.

The first wave might correspond to the reduction of Eqs. (19) and (20).[9] For $x \geq 3$, the reaction of Eq. (21)[9] was predominant, the height of the wave becoming large. The second wave disappeared. This may be caused by the formation of EuI_q^{2-q} which is electroinactive in this potential region.

Eu(III)–Cl⁻ System. For $x<10$, several waves appeared. But a polarogram gave a single reduction wave with a minimum in the diffusion plateau at around −1.0 V *vs.* SCE at $x \geq 10$. The electrocapillary curve of Eu(III)–Cl⁻ system showed a depression in the cathodic range (−0.8——1.0 V *vs.* SCE). The depression was observed at potentials at which a minimum appeared. The hexachloroplatimum(IV) ion[10] produced a minimum similar to that of the complex ion. The minimum may be attributed to the formation of a film of reduction product.

Financial support for this work was given by the Ministry of Education.

References

1) S. Misumi and M. Aihara, *Talanta*, **19**, 549 (1972).
2) S. Misumi and M. Aihara, This Bulletin, **46**, 1674 (1973).
3) S. Misumi, M. Aihara, and S. Kinoshita, *ibid.*, **47**, 127 (1974).
4) I. M. Kolthoff and J. F. Coetzee, *J. Amer. Chem. Soc.*, **79**, 1852 (1957).
5) E. J. Cokal and E. N. Wise, *J. Electroanal. Chem.*, **11**, 406 (1966).
6) J. F. Coetzee, G. P. Cunningham, D. K. McGuire, and G. R. Padmanabhan, *Anal. Chem.*, **34**, 1139 (1962).
7) J. L. Burmeister, S. D. Patterson, and E. A. Deardorff, *Inorg. Chim. Acta*, **3**, 105 (1969).
8) Y. Matsui, R. Kawakado, and Y. Date, This Bulletin., **41**, 2913 (1968).
9) Y. Matsui, Y. Kurosaki, and Y. Date, *ibid.*, **43**, 1707 (1970).
10) P. Kivalo and H. A. Laitinen, *J. Amer. Chem. Soc.*, **77**, 5205 (1955).

Proton Magnetic Resonance Spectra of L- or D-Aspartato (L-2,4-diaminobutyrato)cobalt(III) Complexes

Masatoshi WATABE, Kenji ONUKI,* and Sadao YOSHIKAWA*

General Education Department of Kogakuin University, Hachioji, Tokyo 193

**Department of Synthetic Chemistry, Faculty of Engineering, The University of Tokyo, Hongo, Bunkyo-ku, Tokyo 113*

(Received June 17, 1974)

Three diastereomeric isomers of the L-aspartato(L-2,4-diaminobutyrato)cobalt(III) and two of the D-aspartato (L-2,4-diaminobutyrato)cobalt(III), $Co(N)_3(O)_3$ type were prepared and isolated. The isomers were characterized by their electronic absorption and proton magnetic resonance spectra. Their PMR spectra indicate that the carbon proton adjacent to the coordinated N atom resonates at a higher magnetic field when O atom occupies the site *trans* to the N atom than when N atom occupies the same place.

The preparation and characterization of cobalt(III) complexes containing optically active amino acids which are potentially tridentate ligands have been reported for those with L-2,4-diaminobutyrate ion (L-2,4-dba),[1] D- or L-2,3-diaminopropionate ion (D- or L-2,3-dpa),[2] L-aspartate ion (L-asp)[3,4] and L-histidinate ion (L-his).[5]

However, the assignments are tentative except for that for $[Co(L\text{-}2,3\text{-}dpa)_2]^+$, the exact geometries of which have been determined on the basis of an X-ray diffraction study of one of the *cis* O isomers.[6] An alternative proposal has been given for the isomers for $[Co(L\text{-}asp)_2]^-$.[7] The complexes of bis(L-aspartato)-cobaltate(III) and L-aspartato(iminodiacetato)cobaltate(III) belong to the $[Co(N)_2(O)_4]$ type, and the complexes of bis(L-2,4-diaminobutyrato)cobalt(III) and bis(histidinato)cobalt(III) to the $[Co(N)_4(O)_2]$ type. The aim of the present study was to prepare the mixed complexes [Co(L- or D-asp)(L-2,4-dba)] of the $[Co(N)_3(O)_3]$ type.

Experimental

L-2,4-Diaminobutyric acid was prepared from L-glutamic acid by the Schmidt reaction.[8] All the other materials were of reagent grade.

Three Isomers of [Co(L-asp)(L-2,4-dba)]. To a hot solution (*ca.* 70 °C) containing 1.33 g (0.01 mol) of L-aspartic acid and 1.55 g (0.01 mol) of L-2,4-diaminobutyric acid monohydrochloride in 50 ml of water were added 3.6 g (0.01 mol) of freshly prepared $Na_3[Co(CO_3)_3]\cdot 3H_2O$ and 1 g of activated charcoal. The mixture was stirred on a boiling water bath for *ca.* 30 min. The mixture was then filtered and the charcoal was carefully washed with hot water. The washings and filtrate were combined and concentrated to *ca.* 20 ml on a rotary evaporator at about 40 °C and kept in a refrigerator overnight. Violet powder crystals which appeared were filtered off, washed with a small amount of water and air-dried. The filtrate was passed through a column (3.0×30 cm) containing strong acid cation exchange resin in a hydrogen form(Dowex 50 w×8, 25—50 mesh) and successively through a colum (3.0×30 cm) containing strong base anion exchange resin in a hydroxide form (Dowex 21 k, 25—50 mesh). When water was passed through the column a non-charged complex flowed out. The eluate was concentrated to 10—20 ml. Chromatographic separation was then carried through a column (3.0×110 cm) containing strong acid cation exchange resin in a sodium form (Dowex 50w×8, 100—200 mesh). The adsorbed band was eluted with water at a rate of 0.4 ml/min. Three colored bands, violet (L1), redish violet(L2) and red (L3) were eluted in succession. The three eluates were collected separately and evaporated to dryness in a vacuum desiccator. Each crude product was dissolved in water and reprecipitated with ethanol. Since the amount of L3 was very small. The following alternative method was tried. To a solution containing 1.33 g (0.01 mol) of L-aspartic acid, 1.55 g (0.01 mol) of L-2,4-diaminobutyric acid and 1.0 g (0.025 mol) of NaOH in 30 ml of water were added 2.4 g (0.01 mol) of $CoCl_2\cdot 6H_2O$, 5 ml of 10% of hydrogen peroxide and 1 g of activated charcoal. The mixture was stirred on a boiling water bath for 30 min. Treatment of the reaction was the same as above. By this method the L3 isomer was obtained in a relatively higher yield.

Two Isomers of [Co(D-asp)(L-2,4-dba)]. The isomers were obtained by a similar method to that described above. One of the two meridional isomers was not obtaind. Two isomers were separated and are referred to as D1 and D2 by elution order. Found: (L1) C, 29.55; H, 5.14; N, 12.84%. (L3) C, 29.77; H, 5.15; N, 12.99%. Calcd for $CoC_8H_{14}O_6N_3\cdot 1H_2O$: C, 29.54; H, 4.97; N, 12.92%. Found: (L2) C, 30.38; H, 4.63; N, 13.18%. (D1) C, 29.55; H, 5.23; N, 13.22%. Calcd for $CoC_8H_{14}O_6N_3\cdot 0.5H_2O$: C, 30.39; H, 4.02; N, 13.29%. Found: (D2) C, 28.81; H, 5.78; N, 12.21%. Calcd for $CoC_8H_{14}O_6N_3\cdot 1.5H_2O$: C, 28.75; H, 5.13; N, 12.57%.

Measurements. The electronic absorption spectra were measured with a JASCO ORD-UV-5 spectrometer, proton magnetic resonance(PMR) spectra (100 MHz) in D_2O with a JEOL PS 100 spectrometer. Sodium 2,3-dimethyl-2-silapentane-5-sulfonate (DSS) was used as an internal reference.

Results and Discussion

The possible isomers of [Co(L- or D-asp)(L-2,4-dba)] complexes are shown in Fig. 1. They are denoted by L- or D-series with respect to the asp used. Both series of mixed complexes are composed of two meridional and one facial about $[Co(N)_3(O)_3]$. The two L-*mer* isomers are denoted by L-*trans*O_5 *cis*N_5 (oxygen and nitrogen atoms of the five-membered chelate rings are respectively *trans* and *cis* with each other) and L-*cis*O_5 *trans*N_5. The three [Co(L-asp)(L-2,4-dba)] isomers (L-*trans*O_5 *cis*N_5, L-*fac*, L-*cis*O_5 *trans*N_5) seem to be generated at 120° intervals by an imaginary twist of one coordinated ligand relative to the other about an axis passing through the two ligand occupied triangular faces of the cobalt(III) coordination octahedron. The same kind of relationship exists for the three isomers containing D-aspartate ion.

Separation of the two mixed complexes was accomplished by chromatography on a cation exchange

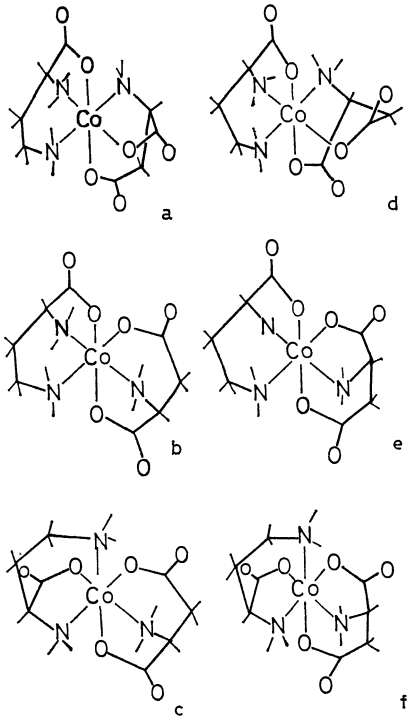

Fig. 1. The six possible geometrical isomers of the [Co(L- or D-asp)(L-2,4-dba)].
a: D-*cis*O_5 *cis*N_5, b: D-*trans*O_5 *trans*N_5, c: D-*fac*, d: L-*trans*O_5 *cis*N_5, e: L-*cis*O_5 *trans*N_5, f: L-*fac*.

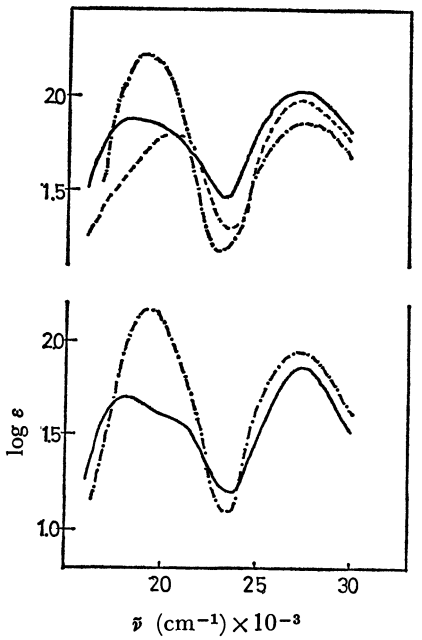

Fig. 2. Absorption spectra of the five isomers of the [Co(L- or D-asp)(L-2,4-dba)].
upper ——, L1; ----, L2; -·-·- L3, lower ——, D1; -·-·- D2.

resin column. Since the complexes exhibit electronic absorption spectra which agree with the crystal field considerations for *mer* and *fac* isomers (Fig. 2), it is possible to assign the *mer* geometry to L1, L2 and D1, and *fac* geometry to L3 and D2.

Assignment of Isomers. It is of significance to

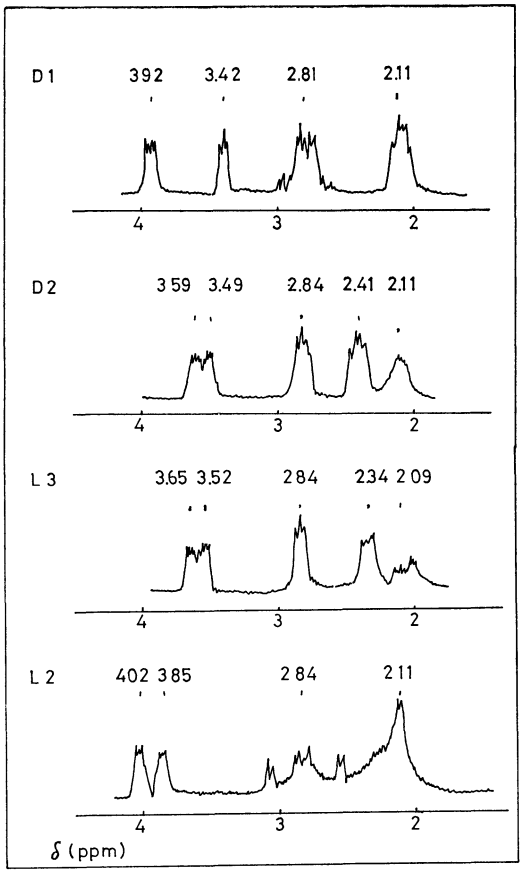

Fig. 3. PMR spectra of the four isomers of the [Co(L- or D-asp)(L-2,4-dba)].

determine the configuration of the *mer* isomers (L1, L2 and D1). Proton magnetic resonance spectra for the four isomers of the [Co(L- or D-asp)(L-2,4-dba)] in D_2O solution are given in Fig. 3. L1 is sparingly soluble in water, and L2, L3, D1 and D2 are soluble in D_2O sufficient for PMR measurements. L1, L3, D1 and D2 are soluble in trifluoroacetic acid, but not L2. Since the PMR specturm of L1 in trifluoroacetic acid resembles that of D1 in the same solvent, the spatial distribution of the ligand atoms (especially N or O atoms) seems to be analogous to that of D1. There is a similarity between the spectra of L3 and D2 in trifluoroacetic acid. The six mixed isomers have C_1 symmetry (Fig. 1). The PMR spectra are thus expected to consist of one ABX pattern due to the CH_2CH moiety of L- or D-asp and one ABMNX pattern due to the CH_2CH_2CH moiety of L-2,4-dba. In order to determine all the resonance lines of these protons, spin decoupling technique was used.

The peak at 2.11 (Fig. 3) can be assigned to the β-methylene protons of L-2,4-dba because of their magnetic shielding and electronegativities. Irradiation of this peak changes the multiplets at *ca.* 3.4—3.5 for D1, D2 and L3 and at *ca.* 3.8 for L2 to a singlet. This indicated that the signals at 3.4—3.5 for D1, D2 and L3 and at *ca.* 3.8 for L2 are attributed to the methine proton of L-2,4-dba moieties. Irradiation of the peak at *ca.* 2.8 makes the lowest field multiplets reduce to a singlet in all the complexes. Thus the lowest field

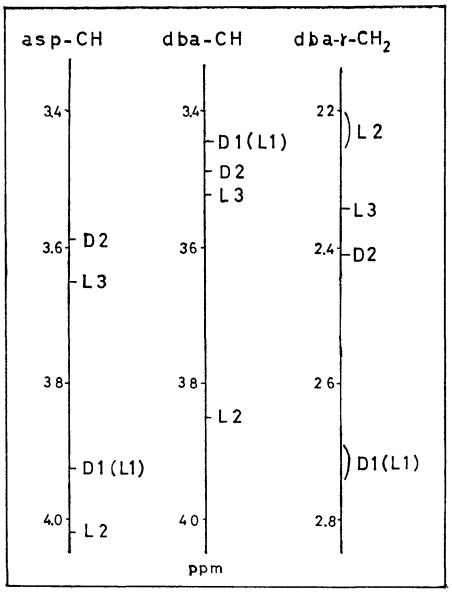

Fig. 4. The distribution of the proton chemical shifts of the [Co(L- or D-asp)(L-2,4-dba)] isomers.

resonance in all of the four spectra should be assigned to the methine proton of aspartic acid and the peak at *ca.* 2.8 to the methylene protons of aspartic acid. Chemical shifts of D1, D2, L2 and L3 are shown in Fig. 4.

The proton resonance peaks of the α-proton of the coordinated asp can be classified into two groups, as can also the chemical shifts of the α-proton and γ-protons of the L-2,4-dba. Although molecular model consideration suggests that the asp and L-2,4-dba coordinated may take several types of conformation, the direction of the C–H bond of α-carbon of both ligands does not seem to change. On the other hand, the difference in conformation of the six-membered chelate ring of L-2,4-dba coordinated seriously affects the orientation of the C–H bonds of γ-carbon, which may give rise to some change in the chemical shifts of γ-carbon protons. As a whole the PMR spectrum of D2 resembles that of L3 (Fig. 3) suggesting that the origin which differentiates the chemical shifts of the α-carbon protons of L-2,4-dba and L- or D-asp into the two magnetic field regions can be ascribed to the effects of the other ligands present, and not to the conformational changes of its own. The bicyclo chelate ring system formed by the coordination of each ligand is common in all six isomers. Because of the identical chelate ring systems, the coupling constant scheme between the eight carbon protons ($OOC-CH_2-\underset{|}{C}HCOO$ and $H_2N\underset{|}{C}H_2-CH_2-CHCOO$) in
NH_2 NH_2
each ligand ring system may be closely resemble each other in the six cases. The geometrical isomers would then reveal themselves mostly in different chemical shifts of the eight carbon-bounded protons in individual cases of the same asp and L-2,4-dba. Different spectra for L2 and L3 and, for D1 and D2 have virtually been observed. For the sake of convenience the three coordination sites occupied by L- or D-asp, situated opposite to the fixed L-2,4-dba, are numbered as indicated

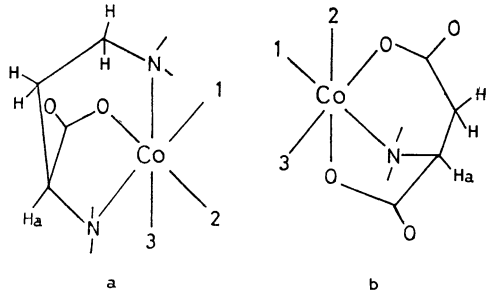

Fig. 5. The relation of the Ha proton chemical shifts and the sites of the other ligand.

in Fig. 5a. For the D2 and L3 isomers the three sites in the order 1,2,3 of the L-2,4-dba are occupied by oxygen, nitrogen and oxygen atoms, respectively (Fig. 5a), while those of the asp are occupied by oxygen, nitrogen and nitrogen atoms, respectively (Fig. 5b). The chemical shift of Ha proton of L-2,4-dba (Fig. 5a) is affected by:[9] 1) the polarity of the amine group due to the polarization of the metal ion induced by the ligand atom of site 1, 2) that of the carboxylate group due to the polarization of the metal ion induced by the ligand atom of site 2, and 3) magnetic anisotropic effects due to site 3. When the chemical shifts of the α-carbon proton of the L-2,4-dba of the complex D2 and L3 are governed by 1), the O atom which occupies site 1 gives rise to a higher field shift of the α-carbon proton of the L-2,4-dba. If this relation holds in the other cases (that is, whenever the O atom occupies site 1 (Fig. 5a), the α-carbon proton adjacent to the N atom *trans* to site 1 resonates at a higher field than when N atom occupies it), the chemical shift of the α-carbon proton of the L-2,4-dba of the D1 isomer which also lies in the higher field suggests that site 1 of D1 is occupied by the O atom. Thus, the isomer is assigned to D-*cis*O_5 *cis*N_5 configuration. The chemical shift of the α-carbon proton of the L-2,4-dba of the L2 isomer which lies in the lower field causes the isomer to be assigned to the L-*cis*O_5 *trans*N_5 configuration, as well. The chemical shift of the α-carbon proton of the L- or D-asp of the L3 and D2 isomer belongs to the higher field group, and site 1 corresponding to these protons should be occupied by the O atom. The chemical shift of the α-carbon proton of the D- or L-asp of the D1 and L2 isomers lies in the lower field, which indicates that site 1 corresponding to these protons is certainly occupied by the N atom. A similar relationship between the chemical shift of the γ-carbon protons of the L-2,4-dba and the atom of the site 1 holds as well (Fig. 4). The relation between PMR chemical shifts of each isomer and the corresponding atom in site 1 is given in Table 1. In the case of sites 2 and 3 no simple explanation for the distinct classification of chemical shifts into two categories of magnetic field region can be given. Thus situation 1) seems to influence the chemical shifts in this case most favorably. The above consideration is in line with the study by Buckingham *et al.*[10] and Clifton and Pratt[11] for pentaammine cobalt(III) complexes $[Co(NH_3)_5X]^{n+}$. The PMR spectra of this series show two NH_3 reso-

TABLE 1. RELATIONSHIP BETWEEN CARBON PROTONS OF EACH ISOMER AND THE ATOM OCCUPYING THE CORRESPONDING SITE 1

	asp-CH	dba-CH	dba-γ-CH_2
D-*cis*O_5*cis*-N_5	N	O	N
D-*fac*	O	O	O
D-*trans*O_5*trans*N_5	N	N	O
L-*trans*O_5*cis*N_5	N	O	N
L-*fac*	O	O	O
L-*cis*O_5*trans*N_5	N	N	O

nances with a 12 : 3 intensity ratio, the intense band being in the lower field. The 12 equivalent protons belong to the NH_3 groups *cis* to the ligand X and the 3 to the *trans* NH_3 group. Clifton and Pratt[11] suggested that the *cis* protons may have been shifted to a lower field than the *trans*, since the polarity of the *trans* ammine group from the metal ion was reduced by ligand X. Our results are regarded as an extension of the above consideration on the reduced polarity of ammine nitrogen atom to that of the carbon proton adjacent to the ammine group. In order to ascertain whether the method of assignment holds for other complex systems or not, the chemical shifts of the PMR spectra of the $[Co(L\text{-asp})_2]^-$,[4] $[Co(L\text{-asp})(ida)]^-$ [12] and $[Co(L\text{-2,4-dba})_2]^+$ complexes (Fig. 6) were investigated. The PMR spectra of the $[Co(L\text{-2,3-dpa})_2]^+$ complexes were similar to those of the $[Co(L\text{-2,4-dba})_2]^+$ complexes except for the peaks due to the β-carbon protons of the L-2,4-dba. The atom (O or N) in parentheses is the atom occupying site 1 (Fig. 6). Since the chemical shift of the γ-carbon protons of the L-2,4-dba coordinated was not distinct, the whole peaks are shown. The geometry of the F isomer of the $[Co(L\text{-asp})_2]^-$ was *trans* N on the basis of the absorption spectrum. The S and L isomers have *cis* N geometries. The chemical shift of the α-carbon proton of L-asp of the F isomer lies in the lower field, which is in line with the fact that site 1 of this complex is occupied by the N atom. The chemical shift of α-carbon protons of the L-asp of the S and L isomers lies in a higher field in accordance with the fact that their site 1 was occupied by oxygen atom. This agrees with the trend found here. The same situation holds in the case of the $[Co(L\text{-asp})(ida)]^-$ isomers. However the two *cis* N isomres cannot be distinguished from each other. In the $[Co(L\text{-2,4-dba})_2]^+$ complexes, each isomer has been assigned by comparing the PMR spectra of $[Co(L\text{-2,4-dba})_2]^+$ with those of $[Co(L\text{-2,3-dpa})_2]^+$, assignments of which were based on X-ray analysis. The α isomer of the complex $[Co(L\text{-2,4-dba})_2]^+$ has the *trans*O geometry and the β and γ isomers the *cis*O geometries. It has not been possible to assign the two *cis*O isomers so far to the *cis,trans,cis* (the isomers were named by considering the spatial relationship of first the two donor oxygens, then the two α-nitrogens, and finally the two γ nitrogens.) or the *cis,cis,trans* geometries without using the analogies of the PMR spectra of the corresponding complexes $[Co(L\text{-2,3-dpa})_2]^+$. Applying the trend we found to this system, we find that since α-proton of the L-2,4-dba of the γ-isomer resonates in a higher field and that of α and β isomers in a lower field, site 1 of the γ isomer should be occupied by an O atom and that of α and of β by N atoms. The same relationship holds between the γ-protons of L-2,4-dba and the corresponding site 1. We can thus assign the β and γ isomers to the *cis,trans,cis* and *cis,cis,trans* geometries respectively. These assignments agree well with the result by Freeman and Liu.[1] For the $[Co(N)_4(O)_2]$ systems, the two *cis*O isomers can be distinguished by comparing their PMR spectra. For the $[Co(N)_3(O)_3]$ system the two meridional isomers are also distinguishable.

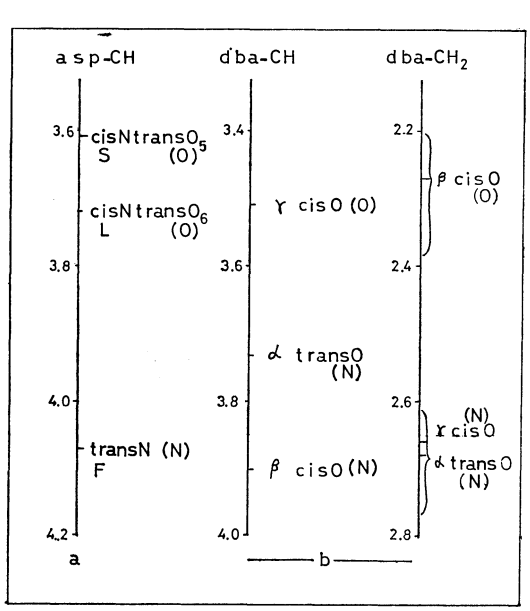

Fig. 6. The distribution of the chemical shifts of the $[Co(L\text{-asp})_2]^-$ isomers (F=first elute, S=second elute, L=last elute) and the $[Co(L\text{-2,4-dba})_2]^+$ (α= first elute, β=second elute, γ=last elute).

The authors wish to thank Drs. M. Saburi and S. Yano for helpful discussions and K. Shimada for measurement of the PMR spectra.

References

1) W. A. Freeman and C. F. Liu, *Inorg. Chem.*, **9**, 1191 (1970).
2) W. A. Freeman and C. F. Liu, *ibid.*, **7**, 764 (1968).
3) S. Yamada, J. Hidaka, and B. E. Douglas, *ibid.*, **10**, 2187 (1971).
4) L. R. Froebe, S. Yamada, J. Hidaka, and B. E. Douglas, *J. Coord. Chem.*, **1**, 183 (1971).
5) L. J. Zompa, *Chem. Commun.*, **1969**, 783.
6) C. F. Liu and J. A. Ibers, *Inorg. Chem.*, **8**, 1911 (1969).
7) J. I. Legg and J. A. Neal, *ibid.*, **12**, 1805 (1973).
8) The Society of Synthetic Organic Chemistry, "Yukikagobutzugoseiho," Vol 5, Gihodo, Tokyo (1968), p. 45.
9) C. J. Hawkins, "Absolute Configuration of Metal complexes," Wiley-Interscience (1971), p. 257.
10) D. A. Buckingham, I. I. Olsen, and A. M. Sargeson, *Aust. J. Chem.*, **20**, 597 (1967).
11) P. Clifton and L. Pratt, *Proc. Chem. Soc.*, **1963**, 339.
12) J. Hidaka, S. Yamada, and B. E. Douglas, *J. Coord. Chem.*, **2**, 123 (1972).

Ionic Equilibria in Mixed Solvents. XI. A Critical Survey of Hydroxo Complexes of Beryllium in Aqueous and Aqueous Mixed Solvents

Hitoshi TSUKUDA, Takayoshi KAWAI, Masunobu MAEDA, and Hitoshi OHTAKI[1)]

Department of Electrochemistry, Tokyo Institute of Technology, O-okayama, Meguro, Tokyo 152

(Received December 4, 1974)

Hydrolytic reactions of beryllium ion were studied in water–methanol, water–ethanol, and water–acetone mixtures, 0.2 mole fraction of an organic component being contained. In all the solutions containing 3M $LiClO_4$ as an ionic medium at 25 °C, we found the Be_2OH^{3+}, $Be_2(OH)_2^{2+}$, $Be_3(OH)_3^{3+}$, and $Be(OH)_2$ complexes. However, in a supplementary work in a 3M $LiClO_4$ aqueous medium in which the solution had been equilibrated with precipitates of beryllium hydroxide and the supernatant was subjected to titration, we found $Be_6(OH)_8^{4+}$ instead of $Be(OH)_2$. From a very slow equilibrium observed in the high pH region, we concluded that the $Be(OH)_2$ complex formed by the addition of an alkaline solution gradually polymerizes to $Be_6(OH)_8^{4+}$ by releasing some OH^- ions. Through these observations a critical survey is described for the species reported by various authors. The solvent effect on the formation constants of hydroxo complexes is also discussed.

According to simple electrostatic theories, an equilibrium constant of a non-isoelectric reaction such as the dissociation of a neutral acid molecule and the hydrolysis of a metal ion might be affected by the dielectric constant of a solvent. However, studies of hydrolytic reactions of beryllium,[2,3)] copper,[4,5)] nickel,[6)] and aluminium[7)] ions in various aqueous dioxane solutions revealed that formation constants of the complexes were very insensitive to the solvent composition over a relatively wide range of the dioxane concentration, 0—85% w/w, in contrast with dissociation constants of carboxylic acids and phenols.[8,9)]

In a reaction in which protons or hydroxide ions are liberated, the acid-base property of a solvent might also contribute to the equilibrium of the reaction beside the dielectric constant and the concentration of water in the solvent. Since studies carried out so far in this series of metal hydrolysis were restricted to aqueous dioxane solutions, we undertake to examine the effect of changing the solvent component on the hydrolysis equilibrium of a metal ion. In the present work we use water–methanol, water–ethanol, and water–acetone mixtures in which 0.2 mole fraction of an organic solvent is contained. The beryllium ion is chosen as an example.

Experimental

Reagents. The methods of preparation and purification of the chemicals used were the same as those described previously.[2,3)] Methanol, ethanol, and acetone (reagent grade) were distilled twice. The solvent mixtures contained 0.2 mole fraction of an organic component, *i.e.*, 30.77% w/w methanol, 38.99% w/w ethanol, and 44.62% w/w acetone, respectively.

Apparatus. Beckman glass electrodes Nos. 40495 and 40498 were used in combination with a silver-silver chloride electrode which was set in an improved type of the "Wilhelm" half-cell (see Fig. 1). An Orion Digital pH Meter 801 was used for emf measurements. A Metrohm *E 211 A* type coulometer was employed as a current source after the current indicator was calibrated with a Yokogawa Decade Resistance Box 2786 as a standard resistance. The method of emf measurements was essentially the same as that in the previous studies.[2,3)]

Results

The plots of Z (average number of hydrogen ions set free per beryllium atom) against $-\log h$ (h denotes the concentration of hydrogen ion at equilibrium) were shown in Figs. 2—4. The concentration of free beryllium ion b was calculated according to the equation[10)]

$$\ln b = \ln B + \int_{\infty}^{\ln h}\left[Z+\left(\frac{\partial Z}{\partial \ln B}\right)_h\right]\mathrm{d}\ln h \qquad (1)$$

where B denotes the total concentration of beryllium ion in solution. The calculation was carried out on the basis of the data in Figs. 2—4 assuming $\int_{\infty}^{-2.0}[2.303Z+(\partial Z/\partial \log B)_h]\,\mathrm{d}\log h=0$.

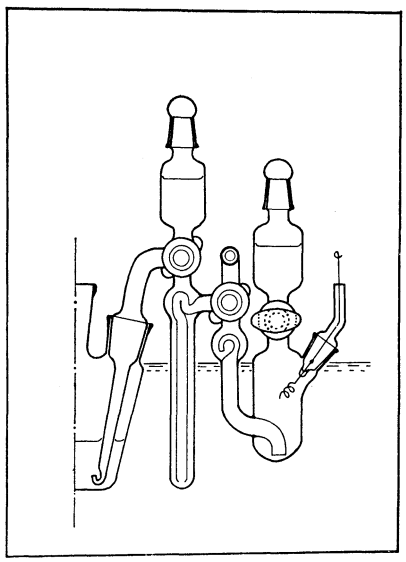

Fig. 1. Cell with silver-silver chloride electrode, salt bridge and titration vessel.

Application of the core-links hypothesis[11)] and calculations of the average numbers of metal and hydroxyl ions in complexes, $\bar{p}$ and $\bar{q}$, respectively, showed that the main product of the reaction was $Be_3(OH)_3^{3+}$. Minor components formed in the lower pH range were estimated by computer calculations.

The plot of $(BZ—3*\beta_{3,3}b^3h^{-3})/2bh^{-2}$ against b in a high pH range gave a straight line independent of the total concentration of beryllium. This shows the formation of the $Be_2(OH)_2^{2+}$ and $Be(OH)_2$ complexes.

Computer calculations also supported the formation

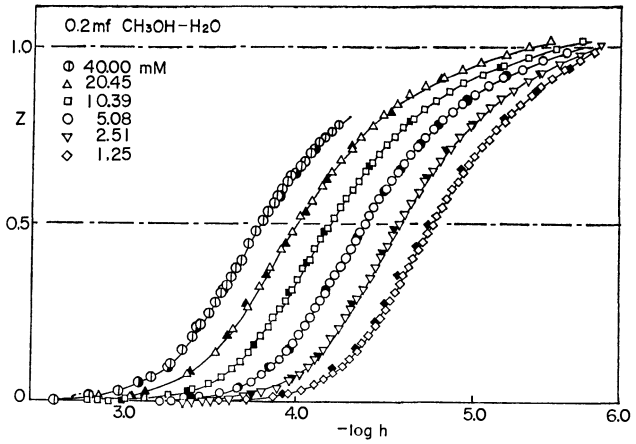

Fig. 2. Z as a function of $-\log h$ in 0.2 mole fraction methanol-water mixture.
Points with open symbols were obtained by forward titrations and points with black symbols, by back titrations. Drawn curves were calculated with the final values of the formation constants listed in Table 4.

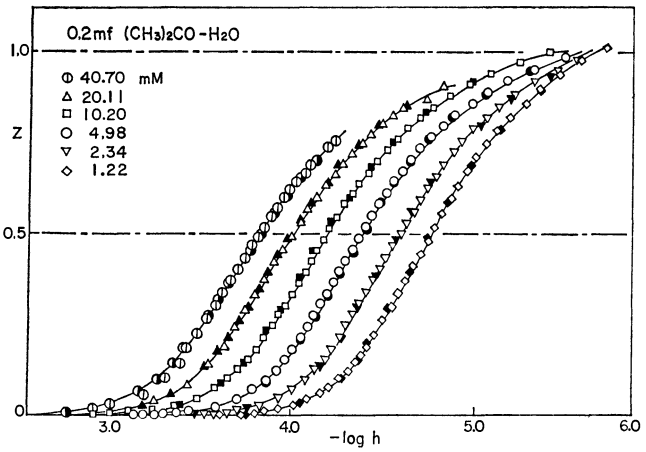

Fig. 4. Z as a function of $-\log h$ in 0.2 mole fraction acetone-water mixture.
The symbols are the same as those in Fig. 2. Drawn curves were calculated with the values of the formation constants listed in Table 4.

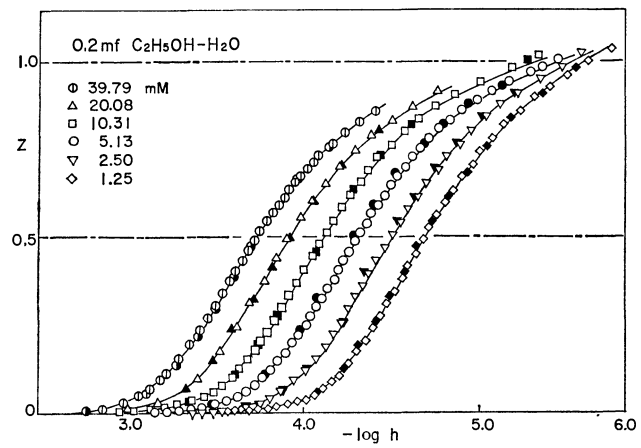

Fig. 3. Z as a function of $-\log h$ in 0.2 mol fraction ethanol-water mixture.
The symbols are the same as those in Fig. 2. Drawn curves were calculated with the values of the formation constants listed in Table 4.

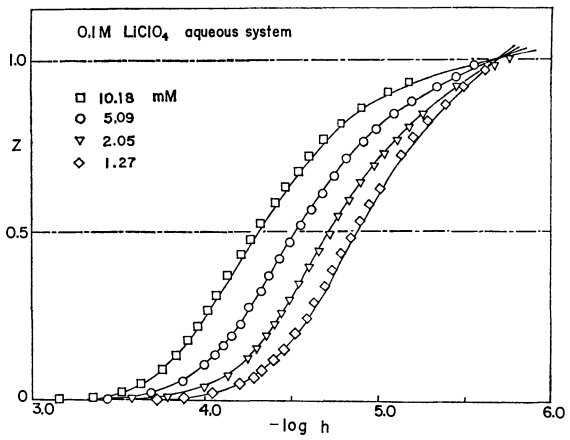

Fig. 5. Z as a function of $-\log h$ in a 0.1 M $LiClO_4$ aqueous solution.
Only the points obtained by forward titrations are shown. Drawn curves were calculated with the values of the formation constants given in Table 5.

Table 1. The error-square sums (U) and the formation constants ($-\log {}^*\beta_{p,q}$) in 0.2 mol fraction methanol-water mixture

$BeOH^+$	Be_2OH^{3+}	$Be(OH)_2$	$Be_2(OH)_2^{2+}$	$Be_3(OH)_3^{3+}$	$Be_3(OH)_4^{2+}$	$Be_6(OH)_8^{4+}$	$U\times10^3$
—	3.52	11.39	7.35	8.54	—	—	3.57
7.44	3.51	11.39	7.34	8.54	—	—	3.58
—	—	11.41	7.22	8.58	—	—	5.67
6.26	—	11.41	7.32	8.57	—	—	5.98
—	3.25	11.33	—	8.46	—	—	7.88
—	3.20	—	—	8.46	14.83	—	10.5
—	3.24	11.46	—	8.46	15.30	—	8.07
—	3.30	—	7.54	8.51	14.82	—	6.26
—	3.24	—	—	8.45	—	26.19	20.5

of these complexes. In Tables 1—3 the results of the calculations of minimum error-square sums are summarized, where $U=\Sigma(Z_{calc}-Z)^2$ and the formation constants in the tables are given as $\log {}^*\beta_{p,q}=\log [Be_q(OH)_p{}^{(2q-p)+}][H^+]^p/[Be^{2+}]^q$.

The final values of the formation constants proposed are tabulated in Table 4, together with those in the aqueous dioxane solution.[2]

A similar experiment was carried out in a 0.1 M $LiClO_4$ aqueous solution. Analysis of the data (see

Table 2. The error square-sums (U) and the formation constants ($-\log {}^*\beta_{p,q}$) in 0.2 mole fraction ethanol–water mixture

$BeOH^+$	Be_2OH^{3+}	$Be(OH)_2$	$Be_2(OH)_2^{2+}$	$Be_3(OH)_3^{3+}$	$Be_3(OH)_4^{2+}$	$Be_6(OH)_8^{4+}$	$U\times10^2$
—	3.39	11.12	7.13	8.31	—	—	0.862
6.41	3.22	11.09	7.50	8.27	—	—	1.17
—	—	11.15	6.97	8.37	—	—	1.09
6.26	—	11.14	7.07	8.35	—	—	1.16
—	3.14	11.06	—	8.23	—	—	1.43
—	3.07	—	—	8.23	14.35	—	1.52
—	3.08	11.45	—	8.23	14.53	—	1.38
—	3.09	—	7.50	8.26	14.33	—	1.13
—	3.13	—	—	8.22	—	25.22	2.66

Table 3. The error square-sums (U) and the formation constants ($-\log {}^*\beta_{p,q}$) in 0.2 mole fraction acetone–water mixture

$BeOH^+$	Be_2OH^{3+}	$Be(OH)_2$	$Be_2(OH)_2^{2+}$	$Be_3(OH)_3^{3+}$	$Be_3(OH)_4^{2+}$	$Be_6(OH)_8^{4+}$	$U\times10^2$
—	3.28	11.24	7.21	8.58	—	—	1.41
8.11	3.30	11.23	7.23	8.57	—	—	1.35
—	—	11.27	7.02	8.67	—	—	1.63
5.64	—	11.25	7.51	8.59	—	—	2.37
—	3.06	11.17	—	8.47	—	—	2.50
—	3.01	—	—	8.47	14.62	—	3.03
—	3.00	11.42	—	8.47	14.92	—	2.61
—	3.07	—	7.42	8.53	14.63	—	2.04
—	3.01	—	—	8.45	—	25.90	5.27

Table 4. The formation constants ($-\log {}^*\beta_{p,q}$) of the hydrolytic reactions of beryllium ions in 0.2 mole fraction methanol, ethanol, acetone, and dioxane-water mixtures[a]

	$BeOH^+$	Be_2OH^{3+}	$Be(OH)_2$	$Be_2(OH)_2^{2+}$	$Be_3(OH)_3^{3+}$
Methanol-water	—	3.50±0.05	11.38±0.03	7.35±0.02	8.541±0.002
Ethanol-water	—	3.39±0.06	11.12±0.04	7.13±0.03	8.310±0.002
Acetone-water	≳8	3.28±0.05	11.24±0.04	7.22±0.02	8.578±0.004
Dioxane-water	≳6.0	3.64±0.05	10.76±0.03	7.11±0.02	8.763±0.005

a) The uncertainties of the formation constants were estimated by multiplying by three the standard deviations.

Table 5. The formation constants ($-\log {}^*\beta_{p,q}$) of the hydrolytic reactions of beryllium ions in aqueous solutions containing various ionic media at 25 °C

	BeOH	Be_2OH^{3+}	$Be(OH)_2$	$Be_2(OH)_2^{2+}$	$Be_3(OH)_3^{3+}$	$Be_3(OH)_4^{2+}$	$Be_6(OH)_8^{4+}$	$Be_6(OH)_9^{3+}$
1 *m* $NaCl$[13]	—	3.42± 0.07	—	—	8.907± 0.007	—	27.46± 0.03	—
2 M KNO_3[14]	—	3.28	—	—	8.900	16.0	27.5	34.5
3 M $NaClO_4$[12]	—	3.24± 0.02	10.9± 0.2	—	8.66± 0.03	—	—	—
3 M $NaClO_4$ (60 °C)[20]	—	2.9± 0.2	—	6.25± 0.05	7.7± 0.1	13.22± 0.15	—	—
3 M $LiClO_4$[3]	≳5.4	3.27± 0.10	11.5± 0.5	—	8.74± 0.05	—	—	—
3 M $LiClO_4$ (this work)	—	3.04± 0.03	—	—	8.671± 0.002	—	27.337± 0.006	—
0.1 M $LiClO_4$ (this work)	≳6.3	3.32± 0.14	11.35± 0.06	—	8.807± 0.005	—	—	—

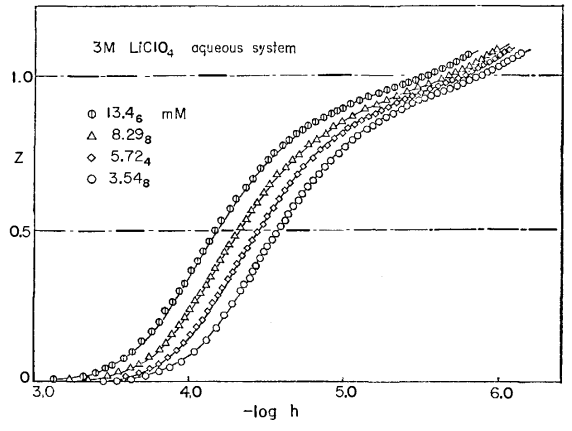

Fig. 6. Z as a function of $-\log h$ in a 3 M $LiClO_4$ aqueous solution.
Only the points obtained by back titrations are shown.
Drawn curves were calculated with the values of the formation constants given in Table 5.

Fig. 5) led to a conclusion of the formation of Be_2OH^{3+}, $Be_3(OH)_3^{3+}$, $Be(OH)_2$, and probably $BeOH^+$. The formation constants obtained are listed in Table 5.

Discussion

In 1967 Mesmer and Baes[13] proposed $Be_5(OH)_7^{3+}$ or $Be_6(OH)_8^{4+}$ instead of $Be(OH)_2$ in 1 *m* NaCl solution at 25 °C. The $Be_6(OH)_8^{4+}$ complex was also found by Lanza and Carpéni.[14] Recently Baes and Mesmer[15] critically reviewed studies on the hydrolysis of beryllium ion and pointed out that the formation constant of $Be(OH)_2$ cannot be so large as reported previously[3,12,16] as long as the solubility data by Gilbert and Garrett[17] and by Schindler and Garrett[18] are accepted. The formation constant of $Be(OH)_2$ determined by means of solvent extraction was $\log {}^*\beta_{2,1} = -13.65$[19], which was consistent with the value expected from the solubility product of $Be(OH)_2$.[17,18] The $Be_2(OH)_2^{2+}$ was not detected by these authors.

Ciavatta and Grimaldi[20] also denied the formation of $Be(OH)_2$ in aqueous solution at an elevated temperature (60 °C) and proposed $Be_3(OH)_4^{2+}$ and $Be_2(OH)_2^{2+}$, together with the main product $Be_3(OH)_3^{3+}$.

In spite of negative conclusions for the formation of $Be(OH)_2$ by some authors, our data could still be well explained in terms of the formation of $Be_2(OH)_2^{2+}$ and $Be(OH)_2$ at a relatively high pH. In order to elucidate the reasons of the diverse conclusions for the minor components at a high pH, we carried out supplementary titrations in a 3 M $LiClO_4$ aqueous medium in which titration procedures were slightly modified.

Test solutions were prepared as follows: pH of a beryllium perchlorate solution (the total concentration of the perchlorate ion was kept constant at 3 M) was increased by reduction of hydrogen ions by electrolysis until beryllium hydroxide precipitated. The solution was left to stand for several days under a nitrogen atmosphere while agitating and the supernatant was subjected to titration by coulometric generation of hydrogen ions. The reverse titration was also performed by alkalifying the solution after the preceding titration over the same pH range. In titrations in which pH decreased (open symbols in Fig. 6) a rapid equilibrium was attained at each point of measurements. On the other hand, a very slow equilibrium was observed at a high pH in the reverse titration (pH of the solution increased), and the emf changed slowly in such a manner that pH increased. It took 10—12 hr until an emf in a reverse titration fell on the titration curve obtained by the preceding titration. The results shown in Fig. 6 were explained in terms of the formation of Be_2OH^{3+}, $Be_3(OH)_3^{3+}$, and $Be_6(OH)_8^{4+}$. Replacement of $Be_6(OH)_8^{4+}$ by any of $Be(OH)_2$, $Be_2(OH)_2^{2+}$, and $Be_3(OH)_4^{2+}$ did not improve values of the error-square sum. Addition of any of these complexes to the set of Be_2OH^{3+}, $Be_3(OH)_3^{3+}$, and $Be_6(OH)_8^{4+}$ did not decrease the error-square sum. The formation of $BeOH^+$ was not conclusive. The final values of the formation constants are tabulated in Table 5, along with values reported by previous authors.

From these observations and the results obtained previously by other workers, we conclude that the $Be(OH)_2$ complex readily formed by the addition of hydroxyl ions is an "over-saturated" species and slowly changes to a polymerized species by releasing some hydroxide ions. The polymerization reaction progresses so slowly that the $Be(OH)_2$ complex is recognized as an equilibrium species in the pH range studied when titrations are carried out with an ordinary speed. Although the equilibrium species at a high pH where $Be(OH)_2$ is detected is expected to be $Be_6(OH)_8^{4+}$ as shown in Table 5, the doubt that the $Be_6(OH)_8^{4+}$ complex could be another intermediate species in the polymerization reaction may hardly be dispelled yet in the present stage of investigation.

Since many hydrolytic reactions proceed very slowly (*e.g.*, as seen in aluminium, iron (III), and even in cadmium[21]), rapid titrations may sometimes cause erroneous conclusions. In order to give a complete scope of hydrolysis equilibria of a metal ion, knowledge of reaction kinetics of slow processes as well as precipitation equilibria and hydrolysis equilibria at low concentrations of the metal ions (where only mononuclear complexes are formed) must be needed.

Although some of the complexes listed in Tables 4 and 5 may not be equilibrium species, the $Be_3(OH)_3^{3+}$ is no doubt the main product and an equilibrium species of the hydrolytic reaction of beryllium ion. The formation constant of the complex practically remained unchanged when an aqueous solvent is replaced with an aqueous organic mixture containing various concentrations of an organic solvent. The change of the organic component in the mixture was also insensitive to the formation constant.

It is widely accepted that the equilibrium constant of an association reaction of a positive and a negative ions increases with an increase in the concentration of an organic solvent in aqueous mixtures. In an isoelectric reaction such as an association reaction of a proton and a neutral molecule, on the other hand, the equilibrium constant is decreased and then steeply increased after passing through a minimum. The

change of the equilibrium constant was accounted for in terms of the medium effect on protons which are distributed in water and organic solvent molecules through the solvation equilibrium.[22] In a non-isoelectric reaction of the hydrolytic reaction of beryllium ion,

$$3Be^{2+} + 3H_2O = Be_3(OH)_3^{3+} + 3H^+$$

as well as those of other metal ions, the free energy change of transfer of three moles of Be^{2+} ion from the aqueous phase to a mixture may not be completely compensated for the sum of the free energy changes of transfer of one mole of $Be_3(OH)_3^{3+}$ and three moles of protons from the mixture to the aqueous phase. The rest of the free energy changes may be further cancelled with the medium effect of protons.

We can rewrite the formation constant of a beryllium hydroxo complex ${}^*\beta_{p,q}$ to $\beta_{p,q}$ as follows:

$$\beta_{p,q} = [Be_q(OH)_p^{(2q-p)+}]/[Be^{2+}]^q[OH^-]^p = {}^*\beta_{p,q}/K_1^p \quad (2)$$

Here K_1 denotes the autoprotolysis constant of a solvent mixture of a constant ionic medium

$$K_1 = [H^+][OH^-] \quad (3)$$

The values of K_1 in the mixed solvents were determined as 14.128 ± 0.003 mol^2 l^{-2} (in 0.2 mole fraction methanol–water mixture) and 14.396 ± 0.008 mol^2 l^{-2} (in 0.2 mole fraction ethanol–water mixture).[23] In the acetone-system K_1 was not determined due to unstable emf's. Acetone may be reduced with hydrogen according to the following equilibrium.[24,25]

$$(CH_3)_2CO + H_2 = (CH_3)_2CH_2O$$

By insertion of the values of K_t into Eq. (2) we see the changes of $\beta_{p,q}$ with the solvent composition. The formation constant $\beta_{p,q}$ markedly increased with the increase in the concentration of an organic solvent from 0 to 0.2 mole fraction. The fact showed that the association reaction

$$qBe^{2+} + pOH^- = Be_q(OH)_p^{(2q-p)+} \quad (4)$$

is subjected to the solvent effect essentially similar to that in the usual ionic association reaction and that the free energy changes due to the distribution of a proton to water and organic solvent molecules must be taken into account as well as the free energy changes of species in the reaction in order to interprete the variation of equilibrium constants with varying solvent compositions.

References

1) To whom correspondence should be addressed.
2) H. Ohtaki, *Inorg. Chem.*, **6**, 808 (1967).
3) H. Ohtaki and H. Kato, *ibid.*, **6**, 1935 (1967).
4) H. Ohtaki, *ibid.*, **7**, 1205 (1968).
5) H. Ohtaki and T. Kawai, This Bulletin, **45**, 1735 (1972).
6) T. Kawai, H. Otsuka, and H. Ohtaki, *ibid.*, **46**, 3753 (1973).
7) H. Ohtaki, *ibid.*, **43**, 2463 (1970).
8) H. Ohtaki, *ibid.*, **42**, 1573 (1969).
9) M. Yasuda, *ibid.*, **32**, 429 (1959).
10) L. G. Sillén, *Acta Chem. Scand.*, **15**, 1981 (1961).
11) L. G. Sillén, *ibid.*, **8**, 299, 318 (1954).
12) H. Kakihana and L. G. Sillén, *ibid.*, **10**, 985 (1956).
13) R. E. Mesmer and C. F. Baes, Jr., *Inorg. Chem.*, **6**, 1951 (1967).
14) E. Lanza and G. Carpéni, *Electrochim. Acta*, **13**, 519 (1968).
15) C. F. Baes, Jr. and R. E. Mesmer, "The Hydrolysis of Cations," Oak Ridge National Laboratory, ORNL-NSF-EATC-3 (1974).
16) S. Hietanen and L. G. Sillén, *Acta Chem. Scand.*, **18**, 1015 (1964).
17) R. A. Gilbert and A. B. Garrett, *J. Amer. Chem. Soc.*, **78**, 5501 (1956).
18) P. Schindler and A. B. Garrett, *Helv. Chim. Acta*, **43**, 2176 (1960).
19) R. W. Green and P. W. Alexander, *Austr. J. Chem.*, **18**, 651 (1965).
20) L. Ciavatta and M. Glimaldi, *Gazzetta Chim. Italiana*, **103**, 731 (1973).
21) H. Matsui and H. Ohtaki, This Bulletin, **47**, 2603 (1974).
22) H. Ohtaki, *ibid.*, **42**, 1573 (1969).
23) The method for determination of the autoprotolysis constants of the aqueous organic mixtures containing 3M $LiClO_4$ will be described elsewhere.
24) G. S. Parks and K. K. Kelley, *J. Phys. Chem.*, **32**, 740 (1928).
25) A. Farkas and L. Farkas, *J. Amer. Chem. Soc.*, **61**, 1336 (1939).

Isomerization of Heptanes over a Palladium-Zeolite Catalyst

Tomoya SAKAI, Masafumi GOTO, Kei-ichiro HATANO, and Manjiro KATO

Faculty of Pharmaceutical Sciences, Nagoya City University, Tanabe-dori, Mizuho-ku, Nagoya 467

(Received October 1, 1974)

The isomerization of heptane isomers, heptane, 2- and 3-methylhexane, 3-ethylpentane, and 2,3- and 2,4-dimethylpentane, was investigated kinetically over a palladium-zeolite catalyst in the presence of hydrogen at 280—350 °C. First-order rate constants of 11 reaction paths were given with their activation energies and pre-exponential factors. The reaction scheme network including 22 isomerization steps among 9 isomers was constructed through the detailed analysis of primary and secondary reaction products from the individual isomers. Finally, the several proposed isomerization mechanisms were examined on the basis of the present experimental results.

The skeletal isomerization of paraffinic hydrocarbons has been extensively studied over the so-called dual functional catalysts.[1-4] The mechanism has been explained as follows: dehydrogenation of paraffins and hydrogenation of isomerized olefins take place on the metallic site and the formation of carbonium ions from olefins and their rearrangements do on the acidic site. However, the isomerization of butane was discovered by Anderson and Avery[5] to occur on the evaporated film of platinum metal. Boudart and Ptak[6] have reported the isomerization of neopentane to occur on the metal surface of platinum, iridium and gold supported on alumina. Corolleur *et al.*[7] have insisted that the isomerization of hexanes takes place exclusively on the metal site of platinum–alumina, although the intermediate postulated by them differs from that by Anderson and Avery.[5] On the structure of the intermediate, it was proposed recently by Lanewala *et al.*[8,9] that hexane isomerized *via* adsorbed dimeric intermediate on a palladium–zeolite catalyst.

Only a few reports,[10,11] however, have been reported on the isomerization mechanism of heptane isomers. Numbers of isomers may make the system complicated, but the informations therefrom will be plenty. The first aim of the present study is to clarify the detailed reaction paths of heptane isomerization on the palladium–zeolite catalyst through the detailed analysis of the products as well as the kinetic examinations of their formations. The second aim is to select the reasonable mechanism among the several proposed mechanisms on the basis that it should not conflict with the obtained results in the present study.

Experimental

Commercially available *n*-heptane (HP; 99.9 mol%), 2-methylhexane (2MHX; 99.4), 3-ethylpentane (3EP; 99.2), 2,4-dimethylpentane (24 DMP; 99.4), 2,3-dimethylpentane (23DMP; 94.7), and 3-methylhexane (3MHX; 96.5) were used without further purifications. Palladium-zeolite catalyst was prepared from Pd(II) tetraammine chloride and Na–13Y zeolite in the aquatic solution by an ion exchange technique.[12] The amount of palladium metal was 3.0 wt%. The Cl ion free dried catalyst sieved 10 to 20 mesh was calcined in the air at 400 °C for 4 hr, followed by the reduction in the dried and deoxygenated hydrogen stream at 500 °C for 6 hr. Thus the composition of the catalyst is expected to be mostly a metallic palladium on H–Y zeolite, although the X-ray diffraction pattern for metallic palladium was not so clearly obtained.

Experiments were conducted by use of two different reaction apparatus. The one was an usual continuous flow-type apparatus. The reactor was made of a pyrex glass tube (18 mm i.d.) furnished with a co-axial thermowell (8 mm o.d.), in which 2.5 g (apparent volume, 5 ml) of the unreduced catalyst was packed. After the reduction of the catalyst, the temperature was settled to begin the isomerization reaction by passing the hydrogen stream through a reactant container which was dipped in an ice–water bath. The concentration of the reactant was maintained at 1.0 mol%. Variations on the concentration were attained by controlling the streaming ratio of hydrogen through the reactant container. The hydrogen pressure was maintained at 770 mmHg. The space velocities* were between 0.2 and 5.0 s^{-1}. The reaction products were analyzed by glc equipped with a flame ionization detector and a capillary column coated with squalane.

The other apparatus was of a conventional micro pulse reactor which was linked directly to a glc equipped with a thermal conductivity detector and a packed column containing dioctylphthalate on celite-545. A small amount (0.25 g) of the unreduced catalyst was placed at the bottom of a U-shaped pyrex tube of 5 mm i.d., then it was reduced. Hydrogen pressure was maintained at 1400 mmHg. Mostly 2.0 μl of the reactant were injected in each run by a microsyringe into the preheated hydrogen stream.

Results

Isomerization of HP and 3MHX with the Continuous Flow-type Apparatus. The experimental results were listed in Table 1. The isomerization of HP was effectively catalyzed on the palladium–zeolite catalyst above 280 °C. The predominant products were 2MHX and 3MHX. The hydrogenolysis products were very small in their amounts. The selectivity for isomerization was found to exceed 97% even at the most severe condition. Among minor isomerized products, 3EP and 23DMP were formed in distinct amounts from the early stage of the reaction.

In the case of 3MHX feed, the predominant products were 2MHX, 3EP, 23DMP, and HP.

Table 2 shows the resulted conversions in the case of HP isomerization at 305 °C by varying the reactant concentration between 0.6 and 2.0 mol%. The invariance of conversion confirms the first-order rate

* The space velocity was defined as the ratio of the volumetric rate of inlet gas at the reaction temperature and pressure to the apparent packed volume of unreduced catalyst. The reciprocal of which was defined as the contact time.

Table 1. Experimental results with the continuous flow-type apparatus

Reactant	Temp. (°C)	1/SV (s)	Obtained hydrocarbons (mol%)										
			C_1-C_3	C_4-C_6	22DMP	24DMP	33DMP	2MHX	23DMP	3MHX	3EP	HP	Others[b]
HP	280	0.66	—	0.04	—	—	—	0.57	0.05	0.78	0.15	98.36	—
		1.31	—	0.04	—	—	—	1.24	0.13	1.62	0.30	96.67	—
		2.62	—	0.04	0.04	—	—	1.96	0.12	2.59	0.19	95.10	—
		5.24	—	0.01	0.14	0.09	0.02	4.04	0.27	4.84	0.41	90.18	—
		10.5	0.04	0.13	0.47	0.41	0.28	7.87	0.71	8.37	0.64	81.08	—
	300	0.32	—	0.04	0.01	—	—	0.86	0.14	1.19	0.06	97.70	—
		0.63	0.01	0.06	0.02	—	—	1.57	0.09	2.20	0.27	95.78	—
		1.27	0.05	0.06	0.02	—	—	2.86	0.18	3.61	0.28	92.94	—
		2.53	0.08	0.13	0.21	0.16	0.11	5.69	0.46	6.91	0.57	85.68	—
	320	0.20	—	0.03	0.03	0.03	—	1.94	0.14	2.52	0.20	94.97	0.14
		0.30	—	0.06	0.08	0.06	—	2.75	0.21	3.52	0.27	92.97	0.08
		0.59	0.08	0.12	0.21	0.20	0.13	5.82	0.52	6.94	0.58	85.26	0.14
		1.18	0.20	0.19	0.48	0.48	0.34	9.16	0.96	10.77	0.86	75.41	1.15
		2.36	0.67	0.70	1.51	1.40	0.96	15.36	2.47	17.57	1.40	57.65	0.31
	340	0.10	0.10	0.04	0.06	0.08	0.08	2.01	0.20	2.48	0.21	94.65	0.09
		0.20	0.14	0.06	0.16	0.17	0.13	3.78	0.45	4.66	0.38	89.98	0.09
		0.30	0.24	0.13	0.26	0.24	0.18	5.46	0.60	6.35	0.46	86.00	0.08
		0.59	0.29	0.35	0.63	0.65	0.46	10.44	1.45	12.00	0.95	72.48	0.30
		1.18	0.91	1.06	1.81	1.85	1.35	10.14	1.74	11.34	1.83	67.39	0.60
3MHX	290	0.32	0.01	0.01	0.16	0.14	0.12	6.54	0.74	85.92	3.51	0.61	2.22
		0.64	0.02	0.02	0.37	0.31	0.20	11.68	1.37	79.17	3.64	1.18	2.09
		1.29	0.06	0.09	0.71	0.64	0.46	18.41	2.20	68.75	4.11	2.40	2.21
		2.57	0.15	0.19	1.31	1.14	0.81	23.75	3.14	58.49	4.28	4.53	2.29
	—[a]	—	—	—	—	—	—	0.18	—	96.50	0.84	—	2.48

a) Feed 3MHX. Unidentified impurities (2.48 mol%) are refractory to the reaction. b) Unidentified substances, presumably cycloalkanes.

Table 2. Effect of concentration of HP upon conversion at 305 °C, 1/SV=2.5 s

Concentration of HP (mol%)	Conversion (%)
0.6	21.3
1.2	21.7
2.0	22.1

equation in respect to HP under the condition of excess hydrogen. Moreover, the first-order rate plots were confirmed to hold for HP isomerization at 280, 300, 320 and 340 °C, and also for 3MHX isomerization at 290 °C, by use of the data in Table 1.

Isomerization of Six Heptane Isomers with the Micro Pulse Apparatus. HP, 3MHX, 2MHX, 3EP, 24-DMP, and 23DMP were subjected to isomerization by use of the micro pulse apparatus. Injection of 2.0 μl of reactants in a hydrogen stream resulted in a constant contact time of 0.2 s. The first-order rate equation was confirmed for all reactants by varying the injection amount and obtaining the same conversions and product distributions. The intrinsic deviations existed for the rate constants of HP and 3MHX isomerizations between the results of the two different apparatus. i.e., average 40.0% lower by the micro pulse reactor than by the continuous flow type one. As the reactant to H_2 molar ratio was sufficiently low, the small deviations could be attributed to the difference of temperature distribution through the catalyst layer. So that the coefficient, 1.40, was introduced for the interconversion between the results obtained with the two apparatus.

The experiments were performed in the range of temperature where the conversions resulted between 2 and 30% of reactant isomers. The followings are the reactants, the temperature necessary to achieve the conversion of 10%, obtained products and their percentages in the total products.

HP	346 °C	3MHX(43.5%), 2MHX(34.2%), 23DMP(4.3%), 3EP(3.7%), 24DMP(1.6%), 22DMP(1.5%)
3MHX	308 °C	2MHX(59.0%), 3EP(30.6%), HP(6.2%), 24DMP(1.0%), 22DMP(1.0%), 33DMP(0.7%)
2MHX	312 °C	3MHX(86.1%), 3EP(4.0%), HP(3.9%), 24DMP(2.3%), 22DMP(2.1%), 33DMP(1.2%)
3EP	277 °C	3MHX(96.5%), 2MHX(2.7%)
24DMP	305 °C	23DMP(74.0%), 33DMP(10.9%), 3MHX(5.3%), 2,2,3-trimethylbutane(3.7%), 3EP(1.9%), 2MHX(1.0%)
23DMP	269 °C	24DMP+22DMP(64.7%), 33DMP(29.0%), 2MHX(5.9%)

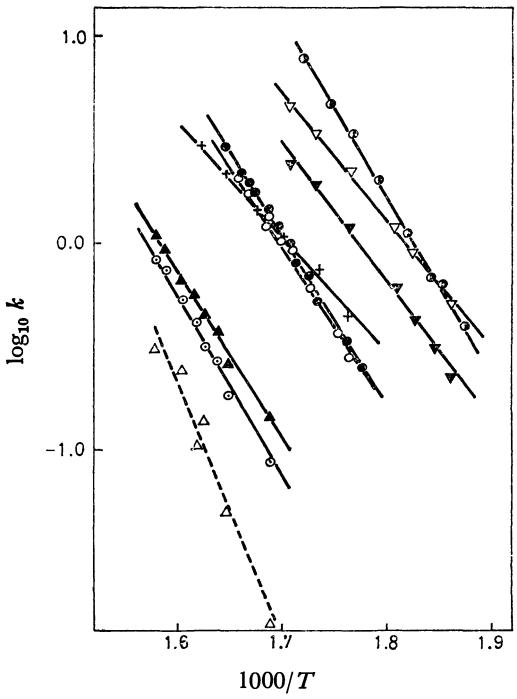

Fig. 1. Arrhenius plots of isomerization of heptane isomers.
⊙, HP → 2MHX; ▲, HP → 3MHX; ●, 2MHX → 3MHX; ○, 3MHX → 2MHX; ◑, 3EP → 3MHX; +, 24DMP → 23DMP; ▼, 23DMP → 33DMP; ▽, 23DMP → 24DMP+22DMP; △, HP → *n*-Hexane.

Arrhenius plots of the 9 main primary reactions including hydrogenolysis of HP were shown in Fig. 1. Activation energies and pre-exponential factors of the reactions above were tabulated in Table 3 along with the rate constants normalized at 320 °C. Obtained data for the two relatively minor reactions, 3MHX→ HP and 2MHX→HP, were also tabulated.

Discussion

The Reaction Scheme. Based on the primary product distributions obtained in the preceding section, the net-work of the reaction path was constructed as shown in Fig. 2. This reaction scheme is composed of 22 isomerization steps among 9 isomers of heptane, neglecting hydrocracking reactions. The characteristic features of the present scheme are that 3EP is generated exclusively from 3MHX and that 23DMP mediates between methylhexanes and other dimethylpentanes. The first proposal is based on the fact that the primary product of 3EP isomerization was solely 3MHX, and that 30.6% of product was 3EP in the reverse reaction of 3MHX. The second proposal is based on the fact that 23DMP is generated prior to other dimethylpentanes in the isomerization of HP and of 3MHX as is seen in Table 1. Besides, the reaction of 23DMP proceeded rapidly to 24DMP, 22DMP, and 33DMP. Although 24DMP and 22DMP were not separated as two distinct gas chromatographic peaks in this case, the amount of them could duly be estimated as one to one from the peak. In the reactions of HP, 3MHX, and 2MHX, the production ratio of 24- to 22-DMP

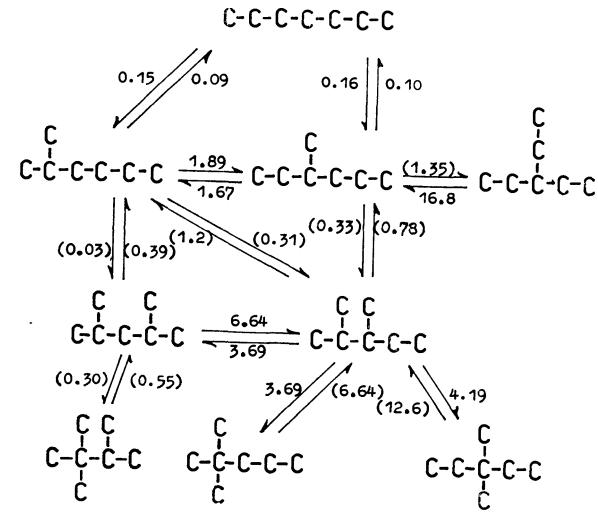

Fig. 2. The proposed isomerization scheme of heptane isomers. Rate constants obtained and (evaluated) at 320 °C.

were almost one to one. In this connection, however, the minor but direct reaction path from 2MHX to 24DMP should exist, because the molar production ratio of 24DMP to 33DMP in the reaction of 2MHX is larger (*ca.* 2.0) than that in the reaction of 3MHX (*ca.* 1.4).

The values of rate constants normalized at 320 °C were prepsented in Figure 2. Those values with parentheses mean the poor reliability of data because of the very small amounts of reaction products and the lack of reverse reactions in the present experiments. They were evaluated not to conflict with the experimental results and the reported equilibrium distribution among 9 isomers.[13] By use of the above values, the numerical integrations of the first-order rate equations were performed by the RUNGE-KUTTA method to examine the validity of the postulated reaction scheme. The results of calculation for the isomerization of HP at 280, 300, 320, and 340 °C, and of 3MHX at 290 °C agreed satisfactorily with the experimental plots of Table 1. Figures 3(a), (b), and (c) show the product distribution *vs.* conversion curves calculated for the reaction of HP at 320 °C together with the experimental results. Figures 4(a) and (b) show the result of examination for the reaction of 3MHX at 290 °C. In this case, product yield *vs.* reciplocal SV curves were adopted.

Examination of Several Proposed Reaction Mechanisms. There have been proposed several mechanisms for the skeletal isomerization of alkanes over acidic and metallic catalysts. Isomerization on the acidic catalysts has been postulated to occur as the carbonium ion mechanism through the 1,2-shift of alkyl anion.[14] Recently, through the examination of the reaction in superacid, the nonclassical protonated cyclopropane was proposed to be an intermediate.[15]

Corolleur *et al.*,[7] and Barron *et al.*[16] adopted the cyclopentane type intermediate on the metal surface. The former used isotope-labeled hexanes on the platinum–alumina catalyst. Anderson and Avery[5] proposed an entity of the 1,3-triadsorbed intermediate by which the skeletal rearrangement was accomplished

Table 3. Kinetic data for the isomerization of heptanes

Reaction	Temperature range (°C)	Activation energy (kcal/mol)	log A	k at 320 °C (V/V/s)
HP ⟶ 3MHX	320—360	38.3	13.3	0.158
HP ⟶ 2MHX	320—360	41.3	14.2	0.153
3MHX ⟶ HP	290—340	32.3	11.1	0.101
3MHX ⟶ 2MHX	290—340	36.5	13.7	1.67
2MHX ⟶ HP	290—340	33.9	11.5	0.092
2MHX ⟶ 3MHX	290—340	37.7	14.2	1.89
3EP ⟶ 3MHX	250—310	38.0	15.2	16.8
24DMP ⟶ 23DMP	270—330	33.1	13.0	6.64
23DMP ⟶ 24DMP+22DMP	260—320	28.2	11.3	7.38
23DMP ⟶ 33DMP	260—320	30.9	12.0	4.19
HP ⟶ n-hexane	320—380	49.0	16.0	0.0093

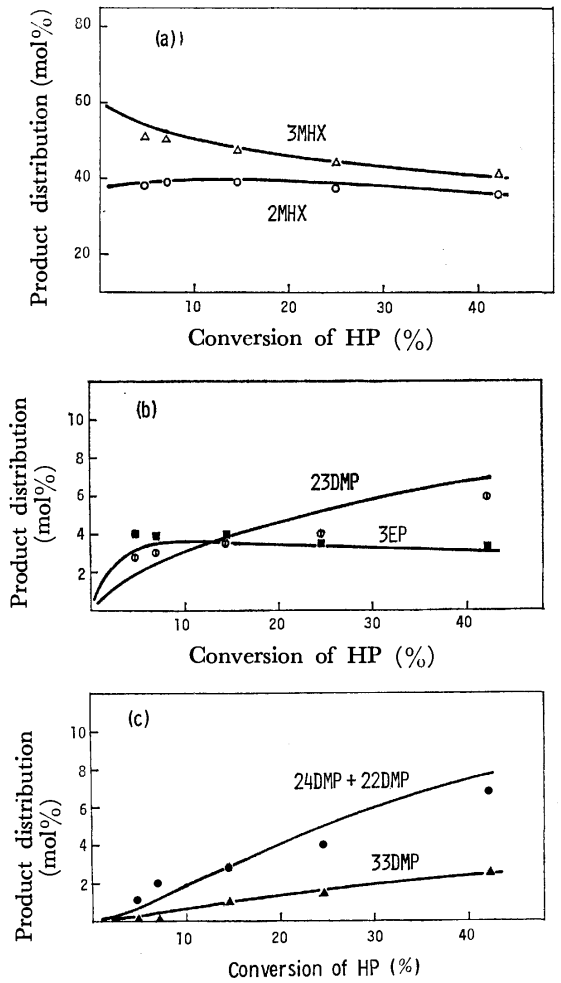

Fig. 3. Calculated (solid lines) and obtained (points) product distribution in the isomerization of HP at 320 °C.

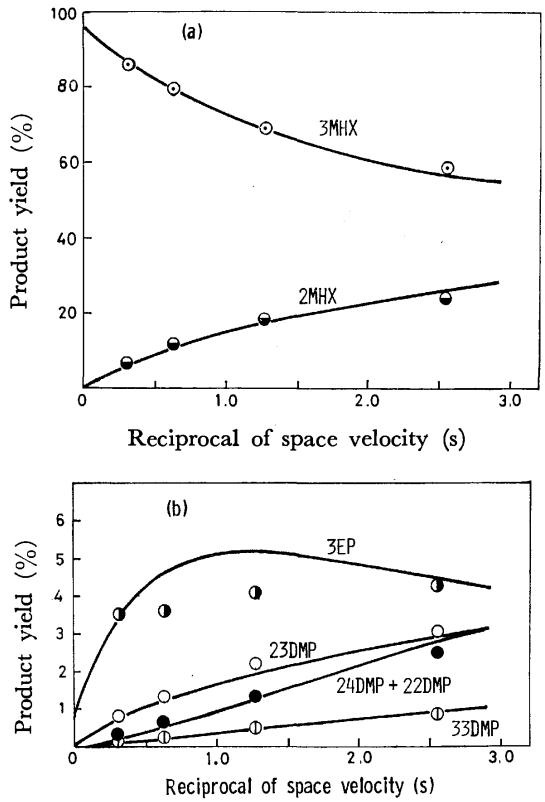

Fig. 4. Calculated (solid lines) and obtained (points) product yield in the isomerization of 3MHX at 290 °C.

via a bridged transition state. The intermediate was considered to be stabilized by transferring a fractional electron from the adsorbed hydrocarbon to the surface metal. This mechanism was supported by themselves through a calculation of the Hückel molecular orbitals.[17] Boudart and Ptak[6] discovered that platinum, iridium and gold, excluding palladium, catalyzed isomerization of neopentane and proposed that metals of sufficient electro-negativity were capable to catalyze the reaction. The intermediate, postulated by them, is a 1,3-triadsorbed species which has some character of the carbonium ion.

Lanewala *et al.*[8,9] conducted the isomerization of hexanes on a palladium–zeolite catalyst. They have proposed a bimolecular mechanism on the surface metal on the basis of their detailed product analyses.

There exists some ambiguity for the supported metal catalysts whether their active sites are metallic or acidic. In the present discussion, the several mechanisms described above will be examined from the point

of proposed intermediates referring to the obtained reaction paths in Fig. 2. Three reaction steps are worth while to consult in the evaluation of the above mechanisms, *i.e.*, (i) simultaneous formations of 2MHX and 3MHX from HP, (ii) reversible isomerization between 3EP and 3MHX, and (iii) reversible reaction between 23DMP and 24DMP.

Formally, the present results are well explained by the carbonium ion mechanism for acidic catalysts if the methyl and ethyl groups shift to the adjacent carbon atom in the reactions (i) and (iii), and in the reaction (ii), respectively. But this mechanism is criticized not to occur on a metal surface.[5]

It seems reasonable that reaction (ii) proceeds *via* the cyclopentane type intermediate.[7,16] However, the reaction (i) and (iii) could not be interpreted by the same intermediate. They require participations of six- and four-membered cyclic intermediates, respectively. The proposal by Lanewala *et al.*[8,9] does not hold in the present results because no trace of octane isomers was detected and no evidence of direct formation of 23DMP from HP was found.

The remaining two mechanisms, those involve 1,3-triadosorbed intermediate[5,6] and the protonated cyclopropane,[15] cannot be distinguished by the present results, because both mechanisms lead to the same conclusion in regard to the cleavage and the formation of C–C bonds. All the reactions in the scheme are interpreted in terms of either of these mechanisms.

Activation energies obtained in the present work for the reactions of six heptane isomers were 30—40 kcal/mol. These values are larger than those found on the acidic catalysts (15—25 kcal/mol)[18–20] and smaller than those on the metallic catalysts (40—50 kcal/mol).[21] Namely, the palladium–zeolite catalyst in the present work exhibits a metallic character in regard to the activation energy and, at the same time, an acidic character in regard to its activity for the isomerization, because the pure palladium metal has been reported not to catalyze the isomerization of hydrocarbons.[6]

References

1) J. H. Sinfelt, H. Hurwitz, and J. C. Rohrer, *J. Phys. Chem.*, **64**, 892 (1960).
2) F. G. Ciapetta and J. B. Hunter, *Ind. Eng. Chem.*, **45**, 147 (1953).
3) J. A. Rabo, P. E. Pickert, and R. L. Mays, *ibid.*, **53**, 733 (1961).
4) S. G. Hindin, S. W. Weller, and G. A. Mills, *J. Phys. Chem.*, **62**, 244 (1958).
5) J. R. Anderson and N. R. Avery, *J. Catal.*, **5**, 446 (1966).
6) M. Boudart and L. D. Ptak, *ibid.*, **16**, 90 (1970).
7) C. Corolleur, S. Corolleur, and F. G. Gault, *ibid.*, **24**, 385, 401 (1972).
8) M. A. Lanewala, P. E. Pickert, and A. P. Bolton, *ibid.*, **9**, 95 (1967).
9) A. P. Bolton and M. P. Lanewala, *ibid.*, **18**, 1 (1970).
10) E. Ogata, Y. Kamiya, and N. Ota, *Kogyo Kagaku Zasshi*, **73**, 2582 (1970).
11) S. W. Csicsery and R. L. Burnett, *J. Catal.*, **8**, 75 (1967).
12) T. Kubo, H. Tominaga, and T. Kunugi, *Nippon Kagaku Kaishi*, **1972**, 1621.
13) F. D. Rossini, *et al.*, "Selected Values of Properties of Hydrocarbons and Related Compounds", API Project 44, Carnegie Institute of Technology, Pittsburgh, Pensylvania (1959).
14) D. M. Brouwer and H. Hogeveen, "Progress in Physical Organic Chemistry", Vol. 9, ed. by A. Streitwieser, Jr., R. W. Taft, John Wiley, New York, N. Y. (1972), p. 179.
15) D. M. Brouwer and J. M. Oelderik, *Rec. Trav. Chim.*, **87**, 721 (1968).
16) Y. Barron, G. Maire, J. M. Muller, and F. G. Gault, *J. Catal.*, **5**, 428 (1966).
17) J. R. Anderson and N. R. Avery, *ibid.*, **7**, 315 (1967).
18) R. E. Dudley and J. B. Malloy, *Ind. Eng. Chem., Process Design Develop.*, **2**, 239 (1963).
19) F. G. Ciapetta and J. B. Hunter, *Ind. Eng. Chem.*, **45**, 1947 (1953).
20) R. Beecher and A. Voorhies. Jr., *Ind. Eng. Chem., Prod. Res. Develop.*, **8**, 366 (1969).
21) E. Kikuchi, M. Tsurumi, and Y. Morita, *J. Catal.*, **22**, 226 (1971).

NOTES

BULLETIN OF THE CHEMICAL SOCIETY OF JAPAN, VOL. 48(2), 701—702 (1975)

Negative Photoconduction in Solution of Aromatic Amine and Benzoquinone by Flash Excitation

Jun-ichi NAKATA, Takeshi IMURA, and Kazuo KAWABE

Electrophysics Laboratory, Department of Electrical Engineering, Faculty of Engineering, Osaka University, Suita, Osaka 565

(Received October 11, 1973)

Synopsis. The conductivity of a solution of benzoquinone and TMPD decreased after being subjected to flash excitation. This is attributed to the decrease of free ions due to the equilibrium shift produced by photo-induced disappearence of the ion pair.

When the absorption of light causes a decrease in the electrical conductivity of a material, the phenomenon is called negative photoconduction. It occurs occasionally in some inorganic solids.[1)]

A new type of negative photoconduction (on continuous excitation) was observed[2)] in organic solution containing both *N,N,N',N'*-tetramethyl-*p*-phenylenediamine (TMPD) and *p*-benzoquinones under the following conditions: (I) In the wavelength range of exciting light 400—500 nm, where *p*-benzoquinone or its chloro-derivatives and small amounts of their semiquinone anion radicals have characteristic absorption bands, the anion radicals are slightly present in the solution due to equilibrated ionic dissociation. (II) For solvents, the negative photoconduction was observed only in appropriately polar ethers such as THF and 1,2-dimethoxyethane, but not in dioxane, a non-polar ether, nor in other moderately polar solvents such as acetone, benzotrifluoride and 1,2-dichloroethane.

We have studied the transient change in the conductivity of a solution after being subjected to flash irradiation for a few μs and the origin of the phenomenon.

Materials,[2)] the apparatus and procedure[3)] are the same as described. The input energy of discharge to obtain a light pulse was 180 J. Two glass filters (Toshiba VY-42 and VB-46) were used. Current signal was read through 10 kΩ resistor; the time constant of the circuit is estimated to be about 1 μs. High purity nitrogen (more than 99.999%) was substituted for dissolved oxygen in the solution. All the experiment were carried out at room temperature.

The conductivity of a THF solution containing both TMPD and chloro-*p*-benzoquinone of the same concentration 1.0×10^{-2} M momentarily increased for *ca.* 15 μs, before the subsequent negative photoconduction was slowly initiated (Fig. 1(a)). Conductivity reached the minimum value at 1.5—2.0 ms, and then recovered exponentially to the original value in the dark within a few seconds. At minimum the decrease in conductivity was a few percent of the original conductivity ($2.3\times10^{-8}\Omega^{-1}$ cm^{-1}).[2)]

The following equilibrium was reached in the solution:

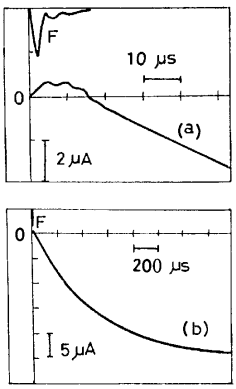

Fig. 1. Photocurrent of THF solution containing both TMPD and chloro-*p*-benzoquinone with the same concentrations of 1.0×10^{-2} M.
Negative photoconduction is shown to begin slowly after the light pulse(F) is over (a), and the minimum value is reached at about 1.5—2.0 ms (b).

$$A + D \rightleftharpoons A\cdot D \rightleftharpoons A^-\cdot D^+ \rightleftharpoons A^- + D^+. \qquad (a)$$

Concentration of the ion pair was estimated to be more than 10^{-6} M from the absorption spectra assuming the molar extinction coefficient of D^+ (mainly in the ion pair) to be 10^4 M^{-1} cm^{-1}; the concentration of free A^- was evaluated to be 10^{-7} M.[2)]

By optical excitation of $A^-\cdot D^+$, an electron will be ejected and subsequently trapped by $A\cdot D^+$:

$$A^-\cdot D^+ + h\nu \rightarrow e_s^- + A\cdot D^+ \rightarrow A\cdot D \text{ or } A + D. \qquad (b)$$

This brings about reduction in the concentration of the ion pair $A^-\cdot D^+$ with subsequent recovery of equilibrium:

$$A^- + D^+ \xrightarrow{k_c} A^-\cdot D^+ \longleftarrow A\cdot D. \qquad (c)$$

According to the left-hand side of (c), the conductivity of the solution decreases. This was verified from the second-order plot of Fig. 1(b). The rate constant k_c was estimated to be of the same order as diffusion limited.

The positive conductivity change appearing within *ca.* 15 μs at the first portion of the responce (Fig. 1(a)) is attributed to the formation of charge carriers according to the left-hand side of (b).

Free anion is also photo-ionized and ejects an electron:

$$A^- + h\nu \rightarrow e_s^- + A. \qquad (d)$$

This is a minor reaction as compared with (b). The electron in (d) will be scavenged by A in a moment. Thus, (d) takes no part in negative photoconduction. We proposed[2] that the origin of the negative photoconduction is attributed to (d) and the subsequent trapping of electron by D^+:

$$e_s^- + D^+ \rightarrow D. \qquad (e)$$

However, the solvated electron is to be scavenged by A in competition with (e):

$$e_s^- + A \rightarrow A^-. \qquad (f)$$

These reactions yields no conductivity change.

Slow recovery from the negative photoconduction was expressed by first order kinetics, and corresponds to ionic dissociation of A·D *via* $A^-\cdot D^+$. The right hand side of (c) might be slow. Slow ionization of quinones by interaction with aliphatic amines was reported[4] by the rapid scan spectrophotometric method.

No solvated electron could be detected spectroscopically with our flash apparatus. The concentration of solvated electron should be 10^{-6} M or less since all A^- is not photo-ionized. Optical path-length of about 100 cm is required if the molar extinction coefficient of solvated electron in THF is about 10^4 M^{-1} cm^{-1}.

References

1) R. H. Bube, "Photoconductivity of Solid," John Wiley & Sons, Inc., New York, (1960), p. 404.
2) T. Imura, J. Nakata, and K. Kawabe, *Chem. Lett.*, **1972**, 421.
3) T. Imura, N. Yamamoto, and H. Tsubomura, This Bulletin, **43**, 1670 (1970).
4) T. Yamaoka and S. Nagakura, *ibid.*, **44**, 1780 (1971).

BULLETIN OF THE CHEMICAL SOCIETY OF JAPAN, VOL. 48(2), 703—704 (1975)

Estimation of Structures and Electronic States of Radicals Using INDO-SCFMO Method. II. Alkylperoxyl Radicals

Katsutoshi OHKUBO and Futoshi KITAGAWA

Department of Synthetic Chemistry, Faculty of Engineering, Kumamoto University, Kurokami, Kumamoto 860

(Received November 16, 1973)

Synopsis. The energetically most stable CH_3OO and CH_3CH_2OO radicals have been found to have the following geometric values: $r(O_\alpha\text{-}O_\beta)=1.12$ Å, $r(O_\alpha\text{-}C)=1.38$ Å for the former and 1.39 Å for the latter, $\angle CO_\alpha O_\beta=112°$ for the former and 115° for the latter, and $r(C\text{-}C)=1.47$ Å for the latter.

Alkylperoxyl radicals (referred to as ROO·) have been postulated as reactive intermediates participating in the oxidation and polymerization reactions. The said radicals are recently believed to play an important role in the air-pollution cycle:

Hydrocarbons such as olefin $+{}^1O_2 \rightarrow$ Hydroperoxide $\xrightarrow{\text{dec.}}$ Radicals such as RO·

$$RO\cdot + {}^3O_2 \rightarrow (RO_3\cdot) \xrightarrow{NO_2} ROO\cdot + NO_2$$

$$ROO\cdot + NO \rightarrow RO\cdot + NO_2$$

The molecular structures and electronic states of ROO·, however, are yet open to question, although aspects of HOO· have been investigated by INDO[1] and *ab initio* SCF[2] methods. There are, therefore, good reasons for embarking on an MO-study of ROO· with a view of estimating how their structures and electronic properties. We wish now to report our results on ROO· (R=CH_3 and CH_3CH_2).

Method of Calculation

The following two systems were investigated in this work: (a) the methylperoxyl radical, CH_3OO· and (b) the ethylperoxyl radical, CH_3CH_2OO·. The geometric parameters of the above species are shown in Fig. 1. All the valence-bond angles except those denoted by θ were uniformly taken to be 109°28′ for the sake of simplicity.

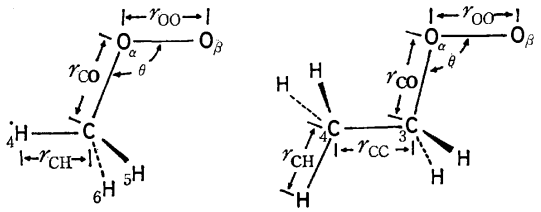

Fig. 1. Geometries used for calculations. ($r(O_\alpha\text{-}O_\beta)$, $r(O_\alpha\text{-}C)$, $r(C\text{-}C)$, $r(C\text{-}H)$, and θ denote geometric parameters.)

The method of calculation is a semiempirical INDO, using the integrals and parametrization in Ref. 3.

Results and Discussion

Methylperoxyl Radical. The INDO calculations were first performed on CH_3OO· with three variables of the bond distances ($r(O_\alpha\text{-}O_\beta)$, $r(O_\alpha\text{-}C)$, and $r(C\text{-}H)$) and one variable of the valence bond angle (θ) by changing $r(O_\alpha\text{-}O_\beta)$, θ, $r(O_\alpha\text{-}C)$, and $r(C\text{-}H)$ in turn.[4] As can be seen from Table 1, the set of $r(O_\alpha\text{-}O_\beta)=1.20$ Å, $r(O_\alpha\text{-}C)=1.38$ Å, $r(C\text{-}H)=1.12$ Å, and $\theta=112°$ gives the lowest SCF total energy (E_{SCF}) for CH_3OO·.[5] The estimated bond length of $O_\alpha\text{-}O_\beta$ (1.20 Å) is very close to that of O_2 (exptl.=1.207 Å[7]), but appreciably shorter than that of HOO·[8] (exptl.=1.30 Å[9]), while the O_α–C length (1.38 Å) is fairly short as compared with the single C–O bonds (1.43 Å). The C–H bond

Table 1. Changes in total energy and electronic state of CH_3OO· as a function of four variables, $r(O_\alpha\text{-}O_\beta)$, θ, $r(O_\alpha\text{-}C)$, and $r(C\text{-}H)$

$r(O_\alpha\text{-}O_\beta)$/Å	θ	$r(O_\alpha\text{-}C)$/Å	$r(C\text{-}H)$/Å	E_{SCF}/a.u.	Q_A		Odd-electron density	μ/D
					O_α	O_β		
1.19	112°	1.44	1.09	−44.3438	−0.036	−0.125	1.218	2.18
1.20	112°	1.44	1.09	−44.3439	−0.043	−0.120	1.207	2.16
1.21	112°	1.44	1.09	−44.3430	−0.048	−0.116	1.200	2.16
1.20	111°	1.44	1.09	−44.3438	−0.042	−0.121	1.208	2.15
1.20	112°	1.44	1.09	−44.3439	−0.043	−0.120	1.207	2.16
1.20	113°	1.44	1.09	−44.3438	−0·043	−0.120	1.208	2.18
1.20	112°	1.37	1.09	−44·3498	−0.039	−0.120	1.205	2.04
1.20	112°	1.38	1.09	−44.350295	−0.040	−0.120	1.206	2.06
1.20	112°	1.39	1.09	−44.350290	−0.040	−0.120	1.207	2.09
1.20	112°	1.38	1.11	−44.3539	−0.039	−0.119	1.205	2.03
1.20	112°	1.38	1.12	−44.3543	−0.038	−0.119	1.208	2.03
1.20	112°	1.38	1.13	−44.3540	−0.038	−0.118	1.205	2.01

(1.12 Å) is also estimated to be longer than the normal C–H distance (1.09 Å). The angle of θ (112 °) also differs by 4° from that of HOO· (exptl.=180°[9]). Moreover, the estimated dipole moment (2.03 D) of $CH_3OO\cdot$, which possesses the slightly negative formal charges (Q_A) of two oxygen atoms, may be close to those of CH_3OH (exptl.=1.69 D[10]; calcd. by INDO=1.94 D[3]) and H_2O (exptl.=1.846 D[11]; calcd. by INDO=2.10 D[3]).

With regard to the g value of the CH_3OO radical, it was evaluated to be 2.003 by means of the Stone equation.[12] The g value is found to be in good agreement with the experimental value of 2.015.[13]

The odd-electron (its density=1.208) is predominantly localized in the following half-occupied MO (−0.5005 a.u.), ϕ_{odd}^{occ}:

$$\phi_{occ}^{odd} = 0.592Z_{O\alpha} - 0.729Z_{O\beta} + 0.150Z_C + 0.223S_{5H} - 0.223S_{6H},$$

while the lowest unoccupied MO (0.1608 a.u), ϕ_{unocc}^{odd}, comes mainly from the following AOs:

$$\phi_{unocc}^{odd} = 0.873Z_{O\beta} - 0.416Z_{O\alpha} - 0.147Z_C + 0.148S_{5H} - 0.148S_{6H}$$

where $Z_{O\alpha}$, Z_C, S_{5H}, *etc.* stand for the p_z of O_α, the p_z of C, the s of 5H, *etc.* respectively.

It is observed that the O_β p_z-orbital contributes distinctly to the formation of both MOs.

Ethylperoxyl Radical. As Fig. 1 indicates, the ethylperoxyl radical, $CH_3CH_2OO\cdot$, has four geometric parameters ($r(O_\alpha$–$O_\beta)$, $r(O_\alpha$–C), r(C–C), and θ) in the present INDO calculations. The calculated results with respect to the most energetically stable $CH_3CH_2OO\cdot$ are summarized in Table 2. The angle of θ (115°) is larger than that of $CH_3OO\cdot$, though the O_α–O_β and O_α–C lengths are just (or nearly) the same as those of $CH_3OO\cdot$. The r(C–C) of 1.47 Å is shorter than the usual single C–C bond (1.54 Å). The INDO calculations, however, sometimes estimate the C–C bond length of hydrocarbons too short; for example, the C–C bond lengths of C_2H_6 (1.46 Å) and C_2F_6 (1.49 Å) are reasonably shorter than those of the experiments (1.536 and 1.51 Å respectively). Moreover, the two oxygen atoms of $CH_3CH_2OO\cdot$ were found to be more positively charged than those of $CH_3OO\cdot$, although the magnitude of the odd-electron density (1.204) is small in comparison with $CH_3OO\cdot$.

Finally, it is worthy of emphasis that, in the INDO calculations, a π-conjugation consisting of the lone-pair p_z-orbital of O_α and the half-occupied p_z-orbital of O_β was recognized in both the radicals (for instance, see the bond-orders of the O_α–O_β bond of $CH_3CH_2OO\cdot$ in Table 2).

The calculations were carried out on a FACOM 230-60 computer at the Data Processing Center of Kyushu University.

Table 2. Molecular structure and electronic state of $CH_3CH_2OO\cdot$

Minimum E_{SCF}/a.u.		−52.803
$r(O_\alpha$–$O_\beta)$/Å		1.20
$r(O_\alpha$–C)/Å		1.39
r(C–C)/Å		1.47
θ/deg		115
μ/D		1.94
g value		2.010
Q_A	O_β	−0.124
	O_α	−0.053
	3C	+0.237
	4C	+0.025
N_{O_β}[a]	s	1.867
	p_x	1.066
	p_y	1.987
	p_z	1.204
N_{O_α}[a]	s	1.661
	p_x	1.154
	p_y	1.470
	p_z	1.769
$P_{O_\alpha-O_\beta}$[b]	p_x–p_x	−0.836
	p_y–p_y	+0.076
	p_z–p_z	+0.399

a) AO population. b) Bond-order.

References

1) M. S. Gordon and J. A. Pople, *J. Chem. Phys.*, **49**, 4643 (1968).

2) D. H. Liskow, H. F. Schaefer III, and C. F. Bender, *J. Amer. Chem. Soc.*, **93**, 6734 (1971).

3) J. A. Pople and D. L. Beveridge, "Approximate Molecular Orbital Theory," McGraw-Hill, New York (1970).

4) A molecule involving N geometric parameters requires at least N^2 SCF evaluations for estimating its minimum SCF energy (for instance, see MINDO/2p program, QCPE program No. 228). The present calculations, however, did not follow this procedure for the simplicity of computations, and the minimum energy of a molecule was determined by changing the parameters in turn until the values of the parameters come to be identical.

5) CNDO/2 calculations[6] gave the best set of $r(O_\alpha$–$O_\beta)$=1.19 Å and θ=111° at the fixed bond distances of $r(O_\alpha$–C)=1.44 Å and r(C–H)=1.09 Å.

6) K. Ohkubo and F. Kitagawa, This Bulletin, **46**, 2942 (1973); K. Ohkubo and F. Kitagawa, *Nippon Kagaku Kaishi*, **1973**, 2147.

7) G. Herzberg, "Diatomic Molecules," D. Van Nostrand, Princeton, N. J. (1950).

8) The INDO calculations of Gordon and Pople[1] on HOO· gave $r(O_\alpha$–$O_\beta)$=1.19 Å similar to that of $CH_3COO\cdot$.

9) T. T. Paukert and H. S. Johnston, Univ. of California, Radiation Laboratory Report, No. UCRL-19109, Nov. (1969).

10) D. G. Burkhard and D. M. Dennison, *Phys. Rev.*, **84**, 408 (1951).

11) G. Burkbaum and S. K. Chatterjie, *J. Appl. Phys.*, **23**, 220 (1952).

12) A. J. Stone, *Mol. Phys.*, **6**, 509 (1963). With regard to the detailed calculation method, see Ref. 13.

13) O. Yamamoto, H. Kato, and T. Yonezawa, *Nippon Kagaku Zasshi*, **91**, 907 (1970).

BULLETIN OF THE CHEMICAL SOCIETY OF JAPAN, VOL. 48(2), 705—706 (1975)

A Method for Determining the Degree of Dissociation of Symmetrical Associated Electrolytes from the Conductivity and Activity Data

Reita TAMAMUSHI

The Institute of Physical and Chemical Research, 2-1 Hirosawa, Wako, Saitama 351

(Received May 13, 1974)

Synopsis. A method is presented for determining the degree of dissociation of symmetrical associated electrolytes from a set of conductivity and activity data. The method was applied to the determination of the dissociation constants of several metal sulfates in aqueous solutions.

In a previous paper,[1] individual ionic activity coefficients were estimated on the basis of the conductivity data by using the correlation between the activity and conductivity equations, in which the effect of the Debye-Hückel interaction is assumed to be represented by a common parameter, χ, on both the activity and the conductivity. A similar consideration provides a new method for determining the degree of dissociation of symmetrical associated electrolytes from a set of conductivity and activity coefficient data. This method does not require an *a priori* assumption of the ion-size parameter.

Let us consider the following dissociation equilibrium of a symmetrical electrolyte, MA, in solution;

$$\mathrm{MA} \rightleftarrows \mathrm{M} + \mathrm{A} \tag{1}$$

with

$$K_c = \frac{\alpha^2 c}{1-\alpha} = K(\gamma_M \gamma_A)^{-1} \tag{2}$$

where α is the degree of dissociation; c, the stoichiometric concentration of MA; γ, the individual ionic activity coefficient; K_c, the conditional dissociation constant, and K, the thermodynamic dissociation constant; the charge of each ionic species is omitted for the sake of simplicity. In Eq. (2) the activity coefficient of the associated electrolyte is assumed to be unity.

The stoichiometric mean activity coefficient, $\gamma_\pm$, of the electrolyte, which can be determined directly from measurements, is given by,[2]

$$\log \gamma_\pm = \log \gamma_\pm^{\mathrm{DH}} + \log \alpha \tag{3}$$

where $\gamma_\pm^{\mathrm{DH}}$ is the activity coefficient due to the Debye-Hückel ionic interaction. In dilute solutions, $\gamma_\pm^{\mathrm{DH}}$ can be represented by the Debye-Hückel equation:

$$\log \gamma_\pm^{\mathrm{DH}} = -A\chi^{-1} \tag{4}$$

where A is the Debye-Hückel limiting slope and where χ is the length which is related to the thickness of the ionic atmosphere (see Eq. (8)). By rearranging the relation obtained by introducing Eq. (4) into Eq. (3), we obtain χ as a function of α and $\gamma_\pm$;

$$\chi^{-1} = (\log \alpha - \log \gamma_\pm)/A \tag{5}$$

On the other hand, the Onsager-Robinson-Stokes

TABLE 1. DEGREE OF DISSOCIATION α, CONDITIONAL DISSOCIATION CONSTANT K_c, AND ION-SIZE PARAMETER a OF SEVERAL METAL SULFATES IN AQUEOUS SOLUTIONS, AS DERIVED BY THE PRESENT METHOD FROM THE CONDUCTIVITY AND ACTIVITY DATA.[4-9]

(Parentheses are used to present the a-values which very much exceed Bjerrum's parameter)

Metal sulfate		Concentration/mM							
		0.5	1	2	3	5	10	20	50
$MgSO_4$ (0 °C)[a]	α	0.951	0.912	0.879	0.855	—	—	—	—
	$-\log(K_c/\mathrm{mol\ dm^{-3}})$	2.04	2.02	1.89	1.82	—	—	—	—
	a/Å	6.7	12.5	8.8	7.9	—	—	—	—
$NiSO_4$ (0 °C)[a]	α	0.920	0.877	0.828	0.795	—	—	—	—
	$-\log(K_c/\mathrm{mol\ dm^{-3}})$	2.28	2.20	2.10	2.03	—	—	—	—
	a/Å	(30.8)	(26.3)	18.4	16.1	—	—	—	—
$CuSO_4$ (25 °C)[b]	α	—	0.828	—	—	0.645	0.593	0.556	0.503
	$-\log(K_c/\mathrm{mol\ dm^{-3}})$	—	2.40	—	—	2.23	2.06	1.86	1.59
	a/Å	—	(74.5)	—	—	(94.2)	(27.5)	11.1	7.5
$ZnSO_4$ (25 °C)[b]	α	—	0.863	0.808	—	0.732	0.665	0.616	0.571
	$-\log(K_c/\mathrm{mol\ dm^{-3}})$	—	2.26	2.17	—	2.00	1.88	1.70	1.42
	a/Å	—	16.7	12.5	—	8.3	7.8	6.0	4.8
$CdSO_4$ (25 °C)[c]	α	—	0.826	0.761	—	0.660	0.596	—	0.496
	$-\log(K_c/\mathrm{mol\ dm^{-3}})$	—	2.41	2.31	—	2.19	2.06	—	1.61
	a/Å	—	(58.1)	(43.0)	—	(24.1)	15.5	—	6.9

a) The conductivity data were taken from Ref. 4, and the activity data from Ref. 5. b) The conductivity data were taken from Ref. 6, and the activity data from Ref. 7. c) The conductivity data were taken from Ref. 8 and 9, and the activity data from Ref. 7.

theory[3] gives the conductivity equation for a symmetrical associated electrolyte;

$$\Lambda = \alpha(\Lambda^{\infty} - S\chi^{-1}) \quad (6)$$

where Λ is the equivalent conductivity; Λ^{∞}, the Λ-value at an infinite dilution, and S, the Onsager limiting slope.

By introducing Eq. (5) into Eq. (6), the relationship among Λ, α, and $\gamma_{\pm}$ is derived;

$$\frac{\Lambda}{\Lambda^{\infty}} = \alpha\left[\left(1+\frac{S}{A\Lambda^{\infty}}\log\gamma_{\pm}\right) - \frac{S}{A\Lambda^{\infty}}\log\alpha\right] \quad (7)$$

This relationship can be used for the determination of α from the conductivity and activity data. It must be noted that, in the derivation of Eq. (7), it is not necessary to know the exact expression of the χ parameter.

Only a small number of experimental data are available in the literature[4-9] for use in estimating the applicability of the present method. Table 1 shows the results obtained with several sulfate salts of divalent metal ions in aqueous solutions.

The thermodynamic dissociation constants, which were determined by the extrapolation of the plot of $\log K_c$ as a function of the square root of the ionic strength, I, as is shown in Fig. 1, are compared in Table 2 with the values reported in the literature.

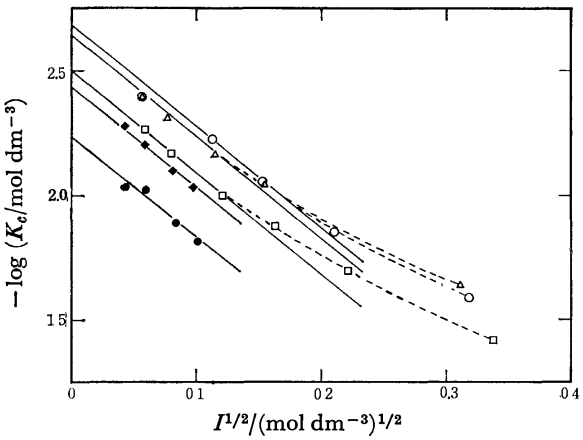

Fig. 1. Plot of $-\log K_c$ as a function of $I^{1/2}$ ($I=4\alpha c$): ● $MgSO_4$ (0 °C), ■ $NiSO_4$ (0 °C), ○ $CuSO_4$ (25 °C), □ $ZnSO_4$ (25 °C), △ $CdSO_4$ (25 °C). The solid lines represent the theoretical slope by the Debye-Hückel limiting equation.

Table 2. Thermodynamic dissociation constants of several metal sulfates in aqueous solutions, as computed by different methods

Metal sulfate	$-\log(K/\text{mol dm}^{-3})$			
	Present method	Cond.[4]	Activ.[5]	Lit.[10]
$MgSO_4$ (0 °C)	2.2_3	2.01[a]	1.66—2.35[c]	1.96—2.39
$NiSO_4$ (0 °C)	2.4_3	2.19[b]	1.80—2.40[c]	2.06—2.39
$CuSO_4$ (25 °C)	2.6_7	—	—	2.10—2.46
$ZnSO_4$ (25 °C)	2.5_0	—	—	2.27—2.38
$CdSO_4$ (25 °C)	2.6_5	—	—	2.29

a) Ion-size parameter $a=5.59$Å. b) Ion-size parameter $a=5.86$Å. c) Depending on the ion-size parameter ($a=3$—4 Å).

In Table 2, the third column gives the log K-values[4] determined by the analysis of the conductivity data according to the Fuoss-Onsager equation, in which a set of log K and the ion-size parameter, a, is obtained in such a way that the theoretical equation gives the best fit to the experimental conductivity data. The fourth column of Table 2 gives the log K-values[5] calculated from the activity data by assuming different values of the ion-size parameter. The present method seems to result in slightly larger values of pK than the values reported in the literature.

It is the advantage of the present method that an *a priori* assumption of ion-size parameter is not required in the determination of the dissociation constant. However, if we assume the Debye-Hückel expression for χ;

$$\chi = a + \kappa^{-1} \quad (8)$$

where κ^{-1} is the Debye-Hückel length of the ionic atmosphere, we can calculate the ion-size parameter, a, by means of Eqs. (5) and (8). The a-values derived in this way at each concentration are shown in Table 1. The present method gives concentration-dependent values for the ion-size parameter; the a-values at lower concentrations are larger than those commonly accepted, and in some cases they exceed Bjerrum's parameter (14 Å for 2 : 2 electrolytes in aqueous solutions). The relatively large pK values obtained by the present method may be correlated with the large ion-size parameters, as has been mentioned above.

Further discussions on the validity of the present method will become possible only when more accurate experimental data have been obtained with various electrolytes.

References

1) R. Tamamushi, This Bulletin, **47**, 1921 (1974).
2) R. A. Robinson and R. H. Stokes, "Electrolyte Solutions," Chap. 2, Butterworths, London (1965); C. W. Davies, "Ion Association," Chap. 3, Butterworths, London (1962).
3) R. A. Robinson and R. H. Stokes, "Electrolyte Solutions," Chap. 7, Butterworths, London (1965).
4) S. Katayama, This Bulletin, **46**, 106 (1973).
5) T. Isono, *Sci. Papers I. P. C. R.*, **65**, 95 (1971).
6) H. S. Harned and B. B. Owen, "The Physical Chemistry of Electrolytic Solutions," Third Edition, Appendix A, Table (6—2—1A), Reinhold, New York (1967).
7) R. Parsons, "Handbook of Electrochemical Constants," Table 19, Butterworths, London (1959).
8) S. Katayama, unpublished data.
9) The Chemical Society of Japan (ed.), "Kagaku Binran," Kisohen II, § 9.8.1, Maruzen, Tokyo (1966).
10) L. G. Sillén and A. E. Martell, "Stability Constants of Metal-Ion Complexes," Special Publication No. 17, The Chemical Society, London (1964); Supplement No. 1, Special Publication 25, The Chemical Society, London (1971).

BULLETIN OF THE CHEMICAL SOCIETY OF JAPAN, VOL. 48(2), 707—708 (1975)

Molecular Vibrations and Force Fields of Alkyl Sulfides. XI. C-S Stretching Vibrations of Some Simple Aliphatic Sulfides

Masaru OHSAKU

Department of Chemistry, Faculty of Science, Hiroshima University, Higashisenda-machi, Hiroshima 730

(Received June 11, 1974)

Synopsis. Infrared spectra of alkyl sulfides were measured. Some correlations of the C–S stretching frequencies to the molecular conformations were proposed.

For alkyl chlorides[1] and alkyl disulfides,[2] the correlations between the C–Cl or C–S stretching frequencies and the molecular conformations have been extensively discussed. In the case of alkyl sulfides, such a relation can also be expected. In the present note, therefore, the observed C–S stretching frequencies of the sulfides will be studied in relation to their molecular conformations.

The infrared spectra of the sulfides were measured in the liquid and solid states by means of a Perkin-Elmer Model 621 spectrophotometer. Table 1 shows the frequencies of the infrared bands, which may be due to the stable form in the solid state. The notations in this table, P_H, P_C, and S_{HH}, are the same as those used in the previous papers.[1,2] From this table we can find the frequency dependence upon the molecular conformations, similar to the C–Cl stretching frequencies of alkyl chlorides[1] and to the C–S stretching frequencies of alkyl disulfides.[2]

A characteristic CH_3–S stretching vibration is observed in the 690—750 cm^{-1} region. The C–S stretching vibrations due to the P_H and P_C conformations appear in the regions of 640—700 cm^{-1} and 710—750 cm^{-1} respectively. In the case of the secondary sulfides, the C–S stretching vibration due to the S_{HH} conformation lies in the 630—660 cm^{-1} region. Our observed frequencies on the alkyl sulfides, therefore, in general correspond very well to the C–Cl stretching frequencies of alkyl chlorides[1] and the C–S stretching frequencies of alkyl disulfides,[2] although we cannot make a straightforward comparison of them with each other, since we could not take into consideration the bands due to the rotational isomers. The CH_3–S stretching frequencies of the fulfides fit the CH_3–Cl stretching frequency of methyl chloride better than the CH_3–S stretching frequencies of alkyl disulfides. Detailed vibrational treatments including the rotational isomers of these sulfides are now in progress; the results will be reported elsewhwere in the near future.

Thanks are due to Professor Hiromu Murata and Associate Professor Yuji Shiro for their valuable comments.

References

1) S. Mizushima, T. Shimanouchi, K. Nakamura, M. Hayashi, and S. Tsuchiya, *J. Chem. Phys.*, **26**, 970 (1957);

TABLE 1. CHARACTERISTIC C–S STRETCHING FREQUENCIES (cm^{-1}) OF ALKYL SULFIDES

Molecule	$\nu(CH_3\text{-}S)$	$\nu(\text{-}CH_2\text{-}S)$		$\nu(\rangle CH\text{-}S)$	Ref.
		P_H	P_C	S_{HH}	
C-S-C	744, 693				3
C-S-C_2	724	655			4
C-S-C_3	745		717		5
C-S-C_4	728		718		5
C_2-S-C_2		692, 656[a]			6
C_2-S-C_3		646	739		5
C_2-S-C_4		657[a]	731[b]		5
C_3-S-C_3			721, 711		5
C_3-S-C_4			744, 734		5
C_4-S-C_4			742, 733		5
C-S-C_3^i	727			638	7
C_2-S-C_3^i		678[a]		632[a]	8
C_3-S-C_3^i			740[a]	635[a]	8
C_4-S-C_3^i			731	652	8
C_3^i-S-C_3^i				658,[a] 655	8
	690—750	640—700	710—750	630—660	
Alkyl chlorides	732	645—690	720—730	605—640	1
Alkyl disulfides	680—700	630—670	700—750	590—640	2

a) Liquid-state bands. b) Average of the doublet-band.

J. J. Shipman, V. L. Folt, and S. Krimm, *Spectrochim. Acta*, **18**, 1603 (1962).
2) H. Sugeta, A. Go, and T. Miyazawa, *Chem. Lett.*, **1972**, 83.
3) M. Ohsaku, Y. Shiro, and H. Murata, This Bulletin, **45**, 113 (1972).
4) M. Ohsaku, Y. Shiro, and H. Murata, *ibid.*, **45**, 954 (1972).
5) M. Ohsaku, *J. Sci. Hiroshima Univ., Ser.* **A38**, 51 (1974).
6) M. Ohsaku, Y. Shiro, and H. Murata, This Bulletin, **45**, 956 (1972).
7) M. Ohsaku, Y. Shiro, and H. Murata, *ibid.*, **45**, 3480 (1972).
8) M. Ohsaku, to be published.

BULLETIN OF THE CHEMICAL SOCIETY OF JAPAN, VOL. 48(2), 709—710 (1975)

The Effect of Partial Deuteration on the Phosphorescence Lifetime of *N,N,N',N'*-Tetramethyl-*p*-phenylenediamine

Nobutoshi YOSHIDA and Nozomu EBARA

Department of Chemistry, College of General Education, The University of Tokyo, Komaba, Meguro-ku, Tokyo 153

(Received June 24, 1974)

Synopsis. A position-dependent deuterium effect on the phosphorescence lifetime of *N,N,N',N'*-tetramethyl-*p*-phenylenediamine was found. Aromatic ring protons and methyl protons were shown to contribute to the radiationless transition independently and differently. Important terms in the decay constant are briefly discussed.

Phosphorescence lifetimes have been measured for *N,N,N',N'*-tetramethyl-*p*-phenylenediamine (TMPD) and its deuterium derivatives;
(I) $(CH_3)_2N$–C_6H_4–$N(CH_3)_2$, (II) $(CH_3)_2N$–$C_6H_2D_2$–$N(CH_3)_2$, (III) $(CH_3)_2N$–C_6D_4–$N(CH_3)_2$ (91%), (IV) $(CD_3)_2N$–C_6H_4–$N(CD_3)_2$ (94%), and (V) $(CD_3)_2N$–C_6D_4–$N(CD_3)_2$ (85%).
II—V were prepared by ammonolysis of *p*-dibromobenzenes in an autoclave under a nitrogen pressure of 25 kbar followed by methylation with dimethyl sulfate in H_2O or D_2O.[1,2] Values in parentheses are the isotopic purities measured by low-voltage mass spectroscopy. II was a mixture of compounds in which deuterium was distributed statistically on the aromatic ring and NMR spectra showed its deuterium content to be ~50%. All samples were dissolved in 3-methylpentane(3MP) or in EPA, degassed with 6—7 freeze-thaw cycles. Phosphorescence lifetimes were measured at 77 K by a standard technique and the triplet decay was displayed on a Riken Denshi High Speed SP-J-5V recorder. The observed decays were exponential over 3—4 lifetimes. The results are listed in Table 1. k_{II} contains a considerable error, as II was a mixture of compounds with different rate constants. It was not discarded because the main part of k_{II} seems to come from the doubly substituted compound.

Following Watts and Strickler,[3] the triplet decay constant was expressed as

$$k = \tau^{-1} = k_d + N_{me}k_{me} + N_{ar}k_{ar},$$

where k_d is the decay constant in the perdeuterated TMPD (V), N_{me} and N_{ar} are the numbers of methyl and aromatic ring protons, and k_{me} and k_{ar} represent changes in the radiationless rate constants when a proton is replaced by a deuteron at the methyl or aromatic ring position, respectively. Our data fitted well to this equation with the least squares values of k_d=0.185, k_{me}=0.0046, and k_{ar}=0.030 s^{-1} in 3MP, and k_d=0.168, k_{me}=0.0038, and k_{ar}=0.029 s^{-1} in EPA. The coincidence is striking as can be seen from the last colume of Table 1. It shows that not only protons at different positions of an aromatic ring, but protons of different groups conform well to Watts' equation. An aromatic ring substitution was 6—8 times more effective in decreasing the decay rate than a methyl substitution. In contrast to toluene in which the methyl protons have a negligible effect,[4] those of TMPD showed a small but difinite effect. Generally lifetimes were longer in EPA than in 3MP.

TABLE 1. TRIPLET DECAY TIMES AND RATE CONSTANTS OF PARTIALLY DEUTERATED TMPD

Solvent	Compound	τ (s)	$k_{obs.}$ (s^{-1})	$k_{calc.}$ (s^{-1})	Δk (%)
3MP	I	2.7	0.37	0.36	−2.7
	II	3.4	0.29	0.30	+3.4
	III	4.2	0.24	0.24	0
	IV	3.3	0.30	0.31	+3.3
	V	5.3	0.19	0.19	0
EPA	I	2.9	0.34	0.33	−2.9
	II	4.0	0.25	0.27	+8.0
	III	4.5	0.22	0.21	−4.5
	IV	3.6	0.28	0.28	0
	V	5.9	0.17	0.17	0

The radiationless rate constant is represented by

$$k = \frac{2\pi}{\hbar}\rho \sum_l \left| \langle f|H_{so}|i\rangle \prod_m \langle \chi^f_{m,l}|\chi^i_m\rangle - \sum_n \frac{\hbar^2}{\mu_n}\left[\sum_j \frac{\langle f|H_{so}|j\rangle\left\langle j\left|\frac{\partial}{\partial Q_n}\right|i\right\rangle}{E_j - E_f} + \sum_k \frac{\left\langle f\left|\frac{\partial}{\partial Q_n}\right|k\right\rangle\langle k|H_{so}|i\rangle}{E_k - E_i}\right] \times \left\langle \chi^f_{n,l}\left|\frac{\partial}{\partial Q_n}\right|\chi^i_n\right\rangle \prod_{m\neq n}\langle \chi^f_{m,l}|\chi^i_m\rangle \right|^2,$$

where i and f denote initial and final pure spin electronic states and j and k are virtual pure spin states. χ^i_i and $\chi^f_{i,l}$ are the vibrational wave-functions coresponding to the normal coordinate Q_s and belonging to the mixed spin initial and final Born-Oppenheimer states, which we were to observe. Here, n refers to the promoting mode and m to the accepting mode. Suffix l runs over the final Born-Oppenheimer manifold Ψ^f_l, isoenergetic with each other and with the initial state, and belonging to a single mixed spin electronic state.

Assuming that a single accepting mode is excited in each of Ψ^f_l and ignoring the contribution of $\chi^f_{n,l}$ to the energy of Ψ^f_l, the sum over l can be replaced by the sum over m, so that the leading term in k becomes

$$k = [\langle S\rangle + \sum_n \langle P_n\rangle] \sum_m \langle A_m\rangle$$

with

$$\langle S\rangle = \frac{2\pi}{\hbar}\rho|\langle f|H_{so}|i\rangle|^2$$

$$\langle P_n\rangle = \frac{\pi\hbar^3}{\mu_n^2}\rho\left|\left[\sum_j \frac{\langle f|H_{so}|j\rangle\left\langle j\left|\frac{\partial}{\partial Q_n}\right|i\right\rangle}{E_j-E_f}\right.\right.$$
$$\left.\left. + \sum_k \frac{\left\langle f\left|\frac{\partial}{\partial Q_n}\right|k\right\rangle\langle k|H_{so}|i\rangle}{E_k-E_i}\right]\left\langle \chi_n^f\left|\frac{\partial}{\partial Q_n}\right|\chi_n^i\right\rangle\right|^2$$

and

$$\langle A_m\rangle = |\langle \chi_m^f|\chi_m^i\rangle|^2$$

where $\chi_{n,i}^f$ has been replaced by χ_n^f in accordance with the selection rule. In TMPD, the first term, $\langle S\rangle$, vanishes by symmetry.[5] For the promoting mode, n, Burland and Robinson[6] claimed that non-totally symmetric in-plane skeletal modes (b_{2u} in benzene) cause radiationless transition by contributing to the π-π Herzberg-Teller matrix elements, whereas Henry and Siebrand[7] stressed the importance of C–H out-of-plane modes which are responsible for σ-π vibronic terms due to breakdown of the Born-Oppenheimer approximation. The latter mechanism was used to account for the position dependent deuterium effect in benzene, naphthalene[7] and anthracene.[8] However, the relative importance of these two mechanisms has not yet been established. From our data we shall make a rough estimate of the relative contribution of two mechanisms. For simplicity, we take only three terms for the promoting modes; skeletal modes, ring C–H out-of-plane modes and ring C–D out-of-plane modes. Notations ⟨CC⟩, ⟨CH⟩ and ⟨CD⟩ stand for the terms $\langle P_n\rangle$ containing these modes. For the accepting mode m, there seems to be little doubt that the C–H stretching modes are most important: we retain only these modes in the present approximation. As the C–H bonds of the ring and those of the methyl group contribute different amounts, we denote their Franck-Condon integrals with ⟨R⟩ and ⟨M⟩, respectively. There are as many terms as there are normal modes, and these symbols represent sums of like terms. The rate of a radiationless transition is expressed by a sum of product terms; ⟨CC⟩⟨R⟩, ⟨CH⟩⟨R⟩, ⟨CD⟩⟨R⟩, ⟨CC⟩⟨M⟩, ⟨CH⟩⟨M⟩, and ⟨CD⟩⟨M⟩. For example $k_I = k_0 + \langle CC\rangle\langle R\rangle + \langle CH\rangle\langle R\rangle + \langle CC\rangle\langle M\rangle + \langle CH\rangle\langle M\rangle$, $k_{III} = k_0 + \langle CC\rangle\langle M\rangle + \langle CD\rangle\langle M\rangle$ and $k_{IV} = k_0 + \langle CC\rangle\langle R\rangle + \langle CH\rangle\langle R\rangle$, where k_0 represents the radiative rate constant. Then $k_I - k_{IV} = 0.070$ (3MP) corresponds to $\{\langle CC\rangle + \langle CH\rangle\}\langle M\rangle$ and $k_{III} - k_V = 0.050$ to $\{\langle CC\rangle + \langle CD\rangle\}\langle M\rangle$. Taking the ratio of these two expressions, we obtain

$$\frac{\langle CC\rangle + \langle CD\rangle}{\langle CC\rangle + \langle CH\rangle} = 0.71\,,$$

According to Siebrand,[7] ⟨CD⟩/⟨CH⟩ is roughly equal to $\omega_D\mu_H/\omega_H\mu_D$, where ω_H and ω_D are the frequencies and μ_H and μ_D are the reduced masses of the corresponding normal modes. Our measurement shows that

$$\frac{\omega_D\mu_H}{\omega_H\mu_D} = \frac{720}{812}\times\frac{7}{13} = 0.48\,,$$

which leads to

$$\frac{\langle CH\rangle}{\langle CC\rangle} = 1.3 \quad \text{(3MP)}\,.$$

A similar calculation gives 0.5 for EPA. The difference may be attributed to the rough approximation employed and to errors in the measured values. We can only infer that neither mechanism can be ignored. To account for the large difference in k_{ar} and k_{me}, we compare $k_I - k_{IV}$ with $k_{IV} - k_V$,

$$\frac{k_I - k_{IV}}{k_{IV} - k_V} = \frac{\langle CC\rangle\langle M\rangle + \langle CH\rangle\langle M\rangle}{\langle CC\rangle\langle R\rangle + \langle CH\rangle\langle R\rangle} = \frac{\langle M\rangle}{\langle R\rangle}.$$

This ratio is 0.6 in 3MP and 0.5 in EPA. Note that there are four terms in ⟨R⟩ and twelve terms in ⟨M⟩. The large difference between k_{ar} and k_{me} may therefore be attributed to the difference in Franck-Condon factors. As the ring protons are attached directly to the carbon atoms which carry π-electrons, it is quite natural that the electronic excitation causes a change in the ring C–H stretching normal modes to give a large k_{ar} value. The absence of contributions to the radiationless rate constant from alkyl groups in alkylbenzenes can be understood as they are separated from the π-electron center. In TMPD, however, the charge density at the nitrogen atom, which carries π-electrons, changes considerably when the molecule is excited, and this may have an inductive effect on methyl C–H bonds giving rise to a moderate deuterium effect.

References

1) A. J. Quick, *J. Amer. Chem. Soc.*, **42**, 1013 (1920).
2) "Organic Syntheses", Vol. 49, p. 107 (1969).
3) R. J. Watts and S. J. Strickler, *J. Chem. Phys.*, **49**. 3867 (1968).
4) D. M. Haaland and G. C. Nieman, *ibid.*, **59**, 1013 (1973).
5) If we assume D_{2h} pseudosymmetry for the molecule, the lowest triplet is B_{3u}. The presence of methyl groups slightly offsets the D_{2h} symmetry, but affects little on the selection rule. The detailed calculation will be presented elsewhere.
6) D. M. Burland and G. W. Robinson, *J. Chem. Phys.*, **51**, 4548 (1969).
7) B. R. Henry and W. Siebrand, *ibid.*, **54**, 1072 (1971).
8) B. R. Henry and W. Siebrand, *Chem. Phys. Lett.*, **7**, **533** (1970).

BULLETIN OF THE CHEMICAL SOCIETY OF JAPAN, VOL. 48(2), 711—712 (1975)

Photolysis of Ethylene at 1470 Å

Hiroshi HARA, Kenji KODAMA, and Ikuzo TANAKA

Department of Chemistry, Tokyo Institute of Technology, Ohokayama, Meguro-ku, Tokyo 152

(Received on July 1, 1974)

Synopsis. Relative quantum yields of the primary processes in the photolysis of ethylene at 1470 Å were determined. No energized vinyl radical was found. Photolysis in the presence of nitric oxide suggests that about 20% of 1-butene is produced through the direct addition reaction of excited ethylene to ground state ethylene, $C_2H_4^* + C_2H_4 \rightarrow 1\text{-}C_4H_8$.

The primary process of the photolysis of ethylene has been reported to be as follows.[1-4]

$$C_2H_4 + h\nu \longrightarrow C_2H_2 + H_2 \qquad \phi_1 \qquad (1)$$

$$\longrightarrow C_2H_2 + 2H \qquad \phi_2 \qquad (2)$$

$$\longrightarrow C_2H_3 + H \qquad \phi_3 \qquad (3)$$

The energized vinyl radical formation was found at 1634 Å.[5]

$$C_2H_4 + h\nu \longrightarrow H + C_2H_3^{**} \xrightarrow{k_d} C_2H_2 + H + H$$

$$C_2H_3^{**} \xrightarrow{k_s[M]} C_2H_3^*$$

$$H + C_2H_3^* \longrightarrow C_2H_3 + H$$

In this investigation, ethylene was photolyzed at 1470 Å in order to examine the existence of the energized vinyl radical and to determine the relative quantum yields of the primary processes.

Experimental

Experimental procedures were almost the same as described previously.[4] The light source of 1470 Å was an electrodeless discharge xenon lamp. The reaction cell was equipped with a LiF window.

Results and Discussion

The products of photolysis at 1470 Å were hydrogen, acetylene, ethane, *n*-butane, and 1-butene, and were the same as those at 1634 Å. No C_4 compounds other than *n*-butane and 1-butene were observed.

If the energized vinyl radical is formed at this wavelength, the ratio of 1-butene to *n*-butane should follow a straight line with a definite slope against ethylene pressure.[5] The ratios plotted as a function of ethylene pressure in Fig. 1 show no pressure dependence. Thus, existence of the energized vinyl radical in the photolysis at 1470 Å can be excluded. This is reasonable for the following reason. If the energized vinyl radical were formed at 1470 Å, the maximum available energy of the vinyl radical would be 89 kcal mol^{-1}, and that at 1634 Å 70 kcal mol^{-1}. At 1470 Å, therefore, the energized vinyl radical would decompose into acetylene and a hydrogen atom before being stabilized by collision.

Relative quantum yields of the primary processes were obtained assuming the same secondary processes as in the photolysis at 1634 Å[4]. The values are given in Table 1 together with other reported ones. Both values are seen to agree. The quantum yields at 1470 Å are shown in Table 2 together with those at 1634 and 1849 Å.[4] The relative quantum yields are wavelength dependent, *viz.*, ϕ_2 decreases and ϕ_3 increases with increasing wavelength, but not ϕ_1.

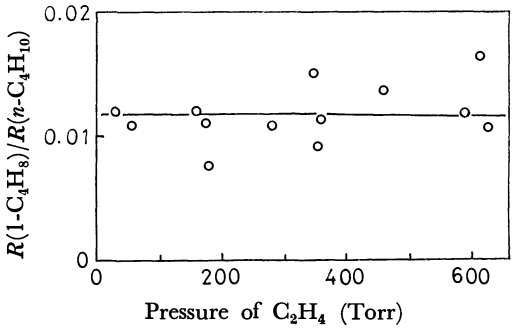

Fig. 1. $R(1\text{-}C_4H_8)/R(n\text{-}C_4H_{10})$ *vs.* pressure of ethylene (Torr).

Table 1. Relative quantum yields at 1470 Å

ϕ_1	ϕ_2	ϕ_3	Ref.
45%	54%	1%	This work
40	59	1	(3)
46	54	—	(6)

Table 2. Quantum yields at 1470, 1634, and 1849 Å

Wavelength	ϕ_1	ϕ_2	ϕ_3
1470 Å	45%	54%	1%
1634	47	48	5
1849	53	33	14

Relative yields of 1-butene and *n*-butane to acetylene were measured at various nitric oxide pressure with a fixed ethylene pressure (350 Torr) as shown in Table 2. On addition of nitric oxide, the yield of 1-butene decreased rapidly by about a factor of 5 and then became constant. On the other hand, the formation of *n*-butane was completely suppressed even at 0.46% nitric oxide. 1-Butene and *n*-butane removed by nitric oxide are formed through the recombination reactions of vinyl and ethyl radicals, and two ethyl radicals, respectively, since nitric oxide scavenges both ethyl[7] and vinyl radicals.[8] However, about 20% of 1-butene can be formed through a nonradical reaction, which is probably the direct addition of excited ethylene to a ground state one:

$$C_2H_4^* + C_2H_4 \longrightarrow 1\text{-}C_4H_8 \qquad (4)$$

The relative quantum yield ϕ_4 of this process, can be roughly estimated as follows.

Table 3. Relative yields of 1-C_4H_8 and n-C_4H_{10} to C_2H_2 in the presence of NO (C_2H_2=350 Torr)

(NO/C_2H_4)%	0	0.46	1.1	1.3	2.7	5.0	9.3
1-C_4H_8	0.0061	0.0011	0.0013	0.0010	0.0016	0.0013	0.0014
n-C_4H_{10}	0.52	0	0	0	0	0	0

$$\phi_4 = \phi(1\text{-}C_4H_8)/5$$
$$= \frac{k_7}{k_5+k_6+k_7} \cdot \frac{\phi_3}{5}$$
$$= 0.08\%$$

where the k's are the rate constants of the reactions.

$$C_2H_3 + C_2H_5 \longrightarrow 2C_2H_4 \quad (5)$$
$$\longrightarrow C_2H_2 + C_2H_6 \quad (6)$$
$$\longrightarrow 1\text{-}C_4H_8 \quad (7)$$

The quantum yield is very small compared with the others. At present, our results do not permit us to speculate on the nature of C_2H_4*.

References

1) Y. Inel, A. Siddiqi, and G. G. Meisels, *J. Phys. Chem.*, **75**, 1317 (1971).
2) P. Borrell, A. Cervenka, and J. W. Turner, *J. Chem. Soc. B*, **1971**, 2293.
3) P. Potzinger, L. C. Glasgow, and G. Von Bunau, *Z. Naturforsch.*, **27a**, 628 (1972).
4) H. Hara and I. Tanaka, This Bulletin, **46**, 3012 (1973).
5) H. Hara and I. Tanaka, *ibid.*, **47**, 1543 (1974).
6) M. C. Sauer, Jr., and L. M. Dorfman, *J. Chem. Phys.*, **35**, 497 (1961).
7) H. Seng and F. W. Lampe, *J. Phys. Chem.*, **76**, 3303 (1972).
8) M. G. Bellas, J. K. S. Wan, W. F. Allen, O. P. Strausz, and H. E. Gunning, *ibid.*, **68**, 2170 (1964).

BULLETIN OF THE CHEMICAL SOCIETY OF JAPAN, VOL. 48(2), 713—714 (1975)

Densities and Molar Volumes of Molten Binary $PrCl_3$–KCl, $PrCl_3$–NaCl, $PrCl_3$–$CaCl_2$, $NdCl_3$–KCl, $NdCl_3$–NaCl, $NdCl_3$–$CaCl_2$ Systems

Junichi Mochinaga and Kazuo Igarashi

Department of Synthetic Chemistry, Faculty of Engineering, Chiba University, Yayoi-cho, Chiba 280

(Received October 3, 1974)

Synopsis. The densities of $PrCl_3$, $NdCl_3$, $PrCl_3$–KCl, $PrCl_3$–NaCl, $PrCl_3$–$CaCl_2$, $NdCl_3$–KCl, $NdCl_3$–NaCl, and $NdCl_3$–$CaCl_2$ melts measured dilatometrically were represented by the empirical equations as functions of temperature. The molar volumes of the melts were calculated from the density data.

Densities and molar volumes of molten salts are the important properties in thermodynamic considerations, and are necessary to calculate the molar quantities. The ideal solution has the additivities of extensive properties except for entropy. Therefore, very few is known to have ideal behavior among the real mixture melts, but there are several molten mixture systems that have approximately the additive behavior for some of the extensive properties. In the previous paper, we reported on the densities and molar volume isotherms of molten YCl_3–KCl, YCl_3–NaCl, YCl_3–KCl–NaCl systems.[1] In the present experiment, the densities of 6 binary mixture systems ($PrCl_3$–KCl, –NaCl, –$CaCl_2$, and $NdCl_3$–KCl, –NaCl, –$CaCl_2$) in the molten state were measured, and the molar volume isotherm equations of these melts at 800 and 1000 °C were calculated.

Experimental

Materials. $PrCl_3$ and $NdCl_3$ were prepared by heating the respective rare-earth oxide with NH_4Cl at 350 and 370 °C, respectively, for 1.5 hr in evacuating with a rotary pump. The mixing ratio of NH_4Cl for each oxide was 2.5 times the theoretical amount. The chlorides were then purified by heating at about 850 °C *in vacuo* to remove the excess amount of NH_4Cl by sublimation. The analysis of impurities in the purified chlorides are shown in Table 1. The ratios of rare-earth and chlorine elements were 1 : 2.96 for both chlorides.

KCl, NaCl, and $CaCl_2$ were dried by heating *in vacuo* for 5 hr or more at the temperature lower by about 50 °C than the melting points of the salts.

Density Measurement. The dilatometric method was used. A dilatometer was made of transparent silica, and the volume of a dilatometer was determined by use of distilled water at room temperature because the thermal expansion coefficient of quartz is very smaller than that of molten salts. In the measurement the meniscus of melt in a dilatometer was read with a cathetometer.

Table 1. Impurities in $PrCl_3$ and $NdCl_3$[a]

$PrCl_3$		$NdCl_3$	
Element	Content (ppm)	Element	Content (ppm)
La	<50	Ce	160
Ce	<30	Pr	<30
Nd	<20	Sm	27
Sm	<20	Eu	<30

a) Fluorescent X-ray analysis.

Results and Discussion

Densities of Molten $PrCl_3$ and $NdCl_3$. Since the change in density of molten salt with increasing temperature is linear, the densities of molten $PrCl_3$ and $NdCl_3$ were represented by the following empirical equations as functions of temperature by use of the method of least squares for the density data observed.

$PrCl_3$; $d=4.139-1.030\times10^{-3}\,t$ $(850\leq t\leq1000)$

$\sigma=0.017$

$NdCl_3$; $d=3.992-0.8047\times10^{-3}\,t$ $(802\leq t\leq1009)$

$\sigma=0.011$

where d is the density of $PrCl_3$ or $NdCl_3$ melt in g/cm^3, t the temperature in °C. σ is the standard error of estimate in density equations in g/cm^3. The results were in fairly good agreement with the densities reported by Cho *et al.*[2]

Densities of Six Binary Systems. The density equations of molten mixtures in various compositions of six binary systems are shown in Table 2.

Molar Volumes of Binary Systems. Molar volume of mixture melt is calculated by the equation, $V_{mix}=\Sigma(X_i\cdot M_i)/d_{mix}$, where V_{mix} is the molar volume of the mixture melt, X_i the mole fraction of i-th component, M_i the molecular weight, and d_{mix} the density of the melt. The molar volume isotherm of $PrCl_3$–KCl system at 800 and 1000 °C are shown in Fig. 1. For six binary systems the molar volume isotherm equations are shown in Table 3.

The phase diagrams of binary $PrCl_3$–NaCl[3], $PrCl_3$–$CaCl_2$, $NdCl_3$–NaCl,[4] and $NdCl_3$–$CaCl_2$[4] systems

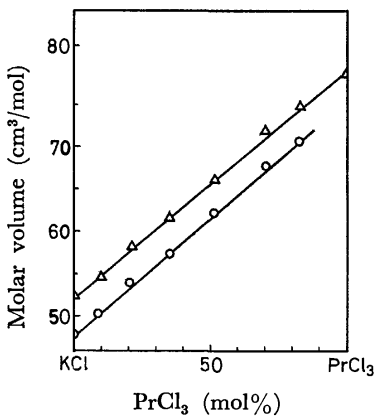

Fig. 1. Molar volume isotherm of $PrCl_3$–KCl system at 800 and 1000 °C: ○—800 °C, △—1000 °C.

TABLE 2. DENSITY EQUATIONS OF MOLTEN SYSTEMS $d=a+b\times10^{-3}t$ d: g/cm³, t: °C

System mol%	System mol%	a	b $\times10^{-3}$	Temp. range (°C)	σ (g/cm³) $\times10^{-2}$
(a) $PrCl_3$-KCl					
0.0	100.0	2.011	−0.609	849—1008	0.123
8.9	91.1	2.131	−0.539	800—958	0.489
20.5	79.5	2.416	−0.571	800—1000	0.701
33.8	66.2	2.777	−0.707	803—1000	0.286
50.3	49.7	3.149	−0.761	800—1000	0.320
68.5	31.5	3.532	−0.898	800—1000	1.07
81.4	18.6	3.721	−0.874	820—1000	1.01
(b) $PrCl_3$-NaCl					
0.0	100.0	2.024	−0.573	838—1021	0.375
11.6	88.4	2.503	−0.666	840—1005	0.678
25.8	74.2	2.772	−0.610	810—1000	0.701
39.4	60.6	3.046	−0.671	830—1000	0.769
61.9	38.1	3.429	−0.708	825—1000	0.311
75.2	24.8	3.648	−0.711	820—1000	0.392
(c) $PrCl_3$-$CaCl_2$					
0.0	100.0	2.473	−0.424	825—1011	0.504
9.7	90.3	2.639	−0.487	800—1000	0.155
20.6	79.4	2.867	−0.518	800—1000	0.132
35.2	64.8	3.143	−0.586	800—1000	0.321
50.7	49.3	3.377	−0.664	800—1000	0.207
66.8	33.2	3.685	−0.820	800—1000	0.512
80.3	19.7	3.844	−0.793	820—1000	0.527
(d) $NdCl_3$-KCl					
0.0	100.0	2.011	−0.609	849—1000	0.123
15.2	84.8	2.377	−0.615	820—1005	0.205
28.4	71.6	2.662	−0.640	832—1010	0.304
42.4	57.6	3.048	−0.738	810—1010	0.695
59.3	40.7	3.433	−0.828	748—1008	1.13
69.7	30.3	3.638	−0.885	772—1010	1.21
86.2	13.8	3.850	−0.875	724—1004	0.821
(e) $NdCl_3$-NaCl					
0.0	100.0	2.024	−0.573	838—1021	0.375
12.5	87.5	2.376	−0.537	858—1011	6.88
26.2	73.8	2.843	−0.692	820—1010	1.03
39.3	60.7	3.154	−0.720	743—1010	0.336
55.3	44.7	3.489	−0.783	750—1009	0.581
68.5	31.5	3.696	−0.857	732—1008	1.94
85.0	15.0	3.890	−0.843	748—1000	0.500
(f) $NdCl_3$-$CaCl_2$					
0.0	100.0	2.473	−0.424	825—1011	0.504
14.4	85.6	2.684	−0.442	820—1003	0.590
27.2	72.8	3.054	−0.623	730—1010	1.12
45.4	54.5	3.356	−0.688	730—1024	1.21
60.8	39.2	3.560	−0.701	733—1009	1.42
74.5	25.5	3.760	−0.794	730—1011	2.28
84.5	15.5	3.837	−0.737	740—1018	0.813

TABLE 3. MOLAR VOLUME ISOTHERM EQUATIONS OF BINARY MIXTURE SYSTEMS IN MOLTEN STATE

Binary system	Temp. (°C)	$V_{mix}=A+BX$ (V_{mix}: cm³/mol, X: mole fraction)	σ (cm³/mol)
$PrCl_3$-KCl	800	$V_{mix}=50.5+25.3X$	1.71
	1000	$V_{mix}=54.2+26.4X$	1.46
$PrCl_3$-NaCl	800	$V_{mix}=37.2+37.7X$	1.07
	1000	$V_{mix}=39.8+39.3X$	1.17
$PrCl_3$-$CaCl_2$	800	$V_{mix}=52.3+21.5X$	1.09
	1000	$V_{mix}=54.4+24.0X$	1.56
$NdCl_3$-KCl	800	$V_{mix}=49.8+25.4X$	0.98
	1000	$V_{mix}=53.7+25.5X$	0.80
$NdCl_3$-NaCl	800	$V_{mix}=37.5+37.2X$	0.51
	1000	$V_{mix}=40.2+38.4X$	0.59
$NdCl_3$-$CaCl_2$	800	$V_{mix}=52.3+22.0X$	0.81
	1000	$V_{mix}=54.6+23.6X$	0.84

X: mole fraction of rare-earth chloride in mixture melt

indicate the simple eutectic melts, and have no intermediate compounds. The linear molar volume isotherms of these systems at 800 and 1000 °C are the reasonable results, which may suggest the random mixing of ions in molten state. But the phase diagrams of $PrCl_3$–KCl[3,5] and $NdCl_3$–KCl[5] systems show the formation of intermediate compounds, and though the existance of complex ions in these mixture melts might be expected, the molar volume isotherms at 800 and 1000 °C have the linear behaviors.

The authors with to thank Mr. Matsuji Sato for assistance in the analysis of materials, and wish to thank Mr. Osamu Ugazin for his capable assistance in this work.

References

1) J. Mochinaga and K. Irisawa, This Bulletin, **47**, 364 (1974).
2) K. Cho, K. Irisawa, J. Mochinaga, T. Kuroda, *Electrochim. Acta*, **17**, 1821 (1972).
3) Z. N. Shevtsova, E. N. Korzina, B. G. Korshunov, *Zh. Neorg. Khim.* **7**, 2596 (1962).
4) I. S. Morzov, Z. N. Shevtsova, L. V. Klyukina, *ibid.*, **2**, 1639 (1959).
5) A. K. Baev, G. I. Novikov, *ibid.*, **6**, 2610 (1961).

BULLETIN OF THE CHEMICAL SOCIETY OF JAPAN, VOL. 48(2), 715—716 (1975)

The Separation and Determination of Chromium(VI) by Reducing Elution Using Anion Exchange Resin and Sodium Sulfite

Takashi YAMASHIGE, Hirofumi IZAWA, and Yasumasa SHIGETOMI*

Miyoshi Health Center, Miyoshi-shi 728

** Department of Chemistry, Okayama College of Science, Okayama-shi 700*

(Received March 14, 1974)

Synopsis. The reducing elution of chromium(VI) by anion exchange using sodium sulfite has been investigated. Chromium(VI) is reduced to chromium(III), which is eluted quickly and easily separated from interfering substances by colorimetry using diphenylcarbazide.

The contamination of an environment by heavy metals has become of interest in recent years. The standards of the content of total and hexavalent chromium for industrial waste water have been established by the Government.

Generally, chromium is determined by atomic absorption spectrophotometry[1] after extraction with MIBK. A simple determination as of JIS can be carried out by spectrophotometry using diphenylcarbazide, but this method necessitates the separation of chromium (VI) to prevent the interference of some metals and that of reducing substances.

Already, several separation methods of chromium such as precipitation by oxidation in basic media[2] and solvent extraction[3] using diethyldithiocarbamate, have been reported. However, it is imposible to determine only chromium (VI) using diphenylcarbazide after separating chromium by these methods. Also, the separation by cation exchange using acetate as the eluent[4] and that by anion exchange using mixed salts of thiocyanate and chloride as the eluent[5] are known.

However, these separation methods are not suitable for spectrophotometry using diphenylcarbazide.

The present authors examined the method of the separation of chromium (VI) by ion exchange, which is suitable for spectrophotometry using diphenylcarbazide. As a consequence of their experiments, the method of ion exchange using mixed solution of sulfuric acid and sodium sulfite as the eluent was found to be suitable for this purpose.

Experimental

A column 0.8 cm in diameter and 10 cm in length was loaded with 5.0 ml of 100—200 mesh Dowex 1X8(hydroxide form).

A Hitachi model 101 spectrophotometer was used for the determination of chromium(VI).

A reagent of a special grade was used without purification.

The elution curves were made of the metal content per 10 ml fraction of the eluate, after demasking by boiling, oxidizing to chromium(VI) and coloring.

Results and Discussion

Concentration of Sulfuric Acid and Sodium Sulfite. The following experiments were performed. Chromium(VI) absorbed on the column of anion-exchange resin is eluted with the mixed solution of sulfuric acid and sodium sulfite. The excess of sulfite in the effluent is decomposed by boiling it for 20 min. The process of adding 2 or 3 drops of 0.3% potassium permanganate solution to the solution and of then boiling it for 5 min is rereated until the color of permanganate is only. After subsequent cooling, 10-ml portion of 20% urea solution is added to 100 ml of the sample solution. Then a 10% sodium nitrate solution is added to the sample solution until the color of the permanganate disappears. Finally, diphenylcarbazide is added to the solution for colorimetry.

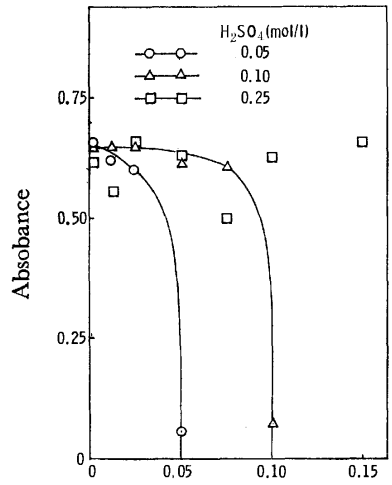

Fig. 1. Effects of concentration of H_2SO_4 and Na_2SO_3 on coloring.

In the above-mentioned experiments, we examined how the concentrations of sulfuric acid and sodium sulfite affected the absorbance. The results are shown in Fig. 1. For instance, when a mixed solution of 0.05 M sulfuric acid and 0.005 M sodium sulfite is used, the absorbance per ppm of chromium (VI) was 0.65, while in the case of 0.05 M sulfuric acid and 0.025 M sodium sulfite, the absorbance of the solution containing one ppm of chromium (VI) was 0.61. This means that, when more than 0.025 M sodium sulfite and 0.05 M sulfuric acid are used, sulfite remains after 20 minutes' boiling and so excess of permanganate has to be added in order to decompose the sulfite. As a result of this, the acidity in the sample solution falls and the absorbance lowered.

The tendency for the absorbance to be lowered is observed when more than 0.075 M sodium sulfite and 0.1 M sulfuric acid are used. Also, when more than

0.25 M sulfuric acid is used, the absorbance varies irregularly. Therefore it was concluded that the concentration of sulfuric acid should be 0.1 M while that of sodium sulfite in an eluent should be between 0.02 M and 0.005 M.

Elution of Chromium (VI) by the Mixed Solution of Sulfuric Acid and Sodium Sulfite. It was found that the direct addition of a mixed eluent leads to uncertain the elution curves, caused by foam generated by the neutralization heat which is brought about by the reaction of hydroxide in resin with sulfuric acid. Therefore, before the elution of chromium, hydroxide in resin was neutralized by introducing 0.1 M sulfuric acid, and then the chromium (VI) was eluted with a mixed solution of sulfuric acid and sulfite.

The metal content in a 10-ml fraction was determined by spectrophotometry using diphenylcarbazide after oxidation by the above-mentioned treatments. The results are shown in Fig. 2. In the first 50-ml effluent eluted by 0.1 M sulfuric acid alone, a slight amount of chromium was contained, but most of the chromium was contained in the next 200-ml fraction, obtained, using the eluent in which more than 0.01 M

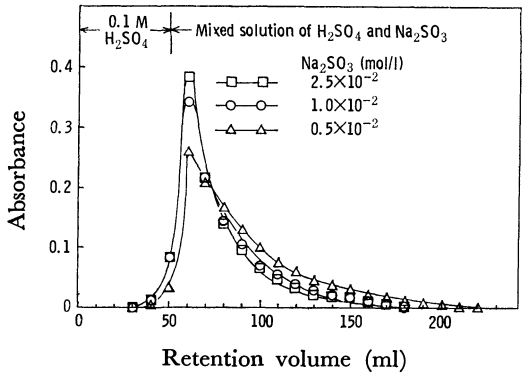

Fig. 2. Elution curves of Cr(VI), using mixed solution of H_2SO_4 and Na_2SO_3.

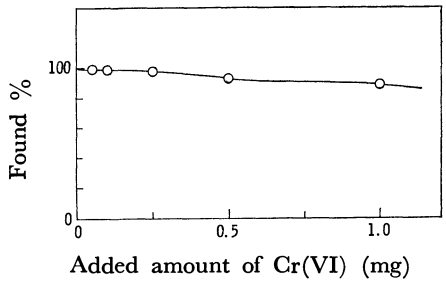

Fig. 3. Relation between found% and added amount.

Table 1. Determination of chromium(VI)[a]

Diverse subs.	ppm of diverse subs.	Cr(VI) ppm, found[b]	Cr(VI) ppm, found[c]
Fe^{+++}	0.5	0.48	0.45
Fe^{+++}	5.0	0.45	0.39
Zn^{++}	0.5	0.50	0.55
Pb^{++}	0.5	0.49	0.50
Cu^{++}	0.5	0.48	0.49
Cd^{++}	0.5	0.49	0.55
HCHO	1%	0.49	0.33
waste water	BOD 50 ppm	0.49	not detected

a) 0.5 ppm Cr(VI), added. b) After the separation. c) By JIS.

of sodium sulfite and more than 0.1 M of sulfuric acid were present.

When various quantities of chromium were added to the column and eluted by the same procedure, the found %, that is, the quantity of chromium in the effluent to that of the added chromium is as shown in Fig. 3. If less than 0.1 mg of chromium is used, most of the chromium is found in the first 250-ml effluent.

Effects of Diverse Substances. A 100-ml fraction of a solution containing 0.5 ppm chromium and various metals or reducing substances was introduced into the column. The chromium, separated by the above-mentioned treatment using 50 ml of sulfuric acid and 200 ml of the solution of 0.1 M sulfuric acid and 0.01 M sodium sulfite, was determined by spectrophotometry using diphenylcarbazide. The results are shown in Table 1 along with those obtained by determination by JIS. The reaction is interfered with by iron, zinc, and cadmium, and much by reducing substances. Especially, in BOD 50 ppm of industrial waste water, no chromium was detected, while chromium could be precisely analysed when this separation method was used.

References

1) T. Kōno, *Bunseki Kagaku*, **22**, 55 (1973).
2) E. B. Sandell, "Colorimetric determination of traces of metals," Interscience Publishers, Inc., New York (1959), p. 388.
3) K. Fukamachi, M. Morimoto, and M. Yanagawa, *Bunseki Kagaku*, **21**, 26, (1972).
4) A. K. De and A. K. Sen, *Talanta*, **13**, 1313, (1966).
5) J. Inczedy, "Analytical Applications of Ion Exchangers," Pergamon Press. (1962), p. 237.

BULLETIN OF THE CHEMICAL SOCIETY OF JAPAN, VOL. 48(2), 717—718 (1975)

Substitution Reaction of Ethylenediaminetetraacetatoaluminate(III) with Indium(III) in Aqueous Solutions

Michiko TSUCHIMOTO

Department of Industrial Chemistry, Tokyo University of Agriculture and Technology, Koganei, Tokyo 184

(Received April 25, 1974)

Synopsis. The kinetics of substitution reaction between the aluminium(III) EDTA complex and the indium-(III) ion has been studied in aqueous solutions of pH 2—10; the aluminium(III) complex is more labile than the gallium(III)[1] and the indium(III)[2] complex.

Previous kinetic studies on the isotopic exchange of ethylenediaminetetraacetatogallium(III),[1] indium-(III)[2] and thallium(III)[3] could not be extended to the corresponding aluminium(III) complex because of lack of suitable radioisotope. Indium(III) complex of EDTA (H_4Y) has a much greater stability constant than that of the aluminium complex $[AlY]^-$ and the following equilibrium shifts towards the right.

$$[AlY]^- + In^{3+} \rightleftarrows [InY]^- + Al^{3+} \quad (1)$$

EDTA complexes of tervalent cations have one mole of coordinated water. The formula would be more complicated than that written in terms of MY^- as done for the sake of simplicity. Determination of the rate of decrease in $[AlY]^-$ concentration is best. For measuring the rate of reaction (1) towards the right. However, $[AlY]^-$ cannot be determined quickly without separation, which takes too long as compared with the progress of the substitution reaction. Thus the concentration of free indium ions was determined by titration with EDTA. Since the liberated aluminium and excessive indium ions give a precipitate in the neutral or basic region, tartrate ions had to be added.

Reaction (1) is very fast below pH 2. The rate was determined in the pH regions 2—4, and 4—9.5 in the absence and the presence of tartrate ion, respectively. When the concentration of the indium ion ($\simeq 10^{-3}$ M) exceeds that of $[AlY]^-$ ($\simeq 10^{-4}$ M), a pseudo first-order kinetic law holds in the initial stages. The apparent first-order rate constant k_1 is a measure for the rate.

$$k_1 = (1/t) \ln (a/a-x) \quad (2)$$

The concentration of $[AlY]^-$ at time t is obtained from $(a-x)$, where x is the decrease in concentration of free indium(III) and a the initial concentration of $[AlY]^-$. The overall dependence of k_1 upon pH is shown in Fig. 1.

Titration of the indium ion took *ca.* 1 min., and had to be carried out at 3—10 min time intervals. The difference $(a-x)$ is relatively small as compared with a and x, and the overall error for k_1 values seems to be *ca.* ±10%. Hence only qualitative discussion was made for the initial stage of the reaction.

In Acid Region. The k_1 values increase almost linearly with increase in indium(III) ion concentration, being independent of the complex concentration at pH 2.8 (Table 1). The apparent Arrhenius activation energy is 13 kcal/mol at pH 2.8. The increase in k_1 below pH 2.5 seems to be due to acid catalysis. Dependence on indium(III) ion concentration can indicate either an electrophilic attack of indium(III) or the retardation of recombination of free acetate branch of partly dissociated $[AlY]^-$. Differentiation of the two mechanisms is difficult. However, the E_A values in acid do not differ from those in neutral or basic region. Hence the rate-determining step seems to lie in the dissociation of $[AlY]^-$, and the dependence on indium ion concentration can be reckoned as Lewis acid catalysis. Indium(III) may give an ion pair or a segment with the complex, retarding the recombination of the free end, $-CH_2COO^-$.

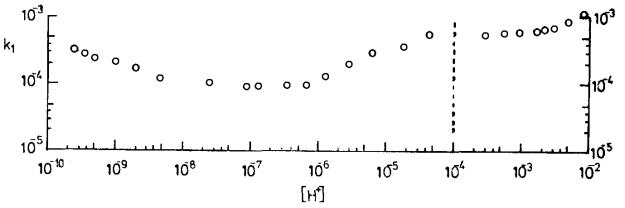

Fig. 1. pH Dependence of the rate constant k_1 in the whole pH region.
20 °C, I=0.2(KNO_3), In^{3+} 4.0×10^{-3} M, Al-EDTA 4.0×10^{-4} M; over pH 4, potassium tartrate 0.02 M, sodium barbiturate 0.002 M.

TABLE 1. RELATIONSHIP BETWEEN THE RATE CONSTANT k_1 AND THE CONCENTRATION OF UNCOMPLEXED INDIUM(III) AND Al-EDTA COMPLEX

[Al-EDTA] 10^{-4} M	[In^{3+}] 10^{-3} M	k_1 (s^{-1}) pH 8.7	pH 7.0	pH 2.8
3.2	4.0	1.5×10^{-4}	7.5×10^{-5}	
3.6	4.0	1.2×10^{-4}	8.1×10^{-5}	5.9×10^{-4}
4.0	4.0	1.3×10^{-4}	8.1×10^{-5}	5.7×10^{-4}
4.8	4.0	1.3×10^{-4}	7.9×10^{-5}	6.1×10^{-4}
5.6	4.0	1.2×10^{-4}	8.0×10^{-5}	6.0×10^{-4}
6.4	4.0	1.0×10^{-4}	5.4×10^{-5}	4.6×10^{-4}
8.0	4.0	1.0×10^{-4}	5.2×10^{-5}	4.5×10^{-4}
4.0	2.0			2.0×10^{-4}
4.0	3.2	1.0×10^{-4}	8.2×10^{-5}	3.5×10^{-4}
4.0	4.0	1.3×10^{-4}	8.1×10^{-5}	5.7×10^{-4}
4.0	4.8			6.8×10^{-4}
4.0	6.0	1.2×10^{-4}	7.9×10^{-5}	8.4×10^{-4}
4.0	8.0	1.2×10^{-4}	8.2×10^{-5}	

20 °C, I=0.2(KNO_3); at pH 7.0 and 8.7, potassium tartrate 0.02 M, sodium barbiturate 0.002 M.

In Neutral and Basic Region. Tartrate ion does not affect titration. k_1 is independent of the free indium(III) ion concentration, but increases linearly

Table 2. Influence of ionic strength(KNO_3) and potassium tartrate upon the rate constant k_1

KNO_3 (M)	Potassium tartrate (M)	k_1 (s^{-1}) pH 8.7	pH 7.0	pH 2.8
0.05	0.02	1.3×10^{-4}	7.5×10^{-5}	6.1×10^{-4}
0.4	0.02	1.4×10^{-4}	8.1×10^{-5}	5.5×10^{-4}
0.2	0.01	1.2×10^{-4}	7.0×10^{-5}	
0.2	0.016	1.4×10^{-4}	8.2×10^{-5}	
0.2	0.03	1.8×10^{-4}	1.5×10^{-4}	
0.2	0.04	2.2×10^{-4}	2.0×10^{-4}	

20 °C, In^{3+} 4.0×10^{-3} M, Al-EDTA 4.0×10^{-4} M; at pH 7.0 and 8.7, sodium barbiturate 0.002 M.

with increase in tartrate ion concentration (Table 2). E_A depends on the tartrate ion concentration; 16 and 13 kcal per mole in the presence of 0.02 M tartrate ion for 4.0×10^{-4} M complex, at pH 7.0 and 8.7, respectively. The buffering agent, barbiturate, does not affect the rate; neither does the ionic strength. k_1 decreases slightly with increase in the complex concentration.

The complex has a coordinated water which dissociates with a $pK\simeq10^{-6}$ and can be replaced by other ligands including tartrate.[4] Substitution of tartrate for the ligand water seems to facilitate the bond break of $[AlY]^-$. With increase in complex concentration, coordinated tartrate may act as a bridging ligand to give a binuclear complex such as $[YAl\cdot tart\cdot AlY]^{4-}$, which may dissociate with slightly greater difficulty than the uninuclear species.

Comparison with Related Reactions. It is remarkable that the dissociation reaction of $[AlY]^-$ is faster than that of the corresponding gallium(III) and indium(III) complex (*e.g.* R/a values are 1.7×10^{-5}, 4.3×10^{-5}, 3.7×10^{-5} and 4.0×10^{-5} s^{-1} for $[GaY]^-$ at pH 1.0 and 8.6 and $[InY]^-$ at pH 1.36 and 10.98, respectively.[1,2]). The lability of $[AlY]^-$ seems to be reflected in the smaller E_A values given above. (The E_A values for the isotopic exchange between MY^- and M^{3+} (M=Ga, In) are 15 to 18, and 25 kcal/mol, M in acid and basic regions respectively.[1,2]) Aluminium(III) is generally understood to be more inert than gallium(III) and indium(III) towards substitution reactions, on the basis of kinetic studies of solvent exchange in water and dimethylformamide,[5] intermolecular ligand isotopic exchange[6] and intramolecular site-exchange of β-diketonato complexes involving one bond break.[7] The present study does not allow more precise discussion because of experimental difficulty. The results, however, suggest remarkable influence of the ligand on the lability, especially of the coordinating atoms in such a multidentate ligand. Figure 1 shows a similar pattern to that of the isotopic exchange of $[GaY]^-$ and $[InY]^-$, although the details are different. Such must be the common pattern for substitution reactions of EDTA complexes of tervalent typical metal ions.

Experimental

Procedure. Aqueous solution (10^{-3} M, 50 ml) of indium(III) nitrate of a given pH containing potassium nitrate (and tartrate whenever necessary) was mixed with the complex[4] solution (10^{-4} M, 50 ml) of the same pH. Ten milliliter portions were withdrawn at appropriate time intervals, diluted with 20 ml of water (and 1 ml of 0.02 M potassium tartrate solution, when the reaction mixture does not contain tartrate ion), and titrated with 0.01 N disodium salt of EDTA with 0.1% xylenol orange solution (1 or 2 drops) as indicator, the pH being adjusted to 4—5 with an acetate buffer. The acid concentration below pH 4 was adjusted with nitric acid.

The free aluminium(III) ion liberated by reaction (1) did not interfere with the titration of free indium(III) in the presence of tartrate ion. Reaction (1) proceeds very slowly at pH 4—5 under the given conditions.

The author wishes to thank Professor Kazuo Saito, Tohoku University, for valuable discussions and suggestions, and Dr. Kazuko Ogino, Tohoku University, for numerical calculations.

References

1) K. Saito and M. Tsuchimoto, *J. Inorg. Nucl. Chem.*, **23**, 71 (1961).
2) K. Saito and M. Tsuchimoto, *ibid.*, **25**, 1245 (1963).
3) M. Tsuchimoto and K. Saito, *ibid.*, **27**, 849 (1965).
4) K. Saito and H. Terrey, *J. Chem. Soc.*, **4701** (1956).
5) Daniel Fiat and R. E. Connick, *J. Amer. Chem. Soc.*, **90**, 608 (1968).
6) K. Saito and M. Masuda, This Bulletin, **43**, 119 (1970).
7) J. J. Fortman and R. E. Sievers, *Coord. Chem. Rev.*, **6**, 331 (1971).

BULLETIN OF THE CHEMICAL SOCIETY OF JAPAN, VOL. 48(2), 719—720 (1975)

The Solubility Parameter of Tetrasulfur Tetranitride

Shuichi HAMADA, Yoshiyuki KUDO, and Masako KAWANO

Department of Chemistry, Faculty of Science, Science University of Tokyo, Kagurazaka, Shinjuku-ku, Tokyo 162

(Received June 3, 1974)

Synopsis. The solubilities of tetrasulfur tetranitride in thirteen organic solvents were measured. The solubility parameter of tetrasulfur tetranitride was estimated from the solubilities and its deduced activity to be 13.$_7$ at 25 °C; we assumed it to be regular.

Only a few solubilities of tetrasulfur tetranitride, S_4N_4, have been reported — for example, those for carbon disulfide, ethanol, dioxane, and benzene.[1] Consequently, the solubility parameter of this compound has not been reported. In this work, the solubilities and the solubility parameter of tetrasulfur tetranitride were estimated.

Experimental

Materials. The tetrasulfur tetranitride was prepared by the method described by Jolly and Goehring[2] and was recrystallized repeatedly from the benzene solution. Thirteen solvents were used to estimate the solubilities, as is shown in Table 1. All the solvents were purified in the usual ways.

Procedure. Suitable amounts of the tetrasulfur tetranitride and an organic solvent were put into a three-necked flask and were then stirred continuously for 2 hr at the temperature range from 20 to 40 °C (from 10 to 30 °C for the dichloromethane) with a precision of ±0.03 °C. An aliquot of the solution was withdrawn through a fine Teflon tube with a glass filter by applying an excessive pressure in the flask. The concentration of the solution was estimated from its optical absorbance at 400 nm, after it has been diluted to a suitable concentration, by using the working curves for the respective solvents previously determined with a double-beam spectrophotometer, model UV-200, from Shimadzu Seisakusho. The solubility was estimated repeatedly, at least three times, under the same conditions; its deviation from an average value was less than ±1.5%.

Results and Discussion

The X-ray powder diffractogram of the sample showed patterns attributable to tetrasulfur tetranitride only.[3] The melting point of the sample was determined microscopically to be 178—179 °C. This value agreed with that of the purified tetrasulfur tetranitride.[4,5]

The solubilities, X_2 (molar fraction), and the heats of solution, ΔH^d, of the tetrasulfur tetranitride in various solvents are shown in Table 1.

The absorption peak in the UV spectra of the tetrasulfur tetranitride was observed at approximately 250 nm in all the solvents except for those with themselves a strong absorption band near 250 nm. In the methanol and the ethanol solutions, a new absorption peak was observed at 420 nm, and the absorbance at 420 and 250 nm decreased with the lapse of time. When the alcoholic solutions were concentrated by heating, the tetrasulfur tetranitride decomposed into sulfate. Though the solubilities in the pyridine and the carbon disulfide at 25 °C (after 2 hr) were estimated to be 1.0×10^{-2} and 4.3×10^{-3} respectively, a black fine precipitate was deposited from the solutions on heating. Consequently, their data are not presented in Table 1.

Table 1. Solubilities, heats of solution, and solubility parameters of tetrasulfur tetranitride at 25 °C

Solvent	X_2 ($\times10^3$)	ΔH^d kcal/mol	δ_1[a]	δ_2
Methanol	0.23	9.9		
Ethanol	0.28	7.6		
Dichloromethane	5.3	4.8	9.7	14.$_0$
1,2-Dichloroethane	5.5	5.5	9.8	14.$_0$
1,1,2,2-Tetrachloroethane	11	4.9	9.7	13.$_3$
n-Hexane	0.32	7.7	7.30	13.$_4$
Cyclohexane	0.64	7.9	8.20	13.$_9$
Cyclooctane	1.2	7.6	8.55	13.$_9$
Benzene	4.9	5.5	9.15	13.$_5$
Chlorobenzene	5.7	5.8	9.5	13.$_7$
Dioxane	8.8	4.9	10.0	13.$_8$
Chloroform	5.7	5.2	9.3	13.$_5$
Carbon tetrachloride	1.7	6.5	8.6	13.$_7$

a) The solubility parameters of the solvents, δ_1, were those at 25 °C.[6]

It is assumed that these solutions are regular solutions,[7] the following equation can be obtained:[8]

$$RT\ln a_2 = RT\ln X_2 + V_2\phi_1^2(\delta_1-\delta_2)^2 \quad (1)$$

where a_2 is the activity of the solute based on its supercooled liquid state at a given temperature; V_2, the molar volume of the solute in the liquid state; ϕ_1, the volume fraction of the solvent; δ_1 and δ_2, the solubility parameters of the solvent and the solute, and R, the gas constant. The activity of the solute can be calculated by means of the following equation:[7]

$$\ln a_2 = -\frac{\Delta H^f}{R}\left(\frac{T_f-T}{T_fT}\right) \quad (2)$$

where ΔH^f is the molar heat of fusion, and T_f, the melting point of the solute.

The molar heat of the fusion of the tetrasulfur tetranitride was deduced approximately as the difference between the molar heat of sublimation, ΔH^s, and that of vaporization, ΔH^v; it could not be estimated because the tetrasulfur tetranitride decomposed with fusion. Sato[9] pointed out that the molar entropy of vaporization of the normal liquids related to their vapor pressures, p (mmHg), at given temperatures as follows:

$$\frac{\Delta H^v}{T} = 23.61\left(\frac{p}{T}\right)^{-0.119} \quad (3)$$

The calculated values agreed with the actual values with a precision of 5%. This relation was derived from the Hildebrand general rule.[10]

The vapor pressure of the tetrasulfur tetranitride at its melting point (178 °C) was calculated to be 10.8 mmHg from the vapor pressure at 90 °C and the molar heat of sublimation (3.51×10^{-2} mmHg and 21.2 kcal/mol),[5] while the temperature change in the molar heat of sublimation was neglected. Assuming that the relation of Eq. (3) is possible on an imaginary liquid tetrasulfur tetranitride, its molar heat of vaporization, ΔH^v, at the melting point was calculated to be 16.6 kcal/mol. From the difference in the ΔH^s and the ΔH^v, the molar heat of fusion of the tetrasulfur tetranitride was obtained to be approximately 4.6 kcal/mol. The activity of the tetrasulfur tetranitride at 25 °C was calculated from Eq. (2) to be approximately 7.2×10^{-2}.

By using the values of the a_2, the X_2, the V_2, the ϕ_1, and the δ_1,[6] the solubility parameter, δ_2, of the tetrasulfur tetranitride at 25°C was calculated from Eq. (1); the results are shown in Table 1. The molar volume, V_2, of the tetrasulfur tetranitride in the supercooled liquid state was deduced from the partial molar volume (86 cm^3/mol), which was itself estimated from the benzene solutions at 25 °C with a precision of ±0.01 °C by using a modified Lipkin-Davison-type pycnometer. The solubility parameter of the tetrasulfur tetranitride at 25 °C was estimated to be 13.$_7$ as an average value.

References

1) A. A. Vosnesenskij, "Solubilities of Inorganic and Organic Compounds," Vol. I, Part 2, ed, by H. Stephen and T. Stephen, Pergamon Press, Oxford (1963), p. 981.
2) W. L. Jolly and M. Becke-Goehring, *Inorg. Chem.*, **1**, 76 (1962).
3) S. Hamada, A. Takanashi, and T. Shirai, This Bulletin, **44**, 1433 (1971).
4) W. L. Jolly, "The Synthesis and Characterization of Inorganic Compounds," Prentice-Hall, Englewood, N. J. (1970), p. 502.
5) S. Hamada, This Bulletin, **46**, 3598 (1973).
6) J. H. Hildebrand and R. L. Scott, "The Solubility of Nonelectrolytes," Dover Publication, New York (1964), p. 435.
7) J. H. Hildebrand and R. L. Scott, *ibid.*, p. 66.
8) J. H. Hildebrand and R. L. Scott, *ibid.*, p. 270.
9) K. Sato, *Kagaku Kikai*, **14**, 270 (1950).
10) J. H. Hildebrand, *J. Amer. Chem. Soc.*, **37**, 970 (1915).

BULLETIN OF THE CHEMICAL SOCIETY OF JAPAN, VOL. 48(2), 721—722 (1975)

Composition of Single Crystal of Iron Sulfide Grown by Normal Freezing

Kohei AMETANI and Tatsuo TAKAHASHI

RCA Research Laboratories, Inc., Zushi-machi, Machida-shi, Tokyo 194-02

(Received July 6, 1974)

Synopsis. The composition of a single crystal of iron sulfide was determined as a function of position along the growth axis using atomic absorption spectrophotometry. The observed composition was consistent with the phase diagram for the iron-iron sulfide pseudo binary system and the results of physical measurements.

Single-crystal ingots of iron sulfide, FeS, are grown from iron-rich nonstoichiometric melts by normal freezing.[1] The maximum size of crystals obtained is 10 mm in diameter and 30 mm in length. To investigate the physical properties of this material, the composition must be determined as a function of position along the growth axis of the crystal. In this paper, a method using 25 mg of samples in each analysis is described. The sample is dissolved in nitric acid containing bromine and sulfur is precipitated as barium sulfate by adding a known amount of barium chloride. After filtration, iron is determined directly by its atomic absorption, and sulfur, indirectly by the atomic absorption of an excess barium content in the filtrate.[2]

Experimental

Reagents. The standard barium solution was prepared by dissolving barium chloride dihydrate in deionized water and standardized by chelatometry using EDTA (5 mg Ba/ml). The standard iron solution was prepared by dissolving iron metals (99.9% up) in hydrochloric acid and stocked as 0.1 M hydrochloric acid solution (1 mg Fe/ml). Reagents used were of analytical reagent grade.

Atomic Absorption Measurements of Iron and Barium. Atomic absorption measurements were made at 372.0 nm for iron and 553.6 nm for barium in a nitrous oxide-acetylene flame using a Hitachi model 208 atomic absorption spectrophotometer and hollow cathode lamps HLA-3. The nitrous oxide-acetylene flame is recommended over an air-acetylene flame for reducing or eliminating the chemical interference by coexisting elements.[3] However, barium has a relatively low ionization potential (5.21 eV) and is readily ionized in the nitrous oxide-acetylene flame, unless a large amount of an easily ionized element is added to suppress the barium ionization.[4] In this work, lanthanum chloride was used as the suppressor. We already described the usefulness of this reagent in the measurements of several rare earths[5] which have ionization potentials (5.67—6.8 eV) similar to barium. As shown in Fig. 1, the barium absorption was increased with an increase of the lanthanum chloride concentration. For example, in the presence of 5000 ppm of lanthanum chloride, the barium absorption is about 2.3 times greater than without this reagent. The iron absorption was not generally affected by the presence of lanthanum chloride. In this lanthanum chloride matrix, iron did not affect the barium absorption and *vice versa*.

Analysis of Single Crystals. Samples, 1.0—2.0 mm thick, were sliced from the single-crystal ingot of iron sulfide perpendicular to the growth axis for each analysis. Twenty-five mg of crystals were dissolved in 2 ml of concentrated nitric acid containing bromine. After the removal of nitric acid by evaporation with hydrochloric acid, the sample solution was diluted to about 40 ml and warmed to about 80 °C. The ferric ions were reduced to ferrous ions by adding ascorbic acid. The solution was adjusted to 0.05 M hydrochloric acid and sulfur was precipitated as barium sulfate by adding 9 ml of the standard barium solution (5 mg Ba/ml). The precipitate was allowed to settle for 1 hr on a hot water bath. After aging for more than 40 hr at room temperature, the precipitate was filtered and washed with six 5-ml portions of boiling water. The filtrate was adjusted to 0.1 M hydrochloric acid and 5000 ppm

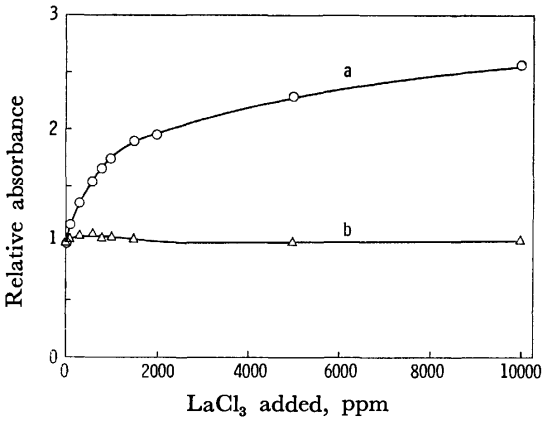

Fig. 1. Effects of lanthanum chloride on atomic absorptions of barium and iron in 0.1 M hydrochloric acid.
a: Ba 50 ppm, b: Fe 20 ppm.

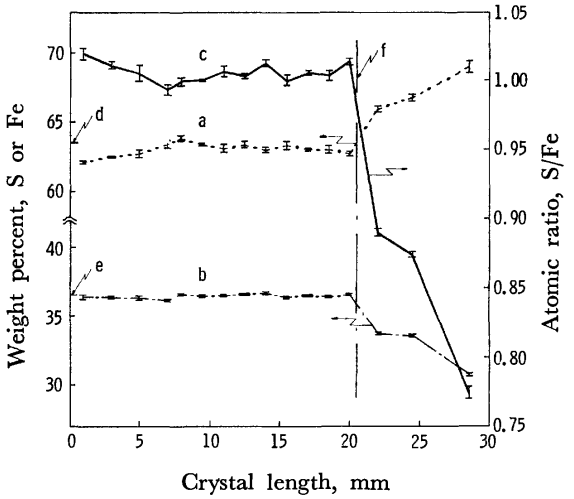

Fig. 2. Composition of the crystal as a function of position along the growth axis.
a: Fe wt%, b: S wt%, c: Atomic ratio S/Fe, d: Fe wt% expected for the composition FeS, e: S wt% expected for the composition FeS, f: Interphase boundary in crystal.

of lanthanum chloride. A similar adjustment was made for the iron and barium standards. Iron was determined directly by atomic absorption, and sulfur, indirectly by the atomic absorption of an excess of barium in the filtrate.

The results are shown in Fig. 2, where the observed wt% values of iron and sulfur are plotted as a function of position along the length of the crystal growth axis. The distance is measured from the bottom of the long single crystal. From the observed wt% values the calculated atomic ratio S/Fe is also plotted. The variation of the observed values for each analysis was usually ± 0.3 wt% for iron and ± 0.1 wt% for sulfur, so that the atomic ratio can be determined within ± 0.004. The sum of the wt% values for iron and sulfur ranged from 98.5 to 100.3 in all analyses. As can be seen in Fig. 2, the chemical composition at the bottom is slightly sulfur rich ($\sim FeS_{1.02}$), but is almost stoichiometric ($FeS_{1.00} \sim FeS_{1.01}$) starting from approximately 7 mm and up to the interphase boundary which appears at a height of 20.5 mm. Above the interphase boundary the composition becomes abruptly iron-rich. This compositional variation is consistent with the solidus curve in the phase diagram for the iron-iron sulfide system,[1,6] and also with the results of physical measurements, such as the transition temperature from hexagonal NiAs structure to distorted NiAs structure and metallographic observations.[1]

References

1) T. Takahashi, O. Yamada, and K. Ametani, *J. Crystal Growth*, **20**, 89 (1973).
2) K. Ametani, *Bunseki Kagaku*, **23**, 745 (1974).
3) M. D. Amos and J. B. Willis, *Spectrochim. Acta*, **22**, 1325 (1966).
4) J. A. Bowman and J. B. Willis, *Anal. Chem.*, **39**, 1210 (1967).
5) K. Ametani, This Bulletin, **47**, 2238 (1974).
6) E. Jensen, *Amer. J. Sci.*, **240**, 695 (1942).

BULLETIN OF THE CHEMICAL SOCIETY OF JAPAN, VOL. 48(2), 723—724 (1975)

The Reactions of Cyclic Sulfilimines with Cyanide Ion and Phosphine: Evidence for Substitution on Trivalent Sulfur

Tetsuo AIDA, Masashi NAKAJIMA, and Teruhiko INOUE

Department of Applied Chemistry, Faculty of Engineering, Osaka City University, Sugimoto-cho, Sumiyoshi-ku, Osaka 558

Naomichi FURUKAWA, and Shigeru OAE

Department of Chemistry, University of Tsukuba, Sakura-mura, Niihari-gun, Ibaraki 300-31

(Received January 18, 1974)

Synopsis. The effect of ring size on the reaction of *N*-*p*-tosylsulfilimine with such nucleophiles as CN^- and *n*-Bu_3P was investigated kinetically and compared with the effect on the reaction of the corresponding cyclic sulfonium salt. The results indicated that the S_N2–S process is more probable than the S_N2–N route.

Recently, we found that the reaction of alkyl aryl *N*-*p*-tosylsulfilimines with such nucleophiles as CN^- and *n*-Bu_3P[1,2] afforded the corresponding sulfides in high yields. We postulated two pathways for the mechanism of this reaction the one involving an initial nucleophilic attack on the trivalent sulfur atom by CN^- or *n*-Bu_3P(S_N2–S), the other proceeding *via* a rate-determining nucleophilic attack on the imine-nitrogen atom(S_N2–N). These two mechanisms are shown in Scheme 1. Although the kinetic and steric observations

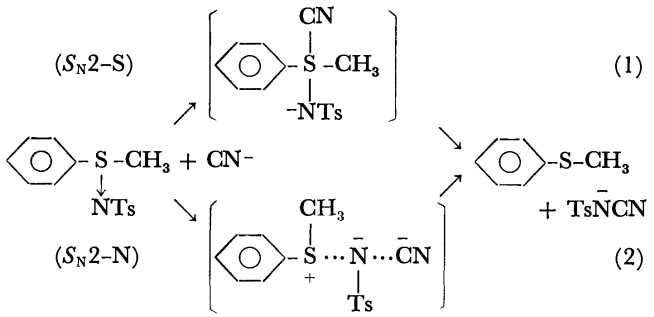

Scheme 1.

seem to support an S_N2 attack on the sulfur atom[3] (S_N2–S), mechanism(2) cannot be ruled out. One way to make choice between these two mechanisms is to compare the effect of ring size on the rate of the nucleophilic substitution reaction of cyclic sulfilimines with that on the analogous reaction of the corresponding cyclic sulfonium salt. Since the following sulfonium salts are known to react with nucleophiles to afford the cyclic sulfides *via* an S_N2 attack on the methyl carbon, the small effect of ring size on reaction(3) should also be found in reaction path(2).

$$(CH_2)_n S^+\text{-}CH_3 + Nu \rightarrow (CH_2)_n S + CH_3\text{-}Nu \quad (3)$$
$$(n=5,6,7;\ Nu=CN^-,\ n\text{-}Bu_3P)$$

In contrast, the effect of ring size would be substantial when the reaction proceeds *via* pathway(1) (S_N2–S), as in S_N2 attacks on sp^3 carbon atom[4] or in S_N2-like reactions of the trivalent sulfur atom.[5,6,7] In the reduction of cyclic sulfoxides by hydroiodic acid[8] which proceeds *via* the S_N2–S path, the reactivities fall in the following order: 5>7>6-membered rings, in keeping with the correlation between the reactivities and the steric effect for the transition complex (I). Johnson and his co-workers[9] also found a similar trend in the reaction of cyclic sulfoxides with sodium hydrogen sulfite, and postulated a transition state or an energetically contiguous intermediate (II) as shown below.

(I) (II)

Thus, we have carried out the reaction of cyclic *N*-*p*-tosylsulfilimines and cyclic sulfonium salts with CN^- or *n*-Bu_3P in DMF (Table 1) and compared the effects of ring size (5, 6, and 7-membered rings) in these systems by means of competition reactions (Table 2).

Inspection of these data indicates that the effect of ring size is a quite different in the two reactions. The effect of ring size on the reaction of sulfilimines with CN^- or *n*-Bu_3P is found to fall in the following order: 5>7>6-membered rings, whereas, for the sul-

TABLE 1. REACTION OF CYCLIC SULFILIMINE OR SULFONIUM SALT WITH NUCLEOPHILES[a]

Nucleophile	Yield of cyclic sulfide (%)					
	$(CH_2)_n S\rightarrow NTs$			$(CH_2)_n S^+\text{-}CH_3\ ClO_4^-$		
	$n=4$	5	6	4	5	6
CN^-	quant	quant	78	quant	quant	quant
n-Bu_3P	quant	quant	81	quant	quant	quant

a) These reactions were carried out in DMF solution.

TABLE 2. RELATIVE REACTIVITIES OF CYCLIC SULFILIMINE AND SULFONIUM SALT[a]

Nucleophile	Molar ratio of sulfide					
	$(CH_2)_n S\rightarrow NTs$			$(CH_2)_n S^+\text{-}CH_3\ ClO_4^-$		
	$n=4$	5	6	4	5	6
CN^-	15.0	1.0	13.0	0.7	1.0	1.5
n-Bu_3P	25.0	1.0	10.0	0.9	1.0	1.7

a) These reaction were carried out in DMF solution.

fonium salts only small differences of the reactivities were found. Therefore, we conclude that the reactions of sulfilimines with CN^- and n-Bu_3P proceed *via* route 1 and not *via* the S_N2–N route.

Experimental

Materials. *Cyclic* N-p-*Tosylsulfilimines*: All the cyclic *N-p*-tosylsulfilimines were prepared by the modified Mann-Pope reaction[10] from the corresponding sulfides and chloramine-T. For the five membered cyclic sulfide a commercial product was used without purification, while the six and seven membered ones were prepared by known methods.[9] All the cyclic *N-p*-tosylsulfilimines were identified by comparing their mp, IR and NMR spectra with those reported earlier.[10]

Cyclic Sulfonium Perchlorates: All the cyclic sulfonium perchlorates were prepared by treating the corresponding sulfides with methyl iodide and silver perchlorate in methanol solution.

Competitive Reaction of Cyclic N-p-*Tosylsulfilimine with Nucleophile*: A typical run was as follows. A mixture of each of the cyclic *N-p*-tosylsulfilimines(5, 6, and 7-membered cyclic sulfilimines, each 0.1 mmol) and NaCN (0.2 mmol) was dissolved in 4 ml of DMF and the whole solution was placed in a sealed tube. It was heated in a constant temperature oil bath at 100°C for 5 hr. The tube contents were then poured into ice-water and the sulfide formed was extracted with petroleum ether. The distribution of the sulfides was determined by gas chromatography; the molar ratio of 5 : 6 : 7-membered cyclic sulfides was 15.0 : 1.0 : 13.0.

Competitive Reaction of Cyclic Sulfonium Perchlorate with Nucleophile: A typical run was as follows. One ml of DMF solution containing all the cyclic sulfonium salts (5, 6, and 7-membered cyclic derivatives, each 0.1 mmol) and 1 ml of DMF solution of tri-*n*-butyl phosphine (0.2 mmol) were prepared. Both solutions were kept at constant temperature (100 °C) in an oil bath before mixing. The reaction was started by mixing the two solutions and continued for 3 hr. The reaction mixture was then poured into 5 ml of water and the sulfides formed were extracted with 1 ml of petroleum ether. The distribution of the sulfides formed in the reaction was determined by gas chromatography: The molar ratio of 5 : 6 : 7-membered cyclic sulfides was 0.9 : 1.0 : 1.7. The reaction of cyclic sulfonium perchlorates with NaCN was carried out at 100 °C for 1 hr and the distribution of sulfides formed in the reaction was determined as described above.

References

1) S. Oae, T. Aida, K. Tsujihara, and N. Furukawa, *Tetrahedron Lett.*, **1971**, 1145.
2) T. Aida, N. Furukawa, and S. Oae, *Chem Lett.*, **1973**, 805; **1974**, 121.
3) S. Oae, T. Aida, and N. Furukawa, *Int. J. Sulfur Chem.*, **8**, 73 (1973).
4) P. J. C. Fierens and P. Verchelden, *Bull. Soc. Chim. Belges.*, **61**, 427 (1952); S. F. Van Straten, P. V. Nicholls, and C. A. Einkler, *Can. J. Chem.*, **29**, 372 (1951).
5) T. Aida, N. Furukawa, and S. Oae, unpublished result.
6) T. Aida, N. Furukawa, M. Nakajima, and S. Oae, *Tetrahedron*, **30**, 947 (1974).
7) T. Aida, N. Furukawa, and S. Oae, unpublished result.
8) S. Tamagaki, M. Mizuno, H. Hirota, and S. Oae, This Bulletin, **44**, 2456 (1971).
9) C. R. Johnson, C. C. Bacon, and J. J. Rigau, *J. Org. Chem.*, **37**, 919 (1972).
10) K. Tsujihara, N. Furukawa, K. Oae, and S. Oae, This Bulletin, **42**, 2631 (1969).

BULLETIN OF THE CHEMICAL SOCIETY OF JAPAN, VOL. 48(2), 725—726 (1975)

The Syntheses of Several Pyrimido[4,5-*e*][1,2,4]triazines

Takashi SUGIMOTO and Sadao MATSUURA

Department of General Education, Nagoya University, Nagoya 464

(Received July 1, 1974)

Synopsis. A new synthetic method for some derivatives of pyrimido[4,5-*e*][1,2,4]triazine, using 5-nitrosopyrimidines as the starting materials, was studied. That is, the condensation of 5-nitrosopyrimidin-2,4,6-trione and its methyl derivative with amino- or alkylamino-guanidine gave several 3-aminopyrimidotriazin-6,8-diones.

The discovery and identification of three naturally-occuring antibiotics, Toxoflavin,[1,2] Fervenulin,[3,4] and MSD-92,[5,6] derivatives of pyrimido[5,4-*e*][1,2,4]triazine, have aroused considerable interest in the syntheses and chemistry of these antibiotics and related compounds.[7-10] The isomeric pyrimido[4,5-*e*][1,2,4]-triazine series is also of increasing interest recently[11-14] because certain derivatives of this series have been found to have antiviral activities.[15,16] In this paper we wish to report a convenient method for the synthesis of several derivatives of the latter series, using readily-available 5-nitrosopyrimidines as the starting material.

Heating 1,3-dimethyl-5-nitrosopyrimidin-2,4,6-trione (**2**) with 2-amino-1-ethylguanidine in dimethylformamide(DMF) under reflux gave 3-ethylamino-5,7-dimethylpyrimido[4,5-*e*][1,2,4]triazin-6,8-dione(**7**) in a single step. A similar procedure afforded its 3-methylamino analogue(**6**), but failed to give their 5,7-demethyl homologues (**9**, **10**); when 5-nitrosopyrimidin-2,4,6-trione(**1**) was boiled in DMF with 2-amino-1-ethyl(or methyl)guanidine, only dark-colored materials were obtained. However, the treatment of **1** in boiling dil. hydrochloric acid with aminoguanidine afforded alloxane guanylhydrazone(**3**) in a good yield; this cyclized to 3-aminopyrimidotriazin-6,8-dione(**8**)[17] in boiling ammonia. Similarly, its 3-methylamino[17] and 3-ethylamino[18] analogues(**9**, **10**) were made from **1** and 2-amino-1-methylguanidine or the ethyl homologue respectively *via* the corresponding guanylhydrazones(**4**, **5**).

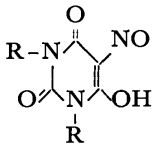

1, R=H
2, R=CH_3

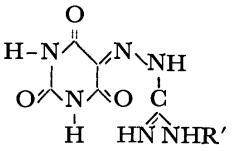

3, R′=H
4, R′=CH_3
5, R′=C_2H_5

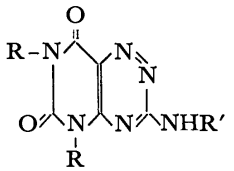

6, R=R′=CH_3
7, R=CH_3, R′=C_2H_5
8, R=R′=H
9, R=H, R′=CH_3
10, R=H, R′=C_2H_5

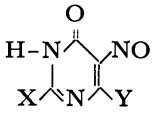

11, X=NH_2, Y=OH
12, X=OH, Y=NH_2
13, X=OH, Y=$NHCH_3$

Attempts to make the 6-amino analogue of **8** from 2-amino-5-nitrosopyrimidin-4,6-dione(**11**) and aminoguanidine in a similar manner resulted only in the formation of **8**; the starting aminopyrimidine inevitably suffered hydrolysis at the initial condensation step under the conditions employed and gave **3**. Similarly, the reaction of 4-amino-5-nitrosopyrimidin-2,6-dione (**12**) or its 4-methylamino analogue(**13**) with aminoguanidine again gave only the same guanylhydrazone (**3**).

Experimental

The analyses were done by the Analytical Section, Meijo University, Nagoya; the UV spectra were measured with a JASCO model ORD/UV-5 spectrophotometer.

*3-Ethylamino-5,7-dimethylpyrimido[4,5-*e*][1,2,4]triazin-6,8-dione (**7**) and its 3-Methylamino Analogue (**6**).* A solution of **2** (3.5 g) and 2-amino-1-ethylguanidine·2HCl (3.5 g) in DMF (40 ml) was boiled under reflux for 1 hr. The subsequent removal of the solvent under reduced pressure and the trituration of the residue with water (10 ml) gave colorless needles (1.3 g) of **7**; mp 267—267.5 °C (from methanol) (Found: C, 45.8; H, 5.0; N, 35.7%. Calcd for $C_9H_{12}N_6O_2$: C, 45.8; H, 5.1; N, 35.6%); λ_{max}^{MeOH} nm (log ε): 338 (3.90), 257 (4.19), and 224 (4.46).

The use of 2-amino-1-methylguanidine·HBr in place of its ethyl homologue in the foregoing condensation gave **6** (36%), mp 290—291 °C (from water) (Found: C, 43.5; H, 4.4; N, 38.0%. Calcd for $C_8N_{10}N_6O_2$: C, 43.2; H, 4.5; N, 37.8%); λ_{max}^{MeOH} nm (log ε); 337 (3.92), 255 (4.19), and 223 (4.49).

*3-Aminopyrimido[4,5-*e*][1,2,4]triazin-6,8-dione (**8**).* A solution of **1** (1.6 g) and aminoguanidine bicarbonate (1.5 g) in 1M–HCl (100 ml) was boiled under reflux for 1 hr. The subsequent concentration under reduced pressure to *ca.* 30 ml and chilling gave **3** as hydrochloride (1.7 g); mp >300 °C (Found: C, 25.6; H, 2.9; N, 36.1%. Calcd for $C_5H_6N_6O_3$·HCl: C, 25.6; H, 3.0; N, 35.8%). The same compound was also obtained from **11** (52% yield), **12** (58% yield), and **13** (55% yield) when these aminopyrimidines were treated with aminoguanidine as above; the structure of the product was confirmed by satisfactory elemental analyses.

A suspension of **3** (hydrochloride, 2.0 g) in 1% ammonia (100 ml) was boiled under reflux for 2 hr. The subsequent acidification with formic acid gave an ivory powder (1.5 g, 93%) of **8**; mp 300 °C (lit,[17] mp>350 °C) (Found: C, 33.1; H, 1.45; N, 46.8%. Calcd for $C_5H_4N_6O_2$: C, 33.1; H, 2.2; N, 46.7%); pK_a 7.08±0.03; λ_{max} nm (log ε) at pH 4.0: 327(3.85) and 244(4.11); at pH 9.3: 335(3.93), 255(sh., 3.93), and 229(4.56).

*3-Methylaminopyrimido[4,5-*e*][1,2,4]triazin-6,8-dione (**9**).* A solution of **1** (3.5 g) and 2-amino-1-methylguanidine·HBr (5.0 g) in 1M–HCl (100 ml) was boiled for 5 hr, and then the solution was treated as above to give **4** as hydrochloride (4.0 g); mp ~300 °C (Found: C, 28.9; H, 3.4;

N, 33.7%. Calcd for $C_6H_8N_6O_3 \cdot HCl$: C, 29.0; H, 3.65; N, 33.8%). Similar treatments of **11**, **12**, and **13** with 2-amino-1-methylguanidine gave the same product (**4**) in 77, 79, and 73% yields respectively.

A suspension of **4** (hydrochloride, 2.5 g) in 1% ammonia (100 ml) was refluxed for 2.5 hr. The resulting solution was acidified with formic acid and chilled to give a colorless powder (1.2 g, 63%) of **9**; mp>300 °C (lit,[17] mp>350 °C) (Found: C, 36.7; H, 3.0; N, 43.5%. Calcd for $C_6H_6N_6O_2$: C, 37.1; H, 3.1; N, 43.3%); pK_a 7.24±0.04; λ_{max} nm (log ε) at pH 4.0: 360(sh., 3.74), 335(3.83), and 254(4.20); at pH 9.6: 360(sh., 3.89), 341(3.96), 265(sh., 3.91), and 235(4.57).

*3-Ethylaminopyrimido[4,5-e][1,2,4]triazin-6,8-dione (**10**).* A solution of **11** (4.0 g) and 2-amino-1-ethylguanidine·HBr (7.0 g) in 1M-HCl (100 ml) was boiled for 5 hr. The subsequent chilling of the solution gave yellow leaflets (2.0 g) of **5** as hydrochloride; mp>300 °C (Found: C, 31.8; H, 4.1; N, 32.3%. Calcd for $C_7H_{10}N_6O_3HCl$: C, 32.0; H, 4.2; N, 32.0%). The heating of **5** with 1% ammonia as above gave **10** (75% yield); mp>300 °C (lit,[18] mp >350 °C) (Found: C, 40.9; H, 3.7; N, 41.2%. Calcd for $C_7H_8N_6O_2$: C, 40.4; H, 3.9; N, 40.4%).

References

1) A. G. van Veen and W. K. Mertens, *Rec. Trav. Chim. Pays-Bas*, **53**, 257 and 398 (1934).

2) G. D. Daves, Jr., R. K. Robins, and C. C. Cheng, *J. Amer. Chem. Soc.*, **84**, 1724 (1962).

3) C. DeBoer, A. Dietz, J. S. Evans, and R. M. Michaels, *Antibiotics Annual*, 220(1959—1960).

4) G. D. Daves, Jr., R. K. Robins, and C. C. Cheng, *J. Org. Chem.*, **26**, 5256(1961).

5) T. W. Miller, L. Chaiet, B. Arison, R. W. Walker, N. R. Trenner, and F. J. Wolf, "Antimicrobial Agents and Chemotrapy," (1963), p. 58.

6) E. C. Taylor and F. Sowinski, *J. Amer. Chem. Soc.*, **91**, 2143(1969).

7) D. J. Brown and R. K. Lynn, *Aust. J. Chem.*, **26**, 1689(1973).

8) G. Blankenhorn and W. Pfleiderer, *Chem. Ber.*, **105**, 3334 (1972).

9) F. Yoneda and T. Nagamatsu, *Tetrahedron Lett.*, **1973** 1577.

10) F. Yoneda and T. Nagamatsu, *J. Amer. Chem. Soc.*, **95**, 5735 (1973).

11) D. J. Brown and J. Kershaw, *J. Chem. Soc., Perkin I*, **1972**, 2316.

12) E. C. Taylor and F. Sowinski, *J. Amer. Chem. Soc.*, **90**, 1374(1968).

13) E. C. Taylor and S. F. Martin, *J. Org. Chem.*, **35**, 3792(1970).

14) E. C. Taylor and S. F. Martin, *ibid.*, **37**, 3958(1972).

15) C. Küchler, W. Küchler, and L. Heinisch, *Arzneim.-Forsch.*, **16**, 1122(1966).

16) F. Yoneda, *Kagaku no Ryoiki*, **24**, 1077(1970).

17) L. Heinisch, W. Ozegowski, and M. Mühlstädt, *Chem. Ber.*, **97**, 5(1964).

18) L. Heinisch, *ibid.*, **100**, 893 (1967).

BULLETIN OF THE CHEMICAL SOCIETY OF JAPAN, VOL. 48(2), 727—728 (1975)

The Synthesis of 24-Norfriedel-4-en-3-one

Hiroshi KAKISAWA, Tsuneyuki HORIE, and Takenori KUSUMI

Department of Chemistry, Tokyo Kyoiku University, Otsuka, Bunkyo, Tokyo, 112

(Received July 1, 1974)

Synopsis. The lead tetraacetate oxidation of 24-hydroxyfriedel-3-ene, prepared from friedelin, afforded a 3-acetoxy-24-norfriedel-4-ene, which was then convered into the title compound.

Pristimerin and celastrol have been shown to have the carbon skeleton of 24-norfriedelane.[1] In connection with the structural investigation of these compounds, we studied the removal of the 24-methyl group from friedelin.

The functionalization of the 24-methyl group in friedelin was studied by Fukuda *et al*;[2] they prepared 3β-hydroxyfriedelan-24-oic acid lactone from 3β-friedelanol (I R=H) by lead tetraacetate–iodine oxidation, followed by chromic oxidation, or by the photolysis of a nitrile (I R=NO), followed by the oxidation of the resulting oxime. Although photoirradiation on 3β-friedelanol (I R=H) in the presence of iodine and mercuric oxide had been reported to form 3β,24-oxidofriedelane (II R=CH_3),[3] Wenkert and Mylari pointed out that the same reaction in the presence of lead tetraacetate instead of mercuric oxide affords 25-iodo-3β,24-oxidofriedelane (II R=CH_2I) besides 3β,24-oxide (II R=CH_3).[4] The formation of the iodo ether seems to be due to an excess of the oxidizing reagent in the photolysis. The photolysis of 3β-friedelanyl hypobromite (I R=Br), which had been prepared from friedelanol, bromine, and mercuric oxide in a dark place, is found to afford 3β,24-oxidofriedelane (II R=CH_3) in a modest yield.

Upon treatment with boron trifluoride-etherate and acetic anhydride, the ether linkage of 3β,24-oxide (II R=CH_3) was cleaved to afford a homoallyl acetate (III R=Ac),[3] which was then further converted into the corresponding alcohol (III R=H) by alkaline hydrolysis. Attempts to remove the hydroxymethyl group of (III R=H) *via* an epoxy derivative (IV) were unsuccessful. However, it was found that the reaction of (III R–H) with lead tetraacetate caused the elimination of the methylol group, affording a norcompound with the composition of $C_{31}H_{50}O_2$. This product showed an acetoxyl absorption band in the IR spectrum at 1730 cm^{-1} and gave a postive test with tetranitromethane. The NMR spectrum indicated a singlet at δ 2.05 due to the methyl group bonded to an olefin group and a multiplet at δ 5.06 assignable to either a carbinyl proton of allyl acetate or a vinyl proton. The product, therefore, appeared to be an unsaturated noracetate, most probably either 3-acetoxy-24-norfriedel-4-ene (V R=Ac) or 5-acetoxy-24-norfriedel-3-ene (VI). The base hydrolysis of the acetate afforded a corresponding allyl alcohol, the NMR spectrum of which showed a new signal at δ 3.86 instead of the signal at δ 5.06 in the original acetate. This change indicates that the signal at δ 5.06 is due to a carbinyl proton of allyl acetate, and

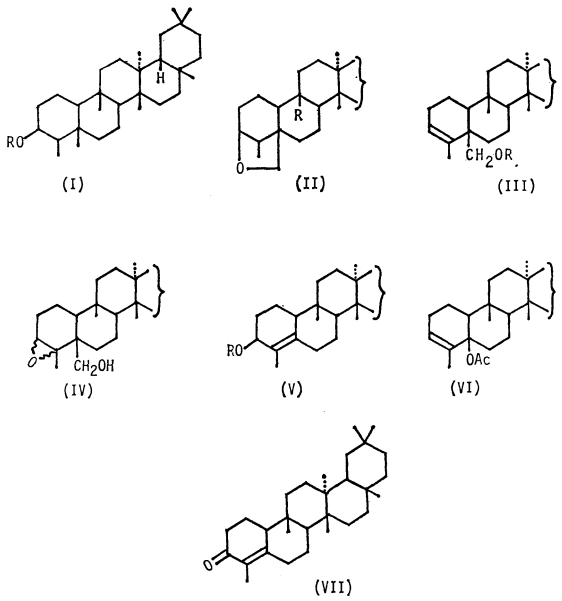

so the structure (V) is assigned to the lead tetraacetate oxidation product. The allyl alcohol (V R=H) was finally converted by oxidation with manganese dioxide into the α,β-unsaturated ketone (VII), which has the desired 24-norfriedelane carbon skeleton.

Experimental

3β-Friedelanol (I R=H). Sodium borohydride (4 g) was added portion by portion to a solution of friedeline (3 g) in diglyme (800 ml), and then the mixture was allowed to stand for 15 hr. After the addition of water (1000 ml), the separated precipitate was collected, washed with water, and dried. The material was recrystallized from chloroform to give 2.2 g of 3β-friedelanol (mp 270—273°C), which was identical with the sample prepared by the authentic method.[1]

3β,24-Oxidofriedelane (II R=CH_3). To a solution of 3β-friedelanol (500 mg) in carbon tetrachloride (1000 ml) containing yellow mercury oxide (900 mg), was added drop by drop a solution of bromine (0.08 ml) in carbon tetrachloride (3 ml) at 0 °C over 1-hr period in a place protected from light. After it had been stirred for 3 hr at 0°C, the mixture was filtered and the filtrate was irradiated with a tungsten lamp (300 W; 15 cm from the liquid level) at 0 °C under a nitrogen atmosphere for 1 hr, after which period the orange color of the solution had faded. The solution was washed with an aqueous sodium chloride solution, dried, and evaporated to give a white solid. The crude product was dissolved in benzene. The solution was purified through a column of alumina (15 g). Elution with benzene yielded 240 mg of pure oxide, which was then recrystallized from chloroform; mp 210—212 °C, ν (KBr) 2980—2850, 1450, 1380 cm^{-1}, $\delta(CDCl_3)$ 3.40(1H,d,J=8 Hz), 3.86(1H,m), 4.24(1H), 4.24(1H,d,J=8 Hz).

24-Hydroxyfriedel-3-ene (III R=H) was prepared from the oxide (II R=CH_3) by the method developed by Courtney and Stern.[3]

3-Acetoxy-24-norfriedel-4-ene (V R=Ac). To a stirred solution of the hydroxyfriedelene (III R=H) (150 mg) in 30 ml of benzene containing 0.07 ml of pyridine, was added 300 mg of lead tetraacetate. The mixture was stirred for 30 min. After subsequent treatment with water, the mixture was extracted with ether. The ether extract was washed successively with aqueous cupric sulfate and an aqueous sodium chloride solution, and dried. The ether was then removed, and the residue was fractionated by the column chromatography of alumina to give white crystals of the allyl acetate (159 mg); mp 172—175 °C, ν(KBr) 1730, 1240 cm^{-1}, $\delta(CDCl_3)$ 2.05(3H,s), 1.68(3H,s), 5.06(1H,m). Found: $(M-HOAc)^+$, 394.36102. Calcd for $C_{29}H_{46}$: 394.35990.

3-Hydroxy-24-norfriedel-4-ene (V R=H). The allyl acetate (V R=Ac, 140 mg) dissolved in ethanol (100 ml) was hydrolysed by means of a reaction with potassium hydroxide (4 g) under an atmosphere of nitrogen to give the allyl alcohol (V R=H, 125 mg); mp 209 °C, ν(KBr) 3430 cm^{-1}, $\delta(CDCl_3)$ 1.78(3H,s), 3.86(1H,bs). Found: $(M-H_2O)^+$, 394.36001. Calcd for $C_{29}H_{46}$: 394.35990.

24-Norfriedel-4-en-3-one (VII). A mixture of the allyl alcohol (V R=H, 45 mg), active manganese dioxide (450 mg), and methylene chloride (5 ml) was stirred for 4 hr. The inorganic substance was removed by filtration, and the filtrate was evaporated *in vacuo* to give a crude α,β-unsaturated ketone (45 mg). A pure compound was obtained by recrystallization from chloroform–methanol; mp 201 °C, ν(KBr) 1675, 1610 cm^{-1}, $\delta(CDCl_3)$ 1,78(3H,s). λ_{max} 252 nm (ε 14900). Found: 410.3566. Calcd for $C_{29}H_{46}O$: 410.3548.

References

1) R. Harada, H. Kakisawa, S. Kobayashi, M. Musha, K. Nakanishi, and Y. Takahashi, *Tetrahedron Lett.*, **1962**, 603; K. Nakanishi, Y. Takahashi, and H. Budzikiewcz, *J. Org. Chem.*, **30**, 1729 (1965).

2) T. Fukuda, T. Tsuyuki, Y. Tanahashi, and T. Takahashi, This Bulletin, **40**, 370 (1969); T. Hoshino, T. Tsuyuki, and T. Takahashi, *ibid.*, **40**, 389 (1969).

3) T. L. Courtney and W. Stern, *Aust. J. Chem.*, **19**, 1709 (1966).

4) E. Wenkert and B. L. Mylari, *J. Amer. Chem. Soc.*, **89**, 174 (1967).

BULLETIN OF THE CHEMICAL SOCIETY OF JAPAN, VOL. 48(2), 729—730 (1975)

Cationic Arylation. VIII. Reactions of Benzenediazonium Tetrafluoroborate with Some Sulfur Compounds

Michio KOBAYASHI, Hiroshi MINATO, Junko FUKUI, and Nobumasa KAMIGATA

Department of Chemistry, Faculty of Science, Tokyo Metropolitan University, Fukazawa, Setagaya, Tokyo 158

(Received July 2, 1974)

Synopsis. Reactions of benzenediazonium tetrafluoroborate (I) with thioanisole in acetonitrile yielded dimethylphenylsulfonium tetrafluoroborate, diphenyl sulfide, methylthiobiphenyls and acetanilide. Reaction of I with cyclohexene yielded 1-cyclohexylcyclohexene and cyclohexyl phenyl ether. Reactions of I with dimethyl sulfide yielded trimethylsulfonium tetrafluoroborate and thioanisole. Mechanisms of these reactions were discussed in terms of the attack of phenyl cation toward the lone electron pair of sulfur atoms and the benzene electrons.

Many papers have described the arylation of aromatic compounds with aryldiazonium tetrafluoroborate (I)[1-3] or some other aryl cation sources.[4-7] However, very few papers have been published on the reaction of aryl cation with compounds other than arenes. Nesmeyanov and his coworkers found that the reaction of I with diaryl sulfides gave triarylsulfonium salts in low yield, but no other products were described.[8]

In order to determine the reactivity of phenyl cation toward compounds other than arenes, the reactions of I with some sulfides, disulfides and cyclohexene have been investigated. The results are described in this paper.

Results and Discussion

I is insoluble in aromatic solvents, but soluble in such aprotic polar solvents as acetonitrile and nitromethane. Therefore, the reaction of I with thioanisole was carried out in acetonitrile. The reaction products were dimethylphenylsulfonium tetrafluoroborate (II), diphenyl sulfide, isomeric methylthiobiphenyls (III), and acetanilide. Methyldiphenylsulfonium tetrafluoroborate (IV) which is the most-likely product from the reaction of phenyl cation with thioanisole was not isolated. The formation of acetanilide in the reaction of phenyl cation with acetonitrile is known.[3,8] Isomer distributions of methylthiobiphenyls formed by the phenylation of the thioanisole nucleus with I were *o*-57%, *m*-14%, *p*-29%; they are similar to those in cationic phenylation of anisole (*o*-64%, *m*-8%, *p*-28%) reported previously.[3]

The formation of products described above can be explained by assuming the following mechanism. Phenyl cation attacks the aromatic nucleus and the sulfur lone pair of the thioanisole competitively, yielding III and IV; the latter further reacted with another molecule of the unchanged thioanisole to give II and diphenyl sulfide. Since IV was not isolated in the reaction mixture, the reaction of IV with thioanisole must be very rapid. In a separate experiment, methyldiphenylsulfonium perchlorate (V) was prepared and treated with thioanisole in acetonitrile. About equal amounts of dimethylphenylsulfonium perchlorate (VI) (33%) and diphenyl sulfide (38%) were found as expected.[9]

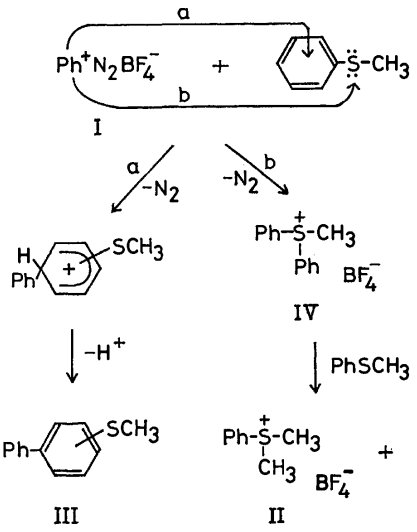

I III II IV

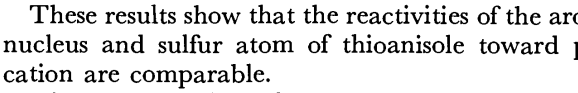

V VI

These results show that the reactivities of the aromatic nucleus and sulfur atom of thioanisole toward phenyl cation are comparable.

Then the reaction of I with cyclohexene was investigated in nitromethane. The products found were 1-cyclohexylcyclohexene and cyclohexyl phenyl ether.

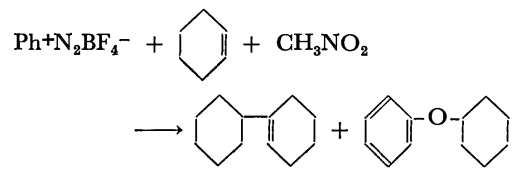

Cyclohexyl phenyl ether was probably formed *via* *O*-phenylation of nitromethane followed by the reaction with cyclohexene. 1-Cyclohexylcyclohexene was probably formed by protonation of cyclohexene, the addition of cyclohexyl cation to cyclohexene, and subsequent deprotonation.

When I was let to react with dimethyl sulfide in acetonitrile, the products found were II, trimethylsulfonium tetrafluoroborate (VII) and thioanisole.

Since II was found in the reaction mixture, the reaction of II with dimethyl sulfide is not so rapid as that of IV with thioanisole.

When I was let to react with dimethyl disulfide in acetonitrile, the only product which was identified was

$$Ph^+N_2BF_4^- + CH_3SCH_3 \xrightarrow{-N_2} Ph\text{-}\overset{+}{S}(CH_3)\text{-}CH_3 \; BF_4^-$$

II

$$\xrightarrow{CH_3SCH_3} CH_3\text{-}\overset{+}{S}(CH_3)\text{-}CH_3 \; BF_4^- + PhSCH_3$$

VII

$$Ph^+N_2BF_4^- + CH_3SSCH_3 \xrightarrow{-N_2} CH_3\text{-}S\text{-}\overset{+}{S}(Ph)CH_3 \; BF_4^-$$

VIII

$$\longrightarrow PhSCH_3 + \overset{+}{(SCH_3)}$$

thioanisole. The reaction probably involved the formation of methylmethylthiophenylsulfonium ion (VIII), which was attacked by some nucleophiles, yielding thioanisole. However, no products other than thioanisole were characterizable.

Experimental

Materials. I,[9] V,[10] and cyclohexene[11] were prepared according to the procedures described in the literature. Thioanisole was prepared by methylation of thiophenol with dimethyl sulfate; bp 75 °/15 mmHg. Dimethyl sulfide and dimethyl disulfide of Tokyo Kasei Co., Ltd. were used without further purification. Acetonitrile was refluxed over phosphorus pentoxide, and then distilled at 81 °C. Nitromethane was dried with calcium chloride and then distilled at 101 °C.

Reaction of I with Thioanisole. A solution of I (4.82 g, 25 mmol) and thioanisole (6.20 g, 50 mmol) in acetonitrile (12.2 g) was stirred at 40°C for 5 hr. After removal of acetonitrile, the ether-insoluble part of the residue was dissolved in aqueous acetone, and eluted through an ion exchange resin column (Amberlite I.R.A.-400) containing perchlorate anions; crystals of dimethylphenylsulfonium perchlorate were obtained (0.56 g, 2.34 mmol). The ether-soluble part was analyzed by glc (Apiezon L, 1 m, 200 °C): diphenyl sulfide (0.33 mmol) and III (isomeric mixture, 0.99 mmol) were found. A very small amount of acetanilide was isolated by the elution chromatography (Florisil) of the ether-soluble part (23 mg, 0.13 mmol).

Reaction of V with Thioanisole. A solution of V (0.60 g, 2.0 mmol) and thioanisole (1.20 g, 11 mmol) in acetonitrile (0.7 g) was stirred at 40 °C for 5 hr. After acetonitrile was evaporated, ether was added to the residue, and the ether-soluble part was analyzed by glc (Apiezon L, 1 m, 190 °C) and the amount of diphenyl sulfide formed was determined (0.76 mmol, 38%). The ether-insoluble part was submitted to NMR analyses, and the amounts of VI formed (0.66 mmol, 38%) and unchanged V (1.34 mmol, 67%) were determined.

Reaction of I with Cyclohexene in Nitromethane. A solution of I (1.01 g, 5.2 mmol) and cyclohexene (5.2 g, 63 mmol) in nitromethane (10 ml) was stirred at 40 °C for 5 hr. After nitromethane was evaporated, the residue was submitted to elution chromatography (Florisil) and the following products were identified by NMR and mass spectroscopy; 1-cyclohexylcyclohexene (82 mg, 0.52 mmol), cyclohexyl phenyl ether (44 mg, 0.25 mmol). Neither phenylcyclohexene nor phenylcyclohexanol was detected.

Reaction of I with Methyl Sulfide. A solution of I (0.96 g, 5 mmol) and methyl sulfide (1.55 g, 25 mmol) in acetonitrile (3.5 g) was stirred at 40 °C for 5 hr. Acetonitrile and methyl sulfide were evaporated, then the reaction products were determined quantitatively by NMR (internal standard: $CHCl_2CHCl_2$). The following products were identified; thioanisole (1.9 mmol, 38%), II (0.48 mmol, 9.6%), and VII (1.63 mmol, 33%).

Reaction of I with Dimethyl Disulfide. A solution of I (1.92 g, 10 mmol) and dimethyl disulfide (1.50 g, 16 mmol) in acetonitrile (8.9 g) was stirred at 40 °C for 5 hr. After acetonitrile was evaporated, the reaction mixture was submitted to elution chromatography (Florisil); thioanisole (196 mg, 1.58 mmol) and acetanilide (177 mg, 1 mmol) were isolated.

References

1) R. A. Abramovitch and S. G. Saha, *Can. J. Chem.*, **43**, 3269(1965).

2) R. A. Abramovitch and F. F. Gadallah, *J. Chem. Soc., B*, **1968**, 497.

3) M. Kobayashi, H. Minato, E. Yamada, and N.Kobori, This Bulletin, **43**, 215(1970).

4) M. Kobayashi, H. Minato, and N. Kobori, *ibid.*, **43**, 219(1970).

5) N. Kamigata, M. Kobayashi, and H. Minato, *ibid.*, **45**, 1231(1972).

6) N. Kamigata, M. Kobayashi, and H. Minato, *ibid.*, **45**, 2047(1972).

7) N. Kamigata, R. Hisada, H. Minato, and M. Kobayashi, *ibid.*, **46**, 1016(1973).

8) A. N. Nesmeyanov, L. G. Makarova, and T. P. Tolustay, *Tetrahedron*, **1**, 145(1957).

9) The incomplete conversion of V can be ascribed to the smaller ratio of PhSMe/V (=5.5) in comparison with that in the reaction of I with thioanisole (PhSMe/V=50/2.34=21.4). It cannot be ascribed to the difference in the counter anion, since the rates of reaction between diethyl sulfide and dibenzylethylsulfonium ion are uninfluenced by the kind of counter anion, ClO_4^- or BF_4^- (D. Van Ooteghem, R. Deveux and E. J. Goethals, *Int. J. Sulfur Chem*, **8**, 33 (1973)).

10) D. T. Flood, "Organic Syntheses," Coll. Vol. II, p. 295(1943).

11) V. Franzen, H. J. Schmidt, and C. Mertz, *Chem. Ber.*, **94**, 2942(1961).

12) L. F. Fieser, "Organic Experiments," D. C. Heath and Company, Boston (1964), p. 96.

BULLETIN OF THE CHEMICAL SOCIETY OF JAPAN, VOL. 48(2), 731—732 (1975)

Photoreaction of Bicyclo[5.3.0]dec-1(7)-en-2-one with Cyclopentene and Cyclohexene

Atsutaka KUNAI, Takeshi OMORI, Koji KIMURA, and Yoshinobu ODAIRA

Department of Petroleum Chemistry, Faculty of Engineering, Osaka University, Suita-shi, Osaka 565

(Received July 2, 1974)

Synopsis. The photoreaction of the enone (I) with cyclopentene gave the radical coupling products, (VII) and (VIII), along with the hydrogen abstraction product (VI), but not [2π+2π] photocycloadduct. On the other hand, the photoreaction of I with cyclohexene proceeded in somewhat different manner to give the [2π+2π] photocycloadduct (V) other than the hydrogen abstraction product (VI) and the radical coupling product (IX).

In the chemistry of α,β-unsaturated carbonyl compounds, much attention has been shown about the photochemistry of cyclic enones. Especially, the [2π+2π] photocycloaddition of some cyclic enones, such as cyclopentenones and cyclohexenones, has been extensively studied[1] and utilized for preparation of a wide variety of poly fused alicyclic compounds.[1,2] On the contrary, cycloheptenone, being a next higher cyclic enone, has been of no consequence. This is because it cannot undergo the crossed photocycloaddition with olefins owing to the facile isomerization to its *trans* isomer.[3] More recently, we reported our preliminary finding concerning the crossed photocycloaddition of a certain cycloheptenone derivative, bicyclo[5.3.0]dec-1(7)-en-2-one (I), having a rigid bicyclic system, with some seven- and eight-membered ring olefins, such as cycloheptene, cyclooctene, and 1,5-cyclooctadiene.[4] In the case of I, the ethylene linkage of cycloheptenone is fixed tightly with five membered ring and, therefore, an unfavorable *cis-trans* isomerization may be entirely inhibited. This situation resulted in the predominant formation of two stereo isomers of the respective cycloadducts IIa, IIb—IVa, IVb.[4] In the present paper, emphasis has been placed on the effect of smaller ring sized olefins, such as cyclopentene or cyclohexene, on the photochemical reaction of I.

Experimental

Generals. The enone (I) was prepared according to the procedure of Dev[5] and Cope and Holzman[6] and purified by fractionation using Taika Kogyo SM-NB spinning band column before use. Irradiation was carried out using a Eikosha Halos 500-W water cooled high pressure mercury lamp. Products were isolated using a Varian Aerograph 90-P gas chromatograph and analyzed by a Hitachi 063 gas chromatograph (column: PEG-20M, SE-30, or FFAP). Yields were based on the enone I reacted. The deuterium exchange reaction was carried out according to the procedure of Pfeffer[7] and Osman and the products were analyzed by mass spectra using a Hitachi RMU-6E mass spectrometer.

I

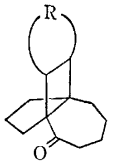

IIa, IIb R=-$(CH_2)_5$-
IIIa, IIIb R=-$(CH_2)_6$-
IVa, IVb R=-$(CH_2)_2CH$=$CH(CH_2)_2$-
V R=-$(CH_2)_4$-

VI R=-H X=H
VII R= X=H
VIII R= X=H
IX R= X=H
X R= X=D
XI R= X=D
XII R= X=D

Photoreaction of I with Cyclopentene. A mixture of I (2.97 mmol) and cyclopentene (29 mmol) placed in a sealed Pyrex tube (1×10 cm) was irradiated with an external mercury lamp at a distance of 2 cm at room temperature for 7 hr. After removal of remaining cyclopentene, residue was distilled *in vacuo* (10^{-3} mmHg) to afford 0.373 g of oil, which consisted of three products (glpc) mainly. Each product was isolated by preparative glpc; yields: VI 22%; VIII 12%; VIII 14%. VII: ν_{max} 1680 cm^{-1} (CO); δ(CCl_4) 1.10—2.15(m,18H), 2.20—2.40(m,2H), 5.55—5.80(m,2H); *m/e* 218(M^+), 152($M-C_5H_6$); 2,4-dinitrophenylhydrazone, mp 171—172 °C; Found: C, 62.98; H, 6.58; N, 13.93%. Calcd for $C_{21}H_{26}O_4N_4$: C, 63.30; H, 6.58; N, 14.06%. VIII: ν_{max} 1675 cm^{-1} (CO); δ(CCl_4) 1.30—2.20(m, 19H), 2.25—2.60(m, 2H), 5.60—5.85(m, 1H); *m/e* 218(M^+), 152($M-C_5H_6$); 2,4-dinitrophenylhydrazone, mp 172—173 °C; Found: C,63.23; H, 6.75; N, 14.26%. Calcd for $C_{21}H_{26}O_4N_4$: C, 63.30; H,6.58; N,14.06%. On treating with the solution of D_2O-dioxane-NaOD twice,[7] both VII and VIII were changed into the deuterated compounds X; *m/e* 220(M^+, $C_{15}H_{20}OD_2$) and XI; *m/e* 220(M^+, $C_{15}H_{20}OD_2$), respectively.

Photoreaction of I with Cyclohexene. A mixture of I (2.76 mmol) and cyclohexene (30 mmol) was irradiated for 3 hr, in a similar manner as described above. After removal of remaining cyclohexene, residue was distilled *in vacuo* (10^{-3} mmHg) to afford 0.444 g of oil, which consisted of three products (glpc) mainly. Each product was isolated by preparative glpc; yields: V 21%; VI 19%; IX 5%. V: ν_{max} 1680 cm^{-1} (CO); δ(CCl_4) 1.20—2.10 (m,22H), 2.20—2.70(m,2H); *m/e* 232(M^+), 151($M-C_6H_9$); Found: C, 82.41; H, 10.61%. Calcd for $C_{16}H_{24}O$: C, 82.70; H, 10.41%; 2,4-dinitrophenylhydrazone, mp 147—148 °C. IX: ν_{max} 1675 cm^{-1} (CO); δ(CCl_4) 1.20—2.40(m, 20H), 2.45—2.90(m, 2H), 5.30—5.85(m, 2H); *m/e* 232(M^+), 152($M-C_6H_8$); 2,4-dinitrophenylhydrazone, mp 163—165 °C; Found: C,63.92; H, 6.61; N, 13.88%. Calcd for $C_{22}H_{28}O_4N_4$: C, 64.06; H, 6.84; N, 13,58%. On treating with the solution of D_2O-dioxane-NaOD twice,[7] IX was changed into the deuterated compound XII; *m/e* 234(M^+, $C_{16}H_{22}OD_2$).

Results and Discussion

As reported previously,[4] the photoreaction of I with some seven- and eight-membered ring olefins, such as cycloheptene, cyclooctene, and 1,5-cyclooctadiene, always afforded two stereo isomers of respective cycloadducts.

Concerning the stereochemistry of above cycloadducts, we assume, presently, that two *trans*-fused isomers of four possible ones are more probable candidates.[8] Interestingly, the photoreaction of I with cyclopentene proceeded in a quite different manner as compared to the reaction with the larger ring sized olefins described above. Namely, the formation of cycloadduct of I with cyclopentene was not observed at all. Instead, two radical coupling products, VII and VIII, and one hydrogen abstraction product VI were obtained in 12%, 14%, and 22% yields. Structural determination of VII and VIII was made on the basis of elemental analyses and spectrometric data in addition to the results of the deuterium exchange reaction. Especially, from the fact that only two hydrogens were always exchanged for deuteriums in each compound, the coupling position of the cyclopentenyl groups was determined to be α-bridgehead to the carbonyl group. On the other hand, the photoreaction of I with cyclohexene proceeded in somewhat different manner to give the cycloadduct V together with the hydrogen abstraction product VI and the radical coupling product IX.

One of the most significant results in these reactions is the finding that the variation in the ring sizes of cyclic olefins has definitive influence on the reaction paths. To account for these results, we would like to make some proposals. It appears that the photo-excited state of I would not be different in a series of the above cyclic olefins, though the excited state of I is uncertain as yet. Moreover, in the case of cyclohexene, three types of products were obtained simultaneously in moderate yields. Taking these points, into consideration it may be reasonable to assume that the photochemical reaction proceeds stepwisely in radical manner through an intermediary 1,4-biradical (XIII), formed between the triplet state of I and cyclic olefins, as shown in Scheme 1. When cyclic olefins are larger ring sized olefins, such as cycloheptene and cyclooctene, the cycloaddition from XIII, according to the path a, smoothly could occur to form the cycloadduct, possessing large strained energy. On the other hand, in the case of smaller ring sized cyclic olefin, such as cyclopentene, the formation of cycloadduct from XIII may be entirely suppressed because of instability of cycloadduct, being highly strained structure.[8] Consequently, two other types of reactions accelerate to give the radical coupling products VII and VIII, and the hydrogen abstraction product VI. Concerning the occurrence of the latter two reactions, it may be also considered that cyclopentene is the substrate having the great hydrogen-donating ability. In the case of cyclohexene, circumstance lies between and the formation of cycloadduct V has barely become feasible. As a result, three types of products are given at the same time.

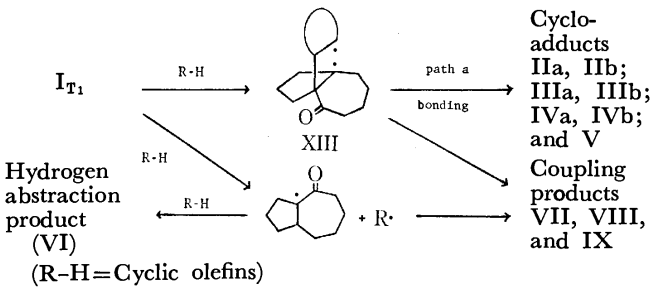

Scheme 1.

Further research for the photoreaction of I in the presence of strained olefins are in progress and will be reported shortly.

References

1a) P. E. Eaton, *Accounts Chem. Res.*, **1**, 50 (1968); b) P. de Mayo, *ibid.*, **4**, 41 (1971), and references cited therein; c) P. E. Eaton and K. Nyi, *J. Amer. Chem. Soc.*, **93**, 2786 (1971); P. E. Eaton and G. H. Temme, *ibid.*, **95**, 7508 (1973); R. L. Cargill, T. E. Jackson, N. P. Peet, and D. M. Pond, *Accounts Chem. Res.*, **7**, 106(1974), and references cited therein.

2) They are utilized also in the syntheses of various natural products: see Ref. 1b); see also, E. J. Corey and S. Nozoe, *J. Amer. Chem. Soc.*, **86**, 1652 (1964); E. J. Corey, R. B. Mitra, and H. Uda, *ibid.*, **86**, 485 (1964): J. D. White and D. N. Gupta, *ibid.*, **90**, 6171 (1968).

3) E. J. Corey, M. Tada, R. LeMahieu, and L. Libit, *J. Amer. Chem. Soc.*, **87**, 2051(1965); P. E. Eaton and K. Lin, *ibid.*, **87**, 2053(1965); H. Nozaki, M. Kurita, and R. Noyori, *Tetrahedron Lett.* **1968**, 2025.

4) A. Kunai, T. Omori, T. Miyata, K. Kimura, and Y. Odaira, *Tetrahedron Lett.*, **1974**, 2517.

5) S. Dev, *J. Indian Chem. Soc.*, **31**, 1(1954).

6) A. C. Cope and G. Holzman, *J. Amer. Chem. Soc.*, **72**, 3062(1950).

7) P. E. Pfeffer and S. F. Osman, *J. Org. Chem.*, **37**, 2425(1972).

8) The structure of cycloadducts, IVa and IVb, is now under study by means of X-ray analysis. At the time, we suppose that, as a plausible structure, the cycloadducts have *trans*-fused structure. In the photocycloaddition of some bicyclic enones with cyclic olefins, the formation of *trans*-fused cycloadducts occasionally dominates. For example, the reaction of bicyclo[4.3.0]non-1(6)-en-7-one with cyclic olefins, such as cyclohexene and cyclooctene, afforded only *trans*-fused cycloadducts which were confirmed by means of X-ray analysis (A. Kunai, H. Omura, K. Kimura, and Y. Odaira, unpublished result, and to be published). On the other hand, the formation of *cis*-fused cycloadduct is observed only when the cycloadduct is substantially free from the repulsion of *syn* overlap. For example, cyclopentenone adds to cyclopentene to afford the corresponding *cis*-fused *anti*-adduct in good yield (P. E. Eaton, *J. Amer. Chem. Soc.*, **84**, 2454 (1962)).

BULLETIN OF THE CHEMICAL SOCIETY OF JAPAN, VOL. 48(2), 733—734 (1975)

On the Mechanism of the Diels-Alder Reaction between 1,3-Cyclopentadiene and 1,3-Cyclohexadiene

Terunobu MAEDA, Sawako HAMANAKA, and Masaya OGAWA

Department of Applied Chemistry, Faculty of Engineering, Kansai University, Suita-shi, Osaka 564

(Received July 8, 1974)

Synopsis. The reaction of 1,3-cyclopentadiene with 1,3-cyclohexadiene, when carried out at 94—118 °C for 5—7 hr, gave tricyclo[4.4.0.$1^{2,5}$]undeca-3,7-diene rather than tricyclo[5.2.2.$0^{2,6}$]undeca-3,8-diene.

In the study of the Diels-Alder reaction, many investigations[1-5] have been carried out in an attempt to elucidate the bonding sequence of two new σ-bonds formed during the reaction. Recently, Salem[3] suggested a new transition structure with secondary attractive force (s.a.f.) like that of the Cope rearrangement and supported a two-stage mechanism postulated by Woodward and Katz.[4] On the other hand, Herndon[5] showed that the prefered *endo*-addition pathway can be interpreted principally in teams of a geometrical relationship rather than s.a.f. and then suggested a one-step mechanism in which the planes of the two reactants are assumed to intersect at an angle of 60°. In our previous work[6] concerning the reaction of 1,3-cyclopentadiene(CP) with 1,3-butadiene, we also imagined a one-step mechanism by considering that the transition state of this reaction is different from that of the Cope rearrangement of one product (*endo*-5-vinyl-2-norbornene) to another (*cis*-3a,4,7,7a-tetrahydroindene). The present work will presents some evidence for the one-step mechanism of the reaction between two different *s*-cisoid dienes, such as CP and 1,3-cyclohexadiene(CH).

The reaction of CP with CH was carried out under N_2 in a sealed tube at a fixed temperature. The reaction products were separated by fractionation into the following fractions; monomers(79—83 °C/760 mmHg), dimers(83—105 °C/66mmHg), trimers(105 °C/5mmHg), and higher polymers(residue). The dimer fraction was analyzed by glc. Two codimers, *A* and *B* (Fig. 1), were isolated from the dimer fraction by preparative glc. The structural assignment of *A* and *B* is based on the following data: *A* —NMR (60 MHz, CCl_4, δ), 1.41 (2H, k, m), 0.95—2.70(4H, a b, m), 2.45(2H, l e, m), 2.80(2H, f i, m), 5.56(2H, c d, m), 5.92(2H, g h, t); (NaCl), 1569 and 1676 cm^{-1}: *B* —NMR(60 HMz, CCl_4, δ), 1.32, 1.44(4H, j k, m), 1.02—2.35(3H, ai, m), 2.48(2H, e h, m), 3.01(1H, d, m), 5.43(2H, b c, t), 6.07(2H, f g, $J_{fg}=4.8$ Hz, $J_{ef}=J_{hg}=3.0$ Hz); IR (NaCl) 1610 and 1645 cm^{-1}.[7] The results of the reaction of CP with CH are shown in Table 1.

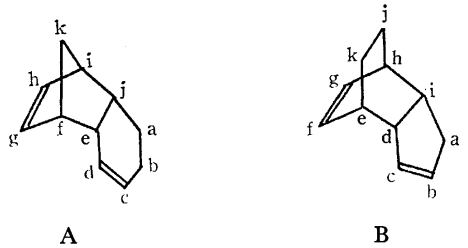

A B

Fig. 1. Reaction products. (Codimer)

Table 1. Reaction of CP with CH

Reaction temp. (°C)		94.4	105.5	118.0	180.0
Reaction time (hr)		5.0	24.0	5.0	5.0
Starting Material	CP (g)	5.5	7.0	5.0	5.0
	CH (g)	4.0	2.0	2.0	3.0
Yield (%)	Monomer	42.1	21.2	25.0	trace
	Homodimer	56.7	77.0	74.2	27.5
	Codimer	1.2	1.8	0.8	27.4
	Trimer	—	—	—	24.4
	Polymer	—	—	—	20.7
Codimer (%)	*A*	70.0	62.8	70.4	4.0
	B	20.1	23.4	16.0	84.2
	Unknown	9.9	13.8	13.6	11.8

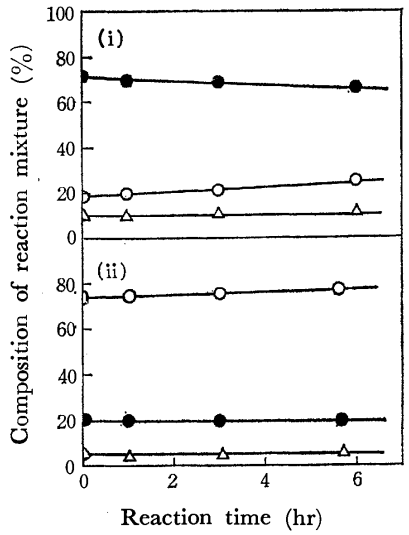

Fig. 2. Rearrangement of codimer.
—●— *A*, —○— *B*, —△— unknown
i) The reaction of *A*-rich fraction
ii) The reaction of *B*-rich fraction

A *n*-hexane solution(10 vol%) of an *A*- or *B*-rich fraction prepared from the reaction products was caused to react by heating at 139.0 °C. The results are shown in Fig. 2. Furthermore, in the reaction of the *A*-rich fraction with acryronitrile at 139.0 °C for 6 hr, no addition product with CH or CP was obtained. Consequently, the decomposition of *A* to CH and CP did not occur at this temperature.

The transition state of the reaction to produce an *A* or *B* codimer is considered to be I* for a one-step me-

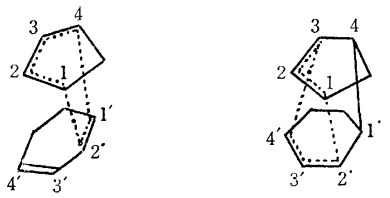

Fig. 3. Hypothetical transition stats.

chanism and *II** for a two-stage mechanism (Fig. 3). In the one-step mechanism, CP probably acts as a diene since the bond distance at C_1—C_4 is shorter than that at the C_1'—C_4' of CH. Therefore, the *A* product can be obtained through *I**. On the other hand, *II** has σ-bond at C_4–C_1' and two weak bonds at C_1—C_2 and C_3—C_4'. As the latter two weak bonds are similar in their reactivity, *II** may give both products, *A* and *B*. According to the additivity rule of strain, the relative stabilities of both *A* and *B* were calculated on the basis of the data estimated by Turner[8] and Alder;[9] *B* was found to be more stable than *A* by 11.4 kcal/mol. Consequently, when the reaction proceeds through the two-stage mechanism, *B* may be predominantly obtained in the products.

As was seen in Table 1 and Fig. 3, the results obviously show that *A* was initially produced and was then converted to *B*. Therefore, the reaction proceeds mainly along the following reaction course;

$$CP+CH \rightarrow I^* \rightarrow A \rightarrow II^* \rightarrow B$$

On the other hand, some portion of *B* may also be formed by the direct reaction of CP with CH, especially at higher temperatures.

Experimental

In glc, the columns used were R-90(0.25 mmϕ) for analysis and PEG-20(25%, 8mmϕ×3 m) for preparation. The measurements of the NMR and IR spectra were performed with JEOL-JNM-3H-60 and Shimadzu-IR-27G apparatuses respectively. All the reactions were carried out in sealed tubes maintained within ±0.1 °C.

References

1) K. Alder and G. Stein, *Angew. Chem.*, **50**, 514 (1937).
2) a) A. Wasserman, *J. Chem. Soc.*, **1935**, 828, 1511; **1936**, 432. b) R. B. Woodward and H. Bear, *J. Amer. Chem. Soc.*, **66**, 645 (1954). c) K. Fukui, "Molecular Orbitals in Chemistry, Physics and Biology," Academic Press, New York (1964), p. 525. d) Y. Kobuke, *Yuki Gosei Kagaku Kyokai Shi*, **30**, 992 (1964). f) W. von E. Ooering, M. Frank-Newmann, D. Hasselmann and R. L. Kaye, *J. Amer. Chem. Soc.*, **94**, 3833 (1972).
3) A. Devaquet and L. Salem, *ibid.*, **91**, 3797 (1969).
4) R. B. Woodward and T. J. Katz, *Tetrahedron*, **5**, 70 (1959).
5) W. C. Herndon and L. Hall, *Tetrahedron Lett.*, **1967**, 3095.
6) T. Maeda, M. Muranaka, S. Hamanaka, and M. Ogawa, *Nippon Kagaku Kaishi*, **1974**, 1587.
7) a) R. G. Foster and M. C. Mclover, *J. Chem. Soc., B*, **1969**, 188. b) L. N. Jackman and S. Sternhell, "Application of NMR Spectroscopy in Organic Chemistry," 2nd, Pergamon Press, London (1969).
8) a) R. B. Turner, W. R. Meador, and R. E. Winkler, *J. Amer. Chem. Soc.*, **74**, 5219 (1951). b) R. B. Turner, D. E. Nettleton, and M. Perelman, *ibid.*, **80**, 1430 (1958).
9) K. Alder and G. Stein, *Ber.*, **67**, 613 (1934).

BULLETIN OF THE CHEMICAL SOCIETY OF JAPAN, VOL. 48(2), 735—736 (1975)

Oxidation by Iron(III) Complexes. IX.[1] The Preparation of α-Diketones by the Oxidation of Enolizable Ketones with the Iron(III) Chloride-Pyridine Complex under Oxygen

Hiroo INOUE, Hiroyuki HATA, and Eiji IMOTO

Department of Applied Chemistry, College of Engineering, University of Osaka Prefecture, Sakai, Osaka 591

(Received August 10, 1974)

Synopsis. The oxidation of deoxybenzoin and *p*-substituted deoxybenzoins with an iron(III) chloride–pyridine complex under air or oxygen was investigated. The reaction afforded the corresponding α-diketones in a satisfactory yield.

We have recently reported that enolizable deoxybenzoin (Ia) is oxidized with iron(III) chloride dispersed in benzene to undergo direct arylation with benzene at the α-position of the carbonyl group.[2] In the course of our studies, we found that the reaction pathway alters in the direction of the formation of an α-diketone, benzil(IIIa), upon the addition of pyridine to the reaction system, and that the reaction proceeds *via* the formation of an intermediate, α-chlorodeoxybenzoin(IIa), followed by the oxidation of IIa with oxygen in the presence of iron(II) chloride and pyridine. We wish to report here a novel method for the preparation of α-diketones from I.

$$\underset{\text{I}}{p\text{-XC}_6\text{H}_4\text{CH}_2\text{COC}_6\text{H}_5} \xrightarrow{\text{FeCl}_3/\text{C}_5\text{H}_5\text{N}} \underset{\text{II}}{p\text{-XC}_6\text{H}_4\overset{\text{Cl}}{\overset{|}{\text{C}}}\text{HCOC}_6\text{H}_5}$$

a; X=H
b; X=Cl
c; X=CH_3

$$\xrightarrow[\text{O}_2]{\text{FeCl}_2/\text{C}_5\text{H}_5\text{N}} \underset{\text{III}}{p\text{-XC}_6\text{H}_4\text{COCOC}_6\text{H}_5}$$

Results and Discussion

The Formation of α-Diketone. When pyridine was added to dry benzene containing the dispersed anhydrous iron(III) chloride (in the pyridine/iron(III) chloride molar ratio of 1:1), the iron(III) chloride solid changed to a black-brown paste which adhered to the wall of the reaction vessel. Ia was then added to the reaction system, and the solution was heated at 80 °C under an atmosphere of air. As the reaction time proceeded, the paste changed to a black-brown solid containing an iron(III) ion and pyridine as the major components. Ia was converted to IIIa, along with the by-products of benzaldehyde, benzoic acid, and 2,2-diphenylacetophenone(IV), as is shown in Table 1. The other products were a high-melting material and a tarry matter, although the structures of the products are still uncertain. In the absence of the iron(III) chloride and/or pyridine, IIIa was not obtained at all. When the reaction was carried out under oxygen, the yield of IIIa became higher than that in the case of air (Table 1). The substituted deoxybenzoins (Ib and Ic) were also converted to the corresponding α-diketones (IIIb and IIIc). In the case of propiophenone, however, the α-diketone was not obtained under similar conditions, although α-chloropropiophenone was produced in a good yield.[2] Thus, the existence of the phenyl group at the α-position of the carbonyl group is required for the formation of the α-diketone.

TABLE 1. THE REACTION OF I WITH AN IRON(III) CHLORIDE-PYRIDINE (1 : 1) COMPLEX UNDER AIR OR OXYGEN[a]

Ketone	Atmosphere	Yield, %	
		III	*p*-XPhCHO
Ia[b]	Air	56	11
Ia	O_2	73	2
Ib	O_2	78	7
Ic	O_2	67	8

a) The reaction time: 24 hr. The remaining I was not detected after 24 hr. b) IV was obtained in 8% yield. In a large scale reaction benzoic acid was isolated in 4% yield.

Catalytic Behavior. The oxidation of Ia with the iron(III) chloride–pyridine complex under air was carried out in the molar ratio of Ia, iron(III) chloride, and pyridine of 10 : 1 : 1. After a reaction of 118 hr, IIIa was produced in a 56% yield (based on Ia). This means that the iron(III) complex acts as a catalyst for the formation of IIIa.

Reaction Pathway. In the initial period of the reaction, IIa was detected by means of glc, although the amount produced was very small. After a long reaction, however, IIa could not be detected at all. This fact suggests that IIa is produced as an intermediate in the formation of IIIa. The reaction of Ia with the iron(III) chloride–pyridine (1: 1) complex under nitrogen at 80 °C for 24 hr afforded only IIa in a 56% yield, with a 35% recovery of Ia. In this reaction, the iron(III) ion was reduced to the iron(II) ion in a 55% yield. In addition, IIa was oxidized with oxygen in the presence of the hydrated iron(II) chloride and pyridine to afford IIIa in a good yield (Table 2), along with an iron(III) complex. In the absence of iron(II) chloride and pyridine, IIIa was not obtained at all. These facts led to the conclusion that IIIa is produced *via* the formation of IIa, followed by the oxidation of IIa with oxygen in the presence of the iron(II) complex produced.

On the other hand, the yields of benzaldehyde and benzoic acid became higher in a homogeneous reaction

Table 2. The reaction of Ia or IIa with the Fe(II) or Fe(III) complex[a)]

Ketone	Fe(II) or Fe(III) complex	Atmosphere	Time hr	Yield, %		Recovery, % Ketone
				IIIa	PhCHO	
Ia[b)]	$FeCl_3/CH_3CN$	Air	24	15	38	10
Ia[c)]	$[Fe(DMF)_3Cl_2][FeCl_4]$	Air	96	26	58	9
IIa[c,d)]	$FeCl_2/C_5H_5N$	O_2	24	83	0	0

a) The molar ratio of Ia or IIa to Fe(II) or Fe(III) ion: 1 : 2. b) IIa and benzoic acid were isolated in 14 and 20% yields, respectively. c) The solvent: benzene. The temperature: 80 °C. d) The Fe(II) ion was oxidized to the Fe(III) ion in 90% yield. The $FeCl_2/C_5H_5N$ molar ratio: 1.

of Ia with iron(III) chloride in acetonitrile under an atmosphere of air. A similar phenomenon was observed in the reaction of Ia with $[Fe(DMF)_3Cl_2][FeCl_4]$[3)] dispersed in benzene (Table 2). Thus, the yields of IIIa and benzaldehyde can be altered by changing the structure of the iron(III) complex. Benzaldehyde and benzoic acid are produced by the carbon-carbon cleavage of the $-CH_2-CO-$ bond, although the mechanism is ambiguous.

Experimental

Materials. The anhydrous iron(III) chloride was prepared by the method described in a previous paper.[1)] The hydrated iron(II) chloride, $FeCl_2 \cdot 5H_2O$, was prepared by the recrystallization of commercial iron(II) chloride from water. The Ia, Ib, Ic, IIa, IIIb, and IIIc were prepared by the methods described in the literature.[4)]

Oxidation. By Iron(III) Chloride-Pyridine Complex: Similar procedures were used for all the reactions. Pyridine (1 mmol) was added to dry benzene (5 ml) containing the dispersed iron(III) chloride (1 mmol). Ia (0.5 mmol) was then added to the solution. The resulting solution was heated at 80 °C under an atmosphere of air, oxygen, or nitrogen for the desired time. In the case of a nitrogen atmosphere, the reaction tube was degassed by the freeze-thaw method and then sealed. After the reaction, 2 ml of water was added to the resulting mixture, and then an internal standard, biphenyl, was added. The benzene layer was analyzed by glc. The products were identified by a comparison of their retention times in glc with those of authentic specimens, and their amounts were determined by means of glc. The products were isolated out by the following method. To dry benzene (40 ml) containing the dispersed iron(III) chloride (1.36 g), we added pyridine (0.64 g) and then Ia (0.85 g), after which the solution was heated at 80 °C under air. After a 24-hr reaction, a black-brown solid (2.08 g) was collected from the brown solution by filtration and washed with benzene. Found: C, 28.08; H, 2.58; N, 5.40; Cl, 38,45; Fe(II), 2.4; Fe(III), 15.27%. The combined benzene solution was extracted with a 10% sodium bicarbonate solution and then subjected to chromatography on alumina. Elution with benzene gave 0.025 g (3%) of the unreacted Ia and 0.1 g (8%) of IV. The formation of benzaldehyde was confirmed by means of glc. Elution with methanol gave 0.47 g (52%) of IIIa (mp 94—95 °C). Elution with methanol-water gave 0.26 g of a white, amorphous product (mp>280 °C), which did not become crystalline, along with a tarry matter. The white product exhibited an IR spectrum with broad peaks at 3050, 1660, 1600, 1550, 1410, 1210, 1180, 1070, 880, 840, 800, 703, and 680 cm^{-1}. The sodium bicarbonate solution was acidified with dilute aqueous hydrochloric acid and extracted several times with benzene. The benzene extracts were then combined and the solvent removed to yield 0.021 g (4%) of benzoic acid. IIIb (mp 71—72 °C) and IIIc (mp 30—31 °C) were isolated and identified by a method similar to that used in the case of IIIa.

By $[Fe(DMF)_3Cl_2][FeCl_4]$: A solution of Ia (0.53 mmol) in benzene (5 ml) containing the iron(III) complex (1.1 mmol) was heated at 80 °C for 96 hr. The amounts of IIIa and benzaldehyde were then determined by means of glc.

By Iron(III) Chloride in Acetonitrile: An acetonitrile solution (30 ml) of a mixture of Ia (3.2 mmol) and iron(III) chloride (6.3 mmol) was refluxed under air for 24 hr. After the subsequent removal of the acetonitrile, the residue was added to benzene. The amounts of the products were determined by means of glc.

Analyses. The iron(II) or iron(III) complex isolated was analyzed by the methods described in a previous paper.[5)] Analytical determinations of the products were carried out using a Hitachi K-53 gas chromatograph fitted with a 3 mm × 1 m stainless steel column packed with 30% high-vacuum silicon grease on Celite 545.

References

1) Part VIII: H. Inoue, M. Izumi, and E. Imoto, This Bulletin, **47**, 1712 (1974).

2) H. Inoue, Y. Kimura, and E. Imoto, *ibid.*, **46**, 3303 (1973).

3) S. Tobinaga and E. Kotani, *J. Amer. Chem. Soc.*, **94**, 309 (1972).

4) C. F. H. Allen and W. E. Barker, "Organic Syntheses," Coll. Vol., II p. 156 (1943); S. S. Jenkins, *J. Amer. Chem. Soc.*, **55**, 703 (1933); H. H. Hatt, A. Pilgrim, and W. J. Hurran, *J. Chem. Soc.*, **1936**, 93.

5) H. Inoue, K. Tamaki, N. Komakine, and E. Imoto, This Bulletin, **40**, 875 (1967).

BULLETIN OF THE CHEMICAL SOCIETY OF JAPAN, VOL. 48(2), 737—738 (1975)

The Synthesis and Polymerization of 2-(*p*-Vinylphenyl)-4,6-diamino-*s*-triazine[1]

Eizo OIKAWA and Kazuya HORIGUCHI

Faculty of Engineering, Niigata University, Nagaoka, Niigata 940

(Received August 23, 1974)

Synopsis. A new olefinic *s*-triazine, that cited in the title, was prepared by the reaction of *p*-cyanostyrene with dicyandiamide. Methyl *p*-vinylbenzoate could provide the triazine in an improved yield. The triazine readily underwent radical polymerization in an aprotic solvent to give a soluble and thermally stable polymer.

The reaction of nitriles with dicyandiamide (DCDA) has long been utilized for the preparation of many guanamines. This method has not, however, been successful in the preparation of olefinic guanamines, which contain an unsaturated group attached directly to the ring. However, the use of this method seems possible if one uses an unsaturated nitrile containing another group or atoms between the unsaturated and cyano group, but very few attempts to do so have thus far been reported.[2] We used *p*-cyanostyrene (*p*-CNSt) as such a nitrile in an attempt to prepare polymerizable *s*-triazine compounds; we could thus prepare the new title compound (VPAT), as is summarized in Table 1. In the actual performance of the reaction, a lower reaction temperature is desirable in order to minimize the polymerization of *p*-CNSt, but the precipitation of the white product did not take place for 2 hr, not until the temperature attained 115 °C. Although the reaction was continued for 2 hr, 1 hr appears to be enough from a comparison of SGH-1 with SGH-4. The amount of potassium hydroxide had an influence on the yield. The optimum molar ratio of the catalyst to *p*-CNSt was about 0.25. A higher amount might give rise to unidentified side reactions to a greater degree.

While *p*-CNSt brought a yield of 20% at best, methyl *p*-vinylbenzoate (MVB) increased the yield of VPAT more than double. A basic catalyst, sodium methoxide, did not markedly affect the reaction.

VPAT readily underwent radical polymerization in a good conversion, as will be described in the Experimental section. Comparable intrinsic viscosities were obtained for heterogeneous polymerization in DMF, but a higher viscosity was obtained for a homogeneous polymerization in DMSO.

Poly(VPAT) has a *s*-triazine ring as a side group in every repeating unit. It is possible to introduce the same side group to a polymer possessing cyano groups, but the complete reaction is generally difficult.[3] In our work, at best about 93% of the cyano group of poly(*p*-CNSt) reacted in DMSO at 100°C for 3 hr. In this respect, poly(VPAT) can be regarded as 100% converted poly(*p*-CNSt).

These polymers were soluble only in DMSO and concentrated sulfuric acid, and were insoluble in other common organic solvents. They showed a relatively good thermal stability in air; the weight losses for PVBG-2 were 10% at 350 °C and 15% at 396 °C; for PVBG-4, they were 10% at 375 °C and 15% at 400 °C.

Experimental

2-(p-Vinylphenyl)-4,6-diamino-s-triazine (VPAT) from p-CNST. *p*-CNSt was prepared from bromobenzene.[4] The reaction was conducted in a 100-ml, three-necked flask fitted with a mechanical stirrer, a condenser, and a thermometer under the conditions listed in Table 1. Thirty or forty min after the reaction started, white solids were precipitated. After the required period, the reaction mixture was cooled to room temperature. The precipitate was filtered and washed with warm water, methanol, and then nitromethane to remove any unreacted materials and the polymer. When the filtrate was poured into water, a white precipitate was obtained. It was treated similarly. Both solids could be purified by either recrystallization from nitromethane or sublimation under reduced pressure, and were found to be the same product from their melting points and the IR spectra; mp 222—223 °C (in a sealed capillary). Found: C, 61.35; H, 5.25; N, 33.75%; Calcd for $C_{11}H_{11}N_5$: C, 61.96; H, 5.20; N, 32.84%. IR (KBr): NH_2 (3520 w, 3320 m, 3130 s, 1680s, 1640s), *s*-triazine ring (1530—50s, 820m), vinyl (900m, 980w, 995w), NMR (DMSO-d_6): *p*-substituted benzene ring (7.91 δ, q, $J=8$, 4H), NH_2 (6.77 δ, s, 4H), vinyl (6.95—5.30 δ, m, 3H).

TABLE 1. REACTION OF *p*-CNSt WITH DCDA[a]

No.	SGH-2	SGH-4[b]	SGH-1	SGH-3
p-CNSt mmol	31.0	31.1	38.8	31.2
DCDA mmol	48.0	48.6	65.0	43.0
KOH mmol	3.7	7.3	10.4	14.8
(mol/l)	(0.46)	(0.91)	(1.04)	(1.85)
[KOH]/[*p*-CNSt]	0.119	0.233	0.268	0.475
Yield %	10.0	19.6	16.0	15.2

a) *p-t*-Butylcatechol: 0.1 g (0.6 mmol); Methyl cellosolve: 8—10 ml, 115 °C, 2 hr. b) 115 °C, 1 hr.

VPAT from MVB. MVB was prepared from β-bromoethylbenzoic acid.[4-6] The reaction was carried out according to the procedure of Ref. 7. The yield in the case of no catalyst was 41.7% (No. SG-1); mp 225—6 °C (in a sealed capillary). Found: C, 62.04; H, 4.95; N, 32.47%. The addition of sodium to methanol or sodium methoxide (16 mol% based on MVB) afforded the same product in a better yield (48.0%, No. SG-2).

Polymerization of VPAT. The polymerization was carried out in a sealed tube with azobisisobutyronitrile (1.05 mol% based on VPAT) at 80 °C for 5 hr. The DMF solution became turbid in a few minutes, and the polymer started to precipitate. The polymer was purified by reprecipitation from DMSO-methanol. One gram of SGH-2 in 5 ml of DMF gave a yield of 73.3% and an intrinsic viscosity of 0.263 at 25 °C in DMSO (No. PVBG-2), and 0.694 g of

SG-2 in 3.5 ml of DMF gave 91.0% and 0.271 (No. PVBG-3). In 1.8 ml of DMSO, 0.365 g of SGH-4 gave 82.5% and 0.325 (No. PVBC-4).

The weight loss was measured with a solenoid-type thermobalance, Model SE-52, of Tokyo Koki Seizosho.

References

1) Polymers containing the *s*-triazine ring. III. Part II: E. Oikawa and H. Tatsuishi, *J. Appl. Polym. Sci.*, **15**, 913 (1971).

2) L. S. Luskin, P. L. de Benneville, and S. Melamed, *J. Org. Chem.*, **23**, 1032 (1958).

3) T. Seo, T. Kakurai, and T. Noguchi, *Kobunshi Kagaku*, **30**, 76, 451 (1973).

4) C. S. Marvel and C. G. Overberger, *J. Amer. Chem. Soc.*, **67**, 2250 (1945); C. G. Overberger and R. E. Allen, *ibid.*, **68**, 722 (1946).

5) E. L. Foreman and S. M. McElvain, *ibid.*, **62**, 435 (1940).

6) P. Jager and E. S. Waight, *J. Chem., Soc.*, **1963**, 1339.

7) J. T. Thurston, US Pat. 2,461,943 (1949).

BULLETIN OF THE CHEMICAL SOCIETY OF JAPAN, VOL. 48(2), 739—740 (1975)

Syntheses and Ring Opening Reactions of 2-Alkyl-3,3-dichlorospiro-[cyclopropane-1,9′-fluorene] Derivatives

Eiji WADA*, Shizuo FUJISAKI, Akiko NAGASHIMA, and Shoji KAJIGAESHI

Department of Industrial Chemistry, Faculty of Engineering, Yamaguchi University, Tokiwadai, Ube 755

(Received September 12, 1974)

Synopsis. 2-Alkyl-3,3-dichlorospiro[cyclopropane-1,9′-fluorene] derivatives (**4**) were obtained by the addition of CCl_2 to 9-alkylidenefluorenes. Ring opening reactions of **4** with bases gave enynes, butadienes, or butatrienes.

Most spiro[cyclopropane-1,9′-fluorene] derivatives have been synthesized from the reactions of 9-diazofluorene with olefins by heating or by irradiation with UV light.[1] In the present paper, we wish to present a convenient method for the syntheses of similar spiro compounds, in which 2-alkyl-3,3-dichlorospiro[cyclopropane-1,9′-fluorene] derivatives (**4**) are prepared in good yields by the reactions of 9-alkylidenefluorenes (**3**) with dichlorocarbene. Furthermore, we wish to report the ring opening reactions of **4** with some bases.

The olefins **3** were obtained by dehydration of the corresponding 9-alkyl-9-fluorenols (**2**) which were prepared from the reaction of fluorenone with alkylmagnesium bromides (**1**). The dichlorocarbene was generated from the reaction of chloroform with aqueous sodium hydroxide solution (50%) in the presence of catalytic amounts of benzyltriethylammonium chloride (method A[2]), or from the reaction of ethyl trichloroacetate with sodium methoxide (method B[3]).

Syntheses of 4. A group $-CH_2-CHR^1R^2$ was chosen as the alkyl group in Grignard reagents **1**, and the syntheses of **2**, **3**, and **4** are shown in Scheme 1. The melting points and yields of the products are summarized in Table 1. All the products had satisfactory

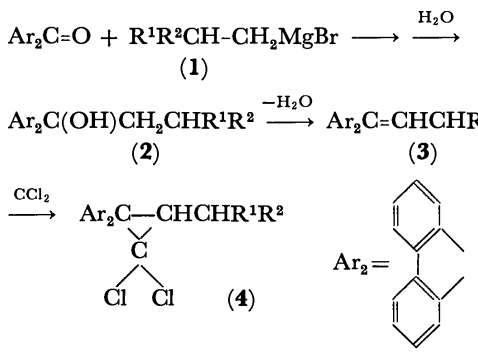

Scheme 1.

elemental analyses (C and H), and the structures of the products were confirmed by their IR and NMR spectra. Compound **4e** was a mixture which was separated into two isomers **4e–1** and **4e–2** by fractional crystallization. The structures of **4e–1** (mp 125—127 °C) and **4e–2** (mp 155—157 °C) were confirmed as *threo* and *erythro* isomers, respectively, from their NMR spectra.[7]

Table 1. Syntheses of **2**, **3**, and **4**

Compd	R^1	R^2	Mp (°C) (Bp:/mmHg)	Yield (%)
2a[4]	H	H	98—99	77
2b	H	CH_3	97—100	76
2c	CH_3	CH_3	112—115	70
2d[5]	H	Ph	56—58	42
2e	CH_3	Ph	89—91	40
3a[4]	H	H	100—103	72
3b	H	CH_3	39—42	91
3c	CH_3	CH_3	(136—138/0.07)	61
3d[5]	H	Ph	88—90	89
3e	CH_3	Ph	74—76	88
3f[6]	Ph	Ph	103—106	44
4a[a]	H	H	110—112	72
4b[a]	H	CH_3	71—72	73
4c[b]	CH_3	CH_3	81—83	57
4d[b]	H	Ph	116—118	88
4e[b]	CH_3	Ph	{125—127 {155—157	82
4f[a]	Ph	Ph	169—170	83

a) CC_2 was generated by the method A.[2] b) CCl_2 was generated by the method B.[3]

Ring Opening Reactions of 4 with Bases. The ring opening reactions of **4a**, **4b**, and **4c** with sodium alkoxides in alcohols or with pyridine gave unidentified polymeric powders or tars in each case. However, the products of the reactions of **4d**, **4e**, and **4f** with bases were derivatives of enynes, butadienes, and butatrienes conjugated with the fluorene moiety. The structures of these derivatives were confirmed by elemental analysis and spectral data. The experimental results are summarized in Table 2.

When pyridine was used as a base, compounds of type **5** were isolated. The reaction of **5f** with sodium

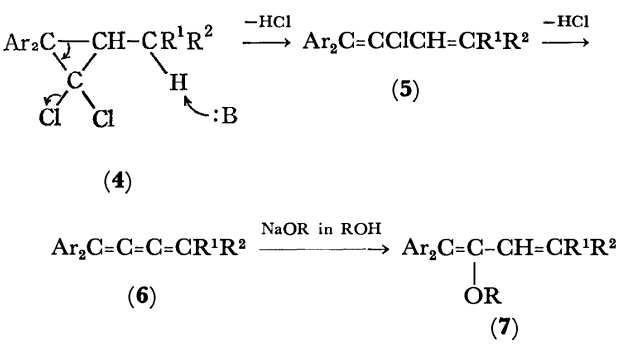

Scheme 2.

* Present address: Research Laboratory of Resources Utilization, Tokyo Institute of Technology, Ookayama, Meguro-ku, Tokyo.

Table 2. Ring opening reactions of **4d**, **4e**, and **4f** with bases

4	Base used	Reaction condition	Product			Yield (%)
			Structure	Mp (°C)	Color	
4d	Pyridine	Δ 48 hr	$Ar_2C{=}CClCH{=}CHPh$ (**5d**)	133—135	Yellow	43
	NaOMe in DMSO	rt 4 hr	$Ar_2C{=}CHC{\equiv}CPh$ (**8d**)	88—90	Yellow	35
	NaOEt in EtOH	Δ 24 hr	$Ar_2C{=}C(OEt)CH{=}CHPh$ (**7d**)	64—67	Yellow	13
4e	Pyridine	Δ 145 hr	$Ar_2C{=}CClCH{=}CMePh$ (**5e**)	91—105	Yellow	24
	NaOEt in EtOH	Δ 28 hr	$Ar_2C{=}C(OEt)CH{=}CMePh$ (**7e**)	147—149	Yellow	18
4f	Pyridine	Δ 96 hr	$Ar_2C{=}CClCH{=}CPh_2$ (**5f**)	162—164	Yellow	60
	NaOMe in DMSO	rt 40 min	$Ar_2C{=}C{=}C{=}CPh_2$[8] (**6f**)	223—224	Orange	90
	NaOMe in DMSO	40 °C 2 hr	$Ar_2C{=}C(OMe)CH{=}CPh_2$ (**7f**)	177—178	Yellow	33

methoxide in MeOH led to **6f**,[8] which was easily converted into **7f** by sodium methoxide in DMSO. Therefore, the following mechanism would account for the formation of products **5**, **6**, and **7** from **4** in the presence of bases.

Experimental

*Syntheses of **4** by Method A.*[2] A typical procedure was as follows. Compound **2a** (5.3 g, 0.028 mol) in $CHCl_3$ (12 ml) was added to a mixture of 50% aq. NaOH (20 ml) and $PhCH_2N(C_2H_5)_3 \cdot Cl$ (0.4 g). The mixture was stirred for 4 hr at 40 °C, and then poured into water (100 ml). The organic layer was separated and the aqueous phase was extracted with ether. The combined organic extracts were washed with water and dried over $MgSO_4$. The dry ether solution was concentrated in a rotary evaporator. Recrystallization of the residue from ethyl alcohol gave **4a**: 5.0 g (72%); mp 110—112 °C.

*Ring Opening of **4** by Bases.*[3] A typical procedure was as follows. Compound **4d** (0.5 g, 0.0014 mol) was reacted with commercial sodium methoxide (0.17 g, 0.003 mol) in DMSO (70 ml) for 4 hr at room temperature. The resulting mixture was poured into water and then extracted with ether. The ether solution was washed with water and dried over $MgSO_4$. Concentration of the dry ether solution gave **8d**: 0.11 g (35%); mp 88—90 °C (from petroleum benzine–benzene (1 : 1 v/v)).

References

1) For example see a) H. K. Reiminger, *Chem. Ind.*, **1966**, 1682; b) G. S. Nikol'skaya and A. T. Troshchenko, *Zh. Org. Khim.*, **3**, 709 (1967); c) S. Murahashi, I. Moritani, and T. Nagai, This Bulletin, **40**, 1655 (1967); d) I. A. D'yakonov, V. P. Dushina, and G. V. Golodnikov, *Zh. Obshch. Khim.*, **39**, 923 (1969); e) H. M. Walborsky, M. S. Aronoff, and M F. Schulman, *J. Org. Chem.*, **36**, 1036 (1971).

2) M. Makosza and M. Wawrzyniewicz, *Tetrahedron Lett.*, **1969**, 4659.

3) W. E. Parham and E. E. Schweizer, *J. Org. Chem.*, **24**, 1733 (1959).

4) F. Ullmann and R. von Wurstemberger, *Ber.*, **38**, 4105 (1905).

5) N. Campbell and K. W. Delahunt, *J. Chem. Soc., C*, **1966**, 1910.

6) R. Kuhn, H. Fischer, F. A. Neugebauer, and H. Fischer, *Ann. Chem.*, **654**, 64 (1962).

7) The NMR data of **4e** are as follows: **4e-1**; δ ($CDCl_3$) 1.65 (d, J=8 Hz, 3, CH_3), 2.76 (d, J=11 Hz, 1, -CH-), 3.55 (two q, J=11 Hz, and J=8 Hz, 1, -CH-CH_3), 6.82 (s, 5, -Ph), 7.0—7.7 (m, 8, fluorene nucleus), **4e-2**; δ ($CDCl_3$) 1.0 (d, J=6.5 Hz, 3, CH_3), 2.76 (d, J=11 Hz, 1, -CH-), 3.55 (two q, J=11 Hz, and J=6.5 Hz, 1, -CH-CH_3), 7.0—7.82 (m, 13, aromatic ring protons). It appeared that both the phenyl protons in the stable conformation of the *threo* form and the methyl protons in the stable conformation of the *erythro* form are located above the fluorene ring. Therefore, these protons above the fluorene ring should be shifted to higher field. From the above NMR data, it may be seen that **4e-1** is the *threo* isomer and **4e-2** is the *erythro* isomer.

8) S. Kajigaeshi, N. Kuroda, G. Matsumoto, E. Wada, and A. Nagashima, *Tetrahedron Lett.*, **1971**, 4887.

BULLETIN OF THE CHEMICAL SOCIETY OF JAPAN, VOL. 48(2), 741 (1975)

Reaction of Benzylic Chlorides with Hexamethylphosphoric Triamide

Seiji ARIMATSU, Ryohei YAMAGUCHI, and Mituyosi KAWANISI

Department of Industrial Chemistry, Faculty of Engineering, Kyoto University, Yoshida, Sakyo-ku, Kyoto 606

(Received April 18, 1974)

Synopsis. Benzyl chloride was converted into benzyldimethylamine (**1**), dibenzylmethylamine (**2**), and benzylpentamethylphosphoric triamide (**3**), when it was heated in hexamethylphosphoric triamide (HMPT). Diphenylmethane (**4**), benzhydrylmethylamine (**5**), and benzophenone methylamine (**6**) were obtained when benzhydryl chloride was used in place of benzyl chloride. Triphenylmethyl chloride afforded triphenylmethane (**7**) as the sole isolable product.

Monson reported that primary and secondary alcohols possessing β-hydrogen atom are readily transformed into the unrearranged olefins in hexamethylphosphoric triamide (HMPT) at 230—240 °C *via* the corresponding alkyl tetramethylphosphorodiamidates,[1] and that primary alkyl halides having β-hydrogen atom afford in HMPT unrearranged 1-alkenes in good yields.[2] In the case of alcohols having no β-hydrogen atom, we found that the reaction proceeds in different ways to give reduction products, substituted products and phosphorodiamidated products.[3] In the reaction of benzyl alcohol with HMPT, we isolated benzyl tetramethylphosphorodiamidate which Monson suggested as an intermediates, and showed that bis(*N*,*N*-dimethylamino) phosphoryl group could behave as a leaving group to give the substituted compounds.

Benzyl chloride has no β-hydrogen atom, but has a chlorine atom which is thought to be a better leaving group than bis(*N*,*N*-dimethylamino)phosphoryl group. We wish to report results (see Table) obtained by the thermal treatment of benzylic chlorides with HMPT.

The results are similar to those of the reaction of benzylic alcohols with HMPT except for two points: i) An additional product was produced—benzylpentamethylphosphoric triamide (**3**) in the case of benzyl chloride, and benzophenone methylimine (**6**) in the case of benzhydryl chloride. ii) The yields of the products were higher than in the case of benzylic alcohols. Triphenylmethyl chloride and triphenylmethanol gave triphenyl methane (**7**) in 83% and 44% yields,[3] respectively. This might be ascribed to the nature of chlorine atom as a better leaving group than that of the bis(*N*,*N*-dimethylamino)phosphoryl group.[5]

TABLE 1. REACTION OF BENZYLIC CHLORIDES WITH HMPT

Substrate	Isolated products (%)
$PhCH_2Cl$	$PhCH_2NMe_2$ (39), $(PhCH_2)_2NMe$ (27), (**1**) (**2**)
	$PhCH_2NMeP(O)(NMe_2)_2$ (23) (**3**)
Ph_2CHCl	Ph_2CH_2 (13), Ph_2CHNMe_2 (40), (**4**) (**5**)
	$Ph_2C{=}NMe$ (6) (**6**)
Ph_3CCl	Ph_3CH (83) (**7**)

Experimental

All the temperatures are uncorrected. The IR and MS spectra were obtained on a Shimadzu IR-27 spectrometer and Hitachi RMS-4 mass spectrometer, respectively. The NMR spectra were obtained on a Varian EM-360 spectrometer, TMS being chosen as an internal standard.

Hexamethylphosphoric Triamide (HMPT). Commercial HMPT was refluxed for 5 hr under N_2 with calcium hydride, and then distilled, bp 110 °C/15 mmHg.

Starting Materials. Commercial benzyl chloride was distilled before use. Benzhydryl chloride and triphenylmethyl chloride were prepared according to the published methods.[6,7]

General Procedure for the Reaction with HMPT. The substrate (0.01 mol) was dissolved in HMPT and heated at 230—240 °C under N_2 for 1 hr. After HMPT had been removed by distillation under diminished pressure, the residue was separated by a combination of vacuum distillation, column chromatography and preparative glc. Each reaction product was identified by comparison with the authentic specimen.[3b,8]

References

1) R. S. Monson, *Tetrahedron Lett.*, **1971**, 567; R. S. Monson and D. N. Priest, *J. Org. Chem.*, **36**, 3826 (1971).

2) R. S. Monson, *Chem. Commun.*, **1971**, 113.

3) (a) M. Kawanisi, S. Arimatsu, R. Yamaguchi, and K. Kimoto, *Chem. Lett.*, **1972**, 881 (b) S. Arimatsu, R. Yamaguchi, and M. Kawanisi, This Bulletin, **47**, 1693 (1974).

4) R. S. Monson and D. N. Priest, *Chem. Commun.*, **1971**, 1018.

5) Since 1- and 2-chloroadamantane did not react with HMPT under similar reaction conditions, the enhanced cationic nature of the benzylic carbon atom can be the driving force for the reactions. (S. Arimatsu, unpublished results.)

6) H. Gilman, *J. Amer. Chem. Soc.*, **48**, 1735 (1926).

7) W. E. Bachmann, "Organic Syntheses," Coll. Vol. 3, p. 841 (1955).

8) S. Arimatsu, R. Yamaguchi, and M. Kawanisi, This Bulletin, **47**, 1553 (1974).

BULLETIN OF THE CHEMICAL SOCIETY OF JAPAN, VOL. 48(2), 742 (1975)

Molecular Vibrations and Force Fields of Alkyl Sulfides. X. Skeletal Bending Vibrations of Several Simple Aliphatic Sulfides

Masaru OHSAKU

Department of Chemistry, Faculty of Science, Hiroshima University, Higashisenda-machi, Hiroshima 730

(Received April 30, 1974)

Synopsis. The skeletal bending vibrations of several normal alkyl sulfides were analysed. It is found that a heterogeneous system as this case can also be explained in the same manner as a homogeneous system.

In recent years, the relations existing between molecular chain lengths and frequencies for the skeletal bending vibrations have been extensively examined on homogeneous oligomer-type molecules, *e.g.*, *n*-paraffines,[1] $CH_3(CH_2)_nCONH_2$[2] and $CH_3(CH_2)_n$-$COND_2$,[2] and $CH_3O(CH_2CH_2O)_nCH_3$.[3] On the other hand, Miyazawa *et al.*[4] treated the relation between the skeletal bending and the phase-difference on such heterogeneous systems as normal alkyl ethers of the same length. The relationships between the frequency and the phase-difference may show a particular behavior, since alkyl sulfides contain a sulfur atom with a fairly large atomic mass in molecules.

In this experiment, we have tried to analyse the skeletal bending vibration by using the frequency-phase difference relation for such heterogeneous system as alkyl sulfides with different lengths.

Results and Discussion

We have recorded the infrared spectra in the liquid and solid states for methyl propyl (MeSPr), methyl butyl (MeSBu), ethyl propyl (EtSPr), ethyl butyl (EtSBu), and dipropyl (PrSPr) sulfides. The observed frequencies of dimethyl (MeSMe),[5] methyl ethyl (MeSEt),[6] diethyl (EtSEt)[6] sulfides, MeSPr, MeSBu, EtSPr, EtSBu, and PrSPr used are those which may be due to the stable form in the solid state, judging on the basis of the normal coordinate treatment. All of the skeletal bending vibrations are infrared-active. Figure 1 shows the observed $\delta_{nk}=k\pi/(n+1)$ plots. The assignments of the k values are shown on the right-hand side, where $n=1$ corresponds to MeSMe, $n=2$ to MeSEt, $n=3$ to MeSPr or EtSEt, $n=4$ to MeSBu or EtSPr, and $n=5$ to EtSBu or PrSPr. The theoretical studies[7] of polyethylene have revealed that the dispersion curve has a ν_{max} of *ca.* 550 cm^{-1} near the phase-difference of $\pi/3$. The plots of the sulfides shifted to a frequency lower region by *ca.* 100 cm^{-1} from that of polyethylene. However, the position of ν_{max} near $\pi/3$ and the shape of the dispersion of the sulfides correspond very well to those of the polyethylene curve. This suggests that the skeltal form in the solid state of the sulfides is the same as that of polyethylene. For the oxygen analogs,[4] the bending vibrations observed are explained well by the theoretical curve of polyethylene. It is, therefore, likely that the effects of the sulfur atom and the methylene group on the vibrational spectra are very different from those of the oxygen atom and the methylene group on the vibrational spectra, since sulfur has a fairly large atomic mass.

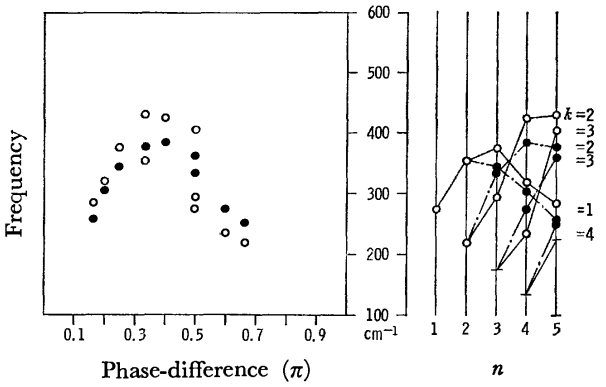

Fig. 1. Frequency-phase difference curve and assignments of k values for the skeletal bending vibrations.
○: MeSMe, MeSEt, MeSPr, MeSBu, EtSBu.
●: EtSEt, EtSPr, PrSPr. —: Calculated.

The skeletal bending vibrations mainly consist of three vibrational modes,—CCC, SCC, and CSC binding, strongly coupled with each other. The bands appearing from the pair of sulfides of the same length are fairly different in frequency, although the regularity is nearly the same in both filled and open circles. These differences arise from the effects of the heavy sulfur atom. Consequently, in the present case it is not simple to explain the relation existing between the chain lengths and the frequencies, but in general it is possible to analyse the band progression in nearly the same manner as in the case of the homogeneous system; rather disperse plots are obtained, though.

The author wishes to thank Professor Hiromu Murata and Associate Professor Yuji Shiro for their helpful advice.

References

1) R. F. Schaufele and T. Shimanouchi, *J. Chem. Phys.*, **47**, 3605 (1967).
2) K. Machida, S. Kojima, and T. Uno, *Spectrochim. Acta*, **28A**, 235 (1972).
3) H. Matsuura, T. Miyazawa, and K. Machida, *ibid.*, **29A**, 771 (1973).
4) K. Kusaki, T. Kitagawa, and T. Miyazawa, Preprints of the 28th Annual Meeting of the Chemical Society of Japan, Vol. **1**, p. 340 (1973).
5) Y. Shiro, M. Ohsaku, M. Hayashi, and H. Murata, This Bulletin, **43**, 609 (1970); M. Ohsaku, Y. Shiro, and H. Murata, *ibid.*, **45**, 113 (1972).
6) M. Ohsaku, Y. Shiro, and H. Murata, *ibid.*, **45**, 954 and 956 (1972); *ibid.*, **46**, 1399 (1973).
7) M. Tasumi and S. Krimm, *J. Chem. Phys.*, **46**, 755 (1967); L. Piseri and G. Zerbi, *ibid.*, **48**, 3561 (1968).

BULLETIN OF THE CHEMICAL SOCIETY OF JAPAN, VOL. 48(2), 743—744 (1975)

Preparation of Tetramethylphthalimide

Koji CHIBA, Eiji ENDO, and Kyoji YAMAKA

Department of Applied Chemistry, Faculty of Engineering, Yamagata University, Yonezawa, Yamagata 992

(Received June 17, 1974)

Synopsis. Treatment of tetramethylphthalic anhydride (I) with 28% aqueous ammonia at room temperature afforded ammonium tetramethylphthalimide (IV) and and 2-cyano-3,4,5,6-tetramethylbenzoate (V). The amount of IV increased by heating at 100 °C, tetramethylphthalimide (VI) being precipitated. A plausible reaction path is proposed.

Of the phthalocyanine group, copper phthalocyanine is the most easily synthesized, but there is difficulty in bringing crude products into acceptable pigments, as well as in preventing a reduction of strength resulting from dispersion in vehicles.

We obtained tetramethylphthalic anhydride (I) by the hydrolysis of bis(nitromethyl)prehnitene.[1] Copper polymethylphthalocyanine synthesized from I might be expected to form more stable dispersion with vehicles, since methyl groups appear to have an affinity to them. However, when a mixture of I, urea and copper salt was heated, no copper phthalocyanine was obtained. It was obtained when tetramethylphthalimide (VI) was used instead of I.

The present study deals with the preparation of VI. We have studied the reaction of I with aqueous ammonia and found a useful procedure.

Phthalimide is formed by heating ammonium phthalate or phthalic anhydride and gaseous ammonia up to 300 °C.[2] Ammonium phthalamidate is formed by heating phthalic anhydride with aqueous ammonia, the dry salt being converted into phthalimide at about 200 °C.[3,4]

By treating I with 28% aqueous ammonia at room temperature for 5 min (Expt. No. 1), ammonium tetramethylphthalimide (IV) and 2-cyano-3,4,5,6-tetramethylbenzoate (V) were obtained in good yields, but neither tetramethylphthalate (VII) nor tetramethylphthalamidate (II) was detected. By warming, IV increased whereas V decreased (Table 1). On continued warming (Expt. No. 4), VI was obtained as a white precipitate, which may have been formed by releasing of ammonia from IV.

VI precipitated when finely powdered VI was dissolved in 28% aqueous ammonia at room temperature and the resulting clear solution was then heated at 100 °C at atmospheric pressure.

Table 1. Experimental results

Expt. No.	Conditions		Products (mol %)			
	Temp.	Time	IV	V	VI[a]	VII
1	Room temp.	5 (min)	61.9	29.5	0.0	0.0
2	100(°C)	1	62.3	31.1	0.0	0.0
3	100	90	56.0	9.5	10.0	14.9
4	100	180	33.8	8.4	40.0	15.3
5	100	240	—	—	70.3	—

a) Obtained as a white precipitate.

IV does not seem to be formed from ammonium tetramethylphthalate (VII) by the removal of water and ammonia, but from intermediary II. Since the repulsion of the four methyl groups on II facilitates cyclization between the amide group and the carboxyl group, IV might be formed as the cyclized product even under mild conditions, and thus II cannot be detected. VII seems to be formed by the hydrolysis of III as a minor product.

A plausible reaction path is shown in the following (Scheme 1).

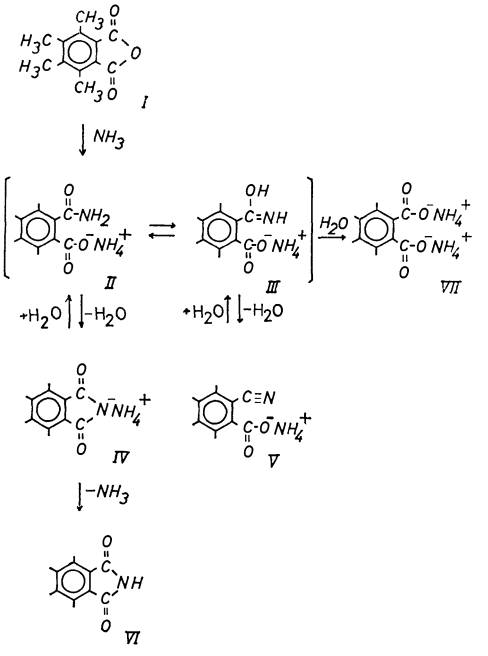

Scheme 1.

Experimental

I was obtained by the hydrolysis of bis(nitromethyl)prehnitene, prepared by the nitration of hexamethylbenzene.[1]

Procedure. I (1.0 g) was added to 250 ml of 28% aqueous ammonia, and the mixture was stirred for a certain time at room temperature or 100 °C. Ammonia gas was allowed to escape through a reflux condenser. The color of the reaction mixture turned from opaque to clear after about 3 min even at room temperature.

Isolation of IV, V, and VII. Excess silver nitrate (100 g/H_2O 70 ml) was added to the above solution (30 ml). The resulting precipitate was filtered off, dried, and refluxed with excess methyl iodide in benzene for 3 hr. After filtration of insoluble material, the filtrate was chromatographed on alumina, and the products were eluted with petroleum and benzene. Each fraction was evaporated and the residue was

recrystallized from chloroform to give three products. The first fraction afforded *N*-methyltetramethylphthalimide (*N*-methylated VI); colorless needles, mp 180—181 °C. Found: C, 71.67; H, 7.05; N, 6.55%. Calcd for $C_{13}H_{15}NO_2$: C, 71.86; H, 6.96; N, 6.45%. IR(KBr, cm^{-1}): 1754, 1697 (C=O), 1440, 1384 (CH_3), 1253, 1105, 1003(C–N) and 757. NMR($CDCl_3$, δ ppm): 2.25 (s, $-CH_3$, 6H), 2.63 (s, $-CH_3$, 6H) and 3.08 (s, $N-CH_3$, 3H).

N-Methylated VI was also obtained by treatment VI with diazomethane in ether. The second fraction afforded methyl 2-cyano-3,4,5,6-tetramethylbenzoate (methylated V); colorless needles, mp 75—76 °C. Found: C, 71.73; H, 7.08; N, 6.51%. Calcd for $C_{13}H_{15}NO_2$: C, 71.86; H, 6.96; N, 6.45%. IR(KBr, cm^{-1}): 2220 (C≡N), 1732 (C=O), 1207 and 1180 (C–O–C). NMR(CCl_4, δ ppm): 2.24(s, $-CH_3$, 6H), 2.30 (s, $-CH_3$, 3H), 2.49(s, $-CH_3$, 3H) and 3.95 (s, $-OCH_3$, 3H). Colorless needles (mp 127.5—128.5 °C) were obtained from the final fraction, and identified as dimethyl tetramethylphthalate (methylated VII) by comparing the retention time in glc and IR spectrum with that of an authentic sample.[1)]

These reaction products were determined by glc (column; 10% Silicone DC 550/Cellite 80—100 mesh, 4 mm×2 m, temp; 215 °C, N_2; 40 ml/min).

Isolation of VI. 1.0 g of I was added to 250 ml of 28% aqueous ammonia, and the mixture was heated at 100 °C. The reaction mixture turned instantly from opaque to clear. On continued heating, a white precipitate was formed. After heating for 3 hr, the mixture was cooled to room temperature and the precipitate was filtered off; yield 0.4 g (40 mol% as VI). Recrystallization from methanol gave colorless needles; mp 289—290 °C. Found: C, 70.74; H, 6.32; N, 7.07%; mol wt (Rast), 206. Calcd for $C_{12}H_{13}NO_2$: C, 70.91; H, 6.45; N, 6.89%; mol wt, 203. IR(KBr, cm^{-1}): 3190 (N–H), 1752, 1696 (C=O), 1127 and 1038 (C–N). NMR (DMF-d_7, δ ppm): 2.24 (s, $-CH_3$, 6H), 2.56 (s, $-CH_3$, 6H) and *ca.* 10.7 (s, NH, 1H).

References

1) K. Chiba and E. Sato, *Nippon Kagaku Kaishi*, **1973**, 1249.
2) W. A. Noyes and P. K. Potter, "Organic Syntheses," Coll. Vol. 1, p. 457 (1941).
3) E. Chapman and H. Stephen, *J. Chem. Soc.*, **127**, 1791 (1925).
5) V. Auger, *Bull. Soc. Chim. Fr.*, **49**, 349 (1889).

Rate of the Dushman Reaction in Iodic Acid at Low Iodide Concentration. Complexity of Iodic Acid

Ryusaburo FURUICHI* and Herman A. LIEBHAFSKY

Department of Chemistry, Texas A&M University, College Station, Texas 77843, U.S.A.

(Received March 20, 1974)

Three rate laws have been postulated for the Dushman reaction, $6H^+ + 5I^- + IO_3^- = 3H_2O + 3I_2$, with total reaction orders of four, five and six, at iodide ion concentrations below 10^{-8} M. New direct measurements of the rate and an examination of thermodynamic data for iodic acid solutions have eliminated some of the confusion. The complexity of iodic acid solutions, with and without added salt, makes it impossible to establish a single reaction order from the radioactive iodine exchange measurements. The new results are best expressed by a quasiempirical rate equation, $-d[IO_3^-]/dt = 8.59 \times 10^4 [H^+]^2(I^-)[IO_3^-]$ mol l^{-1} min^{-1}, which is closely approximated by $-d[IO_3^-]/dt = \gamma_{\pm p}^4 (H^+)^2(I^-)(IO_3^-)\{k' + k''(HIO_3)\}$ mol l^{-1} min^{-1}, with $k' = 2.83 \times 10^5$ mol^{-3} l^3 min^{-1} and $k'' = 6.60 \times 10^6$ mol^{-4} l^4 min^{-1} for 25 °C. The second rate law is interpreted in terms of a reasonable mechanism that takes into account the thermodynamically established polymerization in iodic acid solutions.

A series of preliminary investigations[1-4] into the oscillatory decomposition of hydrogen peroxide by iodine species has shown that the decomposition is accompanied by oscillatory changes in iodine concentration and that the Dushman reaction,

$$6H^+ + 5I^- + IO_3^- = 3I_2 + 3H_2O \qquad (1)$$

participates in the oscillations. For Reaction (1), three rate laws[5-7] have been reported in which the total reaction order is four, five and six, respectively. The first rate law is based on direct rate measurements of iodine formation and an assumption that iodic acid is a strong electrolyte. This rate law gave smaller calculated rate values than those obtained in our experiments. The last two rate laws[6,7] are based on the measurements of rates of radioactive iodine exchange ($I^{131}I + IO_3^- = I_2 + {}^{131}IO_3^-$), which is an indirect method since the measurements are carried out at chemical equilibrium of Reaction (1). These rate laws were derived by using the stoichiometric activity coefficient of iodic acid measured by Abel, Redlich and Hersch[8] which shows unusual change of degree of dissociation with change in concentration of the acid (Fig. 2).

On the other hand, the results of direct rate measurements[9] gave a quasiempirical rate law, satisfactory up to 50 °C.

$$-\frac{d[IO_3^-]}{dt} = k_2'[H^+]^2(I^-)[IO_3^-] \qquad (2)$$

in which concentrations in M actually existing, or calculated to exist are donoted by ( ) and terms for M added to make the reaction mixture are denoted by [ ]. Equation (2) gave calculated rates in sharp conflict with those from the two rate laws established by the radioactive iodine exchange study. However, Eq. (2) does not establish the mechanism of Reaction (1).

The present investigation was undertaken in the hope of explaining some of this disquieting confusion about the Dushman reaction and its mechanism. Emphasis is placed on the thermodynamic complexity of iodic acid solutions, the radioactive exchange data has been re-examined, and new direct rate measurements are made under the simplest possible conditions; *i. e.*, for the most part, in reaction mixtures consisting of iodic acid (0.137—0.833 M) in equilibrium with solid silver iodide and solid silver iodate to maintain the iodide ion concentration constant below 10^{-9} M.

Experimental

Measurements were carried out by a method similar to that already described[9] and are summarized here. Thirty grams of solid AgI, 10 ml of 10^{-2} M-$AgNO_3$ solution and 80 ml of deionized water were mixed in the reaction vessel[10] and stirred at a rate of 1600 rpm in a thermostated water bath. Ten milliliter of HIO_3 solution was then added to start the reaction. The reaction time was measured after 5 ml of the acid has been added. All the reagents were of analytical grade (J. T. Baker Chem. Co.).

Ten seconds prior to each sampling, stirring was stopped and

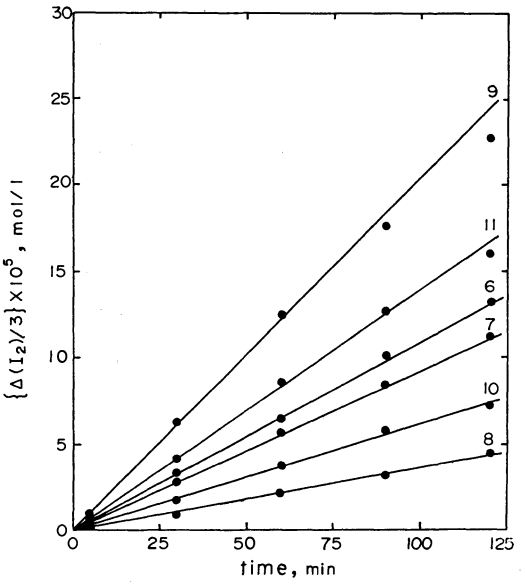

Fig. 1. Rate of the Dushman reaction measured in iodic acid solutions at 25 °C.
Concentrations of iodic acid solutions used are shown in Table 1 for experiments numbered 6—11.
Amount of silver iodide: 30 g/100 ml-solution, Initial silver nitrate concentration: 10^{-3} M, Stirring speed: 1600 rpm.

* Present address: Department of Applied Chemistry, Faculty of Engineering, Hokkaido University, Sapporo 060 Japan.

solid AgI was allowed to settle, which halted the reaction. The solution, 3 ml, was then withdrawn with a syringe and discharged into a small separatory funnel containing 4 ml of CCl_4. The iodine was extracted by shaking for 3 min, and the CCl_4 was transferred to a cuvette and centrifuged for 1.5 min to separate residual solid AgI. The content of I_2 in CCl_4 was spectrophotometrically determined from the absorbance at 500 nm (Hitachi-Perkin-Elmer Double-Beam Type Spectrophotometer).

The iodide ion concentration of the reaction mixture was maintained at constant values below 10^{-9} M by the establishment of the solubility equilibria of AgI[11] and $AgIO_3$[12]. The concentration of H^+ and IO_3^- were also practically constant, since the amount of I_2 formed by the reaction was sufficiently small. The rate of reaction was estimated from the linear relation between the amount of formed I_2 and the time (Fig. 1.). In order to test the salt effect on the rate, five measurements were carried out at 5 °C in solutions containing 1.035 M-$LiClO_4$. In no experiment was formation of solid I_2 observed.

Results and Discussion

Estimation of Rate for 25 °C. The results of the measurements are summarized in Table 1. Rate constant k_2' for Eq. (2) was calculated[13] from the measured rates at 5, 25, 30, and 50 °C.

The reaction order and rate constant should be evaluated from the results of measurements over a sufficiently wide range of iodic acid concentration. However, since the reaction is of high order, an adequate concentration range could not be covered satisfactorily at one temperature. Consequently, the results of measurements carried out at suitably different concentrations over the temperature range 5—50 °C were converted into those at 25 °C for a final test of the different rate laws by the following method.

For each temperature (Table 1), mean values of the k_2' values lie very near the line defined by

$$\log k_2' = \frac{-1.612\times10^3}{T} + 10.339 \qquad (3)$$

The numerical values compare favorably with 1.628×10^3 and 10.504, which appear in the corresponding equation[9] for reaction mixtures prepared by using sodium iodate and perchloric acid instead of iodic acid. Over the temperature range, the two equations obtained by these two sets of values give almost identical values of k_2' since the numerical differences between the equations tend to compensate. There can be no doubt that the conversion of the newly measured k_2' values into those at 25 °C is reliable. Except at high concentrations, constancy of the $k_{2(25°)}'$ values is reasonably good. The mean value of the $k_{2(25°C)}'$ values is 8.59×10^4 mol^{-3} l^3 min^{-1}, to be compared with 11.80×10^4 mol^{-3} l^3 min^{-1}, the corresponding results from the (sodium iodate+perchloric acid) system.[9]

Thermodynamic Complexity of Iodic Acid. Iodic

Table 1. Results of direct rate measurements in iodic acid solution

No.	React. temp.	$[HIO_3]$[a] M	Meas·rate$\times10^7$ mol l^{-1} min^{-1}	$k_2'\times10^{-4}$[b] l^3 mol^{-3} min^{-1}	$k_{2(25°C)}'\times10^{-4}$[c] l^3 mol^{-3} min^{-1}
1		0.343	2.30	4.26	10.42
2		0.595	13.60	3.23	7.90
3	5 °C	0.833	38.10	2.62	6.41
4		0.457	6.50	4.11	10.05
5		0.714	27.00	3.27	8.00
				av. 3.50	av. 8.56
6		0.300	11.00	8.48	8.48
7		0.286	9.35	8.70	8.70
8		0.2285	3.75	8.04	8.04
9	25 °C	0.343	20.50	9.65	9.65
10		0.259	6.25	8.36	8.36
11		0.318	14.00	8.38	8.38
				av. 8.60	av. 8.60
12	30 °C	0.2285	7.20	10.78	8.79
13		0.286	16.00	10.18	8.30
				av. 10.48	av. 8.55
14		0.114	3.60	19.51	7.51
15		0.2285	61.00	23.60	9.67
16	50 °C	0.194	32.50	23.81	9.15
17		0.174	19.80	23.15	8.90
18		0.137	7.80	21.17	8.14
				av. 22.25	av. 8.67
Salt effect measurements					
19		0.343	1.98		
20		0.475	5.80		
21	5 °C	0.595	12.34	$[LiClO_4]=1.035$ M	
22		0.714	20.37		
23		0.833	34.32		

a) Since 10^{-3} M silver nitrate was added to the reaction mixture, iodate ion concentration was less by this amount than hydrogen ion concentration. The difference was taken into account in the calculation. b) Calculated from Eq. (2) and measured rates at each temperature. Values of (I^-) from Ref. 9, Eq. (6) with correct equilibrium constants for each temperature. Constants for 25 °C appear in Table 2, footnote b). c) Calculated from Eq. (3).

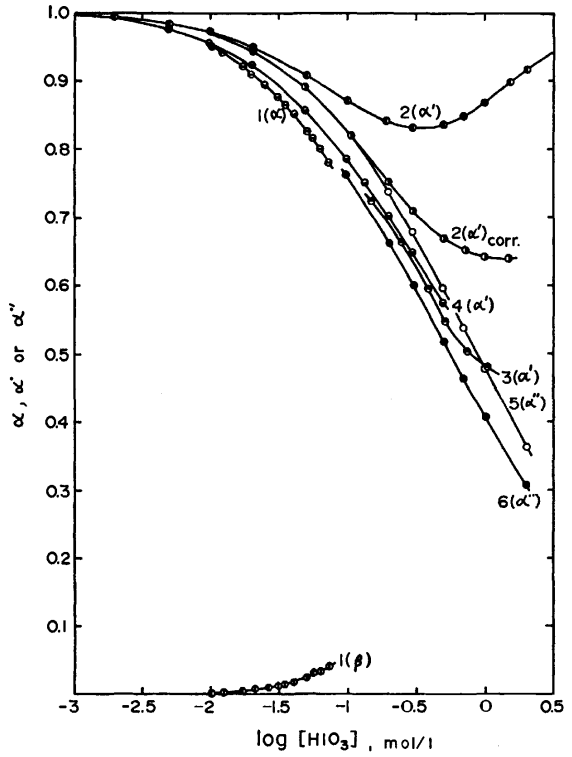

Fig. 2. Degree of dissociation of iodic acid.
$1(\alpha)$ and $1(\beta)$: data of Ref. 14, Table 5, 25 °C (⊖, ⊕), $2(\alpha')$: calculated from γ_s data from Ref. 8, 0 °C, (cryoscopic data) (◐), $2(\alpha')_{corr}$: $2(\alpha')$ corrected for $HI_2O_6^-$ formation (◑), $3(\alpha')$: calculated from data of Ref. 16, 33 °C, (Raman-spectrum data) (◓), $4(\alpha')$: calculated from data of Ref. 8, 18 °C, (conductivity data) (◒), $5(\alpha'')$: calculated with $K=0.258$[9] in Eq. (11), 0 °C (○), $6(\alpha'')$: calculated with $K=0.165$[9] in Eq. (11), 25 °C (●).

acid is an intermediate electrolyte, neither weak nor strong, and the complexity of its aqueous solutions is further increased by the formation of various polymers of pentavalent iodine, *e. g.*, the dimers $H_2I_2O_6$ and $HI_2O_6^-$. The complexity is of thermodynamic and kinetic importance. Results of thermodynamic examination are given in Fig. 2.

Pethybridge and Prue[14] gave a precise thermodynamic treatment of the dissociation equilibrium of iodic acid ($HIO_3 \rightleftarrows H^+ + IO_3^-$) and the formation of polymer ($HIO_3 + IO_3^- \rightleftarrows HI_2O_6^-$), below 0.1 M at 25 °C on the basis of the Debye-Hückel equation and of Eqs. (4)—(6),

$$K = \frac{(\gamma_\pm)^2(H^+)(IO_3^-)}{(HIO_3)} = \frac{\alpha(\alpha-\beta)(\gamma_\pm)^2[HIO_3]}{(1-\alpha-\beta)} = 0.157 \text{ mol l}^{-1} \quad (4)$$

$$K_1 = \frac{(HI_2O_6^-)}{(HIO_3)(IO_3^-)} \quad (5)$$

$$= \frac{\beta}{(\alpha-\beta)(1-\alpha-\beta)[HIO_3]} = 4.1 \text{ mol}^{-1} \quad (6)$$

where K is the acidity constant, K_1 the stability constant of $HI_2O_6^-$, $[HIO_3]$ the formal concentration of iodic acid added to make the solution, α is the degree of dissociation ($(H^+)/[HIO_3]$), β ($(HI_2O_6^-)/[HIO_3]$, and $\gamma_\pm$ the activity coefficient. The values of α and β measured by Pethybridge and Prue are shown in Fig. 2, Curves $1(\alpha)$ and $1(\beta)$.[14]

Three other results for iodic acid solution are expressed by defining the degree of dissociation α' by

$$K = \frac{(\gamma_s)^2[HIO_3]}{(1-\alpha')}, \text{ Cryoscopy}^{8)} \quad (7)$$

where γ_s is the stoichiometric activity coefficient and equal to $\gamma_\pm\alpha'$,

$$\gamma_s = \gamma_\pm\alpha' \quad (8)$$

$$K_c = \frac{(H^+)(IO_3^-)}{(HIO_3)} = \frac{(\alpha')^2[HIO_3]}{(1-\alpha')}, \text{ Conductivity}^{8)} \quad (9)$$

$$(IO_3^-) = \alpha'[HIO_3], \text{ Raman-spectrum}^{16)} \quad (10)$$

The calculated values of α' on the basis of data in Refs. 8 and 16, and of Eqs. (7)—(10) are shown in Fig. 2, Curves $2(\alpha')$, $3(\alpha')$ and $4(\alpha')$.

The minimum of Curve $2(\alpha')$ (Fig. 2) and the high values of α' would be due to polymerization in iodic acid solutions. In the treatment of Pethybridge and Prue,[14] only the dimer $HI_2O_6^-$ was considered giving

$$(\gamma_s)^2 = (\gamma_\pm)^2\alpha(\alpha-\beta). \quad (8a)$$

This equation was used to correct Curve $2(\alpha')$; β is the vertical distance between this curve and Curve $2(\alpha')_{corr}$. Figure 2 shows that the correction is not adequate.

The thermodynamic data for iodic acid solutions above 0.1 M are still uncertain and the solutions are highly complex. Curves $5(\alpha'')$ and $6(\alpha'')$ in Fig. 2 show a degree of dissociation for 0 and 25 °C which was calculated by trial-and-error method by the equation,

$$K = \frac{(\gamma_{\pm p})^2(\alpha'')^2[HIO_3]}{(1-\alpha'')} \quad (11)$$

where $\gamma_{\pm p}$ is the mean activity coefficient of perchloric acid[15] and K the dissociation constant of iodic acid from Ref. 9, Eq. (17). This newly defined α'' is quasi-empirical, but it seems to give reasonable values and a reasonable change with the concentration up to 1 M. Accordingly, for calculating (H^+), (IO_3^-) and (HIO_3), Curves $1(\alpha)$ and $6(\alpha'')$ are used in concentration ranges below and above 0.1 M, respectively. The values of concentrations thus calculated are given in Table 2.

Comparison of Rate Laws. New rate measurements were carried out in order to obtain results that could remove confusion concerning the rate law of the Dushman reaction at iodide ion concentrations below 10^{-8} M. The thermodynamic complexity of iodic acid solutions (Fig. 2) and the lack of thermodynamic data for such solutions containing added salt make the assignment complicated. A comparison of rates calculated for 25 °C from various rate laws is given in Table 3, at each iodic acid concentrations shown in Table 2. In the calculation of rates, it is assumed that $\gamma_{\pm(HIO_3)} = \gamma_{\pm(HI)} = \gamma_{\pm p}$ for a comparison of the different rate laws.

New rates, calculated according to Eq. (2) by use of the $k_2'_{(25°C)}$ values (Table 1) are given in Table 3.

They were calculated from

Table 2. Calculated concentrations for 25 °C

No.	$(H^+)^{a)}$ M	$(IO_3^-)^{a)}$ M	$(HIO_3)^{a)}$ M	$(I^-)\times10^{10}$ b) M	$\gamma_{\pm p}$
1	0.198	0.197	0.145	5.29	0.778
2	0.292	0.291	0.303	7.80	0.769
3	0.362	0.361	0.471	9.66	0.766
4	0.244	0.243	0.213	6.52	0.773
5	0.329	0.328	0.385	8.80	0.767
6	0.180	0.179	0.120	4.80	0.781
7	0.173	0.172	0.113	4.62	0.782
8	0.147	0.146	0.0815	3.93	0.787
9	0.198	0.197	0.145	5.29	0.778
10	0.162	0.161	0.097	4.33	0.784
11	0.195	0.194	0.123	5.20	0.779
12	0.147	0.146	0.0815	3.93	0.787
13	0.173	0.172	0.113	4.62	0.782
14	0.0854	0.0844	0.0289	2.26	0.810
15	0.147	0.146	0.0815	3.93	0.787
16	0.1305	0.1295	0.0638	3.48	0.792
17	0.1184	0.1174	0.0530	3.15	0.795
18	0.0989	0.0979	0.0383	2.63	0.803

a) Calculated by trial-and-error from Eq. (11) with $K=0.165$[9] and $\gamma_{\pm p}$[15] at 25 °C (Column 6). b) Calculated from Eq. (6) in Ref. 9 with $K=0.165$; with 8.591×10^{-17} as the solubility product of silver iodide[11]; and with 3.199×10^{-8} as the solubility product of silver iodate.[12]

Table 3. Comparison of rates calculated for 25 °C from various rate laws

No.	Rate $\times10^7$ mol l^{-1} min^{-1}				
	Eq. (2)[a)]	Eq. (12)	Eq. (13)	Eq. (14)	Eq. (19)
1	22.17	23.80	120.9	4.49	18.57
2	129.54	183.0	1163	62.15	154.57
3	357.27	625.0	4126	177.0	533.93
4	62.39	69.30	408.1	25.31	56.90
5	255.72	357.3	2348	113.0	299.19
6	11.00	14.45	69.61	5.51	11.16
7	9.35	12.04	55.35	4.53	9.11
8	3.75	4.99	21.61	2.01	3.93
9	20.50	23.80	120.9	4.49	18.57
10	6.25	8.37	38.48	3.26	6.38
11	14.00	18.63	110.9	8.24	15.49
12	4.13	4.99	21.61	2.01	3.93
13	9.20	12.04	55.35	4.53	9.15
14	0.25	0.38	0.94	0.13	0.28
15	4.23	4.99	21.61	2.01	3.93
16	2.31	2.50	10.07	1.10	2.13
17	1.40	1.76	6.22	0.68	1.31
18	0.55	0.75	2.34	0.27	0.56

a) Calculated from $k'_{2(25°C)}$ in given Table 1, by use of Eq. (2). For iodic acid solutions, the right-hand side of Eq. (2) equals to $k_2'[HIO_3]^3(I^-)$. This simple form is not quite applicable here. See Table 1, footnote a).

$$-\frac{d[IO_3^-]}{dt} = 11.18\times10^4[IO_3^-](I^-)[H^+]^2 \text{ mol l}^{-1}\text{ min}^{-1} \quad (12)$$

which represents the results of our direct rate measurements[9] on reaction mixtures made from perchloric acid and sodium iodate. The agreement between the two sets of rate is good except at higher concentrations of the acid where thermodynamic complexities are to be expected.

Rates for Eqs. (13) and (14) are based on the results of measurements of the rate of exchange of radioactive iodine at chemical equilibrium (an indirect method); those for Eq. (13) were calculated from

$$-\frac{d(IO_3^-)}{dt} = (\gamma_{\pm p})^6(IO_3^-)(I^-)(H^+)^3\{4.42\times10^8(IO_3^-) + 6.60\times10^6(ClO_4^-)\} \text{ mol l}^{-1}\text{ min}^{-1} \quad (13)$$

which is given by Myers and Kennedy[7] and those for Eq. (14) were calculated from

$$-\frac{d(IO_3^-)}{dt} = 1.1\times10^6(IO_3^-)(I^-)(H^+)^3 \text{ mol l}^{-1}\text{ min}^{-1} \quad (14)$$

which is given by Connick and Hugus.[6]

The rates calculated by Eq. (14) are only a small fraction of those by Eq. (13), which means that the two investigations using radioactive iodine do not agree with each other. The rates obtained from the direct rate measurements all fall between the corresponding data based on the radioactive exchange measurements. In part, the divergences result from different ways of dealing with salt effects. Connick and Hugus[6] assumed that these effects would not vary at constant, high ionic strength; the assumption has not been confirmed. Myers and Kennedy[7] followed Randall and Allen[17] in defining the activity coefficient of iodic acid, and used $\gamma_\pm$ obtained from freezing-point data.[8] The procedure ignores polymerization and relies on the unreasonable α' values of Curve 2(α'). The rate of radioactive iodine exchange in the present system is given by

$$R = k_a(I_2)^{0.6}(IO_3^-)^n(H^+)^p(\gamma_\pm)^{n+p} = k_a(I_2)^{0.6}[HIO_3]^{n+p}(\alpha)^{n+p}(\gamma_\pm)^{n+p} \quad (15)$$

where R is the exchange rate, n and p are the reaction orders. The other symbols were defined previously. This is the starting point for Eq. (13), and the rate

$$R = k_c(I_2)^{0.6}(IO_3^-)^n(H^+)^p = k_c(I_2)^{0.6}[HIO_3]^{n+p}(\alpha)^{n+p} \quad (16)$$

may serve similarly as a starting point for Eq. (14). Since the Dushman reaction (Eq. (1)), with the following equilibrium constant at 25 °C[18]

$$\frac{(I_2)^3}{(\gamma_\pm)^{12}(H^+)^6(I^-)^5(IO_3^-)} = 10^{47.2} \quad (17)$$

was assumed to be in equilibrium during course of the radioactive exchange reaction, the term $(I_2)^{0.6}$ can be eliminated from Eqs. (15) and (16), as follows;

$$(I_2)^{0.6} = 10^{47.2/5}(\gamma_\pm)^{12/5}(IO_3^-)^{1/5}(H^+)^{6/5}(I^-) = 10^{9.44}(\gamma_\pm)^{2.4}(\alpha)^{1.4}[HIO_3]^{1.4}(I^-) \quad (18)$$

Under the simplest conditions, the total order of a reaction is independent of concentration and temperature. Calculations we re carried out to see whether this would hold in the present case when the total order was established according to Myers and Kennedy.[7] Figure 3 shows the logarithm of the exchange rate R as a function of log $\gamma_{\pm p}\alpha''[HIO_3]$ at 0, 25, and 50 °C, the α'' being calculated from Eq. (11) for each temperature.[9] From Eqs. (15) and (18), the total reaction order is given by $(n+p+2.4)$; thus the slopes of the lines in Fig. 3 indicate a change

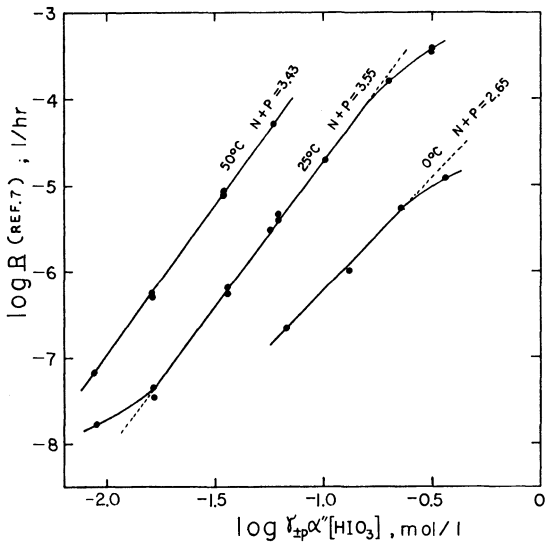

Fig. 3. Re-evaluation of radioactive iodine exchange rate data from Ref. 7.

in total order from 5.05 to 5.95. A similar plot for the rates obtained in direct rate measurements gave a similar result: the total order[19] varied systematically; *i.e.*, 4.7 at 5 °C, 5.04 at 25 °C, 5.14 at 30 °C, and 5.22 at 50 °C.

The most precise way of determining the total order from R values is to use the thermodynamic data of Pethybridge and Prue,[14] which are definitive in the concentration range below $[HIO_3]=0.1$ M, and of R values measured by Myers and Kennedy[7] for solutions of 0.05 and 0.1 M. The thirteen applicable R values were corrected to these iodic acid concentrations and to $(I_2)=10^{-3}$ M. It was found that, at $[HIO_3]=0.1$ M, the mean R value of 4.167×10^{-6} hr^{-1} was obtained for nine data ranging from 3.970×10^{-6} to 4.297×10^{-6} hr^{-1}; at $[HIO_3]=0.05$ M, the mean R value of 0.5916×10^{-6} hr^{-1} was obtained for four data ranging from 0.5510×10^{-6} to 0.6542×10^{-6} hr^{-1}. These means are close to the values of 3.93×10^{-6} and 0.616×10^{-6} hr^{-1}, which were calculated by the equation for R at 25 °C,[7] $R=7.40(\gamma_{\pm p})^{3.6}(I_2)^{0.6}(IO_3^-)^{1.8}(H^+)^{1.8}$ hr^{-1}, in which $n=p=1.8$ was used. Re-evaluation of total order can be made by using these mean R values and Eqs. (15) and (16) with $(\alpha-\beta)^n$ replacing $(\alpha)^n$ to allow for the formation of $HI_2O_6^-$, which was assumed to be inert toward iodide ion. The total order may then be obtained from the ratio between mean R values at $[HIO_3]=0.1$ and 0.05 M, provided that an order with respect to iodate ion concentration is assumed. The results of the calculations are summarized in Table 4, which show total reaction orders not far from six in iodic acid solutions below 0.1 M.

Table 4. Total reaction order ($n+p+2.4$) of radioactive exchange rate estimated from data[14] at $[HIO_3]=0.05$ and 0.1 M.

Assumption[7]	$n=0.8$	$n=p$
Concentration calculation (Eq. (16))	5.87[a]	5.94
Activity Calculation (Eq. (15))	6.24	6.36[b]

a) Corresponding value from Ref. 6 is 5; *i.e.* $(H^+)^3(IO_3^-)(I^-)$. b) Corresponding value from Ref. 7 is 6; *i.e.* $(H^+)^3(IO_3^-)^2(I^-)$.

The radiochemical-exchange results do not give a single, constant total order applicable to the Dushman reaction over a wide range of conditions. The complexity of iodic acid solutions is mainly responsible.

Effect of Added Perchlorate. In order to test the dependence of perchlorate ion concentration required by Eq. (13), five experiments at 5 °C were repeated with reaction mixtures containing 1.035 M of lithium perchlorate (Table 1, Nos. 19—23). The addition of this salt always gave reduced rates: the ratios of rates in the solution containing lithium perchlorate to the corresponding rates obtained from Nos. 1—5 were found to be 0.86, 0.89, 0.91, 0.77, and 0.90, respectively. Furthermore, in the radioactive exchange experiments given in Ref. 7, Table 3, R values of 20.2, 20.4, 20.1, and 14.8×10^{-6} hr^{-1} were obtained for $[HIO_3]=0.2$ M at $[NaClO_4]$ values of 0, 0, 0.053, and 2.000 M, respectively. Both sets of results indicate a 10—25% reduction in rates; this proves that Eq. (13) does not hold. The measured salt effect in this system is small for an ionic reaction of high order.

New Rate Law and Reaction Mechanism. No single, satisfactory reaction order can be found for the Dushman reaction at iodide ion concentration below 10^{-8} M. The quasiempirical rate law, Eq. (2), is the most satisfactory from the results given in Tables 1—3.

The existence of polymeric pentavalent iodine species is indicated by Fig. 2. The work of Pethybridge and Prue[14] supports the existence of a dimeric species, $HI_2O_6^-$, in dilute iodic acid solutions. It is natural to assume that all such species can react with iodide ion. Such reactions would increase the order of the reaction with respect to iodic acid or iodate ion. If only a dimeric species is assumed to react, the expected rate law would have the form

$$-\frac{d[IO_3^-]}{dt}=(\gamma_{\pm p})^4(H^+)^2(IO_3^-)(I^-)\{k'+k''(HIO_3)\} \quad (19)$$

In order to test this equation, the 25 °C rates given for Eq. (2) in Table 3 were divided by $(\gamma_{\pm p})^4(H^+)^2(IO_3^-)(I^-)$, calculated by use of the values in Table 2, and plotted as a function of (HIO_3) at 25 °C. The results (Fig. 4) show a line that gives $k'=2.83\times10^5$ mol^{-3} l^3 min^{-1} and $k''=6.60\times10^6$ mol^{-4} l^4 min^{-1}. The data scatter to some extent at (HIO_3) values above 0.12 M. The rates calculated by use of Eq. (19) with the numerical values of k' and k'' are listed in Table 3. They agree fairly well with those obtained from Eq. (2).

We believe that Eq. (19) gives an improvement on the rate law for the Dushman reaction at low iodide ion concentrations, and that it can replace the other rate laws to establish the reaction mechanism. It should be noted that (HIO_3) can always be replaced by $K(\gamma_\pm)^2(H^+)(IO_3^-)$ because the dissociation of iodic acid is rapid and reversible. It is thus not possible to confirm whether only iodic acid molecule, or only its ions, react; or whether both reaction paths exist. For the sake of simplicity, iodic acid molecule is assumed to be the reacting species, a similar assumption being made for $H_2I_2O_6$. The following

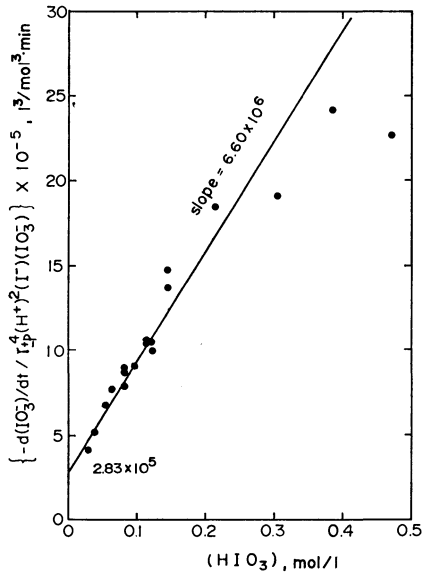

Fig. 4. Plots of Eq. (19) and estimation of the rate constants for 25 °C.
The values of rate, $\gamma_{\pm p}$ and concentrations necessary for the calculations are shown in Table 2, and Table 3, Column 2.

parallel kinetic paths are then postulated to explain Eq. (19);

Monomeric-pentavalent-iodine path (k'; intercept in Fig. 4):

Rapid reversible reaction:

$$H^+ + I^- + HIO_3 \rightleftharpoons H_2I_2O_3 \quad (20)$$

Rate-determining step:

$$H_2I_2O_3 \longrightarrow HIO + HIO_2 \quad (21)$$

Dimeric-pentavalent-iodine path (k''; slope in Fig. 4)
Dimerization equilibrium:

$$2HIO_3 \rightleftharpoons H_2I_2O_6 \rightleftharpoons H^+ + HI_2O_6^- \quad (22)$$

Rate-determining step:

$$H^+ + I^- + H_2I_2O_6 \longrightarrow 3HIO_2 \quad (23)$$

The mechanism should includes the dissociation equilibria of iodic acid. It is completed by the rapid reactions of hydrogen ion and iodide ion with hypoiodous acid and iodous acid to form iodine. The reactive intermediate species $H_2I_2O_3$ has been proved to be useful.[3,10,20–24] The work of Pethybridge and Prue[14] makes $H_2I_2O_6$ (or $HI_2O_6^-$) more logical for the dimeric-pentavalent-iodine path than $IO_2^+IO_3^-$ (closely related to I_2O_5), postulated by Myers and Kennedy.[7] Our mechanism for this path is simpler than that of Edwards,[25] in which iodate ion is assumed to react with I_2O_2 (dehydrated $H_2I_2O_3$) in the rate-determining step.

The present investigation has shown that the confusion concerning the Dushman reaction mainly arises from the complexity of iodic acid solutions, which leads to proposed rate laws that can not be verified by direct measurements of the rate. However, the usefulness of radioactive-exchange measurements in simpler systems is recognized.

We thank Professor J. K. Gladden for helpful discussions and the Robert A. Welch Foundation for supporting the work.

References

1) J. H. Woodson and H. A. Liebhafsky, *Nature*, **224**, 690 (1969).
2) J. H. Woodson and H. A. Liebhafsky, *Anal. Chem.*, **41**, 1894 (1969).
3) I. Matsuzaki, J. H. Woodson and H. A. Liebhafsky, This Bulletin, **43**, 3317 (1970).
4) I. Matsuzaki, R. B. Alexander and H. A. Liebhafsky. *Anal. Chem.*, **42**, 1960 (1970).
5) E. Abel and K. Hilferding, *Z. Phys. Chem.*, **136**, 186 (1928).
6) R. E. Connick and Z. Z. Hugus. Jr., Brookhaven Conf. Report BNL-C-8, Chem. Conf. No. 2, 164 (1948).
7) O. E. Myers and J. W. Kennedy, *J. Amer. Chem. Soc.*, **72**, 897 (1950).
8) E. Abel, O. Redlich and P. Hersch, *Z. Phys. Chem.*, **A170**, 112 (1934).
9) R. Furuichi, I. Matsuzaki, R. Simic and H. A, Liebhafsky, *Inorg. Chem.*, **11**, 952 (1972). Eq. (20) of this reference should read $+2[I_2]/dt = -d[IO_3^-]/dt =$ (numerical terms as in Ref. 9). The approximate iodide ion concentration at which the equality of rates exists is 4.5×10^{-8} M, not 9×10^{-8} M. Correction of the error improves the result.
10) I. Matsuzaki, R. Simic and H. A. Liebhafsky, This Bulletin, **45**, 3367 (1972).
11) L. G. Sillen and A. E. Martell, Chem. Soc. Publ., No. 17, 339, 350 (1964).
12) W. F. Linke, "Inorganic and Metal-Organic Compounds", 4th ed, Van Nostrand, New York, N.Y. (1958), pp. 93 and 101.
13) k_2' was obtained by using Eq. (2) with $[H^+]=[HIO_3]$, $[IO_3^-]=[HIO_3]-[AgNO_3]$, and (I^-). This iodide concentration was calculated from the dissociation constant of iodic acid (Eq. (11)), and the solubility products of silver iodide and silver iodate as in Ref. 9, Eqs. (13) and (14).
14) A. D. Pethybridge and J. E. Prue, *Trans. Faraday Soc.*, **63**, 2091 (1967).
15) "Handbook of Chemistry and Physics," 51st ed, R. C. Weast, The Chemical Rubber Co., Cleveland, Ohio, 1970, p. D–123. The difference between mol/l and mol/kg was usually ignored. In most calculations, the activity coefficients of nitric acid could have been used to replace those of perchloric acid without changing the conclusions.
16) J. R. During, O. D. Binner and W. H. Breazeals, *J. Phys. Chen.*, **69**, 3886 (1965).
17) M. Randall and C. Allen, *J. Amer. Chem. Soc.*, **52**, 1814 (1930).
18) W. O. Lundberg, C. S. Vestling and J. E. Ahlberg, *ibid.*, **59**, 264 (1937). The result was confirmed by recent unpublished measurements of R. D. Spitz and H. A. Liebhafsky.
19) Since iodide ion concentration is proportional to iodate ion concentration in the reaction mixture (Ref. 9, Eq. (6)), the rate could be formally expressed as a function of only hydrogen ion concentration and iodate ion concentration.
20) A. Skrabal, *Z. Elektrochem.*, **40**, 232 (1934).
21) W. C. Bray, *J. Amer. Chem. Soc.*, **52**, 3580 (1930).
22) H. A. Liebhafsky, *ibid.*, **53**, 2074 (1931).
23) W. C. Bray and H. A. Liebhafsky, *ibid.*, **57**, 51 (1935).
24) R. Furuichi and H. A. Liebhafsky, This Bulletin, **46**, 2008 (1973).
25) J. O. Edwards, *Chem. Rev.*, **50**, 455 (1952).

Molecular Structure of 7-Oxanorbornane as Studied by Gas Electron Diffraction

Kazuko OYANAGI, Tsutomu FUKUYAMA, Kozo KUCHITSU,
Robert K. BOHN,* and Shu-tung LI*

Department of Chemistry, Faculty of Science, The University of Tokyo, Bunkyo-ku, Tokyo 113
**Department of Chemistry and Institute of Materials Science, University of Connecticut, Storrs, Connecticut 06268, U.S.A.*

(Received September 24, 1974)

The structure of 7-oxabicyclo[2.2.1]heptane (7-oxanorbornane) in the gas phase has been investigated by making joint use of the electron diffraction intensities measured in the present study and the rotational constants reported by Creswell. The thermal average bond lengths are: $r_g(C_1-C_2)=1.533\pm0.014$ Å, $r_g(C_2-C_3)=1.571\pm0.015$ Å, $r_g(C-O)=1.442\pm0.010$ Å, and $r_g(C-H)=1.117\pm0.008$ Å. The bond angles in the zero-point average structure (r_{av}) are: $\angle C-O-C=94.5\pm2.2°$, θ (the dihedral angle between the $C_1-C_2-C_3-C_4$ and $C_4-C_5-C_6-C_1$ planes)$=113.5\pm0.8°$ and $\angle H-C-H=105\pm5°$. The uncertainties represent the estimated limits of experimental error. The C_2-C_3 bond is longer than the C_1-C_2 bond, and the latter distance is nearly equal to that of a normal C–C single bond. The C–O bond is about 0.02 Å longer, and the C–O–C bond angle is about 17° smaller than the corresponding parameters in dimethyl ether. These trends are analogous to those observed for norbornane and 7-thianorbornane.

As part of our systematic studies of the structures of polycyclic molecules,[1–7] norbornane (bicyclo[2.2.1]-heptane)[4] and 7-thianorbornane[5] have recently been studied by gas electron diffraction. The effect of intramolecular strain is clearly demonstrated in the valence angles of skeletal atoms. In particular, the $C_1-C_7-C_4$ and C_1-S-C_4 angles are both smaller than the corresponding angles in propane and dimethyl sulfide, respectively, by about 19°. Furthermore, the weighted averages of their C–C bond lengths are significantly longer than a normal C–C single bond. A further analysis of the norbornane structure suggested that the C_1-C_7 and C_2-C_3 bonds were appreciably longer than the C_1-C_2 bond, which seemed to be nearly normal. However, it was difficult to precisely determine the individual C–C bond lengths since the rotational constants were not available. Similar circumstances were also encountered in the analyses of thianorbornane,[5] quadricyclene,[6] and nortricyclene[7] using electron diffraction data only. On the other hand, a set of rotational constants for 7-oxanorbornane (Fig. 1) for the normal isotopic species in the ground vibrational state has now become available, and hence, a joint analysis[9–12] of electron diffraction intensities and the rotational constants should be sufficient to uniquely determine the skeletal structure. There is no previous structure work on this molecule except in two theses.[8,13] Thus it is the purpose of the present study to apply this method to a cyclic system for the first time to examine whether there is any significant difference between the C_1-C_2 and C_2-C_3 bond lengths and whether the oxygen valence angle follows the same trend as that observed in the carbon and sulfur valence angles in norbornane and thianorbornane.

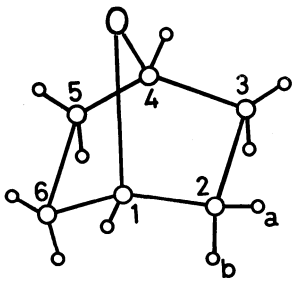

Fig. 1. 7-Oxanorbornane.

Experimental

A commercial sample (Aldrich), kindly supplied by Professor Dewitt Coffey, Jr. of California State University, San Diego, was used after distillation (bp 115 °C). A gas chromatographic analysis indicated that the sample was at least 99.9% pure.

Diffraction photographs were taken at camera lengths of 107.8 and 243.2 mm with an apparatus equipped with an r^3-sector.[14] The accelerating voltage was about 40 kV. During the exposure the sample was maintained in thermal equilibrium with its liquid phase at room temperature. The vapor pressure was about 10 Torr. The scale factors of the diffraction patterns were calibrated to within 0.10% with reference to the r_a(C=O) distance of carbon dioxide (1.1646 Å) measured under nearly the same experimental conditions. Other experimental details are described elsewhere.[14,15]

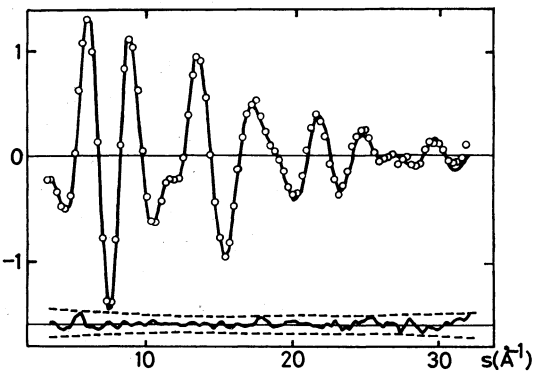

Fig. 2. Molecular intensities for 7-oxanorbornane. Observed values are shown as open circles, and the solid curve represents the best-fit theoretical intensity. The lower solid and broken curves represent the residuals and the error limits, respectively, in the $sM(s)$ to a fractional error of 1×10^{-3} in the original photocurrent.

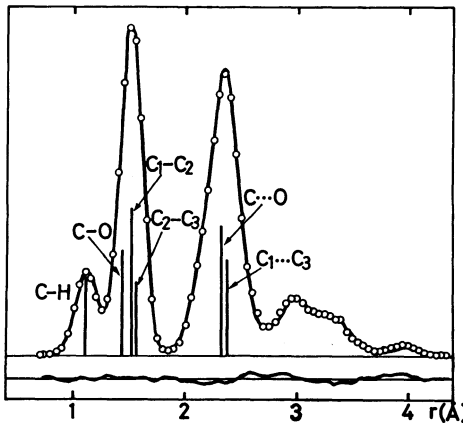

Fig. 3. Experimental (open circles) and the theoretical radial distribution curves for 7-oxanorbornane. Vertical bars represent principal atom pairs. A damping factor, $\exp(-0.0022s^2)$, was used. The residuals are shown below in the same scale.

Two photographic plates taken at the long camera length and three at the short camera length were selected for intensity measurements. Molecular intensities in the ranges $s=3.1$—18.8 and 7.9—32.0 Å^{-1} were obtained from the long and short distance data, respectively, by use of hand-drawn backgrounds. Since they agreed with each other in the overlapping region within experimental error, they were joined at $s=12.6$ Å^{-1}. The elastic and inelastic scattering factors and the phase shifts were taken from the tables prepared by Schäfer *et al.*[16] A typical molecular intensity curve is shown in Fig. 2,** and the corresponding radial distribution curve is shown in Fig. 3. Most of the calculations were carried out on a HITAC 8800/8700 in the Computer Center of the University of Tokyo.

Analysis

Preliminary Analysis of Electron Diffraction Data. The molecular intensities were analyzed by a least-squares method with the following initial assumptions:

1) The molecule had C_{2v} symmetry.
2) The H–C_2–H plane was perpendicular to the C_1–C_2–C_3 plane and bisected the C_1–C_2–C_3 angle, and *vice versa.*
3) The C–C–H angles and the O–C–H angle at the bridgehead were equal to one another, *i.e.*, $\angle C_2$–C_1–H=$\angle C_6$–C_1–H=$\angle$O–C_1–H.
4) All the C–H bond lengths were equal.
5) The C_1–C_2 and C_2–C_3 bond lengths were equal.
6) The H–C–H bond angles were equal to 110°.

With these approximations, the structure was defined by five parameters: the weighted average C–C bond length, the C–O bond length, the weighted average C–H bond length, the C_1–O–C_4 angle and the dihedral angle between the C_1–C_2–C_3–C_4 and C_4–C_5–C_6–C_1 planes (denoted as θ). Assumptions 1—4 were maintained throughout, but constraints 5 and 6 were released in a later stage of the joint analysis of diffraction and spectroscopic data.

** Numerical experimental data of the leveled total intensity and the background have been deposited with the Chemical Society of Japan (Document No. 7503).

Table 1. Estimated force constants for 7-oxanorbornane[a]

K(C–C)	2.3	H(C–C–O)	0.28	F(C–C–O)	0.6
K(C–O)	2.8	H(C–C–C)	0.32	F(C–C–C)	0.2
K(C–H)	4.3	H(C–O–C)	0.53	F(C–O–C)	0.47
Y(C–C)$_g$	0.17[b]	H(H–C–O)	0.26	F(H–C–O)	0.74
Y(C–C)$_c$	0.11[b]	H(H–C–C)	0.2	F(H–C–C)	0.48
Y(C–O)	0.15	H(H–C–H)	0.42	F(H–C–H)	0.07

a) Estimated force constants taken from cyclohexane[18] and ethyl ether.[19] The torsional force constants (Y) are in md·Å, and the others are in md/Å units. b) Symbols g and c represent the C–C axes which have *gauche* and *cis* C···C atom pairs, respectively.

Table 2. Mean amplitudes (l_{ij}) and shrinkage corrections (r_a-r_α) for 7-oxanorbornane[a]

	l_{ij}	r_a-r_α		l_{ij}	r_a-r_α
C_1–C_2	523	10	$C_1\cdots H_{3a}$	1131	22
C_2–C_3	522	23	$C_1\cdots H_{3b}$	1131	22
C_1–O	501	4	$C_2\cdots H_4$	978	15
C_1–H_1	771	78	$C_2\cdots H_{6a}$	1062	31
$C_1\cdots C_3$	609	0	$C_2\cdots H_{6b}$	1501	−11
$C_2\cdots C_6$	727	−1	$C_1\cdots H_4$	916	20
$C_1\cdots C_4$	565	−2	$C_2\cdots H_{5a}$	1054	17
$C_2\cdots C_5$	832	−15	$C_2\cdots H_{5b}$	1659	−38
$C_2\cdots$O	608	1	O$\cdots H_1$	977	24
$C_1\cdots H_2$	1055	47	O$\cdots H_{2a}$	1331	2
$C_2\cdots H_1$	1037	23	O$\cdots H_{2b}$	988	36
$C_2\cdots H_3$	1055	61	$H_{2a}\cdots H_{2b}$	1267	116

a) Calculated at 20°C (in 10^{-4}Å).

The mean amplitudes and the vibrational corrections for shrinkage effects (r_a-r_α)[17,18] for all the internuclear distances were calculated on the basis of an estimated force model using the Urey-Bradley force field listed in Table 1: the force constants were transferred from cyclohexane[19] and ethyl ether.[20] The numerical results listed in Table 2 were used as fixed constants in the analysis. The asymmetry parameter κ for the C–H bond was estimated to be 1×10^{-5} Å^3 by a diatomic approximation.[21] The κ parameters for other atom pairs were ignored.

The r_α structure[18] was determined with a conventional diagonal matrix[22] by a least-squares analysis of molecular intensities. The r_α and r_g structures with estimated limits of error are listed in Table 3.

The estimated error limits contain contributions from several sources:[9,23] 1) random errors estimated from the standard deviations of the least-squares analysis

Table 3. Preliminary analysis of the electron diffraction data for 7-oxanorbornane (in Å and degree)

	r_α	r_g	ε[a]
$(C–C)_{av}$	1.543_1	1.546_3	0.007
C–O	1.440	1.444	0.014
C–H	1.103	1.116	0.012
$\angle$COC	96.2	—	2.6
θ	112.2	—	1.4
$\angle$HCH	(110.0)	—	assumed

a) Estimated limits of error.

and the discrepancies observed in each refined parameter among different plates, 2) experimental systematic errors originating mainly from the uncertainties in the scale factors (0.07%) and sector imperfections (0.05%), 3) the uncertainty in the C–H bond length caused by the assumed value for κ(C–H) (0.002 Å), (The uncertainties in the other κ parameters ignored cause negligible errors.) 4) the effect of the uncertainties in the fixed mean amplitudes, 5) uncertainties originating from assumption 5 on the C–C bond lengths, and 6) those from assumption 6 on the H–C–H bond angle.

In order to estimate the errors due to source 4, the following method[24] was employed. The uncertainties in the calculated mean amplitudes are essentially caused by those in the assumed force constants; they were tentatively assumed to be 10% for bonded atom pairs and 20% for nonbonded atom pairs.[3] Least-squares refinements were carried out by separately varying each of the fixed mean amplitudes systematically to the limit of the estimated uncertainty. This procedure was applied to all the fixed mean amplitudes except for the H···H pairs, which had only a negligible effect. The uncertainties due to sources 5 and 6 were similarly estimated: the maximum difference between the C_1–C_2 and C_2–C_3 bond lengths was estimated to be $\pm$0.03 Å, and the H–C–H bond angle was assumed to be $110\pm5°$. Uncertainties arising from the fixed mean amplitudes are appreciable for all parameters, those from equal C–C bond lengths are appreciable only for the angles, and uncertainties from the assumed H–C–H bond angle are almost negligible.

Joint Analysis of Electron Diffraction Intensities and Rotational Constants. The rotational constants for the ground vibrational state, A_0, B_0, and C_0, determined by Creswell[8] from microwave spectroscopy, were transformed into A_z, B_z, and C_z by making vibrational corrections.[17,24] The uncertainties in A_z, B_z, and C_z (listed in Table 4) mainly originating from the uncertainties in these corrections[12] were tentatively estimated to be 20% of the total vibrational corrections.

The r_a structure determined in the foregoing analysis was extrapolated to zero Kelvin[17,18] by use of a diatomic approximation for bond stretching anharmonicity and the quadratic force constants for the perpendicular amplitudes, and the corresponding rotational constants, A_a^0, B_a^0, and C_a^0, were calculated from the r_a^0 structure. They agree with the corresponding rotational constants derived from microwave spectroscopy within their uncertainties, as shown in Table 4. Therefore, the latter constants were merged into a joint least-squares analysis.[9–12]

Table 4. Observed and calculated rotational constants for 7-oxanorbornane[a] (in cm^{-1})

	0[b]	z[c]	α^0[d]	av[e]
A	0.1309502(2)	0.130916(8)	0.1309(7)	0.130916(5)
B	0.1102560(1)	0.110232(4)	0.1102(2)	0.110232(4)
C	0.0949851(9)	0.094954(6)	0.096 (2)	0.094953(5)

a) Uncertainties attached to the last significant digits are given in parentheses. b) Observed rotational constants for the ground vibrational state. Ref. 8. c) Average rotational constants calculated from A_0, B_0 and C_0 with corrections for vibrational effects. The limits of error are estimated from the uncertainties in the quadratic force constants used for calculating the corrections. d) Rotational constants calculated from the r_a^0 structure given in Table 3. e) Best-fit rotational constants corresponding to the r_{av} structure, listed in Table 5, derived from the combined analysis of diffraction and microwave data. Uncertainties represent 2.5 times the estimated standard deviations.

The weights for the rotational constants were adjusted so that the 2.5 times the standard deviations for the rotational constants were approximately equal to their uncertainties. They were 5×10^9, 7×10^9, and 5×10^9 for A_z, B_z, and C_z, respectively, in comparison with unit weights assigned to the molecular intensities from s=6.3 to 26.7 $Å^{-1}$ taken at $\pi/10$ intervals.

It was now possible to release the constraint on the C–C bond lengths, since the rotational constants A_z and B_z were sensitive to the C_2–C_3 and C_1–C_2 bond lengths, respectively. Furthermore, three mean amplitudes, l(C–C), l(C_2···O), and l(C–H) were also varied: the two C–C amplitudes, l(C_1–C_2) and l(C_2–C_3), were

Table 5. Error matrix for 7-oxanorbornane[a]

	X_1	X_2	X_3	X_4	X_5	X_6	X_7	l_1	l_2	l_3	k_1	k_2
X_1	20	−23	8	−11	33	−20	30	14	10	−19	−20	37
X_2		35	−10	15	−40	28	44	−18	−7	21	36	−19
X_3			19	−7	10	15	47	8	−11	−19	−14	−45
X_4				28	−12	17	55	−7	2	10	17	27
X_5					57	−35	45	24	18	−31	−37	65
X_6						30	58	−14	−13	8	27	−47
X_7							230	24	11	−59	65	62
l_1								14	10	−13	−11	39
l_2									30	11	10	67
l_3										32	27	45
k_1											101	66
k_2												257

a) X_1=C_1–C_2, X_2=C_2–C_3, X_3=C–O, X_4=C–H, X_5=∠C–O–C, X_6=θ, X_7=∠H–C–H, l_1=(C–C), l_2=(C–H), l_3=(C_2···O), k_1, k_2=indices of resolution for the long and short distance data (0.92 ± 0.03 and 1.02 ± 0.07), respectively. Units ($\times10^{-4}$) for the distances and mean amplitudes are Å, those for the angles are rad, and those for the indices are dimensionless.

assumed to be equal to each other. The mean amplitudes l(C–O) and l($C_1 \cdots C_3$) were not varied, however, since they were correlated strongly with the other refined parameters. Therefore, ten independent parameters were now refined. The corresponding error matrix is given in Table 5.

Chiang *et al.*[25] suggested that the methylene group in norbornane could have a structure distorted from local C_{2v} symmetry. However, it was not necessary to release assumption 2) and introduce an additional parameter representing the distortion in any of our analyses of norbornane,[4] thianorbornane[5] and oxanorbornane (the present study) to fit the experimental electron diffraction intensities to within the estimated experimental error.

The error limits were estimated by the method described in the preceding section. Since it was possible to release the constraints 5) and 6) and to vary a part of the mean amplitudes, the systematic uncertainties due to these constraints were eliminated in the present joint analysis. The final structure and mean amplitudes with estimated error limits are listed in Tables 6 and 7.

Table 6. Structure of 7-oxanorbornane from diffraction and microwave data[a]
(in Å and degree)

	r_{av}	r_g	ε[b]		r_{av}[c]	ε[b]
C_1–C_2	1.528_8	1.533	0.014	$\angle C_1C_2C_3$	100.3	0.6
C_2–C_3	1.567_2	1.571	0.015	$\angle C_6C_1C_2$	110.7	0.4
C–O	1.437_5	1.442	0.010	$\angle C_2C_1O$	103.6	1.3
C–H	1.103_7	1.117	0.008	$\angle H_1C_1C_2$	112.7	0.6
$\angle$COC	94.5	—	2.2	$\angle H_2C_2C_1$	113.0	1.5
θ	113.5	—	0.8			
$\angle$HCH	105	—	5			

a) Final result of the present study. b) Estimated limits of error. c) Calculated from the independent parameters.

Table 7. Observed mean amplitudes for 7-oxanorbornane (in Å)

	l_{obsd}[a]	l_{calcd}[a,b]
C–C[c]	0.048 (10)	0.052_3 (5)
C–H	0.071 (19)	0.077_1 (8)
$C_2 \cdots O$	0.076 (18)	0.060_8 (12)

a) Estimated limits of error in 10^{-3}Å are given in parentheses. b) Taken from Table 2. Uncertainties are tentatively estimated to be about 10% for C–C and C–H and about 20% for $C_2 \cdots O$. c) l(C_1–C_2) and l(C_2–C_3) are assumed to be equal to each other.

Discussion

The r_g-r_{av} structure of 7-oxanorbornane determined in the present study is consistent with the rotational constants determined by Creswell.[8] This structure is compared in Table 8 with those of norbornane[4] and 7-thianorbornane.[5] The following points may be noted:

1) Weighted averages of the C_1–C_2 and C_2–C_3 bond lengths in these molecules are essentially equal to one another and about 0.01 Å longer than the normal single C–C bond length.

2) The C_2–C_3 bond in oxanorbornane is longer than the C_1–C_2 bond, which is similar to a normal single bond. The C_2–C_3 bonds of norbornane and bicyclo[2.2.2]octane[1] are also longer than the C_1–C_2 bonds, but in oxanorbornane, the difference appears to be larger (*ca.* 0.04 Å). The C_2–C_3 bond length of 1,4-diazabicyclo[2.2.2]octane[2] is also about 0.02 Å longer than that of cyclohexane.[26]

3) The dihedral angle θ in oxanorbornane is nearly equal to that in norbornane and about 2° less than that in thianorbornane.

Table 8. Comparison of skeletal structures[a]
(in Å and degree)

	b)	c)	d)
$(C–C)_{av}$[e]	1.545 (10)[f]	1.546 (8)	1.549 (3)
C_1–C_2	1.539 (12)	1.533 (14)	—
C_2–C_3	1.557 (25)	1.571 (15)	—
θ	113.1 (18)	113.5 (8)	115.3 (2)
$\angle C_1C_2C_3$[g]	103.3 (7)	100.3 (6)	105.8 (8)

a) Distances in r_g and angles in r_α (r_{av} for c). Uncertainties represent estimated limits of error attached to the last significant digits. b) Bicyclo[2.2.1]heptane, Ref. 4. c) 7-oxanorbornane, the present study. d) 7-thianorbornane, Ref. 5. e) The weighted average value of the C_1–C_2 and C_2–C_3 bond lengths. f) Calculated from the C_1–C_2 and C_2–C_3 bond lengths reported in Ref. 4. g) Calculated from the independent parameters.

Table 9. Comparison of the skeletal structures of related molecules[a]

	29)	28)	b)
C–O	1.418 (3)[c]	1.428 (2)	1.442 (10)
$\angle$COC	111.5 (15)a	106—111[d]	94.5 (22)av
	30)	31)	5)
C–S	1.805 (3)	1.841 (2)	1.837 (6)
$\angle$CSC	99.0 (3)av	93.4 (5)a	80.1 (8)α
	32)	33)	4)
C–C	1.532 (3)	1.546 (1)	1.56_0 (2_4)
$\angle$CCC	112.4 (12)α	102—106[d]	93.1 (17)α

a) r_g distances in Å and r_a (a), r_α (α), and r_{av} (av) angles in degree with the uncertainties quoted in the literature attached to the last significant digits. b) The present study. c) Estimated from the r_a distances reported in the literature by addition of l^2/r_a. d) Pseudorotation.

4) Oxanorbornane has the smallest C_1–C_2–C_3 angle among the three, this angle being about 9° less than the tetrahedral angle.

The structure of oxanorbornane is compared in Table 9 with those of tetrahydrofuran[27,28] (a monocyclic ether), and dimethyl ether[29] (an acyclic ether). The C–O–C bond angle in oxanorbornane is about 17° smaller than that in dimethyl ether and in tetrahydrofuran (nearly free pseudorotation). Also the C–O bond in oxanorbornane is longer than those in tetrahydrofuran and dimethyl ether by about 0.01 and 0.02 Å, respectively.

These trends conform to those observed in the corresponding hydrocarbons and sulfides[30–33] (except that the C–S bond in tetrahydrothiophene seems to be slightly longer than or nearly equal to that in thianorbornane), and present a quantitative basis for semiempirical or empirical calculations[34] of the effect of intramolecular strain in bicyclic compounds.

The authors wish to thank Professor I. M. Mills, the University of Reading, for sending to us information on the rotational constants for 7-oxanorbornane measured by Dr. R. A. Creswell prior to publication. They are also indebted to Dr. Ken-ichi Karakida for his helpful comments on the manuscript.

References

1) A. Yokozeki, K. Kuchitsu, and Y. Morino, This Bulletin, **43**, 2017 (1970).
2) A. Yokozeki and K. Kuchitsu, *ibid.*, **44**, 72 (1971).
3) A. Yokozeki and K. Kuchitsu, *ibid.*, **44**, 1783 (1971).
4) Y. Morino, K. Kuchitsu, and A. Yokozeki, *ibid.*, **40**, 1552 (1967); A. Yokozeki and K. Kuchitsu, *ibid.*, **44**, 2356 (1971).
5) T. Fukuyama, K. Kuchitsu, Y. Tamaru, Z. Yoshida, and I. Tabushi, *J. Amer. Chem. Soc.*, **93**, 2799 (1971).
6) K. Mizuno, T. Fukuyama, and K. Kuchitsu, *Chem. Lett.*, **1972**, 249.
7) R. K. Bohn, K. Mizuno, T. Fukuyama, and K. Kuchitsu, This Bulletin, **46**, 1395 (1973).
8) R. A. Creswell, Ph. D. Thesis, University of Reading (1972), communicated by Professor I. M. Mills. (Note added on November 8, 1974). After the present article was submitted for publication, Dr. Robert A. Creswell of Michigan State University has kindly sent us a preprint of his paper on the microwave spectrum of this molecule (*J. Mol. Spectrosc.*, in press). He determined the $r_s(C_1$–$C_2)$ and $r_s(C_2$–$C_3)$ distances by use of the normal and two singly substituted ^{13}C species. His $r_s(C_2$–$C_3)$ is slightly different from the $r_g(C_2$–$C_3)$ determined in the present study, but the difference is probably due to a systematic difference in the definitions. As discussed in Ref. 18, the r_g-r_{av} parameters determined in the present study have clear physical significance (very likely more clear than the r_s parameters) to within the quoted limits of error.
9) K. Kuchitsu, T. Fukuyama, and Y. Morino, *J. Mol. Struct.*, **1**, 463 (1968).
10) K. Kuchitsu, in G. Allen (editor), MTP International Review of Science, A. Biennial Series, Physical Chemistry, Vol. 2, Medical and Technical Publishers, Oxford (1972), Chap. 6.
11) M. Sugié, T. Fukuyama, and K. Kuchitsu, *J. Mol. Struct.*, **14**, 333 (1972).
12) I. Tokue, T. Fukuyama, and K. Kuchitsu, *ibid.*, **17**, 207 (1973).
13) S. Li, Ph. D Thesis, University of Connecticut (1970).
14) Y. Murata, K. Kuchitsu, and M. Kimura, *Japan. J. Appl. Phys.*, **9**, 591 (1970).
15) M. Tanimoto, K. Kuchitsu, and Y. Morino, This Bulletin, **43**, 2766 (1970).
16) L. Shäfer, A. C. Yates, and R. A. Bonham, *J. Chem. Phys.*, **55**, 3055 (1971).
17) K. Kuchitsu and S. Konaka, *ibid.*, **45**, 4342 (1966).
18) K. Kuchitsu and S. J. Cyvin, "Molecular Structures and Vibrations," ed. by S. J. Cyvin, Chapter 12, Elsevier, Amsterdam (1972).
19) H. Takahashi and T. Shimanouchi, *J. Mol. Spectrosc.*, **13**, 43 (1964).
20) M. Hayashi, *Nippon Kagaku Zasshi*, **78**, 627 (1957).
21) K. Kuchitsu, This Bulletin, **40**, 505 (1967).
22) Y. Morino, K. Kuchitsu, and Y. Murata, *Acta Crystallogr.*, **18**, 549 (1965).
23) K. Kuchitsu, "Molecular Structures and Vibrations," ed. by S. J. Cyvin, Chapter 10, Elsevier, Amsterdam (1972).
24) M. Toyama, T. Oka, and Y. Morino, *J. Mol. Spectrosc.*, **13**, 193 (1964).
25) J. F. Chiang, C. F. Wilcox, Jr., and S. H. Bauer, *J. Amer. Chem. Soc.*, **90**, 3149 (1968).
26) O. Bastiansen, L. Fernholt, H. M. Seip, H. Kambara, and K. Kuchitsu, *J. Mol. Struct.*, **18**, 163 (1973).
27) A. Almenningen, H. M. Seip, and T. Willadsen, *Acta Chem. Scand.*, **23**, 2748 (1966).
28) H. J. Geise, W. J. Adams, and L. S. Bartell, *Tetrahedron*, **25**, 3045 (1969).
29) K. Kimura and M. Kubo, *J. Chem. Phys.*, **30**, 151 (1959).
30) S. Tsuchiya and M. Kimura, to be published.
31) Z. Náhlovská, B. Náhlovský, and H. M. Seip, *Acta Chem. Scand.*, **23**, 3534 (1969).
32) T. Iijima, This Bulletin, **45**, 1291 (1972).
33) W. J. Adams, H. J. Geise, and L. S. Bartell, *J. Amer. Chem. Soc.*, **92**, 5013 (1970).
34) N. L. Allinger, M. T. Tribble, M. A. Miller, and D. H. Wertz, *ibid.*, **93**, 1637 (1971).

Kinetic Studies of Oxygen Chemisorption on the Rutile Single-crystal Surface by Means of Electrical Conductivity

Masayoshi KOMURO*

Faculty of Science, Hiroshima University, Higashisenda-machi, Hiroshima 730

(Received October 30, 1974)

The reaction of oxygen with the surface of a rutile single crystal was studied in the temperature range from 212 to 362 °C and in the pressure range from 10^{-1} to 10^{2} Torr. The process of the surface oxidation was examined by monitoring the electrical conductance change due to oxygen chemisorption. Two types of chemisorption kinetics were found for the rutile which had been reduced to different extents *in vacuo* before the introduction of oxygen. For the low-reduced rutile, the kinetics obeyed the parabolic rate law; this was interpreted by the diffusion-controlled reaction theory. On the other hand, it was found for the high-reduced rutile that the kinetics obeyed the Elovich equation; this could be explained by the boundary layer theory. The apparent activation energy for the former was 14.2 kcal/mol. For the latter, it was 4 kcal/mol and increased with an increase in the chemisorbed surface-charge density. In addition, the rate of oxygen chemisorption in the latter case was proportional to the pressure at a constant density of the chemisorbed surface charge.

It is well known that the electrical properties of semiconductor surfaces are influenced by the change in the ambient atmosphere. The adsorbed active molecules can drastically change the density of charge carriers in the solid and the work function. Since oxygen generally acts as an acceptor-type adsorbate, it is expected that the electrical conductivity of an n-type or p-type semiconductor will decrease or increase, respectively, when oxygen gas is introduced. These phenomena have been extensively studied for many kinds of semiconductor materials by means of the conductivity method.[1-9] It has been reported that the kinetics of oxygen chemisorption on the surfaces of Ge,[10] CdSe,[2,7] CdS,[3] SnO_2,[5] and ZnO[11] follows the Elovich equation and can be explained according to the "boundary layer" theory.[3,12] However, no detailed examinations of the pressure dependence of the chemisorption and the activation energy have been made, and little is known about the oxidation kinetics on the surface of titanium dioxide.[13]

When titanium dioxide is evacuated at a high temperature or treated in a reducing gas, such as hydrogen or carbon monoxide, oxygen atoms tend to be removed from the surface and also from the bulk through the surface region.[14] A reduced rutile exhibits the characteristics of an n-type semiconductor, for the crystal lattice develops defects which act as donors with a low ionization energy.[15] For a reduced rutile, the electrical,[16,17] photoelectric,[18] and dielectric properties[19] have been investigated in order to clarify the electronic structure. On the other hand, the photovoltaic effect has been found for a once-reduced and then reoxidized rutile[20] which has a barrier layer of the Schottky-Mott type in the surface region.[21] It is of interest to examine the surface oxidation, which has much influence on the electrical properties of a reduced rutile. Further, the oxidation process may be expected to be affected by the degree of reduction.

In this paper, the kinetics of oxygen chemisorption was investigated for a single crystal surface of rutile by measuring the electrical conductivity in the temperature range from 212 to 362 °C and in the oxygen pressure range from 10^{-1} to 10^{2} Torr. As a result, it was revealed that the reaction of oxygen with the rutile became remarkable above 200 °C, depending on the temperature and the oxygen pressure, and that the rate of chemisorption followed two types of rate equations because of a difference in the degree of reduction of the rutile.

Experimental

Material. A rutile single crystal grown by the Nakazumi Crystal Co. by means of the Verneuil method was used in this study. A spectroscopic analysis indicated that its purity was above 99.99% and that the main impurity was sodium, the amount of which was less than 0.005%.[22] The crystal was cut into a rectangular wafer $10\times10\times0.18$ mm^3 so as to make large the ratio of the surface to the bulk; the largest face, the (110) plane, was polished mechanically. The sample was then treated with a chromic acid mixture, washed thoroughly with distilled water, and dried at 100 °C. Evaporated gold was used for the electrodes. The distance between the electrodes was 6 mm. The electric contact between the rutile and gold was probably ohmic.[17]

The sample connected with electrodes was mounted on a sample holder, using an insulating spacer of mica so as to facilitate the contact between both (110) planes and the introduced oxygen gas.

Treatment. A rutile single crystal mounted on the sample holder was placed in the apparatus, as is shown in Fig. 1. The measurements of the chemisorption were carried out for the rutile which had been treated by the following two different procedures:

(1) The sample was heated in an atmosphere of oxygen at 450 °C for 10 hr and then evacuated at the same temperature for 5 hr.

(2) The sample was evacuated at 450 °C for 20 hr.

After the measurement of the oxygen chemisorption, the oxidized surface was returned to the initial state by evacuating at 450 °C for 5—8 hr, the residual pressure being about 10^{-6} Torr. The two electrodes were grounded except when the conductivity was checked during the thermal treatment. It was very difficult, however, to get a constant conductivity after the treatment. As a result, the rutile sample had a conductivity varying between 10^{-5} and 10^{-4} mho·cm^{-1} at temperatures between 212 and 362 °C. In order to prevent

* Present address: Maritime Safety Academy, Wakaba-cho, Kure 737.

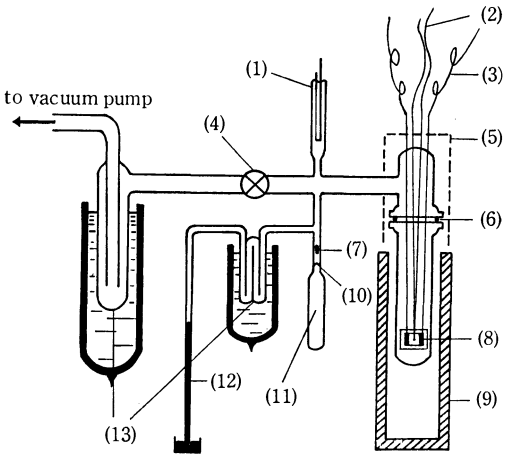

Fig. 1. Experimental apparatus for studying the oxygen chemisorption. (1) Pirani gauge, (2) thermocouple, (3) lead, (4) gleaseless stop-cock, (5) sealed box, (6) O-ring, (7) glass-covered iron core, (8) sample, (9) heater, (10) breakable seal, (11) oxygen gas, (12) Hg manometer, and (13) liquid-nitrogen trap.

any effect of organic contaminants and mercury vapor, liquid-nitrogen traps, an O-ring joint, and a greaseless stop-cock were used, as is illustrated in Fig. 1.

Measurements. The kinetics of the oxygen chemisorption was examined at temperatures between 212 and 362 °C for the rutile treated as has been described above. The sample, an equilibrium state *in vacuo*, was brought into contact with dry oxygen by breaking the glass seal which separated the sample from the oxygen reservoir. Subsequent chemisorption was followed by monitoring the change in the electrical conductivity of the rutile. Electrical conductance measurements were made in the dark by detecting the current between two electrodes, to which a voltage of about 1.2 V was applied by means of a dry battery. The current was measured by means of a Takeda Riken-TR-8651 electrometer connected with a recorder (with a response less than 0.5 s). The pressure of oxygen was measured by means of a mercury manometer at high pressures and a Pirani gauge at low pressures.

Results and Discussion

Oxygen Chemisorption on Low Reduced Rutile. The oxygen-chemisorption measurements were carried out for a sample which had been treated by Procedure (1) and which had a free electron density of about $10^{15}/cm^3$ at the measurement temperature. The conductivity decreased when oxygen gas was introduced at temperatures ranging from 212 to 362 °C. Figure 2 shows some representative results of conductance changes with the time. There was a difference in the initial conductance prior to the introduction of oxygen gas; this was a result of a difference in the temperature or the treatment. However, these results revealed that the conductance change increased with a rise in the temperature of the sample. It was found that the current change was proportional to n powers of time. This current change may be ascribed to a change in the number of free electrons, because the electrons are captured by the oxygen adsorbed on the surface. Therefore, the density of trapped electrons on the

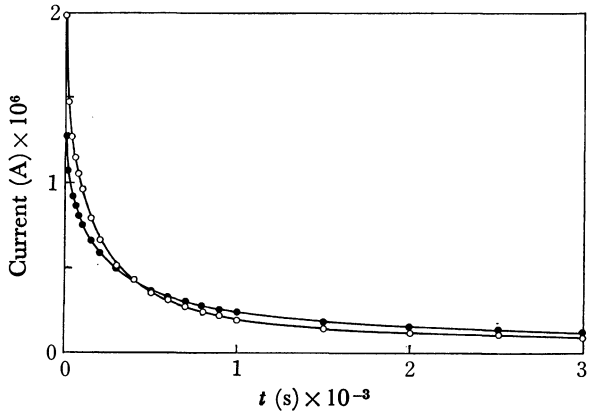

Fig. 2. Conductance change of low reduced rutile with time after the introduction of oxygen at 40 Torr and 212 ° (●) and 262 °C (○).

surface, that is, the chemisorbed surface-charge density, $N_c(t)$, can be estimated from the following equation:[4]

$$N_c(t) = (V/S)n_0(\Delta I/I) \quad (1)$$

where V is the volume of the sample; S, its area in contact with oxygen; n_0, the initial free electron density; I, the initial current at $t=0$, and ΔI, the current change at $t=t$. This equation is obtained by assuming that the electron mobility remains unchanged throughout the run. Since the mobility of the electron in rutile was found to be proportional to $T^{-5/2}$ at temperatures between −196 and 27 °C,[17] the mobility in this study was estimated by extrapolating the relationship in the low-temperature range to 362 °C. By the use of the mobility value thus obtained, the free electron density, n_0, was determined to be about $10^{15}/cm^3$, as has been described above.

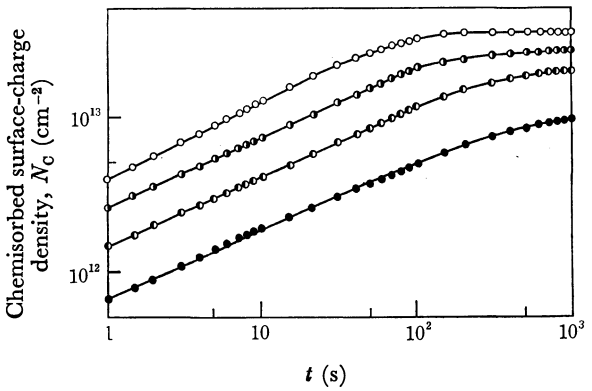

Fig. 3. Surface charge density of low reduced rutile as a function of time on log-log scale after the introduction of oxygen at 40 Torr and 362° (○), 316° (◑), 262° (◐), and 212 °C (●).

The chemisorbed surface-charge density was plotted as a function of the time on the log-log scale, as is shown in Fig. 3. These plots gave approximately straight lines, indicating that the following relationship holds:

$$N_c(t) = Bt^n \quad (2)$$

where B is a constant at a given temperature; n, a constant independent of the temperature and nearly

equal to 1/2, and t, the time after the admission of oxygen. This parabolic rate law has been explained in terms of the diffusion-controlled reaction;[23] the reaction occurs at the gas-solid boundary, forming oxygen ions, and the rate is controlled by the rate of migration of the oxygen ion on the surface. Such phenomena are conceivable, since the surface region of the sample is reduced rather than the bulk. It was estimated from the results of conductivity measurements that more than 95% of the free electrons were trapped by chemisorbed oxygen after 10^3 s. From the ESR studies of oxygen adsorbed on the TiO_2 surface, it has been considered that the chemisorbed oxygen exists in the form of the O^- ion in the temperature range of 140—450 °C.[24] It may be considered, therefore, that the oxygen ion diffuses into the surface region in the form of the O^- ion, resulting in the formation of the O^{2-} ion in the final state.

Activation Energy. It is evident from Fig. 3 that the chemisorption of oxygen requires an activation energy. Murty *et al.* have discussed the estimation of the activation energy, E_a, for a type of kinetic equation such as Eq. (2).[25] Often the B constant in Eq. (2) has an exponential temperature dependence as follows:

$$B = B_0 \exp(-Q/RT) \tag{3}$$

where B_0 is the constant; Q, the term in connection with the activation energy; R, the gas constant, and T, the absolute temperature. From Eq. (2), the rate equation is given by:

$$dN_c/dt = nBt^{n-1} = nN_c/t \tag{4}$$

From Eqs. (2) and (4),

$$nBt^{n-1} = nB^{1/n}N_c^{1-1/n} \tag{5}$$

Thus,

$$\ln(dN_c/dt) = \ln n + 1/n \ln B_0 - Q/nRT + (1-1/n)\ln N_c \tag{6}$$

On the other hand, the Arrhenius equation can be rewritten as:

$$\ln(\text{rate}) = \ln A - E_a/RT \tag{7}$$

By a comparison of Eq. (6) with Eq. (7), we obtain:

$$E_a = Q/n \tag{8}$$

Therefore, the activation energy can be obtained from the plots of ln(rate) *vs.* $1/T$ for a given N_c. From Eqs. (4) and (5), we obtain:

$$N_c/t = B^{1/n}N_c^{1-1/n} \tag{9}$$

The plots of $\ln(N_c/t)$ *vs.* $\ln N_c$ yield a family of parallel lines with the intercepts of $1/n \ln B$ for various temperatures, while the slope of the $1/n \ln B$ *vs.* $1/T$ plots gives the apparent activation energy. Thus, the apparent activation energy was determined to be 14.2 kcal/mol.

Oxygen Chemisorption on High Reduced Rutile. The sample which was treated by Procedure (2) had a free electron density of about $10^{16}/cm^3$ at the measurement temperatures, as estimated in the manner described previously. The changes in the currents after the introduction of oxygen gas are shown in Fig. 4. The kinetics of oxygen chemisorption exhibited the temperature and pressure dependences. However, there

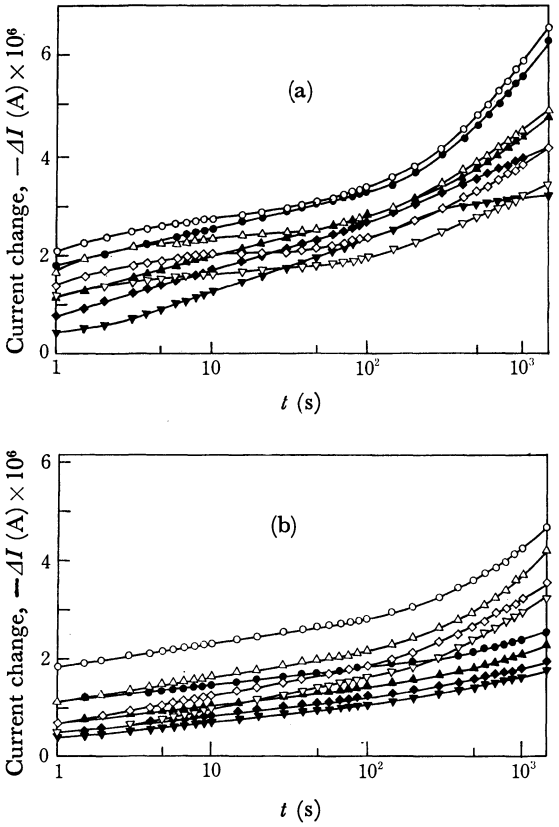

Fig. 4. Current change of high reduced rutile with time after the introduction of oxygen;
(a), at 362 °C and 140 Torr (○), 18.5 Torr (△), 1.6 Torr (◇), and 0.25 Torr (▽) and at 316 °C and 133 Torr (●), 16.0 Torr (▲), 2.0 Torr (◆), and 0.34 Torr (▼).
(b), at 262 °C and 134 Torr (○), 16.5 Torr (△), 2.4 Torr (◇), and 0.52 Torr (▽) and at 212 °C and 148 Torr (●), 17.5 Torr (▲), 2.0 Torr (◆), and 0.44 Torr (▼).

was a difference in the kinetics between the low reduced rutile and the high reduced one; the kinetics for the latter did not obey the parabolic rate law. The plots of ΔI *vs.* $\log t$ gave a family of straight lines until about 200 s, except for the results of chemisorption at 362 °C; these lines for various pressures at a given temperature were nearly parallel to one another. Consequently, these semi-logarithmic plots are in accordance with the Elovich equation:

$$-\Delta I = b \log t + c \tag{10}$$

where b and c are the constants at a given temperature and pressure. This expression can be derived from the boundary layer theory,[12] as will be described below.

Oxygen molecules once physisorbed on the surface are then chemisorbed by combining with free electrons and become negative ions. The charges in the negative ions are compensated for by the positive space-charge region caused by ionized donors near the surface. Thus, the potential-energy barrier, the so-called Schottky barrier, appears in the space-charge region. The chemisorption rate is limited by the arrival rate of electrons to the surface across the barrier, the height of which increases with an increase in the quantity of

negative ions on the surface. Therefore, the rate of increase in the surface-charge density due to the chemisorbed ions is given by:[3,12]

$$dN_c/dt = N_p Cvn \exp(-eV_s/kT) \quad (11)$$

where N_p is the density of the physisorbed oxygen molecules; C, the capture cross section of the physisorbed oxygen molecule for an electron; v, the thermal velocity of the electron; n, the density of the conduction electrons; e, the electronic charge; V_s, the Schottky barrier height, and k, the Boltzmann constant. The height of the Schottky barrier can be expressed as:[12]

$$V_s = (eN_c^2)/(2\varepsilon N_d^+) \quad (12)$$

where ε is the dielectric constant, and N_d^+, the density of the immobile, ionized donors. Assuming that the density of the physisorbed molecules is proportional to $1/m$ power of the pressure with a form such as the Freundlich isotherm,[12] the rate equation is given by:

$$dN_c/dt = P_{O_2}^{1/m} K \exp(-\alpha N_c^2) \quad (13)$$

where P_{O_2} is the oxygen pressure; m, the constant that depends on T, $K=Cvn$, and $\alpha=e^2/(2\varepsilon N_d^+)$. This equation cannot be integrated directly. It should be noted that the current decreases abruptly, followed by a gradual decrease when oxygen is introduced, as is shown in Fig. 4. Thus, the surface density of the trapped electrons increases suddenly to a certain value, N_c°, resulting in a build-up of the potential barrier, V_s, in the surface region. Therefore, the surface-charge density, N, must be increased gradually by the transfer of electrons from the bulk to the chemisorbed surface layer over the potential barrier. Since $N_c^\circ \gg N$, Eq. (13) can be integrated in the region from $N_c=N_c^\circ$ at time $t=t_0$ to $N_c=N_c^\circ+N$ at time $t=t$:

$$P_{O_2}^{1/m} K \Delta t = \exp\{\alpha(N_c^\circ)^2\} \times \{\exp(2\alpha N N_c^\circ) - 1\}/(2\alpha N_c^\circ) \quad (14)$$

After rearrangement, this expression becomes:

$$N_c = \{1/(2\alpha N_c^\circ)\} \ln[2\alpha N_c^\circ P_{O_2}^{1/m} K \Delta t \times \exp\{-\alpha(N_c^\circ)^2\} + 1] \quad (15)$$

When $2\alpha N_c^\circ P_{O_2}^{1/m} K \Delta t \exp\{-\alpha(N_c^\circ)^2\} \gg 1$,

$$N_c = b \ln \Delta t + d + b/m \ln P_{O_2} \quad (16)$$

where $b=1/(2\alpha N_c^\circ)$ and $d=\ln(2\alpha K N_c^\circ)[\exp\{-\alpha \times (N_c^\circ)^2\}]/(2\alpha N_c^\circ)$. If P_{O_2} is constant, this equation can be expressed as Eq. (10).

The deviations from the Elovich equation at 362 °C and above about 200 s may be explained as follows. When oxygen is introduced at 362 °C, the oxygen reacts abruptly with the surface of the rutile, trapping a great number of the free electrons near the surface. As a result, a high potential barrier is formed in the surface region. Any subsequent reaction may be much limited by the barrier. On the other hand, when the reaction time is long, the assumption that $N_c^\circ \gg N$ can not hold, or oxygen ions on the surface may diffuse into the surface region or the bulk in the form of O^{2-} ions.

Activation Energy. The chemisorbed surface-charge density obtained exhibited the temperature dependence shown in Fig. 5. All the terms in Eq. (11) depend on the temperature. By combining Eq. (13) with the

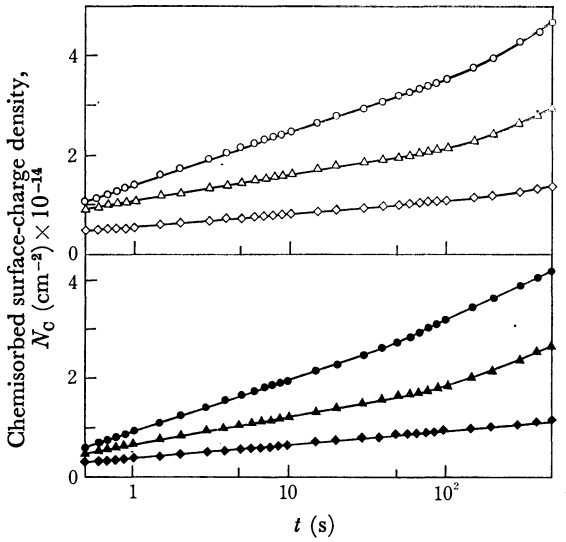

Fig. 5. Surface-charge density of high reduced rutile as a function of time after the introduction of oxygen at 17 Torr and 316 ° (○), 262 ° (△), and 212 °C (◇) and at 2 Torr and 316 ° (●), 262 ° (▲), and 212 °C (◆).

Arrhenius equation, the apparent activation energy, E_a, can be determined at a given chemisorbed surface-charge density and pressure. Instead of Eq. (13), however, the equation obtained by differentiating Eq. (16) by t can be used when the chemisorption kinetics obeys the Elovich equation.[26] The expression for the rate, r, at time t is given by:

$$r = dN_c/dt = b/t \quad (17)$$

where the value of b is determined from the slope of the N_c *vs.* $\ln t$ plots in Fig. 5. Thus the following relationship is obtained:

$$b/t = A \exp(-E_a/RT) \quad (18)$$

The slope of the $\ln b/t$ *vs.* $1/T$ plots for a constant value of N_c is equal to E_a/R, which makes possible the evaluation of the activation energy.

The apparent activation energy in the temperature range of 212—316 °C was obtained in the above manner at various values of the chemisorbed surface-charge density and at the pressures of about 2 Torr and about 17 Torr. Figure 6 shows the apparent activation energy as a function of N_c. It seems that the difference in

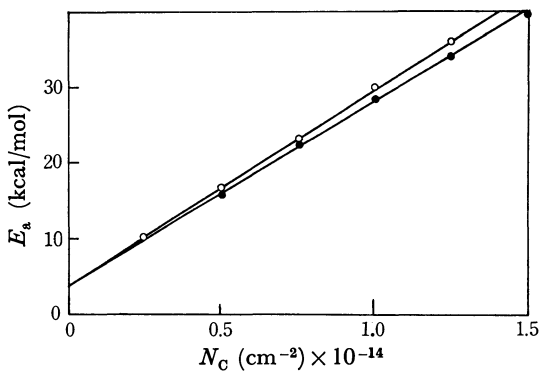

Fig. 6. Apparent activation energy for high reduced rutile as a function of N_c at 2 Torr (○) and 17 Torr (●).

oxygen pressure has scarcely any influence on the activation energy. In this chemisorption, the activation energy can be expressed by:

$$E_a = (25\pm1)\times10^{-14}N_c + 4\,\text{kcal/mol} \quad (19)$$

Pressure Dependence. The straight lines of the N_c *vs.* ln t plots for various pressures at a given temperature were nearly parallel to one another, as can be seen in Fig. 5. By dividing both sides of Eq. (16) by b, the following equation is obtained:

$$N_c/b = \ln t + d/b + 1/m \ln P_{O_2} \quad (20)$$

Plots of N_c/b *vs.* ln P_{O_2} at a given temperature and time give a straight line whose slope is equal to $1/m$. Plots of this type at $t=10$ s for three temperatures are shown in Fig. 7. From these slopes, the value of m was determined to be approximately unity, regardless of the temperature. This suggests that some of the oxygen molecules which strike the surface are physically adsorbed in the manner represented by the Henry law. From Eq. (13), therefore, the rate of oxygen chemisorption is proportional to the pressure at a constant density of the chemisorbed surface charge.

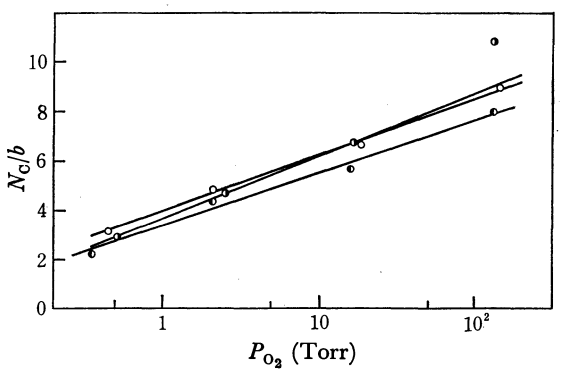

Fig. 7. Plots of N_c/b as a function of the pressure of oxygen at 212 ° (○), 262 ° (◑), and 316 °C (◐).

Conclusions. Two types of chemisorption kinetics were found for reduced rutile. This may be explained as follows: When a well-oxidized rutile is treated at a high temperature *in vacuo* for a relatively short time, only the surface region is reduced by the removal of the oxygen atoms, leaving electrons in the oxygen vacancies or at titanium ions in the neighborhood of the oxygen vacancies. These electrons are not restricted to the surface defects, but are raised to the conduction band at a moderate temperature. As a result, the surface is positively charged and the energy band for the electron bends downwards; the accumulation layer then appears in the surface region. In this case, the free electron density in the bulk is low because the bulk is almost unreduced. When the surface is exposed to oxygen gas in such a state, the oxygen takes free electrons from the accumulation layer and adsorbs chemically on the surface, thus compensating for the positive charge on it. Further, the oxygen ion thus produced tends to migrate toward the oxygen vacancy in the surface region. As a result, the chemical constitution and physical properties of the surface region approach those of the bulk. When most of the surface charges are neutralized by chemisorbed oxygen ions, scarcely any free electrons exist in this solid. Therefore, no potential-energy barrier appears in the surface region, or its height may be low even if one does exist. In such a case, the oxygen chemisorption belongs to the diffusion-controlled reaction and its kinetics obeys the parabolic rate law.

On the other hand, when a rutile is evacuated at a high temperature for a long time, not only the surface region but also the bulk is reduced, and the free electron density is fairly high, even in the bulk. The accumulation layer may also exist. In this case, the chemisorption of oxygen can continue even after the potential barrier appears in the surface region because of the large free electron density in the bulk. However, the reaction is limited by the height of the barrier. The chemisorption kinetics of such a type follows the Elovich equation.

The apparent activation energies were obtained as 14.2 kcal/mol and $(25\pm1)\times10^{-14}$ N_c+4 kcal/mol for the former type and the latter type respectively.

In addition, it was found that, in the latter type, the reaction rate of oxygen with the rutile surface was proportional to the pressure at a constant density of the chemisorbed surface charge.

The author wishes to express his cordial gratitude to Professor Masaji Miura for his continuous guidance and encouragement throughout this work. Thanks are also due to Dr. Toru Iwaki for his stimulating and informative discussions.

References

1) S. R. Morrison, *J. Phys. Chem.*, **57**, 860 (1953).
2) G. A. Somorjai, *J. Phys. Chem. Solids*, **24**, 175 (1963).
3) P. Mark, *ibid.*, **26**, 959 (1965).
4) C. Sébenne and M. Balkanski, *Surface Sci.*, **5**, 410 (1966).
5) H. E. Matthews and E. E. Kohnke, *J. Phys. Chem. Solids*, **29**, 653 (1968).
6) E. Arijs, F. Cardon, and W. Maenhout-Van der Vorst, *Surface Sci.*, **17**, 387 (1969).
7) K. Tanaka and Z. Huruhata, *J. Electrochem. Soc. Jap.*, **37**, 133 (1969).
8) J. P. Legré and S. Martinuzzi, *Phys. Status Solidi, A*, **1**, 689 (1970).
9) L. Surnev and G. Bliznakov, *ibid.*, **7**, 75 (1971).
10) M. Green, J. A. Kafalas, and P. H. Robinson, "Semiconductor Surface Physics," ed. by R. H. Kingston, Univ. of Pennsylvania Press, Philadelphia, N. J. (1957), p. 349.
11) T. I. Barry and F. S. Stone, *Proc. Roy. Soc., Ser. A.* **255**, 124 (1960).
12) P. B. Weisz, *J. Chem. Phys.*, **21**, 1531 (1953); G. A. Somorjai, "Principles of Surface Chemistry," Prentice-Hall, Englewood Cliffs, N. J. (1972).
13) S. Bourasseau, J. R. Martin, F. Juillet, and S. J, Teichner, *J. Chim. Phys.*, **71**, 122 (1974).
14) F. A. Grant, *Rev. Modern Phys.*, **31**, 646 (1959).
15) D. C. Cronemeyer, *Phys. Rev.*, **113**, 1222 (1959); J. B. Wachtman and L. R. Doyle, *ibid.*, **135**, 276 (1964).
16) H. B. Whitehurst, J. J. Morrison, F. L. English, B. M. Warmkessel, and C. J. Kevane, *J. Phys. Chem. Solids*, **28**, 861 (1967); J. Maserjian and C. A. Mead, *ibid.*, **28**, 1971 (1967); T. Goto and T. Okada, *J. Phys. Soc. Jap.*, **25**, 289 (1968).
17) T. Iwaki, This Bulletin, **46**, 1631 (1973).

18) O. W. Johnson, W. O. Ohlsen, and P. I. Kingsbury, Jr., *Phys. Rev.*, **175**, 1102 (1968); A. K. Ghosh, F. G. Wakim, and R. R. Addiss, Jr., *ibid.*, **136**, 284 (1964).
19) L. A. K. Dominik and R. K. McCrone, *ibid.*, **163**, 756 (1967).
20) R. Keezer, *J. Appl. Phys.*, **35**, 1866 (1964); T. Iwaki, M. Komuro, T. Kondo, and M. Miura, *Chem. Lett.*, **1974**, 1185.
21) K. Hauffe and H. Pfeiffer, *Z. Elektrochem.*, **56**, 390 (1952).
22) Y. Nakazumi, *Seramikkusu*, **3**, 731 (1968).
23) T. B. Grimley, "Chemistry of the Solid State," ed. by W. E. Garner, Academic Press, New York (1955), Chap. 14; F. H. Dorer, *J. Catal.*, **13**, 65 (1969).
24) T. Hatsushika, K. Iida, Y. Sashida, and H. Hasebe, *Nippon Kagaku Zasshi*, **89**, 1025 (1968).
25) H. N. Murty, D. L. Biederman, and E. A. Heintz, *J. Phys. Chem.*, **72**, 746 (1968).
26) M. J. D. Low, *Chem. Rev.*, **60**, 267 (1960).

Theoretical Study of Proton Chemical Shifts Induced by the Paramagnetic Anisotropy of Cobaltic Ion

Yoshiaki NAKASHIMA, Ushio SAKAGUCHI,* and Hayami YONEDA*

Department of Physics, Faculty of Education, Wakayama University, Wakayama 640
**Department of Chemistry, Faculty of Science, Hiroshima University, Hiroshima 730*

(Received November 25, 1974)

A new theoretical relation between proton and cobalt-59 chemical shifts in cobalt(III) compounds has been established on the assumption that the proton shift comes primarily from the anisotropy of the second-order paramagnetism of the central cobalt(III) ion. The additivity observed for cobalt-59 chemical shifts in solution is explained and applied to the problem of proton shifts. The relation between ^{1}H and ^{59}Co chemical shifts, coupled with this additivity, allows one to calculate the chemical shift of a proton under the influence of the paramagnetic anisotropy of a cobalt ion.

In previous papers,[1,2] we have reported the chemical shifts of ammine protons of a series of pentaammine cobalt(III) complexes. The shifts have been interpreted as arising primarily from the paramagnetic anisotropy of the central cobalt ions.

In this paper a more rigorous and convenient method of calculating the PMR shifts for cobalt(III) ammines is given. This new result can explain quantitatively the ammine proton chemical shifts. It has already been applied to α-aminocarboxylato cobalt(III) compounds.[3]

The core of the present theory is the use of cobalt-59 chemical shift data. First we establish a relation between the proton chemical shift and the paramagnetic susceptibility tensor of a cobaltic ion using the formulation of Ramsey[4] and McConnell.[5] Next the paramagnetic susceptibility of the central cobalt ion will be shown to be directly proportional to the chemical shift of the cobalt-59 nucleus. Thus, PMR shifts can be obtained from data on cobalt-59 chemical shifts which have been documented for the vast majority of cobaltic complexes. Finally, an additivity of cobalt-59 shifts will be used to show that proton shifts can be calculated very easily.

Theory

Chemical Shift Induced by Paramagnetic Anisotropy. We start with Ramsey's expression for the chemical shift[4]

$$\sigma(^{1}H) = (e^2/2mc^2)\langle 0|\sum_j\{1(r_j^0)^2-r_j^0r_j^0\}/(r_j^0)^3|0\rangle - 2\sum_n(E_n-E_0)^{-1}[\langle 0|\sum_j m_j^0/(r_j^0)^3|n\rangle \times\langle n|\sum_j m_j^0|0\rangle+\text{c.c.}] \quad (1)$$

All notations have their usual significance[1,2] and c.c. denotes the complex conjugate. The origin of the coordinate system is at the proton under consideration. Equation (1) has been simplified by McConnell,[5] using the point dipole approximation, to the form

$$\sigma(^{1}H) = \left(\frac{1}{R^3}-\frac{3\boldsymbol{R}\cdot\boldsymbol{R}}{R^5}\right)\chi \quad (2)$$

Here, the vector $\boldsymbol{R}$ is from the atom exerting the dipole field, in the present case the central cobalt(III) ion, to the proton in question. The magnetic susceptibility tensor of the cobalt(III) ion may be written:

$$\chi = -(1/2)(e^2/2mc^2)\langle 0|\sum_i\{1(r_i)^2-r_ir_i\}|0\rangle + \sum_n(E_n-E_0)^{-1}[\langle 0|\sum_i m_i|n\rangle\langle n|\sum_i m_i|0\rangle+\text{c.c.}] \quad (3)$$

Note that quantities with the superscript 0 refer to the proton and those without 0 to the metal center. We assume that the first term of the right-hand side of Eq. (3) is nearly isotropic and constant over a wide variety of cobaltic complexes and consider only the second term which we denote by $\chi^{p}(^{59}Co)$. The validity of this assumption has been discussed extensively[2,6] and has been well established for many cobalt compounds.[6] With this assumption, we need to treat only the paramagnetic term in proton chemical shift. Thus, we obtain

$$\sigma^{p}(^{1}H) = \left(\frac{1}{R^3}-\frac{3\boldsymbol{R}\cdot\boldsymbol{R}}{R^5}\right)\chi^{p}(^{59}Co) \quad (4)$$

Relation to ^{59}Co Chemical Shifts. The chemical shift of a cobalt-59 nucleus can be calculated from

$$\sigma(^{59}Co) = \sigma^{d}(^{59}Co) + \sigma^{p}(^{59}Co) \quad (5)$$

where

$$\sigma^{p}(^{59}Co) = -2\sum_n(E_n-E_0)^{-1}[\langle 0|\sum_j m_j/r_j^3|n\rangle \times\langle n|\sum_j m_j|0\rangle+\text{c.c.}] \quad (6)$$

For the reasons mentioned above, we need to consider only the term $\sigma^{p}(^{59}Co)$. We use a simple molecular orbital theory, which takes into account the covalency and the anisotropy in chemical shift. The wavefunctions used here are assumed to be well approximated by those appropriate in a crystal field of O_h symmetry, irrespective of the real symmetry of the complex in question. Thus, the theory is similar, in some respects, to that which Yamatera[7] used to explain the absorption spectra of diamagnetic cobalt compounds. This we call the O_h approximation.

The excited state that contributes most to $\sigma_p(^{59}Co)$ is the $^{1}T_{1g}$ state, which corresponds to the first absorption band in cobaltic complexes. In the O_h approximation, it will suffice to investigate the zz component as an example. It is a straightforward matter to show that Eq. (6) can be reduced to

$$\sigma_{zz}^{p}(^{59}Co) = -4(E_E-E_0)^{-1}[\langle\Psi_{t2g(z)}|m_z/r^3|\Psi_{eg(z)}\rangle \times\langle\Psi_{eg(z)}|m_z|\Psi_{t2g(z)}\rangle+\text{c.c.}] \quad (7)$$

for a cobalt(III) ion in a crystal field of O_h symmetry. Here, E_E and E_0 are the energies of the excited state

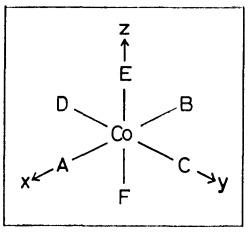

Fig. 1. The coordinate system for a complex [Co(ABCDEF)]. A, B, ···, F stand for ligand molecules.

$^1T_{1g}$ and the ground state $^1A_{1g}$, respectively. Covalency effects can be taken into account by using the molecular orbitals of the form

$$\Psi_{eg(z)} = c_{M1}3d_{x^2-y^2} + c_{L1}\Phi_{L1} \quad (8)$$

$$\Psi_{t2g(z)} = c_{M2}3d_{xy} + c_{L2}\Phi_{L2} \quad (9)$$

Here, the ligand molecular orbitals are defined by linear combinations of atomic orbitals:

$$\Phi_{L1} = (\sigma_A+\sigma_B-\sigma_C-\sigma_D)/2 \quad (10)$$

$$\Phi_{L2} = (\pi_A+\pi_B-\pi_C-\pi_D)/2 \quad (11)$$

The subscripts A, B, C, and D stand for ligand molecules or ions, see Fig. 1. In cases where ligand π^* orbitals are important, molecular orbitals (11) should be replaced by

$$\Psi_{t2g(z)} = c_{M3}3d_{xy}+c_{L3}\Phi_{L3} \quad (12)$$

$$\Phi_{L3} = (\pi_A^*+\pi_B^*-\pi_C^*-\pi_D^*)/2 \quad (13)$$

Substitution of Eqs. (8) and (9) into Eq. (7) yields

$$\sigma_{zz}^p(^{59}Co) = -32\beta^2\langle r^{-3}\rangle(E_E-E_0)^{-1} \times(c_{M1}c_{M2}+c_{M2}c_{L1}S_\sigma+c_{M1}c_{L2}S_\pi)^2 \quad (14)$$

where we have used the relations

$$\Phi_{L1} = S_\sigma 3d_{x^2-y^2} + S_\sigma' 4d_{x^2-y^2} + \cdots \quad (15)$$

$$\Phi_{L2} = S_\pi 3d_{xy} + S_\pi' 4d_{xy} + \cdots \quad (16)$$

in which

$$S_\sigma = \langle 3d_{x^2-y^2}|\Phi_{L1}\rangle \quad (17)$$

$$S_\pi = \langle 3d_{xy}|\Phi_{L2}\rangle \quad (18)$$

We have neglected small terms in S_σ^2 and S_π^2, which do not affect the final result (see below). $\langle r^{-3}\rangle$ is an average of r^{-3} over a metal 3d orbital.

Almost the same calculation leads us to an expression for $\chi_{zz}^p(^{59}Co)$.

$$\chi_{zz}^p(^{59}Co) = 16\beta^2(E_E-E_0)^{-1} \times(c_{M1}c_{M2}+c_{M2}c_{L1}S_\sigma+c_{M1}c_{L2}S_\pi)^2 \quad (19)$$

Thus, we obtain

$$\chi_{zz}^p(^{59}Co) = -\sigma_{zz}^p(^{59}Co)/2\langle r^{-3}\rangle \quad (20)$$

and hence

$$\chi^p(^{59}Co) = -\sigma^p(^{59}Co)/2\langle r^{-3}\rangle \quad (21)$$

This result is quite general and does not depend on the symmetry of the complex in question. In the previous paper,[2] we verified the above relation using molecular orbitals appropriate to C_{4v} symmetry and applied it to the calculation of the proton chemical shift of $[CoX(NH_3)_5]$. From Eqs. (4) and (21), we obtain

$$\sigma^p(^1H) = -\left(\frac{1}{R^3}-\frac{3\boldsymbol{R}\cdot\boldsymbol{R}}{R^5}\right)\sigma^p(^{59}Co)/2\langle r^{-3}\rangle \quad (22)$$

which establishes the relation between the proton and cobalt-59 chemical shifts.

Additivity of ^{59}Co Chemical Shifts. Since the pioneering work of Proctor and Yu,[8] the chemical shift of the cobalt-59 nucleus has been the subject of many investigations.[4,6,9-17] Freeman, Murray, and Richards[14] and Griffith and Orgel[15] have noted that the shift is inversely proportional to the energy of the first absorption band in cobalt(III) complexes. Betteridge and Golding[16] and Fujiwara and coworkers[6] have pointed out that the covalency between the metal and ligand orbitals should be considered. Recently, it has been reported by Fujiwara *et al.*[17] that an additivity holds for shift values of a wide variety of cobaltic compounds, namely, the observed shift value in solution can roughly be given by the sum of contributions from each ligand. To this additivity rule we present an interpretation and an extension, which we believe explains all the above observations. The details are given in the Appendix. The results may be summarized as follows: this rule comes from the additivity valid for each (xx, yy, and zz) component of the shielding tensor.

$$\sigma_{xx}^p(^{59}Co) = \sigma(C) + \sigma(D) + \sigma(E) + \sigma(F) \quad (23)$$

$$\sigma_{yy}^p(^{59}Co) = \sigma(A) + \sigma(B) + \sigma(E) + \sigma(F) \quad (24)$$

$$\sigma_{zz}^p(^{59}Co) = \sigma(A) + \sigma(B) + \sigma(C) + \sigma(D) \quad (25)$$

where $\sigma(X)$ is the contribution from a ligand X to the paramagnetic term of the cobalt-59 shielding. The $\sigma(X)$ values of typical ligands are given in Table 1.

Table 1. $\sigma(X)$ values for some ligands. Data are taken from refs. (10) to (12) and (17).
ox=$C_2O_4^{2-}$, en=ethylenediamine, phen=phenanthroline.

X	σ (X)	Calcd from	
NH_3	−4860 ppm	−19440 ppm of	$[Co(NH_3)_6]$
en	−9205	−18410	$[Co(en)_3]$
Cl	−5910	−20140	$[Co(NH_3)_5Cl]$
Br	−5865	−20110	$[Co(NH_3)_5Br]$
NO_2	−4073	−18915	$[Co(NH_3)_5NO_2]$
CN	−2760	−18040	$[Co(NH_3)_5CN]$
N_3	−5655	−19970	$[Co(NH_3)_5N_3]$
OH	−6345	−20430	$[Co(NH_3)_5OH]$
H_2O	−6255	−20370	$[Co(NH_3)_5H_2O]$
CO_3	−12090	−21020	$[Co(NH_3)_4CO_3]$
ox	−11440	−19900	$[Co(en)_2ox]$
phen	−9135	−18270	$[Co(phen)_3]$

The method for obtaining these values is expounded in the Appendix. Thus, the cobalt-59 chemical shift for a complex [CoABCDEF] in solution is given by

$$\sigma_{iso}^p(^{59}Co) = \sum_i \sigma_{ii}^p(^{59}Co)/3 \quad (26)$$

$$= (2/3)\sum_X \sigma(X) \quad (27)$$

Substituting Eqs. (23) to (25) into Eq. (22), we obtain

$$\sigma_{xx}^p(^1H) = -(1-3\sin^2\theta\cos^2\phi) \times(\sigma(C)+\sigma(D)+\sigma(E)+\sigma(F))/2R^3\langle r^{-3}\rangle \quad (28)$$

$$\sigma_{yy}^p(^1H) = -(1-3\sin^2\theta\sin^2\phi) \times(\sigma(A)+\sigma(B)+\sigma(E)+\sigma(F))/2R^3\langle r^{-3}\rangle \quad (29)$$

$$\sigma_{zz}^p(^1H) = -(1-3\cos^2\theta) \times(\sigma(A)+\sigma(B)+\sigma(C)+\sigma(D))/2R^3\langle r^{-3}\rangle \quad (30)$$

The proton chemical shift in solution is given by

$$\sigma^{p}_{iso}(^1H) = \sum_i \sigma^{p}_{ii}(^1H)/3 \quad (31)$$

Discussion

Hendrickson and Jolly[18] have pointed out, in their interpretation of the PMR spectra of cobalt(III) pentaammines, the importance of the second-order paramagnetism of the central metal ion. However, their explanation for the shifts is only qualitative. They qualitatively explained a gradual change in chemical shifts when the sixth ligand is varied along the spectrochemical series. Buckingham and Stephens[19] were the first to try to treat quantitatively the chemical shift of a proton under the influence of the magnetic anisotropy of metal ions. They considered transition metal hydrides and made an almost *ab initio* calculation. Their calculation was, however, hampered by the paucity of experimental data necessary for the estimation of several parameters, resulting in a qualitative explanation.

We formulated the theory of proton chemical shifts in such a way as to use cobalt-59 chemical shifts. This is because a vast amount of data has been accumulated for many cobaltic compounds. The results obtained here afford a quantitative explanation of proton chemical shifts in cobalt(III) ammines. This we will show in subsequent publications.

Appendix

It seems worthwhile to determine the origin and the implication of the empirical additivity rule for cobalt-59 chemical shifts. As in previous discussions, we use the O_h approximation. The energy levels pertinent to the present discussion are the ground level $^1A_{1g}$ and the excited level $^1T_{1g}$.

Now, the excited state $^1T_{1g}$ is obtained by a one-electron excitation from the t_{2g} to the e_g state. The energy of the $^1T_{1g}$ state may be considered to contain the following terms;[7] $5\times\varepsilon(t_{2g})$, $\varepsilon(e_g)$, the electron repulsion energies, and the configuration interaction energies, where $\varepsilon(t_{2g})$ is the one-electron energy of the t_{2g} state and $\varepsilon(e_g)$ the corresponding energy of the e_g state.

$$E_E = 5\varepsilon(t_{2g}) + \varepsilon(e_g) + \cdots \quad (A1)$$

Similarly, the energy of the ground state $^1A_{1g}$ is given by

$$E_0 = 6\varepsilon(t_{2g}) + \cdots \quad (A2)$$

Contributions from kinetic and potential energies of valence electrons in the field of metal core have been included in $\varepsilon(t_{2g})$ and $\varepsilon(e_g)$. We assume that of these terms only $\varepsilon(t_{2g})$ and $\varepsilon(e_g)$ vary from ligand to ligand and the others remain almost unaltered. This assumption is equivalent to that of Yamatera,[7] who has been successful in explaining the shifts and splittings of the absorption spectra of diamagnetic cobalt complexes. The justification for this assumption can be found in his paper. The change in the denominator of Eq. (14), (E_E-E_0), on going from one complex to another is therefore set equal to the change in $(\varepsilon(t_{2g})-\varepsilon(e_g))$.

In a simple molecular orbital scheme,[20] the energies $\varepsilon(t_{2g})$ and $\varepsilon(e_g)$ are given by

$$\varepsilon(t_{2g}) = H_{MM}(t_{2g}) + S_\pi^2 H_{MM}(t_{2g}) H_\pi (H_{MM}(t_{2g}) - H_\pi)^{-1} \quad (A3)$$

$$\varepsilon(e_g) = H_{MM}(e_g) + S_\sigma^2 H_{MM}(e_g) H_\sigma (H_{MM}(e_g) - H_\sigma)^{-1} \quad (A4)$$

where we define

$$H_{MM}(t_{2g}) = \langle 3d_{xy}|H|3d_{xy}\rangle \quad (A5)$$

$$H_{MM}(e_g) = \langle 3d_{x^2-y^2}|H|3d_{x^2-y^2}\rangle \quad (A6)$$

$$H_\sigma = \langle \Phi_{L1}|H|\Phi_{L1}\rangle \quad (A7)$$

$$H_\pi = \langle \Phi_{L2}|H|\Phi_{L2}\rangle \quad (A8)$$

and

$$H = H_{core} + U \quad (A9)$$

H_{core} is the energy of an electron in the field of the metal core and U the potential energy of an electron in the field of the ligands. In Eqs. (A3) and (A4), the following relations have been used.[20]

$$\langle 3d_{x^2-y^2}|H|\Phi_{L1}\rangle \simeq S_\sigma (H_{MM}(e_g) H_\sigma)^{1/2} \quad (A10)$$

$$\langle 3d_{xy}|H|\Phi_{L2}\rangle \simeq S_\pi (H_{MM}(t_{2g}) H_\pi)^{1/2} \quad (A11)$$

Further, the coefficients c_{M1} and c_{L1} should obey the normalization condition,

$$c_{M1}^2 + 2c_{M1}c_{L1}S_\sigma + c_{L1}^2 = 1 \quad (A12)$$

$$c_{M2}^2 + 2c_{M2}c_{L2}S_\pi + c_{L2}^2 = 1 \quad (A13)$$

If we assume that the value of $H_{MM}(e_g)$ is little influenced by ligand substitution,[7] Eqs. (A3) and (A12) indicate that $\varepsilon(e_g)$, c_{M1}, and c_{L1} are functions of two independent variables, S_σ and H_σ. Likewise, $\varepsilon(t_{2g})$, c_{M2}, and c_{L2} can be considered to be functions of S_π and H_π. Thus, under these conditions $\sigma^{p}_{zz}(^{59}Co)$ is a function of four variables: S_σ, S_π, H_σ, and H_π, the values of which vary of course from ligand to ligand. However, the changes in these values upon going from one complex to another may be assumed to be much smaller than the corresponding values in the parent complex.[7] Therefore, we might as well develop $\sigma^{p}_{zz}(^{59}Co)$ into a power series in these increments. For convenience, we denote the zz component of the shielding tensor for a complex [Co-ABCDEF] as σ^{p}_{zz}(ABCDEF) (see Fig. 1).

$$\begin{aligned}\sigma^{p}_{zz}(ABCDEF) = {} & \sigma^{p}_{zz}(000000) \\ & + \frac{\partial\sigma^{p}_{zz}}{\partial S_\sigma}\sum_X (s_X^\sigma - s_0^\sigma) + \frac{\partial\sigma^{p}_{zz}}{\partial H_\sigma}\sum_X (\varepsilon_X^\sigma - \varepsilon_0^\sigma) \\ & + \frac{\partial\sigma^{p}_{zz}}{\partial S_\pi}\sum_X (s_X^\pi - s_0^\pi) + \frac{\partial\sigma^{p}_{zz}}{\partial H_\pi}\sum_X (\varepsilon_X^\pi - \varepsilon_0^\pi) \\ & + (\text{second-order terms}) \end{aligned} \quad (A14)$$

Note that the summation runs from A to D. We have employed the relation

$$S_\sigma = \sum s_X^\sigma, \quad s_X^\sigma = \langle 3d_{x^2-y^2}|\pm\sigma_X\rangle/2 \quad (A15)$$

$$S_\pi = \sum s_X^\pi, \quad s_X^\pi = \langle 3d_{xy}|\pm\pi_X\rangle/2 \quad (A16)$$

$$H_\sigma = \sum \varepsilon_X^\sigma, \quad \varepsilon_X^\sigma = \langle \sigma_X|H|\sigma_X\rangle/4 \quad (A17)$$

$$H_\pi = \sum \varepsilon_X^\pi, \quad \varepsilon_X^\pi = \langle \pi_X|H|\pi_X\rangle/4 \quad (A18)$$

where X=A, B, C, and D and the subscript o represents some "reference" ligand, *e.g.* NH_3 or ethylenediamine. Equation (A14) can be recast into

$$\sigma^{p}_{zz}(ABCDEF) = \sigma(A) + \sigma(B) + \sigma(C) + \sigma(D) \quad (A19)$$

Here

$$\begin{aligned}\sigma(X) = {} & \tfrac{1}{4}[\sigma^{p}_{zz}(000000) \\ & + \frac{\partial\sigma^{p}_{zz}}{\partial S_\sigma}4(s_X^\sigma - s_0^\sigma) + \frac{\partial\sigma^{p}_{zz}}{\partial H_\sigma}4(\varepsilon_X^\sigma - \varepsilon_0^\sigma) \\ & + \frac{\partial\sigma^{p}_{zz}}{\partial S_\pi}4(s_X^\pi - s_0^\pi) + \frac{\partial\sigma^{p}_{zz}}{\partial H_\pi}4(\varepsilon_X^\pi - \varepsilon_0^\pi)] \\ = {} & \sigma^{p}_{zz}(XXXX00)/4 \end{aligned} \quad (A20)$$

is just one fourth of the zz component of the shielding tensor for a complex [Co(XXXX00)], which is in turn equal, in

the O_h approximation, to that for [Co(XXXXXX)]. Thus, the situation may be visualized simply as

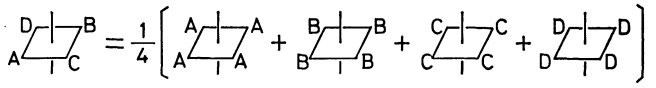

In the O_h approximation, the xx and yy components can be obtained by interchanging the symbols in parentheses.

$$\sigma^p_{xx}(ABCDEF) = \sigma(C) + \sigma(D) + \sigma(E) + \sigma(F) \quad (A21)$$

$$\sigma^p_{yy}(ABCDEF) = \sigma(A) + \sigma(B) + \sigma(E) + \sigma(F) \quad (A22)$$

The cobalt-59 chemical shift for a complex [Co(ABCDEF)] in solution is given by Eqs. (26) and (27) in the text.

Fujiwara *et al.*[6] reported $\sigma^p_{iso}(^{59}Co) = -19440$ ppm for $[Co(NH_3)_6]^{3+}$. This value can be used, along with

$$\sigma^p_{iso}(^{59}Co) = (2/3)6\sigma(NH_3) = 4\sigma(NH_3) \quad (A23)$$

to obtain $\sigma(NH_3) = -4860$ ppm, which is in turn used to evaluate $\sigma(X)$ from data on $[CoX(NH_3)_5]$ ($X = Cl^-$, Br^-, CN^-, OH^-, NO_2^-, N_3^-, and H_2O). These values are summarized in Table 1.

The results obtained here permit us to estimate the chemical shift anisotropy of a cobalt-59 nucleus. It is clear from the procedure that the method used here can be applied to those physical quantities that are closely connected to the optical transitions of six-coordinated metal complexes. In fact, if the physical quantity under consideration is the energy of the electronic transition itself, we can obtain results which are in complete agreement with those reported by Yamatera.[7]

The authors thank Prof. S. Fujiwara and Dr. A. Yamasaki, Tokyo University, for informing them of the cobalt-59 chemical shift data prior to publication and for stimulating discussions.

References

1) H. Yoneda and Y. Nakashima, This Bulletin, **47**, 669 (1974).
2) Y. Nakashima, U. Sakaguchi, and H. Yoneda, *Chem. Lett.*, **1974**, 503.
3) H. Yoneda, U. Sakaguchi, and Y. Nakashima, This Bulletin, **48**, 209 (1975).
4) N. F. Ramsey, *Phys. Rev.*, **78**, 699 (1950); *ibid.*, **86**, 243 (1952).
5) H. M. McConnell, *J. Chem. Phys.*, **27**, 226 (1957).
6) S. Fujiwara, F. Yajima, and A. Yamasaki, *J. Mag. Resonance*, **1**, 203 (1969).
7) H. Yamatera, This Bulletin, **31**, 95 (1958).
8) W. G. Proctor and F. C. Yu, *Phys. Rev.*, **81**, 20 (1951).
9) S. S. Dharmatti and C. R. Kanekar, *J. Chem. Phys.*, **31**, 1436 (1960).
10) C. R. Kanekar, M. M. Dhingra, V. R. Marathe, and R. Nagarajan, *J. Chem. Phys.*, **46**, 2009 (1967).
11) A. Yamasaki, F. Yajima, and S. Fujiwara, *Inorg. Chim. Acta*, **2**, 39 (1968).
12) N. S. Biradar and M. A. Pujar, *Z. Anorg. Allg. Chem.*, **391**, 54 (1972).
13) Y. Koike, F. Yajima, A. Yamasaki, and S. Fujiwara, *Chem. Lett.*, **1974**, 177.
14) R. Freeman, G. R. Murray, and R. E. Richards, *Proc. Roy. Soc. Ser. A*, **242**, 455 (1957).
15) J. S. Griffith and L. E. Orgel, *Trans. Faraday Soc.*, **53**, 601 (1959).
16) G. P. Betteridge and R. M. Golding, *J. Chem. Phys.*, **51**, 2497 (1969).
17) F. Yajima, Y. Koike, A. Yamasaki, and S. Fujiwara, This Bulletin, **47**, 1442 (1974).
18) D. N. Hendrickson and W. L. Jolly, *Inorg. Chem.*, **9**, 1197 (1970).
19) A. D. Buckingham and P. J. Stephens, *J. Chem. Soc.* **1964**, 2747.
20) C. J. Ballhausen and H. B. Gray, "Molecular Orbital Theory," Benjamin Inc., N. Y. (1965).

Proton Magnetic Resonance Spectra of Metal Ammine Complexes. III.* Interpretation of the Chemical Shifts in Cobalt(III) Pentaammines

Yoshiaki NAKASHIMA

Department of Physics, Faculty of Education, Wakayama University, Wakayama 640

(Received November 25, 1974)

The ammine proton chemical shifts of a series of compounds $[CoX(NH_3)_5]^{n+}$ have been explained quantitatively. The shifts are ascribed to the paramagnetic anisotropy of central cobalt(III) ions. The discrepancies between the calculated and the observed shift values, though small, noted for the *trans* ammine protons of complexes with $X=CN^-$ and NO_2^- may be caused by large inductive effects of these ligands.

In the preceding paper,[1] a theory of proton chemical shifts induced by the paramagnetic anisotropy of a central cobalt(III) ion was expounded. This paper is to show how well the above theory can explain the observed shift values of pentaammine cobalt(III) complexes. A qualitative explanation has already been reported.[2]

A pentaammine cobalt(III) ion contains two types of ammonia molecules, *cis* and *trans*. To take the NH_3-rotation into account, we shall slightly modify Eqs. (28)—(30) of Ref. (1). If we take the z-axis as the symmetry axis of $[CoX(NH_3)_5]$, we obtain

$$\sigma_{xx}^{p}(^1H) = -(1-3\sin^2\theta\cos^2\phi) \times (3\sigma(NH_3)+\sigma(X))/2R^3\langle r^{-3}\rangle \quad (1)$$

$$\sigma_{yy}^{p}(^1H) = -(1-3\sin^2\theta\sin^2\phi) \times (3\sigma(NH_3)+\sigma(X))/2R^3\langle r^{-3}\rangle \quad (2)$$

$$\sigma_{zz}^{p}(^1H) = -(1-3\cos^2\theta)(4\sigma(NH_3))/2R^3\langle r^{-3}\rangle \quad (3)$$

For *cis* ammine protons, we take the x-axis as the new z-axis and y- and z-axes as the new x- and y-axes. Thus, the following expressions apply to *cis* protons.

$$\sigma_{xx}^{p}(^1H) = -(1-3\sin^2\theta'\cos^2\phi') \times (3\sigma(NH_3)+\sigma(X))/2R^3\langle r^{-3}\rangle \quad (4)$$

$$\sigma_{yy}^{p}(^1H) = -(1-3\sin^2\theta'\sin^2\phi') \times (4\sigma(NH_3))/2R^3\langle r^{-3}\rangle \quad (5)$$

$$\sigma_{zz}^{p}(^1H) = -(1-3\cos^2\theta') \times (3\sigma(NH_3)+\sigma(X))/2R^3\langle r^{-3}\rangle \quad (6)$$

The definitions of θ, ϕ, θ', and ϕ' are in Fig. 1. After averaging over ϕ and ϕ' for *trans* and *cis* ammonias, respectively, the proton chemical shift in solution may be shown to be

$$\sigma_t^p = (3\cos^2\theta-1)(\sigma(NH_3)-\sigma(X))/6R^3\langle r^{-3}\rangle \quad (7)$$

$$\sigma_c^p = -(3\cos^2\theta'-1)(\sigma(NH_3)-\sigma(X))/12R^3\langle r^{-3}\rangle \quad (8)$$

where the subscripts t and c refer to *trans* and *cis* protons. Note that these equations give shift values relative to the shift of $[Co(NH_3)_6]^{3+}$. It is seen that the shift of *trans* protons with respect to $[Co(NH_3)_6]^{3+}$ is in the opposite direction to and twice that of *cis* protons.

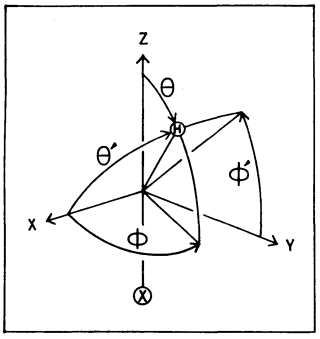

Fig. 1. Definition of the coordinate system.

Method of Calculation

The geometrical factors necessary for the calculation of Eqs. (7) and (8) can be estimated as follows. By taking the Co–N distance as 2.0 Å (3.78 a.u.) and the N–H distance as 1.0 Å (1.89 a.u.),[4] we obtain $R=$ 4.77 a.u. (2.52 Å). If we further assume a tetrahedral configuration for coordinated ammonia molecules, we obtain $\theta=22.0°$ and $\theta'=22.0°$. The value of $\langle r^{-3}\rangle$ is estimated from Eq. (14) of Ref. (1) using the data for $[Co(NH_3)_6]^{3+}$. It is reported that $(E_E-E_0)=(E_{T_{1g}}-E_{A_{1g}})=2.10\times10^4$ cm^{-1},[5] $\sigma_{zz}^{p}(^{59}Co)=-1.91\times10^{-2}$,[3] and $c_{M1}=0.924$, $c_{L1}=-0.61$, $S_\sigma=0.2$, $c_{M2}=1.0$, $S_\pi=0.5$.[5] Substitution of these values into Eq. (14) of Ref. 1 gives 5.77 a.u. for $\langle r^{-3}\rangle$. I asumed the same values of R, θ, θ', and $\langle r^{-3}\rangle$ for all the complexes examined here. As seen from Eq. (14) of Ref. 1, $\sigma_{zz}^{p}(^{59}Co)$ can be considered to be constant over a series of pentaammines.[3] The contribution $\sigma(X)$ from a ligand X to cobalt-59 chemical shifts is summarized in Table 1 of Ref. 1. The relevant quantities in the present study are $\sigma(NH_3)=-4860$, $\sigma(CN)=-2760$, $\sigma(NO_2)=-4073$, $\sigma(H_2O)=-6255$, $\sigma(OH)=-6345$, $\sigma(Cl)=-5910$, and $\sigma(Br)=-5865$ ppm.

Results and Discussion

Clifton and Pratt[6] were probably the first to observe proton resonance spectra of cobalt(III) pentaammines. They found two NH_3 resonances with an intensity ratio of 4 to 1, the intense absorption being at lower field. They suggested that the *cis* protons may be shifted to lower field than the *trans* by (i) intramolecular hydrogen bonding between the *cis* ammine groups and the sixth ligand X, (ii) the effects of magnetic anisotropy of X, and (iii) the reduced polarity of the *trans* ammine group due to polarization of the metal ion by the sixth ligand. As discussed by Lehman and Fung[7] and Hawkins,[8] the magnetic anisotropy effects cannot explain even the

* Part II: Y. Nakashima, U. Sakaguchi, and H. Yoneda, *Chem. Lett.*, **1974**, 503.

sign of chemical shifts. Thus, Lehman and Fung concluded that the point dipole approximation for the magnetic anisotropy of the sixth ligand is too great a simplification to account for the proton shifts. Hawkins argued that since the chemical shift differences were observed for a variety of substituents with widely differing hydrogen bonding capabilities, the intramolecular hydrogen bonding is of minor importance. The polarization effects were suggested as the dominant contributor. Hendrickson and Jolly[9] compared the proton resonance spectra of some pentaammine complexes of cobalt(III) with those of rhodium(III) and iridium(III). Since the latter compounds showed only a single peak, the low-lying paramagnetic states of Co(III) ion were suggested as responsible for the two peaks in cobalt complexes. They qualitatively explained the gradual change in chemical shifts when the sixth ligand was varied along the spectrochemical series.

I consider that the anisotropy in the second-order paramagnetism of the central cobalt ion has the dominant contribution. The calculated proton chemical shifts are illustrated in Fig. 2, together with the observed shift values.[2] The agreement between the calculated and the observed values is remarkably good for complexes with X=H_2O, OH^-, Cl^-, and Br^-. For X=CN^- and NO_2^-, the agreement is also good except for *trans* ammine protons. In view of the extreme approximations used, this agreement may be fortuitous but it is satisfying that correct orders of magnitude could be obtained for the chemical shifts. Therefore, it can be concluded that the proton chemical shifts in pentaammine cobalt(III) complexes can be attributed to the anisotropy in the second-order paramagnetism of the central cobaltic ion. Note that for a weak field ligand X ammine protons *trans* to X appear at higher field than *cis* ammines. If X lies higher in the spectrochemical series than NH_3, the shift pattern is reversed. This behavior is similar to the observation by Watabe *et al.*[10] that in α-aminocarboxylato cobalt(III) complexes the α (to NH_2) C–H proton appear at higher field when it is *trans* to an oxygen atom while it moves to lower field when *trans* to a nitrogen atom.

In a previous communication,[11] the proton shifts in $[CoX(NH_3)_5]$ were treated in the following way. After taking the NH_3-rotation into account, the proton shift in solution may be written

$$\sigma_t^p = [\sigma_{zz}^p(^{59}Co) - \sigma_{xx}^p(^{59}Co)](3\cos^2\theta - 1)/6R^3\langle r^{-3}\rangle \quad (9)$$

$$\sigma_c^p = -[\sigma_{zz}^p(^{59}Co) - \sigma_{xx}^p(^{59}Co)](3\cos^2\theta' - 1)/12R^3\langle r^{-3}\rangle \quad (10)$$

These results are easily obtained from Eq. (22) of Ref. (1). The following equation applies to complexes of C_{4v} symmetry.

$$\sigma_{iso}^p(^1H) = [2\sigma_{xx}^p(^{59}Co) + \sigma_{zz}^p(^{59}Co)]/3 \quad (11)$$

Thus, Eqs. (9) and (10) are reduced to

$$\sigma_t^p = [\sigma_{zz}^p(^{59}Co) - \sigma_{iso}^p(^{59}Co)](3\cos^2\theta - 1)/4R^3\langle r^{-3}\rangle \quad (12)$$

$$\sigma_c^p = -[\sigma_{zz}^p(^{59}Co) - \sigma_{iso}^p(^{59}Co)](3\cos^2\theta' - 1)/8R^3\langle r^{-3}\rangle \quad (13)$$

As stated earlier, $\sigma_{zz}^p(^{59}Co)$ can be considered to be constant for pentaammines. This result indicates that the proton chemical shifts should be directly proportional to the cobalt-59 chemical shifts. Since the details have been reported,[11] it suffices to say that Eqs. (12) and (13) can give almost the same results for pentaammines as those in Fig. 2. However, the above procedure does not allow us to treat complexes of low symmetries.

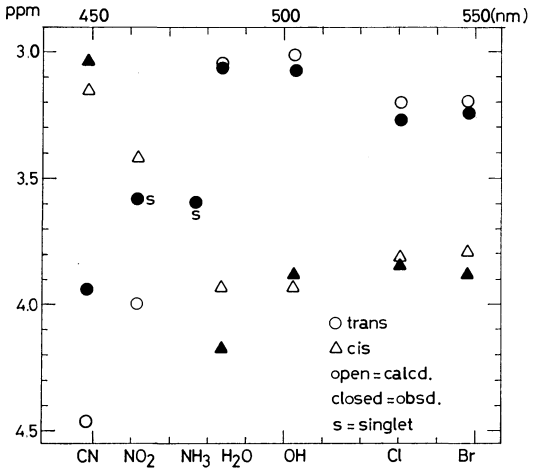

Fig. 2. Comparison of the calculated shift values with the observed values. Shifts are from DSS internal standard and the abscissa is the reciprocal of the excitation energy of the first absorption band ($E_E - E_{A1}$).

Discrepancies between the calculated and the observed shift values, though small, may be noted for *trans* ammines of compounds with X=CN^- and NO_2^-. The cause of these discrepancies may be in the approximations used: disregard of the possible variation of Co–N distances, neglect of several overlap integrals, neglect of the probable change in $\langle r^{-3}\rangle$, or the point dipole approximation itself. Solvent effects may have some contribution.[9] It is also probable that the additivity of cobalt-59 chemical shifts is not sufficiently exact to predict the anisotropy of the shifts. To eliminate several of these possibilities, we are measuring the rate of isotopic deuterium exchange in these complexes. The observed upfield shifts for *trans* ammines of X=CN^- and NO_2^- point to an increase of electron densities on these ammine protons. Thus, it is expected that the *trans* protons are exchanged much more slowly than the *cis* protons. Preliminary results of HD exchange confirmed this expectation. The details will be published in subsequent papers.

I wish to thank Prof. H. Yoneda and Dr. U. Sakaguchi, Hiroshima University, for helpful discussions.

References

1) Y. Nakashima, U. Sakaguchi, and H. Yoneda, This Bulletin, **48**, 762 (1975).
2) H. Yoneda and Y. Nakashima, *ibid.*, **47**, 669 (1974).
3) S. Fujiwara, F. Yajima, and A. Yamasaki, *J. Mag. Resonance*, **1**, 203 (1969).
4) a) M. Iwata and Y. Saito, *Acta Crystallogr.*, **B29**, 822 (1973); b) "International Tables for X-ray Crystallography," Vol. III, The Kynoch Press, Birmingham (1968), p. 270.
5) See, for example, H. Yamatera, *J. Inst. Polytech. Osaka City Univ.*, **5C**, 163 (1956).
6) P. Clifton and L. Pratt, *Proc. Chem. Soc.*, **1963**, 339.

7) J. W. Lehman and B. M. Fung, *Inorg. Chem.*, **11**, 214 (1972).
8) C. J. Hawkins, "Absolute Configuration of Metal Complexes," Wiley-Interscience, N.Y. (1971), Chapt. 6.
9) D. N. Hendrickson and W. L. Jolly, *Inorg. Chem.*, **9**, 1197 (1970).
10) M. Watabe, K. Onuki, and S. Yoshikawa, to be published.
11) Y. Nakashima, U. Sakaguchi, and H. Yoneda, *Chem. Lett.*, **1974**, 503; Part II.

The Reaction of Hydrogen Atoms with Acetylene

Toshio IBUKI and Yoshimasa TAKEZAKI
Institute for Chemical Research, Kyoto University, Gokanosho, Uji, Kyoto 611
(Received December 10, 1973)

The addition of hydrogen atoms to acetylene has been investigated at room temperature. The relative rate constant for

$$H + C_2H_4 \longrightarrow C_2H_5, \quad (1)$$
$$H + C_2H_2 \longrightarrow C_2H_3, \quad (2)$$

was found to be $k_1/k_2=9.99\pm0.16$. The ratios of the rate constant of disproportionation to that of the combination for the same radicals and for different radicals were determined to be as follows:

$$C_2H_5 + C_2H_3 \longrightarrow 1\text{-}C_4H_8, \quad (4)$$
$$\longrightarrow C_2H_6 + C_2H_2, \quad (4a)$$
$$\longrightarrow 2C_2H_4, \quad (4b)$$
$$k_{4a}/k_4 = 0.369,$$
$$k_{4b}/k_4 = 0.68,$$
$$C_2H_3 + C_2H_3 \longrightarrow 1,3\text{-}C_4H_6, \quad (5)$$
$$\longrightarrow C_2H_4 + C_2H_2, \quad (5a)$$
$$k_{5a}/k_5 = 0.087.$$

Although a large amount of quantitative data is now available on the addition of atomic hydrogen to simple olefins,[1-3] comparatively little is known about the reactions of unsaturated radicals, probably because of the difficulty of obtaining clean sources of these radicals, and also because of the problems in analysis, *i.e.*, the polymerization of an unsaturated radical.[4]

Recently, however, Hoyermann, *et al.*[5] have produced a vinyl radical by the addition of a hydrogen atom to acetylene and proposed a rate constant of: 2.3×10^{12} exp(−2500 cal mol$^{-1}/RT$) for the addition reaction. Cowfer, *et al*[6]. have obtained the ratios of the rate constants for H atom-olefin reactions to that for the H atom–acetylene system. In spite of quantitative studies[7-11] which have been published concerning the reactions of vinyl radicals, the data for the ratio of the disproportionation to the combination of the radicals show large discrepancies (see the last column of Table 2), and it remains difficult to say which value should be preferred.

In the present work, we have employed the competitive technique developed for determining the relative rate constants of the reactions of hydrogen atoms with olefins;[3] we have thus determined the relative rate constant of the addition of H atoms to acetylene and the ratio of the disproportionation to the recombination of vinyl radicals. Similar ratios of reactions between vinyl and ethyl radicals have also been obtained.

Experimental

Hydrogen atoms were generated by the Hg6($^3P_1$) sensitized decomposition of H_2. The 2537 Å radiation was obtained from a low-pressure mercury lamp with a Vycor glass filter. A conventional vacuum apparatus was used.

The acetylene and ethylene were purchased from the Takachiho Co.; both gases contained methane and ethane as impurities. The acetylene and ethylene were purified by a gas chromatograph provided with a 1.75 m activated charcoal column at 200 °C, and with a 0.7 m Molecular Sieves 13X column at 200 °C, respectively. The purified gases contained no impurity within the limits of sensitivity of a gas chromatograph with a flame ionization detector; therefore, both gases had a minimum purity of 99.999%. Takachiho research-grade hydrogen (99.999 vol%. O_2 content less than 0.1 ppm) was used without further purification.

The experiments were carried out at 22.7±1.0 °C, and the reactant-product mixture was analyzed by means of a gas chromatograph using a 4 m column of phenylisocyanate on Poracil C (Waters Associates, Inc.,) at 30 °C, and a flame ionization detector. The benzene was measured using a 2 m column of dioctylphthalate, followed by a 2 m column of polyethyleneglycol-4000 on Celite 545 at 80 °C.

In order to compare the rate constant for the H+C_2H_2 reaction with that for the H+C_2H_4 reaction in the photolysis of the H_2–C_2H_2–C_2H_4 system, it is necessary to determine the rate of the formation of the *n*-butane which would be formed if acetylene was absent in the system (denoted by r_B*). Thus, the rate of butane formation was monitored by using two reaction cells, a "mixture" cell (203 ml) and a "reference" cell (204 ml), under identical photolytic conditions. At first, the same pressures of ethylene (3.4—32.5 Torr) and hydrogen (~630 Torr) were admitted simultaneously to both cells, each containing a few drops of mercury, and then the cells were illuminated by an identical light source. Thus, the ratio of the rates of the formation of *n*-butane: $R_{n\text{-}C_4H_{10}}$ (Mixture cell)/$R_{n\text{-}C_4H_{10}}$ (Reference cell), was obtained in the H_2–C_2H_4 system; we define it as the "reference ratio."

Next, in the main run, the same pressures of ethylene (15—30 Torr) and hydrogen (~630 Torr) were put into both cells, while various pressures of acetylene were added to the "mixture cell." Then photolysis was performed in the same way as in the preliminary run. Thus, the value of r_B* was calculated by means of the following relation:

r_B^* = (reference ratio)
× (the rate of *n*-butane formation in the reference cell in the main run).

The reference ratio was checked both before and after the photolysis of the H_2–C_2H_2–C_2H_4 system; if the two values differed, the mean value was used in the calculation.

Table 1. Data for Hg-photosensitized reaction of C_2H_2–C_2H_4–H_2 mixtures

Reactants(Torr at 22.7 °C)			Photolysis time (min)	C_4H_{10} yield (μM)		Reference[a] ratio	Products (n-C_4H_{10}=1.000)			
C_2H_2	C_2H_2/C_2H_4	H_2		Reference cell	Mixture cell		C_2H_6	1-C_4H_8	1,3-C_4H_6	C_6H_6
20.98	2.36	622.9	60[b]		2.197		0.231	0.152	0.091	0.013
25.45	4.50	624.4	60[b]		1.292		0.302	0.363	0.180	0.056
23.8	4.53	630.3	60[b,c]		0		0	0	0	0
0	0	~630	5.0				0.157±0.002[d]			
13.27	0.742	638.0	5.0	2.682	2.365	1.020	0.182	0.074	—	
18.92	1.648	640.9	5.0	2.382	3.979	2.301	0.225	0.076	0.023	
21.37	2.803	629.7	5.0	2.185	1.304	0.988	0.287	0.277	0.090	
21.97	3.898	628.8	5.0	3.162	1.708	0.985	0.323	0.389	0.139	
25.37	4.456	619.5	5.0	2.082	1.063	1.073	0.338	0.413	0.194	
24.96	5.186	634.9	3.0	1.890	0.795	0.971	0.411	0.701	0.260	
27.00	7.105	626.3	5.0	3.538	1.396	1.154	0.436	0.661	0.525	

a) Reference ratio=$R_{C_4H_{10}}$(Mixture)/$R_{C_4H_{10}}$ (Reference). See text. b) Incident light was reduced to about one tenth. c) 2.0 Torr of NO was added. d) Mean value of 15 experiments. Pressure of ethylene was varied from 3.4 to 32.5 Torr.

Results and Discussion

In a series of experiments designed to ascertain the rate measurements, the H_2 pressure was kept higher than 600 Torr and constant. The total olefin pressure was very much smaller than the hydrogen pressure and was also kept approximately constant (~30 Torr). The products were ethane, n-butane, 1-butene, 1,3-butadiene, benzene, and negligible amounts of propane and propylene. The relative rate of the formation of each product is given in Table 1.

Now, if ethylene or acetylene quenches Hg6($^3P_1$) atoms and undergoes chemical reactions, acetylene and benzene should be formed from excited ethylene[12] and acetylene[13] respectively. On the other hand, in the experiments with the mixtures of ethylene (3.4—32.5 Torr) and hydrogen (~630 Torr), no acetylene was detected. Table 1 also shows that benzene formation is suppressed in the H_2–C_2H_2–C_2H_4 system by the addition of a small amount NO, which is known to suppress radical reactions. These observations imply that the excited olefin molecules formed by quenching are efficiently deactivated in collisions with other molecules present, without undergoing a chemical reaction.

The C_2H_6/n-C_4H_{10} ratio in the H_2–C_2H_4 system is very close to the normal ratio of the disproportionation to the combination of ethyl radicals, 0.13—0.14.[14] This shows that the H atom-radical reaction is negligible:

$$H + C_2H_5 \longrightarrow C_2H_6.$$

The formation of products may be explained by the following competitive reactions:[3]

$$Hg6(^1S_0) + h\nu(2537\,Å) \longrightarrow Hg6(^3P_1), \quad (a)$$
$$H_2 + Hg6(^3P_1) \longrightarrow 2H + Hg6(^1S_0), \quad (b)$$
$$H + C_2H_4 \longrightarrow C_2H_5, \quad (1)$$
$$H + C_2H_2 \longrightarrow C_2H_3, \quad (2)$$
$$C_2H_5 + C_2H_5 \longrightarrow n\text{-}C_4H_{10}, \quad (3)$$
$$\longrightarrow C_2H_6 + C_2H_4, \quad (3a)$$
$$C_2H_5 + C_2H_3 \longrightarrow 1\text{-}C_4H_8, \quad (4)$$
$$\longrightarrow C_2H_6 + C_2H_2, \quad (4a)$$
$$\longrightarrow 2C_2H_4, \quad (4b)$$
$$C_2H_3 + C_2H_3 \longrightarrow 1,3\text{-}C_4H_6 \quad (5)$$
$$\longrightarrow C_2H_4 + C_2H_2, \quad (5a)$$
$$C_2H_3 + C_2H_2 \longrightarrow C_4H_5, \quad (6)$$
$$C_4H_5 + C_2H_2 \longrightarrow C_6H_7, \quad (7)$$
$$C_6H_7 \longrightarrow C_6H_6 + H, \quad (8)$$
$$C_4H_5 + nC_2H_2 \longrightarrow \text{polymer}, \quad (9)$$

where Reactions 6—9 have been proposed by Tsunashima and Sato.[13]

In the competitive reaction technique, the basic premise is that the rates of the mutual interaction of the radicals formed are determined statistically:[3]

$$k_5 + k_{5a} = f(k_3 + k_{3a}).$$

If f happens to be unity, and if the simple collision theory of chemical kinetics can be applied to Reactions 3—5a, the activation energies of which are considered to be small,[15] one can get the following equation:

$$k_4 + k_{4a} + k_{4b} = 2(k_3 + k_{3a}) = 2(k_5 + k_{5a}) = 2k. \quad (A)$$

It will be shown below that Eq. (A) is a good approximation.

Table 1 shows that the benzene formation is less than 3% of the products measured at the reduced intensities of the incident light which is favorable for polymerization. Therefore, Reactions 6—9 are neglected in the following kinetic considerations at relatively high intensities.

A steady-state treatment gives the following equation:

$$\frac{[C_2H_2]_{initial}}{[C_2H_4]_{initial}} = \frac{k_1}{k_2}[(r_B^*/r_B)^{1/2} - 1], \quad (1)$$

where r_B^* is the rate of the formation of n-butane in Reaction 3 when ethylene is alone, and where r_B is that when acetylene is added to it.

Cvetanović and Doyle[3] have discussed the case when f is not unity. They have assumed the rate constant of the cross interaction of two radicals to be twice the arithmetic mean of the rates of the self-interaction of the radicals, *i.e.*:

$$k_4 + k_{4a} + k_{4b} = (k_3+k_{3a}) + (k_5+k_{5a}) = (1+f)k. \quad \text{(B)}$$

This seems to be logical.

Under such conditions, the steady-state treatment gives the following expression for k_2/k_1:

$$\left(\frac{k_2}{k_1}\right)^* = \frac{[C_2H_4]}{[C_2H_2]}\left\{\left[\delta\left(\frac{r_B}{r_B^*}\right)^{1/2}\left(1+\frac{(\delta^2-1)r_B}{r_B^*}\right)^{1/2} - \frac{(\delta^2-1)r_B}{r_B^*}\right]^{-1} - 1\right\}, \quad \text{(1a)}$$

where $\delta=(1+f)/2f^{1/2}$.

From Eqs. (1) and (1a), it may be seen that:

$$\rho = \frac{(k_2/k_1)^*}{k_2/k_1} = \left\{\left[\delta\left(\frac{r_B}{r_B^*}\right)^{1/2}\left(1+\frac{(\delta^2-1)r_B}{r_B^*}\right)^{1/2} - \frac{(\delta^2-1)r_B}{r_B^*}\right]^{-1} - 1\right\}\left[\left(\frac{r_B^*}{r_B}\right)^{1/2} - 1\right]^{-1}.$$

They have computed ρ for a wide range of f and r_B^*/r_B values and have shown that even when $f=0.6$, ρ differs from unity by less than 2% in the range of $(r_B^*/r_B)\leq 7$.

In the present case, the rates of the self-interaction of ethyl and vinyl radicals may be almost equal to the collision numbers, so that:

$$f = \frac{k_5+k_{5a}}{k_3+k_{3a}} = \frac{\sigma^2(C_2H_3)}{\sigma^2(C_2H_5)}\left[\frac{M(C_2H_5)}{M(C_2H_3)}\right]^{1/2},$$

where σ and M are the collision cross section and the molecular weight of each radical respectively. The collision diameters are $\sigma(C_2H_3)=4.23$ Å and $\sigma(C_2H_5)=4.33$ Å,[16] which give 0.989 as the value of f. Therefore, we have used Eq. (1) instead of (1a) to obtain k_1/k_2.

The steady-state treatment for the reaction mechanism described above leads to:

$$\frac{R(C_2H_6)}{R(n\text{-}C_4H_{10})} = \frac{k_{4a}}{k_4}\cdot\frac{R(1\text{-}C_4H_8)}{R(n\text{-}C_4H_{10})} + \frac{k_{3a}}{k_3}, \quad (2)$$

$$\frac{R(C_2H_6)}{R(n\text{-}C_4H_{10})} - \frac{k_{3a}}{k_3} = \frac{k_{4a}}{k_3}[(r_B^*/r_B)^{1/2}-1], \quad (3)$$

and

$$\frac{R(1,3\text{-}C_4H_6)}{R(n\text{-}C_4H_{10})} = \frac{k_5}{k_3}[(r_B^*/r_B)^{1/2}-1]^2. \quad (4)$$

Taking the data from Table 1, one can plot Eqs. (1)—(4) as is shown in Figs. 1—4. Good linear plots are obtained, as required by the equations. The slope of each figure gives the relative rate constant.

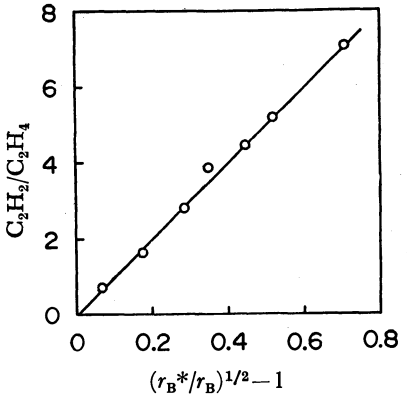

Fig. 1. Experimental plot of Eq. (1).

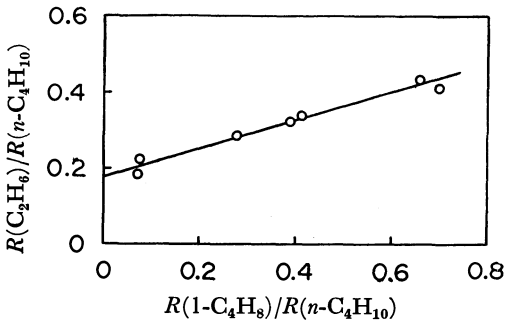

Fig. 2. Experimental plot of Eq. (2).

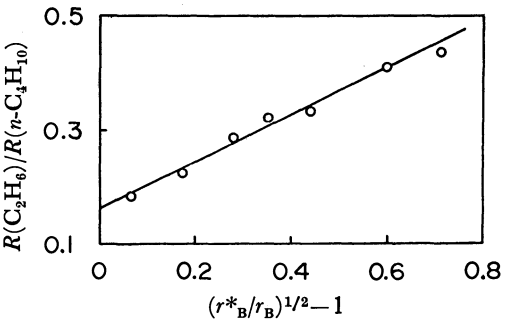

Fig. 3. Experimental plot of Eq. (3).

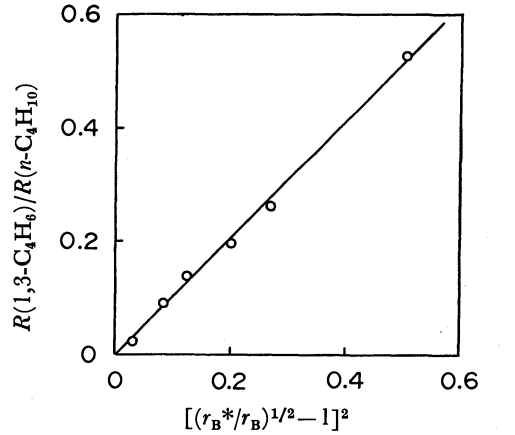

Fig. 4. Experimental plot of Eq. (4).

Using these relative rate constants and Eq. (A), the rate constants of Reactions 3a—5a relative to that of Reaction 3 are calculated to be as is shown in Column 2 of Table 2; they have not been measured hitherto. Column 3 shows the recalculated values expressed in a way similar to the literature values given in the last column.

It can be seen that a good agreement exists between the value of k_1/k_2 obtained in the present work and that of Cowfer, *et al.*[5] though their value has been obtained at total pressures of 10—15 Torr. However, there are some complications involved in obtaining the absolute value of k_2 from the new relative value for acetylene. The main one is that the rate constant for H-atom addition to ethylene is complicated by the redissociation of the vibrationally excited ethyl radical. Therefore, in the region of low pressures the absolute value of k_1 shows a tendency to increase with an increase in the total pressures.[17] Recetnly, Eyre *et al.*,[17j] have obtained the value of k_1

Table 2. Summary of the relative rates of reactions of C_2H_3 and C_2H_5 radicals

Reactions	Relative rate constants: Present results (22.7°C)		Relative rate constants: Literature values	Ref.
1	2	3	4	
$H+C_2H_4 \rightarrow C_2H_5$	9.99±0.16		8.6±1.3	6
$H+C_2H_2 \rightarrow C_2H_3$	1.00		1.00	
$C_2H_5+C_2H_5 \rightarrow n\text{-}C_4H_{10}$	1.00			
$\rightarrow C_2H_6+C_2H_4$	0.157±0.002			
$C_2H_5+C_2H_3 \rightarrow 1\text{-}C_4H_8$	1.13±0.20	1.00	1.00	
$\rightarrow C_2H_6+C_2H_2$	0.417±0.016	0.369	0.115(161—175 °C)	7
$\rightarrow 2C_2H_4$	0.77±0.20	0.68	0.034(161—175 °C)	7
$C_2H_3+C_2H_3 \rightarrow 1,3\text{-}C_4H_6$	1.03±0.04	1.00	1.00	
$\rightarrow C_2H_4+C_2H_2$	0.09±0.04	0.087	0.02(50±0.05 °C)	8
			~0.5(272—301 °C)	9
			1.1(175 °C)	10
			~3	11

Table 3. Absolute rate constant for $H+C_2H_2$

Rate constant cc $mol^{-1}s^{-1} \times 10^{10}$	Temp. °C	Pressure Torr
0.78		0.7—2.1(He)[a]
0.81	17	3.5(H_2)[b]
2.4±0.3	40	1.35—3.00(Ar)[c]
2.7±0.7	room temp.	10—15(He)[d]
3.6	30	0.5—30(He)[e]
5.2	25	1.0—15(H_2)[f]
36		3—17.3(He)[a]
5.5±0.5	22.7	~650(H_2)[g]

a) Ref. 18. b) J. R. Dingle and D. J. Le Roy, *J. Chem. Phys.*, **18**, 1632 (1950). c) Ref. 19. d) Ref. 6. e) Ref. 5. f) E. L. Tollefson and D. J. Le Roy, *J. Chem. Phys.*, **16**, 1057 (1948). g) This work.

$=(5.5\pm0.5)\times10^{11}$ cm^3 mol^{-1} s^{-1}, independent of H_2 pressures of 750—1750 Torr at 298 K; the pressure region and the temperature are close to those used in the present work. If this absolute value is adopted, the relative rate constant obtained in this work leads to $(5.5\pm0.5)\times10^{10}$ cm^3 mol^{-1} s^{-1} as the rate constant for the addition of the H atom to acetylene; it is tabulated in Table 3. Recent studies[5,6,18-20] have indicated that the value of k_2 shows a pressure dependence when determined in the low-pressure region (1 to 50 Torr). This pressure dependence seems to be the reason for the discrepancies in the absolute values given in Table 3. In order to obtain a more reliable value, it may be necessary to study the decomposition of the vibrationally excited vinyl radicals over a wide range of pressures.

The agreements are not good between the literature values and those obtained in the present work for the ratio of the rate constants for the disproportionation to the combination of vinyl and ethyl radicals. There is uncertainty in the analysis of the data to obtain the ratio, as has been mentioned by authors themselves in their papers;[9,11] moreover, the available data are few in number. However, it can be seen at least that the value obtained for the vinyl radical reaction agrees in the order of magnitude with that proposed by Sherwood and Gunning.[7] Though a detailed discussion is impossible at present, it seems safe to conclude that the rate constant of the disproportionation of the vinyl radical does not exceed that of the recombination by one-tenth at room temperature.

References

1) a) E. W. R. Steacie, "Atomic and Free Radical Reactions," 2nd Ed., Reinhold, New York, N.Y., (1954); b) R. J. Cvetanović, "Advances in Photochemistry," Vol. 1, 9. 115 (1963); c) B. A. Thrush, "Progress in Reaction Kinetics," Vol. 3, p. 65 (1965).

2) G. R. Woolley and R. J. Cvetanović, *J. Chem. Phys.*, **50**, 4697 (1969).

3) R. J. Cvetanović and L. C. Doyle, *ibid.*, **50**, 4705 (1969).

4) a) S. W. Benson, "Thermochemical Kinetics," Wiley, New York, N.Y. (1968), p. 156; b) C. M. Drew and A. S. Gordon, *J. Chem. Phys.*, **31**, 1417 (1959).

5) K. Hoyermann, H. Gg. Wagner, and J. Wolfrum, *Ber. Bunsenges. Phys. Chem.*, **72**, 1004 (1968).

6) J. A. Cowfer, D. G. Keil, J. V. Micheal, and C. Yeh, *J. Phys. Chem.*, **75**, 1584 (1971).

7) D. G. L. James and G. E. Throughton, *Trans. Faraday Soc.*, **62**, 145 (1966).

8) A. G. Sherwood and H. E. Gunning, *J. Phys. Chem.*, **69**, 2323 (1965).

9) D. J. Le Roy and A. W. Tickner, *J. Chem. Phys.*, **19**, 1247 (1951).

10) N. A. Weir, *J. Chem. Soc.*, **1965**, 6870.

11) S. Takita, Y. Mori, and I. Tanaka, *J. Phys. Chem.*, **72**, 4360 (1968).

12) A. B. Callear and R. J. Cvetanović, *J. Chem. Phys.*, **24**, 873 (1956).

13) S. Tsunashima and S. Sato, This Bulletin, **41**, 2281 (1968).

14) a) A. F. Trotman-Dickenson and G. S. Milve, "Tables of Bimolecular Gas Reactions," NSRDS-NBS9 (1967); b) E. Ratajczak and A. F. Trotman-Dickenson, "Supplementary Tables of Bimolecular Gas Reactions," NSRDS-NBS9 (1969); c) J. A. Kerr and E. Ratajczak, "Second Supplementary Tables of Bimolecular Gas Reactions," NSRDS-NBS9 (1972).

15) J. A. Kerr and A. F. Trotman-Dickenson, "Progress in Reaction Kinetics," Vol. 1, p. 105 (1961).

16) J. O. Hirschfelder, C. F. Curtiss, and R. B. Bird, "Molecular Theory of Gasses and Liquids," Wiley, New York, N.Y. (1964).

17) a) P. E. M. Allen, H. W. Melvill, and J. C. Robb, *Proc. Roy. Soc., Ser. A*, **218**, 311 (1953); b) W. Braun and M. Lenzi, *Discuss. Faraday Soc.*, **44**, 252 (1967); c) A. B. Callear and J. C. Robb, *Trans. Faraday Soc.*, **51**, 638 (1955); d) K. Yang, *J. Amer. Chem. Soc.*, **84**, 3795 (1962); e) J. M. Brown and B. A. Trush, *Trans. Faraday Soc.*, **63**, 630 (1970); f) J. H. Knox and D. G. Dalgleish, *Int. J. Chem. Kinet.*, **1**, 69 (1969); g) A. A. Westenberg and N. DeHaas, *J. Chem. Phys.*, **50**, 707 (1969); h) M. J. Kurylo, N. C. Peterson, and W. Braun, *ibid.*, **53**, 2776 (1970); i) M. P. Halstead, D. A. Leathard, R. M. Marshall, and J. H. Purnell, *Proc. Roy. Soc., Ser. A*, **316**, 575 (1970); j) J. A. Eyre, T. Hikida, and L. M. Dorfman, *J. Chem. Phys.*, **53**, 1281 (1970); k) J. R. Barker, D. G. Keil, J. V. Michael, and D. T. Osborne, *ibid.*, **52**, 2079 (1970); l) J. V. Michael and D. T. Osborne, *Chem. Phys. Lett.*, **3**, 402 (1969).

18) J. V. Michael and R. E. Weston, *J. Chem. Phys.*, **45**, 3632 (1966).

19) G. G. Volpi and F. Zocchi, *ibid.*, **44**, 4010 (1966).

20) J. V. Michael and N. Niki, *ibid.*, **46**, 4969 (1967).

An MO-theoretical Approach to the Aquation Mechanism of Carboxylatopentaammineruthenium(III) Complexes in Acid Solutions

Kastutoshi Ohkubo, Futoshi Kitagawa, Hiroyuki Sakamoto, and Akira Ohyoshi
Faculty of Engineering, Kumamoto University, Kurokami, Kumamoto 860

(Received March 1, 1974)

The aquation mechanism of carboxylatopentaammineruthenium(III) complexes, $(NH_3)_5RuO_2CR^{2+}$, where R=H, CH_3, C_2H_5, $(CH_3)_2CH$, and CH_2OH, has been investigated with the Wolfsberg-Helmholz-LCAO-MO extended Hückel method augmented by metal d-orbitals. The very weak Ru–O coordination linkage (bond population=0.085—0.092) formed mainly by the antibonding $d_{z^2}p_z$-σ and p_zp_z-σ orbitals facilitates the heterolytic bond-breaking of the Ru–O (dissociation energy=4.61—9.22 kcal/mol), and the order of the bond populations of the Ru–O is well reflected in that of the overall aquation rates. The preferable structure of the protonated complex is $(NH_3)_5RuOHC(=O)R^{2+}$, produced by the interaction between the H^+ catalyst and the non-bonding lonepair orbital of the neighboring oxygen atom attached to the metal. The H_2O solvent was found to play an important role in the bond dissociation of the metal-oxygen linkage from a linear dependence between the reactivity index $(1/2N_{z^2}^{LU})$ of the protonated complex to such nucleophiles as H_2O and the activation energy for the S_N2 aquation reaction. The proposed tetragonal pyramidal intermediate of $(NH_3)_5Ru^{3+}$ combines easily the Ru–O through the lowest unoccupied d_{z^2} Ru-orbital, forming an aquo-complex with the binding energy of with H_2O linkage, 30.25 kcal/mol.

The aquation of carboxylatopentaammineruthenium-(III) complexes (referred to as $(NH_3)_5RuO_2CR^{2+}$, where R=H, CH_3, C_2H_5, $(CH_3)_2CH$, and CH_2OH) has proved to be accelerated by an acid catalyst (H^+), in accordance with:[1]

$$(NH_3)_5RuO_2CR^{2+} + H_2O \underset{E_a=18.58-25.43\ \text{kcal/mol}}{\overset{H^+}{\rightleftharpoons}} (NH_3)_5RuH_2O^{3+} + RCO_2^- \quad (1)$$

where E_a denotes the activation energy. A simulation analysis of the above aquation reaction has led to the proposing of the following reaction sequences of an S_N1 mechanism combined with an S_N2 one:[2]

$$(NH_3)_5RuO_2CR^{2+} \xrightarrow[E_a=18.12-22.22\ \text{kcal/mol}]{H^+} (NH_3)_5Ru^{3+} + RCO_2^- \quad (2a)$$

$$(NH_3)_5RuO_2CR^{2+} \xrightarrow[E_a=21.82-30.29\ \text{kcal/mol}]{} (NH_3)_5Ru^{3+} + RCO_2^- \quad (2b)$$

$$(NH_3)_5Ru^{3+} + H_2O \underset{E_a=6.869\ \text{kcal/mol}}{\overset{E_a=2.094\ \text{kcal/mol}}{\rightleftharpoons}} (NH_3)_5RuH_2O^{3+} \quad (2c)$$

where $(NH_3)_5Ru^{3+}$ stands for a momentarily living five-coordinated intermediate (tetragonal pyramidal structure). The five-coordinated intermediate has also proved to be plausible in an anation study[3] of aquopentaammineruthenium(III) complexes.

In the aquation mechanism of carboxylatopentaammine complexes of Co(III),[4–6] Rh(III),[6] or Ir-(III),[6] however, there remain some obscurities in terms of the structure of the protonated complex, $(NH_3)_5MO_2CR^{n+}$—H^+ (M=central metal), the position of the bond-breaking of the complex (metal-oxygen or acyl-oxygen bond), and the reaction sequences (S_N1, S_N2, *etc.*).

Since the aquation mechanism is still open to question on a molecular level, it seems of interest and significant to reinvestigate the mechanism in connection with the electronic properties of the reactant, the intermediate, and the product in Reactions (2a—c).

Some extended-Hückel-MO-base SCF methods[7] have been used to investigate the electronic structures of metal complexes. However, the reliability of such self-consistent charge and configuration-MO calculation depends directly on the parameters for the diagonal and off-diagonal Hamiltonian matrix elements. In this respect, the EHMO (without SCF) method seems to be useful so long as the parameters are suitably selected to explain such experimental results as d-orbital splittings, electron-excitation energies, *etc.* In our previous EHMO treatment of the pentacyanocobaltate(II) complex,[8] it was found that the EHMO-method produced sufficient calculation results for the electronic property of the metal complex to be discussed qualitatively or quantitatively.

In this paper, we attempted to apply the Wolfsberg-Helmholz-LCAO-EHMO method[9] to explain the electronic structures of ruthenium complexes, in connection with their aquation reactions.

Method of Calculation

The following four systems were investigated in this work: (a) carboxylatopentaammineruthenium(III) complexes, $(NH_3)_5RuO_2CR^{2+}$ (R=H, CH_3, C_2H_5, $(CH_3)_2CH$, and CH_2OH), (b) an interacting system of $(NH_3)_5RuO_2CH^{2+}$ and the acid catalyst (H^+), (c) an intermediate, $(NH_3)_5Ru^{3+}$, and (d) an aquo-complex, $(NH_3)_5RuH_2O^{3+}$.

The diagonal terms for the central ruthenium metal orbitals, H_{ii}, are estimated from the negative of the valence-state ionization energies (VSIE) of Fe, Co, Rh, Ir, *etc.*; That is the VSIE values for the d, s, and p orbitals of Ru were, respectively, taken to be 12.0,[10] 9.0,[10] and 7.0 eV.[10] The off-diagonal terms, H_{ij}, were evaluated by the Wolfsberg-Helmholz approximation:[11]

$$H_{ij} = K(H_{ii}+H_{ij})S_{ij}/2$$

where K is a constant of 1.75 and where S_{ij} is the overlap integral between the i-th AO and the j-th AO. The orbital exponents were taken from Clementi,[12]

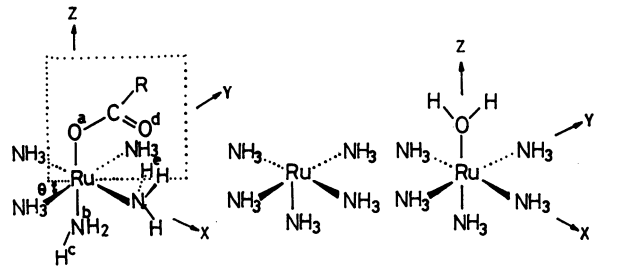

Ru–O=2.5 Å; Ru–N=2.23 Å; N–H=1.031 Å

$(NH_3)_5$-RuO_2CR^{2+} (R)	C–C/Å	C–O/Å	C–O/Å	∠OCO	∠OCC or ∠OCH	∠COH
H	—	1.36	1.23	122.4°	118.8°	
CH_3	1.54	1.43	1.24	130°	120.5°	
C_2H_5	1.54	1.43	1.24	130°	120.5°	
$(CH_3)_2CH$	1.54	1.43	1.24	130°	120.5°	
CH_2OH	1.44	1.28	1.24	124°	120.5°	109°

Cited from L. E. Sutton, editor, "Interatomic Distances," The Chemical Society, London (1958).

Fig. 1. Geometries used for the calculation.

while the VSIE values for H, C, N, and O atoms were supplied by Hinze and Jaffe.[13]

The geometries used for the calculation are illustrated in Fig. 1; for simplicity of computation, the interatomic distances of Ru–O and Ru–N were uniformly taken to be the purely covalent bond lengths of 2.5 and 2.23 Å respectively, and the valence angle of Ru–O–C in the bond between the metal-carboxylato ligand was assumed to be 105° a value which corresponds to that of H–O–C of usual carboxylic acids (RC(=O)OH).

Calculated Results and Discussion

Electronic Property of $(NH_3)_5RuO_2CR^{2+}$. Mention should first be made of the molecular structure of $(NH_3)_5RuO_2CR^{2+}$. In the energetically stable state of $(NH_3)_5RuO_2CR^{2+}$, the RCO_2 ligand has a rotation angle of $\pi/4$ ($\theta=\pi/4$ in Fig. 1) in the direction of d_{xz} Ru-orbital expansion; $(NH_3)_5RuO_2CCH_3^{2+}$ in the case of $\theta=\pi/4$ is, for example, energetically more stable by 18.34 kcal/mol than that in the case of $\theta=0$. In such a situation, an intramolecular hydrogen bonding can be expected between the carbonyl oxygen of the RCO_2 ligand and the hydrogen atom of the ammine group (see Table 1). This hydrogen bond may stabilize the complex molecule.

Now, let us examine the d-orbital splittings and electron-excitation energies of $(NH_3)_5RuO_2CR^{2+}$ in order to check the reliability of the calculation results. The d-orbital separation of $(NH_3)_5RuO_2CR^{2+}$ is very similar to that of usual octahedral metal complexes such as $M(NH_3)_6^{3+}$, and $M(NH_3)_5H_2O^{3+}$; that is, the separation is shown by triply-degenerate d_{xy}, d_{yz}, and d_{xz} (at about −11.95 eV) and by doubly-degenerate d_{z^2} and $d_{x^2-y^2}$ (at about −11.1 eV[14]).

The 10 Dq value for $(NH_3)_5RuO_2CR^{2+}$ is, then, estimated to be 5.36—5.45 kK from the energy difference between the t_{2g} and e_g orbitals.

The 10 Dq value for such octahedral ruthenium complexes as $Ru(NH_3)_5H_2O^{3+}$ and $Ru(NH_3)_6^{3+}$ has been reported to be 1.14 Dq[15] on the basis of the crystal-field theory. Taking into consideration the fact that the Dq for the second transition series is some 50% greater than the first series (Dq=2.10 kK[16]), the value of 1.14 Dq corresponds almost exactly to 3.59 kK, which is approximately in agreement with the above 10 Dq value for $(NH_3)_5RuO_2CR^{2+}$.

In regard to the electron-excitation energies for the CT transition from the central Ru metal to the carboxylato ligand, the CT transition of $(NH_3)_5RuO_2CR^{2+}$ was found from the UV absorption spectra of $[(NH_3)_5$-$RuO_2CR](ClO_4)_2$ in water to occur in the range of 24.9—34.1 kK. The electron-excitation energy calculated from the d_{xz} (or d_{yz}) orbital to the oxygen p_x (or p_y) orbital falls in the range of 27.5—36.0 kK, which is in good accordance with the above experimental results. The present calculation results, thus, seem to be useful for a qualitative or quantitative discussion of electronic property of the ruthenium(III) complex.

Next, let us discuss the charges (of $(NH_3)_5RuO_2CR^{2+}$) calculated by means of Mulliken's electron population analysis.[17]

According to the electronic charge (Q_A) in Table 1, the electron distribution in the complex seems to be somewhat characteristic; the central trivalent ruthenium is negatively charged, as are the neighboring O and N atoms attached to the metal, while the charges of the H atoms in the NH_3 ligands are markedly positive (+0.365). The negativeness of the Ru(III)-charge may be due to the electron-inflowing from the NH_3 ligand through the σ-bond, because the electron-inflowing of the ligand electrons from the NH_3 to the Ru metal cannot be expected through the d-π delocalization. Concerning the Ru–O coordination linkage, the negative charges localized on the neighboring O and N atoms may make the Ru–O bond very weak; in this respect, the weakness of the Ru–O bond is reflected in the very small bond population (M_{AB}) of the Ru–O bond and the small heterolytic bond dissociation energies of 4.61—9.22 kcal/mol.[18] It is of interest here that the order of the M_{Ru-O} values except for that of the glycolato-complex is in satisfactory accordance with that of the E_a values for Reaction (1) (and also with that of the overall aquation rates: formato>acetato>propionate>isobutylato>glycolato) This may suggest qualitatively that the aquation of $(NH_3)_5RuO_2CR^{2+}$ proceeds *via* the S_N1 mechanism in which the bond breaking of the Ru–O linkage is more important than the bond making between the Ru metal and H_2O. It is also noticeable in respect to the Ru–O linkage that the antibonding $d_{z^2}p_z$-σ and p_zp_z-σ orbitals predominantly favor the formation of the Ru–O coordination bond. This implies the nucleophilic attack of such a third body as an electron-releasing solvent or base catalyst on the above antibonding nature of the Ru–O linkage so as to break the bond. In this respect, the order of the AO bond population (N_{Ru-O}) is also in harmony with that of the aquation rates mentioned above.

Table 1. Electronic property of $(NH_3)_5RuO_2CR^{2+}$

$(NH_3)_5RuO_2CR^{2+}$ (R)		Q_A[a]				M_{AB}		
		Ru	O[a]	N[b]	H[c]	Ru–O[a]	Ru–O[b]	O[d]–H[e]
H	(I)	−0.808	−1.167	−0.918	+0.356	0.0854	0.1049	0.0204
CH_3	(II)	−0.817	−1.238	−0.918	+0.356	0.0907	0.1051	0.0172
C_2H_5	(III)	−0.822	−1.236	−0.919	+0.356	0.0912	0.1049	0.0172
$(CH_3)_2CH$	(IV)	−0.829	−1.220	−0.920	+0.356	0.0915	0.1057	0.0171
CH_2OH	(V)	−0.845	−1.107	−0.920	+0.356	0.0851	0.1043	0.0165

$(NH_3)_5RuO_2CR^{2+}$ (R)		Electron densities				N_{Ru-O}		
		d_{xz}	d_{yz}	d_{xy}	$d_{x^2-y^2}$	d_{z^2}	d_{z^2}-p_z	p_z-p_z
H	(I)	1.998	1.993	1.013	0.356	0.294	0.0159	0.0408
CH_3	(II)	1.998	1.990	1.017	0.356	0.296	0.0163	0.0410
C_2H_5	(III)	1.997	1.998	1.021	0.356	0.302	0.0167	0.0411
$(CH_3)_2CH$	(IV)	1.996	1.987	1.022	0.356	0.308	0.0169	0.0417
CH_2OH	(V)	1.998	1.992	1.015	0.356	0.325	0.0185	0.0442

As to the superscripts of a—e, see Fig. 1.
a) The Q_A values for Ru were evaluated on the basis of the trivalent state of Ru (outer-shell electrons=5).

We will now, then, examine whether the above-mentioned antibonding dp-σ or pp-σ orbital plays an important role in the Ru–O bond-breaking in Reaction (2b). In view of the fact that the lowest unoccupied MO (LUMO) of the complexes is predominantly localized by the d_{z^2} Ru-orbital, the net orbital population of the d_{z^2}-orbital at the LUMO (abbreviated by $1/2N_{z^2}^{LU}$) can be taken as the reactivity index to such nucleophiles as H_2O, which is a stronger base than CH_3CO_2H. If H_2O takes part in the bond breaking of the Ru–O through its nucleophilic attack on the LU d_{z^2} Ru-orbital, there should exist a correlation between the $1/2N_{z^2}^{LU}$ values and such kinetic parameters as the E_a values for Reaction (2b). However, there was no parallelism between them. Therefore, the bond-breaking of the Ru–O linkage in Reaction (2b) may easily occur without the direct effect of H_2O on the bond dissociation of the Ru–O linkage, in view of the fairly small heterolytic dissociation energy of the metal-oxygen bond (the E_a values for Reaction (2b) are also small).

Role of the Acid Catalyst in the Dissociation of Metal-Oxygen Bond in $(NH_3)_5RuO_2CR^{2+}$. Up to now, the H^+ catalyst has been considered to participate in the protonated complex formation[19] as follows:

$$(NH_3)_5MO_2CR^{n+} + H^+ \rightleftharpoons \begin{matrix}(NH_3)_5MOC(-OH)R^{(n+1)+} \\ \text{or} \\ (NH_3)_5MOC(=O)R^{(n+1)+} \\ \quad H\end{matrix} \quad (3a)$$

$$\begin{matrix}(NH_3)_5MO(-OH)R^{(n+1)+} \\ \text{or} \\ (NH_3)_5MO(=O)R^{(n+1)+} \\ \quad H\end{matrix} + H_2O \longrightarrow (NH_3)_5MH_2O^{(n+1)+} + RCO_2^- + H^+ \quad (3b)$$

where M means such central metals as Co(III), Rh(III), and Ir(III); the protonated complexes of $(NH_3)_5MOC(-OH)R^{(n+1)+}$ and $(NH_3)_5MOHC(=O)R^{(n+1)+}$ have been supported by Kuroda[5] (and/or Saito *et al.*[20,21]) and Basolo *et al.*[6] respectively.

Let us now discuss the structure and reactivity of the protonated complex. In regard to the interacting system between the complex and the H^+ catalyst, there exist three representative modes of interaction (Modes I, II, and III in Table 2). As may be seen from Table 2, the positive stabilization energy (ΔE_s) favors the formation of the protonated complex, in particular that *via* Mode I. In view of the weakening

Table. 2. Electronic property of the protonated complex.

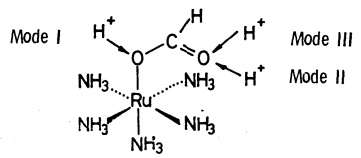

Mode	ΔM_{Ru-O}	HO	LU	$\frac{1}{2}N^{HO}$	$\frac{1}{2}N^{LU}$	ΔE_s/eV[a]	LUMO energy/eV
I	0.012	d_{xy}	d_{z^2}	0.986	0.848	4.46	−11.28
II	0.000	d_{yz} (d_{xz})	d_{xy}	0.827	0.959	2.34	−11.28
III	−0.003	d_{xy}	d_{z^2}	0.985	0.849	3.00	−11.28

a) Stabilization energy was estimated from $E_{EH}((NH_3)_5RuO_2CR^{2+}) + E_{EH}(H^+) - E_{EH}((NH_3)_5RuO_2CR^{2+}-H^+)$ where R=H.

of the Ru–O linkage by the protonation (reflected by the decrease in the M_{Ru-O}, ΔM_{Ru-O}), the protonation probably occurs through Mode I, in which the H^+ reacts with the nonbonding lone-pair oxygen 2p-orbital of the oxygen atom attached to the metal. It is worthy to emphasize that the bond-weakening of the acyl-oxygen linkage by the protonation cannot be expected through Modes I, II, and III. This means that the dissociation of the acyl-oxygen bond would not be promoted by the acid catalyst. It is also of interest to consider the effect of the H_2O solvent on the dissociation of the Ru metal-oxygen bond. In connection with the plausibility of Mode I, there is a noticeable correlation between the reactivity of the protonated complex formed by Mode I and the E_a value for Reaction (2a), in which the direct effect of H_2O on the Ru–O bond dissociation is not emphasized. The reactivity of $(NH_3)_5RuOHC(=O)R^{3+}$ toward such nucleophiles as H_2O can be mainly discussed by taking notice of the interaction between the LU d_{z^2} Ru-orbital of the former and the lone-pair orbitals of the latter.

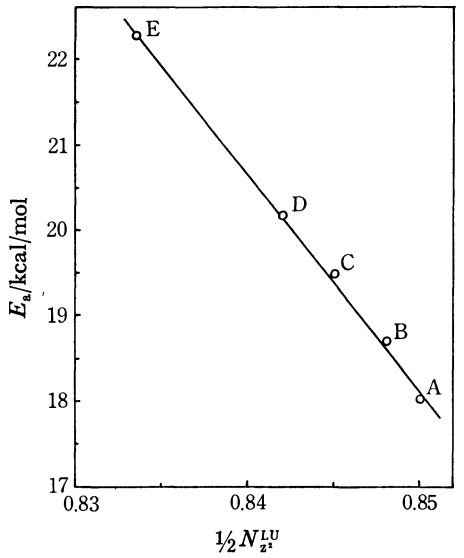

Fig. 2. Plots of E_a values for Reaction (2a) *vs.* $\frac{1}{2}N_{z^2}^{LU}$ values for $(NH_3)_5RuOHC(=O)R^{3+}$.
R: A=H, B=CH_3, C=C_2H_5, D=$(CH_3)_2CH$, E=CH_2OH

Figure 2 shows that there is a linear dependence between the $1/2N_{z^2}^{LU}$ values of $(NH_3)_5RuOHC(=O)R^{3+}$ and the E_a values. It may be deduced, therefore, that the H_2O solvent may promote the bond-dissociation of the Ru–O linkage and that Reaction (2a) can be divided into following steps:

$$(NH_3)_5RuO_2CR^{2+} + H^+ \overset{\text{fast}}{\rightleftharpoons} (NH_3)_5RuOHC(=O)R^{3+} \xrightarrow{H_2O} (NH_3)_5Ru^{3+} + RCO_2^- + H^+ \quad (4)$$

Reaction (4) would then be followed by:

$$(NH_3)_5Ru^{3+} + H_2O \longrightarrow (NH_3)_5RuH_2O^{3+} \quad (5)$$

Reaction (4) proceeds more easily than Reaction (2b), with a lower activation barrier. However, there is, even now, an ambiguity with regard to the presence of $(NH_3)_5Ru^{3+}$, although we can cast doubt on the acyl-oxygen bond-breaking mechanism[22] from the MO-theoretical point of view; that is, there is a possibility of the direct formation of the aquo-complex through the proposed S_N2 mechnism:[4-6,20,21]

$$(NH_3)_5RuO_2CR^{2+} + H^+ \overset{\text{fast}}{\rightleftharpoons} (NH_3)_5RuOC(=O)R^{3+} \xrightarrow{H_2O} (NH_3)_5RuH_2O^{3+} \quad (6)$$

Bearing in mind that, in the aquation of Co(III) complexes in an acid solution, the complexes possessing the NH_3 (or NO_2^-) ligand at the *cis* or *trans* position toward the releasing ligand (in the present case, the RCO_2 ligand) react with a retention of configuration,[23] the five-coordinated tetragonal pyramidal intermediate is selectively formed so long as the bond breaking of the metal-releasing ligand occurs first. Moreover, the seven-coordinated octahedral wedge-type intermediate cannot be excepted so long as the aquation proceeds through the d_{z^2} metal-orbital. Therefore, the nonbonding lone-pair 2p O-orbital of H_2O would start to make a tight bond with the d_{z^2} Ru-orbital of $(NH_3)_5Ru^{3+}$ (LUMO=d_{z^2}) after the releasing of the RCO_2 ligand from the metal, because there is a large steric hindrance to the reaction of H_2O with $(NH_3)_5RuOC(=O)R^{3+}$ before the releasing of the RCO_2 ligand (the orbital overlapping between the above-mentioned orbitals is also small). Taking account of the above discussion, the five-coordination of $(NH_3)_5Ru^{3+}$ seems to be present and seems to be the plausible intermediate, mainly made from Reaction (4) in the aquation mechanism; in the experimental analysis, the concentration of the intermediate was very low (by a factor of approximately $1/10^3$), as compared with that of $(NH_3)_5RuH_2O^{3+}$ under the conditions shown in Refs. 1 and 2.

Electronic Property of $(NH_3)_5Ru^{3+}$ and $(NH_3)_5RuH_2O^{3+}$. From the electronic structure of $(NH_3)_5Ru^{3+}$ shown briefly in Fig. 3, it may be seen that the intermediate does not differ extremely from the parent carboxylato-complexes in terms of the Q_A and M_{AB} values and the frontier orbitals. This is in harmony with the fact that the coordination of RCO_2^- to $(NH_3)_5Ru^{3+}$ with a small binding energy (4.61—9.22 kcal/mol) has no

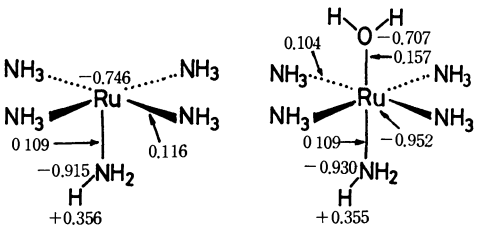

Frontier orbitals	LUMO	d_{z^2}	$d_{x^2-y^2}$
	HOMO	d_{xy}	d_{xy} or d_{xy}
Electron densities	d_{xz}	2.000	1.509
	d_{yz}	1.004	1.524
	d_{xy}	1.010	2.000
	$d_{x^2-y^2}$	0.356	0.356
	d_{z^2}	0.225	0.415

Fig. 3. Electronic structures of $(NH_3)_5Ru^{3+}$ and $(NH_3)_5RuH_2O^{3+}$.

marked effect on the d Ru-orbital separation of $(NH_3)_5RuO_2CR^{2+}$ (only the d_{z^2}-orbital energy was elevated slightly).

The intermediate of $(NH_3)_5Ru^{3+}$ once formed can easily be reconciled with the nucleophilic attack of the H_2O solvent on its d_{z^2}-orbital so as to form the aquo-complex. The coordination of H_2O to the Ru metal is relatively strong as compared with that of RCO_2^- to the metal, in view of the relatively large binding energy of 32.25 kcal/mol. This is reflected in such an electronic structure of $(NH_3)_5RuH_2O^{3+}$ as its Ru–O bond population (0.157).

The calculations were carried out on a FACOM 230-60 computer at the Data Processing Center of Kyushu University.

References

1) A. Ohyoshi, A. Jyo, and N. Shin, This Bulletin, **45**, 2121 (1972).

2) K. Ohkubo, H. Sakamoto, F. Kitagawa, and A. Ohyoshi, *ibid.*, **46**, 2651 (1973); There existed a following kinetic relationship similar to that yielded from the aquations of Co, Rh, and Ir complexes: $k_{obs}=k_{2a}[H^+]+k_{2b}$, where k_{2a} and k_{2b} indicate the rate constants for Reactions (2a) and (2b) respectively.

3) K. Ohkubo, H. Sakamoto, and A. Ohyoshi, *Chem. Lett.*, 969 (1973).

4) F. Basolo, J. G. Bergmann, and R. G. Pearson, *J. Phys. Chem.*, **56**, 22 (1952).

5) K. Kuroda, *Nippon Kagaku Zasshi*, **82**, 572 (1961).

6) F. Monacelli, F. Basolo, and R. G. Pearson, *J. Inog. Nucl. Chem.*, **24**, 1241 (1962).

7) For instance, F. A. Cotton, and T. E. Haas, *Inorg. Chem.*, **3**, 1004 (1964); H. Basch, A. Viste, and H. B. Gray, *J. Chem. Phys.*, **44**, 10 (1966); R. F. Fenske, *Inorg. Chem.*, **4**, 33 (1965); C. J. Ballhausen and H. B. Gray, *ibid.*, **1**, 111 (1962); L. L. Lor and W. N. Lipscomb, *ibid.*, **3**, 22 (1964); S. S. Zumdahl and R. S. Drago, *J. Amer. Chem. Soc.*, **90**, 6699 (1968).

8) K. Ohkubo, H. Kanaeda, and K. Tsuchihashi, This Bulletin, **46**, 3095 (1973).

9) R. Hoffman, *J. Chem. Phys.*, **39**, 1397 (1963); *ibid.*, **40**, 2474 (1964).

10) Assumed values based on L. L. Lohr, Jr., and W. N. Lipscomb, *Inorg. Chem.*, **3**, 22 (1964).

11) M. Wolfsberg and L. Helmholz, *J. Chem. Phys.*, **20**, 837 (1952).

12) E. Clementi and D. L. Raimondi, *ibid.*, **38**, 2686 (1963).

13) J. Hinze and H. H. Jaffé, *J. Amer. Chem. Soc.*, **84**, 540 (1962).

14) Strictly speaking, the energy level of d_{z^2} and $d_{x^2-y^2}$ orbitals are slightly different; the former is -11.28 eV and the latter is -10.93 eV.

15) J. A. Broomhead, F. Basolo, and R. G. Pearson, *Inorg. Chem.*, **3**, 826 (1964).

16) F. Basolo and R. G. Pearson, "Mechanisms of Inorganic Reactions," John Wiley & Sons, Inc., New York (1967), p. 169.

17) R. S. Mulliken, *J. Chem. Phys.*, **23**, 1833 (1955).

18) Calculated from the total energy (E_{EH}) difference: heterolytic dissociation energy$=|E_{EH}((NH_3)_5Ru^{3+})+E_{EH}(RCO_2^-)-E_{EH}((NH_3)_5RuO_2CR^{2+})|$.

19) There is an evidence for the protonation of $(NH_3)_5CoO_2CCH_3^{2+}$ (A. A. Vlcek, "Advances in the Chemistry of Coordination Compounds," Macmillan, New York (1961), p. 590).

20) K. Ogino, T. Murakami, and K. Saito, This Bulletin, **41**, 1651 (1968).

21) T. Murakami, K. Ogino, H. Kobayashi, H. Yamasaki, and K. Saito, *ibid.*, **44**, 120 (1971).

22) J. P. Hunt, A. C. Rutenberg, and H. Taube, *J. Amer. Chem. Soc.*, **74**, 268 (1952). As to the metal-oxygen bond-breaking, there is a tracer study with oxygen-18 in the aquation of acetatopentaamminecobalt(III) complex (C. A. Bunton and D. R. Llewellyn, *J. Chem. Soc.*, 1692 (1953)).

23) F. Basolo and R. G. Pearson, "Mechanisms of Inorganic Reactions," John Wiley & Sons, Inc., New York (1967), p. 258.

Theoretical Considerations of Lower Excited States of *trans*-Polyenecarbaldehydes. II. Radiative and Nonradiative Properties

Kozo Inuzuka

Department of Applied Science, Tokyo Electrical Engineering College, Kanda, Chiyoda-ku, Tokyo 101

(Received March 8, 1974)

The spin-orbit coupling energies between the lowest $^1(n,\pi^*)$ and $^3(\pi,\pi^*)$ states, and between the lowest $^1(\pi,\pi^*)$ and $^3(n,\pi^*)$ states, for the four polyenecarbaldehydes were calculated using the results calculated within the framework of the conventional P–P–P SCF–MO–CI method. In the present paper, the general properties of the emission spectra of polyenecarbaldehyde are theoretically considered using the calculated results for the spin-orbit coupling energy and their lower electronic structure.

In a previous paper,[1] the electronic structures of the lower n,π^* and π,π^* states of planar *trans*-polyenecarbaldehydes (acrolein, 2,4-pentadienal, 2,4,6-heptatrienal, and 2,4,6,8-nonatetraenal) and their oscillator strengths for the π-π^* transition were studied within the framework of the conventional P–P–P SCF–MO–CI method and then discussed. We can not even tentatively discuss the overall features of the emission property of polyenecarbaldehydes, however, because experimental data on the emission spectra of polyenecarbaldehyde are relatively rare except for acrolein[2] and for retinal,[3] which corresponds to 2,4,6,8,10-dodecapentaenal in the skeletal structure of the π electron system. In this investigation, the general features of their radiative and nonradiative properties will be discussed theoretically, using the previous results.[1]

Method of Calculation

When a single-electron operator is used for the spin-orbit Hamiltonian, the coupling of the n,π^* and π,π^* states is as follows:

$$\beta\langle n\pi^*|\pi\pi^*\rangle = \pm(\hbar e^2/4m^2c^2)\langle\pi|H_o|n\rangle \quad (1)$$

where H_o is the orbital part of the spin-orbit coupling operator for molecular systems.[4]

$$H_o = (e^2/2m^2c^2)\sum_{\lambda}\sum_{i} Z_\lambda^* l_i/r_{i\lambda}^3 \quad (2)$$

where Z_λ^* is the Slater effective charge of the nucleus, λ; $r_{i\lambda}$, the distance of the electron, i, from the nucleus, λ and l_i, the orbital moment of the i electron. $<\pi|$ and $<n|$ are the wavefunctions of the π- and n-electrons respectively for the ground state. $<\pi|$ has already been obtained by means of the P–P–P SCF–MO–CI method, and $<n|$ has been assumed in the previous paper[1] to be 2p-type atomic orbital localized on the oxygen atom of the carbonyl group. If we neglect all the two-center integrals, the spin-orbit coupling energy between the n,π^* and the π,π^* states is represented by Eq. (3):

$$\beta\langle n\pi^*|\pi\pi^*\rangle = \pm i(\hbar^2e^2/4m^2c^2)(Z_o^{*4}c_o/3n_o^{*3}a_H^3) \quad (3)$$

where Z_o^* corresponds to the effective nuclear charge of the 2p atomic orbital of the oxygen atom and c_o, to the coefficient of the 2pπ-AO of the oxygen atom of the π-MO; n_o^* is the effective principal quantum number of the n electron, and a_H is the Bohr radius (0.529 Å). In the present calculation the numerical values of $Z_o^*=4.55$ and $n_o^*=2$ were used. When $\alpha=\pm i(\hbar^2e^2Z^{*4}/12m^2c^2n_o^{*3}a_H^3)$ is substituted into Eq. (3), the absolute value of the square of Eq. (3) may be represented as follows:

$$|\beta\langle n\pi^*|\pi\pi^*\rangle|^2 = |\alpha|^2c_o^2 \quad (4)$$

The absolute value of α for the oxygen atom is equal to 52.2 cm^{-1}. The calculation of the spin-orbit interaction matrix element between $^1(\pi,\pi^*)$ and $^3(\pi,\pi^*)$ states or $^1(n,\pi^*)$ and $^3(n,\pi^*)$ states is not as easy as the calculation of the spin-orbit interaction matrix element between the different configurations. However, it is known that this quantity is much smaller than the corresponding one with a different configuration because of the lack of the contribution from the one-center term in the spin-orbit interaction matrix element. Here, this quantity is assumed to be of the order of 1 cm^{-1}.[5] Thus, the spin-orbit coupling between the two states with different configurations is more important than that between those with the same configuration; the former energy may be several orders of magnitude greater than the latter one. Therefore, the efficiency[6] of the intersystem crossing process, $^1(\pi,\pi^*)\rightsquigarrow{}^3(n,\pi^*)$ or $^1(n,\pi^*)\rightsquigarrow{}^3(\pi,\pi^*)$, is larger than that for the $^1(\pi,\pi^*)\rightsquigarrow{}^3(\pi,\pi^*)$ or $^1(n,\pi^*)\rightsquigarrow{}^3(n,\pi^*)$ process.

On the other hand, the energy separation between the lowest π,π^* singlet state, S_1, and the n,π^* triplet state, T_{n,π^*}, decreases, whereas the corresponding one between the n,π^* singlet state, S_{n,π^*}, and the lowest π,π^* triplet state, T_1, increases[1] as the molecular size increases. Therefore, the $S_{n,\pi^*}\rightsquigarrow T_1$ process plays a more important role in the radiationless deactivation of acrolein than does the $S_1\rightsquigarrow T_{n,\pi^*}$ process, but the situation is reversed as the molecular size increases. In order to ascertain the relation between the spin-orbit interaction energy and the energy separation of the two states concerning the radiationless process, the conversion time for the radiationless process was estimated using the Robinson-Frosch equations, (5) and (6):[7]

$$k = 0.71\times10^{12}\times\beta_{ij}^2\times S_{ij} \quad (5)$$

$$S_{ij} = \exp(-0.25\times E_{ij}^{0.4}) \quad (6)$$

where β_{ij} is the matrix element of [the interaction operator between i and j states, and where S_{ij} corresponds to the over-all vibrational factor in their paper.[7] The conversion time can, then, be represented by Eq. (7):

$$\tau_{1/2} = \ln 2/k \quad (7)$$

As Eqs. (5) and (6) were developed for aromatic compounds,[7] the application of these equations to polyenecarbaldehydes might not be justified. The critical comparison of the numerical values might be impossible, but the order-of-magnitude consideration may be useful for the discussion of the intersystem crossing process.

Results and Discussion

The absolute value of the square of the operator matrix elements for the spin-orbit coupling between S_{n,π^*} and T_1, and for that between S_1 and T_{n,π^*}, of the present four molecules and the conversion time were calculated by means of Eqs. (4) and (7), respectively. The calculated results are presented in Table 1. The square of the spin-orbit interaction between S_{n,π^*} and T_1, and/or S_1 and T_{n,π^*}, decreases rapidly with an increase in the number of atoms in the conjugated system. The calculated energy values[1] for the singlet and triplet states are plotted in Fig. 1.

In order to discuss the radiative and nonradiative processes of the excited states of polyenecarbaldehyde, we classified the electronic structures of their lower excited states into the following four groups (see also Fig. 2 for a schematical diagram). Acrolein, whose lowest excited singlet and triplet states are of an n,π^* character, was assigned to *Group* (1), and the remaining three polyenecarbaldehydes, to *Group* (2), for which the lowest excited singlet state is of an n,π^* character, while the lowest excited triplet state is of a π,π^* character. Although the assignment of nonatetraenal to *Group* (2) may be controversial in that its lowest singlet π,π^* state was calculated to be a little lower than the lowest n,π^* singlet state, the lowest π,π^* singlet state of nonatetraenal is estimated to be higher than its n,π^* singlet state on the basis of the experimental results for retinals,[3] as has been discussed in the previous paper.[1] Some polyenecarbaldehydes with longer skeletal chains than nonatetraenal, *e.g.*, dodecapentaenal, were assigned to *Group* (3), for which both the lowest singlet and triplet states of the molecule are of a π,π^* character; other, longer polyenecarbaldehydes whose lowest n,π^* triplet states are higher in energy than their lowest singlet π,π^* states were assigned to *Group* (4).

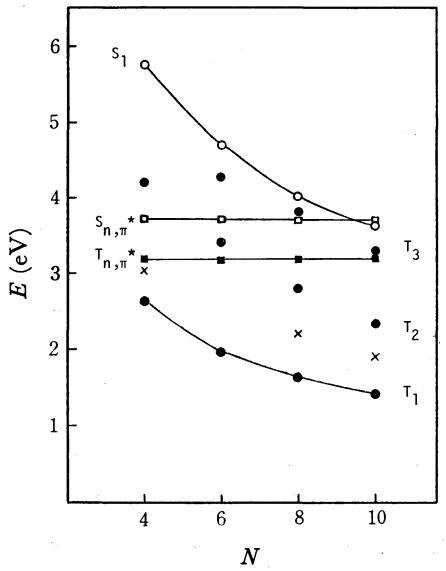

Fig. 1. Calculated lowest n,π^* and π,π^* state energies of *trans*-polyenecarbaldehydes.
N corresponds to the number of atom in the conjugated system of polyenecarbaldehyde. × corresponds to the observed value for the lowest π,π^* triplet state energy (see Ref. 1).

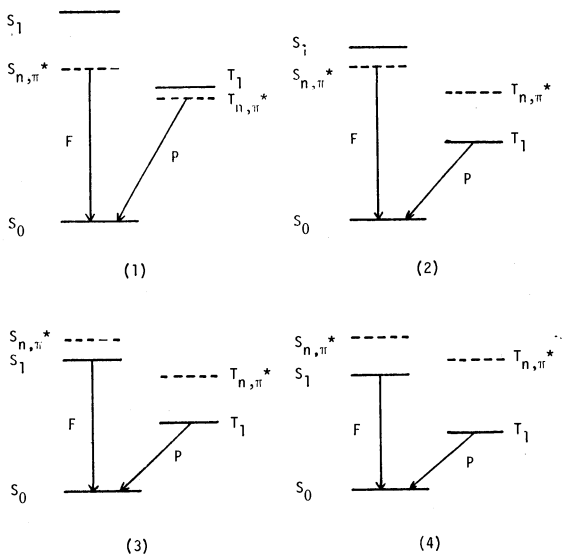

Fig. 2. Schematic energy level diagrams of polyenecarbaldehydes: (1), (2), (3), and (4) correspond to group (1), group (2), group (3), and group (4) (see text).

The general features of radiative and nonradiative properties for each case may be described as follows:

(i) *Group* (1). The observed electronic structure of the lower-lying excited states of acrolein is different in the order of T_{n,π^*} and T_1 states from the calculated

TABLE 1. CALCULATED VALUES FOR THE ABSOLUTE SQUARE OF SPIN-ORBIT COUPLING ENERGY AND CONVERSION TIME[a] BETWEEN S_{n,π^*} AND T_1, OR BETWEEN S_1 AND T_{n,π^*} OF *trans*-POLYENECARBALDEHYDES (in cm^{-2} and s)

	Acrolein	2,4-Pentadienal	2,4,6-Heptatrienal	2,4,6,8-Nonatetraenal
$\lvert\langle S_{n,\pi^*}\rvert H_{SO}\rvert T_1\rangle\rvert^2$	650	280	150	90
$\lvert\langle S_1\rvert H_{SO}\rvert T_{n,\pi^*}\rangle\rvert^2$	430	210	130	80
$\tau(S_{n,\pi^*} \rightsquigarrow T_1)$	3.4×10^{-12}	3.1×10^{-10}	1.4×10^{-9}	3.7×10^{-9}
$\tau(S_1 \rightsquigarrow T_{n,\pi^*})$	3.0×10^{-9}	2.1×10^{-10}	4.0×10^{-11}	0.7×10^{-11}

a) The conversion time was obtained by Eq. (7) in text.

results shown in Fig. 1. The lowest triplet is T_{n,π^*}, lying at 3.01 eV,[8,9] while the next triplet state is of a π,π^* character, lying at 3.05 eV.[10] As the separation between the two states is very small, the lowest n,π^* state may be mixed with the lowest triplet π,π^* state by the vibronic coupling. Excitation to the lowest S_{n,π^*} state may result in fluorescence, internal conversion to S_0, and/or intersystem crossing to the T_1 state. The experimental results[2] for acrolein showed that the fluorescence is very weak ($\Phi_F(77\text{ K})=0.007$) and of an n,π^* character; the phosphorescence is also very weak ($\Phi_P(77\text{ K})=4\times10^{-5}$).

On the other hand, it will be useful to refer to the spectra of testosterone and its derivatives, which contain conjugated systems similar to that of acrolein in their skeletal structures. Their lowest triplet states have been assigned as the π,π^* type, primarily on the basis of the lifetime of the phosphorescence and the separation of the onset of phosphorescence from the observed S_0—T_{n,π^*} excitation spectrum.[11,12] These quantum yields ranged from 0.2—0.3, but no fluorescence was reported. The fluorescences for these compounds are expected to be very weak due to the effective intersystem crossing from S_{n,π^*} to T_1 and the weak intensity of the n-π^* transition. The relationship[13] between the absorption intensity and the fluorescence lifetime of the molecule suggests that the radiative lifetime for the fluorescence with an n,π^* character may be much longer than the nonradiative lifetime for the intersystem crossing process from S_{n,π^*} to T_1 states.

The lowest triplet state of acrolein may be populated mainly *via* the $S_{n,\pi^*}\rightsquigarrow T_1\rightsquigarrow T_{n,\pi^*}$ and $S_1\rightsquigarrow T_{n,\pi^*}$, while the corresponding state of the above-mentioned keto steroid is populated *via* the $S_1\rightsquigarrow T_{n,\pi^*}\rightsquigarrow T_1$ and $S_{n,\pi^*}\rightsquigarrow T_1$ processes. With respect to the efficiency of the lowest triplet population of the two compounds, the keto steroid may have an advantage, because the radiationless lifetime for the $S_{n,\pi^*}\rightsquigarrow T_1$ process is much shorter than that for the $S_1\rightsquigarrow T_{n,\pi^*}$ process, as is shown in Table 1. The reason for the difference in the intensity of phosphorescence of the two compounds may be explained to some extent by the assumption that the following equation holds for the phosphorescence state of the two compounds:

$$[k(T_{n,\pi^*}\rightsquigarrow S_0)/k(T_{n,\pi^*}\rightarrow S_0)] \gg [k(T_1\rightsquigarrow S_0)/k(T_1\rightarrow S_0)] \quad (8)$$

Where the $k(T_i\rightsquigarrow S_0)$ and $k(T_i\longrightarrow S_0)$ notations correspond to the rate constants for the nonradiative and radiative processes respectively from the lowest triplet to the ground state.

However, the above discussion is not enough to explain the difference in the Φ_P values for the two compounds. The difference in the Φ_P may be attributed to the twisting of the carbon-carbon double bond of acrolein[2] in the π,π^* triplet state and to the stability of the cyclic structure of testosterone. Although a restricted twisting is possible in testosterone and its derivatives, the twisting will not give rise to the *cis-trans* isomerization. Also, the intersystem crossing to the ground state is expected to be less than for acrolein because of the restricted twisting. Therefore, the quantum yield of phosphorescence may be considerably larger than for acrolein.

(ii) *Group* (2). There are some higher-lying π,π^* triplet states between the S_{n,π^*} and T_1 states. Accordingly, the radiationless deactivation processes from S_{n,π^*} by spin-orbit coupling include not only $S_{n,\pi^*}\rightsquigarrow T_1$, but also the $S_{n,\pi^*}\rightsquigarrow T_i$ (i-th π,π^* triplet state)$\rightsquigarrow T_1$ process. These processes may compete with the radiative process from S_{n,π^*}. The increase in the fluorescence for *Group* (2) may not be expected. In Table 1, the spin-orbit interaction matrix elements between S_{n,π^*} and T_1 or S_1 and T_{n,π^*} decrease with an increase in the molecular size, but the energy separation between S_1 and T_{n,π^*} decreases rapidly.

The calculated lifetime for the radiationless process, $\tau(S_1\rightsquigarrow T_{n,\pi^*})$, becomes shorter and its process becomes important for the population of the lowest triplet state, T_1. The lowest triplet state for *Group* (2) is populated through the same processes for the keto steroid and the other two processes, $S_{n,\pi^*}\rightsquigarrow T_i\rightsquigarrow T_1$ and $S_1\rightsquigarrow T_{n,\pi^*}\rightsquigarrow T_i\rightsquigarrow T_1$, but the latter two processes may be less efficient than the $S_{n,\pi^*}\rightsquigarrow T_1$ process. The present discussion shows that the efficiency of the population for the lowest triplet state of *Group* (2) may be worse than that of acrolein and the keto steroid. The phosphorescence for *Group* (2) may be expected to be very weak or not emissive if we take into account the twisting effect.

(iii) *Group* (3). The fluorescence has been observed for *trans*-retinal,[3] a model compound of *Group* (3), but no phosphorescence spectrum was observed at 77 K. The calculated value for the radiationless lifetime, $\tau(S_1\rightsquigarrow T_{n,\pi^*})$, for nonatetraenal shows that the radiationless deactivation of the S_1 state becomes dominant. This result suggests that the excitation to the lowest singlet state, S_1, of *trans*-retinal may result in a rapid intersystem crossing to the T_{n,π^*} state before it fluoresces, as long as the lowest singlet state is of a π,π^* character. In a previous paper,[3] the fluorescence quantum yield of retinal was reported to be 0.71 (exciting at 440 nm at 77 K), but the value seems to be too large[14] in view of the above considerations and the comparison with the corresponding value of acrolein ($\Phi_F(77\text{ K})=0.007$). The previous calculation[3] showed that the *cis-trans* isomerization occurs in the lowest π,π^* singlet and triplet states. Its isomerization is one kind of radiationless deactivation process in the excited states. The experimental results for *trans*-retinal[3] suggest that such isomerization plays an important role in the emissibility of polyenecarbaldehyde. Therefore, the phosphorescence of *Group* (3) may be expected to be very weak or not emissive when we take the isomerization in the lowest triplet state into account.

(iv) *Group* (4). The fluorescence of *Group* (4) may become stronger than that of the other groups because of the decrease in the efficiency of the spin-orbit coupling for the $S_1\rightsquigarrow T_1$ radiationless process resulting from the same configuration, although the internal conversion, $S_1\rightsquigarrow S_0$, may increase. As the energy separation between S_1 and T_1 states decreases with an increase in the molecular size, the population of the T_1 state *via* the S_1 state may become relatively better in efficiency

as the molecular length becomes larger.

As the lowest singlet and triplet states of *Group* (4) are all of a π,π^* character, β-carotene[15] and retinyl polyenes[16] may be model compounds for *Group* (4) in lower π electronic structures. These experimental results suggest that the fluorescence of *Group* (4) is much stronger than that of the other groups. In the case of β-carotene,[15] the phosphorescence was observed at 77 K, although it was weak. The conjugated system of the β-carotene is much longer than that of *trans*-retinal. Its energy separation between the S_1 and T_1 states was about 1000—1500 cm^{-1},[15] while the corresponding theoretical value of the model compound for *trans*-retinal was about 1600 cm^{-1}.[3] The delayed emission of β-carotene has been tentatively assigned to the S–T phosphorescence due to the thermal excitation.[15] This type of emission requires a small S–T energy separation. Therefore, such emission can not be expected for the small polyenecarbaldehyde in *Group* (4). As an increase in the conjugated system makes for a small S–T energy separation, there is a possibility that the phosphorescence may be detected for the longer polyenecarbaldehyde. However, the most important factor for the observation of the emission spectra is the twisting effect in the conjugated system of polyenecarbaldehyde through all the groups.

This work was supported by a grant from the Tokyo Electrical Engineering College Research Fund. The author wishes to thank Professor R. S. Becker of the University of Houston for his kind communication regarding retinals.

References

1) K. Inuzuka and R. S. Becker, This Bulletin, **47**, 88 (1974); part I.
2) R. S. Becker, K. Inuzuka, and J. King, *J. Chem. Phys.*, **52**, 5164 (1970).
3) R. S. Becker, K. Inuzuka, J. King, and D. E. Balke, *J. Amer. Chem. Soc.*, **93**, 43 (1971).
4) V. G. Plotnikov, *Opt. Spectry.*, **22**, 401 (1967).
5) D. S. McClure, *J. Chem. Phys.*, **20**, 682 (1952).
6) M. A. El-Sayed, *ibid.*, **38**, 2834 (1963).
7) G. W. Robinson and R. P. Frosch, *ibid.*, **38**, 1187 (1963).
8) J. C. D. Brand and D. G. Williamson, *Discuss. Faraday Soc.*, **35**, 184 (1963).
9) W. H. Eberhardt and H. Renner, *J. Mol. Spectry.*, **6**, 483 (1961).
10) J. M. Hollas, *Spectrochim. Acta*, **19**, 1425 (1963).
11) G. Marsh, D. R. Kearns, und K. Schaffner, *Helv. Chim. Acta*, **51**, 1890 (1968).
12) D. R. Kearns, G. Marsh, and K. Schaffner, *J. Chem. Phys.*, **49**, 3316 (1968).
13) S. J. Strickler and R. A. Berg, *ibid.*, **37**, 814 (1962).
14) R. S. Becker, private communication.
15) R. J. Cherry, D. Chapman, and J. Langelaar, *Trans. Faraday Soc.*, **64**, 2304 (1968).
16) A. J. Thomson, *J. Chem. Phys.*, **51**, 4106 (1969).

Apparent Molal Volumes and Adiabatic Compressibilities of *n*-Alkanols and *α,ω*-Alkane Diols in Dilute Aqueous Solutions at 5, 25, and 45°C. I. Apparent Molal Volumes

Toshio NAKAJIMA, Tsuyoshi KOMATSU, and Tsurutaro NAKAGAWA

Department of Polymer Science, Faculty of Science, Hokkaido University, Sapporo 060

(Received March 15, 1974)

Density measurements have been carried out on a series of dilute aqueous solutions of *n*-alkanols and *α,ω*-alkane diols. The apparent molal volumes, ϕ_V, have been derived, and the ϕ°_V values (V°_2) at an infinite dilution have been estimated. The $\bar{V}^\circ_2$, the $\partial^2\bar{V}^\circ_2/\partial T$, and the $\partial^2\bar{V}^\circ_2/\partial T^2$ of the CH_2, the CH_3, and the CH_2OH groups were obtained from the dependence of the $\bar{V}^\circ_2$ and its temperature behavior upon the alkyl-chain length. It was found that the $\partial^2\bar{V}^\circ_2/\partial T^2$ value well reflects the structural effect.

Much attention has been devoted to the effect of the structural change in water caused by a solute on the thermodynamic properties.[1-4] On the basis of the data of the partial specific volumes, φ_v, of 15 nonelectrolytes in dilute aqueous solutions, Neal and Goring found that the $\partial^2\varphi_v^\circ/\partial T^2$ value of the hydrophobic compounds is positive, while that of the hydrophilic compounds is negative.[5] A similar discussion has been made by Hepler in relation to the pressure dependence of the partial molal heat capacity.[6] Further, Neal and Goring found that the specific expansibility, $\partial\varphi_v^\circ/\partial T$, and the concentration dependence of φ_v is closely related to the hydrophobic-hydrophilic balance in a solute.[5] This difference in the volumetric behavior between the hydrophobic and the hydrophilic compounds is considered to be related to the structural change in water caused by a solute. The purpose of the present paper is to obtain further information about the structural effect on the basis of the effect of the successive addition of the CH_2 group in the series of *n*-alkanols and *α,ω*-alkane diols on the partial molal volume and its temperature and concentration behavior.

Experimental

Materials. The *n*-alkanols from methanol to pentanol and the *α,ω*-alkane diols from 1,2-ethanediol to 1,6-hexanediol were used for the experiments. The best grade available from commercial sources (mostly guaranteed reagents) was dried over calcium sulfate and then fractionally distilled. The 1,6-hexanediol was distilled without such pretreatment. The water used was obtained by the distillation of deionized water by a quartz still and was degassed immediately before use.

Density Measurements. The densities were obtained by a float method analogous to that used by Desnoyers and Arel.[7] The float was suspended to the pan of the balance (Mettler: H20T) by a nylon thread 110 micron in diameter and was immersed in the solution in a thermostated cell. The water circulating in the cell was taken from a well-insulated bath kept at a constant temperature (±0.002 °C). The difference between the density of the solution, d, and that of the water, d_0, is obtained from weights, W and W_0, of the float in the solution and in water by means of this relation: $d-d_0=(W-W_0)/V$, where V is the volume of the float. The volume of the float is about 200 ml. The accuracy of the density measurement is within $\pm 10^{-6}$ g/ml. The density of pure water was taken from Kell's data.[8]

The solution was prepared by adding weighed amounts of a sample into a cell containing a known amount of pure water.

The apparent molal volume, ϕ_v, was obtained from the relation:

$$\phi_v = \frac{1000(d_0-d)}{mdd_0} + \frac{M}{d} \quad (1)$$

where m is the molality and M, the molecular weight of the solute.

Results

Some typical examples of the plot of ϕ_v *vs.* concentration (m) are shown in Fig. 1. The ϕ_v (m) is linearly related to m in the concentration range studied (0.01—0.2 mol/kg). The limiting partial molal volume, $\bar{V}^\circ_2$ ($=\phi^\circ_v$), is obtained from the linear extrapolation of the ϕ_v (m) to an infinite dilution. The experimental error estimated in the $\bar{V}^\circ_2$ is within 0.1 ml/mol. The values of V°_2 of *n*-butanol at 5 and 25 °C are in agreement with the values reported by Franks and Smith[9] within 0.03 ml/mol. The values of $\bar{V}^\circ_2$ and the slope of ϕ_v (m) are summarized in Table 1.

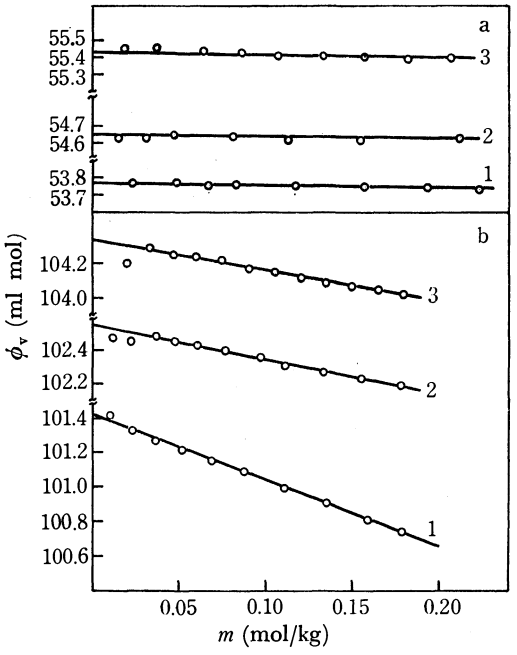

Fig. 1. Apparent molal volumes of 1,2-ethanediol (a) and *n*-pentanol (b) in water at 5 (1), 25 (2), and 45 °C (3).

TABLE 1. VALUES OF $\bar{V}_2^\circ(=\phi_v^\circ)$ AND $\partial\phi_v/\partial m$ AT 5, 25, AND 45 °C

n	$\bar{V}_2$ (mol/ml)			$-\partial\phi_v/\partial m$ (ml kg/mol²)		
	5 °C	25 °C	45 °C	5 °C	25 °C	45 °C
			$H(CH_2)_nOH$			
1	38.10	38.17	38.52	0.3	0.2	0.1
2	55.12	55.08	55.52	0.9	0.6	0.3
3	70.48	70.74	71.56	1.8	1.1	0.6
4	86.00	86.63	87.94	3.0	1.5	0.8
5	101.43	102.55	104.34	3.8	2.1	1.8
			$(CH_2)_n(OH)_2$			
2	53.77	54.65	55.43	0.1	0.1	0.1
3	71.40	71.89	72.55	0.6	0.4	0.3
4	87.81	88.36	89.18	1.2	0.8	0.4
5	103.54	104.43	105.63	1.6	1.2	0.4
6	119.16	120.39	122.05	2.8	1.5	0.7

Discussion

Partial Molal Volumes of CH_2 and CH_3 Groups. The limiting partial molal volume is expressed by the following expression:

$$\bar{V}_2^\circ = \bar{V}_{2,o}^\circ + \Delta\bar{V}_i^\circ + \Delta\bar{V}_h^\circ \qquad (2)$$

where $\Delta\bar{V}^\circ_i$ and $\Delta\bar{V}^\circ_h$ are the volume change, resulting from the iceberg formation around the hydrophobic group and the hydration by the hydrophilic group respectively, and where $\bar{V}^\circ_{2,0}$ is the partial molal volume when the iceberg formation and the hydration do not occur.

The $\bar{V}^\circ_2$ increment per CH_2 group is illustrated in Fig. 2 as a function of the chain length. The increments in the two homologs are different in their dependence upon the chain length, but they approach a common value as the chain length increases. The increment seems to become constant at $n=3$—4 in n-alkanol and at $n=5$—6 in α,ω-alkane diol. The deviation in the $\bar{V}^\circ_2$ increment per CH_2 group in a homologous series is frequently discussed in connection with the range of influence of the polar group on the structure of water.[7,10] This deviation in the V°_2 increment, however, is also observed in the case of the homologous series of n-alkanol in several nonaqueous solvents without the hydrogen-bonded structure, and the dependence of the $\bar{V}^\circ_2$ increment on the chain length partly resembles that in water.[11] In view of this fact, it is difficult to interpret this deviation only in terms of the effect of the polar group on the water structure.

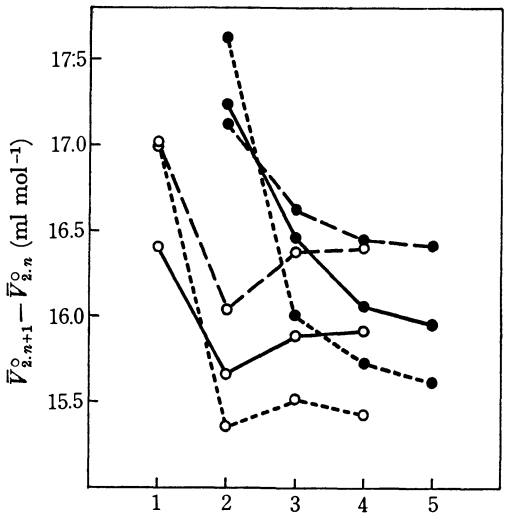

Fig. 2. The $\bar{V}^\circ_2$ increments per CH_2 group as a function of a chain length at 5 (-----), 25 (——), and 45 °C (----). ○: $H(CH_2)_n$-OH, ●: $(CH_2)_n$-$(OH)_2$.

The increment in the case of a longer chain length corresponds to the partial molal volume of the CH_2 group free from the influence of the OH groups. The values are shown in Table 2. The value of $\bar{V}^\circ_2(CH_2)$ is in good agreement with the corresponding value obtained from the homologous organic salts.[7,10]

Since, as may be seen from Fig. 2, the range of influence of the OH group is at most up to the γ-CH_2 group, the $\bar{V}^\circ_2$ values of the $(CH_2)_3OH$ group in n-butanol and in 1,6-hexanediol should be similar. Therefore, the difference between the $\bar{V}^\circ_2$ of n-butanol and a half of that of 1,6-hexanediol corresponds to the $V^\circ_2(CH_3)$ value outside the region of influence of the OH group. The $\bar{V}^\circ_2$ of the CH_2OH group in the long-chain alcohols was estimated by assuming that the $\bar{V}^\circ_2$ values of both the β- and the γ-CH_2 groups are similar to the $\bar{V}^\circ_2(CH_2)$ value free from the influence of the OH groups. The results are shown in Table 2. The $\bar{V}^\circ_2(CH_3)$ value calculated from the data[10] of $CH_3(CH_2)_3COONa$ and $(CH_2)_6(COONa)_2$ at 25 °C is 26.3 ml/mol, in good agreement with our result.

The $\bar{V}^\circ_2$ values of CH_3CH_3 and $CH_3CH_2CH_3$ calculated from the $\bar{V}^\circ_2$ values of the CH_2 and the CH_3 groups are in agreement with the experimental values of 53.3[12] and 51.2[13] for ethane and of 67.0[13] for propane at 25 °C.

Temperature Dependence of the $\bar{V}^\circ_2$. Figure 3 shows the limiting partialmolal expansibilities, $\partial\bar{V}^\circ_2/\partial T(\approx\Delta\bar{V}^\circ_2$

TABLE 2. VALUES OF $\bar{V}^\circ_2$, $\partial\bar{V}^\circ_2/\partial T$, AND $\partial^2\bar{V}^\circ_2/\partial T^2$ OF CH_3, CH_2, AND CH_2OH GROUPS

	V°_2 (ml/mol)			$\partial\bar{V}^\circ_2/\partial T\times10^2$ (ml/mol deg)		$\partial^2\bar{V}^\circ_2/T^2\times10^4$ (ml/mol deg²)
	5 °C	25 °C	45 °C	15 °C	35 °C	25 °C
CH_3	26.3	26.4	26.9	0.0_7	2.3_5	10.2
CH_2	15.5	15.9	16.4	2.1	2.4	2.2
CH_2OH[a]	$28._7$	$28._4$	$28._3$	$-1._3$	$-0._7$	1.0
$1/2(CH_2OH)_2$[b]	26.89	27.33	27.72	2.2	2.0	−1.3

a) CH_2OH group in long chain alcohols. b) CH_2OH group in 1,2-ethanediol.

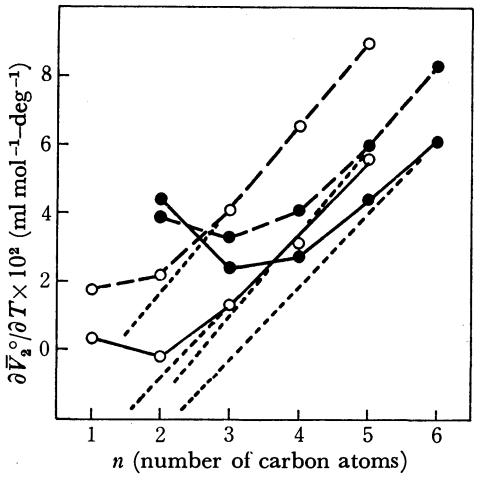

Fig. 3. Plot of the $\partial\bar{V}^{\circ}_2/\partial T$ against a chain length at 15 (——) and 35 °C (– – –), symbols as for Fig. 2.

$/\Delta T$) at 15 and 35 °C as a function of the chain length. The $\partial\bar{V}^{\circ}_2/\partial T$ values seem to fall on straight lines, with a similar slope, as the chain length increases. The $\partial\bar{V}^{\circ}_2/\partial T$ values seem to fall on straight lines when the chain length, n, is 3 for n-alkanol and 5—6 for α,ω-alkane diol. The region of the influence of the OH group on the $\partial\bar{V}^{\circ}_2/\partial T$ increment per CH_2 group seems to be up to the β- or the γ-CH_2 groups. This finding is similar to that observed in the $\bar{V}^{\circ}_2$ increment. The $\partial V^{\circ}_2/\partial T$ value of the CH_2 group free from the influence of the OH group is obtained from the slope of the straight line. By the same procedure as was used in the preceding section, the $\partial\bar{V}^{\circ}_2/\partial T$ values of the CH_3 and the CH_2OH groups were estimated. The values are shown in Table 2.

Neal and Goring found that the temperature dependence of the limiting partial specific volume, $\partial\bar{v}^{\circ}_2/\partial T$-($=\partial\bar{V}^{\circ}_2/\partial T/M$), of hydrophobic compounds is lower than that of hydrophilic compounds at low temperatures, and proposed that the $\partial\bar{v}^{\circ}_2/\partial T$ value is a useful measure of the effect of a nonelectrolyte on the water structure.[5] Figure 4 shows the plot of the $\partial\bar{v}^{\circ}_2/\partial T$ value against the chain length. It is evident from the figure that, contrary to the proposal by Neal and Goring, the $\partial\bar{v}^{\circ}_2/\partial T$ value obviously increases with the increase in the hydrophobic part of a solute. As may be seen from Column 5 in Table 2, the expansibility of the CH_2 group is markedly larger than those of the CH_3 and the CH_2OH groups. The increase in the $\partial\bar{v}^{\circ}_2/\partial T$ value with the increase in the chain length results from the large expansibility of the CH_2 group.

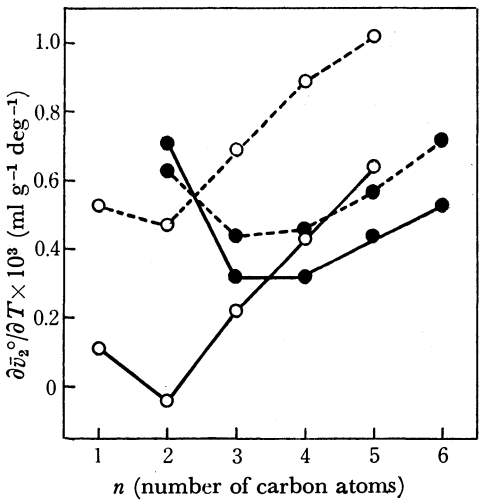

Fig. 4. Plot of the limiting specific expansibility, $\partial\bar{v}_2{}^{\circ}/\partial T^2$ against a chain length at 15 (——) and 35 °C (– – –), symbols as for Fig. 2.

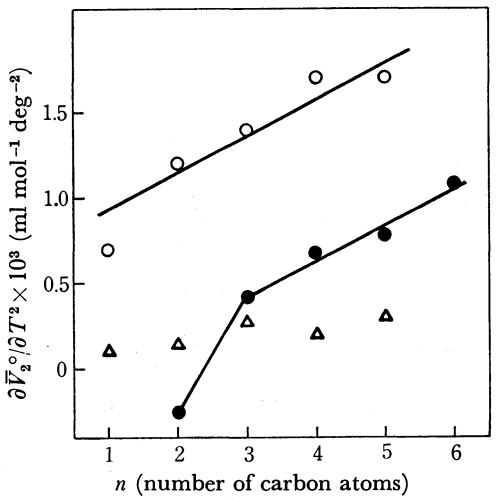

Fig. 5. Plot of the $\partial^2\bar{V}^{\circ}_2/\partial T^2$ against a chain length at 25 °C, symbols as for Fig. 2. △ corresponds to the $\partial^2\bar{V}_2/\partial T^2$ of pure alcohols calculated from the data in Ref. 14.

Figure 5 shows the plot of the $\partial^2\bar{V}^{\circ}_2/\partial T^2$ in solution and the $\partial^2\bar{V}^{\circ}_2/\partial T^2$ of pure alcohols at 25 °C against the chain length. It is noteworthy that the $\partial^2\bar{V}^{\circ}_2/\partial T^2$ of n-alkanol is remarkably high when compared with $\partial^2\bar{V}_2/\partial T^2$. From Eq. (2), $\partial^2\bar{V}^{\circ}_2/\partial T^2$ is given as:

$$\partial^2\bar{V}^{\circ}_2/\partial T^2 = \partial^2\bar{V}^{\circ}_{2,0}/\partial T^2 + \partial^2\Delta\bar{V}^{\circ}_1/\partial T^2 + \partial^2\Delta\bar{V}^{\circ}_h/\partial T^2 \quad (3)$$

Since $\partial^2\bar{V}^{\circ}_{2,0}/\partial T^2$ in Eq. (3) is free from the structural effect caused by a solute, $\bar{V}^{\circ}_{2,0}$ may be expected to be almost linearly related to the temperature; that is, $\partial^2\bar{V}^{\circ}_{2,0}/\partial T^2$ may be expected to be negligible. If this is accepted, the observed $\partial^2\bar{V}^{\circ}_2/\partial T^2$ values of hydrophobic compounds and those of hydrophilic compounds should correspond to the positive $\partial^2\Delta\bar{V}^{\circ}_2/\partial T^2$ and the

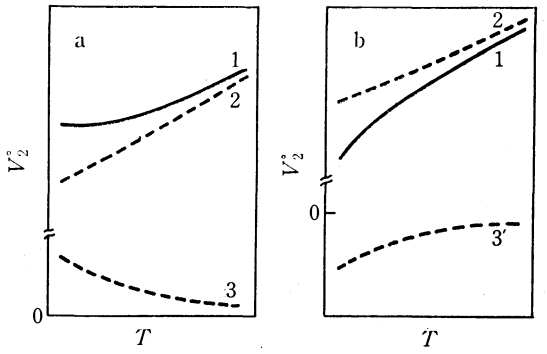

Fig. 6. Schematical figures of the temperature dependence of $\bar{V}^{\circ}_2$, $\bar{V}^{\circ}_{2,0}$, and $\Delta\bar{V}^{\circ}_1$ for hydrophobic compounds (a) and $\bar{V}^{\circ}_2$, $\bar{V}^{\circ}_{2,0}$, and $\Delta\bar{V}^{\circ}_h$ for hydrophilic compounds (b). (1): $\bar{V}^{\circ}_2$, (2): $\bar{V}^{\circ}_{2,0}$ (3): $\bar{V}^{\circ}_1$, and (3′): $\bar{V}^{\circ}_n$.

negative $\partial^2 \Delta \bar{V}^\circ_h/\partial T^2$ respectively.[5] By assuming the linear change of $\bar{V}^\circ_{2,0}$ with the temperature and the monotonous decrease in the structural effect with an increase in the temperature, the temperature dependences of $\bar{V}^\circ_2$, $\bar{V}^\circ_{2,0}$, and $\Delta \bar{V}^\circ_i$ for hydrophobic compounds and of $\bar{V}^\circ_2$, $\bar{V}^\circ_{2,0}$, and $\Delta \bar{V}^\circ_h$ for hydrophilic compounds are schematically shown in Figs. 6a and 6b respectively. It may be seen from the figure that $\Delta \bar{V}^\circ_i$ is positive and that $\Delta \bar{V}^\circ_h$ is negative.

The $\partial^2 \bar{V}^\circ_2/\partial T^2$ values lie on straight lines with the same slope except for 1,2-ethanediol. We note that the distance to the OH group does not significantly affect the $\partial^2 \bar{V}^\circ_2/\partial T^2$ increment per CH_2 group. The present results, therefore, seem to indicate that the water structure[15] around the CH_2 group is only slightly affected by the OH group. A similar result is obtained from the linear dependence of the limiting partial molal heat capacity on the chain length for the different solute series.[16]

The $\partial^2 V^\circ_2/\partial T^2$ value of the CH_2 group is obtained from the slope of the straight lines in Fig. 5. On the basis of the additivity of the $\partial^2 V^\circ_2/\partial T^2$ value for each group, the $\partial^2 V^\circ_2/\partial T^2$ values of the CH_3 and the CH_2OH groups except for 1,2-ethanediol were estimated. These values are given in Column 7 of Table 2. The positive $\partial^2 \bar{V}^\circ_2/\partial T^2$ values of the CH_2 and CH_3 groups reflect the effect of the iceberg formation around these groups.

As is shown in Fig. 5, only the $\partial^2 \bar{V}^\circ_2/\partial T^2$ value of 1,2-ethanediol deviates from the straight line and is negative. Further, Table 2 shows that the $\bar{V}^\circ_2$ and the $\partial \bar{V}^\circ_2/\partial T$ values of the CH_2OH group in 1,2-ethanediol apparently differ from those of the CH_2OH group in long-chain alcohols. These findings suggest that the effect of the adjacent OH groups in 1,2-ethanediol on the water structure differs from that of the OH groups existing relatively apart in higher diols and from those in monovalent alcohols. The negative $\partial^2 \bar{V}^\circ_2/\partial T^2$ values observed in glycerol,[5] glucose,[5] and sucrose[17] may also be attributed to the effect of the adjacent OH groups.

Excess Partial Molal Volume. The excess partial molal volume in an infinite dilution, $\bar{V}^{\circ E}_2$, is defined as:

$$\bar{V}^\circ_2 = V_2 + \bar{V}^{\circ E}_2 \tag{4}$$

where V_2 is the molal volume of a pure solute. It is known that the $V^{\circ E}_2$ value of the hydrophobic compounds is negative and that the absolute value of V°_2 increases as the hydrophobicity increases (*cf.* Fig. 7).[14,18] These facts can be interpreted by the idea that the structural change of water caused by the hydrophobic group results in a volume contraction.[14,18] However, there appear to be some questions in considering the $V^{\circ E}_2$ as a measure of the structural effect, as will be described below.[19] From the view point that the negative $V^{\circ 2}_E$ value is attributable to the iceberg formation, Franks and Smith proposed that the increase in $|V^{\circ E}_2|$ with an increase in the temperature proves the structure promotion by the hydrophobic group.[9] However, this proposal seems to be questionable in view of the conventional concept that the structural effect decreases as the temperature increases. From Eqs. (2) and (4), the $V^{\circ E}_2$ value is given by:

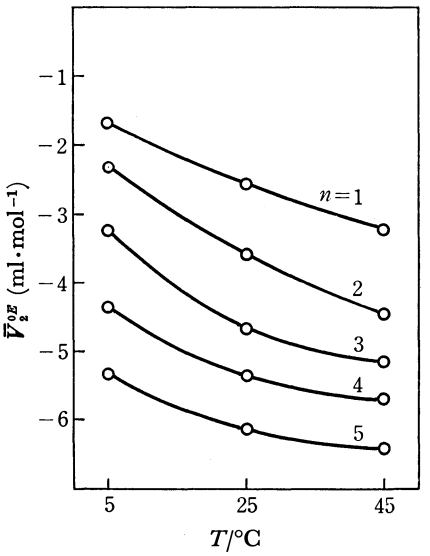

Fig. 7. Plot of the $\bar{V}^{\circ E}_2 (= \bar{V}_2 - V_2)$ of *n*-alkanols, $H(CH_2)_n$–OH, against temperature. The V_2 values were obtained from the data in Ref. 14 and 21.

$$\bar{V}^{\circ E}_2 = (\bar{V}^\circ_{2,0} - V_2) + \Delta V^\circ_i + \bar{V}^\circ_h \tag{5}$$

The $\bar{V}^{\circ E}_2$ does not directly reflect the structural effect unless the $(\bar{V}^\circ_{2,0} - V_2)$ value is negligible. In the previous section we concluded that the ΔV°_i is positive (*cf.* Fig. 6a). Therefore, the $(V^\circ_{2,0} - V_2)$ must be negative in order for $V^{\circ E}_2$ to be negative. Judging from the fact that the V°_2 decreases as the cohesive energy densities of solvents increase,[13,20] the $\bar{V}^\circ_{2,0}$ value can be expected to be small in water, a highly cohesive liquid; therefore, the $(\bar{V}^\circ_{2,0} - V_2)$ is negative. If the negative $(\bar{V}^\circ_{2,0} - V_2)$ value is accepted, the increase in $|V^{\circ E}_2|$ with an increase in the temperature (Fig. 7) can be interpreted in terms of the monotonous decrease in the positive $\Delta \bar{V}^\circ_i$.

Concentration Dependence of the ϕ_V. The slopes of $\phi_V(m)$, $\partial \phi_V/\partial m$, are shown in Table 1. The $\partial \phi_V/\partial m$ value is negative and increases numerically with an increase in the chain length and with a decrease in the temperature. Although the factor determining the slope is of a complicated nature, the above finding appears to indicate that the slope is mainly related to the effect of the hydrophobic groups on the water structure. This tendency of the slope can be interpreted in terms of the overlapping of the icebergs.[22] The contribution of the icebergs to the ϕ_V value, ΔV_i, is positive, as has been shown in the previous section. The decrease in the contribution of the $\Delta \bar{V}_i$ with the increase in the concentration due to the overlapping of the icebergs results in the decrease in the ϕ_V value.

References

1) J. L. Kavanau, "Water and Solute-Water Interaction," Holden-Day, Inc., San Francisco (1964).

2) "Hydrogen-Bonded Solvent Systems," ed. by A. K. Covington and P. J. Jones, Taylor and Francis Ltd., London (1968).

3) "Water and Aqueous Solutions," ed. by R. A. Horne,

John Willy & Sons, Inc., New York (1972).
4) "Water—a Comprehensive Treatise," Vol. 2, ed. by F. Franks, Plenum Press, New York (1973).
5) J. L. Neal and D. A. I. Goring, *J. Phys. Chem.*, **74**, 658 (1970).
6) L. G. Hepler, *Can. J. Chem.*, **47**, 4613 (1969).
7) J. E. Desnoyers and M. Arel, *ibid.*, **45**, 359 (1967).
8) G. S. Kell, *J. Chem. Eng. Data*, **12**, 66 (1967).
9) F. Franks and H. T. Smith, *Trans. Faraday Soc.*, **64**, 2962 (1968).
10) M. Sakurai, This Bulletin, **46**, 1596 (1973).
11) L. A. K. Stavely and B. Spice, *J. Chem. Soc.*, **1952**, 406.
12) E. W. Tieppel and K. E. Gubbins, *J. Phys. Chem.*, **76**, 3044 (1972).
13) W. L. Masterton, *J. Chem. Phys.*, **22**, 1830 (1954).
14) M. E. Friedman and H. A. Scheraga, *J. Phys. Chem.*, **69**, 3795 (1965).
15) H. S. Frank and M. W. Evans, *J. Chem. Phys.*, **13**, 507 (1945).
16) J. Konicek and I. Wadsö, *Acta Chem. Scand.*, **25**, 1541 (1971).
17) J. E. Garrod and T. M. Herrington, *J. Phys. Chem.*, **74**, 365 (1970).
18) F. Franks, *Ann. New York Acad. Sci.*, **125**, 277 (1965).
19) Ref. 2, p. 222.
20) E. W. Lyckman, C. A. Eckert, and J. M. Prausinitz, *Chem. Eng. Sci.*, **20**, 685 (1965).
21) G. C. Benson and H. D. Pflug, *J. Chem. Eng. Data*, **15**, 382 (1970).
22) F. Hirata and K. Arakawa, This Bulletin, **45**, 2715 (1972).

Apparent Molal Volumes and Adiabatic Compressibilities of *n*-Alkanols and *α,ω*-Alkane Diols in Dilute Aqueous Solutions at 5, 25, and 45°C. II. Apparent Molal Adiabatic Compressibilities

Toshio NAKAJIMA, Tsuyoshi KOMATSU, and Tsurutaro NAKAGAWA
Department of Polymer Science, Faculty of Science, Hokkaido University, Sapporo 060
(Received March 15, 1974)

Ultrasonic velocity measurements have been made on a series of dilute aqueous solutions of *n*-alkanols and *α,ω*-alkane diols by means of the sing-around method. The apparent molal adiabatic compressibilities, ϕ_K, have been derived, and the ϕ°_K at an infinite dilution has been estimated. The ϕ°_K values per CH_2 and CH_3 groups were estimated from the additivity of the ϕ°_K value for each group. The values are negative at low temperatures and markedly decrease with a decrease in the temperature. This fact suggests that the iceberg formation makes a negative contribution to the ϕ°_K.

Shigehara,[1] Conway and Verrall,[2] and Laliberte and Conway[3] have discussed the effect of the iceberg formation[4] (the hydrophobic hydration) around CH_2 groups on the adiabatic compressibility in terms of its dependence on the alkyl chain length of organic salts. In view of the fact that the structural effect is sensitive to the temperature, the study of the temperature dependence of the compressibility is of use in order to obtain further information concerning the structural effect. In the present paper we wish to report our findings regarding the apparent molal adiabatic compressibilities, ϕ_K, of a series of *n*-alkanols and *α,ω*-alkane diols in dilute aqueous solutions and their temperature dependence. The ϕ°_K data will be discussed in relation to the ϕ°_V data presented in the previous paper (Part I).[5]

Experimental

Materials. The same samples as were used in Part I, $H(CH_2)_nOH$ (n=1—5) and $(CH_2)_n(OH)_2$ (n=2—6), were used for the experiments.

Ultrasonic Velocity Measurements. The ultrasonic velocity measurements in solutions were made with the sing-around velocimeter developed by Greenspan and Tschieg.[6] Two quartz transducers were mounted at the ends of a glass tube. A pulse from the first transducer travels through the liquid in the time L/u, where u is the sound velocity and L is the effective path length. The pulse received by the second transducer is used to retrigger the first transducer to send another pulse, thus repeating the process. The pulse repetition frequency, f, is determined by the pulse transit time in the liquid, L/u, and the total electronic delay time, t_e, as follows:

$$\frac{1}{f} = \frac{L}{u} + t_e \qquad (1)$$

The f value was measured by using a 6-figure digital electronic counter. The constants, L and t_e, were determined from the best fittings on the sound vilocity of water[7] at various temperatures from 5 to 45 °C. The accuracy of the ultrasonic velocity measurements was within ±1 cm/s.

The solutions were prepared by adding weighed amounts of a sample into a cell containing a known amount of pure water.

The coefficient of the adiabatic compressibility, κ, was calculated from the $\kappa = 1/du^2$ relation, where d is the density and is obtained from the data in Part I. The apparent molal adiabatic compressibility of the solute, ϕ_K, is defined by the $\phi_K = -(\partial\phi_V/\partial T)_s$ relation;[8] it is calculated by means of the following formula:

$$\phi_K = \frac{1000(\kappa-\kappa_0)}{md_0} + \phi_V\kappa \qquad (2)$$

where ϕ_V is the apparent molal volume and is obtained from the data in Part I.

Results

Figure 1 shows the experimental $\phi_K(m)$ results for *n*-butanol and 1,2-ethanediol at 5, 25, and 45 °C. The $\phi_K(m)$ is linearly related to the concentration, as was observed in the case of $\phi_V(m)$ in Part I. The limiting partial molal compressibility, $\bar{K}^\circ_2(=\phi^\circ_K)$, was obtained from the linear extrapolation of the $\phi_K(m)$ to an infinite dilution. The $\bar{K}^\circ_2$ values and slopes of the $\phi_K(m)$ are summarized in Table 1.

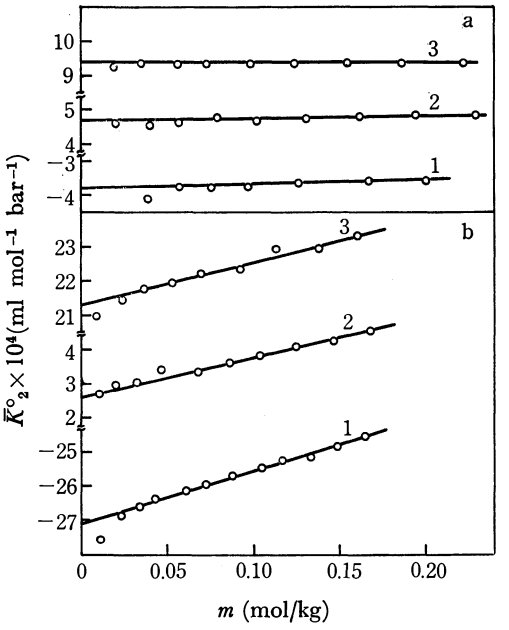

Fig. 1. Apparent molal adiabatic compressibilities of 1,2-ethanediol (a) and *n*-pentanol (b) in water at 5 (1) 25 (2), and 45 °C (3).

Table 1. Values of $\bar{K}^\circ_2$ ($=\phi^\circ_K$) and $\partial\phi_K/\partial m$ at 5, 25, and 45 °C

n	$\bar{K}^\circ_2\times10^4$ (ml/mol bar)			$\partial\phi_K/\partial m$ (ml kg/mol² bar)		
	5 °C	25 °C	45 °C	5 °C	25 °C	45 °C
			$H(CH_2)_nOH$			
1	7.3	12.6	15.9	−1.1	−0.3	−0.1
2	−0.8	10.0	16.5	−1.7	−1.0	−0.4
3	−10.8	6.3	16.9	0.3	0.7	1.0
4	−19.0	4.6	19.0	6.4	1.6	4.1
5	−27.1	2.6	21.3	15.5	11.8	12.6
			$(CH_2)_n(OH)_2$			
2	−3.8	4.7	9.4	1.1	0.7	0.0
3	−0.7	9.5	15.2	1.5	0.3	2.6
4	−5.3	9.4	17.7	1.3	0.0	−0.4
5	−12.2	8.1	19.9	7.5	2.8	1.6
6	−18.9	6.6	21.6	12.1	6.7	3.8

Discussion

Partial Molal Adiabatic Compressibilities of CH_2 and CH_3 Groups. The limiting partial molal adiabatic compressibility is expressed as follows:

$$\bar{K}^\circ_2 = \bar{K}^\circ_{2,0} + \Delta\bar{K}^\circ_i + \Delta\bar{K}^\circ_h \quad (3)$$

where $\Delta\bar{K}^\circ_i$ and $\Delta\bar{K}^\circ_h$ are the compressibility change resulting from the iceberg formation around the hydrophobic group and the hydration by the hydrophilic group respectively, and where $\bar{K}^\circ_{2,0}$ is the partial molal compressibility under the conditions when the iceberg formation and the hydration would not occur.

The $\bar{K}^\circ_2$ increment per CH_2 group is illustrated in Fig. 2 as a function of the chain length. The pattern of the behavior of the $\bar{K}^\circ_2$ increment resembles that of the $\bar{V}^\circ_2$ increment (*cf.* Fig. 2 in Part I). The $\bar{K}^\circ_2$ increments in the two series approach a similar value with the increase in the chain length. This value corresponds to the $\bar{K}^\circ_2$ value of the CH_2 group free from the influence of the OH groups. The $\bar{K}^\circ_2$ values of the CH_3 and CH_2OH groups in long-chain alcohols were estimated by the same procedure as was described in Part I. These results are shown in Table 2. The $\bar{K}^\circ_2(CH_2)$ calculated from the $\bar{K}^\circ_2$ data[2] of n-Pr_4N^+ and n-Bu_4N^+ is -2.6×10^{-4} ml/mol bar at 25 °C. This value is somewhat smaller than our result. The $\bar{K}^\circ_2(CH_2)$ obtained from the compressibility data[1] for a series of surface-active substances is -0.6×10^{-4} ml/mol bar at 30 °C. This value is in agreement with the value estimated from our results at 25 and 45 °C.

It should be noted that the $\bar{K}^\circ_2(CH_2)$ and the $\bar{K}^\circ_2(CH_3)$ values are negative at low temperatures and markedly decrease with a decrease in the temperature. As it is clear that the $\bar{K}^\circ_{2,0}$ value is always positive, the negative value of $\bar{K}^\circ_2$ can be attributed to the negative $\Delta\bar{K}^\circ_i$ value. This suggests that the iceberg is less compressible than bulk water.[2]

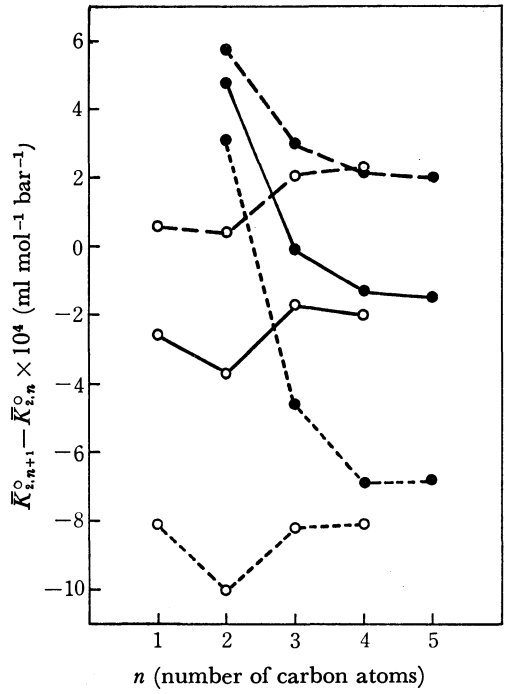

Fig. 2. The $\bar{K}^\circ_2$ increments per CH_2 group as a function of a chain length at 5 (------), 25 (——), and 45 °C (——).
○: $H(CH_2)_nOH$, ●: $(CH_2)_n(OH)_2$.

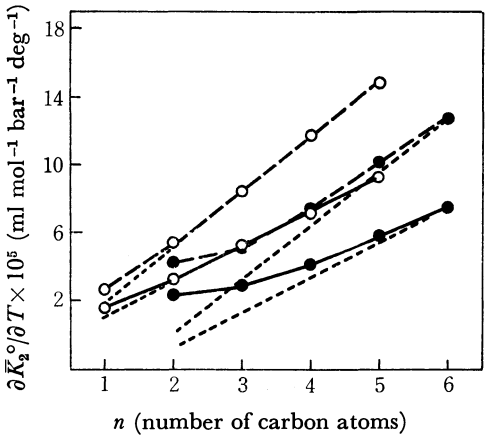

Fig. 3. Plot of the $\partial\bar{K}^\circ_2/\partial T$ against a chain length at 15 (——) and 35 °C (——), symbols as for Fig. 2.

Temperature Dependence of the $\bar{K}^\circ_2$. Figure 3 shows the plot of the $\partial\bar{K}^\circ_2/\partial T(\approx\Delta\bar{K}^\circ_2/\Delta T)$ values at 15 and 35 °C against a chain length. The $\partial\bar{K}^\circ_2/\partial T$ values in both series approach straight lines with the same slope with an increase in the chain length. The pattern of the deviation from the straight lines resembles that of

Table 2. Values of $\bar{K}^\circ_2$, $\partial\bar{K}^\circ_2/\partial T$, and $\partial^2\bar{K}^\circ_2/\partial T^2$ of CH_3, CH_2, and CH_2OH groups

	$\bar{K}^\circ_2\times10_4$ (ml/mol bar)			$\partial\bar{K}^\circ_2/\partial T\times10^5$ (ml/mol bar deg)		$\partial^2\bar{K}^\circ_2/\partial T^2\times10^7$ (ml/mol bar deg²)
	5 °C	25 °C	45 °C	15 °C	35 °C	25 °C
CH_3	-9.5_5	1.3	8.0_5	5.5	3.0	−8.0
CH_2	−8.0	1.8	2.1	3.2	2.1	−5.4
CH_2OH[a]	$6._5$	$6._8$	$6._7$	$-0._2$	$-0._7$	−2.4
$1/2(CH_2OH)_2$[b]	−1.9	2.4	4.7	2.13	1.16	−4.6

a) CH_2OH group in long chain alcohols. b) CH_2OH group in 1,2-ethanediol.

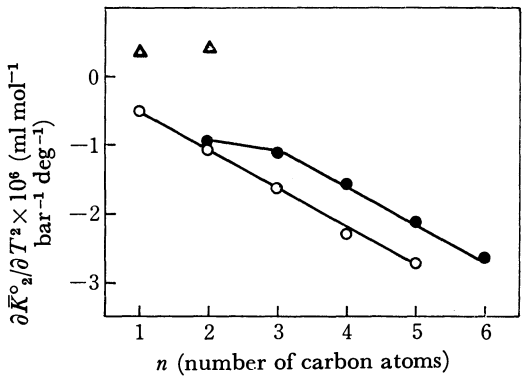

Fig. 4. Plot of the $\partial^2\bar{K}^\circ_2/\partial T^2$ against a chain length at 25 °C, symbols as for Fig. 2. △ corresponds to the $\partial^2 K_2/\partial T^2$ of pure alcohols calculated from the data in Ref. 9, where K_2 is $-(\partial V_2/\partial P)_s$.

$\partial\bar{V}^\circ_2/\partial T$ in Part I. The slope of the straight lines corresponds to the $\partial\bar{K}^\circ_2/\partial T$ value of the CH_2 group outside the region of influence of the OH group. The $\partial\bar{K}^\circ_2/\partial T$ values of the CH_3 and CH_2OH groups in long-chain alcohols were estimated as before. These results are given in Table 2.

Figure 4 shows the $\partial^2\bar{K}^\circ_2/\partial T^2$ value and the $\partial^2 K_2/\partial T^2$ value at 25 °C, where K_2 is $-(\partial V_2/\partial P)_s$, as a function of the chain length. It is noteworthy that the $\partial^2\bar{K}^\circ_2/\partial T^2$ has a large negative value in contrast with the slightly positive value of the $\partial^2\bar{K}_2/\partial T^2$ of pure alcohols From Eq. (3), $\partial^2\bar{K}^\circ_2/\partial T^2$ is given as:

$$\partial^2\bar{K}^\circ_2/\partial T^2 = \partial\bar{K}^\circ_{2,0}/\partial T^2 + \partial^2\Delta K^\circ_i/\partial T^2 + \partial^2\Delta\bar{K}^\circ_h/\partial T^2 \quad (4)$$

Since $\partial^2\bar{K}^\circ_{2,0}/\partial T^2$ in Eq. (4) is free from the structural effect, it can be expected that the $\bar{K}^\circ_{2,0}$ almost linearly relates with the temperature; that is, $\partial^2\bar{K}^\circ_{2,0}/\partial T^2$ is negligible. Therefore, the negative values of $\partial^2\bar{K}^\circ_2/\partial T^2$ shown in Fig. 4 result from the negative values of $\partial^2\Delta\bar{K}^\circ_i/\partial T^2$ and $\partial^2\Delta\bar{K}^\circ_h/\partial T^2$. By assuming a monotonous decrease in the structural effect with an increase in the temperature, the temperature dependences of ΔK°_i and ΔK°_h are schematically shown in Fig. 5. As may be seen from the figure, the negative values of the K°_2 at low temperatures are related to the large negative values of $\partial^2\Delta\bar{K}^\circ_i/\partial T^2$ and $\partial^2\Delta\bar{K}^\circ_h/\partial T^2$.

The $\partial^2\bar{K}^\circ_2/\partial T^2$ values in both series lie on the straight lines with the same slope except for 1,2-ethanediol

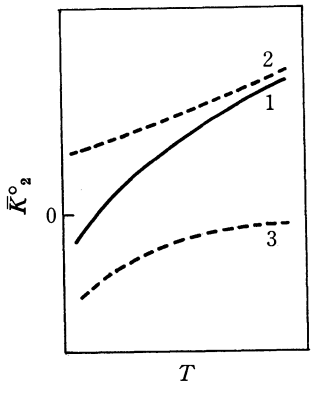

Fig. 5. Schematical figure of the relation between the temperature dependence of K°_2 and $\Delta\bar{K}^\circ_i$(or $\Delta\bar{K}^\circ_h$). (1): $\bar{K}^\circ_2$, (2): $\bar{K}^\circ_{2,0}$, (3): $\Delta\bar{K}^\circ_i$ or $\Delta\bar{K}^\circ_h$.

(Fig. 4). The $\partial^2\bar{K}^\circ_2/\partial T^2$ of the CH_2 group is evaluated from the slope of the straight lines. The $\partial^2\bar{K}^\circ_2/\partial T^2$ values of the CH_3 and the CH_2OH groups except for 1,2-ethanediol are estimated on the basis of the additivity of the $\partial^2\bar{K}^\circ_2/\partial T^2$ value for each group. The values are given in Table 2.

Only 1,2-ethanediol deviates from the straight line, as is shown in Fig. 4; the $\bar{K}^\circ_2$ and the $\partial\bar{K}^\circ_2/\partial T$ of the CH_2OH group in 1,2-ethanediol apparently differ from those of the CH_2OH group in long-chain alcohols, as has been shown in the cases of the $\bar{V}^\circ_2$ and the $\partial\bar{V}^\circ_2/\partial T$ (*cf.* Table 2 in Part I). These results suggest that the effect of the adjacent OH groups in 1,2-ethanediol on the water structure differs from that of the OH groups existing relatively apart in higher diols and those in monovalent alcohols.

Concentration Dependence of the ϕ_K. The slopes of $\phi_K(m)$, $\partial\phi_K/\partial m$, are shown in Table 1. The dependences of the slope upon the temperature and the chain length are not as clear as those for $\phi_v(m)$ presented in Part I, but it appears that the slopes are positive and increase with an increase in the chain length and with a decrease in the temperature, in contrast to the case of the slope of the $\phi_v(m)$. This tendency, as in the explanation of the slope of the $\phi_v(m)$ proposed in Part I, can be interpreted in terms of the overlapping of the icebergs.[10] The value of ΔK°_i resulting from the iceberg formation is negative, as was shown in the previous section. The contribution of the $\Delta\bar{K}^\circ_i$ to the ϕ_K becomes less negative with an increase in the concentration due to the overlapping of the icebergs; this results in the increase in the ϕ_K value.

The authors wish to thank professor Kiyoshi Arakawa, Dr. Nobuo Takenaka, and Dr. Masao Sakurai for their helpful advice. The present work has been supported in part by a Grant for Scientific Research from the Ministry of Education.

References

1) K. Shigehara, This Bulletin, **39**, 2643 (1966).
2) B. E. Conway and R. E. Verrall, *J. Phys. Chem.*, **70**, 3952 (1966).
3) L. H. Laliberté and B. E. Conway, *ibid.*, **74**, 4116 (1970).
4) H. S. Frank and M. W. Evans, *J. Chem. Phys.*, **13**, 507 (1945).
5) T. Nakajima, T. Komatsu, and T. Nakagawa, This Bulletin, **48**, 783 (1975).
6) M. Greenspan and C. E. Tschiegg, *Rev. Sci. Instr.*, **28**, 897 (1957).
7) M. Greenspan and C. E. Tschiegg, *J. Research Natl. Bur. Standards*, **59**, 249 (1957).
8) H. S. Harned and B. B. Owen, "The Physical Chemistry of Electrolytic Solutions," 3rd Edition, New York, N. Y. (1958), p. 375.
9) E. B. Freyer, J. C. Hubbard, and D. H. Andrew, *J. Amer. Chem. Soc.*, **51**, 759 (1929).
10) F. Hirata and K. Arakawa, This Bulletin, **45**, 2715 (1972).

Magnetic Susceptibility of the Solid Oxygen-Fluorine Mixture

Akira SAKAKIBARA,* Yoshihiro MORI,** and Hiroo INOKUCHI
The Institute for Solid State Physics, The University of Tokyo, Roppongi, Minato-ku, Tokyo 106
(Received June 13, 1974)

The magnetic susceptibility of an oxygen–fluorine solid mixture with a 20—75% oxygen content was measured from 12 K to each melting point. The small susceptibility found below 45 K with a 20—60% oxygen content is interpreted in terms of direct- and super-exchange interaction. The supercooling of the cubic phase is suggested in the case of a 75% oxygen content.

Oxygen and fluorine are neighbouring elements of the second row of the Periodic Table, and their molecular sizes and shapes resemble one another: at the 0.002 a.u. contour of the total molecular-charge density, which includes over 95% of the molecular charge, the O_2 molecule is 4.18 Å long and 3.18 Å wide, while the F_2 molecule is 4.18 Å long and 2.86 Å wide.[1] Besides, the packings of the molecules in the solid phase resemble one another: solid oxygen occurs in three phases, α, β, and γ,*** of which the crystal structures are monoclinic (C2/m),[2] rhombohedral ($R\bar{3}m$)[3] and cubic (Pm3n)[4] respectively. On the other hand, the crystal structures of α- and β-fluorine**** are monoclinic (C2/m)[5] and cubic (Pm3n),[6] strikingly similar to those of the α- and γ-solid oxygen. Because of these similarities, we can expect that oxygen and fluorine molecules mix well to form solid solution.

Concerning the physical properties of these solid phases, previous workers[7] have established that antiferromagnetic spin ordering exists in the α-phase, while in the β- and γ-phases the ordering is limited to a short range. As for the magnetic properties of the O_2–Ar solid solution system, Blocker *et al.* have investigated lower concentrations of oxygen molecules in an attempt to determine the exchange interaction between oxygen molecules:[8] argon molecules serve to dilute the oxygen concentration and intercept the magnetic interaction among the oxygen molecules. When there is a higher concentration of O_2 in the O_2–Ar system, however, we have found from our magnetic susceptibility measurements that argon molecules directly affect the antiferromagnetism and also the crystal transformation of the solid oxygen.[9] Therefore, it seemed that it would be interesting to study the magnetic properties of solid solution of oxygen and another molecule such as fluorine, which more strongly interacts with oxygen.

In this paper, the results of the magnetic susceptibilities of oxygen–fluorine mixtures will be presented and discussed in terms of the exchange interaction.

Experimental

The magnetic susceptibility measurements were carried out from 12 K to each melting point of the oxygen–fluorine mixture by the Faraday method, as has previously been described.[10] The magnetic field was set at about 9×10^3 Oe throughout the measurements. The $H(\partial H/\partial x)$ value was calibrated by measuring the susceptibility of sucrose, the mass susceptibility of which was taken to be -0.566×10^{-6} emu/g.

A gaseous mixture of oxygen and fluorine in various ratios, but containing 2—8 mg of oxygen, was thoroughly condensed into a small quartz tube cooled at the temperature of liquid helium, after which the tube was quickly sealed off with an oxyhydrogen flame.

Because of the reactivity of fluorine, especially with even a trace of water, the preparation process was carried out carefully as follows. Each of the oxygen and fluorine gases (commercially obtained) was passed through a liquid-nitrogen trap. Quartz tubes were at first baked for 3 hr at 1050 °C and then treated for a further 12 hr at 500 °C in a vacuum before introducing the sample into the tubes. The tubes and valves for the preparation system, composed of monel metal were also baked at 200 °C. The quartz tube was joined to the monel metal with coval metal, not with a seal using O rings, with attention paid to the resistivity to the heat treatment. The quartz-tube ampoules containing the O_2–F_2 mixture were placed in liquid nitrogen. In spite of the use of such a careful method for preparation and storage, however, the inner wall of the quartz ampoule containing the mixture was partially corroded; therefore, the final molar ratio of oxygen and fluorine is estimated to be larger by at least a few percent.

This quartz ampoule (5 mm in diameter and about 100 mm in length) was suspended by a Pyrex glass string from the arm of a vacuum balance, a Sartorius Electrono Microbalance, and cooled down to about 50 K; warming and cooling were then repeated around the melting point. After this, it was cooled down to 12 K in less than ten minutes. The temperature was measured with an Au: Co–Cu thermocouple placed below the ampoule and calibrated by the phase-transition points of pure oxygen and also by measuring the susceptibilities of the paramagnetic Tutton's salts, $(Fe(NH_4)_2(SO_4)_2\cdot6H_2O)$ and $(Mn(NH_4)_2(SO_4)_2\cdot6H_2O)$. Measurements of the temperature dependence of the magnetic susceptibility were started about three hours later, at a time when the temperature of the sample rose naturally after the evaporation of the liquid helium. The susceptibility was corrected for the diamagnetism of the quartz ampoule, but not for that of the sample itself, which would be negligible in this case.

Results and Discussion

Figures 1—3 show the temperature dependence of the magnetic susceptibilities of the oxygen–fluorine mixture (O_2–F_2). In case of a mixing O_2–F_2 ratio of

* School of Engineering, Okayama University, Okayama 700.
** Faculty of Pharmaceutical Sciences, Toyama University, Gofuku, Toyama 930.
*** α: below 23.88 K, β: 23.88—43.76 K, and γ: 43.76—54.39 K.
**** α: below 45.6 K and β: 45.6—53.5 K.

50: 50 or 60: 40 in Fig. 1, there exists only one phase transition, at 45 K; no transition was found around 24 K, corresponding to the α-β phase transition temperature in pure solid oxygen and also in the 95% O_2–5% Ar mixture.[9] This finding indicates that the solid phases of oxygen and fluorine are not segregated from each other, but that solid solutions are preferably formed below 45 K.

The rapid increase in the susceptibility toward the low-temperature region is due to the free spins of the oxygen molecules isolated in the fluorine matrices. The ratio of the oxygen molecules contributing to this paramagnetism is at most a small percentage at those contents.

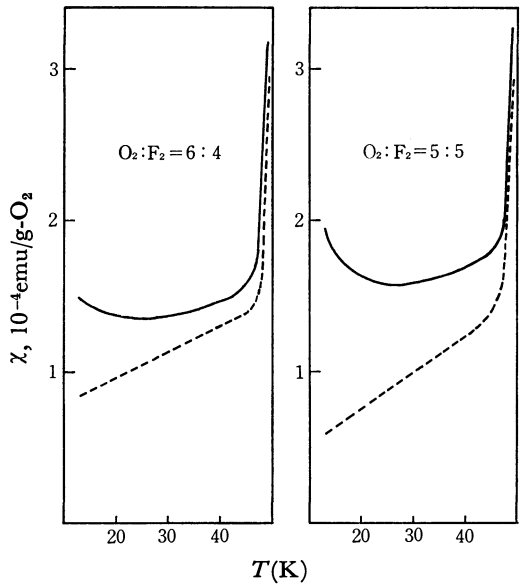

Fig. 1. Magnetic susceptibility for O_2: F_2=60: 40 and 50: 50 mixture as a function of temperature.
——: Measured susceptibility
----: Susceptibility removed of Curie's paramagnetism.

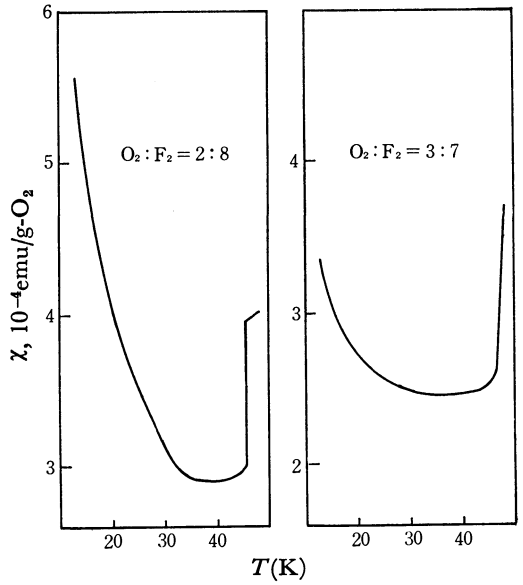

Fig. 2. Magnetic susceptibility for O_2: F_2=20: 80 and 30: 70 mixture as a function of temperature.
——: Measured susceptibility.

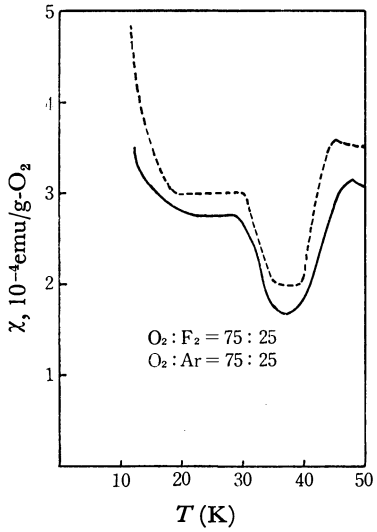

Fig. 3. Magnetic susceptibility for O_2: F_2=75: 25 compared with O_2: Ar=75: 25 mixture as a function of temperature.
——: O_2–F_2, ----: O_2–Ar

The dotted lines in Fig. 1 show the susceptibilities, with their paramagnetism removed by 4% for the 50: 50 mixture and 2% for the 60: 40 mixture according to Curie's law. The exact contribution of this paramagnetic oxygen could not be determined. There appears, then, a monotonously decreasing susceptibility below 45 K (dotted lines in Fig. 1). This temperature dependence of the magnetic susceptibility suggests that there exists a strong antiferromagnetic interaction in these solids, as in the α-phase of pure oxygen. A possible model for this antiferromagnetism of the O_2: F_2=50: 50 solid solution is presented below.

No experimental data for the crystal structure of the O_2–F_2 mixture in the solid phase have been reported. However, considering that the lowest-temperature phases, monoclinic, of both oxygen and fluorine and the molecules resemble each other in shape and size, as has been mentioned above, the crystal structure of the O_2–F_2 solid solution below 45 K can be expected

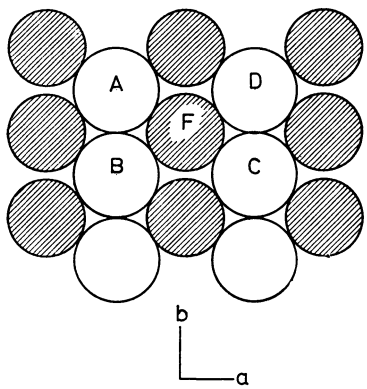

Fig. 4. A possible model for the molecular packing of O_2 and F_2. The contour is at the 0.002 a.u. of the total molecular charge density, which includes over 95% of the total charge. The lattice parameter, a or b, in the model is taken to be an average of that for α-oxygen and α-fluorine. Shadowed are fluorine molecules and non-shadowed are oxygen.

to be monoclinic. In Fig. 4, one of the possible models for the arrangement of oxygen and fluorine molecules in the ab plane is presented. The molecular packing of this arrangement can be predicted to be a nearly closed-packed one judging from that of the α-phase of oxygen and fluorine, and also from the molecular size. Because the fluorine molecule is narrower in width than the oxygen molecule, the distance between A and B may decrease in comparison with that of the same pairs in pure oxygen, 3.43 Å. Then the orbital overlap between them will so increase that the spin of the A oxygen strongly interacts with that of B antiferromagnetically. This direct antiferromagnetic exchange interaction is the most important factor.

The direct-exchange interaction between A and C or A and D can be neglected because of the long distance between them. However, the spin of the A oxygen may indirectly interact with that of the C oxygen through the F fluorine, as there may be a large overlap between the orbitals of A and F and between those of C and F, as is to be expected from their molecular packing shown in Fig. 4. This indirect interaction can be understood in terms of the super-exchange interaction, which has proceeded in some antiferromagnetic ionic compounds. That is, the electron of the $1\pi_g$ orbital of the A oxygen molecule interacts with that of the $1\pi_g$ of the C oxygen molecule, including the electron transfer from fluorine to oxygen. Then the spins of A and C are ordered in antiparallel fashion. The same interaction through F also occurs between A and D. In this case, the spin of A may be ordered parallel to that of D, because the two $1\pi_g$ orbitals of the F fluorine which interact with A and D are orthogonal.

In the ($\bar{2}01$) plane of the monoclinic lattice also, the molecular packing may be nearly closed, as in α-oxygen, in which case exchange interaction will occur directly or indirectly *via* a fluorine molecule.

As a matter of fact, it is still questionable whether or not an ordered distribution of O_2 and F_2 occurs, but in any case, including a randomly distributed model, the antiferromagnetic ordering in this solid solution would be realized by the direct- and also the super-exchange mechanism described above.

The magnetic susceptibilities of the O_2: F_2=20: 80 and 30: 70 mixtures at low temperatures are rather large in comparison with that of the 50: 50 mixture, but the decrease in the susceptibility around 45 K, though a little smaller, was also observed in these mixtures with lower oxygen contents. On the other hand, the susceptibilities of O_2–Ar mixtures of the same ratio do not decrease around 45 K and show a Curie-Weiss paramagnetism in this temperature region.[8] Therefore, in this case of O_2–F_2, oxygen molecules may not be distributed more thinly in one region and may be more concentrated in the other region.

For the case of O_2: F_2=75: 25, the temperature dependence of the susceptibility is very similar to that for O_2–Ar of the same ratio, O_2: Ar=75: 25. The large susceptibility at lower temperature, and the transition at about 27 K are characteristic. For the case of O_2–Ar, there appears a novel phase below 27 K, the crystal structure of which is cubic and very similar to that of the γ-phase.[11] This novel phase can be observed even at a composition and temperature where the monoclinic phase is stable when a rapid cooling quenches the structure of a higher temperature.[9,11] For the case of O_2–F_2 also, supercooling occurs from around 50 K and the cubic lattice is quenched to the lowest temperature.

The authors are much indebted to Drs. G. Fujisawa, M. Iwasaki, and S. Tsujimura of the Tokai Research Establishment, Japan Atomic Energy Research Institute, for preparing the sample and to T. Takeda for his skillful glass work. We are also grateful to Dr. H. Kawamura for helping us to prepare the apparatus.

References

1) R. F. W. Bader, W. H. Henneker, and P. E. Cade, *J. Chem. Phys.*, **46**, 3341 (1967).
2) C. S. Barrett, L. Meyer, and J. Wasserman, *ibid.*, **47**, 592 (1967).
3) E. M. Hörl, *Acta Crystallogr.*, **15**, 845 (1962).
4) T. H. Jordan, W. E. Streib, H. W. Smith, and W. N. Lipscomb, *ibid.*, **17**, 777 (1964).
5) T. H. Jordan, W. E. Streib, and W. N. Lipscomb, *J. Chem. Phys.*, **41**, 760 (1964).
6) L. Meyer, C. S. Barrett, and S. C. Greer, *ibid.*, **49**, 1902 (1968).
7) M. F. Collins, *Proc. Phys. Soc.*, **89**, 415 (1966).
8) T. G. Blocker, C. L. Simmons, and F. G. West, *J. Appl. Phys.*, **40**, 1154 (1969).
9) Y. Mori, A. Sakakibara, and H. Inokuchi, This Bulletin, **46**, 2305 (1973).
10) N. Ohigashi and H. Inokuchi, *ibid.*, **42**, 1212 (1969).
11) C. S. Barrett, L. Meyer, and J. Wasserman, *J. Chem. Phys.*, **44**, 998 (1966).

Ion-Molecule Reactions in Carbonyl Sulfide-Hydrocarbon Mixtures

Akira MATSUMOTO, Satoshi OKADA,* Toshiyuki MISAKI,
Setsuo TANIGUCHI,* and Teruo HAYAKAWA
Department of Chemistry, Faculty of Liberal Aarts and Sciences, University of Osaka Prefecture, Sakai, Osaka 593
**Radiation Center of Osaka Prefecture, Sakai, Osaka 593*

(Received July 15, 1974)

Thermal energy ion-molecule reactions in carbonyl sulfide–hydrocarbon (methane, acetylene and propylene) mixtures were studied using a mass spectrometer equipped with a pulsed ion source. The rate constants for sulfur atom transfer, sulfur ion transfer and sulfur ion addition reactions were measured.

Several papers have been published on ion-molecule reactions in mixtures of hydrocarbons and sulfur-containing compounds.[1-4] However, reactions leading to RHS^+ (RH represents saturated or unsaturated hydrocarbons) have not yet been reported with the exception of ethane studied by Dzidic *et al.*[2] They reported that RHS^+ is produced in a mixture of ethane and carbonyl sulfide exclusively *via* S^+ transfer from COS^+ to ethane, but is not produced in a mixture of methane or ethylene and carbonyl sulfide.

In the present work, further study of the reactions leading to RHS^+ and RS^+ in mixtures of hydrocarbons such as methane, acetylene and propylene and carbonyl sulfide has been carried out using a mass spectrometer equipped with a pulsed ion source. The rate constants of the reactions have been determined.

Experimental

The operating characteristics of a pulsed ion source used in conjunction with a magnetic deflection instrument have been described previously;[5,6] only a brief description need be given here. Primary reactant ions were produced by an electron pulse of 0.2 μs duration and 10—16.3 V amplitude. Ions were extracted for mass analysis by applying a positive pulse of 1 μs duration and 10 V amplitude to the repeller plates. Primary and secondary ion currents were recorded as a function of the delay time between the ionizing pulse and the ion removal pulse. A repetition rate of 100 kHz was used.

In order to avoid the production of the excited ion $S^+(^2D^0)$, measurements were carried out at the electron energies below 16.7 eV (the appearance potential of $S^+(^2D^0)$ from COS).[7]

COS purchased from Matheson was purified by distillation under reduced pressure: analysis showed it to be more than 99.0% pure. H_2S and CS_2 were detected as minor impurities. All other gases were Takachiho high purity grade (99.9%) and were used without further purification.

The rate constants of ion-molecule reactions studied were calibrated with reference to the reported rate constant, $k=1.22\times10^{-9}$ cm^3 mol^{-1} s^{-1}, for the hydrogen transfer reaction $CH_4^+ + CH_4 \longrightarrow CH_5^+ + CH_3$.[8]

Results and Discussion

CH_4–COS System. The ion-molecule reactions for the formation of CH_4S^+ and CH_3S^+ ions in a CH_4–COS mixture were studied at total pressures up to 10^{-4} Torr in the ion source. At electron energies between 10 and 15 eV, the significant primary ions were COS^+, CH_4^+, CH_3^+, and S^+ in the ground state ($^4S^0$).

The ion-molecule reactions forming CH_4S^+ and CH_3S^+ can be discribed by the scheme

$$CH_4 + COS^+ \longrightarrow CH_4S^+ + CO \quad (1)$$
$$CH_4^+ + COS \longrightarrow CH_4S^+ + CO \quad (2)$$
$$CH_4 + S^+ \longrightarrow CH_4S^+ \quad (3)$$
$$CH_4 + COS^+ \longrightarrow CH_3S^+ + HCO \quad (4)$$
$$CH_4^+ + COS \longrightarrow CH_3S^+ + HCO \quad (5)$$
$$CH_3^+ + COS \longrightarrow CH_3S^+ + CO \quad (6)$$
$$CH_4 + S^+ \longrightarrow CH_3S^+ + H \quad (7)$$

The ion intensities of secondary ion CH_4S^+ (m/e=48) and CH_3S^+ (m/e=47) may be written:

$$I_{48} = (k_1 I_{60}[CH_4] + k_2 I_{16}[COS] + k_3 I_{32}[CH_4])t + C_1 \quad (I)$$

$$I_{47} = (k_4 I_{60}[CH_4] + k_5 I_{16}[COS] + k_6 I_{15}[COS] + k_7 I_{32}[CH_4])t + C_2 \quad (II)$$

where I_M is the intensity of ion (m/e=M), k_i the rate constant of the i-th reaction, t the reaction time, and C_1 and C_2 are constants.

In the formation of CH_4S^+, Reactions 1, 2, and 3 may be selected by choosing an appropriate electron energy. However, at lower electron energies (<15.1 eV) where only COS^+ and CH_4^+ are formed as significant primary ions, the amount of the secondary ion, CH_4S^+, formed was too small to determine the rate

TABLE 1. TOTAL RATE CONSTANTS UNDER VARIOUS CONDITIONS IN THE CH_4–COS SYSTEM

Run	Electron energy (eV)	Pressure in reservoir (Torr)		I_{16}/I_{32}	I_{60}/I_{32}	Total rate constant*
		CH_4	COS			
1	15.8	83.08	53.05	4.22	15.1	7.53×10^{-11}
2	16.0	83.08	53.05	4.33	13.7	6.08×10^{-11}
3	14.4	74.55	55.03	10.55	67.1	11.89×10^{-11}
4	15.1	74.55	55.03	6.23	27.1	8.41×10^{-11}
5	14.7	76.66	51.25	10.56	66.4	12.64×10^{-11}
6	15.4	76.66	51.25	7.93	34.5	7.25×10^{-11}
7	15.1	81.57	49.63	8.90	38.6	9.43×10^{-11}
8	15.8	81.57	49.63	5.89	19.9	8.16×10^{-11}
9	15.8	85.76	64.88	4.16	19.4	8.08×10^{-11}
10	16.0	85.76	64.88	4.41	18.1	7.06×10^{-11}
11	14.7	86.50	68.29	7.78	62.5	10.52×10^{-11}
12	15.4	86.50	68.29	6.26	32.2	7.57×10^{-11}

*Total rate constants are expressed by $(k_1 I_{60}/I_{32} + k_2 I_{16}[COS]/I_{32}[CH_4] + k_3)$ in cm^3 mol^{-1}s^{-1}.

constants k_1 and k_2 with sufficient accuracy. Therefore, the experiments were performed in the higher energy region (<16.7 eV) where Reactions 1, 2, and 3 occur simultaneously. From the results of Table 1 obtained under various conditions using least-squares means, the rate constants for Reactions 1, 2, and 3 were calculated to be $(3.8\pm0.1)\times10^{-13}$, $(6.0\pm0.1)\times10^{-12}$, and $(4.42\pm0.02)\times10^{-11}$ cm^3 mol^{-1} s^{-1}, respectively. The rate constant for S atom transfer from COS, k_2, is about 15 times that for S^+ ion transfer from COS^+, k_1. The rate constant for S^+ ion addition reaction, k_3, is about 7 times as large as k_2. It should be pointed that the formation of CH_4S^+, which was not observed by Dzidic *et al.*, has been confirmed. Furthermore, in the formation of RHS^+, S transfer from COS to RH^+ is faster process than S^+ transfer from COS^+ to RH in the CH_4–COS mixture. On the other hand, Dzidic *et al.* concluded that S^+ transfer from COS^+ to RH occurs exclusively in C_2H_6–COS mixture.

In the lower electron energy region (<14.25 eV, A.P. of CH_3^+ from CH_4), CH_3S^+ is produced by Reactions 4 and 5. Using Eq. (II), the rate constants k_4 and k_5 were determined to be $k_4=3.0\times10^{-12}$ and $k_5=1.6\times10^{-11}$ cm^3 mol^{-1} s^{-1}, respectively. However, in the high electron energy region (14.25<E<16.7 eV), Reactions 6 and 7 as well as 4 and 5 take place. The rate constants k_6 and k_7 were determined by substituting in Eq. (II) the above values for k_4 and k_5. Figure 1 shows a plot of $k_6+k_7I_{15}[COS]/I_{32}[CH_4]$ *vs.* $I_{15}[COS]/I_{32}[CH_4]$: the intercept and the slope correspond to $k_6=5.9\times10^{-10}$ and $k_7=9.5\times10^{-10}$ cm^3 mol^{-1} s^{-1}. The rate constant k_6 obtained here is in good agreement with the 5.0×10^{-10} cm^3 mol^{-1} s^{-1} reported by Dzidic and co-workers.[2]

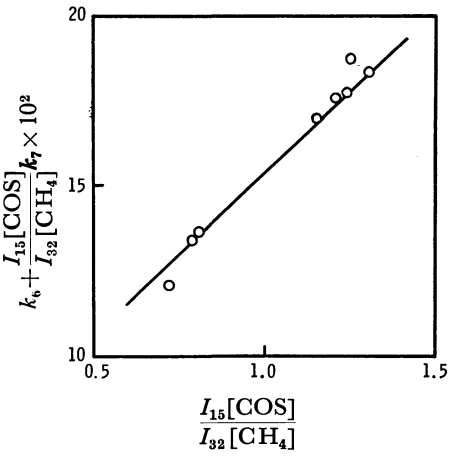

Fig. 1. Plots of $k_6+\frac{I_{15}[COS]}{I_{32}[CH_4]}k_7$ *vs.* $\frac{I_{15}[COS]}{I_{32}[CH_4]}$ in CH_4–COS system.

C_2H_2–COS System. In C_2H_2–COS mixtures, the ion $C_2H_2S^+$ is formed by the reactions such as

$$C_2H_2 + COS^+ \longrightarrow C_2H_2S^+ + CO \quad (8)$$

$$C_2H_2^+ + COS \longrightarrow C_2H_2S^+ + CO \quad (9)$$

$$C_2H_2 + S^+ \longrightarrow C_2H_2S^+ \quad (10)$$

Figure 2 shows the results obtained at lower electron energy where only $C_2H_2^+$ and COS^+ ions are formed as primary ions: the rate constants for Reactions 8 and 9 were determined to be 8.0×10^{-11} and 1.3×10^{-9} cm^3 mol^{-1} s^{-1}, respectively. At higher electron energy, Reaction 10 also yields $C_2H_2S^+$. In Fig. 3 $k_9+k_{10}I_{32}[C_2H_2]/I_{26}[COS]$ is plotted *vs.* $I_{32}[C_2H_2]/I_{26}[COS]$—the value of 8.0×10^{-11} cm^3 mol^{-1} s^{-1} obtained above is used for k_8. From the intercept and the slope $k_9=1.5\times10^{-9}$ and $k_{10}=8.0\times10^{-10}$ cm^3 mol^{-1} s^{-1} were obtained. k_9 determined from Fig. 3 is in good agreement with k_9 obtained at lower electron energy.

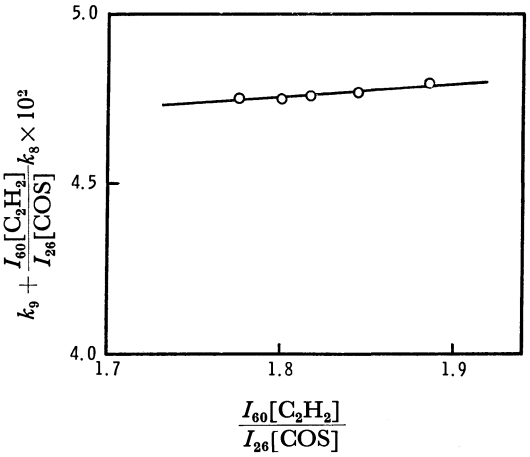

Fig. 2. Plots of $k_9+\frac{I_{60}[C_2H_2]}{I_{26}[COS]}k_8$ *vs.* $\frac{I_{60}[C_2H_2]}{I_{26}[COS]}$ in C_2H_2–COS system.

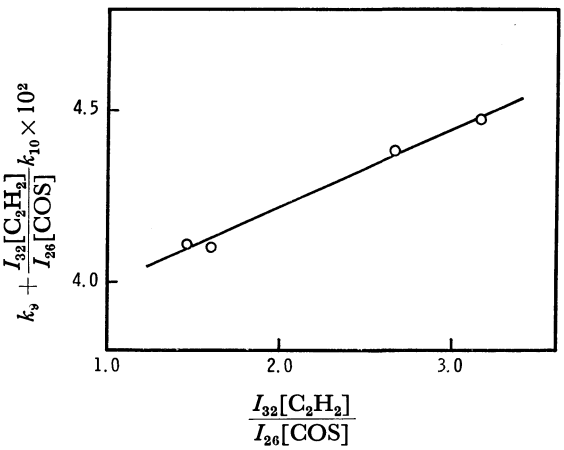

Fig. 3. Plots of $k_9+\frac{I_{32}[C_2H_2]}{I_{26}[COS]}k_{10}$ *vs.* $\frac{I_{32}[C_2H_2]}{I_{26}[COS]}$ in C_2H_2–COS system.

As in the CH_4–COS system, the rate constant k_9 for S atom transfer from COS is about 17.5 times as large as k_8 for S^+ ion transfer from COS^+. On the other hand, the rate constant k_{10} for the S^+ ion addition reaction is smaller than k_9 for S atom transfer reaction. The rate constant of 1.4×10^{-9} cm^3 mol^{-1} s^{-1} for Reaction 9 is surprisingly large compared with the value[2] of 4.7×10^{-11} cm^3 mol^{-1} s^{-1}, reported for the same reaction of the fragment ion $C_2H_2^+$ from C_2H_4. The implication of this difference still remains to be determined.

The possible reactions to account for the formation

of C_2HS^+ are

$$C_2H_2 + COS^+ \longrightarrow C_2HS^+ + CO + H \quad (11)$$

$$C_2H_2^+ + COS \longrightarrow C_2HS^+ + CO + H \quad (12)$$

$$C_2H^+ + COS \longrightarrow C_2HS^+ + CO \quad (13)$$

$$C_2H_2 + S^+ \longrightarrow C_2HS^+ + H \quad (14)$$

Thermochemical data shows that Reactions 11 and 12 are endothermic. Therefore, these processes are expected to occur only slightly. The secondary ion, C_2HS^+ was not detected in the low electron energy region where only COS^+ and $C_2H_2^+$ are observed as primary ions. After all, the formation of C_2HS^+ is attributed to Reactions 13 and 14. Rate constants of 1.1×10^{-10} and 1.5×10^{-9} cm^3 mol^{-1} s^{-1} for Reactions 13 and 14 were obtained from the results shown in Fig. 4.

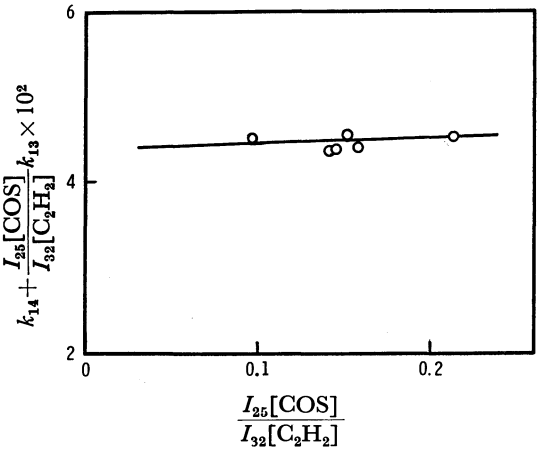

Fig. 4. Plots of $k_{14}+\frac{I_{25}[COS]}{I_{32}[C_2H_2]}k_{13}$ *vs.* $\frac{I_{25}[COS]}{I_{32}[C_2H_2]}$ in C_2H_2–COS system.

C_3H_6–COS System. In C_3H_6–COS mixtures, the following processes yielding $C_3H_6S^+$ were considered:

$$C_3H_6 + COS^+ \longrightarrow C_3H_6S^+ + CO \quad (15)$$

$$C_3H_6^+ + COS \longrightarrow C_3H_6S^+ + CO \quad (16)$$

$$C_3H_6 + S^+ \longrightarrow C_3H_6S^+ \quad (17)$$

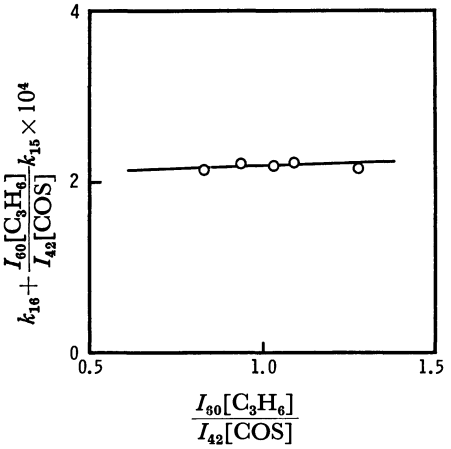

Fig. 5. Plots of $k_{16}+\frac{I_{60}[C_3H_6]}{I_{42}[COS]}k_{15}$ *vs.* $\frac{I_{60}[C_3H_6]}{I_{42}[COS]}$ in C_3H_6–COS system.

From the results shown in Fig. 5, obtained at lower electron energy where $C_3H_6^+$ and COS^+ are the only significant primary ions, the rate constants for Reactions 15 and 16 were determined to be $k_{15}=8.0\times10^{-14}$ and $k_{16}=9.3\times10^{-12}$ cm^3 mol^{-1} s^{-1}. At higher electron energies, the Reaction 17 also occurs. k_{17} was evaluated to be 4.6×10^{-11} cm^3 mol^{-1} s^{-1}, in a manner similar to the case of C_2H_2–COS system.

The following processes involved in the $C_3H_5S^+$ formation are

$$C_3H_6 + COS^+ \longrightarrow C_3H_5S^+ + HCO \quad (18)$$

$$C_3H_6^+ + COS \longrightarrow C_3H_5S^+ + HCO \quad (19)$$

$$C_3H_5^+ + COS \longrightarrow C_3H_5S^+ + CO \quad (20)$$

$$C_3H_6 + S^+ \longrightarrow C_3H_5S^+ + H \quad (21)$$

Since Reactions 18 and 19 are endothermic, $C_3H_5S^+$ formation in C_3H_6–COS systems is attributed to Reactions 20 and 21. From the intercept and the slope of the plot of $k_{20}+k_{21}I_{32}[C_3H_6]/I_{41}[COS]$ *vs.* $I_{32}[C_3H_6]/$

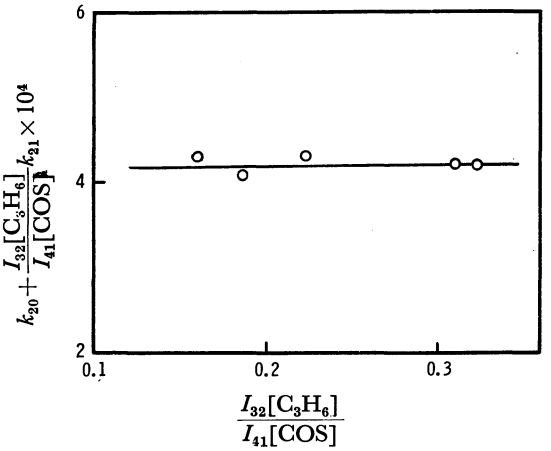

Fig. 6. Plots of $k_{20}+\frac{I_{32}[C_3H_6]}{I_{41}[COS]}k_{21}$ *vs.* $\frac{I_{32}[C_3H_6]}{I_{41}[COS]}$ in C_3H_6–COS system.

TABLE 2. RATE CONSTANTS IN COS-HYDROCARBON SYSTEMS

Reaction	Rate constant cm^{3}mol^{-1}s^{-1}
CH_4–COS system	
$CH_4+COS^+ \rightarrow CH_4S^+ + CO$	$3.8\pm0.1\times10^{-13}$
$CH_4^+ + COS \rightarrow CH_4S^+ + CO$	$6.0\pm0.1\times10^{-12}$
$CH_4+S^+ \rightarrow CH_4S^+$	$4.42\pm0.02\times10^{-11}$
$CH_4+COS^+ \rightarrow CH_3S^+ + HCO$	3.0×10^{-12}
$CH_4^+ + COS \rightarrow CH_3S^+ + HCO$	1.6×10^{-11}
$CH_3^+ + COS \rightarrow CH_3S^+ + CO$	5.9×10^{-10}
$CH_4+S^+ \rightarrow CH_3S^+ + H$	9.5×10^{-10}
C_2H_2–COS system	
$C_2H_2+COS^+ \rightarrow C_2H_2S^+ + CO$	8.0×10^{-11}
$C_2H_2^+ + COS \rightarrow C_2H_2S^+ + CO$	1.4×10^{-9}
$C_2H_2+S^+ \rightarrow C_2H_2S^+$	8.0×10^{-10}
$C_2H^+ + COS \rightarrow C_2HS^+ + CO$	1.1×10^{-10}
$C_2H_2+S^+ \rightarrow C_2HS^+ + H$	1.5×10^{-9}
C_3H_6–COS system	
$C_3H_6+COS^+ \rightarrow C_3H_6S^+ + CO$	8.0×10^{-14}
$C_3H_6^+ + COS \rightarrow C_3H_6S^+ + CO$	9.3×10^{-12}
$C_3H_6+S^+ \rightarrow C_3H_6S^+$	4.6×10^{-11}
$C_3H_5^+ + COS \rightarrow C_3H_5S^+ + CO$	1.8×10^{-11}

I_{41}[COS] shown in Fig. 6, the rate constants for Reactions 20 and 21 were determined to be $k_{20}=1.8\times10^{-11}$ $cm^3\ mol^{-1}\ s^{-1}$ and $k_{21}\leq10^{-13}$ $cm^3\ mol^{-1}\ s^{-1}$, respectively. The small value of k_{21} estimated for the highly exothermic reaction 21 suggests that the product ion, $C_3H_5S^+$ may be followed by fragmentation.

In the low electron energy region, the ion-molecule reactions yielding CH_4S^+, $C_2H_2S^+$, and $C_3H_6S^+$, in methane–COS, acetylene–COS and propylene–COS systems may be classified into three groups; S^+ ion transfer, S atom transfer and S^+ ion addition. As seen in Table 2, the rate constants for S atom transfer are very large compared with those for S^+ ion transfer in methane–COS and propylene–COS mixtures although not in acetylene–COS mixtures. In acetylene–COS mixtures, all the reactions are very fast compared with those in methane–COS and propylene–COS mixtures. This seems to be attributable to the triple bond of acetylene.

References

1) H. Field and F. W. Lampe, *J. Amer. Chem. Soc.*, **80**, 5583 (1958).
2) I. Dzidic, A. Good, and P. Kebarle, *Can. J. Chem.*, **48**, 664 (1970).
3) S. E. Buttrill, Jr., *J. Amer. Chem. Soc.*, **92**, 3561 (1970).
4) W. T. Huntress, Jr., R. F. Pinizzotto, Jr., and J. B. Landenslager, *ibid.*, **95**, 4107 (1973).
5) A. G. Harrison and J. J. Myher, "Ion-Molecule Reactions in the Gas Phase," Advances in Chemistry Series 58, ed. P. J. Ausloos, American Chemical Soc., Washington (1966), p. 150.
6) S. Okada, A. Matsumoto, T. Dohmaru, S. Taniguchi, and T. Hayakawa, *Mass Spectroscopy (Japan)*, **20**, 311 (1972).
7) A. Matsumoto, T. Misaki, S. Okada, S. Taniguchi, and T. Hayakawa, *Chem. Lett.*, **1973**, 1001.
8) S. K. Gupta, E. G. Jones, A. G. Harrison, and J. J. Myher, *Can. J. Chem.*, **45**, 3107 (1967).

Photochromism of 2-Hydroxytriphenylmethanol and Its Derivatives

Sanyo HAMAI and Hiroshi KOKUBUN

Department of Chemistry, Faculty of Science, Tohoku University, Aoba, Aramaki, Sendai 980

(Received July 19, 1974)

2-Hydroxytriphenylmethanol (HM) shows photochromism in air-saturated acetonitrile and other solvents and also in the crystalline state. The colored form has been deduced to be *o*-fuchsone, produced by photochemical dehydration of HM. The photochromism mechanism is entirely different from that of other triarylmethane derivatives. The colored form is the same species as in thermochromism. The reactive state of HM was found to be the excited singlet state from the results of quenching experiments. The quantum yield of the photochemical reaction was determined to be 0.62 in acetonitrile by a method based on the equilibrium between the photochemical and thermal bleaching reactions. Photochromism occurs also at 77 K. At this temperature, HM radical is produced beside the colored form. The ratio of the concentration of HM radical to the colored form increases with irradiation time. Several HM derivatives show photochromism similar to HM.

Photochromism of many triarylmethane derivatives, especially triphenylmethane derivatives, has been studied extensively.[1] In the photochromism of triarylmethane dye leuco derivatives, such as leuco malachite green and leuco crystal violet, the colored forms are the respective cations.[2,3] In the photochromism of *o*-nitrotoluene derivatives, for example 2,4,2′,4′,2″, 4″-hexanitrotriphenylmethane, the colored form is an aci-nitro acid or an anion.[4,5] It has been reported that 2-hydroxytriphenylmethanol[6,7] (HM) and (3-hydroxy-2-naphthyl)-diphenylmethanol[7] show thermochromism. Gomberg and Nishida[6] attributed the thermochromism of HM to the formation of the quinoidal colored form(I), but, Bowden and Beynon[7] suggested the same phenomenon was due to the broadening of the near ultraviolet absorption band. However, both these views do not seem to be fully supported by experimental evidence.

We have found photochromism of HM and its derivatives. The photochromism was studied in various solvents at room temperature as well as at liquid nitrogen temperature. For comparison thermochromism was also studied.

Experimental

Materials. HM was synthesized from methyl salicylate or phenyl salicylate and phenylmagnesium bromide by the Grignard reaction[8] and, after treatment with activated charcoal, recrystallized several times from an ethyl ether–*n*-hexane mixture. 2-Hydroxy-4-methoxytriphenylmethanol (HMM) was also synthesized from 2-hydroxy-4-methoxybenzophenone by the Grignard reaction and, after treatment with activated charcoal, recrystallized several times from ethyl ether–*n*-hexane and methanol–water mixtures. 5-Chloro-2-hydroxytriphenylmethanol and (3-hydroxy-2-naphthyl)-diphenylmethanol were synthesized from 5-chloro-2-hydroxybenzophenone and methyl 3-hydroxy-2-naphthoate by the Grignard reaction and purified by the method used for HM. *o*-Naphthofuchsone was obtained by refluxing dichlorodiphenylmethane, *β*-naphthol and aluminum chloride in carbon disulfide, decomposing the products by ice, steam distilling, and recrystallizing from acetic acid.[9]

Acetonitrile was distilled over phosphorus pentoxide. Ethyl ether was distilled over sodium wire after being stood overnight with calcium chloride and used immediately. Wako G.R. grade acetic acid, methanol and ethanol were used as received.

Piperylene was distilled over sodium wire. Biacetyl was used immediately after distillating three times.

Apparatus. A 6W germicidal lamp was used as a 253.7 nm light source. A Toshiba SHL-100 UV high pressure mercury lamp combined with a Toshiba UV-D2 filter was used for the 365 nm source. An Ushio USH-100 superhigh pressure mercury lamp combined with a photographic plate as a filter was used for the experiment at 77 K. A combination of an Ushio UXL-150 xenon lamp and a Hitachi G-3 grating monochromator was used to obtain 280 nm light for the piperylene quenching experiments.

The absorption spectrum and thermal decay were recorded on a Hitachi EPS-3T spectrophotometer at room temperature. The absorption spectrum at 77 K was measured with a Hitachi 356 Dual-Wavelength spectrophotometer. A JEOL Type P-10 ESR spectrometer was used for measurement of the ESR spectrum.

Results and Discussion

Irradiation of the air-saturated solution of HM in acetonitrile by 253.7 nm light at room temperature turned the colorless solution to a yellowish brown. Photochromism occurs in ethyl ether, 1,2-dichloro-

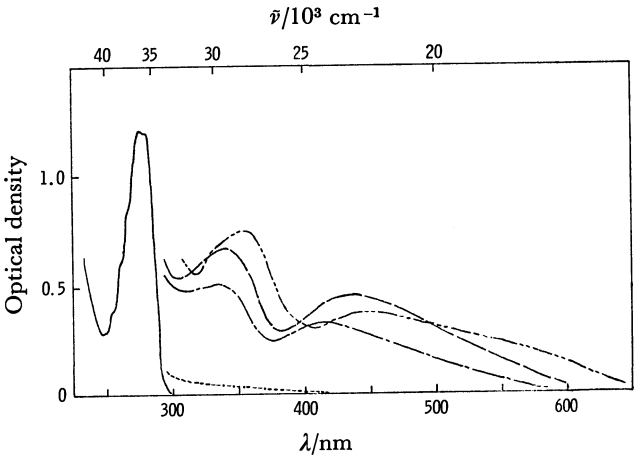

Fig. 1. Absorption spectra of (——) HM in acetonitrile (5.30×10^{-4}M), (----) the colored form in photochromism of HM in acetonitrile, (——) the colored form in photochromism in ethyl ether, and (·····) *ca.* 24 hours aged after the irradiation in acetonitrile ceased. Absorption spectrum of (——) the colored form for thermochromism in acetic acid.

ethane, and benzene and also in the crystalline state. The color bleaches gradually and finally disappears on keeping the solution in the dark. The bleaching, however, is not complete. The absorption spectrum after prolonged storage in the dark indicates the presence of a small amount of the irreversible photoproduct as shown in Fig. 1. The absorption spectra of HM in acetonitrile and its colored form in acetonitrile and ethyl ether are also given in Fig. 1. The absorption maxima of the colored form at 340 (A band) and 440 nm (B band) in acetonitrile shift to 334 and 416 nm respectively in the less polar ethyl ether.

The thermochromic colored form in acetic acid has absorption maxima at 354 and 450 nm. The spectrum closely resembles that of the photochromic colored form as shown in Fig. 1.

The photochromic behavior of HMM in polar solvents is similar to that of HM. In contrast to HM, HMM is photochromic at room temperature in saturated hydrocarbons (*n*-hexane, cyclohexane, methylcyclohexane) in which HM merely decomposes photochemically. Furthermore, thermochromism of HMM was observed in *n*-hexane. Hence, comparison of the absorption spectra of the photochromic and thermochromic forms in the same solvent became possible. As seen from Fig. 2, complete agreement was found between the absorption spectra of the photochromic and thermochromic forms. Consequently, it may safely be concluded that the photochromic form is the same species as the thermochromic one.

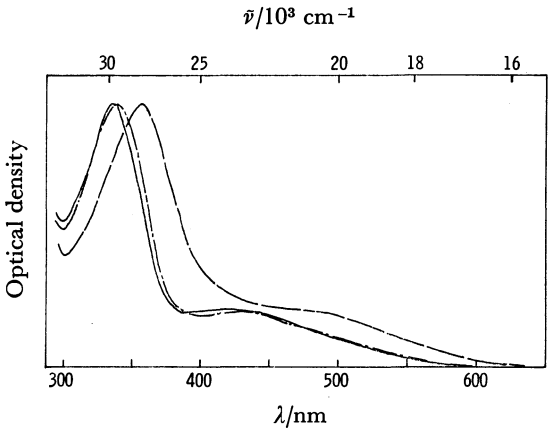

Fig. 2. Absorption spectra (maximum peaks at shorter wavelengths are normalized) of (——) the colorled form in photochromism and thermochromism of HMM in *n*-hexane, (– – –) the colored form in photochromism of HMM in acetonitrile, and (– · –) the colored form in thermochromism of HMM in acetic acid.

The rate of bleaching measured for the A band agreed well with that for the B band. The ratio of the optical density of the A band to that of the B band is little affected by solvent and temperature. These observations strongly support the view that both A and B bands originate from the same species and the colored form in photochromism as well as in thermochromism consists of a single species.

The absorption spectra of the colored form of HMM are shown in Fig. 2. The absorption maxima shifted to longer wavelengths when the solvent was changed from ethyl ether to acetonitrile. In acetic acid, the absorption maxima were located at considerably longer wavelengths than in acetonitrile in spite of the smaller dielectric constant of acetic acid. This implies the existence of a specific interaction between solute and solvent. The most plausible one is hydrogen bond formation.

2-Hydroxytriphenylmethyl cation is not the colored form, since its absorption spectrum has maxima at 410 and 438 nm. The radical, which is produced frequently in the photochemistry of triphenylmethane derivatives, may also be excluded because the colored form in acetic acid does not give an ESR signal.

Compound (I) may be considered as a possible structure of the colored form. However, 2-methoxytriphenylmethanol shows neither photochrmism nor thermochromism indicating that the 2-hydroxy group plays an important role. Therefore, (I) may be excluded.

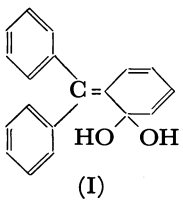

(I)

The thermal bleaching reaction of the colored form of HM obeys first-order kinetics. In acetonitrile the bleaching rate constant is proportional to the concentration of water added, whereas the rate constant is little affected by the addition of *n*-hexane. Similar effects of water and *n*-hexane were observed in ethyl ether solution. The result in acetonitrile is shown in Fig. 3. Thus the first-order kinetics observed in acetonitrile and ethyl ether must be pseudo-first order due to the presence of water as an impurity. In dimethoxyethane, which was so carefully dried over sodium-potassium alloy that the solvent became blue in color due to solvated electrons, the order of the bleaching reaction was found to be close to two. Also, it has been reported that HM dehydrates and then forms 9-phenylxanthene at elevated temperatures.[6] Thus it

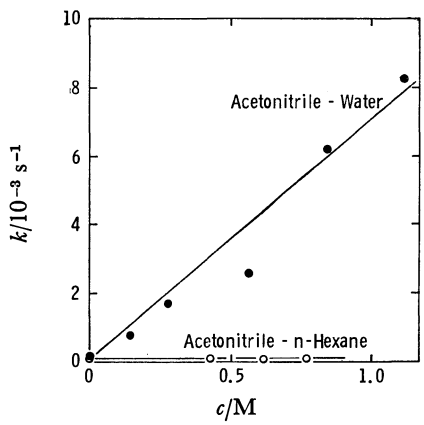

Fig. 3. Effect of added water (●) and *n*-hexane (○) on the first-order bleaching rate constant in acetonitrile.

is evident that the colored form is a dehydrated form of HM.

Compounds (II) and (III) are the possible dehydrated forms of HM. In 2-propanol the absorption spectrum of (III') which has some similarities to (III) in its structure has a maximum at 383 nm,[10] considerably to the blue of the peak for the colored form. The large red shift of the absorption spectrum in acetic acid is not expected for (III). A related compound to (III), xanthene (III'') has absorption maxima at 283 nm and shoulders at 287 and 291 nm in both acetonitrile and acetic acid.

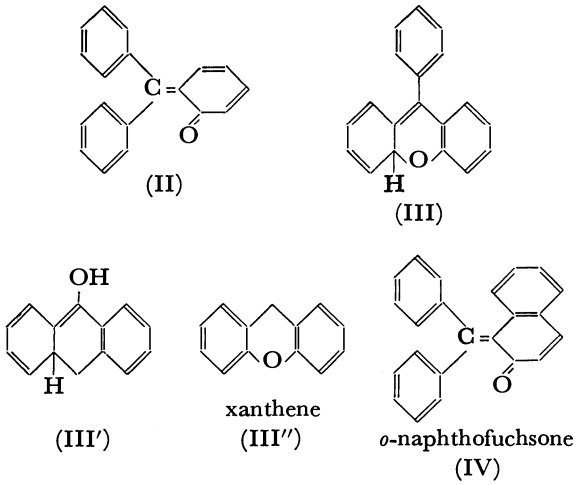

If the colored form is (II), *o*-fuchsone, the observed large red shift in acetic acid can be explained by hydrogen bond formation between (II) and acetic acid. *o*-Naphthofuchsone (IV) is a condensed homologue of *o*-fuchsone, and is stable to be isolated. The absorption spectra of (IV) in two solvents are presented in Fig. 4. The absorption maximum at 360 nm in acetonitrile shifts to 370 nm in acetic acid reflecting the hydrogen bonding with the acetic acid.

Although the colored form can not be isolated for structural determination, spectral and kinetic behavior strongly supports reaction scheme (1) for photochromism as well as thermochromism.

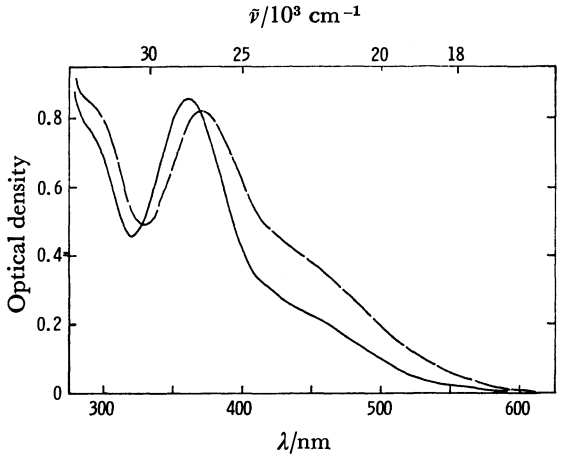

Fig. 4. Absorption spectra of *o*-naphthofuchsone (——) in acetonitrile (1.0×10^{-4}M) and (----) in acetic acid (1.04×10^{-4}M).

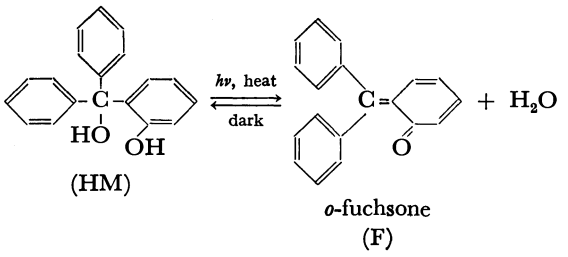

Scheme 1.

This is a new reaction mechanism for photochromism and thermochromism of triarylmethane derivatives.

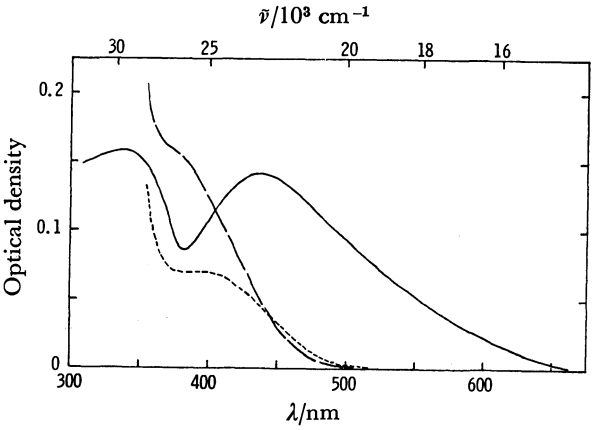

Fig. 5. Absorption spectra of (——) the colored form of ClHM in acetonitrile, (----) after irradiation of HNM, and (·····) *ca.* 24 hours aged after the irradiation in acetonitrile for HNM ceased.

5-Chloro-2-hydroxytriphenylmethanol (ClHM) and (3-hydroxy-2-naphthyl)-diphenylmethanol (HNM) showed the same type of photochromism as HM and HMM. In the case of HNM, however, an irreversible reaction became important. Figure 5 shows absorption spectra of the colored forms of ClHM and HNM.

TABLE 1. EFFECT OF THE CONCENTRATION OF HM ON THE RELATIVE QUANTUM YIELD; $\phi_{rel}=\phi/\phi(1.39\times10^{-4}\text{M})$

[HM]$\times10^4$(M)	ϕ_{rel}
1.39	1.0
5.56	0.92
9.72	0.87
13.9	0.97
Mean value	0.94

TABLE 2. EFFECT OF LIGHT INTENSITY ON THE RELATIVE QUANTUM YIELD

I/I_0(%)	ϕ_{rel}
100	1.0
54	1.0
48	1.0
36	1.0
25.9	0.93

Photochemical Reaction, Photo and Thermal Bleaching at Room Temperature. Tables 1 and 2 show the effect of the concentration and light intensity on the quantum

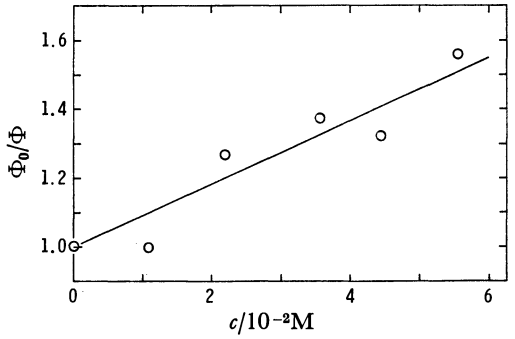

Fig. 6. Quenching by biacetyl in acetonitrile.

yield of the photochemical reaction, HM to F, in acetonitrile. Both concentration and light intensity do not affect the quantum yield, so that the reaction is a one-photon process. The result of the quenching of the photochemical reaction by biacetyl is given in Fig. 6. Quenching by piperylene is very small, if any occurs at all, whereas biacetyl quenches the photochemical reaction significantly. Since piperylene can quench only the triplet state of HM, whereas biacetyl quenches both singlet and triplet states, the state quenched by biacetyl must be the singlet state. The lifetime of the excited singlet state was estimated to be 0.54 ns from the slope of Φ_0/Φ *vs.* concentration of biacetyl in Fig. 6 with the assumption that quenching occurs at the diffusion-controlled rate.

A reactive singlet state with a short lifetime is consistent with the observation that the photochemical reaction occurs even in air-saturated solutions and that no transient intermediate was observed by conventional flash photolysis. Since triphenylmethyl radical is produced from the triplet state,[11,12] HM radical is not a reaction intermediate. Other species, such as phenoxy radical and phenoxy anion derivatives, are not intermediates, since in triphenylmethane derivatives C–H bond cleavage at the central carbon atom generally occurs,[1] and no transient was observed by flash photolysis. Therefore, the photoreaction of HM occurs by a one-step process.

Irradiation by 365 nm light which is absorbed solely by the colored form F accelerates the bleaching of F. This photobleaching occurs not only in air-saturated solutions but also in nitrogen-saturated solutions. The rate constant for thermal bleaching is the same in air and nitrogen-saturated solutions, and also the same before and after the 365 nm irradiation. During the irradiation photo and thermal bleaching occur simultaneously and independently. The rate of bleaching of F is given by

$$-\frac{dC_F}{dt} = \phi'' I_0'(1-10^{-OD})\frac{\varepsilon_F C_F}{OD}\times 10^3 + kC_F \qquad (1)$$

where ε_F is the molar extinction coefficient, OD is the optical density, I_0' is the light intensity at 365 nm, ϕ'' is the quantum yield of photobleaching, k is the thermal bleaching rate constant, and C_F is the concentration of F. Integration of Eq. (1) leads to

$$\ln\frac{OD_F^0}{OD_F} - kt = \phi'' I_0'\varepsilon_F\times 10^3\int(1-10^{-OD})\frac{dt}{OD} \qquad (2)$$

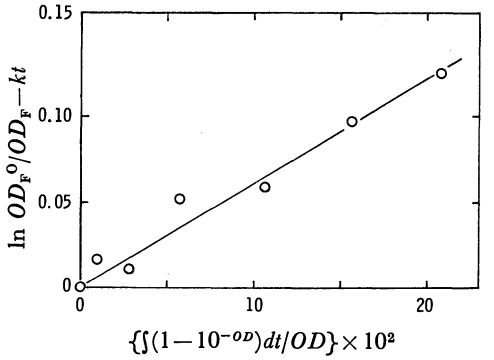

Fig. 7. Plot of $\ln OD_F^0/OD_F - kt$ *vs.* $\{\int(1-10^{-OD})\,dt/OD\}\times 10^2$ in acetonitrile. Suffix, F, stands for the colored form. The exciting wavelength is 365 nm.

where OD_F^0 is the initial optical density. Evaluation of the integral part of Eq. (2) was performed graphically. Plots of $(\ln OD_F^0/OD_F - kt)$ *vs.* $\int(1-10^{-OD})dt/OD$ are presented in Fig. 7. Using ε_F determined by a method described later, ϕ's were estimated to be 0.0079 for air-saturated and 0.12 for nitrogen-saturated solutions. The large discrepancy in the quantum yields means that the reaction of the triplet state of F is the major process in the photobleaching.

When the photochemical reaction of HM is in equilibrium with the photo and thermal bleaching reactions, Eq. (3) holds.

$$I_0(1-10^{-OD})\frac{\varepsilon C}{OD}\times 10^3 = \phi' I_0(1-10^{-OD})\frac{\varepsilon_F' C_F}{OD}\times 10^3 + kC_F \qquad (3)$$

where ε and ε'_F are the molar extinction coefficients of HM and F at 253.7 nm, C is the concentration of HM, ϕ and ϕ' are the quantum yields of photochemical reaction of HM and photobleaching of F, OD is the optical density at 253.7 nm, and I_0, the light intensity at 253.7 nm. Since the irreversible portion of the photochemical reaction of HM is quite small, $C_0 = C + C_F$ holds approximately, where C_0 stands for the initial concentration of HM. Then Eq. (3) is reduced to:

$$\frac{C_0}{OD_F^\lambda} = \frac{1}{\varepsilon_F^\lambda}\left(1+\frac{\phi'\varepsilon_F}{\phi\varepsilon}\right) + \frac{kOD}{\varepsilon_F^\lambda\varepsilon\phi I_0(1-10^{-OD})\times 10^3} \qquad (4)$$

where the superscript λ represents a value at a wavelength λ. Since, it is probable that ϕ' is not so different from the ϕ'' determined already, $\phi'\varepsilon_F/\phi\varepsilon$ may be very small compared to 1. Thus, Eq. (4) may be simplified to

$$\frac{C_0}{OD_F^\lambda} = \frac{1}{\varepsilon_F^\lambda} + \frac{kOD}{\varepsilon_F^\lambda\varepsilon\phi I_0(1-10^{-OD})\times 10^3} \qquad (5)$$

An analysis at 340 nm is given in Fig. 8. ε_F^{340} was determined to be 4.76×10^3. ϕ was found to be 0.62. The same value of ϕ was obtained at 440 nm. The fairly high value of the photochemical quantum yield in aerated solution provides further evidence that the reactive state is predominantly the excited singlet state.

Photochemical Reaction at 77 K. The absorption spectra of the photoproducts from HM in methanol-

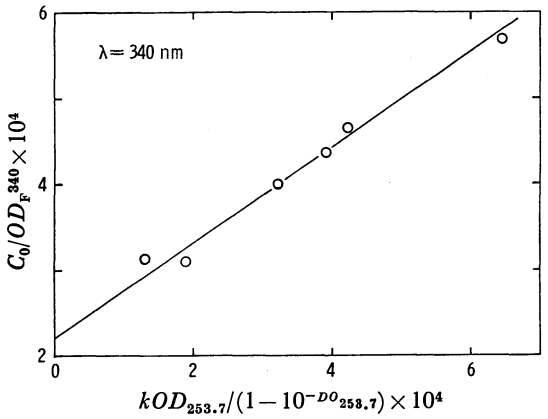

Fig. 8. Plot of $C_0/OD_F^{340}\times10^4$ *vs.* $kOD_{235.7}/(1-10^{-OD_{253.7}})\times10^4$ in acetonitrile. C_0, k, OD^{340} and $OD_{253.7}$ are the initial concentration of HM, the bleaching rate constant, the optical density of the colored form at 340 nm and the optical density at 253.7 nm.

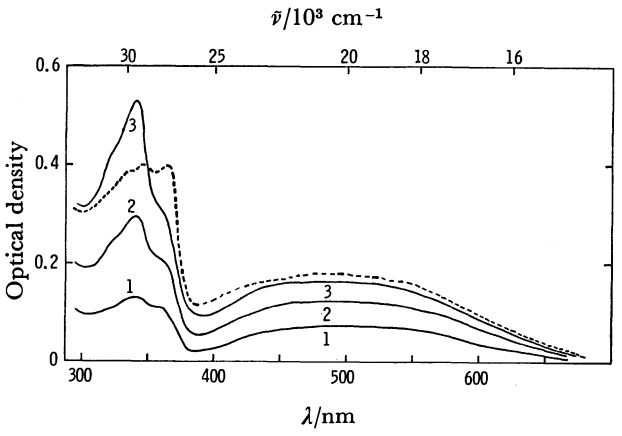

Fig. 9. Absorption spectra of the irradiated HM in methanol–ethanol (1:1) at 77 K; 1— after 10 minute irradiation, 2—35 minutes, 3—115 minutes; ---- cooled to 77 K immediately after melting the solution.

ethanol mixture (1: 1 in volume) at 77 K are shown in Fig. 9 for different irradiation times. The increase in optical density at 340 nm is larger than that at 480 nm indicating that the product is not a single species, since HM has no absorption in this wavelength region. The irradiated glassy solution was allowed to melt and cooled to 77 K again immediately. The resulting absorption spectrum is the dotted curve in Fig. 9. The decrease in optical density around 340 nm is appreciable. 2-Methoxytriphenylmethyl radical obtained by irradiation of 2-methoxytriphenylmethanol under the same conditions as for HM has an absorption maximum at 338 nm. Hence, the absorption around 340 nm belongs to 2-hydroxytriphenylmethyl radical (HM radical) generated photochemically. This conclusion is also supported by the ESR spectra. The irradiated HM solution shows ESR signals which can be assigned to methanol, ethanol, formyl, and HM radicals. All these signals disappear upon melting of the solution, and do not reappear on freezing the solution again.

The solution initially irradiated by 253.7 nm was further irradiated by the light from a superhigh pressure mercury lamp filtered by either a Toshiba VY-43 (transmits longer than —430 nm) or a photographic plate (longer than —300 nm). No change in the absorption spectrum was observed, so that the mechanism by which HM radical is produced by hydrogen atom abstraction of excited F from the surrounding solvent molecules may be almost excluded. It might be possible, however, that F excited by 253.7 nm abstracts hydrogen and that another kind of biphotonic process occurs on 253.7 nm irradiation.

The formation of F is a one-photon process as it is at room temperature, since the yield of F at the early stage of the reaction is proportional to the light intensity.

We are indebted to Prof. N. Suzuki and Mr. H. Watarai, M.S. at Tohoku University for the use of a Hitachi 356 Dual-Wavelength Spectrophotometer.

References

1) G. H. Brown, "Photochromism," Wiley-Interscience, New York, N.Y. (1971), p. 294.
2) E. O. Holmes, Jr., *J. Phys. Chem.*, **61**, 434 (1957).
3) A. H. Sporer, *Trans. Faraday Soc.*, **57**, 983 (1961).
4) G. Wettermark, *Nature*, **194**, 677 (1962).
5) J. D. Margerum, L. J. Miller, E. Saito, M. S. Brown, H. S. Mosher, and R. Hardwick, *J. Phys. Chem.*, **66**, 2434 (1962).
6) M. Gomberg and D. Nishida, *J. Amer. Chem. Soc.*, **45**, 190 (1945).
7) S. T. Bowden and K. I. Beynon, *J. Chem. Soc.*, **1957**, 4244.
8) A. Baeyer, *Ann.*, **354**, 167 (1907).
9) M. Gomberg and F. W. Sullivan, *J. Amer. Chem. Soc.*, **42**, 1864 (1942).
10) E. F. Ullman and K. R. Huffman, *Tetrahedron Lett.*, **1965**, 1863.
11) H. G. Lewis and E. D. Owen, *Chem. Commun.*, **1966**, 216.
12) H. G. Lewis and E. D. Owen, *J. Chem. Soc. (B)*, **1967**, 422.

The Mechanism of the Selective Hydrogenation of 1,3-Butadiene on Copper Surfaces

Eiji NISHIMURA, Yasunobu INOUE, and Iwao YASUMORI

Department of Chemistry, Tokyo Institute of Technology, O-okayama, Meguro-ku, Tokyo 152

(Received August 3, 1974)

The hydrogenation of 1,3-butadiene on copper surfaces was studied in detail. A highly selective formation of 1-butene was observed in the range of temperatures from 27 to 76 °C; the initial rate of the formation was well expressed in terms of the partial pressures of hydrogen, p_h, and butadiene, p_b, as $v=kp_h/(1+Kp_b)^2$ in the pressure range of 5—100 Torr. The reaction with D_2 gave butene-d_0 and -d_1 as the main products, and the butadiene was partly exchanged with D_2 during the hydrogenation. The microwave spectroscopic analysis revealed that the 1-butene produced consisted of $CH_2=CHCH_2CH_2D$, $CH_2=CHCHDCH_3$, and $CHD=CHCH_2CH_3$, without even a trace of $CH_2=CDCH_2CH_3$. Therefore, it was concluded that the reaction proceeds *via* the isobutenyl surface intermediate and that the dissociative adsorption of hydrogen is rate-determining. The structural analysis of the surface suggested that the stable lattice planes, such as (111), (100), and (110), are responsible for the reaction. The origin of the high 1-butene selectivity was discussed on the basis of the surface geometry and the proposed mechanism.

The hydrogenation of 1,3-butadiene has frequently been investigated from the viewpoint of selective catalysis, but it has been studied mainly on such d-metals as Ni,[1] Pd, and Pt.[2,3] Though the reaction on these metals produces 1-butene, *trans*-2-butene, *cis*-2-butene, and a smaller amount of *n*-butane from the initial stage of reaction, the isomer distributions of the produced butenes are considerably different from each other. In order to explain this variation, reaction mechanisms including such surface intermediates as π-allylic or σ-π-bonded species have been proposed. The identification of these adsorbed species, however, has not always been successful because of the complication of the simultaneous formation of butene isomers. On the other hand, it has been found that copper, a typical s-metal, is highly selective in the formation of 1-butene. However, only a few works of the hydrogenation on this metal have been reported,[1] and the features of the reaction are not known in detail. The aim of the present study is to ascertain the mechanism of the reaction and to reveal the origin of the high selectivity on the basis of the structure of the copper surface and the mechanism.

In order to ascertain the detailed mechanism of the reaction, the deuterium distribution in the products and the reactants on the reaction with deuterium were examined mass-spectroscopically; further, the deuterated positions of the produced 1-butene-d_1 and their relative abundances were determined by applying microwave spectroscopic analysis. The adsorbed states of hydrogen and butadiene were analyzed by using the thermal-desorption technique.

In the study of butadiene hydrogenation on Ni, it was found that a drastic change in activity and selectivity occurred when Ni was annealed in the temperature range of 350—400 °C.[4] A similar change in the activity was observed in the acetylene hydrogenation on Pd when the catalyst was annealed at temperatures between 250 and 300 °C. These results show that fine structures such as surface vacancies play an important role in the reactions.[5] In the present study, the effect of annealing on these catalytic properties was examined over a wide range of annealing temperatures, from 180 to 500 °C; the corresponding change in surface structure was followed by means of X-ray and electron diffractions.

Experimental

The kinetic measurements were carried out by using conventional closed systems of 360 or 670 ml incorporating a circulation pump. The reaction was examined in the range of temperature from 27 to 76 °C and in the range of total pressure between 5 and 100 Torr. The pressure change during the course of reaction was followed by means of a glass Bourdon gauge, while the composition of the products was determined by the use of a gas chromatograph connected to the reaction system. A 16 m DMS column was used at room temperature for the separation of butadiene, butenes, and butane.

The copper powder catalyst was prepared in a way similar to the method reported by Hirota *et al.*[6] Copper nitrate, $Cu(NO_3)_2\cdot 3H_2O$ of a guaranteed-reagent grade, was dissolved into distilled water at 80 °C, and then a 20% solution of NaOH was added steadily. The copper oxide thus precipitated was washed several times, calcinated in air at 110 °C for 1 hr, and then evacuated for 1 hr. Prior to the reaction, the oxide was reduced *in situ* with hydrogen of 100 Torr at 180 °C for 3 days and then evacuated for 2 hr at the same temperature. Though a step-by-step decrease in the activity occurred in a repeated run, contact with H_2 at 180 °C prior to each kinetic run could recover the initial activity within a 10% decrease. The catalytic activity was also examined on copper catalysts annealed at 300, 400, and 500 °C *in vacuo* for 1 hr. The surface area was evaluated by means of the BET method, using Kr at 77 K, while the change in surface structure was investigated by means of the X-ray and electron diffractions.

In the reaction of butadiene with D_2, the products were separated gas chromatographically, and the deuterium distributions in respective components were determined by using a mass spectrometer, Hitachi RMU-5B. The relative abundance of 1-butene-d_1 and -d_2 with different deuterium positions was determined by means of microwave spectroscopy.[7] Hydrogen, hydrogen deuteride and deuterium were analyzed gas chromatographically.[8]

The thermal desorption spectra were obtained by using an apparatus which could be pumped out at a constant rate

during the desorption of surface species from the heated catalyst. Copper (1.06 g) was exposed to hydrogen or butadiene of 10 Torr at room temperature for 10 min; then it was cooled and evacuated at −78 °C for several minutes. The temperature of the cell containing copper was raised at a constant rate of 0.14 °C/s by means of an electric furnace. The pressure of the desorbed gases was monitored by means of a Pirani gauge, and the composition of the desorbed gas was determined by using a quadrupole mass spectrometer.

Butadiene (99.6% purity), hydrogen (99.9%), and deuterium (containing 0.3% HD) were obtained from the Takachiho Co., Ltd., and were used without further purification.

Results

A typical time-course of the hydrogenation, when the copper catalyst was reduced at 180 °C, is shown in Fig. 1. The only products at the initial stage were butenes; the absence of butane was evident. The butenes consisted of 1-butene (92%), *t*-2-butene (3%), and *c*-2-butene (5%); this composition was almost unchanged until more than 95% of the butadiene had been consumed. This finding predicts that, in the initial stage of the reaction, each butene is formed directly by the hydrogenation of adsorbed butadiene and that the butenes, once desorbed into the gas phase, hardly participate in the further process of the reaction. After the butadiene in the gas phase had disappeared, however, the isomerization of 1-butene and the slow hydrogenation of butenes took place concurrently, producing 2-butenes and *n*-butane respectively. This selective formation of 1-butene was observed also on the Cu annealed at 500 °C under similar conditions. In the absence of hydrogen, neither the isomerization nor hydrogenation occurred, not even at 76 °C, the highest reaction temperature in the present study.

Kinetics of Hydrogenation. The kinetic measurements were carried out in the temperature range of 27—76 °C, using Cu annealed at 180 and 500 °C. By changing the partial pressure of hydrogen from 13 to 97 Torr, and that of butadiene from 7 to 36 Torr, the initial rate of 1-butene formation, v, was measured. It was found that the rate was proportional to the hydrogen pressure, p_h, and that a linear relationship held between the square root of the reciprocal of v and the butadiene pressure, p_b, as is shown in Fig. 2. Accordingly, the rate was well expressed in this form;

$$v = kp_h/(1+Kp_b)^2 \quad (1)$$

where k and K are constants. From the temperature dependence of the rate, the apparent energy of activation was estimated; it is listed in Table 1, together with that for the reaction with D_2.

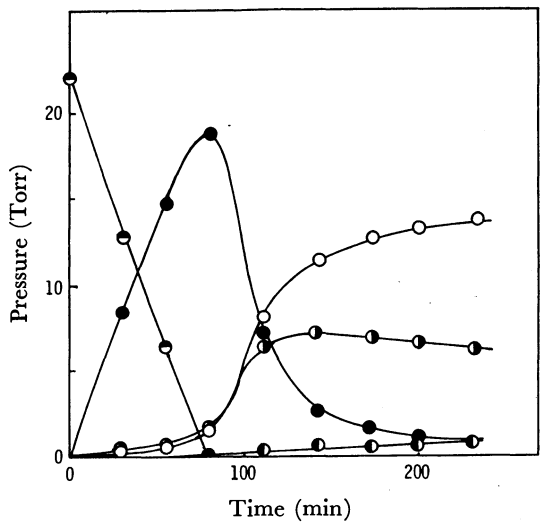

Fig. 1. Hydrogenation of 1,3-butadiene on Cu at 64.5 °C.
p_h=24 Torr, p_b=12 Torr.
◓: 1,3-butadiene, ○: *t*-2-butene, ◑: *c*-2-butene, ●: 1-butene, ◐: *n*-butane.

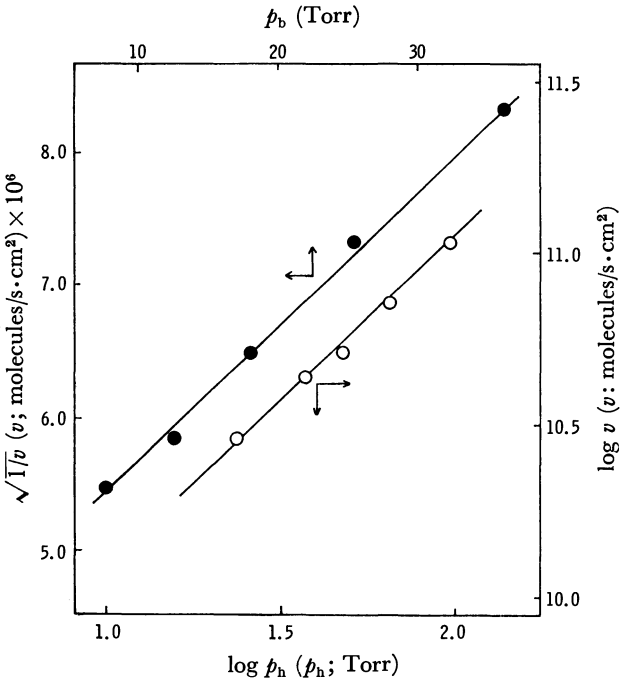

Fig. 2. Dependence of rate on partial pressures at 50 °C.
○: hydrogen (p_b= 12 Torr), ●: 1,3-butadiene (p_h=24 Torr).

TABLE 1. ACTIVATION ENERGIES OF 1,3-BUTADIENE HYDROGENATION ON Cu
(p_D=24 Torr, p_h=24 Torr, p_b=12 Torr)

Annealing temperature	Reaction	Activation energy (kcal/mol)
180 °C	$C_4H_6+H_2$	13.5±0.2
180 °C	$C_4H_6+D_2$	13.8±0.1
500 °C	$C_4H_6+H_2$	13.4±0.2

Deuterium Distributions. The distributions of deuterium in butenes and butadiene were investigated on the reaction with deuterium at 50 °C. Figure 3 shows the changes in the fractions of 1-butene-d_0~-d_3 with the degree of conversion. In the stage of low conversion, the main products were 1-butene-d_0 and -d_1. The decrease in 1-butene-d_0 with an increase in the conversion was counterbalanced by the formation of d_1~d_3 compounds. It should be noted that a considerable amount of butadiene-d_1 appeared as the reaction proceeded; at 40% conversion, the d_1 fraction

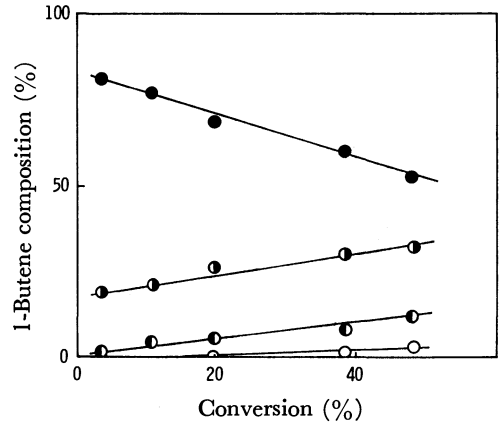

Fig. 3. Deuterium distribution in product from the reaction of butadiene with deuterium at 50 °C.
p_D=24 Torr, p_b=12 Torr
●: 1-butene-d_0, ◑: -d_1, ◐: -d_2, ○: -d_3.

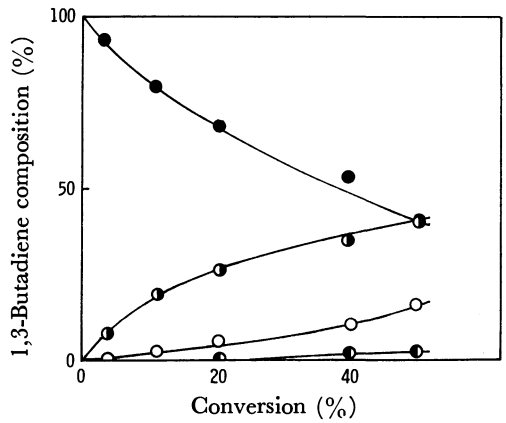

Fig. 4. Deuterium distribution in reactant from the reaction of butadiene with deuterium at 50 °C.
p_D=24 Torr, p_b=12 Torr
●: butadiene-d_0, ◑: -d_1, ○: -d_2, ◐: -d_3.

reached 35% of all the butadienes, as is shown in Fig. 4. It is apparent that the formation of 1-butene-d_2 and -d_3 in the region of high conversion is due to the hydrogenation of deuterobutadiene. On the other hand, a negligibly small amount of HD was found in the gas phase. In the reaction of butadiene with an equi-molar mixture of H_2 and D_2, the amount of HD produced was also negligibly small. These results clearly indicate that the recombination of surface hydrogen into the molecule is very slow.

The microwave spectroscopic analysis was applied to the products at conversions of 15.5 and 48%. The results for butene-d_1 are summarized in Table 2. The deuterium positions of products other than 1-butene-d_1 could not be determined because of their small yields (below the limits of analysis). As may be seen from Table 2, about 54% of the CH_2=$CHCH_2CH_2D$ (4-d_1) and 31% of the CH_2=$CHCHDCH_3$ (3-d_1) were formed at the stage of low conversion. A small fraction, 15%, of CHD=$CHCH_2CH_3$ (1-d_1) was also produced, but CH_2=$CDCH_2CH_3$ (2-d_1) was not detected. The increase in the fraction of the 1-d_1 component was compensated for the decrease in that of the 3-d_1 compound.

Table 2. The relative abundance of 1-butene-d_1 with different deuterium positions
(p_b=12 Torr, p_D=24 Torr, reaction temperature=50°C)

Conversion		15.5%	48.1%	
		%deuterium	% deuterium	
Position[a)]	1c	7.5	12.7	
	1t	7.5	17.5	1-d_1
	2	0	0	2-d_1
	3	30.7(15.4)[b)]	16.3 (8.2)	3-d_1
	4	54.3 (18.1)	53.5 (17.8)	4-d_1

a) H_t, H_c, $C_1=C_2-C_3-C_4$, H, H, H, H, H, H
b) Values in parentheses represent deuterium fraction per hydrogen atom.

The rate of the reaction with H_2 was approximately five times as fast as that of the reaction with D_2 at 50 °C. This isotope effect is mainly attributable to the mass ratio, $(m_D/m_H)^{5/2}$, in the frequency factors of the hydrogen and deuterium adsorption rates, though the difference in activation energy contributes to some extent.

Adsorbed States of Hydrogen and Butadiene. By the use of copper annealed at 180 °C, the adsorption measurement of butadiene was carried out at 50 °C under pressures up to 30 Torr. The adsorption was saturated at equilibrium pressures higher than 7 Torr, and the surface was occupied by 1.9×10^{14} molecules/cm^2, corresponding to about 20% of all the surface Cu atoms. After the evacuation at 50 °C, a considerable amount of the butadiene, 1.3×10^{14} molecules/cm^2, still remained on the surface. The reaction with hydrogen at the same temperature decreased this strongly bound butadiene to 0.47×10^{14} molecules/cm^2, with a slower rate compared to the stationary rate of the hydrogenation.

The thermal desorption spectra of butadiene showed a broad peak which spread over −40~100 °C, with a maximum at 53 °C, indicating that even the most strongly adsorbed butadiene is almost desorbed at temperatures higher than 100 °C. On the other hand, the desorption spectra of hydrogen showed a sharp peak with a maximum at 58 °C; this peak has the characteristic shape of the second-order desorption, indicating a drastic fall on the high-temperature side. This result suggests that the hydrogen is adsorbed dissociatively and exists in a single state on the surface.

Carbon monoxide was added to the reactant up to 22 Torr, but no decay in the activity was observed. However, a preliminary study of ethylene hydrogenation at 50 °C using an equi-molar mixture of ethylene and hydrogen (24 Torr in total pressure) showed that the activity of the copper catalyst decreased proportionally with the pressure of the introduced CO up to about 3 Torr. These results provide evidence of the stronger bond between butadiene and the copper surface than that between ethylene and Cu.

Effect of Annealing on the Activity and the Surface Structure. The effect of annealing on the catalytic activity and the surface area is shown in Fig. 5. It is evident that the decreases in the activity and the surface area are parallel with each other, keeping the specific

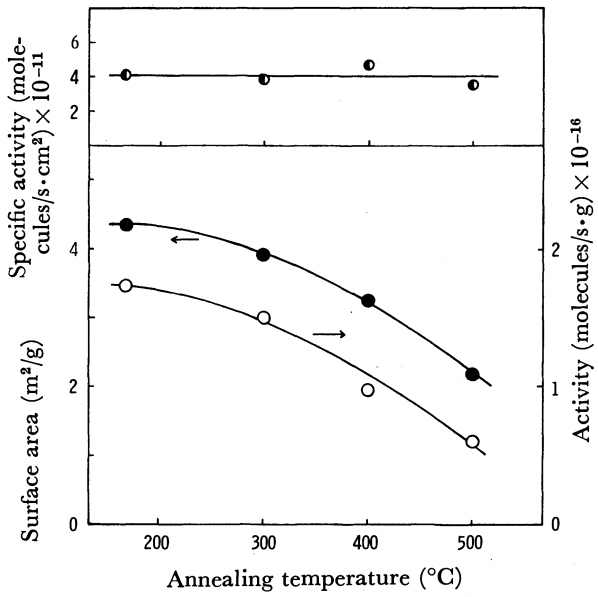

Fig. 5. The changes in activity and surface area with annealing temperature.

activity, the rate per unit area, constant. In the case of the 500 °C-annealed Cu, the selectivity of 1-butene formation was higher than 90% and the activation energy was estimated as 13.4 kcal/mol, as is shown in Table 1. These values coincide with those in the case of the 180 °C-annealed Cu.

X-Ray and electron diffractions of the 180 °C-annealed Cu showed the characteristic patterns due to the (111), (220), and (200) planes. When the copper was annealed at 500 °C, the pattern remained almost unchanged, except that the intensity of the (200) plane became slightly weaker. These findings were in close agreement with those observed by Yamaguchi[9] and by Young *et al.*[10] and showed that the exposed surface was mainly composed of the stable (111), (100), and (110).

Discussion

In the present study using the Cu metal, the high selectivity of 1-butene formation was observed under all the conditions used. The kinetics of the reaction on Cu is not markedly different from those on Pd, Pt, and Ni metals of lower selectivities. However, there were some differences in the activation energy; the value for Cu is considerably higher than those for the other metals. The dissociative adsorption of hydrogen on Cu was also confirmed from a study of the H_2–D_2 equilibration reaction.[11] The adsorption and the thermal-desorption measurements showed that the Cu surface was covered, to a large extent, with butadiene, which is in the reversibly adsorbed and the strongly bound states. The mass analyses showed a considerable formation of butadiene-d_1 and -d_2 during the hydrogenation with deuterium. However, it is clear that the dissociatively adsorbed butadiene scarcely contributes at all to the hydrogenation, since 1-butene-2-d_1 was completely absent in the products, whereas 1-butene-3-d_1 were present in large amounts. Hence, the reversibly adsorbed butadiene and butenyl radicals can be suggested as the intermediates. The following reaction scheme is proposed:

$$C_4H_6 \underset{\overleftarrow{Ia}}{\overset{\overrightarrow{Ia}}{\rightleftharpoons}} C_4H_6(a) \qquad (Ia)$$

$$H_2 \underset{\overleftarrow{Ib}}{\overset{\overrightarrow{Ib}}{\rightleftharpoons}} 2H(a) \qquad (Ib)$$

$$H(a) + C_4H_6(a) \underset{\overleftarrow{II}}{\overset{\overrightarrow{II}}{\rightleftharpoons}} C_4H_7(a) \qquad (II)$$

$$H(a) + C_4H_7(a) \xrightarrow{\overrightarrow{III}} C_4H_8 \qquad (III)$$

where the symbol (a) denotes the adsorbed state which participates in the reaction. The first-order dependence of the rate with respect to the hydrogen pressure leads to the conclusion that either step, $\overrightarrow{Ib}$ or $\overrightarrow{III}$, is rate-determining. In both reactions, with D_2 and with an equimolar mixture of H_2 and D_2, the amount of HD formed was found to be negligibly small. This suggests that the adsorption of hydrogen is irreversible during the hydrogenation. Accordingly, the $\overrightarrow{Ib}$ step is considered to be rate-determining and the rate of hydrogenation is given by:

$$v = k_1 p_h (1-\theta_b)^2 \qquad (2)$$

where θ_b is the fraction of surface coverage of the reversibly adsorbed butadiene and where k_1 is the rate constant of the $\overrightarrow{Ib}$ step. When the pseudo-equilibrium between gaseous and adsorbed butadiene is established, θ_b is expressed as:

$$\theta_b = Kp_b/(1+Kp_b) \qquad (3)$$

where K is the adsorption constant. Then, by substituting Eq. (3) to Eq. (2), the final expression:

$$v = k_1 p_h/(1+Kp_b)^2 \qquad (4)$$

is obtained. The pressure dependence shown by this equation is in accord with the empirical one given by Eq. (1). It should be noted that the same rate-determining step was concluded in the hydrogenation of ethylene on evaporated copper film at low temperatures.[12] No other mechanism which includes the disproportionation between two adsorbed butenyls as the rate-determining step can interpret the observed dependence of the rate on the butadiene pressure.

The remarkable formation of butene-d_0 at the early stage of reaction was quite similar to the formation of ethane-d_0 in the C_2H_4–D_2 reaction on the Ni surface.[13] The present situation of the reaction predicts the following order of the rates of elementary processes: $v(\overrightarrow{Ib}) < v(\overrightarrow{III}) < v(\overrightarrow{Ia}) \simeq v(\overleftarrow{Ia}) \simeq v(\overrightarrow{II}) \simeq v(\overleftarrow{II})$. Thus, it can be understood why the concentration of surface hydrogen becomes reasonably high, because the adsorbed deuterium is quickly consumed through the Ia and II steps by exchanging with hydrogen atoms in the hydrocarbon species. The observed isotope effect on the hydrogenation can be related to the straightforward isotope effect, as is seen in the adsorption of hydrogen and deuterium on copper.[11]

Transition metals of Group VIII, such as Ni,[1] Pd, and Pt,[2,3] provide a considerable amount of *trans*-2-

and *cis*-2-butenes in the products of the hydrogenation. These results can be explained by assuming π-allylic or σ-π bonded intermediates formed by the simultaneous interaction of two double bonds in butadiene with the surface atoms. In the case of copper, however, the absence of 2-butenes predicts that only one double bond of the molecule associates with the surface. The formation of 1-butene-1-d_1, 3-d_1 and 4-d_1 can be well expressed by making use of this adsorbed state:

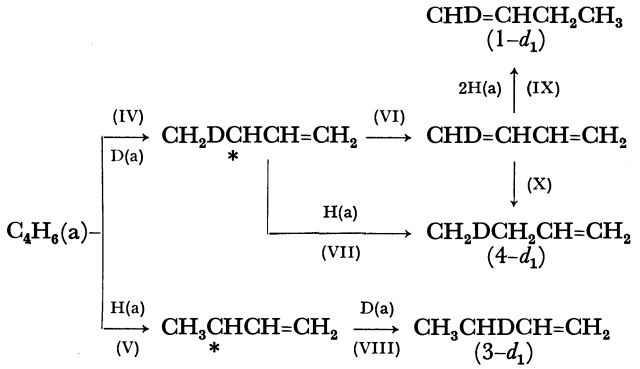

where the asterisk indicates the active site. The attack of the terminal and second carbon atoms of the adsorbed butadiene with D and then H atoms produces butene-4-d_1 (IV and VII). The formation of 3-d_1 is attributed to the hydrogen addition in the reversed order (V and VIII). In the case of 1-d_1 formation, however, deuteriobutadiene-1-d_1 is hydrogenated with two hydrogen atoms (VI and IX). It is clear that no *n*-butenyl such as $\overset{*}{C}H_2CH_2CH=CH_2$ is produced on the surface, since such a formation would result in the formation of butadiene-d_1, $CH_2=CDCH=CH_2$, the subsequent hydrogenation of which would produce both butene-2-d_1 and -3-d_1 in similar amounts. Therefore, it may safely be concluded that the reaction intermediate is isobutenyl, $CH_3\overset{*}{C}HCH=CH_2$. At a high conversion of 48%, the fraction of deuterium at the 1t and 1c positions increases and that of 3-d_1 decreases. As the partial pressure of mono-deuteriobutadiene became higher with an increase in the conversion, the chance of a reaction proceeding *via* Steps (IX) and (X) increases as compared to the chance *via* Step (VIII).

The importance of surface defects in catalysis has been pointed out; Uhara *et al.*[14] reported that the activity of Cu on the decomposition of benzene diazonium chloride was markedly depressed by heat treatment around 350 °C and correlated this depression with the disappearance of dislocations. However, in the present study the decrease in the catalytic activity due to annealing was parallel to that of the surface area. This suggests that the activity of the hydrogenation is not due to the characteristic surface structure of defects, but depends only on the number of exposed metal atoms.[15] The fact that annealing at 500 and 180 °C makes no difference in the activation energy provides other evidence for this conclusion. The present result also supports the previous conclusion that the structural defects in the s-metals are less important in catalysis.[11]

X-Ray and electron diffraction studies indicated that the surfaces of Cu annealed at 180 and 500 °C were mainly composed of low index planes, such as (111), (100), and (110). The valence state of copper is characterized by a half-filled s-band which makes no directed bond. Therefore, the atomic distance in the lattice plane becomes a dominant factor in the interaction with adsorbed molecules. These lattice planes have the closest atomic distance of 2.56 Å; this configuration is not suited to the simultaneous use of two double bonds of butadiene upon adsorption, because the carbon-to-carbon bond length, 1.48 Å, is too short to make a bridge between two copper atoms. As for the isobutenyl radical on the surface, the length of the carbon chain containing a double bond is 1.54 Å. The intermediate can hardly find the copper atom located at a suitable position where the remaining double bond may interact so as to give adsorbed 2-butenes. Accordingly, it seems reasonable that this surface geometry is responsible for the high selectivity of 1-butene formation.

The authors wish to thank Dr. Shuji Saito of the Sagami Chemical Research Center for making the microwave spectroscopic measurements.

References

1) J. J. Phillipson, P. B. Wells, and G. R. Wilson, *J. Chem. Soc., A*, **1969**, 1351.
2) G. C. Bond, G. Webb, P. B. Wells, and J. M. Winterbottom, *J. Chem. Soc.*, **1965**, 3128.
3) P. B. Wells and A. J. Bates, *J. Chem. Soc., A*, **1968**, 3064.
4) Y. Inoue and I. Yasumori, Preprint of the 20th Annual Meeting of the Chemical Society of Japan, Part I, (1967), p. 399: R. G. Oliver, P. B. Wells and J. Grant, *Proc. Vth Int. Cong. on Catalysis*, (1972), North-Holland (1973), p. 659.
5) Y. Inoue and I. Yasumori, *J. Phys. Chem.*, **73**, 1618 (1969); **75**, 880 (1971); I. Yasumori, T. Kabe, and Y. Inoue, *ibid.*, **78**, 583 (1974).
6) K. Hirota, N. Yoshida, S. Teratani, and T. Kitayama, *J. Catal.*, **13**, 306 (1969).
7) Y. Sakurai, Y. Kaneda, S. Kondo, E. Hirota, T. Onishi, and K. Tamaru, This Bulletin, **41**, 1496 (1968), *Trans. Faraday Soc.*, **67**, 3275 (1971); Y. Sakurai, T. Onishi, and K. Tamaru, *Trans. Faraday Soc.*, **67**, 3094 (1971); K. Hirabayashi, S. Saito, and I. Yasumori, *J. Chem. Soc., Faraday I*,**68**, 978 (1972).
8) S. Ohno and I. Yasumori, This Bulletin, **39**, 1302 (1966).
9) N. Yamaguchi, *Kagaku*, **17**, 24 (1947).
10) F. W. Young, Jr. and A. T. Gwathmey, *J. Appl. Phys.*, **31**, 225 (1960).
11) M. Kiyomiya, N. Momma, and I. Yasumori, This Bulletin, **47**, 1852 (1974).
12) M. Sato and K. Miyahara, *Catalyst*, **15**, 134 (1973).
13) T. Keii, *J. Res. Inst. Cat.*, **3**, 36 (1953), *J. Chem. Phys.*, **22**, 144 (1954); I. Matsuzaki and T. Nakajima, *J. Res. Inst. Cat.*, **13**, 44 (1965).
14) I. Uhara, S. Yanagimoto, K. Tani, G. Adachi, and S. Teratani, *J. Phys. Chem.*, **66**, 2691 (1962).
15) M. Boudart, A. Aldag, J. E. Benson, N. A. Doughharty, and C. G. Harkins, *J. Catal.*, **6**, 92 (1966).

Positron Lifetimes in γ-Irradiated Eicosane and Polyethylene

Yasuo Ito and Yoneho Tabata*

National Universities' Laboratory for the Common Use of JAERI Facilities, Japan Atomic Energy Research Institute, Tokai-mura, Ibaraki 319-11

**Nuclear Engineering Research Laboratory, Faculty of Engineering, University of Tokyo, Tokai-mura, Ibaraki 319-11*

(Received August 15, 1974)

The positron lifetimes in a γ-irradiated single crystal of *n*-eicosane and amorphous polyethylene have been measured at -78 °C in a vacuum. The lifetime, τ_2, of the long-lived component decreases upon irradiation in both systems, and the increase in the annihilation rate, λ_2, is proportional to the concentration of free radicals. Assuming that the decrease in τ_2 is entirely due to the reaction of orthopositronium (*o*-Ps) with free radicals, the diffusion constant of *o*-Ps has been estimated to be $D=0.58$—1.75×10^{-5} cm^2 s^{-1}. The intensity, I_2, of the long-lived component decreases markedly in *n*-eicosane, levelling off at about 20%. I_2 in polyethylene does not decrease upon irradiation. Some possible explanations are given.

It is a well-known fact that the lifetime spectra of positrons in solids are influenced both by the chemical properties and by the physical structure.[1] A fraction of the positrons can capture an electron from the surrounding medium and form a bound state called "positronium". The positronium with a total spin number of $S=0$ is called the "parapositronium" (*p*-Ps). The lifetime of *p*-Ps is small ($\tau_p=0.125$ ns), and usually we cannot distinguish, with our conventional time-analyzer, this lifetime component from that of free positrons.

The positronium with a total spin number of $S=1$ is called the "orthopositronium" (*o*-Ps). The lifetime of *o*-Ps is 140 ns in a vacuum, but it is much shortened as a result of the following processes: 1) pick-off quenching, 2) conversion quenching, and 3) chemical quenching.

In a condensed medium, a positron in *o*-Ps has an opportunity to sample an electron in the medium and be annihilated into two gamma quanta. This is called "pick-off quenching." In general, the lifetime of *o*-Ps becomes shorter in a smaller free volume, because, in a smaller free volume, the positron in *o*-Ps has a larger opportunity to sample electrons in the medium. This phenomenon is called the "free volume effect" on *o*-Ps lifetimes.

If the medium contains paramagnetic species, *o*-Ps may be converted to *p*-Ps upon collision with them. The lifetime of *o*-Ps is also reduced by this process. This is called "conversion quenching."

If there are molecules which are reactive toward *o*-Ps to form a positronium compound, the lifetime of *o*-Ps is also reduced, because in a positronium compound the positron has a large opportunity to be annihilated with electrons in the compound. This is called "chemical quenching."

The formation probability of positronium, on the other hand, ranges from 0 to about 50%, depending on the substance. The so-called "Ore model" provides a simple method to estimate the formation probability. This model states that positronium formation is predominant in the region of positron energies from E (the energy of excitation of the first electron level of molecules) to $V-6.8$ eV (V is the ionization potential of molecules, and 6.8 eV is the dissociation energy of positronium). This model, however, must be modified in a condensed phase because of the affinity of the medium to electrons, positrons, and positronium. However, even without these complicating factors, there are cases where the formation of positronium is inhibited due to: 1) the process of the inelastic slowing down of positrons, as a result of which positrons quickly go below the Ore gap and 2) the process of the capture of positrons in the energy region of the Ore gap. Furthermore, in certain circumstances it is possible that positronium is chemically quenched, while it is not thermalized; in this case, the apparent formation probability of positronium may be decreased.

All of the above processes can be affected by radiation-induced changes in solid materials. It has indeed been reported by the present authors[2] and by others[3] that the positron lifetime spectra in various organic solids are altered in various ways by γ-irradiation.

In this paper we wish to report the results of our positron lifetime measurements in γ-irradiated *n*-eicosane (*n*-$C_{20}H_{42}$) and polyethylene. The former has been obtained in the form of single crystals, while the latter is known to contain many amorphous regions and defects. Positron annihilation studies in irradiated polyethylene have been reported by Chandra *et al.*[3a] and J. H. Green *et al.*;[3c] however, since their studies were carried out with samples in air at room temperature, many complex radiation chemical changes should have been taking place and it is difficult to interpret the changes in the lifetime spectra. In order to avoid such complexity, it is advantageous to carry out γ-irradiation and lifetime measurements at a lower temperature *in vacuo*.

Experimental

Sample Preparation. About 15 μCi of ^{22}NaCl was deposited on two single crystals of *n*-eicosane. They were positioned face to face on the deposited side and then placed in a glass ampoule which was subsequently sealed off in a vacuum.

Polyethylene, which had been supplied and named "Takathene" by the Takasaki Radiation Chemistry Research Establishment, JAERI, is the product of the high-pressure radiation-induced polymerization of gaseous ethylene; therefore, it is expected to contain no impurities. This polymer

was pressed in the form of two tablets ($10\phi \times 3$ mm), which were then prepared as a sample for lifetime measurement in the same manner as in the case of *n*-eicosane.

Irradiation and Measurements. Both lifetime measurements and γ-irradiations were carried out at -78 °C, except for those in which the samples were irradiated and measured at room temperature for the sake of comparison.

The lifetime measurements were carried out with a conventional time-analyzer using delayed coincidence technique as has been reported previously.[2] The resolution of the, time-analyzer was 0.34 ns at full width at half maximum of the Co-60 prompt peak for the Na-22 energy selection. It took a run of about 2 days to obtain a single spectrum with a total of approximately 5×10^5 counts. The peak-to-background ratio was greater than 10^4. The lifetime spectra were analyzed by the method of least squares to determine the intensity, I_2, and the lifetime, τ_2, of the long-lived component. The intensity was calculated as the ratio of the area of the long-lived component to that of the total area under the distribution curve.

The concentration of free radicals was measured with an ESR spectrometer (JEOL PE-3X) using a calibrated amount of DPPH in a benzene solution frozen at -78 °C as a standard.

Results and Discussion

Positron Lifetimes in Non-irradiated Samples. The lifetime spectra in *n*-eicosane and polyethylene could be resolved into two components. The mean lifetimes and intensities for non-irradiated samples are given in Table 1. Each datum is the average of at least three measurements carried out under different instrumental conditions—*i.e.*, with different window widths of the wide-channel energy selection and with different time widths per channel (0.05—0.10 ns/channel).

Table 1. Positron annihilation data for *n*-eicosane and takathene before irradiation

	τ_1 (ns)	τ_2 (ns)	I_2 (%)
n-Eicosane (-78 °C)	0.124±0.02	1.15±0.05	52.7±1.5
n-Eicosane (0 °C)	0.28 ±0.03	1.32±0.02	30.4±0.8
Takathene (-78 °C)	0.19 ±0.02	1.71±0.05	29.3±1.0
Takathene (0 °C)	0.36 ±0.04	2.62±0.05	19.2±3

It has often been reported that there are two *o*-Ps components in most polymeric systems, the longer component being attributed to *o*-Ps annihilation in amorphous regions and the shorter one to that in crystalline regions.[4] We could, however, observe only one *o*-Ps component in Takathene. This is natural in view of the special features of this polymer: it has been postulated from the X-ray diffraction and NMR studies of Takathene that the crystal size is small (130—160 Å) and that, moreover, many defects are included in the crystalline regions.[5] In such a structure, *o*-Ps, even if produced in the crystalline regions, may quickly diffuse out to non-crystalline regions or be trapped in crystal defects, since most *o*-Ps has, at the time of its production, a considerable energy above thermal and, therefore, can move a substantial distance. This situation is analogous to the escape of *o*-Ps from inside crystal particles of metal oxides to their surfaces.[6] We will, therefore, assign the long-lived component in Takathene to the annihilation of the *o*-Ps which is thermalized in the non-crystalline regions.

τ_2 in Takathene is larger than that in *n*-eicosane. This is natural in view of the free volume effect, because the density of *n*-eicosane is larger than that of amorphous polyethylene.

I_2 in *n*-eicosane and Takathene is larger at -78 °C than at 0 °C. Since we have not measured the positron lifetimes at temperatures between -78 and 0 °C, it is not clear whether this is connected with the "phase transition effect" on positron lifetimes which has often been reported for various materials.[7]

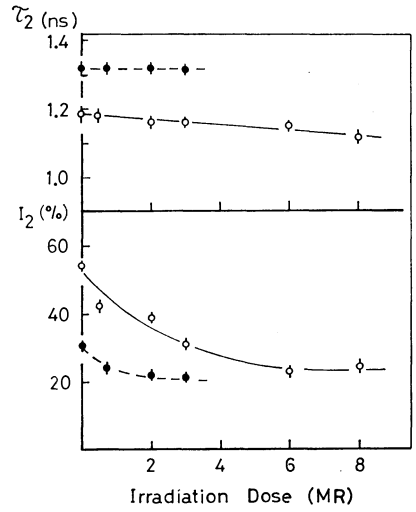

Fig. 1. I_2 and τ_2 in *n*-eicosane at -78 °C (○) and at a room temperature (●) as a function of the dose of γ-irradiation. The vertical bar at each point shows the statistical error of the coincidence counting rate.

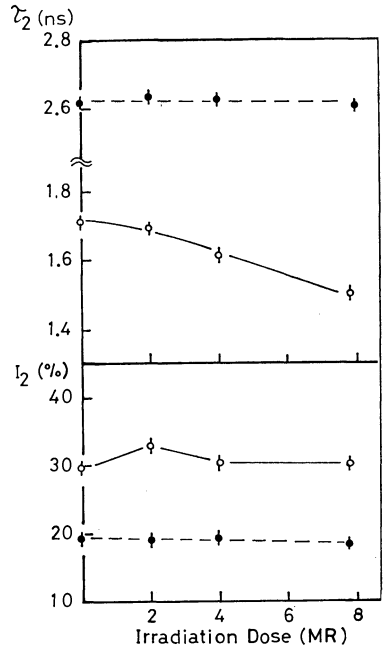

Fig. 2. I_2 and τ_2 in amorphous polyethylene at -78 °C (○) and at a room temperature (●) as a function of the dose of γ-irradiation.

Effect of γ-Irradiation on τ_2. The variations in τ_2 and I_2 are shown in Figs. 1 and 2 as a function of the γ-ray dose. τ_2 decreases upon γ-irradiation in both systems, although the decrease seems smaller in *n*-eicosane than in polyethylene. This may, however, be only apparent, because the radiation yield of free radicals (mainly alkyl radicals $-CH_2\dot{C}HCH_2-$) in *n*-eicosane is approximately one-third that in polyethylene under the present conditions. Moreover, if we plot $\Delta\lambda_2=\lambda_2-\lambda_2^0=1/\tau_2-1/\tau_2^0$ (where λ_2^0 and τ_2^0 are the annihilation rate and the lifetime in a non-irradiated sample respectively) against the spin concentration, it is expressed by a linear relation, as is shown in Fig. 3. From this result, we may assume that the decrease in τ_2 is the result of *o*-Ps reaction with free radicals:

$$o\text{-Ps} + R \xrightarrow{k[R]} PsR \longrightarrow 2\gamma \qquad (1)$$

The fact that τ_2 does not vary when the sample is irradiated at room temperature also supports this assumption, because the spin concentration in samples irradiated at room temperature is far smaller than in those irradiated at −78 °C.

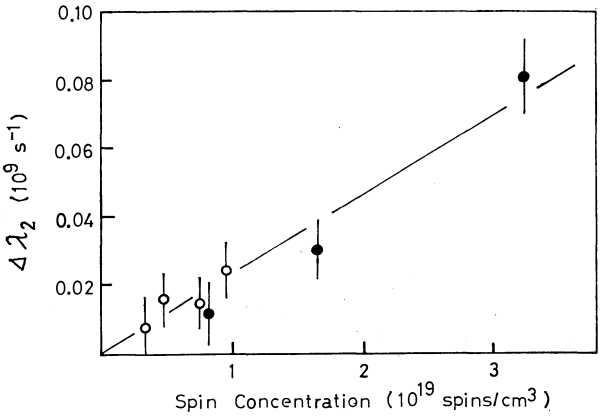

Fig. 3. The increase in the annihilation rate of *o*-Ps ($\Delta\lambda_2=\lambda_2-\lambda_2^0$) in *n*-eicosane (○) and amorphous polyethylene (●) as a function of the concentration of free radicals.

If the observed decrease in τ_2 is entirely due to the reaction of *o*-Ps with free radicals, the rate of Reaction 1 can be calculated to be;

$$k = 0.22\times10^{-11} \quad cm^3\cdot s^{-1}\cdot spin^{-1}$$

This is more than a factor of ten smaller than those for *o*-Ps reactions with various acceptors in organic liquids ($0.1—10\times10^{-10}$ cm^3 s^{-1} $molecule^{-1}$), in which the reaction is believed to be controlled by the diffusion of *o*-Ps.[8] Assuming that the mobility of *o*-Ps in the present substances can also be described in terms of diffusion, the following Smolkovskii formula is given:

$$k = \omega 4\pi(r_{Ps}+r_R)(D_{Ps}+D_R) \qquad (2)$$

where r is the radius, D is the diffusion constant, and ω is the probability factor for the reaction. In applying Eq. (2) we take $r_{Ps}=1$ Å, $r_R=1—2$ Å, $\omega=1$, and $D_R \ll D_{Ps}$. The latter assumption is based on the fact that free radicals can be regarded as immobile in the time scale of the lifetime of *o*-Ps. We thus obtain:

$$D_{Ps} = 0.58-1.75\times10^{-5} \quad cm\cdot s^{-1}$$

This value is as large as that obtained from the reaction of *o*-Ps with DPPH in solid pyridine at −78 °C.[9] It is more than one-third smaller than those previously reported for metal oxides ($\gtrsim 6\times10^{-5}$ cm^2 s^{-1}).[6] However, since the diffusion constants in metal oxides were calculated from the intensity of *o*-Ps or *p*-Ps which has diffused from inside crystal particles to their surfaces, they have been averaged over all the energy spectrum of Ps and therefore, must be larger than those for the thermalized Ps. The fact that our diffusion constant is smaller than those in organic liquids, but is close to those in other solids, supports our assumption that thermalized *o*-Ps can react with free radicals. It must be noted, however, that we have taken $\omega=1$ in Eq. (2), assuming that every encounter of *o*-Ps with free radicals leads to compound formation or conversion quenching. Our diffusion constant is, therefore, a lower limit to the real one. We may conclude either that the mobility of *o*-Ps is small ($\omega=1$) or that the reactivity of *o*-Ps with alkyl radicals is small ($\omega\ll1$).

It must be noted that our diffusion constant is far smaller than those given by Gol'danskii *et al.*,[10] who also applied the Smolkovskii formula for the reaction rate of *o*-Ps with O_2 in solid cyclohexane ($D=1.2\times10^{-3}$ cm^2 s^{-1}) and solid benzene ($D=0.7\times10^{-3}$ cm^2 s^{-1}) at −196 °C, assuming that $\omega=1$. One possible explanation for this discrepancy is that, in solidified cyclohexane and benzene, thermalized *o*-Ps exists in vacancies at the grain boundaries of the polycrystals. Since O_2 molecules may also be selectively concentrated in the grain boundaries, *o*-Ps feels in reality a much larger concentration of O_2 than that averaged over all the volume of the substance. The diffusion constants calculated using the averaged O_2 concentration should be larger than the real ones. Detailed investigations will be required to confirm this, but it may be of great importance to consider in what domain of substances thermalized *o*-Ps exists and how it migrates in it.

Effect of γ-Irradiation and Thermal Annealing on I_2. I_2 decreases upon irradiation in *n*-eicosane and levels off at a value of about 20% (Fig. 1). It is interesting to note that the room temperature value of I_2 also decreases and levels off at 20%. It is expected that

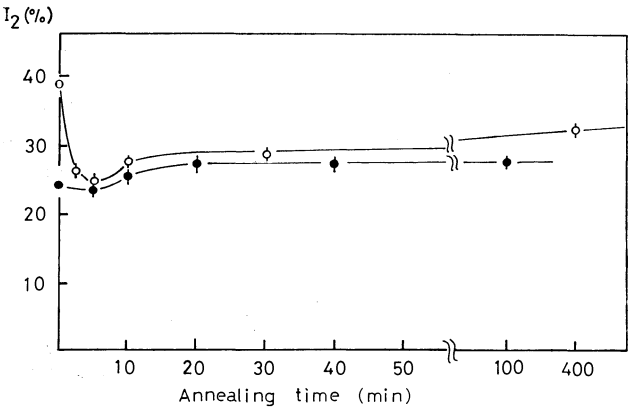

Fig. 4. Effect of thermal annealing at 30 °C on the intensity I_2 in *n*-eicosane irradiated to 2 MR (○) and 8 MR (●).

there is some threshold in the mechanism of the inhibition of thermalized *o*-Ps formation.

I_2 in irradiated *n*-eicosane varies upon thermal annealing, as is shown in Fig. 4. When *n*-eicosane, irradiated to 2 MR, is thermally annealed at 30 °C, I_2 decreases conspicuously to about 20% at first and then increases only slightly. However, in *n*-eicosane irradiated to 8 MR—*i.e.*, to a dose at which the decrease in I_2 levels off at −78 °C, the change due to thermal treatment is small, although it shows a similar tendency. This means that some structural and/or chemical changes which occur after the heat treatment are responsible for the initial decrease in I_2. It may be that, at the dose of 8 MR, such changes have already taken place to a degree sufficient to reduce I_2 to its lowest value and that further heat treatment does not induce any further change in I_2. There are several possibilities to be noted as such changes; the redistribution of free radicals, the conversion of the alkyl radical to the allyl radical (–CH=CH–$\dot{C}$H–CH_2–), *etc.* It remains to be studied which of these possibilities holds true.

Table 2. Effect of thermal annealing on τ_2 and I_2 in amorphous polyethylene

Conditions	τ_2(ns)	I_2 (%)
After irradiation of 8 MR at −78 °C	1.50±0.02	29.3±1.0
Annealed at 0 °C for 1 hr	1.41±0.02	28.8±1.1
Further annealed at 28 °C for 2.5 hr	1.53±0.04	32.3±0.8
Further annealed at 50 °C for 2.5 hr	1.51±0.03	34.5±1.5
Further annealed at RT for 800 hr	1.50±0.02	33.2±1.5

Contrary to the case of *n*-eicosane, I_2 in polyethylene does not decrease upon irradiation at −78 °C, and when thermally treated, it increases only slightly (Fig. 2 and Table 2). This is to be expected because the polyethylene used in the present experiment is quite amorphous, and the structure change due to irradiation or thermal treatment does not affect the positronium formation process as much as in crystalline *n*-eicosane.

Several explanations are possible for the observed decease of I_2 in *n*-eicosane both during γ-irradiation at −78 °C and during thermal treatment. Whatever the explanation may be, however, it must explain (1) the existence of a limit in I_2 reduction, (2) the significant I_2 reduction in annealed *n*-eicosane, and (3) the fact that γ-irradiation is ineffective in reducing I_2 in amorphous polyethylene. One possible explanation is the reaction of energetic *o*-Ps. It is expected that energetic *o*-Ps is rapidly thermalized in amorphous polyethylene by giving its energy to the vibration of molecular chains. Thus, in polyethylene energetic *o*-Ps migrates only a short distance before it is thermalized and has little chance to undergo reaction with acceptors such as free radicals. In crystals of *n*-eicosane, energetic *o*-Ps may migrate a significant distance before thermalization and thus may be able to undergo reaction. It is interesting to recollect in this connection the work by O. Mogensen *et al.*,[11] who showed that positronium moves in a fine crystal of ice as a Bloch wave and that it is rapidly localized in defect sites if such exist in the crystal. They suggested that a higher degree of order in the solid phase will enhance the Ps transport and lead to a stronger interaction. In *n*-eicosane, *o*-Ps may similarly be rapidly transported and localized in defect sites upon collision with them, and since the defect sites are paramagnetic in this case, energetic *o*-Ps may be quenched by the latter, resulting in the reduction of I_2.

If the above explanation is correct, it follows that there is essentially no difference between the mechanism by which τ_2 in *n*-eicosane and polyethylene is shortened and the mechanism by which I_2 in *n*-eicosane is reduced by the irradiation; the reaction of energetic *o*-Ps with free radicals reduces I_2, while the reaction of thermalized *o*-Ps shortens τ_2.

The limits in I_2 reduction might be attributed either to a "cage effect," which confines Ps with an energy below a certain thereshold in a limited region of the substance, or to the presence of some resonance in the mechanism by which *o*-Ps is transported in the crystal of *n*-eicosane.

We cannot, of course, exclude other explanations for the I_2 reduction. The existence of the paramagnetic sites might enhance the direct annihilation of positrons either by narrowing the effective Ore gap or by rapidly moderating the positron energies below the gap. Paramagnetic sites might also capture positrons and form positron compounds, thus inhibiting positronium formation. It seems difficult, however, to explain in terms of these processes why I_2 is not decreased in amorphous polyethylene by the irradiation, while it is decreased in *n*-eicosane.

Our present study involves many problems, and most of them are scarecely understood at present. Further extensive study is needed, but the problems raised in this work will be of importance in understanding the fundamental processes of positronium chemistry in organic solids.

We are grateful to Professor Joseph Silverman and Dr. Naoyuki Tamura, who provided us with single crystal of *n*-eicosane and with Takathene respectively. We are also indebted to Mr. Kiyofumi Sugimoto for helpful assistance.

References

1) See for a general reference, V. I. Gol'danskii, *Atomic Energy Review*, **6**, 3 (1968).

2) Y. Ito and Y. Tabata, This Bulletin, **44**, 1764 (1971); *J. Polym. Sci., A-1*, 1525 (1971).

3) a) G. Chandra, V. G. Kulkarni, R. G. Lagu, and B. V. Thosar, *Phys. Lett.*, **19(3)**, 201 (1965); b) B. V. Tosar, V. G. Kulkarni, R. G. Lagu, and G. Chandra, *Phys. Lett*, **21** (6), 647 (1966); c) J. H. Green and S. J. Tao, *Brit. J. Appl. Phys.*, **12**, 291 (1971); d) J. H. Hadley and F. H. Hsu, *Chem. Phys. Lett.*, **12**, 291 (1971); e) J. H. Hadley and F. H. Hsu, *Phys. Lett.*, **34A**, 317 (1971).

4) See for example, "Positron Annihilation," ed. by Stewart and Roellig, Academic Press, New York (1967), pp. 155—182.

5) N. Tamura, N. Hayakawa, and T. Fijimura, *Rep. Prog. Polym. Phys. Japan*, **13**, 317 (1970).
6) W. Brandt and R. Paulin, *Phys. Rev. Lett.*, **21**, 193 (1968); F. R. Steldt and P. G. Varlashkin, *Phys. Rev.*, **B5**, 4265 (1972).
7) See for example, J. B. Nicholas and H. J. Ache, *J. Chem. Phys.*, **57**, 1597 (1972).
8) S. J. Tao, *J. Chem. Phys.*, **56**, 5499 (1972).
9) Y. Ito and Y. Tabata, Proceedings of 3rd Tihany Symp. on Radiation Chemistry, p. 395.
10) V. I. Gol'danskii, O. V. Mogensen, and V. P. Shantarovich, *Khimiya Vysokikh Energii*, **8**, 124 (1974).
11) O. Mogensen, G. Kvajić, M. Eldrup, and M. Milosević-Kvajić, *Phys. Rev.*, **B4**, 4 (1971).

Semi-empirical SCF-MO Studies of Platinum Hydrides and the Insertion Reaction of Ethylene into the Pt(II)-H Bond

Shigeyoshi SAKAKI, Hiroshi KATO,* Hiroyoshi KANAI, and Kimio TARAMA

Department of Hydrocarbon Chemistry, Faculty of Engineering, Kyoto University, Sakyo-ku, Kyoto 606
**Department of General Education, Nagoya University, Chikusa-ku, Nagoya 464*

(Received August 19, 1974)

Semi-empirical SCF-MO calculations were carried out on *trans*-$PtHX(PH_3)_2$ (X=halogen and CN^-). The absolute value of E_{pt-H} decreases in the following order: F>Cl>Br>I>CN; this agrees with the order of the bond strength of the Pt-H bond. The electron density on the H ligand is remarkably large in all the complexes (*ca.* 1.25 e) and decreases in this order: F>Cl>Br>I>CN. An insertion reaction of ethylene into the Pt-H bond was investigated by the use of the MO method. The intermediate five-coordinate π-olefinic hydride complex has a trigonal bipyramid structure in which Cl and H ligands are positioned *trans* to each other. Three reaction paths of the insertion were investigated, and the following reaction path seems the best: The H ligand starts first to approach ethylene and then the Cl ligand starts to move to the *trans*-position of the H ligand. The reactivities of *trans*-$PtHX(PH_3)_2$ increase in this order: F<Cl<Br<I<CN. MO calculations also reveal that the catalytic ability of *trans*-$PtHX(PH_3)_2$ increases as follows in the hydrogen-deuterium exchange reaction of ethylene: F<Cl<Br<I.

The role of transition metal complexes in homogeneous catalytic reactions is currently a topic of great interest in the fields of both the pure and applied chemistry. In these catalytic reactions, isomerization and hydrogenation of olefins and acetylenes have been particularly studied, as has been reviewed recently.[1,2] It has been accepted in many catalytic isomerizations and hydrogenations that the formation of the metal-hydride (M-H) bond and its reaction with unsaturated compounds are key steps in the overall reaction.[2,3] Many transition metal hydrides have been found and several insertion reactions of olefins into M-H bonds have been reported.[4]

Stable hydride complexes of platinum(II), *trans*-$PtHX(PH_3)_2$ (X=halogen *etc.*), were prepared by Chatt and Shaw.[5] Structural studies have been carried out on *trans*-$PtHX(PEt_3)_2$ (X=Cl and Br),[6,7] and spectroscopic studies such as NMR and IR have been reported.[5,8-11] However, little theoretical study has been done, even though it is necessary in order to investigate the bonding character of the Pt(II)-H bond.

It is wellknown that ethylene reacts with *trans*-$PtHCl(PEt_3)_2$ under vigorous conditions (95°C/80 atm) to give an ethylplatinum(II) complex:[5,12]

$$\textit{trans}\text{-}PtHCl(PEt_3)_2 + C_2H_4 \rightleftarrows \textit{trans}\text{-}Pt(C_2H_5)Cl(PEt_3)_2 \quad (1)$$

Several investigations have been carried out on the insertion reaction of ethylene in order to elucidate the reaction mechanism.[12-17] The suggestion has been accepted that both forward and reverse reactions proceed *via* five-coordinate π-olefinic hydride complexes.[12-13,17]

In this work, we have carried out semi-empirical SCF-MO calculations of hydride complexes of platinum(II) in order to investigate their electronic structures. Studies have also been done of the ethylene insertion reaction into the Pt(II)-H bond. We will discuss the electronic structure of the intermediate five-coordinate π-olefinic hydride complex, $PtHCl(PH_3)_2(C_2H_4)$. The ligand effects and the role of the Pt(II) ion in the ethylene insertion reaction will also be discussed. We have tried to anticipate the ligand effect on the catalytic abilities of *trans*-$PtHX(P_3R)_2$ in the hydrogen-deuterium (H-D) exchange reaction of ethylene.

MO Calculations and Geometries of Complexes

MO Calculations. The MO calculations were performed by the use of the CNDO-type MO method. This method gave reasonable results on tetrachloroplatinate, Zeise's salt, the Pt(0)-ethylene complex, the Pt(0)-acetylene complex, *etc.*[18] The approximations used in this MO method have been reported in detail elsewhere.[18] Here, let us describe important features. (1) The Fock-matrix elements are obtained by the CNDO-type approximations.[19] (2) The resonance integrals are evaluated by the Wolfsberg-Helmholz approximation,[20] where the parameter "K" is taken as 0.90 for AO pairs including a d-orbital and as 0.80 for AO pairs including only s- and p-orbitals.[18] (3) The one-center Coulomb repulsion integrals of the Pt atom are estimated by multiplying a correction factor by nonempirical values calculated by means of single Slater-type orbitals. (4) The two-center Coulomb repulsion integrals are evaluated by the use of a modified Ohno's approximation[18] for AO pairs including only one outer 6s- or 6p-orbital of the Pt atom and by the use of Ohno's original approximation[21] for the other AO pairs.

The quantity of E_{AB}[22,23] is used as the bond index in this work; it is defined as the energy contribution of the AB bond to the total energy. Under the approximations used here, E_{AB} is written as follows;[19]

$$E_{AB} = E_{AB}^{(1)} + E_{AB}^{(2)} + E_{AB}^{(3)} \quad (2)$$

$$E_{AB}^{(1)} = 2.0\sum_r^A\sum_t^B P_{rt}H_{rt} \quad (3)$$

$$E_{AB}^{(2)} = -0.5\sum_r^A\sum_t^B P_{rt}^2\gamma_{rt} \quad (4)$$

$$E_{AB}^{(3)} = \sum_r^A\sum_t^B (P_{rr}-N_r)(P_{tt}-N_t)\gamma_{rt} \quad (5)$$

where $E_{AB}^{(1)} + E_{AB}^{(2)}$ and $E_{AB}^{(3)}$ represent approximately

a covalent bonding interaction and an electrostatic one respectively. The negative value of E_{AB} indicates the bonding interaction. The larger the absolute value of E_{AB}, the greater the interaction between A and B atoms becomes.

Geometries of Complexes. trans-*PtHX*$(PR_3)_2$: The bond lengths of the Pt–Cl and Pt–Br were taken from X-ray studies,[6,7] while those of the other Pt–X bonds were estimated from the covalent bond radii of X's. The bond lengths of the Pt–P and Pt–H bonds were fixed as 2.268 and 1.62 Å respectively for all the complexes. While the ∠PPtCl and ∠PPtBr angles were slightly larger than 90° as a result of the steric effects of Cl and Br ligands,[6,7] ∠PPtX was assumed to be 90° in all the complexes, for the value of this angle had not been known in the other complexes. The PR_3 group (R=phenyl or alkyl group) was replaced by the PH_3 group for the sake of simplicity; its structure was assumed to be the same as that of the uncomplexed one.[24] In spite of these simplifications, MO calculations on these models gave reasonable and sufficient results to enable us to discuss the ligand effect of X, as will be described in the following section.

trans-*PtX*$(C_2H_5)(PH_3)_2$: Since no X-ray study had been carried out on this complex, the bond lengths of the Pt–C and Pt–Cl bonds were taken from the structure of $[Pt(CH_3)_3Cl]_4$,[24] and the Pt–P bond length was fixed in all the complexes. The bond lengths of the other Pt–X bonds were estimated in the same way as those in *trans*-$PtHX(PH_3)_2$. The Pt–P bond length and the structure of the PH_3 group were assumed to be the same as the corresponding ones in *trans*-$PtHX(PH_3)_2$. In these complexes, the structure of the ethyl group was taken from Ref. 24, while only the β-hydrogen atom of the ethyl group was brought slightly close to the Pt atom (β-H–Pt=2.22 Å [25] and β-H–C=1.09 Å) when the abstraction of the β-hydrogen atom was investigated.

Five-coordinate π-Olefinic Hydride Complexes and an Insertion Reaction of Ethylene into the Pt(II)–H Bond. Two types of five-coordinate intermediate complexes were investigated in the insertion reaction of ethylene into the Pt(II)–H bond; they are shown in Fig. 1. In both structures, the structure of the ethylene part was assumed to be the same as the uncomplexed one. The coordination bond of ethylene was also assumed to intercept the double bond of ethylene perpendicularly at its center, and the coordination bond distance was fixed as 2.0 Å by reference to that of Zeise's salt.[26] The A structure can be expected from the substitution reaction of *trans*-$Pt(NO_3)H(PEt_3)_2$ with ethylene which was reported by Deening *et al.*[15] The B structure has been proposed by Uguagliati *et al.*;[14] also, a similar intermediate complex has been isolated by Clark *et al.* in the insertion reaction of tetracyanoethylene with *trans*-$Pt(CH_3)(CN)(PEt_3)_2$.[16]

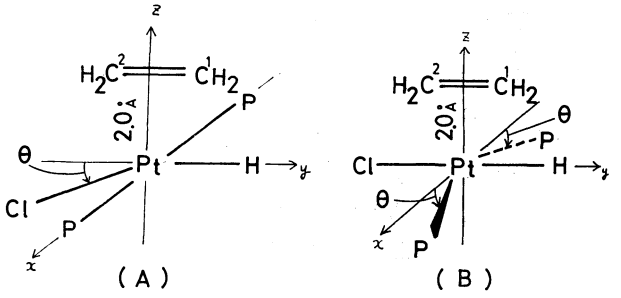

Fig. 1. Five-coordinate π-olefinic hydrido-complexes. P; PH_3. The bond distances of the Pt–P, Pt–H and Pt–Cl and the structure of the PH_3 group are the same as those in the *trans*-$PtHCl(PH_3)_2$.

Since the B structure was more stable than that of A, as will be described below, the insertion reaction was considered to proceed from the B structure (θ=45°); the three reaction paths shown in Fig. 2 were investigated. In the C reaction path, ethylene approaches the hydride ligand parallel with the Pt–H bond. Also, in the D reaction path, ethylene approaches the hydride ligand. In this attack, the δ angle between the coordination bond of ethylene and the z-axis increases, the other part does not vary. In the E reaction path, the hydride ligand attacks ethylene, where the δ angle between the Pt–H bond and the y-axis increases, while the other part does not vary. The states in which hydrogen atoms were displaced out of the original ethylene plane opposite to the Pt atom (10°) were investigated in two reaction paths, D and E; only the $C(1)H_2$ group was bending in the IV state, and both $C(1)H_2$ and $C(2)H_2$ groups were bending in the V state.

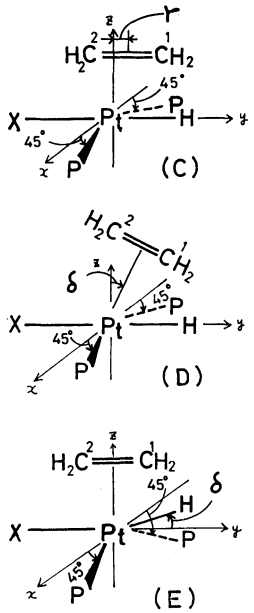

Fig. 2. Insertion reaction paths of ethylene into the Pt(II)–H bond.
P; PH_3. In the reaction paths C and D, the $PtHCl(PH_3)_2$ is the same as the state V of the five-coordinate intermediate B (Fig. 1). In the reaction path E, the H ligand transfers to ethylene and the other part is the same as the state V of the intermediate B.

Results and Discussion

Electronic Structures of trans-*PtHX*$(PH_3)_2$. The results are given in Table 1. The electron density on the Pt atom increases with the decrease in the elec-

TABLE 1. ELECTRONIC STRUCTURES OF *trans*-$PtHX(PH_3)_2$

	Electron density				E_{Pt-H} (eV)	$E^{(1)+(2)}_{Pt-H}$ (eV)	$E^{(3)}_{Pt-H}$ (eV)	ν_{Pt-H}[a] (cm^{-1})
	Pt	H	X	P				
F	9.710	1.289	7.658	5.217	−13.882	−12.783	−1.099	—
Cl	9.846	1.255	7.583	5.222	−13.627	−12.877	−0.750	2183
Br	9.863	1.246	7.584	5.223	−13.585	−12.890	−0.695	2178
I	9.900	1.245	7.541	5.221	−13.480	−12.850	−0.630	2156
CN	9.904	1.242	9.552[b]	5.231	−13.446	−12.833	−0.613	2041

a) Ref. 9. b) The electron density on the CN group.

tronegativity of the X ligand; *i.e.*, F<Cl<Br<I<CN. The H ligand has a remarkably large negative charge, suggesting its hydride character. The electron density on the H ligand decreases with an increase in the electron density on the Pt atom and with a decrease in the electron density on the halogen. This result seems to be similar to the alternative inductive effect;

$$\overset{\delta-}{X}\!\!-\!\!\overset{\delta+}{Pt}\!\!-\!\!\overset{\delta-}{H}$$

Scheme I.

However, this result cannot be explained by hyperconjugation, since the Pt–H bond is not contributed to by hyperconjugation. Because the energy levels of the Pt's valence orbitals decrease as the X ligand goes from F^- to CN^-,[27] the electron transfer increases in this order; F<Cl<Br<I<CN, and the electron density on the H ligand decreases in this order; F>Cl>Br>I>CN.

The absolute value of E_{Pt-H} decreases in this order; F>Cl>Br>I>CN, suggesting that the strength of the Pt–H bond also decreases in this order. From the frequencies of the stretching vibration, ν_{Pt-H}, it is expected that the strength of the Pt–H bond decreases in this order; Cl>Br>I>CN,[9,11] since ν_{Pt-H} gives a measure of the strength of the Pt–H bond. Thus, our finding on the strength of the Pt–H bond agrees qualitatively with the experimental findings. The value of E_{Pt-H} is mainly contributed to by the $E_{Pt-H}{}^{(1)}$ and $E_{Pt-H}{}^{(2)}$, as is shown in Table 1; this suggests the covalent bonding character of the Pt–H bond.

Five-coordinate π-Olefinic Hydride Complexes. The various conformations of the A and B structures (see Fig. 1) were investigated, as is shown in Fig. 3 and Table 2. The increase in θ does not bring about the stabilization of the A structure, but that of the B structure, which is the most stable at $\theta=45°$. In the B structure, the steric repulsion between PH_3 and ethylene decreases greatly. However, it does not change in the A structure, while the streic repulsion between Cl and ethylene decreases. Therefore, the B structure is more favorable than the A structure for the intermediate five-coordinate complex. We will hereafter consider the insertion reaction of ethylene into the Pt(II)–H bond in the B structure.

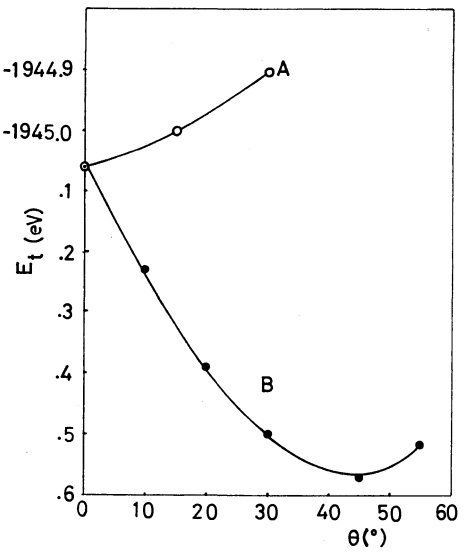

Fig. 3. Total energies of five-coordinate π-olefinic hydrido-complexes, $PtHCl(PH_3)_2(C_2H_4)$.
○: The structure A. ●: The structure B (see Fig. 1.)

An increase in θ brings about an increase in the bonding interaction between the Pt atom and ethylene in both structures, A and B; the absolute value of $E_{Pt-C(1)}+E_{Pt-C(2)}$ also increases with an increase in θ, as is shown in Table 2. In the A structure ($\theta\neq0$), the $5d_{z^2}$ and $5d_{yz}$ orbitals of the Pt atom are bonding

TABLE 2. ELECTRONIC STRUCTURES OF FIVE-COORDINATE π-OLEFINIC HYDRIDO-COMPLEXES

	(a) Structure A			(b) Structure B[d]				
State	I	II	III	II	III	IV	V	VI
θ	0°	15°	30°	10°	20°	30°	45°	55°
$E_{Pt-C(1)}+E_{Pt-C(2)}$	−11.26	−11.46	−11.76	−11.77	−12.35	−12.89	−13.40	−13.72
E_{C-H}[a]	−0.27	−0.29	−0.31	−0.39	−0.44	−0.58	−0.62	−0.63
P_π[b]	0.86	0.86	0.85	0.84	0.82	0.81	0.79	0.78
Δq[c]	0.14	0.13	0.12	0.17	0.21	0.24	0.28	0.29

E_{AB}; eV unit. a) H=the hydride ligand of *trans*-$PtHX(PH_3)_2$. b) The π-bond order of ethylene part. c) The quantity of transferred electrons from ethylene to *trans*-$PtHX(PH_3)_2$ part. d) The state I is the same as that in the structure A.

orbitals, while these are very weak bonding orbitals in the square pyramidal complex. Ethylene donates its electrons to the $5d_{z^2}$ orbital and accepts d-electrons from the $5d_{yz}$ orbital into its π^*-MO, while it scarcely interacts with these d-orbitals in the square pyramidal complex. Of course, ethylene donates its π-electrons to the $6p_z$ orbital of the Pt atom in both the square pyramidal and trigonal bipyramidal complexes. Thus, the interaction between the Pt atom and ethylene is larger in the trigonal bipyramidal complex (A) than in the square pyramidal one; this results in the larger absolute value of $E_{Pt-C(1)}+E_{Pt-C(2)}$ in the former than in the latter. Decreases in the π-bond order of ethylene, P_π, and the quantity of transferred electrons from ethylene, Δq, suggest a greater increase in the π-acceptor bond than in the σ-donor bond, as is shown in Table 2. In the B structure, the $5d_{z^2}$ and $5d_{xz}$ orbitals of the Pt atom also become bonding orbitals. The $5d_{xz}$ orbital can not interact with ethylene, as is shown in Fig. 1. Ethylene donates its π-electrons to the $5d_{z^2}$ orbital of the Pt atom through the σ-donor bond, while it scarcely donates its π-electrons to the $5d_{z^2}$ orbital in the square pyramidal complex. The formation of this interaction brings about increases in the Δq and the $E_{Pt-C(1)}+E_{Pt-C(2)}$ and the decrease in the P_π.

TABLE 3. INSERTION REACTION OF ETHYLENE INTO Pt(II)–H BOND

(a) Reaction path C

State	I	II	III
r(Å)	0.0	0.3	0.6695
E_{total}	−1945.6	−1945.5	−1945.0
E_{C-H} [a]	−0.62	−1.27	−1.86
E_{Pt-H} [a]	−12.59	−12.23	−11.90
E_{C-C}	−29.81	−29.89	−30.27
$E_{Pt-C(1)}$	−6.65	−5.04	−3.01
$E_{Pt-C(2)}$	−6.75	−8.08	−8.66

(b) Reaction path D [b]

State	II	III	IV [c]	V [d]
δ	10°	30°	30°	30°
E_{total}	−1945.7	−1947.7	−1947.7	−1947.7
E_{C-H} [a]	−1.69	−7.83	−8.31	−8.37
E_{Pt-H} [a]	−11.82	−8.44	−8.49	−8.45
E_{C-C}	−29.61	−27.67	−27.57	−27.42
$E_{Pt-C(1)}$	−6.24	−5.68	−5.81	−5.81
$E_{Pt-C(2)}$	−7.25	−8.43	−8.49	−8.74

(c) Reaction path E [b]

State	II	III	IV [c]	V [d]
δ	10°	30°	30°	30°
E_{total}	−1946.1	−1947.7	−1947.6	−1947.6
E_{C-H} [a]	−2.40	−7.39	−7.87	−7.92
E_{Pt-H} [a]	−11.58	−9.04	−9.09	−8.94
E_{C-C}	−29.28	−27.90	−27.79	−27.68
$E_{Pt-C(1)}$	−6.21	−5.76	−5.90	−5.90
$E_{Pt-C(2)}$	−7.14	−7.75	−7.81	−8.02

E_{total} and E_{AB}; eV unit. a) H=the hydride ligand of *trans*-$PtHX(PH_3)_2$. b) The state I is the same as that in the reaction path C. c) Hydrogen atoms bonded to the C(1) atom were displaced out of the original ethylene plane opposite to the Pt atom, while the other parts are unchanged as the state III. d) Hydrogen atoms bonded to the C(1) and C(2) atoms were displaced out of the original ethylene plane opposite to the Pt atom, and the other parts were unchanged.

TABLE 4. LIGAND EFFECT OF HALOGENS IN THE INSERTION REACTION OF ETHYLENE INTO Pt(II)–H

Reaction path D, State III

		F	Cl	Br	I	CN
Electron density	Pt	9.98	10.12	10.15	10.18	10.20
	C(1)	4.09	4.09	4.09	4.09	4.09
	C(2)	4.27	4.25	4.24	4.24	4.23
	H [a]	0.99	0.96	0.95	0.95	0.94
E_{C-H} [a]		−7.78	−7.83	−7.84	−7.86	−7.91
E_{Pt-H} [a]		−8.43	−8.44	−8.44	−8.42	−8.37
E_{C-C}		−27.64	−27.67	−27.67	−27.68	−27.72
$P_{\pi C(2)}$		1.19	1.15	1.14	1.14	1.13
ΔQ [b]		1.13	1.20	1.22	1.22	1.24

E_{AB}; eV unit. a) H=the hydride ligand coordinating to Pt(II). b) The quantity of transferred electrons from the system $C_2H_4+H^-$ to $PtX(PH_3)_2^+$ part.

Inserion Reaction of Ethylene. The results on the reaction paths and those on the ligand effect in this reaction are shown in Tables 3 and 4 respectively.

In the C reaction path, the total energy increases slightly. The absolute values of E_{C-H}, E_{C-C}, and $E_{Pt-C(2)}$ increase as the reaction proceeds from the I state to the III state, while those of $E_{Pt-C(1)}$ and E_{Pt-H} decrease. (In this paper, the H's of the Pt–H and C–H represent the hydride coordinated to the Pt atom.) These results show the increase in the C–H interaction. However, the increase in the absolute value of E_{C-C} suggests an increase in the strength of C–C bond. This rules out the C reaction path, because the C=C double bond must become a C–C single bond after an insertion reaction.

In the D reaction path, the total energy decreases as the reaction proceeds from the I state to the III state.[31] The absolute values of E_{C-H} and $E_{Pt-C(2)}$ increase in this reaction course, while those of E_{Pt-H}, E_{C-C}, and $E_{Pt-C(1)}$ decrease. These results reveal that the C–H and Pt–C(2) interactions become stronger and that the Pt–H, Pt–C(1), and C–C interactions become weaker. This situation agrees with that in the four-center-type reaction;[28]

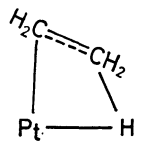

Scheme II.

Therefore, the D reaction path is reasonable for the ethylene insertion reaction.

In the E reaction path, the total energy decreases as the reaction proceeds from the I state to the III state.[31] The bonding interactions of the C–H and Pt–C(2) bonds become stronger and those of the C–C, Pt–C(1), and Pt–H bonds become weaker, similarly to those of

the D reaction path, as the reaction proceeds. The E reaction path also seems reasonable.

In two reaction paths, D and E, the bending of the CH_2 group, in which hydrogen atoms are displaced out of the original ethylene plane opposite to the Pt atom, brings about increases in the absolute values of E_{C-H} and $E_{Pt-C(2)}$, and decreases in those of $E_{Pt-C(1)}$ and E_{C-C}, while it scarcely changes the total energy (see the IV and V states in Table 2). These results suggest the bending of the CH_2 groups is brought about in this reaction course; this corresponds to the C(1) and C(2) atoms becoming sp^3 character from their original sp^2 character.

It is worthwhile to investigate which ligand, ethylene or hydride, transfers in the ethylene insertion reaction. As is shown in Table 3, the II state in the E reaction path has a lower total energy, a larger absolute value of E_{C-H}, and smaller absolute value of E_{Pt-H} and E_{C-C} than that in the D reaction path; that is, the former state has a stronger C–H bonding interaction and weaker Pt–H and C–C bonding interactions than the latter one. From these results, the H ligand can be expected to transfer more easily than ethylene in the initial stage of the reaction. The following states, III—V, in the D reaction path have a larger absolute value of E_{C-H} and smaller ones of E_{Pt-H} and E_{C-C} than those in the E reaction path, while the reaction states in both reaction paths have almost the same total energies. These results suggest, at first glance, that ethylene transfers to the H ligand more favorably than the latter does to the former in the more advanced reaction states. In the E reaction path, however, the Cl ligand should also transfer, as is shown in Scheme III, as the reaction advances, since the final product is the square planar *trans*-$Pt(C_2H_5)Cl(PH_3)_2$.

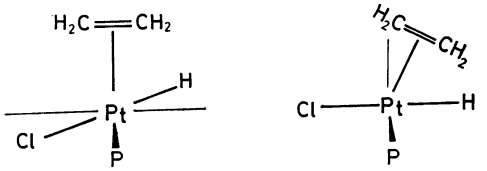

The more advanced reaction state in the reaction path E

The reaction path D

Scheme III.

The transfer of the Cl ligand in the E reaction path results in almost the same intermediate state as that in the D reaction path, while the position of PH_3 is slightly different. The III—V states in the D reaction path can reasonably be considered to be more advanced reaction states in the E reaction path. Thus, our results suggest that the H ligand starts first to attack ethylene and that then the Cl ligand starts to move to the *trans*-position of the H ligand. Of course, this problem should be studied in more detail experimentally and theoretically.

In order to investigate the role of the Pt(II) ion in the insertion reaction, a hypothetical state is studied; it is obtained by removing the $PtCl(PH_3)_2^+$ part from the III state in the D reaction path. This hypothetical state is considered to be a limiting state of the C_2H_4+

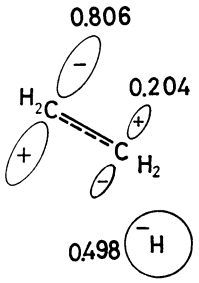

Fig. 4. AO coefficients of the HOMO of the hypothetical state, $C_2H_4+H^-$.

LiH reaction system in which the bond distance of Li–H is infinitely lengthened. This hypothetical state has the following characteristics: (1) The electron density on the C(2) atom is remarkably large (4.64 e); this is a result of the large electron density on its p_π orbital (1.84 e). (2) The highest occupied (HO) MO has a remarkably high orbital energy (−0.345 eV). (3) As is shown in Fig. 4, its HOMO has a non-bonding character; electrons are localized in the $2p_\pi$ orbital of the C(2) atom and the 1s orbital of the H atom. Where the Pt part exists, the MO of this type is obtained at about −10 eV and the $2p_\pi$ orbital of the C(2) atom interacts with the $5d_{z^2}$, 6s, and $6p_\pi$ orbitals of the Pt atom in the D reaction path, as is shown in Fig. 5.

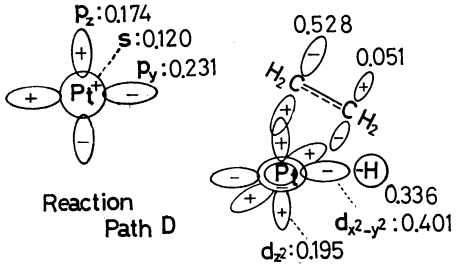

Fig. 5. AO coefficients of an important MO in the interaction between the C(2) and Pt atoms.

As a consequence of these interactions, the electron density on the $2p_\pi$ orbital of the C(2) atom, $P_{\pi C(2)}$, is remarkably reduced in $PtHX(PH_3)_2(C_2H_4)$ relative to the hypothetical state, as is shown in Table 4. Thus, it is the important role of the Pt atom to accept the excess π-electrons on the C(2) atom and to stabilize the HOMO of the hypothetical system. In other words, the insertion reaction mechanism may be represented as follows:

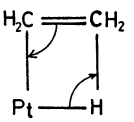

Scheme IV.

The ligand effects on the insertion reaction were studied in the III state of the D reaction path, as is shown in Table 4. In all the reaction systems, the electron density on the C(2) atom and the absolute value of $E_{Pt-C(2)}$ are larger than that on the C(1) atom and that of $E_{Pt-C(1)}$ respectively. The negative values of E_{C-H} in all the systems reveal the C–H bonding

interaction. Its absolute value increases in this order; F<Cl<Br<I<CN, while the absolute values of E_{Pt-H} and E_{C-C} decrease in the same order. Also, the values of ΔQ, which is defined as the quantity of transferred electrons from the $C_2H_4+H^-$ part to the $PtX(PH_3)_2^+$ part, increase, and the values of $P_{\pi C(2)}$ decrease, in this order. From these results, the reactivity of *trans*-$PtHX(PH_3)_2$ in the insertion reaction can be effected to increase in the same order. This order of increase agrees with the order of increase of the *trans*-effect of the X ligand; this is consistent with the experimental results.[29]

The decreasing order of ΔQ of F>Cl>Br>I>CN is the same order as in the electron transfer from the H ligand to the Pt part in *trans*-$PtHX(PH_3)_2$. The results for ΔQ in the former case may also be due to the same reason.[27]

Hydrogen-Deuterium Exchange Reaction. *trans*-$PtHCl(PEt_3)_2$ catalyzes the H–D exchange reaction of ethylene.[30] The H–D exchange reaction is composed of two steps: the ethylene insertion into the Pt(II)–H bond, and the β-hydrogen abstraction in the Pt(II)-ethyl complexes. The transition state in the β-hydrogen abstraction is considered to be the same as that in the ethylene insertion reaction. Therefore, it is only necessary to investigate the interaction between the Pt atom and the β-hydrogen of the ethyl group in the Pt(II)-ethyl complexes. The results are given in Table 5.

TABLE 5. THE INTERACTION BETWEEN Pt AND β-H ATOMS IN *trans*-$PtX(C_2H_5)(PH_3)_2$

		F	Cl	Br	I	CN
Electron density	Pt	9.98	9.96	9.98	10.01	10.03
	β-H[a]	0.82	0.82	0.82	0.82	0.82
E_{C-H}[a]		−0.60	−0.73	−0.75	−0.81	−0.80

E_{AB}; eV unit. a) H=β-H atom of ethyl group.

The absolute values of E_{Pt-H} increase in this order: F<Cl<Br<CN<I, as is shown in Table 5. The β-hydrogen atom is abstracted easily as follows: F<Cl<Br<CN<I. As has been described previously, the ligand effect on the reactivity in the ethylene insertion increases in this order: F<Cl<Br<I<CN. Therefore, the catalytic ability of *trans*-$PtHX(PR_3)_2$ in the H–D exchange reaction increases: F<Cl<Br<I; it is difficult to determine which is more active, the iodo- or the cyano-complex.

These calculations were carried out with Facom 230-75 Computer of the Data Processing Center in Kyoto University.

The authors are grateful to Professor Akio Yamamoto for his creative suggestion. They also wish to thank Dr. Hideyuki Konishi for his help with calculations.

References

1) R. E. Harmon, S. K. Gupta, and D. J. Brown, *Chem. Rev.*, **73**, 21 (1973).
2) F. R. Hartley, *ibid.*, **69**, 799 (1969).
3) R. Cramer, *J. Amer. Chem. Soc.*, **88**, 2272, 3533 (1966).
4) H. D. Kaesz and R. B. Saillant, *Chem. Rev.*, **72**, 231 (1972).
5) J. Chatt and B. L. Shaw, *J. Chem. Soc.*, **1962**, 5075.
6) P. G. Owston, J. M. Partridge, and J. M. Rowe, *Acta Crystallogr*, **13**, 246 (1960).
7) R. Eisenberg and J. A. Ibers, *Inorg. Chem.*, **4**, 773 (1965).
8) J. Powell and B. L. Shaw, *J. Chem. Soc.*, **1965**, 3879.
9) P. W. Atkins, J. C. Green, and M. L. H. Green, *J. Chem. Soc. (A)*, **1968**, 2275.
10) R. R. Dean and J. C. Green, *ibid.*, **1968**, 3047.
11) H. C. Clark and H. Kurosawa, *J. Organometallic Chem.*, **36**, 399 (1972).
12) J. Chatt, R. S. Coffey, A. Gough, and D. T. Thompson, *J. Chem. Soc. (A)*, **1968**, 190.
13) H. C. Clark and W. S. Tsang, *J. Amer. Chem. Soc.*, **89**, 529 (1967).
14) P. Uguagliati and W. H. Baddley, *ibid.*, **90**, 5446 (1968).
15) A. J. Deening, B. F. G. Johnson, and J. Lewis, *Chem. Comm.*, **1970**, 598.
16) H. C. Clark and R. J. Puddephatt *Inorg. Chem.*, **10**, 416 (1971).
17) A. J. Deening, B. F. G. Johnson, and J. Lewis, *J. Chem. Soc. Dalton*, **1973**, 1850.
18) S. Sakaki, H. Kato, and T. Kawamura, This Bulletin, **48**, 195 (1975).
19) S. Sakaki and H. Kato, *ibid.*, **46**, 2227 (1973).
20) H. Wolfsberg and L. Helmholz, *J. Chem. Phys.*, **20**, 837 (1952).
21) K. Ohno, *Theoret. Chim. Acta*, **2**, 219 (1964).
22) M. S. Gordon, *J. Amer. Chem. Soc.*, **91**, 3122 (1969).
23) S. E. Ehrenson and S. Seltzer, *Theoret. Chim. Acta*, **20**, 17 (1971).
24) "Tables of Interatomic Distances and Configuration in Molecules and Ions," by L. E. Sutton, The Chem. Soc., London, (1958).
25) β-H–Pt=2.876 Å in the equilibrium distance.
26) M. Black, R. H. B. Mais, and P. G. Owston, *Acta Crystallogr*, **B25**, 1753 (1969).
27) Under the approximations used here, a diagonal Fock matrix element is written as follows:
$F_{rr} = -I_r + \gamma_{rr} + (0.5 p_{rr} - N_r)\gamma_{rr} + \sum_{s \neq r} (p_{ss} - N_s)\gamma_{rs}$
Going from F to CN$^-$, the values of P_{rr} of the Pt atom increase and those of F_{ss} and γ_{rs} decrease, where r and s represent the valence orbitals of the Pt atom and those of the X ligand respectively. The increase in P_{rr} raises the value of F_{rr} through the third term on the right-hand side. However, the decreases in P_{ss} and γ_{rs} reduce the F_{rr} through the fourth term, since the $P_{rr}-N_{rr}$ is negative in these cases. The change in the value of the third term is less than that of the fourth one, mainly because of the change in the values of γ_{rs}. Thus, the values of F_{rr} decrease as a result of the fourth term as follows: F>Cl>Br>I>CN. This result is not because of our approximations but because of the fundamental nature of the X ligand; the atom which has contracted valence orbitals raises the energy of an electron of the other atom through the electronic repulsion integrals, relative to the atom whose orbitals expand largely.
28) S. Sakaki, H. Kato, H. Kanai, and K. Tarama, This Bulletin, **47**, 377 (1974).
29) R. Cramer and R. V. Lindsey, Jr., *J. Amer. Chem. Soc.*, **88**, 3534 (1966).
30) R. A. Schunn, *Inorg. Chem.*, **9**, 2567 (1970).
31) It has not been ascertained that the MO method used here can give a correct energy difference between the initial state (*trans*-$PtHCl(PH_3)_2+C_2H_4$) and the interacting state ($PtHCl(PH_3)_2(C_2H_4)$). While Table 3 gives us a negative activation enthalpy, it should be studied in more detail.

The Magnetic Properties of Verdazyl Free Radicals. VIII. The Crystal Structure of 1,3,5-Tri-*p*-tolylverdazyl Radical

Nagao AZUMA, Yasuo DEGUCHI, Fumiyuki MARUMO,* and Yoshihiko SAITO**

Department of Chemistry, Faculty of Science, Kyoto University, Kitashirakawa, Sakyo-ku, Kyoto 606
***The Institute for Solid State Physics, The University of Tokyo, Roppongi, Minato-ku, Tokyo 106*

(Received September 2, 1974)

The crystal structure of 1,3,5-tri-*p*-tolylverdazyl has been determined by X-ray diffraction. The crystals are monoclinic, with the space group of $P2_1/m$ and with $a=8.173(3)$, $b=20.23(1)$, $c=6.075(2)$ Å, $\beta=105.4(1)°$, and $Z=2$. The structure was deduced from the sharpened Patterson synthesis and refined by the block-diagonal least-squares method to the final R value of 0.048 for the 1212 non-zero reflections collected by the counter-method. The *sym*-tetrazinyl ring has an asymmetrical boat form. The molecules are arranged approximately parallel to the $(20\bar{1})$ plane. The maximum intermolecular overlap is observed between the *sym*-tetrazinyl and *C*-tolyl groups, suggesting a weak exchange interaction between unpaired electrons.

For studying the magnetic properties of radical solids with an unpaired electron delocalized over the whole molecular frame-work, precise knowledge about both the spin-density distribution and the crystal structure is of great importance. Based on such knowledge, the magnetic properties of 1,3,5-triphenylverdazyl and galvinoxyl radicals were discussed in a previous paper.[1] However, there has thus far been little systematic study in this area. Thereupon, crystal structure analyses were carried out on verdazyls, which exhibit magnetic properties different from one to another in spite of their similar spin-density distributions. Figure 1 shows a generalized canonical formula of the verdazyls of our interest. Their spin distributions have been published elsewhere.[2]

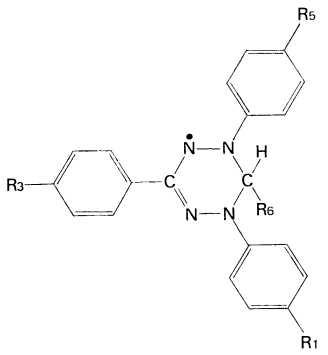

Fig. 1. Constitutional formula of verdazyl radicals. R_1, R_3, and R_5 stand for H, CH_3, and so on. R_6 is H or CH_3.

This and the following papers describe the crystal structures of 1,3,5-tri-*p*-tolylverdazyl (TTV), and 1,3,5-triphenyl-6-methylverdazyl (MeTPV)[3] respectively, whose magnetic susceptibilities indicate, respectively, a weak exchange interaction and a fairly strong isotropic exchange interaction between the unpaired electrons. The details of the magnetic properties of them and of other radicals will be presented in a separate paper.

Experimental

The TTV was prepared from *p*-tolualdehyde, *p*-toluidine, and formaldehyde by a method analogous to that described by Kuhn and Trischmann[4] (Found: C, 78.07; H, 6.65; N, 15.54%; Calcd for $C_{23}H_{23}N_4$: C, 77.72; H, 6.52; N, 15.76%). The crystals used for the structure analysis were obtained by standing a solution of TTV in a mixture of acetone and methanol at room temperature.

Table 1. Crystal data

Molecular formula	$C_{23}H_{23}N_4$
Molecular weight	355.5
Melting point	137—138 °C
Specimen used for the data collection	*ca.* (0.25 mm)^3
Crystal system	Monoclinic
Cell dimensions;	
a	8.173±0.003Å
b	20.23±0.01
c	6.075±0.002
β	105.4±0.1°
V	968.2Å^3
Z	2
Density (calculated)	1.222 g/cm^3
Density (observed by flotation)	1.214
$F(000)$	378
Linear absorption coefficient	0.9 cm^{-1} (Mo$K\alpha$)
Systematic absence	$0k0$: $k=2n+1$
Space group	$P2_1/m$ or $P2_1$

The unit-cell dimensions obtained from Weissenberg photographs were refined by the least-squares method by employing higher-order reflections measured on an automated four-circle diffractometer with Mo$K\alpha$ radiation ($\lambda=0.7107$ Å) monochromated by a graphite crystal. The crystal data are given in Table 1. The intensities of 2321 independent reflections up to $2\theta=55°$ were measured on the same diffractometer using Mo$K\alpha$ radiation. An ω–2θ scan technique was employed. The reflections with $|F_o|$ values of less than $(10/3)\sigma(F_o)$ were measured up to four times. The intensities were corrected for Lorentz and polarization effects. Neither absorption nor extinction corrections were made. A total of 1212 reflections with $|F_o|$ values not less than $2.5\sigma(F_o)$ were regarded as non-zero reflections and were used for the structure analysis.

Structure Determination and Refinement

Wilson's statistics indicated the presence of a center of symmetry. A three-dimensional Patterson map showed 98 resolved peaks in an asymmetric unit. Of

* Present address: Research Laboratory of Engineering Materials, Tokyo Institute of Technology, Ookayama Meguro-ku, Tokyo 152.

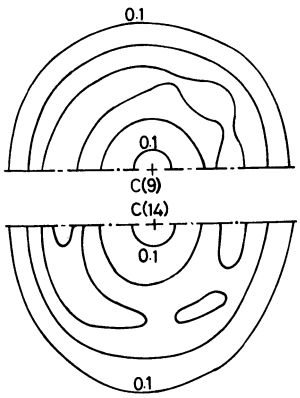

Fig. 2. Difference Fourier maps of the methyl hydrogen atoms. The sections correspond to the planes defined by the methyl hydrogen atoms. The contours are at intervals of 0.1 e/Å^3. The numbering system is referred to Fig. 3.

these, seven prominent peaks were arranged on a line $(0, v, 0)$; this suggested the presence of a plane of symmetry. Accordingly, the space group of $P2_1/m$ was adopted. The starting model was deduced from the Patterson map with the aid of the molecular geometry of 1,3,5-triphenylverdazyl (TPV).[5] This model gave an R value of 0.27.

The block-diagonal least-squares refinement was then undertaken; the R value decreased to 0.12 after four cycles of refinement with individual isotropic thermal parameters. Three further cycles of refinement with anisotropic thermal parameters reduced the R value to 0.095. At this stage, a difference Fourier map was synthesized, from which the positions of the eight ring-hydrogen atoms were located. With anisotropic thermal parameters for the non-hydrogen atoms and isotropic ones for the hydrogen atoms, four cycles of refinement reduced the R value to 0.071. A new difference Fourier map was then computed. As is shown in Fig. 2, there were annular distributions of the residual electron densities near the methyl carbon atoms. The following approximation was then introduced tentatively in order to execute further refinement. The methyl groups ($-CH_3$) were replaced by $-CH_6$, in which the atomic weights for the hydrogen atoms were one half of those for the corresponding ordinary methyl hydrogen atoms. Of course, the $-CH_6$ groups satisfied the symmetry required. The C–H bond length was obtained by inspecting the residual electron-density map. The refinement was continued until all the positional shifts for the non-hydrogen atoms became less than 0.25 σ. The final R value was 0.048 for the 1212 reflections.

Unit weight was given to all the reflections. The atomic scattering factors used were taken from "International Tables for X-Ray Crystallography."[6] The final atomic coordinates and anisotropic thermal parameters of the non-hydrogen atoms are listed in Tables 2 and 3 respectively. The final parameters for the hydrogen atoms are shown in Table 4. The observed and calculated structure factors are compared in Table 5.

TABLE 2. THE FRACTIONAL ATOMIC COORDINATES AND THEIR ESTIMATED STANDARD DEVIATIONS IN PARENTHESES

Atom	x[a]	y[a]	z[a]
C (1)	−606 (6)	2500	−107 (7)
C (2)	−2183 (5)	2500	−4450 (7)
C (3)	433 (4)	3635 (1)	−685 (5)
C (4)	1169 (4)	3725 (2)	1640 (5)
C (5)	2157 (4)	4275 (2)	2389 (5)
C (6)	2431 (4)	4756 (2)	920 (6)
C (7)	1643 (4)	4668 (2)	−1381 (6)
C (8)	680 (4)	4116 (2)	−2178 (5)
C (9)	3485 (5)	5355 (2)	1775 (7)
C (10)	−3460 (5)	2500	−6679 (7)
C (11)	−4060 (4)	3086 (2)	−7763 (5)
C (12)	−5183 (4)	3082 (2)	−9913 (6)
C (13)	−5727 (5)	2500	−11042 (7)
C (14)	−6888 (6)	2500	−13418 (8)
N (1)	−515 (3)	3071 (1)	−1506 (4)
N (2)	−1598 (3)	3090 (1)	−3616 (4)

a) The coordinates have been multiplied by 10^4.

TABLE 3. THE ANISOTROPIC THERMAL PARAMETERS[a] AND THEIR ESTIMATED STANDARD DEVIATIONS IN PARENTHESES[b]

Atom	B_{11}	B_{22}	B_{33}	B_{12}	B_{13}	B_{23}
C(1)	280(11)	23(1)	277(14)		98(10)	
C(2)	149(7)	23(1)	266(12)		68(8)	
C(3)	155(5)	23(1)	287(9)	3(2)	48(5)	−7(2)
C(4)	238(7)	29(1)	285(9)	−3(2)	51(7)	−4(3)
C(5)	213(7)	35(1)	326(11)	−5(2)	24(7)	−26(3)
C(6)	161(6)	28(1)	445(12)	−2(2)	76(7)	−25(3)
C(7)	189(6)	27(1)	410(12)	−3(2)	87(7)	2(3)
C(8)	182(6)	26(1)	300(10)	0(2)	52(6)	2(3)
C(9)	211(7)	35(1)	623(17)	−22(3)	88(9)	−46(4)
C(10)	135(7)	23(1)	278(13)		69(8)	
C(11)	187(6)	23(1)	353(11)	3(2)	20(6)	−7(2)
C(12)	187(6)	26(1)	361(10)	8(2)	21(6)	14(3)
C(13)	136(7)	31(1)	297(14)		48(8)	
C(14)	174(9)	41(2)	324(15)		20(9)	
N(1)	211(5)	23(1)	243(7)	−5(2)	43(5)	−0(2)
N(2)	173(5)	24(1)	267(7)	−2(1)	33(5)	−1(2)

a) The anisotropic thermal parameters are of the form: $\exp[-(B_{11}h^2+B_{22}k^2+B_{33}l^2+2B_{12}hk+2B_{13}hl+2B_{23}kl)]$. b) The values have been multiplied by 10^4.

TABLE 4. THE FINAL PARAMETERS FOR HYDROGEN ATOMS AND THEIR ESTIMATED STANDARD DEVIATIONS IN PARENTHESES

Atom	x[a]	y[a]	z[a]	B_{iso}
H(Cl–1)	−181(6)	250	20(8)	5.5(13)
H(Cl–2)	48(5)	250	125(6)	2.9(8)
H(C4)	106(4)	337(2)	277(5)	4.7(8)
H(C5)	284(3)	430(1)	400(4)	2.7(6)
H(C7)	179(4)	505(2)	−245(5)	4.4(8)
H(C8)	−1(4)	409(1)	−379(5)	3.3(6)
H(C11)	−364(4)	351(1)	−698(5)	3.6(7)
H(C12)	−561(4)	352(2)	−1067(5)	4.2(7)

a) The coordinates have been multiplied by 10^3.

TABLE 5. THE OBSERVED AND CALCULATED STRUCTURE FACTORS ($\times 10$)

K	FO	FC	K	FO	FC	K	FO	FC	K	FO	FC	K	FO	FC	K	FO	FC	K	FO	FC	K	FO	FC
H,L = -1,-7			4	33	29	5	32	26	7	32	23	H,L = 0,-7			5	23	20	H,L = 1,-7			2	27	32
4	30	27	H,L = 2,-7			0	28	32	1	29	28	2	34	34	4	19	25	7	21	20	11	28	22
H,L = 3,-7			7	25	27	8	39	38	11	20	19	H,L = 4,-7			1	32	36	8	44	48			
9	43	47	10	30	36	H,L = 5,-7			1	49	47	2	29	30	6	39	40	H,L = 6,-7			1	51	52
H,L = 7,-7			2	45	51	H,L = -5,-6			1	18	16	5	29	25	8	27	24	0	41	34	8	32	32
9	53	46	H,L = -2,-6			1	14	15	12	26	23	H,L = -1,-6			1	24	22	2	50	53	9	28	26
2	35	39	6	18	9	3	32	32	13	22	24	14	22	19	H,L = 0,-6			0	37	40	2	62	69
3	55	55	4	33	28	5	20	25	6	21	19	7	26	27	12	28	25	14	44	44	15	30	30
4	35	35	H,L = 1,-6			7	22	22	9	29	27	9	34	39	13	28	27	15	30	32	8	32	33
10	21	15	16	20	22	H,L = 2,-6			0	36	35	1	37	33	3	51	55	4	43	46	5	32	31
6	36	39	7	75	74	8	71	73	9	95	97	10	34	38	11	37	39	16	26	26	H,L = 3,-6		
7	36	36	1	36	36	2	30	28	3	70	76	4	101	105	5	26	22	16	62	65	5	55	56
9	32	38	10	62	67	12	32	30	14	37	39	15	31	32	H,I = 4,-6			0	125	127	1	57	61
2	30	32	3	27	25	4	22	22	15	21	25	H,L = 5,-6			0	133	137	1	56	56	2	26	28
3	27	28	14	20	21	H,L = 2,-5			1	29	33	2	30	33	3	124	133	4	82	84	9	30	26
H,L = 7,-6			1	27	26	2	33	32	H,L = 8,-6			5	33	30	H,L = -5,-5			3	47	43	7	32	29
9	69	68	H,L = -4,-5			0	31	30	6	25	23	7	35	29	13	22	19	H,I = -3,-5			0	82	87
1	33	37	19	18	11	2	24	22	15	16	15	H,L = -2,-5			0	96	102	1	60	61	3	51	43
9	37	41	10	57	58	11	26	17	15	28	24	H,L = -1,-5			1	29	33	2	21	30	3	14	16
4	58	60	7	24	23	9	87	87	10	34	36	H,L = 0,-5			0	76	75	1	56	58	2	32	36
3	40	40	5	29	32	6	40	46	7	172	172	8	84	90	9	32	32	10	68	68	11	58	60
15	25	23	16	29	30	17	22	19	18	24	16	H,L = 1,-5			2	24	24	5	82	83	4	95	102
5	54	54	6	188	189	7	120	124	8	105	107	9	29	26	10	101	105	11	53	57	12	124	126
13	48	52	14	20	21	H,L = 2,-5			0	29	33	2	99	91	3	124	133	4	82	84	9	30	26
8	37	42	14	38	37	15	50	48	16	57	59	H,L = 3,-5			0	204	208	2	95	93	3	84	87
4	60	62	7	39	43	8	25	26	9	28	22	10	36	36	11	29	34	12	22	21	14	17	23
15	49	49	16	27	28	18	53	54	1	4,-5		2	113	109	1	25	30	2	60	65	3	51	48
5	27	29	6	33	30	7	37	38	12	43	46	13	29	36	16	27	25	18	32	34	19	28	32
H,L = 3,-5			0	62	63	1	44	44	3	17	17	8	28	30	9	43	46	17	26	30	18	33	33
H,L = 6,-5			1	45	43	4	34	34	7	27	27	9	31	32	11	33	33	H,L = 7,-5			0	34	39
1	40	36	7	47	45	9	42	42	13	13	8	19	17	17	H,L = 8,-5			0	52	52	2	25	24
2	33	32	H,L = 9,-5			1	38	39	3	55	57	H,L = -7,-4			5	31	29	H,L = -6,-4			10	20	19
H,L = -5,-4			2	28	27	3	29	29	4	58	52	7	20	21	14	38	36	H,L = -4,-4			0	113	118
1	31	32	2	17	17	4	6	6	5	27	26	8	46	51	9	31	34	11	14	18	13	51	45
13	28	27	16	55	47	H,L = -3,-4			0	24	23	2	38	40	3	13	12	4	28	29	6	90	95
7	61	61	8	66	66	9	58	58	11	55	55	12	72	70	H,L = -2,-4			0	60	60	1	67	65
2	42	46	3	61	61	5	37	37	6	27	27	7	87	92	7	67	69	9	26	26	10	258	258
10	35	37	12	66	66	13	16	14	14	14	12	16	24	22	18	23	20	H,L = -1,-4			0	50	46
1	13	19	3	19	17	4	38	37	5	27	26	6	225	252	7	46	46	8	199	201	9	250	254
10	195	203	11	29	29	12	109	110	17	29	21	17	12	H,L = 0,-4			0	180	186	1	26	25	28
2	27	29	3	13	19	4	69	71	5	137	138	6	78	85	7	50	53	8	41	44	9	26	24
10	35	39	11	21	21	12	96	94	15	111	112	14	68	65	15	18	22	17	26	27	H,L = 1,-4		
20	206	199	1	21	23	2	149	156	3	61	55	4	23	28	5	108	110	6	101	107	8	49	52
9	41	41	10	31	25	11	32	35	12	109	110	13	81	86	14	27	21	16	92	96	17	29	26
18	37	47	1	H,L = 2,-4		10	93	98	1	129	131	2	30	25	3	61	60	4	170	171	9	28	25
6	25	31	7	58	53	10	22	22	18	12	13	4	14	17	7	67	65	8	18	17	18	38	37
19	27	30	H,L = 3,-4			0	40	43	1	32	36	4	34	36	5	24	20	6	48	48	7	47	49
8	52	55	11	25	32	12	36	42	13	15	20	14	45	48	15	40	37	16	35	30	H,L = 4,-4		
1	50	49	2	55	55	3	55	53	6	116	114	7	21	19	9	30	32	12	26	26	14	26	25
17	51	48	18	21	19	19	36	34	H,L = 5,-4			1	18	15	2	65	71	3	85	87	5	39	40
6	55	52	7	65	66	8	29	31	9	120	122	11	21	29	12	29	29	15	37	36	18	21	15
H,L = 6,-4			0	106	110	1	4	2	3	77	72	5	53	57	7	18	16	8	50	50	12	46	45
15	39	37	18	45	40	H,L = 7,-4			0	109	119	1	118	122	2	16	11	3	40	42	5	20	17
6	24	18	7	29	25	9	42	41	11	26	27	12	29	22	13	33	38	15	36	32	17	56	51
H,L = 8,-4			0	51	55	1	55	55	5	43	43	6	50	54	8	28	24	13	28	25	18	38	37
8	31	26	9	36	31	10	22	6	H,L = 10,-4			1	14	13	5	35	32	H,L = -8,-3			7	21	9
H,L = -7,-3			0	43	42	2	24	24	7	26	18	H,L = -6,-3			0	77	80	1	35	32	2	58	56
3	32	29	4	45	46	8	22	18	10	29	24	13	28	25	14	23	20	15	28	30	16	32	28
16	57	51	H,L = -5,-3			0	49	50	3	57	58	4	122	119	5	72	73	7	57	54	8	32	30
10	14	17	11	64	60	14	65	61	17	16	12	H,L = -4,-3			0	53	47	1	55	53	2	17	22
3	36	37	4	28	26	5	126	126	7	171	173	8	34	33	11	34	33	12	30	34	13	34	34
16	24	23	18	25	19	H,L = -3,-3			0	52	54	1	11	2	2	71	67	4	73	78	5	36	32
6	72	70	7	170	170	8	329	333	9	119	117	10	244	240	11	49	51	22	36	30	H,L = -2,-3		
2	132	133	3	133	131	5	73	71	6	47	44	7	47	41	9	68	67	10	96	97	11	116	114
9	115	115	10	94	92	11	141	141	12	79	82	14	28	27	15	23	18	17	36	37	21	31	31
H,L = -1,-3			0	254	244	1	93	86	2	105	100	3	103	96	4	20	16	5	75	74	6	86	85
7	54	56	8	57	52	9	75	82	10	146	143	11	38	40	12	31	33	13	50	54	14	60	58
16	39	44	17	43	44	18	52	56	H,L = 0,-3			0	129	122	1	343	328	2	284	276	3	125	119
4	79	70	5	31	22	6	25	32	8	38	34	11	68	64	12	111	114	13	66	66	15	80	91
16	97	97	17	88	93	19	49	54	20	15	14	H,L = 1,-3			0	98	94	1	56	56	2	25	22
3	42	44	4	142	138	5	88	83	6	71	66	7	81	74	8	49	39	9	45	43	12	55	58
13	92	92	14	53	55	15	19	11	24	13	14	H,L = 2,-3			1	132	134	2	52	46	3	161	159
4	96	95	5	139	137	6	63	62	7	15	19	8	76	77	9	108	103	10	55	56	12	40	39
13	27	27	14	41	49	15	38	38	16	29	28	21	39	38	23	26	22	1	118	116	2	39	41
1	45	45	2	48	51	3	31	36	4	68	65	5	195	188	6	224	219	7	197	192	8	44	53
9	85	90	10	91	91	11	99	94	12	72	73	13	8	37	14	22	22	18	22	19	23	50	45
H,L = 4,-3			0	107	101	1	37	33	2	159	155	3	47	48	4	44	46	5	27	32	7	92	89
7	37	40	8	21	21	13	66	69	16	48	48	20	26	29	H,L = 5,-3			0	17	11	1	262	263
2	137	141	3	25	22	4	19	14	5	34	29	7	75	74	9	94	91	10	22	27	11	31	38
15	66	62	16	35	36	17	103	102	19	58	54	H,L = 6,-3			0	105	106	2	186	174	3	96	92
4	60	60	5	32	31	6	26	29	7	74	75	8	27	28	10	73	72	11	89	95	12	62	67
4	64	64	15	49	52	16	62	59	18	39	41	20	35	43	H,L = 7,-3			0	47	53	1	41	38
3	76	77	7	22	18	8	78	80	10	57	56	11	52	46	19	21	17	H,L = 8,-3			1	31	33
5	38	34	7	71	68	8	111	106	9	45	48	10	66	68	11	33	38	15	22	12	H,L = 9,-3		
8	24	17	3	20	11	4	44	42	7	30	28	H,L = 10,-3			2	27	27	5	39	34	6	18	14
H,L = -9,-2			0	34	34	1	42	43	2	93	H,L = -8,-2			88	82	3	27	32	4	71	76	H,L = -7,-2		
0	41	40	1	57	57	2	98	96	4	40	42	5	51	51	9	29	27	13	32	28	14	26	27
16	43	43	H,L = -6,-2			0	25	27	1	30	34	3	61	60	4	116	115	5	95	101	10	32	35
13	27	24	14	32	35	H,L = -5,-2			0	73	72	3	24	21	4	63	64	7	51	52	9	149	153
7	95	95	8	236	238	9	57	56	10	158	155	11	52	51	12	57	52	13	33	36	18	29	25

TABLE 5. (Continued)

K	FO	FC	K	FO	FC	K	FO	FC	K	FO	FC	K	FO	FC	K	FO	FC	K	FO	FC	K	FO	FC
H,I = -4,-2			0	42	36	1	92	89	2	79	78	3	61	61	4	133	133	5	174	171	6	72	73
7	28	31	8	56	56	9	17	17	10	20	23	11	44	48	12	29	27	13	27	31	14	54	58
15	28	31	16	25	22	17	36	34	H,L = -3,-2			1	79	77	2	172	168	3	61	61	4	55	56
5	57	58	6	30	30	7	37	37	8	76	75	9	32	30	11	38	41	12	24	19	14	45	47
16	40	43	20	34	34	H,L = -2,-2			0	317	301	1	514	488	2	19	21	3	53	49	4	113	106
8	119	118	6	20	15	8	62	62	10	118	115	13	83	84	14	26	31	15	22	32	17	122	132
18	53	58	19	29	29	H,L = -1,-2			0	152	146	1	52	60	2	159	154	3	143	156	4	65	65
5	25	23	6	68	67	7	82	83	8	27	28	9	152	120	10	99	97	11	86	84	13	23	23
14	19	22	15	39	40	16	23	21	20	28	27	H,L = 0,-2			0	329	313	2	244	234	3	129	128
4	120	120	5	118	111	6	96	92	7	44	37	8	220	209	9	38	41	12	124	11	59	50	
12	15	12	15	25	26	17	44	40	19	66	66	20	22	26	H,L = 1,-2			0	25	28	2	44	44
3	93	92	4	203	200	5	211	209	6	24	24	7	381	366	8	330	315	9	96	92	10	234	229
11	224	215	12	31	33	13	30	28	19	43	42	34	36	36	23	48	45	25	36	36	H,L = 2,-2		
0	72	67	1	22	27	2	164	159	3	179	176	4	211	205	5	160	154	6	13	9	7	56	50
9	23	20	11	54	51	12	20	19	13	41	41	14	104	99	16	107	107	17	46	50	18	31	29
21	21	20	H,L = 3,-2			0	173	172	1	466	462	2	31	22	3	167	153	4	198	183	5	166	140
7	177	175	9	159	159	11	46	55	12	51	48	13	87	79	14	79	79	15	118	116	16	39	41
17	155	150	18	51	52	19	51	60	21	15	17	H,L = 4,-2			0	633	593	2	290	283	3	145	145
4	272	269	5	241	231	6	114	118	8	48	47	9	57	53	10	25	15	12	45	51	13	170	170
14	193	198	16	106	102	18	134	130	19	51	52	20	48	51	21	19	20	H,L = 5,-2			2	54	52
4	68	72	5	138	140	6	93	91	7	37	32	8	45	42	9	99	105	10	70	66	11	75	80
12	42	35	13	79	81	14	44	44	16	43	46	17	21	15	H,L = 6,-2			0	26	27	1	61	56
2	30	33	3	85	81	4	42	40	7	84	89	9	157	159	10	153	151	11	92	96	12	92	91
13	19	19	17	32	26	18	16	12	H,L = 7,-2			0	55	53	6	102	103	7	31	24	8	50	48
9	53	53	12	72	69	H,L = 8,-2			0	71	78	5	16	13	6	30	27	7	32	34	8	44	39
9	40	40	10	52	54	11	42	45	12	38	37	14	25	18	H,L = 9,-2			0	27	27	1	43	43
5	20	18	14	29	22	H,L = 10,-2			1	30	32	H,L = -9,-1			0	63	57	1	55	50	2	23	19
H,L = -8,-1			0	42	40	1	46	46	2	55	55	3	33	36	12	27	28	H,L = -7,-1			2	41	43
3	59	62	8	71	67	11	58	56	12	43	46	13	92	93	14	39	39	15	118	116	16	39	41
H,L = -6,-1			0	63	67	1	55	56	2	27	29	4	98	100	5	16	5	6	37	37	7	168	177
9	60	57	11	113	115	12	41	47	14	21	21	15	37	33	16	15	18	H,L = -5,-1			0	27	26
1	33	30	2	50	43	3	75	71	5	42	40	7	55	58	8	21	29	9	18	19	10	18	18
4	25	29	15	47	48	16	36	37	17	18	17	22	22	25	H,L = -4,-1			0	125	128	1	233	234
2	54	58	5	252	255	6	61	63	6	51	48	7	26	25	9	15	20	10	57	57	12	32	36
15	53	53	16	15	15	18	102	117	19	63	61	20	42	40	19	41	40	1	52	55	H,L = 3,-1		
0	197	188	1	20	16	2	36	32	3	111	108	4	68	68	5	158	148	6	126	115	7	49	48
8	75	77	11	26	19	12	93	89	13	33	36	14	36	33	15	19	17	18	58	57	H,L = -2,-1		
0	113	107	2	66	65	3	82	78	4	107	102	5	159	157	6	139	132	10	34	34	11	28	26
11	137	126	12	53	51	15	61	67	16	46	52	17	36	40	19	34	38	21	42	41	22	36	33
24	27	22	25	15	9	H,L = -1,-1			0	159	119	1	153	158	2	201	192	3	151	141	5	134	132
6	151	150	7	84	88	8	136	112	9	501	468	10	166	164	11	22	12	12	55	48	16	34	32
17	67	69	20	25	30	23	19	42	24	55	60	0	924	915	1	270	268	2	203	198			
3	74	70	4	17	8	5	261	252	6	252	246	7	159	151	8	27	35	9	27	25	10	30	25
11	113	115	12	164	159	15	152	137	14	35	32	15	25	110	19	110	112	21	29	23	H,L = 1,-1		
0	458	454	1	664	659	2	339	317	3	31	37	5	62	60	7	265	260	8	58	52	9	58	52
9	192	189	10	91	86	11	187	178	12	112	109	13	102	104	14	84	81	15	24	27	16	25	22
17	159	140	19	107	115	H,L = 2,-1			0	991	898	1	248	234	2	1430	1421	3	576	568	4	80	75
5	26	29	6	22	19	7	59	65	8	78	78	9	90	31	10	78	74	11	78	58	12	62	62
13	44	39	14	57	40	15	70	87	16	370	367	18	146	145	20	105	107	21	44	51	H,L = 3,-1		
0	261	255	1	81	84	2	183	184	3	357	353	4	76	75	5	174	169	6	215	209	7	197	193
8	41	36	11	50	51	12	118	116	13	151	150	14	16	17	15	58	54	16	44	38	18	38	38
19	23	18	21	45	46	23	17	15	25	25	23	H,L = 4,-1			0	190	115	1	126	124	2	71	65
3	50	44	4	132	132	5	372	372	6	516	510	7	242	246	8	135	136	10	32	38	11	45	44
12	150	151	13	29	29	14	47	51	16	21	24	18	36	32	19	44	38	21	34	34	H,L = 5,-1		
0	61	61	1	55	52	2	69	66	3	34	33	4	165	161	5	48	51	7	61	57	8	39	39
9	212	212	10	57	72	11	21	19	12	26	25	15	29	29	22	46	43	H,L = 6,-1					
0	75	72	1	29	22	2	70	68	3	64	62	4	61	66	7	91	84	8	72	72	9	91	
10	22	17	11	36	35	13	21	16	16	31	31	18	25	20	H,L = 7,-1			0	70	63	2	61	65
3	29	23	4	25	27	6	18	18	8	40	39	11	34	37	13	19	20	16	19	19	H,L = 8,-1		
0	60	57	1	75	75	2	24	27	3	23	22	5	30	31	10	42	38	12	38	34	H,L = 9,-1		
3	25	24	H,L = 10,-1			1	17	15	3	23	22	7	57	60	8	19	18	H,L = -10,0			0	41	39
H,L = -9,0			5	36	35	6	45	47	8	51	45	10	43	42	H,L = -8,0			0	46	41	2	38	42
1	46	46	3	48	51	7	54	53	9	120	121	11	42	38	H,L = -7,0			0	25	26	1	26	22
6	52	48	11	22	18	12	33	36	18	27	26	H,L = -6,0			1	85	105	3	142	147	4	45	47
5	30	34	6	47	48	8	42	42	9	26	30	12	46	51	13	46	46	15	80	80	17	26	32
H,L = -5,0			0	62	64	1	113	123	3	104	102	4	87	83	5	91	96	6	12	15	7	16	22
8	40	41	13	19	24	15	37	39	19	24	25	22	21	12	H,L = -4,0			0	51	55	1	29	33
2	53	53	3	29	25	5	215	213	6	33	36	7	130	126	8	21	20	9	65	66	12	56	61
14	66	65	15	25	24	16	44	39	17	8	9

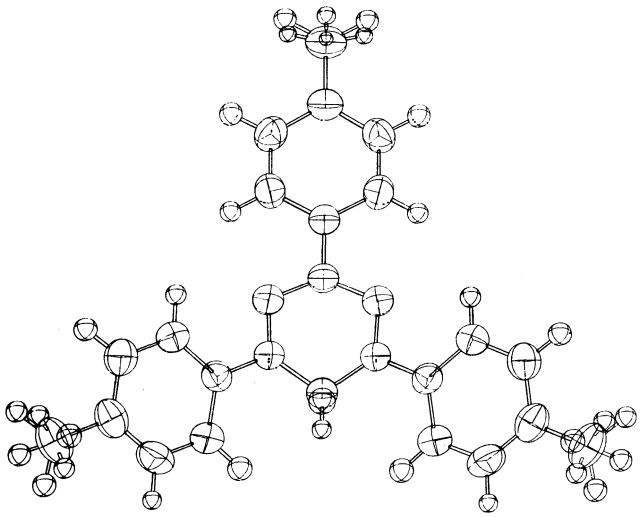

Fig. 4. Molecular structure and thermal ellipsoids.[14] An approximation made on the methyl groups is referred to the text. The thermal ellipsoids enclosing a probability of 50%, except for hydrogen atoms, were viewed approximately along the normal of the nitrogen plane.

Table 6. Bond lengths, pertinent intramolecular contacts, and their estimated standard deviations in parentheses (Å)

Bond	Length	Bond	Length
C(1)–N(1)	1.447(4)	C(7)–C(8)	1.378(4)
N(1)–N(2)	1.352(3)	C(8)–C(3)	1.381(4)
N(2)–C(2)	1.334(3)	C(6)–C(9)	1.496(5)
N(1)–C(3)	1.394(4)	C(2)–C(10)	1.474(5)
C(3)–C(4)	1.393(4)	C(10)–C(11)	1.381(3)
C(4)–C(5)	1.379(5)	C(11)–C(12)	1.382(4)
C(5)–C(6)	1.379(5)	C(12)–C(13)	1.376(4)
C(6)–C(7)	1.387(4)	C(13)–C(14)	1.502(6)
C(1)–H(Cl–1)	1.05(5)	C(7)–H(C7)	1.04(3)
C(1)–H(Cl–2)	1.04(3)	C(8)–H(C8)	1.00(3)
C(4)–H(C4)	1.02(3)	C(11)–H(C11)	1.00(3)
C(5)–H(C5)	0.99(2)	C(12)–H(C12)	1.01(3)
Atoms	**Distance**	**Atoms**	**Distance**
C(1)---C(4)	2.924(4)	C(4)---H(Cl–1)	3.42(3)
C(1)---C(10)	4.054(5)	C(4)---H(Cl–2)	2.54(1)
N(2)---C(8)	2.770(4)	C(10)---H(Cl–1)	4.03(5)
N(2)---C(11)	2.776(3)	H(C4)---H(Cl–1)	3.01(5)
C(1)---H(C4)	2.59(3)	H(C4)---H(Cl–2)	1.98(4)
N(2)---H(C8)	2.42(3)	H(C4)---H(C4′)	3.50(7)
N(2)---H(C11)	2.43(3)	H(C8)---H(C11)	3.29(4)

the configuration of the two *N*-tolyl groups is antipropellor. However, H(C4) and H(C4′) are still staggered betwen H(Cl-1) and H(Cl-2). In comparison with the no-twist case, the configuration mentioned above enlarges the distance between H(C4) and H(C4′) and simultaneously decreases the repulsion between the *N*-tolyl groups and the methylene group. A parallel description holds in the cases of TPV and MeTPV as well.

The equation of the least-squares plane through five atoms, C(1), C(2), C(3), N(1), and N(2), is given by:

Table 7. Bond angles and their estimated standard deviations (in degree)

N(1′)–C(1)–N(1)	105.9(3)	C(1)–N(1)–N(2)	117.2(2)
N(1)–N(2)–C(2)	114.4(1)	N(2)–C(2)–N(2′)	126.8(3)
C(1)–N(1)–C(3)	123.6(2)	N(2)–N(1)–C(3)	118.6(1)
N(1)–C(3)–C(4)	121.3(2)	C(3)–C(4)–C(5)	119.9(2)
C(4)–C(5)–C(6)	122.5(3)	C(5)–C(6)–C(7)	116.7(2)
C(6)–C(7)–C(8)	121.9(2)	C(7)–C(8)–C(3)	120.6(2)
C(8)–C(3)–C(4)	118.4(2)	C(8)–C(3)–N(1)	120.4(2)
C(5)–C(6)–C(9)	121.6(3)	C(7)–C(6)–C(9)	121.6(2)
N(2)–C(2)–C(10)		116.3(2)	
C(2)–C(10)–C(11)		120.9(2)	
C(10)–C(11)–C(12)		120.6(2)	
C(11)–C(12)–C(13)		121.4(2)	
C(12)–C(13)–C(12′)		117.7(3)	
C(11)–C(10)–C(11′)		118.2(3)	
C(12)–C(13)–C(14)		121.1(2)	

Table 8. Comparison of mean bond lengths (Å) and of mean bond angles (degree)

Compound[a]	TTV	TPV	MeTPV	TEAZN	DPAZN
Reference	this work	5	3	8	9
Length;					
N(1)–N(2)	1.352	1.351	1.358	1.321	1.314
N(2)–C(2)	1.334	1.338	1.335	1.334	1.346
C(2)–C(10)	1.474	1.485	1.487		1.454
N(1)–C(3)	1.394	1.414	1.404		
N(1)–C(1)	1.447	1.443	1.457		
C–C single bond			1.517		
Angle;					
N(1)–N(2)–C(2)	114.4	114.4	114.4	116.0	119.1
N(2)–C(2)–N(2′)	126.8	126.8	126.8	127.4	121.8
N(2)–C(2)–C(10)	116.3	116.6	116.5		119.1
N(1)–C(1)–N(1′)	105.9	106.1	104.3		
C(1)–N(1)–C(3)	123.6	122.8	123.8		
N(2)–N(1)–C(3)	118.6	117.4	118.1		
N(2)–N(1)–C(1)	117.2	117.8	117.7		

a) TTV; 1,3,5-tri-*p*-tolylverdazyl, TPV; 1,3,5-triphenyl-verdazyl, MeTPV; 1,3,5-triphenyl-6-methyl-verdazyl, TEAZN; *sym*-tetrazine, DPAZN; 3,6-diphenyl-*sym*-tetrazine.

$$0.8868X - 0.3856Y - 0.2521Z + 2.3566 = 0 \text{ (Å)}, \quad (1)$$

where the Cartesian reference axes are taken as follows: $X=ax+cz\cos\beta$, $Y=by$, and $Z=cz\sin\beta$. The atomic deviations from this plane are C(1)=−0.001, C(2)=0.117, C(3)=0.035, N(1)=0.026, and N(2)=−0.161 Å. The dihedral angle between this and the *N*-tolyl planes is close to that of the twist about the N(1)–C(3) bond. Accordingly, it seems reasonable to divide the TTV molecule into three planes. Two of them are the plane defined by Eq. (1) and its mirror image. The last one covers the *C*-tolyl group and the C(2) atom, at which the three planes intersect. On the other hand, N(2)–C(2)–N(2′) angle is close to that of the ideal trigonal bond. Therefore, the molecular structure of TTV seems to be favorable for the delocalization of an unpaired π-electron. The above consideration holds in both TPV and MeTPV. Actually, the dimensions of the *sym*-tetrazinyl ring of verdazyls are similar to those of TEAZN and DPAZN, both of which are

planar molecules with conjugated double bonds.[8,9]

To summarize, the mutually distinguishable magnetic properties of TTV, MeTPV, and TPV can probably be attributed to the variety of the molecular packing patterns of the respective radicals, taking account of the similarity in molecular structure as well as in this spin-density distribution.[2]

Residual Electron Densities. None of the methyl hydrogen atoms could be located unequivocally, as is shown in Fig. 2. Such annular distributions of the electron densities suggest the rotation of the methyl groups about the C–C bond.

The final difference Fourier map was then calculated. The residual electron densities on this map varied from −0.16 to 0.16 e/Å^3. A composite electron-density map is shown in Fig. 5. The standard deviation of the electron density, $\sigma(\rho)$, was estimated to be 0.02 e/Å^3 following the method of Cruickshank.[10] The residual electron densities at the middle point of every bond exceed $2\sigma(\rho)$; this is probably to be attributed to the aspherical distribution of electrons as a result of the bond formation.

Molecular Packing. The mutual arrangement of the TTV molecules is shown in Fig. 6. The pertinent intermolecular contacts and their estimated standard deviations are listed in Table 9.

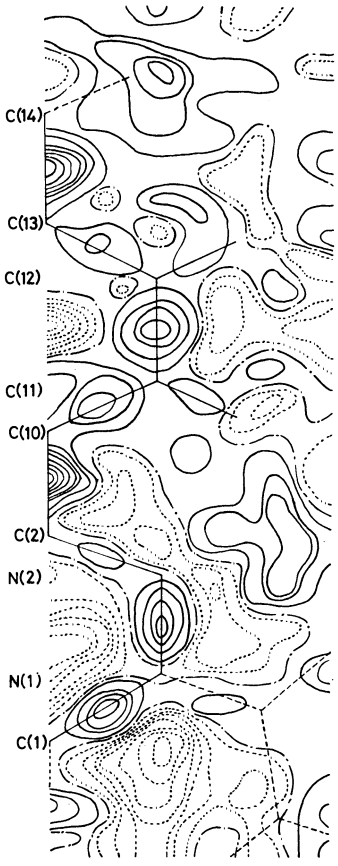

Fig. 5. The final composite residual electron-density sections through the pair of bonds between non-hydrogen atoms and between their counterparts on the opposite side beyond the mirror plane. The contours are at intervals of 0.02 e/Å^3. The solid, dashed, and broken contours indicate positive, zero, and negative values, respectively. The solid and broken straight lines represent the bonds on and out of the section, respectively.

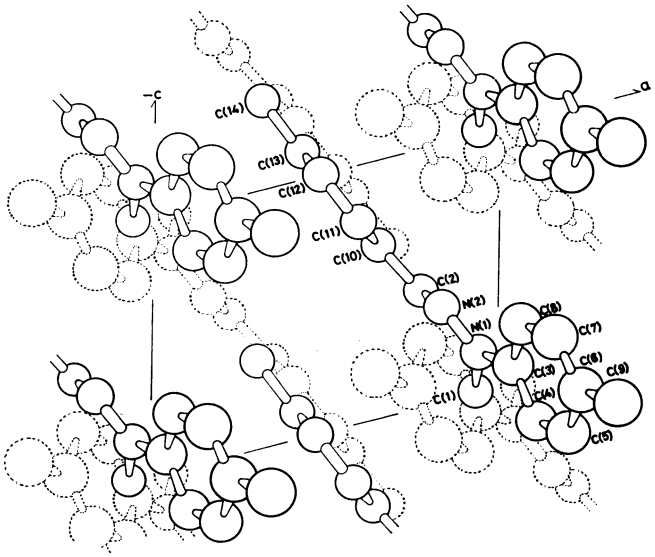

Fig. 6. Mutual arrangement of the molecules viewed along the b-axis. The hydrogen atoms were not drawn.

Table 9. Pertinent intermolecular contacts and their estimated standard deviations

Atom (1) at (x, y, z)	Atom (2)	Distance (Å)	Symmetry operation applied to the second atom
N(1)	C(14)	3.647(6)	$1+x,\ y,\ 1+z$
C(1)	C(10)	3.516(7)	$x,\ y,\ 1+z$
C(10)	C(14)	3.836(7)	$x,\ y,\ 1+z$
H(C1–1)	C(12)	2.99(5)	$x,\ y,\ 1+z$
H(C1–2)	C(10)	2.61(6)	$x,\ y,\ 1+z$
H(C1–2)	C(11)	2.75(5)	$x,\ y,\ 1+z$
C(4)	C(14)	3.891(4)	$1+x,\ y,\ 2+z$
C(3)	C(9′)	3.707(5)	$-x,\ 1/2+y,\ -z$
C(8)	C(9′)	3.638(5)	$-x,\ 1/2+y,\ -z$
C(12)	C(9′)	3.746(5)	$-x,\ 1/2+y,\ -1-z$
C(9)	C(7)	4.053(5)	$1-x,\ 1/2+y,\ -z$
C(9)	C(5′)	4.943(6)	$1-x,\ 1/2+y,\ -z$
C(9)	C(9′)	3.960(9)	$1-x,\ 1/2+y,\ -z$

The shortest C···C, C···N, C···H, and N···H intermolecular distances are 3.516 Å along [001], 3.647 Å along [101], 2.16 Å along [001], and 2.89 Å along [101] respectively. The fairly planar molecules are arranged in sheets approximately parallel to the (20$\bar{1}$) plane. A complete overlap of the molecular plane is observed between the *sym*-tetrazinyl and *C*-tolyl groups, while the other interplanar overlaps are incomplete. The interplanar distance of the complete overlap is roughly 4.2 Å. This maximum overlap leads to a column along the c-axis.

It is worth noting that the TTV crystal contains only two molecules in the unit cell with the center of symmetry. Fortunately, for the purpose of magnetic resonance studies, this means that the so-called similar-dissimilar relation can be disregarded. In general, the resonance spectra consist of contributions from both the single molecules and the whole crystal. However,

it is quite difficult to resolve the spectrum into the component contributions, particularly when dissimilar paramagnetic molecules or different magnetic sites are present. Therefore, we presume that the TTV crystal will give more knowledge peculiar to the verdazyl single molecule in the solid phase than any other verdazyl crystal will give.

Spin Densities and Exchange Interaction. Following the method of Fischer, who has treated the lone pairs on N(1) and N(1′) as π-electrons,[11] the McLachlan spin densities of TTV were calculated. The results are shown in Fig. 3. Those values can explain the qualitative ENDOR (electron nuclear double resonance) spectra of TTV. A considerable amount of spin density can be observed on every atom in the π-electron framework.[2]

On the other hand, the magnitude of the exchange interaction between the π-electron spins may be conjectured on the basis of the spin densities and the molecular packing. For the sake of simplicity, we focus our attention on the column along the c-axis. The exchange interaction of conjugated π-spin radicals being considered, the following two-spin Hamiltonian proposed by McConnell[12] is certainly useful:[1]

$$H^{AB} = -\boldsymbol{S}^{A}\cdot\boldsymbol{S}^{B}\sum_{ij}J_{ij}^{AB}\rho_{i}^{A}\rho_{j}^{B}, \qquad (2)$$

where $\boldsymbol{S}^{A}$ and $\boldsymbol{S}^{B}$ are the total spins on the A and B molecules and where ρ_{i}^{A} and ρ_{j}^{B} are the π-spin densities on the i and j atoms of A and B molecules. The exchange integral, J_{ij}^{AB}, depends on the overlap integral between the $2p_{z}\pi$-orbitals of the i and j atoms, and is certainly negative for all the interatomic contacts in the present case,[1] though we cannot estimate its precise magnitude at present. Using the spin densities in Fig. 3, we consider that the contribution due to the overlap integrals between the *sym*-tetrazinyl and the *C*-tolyl groups is ferromagnetic: that is, the sum in Eq. (2) is positive, while the other contributions are antiferromagnetic. This implies that the effective exchange integral, $|J|$, is small when the summation is carried out over all the atoms in the adjacent molecules. In fact, the magnetic susceptibility of TTV follows the Curie-Weiss law with a negative Weiss constant of *ca.* -1 K down to the lowest temperature reached, 1.8 K. Therefore, we presume that the weak exchange interaction inferred from the susceptibility can be attributed mainly to such competitive contributions.

Computer Programs. All the calculations were carried out on a FACOM 270-30 computer at the Institute for Solid State Physics, the University of Tokyo, with a local version of the Universal Crystallographic Computation Program System, UNICS.[13] The thermal ellipsoids were drawn on a HITAC 5020E computer at the Computer Center, the University of Tokyo.[14]

The authors wish to express their deep thanks to Mr. Kohji Watanabe of the Institute for Chemical Research, Kyoto University, for his kind performance of the molecular orbital calculation, and also to the other colleagues with whom they have done this series of investigations. The present work was supported in part by a Scientific Research Grant of the Ministry of Education, to which the authors' thanks are due.

References

1) N. Azuma, J. Yamauchi, K. Mukai, H. O. Nishiguchi, and Y. Deguchi, This Bulletin, **46**, 2728 (1973).
2) K. Mukai, T. Yamamoto, M. Kohno, N. Azuma, and K. Ishizu, *ibid.*, **47**, 1797 (1974).
3) N. Azuma, Y. Deguchi, F. Marumo, and Y. Saito, *ibid.*, Part IX of the present series, starting with p. 825 of this issue.
4) R. Kuhn and H. Trischmann, *Monatsh. Chem.*, **95**, 457 (1964).
5) D. E. Williams, *Acta Crystallogr.*, **B29**, 96 (1973).
6) "International Tables for X-Ray Crystallography," Vol. III, Kynoch Press, Birmingham (1962), p. 202.
7) M. S. Farag, *Acta Crystallogr.*, **7**, 117 (1954).
8) F. Bertinotti, G. Giacomello, and A. M. Liquori, *ibid.*, **9**, 510 (1956).
9) N. A. Ahmed and A. I. Kitaigorodsky, *ibid.*, **B28**, 739 (1972).
10) D. W. J. Cruickshank, *ibid.*, **2**, 65 (1949).
11) P. H. H. Fischer, *Tetrahedron*, **23**, 1939 (1967).
12) H. M. McConnell, *J. Chem. Phys.*, **39**, 1910 (1963).
13) "Universal Crystallographic Computation Program System (UNICS)," ed. by T. Sakurai, The Crystallographic Society of Japan, Tokyo (1967).
14) "Schematic Drawing of Crystal and Molecular Structures Containing Atomic Thermal Motions," coded by A. Takenaka, Laboratory for Chemistry of National Products, Tokyo Institute of Technology (1972).

The Magnetic Properties of Verdazyl Free Radicals. IX. The Crystal Structure of 1,3,5-Triphenyl-6-methylverdazyl Radical

Nagao AZUMA, Yasuo DEGUCHI, Fumiyuki MARUMO,* and Yoshihiko SAITO**

Department of Chemistry, Faculty of Science, Kyoto University, Kitashirakawa, Sakyo-ku, Kyoto 606

***The Institute for Solid State Physics, The University of Tokyo, Roppongi, Minato-ku, Tokyo 106*

(Received September 2, 1974)

The crystal structure of 1,3,5-triphenyl-6-methylverdazyl has been determined by X-ray diffraction. The crystals are orthorhombic, with the space group of Pnma and with $a=18.25(1)$, $b=16.65(1)$, $c=5.776(2)$ Å, and $Z=4$. The structure was deduced from the sharpened Patterson synthesis and was refined by the block-diagonal least-squares method to the final R value of 0.055 for 960 non-zero reflections collected on an automated four-circle diffractometer. The *sym*-tetrazinyl ring has an asymmetrical boat form, as has been observed in both 1,3,5-triphenylverdazyl and 1,3,5-tri-*p*-tolylverdazyl. The complete intermolecular overlap was observed in a tilted face-to-face array along the c-axis; this accounts for a fairly strong antiferromagnetic exchange interaction between the unpaired electrons.

In the last paper,[1] the present authors have reported the crystal structure of 1,3,5-tri-*p*-tolylverdazyl (TTV), whose electron-spin exchange interaction energy, $|J/k|$, is 1 K at most.[2] The qualitative explanation for the weak exchange interaction has been made on the basis of the crystal structure and π-electron spin densities.[1] On the other hand, the magnetic susceptibility *vs.* temperature curve of 1,3,5-triphenyl-6-methylverdazyl (MeTPV) has a broad maximum in the vicinity of 12 K. This susceptibility can be well described by the linear antiferromagnetic Heisenberg model,[3] and the estimated exchange integral, $|J/k|$, is about 10 K.[2] However, ESR and ENDOR measurements have indicated that the spin-density distribution of MeTPV is almost the same as that of TTV.[4] These facts have made us select MeTPV for the crystal-structure analysis.

Experimental

The crystals of MeTPV prepared by the method of Kuhn and Trischmann[5] were obtained by the recrystallization from an acetone–methanol solution. The results of the elementary analysis showed reasonable values; Found: C, 77.10; H, 5.97; N, 17.03%. The ESR spectrum measured in degassed 2-methyltetrahydrofuran exhibited nine lines, with the nitrogen hyperfine coupling constant of 5.6 gauss. This value was in agreement with the constant of 5.8 gauss (observed in benzene) presented in the literature.[5] However, the melting point of the present sample was higher by ten degrees than the value in the literature;[5] Obs., 193.5—194.5 °C; Lit., 183—184 °C.

The crystal data are shown in Table 1. The lattice constants and intensity data were obtained by using an automatic four-circle diffractometer with Mo$K\alpha$ radiation ($\lambda=0.7101$ Å) monochromated by a graphite crystal. A total 2089 independent reflections were measured up to $2\theta=55°$ by employing the ω-scan technique. Out of these, 960 reflections with $|F_o|$ values not less than $2.5\sigma(F_o)$ were regarded as non-zero reflections and were adopted for the structure determination. The Lorentz and polarization corrections were made as usual, but the correction for absorption was not made in view of the small size of the specimen and the low absorption coefficient.

* Present address: Research Laboratory of Engineering Materials, Tokyo Institute of Technology, Ookayama, Meguro-ku, Tokyo 152.

TABLE 1. CRYSTAL DATA

Molecular formula	$C_{21}H_{19}N_4$
Molecular weight	327.4
Melting point	193.5—194.5 °C
Specimen used for the data collection	*ca.* (0.25 mm)^3
Crystal system	Orthorhombic
Cell dimensions;	
a	18.25±0.01Å
b	16.65±0.01
c	5.776±0.002
V	1755Å^3
Z	4
Density (calculated)	1.233 g/cm^3
Density (observed by flotation)	1.227
$F(000)$	692
Linear absorption coefficient	0.9 cm^{-1} (Mo$K\alpha$)
Systematic absence;	
$0kl$	$k+l=2n+1$
$hk0$	$h=2n+1$
Space group	Pnma or $Pn2_1a$

Structure Determination and Refinement

Wilson's statistics indicated the presence of the center of symmetry; therefore, the Pnma space group was adopted. The crystal structure was solved by the Patterson method. The starting model gave an R value of 0.23. Thereupon, the block-diagonal least-squares refinement was undertaken. Several cycles of the refinement with anisotropic thermal parameters reduced the R value to 0.096. At this stage of the refinement, all the positions of hydrogen atoms were located from a difference Fourier map. With anisotropic thermal parameters for non-hydrogen atoms and isotropic ones for hydrogen atoms, the final R value was 0.055 for 960 non-zero reflections.

Unit weight was adopted for all 960 reflections. The atomic scattering factors used were taken from the International Tables for X-Ray Crystallography.[6] The final parameters for the non-hydrogen atoms are shown in Tables 2 and 3. The positional parameters for the hydrogen atoms are listed in Table 4. The mean

TABLE 2. THE FRACTIONAL ATOMIC COORDINATES AND THEIR ESTIMATED STANDARD DEVIATIONS[a)] IN PARENTHESES

Atom	x	y	z
C(1)	7166(3)	2500	−2248(10)
C(2)	8391(3)	2500	176(9)
C(3)	7542(4)	2500	−4590(11)
C(4)	6929(2)	3871(2)	−543(6)
C(5)	6346(2)	4013(2)	−2051(8)
C(6)	5906(2)	4684(3)	−1698(8)
C(7)	6044(2)	5206(2)	96(9)
C(8)	6628(2)	5064(2)	1589(8)
C(9)	7071(2)	4397(2)	1257(7)
C(10)	9175(3)	2500	878(9)
C(11)	9541(2)	3219(2)	1231(8)
C(12)	10262(2)	3215(3)	1981(8)
C(13)	10617(3)	2500	2362(13)
N(1)	7374(2)	3191(2)	−848(5)
N(2)	8069(2)	3217(2)	−16(5)

a) The coordinates have been multiplied by 10^4.

TABLE 3. THE ANISOTROPIC THERMAL PARAMETERS[a)] AND THEIR ESTIMATED STANDARD DEVIATIONS IN PARENTHESES[b)]

Atom	B_{11}	B_{22}	B_{33}	B_{12}	B_{13}	B_{23}
C(1)	27(2)	23(2)	216(18)		−11(5)	
C(2)	19(2)	22(2)	200(17)		3(5)	
C(3)	45(3)	48(3)	221(20)		12(7)	
C(4)	20(1)	18(1)	256(13)	−0(1)	7(3)	9(4)
C(5)	31(1)	29(1)	323(16)	3(1)	−23(4)	−0(4)
C(6)	31(1)	37(2)	413(19)	8(1)	−22(5)	26(5)
C(7)	30(1)	28(2)	459(19)	6(1)	1(5)	−3(5)
C(8)	27(1)	26(1)	397(17)	−1(1)	5(4)	−17(4)
C(9)	21(1)	23(1)	296(14)	−1(1)	2(4)	−0(4)
C(10)	18(2)	25(2)	215(18)		5(5)	
C(11)	23(1)	28(1)	375(16)	−2(1)	−4(4)	−11(5)
C(12)	24(1)	37(2)	440(19)	−4(1)	−4(4)	−24(5)
C(13)	20(2)	50(3)	359(24)		−5(6)	
N(1)	21(1)	22(1)	248(11)	2(1)	−11(3)	−2(3)
N(2)	19(1)	21(1)	270(11)	0(1)	−3(3)	1(3)

a) The anisotropic thermal parameters are of the form: $\exp[-(B_{11}h^2+B_{22}k^2+B_{33}l^2+2B_{12}hk+2B_{13}hl+2B_{23}kl)]$. b) The values have been multiplied by 10^4.

TABLE 4. THE FINAL PARAMETERS FOR HYDROGEN ATOMS AND THEIR ESTIMATED STANDARD DEVIATIONS IN PARENTHESES[a)]

Atom	x	y	z
H(Cl)	659(3)	250	−232(10)
H(C3–1)	810(3)	250	−469(12)
H(C3–2)	736(2)	296(2)	−551(7)
H(C5)	623(2)	364(2)	−318(7)
H(C6)	550(2)	479(2)	−290(7)
H(C7)	574(2)	572(3)	21(8)
H(C8)	667(2)	544(3)	304(8)
H(C9)	749(2)	428(2)	241(7)
H(C11)	928(2)	373(2)	78(7)
H(C12)	1047(2)	372(2)	220(7)
H(C13)	1110(3)	250	290(10)

The mean thermal parameter is 3.2 Å².

a) The coordinates have been multiplied by 10^3.

TABLE 5. THE OBSERVED AND CALCULATED STRUCTURE FACTORS MULTIPLIED BY 10

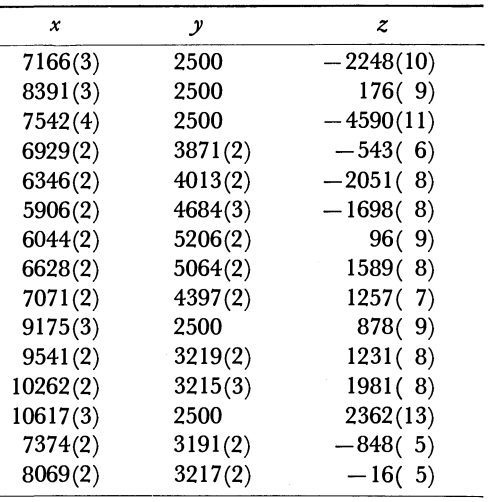

TABLE 5. (Continued)

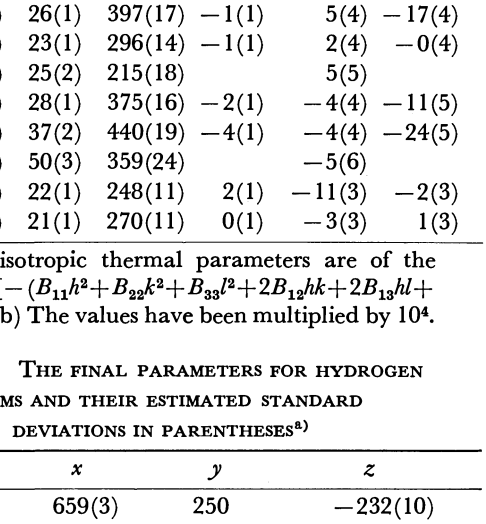

isotropic thermal parameter for the hydrogen atoms was 3.2 Å². The observed and calculated structure factors are compared in Table 5.

Results and Discussion

The molecular structure of MeTPV and the numbering system used in this text are illustrated in Fig. 1. The bond lengths and bond angles are shown in Tables 6 and 7 respectively. The MeTPV molecule has a plane of symmetry and has the molecular structure similar to those of TTV[1)] and TPV.[7)]

C(1) and C(2) are below th N(1)N(2)N(2')N(1') plane (referred to as the N-plane) by 0.622 and 0.105 Å respectively. The corresponding dihedral angles at both ends of the N-plane are 44.1° and 10.1° respectively. Therefore, the conformation of the *sym*-tetrazinyl ring of MeTPV is an asymmetrical boat form, as has been observed in TTV and TPV. The *N*-phenyl ring is above the N-plane by 18.8°, which is the angle between the N-plane and the N(1)–C(4) bond, while the dihedral angle between the plane of the *C*-phenyl ring and the N-plane is 2.6°. The distance of N(1) from the plane through C(1), N(2), and C(4) is 0.055 Å. Accordingly, we can use the following definition for the twist angle about the N(1)–C(4) bond: the twist angle is the dihedral angle between the *N*-phenyl plane and the C(1)N(2)C(4) plane. This twist angle is 21.2°, which is close to the maximum value observed in TPV. The configuration of the *N*-phenyl groups is antipropellor. The two twists of the *N*-phenyls are in opposite directions, since the MeTPV molecule has a plane of symmetry.

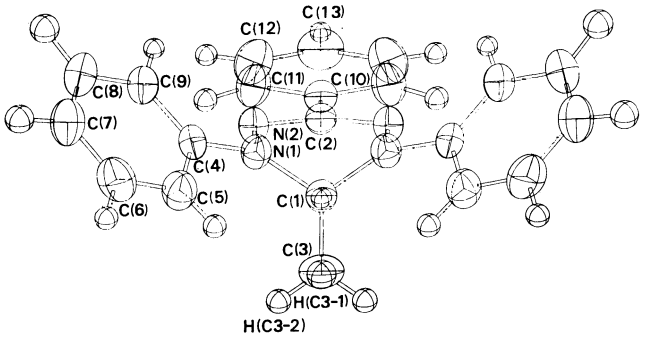

Fig. 1. The molecular structure of MeTPV viewed down the a-axis, along with the numbering system. The thermal ellipsoids enclose a probability of 50%, except for hydrogen atoms. The reflected atom will be represented in terms of its counterpart's symbol followed by a prime, *e.g.* N(1'). The ring hydrogen atom will be labelled by, for example, H(C5) where C5 stands for the ring carbon atom attached by it.

Table 6. Bond lengths, pertinent intramolecular contacts, and their estimated standard deviations in parentheses (Å)

Bond	Length	Bond	Length
C(1)–C(3)	1.517(9)	C(6)–C(7)	1.376(6)
C(1)–N(1)	1.457(4)	C(7)–C(8)	1.392(6)
N(1)–N(2)	1.358(4)	C(8)–C(9)	1.386(5)
N(2)–C(2)	1.335(4)	C(9)–C(4)	1.385(5)
N(1)–C(4)	1.404(4)	C(2)–C(10)	1.487(7)
C(4)–C(5)	1.395(5)	C(10)–C(11)	1.386(5)
C(5)–C(6)	1.392(6)	C(11)–C(12)	1.372(5)
C(1)–H(C1)	1.05(5)	C(8)–H(C8)	1.05(5)
C(3)–H(C3-1)	1.03(6)	C(9)–H(C9)	1.03(4)
C(3)–H(C3-2)	0.98(4)	C(11)–H(C11)	1.01(4)
C(5)–H(C5)	0.93(4)	C(12)–H(C12)	0.93(4)
C(6)–H(C6)	1.03(4)	C(13)–H(C13)	0.93(5)
C(7)–H(C7)	1.02(4)		
Atoms	**Distance**	**Atoms**	**Distance**
N(2)---C(11)	2.781(5)	C(2)---H(C3-1)	2.86(7)
N(1)---H(C3-1)	2.83(6)	C(2)---H(C3-2)	3.86(4)
N(1)---H(C3-2)	2.72(4)	C(10)---H(C3-1)	3.77(4)
N(2)---H(C3-1)	2.95(6)	H(C3-2)---H(C5)	2.72(5)
N(2)---H(C3-2)	3.45(4)	H(C5)---H(C5')	3.79(8)
N(2)---H(C9)	2.49(2)	H(C9)---H(C11)	3.52(5)

Table 7. Bond angles and their estimated standard deviations (in degree)

N(1)–C(1)–N(1')	104.3(4)	C(1)–N(1)–N(2)	117.7(2)
N(1)–N(2)–C(2)	114.4(2)	N(2)–C(2)–N(2')	126.8(4)
N(1)–C(1)–C(3)	112.1(4)	C(1)–N(1)–C(4)	123.8(3)
N(2)–N(1)–C(4)	118.1(2)	N(1)–C(4)–C(5)	120.0(3)
N(1)–C(4)–C(9)	119.8(3)	C(4)–C(5)–C(6)	119.1(3)
C(5)–C(6)–C(7)	120.8(4)	C(6)–C(7)–C(8)	120.0(3)
C(7)–C(8)–C(9)	119.9(3)	C(8)–C(9)–C(4)	120.1(3)
C(9)–C(4)–C(5)	120.3(3)	N(2)–C(2)–C(10)	116.5(3)
C(2)–C(10)–C(11)	120.2(3)		
C(10)–C(11)–C(12)	119.9(2)		
C(11)–C(12)–C(13)	120.2(2)		
C(12)–C(13)–C(12')	120.2(4)		
C(11)–C(10)–C(11')	119.5(4)		
C(3)–C(1)–H(C1)	115(3)		
C(1)–C(3)–H(C3-1)	120(3)		
C(1)–C(3)–H(C3-2)	109(2)		

The methyl group attached to the tetrahedral carbon atom, C(1), occupies the *axial* position of the boat. The *ortho* hydrogen atoms, H(C5) and H(C5'), remain *staggered* between H(C1) and C(3).

A less significant molecular structural difference has been observed among three symmetrically substituted verdazyls, TPV, TTV, and MeTPV. On the other hand, the effect of the methyl groups, introduced in the TTV and MeTPV molecules, upon the spin-density distribution in a molecule has been examined by the ENDOR technique. As was expected, little effect has been revealed by the aid of a comparison of their proton hyperfine coupling constants with those of TPV.[4] Accordingly, these radical solids are optimal for our purpose to correlate the magnetic properties of a neutral radical with a delocalized unpaired electron spin with its molecular packing.

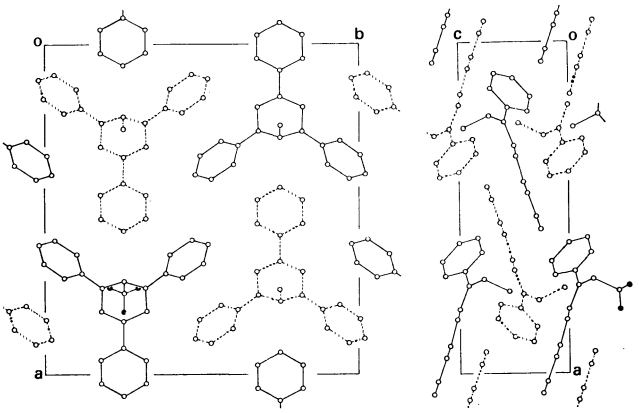

Fig. 2. The mutual arrangement of the MeTPV molecules. The left and the right were viewed along the c- and b-axis, respectively. The doubled circles in the reference molecule stand for the methyl hydrogen atoms, while the other hydrogen atoms were not drawn.

TABLE 8. PERTINENT INTERMOLECULAR CONTACTS AND THEIR ESTIMATED STANDARD DEVIATIONS

Atom (1) at (x,y,z)	Atom (2)	Distance (Å)	Symmetry operation applied to the second atom
C(12)	C(4)	3.381(6)	$1/2+x,\ y,\ 1/2-z$
C(12)	C(5)	3.776(6)	
C(12)	C(6)	3.846(6)	
C(12)	C(7)	3.985(6)	
C(12)	C(9)	3.976(5)	
C(13)	C(1)	3.994(8)	
C(13)	N(1)	3.957(6)	
C(13)	C(4)	3.784(6)	
C(13)	C(5)	3.931(7)	
C(12)	C(5)	3.714(6)	$-1/2+x,\ y,\ -1/2-z$
C(13)	C(3)	3.861(9)	
N(1)	C(3)	3.806(7)	$x,\ y,\ 1+z$
N(2)	C(3)	3.489(7)	
C(2)	C(3)	3.397(8)	
C(10)	C(3)	3.967(8)	
C(8)	N(1′)	3.736(5)	$3/2-x,\ 1/2+y,\ 1/2+z$
C(8)	N(2′)	3.514(5)	
C(8)	C(4′)	3.581(5)	
C(8)	C(9′)	3.703(6)	
C(9)	C(4′)	3.881(5)	
C(9)	C(8′)	3.991(6)	
C(9)	C(9′)	3.849(8)	
C(11)	C(6′)	3.779(6)	
C(11)	C(7′)	3.605(6)	
C(12)	C(7′)	3.979(6)	
C(6)	C(6′)	3.985(9)	$1-x,\ 1/2+y,\ -z$
C(6)	C(7′)	3.681(6)	
C(7)	C(6′)	3.681(6)	
C(7)	C(7′)	3.873(8)	
N(2)	H(C3-2)	2.94(4)	$x,\ y,\ 1+z$
H(C5)	C(12)	2.90(4)	$-1/2+x,\ y,\ 1/2-z$
C(11)	H(C7′)	2.95(5)	$3/2-x,\ 1/2+y,\ 1/2+z$
H(C8)	N(1′)	2.94(4)	
H(C8)	N(2′)	2.55(4)	
H(C8)	C(4′)	2.92(4)	
H(C8)	C(9′)	2.96(4)	
H(C13)	H(C1)	2.71(8)	$1/2+x,\ y,\ 1/2-z$
H(C12)	H(C5)	2.70(6)	$-1/2+x,\ y,\ -1/2-z$
H(C13)	H(C3-2)	2.80(6)	
H(C8)	H(C9′)	2.99(6)	$3/2-x,\ 1/2+y,\ 1/2+z$
H(C11)	H(C6′)	2.61(6)	
H(C11)	H(C7′)	2.77(6)	
H(C12)	H(C7′)	2.96(6)	
H(C6)	H(C7′)	2.88(6)	$1-x,\ 1/2+y,\ -z$

Figure 2 shows the mutual arrangement of the MeTPV molecules. The pertinent intermolecular distances are listed in Table 8. The molecules with a plane of symmetry pack in a tilted face-to-face array along the c-axis. Within the array, the shortest intermolecular distance is 2.94 Å for the N(2)···H(C3-2) contact, and the corresponding N···C distance is 3.489 Å. The intermolecular distance between C(2) and C(3) is 3.397 Å, while the intramolecular distances of the N(1)---C(3) and N(2)---C(3) contacts are 2.468 and 3.054 Å respectively. This intermolecular distance may suggest the deformation of the methyl group from the ordinary tetrahedral conformation.

The melting point of MeTPV is higher than those of its homologues by about 50 °C. This can be mainly attributed to the complete overlap of the adjacent molecules in the array along the c-axis. Such molecular packing will certainly enhance the exchange interaction between the π-electron spins. The magnetic susceptibility of the MeTPV solid is well described by the Heisenberg linear chain model[3] down to the lowest temperature examined so far, 2 K. This fact indicates a less significant coupling of the magnetic chains. The exchange integral estimated from the susceptibility of the MeTPV solid is about -10 K, which corresponds to one of the strongest exchange interactions among those observed in verdazyl free radical solids. The present authors and their colleagues have already interpreted the magnetic properties of TPV, galvinoxyl, and TTV radical solids in terms of both the overlap of $2p_z\pi$-orbitals inferred from the molecular packing and the spin densities.[8,1] From the same point of view, the fairly strong exchange interaction in the MeTPV solid may be attributed to the complete overlap of the molecular planes in the tilted face-to-face array. The excellent magnetic linear chain is also attributable to the uniform intermolecular spacing in the array. The sufficient magnetic insulation between the magnetic chains can be explained by considering the isolation of the chemical chains or the arrays along the c-axis. Speaking in more detail, the interchain contacts occur around the hydrogen atoms or between the atoms whose $2p_z\pi$-orbitals cause a so-called π-overlap and which have small spin densities at that; this will give rise to less significant interchain exchange interactions. The magnetic properties of MeTPV will be discussed quantitatively in a separate paper, together with those of other verdazyls.

The calculations were carried out on a FACOM 270-30 computer at the Institute for Solid State Physics, the University of Tokyo, with a local version of UNICS.[9] The thermal ellipsoids were drawn on a HITAC 5020E computer at the Computer Center, the University of Tokyo.[10] This work was supported in part by a Scientific Research Grant of the Ministry of Education. Thanks are due to authors' colleagues with whom the present authors have done this series of investigations.

References

1) N. Azuma, Y. Deguchi, F. Marumo, and Y. Saito, This Bulletin, Part VIII of the present series, starting with p. 819 of this issue.

2) N. Azuma, The detailed magnetic properties of verdazyl radical solids will be published elsewhere, in preparation.

3) J. C. Bonner and M. E. Fisher, *Phys. Rev.*, **135**, A640 (1964).

4) K. Mukai, T. Yamamoto, M. Kohno, N. Azuma, and K. Ishizu, This Bulletin, **47**, 1797 (1974).

5) R. Kuhn and H. Trischmann, *Monatsh. Chem.*, **95**, 457 (1964).

6) "International Tables for X-Ray Crystallography," Vol. III, Kynoch Press, Birmingham (1962), p. 202.

7) D. E. Williams, *Acta Crystallogr.*, **B29**, 96 (1973).
8) N. Azuma, J. Yamauchi, K. Mukai, H. O. Nishiguchi, and Y. Deguchi, This Bulletin, **46**, 2728 (1973).
9) "Universal Crystallographic Computation Program System (UNICS)," ed. by T. Sakurai, The Crystallographic Society of Japan, Tokyo (1967).
10) "Schematic Drawing of Crystal and Molecular Structures Containing Atomic Thermal Motions," coded by A. Takenaka, Laboratory for Chemistry of National Products, Tokyo Institute of Technology (1972).

Interfacial Capacity between a Silver Bromide Solid Electrolyte and a Blocking Electrode

Noriyoshi KIMURA, Takahisa ŌSAKI, and Shinobu TOSHIMA

Department of Applied Chemistry, Faculty of Engineering, Tohoku University, Aramaki-Aoba, Sendai 980

(Received September 3, 1974)

The interfacial capacity between a silver bromide single crystal and graphite and platinum blocking electrodes was measured using an AC bridge in the potential range 0.05—0.55 V *vs.* Ag/AgBr at 200—400 °C. The observed capacity-potential curves were compared with the calculated values from the space charge layer capacity. In the case of the graphite electrode, the capacity had a minimum value at 0.15—0.20 V *vs.* Ag/AgBr, whereas for the platinum electrode, the capacity was considerably larger and the differential capacity-potential curves were complicated. It is concluded that the space charge layer capacity predominates for the graphite electrode, but for the platinum electrode, its interaction with silver ion must be taken into account.

The structure and polarization capacity of the interface between an electrode and an ionic crystal have been discussed by many researchers.[1-3] In particular, the interfaces of ionic crystals containing excess electrons or positive holes as charge carriers, namely semiconductors, have been extensively investigated both theoretically and experimentally.[4,5] As is well known, in the neighborhood of a semiconductor surface, a space charge layer exists owing to charge excess or depletion, which is analogous to the Gouy-Chapman layer in an ionic aqueous solution.

In the case of an ionic conductive crystal, so called solid electrolyte, lattice defects act as charge carriers, and a space charge layer may be formed at the interface. Such a space charge layer model has been treated theoretically by Grimley and Mott,[6,7] and more recently by Kliewer.[8,9] The real crystal-electrode interface has been discussed many times and although considerable attention has been focussed on the measurements of the interfacial characteristics, we note that the measured values differ appreciably among researchers. This is probably mainly due to the uncertainty of the contact between crystal and solid electrode and partly due to the difficulty in preparing a clean and ordered surface of the crystals. These factors are particularly significant when polycrystalline samples are used.

In the present investigation, single crystals of silver bromide were used. A slight elasticity of the crystal enabled a good contact between the crystal and the electrode to be made. Since silver bromide has a simple crystal structure (NaCl type) and has Frenkel type lattice defects,[10] the interstitial silver ions and silver ion vacancies act as charge carriers in the crystal. Weiss[11] measured polarization current when the electrode potential was changed, and then considered the space charge layer on the basis of the excess electron distribution in the silver bromide. Raleigh treated the interfacial capacity mainly by galvanostatic and potentiostatic charging method.[12-14] We measured the variations of the interfacial capacity with the electrode potential for both graphite and platinum as the blocking electrode in order to consider the interfacial characteristics.

Experimental

Sample Preparation. Silver bromide was prepared by adding hydrobromic acid to silver nitrate solution. All chemicals were of reagent grade and hydrobromic acid was distilled before use. The precipitate was dried under vacuum and melted in a quartz tube. After pinholing, the melted salt was treated in a bromine atmosphere and finally a pure sample was obtained by vacuum distillation. Single crystals were grown by the Bridgeman method. For the sample containing cadmium ion, a given amount of cadmium bromide was added to the silver bromide before vacuum drying. Then it was treated as described above except for the vacuum distillation. The crystal was machined into a disk 15 mm in diameter and 5 mm thick, and then polished. It was etched in 40% sodium thiosulfate and 0.2% potassium cyanide solution, and then washed well in redistillated water followed by heating in vacuum at about 200 °C. The sample preparation and cell assembly were carried out in the dark.

Cell Assembly. The working electrode was either a

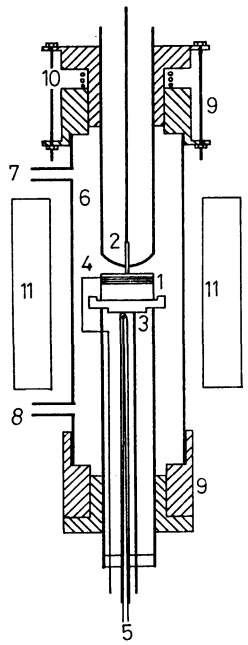

Fig. 1. Cell.
1: Solid electrolyte, 2: Working electrode, 3: Counter electrode, 4: Reference electrode, 5: Thermocouple, 6: Pyrex glass tube, 7: N_2 gas inlet, 8: N_2 gas outlet, 9: Brass holder, 10: Spring, 11: Electric furnace.

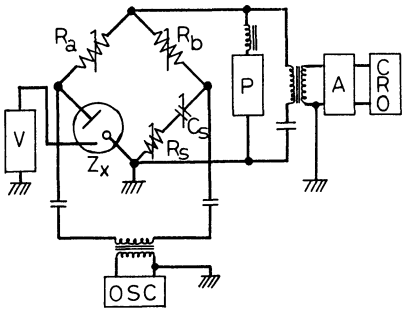

Fig. 2. AC bridge circuit.
P: Potentiometer, A: Tuning amplifier, CRO: Cathode ray oscilloscope, OSC: Oscillator, V: Electrometer.

wire of platinum or a rod of graphite, 1 mm in diameter. These electrodes were polished with γ-alumina (particle size 2 mμ), and were washed in acetone. The counter electrode was prepared by vacuum evaporation of silver on one plane of the cylindrical crystal pellet, and the silver foil was placed on it. For a reference electrode, silver wire was wound around the cylindrical pellet. The cell consisted of a silver bromide crystal pellet spring-loaded between the working and the counter electrodes as shown in Fig. 1. The cell was annealed in a nitrogen atmosphere at 400 °C for half a day before measurement.

An AC bridge shown in Fig. 2 was used for impedance measurements. A potentiometer was included for applying a given potential to the working electrode. The input voltage to the bridge was regulated to be less than 5 mV p-p in the frequency range 0.2 to 10 kHz.

Results

Typical potential sweep curves were shown in Fig. 3. No appreciable rises in current were observed between 0.05 and 0.60 V. The current below 0.05 V is assumed to be due to deposition of silver and that beyond 0.60 V to be due to decomposition of silver bromide. So the differential capacity was measured in the range from 0.05 to 0.60 V. The observed capacity increases to some extent at low frequency, but it becomes almost constant at high frequency at higher temperatures. However, at temperatures below 250 °C, the observed capacity decreases with increasing frequency above 1 kHz. In fact, the resistance of the crystal becomes

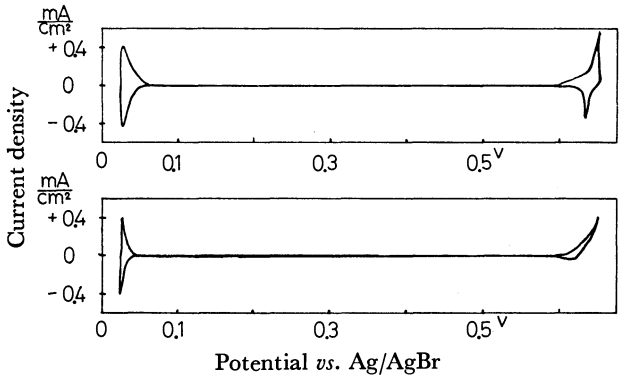

Fig. 3. Typical potential-current curve.
Upper: Pt/AgBr–$CdBr_2$ (0.5 mol%) at 350 °C
Lower: Graphite/AgBr at 345 °C
Potential sweep rate: 480 s/V

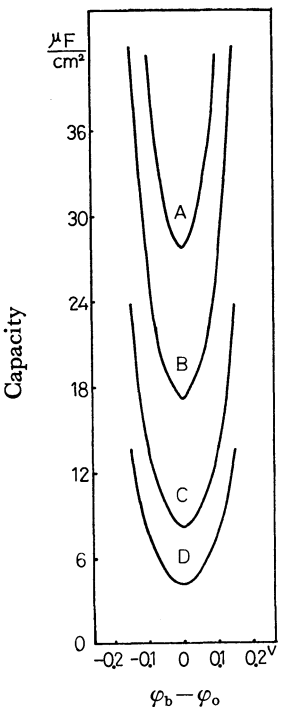

Fig. 4. The calculated value of space charge layer capacity for a silver bromide crystal.
A: 350 °C, B: 300 °C, C: 250 °C D: 200 °C.

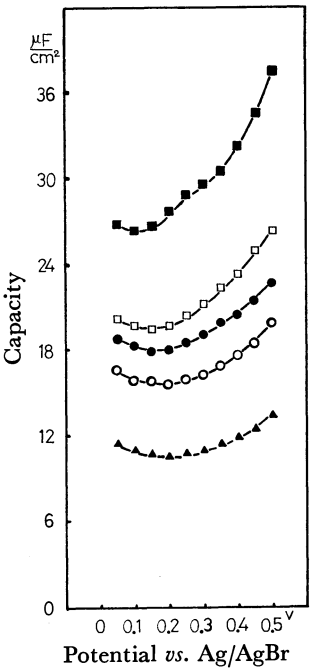

Fig. 5. Observed potential-capacity curves for graphite/AgBr.
■: 395 °C □: 350 °C ●: 301 °C ○: 248 °C
▲: 219 °C

considerable at this temperature, which suggests that the influence of the geometric capacity[15] seems to increase. Therefore, the capacity-potential curves were measured at a frequency of 1 kHz throughout this work.

The capacity-potential curves with graphite electrode are presented in Figs. 5—7 for silver bromide crystals which contained various amounts of cadmium bromide,

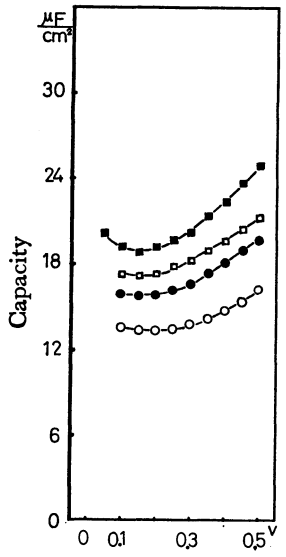

Potential *vs.* Ag/AgBr–$CdBr_2$ (0.1 mol%)

Fig. 6. Observed potential-capacity curves for graphite/AgBr–$CdBr_2$ (0.1 mol%).
■: 402 °C □: 352 °C ○: 305 °C ●: 253 °C

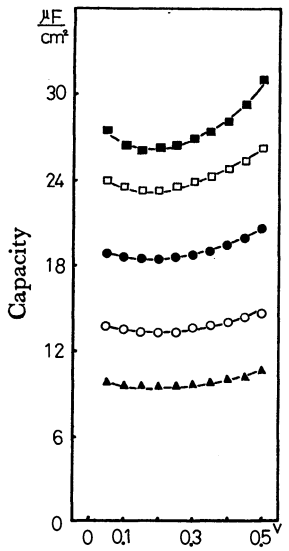

Potential *vs.* Ag/AgBr–$CdBr_2$ (0.5 mol%)

Fig. 7. Observed potential-capacity curves for graphite/AgBr–$CdBr_2$ (0.5 mol%).
■: 397 °C □: 353 °C ●: 305 °C ○: 246 °C
▲: 209 °C

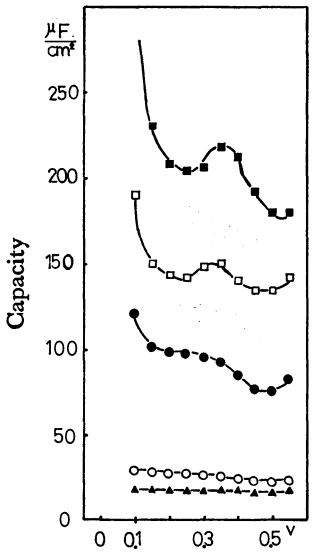

Potential *vs.* Ag/AgBr

Fig. 8. Observed potential-capacity curves for platinum/AgBr.
■: 399 °C □: 355 °C ●: 300 °C ○: 255 °C
▲: 200 °C

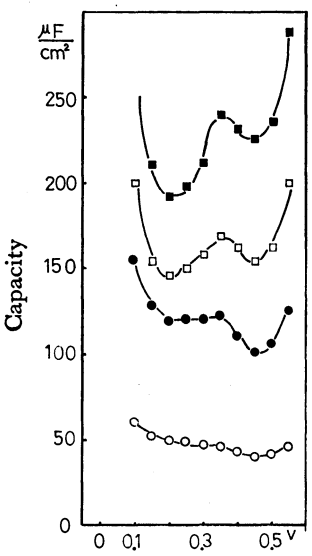

Potential *vs.* Ag/AgBr–$CdBr_2$ (0.1 mol%)

Fig. 9. Observed potential-capacity curves for platinum/AgBr–$CdBr_2$ (0.1 mol%).
■: 400 °C □: 350 °C ●: 302 °C ○: 250 °C

in order to change the amount of silver ion vacancies in them. The corresponding curves with a platinum electrode are shown in Figs. 8—10.

Discussion

Space Charge Layer. Kliewer[9] treated the space charge layer of silver chloride as a typical ionic crystal with Frenkel type defects. The same treatment may be applied to the silver bromide crystal. In a crystal slab of thickness $2L$, the potential φ will obey Poisson's equation with the boundary condition, $\varphi=\varphi_0$ at $x=0$, $x=2L$ (crystal surface) and $d\varphi/dx=0$, $\varphi=\varphi_b$ (in the bulk of crystal),

$$d^2\varphi/dx^2 = -4\pi\rho/\varepsilon, \quad (1)$$

where ε is the static dielectric constant, ρ is the charge density in the crystal. In the silver bromide crystal, the densities of silver ion vacancy (effective charge: $-e$), n_v, and interstitial silver ion (effective charge: $+e$), n_i, are given by

$$n_v = N\exp[\{-F_v+e(\varphi-\varphi_0)\}/kT], \quad (2)$$

$$n_i = N_i\exp[\{-F_i-e(\varphi-\varphi_0)\}/kT]. \quad (3)$$

assuming $n_v \ll N$, the density of silver ion lattice sites, and $n_i \ll N_i$, the density of interstitial sites, and the condition $2N=N_i$ is valid in the silver bromide crystal.

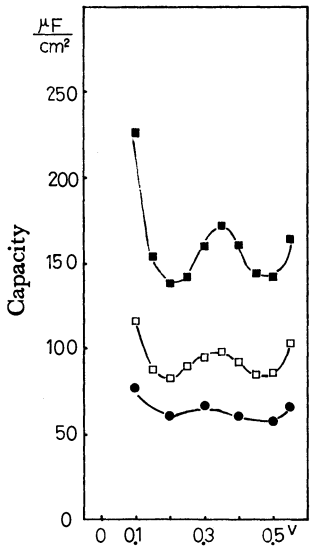

Fig. 10. Observed potential-capacity curves for platinum/AgBr–$CdBr_2$ (0.5 mol%).
■: 399 °C □: 350 °C ●: 303 °C

F_v and F_i are the formation free energy of the vacancy and the interstitial ion. If a divalent cation is introduced into the silver bromide, such a cation has an effective charge $+e$ when it does not associate with the vacancy. The density of unassociated divalent cations may be expressed as

$$n_f = N\exp[\{-\alpha-e(\varphi-\varphi_0)\}/kT], \quad (4)$$

where α is a Lagrange multiplier. Thus, the charge density is given by

$$\rho = e(n_i-n_v+n_f). \quad (5)$$

Within the bulk of the crystal, the condition of electrical neutrality will be satisfied. The condition may be obeyed well when $\kappa L \gg 1$, where $1/\kappa=(\varepsilon kT/8\pi e^2N)^{1/2} \times\exp\{-(eU-F_v)/2kT\}$, substituting $U=\varphi_b-\varphi_0$. This value is about 1×10^{-7} cm, for the silver bromide crystal at 300 °C. For a pure crystal, the equation

$$U = (F_v-F_i+kT\ln 2)/2e \quad (6)$$

may be derived from the condition of electrical neutrality. Substituting Eqs. (2), (3), (4), and (5) into (1), and then integrating it, the electric field is found to be

$$d\varphi/dx = (32\pi kTN/\varepsilon)^{1/2}\exp\{(eU-F_v)/2kT\} \times\sinh\{e(\varphi-\varphi_b)/2kT\}. \quad (7)$$

The surface charge density is given by $\sigma_0=(\varepsilon/4\pi) \times(d\varphi/dx)_{x=0}$. The space charge layer capacity is found to be $C_s=d\sigma_0/d\varphi_0$. In the bulk of the pure crystal, $n_{ib}=n_{vb}=n$ and $n=N\exp\{(eU-F_v)/kT\}$ are derived from the condition of electrical neutrality, so the capacity may be written

$$C_s = (\varepsilon e^2n/2\pi kT)^{1/2}\cosh(eU/2kT). \quad (8)$$

Using Eq. (8), the capacity of the space charge layer for the silver bromide crystal was calculated and the result is shown in Fig. 4. This equation is similar to the space charge layer capacity for an intrinsic semiconductor.

Graphite Electrode. The differential capacity curves measured with the graphite electrode shown in Fig. 5 have a minimum value at a potential 0.15—0.20 V. With increasing temperature, the minimum point appears more sharply and the value of capacity increases, which is similar to the behavior shown in Fig. 4. The observed values of the capacity at minimum points agree fairly well with the calculated values of the space charge layer capacity. The crystals containing cadmium ion show similar characteristics to the pure crystal as shown in Figs. 6 and 7. This seems to be due to the fact that at high temperature intrinsic defects are predominant in the crystal lattice. A structure sensitive region for these crystals appeared in our conductivity-temperature measurements below 250 and 125 °C with crystals containing 0.5 and 0.1 mol% cadmium bromide, respectively. The observed capacity at these temperature varied little with potential in the neighborhood of the capacity minimum point, so that the potential of the capacity minimum was not remarkable.

The potential of zero charge on the silver bromide surface can be considered in connection with the potential of minimum capacity. If the formation energy of defects F_v and F_i were known, the potential of zero charge of the pure crystal can be calculated from the Eq. (6). Trautweiler[16] reported that the surface potential of the silver bromide was −0.14 V in reference to the crystal bulk. The potential of Ag/AgBr was reported to be 1.4 V by Mott and Grimley[6] and recently to be less than 0.6 V by Weiss.[11] Then, the potential of zero charge on the silver bromide may be considered to be less than several hundred millivolts with reference to the potential of Ag/AgBr. In order to obtain a precise value of the zero charge potential in the solid-solid system, it may be difficult to employ the method of Karpachev,[17,18] who studied some fused metal electrodes on stabilized zirconia by potential-surface tension measurements. We would rather regard the observed potential of minimum capacity as the potential of zero charge in the case of the graphite electrode. Therefore, the differential capacity of the graphite in the measured potential range can be considered to be mainly due to the space charge layer capacity, caused by the distribution of the interstitial silver ions and silver ion vacancies.

Platinum Electrode. The observed capacity of the platinum electrode is considerably larger than that of the graphite electrode and the dependence on potential is complicated. The capacity curve had two minimum points at 0.20 and 0.45 V, and a small peak was observed between them. The shape of the differential capacity curve was not changed by addition of cadmium ion, therefore this characteristic was apparently not due to impurities. The same characteristic was observed by Raleigh[12] near the melting point. We consider it difficult to explain this capacity-potential relation by a simple space charge layer model, in which a charge carrier is regarded as an ideal point charge and its interaction with the electrode is not taken into account. In addition, the charge carriers in the real crystal have finite volume, therefore the closest distance of the ion

to the electrode and its interaction must inevitably be considered. This concept is similar to Stern's theory for ionic solutions, except for the solvent action. If an assumption is introduced that the ions interact with the electrode only in the layer adjacent to the surface (first layer), but the ions in the second and the following layer have a distribution determined by the space charge layer model, the electrode potential may be described as

$$\varphi_0 - \varphi_b = (\varphi_0 - \varphi_1) + (\varphi_1 - \varphi_2) + (\varphi_2 - \varphi_b), \quad (9)$$

where φ_1, φ_2, and φ_b represent the potential in the first and second layers and the bulk of the crystal. The surface charge density is given by

$$\sigma_0 = \sigma_1 + \sigma_s, \quad (10)$$

where σ_1 and σ_s denote the charge density in the first layer and the space charge layer. Then the capacity may be written as

$$1/C = \partial(\varphi_0 - \varphi_b)/\partial\sigma_0 = 1/C_{0-1} + (1/C_{1-2} + 1/C_s)(1 - \partial\sigma_1/\partial\sigma_0), \quad (11)$$

where $C_{0-1} = \partial\sigma_0/\partial(\varphi_0 - \varphi_1)$, $C_{1-2} = \partial\sigma_s/\partial(\varphi_1 - \varphi_2)$, and $C_s = \partial\sigma_s/\partial(\varphi_2 - \varphi_b)$. C_s can be determined from Eq. (8), but if any interaction between ion and electrode is present, the observed capacity is not given by the simple space charge layer model. Thus, the platinum electrode is considered to show significant interaction with the silver ion. When there is no interaction, $\partial\sigma_1/\partial\sigma_0 = 0$, and therefore $1/C = 1/C_i + 1/C_s$ is valid, where C_i is the capacity which arises from the finite size of ions. The graphite electrode is considered to have little interaction with the silver ion. When $C_i \gg C_s$, the observed capacity is predominantly due to C_s.

This research was partly supported by the Science Research Fund of the Ministry of Education.

References

1) J. R. Macdonald, *Phys. Rev.*, **92**, 4 (1953).
2) H. Chang and G. Jaffe, *J. Chem. Phys.*, **20**, 1071 (1952).
3) R. J. Friauf, *ibid.*, **22**, 1329 (1954).
4) C. G. B. Garrett and W. H. Brattain, *Phys. Rev.*, **99**, 376 (1955).
5) H. J. Engell and K. Bohnenkamp, "The Surface Chemistry of Metals and Semiconductors", ed. by H. C. Gatos, John Wiley & Sons, New York (1960).
6) T. B. Grimley and N. F. Mott, *Disc. Faraday Soc.*, **1**, 3 (1947).
7) T. B. Grimley, *Proc. Roy. Soc.* (London), **A201**, 40 (1950).
8) K. L. Kliewer and J. S. Koehler, *Phys. Rev.*, **140**, A1226 (1965).
9) K. L. Kliewer, *J. Phys. Chem. Solids*, **27**, 705 (1966).
10) J. Teltow, *Ann. Phys.*, **5**, 63, 71 (1949).
11) K. Weiss, *Ber. Bunsenges. Phys. Chem.*, **76**, 379 (1972).
12) D. O. Raleigh and H. R. Crowe, *J. Electrochem. Soc.*, **118**, 79 (1971).
13) D. O. Raleigh, *J. Phys. Chem.*, **70**, 689 (1966).
14) D. O. Raleigh, *ibid.*, **71**, 1785 (1967).
15) R. D. Armstrong and R. Mason, *J. Electroanal. Chem.*, **41**, 231 (1973).
16) F. Trautweiler, *Phot. Sci. Eng.*, **12**, 98 (1968).
17) A. T. Filyaev, I. D. Remez, and S. V. Karpachev, *Soviet Electrochem.*, **8**, 251 (1972).
18) S. V. Karpachov, V. V. Salnikov, and A. T. Filjayev, *Electrochem. Acta*, **18**, 319 (1973).

A Configuration Analysis of the Electronic States of Aniline

Satoshi SUZUKI and Tsuneo FUJII

Department of Industrial Chemistry, Faculty of Engineering, Shinshu University, Wakasato, Nagano 380

(Received September 11, 1974)

The method of configuration analysis has been applied to the interpretation of the ground and the excited electronic states of aniline. The results of full analysis, including all the singly and the doubly excited configurations, is presented. The electronic wave functions analyzed were obtained by a procedure of the Pariser-Parr-Pople type. The first excited singlet state of aniline is assigned to the ^1L_b. The second, the third, and the fourth excited singlet state are assigned to the mixed state of the ^1L_a and $^1CTS1$ states, the ^1CTA, ^1B_b, and ^1L_b states, and the ^1B_a and ^1L_a states respectively. The lowest triplet state of aniline is assigned to the ^3L_a state. The total weights of all the singly excited configurations range from 88% to 95%, except for the ground state. The inclusion of all the doubly excited configurations improves the weights up to 99.6% or more.

The effects of substitution on electronic spectra have been extensively investigated for benzene derivatives.[1-5] Aniline, which is a typical derivative of benzene with an electron-donating group, has received much attention; numerous papers on its semi-empirical calculations have been published.[6-22] From a chemical point of view, the excited states of substituted compounds have been interpreted in terms of locally excited states and charge-transfer states. In accordance with this standpoint, Murrell,[8] Kimura *et al.*,[15] and Godfrey and Murrell[16] determined the assignment of the excited states of aniline by using the localized-orbital or the composite-molecule description. Using the two-step transformation of the wave functions obtained by the Pariser-Parr-Pople method through natural spin orbitals, Fischer-Hjalmars[11] described the excited states of aniline in terms of locally excited and charge-transfer states. There has also been some discussion of the assignment of the second absorption band of aniline. Kimura *et al.*[15] as well as Murrell[8] assigned the band to a charge-transfer transition, whereas Baba[10] and Fischer-Hjalmars[11] assigned it to a locally excited transition.

The present paper will interpret the excited electronic states of aniline in terms of the locally excited states and the charge-transfer states by the application of configuration analysis.[23,24] A full analysis including all the doubly excited configurations will also be given, and contributions from the doubly excited configurations will be discussed.

Method of Calculation

The Pariser-Parr-Pople method with limited configuration interaction was used for the calculation of the π-electronic states of benzene and aniline. The Coulomb repulsion integrals were obtained by means of the following formula:[24,25]

$$\gamma_{pq} = 14.40/[a \exp(-0.3r^2) + r] \text{ eV}$$

where r is the distance in Å units between a pair of atoms, p and q. The parameter, a, is determined by the following formula:

$$a = 14.40 \Big/ \left\{ \frac{1}{2}[(I_p - A_p) + (I_q - A_q)] \right\} \text{ eV}$$

where I_p and A_p are the ionization potential and the electron affinity of an atom, p, respectively.

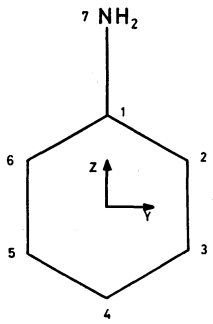

Fig. 1.

The aniline molecule is regarded as being planar and belonging to the C_{2v} symmetry group. The numbering of the atoms and the coordinate axes are shown in Fig. 1. It is assumed that the benzene ring consists of a regular hexagon, with every C–C bond length equal to 1.40 Å, and that the C–N bond length is 1.41 Å. The valence-state ionization potential and the electron affinity for a carbon atom are taken as follows:

$$I_C = 11.16 \text{ eV}, \quad A_C = 0.03 \text{ eV}$$

The resonance integral, β_{CC}, is adjusted to fit the benzene spectrum.

$$\beta_{CC} = -2.48 \text{ eV}$$

In order to discuss the effect of substitution on the electronic spectra, it is reasonable to compare the observed shifts caused by the introduction of a substituent with the calculated shifts, instead of making a direct comparison between the observed and the calculated state energies. From this point of view, the ionization potential, the electron affinity, and the resonance integral related to a nitrogen atom are varied until a satisfactory agreement between the calculated and the observed shifts caused by the introduction of an amino group into benzene is achieved. The best fitted values are as follows:

$$I_N = 26.7 \text{ eV}, \quad A_N = 9.7 \text{ eV}, \quad \beta_{CN} = -1.9 \text{ eV}$$

The SCF MO's are numbered from 1 to 6 for benzene and from 1 to 7 for aniline, in the order of increasing energy. The excited configurations included in the CI calculations are the following one-electron transitions: 2→4, 2→5, 3→4, and 3→5 for benzene and 4→5, 4→6, 3→5, 3→6, 2→5, and 2→6 for aniline.

The ground and the excited state functions of aniline thus obtained are submitted to configuration analysis. The procedure for configuration analysis was presented previously.[23,24] The symbols used in the present paper have the same meanings as in Ref. 24, unless otherwise noted. In the present paper, the reference SCF MO's consist of ϕ°_1, ϕ°_2, $\cdots$, ϕ°_6, which are the SCF MO's of benzene, and ϕ°_N, which represents the π-AO of the substituent of aniline.

Results

Table 1 summarizes the observed and the calculated state energies for benzene and aniline, including the f values. The singlet excited state wave functions are denoted by $^1\Psi_I$, $^1\Psi_{II}$, $\cdots$ in the order of increasing energy, while the ground state function is written as $^1\Psi_G$. The triplet excited wave functions are denoted by $^3\Psi_I$, *etc.*

The results of the configuration analysis for the ground and the excited singlet states of aniline are given in Table 2. The results for the triplet states are given in Table 3. In these and the following tables, the reference-state wavefunctions are indicated by a superscript °. The locally excited states are classified by the group theoretical notation and the Platt notation. The charge-transfer configurations arising from the one-electron excitation from $\phi^\circ_N \rightarrow \phi^\circ_4$, $\phi^\circ_N \rightarrow \phi^\circ_5$, and $\phi^\circ_N \rightarrow \phi^\circ_6$ are denoted by Ψ°_{CTS1}, Ψ°_{CTA}, and Ψ°_{CTS2} respectively. The higher excited configurations, which are not included in the CI calculations of benzene, are written as Ψ°_{15}, which means a one-electron excitation configuration from ϕ°_1 to ϕ°_5, *etc.*

Table 1. Excited states of benzene and aniline

Compound	State function	Energy (eV) Calcd	Energy (eV) Obsd[15]	Oscillator strength Calcd	Oscillator strength Obsd[15]
Benzene	$^1\Psi_G$	0	0		
	$^1\Psi_I$	5.014	4.89	0	0.001
	$^1\Psi_{II}$	6.070	6.17	0	0.126
	$^1\Psi_{III}$	6.898	6.98	1.183	1.035
	$^1\Psi_{IV}$	6.898	6.98	1.183	
	$^3\Psi_I$	3.742	3.88[a]		
	$^3\Psi_{II}$	4.378			
	$^3\Psi_{III}$	4.378			
	$^3\Psi_{IV}$	5.014			
Aniline	$^1\Psi_G$	0	0		
	$^1\Psi_I$	4.539	4.40	0.054	0.028
	$^1\Psi_{II}$	5.328	5.39	0.261	0.140
	$^1\Psi_{III}$	6.253	6.40	0.383	0.510
	$^1\Psi_{IV}$	6.611	6.88	0.889	0.570
	$^1\Psi_V$	7.401	7.87	0.696	0.68
	$^1\Psi_{VI}$	7.542		0.192	
	$^3\Psi_I$	3.392	3.56[a]		
	$^3\Psi_{II}$	3.810			
	$^3\Psi_{III}$	4.166			
	$^3\Psi_{IV}$	5.038			
	$^3\Psi_V$	6.058			
	$^3\Psi_{VI}$	6.621			

a) Estimated values from spectral data.

Table 2. Configuration analysis for aniline (singlet state)

$^1A_1$

Reference state	$^1\Psi_G$	$^1\Psi_{II}$	$^1\Psi_{IV}$	$^1\Psi_{VI}$
$^1\Psi^\circ_G$	0.9352	−0.2422	−0.1042	0.1435
$^1\Psi^\circ_{La}$	−0.0392	−0.6422	0.5619	−0.3965
$^1\Psi^\circ_{Ba}$	0.0200	0.1976	0.6587	0.6440
$^1\Psi^\circ_{CTS1}$	0.3040	0.6104	0.3320	−0.4963
$^1\Psi^\circ_{14}$	−0.0235	−0.1051	−0.0948	0.2709
$^1\Psi^\circ_{36}$	−0.0158	0.0037	0.0017	−0.0029
$^1\Psi^\circ_{CTS2}$	0.1613	−0.0414	−0.0178	0.0244
$^1\Psi^\circ_{16}$	−0.0080	0.0020	0.0008	−0.0011
CT weight (%)	11.84	37.43	11.05	24.69
Sum weight (%)	99.58	89.55	88.00	91.29
Assignment	^1G	(^1L_a+^{1}CTS1)	(^1B_a+^1L_a)	(^1B_a)

$^1B_2$

Reference state	$^1\Psi_I$	$^1\Psi_{III}$	$^1\Psi_V$
$^1\Psi^\circ_{Lb}$	0.7717	0.5172	0.1620
$^1\Psi^\circ_{Bb}$	0.1590	−0.5368	0.7589
$^1\Psi^\circ_{CTA}$	−0.5336	0.5834	0.4825
$^1\Psi^\circ_{15}$	0.0567	−0.1713	−0.2444
$^1\Psi^\circ_{26}$	−0.0003	−0.0004	0.0003
CT weight (%)	28.47	34.04	23.28
Sum weight (%)	90.87	92.54	89.46
Assignment	^1L_b	(^{1}CTA+^1B_b+^1L_b)	^1B_b

Table 3. Configuration analysis for aniline (triplet state)

$^3A_1$

Reference state	$^3\Psi_I$	$^3\Psi_{III}$	$^3\Psi_V$
$^3\Psi^\circ_{La}$	−0.7662	0.4384	−0.3309
$^3\Psi^\circ_{Ba}$	−0.2774	−0.7857	−0.4411
$^3\Psi^\circ_{CTS1}$	0.5230	0.2759	−0.7442
$^3\Psi^\circ_{14}$	−0.0411	−0.0440	0.3059
$^3\Psi^\circ_{36}$	−0.0004	−0.0001	−0.0003
$^3\Psi^\circ_{CTS2}$	0.0003	0.0002	−0.0004
$^3\Psi^\circ_{16}$	0.0000	0.0000	0.0002
CT weight (%)	27.35	7.61	55.38
Sum weight (%)	93.93	88.75	95.16
Assignment	^3L_a	^3B_a	^{3}CTS1

$^3B_2$

Reference state	$^3\Psi_{II}$	$^3\Psi_{IV}$	$^3\Psi_{VI}$
$^3\Psi^\circ_{Bb}$	0.6993	−0.5635	0.2877
$^3\Psi^\circ_{Lb}$	0.3894	0.7520	0.4149
$^3\Psi^\circ_{CTA}$	−0.5089	−0.1924	0.7496
$^3\Psi^\circ_{15}$	0.0320	0.0366	−0.2999
$^3\Psi^\circ_{26}$	0.0001	−0.0006	−0.0001
CT weight (%)	25.90	3.70	56.19
Sum weight (%)	90.07	92.13	90.67
Assignment	(^3B_b)	^3L_b	^{3}CTA

The band assignments are given in Tables 2 and 3. When a single reference state has a weight higher than 50%, the state notation of this state is indicated in the

TABLE 4. CONTRIBUTION FROM DOUBLY EXCITED CONFIGURATIONS (SINGLET STATE)

Configuration	$^1A_1$ $^1\Psi_G$	$^1\Psi_{II}$	$^1\Psi_{IV}$	$^1\Psi_{VI}$	Configuration	$^1B_2$ $^1\Psi_I$	$^1\Psi_{III}$	$^1\Psi_V$
$^1V^\circ_{35.24(1)}$	0.0005	0.0198	−0.0325	0.0024	$^1V^\circ_{35.25}$	−0.0067	0.0001	−0.0067
$^1V^\circ_{35.24(2)}$	−0.0003	−0.0114	0.0188	−0.0014	$^1V^\circ_{35.34}$	−0.0208	0.0004	−0.0206
$^1V^\circ_{35.26(1)}$	0.0002	0.0046	−0.0127	−0.0026	$^1V^\circ_{35.N4(1)}$	0.0207	−0.0226	−0.0187
$^1V^\circ_{35.26(2)}$	−0.0001	−0.0027	0.0073	0.0015	$^1V^\circ_{35.N4(2)}$	0.2020	0.0086	0.2225
$^1V^\circ_{25.25}$	0.0001	0.0046	−0.0125	−0.0025	$^1V^\circ_{35.14(1)}$	−0.0022	0.0066	0.0095
$^1V^\circ_{25.N4(2)}$	−0.0044	−0.1122	0.2753	0.0647	$^1V^\circ_{35.14(2)}$	−0.0152	−0.0035	−0.0218
$^1V^\circ_{25.14(2)}$	0.0003	0.0095	−0.0203	−0.0084	$^1V^\circ_{35.36}$	−0.0079	0.0002	−0.0078
$^1V^\circ_{25.N6(2)}$	−0.0023	−0.0542	0.1489	0.0302	$^1V^\circ_{35.N6(1)}$	0.0078	−0.0086	−0.0071
$^1V^\circ_{25.16(2)}$	0.0001	0.0027	−0.0074	−0.0015	$^1V^\circ_{35.N6(2)}$	0.1090	0.0026	0.1164
$^1V^\circ_{34.34}$	0.0009	0.0268	0.0032	0.0328	$^1V^\circ_{35.16(1)}$	−0.0008	0.0025	0.0036
$^1V^\circ_{34.N4}$	−0.0096	−0.1583	−0.0273	−0.1519	$^1V^\circ_{35.16(2)}$	−0.0052	−0.0013	−0.0076
$^1V^\circ_{34.14}$	0.0007	0.0141	0.0043	0.0044	$^1V^\circ_{25.24}$	0.0044	0.0076	−0.0043
$^1V^\circ_{34.36}$	0.0005	0.0071	0.0008	0.0088	$^1V^\circ_{25.N5}$	0.0055	−0.0060	−0.0049
$^1V^\circ_{34.N6(1)}$	−0.0045	−0.0091	−0.0049	0.0072	$^1V^\circ_{25.15}$	−0.0006	0.0018	0.0025
$^1V^\circ_{34.N6(2)}$	−0.0046	−0.0972	−0.0090	−0.1310	$^1V^\circ_{34.24}$	0.0137	0.0236	−0.0134
$^1V^\circ_{34.16(1)}$	0.0003	0.0016	0.0014	−0.0040	$^1V^\circ_{34.26(1)}$	0.0064	0.0109	−0.0062
$^1V^\circ_{34.16(2)}$	0.0002	0.0042	−0.0002	0.0086	$^1V^\circ_{34.26(2)}$	−0.0037	−0.0063	0.0036
$^1V^\circ_{N4.N4}$	0.0494	0.2112	0.1134	−0.1689	$^1V^\circ_{24.N4}$	−0.0996	−0.1713	0.0970
$^1V^\circ_{N4.14}$	−0.0054	−0.0364	−0.0283	0.0719	$^1V^\circ_{24.14}$	0.0077	0.0132	−0.0075
$^1V^\circ_{N4.N6}$	0.0371	0.0746	0.0405	−0.0606	$^1V^\circ_{24.N6(1)}$	−0.0001	−0.0001	0.0001
$^1V^\circ_{N4.16(1)}$	−0.0035	−0.0157	−0.0142	0.0405	$^1V^\circ_{24.N6(2)}$	−0.0747	−0.1285	0.0728
$^1V^\circ_{N4.16(2)}$	−0.0006	0.0038	0.0053	−0.0191	$^1V^\circ_{24.16(2)}$	0.0037	0.0064	−0.0036
$^1V^\circ_{14.14}$	0.0003	0.0027	0.0024	−0.0068	$^1V^\circ_{N4.N5}$	−0.1227	0.1341	0.1109
$^1V^\circ_{14.16}$	0.0001	0.0006	0.0006	−0.0016	$^1V^\circ_{N4.15(1)}$	0.0116	−0.0127	−0.0105
$^1V^\circ_{36.36}$	0.0001	0.0000	0.0000	0.0000	$^1V^\circ_{N4.15(2)}$	0.0117	−0.0484	−0.0734
$^1V^\circ_{36.N6}$	−0.0019	0.0005	0.0002	−0.0003	$^1V^\circ_{N5.N6}$	−0.0651	0.0712	0.0589
$^1V^\circ_{36.16}$	0.0001	0.0000	0.0000	0.0000	$^1V^\circ_{N5.16(1)}$	0.0085	−0.0256	−0.0365
$^1V^\circ_{N6.N6}$	0.0139	−0.0035	−0.0015	0.0021	$^1V^\circ_{N5.16(2)}$	−0.0003	0.0098	0.0169
$^1V^\circ_{N6.16}$	−0.0010	0.0002	0.0001	−0.0001	$^1V^\circ_{14.15}$	−0.0010	0.0030	0.0043
Sum weight (%)	0.42	10.35	11.66	8.62	$^1V^\circ_{15.16}$	−0.0003	0.0010	0.0015
Total weight (%)	100.00	99.90	99.66	99.91	$^1V^\circ_{N6.26}$	0.0000	−0.0001	0.0000
					Sum weight (%)	8.95	7.39	10.26
					Total weight (%)	99.82	99.93	99.72

TABLE 5. CONTRIBUTION FROM DOUBLY EXCITED CONFIGURATIONS (TRIPLET STATE)

Configuration	$^3A_1$ $^3\Psi_I$	$^3\Psi_{III}$	$^3\Psi_V$	Configuration	$^3\Psi_I$	$^3\Psi_{III}$	$^3\Psi_V$
$^3V^\circ_{35.24(1)}$	−0.0126	0.0316	0.0028	$^3V^\circ_{34.14}$	−0.0118	−0.0030	−0.0194
$^3V^\circ_{35.24(2)}$	0.0048	0.0143	0.0078	$^3V^\circ_{34.36}$	−0.0088	−0.0029	−0.0065
$^3V^\circ_{35.24(3)}$	−0.0131	0.0176	−0.0022	$^3V^\circ_{34.N6(1)}$	−0.0967	−0.0308	−0.0872
$^3V^\circ_{35.26(1)}$	−0.0048	0.0120	0.0011	$^3V^\circ_{34.N6(2)}$	0.0759	0.0258	0.0506
$^3V^\circ_{35.26(2)}$	−0.0017	0.0042	0.0004	$^3V^\circ_{34.N6(3)}$	0.0045	0.0024	−0.0062
$^3V^\circ_{35.26(3)}$	−0.0029	0.0073	0.0007	$^3V^\circ_{34.16(1)}$	0.0046	0.0011	0.0081
$^3V^\circ_{25.N4(1)}$	−0.0917	0.2297	0.0207	$^3V^\circ_{34.16(2)}$	−0.0038	−0.0014	−0.0012
$^3V^\circ_{25.N4(2)}$	0.0649	−0.1624	−0.0146	$^3V^\circ_{34.16(3)}$	−0.0004	−0.0004	0.0026
$^3V^\circ_{25.N4(3)}$	−0.0076	−0.0040	0.0108	$^3V^\circ_{N4.14}$	−0.0002	−0.0052	0.0571
$^3V^\circ_{25.14(1)}$	0.0071	−0.0177	−0.0016	$^3V^\circ_{N4.N6}$	−0.0637	−0.0336	0.0907
$^3V^\circ_{25.14(2)}$	−0.0050	0.0125	0.0011	$^3V^\circ_{N4.16(1)}$	0.0021	0.0043	−0.0379
$^3V^\circ_{25.14(3)}$	0.0006	0.0006	−0.0044	$^3V^\circ_{N4.16(2)}$	0.0046	0.0036	−0.0189
$^3V^\circ_{25.N6(1)}$	−0.0487	0.1219	0.0110	$^3V^\circ_{N4.16(3)}$	0.0035	0.0038	−0.0263
$^3V^\circ_{25.N6(2)}$	0.0344	−0.0862	−0.0078	$^3V^\circ_{14.16}$	−0.0002	−0.0003	0.0019
$^3V^\circ_{25.16(1)}$	0.0024	−0.0061	−0.0005	Sum weight (%)	5.97	10.89	4.79
$^3V^\circ_{25.16(2)}$	−0.0017	0.0043	0.0004	Total weight (%)	99.90	99.64	99.95
$^3V^\circ_{34.N4}$	0.1531	0.0477	0.1490				

(Table 5, continued) $^3B_2$

Configuration	$^3\Psi_{II}$	$^3\Psi_{IV}$	$^3\Psi_{VI}$	Configuration	$^3\Psi_{II}$	$^3\Psi_{IV}$	$^3\Psi_{VI}$
$^3V^{\circ}_{35,25}$	0.0079	0.0014	0.0051	$^3V^{\circ}_{34,26(3)}$	0.0019	−0.0079	−0.0008
$^3V^{\circ}_{35,34}$	0.0244	0.0042	0.0157	$^3V^{\circ}_{24,N4}$	−0.0504	0.2138	0.0207
$^3V^{\circ}_{35,N4(1)}$	0.1857	0.0283	0.1592	$^3V^{\circ}_{24,14}$	0.0039	−0.0165	−0.0016
$^3V^{\circ}_{35,N4(2)}$	−0.1511	−0.0275	−0.0836	$^3V^{\circ}_{24,N6(1)}$	0.0309	−0.1310	−0.0127
$^3V^{\circ}_{35,N4(3)}$	−0.0114	−0.0043	0.0168	$^3V^{\circ}_{24,N6(2)}$	−0.0218	0.0925	0.0089
$^3V^{\circ}_{35,14(1)}$	−0.0146	−0.0014	−0.0211	$^3V^{\circ}_{24,N6(3)}$	0.0000	0.0001	0.0000
$^3V^{\circ}_{35,14(2)}$	0.0116	0.0024	0.0033	$^3V^{\circ}_{24,16(1)}$	−0.0015	0.0065	0.0006
$^3V^{\circ}_{35,14(3)}$	0.0007	0.0008	−0.0067	$^3V^{\circ}_{24,16(2)}$	0.0011	−0.0046	−0.0004
$^3V^{\circ}_{35,36}$	0.0092	0.0016	0.0060	$^3V^{\circ}_{N4,N5}$	−0.1170	−0.0442	0.1723
$^3V^{\circ}_{35,N6(1)}$	0.1014	0.0161	0.0803	$^3V^{\circ}_{N4,15(2)}$	0.0111	0.0042	−0.0163
$^3V^{\circ}_{35,N6(2)}$	−0.0792	−0.0142	−0.0458	$^3V^{\circ}_{N4,15(3)}$	0.0040	0.0095	−0.0881
$^3V^{\circ}_{35,N6(3)}$	−0.0043	−0.0016	0.0064	$^3V^{\circ}_{N5,N6}$	0.0621	0.0235	−0.0914
$^3V^{\circ}_{35,16(1)}$	−0.0049	−0.0004	−0.0076	$^3V^{\circ}_{N5,16(1)}$	−0.0009	−0.0038	0.0370
$^3V^{\circ}_{35,16(2)}$	0.0040	0.0008	0.0010	$^3V^{\circ}_{N5,16(2)}$	−0.0041	−0.0028	0.0186
$^3V^{\circ}_{35,16(3)}$	0.0003	0.0003	−0.0025	$^3V^{\circ}_{N5,16(3)}$	−0.0028	−0.0032	0.0259
$^3V^{\circ}_{25,24}$	−0.0022	0.0095	0.0009	$^3V^{\circ}_{14,15}$	−0.0006	−0.0006	0.0053
$^3V_{25,N5}$	0.0052	0.0020	−0.0077	$^3V_{15,16}$	0.0002	0.0002	−0.0018
$^3V^{\circ}_{25,15}$	−0.0003	−0.0004	0.0031	$^3V^{\circ}_{N6,26}$	0.0000	−0.0001	0.0000
$^3V^{\circ}_{34,24}$	−0.0069	0.0294	0.0028	Sum weight (%)	9.69	7.77	9.13
$^3V^{\circ}_{34,26(1)}$	0.0030	−0.0129	−0.0012	Total weight (%)	99.76	99.90	99.80
$^3V^{\circ}_{34,26(2)}$	0.0011	−0.0045	−0.0004				

column of band assignment. If there is no reference state the weight of which singly exceeds 50%, the state notations for the reference states of the most important contribution are indicated in parentheses.

Configuration analysis including all the doubly excited configurations has been performed for both the singlet and the triplet states. All the doubly excited configurations which have a contribution higher than 0.0001 are given in Table 4 for the singlet states and in Table 5 for the triplet states. The notations concerning the doubly excited configurations are the same as in Ref. 24. The total weight means the sum of the weights of all the singly and doubly excited configurations.

Discussion

The calculated shifts in transition energies caused by the introduction of an amino group are compared with the observed shifts in Table 6. The calculated and the observed shifts agree well. Therefore, the electronic wave functions which were subjected to configuration analysis in the present study are appropriate to a discussion of the effect of substitution on the electronic spectra.

The ground state of aniline may safely be assigned to the ground reference state. The charge-transfer reference states have a weight of 11.84% in the ground state. In the first excited state of aniline, the reference state which has the highest contribution to this state is the ^1L_b, the wight of which is 59.55%. The first excited state of aniline may, therefore, be assigned to the locally excited reference state, ^1L_b. The weight of the charge-transfer contributions to this state is 28.47%. The contribution of the ^1B_b to the first excited state is only 2.53%, but the origin of the absorption intensity of the first absorption band in aniline may be explained by the mixing with the ^1B_b.

In the second excited state of aniline, there is no reference state which alone has a weight of contribution higher than 50%. The reference state of the highest contribution to this excited states is the ^1L_a; however, the weight of the ^{1}CTS1 state is comparable to, and a little lower than, that of the ^1L_a state. It is reasonable that the second excited state of aniline is assigned to the mixed state of the ^1L_a and the ^{1}CTS1 reference state. The ^1B_a reference state has a weight of 3.90%; the intensity of the second absorption band may be derived from the ^1B_a state. The weight of the ground reference state is 5.87%.

In the third excited state of aniline, the reference state with a maximum wight is the ^{1}CTA state. However, there are two other reference states which have weights comparable to that of the ^{1}CTA, namely, the ^1B_b and ^1L_b states. The third excited state of aniline is, therefore, assigned to the mixed state of the ^{1}CTA, ^1B_b, and ^1L_b states. The ^1B_a reference state makes the highest contribution to the fourth excited state of aniline. The ^1L_a reference state also makes a considerable contribution to this excited state. It is found that the higher excited states of aniline are difficult to explain in terms of a single locally excited state or a single charge-transfer state.

Table 6. Comparison of the band shifts caused by the introduction of an amino group into benzene

Band	Band shift (eV)			
	Obsd	This work	Fischer-Hjalmars	Kimura *et al.*
I	−0.49	−0.475	−0.198	−0.17
II	−0.78	−0.742	−0.619	−0.75
III	−0.58	−0.645	−0.501	−0.56
VI	−0.10	−0.287	−0.336	−0.12

In the first excited triplet state, the ^3L_a state alone has a weight higher than 50%; therefore, the first triplet state of aniline may be assigned to the ^3L_a reference state. The ^{3}CTS1 state and the ^3B_a state have weights of 27.35 and 7.70% respectively. The assignments of the higher triplet states of aniline are given in Table 3. It is of interest that the weights of the charge-transfer reference states in the $^3\Psi_V$ and $^3\Psi_{VI}$ states have values higher than 50%, whereas the charge-transfer reference states make little contribution to the $^3\Psi_{III}$ and $^3\Psi_{IV}$ states. In general, it is found that the reference states in the triplet states are mixed together to a lesser extent than those in the singlet states.

All the contributions from the doubly excited configurations were calculated for both the singlet and the triplet states of aniline. The $^1V^\circ_{25.N4(2)}$ reference configuration has a weight of 7.58% relative to the $^1\Psi_{IV}$ state. The reference configurations which have weights higher than 2% are as follows: $^1V^\circ_{35.N4(2)}$ ($^1\Psi_I$); $^1V^\circ_{N4.N4}$ and $^1V^\circ_{34.N4}$ ($^1\Psi_{II}$); $^1V^\circ_{24.N4}$ ($^1\Psi_{III}$); $^1V^\circ_{25.N4(2)}$ and $^1V^\circ_{25.N6(2)}$ ($^1\Psi_{IV}$); $^1V^\circ_{35.N4(2)}$ ($^1\Psi_V$); $^1V^\circ_{N4.N4}$ and $^1V^\circ_{24.N4}$ ($^1\Psi_{VI}$). All the other reference configurations have weights less than 2% relative to the individual singlet states. The contributions of individual doubly-excited configurations are not important, however, the sum weights from all the doubly excited configurations have values ranging between 7.39 and 11.66%, except for the ground state. The sum weight of all the singly excited states or configurations for the ground state has a value of 99.58%, but the sum weights for the excited singlet states have values of about 90% (from 88.00 to 92.54%). The inclusion of all the doubly excited configurations improves the sum weights of the excited states up to 99.66% or more. It may be said that the "accuracy" of the description of the lower excited electronic states of aniline in terms of the locally excited states and the charge-transfer states within the singly excited configurations is approximately 90%. The inclusion of the doubly excited configurations improves the "accuracy" of the description, but the brevity of the description is lost. When the sum weights of all the singly excited configurations are far from 100%, the selection of reference states or configurations should be reconsidered. If a proper selection of reference states is impossible, one should abandon the description of the excited states in terms of locally excited states and charge-transfer states.

The reference states included in the calculation by Kimura *et al.*[15] are the ground state, $^1\Psi^\circ_G$, the four locally excited states, $^1\Psi^\circ_{Lb}$, $^1\Psi^\circ_{La}$, $^1\Psi^\circ_{Bb}$, and $^1\Psi^\circ_{Ba}$, and the two charge-transfer states, $^1\Psi^\circ_{CTS1}$ and $^1\Psi^\circ_{CTA}$. The sum weights of these seven reference states in the present configuration analysis are as follows: 90.55% ($^1\Psi_I$), 88.24% ($^1\Psi_{II}$), 89.59% ($^1\Psi_{III}$), 87.07% ($^1\Psi_{IV}$), 83.50% ($^1\Psi_V$), and 83.89% ($^1\Psi_{VI}$). This implies that a portion of the electronic interactions is neglected in the localized-orbital description compared with the Pariser-Parr-Pople method (10—16% in the case of aniline). In other words, the wave functions of locally excited states or charge-transfer states cannot be regarded as the basis functions of rapid convergence in the expansion of excited states of aniline.

Murrell,[8] Kimura *et al.*,[15] and Godfrey and Murrell[16] obtained the electronic wave functions of aniline as the linear combinations of locally excited and charge-transfer state functions by using the localized-orbital method. On the other hand, Fischer-Hjalmars[11] transformed the excited wave functions obtained by the Pariser-Parr-Pople method into locally excited or charge-transfer state functions through natural spin orbitals. In Table 7, the results of the present configuration analysis are compared with those of the other investigations.

Table 7. Comparison of the results

$^1A_1$

Reference state	$^1\Psi_{II}$ CA[a]	$^1\Psi_{II}$ Fischer-Hjalmars	$^1\Psi_{II}$ Kimura *et al.*	$^1\Psi_{IV}$ CA[a]	$^1\Psi_{IV}$ Fischer-Hjalmars	$^1\Psi_{IV}$ Kimura *et al.*
$^1\Psi^\circ_G$	6.7		3.7	1.3		0.4
$^1\Psi^\circ_{La}$	46.7	57.5	34.9	36.3	26.1	53.1
$^1\Psi^\circ_{Ba}$	4.4	4.2	11.4	49.8	55.4	37.5
$^1\Psi^\circ_{CTS1}$	42.2	38.3	50.0	12.6	18.7	9.0

$^1B_2$

Reference state	$^1\Psi_I$ CA[a]	$^1\Psi_I$ Fischer-Hjalmars	$^1\Psi_I$ Kimura *et al.*	$^1\Psi_{III}$ CA[a]	$^1\Psi_{III}$ Fischer-Hjalmars	$^1\Psi_{III}$ Kimura *et al.*
$^1\Psi^\circ_{Lb}$	65.8	89.5	74.6	29.8	5.7	21.4
$^1\Psi^\circ_{Bb}$	2.8	0.7	2.7	32.2	60.5	39.9
$^1\Psi^\circ_{CTA}$	31.5	9.9	22.6	38.0	33.8	38.7

a) The results of the present work. Weights are normalized to 100% within the states listed in the table.

In the assignment of the first excited state of aniline, a qualitative agreement is found among these results. Kimura *et al.* as well as Murrell assigned the second excited state of aniline to the charge-transfer state, ^{1}CTS1. On the contrary, Baba[10] and Fischer-Hjalmars assigned the band to the locally excited state, ^1L_a. The present study supports the latter assignment rather than the former one, but the weight of the ^1L_a state does not exceed 50%. The third excited singlet state shows a remarkable mixing among the ^1L_b, ^1B_b, and ^{1}CTA states in the present study and in the work of Kimura *et al.*, but it was assigned to the ^1B_b reference state in the work of Fischer-Hjalmars. In the fourth excited state, the result of the present analysis resembles that of Fischer-Hjalmars rather than that of Kimura *et al.* The result obtained by Murrell showed a qualitative resemblance to that obtained by Kimura *et al.*, but the result obtained by Godfrey and Murrell resembled that obtained by Fischer-Hjalmars.

Kimura and Tsubomura[26] calculated the wave functions of the triplet states of substituted benzenes by using the localized-orbital method. They assigned the lowest triplet state of aniline to the ^3L_a, in accordance with the results of the present analysis.

The calculated band shifts caused by the introduction of an amino group into benzene are compared with the

observed shifts as well as the calculated shifts obtained by the other studies in Table 6. Band I of aniline, which was assigned to the locally excited transition of benzene, ^1L_b, shows a considerable red shift compared with Band I of benzene. In the calculation of state energies by the localized-orbital method adopted by Murrell, by Kimura *et al.*, and by Godfrey and Murrell, the observed transition energies of benzene are used as the state energies of the locally excited configurations. Nevertheless, the localized-orbital method can not correctly reproduce the red shift of Band I. The result obtained by Fischer-Hjalmars does not give the red shift of Band I correctly, either. Furthermore, the mixing of the ground state with the excited reference states has been neglected in the work of Fischer-Hjalmars.

References

1) H. H. Jaffé and M. Orchin, "Theory and Applications of Ultraviolet Spectroscopy," Wiley, New York (1962).
2) J. N. Murrell, "The Theory of the Electronic Spectra of Organic Molecules," Methuen, London (1963).
3) J. R. Platt and Co-Workers, "Systematics of the Electronic Spectra of Conjugated Molecules," Wiley, New York (1964).
4) F. A. Matsen, R. S. Becker, and D. R. Scott, Interpretation of Electronic Absorption Spectra in "Chemical Applications of Spectroscopy," Interscience, New York (1968).
5) C. J. Seliskar, O. S. Khalil, and S. P. McGlynn, Luminescence Characteristics of Polar Aromatic Molecules in "Excited States," Vol. 1, Academic Press, New York(1974).
6) K. F. Herzfeld, *Chem. Rev.*, **41**, 233 (1949).
7) F. A. Matsen, *J. Amer. Chem. Soc.*, **72**, 5243 (1950).
8) J. N. Murrell, *Proc. Phys. Soc.* (London), **A68**, 969 (1955).
9) T. E. Peacock, *Mol. Phys.*, **3**, 453 (1960).
10) H. Baba, This Bulletin, **34**, 76 (1961).
11) I. Fischer-Hjalmars, *Ark. Fysik*, **21**, 123 (1962).
12) J. E. Bloor and F. Peradejordi, *Theoret. Chim. Acta*, **1**, 83 (1962).
13) N. Mataga, This Bulletin, **36**, 1607 (1963).
14) J. E. Bloor, P. N. Daykin, and P. Boltwood, *Can. J. Chem.*, **42**, 121 (1964).
15) K. Kimura, H. Tsubomura, and S. Nagakura, This Bulletin, **37**, 1336 (1964); K. Kimura and S. Nagakura, *Mol. Phys.*, **9**, 117 (1965); S. Nagakura and K. Kimura, *Nippon Kagaku Zasshi*, **86**, 1 (1965).
16) M. Godfrey and J. N. Murrell, *Proc. Roy, Soc.*, **A278**, 71 (1964).
17) S. Kwiatkowski, *Acta Phys. Pol.*, **29**, 477, 529 (1966).
18) P. Knowlton and W. R. Carper, *Mol. Phys.*, **11**, 213 (1966).
19) H. Hartmann and J. Fabian, *Ber. Bunsenges. Phys. Chem.*, **73**, 107 (1969).
20) M. Ticky and R. Zahradnik, *J. Phys. Chem.*, **73**, 534 (1969).
21) R. Carbó and S. Fraga, *Anal. Fis.*, **67**, 171 (1971).
22) J. D. Bene and H. H. Jaffé, *J. Chem. Phys.*, **49**, 1221 (1968).
23) H. Baba and S. Suzuki, This Bulletin, **40**, 2457 (1967).
24) H. Baba, S. Suzuki, and T. Takemura, *J. Chem. Phys.*, **50**, 2078 (1969).
25) T. Takemura, K. Hara, and H. Baba, This Bulletin, **44**, 977 (1971).
26) K. Kimura and H. Tsubomura, *Mol. Phys.*, **11**, 349 (1966).

Theoretical Calculation of ^{13}C Chemical Shielding Anisotropy in Some Organic Compounds. II.

Isao ANDO and Atsuo NISHIOKA

Department of Polymer Chemistry, Tokyo Institute of Technology, Ookayama, Meguro-ku, Tokyo 152

(Received September 18, 1974)

The ^{13}C chemical shielding anisotropies of acetic acid and its related compounds were calculated theoretically by the LCGI-MO theory, using the MINDO/2 method; the results were found to agree with the experimental data measured by Pines *et al.* As for acetic acid, a dimer structure was suggested to be preferable to the monomer structure on the basis of the calculated and experimental results.

In our previous paper[1] we calculated theoretically the ^{13}C chemical shielding anisotropies of benzene and its derivatives, and of acetone with a linear combination of the gauge invariant atomic orbitals-molecular orbital (LCGI-MO) theory of Pople,[2] using the MINDO/2 method;[3] we thus obtained good agreement with the experimental data measured by Pines *et al.*[4] In the same way, we will now calculate the ^{13}C chemical shielding anisotropies of acetic acid, taking into account the monomer and dimer structures, and compare our results with Pines' results in order to obtain information on its molecular structure. Further, we will discuss the ^{13}C shielding parameters of its related compounds containing the carbonyl group, acetic anhydride, methyl formate, and acetaldehyde.

Calculation

The ^{13}C chemical shielding is dominated by the paramagnetic terms, σ_{xx}, σ_{yy}, σ_{zz}, which are estimated by the use of the LCGI-MO theory using 2p orbitals, as follows (*e.g.*, σ^p_{xx}):

TABLE 1. THE CALCULATED AND EXPERIMENTAL[4] ^{13}C CHEMICAL SHIELDING PARAMETERS IN ACETIC ACID, ACETIC ANHYDRIDE, METHYL FORMATE, AND ACETALDEHYDE

Compound	Calculated (ppm)				Experimental (ppm)			
	σ^p_{xx}	σ^p_{yy}	σ^p_{zz}	$\Delta\sigma_{calc}$ [a]	σ_{11}	σ_{22}	σ_{33}	$\Delta\sigma_{obs}$ [a]
Acetic acid								
Case I 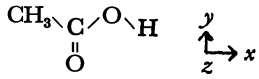 CO	−445.8	−278.5	−223.2	138.9				
Case II 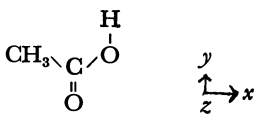 CO	−439.9	−262.8	−238.2	113.2	CO	−140±6	−55±6	19±6	116.5±6
Case III 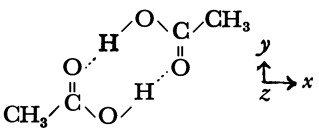 CO	−413.8	−285.2	−229.4	120.1				
Acetic anhydride 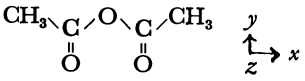 CO	−367.9	−196.2	−215.9	95.7		−152±6	13±6	13±6	82.5±6
Methyl formate 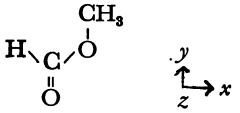 CO	−443.0	−276.5	−228.9	130.8		−124±6	−7±7	22±7	87.5±7
Acetaldehyde 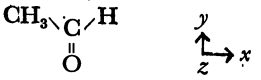 CO	−447.1	−381.8	−221.6	192.8		−147±7	−105±6	42±6	168±6

a) $\Delta\sigma_{calc}$ and $\Delta\sigma_{obs}$ are the calculated and observed shielding anisotropies, respectively.

$$\sigma^{p}_{xx} = -(2e^2\hbar^2/m^2c^2)\langle r^{-3}\rangle_{2p}\sum_{i}^{occ}\sum_{k(\neq i)}^{unocc}\Delta E^{-1}_{k-i} \times (C_{i_{y_A}}C_{k_{z_A}} - C_{i_{z_A}}C_{k_{y_A}})\sum_{B}(C_{i_{y_B}}C_{k_{z_B}} - C_{i_{z_B}}C_{k_{y_B}}) \quad (1)$$

where $C_{i_{x_A}}$ is the coefficient of the $2p_x$ atomic orbital on the A atom of the i-th molecular orbital in the LCAO MO theory, where $\sum_{i}^{occ}$ and $\sum_{k(\neq i)}^{unocc}$ are the summations over occupied and unoccupied orbitals respectively, where $\sum_{B}$ runs over all atomic orbitals in the molecule, and where ΔE_{k-i} is the singlet-singlet excitation energy between the i-th occupied and the k-th unoccupied orbitals. $\langle r^{-3}\rangle_{2p}$ represents the atomic 2p orbital dimension given by:[5]

$$\langle r^{-3}\rangle_{2p} = 34.33a_0^{-3}(1.0-0.323q_A')/24 \quad (2)$$

where a_0 is the Bohr radius and where $-q_Ae$ is the net charge. The MINDO/2 method was used as the molecular orbital method, because the excitation energy for the molecule with π-electrons is said to be interpreted well by this method without taking the configuration interaction into account.

The bond lengths and bond angles used were set at standard values.[6] In the dimer of acetic acid, the distance between the oxygen atoms in the hydrogen bond (C–O–H···O=C) used was 2.76 Å.[7]

The calculations were carried out by means of the HITAC-8800/8700 computer of the Computer Center of the University of Tokyo.

Results and Discussion

First, let us examine the acetic acid molecule. Generally, carboxylic acids are well-known to form hydrogen bonding in the liquid and solid states.[8] Thus, as the molecular structure of acetic acid, we consider the cyclic dimer structure, together with the two monomer structures, as is shown in Table 1. In calculating each component of the chemical shielding, it is necessary to know the direction of the principal axis of the molecule. We assume that the principal axis is along the C=O bond. This seems appropriate approximately for the carbonyl carbon. The principal values, σ^{p}_{xx}, σ^{p}_{yy}, and σ^{p}_{zz}, calculated for the carbonyl carbons are shown in Table 1, together with the experimental values, σ_{11}, σ_{22}, and σ_{33}, measured by Pines *et al.*; the latter are the components of the shielding tensor. The experimental chemical shielding anisotropy is defined as $\Delta\sigma_{obs}=\sigma_{33}-(\sigma_{11}+\sigma_{22})/2$, in which σ_{33} is the most shielded component ($\sigma_{11}<\sigma_{22}<\sigma_{33}$); on the other hand, the calculated anisotropy, $\Delta\sigma_{calc}$, is estimated by taking the most shielded component as the component corresponding to σ_{33} in the experimental results (here, in acetic acid σ^{p}_{yy} is taken as its component). As for the carbonyl carbon, the $\Delta\sigma_{cal}$ values of Cases II and III are found to agree with the experimental ones better than that of Case I. For a more detailed comparison between these, the stick spectra of each shielding tensor are shown in Fig. 1. From this figure the results of Case III are found to agree well with the observed values and also with the results obtained by another method.[8]

Next, let us discuss the $\Delta\sigma$ value of the carbonyl carbon in acetic anhydride. The calculated $\Delta\sigma_{calc}$ value is 95.7 ppm. If the values of σ^{p}_{yy} and σ^{p}_{zz} are averaged with each other by taking into account the observed fact that $\sigma_{22}=\sigma_{33}$, the calculated $\Delta\sigma_{calc}$ value is obtained as 80.9 ppm. This agrees well with the observed value, 82.5 ppm. The stick spectra are shown in Fig. 1. In acetic anhydride, the most shielded component is σ^{p}_{yy}, which is slightly more shielded than σ^{p}_{zz}. This is different from the case of acetic acid, in

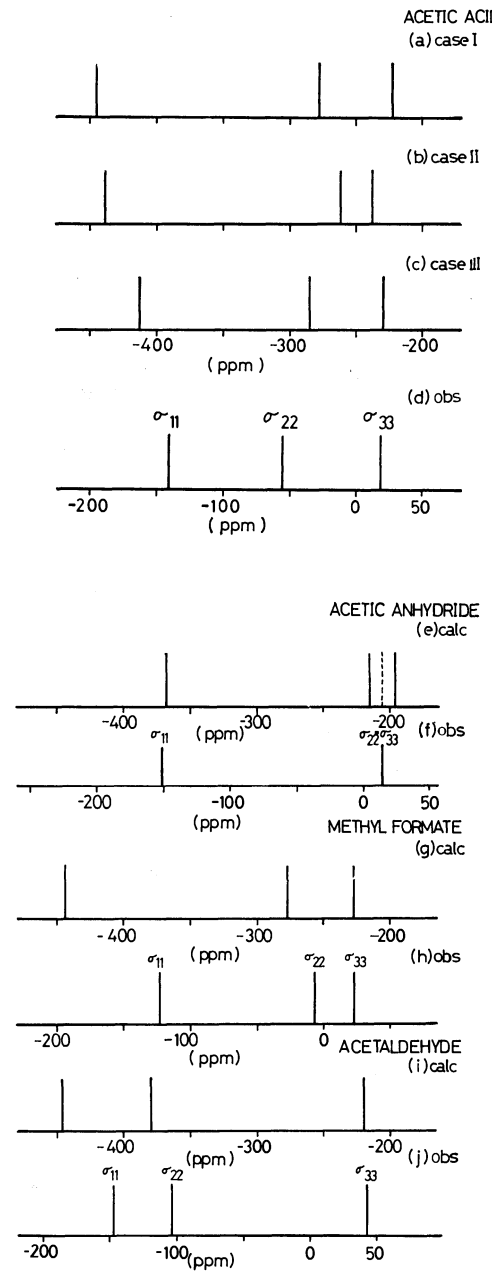

Fig. 1. The calculated and observed[4] stick spectra of acetic acid, acetic anhydride, methyl formate, and acetaldehyde.
acetic acid: calculated, (a)—(c), observed, (d), acetic anhydride: calc, (e). The dash-line is one averaged over σ^{p}_{yy} and σ^{p}_{zz}. observed, (f).
methyl formate: calculated, (g), observed, (h).
acetaldehyde: calculated, (i), observed, (j).

which the most shielded component is σ^{p}_{zz}.

The calculated $\Delta\sigma_{calc}$ values of the carbonyl carbons of methyl formate and acetaldehyde molecules are also shown in Table 1. The calculated results are somewhat larger than the observed ones, but the tendency of the shielding tensors of these carbons is plausible, as is shown in Fig. 1.

If the calculated $\Delta\sigma_{calc}$ values of the carbonyl carbons in all of the molecules are seen as a whole, the order of their magnitutes is found to be; acetaldehyde> methyl formate>acetic acid>acetic anhydride. This order agrees with the observed one. Moreover, we notice the tendency of each shielding tensor through all the compounds. The σ^{p}_{yy} value is found to be especially sensitive to the substituent in the calculated results. This sensitivity is also displayed by the observed results.

Only the most shielded component in acetic anhydride is σ^{p}_{yy}; the other compounds are σ^{p}_{zz}. This may be because the π-electrons of the carbonyl group in acetic anhydride are more delocalized than in the others; therefore, the shielding of the yy component increases in comparison with the other compounds. In acetic anhydride the magnitudes of σ^{p}_{yy} and σ^{p}_{zz} are near to each other, but in other compounds they are not. This would also be qualitatively interpreted by the above reason.

Our theoretical approach to the ^{13}C chemical shielding anisotropy will contribute to obtaining valuable information on the molecular structure in the solid state and to determining the principal axis of the molecule concerned.

References

1) I. Ando, A. Nishioka, and M. Kondo, *Chem. Phys. Lett*, **25**, 212 (1974).
2) J. A. Pople, *J. Chem. Phys.*, **37**, 53 (1962).
3) M. J. S. Dewar and E. Haselbach, *J. Amer. Chem. Soc.*, **92**, 590 (1970).
4) A. Pines, M. G. Gibby, and J. S. Waugh, *Chem. Phys. Lett*, **15**, 373 (1972).
5) J. A. Pople, *Mol. Phys.*, **7**, 301 (1964).
6) J. A. Pople and D. L. Beveridge, "Approximate Molecular Orbital Theory," McGraw-Hill, New York (1970), p. 111.
7) J. Holtzberg, *Acta Crystallogr*, **6**, 127 (1953).
8) P. A. Kollman and L. C. Allen, *Chem. Rev.*, **72**, 283 (1972).

The Role of Anion in the Demethylation Reaction of Methylcobalamin with Mercuric Salts

Haruhiko YAMAMOTO, Takashi YOKOYAMA, Ju-Ling CHEN, and Takao KWAN
Faculty of Pharmaceutical Sciences, University of Tokyo, 7-3-1 Hongo, Bunkyo-ku, Tokyo 113
(Received August 5, 1974)

The demethylation of methylcobalamin with mercuric salts containing ClO_4^-, AcO^-, Cl^-, Br^-, SCN^-, or CN^- was kinetically investigated by a conventional spectroscopic technique. The rates of reaction for mercuric chloride were proportional to $[CH_3\text{–Co}]$ and $[HgCl_2]$ while those for acetate depended little on $[Hg(AcO)_2]$, but increased in proportion with $[AcO^-]$. The rates of reaction varied depending on the concentration and species of anion, and the following sequence was obtained: $AcO^- \gg Cl^- \geq SCN^- \geq Br^- \gg CN^-$. The sequence was reversely correlated with the stability constant of the equilibrium reaction, $HgL_{n-1}+L \rightleftarrows HgL_n$ ($n=1$ or 2), so that it was considered that HgL^+ is an attacking electrophile in the cleavage of cobalt-carbon bond by the mercuric salts. The activity of $HgCl_4^{2-}$ for the reaction was somewhat lower than that of $HgCl_2$ while that of HgClCN was lower to a greater extent.

Mercuric salts are known to be active for the cleavage of cobalt-carbon bond. Halpern and Maher[1] reported, as the first demonstration of this kind of reaction, the formation of methylchloromercury from the reaction of mercuric chloride with methylpentacyanocobaltate(III). Since then, the demethylation reaction of alkylcobalamins and their model compounds with mercuric salts has been investigated by a number of groups,[2–10] especially in connection with organo mercury poisoning.

So far, however, the authors have been primarily concerned with the identification of reaction products, the relationship between the reaction rates and the size of alkyl groups, and/or the influence of the sixth ligand of the alkyl cobalt complexes with respect to the demethylation reaction. Only a little work has been carried out on the effect of mercuric salt species on the reaction by Bertilsson and Neujahr,[9] who described the efficiency of some organo mercuric salts ($HgCl_2$, CH_3HgCl, C_6H_5HgCl, $CH_3COCH_2CH_2HgBr$, C_6H_5-HgOH, CH_3Hg dicyandiamide) for the reaction.

We have therefore studied the effect of anion in mercuric salts on the demethylation reaction. In this paper we describe the reaction features on using ClO_4^-, AcO^-, Cl^-, Br^-, SCN^-, or CN^- as ligands for the mercuric ion, the relationship between the reaction rates and the stability constants of mercuric complexes, and a possible reaction mechanism.

Experimental

Materials. Cyanocobalamin (*Daiichi Pure Chemical*) was used to synthesize methylcobalamin according to the accepted procedure.[11] The methylcobalamin sample was further purified on Amberlite XAD-2 resin. Its purity was checked by paper chromatography on Toyo Filter Paper No. 51 with 1-butanol–2-propanol–acetic acid–water (100-70-1-100, *v/v*) as a solvent.[12]

The concentration of methylcobalamin thus prepared was estimated from spectral data of the Müllers.[13] The sample of methylcalbalamin solution was transferred little by little into a micro tube and preserved in a frozen state. The sample tube was defrosted just before use.

Mercuric chloride and acetate (Koso Chemical GR) were used without further purification. Mercuric perchlorate was prepared from mercuric chloride and silver perchlorate (Kojima Chemical, GR). All the other chemicals used were commercial (GR).

Procedures. Fresh solutions of methylcobalamin and of mercuric salts were made up for a few experiments at a time. The reaction was started by adding a suitable amount of mercuric salt solution to 3 ml of methylcobalamin solution with a micro syringe (Jintan Thermo) and by stirring with a Teflon bar. The spectrum change in the range 340—600 nm was then traced with a Hitachi Recording Spectrophotometer EPS-3T. Finally, the spectrum of completely demethylated sample was obtained by 3 min irradiation of the reaction system with a 100 W projecter lamp.

Demethylation reactions were performed usually with excess mercuric salts over methylcobalamin in the cell of spectrophotometer around room temperature. The concentration range was $40—50\times10^{-6}$ M for methylcobalamin and $400—1600\times10^{-6}$ M for mercuric salts.

Results and Discussion

Mercuric Chloride. Since mercuric chloride reveals no spectral absorption in the region 340—600 nm, it was possible to observe the rates of demethylation of methylcobalamin by measuring the optical absorbance, A, of methylcobalamin at 350 nm. The spectral changes due to the demethylation reaction, $CH_3\text{–Co}\rightarrow H_2O\text{–Co}$, appeared to progress with isosbestic points.

When the natural logarithms of the absorbance change $\ln\{(A-A_\infty)/(A_0-A_\infty)\}$ were plotted against time, a straight line was obtained, A_0 and A being the absorbance at time zero and infinity (or irradiated), respectively. The slope of the straight line, denoted as k_1, will be used as a rate parameter. The dependence of k_1 on the concentration of mercuric chloride was then investigated. It was found that k_1 increases in proportion to the concentration of mercuric chloride. The results are shown in Figs. 1 and 2. Thus, the demethylation rate, r, for mercuric chloride satisfies the following rate law:

$$r = k[CH_3\text{–Co}][HgCl_2] \quad (1)$$

Methylcobalamin is known to conform to different molecular forms depending on the pH.[14] It exists as a "base-on" form in which benzimidazole is axially coordinated while a "base-off" exists at low pH and hence protonated. The corresponding pK_a was re-

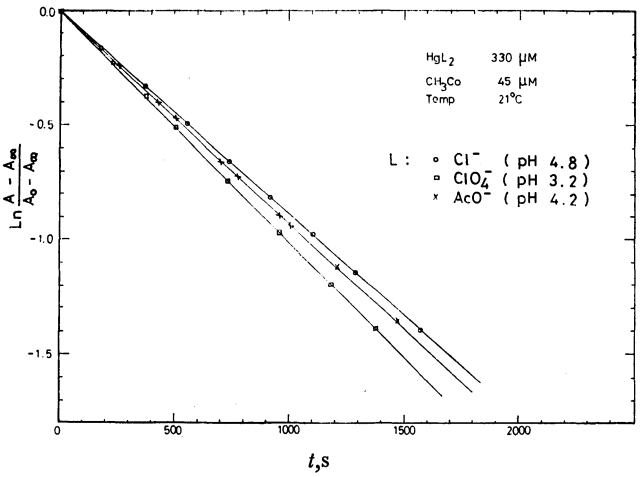

Fig. 1. Representative first-order plots for the demethylation of methylcobalamin with HgL_2.
□: L=ClO_4^-, pH=3.2, ×: L=AcO^-, pH=4.2.
○: L=Cl^-, pH=4.8
[HgL_2]=330 μM, [CH_3–Co]=45 μM, Reaction temperature 21 °C. A: measured at 350 nm

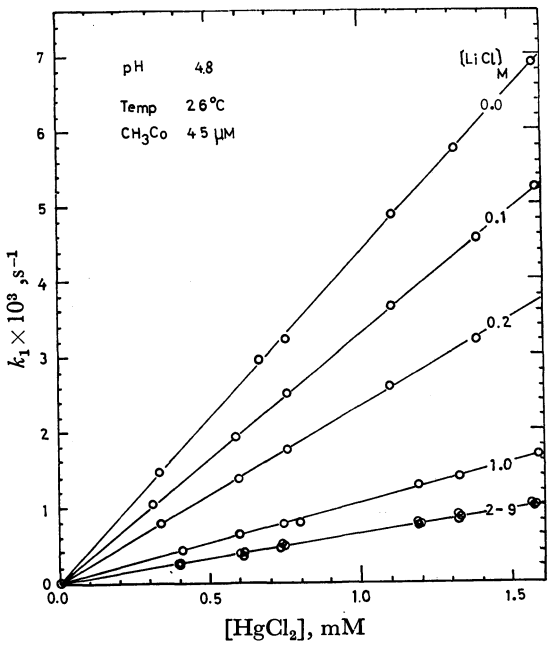

Fig. 2. Dependence of k_1 on the concentration of mercuric chloride and lithium chloride.
[CH_3–Co]=45 μM, pH=4.8. Reaction temperature 26 °C.

ported to be 2.72[14] so that the predominant species should be "base-on" forms above pH 3.5. Thus, the pH dependence of k_1 was investigated in the pH range 1—5 by adding perchloric acid, phosphoric acid or hydrochloric acid to the reaction system.

The spectra of methylcobalamin at the initial stage were explained by the reported pK_a value if pure "base-on" (λ_{max}=520 nm) and "base-off" forms (λ_{max}=460 nm) were respectively present at pH 5.0 and 1.0. Addition of hydrochloric acid to the reaction system usually caused a monotonous decrease of k_1; k_1 was about 25 times larger at pH 4 than at pH 1. A similar tendency was also observed with perchloric acid and phosphoric acid although the decreasing behavior was somewhat peculiar, being associated with the inexplicable action of oxo-acid anions.

The salt effect was investigated under a constant pH. No significant difference in k_1 was observed in 0.1—1 M acetate buffer (pH=4.2), while the effect of lithium chloride was remarkable; k_1 appeared to decrease gradually with increasing [LiCl], falling down to one-seventh of the initial k_1 (Fig. 2). The depression of k_1 at higher [LiCl] (2—9 M) approached a constant value. It might be associated with the formation of $(HgCl_4)^{2-}$.

Mercuric Acetate. The demethylation of methylcobalamin in the presence of mercuric acetate took place similarly as in the case of chloride; the spectral change due to the demethylation progressed with isosbestic points. It was found, however, that the "base-off" type of methylcobalamin is present during the reaction even at pH=4.2. From the results obtained by Desimore *et al.*[10] and by us, an equilibrium between base-off and base-on methylcobalamin upon addition of mercuric acetate can be written as follows:

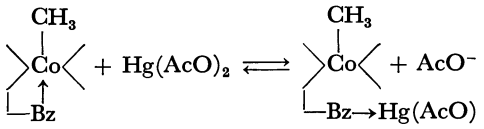

(i)

The demethylation rates, as expressed by $\ln\{(A-A_\infty)/(A_0-A_\infty)\}$ *versus* time, gave a straight line similar to the case of mercuric chloride. However, unlike the chloride case, k_1 was little dependent on the concentration of mercuric acetate (0.2 power), increasing nearly in proportion to the concentration of acetate ion in the acetate buffer (Fig. 3). Thus, 1 mM mercuric acetate is far more active than 1 mM mercuric chloride for the cleavage of cobalt-carbon bond provided that acetate ions were present sufficiently in the solution. The rate of demethylation for mercuric acetate, r', is given by

$$r' \fallingdotseq k'[CH_3\text{–Co}][AcO^-] \quad (2)$$

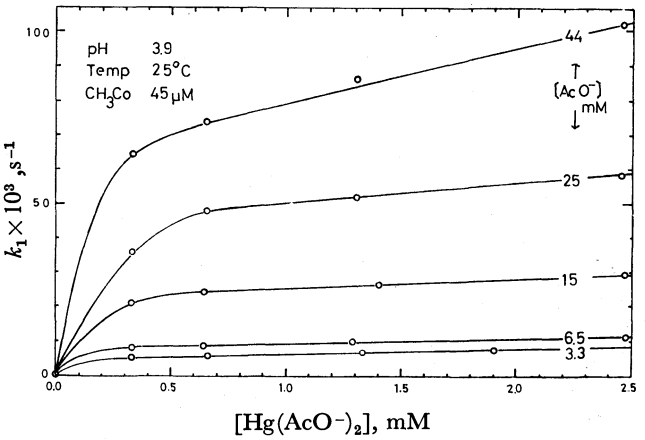

Fig. 3. Dependence of k_1 on the concentration of mercuric acetate and sodium acetate.
[CH_3–Co]=45 μM, pH=3.9, Reaction temperature 25 °C.

The effect of foreign anions was examined. When 3-fold excess of lithium chloride was present over 0.5 mM mercuric acetate in 44 mM acetate buffer, the reactivity of mercuric acetate was found to decrease remarkably, falling down nearly to that of mercuric chloride. Such a phenomenon can be interpreted if the anions of mercuric salt are replaced according to the stability constant of mercury complex (Table 1).

Desimore *et al.*[10] have so far investigated the mechanism of demethylation with mercuric acetate, based on the finding that methylcobiamide (a model compound of base-off methylcobalamin) is far less reactive than base-on methylcobalamin. In the light of their studies and our observations, the following reaction scheme is proposed.

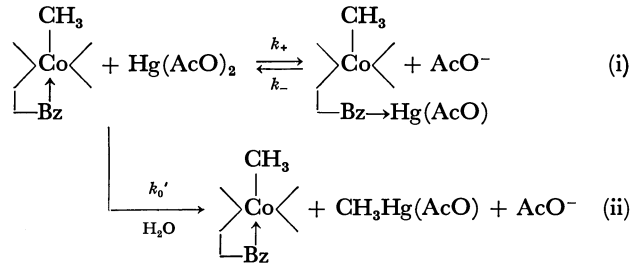

If the equilibration (i) is fast as compared with (ii) and tends to the right-hand side, the rate of demethylation, r', can be approximately given by

$$r' = \frac{k_0'}{K}[CH_3\text{–}Co][AcO^-] \qquad (3)$$

where $K=k_+/k_-$ and $[CH_3\text{–}Co]$ is the total amount of methylcobalamin. The derived expression 3 is essentially the same as the observed one 2.

It is of interest to compare the intrinsic reactivity of mercuric acetate with that of mercuric chloride. For this the ratio k_0'/k was taken into consideration. It follows from Eqs. (1) and (3) that

$$\frac{k_0'}{k} = \frac{r'[CH_3\text{–}Co][HgCl_2]K}{r[CH_3\text{–}Co][AcO^-]} \qquad (4)$$

This can be transformed into an experimentally accessible one by introducing the rate parameter k_1 (k_1' is used for mercuric acetate):

$$\frac{k_0'}{k} = \frac{k_1'}{k_1}\cdot\frac{[HgCl_2]}{[Hg(AcO)_2]}\cdot\frac{K[Hg(AcO)_2]}{[AcO^-]} \qquad (5)$$

The right side of Eq. (5) consists of three factors. The first factor, k_1'/k_1, can be obtained from the observed data in Figs. 2 and 3, and the third one might correspond to the ratio of "base-off" to "base-on" methylcobalamin which can be estimated from the optical absorption.

When the second factor is unity or $[HgCl_2]=[Hg(AcO)_2]=1$ mM at $[AcO^-]=44$ mM, the first factor can be estimated to be *ca.* 20. The major part of methylcobalamin in the case of mercuric acetate was "base-off" so that equilibrium (i) shifted fairly to the right. From an inspection of the optical absorption we see that the third factor, $K[Hg(AcO_2]/[AcO^-]$ is *ca.* 10. Thus, we have

$$\frac{k_0'}{k} \geq 10^2$$

The result shows that mercuric acetate is about 100 times more reactive than mercuric chloride.

Mercuric Perchlorate. Addition of mercuric perchlorate to a methylcobalamin solution caused instantaneous formation of base-off form even at pH 4.5, followed by demethylation reactions. A good first-order plot was obtained in the lower concentration range (below 0.5 mM) as shown in Fig. 1 together with ones for mercuric chloride and acetate. However, at higher concentrations (above 0.5 mM) the plot was found to deviate from linearity, the rate decreasing. The reactivity of mercuric perchlorate was not studied further because of the complicated nature of the reaction.

Mercuric Cyanide, Bromide, and Thiocyanate. Since mercuric salts are less soluble in water, attempts were made to investigate their reactivities indirectly, *viz.* to investigate the effect of potassium cyanide, bromide and thiocyanate added to the reaction system of methylcobalamin and mercuric perchlorate. It was anticipated that mercuric salts in interest would be immediately formed.

30 μl of 0.1 M mercuric perchlorate was added to a 3 ml aqueous or acetate-buffered methylcobalamin solution containing 16 mM potassium salt, namely, CN^-, Br^-, or SCN^-. The role of Cl^- and AcO^- was also investigated in a similar manner. The rate parameter k_1 was obtained for each case (Table 1).

Table 1. Kinetic data for the demethylation of methylcobalamin with mercuric complexes and their stability constants

L	k_1 10^4 s^{-1} a) in H_2O	k_1 10^4 s^{-1} a) in 0.2 M AcO^-	Stability constants M^{-1} b) K_1	K_2	K_3	K_4	
AcO^-	260	$\geq 10^4$	10^5	10^4	—	—	15,16)
Cl^-	32	28	10^7	10^6	10	10	17)
Br^-	7.6	3.5	10^9	10^8	10^2	10^2	18)
SCN^-	8.9	5.4	10^9	10^7	10^3	10^2	15,19)
CN^-	<0.01	<0.01	10^{18}	10^{17}	10^4	10^3	15)

a) $CH_3\text{–}Co=40$ μM, $[L]=16$ mM, $[Hg(ClO_4)_2]=1$ mM, Reaction at 27 °C. b) $HgL_{n-1}+L \rightleftarrows HgL_n$, $K_n = \frac{[HgL_n]}{[HgL_{n-1}][L]}$

In the unbuffered reaction system, k_1 of acetate ion was in good agreement with that derived from mercuric acetate (Fig. 3) while k_1 of chloride ion was slightly less than that of mercuric chloride. It seems that the added anion rapidly combines with mercuric ion.

The k_1 value of Br^- and SCN^- did not differ much from that of mercuric chloride obtainable at high lithium chloride concentrations (≥ 2 M). Addition of CN^- (16 mM) inhibited the demethylation to a considerable extent.

In the 0.2 M acetate buffered solution without the addition of anions, demethylation took place too fast to be followed by a spectroscopic technique in accordance with the finding described. Rate parameter k_1 was also estimated like the unbuffered one for 16 mM Cl^-, Br^-, SCN^-, and CN^-. In these reactions methylcobalamin was of base-on form.

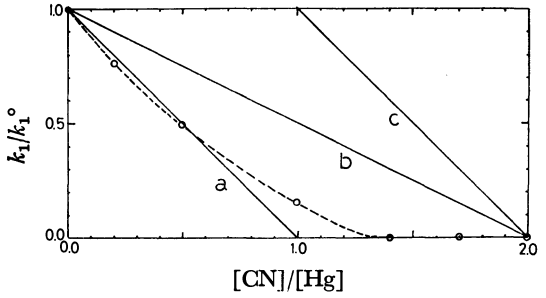

Fig. 4. Inhibition effect by cyanide ion.
···o···: observed values, a, b and c: see text.
$k_1°$: rate parameter for $HgCl_2$
k_1: rate parameter for $HgCl_2$–KCN
$[CH_3\text{–}Co]=45\ \mu M$, $[HgCl_2]=1$ mM, pH=5.0.
Reaction temperature 26 °C.

The inhibition of CN^- was further investigated in the concentration range 0—2 equivalent of KCN for the added $HgCl_2$ (1 mM). The result is shown by the open circles in Fig. 4, and compared with the solid lines a, b, and c which were drawn under the following assumptions (a), (b), and (c) and the anion replacement reactions iii, iv, and v.

$$HgCl_2 + CN^- \longrightarrow HgClCN + Cl^- \quad \text{(iii)}$$

$$HgClCN + CN^- \longrightarrow Hg(CN)_2 + Cl^- \quad \text{(iv)}$$

$$HgCl_2 + 2CN^- \longrightarrow Hg(CN)_2 + 2Cl^- \quad \text{(v)}$$

(a): Reaction iv occurs after the completion of Reaction iii. Reactivities of HgClCN and $Hg(CN)_2$ are negligibly small as compared with that of $HgCl_2$.

(b): Ligation of CN^- occurs according to Reaction v. $HgCl_2$ is much more reactive than $Hg(CN)_2$.

(c): Ligation of CN^- occurs according to (a). Both $HgCl_2$ and HgClCN have the same reactivity, $Hg(CN)_2$ being inactive.

As shown in Fig. 4, assumption (a) is closest to the observed one. It seems that HgClCN and $Hg(CN)_2$ are inactive for the cleavage of cobalt-carbon bond as compared with $HgCl_2$.

Reactivity and Stability Constant of Mercuric Complex. The stability constants of various mercury complexes in the literature[15–19] are shown in Table 1. From these values we can infer the main mercury species in the solution as well as the concentration of anions (shown in parentheses).

$Hg(ClO_4)_2$[15]	Hg^{2+}	ClO_4^- (<1M)
$Hg(AcO)_2$	$Hg(AcO)_2$	AcO^- (1—100 mM)
$HgCl_2$	$HgCl_2$	Cl^- (<100 mM)
$HgCl_2$	$(HgCl_4)^{2-}$	Cl^- (>1 M)
HgBr, $Hg(SCN)_2$, $Hg(CN)_2$	$(HgL_3)^-$ and/or $(HgL_4)^{2-}$	L^- (≥10 mM)

The transformation of $HgCl_2$ into $(HgCl_4)^{2-}$ was inferred when the concentration of Cl^- was increased from 100 mM to 2 M. This is in line with the fact that rate parameter k_1 for mercuric chloride decreased with increasing concentration of lithium chloride as shown in Fig. 2. Addition of mercuric perchlorate or mercuric acetate gave rise to base-off methylcobalamin even at pH 4 while the addition of mercuric chloride retained base-on methylcobalamin. It indicates that the axial benzimidazole can displace the anion in the mercuric complex to yield base-off form when the stability constant K_2 is less than $10^4\ M^{-1}$.

It has been pointed out that the reaction scheme and the type of mercuric complex really depend on the anion species present in the solution. In the light of these observations and in particular from the data shown in Table 1, the reactivities of HgL_2 for the cleavage of cobalt-carbon bond are estimated to be in the following sequence.

$$Hg(AcO)_2 \gg HgCl_2 \geq Hg(SCN)_2 \geq HgBr_2 \gg Hg(CN)_2$$

It is apparent that the above sequence is reverse to the stability constant K_2. It seems to indicate that the elimination of L from HgL_2 is required prior to the cleavage of cobalt-carbon bond. In this connection, it is noteworthy that an equivalent mixture of $HgCl_2$ and KCN is a less active reagent for the cleavage than $HgCl_2$. The cyanide in the mixed ligand complex, HgClCN, might strengthen the Hg–Cl bond.

References

1) J. Halpern and J. P. Maher, *J. Amer. Chem. Soc.*, **86**, 2311 (1964).
2) J. M. Wood, F.S. Kennedy, and C. G. Rosen, *Nature*, **220**, 173 (1968).
3) S. Jensen and A. Jernelov, *Nordforsk*, **14**, 3 (1968).
4) H. A. O. Hill, J. M. Pratt, S. Risdale, F. R. Williams, and R. J. P. Williams, *Chem. Commun.*, **1970**, 341.
5) N. Imura, E. Sukegawa, S. K. Pan, K. Nagao, J. Y. Kim, T. Kwan, and T. Ukita, *Science*, **172**, 1248 (1971).
6) J. Y. Kim, N. Imura, T. Ukita, and T. Kwan, This Bulletin, **44**, 300 (1971).
7) G. N. Schrauzer, J. H. Weber, T. M. Beckham, and R. K. Y. Ho, *Tetrahedron Lett.*, **3**, 275 (1971).
8) A. Adin and W. W. Espenson, *Chem. Commun.*, **13**, 653 (1971).
9) L. Bertilsson and H.Y. Neujahr, *Biochemistry*, **10**, 2805 (1971).
10) R. E. Desimone, M. W. Penley, L. Charbonneau, S. G. Smith, J. M. Wood, H. A. O. Hill, J. M. Pratt, S. Ridsdale, and R. J. P. Williams, *Biochim. Biophys. Acta*, **304**, 851 (1973).
11) H. Weissback, A. Peterkofaky, B. G. Redfield, and H. Dickerman, *J. Biol. Chem.*, **238**, 3318 (1963).
12) H. Y. Neujahr and L. Fries, *Acta Chem. Scand.*, **20**, 347 (1966).
13) O. Müller and G. Müller, *Biochem. Z.*, **336**, 299 (1962).
14) D. H. Dolphin and A. W. Johnson, *Proc. Chem. Soc.* (London), **1963**, 3111.
15) L. G. Sillén and A. E. Martell, "Stability Constants of Metal-Ion Complexes," The Chemical Society, London (1964).
16) D. Banerjea and I. P. Singh, *Z. Anorg. Allgem. Chem.*, **331**, 295 (1964).
17) L. Ciavatta and M. Grimaldi, *J. Inorg. Nucl. Chem.*, **30**, 197 (1968).
18) Y. Marcus, *Acta Chem. Scand.*, **11**, 599 (1957).
19) L. Ciavatta, M. Grimaldi, and A. Mangone, *J. Inorg. Nucl. Chem.*, **32**, 3805 (1970).

Complexes between Nucleotide Base and Amino Acid. I. Crystal Structure of Cytosine: *N*-Formylglycine

Minoru Ohki, Akio Takenaka, Hirotaka Shimanouchi, and Yoshio Sasada

Laboratory of Chemistry for Natural Products, Tokyo Institute of Technology, Ookayama, Meguro-ku, Tokyo 152

(Received September 25, 1974)

Cytosine: *N*-formylglycine complex crystallizes in the space group $Pna2_1$, with cell dimensions of $a=8.444(2)$, $b=21.169(5)$, and $c=5.120(1)$ Å. The structure was solved by the trial-and-error method on the basis of a Patterson map. A full-matrix least-squares refinement led to an R value of 0.035. The difference map revealed the protonation of cytosine by the carboxyl group of *N*-acylamino acid and the involvement of ionic interaction in complex formation. This mode is the same as proposed for cytosine: *N*-benzoylglycine complex in spite of different molecular environment. Such arrangement of cytosine and ionized carboxyl group of amino acid may suggest a mutual recognition scheme between nucleic acid and protein.

Interactions between nucleic acids and proteins take an important part in several processes of protein synthesis, its regulation, the repair of nucleic acids, and so on. In nucleic acid-protein interactions, several kinds of weak bonds must be formed between individual nucleotide and amino acid residues. It is, therefore, interesting to find if there are some specific binding patterns between components of nucleic acids and proteins. They should provide a stereochemical basis for the molecular mechanism of mutual recognition.

Complex formation between nucleotide base and amino acid has been investigated extensively.[1] Tamura, Hata, Sato, and Sakurai[2] showed by an X-ray analysis of cytosine: *N*-benzoylglycine monohydrate (abbreviated hereafter as CBG complex) that the complex is formed by the two hydrogen bonds between the carboxyl group of amino acid and the two nitrogen atoms (amino group and N(3) atom) of cytosine. Recently, we have found a different type of complex formation between cytosine and undissociated acidic side group of glutamic acid.[3] In the former complex, however, the proton migration was deduced from the examination of bond lengths and angles without the direct proof by a difference map. It is well known that cytosine is easily protonated at N(3) by strong acids[4] and the high proton affinity has been justified by the theoretical calculation of π-electron distribution.[5] In view of the nucleic acid-protein interactions, it is important to confirm the protonation of cytosine by amino acid. We have done this by an accurate analysis of the crystal structure of the title complex which is an analogue of the CBG complex.

Experimental

Square-prism crystals were obtained from an aqueous solution containing equimolar cytosine and *N*-formylglycine. The complex formation was confirmed by an elementary analysis and IR spectrum of the crystals. Found: C, 39.1; H, 4.7; N, 25.5%. Calcd for $C_4H_5N_3O \cdot C_3H_5NO_3$: C, 39.3; H, 4.7; N, 26.2%. Laue symmetry and systematic absences of reflexions indicated the space group to be $Pna2_1$ or Pnam. The unti-cell dimensions were determined by least-squares calculation from the spacings of 64 reflexions, $0kl$ and $hk0$, on Weissenberg photographs, calibration being made with superposed silicon lines ($a=5.43075$ Å). The density was measured by flotation in a chloroform-carbon tetrachloride mixture. Crystal data are given in Table 1.

Table 1. Crystal data for cytosine: *N*-formylglycine complex

Crystal system: orthorhombic		
Systematic absences: $0kl$ with $k+l=2n+1$ and $h0l$ with $h=2n+1$.		
Space group: $Pna2_1$.		
$a=8.444(2)$ Å	$b=21.169(5)$ Å	$c=5.120(1)$ Å
$U=915.1(3)$ Å^3	$Z=4$	
$D_x=1.554$ g cm^{-3}	$D_m=1.55_7$ g cm^{-3}	
μ(CuKα)$=11.4$ cm^{-1}		

Intensity data were collected on integrated, equi-inclination Weissenberg photographs ($hk0$-$hk4$ and $0kl$-$6kl$) using Ni-filtered CuKα radiation and the intensities were measured by a TV densitometer.[6] The sizes of crystals used for the a- and c-axis rotations were $0.10\times0.15\times0.40$ mm and $0.15\times0.20\times0.60$ mm, respectively. Corrections were made for Lorentz and polarization factors, but not for absorption. Intensities of both of extended and contracted reflexions on upper layer photographs were corrected by a method proposed by Takenaka and Sasada,[7] and were averaged; a discrepancy index, $R'=\sum||F_{ext}|-|F_{cont}||/\sum|F_{mean}|$, was 0.040, where subscripts ext and cont stand for the extended and contracted spots, respectively. Two sets of intensity data thus obtained were cross-correlated and then placed on an absolute scale by the Wilson's method. A total of 1090 independent reflexions was obtained, of which zero-reflexions numbered 103.

Structure Determination and Refinement

Although $N(z)$ test[8] was not effective, a three-dimensional Patterson map indicated that the space group is $Pna2_1$. The Patterson map also gave the approximate position of the cytosine moiety. The remaining non-hydrogen atoms were found by successive Fourier syntheses. Atomic coordinates and temperature factors, first isotropic and then anisotropic, were refined by the block-diagonal least-squares method; the minimized function was $\sum w\Delta F^2$, where $\Delta F=|F_o|-|F_c|$. After the conventional R factor reached to 0.074, a difference synthesis revealed all the hydrogen atoms. Further refinement including these hydrogen atoms reduced the R factor to 0.037. In the final stage, the full-matrix least-squares method was applied, where the following weight function was used:

$w=\exp(-as^2-bt^2-cst-ds-et-f)$ for $|F_o|\neq 0$, where $s=|F_o|$ and $t=\sin\theta/\lambda$; $w=1/\langle\Delta F^2\rangle$ for $|F_o|=0$. The coefficients, a, b, c, d, e, and f, were evaluated by least-squares at each cycle of the structure refinement so that $\langle w\Delta F^2\rangle=1$; at the final stage, they were 0.001778, 41.00, 0.4658, −0.1752, −42.77, and 8.107, respectively. The refinement was terminated when the largest shift of parameters was less than 0.3σ. The final values of R and R_w, where $R_w=(\sum w\Delta F^2/\sum w|F_o|^2)^{1/2}$, were 0.035 and 0.043, respectively. There were no residual peaks greater than 0.2 e Å^{-3} in the final difference map.

Atomic scattering factors used were taken from "International Tables for X-ray Crystallography".[9]

The computations were done on a HITAC 8800 computer at the University of Tokyo and on a HITAC 8700 computer at Tokyo Institute of Technology. The programs, TLSU for the determination of cell dimensions, TDRW for the data reduction, TFLS for the full-matrix least-squares refinement, and DCMS for the stereo-pair drawing of the crystal and molecular structure, all written by two of the authors (A.T. and Y.S.), and DAPH in the Universal Crystallographic Computation Program System,[10] were used.

The final positional and thermal parameters are given in Table 2. Observed and calculated structure factors are listed in Table 3. Numbering of atoms and thermal ellipsoids are shown in Fig. 1, the crystal structure in Fig. 2, and the bond lengths and angles in Fig. 3. The standard deviations for bond lengths and angles involving C, N, and O are 0.004 Å and 0.4°, respectively, and those involving hydrogen are about ten times of the above values. The hydrogen bonds are listed in Table 4. The least-squares planes of six-membered ring of cytosine, the carboxyl group and the amide group of amino acid are given in Table 5, together with the displacements of atoms from the planes.

Discussion

As shown in Fig. 1, the complex is formed by the two hydrogen bonds between the ionized carboxyl group of amino acid and the two nitrogen atoms, N(4) and the protonated N(3), of cytosine. The present study has proved definitely the protonation of N(3) and the involvement of ionic interaction in complex formation. In this "double hydrogen-bonded system", the two N···O distances are not equal to each other (Fig. 2), contrary to those in CBG complex. The N(4)H···O(3) distance is comparable to the normal distance of NH···O type hydrogen bond,[11] while the

Table 2. Final positional and thermal parameters

Standard deviations are given in parentheses. The anisotropic temperature factor has the form $\exp[-(B_{11}h^2+B_{22}k^2+B_{33}l^2+B_{12}hk+B_{23}kl+B_{31}lh)]$

Atom	x[a]	y[b]	z[a]	B_{11}[a]	B_{22}[b]	B_{33}[a]	B_{12}[a]	B_{23}[a]	B_{31}[a]
N(1)	958(3)	12419(9)	2119(7)	142(3)	115(4)	245(8)	−5(2)	−1(3)	−79(8)
C(2)	1515(3)	18025(10)	3108(7)	127(3)	127(4)	198(9)	−5(2)	6(3)	−76(9)
N(3)	951(3)	23396(9)	1945(6)	129(3)	123(4)	186(7)	−1(2)	7(3)	−88(7)
C(4)	−52(3)	23403(10)	−107(7)	112(3)	151(5)	145(8)	2(2)	8(3)	−29(9)
C(5)	−601(3)	17505(11)	−1090[c]	131(3)	178(5)	192(8)	−12(2)	−11(4)	−84(9)
C(6)	−79(3)	12224(12)	82(7)	143(4)	155(5)	206(9)	−12(2)	−18(3)	−43(9)
O(2)	2465(3)	18192(8)	4900(7)	198(3)	157(4)	350(8)	−2(2)	12(3)	−300(10)
N(4)	−475(3)	28869(11)	−1078(7)	161(3)	177(5)	265(9)	1(2)	24(4)	−156(10)
O(3)	561(3)	40172(8)	1284(7)	184(3)	138(3)	297(8)	10(2)	2(3)	−203(8)
O(4)	1924(2)	34084(7)	4033(7)	191(3)	115(3)	262(7)	3(2)	14(3)	−166(8)
O(5)	3165(2)	52186(8)	347(7)	179(3)	152(3)	273(8)	2(2)	10(3)	128(8)
N(5)	1519(3)	51074(8)	3845(7)	146(3)	111(4)	218(7)	11(2)	−7(3)	52(9)
C(7)	1462(3)	39342(10)	3181(7)	128(3)	115(4)	166(8)	6(2)	10(3)	−12(9)
C(8)	2114(3)	44982(10)	4680(7)	144(4)	131(4)	172(10)	5(2)	1(3)	−15(9)
C(9)	2089(3)	54083(10)	1798(8)	145(3)	106(4)	247(9)	−2(2)	−3(3)	2(10)

Atom	x[d]	y[d]	z[d]	B/Å^2 [e]
H(1)	133(4)	88(2)	297(8)	13(6)
H(3)	133(5)	272(2)	261(9)	25(7)
H(41)	−10(4)	326(2)	−36(10)	25(7)
H(42)	−114(6)	288(2)	−243(12)	36(9)
H(5)	−137(5)	176(2)	−250(10)	25(8)
H(6)	−42(4)	78(2)	−39(8)	18(6)
H(81)	326(4)	450(2)	443(7)	15(6)
H(82)	180(5)	445(2)	649(10)	25(8)
H(9)	163(5)	580(2)	133(10)	28(8)
H(10)	76(5)	528(2)	474(9)	22(7)

a) $\times 10^4$. b) $\times 10^5$. c) The z coordinate of C(5) was fixed from the requirement of the polar space group.
d) $\times 10^3$. e) $\times 10$

TABLE 3. OBSERVED AND CALCULATED STRUCTURE FACTORS ($\times 10$)

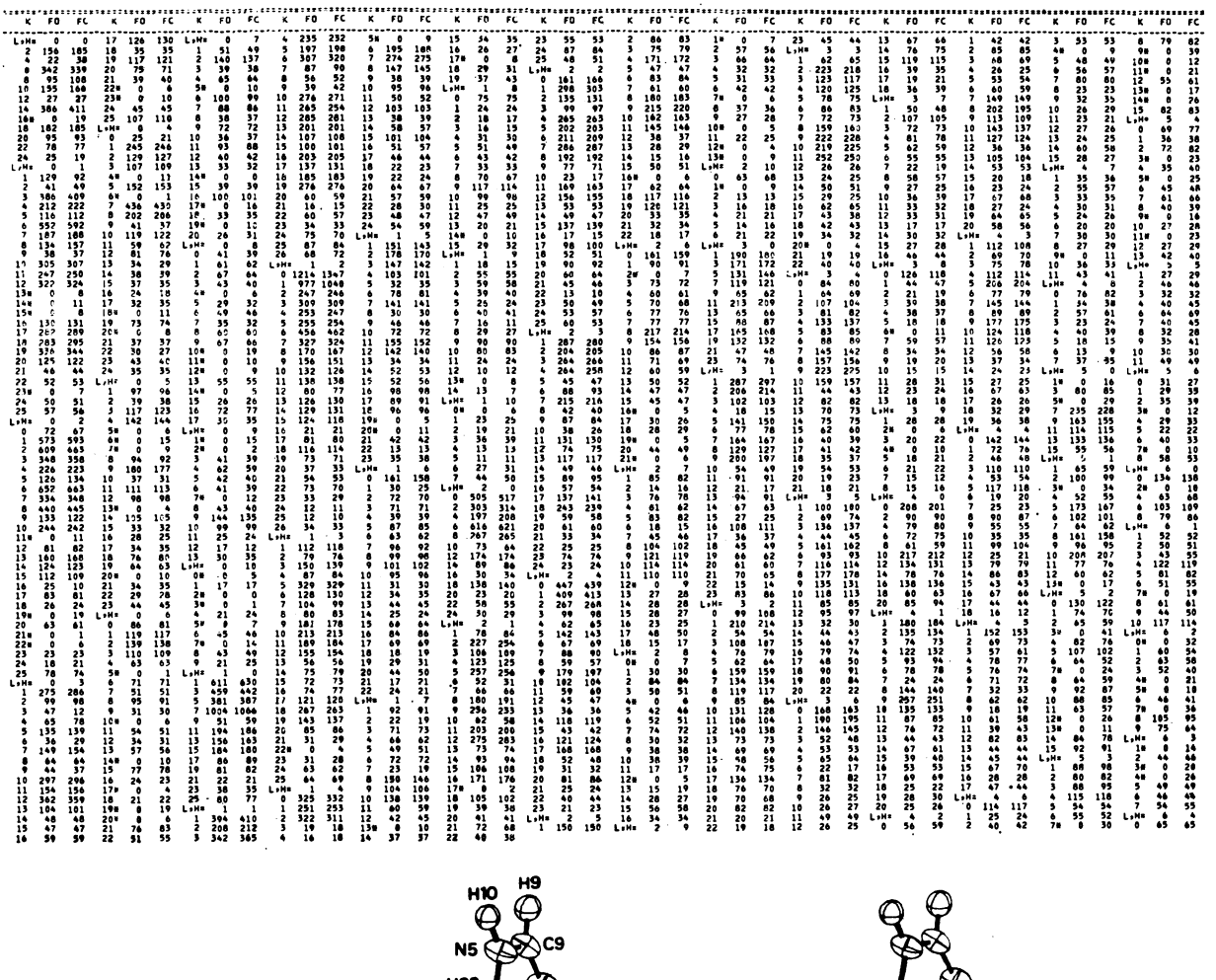

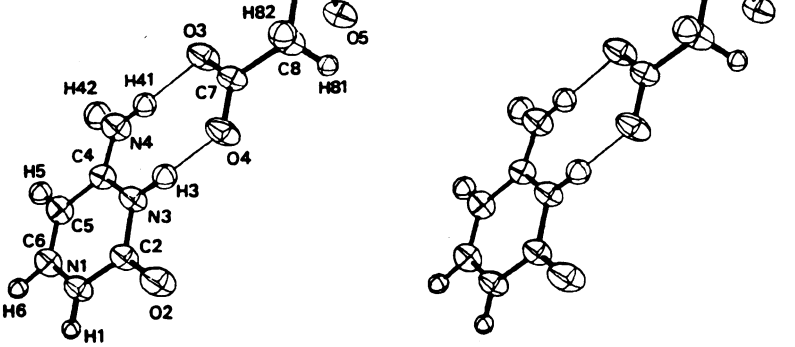

Fig. 1. A stereoscopic view of cytosine: *N*-formylglycine complex. Thermal ellipsoids are drawn at the 50% probability level.

N(3)H···O(4) distance is very close to that between carboxylate oxygen and protonated imidazole nitrogen atoms found in *N*-acetyl-L-histidine monohydrate.[12] This implies that the positive and negative charges are mostly located at N(3) and O(4) atoms, respectively. The differences between the C(7)–O(3) and C(7)–O(4) bond lengths and between the C(8)–C(7)–O(3) and C(8)–C(7)–O(4) angles (Fig. 3) also support this. Other hydrogen bonds are found between the carbonyl O(5) atom of amino acid and the N(1) atom of cytosine, between the N(4) and O(2) atoms of cytosines, and between the O(3) and N(5) atoms of the amino acids. These hydrogen bonds, except for the last one, are schematically the same as those in the CBG complex. The approach of the two amino acids in the CBG complex is impeded by the bulky phenyl groups and they are connected through the hydrogen bonds with the water molecule between them. In the present complex, however, they are linked directly by the N(5)H···O(3) hydrogen bond. The charge distribution in the "double hydrogen-bonded system" seems to be affected by such a different environment.

The closest nonbonding intermolecular contacts are between O(4) of amino acid and C(5) of cytosine at $1/2+x$, $1/2-y$, $1+z$ and between C(9) of amino acid and O(2) of cytosine at $1/2-x$, $1/2+y$, $-1/2+z$.

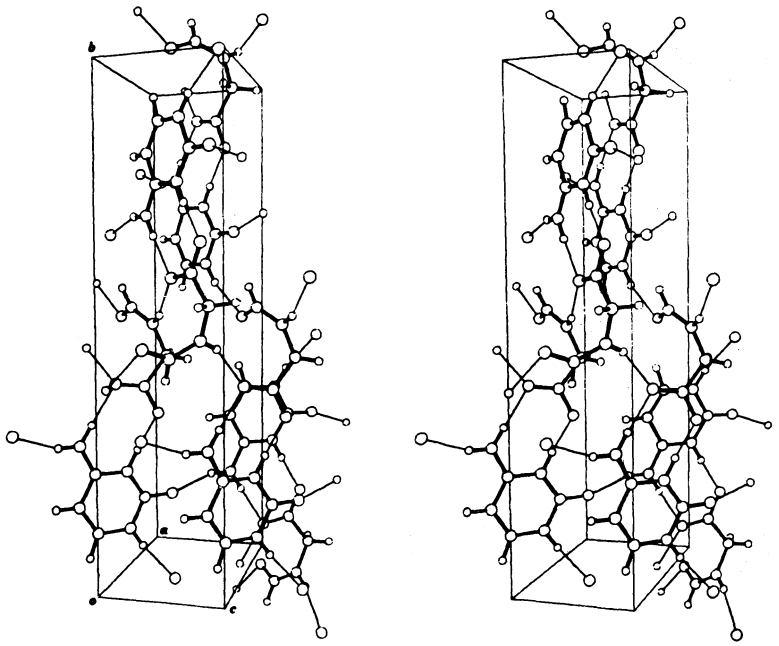

Fig. 2. A stereoscopic view of the crystal structure.

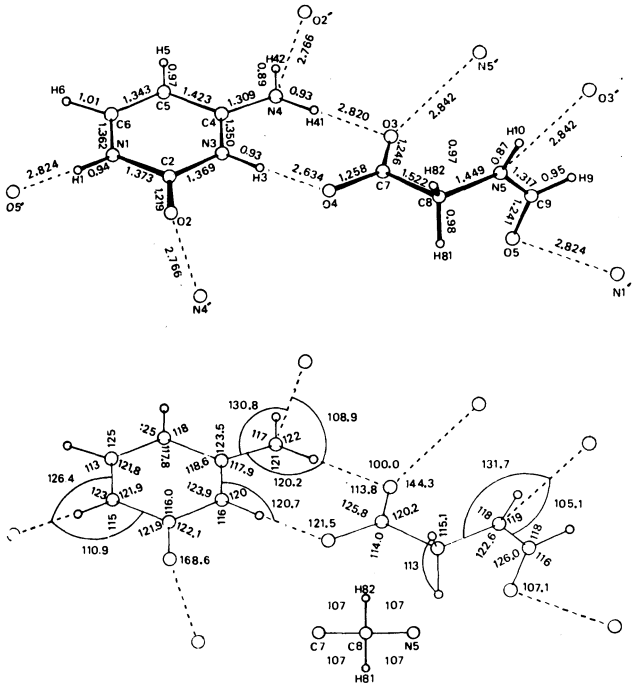

Fig. 3. Distances and angles.
The standard deviations for bond distances and angles are 0.004 Å and 0.4 °, respectively, while those involving hydrogen are about ten times larger.

These distances, 3.274 and 3.164 Å, respectively, are slightly larger than the minimum van der Waals contacts.[13] If the hydrogen atoms are taken into account, however, the H···O distances are somewhat shorter than the sum of these van der Waals radii;[13] H(5)···O(4) 2.32 Å and H(9)···O(2) 2.40 Å. Relevant angle is 170° for C(5)–H(5)–O(4) and 137° for C(9)–H(9)–O(2). It seems that there are some C–H···O interactions, at least in the former.

The bond lengths and angles of amino acid are in good agreement with those found in other amino acids and oligopeptides. The torsion angles of C(7)–C(8)–N(5)–C(9) and of O(3)–C(7)–C(8)–N(5) are −81.1 and 4.2°, respectively, which are close to those found in many dipeptides.[14] The O(5) and C(8) atoms are *cis* around the C(9)–N(5) bond.

Table 4. Distances and angles of the hydrogen bonds

N	H	O	Distance (l/Å) N···O	Distance (l/Å) H···O	Angle (ϕ/°) N–H···O
N(3)	H(3)	O(4) (a)	2.634	1.71	176
N(4)	H(41)	O(3) (a)	2.820	1.89	176
N(4)	H(42)	O(2) (b)	2.766	1.91	160
N(1)	H(1)	O(5) (c)	2.824	1.90	167
N(5)	H(10)	O(3) (d)	2.842	2.03	157
	(a) at		x,	y,	z
	(b) at		$-1/2+x$,	$1/2-y$,	$-1+z$
	(c) at		$1/2-x$,	$-1/2+y$,	$1/2+z$
	(d) at		$-x$,	$1-y$,	$1/2+z$

The protonation to cytosine results in the lengthening of the C(2)–N(3) and N(3)–C(4) bonds, the shortening of the C(2)–O(2) and C(4)–N(4) bonds, and the widening of the C(2)–N(3)–C(4) angle, these features being similar to those in other protonated cytosines as shown in Fig. 4 where the average bond distances and angles are given for the neutral and protonated species.[15–19] The slightly different dimensions between the present and other protonated cytosines are caused by the effects of alkylation at N(1)[20] and hydrogen bond with O(2),[15] since the O(2) atoms of other protonated species are not hydrogen bonded.

The N(3) atom deviates by 0.011 Å from the mean plane of the six-membered ring. The exocyclic atoms, O(2) and N(4), displace in the direction opposite to N(3) by 0.040 and 0.015 Å, respectively. Such a tendency is the same as found in 1-(β-D-arabinofuranosyl)cytosine hydrochloride,[19] but is different from

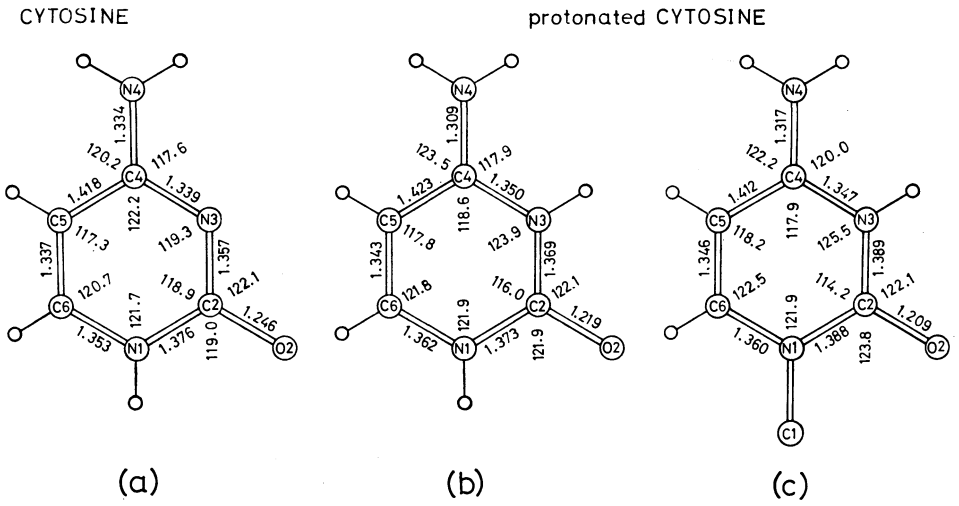

Fig. 4. A comparison of the dimensions of neutral and protonated cytosines.
(a): Average values of cytosine[15] and cytosine monohydrate.[15]
(b): This investigation.
(c): Average values of two forms of cytidylic acid,[16,17] 1-methylcytosine hydrochloride,[18] and 1-(β-D-arabinofuranosyl)-cytosine hydrochloride.[19]

Table 5. Least-squares planes and deviations of the atoms

X, Y, Z are in Å along the crystal axes, respectively.

Plane 1 (cytosine ring)
$0.7703X-0.0281Y-0.6371Z+0.1435=0$

Plane 2 (carboxyl group)
$-0.7884X-0.0335Y+0.6143Z+0.2537=0$

Plane 3 (amide group)
$-0.6740X-0.4542Y-0.5826Z+6.9236=0$

Deviations (l/Å)

Plane 1		Plane 2	
N(1)*	0.001	O(3)*	−0.001
C(2)*	0.008	O(4)*	−0.001
N(3)*	−0.011	C(7)*	0.002
C(4)*	0.005	C(8)*	−0.001
C(5)*	0.004	H(3)	−0.00
C(6)*	−0.007	H(41)	−0.02
O(2)	0.040		
N(4)	0.015	Plane 3	
H(1)	−0.01	N(5)*	0.002
H(3)	−0.01	O(5)*	0.001
H(41)	0.00	C(8)*	−0.001
H(42)	0.02	C(9)*	−0.002
H(5)	−0.04	H(9)	0.02
H(6)	−0.05	H(10)	−0.00

* Atoms included in the calculation of the least-squares plane.

that in other protonated species.[16–18] The dihedral angle between pyrimidine and carboxyl planes, 3.9°, is close to 3.0° found in CBG complex.

In the present and CBG complexes, a common feature of the "double hydrogen-bonded system" is observed, in spite of different molecular arrangements in their crystals. So, this seems to be a specific arrangement between cytosine and ionized carboxyl group of amino acid. The "double hydrogen-bonded system" could be a model for mutual recognition between nucleic acid and protein, such as binding mode between the unpaired cytosine in CCA terminus of *t*RNAs and the *C*-terminal carboxyl group in amino-acyl-*t*RNA synthetase or CCA pyrophosphorylase.

References

1) C. Tamura, N. Sakurai, and S. Sato, This Bulletin, **44**, 1473 (1971).
2) C. Tamura, T. Hata, S. Sato, and N. Sakurai, *ibid*, **45**, 3254 (1972).
3) M. Ohki, A. Takenaka, H. Shimanouchi, and Y. Sasada, *Chem. Lett.*, **1974**, 551.
4) R. F. Bryan and K. Tomita, *Acta Crystallogr.*, **15**, 1174 (1962).
5) B. Pullman and A. Pullman, "Quantum Biochemistry," John Wiley & Sons, New York (1963), p. 117.
6) T. Izumi, *Japan. J. Appl. Phys.*, **10**, 1724 (1971).
7) A. Takenaka and Y. Sasada, presented at the Annual Meeting Cryst. Soc. Japan, Osaka, Japan, Abstracts, p. 27 (1973).
8) E. R. Howells, D. C. Phillips, and D. Rogers, *Acta Crystallogr.*, **3**, 210 (1950).
9) "International Tables for X-Ray Crystallography," Vol. 3, Kynoch Press, Birmingham (1962), p. 201.
10) T. Ashida, "The Universal Crystallographic Computing System (I)," ed. by T. Sakurai, The Crystallographic Society of Japan (1967), p. 76.
11) W. Fuller, *J. Amer. Chem. Soc.*, **81**, 1700 (1959).
12) T. J. Kistenmachen, D. J. Hunt, and R. E. Marsh, *Acta Crystallogr.*, **B28**, 3352 (1972).
13) L. Pauling, "The Nature of the Chemical Bond," Cornell University Press, Ithaca (1960), p. 260.
14) R. E. Marsh and J. Donohue, *Advanc. Protein Chem.*, **22**, 235 (1967).
15) R. J. McClure and B. M. Craven, *Acta Crystallogr.*, **B29**, 1234 (1973).
16) M. Sundaralingam and L. H. Jensen, *J. Mol. Biol.*, **13**, 914 (1965).
17) C. E. Bugg and R. E. Marsh, *ibid*, **25**, 67 (1967).
18) B. L. Trus and R. E. March, *Acta Crystallogr.*, **B28**, 1834 (1972).
19) J. S. Sherfinski and R. E. Marsh, *ibid*, **B29**, 192 (1973).
20) K. Hoogsteen, *ibid*, **16**, 28 (1963).

Lanthanide-Induced Nuclear Magnetic Resonance Shifts and Molecular Structure of L-Azetidine-2-Carboxylic Acid. I. Evaluation of the Shifts Intrinsic to the Lanthanide-Substrate 1:1 Complex

Fuyuhiko INAGAKI, Seizo TAKAHASHI, Mitsuo TASUMI, and Tatsuo MIYAZAWA

Department of Biophysics and Biochemistry, Faculty of Science, The University of Tokyo, Bunkyo-ku, Tokyo 113

(Received November 5, 1974)

The lanthanide-induced PMR shifts (LIS) were observed in D_2O solution of L-azetidine-2-carboxylic acid using europium nitrate as shift reagent. Two series of measurements were carried out with the successive dilution and the incremental dilution methods. The analysis of observed data shows that the formation of 1:2 complex between the lanthanide ion and the substrate molecule should be taken into account in addition to 1:1 complex. The LIS's intrinsic to 1:1 and 1:2 complexes were evaluated. An experimental method appropriate for obtaining the ratio of the LIS's intrinsic to 1:1 complex is proposed.

One of the most important features of the lanthanide-induced nuclear magnetic resonance shift (LIS) lies in its potentiality of giving quantitative information on the structure of molecules in solution. As is well known, however, there are several points to be checked before the observed shift data are utilized for the determination of molecular structures.[1-3] In the first place, it is necessary to evaluate the LIS intrinsic to 1:1 complex formed between a lanthanide ion (or, more generally, a lanthanide shift reagent) and a substrate molecule. This is not a simple task, since the contributions of 1:2 and other complexes to the observed LIS are expected to vary case by case. In this paper we treat the equilibrium between the europium ion and L-azetidine-2-carboxylic acid in aqueous solution and propose a method for evaluating the intrinsic LIS's and the shift ratios for 1:1 complex. This method may be applicable to other systems as well. The results obtained here will be used in a subsequent paper for determining the molecular conformation of L-azetidine-2-carboxylic acid in aqueous solution.

Experimental

L-Azetidine-2-carboxylic acid was kindly provided by Mr. H. Sugano of Tanabe Pharmaceutical Company. Commercially available nitrate of Eu(III) (99.9%) was used without further treatments.

PMR spectra were recorded on a Hitachi R-22 (90 MHz) spectrometer in the frequency-sweep mode. The LIS measurements were performed for D_2O solution at a probe temperature of 37 °C using DSS as an internal standard. The shifts were determined by a frequency counter with the accuracy of ± 0.1 Hz. All the resonance lines shifted to high field in the presence of europium nitrate. The pH value of each sample solution was adjusted to be in the range between 4.6 and 5.0, so that the zwitter ion is the predominant species of the sample molecule.

The computation and curve plotting were carried out at the Computer Centre of the University of Tokyo using HITAC-8800/8700 computers and a Calcomp 563 curve plotter. The programs used for the spectral analysis were NMRTRY, NMRFIT, and NMRPLOT. The curve fitting for the LIS data was carried out with the program SHIFT. All these programs were prepared in our laboratory.

Results and Discussion

PMR Spectrum of L-Azetidine-2-Carboxylic Acid in D_2O Solution. The observed PMR spectrum of L-azetidine-2-carboxylic acid in D_2O solution is shown in Fig. 1, together with the simulated. The absorptions indicated as A, B, C, D, and E in this figure may be assigned to five protons, *viz.*, A and B to the β, C and D to the γ, and E to the α protons (see Fig. 2). The least-square adjustments gave the chemical shifts and spin-spin coupling constants listed in Table 1, which

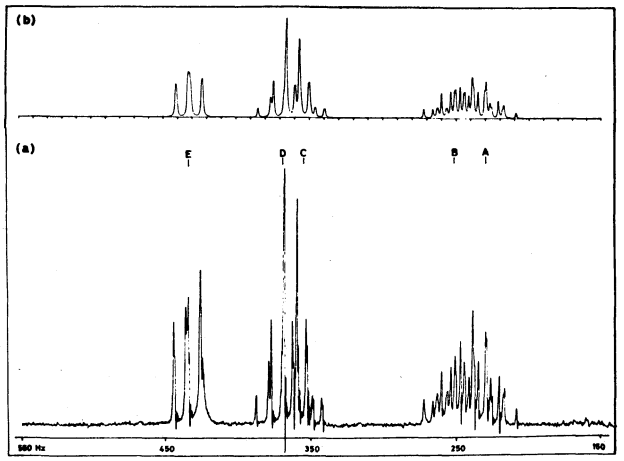

Fig. 1. PMR spectrum (90 MHz) of L-azetidine-2-carboxylic acid in D_2O; (a), observed spectrum; (b) simulated spectrum.

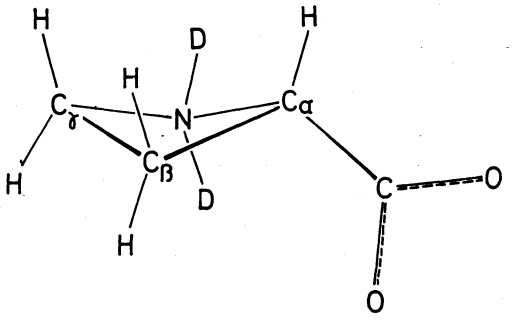

Fig. 2. Molecular structure of L-azetidine-2-carboxylic acid.

Table 1. Chemical shifts (ν) and spin-spin coupling constants (J) of L-azetidine-2-carboxylic acid[a)]

ν_A	229.92±0.03	J_{AD}	9.34±0.05
ν_B	252.16±0.03	J_{AE}	10.02±0.04
ν_C	354.01±0.03	J_{BC}	9.91±0.05
ν_D	368.63±0.03	J_{BD}	8.02±0.05
ν_E	431.64±0.03	J_{BE}	7.96±0.04
		J_{CD}	−10.63±0.04
J_{AB}	−12.17±0.04	J_{CE}	0.79±0.04
J_{AC}	6.06±0.05	J_{DE}	0.23±0.04

a) All values are in Hz.

are essentially in agreement with the values obtained by Thomas and Williams.[4)]

Analysis of the Lanthanide-Induced Shifts. (a) Coordination Site: The measurements of LIS were made in the pH range between 4.6 and 5.0, where L-azetidine-2-carboxylic acid exists as a zwitterion. As LIS was found negligible below $pK_a(=1.7)$ of the carboxylate group, the coordination site for the lanthanide ion must be the carboxylate group of L-azetidine-2-carboxylic acid.

(b) Stoichiometry of the Lanthanide-Substrate Complex and the Evaluation of the LIS Intrinsic to 1:1 Complex: Much work has been done on the stoichiometry of the lanthanide-substrate complex and now the formation of not only 1:1 complex but also 1:2 complex has been established.[2,3)] The equilibria between the lanthanide ion (L) and the substrate molecule (S) may be described by the following schemes (two-step mechanism) under the assumption that the formation of the complex between one lanthanide ion and three (or more) substrate molecules can be neglected.

$$L + S \overset{K_1}{\rightleftharpoons} LS \quad (1)$$

$$LS + S \overset{K_2}{\rightleftharpoons} LS_2 \quad (2)$$

where K_1 and K_2 are the association constants given as

$$K_1 = [LS]/[L][S] \quad (3)$$

$$K_2 = [LS_2]/[LS][S] \quad (4)$$

If the LIS (with respect to the i-th nucleus) intrinsic to LS and LS_2 complexes are expressed as Δ^i_1 and Δ^i_2, respectively, the observed shift ($\Delta\delta^i_{obs}$) may be given as

$$\Delta\delta^i_{obs} = \frac{[LS]}{[S_0]}\Delta_1{}^i + 2\frac{[LS_2]}{[S_0]}\Delta_2{}^i \quad (5)$$

where $[S_0]$ refers to the total concentration of the substrate. Equations (3)—(5) are used to analyse the observed data described below to obtain Δ_1, Δ_2, K_1, and K_2. The following two series of measurements have been made.

(1) Successive Dilution Method:[5)] The changes of chemical shifts are observed with changing $[L_0]$ (total concentration of the lanthanide ion) and $[S_0]$ by successive addition of the solvent (D_2O) to the original solution which contains both the lanthanide ion and the substrate. Accordingly, the mole ratio $\rho(\equiv[L_0]/[S_0])$ is kept constant throughout the measurements. The shifts observed by this method for the five protons of L-azetidine-2-carboxylic acid are shown in Figs. 3 and 5, where ρ was set equal to 1.01.

(2) Incremental Dilution Method:[2)] The changes of chemical shifts are observed with changing $[L_0]$ and ρ by successive addition of the substrate solution to the original solution. The concentration of the substrate solution is made equal to that of the substrate in the original solution, so that no change in $[S_0]$ occurs

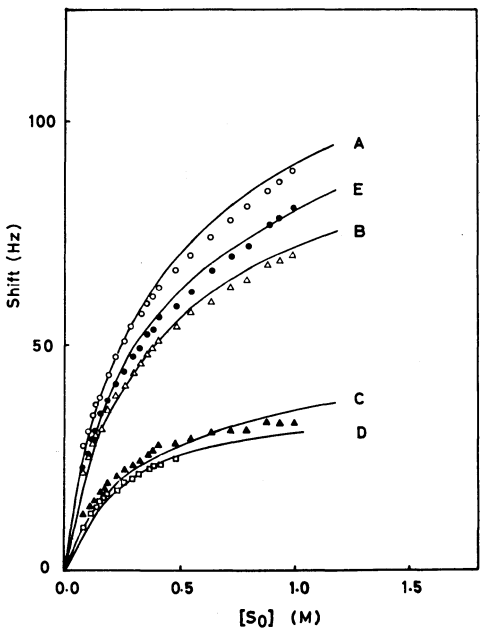

Fig. 3. Eu(III)-induced shifts ($\Delta\delta_{obs}$) of L-azetidine-2-carboxylic acid observed by the successive dilution method *vs.* total substrate concentration ($[S_0]$). D_2O solution, 37 °C, $\rho=1.01$. ○, A; △, B; ▲, C; □, D; ●, E. The curves were obtained by theoretical fitting based on the one-step mechanism.

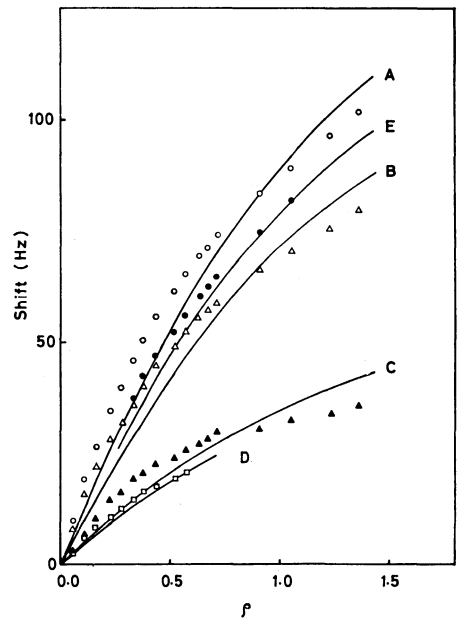

Fig. 4. Eu(III)-induced shifts ($\Delta\delta_{obs}$) of L-azetidine-2-carboxylic acid observed by the incremental dilution method *vs.* the mole ratio (ρ). D_2O solution, 37 °C, $[S_0]=0.991$ M. ○, A; △, B; ▲, C; □, D; ●, E. The curves were obtained by theoretical fitting based on the one-step mechanism.

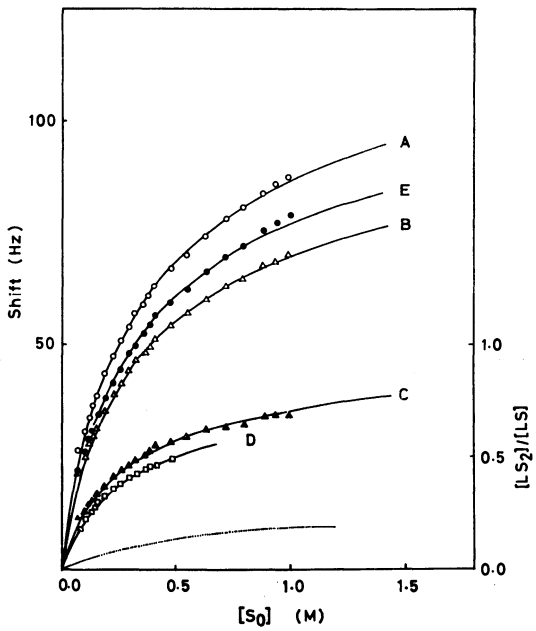

Fig. 5. Eu(III)-induced shifts ($\Delta\delta_{obs}$) of L-azetidine-2-carboxylic acid observed by the successive dilution method *vs.* total substrate concentration ([S_0]). D_2O solution, 37 °C, ρ=1.01. ○, A; △, B; ▲, C; □, D; ●, E. The full curves were obtained by theoretical fitting based on the two-step mechanism. The dotted curve indicates the dependence of the ratio [LS_2]/[LS] upon [S_0].

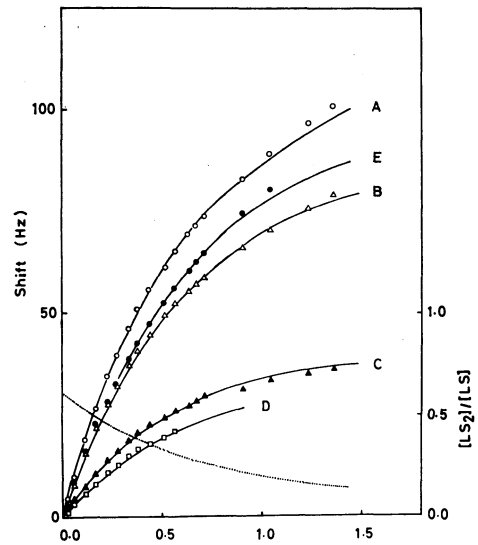

Fig. 6. Eu(III)-induced shifts ($\Delta\delta_{obs}$) of L-azetidine-2-carboxylic acid observed by the incremental dilution method *vs.* the mole ratio (ρ). D_2O solution, 37 °C, [S_0]=0.991 M. ○, A; △, B; ▲, C; □, D; ●, E. The full curves were obtained by theoretical fitting based on the two-step mechanism. The dotted curve indicates the dependence of the ratio [LS_2]/[LS] upon ρ.

throughout the measurements. The shifts observed by this method are shown in Figs. 4 and 6, where [S_0] was chosen to be 0.991 M.

At first the shift data obtained above were analyzed by assuming that only the LS complex was present (one-step mechanism). In this case, $\Delta\delta'_{obs}$ is simply given by the first term in the righthand side of Eq. (5). The best-fit curves obtained by the least-squares adjustments are shown in Figs. 3 and 4. The parameters obtained (Δ_1's and K_1) are given in Table 2. It is noted that in Fig. 3 the calculated curve tends to deviate from the observed data in the high [S_0] region, whereas in Fig. 4 the deviation is found both in the high and low ρ regions. These results indicate the inadequacy of the assumption of one-step mechanism. Then, the analysis in terms of the two-step mechanism has been carried out and the best-fit curves obtained are shown in Figs. 5 and 6. The agreement between the calculated curves and the observed data is now much better, giving a strong support for the LS_2 formation. The parameters obtained (Δ_1's, Δ_2's, K_1, and K_2) are listed in Table 2. The dotted curves in Figs. 5 and 6 indicate the calculated mole ratio [LS_2]/[LS]. The contribution of LS_2 is smaller for the successive dilution method under the present experimental conditions. The contribution of LS_2 decreases with decreasing [S_0] in the successive dilution method (Fig. 5), whereas it increases with decreasing ρ in the incremental dilution method (Fig. 6). These ratios [LS_2]/[LS] explain very well the origin of deviation between the calculated curves and the observed data in Figs. 3 and 4.

Table 2. Lanthanide-induced shifts[a] intrinsic to the LS copmlex (Δ_1) and LS_2 complex (Δ_2) and the association constants[b] for the step L+S⇄LS (K_1) and LS+S⇄LS_2 (K_2)

Proton	One-step mechanism[c]	Two-step mechanism[d]	
	Δ_1, Hz	Δ_1, Hz	Δ_2, Hz
A	160.5	120.7	155.9
B	128.5	97.3	123.2
C	63.5	52.0	50.1
D	58.9	49.8	34.9
E	142.6	110.0	125.2
	K_1=3.2	K_1=3.6	K_2=0.6

a) Shifts for the probe frequency of 90 MHz. b) In the unit of M^{-1}. c) Mechanism involving only L+S⇄LS. d) Mechanism involving L+S⇄LS and LS+S⇄LS_2.

The procedures described above gives the LIS intrinsic to the LS complex quite straightforwardly. The simultaneous use of two series of experimental data, *viz.*, those obtained by the successive dilution and the incremental dilution methods, enhances the reliability of the calculated parameters. However, this method requires much experimental work followed by computer analysis of the data. So it seems desirable to introduce a method convenient for evaluating the LIS intrinsic to the LS complex by an experimental procedure. Taking into account that the shift ratio is a quantity more useful than the absolute shift in treating the structural problem, we show here that the shift ratio for the LS complex can be obtained by extrapolating the ratio of successive dilution data to [S_0]=0. The ratio of the LIS of the i-th nucleus and that of the

s-th nucleus may be expressed from Eqs. (3)—(5) as

$$\frac{\Delta\delta^i_{obs}}{\Delta\delta^s_{obs}} = \frac{\Delta_1{}^i + 2K_2[S_0]\Delta_2{}^i + 2K_2(\Delta_1{}^i - \Delta_2{}^i)[LS]}{\Delta_1{}^s + 2K_2[S_0]\Delta_2{}^s + 2K_2(\Delta_1{}^s - \Delta_2{}^s)[LS]} \quad (6)$$

Then, extrapolating the ratio of successive dilution data to zero substrate concentration, we get

$$\lim_{[S_0]\to 0} (\Delta\delta^i_{obs}/\Delta\delta^s_{obs}) = \Delta_1{}^i/\Delta_1{}^s \quad (7)$$

The ratios of LIS's obtained by the successive dilution method are shown in Fig. 7, where the LIS of the proton A is taken as reference. In Table 3 the observed shift ratios are compared with the values calculated using the parameters for the two-step mechanism listed in Table 2. Satisfactory agreement between the observed and calculated values provides evidence for the consistency between the curve fitting analysis and the shift-ratio extrapolation method. The method of extrapolating the shift ratio obtained by successive dilution to zero substrate concentration would be useful also in other systems for evaluating the ratio of LIS's intrinsic to 1 : 1 complex, particularly in the case with a rather small association constant (K_1). This point will be treated in a separate paper by comparing the two cases with small and large association constants.

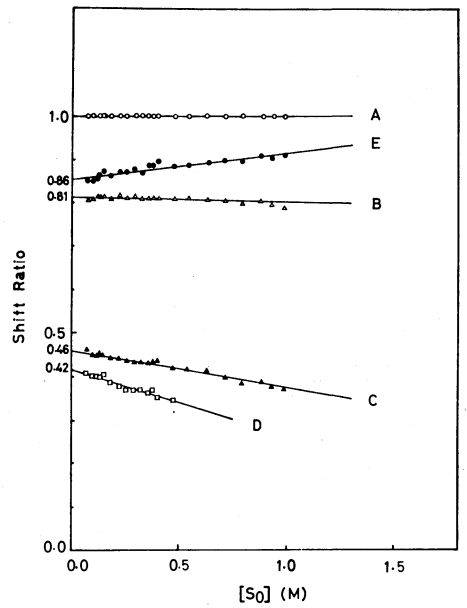

Fig. 7. The ratios of Eu(III)-induced shifts of L-azetidine-2-carboxylic acid observed by the successive dilution method. The shift of proton A was chosen as reference. ○, A; △, B; ▲, C; □, D; ●, E.

TABLE 3. SHIFT RATIOS

Proton	Obsd[a)]	Calcd[b)]
A	1.00[c)]	1.00[c)]
B	0.81	0.81
C	0.46	0.43
D	0.42	0.41
E	0.86	0.91

a) Extrapolated to zero substrate concentration ($[S_0]=0$). b) Calculated using the parameters for the two-step mechanism listed in Table 2. c) Taken as reference.

References

1) B. Bleaney, C. M. Dobson, B. A. Levine, R. B. Martin, R. J. P. Williams, and A. V. Xavier, *Chem. Commun.*, **1972**, 791.

2) B. L. Shapiro and M. D. Johnston, Jr., *J. Amer. Chem. Soc.*, **94**, 8185 (1972).

3) B. L. Shapiro, M. D. Johnston, Jr., R. L. R. Towns, A. D. Godwin, H. L. Pearce, T. W. Proulx, and M. J. Shapiro, "Nuclear Magnetic Resonance Shift Reagents," ed. by R. E. Sievers, Academic Press, New York, N. Y. (1973), pp. 227—245.

4) W. A. Thomas and M. K. Williams, *Org. Mag. Resonance*, **4**, 145 (1972).

5) T. A. Wittstruck, *J. Amer. Chem. Soc.*, **94**, 5130 (1972).

Profiles of the Distribution of Atoms in the Nitrous Oxide-acetylene Flame

Kitao FUJIWARA, Hiroki HARAGUCHI, and Keiichiro FUWA

Department of Agricultural Chemistry, Faculty of Agriculture The University of Tokyo, Tokyo 113

(Received January 7, 1974)

The distributions of neutral atoms in the nitrous oxide–acetylene flame have been measured by nebulizing aquo ions of the following sixteen elements into the flame; cadmium, nickel, zinc, copper, lead, cobalt, manganese, iron, chromium, molybdenum, calcium, tin, gallium, indium, titanium, and boron. The distributions have been figured on the response surfaces on which the changes in distribution are expressed as functions of the flame height and the acetylene flow rate. The response surfaces for the temperature and the OH radical were also investigated. The response surfaces for the atomic absorptions of the elements can be related to the thermodynamic properties of the oxides of the elements. The results have then been used for the discussion of the atomization processes of the elements in the flame. In addition, the sensitivities of absorption spectrometry in the nitrous oxide–acetylene flame have been compared to those in the air–acetylene flame.

In atomic absorption spectrometry, it is important to know the atomization processes of analytical elements, which are reflected in the distribution of atoms in the flame. The distribution of atoms depends on the condition of the flame, particularly on the composition of the flame, which is usually expressed by the ratio of the fuel to the supporting gas.[1–6] However, the relation between the atomic distribution and the properties of the flame has not been well established. Hence, in a previous work a detailed investigation of the atomic distributions of fourteen elements in the air-acetylene flame has been carried out.[7]

In the present study, the absorbances of atoms in the nitrous oxide–acetylene flame are measured as the function of two variables, the acetylene flow rate and the height above the burner, while keeping the flow rate of nitrous oxide constant. The results are shown as a map of the distribution of the atoms, where the abscissa indicates the flow rate of acetylene, and the ordinate the height above the burner. This map of distribution will be refered to as "the response surface" hereafter. The present authors have investigated the response surfaces for atoms of sixteen elements, the OH radical and the temperature, and have discussed the mechanism of atomization in the nitrous oxide-acetylene flame.

Experimental

Reagents. All the reagents used were of an analytical grade and were purchased from the Wako Pure Chemical Ind. Ltd. Sample solutions of metal ions were prepared by dissolving the nitrates of Mn^{2+}, Fe^{3+}, Co^{2+}, Ni^{2+}, Cu^{2+}, Zn^{2+}, Ca^{2+}, Cr^{3+}, In^{3+}, Ga^{3+}, Cd^{2+}, and Pb^{2+} into distilled water containing 0.2% nitric acid. The solutions of ammonium molybdate and boric acid were prepared by dissolving the respective salts into water. The titanyl sulfate was dissolved into a 0.2 N sulfuric acid solution, while the stannic chloride was dissolved into a 0.2% nitric acid solution. The analytical concentrations of the elements are listed in Table 1.

Apparatus. The Hitachi 207 Atomic Absorption Spectrophotometer was used after somewhat modifying the focussing of the light beam so that a single light path with a beam 2—3 mm in diameter was produced at the measuring position in the flame. The details of this modification have already been reported elsewhere.[4]

Most of the hollow cathode lamps which were used in the experiments were produced by Hitachi Ltd.; one for gallium was produced by Westinghouse, and one for tin by Varian Tectron Pty., Ltd., Australia. As the continuous light source, a 200 W deuterium discharge tube, Model HS 200 DS from Dr. Körn Gmbh and Co. was used. For the temperature measurements, a 250 W tungsten lamp, Halogen-bellaphot 64653, of the Osram Co. Ltd., was used as the incandescent light source; a mechanical chopper made by the K. K. Ewig Co. and an optical pyrometer, Model 201 N_1, of the Hokushin Electric Works were also used.

Table 1. Sample solutions and analytical lines

Reagent	Concentration of metal ions (μg/ml)	Analytical line (nm)
$Cd(NO_3)_2 \cdot 8H_2O$	2	228.8
$Ni(NO_3)_2 \cdot 6H_2O$	20	352.4
$Zn(NO_3)_2 \cdot 6H_2O$	1	213.8
$Cu(NO_3)_2 \cdot 3H_2O$	5	327.4
$Pb(NO_3)_2$	20	283.3
$Co(NO_3)_2 \cdot 6H_2O$	20	243.2
$Mn(NO_3)_2 \cdot 4H_2O$	20	403.0
$Fe(NO_3)_3 \cdot 7H_2O$	20	271.9
$Cr(NO_3)_3 \cdot 9H_2O$	20	427.4
$SnCl_4 \cdot 5H_2O$	500	286.3
$Ga(NO_3)_3$	20	287.4
$In(NO_3)_3$	20	303.9
$Ca(NO_3)_2 \cdot 4H_2O$	5	422.6
$(NH_4)_2MoO_4$	20	313.2
$TiOSO_4$	200	364.2
H_3BO_3	1000	249.8

A water-cooled burner with a 50 mm slot was used for the nitrous oxide–acetylene flame.

Procedure. A sample solution was nebulized into the burner at a rate of about 3 ml/min. The light beam was passed through the center of the flame just above the slot of the burner. The absorbances were measured at the positions in the flame, with intervals of 2.5 mm; the positions were adjusted by moving the burner vertically. The conditions of the flame were changed by varying the acetylene flow rate by 0.5 l/min., while the flow rate of nitrous oxide was kept constant at 6 l/min.

The atomic absorption lines for the elements are listed in Table 1.

Temperature Measurement: Temperature of the flame was measured by the sodium 5889 Å line-reversal method.[8,9] Two pin holes were set along the light path, one for obtaining a narrow light beam from the incandescent light source, and the other, behind the flame, for excluding the extra emission

of the flame. The current of the incandescent lamp was controlled by an auto-transformer, while the temperature of the tungsten filament in the lamp was measured by means of the optical pyrometer at the reversal point of absorption and emission. In this measurement, an aqueous solution of 1000 μg Na/ml was nebulized into the flame. The reproducibility of the measurements was within 10 °C.

OH Radical Measurement: The concentration of the OH radical was measured by the molecular absorption method as follows. The luminous intensity of the deuterium discharge was almost constant in the range from 305.0 to 306.7 nm while the flame was not ignited. The absorption spectra of the flame were, therefore, measured by scanning the wavelengths in the above range continuously, and the relative concentrations of OH radicals were evaluated in terms of 305.8 and 306.4 nm. In this measurement, distilled water was nebulized into the flame.

Results

The experimental data for the flame temperature, the concentrations of the OH radical, and the atomic absorptions of Cd, Ni, Zn, Cu, Pb, Co, Mn, Fe, Mo, Ca, Cr, Sn, Ga, In, Ti, and B, which were observed as functions of two variables, such as the acetylene flow rate and the height above the burner, have been indicated in the response surface.

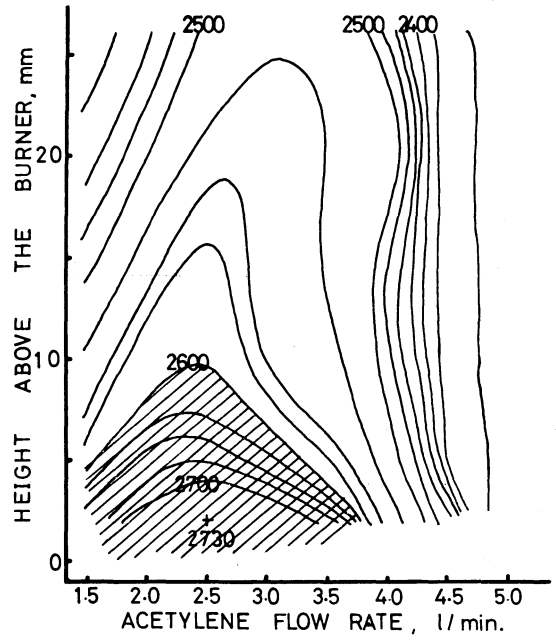

Fig. 1. Response surface of temperature.
Temperature in the hatched region is higher than 2600 °C.

In Fig. 1, the response surface for the flame temperature is shown. The temperatures were measured at 48 positions in the nitrous oxide-acetylene flame; the observed values are plotted in the response surface map. Thus, the isothermal contour lines are obtained with an interval of 25 degrees. In Fig. 1, the areas with a temperature range from 2300 to 2730 °C are shown. The maximal temperature is found at a height of 2 mm and with an acetylene flow rate of 2.5 l/min. The hatched area refers to when the flame temperature is higher than 2600 °C.

In Fig. 2, the response surface for the OH radical is shown. In this case, the absorbances of the molecular absorption of OH at 80 positions in the flame are plotted in the figure; the iso-absorbances are shown as contour lines with an interval of 0.012. The maximal absrobance of OH, 0.036, is found at the position with an acetylene flow rate of 1.5 l/min and a height of 5—20 mm. The absorbance in the hatched region is larger than 0.032.

In Figs. 3—7, the response surfaces for 16 elements are shown in the same way. The absorbances for those elements were measured at 40—72 positions of the

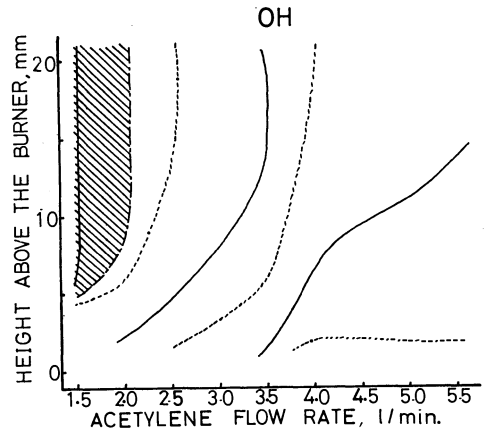

Fig. 2. Response surface of OH radical absorbance.
The absorbance in the hatched region is higher than 0.032.

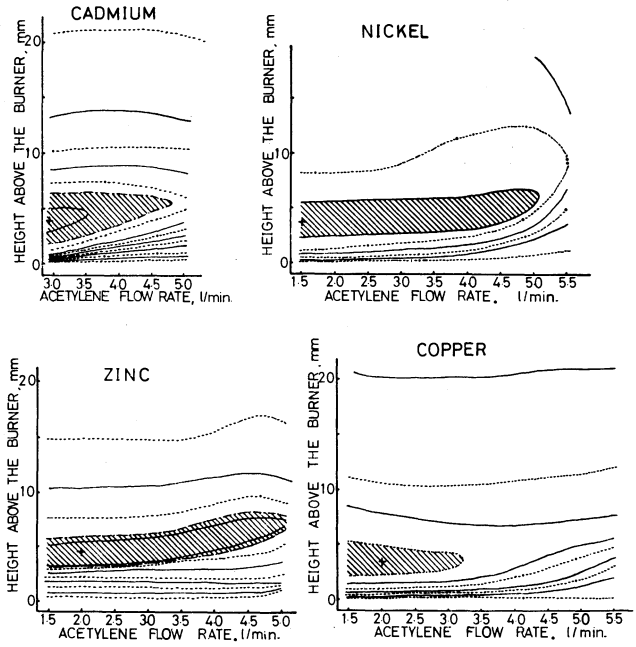

Fig. 3. Response surfaces of absorbances of cadmium, nickel, zinc, and copper.
The absorbances in the hatched regions are higher than 0.056, 0.036, 0.040, and 0.042 for cadmium, nickel, zinc and copper, respectively. The cross point indicates the position that gives the maximal absorbance.

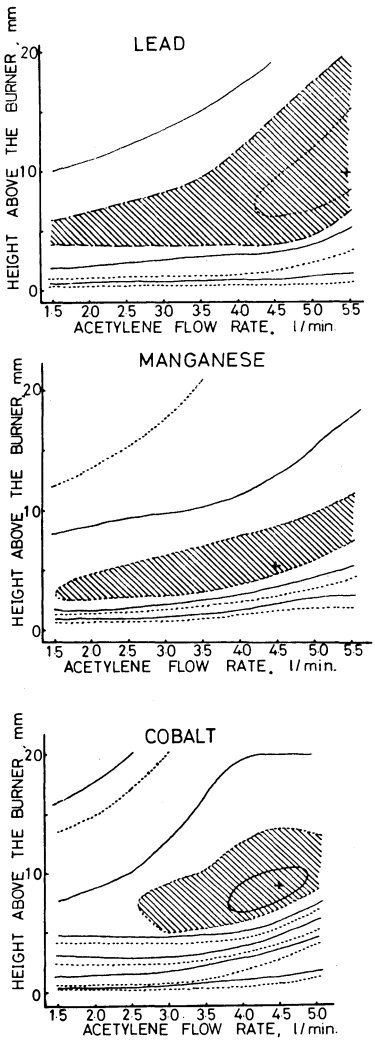

Fig. 4. Response surfaces of absorbances of lead, cobalt and manganese.
The absorbances in the hatched regions are higher than 0.028, 0.054, and 0.030 for lead, cobalt and manganese, respectively. The cross point indicates the position that gives the maximal absorbance.

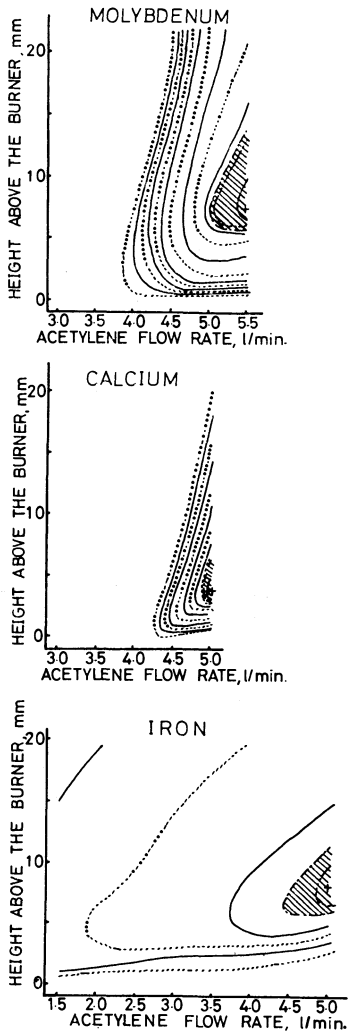

Fig. 5. Response surfaces of absorbances of calcium, molybdenum and iron.
The absorbances in the hatched regions are higher than 0.055, 0.065, and 0.028 for calcium, molybdenum and iron, respectively. The cross point indicates the position that gives the maximal absorbance.

flame. The response surfaces are classified into 5 groups. The basis of this classification will be described later. The maximal absorbances obtained in the nitrous oxide–acetylene flame are summarized in Table 2. The hatched regions in Figs. 3—7 refer to those giving an absorbance larger than nine-tenth of the maximal one. The contour lines giving the highest absorbance in the response surfaces of each element are summarized in Fig. 8.

Discussion

In the normal conditions of the flame in the present experiment system, the acetylene flow rate has been set at 4.0 l/min. This actually corresponds to the ratio of acetylene to nitrous oxide of 2 to 3 in volume. The region where the acetylene flow rate is larger than the normal condition of the flame is conventionally referred to as an acetylene-rich flame, and the smaller one, as an acetylene-lean flame.

Temperature in the Nitrous Oxide–acetylene Flame. The nitrous oxide–acetylene flame has been known as a high temperature flame. In fact, the temperature of this flame, as measured by the method reported previously, is about 300 degrees higher than that in the air–acetylene flame, the range of which is from 1900 to 2300 °C.[7] It should be noted that the highest temperature in the nitrous oxide–acetylene flame, 2730 °C, is observed in the lower part of the acetylene-lean region, and that the flame temperature decreases towards the upper part and the acetylene-rich region.

No distinct correlation in distribution between atoms and temperature in the response surfaces is observed. The sensitive regions of Cu, Ni, Cd, Zn, Co, Pb, and Mn spread from the region with the lowest temperature to that with the highest temperature. In the other elements, the sensitive regions are apart from the highest-temperature region.

OH Radical Distribution. The OH radical is produced by the oxidation of the fuel; it oxidizes the reductive component of the flame and also the metal

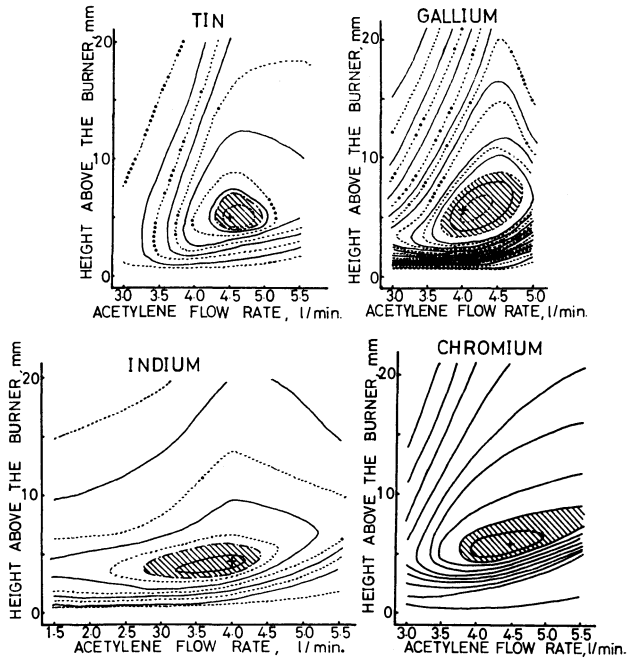

Fig. 6. Response surfaces of absorbances of tin, gallium, indium and chromium.
The absorbances in the hatched regions are higher than 0.050, 0.114, 0.044, and 0.108 for tin, gallium, indium and chromium, respectively. The cross point indicates the position that gives the maximal absorbance.

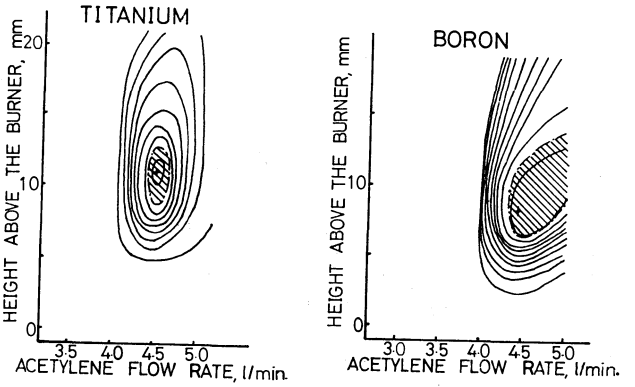

Fig. 7. Response surfaces of absorbances of titanium and boron.
The absorbances in the hatched regions are higher than 0.091 and 0.112 for titanium and boron, respectively. The cross point indicates the position that gives the maximal absorbance.

atoms.[10] Hence, the relative concentration of the OH radical (shown in Fig. 2) has been used as an index of the oxidation potential of the flame. Its concentration becomes higher in the upper part of the acetylene-lean region. On the other hand, the atomic concentrations of all the elements become lower in this region. This suggests that the oxidative reactions are predominant in this region and that the atomization of the analyzed element is prevented by the formation of oxide.

On the other hand, as may be seen in Fig. 8, the absorption maxima of many elements can be observed in the region of the OH radical minimum. This

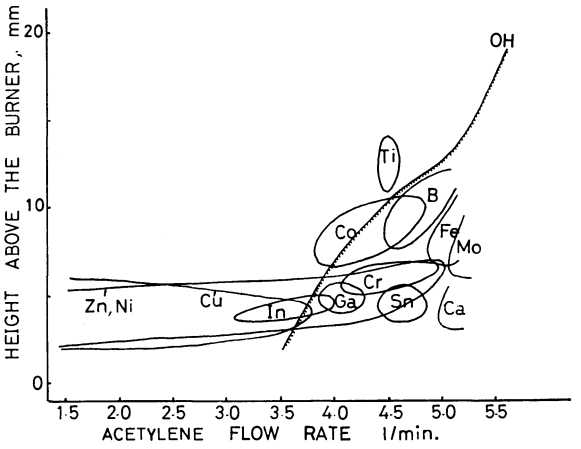

Fig. 8. Locations of higher sensitive regions of elements investigated.
The cited areas refer to those of higher sensitivities. The hatched line, ||||||||, denotes the OH concentration, *i.e.*, the area which is right-hand side of the line refers to that of low concentration, absorbance of OH is lower than 0.012.

region is actually reductive; this suggests that the reductive condition is favorable for the atomization of many elements in the nitrous oxide–acetylene flame.

Sensitivities of the Nitrous Oxide–acetylene Flame and the Air–acetylene Flame. In Table 2 the sensitivities for the analyzed elements in the nitrous oxide–acetylene flame and in the air–acetylene flame are compared; the sensitivity is expressed in terms of the ratio of maximal absorbance. The values in Table 2 refer to those obtained after the normalization with respect to

Table 2.

Element	Heat of formation of M_xO_y (Ref. 15) (eV)		Dissociation energy of MO (Ref. 12, 13, 14, 16) (eV)	Maximum absorbance	Ratio of max. absorbance in N_2O–C_2H_2 flame to that in air–C_2H_2 flame
Cd	CdO	2.6	3.8	0.063	0.61
Ni	NiO	2.5	3.9	0.041	0.34
Zn	ZnO	3.6	2.8	0.052	0.64
Cu	CuO	1.6	3.3—4.1	0.047	0.48
Pb	PbO	2.3	3.9	0.031	0.32
Co	CoO	2.5	—	0.062	0.65
Mn	MnO	4.0	4.0—4.2	0.033	0.46
Ca	CaO	6.6	4.1—4.7	0.064	0.53
Fe	Fe_2O_3	8.5	4.3—4.8	0.031	0.35
Mo	MoO_3	7.7	5.0	0.072	0.83
In	In_2O_3	9.6	3.3	0.049	0.46
Ga	Ga_2O_3	11.1	3.0	0.126	1.6
Sn	SnO_2	6.0	5.4	0.056	1.5
Cr	Cr_2O_3	12.9	4.4—4.9	0.125	1.0
Ti	TiO_2	9.5	6.8—7.2	0.091	a)
B	B_2O_3	13.1	8.0—8.3	0.130	a)

a) Absorbance is not obtained in the air–acetylene flame.

the length of the burner. Those of Ga, Sn, Cr, and B show the ratios larger than one. This indicates the higher sensitivity in the nitrous oxide–acetylene flame. All these elements, except Sn, form stable oxides whose heats of formation are larger than about 10 eV. The results obtained here suggest that the formations and the thermal decompositions of these oxides are essentially important processes for the atomization, which will be discussed later. Sn may form type of oxide other than SnO_2.[11]

Classification of the Elements in Terms of the Response Surface Patterns. The profiles of the response surfaces for 16 elements are shown in Figs. 3—7. Some of the elements are similar to each other. The elements may be classified into the following five groups according to the similarity;
Group A: Cd, Cu, Zn, Ni (Fig. 3); Group B: Pb, Co, Mn (Fig. 4); Group C: Fe, Mo, Ca (Fig. 5); Group D: In, Ga, Cr, Sn (Fig. 6); Group E: Ti, B (Fig. 7).

The characteristics of each group can be summarized as follows.

Group A: The contour lines for the iso-absorbance are almost horizontal and parallel with each other. This indicates that the absorbances of these elements are almost independent of the composition of the flame, although they are slightly more sensitive in the very acetylene-lean region than in the acetylene-rich one.

Group B: The contour lines run from the lower-left to the upper-right, and sensitive regions, expressed by the hatched area, spread towards the acetylene-rich region.

Group C: The contour lines in the response surfaces form half-rounded loop, which open mouth towards the acetylene-rich part. Moreover, the hatched region is very narrow and is located in the most acetylene-rich region. It should be noted that the absorbances of these elements can be hardly detected in the acetylene-lean region. This suggests that the increase in the reductive components of the flame rather than a high temperature is necessary for the atomizations of these elements.

Group D: The hatched regions are in a small circle of the contour line at the lower part of the flame height in the rather acetylene-rich region. The sensitivities of the elements in this group decrease in the relatively-lower-temperature part. This is characteristic of the elements whose oxides have large heats of formation as listed in Table 2.

Group E: The hatched regions are observed in longitudinally elongated loops of the contour lines in the acetylene-rich region. They are located at a upper position of flame height comparing to the other elements. The absorbances of these elements can be observed only in the extreme neighbourhood of the absorption maxima.

Atomization Processes. The thermodynamic properties, the heats of formation of the oxide, M_xO_y, and the dissociation energies of monoxides, MO, with respect to the elements are summarized in Table 2. They are concerned with the atomization processes of elements.

The patterns of the response surfaces obtained show that two different patterns of the atomization process exist. One is independent of the change in the nature of the flame. The response surface of *Group A* is typical of this pattern. The other is directly susceptible to the nature of the flame; *i.e.*, the atomization is promoted by an increase in the fuel flow rate. A typical pattern is *Group C*. *Group B* is intermediate between the former and the latter. For an explanation of this difference, the dissociation energy of the monoxide should be considered. The elements in *Group A* have small dissociation energies of monoxides, lower than 3.9 eV. Therefore, the monoxides of *Group A* elements are easily decomposed, and the monoxide formation does not actually interfere with the atomization of the element. In the case of *Group C*, whose monoxides have dissociation energies larger than 4.5 eV, the reduction of monoxide by the reduction components of the flame is an important process in the atomization. The energies of the monoxides of elements in *Group B* are between those of *Group A* and *C*, 3.9—4.2 eV; this explains why the response surface pattern of *Group B* is intermediate between those of *A* and *C*.

On the other hand, the locations of the sensitive region for the elements in *Group D* and *E* can not be interpreted only in terms of the dissociation energies of their monoxides. The hatched regions of Ga and In are located near the normal flame region, while the dissociation energies of their monoxides are very small. The hatched region of Sn is located in a less fuel-rich region than those of Fe and Mo, while the dissociation energy of SnO is larger than those of FeO and MoO. Those of Ti and B, whose monoxides have the largest dissociation energies among the elements investigated, do not appear in the most acetylene-rich region. It is noted that the sensitive regions of *Groups D* and *E* appear in a temperature region higher than those to be expected from the magnitudes of the dissociation energies of their monoxides. The fact mentioned above seems to be due to the formation of stable oxides, M_xO_y, of these elements in the flame. According to the description given in the previous section, the higher sensitivities are obtained in the higher-temperature flame for the elements whose oxides have heats of formation of more than about 10 eV. This fact suggests that the decomposition of the stable oxide proceeds under high-temperature conditions.

In the case of *Group E* elements, the oxides, TiO_2 and B_2O_3, and monoxides, TiO and BO, are all extremely stable compared to those of other elements. For the atomizations of these elements, a high temperature and a reductive atomosphere are indispensable. The atomic absorption spectrometry of these elements is difficult in the air–acetylene flame. This may be due to the facts that the temperature of the flame is as low as below 2100 °C in the fuel-rich region,[7] and that their oxides are not decomposed. The atomic absorption spectrometry of these elements is also difficult in the hydrogen–oxygen flame even though the temperature of this flame is almost equal to that of the nitrous oxide–acetylene flame.[5] We assume that the carbon components play an important role in the decomposition of the stable monoxide.

In summary, on the basis of the above discussions, the following atomization processes of the elements can be considered in the nitrous oxide–acetylene flame:

$$M(OH_2)_n^{m+} \longrightarrow M_xO_y \quad (1)$$

$$M_xO_y \xrightarrow{\Delta} MO \quad (2)$$

$$MO + C \longrightarrow M + CO \quad (3)$$

where Δ represents the pyrolysis reaction; M, the atom of the analyzed element, and C, the carbon component in the flame. Reaction (2) expresses the pyrolysis of the oxides; it is important for the elements in *Group D* and *E*. Reaction (3) expresses the reduction of monoxide by means of the flame components. This must play a significant role in the atomizations of the elements in the *Group C* and *E*.

References

1) C. S. Rann and A. N. Hambly, *Anal. Chem.*, **37**, 879 (1965).
2) V. A. Fassel, J. O. Rasmuson, R. N. Kniseley, and T. G. Cowley, *Spectrochim. Acta, Part B*, **25**, 559 (1970).
3) R. K. Skogerboe, A. T. Heybey, and G. H. Morrison, *Anal. Chem.*, **38**, 1821 (1966).
4) K. Fujiwara, H. Haraguchi, and K. Fuwa, *ibid.*, **44**, 1895 (1972).
5) K. Fujiwara, H. Haraguchi, and K. Fuwa, *Chem. Lett.*, **1973**, 461.
6) N. V. Mossholder, V. A. Fassel, and R. N. Kniseley, *Anal. Chem.*, **45**, 1614 (1973).
7) K. Fujiwara, H. Haraguchi, and K. Fuwa, *ibid.*, **47**, *no.3* (1975), in press.
8) B. W. Bailey and J. M. Rankin, *ibid.*, **43**, 219 (1971).
9) W. Snelleman, "Flame Emission and Atomic Absorption Spectrometry," ed. by J. A. Dean and T. C. Rains, Marcell Dekker, New York (1969), p. 213.
10) D. R. Jenkins and T. M. Sugden, *ibid.*, p. 151.
11) V. S. Sastri, C. L. Chakrabarti, and D. E. Willis, *Talanta*, **16**, 1093 (1969).
12) "JANAF Tables of Thermochemical Data," prepared by Dow Chem. Corp., Midland, Michigan (1965, 1966, 1967, 1968).
13) P. J. Th. Zeegers, W. P. Townsend, and J. D. Winefordner, *Spectrochim. Acta, Part B*, **24**, 243 (1969).
14) P. J. Padley and T. M. Sugden, *Trans. Faraday Soc.*, **55**, 2054 (1954).
15) "Kagakn Benran," ed. by the Chemical Society of Japan, Maruzen, Tokyo (1966), p. 819.
16) A. G. Gaydon, "Dissociation Energies and Spectra of Diatomic Molecules," 3rd. ed., Chapman and Hall, London (1968).

Studies on Mass Spectrometry of Metal Chelates. III. Mass Spectrometry of 2-, 4-, 5-, 7-Methyl-, and 5-Chloro-oxine Metal Chelates

Shinobu NAGA, Yoshinori KIDANI, and Hisashi KOIKE*

Faculty of Pharmaceutical Sciences, Nagoya City University, Tanabe-dori, Mizuho-ku, Nagoya 467
**School of Medical Technology and Nursing, Fujita Gakuen University, Toyoake, Aichi 470-11*

(Received April 15, 1974)

For application of mass spectrometry to metal chelate chemistry, a group of divalent metal chelates (Co, Ni, Cu, Zn, and Pd) of 2-Me-oxine, 4-Me-oxine, 5-Me-oxine, 7-Me-oxine, and 5-Cl-oxine has been investigated. 2-Methyl-oxine and 4-Me-oxine of these ligands give similar spectra and are considered to have similar fragmentation patterns. The same was found for 5-Me-oxine and 7-Me-oxine. However, the spectra of 2-Me-oxine and 4-Me-oxine metal chelates differ from each other, as do also the spectra of 5-Me-oxine and 7-Me-oxine. Thus fragmentation patterns may vary with the metal chelate formation of the ligands even when they have the same fragmentation patterns. Each metal chelate gave two peaks corresponding to metal-containing ions, a molecular ion (I) of a 2:1 (ligand: metal) chelate, and a fragment ion (II) of a 1:1 chelate due to the loss of a ligand radical from ion I. In the case of Co, Ni, Zn, and Pd chelates of 2-Me-oxine, a peak corresponding to the loss of a methyl radical from I was observed, apparently caused by steric effect. In the metal chelates of 5-Me-oxine, a peak corresponding to the loss of a hydrogen radical from I was also observed. However, the fragmentation pathway of formation of II from I is commonly observed in all metal chelates. Since this pathway is comparable with the second successive formation reaction (k_2) in solution, the peak intensity ratio of the ion of I to that of II was calculated. From the results it was found that the stability of the chelates decreases in the order Zn>Ni>Pd~Co>Cu and that it depends on the charge-radius ratio (e/r) of the central metal ion, or the stability constant (log k_2) observed in solution.

We have studied the divalent metal chelates of 8-quinolinol (oxine)[1] and 8-quinolinethiol (thiooxine)[2] and estimated the stability of these metal chelates under electron impact from the intensity ratio of the peaks. It was found that the stability of these oxine and thiooxine metal chelates is in the order Zn>Ni>Pd~Co>Mn>Cu>Pb and that it depends on the charge-radius ratio (e/r) of the central metal ion.

The results of mass spectral analysis of divalent metal chelates of 2-methyl-8-quinolinol (2-Me-oxine), 4-methyl-8-quinolinol (4-Me-oxine), 5-methyl-8-quinolinol (5-Me-oxine), 7-methyl-8-quinolinol (7-Me-oxine), and 5-chloro-8-quinolinol (5-Cl-oxine) are reported.

Results and Discussion

Mass Spectra of Ligands and Their Fragmentation Patterns. The mass spectra of 2-Me-oxine, 4-Me-oxine, 5-Me-oxine, 7-Me-oxine, and 5-Cl-oxine are shown in Fig. 1.

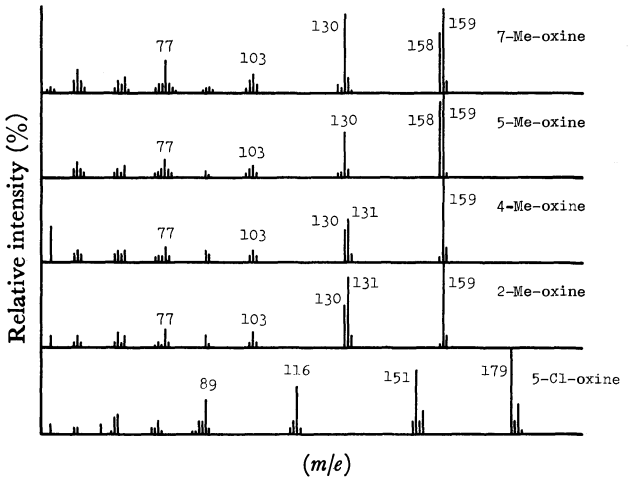

Fig. 1. Mass spectra of oxine derivatives.

Each spectrum gives a strong molecular ion peak (2-, 4-, 5-, and 7-Me-oxine: *m/e* 159; 5-Cl-oxine: *m/e* 179).

The spectrum of 2-Me-oxine is similar to that of 4-Me-oxine, both ligands having fragment ion peaks at *m/e* 131, 130, and 103. The fragmentation patterns of 2-Me-oxine and 4-Me-oxine were reported by Stevenson *et al.*[3] (Scheme 1-a). The molecular ion loses CO to give an ion of *m/e* 131, and then this ion loses H· to produce an azatropylium type ion of *m/e* 130, which in turn loses HCN to produce an ion of *m/e* 103.

Similar spectra are also observed for 5-Me-oxine and 7-Me-oxine, both having the strongest peak, except the molecular ion peak, at *m/e* 158 ($M^{+}-1$); main fragment ion peaks can be observed at *m/e* 130 and 103. The peak at *m/e* 158 is the one corresponding to the loss of H· from the molecular ion, and is due to a tropylium type ion (Scheme 1-b). The peak at *m/e* 130 is due to the ion produced by the loss of CO from the ion of *m/e* 158. The ion of *m/e* 130 might lose HCN to produce an ion of *m/e* 103.

5-Chlorooxine shows main fragment ion peaks at *m/e* 151, 116, and 89. The difference between the molecular ion peak and the peak at *m/e* 151 is 28, corresponding to the loss of CO from the molecular ion. It appears that the peak at *m/e* 116 is due to the ion produced by the loss of Cl· from the ion of *m/e* 151. The peak at *m/e* 89 seems to be due to the ion produced by the loss of HCN from the ion at *m/e* 116. The fragmentation patterns of these oxine derivatives are summarized in Scheme 1-a, b, and c.

In the case of oxine derivatives with a methyl group on its pyridine ring, the molecular ion initially loses CO and then H· to produce an azatropylium type ion. On the other hand, in the case of oxine derivatives with a methyl group on its benzene ring, the molecular ion initially loses H· to produce a tropylium type ion, which then loses CO in succession. A distinct dif-

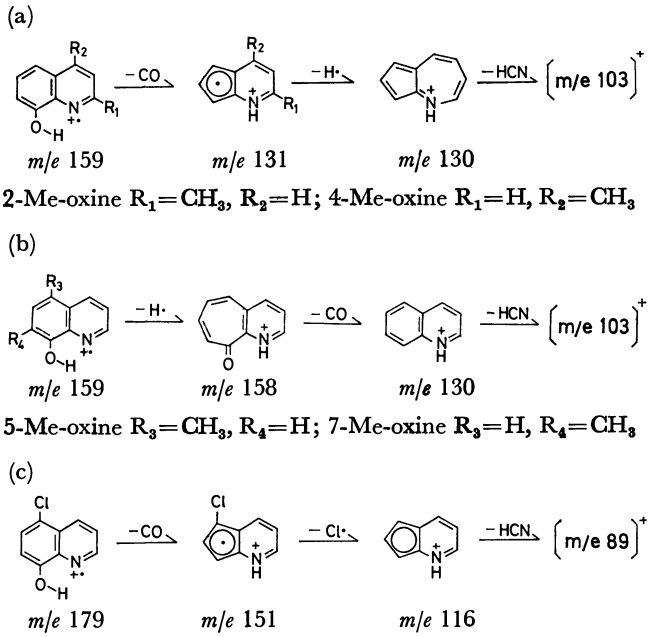

Scheme 1. Fragmentation of oxine derivatives.

ference in fragmentation patterns was found between the two cases. However, it was difficult to find a difference between 2-Me-oxine and 4-Me-oxine and between 5-Me-oxine and 7-Me-oxine from their mass spectra.

The values calculated and found for the metastable ion peaks observed in each fragmentation pathway (Scheme 1) are summarized in Table 1.

TABLE 1. METASTABLE ION PEAKS IN THE MASS SPECTRA OF OXINE DERIVATIVES

Compound	Transition	m* Calcd.	m* Found	Expelled fragment
5-Cl-oxine	179→151+28	127.38	127.1	CO
	151→116+35	89.11	—	Cl·
	116→ 89+27	68.28	68.3	HCN
2-Me-oxine	159→131+28	107.93	108.0	CO
	131→130+ 1	129.01	129.0	H·
	130→103+27	81.61	81.5	HCN
4-Me-oxine	159→131+28	107.93	108.0	CO
	131→130+ 1	129.01	129.0	H·
	130→103+27	81.61	81.5	HCN
5-Me-oxine	159→158+ 1	157.01	157.0	H·
	158→130+28	106.96	107.0	CO
	130→103+27	81.61	81.5	HCN
7-Me-oxine	159→158+ 1	157.01	157.0	H·
	158→130+28	106.96	107.0	CO
	130→103+27	81.61	81.5	HCN

Mass Spectra of Divalent Metal Chelates and Their Fragmentation Patterns. 2-Me-oxine Metal Chelates: Figure 2 shows the spestra of Ni, Co, Cu, Zn, and Pd chelates with 2-Me-oxine. Molecular ion peaks of chelates were observed in the highest mass region of all the spectra, showing that the ligand and metal are combined in a 2: 1 molar ratio. Except for Cu chelate, a fragment ion peak due to the loss of CH_3· from the molecular ion is observed. On the other hand, all spectra have a peak corresponding to the loss of 158

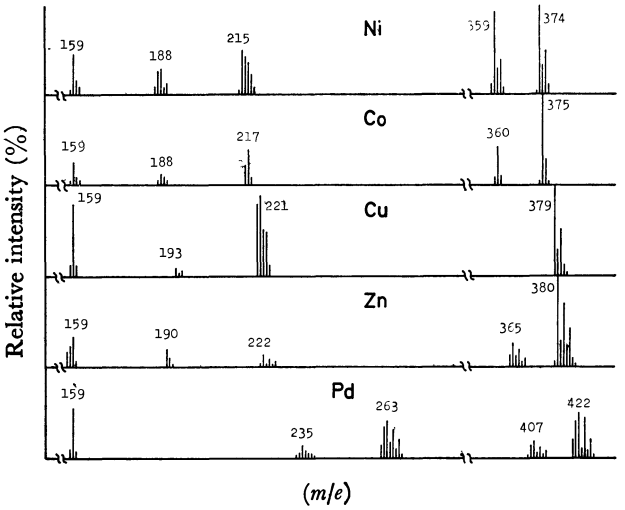

Fig. 2. Mass spectra of 2-Me-oxine metal chelates.

amu (one molecule of 2-Me-oxine) from the molecular ion, the peak due to the ion having a 1: 1 ligand to metal ratio. Another peak due to the loss of H· from this ion, which appears to be azatropylium type ion, is observed. The loss of CO from this ion takes place except for Zn chelate. The fragmentation pattern of 2-Me-oxine metal chelates is shown in Scheme 2.

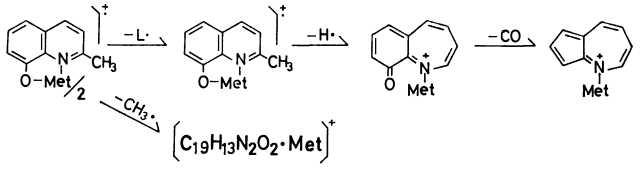

Met=divalent metals

Scheme 2. Fragmentation of 2-Me-oxine metal chelates.

4-Me-oxine Metal Chelates: Figure 3 and Scheme 3 show the spectra of Ni, Co, Cu, Zn, and Pd chelates with 4-Me-oxine and their fragmentation patterns. The molecular ion peak of each chelate corresponding to a 2: 1 ligand to metal ratio was observed in the highest mass region of all the spectra, followed by a fragment ion peak due to the loss of one molecule of 4-Me-oxine

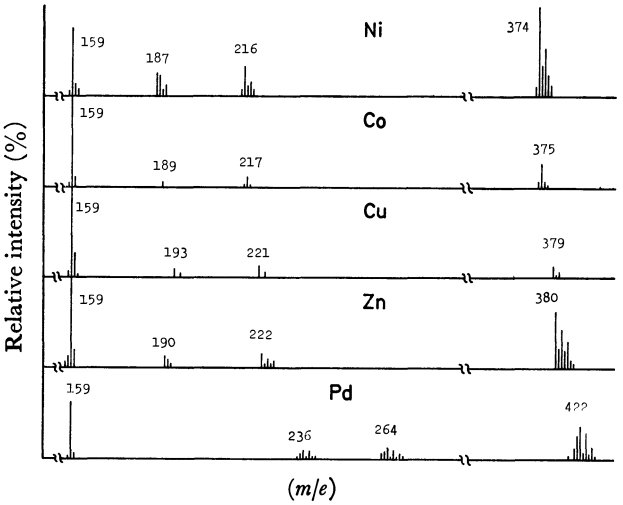

Fig. 3. Mass spectra of 4-Me-oxine metal chelates.

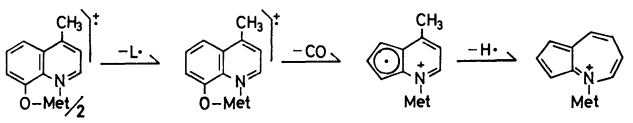

Met=divalent metals

Scheme 3. Fragmentation of 4-Me-oxine metal chelates.

(158 amu), and with a 1:1 ligand to metal ratio. Except for the Zn chelate the peak was followed by another peak corresponding to the loss of CO from the 1:1 chelate ion.

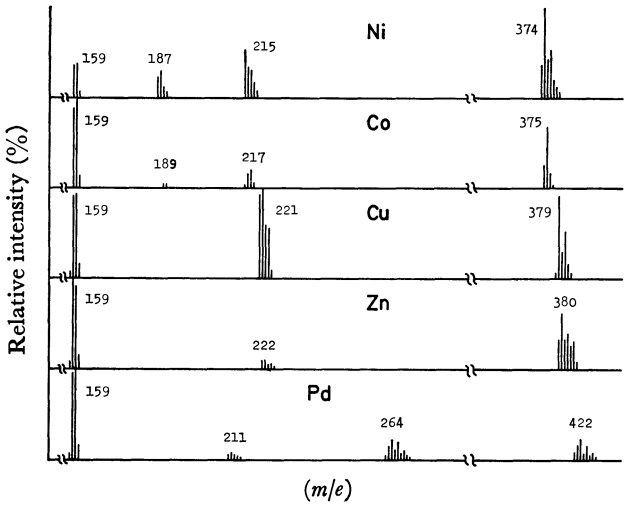

Fig. 4. Mass spectra of 5-Me-oxine metal chelates.

5-Me-oxine Metal Chelates: Figure 4 shows the spectra of Ni, Co, Cu, Zn, and Pd chelates with 5-Me-oxine. The molecular ion peak of each chelate corresponding to a 2:1 ligand to metal ratio was observed in the highest mass region of all the spectra, followed by a peak corresponding to the loss of one amu (corresponding to $H^{\cdot}$). The ion M^{+}–1 would have a mixed ligand complex structure since either of the two ligands can lose a hydrogen to form tropylium type structure. On the other hand, a fragment ion peak corresponding to the loss of 158 amu from the molecular ion also appears with a 1:1 ligand to metal ratio. The peak is followed by another peak, which seems to be a tropylium type ion by the loss of H· from that ion. This is followed by a fragment ion peak corresponding to the loss of CO from tropylium type ion except for Zn chelate, the fragment ion peak being weak (Scheme 4).

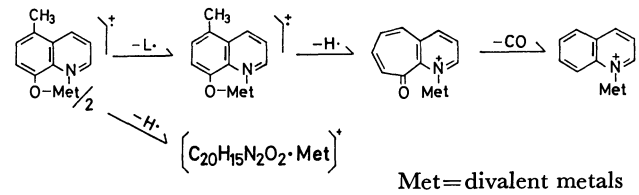

Met=divalent metals

Scheme 4. Fragmentation of 5-Me-oxine metal chelates.

7-Me-oxine Metal Chelates: Figure 5 shows the spectra of Ni, Co, Cu, Zn, and Pd chelates with 7-Me-oxine. The loss of 158 amu, one molecule of 7-Me-oxine, from

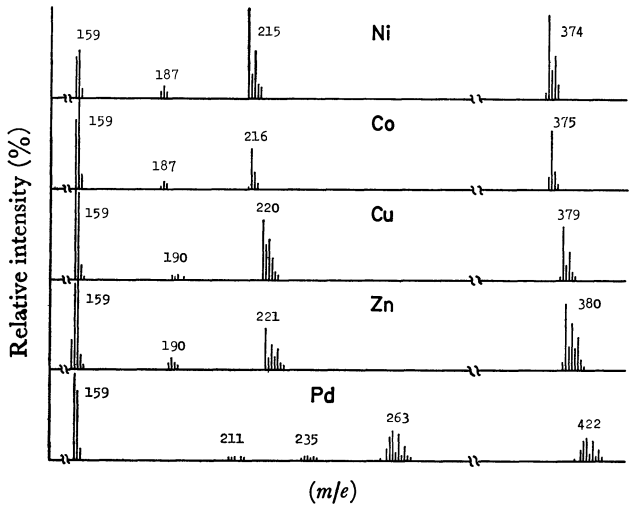

Fig. 5. Mass spectra of 7-Me-oxine metal chelates.

the molecular 2:1 chelate ion appears to give a fragment ion peak corresponding to a 1:1 lignad to metal ratio. This is followed by a peak with high intensity, corresponding to the loss of H· from the 1:1 chelate ion. The peak with low intensity resulting from the loss of 28 amu corresponding to CO is observed in the spectra except for Zn chelate (Scheme 5).

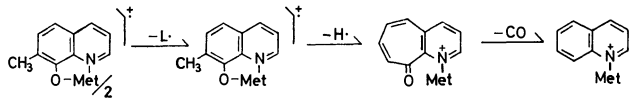

Met=divalent metals

Scheme 5. Fragmentation of 7-Me-oxine metal chelates.

5-Cl-oxine Metal Chelates: Figure 6 shows the spectra of Ni, Co, Cu, Zn, and Pd chelates with 5-Cl-oxine. The molecular ion peak of each chelate was observed in the highest mass region of all spectra corresponding to a 2:1 ligand to metal ratio. A fragment ion peak due to the ion produced by the loss of 178 amu from the molecular ion was also observed. Since 178 amu corresponds to one molecule of 5-Cl-oxine, the ion produced has a 1:1 ligand to metal molar ratio. Except

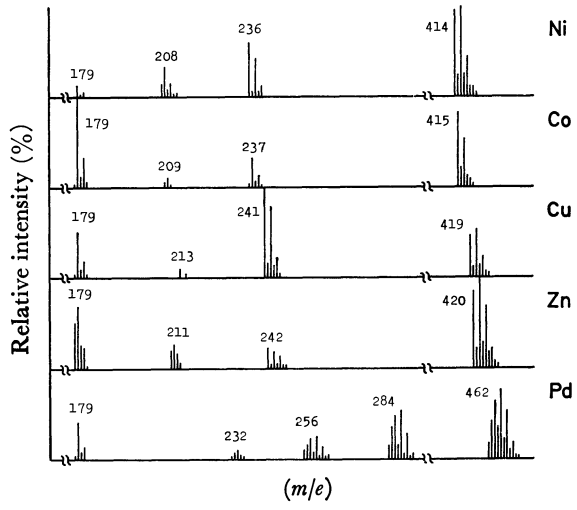

Fig. 6. Mass spectra of 5-Cl-oxine metal chelates.

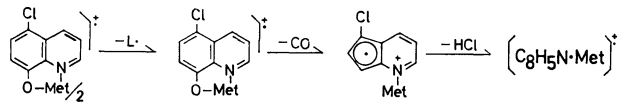

Met=divalent metals

Scheme 6. Fragmentation of 5-Cl-oxine metal chelates.

for Zn chelate, the loss of 28 amu corresponding to CO from the 1:1 chelate ion is observed. The peak is followed by a fragment ion peak which lost HCl. The fragmentation pattern is shown in Scheme 6.

The fragmentation patterns of 2-Me-oxine and 4-Me-oxine and those of 5-Me-oxine and 7-Me-oxine are similar to each other, but the metal chelates of these methyloxine derivatives show fairly different fragmentation patterns. In the case of 2-Me-oxine, a fragment ion peak due to the loss of $CH_3\cdot$ from the molecular ion can be observed, but in that of 4-Me-oxine metal chelates no corresponding fragmentation occurred. A peak corresponding to the loss of H· from the molecular ion was observed in the case of 5-Me-oxine, but not in that of 7-Me-oxine.

In each spectrum the loss of either H· or CO from the 1:1 fragment ion was observed. The fragment ions produced are expected to contain a metal atom combined with the nitrogen atom. Thus, in the 1:1 fragment ion, the metal atom seems to be bound more strongly with the nitrogen atom than with the oxygen atom. However, each Zn chelate shows no loss of CO from the 1:1 fragment ion or from the fragment ion produced by the loss of H· from the 1:1 ion. This may be related to the valence change of the metal in the fragmentation process for acetylacetone metal chelates.[4] According to the classification of metals by Budzikiewicz *et al.*,[5] the valence change in Zn seems to be difficult, and the oxygen-zinc bond might be stronger than the other oxygen-metal bond, resulting in the difficult loss of CO.

The loss of $CH_3\cdot$ from the molecular ion occurs in Co, Ni, Zn, and Pd chelates of 2-Me-oxine only. The fragmentation pathway is not observed for the other methyloxine metal chelates. This may be partly caused by a steric influence of the methyl group at 2-position on the quinoline ring. Thus, in gaseous state the molecular ions of Co, Ni, Zn, and Pd chelates with 2-Me-oxine might take such a sterically hindered structure, which favors the loss of the methyl group.

Each spectrum of the metal chelates includes the peaks due to the ligand itself. It seems that prior to vaporization the chelate is thermally decomposed and the peak due to the ligand itself may be observed together.[1]

Stability under Electron Impact. Various metal chelates of mono-methyl-oxine derivatives show different fragmentation patterns depending on the position of the methyl group. However, a fragmentation pathway common to all the metal chelates can be observed, *i.e.*, the pathway in which a ligand radical is lost initially from a 2:1 molecular ion (I) to transform into a 1:1 fragment ion (II). This fragmentation pathway can be compared with the second successive formation reaction of metal chelates in solution. Thus,

Table 2. Intensity ratios of the molecular ion, I, to the fragment ion, II.

Ligand	Metal				
	Zn	Ni	Pd	Co	Cu
oxine[1]	67	63	61	61	48
thiooxine[2]	52	48	45	45	30
2-Me-oxine	87	77	75	74	55
4-Me-oxine	86	75	75	74	56
5-Me-oxine	75	69	67	65	50
7-Me-oxine	85	77	74	75	57
5-Cl-oxine	65	62	58	57	43

in order to examine the stability of ion I under electron impact, the peak intensity of I was calculated as the intensity ratio of I to the sum of I and II (Table 2). The peak intensity of I for each ligand is in the order: Zn>Ni>Pd~Co>Cu. This suggests that the peak intensity is related to the characteristics of the central metal ions and not to those of the ligands in the chelates. The values in Table 2 are plotted against the charge-radius ratio (e/r) of the central metal ions,[6] *viz.*, charge density, which is known to affect the stability of metal chelate in solution (Fig. 7).[7] We see that the peak intensity of I is proportional to the charge density; even under electron impact the molecular ion of a metal chelate having a central metal ion of high charge density is more stable than that of another chelate having a metal ion of low charge density.

Based on the assumption that the fragmentation pathway from I to II is correlated to the formation process of a 1:1 chelate from a 2:1 chelate in solution, which is expressed in terms of the stability constant,

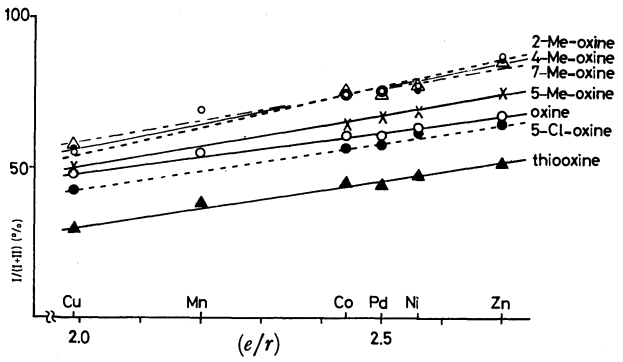

Fig. 7. Correlation between the intensity ratios and the charge-radius ratios of metals.

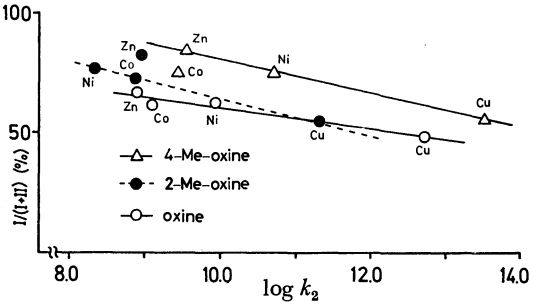

Fig. 8. Correlation between the intensity ratios and stability constants, log k_2.

log k_2, a close relation between the stability of I under electron impact and log k_2, is expected. The values in Table 2 are plotted against log k_2 (Fig. 8).[8] A linear relation holds between the stability of I under electron impact and log k_2 in the metal chelates of 4-Me-oxine, 2-Me-oxine, and oxine. 5-Methyloxine, 7-Me-oxine, and 5-Cl-oxine are not included, since the values of log k_2 are not known.

We can thus distinguish the metal chelates of similar methyl-oxine derivatives, and the molar ratio of ligand to metal in a chelate can be simply determined with a minute quantity of sample. It is possible to identify the metal contained from the isotope ratio in the molecular ion peak. By further detailed examinations of the spectra, the stability of the metal chelates under electron impact can also be studied. All these results indicate that mass spectrometry can be applied effectively to investigations of the metal chelates with methyl-oxine derivatives.

Experimental

Apparatus: Mass spectra were measured with a Hitachi RMU-7 mass spectrometer by means of a direct inlet system, at 70 eV ionization voltage.

Reagents: 2-Methyl-oxine and 5-Cl-oxine (reagent grade, Tokyo Kasei Kogyo Co., Ltd.) were used without further purification. 4-Methyl-oxine,[9] 5-Me-oxine,[10] and 7-Me-oxine[10] were synthesized according to the reported methods.

Syntheses of Metal Chelates: Alcohol solutions of metal chlorides were added to alcohol solutions of the ligands. The mixtures were warmed on a water bath and the resulting precipitates were separated by filtration. After washing with hot alcohol and water several times, the precipitates were dried at *ca.* 110 °C under reduced pressure. The composition of each metal chelate was confirmed by elemental analysis.

The authors' thanks are due to Professor Akira Tatematsu, Faculty of Pharmacy, Meijo University, for use of the apparatus.

References

1) Y. Kidani, S. Naga, and H. Koike, *Chem. Lett.*, **1972**, 507; This Bulletin, **46**, 2105 (1973).
2) Y. Kidani, S. Naga, and H. Koike, *Chem. Pharm. Bull.* (Tokyo), in contribution, "Studies on Mass Spectrometry of Metal Chelates. II. Mass Spectrometry of Thiooxine Metal Chelates."
3) R. L. Stevenson, M. E. Wacks, and W. M. Scott, *Org. Mass Spectrom.*, **2**, 261 (1969).
4) C. G. MacDonald and J. S. Shannon, *Aust. J. Chem.*, **19**, 1545 (1966); S. Sasaki, Y. Itagaki, T. Kurokawa, and K. Nakanishi, This Bulletin, **40**, 76 (1967).
5) H. Budzikiewicz, C. Djerassi, and D. H. Williams, "Mass Spectrometry of Organic Compounds," Holden-Day, Inc., San Francisco, Calif., (1967), p. 663.
6) Pauling's value was taken for ionic radii.
7) A. E. Martell and M. Calvin, "Chemistry of the Metal Chelate Compounds," Prentice-Hall, Inc., Englewood Cliffs, N. J., (1952), p. 191.
8) Stability constants were taken from: W. D. Johnston and H. Freiser, *J. Amer. Chem. Soc.*, **74**, 5239 (1952); *Anal. Chim. Acta*, **11**, 201 (1954).
9) J. P. Phillips, R. L. Elbinger, and L. L. Merritt, Jr., *J. Amer. Chem. Soc.*, **71**, 3986 (1949).
10) E. Noelting and E. Trautmann, *Ber.*, **23**, 3654 (1890).

Thermal Dehydration and Decomposition of Dioxalato Complexes of Be(II), Mn(II), Co(II), Ni(II), Cu(II) and Zn(II) in Solid State

Kenzo NAGASE, Katsuya SATO,* and Nobuyuki TANAKA*

College of General Education, Tohoku University, Kawauchi, Sendai 980

**Department of Chemistry, Faculty of Science, Tohoku University, Aoba, Aramaki, Sendai 980*

(Received July 10, 1974)

The structures of anhydrous dioxalato complexes $K_2[M(C_2O_4)_2]$ (M: Mn(II), Co(II), Ni(II), Cu(II), and Zn(II)) prepared by heating their hydrates, were examined by means of infrared absorption and visible reflectance spectroscopy. It was found that the anhydrous complexes of Mn(II), Co(II), and Zn(II) exist in a polynuclear octahedral form with a bridging oxalate group, and those of Ni(II) and Cu(II), in a monomer form. On further heating, the complexes of Be(II), Mn(II), and Zn(II) decomposed into the corresponding metal oxides and potassium oxalate, and those of Co(II), Ni(II), and Cu(II) into the corresponding metals and potassium oxalate. Except for the beryllium(II) complex, the complexes decomposed at lower temperatures with an increase in $1/r$, where r is the radius of metal ion.

The thermal properties of bivalent metal oxalates-(monooxalato-type complex) and trioxalato-type complexes of tervalent metals have been extensively studied. However, only fragmentary information is available on the thermal decomposition reactions of dioxalato-type complexes of bivalent metals. The TG, DTA, and EG curves for $K_2[Cu(C_2O_4)_2]\cdot 2H_2O$, $K_2[Zn(C_2O_4)_2]\cdot 2H_2O$, $K_2[Pd(C_2O_4)_2]\cdot 3H_2O$, and $K_2[Pt(C_2O_4)_2]\cdot 2H_2O$ were presented and the reaction stoichiometries discussed.[1,2]

Most bivalent metal oxalates(monoxalato-type complexes) exist in a polynuclear form with bridging oxalate groups, the water molecules contained being coordinated directly to the metal ions.[3] Thus, the dehydration temperatures are considerably high (>100 °C). The nature of the metal ions is well reflected not only on the dehydration reactions but also on the decomposition reactions of the anhydrous salts. Trioxalato-type complexes of tervalent metals exist in the mononuclear octahedral form. The coordination number of tervalent metals is usually six, and thus in these complexes, all coordination positions are occupied by the oxygen atoms of three bidentate oxalate groups. All the water molecules contained are crystalline water and dehydration takes place below 100 °C. Interest in the thermal reactions of these complexes has been limited to the decomposition reactions of the anhydrous salts. Dioxalato complexes seem to be of particular interest, since they exist in either a mononuclear or a polynuclear form. The metal ions with coordination number 4 will be mononuclear, whereas those with the number 6 can form both the mononuclear (two of the six positions are occupied by two water molecules) and polynuclear (the bridging oxalate groups act as quadridentate ligand) form complexes. In the case of anhydrous dioxalato complexes, the complexes of the metals with the number 6 should exist in the polynuclear form.

We have examined the structures of the anhydrous dioxalato complexes of Mn(II), Co(II), Ni(II), Cu(II), and Zn(II) prepared by heating their hydrates in solid state by means of infrared absorption and visible reflectance spectroscopies. The thermal properties, as determined by the techniques of TG, DTA, DSC, and EG, are given for $K_2[Be(C_2O_4)_2]$, $K_2[Zn(C_2O_4)_2]\cdot 5H_2O$, $K_2[Mn(C_2O_4)_2]\cdot 2H_2O$, $K_2[Co(C_2O_4)_2]\cdot 6H_2O$, $K_2[Ni(C_2O_4)_2]\cdot 6H_2O$, and $K_2[Cu(C_2O_4)_2]\cdot 2H_2O$.

Experimental

Materials. The dioxalato complexes were prepared as follows: Beryllium(II) complex was obtained by adding $K_2C_2O_4$ to an aqueous solution of $BeSO_4\cdot 4H_2O$. For the other complexes, the corresponding metal oxalates were dissolved in an aqueous solution containing a stoichiometric amount of $K_2C_2O_4$. After filtration, the desired samples were crystallized from the filtrates by addition of methanol. The results of elemental analyses for C and H agreed with the calculated values within $\pm 0.3\%$ for all the complexes.

Measurements. Thermogravimetric (TG) and differential thermal analytic (DTA) curves were obtained in the range from room temperature to 1000 °C with a Shinku Riko TGD-3000, at a heating rate of 5 °C/min in a nitrogen atmosphere with a 50 ml/min flow rate. 20 mg of powdered sample was placed in a platinum crucible and used in each measurement. Heats of dehydration and decomposition were determined with a Rigaku Denki 8002 CS differential scanning calorimeter (DSC) at a 5 °C/min heating rate in a nitrogen atmosphere with a 30 ml/min flow rate. 20 mg of powdered sample was placed in an aluminum crucible, a lid of the same material being then placed inside the crucible. The instrument was calibrated against the heat of transition of KNO_3 which appears at 128 °C with ΔH of 12.28 kcal/mol.

The infrared absorption spectra were measured in the frequency region 2500—400 cm^{-1} with a Hitachi EPI-2G spectrophotometer by the KBr disk method. The sample heated to a given temperature was cooled to room temperature and its spectrum was recorded. A Hitachi EPS-3T spectrophotometer equipped with a standard integrating sphere attachment was used for the measurements of the reflectance spectra in the frequency range 30000—15000 $cm.^{-1}$ MgO was used as a reference material.

The evolved gas (EG) curves were obtained by conductometric technique at a heating rate of 5 °C/min in a helium atmosphere with a 50 ml/min flow rate. Evolved gas analyses (EGA) were carried out for each EG peak with an active charcoal column (2 meters long) and a helium carrier gas (50 ml/min). Procedures for EG and EGA were described previously.[2]

Results and Discussion

TG and DTA Studies. The TG curves for the

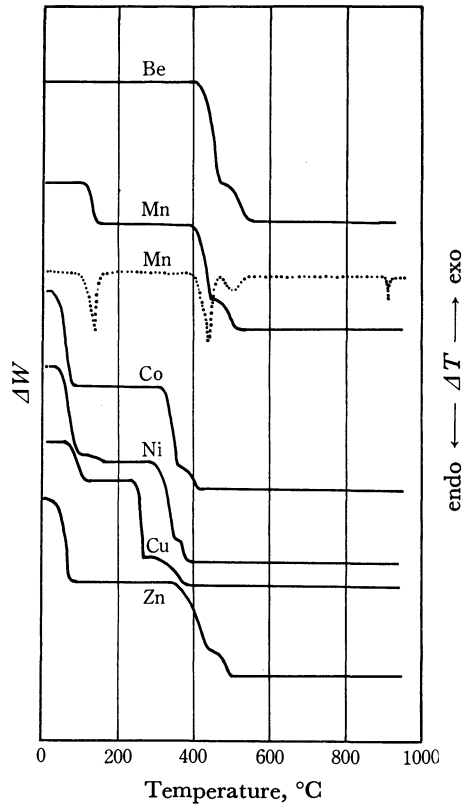

Fig. 1. TG(solid line) and DTA(dotted line) curves of dioxalato complexes in a flowing nitrogen atmosphere.

Be(II), Mn(II), Co(II), Ni(II), Cu(II), and Zn(II) complexes are given in Fig. 1. Curves for Be(II), Mn(II), Co(II), and Ni(II) complexes seem to have been given for the first time. For the sake of comparison, the curves of the remaining complexes[1] were reproduced under the conditions of the present work. The DTA curves were also obtained for all the complexes. As an example, the curve of $K_2[Mn(C_2O_4)_2]\cdot 2H_2O$ is given in Fig. 1. All the complexes decomposed through two or three steps. The initial weight-loss temperatures (t_i) and DTA peak temperatures (t_m) for each stage are summarized in Table 1 and the wieght-loss data (ΔW) in Table 2.

Except for the Be(II) complex, the complexes liberate the water molecules contained in the order of increasing temperature, Zn(II)<Co(II)<Ni(II)<Cu(II)<Mn-(II), giving well-defined plateaus for the anhydrous complexes (dehydration—stage 1) on the TG curves. Dehydration of Ni(II) and Zn(II) complexes gave two

Table 1. Initial weight-loss temperatures (t_i) and DTA peak temperatures (t_m)

Complex	Dehydration (°C)		Decomp. of complex (°C)		Decomp. of $K_2C_2O_4$ (°C)	
	t_i	t_m	t_i	t_m	t_i	t_m
Be(II)	—	—	402	453	469	531
Me(II)	112	129	394	440	450	505
Co(II)	31	68	312	339	364	377
Ni(II)	38	72, 85	295	340	—	375
Cu(II)	63	100	242	270	300	370
Zn(II)	20	40, 70	350	420	—	488

Table 2. Percentage of weight-loss

Complex	Dehydration		Decomp. of complex		Decomp. of $K_2C_2O_4$	
	obsd	calcd	obsd	calcd	obsd	calcd
Be(II)	—	—	27.1	27.4 ($CO+CO_2$)	10.2	10.6 (CO)
Mn(II)	10.8	10.4	20.0	20.9 ($CO+CO_2$)	7.9	8.1 (CO)
Co(II)	23.9	25.6	20.9	20.9 ($2CO_2$)	6.2	6.7 (CO)
Ni(II)	23.1	25.7	20.2	20.9 ($2CO_2$)	6.1	6.7 (CO)
Cu(II)	9.2	10.2	23.4	24.9 ($2CO_2$)	7.2	7.9 (CO)
Zn(II)	22.0	22.0	16.5	17.7 ($CO+CO_2$)	6.3	6.8 (CO)

peaks on each DTA curve, suggesting that all the waters are not held in the same way. The values of t_i of the dehydration varied over the range 18—112 °C with the central metals. The relation between t_i (t_{H_2O}) and $1/r$, where r is ionic radius, is given in Fig. 2. Except for $K_2[Mn(C_2O_4)_2]\cdot 2H_2O$, t_i increased almost linearly with the increase of $1/r$, suggesting that an electrostatic interaction exists to some extent between the water molecules and the central metal ions. Dehydration of the Mn(II) complex took place at the highest temperature, the point (Fig. 2) deviating a great deal from linearity. Thus, two water molecules of the Mn(II) complex might coordinate directly to the metal ion, and the complex should be formulated as $K_2[Mn(H_2O)_2(C_2O_4)_2]$.

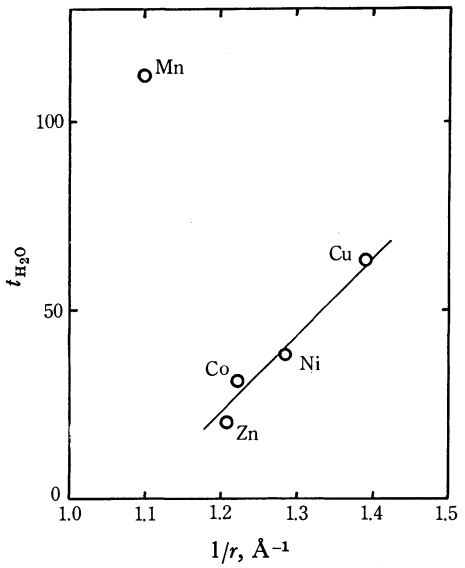

Fig. 2. Relation of initial weight-loss temperatures of the dehydration (t_{H_2O}) with $1/r$ for dioxalato complexes.

The anhydrous complexes then decomposed on further heating to give metal oxides or metals and potassium oxalate (decomposition of anhydrous complex—stage II). The weight-loss data (Table 2) indicate that Be(II), Mn(II), and Zn(II) complexes gave BeO, MnO, and ZnO, respectively, and $K_2C_2O_4$, while Co(II), Ni(II), and Cu(II) complexes gave Co, Ni,

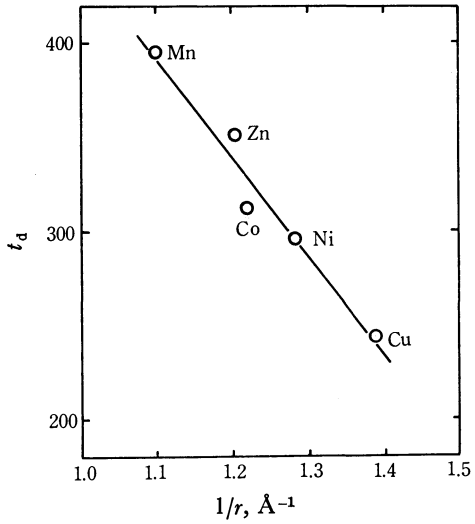

Fig. 3. Relation of initial weight-loss temperatures of the decomposition of the anhydrous dioxalato complexes (t_d) with $1/r$.

and Cu, respectively, and $K_2C_2O_4$. The values of t_i of the anhydrous complexes varied a great deal with the central metals. The plots of $t_i(t_d)$ *versus* $1/r$ are given in Fig. 3. Except for the Be(II) complex, t_i decreased with an increase in $1/r$, irrespective of the metals or the metal oxides formed as a solid decomposition product. This differs from the result obtained for the metal oxalate,[4] where the compounds giving metals decomposed at lower temperatures with an increase in $1/r$, while those giving the metal oxides decomposed in the reverse order.

Stage II which showed no well-defined plateau was followed by the decomposition of $K_2C_2O_4$ formed. The weight-loss data (Table 2) indicate that $K_2C_2O_4$ decomposed to K_2CO_3 to evolve one molecule of carbon monoxide (decomposition of $K_2C_2O_4$—stage III). It should be pointed out that the thermal stability of the potassium oxalate formed was influenced strongly by the metals or the metal oxides included in the decomposition products.

A small endotherm at 916—920 °C without any weight-loss was observed for all the complexes investigated. This corresponded to the melting point of K_2CO_3 formed. Pure K_2CO_3 also gave the same peak at 918 °C.

DSC Study. The enthalpy changes corresponding to the dehydration (ΔH_w), the decomposition of the anhydrous complexes (ΔH_{comp}) and the decomposition of $K_2C_2O_4$ (ΔH_{ox}) are given in Table 3. Since the number of water molecules contained in the complexes varied from 2 to 6, the values given for ΔH_w are the mean value per one mole of water. ΔH_w of the Mn(II) complex, dehydrated at the highest temperature, was the largest. ΔH_w decreased in the order Mn(II)> Cu(II)>Zn(II)>Co(II)>Ni(II), in line with that of ΔH_w of the metal oxalates.[4]

Table 3. Enthalpy changes

Complex	Dehydration ΔH_w, kcal/H_2O	Decomp. of complex $\Delta H_{comp.}$ kcal/comp.	Decomp. of $K_2C_2O_4$ ΔH_{ox}, kcal/$K_2C_2O_4$
Mn(II)	19.9	—	—
Co(II)	14.3	13	7
Ni(II)	13.7	16	6
Cu(II)	16.3	—	—
Zn(II)	14.6	—	—

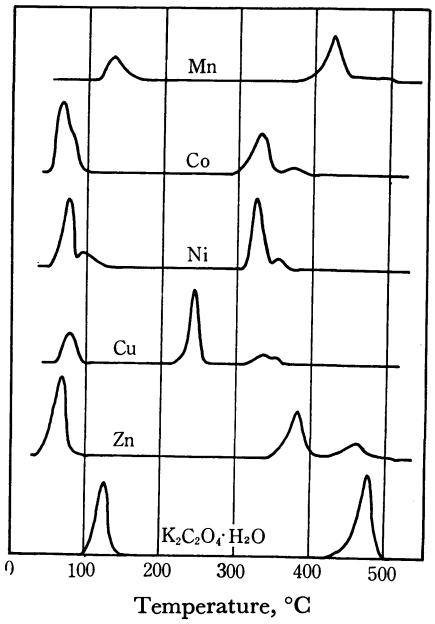

Fig. 4. Evolved gas curves of dioxalato complexes in a flowing helium atmosphere.

Table 4. Evolved gas analyses (mol %)

Complex	Decomp. of complex		Decomp. of $K_2C_2O_4$	
	CO	CO_2	CO	CO_2
Be(II)	40	60	90	10
Mn(II)	55	45	80	20
Co(II)	0	100	50	50
Ni(II)	0	100	40	60
Cu(II)	0	100	84	16
Zn(II)	44	56	82	18

EG and EGA Studies. The EG curves of the complexes in a flowing helium atmosphere are given in Fig. 4, together with the EG curve of pure $K_2C_2O_4$. The evolved gas analyses for each EG peak are given in Table 4. The decomposition of anhydrous complexes can be divided into two types: the complexes of Be(II), Mn(II), and Zn(II) evolved one mole of carbon monoxide and one mol of carbon dioxide, while those of Co(II), Ni(II), and Cu(II) evolved two moles of carbon dioxide. This is consistent with the results from the TG in Table 2.

Although the TG curves indicate that stage III corresponds to the reaction

$$K_2C_2O_4 \longrightarrow K_2CO_3 + CO, \quad (1)$$

the EGA (Table 4) indicate the presence of CO_2 in addition to CO. The compositions of the gaseous mixtures varied with the complexes. For the com-

plexes of Mn(II), Cu(II), Zn(II), and Be(II), the major gaseous product was CO, CO_2 being less than 20% (mol %) of the total products. On the other hand, the percentage of CO_2 for the complexes of Co(II) and Ni(II) reached 50—60%. Thus, the following reaction might be considered in addition to Reaction (1).

$$K_2C_2O_4 \longrightarrow K_2CO_3 + 1/2C + 1/2CO_2 \qquad (2)$$

The presence of carbon in the solid products was confirmed by chemical analyses after removal of K_2CO_3.

Infrared Absorption and Diffuse Reflectance Spectroscopic Studies. The infrared absorption spectra of the hydrated complexes with those of the anhydrous ones are compared in Figs. 5 and 6. For the complexes of Mn(II) and Co(II), the spectra of the hydrated complex differ a great deal from those of the anhydrous complex, suggesting that structural changes occurred in the course of dehydration. In the region 1500—1200 cm^{-1}, $K_2[Mn(C_2O_4)_2]\cdot 2H_2O$ exhibited two C–O stretching vibrations[5] at 1447 and 1303 cm^{-1}, while $K_2[Mn(C_2O_4)_2]$ showed absorptions at 1418, 1387(w), 1332, and 1282 cm^{-1}. The bands of the hydrated complex, and those at 1418 and 1282 cm^{-1} of the anhydrous complex could be assigned to the C–O stretching vibrations of the bidentate oxalate group (I); those at 1387(w) and 1332 cm^{-1} of the anhydrous complex would be due to the quadridentate oxalate group (II).

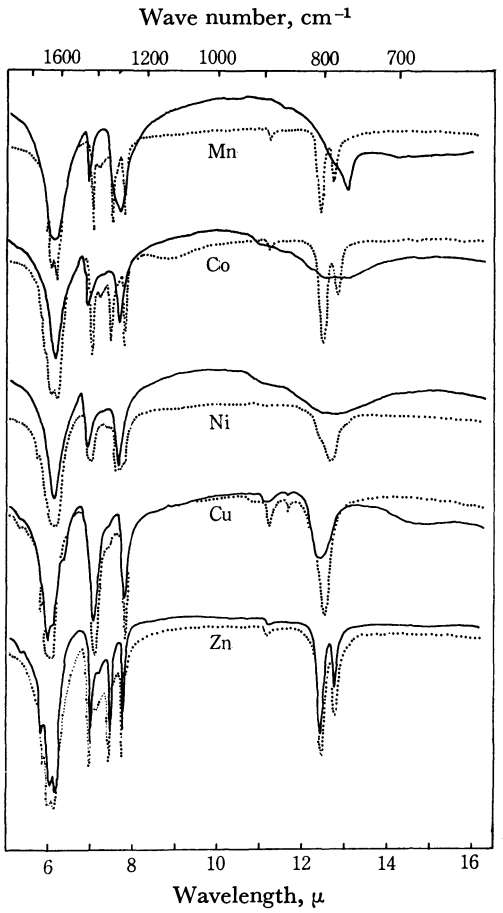

Fig. 5. Infrared absorption spectra of dioxalato complexes before and after the dehydration: —— indicates $K_2[M(C_2O_4)_2]\cdot nH_2O$ and ·····, $K_2[M(C_2O_4)_2]$.

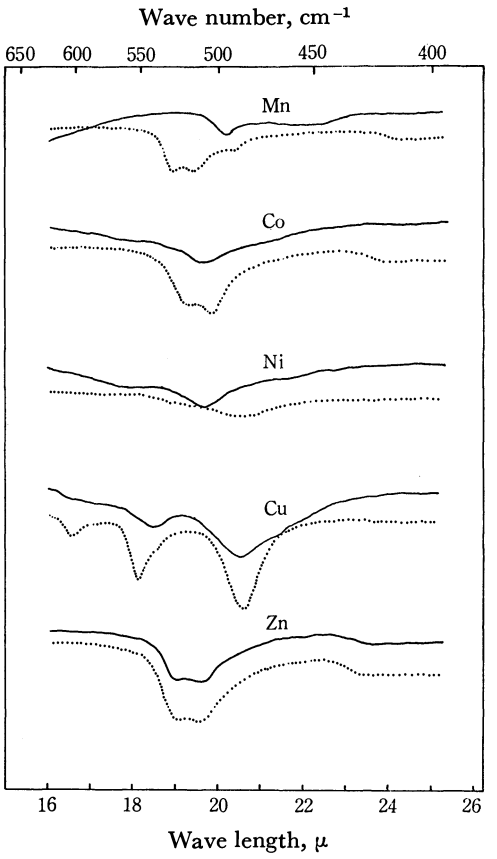

Fig. 6. Infrared absorption spectra of dioxalato complexes before and after the dehydration: —— indicates $K_2[M(C_2O_4)_2]\cdot nH_2O$ and ·····, $K_2[M(C_2O_4)_2]$.

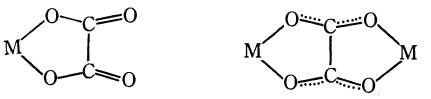

I II

The assignments are supported by comparison of the spectra of the anhydrous complex with those of MnC_2O_4 and $K_6(C_2O_4)_2Mn(OX)Mn(C_2O_4)_2$, where OX denotes a quadridentate oxalate group.[6] The oxalate groups in MnC_2O_4 are also confirmed to act as quadridentate groups by X-ray analysis.[3] Manganese oxalate shows only two bands at 1337(w) and 1319 cm^{-1}, while $K_6(C_2O_4)_2Mn(OX)Mn(C_2O_4)_2$ shows absorptions at 1415, 1385(w), 1310, and 1285 cm^{-1}.[6] In the region 900—650 cm^{-1}, considerable differences were observed in the spectra of $K_2[Mn(C_2O_4)_2]\cdot 2H_2O$ and its anhydrous complex: the hydrated complex gave two broad bands at 766 and 696 cm^{-1}, and the anhydrous complex three narrow bands at 885, 798, and 780 cm^{-1}. The bands at 696 cm^{-1} in the hydrated complex might correspond to coordinated waters; $MnC_2O_4\cdot 2H_2O$ also shows a characteristic band of the coordinated waters at 724 cm^{-1}. This is consistent with results from TG (the hydrated complex should be formulated as $K_2[Mn(H_2O)_2(C_2O_4)_2]$). The bands appearing in the region 600—400 cm^{-1} give direct information on the coordination bond. Oxalato complexes, in general, exhibit M–O stretching modes in this region.[5] The spectrum of the anhydrous complex in this region

differes from that of the hydrated one, suggesting a change of the bonding structure by dehydration.

Comparison of the infrared absorption spectra of the complexes of other metals in a similar way give valuable information on the prediction of the bonding structures of the complexes. The spectra of the anhydrous complexes of Co(II) and Zn(II) and also the hydrated complex of Zn(II) are very similar to that of the anhydrous manganese(II) complex in the range 2000—400 cm^{-1}, indicating that these complexes have essentially the same structure.

The anhydrous complexes of Ni(II) and Cu(II) show no characteristic bands of the bridging oxalate group. Each oxalate ligand might essentially act as a bidentate group.

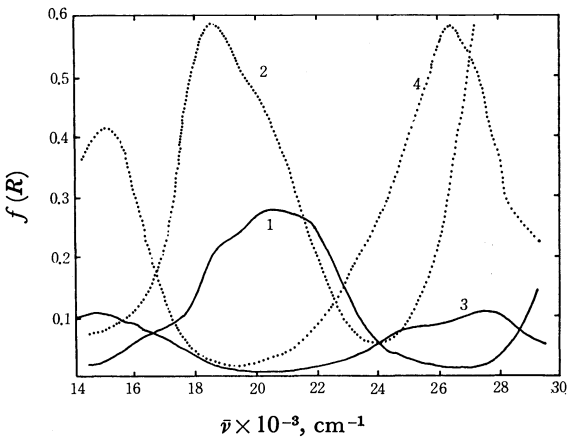

Fig. 7. Reflectance spectra of (1) $K_2[Co(C_2O_4)_2]\cdot 6H_2O$, (2) $K_2[Co(C_2O_4)_2]$, (3) $K_2[Ni(C_2O_4)_2]\cdot 6H_2O$ and (4) $K_2[Ni(C_2O_4)_2]$.

The diffuse reflectance spectra in the visible region (Fig. 7) were obtained in order to study the structures of the colored complexes. The spectrum of the hydrated complex of Ni(II) was similar to that of $NiC_2O_4\cdot 2H_2O$, the nickel ion of which is surrounded octahedrally with six oxygen atoms. $[Ni(H_2O)_6]^{2+}$ in aqueous solution also gives a similar absorption pattern. Thus, the hydrated nickel(II) complex has an octahedral coordination structure. It is blue while the anhydrous nickel(II) complex is bluish green. The spectrum of the latter is similar to that of the hydrated complex, except for the change in apparent intensities and the relatively small shifts of the absorption bands. Thus the Ni(II) ion in the anhydrous complex is also in an approximately octahedral structure, probably due to the formation of weak Ni–O bonds between the non-coordinated oxygen atoms of one $[Ni(C_2O_4)_2]^{2-}$ unit and Ni ions in adjacent units; Appearance of somewhat broad bands of the anhydrous complex might be due to this effect. As to the Co(II) complexes, the spectrum of the hydrated complex is similar to that of $CoC_2O_4\cdot 2H_2O$ and of $[Co(H_2O)_6]^{2+}$, the spectrum of the anhydrous complex not differing very much either. This indicates the essentially octahedral structures of both hydrated and anhydrous complexes. In the case of the copper complex, it seems that there is no remarkable structural change in the course of dehydration. The

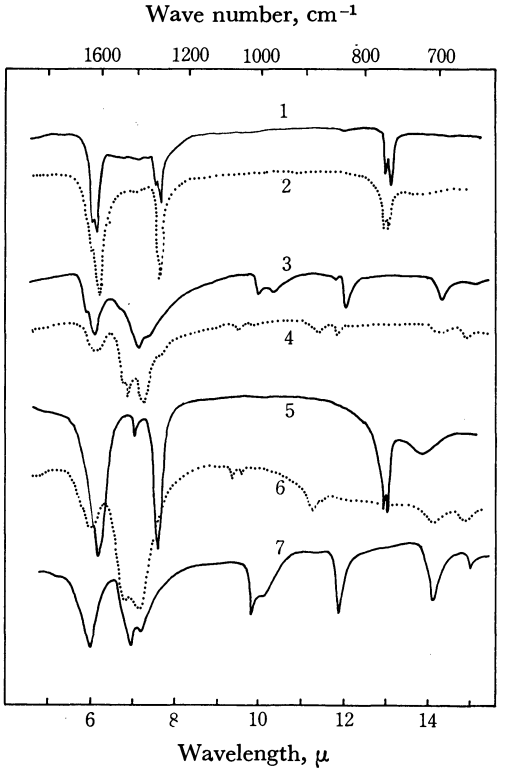

Fig. 8. Infrared absorption spectra of (1) products of the cobalt complex at the stage II, (2) products of the copper complex at the stage II, (3) products of the cobalt complex at the stage III, (4) products of the copper complex at the stage III, (5) $K_2C_2O_4$, (6) K_2CO_3, and (7) $KHCO_3$.

copper(II) ion seems to be surrounded square-planarly with four oxygen atoms of two bidentate oxalate groups, since a copper(II) ion usually tends to form such square planar (or tetragonal distorted) complexes. Thus, the infrared spectrum of the copper(II) complex in the region 600—400 cm^{-1} differs a great deal from that of the anhydrous Ni(II) complex.

The solid products formed at stages II and III were confirmed by means of infrared absorption spectra. The infrared spectra of Co(II) and Cu(II) complexes at each stage are given in Fig. 8, together with those of pure $K_2C_2O_4$, K_2CO_3, and $KHCO_3$. The spectra of the decomposition products at stage II (curves 1 and 2, Fig. 8) were similar to the spectrum of pure $K_2C_2O_4$ (curve 5). The spectra at stage III (curves 3 and 4) showed the presence of $KHCO_3$ in addition to K_2CO_3. Formation of $KHCO_3$ might be due to the reaction between K_2CO_3 formed and H_2O in air, since the spectra were recorded after cooling the heated samples to room temperature in air. The infrared absorption data thus support the results obtained from TG and EGA.

In conclusion, all the spectral data indicate the following structures.

Mn(II) Complexes. The hydrated complex is formulated as $K_2[Mn(H_2O)_2(C_2O_4)_2]$, while the anhydrous one has a polymeric structure with both quadridentate and bidentate oxalate ligands.

Co(II) Complexes. The infrared spectra show a

similar situation to that for the Mn(II) complexes, although the water molecules in the hydrated complex are held only loosely (Fig. 2). Both the complexes containing Co(II) in approximately octahedral environments.

Cu(II) Complexes. Both the hydrated and anhydrous complexes seem to be monomeric. Dehydration causes no remarkable change in the states of the central Cu(II), probably because of the tetragonal distortion of the complexes.

Zn(II) Complexes. Both the hydrated and anhydrous complexes have polymeric structures like $K_2Mn(C_2O_4)_2$; the water molecules are held extremely loosely, so that the dehydration occurs most easily.

Ni(II) Complexes. A similar situation to that for the Cu(II) complexes is seen, but here both complexes have essentially octahedral structures. A certain interaction between the $[Ni(C_2O_4)_2]^{2-}$ units in the anhydride should be postulated.

The authors wish to thank Prof. Kozo Sone for valuable discussions and Mr. Mitsuo Sato for the measurement of infrared absorption spectra. Expenses for the research were defrayed by a grant from the Ministry of Education.

References

1) K. Nagase, This Bulletin, **41**, 2166 (1972).
2) K. Nagase, *ibid.*, **46**, 144 (1973).
3) J. P. Largier, H. Pezernat, and J. Dubernat, *Rev. Chim. Miner.*, **6**, 1081 (1969).
4) K. Nagase, K. Sato, and N. Tanaka, to be published in this Bulletin.
5) K. Nakamoto, "Infrared Spectra of Inorganic and Coordination Compounds," John Wiley and Sons, Inc., New York (1963), pp. 211.
6) G. M. Bancroft, K. G. Dharmavardena, and A. G. Maddoch, *Inorg. Nucl. Chem. Lett.*, **6**, 403 (1970).

Metal Complexes of EDTA and Its Related Compounds. I. Geometric Isomers of [Co(X)(*N*-methyl-trimethylenediamine-*N*, *N'*, *N'*-triacetate)] Complexes with X=H_2O, NH_3, Cl^- or CN^-

Myung-Ki Doh,* Junnosuke Fujita,** Hiroshi Ogino, and Kazuo Saito
Department of Chemistry, Faculty of Science, Tohoku University, Aoba, Aramaki, Sendai 980
(Received August 23, 1974)

Two isomers of the complexes of the type, [Co(X)(*N*-Me-trdtra)] (*N*-Me-trdtra=*N*-methyl-trimethylenediamine-*N*,*N'*,*N'*-triacetate) have been isolated for each X=H_2O, NH_3, and Cl^-. The structures have been assigned from their PMR and absorption spectra and from the results of kinetic studies. The isomers have equatorial-skew and polar-chair structures and no indication of the formation of polar-skew isomer was observed. Isomerization reaction of the aqua complex in an aqueous solution indicated that the polar-chair isomer is more stable than the equatorial-skew isomer. Only the polar-chair isomer of H[Co(CN)(*N*-Me-trdtra)] has been obtained.

When a quinquedentate ligand such as ethylenediaminetriacetate (edtra^{3-}) forms a cobalt(III) complex together with a unidentate ligand, there are two possible geometric isomers as shown in Fig. 1. A similar

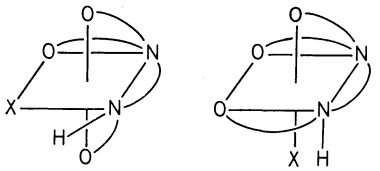

equatorial isomer polar isomer

Fig. 1. Two geometric isomers of [Co(X)(edtra)].

situation arises in ethylenediaminetetraacetate (edta^{4-}) complexes when one acetate group remains uncoordinated. Recent PMR studies,[1] however, have disclosed that all these complexes exist only in the equatorial form. Most recently Bell and Blackmer[2] confirmed this form for K[Co(NO_2)(edtra)]·1.5H_2O by the X-ray analysis. The acetate arm in the plane involving the two amino nitrogen atoms seems to be more strained as compared with that axial to the plane; the Co–O bond length in the plane is 1.919 Å, while that out of the plane, 1.883 Å. A similar difference in the Co–O bond lengths was found in [Co(edta)]$^-$.[3] The differences in the Co–O bond lengths in these complexes may be closely related to the conformation of the ethylenediamine moiety and the valence bond angles of the amino nitrogen atoms. It is, therefore, interesting to examine the geometrical isomerism in cobalt(III) complexes of trimethylenediaminetriacetate, since the trimethylenediamine moiety forms a six-membered chelate ring with conformations different from those of the ethylenediamine moiety of edtra^{3-} ligand.

As a first step of studying such an isomerism, we have attempted to prepare cobalt(III) complexes of *N*-methyl-trimethylenediamine-*N*,*N'*,*N'*-triacetate, [Co(X)(*N*-Me-trdtra)] (X=unidentate ligand). The complexes of this type have three possible geometric isomers as shown in Fig. 2. They are designated as equatorial-skew, polar-skew or polar-chair, depending on the position of the unidentate ligand and on the conformation

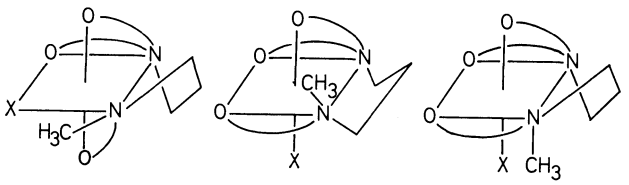

equatorial-skew polar-chair polar-skew

Fig. 2. Three geometric isomers of [Co(X)(*N*-Me-trdtra)].

of the six-membered trimethylenediamine chelate. Other forms involving equatorial-chair or boat conformations of the diamine may not be yielded owing to steric conditions.[4] In the present study, we have obtained two geometric isomers for each [Co(X)(*N*-Me-trdtra)] (X=H_2O, NH_3, and Cl^-) and one isomer of [Co(CN)(*N*-Me-trdtra)]$^-$. This paper deals with the preparation and isolation of these complexes and their geometric structures as determined by PMR and ultraviolet absorption spectroscopy. A kinetic study of the isomerization reaction of [Co(H_2O)(*N*-Me-trdtra)] has also been carried out to give support to the assignment of structures.

Experimental

Preparation of sodium N-*methyl-trimethylenediamine*-N,N',N'-*triacetate* (*Na_3N-Me-trdtra*). Na_3*N*-Me-trdtra was prepared by a method similar to that for *N*-methyl-ethylenediamine-*N*,*N'*,*N'*-triacetate by Van Saun and Douglas.[5] To a cold solution of monochloroacetic acid (37.8 g) in water (100 ml) was added dropwise a cold solution of sodium hydroxide (28 g) in water (70 ml) with steady stirring to keep temperature of the reacting solution below 15 °C. *N*-Methyl-trimethylenediamine (8.8 g) (Tokyo Kasei Co.) was then added. The solution was heated at 80 °C for 40 min, concentrated under reduced pressure at 70 °C and filtered to remove sodium chloride. The filtrate was used directly for the preparation of each cobalt(III) complex without isolating the free ligand. This procedure was justified by analyses of the complexes obtained.

Preparation of Complexes. [*Co(H_2O)(*N*-Me-trdtra)*]·H_2O. An aqueous solution (50 ml) of Co(NO_3)$_2$·6H_2O (29.1 g) was added to the previously prepared *N*-Me-trdtra solution which had been diluted to 500 ml and acidified to pH 6 with conc. hydrochloric acid. Activated charcoal (5 g) and 30% hydrogen peroxide (6 ml) were added and a stream of air was

* On leave from Yeung Nam University, Korea.

** Present address: Department of Chemistry, Faculty of Science, Nagoya University, Nagoya.

bubbled through the mixture for 3 days to complete the oxidation of the cobalt(II). After removal of the charcoal, the solution was diluted to about 20 l and the pH adjusted to about 5 with conc. hydrochloric acid. The solution was passed through a column of Dowex 50 WX8 cation exchange resin in H^+ form (700 ml) and then through a column of Dowex 1X8 anion exchange resin in Cl^- form (700 ml) to remove electrolytes and to obtain hydrochloric acid solution of the chargeless complex [Co(H_2O)(*N*-Me-trdtra)]. The blue violet solution was evaporated to almost dryness under reduced pressure at 50 °C. The residue was again dissolved in 100 ml of water and treated with silver oxide to remove chloride ions. The product was filtered, evaporated to a small volume, and poured carefully on a column ($\phi 3 \times 60$ cm) of Dowex 50 WX8 cation exchange resin in H^+ form. Elution with water gave two separate bands, blue and violet, the former being eluted faster. Blue and violet crystals were obtained by evaporating each eluate to dryness under reduced pressure below 40 °C. The blue complex was highly soluble, but the violet one moderately soluble in water. The latter gave higher yield than the former.

Found: Blue complex, C, 33.43; H, 5.38; N, 7.67%. Violet complex, C, 33.51; H, 5.34; N, 7.95%. Calcd for [Co(H_2O)(*N*-Me-trdtra)]·H_2O, ($C_{10}H_{19}N_2O_8Co$): C, 33.91; H, 5.41; N, 7.91%.

[Co(NH$_3$)(N-Me-trdtra)]·2H$_2$O. Violet and red isomers of the complex were obtained by the same method as that for the aqua complexes except that 28% aqueous ammonia (100 ml) was added to the solution containing cobalt(II) ions and the ligand. On the separation of two isomers by column chromatography (column, $\phi 3 \times 60$ cm), the violet isomer was eluted faster and followed by the red isomer. The former was much more soluble in water than the latter.

Found: Violet complex, C, 32.35; H, 5.71; N, 10.95%. Red complex, C, 32.81; H, 5.80; N, 11.40%. Calcd for [Co(NH_3)(*N*-Me-trdtra)]·2H_2O, ($C_{10}H_{22}N_3O_8Co$): C, 32.35; H, 5.97; N, 11.32%.

H[Co(Cl)(N-Me-trdtra)]·nH$_2$O. Greenish blue and bluish green isomers of the complex were prepared from the blue and the violet aqua complex, respectively, by treating with hydrochloric acid. A solution of each aqua complex in a small amount of conc. hydrochloric acid was warmed at 50 °C for 1 hr, and then evaporated to dryness under reduced pressure. The residue was dissolved in a small amount of water and poured on a column of Dowex 1X8 anion exchange resin in Cl^- form. The column was washed with water, and eluted with 0.5 M hydrochloric acid. The eluate was evaporated to a small volume under reduced pressure and stored in a vacuum desiccator over phosphorus pentoxide and sodium hydroxide. Both chloro complexes were very soluble in water.

Found: Greenish blue complex, C, 29.79; H, 5.65; N, 6.32%. Calcd for H[Co(Cl)(*N*-Me-trdtra)]·3H_2O, ($C_{10}H_{22}N_2O_9ClCo$): C, 29.39; H, 5.43; N, 6.86%.

Found: Bluish green complex, C, 30.60; H, 4.72; N, 6.77%. Calcd for H[Co(Cl)(*N*-Me-trdtra)]·2H_2O, ($C_{10}H_{20}N_2O_8ClCo$): C, 30.74; H, 5.16; N, 7.17%.

H[Co(CN)(N-Me-trdtra)]·2H$_2$O. A dimethylsulfoxide (DMSO) (30 ml) solution containing the violet aqua complex (1×10^{-3} mol) and potassium cyanide (1.5×10^{-3} mol) was warmed at 70 °C for 3 hr. The solution was passed through a column of Dowex 1X8 anion exchange resin in Cl^- form. The column was washed with water and the adsorbed red band was eluted with 0.3 M hydrochloric acid. Red crystals were obtained by evaporating the eluate under reduced pressure. The same cyano complex was obtained by the reaction of the blue aqua complex with potassium cyanide.

Found: C, 34.59; H, 5.17; N, 10.58%. Calcd for H[Co(CN)(*N*-Me-trdtra)]·2H_2O, ($C_{11}H_{20}N_3O_8Co$): C, 34.65; H, 5.29; N, 11.02%.

Measurements. Visible and ultraviolet absorption spectra were recorded with a Hitachi 323 recording spectrophotometer. PMR spectra were recorded with Varian A-60 and Varian HA-100 spectrometers in a deuterium oxide solution containing sodium 3-(trimethylsilyl)-1-propanesulfonate (TMS*) as the internal standard. All the measurements were made at room temperature.

Results and Discussion

Blue and violet complexes which gave correct analytical values as [Co(H_2O)(*N*-Me-trdtra)]·H_2O were obtained as shown in the Experimental part. Since each complex was confirmed to consist of a single species as described later, these complexes will be two of the three possible geometric isomers shown in Fig. 2. As Fig. 3 and Table 1 show, their absorption spectra differ notably from each other in the first absorption band region. However, no structural assignment can be made from the spectra at present, because both complexes belong to the same *cis*-[CoN_2O_4] type. On the other hand, the spectrum of the violet isomer in an aqueous solution was found to change on heating. Figure 4 shows an example of such spectral changes. Two isosbestic points are observed at 520 and 468 nm. Spectrum E in the figure agrees satisfactorily with that of the blue isomer. The spectrum of the blue isomer in water remained unchanged over a prolonged heating of the aqueous solution. These results indicate that the violet isomer isomerizes to the blue isomer and that the reverse reaction can be neglected. The isomerization between the equatorial-skew and the polar-chair isomer will occur by interchanging the coordination sites of one acetate arm and the aqua ligand. On

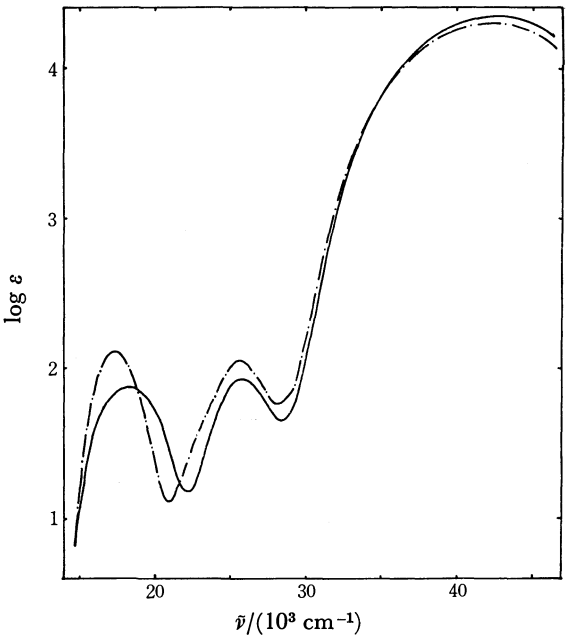

Fig. 3. Absorption spectra of violet (equatorial-skew) (——) and blue (polar-chair) (——) isomers of [Co(H_2O)(*N*-Me-trdtra)] in water.

Table 1. Absorption data of [Co(X)(*N*-Me-trdtra)] complexes $\bar{\nu}/10^3$ cm^{-1} (log ε)

equatorial-skew isomer			
[Co(H_2O)(*N*-Me-trdtra)]·H_2O(violet)	18.27(1.85)	25.81(1.90)	42.56(4.34)
[Co(NH_3)(*N*-Me-trdtra)]·2H_2O(violet)	18.27(1.98)	26.30(2.12)	42.74(4.30)
H[Co(Cl)(*N*-Me-trdtra)]·2H_2O (bluish green)	18.27(1.71)	24.51(1.90)	40.83(4.27)
	16.29sh(1.85)		
polar-chair isomer			
[Co(H_2O)(*N*-Me-trdtra)]·H_2O(blue)	17.39(2.11)	25.64(2.04)	42.40(4.28)
[Co(NH_3)(*N*-Me-trdtra)]·2H_2O(red)	18.80(2.02)	26.46(1.97)	43.10(4.37)
H[Co(Cl)(*N*-Me-trdtra)]·3H_2O(greenish blue)	16.78(2.04)	24.88(2.01)	41.67(4.25)
H[Co(CN)(*N*-Me-trdtra)]·2H_2O(red)	20.16(2.07)	27.33(1.90)	42.56(4.29)

sh: shoulder

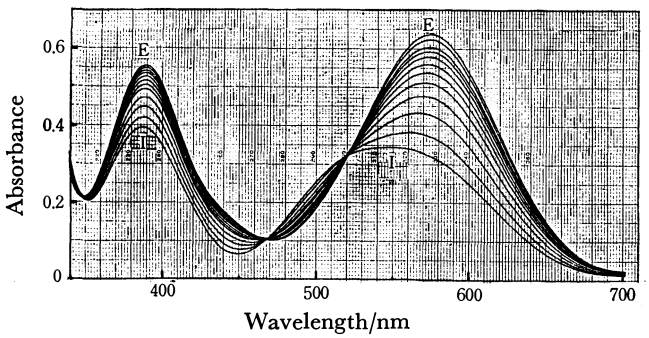

Fig. 4. Spectral change of violet-[Co(H_2O)(*N*-Me-trdtra)] in aqueous solution at 70 °C, pH=1.22 ($HClO_4$) and I=0.10 ($NaClO_4$–$HClO_4$). (I); t=0, (E); $t=\infty$.

the other hand, the isomerization reactions between the equatorial-skew and the polar-skew, and between the polar-chair and the polar-skew isomer will require less feasible change; *i.e.* interchange between the coordination sites of two acetate arms, or the inversion of configuration of the methyl and the acetate groups at the nitrogen atom. The first isomerization would take place more easily than do those of the latter two. Thus, the spectral changes described above may correspond to the isomerization reaction of the equatorial-skew into the polar-chair isomer or *vice versa* and the two isolated isomers can be concluded to have the equatorial-skew and the polar-chair structure.

Kinetic investigation for the isomerization reaction was carried out at an ionic strength (I) of 0.10 ($NaClO_4$–$HClO_4$). The reaction rate was independent of the hydrogen ion concentration over the range from 7×10^{-3} to 0.1 M. The acid independent rate constant was 2.08×10^{-4} s^{-1} at 70 °C, and $\Delta H^{\ddagger}$ and $\Delta S^{\ddagger}$ were 35.0 kcal/mol and +26.5 e.u., respectively.

In order to determine which isomer corresponds to the equatorial-skew or the polar-chair, we have utilized PMR spectroscopy in D_2O. The 100 MHz PMR spectrum of the blue isomer exhibits three AB patterns due to the acetate protons with coupling constants, 16.0, 16.2, and 19.0 Hz (Fig. 5 and Table 2). The grouping of these AB patterns was confirmed by comparison with the spectrum in 60 MHz. In [Co(edta)]$^-$ and its related complexes, it is known that the magnitude of the geminal coupling constant for the in-plane acetate protons is about 16 Hz, while that for the out-of-plane acetate protons about 18 Hz.[1] Therefore, the blue isomer should have two in-plane and one out-of-plane acetate arms and can be assigned to the polar-chair structure. The violet isomer, on the other hand, shows PMR signals corresponding to two out-of-plane acetate arms (J=17.5 and 18.5 Hz) and one in-plane acetate arm (J=16.5 Hz) as shown in Fig. 5 and Table 2, and thus, the violet isomer is assigned to the equatorial-skew structure in agreement with the previous discussion.

Two isomers, violet and red [Co(NH_3)(*N*-Me-trdtra)]·2H_2O were obtained similarly in the present study. Although neither of them isomerized without decomposition under a condition similar to that for the aqua complex, they could be assigned to the equatorial-skew and the polar-chair isomers as in the case of the aqua complexes. Figure 6 shows the absorption

Table 2. Chemical shifts (ν_A, ν_B in ppm) and coupling constants (J_{AB} in Hz) for acetate protons of [Co(X)(*N*-Me-trdtra)] in D_2O (100 MHz)

	out-of-plane			in-plane		
	J_{AB}	ν_A	ν_B	J_{AB}	ν_A	ν_B
equatorial-skew isomer						
[Co(H_2O)(*N*-Me-trdtra)]·H_2O(violet)	18.5	4.26	3.59	16.5	4.27	3.26
	17.5	4.07	3.71			
[Co(NH_3)(*N*-Me-trdtra)]·2H_2O(violet)	17.5	3.68	3.35	16.0	3.99	3.67
	19.0	4.00	3.72			
polar-chair isomer						
[Co(H_2O)(*N*-Me-trdtra)]·H_2O(blue)	19.0	3.67		16.0	3.87	3.09
				16.2	3.87	3.37
H[Co(CN)(*N*-Me-trdtra)]·2H_2O(red)	18.5	4.12	3.35	16.0	3.77	3.49
				16.5	3.88	3.16

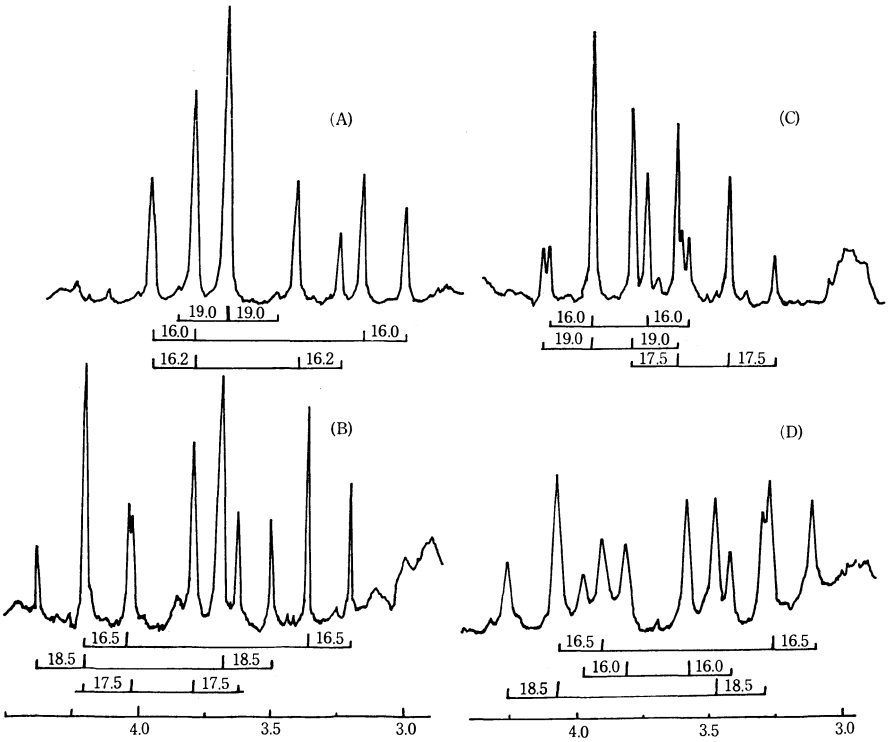

Fig. 5. PMR spectra (100 MHz) of blue (polar-chair) [Co(H_2O)(*N*-Me-trdtra)] (A), violet (equatorial-skew) [Co(H_2O)(*N*-Me-trdtra)] (B), violet (equatorial-skew) [Co(NH_3)(*N*-Me-trdtra)] (C), and [Co(CN)(*N*-Me-trdtra)] (D) in D_2O. Numerical values given in the figure indicate coupling constants in Hz for acetate protons.

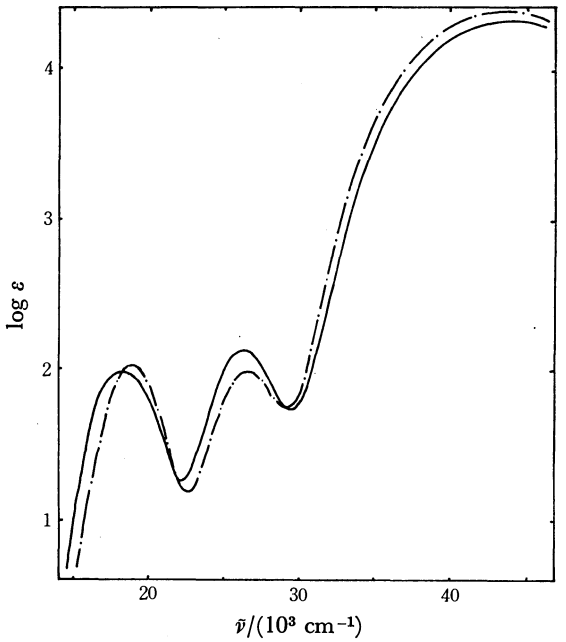

Fig. 6. Absorption spectra of violet (equatorial-skew) (——) and red (polar-chair) (– – –) isomers of [Co(NH_3)(*N*-Me-trdtra)] in water.

spectra of these ammine complexes. The first absorption band of the red isomer is narrower than that of the violet isomer. The polar-chair and the equatorial-skew [Co(NH_3)(*N*-Me-trdtra)] belong to *fac*- and *mer*-[CoN_3O_3] type, respectively, with respect to the configuration of the nitrogen and the oxygen atoms around the metal ion. A *fac*-[CoN_3O_3] complex exhibits a narrow and symmetrical first absorption band as compared with a *mer*-[CoN_3O_3] complexes.[6] Therefore, the red and the violet isomer may be assigned to *fac*-(polar-chair) and *mer*-(equatorial-skew) structure, respectively. This assignment will be supported by the PMR spectra. The PMR spectrum of the highly soluble violet isomer shows three AB patterns with coupling constants, 16.0, 17.5, and 19.0 Hz (Fig. 5 and Table 2). The AB pattern with 16.0 Hz is attributed to the in-plane acetate protons and those with 17.5 and 19.0 Hz to the out-of-plane acetate protons. Thus, the violet isomer is assigned safely to the equatorial-skew structure in agreement with the conclusion obtained from the absorption spectra. The red isomer was not soluble enough in D_2O to obtain PMR spectrum.

Greenish blue and bluish green isomers of H[Co(Cl)-(*N*-Me-trdtra)] have been obtained from the blue and the violet aqua complex, respectively, by warming with hydrochloric acid. The reactions should proceed without isomerization under the given condition, since each chloro complex liberates the chloride ion gradually in a neutral aqueous solution to give the corresponding original aqua complex. Therefore, the greenish blue and bluish green isomer are assigned to the polar-chair and the equatorial-skew structure, respectively. This assignment will be supported by the fact that the shape of the first absorption band of the greenish blue isomer is very similar to that of [Co(Cl)(*R*,*S*-2,4-

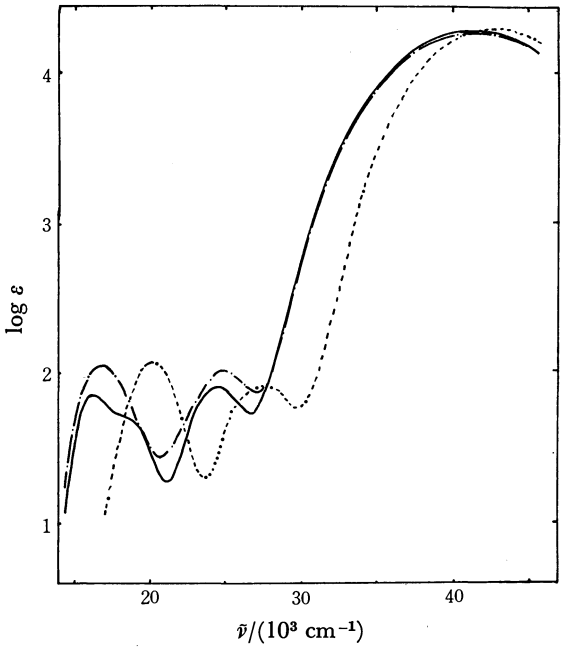

Fig. 7. Absorption spectra of bluish green (equatorial-skew) (——) and greenish blue (polar-chair) (– – –) isomers of [Co(Cl)(*N*-Me-trdtra)]⁻ in 0.1 M HCl and [Co(CN)(*N*-Me-trdtra)]⁻ (– · –) in water.

ptnta)]⁻ (*R,S*-2,4-ptnta=*R,S*-2,4-pentanediaminetetraacetate ion) which takes the polar-chair structure stereospecifically.[4] These polar-chair complexes do not show any splitting in the first absorption band in contrast to the distinct splitting observed for the bluish green, equatorial-skew isomer (Fig. 7). There seems to be a relation between the absorption spectra and the structure of the *N*-Me-trdtra complexes as discussed later.

Only one red complex, H[Co(CN)(*N*-Me-trdtra)]·$2H_2O$ was obtained by the reaction of the violet and the blue aqua complex with potassium cyanide in DMSO. Its PMR spectrum shows three AB patterns due to the acetate protons. The coupling constants are 16.0, 16.5, and 18.5 Hz, and the complex may be assigned to the polar-chair structure (Fig. 5 and Table 2). The complex shows a sharp and symmetrical first absorption band, being identified as the polar-chair structure (Fig. 7). The polar-skew isomer is not likely to be yielded by analogy with other *N*-Me-trdtra complexes.

For each aqua, ammine and chloro complex, no indication for the presence of more than two isomers was found in the present syntheses. The reason why the polar-skew isomers are not produced is not clear at present. The methyl group in the polar-skew structure takes an axial orientation to the chelate ring formed by the diamine moiety in a skew conformation, while that in the equatorial-skew structure an equatorial orientation to the same ring. However, such a difference will not be important in the present complexes, becasue the polar-chair isomer has an axially oriented methyl group to the diamine chelate ring. Further, the equatorial-skew isomer of [Co(H_2O)(*N*-Me-trdtra)] (violet) isomerizes in water into the polar-chair isomer (blue) by heating, and the reverse reaction does not take place under the same condition. This indicates that the polar-chair isomer is more stable thermodynamically than the equatorial-skew isomer. As stated in the Experimental part, the fact that the latter is produced much more than the former, may owe to a kinetically prefered route to form the equatorial-skew isomer favorably. The absence of the polar-skew isomer may also be related to such a prefered route in the complex formation. On the other hand, it should be noted that in the skew isomers the in-plane acetate arm seems to be still more strained than the out-of-plane acetate arm as seen in the [Co(edta)]⁻ and [Co(X)(edtra)] (*vide ante*). It was deduced that the six-membered diamine chelate ring in K[Co(trdta)]·$2H_2O$ (trdta=trimethylenediamine-tetraacetate ion) takes a skew conformation.[7] According to the X-ray analysis, the Co–O distances in the plane and axial to the plane are 1.904 and 1.861 Å, respectively.[8] The difference in these two bond distances is smaller than that reported for [Co(edta)]⁻ (1.912 and 1.833 Å), but it may still be big enough to prevent the formation of the polar-skew isomer.

The absorption spectra of all the complexes we prepared are shown in Figs. 3, 6, and 7. The maximum frequencies of the first and the second absorption bands depend on the kind of the unidentate ligand, and shift in accordance with the spectrochemical series.[9] On the other hand, the first absorption bands of the equatorial-skew isomers are broader than those of the polar-chair isomers. The equatorial-skew isomer of the chloro complex shows the first absorption band split apparently into two components. The origin of the difference in the band shape between the two geometric isomers is not clear at present. Yamatera's theory[6] on the band splitting for a cobalt(III) complex will not be applicable to the present complexes. The first absorption bands of both isomers of the aqua complex differ considerably from each other, although the isomers belong to the same *cis*-[CoN_2O_4] configuration, as stated previously.

One of the authors (M.-K.D.) is grateful to the Ministry of Education for the Japanese Goverment Scholarship.

References

1) G. L. Blackmer and J. L. Sudmeier, *Inorg. Chem.*, **10**, 2019 (1971).
2) J. D. Bell and G. L. Blackmer, *ibid.*, **12**, 836 (1973).
3) H. A. Weakliem and J. L. Hoard, *J. Amer. Chem. Soc.*, **81**, 549 (1959).
4) F. Mizukami, H. Ito, J. Fujita, and K. Saito, This Bulletin, **44**, 3051 (1971).
5) C. W. Van Saun and B. E. Douglas, *Inorg. Chem.*, **7**, 1393 (1968).
6) H. Yamatera, This Bulletin, **31**, 95 (1958).
7) H. Ogino, M. Takahashi, and N. Tanaka, *ibid.*, **43**, 424 (1970).
8) R. Nagao, F. Marumo, and Y. Saito, *Acta Crystallogr.*, **B28**, 1852 (1972).
9) Y. Shimura and R. Tsuchida, This Bulletin, **29**, 311 (1956).

Isomerism of the Metal Complexes Containing Multidentate Ligands. V.[1] Preparation and Properties of Optically Active Tris-(diaminosuccinato)cobaltates(III)

Masaaki KOJIMA, Yuzo YOSHIKAWA, and Kazuo YAMASAKI

Department of Chemistry, Faculty of Science, Nagoya University, Chikusa-ku, Nagoya, 464

(Received August 28, 1974)

Tris(diaminosuccinato)cobaltates(III) with *meso*, *racemic*, and *laevorotatory* ligands were prepared and resolved by column chromatography on DEAE-cellulose and by the use of cinchonidine. The resolved complexes and their absolute configurations, assigned on the basis of the electronic and circular dichroism spectra, and on the basis of the elution order in cellulose column chromatography, are Δ-$(-)_{589}$-$[Co(mdas)_3]^{3-}$, Λ-$(+)_{589}$-$[Co(mdas)_3]^{3-}$, $\Lambda(lel)$-$[Co(ldas)_3]^{3-}$, and $\Lambda(ob)$-$[Co(ldas)_3]^{3-}$.

2,3-Diaminosuccinic acid is able to coordinate to metals with either amino groups or carboxyl groups. The copper and nickel complexes were studied in a previous report.[2] In the present paper, the preparations and properties of tris(diaminosuccinato)cobaltates(III) coordinating with amino groups will be described. The abbreviations $mdasH_2$, $rdasH_2$, and $ldasH_2$ are used for *meso*, *racemic*, and *laevorotatory* (589 nm) 2,3-diaminosuccinic acids respectively. Figure 1 shows three possible isomers of the ligand.

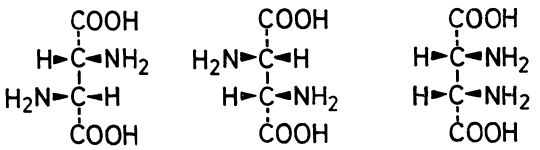

ldas H_2 (2*R*, 3*R*) ddasH_2 (2*S*, 3*S*) mdasH_2 (2*R*, 3*S*)

Fig. 1. Three possible isomers of 2,3-diaminosuccinic acid.

Experimental

Ligands. 2,3-Diaminosuccinic acid was prepared by the method of Toi *et al.*[3], while the *meso* and *racemic* forms were separated by the procedure of Farchy and Tafel.[4] To resolve racemic diaminosuccinic acid, the less soluble diastereoisomer of the benzoylated ligand[5] with cinchonidine was recrystallized several times from a 2:1 mixture of water and ethanol. Then cinchonidine was precipitated by adding aqueous ammonia. The filtrate was acidified to obtain $(-)_{589}$-*N*,*N*′-dibenzoyldiaminosuccinic acid, which was then hydrolyzed with 6 M HCl to give $ldasH_2$.[6]

Preparation of the Complexes. The complexes with mdas, rdas, and ldas were prepared in a similar manner. To 2.4 g (9 mmol) of $[Co(NH_3)_6]Cl_3$ dissolved in 50 ml of water, a 4 g portion (27 mmol) of the ligand dissolved in 100 ml of the 0.5 M NaOH solution was added. After adding 0.5 g of active charcoal, the mixture was stirred for a few days at room temperature. The reaction mixture was then filtered, and the filtrate was subjected to column ($\phi 2.7 \times 120$ cm) chromatography on DEAE-Sephadex (A-25), with a 0.1 M sodium perchlorate as the eluent. A pink band was eluted first; it is a complex probably coordinating through both oxygen and nitrogen atoms of the ligand, but no further investigation of this complex was done. The main orange band, eluted slowly, was collected, and the effluent was evaporated to dryness *in vacuo*. After removing sodium perchlorate by extraction with methanol, the sodium salt was converted to the potassium salt by Dowex 50 W-X8 (K-form). The chemical compositions of the complexes thus prepared are given in Table 1.

Table 1. Chemical compositions of the isomers

Complex	Co (%)	N (%)	H_2O (%)
$K_3[Co(rdas)_3]\cdot 6H_2O$	8.06 (8.16)	11.31 (11.63)	14.57 (14.96)
$K_3[Co(mdas)_3]\cdot 6H_2O$	8.49 (8.16)	11.51 (11.63)	15.11 (14.96)
$(+)_{589}$-$Na_3[Co(ldas)_3]\cdot 6H_2O$	8.49 (8.74)	— —	16.03 (16.02)
$(-)_{589}$-$Na_3[Co(mdas)_3]\cdot 6H_2O$	8.75 (8.74)	12.59 (12.46)	15.88 (16.02)

Calculated values are given in parentheses.

Resolution of the mdas Complex with Cinchonidine. By the fractional crystallization of the diastereoisomers from water, the less soluble $(-)_{589}$-(cinchonidine)$_2$K$[Co(mdas)_3]\cdot 8\frac{1}{2}H_2O$ was obtained; it was then converted into the sodium salt by adsorption on DEAE-Sephadex and by subsequent elution with a 0.5 M sodium perchlorate solution (*cf.* Table 2). The resolved complex has the chemical composition of $(-)_{589}$-$Na_3[Co(mdas)_3]\cdot 6H_2O$ (Table 1).

Table 2. Absorption and circular dichroism spectra

Complex		Absorption $\tilde{\nu}_{max}$ (cm^{-1})	Absorption ε_{max}	CD $\tilde{\nu}_{max}$ (cm^{-1})	CD $\Delta\varepsilon_{max}$
$(+)_{589}$-$Na_3[Co(ldas)_3]\cdot 6H_2O$ Λ (lel) configuration	First Band	21100(473 nm)	110	20300(493 nm)	+3.21
	Second Band	29400(340 nm)	134	29000(345 nm)	−0.14
	CT Band	41700(240 nm)	10900	40000(250 nm)	−18
$(-)_{589}$-$Na_3[Co(mdas)_3]\cdot 6H_2O$ Δ configuration	First Band	21100(474 nm)	113	20300(493 nm)	−3.52
	Second Band	29400(340 nm)	139	29000(345 nm)	+0.15
	CT Band	41700(240 nm)	11000	40000(250 nm)	+12

CT: Charge transfer

Partial Resolution of the mdas Complex by Column Chromatography. The partial resolution of the mdas complex was accomplished by column chromatography on DEAE-cellulose, using a 0.1 M $NaClO_4$ solution as the eluent. The active complex resolved by the use of cinchonidine did not show any further increase in rotation when subjected to column chromatography on DEAE-cellulose, indicating a complete resolution.

The rdas complex too was resolved only partially by column chromatography.

Separation of the ldas Complex into Isomers. When the reaction mixture of $[Co(ldas)_3]^{3-}$ was eluted on a DEAE-cellulose column by the use of a 0.1 M $NaClO_4$ solution, it was separated into the fast-moving isomer I and the slow-moving isomer II. The chemical composition of the isomer II, which shows $(+)_{589}$, is given in Table 1. The isomer I, with a rotation of $(-)_{589}$, was obtained in only a minute amount, and so no chemical analysis has been done.

Measurements. All the measurements were carried out in the way described in previous papers.[1]

Results and Discussion

The mdas Complexes. The absorption (AB) and circular dichroism (CD) spectra of $(-)_{589}$-$Na_3[Co(mdas)_3]\cdot 6H_2O$ are shown in Fig. 2, while the data are listed in Table 2. This complex was tentatively assigned the Δ configuration, because it shows the following features required for that configuration: (a) The tris(diamine)cobalt(III) complex which has five-membered chelate rings and shows a major negative CD peak in the octahedral $^1T_{1g}\leftarrow{}^1A_{1g}$ absorption region and a positive peak in the charge-transfer region generally has the Δ configuration, and (b) The tris(diamine)cobalt(III) complex, which is eluted first by HCl in a P-cellulose column, generally has the Δ configuration.[7]

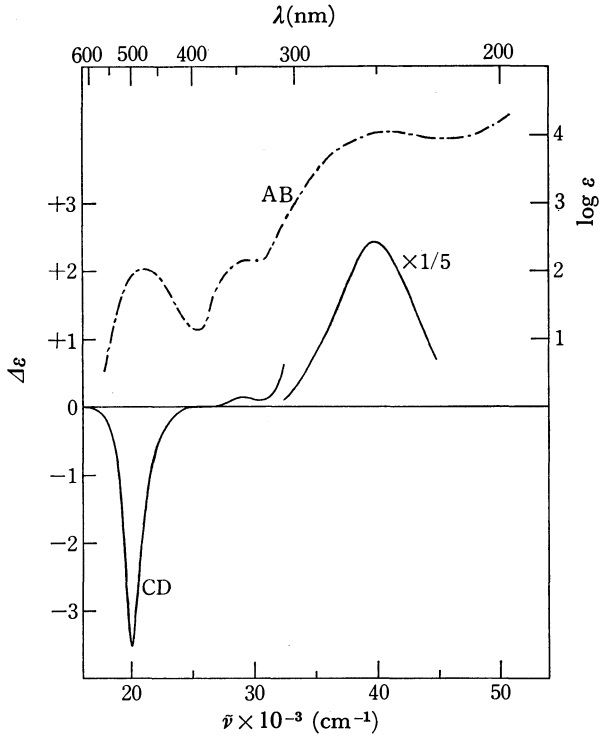

Fig. 2. AB and CD spectra of $(-)_{589}$-$Na_3[Co(mdas)_3]\cdot 6H_2O$.

For the mdas complex, two geometric isomers, *meridional* and *facial*, are possible from the alignment of the asymmetric carbons (*R* and *S*) for each of the absolute configurations, Δ and Λ. These isomers have not been detected by chromatography, although such isomers have been isolated for the tris(*meso*-2,3-butanediamine)cobalt(III) complex, which has a related structure.[8]

The ldas Complex. In Fig. 3 the AB and CD spectra of the isomer II, $(+)_{589}$-$Na_3[Co(ldas)_3]\cdot 6H_2O$, are shown, while the data are listed in Table 2. For the $\Lambda(lel)$-$[Co(d\text{-}pn)_3]^{3+}$ ion, a strong negative peak in the charge-transfer region has been found to be due to the contributions from both the configurational and vicinal effects with the same negative sign.[9] On the basis of this fact, and on the features mentioned above for the mdas complex, the absolute configuration $\Lambda(lel)$ was assigned to the isomer II.

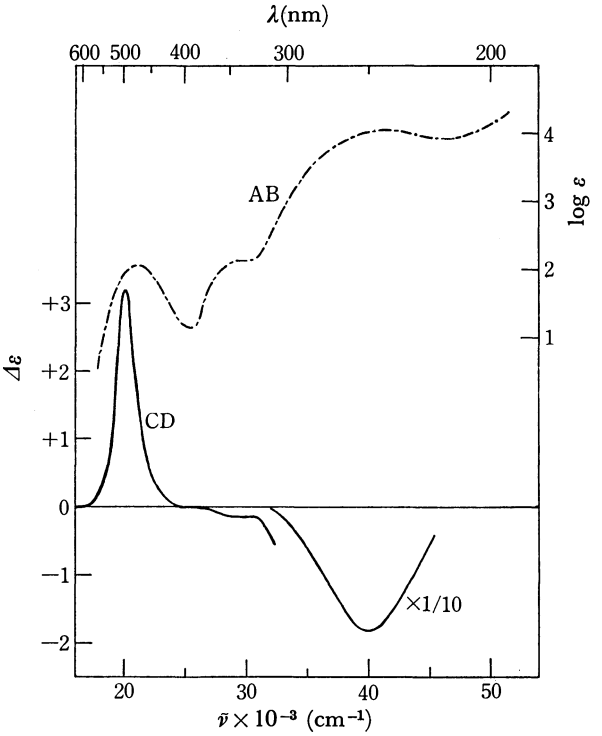

Fig. 3. AB and CD spectra of $(+)_{589}$-$Na_3[Co(ldas)_3]\cdot 6H_2O$.

As the $\Lambda(lel)$ isomer was formed stereoselectively in a predominant amount, the absolute configuration of the ligand, $ldasH_2$, has been determined to be 2*R*,3*R* (Fig. 1). In this $(+)_{589}$-$\Lambda(lel)$ complex, two carboxyl groups of the ligand assume equatorial positions with the $\delta(lel)$ conformation.

The CD spectrum of the isomer I, with the rotation of $(-)_{589}$, shows a negative peak at 480 nm in the d-d absorption region, and a negative and a positive peak in the charge-transfer region at 235 and 215 nm respectively. Taking into account the fact[9] that, in the charge-transfer region, the $\Delta(ob)$-$[Co(d\text{-}pn)_3]^{3+}$ ion has a small negative CD peak at 240 nm and a relatively large positive peak at 212 nm, the isomer I is assigned the $\Delta(ob)$ configuration. The $\Lambda(ob)$-$[Co(l\text{-}pn)_3]^{3+}$ ion

also shows almost the identical CD spectrum with the sign opposite to that of the $\Delta(ob)$-$[Co(d\text{-}pn)_3]^{3+}$ ion.[10]

The CD peak (480 nm) corresponding to the $^1E_a \leftarrow {}^1A_1(D_3)$ transition of the isomer I(*ob*) is at a shorter wavelength than that (493 nm) of the isomer II(*lel*); such a tendency has also been observed for the *lel* and *ob* isomers of the $[Co(d\text{-}pn)_3]^{3+}$ [9] and $[Co(l\text{-}pn)_3]^{3+}$.[10] The spectral data for the isomer I lack the intensity values because it is available in only a minute amount, and so no chemical analysis has been done.

Comparison between the mdas and ldas Complexes. For the tris(2,3-butanediamine)cobalt(III) ion, the $(+)_{589}$-bn complex has an absorption maximum (467 nm)[11] at a shorter wavelength than the *meso*-bn complex (473 nm).[8] This fact is consistent with the forced axial position of one of the two methyl groups for the latter complex, regardless of the chelate-ring conformation (δ or λ). For the das complex, however, the maximum of the octahedral $^1T_{1g} \leftarrow {}^1A_{1g}$ absorption of $\Lambda(lel)$-$[Co(ldas)_3]^{3-}$ is at almost the same wavelength as that of $[Co(mdas)_3]^{3-}$ (Table 2), although the latter has one axial carboxyl group. This spectral feature of the mdas complex is understandable on the basis of a hydrogen-bond formation between the oxygen atom of the axial carboxyl group and the hydrogen atom of the amino group on the adjacent chelate ring. In an acid solution, hydrogen bonds are usually weakened due to protonation. Actually, in 5 M HCl the first band maximum of the mdas complex* is shifted to a longer wavelength (483 nm) than that (479 nm) of the rdas complex.* A similar difference was observed in the solid state as well: 474 nm (mdas complex) and 470 nm (rdas complex).

For the complex, $[Co(ldas)_3]^{3-}$ two carboxyl groups are in the equatorial positions and it is difficult for strong intramolecular hydrogen bonds to be formed between the oxygen atom of the carboxyl group and the hydrogen atoms of the amino groups.

PMR Spectra. The PMR spectra for the mdas and rdas complexes* were measured in D_2O–D_2SO_4 at 60 MHz. The results, however, proved unfruitful, since no signal attributable to carboxyl groups was found down to 15 ppm, and furthermore other signals observed were too complicated and too broad to be analyzed.

* In acid solutions these complexes are converted into the cations, $[Co(mdasH_2)_3]^{3+}$ and $[Co(rdasH_2)_3]^{3+}$ respectively. For the electronic and PMR spectral measurements where it is permissible, the rdas complex was used instead of the ldas complex because it is readily available.

References

1) Parts III and IV were published in This Bulletin, **46**, 1687, 3448 (1973).
2) Y. Yoshikawa and K. Yamasaki, This Bulletin, **40**, 813 (1967).
3) K. Toi, K. Mori, and Y. Izumi, *ibid.*, **33**, 1529 (1960).
4) J. Farchy and J. Tafel, *Ber.*, **26**, 1980 (1893).
5) T. Tamura, *J. Biochem.*, **27**, 335 (1938).
6) R. Kuhn and F. Zumstein, *Ber.*, **59**, 479 (1926).
7) Y. Yoshikawa and K. Yamasaki, Proc. XII I.C.C.C., Sydney, 1969, p. 98.
8) M. Kojima, H. Funaki, Y. Yoshikawa, and K. Yamasaki, to be published.
9) K. Ogino, K. Murano, and J. Fujita, *Inorg. Nucl, Chem. Lett.*, **1968**, 351.
10) M. Kojima, Y. Yoshikawa, and K. Yamasaki, *ibid.*, **9**, 689 (1973).
11) F. Woldbye, "Studier over Optisk Aktivitet," Polyteknisk Forlag, København, 1969, p. 227; *Proc. Roy. Soc., Ser., A*, **297**, 79 (1967).

The Chelation of 3-(*p*-Hydroxybenzylidene)-2,4-pentanedione with the Thallous Ion

Toshio KAWATO, Hajime KANATOMI, Yoichi DEMURA, and Ichiro MURASE

Laboratory of Chemistry, College of General Education, Kyushu University, Ropponmatsu, Chuo-ku, Fukuoka 810

(Received September 4, 1974)

A thallous compound of 3-(*p*-hydroxybenzylidene)-2,4-pentanedione was synthesized and its structure was determined by means of the infrared and proton magnetic resonance spectra. This compound was regarded as a thallous phenolate derivative; however, the effect of chelation by the 2,4-pentanedionate moiety due to a long-range anionotropy was observed. The acetyl proton exchange of the Tl(I) compound in D_2O was observed by a PMR investigation. It was found that the methyl-proton exchange was inhibited by chelation.

Metal chelates of 2,4-pentanedione (acetylacetone), which behaves as an enol, have been well-studied. When two protons at the 3-position of acetylacetone are substituted, no stable metal chelates can be formed, since no such enolization can occur. Although 3-(*p*-hydroxybenzylidene)-2,4-pentanedione (POBAA) has no proton at the 3-position since it is occupied by a benzylidene linkage, it can be drawn as a pair of tautomers, in one of which the 2,4-pentanedione moiety enolizes by a long-range conjugation through the *p*-hydroxyphenyl group, as is shown in Scheme I. It can, therefore, be assumed that the tautomer forms metal chelates as ordinary acetylacetonates.

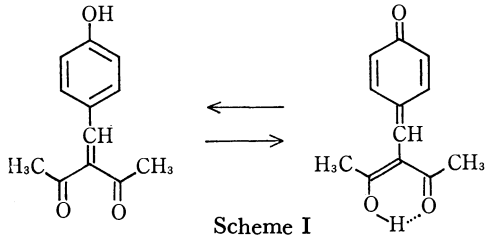

Scheme I

3-(*o*-Hydroxybenzylidene)-2,4-pentanedione was also considered to enolize in the same sense. It had been synthesized by the condensation of salicylaldehyde with acetylacetone.[1] It, however, turned out in our investigation that the product was not the diketo compound but a ketol, *i.e.*, 3-acetyl-2-hydroxy-2-methyl-2*H*-chromene. It is, therefore, omitted from the present investigation; the structure proof will be reported elsewhere.

Several attempts were made to isolate transition metal chelates of POBAA; however, they all resulted in failure. Only a thallous salt was isolated as crystals, and spectroscopic observations of it revealed that it was not a simple phenolate but was characteristic of a complex salt; the Tl(I) ion showed some interaction with the 2,4-pentanedione moiety, as had been expected. This paper will deal with the structure determination of the Tl(I) compound by means of electronic, infrared, and proton magnetic resonance spectroscopy. A thallous salt of 3-(*m*-hydroxybenzylidene)-2,4-pentanedione (MOBAA) was also investigated for the sake of comparison.

Experimental

All the melting points are uncorrected. The IR spectra were determined in potassium bromide disks with a Hitachi EPI-S2 spectrophotometer, while the electronic spectra were measured in ethanol with a Hitachi EPS-3T spectrophotometer. The PMR spectra were recorded at 60 MHz in $CDCl_3$, methanol, dimethylsulfoxide, and a D_2O solution with a Hitachi Model R-24 NMR spectrometer. The chemical shifts are quoted as τ values relative to tetramethylsilane in $CDCl_3$ or DSS (sodium 2,2-dimethyl-2-silapentane-5-sulfonate) in D_2O.

3-(p-Hydroxybenzylidene)-2,4-pentanedione (POBAA). A solution of 12.2 g (0.1 mol) of *p*-hydroxybenzaldehyde and 10.2 g (0.1 mol) of acetylacetone in 30 ml of ethanol was cooled to −15 °C; 30 drops of piperidine were then added to the solution at a temperature below −10 °C. After the solution had stood in a refrigerator for several days, the resulting yellow solid was collected and recrystallized from dilute ethanol to give 11.2 g (55.8%) of pale yellow needles; mp 125—127 °C.

Found: C, 70.86; H, 5.96%. Calcd for $C_{12}H_{12}O_3$: C, 70.58; H, 5.92%.

This compound is hydrolyzed to its original components by repeated recrystallizations from dilute ethanol.

3-(m-Hydroxybenzylidene)-2,4-pentanedione (MOBAA). *m*-Hydroxybenzaldehyde was used in place of *p*-hydroxybenzaldehyde; otherwise the procedure was the same as in POBAA synthesis. The product was recrystallized from ethanol to give 16.7 g (83.2% yield) of colorless crystals; mp 128—129 °C.

Found: C, 70.68; H, 6.07%. Calcd for $C_{12}H_{12}O_3$: C, 70.58; H, 5.92%.

Thallous Salt of POBAA and MOBAA. To a solution of POBAA or MOBAA in absolute ethanol we added an equimolar amount of freshly prepared thallous ethoxide[2] in absolute ethanol at room temperature. The resulting orange or yellow crystals were filtered and washed with absolute ethanol and dried over P_2O_5 at 50 °C in a vacuum.

POBAA-Tl (I), Found: C, 35.14; H, 2.77%. MOBAA-Tl (I), Found: C, 35.08; H, 2.75%. Calcd for $C_{12}H_{11}O_3Tl$: C, 35.34; H, 2.72%.

Results and Discussion

According to the molecular model of 3-benzylidene-2,4-pentanedione (BAA),[3] it seems to be impossible that all the double bonds including the two carbonyl groups are in one conjugated system, because the planarity of the molecule is impaired by the steric hindrance between the benzene ring and the *syn*-acetyl group. The methine proton exhibits a PMR peak in the low magnetic field at τ 2.51. This indicates that the proton and the benzene ring are coplanar.

There are two singlets, at τ 7.72 and τ 7.60, which are due to the two acetyl groups. The peak in the higher magnetic field can be assigned to the conjugation-free acetyl group which is at the *syn*-position to the phenyl group, and the lower one, to another acetyl group which is conjugated with the styryl moiety. In the region of carbonyl and olefinic stretching vibrations, BAA exhibits IR absorptions at 1711 (strong), 1662 (strong), 1620 (medium), and 1576 (weak) cm^{-1}. The absorption at 1711 cm^{-1} is assigned to the conjugation-free acetyl carbonyl, while the others are due to another acetyl carbonyl, an olefinic bond, a benzene ring, or their conjugated stretching vibrations.

In the cases of POBAA and MOBAA, the PMR spectra are shown in Fig. 1. The assignments of the peaks can be understood in the same way as those of BAA; the coplanar methine proton resonance appears at τ 2.60 in the former and at τ 2.50 in the latter. The singlets at τ 7.66 and τ 7.60 for POBAA and the singlets at τ 7.69 and τ 7.60 for MOBAA are assigned to the conjugation-free and the conjugated acetyl groups. The peak due to hydroxyl proton appears at τ 2.89 and at around τ 2.8 respectively. The infrared spectra of POBAA and MOBAA are shown in Fig.2, in which the stretching vibration of the conjugation-free acetyl carbonyl appears at 1705 cm^{-1} for the former and at 1702 cm^{-1} for the latter; in addition, the OH stretching vibrations are at 3350 cm^{-1} and at 3230 cm^{-1} respectively.

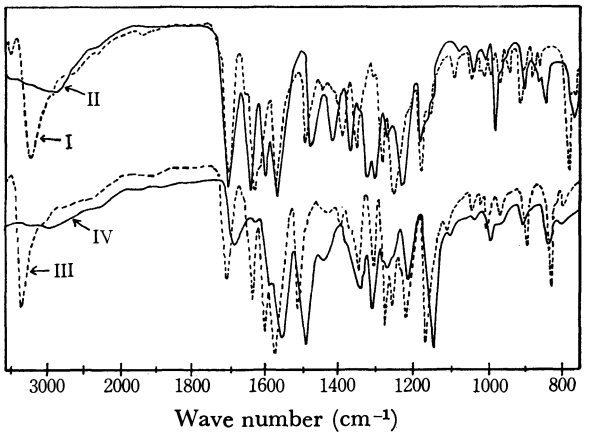

Fig. 1. IR spectra of I: MOBAA, II: MOBAA-Tl(I), III: POBAA, and IV: POBAA-Tl(I).

The ultraviolet absorption maxima of BAA, MOBAA, and POBAA in ethanol are: BAA: 208 nm (log ε: 3.99), 220 (3.92), 284 (4.24); MOBAA: 217 (4.11), 245 (3.98), 287 (4.21), around 330 (shoulder); POBAA: 218 (3.88), 235 (3.96), 327 (4.35). These strong absorptions due to π-π^* transitions indicate the presence of a long conjugated system. Judging from the highest degree of red shift in POBAA, the electronic contribution of the *p*-hydroxyl group is included in the conjugated system.

The Tl(I) salts of POBAA and MOBAA are soluble in polar solvents; however, their electronic absorption spectra in solution resemble those of the parent compounds. It is, therefore, assumed that POBAA-Tl(I) and MOBAA-Tl(I) both dissociate incompletely into the Tl(I) ion and the anion of POBAA or MOBAA in the solution. The PMR spectra of POBAA-Tl(I) and MOBAA-Tl(I) in D_2O are shown in Fig. 2. The PMR pattern of MOBAA-Tl(I) is nearly equal to that of MOBAA except for the absence of the peak due to a hydroxyl proton and the induced chemical shifts of the methine and phenyl peaks by the Tl(I) ion in MOBAA-Tl(I); it also exhibits the methine proton resonance at τ 2.31 and the two acetyl proton resonances at τ 7.67 and τ 7.56 respectively. It can be said that there is no fundamental difference in structure between MOBAA and MOBAA-Tl(I).

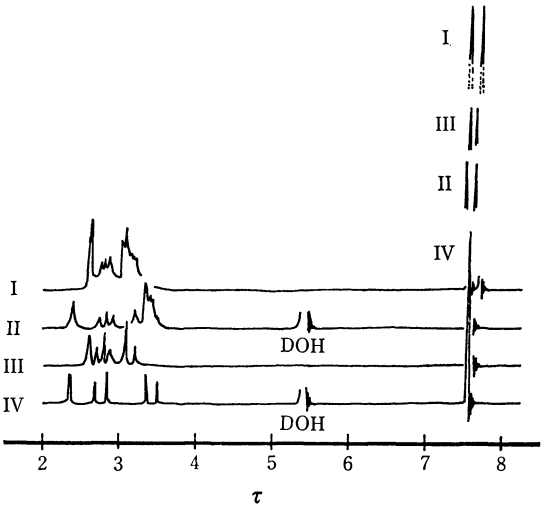

Fig. 2. PMR spectra of I: MOBAA and III: POBAA in $CDCl_3$, and II: MOBAA-Tl(I) and IV: POBAA-Tl(I) in D_2O.

Between the PMR spectrum of POBAA and that of POBAA-Tl(I), a marked difference was observed. Two peaks due to the two kinds of acetyl protons in POBAA became one sharp peak at τ 7.59 in the Tl(I) salt in D_2O, while the methine proton peak shifted to the lower magnetic field and appeared at τ 2.37. The formation of such a singlet at around τ 7.5 was observed in methanol and dimethylsulfoxide as well as in D_2O. This means that all the acetyl protons of POBAA-Tl(I) are equivalent. Judging from the low τ value of the methine peak, the methine proton and the benzene ring are maintained in a coplanar configuration. If the molecule is fixed as a phenolate structure, the steric situation of the two acetyl groups, one of which is in the same plane as the benzene ring, while the other is out of the plane, can not differ from that of POBAA. The equivalence of the acetyl protons can be understood provided the acetyl groups are rapidly interconverted by a flip rotation of the 2,4-pentanedione moiety, as is shown in Scheme II. This explanation leads to the conclusion that the benzylidene C=C bond must have a single-bond character; hence, a long-range anionotropy should exist in the anion of POBAA.

The IR spectra of POBAA-Tl(I) and MOBAA-Tl(I) were compared with those of POBAA and MOBAA (Fig. 1). The band due to a hydroxyl group is necessarily absent in the Tl(I) compounds. Most remarkable is the difference between the IR peaks of POBAA-Tl(I)

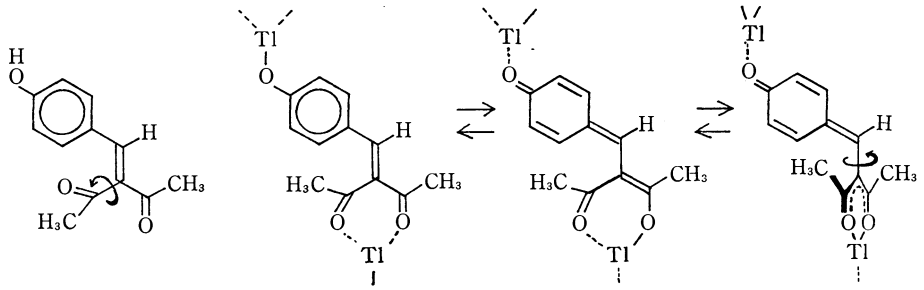

POBAA POBAA–Tl(I)

Scheme II

and those of POBAA in the double-bond stretching region. The peaks of POBAA–Tl(I) are found to be broad and to shift to lower wave numbers compared with those of POBAA. This difference in the absorption pattern clearly reveals a change in the bond character from POBAA to POBAA–Tl(I), in which the electron delocalization or coordination of the diketone moiety to the Tl(I) ion takes part. The structure of POBAA–Tl(I) seems to consist of the planes of the anions of POBAA chained together by the Tl(I) ions. On the contrary, these situations are not observed in MOBAA–Tl(I).

It can thus be concluded that MOBAA–Tl(I) is a simple phenolate, while in POBAA–Tl(I), as a result of a long-range anionotropy, the diketone moiety interacts in part with the Tl(I) ion, as in acetylacetonates.

We also attempted to prepare transition-metal chelates of POBAA. When POBAA was heated in ethanol with each acetate of copper(II), nickel(II), and cobalt(II), or each chloride of cobalt(II) and iron(III), no complexes were obtained, and the hydrolysis of the ligand took place slowly in every case. The metal-ion-exchange reaction with POBAA–Tl(I) was thus examined. A mixture of POBAA–Tl(I) and anhydrous cobalt(II) chloride or anhydrous ferric chloride in absolute ethanol gave white precipitates of thallous chloride; however, all attempts to isolate the desired complex from the resulting filtrate were unsuccessful.

During the course of the PMR investigation of

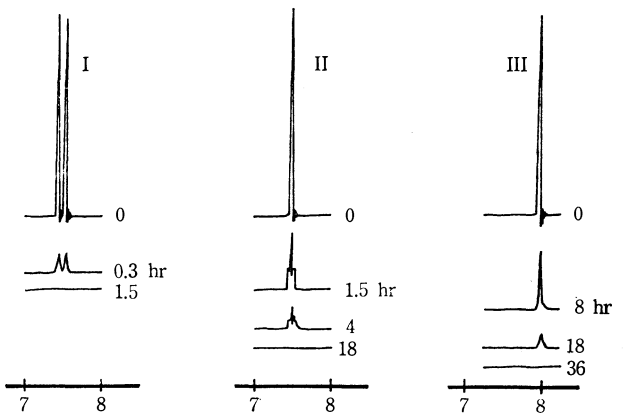

Fig. 3. PMR peaks due to acetyl protons of I: MOBAA–Tl(I), II: POBAA–Tl(I) and III: Tl(I)-acetylacetonate recorded at 35.5 °C at appropriate time intervals (hour) after being dissolved in D_2O.

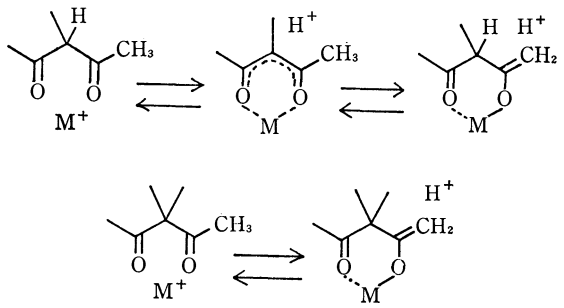

Scheme III

POBAA–Tl(I) in D_2O, a decrease in the intensity of the peak due to acetyl protons were observed with the time. This is clearly due to a hydrogen-deuterium exchange reaction in solution. The exchange rate was, therefore, compared with those of MOBAA–Tl(I) and Tl(I)–acetylacetonate;[4] the results are shown in Fig. 3. The decreasing order of the rate of the acetyl proton exchange is: MOBAA–Tl(I)>POBAA–Tl(I)>Tl(I)–acetylacetonate. This order is opposite to that of the stability of the complexes. From an inspection of the mechanism of the proton dissociation shown in Scheme III, it can readily be understood that the proton dissociation from the methyl group is necessary for MOBAA to form a chelate. In other words, the methyl proton of MOBAA is activated by the neighboring metal ion. On the other hand, acetylacetone forms stable metal chelates by the dissociation of the methylene proton at the 3-position. The methyl-proton activation, therefore, is inhibited by metal-chelate formation. The situation of POBAA–Tl(I) is in between, since the chelate ring stabilization is possible but incomplete because it can take place only with the long-range anionotropy, as has been discussed above. Since the relationship between such a proton exchange rate and the degree of activation of methyl protons has not yet been investigated, the systematic investigation of various thallous compounds is now in progress.

References

1) E. Knoevenagel and R. Arnot, *Ber.*, **37**, 4499 (1904).
2) M. J. Zelesko, E. C. Taylor and A. MacKillop, "Reagents for Organic Synthesis," Vol. 2, ed. by M. Fieser and L. F. Fieser, J. Wiley & Sons, New York, N. Y. (1969), p. 407.
3) E. Knoevenagel, *Ann.*, **281**, 80 (1894).
4) E. C. Taylor, G. H. Hanks, III, and A. MacKillop, *J. Amer. Chem. Soc.*, **90**, 2421 (1968).

The Crystal Structure of α-Barium 12-Tungstosilicate, α-$Ba_2SiW_{12}O_{40}\cdot 16H_2O$

Akiko KOBAYASHI and Yukiyoshi SASAKI

Department of Chemistry, Faculty of Science, The University of Tokyo, Hongo, Tokyo 113

(Received August 1, 1974)

α-$Ba_2SiW_{12}O_{40}\cdot 16H_2O$ is monoclinic, space group C2/c, with $a=25.09(5)$, $b=12.10(2)$, $c=18.79(3)$ Å, $\beta=122.5(3)°$; $D_m=4.95$ g cm^{-3} and $D_x=4.78$ g cm^{-3} for $Z=4$. The crystal consists of the well known Keggin ion $SiW_{12}O_{40}^{4-}$, having a SiO_4 tetrahedron in the center, bound by Ba^{2+} and water molecules to form a three-dimensional framework. Four water molecules could not be located on electron-density maps, which seem to be disordered or "*zeolitic*". The structural relationship of the Keggin ion to its isomer, the β-$SiW_{12}O_{40}^{4-}$ polyanion found in β-$K_4SiW_{12}O_{40}\cdot 9H_2O$, is discussed. Mutual transformation between α- and β-isomers can occur through rotation of a W_3O_{13} group which is a building-unit of both α- and β-polyanions.

It was already known in the last century, that 12-tungstosilicic acid and its salts had two isomers referred to as α- and β-forms (or normal and iso-forms).[1] Acidification of an aqueous solution containing sodium silicate and sodium tungstate gives the α-isomer of the $SiW_{12}O_{40}^{4-}$ ion, while addition of acid to sodium tungstate solution prior to mixing with sodium silicate yields the β-isomer.[2,3]

Recent absorption spectrophotometric and polarographic studies have revealed that a number of related compounds, such as 12-tungstoborate,[2] 12-tungstogermanate,[3] 12-molybdosilicate,[4,5] 12-molybdogermanate,[6] 12-molybdophosphate, and 12-molybdoarsenate,[7,9] show a similar isomerism. In order to clarify the structural relationships between these pairs of isomers, we have undertaken a series of single crystal X-ray diffraction studies.

To start with, we have chosen α- and β-salts of 12-tungstosilicic acid. Owing to the presence of many heavy tungsten atoms, these salts are not suitable for an accurate structure determination. However salts of this acid are favorable for comparative study, since both α- and β-isomers are stable even in aqueous solutions and both can be obtained as separate crystalline samples. Other acids, particularly β-polyanions containing molybdenum atoms, seem to be short lived in aqueous solutions and are quickly converted into the corresponding α-forms.[4-9] The present paper deals with the structure of the α-isomer of 12-tungstosilicate, α-$Ba_2SiW_{12}O_{40}\cdot 16H_2O$. The structure of a β-isomer, β-$K_4SiW_{12}O_{40}\cdot 9H_2O$ was published elsewhere.[10]

The α-salts were widely believed to contain the well known "*Keggin molecules*", or more correctly "*Keggin polyanions*", even though a definite proof was lacking.[11] The guess was based on the fact that $CsHSiW_{12}O_{40}\cdot nH_2O$ ($n=0$ or 2) was isomorphous with $H_3PW_{12}O_{40}\cdot 5H_2O$[13] which was the first example of the "*Keggin structure*".[14]

Experimental

The α-form of 12-tungstosilicate was prepared by mixing a solution of sodium tungstate, sodium silicate and hydrochloric acid.[16] For purification, α-$SiW_{12}O_{40}^{4-}$ was treated with hydrochloric acid and extracted with ether, the extract was then converted to aqueous solution. The barium salt was obtained by neutralization of the polyacid solution with solid barium carbonate. The colorless tabular crystals were obtained from the neutral aqueous solution at >30 °C.

The α-$Ba_2SiW_{12}O_{40}\cdot 16H_2O$ crystals were chosen because of their stability in air and because of the absence of twin formation which is frequently encountered in heteropoly compounds. The crystals are stable at room temperature but begin to loose a part of the water of crystallization at 40 °C.

Thermogravimetric analysis and DTA have shown endothermic reactions at 120, 190 and 250 °C corresponding to the loss of eight, twelve and sixteen water molecules. For the purpose of the X-ray diffraction work a specimen in the form of an irregular rhombus with a maximum dimension of 0.25 mm was used. The intensities of reflections were measured on a Rigaku four-circle diffractometer with Mo$K\alpha$ radiation. The ω-2θ scan technique was employed and 2952 significant independent reflections for which $|F_o|\geq 141.0$ (F_o :absolute scale) up to $2\theta=60°$ were obtained. The data were corrected for Lorentz and polarization effects. No corrections were made for absorption. The crystal data are as follows:

α-$Ba_2SiW_{12}O_{40}\cdot 16H_2O$
F. W. 3438.7
monoclinic
a = 25.09 (5) Å
b = 12.10 (2) Å
c = 18.79 (3) Å
β = 122.5 (3)°
V = 4813 Å^3
space group C2/c
Z = 4 (D_m = 4.95 g cm^{-3}, D_X = 4.78 g cm^{-3})
μ (Mo$K\alpha$: 0.7107 Å) = 320 cm^{-1}

Since Wilson's statistics indicated the presence of a center of symmetry, the space group C2/c was assumed. The structure was solved by the heavy atom method. The atomic positions and anisotropic temperature factors of tungsten, barium and silicon atoms were refined by the block-diagonal least-squares method. At this stage the R-value was reduced to 0.16. After several refinement cycles including oxygen atoms of the anion with isotropic temperature factors, the R value was reduced to 0.14. There are eight crystallographically independent water molecules, of which six were found by a difference Fourier synthesis. After several further cycles, the structure converged to $R=0.13$.

A weighting scheme, $w=0.2$ for $|F_o|\leq 253.0$ and $w=1$, otherwise was employed. Atomic scattering factors were taken from "International Tables for X-ray Crystallography,"[15] and those for W and Ba were corrected for anomalous dispersion.[15]

Results and Discussion

The atomic parameters and their estimated standard deviations are listed in Table 1. The final F_o-F_c table

TABLE 1. ATOMIC PARAMETERS AND THEIR ESTIMATED STANDARD DEVIATIONS

The positional parameters of all the atoms and their anisotropic thermal parameters have been multiplied by 10^4. The anisotropic temperature factor is of the form $\exp[-(h^2B_{11}+k^2B_{22}+l^2B_{33}+2hkB_{12}+2hlB_{13}+2klB_{23})]$.

	x	y	z	$B_{11}(B)$	B_{22}	B_{33}	B_{12}	B_{13}	B_{23}
Si	0(0)	1045(64)	2500(0)	28(17)	80(58)	106(56)	0(0)	47(29)	0(0)
W_1	−205(2)	2967(3)	1045(3)	4(1)	27(2)	19(1)	0(1)	7(1)	4(2)
W_2	1177(2)	2924(3)	3238(3)	5(1)	26(2)	22(1)	−5(1)	9(1)	−2(2)
W_3	−83(2)	−1189(3)	1118(2)	5(1)	25(2)	17(1)	1(1)	8(1)	−2(2)
W_4	1163(2)	−1153(3)	3110(2)	5(1)	24(2)	18(1)	5(1)	9(1)	4(2)
W_5	1011(2)	777(3)	1733(2)	5(0)	25(2)	22(1)	2(1)	10(0)	5(2)
W_6	1298(1)	990(3)	4603(2)	4(1)	23(2)	14(1)	0(1)	5(1)	0(2)
Ba	2757(2)	927(5)	1660(4)	9(1)	24(3)	31(2)	0(2)	14(1)	1(3)
O_1	1754(31)	−2143(63)	3648(44)	1.9(1.1)					
O_2	596(36)	−1883(66)	2023(51)	2.6(1.4)					
O_3	−381(40)	−2167(80)	262(57)	3.3(1.6)					
O_4	1466(31)	−300(58)	2521(44)	1.8(1.1)					
O_5	544(30)	−321(57)	1054(43)	1.5(1.1)					
O_6	1475(38)	1171(77)	1360(54)	3.2(1.5)					
O_7	396(29)	1840(55)	1183(42)	1.5(1.1)					
O_8	1299(36)	1794(70)	2667(52)	2.7(1.4)					
O_9	415(34)	87(64)	2277(48)	2.2(1.2)					
O_{10}	435(29)	3278(53)	2171(42)	1.3(1.0)					
O_{11}	1735(34)	3956(73)	3356(48)	2.8(1.4)					
O_{12}	883(31)	3741(62)	3902(44)	2.1(1.2)					
O_{13}	109(32)	3877(65)	4542(45)	2.3(1.2)					
O_{14}	1682(31)	2126(63)	4293(44)	1.9(1.1)					
O_{15}	900(32)	2213(64)	4820(46)	2.1(1.2)					
O_{16}	1905(27)	695(53)	5583(39)	1.3(1.0)					
O_{17}	1459(32)	25(64)	3942(47)	2.0(1.2)					
O_{18}	682(29)	−47(57)	4482(42)	1.6(1.0)					
O_{19}	500(27)	1717(51)	3297(38)	1.1(0.9)					
O_{20}	496(34)	−1641(65)	3285(48)	2.3(1.3)					
$H_2O(1)$	1788(44)	2064(88)	290(62)	4.2(1.9)					
$H_2O(2)$	2254(34)	4557(64)	2159(48)	2.3(1.3)					
$H_2O(3)$	2171(40)	5997(89)	617(57)	3.9(1.7)					
$H_2O(4)$	1138(49)	4520(90)	678(69)	4.6(2.1)					
$H_2O(5)$	2765(46)	2288(90)	2811(65)	4.4(2.0)					
$H_2O(6)$	980(50)	5772(109)	1967(70)	5.4(2.3)					

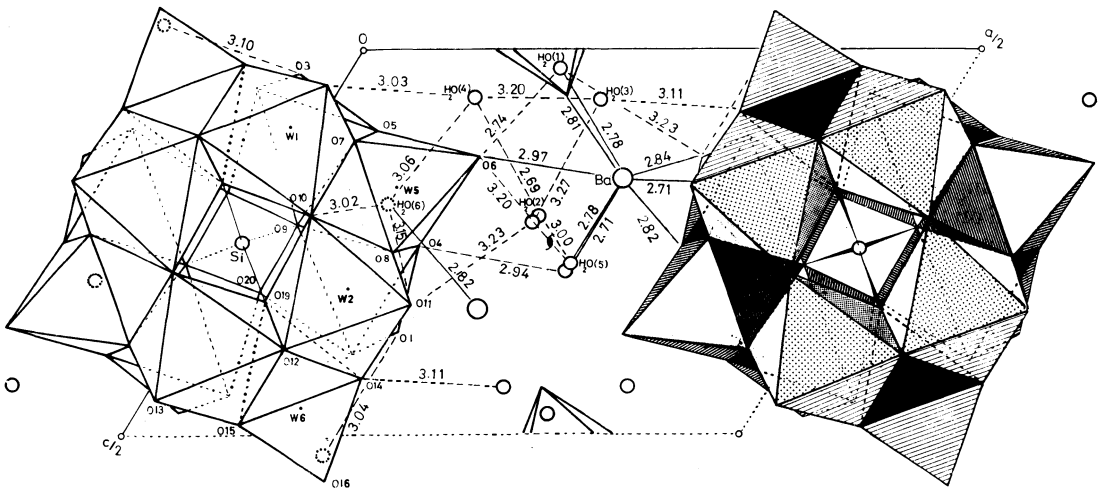

Fig. 1. A view of the structure as projected onto the (010) plane. Large circles represent Ba^{2+} ions and small circles water molecules. The coordination bonds around Ba^{2+} are designated by full lines, other close contacts by dotted lines.

is held by the office of the Chemical Society of Japan as Document No. 7504. The crystal structure projected along the b-axis is shown in Fig. 1. As is shown in this figure, the crystal consists of α-$SiW_{12}O_{40}^{4-}$ anions, Ba^{2+} cations and water molecules of crystallization. The center of the anion lies on a twofold rotation axis at $y=1/4$.

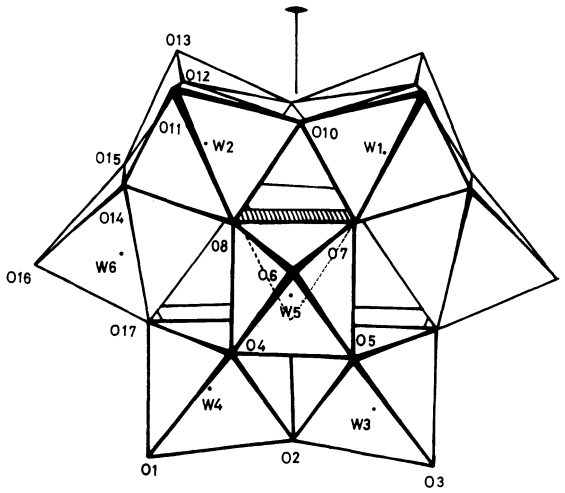

Fig. 2. A perspective view of the α-$SiW_{12}O_{40}^{4-}$ anion. Deformed octahedra represent WO_6 groups. The central SiO_4 tetrahedron, shaded on the figure, is only partly seen.

Table 2. Interatomic distances (Å) and estimated standard deviations[a] within the anion, α-$SiW_{12}O_{40}^{4-}$

W_1-O_{10}	(Ob)[b]	1.88(6)	W_2-O_{10}	(Ob)	1.91(5)
W_1-O_7	(Ob)	1.94(7)	W_2-O_8	(Ob)	1.86(10)
W_1-O_{19}'[c]	(Oa)	2.31(8)	W_2-O_{19}	(Oa)	2.29(7)
W_1-O_{15}'	(Oc)	1.86(6)	W_2-O_{14}	(Oc)	1.94(7)
W_1-O_{12}'	(Oc)	1.99(9)	W_2-O_{12}	(Oc)	2.02(10)
W_1-O_{13}'	(Od)	1.67(9)	W_2-O_{11}	(Od)	1.80(9)
W_3-O_{18}'	(Ob)	1.90(6)	W_4-O_{17}	(Ob)	1.95(8)
W_3-O_{20}'	(Ob)	1.97(11)	W_4-O_{20}	(Ob)	1.96(10)
W_3-O_9	(Oa)	2.40(8)	W_4-O_9	(Oa)	2.25(7)
W_3-O_5	(Oc)	1.95(8)	W_4-O_4	(Oc)	1.94(9)
W_3-O_2	(Oc)	1.84(7)	W_4-O_2	(Oc)	1.96(7)
W_3-O_3	(Od)	1.80(10)	W_4-O_1	(Od)	1.75(7)
W_5-O_7	(Ob)	1.84(6)	W_6-O_{17}	(Ob)	1.90(9)
W_5-O_8	(Ob)	1.94(9)	W_6-O_{18}	(Ob)	1.91(8)
W_5-O_9	(Oa)	2.37(10)	W_6-O_{19}	(Oa)	2.35(5)
W_5-O_5	(Oc)	1.78(6)	W_6-O_{14}	(Oc)	1.94(9)
W_5-O_4	(Oc)	1.84(7)	W_6-O_{15}	(Oc)	1.95(9)
W_5-O_6	(Od)	1.72(12)	W_6-O_{16}	(Od)	1.68(5)
Si-O_9		1.75(11)			
Si-O_{19}		1.57(7)			

a) E.s.d.'s in parentheses in Tables 2 and 3 are in units of the last significant digit. b) Oa: the oxygen atom bound to one silicon and at the same time to three tungsten atoms. Ob: the oxygen atom bridging two tungsten atoms of two neighboring W_3O_{13} moieties. Oc: the bridging oxygen atom shared between two tungsten atoms belonging to a same W_3O_{13} group. Od: the terminal oxygen atom bonded to only one tungsten atom. c) Atoms with a prime are associated with those in Table 1 by a twofold axis.

Structure of α-$SiW_{12}O_{40}^{4-}$ Ion. A perspective drawing of α-$SiW_{12}O_{40}^{4-}$ anion is presented in Fig. 2. Interatomic distances and their e.s.d.'s within the anion are listed in Table 2. The anion consists of a central SiO_4 tetrahedral group in which each of the oxygen atoms is replaced by a W_3O_{13} unit constructed from three WO_6 octahedra sharing edges. Thus, the anion has the expected Keggin structure. This result confirms the proposed model for the structure of this anion in aqueous solution from a liquid X-ray diffraction study.[16] The structural relationships between α- and β-$SiW_{12}O_{40}^{4-}$ are now clear: the α-polyanion has the well known Keggin structure, whereas the β-anion has a lower symmetry and is a geometrical isomer of the Keggin structure. If a model of the α-polyanion is built with idealized polyhedra, a corresponding β-model can be obtained by a 60° rotation of one of the W_3O_{13} groups of the α-model.[10] All the WO_6 octahedra in α-$Ba_2SiW_{12}O_{40}\cdot 16H_2O$ are distorted. The bond lengths of W–Oa, W–Ob, W–Oc, and W–Od are 2.2—2.4, 1.8—2.0, 1.7—2.0, and 1.6—1.8 Å respectively as are listed in Table 2. Oa represents the oxygen atom attached to one silicon atom and to three tungsten atoms, Ob is shared between tungsten atoms of different W_3O_{13} units, Oc is also bound to two tungsten atoms but belonging to the same unit, and Od is the unshared terminal oxygen atom bonded to only one metal atom. These classifications of the oxygen atoms conform to those given by Evans.[17] These data seem to indicate that the octahedra are elongated in the direction of Oa, the oxygen atom attached to the central silicon atom, moreover the tungsten atoms are displaced outward from the diagonal line Oa—Od, as if the tungsten atoms are repulsing each other within a W_3O_{13} group, the Ob–W–Oc diagonal angles being 150(3)—161(3)°. Detailed discussion of the O–O distances was not possible, since the standard deviation was as large as 0.15 Å. The central SiO_4 tetrahedron is not quite regular. The bond distances are listed in Table 2.

Coordination Around Barium Cation. As shown in Table 3 and indicated by broken lines in Fig. 1, each barium ion is coordinated by eight oxygen atoms at distances of 2.7—2.9 Å, four from water molecules and four oxygen atoms (Od) from three adjacent $SiW_{12}O_{40}^{4-}$ anions. Table 3 shows oxygen-oxygen distances around $H_2O(1)$—$H_2O(6)$ and barium-oxygen distances. Six oxygen atoms form a distorted trigonal prism around a barium cation while the other two stick out of two rectangular faces of the prism.

Water of Crystallization. In general, crystals of polytungstates and polymolybdates contain many water molecules. Although it is important to clarify the role of these water molecules in the crystal structure, their position can not always be fixed with sufficient accuracy because of the presence of many heavy atoms. In the present case, twelve out of sixteen water molecules in the chemical formula, could be located while the remaining four are still missing. These water molecules might be "*zeolitic*", having large thermal vibration factors, and be correlated with the loss of water at a temperature as low as 40 °C.[18] Of the twelve water

TABLE 3. INTERATOMIC DISTANCES (Å) LESS THAN 3.5 Å OUTSIDE THE ANION

Ba	O_1	(Od)[a]	2.84(8)			
	O_6	(Od)	2.97(10)			
	O_{11}	(Od)	2.71(9)			
	O_{16}	(Od)	2.81(6)			
	H_2O (1)		2.78(9)			
	H_2O (2)		2.78(9)			
	H_2O (5)		2.71(13)			
	H_2O (6)		2.82(9)			
H_2O (1)	O_1	(Od)	3.04(16)	H_2O (2)	O_4	(Oc) 2.94(12)
	O_1	(Od)	3.23(12)		O_6	(Od) 3.49(10)
	O_3	(Od)	3.10(15)		O_{11}	(Od) 3.23(15)
	O_6	(Od)	2.74(18)		H_2O (3)	3.29(15)
	O_{16}	(Od)	3.37(12)		H_2O (4)	2.69(11)
	O_{17}	(Ob)	3.35(14)		H_2O (5)	3.00(13)
	O_{18}	(Ob)	3.38(12)		H_2O (5)	3.31(13)
	O_{20}	(Ob)	3.44(10)		H_2O (6)	3.36(16)
H_2O (3)	O_{14}	(Oc)	3.11(14)	H_2O (4)	O_3	(Od) 3.35(14)
	O_{17}	(Ob)	3.29(13)		O_{13}	(Od) 3.03(16)
	H_2O (4)		3.20(18)		H_2O (6)	3.06(20)
	H_2O (5)		3.27(17)			
H_2O (5)	O_6	(Od)	3.20(11)	H_2O (6)	O_2	(Oc) 3.02(16)
	H_2O (6)		3.47(18)		O_{10}	(Ob) 3.42(15)
					O_{11}	(Od) 3.15(14)

a) Classification of oxygen atoms in the polyanion: see text and footnote of Table 2.

molecules whose position could be fixed, eight coordinate to two barium cations and at the same time some of them form hydrogen bonds with polyanions. The rest of the water molecules have some close contacts with the polyanion or with water molecules which are coordinated to barium ions. Thus barium cations and polyanions build up a three dimensional framework, accommodating water molecules in interstices.

Comparison of α-$Ba_2SiW_{12}O_{40}\cdot 16H_2O$ *with* α-$K_4SiW_{12}O_{40}\cdot 17H_2O$. The main difference between the crystal structures of the two tungstosilicates is that the barium salt consists of a three dimensional framework with mobile water molecules in interstices, while the potassium salt crystals contain one dimensional spiral chains made of alternate potassium cations and polyanions. There are large channels parallel to the spirals, and the three potassium ions and fifteen water molecules which could not be found by neutron and X-ray diffraction techniques are probably in random or mobile zeolitic state in these spaces; this structure explains the efflorescent nature of the potassium salt.

The calculations were performed on a HITAC 8700/8800 computer at the Computer Center of the University of Tokyo using a local version of UNICS.[20]

The authors wish to thank Dr. Hitoshi Iwasaki for reading through the manuscript and for his criticism. The work was financially supported by a Grant-in-aid for Cooperated Scientific Research of the Ministry of Education.

References

1) C. Marignac, *Ann. Chim. Phys.* [4], **3**, 44 (1864).
2) P. Souchay, *Bull. Soc. Chim. France* [5], **18**, 365 (1951).
3) P. Souchay, A. Tézé, and G. Hervé, *C. R. Acad. Sci. Ser. C*, **275**, 1073 (1972).
4) J. D. H. Strickland, *J. Amer. Chem. Soc.* **74**, 862 (1953).
5) R. Massart, *Ann. Chim.* [14], **3**, 507 (1968).
6) P. Souchay, A. Tézé, and C. Hervé, *Proceedings of XX I.C.C.C. Moscow* 1972.
7) P. Souchay, R. Content, and M. Fruchart, *C. R. Acad. Sci. Ser. C.* **264**, 976 (1967).
8) J. M. Fruchart and P. Souchay, *ibid.* **266**, 1571 (1968).
9) P. Souchay and R. Contant, *ibid.* **265**, 723 (1967).
10) K. Yamamura and Y. Sasaki, *Chem. Communn.*, **1973**, 648.
11) After our measurements were completed, we learned that the Keggin structure of the tungstosilicic acid had been acertained by Smith[12] in his structure determination of $K_4SiW_{12}O_{40}\cdot 17H_2O$ by X-ray and neutron diffraction techniques. However, our computation was continued due to our interest in the roles of divalent barium cation and of water of crystallization in the present polyanion crystals.
12) P. M. Smith, *Dissertation Abstr.*, **32**, 5136-B (1972).
13) J. A. Santos, *Proc. Roy. Soc.* **A150**, 309 (1935).
14) J. F. Keggin, *ibid.*, **A144**, 75 (1934).
15) "International Tables for X-ray Crystallography," Kynoch Press, Birmingham (1962), Vol. III.
16) H. A. Levy, P. A. Agron, and M. D. Danford, *J. Chem. Phys.* **30**, 1486 (1959).
17) H. T. Evans, Jr., *Perspectives Struct. Chem.* **4**, 1 (1971).
18) This kind of water of crystallization is rather common in heteropolymetallate compounds. Apart from $K_4SiW_{12}O_{40}\cdot 17H_2O$,[12] $K_5CoW_{12}O_{40}\cdot 20H_2O$[19] and $(NH_4)_7Na_2[H_2GaW_{11}O_{40}]\cdot 15H_2O$[17] have been known to contain loosely bound water molecules which can not be located by X-ray diffraction techniques.
19) N. F. Yannoni, *Dissertation* (1961).
20) "UNICS: The Universal Crystallographic Computation Program System," Crystallographic Society of Japan (1967).

Structure of Polyvanadotungstates. I. The Crystal Structure of α-$(CN_3H_6)_4V_2W_4O_{19}$

Keiko NISHIKAWA,* Akiko KOBAYASHI, and Yukiyoshi SASAKI

Department of Chemistry, Faculty of Science, The University of Tokyo, Hongo, Bunkyo-ku, Tokyo 113

(Received September 26, 1974)

Crystals of α-$(CN_3H_6)_4V_2W_4O_{19}$ are monoclinic, space group $P2_1$, with the cell dimensions, $a=14.85(2)$, $b=19.48(2)$, $c=9.48(1)$ Å, $\beta=92.6(2)°$. The X-ray structure determination showed that $V_2W_4O_{19}^{4-}$ anion has the hexaniobate-type structure consisting of 6 edge-shared MO_6 octahedra. Each M position is randomly occupied by vanadium and tungsten atoms with a 2:4 probability. This randomness makes it impossible to determine whether $V_2W_4O_{19}^{4-}$ anion has the *cis* or *trans* configuration or both. The final R value was 0.086 with anisotropic temperature factors for metals and isotropic factors for other lighter atoms.

In an acidic aqueous solution, the orthotungstate ion WO_4^{2-} is condensed to isopolytungstate polyanions and the metavanadate ion VO_3^- forms isopolyvanadates. Isopolytungstate anions have no tendency to form an infinite polymer structure in crystals, and the existence of discrete anions with formulas $W_6O_{19}^{2-}$,[1] $W_{10}O_{32}^{4-}$,[2] $H_2W_{12}O_{40}^{6-}$ (metatungstate),[3] and $H_2W_{12}O_{42}^{10-}$ (paratungstate)[4] has been reported in the solid phase. On the other hand, it is known that isopolyanions containing vanadium(V) very often have infinite chain or sheet structures in crystals. The crystals of KVO_3 contain chains of VO_4 tetrahedra connected by sharing corners, and $KVO_3 \cdot H_2O$ has a chain structure made of VO_5 trigonal bipyramids sharing edges.[5]

There are no discrete $V_3O_8^-$ nor $V_5O_{14}^{3-}$ ions in CsV_3O_8[6] and $K_3V_5O_{14}$[7] crystals. In $[V_3O_8^-]_\infty$, VO_6 octahedra form plane sheets by sharing edges, and in $[V_5O_{14}^{3-}]_\infty$, VO_5 square pyramids and VO_4 tetrahedra are bound by sharing corners. The only discrete isopolyvanadate ion which has been reported is $V_{10}O_{28}^{6-}$ built by VO_6 octahedra sharing edges.[8,9] But when vanadium(V) and tungsten(VI) are both present in an acidic solution, crystals of "polyvanadotungstates", which are sometimes called "mixed isopolyanions", may be obtained. It has been reported that the composition of the vanadotungstates varies with the pH and the constitution of the solution.[10–17] Table 1 gives the analytical formulas of vanadotungstate anions so far reported as salts in crystals. No crystal structure work has been published on the vanadotungstate salts and it has not yet known whether these mixed isopolyanions have polymeric structures like the polyvanadates or contain discrete polyanions.

The present paper reports the structure of the guanidinium salt of $V_2W_4O_{19}^{4-}$ polyanion, $(CN_3H_6)_4V_2W_4O_{19}$, obtained from single crystal X-ray diffraction.

Experimental

The guanidinium salt was obtained by mixing a solution of guanidinium perchlorate at pH 4—6 with that of $Na_4V_2W_4O_{19} \cdot 14H_2O$. The sodium salt was prepared by concentration of an aqueous solution at pH 4—6 containing sodium salts of vanadate and of tungstate in the ratio of 1:2.[15]

Repeated preparations revealed the existence of three different guanidinium salts, which are denoted here α, β and γ. The α and β forms, having the same chemical formula $(CN_3H_6)_4V_2W_4O_{19}$, always precipitate together from solution at pH 4—6 as needles-like orange crystals. After several recrystallizations, almost pure α-form was obtained but the β-form could not be prepared in a pure state. The γ form precipitates from the same solution after a week as polyhedral crystals, but loses water of crystallization quickly in air. The crystal data for the α- and β-forms are shown in Table 2.

TABLE 2. CRYSTAL DATA FOR α- AND β-$(CN_3H_6)_4V_2W_4O_{19}$

α-$(CN_3H_6)_4V_2W_4O_{19}$	β-$(CN_3H_6)_4V_2W_4O_{19}$
F.W. 1381.3	F.W. 1381.3
Monoclinic	Orthorhombic
$a=14.85(2)$ Å	$a=14.43$ Å
$b=19.48(2)$	$b=20.49$
$c=9.48(1)$	$c=9.26$
$\beta=92.6(2)°$	
$V=2733$ Å^3	$V=2738$ Å^3
Space group $P2_1$	Space group $Pnm2_1$, $Pn2_1m$ or $Pnmm$
$Z=2$ (for $[(CN_3H_6)_4V_2W_4O_{19}]_2$)	$Z=4$ (for $(CN_3H_6)_4V_2W_4O_{19}$)
$D_m=3.38$ g/cm^3	
$D_x=3.39$ g/cm^3	
μ(MoKα)$=199.0$ cm^{-1}	

Reflection data for a specimen of the pure α-form were collected on a Rigaku four-circle diffractometer with MoKα radiation monochromated by a graphite crystal ($\lambda=0.7107$ Å).

TABLE 1. FORMULAS OF VANADOTUNGSTATE ANIONS REPORTED AS SALTS

$V_3W_{18}O_{72}^{21-}$,	$V_6W_6O_{38}^{10-}$,	$V_6W_{12}O_{57}^{12-}$	Prandtl[10]
$V_2W_4O_{19}^{4-}$	$V_3W_3O_{19}^{5-}$,	$V_3W_7O_{31}^{5-}$	Rosenheim and Pieck[11]
$V_2W_4O_{19}^{4-}$	$V_8W_{16}O_{73}^{10-}$,	$V_4W_{20}O_{75}^{10-}$	Bekturov, Begalieva and I'lyasova[14]
$V_nW_{6-n}O_{19}^{-(n+2)}$ ($n=1,2$): $V_2W_4O_{19}^{4-}$, $VW_5O_{19}^{3-}$			Flynn and Pope[15–17]
$V^tV_nW_{12-n}O_{40}^{-(n+3)}$ ($n=2,3,4$): $V_3W_{10}O_{40}^{5-}$, $V_4W_9O_{40}^{6-}$, $V_5W_8O_{40}^{7-}$			

* Present address: Department of Chemistry, Faculty of Science, Gakushuin University, Mejiro, Toshima-ku, Tokyo 171.

An ω-2θ scan technique was employed and 2362 independent reflections whose intensities are larger than 3σ up to $2\theta=60°$ were obtained. The data were corrected for Lorentz and polarization factors but not for absorption. The dimensions of the specimen used were approximately $0.1\times0.08\times0.14$ mm.

Structure Determination

The structure was solved by the heavy atom method. Twelve metal atoms forming two independent octahedral M_6 units were easily located. The coordinates of these two polyanions are related by pseudo-two fold screw axes parallel to the *a* and *c* axes which cause the observed extra extinction rule: *h*00 and 00*l* are absent or very weak if *h* or *l* is odd.

The positions of oxygen peaks suggested that six MO_6 octahedra are connected in a compact way by sharing edges to form the M_6O_{19} polyanion. Each M_6O_{19} anion must contain two vanadium atoms in either the *trans*- or *cis*-configuration,[18] but it was impossible to distinguish vanadium from tungsten on the Fourier maps. The best agreement between F_o and F_c was obtained by assuming that the twelve metal positions (M1—M6, M1′—M6′) are randomly occupied by vanadium and tungsten atoms with a 2:4 probability. Thus our data could be explained by randomly orientated *trans*- or *cis*-$V_2W_4O_{19}^{4-}$, and no conclusion could be drawn about the configuration of the $V_2W_4O_{19}^{4-}$ anion.

All the 82 atoms—12 metal, 38 oxygen, 8 carbon, and 24 nitrogen (hydrogen atoms were excluded)—are crystallographically independent. Of these, 70 atoms could be located. Three guanidinium ions were omitted as described in the Results and Discussion.

The atomic parameters were refined to $R=0.086$ by the block-diagonal least-squares method, using anisotropic temperature factors for the metal atoms and isotropic ones for the other atoms. The final positional parameters and temperature factors are shown in Tables 3 and 4. The F_o—F_c table is held by the Chemical Society of Japan as Document No. 7505.

The calculations were performed on a HITAC 8700/8800 computer at the Computer Center of the University of Tokyo using a local version of UNICS.[20]

TABLE 3. FINAL POSITION COORDINATES ($\times10^4$) AND ISOTROPIC TEMPERATURE FACTORS FOR O, C AND N ATOMS[a]
(Anisotropic temperature factors for metal atoms are given in Table 4).

	x	*y*	*z*	*B*		*x*	*y*	*z*	*B*
M(1)	−922 (3)	859 (3)	4451 (6)		O(4)′	5672 (44)	−3042 (33)	2935 (72)	2.2 (9)
M(2)	1317 (4)	1238 (3)	1303 (6)		O(5)′	3013 (43)	−1801 (34)	−820 (73)	2.1 (8)
M(3)	−282 (4)	2144 (3)	2436 (7)		O(6)′	6510 (84)	−538 (68)	5240 (74)	2.5 (10)
M(4)	775 (4)	−36 (3)	3244 (6)		O(13)′	3475 (31)	−403 (30)	3061 (53)	0.9 (7)
M(5)	−782 (4)	658 (3)	1012 (7)		O(14)′	4191 (49)	−2158 (39)	3777 (80)	2.5 (9)
M(6)	1166 (4)	1453 (3)	4680 (7)		O(15)′	3138 (54)	−1562 (43)	2094 (88)	2.2 (9)
M(1)′	3689 (4)	−1340 (3)	3836 (6)		O(16)′	4693 (31)	−1061 (25)	4907 (54)	1.1 (7)
M(2)′	5928 (4)	−983 (3)	586 (6)		O(23)′	5289 (43)	−105 (37)	500 (73)	2.4 (7)
M(3)′	4255 (4)	−89 (3)	1767 (6)		O(24)′	6112 (48)	−1886 (37)	931 (79)	2.3 (9)
M(4)′	5394 (4)	−2219 (3)	2550 (7)		O(25)′	4839 (48)	−1329 (40)	−673 (80)	2.2 (9)
M(5)′	3848 (4)	−1559 (3)	369 (7)		O(26)′	6505 (42)	−618 (33)	2358 (71)	1.8 (8)
M(6)′	5773 (4)	−765 (3)	3952 (7)		O(35)′	3594 (32)	−720 (26)	383 (55)	1.0 (7)
O(C)	152 (42)	989 (31)	2855 (69)	1.4 (9)	O(36)′	5201 (37)	52 (29)	3283 (62)	1.1 (7)
O(1)	−1758 (47)	881 (39)	5658 (78)	2.5 (9)	O(45)′	4407 (40)	−2276 (31)	1144 (66)	1.7 (8)
O(2)	2005 (44)	1356 (36)	−211 (73)	2.3 (9)	O(46)′	5979 (60)	−1757 (48)	3996 (85)	2.2 (10)
O(3)	−846 (62)	2888 (48)	1950 (100)	2.5 (10)	C(1)	974 (53)	7425 (48)	2230 (91)	1.0 (9)
O(4)	1070 (53)	−821 (42)	3751 (89)	2.5 (9)	N(11)	490 (84)	7011 (62)	1957 (80)	2.9 (10)
O(5)	−1394 (42)	285 (32)	−247 (71)	2.0 (8)	N(12)	1310 (62)	7589 (51)	3336 (82)	2.2 (10)
O(6)	1787 (35)	1713 (27)	5981 (60)	1.2 (7)	N(13)	1431 (63)	7780 (43)	1236 (78)	1.4 (9)
O(13)	−1169 (30)	1765 (22)	3827 (51)	1.1 (7)	C(2)	3483 (71)	6077 (51)	1657 (83)	0.9 (9)
O(14)	−270 (50)	71 (40)	4636 (82)	2.3 (9)	N(21)	4001 (57)	6068 (45)	566 (74)	1.4 (9)
O(15)	−1461 (40)	701 (31)	2762 (69)	1.8 (8)	N(22)	3160 (66)	6600 (52)	2613 (83)	1.7 (10)
O(16)	−5 (32)	1240 (26)	5518 (54)	1.2 (7)	N(23)	3351 (52)	5424 (39)	2225 (75)	1.1 (10)
O(23)	641 (46)	2092 (36)	1085 (75)	2.4 (8)	C(3)	6340 (71)	5274 (71)	3052 (91)	2.2 (10)
O(24)	1381 (46)	379 (35)	1490 (76)	2.6 (9)	N(31)	6575 (72)	5444 (58)	4391 (90)	2.5 (10)
O(25)	426 (42)	813 (35)	−195 (71)	2.1 (9)	N(32)	5680 (71)	4897 (58)	2541 (88)	2.4 (9)
O(26)	1938 (40)	1534 (31)	3126 (66)	1.7 (8)	N(33)	6710 (70)	5694 (56)	1911 (85)	2.9 (10)
O(35)	−1001 (41)	1580 (33)	1055 (69)	1.9 (7)	C(4)	3880 (74)	2543 (57)	2909 (90)	1.2 (10)
O(36)	464 (40)	2308 (31)	4020 (66)	1.7 (7)	N(41)	3913 (68)	2134 (55)	1600 (81)	1.4 (9)
O(45)	−224 (68)	−185 (55)	1558 (85)	2.7 (10)	N(42)	3606 (90)	2194 (78)	3744 (91)	2.7 (10)
O(46)	1422 (37)	403 (29)	4651 (62)	1.2 (7)	N(43)	4546 (90)	2948 (74)	2999 (100)	2.8 (11)
O(C)′	4790 (51)	−1192 (39)	2219 (83)	1.8 (9)	C(5)	1433 (83)	3754 (68)	2936 (91)	2.1 (9)
O(1)′	2827 (38)	−1529 (29)	4864 (62)	1.3 (7)	N(51)	1032 (82)	3749 (72)	4092 (92)	2.5 (10)
O(2)′	6827 (61)	−739 (48)	−622 (91)	2.4 (9)	N(52)	1738 (83)	3295 (61)	2371 (90)	2.6 (10)
O(3)′	3933 (60)	711 (45)	1678 (94)	2.5 (9)	N(53)	1543 (74)	4265 (58)	2343 (85)	2.3 (9)

a) The estimated standard deviations in parentheses here and elsewhere are in units of the last significant digit.

Table 4. Final anisotropic temperature factors for metals ($\times 10^4$) with their estimated standard deviations in parentheses

(The temperature factor is of the form: $\exp[-(\beta_{11}h^2+\beta_{22}k^2+\beta_{33}l^2+2\beta_{12}hk+2\beta_{13}hl+2\beta_{23}kl)]$)

	β_{11}	β_{22}	β_{33}	β_{12}	β_{13}	β_{23}
M(1)	20 (2)	13 (1)	49 (6)	−1 (1)	11 (3)	0 (2)
M(2)	21 (2)	12 (1)	37 (6)	−1 (1)	11 (3)	−2 (2)
M(3)	33 (3)	16 (1)	80 (8)	1 (2)	13 (4)	0 (3)
M(4)	23 (2)	11 (1)	60 (7)	2 (1)	8 (3)	1 (2)
M(5)	24 (2)	19 (1)	74 (8)	0 (1)	1 (3)	−3 (3)
M(6)	28 (3)	18 (1)	71 (8)	−3 (1)	4 (3)	−2 (3)
M(1)′	21 (2)	13 (1)	36 (6)	−1 (1)	2 (3)	−2 (2)
M(2)′	21 (2)	13 (1)	50 (7)	−1 (1)	11 (3)	0 (2)
M(3)′	24 (3)	11 (1)	60 (8)	2 (2)	9 (4)	2 (3)
M(4)′	40 (3)	17 (1)	78 (8)	3 (2)	11 (3)	1 (3)
M(5)′	27 (2)	18 (1)	75 (7)	−2 (1)	5 (3)	−2 (2)
M(6)′	26 (2)	19 (1)	73 (8)	0 (1)	3 (3)	−5 (3)

The atomic scattering factors were taken from *International Tables for X-ray Crystallography*.[21] A weighting scheme with $w=1$ for $|F_o|\geq 101.3$ and $w=0.4$ otherwise was employed.

Results and Discussion

In Fig. 1, the $M_6O_{19}^{4-}$ ion (M=(2V+4W)/6) is shown as a "coordination polyhedral model" consisting of 6 edge-shared MO_6 octahedra. This is identical with the "hexaniobate structure" found by Lindqvist in $Nb_6O_{19}^{8-}$ [22] and by Henning and Hüllen in $W_6O_{19}^{2-}$.[1]

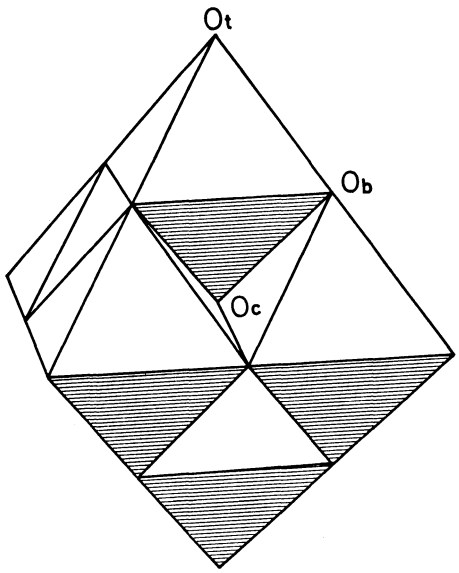

Fig. 1. The coordination polyhedral model of $M_6O_{19}^{4-}$ ion.

The distances between two adjacent metal atoms shown in Table 5 suggest that the M_6 octahedra are slightly deformed, but the reason for this is unknown. The metal atoms are not exactly at the center of each MO_6 octahedron but are displaced outward as if they are repulsing each other.

The oxygen atoms are classified according to the bonding pattern into three groups, Oc, Ob, and Ot. The M–Oc bond length ranges from 2.2 to 2.4 Å,

Table 5. Metal–metal interatomic distances with their estimated standard deviations

M(1)—M(3)	3.316 (9) Å	M(1)′—M(3)′	3.263 (8) Å
M(4)	3.311 (8)	M(4)′	3.334 (9)
M(5)	3.301 (9)	M(5)′	3.335 (8)
M(6)	3.308 (9)	M(6)′	3.288 (9)
M(2)—M(3)	3.185 (8)	M(2)′—M(3)′	3.274 (8)
M(4)	3.215 (8)	M(4)′	3.168 (9)
M(5)	3.316 (9)	M(5)′	3.285 (9)
M(6)	3.248 (8)	M(6)′	3.239 (9)
M(3)—M(5)	3.266 (9)	M(3)′—M(5)′	3.202 (9)
M(6)	3.248 (9)	M(6)′	3.268 (9)
M(4)—M(5)	3.347 (9)	M(4)′—M(5)′	3.282 (9)
M(6)	3.246 (9)	M(6)′	3.169 (9)

Table 6. Metal–oxygen interatomic distances with their estimated standard deviations

(1) The distances of M–Oc			
M(1)–Oc	2.26 (6) Å	M(1)′–Oc′	2.31 (8) Å
M(2)	2.37 (6)	M(2)′	2.33 (8)
M(3)	2.23 (6)	M(3)′	2.21 (8)
M(4)	2.27 (6)	M(4)′	2.31 (8)
M(5)	2.42 (6)	M(5)′	2.38 (8)
M(6)	2.37 (6)	M(6)′	2.30 (8)
(2) The distances of M–Ot			
M(1)–O(1)	1.73 (7) Å	M(1)′–O(1)′	1.69 (6) Å
M(2)–O(2)	1.82 (7)	M(2)′–O(2)′	1.63 (9)
M(3)–O(3)	1.73 (9)	M(3)′–O(3)′	1.69 (7)
M(4)–O(4)	1.66 (8)	M(4)′–O(4)′	1.72 (8)
M(5)–O(5)	1.64 (7)	M(5)′–O(5)′	1.80 (9)
M(6)–O(6)	1.60 (6)	M(6)′–O(6)′	1.66 (8)
(3) The distances of M–Ob			
M(1)–O(13)	1.89 (5) Å	M(2)–O(23)	1.95 (7) Å
O(14)	1.82 (8)	O(24)	1.79 (7)
O(15)	1.78 (6)	O(25)	2.07 (7)
O(16)	1.82 (5)	O(26)	2.01 (6)
M(3)–O(13)	2.05 (5)	M(4)–O(14)	2.09 (8)
O(23)	1.95 (7)	O(24)	2.09 (7)
O(35)	1.98 (7)	O(45)	2.05 (8)
O(36)	1.85 (6)	O(46)	1.82 (6)
M(5)–O(15)	1.98 (6)	M(6)–O(16)	1.99 (5)
O(25)	2.05 (7)	O(26)	1.92 (6)
O(35)	1.90 (8)	O(36)	2.04 (6)
O(45)	1.83 (6)	O(46)	2.05 (6)
M(1)′–O(13)′	1.99 (5)	M(2)′–O(23)′	1.96 (7)
O(14)′	1.86 (7)	O(24)′	1.81 (7)
O(15)′	1.86 (8)	O(25)′	2.08 (8)
O(16)′	1.85 (5)	O(26)′	1.98 (7)
M(3)′–O(13)′	1.83 (5)	M(4)′–O(14)′	2.08 (8)
O(23)′	1.99 (7)	O(24)′	2.02 (7)
O(35)′	2.02 (5)	O(45)′	1.94 (6)
O(36)′	1.98 (6)	O(46)′	1.83 (9)
M(5)′–O(15)′	1.99 (8)	M(6)′–O(16)′	1.96 (5)
O(25)′	1.87 (8)	O(26)′	1.92 (6)
O(35)′	1.78 (5)	O(36)′	1.90 (6)
O(45)′	1.77 (6)	O(46)′	1.96 (9)

M–Ob 1.78—2.08 Å, M–Ot 1.60—1.82 Å (Table 6). The Oc oxygen atoms at the center of the polyanions are bound to six metal atoms, Ob is bound to two metal atoms forming a bridge, and Ot is the terminal oxygen atom and is bonded to only one metal atom.

The bond lengths shown in Tables 5 and 6 should be understood as averaged values of W–W and V–W or V–O and W–O distances because of the randomness

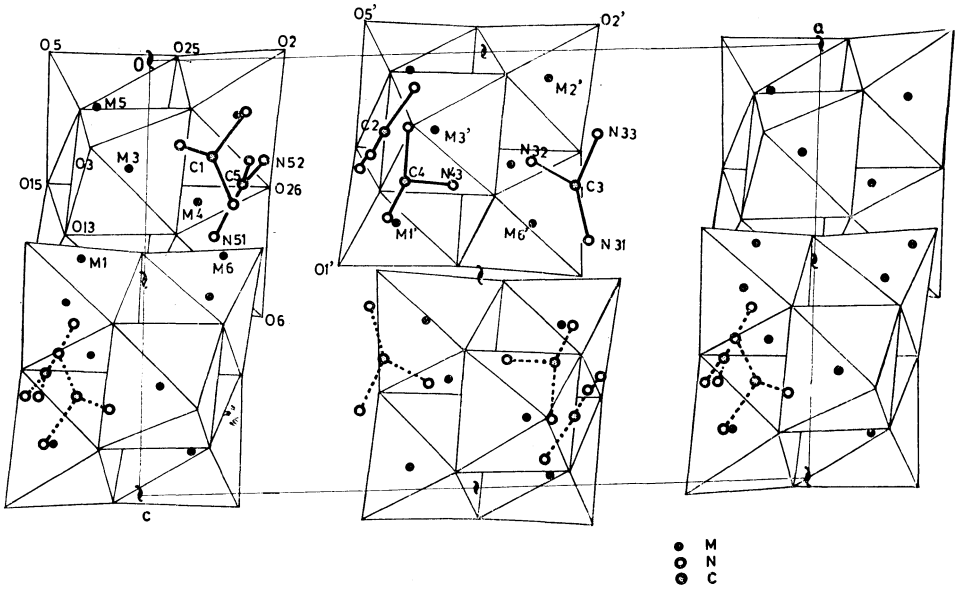

Fig. 2. A view of the structure as projected down the b axis. The dotted lines of guanidinium cations show that they are behind the anions.

already mentioned. In $W_6O_{19}^{2-}$, which has a similar structure, the W–W distances lie between 3.22 and 3.34 Å.[1] The $V_6O_{19}^{8-}$ ion seems to be too unstable to be isolated but V–V distances in the $V_{10}O_{28}^{6-}$ anion range from 3.05 to 3.19 Å.[8,9] It is understandable that the present crystals have intermediate values.

The guanidinium cation, $(CN_3H_6)^+$, has a flat triangular shape. Most of the NH groups form hydrogen bonds to Ob and Ot with O–N distances of 2.7—3.0 Å. Two diffuse peaks corresponding to guanidinium ions found in the Fourier map suggest a rotational disorder around the threefold axis. One of the guanidinium cations could not be found at all.

Flynn and Pope divided the vanadotungstates into two groups, namely the $Nv+Nw=6$ series and the $Nv+Nw=13$ series (Nv: number of vanadium atom, Nw: number of tungsten atom). They proposed the "hexaniobate structure" [22] for the first series, $V_nW_{6-n}O_{19}^{-(n+2)}$, and the Keggin structure $V^tV_nW_{12-n}O_{40}^{-(n+3)}$, for the second series, where V^t is the tetrahedrally coordinated central vanadium atom in a Keggin ion.[23] The present study, together with our unpublished structure determination of $K_7V_5W_8O_{40}\cdot 12H_2O$ crystals having the Keggin structure,[19] provides proof of Flynn and Pope's theory on the composition of vanadotungstates. The isopolytungstate, $W_{16}O_{19}^{2-}$ is unstable in aqueous solution and is easily hydrolyzed.[24] On the other hand, $V_2W_4O_{19}^{4-}$ is stable at pH 4—6 and $VW_5O_{19}^{3-}$ at 4. The latter ion will be isostructural to $W_6O_{19}^{2-}$ and to $V_2W_4O_{19}^{4-}$. The unstable $W_6O_{19}^{2-}$ ion seems to be stabilized by substitution of one or two tungsten atoms by vanadium.

The authors are indebted to Professor J. Fuchs of the Freie Universität Berlin, for his suggestion about Raman spectra, and to Dr. I. Harada of The University of Tokyo for his help in measuring Raman spectra. Thanks are also due to Professor M. T. Pope for his interest in the present work.

References

1) G. Henning and A. Hüllen, *Z. Kristallogr.*, **130**, 162 (1969).
2) J. Fuchs, H. Hartl, and W. Schiller, *Angew. Chem. Int. Edit.*, **12**, 409 (1973).
3) A. Kobayashi and Y. Sasaki, (to be published).
4) R. Allmann, *Acta Crystallogr.*, **B27**, 1393 (1971).
5) H. T. Evans, Jr., *Z. Krist.*, **114**, 257 (1960).
6) H. T. Evans, Jr. and S. Block, *Inorg. Chem.* **5**, 1808 (1966).
7) A. M. Byström and H. T. Evans, Jr., *Acta Chem. Scand.*, **13**, 377 (1959).
8) H. T. Evans, *Inorg. Chem.*, **5**, 967 (1966).
9) A. G. Swallow, F. R. Ahmed, and W. H. Barnes, *Acta Crystallogr.*, **21**, 397 (1966).
10) W. Prandtl, *Z. Anorg. Chem.*, **92**, 198 (1915).
11) A. Rosenheim and M. Pieck, *ibid.*, **98**, 223 (1916).
12) F. Chauveau, *Bull. Soc. Chim. Fr.*, **5**, 834 (1960).
13) F. Chauveau and P. Souchay, *ibid.*, **8**, 561 (1963).
14) A. B. Bekturov, D. U. Begalieva, and A. K. I'lyasova, *Russian J. Inorg. Chem.*, **15**, 1332 (1970).
15) C. M. Flynn, Jr., and M. T. Pope, *Inorg. Chem.*, **10**, 2524 (1971).
16) C. M. Flynn, Jr., and M. T. Pope, *ibid.*, **10**, 2745 (1971).
17) C. M. Flynn, Jr., and M. T. Pope, *ibid.*, **11**, 1950 (1972).
18) The assumption that these two crystallographically independent polyanions might have different chemical formula was ruled out by the aid of Raman spectroscopy. The Raman spectra of the crystals are almost identical to those of $Ag_4V_2W_4O_{19}\cdot 2H_2O$ which contains only one discrete $V_2W_4O_{19}^{4-}$ anion per unit cell.[19]
19) K. Nishikawa, A. Kobayashi, and Y. Sasaki, to be published.
20) "The Universal Crystallographic Computation Program System," Crystallographic Society of Japan (1967).
21) "International Tables for X-ray Crystallography," Kynoch Press, Birmingham (1962), Vol. III.
22) I. Lindqvist, *Arkiv Kemi*, **5**, 247 (1953).
23) J. F. Keggin, *Proc. Roy. Soc.*, **A144**, 75 (1934).
24) K. F. Jahr, J. Fuchs, and R. Oberhauser, *Chem. Ber.*, **101**, 477 (1968).

Thermal Products in the System of $NaPO_3$ Glass-Al_2O_3

Makoto WATANABE, Shoji SATO, and Hajime SAITO*

Department of Industrial Chemistry, Chubu Institute of Technology, Matsumoto-cho, Kasugai-shi, Aichi 487
**Department of Applied Chemistry, Faculty of Engineering, Nagoya University, Chikusa-ku, Nagoya 464*

(Received October 2, 1974)

The glassy and crystalline products were made by heating a mixture of aluminum oxide and sodium metaphosphate glass with P/Al ratios in the range from 1.0 to 300 at 1000 °C for 3 hr. The crystalline substance was present in the products with P/Al ratios smaller than 5.0 and was, except for aluminum oxide, always aluminum orthophosphate. The quantitative analysis and the measurement of the average chain length of the phosphates contained in the soluble parts of the products showed that aluminum oxide reacts with sodium metaphosphate to make Al–O–P linkages. A theoretical treatment of the average chain length of the polyphosphates present in the aluminate-phosphates was also made. By comparing the calculated average chain length with the measured one, it has been concluded that the most reasonable chemical structure of the glassy products of the aluminate-phosphates is $Al(OP)_3$. By the analysis of the infrared spectra of the thermal products, four-way branching points may be said to exist in the glassy products.

From the viewpoint of pure chemistry, the thermal products of arsenate-phosphates,[1] silicate-phosphates,[2] vanadate-phosphates,[3] and borate-phosphates[4,5] have been studied in to obtain some information on the reactivity between these oxo-acid salts at a moderately high temperature and on the chemical structures of the products. By analyzing the hydrolysis products, it has been revealed that there is a P–O–As, P–O–Si, P–O–V, or P–O–B linkage in each of the products. The authors also studied antimonate–phosphates,[6–8] molybdate–phosphates,[9] and tungstate–phosphates;[9] it has been concluded that they have a P–O–Sb, P–O–Mo, or P–O–W linkage respectively. The most reasonable chemical structure of the glassy products has also been reported.

It is well known that aluminum ions react with orthophosphoric acid to form an aggregation polymer, which have three-dimensional networks, in water.[10] In aluminate-phosphates or borate-phosphates, the presence of a four-way branching point was pointed out by Van Wazer.[11] In the present paper, the thermal products of the $NaPO_3$–Al_2O_3 system have been made in an attempt to obtain some information on the structure of the products in connection with the information mentioned above.

Experimental

Materials and Procedure. All the materials used other than sodium metaphosphate were of a commercial grade. The sodium metaphosphate was made by heating monosodium orthophosphate in a platinum crucible at 1000 °C for 3 hr and by then quenching the melt by placing the crucible in ice water. A mixture of sodium metaphosphate and α-aluminum oxide with P/Al ratios in the range from 1.0 to 300 was heated in a platinum crucible at 1000 °C for 3 hr; the resulting product was quenched by the method used in the preparation of sodium metaphosphate.

Paper Chromatography. One-dimensional paper chromatography was used for the separation of phosphate species contained in the products by using acidic and basic solvents. The compositions of the solvents are listed in Table 1. The acidic solvent was used for the separation of ortho-, pyro-, tri-, and long-chain phosphates, while the basic solvent was used for the separation of trimeta- and tetrametaphosphates. About one gram of the product was placed in 50 ml of water, and then the mixture was stirred for one hour at room temperature. The insoluble parts were then filtered off, dried, and weighed for the measurement of the solubility of the product. About 5 μl of the sample solution was spotted on a filter paper of Toyo No. 51A (2 by 50 cm) and developed for 40 hr at 5 °C. After the filter paper had then been dried at 75 °C for more than 30 min, a perchloric acid-molybdate solution was sprayed on the paper. The paper was dried again and exposed to ultraviolet rays until blue spots appeared. The identification of each spot on the chromatogram was made by comparing the spots with those of known phosphates.

TABLE 1. COMPOSITION OF THE SOLVENTS USED FOR THE PAPER CHROMATOGRAPHY

Acidic solvent	Isopropyl alcohol	70 ml
	25% aqueous trichloroacetic acid	20 ml
	Water	10 ml
	28% aqueous ammonia	0.3 ml
Basic solvent	Isopropyl alcohol	38.7 ml
	Isobutyl alcohol	20 ml
	Water	40 ml
	28% aqueous ammonia	0.5 ml

Colorimetric Determination of Phosphates. The determination of the phosphates on a chromatogram was carried out by the colorimetric method described in a previous paper.[6]

The Measurement of the Average Chain Length of Polyphosphates. The method used in our previous paper[6] was adopted for the measurement of the average chain length of polyphosphates contained in the thermal products, but since aluminum ions present in the sample solution strongly affected the pH titration of the solution, the aluminum ions were previously removed by the oxine method.[12]

X-Ray Diffractometry. The samples were ground with an agate mortar until they could pass through a 150 mesh sieve. Their X-ray diffraction patterns were taken by means of a powder method using a Toshiba X-ray diffractometer, ADG-102.

Infrared Spectral Measurement. The infrared spectra of the products were recorded on a JASCO infrared spectrophotometer, model IR-G, by the KBr tablet method.

Results and Discussion

Solubility and Identification of Crystalline Products by X-Ray Diffractometry. The results of the measurement of the solubility of the products and of the identification of the crystalline products by X-ray diffractometry are listed in Table 2. The identification was carried out by comparing the X-ray diffraction peaks of the products with those on ASTM cards. All the X-ray peaks of the products were due to aluminum oxide and/or aluminum orthophosphate. According to the above results, it could be concluded that the P–O–P linkages of high polyphosphate in this system are broken to make aluminum orthophsophate at 1000 °C. The insoluble parts in the products with the P/Al ratios in the range from 7.0 to 15 were amorphous.

TABLE 2. AMOUNT OF WATER-SOLUBLE PARTS OF THE PRODUCTS AND IDENTIFICATION OF THE CRYSTALLINE PRODUCTS BY X-RAY DIFFRACTOMETRY

P/Al	X-Ray diff.	Water-soluble parts (%)
1.0	Al_2O_3, $AlPO_4$	3.1
2.0	Al_2O_3, $AlPO_4$	3.6
2.5	$AlPO_4$	13
3.0	$AlPO_4$	29
5.0	$AlPO_4$	67
7.0	glassy	87
10	glassy	98
15	glassy	99
20—300	glassy	100

TABLE 3. DISTRIBUTION OF PHOSPHATES OF WATER-SOLUBLE PARTS IN THE PRODUCTS

P/Al	Phosphate (P%)					
	Ortho	Pyro	Tri	Tri-meta	Tetra-meta	Higher
1.0	100					
2.0	100					
2.5	100					
3.0	100					
5.0	98.0	2.0				
7.0	11.0	17.9				71.1
10	3.8	2.3	10.5	1.3	1.5	80.6
15	2.9	2.0	3.8	3.3	2.1	85.9
20	2.7	2.4	2.1	2.9	2.4	87.5
30	1.9	1.8	1.8	3.4	2.6	88.5
50	1.4	0.3	0.7	4.5	4.2	88.9
80	0.5	0.3	1.0	2.8	2.1	93.3
100				3.5	2.3	94.2
150				2.6	2.5	94.9
200				2.8	3.1	94.1
300				3.0	2.9	94.1

Distribution of Phosphates. The results of the colorimetric determination of phosphates in the soluble parts of the products are shown in Table 3. The contents of ortho-, pyro-, and tripolyphosphates decrease with an increase in the P/Al ratio, while those of high-polyphosphates increase with an increase in the P/Al ratio. This tendency is the same as that reported in previous papers.[1–4,6–9] By analogy with the previous papers, it can reasonably be concluded that sodium metaphosphate reacts with aluminum oxide to make an Al–O–P linkage at 1000 °C and that the Al–O–P linkage of the water-soluble products is readily hydrolyzed in a water solution. Since the contents of trimeta- and tetrametaphosphates so not change much with the variation in the P/Al ratio, the formation of the metaphosphates may be little affected by aluminum.

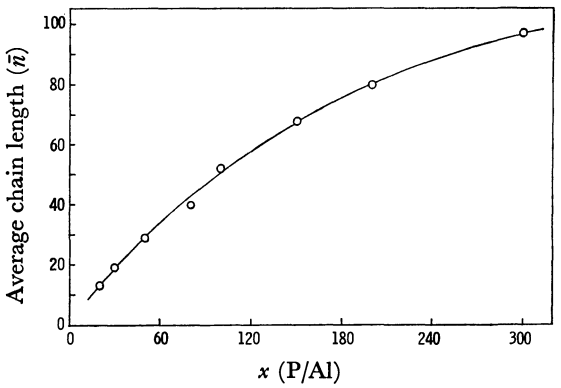

Fig. 1. Variation of average chain length of polyphosphates present in the products with P/Al ratios larger than 20

Average Chain Length of Polyphosphates and the Chemical Structure of Glassy Products. In aluminate-phosphates, the coordination number of aluminum can be four. The behavior of aluminum in the glassy products studied in the present paper can be examined by measuring the correlation between the average chain length of polyphosphates and the P/Al ratio. To obtain the correlation, it is necessary that the thermal product is dissolved completely in water. Therefore, the average chain length of the polyphosphates present in the glassy products with P/Al ratios larger than 20 were measured; the results are shown in Fig. 1. It may clearly be seen that the average chain length of the polyphosphates contained in the glassy products increases with an increase in the P/Al ratio. This tendency is the same as that found in the colorimetric determination of phosphates. The correlation between the coordination number of aluminum and the average chain length of polyphosphates in the thermal products can be considered theoretically by the method described in previous papers.[2,6–9] According to the theory, the relation between the P/Al ratio and the average chain length of polyphosphates can be written as follows:

$$(\bar{n}+2)/\bar{n} = (x+y-z+fx)/x$$

where $\bar{n}$ is the average chain length of polyphosphates, where x, y, and z are, respectively, the number of phosphorus atoms, P–O–Al linkages, and Al–O$^-$ linkages per atom of aluminum, and where f is the factor shortening the chain length of the polyphosphates, given with respect to an atom of phosphorus. It is known by previous experiments[2,6–9] that the value of f is in the range from 0.01 to 0.025 under the conditions employed in this experiment. The bonding formulas

Table 4. Chemical structures of the glassy products with P/Al ratios larger than 20

	A	B	C
I	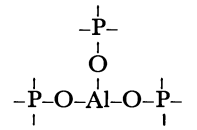	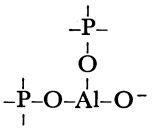	
II	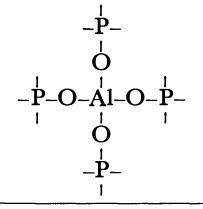	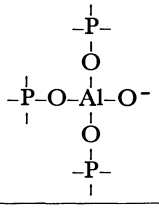	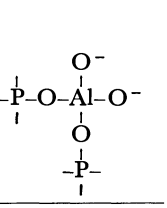

Table 5. Average chain length of polyphosphates of the $NaPO_3$–Al_2O_3 system with P/Al ratios larger than 20

x (P/Al)	$\bar{n}$ Found	$\bar{n}$ calcd. by Eq. (1) (f=0.01) Model[a]				
		IA	IB	IIA	IIB	IIC
20	13	13	33	10	18	200
30	19	18	46	14	26	200
50	29	29	67	22	40	200
80	40	42	89	33	57	200
100	52	50	100	40	67	200
150	68	67	120	55	86	200
200	80	80	133	67	100	200
300	97	100	150	86	120	200

a) The models refer to Table 4.

of aluminum with phosphates in glassy products are shown in Table 4. Other structures could be described for the system, but it can readily be seen in the following discussion that the other structures are unreasonable for the system. The calculated values of $\bar{n}$ based on the chemical structures in Table 4 are listed in Table 5. As may clearly be seen in the table, when the f factor is 0.01, the calculated values of $\bar{n}$ based on the IA structure in Table 4 are very close to the measured ones throughout the range of P/Al ratios from 20 to 300. From these results, it may reasonably be concluded that the chemical structure of the glasses of the Al_2O_3–$NaPO_3$ system with P/Al ratios larger than 20 is the IA structure in Table 4. This also means that the valence of aluminum, which contributes to the shortening of the chain length of polyphosphates, is three.

Infrared Spectra. The infrared spectra of sodium metaphosphate glass and the glassy products with P/Al ratios of 3.0, 5.0, and 7.0 are shown in Fig. 2. Since the infrared spectra of the glassy products with P/Al ratios larger than 7.0 are the same as that of sodium metaphosphate, the existence of the absorption of the Al–O–P linkages in the glassy products with P/Al ratios larger than 20 can not be discussed. According to Corbridge and Lowe,[13] the absorption of 1270 cm^{-1} in the spectrum of sodium metaphosphate may be

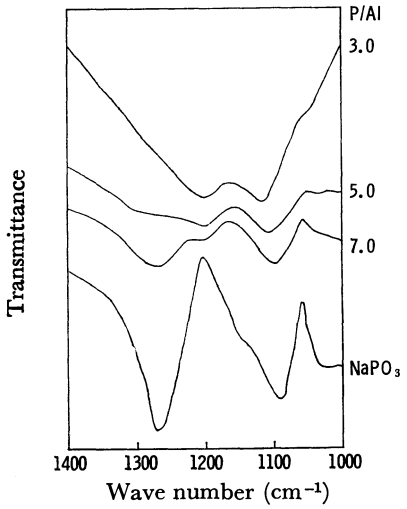

Fig. 2. IR spectra of the products with P/Al ratios from 3.0 to 7.0 and $NaPO_3$ glass

considered to be due to P=O stretching. When the P/Al ratio decreases from 7.0 to lower values, this absorption shifts to lower wave numbers in the spectra of the products. It can be concluded that the bonding force of the P=O bond decreases with a decrease in the P/Al ratio. This phenomenon can be explained as a P=O bond transfers to the P=O=Al bond by the coordination of aluminum. By extending this result to the glassy products with P/Al ratios larger than 10, it can be said that four-way branching points may exist in the glassy products.

References

1) K-H Jost, H. Worzalla, and E. Thilo, *Z. Anorg. Allg. Chem.*, **325**, 98 (1963).
2) S. Ohashi and F. Oshima, This Bulletin, **36**, 1489 (1963).
3) S. Ohashi and T. Matsumura, *ibid.*, **35**, 501 (1962).
4) T. Nakamura and S. Ohashi, *ibid.*, **40**, 110 (1967).
5) K. Honma and K. Honma, *Nippon Kagaku Kaishi*, **1972**, 856.
6) M. Watanabe, K. Tanabe, T. Takahara, and T. Yamada, This Bulletin, **44**, 712 (1971).
7) M. Watanabe and M. Kato, *ibid.*, **45**, 1058 (1972).
8) M. Watanabe, *ibid.*, **46**, 2468 (1973).
9) M. Watanabe, *Nippon Kagaku Kaishi*, **1974**, 1407 and 1412.
10) For example, J. R. Van Wazer, "Phosphorus and Its Compounds," Vol. 1, Interscience Publishers, New York (1958), p. 558.
11) J. R. Van Wazer, *ibid.*, p. 422.
12) For example, Nippon Bunseki Kagakukai, "Bunseki Kagaku Binran," Maruzen, Tokyo (1971), p. 156. In the course of this analysis, it is necessary to heat an acidic sample solution (the pH is near 3) at 70 °C; this causes the scission of the P–O–P linkages. Therefore, the period of heating the sample solution was as short as possible (about 3 min.), and aging was done at room temperature for about 20 min.
13) D. E. C. Corbridge and E. J. Lowe, *J. Chem. Soc.*, **1954**, 493 and 4555.

The Mechanism of the Hydrolysis of Condensed Phosphates. II. The Mechanism of the Degradation of Long-chain Polyphosphates

Makoto WATANABE, Shoji SATO, and Hajime SAITO*

Department of Industrial Chemistry, Chubu Institute of Technology, Matsumoto-cho, Kasugai-shi, Aichi 487
**Department of Applied Chemistry, Faculty of Engineering, Nagoya University, Chigusa-ku, Nagoya 464*

(Received October 22, 1974)

The hydrolysis of long-chain polyphosphates (Graham's salt) was carried out in water and dioxane–water solvents at various pHs in the range from 3.0 to 11.0 and at 30, 50, and 70 °C. The rates of the hydrolytic degradation of the polyphosphates into shorter chains and into trimetaphosphate obeyed the first-order kinetics with respect to the concentration of the polyphosphates. In acidic media, a small solvent effect was perceived on the rates of both the processes. On the other hand, in basic media the effect was very remarkable; that is, the rates of both the processes in the dioxane–water solvent were more rapid than in water. The results show that the rate of the hydrolysis of both the processes in basic media may be very dependent on the step of the nucleophilic attack of a water molecule on the phosphorus atom of phosphates, while in acidic media other factor, for example, the folding of the chains to a helix, may affect the overall rate. The activation energies for the two processes have been found to be 22—26 kcal/mol in the pH range from 3.0 to 7.0.

The hydrolysis of long-chain polyphosphates has been studied by several investigators.[1–4] According to them, there are two processes for the hydrolytic degradation of the polyphosphates. One is the hydrolysis into shorter chains, and the other is the degradation into trimetaphosphate. Both the processes have been found to be pH-dependent and to be catalytically accelerated by metal ions. The catalytic effect increases in this order; K<Na<Li<Ba<Sr<Ca<Mg<Al. Their kinetic studies also prove that the processes follow a first-order law with respect to the concentration of polyphosphates. In our own previous paper,[5] the solvent effect on the hydrolysis of pyro- and tripolyphosphates was examined from the viewpoint of the nucleophilicity of a water molecule. In the present paper, the solvent effect on the hydrolysis of the polyphosphates will be examined by using dioxane–water and water as solvents at various pH values and temperatures. Since the hydrolysis of the polyphosphates at a low temperature is very slow, only the hydrolysis at 70 °C was achieved for all the pH values.

Experimental

Materials and Procedure. All the materials used other than the glassy, high-molecular-weight polyphosphates (Graham's salt) were of a commercial grade. The polyphosphates were prepared by heating monosodium orthophosphate in a platinum crucible at 1000 °C for 3 hr and by then rapidly quenching the resulting melt by placing the crucible in ice water. Since the polyphosphates invariably contained 2—3% (as phosphorus %) of trimetaphosphate, the corresponding adjustment was made to the analytical results of the contents of the hydrolysis products. Water and 15 vol% aqueous dioxane were employed as solvents. The initial concentration of the polyphosphates was 0.025 mol/l. About 25 ml of the solution was transferred into a test tube, and the pH of the solution was controlled at a reaction temperature by adding nitric acid and aqueous tetramethylammonium hydroxide or sodium hydroxide by means of a Hitachi-Horiba pH meter, F-5. The test tube was stoppered to prevent evaporation of the solvent. The tube was then placed in water in a thermostat, and the temperature was maintained at 30, 50, or 70±0.05 °C. A measured sample of this solution was withdrawn by using a microsyringe as soon as the treatment mentioned above was finished; this sample was spotted on to chromatograms. At measured intervals of time, further samples were similarly taken out for quantitative chromatographic analysis. The pH of the solutions was periodically measured and maintained at the required pH by adding nitric acid, aqueous tetramethylammonium hydroxide, or aqueous sodium hydroxide. The pH adjustment of the solution by adding sodium hydroxide was made only at pH 11.0. Since the sodium ion affects the rate of the hydrolysis of the polyphosphates, the quantity of the sodium ion in water and dioxane–water solvents was made identical. The pH adjustment was done within ±0.2 pH unit of the required value.

Chromatography. One-dimensional paper-chromatographic separation were carried out by using filter paper of Toyo No. 51A of 2×50 cm. Sample solutions (8 μl) were placed at the starting point of the filter paper and developed at 3 °C for 50 hr by using an acidic or basic solvent. After the development, the chromatograms were dried in an oven at 75 °C for more than 30 min and then sprayed with a perchloric acid molybdate solution.[6] The papers were subsequently dried for about 10 min at 50 °C and exposed to ultraviolet rays until blue zones appeared. The compositions of the acidic and basic solvents are tabulated in Table 1. The former was used for the separation of ortho-, pyro-, tripoly-, and long-chain polyphosphates, while the latter was used for the separation of trimeta- and tetrametaphosphates.

Quantitative Analysis of Phosphates on Chromatograms. The contents (P%) of phosphates on the chromatograms were determined by means of the same colorimetric method used in our previous paper,[5] using a Hitachi 101 spectrophotometer.

Table 1. Composition of the solvents used for paper chromatography

Acidic solvent	Isopropyl alcohol	70 ml
	25% aqueous trichloroacetic acid	20 ml
	Water	10 ml
	28% aqueous ammonia	0.3 ml
Basic solvent	Isopropyl alcohol	20 ml
	Dimethylformamide	20 ml
	Methyl ethyl ketone	20 ml
	Water	39.1 ml
	28% aqueous ammonia	0.9 ml

Results and Discussion

All attempts to obtain high-molecular-weight polyphosphates free from a trimeta-ring were unsuccessful. The average chain length of the polyphosphates was measured by the pH titration method[7,8] and found to be about 100. The straightforward hydrolytic degradation of the polyphosphate chains into shorter chains and their degradation to trimetaphosphate occurred according to a first-order law with respect to the concentration of polyphosphates under all the conditions studied. The values of the specific rate constants, k_H for the hydrolysis of polyphosphates, and k_D for the splitting out of trimetaphosphate, are listed in Table 2 for the various temperatures and pH values. Since the rates of the hydrolysis of trimetaphosphate at pH 3.0 and 11.0 can not be ignored in comparison with that of the formation of trimetaphosphate from the polyphosphates, k_D was not measured at those pH values. In the case of the hydrolysis of the polyphosphates in a water solvent, both the rate constants decrease with an increase in the pH value at any reaction temperature. This tendency has been well substantiated.[1-4] However, the decrease at 50 and 70 °C in the pH range from 7.0 to 9.0 seems to be less than that obtained by Gill and Riaz.[4] This may be attributed to the difference in cations added to the polyphosphate solutions for the adjustment of the background pH. As for the hydrolysis of the polyphosphates in the dioxane–water solvent, the pH-dependency of both the reaction constants is not the same as that in a water solvent. In an acidic medium, both the rate constants of the reactions in the dioxane–water solvent are the same as, or a little smaller than, those of the reactions in a water solvent at the same pH value. On the other hand, in the polyphosphate solutions with pH values larger than 7.0, the reaction rates of both the processes in the aqueous dioxane are faster than those in a water solvent; the larger the pH value of the solution, the more remarkable is this tendency.

In our previous paper,[5] the solvent effects on the hydrolysis of pyro- and tripolyphosphates have been studied, and it has been concluded that a water molecule in aqueous dioxane has a larger nucleophilicity than in water throughout the pH range from 1.0 to 2.5. From the results of the examination of the catalytic effect of metal cations on the polyphosphate degradation, Wieker and Thilo proposed a mechanism for the degradation.[3] According to them, a positivation of the phosphorus atoms of the polyphosphates may be supposed to be the reason for the catalytic effect of the metal cations. In our previous work,[5] taking into account the findings that the hydrolyses of pyro- and tripolyphosphates are acid-catalyzed reactions, the same positivation of the phosphorus atoms of the phosphates was also proposed for the hydrolysis of the phosphates. On the basis of these results, and considering that the hydrolysis of the polyphosphates is also an acid-catalyzed reaction, one can describe a series of elementary reactions for the hydrolysis of the polyphosphates as follows:

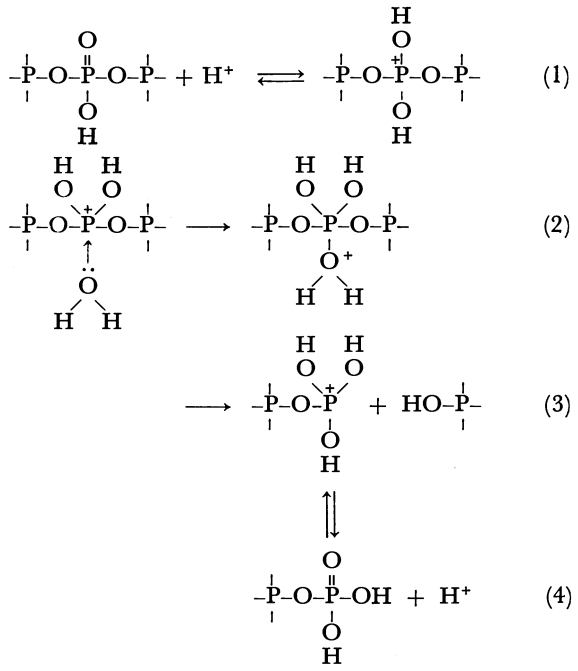

Table 2. Rate constants (min^{-1}) of the degradation of polyphosphates

pH	Solvent[a]	Reaction temp. (°C) 30 k_H	30 k_D	50 k_H	50 k_D	70 k_H	70 k_D
3.0	S_1	2.90×10^{-5}		4.29×10^{-4}		4.74×10^{-3}	
	S_2	2.73×10^{-5}		4.07×10^{-4}		4.39×10^{-3}	
5.0	S_1			1.10×10^{-5}	4.52×10^{-6}	1.97×10^{-4}	5.51×10^{-5}
	S_2			1.14×10^{-5}	3.56×10^{-6}	1.74×10^{-4}	4.40×10^{-5}
7.0	S_1	6.80×10^{-7}	4.04×10^{-7}	6.99×10^{-6}	4.40×10^{-6}	5.50×10^{-5}	3.62×10^{-5}
	S_2	7.80×10^{-7}	5.48×10^{-7}	7.84×10^{-6}	5.31×10^{-6}	6.40×10^{-5}	4.02×10^{-5}
9.0	S_1			6.55×10^{-6}	3.02×10^{-6}	5.40×10^{-5}	3.55×10^{-5}
	S_2			9.79×10^{-6}	5.45×10^{-6}	8.38×10^{-5}	5.41×10^{-5}
11.0	S_1			5.79×10^{-6}		5.31×10^{-5}	
	S_2			1.00×10^{-5}		9.57×10^{-5}	
11.0	S_1Na					1.09×10^{-4}	
	S_2Na					1.95×10^{-4}	

a) S_1 and S_2 stand for water and 15 vol % aqueous dioxane respectively, and Na represents that the pH of the solution is controlled by aqueous sodium hydroxide.

For the hydrolysis of the polyphosphates in a basic solution, the second step can be considered to be the rate-determining step, because the rate of the hydrolysis of both the processes is very dependent on the nucleophilicity of a water molecule.

Because of the formation of ring phosphates larger than trimetaphosphate as hydrolysis products of polyphosphates, it has been concluded that, when polyphosphates are dissolved into water, the folding of the chain into a helix occurs with a random number of PO_4 tetrahedra in the repeating units, and that in the repeating unit of three PO_4 tetrahedra is statistically the most likely. In an acidic medium, it can hardly be considered that the first, second, and fourth steps influence the rate of the overall-hydrolytic reaction of polyphosphates, because the steps may be very rapid reactions. Since no solvent effect as in a basic medium is recognized in acidic systems, the rate of the overall reaction may be little dependent on the third step. Therefore, the overall-reaction rate seems to reflect the effects of other factors—for example, the folding of the chain into a helix. In order to examine the idea, the activation energies and log A (A; frequency factor) at pH 3.0 (for k_H) and 7.0 (for k_H and k_D) were calculated by the use of an Arrhenius plot; they are listed in Table 3. For the overall-hydrolytic degradation of the polyphosphates, in spite of the increase in the reaction rate, the activation energy increases with a decrease in the pH value. This result suggests that the contribution of an entropy term to the rate of the degradation is more important than that of an energy term in an acidic solution, and seems to support the consideration concerning the hydrolytic mechanism of polyphosphates presented above. The activation energies, listed in Table 3, of the degradation of the polyphosphates into trimetaphosphate at pH 7.0 are very similar to that obtained by Gill and Riaz.[4]

Table 3. Activation energy, ΔE_A (kcal/mol) and log A (A; frequency factor) of the hydrolysis of polyphosphates

pH	Solvent[a]	Process[b] P_1 ΔE_A	P_1 log A	P_2 ΔE_A	P_2 log A
3.0	S_1	26.2	14.4		
	S_2	26.2	14.3		
7.0	S_1	22.7	10.2	23.3	10.4
	S_2	22.4	10.0	22.1	9.7

a) S_1 and S_2 represent water and 15 vol% aqueous dioxane respectively. b) P_1 and P_2 stand for the hydrolysis of polyphosphates and the hydrolytic splitting out of trimetaphosphate respectively.

The results of the hydrolytic degradation of the polyphosphates in an aqueous sodium hydroxide solution are also listed on the lowest two lines in Table 2. It can clearly be seen that sodium ions have a catalytical effect on the hydrolysis of polyphosphates and that the solvent effect is also very remarkable.

References

1) E. Thilo and W. Wieker, *Z. Anorg. Allg. Chem.*, **291**, 164 (1957).
2) W. Wieker and E. Thilo, *ibid.*, **306**, 48 (1960).
3) W. Wieker and E. Thilo, *ibid.*, **313**, 296 (1961).
4) J. B. Gill and S. A. Riaz, *J. Chem. Soc., A*, **1969**, 183.
5) M. Watanabe, This Bulletin, **47**, 2048 (1974).
6) The perchloric acid molybdate solution was made by mixing 200 ml of 5% aqueous ammonium molybdate, 10 ml of conc. hydrochloric acid, and 50 ml of 70% aqueous perchloric acid and by then diluting the solution to 1000 ml with water.
7) J. R. Van Wazer, E. J. Griffith, and J. F. McCulough, *Anal. Chem.*, **26**, 1755 (1954).
8) E. J. Griffith, *ibid.*, **28**, 525 (1956).

Analysis of Metals by Solid-Liquid Separation after Liquid-Liquid Extraction. Spectrophotometric Determination of Some Metals by Extraction of Metal Complexes with Molten Naphthalene

Taitiro FUJINAGA, Masatada SATAKE, and Tatsuo YONEKUBO*

Faculty of Science, Kyoto University, Sakyo-ku, Kyoto 606

**Faculty of Engineering, Fukui University, Fukui 910*

(Received October 25, 1974)

A procedure is described for the spectrophotometric determination of metals after extraction with molten naphthalene. Some metal ions react in aqueous solution with complex-forming reagents such as oxine, 2-methyloxine, dimethylglyoxime or α-benzil dioxime to form water-insoluble complexes in certain pH ranges, the complexes being easily extracted into molten naphthalene. The extracted mixture of metal complex and naphthalene is dissolved in dimethylformamide and the amount of each metal is determined spectrophotometrically. The working range of metal ion concentration and effect of various factors such as pH, amount of reagent and naphthalene were studied, and the molar absorptivity, sensitivity and relative standard deviation evaluated.

Spectrophotometric determination of metals in aqueous solution after extraction of their complexes with organic solvent have been widely employed in the analysis of trace amount of metal ions. However, the method is not applicable when the solubility of the complexes in the solvent is small.

We have developed a new method "solid-liquid separation after liquid-liquid extraction," and have applied it to the determination of copper,[1,2] zinc,[3] magnesium,[4] and cadmium[5] with oxine as the complex-forming reagent, and to that of nickel[6] and palladium[7] with dimethylglyoxime. The method is based on the formation of metal complex which is extractable quantitatively with molten naphthalene. After the mixture of solidified complex and naphthalene have been cooled, it is dissolved in adequate organic solvent and the amount of metal in the solution is determined spectrophotometrically. The method is useful for the determination of metals such as zinc, magnesium or cadmium, since direct extraction of the complex with conventional solvents such as benzene or chloroform is very difficult owing to its hydrated structure. Each complex is easily extracted at high temperature merely by being put in contact with molten naphthalene. The extract is easily dissolved in dimethylformamide to develop intense coloration of the stable complex. In the present paper, successful extraction of the following complexes into molten naphthalene is presented: oxine complex of copper, zinc, magnesium and cadmium, 2-methyloxine complex of copper, dimethylglyoxime complex of nickel, and α-benzildioxime complex of nickel.

Experimental

Reagents. Standard 0.01 M metal solutions. Stock solutions of copper, zinc, magnesium, cadmium and nickel were prepared by dissolving copper sulfate, zinc sulfate, magnesium chloride, cadmium chloride and nickel sulfate of reagent grade in water weakly acidified with a few drops of concentrated sulfuric acid or hydrochloric acid and standardized chelatometrically. It was diluted suitably before use.

1% oxine and 2-methyloxine solutions. Prepared by dissolving 1.0 g of oxine or 2-methyloxine in 2 ml of glacial acetic acid on a water bath and diluting to 100 ml with water.

0.5% dimethylglyoxime and 0.02% α-benzil dioxime solutions in ethanol.

Buffer solutions. Mixtures of 1 M acetic acid and 1 M sodium acetate, 0.5 M disodium hydrogen phosphate and 0.5 M potassium dihydrogen phosphate, or 1 M ammonia water and 1 M ammonium chloride.

Redistilled demineralized water was used.

Naphthalene, dimethylformamide and all other reagents were of analytical reagent grade and used without further purification.

Apparatus. A Hitachi Model 124 spectrophotometer was used for the absorbance measurements with matched 10 mm glass cells. A Toa-Dempa HM-6A pH meter equipped with combined glass and calomel electrodes was used for pH measurements.

Procedure. Transfer an aliquot of standard metal solution to a tightly stoppered 80 ml Erlenmeyer flask and

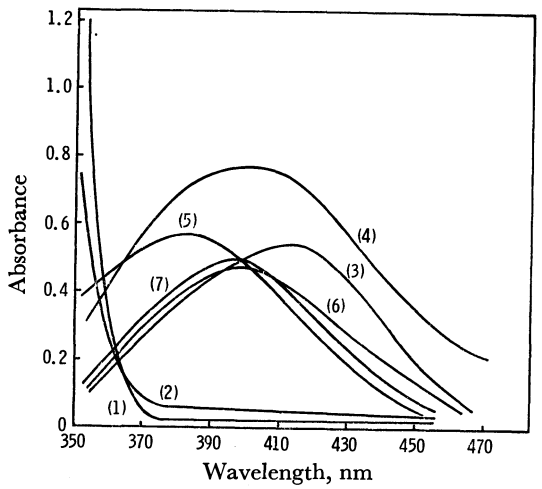

Fig. 1. Absorption spectra of oxine, 2-methyloxine and metal complexes in naphthalene–dimethylformamide solution.
(1) 1% oxine: 1.0 ml; pH: 5.0; against water
(2) 1% 2-methyloxine: 1.5 ml; pH: 5.5; against water
(3) Cu: 64 μg; 1% oxine; 1.0 ml; pH: 5.0
(4) Zn: 262 μg; 1% oxine: 1.0 ml; pH: 8.9
(5) Mg: 73 μg; 1% oxine: 2.0 ml; pH: 9.9
(6) Cd: 100 μg; 1% oxine: 1.5 ml; pH: 7.5
(7) Cu: 64 μg; 1% 2-methyloxine: 1.5 ml; pH: 5.5
Reference: Reagent blank

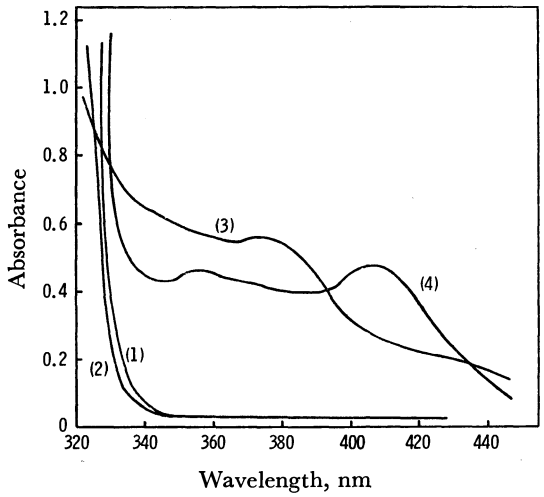

Fig. 2. Absorption spectra of dimethylglyoxime, α-benzil dioxime and metal complexes in naphthalene–dimethylformamide solution
(1) 0.5% dimethylglyoxime: 0.5 ml; pH: 8.6; against water
(2) 0.02% α-benzil dioxime: 3.0 ml; pH: 9.0; against water
(3) Ni: 117 μg; pH: 8.6; 0.5% dimethylglyoxime: 0.5 ml
(4) Ni: 29.4 μg; pH: 9.0; 0.02% α-benzil dioxime: 3.0 ml
Reference: Reagent blank

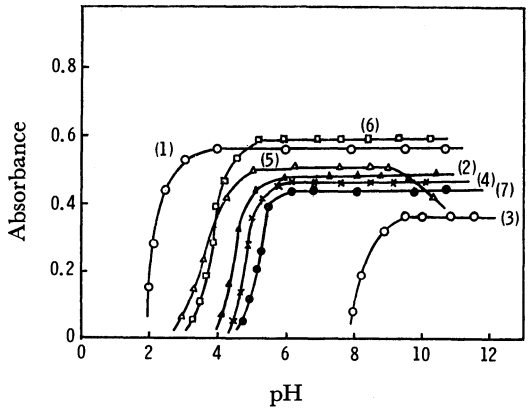

Fig. 3. Effect of pH on absorbance
(1) Cu: 64 μg; 1% oxine: 1.0 ml; Wavelength: 412 nm
(2) Zn: 163 μg; 1% oxine: 1.0 ml; Wavelength: 400 nm
(3) Mg: 49 μg; 1% oxine: 2.0 ml; Wavelength: 384 nm
(4) Cd: 100 μg; 1% oxine: 1.5 ml; Wavelength: 400 nm
(5) Cu: 64 μg; 1% 2-methyloxine: 1.5 ml; Wavelength: 400 nm
(6) Ni: 117 μg; 0.5% dimethylglyoxime: 0.5 ml; Wavelength: 374 nm
(7) Ni: 29 μg; 0.02% α-benzil dioxime: 3.0 ml; Wavelength: 406 nm
Reference: Reagent blank

dilute to about 30 ml with water. Add the complex-forming reagent and then adjust the pH with a buffer solution. Mix the solution well and allow it to stand for 15 min and then warm gently on a water bath at 60 °C until a precipitate of the metal complex appears. Add 2.0 g of naphthalene and heat the mixture to 90 °C. Shake it vigorously till naphthalene solidifies forming fine crystals. Melt it again and shake well, then allow it to cool to room temperature. Warm it again and slowly melt the very fine solidified crystals suspended in the solution, letting them grow to a larger crystalline deposit. After cooling it at room temperature, separate the solidified deposit on a filter paper, wash with water and blot the surplus water with a dry filter paper. Dissolve the deposit with dimethylformamide. Transfer the solution to a 25 ml volumetric flask, fill with dimethylformamide up to 25 ml, and measure the absorbance of the solution in a 10 mm cell against the reagent blank.

Results and Discussion

Figures 1 and 2 show the absorption spectra of metal complexes in naphthalene–dimethylformamide solution against the reagent blank. These complexes have their absorption maxima in the range 370—410 nm, whereas the reagent shows no absorption above 370 nm.

Figure 3 shows the effect of pH on the absorbance of metal complexes in naphthalene–dimethylformamide

TABLE 1. SPECTROPHOTOMETRIC DETERMINATION OF METALS IN NAPHTHALENE-DMF

Metal complexes	Max. wavelength (nm)	pH of extraction	Amount of reagent (ml)	Calibration curve (ppm)	Molar absorptivity ($l \cdot mol^{-1} \cdot cm^{-1}$)	Sensitivity (g/cm^2)	Relative standard deviation (%)
Cu-oxinate	412	3.5—	1% oxine, 0.3—1.5	0.6—10	5.4×10^3	0.012	1.16
Zn-oxinate	400	5.5—10.5	1% oxine, 0.3—3.0	0.7—14	4.6×10^3	0.013	0.45
Mg-oxinate	384	9.5—	1% oxine, 1.5—2.0	0.3— 5	4.5×10^3	0.006	1.40
Cd-oxinate	400	6.0—	1% oxine, 1.0—2.0	1.0—16	5.5×10^3	0.020	1.01
Cu-2-methyl-oxinate	400	5.5—9.0	1% 2-methyloxine, 1.0—3.0	0.6—10	5.2×10^3	0.012	1.06
Ni-dimethyl-glyoximate	374	5.5—	1% dimethylglyoxime, 0.2—1.0	1.0—23	3.0×10^3	0.020	0.92
Pd-dimethyl-glyoximate	370	1.1—7.8	1% dimethylglyoxime, 1.0	3.0—53	1.7×10^3	0.062	0.64
Ni-α-benzil dioximate	406	6.0—	0.02% α-benzil dioxime, 1.5—	0.4— 6	9.0×10^3	0.006	0.88

Naphthalene: 2.0 g, Solvent: Chloroform for Pd, Dimethylformamide for other metals

solution against the reagent blank. The pH values of the aqueous solution after extraction were measured at room temperature. The pH values were adjusted with acetate, phosphate or ammonia buffer solution except for the extraction of cadmium.

The amounts of naphthalene were varied from 0.5 to 3.0 g, extraction operation being carried out by the recommended procedure. Addition of naphthalene above 1.5 g gave no effect on the results. 2.0 g of naphthalene was adequate for complete extraction of each metal complex.

Variation of absorbance with the amount of complex-forming reagent was relatively small over the large amount of the reagent. The amount of buffer solution, 0.5—5 ml, had no effect on the absorbance. Acetate and ammonium salts gave considerable error, both positive and negative, for cadmium determination. Since the speed of extraction of metal complexes into molten naphthalene is great owing to high temperature, extraction is completed merely by contact with molten naphthalene or by slight shaking. It is not necessary to remove water on naphthalene crystals with anhydrous sodium sulfate, since dimethylformamide is miscible with water. The results obtained are summarized in Table 1. The calibration curve for each metal was derived at a proper wavelength against the reagent blank. The molar absorptivity, sensitivity and relative standard deviation on each metal were also calculated for ten determinations.

References

1) T. Fujinaga, T. Kuwamoto, and E. Nakayama, *Talanta*, **16**, 1225 (1969).
2) T. Fujinaga, T. Kuwamoto, T. Yonekubo, and M. Satake, *Bunseki Kagaku*, **18**, 1113 (1969).
3) T. Fujinaga, M. Satake, and T. Yonekubo, *ibid.*, **19**, 217 (1970).
4) M. Satake, Memoirs Fac. Engineering, Fukui University, **18**, 225 (1970).
5) T. Fujinaga, M. Satake, and T. Yonekubo, This Bulletin, **46**, 2092 (1973).
6) T. Fujinaga, M. Satake, and T. Yonekubo, *Bunseki Kagaku*, **20**, 1255 (1971).
7) T. Fujinaga, M. Satake, and T. Yonekubo, *Talanta*, **19**, 689 (1972).

Preparation of *cis*- and *trans*-Dicyanobis(ethylenediamine)chromium(III) Complexes and Optical Resolution of the *cis* Isomer

Sumio KAIZAKI, Jinsai HIDAKA, and Yoichi SHIMURA

Department of Chemistry, Faculty of Science, Osaka University, Toyonaka, Osaka 560

(Received November 11, 1974)

Two geometrical isomers, *cis* and *trans*, of $[Cr(CN)_2(en)_2]^+$ were prepared and the *cis* isomer was resolved into optical isomers. The ligand field absorption and circular dichroism spectra were discussed and the absolute configuration of *cis*-$(+)_{546}$-$[Cr(CN)_2(en)_2]^+$ was determined to Λ on the basis of the circular dichroism sign in the first spin-allowed d-d band region.

There has been known only one series, though incomplete, of mixed cyano chromium(III) complexes, *i.e.*, aquacyano complexes, $[Cr(CN)_n(OH_2)_{6-n}]^{3-n}$,[1-2] which have been studied in solution, but not isolated as solid complexes. No mixed cyanoamine or cyanoammine chromium(III) complexes have been known.

In the present paper, the preparation and characterization of an isomeric pair of dicyanobis(ethylenediamine)chromium(III) perchlorate or chloride, *cis*- and *trans*-$[Cr(CN)_2(en)_2]X$, and the optical resolution of the *cis* isomer will be reported. Their infrared and visible absorption and circular dichroism (CD) spectra will be discussed in connection with the other dianionobis(ethylenediamine)chromium(III) complexes and in comparison with the corresponding mixed cyano cobalt(III) complexes.

Experimental

Preparation of cis- *and* trans-*Dicyanobis(ethylenediamine) chromium (III) Complexes.* Twenty grams of $[Cr(en)_3]Cl_3 \cdot 3.5H_2O$ and 4.8 g of NaCN were dissolved in 80 ml of water and to this solution was added 2 g of activated charcoal. The mixture was kept with stirring at room temperature for a week. After removing the activated charcoal, a yellow compound (*ca.* 6 g) was deposited by adding methanol and acetone to the filtrate. This was filtered off, because the yellow compound was confirmed to be the unreacted complex, $[Cr(en)_3]Cl_3$, by absorption measurement. The filtrate was condensed by a vacuum rotatory evaporator. Then about 4 g of another yellow precipitate was obtained by adding acetone. This yellow compound showed an absorption band at 438 nm. The aqueous solution of the product was poured into a column (300×20 mm) of a strong-acid cation-exchange resin (Dowex 50 W×8, 200—400 mesh, lithium form), and the column was swept with water. When the adsorbed band was eluted with 0.5 M aqueous solution of lithium perchlorate, two yellow bands were eluted. From the first eluate, yellow leaflet crystals were obtained by condensing and cooling. The second eluate was concentrated by a vacuum rotatory evaporator. To the condensed solution was added acetone–methanol mixture. Then yellow powder was obtained. The yield was about 1 g for the first eluate and about 2 g for the second eluate. The product from the second eluate (isomer II) was found to be more soluble than the one from the first eluate (isomer I). These complexes were recrystallized from warm water–methanol mixture. Found for the isomer I (*trans* form): C, 22.64; H, 5.06; N, 25.81%. Found for the isomer II (*cis* form): C, 22.01; H, 5.19; N, 25.48%. Calcd for $[Cr(CN)_2(en)_2]ClO_4$: C, 22.27; H, 4.98; N, 25.96%. In order to obtain more soluble complex salts, the perchlorates were converted to chlorides by using an anion-exchange resin of chloride form. The chlorides of isomer I and II were found to be anhydrous and monohydrated, respectively, from the elemental analyses. Found for the isomer I: C, 27.34; H, 6.28; N, 32.01%. Calcd for $[Cr(CN)_2(en)_2]Cl$: C, 27.75; H, 6.21; N, 32.36%. Found for the isomer II: C, 26.19; H, 6.30: N, 30.69%. Calcd for $[Cr(CN)_2(en)_2]Cl \cdot H_2O$: C, 25.95; H, 6.53; N, 30.26%.

Optical Resolution of the Isomer II. The chloride of isomer II, $[Cr(CN)_2(en)_2]Cl \cdot H_2O$ (0.544 g, 0.002 mol) was dissolved in 5 ml of warm water. To this solution was added $(+)_{589}$-ammonium α-bromocamphor-π-sulfonate (NH_4·*d*-BCS) (0.328 g, 0.001 mol) in 5 ml of water. Then yellow crystals of the least soluble diastereomer were precipitated. The yield was about 0.4 g. $[\alpha]_{546}=+94.7°$, $[\alpha]_{589}=+66.8°$. Found: C, 35.90; H, 5.68; N, 15.70%. Calcd for $[Cr(CN)_2(en)_2]$·*d*-BCS: C, 35.96; H, 5.66; N, 15.73%. The diastereomer was converted to the perchlorate and chloride by the following procedure. The *d*-BCS salt was suspended in a small amount of cold 70% $HClO_4$, and then the perchlorate was deposited by the addition of cold methanol. $[M]_{546}=+19°$. Found: C, 22.09; H, 5.02; N, 25.75%. Calcd for $(+)_{546}$-$[Cr(CN)_2(en)_2]ClO_4$; C, 22.27; H, 4.98; N, 25.96%. The *d*-BCS salt was converted to the chloride by using an anion exchange resin of chloride form. The crude complex obtained was recrystallized from water–ethanol. Found: C, 26.70; H, 6.57; N, 31.01%. Calcd for $(+)_{546}$-$[Cr(CN)_2(en)_2]Cl \cdot 0.5H_2O$: C, 26.83; H, 6.38; N, 31.28%.

Measurements. The visible absorption spectra were obtained with a Shimadzu UV-200 spectrophotometer. The CD spectra were recorded on a Jasco MOE-1 spectropolarimeter. A Yanagimoto spectropolarimeter, Model 185, was used to check optical rotatory power. The infrared spectra in the region of 4000—600 cm^{-1} were measured with a Jasco DS-402G spectrophotometer. The far-infrared spectra in the region of 700—200 cm^{-1} were obtained by a Hitachi FIR-3 far-infrared spectrophotometer.

Results and Discussion

a) The Preparative Method. In general, the syntheses of dianionobis(ethylenediamine)chromium(III) complexes, especially, of the *trans* forms, are rather difficult. Among the known methods a relatively efficient and convenient one is the thermal decomposition of $[Cr(en)_3]X_3$, which yields $[CrX_2(en)_2]X$.[3] O'Brien and Bailar[4] attempted the thermal decomposition of $[Cr(en)_3](CN)_3$, but failed in obtaining $[Cr(CN)_2(en)_2]CN$. Recently the progress has been made of the syntheses of mixed cyano-ammine or -amine complexes of cobalt(III) by four or more methods.[5-8] In the present work, two of them were applied to the chromium(III) analogues. One is based

on the reaction of *cis*- or *trans*-$[CoCl_2(en)_2]Cl$ with NaCN in dimethyl sufoxide,[5] and the other on the reaction of $[Co(en)_3]Cl_3$ with NaCN in an aqueous solution in the presence of activated charcoal.[6] By the application of the latter method $[Cr(CN)_2(en)_2]^+$ was successfully prepared, whereas the application of the former method was unsuccessful. The formation of *cis*-$[Cr(CN)_2(en)_2]Cl\cdot H_2O$, however, was confirmed by Matsumoto *et al.*[9] from the reaction of $[Cr(en)_3]Cl_3$ and NaCN in dimethyl sulfoxide. In the present method, the yield of *cis*-$[Cr(CN)_2(en)_2]^+$ was about twice as high as that of *trans* one. The abundance of *cis* isomer was also found in the corresponding cobalt(III) complexes.[6]

b) Identification. The two isomers isolated in this work have the same chemical composition, but exhibit differences in their solubilities, elution behaviors on cation-exchange column chromatography and crystalline forms.

Although the geometrical isomers of most dianionobis(ethylenediamine) complexes can be distinguished from each other by the spectral behavior in the first absorption band region, the present complexes give quite similar absorption spectra (but with different intensities as in Fig. 1 and Table 1) as in the case of *cis*- and *trans*-$[Cr(NCS)_2(en)_2]^+$.[10] That is, there is no clue for the assignment of geometrical configurations in the absorption spectra. However, since the second eluate (isomer II) was resolved into the enantiomers through its $(+)_{589}$-α-bromocamphor-π-sulfonate, this isomer is the *cis* form, and consequently the first eluate (isomer I) is to be assigned to the *trans* form.

Table 1. Absorption (AB) and CD data for chromium(III) complexes in the d–d transitions
(Wave numbers are in 10^3 cm^{-1})

AB ($\log \varepsilon_{max}$)	CD ($\Delta\varepsilon_{ext}$)
cis-$[Cr(CN)_2(en)_2]^+$	*cis*-$(+)_{546}$-$[Cr(CN)_2(en)_2]^+$
14.24 ($\bar{1}$.41)	14.51 ($+6.5\times10^{-4}$)
14.63 ($\bar{1}$.39)	14.75 (-7.2×10^{-4})
15.02 ($\bar{1}$.43)	
23.10 (1.85)	23.33 (+0.51)
29.48 (1.80)	29.85 (−0.036)
trans-$[Cr(CN)_2(en)_2]^+$	
23.15 (1.69)	
29.67 (1.63)	

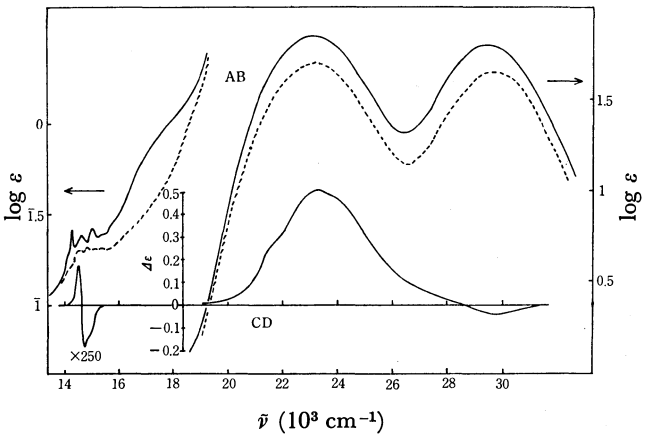

Fig. 1. Absorption curves of *cis*- (——) and *trans*-$[Cr(CN)_2(en)_2]^+$ (– – –), in water. CD curve of *cis*-$(+)_{546}$-$[Cr(CN)_2(en)_2]^+$ (——) in water.

It is generally found that *cis*-dianionobis(ethylenediamine)chromium(III) perchlorate is more soluble than the *trans* one.[11] This is also the case for the present complexes. The column chromatographic elution order also agrees with that generally recognized for *cis*- and *trans*-isomers of bis(ethylenediamine) type complexes.[6,12]

The infrared absorption spectrum of the *trans* isomer exhibits a simpler pattern than that of the *cis* one in the region of 4000—200 cm^{-1}, as in the case of the similar type chromium(III) and cobalt(III) complexes.[13] Particularly, the NH_2 bending near 1600 cm^{-1} and the CH_2 rocking bands at 800—900 cm^{-1} can discriminate between two geometrical isomers of dianionobis(ethylenediamine) complexes. In the isomer II, the former bands are observed at 1582 and 1605 cm^{-1} and the latter at 860 and 880 cm^{-1}, while in the isomer I only one component at 1600 cm^{-1} and undefinitely split ones at about 880 cm^{-1}. Hughes *et al.*[14] measured the far-infrared spectra of various kinds of bis(ethylenediamine) chromium(III) complexes, and found that there is a compatible difference between the spectra of *cis* and *trans* isomers in the region of 550—395 cm^{-1}, where the δ-Cr–N+ring deformation may occur. In fact, four bands are observed for *cis*-$[Cr(CN)_2(en)_2]Cl\cdot H_2O$ in the corresponding region and three bands for the *trans* one. In the Cr–C and Cr–N stretching band region (360—220 cm^{-1}), the *cis* isomer shows more splitting components than the *trans* one as in the other bis(ethylenediamine) complexes.[14] All the facts of the infrared absorption spectra support the present assignment of geometrical configurations. While the corresponding cobalt(III) complexes, *cis*- and *trans*-$[Co(CN)_2(en)_2]^+$, give a strong and sharp CN stretching band near 2100 cm^{-1},[6] the present chromium(III) complexes give very weak bands in this region. It has been revealed that the CN stretching band of $K_3[Cr(CN)_6]$ is about one-nineth as weak in intensity as $K_3[Co(CN)_6]$, probably owing to the difference in the M–CN π-bonding.[15] Thus, it seems plausible that the mixed cyano chromium(III) complexes also show this phenomenon.

c) The Absorption and CD Spsctra. The ligand field absorption spectra of *cis*- and *trans*-$[Cr(CN)_2(en)_2]^+$ are nearly identical with each other as mentioned in b). That is, the first and the second absorption bands of *cis*-$[Cr(CN)_2(en)_2]^+$ locate at 23.1 and 29.48 kK, respectively, while those of the *trans* isomer at 23.15 and 29.67 kK. The molar absorptivities of the *cis* isomer are larger than those of the *trans* isomer for both the first and second band region, as in Fig. 1 and Table 1. This intensity order coincides with the other cases found in literature for the *cis*- and *trans*-dianionobis(ethylenediamine) complexes, for example *cis*- and *trans*-$[Cr(NCS)_2(en)_2]^+$.[10]

The angular overlap model[16] or Yamatera's rule[17] predicts that the first excited quartet state ($^4T_{2g}$) in O_h

symmetry splits into the nondegenerate ($^4A_1$) component at 24.18 kK and the accidentally degenerate ($^4A_2$ and $^4B_2$) one at 23.01 kK for the *cis* isomer of C_{2v} symmetry, while the *trans* isomer of D_{4h} symmetry has the nondegenerate ($^4B_{2g}$) component at 21.85 kK and the degenerate (^4E_g) one at 24.18 kK. On the other hand, Perumareddi[18] has predicted from the ligand field theory the absorption maxima of *cis*- and *trans*-$[Cr(CN)_2(NH_3)_4]^+$, of which the ligand field parameters are very close to those of *cis*- and *trans*-$[Cr(CN)_2(en)_2]^+$; that is, *cis*-$[Cr(CN)_2(NH_3)_4]^+$ has two split components at 24.025 and 22.788 kK and the *trans* one at 23.802 and 21.550 kK. The theoretically predicted energy interval between the degenerate and the nondegenerate components in the first band region of the *trans* dicyano complex is about twice as large as that of the *cis* one and comparable to the splitting of *trans*-$[Cr(OH_2)_2(en)_2]^{3+}$, of which the first band has been reported to split largely.[10] The present *trans* complex, however, exhibits no splitting and its half-width is equal to that of the *cis* one. The absorption maxima of both the *trans*- and *cis*-complexes agree fairly well with the weighted mean value of the predicted components as in Table 2. A discrepancy between the theoretical prediction and observation has also been found for the corresponding *trans* dicyano cobalt(III) complexes.[6] The second absorption band maxima of both the present isomers are close to the value obtained from the weighted mean expression or the rule of the average environment.[19]

TABLE 2. THE PREDICTED POSITIONS OF THE FIRST ABSORPTION BAND IN UNIT OF 10^3 cm^{-1}

Ligand field theory[a]		Yamatera's rule[b]	
cis-$[Cr(CN)_2(en)_2]^+$			Weighted mean
$^4A_2$, $^4B_2$	22.788	23.01	23.40
$^4A_1$	24.025	24.18	
trans-$[Cr(CN)_2(en)_2]^+$			
$^4B_{2g}$	21.550	21.85	23.40
^4E_g	23.802	24.18	

a) The value of the tetraammine complexes after Perumareddi[18] b) Using the parameters, $\delta(en)=0$ and $\delta(CN)=10Dq(CN)-10Dq(en)=4.66$

The CD spectrum of $(+)_{546}$-$[Cr(CN)_2(en)_2]^+$ shows a positive band with an undefined inflection in the first absorption band region and a negative band in the second absorption band region as shown in Fig. 1 and Table 1. Since the positive CD band in the first absorption band region is due to the $^4E(^4T_{2g})$ parentage of the parent trigonal complex, the absolute configuration of this $(+)_{546}$-isomer is assigned to *A*.

In the near-infrared region around 14—15 kK, where the quartet-doublet spin-forbidden transitions occur, the narrow and sharp but weak absorption bands are observed as in Fig. 1. The absorption bands in this region for the *cis* and *trans* isomers differ in their patterns from each other. Three distinct peaks are observed for the *trans* isomer, while some uncertain structural inflections appear for the *cis* one. In the corresponding region, two CD peaks, (+) and (−) from the longer wavelength side, are observed for the *cis*-$(+)_{546}$-isomer. It is found that their CD intensities are about 0.1% of that in the first spin-allowed band region. Provided that the theoretical relationship between rotational strengths for the spin-forbidden and spin-allowed transitions, which has been presented recently for the trigonal chromium(III) complexes,[20] may be applicable also to the *cis*-dianionobis(ethylenediamine) complexes, the positive CD component at the longer wavelength side may be due to the $^2E \leftarrow {}^4A_2$ transition and the remaining negative one to the split component of the $^2T_1$, $\bar{E}_b$. Since the rotational strength for the spin-forbidden transitions is contributed from that for the spin-allowed transitions with same signs,[20] the intensity of negative CD component in the spin-forbidden band region should originate from the negative CD component in the first spin-allowed band region. Therefore, the CD in the first band region may consist of two components with opposite signs, and then it is supposed that a negative minor CD band may be destructively superimposed on the positive major CD band. On the other hand, for the corresponding cobalt(III) complex, $A(+)_{589}$-$[Co(CN)_2(en)_2]^+$, the CD spectra in the first band region give two positive components.[21] Accordingly, it is suggested that the CD behavior of the present chromium(III) complex differs considerably from that of the corresponding cobalt(III) complex, although current CD theories propose that the rotational strengths of low spin cobalt(III) complexes behave analogously to those of chromium(III) complexes.[22]

References

1) W. B. Schaap, R. Krishnamurthy, D. K. Wakefield, and W. F. Coleman, "Coordination Chemistry," S. Kirschner, Ed., Plenum Publishing Co., New York, N. Y. (1969), p. 177.
2) D. K. Wakefield and W. B. Schaap, *Inorg. Chem.*, **8**, 512 (1969).
3) P. Pfeiffer, P. Koch, T. G. Lando, and A. Trieschmann, *Ber.*, **37**, 4255 (1904); C. L. Rollinson and J. C. Bailar, Jr., *J. Amer. Chem. Soc.*, **66**, 641 (1944).
4) T. D. O'Brien and J. C. Bailar, Jr., *ibid.* **67**, 1856 (1945).
5) M. Muto, T. Baba, and H. Yoneda, This Bulletin, **41**, 2918 (1968).
6) K. Konya, H. Nishikawa, and M. Shibata, *Inorg. Chem.*, **7**, 1165 (1968).
7) P. R. Ray and B. Sarma, *J. Indian Chem. Soc*,, **28**, 59 (1951).
8) K. Kuroda, *Nippon Kagaku Zasshi*, **89**, 720 (1968).
9) Y. Matsumoto and Y. Sakabe, The 27th National Meeting of the Chemical Society of Japan, 1973.
10) W. A. Baker and M. G. Phillips, *Inorg. Chem.*, **5**, 1042 (1966).
11) W. W. Fee, J. N. Mac, B. Harrowfield, and W. G. Jackson, *J. Chem. Soc., A*, **1970**, 2612.
12) L. F. Druding, *Coord. Chem. Rev.*, **3**, 409 (1968).
13) K. Nakamoto, "Spectroscopy and Structure of Metal Chelate Compounds," K. Nakamoto and P. J. McCarthy, S. J., Ed., John Wiley & Sons, Inc., New York, N. Y. (1968), p. 216.
14) M. N. Hughes and W. R. McWhinie, *J. Chem. Soc., A*, **1967**, 592.
15) L. H. Jones, *Inorg. Chem.*, **2**, 777 (1963).
16) C. E. Schäffer and C. K. Jørgensen, *Kgl. Danske Videnskab. Selskab. Mat. -fys. Medd.*, **34**, No. 13 (1965).

17) H. Yamatera, This Bulletin, **31**, 95 (1958).
18) J. R. Perumareddi, *Coord. Chem. Rev.*, **4**, 73 (1969).
19) N. Matsuoka, J. Hidaka, and Y. Shimura, This Bulletin, **40**, 1868 (1967).
20) S. Kaizaki, J. Hidaka, and Y. Shimura, *Inorg. Chem.*, **12**, 142 (1973).
21) A. J. McCaffery, S. F. Mason, and B. J. Norman, *J. Chem. Soc.*, **1965**, 5094.
22) W. Moffitt, *J. Chem. Phys.*, **25**, 1189 (1956); F. S. Richardson, *ibid.*, **54**, 2453 (1971).

The Extraction of Bis(8-picolylideneaminoquinoline)iron(II) Perchlorate into Nitrobenzene[1)]

Makoto Otomo and Kazunobu Kodama

Department of Synthetic Chemistry, Nagoya Institute of Technology, Showa-ku, Nagoya 466

(Received November 14, 1974)

The green chelate cation of bis(8-picolylideneaminoquinoline)iron(II) can be extracted into nitrobenzene as the form of the ion-pair with various univalent anions. The extractability with these anions is decreased in the order of $B(C_6H_5)_4^- \approx ClO_4^- > SCN^- > I^- \gg NO_3^- > Br^- > Cl^- \gg CH_3COO^-$. The extractive reaction with perchlorate ions has been applied to the spectrophotometric determination of minute amounts of iron(II). The nitrobenzene extract gives two characteristic charge-transfer ($d \rightarrow \pi^*$) bands at 663 and 569 nm. Under the optimum conditions of pH, ligand concentration and shaking time, Beer's law is obeyed up to 1.2×10^{-4} M iron(II) in the organic phase. The molar absorptivity is 7.04×10^3 l·mol^{-1}·cm^{-1} at 663 nm. The proposed method is selective and can be used for the determination of iron(II) in the presence of fairly large amounts of various ions, provided high concentrations of the ligand or suitable masking agents are used. A kinetic study made to obtain an information on the extraction mechanism of the ion-pair of this type showed that the rate equation can be represented as

$$-\frac{d[Fe^{2+}]}{dt} = k_0[Fe^{2+}][8\text{-PAQ}]_{org}^2(1 + k_1[ClO_4^-])$$

where k_0 and k_1 are respectively the rate constant and a constant.

2,2′,2″-Terpyridine, an important colorimetric reagent for iron(II), has been known as a representative tridentate ligand which contained the functional grouping N=C–C=N–C·C·N (points denote single or double bonds). Lions and his coworkers[2)] reported briefly on the preparation and use of 8-picolylideneaminoquinoline (abbreviated as 8-PAQ) as a tridentate chelating agent with constitutional features similar to those of terpyridine and showed that it coordinated with iron(II) salts similarly to the latter. They also showed that bis(8-PAQ)iron(II) iodide is obtained as a diamagnetic crystalline solid, which gives an intense green color when dissolved in water. Later, Kurmholz[3)] recorded the visible absorption spectra of iron(II) complexes with a series of "terpyridine-like" tridentate imine ligands including 8-PAQ and interpreted the observed spectral patterns on the basis of the molecular models and the geometrical considerations.

We have found that the iron(II) chelate of 8-PAQ can be quantitatively transferred into nitrobenzene as the form of the ion-pair in the presence of such anions as perchlorate, iodide, thiocyanate, or tetraphenylborate ions. This paper deals mainly with the application of 8-PAQ to the extractive spectrophotometric determination of minute amounts of iron(II) in the presence of perchlorate ions. The method proposed here is simple and highly selective for iron(II). The interference from certain metals can be avoided by adding suitable masking agents or by using a large excess of the ligand. The only interfering metal that forms a colored chelate with the ligand is cobalt(II). In order to get a semi-quantitative information on the extraction mechanism of the ion-pair of this type, a kinetic study has also been made spectrophotometrically. The extraction rate was found to be first order with respect to the concentration of iron(II) in the aqueous phase, and second order with respect to the ligand concentration in the organic phase. The rate of the extraction is also affected by the concentration of perchlorate ions in the aqueous phase.

Experimental

Reagents. 8-PAQ and bis(8-PAQ)iron(II) perchlorate were prepared according to the procedures described in the literature. The latter, sparingly soluble black needles, decomposed above 271 °C. Found: C, 49.65; H, 3.24; N, 11.37; Cl, 9.87%. Calcd for $Fe(C_{15}H_{11}N_3)_2(ClO_4)_2 \cdot 0.5H_2O$: C, 49.34; H, 3.17; N, 11.51; Cl, 9.71%.

A stock solution of iron(II) sulfate was standardized complexometrically. Sodium perchlorate was prepared and purified as described previously.[4)] Nitrobenzene obtained from the Katayama Kagaku Co. was distilled under reduced pressure. All the other reagents used were of analytical grade.

Apparatus. The absorbance measurements were made with a Hitachi model 124 double-beam spectrophotometer equipped with quartz cells of 10 mm pathlength. The pH determinations were carried out with a Toa Dempa model HM-6A pH meter.

General Procedure. All of the extraction procedures and the absorbance measurements were made at 25 °C. A centrifuging tube (volume, 50 ml) with a glass stopper was used to equilibrate the organic and aqueous phases. The aqueous phase contained solutions of iron(II) sulfate, ascorbic acid, sodium perchlorate and an acetate buffer. A 5.0 ml portion of the aqueous solution and a 5.0 ml portion of 8-PAQ in nitrobenzene were placed in the tube, and the two phases were agitated vigorously by a mechanical shaker for a required period. When the agitation was stopped, the two phases in the tube were immediately centrifuged for 2 min at 1000 rpm. The iron contents in the two phases were determined from the initial iron concentration and the absorbance of the organic phase at 663 nm.

Results and Discussion

The Extraction of Iron(II) into Nitrobenzene with 8-PAQ in the Presence of Various Anions. In Fig. 1 the extraction behavior of iron(II) on changing counter anion is shown by plotting the percentage extraction of iron(II) as a function of the concentration of the anion. The order of extractability as a measure of half-extrac-

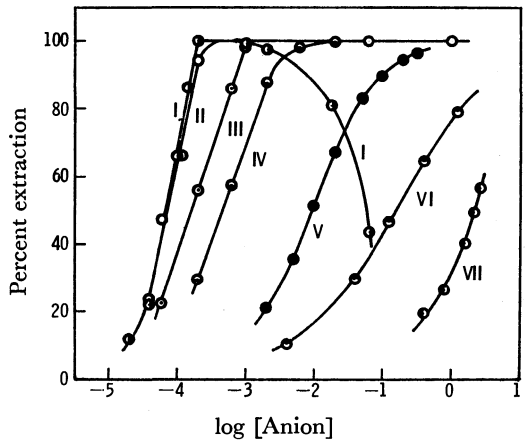

Fig. 1. Extraction of iron(II) as the 8-PAQ chelate with various anions.
Fe^{2+}, 8.0×10^{-5}M; anion ----I, $B(C_6H_5)_4^-$: II, ClO_4^-: III, SCN^-: IV, I^-: V, NO_3^-: VI, Br^-: VII, Cl^-: pH, 3.20; 8-PAQ in $C_6H_5NO_2$, 5.0×10^{-3}M

tion is as follows: $B(C_6H_5)_4^-\approx ClO_4^->SCN^->I^-\gg NO_3^->Br^->Cl^-\gg CH_3COO^-$, SO_4^{2-}. This sequence suggests that the enthalpy of hydration of the anion is the major factor governing the extractability of the iron(II)–8-PAQ chelate cation as the form of the ion-pair. The percentage extraction increases remarkably when the enthalpy of hydration of the anions is below 70—80 kcal/mol. With strongly hydrated anions, such as acetate and sulfate ions, the iron(II) chelate is scarcely extracted at all. This result is in good agreement with those obtained by Gibson and Weatherburn[5] with the quaternary phosphonium and arsonium cations, by Biswas and Mandal[6] with surfactant cations, and by Takamatsu[7] with the tris(1,10-phenanthroline)-ruthenium(II) cation.

In addition, as is evident in Fig. 1, an abnormal decrease in the percentage extraction at higher concentrations of sodium tetraphenylborate is observed.

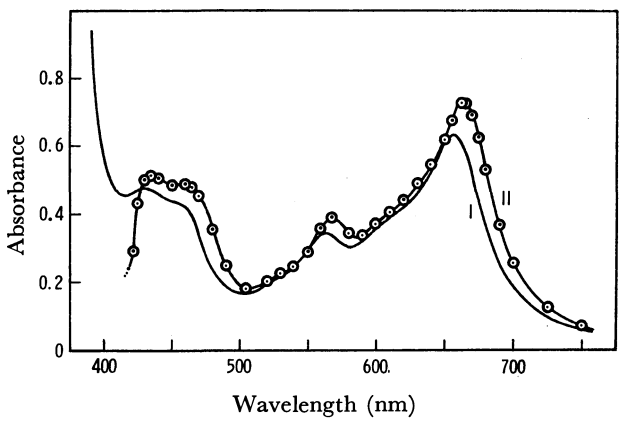

Fig. 2. Visible absorption spectra of 1.03×10^{-4}M $Fe(8\text{-}PAQ)_2(ClO_4)_2$ in 50 v/v % aqueous methanol and nitrobenzene.
I, solid $Fe(8\text{-}PAQ)_2(ClO_4)_2$ dissolved in 50 v/v % aqueous methanol; II, solid $Fe(8\text{-}PAQ)_2(ClO_4)_2$ dissolved in nitrobenzene; —, prepared by extracting 1.03×10^{-4}M iron(II) from a pH 3.2 solution containing 0.02 M $NaClO_4$

A similar result has been obtained in the extraction of tris(1,10-phenanthroline)ruthenium(II) into various organic solvents with tetraphenylborate ions.[7] This phenomenon, therefore, may be explained in terms of the hydrotropism[8,9] which is often encountered in the solution of an electrolyte with a large ion.

Absorption Spectra. The visible absorption spectra of 50 v/v% aqueous methanol and nitrobenzene solutions of bis(8-PAQ)iron(II) perchlorate are shown in Fig. 2.

It has generally been accepted that the visible absorption of diamagnetic iron(II) complexes of tridentate imine ligands as well as that of α-diimine ligands is caused by an electron migration from the filled 3d orbitals of the metal to the lowest vacant molecular orbitals of the ligands. In a 50 v/v% aqueous methanol solution, the main absorption band of the iron(II) complex of 8-PAQ is found at 657 nm (molar absorptivity, $\varepsilon=6.35\times10^3$). This peak is accompanied by a weak shoulder toward shorter wavelengths. A distinct second peak, which is not found in the visible absorption spectrum of the bis(terpyridine)iron(II) complex, is found at 563 nm ($\varepsilon=3.38\times10^3$), also accompanied by a weak shoulder toward shorter wavelengths. The appearance of the second transition has been assigned to the splitting of the filled T_{2g} orbitals by non-cubic field components.[3] An additional absorption band appearing in the 410—470 nm region ($\varepsilon=4.61\times10^3$ at 427 nm) may probably be attributed to the charge-transfer from the 3d orbitals of iron(II) to the second lowest vacant molecular orbitals of the ligand.[10]

In nitrobenzene, as is shown in Fig. 2, the main and the second peaks are shifted toward longer wavelengths along with an increase in intensity. These are found at 663 ($\varepsilon=7.04\times10^3$) and 569 nm ($\varepsilon=3.82\times10^3$) respectively. Figure 2 also shows that the visible absorption spectrum of the nitrobenzene extract obtained according to the general procedure is completely identical with that of the synthesized complex. In both the aqueous methanol and the organic solvent, the free ligand did not show any absorption in the visible region above 450 nm.

The ultraviolet absorption spectrum of the iron(II) complex measured in a 50 v/v% aqueous methanol solution is composed of three intense peaks at 372 ($\varepsilon=4.42\times10^4$), 352 ($\varepsilon=4.24\times10^4$), and 232 nm ($\varepsilon=5.98\times10^4$) and two shoulders at about 332 ($\varepsilon=2.9\times10^4$) and 315 nm ($\varepsilon=1.9\times10^4$). The magnitude of the molar absorptivities suggests that all the absorption bands are caused by $\pi\rightarrow\pi^*$ transitions.

Application to the Spectrophotometric Determination of Iron(II). The Effect of pH: The absorbance of the organic phase was measured as a function of pH of the aqueous phase, the result being shown in Fig. 3. The iron(II)–8-PAQ chelate is formed above pH 1. The absorbance of the extract is at its maximum at pH 2.0—4.2. It is of interest to note that the ion-pair once extracted into nitrobenzene can not be decomposed in the presence of perchlorate ions, unless high concentrations of hydrochloric acid (above 6 M) or sodium hydroxide (above 0.5 M) are used.

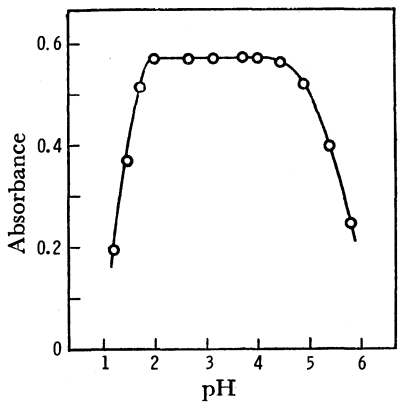

Fig. 3. Effect of pH.
Fe^{2+}, 8.0×10^{-5}M; $NaClO_4$, 0.02 M; 8-PAQ in $C_6H_5NO_2$, 5.0×10^{-3}M

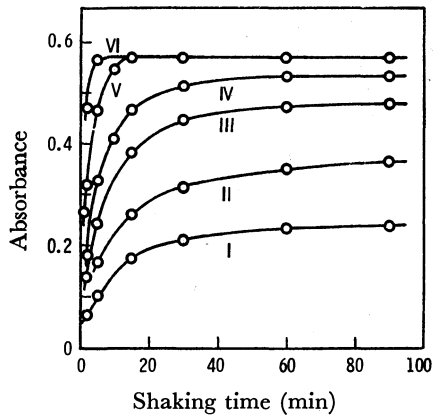

Fig. 4. Effect of the ligand concentration and the shaking time.
Fe^{2+}, 8.0×10^{-5}M; $NaClO_4$, 0.02 M; pH, 3.20; 8-PAQ in $C_6H_5NO_2$——I, 1.25×10^{-3}M: II, 1.59×10^{-3}M: III, 2.01×10^{-3}M: IV, 2.50×10^{-3}M: V, 3.75×10^{-3}M: VI, 6.25×10^{-3}M

The Effects of the Ligand Concentration and the Shaking Time: Figure 4 shows the effects of the ligand concentration and the shaking time on the extraction of iron(II). A shaking period of about 15 min is enough to obtain the maximum extraction, when the initial concentration of the ligand in nitrobenzene is 3.75×10^{-3} M which is about 50 fold molar excess over iron(II). The shaking period can be reduced by using the higher concentrations of the ligand.

The Effect of Solvents and the Stability of the Color: Several organic solvents were examined for their ability to extract the ion-pair. Of all the solvents tested, chloroform, 1,2-dichloroethane and nitrobenzene were capable of extracting the ion-pair, while in the other cases a precipitate was observed at the interface. In chloroform and 1,2-dichloroethane, however, the green color of the ion-pair tended to fade away gradually. The absorbance of the nitrobenzene extract did not change at all for at least 48 hr, indicating that the ion-pair is very stable in nitrobenzene.

The Effect of Volume of the Aqueous Phase: The absorbance of the organic phase was decreased with increasing the volume of the aqueous phase to organic phase, but it could be avoided by using higher concentrations of the ligand or by lengthening the shaking time.

Adherence to Beer's Law: To the series of sample solutions containing up to 34 μg (1.2×10^{-4} M in the final concentration) of iron(II or III), the general procedure described above was applied. The conditions used were: 8-PAQ in nitrobenzene, 5.0×10^{-3} M; sodium perchlorate, 0.02 M; ascorbic acid added as a reducing agent for iron(III), 0.4%; pH of the aqueous phase, 3.20; shaking period, 15 min. It was found that Beer's law is obeyed between the absorbance of the organic phase and the concentration of iron over

Table 1. Effect of diverse ions for the determination of 22.4 μg (0.4 μmol) of iron

Ion	Added (μmol)	Fe found (μg)	Difference (μg)
Zn	2	22.1	−0.3
	4	17.2	−5.2
	10	6.6	−15.8
	10[a)]	22.1	−0.3
Cd	5	20.7	−1.7
	5[a)]	22.4	±0.0
	10	15.6	−6.8
	10[a)]	22.2	−0.2
Co(II)	0.2	22.8	+0.4
	1	24.3	+1.9
	10	24.5	+2.1
Ni	2	22.2	−0.2
	5[a)]	22.7	+0.3
	10	15.6	−6.8
	10[a)]	22.9	+0.5
Cu	4	22.6	+0.2
	10	3.5	−18.9
	10[b)]	22.3	−0.1
Ru(III)	1.2	22.9	+0.5
	6	17.6	−4.8
	6[a)]	22.5	+0.1
Mo(VI)	5	22.1	−0.3
	10	21.1	−1.3
	10[c)]	22.5	+0.1
W(VI)	0.5	20.6	−1.8
	2	15.5	−6.9
	10	4.4	−18.0
	10[c)]	22.0	−0.4
F^-	100	22.4	±0.0
	200	22.4	±0.0
$S_2O_3^{2-}$	200	22.3	−0.1
	500	22.4	±0.0
$C_2O_4^{2-}$	2	22.1	−0.3
	10	21.6	−0.8
	100	16.5	−5.9
$C_4H_4O_6^{2-}$	100	22.4	±0.0
	300	22.4	±0.0
PO_4^{3-}	100	22.2	−0.2
	200	22.0	−0.4
EDTA	0.05	21.9	−0.5
	0.1	21.4	−1.0
	1	12.4	−10.0

a) Reagent concentration: 1.0×10^{-2} M b) 1 ml of 0.2 M sodium thiosulfate solution was added. c) 1 ml of 0.2 M sodium tartrate solution was added.

the entire range examined.

The Effect of Diverse Ions: The extent of interference by a number of metal ions and anions in the determination of 22.4 μg of iron(II) was studied. The following metal ions did not interfere, even if they were present at a concentration level of several ten times that of iron: silver, thallium(I), beryllium, magnesium, calcium, strontium, barium, mercury(II), tin(II), lead, manganese(II), yttrium, lanthanoid, aluminum, gallium, indium, bismuth, chromium(III, VI), osmium(VIII), rhodium, irridium, platinum(II, IV), thorium, titanium, zirconium, vanadium(IV, V), and uranium(VI).

Table 1 shows the effect of several metal ions and anions on the determination of iron. Zinc, cadmium, nickel, copper(II), ruthenium(III), and molybdenum(VI) do not interfere up to concentrations of several times that of the amount of iron. The negative errors observed in the presence of larger amounts of these ions may be due to the consumption of the reagent by the formation of colorless complexes with these cations; the error can be eliminated by the use of a fairly large amount of the reagent, except for copper(II) which still interferes to some extent. The interference from copper(II) can be eliminated by the addition of thiosulfate. The addition of tartrate is also effective to prevent the interference from molybdenum and tungsten. The most difficult interference is that from cobalt(II), which forms an extractable brown complex with the reagent and gives a positive error. The extraction of cobalt(II) seemed to be accompanied by a transformation of $Co(8\text{-}PAQ)_2(ClO_4)_2$ into an inert complex such as $Co(8\text{-}PAQ)_2(ClO_4)_3$. Anions, such as fluoride, tartrate, thiosulfate and phosphate do not interfere, even when they are present at a large concentration. However, as is expected for iron(II), EDTA and a large amount of oxalate interfere with the determination by the formation of complexes with iron(II).

It is clear from these results that 8-PAQ is highly selective for iron(II), and that this reagent, although it is not very stable, can be used as a spectrophotometric reagent for iron in the presence of fairly large amounts of various ions.

A Kinetic Study. Statistical Treatments: Assuming that the diffusion or the transport of materials can be neglected from consideration, the rate of the extraction of iron(II) with the ligand and perchlorate ions may be generally described as follows:

$$-\frac{d[Fe^{2+}]}{dt} = k_0[Fe^{2+}]^a[8\text{-}PAQ]_{org}^b[H^+]^c[ClO_4^-]^d \quad (1)$$

As the concentrations of the ligand and perchlorate ions are in considerably excess to iron(II), and as the aqueous phase is buffered, the rate can be described as follows:

$$-\frac{d[Fe^{2+}]}{dt} = q[Fe^{2+}]^a \quad (2)$$

where q is the multiplication of the rate constant, k_0, and the other concentrations which are kept at certain values. When the reaction order with respect to iron(II) is unity, Eq. (2) can be rewritten by integration as:

$$-\log [Fe^{2+}] = q \cdot t + c_0 \quad (3)$$

where c_0 is a constant. Equation (3) shows that the $\log [Fe^{2+}]$ *vs.* t plot should be a straight line with a slope of $-q$.

The reaction order with respect to the other species can be determined from the rate measurements when two of the concentrations out of these three are kept at certain values. For example, when the concentrations of the hydrogen and perchlorate ions are kept at C and D, then the quantity q_L can be defined as follows:

$$\log q_L = \log k_0 C^c D^d + b \log [8\text{-}PAQ]_{org} \quad (4)$$

Thus, the reaction order with respect to the ligand, b, can be determined by plotting $\log q_L$ *vs.* $\log [8\text{-}PAQ]_{org}$.

By similar treatments, the rest of the values of the c and d reaction orders can be determined from the slope of the plot given by the following equations:

$$\log q_{H^+} = \log k_0 B^b D^d + c \log [H^+] \quad (5)$$

$$\log q_{ClO_4^-} = \log k_0 B^b C^c + d \log [ClO_4^-] \quad (6)$$

However, as will be seen below, the reaction order with respect to the perchlorate ions, d, was not a constant, but changed as the perchlorate concentration was changed; the following equation should therefore be used instead of Eq. (6):

$$\log q_{ClO_4^-} = \log k_0 B^b C^c + \log (1 + k_1[ClO_4^-] + \cdots + k_n[ClO_4^-]^n) \quad (6a)$$

The Reaction Order with Respect to Fe^{2+}: In Fig. 5 are shown some of the experimental values of $-\log [Fe^{2+}]$ as a function of t. It is seen that the points lie on straight lines, indicating that the reaction order with respect to iron(II) is always unity.

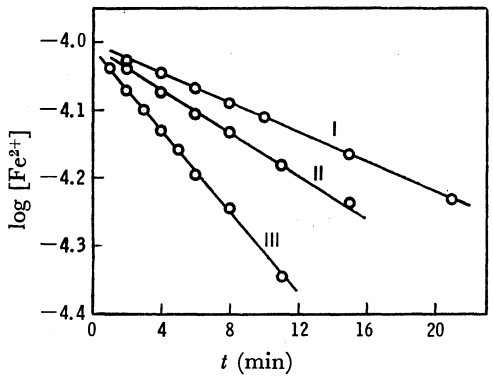

Fig. 5. Dependence of the rate of iron(II) extraction on the Fe^{2+} concentration.
pH, 3.30; $NaClO_4$, 0.1 M; 8-PAQ in $C_6H_5NO_2$——
I, 1.13×10^{-3}M: II, 1.33×10^{-3}M: III, 1.52×10^{-3}M

The Reaction Order with Respect to the Ligand: The rate of extraction was determined in the ligand concentration range between 0.95×10^{-3} M and 2.3×10^{-3} M, the results being plotted in Fig. 6. As may be seen from Fig. 6, the rate of extraction was concluded to be proportional to the square of the ligand concentration under these conditions.

The Reaction Order with Respect to the Hydrogen Ion: The pH of the aqueous phase was varied from 3.02 to 4.50 while the concentrations of the ligand and the perchlorate were kept at 1.35×10^{-3} M and 0.1 M

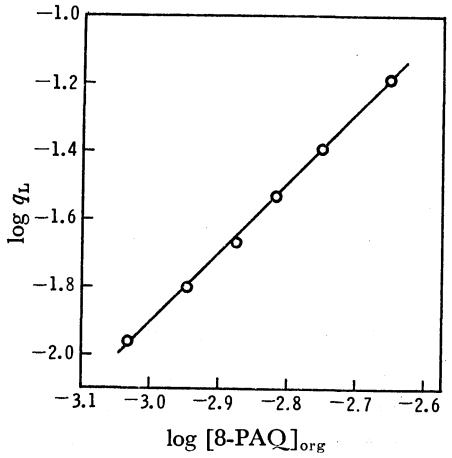

Fig. 6. Dependence of the rate of iron(II) extraction on the 8-PAQ concentration in the organic phase.
pH, 3.30; $NaClO_4$, 0.1 M

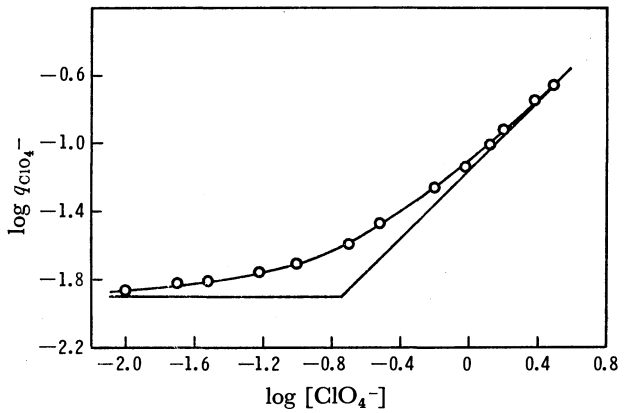

Fig. 7. Dependence of the rate of iron(II) extraction on the perchlorate-ion concentration.
pH, 3.30; 8-PAQ in $C_6H_5NO_2$, 1.35×10^{-3}M. The curve fitted is log $q_{ClO_4^-}=-1.88+\log(1+5.0[ClO_4^-])$. The intersect of the two asymptotes is (−0.72, −1.88).

respectively. As the result, it was found that the rate of extraction was almost independent of the hydrogen ion concentration of the aqueous phase under these conditions.

The Effect of Perchlorate Ions: The rate was determined as a function of the perchlorate-ion concentration in the aqueous phase when the ligand concentration of the organic phase was 1.35×10^{-3} M and when the pH of the aqueous phase was 3.30. Figure 7 gives the log $q_{ClO_4^-}$ *vs.* log [ClO_4^-] plot. The data in this figure were also analysed by the curve fitting method.[11,12] As may be seen from Fig. 7, the slope for the plot approaches zero in the lowest log [ClO_4^-] region, but it increases with the increase in log [ClO_4^-] until it approaches unity. The increase in $q_{ClO_4^-}$ with the perchlorate concentration should not seem to be due to the ionic strength effect. Thus, it was concluded that there are two mechanisms for the extraction and they can be represented by Eq. (6b).

$$\log q_{ClO_4^-} = \log k_0 B^b C^c + \log(1+k_1[ClO_4^-]) \quad (6b)$$

The first order dependence of the rate on the perchlorate concentration is probably due to the first-step association of $Fe(8\text{-}PAQ)_2^{2+}$ chelate cation with perchlorate ions in the aqueous phase. This is contradictory to the conclusion of Yamamoto[13] in a similar study with tris(1,10-phenanthroline)iron(II) perchlorate; he concluded that this ion-pair is completely dissociated in water and also in nitrobenzene. On the other hand, it has also been found that the ion-pairs formed between tris(1,10-phenanthroline)ruthenium(II) and anions such as perchlorate, iodide, and thiocyanate are extracted into various organic solvents mainly as the associated form and that the degree of association is considerable even in water.[7]

The rate equation, therefore, can be expressed as:

$$-\frac{d[Fe^{2+}]}{dt} = k_0[Fe^{2+}][8\text{-}PAQ]_{org}^2(1+k_1[ClO_4^-]) \quad (7)$$

References

1) Heterocyclic Azomethine Compounds and Their Reduction Products as Analytical Reagents. III; Part II: M. Otomo, K. Fukui, and K. Kodama, This Bulletin, **47**, 455 (1974).
2) F. P. Dwyer, N. S. Gill, F. C. Gyarfas, and F. Lions, *J. Amer. Chem. Soc.*, **75**, 3834 (1953); F. Lions and K. V. Martin, *ibid.*, **79**, 2733 (1957).
3) P. Kurmholz, *Inorg. Chem.*, **4**, 612 (1965).
4) M. Otomo and K. Kodama, This Bulletin, **46**, 2421 (1973).
5) N. A. Gibson and D. C. Weatherburn, *Anal. Chim. Acta*, **58**, 159 (1972).
6) H. K. Biswas and B. M. Mandal, *Anal. Chem.*, **44**, 1636 (1972).
7) T. Takamatsu, This Bulletin, **47**, 118 (1974).
8) C. Neuberg, *Biochem. Z.*, **76**, 107 (1916).
9) F. A. Long and W. F. McDerit, *Chem. Rev.*, **51**, 119 (1952).
10) T. Ito and N. Tanaka, This Bulletin, **41**, 365 (1968); **42**, 702 (1969).
11) D. Dyrssen and L. G. Sillen, *Acta Chem. Scand.*, **7**, 663 (1953).
12) T. Sekine and M. Ono, This Bulletin, **38**, 2087 (1965).
13) Y. Yamamoto, *Bunseki Kagaku*, **21**, 418 (1972).

Syntheses and Properties of 2'-Aminobiphenyl-2-ol and Its Copper(II) Complexes

Iwao Mori

Department of General Education, University of the Ryukyus, Naha, Okinawa 903

(Received November 18, 1974)

A new bidentate ligand, 2'-aminobiphenyl-2-ol(Habp), was synthesized. An examination of its behavior toward metal ions proved that, depending on the reaction conditions, the ligand gave mononuclear or polynuclear copper(II) complexes with seven-membered chelate rings. The complexes of the following compositions were thus characterized: $Cu(abp)_2$, $Cu(abp)_2 \cdot H_2O$, $Cu(abp)_2 \cdot C_6H_6$, $Cu(abp)_2 \cdot CH_3COOC_2H_5$, and $Cu_5(abp)_8(OH)_2 \cdot 3H_2O$.

Only a few examples of mononuclear metal complexes[1] with seven-membered chelate rings derived from bidentate ligands have been reported. It is generally accepted that the complexes with chelate rings of more than six members are often unstable and tend to give polynuclear complexes. 2-Aminophenol is a well-known complexing agent, and so the author was tempted to examine the seven-membered analogue of bis-(2-aminophenolato) copper(II) from the above point of view.

The present report will describe the syntheses and characterizations of the new ligand, 2'-aminobiphenyl-2-ol (abbreviated as Habp), and its copper(II) complexes; these studies led to the conclusion that the ligand gives mono- or polynuclear complexes, depending on the reaction conditions.

The aminophenol (**3**) was synthesized according to the scheme shown in Fig. 1. The dissolving-metal reduction of 2-methoxy-2'-nitrobiphenyl (**1**) with Raney alloy led to 2-amino-2'-methoxybiphenyl (**2**), which was then demethylated with boiling hydrobromic acid giving Habp (3) in a fair yield.

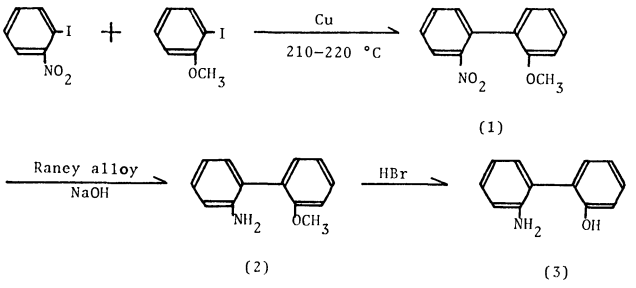

Fig. 1. The synthetic scheme of Habp.

When the ligand was treated with copper(II) ions in an ammoniacal aqueous ethanolic solution, the complex of the composition, $Cu(abp)_2 \cdot H_2O$, was obtained in the form of brown needles. The complex gave $Cu(abp)_2 \cdot C_6H_6$ or $Cu(abp)_2$ when heated with benzene, and $Cu(abp)_2 \cdot CH_3COOC_2H_5$ when heated with ethyl acetate. As will be discussed below, an examination of the IR, UV, and magnetic susceptibilities showed that the complexes had mononuclear structures. On the other hand, however, when the ligand was reacted with copper acetate in an aqueous ethanolic solution, a copper complex of a different composition was obtained; it was confirmed to have a polynuclear, probably a pentanuclear structure, by a study of its elementary analytical, spectral, and magnetic properties.

Experimental

Syntheses. *2-Methoxy-2'-nitrobiphenyl (1)*:[2] *o*-Iodonitrobenzene[3] (200 g), *o*-iodoanisole[4] (200 g), and copper powder[5] (200 g) were mixed and heated at 210—220 °C in an oil bath under stirring for one and a half hour. The reaction mixture was then cooled and extracted with benzene. The benzene solution was distilled, and the fraction between 160—190 °C, 7 mmHg was treated with cold methanol, from which most of the 2,2'-dimethoxybiphenyl crystallized out. The filtrate gave, after concentration and the addition of water, crude methoxynitrobiphenyl (**1**), which was subsequently purified by recrystallization from aqueous methanol. Pale yellow needles; mp 78 °C; 61.2 g, (31.2%). Found: C, 68.09; H, 4.78; N, 6.32%. Calcd for $C_{13}H_{11}O_3N$: C, 68.11; H, 4.84; N, 6.11%.

2-Amino-2'-methoxybiphenyl (2): 2-Methoxy-2'-nitrobiphenyl (**1**) (20 g) was dissolved in a mixture of ethanol (95%, 100 ml) and an aqueous sodium hydroxide solution (20%, 100 ml) by warming. Raney alloy (powder, 20 g) was added, little by little, to the above solution under stirring. After the addition had been completed, the mixture was stirred for a further 20 min and filtered while hot. The subsequent concentration of the filtrate separated an oil which solidified on cooling. It was then distilled under diminished pressure, and the fraction which distilled between 157—159 °C/5.5 mmHg was recrystallized from aqueous methanol. Colorless needles; mp 78—79 °C; 13.6 g (78%). (The yield was 56% when iron powder and hydrochloric acid were used for the reduction.) Found: C, 77.93; H, 6.57; N, 7.83%. Calcd for $C_{13}H_{13}NO$: C, 78.39; H, 6.53; N, 8.04%.

2'-Aminobiphenyl-2-ol (Habp) (3): A mixture of 2-amino-2-methoxybiphenyl (**2**) (10 g) and hydrobromic acid (48%, 40 ml) was gently refluxed for one hour. The mixture was then cooled and poured into water. The aqueous solution was neutralized with a dilute aqueous ammonium hydroxide solution, and the precipitate was collected by filtration and washed with water. The precipitate was then further purified by sublimation under reduced pressure. Colorless needles; mp 91—92 °C; 6.5 g, (70%). IR, Table 1. UV; λ_{max}, 263 nm (no appreciable absorption in the visible region). NMR; δ (ppm) 4.29 (singlet, 3H, $N\underline{H}_2$ and $O\underline{H}$), 7.12 (multiplet, 8H, aromatic protons). Mass Spectrum; *m/e* 186 (M+1, 14% of M+), 185 (M+), 168, 156, 154, 139, 129, 89, 77 and 65. Found: C, 77.84; H, 6.02; N, 7.63%. Calcd for $C_{12}H_{11}NO$: C, 77.81; H, 5.98; N, 7.56%.

$Cu(abp)_2 \cdot H_2O$: Copper acetate (33 mg) was dissolved in water (3 ml) containing an aqueous ammonium hydroxide solution (28%, 0.5 ml) and kept at 50—60 °C. A solution

of Habp (62 mg) in ethanol (1 ml) was then added to the above solution. The precipitate was filtered and washed with water and then with a small amount of ethanol. Reddish orange needles; 65 mg, (91%). Found: C, 64.29; H, 4.82; N, 6.22; Cu, 13.94%. Calcd for $C_{24}H_{20}N_2O_2Cu \cdot H_2O$: C, 64.03; H, 4.93; N, 6.22; Cu, 14.13%.

Cu(abp)$_2$·C$_6$H$_6$: Cu(abp)$_2$·H$_2$O was warmed in benzene at 60 °C for 40 min. The precipitate was filtered, washed with benzene, and air-dried for a short time. Brown needles. Found: C, 70.08; H, 5.10; N, 5.52; Cu, 12.42%. Drying loss (80 °C, 5 mmHg, 8 hr), 14.9%. Calcd for $C_{24}H_{20}N_2O_2Cu \cdot C_6H_6$: C, 70.05; H, 5.10; N, 5.62; Cu, 12.67; C_6H_6, 15.30%.

Cu(abp)$_2$; When Cu(abp)$_2$·H$_2$O was boiled with benzene for one hour, an anhydrous complex was obtained in the form of dark brown needles. Found: C, 66.73; H, 4.70; N, 6.15; Cu, 14.53%. Calcd for $C_{24}H_{20}N_2O_2Cu$: C, 66.74; H, 4.67; N, 6.49; Cu, 14.71%.

Cu(abp)$_2$·CH$_3$COOC$_2$H$_5$: This complex was prepared from Cu(abp)$_2$·H$_2$O by boiling it in ethyl acetate. Glistening brown needles. Found: C, 64.08; H, 5.48; N, 5.35; Cu, 14.50%. Calcd for $C_{24}H_{20}N_2O_2Cu \cdot CH_3COOC_2H_5$: C, 64.66; H, 5.44; N, 5.38; Cu, 14.70%.

Cu$_5$(abp)$_8$(OH)$_2$·3H$_2$O; To a solution of copper acetate (82 mg) in water (4 ml), we added a solution of Habp (122 mg) in ethanol (3 ml), after which the mixture was kept at 50—60 °C. The precipitate was then filtered and washed with water. Brownish green needles; 131 mg (85%). The complex was insoluble in water and slightly soluble in organic solvents. Found: C, 61.36; H, 4.65; N, 5.67; Cu, 16.97%. Calcd for $Cu_5(abp)_8(OH)_2 \cdot 3H_2O$: C, 61.34; H, 4.72; N, 5.69; Cu, 16.90%. Calcd for $Cu_3(abp)_5(OH) \cdot 3H_2O$: C, 60.87; H, 4.90; N, 5.91; Cu, 16.10%.

Measurements; The infrared spectra were taken by means of a Hitachi EPI-S2 spectrophotometer in the 650—4000 cm^{-1} region, mostly on a KBr disk. The electronic spectra in solutions and on solid samples were measured with a Hitachi EPI-3T recording spectrophotometer. The NMR spectrum was taken with a Hitachi R-24 spectrometer (60 MHz, $CDCl_3$, reference TMS), and the mass spectrum, with a Hitachi RMU-6L mass spectrometer.

The magnetic susceptibilities of the complexes were measured by the Faraday method. The temperature variation in the magnetic susceptibility was measured by the Gouy method in the range from the temperature of liquid nitrogen to room temperature. The effective magnetic moments, μ_{eff}, were determined by means of this equation;

$$\mu_{eff} = 2.83\sqrt{(\chi_A - N_\alpha)T}$$

where χ_A is the atomic susceptibility corrected by the use of Pascal's constants[6] for diamagnetism, and N_α, the temperature-independent paramagnetism of the copper(II) ion (60×10^{-6} cgs, emu).[7]

Results and Discussion

An examination of the UV, IR, NMR, and mass spectra of Habp did not reveal any particular deviation from the expected properties as a normal aromatic aminophenol with Structure (3).

In the IR spectrum of Habp, the band due to the O–H stretching vibration of the phenolic hydroxyl group was found at 3400 cm^{-1}. The bands in the 2500—2700 cm^{-1} region cannot be assigned definitely at present. These bands, however, could not be observed in the spectra of the copper(II) complexes. Instead a new band was observed around 1550 cm^{-1}. It is known that such a new band appears when the phenolic oxygen is involved with the coordination. The N–H stretching vibrations were shifted to a lower-frequency region by 65—105 cm^{-1} by the complex formation. These facts indicate that both the phenolic oxygen and amino nitrogen of Habp participate in the coordination, and that Habp acts as a bidentate chelating agent to form copper(II) complexes with seven-membered chelate rings. The band at 685 cm^{-1} for Cu(abp)$_2$·C$_6$H$_6$ and the bands at 1705 and 1380 cm^{-1} for Cu(abp)$_2$·CH$_3$COOC$_2$H$_5$ may be attributed to the benzene and ethyl acetate molecules respectively.

The water molecule in Cu(abp)$_2$·H$_2$O is not considered to be coordinated to the copper(II) ion, since it is easily removable at a relatively low temperature. The reflectance spectrum of this complex (given in Fig. 2) shows the d-d band at 13.9×10^3 cm^{-1}; it is

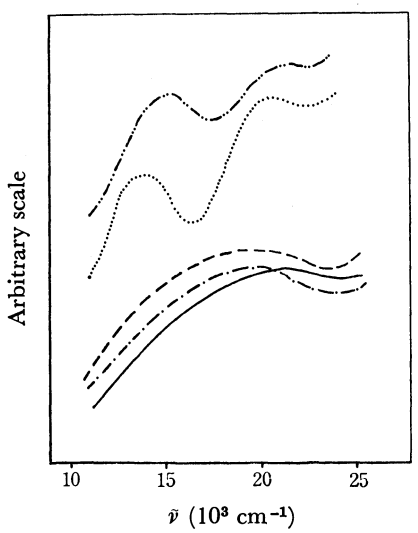

Fig. 2. The reflectance spectra of (abp)–Cu(II) complexes.

-·-·- $Cu_5(abp)_8(OH)_2 \cdot 3H_2O$ ····· $Cu(abp)_2 \cdot H_2O$
---- $Cu(abp)_2 \cdot C_6H_6$ —— $Cu(abp)_2$
-·-· $Cu(abp)_2 \cdot CH_3COOC_2H_5$

Table 1. IR absorption bands of Habp and its complexes

	νOH	νNH$_{as.}$	νNH$_s$.	New bands in the complexes (νC–O)				δC–O	
Habp	3400	3360	3300	2750,	2670,	2570	— — —	1218	KBr disk
Habp	3550	3450	3350	—	—	—	— — —	1230	CCl_4 mull
Cu(abp)$_2$	—	3255	3175	—	—	—	1547	1217	KBr disk
Cu(abp)$_2$·C$_6$H$_6$	—	3300	3200	—	—	—	1550, 685	1215	KBr disk
Cu(abp)$_2$·CH$_3$COOC$_2$H$_5$	—	3275	3195	—	—	—	1550, 1705, 1380	1218	KBr disk
Cu$_5$(abp)$_8$(OH)$_2$·3H$_2$O	—	3300	3225	—	—	—	1555	1235	KBr disk

Table 2. The effective magnetic moments (B.M.) over a temperature range of $Cu_5(abp)_8(OH)_2 \cdot 3H_2O$

T(K)	76.4	96.0	119.1	142.1	170.3	200.0	219.0	241.5	274.7	295.7
$\chi_A \cdot 10^6$	2737	2190	1824	1557	1351	1206	1122	1065	967	925
μ_{eff}	1.27	1.28	1.29	1.30	1.33	1.35	1.36	1.40	1.41	1.43

significantly lower in energy than that of bis-(2-aminophenolato) copper(II) (*ca.* 16×10^3 cm^{-1}). This indicates that the configuration of $Cu(abp)_2 \cdot H_2O$ is considerably distorted from the square-planar structure. Since it is well established that the red shift in the d-d band takes place when the geometry around the copper(II) ion is distorted from planarity,[8] the pseudo-tetrahedral configuration of this complex can also be expected in the examination of the molecular model.

The benzene molecule in $Cu(abp)_2 \cdot C_6H_6$ and the ethyl acetate molecule in $Cu(abp)_2 \cdot CH_3COOC_2H_5$ are also considered to be kept between crystal lattices, since the coordination of benzene to copper(II) ion seems unlikely and since it is clear from the IR spectrum that the ethyl acetate molecule is not coordinated to the copper(II) ion. In fact, the reflectance spectra of $Cu(abp)_2$, $Cu(abp)_2 \cdot C_6H_6$, and $Cu(abp)_2 \cdot CH_3COOC_2H_5$ (given in Fig. 2) are very similar to each other, demonstrating that they have nearly the same molecular structure. Although the d-d bands of these complexes are not well-defined, it is assumed, considering the steric requirement of the ligand, that the complexes have pseudo-tetrahedral structures. The absorption band around the 20×10^3 cm^{-1} region which is common in all these complexes is thought to be a kind of charge-transfer band between the ligand and the copper(II) ion. The effective magnetic moments of $Cu(abp)_2 \cdot H_2O$, $Cu(abp)_2$, $Cu(abp)_2 \cdot C_6H_6$, and $Cu(abp)_2 \cdot CH_3COOC_2H_5$ at room temperature are 1.77, 1.78, 1.88, and 1.85 B.M respectively.

The d-d band of the polynuclear complex appears at 15.1×10^3 cm^{-1}. The effective magnetic moment at room temperature was 1.43 B.M., significantly lower than that of the spin-only value (1.73 B.M.). As can be seen in Table 2, the effective magnetic moment of the complex decreases with a decrease in the temperature and approaches 1.27 B.M. near the temperature of liquid nitrogen. This fact implies that this is a polynuclear copper(II) complex composed of an odd number of copper(II) ions, in which an antiferromagnetic spin-exchange interaction operates (spin-doublet ground state). Therefore, the magnetic property of the polynuclear complex is consistent with the composition of the complex, $Cu_5(abp)_3(OH)_2 \cdot 3H_2O$, as determined by elementary analysis.

The author wishes to express his deep thanks to Professor Yoneichiro Muto of Saga University and Associate Professor Hisashi Okawa of Kyushu University for their help in the physical measurements and for their valuable discussions, and to Professor Masaru Yamaguchi of Kyushu University for his encouragement throughout the work.

References

1) Typical examples are as follows: J.C. Duff, *J. Chem. Soc.*, **119**, 385, 1982 (1921); **123**, 560 (1923); P. Pfeiffer, *Naturwissenschaften*, **35**, 190 (1948); F. Lion and K. V. Martin, *J. Amer. Chem. Soc.*, **79**, 1273 (1957); E. Bayer and E. Breitmaier, *Chem. Ber.*, **101**, 1579 (1968); H. A. Goodwin and F. Lions, *J. Amer. Chem. Soc.*, **82**, 5013 (1960); S. Onaka, This Bulletin, **44**, 2154 (1971).

2) M. Nilsson, *Acta Chem. Scand.*, **20**, 423 (1966); J. C. Colbert, D. Fox, and W. A. Skinner, *J. Amer. Chem. Soc.*, **75**, 2249 (1953). The present author prepared the compound by a modified Colvert's procedure, using 2-iodoanisole in place of 2-bromoanisole, with a slightly improved yield, which is briefly described here.

3) N. Baeyer, *Ber.*, **38**, 2760 (1905).

4) R. G. Bacon and J. R. Wright, *J. Chem. Soc., C*, **1969**, 1978.

5) A. M. VanArendonk, M. E. Cupery, and R. Adams, *J. Amer. Chem. Soc.*, **55**, 4225 (1933); E. C. Kleiderer and R. Adams, *ibid.*, **55**, 4219 (1933).

6) P. W. Selwood, "Magnetochemistry," Interscience, New York (1956), p. 78, 91.

7) B. N. Figgis and R. L. Martin, *J. Chem. Soc.*, **1956**, 3837.

8) S. J. Gruber, C. M. Harris, and E. Sinn, *J. Inorg. Nucl. Chem.*, **30**, 1805 (1968); M. Honda and G. Schwarzenbach, *Helv. Chim. Acta*, **40**, 27 (1957); R. L. Belford and T. S. Piper, *Mol. Phys.*, **5**, 251 (1962): L. Sacconi and M. Ciampolini, *J. Chem. Soc.*, **1964**, 276.

Photo-ethoxycarbonylation of Anisole, Dimethylaniline and Thiophene in Carbon Tetrachloride-Ethanol Solutions*

Takeo AKIYAMA, Osamu IKARASHI, Koji IWASAKI, and Akira SUGIMORI

Department of Chemistry, Faculty of Science and Technology, Sophia University, Kioi-cho 7, Chiyoda-ku, Tokyo 102

(Received February 14, 1974)

UV-Irradiation of anisole, dimethylaniline and thiophene with carbon tetrachloride in ethanol produced ethoxycarbonylated compounds. In general, this photo-ethoxycarbonylation proceeds effectively when a charge transfer complex between aromatic compound and carbon tetrachloride is excited. Attack of trichloromethyl radicals formed by the sensitized decomposition of carbon tetrachloride also occurs in parallel with the charge transfer mechanism.

The authors have reported that ferrocene undergoes photo-ethoxycarbonylation, formylation and ethoxymethylation in carbon tetrachloride–, chloroform–, and dichloromethane–ethanol solutions, respectively.[1a] These photoreactions result from the excitation of the charge transfer complexes of ferrocene with halogenated hydrocarbons.[1b]

Recently, Hirao and Yonemitsu reported the photochemical introduction of formyl group into phenol and diethylaniline during UV-irradiation in chloroform–methanol solutions.[2] They also described the formation of methyl hydroxybenzoates during UV-irradiation of phenol and carbon tetrachloride in aqueous methanol solution.

This paper deals with the photo-ethoxycarbonylation of anisole, dimethylaniline and thiophene in carbon tetrachloride–ethanol solutions.

Experimental

Materials. Commercially available anisole and *N,N*-dimethylaniline (Wako Junyaku E. P. grade reagents) were purified by distillation under reduced pressure and checked by thin layer chromatography after the distillation. Thiophene (Wako Junyaku E. P. grade reagent) was purified by distillation under atmospheric pressure. Carbon tetrachloride was purified as described previously.[1a] Spectro-grade cyclohexane (Wako Junyaku Dotite Spectrosol) was used for the measurement of UV-spectra.

Irradiation. The irradiation procedure was similar to that described previously.[1a]

Separation of the Photoproducts (General Procedure). The irradiated solution was washed with aqueous sodium hydrogen carbonate solution and water after which the organic layer was extracted with ether. The ether solution was dried and then the ether was removed under reduced pressure by a rotary evaporator. The residue was chromatographed on a silica gel column. The eluate was further purified by successive thin layer chromatography on silica gel (Merck, GF-254).

Identification of the Photoproducts. The photoproducts were identified by comparing their IR and NMR spectra, and gas chromatograph retention times with those of authentic samples.

Quantitative Analysis. The products were analyzed with a Yanagimoto GC-550F gas chromatograph equipped with a 1.5 m glass column of Carbowax 20 M on Diasolid L (20%, 60—80 mesh), at 150—184 °C. The analyses listed in Table 1 are the averages of at least three separate experiments.

Measurements. IR spectra were recorded with a Hitachi 215 grating infrared spectrophotometer. UV spectra were recorded with a Hitachi 124 spectrophotometer. NMR spectra were measured with a Hitachi R-24 (60 MHz) or a Hitachi R-22 (90 MHz) spectrometer.

Results and Discussion

The UV-spectra of dimethylaniline, anisole and thiophene in cyclohexane and in carbon tetrachloride are shown in Figs. 1, 2, and 3.

In dimethylaniline, the enhancement of the UV-absorption near 300 nm in the presence of carbon tetrachloride is attributed to the formation of a charge

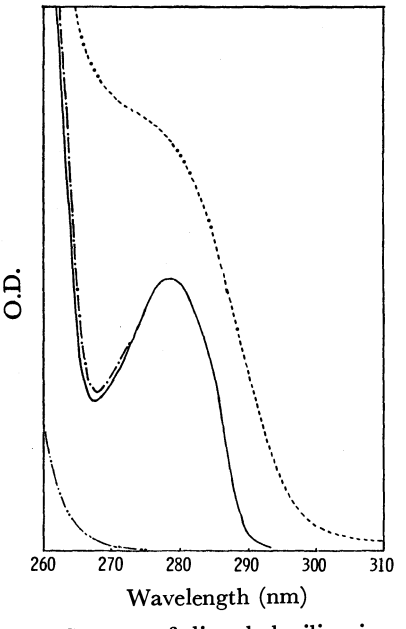

Fig. 1. UV-Spectra of dimethylaniline in cyclohexane and in carbon tetrachloride. (Path length, 1 mm)
(——): Dimethylaniline (3.456×10^{-3}mol·l^{-1}) in cyclohexane.
(– – –): Dimethylaniline (3.456×10^{-3}mol·l^{-1}) in carbon tetrachloride.
(——): Carbon tetrachloride.
(——): The sum of the absorption of dimethylaniline in cyclohexane (3.456×10^{-3}mol·l^{-1}) and that of carbon tetrachloride.

* A part of this work was presented at the Symposium on Photochemistry, Osaka, Japan, November 1—2, 1972.

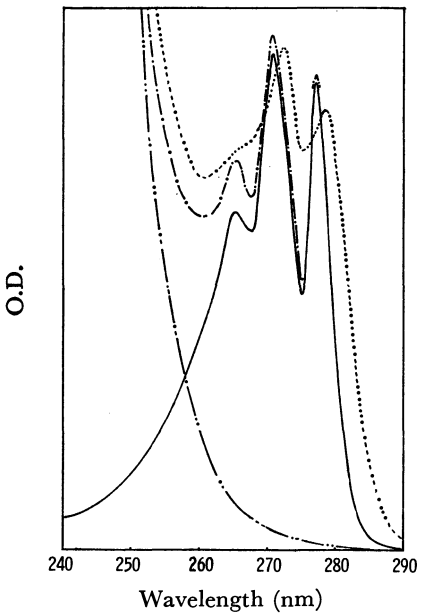

Fig. 2. UV-Spectra of anisole in cyclohexane and in carbon tetrachloride. (Path length, 1 mm)
(——): Anisole (3.456×10^{-3}mol·l^{-1}) in cyclohexane.
(– – –): Anisole (3.456×10^{-3}mol·l^{-1}) in carbon tetrachloride.
(— · —): Carbon tetrachloride.
(· · · ·): The sum of the absorption of anisole in cyclohexane (3.456×10^{-3}mol·l^{-1}) and that of carbon tetrachloride.

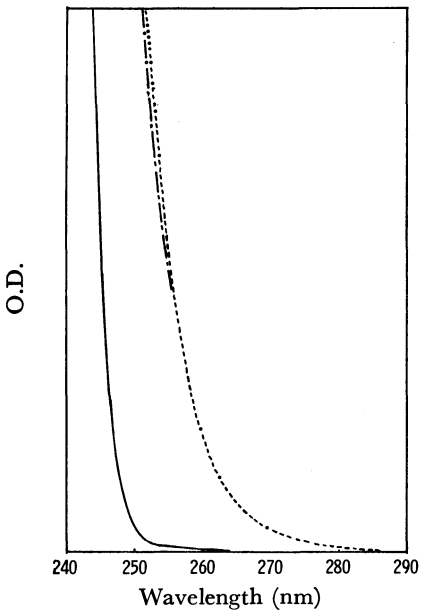

Fig. 3. UV-Spectra of thiophene in cyclohexane and in carbon tetrachloride. (Path length, lmm)
(——): Thiophene (3.456×10^{-3}mol·l^{-1}) in cyclohexane.
(– – –): Thiophene (3.456×10^{-3}mol·l^{-1}) in carbon tetrachloride.
(— · —): Carbon tetrachloride.
The sum of the absorption of thiophene in cyclohexane (3.456×10^{-3}mol·l^{-1}) and that of carbon tetrachloride is smaller than that of thiophene in carbon tetrachloride (3.456×10^{-3}mol·l^{-1}).

transfer complex of dimethylaniline with carbon tetrachloride, as was proposed by Davis and Farmer.[3]

Anisole also shows a slight enhancement of UV-absorption at 250—260 nm and at 270—290 nm. Thiophene also shows a slight enhancement near 250 nm. The linear correlation between ionization potential and wavelength of absorption maximum of the charge transfer band was reported for alkylbenzene-carbon tetrachloride systems.[4,5] Since the ionization potentials of anisole (8.20 eV)[6] and thiophene (8.86 eV)[6] are close to those of hexamethylbenzene (8.15 eV,[7] $h\nu_{CT}$ 240—246 nm[5]) and *m*-xylene (8.9 eV,[7] $h\nu_{CT}$ 232—238 nm[5]), respectively, the enhancement of the UV-absorption of anisole in carbon tetrachloride near 250 nm or that of thiophene in this region can be ascribed to the formation of charge transfer complexes with carbon tetrachloride.

The UV-irradiation of anisole, dimethylaniline and thiophene with carbon tetrachloride in ethanol solution gave the corresponding ethoxycarbonylated compounds, as in the irradiation of the ferrocene–carbon tetrachloride–ethanol system. In the case of anisole and dimethylaniline, the yields of photoproducts and the ratios of isomers obtained are changed significantly by changing the wavelength of irradiating light. The results are summarized in Table 1.

Photoreaction of Dimethylaniline. Irradiation with 254, 313, and 365 nm light gave both *o*- and *p*-dimethylaminobenzoates. Irradiation with 254 nm light resulted in an *o*/*p* ratio of 3.7. An irradiation with 254 nm light, the incident light was mostly absorbed by uncomplexed dimethylaniline. The addition of cyclohexene, a radical scavenger, markedly suppressed the formation of ethyl dimethylaminobenzoates, especially the *ortho* isomer: the *o*/*p* ratio in the presence of cyclohexene was 0.47. Irradiation with light of longer wavelength gave different results: lower *o*/*p* ratio (1.31 and 1.78) were obtained on irradiation with 313 and 365 nm light. The *o*/*p* ratios in the presence of cyclohexene are similar on irradiation with 254 and 313 nm light (0.47 and 0.39). The photo-ethoxycarbonylation of dimethylaniline with 313 nm light, which was not affected by added cyclohexene, can be considered to proceed in the solvent cage. The value of the *o*/*p* ratio, 1.31, obtained on irradiation with 313 nm light is closer to 0.47 and 0.39 than to the 3.7 obtained on irradiation with 254 nm light. In the photo-ethoxycarbonylation of dimethylaniline with 313 nm light, the charge transfer complex between dimethylaniline and carbon tetrachloride contributes greatly to the photo-substitution. Irradiation with 365 nm light also gave an *o*/*p* ratio, 1.78, which is close to that obtained on irradiation with 313 nm light.[8]

Higher yields of the ethoxycarbonylated products were obtained in the presence of cyclohexene than in its absence on irradiation with 313 nm light. The reason for this effect of cyclohexene is still not clear.

The formation of hydrogen chloride during the reaction may cause the decomposition of dimethylaniline to give *N*-methylaniline and an anilinum cation which reacts with dimethylaniline photochemically to give biphenyl derivatives.[9] Although a quantitative analy-

Table 1. Photo-ethoxycarbonylation of aromatic compounds in carbon tetrachloride–ethanol solutions[a)]

Aromatic compound (20 mmol)	CCl_4 (mmol)	Cyclohexene (mmol)	hν/Time (nm)/(hr)	Conversion (%)	Products and Yields[b)]					
					Ethyl methoxybenzoates[c)]				*p*-Chloroanisole	Ethyl salicylate
					o-	*m*-	*p*-	*o*/*p*		
Anisole	40	—	254/48	8.5	4.6	0.6	7.8	[0.59]	18.7	trace
Anisole	40	20	254/48	24.4	3.9	1.1	4.4	[0.88]	24.9	trace
Anisole	40	—	265/48	16.7	8.9	2.2	10.7	[1.71][d)]	5.8	9.4
Anisole	40	20	265/48	13.6	1.3	0.2	2.7	[0.50]	0.1	trace
					Ethyl *N*,*N*-dimethylaminobenzoates[c)]					
					o-	*m*-	*p*-			
Dimethylaniline	40	—	254/48	9.2	14.5 (1.3)	0	3.9 (0.3)	[3.7]		
Dimethylaniline	40	20	254/48	1.3	7.9 (0.1)	0	16.6 (0.2)	[0.47]		
Dimethylaniline	40	—	313/48	4.9	8.4 (0.4)	trace	6.4 (0.3)	[1.31]		
Dimethylaniline	40	20	313/48	14.2	4.9 (0.7)	trace	12.4 (1.7)	[0.39]		
Dimethylaniline	40	—	365/48	3.0	17.8 (0.5)	trace	10.0 (0.3)	[1.78]		
					Ethyl 2-thiophenecarboxylate[f)]					
Thiophene	100	—	254/18		0.8					
Thiophene	100	20	254/18		0.8					
Thiophene	100	—	365/45		0.0					

a) The total volume of the sample solution was 50 ml. b) The values listed in this table are averages of at least three separate experiments. The yields were calculated from glpc data on the basis of starting materials consumed. c) The isomer distributions are as follows: 254 nm, *o*-: *m*-: *p*- =34.8: 5.3: 59.8, 254 nm with cyclohexene, *o*-: *m*-: *p*- =41.4: 11.7: 46.8, 265 nm, *o*-: *m*-: *p*- = 58.4: 7.1: 34.3, 265 nm with cyclohexene, *o*-: *m*-: *p*- =31.7: 4.0: 64.1. d) Ethyl salicylate was taken as an *ortho*-isomer. e) The values in parentheses are the yields on the basis of starting material. f) The yield based on starting material used.

sis was not made, *N*-methylaniline was detected by gas chromatography, but no biphenyl derivatives were detected.

Photoreaction of Anisole. For anisole, the ratio of the photoproducts also changed with the wavelength of the irradiating light; irradiation with 254 nm light gave *p*-chloroanisole and ethyl methoxybenzoates (*o*-: *m*-: *p*-=34.8: 5.3: 59.8) as the main products, whereas irradiation with 265 nm light gave ethyl methoxybenzoates and ethyl salicylate (*o*-: *m*-: *p*-=58.4: 7.1: 34.3, ethyl salicylate was considered as an *ortho*-substituted product) as the main products. The yield of *p*-chloroanisole on irradiation with 265 nm light was nearly one third of that on irradiation with 254 nm light. Cyclohexene was observed to have a marked effect on product formation as in the case of dimethylaniline. The addition of cyclohexene diminished the yields of ethyl methoxybenzoates and *p*-chloroanisole upon irradiation with 265 nm light, whereas the ethoxycarbonylation with 254 nm light was retarded to a lesser extent. In general, the *o*/*p* ratio of the isomers in the free radical substitution of anisole is greater than 1.[10] The *o*/*p* ratio on irradiation with 265 nm light was 1.71 and the addition of cyclohexene lowered the *o*/*p* ratio to 0.50. This indicates that the photoethoxycarbonylation with 265 nm light proceeds mainly *via* a free radical mechanism. On the other hand, the *o*/*p* ratio on irradiation with 254 nm light is less than 1 and the value was affected by cyclohexene to a lesser extent. These results indicate that on irradiation with 254 nm light the ethoxycarbonylated products are not formed *via* free radical attack on anisole but are probably formed by the combination of radical cations of anisole and trichloromethyl radicals produced by the excitation of the charge transfer complex in the solvent cage. This was considered to be the case for dimethylaniline irradiated with 313 nm light which excites mainly charge transfer complexes.

The formation of *p*-chloroanisole on irradiation with 254 nm light can be explained by the attack on anisole by a chlorine atom which is produced either by sensitized decomposition[11] of carbon tetrachloride or by electron transfer between a cation radical and a chloride anion.[12] The possible reaction mechanisms of the

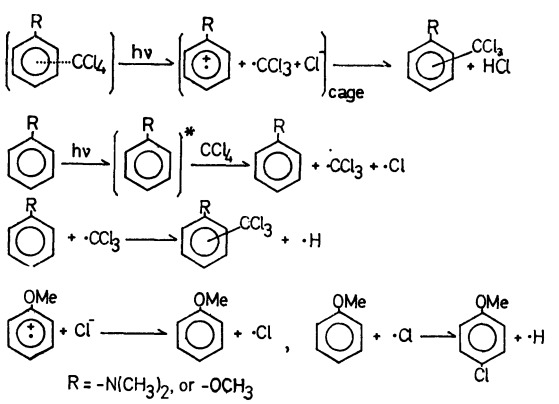

photo-ethoxycarbonylation of dimethylaniline and anisole are shown in the following schemes.

Photoreaction of Thiophene. Thiophene undergoes a similar photo-ethoxycarbonylation upon irradiation with 254 nm light giving ethyl 2-thiophenecarboxylate. In this case, the substitution at the 2-position occurred selectively and no chlorothiophene was detectable. Polymeric substances were also obtained. The addition of cyclohexene did not reduce the yield of ethyl 2-thiophenecarboxylate. The UV-spectrum of thiophene and carbon tetrachloride in ethanol solution showed a slight enhancement of absorption near 254 nm. These results and the effect of cyclohexene on the photoproduct suggest that the trichloromethyl radicals which are formed by the dissociation of the charge transfer complex between thiophene and carbon tetrachloride attack the radical cation of thiophene in the solvent cage.

An attempt to isolate the intermediate trichloromethylthiophene was unsuccessful, but when thiophene was irradiated in carbon tetrachloride and ethanol was then added to the reaction mixture after the irradiation, ethyl 2-thiophenecarboxylate was detected by gas chromatography. As reported,[13] the trichloromethyl group is solvolyzed rapidly during UV-irradiation. The isolation of trichloromethylated compounds may thus be quite difficult. The possible reaction processes for the photo-ethoxycarbonylation of thiophene is shown in the following schemes.

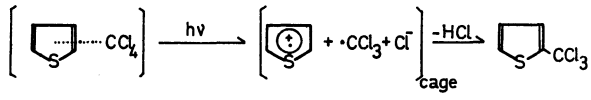

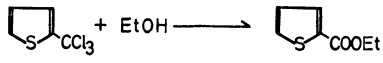

One of the authors, T. A. acknowledges the financial support of the Ministry of Education for this work.

References

1a) T Akiyama, Y. Hoshi, S. Goto, and A. Sugimori, This Bulletin, **46**, 1851 (1973).
1b) T. Akiyama, A. Sugimori, and H. Hermann, *ibid.*, **46**, 1855 (1973).
2) K. Hirao and O. Yonemitsu, *Chem. Commun.*, **1972**, 812.
3) K. M. C. Davis and M. F. Farmer, *J. Chem. Soc., B*, **1967**, 28.
4) R. F. Weimer and J. M. Prausnitz, *J. Chem. Phys.*, **42**, 3463 (1965).
5) D. R. Rosseinsky and H. Kellawi, *J. Chem. Soc., A*, **1969**, 1207.
6) K. Watanabe, *J. Chem. Phys.*, **26**, 542 (1957).
7) F. Meyer and A. G. Harrison, *Can. J. Chem.*, **4**, 2256 (1964).
8) The charge transfer band still has some absorption at 365 nm.
9) C. Pac and H. Sakurai, *Kogyo Kagaku Zasshi*, **72**, 230 (1969).
10) R. A. McClelland, R. O. C. Norman, and C. B. Thomas, *J. Chem. Soc. Perkin I*, **1972**, 562, and M. J. Perkins, "Free Radicals," Vol. II, ed. by J. K. Kochi, John Wiley & Sons, New York, N. Y. (1973), pp. 246—249.
11) J. Klein and G. Laustriat, *J. Chim. Phys.*, **1970**, 310.
12) C. V. Ristagno and H. J. Shine, *J. Org. Chem.*, **36**, 4053 (1971).
13) T. Ishigami, Y. Kinoshita, and A. Sugimori, *Chem. Lett.*, **1974**, 149.

Resins from Formaldehyde. 103.[1] Reaction of Naphthalene with Aqueous Formaldehyde Solution*

Tatsuro OUCHI, Saburo OTSUKA, and Minoru IMOTO

Department of Applied Chemistry, Faculty of Engineering, Kansai University, Senriyama, Suita-shi, Osaka 564

(Received March 7, 1974)

The reaction of naphthalene(N) with formaldehyde(F) was carried out in dioxane or an acetic acid/water solution, using sulfuric acid as the catalyst. The rate of the consumption of F is proportional to $[N]^{1.12}[F]^{1.05}[H_2SO_4]^{1.05}$. The activation energies and entropies of the reaction of N, α- and β-naphthyl carbinol(NC) with F were estimated to be 21.4, 15.3, and 16.0 kcal/mol and −19.1, −36.2, and −33.2 e.u., respectively. The reaction products were isolated and their structures were identified as α-NC, αα′-, αβ′-dinaphthylmethane, three- and four-nuclear compounds, which are linked to each other with methylene or methylene ether bonds at the α- or β-positions; identified was done by means of the IR, NMR, and UV spectra, molecular-weight measurements, elemental analysis, and thin-layer chromatography. In addition to the compounds described above, acetyl esters were obtained when the reaction was carried out in the presence of acetic acid. The reactivities of the α-position of N and its derivatives was larger than those of the β-position. Moreover, the resin formation from N and F was studied by means of gel-permeation chromatography. On the bases of these results, the reaction route of N with F to resin was deduced.

Almost seventy years ago, Bohn[2] found that the condensation resin of naphthalene(N) with formalin gave a resinous matter which could be used as a drying oil. According to his patent, when the molar ratio of formaldehyde(F) to naphthalene becomes larger, the resulting resin has a larger molecular weight, a large melting point, and a lower oxygen content. The resin was assumed to be composed of compounds with methylene linkages.

A German patent[3] in 1918 described that the reaction product of N with F was white resin and could be dissolved in acetone, benzene, solvent naphtha, carbon tetrachloride, and carbon disulfide. In 1962, Imoto *et al.*[4] studied kinetically the reactions of N and methylnaphthalene with F in the presence of perchloric acid, using acetic acid as the solvent.

The present paper will deal with acid-catalyzed reaction of N with an aqueous F solution in dioxane or acetic acid. Moreover, some intermediate compounds to resinous matter were isolated; the reaction mechanism will be discussed.

Experimental

Materials. N of a special grade was purified by sublimation. Formalin containing 41.51% of F and less than 0.8% of methanol, supplied by the Mitsubishi Gas Chemical Co., Ltd., was purified in order to remove the formic acid by passing it through an ion-exchange resin column.

Five kinds of authentic compounds (α-NC, β-NC, αα′-DNM, αβ′-DNM, and ββ′-DNM) were synthesized according to the scheme shown in Fig. 1. Their melting points and their R_f values in thin-layer chromatography (tlc) are listed in Table 1. A thin-layer chromatogram on silica gel (Wakogel B5F) was activated by heating at 130 °C for a period of 4 hr.

Measurement of the Reaction Rate. N or its derivative was dissolved in dioxane. After adding 5 N-sulfuric acid, the measuring flask was warmed at a definite temperature,

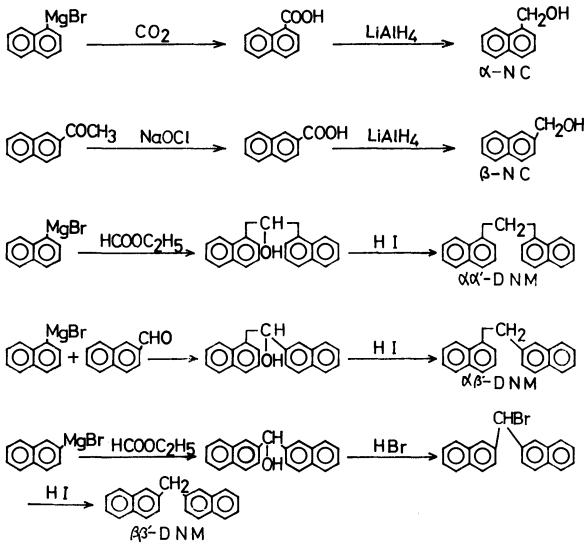

Fig. 1. Syntheses of authentic compounds.

TABLE 1. MELTING POINT AND R_f VALUE OF NAPHTHALENE DERIVATIVES

Compounds	mp (°C) Found	mp (°C) Lit	R_f value[a]
Naphthalene (N)	79.5—80.5	80.2	0.6
α-Naphthylcarbinol (α-NC)	60—61.5	59.5—60[6]	0.1
β-Naphthylcarbinol (β-NC)	80.5—81.5	80—80.5[6]	0.1
α,α′-Dinaphthylmethane (α,α′-DNM)	105—105.5	107—108,[8] 109[9]	0.6
α,β′-Dinaphthylmethane (αβ′-DNM)	94.5—95.5	96[9]	0.6
β,β′-Dinaphthylmethane (ββ′-DNM)	91.5—92.5	93[9]	0.6

a) Benzene–carbon tetrachloride mixture (1: 1) was used as a solvent

an F solution at the same temperature was added, and the solution was diluted to exactly 50 ml with dioxane. The time thirty seconds after the mixing in of F was considered as the starting point of the reaction. An aliquot portion (3 ml) of the reaction mixture was taken up from time to time and quenched with a sufficient volume of a 0.5 M–NaOH solution to neutralize the above mixture. The concentration of the remaining unreacted F was determined by means of the sodium-sulfite method.

Fractionation of the Reaction Product. The reaction products were fractionated by column chromatography and tlc. The R_f values of tlc were obtained by using benzene–CCl_4 (1:1 in vol.) as the developing solvent. The three kinds of DNM showed almost the same R_f values of tlc as that of N. Accordingly, when the separation of DNM from N by tlc was carried out, the chromatogram was allowed to stand under an atmosphere at room temperature for about 20 hr in order to sublime the N. The spot of tlc was determined by the UV-fluorescence method or by coloration with iodine.

Molecular Weights. The molecular weights were determined by the vapor-pressure osmometer (VPO) method at 37 °C, using benzene as the solvent.

Results and Discussion

Kinetics of the Reaction of Naphthalene with Formaldehyde. At first, a kinetic experiment was conducted on the rate of the reaction of N with F in a dioxane–water mixture (1:1) at 80 °C in order to derive the rate equation.

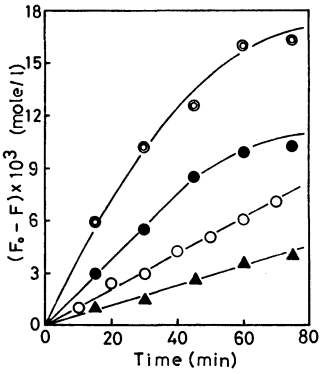

Fig. 2. $[N]_0$ *vs.* consumed [F] at 80 °C. $[F]_0=0.0568$ mol/l, $[H_2SO_4]=0.483$ mol/l, $[N]_0$ ▲: 0.0250 mol/l, ○: 0.0500 mol/l, ●: 0.0750 mol/l, ◎: 0.100 mol/l
solvent: dioxane–water (80:20 in vol)

When the concentration of N was varied from 0.0250 to 0.100 mol/l, while the initial concentrations of F and sulfuric acid were kept at 0.0568 and 0.483 mol/l respectively, the consumption of F increased linearly with the reaction time, as is shown in Fig. 2.

When the F and catalyst concentrations were changed, linear relationships were also obtained between the consumption of F and the reaction time. In addition, the dependence of the initial concentration on the rate was drawn (Fig. 3).

From this figure, the rate equation of the reaction of N with F in aqueous dioxane in the presence of sulfuric acid was concluded to be as follows:

$$R_0 = -\mathrm{d[F]/d}t = k[\mathrm{N}]_0^{1.12}[\mathrm{F}]_0^{1.05}[\mathrm{H_2SO_4}]^{1.05} \quad (1)$$

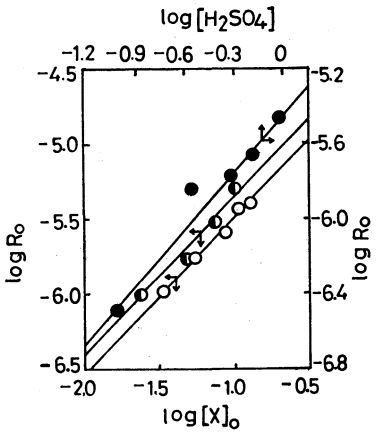

Fig. 3. Dependence of initial concentration on reaction rate.
○: X=N, $[F]_0=0.0568$ mol/l, $[H_2SO_4]=0.483$ mol/l, $[N]_0=0.0250$—0.100 mol/l
◐: X=F, $[N]_0=0.0500$ mol/l, $[H_2SO_4]=0.438$ mol/l, $[F]_0=0.0341$—0.1363 mol/l
●: $[F]_0=0.0568$ mol/l, $[N]_0=0.500$ mol/l, $[H_2SO_4]=$ 0.0966—0.966 mol/l
Solvent: dioxane–water (80:20 in vol) Temp: 80 °C

Equation (1) agreed well with Eq. (2), which was formerly[4] obtained by the acidic reaction of N with F carried out in acetic acid by one of the present authors (M. Imoto). Moreover Eq. (2) is a usual rate equation for the acidic reaction of F with many phenolic compounds and aromatic hydrocarbones.

$$-\mathrm{d[F]/d}t = k[\mathrm{N}]_0[\mathrm{F}]_0[\mathrm{H_2SO_4}] \quad (2)$$

By using Eq. (2), the average value of the rate constant, k, at 80 °C was calculated to be 1.29×10^{-3} $l^2\,mol^{-2}\,s^{-1}$.

Reactivities of Naphthalene and its Derivatives with Formaldehyde. As has been mentioned above, F was concluded to react with N in the presence of sulfuric acid according to Eq. (2). This equation can be also applied to the N derivatives which may be generated as intermediates during the so-called addition-condensation of N with F to from naphthalene-resin.

The reaction was carried out at 80 °C in aqueous dioxane, keepting the initial concentrations of N or its derivatives, F and, H_2SO_4 constant at 0.0500, 0.0568, and 0.483 mol/l respectively.

The experiments to determine the rate constant, k, were repeated twice. The averages of k listed in Table 2 were thus obtained. From the results shown in

Table 2. Reactivities of naphthalene and its derivatives.
$[N]_0$ or [N derivatives]$_0=0.0500$ mol/l, $[F]_0=0.0568$ mol/l, $[H_2SO_4]=0.483$ mol/l; 80 °C
solvent: dioxane–water (80:20 in vol)

Compounds	$k\times10^3$ (l^2/mol^2 s)
N	1.24
α-NC	1.21
β-NC	2.01
αα′-DNM	1.61
αβ′-DNM	3.65
ββ′-DNM	4.62

Table 2, it can be concluded that the α-position of N is more reactive than the β-position. These results are explicable with reactive parameters calculated by means of the molecular-orbital method.

Estimations of E_a and ΔS^* on the Acidic Reactions of Naphthalene and its Carbinols with Formaldehyde. The rate constants of the reaction of N, α-NC, and β-NC with F in aqueous dioxane were determined at 80 °C; they are listed in Table 2. Similarly, the values of the rate constants at 60, 70, and 90 °C were determined. Arrhenius plots were thus drawn, as is shown in Fig. 4. From these lines, the overall activation energies (E_a) and entropies (ΔS^*) were calculated; they are listed in Table 3.

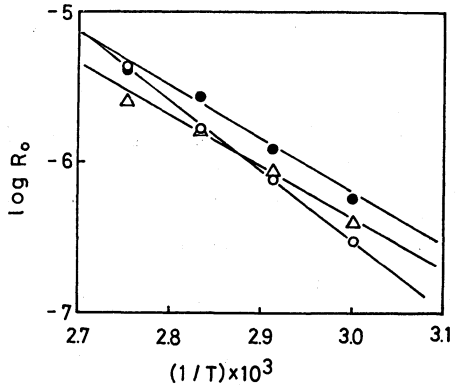

Fig. 4. Arrhenius plots of the reaction of F with N, α-NC and β-NC in aqueous dioxane. ○: N, △: α-NC, ●: β-NC

Table 3. E_a and ΔS^*

Compounds	E_a (kcal/mol)	ΔS^* (80 °C) (e.u.)
N	21.4	−19.1
α-NC	15.3	−36.2
β-NC	16.0	−33.2

The E_a of the reaction of N with F was estimated to be 21.4 kcal/mol. One of the present authors (M. I.) has formerly reported that the activation energies of the reactions of phenol, cresols, and their polynuclear compounds with F were generally close to 23 kcal/mol.[11] It is interesting that the value of 21.4 kcal/mol obtained in the case of naphthalene was also close to 23 kcal/mol.

The E_a and ΔS^* of the reaction of F with NC were found to be smaller than those with N. This may be a result of the activation of the cationic attack on the naphthalene nucleus and the intermolecular hydrogen bond by the introduction of the CH_2OH group into N.

Isolation of Initial Products of the Reaction of Naphthalene with Formaldehyde. Various amount of glacial acetic acid, 12.8 g of N, 5.4 g of 41.51% formalin, and 5 g of 18M-sulfuric acid were mixed thoroughly and warmed (Table 4). After the reaction time has elapsed, the mixture was neutralized with a sodium hydroxide solution and extracted with benzene. The extract was washed repeatedly with water, concentrated to about 100 ml, and then distilled by steam. The unreacted N was then distilled off, and the residue was extracted with benzene. The separation of the components in the extract was carried out by column chromatography, using carbon tetrachloride–benzene (5:1) as the eluent.

Fraction I: Fraction I in Table 4 was fractionated once more into five portions by column chromatography, using the above solvent. The first portion (i) has the largest R_f-value, while the fifth portion (v) has the smallest R_f-value.

Fraction (i): Repeated recrystallizations from an equivolume mixture of benzene and methanol gave needle crystals; mp 104.5—107 °C; R_f of tlc 0.6 (benzene–CCl_4 1:1 in vol.). Mixing with an authentic sample of αα′-DNM showed the same mp, without any depression. IR (KBr disk) 2925, 2875 cm^{-1} (CH_2); NMR (CCl_4) τ 5.16 (s, Ar–CH_2–Ar).

Found: C, 93.81; H, 5.70%; mol wt, 265. Calcd for $C_{21}H_{16}$: C, 93.99; H, 6.10%; mol wt, 268.

Fraction (ii): The powder-like crystals were collected by recrystallization from a benzene–methanol mixture; mp 94.5—95.5 °C; R_f of tlc 0.6. No depression of the mp was observed after mixing with an authentic sample of αβ′-DNM. IR (KBr disk) 2925, 2875 cm^{-1} (CH_2); NMR (CCl_4) τ 5.46 (s, Ar–CH_2–Ar).

Found: C, 94.02; H, 5.79%; mol wt, 263. Calcd for $C_{21}H_{16}$: C, 93.99; H, 6.01%; mol wt, 268.

An alternative reaction of N with F under the conditions shown for Experiment No. 2 in Table 4 was carried out. Fractions (I-i) and (I-ii) were thus isolated. They were distilled under a vacuum (bp 258—265 °C/10 mmHg) and fractionated by recrystallization from a benzene–methanol mixture into αα′-DNM and αβ′-DNM. The quantity of αα′-DNM was assumed to be larger by 15—20 times than that of αβ′-DNM.

Fraction (iii): Repeated fractional recrystallizations from diethyl ether gave powder-like crystals as the most difficultly soluble fraction: mp 137—140 °C; R_f of tlc 0.6; IR (KBr disk) 2925, 2875 cm^{-1} (CH_2); NMR (CCl_4) τ 5.20 (s, Ar–CH_2–Ar–CH_2–Ar).

Found: C, 94.27; H, 5.64%; mol wt, 405. Calcd for $C_{32}H_{24}$: C, 94.08; H, 5.92%; mol wt, 408.

The absorptions due to the methylene group at 2925 and 2875 cm^{-1} very much resembled that of αα′-DNM,

Table 4. Fractionation of reaction products of naphthalene with formaldehyde

Exp. No.	N (g)	F (g)	Acetic acid (ml)	Temp (°C)	Unreacted N (g)	Fractions from column chromatography (g)				
						I	II	III	IV	V
						R_f 0.6	0.4	0.25	0.2	0
1	12.8	5.4	200	90	4.7[a)]	6.1	—	0.1	1.8	—
2	12.8	12.0	150	100	4.8[a)]	6.3	0.04	0.04	1.6	0.4

a) Including the portion of R_f 0—0.1 of the column chromatography.

but the different absorption appeared at about 800 cm^{-1}. By this absorption in IR and a singlet signal due to protons of CH_2 in NMR, it was considered that this compound has a symmetrical structure. Accordingly, it may be concluded that this crystal is a three-nuclear compound linked with methylene groups at the α-positions, as is shown below.

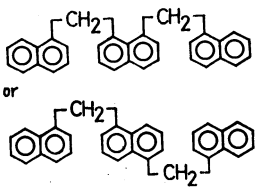

Fraction (iv): Powder-like crystals were obtained by repeated reprecipitations from a benzene solution with methanol; mp 214—220 °C; R_f of tlc 0.6; IR (KBr disk) 2925, 2875 cm^{-1} (CH_2): NMR (CCl_4) 5.15 (s, Ar–CH_2–Ar–CH_2–Ar–CH_2–Ar–CH_2–Ar).

Found: C, 93.27; H, 5.91%; mol wt, 526. Calcd for $C_{43}H_{32}$: C, 94.12; H, 5.88%; mol wt, 549.

From the data of IR and NMR, this fraction was assumed to be composed mainly of the four-nuclear compound, linked with CH_2 groups at the α-positions.

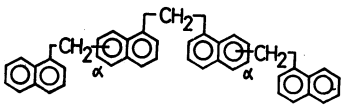

Fraction (v): Repeated reprecipitations from benzene and methanol gave the following five fractions; the mps ranged between 120 and 190 °C, and the R_f values between 0.6 and 0.5; IR (KBr disk) 2925, 2875 cm^{-1} (CH_2).

Found: (a) C, 93.64; H, 5.81%; mol wt, 524; (b) C, 93.38; H, 5.70%; mol wt, 548; (c) mol wt, 649; (d) C, 93.81; H, 5.69%; mol wt, 683; (e) C, 93.16; H, 5.49%; mol wt, 869.

Fraction II: This fraction was obtained as a viscous liquid, with an R_f value of about 0.4. Repeated reprecipitations from benzene and methanol gave a white powder. It started to melt at 78 °C without showing any definite temperature. The IR spectrum has signals at 1730 cm^{-1} (C=O) and 1225 cm^{-1} (C–O), showing that the fraction is composed of an acetylester of NC or DNM.

Found: C, 88.30; H, 6.35%.

Fraction III: This fraction was also assumed to be an ester: mp>117 °C, R_f 0.25. Signals of IR agreed with those of the acetic ester.

Found: C, 89.22; H, 5.58%.

Fraction IV: Fraction IV (R_f 0.2) was a highly viscous liquid. It was purified by reprecipitation from benzene and methanol, and then fractionated by column chromatography, using carbon tetrachloride and chloroform as the solvents. The most abundant fraction was purified by the reprecipitation method, using carbon tetrachloride and methanol. A white powder was thus obtained; mp 142—164 °C; R_f 0.2; IR: 1730 cm^{-1} (C=O), 1225 cm^{-1} (C–O).

Found: C, 90.32; H, 5.63%; mol wt, 600. Calcd for $C_{46}H_{36}O_2$: C, 89.00; H, 5.85%; mol wt, 621.

$C_{46}H_{36}O_2$ corresponds to an acetate of the four-nuclear methylol compound.

Fraction V: A viscous liquid was obtained as a fraction with an R_f value of 0.0—0.06. Reprecipitation from a benzene solution with methanol gave the following three fractions.

Found: (i) C, 88.02; H, 5.40%; mol wt, 790, (ii) C, 86.63; H, 5.38; mol wt, 874, (iii) C, 85.09; H, 5.46; mol wt, 1028.

The oxygen contents of these fractions were very large, and it was assumed from, the IR spectra that oxygen existed as an acetate group or as a dimethylene ether group.

Fraction having R_f of 0.1: In another experiment, the reaction product of N with 41.51% formalin under the same conditions as an Exp. No. 2 in Table 4 was distilled under a vacuum. The fraction boiling at 150—170 °C/15 mmHg was again fractionated by column chromatography, using carbon tetrachloride as the solvent. A fraction with an R_f value of 0.1 was recrystallized from a carbon tetrachloride–methanol solution (1 : 1 in vol.) to give needle crystals: mp 60.5—61.5 °C. IR (KBr disk) 3350, 1000 cm^{-1} (OH), 2925, 2875 cm^{-1} (CH_2).

Found: C, 83.21; H, 6.08%. Calcd for $C_{11}H_{10}O$: C, 83.51; H, 6.37%.

No depression of mp was shown upon mixing with an authentic sample. Accordingly, this crystal may be concluded to be α-naphthyl carbinol.

Formation of Two-nuclear Dimethylene Ether Compound from β-Naphthyl Carbinol. A solution of 2 g of β-NC in 25 ml of dioxane was heated at 100 °C for 22 hr in the presence of 10 ml of 5 M-sulfuric acid. After the reaction, the mixture was extracted with benzene, washed with water, and then neutralized with an 1 M-NaOH solution. The benzene was evaporated almost completely. The residue, diluted with carbon tetrachloride was then submitted to column chromatography. A fraction with an R_f value of 0.35 was recrystallized from a mixture of carbon tetrachloride and petroleum ether. Needle-like crystals were thus obtained; mp 123—125.5 °C (121—123 °C[12]).

Found: C, 88.58; H, 6.23%; mol wt, 292. Calcd for $C_{22}H_{18}O$: C, 88.56; H, 6.08%; mol wt, 298.

From the IR and NMR results, the fraction was concluded to be di-β-naphthylmethylene ether.

Formation of Dinaphthylmethane from Naphthylcarbinol and Naphthalene. Formation of αα′-DNM: α-NC, N, and sulfuric acid were dissolved in acetic acid. Their concentrations were 0.0500, 0.0500, and 0.483 mol/l respectively. After the solution has been warmed at 80 °C for 5 hr, αα′-DNM was isolated from the reaction mixture by column chromatography in a yield of 20 wt% of the α-NC. The αα′-DNM thus isolated was confirmed by comparing its UV spectrum with that of an authentic sample: λ_{max}=285 nm (ε=16200). *Formation of αβ′-DNM*: β-NC was reacted with N in a way similar to that used in the case of α-NC. The yield of αβ′-DNM isolated was about 10 wt%. Its identity as αβ′-DNM was confirmed by studing the UV spectrum: λ_{max}=273 nm (ε=14400).

Assumed Route for the Reaction of Naphthalene with

Formalin to Resin. As has been mentioned above, α-NC, αα'-DNM, αβ'-DNM, and three- and four-nuclear compounds, which are all linked to each other with methylene bonds, predominantly in the positions of α, were isolated. Thus, it was concluded that the formation reaction of naphthalene-formaldehyde resin is also included in the so-called "addition-condensation" reaction. First, NC, especially α-NC, is generated by the reaction of N with F; then NC is condensed with N to give αα'-dNM. These two reactions occur laternatively in preparing a higher nuclear compound. Accordingly, the reaction route may be shown as in Fig. 5.

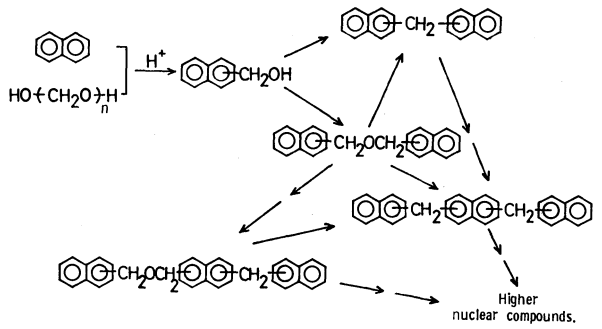

Fig. 5. Reaction route of naphthalene with formaldehyde in acidic medium

Studies of the Resin Formation from Naphthalene and Formaldehyde by Gel-permeation Chromatography. Calibration curve for GPC-analysis: Separation was carried out by means of the apparatus of Waters' Associates, GPC 501, using tetrahydrofuran (THF) as the solvent. The injected samples had an average concentration of 0.1—0.5 wt%. The two columns used were 4 ft long and 1/2 in. in diameter, and were packed with polystyrene gels whose porosities were 100 and 60 Å respectively.

Using synthesized authentic samples and fractionated higher-molecular-weight compounds, a calibration curve was prepared. As is shown in Fig. 6, α- and β-Naphthyl carbinols deviated from the line. Such deviations may be due to the increases in the molecular sizes as a results of the loose complexing of naphthyl carbinol with THF.*

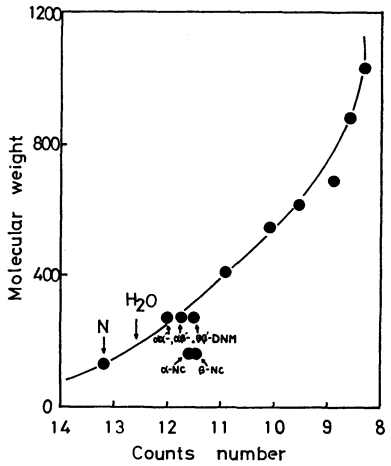

Fig. 6. GPC calibration curve.

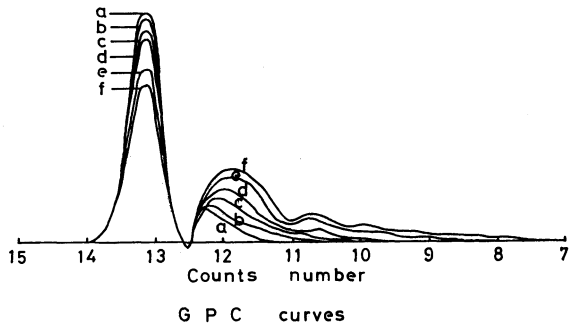

Fig. 7. GPC curves.
Reaction time a: 0 min, b: 30 min, c: 60 min, d: 90 min, e: 150 min, f: 180 min

Change in the GPC-curve of the Reaction Products with Reaction Time: A solution of 19.2 g of N, 9 g of 41.51% formalin, and 7.5 g of 81 M-sulfuric acid in 300 ml of glacial acetic acid was heated at 90 °C. After a definite time, an aliquot of the solution was pipetted

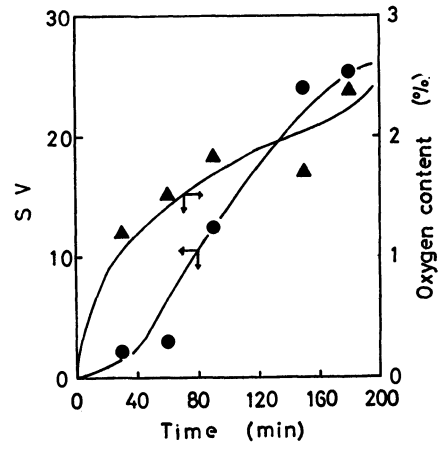

Fig. 8. Saponification values and oxygen contents *vs.* reaction time.

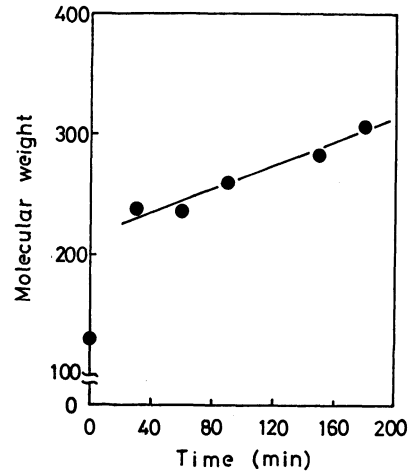

Fig. 9. Molecular weights *vs.* reaction time.

* It had been found that a solution of α- or β-naphthylcarbinol in THF shows a new IR signal of the hydrogen bond at 3420 cm^{-1}.[13]

out, extracted with benzene and carefully washed with water. The benzene layer was then concentrated to almost dryness. The residue was dissolved in THF and used as an injection solution for GPC. The results are shown as Fig. 7. It may be seen that the peak around 13 counts become lower, while the peaks around 12 counts become higher, with the reaction time.

Changes in the Oxygen Contents, Saponification Values and Molecular Weights of the Products with the Reaction Time. The products used for GPC analyses were also submitted to measurements of their oxygen content and saponification value (SV) without and further purification in order to avoid the loss of any components. The oxygen content was estimated by an elemental analysis of the carbon and hydrogen. As the products contained unreacted N, the oxygen contents were not so high as has been expected. The SV was calculated by the usual saponification method, using alcoholic potassium hydroxide in a solvent of benzene–ethanol mixture as the solvent. The molecular weight of the product, after the removal of the unreacted N by steam distillation, was determined by the VPO method, using benzene as the solvent. The results are shown in Figs. 8 and 9.

References

1) Part 102, M. Imoto, T. Ouchi, I. Ueno, and Y. Isayama, *Nippon Kagaku Kaishi*, **1974**, 155.
2) R. Bohn, U.S.P 898, 307 (1908); GP, 207, 743 (1970).
3) Bayer & Co., GP, 349, 741 (1918).
4) M. Imoto, K. Ko, S. Yoshioka, and T. Uehara, *Kogyo Kagaku Zasshi*, **65**, 613 (1962).
5) "Organic Syntheses," Coll. Vol. II, p. 425 (1942).
6) E. D. Bergmann and J. Szmuskovicz, *Bull. Soc. Chim. Fr.*, **1953**, 567; K. Ziegler, *Ber.*, **54**, 739 (1921).
7) "Organic Syntheses," Coll. Vol. II, p. 428 (1942).
8) F. F. Blicke, *J. Amer. Chem. Soc.*, **49**, 2843 (1927).
9) A. E. Tschitschtbabin, *Ber.*, **44**, 443 (1911).
10) T. Yonezawa *et al.*, "Ryoshikagaku Nyumon (Introduction Quantaum Mechanism 2th Ed.)," p. 211.
11) H. Kakiuchi and M. Imoto, *Kobunshi Tenbo*, **8**, 30 (1952); M. Imoto, *J. Inst. Polytechn. Osaka City Univ. Ser.* **C2**, 83 (1952); M. Imoto and T. Tanigaki, *Kogyo Kagaku Zasshi*, **59**, 712 (1956).
12) H. Dahn, U. Solms, and P. Zoller, *Helv. Chim. Acta*, **35**, 2117 (1952).
13) M. Duval, B. Bloch, and S. Kohn, *J. Appl. Polym. Sci.*, **16**, 1585 (1972).

The Photochemical Reaction of Benzo[*c*]cinnoline. I. The Photoreduction and Subsequent Reactions in Acidified Alcohols

Hiroyasu INOUE, Tetsuo SAKURAI, and Fujio TANAKA

Department of Applied Chemistry, Faculty of Technology, Kanagawa University, Kanagawa-ku, Yokohama 221

(Received May 25, 1974)

The photoinduced reaction of benzo[*c*]cinnoline (BCC) in strongly acidic aqueous alcohols, in which BCC exists in a monoprotonated form ($BCCH^+$), was investigated. The initial step of the photoreaction was the hydrogen abstraction, which gave rise to 5,6-dihydro$BCCH^+$, irrespective of the excitation wavelengths and the kind of alcohol (methanol, ethanol, or 2-propanol) used as a solvent. The subsequent reaction occurred upon irradiation by a light longer than 400 nm to afford 2,2′-diaminobiphenyl in ethanol, but not in methanol and 2-propanol. The 1-hydroxyethyl radical formed in the initial photoreduction appeared to participate in this reaction, donating its hydrogen atom to the ground-state 5,6-dihydro$BCCH^+$. On the other hand, ultraviolet irradiation caused the subsequent photoreaction of 5,6-dihydro$BCCH^+$, thus giving carbazole accompanied by the liberation of ammonia.

The photochemistry of a variety of nitrogen heterocyclic compounds has been studied.[1,2] Hitherto, however, little has been known concerning the photochemical behavior of *ortho*-diazines. Chen *et al.*[3] studied the photoreaction of 4-methylcinnoline in ethers, and showed that the 1,4-addition of the ethers occurred. According to Davis and Cohen,[4] benzo[*c*]cinnoline (BCC) undergoes photoreduction to give 5,6-dihydrobenzo[*c*]cinnoline (5,6-dihydroBCC) in benzene containing triethylamine as a hydrogen donor. 5,6-DihydroBCC is very susceptible to oxidation to BCC;[5] hence, it is not isolated. However, in a previous paper[6] it has been found that 5,6-dihydroBCC is fairly stable in a polyvinyl alcohol film, thus permitting the observation of its ultraviolet spectrum, when it is produced photochemically in the film. As has been briefly reported,[7] the ultraviolet irradiation of BCC in strongly acidic aqueous 2-propanol (3.75 M HCl), interestingly, affords carbazole in a fairly high yield. However no carbazole formation is observed when irradiation is carried out on a neutral solution of BCC in 2-propanol.

The purpose of the present paper is to present the experimental results on the photoreaction of $BCCH^+$ in strongly acidic alcohol under nitrogen. Since the photoreaction has been found previously to depend on the excitation wavelengths and on the kind of alcohol used as a solvent (methanol, ethanol, or 2-propanol), particular attention is paid to these points.

Results and Discussion

In an acidic solution stronger than 3 M HCl, BCC exists in the monoprotonated form ($BCCH^+$) and has the absorption spectrum shown in Fig. 1. Although the n-π^* band is at the longest wavelength for BCC,[8] the 420 nm band of $BCCH^+$ is of the π-π^* type. All irradiations were carried out on such strongly acidic solutions of BCC.

Photoreaction of BCC in 2-Propanol and Methanol upon Visible-light Irradiation. A 1.6×10^{-4} M solution of $BCCH^+$ in acidic aqueous 2-propanol was irradiated with visible light longer than 400 nm in an atmosphere of nitrogen at room temperature by using a filter whose percent transmittance is shown in Fig. 1. The spectral change in the solution caused by the irradiation is shown in Fig. 2. The reaction was completed in 180 min of irradiation, giving rise to a compound with absorption bands at 240, 270, and 316 nm. The compound thus produced readily reverted quantitatively to BCC when the irradiated solution was neutralized or bubbled with air, while it was fairly stable in the acidic solution under nitrogen. These facts may indicate that the photoreduction of $BCCH^+$ takes place to give 5,6-dihydroBCC, which is known to be susceptible to oxidation to BCC.[5] The product was identified on the basis of the absorption spectrum. That is to say, as BCC has been found to be photoreduced to 5,6-dihydroBCC in a polyvinyl alcohol film,[6] the absorption spectrum of the acidified film containing 5,6-dihydro$BCCH^+$ was measured. The spectrum thus obtained is almost identical with that of the product under consideration in the acidic solution.

Also, in acidic methanol the visible-light irradiation led to the photoreduction of $BCCH^+$ into 5,6-dihydro-$BCCH^+$. The rate of the reaction in the methanol solution was much slower than that in the 2-propanol solution, in agreement with the difference in the ease

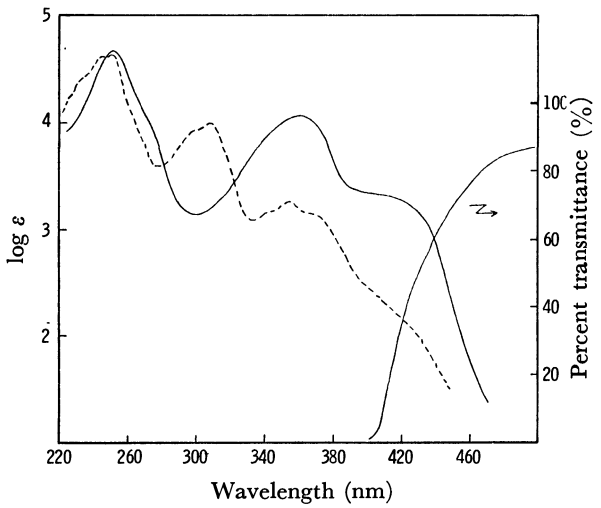

Fig. 1. Absorption spectra of BCC and percent transmittance of a filter used for visible light irradiation.
——: in ethanol, ——: in 4M HCl ethanol-water

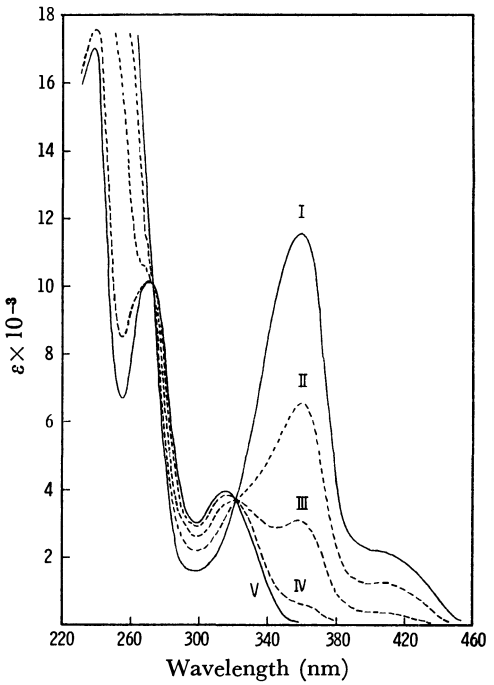

Fig. 2. Spectral change caused by visible light irradiation upon 4M HCl 2-propanol solution.
Initial concentration of BCC: 1.6×10^{-4}M. Irradiation time (min); I: 0, II: 15, III: 30, IV: 60, V: 180.

of photochemical hydrogen abstraction from primary and secondary alcohols.

Judging from the absorption spectrum (Curve V in Fig. 2), 5,6-dihydroBCC seems to be protonated at one of the two nitrogen atoms in the acidic solution. In the methanol and 2-propanol solutions, no subsequent reaction was observed.

Photoreaction of BCC in Ethanol upon Visible-light Irradiation. Figure 3 shows the spectral change in an acidic ethanol solution of $BCCH^+$ (1.0×10^{-4} M) caused by irradiation with visible light longer than 400 nm. As may be seen from this figure, 5,6-dihydroBCCH^+ is formed in the initial stage of the reaction; subsequently, the absorption bands of 5,6-dihydroBCCH^+ decrease in intensity with prolonged irradiation, giving rise to a compound with a tail of a band in the short-wavelength region. When the irradiated solution was neutralized, the absorption band appeared at 294 nm. Therefore, it is evident that the initially produced 5,6-dihydroBCCH^+ takes part in the subsequent reaction. The final product was isolated in the preparative experiments; it was identified as 2,2′-diaminobiphenyl.

By the analysis of the absorption spectra,[9] the changes in the concentrations of BCC, 5,6-dihydroBCC, and 2,2′-diaminobiphenyl with the lapse of irradiation time were determined; the results are presented in Fig. 4. As can be seen from this figure, during the first period of 30 min the formation of 2,2′-diaminobiphenyl is not observed, although the photoreduction of $BCCH^+$ occurs to give 5,6-dihydroBCCH^+ rapidly. This implies that the conversion of 5,6-dihydroBCCH^+ into 2,2′-diaminobiphenyl is initiated after a certain amount of 5,6-dihydroBCCH^+ is produced. The yield of 2,2′-diaminobiphenyl in relation to the BCC used

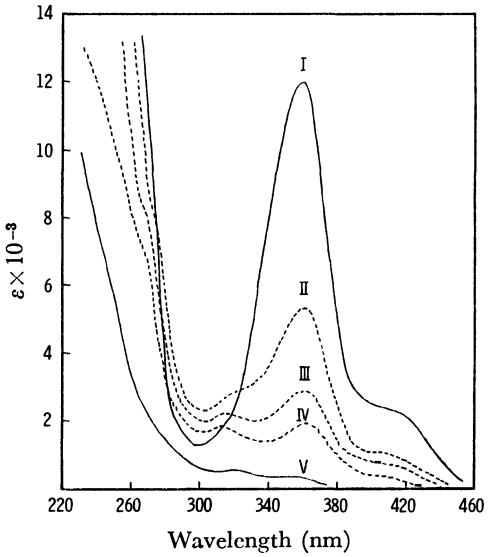

Fig. 3. Spectral change caused by visible light irradiation upon 4N HCl ethanol solution.
Initial concentration of BCC: 1.0×10^{-4}M. Irradiation time (hr); I: 0, II: 1, III: 2, IV: 3, V: 6.

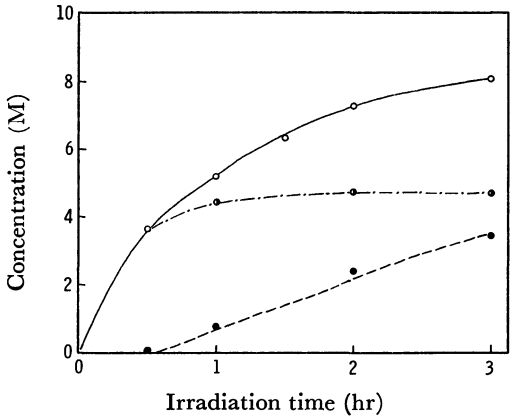

Fig. 4. Rate of the reaction upon visible light irradiation upon 4M HCl ethanol solution.
Initial concentration of BCC: 1.0×10^{-4}M. ○: $BCCH^+$ reacted, ◑: 5,6-dihydroBCCH^+ produced, ●: 2,2′-diaminobiphenyl produced

initially was 34% upon irradiation for 3 hr.

It should be noted that 5,6-dihydroBCCH^+ has no absorption in the visible region longer than 400 nm, as is shown in Fig. 2. Therefore, it can be said that the ground-state 5,6-dihydroBCCH^+ is probably involved in the subsequent reaction. Nevertheless, this reaction did not take place without continued irradiation even after a sufficient concentration of 5,6-dihydroBCCH^+ was reached. In view of this and the fact that 5,6-dihydroBCCH^+ fails to take part in this reaction in the 2-propanol and methanol solutions, the disproportionation between the 5,6-dihydroBCCH^+ molecules can be ruled out as the mechanism of the reaction. Moreover, the ground-state 5,6-dihydroBCCH^+ can not abstract a hydrogen atom from acetaldehyde as well as ethanol; a hydrogen donor participating in the conversion should be a transient species generated in the initial photoreduction of $BCCH^+$. That is to say, the 1-hy-

droxyethyl radical, $CH_3\dot{C}HOH$, is considered to play an essential role in furthering the reaction. Consequently, the mechanism of the 2,2′-diaminobiphenyl formation, which explains the results presented here, can be visualized as is shown in Scheme 1.

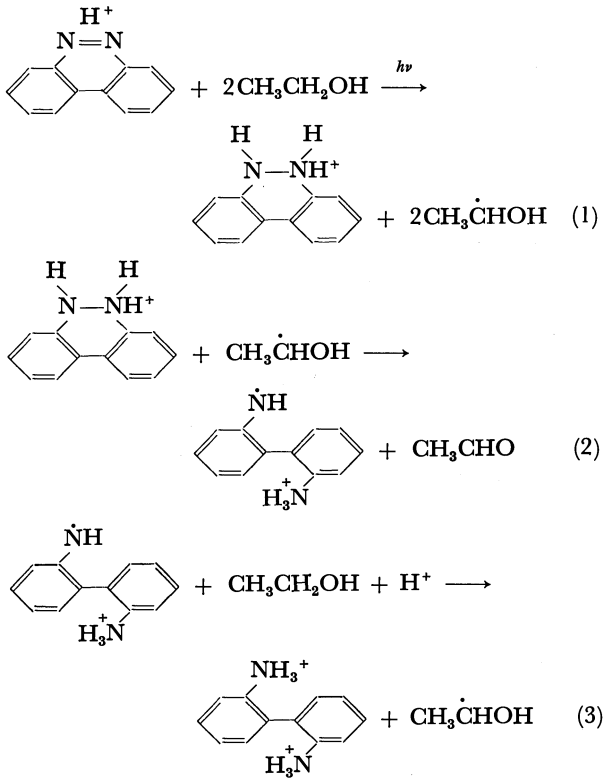

Scheme 1.

The conversion is initiated by the hydrogen abstraction of 5,6-dihydroBCCH$^+$ from the 1-hydroxyethyl radical (Reaction (2)). This reaction does not proceed until a certain amount of 5,6-dihydroBCCH$^+$ is formed, because a relatively short-lived species, $CH_3\dot{C}HOH$, takes part in the reaction. This is the reason for the appearance of the induction period between the first formation of 5,6-dihydroBCCH$^+$ and that of 2,2′-diaminobiphenyl. The successive reproduction of the radical, $CH_3\dot{C}HOH$, is performed in Reaction (3).

The observed solvent dependence of the reaction can be attributed to the different reactivities of the radicals resulting from alcohols in the initial photoreduction. In the cases of 2-propanol and methanol solutions, the resulting radicals are the 1-hydroxy-2-propyl, $(CH_3)_2\dot{C}OH$, and the 1-hydroxymethyl, $\dot{C}H_2OH$, radicals respectively; these radicals apparently have no ability to donate a hydrogen to 5,6-dihydroBCCH$^+$ under the present experimental conditions, probably because other decay processes occur more rapidly than does the hydrogen donation to 5,6-dihydroBCCH$^+$. However, it is a problem to be settled from what such a difference arises.

Photoreaction of BCC upon Ultraviolet Irradiation. In the case of ultraviolet irradiation by light shorter than 380 nm, the main product was carbazole, regardless of the kind of alcohol used here. Figure 5 shows the spectral change of a 1.0×10^{-4} M solution

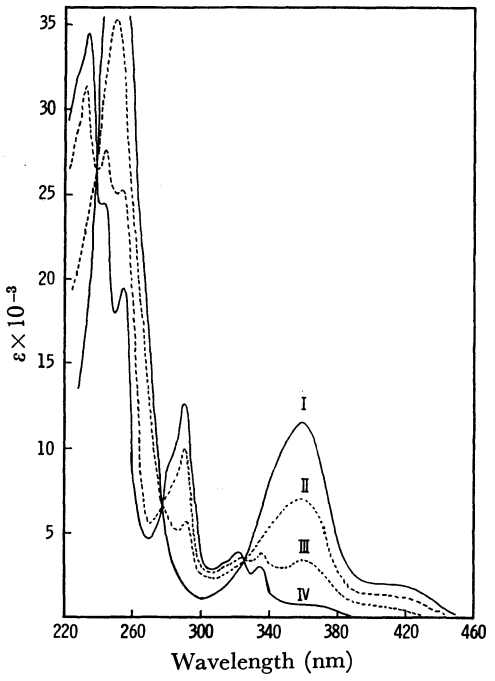

Fig. 5. Spectral change caused by ultraviolet irradiation upon 4M HCl 2-propanol solution.
Initial concentration of BCC: 1.0×10^{-4}M. Irradiation time (hr); I: 0, II: 1, III: 2, IV: 3

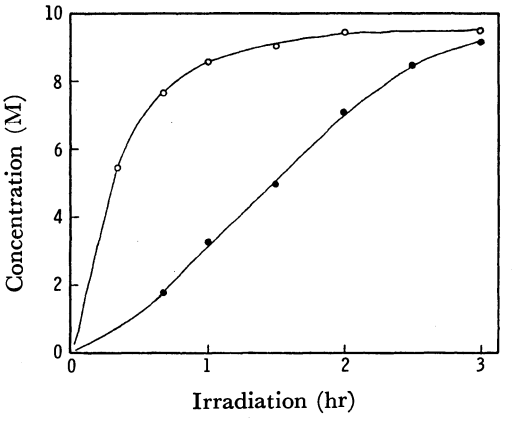

Fig. 6. Rate of the carbazole formation.
●: from BCCH$^+$, ○: from 5,6-dihydro BCCH$^+$

of BCCH$^+$ in acidic 2-propanol upon ultraviolet irradiation by means of a high-pressure mercury lamp. Irradiation for 3 hr resulted in the conversion of BCCH$^+$ into carbazole in about a 92% yield. Although the absorption bands of 5,6-dihydroBCCH$^+$ are apparently not observed in the course of the reaction, as can be seen from Fig. 5, the following fact clearly indicates that this is an intermediate product in the carbazole formation also: when the ultraviolet irradiation was carried out upon a 2-propanol solution in which BCCH$^+$ has previously been photoreduced to 5,6-dihydroBCCH$^+$ with the visible-light irradiation, as has been described above, carbazole was produced much faster than in the case of the ultraviolet irradiation of the BCCH$^+$ solution. The rate of the reactions in these different irradiation manners are compared in Fig. 6.

Consequently, 5,6-dihydroBCCH$^+$ is an intermediate product in the formations of both 2,2′-diaminobiphenyl and carbazole. However, in the case of the latter, the intermediate is considered to participate in the reaction through an excited state, judging from its absorption spectrum (Fig. 2).

It was found that the carbazole formation was attended by the liberation of ammonia. The ammonium ion was detected in the irradiated solution by the Nesler test. Therefore, we may expect that carbazole is produced by photoinduced disproportionation between the excited and ground-state 5,6-dihydroBCCH$^+$ molecules. However, this pausible mechanism can be ruled out, in view of the fact that carbazole is produced in an acidified polyvinyl alcohol film containing the substrate in a concentration of about 10^{-3} M, in which the substrate seems to be very difficult to diffuse. In addition, it is evident that the protonation of 5,6-dihydroBCC is essential for the carbazole formation. In fact, ultraviolet irradiation upon a polyvinyl alcohol film containing 5,6-dihydroBCC not being protonated does not lead to the formation of carbazole.

At the present time, it is considered that carbazole is produced by the photoinduced elimination of an imino radical (N̈H) from 5,6-dihydroBCCH$^+$, and that the resulting radical gives ammonia. The mechanism of the reaction proposed is shown in Scheme 2.

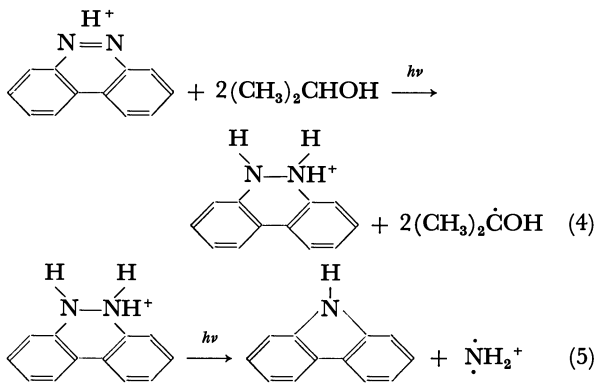

Scheme 2.

Experimental

The ultraviolet absorption spectra were measured with a Shimadzu Spectrophotometer, UV-200, using 1 cm quartz cells. The infrared absorption spectra were recorded on a Hitachi Infrared Spectrophotometer, EPI-G3, in a KBr disk.

Materials. The BCC was prepared from 2,2′-dinitrobiphenyl according to the method of Badger *et al.*;[10] it was purified by repeated recrystallizations from benzene, by treatment with active charcoal, and finally by recrystallization from ethanol; mp 155 °C (lit,[10] 156 °C). 2,2′-Diaminobiphenyl was prepared by the reduction of 2,2′-dinitrobiphenyl with zinc in HCl aqueous ethanol; it was purified by repeated recrystallizations from aqueous ethanol; mp 78.5 °C (lit,[10] 78.5 °C). The polyvinyl alcohol film was prepared from commercially available powder (mean degree of polymerization: 1500).

Irradiation. The irradiation by visible-light longer than 400 nm was carried out by means of a 500 W super-high-pressure mercury arc lamp (Ushio USH-500) and a Corning glass filter CS-3-73 (transmittance percentage shown in Fig. 1). The ultraviolet irradiation was carried out by means of a 450 W high-pressure mercury arc lamp (Ushio UM-452). In the preparative experiment with ultraviolet irradiation, a solution was placed in a 500 ml cylindrical Pyrex vessel, and a high-pressure immersion mercury arc lamp was used as the light source. All the irradiations were carried out at room temperature; the solution of BCCH$^+$ was flushed with nitrogen passed through a pyrogallol solution for 30 min prior to irradiation and continued throughout the irradiation. For the reaction in the polyvinyl alcohol film, the sample film was prepared by the method described elsewhere.[11]

Photoreaction of BCC in Acidic Ethanol upon Visible-light Irradiation. A 2×10^{-3} M solution of BCCH$^+$ in 100 ml of 3.75 M HCl aqueous ethanol was irradiated with visible light longer than 400 nm for 20 hr. After irradiation, the solution was neutralized with an NaOH aqueous solution. The neutral solution was then extracted with diethyl ether. These procedures were carried out for five runs, after which the ethereal solutions were combined. After the solvent has then been evaporated to dryness, the crystalline solid thus obtained was subjected to silica-gel thin-layer chromatography, using a mixture of benzene, cyclohexane, and acetic acid (1:1:1) as the developing solvent. The R_f value for the main product was 0.27. The product thus obtained was further purified by recrystallization from aqueous ethanol; it was identified as 2,2′-diaminobiphenyl; mp 77.0—77.5 °C. Found: C, 77.2; H, 6.6; N, 14.6%. Calcd for $C_{12}H_{12}N_2$: C, 78.2; H, 6.6; N, 15.2%. The UV and IR spectra of the product were identical with those of the authentic sample.

Photoreaction of BCC in Acidic 2-Propanol upon Ultraviolet Irradiation. BCC (120 mg) dissolved in 400 ml of 3.75 M HCl aqueous 2-propanol in a Pyrex vessel was irradiated with a high-pressure immersion mercury arc lamp (Ushio UM-102) for 2 hr. The solvent was then removed by evaporation under reduced pressure to afford a crystalline solid, which was subsequently washed with water. The product thus obtained was dissolved in a mixed solvent of benzene, *n*-hexane, and 2-propanol (2:2:1) and chromatographed on a silica gel column, using the same solvent as the eluent. Final purification was accomplished by recrystallization from ethanol. The product was identified as carbazole; mp 246—247 °C. Found: C, 87.0; H, 5.2%. Calcd for $C_{12}H_9N$: C, 86.2; H, 5.4%. The UV and IR spectra of the product were identical with those of commercially available carbazole.

References

1) M. Mousseron-Canet and J. C. Mani, "Photochemistry and Molecular Reactions," Translated by J. Schmorak, Israel Program for Scientific Translations Ltd., (1972), p. 83.

2) N. J. Turro, "Energy Transfer and Organic Photochemistry," Wiley, New York (1969), p. 275.

3) T. T. Chen, W. Dörscheln, H. Göth, M. Hesse, and H. Schmid, *Helv. Chim. Acta*, **51**, 632 (1968).

4) G. A. Davis and S. G. Cohen, *Chem. Commum*, **1971**, 675.

5) S. D. Ross, G. J. Kahan, and W. A. Leach, *J. Amer. Chem. Soc.*, **74**, 4122 (1952).

6) H. Inoue and M. Matsumoto, *Nippon Kagaku Kaishi*, **1974**, 203.

7) H. Inoue and Y. Matsuka, *Chem. Lett.*, **1972**, 713.

8) G. M. Badger and I. Walker, *J. Chem. Soc.*, **1956**, 122.

9) Both 5,6-dihydroBCCH$^+$ and diprotonated 2,2′-diaminobiphenyl have no absorption at 400 nm, so the reaction

is followed by monitoring the absorbances at 400 nm.

$$\text{BCCH}^+ \text{ reacted (mol)} = \frac{A_0 - A_I}{A_0} \times C_0$$

$$\text{5,6-DihydroBCCH}^+ \text{ produced (mol)} = \frac{A_S - A_I}{A_0} \times C_0$$

$$\text{2,2'-Diaminobiphenyl produced (mol)} = \frac{A_0 - A_S}{A_0} \times C_0$$

where A_0, A_I, and A_S denote the absorbances before irradiation, immediately after irradiation, and after irradiation followed by oxygen bubbling into solution respectively, and C_0 is an initial amount of $BCCH^+$ used.

10) G. M. Badger, J. H. Seidler, and B. Thomson, *J. Chem. Soc.*, **1951**, 3207.

11) H. Inoue, T. Nakamura, and T. Igarashi, This Bulletin, **44**, 1469 (1971).

Studies of the *cis-trans* Isomerization of 3-Aryl-1,2,3-oxathiazolidine-2-oxides

Tomihiro NISHIYAMA and Fukiko YAMADA

Department of Applied Chemistry, Faculty of Engineering, Kansai University, Senriyama, Suita, Osaka 564

(Received July 10, 1974)

The isomerization of the *cis*- or *trans*-3-aryl-1,2,3-oxathiazolidine-2-oxides was investigated under various conditions. The isomerization proceeded in carbon tetrachloride, chloroform, and benzyl chloride solutions at a low temperature. On the other hand, in other organic solvents, such as benzene, acetone, pyridine, *N*,*N*-dimethylformamide, and chlorobenzene, isomerization did not occur. The results can be explained by the mechanism which yields the open-chain halosulfamic acid anion by the attack of a halogen ion on the 5-position. The anion can close to *cis*- or *trans*-oxathiazolidine.

In recent years, a number of studies have been reported on the *cis-trans* isomerization of some heterocyclic compounds. For example, the *cis-trans* isomerization of 3-*t*-butyl-1,2,3-oxathiazolidine-2-oxides in the presence of tetrabutylammonium bromide results in the inversion of sulfoxide, with the preservation of the stereochemistry at the 4- and 5-carbons.[1]

Cyclic sulfoxides have also been inverted by photochemical means or by treatment with hydrogen chloride.[2,3] Cyclic sulfites have been equilibrated thermally.[4]

In a previous paper, we reported that the reaction of *N*-sulfinylanilines with propylene oxide or epichlorohydrin in the presence of catalysts led to 3-aryl-5-methyl- or 3-aryl-5-chloromethyl-1,2,3-oxathiazolidine-2-oxide respectively.[5] These oxathiazolidines exist in the *cis* and *trans* configurations between the S=O group and the methyl or chloromethyl group in the 5-position, and it is possible to determine the substituent geometry of the isomeric pairs by means of NMR spectroscopy.

This paper will describe the *cis-trans* isomerization of oxathiazolidines under various reaction conditions and a possible isomerization mechanism.

Experimental

Measurements. The NMR spectra were recorded at 60 MHz with a Japan Electron Optics JNM-3H-60 spectrometer. The chemical shifts (δ) were described in ppm downfield from the internal TMS. The change in the % age composition of the isomers was followed by the NMR method. A constant-temperature water or oil bath was employed; it was equipped with an immersion heating element that made possible a temperature control of ± 0.2 °C.

Materials. The oxathiazolidines, 3-aryl-5-methyl-1,2,3-oxathiazolidine-2-oxides (R=H **1b**, *o*-CH_3 **2b**, *m*-CH_3 **3b**, *p*-CH_3 **4a**, *o*-Cl **5a**, *m*-Cl **6b**, and *p*-Cl **7b**) and 3-aryl-5-chloromethyl-1,2,3-oxathiazolidine-2-oxides (R=H **8a**, *o*-CH_3 **9a**, *m*-CH_3 **10b**, *p*-CH_3 **11a**, *o*-Cl **12a**, *m*-Cl **13b**, and *p*-Cl **14a**) were prepared by a previously reported method.[5] *Cis* and *trans* isomers are represented by the notations of **a** and **b** respectively. All the reagents used were of an analytical grade.

Results and Discussion

Isomerization. Experiments on the isomerization of oxathiazolidines in chloroform were carried out as follows. A definite amount of oxathiazolidine was dissolved in chloroform (2.0 mol/l). This solution was then divided into test tubes and sealed. The sealed tubes were then shaken at a constant temperature, the progress of the isomerization being periodically checked by measuring the NMR spectrum. The isomerization rate of each oxathiazolidine can be obtained from the integrated data of the *cis* and *trans* 5-methyl or methine proton signals in its NMR spectrum. In the isomerization of the **6b** oxathiazolidine in chloroform, the changes in the NMR spectra with the reaction time are shown in Fig. 1. The NMR spectrum of **6b** exhibits a methyl proton signal at 1.65 ppm (d, J=6.0 Hz), one methylene signal, Ha, at 3.31 ppm (dd, t observed, J *trans*=8.5 Hz), another methylene signal, Hb, at 3.93 ppm (q, J *cis*=5.2 Hz), a methine signal at 5.26—5.68 ppm (m), and a ring proton signal at 6.8—7.34 ppm (m). In the early stages of this isomerization, new peaks appeared at 1.79 ppm (d, J=6.0 Hz), 3.78 ppm (d, J=6.3 Hz), 3.80 ppm (d, J=7.8 Hz), and 4.85—5.23 ppm (m). These new peaks gradually increased with the reaction time, and after about 2 hr the mixture reached equilibrium. These new peaks are the same as those of *cis* 3-(*m*-chlorophenyl)-5-methyl-1,2,3-oxathiazolidine-2-oxide **6a** reported previously.[5] Plots of the conversion *versus* the reaction time for the oxathiazolidines are shown in Fig. 2. These results indicate that the equilibrium

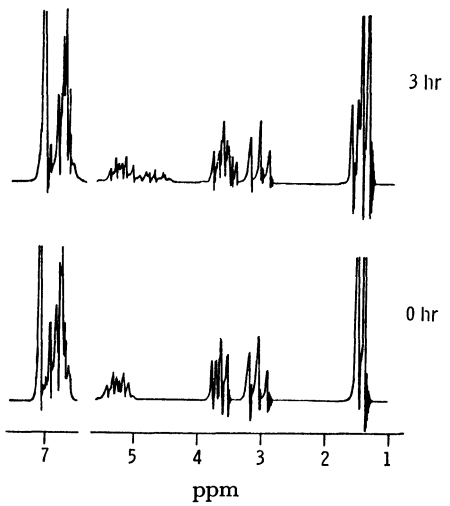

Fig. 1. Changes of the NMR spectra of **6b** with reaction time at 30 °C.

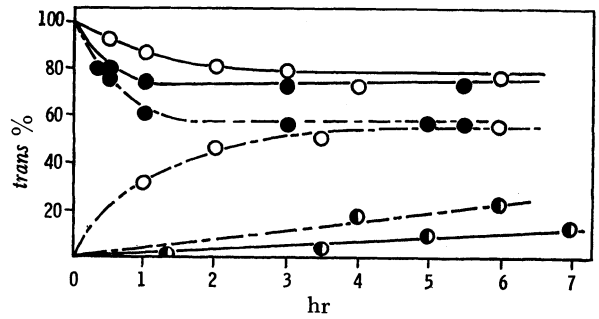

Fig. 2. Time conversion curves at 30 °C in the isomerization of the oxathiazolidines in chloroform (2.0 mol/l).

$R'=CH_3$	$R'=CH_2Cl$
—○— R=*p*-Cl	- -○- - R=*p*-Cl
—◐— R=*p*-CH_3	- -◐- - R=*p*-CH_3
—●— R=*m*-Cl	- -●- - R=*m*-Cl

constant is influenced by the two kinds of substituents, R and R', and that the constants of the 5-chloromethyl-substituted oxathiazolidines are larger than those of the 5-methyl group.

Solvent Effects. The isomerizations of oxathiazolidines at 30 °C in various solvents, such as carbon tetrachloride, chloroform, benzyl chloride, acetone, pyridine, benzene, chlorobenzene, and *N,N*-dimethylformamide, were carried out in sealed tubes. From the results obtained, it was found that the isomerization rates of the oxathiazolidines depend upon the nature of the organic solvent. Figure 3 shows plots of the *trans* content *versus* the reaction time of **6b** in various organic solvents (2.0 mol/l). As is shown in Fig. 3, the isomerization proceeded in carbon tetrachloride, chloroform, and benzyl chloride solutions. On the other hand, in other organic solvents, such as benzene, acetone, pyridine, *N,N*-dimethylformamide, and chlorobenzene, the isomerization did not occur. These facts may indicate, therefore, that the solvents containing active halogen atoms markedly affect the isomerization of the *cis* or *trans* oxathiazolidines. In the case of chlorobenzene, the chlorine atom is stabilized by resonance with the benzene ring. The oxathiazolidine ring interacts with a chlorine atom of the solvent, and then the *cis-trans* isomerization occurs.

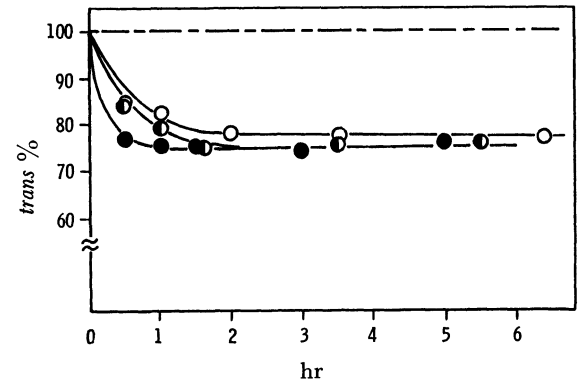

Fig. 3. Time conversion curves in various solvents in the isomerization of **6b**.

—○— $C_6H_5CH_2Cl$
—●— CCl_4
—◐— $CHCl_3$
-—-— C_6H_6, $(CH_3)_2CO$, C_5H_5N, and DMF

TABLE 1. EQUILIBRIUM CONSTANTS FOR *cis* AND *trans* OXATHIAZOLIDINES IN CHLOROFORM IN THE PRESENCE OF NEt_4Br AT 40 °C

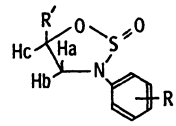

Compd. No.	R	R'	Starting config	*K*
1b	H	CH_3	*trans*	0.47
	H	CH_3	*trans*	0.47[a]
2b	*o*-CH_3	CH_3	*trans*	0.69
4a	*p*-CH_3	CH_3	*cis*	1.53
5a	*o*-Cl	CH_3	*cis*	1.02
6b	*m*-Cl	CH_3	*trans*	0.37
7b	*p*-Cl	CH_3	*trans*	0.40
	p-Cl	CH_3	*trans*	0.39[a]
8a	H	CH_2Cl	*cis*	1.46
10b	*m*-CH_3	CH_2Cl	*trans*	0.68
11a	*p*-CH_3	CH_2Cl	*cis*	1.36
12a	*o*-Cl	CH_2Cl	*cis*	1.20
13b	*m*-Cl	CH_2Cl	*trans*	0.69

a) solvent: *N,N*-dimethylformamide, catalyst: LiCl.

The Effect of Catalysts. Catalytic isomerizations at 40 °C were carried out by a procedure similar to that used in the absence of catalysts. The results under the influence of lithium chloride (LiCl) and tetraethylammonium bromide (NEt_4Br) are given in Table 1 in terms of the equilibrium constants. In all the cases, equilibrium was reached within 20 min. The results indicate that the *trans* isomer is more stable than the *cis* isomer. This is also brought out clearly by a comparison of the values of the equilibrium constants shown in Table 1.

In an *N,N*-dimethylformamide solution, the isomerization did not occur in the absence of a catalyst, but it proceeded rapidly in the presence of LiCl.

It is well known that the chloride ion equilibrates cyclic sulfoxides[6] and alkoxysulfonium salts.[7] It can, therefore, be thought that the halogen ion is related to the isomerization of oxathiazolidines.

The present isomerization is further illustrated by the action of dry HCl. When a sample of oxathiazolidine in a benzene solution was exposed to a trace amount of dry HCl at room temperature, equilibrium was reached within 5 min in all cases. For example, when a sample of the pure *trans* oxathiazolidine, **6b**, was exposed to dry HCl, the equilibrium composition was 74% *trans* and 26% *cis*, based on the integration of the NMR signal of the methyl protons. After the reaction

TABLE 2. *cis-trans* ISOMERIZATION RATIO BY THE ACTION OF DRY HCl

Compd. No.	Before reaction *trans* : *cis*	After reaction *trans* : *cis*
4a	0 : 100	68 : 32
6b	100 : 0	74 : 26
7b	94 : 6	74 : 26
14a	0 : 100	62 : 38

Table 3. Reactions of oxathiazolidines with dry HCl

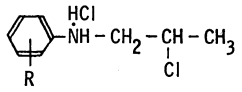

Reaction of dry HCl with	Mp °C	Yield %	% C	% H	% N	% Cl
4a	132—134	79	54.81 (54.54)	6.93 (6.81)	6.41 (6.36)	31.83 (32.27)[a]
6b	104—106	78	44.93 (44.90)	5.10 (4.98)	5.89 (5.82)	44.21 (44.28)
7b	123—127	72	45.25	5.17	5.86	43.85

a) Calcd value.

Table 4. Isomerization for *cis* and *trans* oxathiazolidines at higher temperature

Compd. No.	Solvent	Conditions °C	Time hr	*trans* %	*cis* %
1b	—	100	8	100	0
	—	120	10	66	34
	C_6H_6	100	15	100	0
	C_6H_6	120	13	68	32
	CH_3CN	120	15	100	0
	$(CH_3)_2NCHO$	120	16	67	33
4a	—	100	8	0	100
	CH_3CN	120	4.5	55	45
6b	—	100	7	100	0
8a	—	100	8	0	100
	—	120	12	22	78
	C_6H_6	100	15	0	100
	C_6H_6	120	12	0	100
	CH_3CN	100	3	56	44
	C_5H_5N	100	3	57	43
	$(CH_3)_2NCHO$	100	3	56	44
10b	—	100	14	100	0
	CH_3CN	120	6	100	0
13b	—	100	7	100	0

mixture had reached equilibrium, the temperature was raised to 80 °C. More dry HCl was passed through until a precipitate appeared. The precipitate was subsequently filtered and recrystallized with chloroform to give a colorless crystal (mp 104—106 °C; 78%), which was identified as *N*-(*β*-chloropropyl)-*m*-chloroaniline hydrochloride. These results are summarized in Tables 2 and 3.

Effect of Temperature. The effects of the temperature and of the solvents are given in Table 4. In all of the oxathiazolidines, the isomerization did not occur below about 100 °C. As is shown in Table 4, the isomerization proceeded at about 120 °C.

For the isomerizations of the *trans* oxathiazolidines, **1b** and **10b**, the polar solvents have no appreciable effect. On the other hand, in the *cis* oxathiazolidines, **4a** and **9a**, the isomerization occurs rapidly. Therefore, it is clear that the isomerization is affected by the starting *cis*- or *trans*-form rather than by the R and R′ substituent at higher temperatures.

Possible Isomerization Mechanism. On the basis of the results mentioned above and other considerations,[1] a possible reaction mechanism for the isomerization can be described as follows:

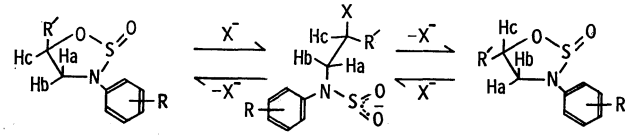

cis-form anion *trans*-form

X: halogen

The above open-chain halosulfamic acid anion may be expected to be formed by the attack of the halogen ion, which is produced from the solvent or the catalyst. Then, this anion can become close to *cis*- or *trans*-oxathiazolidine.

A similar mechanism involving a bromosulfite anion has been proposed in the reaction of oxirans with sulfur dioxide in the presence of NEt_4Br.[8]

References

1) C. L. Moyer, 2-Oxo-1,2,3-oxathiazolidines, Dissertations, II, Harvard University (1968). (Avail. Univ. Microfilms, Ann. Arbor, Mich., Order No. 68-16878), p. 100; *Chem. Abstr.* **70**, 77677d (1969).

2) K. Mislow, M. Axelrod, D. R. Rayner, H. Gotthart, L. M. Coyne, and G. H. Hammond, *J. Amer. Chem. Soc.*, **87**, 4958, (1965).

3) K. Mislow, T. Simmons, J. T. Melillo, and A. L. Ternay, Jr., *ibid.*, **86**, 1452 (1964).

4) C. G. Overberger, T. Kurtz, and S. Yaroslavsky, *J. Org. Chem.*, **30**, 4363 (1965).

5) T. Nishiyama and F. Yamada, This Bulletin, **44**, 3073 (1971).

6) J. J. Rigau, C. C. Bacon, and C. R. Johnson, *J. Org. Chem.*, **35**, 3655 (1970).

7) C. R. Johnson and J. J. Rigaku, *J. Amer. Chem. Soc.*, **91**, 5398 (1969).

8) G. A. Razuvaev, V. S. Etlis, and L. N. Grobov, *Zhur. Obshchei Khim.* **31**, 1328 (1961); *Chem. Abstr.*, **55**, 27011g (1961).

Reactions of 1,8-Dehydronaphthalene with Cyclic Polyenes

Masahiko KATO, Shigeru TAKAOKA, and Toshio MIWA
Faculty of Science, Osaka City University, Sugimoto-cho, Sumiyoshi-ku, Osaka 558
(Received July 18, 1974)

The reactivities of 1,8-dehydronaphthalene (**1**) to cyclic polyenes, *i.e.*, cycloheptatriene, cyclopentadiene, 6,6-dimethylfulvene, furan, and norbornadiene, were examined. It was found that the C–H insertion reaction at the end of the conjugated systems, a new type of reaction of **1**, as well as the 1,2-cycloaddition reaction occurs in every conjugated cyclic polyene. A stepwise mechanism for the formation of the C–H insertion product was proposed.

According to the MO calculations,[1] the peri-electrons of 1,8-dehydronaphthalene (**1**), one of the arynes, occupy an antisymmetric combination of 1,8-dehydro-orbital in the ground state, whereas the *ortho*-electrons of 1,2-dehydrobenzene (**2**) do a symmetric one. Accordingly these two species must show different reactivities towards olefinic compounds, and these were in line with the experimental results by Rees and Storr[2] Thus the reaction of **1** afforded acenaphthene derivatives in a stereospecific manner, whereas the reaction of **2** afforded benzocyclobutene derivatives in a non-stereospecific fashion.[3] As for cyclic polyenes, only the reaction of **1** with cyclopentadiene was reported.[4]

Present authors were interested in the reactivities of **1** to cyclic polyenes compared with those of **2**,[5] because the opposite character of the electronic ground states might be reflected in the difference between the reactivities of these species. By using cycloheptatriene, dimethylfulvene, furan, norbornadiene, and also cyclopentadiene as cyclic polyenes, we found that the insertion of **1** to a C–H bond of a conjugated polyene was also an important pathway as well as the cycloaddition reaction. A kind of such reaction was seen in the reaction of **1** with benzene to give α-phenylnaphthalene.[2]

Reaction Conditions and the Structures of the Products. Compound **1** was generated from 1-aminonaphtho-[1,8-*d*,*e*]triazine (**3**) by oxidation with lead tetraacetate in dichloromethane[2] in the presence of excess substrate under −20 °C or dry ice–acetone temperature, because the substrates were assumed to be susceptible to oxidation near room temperature.[6]

Reaction with Cycloheptatriene: Besides naphthalene, three products, (**4**), (**5**), and (**6**) [**4**: (**5**+**6**)=8: 10] (total yield 5.3%) were characterized as follows after partial separation by column chromatography of the reaction mixture.

The compound **5** was not formed when the separation was carried out in the dark. Catalytic hydrogenation (10% Pd–C) of the oily product **4** (mass spectrum, M^+ *m*/*e* 218) gave 1-cycloheptylnaphthalene which was identical with the authentic sample.[7] The structure **4** was selected among possible structures by consulting the NMR integral ratio of the olefinic proton signals to the aliphatic proton signals and the multiplicity of methylene proton signal. The structure was finally confirmed by the independent synthesis through **5**.

Owing to the difficulty of separation of the compound **6** from **4**, the mixture, enriched in **6** by chromatography in the dark, was subjected to the reaction.

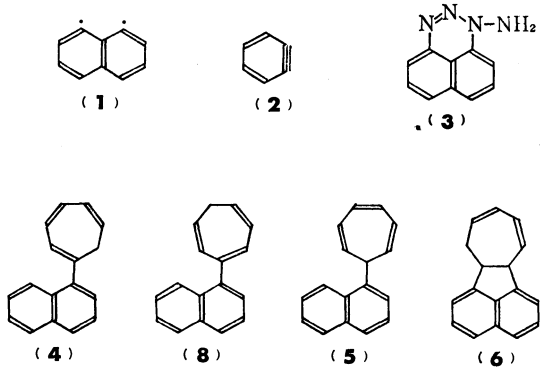

Scheme 1.

Catalytic reduction of the mixture gave, besides 1-cycloheptylnaphthalene originated from **4**, *cis*-1,2-pentamethyleneacenaphthene (**7**), which was identified by comparison with a sample prepared from cycloheptene and **1** and had to be formed from **6**. The NMR spectrum of **6** [δ ppm (CCl_4) 2.20—2.60 (2H, m), 4.21 (2H, m), 5.80—6.04 (2H, m), 6.12—6.20 (2H, m), 7.0—8.0 (6H, m)], obtained by a subtraction of the spectrum of **4** from that of the mixture, is consistent with the unsymmetrical structure rather than the other possible symmetrical ones.

When a mixture of **4** and **6** in carbon tetrachloride was irradiated for a short peirod with a high-pressure mercury lamp through Pyrex filter, it was revealed by NMR spectrum that **4** was transformed almost completely to **5** while **6** remained unaltered. The structure **5**, an isomer of **4**, was obtained directly from consideration of the NMR spectrum and this was confirmed by its synthesis from tropylium fluoroborate[7] and α-naphthylmagnesium bromide. When heated for 15 hr at 125 °C, **5** gave a new compound **8** by 1,5-hydrogen shift, but when the temperature was raised to 160 °C, it gave mainly **4** by two series of 1,5-hydrogen shifts.[9] Irradiation[10] of **4** in carbon tetrachloride using a low pressure mercury lamp for 62 hr gave a mixture of **4** and **5** (4.6: 1).

Reaction with Cyclopentadiene: Meinwald and Gruber reported three kinds of cycloaddition products **9**—**11** from the reaction of **1** with cyclopentadiene.[4] The present authors expected the formation of an insertion product in the reaction as in the case of cycloheptatriene and reexamined the reaction. The resulting hydrocarbon fraction, separated by silicic acid chromatography, was hydrogenated catalytically. Thus, in addition to the products **12** and **13**,[4] 1-cyclopentylnaph-

thalene (**14**)[11] was obtained in almost equal quantity to the total amount of the other products. Although an insertion product (**15**), the precursor of **14**, could not be separated by solution chromatography (tlc or column) and by preparative glc, it was possible by comparing the NMR spectrum of the product mixture with those of **9** and **10** to obtain the spectral data of a new compound **15**. The structure was confirmed by obtaining **15** as a minor product, along with a main product (**16**), (1 : 3) from 1-(1-cyclopentenyl)naphthalene[11] by treatment with NBS in carbon tetrachloride followed by dehydrobromination with triethylamine in ether.

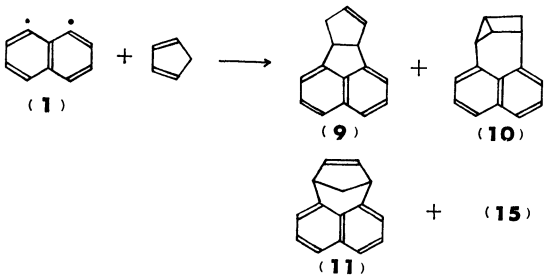

Scheme 2.

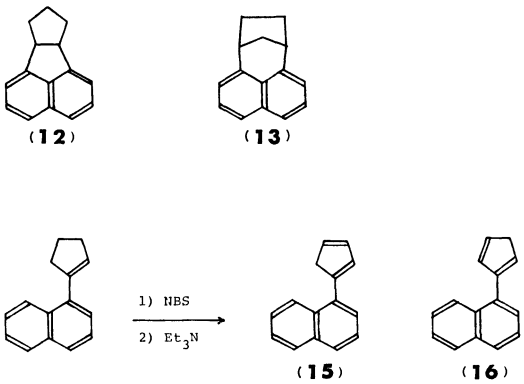

Scheme 3.

Reaction with 6,6-Dimethylfulvene: The reaction afforded compound **17** and **18** (1 : 2) (total yield 3%), which were separated by glc (3% Silicone OV-17, 1/4 in×6 ft, 170 °C). These compounds showed the same molecular ion peak at *m/e* 232 in their mass spectra (1 : 1 adducts of dimethylfulvene and **1**). The proton signal ratio (Ar–H: olefinic–H: benzylic–H: methyl–H=6: 2: 2: 6) and the unsymmetrical feature of the NMR spectrum of **17** supported the structure.

A yellow solid **18**, mp 110—113 °C, showed an NMR spectrum [δ ppm (CCl_4) methyl proton signals at 1.36 (3H, s), 2.18 (3H, s), olefinic at 6.24—6.46 (3H, m) and aromatic at 7.2—7.44 (7H, m)] characteristic to the ring-substituted dimethylfulvene. The position of α-naphthyl group on dimethylfulvene was confirmed by the catalytic hydrogenation to a tetrahydro derivative [M^+ *m/e* 236; δ ppm (CCl_4) 0.90 (6H, d, J= 6 Hz), 1.8—2.9 (7H, m), 7.0—7.8 (7H, m)], which was identical with 1-(α-naphthyl)-2-isopropylcyclopentene (**19**) prepared by dehydration of 1-(α-naphthyl)-2-isopropylcyclopentan-1-ol (**20**).[13]

Reaction with Furan: The reaction was carried out in a usual way, and 2-(α-naphthyl)-furan[14] was obtained in 3% yield as a sole isolable product.

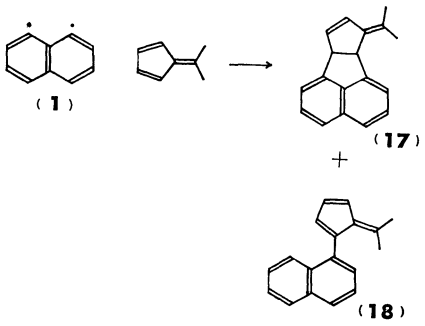

Scheme 4.

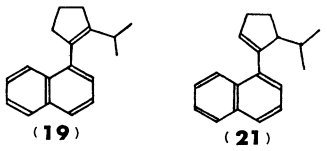

Scheme 5.

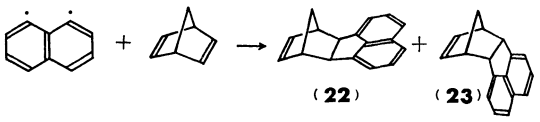

Scheme 6.

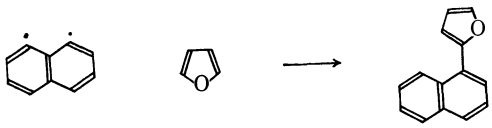

Scheme 7.

Reaction with Norbornadiene: It is known that norbornadiene sometimes reacts with other reagents as a homoconjugated diene owing to the interaction between two double bonds.[5f] Silicic acid chromatography of the reaction mixture gave two products **22** and **23** (total yield 7%), which were reported earlier by Baker and Mason.[15]

Discussion

Since the reactive intermediates like *o*-benzyne or 1,8-dehydronaphthalene are short-lived and react irreversively with other reagents, it may safely assumed that the reactivities are directly reflected to the yields of the products.[16]

Cycloaddition Reactions: It is well known that **2** reacts with cyclic diene to give Diels-Alder reaction products.[5] On the contrary, it is found that **1** gives [$\pi 2_s + \pi 2_s$] cycloaddition product instead of [$\pi 2_s + \pi 4_s$] product as described above.

Cycloheptatriene reacted with **2** rather abnormally to give a 1,2-cycloaddition product and an ene reaction product.[5g,5h,17] With **1**, it reacted to give a 1,2-cycloaddition product (**6**) and an insertion product (**4**). If the products were formed by a stepwise mechanism, the intermediate will be formulated as **24**,

which is stereochemically very similar to the proposed intermediate (**25**) for the reaction of cycloheptatriene and phenalenylidene.[18] The latter forms exclusively a [$_\pi$2+$_\pi$6] product (**26**). From the examination of the molecular model, successive overlap between the electrons on C-6′ of the cycloheptatrienyl and on C-8 of the naphthalene ring is thought to be slightly easier in **24** than in **25**. Nevertheless, the product (**27**), corresponding to **26**, was not detected in the products of **1** with cycloheptatriene. Thus the formation of **6** might occur through another pathway without forming **27**, *via* concerted process rather than the stepwise one. The principal formation of **6**, among 1,2-cycloaddition products, may be explained by the two-fold statistical advantage for the addition to C_1–C_2 compared with that to C_3–C_4 bond in cycloheptatriene and by the thermodynamical stability of **6** over the symmetrical one.

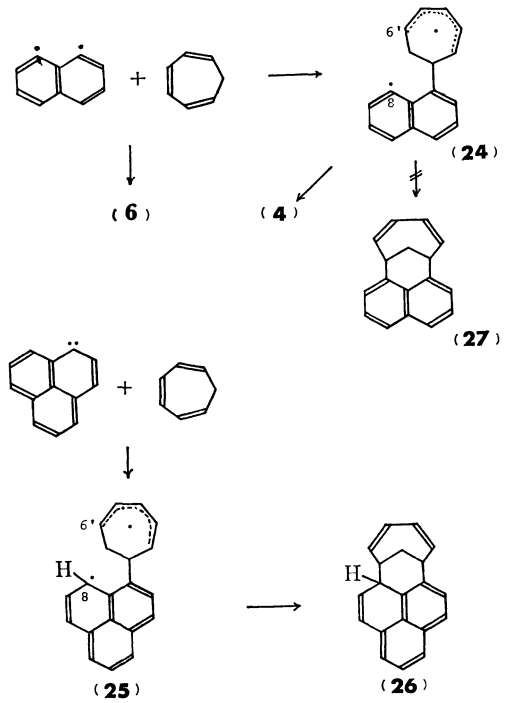

Scheme 8.

Dimethylfulvene with **1** gave a 1,2-cycloaddition product (**17**) and a C–H insertion product (**18**). The exclusive addition to C_1–C_2 double bond rather than the C_5–C_6 double bond is explained also by the same reason discussed above in the case of the formation of **6**, in addition to the steric hindrance to disturb approaching to the tetrasubstituted C_5–C_6 double bond.

With norboranadiene, a homoconjugated diene, **1** reacted exclusively in a manner of [$_\pi$2+$_\pi$2] cycloaddition. Because the rearranged products, as in the case of a radical reaction to substituted norbornadienes,[19] were not detected, the intermediacy of a diradical with a considerable life time cannot be anticipated.

Furthermore, from the steric consideration of the reaction, there is no reason to assume that an *endo*-cycloaddition to 1,2-bond surpasses over a homoconjugate addition to C_1 and C_5 of norbornadiene under a stepwise mechanism. In the concerted mechanism, the orbital symmetry consideration may well conclude the symmetry allowed process for the former and the forbidden process for the latter. The exclusive formation **22** and **23** strongly supports that the reaction might be a concerted one. The abundant formation of **22** over **23** may be recognized by the steric reason, that is, easier approach from the *exo* side than from the *endo* side.

The C–H Insertion Reaction: To clarify whether **1** reacts directly with C_1 carbon atom of cycloheptatriene to form the C–H insertion product or not, its reaction with cycloheptatriene-7-d_1 was carried out and **4**-d_1 was isolated. Investigation of the NMR spectrum revealed that the deuterium in **4**-d_1 was found at a sole position C_7 of the cycloheptatriene ring.

In every conjugated polyene case we examined, the C–H insertion products were formed in considerable amount and this reaction seemed to proceed by the attack of a radical of **1** to a position with the largest value of the free valence in the polyene system.[20]

In the reaction with cycloheptatriene, the intramolecular hydrogen abstraction by an aryl radical in **24**, giving **4**, might occur much faster than the cyclization to **27**. On the other hand, the ability of H-abstraction of allylic radical in **25** could be small owing to the delocalization of the radical electron over the phenalene ring.

In case of dimethylfulvene, two biradical intermediates **28** and **29** are possible, but any products through **29**, which can not be derived to any C–H insertion product, are not observed.

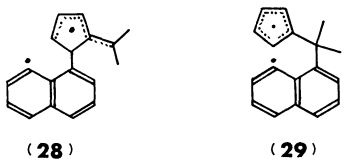

Scheme 9.

Experimental[21]

Reaction of 1,8-Dehydronaphthalene. Reaction with Cycloheptatriene: To a stirred CH_2Cl_2 (5 ml) solution of cycloheptatriene (3.37 g, 37 mmol) cooled externally with dry ice–acetone was added lead tetraacetate (1.5 g, 3.4 mmol) in one portion and followed by dropwise addition of **3** (564 mg, 3.1 mmol) in CH_2Cl_2 (20 ml) over 30 min. After the addition had been completed, the mixture was allowed to come to room temperature and filtered. The filtrate was washed successively with water and saturated salt solution and dried (anhyd. Na_2SO_4). The residue was chromatographed ($CHCl_3$) on silicic acid (60 g) in the dark: Fractions were collected in every 30 ml. Fractions 2—3 contained a liquid (218 mg), which was rechromatographed (*n*-hexane) on silicic acid (20 g) in the dark. Fractions were collected in every 10 ml: Fractions 7—10 contained compounds **4** and **6** (30 mg, 8: 10), which were further chromatographed (*n*-hexane) on neutral alumina (10 g). Fractions were collected in every 10 ml. Fractions 11—13 contained pure **4** (16 mg), which was identical with a sample of **4** described below.

Compound (**4**): NMR δ ppm (CCl_4) 2.76 (2H, d, J=8 Hz), 5.36 (1H, t-d, J=8, 6 Hz), 6.08—6.30 (2H, m), 6.52—6.64

(2H, m), 7—8 (7H, m); mass spectrum *m/e* (%) 218 (100), 217 (94), 215 (38), 203 (63), 202 (63), 152 (21); λ_{max}^{EtOH} nm (log ε) 225.5 (4.54), 295 (3.81).

Reaction with Cyclopentadiene: To a stirred CH_2Cl_2 (30 ml) solution of lead tetraacetate (3.8 g, 8.5 mmol) cooled externally with dry ice–acetone was added cyclopentadiene (5.1 g) in one portion and followed by dropwise addition of CH_2Cl_2 (50 ml) solution of **3** (1.3 g, 7.0 mmol) over 25 min. After stirring at the temperature for 30 min, the mixture was warmed up to 0 °C, treated with ice–water, and then filtered through Hyfrosupercel. The filtrate was washed successively with 5% aq. $NaHCO_3$, H_2O and brine. After drying (anhyd. Na_2SO_4) and concentrating the organic layer, the residue was chromatographed ($CHCl_3$) on silicic acid (40 g), fractions were collected in every 10 ml. Fractions 3—4 (536 mg) were rechromatographed (*n*-hexane) on silicic acid (30 g); fractions were collected in every 10 ml. Fractions 8—12 gave 220 mg of a mixture of **9**, **10** and **15** (1: 0.5: 2). This mixture was characterized by hydrogenation as described below.

Reaction with 6,6-Dimethylfulvene: To a stirred CH_2Cl_2 (15 ml) solution of dimethylfulvene (5.3 g, 50 mmol) cooled at −20 °C was added dropwise alternately a CH_2Cl_2 (40 ml) solution of **3** (916 mg, 5.0 mmol) and a CH_2Cl_2 (15 ml) solution of lead tetraacetate (2.55 g, 5.6 mmol). After usual work-up, the residue was chromatographed (*n*-hexane) on silicic acid (100 g), fractions were collected in every 100 ml. Fractions 8—9 gave a mixture of **17** and **18** (23 mg, 1: 2.8), fraction 10 gave a pure **18** (10 mg). The glc separation of **17** and **18** was carried out using a column of 3% Silicone OV-17 (1/4 in × 5 ft, He 60 ml/min) at 200 °C. Retention time **17**, 8.0 min; **18**, 8.44 min. **17** mp 110—113 °C; mass spectrum *m/e* (%) 232 (86), 217 (100), 202 (46); NMR δ ppm (CCl_4) 1.36 (3H, s), 2.18 (3H, s), 6.24—6.46 (3H, m), 7.2—7.84 (7H, m); λ_{max}^{EtOH} nm (log ε) 222 (4.84), 273 (4.27). **18** mp 119—120 °C; mass spectrum *m/e* (%) 232 (100), 217 (84), 165 (32); NMR δ ppm (CCl_4) 1.84 (3H, s), 2.22 (3H, s), 4.82 (2H, bq), 5.94 and 6.24 (2H, broad AB type), 7.2—7.6 (6H, m).

Reaction with Furan: To a stirred CH_2Cl_2 (30 ml) solution of lead tetraacetate (4.87 g, 11 mmol) cooled externally with dry ice–acetone, was added furan (6.8 g, 100 mmol) in one portion and followed by a dropwise addition of **3** (1.84 g, 10 mmol) in CH_2Cl_2 (40 ml). After usual work-up and chromatography (*n*-hexane/silicic acid 30 g), 2-(α-naphthyl)-furan 56 mg (3.2%) was obtained and identified with an authentic sample;[14] NMR δ ppm (CCl_4) 6.48 (1H, d-d, J=2, 3.5 Hz), 6.64 (1H, d, J=3.5 Hz), 7.32—7.88 (7H, m), 8.28—8.44 (1H, m).

Reaction with Norbornadiene: To a CH_2Cl_2 (20 ml) solution of norbornadiene (5.0 g, 50 mmol) cooled at −20 °C was added dropwise, alternately a solution of **3** (923 mg, 5 mmol) in CH_2Cl_2 (50 ml) and a solution of lead tetraacetate (2.44 g, 5.5 mmol) in CH_2Cl_2 (25 ml) over 45 min. After usual work-up, the product was chromatographed (*n*-hexane) on silicic acid (100 g) to give **22**[15] (75 mg, 7.5%), and **23**[15] (10 mg, 1%).

Reaction with Cycloheptene: To a stirred CH_2Cl_2 (5 ml) solution of cycloheptene (443 mg, 4.5 mmol) cooled externally with dry ice–acetone was added lead tetraacetate (931 mg, 2.1 mmol) in one portion followedby a dropwise addition of CH_2Cl_2 (5 ml) solution of **3** (276 mg, 1.5 mmol) over 15 min. Usual work-up and chromatography (*n*-hexane) on neutral alumina (10 g) gave **7** (10 mg, 3%). [Mass spectrum, *m/e* (%) 222 (100), 179 (53), 166 (25), 165 (66), 153 (20); NMR spectrum, δ ppm (CCl_4) 1.1—2.4 (10H, m), 3.6—3.9 (2H, m), 7.0—7.6 (6H, ABC type); λ_{max}^{EtOH} nm (log ε) $223^{infl.}$ (4.72), 228 (4.84), 244 (3.21), 281 (3.75), 289 (3.80), 301 (3.50), 306 (3.49), 315.5 (3.04), 320 (3.11).

*Catalytic Hydrogenation of a Mixture of Compounds **4** and **6**.* A mixture of **4** and **6** (30 mg), obtained above, was hydrogenated in ethanol over 10% Pd–C (100 mg) at room temperature for 4.5 hr. The mixture was filtered and evaporated *in vacuo*. Repeated chromatography (*n*-hexane/neutral alumina) of the residue gave a mixture (1: 1, 15 mg) of 1-(1-cycloheptenyl)naphthalene[7] and 1-cycloheptylnaphthalene[7] and **7** (16 mg). These were characterized by direct comparison with the authentic samples synthesized independently.

*7-(α-Naphthyl)cycloheptatriene (**5**).* To a stirred suspension of tropylium fluoroborate (2.1 g, 12 mmol) in anhyd. THF (10 ml) was added dropwise α-naphthylmagnesium bromide in ether (8 ml), prepared from α-bromonaphthalene (2.88 g, 11 mmol) and Mg (245 mg, 10 mgatom) at room temperature. Insoluble material was filtered and the filtrate was concentrated *in vacuo* The residue (2.4 g) was chromatographed (*n*-hexane) on silicic acid (70 g), fractions were collected in every 50 ml; fractions 10—18 gave **5** (904 mg, 30%). [Found: C, 93.46; H, 6.54%. Calcd for $C_{17}H_{14}$: C, 93.53; H, 6.47%: Mass spectrum; *m/e* (%) 218 (100), 217 (76), 215 (32), 203 (61), 202 (61): NMR spectrum, δ ppm (CCl_4) 3.36 (1H, t, J=5 Hz), 5.47 (2H, d-d, J=9, 5 Hz), 6.08—6.32 (2H, m), 6.52—6.76 (2H, m), 7.2—8.0 (7H, m): λ_{max}^{EtOH} nm (log ε) 224.5 (4.97), $263^{infl.}$ (3.91), 272 (4.01), 282 (4.06), $292^{infl.}$ (3.91).

*Thermal Rearrangement of 7-(α-Naphthyl)cycloheptatriene (**5**).* When **5** (30 mg) dissolved in DMSO-d_6 (0.4 ml) in an NMR tube was heated at 125 °C for 15 hr.[22] The NMR measurement revealed that **5** was transformed almsot completely to **8**, which was further transformed to **4** by heating it at 160 °C for 4 hr. **8** was isolated by chromatography (*n*-hexane) on neutral alumina (1 g); fractions were collected in every 1 ml. Fraction 5 gave almost pure **8**. Sublimation at 90 °C/1 mmHg. **8** Found: C, 93.35; H, 6.56%. Calcd for $C_{17}H_{14}$: C, 93.53; H, 6.47%. Mass spectrum; *m/e* (%) 219 (19), 218 (100), 217 (71), 215 (33), 203 (54), 202 (56). NMR spectrum; δ ppm (CCl_4) 2.46 (2H, t, J=6 Hz), 5.2—5.6 (2H, m), 6.1—6.4 (2H, m), 6.63 (1H, d, J=5 Hz), 7.2—7.8 (7H, m).

*Photochemical Interconversion of Compounds **4** and **5**.* The CCl_4 solution (0.4 ml) of **5** in a quartz NMR tube was irradiated with a low pressure mercury lamp at room temperature and the reaction was followed by NMR method. The ratios of **4** and **5** in the mixture were observed in the course of the irradiation time as follows; **5**: **4**=16: 1 (18 hr), 5: 1 (38 hr), 4.6: 1 (62 hr).

When a CCl_4 (0.4 ml) solution of **4** (30 mg) was irradiated with a high pressure mercury lamp (UM-452) through Pyrex filter for 30 min, **4** was transformed to **5**, giving a ratio of 23: 1 (**5** to **4**).

*Catalytic Reduction of a Mixture of **9**, **10** and **15**.* A mixture of **9**, **10** and **15** (199 mg, 1: 0.5: 2) dissolved in 95% EtOH (15 ml) was hydrogenated over 10% Pd–C (46 mg) for 2 hr. The glc separation (10% Apiezone L, 1/4 in × 5 ft, 185 °C) of the residue gave almost equal amounts of a mixture of **12** and **13**[4] (4: 3) and **14**, which was identified with the authentic sample[11] [NMR δ ppm (CCl_4) 1.72 (6H, m), 2.0—2.3 (2H, m), 3.5—3.8 (1H, m), 7.12—7.72 (6H, m), 7.8—8.0 (1H, m); λ_{max}^{EtOH} nm (log ε) 225.5 (4.88), 272 (3.79), 283 (3.87), 293 (3.70)].

Dehydrogenation of 1-(1-Cyclopentenyl)naphthalene. 1-(1-Cyclopentenyl)naphthalene[11] (193 mg, 1 mmol), NBS (178 mg, 1 mmol) and benzoylperoxide (10 mg) in CCl_4 (3 ml) was refluxed for 2 hr. The cooled mixture was filtered and the residue dissolved in anhyd. ether (5 ml) was treated with Et_3N (3 ml). After refluxing the mixture for 2 hr and evaporation of the solvent, the residue (261 mg) was chromato-

graphed (*n*-hexane) on silicic acid (3 g); fractions were collected in every 3 ml. Fractions 4 and 5 gave a mixture of **15** and **16** (58 mg, 1:3) [NMR; charasteristic methylene signals at δ 3.38 (q, J=1.1 Hz) and 3.15 (q, J=1.1 Hz) ppm]. The spectral data of the former were identical with the sample obtained from the reaction of cyclopentadiene with **1**. Because of their instability, further purification of **15** was not effected. Catalytic hydrogenation (10% Pd-C/EtOH) of the mixture gave **14** as a sole product.

Catalytic Hydrogenation of 1-(α-Naphthyl)-6,6-dimethylfulvene (18). A solution of **18** (10 mg) in gracial acetic acid (10 ml) was hydrogenated over 5% Pd-C (50 mg) for 3 hr to give a tetrahydro derivative **19** (8 mg), which was identified with the authentic sample described below.

Synthesis of 1-Isopropyl-2-(α-Naphthyl)cyclopentene (19). A solution of **20** (2.3 g, 9.1 mmol)[13] in bromobenzene (20 ml) was heated at 180 °C in the presence of $KHSO_4$ (1.3 g) until the separation of water had ceased. After evaporation of bromobenzene, the residue was chromatographed (*n*-hexane) on silicic acid (25 g); fractions were collected in every 25 ml. Fractions 3—5 gave a mixture of products (1.17 g), which was further chromatographed (*n*-hexane) on neutral alumina (35 g); 20 ml-fractions were collected and fractions 2—5 (948 mg) contained **19** and **21**. The pure samples of **19** and **21** were obtained by glc (5% SE-30, 1/4 in×5 ft, 156 °C, He 40 ml/min). Retention time; **19** 7.2 min, **21** 11.5 min. [**19** Found: C, 91.34; H, 8.55%. Calcd. for $C_{18}H_{20}$: C, 91.47; H, 8.53%. NMR spectrum: δ ppm (CCl_4); 0.90 (6H, d, J=6 Hz), 1.8—2.9 (7H, m), 7.0—7.8 (7H, m). Mass spectrum: *m/e* (%) 236 (62), 221 (100), 193 (41), 179 (30), 178 (24), 165 (37). λ_{max}^{EtOH} nm (log ε) 226 (4.82), $274^{infl.}$ (3.77), 284 (3.86), $293^{infl.}$ (3.79). **21** Found: C, 91.46, H, 8.26%. NMR spectrum: δ ppm (CCl_4); 0.67 (3H, d, J=7 Hz), 0.79 (3H, d, J=7 Hz), 1.6—2.7 (5H, m), 3.1—3.4 (1H, m), 5.82 (1H, bq, J=2 Hz), 7.1—7.42 (4H, m), 7.54—7.8 (2H, m), 7.9—8.16 (1H, m). Mass spectrum: *m/e* (%) 236 (34), 221 (9), 194 (18), 193 (100), 192 (9), 191 (9), 179 (9), 178 (32), 165 (19). λ_{max}^{EtOH} nm (log ε) 226 (4.73), 286 (3.87), 294 (3.86)].

The authors are grateful to Mr. Jun-ichi Goda for the analytical data and Mr. Misao Uegaki for his skillful technical assistance. The authors wish to thank Dr. Yoshio Hirose of the Institute of Food Chemistry for mass spectral measurements.

References and Notes

1) R. Hoffmann, A. Imamura, and W. J. Hehre, *J. Amer. Chem. Soc.*, **90**, 1499 (1968).

2) C. W. Rees and R. C. Storr, *J. Chem. Soc., C*, **1969**, 760.

3) a) M. Jones, Jr. and R. H, Levin, *Tetrahedron Lett.*, **1968**, 5593. b) H. H. Wasserman, A. J. Solodar, and L. S. Keller, *ibid.*, **1968**, 5596.

4) J. Meinwald and G. W. Gruber, *J. Amer. Chem. Soc.*, **93**, 3802 (1971).

5) a) R. Huisgen and R. Knorr, *Tetrahedron Lett.*, **1963**, 1017. b) C. D. Campbell and C. W. Rees, *J. Chem. Soc., C*, **1969**, 748. c) E. Vedejs, R. A. Shepherd, *Tetrahedron Lett.*, **1970**, 1863. d) G. Wittig and R. W. Hoffmann, *Chem. Ber.*, **95**, 2718, 2729 (1962). e) R. Muneyuki and H. Tanida, *J. Org. Chem.*, **31**, 1988 (1966). f) H. Heaney and J. M. Jablonski, *Tetrahedron Lett.*, **1967**, 2733. g) P. Crews, M. Loffgren, and D. J. Bertelli, *Tetrahedron Lett.*, **1971**, 4697. h) M. Kato, T. Sawa, and T. Miwa, *Chem. Commun.*, **1971**, 1635.

6) For example, cyclopentadiene forms a colorless precipitates immediately when mixed with lead tetraacetate at room temperature in dichloromethane.

7) S. I. Khromov and E. S. Balenkova, *Vestnik Moskov Univ., 10, Ser. Fiz. Mat. i Estestven. Nauk*, (**8**) 121 (1955) [*Chem. Abstr.*, **50**, 11305e (1956)]. L. H. Klemm, B. T. Ho, C. D. Lind, B. I. MacGowan, and E. Y. K. Mak, *J. Org. Chem.*, **24**, 949 (1959).

8) a) K. Conrow, "Organic Syntheses," Coll. Vol. **5**, 1138 (1973). b) H. J. Dauben, Jr., L. R. Honnen, and K. M. Harmon, *J. Org. Chem.*, **25**, 1442 (1960).

9) A. P. Ter Borg and H. Kloosterziel, *Rec. Trav. Chim.*, **82**, 741 (1963); *ibid.*, **84**, 245 (1965).

10) T. Tezuka, M. Kimura, A. Sato, and T. Mukai, This Bulletin, **43**, 1120 (1970).

11) W. E. Bachmann and L. H. Klemm, *J. Amer. Chem. Soc.*, **72**, 4911 (1950).

12) We could not detect the 1,4-cycloaddition product (**11**), described by the authors.[4] In the NMR spectrum of the hydrocarbon fraction after chromatography, the signals due to **16** was also found. But as we could not find them just before chromatography, **16** might be formed from **15** by 1,5-sigmatropic hydrogen shift during chromatography.

13) This compound was synthesized from α-naphthylmagnesium bromide and 2-isopropylcyclopentanone in ether.

14) A. W. Johnson, *J. Chem. Soc.*, **1946**, 895.

15) R. Baker and T. J. Mason, *J. Chem. Soc., C*, **1970**, 596.

16) B. H. Klanderman and T. R. Griswell, *J. Org. Chem.*, **34**, 3426 (1969).

17) 7-Phenylcycloheptatriene reacts with *o*-benzyne as a norcaradiene structure to give a [$_{\pi}2+_{\pi}4$] product.[23] Other dienophiles also react with cycloheptatriene itself giving tricyclo[3.2.2.$0^{2,4}$]nonene derivatives.[24]

18) I. Murata, T. Nakazawa, and T. Imanishi, *Tetrahedron Lett.*, 5089 (1972).

19) V. F. Bystrov, V. A. Azovskaya, N. P. Petukhova, A. U. Stepanyants, and E. N. Prilezhaeva, *Izv. Akad. Nauk SSSR, Ser. Khim.*, 318 (1966) [*Chem. Abstr.*, **65**, 8781e (1966)].

20) A. Streitwieser, Jr., "Molecular Orbital Theory for Organic Chemists," John Wiley and Sons Inc., New York (1961), p. 289.

21) All melting points are not corrected. UV spectra were measured on a Hitachi Recording Spectrometer Model 323 and NMR spectra were measured on a JEOL PS-100 spectrometer with TMS as an internal standard. The chemical shifts are expressed in ppm. from TMS.

22) No change was observed when **5** was heated at 100 °C for 18.5 hr or at 120 °C for one hour.

23) M. Kato, T. Sawa, and T. Miwa, Unpublished work.

24) T. Tsuji, S. Teratake, and H. Tanida, This Bulletin, **42**, 2033 (1969).

Bitter Principles of Aquifoliaceae. III.[1] The Structures and Stereochemistry of Three Aglycones Obtained by the Hydrolysis of Latifoloside A, a Bitter Glycoside from *Ilex latifolia* Thunb.

Masamitsu Ochi, Katsumi Ochiai, and Kosho Nagao
Faculty of Arts and Sciences, Kochi University, Asakura, Kochi 780
Takashi Kubota*
Faculty of Science, Osaka City University, Sugimoto-cho, Sumiyoshi-ku, Osaka 558
(Received October 22, 1974)

From the leaves of *Ilex latifolia* Thunb., two new bitter glycosides, latifoloside, A and B, have been isolated. The acid hydrolysis of A afforded three triterpenoid aglycones, which have been formulated by spectroscopic and chemical evidence as I, II, and III respectively.

In the course of an investigation of the bitter principles of Aquifoliaceae plants, the constituents of the leaves of *Ilex latifolia* Thunb., which have an intense bitter taste, have been examined. A methanol extract of fresh leaves was treated with *n*-butanol, the subsequent chromatography of the soluble material over silicic acid led to the isolation of two bitter glycosides, latifoloside A (0.009% yield) (mp 235—236 °C (decomp.), $[\alpha]_D^{25}$ −33° (*c* 1.0, ethanol)) and B (0.001% yield) (mp 210—211 °C (decomp.), $[\alpha]_D^{16}$ −11° (*c* 0.1, pyridine)). Latifoloside A, which has been obtained in a major amount, yielded three triterpenoid aglycones, I, II, and III, on hydrolysis with methanol–1M sulfuric acid. In this paper, we will deal with the structural elucidation of these three compounds.

Results and Discussion

Aglycone I, $C_{31}H_{46}O_4$ (mp 269—270 °C, $[\alpha]_D^{25}$ −110° (*c* 1.0, ethanol)), shows a hydroxylic absorption in the IR spectrum at 3400 cm^{-1} and forms a monoacetate IV, $C_{33}H_{48}O_5$ (mp 272—273 °C), the IR spectrum of which no longer exhibits a hydroxyl group. The NMR spectrum of IV shows signals due to an acetyl group at δ 2.04 and a methoxyl group at δ 3.12. In addition, the signal of the methine proton on the oxygenated carbon of I at δ 3.22 shifts to 4.49 on acetylation. These observations indicate that the hydroxyl group of I is secondary, and the methoxyl group, tertiary.

On the other hand, I exhibits UV maxima at 253 (shoulder), 261, and 270 (shoulder) nm (ε 24500, 30000, and 21500 respectively), an IR band at 1750 cm^{-1}, and NMR signals at δ 1.41 (3H, s), 5.74 (1H, dd, J=11 and 2 Hz), and 6.77 (1H, dd, J=11 and 3 Hz). The similarity of these spectral data to those of the dienelactone V[2] suggests the presence of the partial structure Ia. Further evidence in support of this partial structure was provided by the following chemical transformations. The reduction of I with lithium aluminum hydride, followed by acetylation, gave a monoacetate VI, $C_{33}H_{50}O_4$ (mp 210—211 °C), the UV absorptions of which are quite similar to those of VII.[3] The treatment of the epoxide VIII[4] in the same way as in the formation of V[2] afforded a lactone IX, $C_{34}H_{48}O_6$ (mp 241—242 °C), which exhibits UV maxima at 252, 260, and 269 nm (ε 19300, 23800, and 16600 respectively), an IR band at 1750 cm^{-1}, and NMR signals at δ 1.40 (3H, s), 5.68 (1H, dd, J=11 and 2 Hz), and 6.10 (1H, dd, J=11 and 3 Hz), all supporting the partial structure Ia for aglycone I.

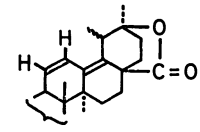

Ia

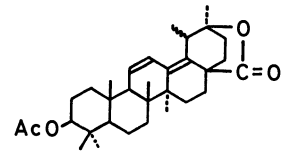

V

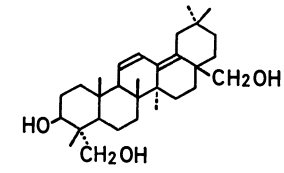

VII

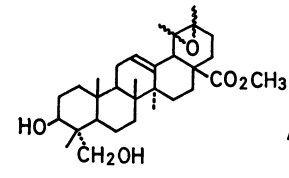

VIII

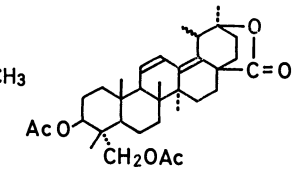

IX

These facts and the analogy with the structures of the congeners isolated from *Ilex latifolia* Thunb.[5] lead to the assignment of the ursane skeleton for I, in which the partial structure Ia would constitute the C, D, and E-rings.

The location and the configuration of the tertiary methoxyl group were proved as follows. In the NMR spectrum of IX, the signal due to the C-19 methyl protons appears as a doublet at δ 1.08 as a result of the coupling with the allylic methine proton, which appears as a quartet at δ 2.66. On the other hand, the NMR spectrum of I does not show the corresponding signals, but a singlet at δ 1.45 assigned to the methyl protons on an oxygenated carbon. Hence, the methoxyl group in question must be located at C-19. In the

* Present address: Kinki University, Kowakae, Higashi-Osaka, Osaka 577.

NMR spectrum of VI, the signal of the C-19 methyl protons shifts to a higher field (δ 1.36) compared with that of IV, while the signal of the methoxyl group appears at a lower field (δ 3.26) than that of IV. Taking account of the anisotropy of the lactonic carbonyl group, these observations indicate that the C-19 methyl group lies near the plane of the carbonyl group (α-oriented) and the methoxyl group above the plane (β-oriented).

On biogenetic grounds, it is most reasonable to place the secondary hydroxyl group in I at the C-3 position. Moreover, the NMR spectrum of IV shows a signal due to the methine proton attached to the carbon atom bearing an acetoxyl group at δ 4.49 (1H, t-like, W1/2 18 Hz), the shape and position of which correspond to those found in the spectra of C-3 equatorial acetates in the polyterpenes.[6]

Finally, the structure was confirmed by correlation with vanguerolic acid lactone, X.[2] The hydrogenolysis of I in glacial acetic acid over a platinum catalyst did give X, $C_{30}H_{46}O_3$ (mp and mixed mp 263—267 °C), along with a dihydro-compound which forms a monoacetate XI, $C_{33}H_{50}O_5$ (mp 247—249 °C). Therefore, the I structure must represent aglycone I.

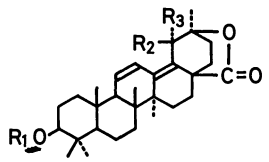

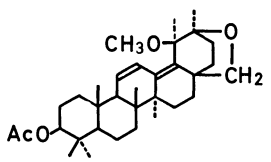

I R_1=H, R_2=OCH_3, R_3=CH_3 VI

II R_1=H, R_2=OH, R_3=CH_3

III R_1=H, R_2=CH_3, R_3=OH

IV R_1=Ac, R_2=OCH_3, R_3=CH_3

XV R_1=Ac, R_2=OH, R_3=CH_3

XVI R_1=Ac, R_2=CH_3, R_3=OH

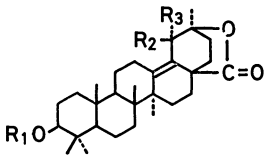

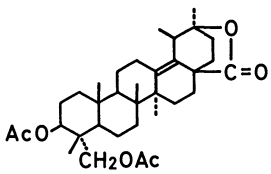

X R_1=H, R_2=CH_3, R_3=H XIX

XI R_1=Ac, R_2=OCH_3, R_3=CH_3

XVII R_1=H, R_2=OH, R_3=CH_3

XVIII R_1=H, R_2=CH_3, R_3=OH

Furthermore, the conversion of I into X determines the configurations at C-19 of not only X, but also V** and IX, which have hitherto remained unknown. Callow and Thompson have reported that the hydrogenolysis of XII over a platinum catalyst gave XIII in glacial acetic acid and XIV in ethyl acetate, with an inversion at C-7 by means of the S_N2 mechanism.[7]

** The hydrogenation of V affords X under the same conditions.[2]

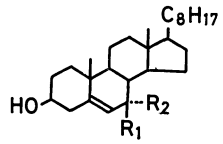

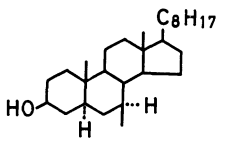

XII R_1=OH, R_2=CH_3 XIII

XIV R_1=CH_3, R_2=H

These facts suggest that C-19 methyl groups of X, V, and IX are β-oriented.

Aglycone II, $C_{30}H_{44}O_4$ (mp 227—229 °C, $[\alpha]_D^{18}$ −90° (c 0.15, ethanol)), exhibits UV maxima at 251 (shoulder), 259, and 268 (shoulder) nm (ε 21000, 26900, and 19100 respectively), IR bands at 3500 and 1730 cm^{-1}, and NMR signals at δ 1.42 and 1.51 (3H each, s), 3.20 (1H, t-like, W1/2 18 Hz), 5.74 (1H, dd, J=11 and 2 Hz), and 6.83 (1H, dd, J=11 and 3 Hz), suggesting the presence of the same partial structure as in I. II forms a monoacetate XV, $C_{32}H_{46}O_5$ (mp 259—261 °C), the IR spectrum of which still shows a hydroxylic absorption at 3420 cm^{-1}. These observations indicate the presence of a hydroxyl group at C-19 in II instead of the methoxyl group in I.

A close structural similarity of aglycone III, $C_{30}H_{44}O_4$ (mp 265—267 °C, $[\alpha]_D^{18}$ −147° (c 0.1, ethanol)), to II is indicated by the spectral data, showing UV maxima at 253 (shoulder), 261, and 270 (shoulder) nm (ε 16500, 20100, and 14200 respectively), IR bands at 3440 and 1720 cm^{-1}, and NMR signals at δ 1.38 and 1.45 (3H each, s), 3.21 (1H, t-like, W1/2 18 Hz), 5.78 (1H, dd, J=11 and 2 Hz), and 6.88 (1H, dd, J=11 and 3 Hz). III forms a monoacetate XVI, $C_{32}H_{46}O_5$ (mp 268—270 °C), the IR spectrum of which still shows a hydroxylic absorption at 3400 cm^{-1}. From these data, it may be concluded that II and III are epimers with respect to C-19.

In order to determine the configuration at C-19, the hydrogenolysis of II and III was attempted in a way similar to that used with I. Thus, II afforded X along with a dihydro-compound XVII, $C_{30}H_{46}O_4$ (mp 247—249 °C), whereas III yielded only a dihydro-compound XVIII, $C_{30}H_{46}O_4$ (mp 259—261 °C). In addition, the UV absorptions of II characteristic of the partial structure Ia disappeared after 4 hr, while those of III disappeared within 1 hr. In the hydrogenolysis reaction of I, which gave X and a dihydro-compound, as has been mentioned above, the disappearance of UV absorptions was observed after 3 hr, while IX gave a dihydro-compound XIX after 1 hr. If we assume that the hydrogenolysis of the allylic C–O bond occurs with inversion by means of the S_N2 mechanism and that the hydrogenation rate is affected only by the ease in approach to the catalyst, these results suggest that the configuration at C-19 of II is similar to that of I, while III and IX have the same configuration at C-19. The catalyst would attack the α-face of the molecule because of the steric hindrance due to the methyl groups at C-8 and C-10. The α-oriented methyl group at C-19 prevents the approach to the catalyst, whereas the α-oriented hydroxyl group promotes the reaction through its affinity for the catalyst metal.

Experimental

The NMR spectra were determined on a JEOL PS-100 (100 MHz) spectrometer in deuterochloroform solutions, with tetramethylsilane as the internal standard. The IR spectra were recorded on a JASCO model IR-S spectrophotometer. The UV data were measured in ethanol solutions with a Hitachi EPS-3T spectrophotometer. A Rex Optical Works apparatus, model NEP-2, was used for the measurement of the rotations. Column chromatography was performed using Mallinckrodt silicic acid. The mps were determined in glass capillaries and are uncorrected.

Isolation. The fresh leaves of *Ilex latifolia* Thunb. (26 kg), collected in Kochi City in July, 1973, were chopped up and extracted with hot methanol (120 l). After treatment with activated carbon, the extract was concentrated up to about 6 l, leaving an aqueous solution. This solution, after filtration, was extracted with ethyl acetate (1.5 l×3) and then with *n*-butanol (1.5 l×3). The *n*-butanol layer, which has an intense bitter taste, was evaporated *in vacuo* to afford a dark brown residue, which was dissolved in methanol (600 ml). The methanol solution was poured into ether (9 l), and the resulting precipitates were collected by filtration, washed with ether, and dried to give a yellowish-white powder (432 g). This powder was repeatedly chromatographed over silicic acid, with chloroform–methanol–water (80:20:2) as the eluent, to give latifoloside A and B.

Latifoloside A. The combined fractions (3.663 g) were recrystallized from acetone–methanol (2:1) at 50—55 °C to give pure latifoloside A as needles (2.256 g); mp 235—236 °C (decomp.), $[\alpha]_D^{24}$ −33° (*c* 1.0, EtOH), Molisch test (+), IR (KBr) 3400, 1720, and 1045 cm^{-1}.

Latifoloside B. The more polar fractions (1.107 g) were recrystallized from methanol to yield pure latifoloside B as needles (255 mg); mp 210—211 °C (decomp.), $[\alpha]_D^{16}$ −11° (*c* 0.1, pyridine), Molisch test (+), IR (KBr) 3400, 1695, and 1075 cm^{-1}.

Hydrolysis of Latifoloside A. To a solution of latifoloside A (2.0 g) in methanol (200 ml), we added 1 M sulfuric acid (200 ml). The mixture was refluxed for 5 hr and then extracted with ether (600 ml). The extract was washed with a sodium bicabonate solution and with water, dried over magnesium sulfate, and evaporated to dryness. The residue (948 mg) was chromatographed over silicic acid; subsequent elution with chloroform gave aglycone I, II, and III, in that order.

Aglycone I. The earliest fractions (284 mg) were recrystallized from methanol to give I as needles (180 mg); mp 269—270 °C, $[\alpha]_D^{25}$ −110° (*c* 1.0, EtOH), UV (EtOH) 253 (shoulder), 261, and 270 (shoulder) nm (ε 24500, 30000, and 21500 respectively), IR (KBr) 3400 and 1750 cm^{-1}, NMR ($CDCl_3$) δ 1.41 and 1.45 (3H each, s, C_{20} and C_{19}–CH_3), 3.12 (3H, s, O–CH_3), 3.22 (1H, t-like, C_3–H), 5.74 (1H, dd, J=11 and 2 Hz, C_{12}–H), and 6.77 (1H, dd, J=11 and 3 Hz, C_{11}–H), (Found: C, 75.45; H, 9.67%. Calcd for $C_{31}H_{46}O_4 \cdot 1/2H_2O$: C, 75.72; H, 9.63%).

Aglycone II. The middle fractions (254 mg) were recrystallized from aqueous methanol to yield II as prisms (168 mg); mp 227—229 °C, $[\alpha]_D^{18}$ −90° (*c* 0.15, EtOH), UV (EtOH) 251 (shoulder), 259, and 268 (shoulder) nm (ε 21000, 26900, and 19100 respectively), IR (Nujol) 3500, 1730, and 1050 cm^{-1}, NMR ($CDCl_3$) δ 1.42 and 1.51 (3H each, s, C_{20} and C_{19}–CH_3), 3.20 (1H, t-like, W1/2 18 Hz, C_3–H), 5.74 (1H, dd, J=11 and 2 Hz, C_{12}–H), and 6.83 (1H, dd, J=11 and 3 Hz, C_{11}–H), (Found: C, 77.34; H, 9.63%. Calcd for $C_{30}H_{44}O_4$: C, 76.88; H, 9.46%).

Aglycone III. The last fractions (300 mg) were recrystallized from aqueous methanol to give III as plates (204 mg); mp 265—267 °C, $[\alpha]_D^{16}$ −147° (*c* 0.1, EtOH), UV (EtOH) 253 (shoulder), 261, and 270 (shoulder) nm (ε 16500, 20100, and 14200 respectively), IR (KBr) 3440, 1720, and 1080 cm^{-1}, NMR ($CDCl_3$) δ 1.38 and 1.45 (3H each, s, C_{20} and C_{19}–CH_3), 3.21 (1H, t-like, W1/2 18 Hz, C_3–H), 5.78 (1H, dd, J=11 and 2 Hz, C_{12}–H), and 6.88 (1H, dd, J=11 and 3 Hz, C_{11}–H), (Found: C, 76.45; H, 9.56%. Calcd for $C_{30}H_{44}O_4$: C, 76.88; H, 9.46%).

Acetylation of I. A solution of I (40 mg) in acetic anhydride (2 ml) and pyridine (1 ml) was allowed to stand at room temperature overnight and then worked up in the usual way to give a white precipitate which was subsequently recrystallized from methanol to yield a monoacetate IV as needles (29 mg); mp 272—273 °C, IR (CCl_4) 1750, 1730, and 1245 cm^{-1}, NMR ($CDCl_3$) δ 1.41 and 1.45 (3H each, s, C_{20} and C_{19}–CH_3), 2.04 (3H, s, O–CO–CH_3), 3.12 (3H, s, O–CH_3), 4.49 (1H, t-like, W1/2 18 Hz, C_3–H), 5.71 (1H, dd, J=11 and 2 Hz, C_{12}–H), and 6.77 (1H, dd, J=11 and 3 Hz, C_{11}–H), (Found: C, 75.38; H, 9.33%. Calcd for $C_{33}H_{48}O_5$: C, 75.53; H, 9.22%).

Acetylation of II. II (37 mg) was treated with acetic anhydride (1 ml) and pyridine (1 ml) as has been described above, and the resulting precipitates were recrystallized from methanol to give a monoacetate XV as needles (30 mg); mp 259—261 °C, IR (Nujol) 3420, 1740, and 1255 cm^{-1}, NMR ($CDCl_3$) δ 1.41 and 1.51 (3H each, s, C_{20} and C_{19}–CH_3), 2.03 (3H, s, O–CO–CH_3), 4.51 (1H, t-like, W1/2 18 Hz, C_3–H), 5.76 (1H, dd, J=11 and 2 Hz, C_{12}–H), and 6.84 (1H, dd, J=11 and 3 Hz, C_{11}–H), (Found: C, 75.20; H, 9.15%. Calcd for $C_{32}H_{46}O_5$: C, 75.26; H, 9.08%).

Acetylation of III. III (50 mg) was treated with acetic anhydride (2 ml) and pyridine (2 ml) as has been described above, and the resulting precipitates were recrystallized from methanol to yield a monoacetate XVI as needles (35 mg); mp 268—270 °C, IR (Nujol) 3400, 1735, 1715, and 1235 cm^{-1}, NMR ($CDCl_3$) δ 1.38 and 1.45 (3H each, s, C_{20} and C_{19}–CH_3), 2.05 (3H, s, O–CO–CH_3), 4.51 (1H, t-like, W1/2 18 Hz, C_3–H), 5.78 (1H, dd, J=11 and 2 Hz, C_{12}–H), and 6.92 (1H, dd, J=11 and 3 Hz, C_{11}–H), (Found: C, 75.33; H, 9.17%. Calcd for $C_{32}H_{46}O_5$: C, 75.26; H, 9.08%).

Reduction of I with Lithium Aluminum Hydride. To a solution of I (50 mg) in tetrahydrofuran (5 ml), we added lithium aluminum hydride (10 mg) in tetrahydrofuran (5 ml). The mixture was stirred at room temperature for 1 hr and then poured into ether floated on water. The organic layer was washed with dilute hydrochloric acid and then with water. The subsequent drying and evaporation of the solution left a residue (48 mg) which no longer showed the lactonic band in the IR spectrum. The acetylation and recrystallization of the product from aqueous methanol afforded a monoacetate VI as needles (19 mg); mp 210—211 °C, UV (EtOH) 244, 253, and 262 nm (ε 18000, 25600, and 16000 respectively), IR (CCl_4) 1735 and 1245 cm^{-1}, NMR ($CDCl_3$) δ 1.16 (3H, s, C_{20}–CH_3), 1.34 (3H, s, C_{19}–CH_3), 2.04 (3H, s, O–CO–CH_3), 3.26 (3H, s, O–CH_3), 3.40 (2H, s, O–CH_2–), 4.51 (1H, t-like, C_3–H), 5.62 (1H, dd, J=11 and 2 Hz, C_{12}–H), and 6.85 (1H, dd, J=11 and 3 Hz, C_{11}–H), (Found: C, 75.60; H, 9.79%. Calcd for $C_{33}H_{50}O_4 \cdot 2/3H_2O$: C, 75.82; H, 9.77%).

Formation of the Lactone IX. The procedure of Barton *et al.*[2] was followed: the epoxide VIII (220 mg) in glacial acetic acid (18 ml) containing concentrated hydrochloric acid (2 ml) was heated at 100 °C for 10 min. The mixture was then worked up in the usual manner, and the resulting precipitates (236 mg) were recrystallized from aqueous methanol

to give a lactone IX as flakes (104 mg); mp 241—242 °C, UV (EtOH) 252, 260, and 269 nm (ε 19300, 23800, and 16600 respectively), IR (CCl_4) 1750 and 1245 cm^{-1}, NMR ($CDCl_3$) δ 1.08 (3H, d, J=7 Hz, C_{19}-CH_3), 1.40 (3H, s, C_{20}-CH_3), 2.02 and 2.06 (3H each, s, O-CO-CH_3), 2.66 (1H, q, J=7 Hz, C_{19}-H), 3.77 (2H, s, O-CH_2-), 4.77 (1H, m, C_3-H), 5.68 (1H, dd, J=11 and 2 Hz, C_{12}-H), and 6.10 (1H, dd, J=11 and 3 Hz, C_{11}-H), (Found: C, 73.92; H, 8.86%. Calcd for $C_{34}H_{48}O_6$: C, 73.88; H, 8.75%).

Hydrogenolysis of I. I (80 mg) and hydrated platinum oxide (40 mg) were stirred in glacial acetic acid (16 ml) under a hydrogen atmosphere at room temperature and normal pressure; after 3 hr, the UV absorptions at 250—270 nm almost disappeared. The catalyst was removed by filtration, and then the filtrate was evaporated. The residue was dissolved in ether, washed with a sodium bicarbonate solution and water, dried over magnesium sulfate, and evaporated to dryness. The residue was chromatographed over silicic acid; subsequent elution with chloroform gave a demethoxy-compound and a dihydro-compound.

The crude demethoxy-compound (32 mg) was recrystallized from aqueous methanol to yield vanguerolic acid lactone X as plates (25 mg); mp and mixed mp with an authentic sample,*** 263—267 °C, $[\alpha]_D^{16}$ −70° (c 0.1, EtOH).

The crude dihydro-compound (43 mg) was acetylated as has been described above, and the product was recrystallized from methanol to give a monoacetate XI as plates (21 mg); mp 247—249 °C, UV (EtOH) 231 nm (ε 5000), NMR ($CDCl_3$) δ 1.39 (6H, s, C_{19} and C_{20}-CH_3), 2.03 (3H, s, O-CO-CH_3), 3.27 (3H, s, O-CH_3), and 4.48 (1H, t-like, W1/2 18 Hz, C_3-H), (Found: C, 75.88; H, 9.72%. Calcd for $C_{33}H_{50}O_5$: C, 75.24; H, 9.57%).

Hydrogenolysis of II. II (78 mg) and hydrated platinum oxide (39 mg) in glacial acetic acid (16 ml) were treated as has been described above; after 4 hr, the UV absorptions at 250—270 nm almost disappeared. The residue was chromatographed over silicic acid; subsequent elution with chloroform–methanol (99: 1) yielded a deoxy-compound and a dihydro-compound.

The crude deoxy-compound (12 mg) was recrystallized from aqueous methanol to give X as plates (8 mg); mp and mixed mp with an authentic sample, 263—267 °C.

The crude dihydro-compound (48 mg) was recrystallized from aqueous methanol to yield XVII as plates (31 mg); mp 247—249 °C, UV (EtOH) 231 nm (ε 8600), IR (nujol) 3560 and 1735 cm^{-1}, (Found: C, 76.61; H, 9.89%. Calcd for $C_{30}H_{46}O_4$: C, 76.55; H, 9.85%).

*** This sample was obtained by the method described in the literature[2] from methyl vanguerolate acetate, which has kindly been provided by Prof. D. H. R. Barton.

The acetylation of XVII (22 mg) and recrystallization of the product from chloroform–methanol afforded a monoacetate as needles (13 mg); mp 325—330 °C, IR (Nujol) 3510 and 1740 cm^{-1}, (Found: C, 75.16; H, 9.05%. Calcd for $C_{32}H_{48}O_5$: C, 74.96; H, 9.44%).

Hydrogenation of III. III (51 mg) in glacial acetic acid (10 ml) was hydrogenated in the presence of hydrated platinum oxide (26 mg) as has been described above; after 1 hr, the UV absorptions at 250—270 nm completely disappeared. The residue was recrystallized from methanol to give XVIII as prisms (39 mg); mp 259—261 °C, UV (EtOH) 229 nm (ε 5100), IR (Nujol) 3440 and 1715 cm^{-1}, (Found: C, 73.03; H, 10.18%. Calcd for $C_{30}H_{46}O_4 \cdot 5/4H_2O$: C, 73.06; H, 9.91%).

The acetylation of XVIII (33 mg) and recrystallization of the product from chloroform–methanol gave a monoacetate as needles (25 mg); mp 320—325 °C, IR (Nujol) 3470, 1740, and 1715 cm^{-1}, (Found: C, 75.02; H, 8.98%. Calcd for $C_{32}H_{48}O_5$: C, 74.96; H, 9.44%).

Hydrogenation of IX. IX (70 mg) and hydrated platinum oxide (35 mg) in glacial acetic acid (14 ml) were treated as has been described above; after 1 hr, the UV absorptions at 250—270 nm almost disappeared. The residue was recrystallized from aqueous methanol to yield XIX as needles (36 mg); mp 226—228 °C, UV (EtOH) 227 nm (ε 5100) IR (Nujol) 1740 cm^{-1}, NMR ($CDCl_3$) δ 1.10 (3H, d, J=7 Hz, C_{19}-CH_3), 1.37 (3H, s, C_{20}-CH_3), 2.01 and 2.05 (3H each, s, O-CO-CH_3), 2.55 (1H, qd, J=7 and 2 Hz, C_{19}-H), 3.70 and 3.86 (1H each, AB q, J_{AB}=12 Hz, O-CH_2-), and 4.77 (1H, t-like, W1/2 18 Hz, C_3-H), (Found: C, 73.60; H, 9.19%. Calcd for $C_{34}H_{50}O_6$: C, 73.61; H, 9.09%).

We are grateful to Professor Takashi Tokoroyama, Osaka City University, for his valuable help and suggestions.

References

1) Part II: N. Ichikawa, M. Ochi, and T. Kubota, *Nippon Kagaku Kaishi*, **1973**, 785.
2) D. H. R. Barton, H. T. Cheung, P. J. L. Daniels, K. G. Lewis, and J. F. McGhie, *J. Chem. Soc.*, **1962**, 5163.
3) J. L. Breton and A. G. Gonzalez, *ibid.*, **1963**, 1401.
4) T. Hase, H. Hagii, M. Ishizu, M. Ochi, N. Ichikawa, and T. Kubota, *Nippon Kagaku Kaishi*, **1973**, 778.
5) a) K. Yagishita, *Bull. Agr. Chem. Soc. Japan*, **21**, 157 (1957); b) S. Yamada, This Bulletin, **39**, 2313 (1966).
6) P. R. Jefferies and R. W. Retallack, *Aust. J. Chem.*, **21**, 1311 (1968).
7) R. K. Callow and G. A. Thompson, *J. Chem. Soc.*, **1964**, 3106.

Effect of Solvent Viscosity on the Decomposition of 1,1,4,4-Tetraphenyl-2-tetrazene

Kazuo SUGIYAMA, Tadao NAKAYA,* and Minoru IMOTO**

Department of Applied Chemistry, Faculty of Engineering, Kinki University, Kure, Hiroshima 737-01

(Received August 9, 1974)

The rate of decomposition of 1,1,4,4-tetraphenyl-2-tetrazene (TPT) was measured in the polyethylene glycol (PEG) thickened dimethylformamide (DMF) of varying viscosities. The observed rate constant for the decomposition of TPT decreases with the viscosity of the DMF/PEG solvent system. A compensating change was found in the enthalpy and entropy of activation. It was also found that the decomposition of TPT occurs by the scission of only one N–N single bond, and undergoes cage return in the solvent system by recombination of radicals.

2-Tetrazenes decompose thermally and photochemically to form two neutral amino radicals and nitrogen.[1] The basic nature of 2-tetrazenes and their reactions with electrophilic reagents have been extensively investigated.[2-4] Nelsen *et al.*[1e] prepared 1,4-dimethyl-1,4-diphenyl-2-tetrazene and several of its bis-*p*-substituted derivatives to obtain information about electronic and thermodynamic factors of the decomposition of 2-tetrazenes. With electron withdrawing substituents, it was found that the decrease in the rate of decomposition is not due to the ΔH^* term, but to the ΔS^* term. However, the rate of decomposition increases with the polarity of the solvent in the radical decomposition of 1,4-dimethoxycarbonyl-1,4-diphenyl-2-tetrazene.[5] The enthalpy of activation is a linear function of the entropy of activation over quite a wide range in various solvents.

There has also been some interest in the effect of viscosity on the rate of bond homolysis.[6] Herk *et al.*[6a] studied the cage reaction of acetyl peroxide and azomethane. Pryor *et al.*[6d] have also investigated the decomposition of a wide variety of free radical initiators in a series of alkane solvents of varying viscosities. However, there has been no systematic investigation of the effect of viscosity on the decomposition of 2-tetrazene.

In earlier works,[1h] we reported that 1,1,4,4-tetraphenyl-2-tetrazene (TPT) acts as an effective inhibitor for the radical polymerization of vinyl monomers. As an extension of our study of the decomposition of TPT, our interests were directed to the effect of solvent viscosity on the decomposition. The present paper is mainly concerned with a detailed study on the decomposition of TPT in polyethylene glycol (PEG) thickened dimethylformamide (DMF) of varying viscosities.

Experimental

Materials. TPT was prepared by oxidizing 1,1-diphenylhydrazine with manganese dioxide, according to the method of Bhatnagar.[8] DMF and PEG were purified in the usual manner.

Viscosity Studies. The stock PEG thickened DMF solution were prepared by dissolving 10 g of PEG of various degrees of polymerization in 100 ml of DMF. The degrees of polymerization of PEG used in this work were 200, 1000, 2000, 4000, 6000, and 20000. The viscosities of the solvent systems, DMF/PEG, were determined at 65, 70, 75, and 80 °C by using an Ostwald viscometer. The rates of decomposition of TPT in DMF and in the six DMF/PEG systems were determined by measuring the amount of nitrogen evolved, according to Overberger *et al.*[9]

Thermodynamic Parameters.[10] The Arrhenius energy of activation E_a, was calculated from a plot of log k_{obsd} *vs.* $1/T$. The enthalpy of activation was obtained from the equation $\Delta H^* = E_a - RT$. ΔS^* was evaluated from the Eyring's equation, $k_{obsd} = T/h \exp(-\Delta H^*/RT)\exp(\Delta S^*/R)$.

Theory for Qualititative Viscosity Test. The mechanism for the decomposition of TPT has been given as follows.[6d]

$$\begin{array}{ccc} & & 2\cdot N(C_6H_5)_2 + N_2 \\ & & \uparrow k_D \\ (C_6H_5)_2N\text{-}\overset{\alpha}{\underset{}{|}}\text{-}N{=}N\text{-}\overset{\beta}{\underset{}{|}}\text{-}N(C_6H_5)_2 & \underset{k_{-1}}{\overset{k_1}{\rightleftharpoons}} & (\text{Cage}) \\ & & \downarrow k_B \\ & & (\text{Cage-B}) + HN(C_6H_5)_2 \end{array}$$

where k_1, k_{-1}, k_D, and k_B represent the rate constants for the bond homolysis, recombination of original geminate radicals, diffusive separation of the geminate radicals, and any other scission that competes with diffusion and cage return. In this case, the observed rate constant for the decomposition of TPT is given as

$$k_{obsd} = k_1(k_D + k_B)/(k_{-1} + k_D + k_B) \quad (1)$$

The viscosity of DMF/PEG may be written as[10]

$$\eta = A_{vis} \exp(E_{vis}/RT) \quad (2)$$

while the temperature dependence of the rate constant for the diffusion, k_D, can be expressed as[6d]

$$k_D = A_D \exp(-E_D/RT) \quad (3)$$

According to Pryor,[6d] the following relationship can be obtained for the decomposition of TPT in high viscosity media

$$1/k_{obsd} = 1/k_1 + (k_{-1}/k_1A_D)(\eta/A_{vis})^{1/2} \quad (4)$$

Equation 4 suggests that the decomposition of TPT maybe divided into two classes.[6d] i) $k_{-1}=0$, TPT decomposes by the synchronous scission of both α- and β-bonds to produce two diphenylamino radicals. The rate of decomposition may be independent of the solvent viscosity. ii) $k_{-1} \neq 0$, TPT decomposes by the scission of the α-bond only to give cage return in whichever solvent system by radical recombination. In this case, the k_{obsd} decreases as the viscosity of the solvent system increases.

* Department of Applied Chemistry, Faculty of Engineering, Osaka City University, Sugimoto-cho, Sumiyoshi-ku, Osaka.

** Department of Applied Chemistry, Faculty of Engineering, Kansai University, Suita, Osaka.

Results and Discussion

In order to use the viscosity test, it is necessary to adopt a solvent system in which the viscosity can be varied without sharply changing any other properties of the solvent. In this work, we chose DMF/PEG. There is no serious difficulty in using DMF/PEG in the application of the viscosity test to TPT, as discussed below.

Measurements of the Viscosity of DMF/PEG. The viscosities of DMF/PEG were measured over a temperature from 60 to 80 °C, and are listed in Table 1.

Arrhenius-like plots of the relative viscosity gave straight lines, from which the activation parameters, E_{vis} and A_{vis}, in Eq. (2) were calculated: they are also listed in Table 1.

Table 1. Activation parameters and relative viscosities of DMF/PEG at various temperatures

Pn of PEG[a]	Temperature 80 °C	75 °C	70 °C	65 °C	E_{vis} (kcal/mol)	A_{vis}
DMF alone	1.000[b]	1.045	1.075	1.128	2.30	0.0189
200(a)	1.022	1.264	1.325	1.406	2.58	0.0146
1000(b)	1.454	1.533	1.617	1.712	2.65	0.0158
2000(c)	1.722	1.817	1.911	2.037	2.79	0.0162
4000(d)	1.994	2.107	2.233	2.359	2.69	0.0220
6000(e)	3.223	3.484	3.669	3.895	3.22	0.0168
20000(f)	7.990	8.525	9.134	9.783	3.47	0.0285

a) Degree of polymerization of PEG as the high viscosity component in DMF. (See Experimental Section)
b) Absolute viscosity 0.507 cps.

Measurements of the Rate of Decomposition of TPT. The kinetics of decomposition of TPT were measured in DMF/PEG at various temperatures. The reaction rate was strictly first-order in TPT-concentration under our conditions.[11] The first-order rate constants are listed in Table 2.

Table 2. First-order rate constants (k_{obsd}) for the decomposition of TPT in DMF and DMF/PEG at various temperatures

Solvent[a]	$k_{obsd} \times 10^5$ (s^{-1}) 80 °C	75 °C	70 °C	65 °C
DMF alone	119	115	102	66.4
(a)	24.3	17.7	16.3	12.6
(b)	19.3	16.7	13.2	10.4
(c)	18.7	15.0	11.9	9.23
(d)	16.3	12.8	11.8	7.91
(e)	15.9	12.4	9.89	8.00
(f)	12.6	10.7	—	7.67

a) See Table 1.

As can be seen from Tables 1 and 2, the observed rate constant for the decomposition of TPT decreases with the viscosity of the solvent system. It may be concluded that the macroscopic viscosity reflects the resistance to translational motion of monomeric radicals in this solvent system.

Arrhenius plots of the data in Table 2 yielded straight lines, from which the thermodynamic parameters were calculated by the method described in the Experimental Section. The results are shown in Table 3.

Table 3. Thermodynamic parameters for the decomposition of TPT in various solvent systems

Solvent[a]	ΔH^* (kcal/mol)	ΔS^* (kcal/mol)	ΔG^* (kcal/mol)
DMF alone	5.40	−58.9	26.2
(a)	8.85	−52.3	27.3
(b)	9.24	−51.7	27.5
(c)	10.1	−49.2	27.5
(d)	10.7	−47.8	27.6
(e)	11.0	−47.2	27.6
(f)	12.5	−43.3	27.8

a) see Table 1.

From the effect of the viscosity of the solvent system on the activation parameters, a compensating change[12] was found in the enthalpy and entropy of activation for the decomposition of TPT, as shown in Fig. 1.

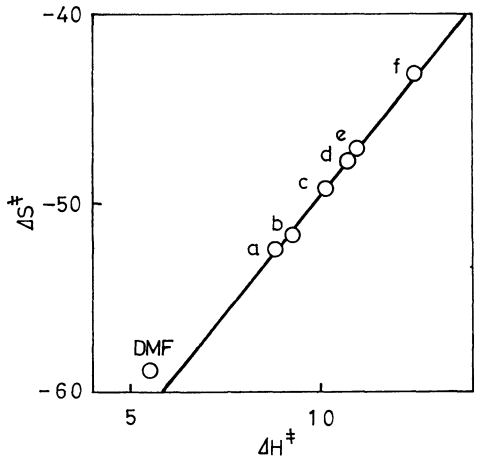

Fig. 1. Relationship between ΔH^* and ΔS^* in the decomposition of TPT
The solvent system are DMF, (a), (b), (c), (d), (e), and (f). (See Table 1.)

This finding suggests that a single mechanism is operative for the thermal decomposition of TPT in the DMF/PEG. Accordingly the variation in k_{obsd} with viscosity is not due to different decomposition mechanisms. It is suggested that the variation in ΔH^* does not depend on the different reaction mode, but depends on the change in apparent rate of decomposition, k_{obsd}.

On the other hand, the factor favoring the dissociation of the N–N single bonds of TPT is mainly responsible for the stability of the nitrogen radical. Large negative entropies of activation were observed in the decomposition of 2-tetrazenes. Nelsen[1e] reported that some 1,4-diaryl-1,4-dimethyl-2-tetrazenes decompose thermally in cumene with negative entropies. In the decomposition of 1,4-dimethoxycarbonyl-1,4-diphenyl-2-tetrazene the entropies were −14.2 cal/K in acetonitrile and −30.5 cal/K in dioxane.[5] It is considered that the delocalization of an odd electron on

nitrogen should compete with that of a lone pair on the diphenylamino group at the time of decomposition of TPT. According to Nelsen,[1e] TPT is in conformation A with the lone pair electrons in a p orbital which overlaps with π system of phenyl ring. But the conformation B is needed for maximum stabilization of the odd electron of the diphenylamino radicals in the decomposition of TPT

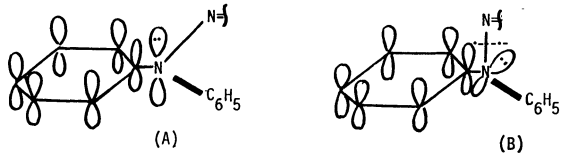

It is obvious that the steric factor plays an important role in the bond homolysis of TPT. The change in $\Delta H^{\ddagger}$ is balanced by a corresponding change in $\Delta S^{\ddagger}$.

Viscosity Test. In order to check whether TPT decomposes by the initial scission of only one N–N bond (α-scission) or the synchronous scission of two single N–N bond (α,β-scission), k_{obsd} was plotted against the viscosity term.

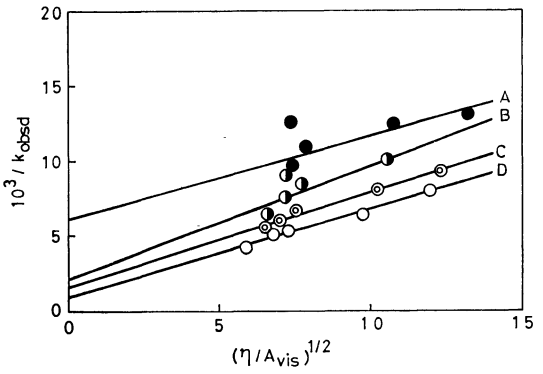

Fig. 2. Relationship between $1/k_{obsd}$ and $(\eta/A_{vis})^{1/2}$ for the decomposition of TPT in DMF/PEG at various temperatures. A; 65, B; 70, C; 75, D; 80 °C.

It was found that k_{obsd} decreased regularly as the solvent changed from low viscosity to high viscosity, as shown in Table 2. As can be seen from Fig. 2, the slopes of the lines are not zero in the decomposition of TPT in DMF/PEG. From Eq. (4), it may be concluded that TPT does not decompose by a concerted mechanism but decomposes by a two step mechanism. That is, TPT decomposes by the scission of only one N–N single bond, and undergoes cage return by recombination of radicals. The following mechanism of the decomposition is proposed to account for our observations:

$$(C_6H_5)_2N\text{–}N{=}N\text{–}N(C_6H_5)_2 \rightleftarrows [(C_6H_5)_2N\text{–}N{=}N\cdot \cdot N(C_6H_5)_2]$$

$$\downarrow$$

$$(C_6H_5)_2N\cdot + N_2 \longleftarrow (C_6H_5)_2N\text{–}N{=}N\cdot + \cdot N(C_6H_5)_2$$

References

1) a) J. S. Watson and A. J. Waring, *Can. J. Chem.*, **38**, 298 (1960); b) B. G. Gowenlock, P. P. Jones, and D. R. Snelling, *ibid.*, **41**, 1191 (1963); c) A. Good and J. C. J. Thyrme, *J. Chem. Soc., B*, **1967**, 684; d) C. J. Michejda and W. P. Hoss, *J. Amer. Chem. Soc.*, **92**, 6298 (1970); e) S. F. Nelsen and D. H. Heath, *ibid.*, **91**, 6452 (1969); f) R. F. Bridger, *J. Org. Chem.*, **35**, 1746 (1970); g) D. W. Jones, *Chem. Commun.*, **1970**, 1084; h) K. Sugiyama, T. Nakaya, and M. Imoto, *J. Polym. Sci.*, Part A, **10**, 205 (1972).

2) W. E. Bull, J. A. Seaton, and L. F. Audrieth, *J. Amer. Chem. Soc.*, **80**, 2516 (1958).

3) W. M. Tolles, D. W. Moore, and W. E. Thun, *ibid.*, **88**, 3476 (1966).

4) a) W. S. Wadworth, Jr., *J. Org. Chem.*, **34**, 2994 (1969); b) D. Romans, W. H. Bruning, and C. J. Michejda, *J. Amer. Chem. Soc.*, **91**, 3859 (1969); c) S. F. Nelsen, *ibid.*, **88**, 5666 (1966); d) S. F. Nelsen, R. B. Metzler, and M. Iwamura, *ibid.*, **91**, 5103 (1969); e) R. C. Kerber and T. J. Ryan, *J. Org. Chem.*, **36**, 1566 (1971); f) C. J. Michejda and D. Romans, *Tetrahedron Lett.*, **44**, 4213 (1969); g) K. Sugiyama, H. Hatanaka, T. Nakaya, and M. Imoto, *Makromol. Chem.*, **165**, 163 (1973).

5) K. Sugiyama, T. Nakaya, and M. Imoto, *ibid.*, **163**, 185 (1973).

6) a) L. Herk, M. Field, and M. Szwark, *J. Amer. Chem. Soc.*, **83**, 2998 (1961); b) H. P. Waits and G. S. Hammond, *ibid.*, **86**, 1911 (1964); c) R. C. Lamb and J. R. Sanderson, *ibid.*, **91**, 5034 (1969); d) W. A. Pryor and K. Smith, *ibid.*, **92**, 5403 (1970).

7) a) T. Nakaya, Y. Maki, and M. Imoto, *Makromol. Chem.*, **113**, 131 (1968); b) K. Sugiyama, T. Nakaya, and M. Imoto, *ibid.*, **161**, 219 (1972); *ibid.*, **166**, 311 (1973).

8) I. Bhatnagar and M. V. George, *J. Org. Chem.*, **33**, 2407 (1968).

9) a) C. G. Overberger, T. M. O'Shaughnessy, and H. Shalit, *J. Amer. Chem. Soc.*, **71**, 2661 (1949); b) C. G. Overberger and M. B. Brenbaum, *ibid.*, **73**, 2618 (1951).

10) S. Glasstone, K. J. Laidler, and H. Eyring, "Theory of Rate Processes," McGraw-Hill Inc., New York (1941).

11) Michejda[1d] found that, at a concentration of 1,1,4,4-tetramethyl-2-tetrazene (TMT) greater than 0.2 M, induced decomposition becomes important in the decomposition of TMT in benzene. Radical induced decomposition was not important for our case. The initial concentration of TPT was 0.0027 M in all cases.

12) J. E. Leffler and E. Grundward, "Rates and Equilibria N. Y. of Organic Reactions," John Wiley & Sons, Inc., New York (1963), Ch. 9.

The Crystal and Molecular Structure of (+)-1,2-Dibromo-2-phenylethyl *p*-Tolyl Sulfoxide

Fujiko IWASAKI, Shuichi MITAMURA,* and Gen-ichi TSUCHIHASHI*

Department of Materials Science, The University of Electro-Communications, Chofu-shi, Tokyo 182
**Sagami Chemical Research Center, Nishi-Ohnuma, Sagamihara, Kanagawa 229*

(Received November 11, 1974)

The crystal structure of (+)-1,2-dibromo-2-phenylethyl *p*-tolyl sulfoxide, a dominant isomer formed by the ionic bromination of (+)-*trans*-*β*-styryl *p*-tolyl sulfoxide, has been determined by the X-ray diffraction method. The crystal is monoclinic; space group, $P2_1$; $a=16.193$, $b=5.706$, $c=8.541$ Å, $\beta=93.51°$, and $Z=2$. The final R value is 0.087 for 792 observed reflections. The absolute configuration has been established to be $S_S, S_{C(1)}, S_{C(2)}$ from the Cu$K\alpha$ anomalous scattering of the bromine and sulfur atoms. The sulfinyl oxygen is *gauche* to the bromine atom across the S–C(1) bond, and the non-bonding distance between the both atoms is 3.13 Å. The bromine atom is *trans* to another bromine across the C(1)–C(2) bond. Based on the assigned structure, a mechanism which involves the preferential formation of an intermediary bromonium ion is elucidated for the bromination. The configuration at the sulfur atom is retained during the reaction.

The ionic bromination of (+)-*trans*-*β*-styryl *p*-tolyl sulfoxide (**1**) results in a dominant formation of one isomer in four diastereomers of (+)-1,2-dibromo-2-phenylethyl *p*-tolyl sulfoxide (**2**). The high selectivity

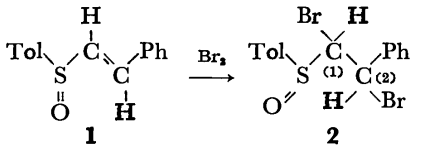

1 **2**

of the addition is attributed to the preferential formation of a bridged bromonium ion by the electronic demand of the adjacent chiral sulfinyl group.[1] In order to elucidate such a specific reaction mechanism, it is important to study the stereochemistry of sulfur centers; however, the steructures of relatively few sulfoxides have been determined. An X-ray study was, therefore, undertaken to establish the absolute configuration and the molecular conformation of **2**.

Experimental

The dominant isomer of **2** was recrystallized from a *n*-hexane–ethanol solution. The crystals are colorless needles and are stable in air. The cell dimensions were calibrated with copper powder lines superposed on Weissenberg photographs (CuK, $\alpha=1.5418$, $\alpha_1=1.5405$ Å).

The crystal data are: $C_{15}H_{14}Br_2SO$, M.W.=402.14; monoclinic, $a=16.193$ (8)[2], $b=5.706$ (12), $c=8.541$ (8) Å, $\beta=93.51$ (5)°, $V=787.6$ Å^3, $Z=2$, $D_x=1.695$ g cm^{-3}, $D_m=1.68$ g cm^{-3}; $F(000)=396$; $\mu=75.7$ cm^{-1} (Cu$K\alpha$); Spase group, $p2_1$; $[\alpha]_D^{22}$ +261.8° (c 0.527, $CHCl_3$); mp 161—163 °C.

The intensity data were collected from integrated equi-inclination Weissenberg photographs around the b and c axes, *h0l*—*h3l* and *hk*0—*hk*5, using Cu$K\alpha$ radiation. The intensities were estimated visually by comparison with a standard scale. A total of 792 non-zero reflections were observed. Lorentz, polarization and spot-shape corrections were made, but because of the size of specimens (max. $\mu R=0.2$) no absorption corrections were applied.

Structure Determination

The positions of the two bromine atoms in an asymmetric unit were found by an inspection of a three-dimensional Patterson map. For the heavy atoms alone, the R value was 0.31. The calculation of Fourier synthesis allowed coordinates to be assigned to all the other atoms. The atomic parameters were refined by least-squares methods, first with isotropic temperature factors to an R value of 0.15 and then with anisotropic temperature factors for all the non-hydrogen atoms to an R value of 0.090. The positions of the hydrogen atoms, other than those of the methyl group, were calculated with a C–H distance of 1.08 Å. These hydrogen parameters were included in the structure-factor calculations, though they were not refined. The isotropic thermal parameters for hydrogen atoms were assumed to be 5.0 Å^2. Further refinement of atomic parameters was carried out for all the non-hydrogen atoms with anisotropic temperature factors. The final R value was 0.087 for all the observed reflections. The weighting scheme used was: $w=0.7$ if $|F_o|<6$, $w=1$ if $6\leq|F_o|\leq25$ and $w=(25/|F_o|)^2$ if $|F_o|>25$. The atomic scattering factors for non-hydrogen atoms were taken from "International Tables for X-ray Crystallography".[3] For the bromine atom, the scattering factor was corrected for dispersion using the expression: $|f|=\sqrt{\{(f_0+\Delta f')^2+(\Delta f'')^2\}}$. For hydrogen, the values given by Stewart, Davidson, and Simpson[4] were used.

The final atomic parameters and their estimated standard deviations are given in Table 1. The observed and calculated structure factors are listed in Table 2.[5]

Absolute Configuration. The absolute configuration has been determined by the anomalous dispersion method, with Cu$K\alpha$ radiation. The values of the real and imaginary dispersion correction terms of the scattering factor were taken as $\Delta f'_{Br}=-0.96$, $\Delta f'_S=0.31$, $\Delta f''_{Br}=1.46$, and $\Delta f''_S=0.58$.[6] The calculated values of the intensity ratio between the Friedel pair of reflections agreed with those observed on the b-axis oscillation photographs if one takes the right-handed coordinate system. A comparison of the observed and calculated intensity ratios is given in Table 3. The figures shown in this paper are drawn with the correct absolute configuration obtained above.

Table 1. Final atomic parameters

(a) Atomic coordinates ($\times 10^4$) and thermal parameters ($\times 10^3$) of non-hydrogen atoms with their estimated standard deviations.[a] The anisotropic temperature factors are of the form:
$\exp\{-2\pi^2(U_{11}h^2a^{*2}+U_{22}k^2b^{*2}+U_{33}l^2c^{*2}+2U_{12}hka^*b^*+2U_{13}hla^*c^*+2U_{23}klb^*c^*)\}$.
The B_{eq} values are the equivalent isotropic temperature factors.[b]

Atom	x	y	z	U_{11}	U_{22}	U_{33}	U_{12}	U_{13}	U_{23}	B_{eq}
Br(1)	3100(2)	2250(9)	3246(4)	83(2)	69(2)	69(2)	−21(2)	−3(1)	18(2)	5.8
Br(2)	531(2)	0(10)	1124(3)	64(1)	99(3)	43(1)	0(2)	5(1)	−6(2)	5.4
S	2117(5)	3429(16)	126(7)	90(5)	39(5)	42(3)	19(5)	25(3)	20(4)	4.4
O	2113(18)	5736(38)	868(22)	246(30)	10(13)	64(10)	20(18)	76(15)	16(11)	8.2
C(1)	2164(17)	1337(52)	1733(25)	84(18)	5(16)	44(12)	−1(14)	9(11)	−6(11)	3.5
C(2)	1373(15)	1405(51)	2615(24)	66(15)	28(18)	37(11)	3(14)	3(9)	19(11)	3.5
C(3)	1378(12)	74(52)	4125(22)	45(11)	20(13)	47(10)	−11(15)	9(8)	6(14)	2.9
C(4)	890(15)	986(56)	5316(25)	59(14)	37(18)	44(11)	−38(15)	17(9)	−6(12)	3.6
C(5)	823(14)	−290(61)	6756(21)	71(14)	61(22)	27(8)	7(20)	15(9)	−18(15)	4.1
C(6)	1267(15)	−2129(65)	6951(27)	55(14)	83(32)	60(14)	−21(18)	18(11)	43(18)	5.2
C(7)	1712(17)	−3213(58)	5846(26)	82(17)	58(24)	46(11)	4(17)	33(11)	44(16)	4.8
C(8)	1776(16)	−2062(47)	4387(32)	65(16)	11(20)	85(17)	13(15)	22(13)	2(14)	4.2
C(9)	3055(17)	2792(62)	−686(28)	74(10)	52(26)	58(14)	4(18)	26(12)	8(15)	6.0
C(10)	3151(22)	757(64)	−1639(36)	108(25)	26(21)	95(21)	22(21)	25(18)	−27(19)	6.0
C(11)	3857(19)	548(58)	−2441(33)	107(23)	31(23)	79(17)	27(20)	25(15)	−21(18)	5.6
C(12)	4513(16)	2045(71)	−2361(32)	58(15)	61(24)	77(16)	−9(20)	11(12)	24(19)	5.2
C(13)	4399(23)	4073(72)	−1351(30)	152(31)	70(29)	56(15)	−76(26)	29(10)	9(18)	7.3
C(14)	3675(20)	4494(77)	−645(29)	130(26)	90(33)	56(15)	−63(29)	39(16)	13(19)	7.2
C(15)	5225(21)	1590(80)	−3330(44)	77(20)	103(40)	121(26)	10(24)	47(19)	−7(26)	7.8

(b) Atomic coordinates for hydrogen atoms ($\times 10^3$).

Atom	x	y	z	Atom	x	y	z
H(1)	225	−42	126	H(7)	213	−279	349
H(2)	126	319	297	H(8)	269	−62	−170
H(3)	55	266	511	H(9)	389	−93	−322
H(4)	46	46	769	H(10)	492	522	−116
H(5)	128	−304	808	H(11)	360	610	−3
H(6)	201	−487	605				

a) The e.s.d.'s are in parentheses and refer to the last significant digits of the respective values in Tables 1 and 5 and in Fig. 1. b) W. C. Hamilton, *Acta Crystallogr.*, **12**, 609 (1959).

Table 3. Determination of the absolute configuration

h	k	l	Calculated $\lvert F(hkl)\rvert^2/\lvert F(h\bar{k}l)\rvert^2$	Observed $I(hkl)/I(h\bar{k}l)$
4	1	2	1.31	>1
6	1	2	1.06	>1
4	1	3	1.06	>1
−4	1	3	0.91	<1
2	1	4	0.87	<1
3	1	4	0.86	<1
−5	1	4	0.90	<1
0	1	5	1.08	>1
4	1	5	0.96	<1
2	2	1	1.16	>1
4	2	1	1.17	>1
−1	2	2	1.15	>1

Results and Discussion

The bond distances and angles are shown in Fig. 1. The three sulfur bonds form a shallow pyramid. The dihedral angle between the planes defined by the C(1)–S–C(9) and O–S–C(9) atoms is 109°. The C(1)–S–O and C(9)–S–O angles are 105 and 107° respectively; the corresponding angles in (+)-methyl *p*-tolyl sulfoxide (**3**) have been reported to be 105.5 and 106.5° respectively.[7] The C(1)–S–C(9) angle is 100°, which agrees well with the values for symmetrical sulfoxides[8] and **3**.[7] The S–O distance is 1.47 Å, which is slightly shorter than those (1.49 and 1.53 Å) in other sulfoxides.[7,8] The S–C(1) and S–C(9) distances are 1.82 and 1.75 Å. They are slightly different from each other, while in **3** the corresponding values for the S–C lengths are 1.796 and 1.797 Å respectively.

The C(1)–C(2) distance is 1.53 Å, and the C(2)–C(3) distance is 1.50 Å. They are similar to the accepted values for single C(sp^3)–C(sp^3) (1.526 Å) and C(sp^3)–C(sp^2) (1.501 Å) bonds.[9] The lengths for C(1)–Br(1) and C(2)–Br(2) are 2.00 and 1.98 Å respectively. They are slightly longer than those for ethyl bromide (1.950 Å),[10] for 2-bromopropane (1.957 Å)[11] in the gas phase, and for hexabromoethane (1.944 Å)[12] in the solid phase.

The average values for C–C bonds in aromatic rings are 1.39 (phenyl) and 1.40 Å (tolyl) respectively. The length of C(12)–C(15), 1.48 Å, is close to the corresponding value for toluene.[13] The least-squares planes are listed in Table 4. The dihedral angle between these planes is 69°.

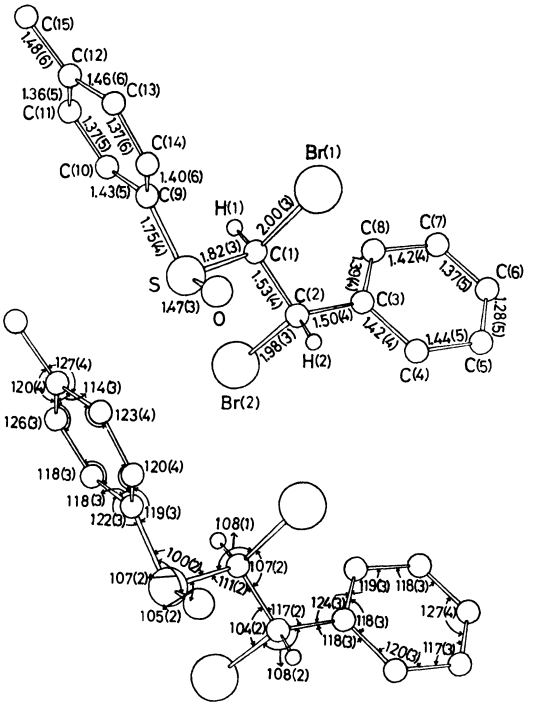

Fig. 1. Bond lengths (Å) and angles (°) with their estimated standard deviations in parentheses.

Table 4. Least-squares planes

Equation of the plane: $AX+BY+CZ=D$, where X, Y, and Z are the coordinates in Å referred to the orthogonal axes a, b, and c*.

		A	B	C	D
(1)	Phenyl ring C(3)—C(8)	0.777	0.502	0.380	2.904
(2)	*p*-Tolyl ring C(9)—C(14)	0.378	−0.482	0.791	0.645

Deviations (Å$\times 10^3$) of atoms from the least-squares planes.

Plane 1		Plane 2	
C(3)	−19	C(9)	−9
C(4)	−4	C(10)	−4
C(5)	39	C(11)	30
C(6)	−48	C(12)	−12
C(7)	15	C(13)	−46
C(8)	18	C(14)	51
C(2)[a]	34	C(15)[a]	60
		S[a]	208

a) Atoms not used to define the least-squares plane.

The conformation of groups across the bonds, C(1)–C(2), S–C(1), S–C(9), and C(2)–C(3), are shown in Fig. 2. The oxygen atom is *gauche* to Br(1) across the S–C(1) bond, and the torsion angle, O–S–C(1)–Br(1), is 45°. The lone-pair orbital of the sulfur atom is *trans* to Br(1). Br(2) is *trans* to Br(1) across the C(1)–C(2) bond. The non-bonding distances, Br(1)···O, Br(1)···C(8), Br(1)···C(9), and O···C(14), are 3.13, 3.44, 3.37, and 2.86 Å respectively.

The absolute configuration is rigorously determined to be *S* at the sulfur atom, *S* at C(1), and *S* at C(2). Therefore the structure of the dominant isomer derived from the ionic bromination of (+)-*trans*-β-styryl *p*-tolyl

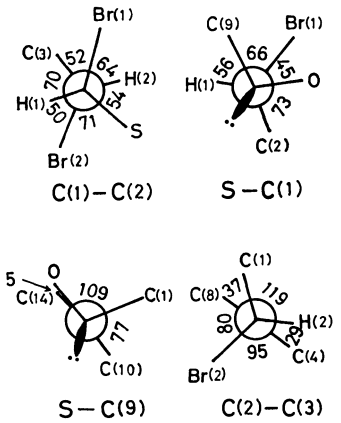

Fig. 2. Torsion angles in the molecule.

sulfoxide (**1**) is (+)-(S_S, $S_{C(1)}$, $S_{C(2)}$)-1,2-dibromo-2-phenylethyl *p*-tolyl sulfoxide (**2**).

(+)-*trans*-β-Styryl *p*-tolyl sulfoxide (**1**)[1a] was obtained by the condensation reaction of benzaldehyde with (+)-(*R*)-methyl *p*-tolyl sulfoxide (**3**), whose configuration has been unequivocally established as *R* by the chemical transformation to sulfoxides of a known absolute configuration[14,15] and by the X-ray diffraction method.[7] Since the **3** to **1** transformation does not involve the chiral center, and since the configuration at the sulfur atom of **2** is *S*, the ionic bromination of **1** proceeds with the retention of the configuration at the sulfur atom.

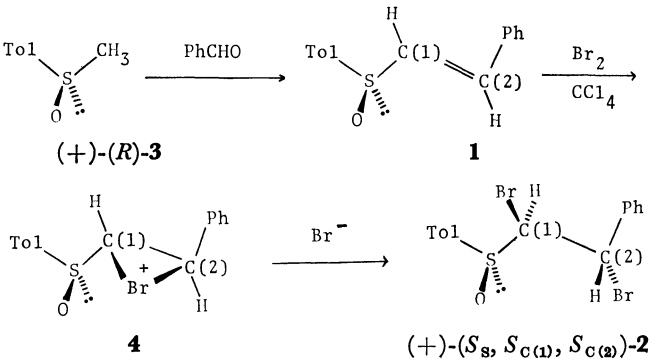

Scheme 1.

An inspection of the molecular structure of (+)-(S_S, $S_{C(1)}$,$S_{C(2)}$)-**2** revealed that the bromination proceeds in the *trans* manner, giving a product in which the bromine atom at C(1) is in the *gauche* position to the oxygen atom in the adjacent sulfinyl group. The formation of this product can be explained in terms of the preferential formation of an intermediary bromonium ion (**4**), followed by the attack of the bromide anion at C(2), as is shown in Scheme 1. The same bromonium ion, **4**, was proposed as an intermediate of the bromo-

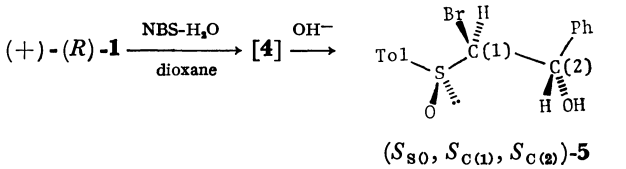

(S_{SO}, $S_{C(1)}$, $S_{C(2)}$)-**5**

and K. Mislow, *J. Amer. Chem. Soc.*, **90**, 4835 (1968).
16) F. Iwasaki, unpublished results.
17) L. Pauling, "The Nature of the Chemical Bond," 3rd ed., Cornell University Press, Ithaca, New York (1960), p. 260.
18) T. Sakurai, Ed., The Universal Crystallographic Computation Program System, The Crystallographic Society of Japan (1967); T. Sakurai, T. Ito, H. Iwasaki, Y. Watanabe, and M. Fukuhara, *Rep. Inst. Phys. Chem. Res.*, **43**, 62 (1967).
19) C. K. Johnson, ORTEP, Report ORNL-3794, Oak Ridge National Laboratory, Oak Ridge, Tennessee (1965).

Dehydrobromination of 16-Bromodihydroenmein-type Compounds

Takahiko Isobe and Takashi Kubota*

Hyogo College of Medicine, Mukogawa-cho, Nishinomiya-shi, Hyogo 663

**Faculty of Medicine, Kinki University, Nishiyama, Sayama-cho, Minamikawachi-gun, Osaka 589*

(Received November 18, 1974)

16-Bromodihydroenmein diacetate (IV) obtained from dihydroenmein diacetate (III) by bromination with *N*-bromosuccinimide was dehydrobrominated with lithium chloride in dimethylformamide to give a product, the structure of which was elucidated as the intermolecular ether (VIII). The dimeric ether compound was also formed by similar reactions from the derivative of isodocarpin.

About 10 years ago, during experiments for structual elucidation of enmein (I),[1] an attempt was made to revert 16-bromodihydroenmein diacetate (IV), obtained by bromination of dihydroenmein diacetate (III),[1,2,3] to enmein diacetate (II) by dehydrobromination. Unexpectedly, however, a structually unknown compound (VIII) of mp 282—283 °C (decompn.) was obtained instead of enmein diacetate (II). On the other hand, the dehydrobromination of VI gave an expected unsaturated compound (VII).[1] In order to elucidate the structure of VIII and to find what kind of reaction had occurred in the case of IV, the following experiments were carried out.

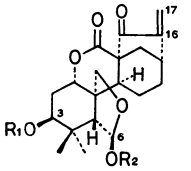

(I) $R_1 = R_2 = H$
(II) $R_1 = R_2 = Ac$
(XIII) $R_1 = Ac$, $R_2 = Et$
(XIV) $R_1 = Ac$, $R_2 = Me$
(XVII) $R_1 = Ac$, $R_2 = H$

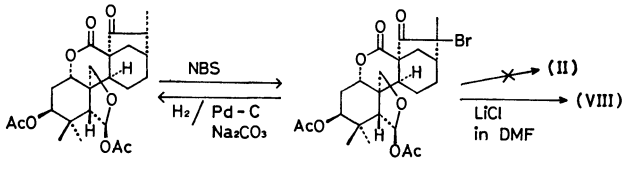

(III) (IV)

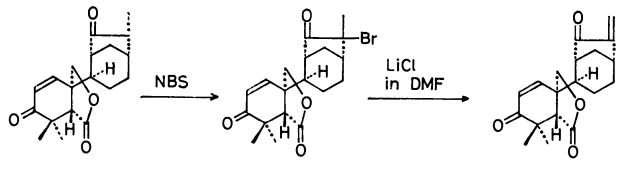

(V) (VI) (VII)

Bromination of dihydroenmein diacetate (III) was carried out repeatedly. But the results were not the same, although the experimental conditions were similar, *i.e.*, the material was treated with *N*-bromosuccinimide in chloroform in the presence of benzoyl peroxide, giving one of the three products (never a mixture of these in one experiment), $C_{24}H_{31}O_8Br$ (IV), mp 235 °C, $C_{24}H_{33}O_7Br$ (IX), mp 223 °C (decompn.), or $C_{23}H_{31}O_7Br$ (X), mp 220—222 °C (decompn.).

In the NMR spectra of IV, IX, and X, the signal for C_{17} secondary methyl present in III was no longer observed, and a signal for tertiary methyl group having a bromine in α-position appeared at δ 1.93, 1.85, and 1.82, respectively. The signal for C_6–H in III was shifted to higher magnetic field in the spectra of IX and X, suggesting an ether linkage in these compounds.[5]

Catalytic reductions of IV, IX, and X over palladium-charcoal–sodium carbonate catalyst afforded dihydroenmein diacetate (III), dihydroenmein 3-acetate 6-ethyl acetal (XI), and dihydroenmein 3-acetate 6-methyl acetal (XII), respectively, which confirmed that bromination had occurred at C_{16} position in these cases. In addition, the acetoxyl group at C_6 position had been converted to ethoxyl or methoxyl group by ethanol or methanol contaminated in chloroform to form IX or X, respectively.

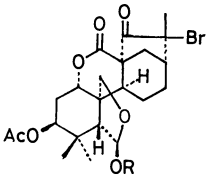

(IX) R=Et
(X) R=Me
(XXII) R=H

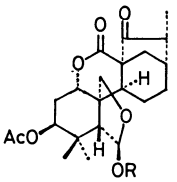

(XI) R=Et
(XII) R=Me

Dehydrobromination of the ethyl- and methyl-acetal type monobromo compound (IX and X) normally gave enmein 3-acetate 6-ethyl acetal (XIII)[5] and enmein 3-acetate 6-methyl acetal (XIV), respectively.

The dehydrobromination of IV with lithium chloride in dimethylformamide was not successful for preparing the expected enmein diacetate (II), but instead gave a high melting substance (VIII). Experiments were also carried out under the following conditions: with (i) pyridine, (ii) collidine, (iii) lithium chloride–pyridine, (iv) lithium carbonate–dimethylformamide, and (v) lithium bromide–dimethylformamide. Under the reaction conditions (i) to (iv) only the starting material was recovered, while in the case of (v) a small amount of VIII was obtained.

The UV, IR, and NMR spectra of VIII were almost identical with those of enmein diacetate (II), with

exception that the peak due to C_6–H in II appearing at δ 6.07 in its NMR spectrum shifted to δ 5.21 in the spectrum of VIII. The compound VIII was not reduced with palladium-carbon catalyst but was reduced to XV over platinum oxide catalyst. Bromination of XV with *N*-bromosuccinimide and dehydrobromination of the bromo compound (XVI), mp 277—278 °C (decompn.), with lithium chloride-dimethylformamide gave VIII.

The reaction and spectral data of VIII suggested etherification of C_6-acetate in II, as in XIII and XIV. Hydrolysis of VIII with acetic acid afforded enmein 3-acetate (XVII).[6] The most plausible explanation for the structure of VIII is an intermolecular ether formation between two molecules of enmein 3-acetate. Molecular weight of VIII was therefore measured by the vapor pressure depression method, as the mass spectral method was not effective, and a value of 794 (calcd 791) was obtained. Consequently, VIII must have been formed from two molecules of enmein 3-acetate (XVII) by ether linkage of the hydroxyl group at C_6 position.

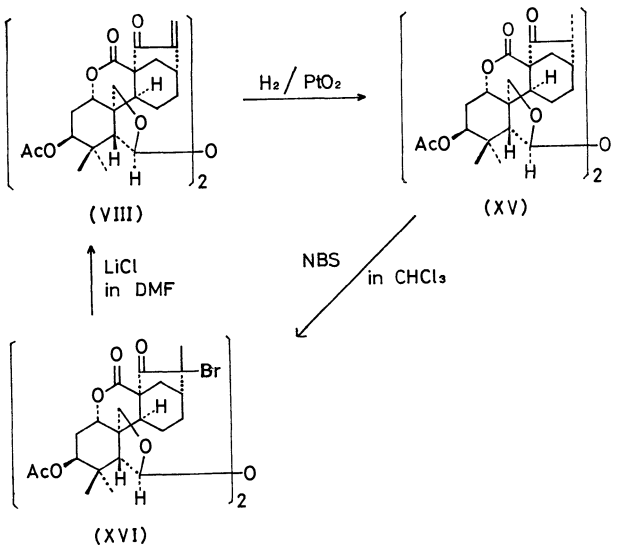

(VIII) (XV) (XVI)

This conclusion is supported from the following experiments. Treatment of dihydroenmein diacetate (III) with lithium chloride-dimethylformamide recovered the starting material, but addition of ethyl bromide in this reaction resulted in etherification to give XV. The same was true in the case of enmein 3-acetate (XVII), recovering the starting material with the use of lithium chloride-dimethylformamide but on addition of ethyl bromide affording VIII.

The same reaction on isodocarpin acetate (XVIII)[5,7] also gave an intermolecular ether (XIX). The IR and NMR spectra did not show the presence of any acetyl group in its molecule, and a diamagnetic shift of C_6–H signal was observed when compared with that of XVIII. (See experimental section.) The mass spectrum of XIX showed the molecular ion peak at *m/e* 674 and characteristic fragment ion peaks at *m/e* 345 and 329, respectively assignable to XX and XXI. Thus, it was confirmed that XIX was an intermolecular ether of two isodocarpin molecules.

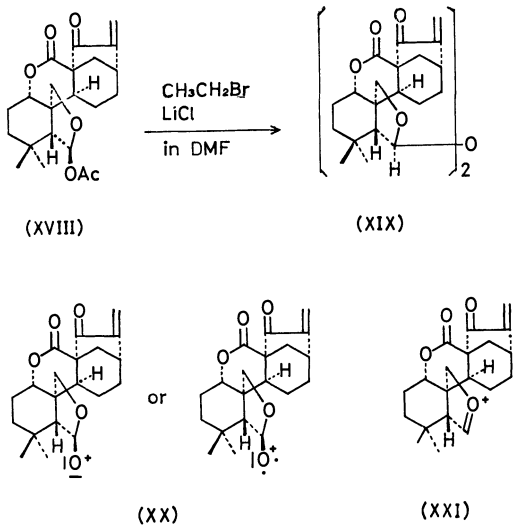

(XVIII) (XIX) (XX) (XXI)

The formation of the dimeric ethers can be accounted for the catalytic action of hydrogen bromide generated *in situ* from ethyl bromide. Thus, the ether (VIII) was also obtained from enmein 3-acetate (XVII) with dry hydrogen bromide in dimethylformamide.

It is concluded from the results of these experiments that, in the bromination of C_{16}–H and dehydrobromination of C_{16}–bromo derivatives in enmein analogs, bromination and dehydrobromination progresses without any abnormal reaction, but a variety of etherification takes place at the acetal-hydroxyl group in C_6 position. Also, the present series of experiments has finally realized a plan made 10 years ago to convert dihydroenmein (II) to enmein (I) *via* 6-acetate derivative.

Experimental

NMR spectra were determined on a JEOL HL-60 (60 MHz) spectrometer in deuterochloroform solutions. IR spectra were recorded on Nujol mull with a Japan Spectroscopic IR-S spectrophotometer. Melting points were measured on a Yanagimoto micromelting point determination apparatus, and uncorrected. Column chromatography was performed with Mallinckrodt silicic acid.

(i) 16-Bromodihydroenmein Diacetate (IV). A mixture of dihydroenmein diacetate (III)[1,2,3] (550 mg), *N*-bromosuccinimide (230 mg), a few mg of benzoyl peroxide, and chloroform (20 ml) was heated under reflux for 3.5 hr. The reaction mixture was chromatographed on silica gel (10 g). Elution with chloroform yielded a crystalline product, which was recrystallised from ethanol to give 16-bromodihydroenmein diacetate (IV) (350 mg) as colorless prisms, mp 235 °C, ν_{max} 1760, 1730, 1240, and 1045 cm^{-1}, δ 1.04 and 1.06 (each 3H, s, *tert*-CMe), 1.93 (3H, s, >C(Br)-CH_3), 1.98 and 2.12 (each 3H, s, OAc), 4.08 (2H, s, -O-CH_2-C<), 4.68 (1H, dd, J=11 and 7 Hz, $H_{1\beta}$), 4.92 (1H, br.s, $H_{3\alpha}$), 6.18 (1H, s, H_6).

(ii) 16-Bromodihydroenmein 3-Acetate 6-Ethyl Acetal (IX). The procedure was same as (i). 16-Bromodihydroenmein 3-acetate 6-ethyl acetal (IX) obtained was colorless plates, mp 223 °C (decompn.), Found: C, 56.11; H, 6.58%. Calcd for $C_{21}H_{33}O_7Br$: C, 56.16; H, 6.50%, ν_{max} 1760, 1730, 1250, and 1045 cm^{-1}, δ 0.95 and 0.99 (each 3H, s, *tert*-CMe), 1.04 (3H, t, J=7.5 Hz, *sec*-CMe), 1.85 (3H, s, >C(Br)-CH_3), 2.06 (3H, s, OAc), 3.52 (2H, q, J=7.5 Hz, -OCH_2CH_3),

3.78 and 3.99 (each 1H, AB-q, $J=10.5$ Hz, $-O-CH_2-C\lessgtr$), 4.60 (1H, dd, $J=11$ and 7 Hz, $H_{1\beta}$), 4.72 (1H, m, $H_{3\alpha}$), 4.81 (1H, s, H_6).

(iii) 16-Bromodihydroenmein 3-Acetate 6-Methyl Acetal (X). The procedure was same as (i). 16-Bromodihydroenmein 3-acetate 6-methyl acetal (X) obtained was colorless prisms, mp 220—222 °C (decompn.), Found: C, 55.29; H, 6.28%. Calcd for $C_{23}H_{31}O_7Br$: C, 55.52; H, 6.26%, ν_{max} 1760, 1730, 1240, and 1045 cm^{-1}, δ 1.00 and 1.04 (each 3H, s, *tert*-CMe), 1.82 (3H, s, $>C(Br)-CH_3$), 2.13 (3H, s, OAc), 3.27 (3H, s, OMe), 3.90 and 4.10 (each 1H, AB-q, $J=9.5$ Hz, $-O-CH_2-C\lessgtr$), 4.70 (1H, dd, $J=11.5$ and 7.5 Hz, $H_{1\beta}$), 4.82 (1H, s, H_6), 4.91 (1H, t, $J=3.5$ Hz, $H_{3\alpha}$).

(iv) Hydrolysis of 16-Bromodihydroenmein 3-Acetate 6-Ethyl Acetal (IX). A mixture of 16-bromodihydroenmein 3-acetate 6-ethyl acetal (IX) (2 g), acetic acid (65 ml), and water (25 ml) was heated at 100 °C for 3 hr. The mixture was extracted with chloroform, and the solution was washed with water, 10% sodium carbonate aqueous solution and water, successively, and dried over anhydrous sodium sulfate. The solvents were removed to give 16-bromodihydroenmein 3-acetate (XXII), ν_{max} 3440, 1760, 1720, 1240, and 1040 cm^{-1}.

(v) Acetylation of 16-Bromodihydroenmein 3-Acetate (XXII). It was carried out with pyridine and acetic anhydride in the usual way. The product was recrystallised from ethanol to give 16-bromodihydroenmein diacetate (IV) as colorless plates, which was identical with an authentic sample derived from dihydroenmein diacetate (III) by bromination in IR.

(vi) Attempted Dehydrobromination of 16-Bromodihydroenmein Diacetate (IV). (a) A mixture of 16-bromodihydroenmein diacetate (IV) (150 mg) and pyridine (5 ml) was refluxed under nitrogen gas for 4 hr. The mixture was extracted with diethyl ether. The solution was washed with 2M-hydrochloric acid and water, and dried over anhydrous sodium sulfate. After evaporation of solvents, the residue was recrystallized from ethanol to give crystals (94 mg), which were identical with IV in IR.

(b) A mixture of 16-bromodihydroenmein diacetate (IV) (200 mg) and collidine (3 ml) was refluxed under nitrogen gas for 1 hr. The mixture was extracted with chloroform. The chloroform layer was washed with 2M-hydrochloric acid and water, and dried over anhydrous sodium sulfate. The solvent was removed and the concentrate was chromatographed on silica gel. Elution with chloroform–methanol (99: 1) yielded a crystalline product (91 mg), which was recrystallised from ethanol. This compound was identical with IV in IR.

(c) A mixture of 16-bromodihydroenmein diacetate (IV) (200 mg), lithium chloride (50 mg), and pyridine (1.5 ml) was heated at 100 °C under nitrogen gas for 2 hr. The mixture was diluted with water. The precipitate formed was collected by filtration, dried and chromatographed on silica gel. Elution with chloroform yielded a crystalline product (114 mg), which was recrystallized from ethanol. This compound was identical with IV in IR.

(d) When the reaction time was extended to 5 hr in the case of (vi-c), 16-bromodihydroenmein diacetate (IV) was recovered.

(e) A mixture of 16-bromodihydroenmein diacetate (IV) (200 mg), lithium chloride (140 mg), and pyridine (4 ml) was heated at 100 °C under nitrogen gas for 3 hr. The mixture was treated in a similar manner as (vi-c) to recover IV.

(f) A mixture of 16-bromodihydroenmein diacetate (IV) (200 mg), lithium carbonate (43 mg), and dimethylformamide (1.5 ml) was heated at 100 °C under nitrogen gas for 5 hr. The mixture was treated in a similar manner as (vi-c) to recover IV.

(g) A mixture of 16-bromodihydroenmein diacetate (IV) (500 mg), lithium chloride (120 mg), and dimethylformamide (3 ml) was heated at 110 °C under nitrogen gas for 3.5 hr. The mixture was treated in a similar manner as (vi-c). The crude product was chromatographed on silica gel (10 g), Elution with chloroform–methanol (99: 1) yielded a crystalline product, which was recrystallised from ethanol to give VIII (198 mg) as colorless prisms, mp over 295 °C, Found: C, 65.97; H, 6.94%; mol wt (vapor pressure depression method), 794. Calcd for $C_{44}H_{54}O_{13}\cdot 1/2H_2O$: C, 66.07; H, 6.93%; mol wt, 790.9, λ_{max} (ethanol) 233 nm (ε 14040), ν_{max} 1750, 1710, 1640, 1230, and 1050 cm^{-1}, δ 0.80 and 0.98 (each 6H, s, *tert*-CMe), 2.03 (6H, s, OAc), 3.08 (2H, m, H_{13}), 3.88 and 4.01 (each 2H, AB-q, $J=10$ Hz, $-O-CH_2-C\lessgtr$), 4.57 (2H, dd, $J=10.5$ and 7 Hz, $H_{1\beta}$), 4.81 (2H, br.s, $H_{3\alpha}$), 5.21 (2H, s, H_6), 5.40 and 5.95 (each 2H, s, $>C=CH_2$).

(h) A mixture of 16-bromodihydroenmein diacetate (IV) (200 mg), lithium bromide (70 mg), lithium carbonate (30 mg) and dimethylformamide (2 ml) was heated at 100 °C under nitrogen gas for 6 hr. Treating in a similar manner as (vi-g) gave a few amount of VIII.

(vii) Catalytic Hydrogenation of VIII. In dioxane (20 ml), VIII (800 mg) was hydrogenated over platinum oxide (93 mg). The crude product was chromatographed on silica gel. Elution with chloroform yielded a crystalline product (346 mg), which was recrystallised from ethanol to give XV as colorless needles, mp over 300 °C, Found: C, 65.12; H, 7.53%. Calcd for $C_{44}H_{58}O_{13}\cdot H_2O$: C, 65.01; H, 7.44%, ν_{max} 1735, 1240, and 1040 cm^{-1}, δ 0.95 and 1.03 (each 6H, s, *tert*-CMe), 1.11 (6H, d, $J=7$ Hz, *sec*-CMe), 2.75 (6H, s, OAc), 3.98 (4H, t, $J=10.5$ Hz, $-O-CH_2-C\lessgtr$), 4.58 (2H, dd, $J=10.5$ and 7 Hz, $H_{1\beta}$), 4.87 (2H, br.s, $H_{3\alpha}$), 5.30 (2H, s, H_6).

(viii) Bromination of XV. A mixture of XV (200 mg), *N*-bromosuccinimide (85 mg), a few mg of benzoyl peroxide, and chloroform (15 ml) was refluxed for 3.5 hr. The mixture was concentrated, and chromatographed on silica gel (5 g). Elution with chloroform yielded a crystalline product (134 mg), which was recrystallised from ethanol to give XVI as colorless needles, mp 277—278 °C (decompn.), ν_{max} 1750, 1725, and 1235 cm^{-1}, δ 0.92 and 1.03 (each 6H, s, *tert*-CMe), 1.87 (6H, s, $>C(Br)-CH_3$), 2.08 (6H, s, OAc), 4.01 (4H, t, $J=11$ Hz, $-O-CH_2-C\lessgtr$), 4.64 (2H, dd, $J=11$ and 7.5 Hz, $H_{1\beta}$), 4.88 (2H, br.s, $H_{3\alpha}$), 5.27 (2H, br.s, H_6).

(ix) Dehydrobromination of XVI. A mixture of XVI (60 mg), lithium chloride (15 mg) and dimethylformamide (0.5 ml) was heated at 110 °C under nitrogen gas for 5 hr. The mixture was diluted with ice–water, and the precipitates collected by filtration were chromatographed on silica gel. Elution with chloroform–methanol (99: 1) yielded a crystalline product (27 mg) which was recrystallized from ethanol to give colorless prisms. This compound was identical with VIII derived from 16-bromodihydroenmein diacetate (IV) by dehydrobromination in IR and NMR.

(x) Hydrolysis of VIII. To VIII (200 mg) acetic acid (10 ml) and water (5 ml) were added, and heated at 110 °C for 45 hr. The mixture was extracted with chloroform, and the extract was washed with water, 10% sodium carbonate aqueous solution, and water, successively, and dried over sodium sulfate. After concentration the residue was recrystallised from ethanol to give enmein 3-acetate (XVII) (63 mg) as colorless needles, ν_{max} 3420, 1750, 1710, 1640, and 1270 cm^{-1}. Enmein 3-acetate (XVII) obtained as above was identical with an authentic sample[6] in IR.

(xi) Reaction of Dihydroenmein Diacetate (III) with Lithium Chloride and Dimethylformamide. A mixture of dihydroenmein diacetate (III) (210 mg), lithium chloride (60 mg), and dimethylformamide (1.5 ml) was heated at 110 °C under

nitrogen gas for 3.5 hr. The mixture was treated in a similar manner for VIII shown in (vi-g). The crude product was chromatographed on silica gel. Elution with chloroform yielded a crystalline product (125 mg), which was recrystallised from ethanol. This compound was identical with III in IR.

(xii) Reaction of Dihydroenmein Diacetate (III) with Lithium Chloride, Dimethylformamide, and Ethyl Bromide. A mixture of dihydroenmein diacetate (III) (250 mg), lithium chloride (60 mg), dimethylformamide (1.5 ml) and ethyl bromide (1.5 ml) was heated at 110 °C under nitrogen gas. After 2 hr, ethyl bromide was added to the mixture and the heating was continued for 2 hr. The mixture was treated in a similar manner for VIII shown in (vi-g), to give XV (71 mg), which was identical with an authentic sample (XV) obtained from VIII by hydrogenation in IR.

(xiii) Reaction of Enmein 3-Acetate (XVII) and Dimethylformamide. Enmein 3-acetate (XVII)[6] (200 mg) in dimethylformamide (1.5 ml) was heated at 110 °C for 4 hr. The product was identical with XVII in IR.

(xiv) Reaction of Enmein 3-Acetate (XVII) with Lithium Chloride, Dimethylformamide, and Ethyl Bromide. A mixture of enmein 3-acetate (XVII) (200 mg), lithium chloride (40 mg), dimethylformamide (1.5 ml), and ethyl bromide (1 ml) was heated at 110 °C under nitrogen gas for 4 hr. After 2 hr, ethyl bromide was added to the mixture and the heating was further continued for 2 hr. The mixture was treated as usual and the crude product was chromatographed on silica gel. Elution with chloroform yielded a crystalline product, which was recrystallized from ethanol to be identical with VIII in IR.

(xv) Reaction of Isodocarpin Acetate (XVIII) with Lithium Chloride, Dimethylformamide and Ethyl Bromide. A mixture of isodocarpin acetate (XVIII)[5,7] (150 mg), lithium chloride (40 mg), dimethylformamide (1.5 ml), and ethyl bromide (1 ml) was heated at 110 °C under nitrogen gas for 4 hr. After 2 hr, ethyl bromide was added to the mixture. The reaction mixture was diluted with water, and the precipitates formed were collected by filtration, dried and chromatographed on silica gel. Elution with chloroform yielded a crystalline product, which was recrystallised from ethanol to give XIX (59 mg) as colorless needles, mp over 300 °C, Found: C, 70.65; H, 7.50%. Calcd for $C_{40}H_{50}O_9 \cdot 1/3H_2O$: C, 70.56; H, 7.50%, *m/e* 674 (M^+), ν_{max} 1750, 1710, 1640, and 995 cm^{-1}, δ 0.85 and 0.96 (each 6H, s, *tert*-CMe), 3.11 (2H, dd, $J=9$ and 4 Hz), 3.87 and 4.07 (each 2H, AB-q, $J=9.5$ Hz, $-O-CH_2-C\lessgtr$), 4.34 (2H, t, $J=8.5$ Hz, $H_{1\beta}$), 5.20 (2H, s, H_6), 5.45 and 5.98 (each 2H, s, $>C=CH_2$).

(xvi) Reaction of Enmein 3-Acetate (XVII) in Dimethylformamide under Hydrogen Bromide Gas. Enmein 3-acetate (XVII) (200 mg) in dimethylformamide (4 ml) was heated at 110 °C under dry hydrogen bromide gas for 2.5 hr. The reaction mixture was diluted with water, and the precipitates collected by filtration were treated by the preparative thin-layer chromatography on silica gel. Elution with chloroform–methanol (9: 1) yielded two crystalline products which were recrystallised from ethanol, respectively. The first product as colorless prisms (44 mg) was identical with VIII in IR, and the second compound as colorless prisms (43 mg) was the starting material (XVII).

We are grateful to Dr. T. Kamikawa, Osaka City University, for valuable discussions.

References

1) T. Kubota, T. Matsuura, T. Tsutsui, S. Uyeo, H. Irie, A. Numata, T. Fujita, and T. Suzuki, *Tetrahedron*, **22**, 1659 (1966).

2) K. Naya, *Nippon Kagaku Zasshi*, **79**, 885 (1958).

3) E. Fujita, T. Fujita, K. Fuji, and N. Ito, *Tetrahedron*, **22**, 3423 (1966).

4) T. Ikeda and S. Kanatomo, *Yakugaku Zasshi*, **78**, 1128 (1958).

5) E. Fujita, T. Fujita, and H. Katayama, *J. Chem. Soc., C*, **1970**, 1681.; Also see the footnote (p. 1682) of this reference on the experiments of the compound (IX), (XI), and (XIII).

6) E. Fujita, T. Fujita, and M. Shibuya, *Yakugaku Zasshi*, **87**, 1076 (1967).

7) T. Isobe, T. Kamikawa, and T. Kubota, *Nippon Kagaku Kaishi*, **1972**, 2143.

The Synthesis of Heterocyclic Compounds by the Reaction of Tin(II) Bis(acetylacetonate) with Isocyanates

Ikuko WAKESHIMA and Ichiro KIJIMA

Department of Industrial Chemistry, Faculty of Engineering, Science University of Tokyo, Kagurazaka, Shinjuku-ku, Tokyo 162

(Received May 2, 1974)

It was found that phenyl isocyanate reacted with tin(II) bis(acetylacetonate) to yield triphenyl isocyanurate, 5-acetyl-6-methyl-2-oxo-3-phenyl-4-phenylimino-3,4-dihydro-2*H*-1,3-oxazine, and *N,N'*-diphenylurea, while ethyl isocyanate reacted with tin(II) bis(acetylaceonate) to afford only 2,4-dioxo-6-ethylimino-1,3,5-triethylhexahydro-1,3,5-triazine.

It has recently been reported that some monomeric tin(II) compounds containing Sn–OC bonds reacted smoothly with *n*-alkyl iodides to give the oxidative addition compounds.[1-2] While there have already been reports on the reaction of tin(II) compounds containing Sn–OC bonds with some isocyanate,[3-5] the reaction with metal acetylacetonate has not yet been studied. It is of interest to investigate the behavior of tin(II) bis(acetylacetonate) toward compounds containing activated double bonds such as isocyanate. In this paper, we will describe the synthesis of heterocyclic compounds by the reaction of tin(II) bis(acetylacetonate) with phenyl and ethyl isocyanates.

From the reaction of phenyl isocyanate (PhNCO) with a catalytic amount of tin(II) bis(acetylacetonate), $Sn(acac)_2$, triphenyl isocyanurate was obtained in a yield of 33%. The product was identified on the basis of the elemental analyses and its IR spectrum. In order to obtain further information on the behavior of $Sn(acac)_2$ toward PhNCO, the reaction was carried out while varying the molar ratio of PhNCO to $Sn(acac)_2$ from 1:1 to 4:1.

The reaction in a molar ratio of 1:1 gave two colorless compounds which were found to be $C_{19}H_{16}N_2O_3$ (I) and $C_{13}H_{12}N_2O$ (II). The infrared spectrum of (I) showed bands ascribable to $\nu_{C=O}$ at 1723, and 1689, to $\nu_{C=C}$ at 1660, to $\nu_{C=N}$ at 1419, to ν_{C-N} at 1345, to δ_{S-CH_3} at 1435, and to δ_{as-CH_3} at 1365 cm^{-1}. Its NMR spectrum in $CDCl_3$ displayed bands at 2.56 (3H, $CH_3C=$) and 2.03 (3H, CH_3CO) ppm, besides the aromatic proton (10H). From these data, (I) was found to be 5-acetyl-6-methyl-2-oxo-3-phenyl-4-phenylimino-3,4-dihydro-2*H*-1,3-oxazine. This assingment was also supported by the mass spectral data—*i.e.*, the peaks of M^+, M^+-1, CH_3CO, and C_6H_5 at *m/e* 320, 319, 43, and 77 respectively. There were also observed fragment ions resulting from the loss of a methyl or carbonyl group from the molecular ion. Compound (II) could also be assinged to *N,N'*-diphenylurea by a comparison of the melting point with that of an authentic sample.

The reaction of $Sn(acac)_2$ with PhNCO in a molar ratio from 1:2 to 1:4 yielded (I) and (II) in equal amounts, which increased with the ratio of PhNCO to $Sn(acac)_2$ (Table 1).

Table 1. Results of the reaction of $Sn(acac)_2$ (0.1 mol) with PhNCO in various molar ratios

Molar ratio PhNCO/$Sn(acac)_2$	Yields (mol)	
	(I)	(II)
1	0.0062	0.0060
2	0.0363	0.0334
4	0.0801[a]	0.0721

a) Triphenyl isocyanurate was detected in a small quantity.

Therefore, as for the formation of (I), (II), and triphenyl isocyanurate, we tentative propose the process depicted in Scheme 1.

Contrary to the reaction with PhNCO, $Sn(acac)_2$ reacted easily with various molar ratios of ethyl isocyanate (EtNCO) at 67—72 °C to give only 6-ethyl-

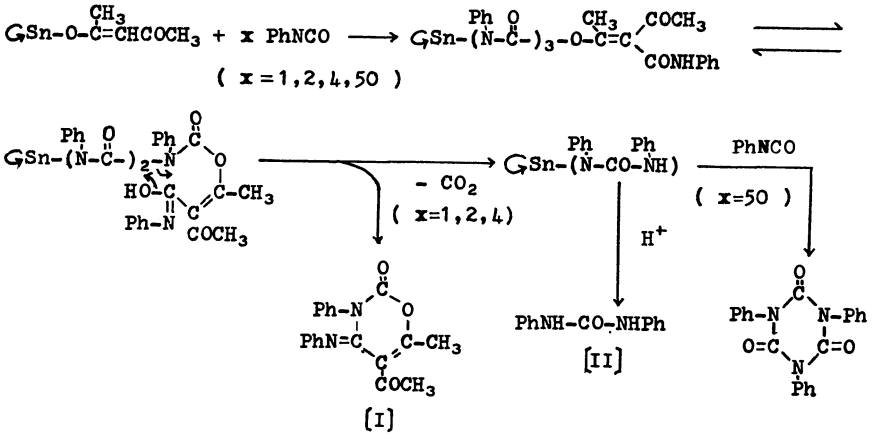

Scheme 1

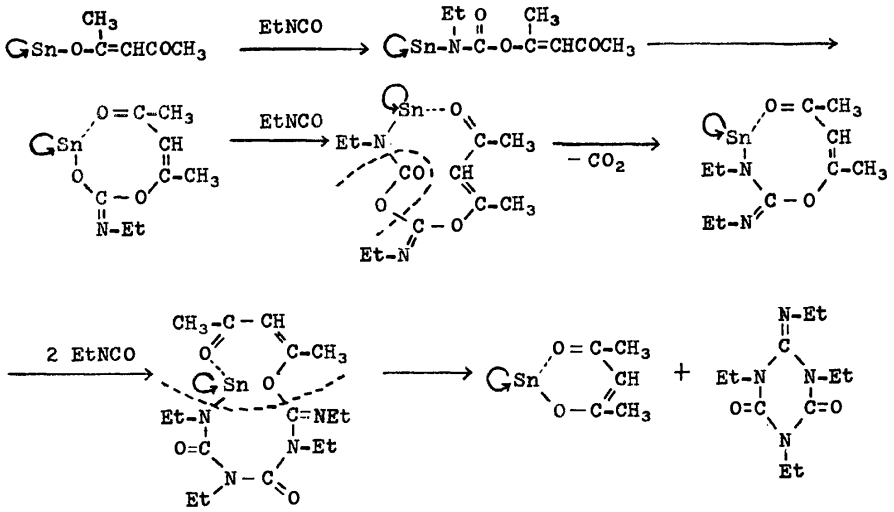

Scheme 2.

imino-1,3,5-triethylhexahydro-1,3,5-triazine in a high yield, with the quantitative recovery of $Sn(acac)_2$. The structure was confirmed by the IR and NMR spectra, by elemental analyses, and by a molecular-weight determination. The IR spectrum exhibited a band at 1672 cm^{-1} which can be ascribed to the carbonyl group. The NMR spectrum showed triplets at 1.18 (9H, $-\underset{|}{N}-CH_2C\underline{H}_3$) and 1.25 (3H, $>C=N-CH_2C\underline{H}_3$) ppm, and quartets at 3.35 (2H, $>C=N-C\underline{H}_2-$), 3.85 (2H, $\begin{matrix}-CO\\-CO\end{matrix}\!\!>\!N-C\underline{H}_2-$), and 3.89 (4H, $\begin{matrix}-CN\\-CO\end{matrix}\!\!>\!N-C\underline{H}_2-$) ppm. A further proof of the structure was provided by its conversion into triethyl isocyanurate by hydrolysis with alcoholic hydrochloric acid. The IR spectrum was identical with that of an authentic sample prepared by the trimerization of EtNCO with a catalytic amount of $Sn(OC_2H_5)_2$. The formation of 6-ethylimino-1,3,5-triethylhexahydro-1,3,5-triazine seems to involve the processes shown in Scheme 2.

Although a detailed explanation cannot be offered for the remarkable difference between the reaction of PhNCO and that of EtNCO with $Sn(acac)_2$, it is clearly possible that the reaction between PhNCO and the methine proton on the C-3 of the Chelate ring leads to the formation of the 1,3-oxazine derivative.

Experimental

The experiments were carried out under a dry nitrogen atmosphere. The IR spectra were recorded on a Hitachi EPI-S2 infrared spectrometer as KBr disks or liquid films. The NMR spectra were determined by means of a Hitachi R-24 spectrometer (60 MHz) in CCl_4 or $CDCl_3$, using TMS as the internal standard. The chemical shifts are expressed in δ values. The mass spectra were measured on a Hitachi RMU-7 model double-focusing spectrometer. The elemental analyses were carried out with a Yanagimoto CHN analyzer, Model MT-2.

Materials. Tin(II) bis(acatylacetonate) was prepared in accordance with the method of a previous paper.[6] The other were commercially available.

Reaction Procedures. *The Reaction of PhNCO in the Presence of a Catalytic Amount of $Sn(acac)_2$*: A solution of PhNCO (46 g, 0.386 mol) and $Sn(acac)_2$ (2.9 g, 9.15 mmol) in benzene (92 ml) was stirred at 80—81 °C for 3 hr. The solids thus precipitated were filtered off and recrystallized from ethanol. Triphenyl isocyanurate was obtained in a 33% yield; mp 269—270 °C (lit, 275 °C[7]). IR (KBr) $\nu_{C=O}$ 1710 cm^{-1}.

The Reaction of PhNCO with $Sn(acac)_2$ in a Molar Ratio of 1: 1—4: 1: Phenyl isocyanate was added, drop by drop, to a *n*-hexane of solution of $Sn(acac)_2$ (0.1 mol) at 26—27 °C, and then the solution was heated with stirring in an oil bath for 3 hr. An evolution of carbon dioxide was observed throughout the reaction. The precipitated yellow solids were isolated by filtration, treated with 2M-HCl at room temperature and extracted with benzene using a Soxhlet extractor. The subsequent evaporation of the benzene from the extract left a solid residue. The recrystallization of the residue from methanol and then acetone gave a product (I) as white crystals; mp 213—213.3 °C (Found: C, 71.54; H, 4.97; N, 8.60%. Calcd for $C_{19}H_{16}N_2O_3$: C, 71.24; H, 5.04; N, 8.75%). IR (KBr): 1723, 1689, 1660, 1435, 1419, 1365, and 1345 (cm^{-1}). NMR ($CDCl_3$): 2.03, 2.56, and 7.0—7.67 ppm. Mass spectra: *m/e* 320 (M^+), 319, 77, and 43. The yellow powders remaining in the Soxhlet extractor were recrystallized from acetone. White needles (II) were thus obtained as the product; mp 234—235 °C (lit, 235 °C[8]). *m/e*: 212 (M^+). IR: 3310 and 1648 cm^{-1}.

On the other hand, $Sn(acac)_2$ was recovered by distilling the evaporation residue of the filtrate in a vacuum.

The Reaction of EtNCO with $Sn(acac)_2$: A mixture of $Sn(acac)_2$ (0.1 mol) and EtNCO (0.2, 0.4, 0.8, and 5.0 mol) in benzene (150 ml) was refluxed for 3 hr at 64—72 °C with stirring in an oil bath. An evolution of carbone dioxide was observed throughout the reaction. After the removal of the solvent in a vacuum, the residue was distilled, giving a mixture of triazine and $Sn(acac)_2$ in a quantitative yield. The mixture was then treated with 1—2 ml of water in acetone (30 ml), and the resulting white solids were separated centrifugally. The acetone solution was distilled *in vacuo* to give a light yellow viscous liquid in an 82—89% yield; bp 84—87 °C/0.5 mmHg (Found: C, 54.52; H, 8.40; N, 21.04%. Mol wt 228 (cryoscopically in benzene). Calcd for $C_{11}H_{20}N_4O_2$: C, 54.99; h, 8.38; N, 21.04%, Mol wt 240). IR (liquid films): 1672 cm^{-1}. NMR (CCl_4): 1.18, 1.23, 1.25, 3.35, 3.85, and 3.89 ppm.

References

1) K. D. Bos, H. A. Budding, E. J. Buten, and J. G. Noltes, *Inorg. Nucl. Chem. Lett.*, **1973**, 9.
2) I. Wakeshima and I. Kijima, *J. Organometal. Chem.*, **76**, 37 (1974).
3) A. J. Bloodworth and A. G. Davies, *J. Chem. Soc.*, **1965**, 5238, 6245, 6858.
4) P. G. Harrison and J. J. Zuckerman, *Chem. Commun.*, **1969**, 321.
5) T. E. Lipatova and Yu. N. Nizel Skii, *Dokl. Akad. Nauk. SSSR*, **175**, 128 (1965).
6) I. Wakeshima and I. Kijima, *Chem. Lett.*, **1972**, 325.
7) "Beilstein," Vol. 26, p. 253.
8) "Beilstein," Vol. 12, p. 352.

Tris(benzimidazo)-1,3,5-triazine from the Thermolysis of 2-Aryloxybenzimidazoles

Sadahiro ISHIDA, Yoshiaki FUKUSHIMA, Shizen SEKIGUCHI, and Kohji MATSUI
Department of Chemistry, Gunma University, Kiryu, Gunma 376
(Received August 23, 1974)

2-Aryloxybenzimidazoles gave tris(benzimidazo)-[1,2-*a*: 1′,2′-*c*: 1″,2″-*e*]-1,3,5-triazine and phenol in almost quantitative yields upon heating at 230—250 °C, while in the reaction in cumene small amounts of 2-aryloxy-1,2′-dibenzimidazole and dicumyl were obtained along with the major products. On the other hand, 2-phenylthiobenzimidazole gave diphenyl disulfide and 1,2′-dibenzimidazole, together with tris(benzimidazo)-1,3,5-triazine. The thermolysis is assumed to proceed by step-by-step radical processes involving the formation of such intermediates as 2-aryloxy-1,2′-dibenzimidazole and 2-aryloxy-1,2′-1′,2″-trisbenzimidazole.

In a previous paper,[1] we reported that 2-aryloxybenzazoles rearrange photochemically to give 2-(2- and/or 4-hydroxyphenyl)benzazoles upon irradiation with a low-pressure mercury lamp, and that 2-(2-aminophenoxy)benzazoles undergo a photo-Smiles rearrangement. During the course of our studies of the reactions of 2-substituted benzazoles, it was found that 2-aryloxybenzimidazoles undergo an interesting thermal reaction. This paper will report on the thermal decomposition of 2-aryloxybenzimidazoles.

Results and Discussion

Thermal Decomposition of 2-Aryloxybenzimidazoles. Ordinary 2-aryloxybenzazoles are thermally stable; in the cases of 2-aryloxy derivatives of benzoxazole and benzothiazole, no decomposition took place upon heating at 200 °C for 5 hr. However, not only 2-aryloxy derivatives of benzoxazole and benzothiazole, but also 2-aryloxybenzimidazoles gradually decomposed above 200 °C, and the TG curves showed a weight loss. Although the weight losses of the derivatives of benzoxazole and benzothiazole during heating were not simple, the TG curves of 2-aryloxybenzimidazoles (I) showed a weight loss, just corresponding to a fission of the phenol moiety; in fact, by heating 2-aryloxybenzimidazoles at 230—250 °C for 5 hr, the corresponding phenol and a product of a high melting point (above 360 °C) were obtained in almost quantitative yields.

The same product with a high melting point was obtained even when benzimidazole derivatives of different aryloxy components (phenol and *p*-cresol were used as the phenol components) were decomposed; it was found to be a cyclic trimer of the benzimidazolyl residue (tris(benzimidazo)-[1,2-*a*: 1′,2′-*c*: 1″,2″-*e*]-1,3,5-triazine) (II) (hereafter we will call the compound merely a trimer), as is shown below:

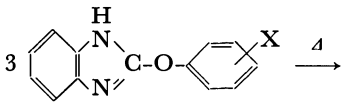

(I)

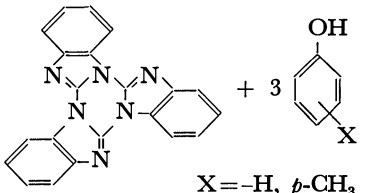

(II)

Recently, similar thermal trimerizations have been observed with 2-chlorobenzimidazole and related derivatives,[2] although the yields of the trimers were quite low. The mechanisms of these reactions, however, have not been investigated.

The thermal trimerization of 2-aryloxybenzimidazoles took place also in various organic solvents, such as cumene, toluene, *o*-dichlorobenzene, and ethanol, as is shown in Table 1; when 2-phenoxybenzimidazole was heated in cumene at 250 °C under pressure, a small amount of dicumyl was obtained along with the trimer and phenol, suggesting that the reaction took place *via* a radical process. However, at present the details of the solvent effect are not clear.

Effect of Substituent on the Thermal Trimerization of 2-Substituted Benzimidazoles. When the substituent of benzimidazole at the 2-position is –OH, –SH, $-NH_2$, or $-NHC_6H_5$, the compounds are thermally very stable; even after heating at 250 °C for a long period, no decomposition to give the trimer was observed. On the other hand, 2-chloro, 2-phenylthio, and 2-phenoxy derivatives gave the trimer under similar reaction conditions, as is shown in Table 2. The derivatives of benzimidazole substituted at the 1-position, such as 1-methyl-2-chlorobenzimidazole, did not yield the trimer upon heating, as might have been anticipated.

From these results, it is obvious that the thermal trimerization of 2-substituted benzimidazoles depends remarkably upon the substituent at the 2-position; when the hetero atom of the 2-substituent possesses an active hydrogen atom, the trimerization became difficult. This is considered to be due to an increase in the bond strength between the ring carbon and hetero

Table 1. Yields of trimer in the thermolysis of 2-phenoxybenzimidazole in organic solvents

Solvent	Yield of trimer (%)[a]
Cumene	81.8
Toluene	38.0
o-Dichlorobenzene	34.4
Ethanol	21.7

a) Yield of trimer when heated at 250 °C for 5 hr.

Table 2. Thermolyses of 2-substituted benzimidazoles

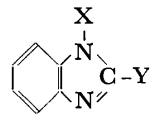

X	Y	Reaction temp. (°C)	Yield of trimer (%)[a]
-H	$-OC_6H_5$	220—230	90<
-H	$-OC_6H_4-CH_3(p)$	220—230	90<
-H	$-SC_6H_5$	220—230	9.7
-H	-Cl	200—210	14.0

a) Yield of trimer after heating for 2.5 hr.

atoms, because these compounds (III) are known to exist as their tautomers (III)', as is shown below:

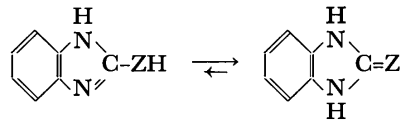

(III) (III')

Z=-S-, -NH-, -O-, $-\overset{|}{N}C_6H_5$, *etc.*

Although 2-Cl, -OAr, and 2-SAr benzimidazoles all underwent the thermal trimerization, the reactivity to give the trimer differed significantly from one to the other; among them, -OAr was the best and -SAr was the worst substituent for the reaction, as can be seen in Table 2. When the 2-phenylthio derivative (IV) was heated at 230 °C for 2.5 hr, the trimer (II) was obtained in a low yield, along with 1,2'-dibenzimidazole (V), diphenyl disulfide (VI), and the undecomposed starting material.

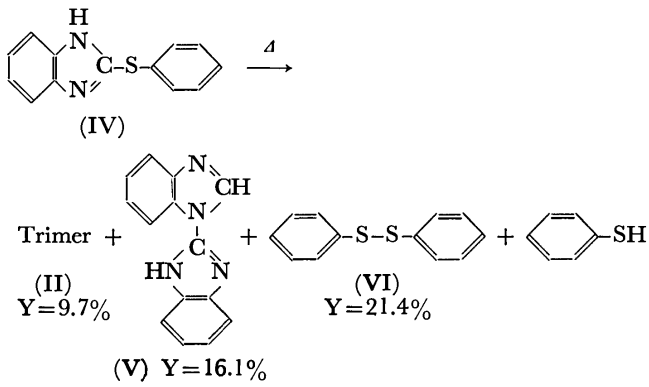

(IV)

(V) Y=16.1%

1,2'-Dibenzimidazole (V) should be formed by a combination between 2- and 1-benzimidazolyl radicals; the former may be produced by a homolytic fission of the C–S bond of the starting material, while the latter may be formed by an intramolecular N→C migration of the hydrogen atom in the former. However, it is unlikely that Compound (V) is a necessary intermediate for the trimerization, and dibenzimidazole of the 1,1'- or 2,2'-type and benzimidazole were not obtained.

On the other hand, in the case of 2-phenoxybenzimidazole, the thermal trimerization took place almost quantitatively, without any appreciable side reaction, and in the reactions in organic solvents, only a small amount of a dimer of the benzimidazolyl residue possessing one phenoxy group (2-phenoxy-1,2'-dibenzimidazole) (X) was obtained, along with the major products (II), as can also be seen in the reaction in cumene; benzimidazole and dibenzimidazole containing no phenoxy group of 1,1'-, 2,2'-, or 1,2'-type were not obtained in this case. 2-Phenoxy-1,2'-dibenzimidazole is considered to be not a mere by-product, but an intermediate for the trimerization, as will be discussed later; the difference in thermal reactivity between phenoxy and phenylthio derivatives is considered to depend mainly upon the difference in readiness for dimerization between the phenoxy and phenylthiyl radicals; the phenylthiyl radical produced by the homolytic fission of the C–S bond would dimerize readily to give diphenyl disulfide. Consequently, in the case of phenylthio derivative, the abstraction of the NH hydrogen would be incomplete in the production of the trimer (II) in a good yield.

On the other hand, in the case of the phenoxy derivative, the phenoxy radical (VIII) once produced by a homolytic cleavage of the C–O bond would rapidly abstract the NH hydrogen atom from the starting material to give phenol and the 1-(2-phenoxy)benzimidazolyl radical (IX), which may then react with the 2-benzimidazolyl radical (VII) to give 2-phenoxy-1,2-dibenzimidazole (X).

However, 2-alkoxy- and 2-alkylthiobenzimidazoles behave in different manners upon heating. For example, 2-ethoxybenzimidazole is known to decompose thermally to give 1-ethyl-2-ethoxybenzimidazole and

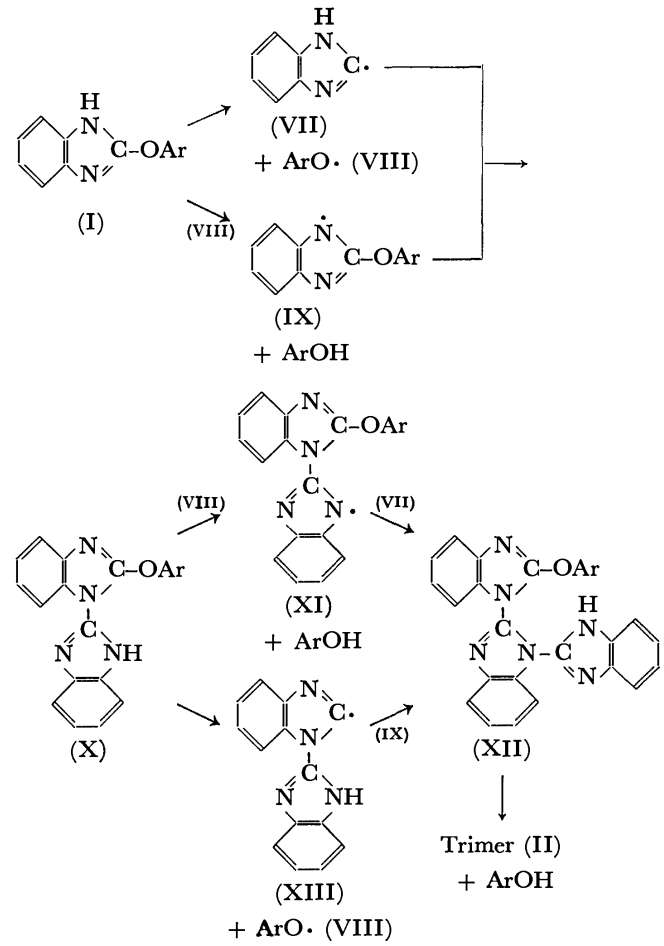

2-(3*H*)-benzimidazolinone upon heating at 200—230 °C,[3] indicating that the bond fission took place at O–C_2H_5. In the case of the aryloxy derivative, the bond fission may occur more readily at C–OAr than at O–Ar, because the O–Ar bond should be stronger than the C–OAr bond as a result of the overlap of the lone pair of electrons on the oxygen with the aromatic π electrons; in addition, the stabilization of the resultant radical by the aryl group may favor the fission at C–OAr. When 2-methylthiobenzimidazole was heated at 230 °C, a decomposition took place to give various decomposition products, although in this case the (II) trimer was not detected in the reaction mixture, showing that substituents at the 2-position consisting of a hetero atom and an alkyl group are not suitable for the thermal trimerization. It can be said that the aryloxy group is the best substituent for the thermal trimerization of 2-substituted benzimidazoles.

Reaction Sequences of the Thermal Trimerization of 2-Aryloxybenzimidazoles. From the results described above, it seems reasonable to assume that the thermal trimerization of 2-substituted benzimidazoles proceeds homolytically by step-by-step processes such as are shown in the case of 2-aryloxybenzimidazoles.

1. The homolytic fission of the C–O bond of 2-aryloxybenzimidazole (I) to give aryloxy (VIII) and 2-benzimidazolyl radicals (VII).

2. The abstraction of the NH hydrogen of I by VIII to give the 1-(2-aryloxy)benzimidazolyl radical (IX) and phenol.

3. The combination of IX and VII to give 2-aryloxy-1,2′-dibenzimidazole (X).

4. From the dimer (X), several possible routes can be considered. A trimer possessing one aryloxy group (2-aryloxy-1,2′-1′-2″-trisbenzimidazole) (XII) is the most probable intermediate, even though it has not been isolated. For the formation of XII, two routes are possible; one is a combination of XIII, produced by a homolytic fission of the C–O bond of X, with IX, while the other is a reaction of XI, formed by an abstraction of the NH hydrogen of X by VIII, with VII. The actual reaction would proceed *via* both of the two routes.

5. The formation of the final product from XII by a fission of the C–O bond and an abstraction of the NH hydrogen by the resulting phenoxy radical therefrom, followed by an intramolecular combination of the resultant biradical.

Experimental

All the melting points are uncorrected. The NMR spectra were taken on a Varian A-60D spectrometer, using tetramethylsilane as the internal standard. The IR spectra were measured in potassium bromide discs on a Jasco D-301 spectrometer. The UV spectra were recorded on a Hitachi-124 UV-VIS spectrometer. The Mass spectra were recorded on a JEOL-JMS-07 mass spectrometer. The elemental analyses were performed in the Micro-analytical Center of Gunma University. The structural assignments of the reaction products were done by means of their NMR, IR, UV, and MS spectra and by elemental analyses.

Materials, Preparation of 2-Substituted Benzazoles; 2-Aryloxybenzazoles were prepared by the condensation of 2-chlorobenzazoles with the equimolar corresponding phenolates.[1] A typical procedure will be described in the case of 2-phenoxybenzimidazole.

After 10.0 g (0.066 mol) of 2-chlorobenzimidazole and 10.0 g (0.086 mol) of sodium phenoxide in 150 g of phenol had been heated at 150 °C for 7 hr, the reaction mixture was steam distilled and the residue was filtered and washed with a 1% aqueous NaOH solution and water. The precipitate was then recrystallized from ethanol to give an analytical sample of 2-phenoxybenzimidazole.

Other 2-substituted benzimidazoles were prepared by the methods described in the literature: 2-OH, mp 312—313 °C (ethanol) (lit,[4] 307—308 °C); 2-SH, mp 302—303 °C (ethanol) (lit,[5] 303—304 °C); 2-NH_2, mp 223—224 °C (ethanol) (lit,[6] 222 °C); 2-NHC_6H_5, mp 190—191 °C (benzene) (lit,[7] 190 °C); 2-OC_6H_5, mp 229—230 °C (ethanol) (lit,[1] 228—229 °C); 2-OC_6H_4–CH_3(p), mp 257—258 °C (dioxane) (lit,[1] 259—260 °C); 2-SC_6H_5, mp 202—203 °C (benzene) (lit,[8] 201—202 °C); 2-Cl, mp 191—193 °C (ethanol–water) (lit,[9] 180 °C, lit,[10] 210—212 °C; Found: C, 55.35; H, 3.33%. Calcd for $C_7H_5ClN_2$: C, 55.11; H, 3.31%); 2-Cl, 1-CH_3, mp 113—115 °C (petroleum ether) (lit,[9] 114—116 °C). 2-Methylthiobenzimidazole was prepared by the condensation of 2-mercaptobenzimidazole with methyl iodide in the presence of potassium hydroxide in a mixture of ethanol and water, as in the case of the 2-nonylthio derivative.[11] Mp 203—204 °C (benzene). Yield, 25%. Found: C, 58.56; H, 4.93%. Calcd for $C_8H_8N_2S$: C, 58.51; H, 4.92%.

Thermolyses of 2-Substituted Benzimidazoles; The thermolyses were carried out both without and with a solvent, as follows.

a) Thermolysis of 2-substituted benzimidazoles without a solvent; A 0.5 g portion of 2-substituted benzimidazole was heated in a small test tube under an atmosphere of nitrogen. The decomposed mixture was then treated with dioxane to give the trimer as a sparingly soluble product. Recrystallization from a large amount of dioxane gave an analytical sample. Mp>360 °C. IR (KBr disc) cm^{-1}, 1624 (–C=N); 1600, 1578, 1480 (phenyl). NMR (in trifluoroacetic acid) δ 7.85 (m, 6H), 8.10 (m, 3H), 8.64 (m, 3H). *M/e* 348.1138 (Calcd for $C_{21}H_{12}N_6$=348.1124). UV $\lambda_{max}^{Dioxane}$ (nm) ($\varepsilon \times 10^4$) 282 (7.8), 260 (9.8). Found: C, 72.61; H, 3.64; N, 24.06%. Calcd for $C_{21}H_{12}N_6$: C, 72.40; H, 3.47; N, 24.12%. The compound is identical with that obtained in the thermolysis of 2-chlorobenzimidazole.[2a]

Decomposed products soluble in dioxane were purified by thin-layer chromatography on silica gel, using benzene as the developing solvent. Thus, in the case of the 2-phenylthio derivative, diphenyl disulfide (yield, 21.4%; mp 60—61 °C) and 1,2′-dibenzimidazole (yield, 16.1%) were obtained from the filtrate. The latter was recrystallized from benzene. Mp 212—213 °C. *m/e* 234 (Calcd for $C_{14}H_{10}N_4$=234). NMR (DMSO-d_6) δ 8.91 (s, 1H), 8.50 (broad, 1H), 7.60 (m, 8H). Found: C, 71.69; H, 4.33; N, 23.98%. Calcd for $C_{14}H_{10}N_1$: C, 71.79; H, 4.30; N, 23.91%.

b) Thermolysis of 2-aryloxybenzimidazoles in organic solvents. A typical run is shown below in the decomposition of 2-phenoxybenzimidazole in cumene. A mixture of 1.0 g of 2-phenoxybenzimidazole and 50 ml of cumene was heated in an autoclave at 250 °C for 5 hr. After the mixture had stood at room temperature for 1 night, the crystals which had separated out were filtered and washed with ether to give the crude trimer (II) in an 81.8% yield. The filtrate was extracted with a 10% aqueous sodium hydroxide solution, and the aqueous layer was acidified with hydrochloric acid to give 2-phenoxy-1,2′-dibenzimidazole (V) in a yield of 13%. Recrystallization from ethanol gave an analytical sample of

(V). Mp 228—230 °C. *m/e* 326 (Calcd for $C_{20}H_{14}N_4O$= 326). NMR (DMSO-d_6) δ 8.20 (broad, 1H), 7.55 (m, 13H). Found: C, 73.36; H, 4.48; N, 17.11%. Calcd for $C_{20}H_{14}N_4O$: C, 73.60; H, 4.32; N, 17.17%.

The cumene layer was evaporated *in vacuo*, and the residue was purified by vacuum sublimation to give 3.0 mg of dicumyl (mp 118—119 °C),[12] which was identified by a mixed-melting-point test with an authentic sample.

References

1) T. Nagai, Y. Fukushima, T. Kuroda, H. Shimizu, S. Sekiguchi, and K. Matsui, This Bulletin, **46**, 2600 (1973).

2) a) E. R. Lavagnino and D. C. Thompson, *J. Heterocycl. Chem.*, **9**, 149 (1972); b) G. I. L. Gofen, Ch. sh. Kadyrov, and M. N. Kosyakovskaya, *Khim. Geterotsikl. Soedin*, **7**, 282 (1971); c) K. Zauer, I. Zauer-Csüllög, and K. Lempert, *Chem. Ber.*, **106**, 1628 (1973); d) G. R. Hansen and F. D. Blake, *J. Heterocycl. Chem.*, **7**, 997 (1970).

3) S. Takahashi and H. Kano, *Chem. Pharm. Bull. Jap.*, **12**, 282 (1964).

4) A. Hartmann, *Ber.*, **23**, 1047 (1890).

5) J. A. Van Allan and B. D. Deacon, "Organic Syntheses," Coll., Vol. 4, 569 (1963).

6) p. Pierron, *Ann.*, **15**, 189 (1908).

7) A. Keller, *Ber.*, **24**, 2499 (1891).

8) D. Harrison and J. T. Ralph, *J. Chem. Soc.*, **1965**, 3132.

9) D. Harrison, J. T. Ralph, and A. C. B. Smith, *ibid.*, **1963**, 2930.

10) N. P. Bednyagina and I. Ya. Postovskii, *Zh. Obshch. Khim.*, **30**, 1431 (1960).

11) Taisho Pharmaceutical Co. Ltd., Jap. 10978 (1961).

12) A. Klages, *Ber.*, **35**, 2638 (1902).

Asymmetric Induction in Friedel-Crafts Reaction with (+)-1,2-Epoxybutane and (−)-2-Chloro-1-butanol

Tadashi NAKAJIMA, Yoshiaki NAKAMOTO, and Sohei SUGA

Department of Industrial Chemistry, Faculty of Technology, Kanazawa University, Kanazawa 920

(Received September 5, 1974)

The alkylation of benzene with (+)-1,2-epoxybutane in the presence of Lewis acid gave a mixture of optically active 2-phenyl-1-butanol (I) and 3-phenyl-1-butanol (II) together with a mixture of optically active 2-chloro-1-butanol (III), 3-chloro-1-butanol (IV) and 1-chloro-2-butanol (V). The formation of (−)-I and (−)-III suggests that the ring opening of the epoxide proceeds with an inversion of configuration, while that of optically active II and IV suggests an asymmetric induction at the carbon adjacent to the terminal methyl group of the epoxide. The reactions with aluminum chloride at 20 °C and with stannic chloride at −20 °C gave (+)-II in 10% and (−)-IV in 56% optical yield, respectively. In the reaction of (−)-III with benzene, such an asymmetric induction was also found to give (+)-II in 21—24% optical yield. The probable mechanism of this induction was discussed on the basis of the stability of the transition state conformations.

The Friedel-Crafts alkylation of aromatic hydrocarbon with 1,2-epoxyalkane is known to give 2-aryl-1-alkanol by fission of the secondary C–O bond in the epoxide.[1,2] A similar reaction of 1,2-epoxybutane with benzene was found to give 2-phenyl-1-butanol (I), 2-chloro-1-butanol (III), and 1-chloro-2-butanol (V) together with 3-phenyl-1-butanol (II) and 3-chloro-1-butanol (IV) as products of the isomerized type.[3]

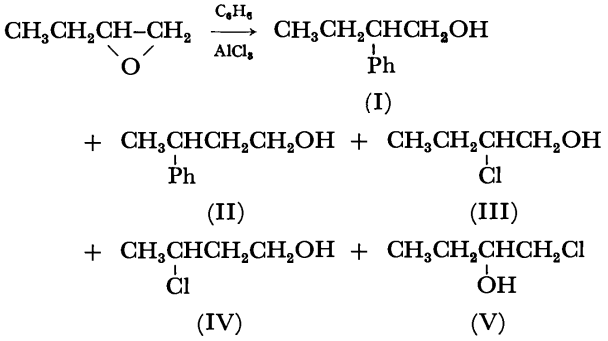

Friedel-Crafts reactions in the presence of Lewis acid are accompanied by isomerization, *e.g.*, the reaction of hex-2-enoic acid, and pent-2-enoic acid with benzene in the presence of aluminum chloride gives a mixture of 3-, 4-, and 5-phenylhexanoic acid,[4] and 3-, and 4-phenyl pentanoic acid,[5] respectively. These results are rationalized on the basis of the mechanism involving the initial carbonium ion formation followed by a series of 1,2-hydride ion shifts. Hata *et al.* reported a similar isomerization in the reaction of 1,2-epoxyoctane with benzene by a Lewis acid catalyst, and concluded that it proceeds through a phenonium ion intermediate.[6] However, the reaction of (+)-propylene oxide in the presence of Lewis acid proceeded with complete inversion of configuration at the secondary carbon atom in the epoxide. Thus the mechanism involving a free carbonium ion should be ruled out in the reaction of epoxide in the presence of Lewis acid.[7]

These studies prompted us to investigate the stereochemistry of the reaction of (+)-1,2-epoxybutane with benzene in the presence of Lewis acid. 3-Phenyl-1-butanol (II) and 3-chloro-1-butanol (IV) were obtained in the reaction in an optically active form, besides (−)-2-phenyl-1-butanol (I) and (−)-2-chloro-1-butanol (III). The formation of optically active II and IV indicates the asymmetric induction at the carbon adjacent to the terminal methyl group of the epoxide. Such an induction in the presence of Lewis acid has not been reported. Its mechanism was discussed on the basis of the stability of the transition state conformations. The stereochemistry of conversion of 2-chloro-1-butanol (III) into 3-phenyl-1-butanol (II) was also investigated.

Results

The reaction of (+)-1,2-epoxybutane with benzene in the presence of Lewis acid was carried out in carbon disulfide at −20—+30 °C. After three hours, the resulting mixture was worked up as reported previously,[3] a mixture of I and II together with a mixture of III, IV, and V being obtained. The structures of these products were identified by comparison of IR and NMR spectra and retention time in gas chromatogram with those of authentic samples. The isomers were separated by means of preparative glpc or recrystallization of the α-naphthylurethane derivatives. The isomer composition in the products was determined by glpc. The results are given in Table 1.

The total yield of the phenylbutanols (I and II) and the relative amount of II to I increased with an increase in temperature, while that of the chlorobutanols (III, IV, and V) decreased with a rise of temperature. The chlorobutanols were scarcely formed at 20—30 °C.

Treatment of III with benzene in the presence of aluminum chloride gave II.[3] In carbon disulfide, the reaction of III with aluminum chloride and bromide gave IV and a mixture of 2-bromo-1-butanol and 3-bromo-1-butanol, respectively (see Experimental). However, no conversion of I into II occurred under these conditions.[3] Thus, if the conversion of III into IV is possible in the reaction of the epoxide with benzene at a higher temperature (0—30 °C), IV formed should react immediately with benzene to afford II, IV thus being scarcely formed.

Stereochemistry. (−)-I and (−)-III, formed by fission of the secondary C–O bond in the (+)-1,2-epoxybutane, were obtained in almost 100% and 55—56% optical yields, respectively (Table 2). The absolute configuration of (+)-1,2-epoxybutane, (−)-I, and (−)-

Table 1. Reaction of (+)-1,2-epoxybutane with benzene in the presence of Lewis acid[a,b] —isomer compositions—

Run	Lewis acid	Temp. (°C)	Phenylbutanol Yield[c] (%)	Phenylbutanol Isomer % I	Phenylbutanol Isomer % II	Chlorobutanol Yield[c] (%)	Chlorobutanol Isomer % III	Chlorobutanol Isomer % IV	Chlorobutanol Isomer % V
1	$AlCl_3$	30	61	13	87	2	trace	0	100
2	$AlCl_3$	20	50	28	72	4	1	trace	99
3	$AlCl_3$	10	25	31	69	38	71	3	26
4	$AlCl_3$	0	33	43	57	35	79	1	20
5	$AlCl_3$	−10	40	51	49	29	81	2	17
6	$AlCl_3$	−30	33	86	14	49	72	17	11
7	$SnCl_4$	−10	41	98	2	34	59	37	4
8	$SnCl_4$	−20	38	98	2	36	61	36	3

a) Mole ratio: (+)-1,2-epoxybutane: Lewis acid: C_6H_6: CS_2=1: 1.2: 20: 10 b) Reaction time, 3 hr.
c) Based on (+)-1,2-epoxybutane used.

Table 2. Stereochemical results of 2-phenyl-1-butanol (I) and 2-chloro-1-butanol (III)[a]

Run	Lewis acid	Temp. (°C)	I $[\alpha]_D^{26}$[b]	I Optical yield (%)[c]	III $[\alpha]_D^{26}$	III Optical yield (%)[d]
1	$AlCl_3$	30	−11.3° (*c* 4.6, C_6H_6)	76		
2	$AlCl_3$	20	−12.6° (*c* 11, C_6H_6)	83		
3	$AlCl_3$	10	−13.5° (*c* 8.7, C_6H_6)	90	−13.0° (neat)	55
4	$AlCl_3$	0	−18.2° (neat)	100		
5	$AlCl_3$	−10	−14.3° (*c* 18, C_6H_6)	96	−13.3° (neat)	56
7	$SnCl_4$	−10	−15.0° (neat)	83	−18.1° (*c* 4.1, C_6H_6)	
8	$SnCl_4$	−20	−15.6° (neat)	87	−14.5° (*c* 28, C_6H_6)[e]	

a) Starting (+)-1,2-epoxybutane: $[\alpha]_D^{26}$ +8.3° (neat), 93% optical purity.[8b] b) Rotations were taken on the samples which contain II in the following percentage; 7, 9, 3, 4, and 4% in run 1, 2, 3, 7, and 8, respectively. c) Calculated from the reported rotation[9] $[\alpha]_D$ −19.5° (neat) or $[\alpha]_D$ −13.8° (*c* 5.9, C_6H_6) of (−)-II, and the optical purity of (+)-1,2-epoxybutane used. These values were uncorrected for the optical rotation due to II contained. d) Calculated from the reported rotation $[\alpha]_D^{25}$ +23.9° (neat)[9] of (+)-III and the optical purity of (+)-1,2-epoxybutane used. e) This fraction contains 4% of V and 2% of IV.

III has been established as *R*,[8] *R*,[9] and *S*,[10] respectively. It is apparent that the formation of (−)-I and (−)-III from (+)-1,2-epoxybutane proceeds with inversion of configuration in analogy with the reaction of (+)-propylene oxide. The lower optical yield of (−)-III obtained can be interpreted by the exchange of chlorine atom. The secondary halohydrin (V) formed by fission of the primary C–O bond in the epoxide was obtained in too low an yield to permit polarimetric measurement. However, V might be optically pure since the asymmetric center of the starting epoxide remains unchanged.

Table 3. Stereochemical results of 3-phenyl-1-butanol (II) and 3-chloro-1-butanol (IV).

Run	Lewis acid	Temp. (°C)	II $[\alpha]_D^{26}$[a]	α-Naphthylurethane $[\alpha]_D^{26}$ (*c* 10, $(CH_3)_2CO$)	α-Naphthylurethane Optical yield (%)[b]	IV $[\alpha]_D^{26}$ (*c* 7, C_6H_6)	IV Optical yield (%)[c]
1	$AlCl_3$	30	+2.3° (neat)	+3.1°	6.9		
2	$AlCl_3$	20	+2.3° (neat)	+4.6°	10.2		
3	$AlCl_3$	10	−0.05° (*c* 14, C_6H_6)	+1.5°	3.3		
4	$AlCl_3$	0	−0.5° (neat)	+1.5°	3.3		
5	$AlCl_3$	−10	−2.2° (*c* 14, C_6H_6)	−0.5°	1.1		
6	$AlCl_3$	−30				+14.6°	21.0
7	$SnCl_4$	−10				+38.8°	51.9
8	$SnCl_4$	−20				+41.8°	55.9

a) Rotations were taken on samples containing (−)-I in the following percentage; 8, 4, 4 and 5% in runs 2, 3, 4, and 5, respectively. b) Calculated from the rotation $[\alpha]_D^{26}$ +8.4° (*c* 10, $(CH_3)_2CO$) of α-naphthylurethane of (+)-II (optical purity 17.2%)[12] and the optical purity of (+)-1,2-epoxybutane used. c) Calculated from the rotation $[\alpha]_D^{25}$ +38.2° (*c* 7, C_6H_6) of (+)-IV (optical purity 51%).

TABLE 4. REACTION OF (−)-2-CHLORO-1-BUTANOL (III) WITH BENZENE IN THE PRESENCE OF ALUMINUM CHLORIDE

Run	(−)-III $[\alpha]_D^{26}$ (neat)	Temp. (°C)	Phenylbutanol Yield (%)	Isomer % I	Isomer % II	α-Naphthylurethane of II $[\alpha]_D^{26}$ (*c* 10, $(CH_3)_2CO$)	α-Naphthylurethane of II Optical yield (%)[c]
10[a]	−17.1°	10	70	trace	100	+8.4°	24.1
11[a]	−12.7°	20	75	10	90	+6.2°	23.7
12[b]	−13.3°	30	74	10	90	+5.5°	21.0

a) Mole ratio; (−)-III: $AlCl_3$: C_6H_6=1: 1.2: 100. b) Reaction was carried out in 1,2-dichloroethane. Mole ratio; (−)-III: $AlCl_3$: C_6H_6: $Cl(CH_2)_2Cl$=1: 1.2: 100: 20. c) See Table 3, footnote c.

Both II and IV were obtained in optically active form (Table 3). The glpc fraction corresponding to II was treated with α-naphthyl isocyanate to give its urethane, since a pure sample of II could not be isolated by means of preparative glpc. After repeated recrystallization of the urethane, the optical rotation was measured to determine the optical yield of II.

In the presence of aluminum chloride at 20 °C, (+)-II was obtained in 10.2% optical yield, while the reaction at −10 °C gave (−)-enantiomer of II in excess (1.1%) and (+)-IV in 20% optical yield. On the other hand, the reaction with stannic chloride gave (+)-IV in 56% optical yield at −20 °C and hardly any II even at elevated temperature. The results suggest that a new chiral center was formed in the carbon adjacent to the terminal methyl group in the epoxide.

In order to ascertain the possibility of asymmetric induction in the reaction of III to II, (−)-III was allowed to react with benzene in the presence of aluminum chloride. (+)-II was obtained in reasonable optical yield (24—25%) (Table 4). When (+)-II was treated with aluminum chloride in benzene under the same conditions, the specific rotation of (+)-II remained unchanged before and after the reaction. Thus successive racemization of (+)-II should not occur in the reaction with (−)-III.

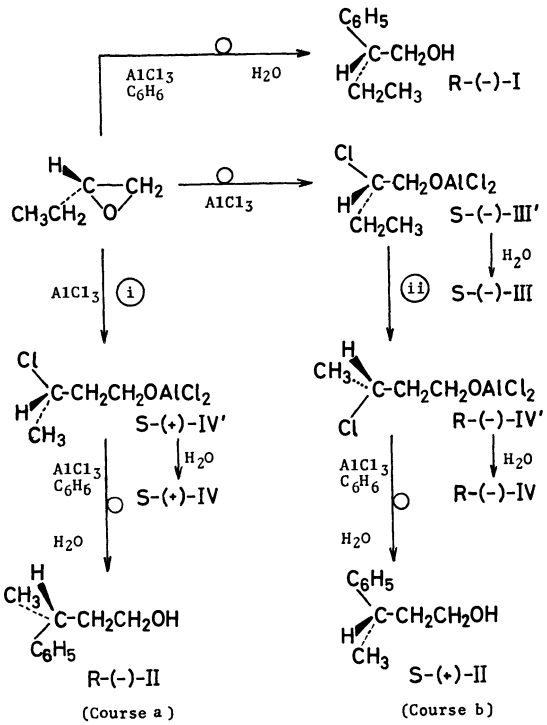

Scheme 1.

Discussion

The reaction of optically active IV with benzene by an aluminum chloride catalyst proceeded with inversion of configuration to give II in 20% optical yield.[11] The absolute configurations of (+)-II and (+)-IV have been established as *S*.[10,12] Thus the aluminum chloride salt of III or IV (III′ or IV′) would play an important role as an intermediate in the reaction of *R*-(+)-1,2-epoxybutane to optically active II.

In the overall reaction, two competing courses for the formation of II would be possible (Scheme 1). In course **a**, the ring opening reaction of *R*-(+)-1,2-epoxybutane yields directly *S*-(+)-IV′ (path i) which alkylates benzene with the inversion of configuration to give *R*-(−)-II. In course **b**, *S*-(−)-III′ was initially formed by the fission of the secondary C–O bond of epoxide, and then converted into *R*-(−)-IV′ (path ii) which reacts with benzene to give *S*-(+)-II. Paths i and ii should involve asymmetric induction at the carbon adjacent to the terminal methyl group of the epoxide. The other pathways, *R*-(+)-1,2-epoxybutane →*R*-IV′ and *S*-III′→*S*-IV′, should be excluded.

Formation of S-(+)-*IV from* R-(+)-*1,2-Epoxybutane.* The free carbonium ion mechanism was ruled out in the ring opening reaction of epoxide by the Lewis acid catalyst. This asymmetric induction may be rationalized as follows. The epoxide reacts initially with aluminum chloride to give a complex in which the secondary C–O bond is released and either of the hydrogens on C_3 migrates to C_2 from the back of the C_2–O bond to form a hydrogen bridge. Thus, the rotation about the C_2–C_3 bond would be restricted, and the chlorine atom of the complexing aluminum chloride would then attack intramolecularly C_3 from the back of the migrating hydrogen. If the C_2–O bond and the

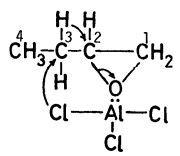

migrating hydrogen are in one plane and *trans* to each

other, the hydrogen on C_3 would migrate easily to C_2 as in the case of E_2 elimination.[13]

The Newman projections **A**, **B**, and **C** show the possible conformations of *R*-(+)-1,2-epoxybutane in the ground state. The conformational stability of **A**

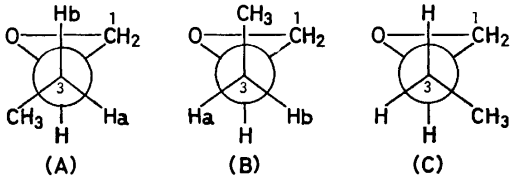

and **C** seems to be nearly equal, while **B** is less stable because of *gauche* interaction between three bulky groups (CH_3–, –O–, and $–CH_2$). However, the conformation **C**, in which the methyl group is *trans* to the C_2–O bond, should not participate in the asymmetric induction since the formation of the hydrogen bridge between C_2 and C_3 is unfavorable. The preferred conformation of epifluorohydrin has also been found to be type **A** by NMR spectroscopy.[14]

Thus the reaction from the stable **A** involves the bond breaking of C_2–O and the hydrogen bridging of Ha between C_2 and C_3, accompanied by an attack of chloride anion at C_3 from the back of Ha to give *S*-(+)-IV′, while the reaction from **B** should form *R*-(−)-IV′ by displacement of Hb from C_3 to C_2.

The enantiomeric product ratio (*S*/*R*) calculated from the optical yield of IV depends on the free energy difference between the two transition states:

$$\Delta\Delta G^{\ddagger} = \Delta G_S^{\ddagger} - \Delta G_R^{\ddagger} = -RT \ln (S/R)$$

where $\Delta G_S^{\ddagger}$ and $\Delta G_R^{\ddagger}$ are the activation free energy for the formation of *S* and *R* enantiomer, respectively. For example, the optical yield (21%) of *S*-(+)-IV in run 6 corresponds to 0.22 kcal/mol of free energy difference. The value implies the difference of steric interaction of the substituents on C_2 and C_3. Since the conformation in the transition state seems to reflect that in the ground state of the epoxide, the reaction from **A** should preferentially proceed to give *S*-(+)-IV in excess.

In the Meerwein-Ponndorf-Verley reduction of methyl isohexyl ketone with (+)-2-butanol to (+)-methylisohexylcarbinol in the presence of aluminum 2-butoxide, the asymmetric induction has been rationalized in terms of an optimal steric fit of the reagents involved, and the free energy difference between the two possible transition states, (a) and (b), have been reported to be 0.2 kcal/mol.[15] Thus, the above value of $\Delta\Delta G^{\ddagger}$ is reasonable.

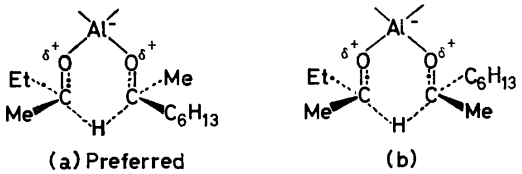

When stannic chloride was used as a catalyst, *S*-(+)-IV was obtained in 56% optical yield ($\Delta\Delta G^{\ddagger}$=0.64 kcal/mol). This might be interpreted in terms of the enhanced steric hindrance in the transition state due to the bulkiness of stannic chloride as compared with the case of aluminum chloride.

Formation of S-*(+)-II from* S-*(−)-III′ (or III).* The Lewis acid salt of *S*-(−)-III (III′) also has three conformations of *gauche* type, **D**, **E**, and **F**, in the ground state. In **D** and **E**, the C_2–Cl bond and the migrating

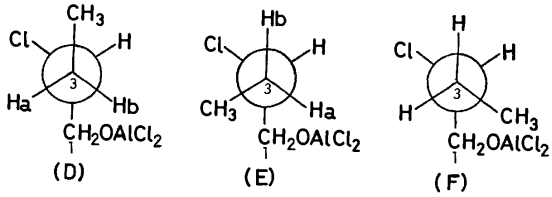

hydrogen are in one plane and *trans* to each other, while the C_2–Cl bond and the methyl group in **F** are *trans* to each other. Thus, the conformation **D** is more stable than **E** because of *gauche* interaction between three bulky groups (Cl–, CH_3–, and $-CH_2OAlCl_2$), and **F** should be ruled out in this asymmetric induction for the same reason as that in the case of conformation **C**.

The first step of the reaction from the stable **D** involves the bond breaking of C_2–Cl and the hydrogen bridging of Hb between C_2 and C_3, accompanied by the attack of chloride anion at C_3 from the back of Hb to give *R*-(−)-IV′. The intermediate then alkylates benzene with inversion of configuration in the presence of aluminum chloride to produce *S*-(+)-II. A similar reaction from **E**, which affords *S*-(+)-IV′ and then *R*-(−)-II, can be ruled out because of its unstable conformation.

On the other hand, *R*-(−)-II could be formed also from *S*-(+)-IV′ in course **a**. The final optical yield of II obtained should therefore be determined by difference of the reaction rate between courses **a** and **b**. Taking into account the preferential formation of *S*-(+)-II in this experiment, the reaction through course **b** would proceed in preference to that through course **a** except at low temperature.

In contrast, at low temperature (run 5, −10 °C) *R*-(−)-II was obtained in 1.1% optical yield. This can be rationalized by considerating that the ability of the catalyst to polarize the C_2–Cl bond of III′ so weakened that the rate of conversion of III′ into IV′ slowed down as compared with the above case.

The reaction with stannic chloride catalyst at low temperature gave two chlorobutanol isomers (III and IV) and 2-phenyl-1-butanol (I), but scarcely any 3-phenyl-1-butanol (II). This might be due to the minor catalytic ability of stannic chloride in the alkylation of benzene with IV (or IV′).

Experimental

All the melting points and boiling points are uncorrected. The optical rotations were taken on a REX photoelectric polarimeter with use of 0.5 and 1 dm tubes. The NMR spectra were determined on a JEOL JNM PS-100 spectrometer operating at a frequency of 100 MHz. Chemical shifts are given in ppm down field from internal TMS. The IR spectra were determined on a JASCO DS-301 spectrometer. Glpc analyses were carried out on a 3 m column of

10% Carbowax 20 M on Diasolid L with a Shimadzu GC-3A instrument. Preparative glpc was carried out on a 3 m column of 25% Carbowax on C-22 with a Yanagimoto GCG-5DH instrument.

Materials. Benzene was washed with concentrated sulfuric acid and distilled after drying on sodium ribbon. Carbon disulfide was distilled over phosphorus pentachloride. Anhydrous aluminum chloride was prepared from high purity aluminum and dry hydrogen chloride. Commercial GR grade stannic chloride was used without further purification.

(+)-1,2-Epoxybutane was prepared by the method of Levene and Walti[8b] and Price and Spector[16] as follows: 1-hydroxy-2-butanone prepared from 1-chloro-2-butanone and potassium formate in methanol, was reduced microbiologically by the reductase of baking yeast to (+)-1,2-butanediol (bp 98—100 °C/18 mmHg, $[\alpha]_D^{26}$ +14.1° (*c* 10, EtOH), lit,[8b] $[\alpha]_D^{25}$ +12.6° (*c* 11, EtOH), 67% yield). The 1,2-butanediol was converted into (−)-1-bromo-2-butanol with dry hydrogen bromide at 0 °C (bp 75—78 °C/20 mmHg, α_D^{26} −8.3° (neat, 1 dm), lit,[8b] α_D^{22} −11.8° (neat, 1 dm), 40% yield). The bromobutanol containing 17% 2-bromo-1-butanol was treated with 50% aqueous solution of potassium hydroxide for conversion into (+)-1,2-epoxybutane. After being dried over anhydrous calcium sulfate (Drierite) and redistillation, the epoxybutane indicated bp 61 °C and α_D^{26} +8.40° (neat, 1 dm) (lit,[8b] α_D^{24} +8.75° (neat, 1 dm)).

Typical Reaction Procedure and Product Indentification. To a stirred mixture of benzene (39 g, 0.5 mol) containing aluminum chloride (8.0 g, 60 mmol) and carbon disulfide (39 g, 0.5 mol) was added a solution of (+)-1,2-epoxybutane (3.6 g, 50 mmol) in benzene (39 g, 0.5 mol). The reaction temperature was maintained at −10 °C throughout the course of addition, which required 1 hr. After the addition the resulting mixture was allowed to stand at −10 °C for 2 hr with stirring and was then poured onto a mixture of crushed ice and 20 ml of concentrated hydrochloric acid. The benzene layer was separated, washed with 6 M hydrochloric acid and then water, and dried over anhydrous sodium sulfate. After removal of solvent, the residue was distilled *in vacuo* to give 0.5 g of a chlorobutanols fraction (bp 82—85 °C/90 mmHg) and 3.9 g of a phenylbutanols fraction (bp 108—115 °C/20 mmHg). After purification by boric ester method,[17] the phenylbutanols fraction showed bp 75—79 °C/4 mmHg. The water layer was extracted five times with 50 ml portions of ether. The combined extracts were dried over anhydrous sodium sulfate. After careful removal of ether, the residue was distilled *in vacuo* to give 0.8 g of a mixture of chlorobutanols (bp 83—95 °C/71 mmHg). The chlorobutanols obtained from benzene and water layer were combined.

Determination of isomer percentages and separation of each isomer by glcp were carried out on a 10% Carbowax column (temperature: 210 °C for the phenylbutanols and 150 °C for the chlorobutanols) and a 25% Carbowax column (temperature: 230 °C for the phenylbutanols and 180 °C for the chlorobutanols), respectively. The isomer percentages and the optical rotations of each isomer are given in Tables 1, 2, and 3.

(−)-2-Phenyl-1-butanol (I): IR(neat); 3340 (νOH), 1050 (νC–OH), 700 and 760 cm^{-1} (δCH, mono-substituted phenyl). NMR ($CDCl_3$, 5%); δ 0.81 (triplet, 3H, $-CH_3$), 1.71 (quintet, 2H, $-CH_2-$), 1.56 (singlet, 1H, −OH), 2.68 (quintet, 1H, −CH=), 3.72 (doublet, 2H, $-CH_2O$), 7.22 (5H, phenyl). α-Naphthylurethane of (−)-I; mp 72 °C; $[\alpha]_D^{26}$ +29° (*c* 1.4, C_6H_6), (Found: C, 78.10; H, 6.70; N, 4.14%).

(+)-3-Phenyl-1-butanol (II): IR(neat); 3340 (νOH), 1050 (νC–OH), 700 and 760 cm^{-1} (δCH, mono-substituted phenyl). NMR ($CDCl_3$, 5%); δ 1.26 (doublet, 3H, $-CH_3$), 1.50 (singlet, 1H, −OH), 1.84 (quartet, 2H, $-CH_2-$), 2.88 (sextet, 1H, −CH=), 3.54 (triplet, 2H, $-CH_2O-$), and 7.20 (5H, phenyl). α-Naphthylurethane of (+)-II; mp 86—87 °C; $[\alpha]_D^{26}$ +4.6 (*c* 10, CH_3COCH_3), (Found: C, 78.47; H, 6.62; N, 4.53%).

(−)-2-Chloro-1-butanol (III): The glpc retention time and IR were identical with those of an authentic sample prepared by the method of Markownikoff[18] and Freudenberg and Lwowski.[10] NMR ($CDCl_3$, 7%); δ 1.06 (triplet, 3H, $-CH_3$), 1.64—1.96 (multiplet, 3H, $-CH_2-$), 2.29 (singlet, 1H, −OH), and 3.56—4.08 (multiplet, 3H, $-CH_2O-$ and −CH=).

(+)-3-Chloro-1-butanol (IV): The glpc retention time and IR were identical with those of an authentic sample prepared by the lithium aluminum hydride reduction of 3-chlorobutanoic acid.[19,20] NMR ($CDCl_3$, 7%); δ 1.56 (doublet, 3H, $-CH_3$), 1.84—2.06 (multiplet, 2H, $-CH_2-$), 2.24 (singlet, 1H, −OH), 3.81 (triplet, 2H, $-CH_2O-$), and 4.25 (sextet, 1H, −CH=).

1-Chloro-2-butanol (V): The glpc retention time and IR were identical with those of an authentic sample prepared by the lithium aluminum hydride reduction of 1-chloro-2-butanone. NMR ($CDCl_3$, 7%); δ 0.98 (triplet, 3H, $-CH_3$), 1.59 (quintet, 2H, $-CH_2-$), 2.27 (singlet, 1H, −OH), and 3.37—3.85 (multiplet, 3H, $-CH_2Cl$ and −CH=).

Reaction of (−)-2-Chloro-1-butanol (III) with Benzene. To a stirred mixture of benzene (29 g, 0.38 mol) containing aluminum chloride (1.81 g, 14 mmol) and carbon disulfide (21 g, 0.28 mol) was slowly added a solution of (−)-III (1.23 g, 11.3 mmol, $[\alpha]_D^{26}$ −12.7—−17.1° (neat)) in benzene (15 g, 0.09 mol). The reaction mixture was maintained at 10—20 °C throughout the course of addition. The resulting mixture was worked up as mentioned above. The results are given in Table 4.

Reaction of a Mixture of 2-Chloro-1-butanol (III) and 1-Chloro-2-butanol (V) with Aluminum Chloride. To a stirred mixture of carbon disulfide (42 g, 0.56 mol) containing aluminum chloride (1.6 g, 12 mmol) was added a solution of III and V (III: V=66: 34, 1.1 g, 10 mmol) in carbon disulfide (10 g, 0.13 mol) at 5 °C. After the resulting mixture was treated as mentioned above, a mixture of III, IV and V was obtained (0.44 g, bp 80—90 °C/70 mmHg, III: IV: V= 1: 58: 41).

Reaction of a Mixture of 2-Chloro-1-butanol (III) and 3-Chloro-1-butanol (IV) with Aluminum Bromide. To a stirred solution of carbon disulfide (42 g, 0.56 mol) containing aluminum bromide (3.2 g, 12 mmol) was added a solution of III and IV (III: IV=58: 42, 1.1 g, 10 mmol) in carbon disulfide (10 g, 0.13 mol) at 5 °C. After the resulting mixture was treated as mentioned above, a mixture of 2-bromo-1-butanol (VI) and 3-bromo-1-butanol (VII) was obtained (1.2 g, bp 90—100 °C/40 mmHg, VI: VII=25: 75).

The authors wish to thank Professor Katsuhiko Ichikawa and Professor Toshio Sugita of Kyoto University for their valuable discussions and encouragement. Financial support from the Saneyoshi Science Foundation is acknowledged.

References

1) S. Suga, T. Nakajima, A. Takagi, and T. Takahashi, *Kogyo Kagaku Zasshi*, **70**, 487 (1967); N. Milstein, *J. Heterocyclic Chem.*, **5**, 337 (1968).

2) S. Hata, H. Matsuda, and S. Matsuda, *Kogyo Kagaku Zasshi*, **70**, 2291 (1967).

3) Y. Nakamoto, T. Nakajima, and S. Suga, *ibid.*, **72**,

2594 (1969).
4) C. D. Nenitzescu, I. Gavat, and C. Cocora, *Ber.*, **73**, 233 (1940); A. M. Glatz, Al. C. Razus, and C. D. Nenitzescu, *Rev. Roumaine Chim.*, **11**, 555 (1966).
5) M. F. Ansell and G. F. Whitfield, *J. Chem. Soc., C*, **1971**, 1098.
6) S. Hata, K. Ono, H. Matsuda, and S. Matsuda, *Kogyo Kagaku Zasshi*, **73**, 1680 (1970).
7) T. Nakajima, S. Suga, T. Sugita, and K. Ichikawa, This Bulletin, **40**, 2980 (1967); T, Nakajima, S. Suga, T. Sugita, and K. Ichikawa, *Tetrahedron*, **25**, 1807 (1969).
8) a) P. A. Levene and H. L. Haller, *J. Biol. Chem.*, **74**, 343 (1927); b) P. A. Levene and A. Walti, *ibid.*, **94**, 369 (1931).
9) W. A. Bonner and T. W. Greenle, *J. Amer. Chem. Soc.*, **81**, 3336 (1959).
10) K. Freudenberg and W. Lwowski, *Ann.*, **597**, 141 (1955).
11) S. Suga, T. Nakajima, Y. Nakamoto, and K. Matsumoto, *Tetrahedron Lett.*, **1969**, 3283.
12) K. Imano and S. Mitsui, *Nippon Kagaku Zasshi*, **85**, 497 (1964).
13) E. L. Eliel, "Stereochemistry of Carbon Compounds," McGraw-Hill Book Co., Inc., New York, N. Y. (1962), p. 140.
14) W. A. Thomas, *J. Chem. Soc., B* , **1968**, 1187.
15) W. von E. Doering and R. W. Young, *J. Amer. Chem. Soc.*, **72**, 631 (1950).
16) C. C. Price and R. Spector, *ibid.*, **88**, 4147 (1966).
17) E. Matsui, *Kogyo Kagaku Zasshi*, **41**, 168 (1941).
18) W. Markownikoff, *Ann.*, **153**, 228 (1870).
19) S. Searles, Jr., *J. Amer. Chem. Soc.*, **79**, 955 (1957).
20) S. Searles, Jr., K. A. Pollart, and F. Block, *ibid.*, **79**, 952 (1957).

Studies of Saturated Heterocyclic Compounds. II.[1] The Preparation and PMR Spectroscopic Study of Mono- and Di-substituted-1,3-dioxolan-4-ones

Yoshihiro ASABE, Shoji TAKITANI, and Yojiro TSUZUKI*

Faculty of Pharmaceutical Sciences, Science University of Tokyo, Ichigayafunagawara-machi, Shinjuku-ku, Tokyo 162
**Department of Chemistry, Science University of Tokyo, Kagurazaka, Shinjuku-ku, Tokyo 162*

(Received November 2, 1974)

The relationship of the configurations and the magnitude of the long-range spin coupling constants between the 2-H and 5-H, $J_{2,5}$, of 1,3-dioxolan-4-ones has been elucidated, the $J_{2,5}(trans)$ value being always larger than the $J_{2,5}(cis)$ value. Geometrical isomers of several 2,5-disubstituted derivatives have been separated by means of preparative tlc and assigned by means of PMR spectroscopy, especially by the use of their $J_{2,5}$ values. The sign of the $J_{2,5}$ values for a 2-trichloromethyl derivative has been determined by a partial decoupling experiment, both $J_{2,5}$ (*cis*) and $J_{2,5}$' (*trans*) being positive.

In a previous paper,[1] we reported that the magnitudes of the long-range coupling constants between 2-H and 5-H, $J_{2,5}$, of 1,3-dioxolan-4-ones may be useful for determining the configurations of geometrical isomers of 2,5-disubstituted derivatives because the derivatives containing phenyl and trichloromethyl groups showed fairly large $J_{2,5}$ values as a result of a dual-path mechanism[2,3] between 2-H and 5-H across the oxygen atoms, $J_{2,5}(trans)$ being larger than $J_{2,5}$ (*cis*).[4] Since stereochemical studies of 1,3-dioxolan-4-ones have been left undeveloped because of the difficulty of the isolation and identification of each isomer,[5–8] the measurement of the $J_{2,5}$ can be expected to be an effective method of their stereochemical assignments. Therefore, a detailed study has now been made with other derivatives.

In this paper, we will first examine whether configurational assignments using differences in phenyl-proton chemical-shifts in some *p*-substituted phenyl derivatives agree with those[1] previously obtained by using the spectral patterns of phenyl protons. Secondly, we will elucidate the relationship between the $J_{2,5}$ values and the configurations of these compounds. Next, the configurational assignments for geometrical isomers of several 2,5-disubstituted derivatives by PMR spectroscopy will be reported. Finally, the determination of the signs of $J_{2,5}(cis)$ and $J_{2,5}(trans)$ for a 2-trichloromethyl derivative by means of a partial decoupling experiment will be described.

Experimental**

*Preparation of Materials.*** 5-Substituted- and 2,5-disubstituted-1,3-dioxolan-4-ones were prepared from the corresponding *dl*-α-hydroxycarboxylic acids and aldehydes; each isomer of the 2,5-disubstituted derivatives was separated from the reaction mixture by means of preparative tlc.[1] The physical constants of these compounds are listed in Table 1. 2-Trichloromethyl-1,3-dioxolan-4-one (Bp 94.5—96 °C/7 mmHg, Mp 40—41 °C) was prepared by the reaction of glycolic acid and chloral.[7,9] All the sample were purified by repeated distillations or by recrystallization from suitable solvents before the measurement, and the 1,3-dioxolan-4-one ring was identified by means of its IR spectra ($\nu_{C=O}$).

Measurements. The PMR spectra were measured with a Varian A-60 spectrometer and a JNM 4H-100 spectrometer at room temperature. Carbon tetrachloride, chloroform-*d*, and acetone-d_6 were used as solvents (concentration: *ca.* 40—50 mg/0.5 ml), and TMS was used as an internal reference. The chemical shifts and coupling constants were recorded in δ and Hz respectively. The solutions were degassed for the partial decoupling experiments, but were not degassed for the other measurements. The mass spectra were measured with a Hitachi RMU-7M spectrometer (ionizing potential: 70 eV; chamber temperature: 150 °C), and the millimass data were calculated against the standard peaks (PFK or *n*-eicosane), using a Hitachi 002-type datalizer connected with the spectrometer. Since, in the low-mass spectra, no distinguishable difference between the geometrical isomers was observed under the present conditions, the measurements of the millimass spectra were carried out with only one of each pair. The IR spectra were measured using a Hitachi-Perkin Elmer 225 spectrometer in a carbon tetrachloride solution (*ca.* 0.2 mol/l, 0.1 mm KRS-5 cell) or KBr discs.

Results and Discussion

Table 2 shows the PMR spectral data for the phenyl protons of several 5-*p*-substituted phenyl derivatives; a higher-field part of the spectrum was used in an approximate analysis of the AA'BB' system in order to avoid complications due to additional larger couplings caused by 5-H. Moreover, the ring protons were assigned by the use of their benzylic couplings with 5-H: the higher-field part of the AA'BB' spectrum was attributable to the protons (A protons) *ortho* to the substituent group, while the lower-field part was attributable to the *meta*-protons (B protons).

By comparing the differences in chemical shifts between the A and B protons $|\Delta\delta_{AB}|$ obtained for the 2-trichloromethyl-5-*p*-substituted phenyl derivatives (Compounds **5** and **6**) in $CDCl_3$, the $|\Delta\delta_{AB}|$ values of the isomers with lower R_f values were found to be larger than those with higher R_f values, which are similar to the $|\Delta\delta_{AB}|$ values of 5-*p*-substituted phenyl derivatives (Compounds **2** and **3**). The same trend continues in the other solvents, although the chemical

** All the melting points and boiling points are uncorrected.

*** All the compounds except for the Compound **1** and the 2-trichloromethyl derivative are unknown.

Table 1. Physical constants of 1,3-dioxolan-4-ones

No.	Compound 2-R	5-R′		Bp, °C/mmHg (Mp, °C)	Millimass, M^+ (*m/e*) Found (Calcd)	$\nu_{C=O}$ cm^{-1}	R_f Value[c]
1	H	C_6H_5		124—125/5	—	1825[a]	0.31
2	H	*p*-Cl·C_6H_4		141/4	198.0084 ($C_9H_7ClO_3$=198.0083)	1825[a] 1790	0.35
3	H	*p*-$CH_3OC_6H_4$		137/1	194.0588 ($C_{10}H_{10}O_4$=194.0576)	1825[a] 1795	0.19
4	H	$C_6H_5CH_2$		112—113/1	178.0638 ($C_{10}H_{10}O_3$=178.0629)	1805[a]	0.31
5	CCl_3	*p*-Cl·C_6H_4	*cis*	needles (105—105.5)	313.9067 ($C_{10}H_6Cl_4O_3$=313.9071)	1837[a]	0.58
			trans	needles (102—102.5)	—	1835[a]	0.69
6	CCl_3	*p*-$CH_3OC_6H_4$	*cis*	needles (110—112)	—	1835[a] 1815	0.40
			trans	powder (52)	309.9581 ($C_{11}H_9Cl_3O_4$=309.9566)	1832[a]	0.51
7	CCl_3	$C_6H_5CH_2$	*cis*	needles (54—55)	293.9601 ($C_{11}H_9Cl_3O_3$=293.9617)	1820[a]	0.55
			trans	plates (54—55)	—	1823[b]	0.61
8	CBr_3	C_6H_5	*cis*	powder (112—113)	411.7969 ($C_{10}H_7Br_3O_3$=411.7947)	1800[b]	0.61
			trans	needles (95—96)	—	1810[b]	0.68
9	CH_3	*p*-Cl·C_6H_4	*cis*	112/2	—	1807[a]	0.37
			trans	needles (60—61)	212.0242 ($C_{10}H_9ClO_3$=212.0240)	1812[a]	0.24
10	CH_3	*p*-$CH_3OC_6H_4$	*cis*	plates (40)	208.0763 $C_{11}H_{12}O_4$=208.0735)	1807[a]	0.22
			trans	plates (58—59)	—	1815[a] 1804	0.17
11	CH_3	C_6H_5	*cis*	98—99/1	—	1805[a]	0.35
			trans	plates (46—47)	178.0632 ($C_{10}H_{10}O_3$=178.0629)	1813[a]	0.26
12	C_2H_5	C_6H_5	*cis*	105—107/1	192.0800 ($C_{11}H_{12}O_3$=192.0786)	1800[a]	0.40
			trans	125—126/2	—	1803[a]	0.32

a) In CCl_4. b) KBr disc. c) R_f values were determined on a silica gel plate, which was coated with silica gel HF_{254} (Merck) at 0.25 mm thickness and activated at 110 °C, 40 min. (developer: benzene; detection: UV light at 254 nm).

shifts (δ) of the phenyl protons in $(CD_3)_2CO$ shift toward a lower-field side than those in CCl_4 or $CDCl_3$. Accordingly, the isomers with lower R_f's, whose phenyl protons show larger $|\Delta\delta_{AB}|$ values, can be assigned to a *cis*-configuration, because the protons should be subject to the larger magnetic anisotropy of the *cis* 2-trichloromethyl group;[4] this assignement is in accordance with those previously reported.[1] In the case of compounds without any highly anisotropic substituent, such as the 2-methyl-5-*p*-methoxyphenyl derivative (Compound **10**), however, the $|\Delta\delta_{AB}|$ values are not useful for assigning the configuration because of an ambiguous difference between the *cis* and the *trans* isomer. Therefore, the $J_{2,5}$ values can be a more significant measure for this purpose, as will be discussed later. In all the compounds, no significant solvent effect on the coupling constants of the phenyl protons is observed.

Table 3 lists the PMR spectral data of the 5-substituted- and 2,5-disubstituted-1,3-dioxolan-4-ones used in this study. The $J_{2,5}$ values of the *trans* forms of Compounds **5** and **6** ($|J|$=1.4—1.6 Hz) are larger than those ($|J|$=1.0—1.2 Hz) of the *cis* forms. These J values are barely affected by the *p*-substituent on the 5-phenyl group or by the solvents. Although the $J_{2,5}$ values of the 5-substituted derivatives (Compounds **1**—**4**) are smaller than those of the 2,5-disubstituted ones, there is a distinguishable difference between the $J_{2,5}$(*trans*) and the $J_{2,5}$(*cis*) values. The assignment based on the $J_{2,5}$ values for the methylene protons of Compounds **1**—**4** are in agreement with that made on the basis of the deshielding effects of their phenyl group. The same relationship between $J_{2,5}$ values has been found in the corresponding compound, with the 2- and the 5-substituents being exchanged for one another,[1] and also in the 2-phenyl[1] and 2-trichloromethyl derivatives. In general, therefore, the isomers with larger $J_{2,5}$ values can be assigned to the *trans*-configuration.

Table 2. PMR Spectral data for phenyl protons of 5-*p*-substituted phenyl derivatives

Compound (2-R, 5-R′)			Chemical shifts (δ) A Protons	Chemical shifts (δ) B Protons	$\lvert\Delta\delta_{AB}\rvert$[a]	Coupling constants (Hz)[b] $\lvert J_{ortho}\rvert$	$\lvert J_{meta}\rvert$	$\lvert J_{para}\rvert$
2 (H, *p*-Cl·C_6H_4)		*a*	7.33		*ca.* 0			
		b	7.38		*ca.* 0			
		c	7.49		*ca.* 0			
5 (CCl_3, *p*-Cl·C_6H_4)	higher[c]	*a*	7.36		*ca.* 0			
		b	7.40		*ca.* 0			
		c	7.52	7.60	7.6	8.8	2.5	0.4
	lower[c]	*a*	7.32	7.50	8.0	8.6	2.5	0.4
		b	7.40	7.49	9.3	8.9	2.5	0.3
		c	7.48	7.63	11.4	9.0	2.5	0.4
3 (H, *p*-$CH_3OC_6H_4$)		*a*	6.83	7.24	41.3	9.0	2.5	0.4
		b	6.93	7.34	40.9	9.0	2.5	0.4
		c	6.98	7.37	39.4	9.0	2.5	0.4
6 (CCl_3 *p*-$CH_3OC_6H_4$)	higher[c]	*a*	6.86	7.26	40.0	8.8	2.5	0.3
		b	6.95	7.32	37.6	8.8	2.5	0.3
		c	7.01	7.46	45.0	8.8	2.5	0.2
	lower[c]	*b*	6.91	7.41	50.1	8.9	2.5	0.3
		c	7.00	7.49	48.8	8.8	2.5	0.2
10 (CH_3, *p*-$CH_3OC_6H_4$)	higher[c]	*a*	6.82	7.26	43.9	8.8	2.5	0.2
		b	6.91	7.34	42.6	8.9	2.5	0.2
		c	6.96	7.36	40.1	8.9	2.4	0.3
	lower[c]	*a*	6.82	7.24	42.0	8.8	2.5	0.3
		b	6.91	7.34	40.1	8.8	2.5	0.3
		c	6.97	7.36	39.2	8.8	2.5	0.3

a) Hz at 100 MHz b) J_{ortho}: $J_{AB}=J_{A'B'}$, J_{meta}: $J_{AA'}=J_{BB'}$, J_{para}: $J_{AB'}=J_{A'B}$ c) higher: isomer of higher R_f value, lower: isomer of lower R_f value *a*: in CCl_4, *b*: in $CDCl_3$, *c*: in $(CD_3)_2CO$.

Table 3. PMR Spectral data of 5-substituted- and 2,5-disubstituted-1,3-dioxolan-4-ones

Compound		Chemical shifts (δ) 2-H *cis*[a]	2-H *trans*[b]	5-H *cis*[c]	5-H *trans*[d]	Phenyl protons	Others	Coupling constant (Hz) $\lvert J_{2,5}\rvert$	$\lvert J_{gem}\rvert$	$\lvert J_{vic}\rvert$
									(2-CH_2)	
1	*a*	5.46(dd)	5.53(t)	5.07(s)		*ca.* 7.32(s)		0.7	0.4	0.4
	b	5.56(t)	5.63(t)	5.15(s)		*ca.* 7.38(c)		0.8	0.5	0.5
	c	5.63(dd)	5.71(t)	5.32(s)		*ca.* 7.42(c)		0.8	0.4	0.5
2	*a*	5.49(dd)	5.56(s)	5.05(s)		7.33(s)		0.9	0.4	0.5
	b	5.58(t)	5.65(t)	5.17(s)		7.38(s)		0.9	0.5	0.4
	c	5.68(dd)	5.80(t)	5.41(s)		7.49(s)		1.1	0.4	0.4
							(OCH_3)		(2-CH_2)	
3	*a*	5.43(dd)	5.51(s)	4.99(s)		6.83 7.24	3.73	0.9	0.4	0.5
	b	5.54(t)	5.62(t)	5.14(s)		6.93 7.34	3.79	0.9	0.5	0.4
	c	5.62(dd)	5.72(t)	5.29(s)		6.98 7.37	3.79	1.0	0.5	0.5
							(5-CH_2)		(5-CH_2)	(5H-CH_2)
4	*a*	5.21(d)	5.12(d)	4.29(m)		7.19(s)	2.95 3.10	1.0	0.5 14.7	6.9 4.0
	b	5.30(d)	5.12(t)	4.43(m)		7.27(s)	3.02 3.19	1.1	0.5 14.7	6.7 3.9
	c	5.39(s)		4.55(m)		7.29(c)	3.00 3.17	—	— 14.7	7.7 3.5
5 *cis*	*a*		5.89(d)		5.44(s)	7.32 7.50		1.0		
	b		5.97(d)		5.53(s)	7.40 7.49		1.0		
	c		6.33(d)		5.93(s)	7.48 7.63		1.0		
5 *trans*	*a*	5.97(d)		5.56(d)		7.36(s)		1.4		
	b	6.06(d)		5.66(d)		7.40(s)		1.6		
	c	6.58(d)		6.00(d)		7.52 7.60		1.4		
							(OCH_3)			
6 *cis*	*b*		5.89(d)		5.44(s)	6.91 7.41	3.80	1.1		
	c		6.24(d)		5.79(s)	7.00 7.49	3.81	1.2		
6 *trans*	*a*	5.92(d)		5.49(s)		6.86 7.26	3.75	1.5		
	b	6.03(d)		5.62(d)		6.95 7.32	3.81	1.6		
	c	6.49(d)		5.86(d)		7.01 7.46	3.82	1.5		

Compound			Chemical shifts (δ) 2-H *cis*[a]	2-H *trans*[b]	5-H *cis*[c]	5-H *trans*[d]	Phenyl protons	Others	Coupling constants (Hz) $\lvert J_{2,5}\rvert$	$\lvert J_{gem}\rvert$	$\lvert J_{vic}\rvert$
								(5-CH_2)		(5-CH_2)	(5H-CH_2)
7	*cis*	*a*		5.66(d)		4.55(m)	7.22(s)	3.13 3.17	1.0	14.6	7.2 5.8
		b		5.77(d)		4.68(m)	7.29(s)	3.20 3.24	1.1	14.6	7.9 5.0
		c		6.09(d)		5.00(m)	7.32(s)	3.20 3.26	1.0	14.6	9.7 3.3
	trans	*a*	5.35(d)		4.88(m)		7.24(s)	3.07 3.19	1.5	14.6	4.7 4.5
		b	5.45(d)		4.97(m)		7.30(s)	3.11 3.25	1.5	14.6	4.8 4.7
		c	5.90(d)		5.16(m)		7.33(s)	3.15 3.28	1.4	14.7	6.1 4.6
8	*cis*	*b*		5.77(d)		5.50(s)	*ca.* 7.41(c)		1.0		
		c		6.09(d)		5.87(s)	*ca.* 7.53(c)		1.0		
	trans	*b*	5.93(d)		5.71(d)		7.42(s)		1.5		
		c	6.40(d)		5.96(d)		*ca.* 7.52(c)		1.6		
								(CH_3)			(2H-CH_3)
9	*cis*	*a*		5.78(dq)		5.24(s)	7.35(s)	1.59(d)	0.8		5.1
		b		5.89(dq)		5.37(s)	7.39(s)	1.62(d)	0.9		5.0
		c		6.07(dq)		5.58(s)	7.49(s)	1.61(d)	0.9		5.0
	trans	*a*	5.70(dq)		5.06(d)		7.34(s)	1.62(d)	1.4		4.9
		b	5.80(dq)		5.19(d)		7.39(s)	1.66(d)	1.4		5.0
		c	5.93(dq)		5.46(d)		7.49(s)	1.64(d)	1.5		5.0
								(CH_3) (OCH_3)			(2H-CH_3)
10	*cis*	*a*		5.74(dq)		5.20(s)	6.82 7.26	1.55(d) 3.74	0.8		5.0
		b		5.87(dq)		5.34(s)	6.91 7.34	1.59(d) 3.78	0.9		5.0
		c		5.99(dq)		5.45(s)	6.96 7.36	1.56(d) 3.78	1.0		5.0
	trans	*a*	5.62(dq)		4.99(s)		6.82 7.24	1.57(d) 3.73	1.0		5.0
		b	5.76(dq)		5.17(s)		6.93 7.33	1.65(d) 3.79	1.3		5.0
		c	5.86(dq)		5.34(s)		6.97 7.36	1.61(s) 3.80	1.3		5.0
								(CH_3)			(2H-CH_3)
11	*cis*	*a*		5.76(dq)		5.26(s)	*ca.* 7.34(c)	1.56(d)	0.8		5.0
		b		5.88(dq)		5.39(s)	*ca.* 7.40(c)	1.60(d)	0.9		5.0
		c		6.04(dq)		5.54(s)	*ca.* 7.44(c)	1.59(d)	1.0		5.0
	trans	*a*	5.67(dq)		5.07(d)		7.35(s)	1.60(d)	1.2		4.9
		b	5.78(dq)		5.21(d)		7.41(s)	1.65(d)	1.4		5.0
		c	5.90(dq)		5.41(d)		7.44(s)	1.63(d)	1.5		5.0
								(CH_2) (CH_3)		(2H-CH_2)	(CH_2-CH_3)
12	*cis*	*a*		5.61(dt)		5.24(s)	7.34(s)	1.84(m) 1.04(t)	0.8	4.5	7.4
		b		5.74(dt)		5.37(s)	7.40(s)	1.89(m) 1.05(t)	1.0	4.6	7.3
		c		5.88(st)		5.52(d)	*ca.* 7.44(c)	1.93(m) 1.02(t)	1.0	4.8	7.4
	trans	*a*	5.51(dt)		5.07(d)		7.33(s)	1.88(m) 1.05(t)	1.2	4.6	7.3
		b	5.62(dt)		5.20(d)		7.40(s)	1.94(m) 1.07(t)	1.3	4.6	7.3
		c	5.75(dt)		5.41(d)		*ca.* 7.43(c)	1.97(m) 1.06(t)	1.3	4.7	7.5

a) *cis* to the 5-substituent group. b) *trans* to the 5-substituent group. c) *cis* to the 2-substituent group. d) *trans* to the 2-substituent group. *a*: in CCl_4, *b*: in $CDCl_3$, *c*: in $(CD_3)_2CO$. s: singlet or almost single peak, c: complicated singals, d: doublet, t: triplet, q: quartet, m: multiplet more than quartet, and for example, dd: doubly doublet.

On this basis, the configurations of the geometrical isomers of several 2,5-disubstituted derivatives (Compounds **7**—**12**) can be confirmed by the $J_{2,5}$ values.

In 2-trichloromethyl (or 2-tribromomethyl)-5-phenyl (or benzyl) derivatives (Compounds **5**—**8**), all of the *trans* isomers show higher R_f values than the *cis* isomers on the tlc coated with silica gel, whereas in the corresponding 2-methyl (or 2-ethyl) derivatives (Compounds **9**—**12**) the isomers with smaller $J_{2,5}$ values appeared at the upper band on the tlc. Thus, in the latter the isomers assigned as *cis* isomers give higher R_f values than those of the *trans* isomers. The R_f values of the methyl (or ethyl) derivatives listed in Table 1 are shown to be lower than those of the corresponding trichloromethyl (or tribromomethyl) derivatives. A different behavior among the methyl (or ethyl) derivatives and the trichloromethyl (or tribromomethyl) derivatives was also observed on the chemical shifts of the 2-H and 5-H signals; the 2-H and 5-H signals in 2-trichloromethyl (or 2-tribromomethyl)-5-phenyl (or benzyl) derivatives (Compounds **5**—**8**) both appear at a slightly higher field in the *cis* than in the *trans* isomer, except for the 2-H signal of Compound **7**. However, in 2-methyl (or 2-ethyl) derivatives (Compounds **9**—**12**) the 2-H and 5-H signals both appear at a higher field in the *trans* than in the *cis* isomer.

Finally, since no report has been found on the signs of the $J_{2,5}$, we aimed at determining them by a partial

decoupling experiment. For this purpose, the 2-trichloromethyl derivative is the most suitable because a further complication due to additional couplings is eliminated; the PMR spectrum of this compound can be analyzed as an ABX system, in which only twelve transitions were observed. The analysis gave the following results by the usual procedure: $\nu_A-\nu_B=15.0$ Hz, $\nu_B-\nu_X=126.9$ Hz, $|J_{AB}|=15.1$ Hz, $|J_{AX}|=0.2$ Hz, $|J_{BX}|=1.4$ Hz (at 100 MHz), and J_{AX} and J_{BX} are of the same sign. Since the J_{AB} value corresponds to a normal J_{gem} value, it is possible to assume a negative sign for the J_{AB}. Thus, a partial decoupling experiment on this spectrum has been carried out according to the usual method.[10] The experiment showed that J_{AX} and J_{BX} are both positive.

Further, on the basis of the magnetic anisotropy of the 2-trichloromethyl group,[7] the signals at the lower field (B proton) were assigned to one of the 5-methylene protons *cis* to the 2-trichloromethyl group, while the signals at the higher field (A proton) were assigned to the *trans* proton. Those assignments are in agreement with those made on the basis of the $J_{2,5}$ values.

The facts that both of the $J_{2,5}$ values have the same positive sign, and that the *trans* coupling constant has a larger value than the *cis* one, are in accordance with the empirical generalization found in 2,5-dihydrofurans[11] and 2,5-dihydropyrroles,[12] which may be considered to be isoelectronic with 1,3-dioxolan-4-ones. Therefore, in view of a resonance contribution, such as

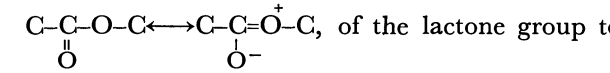

of the lactone group to the ring-planarity, as has been pointed out by Barfield *et al.*[13] the coupling mechanisms may be considered to be the same as those of 2,5-dihydrofurans.

The present work was supported in part by a Grant for the Encouragement of Scientific Research from the Ministry of Education. The authors wish to thank Mr. Hiroshi Toyama and Mr. Teruo Suzuki of the Japan Electron Optics Laboratory Co., Ltd., for their co-operation in the partial decoupling experiments, and also Prof. Nobuo Mori of this University for his helpful advice.

References

1) Part I: Y. Asabe, S. Takitani, and Y. Tsuzuki, This Bulletin, **46**, 661 (1973).
2) M. Barfield, *J. Chem. Phys.*, **41**, 3825 (1963).
3) K. Tori and M. Ohtsuru, *Chem. Commun.*, **1960**, 886.
4) L. A. Cort and R. A. Stewart, *J. Chem. Soc., C*, **1971**, 1386. They reported equal values for the $J_{2,5}$ (*cis*) and $J_{2,5}$ (*trans*) values of the 2-trichloromethyl-5-phenyl derivative. However, our result was different from theirs.
5) E. L. Salmi and A. Pohjolaninen, *Ber.*, **72**, 798 (1939).
6) M. Baron and D. P. Hollis, *Rec. Trav. Chim. Pays-Bas*, **84**, 1109 (1965).
7) M. Farines and J. Soulier, *Bull. Soc. Chim. Fr.*, **1970**, 332.
8) R. Brettle, *J. Chem. Soc., Perkin I*, **1972**, 611.
9) O. Wallach, *Ann.*, **193**, 1 (1878).
10) R. Freeman and D. H. Whiffen, *Mol. Phys.*, **4**, 321 (1961).
11) C. Barbier, D. Gagnaire and P. Vottero, *Bull. Soc. Chim. Fr.*, **1968**, 2330; D. Gagnaire and P. Vottero, *ibid.*, **1970**, 164.
12) T. J. Batterham, N. V. Riggs, A. V. Robertson, and W. R. J. Simpson, *Aust. J. Chem.*, **22**, 725 (1969).
13) M. Barfield, R. J. Spear, and S. Sternhell, *J. Amer. Chem. Soc.*, **93**, 5322 (1971).

Electrical Properties of 1,1-Diphenyl-2-picrylhydrazine and 2,2-Diphenyl-1-picrylhydrazyl Disks

Yoshiro SAKAI and Yoshihiko SADAOKA

Department of Industrial Chemistry, Faculty of Engineering, Ehime University, Bunkyo-cho, Matsuyama, Ehime 790

(Received April 30, 1974)

The electrical properties of 2,2-diphenyl-1-picrylhydrazyl (DPPH) disk were studied in the temperature range 18—60 °C over frequencies 3×10—3×10^6 Hz in comparison with those of 1,1-diphenyl-2-picrylhydrazine (DPPHn). The frequency dependence of conductance (σ_{ac}) for both DPPH and DPPHn can be explained in terms of the hopping conduction caused by localized states and/or shallow traps. At low frequencies, the strong dispersion of the capacitance of DPPH was observed while conductivity remained constant. This was accounted for by hyperelectronic polarization. The difference in electrical properties between DPPH and DPPHn indicates that the unpaired electrons in DPPH play an important role in the frequency independent conductance (σ_{dc}), but not in the frequency dependent conductance (σ_{ac}).

In 1962, Pollak showed[1] that the band type conduction should be essentially frequency-independent, whereas hopping conductivity should increase with increasing frequency of applied field.

It is known[2] that the monotonic increase of conductivity with an increase in frequency can be interpreted in terms of a hopping conduction mechanism in which carriers transit from one localized state to another. The localized states are formed when the interaction between molecules is weak.

Ac measurement is useful for studying the character of conduction since the ac currents are basically different for hopping and band conduction. Many workers have reported[3–5] that the apparent conductivity of aromatic compounds can be expressed as the sum of the frequency independent component (band conduction) and the frequency dependent component (hopping conduction).

2,2-Diphenyl-1-picrylhydrazyl (DPPH) is a well-known solid organic free radical and a semiconductor, but the frequency dependence of both conductivity and dielectric constant has not been studied in detail. We have studied the effects of unpaired electrons in DPPH on the electrical properties by measuring the frequency and the temperature dependence of conductivity and dielectric constant of both DPPH and 1,1-diphenyl-2-picrylhydrazine (DPPHn).

Experimental

DPPH was prepared by the method reported by Inokuchi *et al.*[6] and purified by repeated recrystallization from carbon disulfide which forms no molecular complex with DPPH.[7] DPPHn was purified by repeated recrystallization from ethyl ether. Samples were dried for one day *in vacuo* (about 10^{-5} Torr). Pulverized samples (about 200 mg) were compressed between stainless steel electrodes under pressure of about 220 kg/cm^2 *in vacuo* in order to eliminate the contact resistance and capacitance. The size of a sample was 0.05 cm$\times$3.14 cm^2. The sample was held *in vacuo* (about 10^{-3} Torr) in order to avoid the effect of adsorption of oxygen gas during the course of electrical measurements. Measurements were carried out with an ac bridge TR 10C (Ando Electric. Co. Ltd.). The dc conductivity of the DPPH was measured with an electrometer TR 8651 (Takeda Riken). The temperature of the sample was varied from 15 to 70 °C. It was found by ESR measurement that the purified DPPHn contains trace amounts of paramagnetic substance, probably DPPH, the concentration of which was estimated to be less than 10^{-6} spins/mol. The g value of impurity was determined to be 2.0036 by use of the frequency counter in ESR measurement.

Results and Discussion

In previous papers[8,9] it was shown that the frequency dependence of ac conductivity for aromatic compounds is expressed as

$$\sigma = \sigma_{ac} + \sigma_{dc} = A\omega^n + \sigma_0 \exp(-E/kT) \quad (1)$$

where $\sigma_{ac}(A\omega^n)$ and $\sigma_{dc}(\sigma_0\exp(-E/kT))$ are the frequency dependent and independent components, respectively. ω is the angular frequency ($\omega=2\pi f$). Lakatos and Abkowitz[2] have shown that if hopping takes place between a random distribution of localized states, σ_{ac} should be proportional to ω^n when $0.5<n<1.0$. n takes the lower value for multiple hops and the higher one for a single hop. Multiple hops occur frequently, at a high temperature, while the single hop predominates at a low one.

The frequency dependence of the apparent ac conductivity of DPPHn and DPPH is shown in Figs. 1 and 2, respectively. In the low frequency region

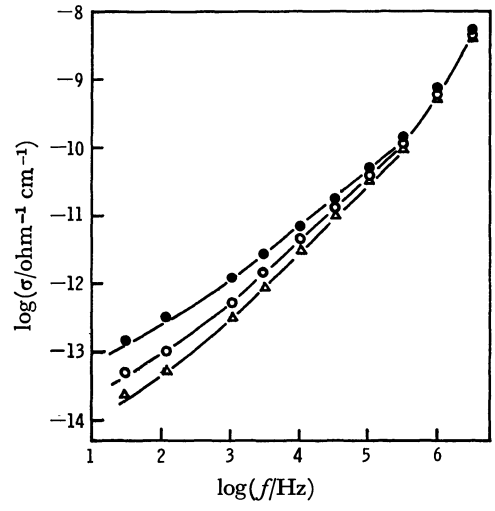

Fig. 1. Frequency dependence of observed conductivity of DPPHn at various temperatures.
(△) 10 °C, (○) 35 °C, (●) 70 °C.

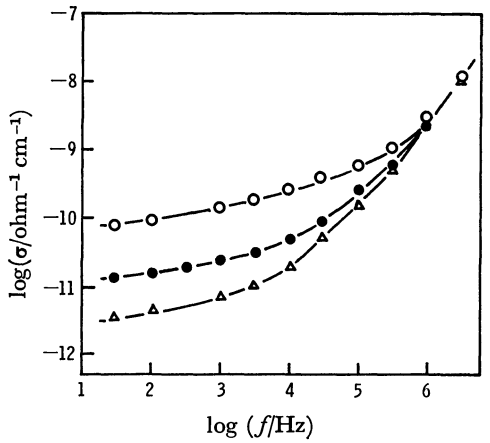

Fig. 2. Frequency dependence of observed conductivity of DPPH at various temperatures.
(△) 10 °C, (●) 32 °C, (○) 60 °C.

(below 3×10^3 Hz) the difference between the observed value for DPPHn and the straight line drawn by extrapolation from the high frequency region (1 kHz—1 MHz), on the assumption that σ_{ac} is proportional to ω^n, is defined as σ_{dc}. The value of σ_{dc} thus obtained is independent of the frequency within experimental error. The dc conductivity of DPPHn could not be measured by the usual dc method because of low conductivity (*i.e.*, specific conductivity $<10^{-13}$ ohm^{-1}·cm^{-1}).

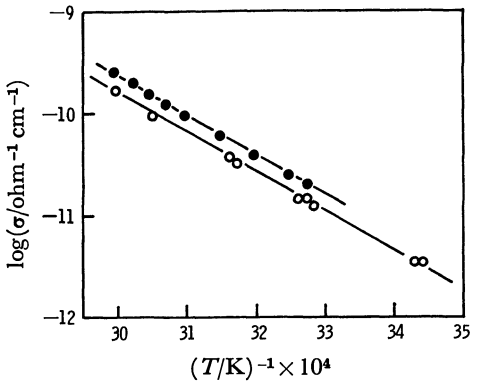

Fig. 3. Temperature dependence of dc and ac (30 Hz) conductivity of DPPH.
(○) ac method (applied frequency: 30 Hz)
(●) dc method (applied voltage: 10 V)
The difference of the conductivity between dc and ac methods is probably due to the difference of the standard resistance.

In the case of DPPH, at 30 Hz frequency the observed conductivity is about 10—10^2 times larger than that obtained by the extrapolation from high frequency region on the assumption that the relation $\sigma_{ac}=A\omega^n$ holds. The observed conductivity at 30 Hz is in good agreement with that obtained by the dc method (Fig. 3). We can thus assume that it is approximately equal to σ_{dc}, *viz.*, the frequency independent component.

The frequency dependence of σ_{ac} of DPPH was obtained by use of the value of σ_{dc}. The values of n in the relation $\sigma_{ac}=A\omega^n$, which were graphically obtained, are given in Table 1 for DPPHn and DPPH. The values are consistent with the thermally assisted hopping conduction mechanism in which n is expected to be between 0.5 and 1.0. The fact that the effect of temperature on σ_{ac} decreases with an increase in frequency indicates that the localized states (and/or shallow traps) are strongly affected by the frequency.

Table 1. Values of n for DPPHn and DPPH disks

DPPHn		DPPH	
Temp. °C	n in σ_{ac}	Temp. °C	n in σ_{ac}
18	0.9_0	18	0.8_0
35	0.8_0	32	0.6_5
70	0.7_5	42	0.5_0
85	0.6_5	54	0.5_0
		60	0.5_0

Since no distinct difference in σ_{ac} of DPPHn and DPPH was observed, the ac conduction of DPPH might be caused by the localized states produced by structural defects, impurities and/or π-electrons but not unpaired electrons.

In the higher frequency region (above 1 MHz) the conductivity is proportional to the square of frequency. This holds when the hopping distance becomes shorter as the frequency increases[10] and in extreme cases it becomes less than the distance between localized states. However, the electrical properties of ω^2 region can not be discussed in detail since the frequency dependence of the conductivity was not measured in a region higher than 3 MHz.

From the results shown in Fig. 3, the activation energy and pre-exponential factor σ_0 in Eq. (1) was estimated to be 0.75 ± 0.05 eV and 10 ohm^{-1} cm^{-1}, respectively. The dc conduction of DPPH should be due to the carriers excited into the localized states at the band edge (E_A) because the value of σ_0 thus obtained is smaller than that expected for the intrinsic band conduction by a factor of 10^2.[11] If the main carriers are thermally excited electrons in DPPH, and conduction is caused by hopping, we have

$$\sigma_{dc}=\sigma_0\cdot\exp\left[-(E_A-E_F+\Delta W_1)/kT\right], \qquad (2)$$

where ΔW_1 is the activation energy for hopping and E_A is the energy at the band edge (Fig. 4), the value of σ_0 being expected to be of the order 10—10^{-2} ohm^{-1}·cm^{-1}.[11] Since the activation energy of the photo-

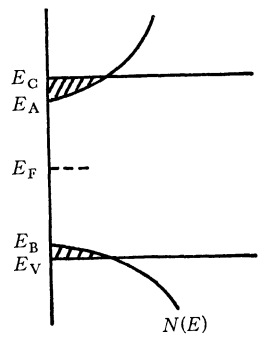

Fig. 4. Density of states as a function of energy in DPPH. Localized states are shown shaded.

Table 2. Dielectric constant for DPPH at 58 °C as a function of thickness and density

Thickness mm	Density g cm^{-3}	Dielectric constant 30 Hz	110 Hz
0.51	1.24	7.30	—
0.76	1.26	7.06	5.08
0.93	1.36	8.38	6.10
0.95	1.33	8.09	5.74
1.15	1.39	8.12	6.50
1.22	1.31	8.05	5.86

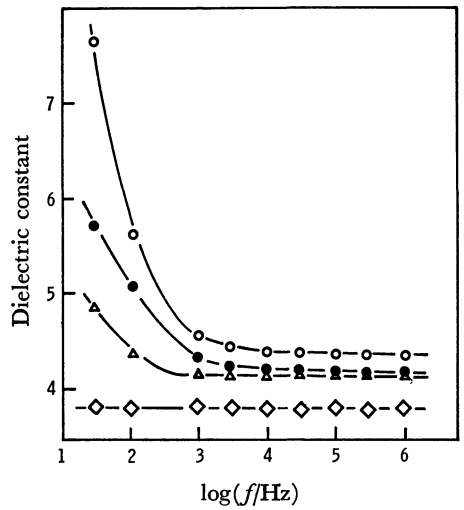

Fig. 5. Frequency dependence of dielectric constant of both DPPH and DPPHn at various temperatures. (○) DPPH 60 °C, (●) DPPH 54 °C, (△) DPPH 40 °C, (◇) DPPHn 18—70 °C.

conduction of DPPH film prepared by solvent evaporation has been estimated to be 0.16 eV by Eley and his co-workers,[12] it is expected that the activation energy for hopping (ΔW_1) takes the value of the order 0.1 eV.

On the other hand, the dielectric constant of DPPH shows a strong dispersion for frequency of the applied field and increases with increasing temperature while that of DPPHn remains constant (Fig. 5). The fact that in the case of DPPH the dielectric constant shows a strong dispersion in the low frequency region but conductivity does not can be explained in terms of interfacial polarization and/or hyperelectronic polarization. Since the observed dielectric constant is not a function of sample thickness (Table 2) and σ_{dc} obeys Ohm's law up to 10^3 V cm^{-1} at 50 °C, it is expected that the hyperelectronic polarization rather than the interfacial polarization takes place for DPPH.

Pohl *et al.*[13] showed that the strong dispersion of dielectric constant at low frequency can be explained by hyperelectronic polarization. Large molecules are expected to give high values of dielectric constant if the transit of electrons is more unlikely to occur between molecules than within molecules. The low value of σ_0 obtained above is in line with the assumption of hyperelectronic polarization since the thermally excited unpaired electron must pass over the activation energy for hopping. It is expected that the observed mobility takes a lower value than that expected for intrinsic band conduction. The assumption of hyperelectronic polarization can be confirmed by the fact that the conductivity is strongly dependent on pressure[14] and weakly dependent on frequency of the applied field. Hyperelectronic polarization is most likely to occur for DPPH in the low frequency region and low mobility may be explained by the electronic hopping between DPPH molecules. Since no similar tendency could be observed for DPPHn, the hyperelectronic polarization should be due to the unpaired electrons in DPPH.

References

1) M. Pollak, "Proc. International Conference on the Physics of Semiconductors," The Institute of Physics and the Physical Society, London, (1962) p. 86.
2) A. I. Lakatos and M. Abkowitz, *Phys. Rev.*, **B3**, 1791 (1971).
3) M. Kawabe, K. Masuda, and J. Yamaguchi, *J. Phys. Soc. Jap.*, **24**, 1281 (1968).
4) Y. Sakai and Y. Sadaoka, *Japan. J. Appl. Phys.*, **12**, 1463 (1973).
5) J. J. Fendley and A. K. Jonscher, *J. Chem. Soc. Faraday* I, 1213 (1973).
6) H. Inokuchi, Y. Harada, and Y. Maruyama, This Bulletin, **35**, 1559 (1962).
7) H. Inokuchi and M. Kinoshita, *ibid.*, **33**, 1627 (1960).
8) Y. Sakai and Y. Sadaoka, *Japan J. Appl. Phys.*, **12**, 1952 (1973).
9) Y. Sakai, Y. Sadaoka, and H. Yokouchi, This Bulletin, **47**, 1886 (1974).
10) M. Pollak, *Discuss. Faraday Soc.*, **50**, 13 (1970).
11) N. F. Mott and E. A. Davis, "Electronic Processes in Non-Crystalline Materials," Clarendon Press, Oxford, (1971), p. 200.
12) D. D. Eley, K. W. Jones, J. G. F. Littler, and M. R. Willis, *Trans. Faraday Soc.*, **62**, 3192 (1966).
13) H. A. Pohl, A. Rembaum, and A. Henry, *J. Amer. Chem. Soc.*, **84**, 2699 (1962).
14) H. Inokuchi, I. Shirotani, and S. Minomura, This Bulletin, **37**, 1234 (1964).

Nuclear Magnetic Resonance Studies of Bicyclic Thiophene Derivatives. II. Through Space H-F Coupling in *o*-Fluorophenyl Derivatives of Benzoylthiophene, Thienopyrimidine and Thienodiazepine Derivatives

Toshiyuki HIROHASHI, Shigeho INABA, and Hisao YAMAMOTO

Takarazuka Research Laboratories, Sumitomo Chemical Co., Takatsukasa, Takarazaka, Hyogo 665

(Received June 27, 1974)

Proton–fluorine coupling over six bonds has been observed between fluorine and H_β of the thiophene ring in *ortho* fluorophenyl derivatives of 4-phenylthienopyrimidines (**1**), 2-acetylamino-3-benzoylthiophenes (**2**), 5-phenyl-1,4-thienodiazepines (**3**) and 5-phenyl-1,4-thienodiazepine-4-oxides (**4**). The solvent effect and the *N*-methylation effect on the coupling constant can be explained by considering that the H–F coupling is a through space coupling. The value of coupling constant (J_{HF}: 0.5 Hz to 4.1 Hz) depends upon the geometry of the ring system condensed at 2-C and 3-C of thiophene ring, decreasing in the order of **1**>**2**>**3**>**4**. A discussion is given on the manner of steric repulsion between the benzene ring and some atoms on the other moiety of these compounds.

In a previous paper,[1] we reported on the ring current effect of the benzene ring on H_β and H_α (when Y=H_α) of the thiophene ring in 4-phenylthienopyrimidines (**1**), 2-acetylamino-3-benzoylthiophenes (**2**), 5-phenyl-1,4-thienodiazepines (**3**) and 5-phenyl-1,4-thienodiazepine-4-oxides (**4**).

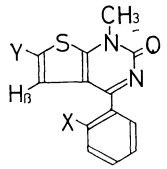

(1)

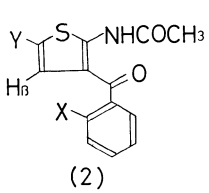

(2)

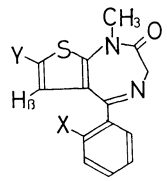

(3)

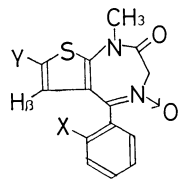

(4)

We have found that the H_β signal exhibits an extra splitting only when *ortho* substituent (X) of the benzene ring is fluorine, and that the amount of splitting is independent of the field. This indicates that there is a long range coupling over six bonds between H_β of the thiophene ring and fluorine on the benzene ring. Martin *et al.* did not mention such a H–F coupling between H_3 and fluorine in their NMR study of 2-(*o*-fluorobenzoyl)-thiophene (**5**).[2-3] The H–F coupling

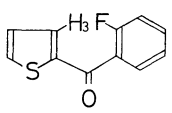

(5)

found in compounds (**1**)—(**4**) is considered to be a through space coupling. Compounds (**1**)—(**4**) are suitable for obtaining information on a H–F through space coupling, because each has a ring system condensed at 2-C and 3-C of the thiophene ring (*i.e.* compound (**2**) has a ring system by an intramolecular hydrogen bonding; see formula [IV] as well as Part I[1]) and has only one degree of freedom of internal rotation

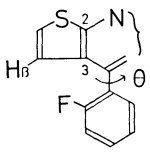

[I]

(*i.e.* torsional angle between the benzene ring plane and the thiophene ring plane; θ in formula [I]). The internuclear distance between H_β and fluorine in each of these compounds is simply related with θ, and the value of θ was estimated on the basis of ring current effect of the benzene ring on H_β.[1]

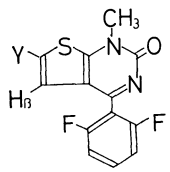

1aI (Y=H)
1bI (Y=Cl)

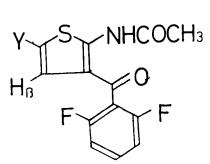

2aI (Y=H)
2bI (Y=Cl)

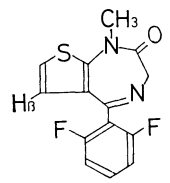

3aI

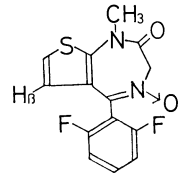

4aI

We have prepared *o,o'*-difluorophenyl derivatives (**1aI**, **1bI**, **2aI**, **2bI**, **3aI**, and **4aI**), and also 2-acetylamino-3-(*o*-fluorobenzoyl)thiophene derivatives (**2iB**, **2jB**, and **2kB**). They also supply information on the H–F through space coupling. Long range proton–fluorine through space coupling over five bonds or more has been a subject of interest.[4-10] Investigations have

2iB (Y = NO_2, R_1 = H)
2jB (Y = NO_2, R_1 = CH_3)
2kB (Y = Cl, R_1 = CH_3)

been made on the relation between J_{HF} and the spacial proximity of the coupled nuclei.[4,8–10] In this paper, we present our experimental results of these new compounds.

Results

NMR data for the fluorophenyl derivatives of compounds (**1**)—(**4**) are collected in Table 1. We see that the J_{HF} of *o*-fluorophenyl derivatives of compounds (**1**)—(**4**) is independent of substitution Y. The J_{HF} of compound (**3**) is also independent of the kind of substitution R_1. It depends, however, greatly upon the kind of ring system condensed at 2-C and 3-C of the thiophene ring. Thus, in the *o*-fluorophenyl derivatives, it is 0.5 Hz in compound (**4**), 1.2 Hz in compound (**3**), 2.7 Hz in compound (**2**) and 4.1 Hz in compound (**1**). In the *o,o'*-difluorophenyl derivatives, the H–F coupling is observed as a triplet. This may be explained by considering that H_β couples with two

Table 1. NMR data[a] for fluorine substituted compounds (**1**)—(**4**)

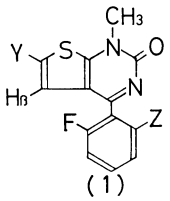

(1)

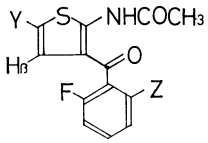

(2)

(3)

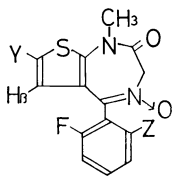

(4)

Compound	Y	Z	R_1	δ (ppm) H_α	δ (ppm) H_β	$J_{H_\beta, F}$ (Hz)
1aB	H	H	—	6.94[b]	7.07[b]	4.0 d[c]
1bB	Cl	H	—	—	6.93[b]	4.2 d
1aI	H	F	—	6.94	6.94	nv[d]
1bI	Cl	F	—	—	6.77	1.6 t[e]
2aB	H	H	—	6.66[b]	6.88[b]	2.6 d
2bB	Cl	H	—	—	6.74[b]	2.7 d[f]
2aI	H	F	—	6.67[g]	6.79[g]	1.3 t
2bI	Cl	F	—	—	6.63	1.5 t
3aB	H	H	CH_3	6.94[b]	6.68[b]	1.3 d[h]
3bB	Cl	H	CH_3	—	6.54[b]	1.2 d
3cB	H	H	H	6.83[b]	6.66[b]	1.2 d
3aI	H	F	CH_3	6.92[i]	6.65[i]	0.8 t
4aB	H	H	—	7.01[b]	6.52[b]	0.6 d
4bB	Cl	H	—	—	6.38[b]	0.5 d
4aI	H	F	—	7.03[i]	6.55[i]	bs[j]

a) See Experimental for protons not given here. b) Reported in Part I. c) Doublet. d) Not visible due to overlapping. e) Triplet. f) The observed splitting is field independent; $J=2.7$ Hz at 100 MHz ($CDCl_3$). g) $J_{H_\alpha, H_\beta}=5.8$ Hz. h) The observed splitting is field independent; $J=1.3$ Hz at 100 MHz ($CDCl_3$). i) $J_{H_\alpha, H_\beta}=5.7$ Hz. j) Broad singlet.

Table 2. Effect of *N*-methylation on $J_{H_\beta, F}$ (Hz)

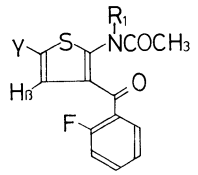

Compound	R_1	Y	$J_{H_\beta, F}$	$J_{HF(N-CH_3)}/J_{HF(N-H)}$
2iB	H	NO_2	3.0	60%
2jB	CH_3	NO_2	1.8	
2bB	H	Cl	2.7	59%
2kB	CH_3	Cl	1.6	

Table 3. Solvent effect on $J_{H_\beta, F}$ (Hz)

Compound	Solvent $CDCl_3$	Solvent DMSO-d_6
1bB	4.2	3.4
2aB[a]	2.6	2.1
3aB	1.3	1.2
4aB	0.6	0.5

a) $J_{NH, H_\alpha}=0.8$ Hz in $CDCl_3$ and 0.7 Hz in DMSO-d_6.

equivalent fluorine nuclei.[11] In compound **4aI**, H_β signal is observed as a broad singlet instead of a triplet. This suggests that the coupling constant is smaller than 0.5 Hz. In Table 2, the effect on J_{HF} by *N*-methylation of compound (**2**) is summarized. Each *N*-methyl compound (**2**) shows a smaller J_{HF} than the corresponding *N*-hydrogen compound. The solvent effect on J_{HF} of compounds (**1**)—(**4**) is summarized in Table 3. When the *o*-fluorophenyl derivatives of compounds (**1**)—(**4**) are measured in dimethylsulfoxide-d_6 solution, J_{HF} is found to be smaller than that in chloroform-*d* solution. In compound **2aB**, H_α couples with amide proton not only in chloroform-*d* but also in dimethylsulfoxide-d_6. This indicates that the carbonyl oxygen forms intramolecular hydrogen bonding with an amide proton to form a six membered ring also in dimethylsulfoxide-d_6, as well as in chloroform-*d* (see formula [IV] as well as Part I[1]).

Discussion

In order to explain the results of J_{HF}, let us assume as follows: of the two possible conformers [II] and [III], [II] is much more predominant in the *o*-fluorophenyl derivatives of Compounds (**1**)—(**4**). This is understandable, since [III] should be much less stable because of the Coulombic repulsion between the fluorine and imino nitrogen in compounds (**1**) and (**3**), carbonyl oxygen in compound (**2**), or oxygen atom of *N*-oxide in compound (**4**).[4] The assumption does not mean

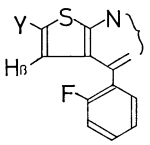

[II]

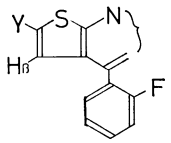

[III]

that the torsional angle θ between the benzene ring plane and thiophene ring plane is exactly zero degree in [II]. Let us define that [II] is a conformer in which $0° \leqq \theta < 90°$ and that [III] is a conformer in which $90° \leqq \theta < 180°$.

Proton-fluorine through Space Coupling. The observed proton-fluorine coupling is considered to be a through space coupling on the basis of the following observations.

Solvent Effect on J_{HF}: We see from Table 3 that changing the solvent from chloroform-*d* to dimethylsulfoxide-d_6 causes a significant reduction in the J_{HF} of the *o*-fluorophenyl derivatives of compounds (**1**)—(**4**). According to Adcock *et al.*,[4] such a solvent effect can be taken as indicating that the proton-fluorine coupling is a through space coupling; changing the solvent from chloroform-*d* to dimethylsulfoxide-d_6 should cause an increase in the dielectric of the medium as well as dipole-dipole interaction, and therefore, should cause dampening of the intramolecular Coulombic repulsion which controls conformational preference. Thus, the population of conformer [III] should increase on changing the solvent. Since in [III], the internuclear distance between H_β and fluorine is much greater than that in [II], the J_{HF} value should decrease by changing the solvent, if the coupling takes place through space. This is what was actually found.

Effect of N-Methylation on J_{HF}: *N*-Methylation of every compound in the series of compound (**2**) causes a lowering of the J_{HF} value to 60%. On the other hand, *N*-methylation of compound (**3**) causes no change in the J_{HF} value (*i.e.* compound **3cB**, $J=1.2$ Hz; compound **3aB**, $J=1.3$ Hz; see Table 1). The NH group of compound (**2**) forms an intramolecular hydrogen bonding with the carbonyl oxygen, so that a six membered ring is formed, as shown in formula [IV].

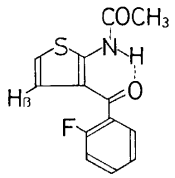

[IV]

On *N*-methylation, however, this hydrogen bonding is broken and there would be two possible conformers [V] and [VI]. In [VI], the internuclear distance

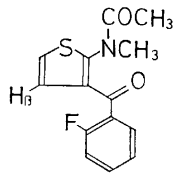

[V]

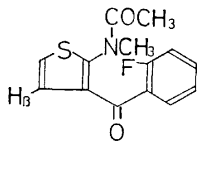

[VI]

between H_β and fluorine is much greater than in [V] or [IV]. In compound (**3**), on the other hand, no conformational change is expected by *N*-methylation. Thus it is understandable that no change in J_{HF} was observed.

Torsional Angle (θ) between the Benzene Ring Plane and Thiophene Ring Plane. The internuclear distance between H_β and fluorine in each of compounds (**1**)—(**4**) is considered to be related with the torsional angle between the thiophene and benzene ring planes (θ in formula [I]). The shielding effect of the benzene ring on H_β is also considered to be related with the torsional angle θ (see Part I[1]).

o-Fluorophenyl Derivatives of Compounds (1)—(4): As is seen from Table 1, J_{HF} of the *o*-fluorophenyl derivatives of compounds (**1**)—(**4**) decreases in the order of **1** ($J=4.1$ Hz)>**2** ($J=2.7$ Hz)>**3** ($J=1.2$ Hz)>**4** ($J=0.6$ Hz). As has been discussed in Part I,[1] the ring current effect of the benzene ring on H_β increases on going from compound (**1**) to compound (**4**) through compounds (**2**) and (**3**). It was thus assumed that the torsional angle θ increases in the order of **1**→**2**→**3**→**4**. Therefore, the internuclear distance between H_β and fluorine should increase in the order of **1**<**2**<**3**<**4**, and the J_{HF} value should decrease in this order, which is what was actually observed. This may be taken as an additional piece of evidence that the coupling between H_β and fluorine takes place through space. It also supports our previous conclusion that the torsional angle θ increases in the order of **1**<**2**<**3**<**4**.

TABLE 4. COMPARISON OF THE BENZENE RING CURRENT EFFECT ON H_β AND $J_{H_\beta \cdot F}$ BETWEEN *o*-FLUOROPHENYL COMPOUND AND *o,o'*-DIFLUOROPHENYL COMPOUND

Compound	**1b**	**2**[a]	**3a**	**4a**
J_{HF}(F) (Hz)	4.2	2.7	1.3	0.6
J_{HF}(FF) (Hz)	1.6	1.4	0.8	—
$J_{HF}(FF)/J_{HF}(F)$	38%	52%	62%	—
$\Delta\delta'$ (ppm)	0.16	0.10	0.03	−0.03

a) Average value of compounds **2a** and **2b**.

o,o'-Difluorophenyl Compounds (1)—(4): Let us next compare the J_{HF} value of *o,o'*-difluorophenyl compounds (**1**)—(**4**) (*i.e.* J_{HF}(FF)) with the one of the corresponding *o*-fluorophenyl compounds (*i.e.* J_{HF}(F)) (Table 4). J_{HF}(FF) is always smaller than the corresponding J_{HF}(F). This can be explained by considering that the torsional angle θ in the *o,o'*-difluorophenyl compound is greater than that in the corresponding *o*-fluorophenyl compound. The greater θ causes greater internuclear distance between H_β and fluorine, and therefore should cause a smaller J_{HF} value. This phenomenon can be explained by considering that the steric and Coulombic repulsion should be greater in *o,o'*-difluorophenyl compound than in *o*-fluorophenyl compound.[4] Let us examine the amount of decrease in the J_{HF} value on going from a *o*-fluorophenyl compound to the corresponding *o,o'*-difluorophenyl compound. The $J_{HF}(FF)/J_{HF}(F)$ values are given in Table 4 for compounds (**1**)—(**3**). The value becomes greater in the order of **1** (38%)<**2** (52%)<**3** (62%). Let us define $\Delta\theta$ as the amount of increase in θ on going from a *o*-fluorophenyl compound to the corresponding *o,o'*-difluorophenyl compound. Then, what has just been observed may be taken as indicating that the $\Delta\theta$ value is the greatest for compound (**1**).

For a comparison of the chemical shift of H_β of *o,o'*-difluorophenyl compounds (**1**)—(**4**) (*i.e.* δH_β(FF)) with that of the corresponding *o*-fluorophenyl com-

pounds (*i.e.* $\delta H_\beta(F)$), let us define $\Delta\delta'$ as $\Delta\delta' = \delta H_\beta(F) - \delta H_\beta(FF)$. As may be seen from Table 4, the $\Delta\delta'$ value becomes smaller in the order of **1**>**2**>**3**>**4**. This order of the $\Delta\delta'$ value must mean that the $\Delta\theta$ value becomes smaller in this order. Thus, the result is in accordance with that obtained from the $[J_{HF}(FF)/J_{HF}(F)]$ value.

The Steric Effect by the Ring System Condensed at 2-C and 3-C of the Thiophene Ring. It has become clear that the torsional angle between the benzene ring plane and thiophene ring plane increases in the order of **1**<**2**<**3**<**4**. This fact should be taken as indicating that the amount of steric hindrance depends on the geometry of the ring system condensed at 2-C and 3-C of the thiophene ring in each molecule.

The difference in steric hindrance between compounds (**3**) and (**4**) can be explained as follows. From a comparison of 5-phenyl-1,4-thienodiazepine (**3**) with the corresponding *N*-oxide compound (*i.e.* compound (**4**)), we see that the torsional angle between the benzene and thiophene ring planes should be greater for (**4**), since in compound (**4**) the steric hindrance exists between the benzene ring and oxygen atom of *N*-oxide, which is near the benzene ring. This extra steric repulsion forces the benzene ring out of the plane of the thiophene ring. An analogous steric hindrance was reported in the case of *p*-bromobenzophenone oxime *o*-picrylethers.[12]

It should be mentioned that in the preceding discussion we assumed that the ring system condensed at 2-C and 3-C of the thiophene ring is in the same plane as the thiophene ring plane in each series of compounds (**1**)—(**4**) (see Part I[1]). On the basis of this assumption, we have defined the torsional angle between the benzene ring plane and the thiophene ring plane as θ (see formula [I]). This assumption should be true for compound (**1**); the thienopyrimidine ring is considered to be flat. However, in compounds (**2**)—(**4**), it seems that the ring system condensed at 2-C and 3-C of the thiophene ring is not completely flat and that the thiophene ring plane is to some extent twisted out of the C–CO–C or C–(C=N)–C plane. Thus in order to discuss the degrees of the torsional angle between the benzene ring plane and the thiophene ring plane in more detail, it is necessary to define the torsional angle more correctly. Let us define the torsional angle between the thiophene ring plane and C–CO–C or C–(C=N)–C plane as θ_1 and the torsional angle between the benzene ring plane and C–CO–C or C–(C=N)–C plane as θ (see formula [VII] as well as formula [I]).

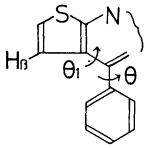

[VII]

In the subsequent discussion, the following point is tacitly assumed. Conformations where the benzene ring and the carbonyl group or imino group are coplanar (maximum π-π overlap) become strongly preferred whenever structurally possible.[17]

In compound (**2**), the thiophene ring plane is considered to be to some extent twisted out of the C–CO–C plane by a steric hindrance between H_β of the thiophene ring and the benzene ring, because the six membered ring by the intramolecular hydrogen bonding may not be so rigid. An analogous steric hindrance was reported in the case of 2-amino-*p*-bromobenzophenone.[13] Thus, there may be some freedom of rotation around C–C bond (expressed as θ_1 in formula [VIII]). Accordingly, in compound (**2**), the torsional angle between the benzene and thiophene ring planes can be expressed as θ_1 plus θ. In compound (**1**), θ_1 (see formula [VII]) is considered to be zero and thus the torsional angle can be expressed as θ (see formula [VII]). From experimental results, we can state that θ_1 plus θ in compound (**2**) is greater than θ in compound (**1**). The reason for this is as follows. Dreiding models of compounds (**1**) and (**2**) indicate that the bond angle C–CO–C or C–(C=N)–C (expressed as θ' in formula

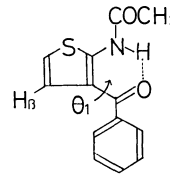

[VIII]

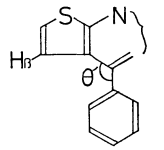

[IX]

[IX]) is a little smaller in compound (**2**). This should cause greater steric hindrance between H_β of the thiophene and benzene rings, thus causing a greater torsional angle between the benzene and thiophene ring planes in compound (**2**) than in compound (**1**).

Compound (**3**) is considered to take a boat form known in benzodiazepines.[14] In this conformation, the thiophene ring plane is considered to be to some extent twisted out of the C–(C=N)–C plane by θ_1 (see formula [X]). Accordingly, the torsional angle

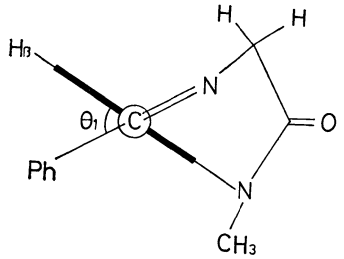

[X]

between the benzene and thiophene ring planes can be expressed as θ_1 plus θ. Experimental results suggest that θ_1 plus θ in compound (**3**) is greater than θ in compound (**1**). Presumably, θ_1 in compound (**3**) may be greater than θ in compound (**1**), and therefore θ_1 plus θ in compound (**3**) is greater than θ in compound (**1**).

Experimental

^{1}H NMR spectra were recorded at 60 MHz on a Hitachi NMR spectrometer R-20-B or 100 MHz on a JNM-4H-100 (Japan Electron Optics Lab.) in dilute deutero chloroform solution (about 10% w/v). The probe temperature was 35 °C. TMS was used as an internal reference standard. The chemical shifts are expressed in δ-values (ppm) downfield from TMS, and were measured directly from the spectra or from a frequency counter with a precision of $\pm$0.01 ppm. The coupling constants, measured by repeated sweeping at an expanded width (60 or 120 Hz), are expressed numerically in Hz with an accuracy of $\pm$0.1 Hz. IR spectra were recorded as Nujol mulls on a Hitachi Infrared Spectrophotometer, EPI-G-3 and are expressed as wave numbers. UV spectra were determined in 95% ethanol with an ultraviolet spectrophotometer, Hitachi-323, being expressed as λ_{max} mμ (ε). Melting points were measured on a Thomas-Hoover melting point apparatus and are uncorrected.

The synthetic procedures for the following compounds were reported in Part I.[1] 4-(*o*-Fluorophenyl)-1-methyl-1,2-dihydrothieno[2,3-*d*]-pyrimidin-2-one (**1aB**). 6-Chloro-4-(*o*-fluorophenyl)-1-methyl-1,2-dihydrothieno[2,3-*d*]-pyrimidin-2-one (**1bB**). 2-Acetamido-3-(*o*-fluorobenzoyl)-thiophene (**2aB**). 2-Acetamido-5-chloro-3-(*o*-fluorobenzoyl)-thiophene (**2bB**). 5-(*o*-Fluorophenyl)-1-methyl-1,3-dihydro-2*H*-thieno[2,3-*e*]-1,4-diazepin-2-one (**3aB**). 7-Chloro-5-(*o*-fluorophenyl)-1-methyl-1,3-dihydro-2*H*-thieno[2,3-*e*]-1,4-diazepin-2-one (**3bB**). 5-(*o*-Fluorophenyl)-1,3-dihydro-2*H*-thieno[2,3-*e*]-1,4-diazepin-2-one (**3cB**). 5-(*o*-Fluorophenyl)-1-methyl-1,3-dihydro-2*H*-thieno[2,3-*e*]-1,4-diazepin-2-one-4-oxide (**4aB**). 7-Chloro-5-(*o*-fluorophenyl)-1-methyl-1,3-dihydro-2*H*-thieno-[2,3-*e*]-1,4-diazepin-2-one-4-oxide (**4bB**).

The other compounds were prepared by the following methods.

*2-Acetamido-3-(o,o'-difluorobenzoyl)-thiophene (**2aI**).* This was prepared from 2-methyl-4*H*-thieno[2,3-*d*][1,3]-oxazin-4-one and *m*-difluorobenzene with *n*-buthyllithium according to the procedure applied to the synthesis of 2-acetamido-5-chloro-2',6'-difluorobenzophenone reported by Lemke *et al.*,[15] Yield 7.4%: mp 129—130 °C (from ether). IR: 3250, 3100, 3050, 1686, 1624. NMR: 2.33 (3H, s, $COCH_3$). UV: 238 (14100), 276 (11700), 346 (9500). Found: C, 55.69; H, 3.26; N, 4.84%. Calcd for $C_{13}H_9NO_2SF_2$: C, 55.51; H, 3.22; N, 4.98%.

2-Amino-3-(o,o'-difluorobenzoyl)-thiophene. (Method: see Part I, Experimental part, Method 1B). Yield 39.9%: mp 128.5—129.5 °C (from IPA). IR: 3350, 3250, 3150, 1620, 1590.

*2-Acetamido-5-chloro-3-(o,o'-difluorobenzoyl)-thiophene (**2bI**).* (Method: see Part I, Method 3). Yield 25.9%: mp 135—137 °C (from *n*-hexane–ether). IR: 3260, 3120, 1697, 1640, 1633. NMR: 2.32 (3H, s, $COCH_3$). UV: 245 (19300), 335 (9400). Found: C, 49.31; H, 2.43; N, 4.20%. Calcd for $C_{13}H_8NO_2SClF_2$: C, 49.46; H, 2.55; N, 4.44%.

4-(o,o'-Difluorophenyl)-1,2-dihydrothieno[3,2-d]-pyrimidin-2-one. (Method: see Part I, Method 4A). Yield 44.4%: It was used to the next step without further purification.

*4-(o,o'-Difluorophenyl)-1-methyl-1,2-dihydrothieno[2,3-d]pyrimidin-2-one (**1aI**).* (Method: see Part 1, Method 4A). Yield 11.6%: mp 212—213 °C (from ether). IR: 3055, 1645. NMR: 3.79 (3H, s, *N*-CH_3). UV: 245 (31300), 347 (5800). Found: C, 56.09; H, 2.90; N, 10.12%. Calcd for $C_{13}H_8N_2OSF_2$: C, 56.11; H, 2.90; N, 10.07%.

*6-Chloro-4-(o,o'-difluorophenyl)-1-methyl-1,2-dihydrothieno[2,3-d]-pyrimidin-2-one (**1bI**).* (Method: see Part 1, Method 5) Yield 22.2%: mp 150.5—151.5 °C (from Ethanol–Ether). IR: 3080, 3050, 1670. NMR: 3.72 (3H, s, *N*-CH_3). UV: 250.5 (28600), 355 (6400). Found: C, 49.94; H, 2.17; N, 8.91%. Calcd for $C_{13}H_7N_2OSClF_2$: C, 49.93; H, 2.66; N, 8.96%.

3-(o,o'-Difluorophenyl)-2-(N-phthalimidoacetyl)-aminothiophene. (Method: see Part I, Method 7B). Yield 73.2%: mp 184—189 °C (from acetone). IR: 3200, 1775, 1620.

3-(o,o'-Difluorophenyl)-2-(N-methyl-N-phthalimidoacetyl)-aminothiophene. (Method: see Part 1, Method 7B). Yield 54.7%: mp 192—193 °C (from acetone). IR: 3110, 3060, 1775, 1715, 1685, 1660, 1615.

*5-(o,o'-Difluorophenyl)-1-methyl-1,3-dihydro-2H-thieno[2,3-e]-1,4-diazepin-2-one (**3aI**).* (Method: see Part I, Method 7B). Yield 54.7%: mp 97.5—99.5 °C (from ether). IR: 3125, 3060, 1701, 1669, 1616. NMR: 3.54 (3H, s, *N*-CH_3), 4.52 (2H, s, CH_2). UV: 240 (22700), 315 (3000). Found: C, 57.50; H, 3.39; N, 9.69%. Calcd for $C_{14}H_{10}N_2OSF_2$: C, 57.53; H, 3.45; N, 9.58%.

2-(N-Acetyl-N-methyl)-amino-3-(o-fluorobenzoyl)-thiophene. (Method: see Part I, Method 4B). Yield 56.9%: mp 94—95 °C (from ether). IR: 3100, 1660, 1640, 1600.

*2-(N-Acetyl-N-methyl)-amino-5-chloro-3-(o-fluorobenzoyl)-thiophene (**2kB**).* (Method: see Part I, Method 3). Yield 71.4%: oil. IR: 1670, 1605. NMR: 1.98 (3H, s, $COCH_3$), 3.13 (3H, s, *N*-CH_3), 6.93 (1H, d, H_β).

*2-Acetamido-3-(o-fluorobenzoyl)-5-nitrothiophene (**2iB**).* This was prepared from 2-acetamido-3-(*o*-fluorobenzoyl)-thiophene (**2aB**) (already reported in Part I) with fuming nitric acid in the presence of acetic acid and acetic anhydride, according to the procedure applied to the synthesis of 2-nitrothiophene.[16] Yield 31.0%: mp 162—164 °C (from ethanol). IR: 3210, 3120, 1691, 1642, 1614. NMR: 2.39 (3H, s, $COCH_3$), 7.79 (1H, d, H_β), 12.12 (1H, s, NH). UV: 247 (15500), 343 (14400). Found: C, 50.35; H, 3.25; N, 8.93%. Calcd for $C_{13}H_9N_2O_4SF$: C, 50.65; H, 2.94; N, 9.09%.

*2-(N-Acetyl-N-methyl)-3-(o-fluorobenzoyl)-5-nitrothiophene (**2jB**).* This was prepared by the same method as that for **2iB** from 2-(*N*-acetyl-*N*-methyl)-amino-3-(*o*-fluorobenzoyl)-thiophene with fuming nitric acid. Yield 75.5%: mp 123—124.5 °C (from ethanol). IR: 3090, 1680, 1665, 1605. NMR: 2.11 (3H, s, $COCH_3$), 3.29 (3H, s, *N*-CH_3), 7.85 (1H, d, H_β). UV: 247 (16000), 323 (7100). Found: C, 52.02; H, 3.43; N, 8.62%. Calcd for $C_{14}H_{11}N_2O_4SF$: C, 52.17; H, 3.44; N, 8.69%.

*5-(o,o'-Difluorophenyl)-1-methyl-1,3-dihydro-2H-thieno[2,3-e]-1,4-diazepin-2-one-3-oxide (**4aI**).* (Method: see Part I, Method 9). Yield 54.9%: mp 104—107 °C (from ethanol). IR: 1682, 1627. NMR: 3.61 (3H, s, CH_3), 4.83 (2H, s, CH_2). UV: 248 (20500), 264 (17700), 310 (6400). Found: C, 54.60; H, 3.33; N, 8.92%. Calcd for $C_{14}H_{10}N_2O_2SF_2$: C, 54.54; H, 3.27; N, 9.09%.

The authors express their deep gratitude to Prof. Masamichi Thuboi, the University of Tokyo, and Dr. Makoto Sunagawa of this laboratory for their guidance and encouragement throughout this work. They are also indepted to Mr. Koichi Moriguchi for the measurement of 100 MHz NMR spectra and to Mr. Hiromi Sato for his co-operation in the synthetic experiments.

References

1) Part I: T. Hirohashi, S. Inaba, and H. Yamamoto, This Bulletin, **48**, 147 (1975).

2) M. L. Martin, C. Andrieu, and G. J. Martin, *Tetrahedron Lett.*, **1966**, 921.
3) C. Andrieu, M. L. Martin, and G. J. Martin, *Bull. Soc. Chim. Fr.*, **1967**, 698.
4) W. Adcock, D. G. Matthews, and S. Q. A. Rizvi, *Aust. J. Chem.*, **24**, 1829 (1971), and references therein.
5) W. Adcock and S. Q. A. Rizvi, *ibid.*, **26**, 2659 (1973).
6) P. A. Lehmann F., *Org. Magn. Resonance*, **5**, 61 (1973).
7) T. Kobayashi and M. Hirota, *Chem. Lett.*, **1972**, 975.
8) P. Martinson, *Acta Chem. Scand.*, **26**, 3529 (1972).
9) E. Abushanab, *J. Amer. Chem. Soc.*, **93**, 6532 (1971).
10) D. J. Gale and J. F. K. Wilshire, *Aust. J. Chem.*, **25**, 2145 (1972).
11) J. Burdon, *Tetrahedron*, **21**, 1101 (1965).
12) J. D. Mc Cullough, Jr., I. C. Paul, and D. Y. Curtin, *J. Amer. Chem. Soc.*, **94**, 883 (1972).
13) J. D. Misovic and S. M. Ramaseshan, *Glas. Hem. Drus. Beograd*, **32**, 253 (1976).
14) A. Camerman and N. Camerman, *J. Amer. Chem. Soc.*, **94**, 268 (1972).
15) T. L. Lemke, J. B. Hester, and A. D. Rudzik, *J. Pharmaceutical Sci.*, **61**, 275 (1972).
16) V. S. Babasinian, "Organic Synthesis," Coll. Vol. II p. 466 (1943).
17) G. Montaudo, P. Finocchiaro, and P. Maravigna, *J. Amer. Chem. Soc.*, **93**, 4214 (1971).

CNDO/2 Calculations of the Ionization Potentials and Electronic Spectra of Some Unsaturated Hydrocarbons

Toshio HAYASHI and Takeshi NAKAJIMA

Department of Chemistry, Faculty of Science, Tohoku University, Sendai 980

(Received July 23, 1974)

A modified CNDO/2 method in which local core matrix elements are taken to be empirical parameters is presented. Using this method, the ionization potentials and electronic spectra of some unsatutated hydrocarbons, ethylene, *trans*-, *cis*-1,3-butadienes, cyclobutene, cyclopentadiene, benzene and naphthalene, were calculated. The results are in general agreement with the previously available experimental information.

SCF MO methods including all valence-shell electrons have already been advanced by many authors.[1] It is, however, known that the traditional SCF calculations in *ab initio* and semiempirical frameworks are not always reliable in reproducing the electronic spectra and the ionization potentials at the same time.

The Complete Neglect of Differential Overlap method (CNDO), which is the simplest one among the SCF methods including all valence-shell electrons, was developed by Pople and his co-workers.[2-4] Although this method is quite successful in predicting ground-state geometries, it is not so useful in calculating electronic spectra and in interpreting ionization potentials through the use of Koopmans' theorem.[5]

In view of these facts, Tinland,[6] Clark,[7-8] and Del-Bene and Jaffé[9-11] have introduced empirical elements into the original CNDO/2 method and have thus obtained results which reproduce well the observed excitation energies. A new parameter set for reproducing ionization potentials has recently been proposed by Ohno *et al.*[13] It should be noted, however, that these modifications do not lead to a good result in predicting both the electronic spectra and the ionization potentials at the same time.

Under these circumstances, we wish now to propose a new parameter set to calculate both the ionization potentials and the electronic spectra within the framework of the CNDO approximation. We will apply this method to some unsaturated hydrocarbons and will compare the predicted electronic spectra with those obtained using the π-electron approximation and the calculated ionization potentials with those of other SCF MO calculations.

Method of Calculation

Tajiri *et al.*[14] and Ohmichi *et al.*[15] have calculated the electronic spectra of a number of saturated and unsaturated compounds using a modified CNDO/2 method which is a compromise between the methods of Bene-Jaffé[9-11] and of Sichel-Whitehead.[12]

Our method differs from the above one in the following points:

1) In the above method, as in the original CNDO/2 scheme, the local core matrix element, $U_{\mu\mu}$, of the atomic orbital, μ, is estimated from the atomic data:

$$U_{\mu\mu} = -\frac{1}{2}(I_\mu + A_\mu) - \left(Z_A - \frac{1}{2}\right)\gamma_{AA}$$

where I_μ and A_μ are the ionization potential and the electron affinity of the appropriate average atomic state respectively and where γ_{AA} is the average interaction energy between two electrons in any valence atomic orbital of the A atom. We consider this matrix element as an additional empirical parameter and adjust its value, together with the selected values of the bonding parameters and the separation constant (*vide infra*), so that a wide range of ionization potentials for ethylene may be reproduced.

2) According to the approximation proposed by Del Bene and Jaffé.[9-11] the core matrix element, $\beta_{\mu\nu}$, between the orbitals, μ and ν, on the A and B atoms respectively is assumed to be proportional to the overlap between them and is given by:[17]

$$\beta_{\mu\nu} = -\frac{1}{2}(\beta_A^\circ + \beta_B^\circ)(S_{\mu\nu}^\sigma + kS_{\mu\nu}^\pi)$$

where β_A° is the bonding parameter, which depends only on the nature of the A atom. $S_{\mu\nu}^\sigma$ is a σ component of the overlap which arises from the projection of the orbitals, μ, and ν, onto the bond axis, and $S_{\mu\nu}^\pi$ is a π component of the overlap which arises from the projections of μ and ν normal to the bond axis. k is the σ-π separation constant. The values of the parameters, $U_{\mu\mu}$, β_A°, and k, adopted in this paper are summarized and compared with those of previous authors in Table 1.

Table 1. Parameter values[a]

Parameter	Method	H	C
U_{ss}	CNDO/2[b]	−17.38	−70.3
	Ohmichi *et al.*[c]	−13.60	−50.69
	This method	−13.60	−42.0
U_{pp}	CNDO/2		−61.8
	Ohmichi *et al.*		−41.53
	This method		−40.0
β_A°	CNDO/2	9	21
	Ohmichi *et al.*	8	15
	This method	9	15
k	Ohmichi *et al.*		0.75
	This method		0.70

a) Values for U_{ss}, U_{pp} and β_A° are in eV units. b) Ref. 2—4. c) Ref. 15.

The molecular geometries used in this calculation were mostly taken from Sutton's tables;[18] the co-ordinates are shown in Fig. 1.

All the calculations were carried out on the NEAC 2200 model 700 computer of TOHOKU University, using the program of our modification of the CNDO/2

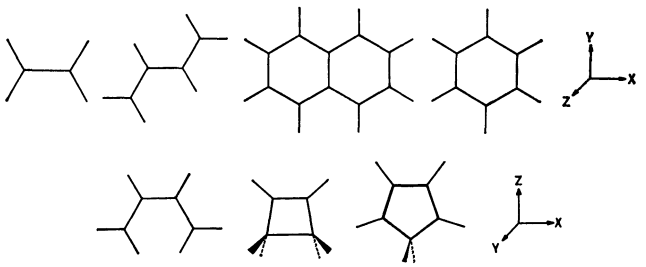

Fig. 1. Co-ordinate systems for calculated molecules.

method, including configuration interactions restricted to the 28 lowest singly excited configurations.

Results and Discussion

In Tables 2—7, the calculated orbital energies are given in comparison with the observed vertical ionization potentials (I.P.'s) and with the other calculated values.

Table 2. Ionization potentials of ethylene (eV)

Obsd[19]	Orbital	This work	CNDO[13]	MINDO[20]	*ab initio*[21]
10.51π	b_{1u}	10.59π	10.61π	10.39π[b]	10.05π
12.38	b_{1g}	12.95	12.96	11.47	13.91
14.47	a_g	14.41	14.51	11.65	15.88
15.68	b_{2u}	18.52	18.61	14.37	17.48
18.87	b_{3u}	19.74	21.21	19.21	21.70
23, 24.5[a]	a_g	26.63	29.54	28.01	27.97

a) T. Darrah Thomas, *J. Chem. Phys.*, **52**, 1373 (1970).
b) The orbital symmetries are not given in Ref. 20.

For ethylene (Table 2) the calculated energy of the lowest occupied orbital with the a_g symmetry is rather closer to the observed value than other calculations. This may be due to the facts that the main contribution to this orbital is by carbon 2s atomic orbitals and that the value of U_{ss} for the carbon atom chosen here is considerably smaller than that used in other methods (see Table 1). Both the present method and the earlier CNDO method by Ohno *et al.*[13] lead to a predicted energy of the b_{2u} orbital larger by about 3 eV than the observed value. It seems that this is due to the large relaxation energy of the ionized state inherent in this orbital. We have actually calculated the relaxation energies of the various ionized states of ethylene using the second-order perturbation method, and have

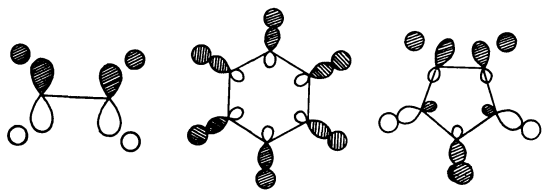

(a) (b) (c)

Fig. 2. The atomic-orbital arrangement of; a) the b_2-orbital of ethylene predicted at 18.52 eV, b) the a_1-orbital of benzene predicted at 20.50 eV and c) the a_1 orbital of cyclopentadiene predicted at 18.50 eV.

shown that the relaxation energy of this orbital is considerably larger than those of the other orbitals.[24] This is probably related to the atomic-orbital arrangement characteristic of this orbital, shown in Fig. 2; in this orbital, carbon 2p orbitals which are normal to the bond axis and which lie in the molecular plane are mutually bonding: at the same time, they are also bonding with the nearest hydrogen 1s orbitals.

Table 3. Ionization potentials of *trans*-1,3-butadiene (eV)

Obsd[20]	Orbital	This work	CNDO[13]	CNDO[8]	*ab initio*[23]
9.07π[a]	b_g	9.07π	9.78π	9.40π	9.74π
11.27	a_g	11.95	11.97	10.00	13.99
12.17π[a]	a_u	12.39π	11.47π	12.69π	12.98π
13.11	a_g	12.82	13.03	11.47	15.62
(13.9)[a]	b_u	13.57	13.99	12.20	15.48
15.16	b_u	16.13	16.85	14.90	17.96
17.78	a_g	17.43	17.63	16.33	18.07
19.02	a_g	20.15	22.18	19.30	22.80
20.56	b_u	20.96	21.42	19.71	21.09
	b_u	25.38	27.93	24.45	27.78
	a_g	29.27	31.92	27.62	30.18

a) Taken from the He I spectrum by Brundle and Robin (Ref. 22)

Table 3 shows that the first three bands of *trans*-1,3-butadiene are attributed to the π, σ, and π electrons, in the order of increasing energy. This interpretation differs from those of the earlier SCF MO calculations, but is consistent with the analysis of Brundle and Robin, who observed that the second ionization potential should be attributed to the σ electron because it suffers a large shift to a higher energy on fluorination (the perfluoro-effect).[22] Indeed, using the present method, we found that the second highest orbital with the symmetry, a_g, of *trans*-1,3-butadiene shifts to a

Table 4. Ionization potentials of *cis*-1,3-butadiene and cyclobutene (eV)

cis-1,3-Butadiene[a]			Cyclobutene[b]			
This work	Orbital	*ab initio*[23]	This work	Orbital	Calcd[28]	Obsd[27]
9.03π	a_2	9.63π	9.56π	b_1	$10.33(\pi)$	9.43π
12.25	a_1	14.31	10.72	b_2	12.03	10.9
12.33	b_2	14.61	11.22	a_1		
12.41π	b_1	12.98π	13.73	a_2		
13.84	b_2	16.38	14.51	a_1		
15.57	a_1	17.12	17.04	b_2		
17.53	b_2	20.24	18.25	a_1		
19.55	a_1	19.24	19.07	b_1		
21.97	a_1	23.32	21.99	b_2		
24.38	b_2	27.51	22.36	a_1		
30.23	a_1	30.34	34.29	a_1		

a) The bond lengths and the bond angles except the dihedral angle were assumed to be those of *trans*-1,3-butadiene. b) The geometry was assumed to be (in Å unit); C_1, C_4 (± 0.77, -1.5167); C_2, C_3 (± 0.67, 0); H_1, H_2, H_5, H_6 (± 1.2463, -1.7917, ± 0.9526); H_3, H_4, (± 1.22, 0.9526).

lower energy on fluorination,[25] while the first and third highest orbitals suffer no substantial change.

In Table 4, the results for *cis*-1,3-butadiene and cyclobutene, which are isomers of *trans*-1,3-butadiene, are given. The first I.P. of the *trans*-1,3-butadiene obtained is higher by about 0.04 eV than that of its planar *cis* form. This result is in agreement with that of the *ab initio* calculation by Buenker,[23] while the calculations of the MINDO and the π-electron approximation[26] show that the first I.P. of the *cis* form is higher by 0.03 eV than that of the *trans* form. The first two I.P.'s of cyclobutene obtained are attributed to the π and σ electrons, in good agreement with the experimental results.[27]

TABLE 5. IONIZATION POTENTIALS OF BENZENE (eV)

Obsd[29]	Orbital	This work	CNDO[13]	CNDO[7]	*ab initio*[31]
9.3π	e_{1g}	9.41π	9.77π	9.40π	10.31π
11.4	e_{2g}	11.34	11.48	9.79	14.30
12.1π	a_{2u}	13.93π	12.55π	12.99π	14.64π
13.8	e_{1u}	13.95	14.68	13.81	17.04
14.7	b_{2u}	14.79	15.30	14.26	17.96
15.4	b_{1u}	15.27	16.34	15.15	18.33
16.9	a_{1g}	20.50	20.93	19.64	20.16
19.2	e_{2g}	20.77	22.50	20.10	23.09
	e_{1u}	25.21	28.18	24.81	28.38
	a_{1g}	33.14	35.74	31.18	31.94

In Table 5, the calculated results of benzene are given, together with those of the photoelectron spectra which were studied and discussed by Lindholm and Jonsson;[29] also given are the results obtained from the viewpoint of the angular distribution by Carlson and Anderson.[30] The calculated order of orbitals is in general agreement with the experimental results, but the energies of the two levels are predicted to be rather larger than the observed values. One is the lower nondegenerate π orbital with the symmetry, a_{2u}, predicted at 13.93 eV, while the other is the a_{1g} orbital predicted at 20.50 eV, which is larger by about 3 eV than the experimental value. In case of the a_{1g} orbital, the disagreement may be related to the fact that the atomic-orbital arrangement of this orbital resembles that of the b_{2u} orbital of ethylene, for which the predicted I.P. is larger by 3 eV than the observed one (see Fig. 2).

TABLE 6. IONIZATION POTENTIALS OF CYCLOPENTADIENE (eV)

Obsd[32]	Orbital	This work	SPINDO[33]	EH[32]
8.57	a_2	8.77π	9.20π	12.6π
10.72	b_1	11.32π	10.68π	13.8π
12.2	a_1	11.63	12.24	13.5
12.6	b_2	12.05	12.38	13.8
13.2	b_2	12.81	13.30	14.0
13.8	a_1	13.21	12.87	13.9
14.8	b_1	16.85π	14.54π	15.6π
16.4	a_1	18.50	16.55	16.4
17.5	b_2	18.63	16.98	17.5
18.4	a_1	19.44	17.75	18.1
22.0	b_2	23.29	22.03	22.5
22.3	a_1	24.28	21.51	22.3
	a_1	33.85	26.17	26.5

As is shown in Table 6, the present results for cyclopentadiene are in good agreement with the values of the photoelectron spectra observed by Derrick *et al.*[32] and by Fridh *et al.*,[33] and also with those of the SPINDO calculation by Fridh *et al.*[33] except for the orbital symmetries of the two levels, which are found experimentally at 13.2 and 13.8 eV. The lowest π-orbital (b_1) predicted at 16.85 eV should correspond to the band observed at 14.8 eV, since, in our method, the energy of the lowest π-orbital is usually calculated to be larger by about 2 eV than the observed one. Furthermore, considering that the calculated energies for the b_{2u} orbital of ethylene and the a_{1g} orbital of benzene are higher by about 3 eV than the observed values, the a_1 orbital predicted at 18.50 eV may be assigned to the observed band at 16.4 eV, since this orbital includes the part resembling the b_{2u} orbital of ethylene (see Fig. 2).

The photoelectron spectra of naphthalene are more complicated, and the assignment of the higher I.P.'s is considerably difficult. From the discussion for the lowest π orbitals in benzene and cyclopentadiene, it seems that the lowest π orbital with the symmetry, b_{1u}, of naphthalene corresponds to the band at about 13 eV (Table 7).

TABLE 7. IONIZATION POTENTIALS OF NAPHTHALENE (eV)

Obsd[19,34]	Orbital	This work	CNDO[13]	*ab initio*[36]
8.11	a_{1u}	8.11π	9.21π	9.30π
8.79	b_{1u}	9.05π	9.48π	10.20π
9.96	b_{3g}	10.36π	10.49π	11.84π
10.90	b_{1g}	10.47	10.62	14.41
11.35	a_{1g}	10.69	10.83	14.20
11.90	b_{3u}	12.15	12.43	15.43
12.26	b_{2g}	12.16π	11.56π	13.51π
13.22	b_{2u}	12.79	13.62	16.57
	b_{3u}	13.13	13.52	17.15
	b_{1g}	13.72	14.56	17.26
	b_{2u}	14.42	15.77	18.19
	a_{1g}	14.66	15.25	17.99
	b_{1u}	14.98π	13.13π	15.66π
15.73	b_{1g}	15.69	17.81	20.36
	a_{1g}	17.10	17.86	19.52
18.65	b_{3u}	18.89	20.03	20.25
21.03	b_{2u}	21.09	22.90	23.71
	b_{3u}	21.81	23.39	24.11
	a_{1g}	22.16	23.37	23.15
	b_{1g}	23.76	26.89	27.88
	a_{1g}	24.89	27.76	28.47
	b_{2u}	26.86	29.97	29.64
	b_{3u}	31.41	33.89	31.16
	a_{1g}	34.33	37.18	33.00

The calculated transition energies were compared with the available experimental values and also with those obtained by the π-electron approximation. The lower ten singly excited states and the corresponding oscillator strengths are listed in Table 8. It may be seen that the calculated values are in good agreement

Table 8. The calculated and experimental transition energies (eV)

Compound	Type	Symmetry	Transition energy (f) This work	π-Approxn.[a]	Obsd
Ethylene	σ–π^*	$^1B_{3g}$	7.08		
	σ–π^*	$^1B_{2g}$	7.60		
	π–π^*	$^1B_{3u}$	7.64 (0.72)	7.6	7.64[b] (0.29)[c]
	π–σ^*	$^1B_{3g}$	8.73		
	⋮	⋮	⋮		
	σ–σ^*	$^1B_{3u}$	12.68 (0.2)		
trans-1,3-Butadiene	π–π^*	^1B_u	5.87 (1.07)	6.21	5.93[d] (0.53)[e]
	σ–π^*	^1A_u	5.94		
	σ–π^*	^1A_u	6.74		
	π–π^*	^1A_g	6.93 (0.0)	7.87	7.14
	σ–π^*	^1B_g	7.21		
	⋮	⋮	⋮		
	π–π^*	^1A_g	8.58 (0.0)	8.51	
	⋮	⋮	⋮		
	π–π^*	^1B_u	10.07 (0.42)	9.50	
cis-1,3-Butadiene	π–π^*	$^1B_2$	5.35 (0.404)	5.91	
	σ–π^*	$^1A_2$	6.28		
	σ–π^*	$^1B_1$	6.35		
	π–π^*	$^1A_1$	6.86 (0.114)	8.29	
	σ–π^*	$^1A_2$	7.23		
	⋮	⋮	⋮		
	π–π^*	$^1A_1$	8.89	8.34	
	⋮	⋮	⋮		
	π–π^*	$^1B_2$	9.92	9.25	
Cyclobutene	σ–π^*	$^1B_1$	5.48 (0.001)		
	σ–π^*	$^1A_2$	5.84		
	π–π^*	$^1B_2$	6.48 (0.328)	6.10[f]	6.32 (0.28)[g]
	π–σ^*	$^1A_2$	8.40		
	π–σ^*	$^1B_1$	8.69		
Cyclopentadiene	π–π^*	$^1B_2$	5.11 (0.23)	4.8 (0.105)[h]	4.8 (0.07)[i]
	σ–π^*	$^1B_1$	6.01 (0.002)		
	σ–π^*	$^1A_2$	6.29		
	π–π^*	$^1A_1$	6.36 (0.016)	6.3 (0.049)	6.3(s)
	σ–π^*	$^1A_2$	6.94		
	π–π^*	$^1B_1$	7.27 (0.004)	7.4 (0.002)	7.4(s)
	σ–π^*	$^1A_2$	8.03		
	π–π^*	$^1A_1$	8.12 (1.23)	7.9 (0.468)	7.9(vs)
	π–σ^*	$^1A_2$	8.34		
Benzene	π–π^*	$^1B_{2u}$	4.93 (0.0)	4.9	4.89[j]
	π–π^*	$^1B_{1u}$	6.03 (0.0)	5.3	6.14
	σ–π^*	$^1A_{2u}$	6.46		
	σ–π^*	$^1E_{2u}$	6.49		
	σ–π^*	$^1A_{2u}$	6.52		
	π–π^*	$^1E_{1u}$	6.89 (1.18)	7.0	6.76 (0.88)[c]
	σ–π^*	$^1B_{2g}$	7.80		
	π–π^*	$^1E_{2g}$	8.08 (0.0)		
	π–π^*	$^1E_{2g}$	10.25 (0.0)		
Naphthalene	π–π^*	$^1B_{3u}$	4.21 (0.0)	4.02 (0.0)[k]	3.97 (0.002)[l]
	π–π^*	$^1B_{2u}$	4.46 (0.23)	4.49 (0.256)	4.46 (0.18)
	σ–π^*	$^1B_{3g}$	5.40		
	π–π^*	$^1B_{1g}$	5.63 (0.0)	5.51 (0.0)	
	π–π^*	$^1B_{3u}$	5.70 (2.02)	5.94 (2.115)	5.63 (1.70)
	σ–π^*	$^1B_{2g}$	5.74		
	π–π^*	$^1A_{1g}$	5.75 (0.0)	7.10 (0.0)	
	σ–π^*	$^1B_{2g}$	6.19		
	π–π^*	$^1B_{2u}$	6.23 (0.59)	6.31 (0.966)	6.51 (0.21)
	π–π^*	$^1B_{1g}$	6.34 (0.0)	5.99 (0.0)	

a) Ref. 37, b) Ref. 38, c) Ref. 39, d) Ref. 40, e) Ref. 41, f) Ref. 28, g) Ref. 42, h) Ref. 10, i) Ref. 43, 44, j) Ref. 45, k) Ref. 46, l) Ref. 47.

with the observed ones. It may be noted here that the first two excited states of ethylene calculated are attributed to σ-π^* transitions, whereas the first excited state was observed as the Rydberg state by Willkinson.[36] If an extended basis set is used, then the Rydberg state might be calculated as the first excited state.

In our calculations, the triplet states are generally found to be lower by 0.5—1.0 eV than the experimental values. This point will not be discussed here.

In the following papers we will apply this method to the calculation of the electronic spectra and the ionization potentials of the unsaturated compounds containing O, N, and F atoms.

References

1) O. Sinanoğlu and K. B. Wiberg, "Sigma Molecular Orbital Theory," Yale University Press, New Haven and London (1970).
2) J. A. Pople, P. P. Santry, and G. A. Segal, *J. Chem. Phys.*, **43**, 129 (1965).
3) J. A. Pople and G. A. Segal, *ibid.*, **43**, 136 (1965).
4) J. A. Pople and G. A. Segal, *ibid.*, **44**, 3289 (1966).
5) T. Koopmans, *Physica*, **1**, 104 (1933).
6) B. Tinland, *Molec. Phys.*, **16**, 413 (1969).
7) P. A. Clark and J. L. Ragle, *J. Chem. Phys.*, **46**, 4235 (1967).
8) P. A. Clark, *ibid.*, **54**, 45 (1971).
9) J. Del Bene and H. H. Jaffé, *ibid.*, **48**, 1807 (1968).

10) J. Del Bene and H. H. Jaffé, *J. Chem. Phys.* **48**, 4050 (1968).
11) J. Del Bene and H. H. Jaffé, *ibid.*, **49**, 1221 (1969).
12) J. M. Sichel and M. A. Whitehead, *Theoret. Chim. Acta*, **7**, 32 (1967).
13) K. Ohno, T. Hirooka, Y. Harada, and H. Inokuchi, This Bulletin, **46**, 2353 (1973).
14) A. Tajiri, N. Ohmichi, and T. Nakajima, *ibid.*, **44**, 2347 (1971).
15) N. Ohmichi, A. Tajiri, and T. Nakajima, *ibid.*, **45**, 3026 (1972).
16) K. Nishimoto and N. Mataga, *Z. Phys. Chem.* **13**, 140 (1957).
17) R. L. Ellis, G. Kuehnlenz, and H. H. Jaffé, *Theoret. Chim. Acta*, **26**, 131 (1972).
18) L. E. Sutton, "Tables of Interatomic Distances," The Chemical Society, London (1958).
19) D. W. Turner, C. Baker, A. D. Baker, and C. R. Brundle, "Molecular Photoelectron Spectroscopy." John Wiley & Sons, New York (1970).
20) M. J. S. Dewar and S. D. Worley, *J. Chem. Phys.*, **50**, 654 (1969).
21) I. Fischer-Hjalmars and P. Siegbahn, *Theort. Chim. Acta* (Berl.), **31**, 1 (1973).
22) C. R. Brundle and M. B. Robin, *J. Amer. Chem. Soc.*, **92**, 5550 (1970).
23) R. J. Buenker and J. L. Whitten, *J. Chem. Phys.*, **49**, 5381 (1968).
24) K. Deguchi and T. Hayashi (unpublished).
25) T. Hayashi and T. Nakajima, to be published.
26) M. J. S. Dewar and S. D. Worley, *J. Chem. Phys.*, **49**, 2454 (1968).
27) P. Bischof and E. Heilbronner, *Helv. Chim. Acta*, **53**, 195 (1970).
28) F. H. Watson, Jr., A. T. Armstrong, and S. P. McGlynn, *Theoret. Chim. Acta* (Berl.), **16**, 75 (1970).
29) E. Lindholm and B. O. Jonsson, *Chem. Phys. Lett.*, **1**, 501 (1967).
30) T. A. Carlson and C. P. Anderson, *ibid.*, **10**, 561 (1971).
31) R. J. Buenker, J. L. Whitten, and J. D. Petke, *J. Chem. Phys.*, **49**, 2261 (1968).
32) P. J. Derrick, L. Asbrink, O. Edqvist, B. O. Jonsson, and E. Lindholm, *Intern. J. Mass Spec. Ion Phys.*, **6**, 203 (1971).
33) C. Fridh, L. Asbrink, and E. Lindholm, *Chem. Phys. Lett.*, **15**, 408 (1972).
34) J. H. D. Eland, Inter. *J. Mass Spec. Ion. Phys.*, **9**, 124 (1972).
35) R. J. Buenker and S. D. Peyerimhoff, *Chem. Phys. Lett.*, **3**, 37 (1969).
36) P. G. Willkinson, *Can. J. Phys.*, **34**, 643 (1956).
37) R. Pariser and R. G. Parr, *J. Chem. Phys.*, **21**, 767 (1953).
38) P. G. Willkinson and R. S. Malliken, *ibid.*, **23**, 1895 (1955).
39) V. J. Hammond and W. C. Price, *Trans. Faraday Soc.*, **51**, 605 (1955).
40) R. S. Mulliken, *Rev. Mod. Phys.*, **14**, 265 (1942).
41) R. S. Mulliken and C. A. Rieke, *Rep. Prog. Phys.*, **8**, 23 (1941).
42) B. B. Loeffler, E. Eberlin, and L. W. Pickett, *J. Chem. Phys.*, **28**, 345 (1958).
43) L. W. Pickett, E. Paddock, and E. Sackter, *J. Amer. Chem. Soc.*, **63**, 1073 (1941).
44) W. C. Price and A. D. Walsh, *Proc. Roy. Soc.*, **179A**, 201 (1941).
45) J. Petruska, *J. Chem. Phys.*, **34**, 1120 (1961).
46) R. Pariser, *ibid.*, **24**, 250 (1956).
47) H. B. Klebens and J. R. Platt, *ibid.*, **17**, 470 (1949).

Photochemistry in the Adsorbed Layer. III. Photolysis of Acetone Adsorbed on Porous Vycor Glass

Masakazu ANPO, Sōzi HIROHASHI, and Yutaka KUBOKAWA

Department of Applied Chemistry, College of Engineering, University of Osaka Prefecture, Mozu-Umemachi, Sakai, Osaka 591

(Received September 9, 1974)

Photolyses of acetone adsorbed showed that the ratio of ethane to methane in the products as well as the kinetic isotope effect for the methane formation is much smaller than that in the gas phase photolysis. The methane formed from acetone-d_6 contains a considerable amount of CD_3H. Ethane formation is quenched more efficiently by nitric oxide than methane formation. It is proposed that there are two types of methyl radicals, *i.e.*, long- and short-lived ones, the ethane resulting from the long-lived radicals. The results suggest that methane arises from hydrogen abstraction from surface OH groups as well as disproportionation reaction $CH_3+CH_3CO \longrightarrow CH_4+CH_2CO$, in addition to hydrogen abstraction from acetone molecules.

Studies were carried out on the photochemistry of alkyl ketones adsorbed on porous Vycor glass, general characteristics of the photochemistry in the adsorbed layer being found.[1] In the case of 2-pentanone the photolysis was seriously affected by the surface OH groups. The studies are concerned mainly with 2-pentanone and methyl ethyl ketone and very little with acetone. In the present work a detailed study has been made of acetone photolysis. We carried out nitric oxide quenching as well as isotopic studies in order to obtain information on the nature of the methane and ethane formation processes. The role of surface OH groups in the photolysis has been clarified by the study of acetone-d_6 photolysis.

Experimental

A conventional vacuum system was used in conjunction with a special quartz cell for studying the spectra and photolysis in the adsorbed layer. The specimen of porous Vycor glass (Corning, No. 7930) which had been heated in oxygen to remove carbonaceous impurities was placed inside the cell and degassed at 500 °C for 7 hr. After acetone had been adsorbed on the specimen at room temperature, photolysis was carried out with an ultra high pressure mercury lamp without filter. Prior to this, a small amount of acetone remaining in the gas phase was removed by means of a liquid nitrogen trap. When photolysis was completed, the reaction products were desorbed together with unreacted acetone and analyzed by gas chromatography. The BET surface area of the adsorbent was found to be 160 m^2/g. The amount of adsorbed acetone of 1.0 cm^3/g corresponded to $\theta=0.05$ using 25 A^2 as the area occupied by each molecule.

Acetone (Tokyo Kasei Kogyo Co., Ltd., Grade SG. 99.5 mol%) was dried by well-degassed molecular seive 4A and purified by bulb to bulb distillation. Acetone-d_6 of 99.5 mol% isotopic purity (E. Merck, Darmstadt.) was used without further purification.

Isotopic analysis of the deuterated methane was carried out with a Shimadzu MASPEQ-070 mass spectrometer using low-voltage electron (10—20 eV) in just sufficient amount to produce the ion of the parent mass. The CD_4/CD_3H ratio was determined by measurement of the parent peaks at $m/e=19$ [CD_3H^+] and $m/e=20$ [CD_4^+].

Results

1) Products of Acetone Photolysis in the Adsorbed Layer. The rates of methane and ethane formation plotted against the amount of acetone adsorbed are given in Fig. 1. It is seen that methane formation increases with an increase in the amount of acetone adsorbed. Ethane formation appears to level off to a constant value. The ratio of the amount of methane to that of ethane ranged from 0.6 to 4.3, being larger than the corresponding value in the gas phase photolysis.[2] Our results with acetone-d_6 photolysis (25 °C, 5.05 Torr) showed this ratio to be 0.067. This suggests that the recombination of methyl radicals was suppressed and their hydrogen abstraction reaction enhanced in the adsorbed layer. A slight formation of carbon monoxide as well as greatly reduced efficiency of photolysis compared to the gas phase are other features of acetone photolysis in the adsorbed layer.

2) Isotopic Analysis of the Methane Formed. The CD_3H content of methane formed by the photolysis of acetone-d_6 adsorbed is shown in Fig. 2. A large frac-

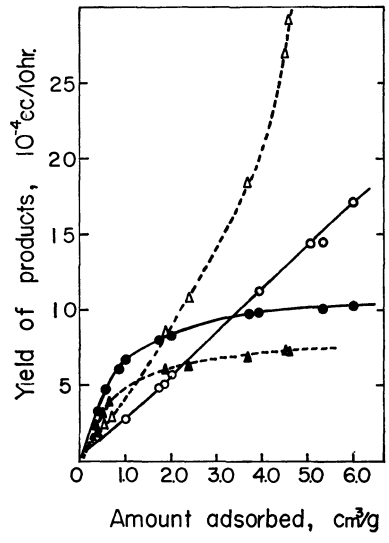

Fig. 1. Yield of products from the acetone photolysis. Irradiation time, 10 hr.; Temperature, 25 °C; △: methane, ▲: ethane (acetone), ○: methane, ●: ethane (acetone-d_6).

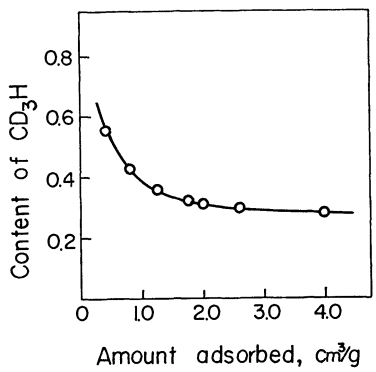

Fig. 2. The CD_3H content of the methane formed from the photolysis of acetone-d_6.

tion of the methane consists of CD_3H, decreasing with increasing amount of acetone-d_6 adsorbed. It appears that light hydrogen in the methane comes from the surface OH groups. The hydrogen atom abstraction reaction from the surface OH groups by methyl radicals, *i.e.*, $CD_3+[Si-OH]\rightarrow CD_3H+[Si-O]$, should be mentioned as the most probable process. Its activation energy is less than 9 kcal/mol,[3] being smaller than the corresponding value for the hydrogen atom abstraction from acetone molecules.[4] Thus, the hydrogen atom abstraction from the OH groups is expected to occur more easily. There is some possibility that light hydrogen atom is transferred according to the following steps:

$$CD_3COCD_3 + [Si-OH] \longrightarrow CD_2HCOCD_3 + [Si-OD] \text{ (Exchange Reaction)},$$

$$CD_2HCOCD_3 + h\nu \longrightarrow \dot{C}D_2H + CD_3\dot{C}O,$$

$$\dot{C}D_2H + CD_3COCD_3 \longrightarrow CD_3H + \dot{C}D_2COCD_3.$$

However, this could be excluded since the exchange reaction was found to be slow even under irradiation.[5] The occurrence of hydrogen atom abstraction from the surface OH groups suggests that porous Vycor glass should be regarded not only as an adsorbent but also as a photochemical reactant in the adsorbed layer.

3) Kinetic Isotope Effects for Methane Formation. In order to clarify the nature of the methane formation, the primary kinetic isotope effect for the photolysis of acetone adsorbed was investigated. The values of $R_{methane}/\sqrt{R_{ethane}}=A$[6] are plotted against the amounts of acetone adsorbed (Fig. 3). Marked isotope effects can hardly be expected for the recombination of methyl radicals in the adsorbed layer, suggesting that the observed isotope effects are attributable to the methane formation reaction. The difference in A values is negligibly small at very small amounts adsorbed, but increases with increasing amount adsorbed, the ratio k_H/k_D approaching 3~4. It has been reported that the ratio k_H/k_D for the hydrogen atom abstraction reaction from acetone molecules by methyl radical in the gas phase is more than 10,[7] which is much larger than the corresponding value in the adsorbed layer. This indicates that in the photolysis of acetone adsorbed the mechanism of methane formation differs from that in the gas phase. It appears that hydrogen atom abstraction from acetone molecules is not the main reaction leading to methane formation especially in the range of small amounts of acetone adsorbed.

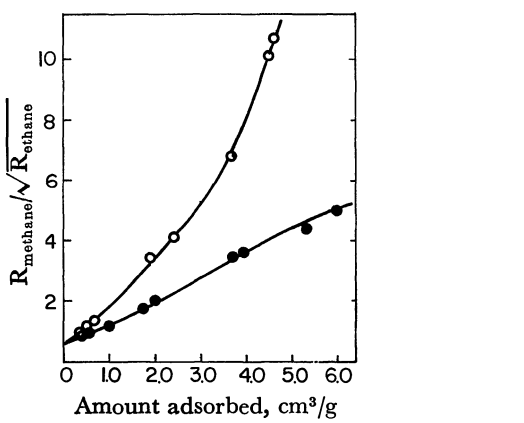

Fig. 3. The primary kinetic isotope effects for the photolysis of acetone adsorbed.
○: for acetone, ●: for acetone-d_6.

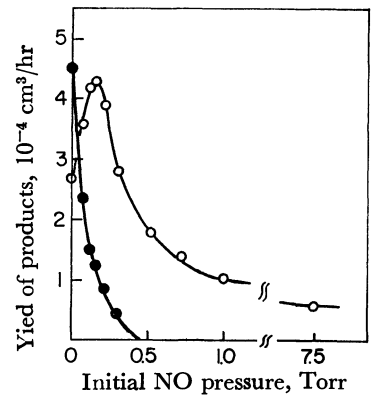

Fig. 4. Effect of nitric oxide upon the photolysis of acetone.
Amount of acetone-d_6 adsorbed, 1.91 cm³ S.T.P./g.
○: methane, ●: ethane.

4) Effect of Nitric Oxide upon Photolysis. Figure 4 shows the change in the rate of methane and ethane formation caused by added nitric oxide. The rate of ethane formation approaches zero with increasing pressure of nitric oxide, while the rate of methane formation increases at first, passes through a maximum and then decreases. Apart from a rate maximum observed in methane formation the rate decrease caused by added nitric oxide is attributable to its scavenging action of methyl radicals.[8] The pressure range in which the rate decreases is higher for methane formation than for ethane formation, suggesting that different types of

Table 1. Effect of nitric oxide upon the content of CD_3H

NO Pressure Torr	Content of CD_3H %
0.00	35.0
0.30	27.2
0.47	24.5
0.80	22.0
1.00	20.5

Amount of acetone-d_6 adsorbed, 1.91 cm³ S.T.P./g.

methyl radicals are operative in both formations. It was found that the CD_3H content in the methane formed decreased with increasing pressure of nitric oxide (Table 1).

Discussion

The following interpretation might be given as regards the two types of methyl radicals. Geminate radical pairs are held in a fixed position for a relatively long time before they separate from each other. The methyl radicals present in such radical pairs would be short-lived because of an efficient radical recombination leading to acetone formation. This primary recombination has been discussed in solution phase photochemistry. Leermakers *et al.*[9] postulated the occurrence of such phenomena in the adsorbed layer. Under such circumstances, a disproportionation reaction such as $CD_3+CD_3CO\rightarrow CD_4+CD_2CO$ would be expected to occur in addition to the recombination reaction. Such a reaction has been reported to take place to a small extent in gas[2] and solution phase[10] photolyses of acetone. The small kinetic isotope effect in methane formation (Fig. 3) suggests that methane is formed *via* a process having a small activation energy such as disproportionation of radicals. A small amount of ketene was found by mass spectroscopy in the reaction products, supporting the above conclusion. Methane formation is expected to be quenched less efficiently than reactions originated from other types of methyl radicals described below.

A methyl radical separated from its partner radical would be long-lived since it is sensitive to quenching by nitric oxide. Such methyl radicals would react in two ways, recombination to from ethane and hydrogen abstraction from acetone molecules. In cases where the abstraction reaction is the sole methane source, the rate of methane formation is expected to be larger for undeuterated acetone than for acetone-d_6 owing to its lower activation energy. As a result the rate of ethane formation will be larger for acetone-d_6. Such a behavior has been observed in the range of the amounts of acetone adsorbed above 1.0 cm^3/g (Fig. 1).

Hydrogen abstraction from the surface OH groups would be associated with both types of methyl radicals, since on addition of nitric oxide there is no marked change in the CD_3H content of the methane formed, its value decreasing from 35 to 20%.

The contribution of the three processes to the overall methane formation varies with the amount of acetone adsorbed. The contribution of hydrogen abstraction from the surface OH groups decreases with increasing amount of acetone-d_6 adsorbed (Fig. 2). Some information on the contribution of the disproportionation reaction to the overall methane formation would be obtained from the isotope effects in the formation reaction, since little or no isotope effect is expected for the disproportionation reaction as well as the hydrogen abstraction from surface OH groups in contrast with the large isotope effect for hydrogen abstraction from acetone molecules. From the marked change in isotope effects with the amount of acetone adsorbed (Fig. 3), it is concluded that below the amount adsorbed of 0.3 cm^3/g little or no hydrogen abstraction from acetone molecules takes place. Most of the CD_4 results from the disproportionation reaction, while above the amount adsorbed of 3.0 cm^3/g the predominant process in the CD_4 formation may be the hydrogen abstraction from acetone molecules.

References

1) Y. Kubokawa and M. Anpo, *J. Phys. Chem.*, **78**, 2442 (1974). M. Anpo and Y. Kubokawa, *ibid.*, **78**, 2446 (1974).

2) P. Ausloos and E. W. R. Steacie, *Can. J. Chem.*, **33**, 47 (1955). W. A. Noyes, Jr., G. B. Porter, and J. E. Jolley, *Chem. Rev.*, **56**, 49 (1956).

3) N. H. Sagert, J. A. Reid, and R. W. Robinson, *Can. J. Chem.*, **48**, 17 1970).

4) A. F. Trotman-Dickenson and E. W. R. Steacie, *J. Chem. Phys.*, **18**, 1097 (1950).

5) The fraction of the CD_3H yield attributable to the photoexchange reaction was below 0.08.

6) The precursor of ethane is confined only to some fraction of methyl radicals. However, on isotopic substitution no marked change appears in the value of the fraction.

7) P. Gray and A. A. Herod, *Trans. Faraday Soc.*, **64**, 1568 (1968). P. Gray, A. A. Herod, and A. Jones, *Chem. Rev.*, **71**, 247 (1971).

8) The quenching of the triplet excited acetone molecules by nitric oxide appears to be negligible below 1 Torr nitric oxide pressure.

9) P. A. Leermakers, L. D. Weis, and H. T. Thomas, *J. Amer. Chem. Soc.*, **87**, 4403 (1965).

10) R. Pieck and E. W. R. Steacie, *Can. J. Chem.*, **33**, 1304 (1955).

The Viscosity of Gaseous Sulfur Dioxide

Hiroji IWASAKI and Mitsuo TAKAHASHI

The Chemical Research Institute of Non-Aqueous Solutions, Tohoku University, Katahira, Sendai 980

(Received September 19, 1974)

The viscosity of sulfur dioxide was measured in the range from 25 to 160 °C over the pressure range from 1 atm to near the saturation pressure at 25—150 °C and up to 80 atm at 160 °C by means of the oscillating-disk method. The accuracy of the measurement is, at worst, ±0.25%, except that the accuracy is ±0.3% for the range above 66 atm at 160 °C. It is found that, at temperatures from 25 to 75 °C, the viscosity of sulfur dioxide shows a steady decrease with the pressure (or density) and that at 100 and 125 °C it passes through a minimum. On the contrary, the isotherms at 150 and 160 °C show a steady increase with the pressure (or density). The data were fitted to the polynomials of the density at each temperature investigated. The coefficient of the first-order density term in the equation, which indicates the degree of the initial density dependence, changes its sign from negative to positive at a temperature of about 135 °C.

The present paper continues the work on the experimental determination of the viscosity of polar gases and constitutes a sequel to our paper on ammonia.[1] Investigations of the effect of the pressure on the viscosity of sulfur dioxide have been made by several investigators,[2-4] but the results have not indicated any definite relation between the viscosity of sulfur dioxide and the pressure (or density). Therefore, the measurements of the viscosity of sulfur dioxide were undertaken in the range from 25 to 160 °C over the pressure range from 1 atm to near the saturation pressure at 25—150 °C and up to 80 atm at 160 °C.

TABLE 1. CHARACTERISTICS OF SUSPENSION SYSTEM (25 °C)

Total separation between plates		$D=0.1732_4$ cm
Upper separation		$b_1=0.0386_6$ cm
Lower separation		$b_2=0.0386_6$ cm
Radius of disk		$R=1.3955_7$ cm
Thickness of disk		$d=0.0959_1$ cm
Moment of inertia of suspension system		$I=4.5119$ g·cm²
Damping decrement and natural period of oscillation		
25 °C	$\Delta_0=2.73\times10^{-5}$	$T_0=30.00$ s
50 °C[a]	$\Delta_0=2.52\times10^{-5}$	$T_0=26.20$ s
75 °C	$\Delta_0=4.54\times10^{-5}$	$T_0=30.09$ s
100 °C	$\Delta_0=7.61\times10^{-5}$	$T_0=30.13$ s
125 °C	$\Delta_0=12.74\times10^{-5}$	$T_0=30.13$ s
150 °C	$\Delta_0=20.92\times10^{-5}$	$T_0=30.15$ s
160 °C	$\Delta_0=24.92\times10^{-5}$	$T_0=30.03$ s

a) Suspension wire used for 50 °C is different from that used for other temperatures.

Experimental

Measurements were made by the Maxwell-type oscillating-disk method. The apparatus as well as the experimental procedures was identical with those described in Ref. 1 and so need not be repeated here.

The characteristics of the suspension system are recorded in Table 1.

Materials. The sulfur dioxide was obtained from the Showa Denko Co., which reported a purity of about 99.9%. It was purified and dried by several distillations, with a generous rejection of the head and tail fractions, and finally by distillation through phosphorus pentoxide tubes.

Evaluation of Results

The results of measurements were evaluated with the aid of Newell's theory in a manner similar to, but not quite identical with, that used in Ref. 1. In this experiment, the evaluations were made by means of Eqs. (1) and (2), not by Eq. (4) as in Ref. 1. This was because the neglect of the terms containing a, f, and h in Eq. (2) in Ref. 1 was found to cause a discrepancy over 0.3% in the results evaluated by Eqs. (1) and (2) in Ref. 1 in the high-density region at temperatures over 125 °C.

It was confirmed that the present measurements satisfactorily fulfill the conditions under which Eqs. (1) and (2) in Ref. 1 will yield the required accuracy

TABLE 2. EXPERIMENTAL RESULTS AT 150 °C

Pressure P atm	Density ρ g/cm³	Period T s	Decrement $\Delta\cdot10^2$	Viscosity η μpoise	Boundary layer thickness δ, cm	δ/b
1.00	0.00185	30.235	3.4264	182.55	0.6876	17.764
3.30	0.00619	30.202	3.4262	182.79	0.3766	9.729
6.53	0.01244	30.242	3.4328	182.95	0.2657	6.864
9.683	0.018758	30.181	3.4320	183.33	0.2166	5.594
14.036	0.027854	30.188	3.4420	183.88	0.1780	4.598
19.759	0.040551	30.194	3.4570	184.71	0.1478	3.819
24.917	0.052812	30.200	3.4803	186.00	0.1300	3.358
34.909	0.079639	30.342	3.5492	188.95	0.1067	2.756
43.707	0.10884	30.298	3.6268	193.53	0.0924	2.386
53.640	0.14859	30.384	3.7875	201.77	0.0807	2.085
60.677	0.18891	30.468	4.0019	212.86	0.0735	1.900
67.291	0.25354	30.533	4.4360	235.93	0.0668	1.726

of 0.1%. For example, the experimental results at 150 °C are shown in Table 2. All of the δ/b values were larger than 1.25.

The apparatus constant, C_N, was determined experimentally using air and nitrogen at 1 atm and 25 °C respectively. The values of C_N obtained by the two methods showed a good agreement, the discrepancy being only 0.04%.

The mean value of

$$C_N = 1.13124$$

was adopted for further calculation. However, for the measurement at 50 °C the suspension wire was different from that for the other temperatures and the check measurements of the instrument constant, C_N, were made following the method described above. The following value was obtained, showing a very slight discrepancy from the above value, and was used for the calculation at 50 °C:

$$C_N = 1.12881.$$

The accuracy of the present experiments is at worst ±0.25%, considering the uncertainty in the determination of Δ and T, and other sources of error, except that the accuracy is ±0.3% for the range above 66 atm at 160 °C for a reason to be described later.

Results and Discussion

The experimental results are presented in Table 3 and in Figs. 1 and 2. The density of sulfur dioxide was calculated using the compressibility data given by Kang *et al.*[5]

The densities marked * in Table 3 have an uncertainty of 10% at most, because of the difficulty of the estimation by the interpolation of the P–V–T data given by Kang *et al.*, the region being near the critical state. Therefore, the viscosity data in this range were

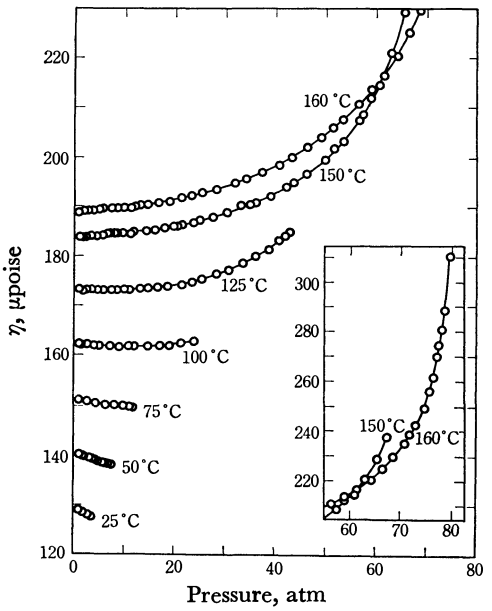

Fig. 1. Effect of pressure on viscosity of sulfur dioxide.

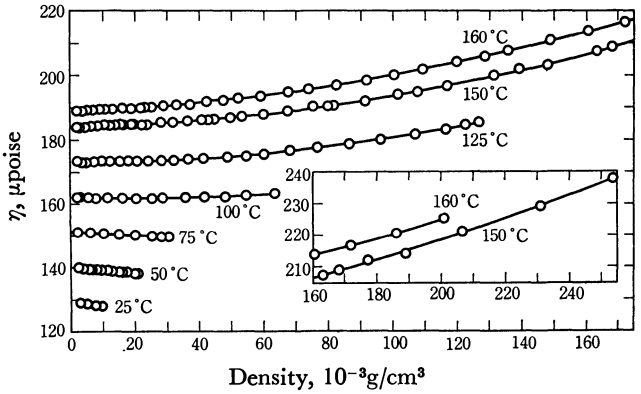

Fig. 2. Effect of density on viscosity of sulfur dioxide.

Table 3. Experimental results

Pressure atm	Density g/cm³	Viscosity μpoise	Pressure atm	Density g/cm³	Viscosity μpoise
	25 °C		4.30	0.01006	149.37
1.00	0.00267	127.93	6.18	0.01476	149.14
1.74	0.00471	127.51	8.00	0.01953	148.90
2.67	0.00738	127.12	9.870	0.024634	148.83
3.36	0.00941	126.79	11.107	0.028170	148.52
	50 °C		11.841	0.030340	148.55
1.00	0.00245	139.26		100 °C	
1.67	0.00411	138.94	1.00	0.00211	161.02
2.12	0.00526	138.89	1.50	0.00317	160.92
3.08	0.00775	138.74	2.61	0.00557	160.96
3.74	0.00950	138.41	3.86	0.00833	160.76
4.40	0.01128	138.35	5.18	0.01127	160.67
4.90	0.01265	138.18	7.13	0.01579	160.58
5.59	0.01457	137.79	8.94	0.02011	160.49
6.09	0.01601	137.72	10.933	0.025029	160.56
6.57	0.01740	137.55	12.227	0.028336	160.57
7.32	0.01960	137.43	14.824	0.035273	160.72
7.68	0.02069	137.26	16.969	0.041331	160.88
	75 °C		19.222	0.048078	160.92
1.00	0.00226	150.03	21.196	0.054347	161.34
2.67	0.00591	149.82	23.867	0.063443	161.87

TABLE 3. (Continued)

Pressure atm	Density g/cm³	Viscosity μpoise	Pressure atm	Density g/cm³	Viscosity μpoise
	125 °C		43.707	0.10884	193.53
1.00	0.00197	172.03	46.143	0.11667	195.14
1.55	0.00307	171.85	49.797	0.13118	198.29
2.47	0.00492	171.92	51.686	0.13938	200.30
3.52	0.00704	171.97	53.640	0.14859	201.77
4.61	0.00930	171.95	56.505	0.16332	205.82
5.87	0.01194	171.91	57.348	0.16796	207.07
7.36	0.01512	172.06	58.870	0.17706	210.37
8.55	0.01770	172.03	60.677	0.18891	212.86
9.820	0.020506	172.06	62.986	0.20637	219.37
11.217	0.023650	172.16	65.526	0.23090	227.27
13.082	0.027952	172.20	67.291	0.25354	235.93
14.740	0.031884	172.45		160 °C	
16.470	0.036517	172.62	1.00	0.00181	187.50
18.463	0.041127	172.88	2.11	0.00384	187.63
21.252	0.048469	173.39	2.72	0.00497	187.68
23.421	0.054442	173.78	3.78	0.00692	187.73
25.378	0.060059	174.30	4.90	0.00904	188.03
28.073	0.068225	175.28	5.63	0.01042	188.06
30.627	0.076528	176.07	6.98	0.01299	188.11
33.507	0.086641	177.42	8.40	0.01575	188.29
35.998	0.096125	178.75	9.862	0.018622	188.39
38.574	0.10694	180.24	11.406	0.021702	188.46
40.567	0.11633	182.01	11.917	0.022731	188.56
41.760	0.12231	183.11	13.006	0.024941	188.83
42.611	0.12691	183.79	14.725	0.028489	189.07
	150 °C		16.693	0.032619	189.42
1.00	0.00185	182.55	18.766	0.037087	189.82
1.55	0.00288	182.44	21.143	0.042328	190.46
1.69	0.00315	182.74	23.273	0.047164	190.95
2.31	0.00430	182.56	25.317	0.051925	191.48
3.30	0.00619	182.79	28.166	0.058765	192.08
4.46	0.00842	182.70	31.663	0.067523	193.41
5.47	0.01036	182.99	34.051	0.073768	194.18
5.53	0.01049	182.95	37.161	0.082266	195.46
6.53	0.01244	182.95	40.478	0.091866	197.03
7.18	0.01372	183.24	43.207	0.10026	198.50
8.05	0.01546	183.19	46.207	0.10994	200.63
8.35	0.01607	183.28	49.011	0.11957	202.54
9.683	0.018758	183.33	51.445	0.12847	204.32
9.990	0.019389	183.28	53.299	0.13564	206.08
11.217	0.021911	183.10	56.391	0.14845	209.28
12.068	0.023684	183.49	59.097	0.16062	212.18
14.036	0.027854	183.88	61.396	0.17171	214.82
15.938	0.031742	184.00	64.123	0.18622	218.68
16.052	0.031987	183.81	66.537	0.20089	223.38
17.821	0.036153	184.18	68.600	0.21539*	227.87
19.759	0.040551	184.71	70.824	0.23379*	233.31
20.621	0.042543	184.73	71.807	0.24313*	236.91
21.509	0.044615	185.00	73.068	0.25666*	241.05
23.554	0.049491	185.58	74.769	0.27895*	247.40
24.917	0.052812	186.00	75.717	0.29330*	254.49
27.577	0.059539	186.68	76.522	0.30704*	259.97
30.461	0.067133	187.61	77.094	0.31776*	264.50
33.224	0.074786	188.85	77.521	0.32677*	272.68
34.909	0.079639	188.95	78.278	0.34404*	278.11
35.582	0.081619	189.34	78.609	0.35220*	286.09
38.763	0.091347	190.75	79.792	0.38631*	308.04
41.877	0.10153	192.54			

TABLE 4. EFFECT OF ERROR IN DENSITY UPON THE CALCULATION OF VISCOSITY (160 °C)

Pressure P atm	Viscosity η μpoise Density from Table 3	Viscosity η' μpoise Density increased by 5%	% difference in viscosity $\frac{\eta'-\eta}{\eta}\times 100\%$	Viscosity η'' μpoise Density increased by 10%	% difference in viscosity $\frac{\eta''-\eta}{\eta}\times 100\%$
68.600	227.87	227.91	0.019	227.95	0.038
70.824	233.31	233.36	0.021	233.40	0.040
71.807	236.91	236.96	0.021	237.01	0.041
73.068	241.05	241.10	0.022	241.15	0.042
74.769	247.40	247.45	0.023	247.51	0.045
75.717	254.49	254.55	0.024	254.61	0.047
76.522	259.97	260.03	0.025	260.09	0.049
77.094	264.50	264.57	0.026	264.63	0.051
77.521	272.68	272.75	0.028	272.83	0.054
78.278	278.11	278.20	0.029	278.27	0.056
78.609	286.09	286.18	0.031	286.26	0.060
79.792	308.04	308.15	0.035	308.26	0.070

excluded from the viscosity *vs.* density curves (Fig. 2).

In order to assess the extent of the deviations in viscosity values resulting from the uncertainty in the density, it will be necessary to refer to the effect of the density on the calculation of the viscosity using Eqs. (1) and (2) in Ref. 1. The density of the gas appears in the final, working equation (1) in Ref. 1. However, for this purpose the value of the density need not be known extremely accurately, because it affects the value of β^2 taken from Eq. (2) in Ref. 1 approximately proportionately, thus nearly cancelling the direct effect upon the viscosity, η, in Eq. (1). A test calculation was performed for the range of pressures higher than 66 atm at 160 °C in the case of the densities increased by 5% and then by 10% of those listed in Table 3. The results are recorded in Table 4. Thus, considering the uncertainty of the density, the accuracy of the viscosity in the range discussed above is assumed to be better than ±0.3%.

The diagram in Fig. 1 represents the variation in the viscosity of sulfur dioxide with the pressure for the given temperatures. The viscosity of sulfur dioxide shows a steady decrease with the pressure at the temperatures from 25 to 75 °C. The viscosities at 100 and 125 °C pass through a minimum. On the contrary, the isotherms at 150 and 160 °C show a steady increase with the pressure; $(\delta\eta/\delta T)_P>0$ at low pressures and $(\delta\eta/\delta T)_P<0$ at high pressures.

The diagram in Fig. 2 representing the variation in the viscosity of sulfur dioxide with the density is similar to that in Fig. 1, but $(\delta\eta/\delta T)_\rho>0$ under the present experimental conditions.

Figures 1 and 2 show that the initial pressure (or density) dependency of the viscosity of sulfur dioxide changes its sign from negative to positive as the temperature increases. This relation can be clarified by representing the viscosity of sulfur dioxide in the polynomials of density as follows:

$$\eta = \eta_0 + b\rho + c\rho^2 + d\rho^3. \quad (1)$$

The constants of Eq. (1), η_0, b, c, and d, were evaluated using the measured values of the viscosity at each temperature; they are recorded in Table 5. These equations reproduce the measured values with a deviation not exceeding ±0.1% except for the several measured values in the high-pressure region at 150 °C, which were also reproduced within the limits of experimental error. The initial density dependence of the viscosity of sulfur dioxide, b, and the viscosity at zero density, η_0, are both given against the temperature in Fig. 3. This figure shows that the relation between the

TABLE 5. VALUES OF CONSTANTS IN Eq. (1)[a]

Temp. °C	η_0	b	$c\cdot 10^3$	$d\cdot 10^6$
25	128.38	−0.169		
50	139.51	−0.112	0.18	
75	150.24	−0.090	1.12	
100	161.09	−0.044	0.885	
125	172.03	−0.020	1.053	−1.26
150	182.54	0.0243	0.720	0.067
160[b]	187.52	0.0304	0.877	−0.717

a) $\eta=\eta_0+b\rho+c\rho^2+d\rho^3$. η: poise, ρ: 10^{-3}g/cm^3
b) Density up to 0.20089 g/cm^3.

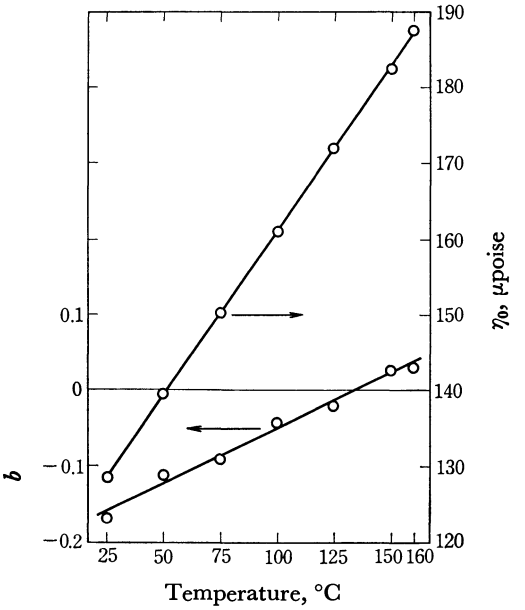

Fig. 3. Effect of temperature on η_0 and b in Eq. (1).

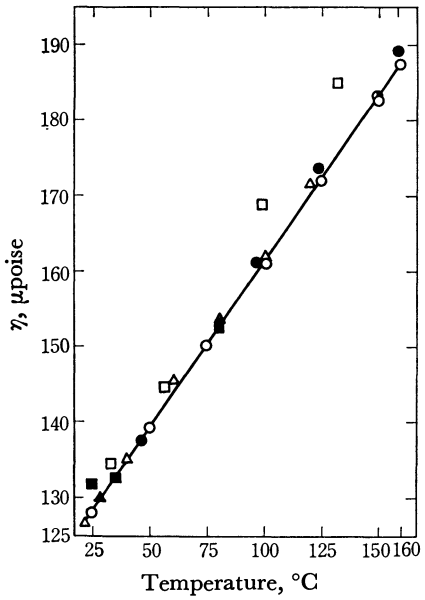

Fig. 4. Comparison of results for sulfur dioxide at 1 atm.
●, Trautz and Weizel[6]; △, Titani[7]; ◑, Trautz and Winterkorn[8]; ■, Chakraborti and Gray[9]; □, Pal and Barua[10]; ▲, Stewart and Maass[11]; ○, present work.

initial density dependence and the temperature is linear and changes its sign from negative to positive at about 135 °C, and that the relation between the viscosity at zero density and the temperature is also linear.

The measurements of the viscosity of sulfur dioxide at high densities were performed by Awbery and Griffiths[2] for the liquid region, by Shimotake and Thodos[3] at 200 °C, and by Stakelbeck.[4] The measurements by Stakelbeck were performed not only for the liquid region but also for the gaseous region up to 40 °C, using the falling-body method, and so can be compared directly. However, his data indicate a rapid increase in the viscosity with an increase in the pressure, in disagreement with the present measurements.

In Fig. 4, the relation between the viscosity of sulfur dioxide at 1 atm and the temperature is given. Here, the data given by other investigators[6-11] are limited to those obtained in the same temperature range as that of the present measurement, thus making it possible to compare directly.

The data plotted show a good agreement within 1% among all the investigators, except that the value at 25 °C by Chakraborti and Gray[9] and those by Pal and Barua[10] show a large discrepancy.

References

1) H. Iwasaki and M. Takahashi, *Rev. Phys. Chem. Japan*, **38**, 18 (1968).
2) J. H. Awbery and E. Griffiths, *Proc. Phys. Soc.* (London), **48**, 372 (1936).
3) H. Shimotake and G. Thodos, *J. Chem. Eng. Data*, **8**, 88 (1963).
4) H. Stakelbeck, *Z. ges. Kälte-Ind.*, **40**, 33 (1933).
5) T. L. Kang, L. J. Hirth, K. A. Kove, and J. J. McKetta, *J. Chem. Eng. Data*, **6**, 220 (1961).
6) M. Trautz and W. Weizel, *Ann. Phys.*, **78**, 305 (1925).
7) T. Titani, This Bulletin, **5**, 98 (1930).
8) M. Trautz and H. Winterkorn, *Ann. Phys.*, **10**, 511 (1931).
9) P. K. Chakraborti and P. Gray, *Trans. Faraday Soc.*, **61**, 2422 (1965).
10) A. K. Pal and A. K. Barua, *ibid.*, **63**, 341 (1967).
11) W. W. Stewart and O. Maass, *Can. J. Res.*, **6**, 453 (1932).

Dielectric Relaxation and Molecular Structure. XIII. The Dielectric Behavior of Mixtures of 1-Propanol with Hydrogen-bonding and Non-hydrogen-bonding Solvents

Taro KOSHII, Hiroaki TAKAHASHI, and Keniti HIGASI
Department of Chemistry, Waseda University, Shinjuku, Tokyo 160
(Received September 26, 1974)

The dielectric constants and losses of 1-propanol and its mixtures with benzene, chlorobenzene, 1,4-dioxane, and pyridine have been measured in the frequency range of 1—0.35 GHz in the temperature range of 10—40 °C. The concentrations of the mixture lie between 1—0.6 mol fractions of the alcohol. The dielectric relaxations of the observed systems in the above frequency range are all of the Debye type. The measured data were used to calculate the activation enthalpy, ΔH^*, and the entropy, ΔS^*. The dependence of ΔH^* and ΔS^* upon the concentration differs with the nature of the solvent. Both ΔH^* and ΔS^* decrease upon the addition of a hydrogen-bonding solvent, while they increase slightly upon the addition of a non-hydrogen-bonding solvent. The mechanism of the principal relaxation of 1-propanol is discussed on the basis of these observations.

Since Mizushima[1] made his classic study of alcohols, the dielectric properties of mono-alcohols have been extensively investigated by a number of workers using a wide range of both frequencies and temperatures. The dielectric dispersions of primary aliphatic alcohols in the liquid state are now known to have three different absorptions.[2] The most important of these absorptions is the principal Debye-type dispersion on the low-frequency side; it is regrettable, however, that we have still no reliable explanation for the true mechanism of this principal dispersion.

The activation enthalpy, ΔH^*, and the entropy, ΔS^*, have been well studied for liquid alcohols,[3,4] but seldom for solutions except for those in non-polar solvents.[5,6]

In the preceding papers,[7,8] dielectric measurements at 25 °C were described. In this report, we shall deal with the dielectric measurements of 1-propanol in the same set of solvents (benzene, chlorobenzene, 1,4-dioxane, and pyridine) and in the same frequency range at four or three temperatures; we shall also discuss the ΔH^* and ΔS^* derived therefrom. Emphasis will be placed upon the solvent interactions of the alcohol with hydrogen-bonding solvents.

Experimental

The experimental materials were purified as described previously.[7] The dielectric constants and losses were measured by the use of a UHF apparatus of the coaxial-slotted-line type, the details of which were given in a preceding report.[7] The relaxation time, τ, and the limiting low- and high-frequency dielectric constants, ε_0 and ε_∞ respectively, were calculated from the Debye equation (1):

$$\varepsilon' - j\varepsilon'' = \varepsilon_\infty + \frac{\varepsilon_0 - \varepsilon_\infty}{1 + j\omega\tau} \qquad (1)$$

by an iterative method using an electronic computer. In order to determine the activation enthalpy, ΔH^*, and the entropy, ΔS^*, from the temperature dependence of the relaxation time, τ, $\log_{10}(\tau T)$ was plotted against $1/T$ using Eq. (2)[9]:

$$\tau = \frac{h}{kT} \exp\left(\frac{\Delta H^* - T\Delta S^*}{RT}\right) \qquad (2)$$

where h, k, and R are the Planck, the Boltzmann, and the gas constants respectively, and where T is the absolute temperature. A straight line fitting best with the points was obtained by the use of the least-square method. ΔH^* was obtained from the slope of this line, and ΔS^*, from its intercepts with the $\log_{10}(\tau T)$ axis.

Results

The Cole-Cole plots[10] for 1-propanol mixtures with benzene and pyridine are shown in Fig. 1. It may be seen that almost all the measured points lie exactly on the Debye semicircles; hence, they can be considered to be associated with the principal dispersions of the alcohols.[7]

The low- and the high-frequency intercepts of the Debye semicircle with the ε' axis, ε_0 and ε_∞, are compared with the static dielectric constants, ε_0, and the square of refractive indices, n^2 (for the H_α-line) in the literature respectively, in Tables 1 and 2. The low-frequency intercepts, ε_0, obtained in this work are in fair agreement with the real static dielectric constants, ε_0 (Table 1), while the high-frequency intercepts, ε_∞, are much larger than the squares of the refractive indices, n^2 (Table 2). The appreciable differences, $\varepsilon_\infty - n^2$, are due to the existence of minor dispersions of alcohols in the higher-frequency range.[2] In Fig. 1(a), we find that the limiting high-frequency dielectric constants, ε_∞, remain almost constant with an increase in

TABLE 1. LIMITING LOW FREQUENCY DIELECTRIC CONSTANTS ε_0 OF LIQUID 1-PROPANOL

Temp. (°C)	ε_0 (This work)	ε_0 (Literatures)			
10.0	21.0±0.2	(22.2)[11]	(22.6)[12]	(22.8)[13]	
20.0	20.9±0.5	20.8[11]	21.1[12]	(21.2)[13]	21.3[3]
30.0	19.6±0.2	19.4[11]	(19.8)[12]	19.7[13]	
40.0	18.9±0.3	18.2[11]	18.5[12]	18.4[13]	

The values in parentheses were obtained from the literature by inter- or extrapolation of values given at different temperatures.

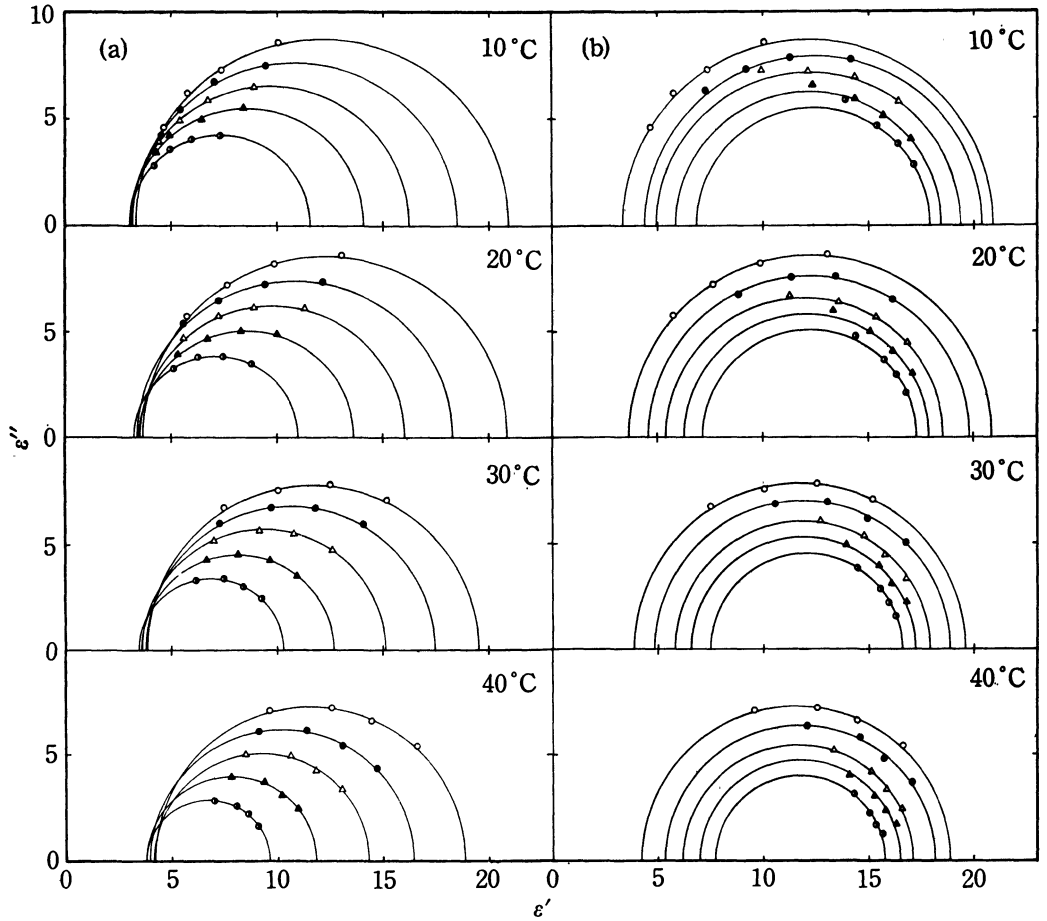

Fig. 1. Cole-Cole plots for 1-propanol mixtures with (a) benzene and (b) pyridine at 10, 20, 30, and 40 °C. ○, 1.0; ●, 0.9; △, 0.8; ▲, 0.7; ◑, 0.6 in mole fraction of 1-propanol. Frequencies of the measurement, right to left; 0.356, 0.515, 0.697, 1.00 GHz.

Table 2. Limiting high frequency dielectric constants ε_∞ of liquid 1-propanol

Temp. (°C)	ε_∞ (This work)	n^2 (Literature)
10.0	3.3±0.1	1.9[14]
20.0	3.6±0.1	1.9[14]
30.0	3.8±0.1	1.9[14]
40.0	4.2±0.1	1.9[14]

Table 3. Relaxation times τ ($\times 10^{-2}$ ps) of liquid 1-propanol

Temp. (°C)	τ (This work)	τ (Literatures)	
10.0	5.7±0.2	(6.50)[12]	
20.0	4.1±0.3	4.30[12]	5.31[3]
30.0	2.8±0.2	(3.34)[12]	
40.0	2.0±0.2	2.86[12]	

Regarding the values in parentheses see the note below Table 1.

the amount of non-polar solvent (benzene), while in Fig. 1(b) they increase considerably with an increase in the polar solvent (pyridine). The difference in the latter parallels the amount of pyridine added and must be due largely to the main dispersion of pyridine* in the high-frequency region.[11]

The dependence of the dielectric relaxation time, τ, upon the concentration is examined in Fig. 2. The relaxation times, τ, decrease gradually and linearly in mixtures with benzene (a), while they decrease sharply in mixtures with pyridine (b), the curves becoming concave in the latter mixtures. The dependence of the relaxation time upon the concentration in mixtures with chlorobenzene (●) seems to coincide with that in mixtures with benzene (○), while the points for mixtures with 1,4-dioxane (▲) lie on the curves for mixtures with pyridine (△).

The principal relaxation times, τ, of liquid 1-propanol are recorded in Table 3, together with those obtained by other workers. The disagreement with the literature[12] values might be due to the difference in the frequency ranges; the frequency range of this study is higher than in most of the works concerned.

Some representative plots of $\log_{10}(\tau T)$ against $1/T$ are shown in Fig. 3. The ΔH^* and ΔS^* values obtained are plotted against the concentration of the alcohol in Fig. 4. For liquid 1-propanol, ΔH^* is obtained as 5.5 kcal/mol, which compares well with the literature values of 5.0,[12] 5.3,[3] 5.4,[5] 5.5[4] kcal/mol, while the ΔS^* of the present work, 1.7 e.u., lies between the values of 1.2[12] and 2.1[3]—3.0[5] e.u. of the other workers.

* See also the first footnote on errors on page 621 in a preceding report.[7]

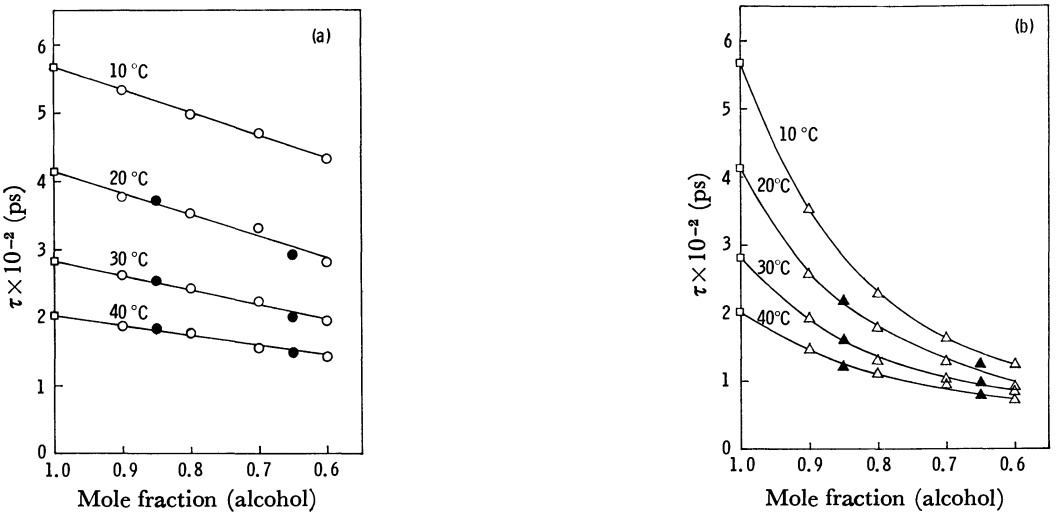

Fig. 2. Variation of relaxation time τ with concentration (for 1-propanol mixtures with solvents). (a) Non-hydrogen-bonding: ○, benzene; ●, chlorobenzene; (b) hydrogen-bonding: ▲, 1,4-dioxane; △, pyridine. □, Pure alcohol.

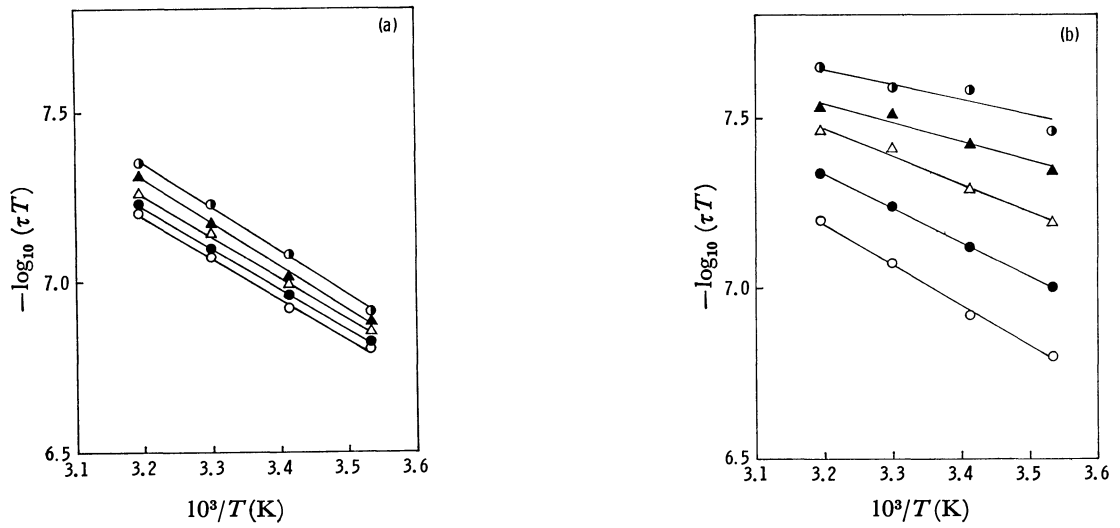

Fig. 3. Plots of $\log_{10}(\tau T)$ against $1/T$ for 1-propanol mixtures with (a) benzene and (b) pyridine. ○, 1.0; ●, 0.9; △, 0.8; ▲, 0.7; ◑, 0.6 in mole fraction of alcohol.

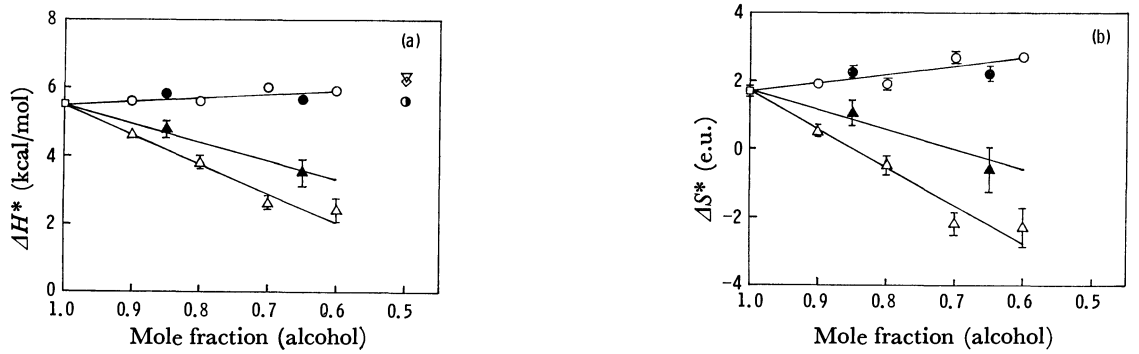

Fig. 4. Variation of (a) ΔH^* and (b) ΔS^* with the concentration (for 1-propanol mixtures with a variety of solvents). This work: ○, benzene; ●, chlorobenzene; △, pyridine; ▲, 1,4-dioxane; □, pure alcohol. From Gemert[5]: ◇, benzene; ◑, hexane; ▽, cyclohexane and carbon tetrachloride. N. B., ⊕ indicates limits of assessed accuracy of measurement.

Discussion

The activation enthalpies, ΔH^*, and the entropies, ΔS^*, obtained in the present experiment are plotted against the concentration of propyl alcohol, in Fig. 4. We find that both ΔH^* and ΔS^* increase slightly upon

the addition of benzene or chlorobenzene. On the contrary, though, these two parameters decrease rapidly with the amount of hydrogen-bonding solvent; moreover, the decrease upon dilution with pyridine is more pronounced than that with 1,4-dioxane.

Polar chlorobenzene ($\mu=1.7$ D) has a high dielectric constant ($\varepsilon_0=5.62$), while non-polar benzene has a low dielectric constant ($\varepsilon_0=2.27$). 1,4-Dioxane is similar to benzene in having a low dielectric constant ($\varepsilon_0=2.21$) and a low polarity ($\mu=0$—0.4 D), while pyridine has $\varepsilon_0=12.3$ and $\mu=2.25$ D. It is evident at a glance at Fig. 4 that neither the static dielectric constant nor the polarity of the solvent play any important role in the relaxation processes.

The size of the solvent relative to that of the alcohol will be considered next. Since the molar volumes of benzene (M.V.=89) and chlorobenzene (M.V.=102) are larger than that of 1-propanol (M.V.=75), a larger size of the solvent might be expected to increase these parameters.[5,6] However, this expectation is not supported here; the two hydrogen-bonding solvents also have larger molar volumes than 1-propanol—*i.e.*, 1,4-dioxane has M.V.=85 and pyridine M.V.=81. The size of the solvent relative to that of the alcohol is, thus, not an important factor in the observed relaxation processes.

Changes in the ΔH^* on the addition of non-polar solvents have been well studied. For a number of normal alcohols (methanol, ethanol, 1-propanol, 1-butanol, and 1-heptanol), Gemert *et al.*[5] found that ΔH^* becomes higher on the addition of non-polar, inert solvents (benzene, carbon tetrachloride, cyclohexane, and hexane); their finding on a benzene solution for propyl alcohol is in good agreement with the present observation. A similar increase in the ΔH^* on dilution with cyclohexane was observed,[6] while decreases on dilution with non-polar solvents have also been reported and discussed.[15–17]

Recently, the dielectric properties of solutions of water in straight-chain heptanols were studied by Tjia,[18] who concluded that the relaxation times of these alcohols decrease upon an addition of a small amount of water and that the energy of activation also decreases with an increase in the quantity of water added—the latter statement was definitely proved for both heptanol-2 and heptanol-4. His observation seems to be parallel with our results for propanol mixtures with hydrogen-bonding solvents.

In order to explain why the principal dielectric relaxation of mono-alcohols is of a pure Debye type, Brot,[19,20] and Bauer and Magat[21] introduced a hypothesis that hydrogen-bond breaking is the controlling step in this relaxation and that the activation energy for the principal lower-frequency relaxation must be identical with the energy necessary to break the hydrogen bond.

The so-called switch-over mechanism was introduced by Sagal,[6] who stated: "The hydrogen bond will break when another molecule approaches with its oxygen atom oriented favorably for a switch. It is reasonable to assume that the presence of this third oxygen atom will lower the energy barrier for breaking the hydrogen bond." According to this assumption, the addition of a non-hydrogen-bonding solvent (benzene or chlorobenzene) to alcohols would increase the energy necessary to break the hydrogen bond, because it would decrease the possibility of the approach of a third oxygen atom for a switch over. Contrary to this, the addition of a strongly hydrogen-bonding solvent (1,4-dioxane or pyridine) would provide a new possibility of a switch over to the electronegative atom of the solvent; hence, this would help lower the energy of activation. Sagal's mechanism seems to agree partially with the observations of this work. Furthermore, we note that the variations in ΔH^* and ΔS^* with the two different kinds of solvents are all in the same direction with those of the g factors and the reduced relaxation times, τ/η.[8] However, we shall have to refrain from discussing the possible mechanism in detail since we do not have sufficient evidence at present.

We wish to thank the Science and Engineering Research Laboratory, Waseda University, for its financial aid.

References

1) S. Mizushima, This Bulletin, **1**, 163 (1926).
2) R. H. Cole and D. W. Davidson, *J. Chem. Phys.*, **20**, 1389 (1952).
3) C. Brot, M. Magat, and L. Reinisch, *Kolloid-Z.*, **134**, 101 (1953).
4) W. Dannhauser and R. H. Cole, *J. Chem. Phys.*, **23**, 1762 (1955).
5) M. J. C. van Gemert, G. P. de Loor, P. Bordewijk, P. A. Quickenden, and A. Suggett, *Advan. Mol. Relaxation Processes*, **5**, 301 (1973).
6) M. W. Sagal, *J. Chem. Phys.*, **36**, 2437 (1962).
7) T. Koshii, E. Arie, M. Nakamura, H. Takahashi, and K. Higasi, This Bulletin, **47**, 618 (1974).
8) T. Koshii, E. Arie, M. Nakamura, H. Takahashi, and K. Higasi, This Bulletin, **47**, 623 (1974).
9) W. Kauzmann, *Rev. Mod. Phys.*, **14**, 12 (1942).
10) K. S. Cole and R. H. Cole, *J. Chem. Phys.*, **9**, 341 (1941).
11) A. A. Maryott and E. R. Smith, "Table of Dielectric Constants of Pure Liquids," NBS Circular 514 (1951).
12) S. K. Garg and C. P. Smyth, *J. Phys. Chem.*, **69**, 1294 (1965).
13) W. Dannhauser and L. W. Bahe, *J. Chem. Phys.*, **40**, 3058 (1964).
14) J. Timmermans, "Physico-Chemical Constants of Pure Organic Compounds," Elsevier Pub. Co., Inc., (1950).
15) P. Bordewijk, *Ph. D. Thesis*, Leiden, Holland 1968.
16) G. Klages and D. Roth, *Z. Naturforsch.*, **14a**, 628 (1959).
17) F. F. Hanna and I. K. Hakim, *ibid.*, **26a**, 1194 (1971).
18) T. H. Tjia, *Ph. D. Thesis*, Leiden, Holland 1974.
19) C. Brot, *Ann. Phys. (Paris)*, (**13**)**2**, 714 (1957).
20) C. Brot, "Molecular Relaxation Processes," Chem. Soc., Spec. Publ., Vol. 20, Discussion, p. 75, (1966).
21) E. Bauer and M. Magat, *Bull. Soc. Chim. Fr.*, **1949**, 341.

Adsorption of Neutral Organic Substances Evaluated from Electrocapillary Curves and Double Layer Capacities

Katsumi NIKI

Department of Electrochemistry, Yokohama National University, Ohoka, Minami-ku, Yokohama 233

(Received November 30, 1974)

Adsorption of neutral organic substances on mercury electrode was evaluated from both electrocapillary curves and differential capacities of the double layer. The results were compared for the adsorption of *n*-aliphatic alcohols, phenol, and *o*-cresol in 0.5 M H_2SO_4. There was some evidence that the electrode potential was more favorable than the charge on the electrode as an electrical variable in the adsorption of the *n*-aliphatic alcohols. However, the values deduced from the Frumkin model were generally larger than the θ's obtained from the electrocapillary curves. This discrepancy is probably due to the deviation from the two-condensers-in-parallel model, because, the two condensers were not independent in an actual system. Neither the two-condensers-in-parallel model nor the three-condensers-in-parallel model were applicable to the adsorption of aromatic compounds.

It is well known that there are two methods to evaluate the adsorption of organic molecules on mercury electrodes. One is purely thermodynamic, while the other, proposed by Frumkin[1] in 1926, is non-thermodynamic.

The surface excess Γ can be determined thermodynamically from the electrocapillary cruves; that is;

$$\Gamma_A = -(\partial\gamma/\partial\mu_A)_E \quad (1)$$

where γ is the interfacial tension at the mercury electrode-solution interface and μ is the chemical potential of the surface active organic molecules in the solution. The activity coefficient of organic substances in the electrolyte solution is assumed to be unity.

Frumkin's model treated the electrical double layer as a two-plate-condensers-in-parallel, which is strictly equivalent to a potential congruency isotherm at a constant amount adsorbed (Frumkin isotherm);

$$C_\theta = C_0(1-\theta) + C'\theta \quad (2)$$

where C_0 and C' are the differential capacities of the uncovered and fully covered electrode, respectively. The differential capacity of the electrode, C_θ, varies linearly with the surface coverage, θ. A potential-congruent isotherm leads to the equation for the charge on the electrode as a sum of the charges on the covered and uncovered parts of the electrode

$$q_\theta = q_0(1-\theta) + q'\theta \quad (3)$$

where q_0 is the electrode charge when $\theta=0$ and q' is the charge at $\theta=1$. Differentiation of Eq. (3) gives:

$$C_\theta = C_0(1-\theta) + C'\theta\,(q'-q_0)\mathrm{d}\theta/\mathrm{d}E \quad (4)$$

The capacity at a constant amount adsorbed Eq. (4) gives Eq. (2).

Breiter and Delahay[2] compared values of θ calculated from Eq. (3) with the thermodynamic surface excess for the adsorption of *n*-amyl alcohol from 1 M $NaClO_4$+ 0.001 M $HClO_4$ and found that the two sets of θ's are comparable but the values deduced from Eq. (3) are generally larger than the θ's obtained from the surface excess. The two methods for the evaluation of θ from the charge computed by graphical integration of the differential capacity curves at zero frequency and differential capacities compliment each other; *i.e.*, the differential capacity method (Eq. (2)) can be applied in the region of the adsorption maximum, in which the charge method becomes very uncertain. Hansen and his co-workers[3] confirmed that the double layer capacitance was linear in Γ for all the Γ's near the electrocapillary maximum for both the *n*-amyl alcohol- and phenol-containing systems in 0.1 M $HClO_4$. When the electrode charge was chosen as an independent variable, as has been shown by Parsons,[4] a charge-congruent isotherm is analogous to Eq. (3);

$$E_\theta = E_0(1-\theta) + E'\theta \quad (5)$$

where E_0 and E' are the potentials corresponding to $\theta=0$ and $\theta=1$ respectively at a constant charge. On differentiation, the differential capacity at a constant amount adsorbed is given by:

$$1/C_\theta = (1-\theta)/C_0 + \theta/C' \quad (6)$$

The charge congruent model shows a linear dependence of E on θ, as is shown by Eq. (5). On the other hand, in the case of the potential congruent model, the dependence of E on θ is not linear. This is shown by rewriting Eq. (2) as Eq. (7).

$$E = (q+C'E_N\theta)/[C'\{C_0(1-\theta)/C'+\theta\}] \quad (7)$$

where the potential E is referred to the potential of zero charge for $\theta=0$ and E_N is the shift of the point of zero charge (p.z.c.) as θ changes from 0 to 1. Frumkin *et al.*[5] found that the experimental evidence of Eq. (7) holds at $q=0$ for the case of the adsorption of *n*-propanol and *n*-caproic acid on mercury, in which the θ's were evaluated by using both thermodynamic and differential capacitance methods. A direct comparison of Eqs. (3) and (5) was made by Dutkiewicz *et al.*[6] for simple aliphatic compounds with four carbon atoms. It was found that, for 1,4-butanediol and 2-butyne-1,4-diol, both equations, (3) and (5), fit equally well. On the other hand, neither equation can represent the data for *n*-butanol and diethyl ether. However, Frumkin *et al.*[5] showed that the isotherms obtained for *n*-butanol are congruent with respect to charge. The discrepancy between these results is probably due to the fact that Frumkin *et al.*[5] used Eqs. (3) and (5) for calculating the adsorption isotherm (or Eqs. (2) and (6) were used at the p.z.c.) in the θ *vs.* concentration of *n*-butanol plots both at E=const. and q=const. On the other hand, Dutkiewicz *et al.*[6] used the thermodynamical method to evaluate the surface excess. As has already

been mentioned by Breiter and Delahay in their pioneer work[2] and in our previous work,[7] the surface coverages deduced from Eq. (3) are generally larger than the θ's obtained from Eq. (1) for *n*-amyl alcohol.

In the present work, (i) the reproducibility of the values is examined by comparing the results of previous works with those of the present work and (ii) the validity of Eq. (2) at a constant amount adsorbed is studied by a comparison of the values of θ directly obtained from Γ.

Experimental

The Lipmann electrometer used in the present experiment has been described previously.[8] The double layer capacitance was measured with a Yokogawa BV-Z-103-A universal bridge at 1000 Hz. The surface active organic substances were of an analytical reagent grade (Tokyo Kasei); no further purification was made. Solutions were made up of 0.5 M H_2SO_4 solution. The solutions were de-aerated with nitrogen purified by passing through a vanadous solution. The purified nitrogen was pre-saturated by passing it through a solution identical with that being studied and then to the cell. The radius of the capillary at the null point was determined by standardization against a solution of known surface tension.[9] All measurements were made at 25±0.1 °C. The potentials were measured against a saturated calomel electrode.

Results and Discussion

n-*Amyl Alcohol.* Electrocapillary curves for the solutions of *n*-amyl alcohol and the interfacial tension *vs.* the logarithm of the concentration of *n*-amyl alcohol are shown in Figs. 1 and 2, respectively. Reproducibility of these electrocapillary curves was studied by comparing the results obtained independently by two persons with a different capillary. The difference between these results was, at most, 1.1 dyne/cm in the potential range between −0.4 and −0.8 V (*vs.* SCE). The surface excess of the alcohol was determined by graphical differentiation of the electrocapillary curves. The error in the surface excess was within 10%. The adsorption isotherm of *n*-amyl alcohol at the potential of electrocapillary maximum in 0.5 M H_2SO_4 is shown in Fig. 3; it is generally in accord with that obtained by Hansen *et al.*[3]

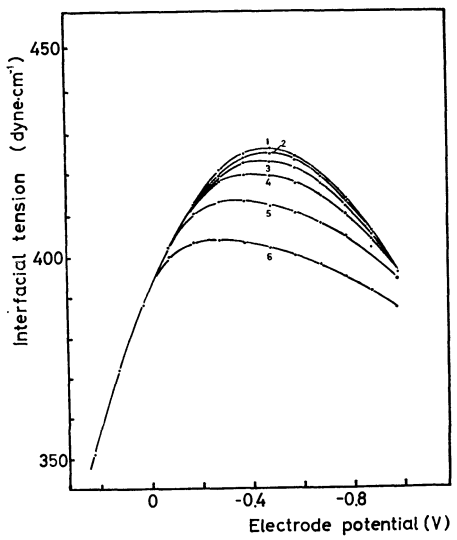

Fig. 1. Electrocapillary curves for *n*-amyl alcohol at various concentrations in 0.5 M H_2SO_4. (1) base solution; (2) 2.0 mM; (3) 5.0 mM; (4) 10 mM; (5) 20 mM; (6) 50 mM.

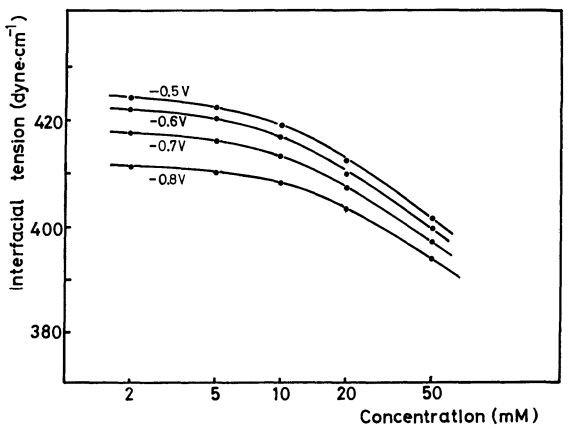

Fig. 2. Variation of interfacial tension with the logarithm of concentration of *n*-amyl alcohol at various electrode potentials in 0.5 M H_2SO_4.

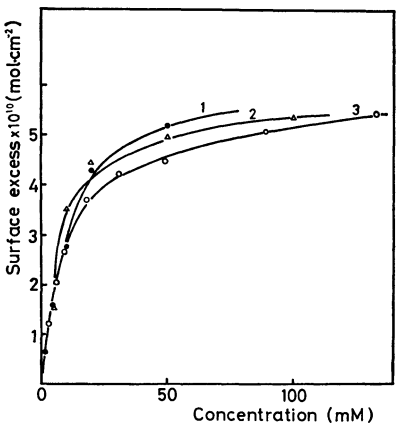

Fig. 3. Adsorption isotherms of *n*-amyl alcohol on mercury electrode calculated from the electrocapillary measurement at p.z.c. in the base solution. (1) present work I; (2) present work II; (3) Hansen *et al.*[3]

The adsorption isotherms determined by both electrocapillary and differential capacitance measurements at the potential of electrocapillary maximum for the base solutions are shown in Fig. 4. We should notice that the agreement between the isotherms evaluated by the same method is very good regardless of the type of supporting electrolyte in the solution. This is probably because neither sulfate ions nor perchlorate ions were adsorbed specifically on mercury electrode near the p.z.c. On the other hand, the isotherms obtained by the electrocapillary measurement agreed poorly with those determined by the differential capacitance method, as is shown in Fig. 4.

Equation (6) was tested by plotting the shift of the electrocapillary maximum against Γ (Fig. 5). In this

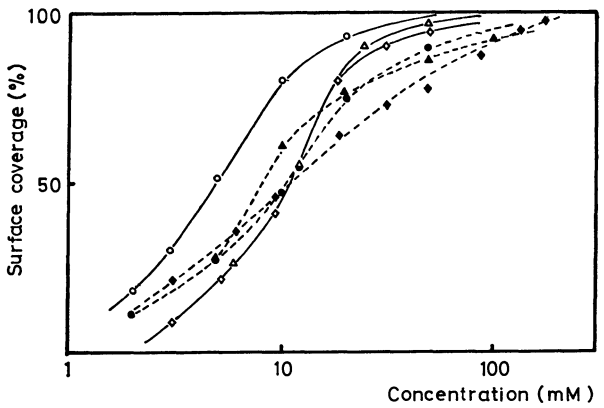

Fig. 4. Adsorption isotherms of *n*-amyl alcohol on mercury electrode. Dotted lines are calculated from the electrocapillary measurement and solid lines are from the differential capacity measurement at p.z.c. in the base solution. —●— present work I; —▲— present work II; —◆— Hansen *et al.*[3]; —◇— Hansen *et al.*[10]; —△— Breiter and Delahay[2]; —○— present work III.

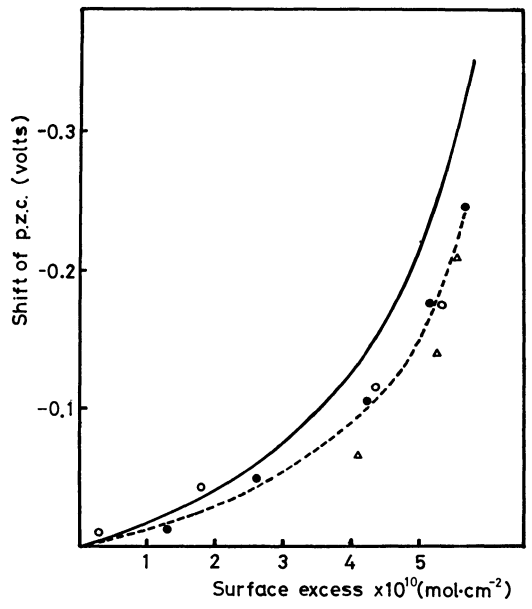

Fig. 5. Dependence of p.z.c. on amount of adsorbed *n*-amyl alcohol. Solid line is calculated from the data taken from ref. (2) and dotted line is calculated from the present work. (△) Breiter and Delahay[2] (differential capacity measurement); (●) present work (electrocapillary curve); (○) present work (differential capacity measurement).

case, the surface excess was evaluated by using the Gibbs equation (Eq. (1)) for the electrocapillary measurements and by using Eq. (2) for the differential capacitance measurements. The experimental values of the electrocapillary measurements agreed well with the calculated values using Eq. (7), where the parameters were $C/C'=4.03$ and $E_N=0.245$ V. The values obtained by the differential capacitance measurement, however, showed a systematical deviation from the calculated curve (*i.e.*, from the values determined by the electrocapillary measurement). That is, at lower concentrations of *n*-amyl alcohol the coverage evaluated by the differential capacitance measurement showed a smaller value than that evaluated by the electrocapillary measurement. On the other hand, at higher concentrations of the alcohol it showed a larger value; agreed with the statement of Breiter and Delahay.[2] This result also agreed with the observation by Frumkin *et al.* for *n*-butyl alcohol.[5]

The systematic deviation of the measured values, as determined by means of the differential capacitance measurement, from those of the calculated values by using Eq. (7) can be explained as follows. When the surface excess of the adsorbed species is small, the adsorbed molecules can move rather freely and they are not necessarily oriented perpendicularly to the electrode. Some of them may be flat, some in a vertical position, and some in intermediate position. The center of the dipole of these adsorbed molecules (the -OH group) is, as the average, closer to the electrode surface than that of the perpendicularly oriented molecules. The contribution to the displacement of the p.z.c. by these molecules becomes larger than that by the perpendicularly oriented molecules. That is, the capacitance of the condenser filled with randomly oriented molecules, C_1', must be greater than that filled with molecules with a fixed orientation (perpendicularly oriented to the electrode), C'. Accordingly, C_0/C_1' with the configuration of the low coverage type becomes smaller than C/C' for the saturated adsorption. This leads to a negative deviation of the measured values from the calculated values according to Eq. (7).

At higher coverages, on the other hand, the positive deviation of the measured values suggests a larger value for C_{0h}/C' than for C_0/C', where C_{0h} is the double layer capacitance of the uncovered part of the electrode at a higher coverage. The capacitance of the condenser filled with water molecules in the presence of a large amount of the adsorbed *n*-amyl alcohol, C_{0h}, is con-

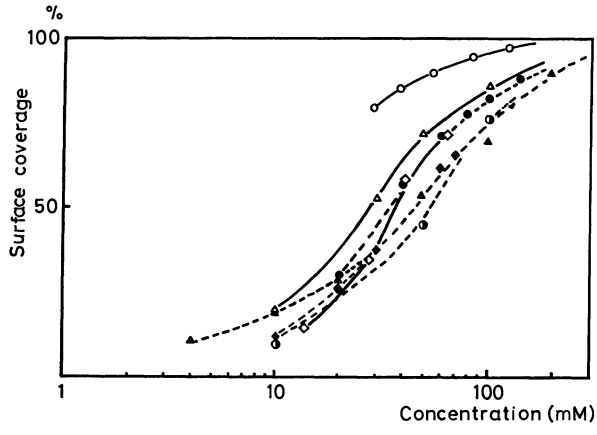

Fig. 6. Adsorption isotherms of *n*-butyl alcohol on mercury electrode at p.z.c. in the base solution. Dotted lines are for the electrocapillary measurement and solid lines for the differential capacity measurement. —▲— present work I; —◆— present work II; —●— Frumkin *et al.*[5]; —◑— Blomgren *et al.*[12]; —△— present work III; —◇— Biegler and Laitinen[13]; —○— Sathyanarayana.[14]

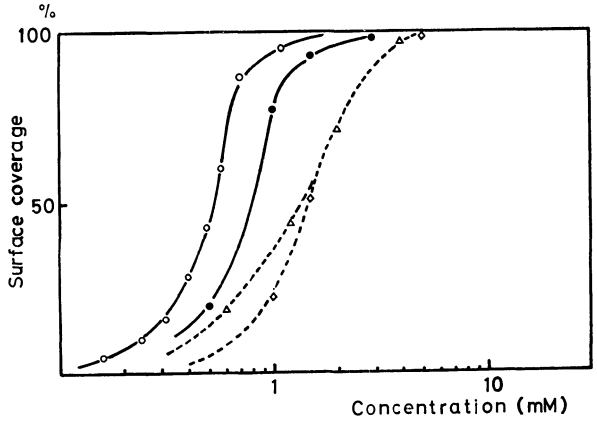

Fig. 7. Adsorption isotherms of *n*-hexyl alcohol on mercury electrode at p.z.c. in the base solution. Dotted lines are for the electrocapillary measurement and solid lines for the differential capacity measurement. —△— present work I; —◇— present work II; —●— present work III; —○— Ohsumi.[15]

sidered to be larger than that at the electrode without an adsorbed species on the electrode. At the electrode with higher coverages by *n*-amyl alcohol, the hydrocarbon end is in contact with the electrode surface and the molecule is normal to the surface. The inductive effect by the oriented alcohol molecules may influence the orientation of water molecules at the electrode surface. As in the case of the repulsive interaction between the dipoles at the electrode surface,[11] this effect causes an increase in the capacitance of the condenser filled with water molecules from C_0 to C_{0h}.

The adsorption isotherms for *n*-butyl alcohol and *n*-hexyl alcohol are shown in Figs. 6 and 7. These isotherms also showed the same tendency as in the case of *n*-amyl alcohol. The negative deviation from Eq. (7) at lower coverages decreased with an increase in the chain length of the alcohol molecule, and the positive deviation increased with the chain length. This behavior can easily be explained by the arguments used in the case of *n*-amyl alcohol. The plot of the shift of the p.z.c. against the surface excess of the alcohol showed an excellent agreement with Eq. (7) for both *n*-butyl and *n*-hexyl alcohols when the surface excess was determined thermodynamically.

Phenol. The adsorption isotherms of phenol from 0.5 M H_2SO_4 solution at the potential of electrocapillary maximum of the base solution are shown in Fig. 8, together with the adsorption isotherms obtained by Hansen *et al.*[3] and by Blomgren *et al.*[12] All of these isotherms were determined from the electrocapillary measurements, and they showed a good agreement between them. The adsorption isotherms for phenol

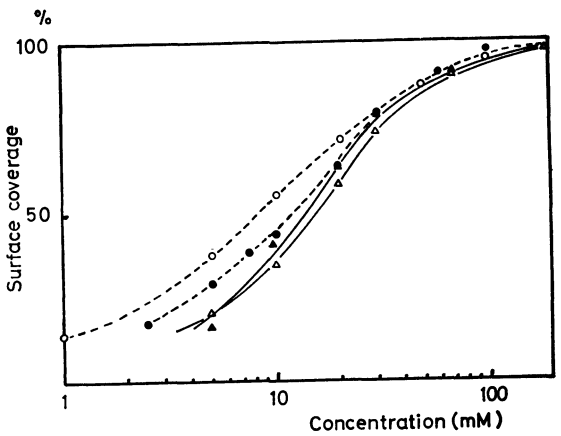

Fig. 9. Adsorption isotherms of phenol on mercury electrode at p.z.c. in the base solution. Dotted lines are for the electrocapillary measurement and solid lines for the differential capacity measurement. —▲— present work I; —●— Hansen *et al.*[3]; —△— present work II; —○— Hansen *et al.*[3]

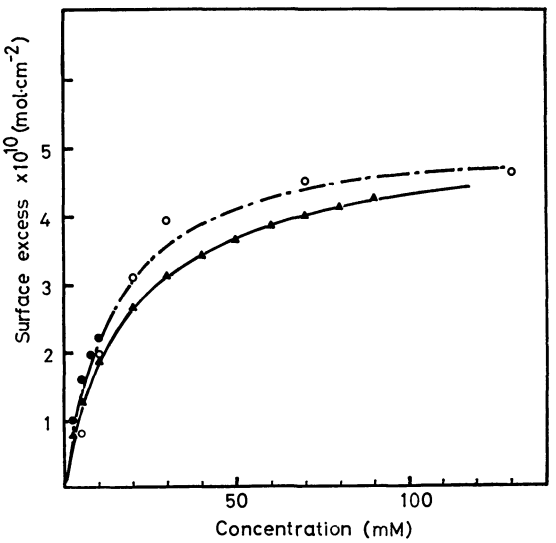

Fig. 8. Adsorption isotherms of phenol on mercury electrode at p.z.c. in the base solution calculated from electrocapillary curves. —○— present work; —▲— Hansen *et al.*[3]; —●— Blomgren *et al.*[12]

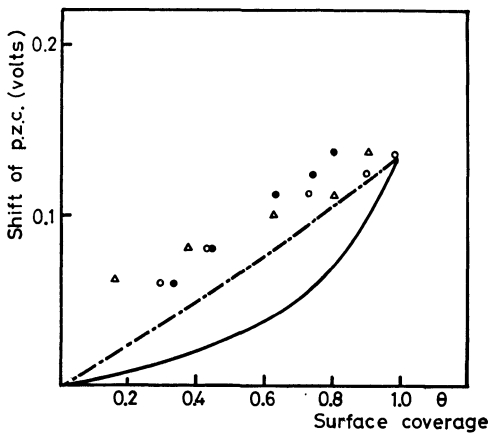

Fig. 10. Dependence of p.z.c. on amount of adsorbed phenol. The solid line is calculated from the present work and the dotted line corresponds to the three condenser model (*cf.* text). (△) present work and (○) Hansen *et al.*[3] for the electrocapacillary measurement; (●) Hansen *et al.*[3] for the differential capacity measurement.

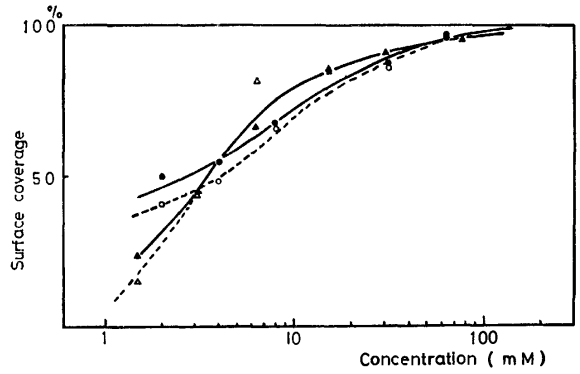

Fig. 11. Adsorption isotherms of *o*-cresol on mercury electrode at p.z.c. in the base solution. Dotted lines are for the electrocapillary measurement and solid lines for the differential capacity measurement.
—○— present work I; —△— Manohar and Sathyanarayana[19]; —●— present work II; —▲— Manohar and Sathyanarayana.[19]

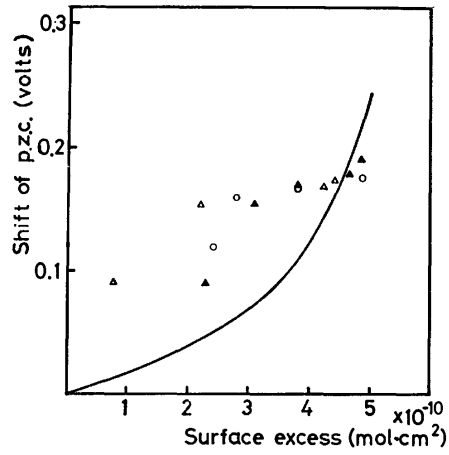

Fig. 12. Dependence of p.z.c. on amount of adsorbed *o*-cresol. (○) present work I; (△) Manohar and Sathyanarayana[19] (electrocapillary measurement); (▲) Manohar and Sathyanarayana[19] (differential capacity measurement).

calculated by using Eq. (2) at the p.z.c. for the base solution are shown in Fig. 9. The surface coverages determined by the electrocapillary measurement coincided with those determined by the differential capacitance measurement. This agreement has also been reported by Elliott.[17]

The two-condensers-in-parallel model was tested by plotting the shift of the potential of zero charge against Γ, as is shown in Fig. 10. The plots were far from this model. The shift of the electrocapillary maximum was nearly linear with respect to the surface excess of phenol. Similar behavior was also observed in the case of *o*-cresol in 0.5 M H_2SO_4, as is shown in Figs. 11 and 12. The surface excess evaluated from Eq. (2) coincided with the values evaluated thermodynamically. The two-condensers-in-parallel model was also inapplicable to this model, as is shown in Fig. 12.

The displacement of the potential of zero charge with respect to the surface excess was analyzed by using a three-condensers-in-parallel model[17] (the orientation of the adsorbed aromatic molecule changes from flat to vertical upon an increase in the concentration of the adsorbed species). The shift of the potential of zero charge is given by:

$$E = \theta E_{N1} \frac{(E_{N2}/E_{N1})(1-\theta)+\theta}{(C_0/C')(1-\theta)+\theta} \tag{8}$$

where E_{N1} and E_{N2} are, respectively, the shift of the potential of zero charge upon transition from the base solution to $\theta_1=1$ (when the electrode is fully covered by the vertically oriented molecules) and to $\theta_2=1$ (when the electrode is fully covered with the molecules of a flat orientation). E_{N2} was calculated by using this equation[17]

$$\beta = -\frac{C_1(E_{N1}-E_{N2})}{A} \tag{9}$$

where C_1 is the differential capacitance when $\theta_1=1$. The parameters used for the calculation were $\beta=-2.05\ V^{-1}$,[18] $A=1.22\ \mu J/cm^2$ ($A=RT\Gamma_{max}$, $\Gamma_{max}=4.93\times10^{-10}$ mol/cm^2), $C_1=7.00\ \mu F/cm^2$, and $E_{N1}=-0.140$ V. The calculated $E_{N2}=-0.498$ V. The plot of the three-condensers-in-parallel model is shown in Fig. 10. The plot showed a linear dependence of the displacement of the potential of zero charge on Γ. The three-condensers-in-parallel model does not explain the large displacement of the p.z.c. at lower coverages of the electrode with phenol. As has been stated by Damaskin,[17] the shape of the E *vs.* θ curve varies with the values of (E_{N2}/E_{N1}) and (C_0/C_1); that is, its convex or concave side is turned toward abscissa axis. Equation (8), however, does not explain the large shift of the p.z.c. at low θ values regardless of the values of (E_{N2}/E_{N1}) and (C_0/C_1). This has also been reported by Damaskin on the basis of their data.[18] *o*-Cresol behaved much like to phenol.

The author wishes to thanks Messrs. Y. Inoue, Y. Akimoto, and Y. Yamada for their extensive assistance during this work. This work was supported by the Ministry of Education of Japan for a Scientific Research Grant-in-aid.

References

1) A. N. Frumkin, *Z. Phys.*, **35**, 792 (1926).
2) M. Breiter and P. Delahay, *J. Amer. Chem. Soc.*, **81**, 2938 (1959).
3) R. S. Hansen, D. J. Kelsh, and D. H. Grantham, *J. Phys. Chem.*, **67**, 2316 (1963).
4) R. Parsons, *Trans. Faraday Soc.*, **51**, 1518 (1955); **55**, 999 (1959).
5) A. N. Frumkin, B. B. Damaskin, and A. A. Survila, *J. Electroanal. Chem.*, **16**, 493 (1968).
6) E. Dutkiewicz, J. D. Granish, and R. Parsons, *ibid.*, **16**, 505 (1968).
7) K. Niki and N. Hackerman, *ibid.*, **32**, 257 (1971).
8) Y. Inoue and K. Niki, *Rev. Polarogr.* (Kyoto), **18**, 49 (1972).
9) C. A. Smolders and E. M. Duyvis, *Rec. Trav. Chim.*, **80**, 635 (1961).
10) R. S. Hansen, R. E. Minturn, and D. A. Hickson, *J. Phys. Chem.*, **61**, 953 (1957).

11) J. O'M. Bockris, M. A. V. Devanathan, and K. Müller, *Proc. Roy. Soc.*, **A279**, 55 (1963).
12) E. Blomgren, J. O'M. Bockris, and C. Jesch, *J. Phys. Chem.*, **65**, 2000 (1961).
13) T. Biegler and H. A. Laitinen, *J. Electrochem. Soc.*, **113**, 852 (1966).
14) S. Sathyanarayana, *J. Electroanal. Chem.*, **10**, 119 (1965).
15) K. Ohsumi and K. Takahashi, private communication.
16) D. Elliott, *J. Electroanal. Chem.*, **22**, 301 (1968).
17) B. B. Damaskin, *Elektrokhimiya*, **4**, 675 (1968).
18) B. B. Damaskin, V. M. Gerovich, I. P. Gladkikh, and R. I. Kaganovich, *Zhur. Fiz. Khim.*, **38**, 2495 (1965).
19) G. Manohar and S. Sathyanarayana, *J. Electroanal. Chem.*, **30**, 301 (1971).

Radiation Synthesis of Ethylamine from Ethane-Ammonia Systems. Effect of Nitric Oxide Addition

Saburo SHIMIZU, Yasumasa IKEZOE, and Shoichi SATO
Japan Atomic Energy Research Institute, Tokai-mura, Ibaraki 319-11
(Received August 1, 1974)

Formation of ethylamine was observed in the γ-radiolysis of the ethane–ammonia system: the maximum G value was 0.5. Using oxygen as a radical scavenger, it was found that the ethylamine was formed *via* radical and ion intermediates. Addition of excess nitric oxide suppressed the ethylamine yield, but $G(C_2H_5NH_2)$ increased to 1.2 on addition of an optimum amount. This was attributed to the reduction of acetaldoxime by hydrogen atoms or alkyl radicals, after acetaldoxime had been formed by the reaction between ethyl radicals and the nitric oxide added as a scavenger.

Radiolysis of mixtures of hydrocarbons and ammonia has been studied by many workers. Ethylamine was produced in the irradiated ethylene–ammonia system[1] and propylamine was reported to be formed in the *n*-butane–ammonia system.[2]

In this study, the radiolysis of the ethane–ammonia system and especially the mechanism of ethylamine formation was examined. When an optimum amount of nitric oxide was added to the ethane–ammonia system, the ethylamine yield was enhanced, but when added in excess, the usual radical scavenging action of nitric oxide was observed. A mechanism was proposed for the formation of the amine in the presence of the additive.

Experimental

Ethane (99.7%, Takachiho Chemical) was used after purification by trap to trap distillation in a vacuum line. Ammonia (99.99%, Matheson) was dried with sodium metal and purified likewise. Nitric oxide (99.8%, Takachiho Chemical) was used after removal of non-condensible gases at −196 °C. Oxygen (99.7%) was used without further purification.

Gases were irradiated at room temperature by ^{60}Co gamma rays at 5.4×10^5 R/hr, in 40 ml Pyrex glass ampoules. The dose of gamma rays was measured with a Fricke dosimeter. The G value was calculated assuming that the mass absorption coefficient was proportional to the total number of electrons in the system.

Radiolysis products, amines and hydrocarbons were analyzed by a gas chromatograph equipped with a flame ionization detector at 70 °C. To obtain reproducible results with ethylamine, grease, metal and rubber were eliminated as much as possible, and nitrogen gas mixed with 10% ammonia was used as carrier gas. The column consisted of a 2 m (10% KOH+10% TEPA on Porapak Q) and a 1 m (10% KOH+10% Quadrol on Porapak Q) column. Nitric oxide, hydrogen and methane were analyzed by volumetry and mass spectrometry.

Results and Discussion

Ethylamine Formation from Ethane–Ammonia System. When ethane–ammonia mixtures were irradiated, hydrogen, nitrogen methane, propane, *n*-butane and methylamine were formed besides ethylamine. Yield of ethylamine, *n*-butane and others are shown in Fig. 1 as a function of the mixing ratio. The yield of *n*-butane increased with increasing ammonia concentration until $C_2H_6/NH_3=90/10$, then decreased almost linearly on further addition of ammonia. The yield of ethylamine showed similar characteristics with a maximum G value of 0.5 at the same ammonia content.

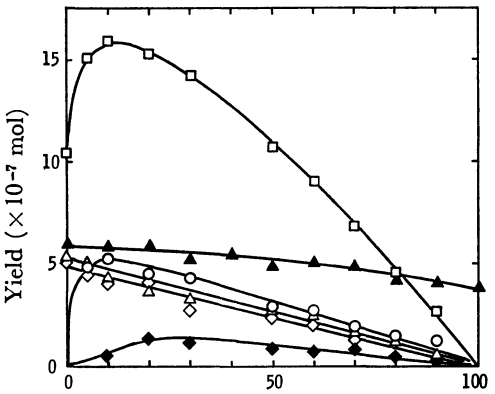

Fig. 1. Composition dependence of product yields.
○; ethylamine, □; *n*-butane, ◆; methylamine, △; methane, ◇; propane, ▲; hydrogen (×0.1)
Gamma rays; total dose 10 Mrad. Irradiated gas; total amount $C_2H_6+NH_3=3.43\times10^{-3}$ mol, pressure 2 kg/cm², in 40 ml glass ampoules.

The effect of addition of oxygen to this system was studied. The yield of *n*-butane was effectively reduced on addition of the radical scavenger, oxygen, as shown in Table 1. Therefore, *n*-butane should be formed predominantly by the following radical reaction:

Table 1. Effect of added oxygen in the radiolysis of the ethane–ammonia system

% added oxygen	Yields	
	ethylamine ($\times10^{-7}$ mol)	*n*-butane ($\times10^{-7}$ mol)
0	4.90	13.65
0.48	4.45	4.10
1.20	3.63	1.10
3.12	3.02	0.75
6.72	3.37	0.73
12.72	3.30	0.75

Gamma rays; total dose=8.64 Mrad; Irradiated gas; composition $C_2H_6/NH_3=90/10$, pressure=2 kg/cm, in 40 ml glass ampoules.

$$C_2H_5\cdot + C_2H_5\cdot \longrightarrow n\text{-}C_4H_{10} \quad (1)$$

On the other hand, the ethylamine formation was considerably suppressed by addition of 3.12% oxygen, but not further affected by further addition of oxygen. This suggests the following two reactions for ethylamine formation: the radical reaction 2, which is inhibited by the presence of oxygen, and the ionic reaction 3, which is not.

$$C_2H_5\cdot + NH_2\cdot \longrightarrow C_2H_5NH_2 \quad (2)$$

$$C_2H_5^+ + NH_3 \longrightarrow C_2H_5NH_3^+ \xrightarrow{e^-} C_2H_5NH_2 + H \quad (3)$$

In the radiolysis[1] and the photolysis[3] of the ethylene–ammonia system, ethylamine formation has been attributed to the radical reaction. An ionic reaction similar to Reaction 3 has been suggested for propylamine formation in the radiolysis of the *n*-butane–ammonia system.[2]

Ethylamine Formation in the Presence of Nitric Oxide. The effect of added nitric oxide on the radiolysis of the ethane–ammonia system was studied for the mixture containing 10% ammonia (the composition at which the maximum yield of ethylamine was observed (Fig. 2)).

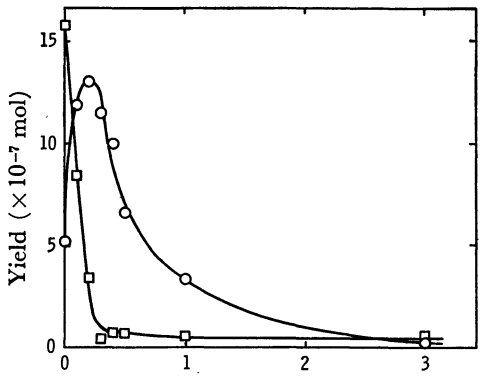

Fig. 2. Effect of added nitric oxide on product yields.
○; ethylamine, □; *n*-butane
Gamma rays; total dose 10 Mrad. Irradiated gas; composition $C_2H_6/NH_3=90/10$, pressure 2 kg/cm², in 40 ml glass ampoules.

The yield of ethylamine increased significantly on adding small amounts of nitric oxide, then decreased on further addition, while the yield of *n*-butane decreased monotonically. The maximum $G(C_2H_5NH_2)$ value, 1.2, obtained with 0.2% added NO was 2.4 times larger than that obtained without the additive.

It is difficult to interpret the increase of the ethylamine yield with a slight addition of nitric oxide according to the mechanisms (2) and (3). Nitric oxide addition should suppress ethylamine formation by either the radical or ionic reaction 2 or 3, because nitric oxide is able to scavenge ethyl and amino radicals, or because it interacts with ethyl cations due to its very low ionization potential (IP=9.24 eV). Therefore, a third mechanism must be considered for the enhanced formation of amine (See following section).

Effect of Dose in the Presence of Nitric Oxide. At

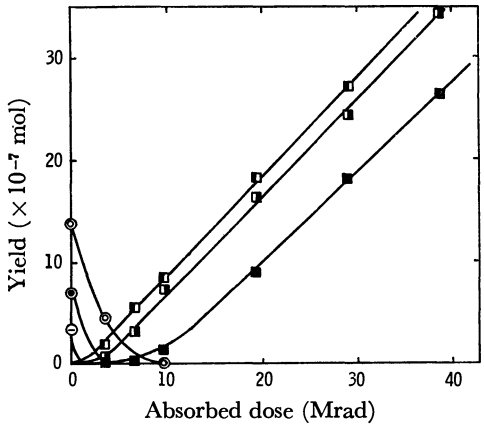

Fig. 3. Effect of absorbed dose on *n*-butane formation and nitric oxide consumption.
n-butane yield for added nitric oxide concentration, ◧; 0.1%, ◨; 0.2%, ■: 0.4%, residual amount of nitric oxide (×0.1) for initial concentration, ⊖; 0.1%, ⊙; 0.2%, ◎; 0.4%.
Gamma rays; dose rate 5.4×10⁵ R/hr. Irradiated gas; composition $C_2H_6/NH_3=90/10$, pressure 2 kg/cm², in 40 ml glass ampoules.

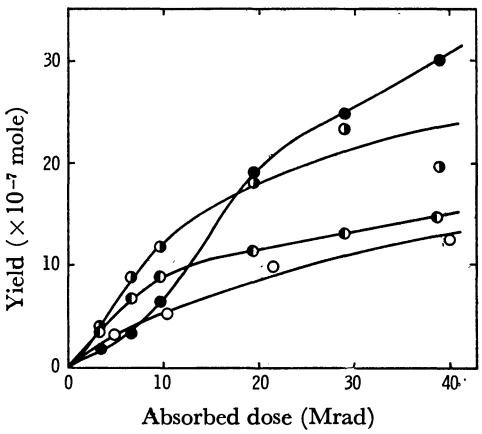

Fig. 4. Effect of absorbed dose on ethylamine yield.
initial concentration of nitric oxide, ○; 0%, ◐; 0.1%, ◑; 0.2%, ●; 0.4%.
Experimental conditions; same as in Fig. 3.

nitric oxide concentrations of 0.1, 0.2, and 0.4%, the effect of absorbed dose on the radiolysis of the ethane–ammonia–nitric oxide system was studied. The yield of *n*-butane and the amount of nitric oxide which remained are shown in Fig. 3, and the yield of ethylamine in Fig. 4. In each system, the nitric oxide concentration decreased rapidly. An initial $G(-NO)$ value of 22.5 was obtained for the system containing 0.4% nitric oxide.

In the formation of *n*-butane, induction periods appeared. Their length was closely related to the initial concentration of nitric oxide. The longest period was observed with 0.4% nitric oxide. Reaction 1 is suppressed during the induction period when nitric oxide is present. After all the nitric oxide is consumed, the amount of *n*-butane formed increases linearly with the absorbed dose.

The ethylamine yield in the absence of nitric oxide

increased linearly with the absorbed dose at relatively low doses and was close to saturation at about 30 Mrad. On addition of 0.1 and 0.2% nitric oxide, the yield over the whole range of absorbed dose was about 1.2 and 2 times larger, respectively, than in the system without the additive. On addition of 0.4% nitric oxide, the yield of ethylamine was smaller than that of the system without nitric oxide up to an absorbed dose of 10 Mrad. The region where the yield of ethylamine was smaller may be regarded as the induction period for ethylamine formation. After the induction period, *i.e.* after the nitric oxide had disappeared, the yield of ethylamine increased significantly. It must be noted that this phenomenon is similar to that in the *n*-butane formation.

Again, this increase in the amine yield at high dose for large initial nitric oxide concentration can not be explained by the two amine formation mechanisms (2) and (3). After the induction period, the nitric oxide may be assumed to be exhausted and alkyl radicals be formed without being scavenged. Therefore, a third mechanism was studied which explained the increased amine formation with these assumptions.

Role of Acetaldoxime in Ethylamine Formation. It has been known that a nitroso compound or its oxime tautomer is formed when an alkyl radical is scavenged by nitric oxide.[4] The formation of cyclohexylamine has been reported in the radiolysis of liquid cyclohexane with nitric oxide added.[5] The reaction pathway consisted of the scavenging of a cyclohexyl radical by nitric oxide and the reduction of the tautomer, cyclohexanonoxime, by alkyl and hydrogen radicals. Similarly, the following reactions may be expected to give ethylamine in the ethane–ammonia system;

$$C_2H_5\cdot + NO \longrightarrow C_2H_5NO \quad (4)$$

$$C_2H_5NO \rightleftarrows CH_3CH{=}NOH \quad (5)$$

$$CH_3CH{=}NOH \xrightarrow{R\cdot,\ H\cdot} C_2H_5NH_2 \quad (6)$$

Table 2. Effect of additives on $G(C_2H_5NH_2)$

Reaction system	$G(C_2H_5NH_2)$
$C_2H_6(90)+NH_3$ (10)	0.5
$C_2H_6(90)+NH_3(10)+NO$ (0.2%)	1.2
$C_2H_6(100)+NO$ (0.1–1%)	<0.1
$C_2H_6(90)+NH_3(10)+CH_3CH{=}NOH$ (2%)	1.2
$C_2H_6(100)+CH_3CH{=}NOH$ (2%)	≈ 0.1
$NH_3(100)+CH_3CH{=}NOH$ (2%)	0.3

Gamma rays; total dose=10 Mrad. Irradiated gas; pressure 2 kg/cm, in 40 ml glass ampoules.

Reaction 6 could occur in the gas phase, since the vapor pressure of acetaldoxime is 10.0 Torr at 25.8 °C.

Table 2 shows the $G(C_2H_5NH_2)$ values which were obtained for various combinations of the reactants, ethane and ammonia, as well as the additives, nitric oxide and acetaldoxime. For ethane–ammonia mixtures above, the maximum G value was 0.5, but was 1.2 in the presence of 0.2% nitric oxide. The value was also 1.2 for the ethane, ammonia and 2% acetaldoxime mixture.

The direct reaction between ethane and nitric oxide or acetaldoxime and that between ammonia and acetaldoxime can be excluded from the mechanism for the enhanced ethylamine formation. Acetaldoxime added to the ethane–ammonia mixture plays the role of the intermediate in ethylamine formation as effectively as nitric oxide does. Thus, the third mechanism (expressed by Reactions 4, 5, and 6) seems plausible from these qualitative results. As shown in Figs. 2 and 4, the ethylamine yield increased at an optimum amount of nitric oxide, and decreased with addition of excess. These observations are also consistent with the proposed mechanism.

Nitric oxide has been used as a radical scavenger in radiolysis. However, it has been noted that its use sometimes makes the main reaction scheme more complex.[6] This study exemplifies a case in which the scavenging reaction of nitric oxide results in yields of the product that are the same as those obtained without the additives, clearly showing the necessity of taking care in using this compound in the study of radiolysis. At the same time, it has been demonstrated that a radical scavenger could be used to enhance the formation of a reaction product, as has been shown in one other system.[7] This point is of interest for preparative radiation chemistry.

References

1) O. Tokunaga, K. Hamanoue, J. Okamoto, and A. Danno, This Bulletin, **45**, 1050 (1972).
2) T. Miyazaki and S. Shida, *ibid.*, **38**, 2114 (1965).
3) U. Schurath, P. Tiedeman, and R. N. Schindler, *J. Phys. Chem.*, **73**, 456 (1969).
4) G. L. Pratt and J. H. Purnell, *Trans. Faraday Soc.*, **60**, 371 (1964).
5) A. Henglein, *Int. J. Appl. Radiat. Isotopes*, **8**, 149 (1960).
6) For example, L. W. Sieck, "Fundamental Processes in Radiation Chemistry," ed. by P. Ausloos, Interscience Publ., New York, N. Y. (1968), p. 135.
7) Y. Ikezoe, S. Sato, and K. Oshima, This Bulletin, **47**, 1559 (1974).

Properties of Protective Films Formed on an Iron Surface by Dialkyl Phosphate as a Corrosion Inhibitor

Satoru NAKAGAWA and Genzo HASHIZUME

Industrial Research Institute of Hyogo Prefecture, Suma-ku, Kobe 654

(Received October 18, 1974)

The properties of films formed on an iron surface by di-*n*-dodecyl phosphate were studied. The inhibition effects for iron specimens treated with dodecyl phosphate were estimated from the losses in weight of iron specimens in 5% NaCl aqueous solutions. The Fe L_α, L_β X-ray emission spectra of the iron surface were obtained by electron microprobe X-ray analysis. The value of the intensity ratio, Fe L_β/L_α, of the untreated iron specimen was 0.17, while that of the treated iron specimen was 0.28. The infrared spectrum of the treated iron surface was similar to that of tribasic orthophosphate. The content of Fe in the film formed on the iron surface by di-*n*-dodecyl phosphate was from 4.3% to 6.98%. From these results, it was inferred that di-*n*-dodecyl phosphate reacted with iron atoms at the iron surface in a cyclohexane solution and that the main component of the film formed on the iron surface was $[(RO)_2POO]_2Fe$ or $[(RO)_2POO]_3Fe$.

Corrosion inhibitors for recirculating cooling water are grouped into three classes—that is, inhibitors which passivate the metal surface, those which precipitate on the metal surface, and those which are adsorbed on the metal surface, by the formation mechanism of the film on the metal surface.[1] It is thought[2] that dialkyl phosphate is adsorbed on an iron surface with the orthophosphate ion, but the mechanism of film formation by dialkyl phosphate has not yet been studied in detail. In this paper, the properties of the films formed on an iron surface by di-*n*-dodecyl phosphate $(C_{12}H_{25}O)_2PO(OH)$ were studied by measurements of the Fe L_α, and L_β X-ray emission spectra, the infrared spectra, and the contents of the film formed on the iron surface.

Experimental

Materials. The iron specimens used were the same as those used in the previous work.[3] The di-*n*-dodecyl phosphate was synthesized by a known procedure[4] and was purified by recrystallization. No significant impurities were detected in the mass spectrum of the di-*n*-dodecyl phosphate used in these experiments.

Procedures. Iron specimens were placed in C_6H_{12}, CCl_4 and $CHCl_3$ solutions of dodecyl phosphate at 35 °C; then they were taken out of the solutions, washed in the solvent, and wiped with gauze. The inhibition effects of dodecyl phosphate on iron specimens were estimated from the losses in weight of the iron specimens (55×15×0.7 mm) in 5% NaCl aqueous solutions (15 ml) during 24 hr at 35 °C and from the percentage of the rusted surface as estimated by a visual observation of the iron specimens (30×80×1.0 mm) after a humidity test at 40 °C and 95% RH for 48 hr. The Fe L_α, and L_β spectra of the surfaces of iron specimens (10×10×1.0 mm) were measured by means of a Shimadzu-ARL electron microprobe X-ray analyzer EMX-SM with RAP crystals. When the iron specimens were placed in a C_6H_{12} solution of dodecyl phosphate at 35 °C for 7 days, a viscous liquid material adhered to the iron surface. Therefore, the iron specimens were taken out of the solution, as they were, and were placed in a desiccator without washing and wiping; they were then dried at room temperature in the evacuated desiccator. A white film was thereupon separated from the iron surface. The infrared spectra of these films were measured by the tablet method with KBr, and the contents of Fe and P in the C_6H_{12} solutions dissolved from these films were determined by fluorescent X-ray analysis. The preparation of the sample for the analysis was carried out as follows; 200 μl of a solution was dropped onto the miller film and then evaporated to dryness by using an infrared lamp. The intensity of Fe K_α was measured at 57.50° with an LiF crystal and a Cr target, while that of P K_α was measured at 141.05° with a Ge crystal and a Cr target. The infrared spectra of the surfaces of iron specimens (19×56×1.0 mm and 19×47×1.0 mm) treated with dodecyl phosphate were measured by the ATR method.

Results and Discussion

Inhibition Effects of di-n-Dodecyl Phosphate. The inhibition efficiencies of dodecyl phosphate, as estimated from the losses in weight of the iron specimens and from visual observations of the iron surface, are shown in Table 1. The inhibition effects on iron specimens treated in C_6H_{12} solutions of dodecyl phosphate were more than those on iron specimens treated in other solutions. On the basis of these data, subsequent experiments were carried out in the cyclohexane solutions.

TABLE 1. THE EFFECTS OF SOLVENTS ON THE INHIBITION EFFICIENCIES OF DI-*n*-DODECYL PHOSPHATE FOR IRON SPECIMENS

Solvent[a]	Percent inhibition[b] %	Rusted surface[c] %
C_6H_{12}	66	10
CCl_4	33	70
$CHCl_3$	0	100

a) Concentration of inhibitor is 0.5%. b) By total immersion tests in test tube (15×110 mm, in aerated 5% NaCl solution) at 35 °C for 24 hr. c) By humidity tests in desiccator at 40 °C and 95% RH for 48 hr.

Adsorption-Time Curve of the Dodecyl Phosphate for Iron. The intensity of the P K_α line of the iron surface treated with dodecyl phosphate, as measured by fluorescent X-ray analysis, was introduced instead of the amount of dodecyl phosphate adsorbed on the iron surface. The P K_α intensities of the iron surface are plotted as a function of the time in Fig. 1. The P K_α intensity of the iron surface reached a maximum after 7 days. Therefore, subsequent experiments were carried out by treating the surface fors 7 days; the concentration was 0.5%.

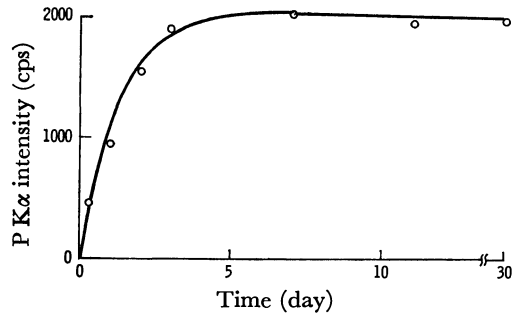

Fig. 1. Adsorption-time curve of di-*n*-dodecyl phosphate for iron specimen, in 0.5% cyclohexane solution at 35 °C.

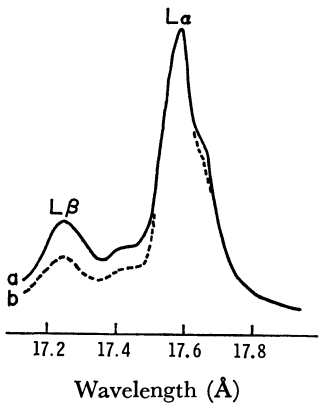

Fig. 2. Fe Lα, Lβ band spectra for iron specimens.
(a) Iron specimen treated with di-*n*-dodecyl phosphate,
(b) non treated iron specimen.

Fe L_α and L_β X-Ray Emission Spectra of an Iron Surface. The Fe L_α and L_β spectra of an untreated iron surface and a treated iron surface are shown in Fig. 2. These spectra differ from one another in the Fe L_β/L_α intensity ratio. This intensity ratio varies with the Fe-oxidation state.[5] For example,[6] the Fe L_β/L_α intensity ratio of Fe-metal is 0.17, while that of Fe-oxide (Fe_3O_4) is 0.51. The spectra in Fig. 2 show that the ratio for the untreated iron surface is 0.17, while the ratio for the treated iron surface is 0.28. The ratio varies not only with the Fe-oxidation state, but also with the self-absorption effect or with the absorption effects of elements in the film on the surface. The spectra in Fig. 2 were obtained under the same conditions at 10 kV and 0.04 μA, so the self-absorption effect is negligible. The value of the ratio for an iron surface is obtained as only 0.18 instead of 0.17 by the correction of the absorption effects of the components in the film on the iron surface, carbon, oxygen, and phosphorus atoms in dodecyl phosphate. Therefore, the increase in the ratio observed in this experiment shows that the chemical state of the iron atom at the surface is made to vary by the treatment with dodecyl phosphate.

Infrared Spectra. The infrared spectrum of the surface of an iron specimen treated with dodecyl phosphate, as obtained by the ATR method, is shown in Fig. 3, together with the spectrum of the surface of phosphating steel obtained by Sato.[7] Both spectra show broad peaks at about 1100 cm^{-1}. The infrared

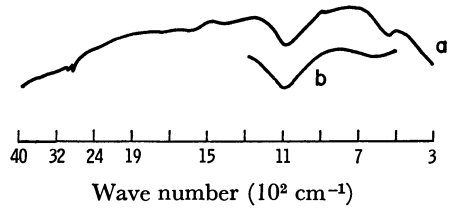

Fig. 3. IR spectra of iron treated with di-*n*-dodecyl phosphate by ATR method (a) and phosphating steel by Sato (b).

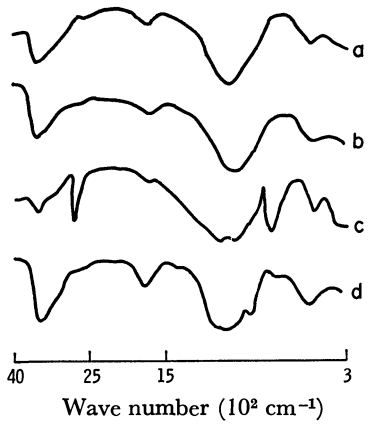

Fig. 4. IR spectra of the products obtained by precipitation reactions of $FeCl_3$ with NaH_2PO_4 (a), Na_2HPO_4 (b), NaH_2PO_4 (c) and $Na_4P_2O_7$ (d).

spectra of the products obtained by the precipitation reactions of ferric chloride with monosodium phosphate, disodium phosphate, sodium hypophosphite, or sodium pyrophosphate are shown in Fig. 4. The spectrum (a) in Fig. 3 is similar to the (a) and (b) spectra in Fig. 4—that is, the spectra of orthophosphate. The spectra of tribasic, dibasic and monobasic orthophosphate were reported by Miller and Wilkins.[8] The (a) spectrum in Fig. 3 is similar to the spectrum of tribasic orthophosphate, which has no OH group. The infrared spectrum of a white film separated from the iron surface, as obtained by the tablet method with KBr, is shown in Fig. 5, together with the spectrum of the di-*n*-dodecyl phosphate used in this experiment. In the (a) spectrum in Fig. 5, a peak at about 1200 cm^{-1} disappears and a peak at about 1150 cm^{-1} appears. These peaks cannot be definitely assigned for the present, but the spectra show that dodecyl phosphate varies at the iron surface. From these infrared spectra, it can be thought that the iron atom is substituted for

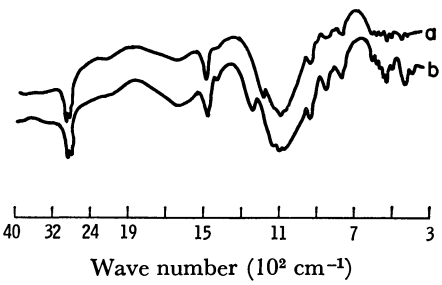

Fig. 5. IR spectra of white film separated from iron surface (a) and di-*n*-dodecyl phosphate (b).

TABLE 2. THE CONTENT OF Fe AND P IN THE SOLUTION DISSOLVED FROM WHITE FILM SEPARATED FROM THE IRON SURFACE[a)]

Sample	Fe mg/cm³	dodecyl phosphate mg/cm³	Fe content in phosphate %
film A	0.025	0.575[b)]	4.30[c)]
film B	0.030	0.425[b)]	6.98[c)]
dodecyl phosphate	0.0013	1.50	0.08

a) Film separated from iron surface was dissolved in cyclohexane b) Content of dodecyl phosphate was calculated from the PK_α intensity. c) Weight of film separated from iron surface was calculated from content of dodecyl phosphate, supposing that film consisted of dodecyl phosphate.

one hydrogen atom in dodecyl phosphate at the iron surface.

Determination of Fe and P. The contents of Fe and P in the films separated from the iron surface are shown in Table 2. The content of the Fe impurity in the dodecyl phosphate used in this experiment is 0.08%. The content of Fe in the white film separated from the iron surface is between 4.3 and 6.9%. The composition in the films was not constant, but the Fe content in the films showed values in the range from about 4.3 to 6.9% in several experiments. The calculated value of the Fe content in the film is 4.3%, supposing that two molecules of dodecyl phosphate combine with the iron atom as Fe^{2-}, while the value is 6.4%, if we suppose that three molecules of dodecyl phosphate combine with the iron atm as Fe^{3-}. From these results, it was inferred that di-*n*-dodecyl phosphate reacted with the iron atom at the iron surface in the C_6H_{12} solution, that the iron atom was substituted for two or three molecules of dodecyl phosphate, and that the main component of the film formed on the iron surface was $[(RO)_2POO]_2Fe$ or $[(RO)_2POO]_3Fe$.

References

1) R. Sugano, *Boshoku Gijutsu*, **22**, 367 (1973).
2) D. A. Carter and C. C. Nathan, *Mater. Prot.*, **8**, No. 9. 61 (1969).
3) S. Nakagawa and G. Hashizume, *Denki Kagaku*, **37**, 598 (1969).
4) R. S. Cooper, *J. Amer. Oil Chem. Soc.*, **40**, 642 (1963).
5) D. G. W. Smith and R. K. O'Nions, *Brit. J. Appl. Phys.*, **4**, 147 (1971).
6) W. Reuter, *Surface Sci.*, **25**, 80 (1971).
7) K. Sato, *Jasco Report*, **8**, 122 (1971).
8) F. A. Miller and C. H. Wilkins, *Anal. Chem.*, **24**, 1253 (1952).

The Crystal Structure of Sodium Molybdate Dihydrate, $Na_2MoO_4 \cdot 2H_2O$

Kazuko MATSUMOTO, Akiko KOBAYASHI, and Yukiyoshi SASAKI

Department of Chemistry, Faculty of Science, The University of Tokyo, Hongo, Tokyo 113

(Received August 1, 1974)

$Na_2MoO_4 \cdot 2H_2O$ is orthorhombic, with the space group of Pbca and with cell constants of $a=8.463(3)$, $b=10.552(3)$, and $c=13.827(6)$ Å; $U=1234.8$ Å^3; $Z=8$. The crystals are composed of alternate layers of MoO_4^{2-} tetrahedra and water molecules. The layers are connected by interlinking sodium cations and hydrogen bonds. The MoO_4^{2-} tetrahedron is slightly elongated in the direction of the hydrogen bonds.

Recent structure determinations of $Na_6Mo_5P_2O_{23} \cdot 13H_2O$,[1] $Na_4H_2Mo_5P_2O_{23} \cdot 10H_2O$,[2] and $Na_6Mo_7O_{24} \cdot 14H_2O$[3] have revealed the remarkable basic character of the oxygen atoms, which are octahedrally attached to the molybdenum atoms to form not only hydrogen bonds with water, but also coordination bonds with sodium ions.

Our main interest in the present structural study of $Na_2MoO_4 \cdot 2H_2O$ lies in the coordination of the oxygen atoms in the tetrahedral MoO_4^{2-} anion to Na^+ cations in comparison with those in octahedral MoO_6 groups in the heteropoly- and isopoly-anions.

About $Na_2MoO_4 \cdot 2H_2O$, the unit-cell dimensions and the space group,[4] the Raman spectra, and the infrared spectra data[5] have already been reported.

Experimental

Suitable crystals of $Na_2MoO_4 \cdot 2H_2O$ were selected from the reagent-grade chemicals commercially available from the KOSO Wako Company. Preliminary oscillation and Weissenberg photographs showed that the crystals were orthorhombic, with the space group Pbca; this confirmed the results of the preliminary measurements made by Poljak and Becka.[4]

The intensities of the reflections were measured on a Rigaku automated four-circle diffractometer. Graphite monochromatized Mo$K\alpha$ radiation was used. The ω-2θ scan technique was employed. The scan range was calculated from this formula: $1.2+0.5\tan\theta$; the scan speed was 0.5° per min in ω, and background counts of 10 s were taken at both limits of the scan. Three reference reflections, 220, 020, and 002, were measured for every 50 reflections. The net counts of these reflections altered only within 1% over the period of data collection. A total of 2104 independent intensities were measured up to $2\theta=60°$ ($0\leq h\leq 11$, $0\leq k\leq 14$, $0\leq l\leq 19$); those reflections of which the $|F_o|$ value was less than 7.9 (absolutely scaled value) were regarded as unobserved in view of the accuracy of the measurement. The remaining 1497 reflections were adopted for the structure determination. The unit-cell dimensions and their standard deviations, as measured on the Rigaku diffractometer (Mo$K\alpha$, $\lambda=0.71069$ Å), were $a=8.463$ (3), $b=10.552$ (3), $c=13.827$ (6) Å; $U=1234.8$ Å^3 at 23 °C; $D_m=2.51$ and $D_x=2.60$ g cm^{-3} for $Z=8$; M.W.=241.9 and μ for Mo$K\alpha=23.2$ cm^{-1}. As the dimensions of the specimen used were approximately $0.15\times 0.1\times 0.2$ mm, the absorption correction was not made.

Structure Determination

The structure was solved by the heavy-atom technique and was refined by the least-squares method, the function minimized being $\sum\omega(|F_o|-k|F_o|)^2$. A weighting scheme, $w=0.2$ for $|F_o|<11.9$ and otherwise $w=1$, was employed. The refinements of the parameters of all the non-hydrogen atoms were carried out by the block-diagonal least-squares method. In the last cycle

Table 1. Final fractional atomic coordinates ($\times 10^4$) with their estimated standard deviations in parentheses

	x	y	z
Mo	5149(1)	1982(1)	5233(0)
Na(1)	6565(4)	4952(3)	4145(2)
Na(2)	7424(4)	4492(3)	6482(2)
O(1)	5573(6)	3602(5)	5431(4)
O(2)	4505(7)	1759(5)	4013(4)
O(3)	6877(7)	1090(6)	5393(4)
O(4)	3716(6)	1486(5)	6097(4)
H_2O(1)	2288(7)	1416(6)	2011(4)
H_2O(2)	4617(8)	4077(6)	2996(4)

Table 2. Final temperature factors ($\times 10^4$) with their estimated standard deviations in parentheses

(The temperature factor is of the form: $\exp[-(\beta_{11}h^2+\beta_{22}k^2+\beta_{33}l^2+\beta_{12}hk+\beta_{13}hl+\beta_{23}kl)]$)

	β_{11}	β_{22}	β_{33}	β_{12}	β_{13}	β_{23}
Mo	31(1)	16(0)	13(0)	0(1)	1(1)	0(1)
Na(1)	40(4)	24(3)	18(2)	8(5)	−3(4)	−3(3)
Na(2)	43(4)	29(2)	16(1)	−9(5)	−5(5)	4(3)
O(1)	34(6)	12(4)	20(3)	−3(8)	−3(7)	−4(5)
O(2)	42(7)	26(4)	23(3)	26(10)	−3(7)	8(6)
O(3)	44(7)	25(4)	17(3)	−24(9)	11(7)	−2(6)
O(4)	40(7)	28(4)	14(3)	−4(9)	−7(7)	−7(5)
H_2O(1)	55(8)	33(5)	16(3)	0(10)	−10(8)	8(6)
H_2O(2)	71(8)	29(5)	21(3)	7(11)	−9(8)	−5(6)

of least-squares refinement with anisotropic temperature factors, the R index ($R=\Sigma||F_o|-|F_o||/\Sigma|F_o|$) converged to 0.037. A difference Fourier synthesis was calculated at this stage; some faint electron density peaks were detected, but their positions were inadequate for hydrogen atoms. The atomic scattering factors used were taken from the International Tables for X-ray Crystallography Vol. III.[19] Corrections for the anomalous dispersion were not made. The atomic coordinates and temperature factors are listed in Tables 1 and 2. The F_o-F_o table is kept at the office of this Bulletin as Document No. 7507.

Results and Discussion

Description of the Structure. The crystal structure

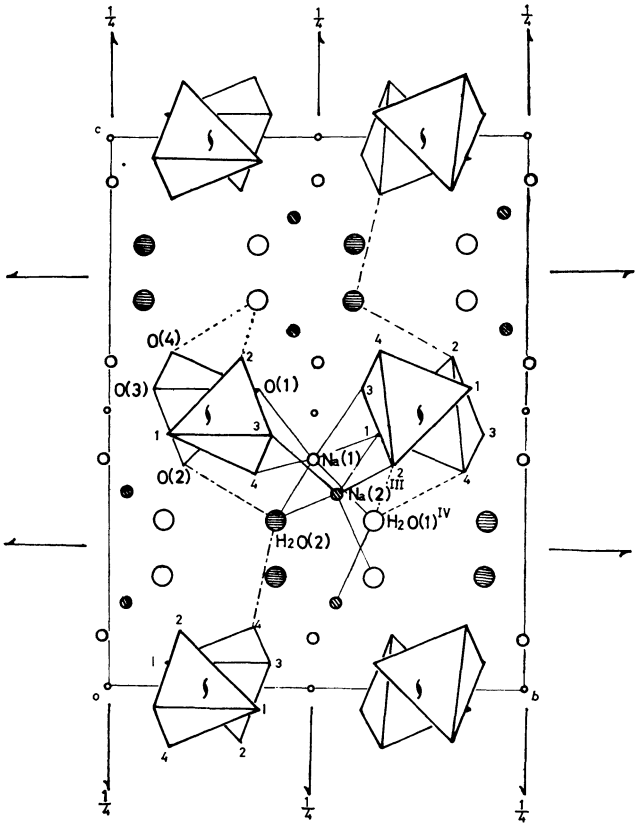

Fig. 1. The structure viewed along the a axis. Water layers and molybdate anion layers are seen alternately. Tetrahedra represent MoO_4^{2-} anions. The coordination bonds around Na^+ cations are shown with full lines. Dotted lines are O(2)···H_2O(1)···O(4) hydrogen bonds between two MoO_4^{2-} anions in the same layer. Dot-dash lines are O(2)—·—H_2O(2)—·—O(4) type hydrogen bonds bridging adjacent layers. The small letters 1, 2, 3, and 4 represent oxygen atoms equivalent to O(1), O(2), O(3), and O(4). The Na(2) atoms are shaded only in Fig. 1. Parameter transformations are as follows.

I	$1/2+x$	$1/2-y$	$-z$
II	$1/2-x$	$1/2+y$	z
III	$-x$	$-y$	$-z$
IV	$-x$	$1/2+y$	$1/2-z$
V	x	$1/2-y$	$1/2+z$
VI	$1/2+x$	y	$1/2-z$
VII	$1/2-x$	$-y$	$1/2+z$

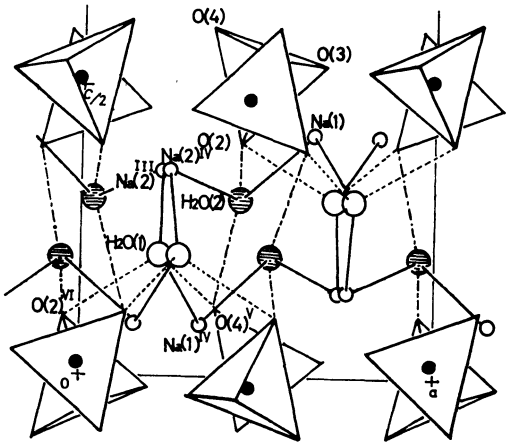

Fig. 2. The structure viewed along the b axis. Full lines represent Na–O(H_2O) bonds, Na–O(MoO_4) bondings are omitted. See the caption of Fig. 1.

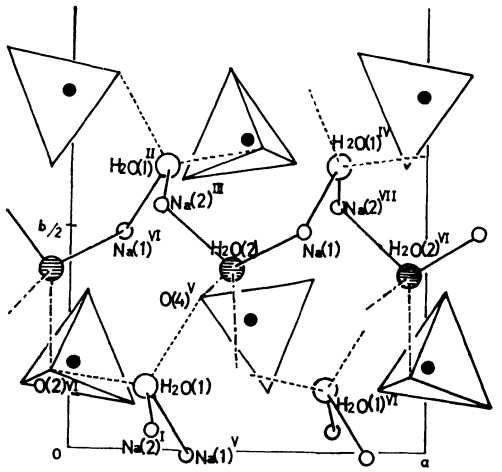

Fig. 3. The structure viewed along the c axis. Only the structure in the range of $0\leqq z\leqq 0.5$ is depicted. Bonds between Na^+ and MoO_4^{2-} are omitted. See the caption of Fig. 1.

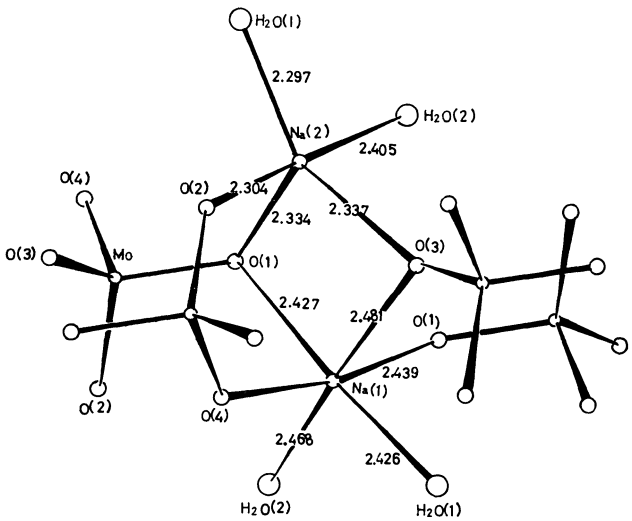

Fig. 4. Oxygen coordinations around the two sodium cations. Na(1) is hexacoordinated and Na(2) is pentacoordinated.

Table 3.

	The number of water oxygens coordinated to Na atom, with the range of Na–O distances in parentheses (Å)	The number of non-water oxygens coordinated to Na atom, with the range of Na–O distances in parentheses (Å)	Reference
$Na_2SO_4 \cdot 10H_2O$	6 (2.39—2.47)	0	6)
$Na_2H_2P_2O_6 \cdot 6H_2O_6$	4 (2.329—2.485)	2 (2.325—2.459)	7)
$Na_2H_2P_2O_7 \cdot 6H_2O$	4 (2.350—2.507)	2 (2.332—2.434)	7)
$Na_2Zn(SO_4)_2 \cdot 4H_2O$	2 (2.43—2.75)	4 (2.32—2.38)	8)
$NaHC_2O_4 \cdot H_2O$	2 (2.311—2.403)	4 (2.328—2.475)	9)
$Na_2HAsO_4 \cdot 7H_2O$	6 (2.365—2.509)	0	10)
$Na_2HPO_4 \cdot 7H_2O$	6 (2.341—2.486)	0	10)
Na_2SiO_3	0	5 (2.282—2.549)	11)
$Na_2H_2SiO_4 \cdot 4H_2O$	1 (2.38)	4 (2.31—2.40)	12)
$NaOH \cdot 4H_2O$	5 (2.36—2.37)		13)

is considered to consist of alternate layers of MoO_4^{2-} tetrahedra parallel to (001) and of water molecules; it is shown in three projections in Figs. 1, 2, and 3. The MoO_4^{2-} tetrahedra within a layer are connected by interlinking Na(1) and Na(2), as well as by the hydrogen bonding, O(2)···H_2O(1)···O(4). The adjacent layers are bridged by interlinking cations and hydrogen-bonding O(2)-·-·-H_2O(2)-·-·-O(4) linkages, as is shown in Figs. 1 and 2.

Coordination around Sodium Ions. The oxygen coordinations around the two crystallographically-independent sodium atoms are remarkably different, as is shown in Fig. 4. The Na(1) ion is surrounded by two water oxygen atoms and four MoO_4^{2-} oxygen atoms, each of which belongs to a different MoO_4^{2-} group, thus form a distorted octahedron. The Na(2) ion is surrounded by two water oxygen atoms and three MoO_4^{2-} oxygen atoms in the form of a distorted trigonal bipyramid. The mean distance of Na(1)–O is 2.439 Å, while that of Na(2)–O is 2.335 Å; the difference is presumably attributable to the different coordination numbers, 6 and 5.

Table 3 gives the coordination numbers of the sodium atoms and the Na–O distances in some hydrated sodium salts of oxyacids. It shows that the most common coordination number of sodium atoms is six and that the pentacoordinated sodium ion as in $Na_2MoO_4 \cdot 2H_2O$ is rare.[12,13] Another example is found in Na_2SiO_3,[11] where the sodium ion is coordinated to form a distorted trigonal bipyramid and where the Na–O distances are 2.370, 2.303, 2.282, 2.549, and 2.404 Å. The Na(2)–H_2O(1) distance, 2.297 Å, in $Na_2MoO_4 \cdot 2H_2O$ is, along with the Na–O distance in the above-mentioned Na_2SiO_3 and along with that of the hexacoordinated sodium ion in $Na_2OGeO_2 \cdot 6H_2O$, 2.28 Å,[14] one of the shortest Na–O distances reported thus far. Some of the compounds listed in Table 3 have sodium ions coordinated entirely by water oxygens. In hydrated sodium salts of oxyacids which contain elements of Group 4, 5, or 6 in the periodic table and which have sodium ions coordinated both by water and anion oxygens, the Na–O(H_2O) distance is generally a little longer than that of the Na–O(anion). However, in $Na_2MoO_4 \cdot 2H_2O$ there is no appreciable difference between the Na–O(H_2O) and Na–O(anion) distances.

Table 4. Interatomic distances and angles in hydrogen bonding and in coordination bonding

$H_2O(1)$·····$O(2)^{VI}$	2.772(8) Å
$H_2O(1)$·····$O(4)^{V}$	2.821(8)
$H_2O(1)$——$Na(2)^{I}$	2.297(7)
$H_2O(1)$——$Na(1)^{V}$	2.426(7)
$O(2)^{VI}$·····$H_2O(1)$·····$O(4)^{V}$	91.9(2)°
$Na(1)^{V}$——$H_2O(1)$——$Na(2)^{I}$	108.2(3)
$H_2O(2)$——O(2)	2.824(8) Å
$H_2O(2)$——O(4)^{V}	2.798(8)
$H_2O(2)$——Na(1)	2.468(7)
$H_2O(2)$——$Na(2)^{III}$	2.405(7)
O(2)——$H_2O(2)$——O(4)^{V}	105.9(3)°
Na(1)——$H_2O(2)$——$Na(2)^{III}$	93.0(2)

Table 5. Interatomic distances in MoO_4^{2-} and sodium-oxygen polyhedra, with their estimated standard deviations

Mo—O(1)	1.768(5) Å	$Na(2)^{III}$—$O(1)^{III}$	2.334(6) Å
Mo—O(2)	1.788(6)	$Na(2)^{III}$—$O(2)^{II}$	2.304(6)
Mo—O(3)	1.752(6)	$Na(2)^{III}$—$O(3)^{I}$	2.337(7)
Mo—O(4)	1.781(6)	$Na(2)^{III}$—$H_2O(1)^{II}$	2.297(7)
O(1)—O(2)	2.906(8)	$Na(2)^{III}$—$H_2O(2)$	2.405(7)
O(1)—O(3)	2.872(8)	Na(1)—O(1)	2.427(6)
O(1)—O(4)	2.882(8)	Na(1)—$O(4)^{I}$	2.393(7)
O(2)—O(3)	2.858(8)	Na(1)—$O(3)^{II}$	2.481(7)
O(2)—O(4)	2.972(8)	Na(1)—$O(1)^{III}$	2.439(6)
O(3)—O(4)	2.877(8)	Na(1)—$H_2O(1)^{IV}$	2.426(7)
		Na(1)—$H_2O(2)$	2.468(7)

Table 6. Angles in MoO_4^{2-} and sodium-oxygen polyhedra, with their estimated standard deviations

O(1)—Mo—O(2)	109.6(3)°	$O(4)^{I}$—Na(1)—$H_2O(2)$	100.4(2)°
O(1)—Mo—O(3)	109.3(3)	$O(3)^{II}$—Na(1)—$O(1)^{III}$	85.7(2)
O(1)—Mo—O(4)	108.6(3)	$O(3)^{II}$—Na(1)—$H_2O(1)^{IV}$	86.4(2)
O(2)—Mo—O(3)	107.6(3)	$O(1)^{III}$—Na(1)—$H_2O(1)^{IV}$	93.2(2)
O(2)—Mo—O(4)	112.7(3)	$O(1)^{III}$—Na(1)—$H_2O(2)$	83.9(2)
O(3)—Mo—O(4)	109.0(3)	$H_2O(1)^{IV}$—Na(1)—$H_2O(2)$	94.7(2)
		$O(4)^{I}$—Na(1)—$O(1)^{III}$	174.2(2)
O(1)—Na(2)—$O(2)^{I}$	95.6(2)	O(1)—Na(1)—$H_2O(1)^{IV}$	174.0(2)
O(1)—Na(2)—$O(3)^{II}$	93.4(2)	$H_2O(2)$—Na(1)—$O(3)^{II}$	169.5(3)
O(1)—Na(2)—$H_2O(1)^{I}$	111.3(2)	O(1)—Na(1)—$O(4)^{I}$	89.6(2)
O(1)—Na(2)—$H_2O(2)^{III}$	87.6(2)	O(1)—Na(1)—$O(3)^{II}$	87.6(2)
$O(2)^{I}$—Na(2)—$O(3)^{II}$	91.6(2)	O(1)—Na(1)—$H_2O(2)$	91.2(2)
$O(2)^{I}$—Na(2)—$H_2O(1)^{I}$	94.0(2)	O(1)—Na(1)—$O(1)^{III}$	86.3(2)
$O(3)^{I}$—Na(2)—$H_2O(2)^{III}$	175.9(3)	$O(4)^{I}$—Na(1)—$O(3)^{II}$	90.0(2)
$O(3)^{II}$—Na(2)—$H_2O(1)^{I}$	153.9(3)	$O(4)^{I}$—Na(1)—$H_2O(1)^{IV}$	90.4(2)
$O(3)^{II}$—Na(2)—$H_2O(2)^{III}$	85.5(2)		
$H_2O(1)^{I}$—Na(2)—$H_2O(2)^{III}$	87.3(2)		

Water of Crystallization. The hydrogen bondings and H_2O–Na coordinations are depicted in Figs. 2 and 3. Table 4 shows their distances and angles. Around $H_2O(1)$ and $H_2O(2)$, oxygen atoms from two MoO_4^{2-} anions and two sodium cations construct a distorted tetrahedron; this suggests that two lone pairs of a water oxygen atom point to the two sodium ions. The $O(2)^{vi}\cdots H_2O(1)\cdots O(4)^{v}$ angle differs noticeably from the water H–O–H angle in gas phase, 104.5°; this implies that the O–H···O hydrogen bonding is not linear. The $O(2)$–$H_2O(2)$–$O(4)^{v}$ angle is near to 104.5°, and O–H···O in this case can be considered to be almost linear. Judging from the infrared spectra data, it would seem that the O–H···O distances of 2.78 and 2.87 Å can be predicted from the O–H stretching frequencies, 3250 and 3450 cm^{-1},[5] by the aid of the empirical relationships proposed by Nakamoto.[15] Actually, these values agree fairly well with the present structural data.

The Structure of the MoO_4^{2-} Anion. The Mo–O distances and O–Mo–O angles are listed in Tables 5 and 6. The shape of the anion is a slightly deformed tetrahedron, and the Mo–O distances in the MoO_4^{2-} anion are almost equal to those found in the anhydrous K_2MoO_4 crystals (1.74(1) and 1.78(1) Å).[16] The four oxygen atoms in MoO_4^{2-} are crystallographically unique. The O(2) atom which is coordinated to the Na(2) cation forms two hydrogen bonds with two water molecules, and O(4) also accepts two hydrogen bonds and is attached to Na(1); on the other hand, O(1) and O(3) form no hydrogen bonding, each oxygen atom being coordinated to Na(1) and to Na(2). The bond lengths, Mo–O(2) (1.788(6) Å) and Mo–O(4) (1.781(6) Å), appear to be significantly longer than Mo–O(1) (1.768(5) Å) and Mo–O(3) (1.752(6) Å). The O(2)–Mo–O(4) angle (112.74(26)°) is larger than any other O–Mo–O angle by 3.23—5.12(26)°. The MoO_4^{2-} tetrahedra appear to be elongated, as if pulled by the hydrogen bonds, on pushed by sodium cations. However, an example of the deformation of SO_4^{2-} anions in the opposite direction was found in the $CaSO_4\cdot 2H_2O$ crystal,[17] containing two kinds of crystallographically independent sulfate oxygens, O_I and O_{II}, the former one with two hydrogen bonds to water molecules, and the later one with a close Ca^{2+} neighbor. Here elongation is observed in the direction of the Ca^{2+} cations, and the hydrogen bonds to the water molecules do not seem stretch the SO_I bond. Therefore, we need still more examples before we can undertake a general discussion of the effect of hydrogen-bond or coordination-bond formation on the shape of tetrahedral oxyanions.

Comparison with Octahedral MoO_6 Unit in Polymolybdates. In the present study, the Na–O (belonging to tetrahedral MoO_4^{2-}) bond lengths were found to lie between 2.29 and 2.48 Å, and in the literature those of the Na–O (belonging to MoO_6 unit) in the polymolybdates, $Na_6Mo_5P_2O_{23}\cdot 12H_2O$,[1] $Na_4H_2Mo_5P_2O_{23}\cdot 12H_2O$,[2] and $Na_6Mo_7O_{14}\cdot 14H_2O$,[3] range from 2.27 to 2.55 Å. These ranges agree with that of the Na–O(H_2O) bond lengths found in the above-mentioned four compounds. It seems that there is no distinct difference between the oxygen atoms in the MoO_4^{2-} anion and those of the MoO_6 unit in polymolybdate anions and water molecules in the coordination-bond distance to the Na^+ cation.

Crystal Structure of $Na_2WO_4\cdot 2H_2O$. The structure determination of $Na_2WO_4\cdot 2H_2O$ was also started at the same time in this laboratory; it was found that the crystals were exactly isostructural, with slightly larger unit-cell dimensions. However, it was impossible to find well-formed crystals for accurate experiments, and so further detailed computation was abandoned. Later the structure was reported by Okada, Morikawa, Iwai, and Marumo[18] independently.

The calculations were performed on a HITAC 8700/8800 computer at the Computer Centre of the University of Tokyo, using a local version of UNICS.[20]

The authors are indebted to Professor N. Ingri of the University of Umeå for sending us papers from his Institute prior to publication.[1-3] Thanks are also due to Professors H. Kuroya and S. Ooi of the Osaka City

University for reading through the manuscript and for their advice.

References

1) R. Strandberg, *Acta Chem. Scand.*, **27**, 1004 (1973).
2) B. Hedman, *ibid.*, **27**, 3335 (1973).
3) K. Sjoblom and B. Hedman, *ibid.*, **27**, 3673 (1973).
4) R. J. Poljak and L. N. Becka, *Ann. Asoc. Quim. Argent.*, **46**, 199 (1958).
5) R. H. Busey and O. L. Keller, *J. Chem. Phys.*, **41**, 215 (1964).
6) H. W. Ruben, D. H. Templeton, R. D. Rosenstein, and I. Olovsson, *J. Amer. Chem. Soc.*, **83**, 820 (1961).
7) L. Collin, M. Willis, *Acta Crystallogr.*, **B27**, 291 (1971).
8) M. Giglis, *ibid.*, **11**, 789 (1958).
9) R. Tellgren and I. Olovsson, *J. Chem. Phys.*, **54**, 127 (1971).
10) W. H. Baur and A. A. Khan, *Acta Crystallogr.*, **B26**, 1584 (1970).
11) W. S. McDonald and D. W. J. Cruickshank, *ibid.*, **22**, 37 (1967).
12) K. H. Jost and W. Hilmer, *ibid.*, **21**, 583 (1966).
13) G. Beurskens and G. A. Jeffrey, *J. Chem. Phys.*, **41**, 924 (1964).
14) P. B. Jamieson and L. S. D. Glasser, *Acta Crystallogr.*, **22**, 507 (1967).
15) K. Nakamoto, M. Margoshes, and R. E. Rundle, *J. Amer. Chem. Soc.*, **77**, 6480 (1955).
16) B. M. Getehouse and P. Leverett, *J. Chem. Soc., A*, **1969**, 849.
17) W. F. Cole and C. J. Laucucki, *Acta Crystallogr.*, **B30**, 921 (1974).
18) K. Okada, J. Morikawa, S. Iwai, and F. Marumo, *Bull. Tokyo Institute of Technology*, **7**, (1974).
19) "International Tables for X-ray Crystallography" Kynoch Press, Birmingham (1962), Vol. III.
20) "The Universal Crystallographic Computation Program System," Crystallographic Society of Japan (1967).

Infrared Spectra and Structure of Substituted Unsaturated Carbonyl Compounds. XVIII. *N*-Alkyl-enamino Thiones

Urszula DABROWSKA and Janusz DABROWSKI
Institute of Organic Chemistry, Polish Academy of Sciences, 00-961 Warsaw, Poland
(Received January 7, 1974)

Skeletal and N–H bending vibrations have been investigated in enamino thiones having the general formula $R^1C(S)CH=C(R^3)NHR^4$ (R=alkyl) and compared with those of the oxygen analogues (enamino ketones).

Previous work[1] has shown that the interpretation of IR spectra of enamino ketones, in the region where absorptions due to skeletal vibrations occur, is made very difficult by the presence of strong vibrational coupling. The effect encompasses all the bonds present in the main chain of molecules of this type (O=C–C=C–N<H). This also applies to bending vibrations of the amino group: these are uncharacteristic, due undoubtedly to strong vibrational interactions with the skeleton.

Replacing oxygen by sulphur, whilst effectively not changing the mesomerism within the molecule, does lead to a change in the frequencies of skeletal vibrations. It seemed likely that this would afford a better opportunity of studying the absorptions corresponding to bending vibrations of the >NH group. Such was the main reason why the present work on the IR spectra of a number of secondary enamino thiones and their deuterated derivatives (listed in Table 1) was undertaken. Their oxygen analogues (enamino ketones) have been included for comparison. Moreover, an attempt has been made to assign the absorption bands for other vibrations of the above system, especially the stretching vibrations of the thione group. Previous assignments[2] with $\nu_{C=S}$=1260—1300 cm^{-1} are incorrect.[3]

TABLE 1. ALIPHATIC ENAMINO THIONES AND ENAMINO KETONES $R^1C(X)CHCR^3–NR^4R^{4'}$

Compound No	X	R^1	R^3	R^4	$R^{4'}$
I	S	CH_3	H	H	C_2H_5
Ia	O	CH_3	H	H	C_2H_5
Id_1	S	CH_3	H	D	C_2H_5
II	S	C_2H_5	H	H	CH_3
IIa	O	C_2H_5	H	H	CH_3
IId_1	S	C_2H_5	H	D	CH_3
III	S	CH_3	H	H	C_3H_7
IIIa	O	CH_3	H	H	C_3H_7
IIId_1	S	CH_3	H	D	C_3H_7
IV	S	CH_3	CH_3	H	C_3H_7
IVa	O	CH_3	CH_3	H	C_3H_7
IVd_1	S	CH_3	CH_3	D	C_3H_7

Experimental

The syntheses of 4-ethylaminobuten-3-thione-2 (I) and 1-methylaminopenten-1-thione-3 (II) have been described in a previous paper.[2] 4-Propylaminobuten-3-thione-2 (III) and 4-propylaminopenten-3-thione-2 (IV) were obtained in a similar way. Infrared spectra were recorded on a VEB Carl Zeiss (Jena) UR-20 double beam spectrometer using NaCl and KBr prisms. Solvents and concentrations are reported in Tables 2 and 3.

Results and Discussion

The >NH stretching region is specifically dealt with in a separate paper;[4] in the present work the 1800—400 cm^{-1} region has been studied. Here, in theory, four bands due to skeletal stretching vibrations of the S=C–C=C–N< system are to be expected, together with two bands derived from >NH bending (assuming there is no strong interaction with other oscillators).

It has been considered appropriate to retain the nomenclature previously used for the skeletal bands, *i.e.* "Amide Vinylogue Bands," AV-I, AV-II, AV-III, and AV-IV.[1] However, whereas in enamino ketones the AV-I frequency (mainly $\nu_{C=O}$) was the highest the analogous AV-I frequency in the thiones is the lowest of the four (Tables 2 and 3). AV-II is a skeletal vibration, chiefly of $\nu_{C=C}$ character but with a significant contribution from NH bending. AV-III and AV-IV are coupled vibrations dominated by C–C and C–N stretching. Apart from these four bands one other due to a vibration dominated by N–H bending has been identified. In recent papers Taylor[5,6] has discussed our previous results, and in particular our nomenclature, obviously without being aware of some of the arguments presented in the references cited by him, and also of our subsequent papers[1c–h] where the infrared spectroscopy of enamino carbonyl compounds has been further discussed. Thus, in contrast to Taylor's assesment,[5] we were able in many cases to obtain a complete separation of isomers[1a,d,e] and there is really no ground for the statement[5] that: "Up to the present time no detailed infrared study based on compounds of known configuration has appeared." As to the nomenclature, Taylor supposed that our reason for not naming directly the bands $\nu_{C=O}$ and $\nu_{C=C}$ was due possibly to the "··· prejudice that existed, and still exists, against assigning the strongest band in the 6 μm region to anything other than carbonyl".[6]

In fact we did not consider intensity as a factor in the discrimination between the $\nu_{C=O}$ or $\nu_{C=C}$ character of any of the bands under discussion. On the contrary, we showed, that a band, which is conventionally assigned $\nu_{C=C}$, can be both more intense than "$\nu_{C=O}$" (for the *trans-s-cis*[1c] and *cis-s-cis* forms[1c,e]) as well as less intense (for the *trans-s-trans* form[1e]). The main reason for proposing a nomenclature similar to that employed for amides (*i.e.* the avoidance of a simplified

TABOE 2. THE MAIN INFRARED ABSORPTION BANDS OF ENAMINO THIONES AND THEIR *N*-DEUTERATED DERIVATIVES IN THE 1700—700 REGION

Compound No.	Solvent	Concn. mol/l	AV-II[a]	δ_{NH}	AV-III[a]	AV-IV[a]	δ_{ND}	AV-I[a] *trans*	AV-I[a] *cis*	γ_{NH}
	MeC(S)CH=CHNHEt									
I	—	—	1628s	1585m	1497s	1271s	—	—	1107m	790s[e]
Id_1	—	—	1592s	—	1487s	1290s	1158m	—	1074w	
I	C_2Cl_4	0.4	1622s	—	1492s	1266s	—	—	1110m	
Id_1	C_2Cl_4	0.4	1590s	—	1485s	1287s	1160w[c]	—	1074w	
Id_1	CCl_4	0.2	1590s	—	1484s	1287s	1162w[c]	—	1074w	
I	$(CH_3)_2SO$	1.5	1626s	1588s[b]	1503s	1270s	—	1130sh[d]	1108w[c]	
	EtC(S)CH=CHNHMe									
II	—	—	1628s	1587m	1498s	1296s	—	—	1115m	802s[e]
IId_1	—	—	1599s	—	1488s	1267m	1160w	—	1050w	
II	C_2Cl_4	0.4	1631s	—	1495s	1291s	—	—	1119m	
IId_1	C_2Cl_4	0.4	1597s	—	1486s	1262m	—	—	1050w	
II	$(CH_3)_2SO$	1.5	1630s	1593s[b]	1503s	1285s	—	1135sh[d]	1113w[c]	
	MeC(S)CH=CHNHPr									
III	—	—	1628s	1587m	1498s	1276s	—	—	1106m	786s[e]
IIId_1	—	—	1592s	—	1486s	1288s	1156w	—	1076w	
III	C_2Cl_4	0.4	1626s	—	1495s	1268s	—	—	1110m	
IIId_1	C_2Cl_4	0.4	1591s	—	1483s	1287s	1160w[c]	—	1076w	
III	$(CH_3)_2SO$	1.5	1624s	1588s[b]	1501s	1275s	—	1135sh[d]	1105w[c]	
	MeC(S)CH=C(Me)NHPr									
IV	—	—	1602s	1537s	—	1310s	—	—	1108m	786m[e]
IVd_1	—	—	1556s	—	1476s	1305s	1216m	—	1133m	
IV	C_2Cl_4	0.4	1601s	1531s	—	1293s	—	—	1116m	

a) For nomenclature see text. b) The band is of higher intensity than in the neat compound. c) The band is of lower intensity than in the neat compound. d) Shoulder on a band with its maximum at about 1145 cm^{-1}. e) Intensity diminishes upon deuteration.

TABLE 3. THE MAIN BANDS OF ENAMINO KETONES IN THE 900—1700 cm^{-1} REGION; SOLUTIONS IN C_2Cl_4

Compound No.	AV-I	AV-II	AV-III	AV-IV	γ_{NH}[a]
Ia	1644s	1583s	1486s	1261s	740s
IIa	1643s	1584s	1483s	1290s	730s
IIIa	1645s	1581s	1486s	1277s	740s
IVa	1616s	1586s	1519m	1288s	736s

a) Band position was determined for neat compounds.

group frequency nomenclature) was the pronounced vibrational coupling in amide vinylogues; the coupling manifests itself in both isotopic[1a,c-h] and solvent shifts[1a,b] of the bands and is unexplanable within a simple concept of characteristic group frequencies.

The skeletal bands of compounds I, II, and III manifest themselves as described below.

AV-II, dominated by C=C coordinate, appears in solution spectra (in C_2Cl_4) at frequencies between 1622—1631 cm^{-1}, *i.e.* 39—47 cm^{-1} higher than in the case with the oxo analogues (comparison of I, II, and III with Ia, IIa, and IIIa in Tables 2 and 3). This can be explained in terms of a "repulsive" interaction between C=O and C=C oscillators in the oxo compounds. At the same time, this frequency is lower by some 30 cm^{-1} than $\nu_{C=C}$ is in olefins since the conjugation with the thione group is comparable to that with the carbonyl group.

The positions of bands AV-III at 1492—1495 cm^{-1} and AV-IV at 1266—1291 cm^{-1} differ little from those of the corresponding bands in the enamino ketones. This is to be expected since, as has already been stated, there is no inherent difference in the bond orders within the two skeletons being compared. It should be added that under the conditions described above, both classes of compounds exist in the *cis* form.

As for the bending vibrations of the >NH group, with solution spectra (in C_2Cl_4) of the thioketones I, II, and III the appropriate band is not observed as a separate entity. On the other hand, the pure substances (which according to NMR data, also exist exclusively in the *cis* form) exhibit an additional band in the region 1585—1587 cm^{-1}. This disappears on deuteration while a new band arises at 1156—1160 cm^{-1} (see Figs. 1 and 2). This band is also absent in the Ni(II) complex of I. Another consequence of deuteration is the shift of AV-II to 1592—1599 cm^{-1}, *i.e.* 29—36 cm^{-1} towards lower frequencies.

The fact that two bands are affected by deuteration permits us to assume that both represent some complex form of vibration with contributions from skeletal and NH bending modes. In the deutero derivative these

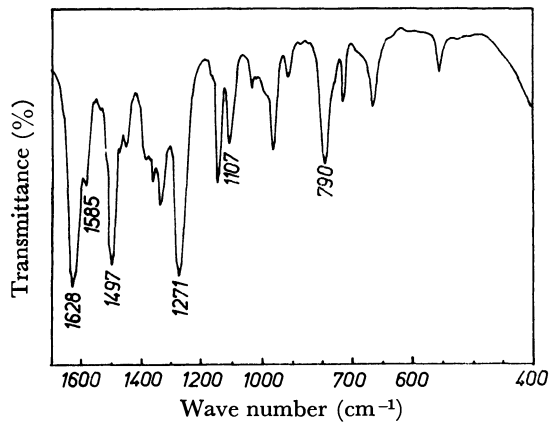

Fig. 1. Infrared spectrum of 4-ethylaminobuten-3-thione-2 (I); capillary film.

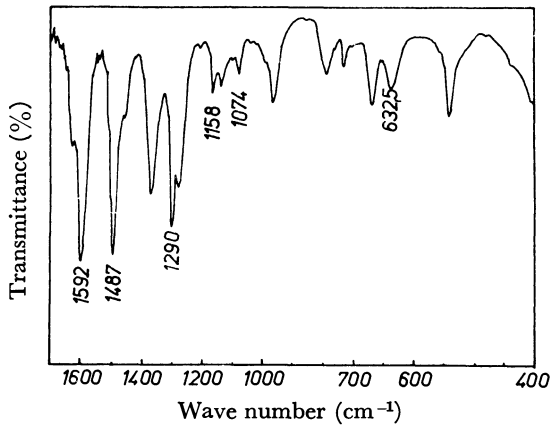

Fig. 2. Infrared spectrum of deuterated 4-ethylaminobuten-3-thione-2 (Id_1): capillary film.

vibrations are no longer coupled to an appreciable degree; thus, the band above 1500 cm^{-1} corresponds to a large extent to sketetal vibrations and the 1156—1160 cm^{-1} band to δ_{N-D} vibrations.

Remarkably, compound IV (having, β to the thiocarbonyl group, a methyl group instead of hydrogen) exhibits spectral characteristics which differ somewhat from those of compounds I, II, and III. The AV-II frequency is lowered by 26 cm^{-1} (for neat liquid) which indicates a lowered C=C bond order. Instead of two separate bands of the δ_{N-H} and AV-III type one band was found at 1537 cm^{-1} which exhibits features characteristic of both the skeletal stretching and NH bending vibrations. This assignment is based on the results of deuteration of the compound IV: in place of the disappeared 1537 cm^{-1} band two bands, *viz.*, a strong AV-IIId_1 band at 1476 cm^{-1} and a δ_{N-D} one at 1216 cm^{-1} occur. Obviously, a decoupling of the complex AV-III$+\delta_{N-H}$ vibration resulted from deuteration.

In order to understand the unusual spectral behaviour of compound IV one must take into account the great degree of stabilization achieved by the *cis* form. There is then a complementary increase in the strength of the intramolecular hydrogen bonding as compared with compounds I, II, and III (this has been shown in a previous paper[4]). We can thus postulate greater intramolecular charge delocalization and further, an equalization of the bond energies within the skeleton. This may be the reason for the exceptional nature of the IR absorption of compound IV.

In the literature[7,8] dealing with the absorptions of the thiocarbonyl group it is stated that the C=S band appears at 1170—1220 cm^{-1} in aromatic thioketones and at 1244—1270 cm^{-1} in aliphatic thioketones.[8] Clearly the position of the band depends on the coupling present (assuming, of course, that the assignments are correct).

The problem is particularly difficult in the compounds here investigated because, due to the strong coupling of the skeletal vibrations, there cannot exist a vibration localized solely within the C=S group. For this same reason no resemblance to the spectra of thiones described in the literature is expected.

For the purpose of detecting such a band in which the contribution of C=S stretching predominates, (designated AV-I, according to our nomenclature) we utilized the changes that take place in the spectrum when, in a medium of dimethylsulphoxide, the *cis* form changes to the *trans*. NMR spectra have confirmed, unequivocally, that a partial *cis-trans* isomerisation takes place under these conditions. In the IR spectrum a new AV-I band is expected at higher frequencies, the hydrogen bonds, >N–H···S=C< having been broken by dimethylsulphoxide. In the region under discussion the 1106—1115 cm^{-1} band undergoes a definite change (*cf.* the spectra in Table 2). In dimethylsulphoxide solution this band contracts while at the same time a new band appears at higher frequencies (1130—1135 cm^{-1}). The first of these would thus correspond to the AV-I vibration of the *cis* form and the second to that of the *trans* form. As we have already communicated[3] our previous assignments[2] of the AV-I ("$\nu_{C=S}$") band were incorrect.

Another characteristic feature of the spectra of enamino thiones, found in all the examples studied is the presence of intense wide band in the region 786—802 cm^{-1}. This is probably an out-of-plane deformation of the NH group since deuteration causes a decrease in the intensity of the band together with the appearance of a new band at 630 cm^{-1}.

The authors thank Dr. Jacek Chudy (University of London) for assistance in preparing the manuscript. The work carried out is part of the Polish Academy of Sciences programme for structural research (PAN-3).

References

1) a) J. Dabrowski, *Spectrochim. Acta*, **19**, 475 (1963). b) J. Dabrowski and K. Kamieńska-Trela, *ibid.*, **22**, 211 (1966). c) J. Dabrowski and U. Dabrowska, *Chem. Ber.*, **101**, 2365 (1968). d) J. Dabrowski and U. Dabrowska, *ibid.*, **101**, 3392 (1968). e) J. Dabrowski, *J. Mol. Struct.*, **3**, 227 (1969). f) J. Dabrowski and J. Terpiński, *Roczniki Chem.*, **43**, 555 (1969). g) J. Dabrowski and J. Terpiński, *ibid.*, **43**, 1677 (1969). h) J. Terpiński and J. Dabrowski, *J. Mol. Struct.*, **4**, 285 (1969).

2) K. Kamieńska-Trela, U. Dabrowska, and J. Dabrowski, *Bull. Acad. Polon. Sci., Ser. Sci. Chim.*, **19**, 549 (1971).

3) J. Dabrowski and K. Kamieńska-Trela, *Org. Magn. Resonance*, **4**, 421 (1972).

4) U. Dabrowska and J. Dabrowski, *Advan. Mol. Relaxation Processes*, **5**, 81 (1973).
5) P. J. Taylor, *Spectrochimica Acta*, **26A**, 153 (1970).
6) P. J. Taylor, *ibid.*, **26A**, 165 (1970).
7) O. Korner, J. U. Veenland, and Th. J. de Boer, *Rec. Trav. Chim.*, **84**, 310 (1965).
8) C. Andrieu and Y. Mollier, *Tetrahedron Lett.*, **1971**, 1573.

Dithiocarbamate Complexes of Rhodium(III), Iridium(III), Palladium(II) and Platinum(II)

G. MARCOTRIGIANO, G. C. PELLACANI, C. PRETI,* and G. TOSI
Istituto di Chimica Generale ed Inorganica, University of Modena, 41100 Modena, Italy
(Received June 12, 1974)

The complexes of rhodium(III), iridium(III), palladium(II) and platinum(II) with piperidine-, piperazine-, *N*-methylpiperazine-, morpholine- and thiomorpholine-dithiocarbamate have been prepared and characterized by spectroscopic methods. From the electronic absorption spectra the values of the ligand field parameters were determined. The nephelauxetic parameters are indicative of a strong covalency in the metal-ligand bond. A monomeric structure for the complexes is suggested. All the new compounds here reported are diamagnetic.

In a previous paper[1] we have discussed the complexes of many transition metals with piperidine-, thiomorpholine- and *N*-methylpiperazine-dithiocarbamate. We report now the preparation and the characterization of new complexes of rhodium(III), iridium(III), palladium(II) and platinum(II) with:

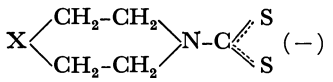

X=CH_2	Pipdtc
X=NH	Pzdtc
X=N-CH_3	CH_3-Pzdtc
X=O	Morphdtc
X=S	Timdtc

in order to investigate particularly the spectrochemical properties of these compounds. This paper is the extension of the previously reported studies on the dithiocarbamates in order to further our present knowledge and to gain new informations concerning the behaviour of the different ligands by substituting the dialkyl derivatives for the heterocyclic dithiocarbamates.

The complexes have been characterized on the basis of vibrational (conventional and far infrared) and electronic spectroscopy and magnetic measurements.

During the first draft on this manuscript Sceney and Magee[2] reported the complexes $Pd(Pipdtc)_2$ and $pd(Morphdtc)_2$ that we have included for comparison purposes only.

Results and Discussion

The complexes obtained and some physical properties are reported in Table 1. Solid state electronic spectra are given in Tables 2 and 3. The most important infrared bands are summarized in Table 4.

The metal dithiocarbamates were prepared using the appropriate sodium dithiocarbamate and rhodium trichloride, ammonium esachloroiridate(III), palladium(II) nitrate and potassium tetrachloroplatinate(II) according to the methods described in the experimental section.

The compounds are micro-crystalline, soluble in acetone, *N*,*N*-dimethylformamide and chloroform.

The trisdithiocarbamate derivatives of rhodium(III) and iridium(III) are low-spin type (t^6_{2g}). Solid state electronic spectra confirm an octahedral configuration

TABLE 1. ANALYTICAL DATA AND OTHER PHYSICAL PROPERTIES

Compound	Color	Calcd %		Found %		Dec. point
		C	H	C	H	°C
$[Rh(Pipdtc)_3]$	Orange	37.03	5.18	37.31	5.38	298—300
$[Rh(Pzdtc)_3]$	Orange	30.70	4.64	30.76	4.63	293—295
$[Rh(CH_3\text{-}Pzdtc)_3]$	Orange	34.38	5.30	34.31	5.36	315—317
$[Rh(Morphdtc)_3]$	Orange	30.55	4.10	30.53	4.07	232—234[a]
$[Rh(Timdtc)_3$	Orange	28.24	3.79	28.60	3.64	265—267
$[Ir(Pipdtc)_3]$	Orange-yellow	32.13	4.50	32.06	4.51	318—320
$[Ir(Pzdtc)_3]$	Orange-yellow	26.65	4.03	26.62	3.64	314—316
$[Ir(CH_3\text{-}Pzdtc)_3]$	Orange-yellow	30.10	4.63	29.97	4.40	330—332
$[Ir(Morphdtc)_3]$	Orange-yellow	26.53	3.56	26.58	3.65	318—320[a]
$[Ir(Timdtc)_3]$	Orange-yellow	24.77	3.33	24.34	3.26	288—290
$[Pd(Pzdtc)_2]$	Yellow	28.00	4.23	28.11	4.23	298—300
$[Pd(CH_3\text{-}Pzdtc)_2]$	Yellow	31.53	4.85	31.70	4.44	302—304
$[Pd(Timdtc)_2]$	Yellow	25.94	3.48	26.35	3.34	>350
$[Pt(Pipdtc)_2]$	Bright yellow	27.90	3.90	28.12	3.72	318—320
[Pt(Pzdtc)	Bright yellow	23.20	3.51	22.86	3.21	>350
$[Pt(CH_3\text{-}Pzdtc)_2]$	Bright yellow	26.41	4.06	26.72	4.08	>350
$[Pt(Morphdtc)_2]$	Bright yellow	23.12	3.10	23.66	2.89	>350
$[Pt(Timdtc)_2]$	Bright yellow	21.77	2.92	22.10	2.86	>350

a) Melting point.

* All the correspondence should be addressed to this author.

Table 2. Electronic spectra (cm^{-1})

Compound	$^1A_{1g}\rightarrow{}^1T_{1g}$	$^1A_{1g}\rightarrow{}^1T_{2g}$	C. T.	ν_2/ν_1	Δ	B'	β	Z^*
[Rh(Pipdtc)$_3$]	24100	28735		1.19	24840	310	0.43	0.27
[Rh(Pzdtc)$_3$]	23365	28170		1.21	24140	323	0.45	0.31
[Rh(CH$_3$-Pzdtc)$_3$]	24100	29240		1.21	25400	346	0.48	0.38
[Rh(Morphdtc)$_3$]	23420	28820		1.23	24580	366	0.51	0.45
[Rh(Timdtc)$_3$]	23640	29150		1.23	25520	373	0.52	0.47
[Ir(Pipdtc)$_3$]	27250	28820	31750	1.06	28000	100	0.15	
[Ir(Pzdtc)$_3$]	27400	28985	31750	1.06	27640	101	0.15	
[Ir(CH$_3$-Pzdtc)$_3$]	27320	28890	31750	1.06	28000	100	0.15	
[Ir(Morphdtc)$_3$]	27320	28890	—	1.06	28000	100	0.15	
[Ir(Timdtc)$_3$]	27400	29000	30950	1.06	27310	102	0.15	

B is taken to be 720 cm^{-1} for the Rh^{3+} free ion and 660 cm^{-1} for the Ir^{3+} free ion.

Table 3. Electronic spectra (cm^{-1})

Compound	d-d band	C. T.	Δ_1
[Pd(Pipdtc)$_2$][a)]	22200	—	24300
[Pd(Pzdtc)$_2$]	22330	28010	24430
[Pd(CH$_3$-Pzdtc)$_2$]	22470	27780	24570
[Pd(Morphdtc)$_2$][a)]	22000	—	24100
[Pd(Timdtc)$_2$]	22730	27550	24830

a) Ref. 2

Table 4. Infrared absorption bands (cm^{-1})

Compound	ν(C=N)	ν(C=S)	ν(M-S)
PipdtcNa	1465 vs	965 vs	—
PzdtcNa	1460 vs	1000 vs	—
CH$_3$-PzdtcNa	1450 vs	995 s	—
MorphdtcNa	1440 vs	990 s	—
TimdtcNa	1458 vs	995 s	—
[Rh(Pipdtc)$_3$]	1495 vs	985 m	330 m
[Rh(Pzdtc)$_3$	1485 vs	1000 s	330 m
[Rh(CH$_3$-Pzdtc)$_3$]	1490 vs	1000 vs	335 ms
[Rh(Morphdtc)$_3$]	1490 vs	1000 s	330 ms
[Rh(Timdtc)$_3$]	1470 vs	1005 m	335 m
[Ir(Pipdtc)$_3$]	1500 vs	982 ms	323 m
[Ir(Pzdtc)$_3$]	1495 vs	1000 vs	320 m
[Ir(CH-Pzdtc)$_3$]	1495 vs	1000 s	325 m
[Ir(Morphdtc)$_3$]	1495 vs	1000 s	320 m
[Ir(Timdtc)$_3$]	1490 vs	1000 m	320 mw
[Pd(Pipdtc)$_2$][a)]	1510 vs	972 w	353 m
[Pd(Pzdtc)$_2$]	1500 vs	1010 ms	350 ms
[Pd(CH$_3$-Pzdtc)$_2$]	1505 vs	1000 vs	340 s
[Pd(Morphdtc)$_2$][a)]	1493 vs	—	346 m
[Pd(Timdtc)$_2$]	1500 vs	1000 m	340 ms
[Pt(Pipdtc)$_2$]	1515 vs	970 m	360 mw, 300 w
[Pt(Pzdtc)$_2$]	1510 vs	1000 vs	350 m, 290 w
[Pt(CH$_3$-Pzdtc)$_2$]	1505 vs	1010 s	380 w, 290 w
[Pt(Morphdtc)$_2$]	1500 vs	1005 s	345 s, 290 ms
[Pt(Timdtc)$_2$]	1510 vs	1005 m	380 vs, 290 mw

a) Ref. 2

of the central atom, Table 2.

The bands positions are similar to those reported with other sulphur coordinating ligands.

The band at somewhat higher energies in the iridum derivatives, *ca.* 31000 cm^{-1}, can be attributed to a charge transfer transition[3,4].

Studies on the electronic spectra of IrS_6 complexes are rare, the assignments of the transitions in our complexes were made with the aid of previous reports.[5,6]

The ratios ν_2/ν_1 are in the range 1.19—1.23 and are equal to 1.06 for rhodium and iridium complexes respectively, in very good agreement with the literature data of diethyldithiophosphate derivatives.[7]

The ligand field parameters Δ, B′ and β have been calculated by means of the equations

$$\nu_1 = \Delta - 4B' + 86(B')^2/\Delta \quad \nu_2 = \Delta + 12B' + 2(B')^2/\Delta$$

and are reported in Table 2. The B' values are of the order of 40—50% of the free ion value in rhodium complexes, and of 15% of the free ion value in iridium derivatives. This fact suggests that there is a considerable orbital overlap with a strong covalency in the metal-ligand σ bond.

The nephelauxetic effect is quite in line with other sulphur-containing chelating agents, which give a very pronounced nephelauxetic decrease of β[6]. It is well known that decreasing values of β are associated with a reduction in the effective positive charge of the metal ion and with an increasing tendency to be reduced to the next lower oxidation state. For the second-row transition metals the variation of the Racah interelectronic repulsion parameter with cation charge Z*, and the number q of electrons in the partly filled d shell, is well-expressed by the relation:

$$B'(cm^{-1}) = 472 + 28q + 50(Z^*+1) - 500/(Z^*+1)$$

The effective ionic charges of the rhodium complexes have been found (Table 2) to lie in the range 0.27—0.47, considerably below the formal +3 oxidation state of rhodium. Rhodium(III) complexes with oxygen donors have effective charges[8] in the range 1.65—2.03.

In the electronic spectra of palladium(II) derivatives, recorded in solid state as nujol mulls, only the first band, mostly a shoulder, at 22300—22700 cm^{-1}, can be considered a d-d transition. The great intensity of the second band suggests that it may be charge-transfer in character rather than ligand-field. The d-d band can be assigned to the $^1A_g\rightarrow{}^1B_{1g}$ (x^2–$y^2\rightarrow xy$) transition.[9] By assuming a value of $F_2=10F_4=$ 600 cm^{-1} for the Slater-Condon interelectronic repulsion parameters,[10] it is possible to derive from the first spin-allowed d-d transition the value of Δ_1 being

$\nu_1+3.5F_2=\Delta_1$ (Table 3). The fact that the first d-d band is at higher energy for palladium(II) (22300—22700 cm^{-1}) than for nickel(II) (16000—16100 cm^{-1})[1] agrees with the spectrochemical order of these metal ions.

Infrared spectral studies of dithiocarbamates have not been carried out in detail, it is quite difficult to assign the bands being most of them very highly coupled. A normal coordinate analysis has been carried out by Nakamoto[11] for the complex $[Pt(S_2CNH_2)_2]$ and by Dugarprased[12] for the derivative $[Ni(Me_2dtc)_2]$.

The ν(C=N) and ν(C=S) stretching frequencies for the free ligand sodium salts and for our complexes are reported in Table 4. The medium band present in all the studied complexes in the range 835—790 cm^{-1} is assigned to a C–S stretching coupled with the NH_2 rocking mode.

Very little differences have been observed in the infrared spectra of the complexes on changing the heterocyclic ring in the system.

The ν(C=N) stretching mode of the dithiocarbamate used as ligands in this work is at lower wave numbers than ν(C=N) of diethyldithiocarbamate, 1477 cm^{-1}. This difference is reflected in the complexes too, in fact if we compare the dithiocarbamates of iridium, palladium and platinum we observe that ν(C=N) follows the order: $Me_2dtc>Et_2dtc>Pipdtc>nPr_2dtc>nBu_2dtc>CH_3$-Pzdtc>Pzdtc>Morphdtc > Timdtc $>iPr_2dtc>iBu_2dtc>CycHex_2dtc$.

The structure of the dithiocomplexes can be represented by the following formalism:

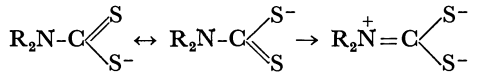

(a) (b) (c)

The extent to which resonance form (c) contributes to the structure and its effects on the physical and chemical properties of the complexes has been extensively studied. Chatt and co-workers[13] concluded that resonance form (c) does indeed contribute to the structure to a considerable extent.

From the above reported sequence of ν(C=N) we could conclude that the contribution of structure (c) is greatest for the corresponding dialkyl complexes, lower for more complex aliphatic chain and it is relatively small for heterocyclic derivatives. Perhaps because of the rigid heterocyclic ring system which shows less tendency to release electrons to the nitrogen-carbon bond and, as consequence, this bond has a less double-bond character.

In the far infrared region the bands of the ligands appear unchanged in the complexes spectra. New bands appear in the rhodium derivatives at *ca.* 330 cm^{-1} and at *ca.* 325 cm^{-1} in iridium complexes (Table 4). These absorption bands, absent in the spectra of the free ligand and in the spectra of palladium and platinum derivatives, are to be due to a metal ligand interaction. We could tentatively assign these values to a ν(Rh-S) and ν(Ir-S) stretching vibrations respectively.

According to Sceney[2] and Nakamoto[11] we can assign the palladium-sulphur and platinum-sulphur vibration modes in the ranges 353—340 cm^{-1} and 380—345 cm^{-1}, 300—290 cm^{-1} respectively, the bands at 300—290 cm^{-1} in platinum complexes being coupled with a ring deformation mode.

Experimental

Preparation of the Ligands. The sodium salt of the piperidine-, thiomorpholine- and *N*-methylpiperazinedithiocarbamate have been prepared as previously described.[1] The sodium morpholinedithiocarbamate has been prepared by treating morpholine in dry ethyl ether with carbon disulphide and adding under vigorous stirring sodium hydroxide during four hr. Molar ratios amine : CS_2 : NaOH= 1 : 1 : 1. The crude product was recrystallized from isopropyl alcohol. The sodium piperazinedithiocarbamate has been prepared by the same method, starting with piperazine dissolved in dry ethyl ether and isopropyl alcohol. The crude product was recrystallized from methanol/ethyl ether.

Preparation of the Complexes. The complexes have been obtained by adding an aqueous solution of rhodium trichloride, ammonium esachloroiridate(III), palladium nitrate, potassium tetrachloroplatinate(II) to the dithiocarbamate dissolved in methanol or water, at room temperature. The precipitate was filtered, washed with methanol and dried over P_4O_{10}.

Infrared Spectra. The IR spectra have been recorded in the range 4000—200 cm^{-1} with Perkin-Elmer 457 and 225 spectrophotometers as KBr discs and nujol mulls between polyethylene sheets. Atmospheric water was removed from the spectrophotometer housing by flushing dry nitrogen.

Visible and UV Spectra. Solid state electronic spectra have been recorded with a Shimadzu MPS-50L spectrophotometer.

Magnetic Susceptibility Measurements. These were carried out by Gouy's method. Molecular susceptibilities were corrected for diamagnetism of the component atoms by use of the Pascal's constants. All the complexes resulted diamagnetic.

We thank Dr. G. P. Benassi for his experimental work and the National Research Council (C.N.R.) of Italy for financial support.

References

1) G. Marcotrigiano, G. C. Pellacani, and C. Preti, *J. Inorg. Nucl. Chem.*, **36**, 3709 (1974).
2) C. G. Sceney and R. J. Magee, *Inorg. Nucl. Chem. Lett.*, **10**, 323 (1974).
3) C. K. Jorgensen "Absorption Spectra and Chemical Bonding in Complexes", Pergamon Press, London (1964).
4) J. A. Broomhead and W. Grumley, *Inorg. Chem.*, **10**, 2002 (1971).
5) C. Furlani and M. L. Luciani, *ibid.*, **8**, 1586 (1968).
6) C. K. Jorgensen, *J. Inorg. Nucl. Chem.*, **24**, 1571 (1962).
7) Ref. 3 p. 295.
8) E. Bertelli, C. Preti and G. Tosi, *J. Inorg. Nucl. Chem.*, in press.
9) S. I. Shupack, E. Billig, R. J. H. Clark, R. Williams and H. B. Gray, *J. Amer. Chem. Soc.*, **86**, 4594 (1964).
10) A. R. Latham, V. Hascall and H. B. Gray, *Inorg. Chem.*, **4**, 788 (1965).
11) K. Nakamoto, J. Fujita, R. A. Condrate and Y. Morimoto, *J. Chem. Phys.*, **39**, 423 (1963).
12) G. Dugarprased, D. Sathyanarayana, and C. Patel, *Can. J. Chem.*, **47**, 631 (1969).
13) J. Chatt, L. A. Duncanson and L. M. Venanzi, *Suomen Kemi.*, **B29**, 75 (1956).

ESR Study of MoO_3 Obtained from Thermal Decomposition of Ammonium Molybdate

R. S. MANN and K. C. KHULBE

Department of Chemical Engineering, University of Ottawa, Ottawa, Canada

(Received August 7, 1974)

The thermal decomposition of ammonium molybdate, between 100—600°C was studied by ESR technique. At 250 °C all ammonium molybdate was decomposed into molybdenum trioxide. Samples taken at 250, 300, 350, 400 and 450 °C all gave ESR signals. Samples at other temperatures (higher and below of this temperature range) did not give any ESR signal. The ESR signals were due to the formation of Mo^{5+} and Mo^{3+} ions. The maximum ESR intensity was observed for the sample (MoO_3) at 300 °C. The different colouration of molybdenum trioxide formed at different temperature, was due to Mo^{5+} and Mo^{3+} ions.

Molybdenum trioxide catalyst is usually prepared in the laboratory by thermal decomposition of ammonium molybdate. Onchi and Ma[1] studied the gases evolved during thermal decomposition of ammonium molybdate by using the omegatron mass spectrometer at 395°C. No electron spin resonance (ESR) study has been reported during the formation of MoO_3 from thermal decomposition of ammonium molybdate. It is well known that pure MoO_3 does not give ESR spectra being a higher oxide[2]. In the present paper we report the formation of Mo^{5+} and Mo^{3+} during the MoO_3 formation from ammonium molybdate at different temperature.

Experimental

The MoO_3 was prepared by heating ammonium molybdate (B.D.H.A.R. Grade). Ammonium molybdate was dissolved in minimum quantity of warm water and the solution evaporated over a hot plate with a magnetic stirrer at low heat. The residue was dried for 12 hr at 60°C. The temperature was increased and maintained successively for 24 hr at 100, 150, 200, 250, 300, 350, 400, 450, 500, and 600°C. The samples were taken from the bulk before increasing the temperature. The ESR measurements were carried out by using Bruker 416 spectrometer in which the microwave frequency was in the X band. All measurements were made at room temperature. The Phillips difractometer was used for X-ray analysis of the samples. Measurements were carried out by Debye Sherrer method at room temperature using a cobalt target and an iron filter.

Results

a) X-Ray Analysis. The following table (Table 1) gives the results of X-ray analysis of the thermal decomposition of ammonium molybdate at different temperatures. At 250°C all ammonium molybdate was decomposed and pure MoO_3 formed. There were no other phases (other molybdenum oxides) present except molybdenum trioxide. The colour of the mass changed from white to bluish or gray and again to white as the temperature was raised. The colour of the molybdenum trioxide obtained at 300 °C was sharper than other samples of molybdenum trioxide obtained at other temperature.

b) ESR Measurements. Samples taken at 250, 300, 350, 400, and 450 °C all gave ESR signals. Samples at other temperatures (higher and below this range) did not give any ESR signals. Well resolved hyperfine structure was obtained for molybdenum trioxide at 300 °C obtained from the thermal decomposition of ammonium molybdate (Fig. 1), after which the individual hyperfine line broadened out

TABLE 1. RESULTS OF THE PHASE ANALYSIS

Sample at °C	Identified by	Colour
100	Molybdenum-Ammonia-Oxide-Hydrate (NH_3), $Mo_5O_{15}2H_2O$	White
150	$(NH_3)_4Mo_5O_{15}2H_2O$	White
200	$(NH_4)Mo_8O_{26}$ [b]	Grayish white
250	Molybdite, (MoO_3) [c]	Grayish white
300	Molybdite	Gray or bluish
350	Molybdite	Gray or bluish
400	Molybdite	Grayish white
450	Molybdite	Grayish white
500	Molybdite	Grayish white
550	Molybdite	Yellowish white
600	Molybdite	White

a) ASTM-21-971. b) ASTM-18-117. c) ASTM-5-508.

TABLE 2. ESR INTENSITY WITH TEMPERATURE

Sample at 0 °C	ESR signal intensity (main line) rel. units
100	0
150	0
200	4
250	11
300	54
350	13
400	6
450	2.5
500	2.0
550	~0
600	~0

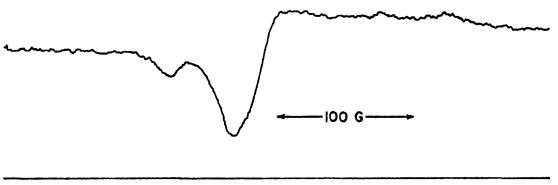

Fig. 1. ESR spectrum of MoO_3 formed at 300 °C.

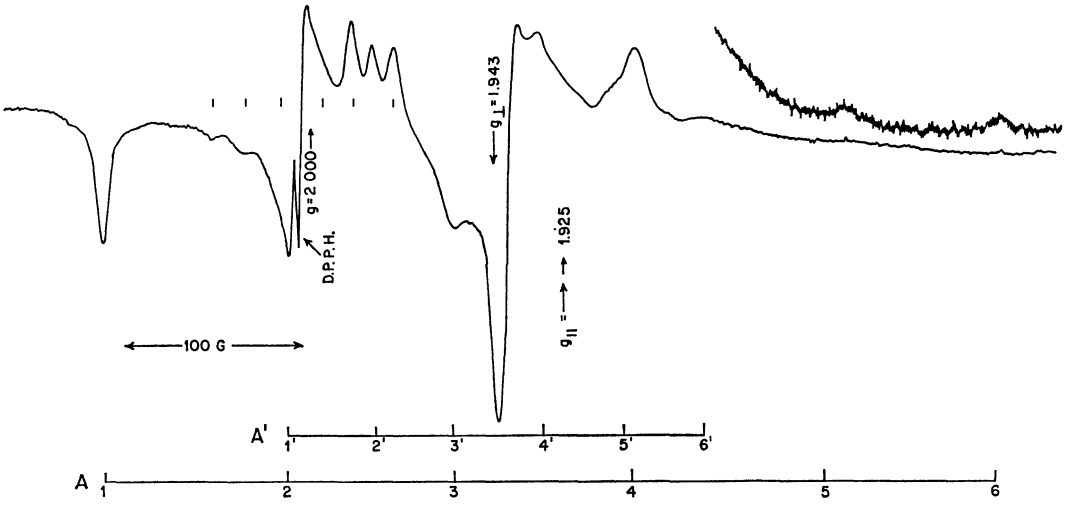

Fig. 2. ESR spectrum of MoO_3 formed at 450 °C.

to form a single broad line near the centre of the spectral pattern (Fig. 2). On the spectrum of the even numbered isotopes there is superimposed hyperfine structure from the uneven numbered isotopes ^{95}Mo and ^{97}Mo (Fig. 1). The quantum number which describe the spectrum are $S=1/2$ and $I=5/2$, and the appropriate axial spin Hamiltonian is:

$$H = \beta[g_{\parallel} H_z S_z + g_{\perp}(H_x S_x + H_y S_y)] + A I_z S_z + B(I_x S_x + I_y S_y)$$

where the terms have their usual meaning. The spin Hamilton parameters were calculated as shown in Table 3.

TABLE 3. A COMPARISON OF RESULTS OBTAINED

Ref.	g_1	$g_{\parallel}$	A	B
Maksimovskya *et al.*[5]	1.932	1.88	98±3	52±3
Sultanov *et al.*[6]	1.93	1.88		
Present case	1.943	1.925	100±6	49±2

The effect of the temperature on the ESR signal was investigated. It is apparent from Table 1 and Table II that the maximum signal intensity is observed for a sample at 300 °C when the colour of the molybdenum trioxide was sharper (bluish) than others.

Discussion

Natural molybdenum is a mixture of isotopes, 25% of which consists of two isotopes (^{95}Mo—15.7 and ^{97}Mo—9.4) with nuclear spin of 5/2. The interaction of an unpaired electron with the nuclear magnetic moments of these two isotopes should lead to hyperfine splitting of the spectrum into six components. The remaining isotopes do not have nuclear spins, and should give a spectrum consisting of one line only. Accordingly, the ESR spectrum of the Mo ion should consist of seven lines, the central line being about 25 times as intense as others.

Molybdenum can exist in any of four valency, 6^+, 5^+, 4^+ and 3^+ corresponding to d^0, d^1, d^2 and d^3 configuration. Hexavalent molybdenum if diamagnetic and, therefore gives no ESR signal. The tetravalent molybdenum, even if it were paramagnetic would not be observed except at very low temperatures. Also it would be expected that any observed resonance due to d^2, would have a large zero field splitting and therefore would give a very broad signal. Hence the observed signals must be due to Mo(V) and Mo(III).

The patterns of line shown in Fig. 1 are characteristic of Mo^{5+} ion and Mo^{3+}. Landry[3] studied Mo(III) in Al-Zn-phosphate-glass and reported a very broad spectrum at g_{eff} of 4.19. Griffiths, Owen and Ward[4] studied hydrated and unhydrated chloro and fluro complexes of Mo(III) and have reported isotropic g value around 1.96. In the present spectra there are six hyperfines including the main signal at around $g=2.000$. Further the hyperfine lines are approximately at equal spacing *i.e.* around 20±.5 G. Thus it is confirmed that this line *i.e.* at around $g=2.000$ with 6 hyperfine lines is due to Mo^{3+} ion and is not from a free electron.[5] The rest of the spectra is due to Mo^{5+} ion. The g value and other parameters are calculated and are given in Table 3. These are approximately the same as observed by others.[6,7] Thus it is confirmed that the Mo^{5+} and Mo^{3+} are formed during the thermal decomposition of ammonium molybdate.

It is well known that molybdenum trioxide (MoO_3) forms a number of nonstoichiometric oxides on heat treatment in vacuum or in a reducing atmosphere. The departure from stoicheometry is generally associated with the formation of colour centre or can acquire a blue colouration, the so called "Molybdenum blue". The general interpretation had been that the colouration is due to crystal field spectra of electrons in the Mo^{5+} state. The mechanism of the colouration process is not well understood. Deb and Chopoorian[5] suggested that the colour centres in MoO_3 are formed as a result of the free electrons being trapped in oxygen ion vaccancies. An attempt to detect the presence of a one electron centre by the ESR studies on UV irradiated thin film of MoO_3 had failed. In the repeated

experiment[8] a new weak ESR absorption at $g=2.000\pm0.005$ was observed which is close to the free electron value. In the present study the absorption at $g=2.00$ has six hyperfine lines (Fig. 1) which are due to Mo^{3+} not a free electron. The maximum ESR intensity was observed for the sample MoO_3 at 300 °C (Table 2) and also the colour of the sample was sharper than others (Table 1). The intensity of the ESR signals and the colour decreased with the increase of temperature. It may be possible that the colouration is due to Mo^{5+} and Mo^{3+} (may be Mo^{4+} ion too) ions, and not due to the trapped electrons at anion vaccancies as suggested by Deb and Chopoorian.[5]

We are greatly indebted to Dr. A. Manoogian (Physics Department, University of Ottawa, Ottawa) for discussion and encouragement. The authors are also grateful to National Research Council for financial assistance for the project.

References

1) M. Onchi, and E. Ma, *J. Phys. Chem.*, **67**, 2240 (1963).
2) Y. I. Petcherskaya, V. B. Kazansky, and V. V. Veovodsky, Proc. 2nd Inter. Cong. Cat. Paris, 2nd Edition, Technip 1961, 2121—2134.
3) R. J. Landry, *J. Chem. Phys.*, **48**, 1422 (1968).
4) J. H. E. Griffiths, J. Owen, and I. M. Ward., *Proc. Roy. Soc. Ser. A*, **219**, 526 (1953).
5) S. K. Deb, and J. A. Chopoorian, *J. Appl. Phys.*, **37**, 4817 (1966).
6) R. I. Maksimovskaya, V. F. Anufrienko, and G. D. Kolovertnov, *Kinet. Katal.*, **9**, 1186 (1968).
7) A. S. Sultanov, G. Talipore, M. Inoyatore, V. P. Tatarskii, and K. A. Samigov, *ibid.*, **12**, 1259 (1971).
8) S. K. Deb, *Proc. Roy. Soc., Ser. A*, **304**, 211 (1968).

Complexing Behaviour of 5-Amino-1,3,4-Thiazole-2-thiol. II. Complexes of Ni(II), Rh(I), Pd(II), Pt(II), Au(III) and Cu(II)

M. R. GAJENDRAGAD and U. AGARWALA*

Department of Chemistry, Indian Institute of Technology, Kanpur-208016, India

(Received July 30, 1974)

Complexes of Ni(II), Rh(I) Pd(II), Pt(II), Au(III) and Cu(II) with 5-Amino-1,3,4-thiadiazole-2-thiol have been prepared. Probable structures have been proposed for the complexes on the basis of visible and infrared spectral and magnetic susceptibility data and results of chemical analysis. Crystal field parameters have been calculated wherever possible.

In our previous communication[1] we had indicated our interest in the study of metal complexes with 5-amino-1,3,4-thiadiazole-2-thiol (I).

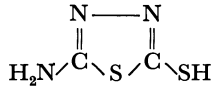

(I)

This has been used earlier as an analytical reagent.[2-4] Structure elucidation of the metal complexes of this ligand have not so far been done and the present work is an attempt an investigating the structural aspects of metal complexes with this ligand. In this communication, we report the preparation and characterisation of the complexes of Ni(II), Rh(I), Pd(II), Pt(II), Au(III) and Cu(II) with the ligand in question.

Experimental

The chemicals used were all of Analar or chemically pure grade.

I *Preparation of the Ligand.* *(a) 5-Amino-1,3,4-thiadiazole-2-thiol*: This was prepared by the method given by Sandstrom.[5] The ligand is hereafter referred to as (Htta) in the abbreviated form.

(b) Deuterated form of 5-Amino-1,3,4-thiadiazole-2-thiol: About 0.1 g of (I) was dissolved in 25 ml hot D_2O and the resulting solution refluxed for 6 hr under dry nitrogen. On cooling, the deuterated ligand crystallized. The crystals were separated by centrifugation and dried in a vacuum desiccator overnight, and finally in an oven at 105°C for 4 hr.

II *Preparation of the Metal Complexes.* *(a) Bis(5-amino-1,3,4-thiadiazole-2-thiolato)diaquonickel (II)*: A solution of 1.8 g (~5 mmol) of $NiCl_2 \cdot 6H_2O$ in 25 ml water was added to a solution of 1.4 g (~10 mmol) of (I) in about 60 ml mixture of alcohol and water (1 : 1), neutralised with NH_4OH solution. A bluish green complex was immediately formed. The product was digested on a water bath for an hour, centrifuged, washed repeatedly with hot water, warm alcohol and finally with ether. The residue was dried in a vacuum desiccator about 6 hr.

(b) Chloro(5-amino-1,3,4-thiadiazole-2-thiolato)dipyridinenickel(II): About 10 ml of pyridine was added to a solution of 1.8 g (~5 mmol) of $NiCl_2 \cdot 6H_2O$ in 25 ml water. A deep blue solution resulted. This was then added to a solution of 1.4 g (~10 mmol) of (I) in about 60 ml mixture of alcohol and water (1 : 1), neutralised with NH_4OH solution. A greyish green complex was slowly formed on heating the solution on a water bath. The product was digested on the water bath for an hour, centrifuged, washed and dried as described in II(a).

(c) Chlorobis(5-amino-1,3,4-thiadiazole-2-thiol)triphenylphosphine rhodium(I): Chlorotris(triphenylphosphine)rhodium(I) was first prepared by the method given in literature.[6]

A solution of 0.6 g (~0.67 mmol) of $Rh(P\emptyset_3)_3Cl$ in 25 ml warm benzene was added to a solution of 0.4 g (~3 mmol) of (I) in 50 ml alcohol. The resulting solution was digseted on a water bath for an hour when a reddish brown complex was formed. The product was centrifuged, washed repeatedly with hot benzene, warm alcohol and finally with ether. The residue was dried in a vacuum desiccator overnight.

(d) Bis(5-amino-1,3,4-thiadiazole-2-thiolate)palladium(II): A solution of 0.35 g (~2 mmol) of $PdCl_2$ was prepared in 50 ml warm water containing KCl. This was added to a solution of 0.35 g (~4 mmol) of (I) in a 50 ml mixture of alcohol and water (1 : 1). A chocolate red complex was immediately formed. It was digested on a water bath, centrifuged, washed and dried as described in II(a).

(e) Bis(5-amino-1,3,4-thiadiazole-2-thiolate)platinum(II): K_2PtCl_4 was first prepared by the method given in the literature.[7]

A solution of 0.4 g (~1 mmol) of K_2PtCl_4 in 20 ml water was added to a solution of 0.30 g (~2 mmol) of I in 25 ml alcohol. A rose red complex was formed when the solution was heated on a water bath. The rest of the procedure was the same as that described in II(a).

(f) Tris(5-amino-1,3,4-thiadiazole-2-thiolate)gold(III): A solution of 0.45 g (~1 mmol) $AuCl_3$ in about 10 ml water was added to a solution of 0.4 g (~3 mmol) of (I) in 30 ml alcohol. A pale yellow complex was immediately formed. The product was digested on a water bath for an hour, centrifuged, washed and dried as described in II(a).

(g) Bis(5-amino-1,3,4-thiadiazole-2-thiolato)copper(II): A solution of 0.8 g iodine in 50 ml alcohol was added to a solution of 1.2 g (~6 mmol) of $CuCl_2\ 2H_2O$ in 30 ml alcohol. The resulting solution was then added to a solution of 1.6 g (~12 mmol) of (I) in 100 ml alcohol. A green complex was immediately formed on mixing. The product was digested on a water bath, centrifuged, washed and dried as described in II(a).

Analyses. The sulphur, phosphorus and chloride (wherever present) in the ligand and the complexes were estimated by standard method.[8,9] The analyses of the metal ions in the complexes were carried out by the methods given in literature.[9,10]

Carbon, hydrogen and nitrogen were analysed by the microanalytical section of the Indian Institute of Technology, Kanpur.

The results of all the analyses are given in Table 1.

Magnetic Susceptibilities. Magnetic susceptibilities of the complexes were determined at room temperature with a Guoy balance. Mercurytetrathiocyanatocobaltate(II) was used as a magnetic susceptibility standard. Diamagnetic

* To whom all correspondence should be addressed.

corrections were calculated by the method given in literature.[11] The values of the magnetic moments are given in Table 1.

Spectra. *(i) Visible and Ultraviolet*: The absorption spectra of the ligand and the complex were recorded with a Cary-14 recording spectrophotometer in alcoholic solution and nujol mull respectively in the range 1600—300 nm. The absorption bands are given in Table 2.

(ii) Infrared: The infrared spectra of the ligand and the complexes were taken with the help of a Perkin-Elmer 521 Grating Infrared Spectrophotometer in the range 4000—250 cm^{-1}, using KBr pellets of the samples. The major infrared bands are given in Table 3.

Results and Discussion

Magnetic moments. *(i) Complexes of Ni(II)*: The experimental values of the magnetic moments of $Ni(tta)_2(H_2O)_2$ and $Ni(py)_2(tta)Cl$ as given in Table 1 are close to those reported in literature for other octahedral Ni(II) complexes.

(ii) Complexes of Rh(I), Pd(II), Pt(II), and Au(III): All these complexes are found to be diamagnetic. The diamagnetism of these complexes supports the square planar arrangement of the ligand molecules around the central metal ion.

(iii) Cu(II) Complexes: This complex is diamagnetic. Only in a few Cu(II) complexes, the paramagnetism equivalent to one unpaired electron is completely quenched ($\mu_{eff}=0$) at room temperature,[12,13] as against partial quenching observed in the case of several Cu(II) complexes.[14–16]

Since the complex is prepared in the presence of stoichiometric amounts of I_2, reduction of Cu^{2+} to Cu^{+} and hereby the diamagnetic behaviour of the complex appears to be highly unlikely. Also the complex of Cu(I), prepared (and reported elsewhere)[17] by reducing Cu^{2+} ions with SO_2 solution followed by treatment with the ligand, has totally different physical porperties and stoichiometry in contrast to the Cu(II) complex.

With a view to knowing the oxidation state of the metal ion in the Cu(II) complex, the authors dissolved the Cu(II) complex in pyridine and determined the magnetic susceptibility of the solution, when the complex showed a magnetic moment of 1.77 B.M. Since pyridine is not an oxidising agent is it unlikely that the Cu^{+} ions, if present at all, in the complex, could have been oxidised to Cu^{2+} to account for the observed paramagnetism in pyridine solution.

The spin-pairing in the complex may be explained by the overlap of the d_{z^2} or $d_{z^2-y^2}$ orbitals of the Cu^{2+} ions resulting in σ or δ bond formation,[18–20] or by super-exchange mechanism.[21] In complexes with ligands containing sulphur as donor atom, bonding of the metal ion with the easily polarizable sulphur atom of the ligand may result in a large transfer of electron density from sulphur to the metal ions with the consequent increase in the overlap of the metal orbitals.[22] Hence a direct metal-metal bond is preferred for the quenching of the paramagnetism over super exchange mechanism. However, it is only tentative.

Electronic Spectra. *(i) Complexes of Ni(II)*: The visible spectrum of $Ni(tta)_2(H_2O)_2$ shows three bands whose positions are characteristic of those found for other octahedral complexes of Ni(II). In the spectrum of $Ni(py)_2(tta)Cl$, only two bands are seen. The third band, expected around 27000 cm^{-1}, may be masked by the intense charge transfer band due to pyridine molecule. The positions of these bands together with their assignments are given in Table 2. These are taken as evidence in support of the octahedral geometry of the ligand molecules around the central metal ion.

Besides these bands, a shoulder appears at 875 nm

Table 1. Analytical data, magnetic moments and solubilities of the ligand and the complexes

	Compound		C	H (or D)	N	S	Cl	P	M	Magnetic moment	Solubility
I(a)	Ligand	Calcd	18.0	2.26	31.6	48.1	—	—	—	—	s in water
	$C_2H_3N_3S_2$	Found	17.8	2.40	31.8	47.7	—	—	—		S in alcohol
(b)	Ligand(deuterated)	Calcd	17.7	4.41	30.9	47.1	—	—	—	—	s in water
	$C_2D_3N_3S_2$	Found	17.9	2.7	31.3	46.9	—	—	—		S in alcohol
II(a)	$Ni(C_2H_2N_3S_2)_2(H_2O)_2$	Calcd	13.4	2.23	23.4	35.7	—	—	16.4	3.01 BM	I
		Found	13.1	2.00	23.3	35.2	—	—	16.1		
(b)	$Ni(C_5H_5N)_2(C_2H_2N_3S_2)Cl$	Calcd	37.5	3.13	18.2	16.7	9.2	—	15.3	2.97 BM	I
		Found	37.8	3.40	18.0	16.2	8.5	—	15.1		
(c)	$Rh(P(C_6H_5)_3)(C_2H_3N_3S_2)Cl$	Calcd	39.6	3.06	12.6	19.3	5.2	4.7	15.5	D	s in alcohol
		Found	39.6	3.00	12.7	19.0	4.5	4.0	15.0		
(d)	$Pd(C_2H_2N_3S_2)_2$	Calcd	13.0	1.08	22.7	34.6	—	—	28.7	D	I
		Found	12.8	1.50	23.1	34.2	—	—	28.6		
(e)	$Pt(C_2H_2N_3S_2)_2$	Calcd	10.5	0.87	18.3	27.9	—	—	42.5	D	I
		Found	10.2	1.01	18.0	28.0	—	—	41.7		
(f)	$Au(C_2H_2N_3S_2)_3$	Calcd	12.1	1.01	21.2	32.4	—	—	33.2	D	I
		Found	11.9	1.00	20.5	31.2	—	—	32.0		
(g)	$Cu(C_2H_2N_3S_2)_2$	Calcd	14.7	1.22	25.7	39.1	—	—	19.4	D	I
		Found	14.3	1.09	25.4	38.6	—	—	19.1		

s=slightly soluble; S=soluble; D=diamagnetic; I=insoluble in water and other common non-coordinating organic solvents.

TABLE 2. ELECTRONIC SPECTRAL BANDS, THEIR ASSIGNMENTS AND CRYSTAL FIELD PARAMETERS[a]

Complex		Band position nm	Band position cm^{-1}	Assignment	A_q^A cm^{-1}	D_q^E cm^{-1}	D_t cm^{-1}	B cm^{-1}	β	Δ_1 cm^{-1}	Δ_2 cm^{-1}	C cm^{-1}
1		2	3	4	5	6	7	8	9	10	11	12
1. $Ni(tta)_2(H_2O)_2$	ν_1	1050	9524	$^3B_{1g}\rightarrow{}^3B_{2g}$								
	ν_1'	875	11430	$^3B_{1g}\rightarrow{}^3E_g$								
	ν_2	625	16000	$^3A_{2g}\rightarrow{}^3T_{1g}(F)$	775	1143	218	762	0.75			
	ν_2'	—	—	—								
	ν_3	400	25000	$^3A_{2g}\rightarrow{}^3T_{1g}(P)$								
2. $Ni(Py)_2(tta)Cl$	ν_1	1050	9524	$^3B_{1g}\rightarrow{}^3E_g$								
	ν_1	970	10310	$^3B_{1g}\rightarrow{}^3B_{2g}$								
	ν_2	600	16667	$^3A_{2g}\rightarrow{}^3T_{1g}(F)$	1010 (Py)	952 (Cl+tta)	−90	866	0.85			
	ν_2	625 sh	16000	due to departure from O_h symmetry								
	ν_3	—	—	—								
3. $Rh(P\emptyset_3)(Htta)_2Cl$	Charge transfer band only											
4. $Pd(tta)_2$	ν_1	500	18200	$^1A_{1g}\rightarrow{}^3E_g$				750		20820	4852	2620
	ν_2	480	21000	$^1A_{1g}\rightarrow{}^1A_{2g}$								
5. $Pt(tta)_2$	ν_1	740	13500	$^1A_{1g}\rightarrow{}^3A_{2g}$				750		25200	9250	3900
	ν_2	625	16000	$^1A_{1g}\rightarrow{}^1E_g$								
	ν_3	470	21300	$^1A_{1g}\rightarrow{}^1A_{2g}$								
6. $Au(tta)_3$	ν_1	600	16667	$^1A_{1g}\rightarrow{}^3A_{2g}$				750		25116	7995	2816
	ν_2	520	19230	$^1A_{1g}\rightarrow{}^3E_g$								
	ν_3	445	22300	$^1A_{1g}\rightarrow{}^1A_{2g}$								
7. $Cu(tta)_2$	ν_1	700	14285	$d_{xy}\rightarrow d_{z^2}$								
	ν_2	620	16130	$d_{xy}\rightarrow d_{x^2-y^2}$								

a) Calculations based on expressions given in Ref. 23 (pp. 310 and 338) for Ni and Ref. 28 (p. 69) for others.

TABLE 3. MAJOR INFRARED SPECTRAL BANDS AND THEIR ASSIGNMENTS IN THE CASE OF LIGAND AND THE COMPLEXES

Ligand cm^{-1}	Ligand (Deuterated) cm^{-1}	Ni(II) Complexes cm^{-1}	Rh(I) Complex cm^{-1}	Au(III) Complex cm^{-1}	Other Complexes cm^{-1}	Assignments
		3500[a] m				$\nu_{(O-H)}$
		3400[b] m				Characteristic of Py
2900—3400[c] s	3000—3400[d] m	3160—3400 mb	2900—3380 mb	3080—3380 mb	3080—3280 mb	$\nu_{(N-H)}$
2570 m	—	—	2570 w	—	—	$\nu_{(S-H)}$
—	2300—2450 m	—	—	—	—	$\nu_{(N-D)}$
—	1750 w	—	—	—	—	$\nu_{(S-D)}$
1600 s	1580 sh	1605±5 s	1600 s	1634 s	1630±10 s	
1535 s	1550 s			1590 sh	1590[e]±10 s	Thioamide band I[g]
1500 s	1530 s	1525±5 s	1515 s	1500 s	1525[f]	
	1460 m				1490±10 s	
1365 s	1365 s	1400±10 m	1335—1370 mb	1420 w	1390±5 m	
1335 m	1335 s	1350±10 m		1390 m	1310±10 w	Thioamide band II[h]
				1320 w		
1080 sh	1030—80 sb	1050±5 sb	1050 m	1060 mb	1040±10 m	
1070 sh				1040 wb		Thioamide band III[i]
1060 s						
750 m	—	750 w	750 m	740—700 mb	690±10 m	$\tau_{(N-H)}$
—	730 sh	—	—	—	—	$\tau_{(N-D)}$
735 m	720 m	635±5 w	700 s	630 w	630±10 m	Thioamide band IV[j]
		450—350 w (two bands)	400 w	450—350 w (two bands)	450—350 w (two bands)	$\nu_{(M-N)}$ $\nu_{(M-S)}$

a) present in $Ni(tta)_2(H_2O)_2$. b) present in $Ni(Py)_2(tta)Cl$. c) multiple bands well resolved. d) perhaps due to some protons remaining over unexchanged with deuterium. e) present in Pt(II) and Cu(II) complexes. f) present in Pd(II) complex. g) due to $\delta_{(NH)}$ (major contribution)+$\nu_{(CN)}$ (minor contribution. h) due to $\delta_{(HH)}$ (minor contribution)+$\nu_{(C=N)}$ (major contribution). i) due to $\nu_{(C-N)}$; j) due to $\nu_{(C=S)}$.
s=strong, m=medium, mb=medium broad, w=weak, shoulder.

in the case of the aquo complex and 970 nm in the case of the pyridine complex. These could be assigned to departure from O_h towards D_{4h} symmetry, on the assumption that the water or the pyridine molecules are *trans* to each other in the respective complexes. In the D_{4h} symmetry, all the three bands should split. But the spectrum of the aquo complex does not show any such splitting of the bands at 625 nm and 400 nm. This may be because both the terms $^3T_{1g}(F)$ and $^3T_{1g}(P)$ yield $^3A_{2g}$ and ^3E_g terms in D_{4h} symmetry. In the strong fields the components of the $^3T_{1g}(F)$ level lies in the sequence $^3A_{2g}<{}^3E_g$, while those of the $^3T_{1g}(P)$ level are inverted ($^3E_g<{}^3A_{2g}$). Thus, when configurational interactions are taken into consideration, the splittings tend to cancel out[23] and it would be difficult to resolve the bands due to these transitions. The amount of splitting in the 1050 nm band may be taken as a measure of the degree of distortion.[24,25]

The values of D_q^E, D_q^A and D_t have been calculated using the expressions given in the literature[23] (Table 2). In these calculations the field strengths due to water and pyridine have been assumed respectively to be less than and greater than that due to ligand.

It may be noted that the values of B and β are quite low. This puts the ligand towards the strong end of the nephelauxetic series. As was pointed out by Schaffer[26] and later on by Jørgensen[27] the low value of β independently suggests bonding through sulphur.

(ii) Complexes of Rh(I), Pd(II), Pt(II) and Au(III): Metal ions of d^8 system exhibit square planar structure in most of their complexes.[28] In D_{4h} symmetry of the field, the d orbitals split into four levels, *viz.*, b_{1g}, b_{2g}, a_{1g}, and e_g. The ground state for the low spin d^8 system is $^1A_{1g}$ ($=a_{1g}^2 \cdot e_g^4 \cdot b_{2g}^2$).[28] The ligand field excited states are $^3A_{2g}$, $^1A_{2g}$ ($b_{2g}\rightarrow b_{1g}$), ^3E_g, ^1E_g($e_g\rightarrow b_{1g}$) and $^3B_{1g}$, $^1B_{1g}$ ($a_{1g}\rightarrow b_{1g}$). Therefore, one should expect three spin allowed and three spin forbidden transitions in these cases. In the electronic spectra of the Rh(I), Pd(II), Pt(II) and Au(III) complexes, the bands obtained together with their probable assignments are given in Table 2. Owing to the forbidden nature of the singlet→triplet transitions, it is quite probable that they may not appear at all in the electronic spectra some of the complexes in nujol mull.

The low intensity bands arising out of transition, $a_{1g}\rightarrow b_{1g}$ could not be assigned unambiguously, since the intense charge transfer bands (L→M) masks the forbidden d–d transition bands. The shift of the intense charge transfer bands in the spectra of some of the complexes is in accordance with the optical electronegativity values,[29] with the result that all the d–d transition bands in the case of Rh(I) complex are masked by the charge transfer bands. The metal ions with next higher optical electronegativity values are Pt(II) and Au(III). Charge transfer bands in the case of complexes of these metal ions start from 450 nm, with the result that the d–d transition bands in these cases appear only as shoulders. The spectrum of Pd(II) ion having highest value of the optical electronegativity exhibits bands due to d–d transition in the visible region.

Assuming the value of B to be 750 cm^{-1}, the values of C, Δ_1 and Δ_2 were calculated on the basis of the assignments given in Table 2. These values compare quite well with those cited in literature for other complexes of these metal ions. This suggests that the field around the metal ion should be tetragonal (D_{4h}-symmetry). This is also in conformity with the preferred orientation of the ligand molecules in the complexes of these metal ions.[30]

It is interesting to note that the value of Δ_1 is much larger than that of Δ_2. This means that similar to other σ or π donor molecules, the ligand molecules cause a marked destabilization of the b_{1g} level ($d_{x^2-y^2}$ orbital) as compared to other d orbitals. This is what one should expect in the square planar geometry.

The value of Δ_1 depends on the relative energy of $b_{1g}(d_{y^2-x^2})\sigma^*$ and $b_{2g}(d_{xy})\pi^*$ levels and therefore, both σ and π bonding are the contributing factors (π acceptor ligands cause destabilization of the b_{1g} level, keeping the b_{2g} level essentially non-bonding). Table 2 also shows Δ_1 value of the Pd(II) complex to be less than the Δ_1 value of Pt(II) complex. The increase in the value of Δ_1 for Pt(II) complex may be due to the increasing σ-bond strength in the order $4d\sigma < 5d\sigma$. This result is quite in conformity with existing results. Also the values of Δ_1 for Pt(II) and Au(III) complexes are nearly the same. This reslt is also in agreement with the results of molecular orbital calculations.[31]

(iii) Cu(II) Complex: As already discussed, the Cu(II) complex is diamagnetic. Harris, *et al.*[32] have proposed a structure for the diamagnetic Cu(II) complex of diazoaminobenzene in which there is metal-metal interaction and the Cu^{2+} ion has squareplanar geometry. The electronic spectrum of this complex shows two bands at 670 nm and 530 nm. These were assigned by them tentatively to $d_{xy}\rightarrow d_{z^2}$ and $d_{xy}\rightarrow d_{x^2-y^2}$ transitions. Tsuchida *et al.*[33,34] have observed a band around 375 nm in all the diamagnetic carboxylate complexes of Cu(II). They have suggested that these bands are characteristic of metal-metal interaction.

The Cu(II) complex reported here has in its electronic spectrum, a shoulder at 700 nm, a weak and broad band at 620 nm and a well defined band at 425 nm. Assuming a square planar arrangement of the ligand molecules around Cu^{2+} ion, these bands are assigned to $d_{xy}\rightarrow d_{z^2}$, $d_{xy}\rightarrow d_{x^2-y^2}$ and metal-metal bond respectively. The assignments, however, are tentative.

Infrared Spectra. From the analytical, electronic spectral and magnetic susceptibility data given in Tables 1 and 2, it appears that the ligand is acting as bidentate in most of the complexes reported here. This is quite in keeping with the preferred geometries the metal ions would take in their complexes.

In solution the ligand can exist either in the thiol form or in the thione form or both. It is believed that it exists as tautomers. Infrared spectral studies were made, with a view to ascertaining the existence of tautomerism and to know the mode of linkage with metal ions in the complexes.

In order to confirm our assignments, the IR spectrum of the deuterated ligand was also studied. Since shifts due to isotopic effect could be expected in the positions of only those bands which arise due to fun-

damental modes of vibration of the NH and the SH groups, comparison of these two spectra confirms not only the assignment but also the existence of the ligand in the thiol form (Table 3).

A close look at the infrared spectra of the complexes suggests that the complexes can be classified into groups on the basis of the direction of shifts in the positions of the major bands in their spectra. The spectra of all the complexes in any group are similar so far as the direction of shifts in the band positions is concerned. It is reasonable to expect the bonding scheme in these complexes to be the same. The following is a brief groupwise discussion regarding the shifts in the positions of the major bands in the spectra of the complexes.

(i) Complexes of Ni(II). The major shifts in the positions of bands were found to be similar to those of cobalt(II)[1] and therefore, the mode of bonding in nickel complex (Fig. 1) should be the same as that of cobalt complex.[1]

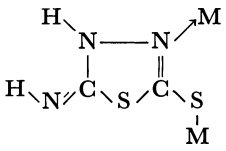

Fig. 1.

(ii) Complexes of Pd(II), Pt(II), and Cu(II). In the spectra of this group of complexes, the shifts in the position of the bands are similar to those found in the spectra of the complexes of Ru(III), Rh(III), Ir(III), Pd(IV).[1] Thereby the mode of linkage in these complexes as shown in Fig. 2 should be identical with those in Rh(III), Ru(III), Ir(III) and Pd(IV) complexes.[1]

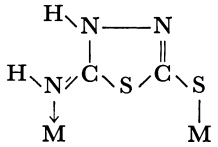

Fig. 2.

(iii) Rh(I) Complexes. (a) The band at 2750 cm^{-1} in the spectrum of the ligand is also seen in that of the complex. (b) Bands due to $\nu_{(N-H)}$, $\delta_{(N-H)}$ and $\tau_{(N-H)}$ appear in the spectrum of the complex at about the same positions as in the spectrum of the ligand. (c) Thioamide band II shifts slightly towards higher wave number side. (d) Thioamide band III remains practically unchanged. (e) Thioamide band IV shifts towards lower wave number side. (f) New bands appear in the region of 400 cm^{-1}. (g) All bands due to triphenylphosphene molecule appear in the spectrum of the complex with slight shifts in their positions.

These results can be explained if the mode of bonding is as shown in Fig. 3.

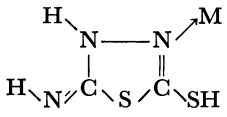

Fig. 3.

From this type of bonding it is evident that the positions of the bands due to (a) $\nu_{(S-H)}$ should not disappear and (b) $\nu_{(N-H)}$, $\delta_{(N-H)}$ and $\tau_{(N-H)}$ should not shift. The bond order of (C=N) should increase, while that of (C=S) should decrease and $\nu_{(M-N)}$ coupled with other bending modes of vibration of the ligand molecule should appear.

(iv) Au(III) Complex. The infrared spectrum of this complex is quite complicated because most of the bands are either split or broadened. In the spectrum of the Au(III) complex, the positions of most of the major bands are the same as those present in the spectra of Pd(II) and Ni(II) complexes (except those of water or pyridine in the latter complex). This behaviour is not quite unexpected because three ligand molecules as required by stoichiometry can be arranged in a square planar geometry around the metal ion (as determined from magnetic and visible spectral data) only in one way and that is two of the ligand molecules act as monodentate whereas the third one, as bidentate as shown in Fig. 4.

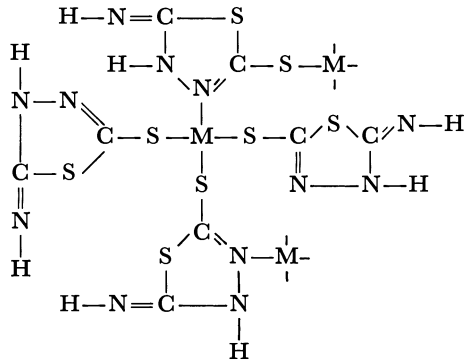

Fig. 4.

It is evident from this mode of bonding that the bond orders of (C=N) of the bonded N=C–SH and the unbonded H–N–C=N–H groups in the mono and bidentate ligand molecules should be different (next page).

It is reasonable to expect that the fundamental modes of vibrations of (C=N) bonds with different bond orders in the same ligand molecule interact strongly while those in different ligand molecules would interact rather weakly. As a result of these interactions, thioamide band II would appear considerably split bands should appear at higher wave number, one at slightly higher wave number and one at lower wave number. The appearance of bands at 1420, 1390, and 1320 cm^{-1}, assigned to thioamide band II is in keeping with the results expected. Besides, the shift of thioamide band IV towards lower wave number side lends support to the bonding scheme proposed. (next page)

With the exception of Rh(I) complex which is very slightly soluble in alcohol, all the other complexes reported here are insoluble in water and other common non-coordinating organic solvents. This suggest that they are polymeric in nature.

Therefore, on the basis of the analytical, magnetic and spectral data as well as the preferred geometries the metal ions would take in their complexes, the following plausible polymeric structures are proposed for the complexes.

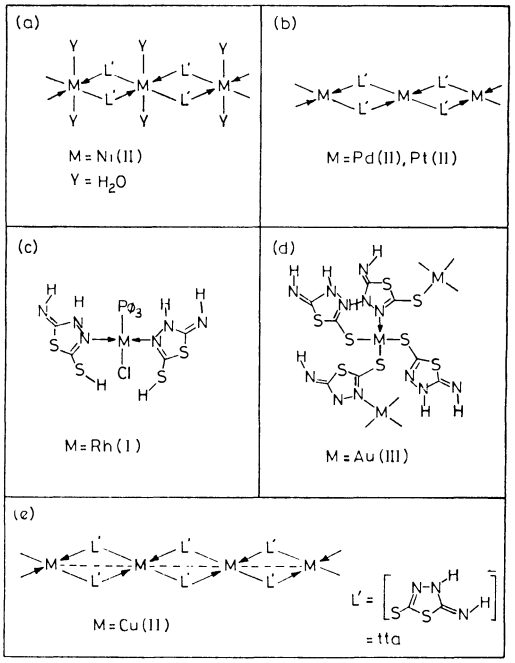

Scheme.

The authors are thankful to Dr. S.N. Tandon, Reader in Chemistry, Roorkee University (India) for providing a sample of the ligand. One of the authors (MRG) grateful to the Govt. of India and the Karnataka Regional Engineering College, Suratkal (India) for the Fellowship under the Quality Improvement Programme for serving teachers in Engineering colleges. He is indebted to the Director, Indian Institute of Technology, Kanpur for providing research facilities.

References

1) M. R. Gajendragad and U. Agarwala, *J. Inorg. Nucl. Chem.*, in press.
2) E. Domagalina and L. Przyborowski, *Z. Anal. Chem.*, **207**, 411 (1965).
3) E. Domagalina and L. Przyborowski, *Chem. Anal.* (Warsaw), 1087 (1966).
4) S. R. Joshi, C. B. Gupta, and S. N. Tandon, *Acta Chem.* (Budapest), **77**, 147 (1973).
5) J. Sandstrom, *Acta Chem. Scand.*, **15**, 1300 (1961).
6) J. A. Osborn, F. H. Jardine, J. F. Young, and G. Wilkinson, *J. Chem. Soc.*, **A**, **1966**, 1711.
7) G. Brauer, "Handbook of Preparative Inorganic Chemistry", Vol. II, Academic Press, New York (1963), p. 1572.
8) F. P. Treadwell and W. T. Hall, "Analytical Chemistry" Vol. II, John Wiley & Sons Inc., New York, N.Y. (1958), pp. 77, 199.
9) A. I. Vogel, "A Text Book of Quantitative Inorganic Chemistry", Longmans Green & Co. Ltd., III Ed., (1961), pp. 460, 462, 480, 497, 509, 511, 513, 575.
10) F. E. Beamish, "The Analytical Chemistry of the Noble Metals", Vol. 24, Pergamon Press, Oxford (1966), pp. 273, 286, 308, 314.
11) A Earnshaw, "Magnetochemistry", Academic Press, New York (1968), pp 6—7.
12) T. Norita, *Suomen Kem.*, **33**, 161 (1960).
13) B. Singh, Lakshmi, and U. Agarwala, *Inorg. Chem.*, **8**, 2341 (1969).
14) B. N. Figgis and D. J. Martin, *ibid.*, **5**, 100 (1966).
15) E. J. Duff, M. N. Hughes, and K. J. Rutt, *J. Chem. Soc., A*, **1969**, 210–5.
16) J. S. Dwivedi and U. Agarwala, *J. Inorg. Nucl. Chem.*, **35**, 2229 (1973).
17) M. R. Gajendragad and U. Agarwala, *J. Prakt. Chem.*, in press.
18) I. G. Ross and Y. Yates, *Trans. Faraday Soc.*, **55**, 1064 (1959).
19) E. A. Boudreaux, *Inorg. Chem.*, **3**, 506 (1964).
20) L. S. Forster and C. J. Hallhause, *Acta Chem. Scand.*, **16**, 1385 (1962).
21) D. L. Kepert and K. P. Vrieze, "Comprehensive Inorganic Chemistry", Vol. IV, ed. by J. C. Bailer *et al.*, Pergamon Press, Oxford (1973), p. 300.
22) R. S. Nyholm, *Proc. Chem. Soc.* **1961**, 273.
23) A. P. B. Lever, "Inorganic Electronic Spectroscopy", Elsevier Publishing Co., New York (1968), p. 338.
24) C. R. Hare and C. J. Ballhausen, *J. Chem. Phys.*, **40**, 788 (1964).
25) G. R. Brubaker and D. H. Bush, *Inorg. Chem.*, **5**, 2114 (1966).
26) C. E. Schaffer, 'Abstracts, 140th National Meeting of the American Chemical Society, Chicago (Ill.), Sept. 1961, p. 24N.
27) C. K. Jørgeysen, *Acta Chem. Scand.*, **16**, 2017 (1962).
28) C. J. Ballhausen and H. B. Gray, "Coordination Chemistry", Vol. I, Edited by A. E. Martel, Van Nostrand Reinhold Co., New York (1971), p. 66.
29) A. P. B. Lever, "Inorganic Electronic Spectroscopy", Elsevier Publishing Co., New York (1968), p. 245.
30) F. A. Cotton and G. Wilkinson, "Advanced Inorganic Chemistry", II Edition, John Wiley & Sons, Inc., New York (1966), Chapter 30.
31) H. Basch and H. P. Gray, *Inorg. Chem.*, **6**, 365 (1967).
32) C. M. Harris, B. F. Hoskins, and R. L. Martin, *J. Chem. Soc.*, **1951**, 3728.
33) Y. Yamada, H. Nakamura, and T. Tsuchida, This Bulletin, **31**, 303 (1958).
34) S. Yamada, H. Nishikawa, and T. Tsuchida, *ibid.*, **33**, 1278 (1960).

NOTES

BULLETIN OF THE CHEMICAL SOCIETY OF JAPAN, VOL. 48 (3), 1030 (1975)

Synthesis of Dialkylaminomethylenediphosphonic Acids

Masahiro FUKUDA, Yoshiki OKAMOTO, and Hiroshi SAKURAI

The Institute of Scientific and Industrial Research, Osaka University, Yamada-kami, Suita shi, Osaka 565

(Received May 10, 1974)

Synopsis. *N,N*-Dialkylformamides reacted with phosphorus trichloride or phosphorus tribromide to give the corresponding dialkylaminomethylenediphosphonic acids.

Although the reaction of amides with phosphoryl chloride has been studied as Vilsmeiyer reaction,[1] little is known concerning of the reaction of amides with phosphorus trichloride or phosphorus tribromide. In this paper, we wish to report the synthesis of dialkylaminomethylenediphosphonic acids by successive treatment of *N,N*-dialkylformamides with phosphorus trichloride and with acetic acid. In this experiment, the following amides were employed; *N,N*-dimethylformamide (Ia), *N,N*-diethylformamide (Ib), *N,N*-dipropylformamide (Ic), *N*-formylpyrrolidine (Id), *N*-formylpiperidine (Ie), and *N*-formylmorpholine (If). Phosphorus tribromide reacted also with the formamides to give the same products.

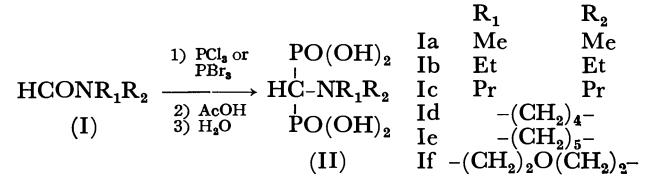

(I) (II)

	R_1	R_2
Ia	Me	Me
Ib	Et	Et
Ic	Pr	Pr
Id	$-(CH_2)_4-$	
Ie	$-(CH_2)_5-$	
If	$-(CH_2)_2O(CH_2)_2-$	

These results are summarized in Table 1.

TABLE 1. PROPERTIES OF DIALKYLAMINOMETHYLENEDIPHOSPHONIC ACIDS

Product	Yield (%)	Dp(°C)	pK_{a_1}	pK_{a_2}	pK_{a_3}
IIa	53.5	255	2.5	5.2	9.5
IIb	39.6	190—200	2.5	5.2	9.0
IIc	33.9	195—200	3.2	5.6	9.2
IId	44.0	220—225	2.7	5.3	9.5
IIe	28.9	250—255	3.0	5.5	9.4
IIf	15.7	250—260	3.0	5.2	9.0

The structure of IIa was confirmed to be dimethylaminomethylenediphosphonic acid by direct comparison with an authentic sample[2] by NMR and by dissociation constant (pK_a). The structures of the other products (IIb—IIf) were identified by elemental analysis and by alkalimetry.

Experimental

Preparation of Dimethylaminomethylenediphosphonic Acid (IIa). General Procedure: *N,N*-Dimethylformamide (7.3 g) was added dropwise to phosphorus trichloride (68.5 g) under cooling with ice-water. After stirring for an hour, the mixture was treated with 100 ml of glacial acetic acid. This was allowed to stand for several hours at room temperature with protection from moisture. After removal of the upper layer containing acetyl chloride by decantation, the lower layer was poured into 150 ml of ice-water, and this was concentrated to syrup under reduced pressure. After addition of absolute ethanol (300 ml), precipitate separated and it was filtered (17.5 g) and recrystallized from water. Mp 255 °C (dec.). NMR (D_2O): δ 3.12 (s, 6H, N-CH_3), 3.74 (t, 1H, P_2C-H, J_{PCH} 20 Hz). pK_{a1} 2.5, pK_{a2} 5.2, and pK_{a3} 9.5. Found: C, 15.22; H, 5.98; N, 5.87; P, 26.20%. Calcd for $C_3H_{11}NP_2O_6 \cdot H_2O$: C, 15.19; H, 5.49; N, 5.91; P, 26.16%.

In a similar manner, compounds IIb, IIc, IId, IIe, and IIf were obtained, as shown in Table 1.

References

1) H. H. Bosshard, R. Mory, M. Schmid, and H. Zollinger, *Helv. Chim. Acta*, **42**, 1653 (1959); H. H. Bosshard and H. Zollinger, *ibid.*, **42**, 1659 (1959); H. Bredereck, F. Effenberger, and G. Simchen, *Chem. Ber.*, **97**, 1403 (1964); M. Ochiai, *Kagaku no Ryoiki*, **19**, 900 (1965).

2) The synthetic sample was prepared by the procedure of Gross [H. Gross and B. Costisella, *Angew. Chem.*, **80**, 364 (1968).].

BULLETIN OF THE CHEMICAL SOCIETY OF JAPAN, VOL. 48 (3), 1031—1032 (1975)

Molten-state Absorption Spectra of Weakly Interacting Donor-Acceptor Mixtures[1)]

Jun-ichi AIHARA

Department of Chemistry, Faculty of Science, Hokkaido University, Sapporo 060

(Received February 14, 1974)

Synopsis. Absorption spectra of equimolecular mixutres of bulky electron donors, such as triphenylamine, and typical electron acceptors, such as *sym*-trinitrobenzene (TNB) and chloranil, in the molten state are reported. Though the components do not interact in the solid, the melts display distinct charge-transfer absorption bands in the visible region.

Several years ago, Hammond and Burkardt studied extensively various aspects of a series of weak donor-acceptor complexes.[2)] According to their visual observations, some electron-donating molecules having bulky substituents do not form charge-transfer complexes with any of the typical electron acceptors in the solid state. A mixture of a bulky electron donor, such as triphenylamine, with most electron acceptors, however, has a deep color in the melt. The color of the melt vanishes on freezing, and the cycle can be repeated many times. In order to extend our understanding of this phenomenon, we measured the electronic spectra of this kind of donor-acceptor mixtures in the molten state.

Two bulky donor compounds, triphenylamine (TPA) and diphenylamine (DPA), were used in this study. The samples for the measurements of the solid- and molten-state spectra were prepared by solidfying the molten mixtures of the bulky electron donors with equimolar amounts of electron acceptors. The molten-state absorption spectra were taken near 150 °C at which temperature the mixtures were sure to be totally molten. The absorption spectra of the methylene chloride solutions were taken for comparison. A Beckman DK-2A spectrophotometer was used.

Figures 1–5 show the visible absorption spectra of mixtures of TPA with five electron acceptors. TPA is a pronounced example of a bulky electron donor. The gaseous ionization potential (I_g) of this compound is as low as 6.84 eV,[3)] and it is customarily considered as an excellent electron donor. Furthermore, this compound is very suitable for the present experiment because it is thermally stable.

In general, the solution spectrum of the donor-acceptor mixture in the visible region displays an absorption band characteristic of a charge-transfer complex. Fortunately, absorption peaks of the charge-transfer bands were observed in the solution spectra of the two mixtures, the TPA-chloranil and the TPA-TNB. These absorption peaks ($h\nu_{CT}$) should be re-

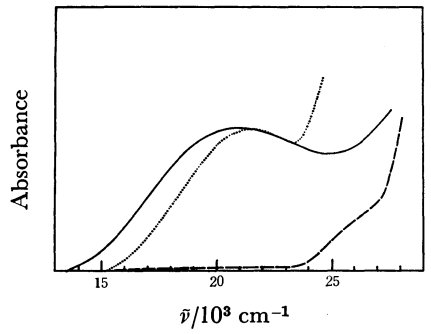

Fig. 1. The absorption spectra of the TPA-TNB mixture in the solid state (——), in the molten state (——), and in solution (·····).

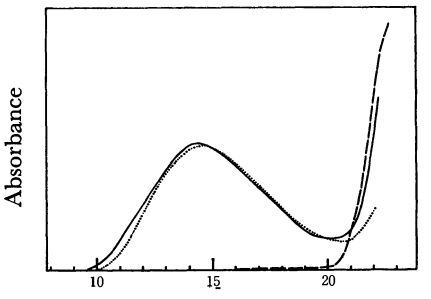

Fig. 2. The absorption spectra of the TPA-chloranil mixture in the solid state (——), in the molten state (——), and in solution (·····).

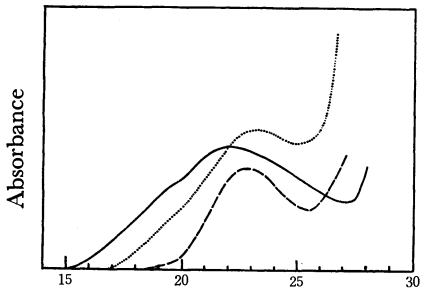

Fig. 3. The absorption spectra of the TPA-DMBQ mixture in the solid state (——), in the molten state (——), and in solution (·····).

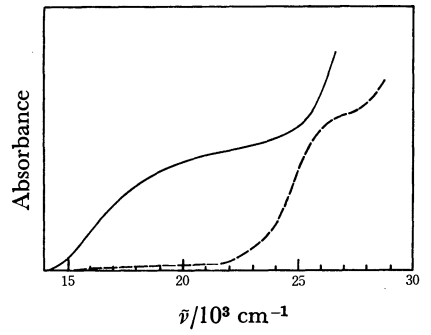

Fig. 4. The absorption spectra of the TPA-picric acid mixture in the solid state (——-), and in the molten state (——).

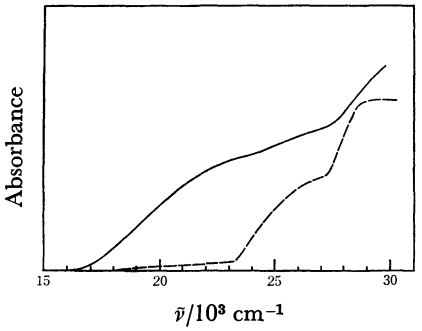

Fig. 5. The absorption spectra of the TPA-*m*-dinitrobenzene mixture in the solid state (——), and in the molten state (——).

produced by the empirical expressions such as:

$$h\nu_{CT} = aI_g - b, \quad (1)$$

where a and b are constants associated with a given electron acceptor. For example, a and b are 0.853 and 3.51 eV, respectively, for a group of TNB complexes in chloroform. The absorption maximum of the TPA-TNB system in chloroform is located at 2.60 eV, whereas the value estimated from Eq. (1) is 2.32 eV. The deviation of the observed value from the estimated one is 0.28 eV. A deviation of this extent is properly ascribed to the bulky substituent effect, as was suggested before for the tetracyanoethylene complexes of methylbenzenes.[4]

On the other hand, the solid donor-acceptor mixtures appear almost colorless, indicating that the intermolecular charge-transfer interaction is substantially suppressed even in the domains of the solid solutions which may be present in the mixtures. The weak absorption tail which often appears in the energy region where there should be a charge-transfer band is supposedly due to incidental formation of a charge-transfer complex in the mixture.

An almost colorless mixture of TPA with TNB turned deep red on melting, and a mixture of TPA with chloranil was deep green in the molten state. Other molten mixtures were all reddish. This is in marked contrast to the behavior observed for ordinary charge-transfer complexes on raising the temperature above the melting point; in this case, the colored solid melts with little color change.[5]

As is shown in Figs. 1–5, the color change of the present mixtures is in accord with the appearance of the charge-transfer bands in the molten state. The absorption peaks are located at 20700 cm^{-1} for the molten TPA-TNB and at 14300 cm^{-1} for the molten TPA-chloranil. The astonishing coincidence of the spectral shapes between the molten-state and solution spectra strongly suggests that the colored species in the melt is similar to that in solution. In addition, the coincidence of the absorption peaks of the TPA-chloranil mixture in the melt and in solution suggests that the dielectric properties of the mixture, which are presumably associated with the solvatochromism of the charge-transfer band, are quite similar to those of the solvent (methylene chloride). Therefore, the intermolecular interactions appear to be still very weak in the melt. As was suggested by Lower for the solid complex,[6] the excitation might be localized in each donor-acceptor pair in the melt.

For the other molten mixtures containing TPA, the charge-transfer bands are found to overlap more or less with the absorption bands of the component molecules. For example, in the molten-state spectrum of the TPA-DMBQ (2,5-dimethyl-*p*-benzoquinone) system, the charge-transfer band is located above 15000 cm^{-1}, partially overlapping with the n-π^* transition of the benzoquinone. Since the relative intensities of both absorption bands are apparently comparable in the melt, the extinction coefficient of the charge-transfer band is estimated to be of the same order of magnitude as that of the n-π^* transition ($\varepsilon_{max}=\sim 20$).[7] Such a small extinction coefficient is consistent with weak intermolecular interactions which are insufficient to form a complex in the solid state.

Mixtures of DPA with various electron acceptors display similar spectral changes on melting. However, they are very reactive in the molten state, and readily decompose. An absorption spectrum could be obtained of only the DPA-DMBQ mixture. Every aspect of the molten-state spectrum resembles that of the spectrum of the TPA-DMBQ mixture.

In a previous paper, we suggested that the charge-transfer interaction is not always a primary factor in determining the structure of the condensed phase.[8] It is noteworthy that the self-complex formation which is often attained to 100 percent in the *o*-anisyl-*p*-benzoquinone crystal is completely disturbed by the fluidity of the melt.[9] On the contrary, the fluidity of the melt is needed to allow the intermolecular charge-transfer interaction in the present donor-acceptor mixtures. Since the heat of complex formation (~0.30 kcal/mol)[2] is much less than the typical heat of sublimation (~30 kcal/mol),[10] the charge-transfer interaction, at all events, seems to be of secondary importance in the solid mixtures.

References

1) This work was financially supported by the Fuji Photo Film Co., Ltd.
2) P. R. Hammond and L. A. Burkardt, *J. Phys. Chem.*, **74**, 639 (1970).
3) F. I. Vilesov and V. M. Zaitsev, *Dokl. Phys. Chem. Proc. Acad. Sci. USSR*, **154**, 117 (1964).
4) J. Aihara, M. Tsuda, and H. Inokuchi, This Bulletin, **40**, 2460 (1967).
5) J. Aihara, A. Sasaki, and Y. Matsunaga, *ibid.*, **43**, 3323 (1970).
6) S. K. Lower, *J. Phys. Chem.*, **74**, 2733 (1970).
7) E. A. Braude, *J. Chem. Soc.*, **1945**, 490.
8) J. Aihara, G. Kushibiki, and Y. Matsunaga, This Bulletin, **46**, 3584 (1973).
9) J. Aihara, *ibid.*, **47**, 2063 (1974).
10) H. Inokuchi, S. Shiba, T. Handa, and H. Akamatu, *ibid.*, **25**, 299 (1952).

BULLETIN OF THE CHEMICAL SOCIETY OF JAPAN, VOL. 48 (3), 1033—1034 (1975)

A Flash Photolytic Investigation of the Interaction between Halide Anions and the Triplet Eosin

Takeshi AKIYAMA,* Mamoru KAMIYA, and Yukio AKAHORI
Shizuoka College of Pharmacy, Oshika, Shizuoka-shi 421
(Received may 16, 1974)

Synopsis. The quenching effect of the iodide ion to the triplet eosin in oxygen-free aqueous solution was strongly enhanced at 10^{-1}—10^{-2} M, but the effects of bromide and chloride ions were negligibly small at 10^{-1}—10^{-4} M. The above-mentioned results were found directly by means of a flash photolytic method.

Halide anions work as typical quenchers of the fluorescence of an eosin aqueous solution. In this case, the quantity of the quenching rate constant suggests that the energy transfer from the photoexcited eosin to the halide anion is a diffusion-controlled process.[1] It has also been found that the iodide ion strongly quenches the dye phosphorescence in a viscous glycerol solution.[2] Hence, we can expect that the halide anion quenches the triplet eosin as well as the singlet eosin. This postulation is supported also by the intermolecular heavy-atom effect of the halogen atom.

Experimental

Commercial eosin-Y was purified chromatographically according to the method of Koch.[3] A 6.2 μM eosin solution was prepared using a 1/15 M phosphate buffer at pH=7.0. Sodium iodide, sodium bromide, and sodium chrolide (G.R.) were used without further purification. Repeated cycles of freezing and thawing under a high vacuum were adopted in order to degass the sample solutions. The flash irradiation source consisted of two xenon lamps, Ushio-103 type. The lamps were used at 2 μF and 6 kV. A cylindrical quartz cell 20 cm in length and 2 cm in diameter was used. The monitoring lamp was a 500-W xenon arc lamp, Ushio-UXL-500D. The changes in the optical density after the flash irradiation were followed by means of a 1P28 photomultiplier coupled to a Hitachi QV-50 spectrophotometer. The decay of the triplet eosin was followed by selecting the wavelength of 436 nm, according to the method of Zwicker and Grossweiner.[4] The kinetic data were taken only from the initial flash irradiation of a freshly-prepared solution.

Results

Figures 1 and 2 show the decay curves of the transient absorbance of the triplet eosin. The initial decays were well fitted by exponential decay curves, which gave first-order decay constants. Without the quencher, the decay constant is of the same order as that obtained by Zwicker and Grossweiner.[4] The origin of the irreversible absorbance change which is seen at the period of ms order after the flash irradiation is not known. We consider, however, that it can not necessarily be attributed to another transient product whose spectrum overlaps that of the triplet eosin, because a permanent increase in the absorbance in this wavelength region is observed. It is of interest to note that

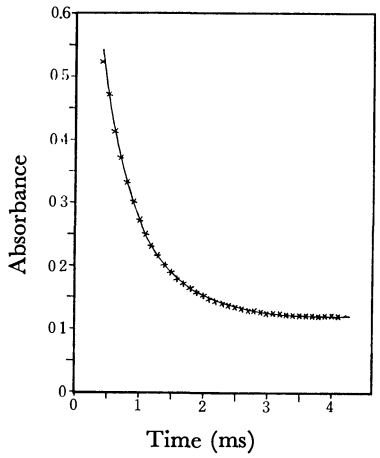

Fig. 1. Time-dependence of absorbance at 436 nm as measured by Flash-photolysis of eosin-Y in buffer solution (pH=7.0).
Concentration of eosin-Y: 6.19×10^{-6} mol/l.

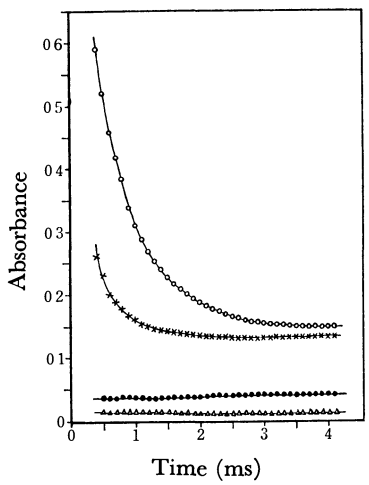

Fig. 2. Time-dependence of absorbance at 436 nm as measured by flash-photolysis of eosin-Y and quencher (NaI) in buffer solution (pH=7.0).
Concentration of eosin-Y: 6.19×10^{-6} mol/l.
Concentration of NaI
△: 1.03×10^{-1} mol/l ●: 1.08×10^{-2} mol/l
×: 1.08×10^{-3} mol/l ○: 1.06×10^{-4} mol/l

the quenching effect of the iodide ion is enhanced at 10^{-1}—10^{-2} M to such an extent that the triplet eosin can not be observed within ms time after the flash irradiation. The quenching effects of the bromide and chloride ions are negligibly small at 10^{-1}—10^{-4} M.

* Present address: Japan IBM Co. Inc., 2-6-1, Nishishinjuku, Shinjuku-ku, Tokyo 160.

The remarkable concentration dependence of the quenching effect of the iodide ion gives definitive evidence of a specific interaction between the triplet eosin and the iodide ion. This finding is in accord with the earlier suggestion of a charge-transfer interaction between the photoexcited eosin and the iodide ion.[5]

Table 1. The kinetic data of the decay constants of the triplet eosin

Quencher	Concentration of quencher (mol/l)	First-order decay constant (s^{-1})
None	—	406.5
NaI	1.03×10^{-1}	—
	1.08×10^{-2}	—
	1.08×10^{-3}	347.4
	1.06×10^{-4}	429.9
NaBr	1.00×10^{-2}	420.5
	1.02×10^{-3}	410.3
	1.05×10^{-4}	399.3
NaCl	1.69×10^{-1}	433.3
	1.08×10^{-3}	451.3
	1.11×10^{-4}	411.7

References

1) G. Oster and A. H. Adelman, *J. Amer. Chem. Soc.*, **78**, 913 (1956).
2) F. Perrin, *C. R. Acad. Sci. Paris*, **184**, 1121 (1927); S. Boudin, *J. Chem. Phys.*, **27**, 285 (1930).
3) L. Koch, *J. Assoc. Offic. Agr. Chemists*, **39**, 397 (1956).
4) E. F. Zwicker and L. I. Grossweiner, *J. Phys. Chem.*, **67**, 549 (1963).
5) J. Q. Umberger and D. K. LaMer, *J. Amer. Chem. Soc.*, **67**, 1099 (1945).

BULLETIN OF THE CHEMICAL SOCIETY OF JAPAN, VOL. 48 (3), 1035—1036 (1975)

The Formation of Crystalline Molecular Complexes between Inosine and Several Phenols

Yoshihisa SUZUKI, Kentaro HARA, and Tsuneo HIRAHARA

Central Research Laboratories, Ajinomoto Co., Inc., Suzuki-cho, Kawasaki 210

(Received July 4, 1974)

Synopsis. Inosine has been found to form 1:1 crystalline molecular complexes with phenol, *p*-nitrophenol, and 1,2,3-trihydroxybenzene respectively, and to be inactive with *o*-, *m*-nitrophenol, 1,2,4-, 1,3,5-benzenetriol, benzenediols, aminophenols, and cresols.

Since the formation of a crystalline molecular complex between inosine and tryptophan was shown for the first time between 1968 and 1970 by Suzuki *et al.*,[1,2] inosine is known to have a strong ability of complex-formation among several ribonucleosides. The formation of a specific crystalline molecular complex is useful for industrial isolation processes. It is also known that flavins with indoles[3] including tryptophan form molecular complexes similar to the flavin-phenol complexes.[4] Indoles are considered to be poorer electron donors to flavins than are phenols. These facts suggested the probability of some crystalline complex-formation of inosine with phenols. This paper will deal with the formation of molecular complexes between inosine and several phenols, which are of interest in relation to the above background.

Results and Discussion

Table 1 shows the results of the crystalline complex formation between inosine and several phenols. Phenol, *p*-nitrophenol, and 1,2,3-benzenetriol (pyrogallol) were confirmed to form 1:1 complexes with inosine. Table 2 shows their X-ray powder diffraction data.

The inosine-*p*-nitrophenol complex is easily obtained from an equimolecular aqueous solution of inosine and *p*-nitrophenol. However, both inosine–phenol and inosine–pyrogallol complexes are incongruent and could not be obtained in a pure form from an equimolecular aqueous solution of the two components, from which the crystals of inosine were usually precipitated with or without those of the complexes. The crystallization of the complex without any contamination of the inosine crystals was performed from an aqueous solution which contained 1 mol of inosine and 2 mol (or more) of phenol, or 1 mol of inosine and 4 mol (or more) of pyrogallol, respectively.

Table 1. The crystalline complex formation between inosine and several phenol compounds

Phenol	+
o-Nitrophenol	−
m-Nitrophenol	−
p-Nitrophenol	+
o-Aminophenol	−
m-Aminophenol	−
p-Aminophenol	−
o-Cresol	−
m-Cresol	−
p-Cresol	−
o-Benzenediol	−
m-Benzenediol	−
p-Benzenediol	−
1,2,3-Benzenetriol (Pyrogallol)	+
1,2,4-Benzenetriol	−
1,3,5-Benzenetriol	−

Table 2. The X-ray powder diffraction data of several inosine–phenol complexes

Inosine–phenol complex		Inosine–*p*-nitrophenol complex		Inosine–pyrogallol complex	
d(Å)	I/I_0[a]	d(Å)	I/I_0[a]	d(Å)	I/I_0[a]
7.73	20	7.83	10	7.83	30
6.66	70	6.92	10	6.97	10
5.70	20	5.87	10	6.37	20
5.59	20	5.50	30	5.87	20
5.45	40	4.90	20	5.19	20
4.87	50	4.29	10	4.93	10
3.44	50	3.75	10	4.31	20
3.33	100	3.62	20	4.02	20
3.29	30	3.44	100	3.92	100
3.02	50	3.28	30	3.40	40
				3.33	30

a) The scale of the intensity is so chosen as to make the most intense line have the value 100.

Inosine is known to crystallize with such solvents of crystallization as water,[5] pyridine,[6] *N,N*-dimethylformamide,[6] and dimethyl sulfoxide.[7] Among the several phenols investigated in the present study, only phenol is liquid at room temperature and can be used as a solvent of inosine. The complex between inosine and phenol was also obtained from a pure phenol solution of inosine as well as from the aqueous phenol solution described above. Considering these facts, the phenol in the complex may be interpreted as a solvent of crystallization.

The presence of the specific interactions of inosine with *p*-nitrophenol and phenol in the present study, and the absence of that with *o*-nitrophenol, are of interest in view of the facts that *p*-nitrophenyl phosphate and phenyl phosphate were good donors, while *o*-nitrophenyl phosphate was not, in the phosphorylation of inosine by the bacterial nucleoside phosphotransferase.[8,9]

The information now available to us is insufficient to explain why these three phenols form crystalline complexes with inosine from among many other phenol

compounds. The ionization constants of phenol (1.3×10^{-10})[10] and pyrogallol (9.68×10^{-10})[11] are of the same order as those of unreacted phenols, such as 1,3,5-benzenetriol (4.5×10^{-10}),[10] *o*-aminophenol (2.18×10^{-10})[12] and benzenediol ($1.1—3.6\times10^{-10}$).[10] *p*-Nitrophenol has an ionization constant (6.5×10^{-8})[13] similar to those of the *o*-isomer (7.5×10^{-8})[13] and *m*-isomer (1.0×10^{-8}).[13] These facts suggest that acid-base interaction makes little contribution to these molecular complex-formations. The effect of hydrogen bonding or sterical arrangement may be proposed.

Experimental

Examination of the Complex-Formation. Inosine and one of the phenols were dissolved (in a molar ratio of 1:1) into water, and the mixture was evaporated to dryness in a desiccator. The resultant solids were examined with the X-ray (CuK_α) powder diffraction method. When their data did not coincide with those of the mechanical mixture of the two components, the complex may be formed; further confirmation was done.

The Crystallization of the Complexes. *Inosine–Phenol Complex*: Inosine (3.3 g) was dissolved in a mixture of water (6 ml) and 90% aqueous phenol (15 ml) with heating. When the resultant solution was cooled to room temperature, prism crystals were precipitated. They were filtered and analyzed.

Inosine–p-Nitrophenol Complex: Inosine (6.7 g) was dissolved in water (80 ml) with heating, and then *p*-nitrophenol (3.25 g) was stirred into this solution at 40 °C over a 2-hr period. The crystals thus precipitated were filtered and analyzed.

Inosine–Pyrogallol Complex: Inosine (13.4 g) was dissolved in water (160 ml) with heating, and then pyrogallol (25.2 g) was added to this solution. The resultant mixture was stirred for 2 hr at 5 °C. The crystals thus precipitated were filtered and analyzed.

Paper Chromatography. The components of the crystals were determined by paper chromatography on Toyo-Roshi No. 51A, with the *n*-butanol–acetic acid–water (4:1:1) solvent system. The UV absorbance of the spots was determined at the maximum wavelength compared with that of the standard references.

Analysis. *Inosine–Phenol Complex*: Mp 143—145 °C. Found: C, 53.02; H, 5.07; N, 15.28%. Calcd for $C_{10}H_{12}N_4O_5\cdot C_6H_6O$: C, 53.03; H, 5.01; N, 15.46%.

Inosine–p-Nitrophenol Complex: Mp 189—191 °C. Found: C, 47.18; H, 4.21; N, 17.15; Inosine, 66.3; *p*-Nitrophenol, 33.4%. Calcd for $C_{10}H_{12}N_4O_5\cdot C_6H_5NO_3$: C, 46.91; H, 4.31; N, 17.19; Inosine, 65.9; *p*-Nitrophenol, 34.1%.

Inosine–Pyrogallol Complex: Mp 167—171 °C. Found: C, 51.22; H, 4.58; N, 14.33; Inosine, 70.4; Pyrogallol, 30.4%. Calcd for $C_{10}H_{12}N_4O_5\cdot C_6H_6O_3$: C, 51.80; H, 4.60; N, 14.21; Inosine, 68.1; Pyrogallol, 31.9%.

References

1) Y. Suzuki, T. Hirahara, and T. Nakamura, Japanese Pat. 43-29010 (1968).
2) Y. Suzuki, T. Hirahara, T. Akashi, and T. Nakamura, U.S. Pat. 3532684 (1970).
3) J. F. Pereira and G. Tollin, *Biochim. Biophys. Acta.* **143**, 79 (1967).
4) D. E. Fleischman and G. Tollin, *Proc. Natl. Acad. Sci. U.S.*, **53**, 237 (1965).
5) C. E. Bugg, U. T. Thewalt and R. E. Marsh,, *Biochem. Biophys. Res. Commun.*, **33**, 436 (1968).
6) Y. Suzuki, K. Hara, and T. Hirahara, Japanese Pat. 46–18758 (1971).
7) Y. Suzuki and K. Hara, This Bulletin, **47**, 2551 (1974).
8) K. Mitsugi, *Agr. Biol. Chem.*, **28**, 659 (1964).
9) K. Mitsugi, A. Kamimura, M. Kimura, and S. Okumura, *ibid.*, **29**, 1109 (1965).
10) "Kagakudaijiten," Vol. 7, Kyoritsu Shuppan, Tokyo (1960), p. 727.
11) C. T. Abichandani and S. K. K. Jatkar, *J. Indian Inst. Sci.*, **21A**, 417 (1938).
12) "Kagakudaijiten," Vol. 1, Kyoritsu Shuppan, Tokyo (1960), p. 290.
13) "Kagakudaijiten," Vol. 6, Kyoritsu Shuppan, Tokyo (1960), p. 788.

BULLETIN OF THE CHEMICAL SOCIETY OF JAPAN, VOL. 48 (3), 1037—1038 (1975)

Molecular Vibrations and Force Fields of Alkyl Sulfides. XII. Skeletal Conformations of Several Simple Aliphatic Sulfides

Masaru OHSAKU

Department of Chemistry, Faculty of Science, Hiroshima University, Higashisenda-machi, Hiroshima 730

(Received July 9, 1974)

Synopsis. A normal coordinate treatment of methyl propyl, methyl butyl, ethyl propyl, ethyl butyl, and dipropyl sulfides has been carried out. From the observed and calculated frequencies, the conformation about each of six C–C bonds—CSC–CC, CSC–CCC, CCSC–CC, CCSC–CCC, and CC–CSC–CC— was confirmed to be the T form in the annealed crystalline state.

It is very difficult to analyse completely the skeletal conformations for longer molecules. In the present study, we have determined the conformations about the C–C bonds adjacent to the C–S bonds for five sulfides: methyl propyl (CSCCC), methyl butyl (CSCCCC), ethyl propyl (CCSCCC), ethyl butyl (CCSCCCC), and dipropyl (CCCSCCC) sulfides.

A normal coordinate treatment has been carried out, using a modified Urey-Bradley force field. The molecular parameters, the potential terms—except the bending and repulsion constants, H(CCC) and F(CCC), and the bond-interaction term, p_C, between the adjacent C–C bonds— and the force constants used were all the same as those of the previous paper.[1] The additional constants were assumed to be H(CCC)=0.275 mdyn/Å, F(CCC)=0.335 mdyn/Å, and $p_C=-0.100$ mdyn/Å. For the longer sulfides, except for CSCCC, normal coordinates were treated here only in the cases of the typical forms.

The observed infrared and calculated frequencies of the C–S stretching and skeletal deformation regions are shown in Fig. 1.

CSCCC. The C–S stretching frequencies observed in the solid state are reproduced well by those calculated for the TT or GT form. The frequencies of the skeletal deformation bands appearing in the solid state are also explained well by these forms.

CSCCCC. The frequencies of the two solid-state bands observed in the C–S stretching region can be explained by the frequencies calculated for the TTT, GTT, TTG, or GTG form. From the data of the skeletal deformation region, however, we cannot obtain any clear and conclusive information on the skeletal

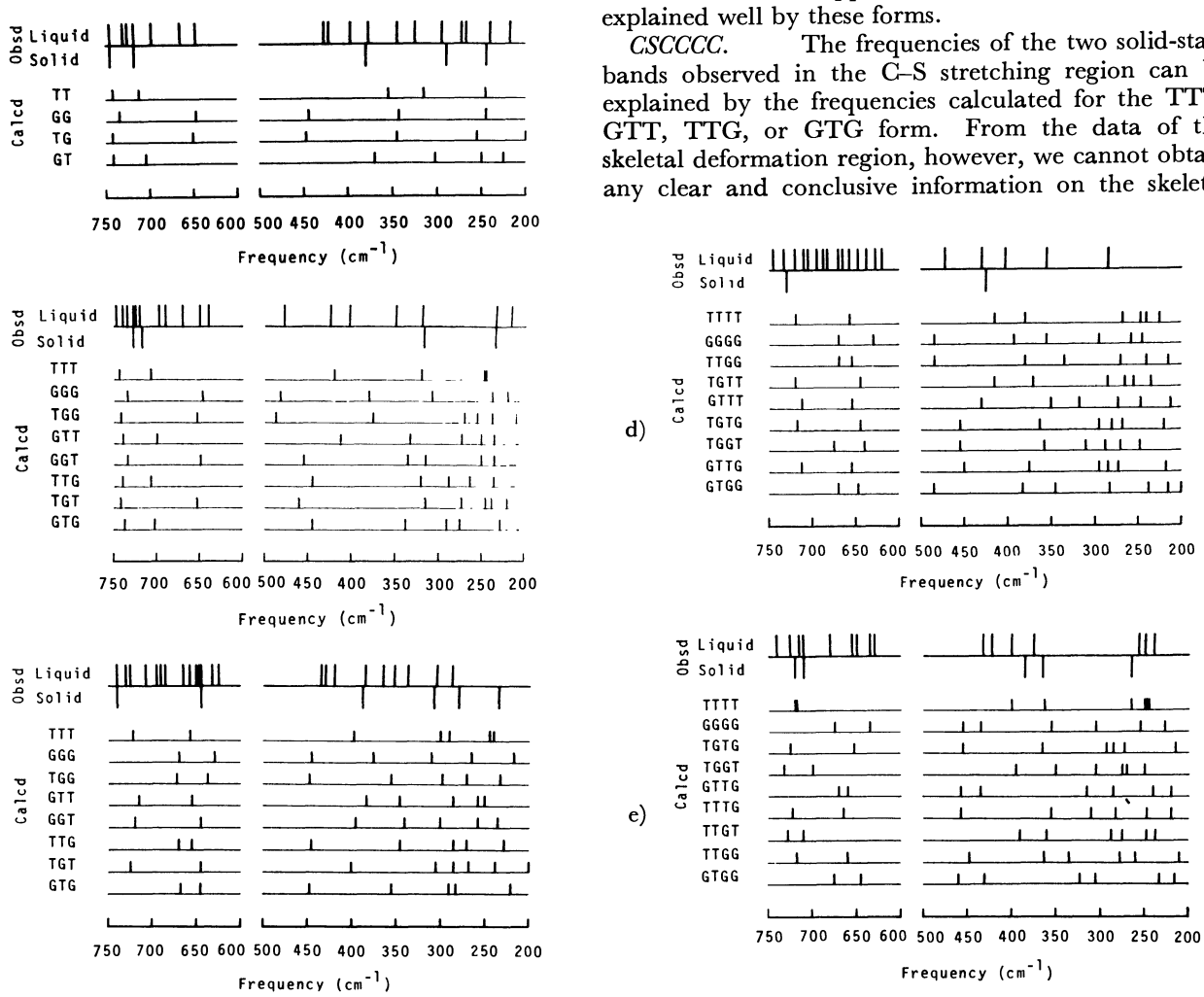

Fig. 1. Observed and calculated frequencies in the C–S stretching and skeletal deformation regions of a) CSCCC, b) CSCCCC, c) CCSCCC, d) CCSCCCC, and e) CCCSCCC.

forms.

CCSCCC. The observed frequencies in the C–S stretching region in the solid state are reproduced well by the frequencies calculated for the TTT, GTT, GGT, or TGT form. The frequencies of the four bands observed in the skeletal deformation region in the solid state can also be reproduced well by those calculated for one of these forms.

CCSCCCC. One each of the bands appeared in the C–S stretching and skeletal deformation regions in the solid-state spectra. The frequencies of these bands are reproduced well by the frequencies calculated for the TTTT, TGTT, GTTT, TGTG, or GTTG form.

CCCSCCC. Two and three bands appeared in the C–S stretching and skeletal deformation regions respectively in the solid-state spectra. The frequencies of these bands fit well to those calculated for the TTTT, TGGT, or TTGT form.

In this note, we are concerned with the skeletal conformations about the C–C bonds adjacent to the C–S bond, *i.e.*, CSC–CC, CSC–CCC, CCSC–CC, CCSC–CCC, and CC–CSC–CC. As we have mentioned above, the frequencies of the C–S stretching and skeletal deformation vibrations can be reasonably explained by the frequencies calculated only for the forms which have the *trans* conformation about the C–C bonds. We may, therefore, conclude that the stable forms in the crystalline state for these sulfides are as follows:

$$CSC_{\bar{T}}CC,\ CSC_{\bar{T}}CCC,\ CCSC_{\bar{T}}CC,\ CCSC_{\bar{T}}CCC,$$

$$\text{and } CC_{\bar{T}}CSC_{\bar{T}}CC.$$

Let us consider in some detail the relation between the C–S stretching frequency and the conformation about the C–C bond adjacent to the C–S bond. The frequencies and separations of two C–S stretching bands observed in the solid state are closely related to the conformation about this bond. The conformations about the other bonds do not much affect the C–S stretching frequencies. From the Jacobian matrix, the force constants which affect the C–S stretching frequencies with different conformations about these C–C bonds are, in general, H(CCC), H(CCH), H(SCC), F(SCH), Y_{C-C}, and p'. There are three questions which arise from these results: a) why do these force constants mainly affect the C–S stretching frequency?, b) why is the C–S stretching frequency affected by the conformation about the C–C bond adjacent to the C–S bond?, and c) why is the C–S stretching frequency not so much affected by the conformation about the C–S bond?

The ***F***-matrix elements themselves do not vary much with the different conformations. On the other hand, for some ***G***-matrix elements, different values appear with different conformations. Now let us consider the values of these elements, taking CCSCCC as an example. A part of the ***G***-elements now of interest are shown above, along with the coordinate numbering. In the off-diagonal elements, *e.g.*, R_8–R_{24}, R_8–R_{25}, R_8–R_{37}, and R_8–R_{41}, and also in the diagonal and off-diagonal elements in relation to the coordinates of C–S and C–C torsions, a different value appears with the T or G conformation about the C–C bond—R_9. These elements are directly related to the force constants, as has been mentioned above. Therefore, the main parts of the first two questions, a) and b), can be explained reasonably. The values of, for example, R_8–R_{24}, R_8–R_{25}, and R_8–R_{27} are much smaller than those of R_8–R_{37}, R_8–R_{41}, and R_8–R_{39}, since the atomic mass of the sulfur atom is much larger than that of carbon. This gives an answer to the c) question. As a result, it seems that most of the contribution to the C–S stretching frequency is due to the conformation about the 9—bond.

	TTT	GGG	
R_8–R_{24}	−1.7019	0.8509	($\times 10^{-2}$)
R_8–R_{25}	0.8509	−1.7019	
R_8–R_{27}	0.8509	0.8509	
R_8–R_{37}	−5.0970	2.5485	
R_8–R_{41}	2.5485	−5.0970	
R_8–R_{39}	2.5485	2.5485	
R_8–R_{52}	−0.0000	−0.0442	

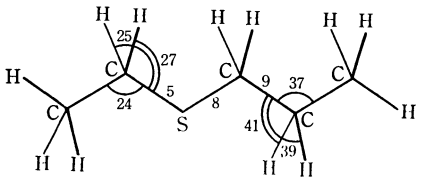

52: torsion—9

The stable conformations in the solid state about the C–S bonds[1] for CS–CC and CC–S–CC and about the C–C bonds[2] for *n*-alkanes were established to be *trans*. Consequently, it can be expected that the stable conformations in the solid state for these sulfides are all of the *trans* form. However, we cannot decide exactly the whole conformation for these sulfides at present. Detailed treatments are now in progress; the results will be published elsewhere in the near future.

Thanks are due to Professor Hiromu Murata and Associate Professor Yuji Shiro for their valuable comments.

References

1) M. Ohsaku, Y. Shiro, and H. Murata, This Bulletin, **46**, 1399 (1973).

2) For example: R. G. Snyder, *J. Chem. Phys.*, **47**, 1316 (1967).

BULLETIN OF THE CHEMICAL SOCIETY OF JAPAN, VOL. 48 (3), 1039—1040 (1975)

An EMF Study of Certain Orthoferrites: $YFeO_3$, $GdFeO_3$ and $SmFeO_3$

Shigeru YAMAUCHI, Kazuo FUEKI,* Takashi MUKAIBO, and Chiaki NAKAYAMA

Department of Industrial Chemistry, Faculty of Engineering, The University of Tokyo, Bunkyo-ku, Tokyo 113
Department of Synthetic Chemistry, Faculty of Engineering, The University of Tokyo, Bunkyo-ku, Tokyo 113

(Received August 20, 1974)

Synopsis. The EMF of a solid electrolyte galvanic cell on the formation of orthoferrites, $LnFeO_3$, was measured for Ln=Y, Gd and Sm at 1200—1400 K. The free energy change of the $(1/2)Fe_2O_3+(1/2)Ln_2O_3 \rightarrow LnFeO_3$ reaction was calculated.

Since the pioneering work by Kiukkola and Wagner,[1] many studies have been carried out in an effort to obtain free energy data from the EMF of a solid electrolyte galvanic cell. The present investigation aims to obtain, by means of the EMF method, thermodynamic data relevant to the formation of orthoferrites, which have attracted much attention as magnetic materials.

Experimental

The orthoferrites were synthesized by a solid-state reaction of ferric oxide and rare earth sesquioxide. A pellet of a mixture of 99.99% pure Fe_2O_3 and Ln_2O_3 was fired at 1300 °C to form orthoferrite. The product was ground to powder and pressed to a pellet at 5 kg/cm^2. Then it was fired again at 1400 °C.

A high-temperature galvanic cell was constructed by using a stabilized zirconia tube as an electrolyte. The arrangement of the cell is shown in Fig. 1. The open end of the stabilized zirconia tube(e) was kept at room temperature and connected to a stainless steel head(h) with a O-ring vacuum seal fitting(g). A mixture of Ni and NiO powders was used as a reference electrode (b), which was placed inside the zirconia tube. The test electrode of mixed powders(a) was placed outside the electrolyte. O-ring vacuum seal fittings(g) were used to separate the gas atmospheres inside and outside the zirconia tube(e) and the quartz glass tube (c). After the cell was arranged as is shown in Fig. 1, the whole system was evacuated to 10^{-4}—10^{-5} Torr through Pyrex tubings(i,j). Then the cell was vacuum-sealed and disconnected from the evacuation system.

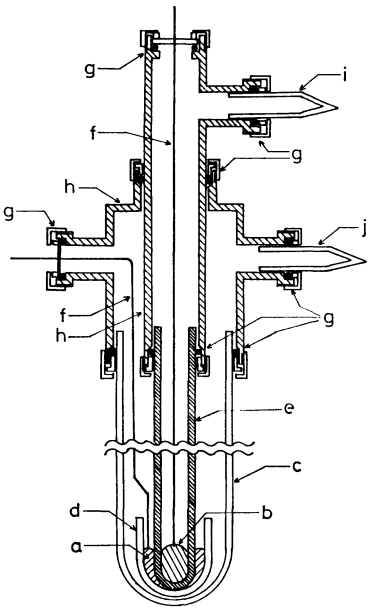

Fig. 1. Arrangement of cell.
a: test electrode powder, b: reference electrode powder, c: quartz glass tube, d: quartz glass container of test electrode powder, e: calcia-stabilized zirconia tube, f: platinum lead wire, g: O-ring vacuum seal fittings, h: stainless steel head, i: Pyrex tubing for an evacuation of reference electrode compartment, j: Pyrex tubing for an evacuation of test electrode compartment.

The cell was heated in a resistance furnace, controlled to ±0.5 °C. The cell temperatures were measured using a Pt/0.13Rh+Pt thermocouple. The EMF of the cell and that of the thermocouple were measured by using a Yokogawa high-precision potentiometer, Model 2722.

As a preliminary run, the EMF of the

$$Pt|Fe, FeO|ZrO_2\text{-}CaO|Ni, NiO|Pt \text{ cell} \quad (I)$$

was measured. The observed values agreed within 0.5 mV with the reported ones.[2-5]

Results

The EMF of the

$$Pt|Fe, Ln_2O_3, LnFeO_3|ZrO_2\text{-}CaO|Ni, NiO|Pt \text{ cell} \quad (II)$$
$$(Ln=Y, Gd \text{ and } Sm)$$

was reproducible at 1200—1400 K. The results are given in Fig. 2 and the first column of Table 1.

From the EMF data of the cell (II), the free energy change, ΔG°_1, of the reaction:

$$Fe + (3/2)NiO + (1/2)Ln_2O_3 \longrightarrow (3/2)Ni + LnFeO_3 \quad (1)$$

was calculated. The results are shown in the second

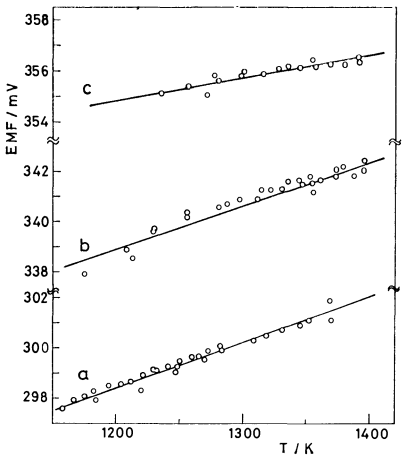

Fig. 2. EMF of cell (II).
a: $YFeO_3$, b: $GdFeO_3$, c: $SmFeO_3$.

Table 1. The EMF data and the derived Gibbs free energy changes

Ln	EMF[a] / mV	ΔG_1°[b] / cal	ΔG_2° / cal
Y	$277.1+0.0178T$ (± 0.2)	$(-19170\pm 40)-(1.23\pm 0.04)T$	$-6250-0.31T$
Gd	$318.3+0.172T$ (± 0.4)	$(-22000\pm 70)-(1.19\pm 0.07)T$	$-9105-0.27T$
Sm	$344.1+0.0089T$ (± 0.4)	$(-23800\pm 140)-(0.61\pm 0.13)T$	$-10900+0.32T$

a) The values in parentheses are square roots of invariant variances. b) Uncertainties in ΔH_1° and ΔS_1° are the standard variations.

column of Table 1, where the constant term and the temperature coefficient correspond to $\Delta H^{\circ}_{1,\,1300\mathrm{K}}$ and $\Delta S^{\circ}_{1,\,1300\mathrm{K}}$ respectively. The standard deviations of these values were also calculated.

The oxygen partial pressure at the test electrode was the lowest for Reaction (1) of $SmFeO_3$. It was $10^{-17.5}$ atm at 1200 K and $10^{-13.6}$ atm at 1400 K. According to Tretyakov and Muan,[6] the electronic transport number of the calcia-stabilized zirconia electrolyte, t_e, is $10^{-4.5}$ at these temperatures and oxygen partial pressures. Etsell and Flengas[7] have reported that the t_e value is still as low as 10^{-3} at these oxygen partial pressures. Thus, the systematic error due to the electronic conduction is negligibly small.

The values of ΔG°_2, the free energy change of the reaction

$$(1/2)Fe_2O_3 + (1/2)Ln_2O_3 \longrightarrow LnFeO_3 \qquad (2)$$

were calculated from ΔG_1°. In this calculation, the equation reported by Charette and Flengas[2] was used for the free energy of the formation of NiO. An approximation was made in the calculation of the free energy of the formation of Fe_2O_3 by using this equation:

$$\Delta G^{\circ}_{f.Fe_2O_3.1200-1400\mathrm{K}} = \Delta H^{\circ}_{f.1300\mathrm{K}} - T\cdot\Delta S^{\circ}_{f.1300\mathrm{K}}$$
$$= -193373 + 59.05T \text{ (cal/mol)}$$

The values of $\Delta H_f^{\circ}{}'_{1300\mathrm{K}}$ and $\Delta S_f^{\circ}{}'_{1300\mathrm{K}}$ were taken from the JANAF Thermochemical Tables.[8] The calculated values of ΔG_2° are given in the third column of Table 1. As may easily be seen, the absolute values of ΔS°_2 are very small, as is to be expected from Neumann-Kopp's rule on the ΔC_p of a solid-state reaction.

References

1) K. Kiukkola and C. Wagner, *J. Electrochem. Soc.*, **104**, 308, 379 (1957).
2) G. G. Charette and S. N. Flengas, *ibid.*, **115**, 796 (1968).
3) B. C. H. Steel and C. B. Alcock, *Trans. Amer. Inst. Min. (Metall.) Engrs.*, **233**, 1359 (1965).
4) Ju. D. Tretyakov and H. Schmalzried, *Z. Elektrochem.*, **69**, 396 (1965).
5) J. Chipman, *Pure Appl. Chem.*, **5**, 669 (1962).
6) Ju. D. Tretyakov and A. Muan, *J. Electrochem. Soc.*, **116**, 331 (1969).
7) T. H. Etsell and S. N. Flengas, *ibid.*, **118**, 1980 (1971).
8) JANAF Thermochemical Tables, NSRDS-NBS 37, Office of Standard Reference Data, National Bureau of Standards, Washington, D. C. (1971).

BULLETIN OF THE CHEMICAL SOCIETY OF JAPAN, VOL. 48 (3), 1041—1042 (1975)

Formation of Hydrogen Gas with an Electrochemical Photo-cell

Akira FUJISHIMA, Koichi KOHAYAKAWA, and Kenichi HONDA*

Department of Applied Chemistry, Kanagawa University, Rokkakubashi, Yokohama 221
**Institute of Industrial Science, The University of Tokyo, Roppongi, Tokyo 106*

(Received September 19, 1974)

Synopsis. In an electrochemical photo-cell the use of a basic electrolyte solution in the TiO_2 electrode compartment and an acidic one in the Pt cathode compartment can produce a high yield of hydrogen gas.

In a previous paper[1] we reported on an electrochemical photo-cell which consists of a titanium dioxide single crystal semiconductor as an anode, platinum black as a cathode and water as the electrochemically active species. The cell works only under irradiation on the TiO_2 electrode, generating oxygen gas at the surface of the semiconductor and hydrogen on the platinum cathode (Fig. 1). Since the forbidden gap width of TiO_2 is 3.0 eV, the effective wavelength of the irradiated light is restricted to 413 nm or less. The photo-cell produces hydrogen, which can be a source of a "clean energy", through the decomposition of water by means of solar energy.

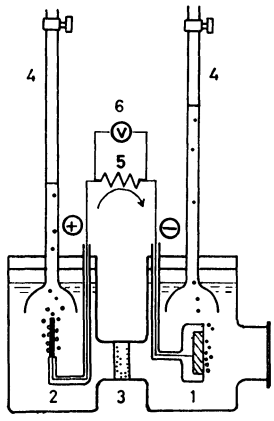

Fig. 1. Schematic diagram of electrochemical photo-cell.
1: TiO_2 electrode, 2: Platinum electrode, 3: Diaphragm (agar salt bridge), 4: Gas burette, 5: External resistance, 6: Voltmeter.

In order to increase the electro-motive force of the cell (and consequently the amount of hydrogen generated), the potential for hydrogen evolution at the cathode should be made more positive, and that for oxygen evolution at the anode more negative. The former can be attained by increasing the proton concentration, the latter by increasing the pH value of the solution, as supported by the fact that the flatband potential of TiO_2 electrode varies linearly with the pH of the solution, with the slope of *ca.* -60 mV/ΔpH.[2] The use of an alkaline solution in the TiO_2 electrode compartment and an acidic solution in the Pt cathode compartment thus brings about a higher e.m.f. of the photo-cell.

Since the potential difference at the semiconductor-electrolyte interface falls normally within the space charge region at the surface of the semiconductor, the increase in the e.m.f. leads to an enhancement of the separation efficiency for electron-hole pairs created by the irradiation in the space charge region. Under irradiation of monochromatic light (380 nm), a quantum efficiency as high as 0.3 or more is attained when the pH value of the anode compartment is higher and that of the cathode compartment is lower; it does not exceed 0.01 in the case of a common neutral electrolyte (*e.g.*, KCl) solution.

In the present study, a wafer of single crystal TiO_2, 1.5 mm in thickness and 1.0 cm^2 in area, treated under a reducing atmosphere before use, was employed. Its donor density calculated from the slope of the Mott-Schottky plot[3] was *ca.* 2.5×10^{17} cm^{-3}. The (001) face of the crystal was exposed to the electrolyte solution. A 500 W xenon lamp was used as a light source. With the use of a colored glass filter (Toshiba Kasei VV40 filter), the number of the incident quanta per second per square centimeter at the surface of the TiO_2 electrode was measured by means of the chemical actinometry using a potassium ferrioxalate system,[4] and found to be *ca.* 2×10^{17}. A platinum black electrode having the surface area of 1.0 cm^2 served as a cathode.

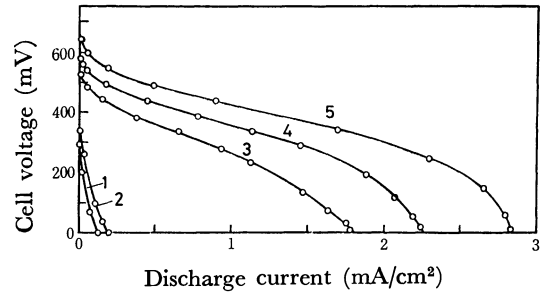

Fig. 2. Relation between the cell voltage and the discharge current.

TiO_2 anode compartment	Pt cathode compartment
1: 1 M NaOH,	1 M NaOH
2: 1 M NaOH,	1 M Na_2SO_4
3: 1 M NaOH,	0.005 M H_2SO_4
4: 1 M NaOH,	0.05 M H_2SO_4
5: 1 M NaOH,	0.5 M H_2SO_4

Figure 2 shows the relations between the cell voltage and the discharge current under irradiation, as a function of the composition of the anodic and cathodic electrolyte solutions. The curves were obtained by adjusting the external resistance. The maximum efficiency was attained by a combination of strong basic and strong acidic solutions (curve 5) as expected, the open-circuited cell voltage being *ca.* 0.64 V. The amounts of hydrogen and oxygen evolved were proportional to the intensity of light and the surface area

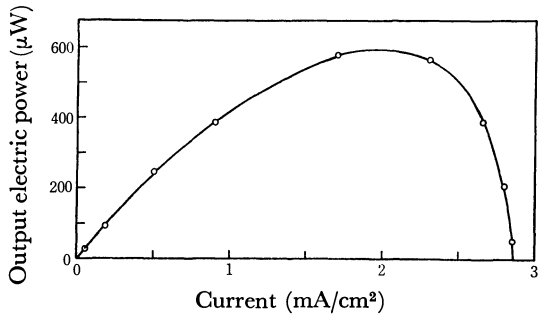

Fig. 3. Relation between the electric power output at the external resistance and the cell current.
The solutions are 1 M NaOH in the TiO_2 anode compartment and 0.5 M H_2SO_4 in the platinum black cathode compartment, respectively. The number of quanta per second per square centimeter: 2×10^{17}.

of the TiO_2 electrode, when the cross section of the incident light flux was sufficiently large as compared with the surface area of TiO_2. The rate of generation of hydrogen amounted to *ca.* 1.1 ml/hr when the cell was short-circuited, indicating the current efficiency of about 100%.

Figure 3 shows the relationship between the cell current and the output electric power at the external resistance (calculated from curve 5, Fig. 2). The apparent over-all internal resistance of the cell is estimated to be about 140 Ω from the slope of curve 5. The maximum output electric power was obtained using an external resistance of 140 Ω, as predicted by a simple theory. The quantity appearing on the abscissa in Fig. 3, *i.e.*, the current density, can be interpreted as representing the amount of hydrogen evolved, since these two quantities are proportional to each other. We see that a fairly large amount of hydrogen is obtained when the maximum output power is attained.

The fact that, when the acidic and basic solutions are used in each compartment, the electro-motive force arising from the concentration difference of hydrogen ions is involved in the cell voltage should be taken into consideration. The electro-motive force is estimated to be *ca.* 0.77 V for a pH difference of 13. In view of the theoretical decomposition voltage of water of *ca.* 1.23 V and the practical one of more than 1.6 V and the heat of combustion of hydrogen (68 kcal/mol), the observed results support the effectiveness of the combined utilization of acid-base electrolyte solutions. The liquid junction potential was actually lower than 0.05 V since a salt bridge consisting of agar containing KCl was used. Use of an ion-exchange membrane of low resistance and long durability could increase the efficiency of hydrogen evolution.

Since the electrode reactions are $4OH^- + 4p^+ \rightarrow O_2 + 2H_2O$ at the TiO_2 electrode, and $4H^+ + 4e^- \rightarrow 2H_2$ at the Pt electrode, after a long run the solution in the TiO_2 compartment will become less alkaline, and that in the Pt compartment less acid.

References

1) A. Fujishima and K. Honda, *Nature*, **238**, 37 (1972).
2) A. Fujishima, A. Sakamoto, and K. Honda, *Seisan Kenkyu*, **21**, 450 (1969).
3) J. F. Dewald, *J. Phys. Chem. Solids*, **14**, 155 (1960).
4) C. G. Hatchard and C. A. Parker, *Proc. Roy. Soc. Ser. A*, **235**, 518 (1956).

BULLETIN OF THE CHEMICAL SOCIETY OF JAPAN, VOL. 48 (3), 1043—1044 (1975)

The Dimerization of the Phenoselenazine and Benzo[c]-phenoselenazine Cation-radicals

Yoshio MATSUNAGA and Tomio TANAKA

Department of Chemistry, Faculty of Science, Hokkaido University, Sapporo 060

(Received October 7, 1974)

Synopsis. The equilibrium constants and the heats of dimerization and the monomer and dimer spectra were determined for the phenoselenazine and benzo[c]phenoselenazine cation-radicals in aqueous sulfuric acid (1:1 by volume).

In connection with our work on the phenoselenazine-iodine complex,[1] attempts were made to measure the ESR absorption spectrum of the phenoselenazine cation-radical produced in sulfuric acid at various dilutions and temperatures, but all without success. During the course of such attempts, however, a reversible color change from brown to pink occurred upon warming, suggesting that the cation-radical is in the monomer-dimer equilibrium. As the monomer and dimer spectra are important tools for speculating on the mode of intermolecular interaction in solid ion-radical salts,[2] we analyzed the temperature- and concentration-dependences of the solution spectrum.

The phenoselenazine and its semiquinoid bromide employed here were prepared in our previous work.[1] The preparation of benzo[c]phenoselenazine was carried out by a method analogous to that for phenoselenazine reported by Müller *et al.*[3] The phenoselenazine bromide was dissolved in aqueous sulfuric acid (1:1 by volume). The absorption spectra of eight solutions, ranging from 5.05×10^{-5} to 6.12×10^{-4} mol/l, were recorded on a Beckman DK 2A spectrophotometer at 20, 35, and 50 °C with the aid of a temperature-regulated cell holder. As the composition of the oxidation product of benzo[c]phenoselenazine with bromine did not agree with the calculated one, the compound was directly dissolved in concentrated sulfuric acid. Then, one volume of the solution was slowly diluted, avoiding excessive heating, with one volume of water. For this radical, we prepared fifteen solutions, the concentrations of which were in the range from 1.27×10^{-5} to 1.64×10^{-3} mol/l. The spectra were then examined at 20, 35, 50, and 65 °C. The spectral change in the phenoselenazine cation-radical was found to be slightly irreversible if the solution was heated to 65 °C.

Upon heating, the intensities at 400, 475, and 733 nm in the spectrum of the phenoselenazine radical become weaker and those at 433 and 513 nm become stronger. The locations of the six isosbestic points observed are as follows: 358, 411, 438, 493, 559, and 868 nm. We assumed that the observed spectral change can be interpreted in terms of the monomer-dimer equilibrium; that is, $2(A^+)\rightleftarrows(A_2)^{2+}$. This formula does not exclude the possibility of the presence of an anionic species in the dimer. Since the absorption bands assignable to the monomer and dimer overlap considerably, the values of the true extinction coefficient of the monomer, ε_M, and that of the dimer, ε_D, were determined by the extrapolation procedure described by Boyd and Phillips.[4] The monomer band at 513 nm and the dimer band at 733 nm were chosen for this purpose. The best sets of values of ε_M and ε_D were as follows:

$\varepsilon_M = 9.50\times10^3$, $\varepsilon_D = 5.55\times10^3$ at 513 nm and

$\varepsilon_M = 0.75\times10^3$, $\varepsilon_D = 11.0\times10^3$ at 733 nm.

The average equilibrium constants evaluated from the data at the monomer and dimer bands were $K(20\ ^\circ\mathrm{C}) = 3.7\times10^3$, $K(35\ ^\circ\mathrm{C}) = 1.6\times10^3$, and $K(50\ ^\circ\mathrm{C}) = 0.72\times10^3$ l/mol. From the temperature dependence of K, the heat of dimerization of the phenoselenazine cation-radical was estimated as −9.9 kcal/mol.

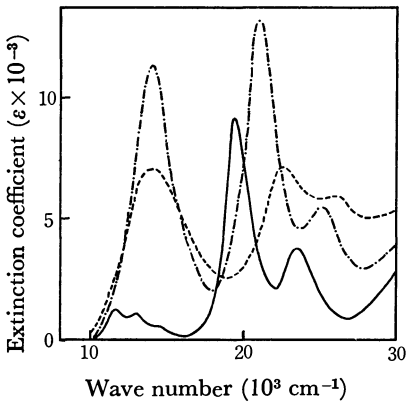

Fig. 1. Absorption spectra of the monomer (——) and dimer (– – –) of phenoselenazine cation-radical and reflection spectrum of the semiquinoid bromide (——).

The monomer and dimer spectra were constructed by plotting the measured apparent extinction coefficient, ε, at about thirty wavelengths *versus* the fraction of the stoichiometric concentration existing as a monomer calculated from the above-mentioned equilibrium constants for each concentration. They are presented in Fig. 1, along with the spectrum of the solid semiquinoid bromide, as measured by the diffuse-reflectance method. The similarity between the dimer spectrum and the solid-state spectrum provides strong evidence that the intermolecular interaction in the solid bromide is predominantly pair-by-pair.

Although phenothiazine bromide dissolved in aqueous sulfuric acid shows a spectrum essentially the same as the monomer spectrum given in Fig. 1, the dimerization has been demonstrated by Kagiya *et al.* at temperatures as low as −70 °C in an ethanol–ether–sulfuric acid solution.[5] The enthalpy change estimated by them is about −5 kcal/mol. There seems to be appreciably more shift of the equilibrium towards the dimer in the phenoselenazine cation-radical as compared with

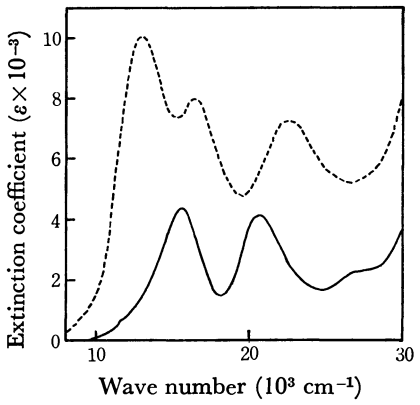

Fig. 2. Absorption spectra of the monomer (——) and dimer (– – –) of benzo[*c*]phenoselenazine cation-radical.

the sulfur-analogue. A similar marked difference in the dimerization behavior between the cation-radical of phenoxathiin and that of phenoxaselenine, as judged from the spectral and magnetic properties, has been reported by Hillebrand *et al.*[6]

Upon the introduction of an extra benzene nucleus into phenoselenazine, the temperature-dependence of the spectrum of the cation-radical becomes less pronounced. The extrapolation procedure could be applied only to the dimer band appearing at 788 nm. We obtained the following values; $\varepsilon_M = 1.25 \times 10^3$, $\varepsilon_D = 9.95 \times 10^3$, $K(20\ ^\circ\mathrm{C}) = 9.9 \times 10^4$, $K(35\ ^\circ\mathrm{C}) = 3.4 \times 10^4$, $K(50\ ^\circ\mathrm{C}) = 1.3 \times 10^4$, and $K(65\ ^\circ\mathrm{C}) = 0.48 \times 10^4$ l/mol. The heat of dimerization of -13.3 kcal/mol estimated for this cation-radical is about 30% higher than that of the phenoselenazine cation-radical; that is, the heat is approximately proportional to the size of the molecules within this pair. For such a comparison, it may be more appropriate to use the heat of the dimerization of the phenoselenazine cation-radical, evaluated only on the basis of the data taken at the dimer band. The required value is a little larger than the aforementioned value—that is, -10.7 kcal/mol. The constructed spectra of the monomeric and dimeric benzo[*c*]phenoselenazine cation-radical are presented in Fig. 2. The difficulty in analyzing the spectrum of this radical apparently arises not only from the large equilibrium constant but also from the overlap of the monomer and dimer spectra.

We attempted to extend our study to the dibenzo[*c*,*h*]phenoselenazine cation-radical; however, the dilution of a concentrated sulfuric acid solution in the desired range of concentration with an equal volume of water resulted in the formation of a dark green precipitate, and the recording of the spectrum was not possible.

The authors wish to express their thanks to Mr. Yukio Suzuki for providing them with the results of his preliminary spectral measurements of the phenoselenazine cation-radical.

References

1) Y. Matsunaga and Y. Suzuki, This Bulletin, **45**, 3375 (1972).
2) Y. Iida and Y. Matsunaga, *ibid.*, **41**, 2615 (1968).
3) P. Müller, N. P. Buu-Hoï, and R. Rips, *J. Org. Chem.*, **24**, 37 (1959).
4) R. H. Boyd and W. D. Phillips, *J. Chem. Phys.*, **43**, 2927 (1965).
5) T. Kagiya, K. Nakai. S. Nakayama, and K. Suzuki, Paper presented at the 23rd Annual Meeting of the Chemical Society of Japan, Tokyo, April, 1970.
6) M. Hillebrand, O. Maior, and V. E. Sahini, *Rev. Roum. Chim.*, **16**, 1489 (1971).

BULLETIN OF THE CHEMICAL SOCIETY OF JAPAN, VOL. 48 (3), 1045—1046 (1975)

An Electron Paramagnetic Resonance Study of Low-Spin Five-coordinate Cobalt(II) Complexes[1)]

Yuzo NISHIDA and Sigeo KIDA

Department of Chemistry, Faculty of Science, Kyushu University, Hakozaki, Higashi-ku, Fukuoka 812

(Received August 13, 1974)

Synopsis. EPR spectra were measured for the five-coordinate cobalt(II) complexes, $[CoCldpe_2]SnCl_3$ and $[CoCldpe_2]SnCl_3 \cdot C_6H_5Cl$, which had been determined by X-ray analyses to have a tetragonal pyramidal and trigonal bipyramidal structures, respectively. The observed g-values showed a satisfactory agreement with the previously reported prediction.[6)]

Recently, several EPR studies were reported on five-coordinate low-spin cobalt(II) complexes.[1-6)] In all those studies EPR spectra of tetragonal pyramidal complexes were interpreted on the basis of the ground state configuration $(d_{xz})^2(d_{yz})^2(d_{x^2-y^2})^2(d_{z^2})^1$, where the Z-axis conincides with the tetragonal axis and X-axis divides the planar P–Co–P bond angle. On the other hand, the ground state configuration for the trigonal bipyramidal complexes has been assumed to be $(d_{xz})^2(d_{yz})^2(d_{x^2-y^2})^2(d_{xy})^1$. On this basis Maher[2)] and Kimball *et al.*[4)] theoretically calculated $g_{//}$ and $g_\perp$ values to be 4.0 and 0, respectively. However, no EPR data to support their conclusion have yet been reported. Nishida and Shimohori investigated a series of penta-coordinated low-spin cobalt(II) complexes, $[CoXdpe]_2Y$ ($X=Cl^-$, Br^-, NCS^-, NO_3^- and $Y=ClO_4^-$, NO_3^-) and reached a different conclusion for g-values ($g_z > g_x \approx g_y > 2$) for trigonal bipyramidal complexes, assuming that the orbital degeneracy is removed by the distortion from regular trigonal symmetry, (probably due to, *e.g.*, the Jahn-Teller effect or a steric requirement of the crystal, *etc.*). On this basis they showed that the two possible geometries, *i.e.*, tetragonal pyramid and trigonal bipyramid, can be discriminated by the use of EPR data. Recently, it was demonstrated by X-ray analyses that $[CoCldpe_2]SnCl_3$ and $[CoCldpe_2]SnCl_3 \cdot C_6H_5Cl$ have tetragonal pyramidal and trigonal bipyramidal structures, respectively,[7)] where dpe denotes 1,2-bis-(diphenylphosphino)ethane. Accordingly, we have carried out an EPR study on these compounds in order to confirm the previously derived criterion for the discrimination of the geometrical isomers.[6)]

Experimental

Preparation. 1,2-Bis(diphenylphosphino)ethane(=dpe) was prepared according to Hewertson's method.[8)] The complexes, $[CoCldpe_2]SnCl_3$ and $[CoCldpe_2]SnCl_3 \cdot C_6H_5Cl$ were prepared by the method described in the literature.[7)]

EPR Measurements. EPR spectra were measured using X-band at room temperature with a JEOL ESR apparatus model JES-ME-3X, DPPH being used as a standard for magnetic field strength.

* In this model the d_{xy} and $d_{x^2-y^2}$ orbitals are not degenerate, $d_{x^2-y^2} > d_{xy}$ in energy being assumed.

Results and Discussion

Powder EPR spectra of $[CoCldpe_2]SnCl_3 \cdot C_6H_5Cl$ and $[CoCldpe_2]SnCl_3$ were shown in Figs. 1 and 2, respectively. The former shows an axial symmetry, and $g_{//}$ and $g_\perp$ were evaluated from the spectra following Sands[9)] and Kneubuhls'[10)] method. On the other hand, the latter spectrum shows a rhombic symmetry, and g_1, g_2, and g_3 were evaluated at 2.357, 2.276, and 2.003, respectively, by the same method.

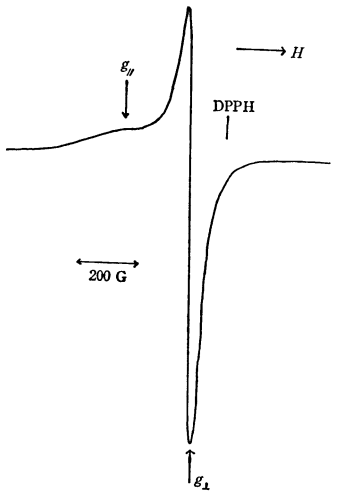

Fig. 1.

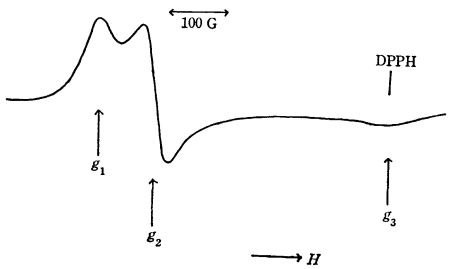

Fig. 2

As was shown in the preceeding paper,[6)] g-values for the low-spin cobalt(II) complexes of a distorted trigonal bipyramidal symmetry* were calculated in the first order as,

$$g_z = 2(1-4a_1)$$
$$g_x = 2(1-a_2)$$
$$g_y = 2(1-a_3)$$

where

$$a_1 = \zeta/\Delta\{(x^2-y^2)-(xy)\}$$

$$a_2 = \zeta/\Delta\{(x^2-y^2)-(yz)\}$$
$$a_3 = \zeta/\Delta\{(x^2-y^2)-(xz)\}$$

ζ: one electron spin-orbit coupling const.
$\Delta\{(x^2-y^2)-(xy)\}$: the energy difference between the $(d_{z^2})^2(d_{x^2-y^2})^1$ and the $(d_{z^2})^2(d_{xy})^1$ states (in terms of electron-hole formulism), and so on.

From these equations the following relation was derived for this type of complexes.

$$g_z > g_x \approx g_y > 2.0 \quad (1)$$

For the complexes of tetragonal pyramidal symmetry,

$$g_z = 2.0$$
$$g_x = 2(1-3b_1)$$
$$g_y = 2(1-3b_2)$$

where

$$b_1 = \zeta/\{\Delta(z^2)-(yz)\}$$
$$b_2 = \zeta/\{\Delta(z^2)-(xz)\}$$

$\Delta\{(z_2)-(xz)\}$: the energy difference between the $(d_{xy})^2(d_{z^2})^1$ and the $(d_{xy})^2(d_{xz})^1$ states, and so on.

From these equations the relation

$$g_x \geqq g_y > g_z \approx 2.0 \quad (2)$$

was derived.

In fact, the present EPR data** show a satisfactory agreement with the above theoretical prediction. The trigonal bipyramidal complex, $[CoCldpe_2]SnCl_3 \cdot C_6H_5Cl$ gives the g-values ($g_{//}=2.258$, $g_{\perp}=2.062$) conforming to the relation (1), and the tetragonal pyramidal one, $[CoCldpe_2]SnCl_3$, gives the g-values ($g_1=2.357$, $g_2=2.276$, $g_3=2.003$) conforming to the relation (2). This result is also quite compatible with the previous conclusion for $[CoXdpe_2]Y$.

Thus, we can conclude that the assumption on which our theoretical calculation are based[6] is valid and the two possible geometries for low-spin five-coordinate cobalt(II) complexes can be discriminated on the criterion based on the relations (1) and (2) for which numerical values are obtainable from EPR spectra.

** The effect of the intermolecular magnetic interaction on the observed g-values can be neglected in this discussion, since according to Stalick *et al.*,[7] the shortest Co–Co distance are 11.4 Å and 9.49 Å in $[CoCldpe_2]SnCl_3$ and $[CoCldpe_2]SnCl_3 \cdot C_6H_5Cl$, respectively.

References

1) Part IV of the series "Investigation on Low-Spin Cobalt(II) Complexes".
2) J. P. Maher, *J. Chem. Soc., A*, **1968**, 2918.
3) F. Tsay, H. B. Gray, and J. Danon, *J. Chem. Phys.*, **54**, 3760 (1971).
4) M. E. Kimball, D. W. Pratt, and W. C. Kaska, *Inorg. Chem.*, **7**, 2006 (1968).
5) T. Nowlin, S. Subramanian, and K. Cohn, *ibid.*, **11**, 2907 (1972).
6) Y. Nishida and H. Shimohori, This Bulletin, **46**, 2406 (1973).
7) J. K. Stalick, P. W. R. Corfield, and D. W. Meek, *Inorg. Chem.*, **12**, 1668 (1973).
8) W. Hewertson and H. R. Watson, *J. Chem. Soc.*, **1962**, 1490.
9) R. H. Sands, *Phys. Rev.*, **99**, 1222 (1955).
10) F. K. Kneubühl, *J. Chem. Phys.*, **33**, 1074 (1960).

BULLETIN OF THE CHEMICAL SOCIETY OF JAPAN, VOL. 48 (3), 1047—1048 (1975)

Atomic Absorption Spectrophotometry of Titanium in the Iron Sulfides of NiAs Type

Kohei AMETANI

RCA Research Laboratories, Inc., Zushi-machi, Machida-shi, Tokyo 194-02

(Received August 15, 1974)

Synopsis. A method is described for the atomic absorption spectrophotometric determination of titanium in the sulfides, $Fe_{1-x}Ti_xS$ ($x \leq 0.3$), of NiAs type. Potassium sulfate was added to both sample and standard solutions to suppress the iron interference. The powder and single crystal samples were successfully analyzed using 10 mg of samples.

The atomic absorption spectrophotometry of titanium is carried out on iron ores,[1] cast iron,[2] ferric oxides,[3] steels,[2,3] and alloys[2-4] using a high temperature flame of nitrous oxide–acetylene. However, titanium forms refractory oxides in the flame and various interference effects are encountered.[3-5] Therefore, some workers described the necessity of several additives such as aluminium,[1,3] potassium chloride,[4] and organic compounds[3] to suppress the interference of foreign elements in each sample. Iron is known to be one of the interfering elements in the atomic absorption spectrophotometric analysis of titanium.[3-5] In the present work on the analyses of titanium in the iron sulfides, $Fe_{1-x}Ti_xS$ ($x \leq 0.3$), of NiAs type, the usefulness of the following reagents was examined to suppress the iron interference; hydroxylamine hydrochloride, ammonium fluoride, diammonium salt of EDTA, sodium chloride, potassium chloride, sodium sulfate, and potassium sulfate. Among these reagents, sodium or potassium sulfate was the most effective in suppressing the iron interference. Finally the results of the determination of titanium in the actual samples by a method using potassium sulfate are presented. Ten mg of samples were used for the analysis.

Experimental

Reagents. The standard solution (1 mg Ti/ml) was prepared by dissolving sponge metal (99.5% up) in hydrochloric acid. The solution was stocked as 1 M hydrochloric acid solution. The reagents to be examined as a suppressor for the iron interference were dissolved in deionized water. Reagents used were of analytical reagent grade.

Measurements of Titanium Absorption. The titanium absorption was measured in a nitrous oxide–acetylene flame using a Hitachi model 208 Atomic Absorption Spectrophotometer and a hollow cathode lamp HLA-3. Working conditions used are listed in Table 1. Figure 1 shows effects of

TABLE 1. WORKING CONDITIONS

Wavelength	364.3 nm
Lamp current	15 mA
Slit setting	Entrance 1 (0.18 mm), Exit 1 (0.18 mm)
Burner height	Scale position 2 (beam height above burner, approximately 20 mm)
Nitrous oxide	1.8 kg/cm², 8.0 l/min
Acetylene	0.8 kg/cm², 6.0 l/min

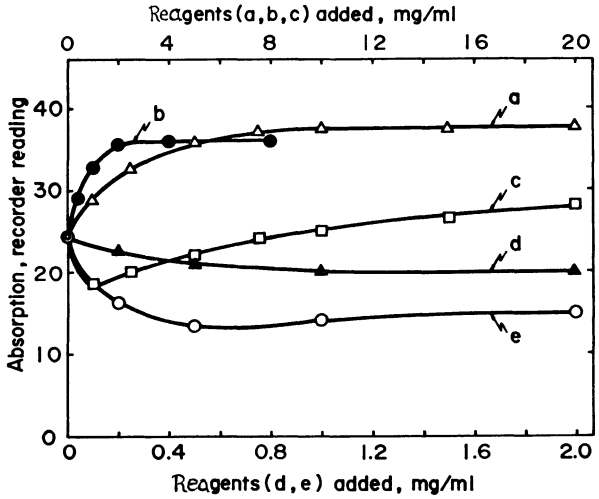

Fig. 1. Effects of several reagents on titanium absorption.
a: $NH_2OH \cdot HCl$, b: NH_4F, c: EDTA·$2NH_4$, d: NaCl or KCl, e: Na_2SO_4 or K_2SO_4. Ti: 100 ppm.

the reagents described above on the titanium absorption, where the solutions, except for diammonium salt of EDTA, are adjusted to 0.5 M hydrochloric acid. EDTA solutions are adjusted to pH 4 by adding a minimum amount of ammon-

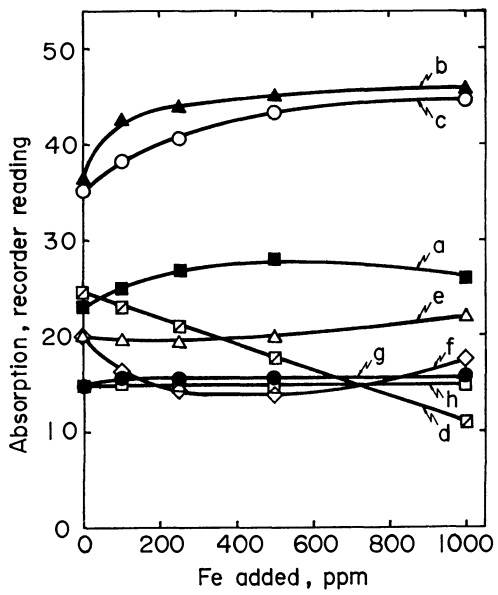

Fig. 2. Effects of iron on titanium absorption in several matrixes.
a: Without other reagents, b: $NH_2OH \cdot HCl$ 20 mg/ml, c: NH_4F 4 mg/ml, d: EDTA·$2NH_4$ 10 mg/ml, e: NaCl 2 mg/ml, f: KCl 2 mg/ml, g: Na_2SO_4 2 mg/ml, h: K_2SO_4 2 mg/ml. Ti: 100 ppm.

Table 2. Results of analyses

Sample (Nominal composition)	Analyte, wt% Fe calcd	Fe obsd	Ti calcd	Ti obsd	S calcd	S obsd	Recovery[a] (%)
Powder 1 ($Fe_{0.90}$ $Ti_{0.10}$ S)	57.70	58.0	5.50	5.0	36.80	36.5	99.5
Powder 2 ($Fe_{0.80}$ $Ti_{0.20}$ S)	51.76	51.8	11.10	11.3	37.14	37.3	100.4
Powder 3 ($Fe_{0.75}$ $Ti_{0.25}$ S)	48.75	47.8	13.94	14.1	37.31	37.5	99.4
Crystal 1		58.8		0.2		40.2	99.2
Crystal 2		54.5		4.6		40.4	99.5
Crystal 3		46.8		11.6		41.6	100.0

a) Sum of the observed values for three components.

nium acetate. Reagents which increase the titanium absorption were hydroxylamine hydrochloride and ammonium fluoride. Alkali metal salts such as sodium chloride, potassium chloride, sodium sulfate, and potassium sulfate reduced the titanium absorption. However, at the higher concentration of these reagents the titanium absorption remained constant. At the lower concentration of EDTA the titanium absorption was decreased but the absorption was gradually increased with an increase of the concentration of this reagent.

To suppress the iron interference the effects of these reagents were examined by adding the reagents to the titanium solution containing iron. The concentrations of the reagents added were chosen by the value at which the titanium absorption remained constant (*cf.* Fig. 1). Ferric ions were added as chlorides. The results are shown in Fig. 2. The titanium absorption was increased in the presence of ferric ions in the solution without other reagents. The absorption was higher in hydroxylamine hydrochloride or ammonium fluoride solutions than in the other solutions examined. Though the two reagents highly enhanced the titanium absorption in the presence of ferric ions, they did not suppress the iron interference. EDTA decreased the titanium absorption linearly with an increase of ferric ion concentration. Alkali metal salts reduced the titanium absorption. However, sodium and potassium sulfates gave a constant titanium absorption over a wide range of iron concentrations. In this work, potassium sulfate was used as the suppressor for iron interference.

Analysis of Samples. The powder samples were synthesized by sintering a mixture of the respective elements with the nominal compositions shown in Table 2 at a high temperature, and the crystal structure was identified by X-ray diffraction. The single crystal samples (unknown compositions) were grown by chemical vapor transport. Ten mg of the powder or single crystal samples were dissolved in *aqua regia* containing bromine. After removal of the excess nitric acid by evaporation with hydrochloric acid, the final solution was made up to 25 ml, where the acidity was adjusted to 0.5 M hydrochloric acid and the concentration of potassium sulfate, 2000 ppm. The same adjustment was carried out for standards containing 10 to 100 ppm titanium and the atomic absorption was then measured. The results of the analyses are shown in Table 2, together with the contents of iron and sulfur obtained in separate experiments.[6] For the powder samples, the observed values are in agreement with the calculated values. All the observed values are satisfactory, as the sum of the observed values for three components is close to 100% in all cases.

The author thanks Dr. Tatsuo Takahashi of this laboratories for providing the samples.

References

1) Y. Endo, T. Hata, and Y. Nakahara, *Bunseki Kagaku*, **18**, 833 (1969).
2) J. B. Headridge and D. P. Hubbard, *Anal. Chim. Acta*, **37**, 151 (1967).
3) T. Nakahara, M. Munemori, and S. Musha, This Bulletin, **46**, 1172 (1973).
4) R. A. Mostyn and A. F. Cunningham, *At. Abs. Newslett.*, **6**, 86 (1967).
5) M. D. Amos and J. B. Willis, *Spectrochim. Acta*, **22**, 1325 (1966).
6) K. Ametani, *Bunseki Kagaku*, **23**, 745 (1974).

BULLETIN OF THE CHEMICAL SOCIETY OF JAPAN, VOL. 48 (3), 1049—1050 (1975)

A New Optically Active Co(II) (salen) Type Complex Containing a Pentadentate Schiff-Base Ligand

Haruhiko Aoi and Sadao Yoshikawa

Department of Synthetic Chemistry, Faculty of Engineering, University of Tokyo. Bunkyo-ku, Tokyo 113

(Received September 19, 1974)

Synopsis. A new optically active square-pyramidal cobalt(II) complex, *N,N'*-bis(salicylaldehyde)-2-(*S*)4-*S*-methyl-4-thio-1,2-butanediiminatocobalt(II), was synthesized. The structure of this complex was examined.

The square-planar tetradentate Schiff-base complexes of cobalt such as cobaloxime, Co(salen), *etc.* have been widely studied as model compounds for coenzyme B_{12} and as oxygen carriers. Terent'ev[1] and Hipp[2] reported the conformation of *N,N'*-bis(salicylaldehyde)-(—)-propylenediiminatocobalt(II) based on analysis of the CD spectra in solution, stating that the δ conformation about the central chelate ring was preferred. It is well-known in the case of cobalamin that the spin state of Co(II) is low-spin and that the corrin ring is in-plane. Some data are available on Co(II) complexes containing a pentadentate Schiff-base ligand,[3] but in almost all cases the spin state of Co(II) was found to be high-spin. The two chelate rings composed of phenolic oxygen and the Schiff-base were not in-plane because of steric hindrance. It is therefore of interest to prepare a low-spin Co(II) complex containing a pentadentate Schiff-base ligand maintaining planarity and to examine the behavior of the atom coordinated in the apical position.

In this report we will describe the synthesis and structure of *N,N'*-bis(salicylaldehyde)-2(*S*)-4-*S*-methyl-4-thio-1,2-butanediiminatocobalt(II), Co(II)[sal$_2$-2(*S*)-SMT-BDA], [A], and its properties will be compared with those of *N,N'*-bis(salicylaldehyde)-1(*R*),2(*R*)-1,2-*trans*-cyclohexanediiminatocobalt(II), Co(II)[sal$_2$-(*R*)-CHXDA], [B], which has been discussed in the preceeding paper.[4]

Experimental

Preparation of Ligands: 2(*S*)-4-S-methyl-4-thio-1,2-butanediamine, [D], was prepared from (*S*)-methionine by the usual method. Bp/2 mmHg=81 °C; $[\alpha]_{589}^{30}=-12.3°$ (in 3% methanolic solution). NMR: (in d_4-MeOH) 1.63 (m, 2H, $-CH_2-$), 2.09 (s, 3H, $-CH_3$), 2.57 (t, 2H, $-CH_2-S$), 2.59 (d, 2H, $-CH_2-N$), 2.60 (m, 1H, $=CH-N$). *N,N'*-bis(salicylaldehyde)-2(*S*)-4-S-methyl-4-thio-1,2-butanediimine, [E], was prepared from salicylaldehyde and diamine [D] in a molar ratio of 2 : 1 in ethanol.

Co(II)[sal$_2$-2(S)-SMT-BDA], [A]: 1.56 g of anhydrous cobalt acetate and 3.01 g of ligand [E] were reacted in 40 ml of 1-propanol at 60 °C under a nitrogen atmosphere for 20 min with stirring. After concentrating the solvent to about 10 ml, 20 ml of THF was added with stirring at 60 °C. Brown needle-like crystals precipitated when cyclohexane was added. These were filtered off and washed with cyclohexane. Found: C, 57.16; H, 5.29; N, 6.71%. Calcd. for $C_{19}H_{20}N_2O_2SCo$: C, 57.14; H, 5.05; N, 7.01%. IR: (KBr) 1600 (C=N), 1525 cm^{-1} (C=C).

Co(II)[sal$_2$-2(S)-SMT-BDA]·2H$_2$O, [C]: Similar method to that of complex [A] was used but aqueous ether was added instead of cyclohexane. Found: C, 51.54; H, 5.05; N, 6.43%. Calcd for $C_{19}H_{24}N_2O_4SCo$: C, 52.41; H, 5.56; N, 6.43%. IR: (KBr) 3400 (OH), 1634 and 1603 (C=N), 1537 cm^{-1} (C=C).

Results and Discussion

The main purpose of this study was to synthesize a low-spin square-pyramidal Co(II) complex containing a pentadentate Schiff-base ligand. It is generally accepted that the values of μ_{eff} of low-spin square-planar Co(II) complexes and the low-spin octahedral Co(II) complexes fall in the range 2.1—2.9 and 1.8—1.9 B.M., respectively, while the values of μ_{eff} of high-spin five-coordinated Co(II) complexes fall in the range 4.5—4.8 B.M.[5,6]

The planarity of the ligand can be discussed in terms of the shape of the CD spectrum at the π-π^* transition

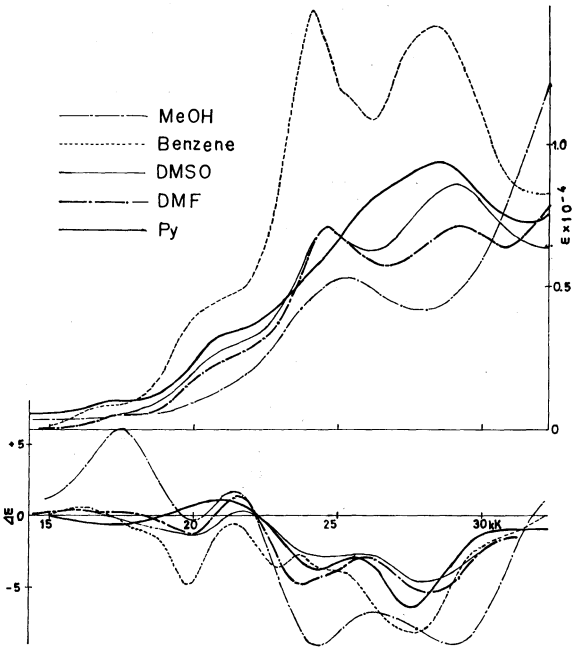

Fig. 1. The CD and absorption spectra of Co(II) [sal$_2$-2(*S*)-SMT-BDA] in various solvents.

region.[2,7,8] The π-π^* transition appears at about 28 kK and shows only one component in the cases of Co(II) and Ni(II) complexes with tetradentate Schiff-base ligands while in the corresponding Zn(II) complex the π-π^* transition contains two components with nearly equal magnitudes of positive and negative CD due to the T_d symmetry.

The magnetic moment, μ_{eff}, of complex [A] measured

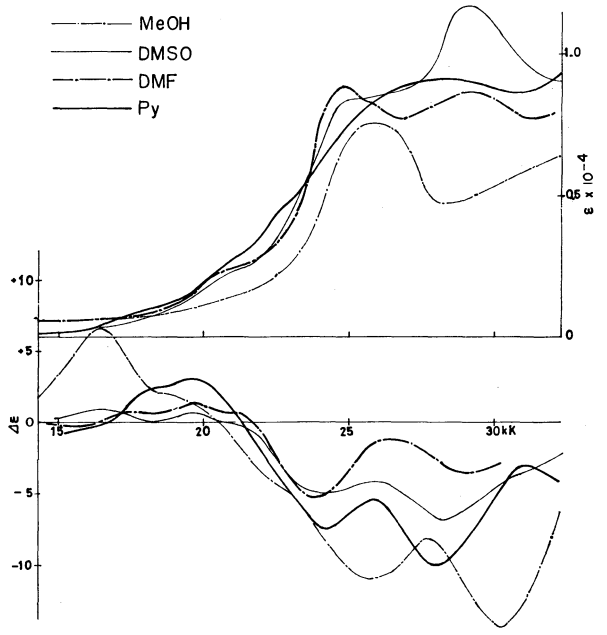

Fig. 2. The CD and absorption spectra of Co(II) [Sal_2-(*R*)-CHXDA] in various solvents.

by the method of Guoy was 1.99 B.M.; it was 2.41 B.M. in complex [B].[4] This shows that the spin state of complex [A] is low-spin, suggesting that complex [A] is square-pyramidal. The CD and associated absorption spectra of complex [A] were measured in various solvents and are given in Fig. 1. Those of complex [B] are given in Fig. 2. All the CD spectra in Fig. 1 show only one component at about 28 kK. These results suggest that the two chelate rings, composed of phenolic oxygen and Schiff-base, are coplanar in complex [A]. In complex [B] the central chelate ring is locked in the λ conformation.[4] Comparing the CD spectra of complex [A] and [B], shown in Figs. 1 and 2, the shapes of spectra are similar. Nevertheless, the CD spectra of the ligands [E] and [F][9] are almost opposite in sign, reflecting the difference of chirality of the asymmetric carbon. This would be attributed to the similarity of the central chelate ring conformation in complexes [A] and [B]. These results in the measurements of the CD spectra support the view that complex [A] is a low-spin square-pyramidal Co(II) complex. A possible structure of complex [A] is shown

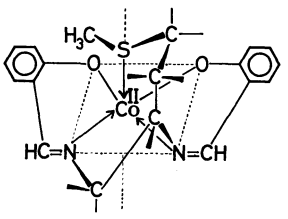

Fig. 3. The structure of Co(II) [sal_2-2(*S*)-SMT-BDA]

in Fig. 3.

A drastic change was observed in the CD spectrum of complex [A] in Py solution after dissolving complex [A] in aqueous methanol and evaporating off the solvent. This change would depend on whether or not H_2O coordinates in the *trans* position of the sulfur atom. When the *trans* position of the sulfur atom is occupied by H_2O, a Py molecule would attack at the coordinated sulfur atom, resulting in substitution of the sulfur atom. On the other hand, the Py molecule would simply interact with the vacant site in the *trans* position of the sulfur atom if no H_2O molecule was present in this position.

The complex [C], Co(II)[sal_2-2(*S*)-SMT-BDA]·$2H_2O$, was synthesized to confirm such a drastic change in the CD spectrum in Py solution. The CD spectra of complex [C] were measured in various solvents (Fig. 4). A drastic change in the CD spectrum was observed in Py solution, while similar CD spectra were seen in DMF, DMSO and methanol solutions. This drastic change also supports the view that complex [A] is a square-pyramidal Co(II) complex.

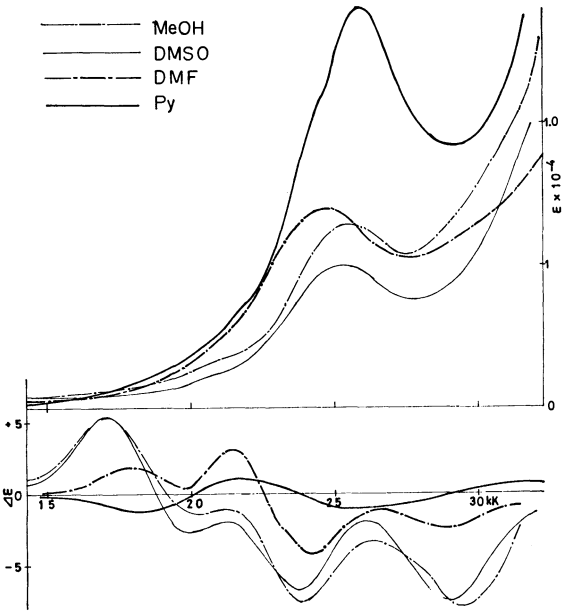

Fig. 4. The CD absorption spectra of Co(II) [sal_2-2(*S*)-SMT-BDA]·$2H_2O$ in various solvents

References

1) A. P. Terent'ev, E. G. Rukhadge, G. V. Panova, and N. M. Voktorova, *Zh. Obshch. Khim.*, **34**, 3025 (1964).
2) C. J. Hipp and W. A. Baker, *J. Amer. Chem. Soc.*, **92**, 792 (1970).
3) W. M. Coleman and L. T. Taylor, *ibid.*, **93**, 5446 (1971).
4) H. Aoi, M. Ishimori, S. Yoshikawa, and T. Tsuruta, *J. Organometal. Chem.*, **85**, 241 (1975).
5) M. Hariharan and F. L. Urbach, *Inorg. Chem.*, **8**, 556 (1969).
6) R. L. Carlin, "Transition Metal Chemistry," Vol. 1, Marcel Dekker, New York, (1966). p. 28.
7) B. Bosnich, *J. Amer. Chem. Soc.*, **90**, 627 (1968).
8) M. D. Hobday and T. D. Smith, *Coord. Chem. Rev.*, **9**, 311 (1972).
9) ligand [F]: *N,N'*-bis(salicylaldehyde)-1(*R*),2(*R*)-1,2-*trans*-cyclohexanediimine.

BULLETIN OF THE CHEMICAL SOCIETY OF JAPAN, VOL. 48 (3), 1051—1052 (1975)

Tetracyanoethylene Complexes of Ni(0) and Co(−1) Containing Isocyanides and Nitrosyl

Katsuhiko KAWAKAMI, Kazuhiro ISHII, and Toshio TANAKA

Department of Applied Chemistry, Faculty of Engineering, Osaka University, Yamada-kami, Suita, Osaka 565

(Received September 30, 1974)

Synopsis. The magnetic equivalence of the isocyanides in $Ni(RNC)_3(TCNE)$ and $Co(NO)(RNC)_2(TCNE)$ is more likely to be due to the free rotation of TCNE in solution than to the dissociative exchange of ligands.

Many phosphine and/or carbonyl complexes of transition metals are known to react with tetracyanoethylene (TCNE) to afford complexes with a rigidly bonded TCNE.[1,2] Recently we have reported for the first time the free rotation of TCNE in its adducts with some tetrakis(isocyanide)rhodium salts.[3] On the other hand, activated olefins were found to replace one molecule of phosphine from tetrahedral tris(triphenylphosphine)-(nitrosyl)-cobalt, -rhodium, and -iridium to form a square pyramidal complex with the rigidly bonded TCNE in the basal plane.[4] In connection with these results, it seemed that it would be of interest to investigate the reactions of TCNE with tetrahedral nickel- and cobalt-isocyanide complexes.[5,6]

Here we wish to report the synthesis and some spectroscopic studies of two types of complexes, $Ni(RNC)_3(TCNE)$ and $Co(NO)(RNC)_2(TCNE)$.

Experimental

All the tetrakis(isocyanide)nickel[5] and bis(isocyanide)-(carbonyl)(nitrosyl)cobalt[6] complexes were synthesized by the literature methods, including the previously unknown 2,4,6-trimethylphenyl isocyanide complexes. The reactions were carried out under nitrogen, and the recrystallizations were done in air, unless otherwise noted.

Preparation of Tris(p-methoxyphenyl isocyanide)(tetracyanoethylene)nickel, $Ni(p\text{-}CH_3OC_6H_4NC)_3(TCNE)$ (1a). TCNE (128 mg, 1 mmol) was added to a stirred suspension of $Ni(p\text{-}CH_3OC_6H_4NC)_4$ (592 mg, 1 mmol) in petroleum ether (20 ml). The color of the suspension gradually changed from bright yellow to brown. The suspension was then stirred overnight at the ambient temperature. The resultant powder was filtered and recrystallized from CH_2Cl_2/petroleum ether to yield black crystals of **1a** (350 mg, 61%).

Other nickel complexes were prepared in similar manners. Only the $2,4,6\text{-}(CH_3)_3C_6H_2NC$ complex was recrystallized from ligroin.

Preparation of Bis(p-methoxyphenyl isocyanide)(nitrosyl)(tetracyanoethylene)cobalt, $Co(NO)(p\text{-}CH_3OC_6H_4NC)_2(TCNE)$ (2a). A reaction of $Co(NO)(CO)(p\text{-}CH_3OC_6H_4NC)_2$ (383 mg, 1 mmol) with TCNE (128 mg, 1 mmol) in a manner similar to that described for **1a** afforded a brown powder, which was then filtered and recrystallized from CH_2Cl_2/petroleum ether under nitrogen to yield brown crystals of **2a** (310 mg, 64%).

Other cobalt complexes were obtained in analogous manners; only the $p\text{-}ClC_6H_4NC$ complex was recrystallized from C_6H_6/petroleum ether under nitrogen.

The physical measurements were performed as has been described elsewhere.[3a] The analytical data and molecular weights of the complexes are collected in Table 1, and the IR and PMR data are summarized in Table 2.

Results and Discussion

The tetrakis(aryl isocyanide)nickel series reacts with an equimolar amount of TCNE to give tris(isocyanide)-(tetracyanoethylene)nickel, with the substitution of one molecule of isocyanide, as has been reported for the *t*-butyl isocyanide analog.[7] Bis(isocyanide)(carbonyl)-(nitrosyl)cobalt also reacts with TCNE to afford bis-(isocyanide)(nitrosyl)(tetracyanoethylene)cobalt, with the evolution of carbon monoxide. All the TCNE complexes of Ni and Co are dark brown or black in color and are stable in air in the solid state over an extended period of time. Some of them are, however, unstable in solution and were recrystallized under nitrogen.

TABLE 1. ANALYTICAL DATA AND MOLECULAR WEIGHTS OF COMPLEXES

No.	Complexes	Anal. (%) Found (Calcd) C	H	N	Mol. wt. Found	Calcd
1a	$Ni(p\text{-}CH_3OC_6H_4NC)_3(TCNE)$	61.42 (61.46)	3.63 3.61	16.74 16.73)	626[a]	586
1b	$Ni(p\text{-}CH_3C_6H_4NC)_3(TCNE)$	67.01 (66.93)	3.77 3.94	18.26 18.22)	564[a]	538
1c	$Ni(C_6H_5NC)_3(TCNE)$	65.44 (65.35)	3.00 3.05	19.79 19.76)	524[a]	496
1d	$Ni(p\text{-}ClC_6H_4NC)_3(TCNE)$	53 64 (54 09	2.28 2.02	15 33 16.36)	628[a]	599
1e	$Ni(2,4,6\text{-}(CH_3)_3C_6H_2NC)_3(TCNE)$	69.64 (69.47	5.37 5.34	15.91 15.76)	602[b]	622
2a	$Co(NO)(p\text{-}CH_3OC_6H_4NC)_2(TCNE)$	54.75 (54.67	2 94 2.92	20.00 20 54)	492[b]	483
2b	$Co(NO)(p\text{-}CH_3C_6H_4NC)_2(TCNE)$	58 82 (58.55	3.18 3.13	21.76 21.72)	464[b]	451
2c	$Co(NO)(p\text{-}ClC_6H_4NC)_2(TCNE)$	48.98 (48.81	1.62 1.64	19.63 19.93)	534[b]	492
2d	$Co(NO)(2,4,6\text{-}(CH_3)_3C_6H_2NC)_2(TCNE)$	61.82 (61.54	4.36 4.37	19.13 19.33)	522[b]	507

a,b) Measured by a vapor pressure osmometer in $CHCl_3$ at 25 °C (a) or in C_6H_6 at 37 °C (b).

TABLE 2. RELEVANT IR AND PMR DATA OF COMPLEXES

	Complexes	IR,[a] cm^{-1} $\nu(NC)$[b]	$\nu(NO)$	$\nu(CN)$[c]		PMR, δ(ppm)[f] $\delta(-C_6H_n-)$[g]		$\delta(CH_3)$
	$Ni(p\text{-}CH_3OC_6H_4NC)_4$	2035	2010	—	—	7.12	6.98	3.79
1a	$Ni(p\text{-}CH_3OC_6H_4NC)_3(TCNE)$	2166	2139	—	2215	7.48	6.91	3.81
1b	$Ni(p\text{-}CH_3C_6H_4NC)_3(TCNE)$	2166	2137	—	2215	7.41	7.23	2.36
1c	$Ni(C_6H_5NC)_3(TCNE)$	2173[d]	2142[d]	—	2217[d]	7.48s		—
1d	$Ni(p\text{-}ClC_6H_4NC)_3(TCNE)$	2166	2135	—	2217	7.46s		—
	$Ni(2,4,6\text{-}(CH_3)_3C_6H_2NC)_4$	—	2011	—	—	6 84s		2.36(*o*) 2.24(*p*)
1e	$Ni(2,4,6\text{-}(CH_3)_3C_6H_2NC)_3(TCNE)$	2156	2122	—	2214	6.91s		2.42(*o*) 2.29(*p*)
	$Co(NO)(p\text{-}CH_3OC_6H_4NC)_2(CO)$	2135	2091	1733	1985[e]	7 36	6.90	3.82
2a	$Co(NO)(p\text{-}CH_3OC_6H_4NC)_2(TCNE)$	2177	2161	1812	2219	7.56	6.99	3.86
2b	$Co(NO)(p\text{-}CH_3C_6H_4NC)_2(TCNE)$	2174	2159	1813	2215	7.49	7.30	2 41
2c	$Co(NO)(p\text{-}ClC_6H_4NC)_2(TCNE)$	2174	2157	1807	2217	7.55	7.47	—
2d	$Co(NO)(2,4,6\text{-}(CH_3)_3C_6H_2NC)_2(TCNE)$	2173	2152	1810	2218	6.96s		2.45(*o*) 2.33(*p*)

a) Measured in C_6H_6 (0.03 M or less) unless otherwise noted. b) Isocyanide vibration. c) TCNE vibration. d) Measured in Nuiol mulls. e) $\nu(CO)$. f) Measured in CH_2Cl_2 (0.04 M) at 25°C. g) A_2B_2-type quartet with a coupling constant of about 9 Hz unless otherwise noted; s=singlet.

The IR spectra of the TCNE complexes show a weak ν(CN) band around 2220 cm^{-1}, which indicates TCNE π-bonded through the C=C bond.[1,7] The ν(NC) frequency of the isocyanides is always higher in the TCNE complexes than in the starting complexes about 130 and 110 cm^{-1} (the differences between the averaged values of two frequencies) for the Ni and Co complexes respectively, indicating a charge transfer from the isocyanide ligands to the TCNE moiety. Moreover, in the Co series in $Co(NO)(RNC)_2(TCNE)$ the ν(NO) bands shift to frequencies higher by about 80 cm^{-1} than those in $Co(NO)(RNC)_2(CO)$. In the PMR spectra the isocyanide protons are always shifted to lower magnetic fields upon complex formation. These results indicate that TCNE is a stronger π-acid than carbon monoxide and isocyanides.

The electronic spectrum of $Ni(p\text{-}CH_3C_6H_4NC)_4$ shows an absorption maximum at 363 nm (ε 2.3×10^4); it is probably a charge transfer band from Ni to isocyanides. On the other hand, the corresponding band of **1b** may be blue-shifted and hidden under the strong band due to the isocyanide ligands. However, a new band appears at 452 nm (ε 2×10^3); its ε value suggests that this is a charge transfer band from Ni to TCNE. This is consistent with the stronger π-acceptor capacity of TCNE than those of isocyanides.

The IR spectrum of **1a** in C_6H_6 shows two strong ν(NC) bands of the isocyanides, indicating a C_{3v} local symmetry for the three isocyanides. The PMR spectrum in CH_2Cl_2 at 25 °C displays one sharp singlet and one A_2B_2-type quartet for the CH_3O and phenyl ring protons respectively; the magnetic equivalence of the three isocyanides is consistent with either the intramolecular rotation of TCNE (averaging the anisotropic effect of TCNE) or the rapid dissociative exchange of the ligands.

The molecular-weight determination reveals the essentially monomeric nature of **1a** (Table 1). The chemical shifts of the isocyanide protons were only slightly changed (0.02 ppm) when the concentration of **1a** in CH_2Cl_2 was changed from 0.20 to 0.008 M. The temperature dependence of the chemical shifts of **1a** in CH_2Cl_2 was found to be small (0.02 ppm) over the wide temperature range between −88 and 25 °C. These results suggest only a slight dissociation of ligands, if any. The addition of one molar equivalent of free TCNE to **1a** in CH_2Cl_2 at 25 °C did not affect the PMR spectrum; this eliminates the dissociative exchange of TCNE. On the other hand, the addition of three molar equivalents of free $p\text{-}CH_3OC_6H_4NC$ to **1a** in CH_2Cl_2 at 25 °C caused changes in the chemical-shift values; the isocyanide protons appeared at the averaged field between those of the complex and the free ligand. However, at −50 °C there occurred two sets of signals which exactly correspond to the complexed and free isocyanides, as is depicted in Fig. 1. This indicates a negligible dissociative exchange of isocyanides below −50 °C on the NMR time scale. However, no signal pattern indicative of the rotation being slowed down[3] was observed as low as −115 °C in a 1:4 mixture of CH_2Cl_2 and $CHClF_2$. This is also the case with the 2,4,6-$(CH_3)_3C_6H_2NC$ derivative, which is considered to be sterically most hindered. Thus, no direct evidence for the rotation being slowed down on the NMR time scale could be obtained. However, since the possibility of the rapid dissociative exchange of the ligands has been eliminated, the magnetic equivalence of the three isocyanides is more likely to be due to the free rotation of TCNE over a very low energy barrier.[8] Similar experiments were performed for some of the other Ni and Co complexes (**1b** and **2a**); the magnetic equivalence of the isocyanides observed for these complexes is also likely to be due to the free rotation of TCNE.

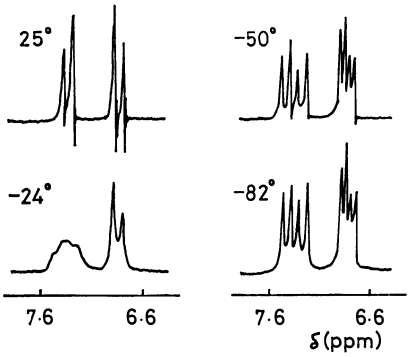

Fig. 1. Temperature-dependent PMR spectra of the phenyl ring protons of $Ni(p\text{-}CH_3OC_6H_4NC)_3$ (TCNE) (**1a**) in the presence of three molar equivalents of $p\text{-}CH_3OC_6H_4NC$ in CH_2Cl_2.

References

1) W. H. Baddley, *Inorg. Chim. Acta Rev.*, **2**, 7 (1968).
2) J. H. Nelson and H. B. Jonassen, *Coord. Chem. Rev.*, **6**, 27 (1971).
3) a) T. Kaneshima, K. Kawakami, and T. Tanaka, *Inorg. Chem.*, **13**, 2198 (1974); b) K. Kawakami, T. Kaneshima, and T. Tanaka, *J. Organometal. Chem.*, **34**, C21 (1972).
4) G. La Monica, G. Navazio, and P. Sandrini, *ibid.*, **31**, **89** (1971).
5) F. Klages and K. Mönkemeyer, *Chem. Ber.*, **83**, 501 (1950).
6) L. Malatesta and A. Sacco, *Z. Anorg. Allg. Chem.*, **274**, 341 (1953).
7) S. Otsuka, T. Yoshida, and Y. Tatsuno, *J. Amer. Chem. Soc.*, **93**, 6462 (1971).
8) The magnetic equivalence of the three $t\text{-}C_4H_9NC$ in $Ni(t\text{-}C_4H_9NC)_3(TCNE)$ was attributed to a slight dissociative exchange of the isocyanides without low-temperature PMR spectral measurements in the presence of free $t\text{-}C_4H_9NC$.[7]

BULLETIN OF THE CHEMICAL SOCIETY OF JAPAN, VOL. 48 (3), 1053—1054 (1975)

Fourier Analysis of AC Polarogaphy: Kinetic Parameters for Zn(II)-1 M $NaClO_4$ and KCl Systems

Michio HIROTA, Yoshio UMEZAWA, and Shizuo FUJIWARA
Department of Chemistry, Faculty of Science, The University of Tokyo, Hongo, Tokyo 113

(Received October 8, 1974)

Synopsis. The fundamental and second harmonic responses of the Zn(II)/Zn(Hg) electrode agreed with the theory with respect to the phase angle. Th ekinetic parameters of the systems were: $k_s=(2.8\pm0.3)\times10^{-3}$cm/s, $\alpha=0.30\pm0.05$ in 1 M $NaClO_4$ and $k_s=(3.3\pm0.3)\times10^{-3}$ cm/s, $\alpha=0.27\pm0.03$ in 1 M KCl.

Fourier transform AC polarography has the advantage of allowing the simultaneous measurement of the amplitude and phase angle for the components of the fundamental and higher harmonic AC current.[1-8] This opens a way to investigate the reaction at the electrode surface with different time scales, and it would probably be very useful for kinetic investigations.

The purpose of the present paper is to examine, taking the Zn(II) ion as an example, whether or not any discrepancy exists between the fundamental(1st) and second(2nd) harmonic responses under the same experimental conditions.

The apparatus and experimental procedures were the same as those of the previous paper.[8] The frequencies, f, of the applied AC potentials were 27.9, 55.8, 111.6, and 173.6 Hz, each with an amplitude, ΔE, of 5 mV. All the chemicals used were of analytical reagent grade, except for $Zn(ClO_4)_2\cdot6H_2O$, which was prepared by the usual method.

The actual steps of the measurements were as follows: 1) The kinetic parameters were first roughly estimated, by which the computer simulation of Procedure 2) was started. 2) Simulation was continued by varying the kinetic parameters until the calculated curve for cot ϕ *vs.* $\sqrt{w}$ at peak potential, E_p, of the 1st harmonic AC polarogram coincided with the experimental curves, where ϕ is the phase angle and ω is $2\pi f$. 3) The 2nd harmonic AC polarogram was then calculated by the use of the kinetic parameters which had just been obtained by the preceding procedure, after which the polarogram was compared with the experimental curve.

1) The standard rate constants of the electrode reaction, k_s, were calculated by means of Eq. (1);

$$\cot\phi = \frac{1}{k_s}\sqrt{\frac{\omega D}{2}},$$
$$D = D_o^{1-\alpha}\cdot D_r^{\alpha} \qquad (1)$$

where ϕ is the phase angle between the 1st harmonic AC current and the applied AC potential at the reversible half-wave potential, $E^r_{1/2}$. D_o and D_r are the diffusion coefficients of the oxidized and reduced forms respectively, and α, the transfer coefficient. By plotting cot ϕ against the frequency of the AC potential, k_s is calculated from the slope of the cot ϕ *vs.* $\sqrt{\omega}$ curve, with the intercept of 1.[14] In the present case, the cathodic peak potential, E_p^c, of the 2nd harmonic AC polarogram was used as the $E^r_{1/2}$ value, and α was roughly taken as 0.3 for both systems. These values of $E^r_{1/2}$ and α were actually the averages of the values in the literatures.[9-11,16] The observed values of k_s were $(3.5\pm0.9)\times10^{-3}$ cm/s for the Zn(II)–1 M $NaClO_4$ system and $(3.7\pm0.5)\times10^{-3}$ cm/s for the Zn(II)–1 M KCl system.

2) Simulation was performed by varying the values of k_s and α, until the calculated curve (cotϕ *vs.* $\sqrt{\omega}$) coincided with the experimental curves within the limit of experimental error, where theoretical calculation was based on the expanding-plane model.[13] The experimental values of cot ϕ used in this procedure were those obtained at E_p, where the current intensity is larger than that at $E^r_{1/2}$, which improved the precision of the phase angle. The kinetic parameters thus obtained for these systems were as follows: $k_s=(2.8\pm0.3)\times10^{-3}$ cm/s and $\alpha=0.30\pm0.05$ for Zn(II)–1 M $NaClO_4$ ($[H^+]=1$ mM), and $k_s=(3.3\pm0.3)\times10^{-3}$ cm/s and $\alpha=0.27\pm0.03$ for Zn(II)–1 M KCl($[H^+]=1$ mM). In these cases, D_o was obtained experimentally, and D_r was taken from Ref. 15.

3) Using the kinetic parameters obtained from the above procedure, the theoretical curves of the 2nd harmonic AC polarogram were described (Fig. 1). The frequency dependence of the several parameters, *i.e.*, the phase angles (Fig. 2), the ratio of I_p^c to I_p^a

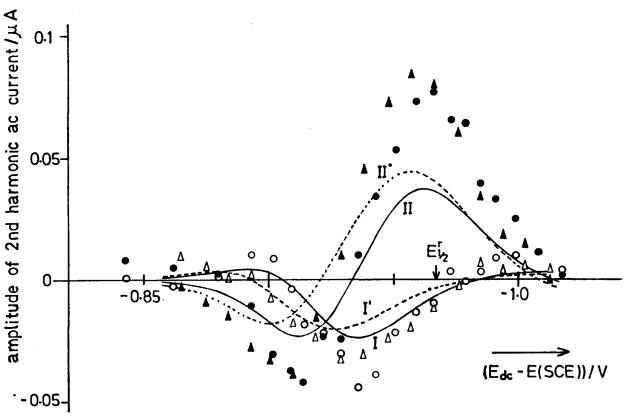

Fig. 1. 2nd harmonic AC polarogram of Zn(II)-1 M $NaClO_4$ ($[H^+]=1$ mM) system.
$f=27.9$ Hz; ○—in-phase component
●—quadrature component
$f=111.6$ Hz; △—in-phase component
▲—quadrature component
simulation curves for $k_s=2.8\times10^{-3}$ cm/s and $\alpha=0.30$
$f=27.9$ Hz (——), $f=111.6$ Hz (——)
I,I'=in-phase component
II,II'=quadrature component
$\Delta E=5$ mV, $n=2$, $[Zn(II)]=1.01$ mM, $D_o=0.71\times10^{-5}$ cm²/s, $D_r=1.70\times10^{-5}$ cm²/s, drop time=3.58 s, electrode area=0.015 cm².

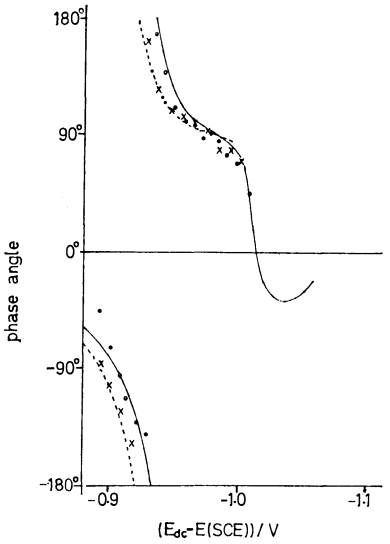

Fig. 2. Phase angle of the 2nd harmonic AC polarogram of Zn(II)–1 M $NaClO_4$([H^+]=1 mM) system.
o: f=27.9 Hz, x: f=111.6 Hz
simulation curves
f=27.9 Hz (——), f=111.6 Hz (——)
same parameters as Fig. 1.

(cathodic and anodic peak currents respectively), and the separation between E_p^c and E_p^a (the anodic peak potential), were consistent with the theoretical predictions. However, the amplitude of the experimental curve was considerably (about twice) larger than that of the theoretical one in both systems. To confirm that the discrepancy was larger than the experimental error, the D_0 of Zn(II) (for the case of 1 M KCl solution) was measured by using different starting materials ($ZnCl_2$ and zinc metal). The D_0 found after four measurements was $(0.73\pm0.02)\times10^{-5}$ cm^2/s; its error gave only an error of less than 2% in the amplitude.

In conclusion, the results for the 1st and 2nd harmonic AC polarograms for the present systems agree with each other with respect to the phase angle. The kinetic parameters obtained from the phase angle of the 1st and 2nd harmonic responses are in good agreement with those previously reported.[9–11,16]

The observed amplitude, which was larger than the theoretical one, is assumed to be due to the effect of the spherical diffusion. In the present systems, the departure of the measured amplitude from the theoretical amplitudes was larger than in the cadmium system.[8] This may be qualitatively interpreted in terms of the fact that the spherical diffusion influences both the surface concentration and the deviation from the electrochemical equilibrium.[17]

References

1) H. Kojima and S. Fujiwara, This Bulletin, **44**, 2158 (1971).
2) S. C. Creason and D. E. Smith, *J. Electroanal. Chem.*, **36**, Al (1972).
3) *ibid.*, **40**, Al (1972).
4) B. J. Huebert and D. E. Smith, *Anal. Chem.*, **44**, 1179 (1972).
5) S. C. Creason and D. E. Smith, *J. Electroanal. Chem.*, **47**, 9 (1973).
6) D. E. Glover and D. E. Smith, *Anal. Chem.*, **45**, 1869 (1973).
7) S. C. Creason and D. E. Smith, *ibid.*, **45**, 2401 (1973).
8) M. Hirota, Y. Umezawa, H. Kojima, and S. Fujiwara, This Bulletin, **47**, 2486 (1974).
9) T. G. McCord and D. E. Smith, *Anal. Chem.*, **42**, 126 (1970).
10) J. H. Sluyters and J. J. C. Oomen, *Rec. Trav. Chim. Pays-Bas*, **79**, 1101 (1960).
11) P. Teppema, M. Sluyters-Rehbach, and J. H. Sluyters, *J. Electroanal. Chem.*, **16**, 165 (1968).
12) D. E. Smith and A. J. Bard "Electroanalytical Chemistry," M. Dekker, New York, N. Y. (1966).
13) T. G. McCord and D. E. Smith, *Anal. Chem.*, **40**, 289 (1968).
14) J. K. Frischman and A. Timnick, *ibid.*, **39**, 507 (1967).
15) N. H. Furman and W. C. Cooper, *J. Amer. Chem. Soc.*, **72**, 5667 (1950).
16) P. J. Lingane and J. H. Christie, *J. Electroanal. Chem.*, **10**, 284 (1965).
17) J. R. Delmastro and D. E. Smith, *Anal. Chem.*, **38**, 169 (1966).

BULLETIN OF THE CHEMICAL SOCIETY OF JAPAN, VOL. 48 (3), 1055—1056 (1975)

A Convenient Method for the Preparation of Aminoethyliminodiacetatocobalt(III) Complexes

Kashiro KURODA, Shuji OHTSUKA, and Noriko MATSUMOTO

Department of Chemistry, Faculty of Science, Ehime University, Matsuyama, Ehime 790

(Received October 31, 1974)

Synopsis. Sodium dinitro(aminoethyliminodiacetato)-cobaltate(III) has been obtained by the oxidation of an aqueous mixture of cobalt(II) chloride, sodium nitrite, and a reaction product between ethylenediamine and sodium monochloroacetate. Several other complexes with the tetradentate ligand have also been derived from the dinitro complex.

Schwarzenbach *et al.*[1] prepared β-aminoethyliminodiacetic acid, NH_2–CH_2–CH_2–$N<^{CH_2\text{–}COOH}_{CH_2\text{–}COOH}$ (abbreviated as aeidaH_2 in this report), and measured the formation constants with various metal ions in aqueous solutions. Chu *et al.*[2] prepared the tetradentate ligand by Schwarzenbach's method and synthesized *cis*(*O*)- and *trans*(*O*)-isomers of [Co(aeida)(en)]X (X=Cl, ClO_4). Their preparation route for the ligand requires several reaction steps, however, and so is not very convenient. It has been reported that the main product of the reaction between 1 mol of ethylenediamine and 2 mol of the monochloroacetate ion is not the aeida or the ethylenediamine-*N*,*N*′-diacetate ion (EDDA), but the ethylenediaminetetraacetate ion (EDTA) with the unreacted diamine.[3] However, we supposed that there might be some aeida in the reaction mixture and that there might be a possibility for a cobalt(III) complex with the tetradentate ligand to be separable, together with the coordination of a unidentate or a bidentate ligand. Thus, the reaction mixture was combined with cobalt(II) chloride and sodium nitrite, and the mixture was oxidized by air bubbling. As a result, sodium dinitro(aminoethyliminodiacetato)cobaltate(III) was obtained. This substance and a few complexes derived from it were identified, as will be described below.

Experimental

Sodium Dinitro(aminoethyliminodiacetato)cobaltate(III), Na[Co(aeida)(NO_2)$_2$]. Ethylenediamine (6.0 g) was placed in a 150 ml flask furnished with a reflux condenser and a dropping funnel, and the flask was set in an oil bath at 110 °C. A sodium monochloroacetate solution, which had been prepared by mixing monochloroacetic acid (18.9 g in 25 ml) with sodium hydroxide (8.0 g in 25 ml) below 20 °C, was added, drop by drop, from the funnel into the flask, taking about 2 hr. A sodium hydroxide solution (8.0 g in 25 ml) was then added, taking about 30 min. After this addition, the heating was continued for a further 2 hr. The product solution was then adjusted to be slightly alkaline by the addition of hydrochloric acid, and was combined with a solution of cobalt(II) chloride hexahydrate (24 g in 50 ml). While vigorous air bubbling into the mixture was started, a sodium nitrite solution (14 g in 25 ml) was added, drop by drop, from the inlet of the air stream. The solution, dark violet at the early period of the oxidation, gradually turned dark brown; at the same time, bright brown crystals began to come out. The air bubbling was continued for 5 hr. After the product had been placed in a refrigerator overnight, the crystals were collected and then recrystallized from 50 ml of warm water. The purified crystals were washed with methanol and ether. Yield, 7.5 g. Found: C, 20.76; H, 2.95; N, 15.99%. Calcd for Na[Co(aeida)(NO_2)$_2$]=$CoC_6H_{10}O_8N_4Na$ (348.09): C, 20.70; H, 2.90; N, 16.10%.

trans(O)-*Aminoethyliminodiacetato(ethylenediamine)cobalt (III) Perchlorate,* trans(O)-[*Co(aeida)(en)*]ClO_4. In an evaporating dish, 1.0 g of the dinitro complex was mixed with 10 ml of acetic acid and 2 ml of water. The dish was covered with a watch-glass and was heated on a boiling-water bath until the solid had been completely dissolved. Nitric oxides were evolved during the dissolution, and a red-violet solution was formed. Then the solution was concentrated with the aid of an air stream to obtain a tarry residue. After it had then been dissolved in 5 ml of water, the solution was concentrated again to the tarry state; the odor of acetic acid thereupon vanished. The product was dissolved in 5 ml of water again, and 1.0 g of 20%-ethylenediamine solution was added. The heating of the mixture on the bath for 30 min, followed by cooling and the addition of 1 ml of 6 M $HClO_4$, produced a red precipitate. The precipitate was recrystallized from 20 ml of warm water with the addition of a few drops of 6 M $HClO_4$. Yield, 0.4 g. Found: C, 24.32; H, 4.65; N, 14.10%. Calcd for [Co(aeida)(en)]ClO_4=$CoC_8H_{18}O_8N_4Cl$ (392.64): C, 24.47; H, 4.62; N, 14.27%.

trans(O)-*Aminoethyliminodiacetato(trimethylenediamine)cobalt-(III) Perchlorate,* trans(O)-[*Co(aeida)(tn)*]ClO_4. This complex was isolated by the use of trimethylenediamine instead of ethylenediamine in the above preparation. Yield, 0.4 g. Found: C, 26.50; H, 5.02; N, 13.60%. Calcd for [Co(aeida)(tn)]ClO_4=$CoC_9H_{20}O_8N_4Cl$ (406.67): C, 26.58; H, 4.96; N, 13.78%.

trans(O)-*Aminoethyliminodiacetato(diammine)cobalt(III)Perchlorate,* trans(O)-[*Co(aeida)(NH_3)$_2$*]ClO_4. One gram of the dinitro complex was treated with acetic acid and then with water, such as in the preparation of the ethylenediamine complex. Then, 5 ml of aqueous ammonia (6M) and 0.1g of active charcoal were added. After the mixture had been concentrated to dryness at ~60 °C, the residue was extracted with 20 ml of warm water. The addition of 1 ml of 6M $HClO_4$ to the extract, followed by cooling, produced a red-violet precipitate. It was recrystallized from 15 ml of warm water with the addition of a few drops of 6M $HClO_4$. Yield, 0.3 g. Found: C, 19.67; H, 4.51; N, 15.11%. Calcd for [Co(aeida)(NH_3)$_2$]ClO_4=$CoC_6H_{16}O_8N_4Cl$ (366.60): C, 19.66; H, 4.40; N, 15.28%.

Discussion

Identification. Figure 1 shows the absorption spectra of the diammine- and the diamine-complexes, in which a splitting is observable in each first band. Thus, the spectra clearly indicate that their configurations are *trans*-[CoN_4O_2]. The numerical values of the

Table 1. Absorption maxima of the electronic spectra of some Co(III)-aeida complexes

	I $\bar{\nu}$ (kK) (ε)		II or Sp $\bar{\nu}$ (kK) (ε)
	Ia	Ib	
Na[Co(aeida)$(NO_2)_2$]	21.28 (224.0)		29.80 (5640) [a]
trans(*O*)-[Co(aeida)(en)]ClO_4	18.97 (142.4)	sh	28.20 (172.0)
trans(*O*)-[Co(aeida)(tn)]ClO_4	18.62 (146.0)	sh	27.86 (186.2)
trans(*O*)-[Co(aeida)$(NH_3)_2$]ClO_4	18.73 (145.0)	sh	27.93 (178.2)

a) Ligand specific band.

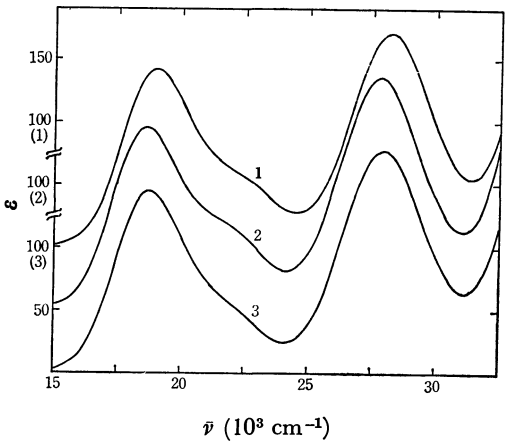

Fig. 1. Absorption spectra of some Co(III)-aeida complexes.
1: *trans*(O)-[Co(aeida)(en)]ClO_4
2: *trans*(O)-[Co(aeida)(tn)]ClO_4
3: *trans*(O)-[Co(aeida)$(NH_3)_2$]ClO_4

absorption maxima (Table 1) of our ethylenediamine complex agree satisfactorily with those of the *trans*(*O*)-isomer prepared by Chu *et al.*[2] Each of the spectra is definitely different from the spectrum of the Co(III)-EDDA complex with the corresponding ligand.[4] (An aeida-complex has the same elemental composition as the EDDA-complex with the same additional ligand.) Thus, on the basis of the absorption spectra as well as the elemental analyses, there remains no question as to the identification of the complexes.

Notes on the Preparations. Following are some notes on things observed qualitatively during the preparations:

(1) The solubility of the dinitro complex varies greatly with the temperature. The growth of the crystals from the reacting mixture is relatively slow. Thus, cooling the mixture during the later half of the air oxidation makes the preparation time shorter.

(2) In the preparations of cobalt(III) complexes with another multidentate ligand, such as trien or DTMA, a nitro complex is usually treated with hydrochloric acid to convert it into the chloro complex.[5] A similar treatment was attempted here. However, it appeared to decompose the complex itself. A large excess of acetic acid, as has been described above, is useful in expelling the nitro groups. Perchloric acid is not useful, since there is no proper means to remove the excess of the acid after the reaction.

(3) For the preparation of the diammine complex, it is necessary to add charcoal to the reacting mixture; otherwise, an aquoammine complex arises. Many other unidentate and bidentate ligands, such as SCN^-, N_3^-, phen, and dipy, also react with the product from the dinitro complex treated with acetic acid. The aquoammine complex as well as the other species in this series will be reported on elsewhere.

References

1) G. Schwarzenbach, G. Anderegg, W. Schneider, and H. Senn, *Helv. Chim. Acta*, **38**, 1147 (1955).
2) M. W. S. Chu, D. W. Cooke, and C. F. Liu, *Inorg. Chem.*, **7**, 2453 (1968).
3) I. Murase, "Syntheses of Metal Complexes and Reactivities of Ligands," ed. by A. Nakahara and M. Shibata, Nankodo, Tokyo (1970), p. 126.
4) K. Kuroda, This Bulletin, **45**, 2176 (1972); *Chem. Lett.*, **1974**, 17.
5) A. M. Sargeson and G. H. Searle, *Inorg. Chem.*, **6**, 787 (1967); P. W. Schneider and J. P. Collman, *ibid.*, **7**, 2010 (1968).

BULLETIN OF THE CHEMICAL SOCIETY OF JAPAN, VOL. 48 (3), 1057—1058 (1975)

Ketyl Radical Formed in the Grignard Reaction of 2-Methylbenzophenone

Masao Ōkubo

Department of Chemistry, Faculty of Science and Engineering, Saga University, Honshō-chō, Saga 840

(Received December 6, 1973)

Synopsis. The radical in the title reaction gave an ESR spectrum different from that of potassium-ketyl. From studies using the deuterium label technique, the reason for this difference was ascribed to the suppression of the twisting vibration caused by aggregate-formation.

The scheme for the reaction of Grignard reagents with benzoyl peroxide in tetrahydrofuran (THF) was recently established to be that shown in formula 1.[1]

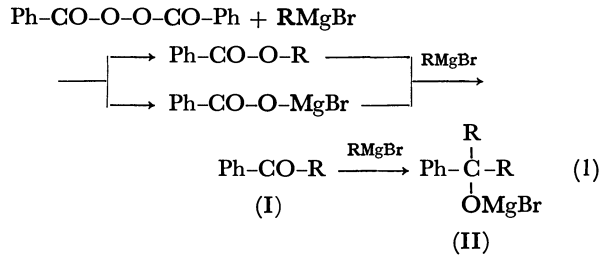

In the course of a study of this reaction, a large excess of *o*-tolyl-MgBr was found to change the reaction solution from colorless to purple and an exceptionally long-lived radical species was detected.[2] As this radical is considered by the author to be related to the ketone (I, R=*o*-tolyl in formula 1), the radical produced in the Grignard reaction of 2-methylbenzophenone itself was studied in detail.

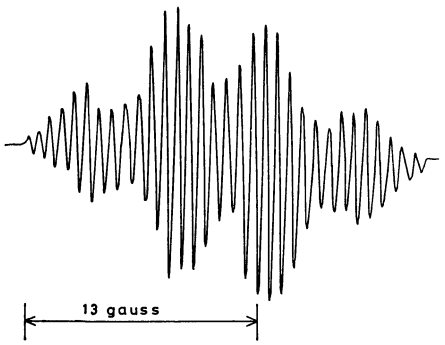

Fig. 1. ESR spectrum (A) of the radical species obtained in the reaction of 2-methylbenzophenone with *o*-tolyl-MgBr in THF.

The ESR spectrum (A) obtained in the reaction of I with *o*-tolyl-MgBr is shown in Fig. 1. As the spectrum obtained in the reaction of I with phenyl-MgBr was identical with spectrum A, the radical seemed to be a ketyl-type.[3] This radical existed even after the evacuated sample solution had been allowed to stand for several months at room temperature. This Grignard-ketyl, if that is what it is, is anomalous because of its long life[4] in comparison with the Grignard-ketyl of benzophenone which gave a measurable (by ESR) radical concentration only at temperatures lower than −20 °C.[5,6] Considering this anomaly, one might suspect that spectrum A is not that of a ketyl radical but that of triarylmethyl radical derived from the final product (II). The latter possibility, however, can be excluded by examining the calcium-ketyl of I prepared by using Ca-amalgum in THF. Spectrum B shown in Fig. 2 was obtained when the solution of Ca-ketyl was not fully diluted. Resemblance of spectrum A to B is obvious.

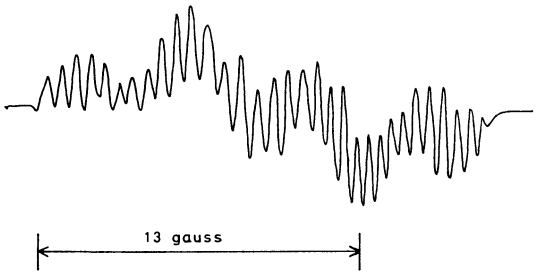

Fig. 2. ESR spectrum (B) of Ca-ketyl of 2-methylbenzophenone prepared in THF.

Spectrum A (total width 23.5 G) consists of four broad lines (a_1=5.86 G), each of which splits into eight lines (a_2=0.73 G). This spectrum differs from that of the potassium-ketyl of the same ketone, which is known to give a spectrum made up of only four broad lines.[7] In order to explain why the hyperfine splittings are observed in the Grignard reaction and not observed in the alkali metal reduction, the assignment of the splitting constants a_1 and a_2 is necessary. As no fruitful result is obtained if the numbers of equivalent hydrogen atoms are taken into account, the deuterium label technique was applied. When d_5-phenyl *o*-tolyl ketone (III) was treated with phenyl-MgBr, a broad single line

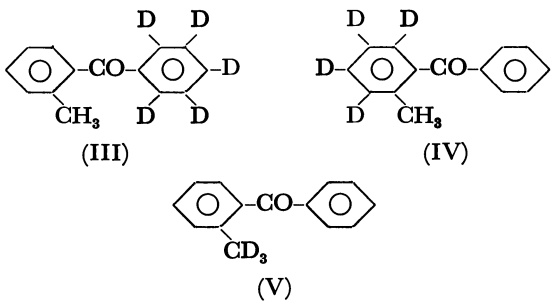

with the total width of 9.4 G was observed. The splitting constant a_1 is thus ascribed to the equivalent coupling of the two *ortho*- and one *para*-hydrogen atoms of the phenyl group with the free electron.[7] 2-Methyl-3,4,5,6-d_4-phenyl phenyl ketone(IV) gave four broad lines. In the case of 2-(d_3-methyl)phenyl phenyl ketone (V), spectrum C, composed of 32 lines, was observed but the relative strength of each line varied as shown in Fig. 3. The hyperfine splitting constant a_2 can thus be assigned mainly to the coupling of the nuclear

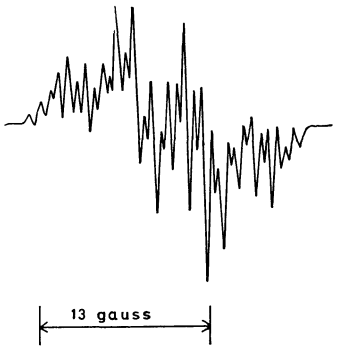

Fig. 3. ESR spectrum (C) of radical species obtained in the reaction of 2-(d_3-methyl)phenyl phenyl ketone with PhMgBr.

hydrogen atoms of the *o*-tolyl group and partly to that of the *o*-methyl hydrogen atoms with free spins.

The difference between the spectrum of the Grignard-ketyl and that of the K-ketyl can be ascribed to "aggregate-formation". The divalent calcium ion favors the formation of dimeric ketyl, which may aggregate further when the solution is less than fully diluted. During the dilution of the solution of the Grignard-ketyl in an evacuated sample tube, a portion of the deeply colored concentrated solution was observed to form a heavy layer at the bottom of the tube and some difficulty was found in obtaining a homogeneously diluted solution. This must be due to the formation of dimeric or polymeric aggregates. Resemblance of spectrum A to B suggests that the Grignard–ketyl exists in an aggregated state even in a fully diluted solution, although a description of this state cannot be given at present. The dimer- or aggregate-formation may suppress the twisting vibration of the *o*-tolyl group out of the plane of the benzoyl group, and thus the interaction of *o*-tolyl hydrogen atoms with free spins can be observed even though the spin density on the *o*-tolyl group is low. In the case of the K-ketyl, in which aggregate formation is not favored at low concentrations, the twisting vibration of the *o*-tolyl group may be rapid and the interaction of its hydrogen atoms with free spins could not be observed.

The large effect of deuterium label of the phenyl group on the total width of the Grignard-ketyl spectrum is remarkable. The spectrum width is reduced from 23.5 to 9.4 G while that of the K-ketyl is reduced from 21.7 to 18.5 G.[7] This indicates that the free spin density on the phenyl group is much higher in the Grignard-ketyl than in the K-ketyl. It is therefore concluded that the twisting angle of the *o*-tolyl group is larger in the former and the twisting vibration of the *o*-tolyl group is more rapid in the latter.

The reason for the exceptionally long life of the Grignard-ketyl is not yet clear, and further studies of Grignard-ketyls of 2-substituted benzophenones are now in progress.

Experimental

Materials. 2-Methylbenzophenone was prepared as usual. The ketone III was prepared from *o*-tolyl chloride and benzene-d_6 in CS_2 using $AlCl_3$. The ketone IV was prepared by the reaction of PhCOCl with the Grignard reagent derived from 2-methyl-3,4,5,6-d_4-phenyl bromide, which was obtained by repeated treatment of *o*-bromotoluene with 95% D_2SO_4.[9] The ketone V was prepared by the reaction of PhCOCl with the Grignard reagent derived from 2-(d_3-methyl)phenyl bromide, which was obtained from the following sequence of reactions. Anthranilic acid was converted to *o*-bromobenzoic acid by Sandmeyer reaction. By treatment of the acid with $LiAlD_4$, *o*-bromo-α,α-d_2-benzyl alcohol was obtained. The alcohol was then converted to the chloride by treatment with $SOCl_2$, and the Cl-atom was replaced by deuterium by using Zn-powder and CH_3COOD. Grignard reagents in THF were prepared as usual and transferred under N_2 to storage bottles.

ESR Measurement. Evacuated samples were prepared as previously described.[8] The molar ratio of phenyl-MgBr to ketones was 5: 1. After mixing by breaking the seal, the resulting purple solution was diluted by low-temperature-distillation in order to obtain a sufficiently resolved spectrum. A JEOL JES-ME-3X ESR spectrometer was used.

References

1) M. Ōkubo, K. Maruyama, and J. Ōsugi, This Bulletin, **44**, 125 (1971).
2) See foot-note 3) of Ref. 1.
3) If these spectra are not identical with each other, the possibility of formation of a triarylmethyl-type radical should be considered. See the following discussions.
4) E. C. Ashby, J. Laemmle, and H. M. Neumann, *J. Amer. Chem. Soc.*, **94**, 5421 (1972).
5) K. Maruyama, This Bulletin, **37**, 897 (1964).
6) C. Blomberg and H. S. Mosher, *J. Organometal. Chem.*, **13**, 519 (1968).
7) K. Maruyama, R. Tanikaga, and R. Gotō, This Bulletin, **36**, 1141 (1963).
8) K. Maruyama, *ibid.*, **37**, 1013 (1964).
9) R. N. Renaud, D. Kovachic, and L. C. Leitch, *Can. J. Chem.*, **39**, 21 (1961).

BULLETIN OF THE CHEMICAL SOCIETY OF JAPAN, VOL. 48 (3), 1059—1060 (1975)

The Transisopropylation of Naphthalene[1)]

Keizo SHIMADA and Shizuo NAGAHAMA

Central Research Institute, Teijin Limited, 4-3-2 Asahigaoka, Hino, Tokyo 191

(Received June 2, 1974)

Synopsis. The transisopropylation of naphthalene with *p*-cymene and isopropylxylenes in the presence of aluminum chloride–nitromethane complex as a catalyst was studied. It was observed that the α-isomer initially formed was isomerized to the β-isomer in the reaction with isopropyl-*p*-xylene. However, when *p*-cymene or isopropyl-*o*-xylene was used, the isomer distribution was almost constant from the beginning to the end of the reaction. This was attributed to the fact that the hydride abstraction mechanism plays a role in the latter case.

In the case of the isopropylation of naphthalene, the exclusive or predominant formation of the β-isomer has been reported; this result has been explained as the isomerization of the initially formed α-isomer.[2)]

Farberov *et al.*[3)] showed that the isomeric composition depended on the alkylation conditions, especially on the temperature.

The equilibrium mixture seems to contain 95—96% of the β-isomer.[3,4)]

The isopropylation of naphthalene by transalkylation has also been reported.[5)] Several patents[6)] have claimed that the transalkylation of naphthalenes gave as product the β-isomer predominantly.

Recently, Yumoto[7)] obtained a product of transisopropylation in which the ratio of the α: β isomers was 8.4: 91.6.

One of the present authors (K. S.)[8)] has previously showed that the migration of an isopropyl group of alkylbenzene to another aromatic nucleus proceeded by two different mechanisms according to the structure of the isopropylbenzenes. That is, the transisopropylation of toluene by 1,4-dimethyl-2-isopropylbenzene in the presence of the $AlCl_3$–CH_3NO_2 catalyst gave a product which had a isomer distribution similar to that obtained by the isopropylation with isopropyl bromide. Thus, both reactions seem to proceed by means of the formation of the isopropyl cation. On the other hand, the transisopropylation of toluene with 1,2-dimethyl-4-isopropylbenzene or especially *p*-diisopropylbenzene gave a product rich in *p*-cymene.

In this case, an alkyl substituent on the *p*-position to the isopropyl group may stabilize the *tert*-carbonium ion produced by hydride abstraction from the isopropyl group, and the attack of the bulky phenyldimethyl cation on the *ortho* position of the methyl group of toluene becomes unlikely.

We wish now to report the effect of the structure of isopropylalkylbenzene as a transalkylation reagent on the isomer distribution of the isopropylnaphthalene obtained by the transisopropylation with the $AlCl_3$–CH_3NO_2 catalyst.

Experimental

Materials. The naphthalene was purified by sublimation and was 99.7% pure. The 1,4-dimethyl-2-isopropylbenzene was synthesized from *p*-xylene (purity 99.5% up) and isopropyl bromide with $AlCl_3$ and was distilled twice; 99.0% pure. The 1,3-dimethyl-5-isopropylbenzene was synthesized from m-xylene (purity 99.0% up) and isopropyl bromide as above (purity 96.7%). The 1,2-dimethyl-4-isopropylbenzene was synthesized from *o*-xylene (purity 99.0% up) and isopropyl bromide as above (purity 99.0%).

Commercial *p*-cymene and nitromethane (special grade reagent, Wako Pure Chemical Ind., Ltd.) were used. The *p*-cymene was purified by distillation and was 99.0% pure. The nitromethane was used without further purification.

Reactions. A mixture of 0.1 mol each of naphthalene and one of the isopropylbenzenes in 20 g of *n*-heptane was stirred at 50 °C. To this mixture was then added a catalyst prepared from 0.02 mol of $AlCl_3$ and 0.05 mol of nitromethane. Aliquots of samples were taken off in appropriate times, poured into ice water and ether to decompose the catalyst, washed, and dried. Finally, 0.05 mol of $AlCl_3$ was added to the reaction mixture at 20 °C and the mixture was stirred until the α- and β-isomer composition was equilibrated.

The samples were analyzed by gas chromatography, using an MBMA Golay column (45 m) at 140 °C.

Results and Discussion

1,4-Dimethyl-2-isopropylbenzene: The isomer distribution and the reaction time are shown in Table 1. The data clearly show the initial attack favorable to the α-position, followed by isomerization to the β-position.

Table 1. Isomer distribution in the isopropylation of naphthalene with 1,4-dimethyl-2-isopropylbenzene

Time (min)	Isopropylnaphthalene (%)		Conversion[a)] (%)
	α	β	
10	72	28	1
30	50	50	2
60	38	62	4
180	18	82	11
One day after addition of further cat.	2.9	97.1	50

a) Calculated from the peak area of gas chromatogram Isopropylnaphthalene/naphthalene + isopropylnaphthalene + diisopropylanphthalene

By extrapolation to the time zero, an initial isomer distribution of about 90% α- and 10% β-position was obtained. Isopropylation by isopropyl alcohol with sulfuric acid gave 80% α- and 20% β-isomer.

Thus, the attacking species of the transalkylation in this case was similar to that of the alkylation. That is, the isopropyl cation formed by proton attack on the

Table 2. Isomer distribution in the isopropylation of naphthalene with 1,2-dimethyl-4-isopropylbenzene

Time (min)	Isopropylnaphthalene (%) α	Isopropylnaphthalene (%) β	Conversion (%)
10	2.8	97.2	2
30	2.8	97.2	4
60	2.8	97.2	8
One day after addition of further cat.	2.5	97.5	44

Table 3. Isomer distribution in the isopropylation of naphthalene with *p*-cymene

Time (min)	Isopropylnaphthalene (%) α	Isopropylnaphthalene (%) β	Conversion (%)
10	2.5	97.5	0.4
30	2.7	97.3	2
60	2.6	97.4	6
180	2.9	97.1	18
2 hr after addition of further cat.	2.1	97.9	27

Table 4. Isomer distribution in the isopropylation of naphthalene with 1,3-dimethyl-5-isopropylbenzene

Time (min)	Isopropylnaphthalene (%) α	Isopropylnaphthalene (%) β	Conversion (%)
15	48	52	0.1
30	38	62	0.7
60	28	72	2
180	12	88	6
One day after addition of further cat.	2.4	97.6	35

1,4-dimethyl-2-isopropylbenzene reacts mainly with the α-position of naphthalene.

1,2-Dimethyl-4-isopropylbenzene and p-*Cymene*: The isomer distribution and the reaction times are shown in Tables 2 and 3.

The data of the Tables 2 and 3 are quite different from those of Table 1. The ratio of α- and β-isomer was almost constant from the beginning to the end of the reaction.

This means that the attacking species must be a bulky and sterically hindered group. That is, the phenyldimethyl carbonium ion formed by hydride abstraction from the isopropyl group of 1,2-dimethyl-4-isopropylbenzene or *p*-cymene reacts with the β-position of naphthalene.

1,3-Dimethyl-5-isopropylbenzene: The results of the reaction are shown in Table 4.

The results show the two reaction mechanisms work simultaneously.

Thus, it was further confirmed that two different mechanisms, namely, the proton addition and the hydride abstraction mechanism, operated according to the structures of alkylbenzenes, in the transalkylation of such *sec*-alkyl groups as isopropyl.

The authors are indebted to Dr. Shoichi Sakajiri, Director of the Central Research Institute, Teijin Limited, for his permission to publish this article.

References

1) The Alkylation and Transalkylation Reaction of Aromatic Hydrocarbons III.

2) For references on the previous researches, see S. H. Patinkin and B. S. Friedman in "Friedel-Crafts and Related Reactions," Vol. II, ed. by G. A. Olah, Interscience Publishers New York, N. Y. (1964), Part 1, p. 68—71.

3) M. I. Farberov, A. V. Bondarenko, V. M. Obukhov and G. I. Karakuleva, *Dokl. Akad. Nauk SSR*, **179**, 1359 (1968).

4) a) G. Suld, U.S. 3,458,587 (1969). b) J. S. Marchese, J. C. Hamilton, Fr. 1,540,716 (1968).

5) G. I. Karakuleva, A. V. Bondarenko, M. I. Farberov, and Z. V. Smirnova, *Neftekhimiya*, **5**, 856 (1965).

6) a) A. P. Lien and D. A. McCaulay, U.S. 2,837,583 (1958). b) H. Binder and J. Sulo, Ger. 1,274,097 (1968). c) I. I. Tokarskaya, L. Kh. Bikchurina, A. S. Shmelev, S. Z. Akhmetova, Z. I. Abramovich, and T. M. Kannanov, U.S.S.R. 263,583 (1970). d) K. Ito, H. Uenaka, N. Kotera, S. Yamamoto, I. Dogane, Y. Shigehiro, H. Kuruma, T. Chinuki, H. Yoshitake, K. Tanimoto, S. Hasegawa, and N. Kobayashi, Japan, 71—9576 (1971). e) K. Shimada, S. Nagahama, T. Nishikawa, and T. Harada, Japan, 73—1067 (1973).

7) T. Yumoto, *Nippon Kagaku Kaishi*, **1973**, 2240.

8) K. Shimada, *ibid.*, **1972**, 616.

BULLETIN OF THE CHEMICAL SOCIETY OF JAPAN, VOL. 48 (3), 1061—1062 (1975)

The Structure of Tedanin, a New Carotenoid of *Tedania digitata* (O. Schmidt)

Nobuhisa OKUKADO

Department of Chemistry, Faculty of Science, Kyushu University, Higashi-ku, Fukuoka 812

(Received July 17, 1974)

Synopsis. A new carotenoid, tedanin, which was isolated as a main pigment from a sea sponge, "*Tedania digitata* (O. Schmidt)," was shown to have the (I) structure by means of spectroscopic and chemical evidence.

The carotenoids of sponges have been the subject of many investigations;[1] for instance, a novel class of carotenoids with aromatic end-groups has been discovered.[2] However, the pigments of one sea sponge, "*Tedania digitata* (O. Schmidt)," have not so far been reported. This paper will describe the isolation of a new carotenoid named tedanin from the sponge and structural studies which showed that the pigment has the structure represented by Formula (I).

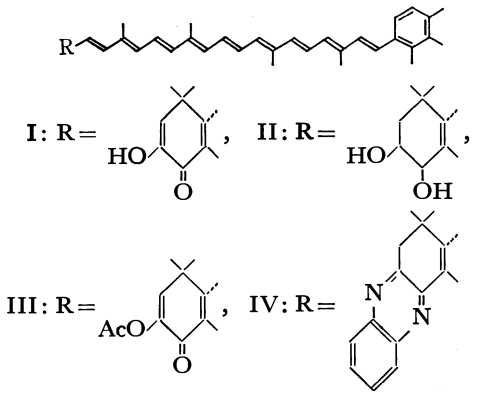

Results and Discussion

Tedanin crystallizes in the form of purplish-black prisms with a mp of 188—190 °C. The molecular formula, $C_{40}H_{48}O_2$, was established by high-resolution mass spectrometry and by elemental analysis. The UV spectrum shows a single round absorption at 490 nm in benzene and one at 500 nm in pyridine, as is shown in Fig. 1. The location and the curve of the

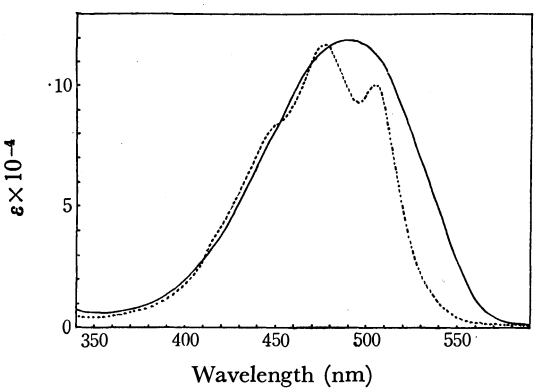

Fig. 1. Absorption spectra of tedanin (I) (——) and tetrahydrotedanin (II) (——) (benzene)

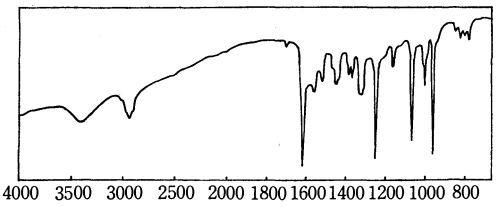

Fig. 2. IR Spectrum of tedanin (I) (KBr disk).

absorption are very similar to those of astacene.[3] Other properties, such as chromatographic behaviour, solubility, and solvent partition, also resembled those of astacene.[3] These facts seem to indicate the structural similarity of these two pigments. The IR spectrum of this pigment is shown in Fig. 2. The occurrence of peaks at 1620, 1250, 1060, 1380, and 1365 cm^{-1}, which are also present in the spectrum of astacene[4] suggests the presence of a diosphenol grouping. In addition to the ion peaks characteristic of the polyene chain of typical carotenoids [*m/e* 560(M), 468(M−92), 454(M−106), 106, and 91],[5] the mass spectrum of the pigment gives peaks at *m/e* 408(M−152), 203, 152, and 137, which are also considered to be evidence for the presence of a diosphenol end-group.[6] Furthermore, a diagnostically important peak was observed at *m/e* 133; this clearly indicates the presence of a trimethylphenyl end-group.[7] Further evidence of the presence of these end-groups was obtained from the NMR spectral study. The signals at δ 1.32(6H) and 2.11(3H) can be assigned to the 1,1-dimethyl and 5-methyl protons of the diosphenol group respectively.[8] The signals appearing at the lower field [δ 2.22(3H) and 2.31(6H)] are considered to arise from the three methyl groups attached to the aromatic nucleus, and a comparison of the chemical shifts with those of three aryl methyl groups of okenone[9] and 4′-desoxo-okenone[10] suggests that the second end-group is 2,3,4-trimethylphenyl. This was confirmed by the presence of the double doublet signal centered at δ 6.97(1H) and δ 7.27(1H) (J=7.2 Hz), which is characteristic of aromatic protons at the 5- and 6-positions of this end-group.[1c] The IR absorption at 800 cm^{-1} attributable to two adjacent aryl hydrogens is in agreement with this conclusion.

From the above evidence, the structure of tedanin can be formulated as is shown in Formula (I). The all-*trans* configuration of I was based on the absence of the *cis*-peak in the UV spectrum[11] and the presence of a sharp singlet at 960 cm^{-1} in the IR spectrum.[12]

Further evidence supporting the (I) structure comes from chemical studies. The reduction of tedanin with sodium borohydride resulted in a hypsochromic shift, accompanied by the new formation of fine structures

in the UV spectrum (Fig. 1). This is in accordance with the formation of a tetrahydro compound (II). The UV spectral data of II [λ_{max}, 496 nm (CS_2)] are very similar to those of β-renierapurpurin [λ_{max}, 497 nm (CS_2)][13] but differ from those of β-isorenieratene [λ_{max}, 487 nm (CS_2)].[13] This apparently shows that the chromophore of this reduction product (II) is not of the β,φ-carotene-type but of the β,χ-carotene-type. The acetylation of tedanin with acetic anhydride and pyridine afforded an acetate (III). Finally, the quinoxaline derivative (IV) was prepared by a reaction with *o*-phenylenediamine. The structures of these derivatives were confirmed by the fact that the mass spectra of these derivatives showed the expected molecular ion and a regular pattern of fragmentations.[14] These facts strongly support the conclusion that the structure of tedanin is 3-hydroxy-2,3-didehydro-β,χ-carotene-4-one (I).

However, it is not clear whether tedanin originally occurs in the sponge or whether it is an artifact formed by the oxidation of a ketol compound.

Experimental

All the melting points are uncorrected. The solutions were concentrated under reduced pressure below 45 °C under nitrogen. The instruments used for the measurements of the spectra were as follows. UV spectra; Hitachi, Model EPS-3T. IR spectra; Hitachi, Model 215. NMR spectra; Hitachi, Model R-22. Mass spectra; Hitachi, Model RMU-4 and JEOL, Model JMS-01SG.

Isolation of Tedanin (I). Specimens of the sponge, (80 g, dry weight), collected at Amakusa in Kumamoto Prefecture in November, 1972, were repeatedly extracted with acetone, and the pigments were transferred into benzene by the addition of water. After the evaporation of the solvent, the pigments were saponified with 10% methanolic potassium hydroxide in petroleum benzine at room temperature for 12 hr and then separated into epiphasic and hypophasic fractions by repeated partitioning between 90% methanol and petroleum benzine. The hypophasic methanol solution was then diluted with water, and the pigments were extracted again with benzene. The evaporation residue was treated with acetone, and the insoluble colorless impurities were removed repeatedly as completely as possible. The residue was finally diluted with a small quantity of petroleum benzine and left to stand in an ice-box. Repeated recrystallizations of the precipitate from methylene chloride–ethanol gave tedanin (I, 5 mg) as purplish-black prisms; mp 188—190 °C. Found: C, 85.20; H, 8.56%. Calcd for $C_{40}H_{48}O_2$: C, 85.66; H, 8.63%. UV spectra: λ_{max}, 490 nm ($\varepsilon=1.19\times10^5$)($C_6H_6$); 500 nm (pyridine). IR spectrum; Fig. 2. NMR spectrum: δ ($CDCl_3$) 1.32 (6H, s, 1,1-dimethyl); 2.00 and 2.03 (each 6H, s, chain methyl); 2.11 (3H, s, 5-methyl); 2.22 and 2.31 (3H, and 6H, respectively, s, arylmethyl); 6.03—6.90 (15H, m, olefinic protons); 6.97 and 7.27 (2H, dd($J=7.2$ Hz), aromatic protons). Mass spectrum: 560.3579 (M. Calcd for $C_{40}H_{48}O_2$, 560.3655), 408(M−92), 454 (M−106), 408(M−152), 203, 152, 137, 133, 106, 105, 92, 91, 77, 44, 28, 18.

Reduction of Tedanin to Tetrahydrotedanin (II). Tedanin (I, 1 mg) dissolved in ethanol (10 ml) was treated with sodium borohydride (40 mg) for 1 hr at room temperature. The mixture was diluted with water and extracted with benzene. The extract was washed with dilute hydrochloric acid, an aqueous sodium bicarbonate solution, and then water, dried, and evaporated. Recrystallizations of the residue from methylene chloride–ethanol gave II as red prisms (0.6 mg); mp 186 °C. UV spectra: λ_{max}, 446_{sh}, 475 ($\varepsilon=1.17\times10^5$), 506 nm ($C_6H_6$); 453_{sh}, 496, 524 nm (CS_2). Mass spectrum; 564 (M), 546, 528 472, 458, 440, 422, 408 395, 348, 329, 289, 249, 221, 133, 106, 105, 92, 91, 77, 44, 28, 18.

Acetylation of Tedanin to Tedanin Acetate (III). To a solution of tedanin (I, 1 mg) in dry pyridine (10 ml), was added acetic anhydride (1 ml). The reaction mixture was then left to stand at room temperature for 6 hr and extracted with benzene. The treatment of the extract by the usual procedure gave III as black prisms (0.65 mg); mp 172—173 °C. UV spectrum: λ_{max}, 487 nm ($\varepsilon=1.28\times10^5$)($C_6H_6$). Mass spectrum: 602 (M), 560, 510, 496, 454, 404, 362, 347, 329, 289, 133, 106, 105, 92, 91, 77, 51, 44, 28.

Preparation of Quinoxaline Derivative (IV). To a solution of tedanin (I, 1.8 mg) in glacial acetic acid (1 ml), was added *o*-phenylenediamine (15 mg). The mixture was kept at 100 °C on a water bath for 2 hr and then extracted with benzene. The treatment of the extract by the usual procedure gave IV as reddish-purple crystals (0.3 mg); mp 150—151 °C. UV spectrum: λ_{max}, 493 nm ($\varepsilon=1.16\times10^5$)($C_6H_6$). Mass spectrum: 632 (M), 617, 540, 526, 511, 434, 419, 393, 355, 343, 329, 289, 277, 275, 259, 249, 133, 105, 91, 77, 55, 41.

The author wishes to express his deep gratitude to Professor Masaru Yamaguchi for his many helpful discussions and suggestions during this work. The author also wishes to thank Dr. Michio Nakanishi of the Yoshitomi Pharmaceutical Co., Ltd., for the help he gave him in the measurement of the mass spectrum and Dr. Takaharu Hoshino of the Mukaijima Marine Station, Hiroshima University, for the identification of the sponge.

References

1) a) P. Karrer and E. Jucker, "Carotenoids,." translated by E. A. Braude, Elsevier, New York (1950), p. 88. b) T. W. Goodwin, "Carotenoids," Chemical Publishing Co., New York (1954), p. 155. c) T. Hamasaki, N. Okukado, and M. Yamaguchi, This Bulletin, **46**, 1884 (1973).

2) M. Yamaguchi, This Bulletin, **30**, 111, 979 (1957); **31**, 51, 739 (1958); **33**, 1560 (1960).

3) Ref. 1a, p. 237.

4) R. R. Upadhyay and S. Liaaen-Jensen, *Acta Chem. Scand.*, **24**, 3055 (1970).

5) W. Vetter, G. Englert, N. Rigassi, and U. Schwieter, "Carotenoids," ed. by O. Isler, H. Gutmann, and U. Solms, Birkhauser, Basel (1971), p. 248.

6) J. Baldas, Q. N. Porter, A. P. Leftwick, R. Holzel, B. C. L. Weedon, and J. Szabolcs, *Chem. Commun.*, **1969**, 415.

7) C. R. Enzell, G. W. Francis, and S. Liaaen-Jensen, *Acta Chem. Scand.*, **23**, 727 (1969).

8) Ref. 5, p. 207.

9) S. Liaaen-Jensen, *Acta Chem. Scand.*, **21**, 961 (1967).

10) A. J. Aasen and S. Liaaen-Jensen, *ibid.*, **21**, 970 (1967).

11) L. Zechmeister, A.L. LeRosen, W. A. Schroeder, A. Polgar, and L. Pauling, *J. Amer. Chem. Soc.*, **65**, 1940 (1943).

12) K. Lunde and L. Zechmeister, *ibid.*, **77**, 1647(1955).

13) R. D. G. Cooper, J. B. Davis, and B. C. L. Weedon, *J. Chem. Soc.*, **1963**, 5637.

14) G. W. Francis, S. Hertzberg, R. R. Upadhyay, and S. Liaaen-Jensen, *Acta Chem. Scand.*, **26**, 1097 (1972); S. Hertzberg, S. Liaaen-Jensen, C. R. Enzell, and G. W. Francis, *ibid.*, **23**, 3290 (1969).

BULLETIN OF THE CHEMICAL SOCIETY OF JAPAN, VOL. 48 (3), 1063—1064 (1975)

Reaction of Benzyne with *N*-Benzylideneaniline

Jyuzo NAKAYAMA, Hiroshi MIDORIKAWA, and Masayuki YOSHIDA*

The Institute of Physical and Chemical Research, Wako-shi, Saitama 351

**Department of Chemistry, Faculty of Science, The University of Tokyo, Hongo, Tokyo 113*

(Received July 18, 1974)

Synopsis. Benzyne, generated from benzenediazonium-2-carboxylate and 2-carboxybenzenediazonium chloride, reacted with *N*-benzylideneaniline to give *N*-(*o*-anilinobenzhydryl)aniline (I) and 5,6-dihydro-5,6-diphenylphenanthridine (II) as final products.

Although benzyne is known to undergo 1,2-cycloadditions with carbon-carbon double bonds,[1] its reactions with carbon-heteroatom double bonds are scarce and only carbonyl groups have been shown to react with benzynes.[2,3] In this paper we wish to report the first example of reaction of benzyne with an azomethine group.

Heating benzenediazonium-2-carboxylate[4] with *N*-benzylideneaniline under reflux in methylene chloride yielded *N*-(*o*-anilinobenzhydryl)aniline[5] (I, 18%[6]) and 5,6-dihydro-5,6-diphenylphenanthridine (II, 8%[6]) together with small amounts of a few unidentified products. Similarly, 2-carboxybenzenediazonium chloride[7] was decomposed with *N*-benzylideneaniline in boiling 1,2-dichloroethane in the presence of propylene oxide to afford the diamine (I, 35%[6]) and the dihydrodiphenylphenanthridine (II, 11%[6]).

In the reaction of benzyne with *N*-benzylideneaniline, the initial formation of a benzazetine (III) by a 1,2-cycloaddition of benzyne to the azomethine group of *N*-benzylideneaniline seems most probable and this benzazetine (III) is converted by ring-opening into a valence tautomer (IV), which undergoes a 1,4-cycloaddition with *N*-benzylideneaniline to yield a tetrahydroquinazoline (V). The formation of the diamine (I) from V during its isolation by chromatography is feasible because of the known susceptibility of 1,2,3,4-tetrahydroquinazolines to acid hydrolysis.[8] Evidence in support of the above reaction courses is found in the reaction of *N*-phenylbenzazetine with *N*-phenylmaleimide.[9] We have also postulated such cycloaddition and ring-opening in the formation of 2,4-diphenyl-1,3-benzodioxin from benzyne and benzaldehyde.[3] The formation of the dihydrodiphenylphenanthridine (II) may be explained in terms of a 1,4-cycloaddition of benzyne with *N*-benzylideneaniline followed by aromatization to 5,6-dihydrophenanthridine (VI) and subsequent *N*-phenylation with benzyne.[10] The last course of the *N*-phenylation was confirmed by a separate synthesis of II by heating benzenediazonium-2-carboxylate with 5,6-dihydro-6-phenylphenanthridine[11] (VI) and thus, the structure of II was confirmed.

5,6-Dihydro-5-phenylphenanthridine (VII), which might be formed by an alternative way of a 1,4-cycloaddition of benzyne with *N*-benzylidneaniline, was not observed in the reaction products. Since steric hindrance exerted in the transition states producing VI and VII seems to be the same, the selective formation

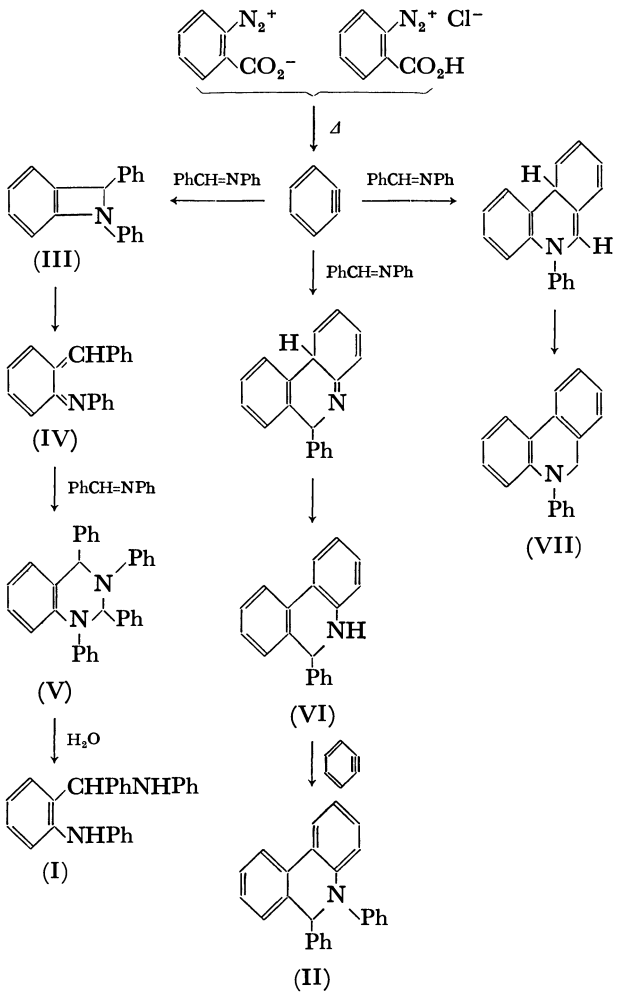

of VI may suggest that the concerted formation of two carbon-carbon bonds in the 1,4-addition is preferable to that of carbon-carbon and carbon-nitrogen bonds.

All other attempts to isolate similar products in the reaction of benzyne with substituted *N*-benzylideneaniline such as *N*-(4′-methylbenzylidene)-4-toluidine, *N*-(4′-methoxybenzylidene)-4-anisidine, and *N*-(4′-chlorobenzylidene)-4-chloroaniline have failed.

Experimental

Reaction of N-*Benzylideneaniline with Benzyne Generated from Benzenediazonium-2-carboxylate.* A suspension of benzenediazonium-2-carboxylate, prepared from 20 mmol of anthranilic acid according to the procedure described in the literature,[12] in methylene chloride (120 ml) was dried over Molecular Sieves (10 g) at 0 °C with stirring for 5 hr. To the suspension *N*-benzylideneaniline (12 mmol) was added and the mixture was heated under reflux for 1.5 hr. The dark brown reaction mixture was filtered and the filtrate, upon

evaporation of the solvent, gave a brown oily residue, which was chromatographed on silica gel (120 g). Elution with cyclohexane gave a pale yellow oil (0.48 g), which, after rechromatography, afforded 0.27 g (8%) of 5,6-dihydro-5,6-diphenylphenanthridine (II) as colorless needles and small amounts of two unidentified products (mp 146—152 °C and 128—130 °C). Elution with cyclohexane–benzene (9: 1) afforded a small amount of crystallines (mp 117—138 °C), while elution with cyclohexane–benzene (5: 1) afforded 0.38 g (18%) of *N*-(*o*-anilinobenzhydryl)aniline (I), mp 134—135 °C (lit,[5] 134—135 °C). Further elution with cyclohexane–benzene (1: 1) gave aniline and benzaldehyde.

5,6-Dihydro-5,6-diphenylphenanthridine (II) (Found: C, 90.02; H, 6.03; N, 4.30%. Calcd for $C_{25}H_{19}N$: C, 90.05; H, 5.74: H, 4.20%), mp 138—140 °C, ν_{max} (Nujol) 3070, 3040, 1592, 1496, 1438, and 1260 cm^{-1}, *m/e* 333 (M^+), δ ($CDCl_3$) 5.93 (1H, s), 6.84—7.50 (16H, m), and 7.68—7.90 (2H, m).

Chromatography of the brown oily residue over basic alumina or florisil gave similarly compounds I and II, but no tetrahydroquinazoline (V) was isolated in any experiments. The reaction carried out in the absence of Molecular Sieves yielded I and II in somewhat decreased yield along with a small amount of triphenylamine, the reaction product of benzyne with aniline, which may be formed by hydrolysis of *N*-benzylideneaniline. When the reaction was carried out in methylene chloride not strictly dried, only diphenyl- and triphenylamines were obtained, and neither I nor II was isolated.

Reaction of N-*Benzylidneaniline with Benzyne from 2-Carboxybenzenediazonium Chloride.* 2-Carboxybenzenediazonium chloride[7] (10 mmol) was heated under reflux for 1 hr with *N*-benzylideneaniline (7 mmol) in the presence of propylene oxide (1.7 ml) in 1,2-dichloroethane (100 ml). The red reaction mixture was concentrated under reduced pressure and the residue was chromatographed on silica gel. Compounds I (35%) and II (11%) were isolated in a similar way described before.

5,6-*Dihydro*-5,6-*diphenylphenanthridine (II).* Benzenediazonium-2-carboxylate, prepared from 5 mmol of anthranilic acid, was heated with 5,6-dihydro-6-phenylphenanthridine[11] (VI, 3 mmol) in methylene chloride (50 ml) under reflux for 1 hr. The brown reaction mixture was concentrated and the residue was submitted to purification by chromatography on silica gel to give 5,6-dihydro-5,6-diphenylphenanthridine (II, 35%), mp 138—140 °C, which was identical (mixed melting point) with the product obtained from benzyne and *N*-benzylideneaniline.

References

1) R. W. Hoffmann, "Dehydrobenzene and Cycloalkynes," Academic Press, New York, N. Y. (1967).

2) H. Heaney, J. M. Jablonski, and C. T. McCarty, *J. Chem. Soc., Perkin I*, **1972**, 2903.

3) J. Nakayama, M. Yoshida, and O. Simamura, *Chem. Lett.*, **1973**, 451.

4) M. Stiles and R. G. Miller, *J. Amer. Chem. Soc.*, **82**, 3802 (1960); M. Stiles, R. G. Miller, and U. Burckhardt, *ibid.*, **85**, 1792 (1963); R. G. Miller and M. Stiles, *ibid.*, **85**, 1798 (1963).

5) H. Hoberg and A. Milchereit, *Anal. Chem.*, **766**, 146 (1972).

6) Yield of I was based on *N*-benzylideneaniline used and that of II based on anthranilic acid or 2-carboxybenzenediazonium chloride.

7) B. H. Klanderman and T. R. Criswell, *J. Org. Chem.*, **34**, 3426 (1969); F. M. Logullo, Ph. D. Dissertation, Case Institute of Technology, 1965.

8) See for example, H. M. Fales, *J. Amer. Chem. Soc.*, **77**, 5118 (1955); L. Crombie, A. H. A. Krasinski, and M. Manzoor-i-Khuda, *J. Chem. Soc.*, **1963**, 4970.

9) E. M. Burgess and L. McMullagh, *J. Amer. Chem. Soc.*, **88**, 1580 (1966).

10) An alternative way of formation of II which involves the direct *N*-phenylation by benzyne to the initial 1,4-adduct of benzyne and *N*-benzylideneaniline (*ene* reaction) was suggested by a referee.

11) C. A. Bartram, D. Harrison, and W. F. Short, *J. Chem. Soc.*, **1958**, 1158.

12) F. M. Logullo, A. H. Seitz, and L. Friedman, "Organic Syntheses," Vol. 48, p. 12 (1968).

BULLETIN OF THE CHEMICAL SOCIETY OF JAPAN, VOL. 48 (3), 1065—1066 (1975)

Steric Interaction between the 1-Methyl and 9-Hydrogen of 1,2,3,4-Tetramethyldibenzofuran[1)]

Takashi KEUMI, Yoshibumi OSHIMA, and Niichiro TOKURA*

Department of Fiber and Dyestuff, Faculty of Engineering, Fukui University, Bunkyo, Fukui 910

**Department of Applied Chemistry, Faculty of Engineering, Osaka University, Yamadakami, Suita, Osaka 565*

(Received July 18, 1974)

Synopsis. 1,2,3,4-Tetramethyldibenzofuran was newly synthesized and the steric interaction between the hydrogen atom at the 9-position and the methyl group at the 1-position was examined from the nuclear Overhauser effects.

Recently, we have reported that the electrophilic substitution on the 1-position of dibenzofuran was hindered sterically by the hydrogen at the 9-position.[2)] This kind of the steric hindrance has never been pointed out in the heteroaromatic compounds such as dibenzofuran, dibenzothiophene, *etc.* In this paper, we wish to report the synthesis of 1,2,3,4-tetramethyldibenzofuran (**5**) and the measurements of the intramolecular nuclear Overhauser effects (NOE) in order to confirm the steric interaction between the hydrogen at the 9-position and the substituent at the 1-position. New compound **5** was synthesized in a 54.4% total yield according to the procedures described in the experimental section. The NMR chart of this compound and the results of the NOE are shown in Fig. 1 and Table 1, respectively. The assignments of the methyl signals were made by the comparison of the spectrum of **5** with those of mono- and polymethyldibenzofurans. The proton or methyl-protons at the 1- and 9-positions of dibenzofuran are most deshielded by the induced ring currents of the outer aromatic and furan rings, followed by those at 4- and 6-positions. For example, the methyl signals of 1-, 2-, 3-, and 4-methyldibenzofurans were observed at δ 2.72, 2.50, 2.48, and 2.58 respectively.[3)]

Saturation of 1-methyl signal resulted in an enhancement of 38% of the integrated area of the multiplet of 9-hydrogen, leaving the other parts of the spectrum unaltered, whereas saturations of [2-methyl+3-methyl] and 4-methyl frequencies had no effect on the signals of the aromatic protons. Irradiation at the [2-methyl+3-methyl] frequencies gave a small increase

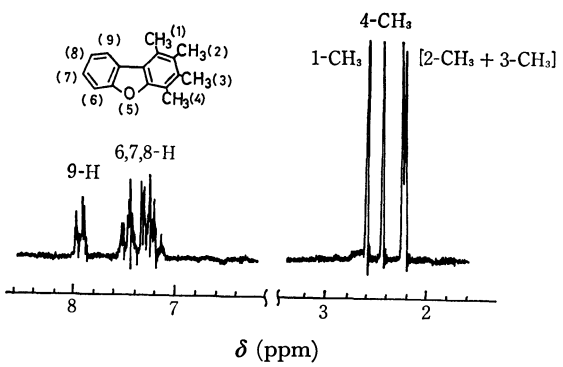

Fig. 1. NMR spectrum of 1,2,3,4-tetramethyldibenzofuran in $CDCl_3$.

TABLE 1. THE RESULTS OF THE NOE MEASUREMENTS

Irradiation protons (δ in $CDCl_3$)	Enhancements of the observed protons[a)] (%)		
	9-H	1-CH_3	6,7,8-H
1-CH_3 (2.63)	+38		—
[2-CH_3+3-CH_3] (2.26) (2.24)	+ 3	+12	—
4-CH_3 (2.46)	—	—	—

a) Average of 3 runs.

in the integrated area of the 1-methyl signals. It is clear, from these results, that the methyl group at the 1-position of dibenzofuran affects significantly the hydrogen at the 9-position in the NOE. Martin and Nouls have reported[4)] in the studies on the NOE of overcrowded aromatic hydrocarbons that the proton signals at the 5-position of phenanthrene increased in intensity by 33.5% on saturation of the methyl signal at the 4-position. The steric interaction between the 1- and 9-positions of dibenzofuran is comparable to that between the 4- and 5-positions of phenanthrene. Consequently, we should consider that not only the increase in the electronegativity of the 1-carbon by a strain effect[5)] of the fused ring and the steric hindrance by the hydrogen at the 9-position are responsible for the low reactivity[6)] of the 1-position in electrophilic substitutions of dibenzofuran derivatives.

Experimental

Measurements. NMR spectra were measured at 100 MHz on JEOL Co. Model PS-100 spectrometer using TMS as an internal standard. IR and UV spectra were measured with Hitachi EPI-S2 and EPS-2U spectrophotometers, respectively. For NOE measurements, 13% $CDCl_3$ solutions of freshly sublimed **5** were thoroughly degassed under high vacuum. These solutions were studied at 100 MHz by a frequency sweep method. The enhancements of the quotient of the integrated intensities of the observing protons with and without irradiation of the another proton signals.

Synthesis of **5**. *2-(2,3,5-Trimethylphenoxy)cyclohexanone* (**1**): A solution of α-bromocyclohexanone (prepared from 20 g of cyclohexanone and 36.4 g of *N*-bromosuccinimide in carbon tetrachloride) and sodium 2,3,5-trimethylphenoxide (prepared from 28 g of 2,3,5-trimethylphenol and 4.7 g of sodium) in benzene (200 ml) was shaken for 5 hr at room temperature. The reaction mixture was washed with water, dilute alkali, and water and the solvent was removed. Recrystallization of the residue from methanol gave 31.5 g (66.9%) of **1**. Mp 75—76 °C. IR (cm^{-1}, KBr): 1728, 1157, and

838. Found: C, 77.82; H, 8.52%. Calcd for $C_{15}H_{20}O_2$: C, 77.55; H, 8.68%.

1,3,4-Trimethyl-6,7,8,9-tetrahydrodibenzofuran (2): A mixture of **1** (20 g), polyphosphoric acid (200 ml), and phosphorus pentaoxide (100 g) was shaken at 100 °C for 3 hr, poured into ice-water, and filtered out. Recrystallization of the product from methanol gave 19.5 g (quantitatively) of **2**. Mp 95—96 °C. IR (cm^{-1}, KBr): 1450, 1215, 1100, and 860. NMR (CCl_4, δ): 6.52 (2-H, s, 1H), 2.60—2.80 (m, 4H), 2.39 (1-CH_3, s, 3H), 2.26 (4-CH_3, s, 3H), 2.22 (3-CH_3, s, 3H), and 1.70—1.90 (m, 4H). Found: C, 84.03; H, 8.54%. Calcd for $C_{15}H_{18}O$: C, 84.07; H, 8.47%.

1,3,4-Trimethyl-2-chloromethyl-6,7,8,9-tetrahydrodibenzofuran (3): **2** (5.0 g) was added to a solution of zinc chloride (0.3 g), formaldehyde (3.0 g, 37%), and concd hydrochloric acid (20 ml) with vigorous stirring. The mixture was kept at 75—80 °C for 10 hr under an introduction of hydrogen chloride, and then, it was filtered out. Recrystallization of the product from ethanol gave 5.8 g (94.8%) of **3**. Mp 131—131.5 °C. IR (cm^{-1}, KBr): 1448, 1322, 1096, and 713. NMR (CCl_4, δ): 4.68 (CH_2Cl, s, 2H), 2.60—2.88 (m, 4H), 2.56 (1-CH_3, s, 3H), 2.37 (4-CH_3, s, 3H), 2.36 (3-CH_3, s, 3H), and 1.80—2.00 (m, 4H). Found: C, 73.25; H, 7.44%. Calcd for $C_{16}H_{19}OCl$: C, 73.13; H, 7.29%.

1,2,3,4-Tetramethyl-6,7,8,9-tetrahydrodibenzofuran (4): A solution of **3** (2.0 g) in dry ether was added to a suspension of lithium aluminum hydride (0.4 g) in dry ether (20 ml) with stirring. The mixture was refluxed for 2 hr, poured into dilute hydrochloric acid, and the ether solution was evaporated to dryness. Recrystallization of the residue from ethanol gave 1.6 g (92%) of **4**. Mp 94—95 °C. IR (cm^{-1}, KBr): 1194 and 1094. NMR (CCl_4, δ): 2.60—2.90 (m, 4H), 2.40 (1-CH_3, s, 3H), 2.33 (4-CH_3, s, 3H), 2.22 (2-CH_3, s, 3H), 2.18 (3-CH_3, s, 3H), and 1.70—2.00 (m, 4H). Found: C, 84.12; H, 8.96%. Calcd for $C_{16}H_{20}O$: C, 84.16; H, 8.83%.

1,2,3,4-Tetramethyldibenzofuran (5): A mixture of **4** (5.0 g) and 5% palladium–charcoal (2.5 g) was heated at 220—230 °C for 3 hr under a slow stream of dry nitrogen, extracted with ether, and the solvent was removed. Recrystallization of the residue from ethanol gave 4.5 g (91%) of **5**. Mp 111—112 °C. IR (cm^{-1}, KBr): 1452, 1223, 1084, and 744. NMR (CCl_4, δ): 7.94 (9-H, m, 1H), 7.00—7.60 (6,7,8-H, m, 3H), 2.63 (1-CH_3, s, 3H), 2.46 (4-CH_3, s, 3H), 2.26 (2-CH_3, s, 3H), and 2.24 (3-CH_3, s, 3H). UV (cyclohexane, nm (log ε)): 311.8 (3.53), 287 (4.32), 257.6 (4.24), 228.5 (4.59), and 214.6 (4.53). Found: C, 85.52; H, 7.20%. Calcd for $C_{16}H_{16}O$: C, 85.68; H, 7.19%.

The authors are grateful to Professor A. Yoshikoshi and Mrs. R. Tanaka of the Chemical Research Institute of Non-Aqueous Solutions of Tohoku University for the measurements of NOE.

References

1) Studies on Dibenzofuran and Its Derivatives. XXI. For XX; T. Keumi, N. Mochinaga, and Y. Oshima, *Nippon Kagaku Kaishi*, **1974**, 2243.

2) T. Keumi, S. Yamada, and Y. Oshima, *ibid.*, **1972**, 1438.

3) T. Keumi, Unpublished results.

4) R. H. Martin and J. C. Nouls, *Tetrahedron Lett.*, **1968**, 2727.

5) R. Taylor, *J. Chem. Soc., B*, **1968**, 1559.

6) C. Eaborn and J. A. Sperry, *J. Chem. Soc.*, **1961**, 4921. R. Baker and C. Eaborn, *ibid.*, **1961**, 5077.

BULLETIN OF THE CHEMICAL SOCIETY OF JAPAN, VOL. 48 (3), 1067—1068 (1975)

Reaction of Ethyl α,α-Dichloroacetoacetate with Aldehydes

Akira TAKEDA, Sadao TSUBOI, and Isao NAKASHIMA

Department of Synthetics Chemistry, School of Engineering, Okayama University, Tsushima, Okayama 700

(Received August 12, 1974)

Synopsis. Ethyl α,α-dichloroacetoacetate reacted with aldehydes in the presence of sodium ethoxide to give α-chloropyruvate and/or α-chloroglycidate. 2,5-Bis(1'-chloroalkylidene)-1,4-cyclohexanedione (**4**) was obtained as a by-product in a low yield.

Previously, one of the present authors (A. T.) has reported the base-catalyzed condensation of dichloroacetate with aldehydes to give α-chloropyruvate (**1**) and/or α-chloroglycidate (**2**), which are useful synthetic intermediates.[1]

$$RCHO + CHCl_2CO_2R' \xrightarrow{NaOEt} \underset{\mathbf{1}}{RCH(O)C(Cl)CO_2R'} + \underset{\mathbf{2}}{R\text{-}CH(Cl)COCO_2R'}$$

As an extension of the previous work, we carried out the base-catalyzed condensation of ethyl dichloroacetoacetate (**3**) with aldehydes to give esters **1** and **2**. This reaction can be well explained by assuming the formation of enolate anion of dichloroacetate, since the ester **3** is known to undergo retro acetoacetate reaction to afford dichloroacetate in the presence of alkoxide.[2] The yields and boiling points of the products **1** and **2** are listed in Table 1.

$$\underset{\mathbf{3}}{CH_3COCCl_2CO_2Et} \xrightarrow{EtO^-} CH_3\text{-}C(=O)(OEt)\text{-}CCl_2CO_2Et \xrightarrow{-CH_3CO_2Et} \bar{C}Cl_2CO_2Et \xrightarrow{RCHO} \mathbf{1} \text{ or } \mathbf{2}$$

The identification of the products was done by comparison of spectral data with those of authentic samples.[1,3] In contrast with the reaction of dichloroacetate, the present reaction afforded a small amount of crystalline by-products, which were identified as 2,5-bis(1'-chloroalkylidene)-1,4-cyclohexanedione (**4**) or its geometrical isomers on the basis of IR, NMR, MS spectral data, and elemental analyses (see Tables 2 and 3). The mass spectra of these products as well as their analyses supported the composition of $C_8H_4Cl_2O_2R_2$.

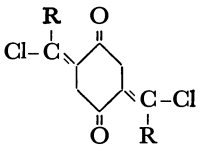

4 (R=alkyl or aryl)

IR spectra exhibited absorptions due to conjugated C=O stretching at 1692—1705 cm^{-1} and those due to C=C stretching at 1660—1665 cm^{-1}.

Possible route of the formation of dione **4** can be explained by the following mechanism, involving the condensation of two molecules of **6**, which may be derived from the reaction of dichloroacetonyl anion (**5**) with the aldehyde.

$$\underset{\mathbf{5}}{CH_3COCCl_2CO_2Et} \longrightarrow CH_3COC\bar{C}l_2 \xrightarrow[-Cl^-]{RCHO}$$

$$\left[RCH(Cl)\text{-}C(=O)\text{-}C(Cl)(=O)\text{-}CH_3 \longrightarrow \underset{\mathbf{6}}{RCH(Cl)\text{-}C(=O)\text{-}C(=O)\text{-}CH_3} \right]$$

$$\xrightarrow{-H_2O} \left[R\text{-}CH(Cl)\text{-}C(=O)\text{-}CH=C(Cl)\text{-}C(=O) \right] \longrightarrow \mathbf{4}$$

Table 1. Products from the reaction of **3** with aldehydes

$$R\text{-}CH(Cl)\text{-}C(=O)\text{-}CO_2Et \ (\mathbf{1}) \text{ or } R\text{-}CH(Cl)\text{-}C(Cl)(=O)\text{-}CO_2Et \ (\mathbf{2})$$

Compound Code	R	Yield, %	Bp(lit,), °C/mmHg
1a	C_2H_5	69	99—105/17 (94—98/18[1])
1b	$(CH_3)_2CH$	25	76—86/6 (104—106/20.5[1])
2c	n-C_6H_{13}	15	120—130/7 (134—136/13[1])
2d	C_6H_5	17	130—136.5/8 (165—167/18.5[3])

Table 2. By-products from the reaction of **3** with aldehydes

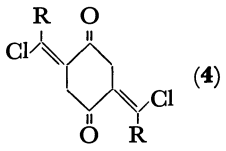

(**4**)

Compound Code	R	Yield, %	Mp, °C	Found (%) (Calcd (%)) C	H
4a	C_2H_5	6.1	141—142	54.93 (55.19	5.46 5.40)
4b	$(CH_3)_2CH$	3.7	197	58.13 (58.14	6.36 6.27)
4c	n-C_6H_{13}	7.9	105.5—106	64.55 (64.33	8.25 8.10)
4d	C_6H_5	5.9	218	67.41 (67.24	3.78 3.95)

Table 3. Spectral data of compound **4**.

Compound	IR (Nujol) cm^{-1}	NMR, δ (solvent)	MS (70 eV) *m/e* (rel. intensity)
4a	1700 (C=O), 1660 (C=C), 1150, 930, 900, 880, 795	($CDCl_3$) 1.12 (br. t, 6H, J=6 Hz, $2CH_3$), 1.50—2.90 (m, 8H, $4CH_2$)	260 (12, M^+, 2Cl), 231 (14), 225 (100, M^+–Cl, 1Cl), 197 (57), 183 (50), 155 (30), 115 (32)
4b	1705 (C=O), 1668 (C=C), 1293, 1180, 1156,1103, 1030, 882, 695	($CDCl_3$) 1.06 (d, 6H, J=5.5 Hz, $2CH_3$), 1.16 (d, 6H, J=5.5 Hz, $2CH_3$), 1.30—1.80 [m, 4H, $2C\underline{H}(CH_3)_2$ and $2\underline{H}>\dot{C}-CO-$], 2.25 (d, 2H J=6 Hz, $2\underline{H}>\dot{C}-CO-$)	288 (1, M^+, 2Cl), 253 (14, M^+–Cl, 1Cl), 245 (4), 233 (21), 211 (12),197 (100)
4c	1692 (C=O), 1660 (C=C), 1100, 940, 880, 730, 680	(CCl_4) 0.9 (br. t, 6H, J=6 Hz, $2CH_3$), 1.10—2.11 (m, 24H, $12CH_2$)	372 (7, M^+, 2Cl), 337 (30, M^+–Cl, 1Cl), 253 (73), 239 (30), 191 (100), 157 (60), 115 (47), 97 (50)
4d[a]	1703 (C=O), 1665 (C=C), 1603 (benzene ring), 945, 866, 760, 700, 680		356 (18, M^+, 2Cl), 321 (82, M^+–Cl, 1Cl), 293 (23), 285 (23, M^+–2Cl), 258 (45, M^+–2Cl–CO), 178 (100), 105 (98)

a) NMR spectrum of this compound could not be measured, because it was almost insoluble in usual solvents such as acetone, chloroform, methanol, and dimethyl sulfoxide.

Experimental

The melting points and boiling points are uncorrected. Elemental analyses were carried out by Mr. Eiichiro Amano. We are indebted to Mr. Hiroshi Ooyama of Hokko Chemical Industry Co., Ltd. for the NMR measurements, and also to Mr. Shinichi Ninomiya for technical assistance. Ethyl α,α-dichloroacetoacetate (**3**) was obtained by the reaction of ethyl acetoacetate with sulfuryl chloride, yield 63%: bp 91.5—92 °C/13 mmHg (lit,[4] 106—108 °C/30 mmHg). Aldehydes were distilled just before use.

The following experiment is shown as a typical run.

*Reaction of **3** with 2-Methylpropanal.* To a solution of 103 g (0.52 mol) of **3** and 37.3 g (0.52 mol) of 2-methylpropanal in 104 ml of dry ether was added 40.8 g (0.6 mol) of dry, powdered sodium ethoxide in several portions at 0—5 °C. After complete addition, the mixture was allowed to warm up at room temperature and then refluxed for 2 hr. It was poured into a large excess of water. Precipitated crystals collected by filtration were washed with water and ether successively, and dried. Recrystallization of the white crystals from ethanol gave 2.8 g (3.7%) of **4b**: mp 197 °C.

The ethereal layer was washed with water several times, and dried over $MgSO_4$. After removal of the solvent, the residue was distilled to give 24.6 g (25%) of **1b**: bp 76—86 °C/6 mmHg (lit.[1] 104—106 °C/20.5 mmHg). Its IR and NMR spectra were identical with those of the authentic sample.[1]

References

1) A. Takeda, S. Wada, M. Fujii, and H. Tanaka, This Bulletin, **43**, 2997 (1970).

2) This mechanism was substantiated by Gupta's work. In the course of our study on the reaction of **3** with aldehyde, he has reported that ester **3** reacts with base to give ethyl dichloroacetate: S. K. Gupta, *J. Org. Chem.*, **38**, 4081 (1973).

3) A. Takeda, S. Wada, and T. Uno, *Memoirs of the School of Engineering Okayama Univ.*, **2**, 80 (1967).

4) D. P. Wyman, *J. Org. Chem.*, **29**, 2709 (1964).

BULLETIN OF THE CHEMICAL SOCIETY OF JAPAN, VOL. 48 (3), 1069—1070 (1975)

The Cyclic Trimerization of Isocyanates by Organic Tin(II) Compounds Containing Sn-O-C Bonds

Ikuko WAKESHIMA, Hiroshi SUZUKI, and Ichiro KIJIMA

Department of Industrial Chemistry, Faculty of Engineering, Science University of Tokyo, Kagurazaka, Shinjuku-ku, Tokyo 162

(Received September 4, 1974)

Synopsis. Organic tin(II) compounds containing Sn–O–C bonds were found to be effective catalysts for the cyclic trimerization of phenyl and ethyl isocyanate. The cyclic trimerization mechanism is discussed.

There have been a number of papers[1–3] describing the addition of Sn–O–C bonds of organotin(IV) oxides and alkoxides to compounds containing such activated double bonds as isocyanate, isothiocyanate, and carbodiimide. However, no similar reactions of organic tin(II) compounds have been investigated except for two reports by P. G. Harrison and J. J. Zuckerman on the reaction between phenyl isocyanate and organic tin(II) compounds.[4–5] For the purpose of investigating the reactivity of organic tin(II) compounds containing Sn–O–C bonds towards heterocumulenes, we have examined the reaction of phenyl and ethyl isocyanate with $Sn(OC_2H_4N(CH_3)_2)_2$ (A), $Sn(OC_2H_4OCH_3)_2$ (B), $Sn(OC_2H_5)_2$ (C), $Sn(OC(CH_3)=CHCOCH_3)_2$ (D), $Sn(OC(CH_3)=CHCO_2C_2H_5)_2$ (E), and $Sn(O\text{-}C_6H_4\text{-}CO_2C_2H_5)_2$ (F). The above tin(II) compounds showed different degrees of association, that is (A), (D), (E), as well as (F) are monomeric, (B) is dimer or trimer, and (C) is an associated solid.[6]

Results and Discussion

It was found that tin(II) compounds (A—F) were effective catalysts for the cyclic trimerization of phenyl isocyanate (PhNCO) and ethyl isocyanate (EtNCO), with the formation of the corresponding isocyanurates; the catalytic activity of (A) was the best, while that of (F) was least effective (Table 1).

However, similar reactions did not occur between PhNCO and tetravalent tin alkoxide, such as $Sn(OC_4H_9^t)_4$ and $n\text{-}C_4H_9Sn(OC_4H_9^t)_3$, under the same conditions; Rather, they stopped at the stage of the adduct-formation to give simply the corresponding *t*-butyl *N*-phenylcarbamatotin(IV) derivatives.

It may be concluded from these results that: i) the nucleophilicity of the oxygen atom of Sn(II)–OR bonds, which was expected from the I- and M-effects of R and the degree of association of $Sn(OR)_2$, has a marked effect on the catalytic action of Sn(II) compounds; ii) the reactivity of PhNCO toward Sn(II)–OR bonds is less than that of EtNCO; and iii) the divalent tin compounds are far better than the tetravalent tin tetraalkoxide and monoalkyltin trialkoxide as catalysts for the cyclic trimerization of isocyanates.

When a benzene solution of PhNCO and (C) in a molar ratio of 2: 1 was treated at room temperature for 40 min, the IR spectrum of the mixture showed no absorption band assigned to the NCO group. The hydrolysis products were ethyl *N*-phenylcarbamate and triphenyl isocyanurate in yields of 63 and 8% respectively. On the other hand, when the benzene solution was heated at 80—81 °C for 3 hr, the yields of the above hydrolysis products changed to 47 and 40% respectively after the hydrolysis of the reaction mixture.

Although the organotin(IV) compound-catalyzed reaction has been explained by a proposed mechanism[7] involving the successive insertion of three isocyanate units between the tin atom and the heteroatom of the attached group, followed by the elimination of the trimer from 1: 3 adducts, the change in the yields of the hydrolysis products suggests an alternative reaction route involing the four-centered intermolecular co-ordination of the divalent tin intermidiates, as is shown in the following scheme;

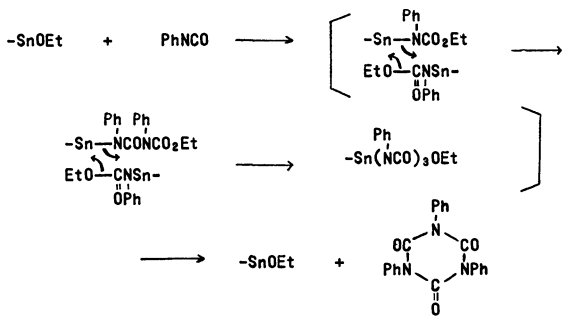

Scheme

This reaction route was supported by the finding that the nucleophilicity of the nitrogen atom of the *N*-phenyl urethano group in $Sn(N(Ph)CO_2C_2H_5)_2$ is more depressed than that of the *N*-ethyl urethano group in $Sn(N(Et)CO_2C_2H_5)_2$; when a mixed solution of (C) (0.1 mol)–PhNCO (0.2 mol) in benzene and (C) (0.1 mol)–EtNCO (0.2 mol) in benzene, neithere of which showed any characteristic infrared absorption band of the NCO group, was heated at 80—81 °C for 3 hr, and then hydrolyzed, ethyl *N*-phenyl-*N'*-ethylallophanate ($C_6H_5NHCON(C_2H_5)CO_2C_2H_5$) and *N*-phenyl-*N'*,*N''*-diethyl isocyanurate were obtained in yields of 51 and 6.2% respectively.

Therefore, the four-centered intermolecular co-ordination mechanism may be proposed for the reaction

Table 1. Yields of isocyanurate by the action with $Sn(OR)_2$ on R'NCO at 80 °C[a]

$Sn(OR)_2$[d,e]	(A)[b]	(B)	(C)	(D)	(E)	(F)	(C)[b]
	$R'=C_6H_5$						$R'=C_3H_5$
Yields (%) of $(R'NCO)_3$	100	100	66	33	27	0[c]	100

a) [R'NCO]: [$Sn(OR)_2$]=50: 1 (3 hrs in benzene) b) IR spectroscopy demonstrated the absence of the characteristic absorption band of NCO group within 2 hr. c) Triphenyl isocyanurate was obtained almost quantitatively by removing benzene under reduced pressure (water pump). d) R: (A); $C_2H_4N(CH_3)_2$ (B); $C_2H_4OCH_3$ (C); C_2H_5, (D); $C{=}CHCOCH_3$ (E); $C{=}CHCO_2C_2H_5$ and (F); 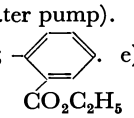 . e) Ref. 6.

with organotin(II) compounds containing an Sn–O–C bond, in addition to the conventional view of the successive insertion of isocyanate unites. The mechanism is based on the structural analogy of tin(II) compounds with carbene.

Experimental

Reaction Procedures.[8] *Reaction of Organic Tin(II) Compounds with PhNCO in a 1: 50 Molar Ratio*: To a suspension of C (0.4 g, 1.8 mmol) in benzene (20 ml), PhNCO (10.1 g, 90 mmol) was added, after which the mixture was heated at 80—81 °C for 3 hr. During the reaction, white crystals precipitated. After cooling, the crystals were filtered off, washed with benzene, and then recrystallized from acetone afford triphenyl isocyanurate; mp 269.2—270 °C. IR: 1710 cm^{-1} ($\nu_{C=O}$). Found: C, 70.58; H, 4.31; N, 11.55%. Calcd for $C_{21}H_{15}N_3O_3$: C, 70.58; H, 4.23; N, 11.76%.

The other organic tin(II) compounds were reacted with PhNCO similarly.

Reaction of C with EtNCO in a 1: 50 Molar Ratio. Ethyl isocyanate (7.8 g, 110 mmol) was added to a suspension of C (4.8 g, 2.3 mmol) in benzene (26 ml), and then the mixture was refluxed for 2 hr. The reaction mixture showed no characteristic absorption band ascribable to the NCO group. After the reaction mixture has been concentrated and then hydrolyzed with aqueous acetone, the insoluble parts of the hydrolyzate were separated centrifugally and concentrated again under reduced pressure. The precipitates were then filtered and recrystallized from *n*-hexane to give 7.6 g (97.4%) of white crystals; mp 94—95 °C. IR: 1680 cm^{-1} ($\nu_{C=O}$). NMR (CCl_4): δ 1.20 (3H, t, CH_3), 3.86 (2H, q, CH_2). Found: C, 50.29; H, 7.16; N, 19.59%. Calcd for $C_9H_{15}N_3O_3$: C, 50.69; H, 7.09; N, 19.71%.

Reaction of $Sn(OC_4H_9^t)_4$ with PhNCO in a 1: 50 Molar Ratio. Phenyl isocyanate (27.8 g, 231 mmol) was added, drop by drop, to a solution of $Sn(OC_4H_9^t)_4$ (1.9 g, 4.6 mmol) in benzene (55 ml), and then the mixture was refluxed for 3 hr. After the removal of solvent and the unreacted PhNCO *in vacuo*, the residue was recrystallized from benzene to give 3.4 g (83%) of tetrakis(*t*-butyl *N*-phenylcarbamato)tin(IV) as white crystals; mp 151 °C (dec). IR: 1647 cm^{-1}. NMR (C_6H_6): δ 1.45 (s, CH_3). Found: C, 60.11; H, 6.32; N, 6.38; Sn, 12.95%. Mol wt; 850. Calcd for $C_{44}H_{56}N_4O_8Sn$: C, 59.54; H, 6.36; N, 6.31; Sn, 13.37; Mol wt, 888.

The reaction of n-$C_4H_9Sn(OC_4H_9^t)_3$ with PhNCO was carried out in a similar way. The tin compound thus obtained was identified on the basis of the IR spectrum and its hydrolysis product.

Reaction of C with PhNCO in a 1: 2 Molar Ratio. *Reaction at 80—81 °C*: Phenyl isocyanate (19.8 g, 166 mmol) was added, drop by drop, to a suspension of C (17.2 g, 82.3 mmol) in benzene (69 ml) at 23—25 °C. After the disappearance of the NCO absorption band in their spectrum (40 min), the solution was refluxed for 3 hr. The white crystals thus precipitated were removed by filtration and then recrystallized from benzene to give triphenyl isocyanurate in a yield of 40%. The mother liquor was concentrated and then hydrolyzed with aqueous acetone. After the centrifugal removal of the insoluble parts, the acetone solution of the hydrolyzate was distilled *in vacuo*. *N,N'*-Diphenylurea (mp 234 °C) and ethyl *N*-phenylcarbamate (bp 140.5 °C/10.5 mmHg) were obtained in yields of 12% and 47% respectively.

Reaction at Room Temperature: After the disappearance of the NCO absorption band in the IR spectrum, the reaction mixture was hydrolyzed with aqueous acetone. Triphenyl isocyanurate, *N,N'*-diphenylurea, and ethyl *N*-phenylcarbamate were thus obtained in yields of 8%, 8%, and 63% respectively.

Similarly, the reaction of C with EtNCO in a molar ratio of 1: 2 was carried out.

Reaction of a Solution of C-PhNCO in Benzene with a Solution of C-EtNCO in Benzene. To a solution of C (15.0 g, 72 mmol) and EtNCO (10.2 g, 144 mmol) in benzene (34 ml), a solution of C (15.0 g, 72 mmol) and PhNCO (17.1 g, 144 mmol) in benzene (34 ml) was added, and then the mixture was heated at 80—85 °C for 3 hr. After the distillation of the solvent, the concentrated residue was hydrolyzed with aqueous acetone and the insoluble parts of the hydrolyzate were removed centrifugally. The vacuum distillation of the acetone solution afforded 17.3 g of ethyl *N'*-ethyl-*N*-phenylallophanate [Bp 91 °C/0.25 mmHg. IR: 1691, 1710 (sh), 1725 (sh), 1743 ($\nu_{C=O}$) and 3350 (ν_{N-H}). NMR: δ 1.15 (NCH_2CH_3), 1.20 (OCH_2CH_3), 3.83 (NCH_2), 4.08 (OCH_2), and 6.7—7.13 (C_6H_5). Found: (Calcd for $C_{12}H_{16}N_2O_3$): C, 60.54 (61.00); H, 6.80 (6.82); N, 11.88 (11.86)] and 1.58 g of *N*-phenyl-*N',N''*-diethyl isocyanurate [Mp 94.5—96.8 °C. IR: 1674 and 1697 ($\nu_{C=O}$). NMR: δ 1.26 (CH_3), 3.97 (CH_2), and 7.1—7.65 (C_6H_5). Found: (Calcd for $C_{13}H_{15}N_3O_3$): C, 59.67 (59.75); H, 5.81 (5.78); N, 16.30% (16.08%)].

References

1) A. J. Bloodworth and A. G. Davies, *J. Chem. Soc.*, **1965**, 5238, 6245.
2) A. J. Bloodworth, A. G. Davies, and S. C. Vasishtha, *J. Chem. Soc., C*, **1967**, 1309.
3) A. G. Davies and P. G. Harrison, *ibid.*, **1967**, 1313.
4) P. G. Harrison and J. J. Zuckerman, *Chem. Commun.* **1969**, 321.
5) P. G. Harrison and J. J. Zuckerman, *Inorg. Chim. Acta*, **7**, 235 (1967).
6) I. Wakeshima and I. Kijima, *Chem. Lett.* **1972**, 325. *Nippon Kagaku Kaishi*, **1974**, 537.
7) A. J. Bloodworth and A. G. Davies, *J. Chem. Soc.*, **1965**, 6858.
8) I. Wakeshima and I. Kijima, This Bulletin, **43**, 953 (1975).

BULLETIN OF THE CHEMICAL SOCIETY OF JAPAN, VOL. 48 (3), 1071—1072 (1975)

Synthesis of 1,3-Diaryl-1,2-propanedione by Dehydrochlorination of 3-Chloro-2-hydroxy-1,3-diaryl-1-propanone Catalyzed by Hydrogen Chloride

Takane UCHIDA, Yo MIYAGI,* and Kazuhiro MARUYAMA*

Department of Chemistry, Faculty of Education, Fukui University, Bunkyo, Fukui 910

**Department of Chemistry, Faculty of Science, Kyoto University, Sakyo-ku, Kyoto 606*

(Received September 17, 1974)

Synopsis. Dehydrochlorination of 3-chloro-2-hydroxy-1,3-diaryl-1-propanone proceeds to give 1,3-diaryl-1,2-propanedione in a high yield on heating its dioxane solution with a catalytic amount of hydrogen chloride. Kinetic studies were carried out.

α-Diketones have usually been prepared by oxidation of the corresponding ketones with selenium oxide. However, when the α-diketone to be synthesized has another methylene group at the α-position, the α-diketone produced is further oxidized to polyketones and the yield of α-diketone is, in general, not satisfactory because of the production of tarry matter.

We found a novel method for synthesis of α-diketones by chloride ion catalyzed dehydrochlorination in an acidic medium. *erythro-* and *threo*-3-Chloro-2-hydroxy-1,3-diaryl-1-propanones, (*erythro*-**1a**—**c**) and (*threo*-**1a**—**f**), underwent dehydrochlorination to give 1,3-diaryl-1,2-propanediones (**2a**—**f**) in good yields on heating their dioxane solutions containing hydrogen chloride at 70—90 °C for 20—40 hr (Scheme 1). The products (**2a**—**f**) were identified as 2-aryl-3-aroylquinoxalines (**3a**—**f**) which were produced by reaction with *o*-phenylenediamine. The yields of **3** were 80—90% (Table 1).

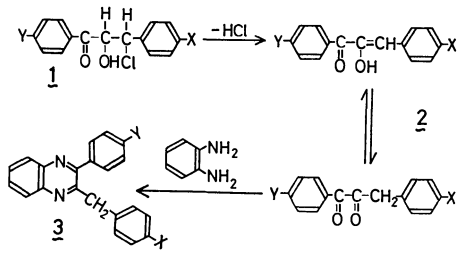

1—**3**: **a**, X=Y=H; **b**, X=Cl, Y=H; **c**, X=H, Y=Cl; **d**, X=CH_3, Y=H; **e**, X=H, Y=CH_3; **f**, X=H, Y=CH_3O

Scheme 1.

The significant feature of this reaction is the use of acidic medium since halide ion catalyzed dehydrohalogenation[1] is usually carried out in an aprotic solvent in the presence of amine, that is, in slightly basic medium in which carbonyl compounds are not stable enough to be isolated.

House[2] also obtained **2a**, identified as **3a**, by reaction of *erythro*-**1a** (10% yield) and *threo*-**1a** (26% yield) with sodium acetate in ethanol.* He assigned the diastereomeric configurations of *erythro-* and *threo*-**1a**, supposing that the phenyl and benzoyl groups of *erythro*-**1a** were eclipsed at the transition state for the *trans* elimination. We confirmed the diastereomeric configurations of *erythro-* and *threo*-**1a** by their NMR spectra. The reactants, *erythro*-**1b**—**c** and *threo*-**1b**—**f**, were prepared in the same manner as *erythro*-**1a**[2] and *threo*-**1a**.[3]

Some details of the kinetics of the reaction were investigated. The rate of the reaction was first order in both reactant and hydrogen chloride.** It was established that the reaction was promoted by chloride ion but not by protons, since no reactions were detectable when *p*-toluenesulfonic acid was used instead of hydrogen chloride (at 80.0 °C for 8 hr).

The kinetic results are listed in Table 2 and can be

Table 1. Yields, melting points, and elemental analyses of 2-benzyl-3-phenylquinoxalines **3a**—**f**

Starting material	Products	Yield (%)	Mp[a] (°C)	Found (%) C	H	N	Cl	Calcd (%) C	H	N	Cl
erythro-**1a**	**3a**	84	96[b]	85.22	5.36	9.46		85.11	5.44	9.45	
threo-**1a**	**3a**	84						($C_{21}H_{16}N_2$)			
erythro-**1b**	**3b**	82	146	75.09	4.57	8.36	10.59	76.25	4.57	8.47	10.72
threo-**1b**	**3b**	85						($C_{21}H_{15}N_2Cl$)			
erythro-**1c**	**3c**	78	137	76.44	4.57	8.37	10.82				
threo-**1c**	**3c**	88									
threo-**1d**	**3d**	80	133	84.97	6.03	8.89		85.12	5.85	9.03	
threo-**1e**	**3e**	89	113	85.31	5.96	9.06		($C_{22}H_{18}N_2$)			
threo-**1f**	**3f**	87	141	81.03	5.37	8.63		80.95	5.56	8.58	
								($C_{22}H_{18}N_2O$)			

a) Uncorrected. b) Lit,[2] 96 °C.

* The reaction time was indicated as appropriate.

** The rate constants were calculated from $kt=(1/a+b)\times \ln a(b+x)/b(a-x)$; where a and b are initial concentrations of hydrogen chloride and reactant respectively, and x is the variation in reactant concentration.

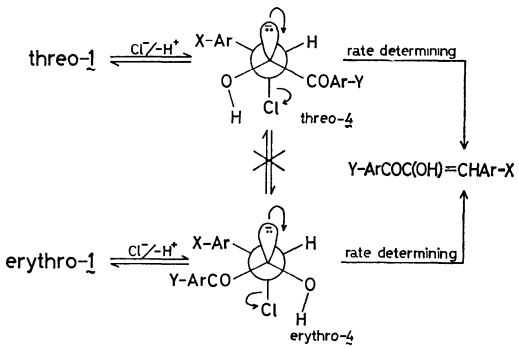

Scheme 2.

Table 2. Rate constants of elimination reactions of *erythro*- and *threo*-**1**

Reactant	Temp[a]	$k\times10^{2}$[b]	$k_{threo}/k_{erythro}$
erythro-**1a**	60.0	0.481	
	70.0	0.780	
	80.0	1.45[c]	
erythro-**1b**	80.0	1.49	
threo-**1a**	70.0	2.42	3.1
	80.0	4.82[d,e]	3.3
	90.0	6.55	
threo-**1b**	80.0	5.26[e]	3.5
threo-**1c**	80.0	2.59[e]	
threo-**1d**	80.0	5.04[e]	
threo-**1e**	80.0	7.89[e]	
threo-**1f**	80.0	11.4[e]	

a) °C. b) l/mol min; initial concentrations: reactant, 5.00×10^{-2} M; HCl, 5×10^{-2} M. c) $\Delta H=12.9$ kcal/mol, $\Delta S=40.8$ eu at 80.0 °C. d) $\Delta H=12.4$ kcal/mol, $\Delta S=39.9$ eu at 80.0 °C. e) $\rho=-1.3$ *vs.* σ.

summarized as follows; i) the reaction of a *threo* isomer is faster than that of the corresponding *erythro* isomer; ii) the reaction rate is enhanced by electron donating substituents (Y) on the aroyl group, whereas substituents (X) on the aryl group show little effect on the rate. From these results the reaction mechanism shown in Scheme 2 can be suggested as a plausible one.

Substituents, (X) and (Y), may not affect the equilibrium of intermediate **4** formation but the rate of C–Cl bond rupture of **4**. The formation of *erythro*-**4** may not be preferred because of eclipsing of the aryl and aroyl groups. The diastereomeric configurations of *erythro*- and *threo*-**4** may be retained, because, if they invert, the reaction rates of an *erythro* compound and the corresponding *threo* compound should become similar as the reaction proceeds but this was not the case.

Experimental

erythro-*3-Chloro-1,3-diaryl-2-hydroxy-1-propanones* (erythro-***1a-c***). *erythro*-**1a-c** was prepared by a method similar to the one described by House.[2] To a solution of 1-aroyl-2-arylethylene oxide[4] (10 g) in methanol (100 ml), cooled by ice, concentrated hydrochloric acid (100 ml) was added. After two hours' stirring, the mixture was stored in a refrigerator overnight. Precipitated crystals were filtered and recrystallized from benzene. Yields, melting points, and elemental analyses of *erythro*-**1a-c** are shown in Table 3.

threo-*3-Chloro-1,3-diaryl-2-hydroxy-1-propanones* (threo-***1a-f***). Using the same method as for *threo*-**1a**,[3] *threo*-**1b-f** was prepared from 1-aroyl-2-arylethylene oxide.[4] Yields, melting points, and elemental analyses of *threo*-**1a-f** are shown in Table 3.

NMR Spectra of erythro- *and* threo-**1a**. NMR signals of the aliphatic protons of *erythro*- and *threo*-**1a** in $CDCl_3$ were observed at $\delta=5.23$ (1H, d, $J=3.5$ Hz), 5.48 (1H, d, $J=3.5$ Hz), and 3.60 (OH, s), and 5.26 (1H, d, $J=1.8$ Hz), 5.42 (1H, d, $J=1.8$ Hz), and 3.98 (OH, s, broader than the signal of *erythro*-**1a** at 3.60). The larger coupling constant of *erythro*-**1a** than that of *threo*-**1a** supports the assignment of their diastereomeric configurations.[2]

*Products (2-Aryl-3-aroylquinoxalines (**3a-f**)).* A reactant (**1**) (*ca.* 0.5 mmol) was dissolved in 0.05 M HCl-dioxane (10 ml). The solution was heated at 80.0 °C for 20—40 hr in an ampoule and then poured into an ethanol solution of *o*-phenylenediamine (*ca.* 0.075 mmol). After standing overnight, the solution was concentrated under reduced pressure. The residue was crystallized from aqueous ethanol. Yields, melting points, and elemental analyses of products (**3**) are shown in Table 1.

Kinetics. Kinetic measurements were carried out as usual using ampoules. The acid was titrated with methanolic sodium methoxide solution.

References

1) W. H. Saunders, "Mechanisms of Elimination Reactions," John Wiley & Sons, New York, N. Y., (1973), p. 345.
2) H. O. House, *J. Org. Chem.*, **21**, 1306 (1956).
3) H. O. House, *J. Amer. Chem. Soc.*, **76**, 1235 (1954).
4) H. O. House and G. D. Ryerson, *ibid.*, **83**, 979 (1961).

Table 3. Yields, melting points, and elemental analyses of *erythro*- and *threo*-**1**

Compound	Yield (%)	Mp[a] (°C)	Found (%) C	H	Cl	Calcd (%) C	H	Cl
erythro-**1a**	50	106.8[b]	68.77	5.24	13.63	69.10	5.03	13.60
threo-**1a**	43[d]	72.5[c]				($C_{15}H_{13}O_2Cl$)		
erythro-**1b**	52	99.5—101	60.99	4.02	23.84			
threo-**1b**	88	129	60.80	4.38	24.28	61.03	4.09	24.02
erythro-**1c**	52	93—96	61.30	4.34	24.05	($C_{15}H_{12}O_2Cl_2$)		
threo-**1c**	86	104	61.03	4.20	24.36			
threo-**1d**	50	121	70.07	5.45	12.73	69.94	5.50	12.90
threo-**1e**	89	94.6	70.20	5.60	13.18	($C_{16}H_{15}O_2Cl$)		
threo-**1f**	73	112.5	65.84	5.47	12.22	66.09	5.20	12.19
						($C_{16}H_{15}O_3Cl$)		

a) Uncorrected. b) Lit,[2] 105—107 °C. c) Lit,[2] 71—72 °C. d) Ref. 2.

BULLETIN OF THE CHEMICAL SOCIETY OF JAPAN, VOL. 48 (3), 1073—1074 (1975)

Photochemical Reaction of Friedelin. Formation of an ε,ζ-Unsaturated Aldehyde

Hidekazu SHIRASAKI, Reiko AOYAGI, Takahiko TSUYUKI, Takeyoshi TAKAHASHI, and Robert STEVENSON*

Department of Chemistry, Faculty of Science, The University of Tokyo, Hongo, Bunkyo-ku, Tokyo 113

**Department of Chemistry, Brandeis University, Waltham, Massachusetts 02154, U.S.A.*

(Received September 20, 1974)

Synopsis. Friedelin (**1**) in *n*-pentane or ethanol was irradiated using a high pressure mercury lamp under a nitrogen atmosphere. From the aldehydic fraction of the photolysate, an ε,ζ-unsaturated aldehyde, 10β-(2-formylethyl)-5α-vinyl-des-*A*-friedelane (**5**) has been isolated. Upon oxidation with silver oxide, **5** afforded putranjivic acid (**6**).

Previously we reported the formation of the seco-nor saturated aldehyde (**4**), an autoxidation product of the ketene (**3**) which was formed by photoreaction of friedelin (**1**) in aprotic solvents, together with the mechanistic elucidation of the formation of **4**.[1] Attention was drawn to the fact that since there is no hydrogen atom on the δ-carbon atoms in the seco-friedelin skeleton (**2**), the usual formation of a δ,ε-unsaturated aldehyde by α-cleavage, followed by transfer of the δ-hydrogen atom through a six-membered transition state, is not feasible.

In this paper we wish to describe the formation of an ε,ζ-unsaturated aldehyde on the photolysis of friedelin (**1**). An aldehydic fraction of the photolysate of friedelin (**1**) in *n*-pentane or ethanol was reinvestigated and an unsaturated aldehyde was isolated in 2 and 0.4% yields, respectively. The unsaturated aldehyde (**5**), mp 133.5—135 °C, $[\alpha]_D$ +10° ($CHCl_3$), had a molecular formula $C_{30}H_{50}O$, determined by high resolution mass spectrometry. The PMR and IR spectra showed the presence of the groupings $-CH_2CHO$ and $-CH{=}CH_2$ (*cf.* Experimental). These data suggested that the unsaturated aldehyde (**5**) should be 10β-(2-formylethyl)-5α-vinyl-des-*A*-friedelane. This was confirmed by oxidation of **5** with silver oxide to give putranjivic acid (**6**).[2]

The formation of ε,ζ-unsaturated aldehydes is not frequently encountered.[3-5] It seems to be more likely that the ε,ζ-unsaturated aldehyde (**5**) was produced by intramolecular transfer of a hydrogen atom from a ζ-carbon atom (C-23) to the acyl radical through an eight-membered transition state,[3] rather than by intermolecular mechanisms with solvent participation. In the case of ethanol as a solvent, it would be expected that the acylalkyl biradical (**2**) undergoes a preferential hydrogen transfer reaction from C-2 to the alkyl radical through a six-membered transition state to yield the ketene (**3**), which is immediately stabilized by the reaction with ethanol yielding a seco-ester (**7**). It is therefore suggested that the acylalkyl biradical (**2**) in such circumstances undergoes a hydrogen transfer reaction *via* the eight-membered transition state to give the ε,ζ-unsaturated aldehyde (**5**).

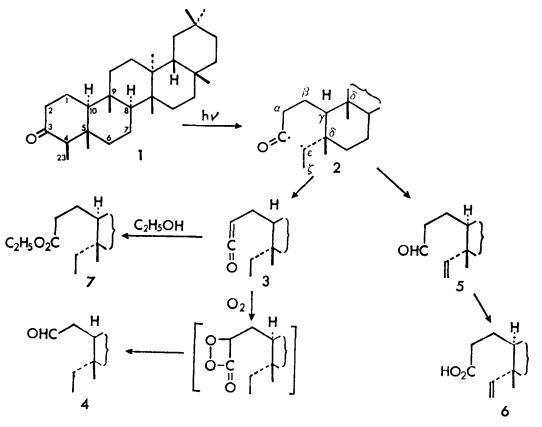

Experimental

IR spectra were measured on a Hitachi EPI-G2 spectrometer. Mass spectra were taken on a Hitachi RMU-6-Tokugata mass spectrometer operating at 70 eV with a direct inlet system. High resolution mass spectra were taken using a Hitachi RMH-2 mass spectrometer at 70 eV. PMR spectra were measured using a Hitachi R-24 (60 MHz) spectrometer. Chemical shifts were expressed in ppm downfield from TMS as an internal standard and coupling constants in Hz. Optical rotation was measured with a JASCO DIP-SL polarimeter. Melting points were determined using a Mel-temp (Laboratory Devices) and are reported uncorrected.

Photolysis of Friedelin (1). *In* n-*Pentane*: A solution of friedelin (**1**; 1.05 g) in *n*-pentane (850 ml) was irradiated with a high pressure mercury lamp (100 W) under a nitrogen atmosphere for 9 hr at room temperature. After the irradiation, dry oxygen was passed through the solution in the dark for 14 hr at room temperature.

A part (250 ml) of the solution, on evaporation of the solvent under reduced pressure, afforded a residue (346 mg), which was separated on a silica gel (300 g) column and eluted with the following solvents (each fraction 200 ml): frs 1—7, light petroleum; frs 8—10, light petroleum–benzene (10:1); frs 11—16, light petroleum–benzene (5:1); frs 17—35, light petroleum–benzene (3:1). From fractions 27 and 28, the seco-nor aldehyde (**4**; 9 mg) was obtained and was shown to be identical with an authentic specimen.[1] Fractions 31 to 34, on evaporation, gave white crystals (6 mg; 2% yield from **1**). Mp 133.5—135 °C (from light petroleum); $[\alpha]_D$ +10° (*c*, 0.78; $CHCl_3$); MW (by high resolution mass spectrometry) 426.3887. Calcd for $C_{30}H_{50}O$: 426.3859; IR (Nujol) 2700, 1725, 1630, 1005, and 910 cm^{-1}; PMR ($CDCl_3$) δ 2.15—2.60 (2H, m, $-C\underline{H}_2-CHO$), ABX type signals due to vinyl protons $\left[H_X\rangle C{=}C\langle {H_A \atop H_B} \right]$ δ_A 4.92 (J_{AX}=18 Hz, J_{AB}=1.6 Hz), δ_B 4.96 (J_{BX}=10 Hz, J_{AB}=1.6 Hz), and δ_X 5.71 (J_{AX}=18 Hz, J_{BX}=10 Hz)], and δ 9.65 (1H, t, J=2.5 Hz,

$-CH_2-C\underline{H}O$); Mass *m/e* 426 (M^+, 8%*), *m/e* 411 [$(M-15)^+$, 12%], *m/e* 301 [$(M-C_8H_{13}O)^+$, a fragment ion due to fissions of C_5–C_6 and C_9–C_{10}, 8%], *m/e* 273 (24%), *m/e* 218 (32%), 205 (90%), and 109 (100%).

In Ethanol: Friedelin (**1**; 500 mg) in ethanol (750 ml) was irradiated for 30 hr by the same procedure as above. The reaction products, after removal of the solvent, were chromatographed on a silica gel column. The ethyl ester (**7**) was eluted with light petroleum–benzene (5:1) (66% yield from **1**) and then the unsaturated seco aldehyde (**5**; 0.4% yield from **1**) was eluted with the same eluent. This was purified by repetitive chromatography on silica gel.

Oxidation of 10β-(2-Formylethyl)-5α-vinyl-des-A-friedelane (5). To a solution of the unsaturated aldehyde (**5**; 25 mg) in ethanol (10 ml), silver nitrate (50 mg) in water (1 ml) and 0.05 M sodium hydroxide solution (20 ml) were added in turn, and the reaction mixture was stirred overnight. Usual work-up and extraction with ether afforded a residue, which was chromatographed on silica gel (50 g) and eluted with benzene–ether (10:1, each fraction 30 ml). Fractions 7 and 8, on evaporation of the solvents, afforded 8 mg (31% yield from **5**) of crystals, which was identified by direct comparison (IR, tlc (SiO_2–$AgNO_3$), and Mass) with the authentic putranjivic acid (**6**), prepared by the photoxidation of friedelin (**1**).[2e] MW (by high resolution mass spectrometry) 442.3816. Calcd for $C_{30}H_{50}O_2$: 442.3808.

* Relative intensities of peaks above *m/e* 100.

References

1) R. Aoyagi, T. Tsuyuki, M. Takai, T. Takahashi, F. Kohen, and R. Stevenson, *Tetrahedron*, **29**, 4331 (1973), and references cited therein.

2) a) G. R. Chopra, A. C. Jain, and T. R. Seshadri, *Curr. Sci.*, **37**, 301 (1968); *Chem. Abstr.*, **69**, 93685q (1968). b) G. R. Chopra, A. C. Jain, T. R. Seshadri, and G. R. Sood, *Indian J. Chem.*, **8**, 776 (1970); *Chem. Abstr.*, **74**, 1024a (1971). c) G. R. Chopra, A. C. Jain, and T. R. Seshadri, *ibid.*, **7**, 1179 (1969); *Chem. Abstr.*, **72**, 67139g (1970). d) P. Sengupta and A. K. Dey, *Tetrahedron*, **28**, 1307 (1972). e) R. Aoyagi, T. Tsuyuki, and T. Takahashi, This Bulletin, **46**, 692 (1973).

3) K. Kojima, K. Sakai, and T. Tanabe, *Tetrahedron Lett.*, **1969**, 3399. In this paper, the photochemical reaction of 4,4-di(trideuteriomethyl)-19-norandrost-5-en-3-one in benzene has been reported and the intramolecular nature of the transformation *via* an eight-membered transition state has been suggested.

4) J. M. Beard and R. H. Eastman, *Tetrahedron Lett.*, **1970**, 3029.

5) H. Hirota, T. Tsuyuki, Y. Tanahashi, and T. Takahashi, This Bulletin, **47**, 2283 (1974).

BULLETIN OF THE CHEMICAL SOCIETY OF JAPAN, VOL. 48 (3), 1075—1076 (1975)

A Novel Reduction of the *O*-(3,5-Dinitrobenzoyl)-*N*,*N*-(aroylaryl)hydroxylamines by the Cyanide Ion in Dipolar Aprotic Solvents

Shigeru OAE and Tadamitsu SAKURAI*

Department of Chemistry, University of Tsukuba, Sakuramura, Niihari-gun, Ibaraki 300-31

**Department of Applied Chemistry, Faculty of Engineering, Osaka City University, Sugimoto-cho, Sumiyoshi-ku, Osaka 558*

(Received September 20, 1974)

Synopsis. The reaction of *O*-(3,5-dinitrobenzoyl)-*N*,*N*-(aroylaryl)hydroxylamines with the cyanide ion in dipolar aprotic solvents was found to afford the corresponding reduction products, *i.e.*, *N*-aroylarylamines, in good yields *via* decarboxylation. The mechanism of this novel reduction was discussed.

In the preceding paper we have shown that *N*,*N*-dibenzyl-*O*-(*p*-nitrobenzoyl)hydroxylamine is a good model compound for studying both nucleophilic substitution and elimination reactions on the trivalent nitrogen atom.[1)]

As an extension of the earlier study, we have now prepared *O*-(3,5-dinitrobenzoyl)-*N*,*N*-(aroylaryl)hydroxylamines and allowed them to react with various nucleophiles in dimethyl sulfoxide (DMSO), expecting that the reaction would proceed *via* nucleophilic substitution on the nitrogen atom as follows:

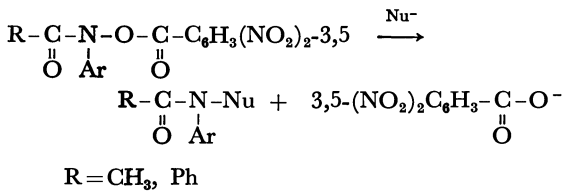

R = CH_3, Ph

Results and Discussion

The reaction of *O*-(3,5-dinitrobenzoyl)-*N*,*N*-acetyl-(*p*-chlorophenyl)hydroxylamine (I) with nucleophiles in DMSO or DMF at room temperature was found to give products which appear to be formed by the attack of the nucleophile upon the carbonyl-carbon of the reactant, as is shown below, except for the reaction with cyanide ion, as is indicated in Table 1. When the cyanide ion was allowed to react with I, an unexpected reduction product was obtained in a substantial yield, while no substitution product was detected.

Thus, the effects of substituent on the yields of the reduction products and on the course of the reaction were investigated in order to clarify the mechanism of

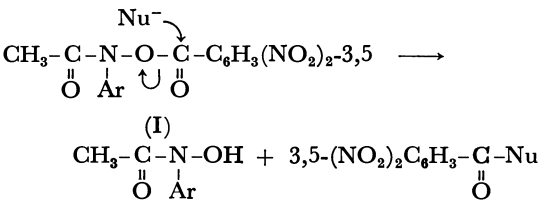

Ar = *p*-ClC_6H_4

this novel reduction by the cyanide ion. The results are listed in Table 2. An inspection of the data in Table 2 clearly indicates that the novel reduction occurred only when the leaving group was 3,5-dinitrobenzoyloxy group, since no hydroxylamine (V) with *p*-nitrobenzoyloxy group as the leaving group gave the reduction product in the reaction. Moreover, the yield of the reduction tends to increase with the increase in the electron-withdrawing ability of the substituent which is attached directly to the nitrogen atom.

One mechanism to explain the product distribution of the reaction with the cyanide ion may involve the

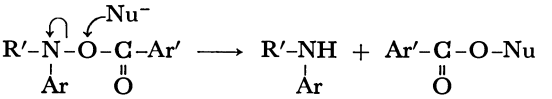

R′ = CH_3CO (II), PhCO (III), *p*-$CH_3C_6H_4SO_2$ (IV); Ar = Ph

R′ = CH_3CO; Ar = *p*-ClC_6H_4 (I); Ar′ = $-C_6H_3(NO_2)_2$-3,5

nucleophilic substitution on the oxygen atom which has been observed in the reactions of peroxides with nucleophiles.[2)] This mechanism, however, seems un-

Table 1. Reaction of I with various nucleophiles at room temperature

Nucleophile	Solvent	Product (Yield %)	Reaction time (hr)
NaN_3	DMSO	Ac–N(OH)–Ar (66), Ar′CO_2Na (12)	26
NaSPh	DMSO	Ac–N(OH)–Ar (74), Ar′CO_2Na (27), PhSSPh (67)	25
p-$CH_3C_6H_4SH$	DMF	Ac–N(OH)–Ar (96), *p*-$CH_3C_6H_4$–S–C(=O)–Ar′ (83)	48
$NaOCH_3$	DMSO	Ac–N(OH)–Ar (57), Ar′CO_2CH_3 (41)	25
NaCN	DMSO	Ac–N(H)–Ar (52)	26

Ac = CH_3CO Ar = *p*-ClC_6H_4 Ar′ = $-C_6H_3(NO_2)_2$-3,5

Table 2. Reaction of R′–N(Ph)–O–C(=O)–Ar′ with sodium cyanide at room temperature

Substituent R′	Solvent	Yield of reduction product (%)	Reaction time (hr)
CH_3CO (II)	DMSO	63	26
PhCO (III)	DMSO	90	26
PhCO (III)	DMF	76	26
p-$CH_3C_6H_4SO_2$ (IV)	DMSO	94	26
Ac–N(Ar)–O–C(=O)–C_6H_4–NO_2–*p* (V)	DMSO	Ac–N(Ar)–OH (81), *p*-$NO_2C_6H_4CO_2Na$ (37)	25

Ac=CH_3CO Ar=*p*-ClC_6H_4 Ar′=$-C_6H_3(NO_2)_2$-3,5

likely because the reduction product of (IV) was obtained in a high yield in spite of the large steric and electronic repulsions between the sulfonyl oxygen and charged nucleophiles, serving to suppress the reduction.

A more probable mechanism is that the reduction proceeds *via* the decarboxylation of a Meisenheimer-type complex formed as an intermediate as in the displacement reaction of polynitroaromatics.[3] This mechanism explains the observation that the reduction proceeds more readily when the electron-withdrawing power of the R′ substituents increases. Another strong support for this mechanism is that carbon dioxide was trapped as barium carbonate by bubbling through an aqueous solution of barium hydroxide, with nitrogen gas as a carrier gas, in the reaction of hydroxylamine (III) with the cyanide ion in DMSO at room temperature, though the yield of carbon dioxide thus evolved was relatively low (*ca.* 10%).

$$\text{R′–N(Ar)–O–C(=O)–Ar′} \xrightarrow[CN^-]{} [\text{Meisenheimer Complex}] \xrightarrow[-CO_2]{} \text{R′–NH(Ar)} + \text{Amorphous Solid}$$

R′=CH_3CO (II), PhCO (III), *p*-$CH_3C_6H_4SO_2$ (IV); Ar=Ph

R′=CH_3CO; Ar=*p*-ClC_6H_4 (I); Ar′=$-C_6H_3(NO_2)_2$-3,5

It has been recently established that the species more readily formed in the interaction of aromatic polynitro compounds with the cyanide ion in a dipolar aprotic solvent than in alcoholic or ketonic solvents, may be formulated as Meisenheimer complexes on the basis of their UV, IR, and NMR spectra.[4] Therefore, the intermediate whose strong absorption band appeared at λ_{max}=576 nm may safely be ascribed to the Meisenheimer-type complex formed by the interaction of (III) with sodium cyanide in DMF.

Table 3. Physical properties of I, II, III, IV, and V

Compound	Mp (°C)	IR (KBr, cm^{-1})
(I)	137—138	3100, 1780, 1690, 1540, 1340, 1250
(II)	103—104	3060, 1770, 1675, 1530, 1340, 1245
(III)	---[a]	3100, 1780, 1680, 1545, 1350, 1250
(IV)	---[a]	3100, 1780, 1550, 1365, 1340, 1255, 1170
(V)	135—136	1770, 1705, 1530, 1340, 1240

a) The melting points could not be precisely determined because thermal rearrangement occurred before melting.

Experimental

Materials. The *O*-(3,5-dinitrobenzoyl)-*N*,*N*-(aroylaryl)-hydroxylamines used were prepared from 3,5-dinitrobenzoyl chloride and the corresponding *N*,*N*-aroylarylhydroxylamines under the usual Schotten-Bauman conditions. The *O*-(*p*-nitrobenzoyl)-*N*,*N*-acetyl-(*p*-chlorophenyl)hydroxylamine was synthesized similarly. The mp and the IR spectrum of these hydroxylamines are shown in Table 3.

General Procedure for the Reaction of I, II, III, IV and V with Nucleophiles. A small excess of a nucleophile (1.1—1.7 mM) was added to 6 ml of a DMSO solution of I—V (0.9—1.6 mM) in a reaction vessel, after which the whole solution was stirred with a magnetic stirrer at room temperature for 25—48 hr. After the reaction, the contents were poured into a large excess of water, and then the products were extracted with $CHCl_3$. The $CHCl_3$ solution was washed with water several times and dried over Na_2SO_4. The subsequent evaporation of $CHCl_3$ afforded a residue, which was then subjected to column chromatography through silica gel, using CH_2Cl_2 as the eluent. The water solution was acidified slightly with a dil-HCl aqueous solution, and the aqueous solution was extracted with $CHCl_3$. The evaporation of $CHCl_3$ gave the crude *p*-nitro- and 3,5-dinitrobenzoic acids respectively. The structures of the products isolated were determined by comparison with authentic samples.

References

1) S. Oae, T. Sakurai, and S. Kozuka, *Chem. Lett.*, **1974**, 621.

2) J. O. Edwards, "Peroxide Reaction Mechanism," ed. by J. O. Edwards, Wiley-Interscience, New York (1962), pp. 67—106.

3) Th. J. de Boer and I. P. Dirks, "The Chemistry of the Nitro and Nitroso Groups," ed. by H. Feuer, Part 1, Interscience Publishers, New York (1969), pp. 487—612.

4) B. Vickery, *Chem. Ind.* (London), **1967**, 1523; E. Buncel, A. R. Norris, and W. Proudlok, *Can. J. Chem.*, **46**, 2759 (1968).

BULLETIN OF THE CHEMICAL SOCIETY OF JAPAN, VOL. 48 (3), 1077—1078 (1975)

A Novel Method for the Synthesis of Cytidine Diphosphate-Choline

Takashi KURIHARA, Isamu YAMAMOTO, and Tsujiaki HATA*

Laboratory of Chemistry for Natural Products, Faculty of Science, Tokyo Institute of Technology, Ookayama, Meguro-ku, Tokyo 152

(Received November 18, 1974)

Synopsis. Cytidine diphosphate choline was synthesized by the reaction of cytidine 5′-phosphate with 2-bromoethyl 2′-(chloromethyl)-4′-nitrophenyl phosphate in the presence of trimethylamine.

Derivatives of cytidine 5′-phosphate are known to participate in the biosynthesis of phospholipids. Cytidine diphosphate choline (CDP-choline) is one of the important intermediates for the enzymatic incorporation of choline phosphate into lecithin. Although several methods for the synthesis of CDP-choline are described in the literature,[1] most synthetic methods give many by-products that are difficult to remove. An important consideration in the synthesis of CDP-choline is the method of introduction of the choline residue. Sanno and Tanaka synthesized CDP-choline with a 35% yield by the ring-opening reaction of ethyleneimine with cytidine 5′-diphosphate followed by methylation.[1b]

In this paper, we wish to report a novel method for the synthesis of CDP-choline using 2-bromoethyl 2′-(chloromethyl)-4′-nitrophenyl phosphate (**1**) as a precursor for choline phosphate as shown in Scheme 1.

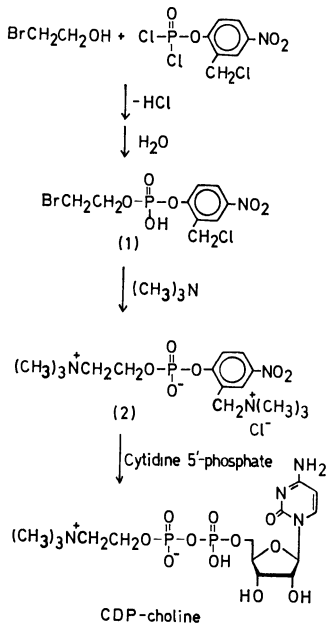

Scheme 1.

In this method, the 2-(chloromethyl)-4-nitrophenoxy group is activated and the choline residue is formed by attack of trimethylamine together with the corresponding ammonium derivative (**2**), which in turn reacts with cytidine 5′-phosphate to afford CDP-choline.[2]

In addition, it should be noted that the intermediate (**2**) reacts selectively with the phosphate, leaving the amino group on the cytosine residue and the hydroxyl groups on the sugar moiety of the cytidine 5′-phosphate. Further, it was found that P^1-(2-bromoethyl) P^2-cytidine 5′-pyrophosphate and unreacted cytidine 5′-phosphate were only detected as the by-products which were easily separated from CDP-choline.

Experimental

Methods. For paper chromatography, the descending technique using Toyo Roshi No. 51 and No. 51A papers was employed. The solvent system was ethanol–1 M ammonium acetate (7: 3 v/v). Paper electrophoresis was carried out with an apparatus similar to that described by Markham and Smith.[3] The buffer solution was 0.05 M phosphate (pH 8.0). The yields of the reported compounds were most frequently estimated spectrophotometrically after elution of spots from paper chromatograms run. The preparation of 2-(chloromethyl)-4-nitrophenyl phosphorodichloridate has been described previously.[4] Commercial 2-bromoethanol was purified by distillation. Cytidine 5′-phosphate was purchased from Yamasa Shoyu co. A dry solution of trimethylamine in dimethylformamide (DMF) was prepared as follows: Gaseous trimethylamine generated from the commercially available aqueous solution by adding sodium hydroxide was passed through a soda-lime tube and bubbled into dry DMF.

Preparation of 2-Bromoethyl 2′-(Chloromethyl)-4′-nitrophenyl Phosphate (1). A mixture of 2-bromoethanol (62.4 mg, 0.5 mmol) and pyridine (39.6 mg, 0.5 mmol) was added to a solution of 2-(chloromethyl)-4-nitrophenyl phosphorodichloridate (1.52 g, 0.5 mmol) in 10 ml of tetrahydrofuran (THF) cooled to 0 °C for 2 hr. Then, it was allowed to stand at room temperature for 7 hr. The mixture was poured into an aqueous solution containing pyridine (39.6 mg, 0.5 mmol) and stirred for 30 min. After removal of THF under reduced pressure, the aqueous solution was washed with three 40 ml portions of chloroform and then with two 20 ml portions of chloroform. The chloroform extracts were combined and washed with water (5 ml) and the aqueous solution was washed again with chloroform. All of the chloroform extracts were combined and finally dried over sodium sulfate. After evaporation of chloroform, 2-bromoethyl 2′-(chloromethyl)-4′-nitrophenyl phosphate (1.66 g, 89%) was obtained as a pale yellowish oil which was homogeneous on a paper chromatogram.

Synthesis of CDP-choline. Compound **1** (0.5 mmol) was dissolved in 7 ml of DMF saturated with dry trimethylamine and containing a catalytic amount of sodium iodide. The solution was stirred at room temperature in a pressure bottle for 3 hr and then heated at 55 °C for 1 hr. After evaporation of the DMF under reduced pressure, further anhydrous trimethylamine in DMF was added and evaporation was repeated. A hot (75 °C) solution of the 4-morpholine *N,N′*-dicyclohexylcarboxamidinium salt of cytidine

* To whom correspondence should be addressed.

5′-phosphate (0.1 mmol) in dry DMF (5 ml) was added to the residue. The mixture was heated at 95 °C for 10 hr. After addition of water, the precipitate was removed. The aqueous solution was concentrated and chromatographed on a DEAE cellulose column. First, CDP-choline was eluted with a linear gradient of triethylammonium bicarbonate solution from 0 to 0.1 M. The eluate was concentrated. CDP-choline was obtained in 54% yield based on cytidine 5′-phosphate. It was homogeneous on a paper chromatogram. The CDP-choline was characterized by its electrophoretic mobility (0.25 at pH 8.0) relative to cytidine 5′-phosphate and by phosphorus analysis (phosphorus: cytidine=2.00: 1.00).

The authors wish to heartily thank Professor Teruaki Mukaiyama for his encouragement and comments throughout the investigation and to Dr. Yoshitaka Mushika for his kind advice given during the course fo this experiment.

References

1) a) E. P. Kennedy, *J. Biol. Chem.*, **222**, 185 (1956); b) Y. Sanno and K. Tanaka, *Chem. Pharm. Bull.* (Tokyo), **10**, 231 (1962); c) A. M. Michelson and R. Letters, *Bull. Soc. Chim. Belg.*, **45**, 1353 (1963).

2) A few years ago, we reported a similar type of reaction for the synthesis of mixed diesters of phosphoric acid: T. Hata, Y. Mushika, and T. Mukaiyama, *Tetrahedron Lett.*, **1970**, 3505. Also Mushika and Yoneda synthesized α-glycerophosphoryl choline by the reaction of 2-chloroethyl 2′-(chloromethyl)-4′-nitrophenyl isopropyridene-α-glyceryl phosphate with aqueous trimethylamine: Y. Mushika and N. Yoneda, *Chem. Pharm. Bull.* (Tokyo), **19**, 696 (1971).

3) R. Markham and J. D. Smith, *Biochem. J.*, **52**, 552 (1952).

4) T. Hata, Y. Mushika, and T. Mukaiyama, *J. Amer. Chem. Soc.*, **91**, 4532 (1969).

BULLETIN OF THE CHEMICAL SOCIETY OF JAPAN, VOL. 48 (3), 1079—1080 (1975)

Catalytic Function of Metal Salts on the Reduction of Pyridine-2-carbaldehyde by 1-Benzyl-1,4-dihydronicotinamide

Masamitsu SHIRAI, Taizo CHISHINA, and Makoto TANAKA

Department of Applied Chemistry, Faculty of Engineering, University of Osaka Prefecture, Sakai, Osaka 591

(Received December 12, 1974)

Synopsis. A catalytic function of metal salts on the reduction of pyridine-2-carbaldehyde by 1-benzyl-1,4-dihydronicotinamide was discussed kinetically. The reduction rate was affected not only by the nature of metal cation but by that of counter anion.

Because of a biochemical significance the reactions of 1,4-dihydronicotinamide derivatives, as a model for the reduced nicotinamide-adenine dinucleotide, have been studied by many workers.[1] Although it was known that zinc ion was essential for the activity of alcohol dehydrogenase,[2] only few investigations were reported about the catalytic function of metal ions for the reactions to which 1,4-dihydronicotinamide derivatives participated. Sigman *et al.*[3] reported that zinc ion efficiently catalyzed the reduction of 1,10-phenanthroline-2-carbaldehyde to 1,10-phenanthrolin-2-ylmethanol by 1-propyl-1,4-dihydronicotinamide. Shinkai *et al.*[4] presented that pyridoxal derivatives were reduced by 1,4-dihydropyridine derivatives and that the reductions were facilitated by metal ions. In the present study the reduction of pyridinecarbaldehyde (2-, 3-, 4-) by 1-benzyl-1,4-dihydronicotinamide(NBNH)[5] was attempted and the catalytic function of some metal salts (metal cations and their counter anions) was discussed.

Results and Discussion

Pyridine-2-carbaldehyde(2-PCHO) was found to be reduced to 2-(hydroxylmethyl)pyridine by NBNH in the presence of $Zn(OAc)_2$. The reaction rate was evaluated kinetically. 3-PCHO was not reduced and 4-PCHO was reduced with difficulty, the pseudo first-order rate constant(k) of which was twenty eight times smaller than that of 2-PCHO. This implies that a direct activation of carbonyl group by Zn^{2+} which was fixed in the neighborhood of the carbonyl group by coordination with the nitrogen atom of pyridine ring is an important factor for the reduction of PCHO, though the reaction mechanism is not obvious. Suggestive evidences for the direct activation were obtained from the UV and NMR spectra of methanolic solution of PCHO–$Zn(OAc)_2$ mixture. The UV spectrum of the mixture for 2-PCHO showed a new absorption peak at 390 nm, while that of 3- and 4-PCHO did not show any appreciable change. The difference in $\Delta\tau$ for the

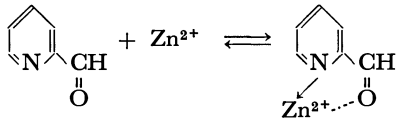

TABLE 1. PSEUDO FIRST-ORDER RATE CONSTANTS CATALYZED BY BIVALENT METAL CATIONS

	Zn^{2+}	Pb^{2+}	Cb^{2+}	Cu^{2+}
Metal[a] $\times 10^3$ M	6.95	7.18	7.04	0.70
2-PCHO $\times 10^2$ M	3.48	3.43	3.43	3.52
k[b] $\times 10^5$ s^{-1}	7.31	2.23	2.06	10.10

a) Counter anion is OAc^-. b) At 29 °C in methanol, $[NBNH]=7.0\times10^{-5}$ M.

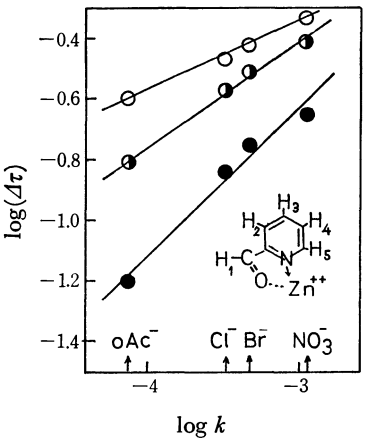

Fig. 1. Relation between log k and log ($\Delta\tau$) at 29 °C in methanol.
In pseudo first-order rate constants measurement, $[Zn^{2+}]=7.45\times10^{-3}$ M, $[2\text{-PCHO}]=3.50\times10^{-2}$ M, $[NBNH]=7.01\times10^{-5}$ M.
In NMR spectra measurement, $[Zn^{2+}]=0.25$ M, [2-PCHO]=0.50 M, $\Delta\tau=\tau$ (none)—τ (added Zn^{2+} salts)
—●—: H_2, —○—: H_3, —◑—: H_4

ring protons among the three isomers did not give any useful information but the magnitude of the diminution of aldehyde proton peak was in the order, 2-PCHO> 4-PCHO>3-PCHO≃0.

The reduction of 2-PCHO was catalyzed by other bivalent metal salts than $Zn(OAc)_2$, such as $Pb(OAc)_2$, $Cd(OAc)_2$, and $Cu(OAc)_2$, each of which was unreactive to NBNH. As shown in Table 1, the k values for these salts as catalyst decreased in the order, $Cu^{2+}>Zn^{2+}>Pb^{2+}>Cd^{2+}$, agreeing with the order of the stability constants of the complexes between pyridine-2-carboxylic acid and the corresponding metal ions.[6] Interestingly the k values were altered by change of the counter ions of Zn^{2+}, decreasing in the order, $NO_3^->Br^->Cl^->OAc^-$. The $\Delta\tau$ in the NMR spectra of the 2-PCHO–zinc salts mixture was varied by change of the counter anion. A good linear relationship, as shown in Fig. 1, was observed between log($\Delta\tau$) and

log k. This shows that the catalytic function of metal salts for the reduction of 2-PCHO by NBNH results from their strong coordination to the substrate and that the coordination strength depends not only on the nature of metal cation but on that of counter anion. Salicylaldehyde, thiophene-2-carbaldehyde and furfural were not reduced by NBNH in the presence of $Zn(OAc)_2$. This suggests the coordination of Zn^{2+} to oxygen atom or sulfur atom is too weak to fix the Zn^{2+} in the proximity of the carbonyl group.

Experimental

Kinetic Procedures. Reaction was started by mixing methanol solutions of 2-PCHO, metal salt and NBNH in a quartz cell which was placed in a water jacket maintained at a working temperature. The rate was determined spectrophotometrically by following the decrease in the absorbance at 355 nm due to NBNH. To eliminate an increment of the absorbance due to 2-PCHO–metal ion complexes which showed a weak absorbance at 355 nm, differential spectra were taken by employing a solution of 2-PCHO–metal ion mixture as a reference. An obvious isosbestic point was observed at 310 nm. Under the condition where aldehyde and metal ion were present in great excess with respect to NBNH, the rate of disappearance of NBNH depended on first order of its concentration. The pseudo first-order rate constant (k) was obtained from the slope of the plot of log [(NBNH)] against time. Metal salts were used as hydrate except $ZnCl_2$ and $ZnBr_2$; $Zn(OAc)_2 \cdot 2H_2O$, $Pb(OAc)_2 \cdot 3H_2O$, $Cd(OAc)_2 \cdot 2H_2O$, $Cu(OAc)_2 \cdot H_2O$, and $Zn(NO_3)_2 \cdot 6H_2O$.

Products Analysis. 2-PCHO (5.0 g; 0.047 mol), NBNH (1.5 g; 0.070 mol) and $Zn(OAc)_2$ (6.6 g; 0.023 mol) were dissolved into methanol (100 ml) and the solution was allowed to stand for two days at 40 °C. The methanol was removed by vaccum distillation from the reaction mixture. After dissolving the residue in water, enough amount of EDTA tetra sodium salt was added to chelate the all zinc ion and filtered. The filtrate was extracted with ether. The ether solution was dried over sodium sulfate and then the ether was evaporated. The gas chromatographic analysis (Apiezone grease L-30, 150 °C: retension time 2.45 min) and the picrate (mp 158 °C, lit.[7] 159 °C) confirmed the formation of 2-(hydroxymethyl)pyridine. A part of the aqueous filtrate was passed through an anionic resin (Amberlite IRA-400). The eluted solution showed the same UV spectrum as that of an authentic 1-benzyl-3-carbamoylpyridinium chloride (λ_{max} 265 nm in H_2O).

References

1) D. J. Creighton, J. Hujdu, G. Mooser, and D. S. Sigman, *J. Amer. Chem. Soc.*, **95**, 6855 (1973). S. Shinkai and T. Kunitake, *Chem. Lett.*, **1974**, 1113.

2) B. L. Vallee and F. L. Hoch, *J. Biol. Chem.*, **225**, 185 (1957).

3) D. J. Creighton and D. S. Sigman, *J. Amer. Chem. Soc.*, **93**, 6314 (1971).

4) S. Shinkai and T. C. Bruice, *ibid.*, **94**, 8258 (1972).

5) A. G. Anderson and G. Beykelhammer, *ibid.*, **80**, 996 (1968).

6) K. Suzuki, M. Yasuda, and K. Yamasaki, *J. Phys. Chem.*, **61**, 229 (1957).

7) Beilstein Handbuch, **2**, (I), 203.

BULLETIN OF THE CHEMICAL SOCIETY OF JAPAN, VOL. 48 (3), 1081—1082 (1975)

Fundamental Studies of Solvent Dyeing with Tetrachloroethylene. II. The Diffusion of 1,4-Diaminoanthraquinone in Nylon 6

Zenzo MORITA, Koji UCHIMURA,* and Hiromi MOTOMURA

Department of Textiles and Polymer Science, Faculty of Engineering, Tokyo University of Agriculture and Technology, Koganei, Tokyo 184

(Received October 5, 1974)

Synopsis. The diffusion and sorption of 1,4-diaminoanthraquinone in nylon 6 were investigated using a cylindrical film-roll. The diffusion of the penetrant in nylon 6 from the aqueous dyebath was much faster than that from the tetrachlororoethylene (TCE) dyebath. The surface concentration from water was larger than that from TCE. The water added to the TCE dyebath accelerated the diffusion of the penetrant in nylon 6.

Solvent dyeing with halogenated hydrocarbons, especially tetrachloroethylene (TCE), has attracted considerable attention, and many publications on this subject have appeared in the recent literature.[1-6] In the solvent dyeing of poly(ethylene terephthalate) (PET) with disperse dyes, the diffusion from the TCE dyebath is faster than that from the aqueous one,[7] and the partition coefficient in the TCE system becomes smaller than in the aqueous system, as the solubility of dye in TCE is larger than that in water.[1]

In a previous paper, some comparisons of the diffusion of disperse dyes in PET have been made between the systems of water and of TCE.[7] The results obtained have confirmed the above facts and have shown that TCE affected the properties of PET. The glass transition temperature, T_g, of PET has been reduced and disperse dyes have been diffused into PET at lower temperatures than 80 °C.

In this paper, some comparisons will be made between the systems of water and TCE in the diffusion and sorption behavior of 1,4-diaminoanthraquinone in nylon. The effect of water added to the TCE dyebath will also be studied.

Experimental

Films. Biaxial oriented nylon 6 film (Emblem, Unitica Co., Ltd.) was used. It was cut 4 cm wide and 55 cm long, scoured with hot water, and heat-set at 95 °C in water for 24 hr. The film was wound so tightly on a glass tube (ϕ=1 cm) in the same solvent of the dyebath that there were no bubbles between the consecutive layers. The thickness of these films was measured by a thickness gage (Peacock Upright Dial Gage, Ozaki Manufacturing Co., Ltd.) to be 30.0 μm.

Chemicals. 1,4-Diaminoanthraquinone, supplied by Nippon Kayaku Co., Ltd., was crystallized by aqueous acetic acid and dried in a vacuum dryer for more than a week. The absence of impurities was checked by thin-layer chromatography. TCE of a technical grade (Toa Gosei Kagaku Kogyo Co., Ltd.) was used throughout without purification.

Diffusion and Sorption. The diffusion experiments were carried out in a 500 ml or 100 ml diffusion bottle with a reflux condenser. The dyeing conditions are shown in Table 1. Diffusion was carried out after the solution equilibrium of penetrant has been reached in the dyebath. After diffusion, the optical densities of the respective layers at the wavelength of 605 nm were measured by means of a Shimadzu MPS-50L Recording Spectrophotometer. The optical density of the penetrant on film was confirmed to obey Beer's law. The diffusion coefficient and surface concentration were calculated by the method of Sekido-Matsui from the concentration profile obtained experimentally.[8] The surface concentration was assumed to be equal to the equilibrium sorption.

Results and Discussion

The concentration profiles in the substrate are shown in Figs. 1—3. The plots are superimposed by a

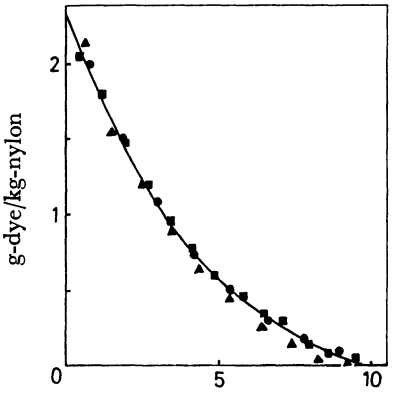

Fig. 1. Diffusion profile in nylon 6 from the water dyebath at 80 °C. (diffusion time, ■: 300 min, ▲: 180 min, ●: 120 min)

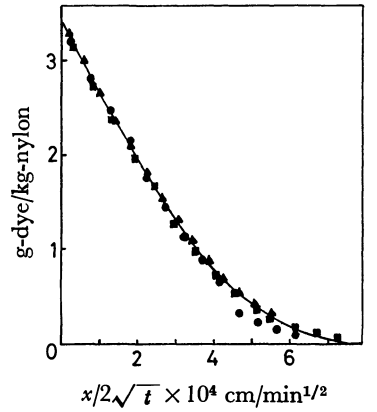

Fig. 2. Diffusion profile in nylon 6 from the 100 ml TCE+1.0 ml water dyebath at 80 °C. (diffusion time, ▲: 1050 min, ●: 720 min, ■: 600 min)

* Present address: Shikishima Spinning Co., Ltd., Higashi-ku, Osaka 541.

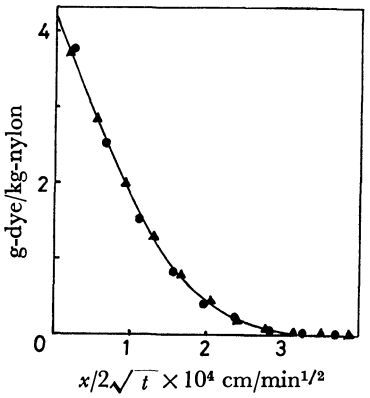

Fig. 3. Diffusion profile in nylon 6 from the 100 ml TCE+0.3 ml water dyebath at 80 °C. (diffusion time, ▲: 1260 min, ●: 900 min)

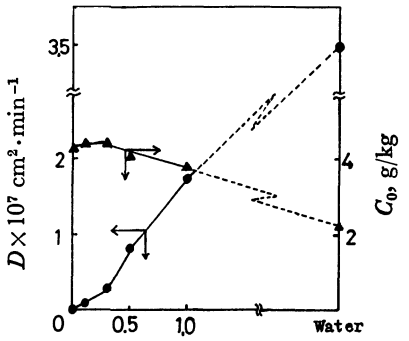

Fig. 4. The effect of water added to the TCE dyebath on the surface concentration C_0 and diffusion coefficient D in nylon 6 at 80 °C.

Boltzmann transformation ($x/2\sqrt{t}$), where x is the diffusion distance and where t is the time. These figures show that the dyeing system (nylon 6+water and/or TCE+dye) does not change during diffusion, even when more water than solubility in TCE was added, and that the diffusion obeys Fick's law. The diffusion coefficients from water were 300 times larger than those from TCE (Table 1). As the concentration in the aqueous dyebath was much smaller than that in the TCE one, the partition coefficient from the aqueous dyebath was larger than that from the TCE one.

The effect of additive water to the TCE dyebath is shown in Fig. 4. The diffusion coefficients increased with an increase in the additive water. The effect on the surface concentration was small. The solubility of water in TCE at 80 °C is estimated to be about 0.08 g in 100 ml of TCE.[9] The essential effect of such excess water is not clear.

Table 1. Diffusion in nylon 6 at 80 °C

Dyebath composition			Time of diffusion hr	Diffusion coefficient cm²/min
TCE ml	Water ml	Dye g		
0	500	0.1	2	3.79×10^{-7}
			3	3.57
			5	3.75
100	1.0	0.1	10—17.5	1.76×10^{-7}
	0.5		10—21	8.55×10^{-8}
	0.3		15—21	2.90
	0.1		20	1.04
	0		168	1.13×10^{-9}

The authors should like to thank Professor Kenzo Nishida for his helpful discussion. Acknowledgements are also due to the Nippon Kayaku Co., Ltd., for its staff's assistance in the preparation of this paper.

References

1) K. V. Datye, S. C. Pitkar, and U. M. Purao, *Textilveredlung*, **6**, 593 (1971).
2) B. Milićević, *ibid.*, **4**, 213 (1969).
3) B. Milićević, *J. Soc. Dyers Colour.*, **87**, 503 (1971).
4) B. Milićević, *Text. Chem. Color.*, **2**, 87 (1970); *Pev. Prog. Color.*, **1**, 49 (1970).
5) K. Gebert, *Melliand Textilber.*, **52**, 710 (1971); *J. Soc. Dyers Colour.*, **87**, 509 (1971).
6) J. Mecheels, *Textilveredlung*, **4**, 749 (1969).
7) Z. Morita, R. Kobayashi, K. Uchimura, and H. Motomura, *J. Appl. Polym. Sci.*, in press.
8) M. Sekido and K. Matsui, *Sen-i Gakkaishi*, **20**, 778 (1964).
9) E. W. McGovern, *Ind. Eng. Chem.*, **35**, 1230 (1943).

BULLETIN OF THE CHEMICAL SOCIETY OF JAPAN, VOL. 48(3), 1083—1084 (1975)

The Spin-Statistical Contribution in Redox Chemiluminescence Quantum Efficiency

Csaba P. Keszthelyi

Department of Chemistry, Louisiana State University, Baton Rouge, Louisiana 70803, U.S.A.

(Received June 18, 1974)

Synopsis. The theoretical upper limit of the quantum efficiency of Redox Chemiluminescence is shown to be 1.0 for both energy sufficient and energy deficient systems; whether the oxidant and reductant are generated *in situ* (as in ECL) has no effect on the chemiluminescence efficiency.

Electron transfer or redox chemiluminescence involves the conversion of chemical energy to light. The early experimental inquiries[1] were augmented by the theoretical considerations put forth by Marcus[2] and Hoytink.[3] The most common light producing sequence involves radical ions ($A^{\cdot-}$ and $D^{\cdot+}$) undergoing a homogeneous electron transfer reaction in fluid solution:

$$A^{\cdot-} + D^{\cdot+} \rightarrow A + D + h\nu. \quad (1)$$

The nature of the emitted light ($h\nu$) has allowed identification of the luminescors in many systems as $^1A^*$, $^1D^*$, $(AD)^*$ or $(A)_2^*$.[4,5] It is convenient to classify redox chemiluminescence systems as energy sufficient or energy deficient, depending on whether the enthalpy of Eq. 1 is greater or smaller than the first excited singlet energy (E_s) of the luminescor parent compound. Ways for obtaining singlet emission from an energy deficient system will be discussed further on in this paper.

An important property of all useful redox chemiluminescent systems is the quantum efficiency, Φ_{CL}, defined as the number of photons emitted per radical ion annihilation. It has recently been demonstrated that Φ_F, the fluorescence quantum efficiency determined from optical excitation, does not represent an upper limit for Φ_{CL}, because the chemiluminescence excitation reaction path may be more efficient than the optical excitation route.[6]

Recent papers dealing with redox chemiluminescors have examined their practical applicability as display devices[7-9] or a new type of laser.[10,11] While exploring practical applicability, some of the new papers have introduced a number of contradictory claims which involve erroneous interpretation of the theoretical work of Hoytink and Marcus. For example, the paper by Schwartz, Blakeley, and Robinson[8] claims that the maximum theoretical efficiency of an energy sufficient ECL system is 0.828, while that of an energy deficient (T-route) system is 0.414. This is contradicted by Pighin[9] who reported that the maximum theoretical efficiency of an energy deficient system is 6.6% (based on photons/electron). Rather than retracing the lines of thought that lead to the erroneous numbers 0.828 0.414, and 0.066, which are amply documented in the original papers themselves, we should briefly establish the correct conclusions based on the work of Marcus and Hoytink primarily.

The radical ions themselves are doublets, hence the pure spin-statistical prediction for Eq. 1 is

$$A^{\cdot-} + D^{\cdot+} \rightarrow \frac{1}{4}S + \frac{3}{4}T, \quad (2)$$

where S stands for singlet and T stands for triplet. Although it is possible to trace the quantum efficiency from Eq. 2, it would, in effect, be totally unwarranted. In the theory of Marcus the spin-statistical contribution is subject to the rate constant k for the electron transfer

$$k = \mathscr{Z}_\rho Z \exp\{-\Delta G^{\neq}/k_b T\}, \quad (3)$$

and the potential energy curves (G *vs.* Reaction Coordinate) incorporate the 'orientation polarization' factor. The activation barrier in the electron transfer step is strongly affected by the 'orientation polarization', which in turn may involve a transition state with a virtual charge distribution corresponding to $(A^{2-}\cdots D^{2+})$ for example.[2] Not only does Marcus' theory mitigate against blind reliance on the simplicistic spin-statistical approach when dealing with fluid solution media, but it would specifically make quick dissipation of ~3 eV unlikely by non-radiative means – such as required by Eq. 2 in case of an energy deficient system for 25% of the redox events; *i.e.*, producing $^1S_0$ rather than $^1S^*$ in the present notation.

Hoytink expresses the rate constants as

$$K_{singlet^*} = \frac{1}{4}K_d \exp\{-\Delta H_s^*/kT\} \quad (3a)$$

and

$$K_{triplet} = \frac{3}{4}K_d \exp\{-\Delta H_t^*/kT\} \quad (3b)$$

Hence only for the special case when the exponential terms are equal would Hoytink's work support Eq. 2. Once we emphasize the importance of specific terms that vary from system to system, we can proceed to set maximum quantum efficiency limits.

Considering Eq. 1 in some detail, we find that the over-all light production scheme involves competing reaction paths:

$$\left.\begin{aligned} A^{\cdot-} + D^{\cdot+} &\xrightarrow{k_S} {}^1S^* + {}^1S_0 \\ &\xrightarrow{k_t} {}^3T^* + {}^1S_0 \\ &\xrightarrow{k_Q} {}^1S_0 + {}^1S_0 \end{aligned}\right\} \quad (4)$$

For an energy sufficient system utilizing an efficient fluorescor parent compound, the upper limit of Φ_{CL} or Φ_{ECL} is 1.0 when $k_s \gg k_t + k_Q$. For an energy deficient system when $k_t \gg k_s + k_Q$, the number of redox events also represents the upper limit of triplets produced. In this case, corresponding to E-Type delayed fluorescence,[12] thermal activation of $^3T^*$ gives

$$^3T^* \xrightarrow[\text{activation}]{\text{thermal}} {}^1S^* \quad (5)$$

Consequently the maximum quantum efficiency of an energy deficient system is also 1.0.

We must emphasize the tenacious nature of Eq. 5 at this point; the type of thermal activation occurring in the case of eosin is not characteristic of many other systems. Also, and this is perhaps even more important, the presence of ionic species in the chemiluminescence solution (and the additional presence of a large excess of supporting electrolyte ions in an ECL system) can be expected to quench some of the triplets, hence cut the efficiency of possible thermal activation. Therefore, we should consider an alternative 'energy-doubling' process, triplet-triple annihilation or TTA:[12]

$$^3T^* + {}^3T^* \rightarrow {}^1S^* + {}^1S_0. \quad (6)$$

This would lead to the production of one excited singlet per two redox events, giving Φ_{CL} or $\Phi_{ECL}=0.5$ as the maximum value. Reliance on spin-statistics only (ignoring quintets) gives $1/4\ ^1S^*+3/4\ ^3T^*$ per TTA, a prediction which is once again unwarranted.

In closing, we should re-emphasize that various types of losses do occur in actual chemiluminescence and ECL systems. One loss that does not occur at practical concentrations of luminescor parents is electrochemical destruction of cations at the anion-generating pulse and *vice-versa* (except at the very first instant when the pulse is switched). The losses in the 'triple step' experiments of Faulkner[13] do not carry over to the typical double potential step mode of electrogeneration.

Combining the recent calculations of Measures[11] with the 20% efficient ECL system available,[10,14] one finds that laser action is not improbable in these systems; further investigations and improvements should be conducted, nevertheless, by observing the proper relationship between spin-statistics and chemiluminescence quantum efficiency.

Support of this work by the Louisiana State University Council on Research is gratefully acknowledged.

References

1) (a) D. M. Hercules, *Science*, **145**, 808 (1964); (b) R.E. Visco and E. A. Chandross, *J. Amer. Chem. Soc.*, **86**, 5350 (1964); (c) K. S. V. Santhanam and A. J. Bard, *ibid.*, **87**, 139 (1965). (d) A. Weller and K. Zachariasse, *J. Chem. Phys.*, **46**, 4984 (1967).

2) R. A. Marcus, (a) *Ann. Rev. Phys. Chem.*, **15**, 155 (1964); (b) *J. Chem. Phys.*, **43**, 679, 2654 (1965).

3) G. J. Hoytink, *Discus. Faraday Soc.*, **45**, 14 (1968).

4) (a) T. Matsumoto, M. Sato, S. Hirayama, and S. Uemura, This Bulletin, **44**, 1450 (1971); (b) T. Matsumoto, M. Sato, and S. Hirayama, *ibid.*, **46**, 369 (1973).

5) C. P. Keszthelyi, H. Tachikawa, and A. J. Bard, *J. Amer. Chem. Soc.*, **94**, 1522 (1972); C. P. Keszthelyi and A. J. Bard, *Chem. Phys. Lett.*, **24**, 300 (1974); *J. Org. Chem.*, **39**, 2936 (1974).

6) C. P. Keszthelyi, *J. Amer. Chem. Soc.*, **96**, 1243 (1974).

7) C. P. Keszthelyi and A. J. Bard, *Extended Abstracts*, **72—1**, p. 275; *J. Electrochem. Soc.*, **120**, 241 (1973).

8) P. M. Schwartz, R. A. Blakeley, and B. B. Robinson, *J. Phys. Chem.*, **76**, 1868 (1972).

9) A. Pighin, *Can. J. Chem.*, **51**, 3467 (1973).

10) (a) C. P. Keszthelyi, *J. Electrochem. Soc.*, **120**, 39C (1973); (b) *Appl. Optics*, **14** (1975—in press).

11) R. M. Measures, *Appl. Optics*, **13**, 1121 (1974).

12) C. A. Parker, "Photoluminescence of Solutions," Elsevier Publ. Co., (1968), Chapter 2.

13) R. Bezman and L. R. Faulkner, *J. Amer. Chem. Soc.*, **94**, 3699, 6317, 7324, 7331 (1972).

14) C. P. Keszthelyi, N. E. Tokel, and A. J. Bard, *Anal. Chem.*, **47**, 249 (1975).

BULLETIN OF THE CHEMICAL SOCIETY OF JAPAN, VOL. 48 (3), 1085—1086 (1975)

Microdetermination of Olefinic Linkage by *N*-Bromosuccinimide

Alfy Badie SAKLA,* Sadek Elsayed ABDOU, and Olfat Ahmed EL-KHADRAWY

Microanalytical Unit, Faculty of Science, University of Cairo, Giza, A. R. Egypt

(Received February 26, 1974)

Synopsis. A simple, accurate, and relatively rapid procedure for the estimation of olefinic linkage with *N*-bromosuccinimide has been presented.

Numerous methods have been developed for the determination of carbon to carbon unsaturation.[1] One of the problems is the development of a method for the determination of olefinic unsaturation, and the wide variation in reactivity of this group in different environments has resulted in the publication of some 3000 analytical methods to cover the whole range of olefinic compounds.[2] The halogenation methods are the most generally employed procedures for the determination of unsaturation in known compounds as well as mixtures. While standard bromine solution is a convenient and relatively stable reagent in macro scale analysis, yet its adaptation to the micro scale is difficult because 0.01 M bromine deteriorates rapidly.[3a]

It is now shown that *N*-bromosuccinimide (NBS) is stable, reactive, and convenient for routine microdetermination of olefinic linkage. The reaction with NBS is at least twenty five times faster than that with bromine.[4] An excess amount of a 1% aqueous solution of NBS is added to the unsaturated organic compound (2—4 mg) in glacial acetic acid at room temperature and kept for 10 min. Excess of NBS is determined titrimetrically against standard sodium thiosulphate. The results are given in Table 1 and are shown to be quite satisfactory (mean error $\pm 0.3\%$). The present procedure is simple, accurate and relatively rapid for the estimation of olefinic linkage.

It should be noted, however, that (a) none of the procedures described in the literature is applicable to all types of compounds containing the alkene function, and (b) a method yielding consistently reproducible results does not necessarily give the true unsaturation values of the substance under investigation.[3b] Estimation of tetraphenylethylene with NBS gives zero result and the starting material is recovered unchanged. This may be attributed to the absence of hydrogen atoms in the olefinic linkage. The nature of the *para*-substituent in the 1,1-diarylethylenes Ia—g has an influence on their reaction with NBS. In the presence of *para*-alkoxy groups Ia—c the corresponding 2-bromo-

TABLE 1. MICRODETERMINATION OF OLEFINIC LINKAGE BY NBS

Compound	Weight of sample (mg)		Calcd >C=C<	Found >C=C<		% error	
Cinnamic acid	2.985	2.395	16.20	16.17	16.00	−0.03	−0.20
	2.715	2.200		16.09	16.40	−0.11	+0.20
	3.430	2.900		16.30	16.50	+0.10	+0.30
Cinnamyl alcohol	2.580	2.655	17.90	18.00	17.60	+0.10	−0.30
	2.900	3.210		18.20	17.80	+0.30	−0.10
Stilbene	1.890	2.000	13.30	13.00	13.50	−0.30	+0.20
	3.150	2.515		13.09	13.20	−0.21	−0.10
	2.550			13.60		+0.30	
Styrene	2.890	3.150	23.06	23.20	22.90	+0.14	−0.16
	2.950	3.810		23.09	22.90	+0.03	−0.16
p-Bromostyrene	2.050	1.815	12.90	13.08	12.85	+0.18	−0.05
	3.805			12.60		−0.30	
Diphenylethylene	2.070	2.370	13.30	13.20	13.00	−0.10	−0.30
	1.135			13.00		−0.30	
Triphenylethylene	4.055	3.200	9.20	9.00	8.99	−0.20	−0.21
	2.545	2.725		9.09	9.10	−0.11	−0.10
	3.050			9.50		+0.30	
2-Bromo-1,1-diphenylethylene	2.015	3.090	9.20	9.00	8.90	−0.20	−0.30
	4.010	3.250		8.90	9.10	−0.30	−0.10
1,1-Bis(*p*-bromophenyl)ethylene	1.830	2.280	7.10	7.30	7.20	+0.20	+0.10
	2.180	1.936		7.00	7.15	−0.10	+0.05
1,1-Bis(*p*-chlorophenyl)ethylene	2.450	3.010	9.60	9.50	9.30	−0.10	−0.30
	2.350			9.80		−0.20	
1,1-Bis(*p*-tolyl)ethylene	1.440	1.925	11.53	11.50	11.40	−0.03	−0.13
	1.680	2.132		11.60	11.40	+0.07	−0.13

* The author to whom the correspondence should be directed.

Table 2. Reactions of 1,1-diarylethylenes with NBS

(I, 0.01 mol)	R	NBS mol	II %	II Mp (°C)	III %	III Mp (°C)	IV %	IV Mp (°C)
a	MeO[6]	0.01	99.6	48[6]	—	—	—	—
		0.02	—	—	99.3	91[6]	—	—
		0.005	—	—	—	—	1000	204[7]
b	EtO[8]	0.01	99.5	64[8]	—	—	—	—
		0.02	—	—	99.5	118[6]	—	—
		0.005	—	—	—	—	100	207[8]
c	*i*-PrO[8]	0.01	99.55	52[8]	—	—	—	—
		0.02	—	—	99.56	62[a]	—	—
		0.005	—	—	—	—	100	187[9]
d	H[10]	0.01	99	42[10]	—	—	—	—
		0.02	99.2		—	—	—	—
e	Me[11]	0.01	99.3	64[11]	—	—	—	—
		0.02	99.6		—	—	—	—
f	Br[12]	0.01	99.5	104[13]	—	—	—	—
		0.02	99.5		—	—	—	—
g	Cl[14]	0.01	99.4	71[13]	—	—	—	—
		0.02	99.4		—	—	—	—

Reaction period 10 min. Solvent in all experiments, chloroform, 15 ml.

a) Found: C, 52.70; H, 4.80; Br, 35.30%. Calcd for $C_{20}H_{22}Br_2O_2$: C, 52.85; H, 4.84; Br, 35.24%.

ethylene IIa—c, 2,2-dibromoethylene IIIa—c and 1,1,4,4-tetra-arylbuta-1,3-diene IVa—c are isolated with equimolecular, dimolecular, and half-molecular quantities of NBS respectively.

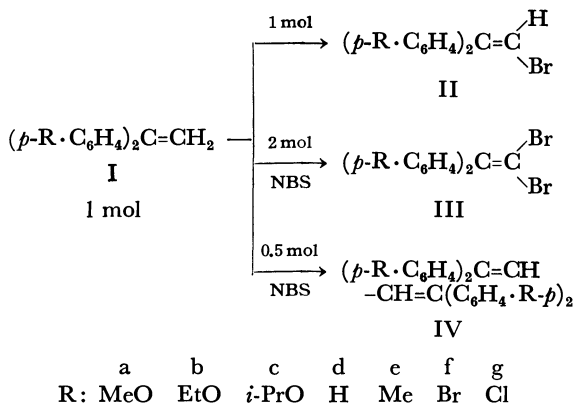

The mechanism of formation of 1,1,4,4-tetra-arylbuta-1,3-dienes IVa—c is apparently the same as previously described.[5] On the other hand, the other compounds Id—g gave 2-bromoethylenes IId—g as the only product (Tables 1 and 2).

Experimental

Procedure. Introduce an exactly weighed amount (2—4 mg) of the olefinic compound in a 50 ml Erlenmeyer flask charged with 4 ml of glacial acetic acid. Stirr until the organic compound is dissolved. Add accurately 1 ml of a 1% (w/v) aqueous solution of *N*-bromosuccinimide. The flask is stoppered, shaken and left in the dark for 10 min. Add 4 ml of 10% potassium iodide and titrate the liberated iodine with standard sodium thiosulphate solution (0.02 N) to the starch end-point.

The olefinic linkage is determined by the following equation:

$$\% \text{ C=C} = \frac{(a-b)(\text{normality of } Na_2S_2O_3)(24.02)(100)}{(\text{weight of sample in mg})(2)}$$

a = ml of $Na_2S_2O_3$ for blank, and

b = ml of $Na_2S_2O_3$ for sample.

Reactions of 1,1-Diarylethylenes Ia—g with NBS: This is exemplified by the following:

A solution of 1,1-bis(*p*-methoxyphenyl) ethylene[6] (Ia, 2.4 g, 0.01 mol) in chloroform (15 ml) and NBS (1.78 g, 0.01 mol) in the same solvent (15 ml) was heated to boiling for 10 min. The residue obtained after removal of the solvent was washed with water and then crystallised from 95% ethanol to give 2-bromo-1,1-bis(*p*-methoxyphenyl)ethylene IIa (3.15 g) with mp and mixed[6] mp 84 °C.

References

1) F. E. Critchfield, "International Series of Monographs on Analytical Chemistry," Vol. **8**, Organic Functional Group Analysis, Pergamon Press, New York (1963), p. 108.
2) R. Belcher and B. Fleet, *J. Chem. Soc.*, **1965**, 1740.
3) N. D. Cheronis and T. S. Ma, "Organic Functional Group Analysis by Micro and Semimicro Methods", Interscience Publishers, New York (1964), (a) p. 362, (b) p. 360.
4) S. D. Ross, M. F. Finkelstein, and R. C. Petersev, *J. Amer. Chem. Soc.*, **80**, 4327 (1958).
5) W. Tadros and A. B. Sakla, *J. Chem. Soc.*, **1957**, 3210.
6) P. Pfeiffer and R. Wizinger, *Ann. Chem.*, **461**, 132 (1928).
7) F. Bergmann, J. Szmuszkowicz, and E. Dimant, *J. Amer. Chem. Soc.*, **71**, 2968 (1949).
8) W. Tadros and G. Aziz, *J. Chem. Soc.*, **1951**, 2553.
9) W. Tadros, *ibid.*, **1954**, 2966.
10) R. Anschutz, *Ann. Chem.*, **235**, 159, 151 (1886).
11) R. Anschutz and A. Hilbert, *Ber.*, **57**, 1697 (1924).
12) T. N. Ashely, J. F. Grove, and T. Henshall, *J. Chem. Soc.*, **1948**, 261.
13) W. Tadros, A. B. Sakla, and Y. Akhnookh, *ibid.*, **1956**, 2070.
14) O. Grummutt, A. C. Buck, and E. I. Becker, *J. Amer. Chem. Soc.*, **67**, 2265 (1945).

BULLETIN OF THE CHEMICAL SOCIETY OF JAPAN, VOL. 48 (3), 1087—1088 (1975)

Magneto-chemistry and Infrared Spectra of Ammonia and Primary Aliphatic Amine Complexes of Copper(II) Chromate

Babu Ram S. SENGAR* and Gopal NARAIN**

Department of Chemistry, University of Sagar, Sagar (M.P.), India

(Received April 1, 1974)

Synopsis. Complexes of divalent copper of the type $CuCrO_4 \cdot 4Am$ and $CuCrO_4 \cdot 2Am \cdot 2H_2O$ with Am=ammonia or primary aliphatic amine, have been prepared and characterized. All the compounds reported are paramagnetic and values of μ_{eff} in the range 1.77—1.86 B.M. The assignment of the vibrational bands of the ligands and their shifts in frequency on co-ordination with copper(II) ion are discussed.

Many complexes of copper(II) have been described in literature and in particular complexes with ammonia and primary aliphatic amines. Relatively, very little work has been done on copper(II)chromate.[1] So far, most studies have been concerned with synthesis of copper(II) chromate–ammonia complexes and apart from few isolated examples, there have been no reports of magnetic data or absorption spectra. In the present communication, we report the results of an investigation into preparation, characterization, magnetic properties and infrared spectra of several complexes of copper(II)chromate with ammonia and primary aliphatic amines.

Experimental

The complexes were prepared by the following two methods:

(a) Shaking Method. About 5 g of copper(II) chromate was suspended in 40 ml of acetone with calculated quantity of liquor ammonia in a 250 ml conical flask. The contents were shaken for about two days. The complex formed was filtered, washed with acetone and dried over P_4O_{10}.

(b) Vapor Method. About 5 g of copper(II) chromate was placed in a calcium chloride tube fitted with a glass wool plug at the bottom. This tube was fitted in a conical flask containing the anhydrous primary aliphatic amine, thereby exposing the solid to vapors for about thirty hours. The complex formed was dried over P_4O_{10}.

1. Tetraaminecopper(II) Chromate. Prepared by Method a. The complex is green in color. Found: Cu, 25.59; N, 22.58; H, 6.88%. Calcd for $H_{16}O_4CrN_4Cu$: Cu, 25.23; N, 22.25; H, 6.40%.

2. Tetramethylaminecopper(II) Chromate. Prepared by Method b. Green. Found: Cu, 21.00; N, 18.42; C, 16.10; H, 6.14%. Calcd for $C_4H_{20}O_4CrN_4Cu$: Cu, 20.92; N, 18.44; C, 15.82; H, 6.58%.

3. Tetraethylaminecopper(II) Chromate. Prepared by Method b. Green. Found: Cu, 17.62; N, 15.40; C, 26.68; H, 7.49%. Calcd for $C_8H_{28}O_4CrN_4Cu$: Cu, 17.67; N, 15.58; C, 26.70; H, 7.78%.

4. Diaquodi-n-propylaminecopper(II) Chromate. Prepared by Method b. Green. Found: Cu, 18.98; N, 8.35; C, 21.86; H, 6.19%. Calcd for $C_6H_{22}O_6CrN_2Cu$: Cu, 19.06; N, 8.39; C, 21.59; H, 6.59%.

5. Diaquodi-n-butylaminecopper(II) Chromate. Prepared by Method b. Green. Found: Cu, 17.52; N, 7.61; C,

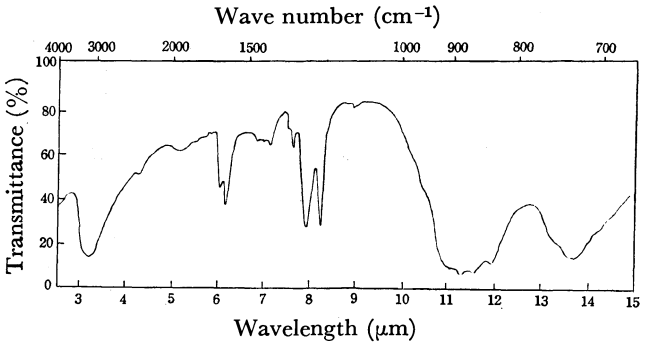

Fig. 1. Infrared spectrum of tetraamminecopper(II) chromate.

TABLE 1. MAGNETIC MOMENTS AND INFRARED BADNS (cm^{-1})

Compound	μ_{eff} (B.M.)	ν(NH)	NH_2 deform.	ν(CN)	Symm. C–N–H bend.	Asymm. C–N–H bend.	ν(OH)	νδ (Cr–O)
1. Tetraamminecopper(II) chromate	1.86	3205br	1646m	—	—	—	—	880br
2. Tetramethylaminecopper(II)-chromate	1.77	3325m	—	1075s 1037w	750m	837w	—	885s
3. Tetraethylaminecopper(II)-chromate	1.82	3230m	—	1078m 1042w	745m	839w	—	886s
4. Diaquodi-*n*-propylaminecopper(II)chromate	1.81	3240m	—	1085m 1051w	745m	851w	3480m	889s
5. Diaquodi-*n*-butylaminecopper(II) chromate	1.84	3365sh 3250m	1586s	1100w 1073vw	743s	845s	3490m	888s
6. Diaquodi-*n*-amylaminecopper(II) chromate	1.81	3368sh 3252m	1586s	1095w 1075vw	741s	845m	3485w	889s
7. Free aliphatic amine	—	3400	1620±30	1079±11	778±15	825±15	—	—

s, strong; m, medium; w, weak; vw, very weak; sh, shoulder; br, broad.

* Abstracted in part from thesis of B. S. Sengar.

** Author to whom correspondence should be directed.

26.33; H, 6.88%. Calcd for $C_8H_{26}O_6CrN_2Cu$: Cu, 17.58; N, 7.74; C, 26.56; H, 7.19%.

6. Diaquodi-n-amylaminecopper(II) Chromate. Prepared by Method b. Green. Found: Cu, 16.27; N, 7.16; C, 31.20; H, 7.32%. Calcd for $C_{10}H_{30}O_6CrN_2Cu$: Cu, 16.31; N, 7.19; C, 30.81; H, 7.70%.

Magnetic Measurements. The absolute values of magnetic moments of the compounds were measured at room temperature (304 K) using Gouy's method. (Table 1). The infrared spectra were obtained on a Infracord Model 137 spectrophotometer with the samples mounted as KBr disks. (Table 1, Fig. 1.)

Results and Discussion

The copper(II) chromate complexes possess general molecular formulae $[Cu(Am)_4]CrO_4$ and $[Cu(Am)_2(H_2O)]CrO_4$, where Am in the former represents either ammonia, methylamine or ethylamine and in the latter either *n*-propylamine, *n*-butylamine or *n*-amylamine.

All the complexes have been found to be paramagnetic and the value of effective magnetic moment is between 1.77—1.86 B.M. The four co-ordinate planar copper(II) complexes should have a value close to spin-only value of 1.73 B.M.[2] The magnetic moments of tetrahedral copper(II) complexes are expected to be around 2.2 B.M.[3] The tetrahedral arrangement of ligands has been found to be extremely rare for all copper(II) complexes, as a perfectly tetrahedral complex is orbitally triply degenerate and hence unstable.[4]

The ν(NH) in all complexes is observed in the range 3205—3368 cm^{-1}, whereas in ammonia and free aliphatic amines the band is observed at 3414 and 3400 cm^{-1}, respectively. The ν(NH) shifts to a lower value on co-ordination due to drainage of electrons from the nitrogen atom, thereby weakening N–H bond and resulting in a highly covalent metal–nitrogen bond.[5] The magnitude of the negative shift decreases as the molecular weight of the amine increases, which indicates that covalency of metal–nitrogen bond and stability of complexes decrease in the above order.[6] The position of all other bands are affected by co-ordination when compared with free amines.[7–9]

The O–H stretching band near 3485 cm^{-1} has been observed in all aquo complexes. There is a decrease in O–H stretching frequency due to co-ordination of water molecule with metal atom.[10–12] In addition to ν(OH), a characteristic band of co-ordinated water at 795 cm^{-1} in all aquo complexes has been observed.[13–15]

The $\nu\delta$(Cr–O) band in all complexes has been observed near 884 cm^{-1} indicating the presence of ionic chromate.[16]

We thank Professor S. S. Nigam for his keen interest and help throughout this research.

References

1) H. Hartford, *J. Amer. Chem. Soc.*, **66**, 312 (1944).
2) P. Ray and D. N. Sen, *J. Ind. Chem. Soc.*, **25**, 473 (1948).
3) K. Ito and T. Ito, *Aust. J. Chem.*, **11**, 406 (1958).
4) L. Sacconi, M. Ciampolini, F. Maggio, and F. P. Cavasino, *J. Inorg. Nucl. Chem.*, **19**, 73 (1961).
5) J. Fujita, K. Nakamoto, and M. Kobayashi, *J. Amer. Chem. Soc.*, **78**, 3295 (1956).
6) K. Nakamoto, "Infrared Spectra of Inorganic and Co-ordination Compounds," Pergamon Press, New York (1962), p. 146.
7) J. E. Stewart, *J. Chem. Phys.*, **30**, 1259 (1959).
8) P. J. Krueger and D. W. Smith, *Can. J. Chem.*, **45**, 1605 (1967).
9) L. J. Bellamy and R. L. Williams, *Spectrochim. Acta*, **9**, 341 (1957).
10) W. F. Griffith, *J. Chem. Soc.*, **1965**, 3694.
11) W. R. McWhinnie, *J. Inorg. Nucl. Chem.*, **27**, 1063 (1965).
12) G. Narain, *ibid.*, **28**, 2403 (1966).
13) J. Fujita, K. Nakamoto, and M. Kobayashi, *J. Amer. Chem. Soc.*, **78**, 3963 (1956).
14) I. Gamo, This Bulletin, **34**, 760, 765, 1430, 1433 (1961).
15) G. Sartori, C. Furlani, and A. Damiani, *J. Inorg. Nucl. Chem.*, **8**, 119 (1958).
16) D. Bassi and O. Sala, *Spectrochim. Acta*, **12**, 403 (1958).

BULLETIN OF THE CHEMICAL SOCIETY OF JAPAN, VOL. 48 (3), 1089—1090 (1975)

Amperometric Titration of Lead with Potassium Dithiotrihydroxymethyl Aminomethane and Its Determination in Presence of Mercury and Silver

G. S. DESHMUKH, H. CHAUDHURI, and H. S. MAHANTI*
Analytical Chemistry Division, Banaras Hindu University, Varanasi, India

(Received April 2, 1974)

Synopsis. Amperometric titration of lead with potassium dithiotrihydroxymethyl aminomethane at −0.2 V (*vs.* SCE) in ammoniacal ammonium tartrate–potassium nitrate base electrolyte (pH 8.0) has been carried out with a dropping mercury electrode. Lead has also been estimated in binary solutions with silver and mercury. The accuracy of the procedure is comparable to that obtained with classical methods.

Electrometric determination of lead by precipitating with sulphate ion was first introduced by Majer.[1] Later Kolthoff and Pan[2] titrated lead with dichromate amperometrically. Lead estimation with EDTA was carried out by Tanaka *et al.*[3] The use of mercaptobenzothiazole in the amperometric estimation of lead was reported by Cihalik *et al.*[4] Diethyldithiocarbamate[5] was also reported as a successful reagent in amperometric titration for lead.

Potassium dithiotrihydroxymethyl aminomethane has now been used as a precipitating agent in the amperometric determination of lead, which has also been estimated in presence of mercury and silver. This reagent with the structural formula, $(CH_2OH)_3$ C–NH–C(SK)=S, having two sulphur and one nitrogen which can act as donors, forms insoluble complexes with metal ions. Polarographic characteristics of this compound revealed an anodic wave at dropping mercury electrode extending over a wide span of potential (−0.7 V *vs.* SCE) in ammoniacal ammonium tartrate and potassium nitrate base electrolyte (pH 7.0—10.5). The diffusion current was found to be proportional to the concentration. Two methods have been developed for the amperometric titrations. The first is based on the measurement of the anodic current of excess titrating agent after complete precipitation of lead. In the second procedure dealing with the analysis of binary mixtures, the applied potential was so chosen that one of the two components is reduced at that potential. This also being the oxidation potential of the titrant, the current readings include the cathodic current of the reducible ion as well as the anodic current of the reagent. With the addition of the reagent, the ion reducible at the applied potential is preferentially precipitated and the cathodic current is decreased. When whole of the metal ion is precipitated, the current is reduced to residual current value, and the second component starts getting precipitated. The current remained steady during this stage, and after the complete precipitation of the second cation the anodic current of the excess reagent begins to increase.

* Present address: National Institute of Foundry and Forge Technology, Hatia, Ranchi-3, India.

Solutions. Stock solutions of various metal ions were prepared from E. Merck's guaranteed reagents and standardized by gravimetric procedures.[6] All other reagents used were of AnalaR variety. The preparation and standardization[7] of potassium dithiotrihydroxymethyl aminomethane were carried out as follows: 200 ml of saturated solution of trihydroxymethyl aminomethane was taken in a beaker and 5 g of KOH was added. The beaker was cooled in ice, and then 10 ml of carbon disulphide was added, and stirred thoroughly with magnetic stirrer for 16 hr. The excess carbon disulphide was then removed by thorough shaking with double distilled pure benzene and the liquid was separated using a separating funnel. It was then evaporated little by heating on water bath and cooled in ice. Highly hygroscopic crystalline solid was separated. An aqueous solution of the reagent was standardized with potassium ferricyanide in alkaline medium in presence of osmium tetroxide as catalyst by amperometric titration at a potential of +0.2 V (*vs.* SCE) using rotating platinum micro-electrode.

Apparatus. A Fisher Electropode in conjunction with dropping mercury electrode and saturated calomel electrode was used for the titration. The pH measurements were made with a line operated Beckmann Zeromatic pH meter.

Experimental

The appropriate operative conditions for quantitative estimation of lead were established by trial experiments and it was observed that reproducible results were obtained in a base electrolyte consisting of ammoniacal ammonium tartrate and potassium nitrate (overall concentration 0.05—0.25 M) and pH range 7.0—9.0. In the actual procedure an aliquot of lead solution was taken in a titration cell containing 0.1 M base electrolyte. The pH of the solution was adjusted to 8.0 by adding ammonia. Pure nitrogen was passed into the solution to remove oxygen. A potential of −0.2 V (*vs.* SCE) was applied, the galvanometer reading was noted initially and after each addition of the titrant. After complete precipitation of lead, excess reagent gave the anodic

TABLE 1. AMPEROMETRIC DETERMINATION OF LEAD WITH POTASSIUM DITHIOTRIHYDROXYMETHYL AMINOMETHANE

Amount (mg) of Pb^{2+}		% Error
Taken	Found	
0.5084	0.5083	−0.02
1.0170	1.0170	—
0.6355	0.6325	−0.47
2.2330	2.2330	—
2.9770	2.9840	+0.23

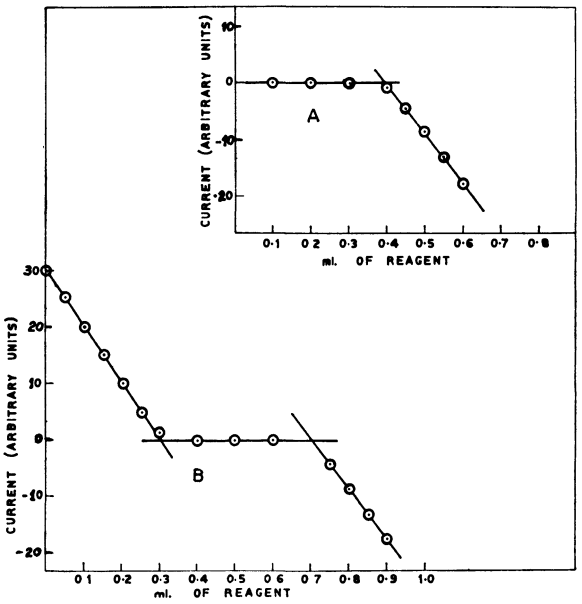

Fig. 1. Typical amperometric titration curves.

diffusion current of its own resulting in a regular rise in the current. The end point was located graphically (Fig. 1, Curve A). The results of estimations are given in Table 1.

For the determination of lead+silver and lead+mercury in a binary mixture, the titrations were carried out in ammoniacal ammonium tartrate and potassium nitrate base electrolyte of pH 8.0 at an applied potential of −0.2 V (*vs.* SCE). At this potential silver or mercury had its cathodic current while lead remained unreduced. During the titration the current decreased with the precipitation of silver or mercury and remained constant with the commencement of lead precipitation and increased with the anodic diffusion current of the excess reagent. The end points were located graphically (Fig. 1, Curve B), the first point of intersection gave the end point for silver or mercury and second point of intersection gave the end point for lead. The results of these titrations are given in Table 2.

Sincere thanks of the authors are due to Council of Scientific and Industrial Research, Government of India for research grants.

Table 2. Amperometric determination of the two components of binary mixtures with potassium dithiotrihydroxymethyl aminomethane

Mixture of Pb^{2+} and Ag^+					
Amount taken (mg)		Amount found (mg)		% Error	
Pb^{2+}	Ag^+	Pb^{2+}	Ag^+	Pb^{2+}	Ag^+
1.3460	0.8754	1.3510	0.8584	+0.37	−1.94
1.2430	1.1670	1.2430	1.1620	—	−0.42
1.6576	1.4590	1.6510	1.4470	−0.40	−0.82
2.0720	1.7508	2.0720	1.7508	—	—
1.4890	1.1670	1.4890	1.1570	—	−0.86
Mixture of Pb^{2+} and Hg^+					
Amount taken (mg)		Amount found (mg)		% Error	
Pb^{2+}	Hg^+	Pb^{2+}	Hg^+	Pb^{2+}	Hg^+
1.8650	1.7620	1.8320	1.7620	−0.16	—
2.0720	1.1740	2.0740	1.1730	+0.09	−0.08
3.1080	0.5872	3.1120	0.5851	+0.13	−0.35
4.1440	2.3490	4.1500	2.3460	+0.14	−0.13
1.6580	0.5872	1.6580	0.5851	—	−0.35

References

1) V. Majer, *Z. Electrochem.*, **42**, 120 (1936).
2) I. M. Kolthoff and Y. D. Pan, *J. Amer. Chem. Soc.*, **61**, 3402 (1939).
3) N. Tanaka, M. Kodama, M. Sasaki, and M. Sugino, *Bunseki Kagaku*, **6**, 86 (1957).
4) J. Cihalik and E. K. Pavlikova, *Chem. Listy*, **49**, 1640 (1955).
5) W. Stricks and S. K. Chakravarty, *Anal. Chem.*, **34**, 508 (1962).
6) A. I. Vogel, "A Text Book of Quantitative Inorganic Analysis," Longmans, Green & Co, London (1961), pp. 482, 486.
7) H. Chaudhuri, S. S. Chatterjee, and H. S. Mahanti, *Technology*, **10**, 4 (1973).

BULLETIN OF THE CHEMICAL SOCIETY OF JAPAN, VOL. 48 (3), 1091—1092 (1975)

Synthesis of α,β-Ethylenic Sulfones

M. SESHAPATHI RAO NAIDU and D. Bhaskar REDDY

Department of Chemistry, Post-Graduate Centre, Sri Venkateswara University, Anantapur 515003, India

(Received June 24, 1974)

Synopsis. A series of new α,β-ethylenic sulfones were prepared by the condensation of *p*-chlorophenylsulfonylacetic acid with various aryl aldehydes. The UV and IR spectra of all these compounds were recorded. Their IR spectra exhibited medium to strong bands in the region 1000—975 cm^{-1}, characteristic of *trans* ethylenic compounds.

The preparation of α,β-ethylenic sulfones by several routes has been reported.[1–5] For our current investigation on aryl cyclopropyl sulfones we were interested in preparing a series of unsaturated sulfones as intermediates. A number of new α,β-ethylenic sulfones prepared (see Table 1) by a slightly improved procedure of Baliah and Seshapathirao[1] are reported in this paper. Aromatic aldehydes were condensed with *p*-chlorophenylsulfonylacetic acid in glacial acetic acid solution in the presence of catalytic amounts of benzylamine. The synthetic utility of this procedure appears to be more elegant and convenient under simpler experimental conditions, affording fairly high yields of the unsaturated sulfones.

The UV spectra of all these unsaturated sulfones exhibited a long wavelength band around 245—320 nm, a second band around 220—236 nm and a third band with high intensity at 200 nm region.

The IR spectra of most of these sulfones showed a band in the region 1680—1620 cm^{-1} (ν C=C) and a strong band in the region 1000—975 cm^{-1} (δ CH out-of-plane) characteristic of *trans* ethylenic compounds.[4] In case of compounds containing polynuclear and heterocyclic substituents this band has

TABLE 1. *p*-$ClC_6H_4SO_2CH$=CHR

Sl. No.	R	Yield %	Mp °C	Formula	Analysis (%) Calcd C	Calcd H	Calcd Cl	Found C	Found H	Found Cl
1	4-$CH_3CONHC_6H_4$	69.0[a]	206—208	$C_{16}H_{14}ClNO_3S$	57.24	4.21		56.99	4.33	
2	2-BrC_6H_4	60.4[b]	149—150	$C_{14}H_{10}BrClO_2S$	47.01	2.82		46.62	2.57	
3	4-BrC_6H_4	75.0[c]	184—185	$C_{14}H_{10}BrClO_2S$	47.01	2.82		47.02	2.83	
4	3-Br-4-$OCH_3C_6H_3$	62.0[d]	149—150	$C_{15}H_{12}BrClO_3S$	46.48	3.12		46.40	3.07	
5	2-ClC_6H_4	87.9[b]	139.5—140.5	$C_{14}H_{10}Cl_2O_2S$	53.70	3.22	22.64	53.43	3.17	22.90
6	3-ClC_6H_4	84.7[d]	130—131	$C_{14}H_{10}Cl_2O_2S$	53.70	3.22	22.64	53.77	3.21	22.80
7	4-ClC_6H_4	57.5	167—167.5[f]							
8	2,4-$Cl_2C_6H_3$	79.3[d]	153—154	$C_{14}H_9Cl_3O_2S$	48.38	2.61		48.43	2.65	
9	3,4-$Cl_2C_6H_3$	57.6[d]	164—165	$C_{14}H_9Cl_3O_2S$	48.38	2.61		48.27	2.59	
10	4-$(CH_3)_2NC_6H_4$	81.0	158—159[g]							
11	2,3-$(CH_3O)_2C_6H_3$	80.6[d]	125—126	$C_{16}H_{15}ClO_4S$	56.72	4.46		56.73	4.41	
12	2,5-$(CH_3O)_2C_6H_3$	44.3[c]	114—115	$C_{16}H_{15}ClO_4S$	56.72	4.46		57.09	4.40	
13	3,4-$(CH_3O)_2C_6H_3$	45.9	147—147.5[h]							
14	2-$C_2H_5OC_6H_4$	42.1[e]	110—111	$C_{16}H_{15}ClO_3S$	59.53	4.68		59.18	4.58	
15	2-FC_6H_4	92.3[d]	103—104	$C_{14}H_{10}FClO_2S$	56.66	3.39	11.95	56.90	3.45	12.10
16	4-FC_6H_4	51.8[b]	118—118.5	$C_{14}H_{10}FClO_2S$	56.66	3.39		56.78	3.55	
17	4-$(CH_3)_2CHC_6H_4$	42.4[d]	97—97.5	$C_{17}H_{17}ClO_2S$	63.66	5.34		63.54	5.32	
18	2-$CH_3C_6H_4$	78.8[b]	135.5—136	$C_{15}H_{13}ClO_2S$	61.55	4.47		61.47	4.49	
19	4-$CH_3C_6H_4$	66.9[d]	124—125	$C_{15}H_{13}ClO_2S$	61.55	4.47		61.61	4.59	
20	4-$CH_3OC_6H_4$	62.2	144—145[i]							
21	2-$NO_2C_6H_4$	77.4[c]	174—175	$C_{14}H_{10}ClNO_4S$	51.94	3.11	10.95	52.11	3.11	10.90
22	3-$NO_2C_6H_4$	80.5[d]	141—142	$C_{14}H_{10}ClNO_4S$	51.94	3.11	10.95	52.14	3.07	10.80
23	4-$NO_2C_6H_4$	76.7[c]	197—198	$C_{14}H_{10}ClNO_4S$	51.94	3.11	10.95	51.69	3.17	11.20
24	1-Naphthyl	63.4[d]	136.5—137	$C_{16}H_{13}ClO_2S$	65.75	3.98	10.78	65.85	3.95	10.80
25	2-Naphthyl	61.0[c]	182—183	$C_{18}H_{13}ClO_2S$	65.75	3.98		65.81	4.02	
26	9-Anthryl	82.0[e]	184—185	$C_{22}H_{15}ClO_2S$	69.72	3.99		69.45	3.91	
27	1-Pyrene	84.4[c]	204—205	$C_{24}H_{15}ClO_2S$	71.37	3.75		70.98	3.57	
28	2-Thienyl	90.1	134.5—135.5[j]							

Products recrystallized from (a) aqueous acetone, (b) methanol, (c) glacial acetic acid, (d) 95% ethanol and (e) 2-propranol. W.L. Nobles and B.B. Thomson [*J. Pharm. Sic.*, **54**, 709, 576 (1965)] report (f) mp 163—164 °C, yield 30.2%; (h) mp 144—146 °C, yield 10.2%; (i) mp 142.5—143.5 °C, yield 19%; (g) mp 162—164 °C, yield 1.8%. W.P. Thompson and H.O. Huisman [*Rec. Trav. Chim.*, **85**, 175 (1966)] report (j) mp 135—136.5 °C, yield 19%.

Table 2. UV and IR spectra of α,β-ethylenic sulfones

Compd. No.	IR (cm^{-1}) Nujol					UV, nm, 95% ethanol λ_{max} (ε_{max})
	ν C=C	δ CH in-plane	δ CH out-of-plane	ν SO_2		
1	1672	1290	978	1310	1140	317(26470), 235(15410), 203(20850)
2		1282	980	1319	1150	276(17820), 232(13410), 203(17070)
3		1280	983	1316	1145	286(25540), 220(13300), 202(17860)
4	1680	1296	992	1320	1150	311(24680), 295(23910), 239(26110), 202(27490)
5		1278	962	1320	1144	276(19390), 226(14280), 203(21280)
6	1624	1297	1000	1315	1160	275(23700), 205(21040)
7		1272	975	1300	1135	285(29830), 219(18660), 203(23600)
8		1284	979	1323	1150	282(27800), 228(20870), 204(26020)
9	1660	1272	972	1310	1130	283(26260), 230(19050), 204(18990)
10	1665	1278	980	1316	1142	240(15490), 203(25230)
11	1660	1285	998	1312	1140	285(23810), 219(24340), 203(25520)
12	1664	1287	992	1308	1148	279(12480), 236(13070), 203(17440)
13	1686	1286	978	1302	1133	325(20040), 296(13520), 238(18330), 203(20690)
14	1680	1285	988	1305	1138	325(8349), 277(18050), 232(17330), 203(22980)
15	1674	1275	960	1303	1132	272(26570), 235(12040), 203(24290)
16	1640	1285	1005	1307	1132	279(23860), 236(11270), 224(12800), 203(20790)
17		1280	987	1315	1148	289(27130), 226(15360), 203(21280)
18		1266	980	1294	1127	282(21380), 226(14370), 204(25720)
19		1267	974	1305	1138	288(24960), 227(15970), 203(20760)
20		1290	974	1308	1158	310(28980), 233(22710), 203(26360)
21	1623	1282	980	1320	1144	247(19950), 203(22410)
22	1647	1276	982	1319	1146	265(35560), 233(19430), 202(23940)
23		1275	978	1316	1140	294(16780), 225(14970), 203(27490)
24		1295	986	1322	1159	320(7474), 222(47760), 204(37670)
25	1660	1283	990	1320	1160	308(27110), 271(35300), 232(30740), 203(25360)
26	1660	1280	972	1309	1125	256(111000), 221(27040), 203(37070)
27		1275	959	1302	1136	280(22580), 235(50240), 203(38900)
28	1650	1274	962	1310	1140	311(20790), 241(10660), 202(15990)

shifted to around 960 cm^{-1}.[5] These compounds also exhibited bands in the region 1295—1275 cm^{-1} [6] (δ CH in-plane). From the spectral data it may be concluded that all these compounds are *trans* isomers. They have also showed very strong peaks in the regions 1320—1300 and 1160—1120 cm^{-1} which are characteristic of sulfone groups.[7,8]

Experimental

All melting points were determined on a Mel-Temp apparatus and are uncorrected. The elemental analyses were performed by Dr. R. D. MacDonald, Australian Microanalytical Service. UV absorption measurements were determined in 95% ethanol with a Beckmann model DU-2 Ultraviolet Spectrophotometer and IR spectra were recorded on a Perkin-Elmer model 700 in nujol mulls. *p*-Chlorophenylsulfonylacetic acid[9] and 9-anthraldehyde[10] were prepared by published procedures and other aldehydes were obtained from commercial sources.

General Procedure. A solution of *p*-chlorophenylsulfonylacetic acid (0.01 mol) in acetic acid (6 ml) was mixed with an aryl aldehyde (0.01 mol) and benzylamine (0.2 ml), and refluxed for 90 min. The reaction mixture was cooled, treated with dry ether (50 ml) and any product separated was collected by filtration. The filtrate was diluted with more ether and washed successively with a saturated solution of $NaHCO_3$ (15 ml), $NaHSO_3$ (15 ml), dilute HCl (20 ml) and a finally with water. Evaporation of the dried etherial layer yielded in many cases a solid product. However, in some instances a syrupy substance separated was solidified on treatment with a small amount of methanol or 2-propanol. The relevant data on the compounds synthesized are given in Tables 1 and 2.

References

1) V. Baliah and M. Seshapathirao, *J. Org. Chem.*, **24**, 867 (1959).
2) W. E. Truce and C. T. Goralski, *ibid.*, **36**, 2536 (1971).
3) G. H. Posner and D. J. Brunelle, *ibid.*, **37**, 3547 (1972) and references cited therein.
4) V. Baliah and T. K. Rathinasamy, *Indian J. Chem.*, **9**, 220 (1971).
5) W. P. Trompen, C. Kruk, P. J. van Der Haak, and H. O. Huisman, *Rec. Trav. Chim.*, **85**, 185 (1966).
6) N. Sheppard and G. B. B. M. Sutherland, *Proc. Roy. Soc., Ser. A*, **196**, 195 (1949).
7) D. Bernard, J. M. Fabian, and H. P. Koch, *J. Chem. Soc.*, **1949**, 2442.
8) P. M. G. Bavin, G. W. Gray, and A. Stephenson, *Spectrochim. Acta*, **16**, 1312 (1960).
9) Gabriel, *Ber.*, **14**, 834 (1881).
10) L. Fieser and J. L. Hartwell, *J. Amer. Chem. Soc.*, **60**, 2555 (1938).

BULLETIN OF THE CHEMICAL SOCIETY OF JAPAN, VOL. 48 (3), 1093 (1975)

The Carbon-13 Nuclear Magnetic Resonance Spectra of Isomers of the Tris(*l*-propylenediamine)cobalt(III) Ion

Masaaki KOJIMA and Kazuo YAMASAKI

Department of Chemistry, Faculty of Science, Nagoya University, Chikusa-ku, Nagoya 464

(Received August 22, 1974)

Synopsis. The proton-decoupled carbon-13 NMR spectra were measured for the *mer*-$\Lambda(ob)$, *facial*-$\Lambda(ob)$, and *facial*-$\Delta(lel)$[Co(*l*-pn)$_3$]$^{3+}$ ions using the Fourier transform technique. There was a clear difference between the Λ and Δ configurations. However, no appreciable difference was observed between the *mer* and *facial* isomers of $\Lambda(ob)$-[Co(*l*-pn)$_3$]$^{3+}$.

Since the proton NMR spectra of tris(diamine)-cobalt(III) complexes are broad as a result of the spin-spin coupling of protons with ^{59}Co (I=7/2, 100% natural abundance), ^{59}Co decoupling is necessary to get a sufficient resolution for accurate analysis and to detect, for instance, the *mer* and *facial* isomers of the $\Delta(lel)$-[Co(*l*-pn)$_3$]$^{3+}$ ion.[1] We have separated the *mer* and *facial* isomers of $\Lambda(ob)$-[Co(*l*-pn)$_3$]$^{3+}$ by column chromatography on SP-Sephadex (Fig. 1) and measured the 100 MHz PMR spectra in DMSO-d_6; the spectra were similar for these two isomers except for the amine-proton signals.[2]

As recent developments in the carbon-13 NMR technique have made valuable contributions to the analysis of conformations[3] and to the determination of stereochemical structures,[4] this method has been applied to these isomers. Figure 2 shows an illustrative example of the 22.63 MHz ^{13}C-NMR spectra, including the assignment of the signals. Table 1 gives the results, together with that of *facial*-$\Delta(lel)$-[Co(*l*-pn)$_3$]Br$_3$. As the uncertainty of peak positions is about 0.1 ppm, there is a clear difference between the δ-positions of the Λ and Δ isomers. The *facial* isomer has a three-fold axis of rotation and its chelate rings are equivalent, whereas the chelate rings of the *mer* isomer are non-equivalent (*cf.* Fig. 1). Consequently, three signals can be expected for each carbon atom of the latter. The spectrum obtained, however, showed only one signal for the *mer* isomer as well as for the *facial* isomer (Fig. 2). Therefore, neither the ^{13}C-NMR nor the 100 MHz PMR technique is effective in distinguishing the *mer* isomer from the *facial* isomer of $\Lambda(ob)$-[Co(*l*-pn)$_3$]$^{3+}$. The cobalt-59 NMR spectra, however, showed a difference in chemical shift in the *mer-facial* isomerism.[5]

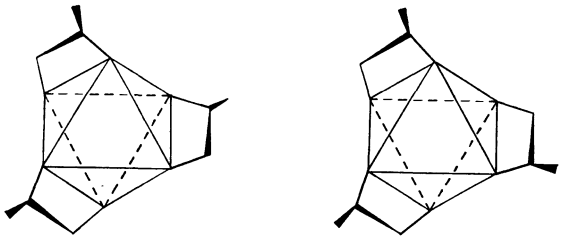

mer *facial*

Fig. 1. Geometric isomers of $\Lambda(ob)$-[Co(*l*-pn)$_3$]$^{3+}$.

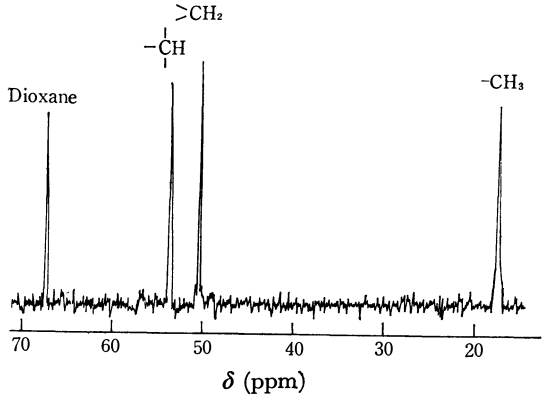

Fig. 2. ^{13}C-NMR spectrum of *mer*-$\Lambda(ob)$-[Co(*l*-pn)$_3$]Cl$_3$·4H$_2$O.

Table 1. ^{13}C-NMR Chemical shifts of the isomers of [Co(*l*-pn)$_3$]$^{3+}$ (in δ ppm)

Complex	$-CH_3$	$>CH_2$	$-\overset{\vert}{C}H$
mer-$\Lambda(ob)$-[Co(*l*-pn)$_3$]Cl$_3$·4H$_2$O	17.5	50.4	53.7
facial-$\Lambda(ob)$-[Co(*l*-pn)$_3$]Cl$_3$·3H$_2$O	17.6	50.2	53.7
facial-$\Delta(lel)$-[Co(*l*-pn)$_3$]Br$_3$	17.8	50.7	55.0

Experimental

Measurement of the ^{13}C-NMR Spectra. The proton-decoupled 22.63 MHz ^{13}C-NMR spectra were obtained by means of a Bruker WH 90 spectrometer, using the Fourier transform technique, which allows the measurement of samples with ^{13}C in natural abundance (1.1%). The solvent was D_2O, and the spectra were run at an ambient temperature. Dioxane (δ=67.40) served as an internal standard; the δ-values are given relative to TMS.

The ^{13}C-NMR spectra were measured by Dr. Sven Bagger and Prof. Woldbye, Chemistry Department A, The Technical University of Denmark. We wish to express our deep gratitude for their kindness.

References

1) J. L. Sudmeier, C. L. Blackmer, C. H. Bradley, and F. A. L. Anet, *J. Amer. Chem. Soc.*, **94**, 757 (1972).
2) M. Kojima, Y. Yoshikawa, and K. Yamasaki, *Inorg. Nucl. Chem. Lett.*, **9**, 689 (1973).
3) S. Bagger, O. Bang, and F. Woldbye, *Acta Chem. Scand.*, **27**, 2663 (1973).
4) O. W. Howarth, P. Moore, and N. Winterton, *Inorg. Nucl. Chem. Lett.*, **10**, 553 (1974).
5) Y. Koike, F. Yajima, A. Yamasaki, and S. Fujiwara, *Chem. Lett.*, **1974**, 177.

BULLETIN OF THE CHEMICAL SOCIETY OF JAPAN, VOL. 48 (3), 1094 (1975)

A Novel Route to Menthyldiphenylphosphine

Masato TANAKA and Ikuei OGATA

National Chemical Laboratory for Industry (Tokyo Kogyo Shikensyo), Hon-machi, Shibuya-ku, Tokyo 151

(Received September 2, 1974)

Synopsis. As evidence of a novel, configurationally-stable Grignard reagent, menthyldiphenylphosphine (MDPP) has been obtained by the reaction of diphenylphosphinous chloride with the Grignard reagent derived from menthyl chloride.

During the past several years, a variety of optically active phosphines have been used in asymmetric syntheses by homogeneous phosphine–transition metal complex catalysts. Neomenthyldiphenylphosphine (NMDPP) and menthyldiphenylphosphine (MDPP) have also been examined as chiral ligands in asymmetric hydrogenation,[1] hydroformylation,[2] and hydrosilylation.[3]

Since it has been believed that the preparation of a Grignard reagent from an optically active halide where halogen is attached to the asymmetric carbon results in significant racemization,[4] MDPP has been prepared according to the same procedure as was used in the case of NMDPP by

$$NaP(C_6H_5)_2 + \text{Neomenthyl chloride} \longrightarrow (\text{Menthyl})P(C_6H_5)_2$$

the reaction of sodium diphenylphosphide with neomenthyl chloride, whose preparation is fairly difficult.[5] The present authors, however, have found, as a rare example, that MDPP can be easily prepared by the reaction of diphenylphosphinous chloride with a Grignard reagent derived from menthyl chloride:

$$\text{Menthyl chloride} + Mg \longrightarrow \xrightarrow{P(C_6H_5)_2Cl} (\text{Menthyl})P(C_6H_5)_2$$

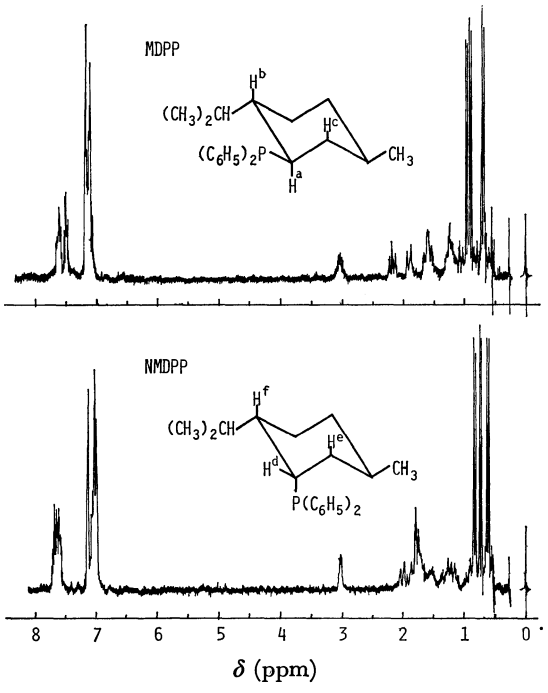

Fig. 1. The PMR spectra of MDPP and NMDPP at 220 MHz (benzene-d_6 solution).

The PMR spectra of the MDPP thus prepared is distinctly different from that of NMDPP, as is shown in Fig. 1; this indicates that MDPP is not contaminated by NMDPP. MDPP has an axial α-hydrogen (H^a) and two axial β-hydrogens (H^b and H^c) in the most stable conformation, and therefore MDPP exhibits an α-hydrogen multiplet with relatively large coupling constants. On the other hand, NMDPP has an α-hydrogen in the equatorial position, coupling and so the constant between H^d and H^e, and that between H^d and H^f, are much smaller.

The new route also offers a convenient way to prepare dimenthylphosphines and possibly even trimenthylphosphine.

Experimental

Neomenthyldiphenylphosphine was prepared by the method outlined in the literature.[1] The PMR spectra were recorded on a Varian HR-220 NMR spectrometer.

Menthyldiphenylphosphine. Menthyl chloride was prepared according to the method reported by Smith and Wright,[6] $[\alpha]_D$ −45.0° (neat). Magnesium (3.4 g, 0.14 mol) and 35 ml of dry tetrahydrofuran were placed in a 200 ml flask, and the mixture was treated with ethyl bromide (0.5 ml). Then, a solution of 20 ml of menthyl chloride (0.11 mol) in 40 ml of tetrahydrofuran was added, portion by portion, over a period of 4 hr at 50 °C, followed by reflux for 30 min. To the filtrate of the mixture, a 20 g portion of diphenylphosphinous chloride (0.091 mol) was added at 0 °C over a 10 min period. The resultant mixture was refluxed for 20 min, hydrolyzed by the cautious addition of 50 ml of water, and then extracted with hexane–ether. The organic layer was washed with water, dried over calcium sulfate, and concentrated. Through an agitated pot-still molecular distillation under $4—5\times10^{-4}$ mmHg, a fraction boiling at 110—120 °C (bath temperature) was collected, yield; 15 g (51%). A viscous oily substance solidified in several days and was then recrystallized from methanol to give large colorless needles; mp 52.9—54.0 °C (under nitrogen, corrected), $[\alpha]_D$ −93.5° (*c* 1.56, CH_2Cl_2).

Found: C, 81.60; H, 8.75%. Calcd for $C_{22}H_{29}P$: C, 81.44; H, 9.01%.

References

1) J. D. Morrison, R. E. Burnett, A. M. Aguir, C. J. Morrow, and C. Phillip, *J. Amer. Chem. Soc.*, **93**, 1301 (1971).

2) M. Tanaka, Y. Watanabe, T. Mitsudo, and Y. Takegami, *Chem. Lett.*, **1972**, 483.

3) Y. Kiso, K. Yamamoto, K. Tamao, and M. Kumada, *J. Amer. Chem. Soc.*, **94**, 4373 (1972).

4) H. M. Walborsky and A. E. Young, *ibid.*, **86**, 3288 (1964), and the referenced cited therein.

5) J. D. Morrison and W. F. Masler, *J. Org. Chem.*, **39**, 271 (1974).

6) J. G. Smith and G. F. Wright, *ibid.*, **17**, 1116 (1952).

BULLETIN OF THE CHEMICAL SOCIETY OF JAPAN, VOL. 48 (3), 1095—1096 (1975)

Syntheses of Trinuclear Ruthenium(III) Complexes with Dichloroacetato Ligands

Masao MUKAIDA, Mitsumasa KUSAKARI, Tadashi TOGANO, Toshihiro ISOMAE, Terunosuke NOMURA, and Tatsujiro ISHIMORI*

Department of Chemistry, Sophia University, Chiyoda, Tokyo 102

**Department of Chemistry, Rikkyo (St. Paul's) University, Ikebukuro, Tokyo 171*

(Received August 13, 1974)

Synopsis. Trinuclear ruthenium(III) complexes were prepared by the reaction of the dinuclear ruthenium(II, III) acetato complex with dichloroacetic acid. On the basis of chemical and thermal analyses, and on the basis of observations of the magnetic properties, the conductivities, the molecular weight, the alkalimetry, the infrared spectra and the electronic spectra, the complexes prepared here were formulated as $[Ru_3O(CHCl_2COO)_6(CH_3OH)_3](CHCl_2COO)$ and $[Ru_3O(CHCl_2COO)_6(OH)(H_2O)_2]$.

Some years ago, tetra-μ-monocarboxylato-chlorodiruthenium(II, III) complexes, $[Ru_2(RCOO)_4Cl]$ (R= H, CH_3, C_2H_5, *n*-C_3H_7, *n*-C_4H_9, C_6H_5), were prepared.[1,2] The structure of the butyrato complex was determined to have $[Ru_2(C_4H_9COO)]^+$ units linked into chains by Ru–Cl–Ru bridges.[3] Trinuclear acetato ruthenium(III) complexes, $[Ru_3O(CH_3COO)_6X_3]^{n+}$ (X=H_2O, py, CH_3OH, *n*=0 or 1), which contain an oxygen-centred structure, have recently been prepared.[4,5] Monochloro- and trichloroacetato ruthenium complexes have also been prepared.[2] However, no ruthenium complex with dichloroacetato ligands has yet been reported. This paper will describe the preparation and the properties of two dichloroacetato ruthenium complexes, $[Ru_3O(CHCl_2COO)_6(CH_3OH)_3](CHCl_2COO)$ and $[Ru_3O(CHCl_2COO)_6(OH)(H_2O)_2]$. The complexes prepared here were thought to have a skeletal structure similar to those of μ_3-oxo-trinuclear metal (Fe, Cr, Ru) acetato complexes.

Experimental

Preparation of $[Ru_3O(CHCl_2COO)_6(CH_3OH)_3](CHCl_2COO)$, *(1).* To a solution of tetra-μ-acetato-chlorodiruthenium(II, III) (1500 mg) in a mixture of CH_3OH (150 ml) and H_2O (150 ml), was added dichloroacetic acid (60 ml), after which the solution was left standing at room temperature.

After one or two weeks, the solution separated into two layers. The under layer (dark green) was transferred to a beaker, after which it was again kept standing for about a month. The dark green crystals thus obtained were filtered, washed with petroleum ether, and dried *in vacuo*, giving 350 mg. The crystals were recrystallized from CH_3OH. Found: Ru, 23.2; C, 15.34; H, 1.46%. Calcd for $[Ru_3O(CHCl_2COO)_6(CH_3OH)_3](CHCl_2COO)$: Ru, 23.1; C, 15.55; H, 1.45%.

The same complex was also obtained when tetra-μ-acetato-nitratodiruthenium(II, III) was used as the starting material in place of tetra-μ-acetato-chlorodiruthenium (II,III).

Preparation of $[Ru_3O(CHCl_2COO)_6(OH)(H_2O)_2]$, *(2).* The preparation was very similar to that described above, except that ethanol was used as the reaction solvent in place of methanol. Attempted recrystallization from methanol and ethanol were unsuccessful. Found: C, 12.54; H, 1.13; Cl, 37.12; H_2O, 3.3%. Calcd for $[Ru_3O(CHCl_2COO)_6(OH)(H_2O)_2]$: C, 12.64; H, 0.97; Cl, 37.32; H_2O, 3.16%.

The binuclear acetato ruthenium complexes used as the starting materials in these syntheses were prepared by methods described previously.[2]

Results and Discussion

The compositions were consistent with the formulae given in Table 1. The presence of two molecules of the coordinating water in **2** were determined by DTA and TG measurements. No endothermic peak due to the deaquation was found for **1**. The trimeric structure of the complexes was indicated by the molecular-weight measurement of **1** (Table 1). X-Ray single crystal photographs of **1** showed that the cell volume of the complex was about 4200×10^{-24} cm^3. The density calculated using the assumption of four molecules per cell was 2.07 g·cm^{-3} while the observed density was 2.03 g·cm^{-3} (by the flotation method in CCl_4 and CH_2I_2).

The unipositive cation assumed for **1** was supported by the absorbing behavior toward cation-exchange resin(Dowex 50W-X 8) in a methanolic solution, although the molar conductivities observed were quite small compared to those found for ordinary complexes of 1 : 1-type electrolytes. In the titration of a methanolic solution of **1** with a sodium hydroxide solution, two infliction points were observed, as is shown in Fig. 1. This is probably due to the ligand substitution between the coordinated methanol in **1** and the hydroxide ion.

Table 1. CHEMICAL FORMULAE AND THEIR PROPERTIES

	Complex	Λ_M in 10^{-3} M S cm^2	M.W.[c]	μ_{eff}[d] (B.M.)	λ nm[a] (ε)
1,	$[Ru_3O(CHCl_2COO)_6(CH_3OH)_3](CHCl_2COO)$	16[a]	1455[a]	2.16 (293 K)	715—690 (*ca.* 1570) 610—600 sh —420 sh
		12[b]	1366[b]		
2,	$[Ru_3O(CHCl_2COO)_6(OH)(H_2O)_2]$	20[a]		2.04 (298 K)	730—700 (*ca.* 2950) 630—600 sh —420 sh

a) in CH_3OH. b) in DMF. c) by vaper pressure osmometry. d) by Gouy method.

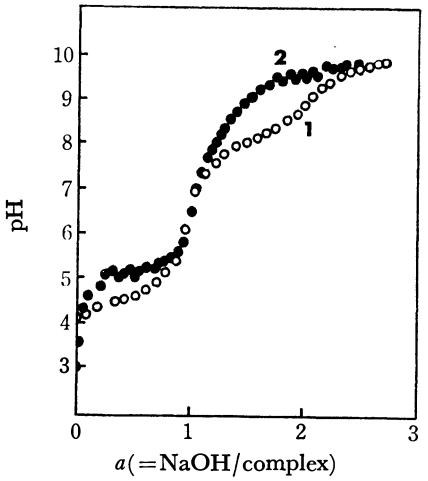

Fig. 1. pH titration curves for **1** and **2** in methanolic solution.
Complexes: 3×10^{-4} M.

On the other hand, **2** in a methanolic solution was absorbed by anion-exchange resin(Dowex 1-X 4), and only one infliction point was observed in its pH titration curve. This behavior seem to be evidence for the proton-dissociation of the aqua ligand in **2**:

$$[Ru_3O(CHCl_2COO)_6(OH)(H_2O)_2] \text{ (in solid)} \longrightarrow$$
$$[Ru_3O(CHCl_2COO)_6(OH)_2(H_2O)]^- + H^+ \text{ (in } CH_3OH)$$

The presence of methanol in **1** was ascertained by infrared spectroscopy. The IR spectra of the two complexes were almost identical except for the bands in the 1000 cm^{-1} region. In this region, two absorption bands at 996 and 968 cm^{-1} were observed for **1**, while only one absorption band, at 967 cm^{-1}, was found for **2**. The band at 996 cm^{-1} in **1** can be assigned to the methyl rocking vibration.

It has been reported that the observations of the electronic absorption spectra can serve as a guide for the characterization of μ_3-oxo-trinuclear acetato ruthenium complexes.[5] The electronic absorption spectra and the effective magnetic moments of **1** and **2** were similar to those of the complexes mentioned above.[5] The observed magnetic moments may also suggest an oxygen-centred structure in which marked spin-spin interaction occurs *via* the central oxygen atom in the Ru_3O unit.[6]

In the present study, **1** and **2** were obtained under the same reaction conditions. It is interesting to note that the formation of these species depends on the kind of alcohol used as a solvent in the syntheses. As has been noted in the Experimental section, attempts to recrystallize **2** from ethanol were unsuccessful. However, when **2** was treated by a mixture of methanol and water containing dichloroacetic acid, a crystalline material, which is thought to be $[Ru_3O(CHCl_2COO)_6(H_2O)(CH_3OH)_2](CHCl_2COO)$ on the basis of its composition and infrared spectrum, was obtained. This finding indicates a fairly strong coordinating nature of methanol in the complexes.

References

1) T. A. Stephenson and G. Wilkinson, *J. Inorg. Nucl. Chem.*, **28**, 2285 (1966).
2) M. Mukaida, T. Nomura, and T. Ishimori, This Bulletin, **40**, 2462 (1967); *ibid.*, **45**, 2143 (1972).
3) M. J. Bennett, K. G. Caulton, and F. A. Cotton, *Inorg. Chem.*, **8**, 1 (1969).
4) F. A. Cotton, J. G. Norman, A. Spencer, and G. Wilkinson, *Chem. Commun.*, **1971**, 967.
5) A. Spencer and G. Wilkinson, *J. Chem. Soc., Dalton*, **1972**, 1570.
6) A. Earnshow, B. N. Figges, and J. Lewis, *J. Chem. Soc., A*, **1966**, 1656.

Epoxide Rearrangement II.† Isomerization of 1-Methylcyclohexene Oxide over Solid Acids and Bases

Kazushi ARATA, Susumu AKUTAGAWA,* and Kozo TANABE**

Department of Chemistry, Hokkaido University of Education, Hachiman-cho, Hakodate 040
**Central Research Laboratory, Takasago Perfumery Co., Kamata 5, Ota-ku, Tokyo 144*
***Department of Chemistry, Faculty of Science, Hokkaido University, Sapporo 060*

(Received October 26, 1974)

The reaction of 1-methylcyclohexene oxide over solid acids and bases at 108 °C was found to give five main products, 2-methylcyclohexanone (III), 1-methylcyclohexanol (IV), 2-methyl-2-cyclohexene-1-one (V), 2-methylenecyclohexanol (VIa), and 2-methyl-2-cyclohexene-1-ol (VIb), with a small amount of 1-methylcyclohexene (I) and unidentified compound (II). The ketone (III) was formed predominantly over zeolite, SiO_2–Al_2O_3, H_2SO_4/SiO_2, $AlCl_3$, and BBr_3, while the allyl alcohol (VI) was given by Al_2O_3 and TiO_2. HCl/SiO_2 and solid H_3PO_4 calcined at 400—900°C gave both products, III and VI, in the same amounts, though the latter calcined at 200—300 °C formed almost 100% ketone. Solid lithium perchlorate was surprisingly active for the formation of ketone, but other metal perchlorates and lithium salts were quite inactive. Alkaline earth metal oxides and $NaOH/SiO_2$ were almost inactive. The catalytic activity and selectivity as well as the reaction path and mechanism are briefly discussed mainly in connection with acid-base property of solid catalysts.

Since Cope and Tiffany[1] observed an unusual base-catalyzed rearrangement of cyclooctatetraene oxide, much work has been done on the rearrangements of both cycloalkene oxide and open-chain oxide with strong bases, usually lithium dialkylamide.[2-6] The isomerization reactions of various epoxides with Lewis acid catalysts such as BF_3,[7,8] $ZnBr_2$,[9] $MgCl_2$,[10] and solid acid catalyst, Al_2O_3[11,12] have also been investigated.

Recently, Imanaka *et al.*[13,14] have studied the activity and selectivity of several solid acids and bases for the isomerization of propylene oxide. However, no work has been reported on the isomerization of epoxides other than propylene oxide and ethylethylene oxide[15,16] over solid acids or bases.

Cyclohexene oxide, one of the simplest cycloalkene oxides, seems suitable to study the selectivity and activity of solid acid or base catalysts and the effect of ring structure on the reaction. However, the reaction rate was extremely slow even over SiO_2–Al_2O_3. Thus, 1-methylcyclohexene oxide was chosen, because the reaction rate was much faster due to the electronic effect of methyl group and the selectivity for the formation of allyl alcohol with exo- or endo-double bond can be investigated.

In the present work, the activity and selectivity of several solid acids and bases and some salt catalysts for the isomerization of 1-methylcyclohexene oxide have been studied in a heterogeneous solid-liquid system.

Experimental

Catalysts and Materials. 1-Methylcyclohexene oxide, supplied from Takasago Perfumery Co., was fractionally distilled to purify to more than 98% and toluene, a guaranteed reagent, used as a solvent was redistilled over sodium metal.

The zeolite H-F9 was prepared from zeolite F-9, supplied from Tekkosha Co., by a conventional ion-exchange method using NH_4Cl and by calcining at 500° C. Al_2O_3 was KAT6 of Nishio Chemical Co. and SiO_2–Al_2O_3 was N631(L) (Al_2O_3; 15 wt. %) of Nikki Chemical Co. Both catalysts were calcined at 500 °C. H_2SO_4/SiO_2 was prepared as follows: 10 g of granular silica gel (White, Kanto Chemical Co.) was immersed in 12 ml of 0.5 M H_2SO_4, evaporated, dried and then calcined at 150 °C. HCl/SiO_2 was prepared by the same method. TiO_2 was prepared by the hydrolysis of titanium tetrachloride with 28% ammonia water at pH=9.4, followed by washing the precipitate, drying at 110 °C for 14 hr and calcining at 500 °C for 3 hr. ZnO was prepared by the hydrolysis of zinc nitrate with 28% ammonia water similarly as in the case of TiO_2.

Anhydrous $AlCl_3$ and BBr_3 were guaranteed reagents of Wako Pure Chemical Co. Solid phosphoric acid was N501 of Nikki Chemical Co. $LiClO_4 \cdot 3H_2O$, a guaranteed reagent of Nakarai Chemical Co., was used without any pretreatment. $LiClO_4$, $KClO_4$, LiCl, and $LiNO_3$, guaranteed reagents of Nakarai Chemicals Co., and $NaClO_4$ and Li_3PO_4, reagents of Wako Pure Chemical Co., were dried at 120 °C for 3 days. $NaOH/SiO_2$ was prepared by following the procedure of Malinowski and Czczepanska[17]: 10 g of granular silica gel was immersed in 12 ml of 1 M NaOH, dried and calcined at 500 °C. CaO and MgO were prepared by calcining their hydroxides in air at 550 °C or by calcining further the oxide *in vacuo* (10^{-4}—10^{-5} mmHg) in quartz tubes at 600 °C for 2 hr and at 640 °C for 3 hr, respectively. All the catalysts prepared were stored in sealed ampoules.

Procedure and Analysis of Products. In general, the reaction was carried out in the presence of toluene as a solvent at 108 °C for 2 hr. A mixture of 0.5 ml of the epoxide, 2.5 ml of toluene, and about 0.3 g of catalyst below 100 mesh was stirred in a reaction vessel by a magnetic stirrer, At appropriate time intervals, a small amount of the sample was taken out by a 1 ml syringe, separated from catalyst and analyzed by a gas chromatograph with a hydrogen-flame detector using a 3 m column of polyethylene glycol 20 M on celite 545 SK (150 °C; N_2, 0.9 kg/cm²). For the separation of two allyl alcohols, a 45 m capillary column of Ucon LB-550-X (100 °C; N_2, 1.2 kg/cm²) was used. The yields of products were calculated from VPC peak areas (uncorrected).

In the experiment where $AlCl_3$ was used as a catalyst, 0.5 g of the catalyst was added into a mixture containing 0.5 ml of the epoxide and 2.5 ml of toluene with vigorous stirring at room temperature and the reaction was continued for 15 min. Then, the reaction mixture was poured into

† Part I: K. Arata and K. Tanabe, *Chem. Lett.*, **1974**, 923.

50 ml of 5% hydrochloric acid. The organic layer was separated, washed with water twice and then dried over anhydrous calcium chloride. In the case of BBr_3, 0.3 ml of BBr_3 was poured into the same reaction mixture cooled in ice and the reaction was continued for 10 min. The subsequent procedure was the same as in the case of $AlCl_3$.

The reactions catalyzed by MgO and CaO calcined *in vacuo* were carried out by the procedure of Ohnishi and Tanabe.[18] The catalyst prepared *in vacuo* was introduced into an evacuated and sealed reaction vessel through a breakable joint to prevent the contact with air. Then, the reaction was followed by the general procedure.

The main reaction products, III–VI, were isolated by a column chromatograph on silica gel eluted with petroleum ether-diethyl ether (1 : 1) and analyzed by NMR and IR. Compound III was easily identified as 2-methylcyclohexanone by its IR spectrum and by glc comparison with the authentic sample; IR (neat): 2940, 2860, 1710, 1445, 1370—1330, 1310, 1210, 1120, 860, 810, and 720 cm^{-1}. Compound IV was identified as 1-methylcyclohexanol by IR and NMR; IR (neat): 3400—3200, 2950—2850, 1450, 1370, 1320, 1050, 1020, and 380 cm^{-1}; NMR (δ): 3.4 (s, 1H, OH), 1.7—1.1 (m, 10H, CH_2) and 1.0 ppm (s, 3H, CH_3). Compound V was recognized as 2-methyl-2-cyclohexene-1-one by its IR and by glc comparison with the authentic sample; IR (neat): 3500—3300, 2594, 2586, 2660, 1450, 1360, 1180, 1110, 1020, and 900 cm^{-1}. Compound VI was revealed to be a mixture of two allylic alcohols by its glc analysis with a capillary Golay column, IR, and NMR; IR (neat): 3180, 990 cm^{-1} assigned to hydroxyl group and 890 cm^{-1} to methylene group; NMR (δ): 5.1—5.3 ppm assigned to olefinic protons. The mixture is considered to consist of 2-methyl-2-cyclohexene-1-ol and 2-methylenecyclohexanol in view of mechanistic considerations. The hydrogenated compound of VI was identical in glc, IR and NMR spectra to those of the synthesized and hydrogenated compound of 2-methyl-2-cyclohexene-1-ol and identified to be 2-methyl-cyclohexanol. Both allylic alcohols were synthesized as follows in order to identify compound VI in glc.

(1) *2-Methyl-2-cyclohexene-1-ol.* 1-Methylcyclohexene (1.0 g) was oxidized with $Hg(OCOCH_3)_2$ (3.2 g) in 10 ml CH_3COOH at 80 °C for 2 hr to form 1-acetoxy-2-methyl-2-cyclohexene (0.90 g): bp 85 °C/15 mmHg, which was hydrolyzed with NaOH–CH_3OH to yield its allyl alcohol (0.5 g): bp 90 °C/18 mmHg; IR (neat); 3180, 990 cm^{-1} (-OH); NMR (δ): 5.4 (t, 1H, C=CH), 4.1 (s, 1H, OH), 3.8 (t, 1H, CHOH), and 1.7 ppm (s, 3H, $C=CCH_3$), which were identical with the literature values.[19] This sample showed the second peak of compound VI in glc.

(2) *2-Methylenecyclohexanol.* Methylenecyclohexane (0.5 g) synthesized by Wittig reaction from cyclohexanone, $(C_6H_5)_3PCH_3Br$ and BuLi[20] was oxidized with SeO_2 (1.1 g) in 8 ml AcOH and 2 ml Ac_2O at 60 °C for 2 hr, followed by the saponification with aqueous NaOH to give its allyl alcohol (75 mg); IR (neat): 3170, 995 cm^{-1} (-OH) and 890 cm^{-1} ($CH_2=C$); NMR (δ): 5.3 (s, 2H, $CH_2=C$), 4.1 (s, 1H, OH), and 3.8 ppm (t, 1H, CHOH), which were identical with the literature values.[21] This sample gave the first peak of compound VI in glc.

Results and Discussion

The reaction of 1-methylcyclohexene oxide over solid acids and bases gave five main products, 2-methylcyclohexanone (III), 1-methylcyclohexanol (IV), 2-methyl-2-cyclohexene-1-one (V), 2-methylenecyclohexanol (VIa), and 2-methyl-2-cyclohexene-1-ol (VIb), with a small amount of 1-methylcyclohexene (I) and unidentified compound (II).

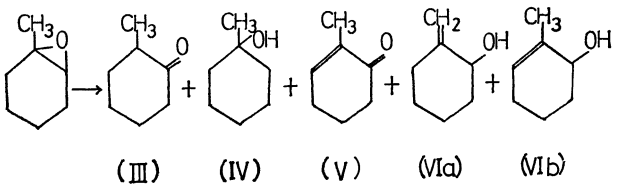

II was possibly the dehydrated diene-compound of VI, because cyclohexene oxide also rearranged under the same reaction conditions with extended periods to yield a small amount of cyclohexene and 1,3-cyclohexadiene, presumably formed by the dehydration of cyclohexenol. Their RRT (Relative Retention Time) in GLC was quite close to that between I and II.[22]

The relation between the yields of the products and reaction time is shown in Fig. 1, where the catalyst was solid H_3PO_4 calcined at 900 °C. The yields of III and VI increased almost parallel with each other during the course of reaction. The similar time-variation of the products was also observed in the case of TiO_2. This suggests that they are not intermediate species for each other. Since other products, IV and V, are presumably formed by hydrogenation and dehydrogenation of the starting epoxide, respectively, these two materials can not be intermediate species for III or VI formation. Consequently, it seems likely that ketone and allyl alcohol are formed by different mechanisms. However, there is a report implying the possibility of the carbonyl compound formation from the corresponding allyl alcohol on the base-induced conversion of epoxides.[5] This possibility seems to be very small, judging from the product distribution during the course of reaction in the present work.

Table 1 shows the catalytic activity and selectivity of several solid acid catalysts in 2 hr at 108 °C, and those of solid H_3PO_4 calcined at different temperatures are given in Table 2. The products are mainly divided into two categories, ketone (III) and allyl alcohol (VI). The former was formed predominantly

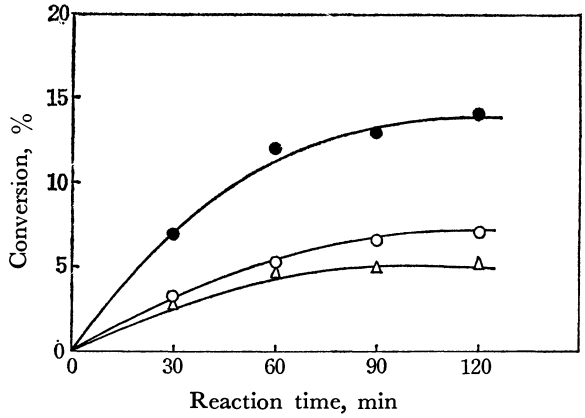

Fig. 1. Isomerization of 1-methylcyclohexene oxide over solid phosphoric acid calcined at 900 °C.
Reaction temp.: 108 °C, (-●-) Total conversion, (-○-) Allyl alcohol (VI), (-△-) ketone (III).

Table 1. Catalytic activity and selectivity of solid acid catalyst for isomerization of 1-methylcyclohexene oxide at 108 °C

Catalysts	Amount of catalyst (g)	Conversion (%)	Products (%)[d]					
			I	II	III	IV	V	VI (a,[e] b[f])
Zeolite H-F9[a]	0.343	35.8		1.7	23.2	0.6	0.9	8.6 (6.7, 1.9)
SiO_2-Al_2O_3[a]	0.473	42.3			42.3			
Al_2O_3	0.340	90.4	trace	2.4	5.6	4.8	2.4	74.6(51.1, 23.5)
Al_2O_3[b]	0.340	75.2			4.2	trace		69.6
H_2SO_4/SiO_2	0.413	100.0	0.8		99.2			
H_2SO_4/SiO_2[b]	0.413	98.4	0.8		97.6			
HCl/SiO_2	0.453	37.1	0.6		18.0			14.5 (3.9, 10.6)
TiO_2	0.435	27.3		0.2	2.0		0.2	24.9(13,9, 11.0)
ZnO	0.190	2.4						2.4
$AlCl_3$[c]	0.5	95.5	1.4	1.0	79.6	1.7	3.1	1.9
BBr_3[c]	0.3(ml)	93.4	3.6	28.3	31.3	3.0	1.0	2.0

a) A mixture of 1 ml of the epoxide and 5 ml of toluene was reacted at 100 °C. b) Reaction time: 30 min. c) The reactions were carried out at room temperature for 15 min in a heterogeneous state and at 0 °C for 10 min in a homogeneous state for $AlCl_3$ and BBr_3, respectively. Both catalysts gave several small peaks of unexpected and unidentified compounds in glg. d) See text. e) 2-methylenecyclohexanol. f) 2-methyl-2-cyclohexene-1-ol.

Table 2. Catalytic activity and selectivity of solid phosphoric acid for isomerization of 1-methylcyclohexene oxide at 108 °C

Temperature of calcination (°C)	Amount of catalyst (g)	Conversion (%)	Products (%)[b]					
			I	II	III	IV	V	VI (a, b)
200	0.440	98.0	0.5		96.8		trace	
200[a]	0.440	78.8	0.5	0.6	76.2			
300	0.370	87.7		1.2	86.5			
300[a]	0.370	85.1			57.9	8.1		17.6(12.8, 4.8)
400[c]	0.508	45.2		4.7	19.7		0.9	17.5 (9.2, 8.3)
900	0.380	12.4			5.3			7.2 (4.4, 2.8)

a) Reaction time: 30 min. b) See text. c) A mixture of 1 ml of the epoxide and 5 ml of toluene reacted at 100 °C.

over zeolite, SiO_2–Al_2O_3, H_2SO_4/SiO_2, $AlCl_3$, BBr_3 and solid H_3PO_4 calcined at 200 and 300 °C, while the latter was given by Al_2O_3 and TiO_2. HCl/SiO_2 and solid H_3PO_4 calcined at 400 and 900 °C gave both products in the same amounts, though their catalytic activities were not high. It is especially interesting that SiO_2–Al_2O_3, H_2SO_4/SiO_2 and low-temperature calcined solid H_3PO_4, which are known to have strong acid sites,[23,24] formed almost 100% ketone, whereas Al_2O_3 and TiO_2 gave more than 80% of allyl alcohol.

$AlCl_3$ and BBr_3, which are typical Lewis acid catalysts, showed the almost similar selectivity for ketone to those of H_2SO_4/SiO_2 and solid H_3PO_4 calcined at low temperature, which are Brönsted acids. Accordingly, it is considered that the selectivity does not depend on the type of acid sites, Brönsted and Lewis acids. BBr_3 produced a large amount of the unidentified compound (II) and many products other than those listed in the table, probably owing to its very high acid strength.[25]

A number of authors have reported that ketone is formed from epoxides with various acid catalysts; for example, from *p*-menthene and *d*-limonene oxide with $ZnBr_2$,[26] 2,3-butene oxide with BF_3-etherate,[27] *d*-limonene oxide with CH_3COOH,[28] propylene oxide over zeolite.[29] Our observations also substantiate the ketone formation with acid catalysts.

The pronounced activity of Al_2O_3 for the allyl alcohol formation was quite similar to Nigam and Levi's results,[30] where limonene and α-pinene oxides isomerized to the corresponding α, β-unsaturated alcohols, the yields being increased in order of acidic< neutral<basic alumina. Okamoto *et al.* have investigated the isomerization of propylene oxide over SiO_2–MgO catalysts using a pulse reactor and concluded that allyl alcohol was formed by acid-base bifunctional catalysts, where the oxygen of the epoxide was adsorbed on an acidic site and β-hydrogen on a basic site and that even very weak acid site was favorable for its formation.[14] Taking into account both observations, our results of Al_2O_3 could be explained by the bifunctional mechanism. The same mechanism seems to operate over TiO_2, since it has basic sites[31] as well as acidic sites.[32] The catalytic activities of solid H_3PO_4 calcined at various temperatures correlate well with their acidities, which are 4.5 mmol/g for 250 °C, 1.6 for 400, and 0.4 for 980 at $pK_a = 1.5$.[24] The formation of allyl alcohol over the catalyst calcined at high temperature suggests that basic sites appear on the surface and the reaction takes place by acid-base bifunctional mechanism,

Table 3. Catalytic activity and selectivity of solid metal perchlorates, lithium salts and solid base catalysts for isomerization of 1-methylcyclohexene oxide at 108 °C

Catalysts	Amount of catalyst (g)	Conversion (%)	Products (%)[d]					
			I	II	III	IV	V	VI
$LiClO_4 \cdot 3H_2O$	0.301	75.7		0.5	70.3			
$LiClO_4 \cdot 3H_2O$[a]	0.301	86.9		0.7	80.3			
$LiClO_4$	0.290	87.3	0.5	0.3	86.5			
$LiClO_4$[b]	0.290	86.7	0.4	0.6	85.7			
$KClO_4$	0.383	1.6			1.1		0.2	
$NaClO_4$	0.656	8.4		0.6	5.5			2.3
Li_3PO_4	0.351	2.9			1.8			1.1
LiCl	0.327	2.2			0.6			0.8
$LiNO_3$	0.355	2.4			0.4			0.3
$NaOH/SiO_2$	0.365	2.8		0.2	1.3		trace	1.2
CaO	0.270	2.8		0.2	1.5	1.1		
MgO	0.238	2.3		trace	1.3	0.9		
CaO[c]		0						
MgO[c]		0						

a) Reaction time: 15 min. b) Rection time: 30 min. c) Calcined *in vacuo*. d) See text.

In allyl alcohol formation, VIa generally exceeded VIb. This seems to be caused by the competition between primary and secondary proton abstraction. The preference for primary proton abstraction is due to the more enhanced acidity of primary hydrogen by the electronic effect and the preferred geometry, *i.e.*, less strain of cyclohexane ring containing the exo-double bond. The similar observations were demonstrated by Rickborn and Thummel,[5,6] in which the relative rates of proton abstraction were in order of primary>secondary> tertiary in the rearrangement of both cycloalkene and open-chain oxides catalyzed by a strong base, lithium diethylamide. Only in the case of HCl/SiO_2, VIb exceeded VIa against the above rule. This is probably due to the absence of appropriate basic sites on the catalyst.

Table 3 shows the catalytic activity and selectivity of solid metal perchlorates, lithium salts and solid base catalysts. Solid lithium perchlorate was surprisingly active for the formation of ketone, but other metal perchlorates and lithium salts were quite inactive. The high polarisability of lithium cation, the smallest cation of alkali metals, combined with perchlorate ion in which negative charge is dispersed seems to be necessary as the active sites for the rearrangement. Another reason for the high activity of $LiClO_4$ is considered to be the partial dissolution of the catalyst or its complex with the epoxide. Rickborn and Gerkin[33] reported that lithium perchlorate partially dissolved in benzene solution of epoxides gave rise to the rapid rearrangement. They obtained 80% of 2-methyl-cyclohexanone from 1-methylcyclohexene oxide over $LiClO_4$ in agreement with our findings. They also found that 1,2-dimethylcyclohexene oxide gave 91—98% of 1-acetyl-1-methylcyclopentane and 2—9% of 2,2-dimethylcyclohexanone,[33] which were formed with the same amount in the $HClO_4$-catalyzed pinacolone rearrangement.[34] In both reactions, the product formation can be best interpreted by assuming a planar carbonium ion intermediate. Thus, the cyclohexanone products from 1-methyl- and 1,2-dimethylcyclohexene oxide are considered to be formed by a process which allows the development of a planar carbonium ion at the cleaved tertiary center.

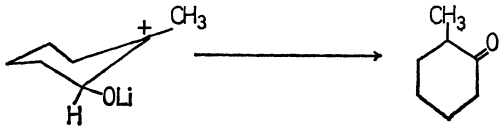

Sodium-silica gel, calcium and magnesium oxides calcined in air, which have basic characters,[17,35] were almost inactive for this reaction. The alkaline earth metal oxides calcined *in vacuo*, which were found recently to show strong basic character and high catalytic activity for the isomerizations of 1-butene to 2-butenes and α-pinene to β-pinene,[18,36,37] were not active at all at the mild reaction condition in the present work. However, a small amount of ketone was formed over these basic catalysts calcined in air. The formation of ketone may be due to the weak interaction between the alkaline earth metals as soft acids and the oxygen atom of the reactant as reported by Matsumoto *et al.*[38] Since MgO was active for the isomerization of propylene oxide at 260—270 °C in a gas phase,[14] the experiment at more severe condition is being planned in order to clarify the activity difference for different epoxides.

References

1) A. C. Cope and B. D. Tiffany, *J. Amer. Chem. Soc.*, **73**, 4158 (1951).
2) R. P. Thummel and B. Rickborn, *J. Org. Chem.*, **37**, 4250 (1972).
3) R. P. Thummel and B. Rickborn, *ibid.*, **37**, 3919 (1972).
4) C. L. Kissel and B. Rickborn, *ibid.*, **37**, 2060 (1972).
5) B. Rickborn and R. P. Thummel, *ibid.*, **34**, 3583 (1969).
6) R. P. Thummel and B. Rickborn, *ibid.*, **36**, 1365 (1971).

7) B. N. Blackett, J. M. Coxon, M. P. Hartshorn, and K. E. Richards, *J. Amer. Chem. Soc.*, **92**, 2574 (1970).
8) J. M. Coxon, E. Dansted, M. P. Hartshorn, and K. E. Rickards, *Tetrahedron*, **25**, 3307 (1969).
9) R. L. Settine and C. McDaniel, *J. Org. Chem.*, **32**, 2910 (1967).
10) S. M. Naqui, J. P. Horwitz, and R. Filler, *J. Amer. Chem. Soc.*, **79**, 6283 (1957).
11) V. S. Joshi, N. P. Damodaran, and S. Dev, *Tetrahedron*, **24**, 5817 (1968).
12) V. S. Joshi, N. P. Damodaran, and S. Dev, *ibid.*, **27**, 459 (1971).
13) T. Imanaka, Y. Hayashi, and S. Teranishi, *Nippon Kagaku Kaishi*, **1973**, 889.
14) Y. Okamoto, T. Imanaka, and S. Teranishi, This Bulletin, **46**, 4 (1973).
15) M. Nitta, S. Matsumoto, and K. Aomura, *Nippon Kagaku Kaishi*, **1973**, 1839.
16) S. Matsumoto, M. Nitta, and K. Aomura, *ibid.*, **1973**, 2028.
17) S. Malinowski and S. Szczepanska, *J. Catal.*, **2**, 310 (1963).
18) R. Ohnishi and K. Tanabe, *Chem. Lett.*, **1974**, 207.
19) A. Mrion, *C. R. Acad. Sci., Paris.*, **199**, 363 (1934).
20) "Organic Syntheses," Coll. Vol. V, p. 751.
21) M. Mousseron, *Bull. Soc. Chim. Fr.*, **1948**, 878.
22) The rearrangement reactions of both epoxides were also examined in a gas phase using a usual pulse method and found to give large amounts of 1, 3-cyclohexadiene from cyclohexene oxide and the unidentified compound, very close to II in RRT, from 1-methylcyclohexene oxide.
23) H. A. Benesi, *J. Phys. Chem.*, **61**, 970 (1957).
24) K. Mitsutani and Y. Hamamoto, *Kogyo Kagaku Zasshi*, **67**, 1231 (1964).
25) D. Cook, *Can. J. Chem.*, **41**, 522 (1963).
26) R. L. Settine, G. L. Parks, and G. L. K. Hunter, *J. Org. Chem.*, **29**, 616 (1964).
27) J. M. Coxon, M. P. Hartshorn, A. J. Lewis, K. E. Richards, and W. H. Swallow, *Tetrahedron*, **25**, 4445 (1969).
28) E. E. Royals and L. L. Harrell, Jr., *J. Amer. Chem. Soc.*, **77**, 3405 (1955).
29) T. Imanaka, Y. Okamoto, and S. Teranishi, This Bulletin, **45**, 3251 (1972).
30) I. C. Nigam and L. Levi, *Can. J. Chem.*, **46**, 1944 (1968).
31) M. Ito, H. Hattori, and K. Tanabe, *J. Catal.*, in press.
32) K. Tanabe, C. Ishiya, I. Matsuzaki, I. Ichikawa, and H. Hattori, This Bulletin, **45**, 47 (1972).
33) B. Rickborn and M. Gerkin, *J. Amer. Chem. Soc.*, **93**, 1963 (1971).
34) C. A. Bunton and M. D. Carr, *J. Chem. Soc.*, **1963**, 5854.
35) T. Iizuka, H. Hattori, Y. Ohno, J. Sohma, and K. Tanabe, *J. Catal.*, **22**, 130 (1971).
36) J. Take, N. Kikuchi, and Y. Yoneda, *ibid.*, **21**, 164 (1971).
37) K. Tanabe, N. Yoshii, and H. Hattori, *Chem. Commun.*, **1971**, 464.
38) H. Matsumoto, Y. Saito, and Y. Yoneda, *Shokubai*, **11**, 202p (1969).

Optically-active Vibrations and Effective Charges of Calcite and Magnesite[1)]

Akio YAMAMOTO, Yuji SHIRO*, and Hiromu MURATA

Department of Chemistry, Faculty of Science, Hiroshima University, Higashisenda-machi, Hiroshima 730

** Shinonome Branch School, Faculty of Education, Hiroshima University, Shinonome-3-chome, Hiroshima 734*

(Received December 10, 1973)

A rigid-ion model analysis was made for the optically-active crystal vibrations of calcite ($CaCO_3$) and magnesite ($MgCO_3$) with reference to the previous vibrational treatments. The effects of the effective charge distribution on the TO–LO splittings of the lattice modes were examined on the proposed distribution model, and the effective charges have been found: $Z_{Ca}=1.21$, $Z_C=0.20$, and $Z_O=-0.47$ in calcite, and $Z_{Mg}=1.28$, $Z_C=0.21$, and $Z_O=-0.50$ in magnesite, all in electron units. The force fields and effective charges determined in the present study reproduce satisfactorily the observed transverse and longitudinal frequencies of the optically-active lattice vibrations.

The vibrational spectra of calcite and magnesite have been studied by many investigators[2–14)] in connection with those of the isomorphic crystals with the calcite structure. In this work, our attention will be confined to the optically-active vibrations of calcite and magnesite; the vibrations will be analyzed on the basis of the rigid-ion model.[15)] In the rigid-ion formulation, account is taken only of the long-range Coulomb interactions of vibrationally-induced dipoles as those of rigid point dipoles; any contribution originating in the distortion of the electronic distribution is implicitly neglected. The model has been extensively applied to the vibrational analysis of relatively simple crystals[16,17)] and has been found to give less good results for the explanation of phonon-dispersion relations[18)] than the more elaborate models.[19,20)] We will, however, apply the model to the vibrational analysis of the calcite-type crystals, since only a small number of unknown parameters are introduced in taking the Coulomb interactions, and since a fairly good agreement can be obtained at least between the calculated and observed optically-active vibration frequencies.[21)]

Method of Calculation

Crystal Structure. Calcium carbonate and magnesium carbonate crystallize in a calcite structure. The primitive unit cell is trigonal, and two formula units are present in it. The space group is $D_{3d}{}^6$–$R\bar{3}c$, and the cell constants[22)] of calcite and magnesite are $a_{rh}=6.375$ Å and $\alpha=46°5'$, and $a_{rh}=5.675$ Å and $\alpha=48°11'$ respectively. In the calcite-type lattices, each metal atom is coordinated by six oxygen atoms of different carbonate groups, and each such atom is bound to two metal atoms, as is illustrated in Fig. 1.

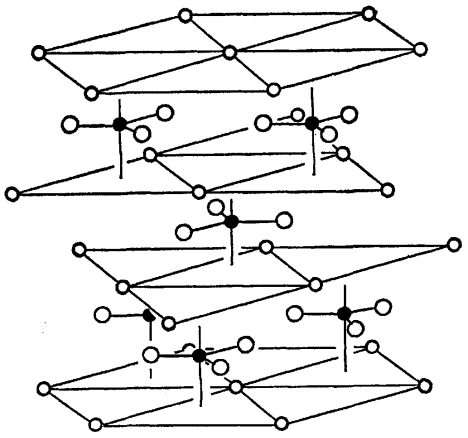

Fig. 1. Crystal structure.
○, Ca or Mg; ●, C; ○, O.

Normal Coordinate Treatment. A dynamical matrix is composed of two constituents:[15)]

$$\boldsymbol{D} = \boldsymbol{D}^s + \boldsymbol{D}^c,$$

where $\boldsymbol{D}^s$ and $\boldsymbol{D}^c$ are the short-range non-Coulomb and the long-range Coulomb interaction parts respectively; $\boldsymbol{D}^c=\boldsymbol{ZCZ}$, where $\boldsymbol{C}$ represents the long-range Coulomb interactions and $\boldsymbol{Z}$ is a diagonal matrix, the elements of which are effective charges.

Short-range Part: An application of the *GF*-matrix method[23)] to the analysis of optically-active crystal vibrations was previously reported by Shimanouchi *et al.*[24)] In the present study, a modified Urey-Bradley force field[25)] was applied to the intramolecular vibrations of carbonate groups, the correction terms of which were the bond interaction term, p, and the angle interaction term, n. On the other hand, a central force field was used for the lattice vibrations,

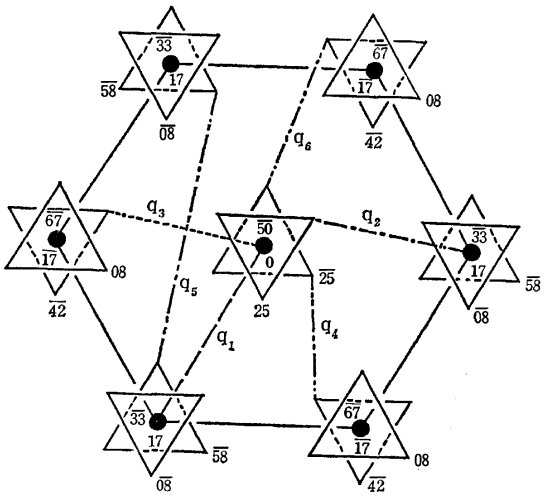

Fig. 2. Short-range interactions, projected on a plane perpendicular to the z axis of the hexagonal cell. The heights of atoms or carbonate groups are expressed in units of $100/c_0$.
(——), Ca or Mg···C; (·····), C···O; (—·—), Ca or Mg···O; (—··—), O···O.

Table 1. Internal coordinates in calcite and magnesite

Coord.[a]	F. C.[b]	Distance (Å)	
		Calcite	Magnesite
R	K(C-O)	1.294	1.286
θ	H(O-C-O)	(120°)	(120°)
	F(O···O)		
ϕ[c]	$\alpha(CO_3)$		
	p[d]		
	n[d]		
q_1	f_1(M···C)[e]	3.213	2.953
q_2	f_2(M···O)[e]	2.353	2.102
q_3	f_3(C···O)	3.406	3.019
q_4	f_4(O···O)	3.189	2.849
q_5	f_5(O···O)	3.249	2.924
q_6	f_6(O···O)	3.406	3.019

a) Notations are the same to Fig. 2. b) Force constants. c) Out-of-plane angle deformation coordinate. d) Correction terms. See text. e) M: Ca or Mg.

where only the pairs that lie within 3.5 Å were taken into consideration as effective short-range terms. As is shown in Fig. 2, there are six kinds of pairs in these crystals; the interatomic distances are given in Table 1.

Long-range Coulomb Part: In ionic crystals, the long-range Coulomb interactions are considered to play an important role in the splitting of a longitudinal mode frequency, ν_l, from the transverse ν_t. The Coulomb interaction part, $\boldsymbol{D}^c$, was calculated with the expression established by Born and Huang,[15] where the magnitude of the wave vector must be set at zero for the optically-active vibrations. In the Born and Huang expression, the $\boldsymbol{Q}$ term is a tensor of the second rank, the elements of which are called "the dipole lattice sum." The evaluation of the sum has been discussed in several places;[15,26,27] the actual calculations were performed by the use of the computer program PEG0.[28]

In contrast with simple crystals, some additional charge parameters must be introduced into these crystals, since the distribution of the effective charges in the unit cell is not known in advance. As is shown in Fig. 3, we have assumed the charge distribution on the carbonate groups under electrically neutral conditions.

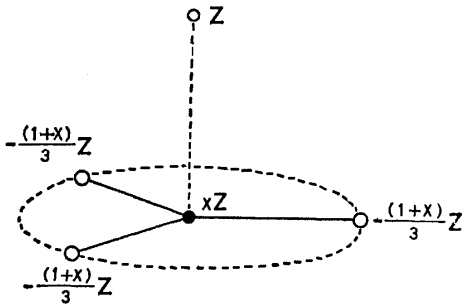

Fig. 3. Charge distribution.
○, O; ○, Ca or Mg; ●, C; Z, magnitude of effective charge in electron units; x, charge distribution parameter.

In the same manner as with short-range force constants,[29] one of the Coulomb parameters, *i.e.*, Z, can be refined by the least-squares method, since the Coulomb part has a common factor, Z^2, for a fixed distribution parameter, x.

The actual calculations were carried out on the TOSBAC 3400 TOPS 14 electronic computer at the Computing Center of Hiroshima University.

Table 2. Observed and calculated frequencies (cm^{-1})[a]

Sym.	Calcite				Magnesite			
	ν_t^{obsd}	ν_l^{obsd}	ν_t^{calcd}	ν_l^{calcd}	ν_t^{obsd}	ν_l^{obsd}	ν_t^{calcd}	ν_l^{calcd}
A_{1g}	1086		1086		1096		1095	
A_{1u}	—		1088		—		1101	
	—		255		—		345	
A_{2g}	—		884		—		906	
	—		254		—		349	
	—		192		—		315	
A_{2u}	872	890	874	885	876	911	881	899
	303	387	321	375	362	459	363	458
	92	136	93	133	230	281	236	268
E_g	1434		1424		1460		1451	
	712		714		735		745	
	284		262		332		332	
	156		165		212		213	
E_u	1407	1549	1424	1429	1436	1599	1451	1459
	712	715	712	713	747	783	743	745
	297	381	296	357	356	475	353	464
	223	239	226	234	301	315	310	314
	102	123	101	123	225	241	226	239

a) Observed frequencies are taken from Refs. 4, 5, and 11. ν_t, transverse frequency; ν_l, longitudinal frequency.

Results and Discussion

In calcite and magnesite, only the E_u and A_{2u} modes are infrared-active. The non-zero dipole moment is induced parallel to the z axis in the A_{2u} modes and normal to the axis in the E_u modes. When the wave vector $\mathbf{y}\rightarrow\mathbf{0}//z$, the A_{2u} modes are identified as the longitudinal modes, and the E_u, as the transverse. On the other hand, when $\mathbf{y}\rightarrow\mathbf{0}\perp z$, the E_u modes are longitudinal and the rest transverse.

Intramolecular Vibration. The intramolecular vibration modes have the following irreducible representations:[3]

$$\Gamma_n = A_{1g} + A_{1u} + A_{2g} + A_{2u} + 2E_g + 2E_u.$$

The observed[4,5,11] and calculated vibrational frequencies are compared in Table 2. It is shown that the interactions between the induced dipoles and the macroscopic field appear to exert little effect on the intramolecular modes. Since an out-of-plane angle deformation mode is accompanied by translational motions along the direction perpendicular to the tightly binding plane, the interactions may be fairly well approximated by the present model as compared with those of the other intramolecular modes. In an in-plane vibrational mode, however, the vibrational motions in the tightly binding regions should be actually followed by an intense electronic polarization originating in the distortion of the electronic distribution. Therefore, the polarization due to the electronic interactions between tightly binding atoms is likely to contribute predominantly to the total polarization rather than that due to the long-range electrostatic interactions between rigid dipoles in the above regions. It may be concluded that the rigid-ion approximation is not suitable for the interpretation of the dynamical properties of tightly-bonded systems, *e.g.*, the in-plane intramolecular vibration modes in these crystals. These subjects have been in part discussed by Decius *et al.*,[30-34] by Ishigame *et al.*,[35] and by Donoghue *et al.*[36] No quantitative explanation of the experimental results seems to have been made, though their discussions are quite suggestive. Further study based on some elaborate models will, therefore, be essential in order to obtain a satisfactory agreement with these experimental results.

Lattice Vibration. It can be shown from the factor-group theory[3] that the optical lattice modes are: $2A_{2g}+2E_g+A_{1u}+2A_{2u}+3E_u$. The observed[11] and calculated vibration frequencies are listed in Table 2, showing that the calculated frequencies for the lattice modes are in good agreement with the observed frequencies. The reason for this may be that the lattice vibration is considered to be essentially concerned with the relative motions of weakly interacting groups; therefore, the dynamical properties of these systems can be fairly well approximated by the rigid-ion model.

An introduction of the Coulomb interaction terms will change some vibrational modes from the corresponding non-Coulomb interaction modes; it has been found in some critical cases[37] that the changes are so serious that even the vibrational assignments of the fundamental bands must be modified from those determined from the non-Coulomb point of view. By examining the calculated eigenvectors carefully, it is found that there is not such a significant change in TO modes as in the above critical cases. Small changes, however, are noticeable in the LO modes, especially in the "polar" modes, which give rise to a large polarization. For instance, two polar modes, the modes which have high LO frequencies about 400 cm^{-1} in the A_{2u} and E_u symmetry, are seen to become more translational along the macroscopic field than the corresponding TO modes through additional interactions with the field.

Normal coordinate treatments have been made for calcite[38-41] on the basis of the short-range interaction models. In addition to these treatments, the long-range Coulomb interactions have been introduced by two groups of workers. First, both the interactions between the vibrationally-induced dipoles and the influence of the electronic distortion have been taken into account in the shell model by Plihal and Schaack.[42] They regarded a carbonate group as one bulky ion whose charge is located at the center of the group; they analyzed the optically-active vibrations of the three minerals of the calcite structure. Their rigid-ion model corresponds essentially to the present distribution model with $x=-1$; however, the results on these crystals were not given in their paper. If one assumes this charge distribution, any influence of the long-range interactions appears in the translational lattice modes; consequently, the Z-dependency of the lattice vibration is monotonic. In spite of their rather crude approximation, the calculated frequencies are in fair accord with the experimental results. Recently, phonon-dispersion relations were calculated for calcite by Plihal[43] by using the same model; however, the results have not been compared in detail with the observed results. Secondly, a rigid-ion model analysis was made for calcite by Onomichi.[44] He took, for the sake of simplicity, only four short-range force constants into consideration; therefore, the agreement with his observed values was seen to be less good. The effective charges attributed to the constituent atoms are read as $Z_{Ca}=1.86$, $Z_O=0.074$, and $Z_C=-2.08$ respectively in electron units; a positive value, though relatively small, was given on the most electrically-negative oxygen atom. The present authors have allowed only a negative charge on oxygen atoms from the chemical point of view.

Force Constants and Effective Charges. The short-range force constants and the effective charges are shown in Table 3. In the present study, account is taken separately of the long-range Coulomb interactions, and all of the short-range force constants need not have positive values; therefore, the physical meaning of the force constants is considered to be different from that in the previous short-range force models.

In performing the optimization procedures, some force constants were changed appreciably with the distribution models; however, the magnitude term, Z, was found to fall mostly into the range from 1.0 to 1.3, regardless of the distribution. Though the calculated TO–LO splittings seem to depend critically on the Z

Table 3. Short-range force constants (mdyn/Å) and effective charges (electron unit)

F. C.[a]	Calcite	S. D.[b]	Magnesite	S. D.[b]
K	5.647	0.008	5.758	0.035
H	0.340	0.000	0.340	0.015
F	1.720	0.001	1.720	0.013
α	0.444	0.003	0.447	0.002
p	−0.012[c]		−0.092	0.019
n[d]	0.043	0.000	0.032	0.016
f_1	0.030[c]		0.091[c]	
f_2	0.605	0.005	0.642	0.003
f_3	0.000[c]		0.000[c]	
f_4	0.074[c]		0.168	0.009
f_5	−0.016	0.001	0.081	0.002
f_6	−0.021	0.002	0.056	0.001
Z_M[e]	1.21	0.08	1.28	0.01
Z_C	0.20		0.21	
Z_O	−0.47		−0.50	

a) Notations are the same as those in Table 1. b) Standard deviation. c) Fixed force constants. d) Unit of n in mdyn·Å. e) Effective charge of metal atom.

term rather than on the x term, the x-dependency of the calculated splittings changes slightly from model to model[21] through the oxygen-oxygen interactions.

A careful comparizon of the calculated and found frequencies has given a fairly good agreement for $x=1/6$, though the lattice-mode frequencies are not so sensitive to the distribution parameter, x, in the range from −1.0 to 0.75 as to the Z parameter. Those distribution models which have values of x larger than unity were seen to give poorer results. The effective charge of the cation in magnesite is larger than that in calcite; the order of magnitude is consistent with the expectation based on the experimental TO–LO separations, and also with that of the effective charges determined for oxide crystals.[45]

In general, effective charges which interpret the sums of the observed TO–LO splittings may, in principle, be estimated for each infrared-active symmetry species by this relation:[17]

$$\sum\omega_l^2 - \sum\omega_t^2 = \mathrm{Trace}\{\boldsymbol{D}_l - \boldsymbol{D}_t\},$$

where ω and $\boldsymbol{D}$ are the circular frequency of the vibration and the dynamical matrix respectively, where the subscripts l and t specify longitudinal and transverse properties respectively, and where the summations are extended over the infrared-active modes. All the charges obtained by using the relation are, however, considered not to be reasonable: for instance, when the frequencies are distributed separately with wide gaps, the TO–LO splittings of the lower frequency modes are essentially neglected in the course of calculation. In these crystals, the charges which may explain appropriately the observed TO–LO separations of the modes around 1400 cm^{-1} were calculated to be extraordinary values about 5 in electron units; with these values, it is quite difficult to explain the TO–LO splittings of the lattice modes. The reason may be that the intense electronic polarization can hardly be reproduced by the point-dipole approximation, as has been mentioned above. However, its utility can best be appreciated by reference to the limitations of the rigid-ion model. Since the contribution of the lattice modes can be estimated fairly well, appropriate change parameters can be obtained when the lattice-mode frequencies are used.

A recent neutron inelastic scattering study will now be discussed briefly. Cowley and Pant[46] performed a simple shell-model analysis of the phonon-dispersion relations for the lowest-ten external branches and for the wave vectors along the optic axis; they obtained the following effective charges: $Z_{Ca}=2.3$, $Z_C=0.27$, and $Z_O=-0.87$, all in electron units. The value of Z_{Ca} is the largest of all the values[42,44] reported thus far. It is not clear at present whether the discrepancy among them depends on the electronic polarizability or on the choice of parameters. Since the intramolecular modes of vibration are influenced by the electronic polarizability [30–34] as well as the lattice modes, the effects of the Coulomb interactions must be estimated so as to reproduce simultaneously both types of vibration. Special attention should also be given to the fact that the two vibrational frequencies of the optically-inactive modes were determined to be 309 cm^{-1} and 172 cm^{-1}.

The charge distribution on molecules or groups has been estimated from the cohesive energies of crystals[47] or from the electronegativities[48,49] of constituent atoms. Those obtained are, however, considered to be static by nature; consequently, they need not always coincide with the present dynamically-effective charges. Even in these studies, the resulting distributions are seen to differ considerably with either investigators or methods.

The authors wish to express their thanks to Mr. Masaru Ohsaku of Hiroshima University for his kind and useful suggestions, and also to Mr. Tamaki Utida of Hiroshima University for permitting them the use of his computer program PEG0 and his helpful discussion.

References

1) Presented in part at the 29th Annual Meeting of the Chemical Society of Japan, Hiroshima, October (1973).
2) C. Schafer, F. Matossi, and H. Aderhold, *Z. Phys.*, **65**, 289 (1930).
3) S. Bhagavantam and T. Venkatarayudu, *Proc. Indian Acad. Sci.*, **9A**, 224 (1939).
4) A. K. Ramdas, *ibid.*, **37A**, 441 (1953).
5) D. Krishnamurti, *ibid.*, **43A**, 210 (1956).
6) D. Krishnamurti, *ibid.*, **44A**, 183 (1957).
7) J. Louisfert, *C. R. Acad. Sci. Paris*, **248**, 1150 (1959).
8) C. E. Weir and E. R. Lippincott, *J. Res. Nat. Bur. Std.*, **65A**, 173 (1961).
9) J. Morandat and J. Lecomte, *C. R. Acad. Sci. Paris, Ser. B*, **263**, 735 (1966).
10) W. P. Griffith, *J. Chem. Soc., A*, **1970**, 132.
11) K. H. Hellwege, W. Lesch, M. Plihal, and G. Schaack, *Z. Phys.*, **232**, 61 (1970).
12) M. Onomichi, K. Kudo, and T. Arai, *J. Phys. Soc. Japan*, **31**, 1837 (1971).
13) P. J. Ring, *Infrared Phys.*, **12**, 237 (1972).

14) J. C. Decius, R. Frech, and P. Bruesch, *J. Chem. Phys.*, **58**, 4056 (1973).
15) M. Born and K. Huang, "Dynamical Theory of Crystal Lattices," Oxford University Press, London (1954).
16) See, for example, E. W. Kellerman, *Phil. Trans. Roy. Soc.*, **238A**, 513 (1940) or I. Nakagawa, *Spectrochim. Acta*, **29A**, 1451 (1973).
17) J. Hiraishi, This Bulletin, **46**, 1334 (1973).
18) See, for example, T. Toya, *Bussei*, **6**, 121 (1966).
19) "Lattice Dynamics," ed. by R. F. Wallis Pergamon Press, Oxford (1965).
20) R. A. Cowley, *Proc. Roy. Soc.*, **268A**, 109 (1962).
21) A. Yamamoto, Y. Shiro, and H. Murata, This Bulletin, **47**, 1108 (1974).
22) D. L. Graí, *Amer. Minerallogist*, **46**, 1283 (1961).
23) E. B. Wilson, Jr., *J. Chem. Phys.*, **7**, 1047 (1939).
24) T. Shimanouchi, M. Tsuboi, and T. Miyazawa, *ibid.*, **35**, 1597 (1961).
25) T. Shimanouchi, *Pure Appl. Chem.*, **7**, 131 (1963).
26) P. P. Ewald, *Ann. Phys.*, **54**, 519 (1917).
27) J. J. Sullivan, *J. Phys. Chem. Solids*, **25**, 1039 (1964).
28) The computer program PEG0 was originally written by Mr. Tamaki Utida of Hiroshima University for the calculation of the dipole lattice sum.
29) T. Miyazawa, *Nippon Kagaku Zasshi*, **76**, 1132 (1955).
30) J. C. Decius, *J. Chem. Phys.*, **49**, 1387 (1968).
31) R. Frech and J. C. Decius, *ibid.*, **51**, 1536 (1969).
32) R. Frech and J. C. Decius, *ibid.*, **51**, 5315 (1969).
33) R. Frech and J. C. Decius, *ibid.*, **54**, 2374 (1971).
34) R. E. Carlson and J. C. Decius., *ibid.*, **58**, 4919 (1973).
35) M. Ishigame, T. Sato, and T. Sakurai, *Phys. Rev.*, **3B**, 4388 (1971).
36) M. Donoghue, P. H. Hepburn, and S. D. Ross, *Spectrochim. Acta*, **27A**, 1065 (1971).
37) See, for example, I. Nakagawa, *Bussei*, **13**, 541 (1972).
38) L. Giulotto and A. Loinger, *Nuovo Cimento*, **8**, 475 (1951).
39) M. Tsuboi, Presented at the International Symposium on Molecular Structure and Spectroscopy, Tokyo (1962).
40) K. Venkateswarlu and K. Ramaswamy, *Indian J. Pure Appl. Phys.*, **2**, 209 (1964).
41) Y. Shiro, *J. Sci. Hiroshima University, Ser. A-II*, **32**, 77 (1968).
42) M. Plihal and G. Schaack, *Phys. Status Solidi*, **42**, 485 (1970).
43) Plihal, *ibid.*, **56B**, 495 (1973).
44) M. Onomichi, *Sci. Light* (Tokyo), **22**, 47 (1973).
45) B. Szigeti, *Trans. Faraday Soc.*, **45**, 155 (1949).
46) E. R. Cowley and A. K. Pant, *Phys. Rev.*, **8B**, 4795 (1973).
47) H. D. P. Jenkins and T. C. Waddington, *J. Chem. Phys.*, **56**, 5323 (1972).
48) S. S. Batsnov, *Zh. Neorg. Khim.*, **9**, 1323 (1964).
49) R. T. Sanderson, "Inorganic Chemistry," Reinhold, New York (1967).

Electron Scavenging Study on the Photobleaching of Trapped Electrons in 3-Methylhexane Matrices at 77 K

Koichi OKA, Hideo YAMAZAKI, and Yoshihiko HATANO

Laboratory of Physical Chemistry, Tokyo Institute of Technology, Meguro-ku, Tokyo 152

(Received December 11, 1973)

The effect of addition of sulfur hexafluoride as an electron scavenger on quantum efficiency was investigated for the decay of trapped electrons in 3-methylhexane matrices at 77 K during photobleaching in the wavelength range 700—1900 nm. Since the quantum efficiency for the decay of trapped electrons in pure matrices is independent of the initial concentration, almost all the recombination of liberated electrons with the cations is geminate. The increase in quantum efficiency for the decay of trapped electrons by the addition of the electron scavenger SF_6 was analyzed quantitatively. The quantum efficiency for the photoliberation of trapped electrons from the trapping sites may be about unity. The liberated electrons in the absence of the electron scavenger are retrapped or neutralized. The ratio of the former process to the latter at a wavelength greater than 1500 nm is much larger than that at a shorter wavelength. The wavelength dependence of the ratios of the electron scavenging process to these processes has also been discussed.

The trapped electrons (e_t^-) produced by γ-irradiation in organic glasses at low temperature in the dark decay with infrared illumination (photobleaching)[1-4] or in the course of annealing (thermal bleaching).[5-7] The recombination-luminescence[8,9] and electric conductivity[10-12] have been measured during the course of bleaching. There are two states for electrons in glassy matrices, trapped electrons e_t^- and mobile electrons e_m^-, the former being stable and observable by optical absorption measurement or ESR, and the latter undergoing rapid retrapping or neutralization and not observable by the usual methods. Neutralization is either geminate or random. The decay of e_t^- might be due to either kind. The part of e_t^- geminately neutralized can not contribute to electric conductivity. The presence of electron scavengers suppresses the formation of e_t^-,[13] and increases the decay rate of e_t^- during the course of photobleaching.[1] More quantitative analysis of the photobleaching of e_t^- in 3-methylhexane glass (3MHX) and the effect of the addition of SF_6 as an electron scavenger have been carried out in order to estimate the quantum efficiency of the photoliberation of e_t^- from the trapping sites. The wavelength dependence of the fate of the photoliberated electrons has been examined in both the absence and presence of SF_6. The fate has been discussed in terms of the competition between the retrapping, neutralization and scavenging processes.

Experimental

3MHX (pure grade, Aldrich Chemical Co.) was purified by passing through an activated silica gel column. It was degassed by the freeze-pump method and trap-to-trap distillation, and stored on sodium-potassium alloy for more than a day before use. SF_6 (Matheson Co.) was used without purification.

In a mercury-free vacuum system, a constant volume (0.35 ml at room temperature) of 3 MHX was measured with a capillary of 2 mm diameter. The amounts of gaseous material added were determined by means of an oil manometer with a flask of a constant volume. The Ostwald absorption coefficient of SF_6 in liquid 3MHX at room temperature was about 1.3 and was used to determine the concentration of the solute in 3MHX glass at 77 K. The sample was sealed in a Suprasil quartz ESR tube (diameter 5 mm, volume 0.4 ml) and irradiated for 2.5—30 min with ^{60}Co γ-rays at 77 K in the dark at the dose rate $(1.0—5.4)\times 10^5$ r/hr. An aluminum foil was used to intercept the light emitted from Pyrex glass of a Dewar vessel during the course of γ-irradiation. After γ-irradiation, the ESR spectra of the samples were immediately measured in the dark with a JEP-1 X-band ESR spectrometer (JEOL) with field modulation 100 kHz. During repeated measurements by forward and backward scanning of the magnetic field, bleaching experiments were performed with monochromatic infrared light from a light source of QR-50 photospectrometer (Shimadzu). Actinometry was carried out with a photometer of thermocouple (JASCO) corrected by total light-intensity of a tungsten lamp (30 W; efficiency of the light emission 60%).

Results

The trapped electrons in γ-irradiated 3MHX matrices at 77 K were measured by ESR. The signal intensity of e_t^- decreased during the course of photo bleaching by infrared light, but not that of 3-methylhexyl radical. At a small microwave power of ESR, the saturation factor of the signal of e_t^- was almost constant during the course of photobleaching. The effect of photobleaching on the ESR signal intensity

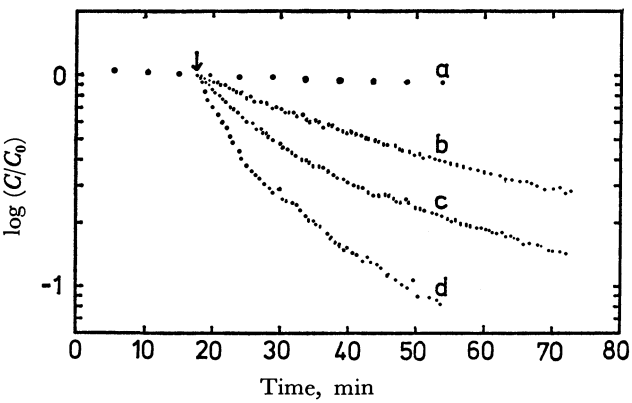

Fig. 1. The decay plots of log (C/C_0) against time in 3MHX after γ-irradiation: a) natural decay in the dark (dose$=1.1\times 10^{19}$ eV/g), and the decay due to photobleaching at $\lambda=1500$ nm after elapse of the time indicated by arrow. The slit of the monochrometer was opened to various widths, namely b) 0.2, c) 0.3, d) 0.5 mm (dose$=2.8\times 10^{18}$ eV/g).

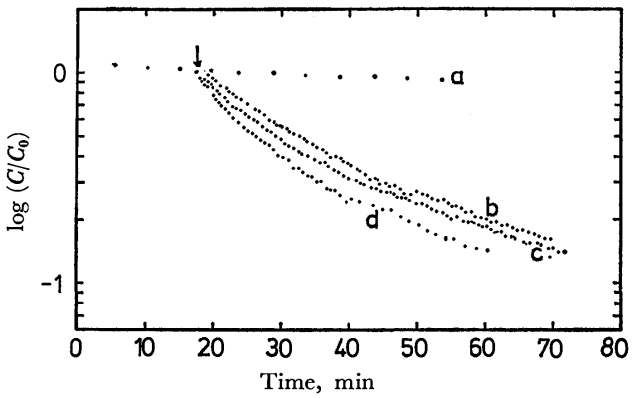

Fig. 2. The decay plots of log (C/C_0) against time after γ-irradiation: a) natural decay in the dark (γ-irradiation dose 1.1×10^{19} eV/g), and the decay due to photobleaching at $\lambda=1500$ nm with slit width 0.3 mm, in which the samples were γ-irradiated to various doses, namely b) 5.6, c) 2.8, d) 1.4 (10^{18} eV/g). The arrow on the curve indicates the starting point of infrared irradiation.

of e_t^- is given by C/C_0, the ratio of the concentration of e_t^- after and before photobleaching. Semilogarithmic plots of the decay of C/C_0 in the dark or under illumination of infrared light at $\lambda=1500$ nm are given in Fig. 1. The natural decay in the dark is negligibly small as compared with the decay due to photobleaching. At each slit width, the time necessary for C/C_0 to decay to the same value is roughly proportional to the light intensities which are proportional to the square of the slit width. At a fixed light intensity the decay rate decreased slightly with increasing doses of γ-irradiation (Fig. 2). This might be due to the nonuniformity of light intensity in a sample tube. The intensity of the light flux near the inlet of the light path is larger than that near the outlet because of the light absorption of e_t^-. Thus, the quantum efficiency for the decay of e_t^- during photobleaching Φ is given by[14]

$$-\frac{\mathrm{d}\log C}{\mathrm{d}t}=I\varepsilon\Phi\bar{Q} \qquad (1)$$

where I is light intensity, ε the extinction coefficient of e_t^- and $\bar{Q}$ the correction term attributed to the nonuniformity of light intensity in a sample tube. Assuming that the light flux is parallel in the cylindrical sample tube, $\bar{Q}$ is given as a function of D:

$$\bar{Q}=\frac{2}{\pi D\ln 10}\int_{-1}^{1}[1-\exp\{(-\ln 10)\,D\sqrt{1-y^2}\}]\mathrm{d}y \qquad (2)$$

where D $(=2\varepsilon CR)$ is the optical density of e_t^-, and R the radius of the cylinder. The value of $\bar{Q}$ approaches unity for a small value of D, namely for a small value of C or ε. The values $\varepsilon=3.0\times10^4$ l mol^{-1} cm^{-1} at 1700 nm, which is assumed to be equal to that in 3-methylpentane glass,[15] and $G(e_t^-)=0.9$,[16] are used for the calculation of Φ. An appropriate coefficient is necessary for the right term of Eq. 1.

If Φ is constant during the course of photobleaching, the plots of log (C/C_0) against time are nearly on a straight line. Actually, however, the slope or the value $(-\mathrm{d}\log C/\mathrm{d}t)$ decreases with increasing time

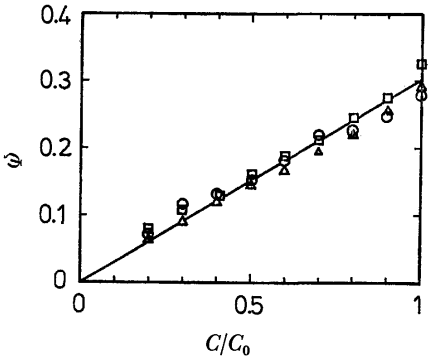

Fig. 3. Relation between Φ and C/C_0 at $\lambda=1500$ nm with slit width 0.3 mm in 3 MHX. Samples were γ-irradiated to various doses (10^{18} eV/g): ○ 1.4, △ 2.8, □ 5.6.

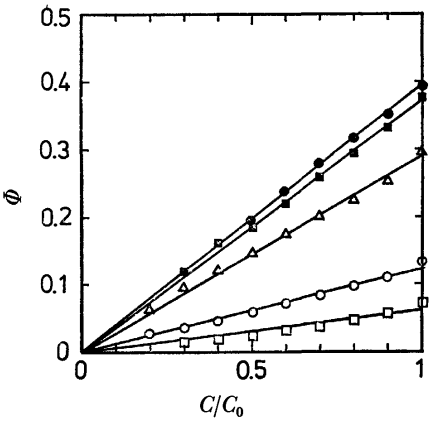

Fig. 4. Relation between Φ and C/C_0 at various wavelengths: ● 700, ■ 1300, △ 1500, ○ 1700, □ 1900 nm. This relation is also dose-independent as in Fig. 3.

(Fig. 1). The quantum efficiency for the decay of e_t^- calculated from the slopes by means of Eq. 1 decreases steadily with decreasing C/C_0. The values of Φ calculated from three series of measurements at different light intensities are almost the same for the same value of C/C_0. This shows that the main part of the primary act is a one-photon process.[17]

The efficiency Φ at 1500 nm is independent of γ-irradiation doses (Fig. 3). Also at $\lambda=1300$ nm, Φ is independent of γ-irradiation doses of $(0.28—5.7)\times10^{18}$ eV/g within 10% error. The dose-independence of γ-irradiation may support the validity of the correction term $\bar{Q}$. The relation between Φ and C/C_0 at various wavelengths is shown in Fig. 4. The plots are approximately on straight lines through origin, and represented approximately by

$$\Phi=\Phi_0(\lambda)C/C_0 \qquad (3)$$

where $\Phi_0(\lambda)$ is the initial quantum efficiency for the photobleaching at the wavelength λ, obtained from the value of Φ at $C/C_0=1$ (Fig. 4) and shown in Fig.9 as a function of the wavelength. The value of $\Phi_0(\lambda)$ is about 0.4 at 700—1300 nm. It decreases with increasing wavelength above 1300 nm. From Eqs.1 and 3 we obtain

$$-\frac{\mathrm{d}C/\mathrm{d}t}{C}=(\ln 10)I\varepsilon\bar{Q}\Phi_0\frac{C}{C_0} \qquad (4)$$

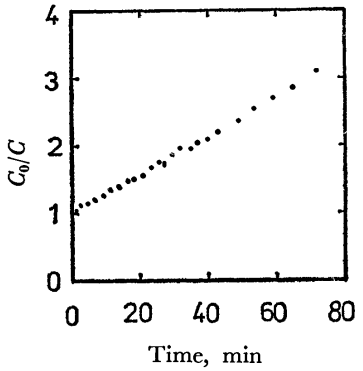

Fig. 5. Relation between C_0/C and time during photobleaching of e_t^- at $\lambda=700$ nm with slit width 1 mm (dose$=2.9\times10^{18}$ eV/g).

Since $\bar{Q}$ is regarded to be constant when either the concentration of e_t^- or the value ε is small, the solution of Eq. 4 is approximately given by

$$\frac{C_0}{C}=\Phi_0\left\{(\ln 10)I\varepsilon\bar{Q}t+\frac{1}{\Phi_0}\right\} \tag{5}$$

Substituting this into Eq. 3, we get

$$\Phi(t)=\left\{(\ln 10)I\varepsilon\bar{Q}t+\frac{1}{\Phi_0}\right\}^{-1} \tag{6}$$

The relation between C_0/C and time at wavelength 700 nm for small values of ε (Fig. 5) is in line with Eq. 5.

Since the time scale in the decay plots is influenced by both the light intensity and concentration of e_t^- (Figs. 1 and 2), we introduce a new variable T ($=\int(\ln 10)\,I\varepsilon\bar{Q}\,dt$). This is nearly proportional to t and experimentally approximated as

$$T=\sum_{j=1}^{n}(\ln 10)I\varepsilon\langle\bar{Q}\rangle_j\Delta t_j \tag{7}$$

where $C/C_0=1-j/10$ at t_j (j: integer), $\Delta t_j=t_j-t_{j-1}$, $\langle\bar{Q}\rangle_j$ is an average of $\bar{Q}$ between t_{j-1} and t_j. The exact solution of Eq. 4 is

$$\Phi(T)=\frac{1}{T+1/\Phi_0(\lambda)} \tag{8}$$

Thus the introduction of T gives a simple solution useful for the analysis of the results particularly in the presence of SF_6.

In the semilogarithmic decay plots (Fig. 6) of e_t^- in 3MHX containing SF_6, the γ-irradiation doses are controlled in order to obtain the same initial concentration of e_t^-. Although the natural decay of e_t^- in the dark is accelerated by the addition of SF_6, the slope is less than 5% of that of the photobleaching even at the highest concentration of SF_6. During photobleaching, the decay time at the same value of C/C_0 decreases with increasing concentration of SF_6, the decay curve becoming almost linear at high concentrations. Figure 7 shows Φ calculated from the slopes (Fig. 6) by means of Eq. 1. The efficiency is enhanced by the addition of SF_6. The decrement of Φ with decreasing C/C_0 is smaller in the presence than that in the absence of SF_6. At the same concentration of SF_6, Φ is smaller for high γ-irradiation

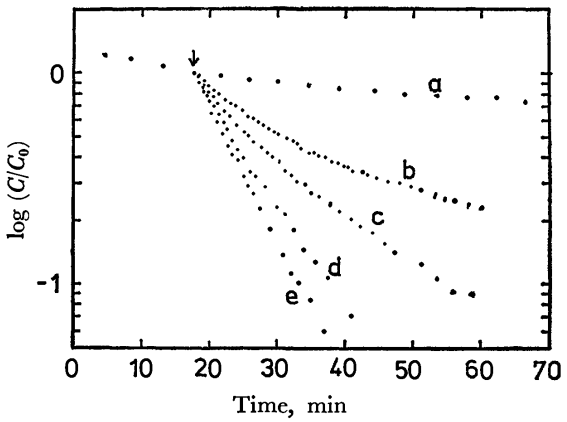

Fig. 6. The decay plots of log (C/C_0) against time in the dark and the decay due to photobleaching in the presence of SF_6 at $\lambda=900$ nm with slit width 0.7 mm: a) natural decay in the dark, $[SF_6]=9.7\times10^{-4}$ mol/l, irradiation dose$=5.6\times10^{18}$ eV/g, and the decay due to photobleaching, b) $[SF_6]=0$ mol/l, dose$=2.9\times10^{18}$ eV/g; c) $[SF_6]=1.7\times10^{-4}$ mol/l, dose$=2.1\times10^{18}$ eV/g; d) $[SF_6]=5.2\times10^{-4}$ mol/l, dose$=3.4\times10^{18}$ eV/g; e) $[SF_6]=9.7\times10^{-4}$ mol/l, dose$=7.7\times10^{18}$ eV/g. The initial concentrations of e_t^- (10^{-5} mol/l) are: a) 1.4; b) 3.8; c)d)e) 1.9. The arrow on the curve indicates the starting point of infrared irradiation.

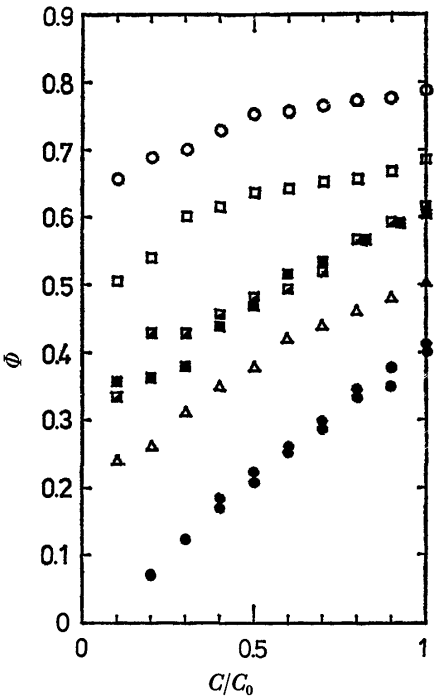

Fig. 7. Relation between Φ and C/C_0 in 3MHX γ-irradiated to various doses in the presence of various concentrations of SF_6 at $\lambda=900$ nm: ● $[SF_6]=0$ mol/l, dose$=2.9\times10^{18}$ eV/g; △ $[SF_6]=1.75\times10^{-4}$ mol/l, dose$=2.1\times10^{18}$ eV/g; □◪■ $[SF_6]=5.2\times10^{-4}$ mol/l, doses$=3.4,\ 6.9,\ 21\times10^{18}$ eV/g; ○ $[SF_6]=9.7\times10^{-4}$ mol/l, dose$=7.7\times10^{18}$ eV/g. The initial concentrations of e_t^- (10^{-5} mol/l) are: △□○ 1.9; ●◪ 3.8; ■ 12.

doses than that for the lower doses.

The effect of the addition of SF_6 on the relation between Φ and T is shown in Fig. 8. The samples were γ-irradiated in the two series of doses at various concentrations of SF_6. Efficiency Φ decreases gradually with increasing T calculated by means of Eq. 7. In pure matrices the plots almost fit the solid line given by Eq. 8. The initial concentration of e_t^- is 3.8×10^{-5} mol/l in the series of high γ-irradiation doses, and 1.9×10^{-5} mol/l in the series of low γ-irradiation doses. At each concentration of SF_6, Φ observed in the series of high irradiation doses is smaller than that of the low irradiation doses. The dose dependence of γ-irradiation in the presence of SF_6 (Figs. 7 and 8) suggests that SF_6 decomposes and produces less reactive molecules than SF_6 in electron scavenging reactions.

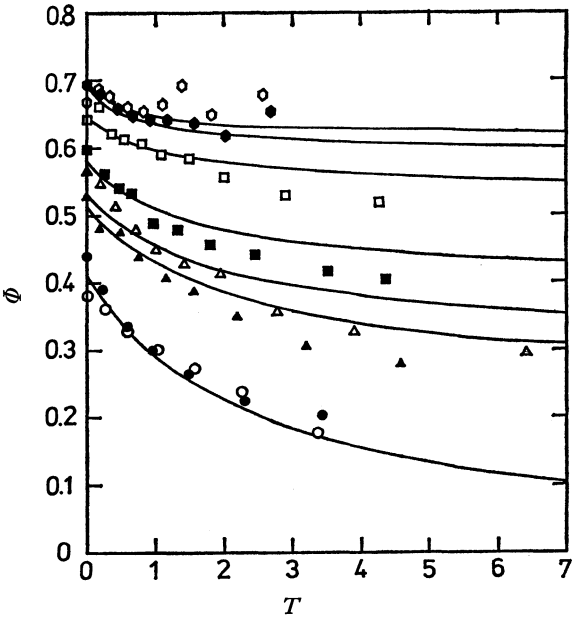

Fig. 8. Relation between Φ and T at $\lambda=1100$ nm in 3MHX containing various concentrations of SF_6 for various doses of γ-irradiation: ○● $[SF]_6=0$ mol/l, doses=1.4, 2.9×10^{18} eV/g; △▲ $[SF_6]=1.75\times10^{-4}$ mol/l, doses=2.3, 4.5×10^{18} eV/g; □■ $[SF_6]=5.2\times10^{-4}$ mol/l, doses=3.4, 6.9×10^{18} eV/g; ○● $[SF_6]=9.7\times10^{-4}$ mol/l, doses=7.7, 15.5×10^{18} eV/g. The initial concentration of e_t^- for the curves obtained by ○△□ and ○ is 1.9×10^{-5} mol/l, and for those by ●▲■ and ● 3.9×10^{-5} mol/l. The solid lines are the theoretical curves given by Eq. 13 when σ is 1, and b is selected to fit the experimental plots.

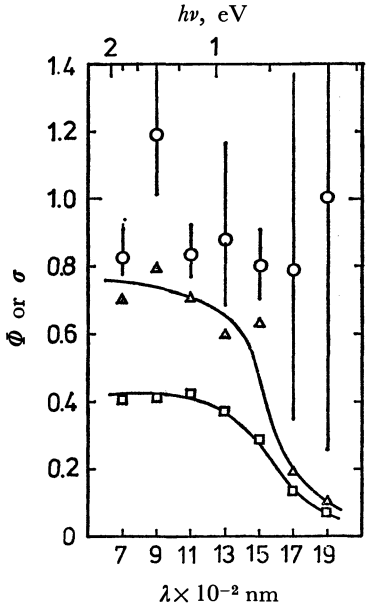

Fig. 9. Wavelength dependence of Φ or σ in the absence and presence of SF_6: □ Φ_0 in pure matrices, △ the initial value of Φ in the presence of SF_6 (9.7×10^{-4} mol/l); ○ σ obtained from the plots of Eq. 14.

The initial quantum efficiency for the decay of e_t^- is enhanced by the addition of SF_6 in the wavelength range 700—1900 nm (Fig. 9). At 700—900 nm, Φ becomes about 0.7 and can approach unity with increasing concentration of SF_6. At a wavelength greater than 1700 nm, the effect of the addition of SF_6 on the enhancement of Φ becomes less severe than that at shorter wavelength. It is difficult to know experimentally whether Φ approaches unity or not, since the ESR signal of e_t^- could not be observed at a high concentration of SF_6.

Discussion

The trapped electrons absorb the light in the infrared region and are liberated from the trapping sites in the following process.

$$e_t^- + h\nu \xrightarrow{\sigma} e_m^- \qquad (A)$$

where σ is the quantum efficiency of the primary photoliberation. Photo-liberated electrons or mobile electrons e_m^- move in matrices preceding neutralization with cations or preceding the retrapping into trapping sites (T.S.).

$$e_m^- + RH^+ \longrightarrow RH \qquad (B)$$

$$e_m^- + T.S. \xrightarrow{k_t} e_t^- \qquad (C)$$

Since the right term of Eq. 5 is independent of the initial concentration of e_t^-, the decay of e_t^- during photobleaching is a pseudo-second order process. The linear relation between C_0/C and time (Fig. 5) agrees with what is expected from Eq. 5. Since Φ_0 is not influenced by the change of initial concentration of e_t^-, the main part of the neutralization of e_t^- is geminate. The pseudo-second order processes depend probably on the probability distribution of the separation between e^-_t and cations. The main part of ion-pair separation should be smaller than the average ion-pair separation 230—600 Å, calculated from γ-irradiation doses assuming uniform distribution.

The relation between Φ and C, classified according to the type of neutralization, is given as a function of T in Table 1. The empirical relation of (2) represented by Eqs. 3 and 5 is applicable only to the non-polar hydrocarbon matrices.[1] Φ could be obtained as a function of C from the following factors characterizing the movement of electrons, *viz.*, the distribution of ion-pair separation, the range of Coulombic force of the parent cations and the mobility of e_m^-. The attractive force between electrons and cations pre-

Table 1. Φ as a function of C/C_0, and C as a function of T

Class number	Class of neutralization	$\Phi=-(dC/dT)/C$[a,b]	C/C_0[a,b]
1	geminate (strong attraction)	$\alpha(C/C_0)^{1/m}$; $m>1$	$(1+\alpha T/m)^{-m}$
2	geminate (intermediate attraction)	$\alpha C/C_0$	$(1+\alpha T)^{-1}$
3	geminate (weak attraction)	$\alpha C/C_0-\beta$; $C/C_0>\beta/\alpha$	$\left\{\frac{\alpha}{\beta}-\frac{\alpha-\beta}{\beta}\exp(-\beta T)\right\}^{-1}$
		0; $C/C_0<\beta/\alpha$	
4	random	αC	$(1+C_0\alpha T)^{-1}$

a) Classified according to the type of neutralization (see Appendix). b) α, β and m are constants.

scribed by the above factors might decrease in the order given. In (1) most of e_m^- is geminately neutralized and most of e_t^- can be easily photobleached. In (3), for a small concentration of ions, e_m^- escapes from a cation and cannot be neutralized randomly. In (4) random neutralization takes place because of uniform distribution of electrons and cations, the decay processes being of real-second order. The neutralization of e_m^- in a 2-methyltetrahydrofuran[3] glass is in an intermediate state between (3) and (4). (2) is distinguished from (4) by the role of C_0 in the equations. Experimentally the effect of γ-doses on Φ can differentiate the two types.

Diminution of Φ with the progress of photobleaching suggests that the neutralization process (B) decreases gradually as compared with the retrapping process (C). Since the rate of the geminate neutralization process is proportional to the probability density of e_m^- in the vicinity of the cations, and the position of e_t^- changes with repetition of photoliberation and reprapping, the gradual decrease of the role of recombination process may be caused by the gradual decrease of the probability density. A theoretical consideration is possible by means of prescribed diffusion approximation for an extended form[18] of the Smoluchowski equation.[19] In this approximation the rate of process (B) is given by KW, where K is a constant and W is the probability density of e_m^- in the vicinity of cations. The rate of process (C) is given by k_tS_t, where k_t is the rate constant and S_t is the concentration of the trapping sites. For the competition between (B) and (C), the quantum efficiency for the decay of e_t^- is given by

$$\Phi=\frac{\sigma KW(T)}{KW(T)+k_tS_t} \tag{9}$$

where $W(T)$ is a function of T, since the distribution of ion-pair separation changes with the progress of photobleaching. From Eqs. 8 and 9, we get

$$KW(T)=\frac{KW(0)}{(\sigma KW(0)/k_tS_t)T+1} \tag{10}$$

and

$$\frac{k_tS_t}{KW(0)}=\frac{\sigma}{\Phi_0}-1 \tag{11}$$

where k_t, K, σ, and Φ_0 are functions of λ.

In the presence of SF_6, the electron scavenging reaction competes with processes (B) and (C):

$$e_m^- + SF_6 \xrightarrow{k_s} SF_6^- \tag{D}$$

Since process (D) interrupts process (C), the value of Φ for a very large concentration of SF_6 might give the quantum efficiency σ. However, σ cannot be obtained by this method, since e_t^- is not formed at a very high concentration of SF_6. Efficiency Φ in the presence of SF_6 is given by

$$\Phi=\frac{\sigma(KW(T)+k_s[SF_6])}{KW(T)+k_tS_t+k_s[SF_6]} \tag{12}$$

Assuming that $KW(T)$ is given by Eq. 10 used in the case of pure 3MHX matrices, the following equations are obtained from Eqs. 10, 11 and 12:

$$\Phi(T)=\frac{(1-b/\sigma)^2}{T+1/\Phi_0-b/\sigma^2}+b \tag{13}$$

$$\frac{1}{b}=\frac{1}{\sigma}(1+k_tS_t/k_s[SF_6]) \tag{14}$$

The solid lines in Fig. 8 are given by Eq. 13 for the values of b selected to fit the plots at $\sigma=1$. Although the experimental data are scattered, the intercept of a straight line in plots of $1/b$ against $1/[SF_6]$ gives σ (Fig. 9). When σ is smaller than unity,

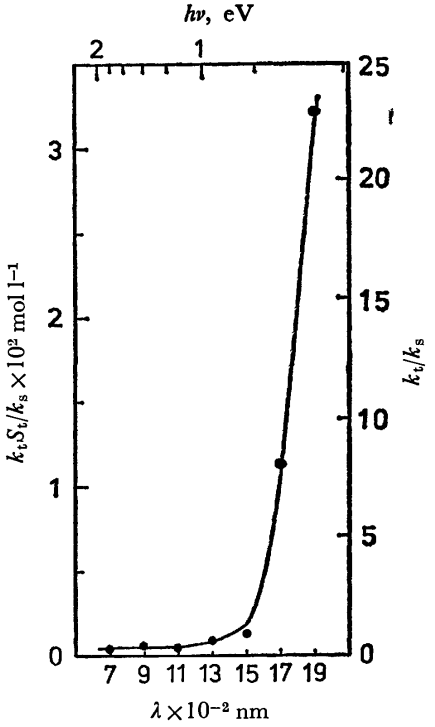

Fig. 10. Wavelength dependence of k_tS_t/k_s or k_t/k_s observed from the plots of Eq. 14 assuming that S_t is 1.4×10^{-3} mol/l.

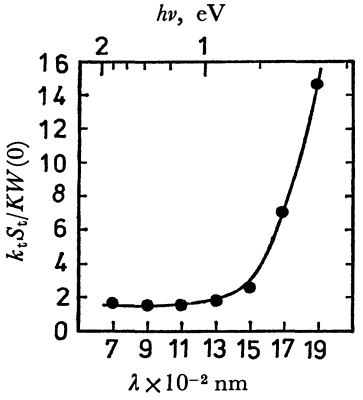

Fig. 11. Wavelength dependence of $k_tS_t/KW(0)$ estimated by means of Eq. 11.

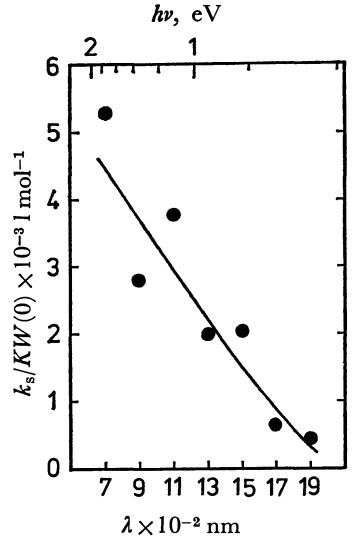

Fig. 12. Wavelength dependence $k_s/KW(0)$ calculated by means of Eq. 11 and the slope of the plots of Eq. 14.

Eq. 13 deviates from the plots to a greater extent than that at $\sigma=1$. Thus, σ might be about unity for wavelengths in the range 700—1900 nm.

Figure 10 shows the wavelength dependence of k_tS_t/k_s obtained from the slope of the straight line in the plots $1/b$ *vs.* $1/[SF_6]$. The minimum value of S_t is 1.4×10^{-3} mol/l which is estimated from the dose effect of γ-irradiation of the formation of e_t^-. The value of k_t/k_s is calculated by using this value of S_t. At a wavelength greater than 1500 nm, k_t/k_s becomes greater than that at a shorter wavelength. The value of $k_tS_t/KW(0)$ obtained from Eq. 11 becomes great at a wavelength greater than 1500 nm (Fig. 11). The value of $k_s/KW(0)$, calculated from the values of k_tS_t/k_s and $k_tS_t/KW(0)$, decreases gradually with increasing wavelength (Fig. 12). Because of a strong resemblance between Figs. 10 and 11, k_t increases markedly at a wavelength greater than 1500 nm. This wavelength dependence of k_t might show a relation between the translational energy of e_m^- and the track length of e_m^- from photoliberation to retrapping. The wavelength dependence of $k_s/KW(0)$ may be caused by the diffusion of e_m^- which separates electrons from cations.

The authors are gratefull to Professor Shoji Shida for his helpfull discussion.

Appendix

Calculation of Φ from the Decay Plot. During photobleaching, the concentration of e_t^-, C, decreases with time t. The rate of decay in a rectangular cell is given by

$$-\frac{dC}{dt}=\frac{I\Phi}{l}\{1-\exp(-\alpha lC)\} \tag{15}$$

where I is a light flux, $\alpha(=\varepsilon\ln 10)$ the extinction coefficient of e_t^-, Φ the quantum efficiency for the decay of e_t^- during photobleaching, and l the length of the cell. With the progress of photobleaching, the value of C at the inlet of light flux in the sample becomes smaller than that at the outlet, and the concentration becomes nonuniform. Equation 15 can be applied to this nonuniform sample by substituting the average concentration of e_t^- into C. The solution is found to be

$$\ln(\exp\alpha lC-1)=-I\int_{t_n}^{t}\Phi\alpha dt+\ln(\exp\alpha lC_n-1) \tag{16}$$

where C_n is the concentration of e_t^- at time t_n. Under conditions of a small αlC and a constant value of Φ, C is approximately given by exponential function:

$$C=C_n\exp\{-I\Phi\alpha(t-t_n)\} \tag{17}$$

For a large αlC, Eq. 16 is reduced to

$$C=-I\Phi(t-t_n)/l+C_n \tag{18}$$

At time t_n, Eq. 15 is given by

$$\left[\frac{d\ln C}{dt}\right]_{t_n}=-\frac{I\Phi\{1-\exp(-\alpha lC_n)\}}{lC_n} \tag{19}$$

which can be transformed into

$$\left[\frac{d\log C}{dt}\right]_{t_n}=-\varepsilon I\Phi Q \tag{20}$$

and

$$Q=\frac{1-\exp(-\alpha lC_n)}{\alpha lC_n} \tag{21}$$

In the case of a cylindrical tube, the parallel light flux is transmitted in the direction at right angle to the axis of the cylinder, and the length of light path is $l=2R\sqrt{1-y^2}$, where R is a radius of the cylinder. The effective Q is an averaged value such as

$$\bar{Q}=\int_{-1}^{1}Q\frac{2\sqrt{1-y^2}}{\pi}dy$$
$$=\frac{2}{\pi D\ln 10}\int_{-1}^{1}[1-\exp\{-D(\ln 10)\sqrt{1-y^2}\}]dy \tag{22}$$

where $D(=2\varepsilon C_nR)$ is the optical density of e_t^-.

Classification of the Geminate Reactions The experimental relation between Φ and C/C_0 can be classified as shown in Fig. 13. A speculative case given by curve (1) is expressed by

$$\Phi=\alpha(C/C_0)^{1/m},\quad m>1 \tag{23}$$

where the quantum efficiency of photobleaching is almost constant at the beginning of the photobleaching. Curve (1) corresponds to the photobleaching process of the trapped electrons, in narrow spatial distribution, in strong Coulombic field of parent ions and in weak diffusional movement. Curve (2) is given by

$$\Phi=\alpha(C/C_0) \tag{24}$$

The quantum efficiency of photobleaching is proportional to the value of C/C_0 as shown in Fig. 3. Curve (2) is observed

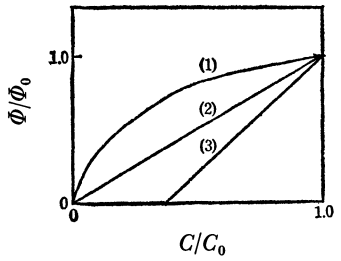

Fig. 13. Relation between Φ/Φ_0 and C/C_0 for the various types of geminate reaction: curve (1) strong attraction; curve (2) intermediate attraction; curve (3) weak attraction.

in the photobleaching process of the trapped electrons in nonpolar materices. Curve (3) can be written as

$$\Phi = \alpha(C/C_0) - \beta, \qquad C/C_0 > \beta/\alpha \qquad (25)$$
$$\Phi = 0, \qquad C/C_0 < \beta/\alpha$$

The quantum efficiency of photobleaching decreases with decreasing value of C/C_0 and becomes zero at a finite value of C/C_0. Therefore, as in the case of the neutralization in 2-methyltetrahydrofuran glass[3], it is difficult to observe a complete photobleaching. The functions in the last column of Table 1 can be obtained by integrating Eqs. 23—25.

References

1) D. W. Skelly, and W. H. Hamill, *J. Chem. Phys.*, **44**, 2891 (1966).
2) P. Hamlet and L. Kevan, *J. Amer. Chem. Soc.*, **93**, 1102 (1971).
3) P. J. Dyne and O. A. Miller, *Can. J. Chem.*, **43**, 2696 (1965).
4) H. B. Steen and J. Moan, *J. Phys. Chem.*, **76**, 3366 (1972).
5) J. B. Gallivan and W. H. Hamill, *J. Chem. Phys.*, **44**, 1279 (1966).
6) D. Soulter and J. E. Willard, *J. Phys. Chem.*, **76**, 3167 (1972).
7) F. S. Dainton, G. A. Salmon, and J. Teply, *Proc. Roy. Soc. Ser. A*, **286**, 27 (1965).
8) K. Funabashi, C. Herbert, and J. L. Magee, *J. Phys. Chem.*, **75**, 3221 (1971).
9) H. Yamazaki, K. Oka, M. Sato, and S. Shida, This Bulletin, **47**, 31 (1974).
10) L. Kevan, *J. Phys. Chem.*, **76**, 3830 (1972).
11) A. K. Munjal, and L. Kevan, *ibid.*, **76**, 2781 (1972).
12) B. Wiseal and J. E. Willard, *J. Chem. Phys.*, **46**, 4387 (1967).
13) a) T. Wakayama, T. Kimura, T. Miyazaki, K. Fueki, and Z. Kuri, This Bulletin, **42**, 266 (1969).
b) J. R. Miller, *J. Chem. Phys.*, **56**, 5173 (1972).
c) K. Oka, H. Yamazaki, and S. Shida, This Bulletin **46**, 2347 (1973).
14) Derivations are given in the Appendix.
15) W. H. Hamill, "Radical Ions," ed. by E. T. Kaiser and L. Kevan, Wiley-Interscience, New York, p. 353 (1968).
16) J. Lin, K. Tsuji, and F. Williams, *J. Amer. Chem. Soc.*, **90**, 2766 (1968).
17) A two photon process can occur to some extent in addition to the one photon process (Ref. 10).
18) A. Mozumder, *J. Chem. Phys.*, **55**, 3020 (1971).
19) M. V. Smoluchowski, *Ann. Phys.*, **48**, 1103 (1915).

Some Remarks on the Reaction Mechanism and Kinetic Rate Constants for the Pentacyanocobaltate(II)-catalyzed Hydrogenation of Olefins Using the Iterative Simulation Technique

Katsutoshi OHKUBO, Kohji TSUCHIHASHI, Hiromichi IKEBE, and Hiroyuki SAKAMOTO

Department of Synthetic Chemistry, Faculty of Engineering, Kumamoto University, Kurokami, Kumamoto 860

(Received March 11, 1974)

The reaction mechanism and kinetic-rate constants of the pentacyanocobaltate(II)-catalyzed hydrogenation of olefins were investigated. The present study with an iterative simulation technique supported the $Co(CN)_5^{3-}+H_2 \rightarrow Co(CN)_5H^{3-}+H\cdot$ and $Co(CN)_5^{3-}+H\cdot \rightarrow Co(CN)_5H^{3-}$ reactions for the uptake of H_2 by the cobaltate(II) during the initial stage of the reaction. An examination was also made of the stationary-state approximation used for the kinetic analysis of the reaction.

It is well known that pentacyanocobaltate(II) takes part in the reductive cleavage of covalent molecules:

$$2Co(CN)_5^{3-} + X\text{–}Y \rightarrow Co(CN)_5X^{3-} + Co(CN)_5Y^{3-} \quad (1)$$

where X–Y means such molecules as H_2,[1–5] H_2O,[2] Br,[6] I_2[6] H_2O_2,[7] $HONH_2$[8] ICN,[8] and organic halides.[9–11]

In the hydrogenation of olefins (denoted as A) with $Co(CN)_5^{3-}$, the molecular hydrogen has been considered, on the basis of the kinetic investigations,[4,12] to participate in the formation of hydropentacyanocobaltate(III), $Co(CN)_5H^{3-}$, through Reaction (2):

$$2Co(CN)_5^{3-} + H_2 \xrightarrow{k_1} 2Co(CN)_5H^{3-} \quad (2)$$

Reaction (2) is followed by:

$$Co(CN)_5H^{3-} + A \xrightarrow{k_2} Co(CN)_5^{3-} + AH\cdot \quad (3)$$

$$Co(CN)_5H^{3-} + AH\cdot \xrightarrow{k_3} Co(CN)_5^{3-} + HAH \quad (4)$$

where AH· and HAH denote a momentarily living radical intermediate and a saturated hydrocarbon respectively.

Although the mechanism expressed by Reactions (2—4) (named Mechanism I) has hitherto been accepted as the most plausible one for the $Co(CN)_5^{3-}$-catalyzed hydrogenation of olefins, the following mechanism (named Mechanism II) can also be considered in view of the fact that the uptake of H_2 by $Co(CN)_5^{3-}$ is between first- and second-order in cobalt from 0 to 25 °C[13] and that $Co(CN)_5^{3-}$ takes part in the reductive cleavage of such X–Y as organic halides by the two-step reaction ($Co(CN)_5^{3-}+X\text{–}Y \rightarrow Co(CN)_5X^{3-}+Y\cdot$ and $Co(CN)_5^{3-}+Y\cdot \rightarrow Co(CN)_5Y^{3-}$):

$$Co(CN)_5^{3-} + H_2 \xrightarrow{k_1} Co(CN)_5H^{3-} + H\cdot \quad (5)$$

$$Co(CN)_5^{3-} + H\cdot \xrightarrow{k_2} Co(CN)_5H^{3-} \quad (6)$$

$$Co(CN)_5H^{3-} + A \xrightarrow{k_3} Co(CN)_5^{3-} + AH\cdot \quad (7)$$

$$Co(CN)_5H^{3-} + AH\cdot \xrightarrow{k_4} Co(CN)_5^{3-} + HAH \quad (8)$$

Reactions (5, 6) indicate a first-order dependence on cobalt for the formation of $Co(CN)_5H^{3-}$, which corresponds to $[Co^{II}(CN)_5(\cdot H)]^{3-}$ rather than $[Co^{III}(CN)_5(:H)]^{3-}$.[14]

In Reaction (6), the highest singly-occupied d_{z^2} Co-orbital (at -11.01 eV)[15] of $Co(CN)_5^{3-}$ seems to play an important role in the reaction with the H radical.

In this paper, we will discuss the reaction mechanism and rate constants for the $Co(CN)_5^{3-}$-catalyzed hydrogenation of olefins on the basis of Mechanisms I and II, using an iterative simulation technique involving least-squares error analysis.

Computation Method

The rate constants in systems of nonlinear differential equations such as those derived from Reactions (2—4) or (5—8) can be estimated by means of such numerical integration methods as the Runge-Kutta integration,[16] the Marquardt method,[17] and Taylor's series expansions.[18] These methods, however, require very dense data, much computation time, and highly developed mathematical techniques to estimate the rate constants directly. Therefore, we will use an iterative simulation technique combined with the least-squares error analysis in the present paper. Here, we will briefly describe the present technique.

The differential equations (rate equations) can be simply expressed on the basis of the law of mass action as:

$$d(C_s)/dt = f(k_i, (C_r))$$

where (C_s) and (C_r) denote the concentrations of C_s (s=species number) and C_r (r=species number) respectively, and where $f(k_i, (C_r))$ means a function made by the rate constants, k_i ($i=1-3$ or $1-4$ for Mechanism I or II respectively) and (C_r). The reaction increments of (C_s), $D(C_s)$, are shown with a very short time interval, Δt[19]:

$$D(C_s) = f(k_i, (C_r))\Delta t \quad (10)$$

The concentrations of C_s at the reaction time of t, $(C_s)_{t,\mathrm{calcd}}$, are evaluated by means of the trapezoidal average method:[20]

$$(C_s)_{t,\mathrm{calcd}} = (C_s)_0 + \sum^{n} D(C_s)_{\mathrm{av}}\Delta t \quad (n\Delta t = t) \quad (11)$$

where $(C_s)_0$ and $D(C_s)_{\mathrm{av}}$ indicate the initial concentrations and the average increments of C_s respectively.

In the evaluation of the $(C_s)_{t,\mathrm{calcd}}$ values, the rate constants, k_i, are inserted into Eq. (11) in accordance with our previous technique:[17,19]

$$k_i = \min k_i + \sum^{m} 10^{(\gamma-\beta)} \min k_i,\ \gamma = \mathrm{gauss}\left[\frac{m-1}{9\alpha}\right] \quad (12)$$

$$(m=1,2,\cdots\cdots;\ \beta=0,1,2,\cdots\cdots;\ \alpha=10)$$

where the notations have the same meanings as those in previous papers.[19,21]

in order to check the reliability of the selected best set of k_i. We will simulate the time-dependence of the hydrogen absorption in both the mechanisms with the following different initial specifications: $(Co(CN)_5^{3-})_0=0.005$ M and $(A)_0=0.20$ M. The simulation results are shown in Fig. 1. As can be seen from Fig. 1, the predicted $(H_2)_{t,absd}$ curves for Mechanism II accord more satisfactorily with the observed $(H_2)_{t,absd}$ curves than those for Mechanism I.

It is of interest here to notice the time conversions of the concentrations of species participating in Mechanism II. From the time conversions of the species shown in Fig. 2, we can observe that the concentrations of the H and AH radicals ($(H\cdot)/(AH\cdot)\simeq 10$) seem to be relatively high despite their momentary lives, in comparison with those of $Co(CN)_5H^{3-}$ and HAH; the $(H\cdot)$ and $(AH\cdot)$ values are almost constant at $t\gtrsim 10$ min. Under these conditions, it seems that the stationary-state approximation can be used for the concentrations of both the intermediates. Then, we will test the stationary-state approximation in order to estimate the rate constants in Mechanism II. From the rate equations (differential equations) derived from Eqs. (5—8) and (16a, b), the rate of H_2 absorption, $R_{t,calcd}$, can be expressed by the following kinetic relationships:

$$R_{t,calcd} = d(H_2)_{t,absd}/dt = ae^{-2at}((Co(CN)_5^{3-})_0-b/a) - k_1(H_2)be^{-2at}/a+k_1(H_2)(A)(Co(CN)_5^{3-})_0/a \quad (17)$$

$$(H_2)_{t,absd} = (1-e^{-2at})((Co(CN)_5^{3-})_0-b/a)/2 + k_1k_3(H_2)(A)(Co(CN)_5^{3-})_0t/a + k_1(H_2)b(e^{-2at}-1)/2a^2 + k_1(H_2)/2k_2+k_3(A)/2k_4 \quad (18)$$

where $a=k_1(H_2)+k_3(A)$ and $b=k_3(A)(Co(CN)_5^{3-})_0$.

Let us estimate the k_1 and k_3 values in Eq. (17) by means of the present technique under the following condition:

$$F' = \text{minimize}\sum_{p=1}^{p}\varepsilon_p' = \text{minimize}|R_{t,calad}-R_{t,given}|^2 \quad (19)$$

where $R_{t,calcd}$ and $R_{t,given}$ indicate the calculated and observed rates of H_2 absorption respectively.

The above procedure gave $k_1=1.0\times10^{-3}$ and $k_3=1.0\times10^{-1}$ M^{-1} s^{-1} as the best set of rate constants, appreciably different from those ($k_1=1.2\times10^{-3}$ and $k_3=2.4\times10^{-3}$ M^{-1} s^{-1}) shown in Table 1. The computer simulations with the sets of both k_1 and k_3 values obtained by means of Eq. (17) indicate that the former set of rate constants gives a more precise fit to the $R_{t,given}$ values than the latter one. However this is not a surprising phenomenon for the following reasons: (a) strictly speaking, the concentration of neither radical intermediate is constant; (b) the stationary-state approximation which neglects the rate constants of k_2 and k_4 (not extremely large rate constants) may bring about the apparent difference between the k_3 values mentioned above, and (c) the $R_{t,calcd}$-value evaluation by means of Eq. (17), derived from the stationary-state approximation with only the set of k_1 and k_3 values for Mechanism II (see Table 1), cannot give an accurate time-conversion of the H_2 absorption rate. This discussion is reasonable if we notice that the $(H_2)_{t,absd}$ values obtained from the present simulation with $k_1=1.0\times10^{-3}$, $k_2=1.0$, $k_3=1.0\times10^{-1}$, and $k_4=1.0\times10^2$ M^{-1} s^{-1} are very small compared with the observed values. Furthermore, Eq. (18) brings about somewhat large $(H_2)_{t,absd}$ values under $k_1=1.0\times10^{-3}$, $k_3=1.0\times10^{-1}$, and $k_4=1.0\times10^2$ M^{-1} s^{-1} (Eq. (18) excludes k_2), while the simulation with the best set of k_i ($i=1$—4) values for Mechanism II indicates satisfactorily precise fits to the experimental results. It may be deduced, therefore, that the kinetic analysis by means of the present iterative simulation technique, which does not include any stationary-state approximation, gives more reliable information about the unknown rate constants in elementary reactions.

Table 1. The best sets of rate constants and the least-squares error for Mechanisms I and II

Mechanism I	Mechanism II
$k_1=1.3\times10^{-1}$ M^{-1} s^{-1}	$k_1=1.2\times10^{-3}$ M^{-1} s^{-1}
$k_2=9.0\times10^{-4}$	$k_2=1.0$
$k_3=1.0\times10^2$	$k_3=2.4\times10^{-3}$
	$k_4=1.0\times10^2$
$\varepsilon_p=7.121\times10^{-11}-2.837\times10^{-7}$ M^2	$\varepsilon_p=6.713\times10^{-12}-2.360\times10^{-8}$ M^2
$F=1.466\times10^{-6}$ M^2	$F=1.345\times10^{-7}$ M^2

In conclusion, we have demonstrated that, in the $Co(CN)_5^{3-}$-catalyzed hydrogenation of olefins, the two-step reaction of the complex and molecular hydrogen may play an important role in the formation of hydropentacyanocobaltate(III), especially during the initial reaction state.

The calculations were carried out on a FACOM 230—60 computer at the Data Processing Center of Kyushu University.

References

1) N. K. King and M. E. Winfield, *J. Amer. Chem. Soc.*, **83**, 3366 (1961).
2) B. De Vries, *J. Catal.*, **1**, 489 (1962).
3) L. Simandi and F. Nagy, *Acta Chim. Akad. Hung.*, **46**, 101 (1965).
4) M. G. Burnett, P. J. Connolly, and C. Kemball, *J. Chem. Soc., A*, **1967**, 800.
5) R. G. S. Banks and J. M. Pratt, *ibid.*, **1968**, 854.
6) A. W. Adamson, *J. Amer. Chem. Soc.*, **78**, 4260 (1956).
7) A. Haim and W. K. Wilmarth, *ibid.*, **86**, 2311 (1964).
8) P. B. Chock, R. B. K. Dewar, J. Halpern, and Lai-Yoong Wong, *ibid.*, **91**, 82 (1969).
9) J. Halpern and J. P. Maher, *ibid.*, **86**, 2311 (1964).
10) J. Halpern and J. P. Maher, *ibid.*, **87**, 5361 (1965).
11) J. Kwiatek and J. K. Seyler, *J. Organometal. Chem.*, **3**, 421 (1965).
12) J. Halpern and M. Pribanic, *Inorg. Chem.*, **9**, 2616 (1970).
13) W. Strohmeier and N. Iglauer, *Z. Phys. Chem.*, **51**, 50 (1966).
14) $[Co^{II}(CN)_5(\cdot H)]^{3-}$ was also suggested by Simandi and Nagy (see Ref. 3).

15) K. Ohkubo, H. Kanaeda, and K. Tsuchihashi, This Bulletin, **46**, 3095 (1973).
16) For instance, H. Margenau and G. H. Marphy, "The Mathematics of Physics and Chemistry," D. van Nostrand, New York (1943), p. 450.
17) D. W. Marquardt, *J. Soc. Ind. Appl. Math.*, **11**, 431 (1963).
18) I. G. Darvey, S. J. Prokhovnik, and J. F. Williams, *J. Theoret. Biol.*, **11**, 459 (1966).
19) In regard to the effect of Δt on the computation results, the brief discussion can be seen in K. Ohkubo, K. Tsuchihashi, and H. Sakamoto, This Bulletin, **47**, 579 (1974).
20) K. Ohkubo and T. Hashimoto, This Bulletin, **45**, 3350 (1972).
21) K. Ohkubo, H. Sakamoto, and K. Tsuchihashi, *ibid.*, **47**, 2141 (1974).
22) M. Takahashi, Y. Hisamatsu, and M. Iguchi, *Nippon Kagaku Zasshi*, **91**, 46 (1970).
23) J. Halpern and Lai-Yoong Wong, *J. Amer. Chem. Soc.*, **90**, 6665 (1968).

Electronic Structures of Excited States of Benzoquinolines[1)]

Hiroyuki YAMAGUCHI, Teruki IKEDA, and Hiroaki MAMETSUKA
Department of Chemistry, Kumamoto University, Kumamoto 860

(Received May 2, 1974)

Measurements of the dipole moments and acidity constants in the lowest excited singlet states for benzo[*c*]quinoline, benzo[*f*]quinoline, and benzo[*h*]quinoline have been carried out by spectrophotometry. The electronic structures of excited states have been calculated by using the semi-empirical SCF–π–MO CI method, which allows for a bond order-bond length relationship at each iteration. The experimentally-determined dipole moments and acidity constants can not be correlated to the calculated electronic structures of the Franck-Condon states, but they can be correlated to the calculated structures of the equilibrium states for the lowest excited singlet states of three isomeric benzoquinolines.

Many phenomena occurring in the electronically-excited states of molecules, such as photochemical reactions, are dependent on the changes in the electronic structures. Electronic excitation in molecules leads to a new electron density distribution and, consequently, to changes in the dipole moment and in the reactivity. For example, aminonaphthalenes, which are weak bases in the ground state, lose their basic properties in the lowest excited-singlet state and become weak acids, dissociating in alkaline solutions.[2)] Furthermore, some unusual photochemical reactions of aromatic substitution seem to correlate with the electron-density distribution in the excited states.[3,4)] Numerous quantitative data are already known on the protolytic equilibria[5)] and on the dipole moments[6)] of molecules in their excited states. A comparison of the two sets of experimental data has, however, been done only exceptionally from the point of view of the electron-density distribution in the excited molecules.[7)]

It is the purpose of this paper to determine experimentally the acidity constants and dipole moments in the lowest excited singlet states of benzo[*c*]quinoline (I), benzo[*f*]quinoline (II), and benzo[*h*]quinoline (III) and to investigate the possible correlation between the experimental results and the theoretical π-electron indices.

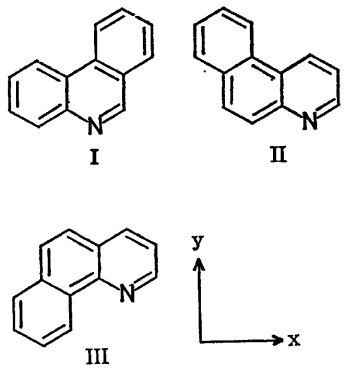

Fig. 1. Numbering of benzoquinolines and choice of axes.

Experimental

Materials. Substance I was obtained from the Dōjindō Chemicals Co. It was purified by recrystallization from light petroleum and by subsequent sublimation *in vacuo*.[8)] II and III were purchased from the Tokyo Kasei Co. According to the procedure described by Kanda and Shimada,[9)] the purification was done in the same way for both compounds. The solvents used were carefully purified according to the descriptions in Ref. 10.

Measurements. The dielectric constants were determined with a home-made resonance-method apparatus which used the electric circuit reported by Nakagawa.[11)] A dielectric-constant-measurement cell with cylindrical platinum electrodes was used. The refractive indices were measured by means of a Pulfrich refractometer. The static dielectric constant (ε) and the refractive index (n_D) at the sodium D line of the solvents agreed with the values cited in Ref. 10. The densities of the solutions were measured by the use of a pycnometer[12)] for volatile liquids.

The absorption spectra were measured with a Hitachi EPS-3T spectrophotometer. The fluorescence spectra were recorded on a Shimadzu RF-502 spectrophotometer. The wave numbers of the emission-band maxima were determined from the emission spectra, as corrected for the spectral sensitivity of the instrument. The concentration of I, II, and III was kept less than 10^{-5} mol/l for all solutions prepared, so that the system was free from any undesired concentration quenching. The measurements were made on deaerated samples at 20 °C.

Calculation

The method used in predicting the energetically most favorable nuclear arrangement for an electronically-excited state of a conjugated molecule, which is assumed to be planar, is a modified version[13)] of the semi-empirical SCF MO CI method used in combination with the variable bond-length technique, which has proved to be quite successful in predicting the ground-state electronic structures of a variety of conjugated molecules.[14)]

Assuming a certain nuclear arrangement for a conjugated molecule, we carry out the SCF MO CI calculation in the framework of the Pariser-Parr-Pople approximation.[15,16)] Using the wave function for an excited state obtained after the inclusion of the configuration mixing all the singly-excited states, we then calculate the bond length for the excited state by the aid of a suitable bond order-bond length relationship (*vide infra*). The new nuclear arrangement is taken as the geometrical structure for the next SCF MO calculation, and the process is repeated until the bond lengths for the excited state converge.

The one-center repulsion integrals were found from the corresponding valence-state ionization potentials, (W), and electron affinities, (E), by the Pariser-Parr method,[15)] the W and E being determined from the

spectroscopic data using the promotion energies of Hinze and Jaffé.[17] The two-center repulsion integrals were estimated by using the Mataga-Nishimoto method.[18]

Resonance integrals were included only between nearest neighbors. These resonance integrals were estimated by using the Wolfsberg-Helmholtz overlap approximation:[19]

$$\beta_{\mu\nu} = -0.5K_{\mu\nu}(W_\mu + W_\nu)S_{\mu\nu} \quad (1)$$

where the overlap integral, S, was calculated from Roothaan's formulas[20] using the effective nuclear charges of 3.25 and 3.90 for carbon and nitrogen respectively.

Only the nearest-neighbor two-center integrals were allowed to change, using a bond distance calculated by the aid of this relationship:

$$r_{\mu\nu} = \alpha - 0.186p_{\mu\nu} \quad (2)$$

where p is the π-bond order. The nonbonded distances were calculated assuming the ring to be regular and were kept constant for the sake of simplicity.

The values of K in Eq. (1) and α in Eq. (2) were determined as follows.

C–N Bond. The best value of K for the C–N bond was determined from the β value so adjusted that the theoretical excitation energies and intensities of the reference molecule, *s*-triazine,[21,22] which were calculated using a bond distance obtained by the X-ray technique[23] in the framework of the SCF MO CI method, might reproduce the experimental excitation energies and intensities of this molecule. We thus obtained $K=0.97$. From the bond order of the C–N bond that was calculated by using the best value of K obtained by means of the SCF MO CI method, the bond order-bond length relationship for this bond was determined. This procedure yielded $\alpha=1.459$ Å.

C–C Bond. The value of α which had been proposed by Nakajima and Katagiri,[24] was used. The value of K for this bond was determined from the value so adjusted as to reproduce the experimental excitation energies of such reference molecules as butadiene and naphthalene.[25–27] We thus obtained $K=0.85$.

Using these values for K and α, we calculated the transition energies and intensities of pyridine and pyrazine. The calculated transition energies and intensities of these molecules are in good agreement with the experimental values.[28,29]

The dipole moments of the ground and excited states for I, II, and III are calculated by using the moment due to the C–N localized bonds, 1.77 D,[30] and the C–H moment, 0.4 D.[31]

Results and Discussion

Ground-state Dipole Moments, $\vec{\mu}_0$. The dipole moment, $\vec{\mu}_0$, of I has already been measured in benzene solutions.[8] The dipole moments, $\vec{\mu}_0$, of II and III were measured in carbon tetrachrolide by the use of the ordinary Halverstadt-Kumler method.[32] The molecular refractions, $[R_L]_D$, were obtained from this expression: $[R_L]_D=M[r_2+(r_{12}-r_2)/\omega_1]$. Here, ω_1 is the weight fraction of the solute, whose molecular weight is M, and r_2 and r_{12} are the specific refractions of the solvent and the solution respectively. These results are summarized and compared with the calculated results in Table 1. The predicted values agree well with the experimental values.

Table 1. Ground-state dipole moments $\vec{\mu}_0$ and molecular refractions $[R_L]_D$ of benzoquinolines

Molecule	$[R_L]_D$ (cm^3)	μ_0 (D)[a]	
		Calcd	Obsd
I	60.82[b]	2.74 (75°)	2.39[b]
II	60.51[c]	2.52 (93°)	2.19[c]
III	60.32[c]	2.28 (91°)	1.81[c]

a) Numbers in parenthesis represents the angle that the dipole moment makes with X-axis in the counter-clockwise sense in the coordinate system of Fig. 1. b) Measured in benzene. See Ref. 8. c) Measured in carbon tetrachloride.

Excited-state Dipole Moments, $\vec{\mu}_1$. The difference between the dipole moments in the lowest singlet excited state ($\vec{\mu}_1$) and the ground state ($\vec{\mu}_0$), $|\Delta\vec{\mu}_1| = |\vec{\mu}_1-\vec{\mu}_0|$, can be estimated by measuring the wave numbers of the band maxima of the fluorescence (ν_f^m) and the absorption (ν_a^m) spectra in various solvents and by using the following equation:[33]

$$\nu_a^m - \nu_f^m = \text{Const.} + F(\varepsilon, n_D)\delta$$
$$F(\varepsilon, n_D) = \frac{\varepsilon-1}{\varepsilon+2} - \frac{n_D^2+1}{n_D^2+2} \quad (3)$$
$$\delta = \frac{2|\Delta\vec{\mu}_1|^2}{a^3hc}$$

where a is the cavity radius in Onsager's theory[34] of the reaction field.

The observed $(\nu_a^m-\nu_f^m)$ *versus* $F(\varepsilon,n_D)$ relations are shown in Figs. 2, 3, and 4. The straight lines in the figures were obtained by the least-squares method. The $\Delta\vec{\mu}_1$ values for I, II, and III were determined by using the slopes (A) of these lines.

These results are summarized and compared with the theoretical results in Table 2. Table 2 shows that the difference between the dipole moments for the equilibrium state of the lowest singlet excited state ($\vec{\mu}_E$) and for the ground state ($\vec{\mu}_0$), $|\Delta\vec{\mu}_E| = |\vec{\mu}_E-\vec{\mu}_0|$, is in better agreement with the experimental $|\Delta\vec{\mu}_1|$ value than the difference between the dipole moments for the Franck-Condon state of the lowest excited state ($\vec{\mu}_F$) and for the ground state, $|\Delta\vec{\mu}_F| = |\vec{\mu}_F-\vec{\mu}_0|$. This agreement of the experimental and computed results on the dipole moments indicates a good approximation of the electronic structures for the equilibrium states of the lowest singlet excited states.

Excited Singlet-state Acidity Constants. The pK_a values in the ground states (S_0) were previously meas-

TABLE 2. EXCITED-STATE DIPOLE MOMENTS OF BENZOQUINOLINES[a)]

Molecule	a(Å)[b)]	A (cm^{-1})	Calcd (D)				Exptl. (D)
			$\vec{\mu}_F$	$\lvert\Delta\vec{\mu}_F\rvert$	$\vec{\mu}_E$	$\lvert\Delta\vec{\mu}_E\rvert$	$\lvert\Delta\mu_1\rvert$
I	3.91[c)]	193	3.84 (137°)	3.51	3.34 (97°)	1.30	0.77
II	3.86[d)]	397	4.29 (127°)	2.53	3.75 (120°)	1.89	1.24
III	3.94[d)]	268	3.18 (155°)	2.99	2.66 (127°)	1.57	1.08

a) Numbers in parenthesis represent the angle that the dipole moment makes with the positive X-axis in the counterclockwise sense in the coordinate system of Fig. 1. b) Estimated from the apparent molal volume ϕ_v. The ϕ_v is defined by the relation, $\phi_v = 1000(d_2 - d_{12})/(m_1 d_2 d_{12}) + M_1/d_{12}$, where d_2 and d_{12} are the densities of the solvent and the solution of molality m_1 of the solute having molecular weight M_1, respectively. c) Estimated from the tabulated data of Ref. 8. d) Measured in carbon tetrachloride.

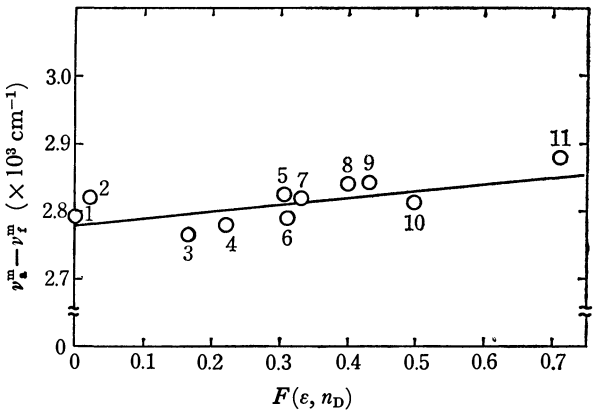

Fig. 2. The plot of $(\bar{\nu}_a^m - \bar{\nu}_f^m)$ against $F(\varepsilon, n_D)$ for benzo[*c*]quinoline. Here numbers denote the solvents as (1): cyclohexane, (2): carbon tetrachloride, (3): *n*-butyl ether; (4): anisole, (5): isoamyl acetate, (6): ethyl ether, (7): *n*-butyl acetate, (8): ethyl acetate, (9): methyl acetate, (10): benzonitrile, (11): acetonitrile.

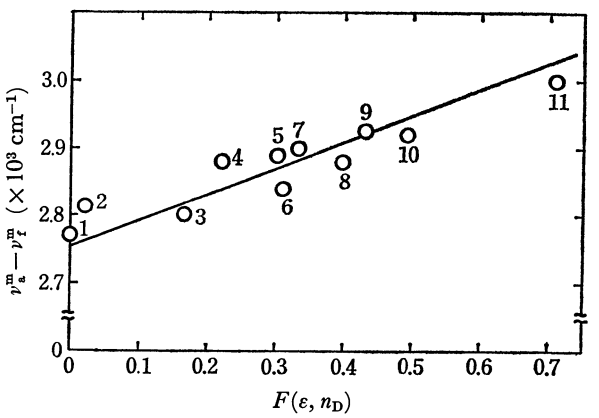

Fig. 3. The plot of $(\bar{\nu}_a^m - \bar{\nu}_f^m)$ against $F(\varepsilon, n_D)$ for benzo[*f*]quinoline. The numbers are the same as described in Fig. 2.

ured at 20 °C in an aqueous ethanol solution (50 vol. percent ethanol solution).[35)] The pK_a (S_1) values were estimated by means of the Förster cycle, as in the following relation:[2)]

$$pK_a(S_0) - pK_a(S_1) = \frac{\Delta E_{HB} - \Delta E_B}{2.303\,RT} \qquad (4)$$

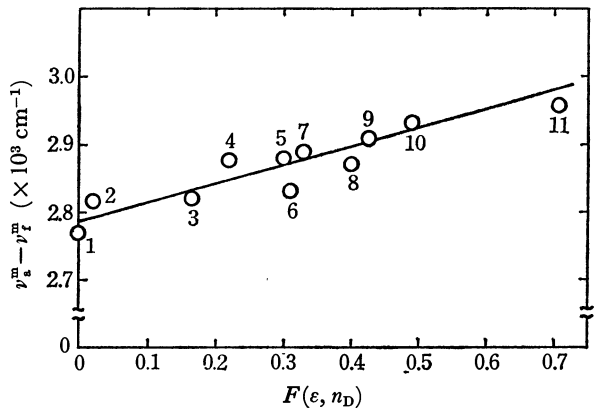

Fig. 4. The plot of $(\bar{\nu}_a^m - \bar{\nu}_f^m)$ against $F(\varepsilon, n_D)$ for benzo[*h*]quinoline. The numbers are the same as described in Fig. 2.

where ΔE_{HB} and ΔE_B are the energy differences between the ground and excited states of the protonated and unprotonated molecules respectively. The p$K_a(S_0)$ and p$K_a(S_1)$ denote the pK_a values in S_0 and the excited state (S_1) respectively. R and T are the gas constant and the absolute temperature respectively. In the present work, the energy difference between the S_0 and S_1 states was evaluated by means of the absorption and fluorescence spectra.

The absorption and fluorescence spectra of I, II, and III and of their conjugated acids were measured at 20 °C in an aqueous ethanol solution (50 vol. percent ethanol solution) for the unprotonated molecules (B) and in an aqueous ethanol solution with sulfuric acid added for the protonated molecules (BH^+). In Table 3, the p$K_a(S_1)$ values obtained by the application of the Förster cycle are collected, along with the pK_a (S_0) values.

It has been shown that there is a good correlation between the pK_a value of heterocyclic molecules containing a nitrogen atom and the electron density (q_N) of the atom.[36)] In a series of molecules where the molecular skeleton changes, the relation between pK_a and q_N is much less direct. Besides q_N, the interactions with all the π-electron charges, located at various distances from the reactive center, also influence the pK_a values.[37,38)] A large q_N value may be compensated for by the influence of positive charges located on neighboring carbon atoms. For the ground

Table 3. $S_1 \leftarrow S_0$ transition energies, $pK_a(S_0)$, and $pK_a(S_1)$ values

Molecule	Absorption (eV)		Fluorescence (eV)		0-0 Transition energy (eV)[a]		$pK_a(S_1)$	$pK_a(S_0)$[b]
	B	BH^+	B	BH^+	B	BH^+		
I	3.58	3.37	3.53	3.06	3.56	3.22	9.16	3.36
II	3.57	3.38	3.52	2.89	3.54	3.14	10.2	3.90
III	3.57	3·41	3.53	2.90	3.55	3.16	10.7	3.15

a) Evaluated by means of the absorption and fluorescence spectra. b) Measured by using the potentiometric method. See Ref. 35.

Table 4. Calculated electron densities (q_N) and interaction terms ($\sum_p Q_p(l_N l_N|pp)$) (eV) of various states

Molecule	S_0 state		S_1 state			
			Frack-Condon		Equilibrium	
	q_N	$\sum_p Q_p(l_N l_N\|pp)$	q_N	$\sum_p Q_p(l_N l_N\|pp)$	q_N	$\sum_p Q_p(l_N l_N\|pp)$
I	1.234	−1.71	1.285	−2.28	1.262	−2.01
II	1.238	−1.73	1.280	−2.27	1.260	−2.05
III	1.237	−1.70	1.288	−2.33	1.263	−2.07

state, Nakajima and Pullman[37] have proposed this relationship between the pK_a values and the interactions:

$$pK_a \propto \sum_p Q_p(l_N l_N|pp) + \text{Const.} \quad (5)$$

In Eq. (5), Q_p is the formal charge on the p atom and $(l_N l_N|pp)$ is the Coulomb repulsion integral between the lone-pair electrons of the nitrogen atom and the π-electron on the p atom. The $(l_N l_N|pp)$ integral was calculated from Roothaan's formulas[20] using the effective nuclear charges of 3.25 and 3.90 for carbon and nitrogen respectively.

The calculated q_N and $\sum_p Q_p(l_N l_N|pp)$ values for the S_0 and S_1 states are listed in Table 4. From Tables 3 and 4, no relationship can be found between the q_N and the variation in the pK_a values of both the states. In the S_0 state and the equilibrium state of the S_1 state, however, it seems that there is a good correlation between the pK_a value and the first term in Eq. (5) for both the states. Such a correlation can not be found in the Franck-Condon state of the S_1 state.

One of the present authors (H.Y.) especially wishes to thank Professor Takeshi Nakajima of Tohoku University for his helpful discussions and encouragement. Throughout this work, a FACOM 230—60 computer of the Kyushu University Computer Center was used. The investigation was supported in part by a Scientific Research Grant from the Ministry of Education.

References

1) This work was presented at the lst International Congress of Quantum Chemistry, Menton, France, July 4, 1973.
2) Th. Förster, *Z. Elektrochem.*, **54**, 42, 531 (1950).
3) E. Havinga and M. E. Kronenberg, *Pure Appl. Chem.*, **16**, 137 (1968).
4) J. A. J. Vink, C. M. Lok, J. Cornelisse, and E. Havinga, *Chem. Commun.*, **1972**, 710.
5) E. L. Wehry and L. B. Rogers, *J. Amer. Chem. Soc.*, **87**, 4234 (1965).
6) W. Liptay, *Z. Naturforsch.*, **A20**, 1441 (1965).
7) M. B. Ledger and P. Suppan, *Spectrochim. Acta*, **23**, 641 (1967).
8) C. W. N. Cumper, R. F. A. Ginman, and A. I. Vogel, *J. Chem. Soc.*, **1962**, 4518.
9) Y. Kanda and R. Shimada, *Spectrochim. Acta*, **15**, 211 (1959).
10) J. A. Riddick and W. B. Bunger, "Organic Solvent," Vol. II, ed. by A. Weissberger, John Wiley & Sons, Inc., New York (1970).
11) I. Nakagawa, *Nippon Kagaku Zasshi*, **79**, 1353 (1958).
12) M. R. Lipkin, J. A. Davison, W. T. Harvey, and S. S. Kurtz, Jr., *Anal. Chem.*, **16**, 55 (1944).
13) Y. Fujimura, H. Yamaguchi, and T. Nakajima, This Bulletin, **45**, 384 (1972).
14) H. Yamaguchi, T. Nakajima, and T. L. Kunii, *Theor. Chim. Acta*, **12**, 349 (1968).
15) R. Pariser and R. G. Parr, *J. Chem. Phys.*, **21**, 446, 767 (1953).
16) J. A. Pople, *Trans. Faraday Soc.*, **49**, 1375 (1953).
17) J. Hinze and H. H. Jaffé, *J. Amer. Chem. Soc.*, **84**, 540 (1962).
18) N. Mataga and K. Nishimoto, *Z. Phys. Chem.* (Leipzig), **13**, 140 (1957).
19) M. Wolfsberg and L. Helmholtz, *J. Chem. Phys.*, **20**, 837 (1952).
20) C. C. J. Roothaan, *ibid.*, **19**, 1445 (1951).
21) G. Favini, I. Vandoni, and M. Simonetta, *Theor. Chim. Acta*, **3**, 418 (1965).
22) J. S. Brinen, R. C. Hirt, and R. C. Schmitt, *Spectrochim. Acta*, **18**, 863 (1962).
23) J. E. Lancaster and B. P. Stoicheff, *Can. J. Phys.*, **34**, 1016 (1967).
24) T. Nakajima and S. Katagiri, *Mol. Phys.*, **7**, 149 (1964).
25) American Peteroleum Institute, Research Project 44, "Ultraviolet Absorption Spectra Data," Carnegie Institute of Technology.

26) R. S. Mulliken, *Rev. Mod. Phys.*, **14**, 265 (1942).
27) J. N. Murrell, "The Theory of The Electronic Spectra of Organic Molecules," London, Methuen (1963).
28) F. Halverson and R. C. Hirt, *J. Chem. Phys.*, **19**, 711 (1951).
29) L. W. Pickett, M. E. Corning, G. M. Wieder, D. A. Semenov, and J. M. Buckley, *J. Amer. Chem. Soc.*, **75**, 1618 (1958).
30) R. D. Brown and B. A. W. Coller, *Theor. Chim. Acta*, **7**, 259 (1967).
31) R. Daudel, R. Lefebvre, and C. Moser, "Quantum Chemistry, Methods and Applications," Interscience Publishers, New York, N. Y. (1959), p. 206.
32) I. F. Halverstadt and W. D. Kumler, *J. Amer. Chem. Soc.*, **64**, 2988 (1942).
33) E. G. McRae, *J. Phys. Chem.*, **61**, 562 (1957).
34) L. Onsager, *J. Amer. Chem. Soc.*, **58**, 1486 (1936).
35) A. Albert, R. Goldacre, and J. Phillips, *J. Chem. Soc.*, **1948**, 2240.
36) H. C. Longuet-Hinggins, *J. Chem. Phys.*, **18**, 275 (1950).
37) T. Nakajima and A. Pullman, *J. Chim. Phys.*, **55**, 793 (1958).
38) A. K. Chandra and C. A. Coulson, *J. Chem. Soc.*, **1965**, 2210.

TABLE 1. SPECIFIC SURFACE AREA AND PORE VOLUME OF METAL OXIDES

	Pretreatment temperature (°C)	Aerosil	Porous silica glass[a)]	Silica gel	Alumina	Silica-alumina
Surface area (m^2/g)	100	203	212	477	178	382
	300	205	204	536	185	386
	500	208	199	559	182	391
	800	197	177	509	166	349
	1000	175				
Pore volume (ml/g)	100		0.251	0.591	0.402	0.789
	800		0.224	0.543	0.387	0.747

a) 65—100 mesh

magnesium iodide and the successive-ignition-loss method. On analysing active hydrogen by means of Zerewitinoff's method, 0.2—0.5 g of a finely divided solid sample was evacuated in a small ampoule at elevated temperatures for 4 hr, sealed off *in vacuo*, and allowed to react with methylmagnesium iodide at 25 °C after breaking the ampoule in a *n*-butylether solution containing the Grignard reagent. The amount of methane gas evolved was measured by means of a gas burette. In the measurement of water content by means of the successive-ignition-loss method, the amount of water vapor expelled by heating at successively elevated temperatures was measured volumetrically; the water content in a sample treated at a certain temperature was obtained by summing up the amounts of water vapor expelled at temperatures higher than that indicated.

Measurement of Surface Area and Porosity. The adsorption-desorption isotherms of nitrogen were determined for each sample at the temperature of liquid nitrogen. The specific surface area was computed by applying the BET method to the nitrogen adsorption isotherm in the relative pressure range 0.05—0.30, in which the cross-sectional area of a nitrogen molecule was assumed to be 16.2 Å^2.

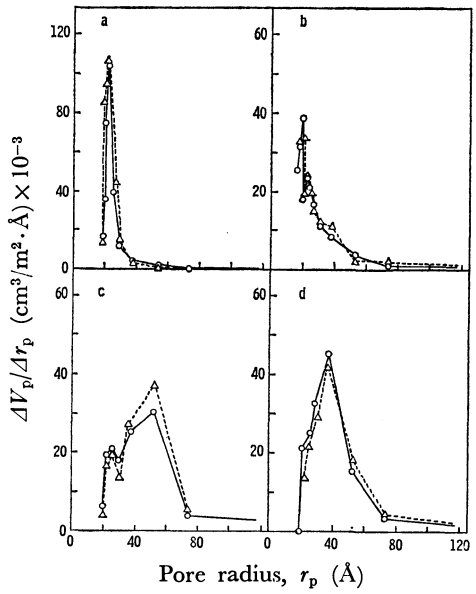

Fig. 2. Pore size distribution curve of porous silica glass (a), silica gel (b), alumina (c), and silica-alumina (d). Solid and broken lines indicate the values on the sample trated at 100° and 800 °C respectively.

The adsorption isotherms of nitrogen and the calculated specific surface area are shown in Fig. 1 and Table 1, respectively.

The porosity of the samples was calculated by applying the Kelvin equation to the desorption branch in the nitrogen isotherms,[18] where a correction for the thickness of the adsorbed layer on the walls was carried out by the method used by Clanston and Inkley.[19] The pore size distribution curves thus calculated for four samples except for Aerosil are illustrated in Fig. 2; the latter sample may be considered to have no pores in the sense of "transitional" range of Dubinin[18] because of the absence of hysteresis (Fig. 1). In Fig. 2 it can be seen that porous silica glass and silica gel have considerably small pores, both distribution curves exhibiting peaks at radii 22 and 19 Å, respectively; the latter has a broader distribution of pores than the former. The pores in alumina and silica-alumina are larger than those in the two kinds of silicas stated above, the distribution curves representing peaks at 53 and 37 Å, respectively. The pore volume can be calculated by assuming the saturated value in nitrogen adsorption isotherms of Type IV to correspond to the amount of nitrogen condensed in the pores (Table 1).

Results and Discussion

Reaction Rate of Methylmagnesium Iodide. One molecule of methylmagnesium iodide reacts with one hydroxyl group or physisorbed water molecule to liberate one molecule of methane gas.[16] The amount of methane gas evolved from one gram of metal oxides is plotted against time (Fig. 3). We see that the evolution of methane gas is rapid in the case of Aerosil, and stops in *ca.* 20 min (Fig. 3a). The reaction is extremely slow on the surface of porous silica glass, being completed after 17 hr (Fig. 3b). The results for two kinds of porous silica glass samples having different particle sizes (65—100 and 270<mesh) are essentially the same. In the case of silica gel, the rate of reaction is as slow as that on porous silica glass (Fig. 3c). In alumina and silica-alumina (SA-50), the liberation of methane gas proceeds at a

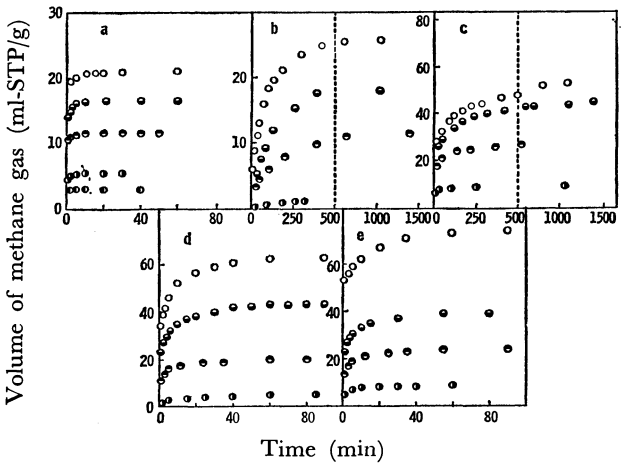

Fig. 3. Reaction of CH_3MgI with active hydrogen on Aerosil-200 (a), porous silica glass (65—100 mesh) (b), silica gel (c), alumina (d), silica-alumina (SA-50) (e); pretreatment temperature, ○: 100°, ◒: 300°, ◓: 500°, ◑: 800°, ◐: 1000 °C.

moderate rate, and ends in *ca.* 60 min (Figs. 3d and e).

A comparison of Figs. 1, 2 and 3 shows that the reaction rate of methylmagnesium iodide is closely related to the pore size distribution of metal oxides. In Aerosil samples, in which no hysteresis appears in the adsorption isotherm, the reaction is completed very rapidly (20 min), while in those having small pores the completion for the reaction requires a longer time. It takes about 60 min on alumina and silica-alumina having a peak at radii 53 and 37 Å, respectively, and about 1000 min on porous silica glass and silica gel having a peak at radii 22 and 19 Å, respectively. We can thus conclude that the rate of reaction of methylmagnesium iodide with active hydrogen on metal oxides is determined by the diffusion of the reagent into pores. The time required for the completion of the reaction gives a measure for the porosity of powders.

Dependence of Water Content upon the Nature and Origin of Samples. The water content obtained from the extreme value of methane gas evolved (Fig. 3) is plotted against pretreatment temperature (Figs. 4 and 5), along with those obtained from the successive-ignition-loss method. Figures 4 and 5 show that the values of water content measured by the two methods on each sample are in fairly good agreement with each other, as in other examples.[16] This indicates that the two methods tested here give mutually reliable data on surface water content in spite of their difference, even when the samples have pores of transitional sizes; a prolonged reaction time is required for the measurement by methylmagnesium iodide. It should be noted that the water contents in three kinds of silica are in fairly good agreement with each other, in spite of large differences in their origin and also in surface properties such as area and porosity. The

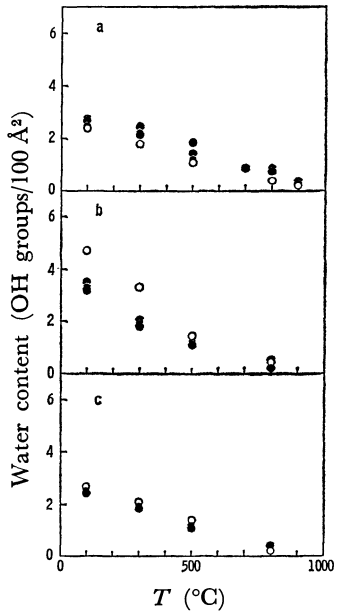

Fig. 4. Water content on Aerosil (a), porous silica glass (65–100 mesh) (b), silica gel (c), measured by the active hydrogen analysis (●) and the successive-ignition-loss method (○).

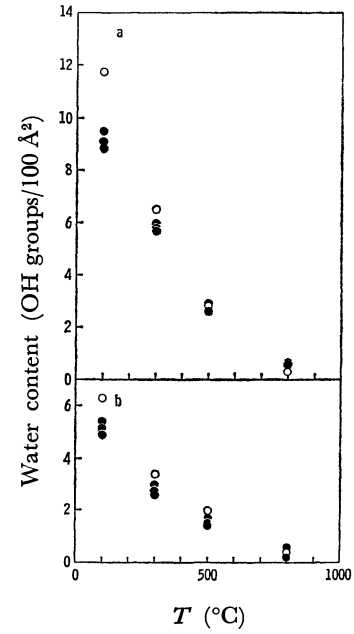

Fig. 5. Water content on alumina (a) and silica-alumina (SA-50) (b), measured by the active hydrogen analysis (●) and the successive-ignition-loss method (○).

water content in three kinds of 100 °-treated silica is *ca.* 3 OH/100 Å² (Fig. 4) which is much smaller than the values in the other oxides, but approximate to values estimated theoretically.[20]

A discrepancy between the two methods appears on porous silica glass treated at relatively lower temperatures: the successive-ignition-loss method gives a larger value. This might be due to the existence of extremely small pores which impede the diffusion of methylmagnesium iodide molecules, but permit the passage of condensed water molecules on outgassing. A similar discrepancy in the values of water content is observed on alumina and silica-alumina, when treated at lower temperatures (Figs. 5a and b). The same interpretation will also hold in these samples from the existence of pores of critical size. It can be expected that alumina and silica-alumina are easily hydrated to form aluminum atoms coordinated with water molecules or structural hydroxyl groups in the surface layer because of the well-known hydrophilic nature of aluminum ion. The latter situation will bring about a fairly large amount of observed water content on alumina as seen in Fig. 5a and also from previous results.[14,15]

It should be noted that the two methods give reliable values of water content in the process of heating the samples, especially in a range of smaller value of water content such as <2 OH/100 Å². From the fact that water evolution from the metal oxide surface at higher temperatures arises from the condensation dehydration of surface hydroxyls, it can be inferred that isolated surface hydroxyl groups which might remain on metal oxides at elevated temperatures can migrate to meet with each other on the surface, and that the migration occurs in the form of active hydrogens rather than hydroxyl groups themselves.

References

1) T. Morimoto, M. Nagano, and F. Tokuda, This Bulletin, **41**, 1533 (1968).
2) G. J. Young, *J. Colloid Sci.*, **13**, 67 (1958).
3) T. Morimoto, M. Nagao, and F. Tokuda, *J. Phys. Chem.*, **73**, 243 (1969).
4) T. Morimoto and M. Nagao, This Bulletin, **43**, 3746 (1970).
5) T. C. Franklin and M. Kawamata, *J. Phys. Chem.*, **71**, 4213 (1967).
6) J. N. Finch and A. Clark, *ibid.*, **73**, 2234 (1969).
7) G. A. Parks, *Chem. Rev.*, **65**, 177 (1965).
8) T. Morimoto and S. Kittaka, This Bulletin, **46**, 3040 (1974).
9) J. J. Fripiat and J. Uytterhoeven, *J. Phys. Chem.*, **66**, 800 (1962).
10) J. Uytterhoeven and H. Naveau, *Bull. Soc. Chim. Fr.*, **1962**, 27.
11) J. Uytterhoeven, M. Sleen, and J. J. Fripiat, *ibid.*, **1965**, 1800.
12) H. P. Boehm, *Angew. Chem. Int. Ed. Engl.*, **5**, 533 (1966).
13) R. Flaig-Baumann, H. D. Neuwinger, and H. P. Boehm, *Fortsch. Kolloid Polym.*, **55**, 7 (1971).
14) T. Morimoto, K. Shiomi, and H. Tanaka, This Bulletin, **37**, 392 (1964).
15) T. Morimoto, M. Nagao, and J. Imai, *ibid.*, **44**, 1282 (1971).
16) T. Morimoto and H. Naono, *ibid.*, **46**, 2000 (1973).
17) T. Morimoto, J. Imai, and M. Nagao, *J. Phys. Chem.*, **78**, 704 (1974).
18) S. J. Gregg and K. S. W. Sing, "Adsorption Surface Area and Porosity," Academic Press, London (1967).
19) R. W. Clanston and F. A. Inkley, *Advan. Catal.*, **9**, 143 (1957).
20) M. Schneider, Ph. D. Thesis, University of Heidelberg, Germany (1962); H. P. Boehm, *Advan. Catal.*, **16**, 179 (1966).

The Absorption and Fluorescence Spectra of 2-Methyl-1-aceanthrenone and Its Cation. A Comparison with 9-Anthracenecarboxaldehyde

Satoshi HIRAYAMA

Faculty of Textile Science, Kyoto Technical University, Matsugasaki, Sakyo-ku, Kyoto 606

(Received June 15, 1974)

The fluorescence and absorption spectra of 2-methyl-1-aceanthrenone (I) and its cation were investigated. The spectra showed well-defined vibrational structures in a wide variety of solvents, but not in ethyl alcohol and acetic acid. The existence of the ^1L_b absorption band on the shorter-wavelength side of the ^1L_a band was strongly supported by the different solvent effects of these bands. In non-polar solvents, (I) formed a strongly fluorescent, 1 : 1, hydrogen-bonded complex with a trichloroacetic acid molecule. The formation constant in *n*-hexane was determined spectrophotometrically as $3.1 \times 10^2\ M^{-1}$ at 20 °C. In acidic solutions, pK_a and pK_a^*, were determined as -5.1 and 1.3 for the ground and first excited singlet states respectively. These values are the same as the corresponding values of 9-anthracenecarboxaldehyde (9-CHO-A), reflecting a marked resemblance in the electronic nature of the carbonyl groups of the two compounds. The broad absorption spectra of 9-CHO-A, in contrast to the highly structured spectra of (I), are due to a feasible torsional motion of the carbonyl group of the former compound.

The photochemical and photophysical processes of the carbonyl derivatives of anthracene have long attracted our attention, and several new features have been revealed by the present author and his co-workers.[1-4]

In spectroscopic studies of the carbonyl derivatives, an unavoidable complexity is met in elucidating the electronic nature of the excited states, because all these compounds have $n\rightarrow\pi^*$ states in addition to $\pi\rightarrow\pi^*$ states in the energy region attainable by usual photo-excitation. Before any detailed discussion of the photochemical and photophysical behavior of these compounds, threfore, it is necessary not only to determine the energy levels of four states—$S_{1\pi\pi^*}$, $S_{n\pi^*}$, $T_{1\pi\pi^*}$, and $T_{n\pi^*}$—at least, but also to elucidate the principal pathways of the internal conversion and intersystem crossing processes between any two states chosen from these states and the ground state. Actually, however, it is quite rare for all the above-mentioned matters to be made sufficiently clear. In this sense, 9-anthracenecarboxaldehyde (9-CHO-A) is a typical compound; its unusual photochemical reactivity has long been the subject of dispute, but no unambiguous conclusion has yet been obtained as to its reactive excited state. Several investigators, including Yang,[5-8] have proposed that the reactive excited states are the upper triplet $n\rightarrow\pi^*$ and/or the singlet $n\rightarrow\pi^*$ states. On the contrary, Suppan recently asserted that the reactive excited state was the lowest excited singlet $\pi\rightarrow\pi^*$ state.[9] The reason for this discrepancy can be ascribed to the shortage of useful spectroscopic data because of the broadness of the absorption and fluorescence spectra of 9-CHO-A.

A few studies of the molecular structure of 9-CHO-A have revealed that the angle between the anthracene ring and the plane containing the aldehyde group is approximately 25 °,[10] whereas for the other 9-carbonyl derivatives of anthracene this angle is believed to be close to 90 ° as a result of the large steric effect of the peri hydrogen atom.[11] Therefore, except for a characteristic non-fluorescent property common to these carbonyl derivatives,[1,2,12] they hardly differ from the 9-alkyl substituted anthracenes in UV absorption spectrum. Thus, the unusual photochemical reactivity and the broadness in the absorption and fluorescence spectra of 9-CHO-A may be supposed to arise from the approximate co-planarity of the anthracene ring and the plane of the aldehyde group.

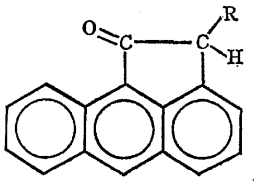

(I): R=CH_3

(II): R=H

In 2-methyl-1-aceanthrenone (I) and 1-aceanthrenone (II), which are the main photo-products of 9-α-bromopropionylanthracene[13] and 9-ω-bromoacetylanthracene[4] respectively, it is quite evident that the planes of the carbonyl groups lie on the same plane as the anthracene ring. Considering the approximate co-planarity seen in both (I) and 9-CHO-A, we may expect a very similar behavior of these two compounds in various points. Therefore, detailed investigations of the spectroscopic properties and photochemical reactions of (I) or (II) should aid in clarifying the unusual photochemistry of 9-CHO-A.

The intention of this paper is to report for the first time on the fluorescence and absorption spectra of (I) and its cation and to discuss the results in comparison with the spectroscopic properties of 9-CHO-A as reported by Schulman and Young.[14]

Experimental

Materials. Compound (I) was obtained as the main product of the photolysis of 9-α-bromopropionylanthracene.[13] It was purified by column chromatography and then sublimated twice *in vacuo*. Obviously, (I) and (II) are quite similar in their structural and spectroscopic properties. (I) was employed in this paper simply because it was readily available.

9-CHO-A was prepared according to the well-known method[15] and was recrystallized from acetic acid and purified by sublimation *in vacuo*.

Among the solvents used for the spectroscopic measurements, *n*-hexane and cyclohexane were of a spectro grade (Nakarai Chem. Co., Ltd.). The other solvents (guaranteed

grade) were either distilled before use on a 1-ft Widmar column or were used as received. Tetrahydrofuran, *n*-hexane, and methylenedichloride employed to study the effect of a small amount of oxygen or moisture on the spectra were distilled from a Widmar column and then dried over sodium-potassium amalgam. All these solvents were transferred into an optical cell *in vacuo*. Sulfuric acid (s.g. 1.86) and trichloroacetic acid obtained from the Nakarai Chem. Co., Ltd., were used without further purification. Deionized and distilled water was used.

Optical Measurements. The absorption spectra at room temperature were taken on a Hitachi 124 Spectrophotometer. The fluorescence and excitation spectra were recorded on a Shimadzu Corrected Spectrofluorophotometer, RF 502. To produce corrected spectra, the time- and wavelength-dependent variation in the irradiation-source intensity was corrected automatically by using a rhodamine B quantum counter, while the response of the monochromator-photomultiplier combination was calibrated by means of the manufacturer's electrical compensator. The correctness of the calibration was checked with a dilute standard solution of quinie bisulfate (5×10^{-5} M in 0.5 M sulfuric acid). To record the fluorescence spectra at 77 K, a Dewar vessel and a sample cell made for ordinary ESR measurements at 77 K were used after a slight modification; the Dewar vessel was set in the cell holder of the spectrofluorophotometer, RF 502. Therefore the fluorescence spectra obtained thus at 77 K were uncorrected. The absorption spectra at low temperatures were taken by using a modified Beckman-type spectrophotometer equipped with an EMI 9558 QB photomultiplier. Constant low temperatures were obtained by circulating cold nitrogen gas.

Determination of the Acid Dissociation Constants. The acid dissociation constant, pK_a^*, of the first excited singlet state of (I) was determined by an approximate procedure, *i.e.*, by the fluorimetric pH titration in water-sulfuric acid mixed solvents and buffer solutions.[16] Sørensen's buffer solutions were used, and the pH measurements were made on a Takeda Riken pH-meter, Model HG-2. Sample solutions were prepared by adding a buffer or an acid solution to each 1.0 ml ethanol solution of (I) (*ca.* 10^{-4} M) in a 50 ml volumetric flask. The fluorescence intensities were measured at the wavelength where the fluorescence intensity of the neutral molecule reaches its maximum value.

The acid dissociation constant, pK_a, of the ground state of (I) was determined spectrophotometrically according to the method of Davis and Geissman.[17] The corrected Hammett acidity scale of Jorgenson and Hartter[18] was adopted here. To prepare the sample solutions, the solvent was removed from the 1.0 ml ethanol solution of (I) (*ca.* 1.2×10^{-2} M) in a 25 ml volumetric flask, and then an acidic solution of a known H_0 was poured into the flask until the volume reached 25 ml. The H_0 values were determined by weighing each solvent before mixing. Since, above $H_0=-5.3$, (I) became insoluble in water–sulfuric acid mixed solvents, a small amount of ethanol (2% by volume) was added. All the measurements were carried out at 20 °C.

Results

Neutral Molecule. In Fig. 1 are shown the absorption and fluorescence spectra of (I) observed at room temperature in *n*-hexane and ethanol. The fluorescence yield in *n*-hexane is so low that the spectrum in *n*-hexane is enlarged approximately 44 times. In relation to the photochemistry of 9-ω-bromoacetylanthracene, the absorption spectra of (II) in cyclohexane and ethanol have already been reported.[4] They are very similar to those of (I). In Fig. 2 the fluorescence and excitation spectra of (I) in EPA (5 : 5 : 2 by volume) at 77 K are shown. The fluorescence intensity is rather weak and does not increase very much when the temperature is lowered to 77 K.

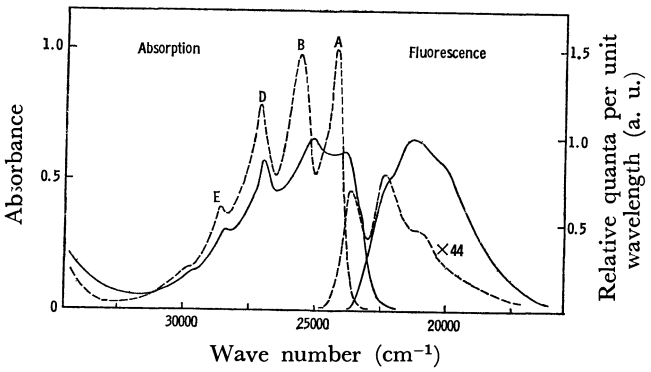

Fig. 1. Absorption and fluorescence spectra of (I) at room temperature.
——: ethanol (8.3×10^{-5} M),
----: *n*-hexane (1.0×10^{-4} M).
The fluorescence spectra were observed at the concentration of *ca.* 5×10^{-5} M in both media. The fluorescence intensity in *n*-hexane is enlarged approximately 44 times. The symbols A to E denote the vibrational band maxima (see also Table 1).

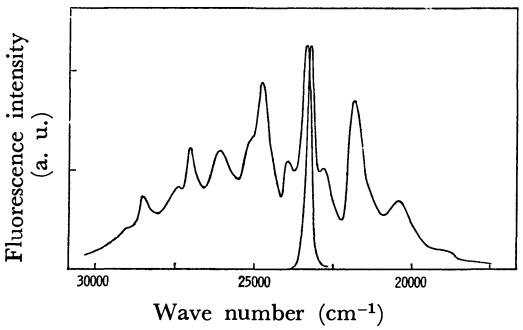

Fig. 2. Fluorescence and excitation spectra of (I) (*ca.* 5×10^{-5} M) in EPA at 77 K.
The excitation spectrum accords well with the absorption spectrum observed at 77 K in the same medium. Comparing the fluorescence and excitation spectra, the existence of the ^1L_b band with sharp band maxima at 351 and 369 nm is evident.

The absorption spectrum of 9-CHO-A in *n*-hexane is shown in Fig. 3 for the sake of comparison. Practically, 9-CHO-A is non-fluorescent in this solvent. The absorption spectrum of 9-CHO-A is inherently broad and does not differ much in a wide variety of solvents.[3] Its fluorescence spectrum at 77 K is also less structured than that of (I), and the fluorescence intensity varies little with the temperature. In contrast, the shape and the position of the absorption spectrum of (I) depend greatly on the solvents. The wave numbers of the absorption band maxima observed for (I) in various solvents are collected in Table 1 (see also Fig. 1). In such polar solvents as dimethylformamide and methylenedichloride, the red shifts were so large that the new absorption maxima (Band

TABLE 1. UV ABSORPTION BAND MAXIMA OF (I)

Solvent	^1L_a (cm^{-1})			^1L_b (cm^{-1})	
	A	B	C	D	E
n-Hexane	24270	25640	—	27170	28650
Triethylamine	24210	25580	—	27100	28570
Carbon tetrachloride	23920	25320	shoulder	27030	28490
Acetonitrile	23920	25250	flat	27170	28650
Benzene	23810	25190	26460	27100	28490
Methylenedichloride	23810	25130	26460	27030	28570
Dimethylformamide	23700	25000	26320	27100	28570
Pyridine	23640	24940	26250	27030	28490
Benzonitrile	23580	24940	26250	27030	28410
n-Hexane+*ca.* 1% trichloroacetic acid[a)]	23200	24390	25640	26880	28250

a) Absorption maxima for the hydrogen-bonded complex.

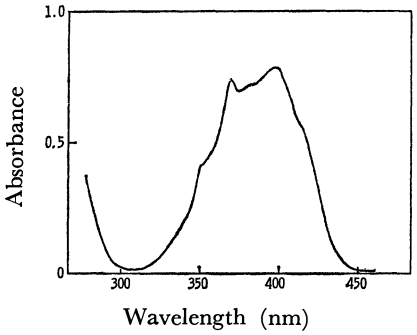

Eig. 3. Absorption spectrum of 9-CHO-A (1.2×10^{-4} M) in *n*-hexane.
The spectrum should be compared with that of (I) shown in Fig. 1. The shoulder observed at around 420 nm is attributed to the 0-0 band.

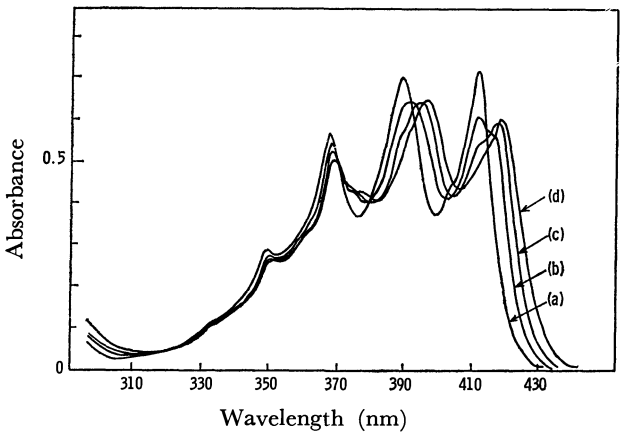

Fig. 4. Absorption spectrum change upon the addition of methylenedichloride to a *n*-hexane solution of (I). The concentrations of the additive by volume are; (a) 0%, (b) 9.1%, (c) 23.1%, (d) 50%. The concentration of (I) is the same (7.2×10^{-5} M) for (a) to (d).

C) appeared clearly between Bands B and D. Despite the large solvent effect in these solvents, the absorption spectra are highly structured and the band widths of A, B, and C are comparable to those obtained in non-polar solvents. It should also be noted that, in any of the solvents studied here, the band widths of D and E are narrower than those of A, B, and C.

On the basis of the different solvent effects on the two band groups, the A, B, and C absorption bands are considered to originate from a different electronic transition from that of the D and E bands. The former band group showed a larger red shift in polar solvents than did the latter band group. Furthermore, the energy separations between B and D, and between D and E, are not the same, so these bands are not considered to belong to the same vibrational manifold of the same excited singlet state. The A, B, and C bands could be assigned to the vibrational manifold of the ^1L_a band, and D and E, to that of ^1L_b. The fact that the fluorescence spectrum shown in Fig. 2 lacks the vibrational progression (corresponding to the bands at 28,490 and 27,100 cm^{-1}) seen in the excitation spectrum also supports this.

As an example of a large solvent effect on the absorption spectrum of (I), the absorption spectrum change in *n*-hexane–methylenedichloride mixed solvents is shown in Fig. 4. Although no clear isosbestic points can be seen, the spectrum changes as if (I) and methylenedichloride form a certain complex; two clear absorption peaks can be recognized at around 410 nm even at a high concentration of methylenedichloride. The fluorescence intensity was observed to increase as the fraction of methylenedichloride increased. In general, the fluorescence yield was larger in polar solvents than in non-polar solvents; *i.e.*, (I) showed a so-called fluorescence activation. Dissolved oxygen and moisture did not affect the fluorescence yield appreciably, as evidenced by a comparison of the fluorescence intensities observed in dry and degassed and aerated solvents.

Figure 5 shows the absorption spectrum change when a small amount of trichloroacetic acid is added to a *n*-hexane solution of (I). In this case, clear isosbestic points are seen at 415, 395.5, 377.5, 371, 355.5, and 352.5 nm, indicating the formation of a hydrogen-bonded complex. The detailed analysis of the spectra showed it to be a 1 : 1 complex with the formation constant of 3.1×10^2 M^{-1} at 20 °C.

Figure 6 shows how the fluorescence spectrum and its intensity change upon the addition of trichloroacetic acid. Compared with the fluorescence spectra shown in Fig. 1, the fluorescence spectra in Fig. 6

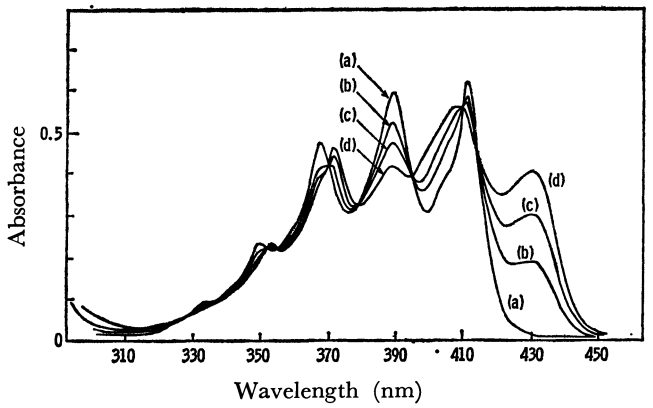

Fig. 5. Absorption spectrum change upon the addition of a small amount of trichloroacetic acid to a *n*-hexane solution of (I).
The concentrations of the additive are;
(a) 0 M, (b) 2.4×10^{-3} M, (c) 6.6×10^{-3} M,
(d) 4.4×10^{-2} M.
The isosbestic points are seen at 415, 395.5, 377.5, 371, 355.5, and 352.5 nm, indicating the formation of the 1 : 1 hydrogen-bonded complex.

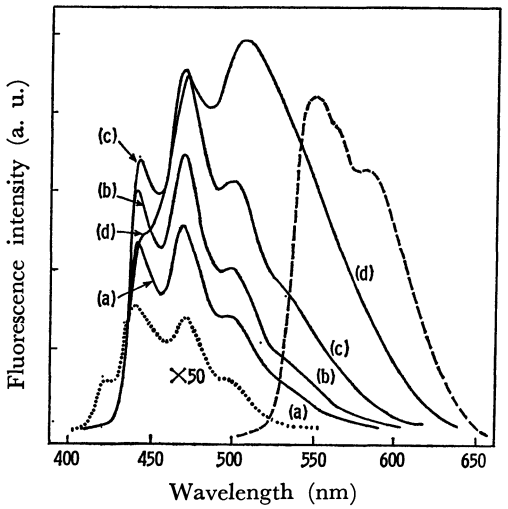

Fig. 6. Fluorescence spectra observed for the 1 : 1 hydrogen-bonded complex of (I).
The spectra denoted by (b) to (d) were observed for the solutions showing the absorption spectra represented by Fig. 5(b) to (d) respectively. The spectrum (a) was observed for the 1.2×10^{-3} M solution of trichloroacetic acid.
The excitation wavelength was 370±10 nm. The fluorescence at the longer wavelength is emitted from the cation. In a much more concentrated solution of trichloroacetic acid (*ca.* 0.5 M), the fluorescence band maximum lies at 532 nm. The broken line represents the fluorescnece spectrum of the cation in conc. sulfuric acid.
In a very dilute solution of trichloroacetic acid (*ca.* 10^{-6} M), fluorescences from the two species (hydrogen-bonded and non-hydrogen-bonded molecules) can be observed as shown by the dotted line.

differ in their position, intensity, and vibrational structure. Thus, the fluorescence spectrum observed in *n*-hexane with a small amount of trichloroacetic acid can be attributed to the hydrogen-bonded molecule. A further increase in the concentration of trichloroacetic acid greatly shifted the fluorescence spectra to the red and caused the loss of a vibrational structure. A comparison with the fluorescence spectrum observed in sulfuric acid (broken line in Fig. 6) revealed that the fluorescence in a concentrated trichloroacetic acid solution was due to a fluorescence from the cation of (I).

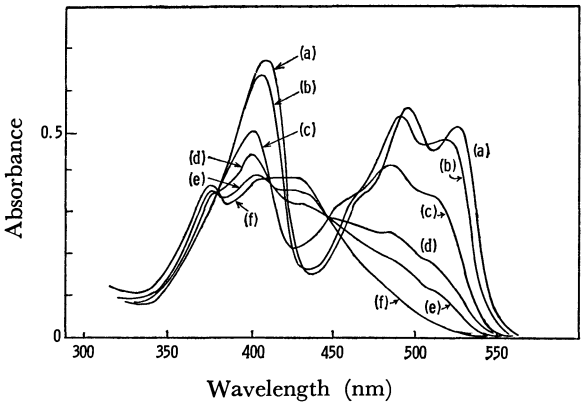

Fig. 7. Absorption spectra of (I) (5.7×10^{-5} M) in acidic solutions.
(a) conc. sulfuric acid, (b) $H_0=-7.74$,
(c) $H_0=-5.32$, (d) $H_0=-4.45$, (e) $H_0=-4.23$,
(f) $H_0=-4.03$.
In the $H_0\geqq-5.0$ range rather good isosbestic points are seen at 379 and 441 nm.

Although 9-CHO-A behaved in a way analogous to (I) upon the addition of trichloroacetic acid, the observed spectra lacked a clear vibrational structure. Consequently, the spectroscopic discrimination of the existence of a non-hydrogen-bonded state and a hydrogen-bonded state is not so feasible as in the case of (I).

Cation. Figure 7 shows the absorption spectra of (I) observed in water-sulfuric acid mixed solvents. The cation formed in sulfuric acid emitted a fluorescence with a band maximum at 550 nm. Although the cation, which naturally showed no ESR signal, was comparatively stable, it could not be set aside for a long time. The absorption at around 520 nm gradually became broader, indicating a decomposition of (I).

Schulman and Young[14] have reported on the absorption and fluorescence spectra of 9-CHO-A under similar conditions; they obtained the values of the acid dissociation constants, pK_a and pK_a^*, as −5.1 and 1.3 for the ground and the lowest excited singlet states respectively. The cations of (I) and 9-CHO-A resemble each other in their absorption spectra, though the latter cation absorbs at wavelengths a little longer. Compared with the absorption spectra observed at high H_0 values, the bands at 410 nm and in the range from 450 to 550 nm in sulfuric acid are assigned to the ^1L_b band and the ^1L_a band respectively. It should be noted here that the ^1L_b band of the cation of (I) is structureless and is as broad as that of the cation of 9-CHO-A.

pK_a and pK_a^*. An approximate value of pK_a^*[16] was obtained by observing the fluorescence intensities of the neutral molecule at 495 nm (excitation: 420±10 nm) at various pH's. The fluorescence inten-

sity *vs.* pH curve gave 1.3 as the approximate value of pK_a^*. Since the fluorescence intensity depends on the kind of buffer solution used, the error in pK_a^* determination may be considerable.

The value of pK_a was determined spectrophotometrically according to the method of Davis and Geissman.[17] The difference in the absorbances at the wavelengths of the absorption peaks of the cation and the neutral molecule were plotted against H_0. The inflection point of this curve gave the value of pK_a as -5.1. As may be seen in Fig. 7, in a strict sense no isosbestic point was observed when H_0 was varied over a wide range; hence, the obtained value of pK_a may again have an appreciable error. In the $H_0 \geqq -5.0$ range, however, rather good isosbestic points were observed at 379 and 441 nm.

The obtained values of pK_a^* and pK_a are in good agreement with those of 9-CHO-A determined by Schulman and Young,[14] indicating a close similarity of the electronic natures of the two carbonyl groups.

Using the equation based on the Förster cycle: $pK_a^* = pK_a + (0.625/T)\,(\bar{\lambda}_N^{-1} - \bar{\lambda}_C^{-1})$, the difference $\Delta pK = pK_a^* - pK_a$ was calculated as 6.7; it showed good agreement with the experimental value of 6.4. The terms in the parentheses are the 0–0 frequencies (in cm^{-1}) estimated from the mean of the positions of the wavelengths of the absorption and fluorescence maxima for the neutral molecule and the cation respectively.

Photolysis of (I). Neither the photochemical reduction of (I) in isopropanol, dimethylaniline, and triethylamine nor the photocycloaddition reaction in 2-methylpentene was observed. That is, both photochemical reactions noted for 9-CHO-A[3,5-8] did not proceed. On the irradiation of (I), however, the absorbance of the p-band gradually decreased; this indicates the occurrence of photochemical reactions presumably including a photodimerization reaction.

Discussion

Similarity and Dissimilarity in the Spectroscopic Properties of (I) and 9-CHO-A. Both compounds bear a marked resemblance to each other in various properties, such as the basicity of the carbonyl groups (pK_a^* and pK_a), a large red shift of the ^1L_a band compared with those of the other 9-carbonyl derivatives of anthracene, fluorescence activation, and the ability of hydrogen-bonding. It is quite evident that the cause for this resemblance is attributable to the fact that the planes of the carbonyl groups and the anthracene ring are approximately coplanar; *i.e.*, the increased conjugation between the carbonyl groups and the anthracene ring endows these compounds with similar properties. This is also supported by the fact that it is impossible to find such a similarity among the other 9-carbonyl derivatives: 9-RCO-A (*e.g.*, R=CH_3–, CH_3CH_2–, $CH_3CH_2CH_2$–, ph–, CH_2=CH–, NH_2– CH_3O–, HO–,) where the carbonyl groups are supposed to make almost right angles with the anthracene ring at the ground states. From this resemblance between (I) and 9-CHO-A, it can also be said that the unusual spectroscopic behavior of 9-CHO-A can not necessarily be ascribed to the fact that its carbonyl group is aldehyde.

On the other hand, a distinct difference in the spectra of (I) and 9-CHO-A lies in the sharpness and the vibrational structure of the absorption and fluorescence bands. Schulman and Young[14] have attributed the lack of a vibrational structure in the absorption spectrum of 9-CHO-A to the loss of vibrational quantization in ^1L_a band. To explain the loss of quantization, they assumed that, since the $^1L_a \leftarrow {}^1A$ transition bore a CT character to some extent, the solvent-relaxation process and the functional rehybridization (the rotation of the aldehyde group) had to occur during the electronic transition, particularly in polar fluid solvents. In comparison with the absorption spectra of (I), however, we see that Schulman's proposal has several difficulties. First, (i) it is questionable whether the rotation of the carbonyl group of 9-CHO-A competes well with the electronic transition. Second, (ii) the broadening in the UV spectrum of 9-CHO-A should be strongly solvent-dependent if solvent relaxation process alters the vibrational sublevels of the Franck-Condon-excited state. On the contrary, though, the broadening is nearly insensitive to solvents. Third, (iii) if the CT character of the ^1L_a band is partly responsible for the broadening, a similar broadening should be observed for (I) and 9-CHO-A. Fourth, (iv) even if the rotation of the carbonyl group is forbidden as in (I), its absorption and fluorescence spectra are quite broad in alcohols. (This will be discussed in a later section.) Fifth, (v) the ^1L_b band of the cation of (I), for which a non-Franck-Condon electronic transition is not to be expected because of the structurally fixed carbonyl group, is also broad and vibrationally structureless, as has been observed for the cation of 9-CHO-A. Furthermore, it should be noted that the absorption spectrum of 9-CH_3OCO-A, whose substituent is supposed to rotate into a coplanar configuration at the excited state, has been reported by Werner and Hoffman[19] to retain an anthracene-like structure. Thus it seems inappropriate to interpret the spectrum broadening observed for 9-CHO-A in terms of a non-Franck-Condon transition to the ^1L_a state.

A comparison of the ^1H spectra of 9-CHO-A and (I) implies the occurrence of a torsional motion of the carbonyl group of 9-CHO-A in the ground state.[20] Therefore, in the present author's opinion, the breadth of the absorption spectrum of 9-CHO-A can be explained as follows, without introducing the concept of a non-Franck-Condon transition to the ^1L_a state. The transition energy changes as the extent of the conjugation of the substituent varies; *i.e.*, the transition energy is a function of the angle made by the carbonyl group and the anthracene ring. Hence, if the electronic transition is supposed to occur from the various ground states with respect to the angle, this will naturally lead to the spectrum broadening, which will be almost insensitive to solvents.

The sharpness of the ^1L_b bands of (I) and 9-CHO-A can also be understood when it is noted that the energy of the ^1L_b band, which is polarized to the long axis of the anthracene ring, is not appreciably affected by meso-substitution, so the transition energy does not

depend on the extent of conjugation of the carbonyl group. This is substantiated by the approximate invariance of the values of the $^1L_b \leftarrow ^1A$ transition energy observed for several 9-substituted anthracenes.[21]

Energy Levels. The electronic states of (I) are well defined. The A, B, and C bands belong to the ^1L_a band, and D and E, to the ^1L_b band, as has been described already. Since, in general, the ^1L_a band does not suffer significantly any substituent effect due to the 1- or 2-position, the large red shift of the 0–0 band of the ^1L_a band may be regarded as being due to the conjugation effect of the carbonyl group. Though the position of the 0–0 band of the ^1L_a band of 9-CHO-A is not clear, a comparison of the absorption spectra of (I) and 9-CHO-A implies that the shoulder observed at around 420 nm in Fig. 3 is due not to the $n \rightarrow \pi^*$ transition, but to the 0–0 band of the ^1L_a band. The lowest excited singlet state of (I) is undoubtedly the $\pi \rightarrow \pi^*$ state, as can be seen from Fig. 1, so the lowest excited singlet state of 9-CHO-A, which has long been in dispute, should also be the $\pi \rightarrow \pi^*$ state. Therefore, the phenomenon of fluorescence activation found for 9-CHO-A as well as for (I) should be explained by a mechanism other than the level inversion between $S_{1\pi\pi^*}$ and $S_{n\pi^*}$ states,[22] as has been suggested by the present author in a previous paper.[3] Instead, two triplet states, $T_{2\pi\pi^*}$ and more particularly, $T_{n\pi^*}$, seem to play an important role in the fluorescence activation phenomenon. However, it is impossible at present to determine the energy levels of these states experimentally. The best way to do so would be to estimate the energy levels from the spectroscopic data accumulated for various carbonyl derivatives of anthracene.[3] All we can say now, on the basis of the present results, is that the fluorescence activation process can more reasonably be explained in terms of the level inversion between $S_{1\pi\pi^*}$ and $T_{n\pi^*}$ states, which may be caused by the increased solvent polarity or by the formation of a hydrogen-bond with a solvent molecule. The fact that abnormal photo-reactivity was not found for (I) may reflect either an unsuitable energy level of the $T_{n\pi^*}$ state relative to the $T_{2\pi\pi^*}$ state (*i.e.*, the lifetime of $T_{n\pi^*}$ is too short for its state to participate in the reactions because of an efficient internal conversion to $T_{2\pi\pi^*}$) or a steric prohibition of the reactions.

Explanation of the Absorption Spectra of (I) in Alcoholic Solvents. The absorption and fluorescence spectra of (I) observed in alcoholic solvents differ much in their breadth from those in non-alcoholic polar solvents, such as dimethylformamide and acetonitrile. The non-hydrogen-bonded neutral molecule of (I) and also the hydrogen-bonded molecule show pronounced vibrational structures in both the fluorescence and absorption spectra, as is indicated in Figs. 1 and 6. The broadening observed in alcoholic solvents can not, therefore, be explained in terms of a simple solvent effect on the spectra. When the temperature was lowered to *ca.* −80 °C, the absorption band at 418 nm sharpened, became more pronounced, and shifted to 420 nm. At the same time, the new bands with peaks at 430 (shoulder), 412, and 388 nm, which correspond well with the absorption peaks observed for a hydrogen-bonded molecule, appeared. Since the band at 418 nm corresponds to the non-hydrogen-bonded molecule, the above-mentioned fact is indicative of the coexistence of at least two species. Thus, the apparent broadening in alcoholic solvents can be reasonably explained in terms of the coexistence of hydrogen-bonded and non-hydrogen-bonded molecules, which absorb light at slightly different wavelengths. A part of the broadening observed for 9-CHO-A may be attributed to such a coexistence, but an experimental proof is need. In order to confirm these things, further studies are now in progress.

References

1) T. Matsumoto, M. Sato, and S. Hirayama, *Chem. Phys. Lett.*, **13**, 13 (1972).
2) T. Matsumoto, M. Sato, and S. Hirayama, *ibid.*, **18**, 563 (1973).
3) S. Hirayama, *Rev. Phys. Chem. Japan*, **42**, 49 (1972).
4) T. Matsumoto, M. Sato, and S. Hirayama, This Bulletin, **47**, 358 (1974).
5) N. C. Yang and R. L. Loeschen, *Tetrahedron Lett.*, **1968**, 2571.
6) N. C. Yang, R. L. Loeschen, and D. Mitchell, *J. Amer. Chem. Soc.*, **89**, 5465 (1967).
7) D. A. Warwick and C. H. J. Wells, *Tetrahedron Lett.*, **1968**, 4401.
8) D. A. Warwick and C. H. J. Wells, *ibid.*, **1969**, 4955.
9) P. Suppan, *ibid.*, **1971**, 4469.
10) R. J. LeFèvre, L. Radom, and G. L. D. Ritchie, *J. Chem. Soc. (B)*, **1968**, 775.
11) (a) T. C. Werner and D. M. Hercules, *J. Phys. Chem.*, **73**, 2005 (1969).
(b) M. Martynoff, *Bull. Soc. Chim. France*, **25**, 164 (1958).
12) S. Hirayama, unpublished results.
13) T. Matsumoto, M. Sato, and S. Hirayama, *Chem. Phys. Lett.*, **27**, 237 (1974). Details of the photochemistry of 9-α-bromopropionylanthracene will be published elsewhere. To the author's knowledge, (I) is a new compound.
14) J. F. Young and S. G. Schulman, *Talanta*, **20**, 399 (1973).
15) L. F. Fieser and J. L. Hartwell, *J. Amer. Chem. Soc.*, **60**, 2555 (1938).
16) (a) H. Kokubun, *Z. Elektrochem.*, **62**, 599 (1958). (b) A. R. Watkins, *J. Chem. Soc. Faraday Trans. I*, **68**, 28 (1972).
17) C. T. Davis and T. A. Geissman, *J. Amer. Chem. Soc.*, **76**, 3507 (1954).
18) M. J. Jorgenson and D. R. Hartter, *ibid.*, **85**, 878 (1963).
19) T. C. Werner and R. M. Hoffman, *J. Phys. Chem.*, **77**, 1611 (1973).
20) The chemical shift of the peri hydrogen atom of (I) is 8.93 ppm (1H multiplet) in carbon disulfide, while the two-peri hydrogen atoms of 9-CHO-A show a very similar multiplet absorption (2H multiplet) at 8.75 ppm, indicating the equivalence of the two hydrogen atoms of this molecule. This equivalence can be explained only by the torsional motion of the aldehyde group.
21) For example, 364, 372, and 370 nm for 9-CN-A, 9-NH_2-A[22], and 9-CHO-A respectively.
22) S. G. Schulman, P. J. Kovi, G. Torosian, H. McVeigh, and D. Carter, *J. Pharm. Science*, **62**, 1823 (1973).
23) K. Bredereck, T. Förster, and H. G. Oesterlin, "Molecular Luminescence of Organic and Inorganic Materials," ed. by H. Kallman and G. M. Spruch, Wiley, New York (1962), p. 104.

Photoemission from Pyrene and its Derivatives

Shojun HINO, Tomohiko HIROOKA*, and Hiroo INOKUCHI

The Institute for Solid State Physics, The University of Tokyo, Roppongi, Minato-ku, Tokyo 106

**Department of Chemistry, Faculty of Science, The University of Tokyo, Hongo, Tokyo 113*

(Received July 11, 1974)

Photoemissions from pyrene and its derivatives, 1,3,6,8-tetrachloropyrene(TClP), 1,3,6,8-tetrabromopyrene(TBrP), 1,6-dicyanopyrene(CDNP), 1,3,6,8-tetracyanopyrene(TCNP), and 1,3,6,8-tetranitropyrene (TNO_2P), were measured. Their photoelectron energy distribution curves(EDCs) were thus obtained; the peaks or shoulder appearing on the EDCs correspond to the ionization potentials of the pyrene molecule. Further, the spectral dependences of their quantum yields(SDQYs) were measured. The ionization potentials obtained from their threshold values were 5.8 eV(pyrene), 6.3 eV(TClP), 6.0 eV (TBrP), 6.3 eV(DCNP), 6.2 eV(TCNP), and 6.6 eV(TNO_2P).

Changes in photoelectron spectra have often been investigated by introducing some functional groups into the π-electron conjugated system, mostly benzene[1]; these photoelectron spectroscopic studies have been carried out in the gaseous state, but not in the solid state. However, as the material property of the solid state is our great concern, the photoemission will give us useful information on the materials in the solid state. As is well known, the photoemission from a solid material consists of three steps:

1) optical excitation process in the solid,
2) transport process in the solid, and
3) escape process from the surface

As the photoemission is a mixed phenomenon of such processes, the information obtained does not always reflect the electronic states of the materials.

The photoemission from organic molecular crystals has been measured by several workers.[2-5] Schechtman and Spicer[6] used Spicer's **k**-independent indirect-transition model[7] (disregarding photoelectron scattering in the bulk and at the surface) and succeeded in determining the energy structures of phthalocyanine and protoporphyrin. Applying a band theory to organic crystals, and also assuming that the state density of the conduction band is constant in molecular crystals, Spicer's model is effective in these materials.[8]

In this paper, we wish to present the photoelectron energy distribution curves and the spectral dependences of the quantum yields of pyrene and its derivatives.

Experimental

Samples. The samples used in this work are pyrene, 1,3,6,8- tetrachloropyrene (TClP), 1,3,6,8- tetrabromopyrene (TBrP), 1,3,6,8- tetracyanopyrene(TCNP), 1,6- dicyanopyrene(DCNP), and 1,3,6,8-tetranitropyrene(TNO_2P). The pyrene derivatives were prepared by Iwashima,[9] as has already been reported.[10]

In order to prepare the specimens for the photoemission measurement, pyrene and its derivatives were deposited onto a small copper disk (12 mm in diameter) by the sublimation method. The deposition was carried out *in vacuo* better than 10^{-5} Torr. However, the vapour pressure of pyrene was too high to deposit in such a vacuum, therefore, we were obliged to make the specimen on the cooled copper disk in a low vacuum ($\sim 10^{-4}$ Torr).

Measurements. The photoemission was measured with a half-meter Seya-Namioka-type vacuum ultraviolet monochromator. The details of the equipment attached to the monochromator were reported previously.[4] The collector of the photocell was a spherical glass one; the inside was coated with colloidal graphite, "Aquadag."

The energy distribution curves(EDCs) were obtained by recording the derivative of the photoelectron current, with respect to the retarding potential, V. Differentiation was performed by superimposing a small sinusoidal potential, ΔV (200 mV p-p, 4 Hz), upon V; the details of this have also been reported already.[5]

The quantum yield, Y, is the ratio between the number of the photoemitted electrons and the incident photons. When the quantum yield was measured, an accelerating potential was applied between the emitter and the collector enough to collect all the electrons emitted. The spectral response of the quantum yield was observed at intervals of 1 nm.

Results and Discussion

Energy Distribution Curves. Figures 1—6 are the EDCs of pyrene and its derivatives plotted as functions of the retarding potential. The numerical value beside each EDC is the energy of the incident photon. As a whole, only a few structures were found in the curves, and the dominant peaks were located at about 0 eV. These peaks grew rapidly with an increase in the incident photon energy.[11] These peaks, independent of the incident photon energy, are so-called "stationary peaks."

During the operation, the retarding potential was swept from minus voltage to plus one. The potential when the peak takes off from the base line is the stopping voltage, V_0, and the potential when the peak falls down to the base line is the saturation voltage, V_s. When the EDC has a tail, V_0 and V_s were determined by approximating the edges of the EDCs by straight lines. The EDCs of pyrene derivatives, especially TClP (Fig. 2), have long tails on the V_s side: this phenomenon is, perhaps, produced by the potential drop between the sample surface and the copper disk, since a charge-up takes place. Moreover, the V_s-value changes with the energy of the incident photons. From these effects, both values, V_0 and V_s, have some ambiguities; these values are summarized in Tables 1 and 2.

When the EDCs are rewritten against the initial energy of the emitted electrons, measured with respect to the stopping potentials, V_0, this revised EDC is appropriate for organic crystals, since it is uncertain whether these materials are conductors or insulators. That is, there is no need to consider the Fermi level

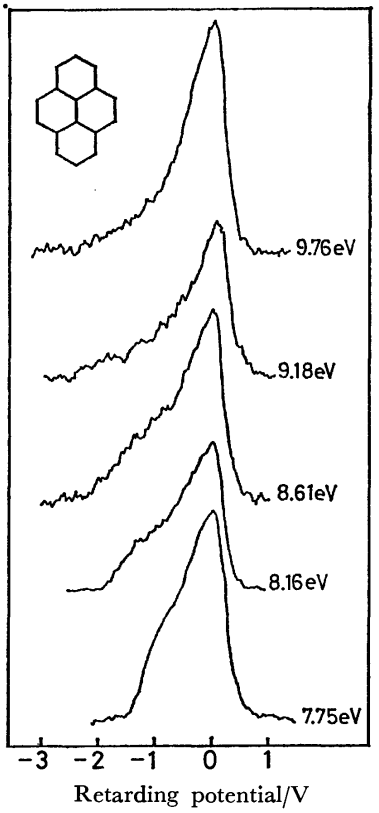

Fig. 1. Energy distribution curves of pyrene, plotted as a function of retarding potential, V, in arbitrary unit. Numerical values beside each curves (7.75 eV, 8.16 eV, 8.61 eV, 9.18 eV and 9.76 eV) are the energies of incident photon.

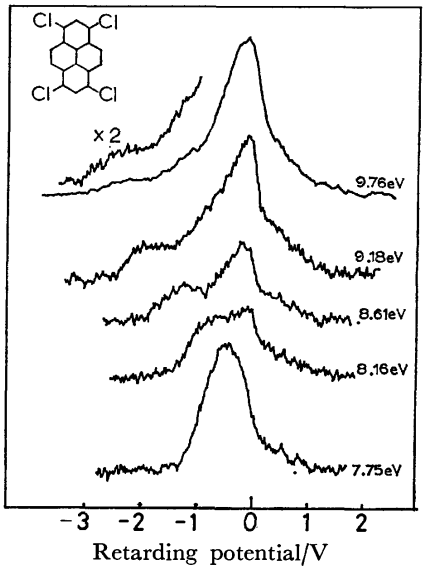

Fig. 2. Energy distribution curves of TClP. (The experimental condition is the same as Fig. 1)

in plotting.[12] Adding the threshold energy to the energy value of each peak or shoulder in EDC, which is independent of the incident photon energy in the revised plot,[13] we can find the positions of the valence bands from the vacuum levels.

In Table 3, as the peak or shoulder positions, the

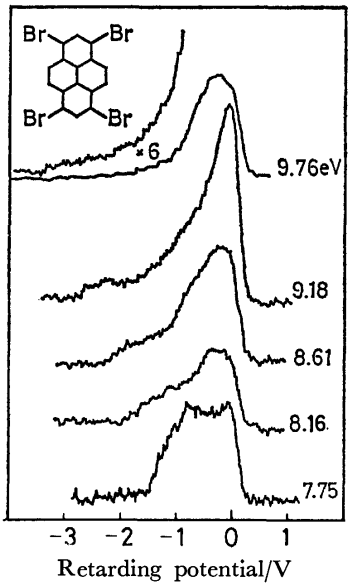

Fig. 3. Energy distribution curves of TBrP.

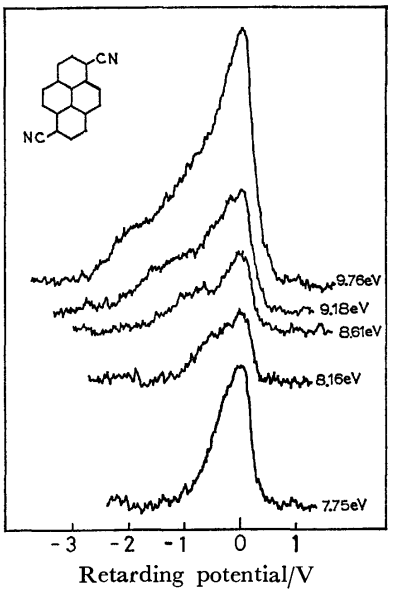

Fig. 4. Energy distribution cruves of DCNP.

energies of the optical state densities of the valence bands are listed, and the ionization potentials of pyrene in the gas phase obtained by Boschi and Schmidt[14] are also quoted. Moreover, the energy differences between the first band and the other bands are shown in Table 4.

The energy differences between the first band and the other were in good agreement with the values of Boschi's work.[14] This indicates that the locations of the first few π-bands of polycrystalline pyrene and its derivatives are similar to those of the pyrene free molecule. However, there are large differences in the shapes of their EDCs. This shape difference can be understood by considering the following several reasons:

1) The electron-attenuation lengths differ from each other; that is, the numbers of the scattering centres (π-electrons[15]) are different.

Table 1. Stoppong potentials, V_0, obtained from EDCs in V

Incident photon energy (eV)	Samples					
	Pyrene	TClP	TBrP	DCNP	TCNP	TNO_2P
7.75	−1.49	−1.25	−1.53	−1.10	−1.05	−0.82
8.16	−1.97	−1.46	−1.98	−1.46	−1.40	−1.21
8.61	−2.30	−1.91	−2.36	−1.83	−1.80	−1.81
9.18	(−2.47)	−2.43	−2.84	−2.42	−2.36	−2.38
9.76	—	−3.09	−3.42	−2.90	(−2.50)	−2.78

The values in parentheses are vague, because the determination of the onsets of the EDCs is difficult. Experimental errors were ±0.05 *V*.

Table 2. Saturation potentials, V_s, obtained from EDCs in V

Incident photon energy (eV)	Samples					
	Pyrene	TClP	TBrP	DCNP	TCNP	TNO_2P
7.75	0.42	(0.24)	0.25	0.32	0.49	0.37
8.16	0.41	(0.30)	0.25	0.38	0.50	0.38
8.61	0.34	(0.24)	0.25	0.35	0.53	0.30
9.18	0.41	(0.28)	0.23	0.42	0.59	0.36
9.76	0.42	(0.44)	0.27	0.48	0.55	0.34
Average	0.41	(0.27)	0.25	0.39	0.53	0.35

As the EDCs of TClP have long tails in V_s side, the values in this Table are the cross points of the straight parts of the EDCs and base line. Experimental errors are in ±0.05 *V*.

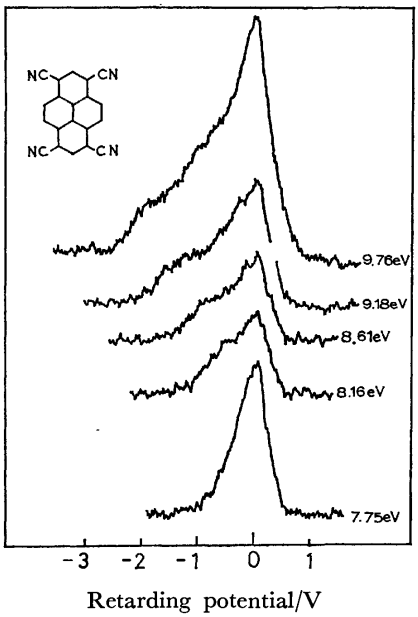

Fig. 5. Energy distribution curves of TCNP.

2) There are changes in crystal structures; that is, the escape probabilities of photoexcited electrons from the surface of the polycrystallines are different.

3) The surface cleanness differs, since their vapour pressures are not equal; that is, contamination of the surface by residual gas occurs.

4) Their electronic structures are changed by the functional groups; that is, the numbers of photo-

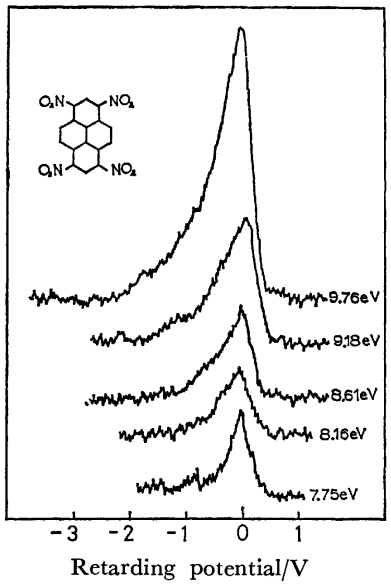

Fig. 6. Energy distribution curves of TNO_2P.

excitable electrons are affected by such functional groups.

As for the first and second reasons, no data on the electron-attenuation lengths and crystal structures of these compounds are to be found, therefore, further discussion is difficult. As for the third reason, it is known that the surface of organic compounds with high vapour pressures are fairly clean in an ordinary vacuum because of their successive sublimation. This factor is useful in comparing halogen derivatives and cyano- and nitro-derivatives. From the view point of the vapour pressure, we can expect the surface of pyrene film to be clean, since its vapour pressure is the highest among these materials. On the other hand, it is also known that a contaminated surface reduces high-energy electrons to low-energy electrons; in this case, the EDCs become structureless. As the EDCs of pyrene show less structure than those of halogenized pyrenes, contamination must take place on the pyrene film. This fact is inconsistent with self-cleaning by successive sublimation. However, practically, as the spectroscopical observation was carried out in a low vacuum and with a cooled emitter, it is feasible that the surface of pyrene film is contaminated with residual gases.

In considering the fourth reason, a well-known phenomenon, mesomeric or inductive effect, is useful. Cyano- and nitro-groups are electron-withdrawing

Table 3. Peak (shoulder) positions from vacuum level in eV

	Pyrene	TClP	TBrP	DCNP	TCNP	TNO_2P	Pyrene[a)]
1st peak	(6.5_5)	6.1_5	6.7_5	(7.3_0)	(7.2_0)	7.5_0	7.41
2nd peak	(7.3_5)	(6.8_5)	(7.6_5)	(8.3_0)	(8.0_5)	(8.5_5)	8.26
3rd peak	—	(7.4_0)	(8.3_0)	—	—	—	9.00

The values in parentheses are shoulder positions. a) Ionization potentials in gas phase in Ref. 14.

Table 4. The energy differences between the first peak and the others in eV

	Pyrene	TClP	TBrP	DCNP	TCNP	TNO_2P	Pyrene[a)]
2nd	0.8_0	0.7_0	0.9_0	1.0_0	0.8_5	1.0_5	0.85
3rd	—	1.2_5	1.5_5	—	—	—	1.59

a) gas phase pyrene

functional groups (mesomeric effect). Halogen atoms have two effects: a plus mesomeric effect and a minus inductive effect. These effects increase or decrease the electron density of the pyrene-ring system; its increase or decrease may change the number of photoexcitable electrons.

Spectral Dependence of the Quantum Yield. Figure 7 shows the spectral dependences of the quantum yields (SDQYs) of pyrene and its derivatives. As may clearly be seen, pyrene has a higher photoelectron efficiency in the whole spectral region compared to those of the others. The SDQY of pyrene is about 3×10^{-2} electrons/photon at 10 eV; it gradually decreases to 7 eV, and then falls down steeply to 7×10^{-5} electrons/photon. On the other hand, the SDQYs of the substituted pyrenes show almost the same inclinations above 9 eV. However, below 9 eV those SDQYs are classified into three groups. One group (A) consists of halogen-substituted pyrenes; Group B consists of cyano-substituted pyrenes, and Group C is nitro-substituted. The SDQYs of Group A resemble those of pyrene except for the absolute value of the quantum yield; the decrease in the absolute quantum yield can be understood in terms of a deepening of the threshold energies upon the introduction of halogen atoms. The SDQYs of Groups B and C are monotonously decreasing curves, and their inclinations are steeper than those of pyrene and Group A. The quantum yield of Group C is smaller than those of Group B. These results support the fourth reason described at the EDC shape differences. Cyano- and nitro-groups induce a decrease in the cross section (the number of photoexcitable π-electrons in the pyrene-ring system) of photoemission largely by withdrawing the electrons from the pyrene-ring system. The effect of halogen atoms is not so large comparatively.

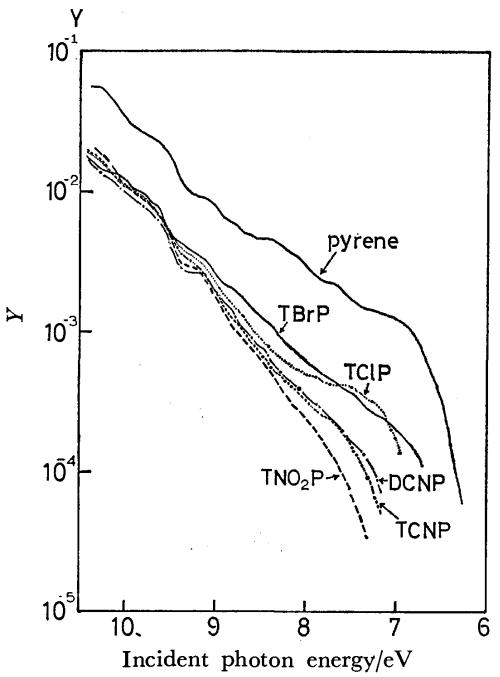

Fig. 7. Spectral dependences of quantum yields, Y, of pyrene and its derivatives, plotted as a function of incident photon energy.

Threshold Energy. To determine the ionization potential of these aromatic crystals, the threshold energy, E_{th}, is estimated by the following methods.

1) From the EDCs, with the values of V_0 and V_s, using this relations:

$$E_{th} = h\nu - V_s + V_0$$

where $h\nu$ is the incident photon energy.

2) From the SDQYs, as used by Lyons and Morris,[16] E_{th} is determined as the lowest detectable current photon energy, usually the order of $10^{-7}\sim10^{-8}$ electrons/photon as the quantum yield.

3) From the relation between the quantum yield and the incident photon energy near the threshold energy region as:

$$Y \propto (h\nu - E_{th})^3$$

In our measurments, however, there were some cases where the methods described above could not be used. The second method was especially invalid, because the lowest detectable quantum yields were in the order of $10^{-4}\sim10^{-5}$ electrons/photon, far from the order of $10^{-7}\sim10^{-8}$. The first method has some ambiguities when it is difficult to determine V_s and V_0. Moreover, as high-energy electrons often lose their energy, the determination of V_0 excited with a high-energy photon is difficult. Therefore, in this work, we adopted V_s and V_0 from the EDCs excited with 7.75 eV photons.

In the halogen-substituted pyrenes, the third method was not used, because we could not find any linear relation between $Y^{1/3}$ and $(h\nu - E_{th})$.[17] The cube-root plots of the other compounds are shown in Fig. 8.

The threshold energies obtained from the first and third methods are listed in Table 5. Batley and Lyons[18] reported the threshold energy of 1,6-diamino-

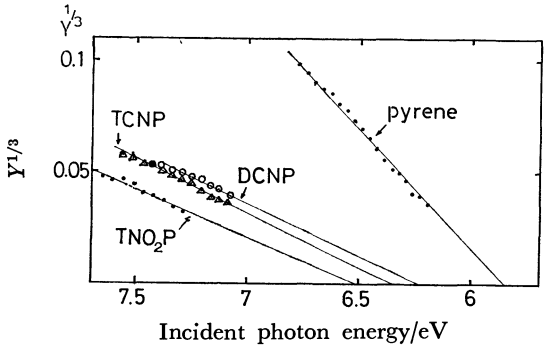

Fig. 8. Cube root of quantum yield plotted as a function of incident photon energy.

pyrene as 4.71 eV. This value is smaller than that of pyrene by more than 1 eV. As the amino group is electron-donating, the E_{th} of the amino derivative becomes small, because an electron is easily emitted from the pyrene-ring system. As for the cyano- and nitro-groups, on the other hand, the E_{th} of such substituted pyrene becomes large, because these groups are electron-withdrawing.

The authors wish to thank to Professor Satoshi Iwashima for his preparation of the materials used in this experiment.

Table 5. Threshold energies of pyrene and its derivatives in eV

	E_{th}[a)]	E_{th}[b)]
Pyrene	5.84	5.85
TClP	(6.26)	—
TBrP	5.97	—
DCNP	6.33	6.23
TCNP	6.21	6.35
TNO_2P	6.56	6.52
1,6-Diaminopyrene[c)]	4.71	

a) obtained from EDCs. b) obtained from cube root plot. c) the work of Batley and Lyons.[17)]
E_{th} of TClP has some ambiguities.
Experimental errors are in ±0.05 eV.

References

1) For example, "Molecular Photoelectron Spectroscopy," D. W. Turner, C. Baker, A. D. Baker, and C. R. Brundle, Wiley-Interscience, London (1970).
2) A. A. Zagrubskii and F. I. Vilesov, *Fiz. Tverd. Tela*, **13**, 2300 (1971).
3) T. Hirooka, M. Kochi, J. Aihara, H. Inokuchi, and Y. Harada, This Bulletin, **42**, 1481 (1969).
4) M. Kochi, Y. Harada, T. Hirooka, and H. Inokuchi, *ibid.*, **43**, 2690 (1970).
5) T. Hirooka, K. Tanaka, K. Kuchitsu, M. Fujihira, H. Inokuchi, and Y. Harada, *Chem. Phys. Lett.*, **18**, 390 (1973).
6) B. H. Schechtman and W. E. Spicer, *ibid.*, **2**, 207 (1968).
7) W. E. Spicer, *Phys. Rev. Lett.*, **11**, 243 (1963).
8) W. E. Spicer, in F. A. Abeles (editor), "Optical Properties of Solids," North-Holland Publ. Co., Amsterdam (1972).
9) Meisei University.
10) K. Ogino, S. Iwashima, H. Inokuchi, and Y. Harada, This Bulletin, **38**, 473 (1965).
11) In Figs. 1—6, each EDC is plotted in arbitrary unit. Then, to recognize this behaviour, we must normalized each EDC with a photon intensity.
12) If Fermi level is decided by the method described in Ref. 3, obtained value for Fermi energy is changed by impurities. As impurities easily make donor and/or acceptor levels in band gap, there is an ambiguity in plot using Fermi level.
13) As the obtained EDCs were almost structureless, it is difficult to apply a Spicer's **k**-independent indirect transition model to our EDCs. It is, however, reasonable that the obtained EDCs represent the state density of the valence band, since the peak positions of our EDCs were in good agreement with orbital energies of pyrene free molecule.
14) R. Boschi and W. Schmidt, *Tetrahedron Lett.*, **25**, 2577 (1972).
15) W. Pong and J. A. Smith, *J. Appl. Phys.*, **44**, 174 (1973).
16) L. E. Lyons and G. C. Morris, *J. Chem. Soc.*, **1960**, 5192.
17) This fact should be caused purely by experimental defects. In these cases, quantum yields could be measured till about 10^{-4} electrons/photon, and the observed values were far from the regions where above relation held good.
18) M. Batley and L. E. Lyons, *Mol. Cryst.*, **3**, 357 (1968).

The Analysis of the Molecular Vibration by the Molecular Orbital Method. I. Application to HCN

Tomoo MIYAZAKI, Masaru IKEDA, and Masayuki SHIBATA

Department of Applied Chemistry, Faculty of Science and Engineering, Waseda University, Nishi-Ohkubo, Shinjuku-ku, Tokyo 160

(Received July 24, 1974)

The approximate self-consistent molecular orbital method has been applied to the analysis of the vibrational spectrum of HCN. The frequencies of the fundamental, overtone, and combination bands in the region from about 700 to 12000 cm^{-1} have been calculated, and their absolute infrared absorption intensities have been estimated, the variational method being used in this calculation. Also, the frequencies and absorption intensities of hot bands, referring to the bending vibration, have been calculated. In comparison with the experimental results, the calculated frequencies were not always appropriate. However, it was found that these results are effective in the analysis of the molecular vibration if the calculated frequencies are discussed along with their infrared absorption intensities.

There have been reports in which the force constant and $\partial\mu_i/\partial S_j$ have been calculated on the basis of the results of molecular orbital calculations, where μ_i is the component of the molecular dipole moment and where S_i is an appropriate vibrational coordinate.[1-18] However, these results are not always desirable in comparison with the values from the experimental results. The main reason for the undesirable results is that the following requirement is hard to put into practice: the semi-empirical molecular orbital method adopted in the estimation of those values has to lead simultaneously to many appropriate values for the molecular constants, such as the bond length, the bond angle, the force constant, the dipole moment, and its derivative $(\partial\mu_i/\partial S_j)$. For example, the CNDO/2 method[1] proposed by Pople *et al.* can obtain reasonable values for the moleculr geometry, the dipole moment, and its derivative, but the calculated stretching force constant tends to be larger than that generally found. The MINDO/2' method[20] proposed by Dewar *et al.* leads to appropriate values for the molecular geometry and the stretching force constant, but adequate values for the bending force constant and the dipole-moment derivative with the bending coordinate cannot be obtained.

In previous papers,[14,15] the present authors discussed the abnormal infrared absorption intensity of the C–H stretching vibration band in chloroform on the basis of the dipole-moment derivative and the potential function calculated from the CNDO/2 method. In these calculations, the mechanical and electrical anharmonicities were considered and the variational method was used to estimate the energy and wave function of the vibrating system. At that time, some substantial modification for the potential function had to be made, although there was a problem to be solved in the method of modification.

In this work, the frequencies of the fundamental, overtone, and combination bands in the vibrational spectrum of HCN in the region from about 700 to 12000 cm^{-1} have been calculated by the use of the potential function obtained by the MINDO/2' method. Moreover, their absolute infrared absorption intensities have been estimated from the dipole-moment derivative calculated by the CNDO/2 method. Also, the frequencies and absorption intensities of the hot bands, referring to the bending vibration, have been calculated. In comparison with the experimental results, the calculated frequencies were not always appropriate. However, it was found that these results are effective in the analysis of the molecular vibration if the calculated frequencies are discussed along with their infrared absorption intensities. Furthermore, the effect of the different level of approximation for the bending coordinate on the calculated results was discussed.

Methods of Calculation

The Potential Energy Function. The total energies of the molecule required to determine the potential energy function for the molecular vibration have been calculated by the MINDO/2' method. In this calculation, the values of the parameters, B_{AB}, in the following approximate equation for the resonance integral, $\beta_{\mu\nu}$, were slightly modified:

$$\beta_{\mu\nu} = B_{AB}(I_\mu + I_\nu)S_{\mu\nu} \quad (1)$$

where I_μ and I_ν are the valence-state ionization potentials of the atomic orbitals, χ_μ and χ_ν, where $S_{\mu\nu}$ is the corresponding overlap integral, and where B_{AB} is a parameter characteristic of the A—B atom pair. The values of B_{CH} and B_{CN} were taken to be 0.3021 and 0.3522 respectively (the original values in the MINDO/2' method: $B_{CH}=0.2823$ and $B_{CN}=0.3453$). The calculated bond lengths of HCN, which is a linear structure, were 1.0445 Å and 1.1739 Å for r_{CH} and r_{CN} respectively (the observed values: $r_{CH}=1.06317$ Å and $r_{CN}=1.15535$ Å). According to the method of least-squares, the potential energy function, V, was obtained by fitting the increase in the total energy calculated for the distorted molecule to the 5th-order function with respect to the internal coordinates, R_i (the 6th order for the bending coordinate), but the 5th-order terms were omitted in the succeeding calculations.

$$V(R) = \sum_{i\leq j} K_{ij}R_iR_j + \sum_{i\leq j\leq k} K_{ijk}R_iR_jR_k + \sum_{i\leq j\leq k\leq l} K_{ijkl}R_iR_jR_kR_l. \quad (2)$$

For the HCN molecule, the internal coordinates are two bond-stretching coordinates, $R_1=\Delta r_{CH}$ and $R_2=$

Δr_{CN}, and two bending coordinates perpendicular to each other, $R_3=\Delta\theta_{(y)}$ and $R_4=\Delta\theta_{(z)}$. Generally, doubly degenerate vibrations, such as the bending coordinates in HCN, are treated as superpositions of these vibrations by the introduction of the polar coordinates. In this work, such a general treatment was avoided because the treatment was inconvenient in calculating collectively, by the variational method, the frequencies of all the vibrations in the molecule in view of the mechanical anharmonicity. In this calculation, the superposed system was described by a product of the wave functions of the doubly degenerate vibrations.

The calculations of the energy-increase arising from the bending deformation were performed for the different cases by the following methods, I and II. In these calculations, it was prescribed that we employ the B matrix, generally used, which is derived from the approximate linear-relation between the internal and the Cartesian coordinates. In Method I, the molecule was distorted according to the rectilinear bending deformation. The conformation of the distorted HCN molecule required to calculate the cross terms between bending and stretching vibrations was decided by the Δr_{CH}, Δr_{CN}, and $\Delta\theta$ values, which are related with one another as is shown in Fig. 1. In

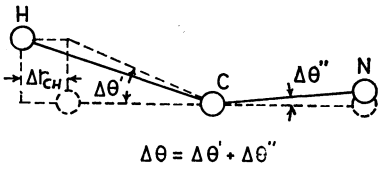

Fig. 1. Conformation of the distorted HCN referring to the C-H stretching and the rectilinear bending coordinates.

Method II, the molecule was distorted according to the curvilinear bending coordinate indicated in the potential surface of HCN, illustrated by Suzuki *et al.*[22] In this treatment, the conformation of the distorted HCN can be determined without trouble by Method I. Finally, the potential energy function represented by the internal coordinates was transformed to a function with the normal coordinates by the use of the L_R matrix elements:

$$V(Q)=\sum_i\frac{1}{2}\lambda_{ii}Q_i^2+\sum_{i\leq j\leq k}g_{ijk}Q_iQ_jQ_k+\sum_{i\leq j\leq k\leq l}h_{ijkl}Q_iQ_jQ_kQ_l. \quad (3)$$

The variational Treatment. The variational method has been used to calculate the energy levels of vibrations in view of the mechanical anharmonicities.

The total wave function, Ψ^{total}, for the molecular vibration is described as a linear combination of ψ's, each of which is written as a product of the harmonic oscillator wave functions, φ's, of all the vibrations in the molecule:

$$\Psi^{\text{total}}=\sum_i C_i\psi_i, \quad (4)$$

$$\psi_i=\varphi_l^{\,1}\varphi_m^{\,2}\varphi_n^{\,3}\varphi_o^{\,4}, \quad l,m,n, \text{ and } o=0,1,2,3\cdots\cdots \quad (5)$$

where $\varphi_n^{\,k}$ indicates the n-th harmonic oscillator wave function, referring to the normal coordinate, Q_k (here, n is the principal quantum number of the vibration), and ψ_i is decided by the variety of the combination of the quantum numbers, l, m, n, and o.

The variational treatment of the coefficient, C_i, leads to this equation:

$$\sum_{j=0}^{k}C_j(H_{ij}-E\delta_{ij})=0, \qquad i=0,1,2,3,\cdots\cdots k, \quad (6)$$

$$H_{ij}=\langle\psi_i|\hat{T}+\hat{V}|\psi_j\rangle, \quad (7)$$

where δ_{ij} is the Kronecker delta symbol, $\hat{T}$ is the operator of the kinetic energy, $-\frac{h^2}{8\pi^2}\sum_k\frac{\partial^2}{\partial Q_k^{\,2}}$ and $\hat{V}$ is the operator referring to the potential function (3) with the normal coordinates. The energy, E, is the root of the secular equation:

$$|H_{ij}-E\delta_{ij}|=0.$$

Generally, the accuracy of the wave function improved by this treatment is restricted by the maximum values of the quantum numbers, l,m,n, and o. The upper limits of the quantum numbers are determined by the ability of the computer and the other restrictions. On the other hand, in order to obtain the improved wave function in the quantum numbers from 0 to 3, we have to consider the harmonic wave functions in the quantum numbers from 0 to 10 for each vibration in Eq. (5) at least. Therefore, we divided the variational treatment into the following two steps.

The First Step: The wave function of a specified normal vibration (k) was modified in view of the principal terms of the mechanical anharmonicity, without cross terms. In this treatment, the modified wave function, Φ^k, was described by a linear combination of harmonic oscillator wave functions, φ^k's, as follows:

$$\Phi^k=\sum_i C_i^k\varphi_i^k, \qquad i=0 \text{ to } 11. \quad (8)$$

The operator, $\hat{H}'$ (k), used in this calculation was as follows:

$$\hat{H}'(k)=-\frac{h^2}{8\pi^2}\frac{\partial^2}{\partial Q_k^{\,2}}+\frac{1}{2}\lambda_{kk}Q_k^{\,2}+g_{kkk}Q_k^{\,3}+h_{kkkk}Q_k^{\,4}. \quad (9)$$

The wave function and their energies can be obtained from the appropriate set of the secular equation and the equation corresponding to Eq. (6).

The Second Step: The total wave function, Ψ^{total}, was described as a linear combination of ψ's, each of which was written as a product the wave functions, Φ's, obtained from the first-step treatment:

$$\Psi^{\text{total}}=\sum_i C_i\psi_i, \quad (10)$$

$$\psi_i=\Phi_l^{\,1}\Phi_m^{\,2}\Phi_n^{\,3}\Phi_o^{\,4}, \qquad l,m,n, \text{ and } o=0 \text{ to } 4. \quad (11)$$

The variety of combinations in ψ_i was restricted by the condition that $l+m+n+o\leqslant 4$. The calculations in the subsequent treatment were the same as those described above.

The Dipole Moment and its Expansion. It is desirable for the dipole moment of molecule to be calculated according to the method used to determine

the potential function. However, the values of the dipole-moment derivative with the bending coordinate obtained from the MINDO/2' method which was used to determine the potential function were not desirable in calculating the infrared absorption intensity; the detailed reasons why will be indicated later (see "Discussion"). Therefore, in this work, the component of the dipole moment was expanded by the normal coordinates on the basis of the results of the CNDO/2 calculations for the molecule which was distorted according to the L_x matrix elements, the values of equilibrium distances calculated by the MINDO/2' method being employed. The function of the dipolemoment component, μ_x, was obtained as the 5th-order expansion with the normal coordinates, but the 4th- and 5th-order terms were omitted in the calculation of the absorption intensities:

$$\mu_x = \mu_x{}^0 + \sum_i M_i Q_i + \sum_{i\leq j} M_{ij} Q_i Q_j + \sum_{i\leq j\leq k} M_{ijk} Q_i Q_j Q_k. \quad (12)$$

The Absolute Infrared Absorption Intensity. The method of the calculation of the absolute infrared absorption intensity in [$cm^2 s^{-1}$ $molecule^{-1}$] units was described in detail in a previous paper.[15] Practically, though, there is a difference in the integrals involving the cross terms in comparison with the previous calculation. The equation required to calculate the absolute absorption intensity, A, is as follows:

$$A_{v+n\leftarrow v} = \frac{8\pi^3}{3ch}\left(\frac{N_v}{N_t} - \frac{N_{v+n}}{N_t}\right)\nu_{v+n,v} \sum_{i=x,y,z} |(\mu_i)_v{}^{v+n}|^2, \quad (13)$$

$$N_v = N_0 \exp\left(-(E_v - E_0)\right)/kT, \quad (14)$$

$$N_t = N_0 \sum_{v=0}^{\infty} \exp(-(E_v - E_0))/kT, \quad (15)$$

$$(\mu_i)_v{}^{v+n} = \langle \Psi_v{}^{\text{total}} | \hat{\mu}_i | \Psi_{v+n}{}^{\text{total}} \rangle, \quad (16)$$

where N_0 and N_v are the numbers of the molecules per unit volume in the E_0 and E_v states of the total energies respectively; N_t is the total number of molecules, c is the velocity of light, h is Planck's constant, k is Boltzmann's constant, $\hat{\mu}_i$ is the operator corresponding to the function of the dipole-moment component with the normal coordinates (12), and $\nu_{v+n,v}$ is the transition energy in [s^{-1}] units between the E_v and E_{v+n} states of total energies. In this calculation, the absolute temperature, T, was taken to be 300 K. The absorption intensities of the hot bands, referring to the bending vibration, were also calculated.

Table 1. Coefficients of potential function, $V(R)$, for HCN

	Units	Method I	Method II	Ref.[22]
K_{11}	mdyn/Å	3.00985	3.00908	3.1150
K_{22}	mdyn/Å	9.35171	9.35063	9.3872
K_{33}, K_{44}	mdyn·Å/rad²	0.12100	0.12040	0.1296
K_{12}	mdyn/Å	0.40217	0.40050	−0.2160
K_{111}	mdyn/Å²	−4.39913	−4.39595	−6.0848
K_{222}	mdyn/Å²	−16.34869	−16.28970	−19.2273
K_{112}	mdyn/Å²	−0.15529	−0.21974	−0.3215
K_{122}	mdyn/Å²	0.16522	−0.36209	−1.3345
K_{133}, K_{144}	mdyn/rad²	2.04294	−0.03181	−0.1341
K_{233}, K_{244}	mdyn/rad²	−0.18322	−0.49783	−0.2716
K_{1111}	mdyn/Å³	4.25730	+4.27731	+8.7854
K_{2222}	mdyn/Å³	17.43130	17.39006	17.5164
K_{3333}, K_{4444}	mdyn·Å/rad⁴	0.40753	0.00552	0.0029
K_{1122}	mdyn/Å³	2.93309	2.41937	1.1719
K_{1133}, K_{1144}	mdyn/Årad²	−7.46997	+0.01205	+0.2008
K_{2233}, K_{2244}	mdyn/Årad²	−0.84781	0.16097	−0.1889
K_{3344}	mdyn·Å/rad⁴	0.81506	0.01104	
K_{1112}	mdyn/Å³	0.42934	0.61351	1.0544
K_{1222}	mdyn/Å³	4.56675	2.83037	4.7149
K_{1233}, K_{1244}	mdyn/Årad²	0.94222	0.93988	0.1962

Results and Discussion

In this work, trial calculations were performed by the use of several semi-empirical molecular orbital methods, such as the CNDO/2'[11] CNDO/BW,[19] and MINDO/2'[20] methods. We expected that any method would serve the purpose of determining the frequencies and intensities for the infrared absorption bands of HCN. Unfortunately, not every method answered to our expectations.* Elaborate parametrizations in any method would be able to satisfy our requirements, but such treatment is intricate and tedious, for universal validity is required for the values of parameters. For this reason, the MINDO/2' and CNDO/2 methods were used to calculate the total energy and the dipole moment of HCN respectively. *However, it should be emphasized that this treatment is an expediency.* The parameters in the MINDO/2' method were slightly modified in order to obtain agreement between the calculated frequencies and observed ones.

The coefficients of the potential function, $V(R)$, as calculated from Methods I and II, are indicated in Table 1; the values obtained by others[22] are also included. The large values of the cross terms between the stretching and the bending vibrations were obtained by Method I. In view of the level of approximation of the B matrix used in this work, the

* The force constants, k's, calculated by means of the CNDO/2 method were larger than those generally found:

$k_{11}=2K_{11}=12.861$ mdyn/Å, $k_{22}=2K_{22}=41.434$ mdyn/Å,
$k_{12}=K_{12}=0.42583$ mdyn/Å, $k_{33}=k_{44}=2K_{33}=2K_{44}=0.57394$ mdyn·Å/rad².

These values of the force constants led to undesirable results for the calculated frequencies of the absorption bands.

On the other hand, the coefficients, M's, of the $\mu_i(Q)$ function calculated from the MINDO/2' method were as follows:

$$\mu_x(Q): \quad M_{33}=M_{44}=68.969\times10^{20} \text{ esu}/(g\cdot c),$$
$$\mu_y(Q),\ \mu_z(Q): \begin{cases} M_3=M_4=10.020\times10 \text{ esu}/\sqrt{g} \\ M_{333}=M_{444}=-117.43\times10^{40} \text{ esu}/(\sqrt{g^3}c^2). \end{cases}$$

These values led to abnormal absorption intensities of the bending vibration; the intensities of the fundamentals, $A(0001)$ and $A(0010)$, are weak, and the intensity of the first overtone, $A((0002)+(0020))$, is much stronger than that of the former:

$A(0001)=A(0010)=57.379\times10^{-10}$ cm^2 s^{-1} $molecule^{-1}$,
$A((0002)+(0020))=504.38\times10^{-10}$ cm^2 s^{-1} $molecule^{-1}$.

TABLE 2-a. COEFFICIENTS OF $V(Q)$ AND $\mu_x(Q)$ FOR HCN
(V: [erg], μ_x: [esu·cm], Q: [$\sqrt{g}$·cm])

	Units	Coefficients[a)]		Units	Coefficients[b,c)]
$\frac{1}{2}\lambda_{11}$	$1/s^2$	19.7909×10^{28}	Const.	esu·cm	-2.47862×10^{-18}
$\frac{1}{2}\lambda_{22}$	$1/s^2$	8.20873×10^{28}	M_1	esu/$\sqrt{g}$	-1.42897×10
$\frac{1}{2}\lambda_{33}, \frac{1}{2}\lambda_{44}$	$1/s^2$	0.89465×10^{28}	M_2	esu/$\sqrt{g}$	-3.58430×10
			M_{11}	esu/($g\cdot c$)	23.5191×10^{20}
g_{111}	$1/(\sqrt{g}\cdot c\cdot s^2)$	-2.22583×10^{49}	M_{22}	esu/($g\cdot c$)	0.36093×10^{20}
g_{222}	$1/(\sqrt{g}\cdot c\cdot s^2)$	-0.40414×10^{49}	M_{33}, M_{44}	esu/($g\cdot c$)	31.5773×10^{20}
g_{112}	$1/(\sqrt{g}\cdot c\cdot s^2)$	-0.89214×10^{49}	M_{12}	esu/($g\cdot c$)	-55.4788×10^{20}
g_{122}	$1/(\sqrt{g}\cdot c\cdot s^2)$	0.27610×10^{49}	M_{111}	esu/($\sqrt{g}^3\cdot c^2$)	0.60743×10^{40}
g_{133}, g_{244}	$1/(\sqrt{g}\cdot c\cdot s^2)$	0.01609×10^{49}	M_{222}	esu/($\sqrt{g}^3\cdot c^2$)	-11.8450×10^{40}
g_{233}, g_{244}	$1/(\sqrt{g}\cdot c\cdot s^2)$	-0.10941×10^{49}	M_{112}	esu/($\sqrt{g}^3\cdot c^2$)	-23.5586×10^{40}
h_{1111}	$1/(g\cdot c^2\cdot s^2)$	1.73513×10^{69}	M_{122}	esu/($\sqrt{g}^3\cdot c^2$)	45.0192×10^{40}
h_{2222}	$1/(g\cdot c^2\cdot s^2)$	0.13131×10^{69}	M_{133}, M_{144}	esu/($\sqrt{g}^3\cdot c^2$)	-81.5843×10^{40}
h_{3333}, h_{4444}	$1/(g\cdot c^2\cdot s^2)$	0.00305×10^{69}	M_{233}, M_{244}	esu/($\sqrt{g}^3\cdot c^2$)	-7.93415×10^{40}
h_{1122}	$1/(g\cdot c^2\cdot s^2)$	0.29456×10^{69}			
h_{3344}	$1/(g\cdot c^2\cdot s^2)$	0.00609×10^{69}			
h_{1133}, h_{1144}	$1/(g\cdot c^2\cdot s^2)$	-0.04606×10^{69}			
h_{2233}, h_{2244}	$1/(g\cdot c^2\cdot s^2)$	0.02798×10^{69}			
h_{1112}	$1/(g\cdot c^2\cdot s^2)$	0.77069×10^{69}			
h_{1222}	$1/(g\cdot c^2\cdot s^2)$	-0.07116×10^{69}			
h_{1233}, h_{1244}	$1/(g\cdot c^2\cdot s^2)$	0.15097×10^{69}			

a) The values were obtained from the method II. b) Cartesian axis used in this calculation is as follows:

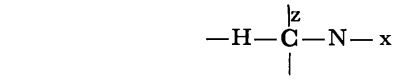

c) Negative dipole corresponds to $^+$(H–C–N)$^-$.

TABLE 2-b. COEFFICIENTS, $M^{(y)}$ AND $M^{(z)}$, FOR $\mu_y(Q)$ AND $\mu_z(Q)$. (μ_y, μ_z: [esu·cm], Q: [$\sqrt{g}$·cm])

$M^{(y)}$	$M^{(z)}$	Units	Coefficients	$M^{(y)}$	$M^{(z)}$	Units	Coefficients
M_3	M_4	esu/$\sqrt{g}$	5.51851×10	M_{113}	M_{114}	esu/($\sqrt{g}^3\cdot c^2$)	27.5416×10^{40}
M_{13}	M_{14}	esu/($g\cdot c$)	-47.2999×10^{20}	M_{223}	M_{224}	esu/($\sqrt{g}^3\cdot c^2$)	7.20507×10^{40}
M_{23}	M_{24}	esu/($g\cdot c$)	29.3334×10^{20}	M_{123}	M_{124}	esu/($\sqrt{g}^3\cdot c^2$)	22.2784×10^{40}
M_{333}	M_{444}	esu/($\sqrt{g}^3\cdot c^2$)	16.0836×10^{40}	M_{344}	M_{334}	esu/($\sqrt{g}^3\cdot c^2$)	16.0836×10^{40}

TABLE 3. ENERGY LEVELS AND WAVE FUNCTIONS OF VIBRATION WITH C-H STRETCHING MODE AS THE MAIN CONSTITUENTS.
(ε_v and $\Phi_v=\sum_i C_{vi}\varphi_i$)

The values were obtained from the method II.

v	0	1	2	3	4
ε[erg]$\times10^{13}$	3.30722	9.84286	16.3074	22.7325	29.1481
C_{v0}	**0.99695**	−0.07500	0.00426	−0.01787	0.01014
C_{v1}	0.07518	**0.97448**	−0.20456	0.02843	−0.03528
C_{v2}	0.00418	0.20544	**0.90684**	−0.35004	0.07883
C_{v3}	0.02013	0.02676	0.35323	**0.77630**	−0.47987
C_{v4}	0.00293	0.04099	0.07313	0.48879	**0.58106**
C_{v5}	−0.00006	0.01244	0.06820	0.14252	0.58408
C_{v6}	0.00078	0.00146	0.03063	0.10312	0.22695
C_{v7}	0.00014	0.00202	0.00670	0.05843	0.14542
C_{v8}	−0.00003	0.00074	0.00440	0.01810	0.09488
C_{v9}	0.00003	0.00003	0.00214	0.00888	0.03717
C_{v10}	0.00001	0.00009	0.00037	0.00483	0.01662
C_{v11}	−0.00000	0.00004	0.00017	0.00121	0.00815

$\Delta\varepsilon_{0,1}=3291.28\ \mathrm{cm}^{-1}$, $\Delta\varepsilon_{0,2}=6546.75\ \mathrm{cm}^{-1}$, $\Delta\varepsilon_{0,3}=9782.35\ \mathrm{cm}^{-1}$, $\Delta\varepsilon_{0,4}=13013.19\ \mathrm{cm}^{-1}$.
The $\Delta\varepsilon_{0,1}$ in the harmonic oscillator model was $3339.76\ \mathrm{cm}^{-1}$.

Table 4. Energy levels and wave functions of vibration with C-N stretching mode as the main constituents.
(ε_v and $\Phi_v=\sum_i C_{vi}\varphi_i$)

The values were obtained from the method II.

v	0	1	2	3	4
ε[erg]$\times 10^{13}$	2.13383	6.38356	10.6117	14.8199	19.0097
C_{v0}	**0.99906**	−0.04184	0.00102	−0.01085	0.00354
C_{v1}	0.04183	**0.99190**	−0.11729	0.00822	−0.02132
C_{v2}	0.00150	0.11722	**0.96923**	0.21138	0.02510
C_{v3}	0.01136	0.00939	0.21113	**0.92178**	−0.31458
C_{v4}	0.00101	0.02303	0.02689	0.31405	**0.84221**
C_{v5}	0.00002	0.00434	0.03760	0.05646	0.41590
C_{v6}	0.00028	0.00041	0.01105	0.05588	0.09900
C_{v7}	0.00003	0.00075	0.00175	0.02219	0.07873
C_{v8}	−0.00000	0.00018	0.00162	0.00493	0.03860
C_{v9}	0.00000	0.00002	0.00056	0.00317	0.01098
C_{v10}	0.00000	0.00003	0.00010	0.00136	0.00586
C_{v11}	−0.00000	0.00001	0.00007	0.00030	0.00267

$\Delta\varepsilon_{0,1}=2140.12$ cm^{-1}, $\Delta\varepsilon_{0,2}=4269.37$ cm^{-1}, $\Delta\varepsilon_{0,3}=6388.55$ cm^{-1}, $\Delta\varepsilon_{0,4}=8498.49$ cm^{-1}.
The $\Delta\varepsilon_{0,1}$ in the harmonic oscillator model was 2150.90 cm^{-1}.

Table 5. Energy levels and wave functions of vibration with bending mode as the main constituents.
(ε_v and $\Phi_v=\sum_i C_{vi}\varphi_i$)

The values were obtained from the method II.

v	0	1	2	3	4
ε[erg]$\times 10^{13}$	0.70669	2.12287	3.54463	4.97192	6.40467
C_{v0}	**0.99999**	0	0.00141	0	0.00041
C_{v1}	0	**0.99999**	0	0.00404	0
C_{v2}	−0.00141	0	**0.99997**	0	0.00796
C_{v3}	0	−0.00406	0	**0.99990**	0
C_{v4}	−0.00040	0	−0.00799	0	**0.99977**
C_{v5}	0	−0.00088	0	−0.01321	0
C_{v6}	0.00000	0	−0.00148	0	−0.01968
C_{v7}	0	0.00002	0	−0.00220	0
C_{v8}	0.00000	0	0.00004	0	−0.00299
C_{v9}	0	0.00000	0	0.00007	0
C_{v10}	−0.00000	0	0.00000	0	0.00013
C_{v11}	0	−0.00000	0	0.00001	0

$\Delta\varepsilon_{0,1}=713.17$ cm^{-1}, $\Delta\varepsilon_{0,2}=1429.15$ cm^{-1}, $\Delta\varepsilon_{0,3}=2147.91$ cm^{-1}, $\Delta\varepsilon_{0,4}=2869.42$ cm^{-1}.
The $\Delta\varepsilon_{0,1}$ in the harmonic oscillator model was 710.08 cm^{-1}.

Table 6. Wave numbers, $\tilde{\nu}$, and absorption intensities, A, of vibrational spectrum of HCN
($\tilde{\nu}$: [cm^{-1}], A: [cm^2 s^{-1} molecule^{-1}], $T=300$ K)

Method I			Method II			Ref.[21,22]
$\tilde{\nu}$	$A\times 10^{10}$	Vibrational Modes[a] (v^1, v^2, v^3, v^4)[b]	$\tilde{\nu}$	$A\times 10^{10}$	Vibrational Modes[a] (v^1, v^2, v^3, v^4)[b]	$\tilde{\nu}$ (obsd)
738.95	1148.6[c]	(0001)	704.65	1065.7[c]	(0001)	713.74 ($00^{0}1^{1}$)
738.95	1148.6	(0010)	704.65	1065.7	(0010)	
1540.73	0	(0011)	1410.23	70.400	(0002) + (0020)	1411.42 ($00^{0}2^{0}$)
1552.64	221.28	(0002) + (0020)	1411.55	0	(0011)	
1556.89	0	(0002) − (0020)	1411.58	0	(0002) − (0020)	
2147.11	378.48[c]	(0100)	2113.61	4.537	(0003) + *(0021)*	2115.00 ($00^{0}3^{1}$)
2340.14	2.511	(0030) − *(1030)*	2113.61	4.537	(0030) + *(0012)*	
2340.14	2.511	(0003) − *(1003)*	2116.54	0.032	(0012) − *(0030)*	
2473.26	5.500	(0021) − *(1021)*	2116.54	0.032	(0021) − *(0003)*	
2473.26	5.500	(0012) − *(1012)*	2136.24	485.26[c]	(0100)	2096.68 (010)
2919.03	19.666	(0110)	2841.83	10.386	(0110)	2807.06 ($01^{1}1$)
2919.03	19.666	(0101)	2841.83	10.386	(0101)	
3286.20	76.198[c]	(1000)	2852.85	0.006	(0004) + (0040) + *(0022)*	
3743.36	0	(0111)	2854.24	0	(0004) − (0040)	
3756.94	0.023	(0102) + (0120)	2854.30	0	(0013) + (0031)	

Table 6. (Continued)

Method I			Method II			Ref.[21,22]
$\bar{\nu}$	$A\times10^{10}$	Vibrational Modes[a] (v^1, v^2, v^3, v^4)[b]	$\bar{\nu}$	$A\times10^{10}$	Vibrational Modes[a] (v^1, v^2, v^3, v^4)[b]	$\bar{\nu}$ (obsd)
3759.21	0	(0102) − (0120)	2858.52	0	(0022) − (*0004*) − (*0040*)	
3892.25	3.470	(0022)	2858.55	0	(0013) − (0031)	
3968.86	0	(0013) + (0031) − (*1011*)	3278.82	144.58[c]	(1000)	3311.47 (100)
3994.55	0	(0004) − (0040)	3545.09	0.827	(0120) + (0102)	3504.07 (012^0)
4011.60	2.446	(0004) + (0040)	3545.36	0	(0102) − (0120)	
4037.60	7.671	(1010)	3545.37	0	(0111)	
4037.60	7.671	(1001)	3981.36	31.087	(1001)	4005.64 (101^1)
4041.92	0	(0013) − (0031)	3981.36	31.087	(1010)	
4299.03	1.061	(0200)	4265.53	0.816	(0200)	4173.02 (020)
4963.09	0	(1002) − (1020)	4280.37	0.080	(0103) + (*0121*)	4202.77 (013^1)
4979.27	0.080	(0112) − (*0210*) + (*0130*)	4280.37	0.080	(0130) + (*0112*)	
4979.27	0.080	(0121) − (*0201*) + (*0103*)	4288.03	0	(0112) − (*0130*)	
5026.02	0.051	(0130) − (0112)	4288.03	0	(0121) − (*0103*)	
5026.02	0.051	(0103) − (0121)	4682.12	22.461	(1002) + (1020)	4684.61 (102^0)
5077.55	0	(1011) + (*0013*) + (*0031*)	4682.95	0	(1011)	4705.25 (102^2)
5090.37	4.573	(1002) + (1020) + (*0022*)	4683.06	0	(1002) − (1020)	
5104.86	0.029	(0210) + (*0130*)	4968.20	0.030	(0210)	4879.73 (021^1)
5104.86	0.029	(0201) + (*0103*)	4968.20	0.030	(0201)	
5442.91	16.746	(1100)	5419.36	17.333	(1100)	5393.70 (110)
6136.38	0	(0202) − (0220)	5426.37	0.005	(1003) + (*1021*)	5368.62 (103^1)
6142.34	0.011	(0202) + (0220)	5426.37	0.005	(1030) + (*1012*)	
6144.94	0	(0211)	5428.52	0	(1012) − (*1030*)	
6161.04	0.120	(1021) + (*0021*)	5428.52	0	(1021) − (*1003*)	
6161.04	0.120	(1012) + (*0012*)	5695.67	0.078	(0202) + (0220)	5572.17 (022^0)
6256.26	0.013	(1101) − (*1003*)	5701.50	0	(0202) − (0220)	
6256.26	0.013	(1110) − (*1030*)	5701.54	0	(0211)	
6286.34	1.294	(1003) + (*1101*) + (*0003*)	6119.67	0.478	(1110)	6084.81 (111^1)
6286.34	1.294	(1030) + (*1110*) + (*0030*)	6119.67	0.478	(1101)	
6428.36	0.227	(0300)	6393.20	0.360	(0300)	
6475.71	8.920	(2000)	6521.45	13.911	(2000)	6519.61 (200)
7245.87	0	(1102) − (1120)	6874.74	0.147	(1102) + (1120)	6761.30 (112^0)
7260.38	0	(1111)	6877.89	0	(1102) − (1120)	6781.74 (112^2)
7261.11	0.032	(1102) + (1120)	6877.92	0	(1111)	
7265.98	0.330	(2001) + (*1003*)	7112.88	0.001	(0301)	
7265.98	0.330	(2010) + (*1030*)	7112.88	0.001	(0310)	
7328.52	0.002	(0310)	7218.98	1.153	(2010)	7194.22 (201^1)
7328.52	0.002	(0301)	7218.98	1.153	(2001)	
7590.84	0.773	(1200)	7551.44	0.312	(1200)	
8181.18	0	(2002) − (2020)	7966.51	0.143	(2002) + (2020)	
8192.38	0	(2011) + (*1011*)	7967.18	0	(2011)	
8212.82	0.004	(2002) + (2020)	7967.21	0	(2002) − (2020)	
8437.54	0	(1201)	8308.91	0.001	(1210)	
8437.54	0	(1210)	8308.91	0.001	(1201)	
8602.53	0.056	(0400)	8651.19	0.063	(0400)	
8637.94	0.252	(2100)	8666.64	0.015	(2100)	8585.57 (210)
9435.06	0.055	(2101)	9435.47	0.013	(2101)	9257.56 (211^1)
9435.06	0.055	(2110)	9435.47	0.013	(2110)	
9624.93	0.175	(3000)	9734.39	0.001	(1300)	
9738.53	0.030	(1300)	9747.54	0.390	(3000)	9627.02 (300)
10344.30	1.429	(3001)	10486.50	0.037	(3010)	10282.03 (301^1)
10344.30	1.429	(3010)	10486.50	0.037	(3001)	
10814.66	0.004	(2200)	10884.85	0	(2200)	
11807.75	0.046	(3100)	11948.97	0.003	(3100)	11674.46 (310)
12236.33	0.025	(4000)	12969.68	0.013	(4000)	12635.90 (400)

a) The italics indicate the additional modes. b) The v^k indicates the quantum number of energy level for the molecular vibration k. c) The observed values are as follows:[23] $A(0001)=1140\times10^{-10}$, $A(0100)=7.2\times10^{-10}$, $A(1000)=2700\times10^{-10}$ in unit [$cm^2\,s^{-1}$ molecule^{-1}].

Table 7. Wave numbers, $\tilde{\nu}$ and absorption intensities, A, of hot bands of HCN
The values were calculated by the method II.
($\tilde{\nu}$: [cm^{-1}], A: [cm^2 s^{-1} molecule^{-1}], T=300 K)

$\tilde{\nu}$	$A\times10^{10}$		Vibrational Modes	Ref.[21] $\tilde{\nu}$ (obsd)	$\tilde{\nu}$	$A\times10^{10}$		Vibrational Modes	Ref.[21] $\tilde{\nu}$ (obsd)
	G: $(0001)^z$	G: $(0010)^y$				G: $(0001)^z$	G: $(0010)^y$		
705.57	40.110(z)	40.110(y)	(0002) + (0020)		4723.86		0.001	(1012) − (1030)	
706.89	38.220(y)	38.220(z)	(0011)		4723.86	0.001		(1021) − (1003)	
706.92	38.227(z)	38.227(y)	(0002) − (0020)		4991.02	0.001(z)	0.001(y)	(0202) + (0220)	4858.43 (022^0)
1408.95	4.740		(0003)		4996.84	0.001(z)	0.001(y)	(0202) − (0220)	
1408.95		4.740	(0030)		4996.88	0.001(y)	0.001(z)	(0211)	
1411.88		0.032	(0012)		5415.01		0.480	(1110)	5371.35 (111^1)
1411.88	0.032		(0021)		5415.01	0.480		(1101)	
1431.58	0.013(z)	0.013(y)	(0100)		5688.55	0	0	(0300)	
2137.17		17.794	(0110)		5816.79	0.029(z)	0.029(y)	(2000)	
2137.17	17.794		(0101)		6170.08	0.030(z)	0.030(y)	(1102) + (1120)	6047.56 (112^0)
2148.19	0.393(z)	0.393(y)	(0004) + (0040)		6173.23	0.021(z)	0.021(y)	(1102) − (1120)	6068.00 (112^2)
2149.58	0.298(z)	0.298(y)	(0004) − (0040)		6173.26	0.021(y)	0.021(z)	(1111)	
2149.64	0.286(y)	0.286(z)	(0013) + (0031)		6408.23	0.015		(0301)	
2153.86	0	0	(0022)		6408.23		0.015	(0310)	
2153.89	0	0	(0013) − (0031)		6514.33		0.550	(2010)	6480.76 (201^1)
2574.16	0.701(z)	0.701(y)	(1000)	2598.01 (100)	6514.33	0.550		(2001)	
2840.43	0.271(z)	0.273(y)	(0120) + (0102)	2788.85 (012^0)	6846.78	0	0	(1200)	
2840.70	0.333(z)	0.332(y)	(0102) − (0120)		7261.85	0.034(z)	0.034(y)	(2002) + (2020)	
2840.71	0.333(y)	0.333(z)	(0111)		7262.52	0.038(y)	0.038(z)	(2011)	
3276.70	8.642		(1001)	3292.17 (101^1)	7262.56	0.038(z)	0.038(y)	(2002) − (2020)	
3276.70		8.642	(1010)		7604.25		0.011	(1210)	
3560.87	0.004(z)	0.004(y)	(0200)		7604.25	0.011		(1201)	
3575.71	0.074		(0103)		7946.53	0	0	(0400)	
3575.71		0.074	(0130)		7961.98	0.001(z)	0.001(y)	(2100)	
3583.37		0	(0112)		8730.81	0.002		(2101)	
3583.37	0		(0121)		8730.81		0.002	(2110)	
3977.46	1.003(z)	1.003(y)	(1002) + (1020)	3970.87 (102^0)	9029.73	0	0	(1300)	
3978.30	1.037(y)	1.037(z)	(1011)	3991.51 (102^2)	9042.88	0.001(z)	0.001(y)	(3000)	
3978.40	1.037(z)	1.037(y)	(1002) − (1020)		9781.84		0.019	(3010)	9568.29 (301^1)
4263.54		0.026	(0210)		9781.84	0.019		(3001)	
4263.54	0.026		(0201)		10180.19	0	0	(2200)	
4714.70	0.024(z)	0.024(y)	(1100)		11244.31	0.002(z)	0.002(y)	(3100)	
4721.71	1.566		(1003) + (0121)	4654.88 (103^1)	12265.02	0	0	(4000)	
4721.71		1.566	(1030) + (0112)						

treatment in Method I may be considered to be more reasonable than that in Method II. However, the final result from Method I was undesirable in comparison with the observed values. Therefore, we are especially interested in the treatment of Method II, which brings better results. The results calculated by Method II are mainly indicated in Tables 2 to 5.

The variational treatment was divided into two steps because of the technical counterplan. However, this treatment was effective in obtaining additional information. For example, we thus learned that the wave functions of molecular vibration can be specified in view of the principal terms of anharmonicity, without cross terms, as is indicated in Tables 3,4, and 5.** It is recognized that the mechanical anharmonicity of the C–H vibration is as large as that generally found. Moreover, the effects of cross terms in anharmonicity on the frequencies of the absorption bands can be confirmed. The coefficients of the function of the dipole-moment component with the normal coordinates are indicated in Table 2. In Table 6, the final results involving the frequencies and the absorption intensities of the vibrational spectrum of HCN are indicated, and the principal and additional modes of vibration are clarified. It should be noted that the representation of the vibrational mode is indicated by the quantum number of the energy level of vibration, considering the principal terms of anharmonicity without cross terms. The frequencies and the absorption intensities of the hot bands, referring to the bending vibration, are listed in Table 7. In Tables 6 and 7, the calculated frequencies and the intensities of the absorption bands are not always appropriate. However, it was found that the calculated intensities are effective in clarifying the assignment of the observed absorption bands. In comparison with the results in the references,[21,22] we can make the following statements: the absorption intensities of (1011), (1002)—(1020), (1111), and (1102)—(1120) are equal to zero, and the order of intensities of (0300), (1200), and (2002)+(2020) is 10^{-11} degree in [$cm^2\ s^{-1}$ $molecule^{-1}$] units. The absorption intensity of the degenerate hot band {(0111), (0102)−(0120)} is larger than the intensity of (0102)+(0120), and also {(0211), (0202)—(0220)} is larger than (0202)+(0220).

The results presented above show that the molecular orbital calculations are effective in the analysis of the vibrational specturm if the absorption intensities are slso calculated.

The authors would like to acknowledge the continuing encouragement of Professor K. Higasi. In their calculation, they were helped by the "University Contribution" of UNIVAC Japan, Ltd.

** There remains a further question as to the number of harmonic wave-functions used in Eq. (8). Therefore, the wave numbers, $\tilde{\nu}$, and the absorption intensities, A, were calculated under different restrictions. The results calculated on the basis of the condition ($i=0$ to 13) are as follows:

$\tilde{\nu}$		$A\times10^{10}$
704.92	(0001)	1065.7
1410.76	(0002) + (0020)	70.400
2114.40	(0003)	4.537
2137.04	(0100)	485.26
2853.91	(0004) + (0040)	0.006
3280.05	(1000)	144.58
4267.12	(0200)	0.816
6395.59	(0300)	0.360
6523.88	(2000)	13.911
8654.41	(0400)	0.063
9751.18	(3000)	0.390
12974.26	(4000)	0.013

($\tilde{\nu}$: cm^{-1}, A: $cm^2\,s^{-1}$ $molecule^{-1}$)

In comparison with the values shown in Table 6, there is no difference in the absorption intensity and the difference in the wave numbers is not a serious problem in this work.

References

1) J. A. Pople and G. A. Segal, *J. Chem. Phys.*, **44**, 3289 (1966).
2) D. P. Santry and G. A. Segal, *ibid.*, **47**, 158 (1967).
3) G. A. Segal, *ibid.*, **47**, 1876 (1967).
4) G. A. Segal and M. L. Klein, *ibid.*, **47**, 4236 (1967).
5) K. Machida, H. Nakatsuji, H. Kato, and T. Yonezawa, *ibid.*, **53**, 1305 (1970).
6) N. Boder, M. J. S. Dewar, A. Harget, and E. Haselbach, *J. Amer. Chem. Soc.*, **92**, 3854 (1970).
7) R. E. Bruns and W. B. Person, *J. Chem. Phys.*, **53**, 1413 (1970).
8) T. P. Lewis and I. W. Levin, *Theoret. Chem. Acta* (Berl.), **19**, 55 (1970).
9) P. Pulay, *Mol. Phys.*, **21**, 329 (1971).
10) I. W. Levin and O. W. Adams, *J. Mol. Spectrosc.*, **39**, 380 (1971).
11) I. W. Levin, *J. Chem. Phys.*, **55**, 5393 (1971).
12) R. E. Bruns and W. B. Person, *ibid.*, **55**, 5401 (1971).
13) G. A. Thomas, G. Jalsovszky, J. A. Ladd, and W. J. Orville-Thomas, *J. Mol. Struct.*, **8**, 1 (1971).
14) T. Miyazaki, T. Shigetani, and H. Yamamoto, This Bulletin, **45**, 678 (1972).
15) T. Miyazaki and H. Yamamoto, *ibid.*, **45**, 1669 (1972).
16) M. J. A. Dewar and H. Metiu, *Proc. Roy. Soc. London, A* **330**, 173 (1972).
17) R. J. Boyd and M. A. Whitehead, *J. Chem. Soc. Dalton*, **1972**, 81
18) Tae-Kyu Ha, R. Meyer, and H. H. Gunthard, *Chem. Phys. Lett.* **22**, 68 (1973).
19) R. J. Boyd and M. A. Whitehead, *J. Chem. Soc. Dalton*, **1972**, 73.
20) M. J. S. Dewar and D. H. Lo., *J. Amer. Chem. Soc.*, **94**, 5296 (1972).
21) D. H. Rank, G. Skorinko, D. P. Eastman, and T. A. Wiggins, *J. Opt. Soc. Amer.*, **50**, 421 (1960).
22) I. Suzuki, M. A. Pariseau, and J. Overend, *J. Chem. Phys.*, **44**, 3561 (1966).
23) G. H. Hyde and D. F. Horing, *ibid.*, **20**, 647 (1952).

An ESR study of the Role of CoO and NiO in Al_2O_3–MoO_3–CoO (or NiO) Desulfurization Catalysts

Hisashi UEDA and Naoyuki TODO

National Chemical Laboratory for Industry, Mita, Meguro-ku, Tokyo 153

(Received July 25, 1974)

The ESR spectra from the catalyst/perylene/purified-benzene system were studied. The surface equilibria, $Co^{3+}+P \rightleftharpoons Co^{2+}+P^+$, $Ni^{3+}+P \rightleftharpoons Ni^{2+}+P^+$, and $Mo^{6+}+P \rightleftharpoons Mo^{5+}+P^+$, have been established, with the equilibrium constants at 20°C, 3.3×10^{15}, 3.0×10^{14}, and 6.8×10^{9} respectively. In Al_2O_3–MoO_3–CoO, $Mo^{6+}+Co^{2+} \rightleftharpoons Mo^{5+}+Co^{3+}$, is attained; the equilibrium constant obtained was 2.0×10^{-6}, and the corresponding value for $Mo^{6+}+Ni^{2+} \rightleftharpoons Mo^{5+}+Ni^{3+}$ was 2.3×10^{-5}. These results indicate that the roles of NiO and CoO in these catalysts are essentially the same. It has been found that the supporting order was important when CoO and MoO_3 were supported together, but unimportant when NiO and MoO_3 were supported together. Considering the known fact that CoO is a more efficient Co-catalyst of MoO_3 than NiO at lower supported concentrations (less than 2%), it has been concluded that CoO is incorporated in the alumina-carrier surface less stereospecifically, but more effectively, than NiO.

Numerous papers have been written on Al_2O_3–MoO_3–CoO–type catalysts, including several reviews.[1] In only a few papers, however, have the catalytic roles of MoO_3, CoO, and alumina as the carrier been cosidered, particularly in the form of a discussion of the reaction mechanism.[2] This is probably because of the fact that, when handling this type of catalyst, the researchers are more concerned with the practical usefulness, high activity, or long life of the catalyst. The present authors have been studying this catalyst by means of the ESR method in an attempt to get some knowledge about the catalytic reaction mechanism. As one way of approaching this problem, the surface concentrations of the paramagnetic species have been observed.[3]

In the present paper, the surface concentrations of the paramagnetic species formed in the oxide catalysts, if they are in contact with a dehydrated and degassed perylene/benzene solution, were measured by a quantitative ESR method.[4] Particular attention had been paid to the roles which CoO and NiO play in the catalysis reaction.

The present authors have always thought it most desirable to make measurements of the properties of a catalyst under the circumstances in which the catalyst is actually used. In some of our past papers, a few such efforts have been described.[3] Comparisons of the concentrations of the paramagnetic species to be formed in the catalyst studied in the present work at, say, 400 °C and 100 atm of H_2 are very desirable, too. However, before trying such rather difficult experiments, it will be helpful to try some less difficult experiments and to find a few of the essential differences between the effects of cobalt and nickel, if possible. For this reason, the following experiments were carried out.

Experimental

Purity of the Carrier. It is often advisable to use as simple a system as possible to find the mutual interactions between the components being considered in the system. Accordingly it is better to use the purest available γ-alumina carrier in order to study the roles of the supported transition metal ions than to use a commercial-grade one. However, when some time-consuming experimental data, such as those of catalyst-activity measurements, have already been obtained using a certain commercially available carrier, a comparison between those data and the ESR results is possible by using the same commercial carrier in the sample preparation for the ESR measurements. It is for this reason that a commercial γ-alumina carrier (Shokubai Kasei Co.) was used in the experiments in this work. The ESR spectrum of the carrier used and of a relatively pure one (Baikowski A 125 AS-2; Fe 20 ppm, Si 18 ppm, Cr 8 ppm, V and Mn 3 ppm, *etc.*) are both shown in Fig. 1. It should be noted that some "built-in acid points" due to impurities already exist on the carrier surface, even when nothing is supported. The surface area of the carrier used was 200 m^2/g.

Supporting Method and Analysis. MoO_3 was supported on alumina by immersing the carrier in a solution of ammonium molybdate (impregnation method). It was then

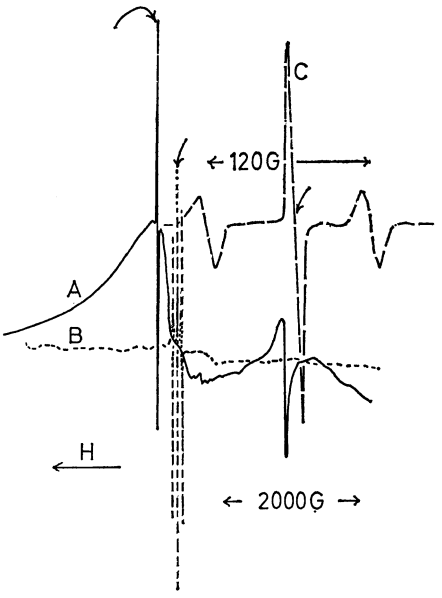

Fig. 1. ESR of the alumina carrier used. The right end of each spectrum is for 500 G, and the left end is for 5500 G of static magnetic field. The pointed arrows indicate $g=2.003$.
The modulation width used was 10 G. A: the γ-alumina used (Shokubai Kasei Co.). B: γ-alumina of Baikowski (France). The amplification of signal is 10 times of A. C: The central part of B, the amplication 1.6 times of A.

agitated for one hour at 40 °C, dried by means of a centrifuge, heated at 100 °C in an air bath, and then calcined at 550 °C for one hour. The mixed oxide thus prepared was denoted Al_2O_3–MoO_3. If a second ingredient (CoO or NiO) was supported, Al_2O_3–MoO_3 was then immersed in a solution of cobalt (or nickel) nitrate, dried, and calcined in the same way. This mixed oxide was denoted Al_2O_3–MoO_3–CoO (or NiO). If only CoO (or NiO) was supported, the supporting process for MoO_3 in the above processes was omitted. This was denoted Al_2O_3–CoO (or NiO). In the past works, the supporting order was always from MoO_3 to CoO (or NiO). In the present work, the reverse supporting order was also attempted. In this preparation, MoO_3 was supported on Al_2O_3–CoO or Al_2O_3–NiO. This was denoted Al_2O_3–CoO–MoO_3 (or Al_2O_3–NiO–MoO_3).

The analysis of the mixed oxides was done as follows: 1 g of the mixed oxide sample was heated to 130 °C with 10 ml of 1 : 1 H_2SO_4. After dissolution has been completed, it was cooled and diluted to 100 ml. The Co and Ni were analysed by means of an X-ray fluorescence analyser. The Mo was analysed by reducing all the Mo ions to Mo^{3+} and was then titrated with a $KMnO_4$ solution.

Preparation of the Sample and Measurements of ESR. By the same procedure as in a previous paper,[4] sample systems composed of oxide/perylene/purified-benzene were prepared and measurements were made after 10 min. The benzene pretreatment of the oxide was included.

Results

Figure 2 shows the concentrations of the perylene cation with the 9-line hyperfine structure, denoted as Pn^+, and those of the perylene cation without a hyperfine structure, denoted as Ps^+ (which has been denoted as P^+O^{*2-} in previous papers)[4,5] obtained by the use of Al_2O_3–CoO. The same values for Al_2O_3–NiO are shown in Fig. 3. In Fig. 3, the concentrations of Pn^+ and Ps^+ decrease when a relatively small amount of NiO is supported, probably because of some surface reactions between Ni^{3+} and the impurities. In Fig. 4, the concentrations of Pn^+, Ps^+, and Mo^{5+} obtained by Al_2O_3–MoO_3 are shown. In Figs.

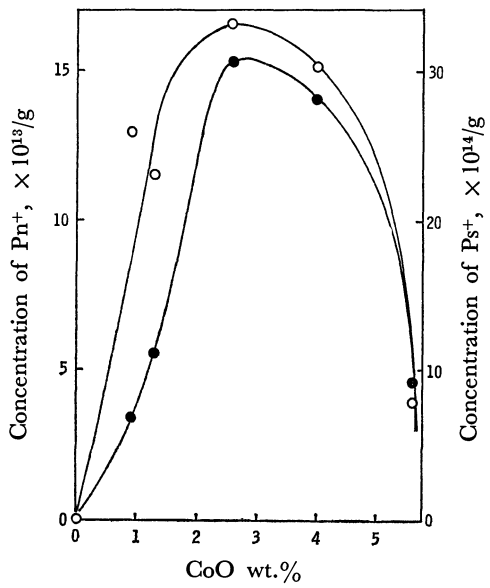

Fig. 2. P^+ concentrations obtained from Al_2O_3-CoO. ○ is for Pn^+ (left scale), and ● is Ps^+ (right scale).

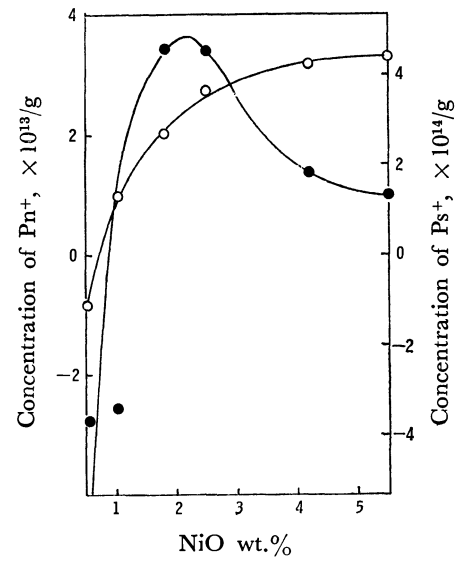

Fig. 3. P^+ concentions obtained from Al_2O_3-NiO. ○ is for Pn^+ (left scale), and ● is for Ps^+ (right scale).

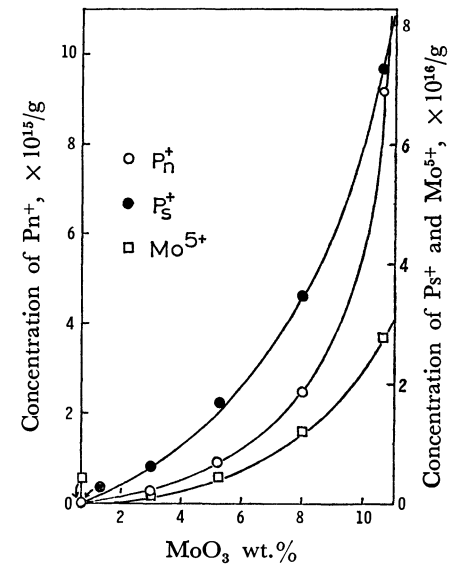

Fig. 4. P^+ and Mo^{5+} concentrations from Al_2O-MoO_3. ○ is for Pn^+ (left scale), ● is Ps^+ (right scale), and □ is for Mo^{5+} (right scale).

2 and 4, the concenrations of Pn^+ and Ps^+ formed on the unsupported carrier have been subtracted from the concentrations observed by supported catalysts; therefore, the curves pass the original point. In Table 1, the concentrations of Pn^+, Ps^+, and Mo^{5+} obtained by the use of Al_2O_3–MoO_3–CoO are shown. Table 2 is for Al_2O_3–MoO_3–NiO. In Fig. 5 the decay curves of the Pn^+ concentration obtained by the carrier and singly supported catalysts are shown. In Fig. 6, the decay curves of Pn^+ concentrations obtained by doubly supported catalysts are shown. In Fig. 7 the formation curves of the Mo^{5+} concentration obtained by doubly supported catalysts are shown.

Discussion

Surface Reaction Constants and the Role of CoO and NiO,

Table 1. Concentration of Pn^+, Ps^+, and Mo^{5+} in Al_2O_3-MoO_3-CoO ($\times 10^{13}$/g)

CoO%		0.4—0.9	1.5—2.5	3.6—5.6
MoO%	Species			
0.7	Pn^+	6.1[a]	10.2[d]	13.4[g]
	Ps^+	109	277	236
	Mo^{5+}	20	5.9	5.0
5.2	Pn^+	120[b]	153[e]	263[h]
	Ps^+	1,570	2,940	3,480
	Mo^{5+}	283	61.4	10.0
10.6	Pn^+	1,020[c]	1,070[f]	675[i]
	Ps^+	9,210	11,400	6,740
	Mo^{5+}	2,180	1,570	600

(MoO_3%)/(CoO%): a) 0.66/0.85. b) 5.18/0.60. c) 10.60/0.39. d) 0.65/2.47. e) 5.12/1.95. f) 10.48/1.54. g) 0.64/4.26. h) 5.01/4.19. i) 10.27/3.63.

Table 2. Concentration of Pn^+, Ps^+, and Mo^{5+} in Al_2O_3-MoO_3-NiO ($\times 10^{13}$/g)

NiO%		0.2—0.6	1.0—1.8	2.6—4.2
MoO_3%	Species			
0.67	Pn^+	2.8[a]	2.1[d]	5.7[g]
	Ps^+	69.8	123	226
	Mo^{5+}	18.2	15.5	4.5
5.22	Pn^+	73.9[b]	39.4[e]	40.5[h]
	Ps^+	1,220	1,420	1,050
	Mo^{5+}	251	188	6.5
10.65	Pn^+	1,170[c]	378[f]	85.6[i]
	Ps^+	13,900	5,400	2,870
	Mo^{5+}	3,870	2,510	361

(MoO_3%)/(NiO%): a) 0.66/0.50. b) 5.20/0.34. c) 10.62/0.20. d) 0.66/1.47. e) 5.15/1.26. f) 10.54/1.01. g) 0.65/3.22. h) 5.06/3.00. i) 10.37/2.62.

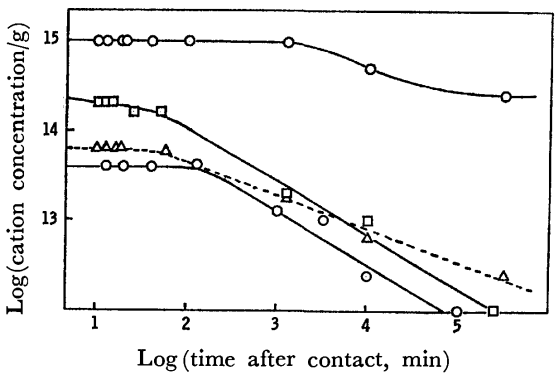

Fig. 5. Decay curves of Pn^+. ○ (bottom ones) are for Al_2O_3. △ (dotted line) are for Al_2O_3-NiO (98.2—1.8%), □ are for Al_2O_3-CoO (97.4—2.6%), and ○ (top ones) are for Al_2O_3-MoO_3 (94.8—5.2%).

As has already been discussed in previous papers, surface concentration equilibria are attained among surface redox species on an oxide surface;[5]

$$Co^{3+} + P \rightleftharpoons Co^{2+} + P^+ \quad (1)$$

$$Ni^{3+} + P \rightleftharpoons Ni^{2+} + P^+ \quad (2)$$

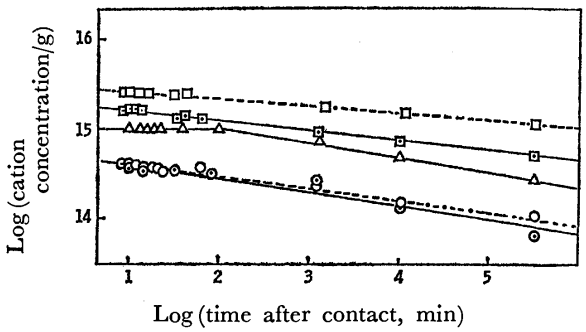

Fig. 6. Decay curves of Pn^+. △ are for Al_2O_3-MoO_3 (94.8—5.2%).
⊡ are for Al_2O_3-MoO_3-CoO (92.9—5.1—2.0%),
□ are for Al_2O_3-CoO-MoO_3 (92.8—1.9—5.3%),
⊙ are for Al_2O_3-MoO_3-NiO (93.5—5.2—1.3%),
and ○ are for Al_2O_3-NiO-MoO_3 (92.3—2.0—5.7%).

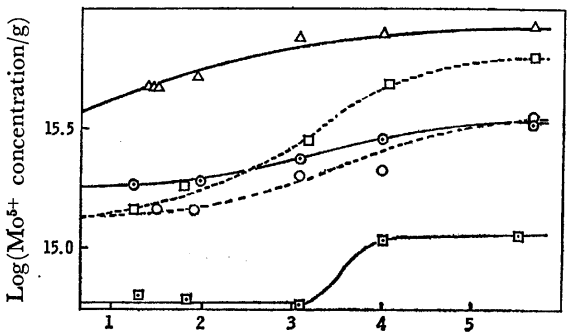

Fig. 7. Formation of Mo^{5+}. Symbols are the same as in Fig. 6.

The formation of P^+ (here, P^+ denotes both Pn^+ and Ps^+; therefore, $[P^+]=[Ps^+]+[Pn^+]$), as is shown in Figs. 2, 3, and 5, proves the existence of Co^{3+} and Ni^{3+} on the oxide surface. It is reasonable to use the activity coefficients, f_c, f_n, and f_m, for Co^{2+}, Ni^{2+}, and Mo^{6+} because it can easily be assumed that not all the metal ions supported on the oxide surface are actively working in the surface reactions. Actually, the activity of a catalyst depends not only on the amount of supported salts, but also on the method of preparation. Therefore, f_c = (concentration of active Co^{2+})/(concentration of total Co^{2+} supported). In an extreme case, in which only one Co^{2+} ion is supported on a 200 m^2 surface area (*i.e.*, one gram carrier), the Co^{2+} ion should be 100% active; in other words, $f_c = 1.0$. Therefore,

$$\frac{f_c \cdot [Co^{2+}] \cdot [P^+]}{[Co^{3+}] \cdot [P]} = K_1 \quad (3)$$

Let K be equal to the following value;

$$K = \frac{[Co^{2+}] \cdot [P^+]}{[P]} = \frac{K_1 \cdot [Co^{3+}]}{f_c} \quad (4)$$

If $[Co^{3+}] \rightarrow 1$ (ion/g catalyst) is considered, $[Co^{2+}]$ should also be close to 1 (ion/g catalyst), or $f_c \rightarrow 1.0$. Therefore, the limiting value of K_1 is K. The values of K are plotted against $[Co^{2+}]$ in Fig. 8-A. The value of K for $[Co^{2+}] \rightarrow 0$ gives $K_1 = 3.3 \times 10^{15}$ for CoO. For NiO, K_1 of 3.0×10^{14} is obtained from Fig. 8-B.

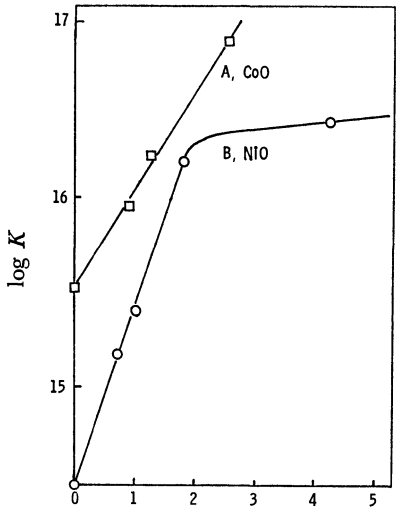

Fig. 8. Log K plotted against CoO (A) or NiO (B) concentration.

In the mixed oxide, Al_2O_3–MoO_3–CoO, there are those equilibria:

$$Mo^{6+} + Co^{2+} \rightleftharpoons Mo^{5+} + Co^{3+} \; ; \; K_r \qquad (5)$$

$$Mo^{6+} + P \rightleftharpoons Mo^{5+} + P^{+} \; ; \; K_f \qquad (6)$$

The constants are:

$$K_r = \frac{[Co^{3+}]\cdot[Mo^{5+}]}{f_c\cdot[Co^{2+}]\cdot f_m\cdot[Mo^{6+}]}, \quad K_f = \frac{[Mo^{5+}]\cdot[P^{+}]}{f_m\cdot[Mo^{6+}]\cdot[P]}.$$

Then, $K_f = K_1\cdot K_r$. At the limit of $[Mo^{6+}]\rightarrow 1$ (ion/g catalyst), $f_m \rightarrow 1.0$. Then, in the same way as in (4), the value of K_r is obtained as the limiting value of K' at $[Mo^{6+}]\rightarrow 0$:

$$K' = \frac{[Mo^{5+}]\cdot[P^{+}]}{[P]} \rightarrow K_f \text{ (when } [Mo^{6+}] \rightarrow 1).$$

From Fig. 9, 9.93×10^{9} (for Al_2O_3–MoO_3–CoO), 5.62×10^{9} (for Al_2O_3–MoO_3–NiO), and 6.31×10^{9} (for Al_2O_3–MoO_3) are obtained as the K_f values. The average value of these three values is 6.82×10^{9}. The K_r values calculated from K_f and K_1 are 2.06×10^{-6} for Al_2O_3–MoO_3–CoO, and 2.27×10^{-5} for Al_2O_3–MoO_3–NiO.

From (4), $f_c = (K/K_1)\cdot[Co^{3+}]$. Under the condition $[Co^{3+}]\simeq 1$, meaning that Co^{3+} has almost completely reacted, f_c values of 0.37,0.20,0.05, and 0.05 are obtained for 0.88, 1.27, 2.58, and 5.61% of CoO supported in Al_2O_3–CoO. In the same way, f_n values of 0.20, 0.12, 0.02, and 0.01 are obtained for 0.67, 1.02, 1.87, and 4.16% of NiO supported in Al_2O_3–NiO. f_m is obtained as $[P^{+}]$/(total $[Mo^{6+}]$ supported); the values are 2.8×10^{-5}, 8.4×10^{-5}, and 1.8×10^{-4} for 0.67, 5.22, and 10.65% of MoO_3 supported in Al_2O_3–MoO_3. The effective Mo^{6+} concentrations, $f_m\cdot[Mo^{6+}]$, are 7.8×10^{14}, 1.8×10^{16}, and 8.0×10^{16} (ion/g oxide). The $[Co^{3+}]$ value in Al_2O_3–MoO_3–CoO (CoO 1.5%, MoO_3 10.5%) was estimated by these values; it is 2.5×10^{14} (ion/g oxide), some 1 ppm of the total Co^{2+} supported concentration.

In the present catalyst, it has been established that MoO_3 plays the main role, while CoO plays the auxiliary

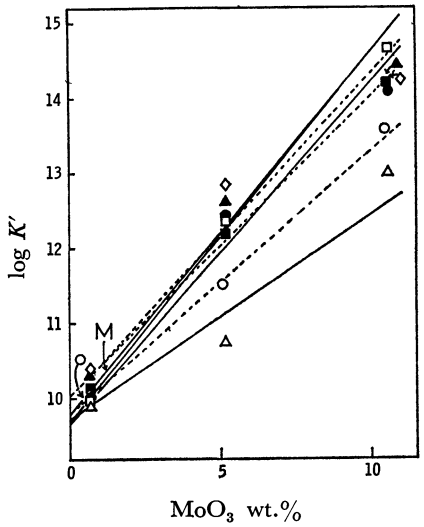

Fig. 9. Log K' plotted against MoO_3 concentration. The seven lines were obtained by, from top to bottom (viewed at 10% position), ◇, (marked M at left) Al_2O_3–MoO_3. □, NiO (0.2—0.6%). ▲, CoO (0.4—0.9%). ●, NiO (1.0—1.8%). ■, CoO (1.5—2.5%). ○, CoO (3.6—5.6%), and △, NiO (2.6—4.2%).

part. The following three results obtained by our study make possible a theoretical interpretation for those facts: (1) In the Mo^{6+}–Mo^{5+} equilibrium, the higher oxidation state is relatively more stable than the lower oxidation state; therefore, it is more suitable to activate the hydrocarbon substrate. In the Co^{2+}–Co^{3+} equilibrium, the lower oxidation state is more stable than the higher oxidation state; therefore, it does not activate the hydrocarbon. However, it oxidizes Mo^{5+} to Mo^{6+}. (2) The K_1 values are far larger than K_f; therefore, the recovery of the lower oxidation state (*e.g.*, the reversely directed reaction (5) with respect to the Mo ions) after the activation reactions, (1), (2) or (6), proceeds more easily with $Mo^{5+}\rightarrow Mo^{6+}$ than with $Co^{2+}\rightarrow Co^{3+}$. (3) There is another point which should be considered for a complete understanding of this problem — the rate constants of the following reactions:[3] $H^{+}+Co^{2+}\rightarrow H+Co^{3+}$ and $H^{+}+Mo^{5+}\rightarrow H+Mo^{6+}$. These constants must be compared in future studies.

The carrier effects have been studied with the desulfurization catalysts, and it has shown that the γ-alumina carrier used in this type of catalyst stabilizes the metal ions supported on it.[3] For this reason, it is not unreasonable to assume the existence of the higher oxidation state of Co and Ni ions at elevated temperatures and under high pressures of H_2, though this point, too, must be confirmed by future studies.

Some Results Related to the Stereochemistry of the Catalysts.

In Eq. (1) through (5), the sum of $[Pn^{+}]$ and $[Ps^{+}]$, or $[P^{+}]$, have been used instead of any one of these two components. This has been done because both species are to be counted as cations.[3,5,6] If the $[Pn^{+}]/[Ps^{+}]$ ratio is written as r, this value depends on the solvent used.[4] In Table 3 the r values are shown. It will be found that, in Al_2O_3–CoO and Al_2O_3–NiO,

TABLE 3. $[Pn^+]/[Ps^+]$, OR r-VALUE

MoO_3% =0		MoO_3% =0.67		MoO_3% =5.22		MoO_3% =10.65	
CoO%	r	CoO%	r	CoO%	r	CoO%	r
0.00	0.061	0.00	0.055	0.00	0.053	0.00	0.125
0.88	0.126	0.85	0.056	0.60	0.076	0.39	0.111
1.27	0.088					1.54	0.094
2.58	0.055	2.47	0.037	1.95	0.052		
5.61	0.050	4.26	0.057	4.19	0.076	3.63	0.100
NiO%	r	NiO%	r	NiO%	r	NiO%	r
0.60	0.106	0.50	0.040	0.34	0.061	0.20	0.084
1.02	0.155			1.26	0.028	1.01	0.070
1.80	0.050	1.47	0.027				
4.16	0.086	3.22	0.025	3.00	0.038	2.62	0.030

the less the amount of the support, the higher the r value. In contrast, in Al_2O_3–MoO_3, the more the amount of the support, the higher the r value. In doubly supported Al_2O_3–MoO_3–CoO and Al_2O_3–MoO_3–NiO, no clear-cut tendency is found. However, the general tendency is the same as that in singly supported cases. These results can be understood if it is assumed that the supporting sites of Co^{2+} (or Ni^{2+}) and of Mo^{6+} are different. The assumption here agrees quite well with the conclusions of past literature that effective CoO and NiO are supported at the octahedral sites in the β-phase, while MoO_3 is supported at the tetrahedral sites in the δ-phase.[7,8] It has been shown that an analysis of the P^+ spectrum may give some knowledge about the stereochemistry of the catalyst surface.

Since the effective MoO_3 and the effective CoO (or NiO) seem to be occupying different surface sites, the catalyst prepared by the use of the reverse supporting order may have a different nature compared with the one made by the use of a normal supporting order. Such differences will be found in Figs. 6 (Pn^+ concentrations) and 7 (Mo^{5+} concentrations). In Fig. 7, the rates of the formation of Mo^{5+} before and after approximately 3×10^3 min. (the middle points of the curves) are different. Though each catalyst surface should be handled as one integrated system of Al^{3+}–Mo^{6+}–Co^{2+}–O^{2-}–*etc.* in the equilibrium state ($t=10^5$ min or more), in the initial period (t, less than 10^3 min.) the more reactive Co^{3+} may be receiving an electron from a perylene molecule faster than Mo^{6+}, thus making the initial part of the lowest curve (⊡) parallel to the time axis. It seems that this reactivity of Co^{3+} is faster for Al_2O_3–MoO_3–CoO than for Al_2O_3–CoO–MoO_3 (□). However, the equilibrium Mo^{5+} concentration must be estimated by the use of Eq. (5), not Eq. (6). The K_r value in (5) for Al_2O_3–CoO–MoO_3 is some 10 times larger than that for Al_2O_3–MoO_3–CoO. This difference may be explained as follows. If Mo^{5+} in the tetrahedral coordination is more efficiently oxidized by Co^{3+} than that in the octahedral coordination, and if a relatively larger portion of Co^{2+} ions is distributed to tetrahedral sites when CoO is supported prior to MoO_3 (Al_2O_3–CoO–MoO_3), and if, therefore, a relatively larger portion of Mo^{6+} is in this case coordinated to octahedral sites, the rsults in Fig. 7 may be interpreted by saying that the number of the combination sites, Mo^{6+} (tetrahedral)–Co^{2+}(octahedral), is smaller in Al_2O_3–CoO–MoO_3 than in Al_2O_3–MoO_3–CoO, although the overall compositions of the oxides are almost equal.

In the cases of Al_2O_3–MoO_3–NiO and Al_2O_3–NiO–MoO_3, the curves in Figs. 6 and 7 are quite similar. This may be interpreted by means of a hypothesis that Ni^{2+} is incorporated into the carrier more stereospecifically, but less effectively (for example, the number of Ni^{2+} ions in one NiO colony on the carrier surface is different from the number of Co^{2+} ions in one CoO colony), than Co^{2+} is. The ratios of the catalyst activity *vs.* the CoO and NiO content in the Al_2O_3–MoO_3–CoO (or NiO) curves are different.[9] CoO is quite efficient at 1%, and the activity reaches its maximum value at 2%, while NiO is quite inefficient at 1%, but the activity increases until the NiO content reaches 4% or more. These results show that the supporting order can be used to get information on the stereochemical interactions between the support and the carrier surface.

ESR as an Analysing Method of a Solid Catalytic Reaction System.

There are several advantages of the ESR method when it is used to analyse catalytic reaction systems. In this section, only its sensitivity will be considered as an advantage. If only 1% of CoO is supported on Al_2O_3, some 4×10^{13}/g of Pn^+ and 2×10^{15}/g of Ps^+ are formed. If all the Co^{3+} had been converted to either Pn^+ or Ps^+, $[Co^{3+}]$ should have been 2×10^{15}/g. As the $[Co^{2+}]$ supported is 8×10^{19}/g, the abundance of Co^{3+} ions in the supported cobalt salt is only 25 ppm. If only those Co^{3+} ions which produce Pn^+ are considered, their abundance is only 0.5 ppm in supported cobalt salt. No method other than ESR can detect such a very small quantity. For example, by magnetic susceptibility measurements, the contribution of $\mu(Co^{3+})$ to the observed average μ value at 25 ppm is completely negligible; this then leads to the wrong conclusion that Co^{3+} does not participate in the catalytic reactions.[10] Though their concentrations are quite small, Co^{3+} and Ni^{3+} play important roles in the dynamic reaction process of desulfurization. The detection of such dilute but reactive species can be done only either by a fast detection of a created transient state or by a trapping method. In the present application, those transient species have been transformed to Pn^+ and Ps^+ and have been measured as semistable paramagnetic species.

The authors wish to thank Mr. K. Ogawa of their Institute and Mr. K. Fujita of Kanagawa University for their cooperation in the preparation and analysis of the oxide catalysts.

References

1) P. C. H. Mitchell, "The Chemistry of Some Hydrocarbon Desulfurization Catalysts Containing Molybdenum," Climax Molybdenum Company, 1967. G.C.A. Schuit and

B. C. Gates, *A. I. Ch. E. Journal*, **19**, 417 (1973). K. Wakabayashi, *Nenryo Kyokaishi*, **49**, 825 (1970).

2) J. M. J. G. Lipsch and G. C. A. Schuit, *J. Catal.*, **15**, 179 (1969).

3) H. Ueda and N. Todo, This Bulletin, **43**, 3698 (1970). H. Ueda and N. Todo, *J. Catal.*, **27**, 281 (1972). H. Ueda, N. Todo, and M. Kurita, *J. Less-Common Metals*, **36**, 387 (1974).

4) H. Ueda, This Bulletin, **47**, 1338 (1974).

5) H. Ueda, *ibid.*, **43**, 319 (1970).

6) H. Ueda, *Can. J. Chem.*, **46**, 891 (1968).

7) J. H. Ashley and P. C. H. Mitchell, *J. Chem. Soc., A*, **1968**, 2821, **1969**, 2730.

8) P. E. Jacobson and P. W. Selwood, *J. Amer. Chem. Soc.*, **76**, 2641 (1954), G. T. Rymer, J. M. Bridges, and J. R. Tomlinson, *J. Phys. Chem.*, **65**, 2152 (1961).

9) N. Todo, K. Muramatsu, M. Kurita, K. Ogawa, T. Sato, M. Ogawa, and Y. Kotera, *Bull. Japan Pet. Inst.*, **14**, 89 (1972).

10) J. T. Richardson, *I. E. C. Fundamentals*, **3**, 154 (1964).

On the Stable Molecular-shapes of C_mH_{m-4} Cata-condensed Nonalternant Hydrocarbons

Azumao TOYOTA

Department of Chemistry, Faculty of General Education, Yamagata University, Koshirakawa, Yamagata 990

(Received July 31, 1974)

The energetically most favorable molecular-symmetry groups and geometrical structures of C_mH_{m-4} cata-condensed nonalternant hydrocarbons were examined systematically on the basis of the symmetry rule and the semiempirical SCF MO method. The first excitation energies in the fully-symmetrical nuclear arrangements were found to decrease with increasing the number of carbon atoms, showing a tendency to converge to a certain limiting value, *ca.* 0.8 eV. Molecules larger than a certain critical size ($m\sim10$) were predicted to suffer the second-order Jahn-Teller distortion, exhibiting a double-bond fixation in the peripheral carbon skeleton. Using the most stable geometrical structures obtained, the electronic spectra of these molecules were calculated. Furthermore, the predictions of the stable molecular-shapes in the lowest excited singlet states were briefly mentioned.

Recently, we have developed the symmetry rule[1-3] for predicting the stable molecular shapes of conjugated hydrocarbons.[4,5] This rule is based on the pseudo, or the second-order Jahn-Teller effect,[6,7] which is due to the stabilization, occuring when a certain bond distortion mixes two electronic states nearly degenerate in the fully-symmetrical nuclear arrangement. On the basis of this rule, we examined systematically, in a previous paper,[8] the problem of the molecular-symmetry reduction in C_mH_{m-2} cata-condensed nonalternant hydrocarbons. As a result, we found that there is a good correlation between the molecular-symmetry reduction and the number of carbon atoms(m): in the $4n$ π-electron systems the first excitation energies in the fully-symmetrical nuclear arrangements were predicted to be significantly smaller than a certain critical value, and the molecular-symmetry reduction accompanied by a marked double-bond fixation in the peripheral carbon skeleton to occur. On the other hand, in the $4n+2$ π-electron systems, such energies were found to be considerably large for small members and to decrease rapidly with the number of carbon atoms, resulting in the molecular-symmetry reduction for members larger than a certain critical molecular size($m=14$).

The purpose of this paper is to examine further the possibility of a relationship between the number of carbon atoms and the molecular-symmetry reduction in C_mH_{m-4} cata-condensed nonalternant hydrocarbons considered as formed by the introduction of two cross-links between the carbon atoms of like parity of C_mH_m cyclic polyenes. Moreover, we investigate the second-order Jahn-Teller effects on the bond-length distributions and the excitation energies of these nonalternant hydrocarbons.

Theoretical

The method employed for predicting the energetically most favorable molecular-symmetry groups of conjugated hydrocarbons is the symmetry rule based on the second-order Jahn-Teller theorem.[7] We outline this rule briefly. Let us start by assuming for a conjugated molecule a fully-symmetrical nuclear arrangement as the unperturbed configuration. We assume that in the unperturbed nuclear configuration all the symmetrical bond distortions have taken place until the first-order energy equilibrium is reached. The unperturbed electronic wave functions ψ_0, ψ_1,$\cdots$, ψ_n,$\cdots$ and the corresponding eigenvalues E_0, E_1,$\cdots$, E_n,$\cdots$ are assumed to be known. We now distort the nuclei from the symmetrical first-order nuclear arrangement by means of the ith normal coordinate of nuclear motion Q_i. On the basis of the same approximation as used previously,[1] the energy of the ground state after deformation may be written as

$$E(Q_i) = E_0 + \frac{1}{2}\left\{k - 2\sum_n{}' \frac{|\langle\psi_n|(\partial H_\pi/\partial Q_i)_0|\psi_0\rangle|^2}{(E_n-E_0)}\right\}Q_i^2$$

where k and H_π represent the force constant for an sp^2 hybridized C–C σ-bond and the Hamiltonian for π-electrons, respectively.

According to the above equation, the force constant associated with the normal vibration Q_i should be regarded as $\{k-2\sum_n{}'|\langle\psi_n|(\partial H_\pi/\partial Q_i)_0|\psi_0\rangle|^2/(E_n-E_0)\}$ and can be negative if a given matrix element $\langle\psi_n|(\partial H_\pi/\partial Q_i)_0|\psi_0\rangle$ is nonvanishing and the associated energy gap E_n-E_0 is sufficiently small. If the force constant, *i.e.*, the curvature of $E(Q_i)$ with respect to Q_i, is negative, the energy should be lowered by the nuclear deformation Q_i, and a pseudo Jahn-Teller distortion from the symmetrical nuclear arrangement would occur spontaneously.

In order to estimate the value of the force constant, we have to take into account the infinite sum over the excited states in the above equation. However, to derive the symmetry rule we made the following drastic approximation: from the viewpoint of energy gap law, the infinite sum over the excited states is replaced by one term corresponding to the lowest excited state. In spite of the very crude approximation, Pearson and we have shown that this is justified in a variety of small molecules, complex ions and conjugated hydrocarbons.[1-5]

The symmetry rules[1] for predicting the stable molecular shapes in the closed-shell ground states are as follows: the symmetry of the nuclear displacement with the smallest force constant is identical with that of the lowest excited state, ψ_1. If the energy gap E_1-E_0 is smaller than the critical value, *ca.* 1.2 eV, the molecule would be distorted into a less symmetrical nuclear configuration. The most favorable type of bond distortion is predicted by examining the distribution of the transition density ρ_{01} over the molecular

skeleton. When the excited state is represented by a one-electron transition between molecular orbitals ϕ_i and ϕ_j, the transition density ρ_{01} between the ground and the lowest excited state is given by $\sqrt{2}\,\phi_i\phi_j$.[6]

Eigenvalues and wavefunctions for the fully-symmetrical nuclear arrangements are calculated using the self-consistent configuration interaction formalism of the Pariser-Parr-Pople method.[9-11]

Results and Discussion

Ground-state Molecular-symmetry Groups and Geometries. The symmetries and the energies of the lowest excited singlet states of C_mH_{m-4} cata-condensed nonalternant hydrocarbons (Fig. 1) obtained by assuming the fully-symmetrical nuclear arrangements are listed in Table 1. The first excitation energies for the fully-symmetrical nuclear arrangement of C_mH_{m-4} systems are shown in Fig. 2, in which those of C_mH_{m-2} systems are also shown by the open circles. It is seen that the dependence of the energy gap on the number of carbon atoms is remarkably different between C_mH_{m-2} systems. That is, in the former systems there is no such a sharp distinction of the energy gap dependence between $4n$ and $4n+2$ π-electron systems as that observed in the latter systems: the energy gaps are intermediate of those for the $4n$ and $4n+2$ π-electron systems of C_mH_{m-2}, decreasing as the number of car-

Table 1. Symmetries and energies of first and second excited singlet states of cata-condensed nonalternant hydrocarbons

Molecule[a] (Point group)[b]	First excited state		Second excited state	
	E_1-E_0 (eV)	Symmetry	E_2-E_1 (eV)	Symmetry
I(D_{2h})	2.41	B_{2u}	2.39	B_{3g}
II(D_{2h})	1.32	B_{3g}	2.29	B_{1u}
III(C_{2v})	1.57	B_2	2.11	A_1
IV(D_{2h})	1.22	B_{2u}	2.15	B_{1u}
V(C_{2v})	1.42	B_2	2.19	A_1
VI(D_{2h})	1.75	B_{2u}	1.78	B_{1u}
VII(C_{2v})	1.30	B_2	2.20	A_1
VIII(D_{2h})	1.00	B_{3g}	1.54	B_{1u}
IX(C_{2v})	1.07	B_2	1.51	A_1
X(C_{2v})	1.00	B_2	1.62	A_1
XI(C_{2v})	1.04	B_2	1.71	A_1
XII(C_{2v})	1.15	B_2	1.64	A_1
XIII(D_{2h})	0.81	B_{2u}	1.75	B_{1u}
XIV(D_{2h})	0.98	B_{2u}	1.51	B_{3g}
XV(C_{2v})	0.81	B_2	1.62	A_1
XVI(D_{2h})	0.82	B_2	1.75	A_1
XVII(C_{2v})	1.00	B_2	1.52	A_1
XVIII(C_{2v})	0.98	B_2	1.63	A_1
XIX(D_{2h})	0.83	B_{3g}	1.20	B_{1u}
XX(C_{2v})	0.84	B_2	1.25	A_1
XXI(C_{2v})	0.81	B_2	1.20	A_1
XXII(C_{2v})	0.83	B_2	1.23	A_1
XXIII(C_{2v})	0.85	B_2	1.34	A_1

a) See Fig. 1. b) The apparent fully-symmetrical point group.

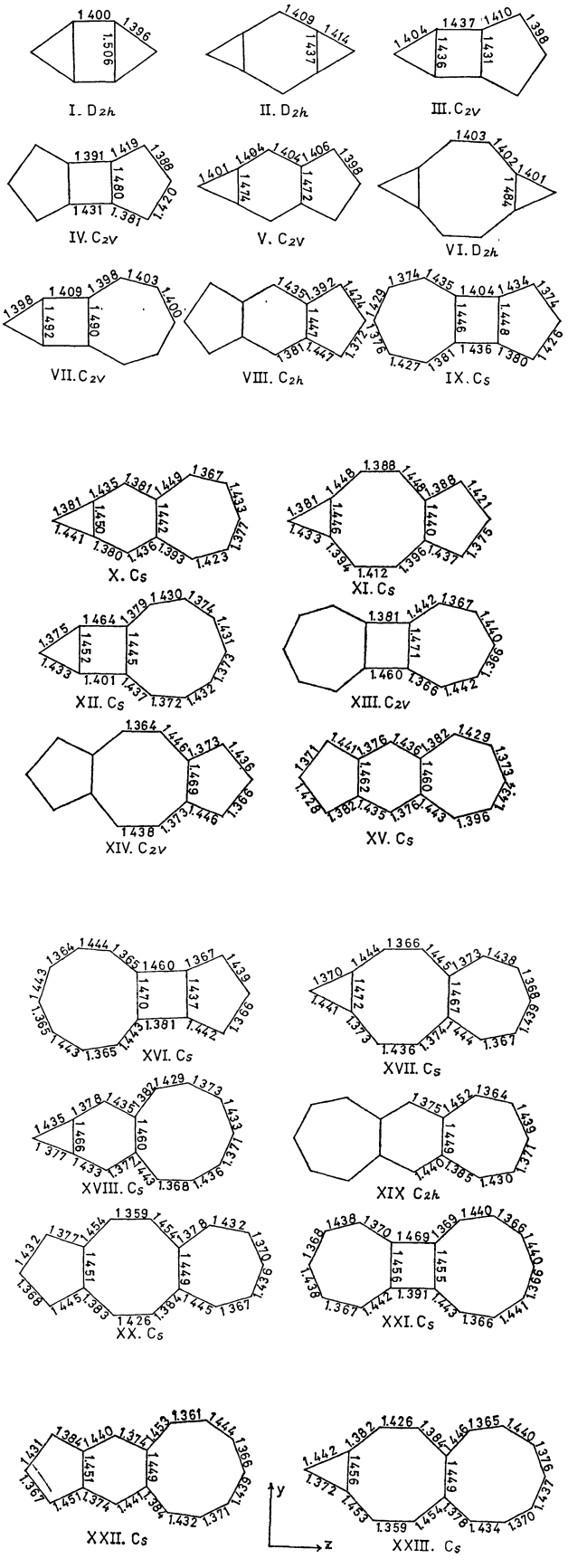

Fig. 1. Predicted stable molecular-symmetry groups and equilibrium bond lengths (in Å unit) and choice of axes.

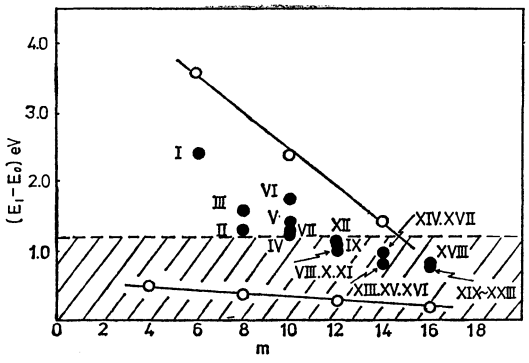

Fig. 2. Dependence of the first excitation energies for the fully-symmetrical nuclear configurations on the number of carbon atoms (m) in C_mH_{m-4} systems. Open circles mean values in C_mH_{m-2} systems.

bon atoms increases, and showing a tendency to converge to a certain limiting value, *ca.* 0.8 eV. This may be explained qualitatively by considering the orbital energy changes due to the introduction of cross-link into the unperturbed cyclic polyene. In the Hückel MO description, the energy change of the ith molecular orbital may be evaluated using the first-order perturbation theory:

$$\delta\varepsilon_i = \sum_{\mu\nu} 2C_{\mu i}C_{\nu i}\beta$$

where C_μ and C_ν are atomic-orbital coefficients for atoms μ and ν between which a cross-link is introduced. As an illustration, we show in Fig. 3 the correlation of the Hückel molecular orbitals of benzene(C_6H_6) with those of C_6H_4 and C_6H_2 (I) and in Fig. 4 that of molecular orbitals of cyclic polyene(C_8H_8) with those of C_8H_6 and C_8H_4(III). That energy gaps E_1–E_0 for C_mH_{m-4} are smaller than those for C_mH_{m-2} systems with $4n+2$ π-electrons is due to the fact that the separation between the highest occupied and the lowest vacant molecular orbitals becomes smaller by increasing the number of the cross-link between the like parity of carbon atoms of cyclic polyene. On the other hand, energy gaps for C_mH_{m-4} larger than those for C_mH_{m-2} systems with $4n$ π-electrons is ascribable to the fact that the separation between the highest occupied and the lowest vacant orbitals becomes larger by increasing the number of the cross-link, in contrast to the case of the above mentioned $4n+2$ π-electron systems.

The problem of the molecular-symmetry reduction can now be discussed on the basis of the symmetry rules and Table 1. The dashed line in Fig. 2 represents the critical value for the molecular-symmetry reduction, and in the hatched area the molecule should distort into a less symmetrical nuclear configuration.

As to the smallest member of C_mH_{m-4} systems, *i.e.*, I(m=6), the lowest excited state is of B_{2u} symmetry and the energy gap is considerably larger than the critical value. We may predict that this molecule undergoes no molecular-symmetry resuction to C_{2v} from D_{2h}. It is, however, of interest to note that the type of the nuclear displacement with the smallest force constant is that of bond-length alternation in the peripheral carbon skeleton. A similar situation

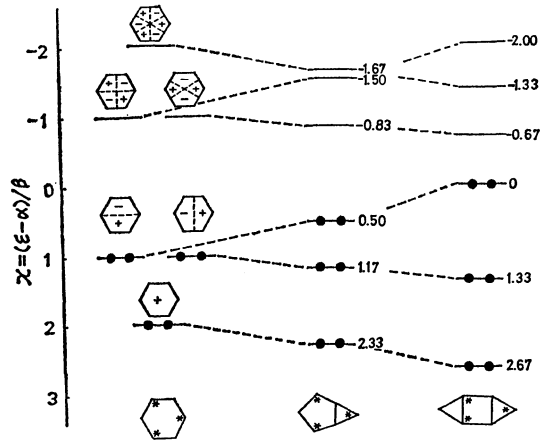

Fig. 3. Correlation of molecular orbitals of benzene (C_6H_6) with those of C_6H_4 and C_6H_2(I).

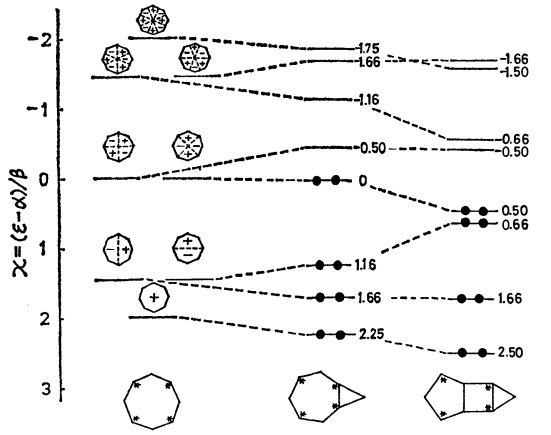

Fig. 4. Correlation of molecular orbitals of cyclic polyene (C_8H_8) with those of C_8H_6 and C_8H_4(III).

is also seen in the unperturbed cyclic polyene, benzene.

As for molecules (m=8), II and III, the energy gaps are relatively larger than the critical value and the symmetries of the lowest excited states are B_{3g} and B_2, respectively. From the view-point of energy gap law, there is no possibility for the molecular-symmetry reduction to occur in both molecules.

In case of m=10 (IV—VII), the energy gaps are predicted to be slightly large as compared with the critical value, and all these molecules, except bowtine (IV), do not suffer the second-order Jahn-Teller distortion.

Of the molecules with 12 carbon atoms, only *s*-indacene (VIII) has been synthesized by Hafner's group.[12] It is of interest to note that in these valence isomers the energy gaps are nearly the same, *i.e.*, about 1.0 eV, which are smaller than the critical value. Thus, these molecules may undergo the second-order bond distortions, reducing their ground-state molecular-symmetry groups to C_{2h}(VIII) and C_s (IX—XII) from D_{2h} and C_{2v}, respectively.

In case of m=14 (XIII—XVIII), the energy gaps are smaller than the critical value, so that these molecules are predicted to lower their ground-state molecular-symmetry groups to C_{2v}(XIII and XIV) and C_s (XV—XVIII) from D_{2h} and C_{2v}, respectively, by

Table 2. Singlet transition energies and intensities

Molecule (Point group)	Transition symmetry[a]	ΔE (eV)	f (c. g. s)	Molecule (Point group)	Transition symmetry[a]	ΔE (eV)	f (c. g. s)
IV(C_{2v})	A_1	1.32	0.01		A′	2.68	0.02
	B_2	3.36	0.01		A′	3.45	0.48
	B_2	3.59	0.18	XVI(C_s)	A′	1.53	0.01
VIII(C_{2h})	A_g	1.39(1.77)[b]	Forb. (log ε=2.59, tailing)[b]		A′	2.83	0.17
					A′	3.15	0.08
	B_u	2.62(2.42)	0.59(4.63)	XVII(C_s)	A′	1.52	0.03
	B_u	3.78(3.61)	0.21(4.81)		A′	2.74	0.01
IX(C_s)	A′	1.48	0.02		A′	3.13	0.02
	A′	2.77	0.01	XVIII(C_s)	A′	1.44	0.09
	A′	3.34	0.16		A′	2.82	0.15
X(C_s)	A′	1.41	0.01		A′	3.56	0.42
	A′	2.70	0.64	XIX(C_{2h})	A_g	1.49	Forb.
	A′	3.98	0.13		B_u	2.20	0.66
XI(C_s)	A′	1.39	0.01		B_u	3.20	0.30
	A′	2.90	0.10	XX(C_s)	A′	1.54	0.03
	A′	3.52	0.28		A′	2.48	0.04
XII(C_s)	A′	1.58	0.03		A′	2.88	0.50
	A′	2.93	0.10	XXI(C_s)	A′	1.68	0.06
	A′	3.82	0.43		A′	2.49	0.00
XIII(C_{2v})	A_1	1.50	0.01		A′	3.02	0.46
	B_2	2.79	0.14	XXII(C_s)	A′	1.53	0.00
	B_2	3.01	0.13		A′	2.24	0.61
XIV(C_{2v})	A_1	1.54	0.02		A′	3.33	0.26
	B_2	2.72	0.00	XXIII(C_s)	A′	1.56	0.03
	B_2	2.91	0.04		A′	2.51	0.23
XV(C_s)	A′	1.34	0.08		A′	3.20	0.50

a) For molecules which belong to the point group C_{2h}, the z axis is taken to be perpendicular to the molecular plane. b) The spectrum of a hexacarbometoxydihydroxy derivative; E. LeGoff and R. B. LaCount: *Tetrahedron Lett.*, **1964**, 1161.

the interaction of the ground-state with the lowest excited state through the unsymmetrical C–C stretching vibration.

Finally, in case of m=16 (XIX—XXIII) all the valence isomers have almost the same energy gaps, *i.e.*, about 0.8 eV, and it is predicted that these molecules undergo the second-order Jahn-Teller distortion, and their molecular-symmetry groups are reduced to C_{2v} (XIX) and C_s (XX—XXIII) from D_{2h} and C_{2v}, respectively.

The ground-state molecular-shapes for the energetically most favorable nuclear arrangements are predicted from the distribution of the two-center components of transition densities between the ground and the lowest excited singlet states, some of which are shown in Fig. 5.

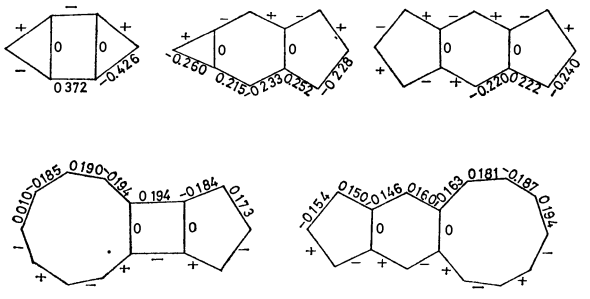

Fig. 5. Distribution of two-center components of transition densities (ρ_{01}).

In order to obtain the information on the actual magnitude of distortions or the equilibrium nuclear configurations with respect to C–C bond lengths at which the real molecule will settle, we performed the calculation using the variable bond-length SCF MO method, taking into account the distorted structures as a starting geometry.[11,13]

Results of SCF MO calculations show that almost all molecules undergo the second-order Jahn-Teller distortion, as predicted from the symmetry rule.

As to the distribution of C–C bond length, it should be noted that the second-order double-bond fixation, *i.e.*, the bond-length alternation in the peripheral carbon skeleton, is the common phenomenon in these cata-condensed nonalternant hydrocarbons (Fig. 1).

Stabilization Energies. Figure 6 shows the correlation of stabilization energies with the energy gaps calculated assuming the fully-symmetrical nuclear arrangements. We define the stabilization energy ΔE_s as the difference in total energy between the fully-symmetrical and the reduced molecular geometries. The total energy is assumed to be the sum of π-bond

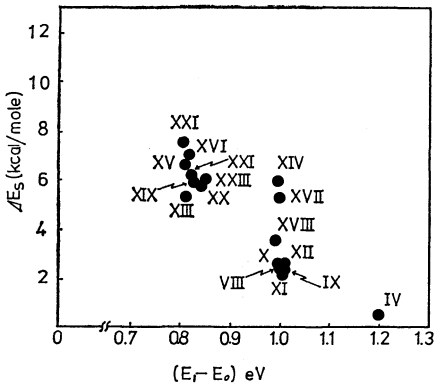

Fig. 6. Correlation of stabilization energies ΔE_s with energy gaps(E_1-E_0).

and σ-bond energies, the latter being calculated using harmonic oscillator model with the force constant equal 714 kcal mol^{-1} Å^{-2}.[14] As is seen in this figure, there is a fairly good correlation between ΔE_s and the energy gaps E_1–E_0. Particularly, it is noticed that in the valence isomers with 12 carbon atoms, the ΔE_s are almost the same.

Electronic Spectra. We calculated the excitation energies using the bond-lengths for the energetically favorable equilibrium configuration. The employed method is based on the semiempirical Pariser-Parr-Pople SCF MO CI method, and the configuration mixing of 28 singly excited states is included.

It is shown that the lowest excitation energies for the reduced molecular geometries are larger than those for the fully-symmetrical ones, and are almost constant (1.4—1.6 eV) from molecule to molecule. On the other hand, the next lowest excited states would not be remarkably changed by the molecular-symmetry reduction, lying in the region about 2.2 eV (compare Table 1 with Table 2).

Excited-state Molecular-symmetry Groups. In connection with the ground-state molecular-symmetry groups, we briefly mention the stable molecular shapes in the first excited singlet states. The criterion for the molecular-symmetry reduction in an excited state is that the energy gap E_2–E_1 is less than the critical value, *ca.* 0.6 eV.[1] From this criterion and Table 1 we may predict that all the molecules examined do not reduce their molecular-symmetry groups in the first excited singlet states. That is, the stable molecular shapes in the excited states belong to their fully-symmetrical nuclear arrangements.

Conclusion

On the basis of the symmetry rule and the semiempirical SCF MO method, the problem of the molecular-symmetry reduction in C_mH_{m-4} cata-condensed non-alternant hydrocarbons was systematically examined. It was revealed that there is a fairly good correlation between the molecular-symmetry reduction and the number of carbon atoms: that is, the molecular-symmetry reduction should set in about $m\sim10$. In these systems, there is no such a sharp distinction of molecular-symmetry reduction between $4n$ and $4n+2$ π-electron systems as that seen in C_mH_{m-2} systems. The predicted types of the energetically most favorable bond distortion, determined by examining the two-center components of transition densities, are in good agreement with the results of variable bond-length SCF MO calculations. The obtained stable molecular shapes are found to correspond to one of the Kekulé-like structures. It is concluded that such phenomena in these non-alternant hydrocarbons arise from the fact that the type of the symmetry of the lowest excited state in the fully-symmetrical nuclear arrangement is that of bond-length alternation in the peripheral carbon skeleton, and that the lowest excited state is very close to the ground state.

The auther is very grateful to Professor T. Nakajima of Tohoku University for reading the manuscript and helpful discussions.

The numerical calculation was carried out at Tohoku university with a NEAC 2200—700 computer.

References

1) T. Nakajima, A. Toyota, and S. Fujii, This Bulletin, **45**, 1022 (1972).
2) R. F. Bader, *Mol. Phys.*, **3**, 137 (1960).
3) R. G. Pearson, *J. Amer. Chem. Soc.*, **91**, 4947 (1969).
4) T. Nakajima, "Topics in Current Chemistry," Vol. 32, Spring-Verlag, Heidelberg (1972), p. 1.
5) A. Toyota and T. Nakajima, This Bulletin, **46**, 2284 (1973).
6) L. Salam, "The Molecular Orbital Theory of Conjugated Systems," Benjamin, New York (1966).
7) H. A. Jahn and E. Teller, *Proc. Roy. Soc.* (London), **A161**, 220 (1937).
8) A. Toyota and T. Nakajima, This Bulletin, **46**, 3681 (1973).
9) R. Pariser and R. G. Parr, *J. Chem. Phys.*, **21**, 446 (1953).
10) J. A. Pople, *Trans. Faraday Soc.*, **49**, 1357 (1953).
11) H. Yamaguchi, T. Nakajima, and T. L. Kunii, *Theor. Chim. Acta*, **12**, 349 (1968).
12) K. Hafner, K. Häfner, C. Konig, M. Kreuder, G. Ploss, G. Schulz, E. Strum, and K. H. Vopel, *Angew. Chem.*, **75**, 35 (1963): *Angew. Chem. Int. Ed. Engl.*, **2**, 123 (1963).
13) T. Nakajima and A. Toyota, *Chem. Phys. Lett.*, **3**, 272 (1969).
14) L. C. Snyder, *J. Chem. Phys.*, **66**, 2299 (1962).

The Crystal and Molecular Structure of Nagilactone A Diacetate[1)]

Ken HIROTSU, Taiichi HIGUCHI, Akira SHIMADA,† Yuji HAYASHI, and Takeo SAKAN

Department of Chemistry, Faculty of Science, Osaka City University, Sugimoto-cho, Sumiyoshi-ku, Osaka 558

(Received August 14, 1974)

The title compound crystallizes in the orthorhombic space group $P2_12_12_1$, with cell dimensions of $a=10.43$, $b=15.45$, $c=13.65$ Å, and $Z=4$. The structure was determined by direct methods from photographic data, and was refined by the least-squares method to a final R of 0.098 for 2581 reflections. Rings A and B are subject to steric strains resulting from the formation of a lactone ring. This is reflected in the abnormal values for some bond lengths, angles, and dihedral angles.

Nagilactones were the first reported compounds of novel tricyclic nor- or bisnor-diterpenoid constituents which originate in *Podocarpus* plants. Since four nagilactones, A, B, C, and D, were isolated from *P. nagi* zoll. et Moritzi in 1968,[2)] more than twenty components have been found in various *Podocarpus* species as important biologically active principles: plant-growth regulators,[3)] anti-termite substances,[4)] and insect toxins for house-fly larvae.[5)] Although the structures of all the lactones have been assigned and correlated on the basis of chemical or spectral evidence, it has become increasingly important to determine the exact structure of any congener in this group of compounds by means of X-ray crystallography. This article will report the details of the X-ray analysis of nagilactone A diacetate. The present results completely support the structure as assigned in the preliminary communication.[1)]

Experimental

Nagilactone A diacetate crystallizes from chloroform as colorless prisms. All the data were obtained from a specimen with dimensions of $0.2\times0.3\times0.4$ mm, cut from the above crystal.

Crystal Data. $C_{23}H_{28}O_8$, $M=432.5$, orthorhombic, $a=10.43(1)$, $b=15.45(1)$, $c=13.65(1)$ Å, $U=2200$ Å^3, $D_c=1.32$ g·cm^{-3} $Z=4$, $F(000)=920$, $\mu=$(Cu-$K\alpha$, $\lambda=1.542$ Å)$=6.9$ cm^{-1}; space group $P2_12_12_1(D_2^4)$; systematic absences: $h\,0\,0$ when $h\neq2n$, $0\,k\,0$ when $k\neq2n$, and $0\,0\,l$ when $l\neq2n$.

Crystallographic Measurements. The unit-cell dimensions were evaluated from zero-layer Weissenberg photographs, the spacings of the reflections being calibrated with superimposed Al powder lines. The intensity data for the $0\,k\,l$~$10\,k\,l$ and $h\,0\,l$~$h\,3\,l$ layers were recorded by equi-inclination Weissenberg photography using Cu-$K\alpha$ radiation. The intensities were estimated visually and corrected for spot shape and for Lorentz and polarization factors. No correction was applied for absorption and extinction. The resulting data were correlated and reduced to structure-factor amplitudes using the method of Hamilton, Rollet, and Sparks.[6)] A total of 2581 independent structure factors were obtained; 292 were too weak to be measured.

Structure Determination and Refinement. The normalized structure factors, E's, were calculated with a scale factor and a mean isotropic temperature factor derived from a Wilson plot.[7)] The structure was solved by direct phase-determining methods.[8)] Using 600 reflections with $E>1.21$, the $\sum_2$ relations were listed. Four zonal reflections (Table 1), having large $|E|$ values and appearing in many $\sum_2$ interactions, were chosen to define the origin and the enantiomorph. In addition, three symbolic phases (A, B, and C) were assigned. The starting set, together with the final refined values of A and B, is listed in Table 1. The manual symbolic addition procedure indicated that $B=\pi/2$ and $C=-\pi/2$, or that $B=-\pi/2$ and $C=\pi/2$. No information was obtained for the A symbol. In order to apply the tangent formula,[9)] the numerical phases from 0 ° to 315 °, in steps of 45 °, were assigned to the A symbol. Tangent refinement was carried out for each of the 16 possible phase combinations. The values of R_{Karle}[8)] ranged from 0.25 to 0.33, and those of Z,[10)] from 5602 to 7710. A reasonable structure was obtained from an E-map calculated with the phases in the most consistent set ($R_{Karle}=0.25$ and $Z=7710$). All the atoms, except for C(16) and C(17) of the isopropyl group, were located. Three cycles of block-diagonal least-squares refinement of the positions and isotropic thermal parameters for these 29 atoms reduced the R from 0.402 to 0.243. The two remaining carbon atoms were located in a difference synthesis. A further five cycles including all the non-hydrogen atoms reduced the R to 0.135. In the anisotropic least-squares calculations, the following weighting scheme was used:

$$w = 0.1 \quad \text{for } |F_o|\leq2.0$$
$$w = 1.0 \quad \text{for } 2.0<|F_o|\leq12.0$$
$$w = (12.0/F_o)^2 \quad \text{for } |F_o|>12.0.$$

Seven rounds of least-squares with block-diagonal approximation brought the refinement to convergence at 0.112. The hydrogen atoms, except for those bonded to C(22),

TABLE 1. STARTING SET OF REFLECTIONS, TOGETHER WITH FINAL REFINED PHASES FOR THE SYMBOLS

h	k	l		$\phi(h)$ initial	$\phi(h)$ final
0	10	5		0	fixing origin and enantiomorph
0	3	6		$\pi/2$	
9	2	0		$\pi/2$	
2	0	1		$\pi/2$	
4	1	10	A	$\pm\pi/4$, $\pm3\pi/4$, 0, π, $\pm\pi/2$	-2.83
4	1	11	B	$\{\pi/2\}$, $\{-\pi/2\}$	1.85
1	14	0	C	$\{-\pi/2\}$, $\{\pi/2\}$	$-\pi/2$

† Deceased 5 August 1973.

Table 2. Fractional atomic co-ordinates and anisotropic thermal parameters with estimated standard deviations in parentheses

(a) Fractional co-ordinates

Atom	x/a	y/b	z/c	Atom	x/a	y/b	z/c
C (1)	−0.0776(7)	0.0602(5)	−0.1621(5)	C (22)	0.1238(9)	0.0035(7)	−0.3784(6)
C (2)	−0.0507(9)	0.1582(5)	−0.1506(6)	C (23)	0.0020(7)	−0.0705(4)	0.2769(5)
C (3)	−0.1358(9)	0.2010(5)	−0.0792(6)	C (24)	0.1356(7)	−0.0846(5)	0.3213(5)
C (4)	−0.1627(8)	0.1525(4)	0.0168(5)	O (25)	0.0101(6)	0.2198(3)	0.1152(4)
C (5)	−0.1704(6)	0.0544(4)	0.0052(4)	O (26)	−0.0599(5)	0.0870(3)	0.1513(3)
C (6)	−0.1550(6)	0.0267(4)	0.1112(4)	O (27)	−0.1681(7)	−0.2683(3)	−0.2052(4)
C (7)	−0.1140(6)	−0.0691(5)	0.1270(4)	O (28)	0.0249(4)	0.0259(3)	−0.2262(3)
C (8)	−0.1098(7)	−0.1224(4)	0.0331(5)	O (29)	−0.0844(5)	0.0700(4)	−0.3588(4)
C (9)	−0.0951(6)	−0.0817(4)	−0.0616(4)	O (30)	0.0084(5)	−0.0781(3)	0.1778(3)
C (10)	−0.0619(6)	0.0136(4)	−0.0610(4)	O (31)	−0.0948(5)	−0.0554(4)	0.3195(3)
C (11)	−0.1129(7)	−0.1306(4)	−0.1440(5)	H (C1)	−0.169(9)	0.048(6)	−0.188(7)
C (12)	−0.1437(7)	−0.2193(5)	−0.1368(5)	H (C2)	−0.061(8)	0.183(6)	−0.226(6)
O (13)	−0.1418(6)	−0.2553(3)	−0.0461(3)	H (C2a)	0.044(8)	0.154(6)	−0.116(6)
C (14)	−0.1296(8)	−0.2059(4)	0.0383(5)	H (C3)	−0.229(8)	0.199(6)	−0.110(7)
C (15)	−0.1344(10)	−0.2641(5)	0.1267(6)	H (C3a)	−0.100(8)	0.248(6)	−0.061(6)
C (16)	−0.2684(13)	−0.3104(7)	0.1332(8)	H (C5)	−0.245(8)	0.036(6)	−0.026(7)
C (17)	−0.0136(13)	−0.3284(7)	0.1223(8)	H (C6)	−0.240(7)	0.031(5)	0.147(6)
C (18)	−0.2922(8)	0.1882(6)	0.0592(7)	H (C7)	−0.190(8)	−0.102(6)	0.182(7)
C (19)	−0.0604(7)	0.1609(5)	0.0944(5)	H (C11)	−0.103(8)	−0.115(6)	−0.213(7)
C (20)	0.0772(6)	0.0217(5)	−0.0213(5)	H (C15)	−0.125(7)	−0.226(5)	0.187(6)
C (21)	0.0062(8)	0.0373(5)	−0.3227(5)				

(b) Anisotropic thermal parameters ($\times 10^4$)[a]

Atom	β_{11}	β_{22}	β_{33}	β_{12}	β_{13}	β_{23}
C (1)	40(7)	28(3)	33(4)	0(8)	4(8)	11(7)
C (2)	121(11)	17(3)	43(5)	−31(9)	34(12)	5(7)
C (3)	138(12)	25(3)	36(4)	−2(11)	12(13)	23(7)
C (4)	83(8)	12(3)	32(4)	13(8)	11(10)	−6(6)
C (5)	39(6)	13(3)	22(3)	3(7)	−3(7)	−8(5)
C (6)	36(6)	16(3)	26(3)	−15(7)	−5(8)	5(6)
C (7)	37(6)	30(3)	15(3)	−3(8)	−3(7)	−7(6)
C (8)	62(7)	17(3)	20(3)	−7(7)	−7(9)	3(5)
C (9)	32(6)	24(3)	19(3)	3(7)	4(7)	−5(6)
C (10)	20(5)	17(3)	21(3)	−2(7)	1(7)	3(5)
C (11)	65(7)	19(3)	24(3)	−3(8)	16(9)	−8(6)
C (12)	66(8)	28(3)	28(4)	−15(9)	−21(9)	−16(6)
O (13)	114(7)	19(2)	30(3)	−28(7)	−15(8)	−10(4)
C (14)	94(9)	20(3)	34(4)	−34(9)	2(11)	−18(7)
C (15)	213(15)	22(3)	30(4)	−54(13)	−35(14)	8(7)
C (16)	261(20)	64(6)	79(8)	−191(20)	73(23)	15(12)
C (17)	281(20)	60(6)	74(8)	185(20)	−47(23)	40(11)
C (18)	90(9)	41(4)	68(6)	95(10)	13(13)	−28(9)
C (19)	73(8)	21(3)	34(4)	0(9)	13(10)	5(7)
C (20)	11(5)	32(3)	30(3)	−22(7)	−17(7)	−9(6)
C (21)	81(8)	45(4)	29(4)	−31(11)	37(10)	15(8)
C (22)	94(10)	70(6)	44(5)	68(13)	76(11)	−20(9)
C (23)	75(7)	19(3)	23(3)	−4(9)	−11(9)	−2(6)
C (24)	60(8)	43(4)	35(4)	3(9)	−38(9)	−7(8)
O (25)	125(8)	24(2)	58(4)	−61(7)	−22(10)	−13(5)
O (26)	72(5)	13(2)	25(2)	−19(5)	−21(6)	−6(4)
O (27)	132(8)	31(2)	37(3)	−21(7)	−21(8)	−34(5)
O (28)	47(5)	33(2)	22(2)	−12(5)	19(6)	5(5)
O (29)	61(6)	80(4)	33(3)	−21(8)	−21(8)	31(6)
O (30)	45(4)	22(2)	23(2)	3(5)	−7(6)	2(4)
O (31)	63(6)	57(3)	25(2)	13(7)	19(7)	−28(5)

a) in the form $\exp[-(\beta_{11}h^2+\beta_{22}k^2+\beta_{33}l^2+\beta_{12}hk+\beta_{13}hl+\beta_{23}kl)]$.

C(16), C(17), C(24), and C(20), appeared in a difference map.

The inclusion of these in a structure-factor calculation, with each assigned an isotropic temperature factor of 4.0 Å^2, followed by six cycles, gave an R value of 0.098. The atomic scattering factors were taken from Ref. 11. At the end of the refinement, an analysis of the distribution of $\langle W\Delta^2 \rangle$ against $|F_o|$ and $\sin\theta$ confirmed that the weighting scheme was adequate. The final positional and thermal parameters for the atoms are listed in Table 2. The final structure factors are given in Table 3.*

Results and Discussion

A perspective view of the molecule, together with the numbering scheme, is shown in Fig. 1. The molecular structure of nagilactone A diacetate derived from X-ray analysis, as shown in (I), was consistent with that previously proposed on the basis of the chemical and spectroscopic data.[5]

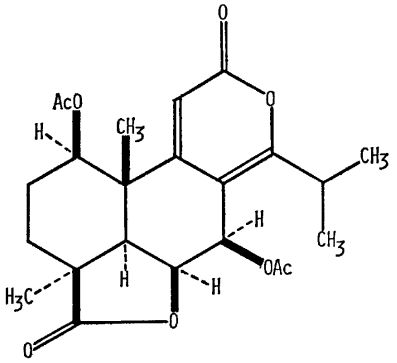

(I)

The A/B ring junction is *trans*, and H(5)/H(6) and H(6)/H(7) are *cis*. The O(30) atom at the 7-position is *cis* to C(20) at the 10-position and the γ-lactone ring. O(28) is in an equatorial position.

The equations of the least-squares planes and the deviations of individual atoms from these planes are given in Table 4. The torsional angles are shown in Fig. 2.

Ring A adopts a distorted chair conformation. The deviations from the least-squares plane (Plane I of Table 4) range from 0.096 Å (C(3)) to 0.324 Å (C(10)). For a closer examination of the chair, several planes consisting of four atoms and the deviations of the atoms from them are given in Table 4. These results and the torsional angles indicate that a flattening of the chair conformation occurs at C(3) and C(4), while puckering occurs at C(1) and C(10). The distortion of Ring A from a chair conformation may be mainly attributed to the formation of a lactone ring and to the 1,3-diaxial steric strains between C(20) and C(19), and between C(20) and O(26). In spite of the deformation, the C(20)···C(19) and C(20)···O(26) distances (3.028 Å and 2.934 Å respectively) are still shorter than the sum of the van der Waals radii, although these are larger from those expected from the dreiding molecular models.

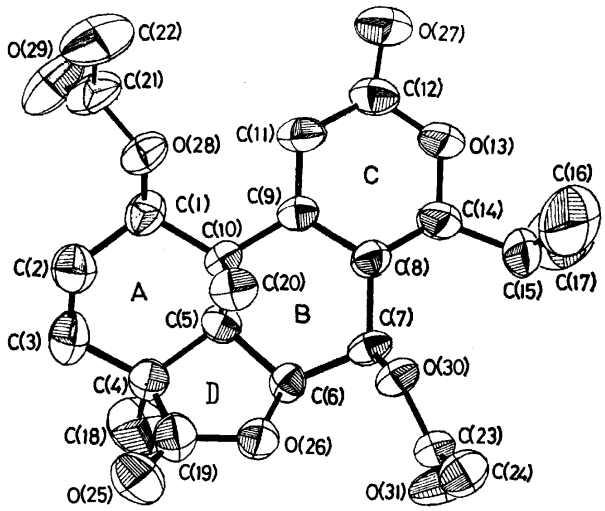

Fig. 1. Molecular structure and atomic numbering in nagilactone A diacetate. The thermal ellipsoids are scaled to include 50% probability.

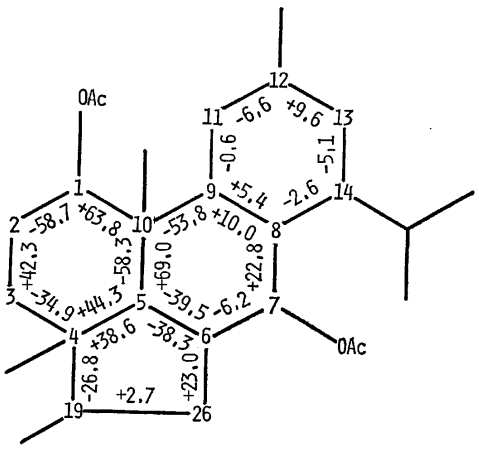

Fig. 2. Ring torsional angles in nagilactone A diacetate.

In Ring B, C(7), C(8), C(9) and C(10) are coplanar within 0.047 Å, with C(5) and C(6) deviating by 1.113 Å and 0.736 Å respectively in the same direction from this plane (Plane V). Upon the ABD ring fusion, Ring B adopts a conformation distorted from the energetically preferred half-chair form.[12] Ring C (α-pyrone ring) is nearly planar, although the deviations from Plane VI show a slight bending of the α-pyrone ring along the C(8)···C(12) vector. C(7) and O(27) deviate from Plane VI by +0.263 Å and +0.136 Å respectively in the same direction as C(12) and C(8), while C(10) and C(15) deviate by −0.093 Å and −0.090 Å respectively in the opposite direction.

In Ring D (γ-lactone ring), the C·C(O)·O·C moiety is planar with C(5), by 0.626 Å out of the plane.

The bond lengths and angles, together with their estimated standard deviations, are listed in Table 5. The mean C(sp^3)–C(sp^3) bond is 1.546 Å; however, there are a number of significant departures from

* Table 3 has been submitted to, and is kept by, the office of the Chemical Society of Japan, 1–5 Kanda-Surugadai, Chiyoda-ku, Tokyo 113. (Document No. 7509).

Table 4. Least-squares planes and deviations

The atoms indicated with asterisks were included in the calculation of the least-squares planes.

Plane I	$-0.8956x - 0.1300y - 0.4254z = 1.2292$
Plane II	$-0.8957x + 0.1506y - 0.4145z = 1.7385$
Plane III	$-0.7386x - 0.2514y - 0.6255z = 1.0017$
Plane IV	$-0.9448x - 0.2694y - 0.1867z = 0.8165$
Plane V	$-0.9780x + 0.1844y - 0.0976z = 0.7739$
Plane VI	$-0.9822x + 0.1865y + 0.0237z = 0.7486$
Plane VII	$-0.6829x + 0.3907y + 0.6173z = 2.2116$

Deviations from planes

Plane I		Plane II		Plane III		Plane IV	
C (1)*	0.316 Å	C (1)*	0.045 Å	C (1)	0.747 Å	C (1)*	0.111 Å
C (2)*	−0.199	C (2)*	−0.044	C (2)*	0.060	C (2)	−0.592
C (3)*	0.096	C (3)	0.449	C (3)*	−0.060	C (3)*	−0.113
C (4)*	−0.113	C (4)*	0.044	C (4)	−0.484	C (4)*	0.109
C (5)*	0.224	C (5)*	−0.046	C (5)*	0.056	C (5)	0.624
C (10)*	−0.324	C (10)	−0.782	C (10)*	−0.056	C (10)*	−0.107

Plane V		Plane VI				Plane VII	
C (5)	1.113 Å	C (7)	0.263 Å	C (15)	−0.090 Å	C (4)*	0.009 Å
C (6)	0.736	C (8)*	0.036	O (27)	0.136	C (5)	−0.626
C (7)*	0.023	C (9)*	−0.028	C (5)	1.158	C (6)*	−0.009
C (8)*	−0.047	C (10)	−0.093	C (6)	0.955	C (19)*	−0.015
C (9)*	0.046	C (11)*	−0.013			O (26)*	0.015
C (10)*	−0.022	C (12)*	0.050			O (25)	0.014
C (11)	0.197	O (13)*	−0.044				
C (14)	−0.090	C (14)*	0.000				

this mean. The C(2)–C(3) bond length (1.478 Å) is shorter by 6σ than the average value of the other C–C distances of Ring A. The lengthening of the C(5)–C(10) bond (1.580 Å) may be due to intramolecular steric strains between C(20) and C(19) and between C(20) and O(26). The same type of bond lengthening has been found in the crystal structures of levopimaric acid,[13] mebadonin,[14] and prerotundifuran.[15]

In Ring D, C(19)–O(26) [1.380 Å] is short and C(6)–O(26) [1.467 Å] long. Differences between C(sp^2)–O and C(sp^3)–O single-bond lengths in lactone groups have been found in many other structures.[16] A similar trend is found between C(21)–O(28) and C(1)–O(28), and between C(23)–O(30) and C(7)–O(30). The geometry observed in the C·C(O)·O·C moiety of Ring D or OAc may be ascribed to the contribution from the resonance form (II):

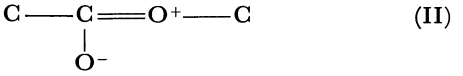

(II)

In Ring C (α-pyrone ring), the two C–O lengths (C(12)–O(13) and C(14)–O(13)) indicate a contribution from two resonance forms (IIIa and IIIb):

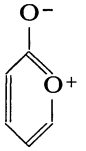

(IIIa)

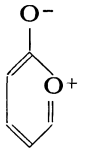

(IIIb)

The slight shortening of C(12)–O(13) is probably due to the larger electronegativity of the C(12) bonded to O(27) than that of C(14).

The C(8)–C(9), C(11)–C(12), C(12)–O(13), and C(14)–O(13) bond lengths show that considerable delocalization occurs in Ring C.

Most of the bond angles around the C(sp^3) atoms in Rings A and B deviate greatly from the tetrahedral angle as a result of the formation of the γ-lactone ring and the 1,3-diaxial interactions. The values range from 100.1° (C(4)–C(5)–C(6)) to 117.0° (C(2)–C(3)–C(4)). The C(4)–C(19)–O(25)=131.5° bond angle is largest for those around the C(19) atom of Ring D. The same trend was observed in the bond angles around the C(12) atom of the α-pyrone ring; C(11)–C(12)–O(27) is largest.

The shorter intermolecular contacts (less than 4.0 Å) are given in Table 6. The packing of nagilactone A diacetate molecules in the crystal structure is illustrated in Fig. 3. The mean plane of the four-ring nucleus is roughly parallel to the crystallographic bc plane. The intermolecular contacts correspond to van der Waals interactions.

Computer Programs

All the calculations were performed on a FACOM 270/30 computer at the Computer Center of Osaka City University using the following programs: RSLC-3,[17] RSSFR-3,[17] HBLS-IV,[17] SCALE (film factor, Lp and layer scaling),[18] TECS (stereoscopic drawing

TABLE 5. BOND LENGTHS (Å) AND ANGLES (deg.), WITH STANDARD DEVIATIONS IN PARENTHESES

(a) Bond distances

C (1) - C (2)	1.549 (10)	C (5) - C (10)	1.580 (9)	C (21) - C (22)	1.536 (13)	O (30) - C (23)	1.361 (8)
C (2) - C (3)	1.478 (12)	C (10) - C (1)	1.565 (9)	C (21) - O (29)	1.179 (11)	C (23) - C (24)	1.535 (11)
C (3) - C (4)	1.536 (11)	C (9) - C (11)	1.367 (9)	C (4) - C (19)	1.510 (11)	C (23) - O (31)	1.188 (10)
C (4) - C (5)	1.526 (9)	C (11) - C (12)	1.410 (11)	C (19) - O (26)	1.380 (8)	C (10) - C (20)	1.554 (9)
C (5) - C (6)	1.518 (9)	C (12) - O (13)	1.358 (9)	C (6) - O (26)	1.467 (8)	C (12) - O (27)	1.229 (9)
C (6) - C (7)	1.556 (9)	O (13) - C (14)	1.389 (9)	C (4) - C (18)	1.571 (12)	C (14) - C (15)	1.506 (11)
C (7) - C (8)	1.524 (9)	C (8) - C (14)	1.308 (10)	C (19) - O (25)	1.205 (9)	C (15) - C (16)	1.572 (18)
C (8) - C (9)	1.446 (9)	C (1) - O (28)	1.480 (8)	C (7) - O (30)	1.460 (8)	C (15) - C (17)	1.606 (17)
C (9) - C (10)	1.512 (9)	O (28) - C (21)	1.344 (9)				

(b) Valency angles

C (2) - C (1) - C (10)	110.0 (6)	C (3) - C (4) - C (19)	115.3 (7)
C (2) - C (1) - O (28)	106.2 (6)	C (5) - C (4) - C (18)	110.0 (6)
C (10) - C (1) - O (28)	106.3 (5)	C (5) - C (4) - C (19)	101.3 (5)
C (1) - C (2) - C (3)	113.3 (7)	C (18) - C (4) - C (19)	108.6 (6)
C (2) - C (3) - C (4)	117.0 (7)	C (4) - C (5) - C (6)	100.1 (5)
C (3) - C (4) - C (5)	114.0 (6)	C (4) - C (5) - C (10)	114.7 (5)
C (3) - C (4) - C (18)	107.5 (6)	C (6) - C (5) - C (10)	111.0 (5)
C (5) - C (6) - C (7)	115.4 (5)	O (13) - C (12) - O (27)	116.3 (7)
C (5) - C (6) - O (26)	104.4 (5)	C (12) - O (13) - C (14)	122.2 (6)
C (7) - C (6) - O (26)	111.5 (5)	C (8) - C (14) - O (13)	120.8 (7)
C (6) - C (7) - C (8)	114.0 (5)	C (8) - C (14) - C (15)	129.7 (7)
C (6) - C (7) - O (30)	113.4 (5)	O (13) - C (14) - C (15)	109.5 (6)
C (8) - C (7) - O (30)	108.8 (5)	C (14) - C (15) - C (16)	110.3 (8)
C (7) - C (8) - C (9)	121.4 (6)	C (14) - C (15) - C (17)	108.4 (8)
C (7) - C (8) - C (14)	118.8 (7)	C (16) - C (15) - C (17)	114.7 (8)
C (9) - C (8) - C (14)	119.6 (7)	C (4) - C (19) - O (25)	131.5 (7)
C (8) - C (9) - C (10)	116.3 (6)	C (4) - C (19) - O (26)	109.0 (6)
C (8) - C (9) - C (11)	118.7 (6)	O (25) - C (19) - O (26)	119.4 (7)
C (10) - C (9) - C (11)	125.0 (6)	C (22) - C (21) - O (28)	109.0 (7)
C (1) - C (10) - C (5)	104.2 (5)	C (22) - C (21) - O (29)	125.4 (7)
C (1) - C (10) - C (9)	114.8 (5)	O (28) - C (21) - O (29)	125.6 (8)
C (1) - C (10) - C (20)	111.6 (5)	C (24) - C (23) - O (30)	109.6 (6)
C (5) - C (10) - C (9)	103.2 (5)	C (24) - C (23) - O (31)	127.3 (7)
C (5) - C (10) - C (20)	115.9 (5)	O (30) - C (23) - O (31)	123.1 (7)
C (9) - C (10) - C (20)	107.1 (5)	C (6) - O (26) - C (19)	108.3 (5)
C (9) - C (11) - C (12)	120.7 (6)	C (1) - O (28) - C (21)	115.3 (6)
C (11) - C (12) - O (13)	117.2 (6)	C (7) - O (30) - C (23)	114.9 (5)
C (11) - C (12) - O (27)	126.4 (7)		

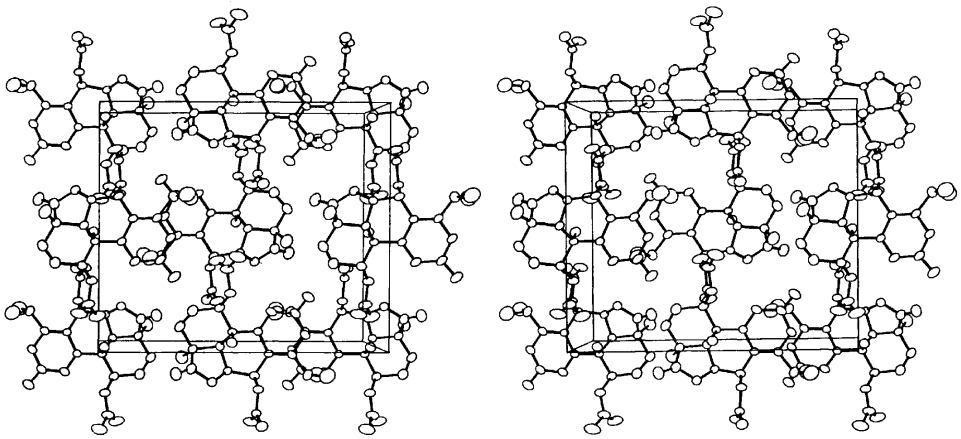

Fig. 3. Stereoscopic view of the packing in the crystal of nagilactone A diacetate looking along the a axis. The b axis is horizontal and the c axis is vertical. The atoms are represented by 50% probability thermal ellipsoids.

Table 6. Intermolecular distances less than 4.0 Å

C (1)	O (31, a)	3.427 Å	C (3)	O (25, g)	3.922 Å
C (3)	O (31, a)	3.856	C (2)	C (18, h)	3.803
C (4)	O (31, a)	3.987	C (3)	C (18, h)	3.981
C (5)	O (31, a)	3.525	C (18)	O (25, g)	3.456
C (10)	O (31, a)	3.988	O (13)	C (21, i)	3.935
C (6)	C (21, b)	3.900	O (13)	C (22, i)	3.872
C (18)	O (27, b)	3.471	O (13)	O (29, i)	3.813
C (5)	O (29, b)	3.699	C (2)	O (27, j)	3.220
C (6)	O (29, b)	3.129	C (21)	O (27, j)	3.467
C (7)	O (29, b)	3.152	C (22)	O (27, j)	3.735
C (8)	O (29, b)	3.607	O (27)	O (28, i)	3.636
C (14)	O (29, b)	3.910	O (27)	O (29, i)	3.734
C (20)	C (24, c)	3.812	C (15)	O (25, k)	3.762
C (20)	C (22, d)	3.699	C (17)	C (19, k)	3.947
C (22)	C (24, c)	3.912	C (17)	C (23, k)	3.987
C (24)	O (28, d)	3.712	C (17)	O (25, k)	3.660
C (12)	C (17, e)	3.933	C (17)	O (26, k)	3.443
C (9)	C (16, f)	3.918	C (17)	O (31, k)	3.771
C (11)	C (16, f)	3.710	C (23)	O (25, k)	3.561
C (12)	C (16, f)	3.942	C (24)	O (25, k)	3.493
C (16)	C (20, e)	3.948	O (25)	O (31, k)	3.692
C (24)	O (27, f)	3.446			

The letters refer to the following transformation relative to the reference molecule at x, y, z:

(a)	$-1/2-x$,	$-y$,	$-1/2+z$
(b)	$-1/2-x$,	$-y$,	$1/2+z$
(c)	$1/2-x$,	$-y$,	$-1/2+z$
(d)	$1/2-x$,	$-y$,	$1/2+z$
(e)	$-1/2+x$,	$-1/2-y$,	$-z$
(f)	$1/2+x$,	$-1/2-y$,	$-z$
(g)	$-1/2+x$,	$1/2-y$,	$-z$
(h)	$1/2+x$,	$1/2-y$,	$-z$
(i)	$-x$,	$-1/2+y$,	$-1/2-z$
(j)	$-x$,	$1/2+y$,	$-1/2-z$
(k)	$-x$,	$-1/2+y$,	$1/2-z$

of crystal and molecular structure),[19] PHASE-I, II and III (direct method),[20] and BOND (bond length and angle, best plane, dihedral angle and intermolecular distance).[21]

References

1) Preliminary communication, Y. Hayashi, T. Sakan, K. Hirotsu, and A. Shimada, *Chem. Lett.*, **1972**, 349.

2) Y. Hayashi, S. Takahashi, H. Ona, and T. Sakan, *Tetrahedron Lett.*, **1968**, 2071.

3) M. N. Galbraith, D. H. S. Horn, S. Ito, M. Kodama, and J. M. Sasse, *Agr. Biol. Chem.*, **36**, 2393 (1972); Y. Hayashi and T. Sakan, Proc. of the 8th International Conference on Plant Growth Substances (1973), in press, and the references cited therein.

4) I. Saeki, M. Sumimoto, and T. Kondo, *Holzforschung*, **24**, 83 (1970)

5) G. B. Russell, P. G. Fenemore, and P. Singh, *Chem. Commun.*, **1973**, 166.

6) W. C. Hamilton, J. S. Rollet, and R. A. Sparks, *Acta Crystallogr.*, **18**, 129 (1965).

7) A. J. C. Wilson, *Nature*, **150**, 152 (1942).

8) J. Karle and I. L. Karle, *Acta Crystallogr.*, **21**, 849 (1966).

9) J. Karle and H. Hauptman, *ibid.*, **9**, 635 (1956).

10) G. Germain, P. Main, and M. M. Woolfson, *ibid.*, **A27**, 368 (1971).

11) International Tables for X-ray Crystallography Vol. III. Birmingham: Kynoch Press (1962).

12) F. R. Jensen and C. H. Bushweller, *J. Amer. Chem. Soc.*, **91**, 5774 (1969).

13) I. L. Karle, *Acta Crystallogr.*, **B28**, 2000 (1972).

14) K. Hirotsu, T. Kamikawa, T. Kubota, A. Shimada, and T. Isobe, *Chem. Lett.*, **1973**, 255.

15) K. Hirotsu and A. Shimada, *ibid.*, **1973**, 1035.

16) P. C. Riche, *Acta Crystallogr.*, **B29**, 2147 (1973).

17) The Universal Crystallographic Computing System (I) ed. by T. Sakurai, The Crystallographic Society of Japan (1967).

18) H. Yoshioka, K. Hirotsu, and F. Takusagawa, unpublished work.

19) F. Takusagawa, unpublished work.

20) K. Nakatsu and K. Hirotsu, unpublished work.

21) H. Yoshioka, unpublished work.

X-Ray Photoelectron Spectroscopic Studies of Catalysts — Supported Cobalt Catalysts —

Yasuaki OKAMOTO, Hajime NAKANO, Toshinobu IMANAKA, and Shiichiro TERANISHI

Department of Chemical Engineering, Faculty of Engineering Science, Osaka University, Toyonaka, Osaka 560

(Received August 24, 1974)

XPS techniques were used to clarify the state of supported cobalt catalysts. In order to characterize Co^{2+} and Co^{3+}, the spin-orbit splitting of the 2p level, which is considered to be affected by the exchange interaction between the unpaired 3d electrons and 2p electrons, was found to be very useful. The interaction between catalyst and support was investigated. The state of supported cobalt was determined: Co_2O_3 on SiO_2, Co_2O_3+ $CoAl_2O_4$ on γ-Al_2O_3, and $LaCoO_3$ on La_2O_3. The order of the strength of the chemical interaction between cobalt and support is as follows:

$$La_2O_3 > \gamma\text{-}Al_2O_3 > SiO_2.$$

This fact was also confirmed by reduction experiments.

Recently, X-ray photoelectron spectroscopy (XPS or ESCA) techniques have been used in the studies of catalysts by many workers.[1-8] The advantage of XPS over the other techniques is that, in principle, it is capable of determining different valencies of supported metal on the surface layer simultaneously and of detecting the presence of any interaction between catalyst and support.

From XPS measurements for catalysts, we can obtain three important pieces of information–that is, information about the binding energy, the satellite, and the relative intensity of each level. On the basis of the binding energy of some inner level of an atom concerned (chemical shift), we can obtain information about the charge density of the atom and, therefore, the valence state of the atom. However, atoms with the same formal charge have different binding energies according to different circumstances, and, in some cases (for example, Ni compounds[9]), we cannot determine the valence states of the atom by the chemical shift alone.

The origins of satellite peaks have been investigated from the physical point of view by many workers.[10,11] According to their results, the paramagnetic species of some first transition-metal compounds show satellites on some levels; the satellites on the 2p-level are conidered to originate from shake-up processes (3d→4s transition), while the 3s-satellites are concluded to result from multiplet splittings by means of exchange interaction with 3d-unpaired electrons. However, the diamagnetic compounds show no such satellites. On the basis of these results, we can determine the magnetic properties of metal complexes or supported metal catalysts. The information about satellites is very useful in order to elucidate the valence state of the metal ion, especially in cases where it is difficult to determine its state by means of the binding energy alone.

From the relative intensities of the peaks for different level, we can obtain information about the surface composition of a catalyst or the surface coverage of the catalyst.[8]

According to the ESR spectra of supported cobalt catalysts,[12] it seems to be difficult to study the valence state of the supported cobalt because of the large spin-orbital interactions. Only very broad and ambiguous signals are obtained by ESR measurements for supported cobalt catalysts, and the cobaltic species are ESR-inactive. Moreover, only the bulk state of a catalyst is given by ESR and other techniques. Therefore, it seems that it would be interesting to investigate these catalysts by means of the XPS technique in order to characterize the surface state of the supported cobalt catalysts.

In this paper, on the basis of the results obtained by XPS measurements, the surface properties of the cobalt catalysts will be discussed. Moreover, we found that the energy differences between the $2p_{1/2}$ and $2p_{3/2}$ subshells of some first-transition metals are sensitive to the magnetic properties of the metal ion, and also that, in some cases, such information is more useful in the study of elucidating the valence state (magnetic properties) of the metal ion than the satellite is. We also studied the interaction between cobalt and support in order to ascertain the role of the support.

Experimental

Materials. The cobalt catalysts were prepared by a conventional impregnation technique using cobaltous nitrate. After drying at 100 °C, the catalysts were calcined at various temperatures for 5 hr in air. The supports examined were γ-Al_2O_3, SiO_2, and La_2O_3; and their surface areas were 235, 390, and 2 m^2/g respectively. The compounds used in this study were all supplied by Nakarai Chemical, Ltd., and Wako Pure Chemical, Ltd., except for the cobaltic compounds and $Co(CN)_2$, which were prepared and characterized according to published methods.[13] The CoO was obtained by the reduction of Co_2O_3 with H_2 or CO *in situ*.

Procedure. The photoelectron spectra were measured on a Hitachi 507 photoelectron spectrometer using AlKα or MgKα radiation. Powdered samples were held on a sample holder made of copper metal. The binding energies were corrected by using the value of 285.0 eV for the Cls level resulting from the contaminated carbon. The reproducibilities of the values thus obtained were within $\pm$0.2 eV; the energy differences were determined with an accuracy of $\pm$0.1 eV.

The reduction of the cobalt catalysts was carried out *in situ* using hydrogen with a pressure of 10 mmHg.

Results and Discussion

Spin-orbit Splitting of the 2p Level. There have been only a few reports of X-ray photoelectron spec-

Table 1. Binding energy, satellite splitting of 2p level, satellite type, and ΔE for cobalt compounds

	Compound	Satellite type[a]	Co2p$_{1/2}$		Co2p$_{3/2}$		ΔE[d]
			B. E.[b]	S. S.[c]	B. E.[b]	S. S.[c]	
1	CoF_2	B	798.1	6.0	782.1	4.6	16.0
2	$Co(NO_3)_2$	B	797.6	5.5	781.8	4.8	15.8
3	$CoSO_4$	A	797.5	5.0	781.4	3.7	16.1
4	$Co(CH_3COO)_2$	B	797.0	5.2	781.1	4.8	16.1
5	$Co_3(PO_4)_2$	A	797.0	5.2	781.0	4.8	16.0
6	$CoCrO_4$	B	796.8	6.5	780.9	5.6	15.9
7	$Co(CN)_2$	D	796.0	—	780.9	—	15.1
8	$CoCl_2$	A	796.6	6.2	780.7	5.6	15.9
9	$2CoCO_3 \cdot 3Co(OH)_2$	B	796.7	5.7	780.7	4.5	16.0
10	$CoBr_2$	A	796.3	6.7	780.3	5.2	16.0
11	CoO	B	796.0	6.1	780.3	5.5	15.7
12	Co_3O_4	C	794.6	9.2	779.6	9.5	15.0
13	Co_2O_3	C	794.5	9.3	779.4	8.9	15.1
14	$K_3Co(CN)_6$	D	796.7	—	781.7	—	15.0
15	$[(NH_3)_5Co(O_2)Co(NH_3)_5](NO_3)_4$	C	796.3	6.9	781.2	9.5	15.1
16	$[(NH_3)_5Co(O_2)Co(NH_3)_5]Cl_5$	C	796.5	9.3	781.5	9.4	15.0
17	$[Co(NH_3)_6]Cl_3$	C	796.7	8.4	781.7	9.6	15.0
18	$[Co(NH_3)_6]Br_3$	C	796.3	9.0	781.3	10.3	15.0
19	$[Co(NH_3)_5Br]Br_2$	C	796.1	8.0	781.0	8.9	15.1
20	$[Co(NH_3)_6](NO_3)_3$	C	796.4	8.7	781.5	9.4	14.9
21	$[Co(en)_3]Cl_3$	C	794.9	8.9	780.2	9.3	14.7
22	$[Co(en)_2Cl_2]Cl$	C	794.9	8.7	780.0	8.2	14.9
23	Co-metal	D	792.9	—	777.8	—	15.1

a) see Fig. 1. b) binding energy (eV). c) satellite splitting (eV). d) spin-orbit splitting of 2p level (eV).

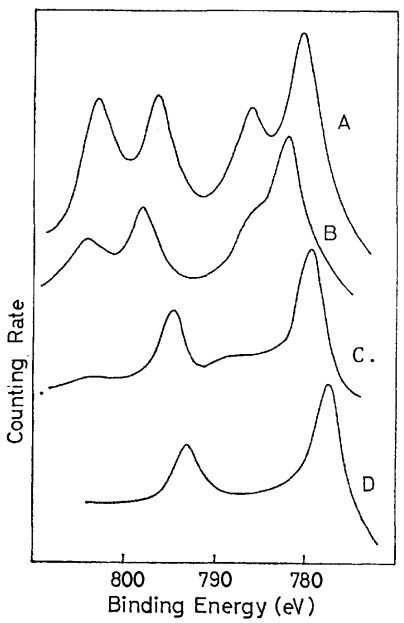

Fig. 1. XPS spectra of Co2p level for cobalt compounds, A~D indicate satellite type, A: $CoCl_2$, B: CoF_2, C: Co_2O_3, D: Co-metal.

troscopic measurements of cobalt compounds.[14] The binding energies of the cobalt compounds examined are listed in Table 1. The chemical shift is generally used to distinguish the oxidation states of the atom. However, as is shown in Table 1, the binding energies of the cobaltous compounds (Co^{2+}) examined are distributed between 782.1 eV for CoF_2 and 780.3 eV for $CoBr_2$, while those of cobaltic compounds (Co^{3+}) are distributed between 781.7 eV for $K_3Co(CN)_6$ and 779.4 eV for Co_2O_3, according to their chemical environments. Therefore, from the binding energy alone, we cannot clarify the oxidation state of these cobalt compounds. In the case of copper compounds, cuprous and cupric compounds can be distinguished by the chemical shift alone, as has been reported by Frost *et al.*,[15] whereas, in the case of cobalt compounds, as has been reported for nickel compounds,[9] the chemical shift is not a useful measure for discriminating the valence states.

The photoelectron spectra of the 2p level for some representative cobalt compounds are shown in Fig. 1. In some cases of a first-transition metal, it is well known that paramagnetic compounds show satellite(s) on the 2p level as a result of a shake-up process, while diamagnetic compounds do not. According to our systematic studies of cobalt compounds, all the cobaltous compounds except $Co(CN)_2$ have intense satellites, as is shown in Fig. 1, but none of the cobaltic compounds examined, cobalt metal, or $Co(CN)_2$ showed any such strong satellite. According to the intensity of the satellite, we classified the spectra into 4 types(A–D), as is shown in Fig. 1. The intensity ratio of the satellite and its main peak ($2p_{3/2}$) is >0.8 for Type A, >0.6 for Type B, ~0.1 for Type C, and ~0 for Type D. In Table 1, the satellite splittings and types are summarized for the cobalt compounds studied. Negative relations were observed between the satellite splittings and the binding energies for both

the $2p_{1/2}$ and $2p_{3/2}$ subshells of cobaltous compounds, as has been reported by Frost *et al.*[15] for cupric compounds. That is, when the covalency becomes smaller or the electronegativities of ligands become larger, the satellite splittings become smaller. These facts can be explained in terms of a shake-up process under the influence of the chemical environment, as has been indicated by Frost and his co-workers.[15] Therefore, the information about satellites may be used in conjunction with binding energy to predict the relative degree of covalency between the ligand and the central ion.

In the case of $Co(CN)_2$, the electronic configuration of this compound is a low-spin state; that is, $Co(CN)_2$ has one unpaired electron and the magnetic moment (μ_{eff}) of this compound is 3.11.[16] The other cobaltous compounds examined have high-spin configurations ($\mu_{eff} \fallingdotseq 5.2$). Moreover, the unpaired spin must be distributed over cyano ligands because of their large nephelauxetic effect. Therefore, $Co(CN)_2$ may behave like diamagnetic compounds in the XPS study of 2p satellites, since the spin density of the cobalt ion in $Co(CN)_2$ is low. The cobalt complex $[(NH_3)_5Co(O_2)Co(NH_3)_5]\ Cl_5$ is paramagnetic; it contains Co^{3+} and Co^{4+} and has one unpaired electron.[17] However, this compound also behaves in a diamagnetic manner for the 2p satellite, for the same reason as $Co(CN)_2$. However, an ambiguous weak satellite can be observed on the 3s level for both compounds; this indicates that the compounds are paramagnetic, as estimated from the magnetic properties.[16] It is considered that the different behavior of 2p and 3s satellites is a result of their different interaction strengths with 3d unpaired electrons.

Cobaltous compounds cannot be distinguished from cobaltic compounds by the chemical shift alone, but they can be discriminated by the satellite structure (magnetic properties). Since the chemical shift reflects the over-all electron density, and since the satellite structure shows the electronic configuration of the 3d level, it may be considered that the electron densities of the central metal ions, which are, of course, affected by the electronegativities of the ligands, are similar for cobaltous and cobaltic compounds, but that the electron configurations of the 3d levels for these compounds are influenced only very slightly by the ligands. It is estimated that the electrons of level higher than 3d (4s, 4p electrons) are responsible to a considerable degree for the bonding to the surrounding ligands.

From the XPS measurments, Co_2O_3 and Co_3O_4, which contains both Co^{2+} and Co^{3+}, could not be distinguished by chemical shift or satellite. This suggests that the surface layer of Co_3O_4 is similar to that of Co_2O_3.

As has been discussed above, the chemical shift and satellite peaks give information about the oxidation state and the chemical environment of a metal ion or a catalyst surface. However, in the studies of supported catalysts, the spectra obtained are usually weak, especially when the concentration of the catalytic components is low. Therefore, the information about the satellite is sometimes ambiguous, and it becomes difficult to characterize the catalyst.

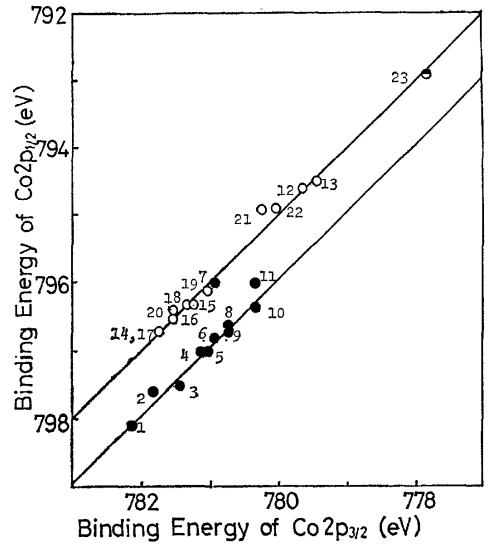

Fig. 2. Correlations of the binding energies of $Co2p_{3/2}$ and those of $Co2p_{1/2}$ for cobalt compounds. See Table 1 for a listing of the compounds

Table 2. ΔE values for Ni, Cr, and Cu compounds observed

Metal	ΔE (eV)	Compounds
Ni	17.6	Ni^{2+} compounds[1]
	17.2	Ni-metal
Cr	9.2	Cr^{6+} compounds
	9.7	Cr^{3+} compounds
	9.1	Cr-metal
Cu	20.1	Cu^{2+} compounds
	20.0	Cu^{+} compounds, Cu-metal

1) Paramagnetic compounds.

The spin-orbit splittings of the 2p level (ΔE) of the cobalt compounds examined are shown in Table 1. The relation between the binding energies of the $2p_{1/2}$ subshells and those of the $2p_{3/2}$ subshells is shown in Fig. 2. It is interesting that two different linear corelations are obtained for the cobaltous and cobaltic compounds. It is clear from Fig. 2 that, for cobaltous compounds, $\Delta E = 16.0$ eV, while for cobaltic compounds, $Co(CN)_2$, and cobalt metal, $\Delta E = 15.0$ eV. Hence, we can distinguish the oxidation states of the cobalt compounds by means of the value of ΔE. Recently, such correlations between the oxidation state and ΔE have been reported for several cobalt compounds by Frost *et al.*[14] The ΔE values for nickel, chromium, and copper compounds are shown in Table 2.

On the basis of these results, it seems to be established that the ΔE values for paramagnetic compounds are larger than those for diamagnetic compounds or metal, and that the energy difference in ΔE between paramagnetic and diamagnetic (or metal) compounds depends on the number of the unpaired electrons of the paramagnetic compounds. These results suggest that the origin of the change in ΔE is as follows. In the case of a paramagnetic 3d transition metal, the

satellite peaks of the 3s level are generally observed and the origin of the satellite is considered to be due to the exchange interaction between the 3s electron and the 3d unpaired electrons.[10] According to Basch,[10] the satellite splitting due to the exchange interaction is given as follows:

$$\Delta\varepsilon_\mu = \sum(N_t^\alpha - N_t^\beta)K_{\mu t} \quad (1)$$

where $\Delta\varepsilon_\mu$ is a satellite splitting of the μ-level, where N_t^α and N_t^β are the numbers of α and β spins respectively in the t-level, and where $K_{\mu t}$ is the exchange integral between t- and μ-levels. Such an effect of unpaired spins in the 3d band has been clearly observed on the 3s and 3p levels,[18] but for the 2p-level no such clear evidence of multiplet splitting has been found because of the smaller value of $K_{2p,3d}$ relative to $K_{3s,3d}$. According to the UHF calculations by Moskowitz *et al.*,[19] which predict a 3s-level splitting of 5.2 eV (compared to the 4.0 eV observed), the exchange splitting of the 2p level of NiF_6^{4-} is calculated to be about 2 eV. Therefore, the expected splitting of less than 2 eV would be difficult to observe with non-monochromatized X-ray sources, which give spectra with band widths at half height, typically about 2.5 eV. Recently, however, Frost *et al.*[15] reported that the widths of the main peaks of the 2p level from the cuprous compounds are narrower than that of cupric. These facts can be considered to be indirect evidence in favor of such splitting.

If we consider the case in which one unpaired electron exists in the 3d level and the orbital angular momentum, l, of the electron is spherically averaged (its state is expressed by $^2S_{1/2}$), for the sake of simplicity, the hole state of $2p_{1/2}$ and $2p_{3/2}$ subshells, after the emission of photoelectrons (whose states are expressed by $^2P_{1/2}$ and $^2P_{3/2}$ respectively), is split by exchange interaction with the 3d unpaired electron into two terms[20]:

$$^2S_{1/2}{}^2P_{1/2} \rightarrow {}^3P_0 \text{ and } {}^3P_1$$

$$^2S_{1/2}{}^2P_{3/2} \rightarrow {}^3P_2 \text{ and } {}^1P_1$$

In Fig. 3, some schematic spectra are shown. From Eq. (1), the energy differences between $^3P_0$ and $^3P_1$, or between $^3P_2$ and $^1P_1$ are given. The energy diagram of the sp configuration in an intermediate coupling[20] must be inverted in our case, since the hole states are involved in the XPS. From Fig. 3, we can expect a larger ΔE value for a paramagnetic compound than for a diamagnetic one. In real systems, the conditions are much more complicated, but the ΔE value for a paramagnetic compound may be expected to be larger than that for a diamagnetic compound. As has been discussed above, the change in ΔE is considered to be due to the multiplet splitting of the 2p level and to be indirect evidence for exchange interaction between the 2p and 3d levels. The dependence of the difference in the ΔE values between paramagnetic and diamagnetic compounds upon the number of unpaired spins can be explained by Eq. (1)

If the spin-orbit splitting of the 2p level is considered to be due to the multiplet splitting by the exchange

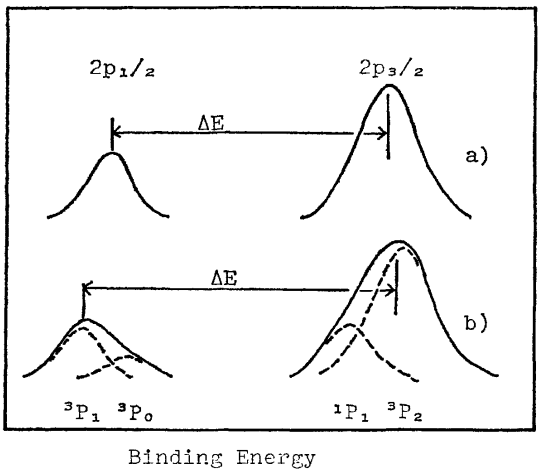

Fig. 3. Schematic spectra with and without exchange interaction between 2p and 3d levels.
a) without interaction b) with interaction.

Table 3. Binding energy of $2p_{3/2}$ level and ΔE for supported cobalt catalyst

Support	wt%	Calcination temperature (°C)	B. E. (eV)	ΔE (eV)
γ-Al_2O_3	5.0	100	780.8	15.8
	5.0	500	780.7	15.6
	5.0	1000	780.4	15.3
	10.0	500	781.0	15.1
La_2O_3	5.0	100	780.5	15.7
	5.0	500	779.7	15.0
	5.0	1000	779.6	15.0
	10.0	500	780.2	15.0
SiO_2	10.0	500	779.1	15.3

interaction with 3d unpaired electrons, the widths of the 2p-level spectra for paramagnetic cobaltous compounds must be broader than those for diamagnetic cobaltic compounds. In fact, the full widths at half height are about 3.4 eV and 2.9 eV for cobaltous and cobaltic compounds respectively. These facts support the multiplet splitting mechanism.

Consequently, in the study of catalysts with XPS, we can also use the ΔE value as a useful piece of information for elucidating the oxidation state of a catalyst component as well as the binding energy and the satellite.

Supported Cobalt Catalysts. The cobalt catalysts supported on γ-Al_2O_3, SiO_2, and La_2O_3 were also investigated. The catalysts examined are shown in Table 3; their binding energies of the $2p_{3/2}$ subshell and the ΔE values are also listed. In the case of cobalt catalysts, the ΔE values fall between 15.0 and 16.0 eV. This fact indicates the coexistence of Co^{2+} and Co^{3+} on the surface of cobalt catalysts.

In Fig. 4, the spectra of the 2p level for the supported cobalt (5 wt%) on γ-Al_2O_3 (a) are shown. As with the cobalt-alumina catalysts, after drying at 100°C the oxidation state of a large proportion of the cobalt is considered to be Co^{2+}, as expected, on the basis of the satellite and ΔE value, listed in Table

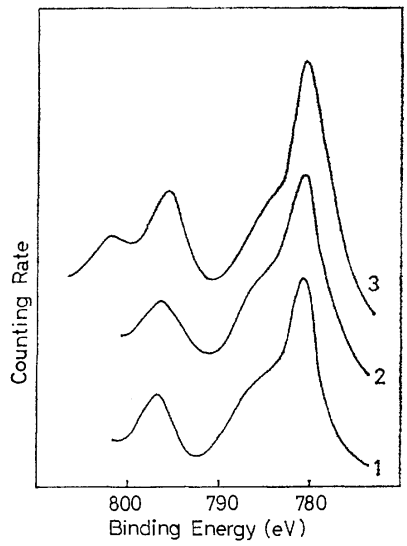

Fig. 4a. XPS spectra of Co2p level for cobalt supported (5 wt%) on γ-Al_2O_3, 1) after drying at 100 °C, 2) after calcination at 500 °C for 5 hr, 3) after calcination at 1000 °C for 5 hr.

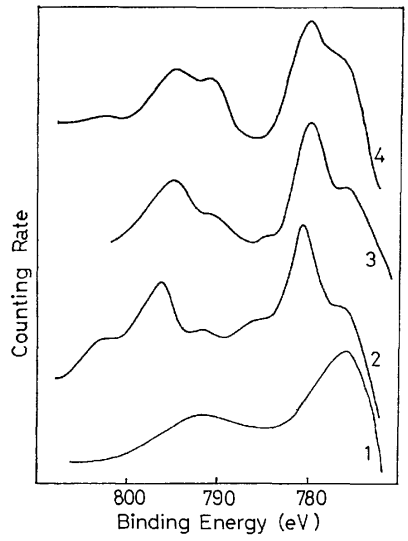

Fig. 4b. XPS spectra of Co2p level for cobalt supported (5 wt%) on La_2O_3, 1) back ground spectrum of La_2O_3, 2) after drying at 100 °C, 3) after calcined at 500 °C for 5 hr, 4) calcined at 1000 °C for 2 hr.

3. After the catalysts were calcined in air at 500 °C or 1000 °C, only very small chemical shifts for the $2p_{3/2}$ sublevel are observed, but ΔE changes 0.5 eV among these catalysts. In the case of the catalyst calcined at 500 °C, a weak satellite is observed (Fig. 4a) and the spin-orbit splitting is about 15.6 eV. Therefore, both Co^{2+} and Co^{3+} exist in comparable amounts on the 500 °C-calcined catalyst. However, with regard to the cobalt-alumina catalyst calcined at 1000 °C, it is considered that a large proportion of the cobalt is Co^{3+}, while only a small amount of Co^{2+} is present. This is confirmed by the ambiguous satellite peak for this catalyst shown in Fig. 4a. It may be concluded from Table 3 that the Co^{3+} content

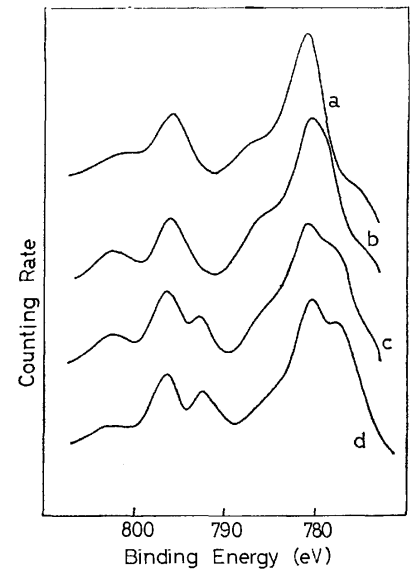

Fig. 5. XPS spectra of Co2p level for cobalt-alumina catalyst (10 wt%) reduced by H_2 (10 mmHg) at 400 °C.
a) after calcination at 500 °C for 5 hr, b) 20 min reduction, c) 80 min reduction, d) 250 min reduction

becomes larger with calcination at higher temperatures and with an increase in the amount of supported cobalt. It may be of interest to mention here that all the Co–Al_2O_3 catalysts calcined above 800 °C were blue in color, revealing the presence of Co^{2+} ions in a tetrahedral surrounding of O^{2-} ions,[21] and that X-ray diffraction analysis of this catalyst suggests the presence of $CoAl_2O_4$. Contrary to these results, a large proportion of the cobalt is Co^{3+}, as is shown by XPS measurements. The discrepancy between these results is considered to be due to different types of information about the catalyst; that is, the information about the surface layer is obtained by XPS (<20Å), about the much thicker layer, by means of the visible spectra ($<1\,\mu$), and about the "bulk" of the catalyst, by X-ray diffraction analysis. Comparing the chemical shift data in Tables 1 and 3, it is considered that the state of cobalt over γ-alumina calcined at 100°C is more covalent than that of cobaltous oxide. Moreover, after calcination at 500 °C or 1000 °C, the binding energies of $Co2p_{3/2}$ for these catalyst do not fall between those for CoO and Co_2O_3. These facts indicate an interaction (chemical or physical) between cobalt and γ-alumina, even after drying at 100 °C.

Such an interaction is supported by such reduction experiments as are shown in Fig. 5. After calcination at 500 °C (a), the cobalt-alumina catalyst (10 wt%) contains mainly Co^{3+}, as is to be expected from its spectrum (weak satellite) and ΔE value (15.1 eV). However, after a 20-min reduction at 400 °C (b), the main peak of the $2p_{3/2}$ subshell becomes broader, the satellite intensity becomes larger relative to the main peak, and the ΔE value increases to 15.5 eV. That is, the appearance of Co^{2+} can be expected. After further reduction (80 min) at 400 °C (c), a metal peak ap-

pears as a shoulder at about 778.1 eV. The higher binding energy peak of the $2p_{3/2}$ subshell with an ambiguous satellite is considered to be that of Co^{2+}, probably due to $CoAl_2O_4$, judging from the ΔE value (15.8 eV). No further intense change in the spectrum was observed even after a 250-min reduction at the same temperature (d). However, in the case of unsupported Co_2O_3, a peak due to CoO appeared after a 10-min reduction at 400 °C and a metal peak appeared clearly after a 15-min reduction at the same temperature. The spectrum of a pure metal was obtained after only a 40-min reduction. These facts indicate a strong interaction between cobalt and γ-Al_2O_3.

In the case of silica gel, it is considered that Co_2O_3 is formed on the surface; it is then easily reduced to cobalt metal as Co_2O_3. Therefore, no specific interaction between cobalt and silica gel is found.

As regards the cobalt catalysts supported on La_2O_3, a cobaltic compound can be expected after calcination over 500 °C. Comparing the chemical shifts of cobaltic compounds in Table 1, the chemical environment of cobaltic compounds on La_2O_3 is considered to be similar to that of Co_2O_3. It is clear from Fig. 4b the intensity of the cobalt 2p level, compared to the background peak of La_2O_3, becomes weaker with the calcination temperature; this indicates that the cobalt ion diffuses into La_2O_3 or that new compounds of cobalt and La_2O_3 are formed. In the cases of alumina and silica gel, no such intense change in the intensity of the cobalt peaks was observed upon treatment. On the basis of the X-ray diffraction studies, it is found that $LaCoO_3$ is formed. To confirm this conclusion, reduction experiments were carried out. After a 1-hr reduction, Co^{2+} appeared (ΔE=15.5 eV); no metal peak was observed clearly until after a 2-hr reduction at 400 °C. Therefore, cobalt on La_2O_3 is the most difficult to reduce among the cobalts on all the supports examined. These facts confirm that the new compound ($LaCoO_3$) is formed on the catalyst surface.

Summarizing these results, it is determined that the states of supported cobalt are; Co_2O_3 on SiO_2, Co_2O_3+$CoAl_2O_4$ on γ-Al_2O_3, and $LaCoO_3$ on La_2O_3. Consequently, it is concluded that the chemical interaction between support and cobalt catalyst decreases as follows:

$$La_2O_3 > \gamma\text{-}Al_2O_3 > SiO_2$$

References

1) W. N. Delgass, T. R. Hughes, and C. S. Fadley, *Catal. Rev.*, **4**, 179 (1970).
2) A. W. Miller, W. Atkinson, M. Barber, and P. Swift, *J. Catal.*, **22**, 140 (1971).
3) D. A. Whan, M. Barber, and P. Swift, *Chem. Commun.*, **1972**, 198.
4) J. S. Brinen and A. Melera, *J. Phys. Chem.*, **76**, 2525 (1972).
5) P. Biloen and G. T. Pott *J. Catal.*, **30**, 169 (1973).
6) J. Escard, C. Leclere, and J. P. Contour *ibid.*, **29**, 31 (1973).
7) Y. Okamoto, K. Adachi, T. Imanaka, and S. Teranishi, *Chem. Lett.*, **1974**, 241.
8) Y. Okamoto, M. Fujii, T. Imanaka, and S. Teranishi, unpublished.
9) L. J. Matienzo, L. I. Yin, S. O. Grim, and W. E. Swartz, *Inorg. Chem.*, **12**, 2762 (1973).
10) H. Basch, *Chem. Phys. Lett.*, **20**, 233 (1973) and the literature therein.
11) L. Yin, I. Adler, T. Tsang, L. J. Matienzo, and S. O. Grim, *Chem. Phys. Lett.*, **24**, 81 (1974) and the literature therein.
12) H. Ueda, *J. Catal.*, **27**, 281 (1972).
13) "Inorganic Synthesis," Vol 1–12, McGraw-Hill Book Comp. New York and London (1939–1970).
14) D. C. Frost, C. A. McDowell, and I. S. Woolsey *Mol. Phys.* **27**, 1473 (1974).
15) D. C. Frost, A. Ishitani, and C. A. McDowell *ibid.*, **24**, 861 (1972).
16) "American Institute of Physics Handbook," 3rd Ed. McGrow-Hill Book Company, New York (1972).
17) F. A. Cotton and G. Wilkinson "Advanced Inorganic Chemistry," 2nd Ed. Interscience Publishers, New York, London, Sydony, 1966.
18) C. S. Fadley and D. S. Shirley, *Phys. Rev.*, **2A**, 1109 (1970).
19) J. W. Moskowitz, C. Hollister, C. J. Hornback, and H. Basch, *J. Chem Phys.*, **53**, 2570 (1970)
20) E. C. Condon, and G. H. Shortley "The Theory of Atomic Spectra," Cambridge University Press (1970), p. 272.
21) J. H. Ashley and P. C. Mitchell, *J. Chem. Soc. Ser. A*, **1968**, 2821.

Studies of the Catalytic Properties of Synthetic Zeolite A. IV.[1,2] The Thermal Stability of Silver-exchanged Zeolite A

Shigemi MATSUMOTO,* Masahiro NITTA, Kiyoshi OGAWA, and Kazuo AOMURA

Faculty of Engineering, Hokkaido University, Sapporo 060

(Received September 11, 1974)

The effects of the degree of exchange and the dehydration upon the structural stability of silver-exchanged forms of the synthetic zeolite Linde 4A have been investigated by means of DTA, X-ray diffraction, and adsorption studies. The relative intensity of the X-ray powder diffraction decreased with an increase in the extent of Ag^+-exchange, though it indicated no accurate information on the crystallinity. An exotherm on the DTA curves which shifted to a lower temperature with the degree of exchange became an indication of the collapse of the structure; this was in good agreement with the specific surface area of the sample heated at a higher temperature. From these results, the silver-exchanged zeolite A was concluded to be thermally unstable and to lose its crystal structure at a lower temperature than the original sodium form. It is also proposed that the comparison of the X-ray powder diffraction intensity is not suitable as a method for judging the crystallinity of zeolites A.

In the previous papers of this series,[3,4] the instability of silver-exchanged zeolites A [(Ag^{ex}, Na)-A and (Ag^{ex}, Ca)-A]** was pointed out on the basis of the low intensities of the X-ray diffraction patterns and on the basis of their catalytic properties, which are quite different from those of other cation-exchanged forms. No study of the thermal stability of Ag^{ex}-A is found in the literature except that of the reduction of silver ions in zeolite. Earlier studies of zeolite A reported that the instability of zeolite A was observed in ion-exchanges involving H^+, Ba^{2+}, Zn^{2+}, Ni^{2+}, Co^{2+}, Cu^{2+} and Fe^{3+} by means of X-ray study, and that Ag^{ex}-A was stable.[5,6] However, the influence of the degrees of exchange and dehydration (heat-treatment) on the structural stability has not been systematically investigated; also, there are many ambiguous statements in the method for determining the crystallinity of cation-exchanged zeolite in the reports.

The object of this investigation was to study the thermal stability of (Ag^{ex}, Na)-A in relation to the degree of exchange. The propriety of the method for determining the crystallinity will also be discussed in relation to DTA, X-ray-diffraction, and adsorptive studies.

Experimental

Materials. The original sodium-form of zeolite A was Linde Molecular Sieves 4A (Na–A) powder. The ion exchange was carried out at 85±1 °C with a 0.1 M solution of $AgNO_3$, according to a method described before.[4] Precautions were taken to shied it from bright light during operations as much as possible, since silver-exchanged zeolite was somewhat unstable to light. The higher exchanged sample was colored only a slight gray. The (Ag^{ex}, Na)-A samples, after having been dried at 120 °C for 10 hr, were all kept over saturated NH_4Cl solutions for at least 2 weeks at room temperature to maintain the moisture content constant. The degree of exchange was determined by a method described before.[4]

X-Ray Diffraction. The X-ray powder diffraction patterns were obtained on a scintillation counter spectrometer (Rigaku-Denki Geiger flex D-9C unit) with a pen recorder, using filtered Cu $K\alpha$ radiation. The hydrated and the dehydrated samples were exposed to air while their spectra were measured. Visual comparisons of the peak intensities of certain planes were made. The (311), (321), and (322, 410) planes were chosen, as they have suitable intensities in the original Na-A.

DTA. The differential thermal analysis was performed in air using a Rigaku-Denki 8001 DTA unit, in which the temperature was raised at the rate of 10 °C/min up to 1000 °C. The α-alumina was used as the reference material.

Specific Surface Area. The specific surface areas of the samples, which were activated at various temperatures for 3 hr, were measured by a standard volumetric method, using oxygen as an adsorbate, at −196 °C. The samples were activated in two different atmospheres, *i.e.*, *in vacuo* and in air.

Results and Discussion

First, the crystallinity of Ag^{ex}-A was estimated from the X-ray diffraction patterns. The sum of the peak intensities of the (311), (321), and (322, 410) planes of Ag^{ex}-A was compared with that of the other cation forms. As is shown in Table 1, all but Ag^{ex}-A have almost the same intensity. This shows that, after ion exchange, all the hydrated samples except Ag^{ex}-A retain their primary crystal structure, as has been reported in the literature.[5,6] In many studies of zeolites, the crystallinity has thus been determined by comparing the intensities of selected X-ray powder reflections.[7]

TABLE 1. RELATIVE X-RAY CRYSTALLINITY OF HYDRATED ZEOLITES A

Cation form[a]	% Exchanged	X-ray intensity[b]
Na^+	100	164
K^+	79	143
Mg^{2+}	76	170
Ca^{2+}	82	148
Zn^{2+}	81	137
Ag^+	99	59

a) Cation forms other than Ag^+ were prepared in Part II.[4] b) Arbitrary units.

* Present address: Kanegafuchi Kagaku Kogyo Co., Takasago-shi, Hyogo.

** The nomenclature of the synthetic zeolites exchanged with various cations is based on the suggestions given by Barrer in the Proceedings of the 3rd International Conference on Molecular Sieves, Zurich 1973.

TABLE 2. RELATIVE INTENSITY OF (Ag^{ex}, Na)-A POWDER DIFFRACTIONS

% Exchanged $Ag^+/(Ag^+ + Na^+)$	X-ray intensity[a] Hydrated	300 °C[b]	600 °C[c]
0	164	173	166
28	119		
38	105		
50	83		
57	72	61	58
84	58		
99	59	49[d] 48	71 0[e]
46[f]	118		

a) Arbitrary unit. b) After heated for 3 hr *in vacuo*. c) After heated for 3 hr in air. d) 250 °C. e) 700 °C. f) $Na^{ex}_{0.54}$ $Ag^{ex}_{0.46}$-A reexchanged from uncalcined $Ag^{ex}_{0.99}$ $Na_{0.01}$-A.

The trouble is that the pattern of Ag^{ex}-A was very weak. As is shown in Table 2, the relative X-ray crystallinity of (Ag^{ex}, Na)-A decreased with an increase in the extent of Ag^+ exchanged; this trend was found also in the samples calcined at higher temperatures (up to 600 °C). This generally implies that ion exchange of Na-A with Ag^+ destroys the crystal structure, and it is contrary to Barrer's report.[6] However, in spite of the low intensities of all the peaks every major peak of the Na-A pattern ($5<2\theta<35°$) was present in the pattern of Ag^{ex}-A. We felt, therefore, that the low intensity of Ag^{ex}-A was a result of interference based on the high scattering power of silver for X-rays. This suspicion was verified by the fact that, when a sample of Ag^{ex}-A, which had never been dehydrated above 120 °C, was re-exchanged with an $NaNO_3$ solution, the Na^{reex}-A showed its peak intensity close to the original Na-A (See Table 2). It may, therefore, be concluded that the silver-exchange

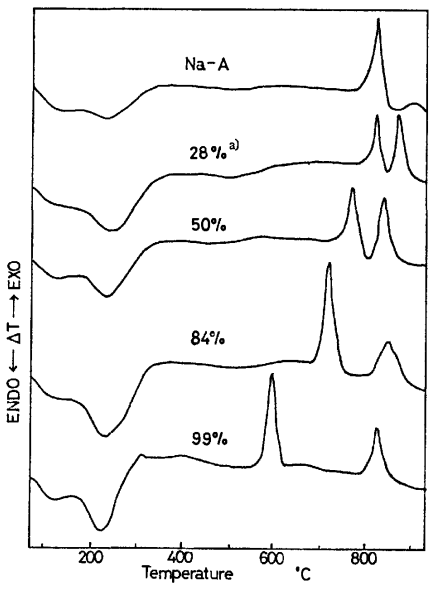

Fig. 1. DTA curves for (Ag^{ex}, Na)-A
a) The degree of exchange, $Ag^+/(Na^+ + Ag^+)$

of Na-A does not cause the crystal to collapse and that Ag^{ex}-A may be stable thermally up to 600 °C. The most important point is that a conventional X-ray powder diffraction study (*i.e.*, a comparison of the peak intensity) of cation-exchanged zeolites A does not give accurate information on the crystallinity. A similar conclusion may also be drawn from recent reports on the stability of Ba^{ex}-A.[8,9]

Then, more detailed information on the stability of Ag^{ex}-A was obtained by a thermographic method. The DTA results on (Ag^{ex}, Na)-A are shown in Fig. 1. A pronounced endothermal effect (130—230 °C) and two high-temperature exothermal effects (600—910 °C) were observed in all the samples. The endothermal effect corresponds to the removal of water from the zeolite.[10] The beginning of the first high-temperature exotherm, which is due to the loss of the structure, shifted from 780 to 560 °C with an increase in the extent of silver. In fact, the additional X-ray measurement revealed that the zeolite structure of $Ag^{ex}_{0.99}Na_{0.01}$-A is maintained until the beginning of the first exoeffect (~600 °C) and that, at 700 °C, the structure converts to the amorphous phase. This exoeffect may be considered to be due to the following reaction, caused by dehydration from structural hydroxyl groups:

$$\underset{\text{I}}{Ag(H_2O)_n\text{-Zeolite}} \overset{\Delta}{\rightleftarrows} \underset{\text{II}}{\{Ag(OH)_m\text{-Z}+AgO_x\text{-Z}+\underset{\text{IV}}{\text{H-Z}}\}}$$

$$\overset{\Delta}{\rightleftarrows} \underset{\text{III}}{AgO_x\text{-Z} + \text{amorphous phase}}$$

That is to say, the dissociation of coordinated water molecules by the polarizing power of Ag^+ and by heating releases protons, thus forming the structural hydroxyls (IV). The dehydration of IV at a higher temperature destroys the lattice structure. Since the polarizing power of Ag^+ is larger than that of Na^+, the dissociation of the protons and the hydroxyl dehydration may be promoted at lower temperatures with an increase in the extent of Ag^+ in zeolite. The process of the dehydration of IV appears on the first exotherm. This trend was in good agreement with the results obtained from the X-ray study and with the below-mentioned specific surface area.

The other exotherm appears at 850—910 °C. It is known that, at 800 °C, zeolite A recrystallizes to a β-crystobalite-type structure. The latter exoeffect, therefore, may indicate this. From these results, it may be concluded that the thermal stability of Ag^{ex}-A is lower then that of Na-A.

The specific surface area of (Ag^{ex}, Na)-A was determined from the oxygen adsorption for samples calcined at various temperatures in different atmospheres. The stability of (Ag^{ex}, Na)-A to the degree of exchange and to heat-treatment is shown in Table 3. The Ag^{ex}-A calcined at 200 °C did not adsorb oxygen. This is because of the residual water molecules coordinated strongly to Ag^+; the evidence is supported by the endotherm being sharp and larger than that of Na-A in Fig. 1. It seems that the loss of the crystallinity is slightly greater in the case of air calcination

TABLE 3. THE SPECIFIC SURFACE AREA OF (Ag^{ex}, Na)-A

% Exchanged	Specific surface area, m^2/g, Calcination temp. *in vacuo*				
	200 °C	250 °C	300 °C	400 °C	600 °C
0	385	689	659	616	237[a]
			631[a]		36[a,b]
28	*	664	686		
38			638		
50			653		
57			661	527	
84			451		
99	*	669	403	361	71.2[a]
			326[a]	308[a]	<10[a,b]

a) Recalcined at 250 °C for 30 min *in vacuo* after calcined for 3 hr in air. b) 750 °C. * Impossible to measure.

above 300 °C was smaller than that at 250 °C. This effect increases with the extent of silver exchange. We estimate that a degradation of the structure occurred to some degree, resulting in a partial obstruction of the zeolite pores to the oxygen adsorbate. Below 600 °C, however, this structural change is too samll to appear on the DTA curves. The specific surface area of Na-A calcined at 600 °C in air was still about 35% of the value at 250 °C, whereas $Ag^{ex}_{0.99}Na_{0.01}$-A calcined at 600 °C in air retained only about 10% of its original crystallinity. The latter change is very large, and it appears on the DTA curve (see the 99% value in Fig. 1).

The results in Table 3 (column of 300 °C) suggest that Ag^+ enters into sites unfavorable to maintaining the structure when the degree of exchange exceeds about 57%, since the specific surface area suddenly decreases at 84%. Zeolite A has three kinds of cation sites.[11] Details on the site selectivity of Ag^+ have been reported by Nitta *et al.*[12]

On the other hand, it is known that the Ag^+-exchanged zeolites are relatively reducible, easily in the dehydrated state. It was first pointed out by Habgood[13] that the reduced Ag^{ex}-X has a partial loss of crystallinity with the appearance of metallic silver. Huang[14] reported also that Ag^{ex}-X and Ag^{ex}-Y were reduced after treatment with CO at 350 °C. In the present case, Ag^{ex}-A exchanged highly has colored only a slight gray in the hydrated state. This may indicate a slight reduction of Ag^+ by light or CO in air during drying at 120 °C. However, it is considered that the reduction resulting in a collapse of the structure did not occur, because the specific surface area was retained almost the same as in Na-A and because the X-ray diffraction pattern, though low in intensity, was unchanged. Giordano[15] also reported, from the results of DTA, that the collapse of the structure for Ag^{ex}-A calcined at 400 °C and reduced by hydrogen at 250 °C was negligible.

Furthermore, with regard to the color of Ag^{ex}-A, the sample was a white color and a slight grayish white color; it first turned a deep yellow-red color on dehydration *in vacuo* and in air at elevated temperatures. It changed to a bright yellow while cooling in air and ultimately back to the original white at room temperature. This color change occurred reversibly. Therefore, it is due to the alteration of the ligands of Ag^+ on dehydration, as has been described above. A study[16] of the UV spectra of Cu^{ex}-Y at different hydration levels has revealed that, in the below reaction, the absorption band corresponding to VI appears in a longer wavelength region compared with that of V:

$$\underset{\text{V}}{Cu(H_2O)_6} \overset{\Delta}{\rightleftarrows} CuO_3(OH)_3 \overset{\Delta}{\rightleftarrows} \underset{\text{VI}}{CuO_6}$$

In the present case, three distinct complexes exist at several degrees of hydration; *i.e.*, the I, II and III described above correspond to them. According to the spectrochemical series, the absorption spectrum of Ag^+ in II should shift to a wavelength longer than that of I (*i.e.*, from the ultraviolet to the visible region); probably that of III would also shift to a longer wavelength region. Consequently, the Ag^{ex}-A changes from colorless to yellow-red when it is dehydrated at elevated temperatures.

We wish to thank Professor Jiro Ishii of Tokai University for his help in the X-ray measurment, Mr. Takeshi Tsuchida of Hokkaido University for his help in DTA analysis, and Dr. Takao Yotsuyanagi of Hokkaido University for his valuable discussion on the color of metal ion.

References

1) Part III: S. Matsumoto, M. Nitta, and K. Aomura, This Bulletin, **47**, 1537 (1974).
2) Presented at the Summer Meeting of the Hokkaido Branch of the Chemical Society of Japan, Kitami, July, 1974.
3) M. Nitta, K. Tanabe, and H. Hattori, *Bull. Japan Petrol. Inst.*, **15**, 113 (1972).
4) M. Nitta, S. Matsumoto, and K. Aomura, *Nippon Kagaku Kaishi*, **1973**, 1839.
5) D. W. Breck, W. G. Eversole, R. M. Milton, T. B. Reed, and T. L. Thomas, *J. Amer. Chem. Soc.*, **78**, 5963 (1956).
6) R. M. Barrer and W. M. Meier, *Trans. Faraday Soc.*, **54**, 1074 (1958).
7) D. W. Breck, "Zeolite Molecular Sieves," John Wiley & Sons, New York (1974), p. 493.
8) H. S. Sherry and H. F. Walton, *J. Phys. Chem.*, **71**, 1457 (1967).
9) A. Dyer, R. B. Gettins, and A. Molyneux, *J. Inorg. Nucl. Chem.*, **30**, 2823 (1968).
10) R. M. Barrer and D. A. Langley, *J. Chem. Soc.*, **1958**, 3817
11) R. Y. Yanagida, A. A. Amaro, and K. Seff, *J. Phys. Chem.*, **77**, 805 (1973).
12) M. Nitta, S. Matsumoto, and K. Aomura, *J. Catal.*, **35**, 317 (1974).
13) H. W. Habgood, *Can. J. Chem.*, **42**, 2340 (1964).
14) Y. Y. Huang, *J. Catal.*, **32**, 482 (1974).
15) N. Giordano, S. Motelatici, and C. Zen, Recent Prog. Report, 3rd International Conf. Molecular Sieves, 1973, p. 449.
16) N. M. Kuzmenko and V. I. Lygin, *ibid.*, p. 347.

The Quenching of the Cadmium Resonance Radiation at 326.1 nm by Ammonia and the Emission from the Complex between Excited Cadmium Atoms and Ammonia in the Presence of Argon

Shunzo YAMAMOTO, Shigeru TSUNASHIMA, and Shin SATO

Department of Applied Physics, Tokyo Institute of Technology, Ookayama, Meguro-ku, Tokyo 152

(Received October 3, 1974)

The pressure dependences of the emission intensities at 326.1 and 432 nm in the cadmium-photosensitized reaction of ammonia have been measured. In order to interpret the nonlinear Stern-Volmer plots for the quenching of the 326.1 nm resonance line, the following reactions have to be taken into account in the reaction scheme: $Cd^*+NH_3 \rightleftharpoons CdNH_3{}^*{}_v$, $CdNH_3{}^*{}_v+M \rightarrow CdNH_3{}^*+M$. The pressure dependence of the emission from the $CdNH_3{}^*$ complex (at 432 nm) was also well explained in terms of a reaction scheme involving the above reactions.

It is well known that excited mercury atoms form complexes with some molecules (NH_3, H_2O, *etc.*) and that these complexes fluoresce.[1-3] Since the electronic character of cadmium atoms is similar to that of mercury atoms except for the amount of energy involved, the complexes of excited cadmium atoms with some molecules are expected to fluoresce. Recently, two groups, including one in our laboratory,[4,5] have reported a cadmium-photosensitized emission of ammonia at the wavelength of 432 nm; this emission has been attributed to that from the complex between excited cadmium atoms and ammonia. In a short communication,[4] Morten *et al.* assigned the emitting complex to that formed between $Cd(^3P_0)$ atoms and ammonia, by analogy with the Hg–NH_3 system.

As was mentioned in a previous paper,[6] the absorption intensity at 326.1 nm ($5^3P_1 \leftarrow 5^1S_0$) is dependent upon the pressure of foreign gases through the pressure broadening of the absorption line. In a previous study[5] of the cadmium-photosensitized luminescence of ammonia, however, this effect was not taken into account. The present paper will report the results of a study of the cadmium-photosensitized luminescence and of the quenching for the 326.1 nm resonance line under the conditions of the ammonia being diluted with argon and the total pressure being kept constant in order to minimize the effect of the pressure broadening. These results will reveal a somewhat detailed mechanism of the complex-formation between the excited cadmium atoms and ammonia.

Experimental

The apparatus and procedure were almost the same as those previous described.[5] The reaction cell and the cadmium resonance lamp were kept in an electric furnace at 220±1 °C. The vapor pressure of cadmium at 220 °C is 1.04×10^{-3} Torr. The lamp was operated by an alternating current (50 Hz).[6]

The cadmium metal used was high-purity cadmium (99.9999%) manufactured by the Osaka Asahi Metal Co. Pure-grade ammonia (Takachiho Shoji Co.) was used after degassing at the temperature of liquid nitrogen. Pure-grade argon purchased from the Takachiho Shoji Co. was used after repeated adsorption and desorption on a molecular sieve at the temperature of liquid nitrogen.

Results

When the empty cell was illuminated by means of the cadmium lamp, line spectra were observed at 326, 340, 347, 361, 468, 480, and 509 nm. In the presence of the cadmium vapor in the cell at 220 °C, the intensity of the 326.1-nm emission increased, but those of the other lines remained unchanged. When argon was added, the intensity of the 326.1-nm emission increased with the increase in the pressure, as is shown in Fig. 1. This increase has been attributed to the increase in the absorption of the exciting light on the basis of the pressure broadening of the absorption line.[6]

When an ammonia–argon mixture was added, the intensity of the emission at 326.1 nm decreased with the increase in the partial pressure of ammonia, while the total pressure was kept constant, and a new band emission was observed at 432 nm. The position and the profile of the new band emission at 432 nm were independent both of the total pressure examined and of the pressure ratio of ammonia to argon, while the intensity changed with the increase in the partial pressure of ammonia, as is shown in Fig. 2. As the intensity of the 432-nm emission decreased with the increase in the irradiation time, the emission intensities shown in Fig. 2 were obtained by extrapolation to zero irradiation time.

The Stern-Volmer plots for the quenching of the 326.1-nm resonance line are shown in Fig. 3, where $I^0_{326.1}$ and $I_{326.1}$ are the emission intensities at 326.1 nm in the absence and in the presence of ammonia

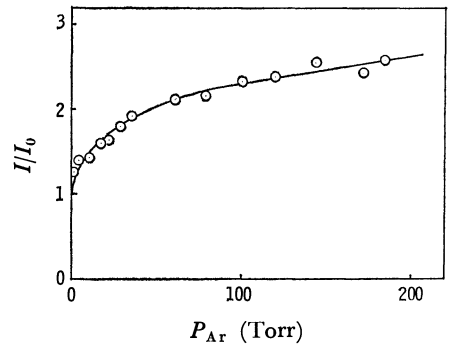

Fig. 1. The intensity of the resonance radiation at 326.1 nm as a function of the pressure of argon.

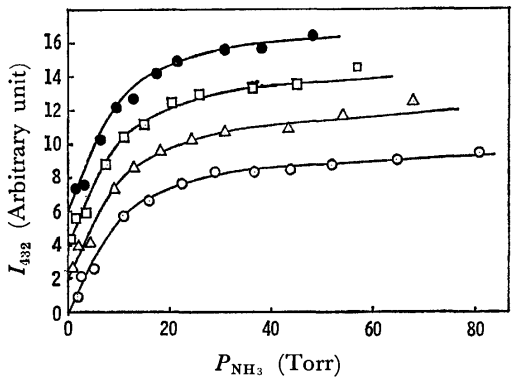

Fig. 2. The emission intensity at 432 nm as a function of the partial pressure of ammonia. The total pressures are 208 (○), 175 (△), 147 (□), and 123 (●) in Torr. Solid lines show the values calculated according to Eq. (2). The plots are displaced upwards by 2 units of I_{432} for clarity in the above order of the total pressure.

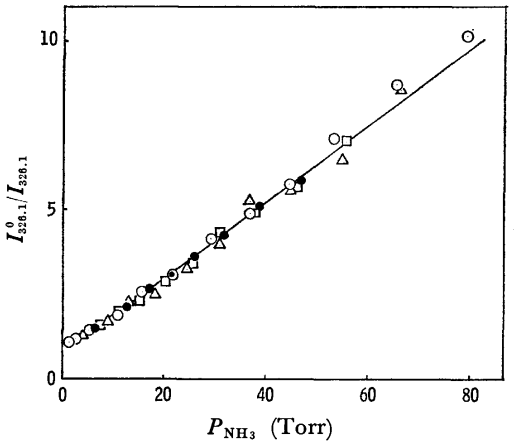

Fig. 3. Stern-Volmer plots for the quenching of the resonance radiation at 326.1 nm by ammonia diluted with argon. The total pressures are 208 (○), 175 (△), 147 (□), and 123 (●) in Torr. Solid line shows the values calculated according to Eq. (1).

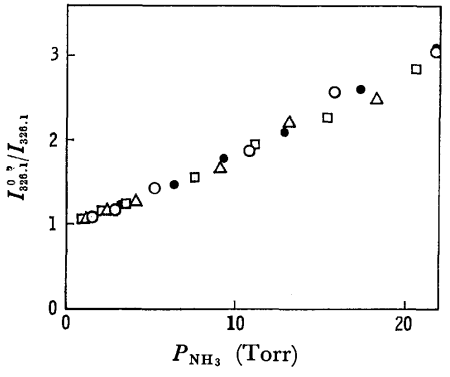

Fig. 4. Stern-Volmer plots in the low pressure region. The total pressures are 208 (○), 175 (△), 147 (□), and 123 (●) in Torr.

respectively. On the assumption that 100 Torr carbon dioxide quenches the $Cd(^3P_1)$ atoms completely,[6] the scattered light intensity at 326.1 nm was estimated to be less than 0.2% of $I^0_{326.1}$; hereafter, it was neglected. The emission intensity at 326.1 nm hardly changed with the irradiation time. As is shown in Fig. 3, the plots obtained at various total pressures lie on one curve, and no total pressure dependence can be seen. The intercept of the Stern-Volmer plots at zero pressure of ammonia obtained in the previous paper[5] was less than unity, but that in Fig. 3 was equal to unity. This discrepancy can be attributed to the neglect of the effect of the pressure broadening in the previous study. The plots obtained with ammonia were previously regarded as lying on a straight line; however, the plots shown in Fig. 3 deviate from a straight line, especially in the low-pressure region. The deviation is observed more clearly in Fig. 4. This finding forced us to modify the reaction scheme previously proposed.[5]

Discussion

The energy difference between the 5^3P_1 and 5^3P_0 states of cadmium atoms is only 1.6 kcal/mol. In the presence of foreign gases, for example, 5 Torr of Ar or 0.1 Torr of ammonia,[7] the equilibrium between the two electronic states is readily established. Consequently, we cannot discriminate the reactions of two states. Morten *et al.* used the phase-shift technique to observe the emission at 432 nm and said that the emitting species is produced by the reaction between the 5^3P_0 state of cadmium atoms and ammonia; however, if the equilibration reaction between 5^3P_1 and 5^3P_0 states is very fast, their assignment is not necessarily unique. In the following treatment, therefore, we will consider both $Cd(^3P_1)$ and $Cd(^3P_0)$ as precursors of the emitting species and will use the symbol Cd* to express either $Cd(^3P_1)$ or $Cd(^3P_0)$.

Quenching of the 326.1-nm Resonance Line. As was mentioned in the "Results" section, the Stern-Volmer plots for the quenching of the 326.1-nm resonance line by ammonia do not lie on a straight line. In order to explain such Stern-Volmer plots, the following reaction mechanism was considered:

$Cd + h\nu \longrightarrow Cd(^3P_1)$	I_a
$Cd(^3P_1) \longrightarrow Cd + h\nu$	k_0
$Cd(^3P_1) + M \rightleftharpoons Cd(^3P_0) + M$	k_1, k_{-1}
$Cd(^3P_1) + NH_3 \longrightarrow$ products	k_2
$Cd(^3P_0) + NH_3 \longrightarrow$ products	k_3
$Cd^* + NH_3 \rightleftharpoons CdNH_3^*{}_v$	k_4, k_{-4}
$CdNH_3^*{}_v + NH_3 \longrightarrow CdNH_3^* + NH_3$	k_5
$CdNH_3^*{}_v + Ar \longrightarrow CdNH_3^* + Ar$	k_5'
$CdNH_3^* \longrightarrow Cd + NH_3 + h\nu'$	k_6
$CdNH_3^* + NH_3 \longrightarrow Cd + 2NH_3$	k_7
$CdNH_3^* + Ar \longrightarrow Cd + NH_3 + Ar$	k_7'

Here, M stands for Ar or NH_3. $CdNH_3^*{}_v$ and $CdNH_3^*$ represent, respectively, an unstabilized and a stabilized complex between the triplet cadmium and ammonia. In this mechanism, it is assumed that the unstabilized complex does not fluoresce, because the profile of the emission band is independent of the pressures of ammonia and argon.

A steady-state treatment on the assumptions that the equilibration reaction between the 5^3P_1 and 5^3P_0 states is very fast and that either the $^3P_1$ or the $^3P_0$ state is the precursor of the emitting species gives the following relation:

$$\frac{I^0_{326.1}}{I_{326.1}} = 1 + a[NH_3] + \frac{b[NH_3]}{1+\dfrac{1}{c+d[NH_3]}} \quad (1)$$

Here, $I^0_{326.0}$ and $I_{326.1}$ are the emission intensities at 326.1 nm in the absence and in the presence of ammonia respectively. a, b, c, and d are constants depending only on the total pressure. When Cd* = Cd($^3P_1$), then

$$a = \frac{1}{k_0}\left(k_2+\frac{k_1}{k_{-1}}k_3\right), \quad b = \frac{k_4}{k_0}, \quad c = \frac{k_5'}{k_{-4}}[M],$$

and

$$d = \frac{k_5-k_5'}{k_{-4}}$$

In the case of Cd* = Cd($^3P_0$), a, c, and d are expressed in the same manner as above, while

$$b = \frac{k_1}{k_{-1}}\frac{k_4}{k_0}.$$

At the temperature of 220 °C, the equilibrium constant between $^3P_1$ and $^3P_0$ states is 1.68 ($=1/3 \exp(1.6/RT)=K=k_1/k_{-1}$).

According to Eq. (1), the $I^0_{326.1}/I_{326.1}$ ratio should have a linear dependence on the pressure of ammonia in the high-pressure region and a second-order dependence in the low-pressure region. These tendencies agree with the observations. By applying Eq. (1) to the observed values, the constants, a, b, c, and d, could be obtained by trial and error. The results are summarized in Table 1. The solid line in Fig. 3 was

Table 1. The constants involved in Eq. (1)

a = 0.010 ± 0.002	Torr^{-1}
b = 0.103 ± 0.002	Torr^{-1}
c/[M] = 0.0024	Torr^{-1}
d = 0.30	Torr^{-1}

drawn by introducing these values into Eq. (1). The c term is so small that the $I^0_{326.1}/I_{326.1}$ ratios calculated are scarcely dependent at all on the total pressure.

The Pressure Dependence of the Emission at 432 nm. The steady-state treatment of the above mechanism gives the following relation for the intensity of the emission at 432 nm:

$$\frac{I_{326.1}[NH_3]}{I_e} = (e+f[NH_3])\left(1+\frac{g}{h+[NH_3]}\right) \quad (2)$$

Here, I_e represents the total emission intensity arising from the stabilized complex. Since the emission profile was the same at all pressures and compositions examined, the observed emission intensity at 432 nm (I_{432}) should be proportional to the total emission intensity; *i.e.*, $I_e=\alpha I_{432}$. The proportional factor, α, depends on the geometry of the apparatus, the slit width, and the sensitivity of the photomultiplier used. e, f, g, and h are constants depending only on the total pressure; when Cd* = Cd($^3P_1$),

$$e = \frac{k_0}{k_4}+\frac{k_0}{k_4}\frac{k_7'}{k_6}[M], \quad f = \frac{k_0}{k_4}\frac{k_7-k_7'}{k_6},$$

$$g = \frac{k_{-4}}{k_5-k_5'}, \quad \text{and} \quad h = \frac{k_5'}{k_5-k_5'}[M].$$

In the case of Cd* = Cd($^3P_0$), k_4 should be replaced by $(k_1/k_{-1})k_4$. These constants have been evaluated by the method given in the Appendix and are listed in Table 2. The solid lines in Fig. 2 were drawn

Table 2. The constants involved in Eq. (2)

[M] (Torr)	αe (Torr)	αf	g (Torr)	h/[M]
208	2.17	0	3.20	0.0072
175	1.99	0	3.23	0.0072
147	1.87	0	2.78	0.0072
123	1.74	0	2.52	0.0072

by substituting the values in Table 2 into Eq. (2). The agreement between the calculated values and the observed ones is good at all the pressures examined.

The lifetime (τ_0) of Cd($^3P_1$) has been reported to be 2.39×10^{-6} s.[8] As was mentioned in a previous paper,[6] the effective lifetime is independent of the pressure of foreign gases in the range we are studying. Therefore, k_0 may be set equal to $1/\tau_0$. On the other hand, several ratios of the rate constants can be evaluated from the relationships between the constants, a, b, c, d, e, f, g, and h, and the total pressure ([M]). The results are summarized in Table 3. A comparison of

Table 3. Several rate constants and ratios between the rate constants

$k_2 + 1.68\,k_3 = (2.1\pm0.4)\times10^{-13}$ cm^3 molecule^{-1} s^{-1}
k_4 (or $1.68\,k_4$) $= (2.2\pm0.4)\times10^{-12}$ cm^3 molecule^{-1} s^{-1}
$k_5/k_{-4} = 0.336\pm0.012$ Torr^{-1}
$k_5/k_5' = 139$
$k_7/k_6 = (4.9\pm0.2)\times10^{-3}$ Torr^{-1}
$k_7/k_7' = 1$

k_4 with $(k_2+1.68\,k_3)$ indicates that the cross section for the quenching of the excited cadmium atoms through the formation of the complex is about 10 times that for the quenching through other processes, such as the abstraction of the hydrogen atom. The half-quenching pressure of ammonia is calculated to be 12.6 Torr. This value is less than a half that reported previously (29.8 Torr).[5] The latter value, however, was obtained while paying no attention to the pressure broadening of the absorption line. Therefore, the value obtained here should be more reliable.

On the basis of the data obtained by using a flash technique, Callear and McGurk[3] proposed two types of the formation of the emitting complex in the system of Hg and NH_3:

$$Hg^* + NH_3 \longrightarrow HgNH_3^* \qquad k_b$$

$$Hg^* + NH_3 + M \longrightarrow HgNH_3^* + M \qquad k_t$$

The lifetime of Hg*, therefore, was expressed as follows:

$$\tau^{-1} = \tau_M^{-1} + k_b[NH_3] + k_t[NH_3][M]$$

where τ_M is the lifetime of Hg* in the absence of foreign gases. Morten *et al.*[4] assumed a similar mechanism for the formation of the emitting cadmium complex

and estimated that $k_b=(1.7\pm0.3)\times10^{-12}$ cm^3 molecule^{-1} s^{-1} at 560 K. In our treatment, the lifetime of Cd($^3P_1$) may be expressed in this form:

$$\tau^{-1}=\tau_M^{-1}\left(1+a[NH_3]+\frac{b[NH_3]}{1+\frac{1}{c+d[NH_3]}}\right)$$

As is shown in Table 1, we obtained d=0.3 Torr^{-1}. The experiment of Morten *et al.* was carried out at more than a few Torr of NH_3. Therefore, the k_b value obtained by Morten *et al.* may be compared with the value of $(a+b)/\tau_M$. The calculated value is 2.4×10^{-12} cm^3 molecule^{-1} s^{-1} at 493 K. It may be said that these two values are in good agreement.

By assuming the cross section of 9 Å^2 for Reaction (5), which corresponds to $k_5=2.36\times10^{-10}$ cm^3 molecule^{-1} s^{-1} at 220 °C, the lifetime of the unstabilized complex was calculated to be 7.4×10^{-8} s. This is the shortest possible lifetime of the unstabilized complex. Therefore, if other molecules which are more complex than ammonia can form emitting species, and if the back reaction is not important, we shall not be able to observe the second order pressure dependence of the Stern-Volmer plots in the low-pressure region, as was observed in the present case of ammonia.

The ratio of $k_5'/k_5=0.0072$ shows that the stabilization of the unstabilized complex by ammonia is about 140 times as efficient as that by argon. On the other hand, $k_7'/k_7=1$ suggests that the efficiency of the deactivation of the stabilized complex is almost the same for both quenchers. Morten *et al.* estimated the lifetime of the emitting complex to be $(4.9\pm0.2)\times10^{-7}$ s. This suggests that Reactions (7) and (7′) are extremely inefficient.

Appendix

At the pressure of ammonia high enough for $1+\frac{g}{h+[NH_3]}\approx1$, Eq. (2) can be reduced to this form:

$$\frac{I_{326.1}[NH_3]}{I_{432}}=\alpha e+\alpha f[NH_3] \quad (3)$$

The left-hand side of Eq. (3) is plotted against the pressure of ammonia, and the constants, αe and αf, are evaluated from the intercept and the slope of the straight line obtained in the high-pressure region.

Equation (2) can be rewritten as follows:

$$\frac{I_{326.1}[NH_3]}{I_{432}}\frac{1}{\alpha(e+f[NH_3])}=1+\frac{g}{h+[NH_3]} \quad (4)$$

The left-hand side of Eq. (4) can be calculated by using the values of αe and αf obtained above. The g and h constants are determined by using the method of curve-matching. Then, according to Eq. (2), the αe and αf constants can be determined in turn by using the values of g and h just obtained. These constants should be equal to the values obtained above. We, therefore, used the circulating procedure until a self-consistent set of constants was obtained. The final values are listed in Table 2.

References

1) S. Penzes, O. P. Strausz, and H. E. Gunning, *J. Chem. Phys.*, **45**, 2322 (1966); H. E. Gunning, S. Penzes, H. S. Sandhu, and O. P. Strausz, *J. Amer. Chem. Soc.*, **91**, 7684 (1969).

2) C. G. Freeman, M. J. McEvan, R. F. C. Claridge, and L. F. Phillips, *Chem. Phys. Lett.*, **5**, 555 (1970); **6**, 482 (1970); **8**, 226 (1971); **9**, 578 (1971); *Trans. Faraday Soc.*, **66**, 2974 (1970); **67**, 2004, 2565 (1971); R. H. Newman, C. G. Freeman, M. J. McEvan, R. F. C. Claridge, and L. F. Phillips, *ibid.*, **66**, 2827 (1970); **67**, 1360 (1971).

3) A. B. Callear and J. McGurk, *Chem. Phys. Lett.*, **7**, 491 (1970); J. Koskikallio, A. B. Callear, and J. H. Conner, *ibid.*, **8**, 467 (1971); A. B. Callear and J. H. Conner, *ibid.*, **13**, 245 (1972).

4) P. D. Morten, C. G. Freeman, M. J. McEvan, R. F. C. Claridge, and L. F. Phillips, *ibid.*, **16**, 148 (1972).

5) S. Tsunashima, T. Toyono, and S. Sato, This Bulletin, **46**, 2654 (1973).

6) S. Yamamoto, M. Takaoka, S. Tsunashima, and S. Sato, *ibid.*, **48**, 130 (1975).

7) M. Takaoka, S. Yamamoto, S. Tsunashima, and S. Sato, *Chem. Lett.*, **1974**, 343.

8) F. W. Byron, Jr., M. N. McDermott, and R. Novick, *Phys. Rev.*, **134**, A615 (1964).

Solution Properties of Phycocyanin. II. Studies of the Molecular Shape and Size by Using the Shell Model**

Akira KOTERA*, Takahide SAITO, Naomichi ISO, Haruo MIZUNO, and Nobuo TAKI*

Department of Food Science and Technology, Tokyo University of Fisheries, Konan, Minato-ku, Tokyo 108

(Received October 5, 1974)

The number-average molecular weight and intrinsic viscosity of phycocyanin, isolated from *Porphyra tenera*, have been determined by osmotic pressure and viscosity measurements at various values of pH and ionic strength. The molecular shape and size for phycocyanin aggregates were also discussed by comparing the experimental values of sedimentation coefficient and intrinsic viscosity with the calculated results obtained by using the shell model theory. It is shown that the aggregate of phycocyanin at pH 5.4 is a hexamer of molecular weight 256000 and the structure consists of six juxtaposed monomers. The monomer is a prolate ellipsoid of 35 Å in diameter and 105 Å length. This structure for the hexamer is consistent with the model proposed by Jennings. At pH 6.8, it is shown that the number-average molecular weight of phycocyanin depends on the ionic strength in solution.

In a previous paper,[1] we studied the dissociation-association equilibrium of phycocyanin, isolated from red algae, *Porphyra tenera*, by sedimentation transportation measurements at pH 6.8 and 5.4 and ionic strengths of 0.1 and 0.2. The sedimentation velocity data indicated that the predominant phycocyanin aggregate was a trimer at pH 6.8 and a hexamer at pH 5.4. Moreover, the dissociation-association system of phycocyanin was presumed to be trimer⇌monomer at pH 6.8 and hexamer⇌monomer at pH 5.4.

Berns and Edwards[2] observed phycocyanin aggregates with an electron microscope. They suggested that the higher aggregate of phycocyanin consisted of six globular particles, and, also, that the shape of the hexagonal aggregate was that of an oblate or prolate ellipsoid with an axial ratio of approximately 4 : 1. Scott and Berns[3] performed diffusion and viscometric measurements on phycocyanin solutions, and proposed a round structure with a central hole for the phycocyanin aggregate. Jennings[4] discussed the size and shape of the phycocyanin aggregate on basis of an amino acid composition analysis reported by Berns *et al.*[5] and proposed that the hexamer was an aggregate of six monomers, in juxtaposition, with their major axes parallel so as to form a ring structure, as shown in Fig. 1. Although some investigators proposed a trimer for the lower aggregate of phycocyanin, the shape and size of this aggregate have not been discussed.

Bloomfield *et al.*[6,7] reported a method of estimating the size and conformation of macromolecules in terms of the number of equivalent spherical subunits. In this procedure, the complex structures are replaced by a surface shell consisting of many small spheres, and hence this approximation for a macromolecular complex structure is called the "shell model." Bloomfield *et al.*[7] studied the size of phycocyanin using their theory and proposed that the phycocyanin monomer was a single sphere having a 26 Å radius or a linear array of three spheres, each having an 18 Å radius.

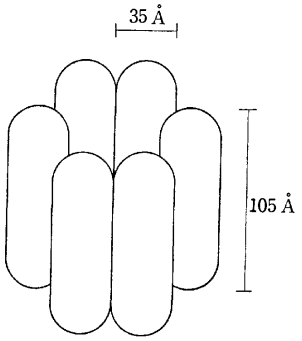

Fig. 1. Schematic model of the phycocyanin hexamer proposed by Jennings[4].

Tsuda[8,9] presented an expression for the intrinsic viscosity of macromolecules based on Kirkwood's approximation for the frictional coefficient. It was found that the experimental results obtained from the measurements of sedimentation coefficient and intrinsic viscosity for many biological macromolecules, such as fibrinogen, hemoglobin and hemocyanin, can be reasonably explained by the shell model.[7,8]

In this paper, the molecular weight and the intrinsic viscosity were measured in phycocyanin solutions under several sets of conditions, that is, pH 6.8 and 5.4, and ionic strength (μ) 0.01, 0.1 and 0.2. The molecular size and shape of this protein were discussed by using the theory of the frictional coefficient of the multi-subunit structure reported by Bloomfield *et al.*[7] and Tsuda.[8,9]

Experimental and Calculation

Treatment of Phycocyanin. The phycocyanin used in this study was obtained from dried *Porphyra tenera* by repeated precipitation with ammonium sulfate, and the process for sample preparation and the concentration determination of the protein solution were described in detail in part I.[1].

Osmotic Pressure Measurements. Osmotic pressure measurements of phycocyanin were conducted in buffer solution at 25.0 °C with a Model 502 High Speed Membrane Osmometer. Phosphate (pH 6.8, μ 0.01, 0.1 and 0.2) and acetate (pH 5.4, μ 0.1 and 0.2) buffer solutions were used in these determinations. The membrane was Gel-cellophane #600 supplied by Tokyo Cellophane, and was conditioned by the

* Department of Chemistry, Tokyo Kyoiku University, Otsuka, Bunkyo-ku, Tokyo 112.

** Some of the experimental results in this paper were represented at the 22nd Annual Meeting of The Society of Polymer Science, Japan, Kyoto, May 30, 1973 and 23rd Annual Meeting of the Socity of Polymer Science, Japan, Tokyo, June 6, 1974.

"subsequent transfer method" from water to buffer solution. Prior to use, the membrane was equilibrated overnight in the appropriate buffer solutions. The number-average molecular weight and the second virial coefficient were obtained by the usual method.

Viscosity Measurements. Viscosity measurements were made in the buffer solution at 25.0 °C, under the following conditions: pH 6.8 and 5.4; μ 0.1 and 0.2. An Ubbelohde dilution type viscometer was used for the measurements. Kinetic energy corrections were not made. The intrinsic viscosity was obtained by using Huggins' equation.

Results and Discussion

The osmotic pressure data are shown in Fig. 2, plotted as π/c *versus* c. As shown in this figure, the concentration dependence of π/c was small for all systems. Therefore, the second virial coefficients of all systems were considered to be nearly zero. The values of π/c at pH 5.4 show the same value irrespective of the ionic strength (0.1 or 0.2), while the π/c values at pH 6.8 increased with decreasing ionic strength of the solution.

The number-average molecular weight at pH 5.4 was 256000. At pH 6.8, the number-average molecular weights were 228000 for μ 0.2, 172000 for μ 0.1 and 154000 for μ 0.01.

We consider that the change in the molecular weight of phycocyanin with the variation of ionic strength at pH 6.8 arises from the difference in the dissociation-association reaction of the protein. In the previous paper, it was shown that the sedimentation coefficient of phycocyanin did not change markedly with changing ionic strength.[1] The results seem to be a consequence of measuring the sedimentation coefficient at too low concentration. As pointed out previously,[1] the dissociation-association equilibrium for phycocyanin at low concentration was trimer$\rightleftarrows$monomer, and the predominant species was a trimer. However, the results from the present study suggest that various aggregates, having different molecular weights, coexist in higher concentration regions. At pH 5.4, the phycocyanin molecule seems to be relatively stable in solution.

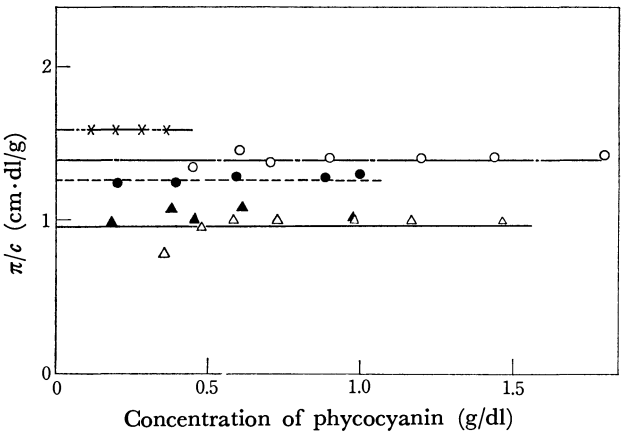

Fig. 2. Plots of π/c *versus* phycocyanin concentration in five different buffer solutions at 25.0 °C. ○, phosphate buffer, pH 6.8 and μ=0.1; ●, phosphate buffer, pH 6.8 and μ=0.2; ×, phosphate buffer, pH 6.8 and μ=0.01; △, acetate buffer, pH 5.4 and μ=0.1; ▲, acetate buffer, pH 5.4 and μ=0.2.

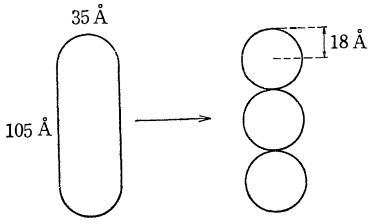

Fig. 3. Monomer model proposed by Jennings[4] treatment according to the shell model.

Figure 3 shows the model of the phycocyanin monomer for the calculation of theoretical values of sedimentation coefficient and intrinsic viscosity. This model is the same one as that proposed by Jennings[4]. The monomer structure was assumed to be an array of three identical spheres of radius of 18 Å as shown in Fig. 3. Also the molecular weight of the monomer was estimated to be 42000. This value was about 1/6 of 256000, which was the molecular weight of hexamer obtained from an osmotic pressure measurements.

Viscosity data for phycocyanin in various buffer solutions at 25.0 °C are shown in Fig. 4. All plots of η_{sp}/c against c under various conditions (pH 6.8, μ 0.2, and pH 5.4, μ 0.1 and 0.2) displayed an increase with decrease in concentration in lower concentration regions. This viscosity behavior is generally found for polyelectrolyte solutions. The viscosity characteristic for phycocyanin may be attributed to the charge effects on the protein molecule. Intrinsic viscosities of phycocyanin reported in this paper were determined by linear extrapolation of plots of η_{sp}/c against c in a higher concentration range to infinite dilution. From this extrapolation the values of $[\eta]$ for phycocyanin aggregates were found to be 3.92 ml/g at pH 5.4 and 4.32 ml/g at pH 6.8.

According to the shell model theory, the translational frictional coefficient, f, of a molecule composed of n identical spherical subunits, may be expressed by following equation[8] which is derived from the Kirkwood theory for irreversible processes in solutions of macromolecules.[10]

$$f = \frac{6\pi\eta_0 n^2 r}{n + r\sum_i \sum_{j(\neq i)} R_{ij}^{-1}} \tag{1}$$

where r is the radius of the sphere, η_0 the solvent viscosity and R_{ij} the distance between the i-th and j-th subunit.

In a fluid medium, the rate of sedimentation for solute depends on the translational frictional coefficient, f. Therefore, the sedimentation constant, s_0, is a function of the frictional coefficient and may be expressed by Eq. (2):

$$s_0 = \frac{M(1-\bar{v}\rho)}{fN_A} \tag{2}$$

where M is the molecular weight, $\bar{v}$ the partial specific volume of solute, ρ the density of solvent and N_A Avogadro's number.

On the other hand, the intrinsic viscosity of a macro-

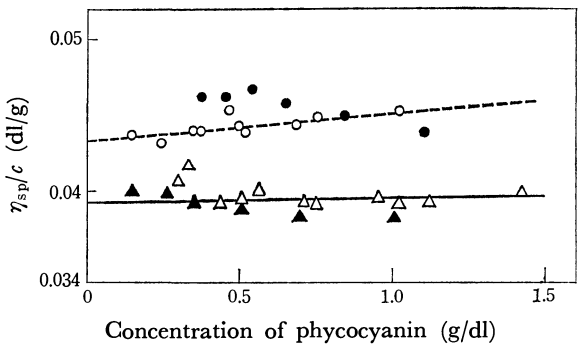

Fig. 4. Plots of η_{sp}/c *versus* concentration of phycocyanin in four different buffer solutions at 25.0 °C. ○, phosphate buffer, pH 6.8 and $\mu=0.1$; ●, phosphate buffer, pH 6.8 and $\mu=0.2$; △, acetate buffer, pH 5.4 and $\mu=0.1$; ▲, acetate buffer, pH 5.4 and $\mu=0.2$.

molecule is related to the rotational frictional property. A general expression for intrinsic viscosity of a complex structure composed of different subunits is

$$[\eta] = \left(\frac{4\pi}{3}\right)\left(\frac{N_A}{M}\right)B \tag{3}$$

where B is a parameter related to the molecular shape and size of a complex macromolecule and its form is given by Eqs. (29)—(33) of Ref. 8.

The intrinsic viscosity and sedimentation constant for various model structures of phycocyanin aggregate were calculated by a computer using Eqs (1), (2) and (3). In these calculations, the monomer structure was assumed to be an array of three identical spheres with a radius of 18 Å, and the monomer molecular weight of 42000, estimated from the osmotic pressure measurements, was used.

For the monomer model the intrinsic viscosity was calculated to be 4.2 ml/g, and the sedimentation constant to be 3.5×10^{-13} s, respectively. The s_0-value of 3.5×10^{-13} s agrees with the experimental value (3.2×10^{-13} s) obtained by Hattori *et al.*[11] Therefore, the shape of the phycocyanin monomer may be a prolate spheroid with an axial ratio of approximately 3 : 1. Since the experimental value of $[\eta]$ for the monomer has not yet been reported, the calculated value of the intrinsic viscosity cannot be compared with the experimental value.

The values of $[\eta]$ and of s_0 for Jennings' model and other assumed hexameric structure of phycocyanin were calculated by the shell theory. An $[\eta]$ value of 4.08 ml/g and an s_0-value of 11.8×10^{-13} s were calculated for Jennings' model. These values are in reasonable agreement with the exprimental values ($[\eta]=$ 3.92 ml/g and $s_0=10.8\times10^{-13}$ s[1]) obtained at pH 5.4. Therefore, the aggregate of the protein seems to be a hexamer at pH 5.4. The hexamer of phycocyanin can be considered to be an aggregate of six prolate monomers. The prolate monomers are associated side by side with their major axes parallel to the hollow core of the hexamer. Such a structure for hexamer would have an axial ratio close to unity.

From the results of osmotic pressure measurements at pH 6.8, it might be supposed that the aggregate at this pH value is a tetramer. However, the results of the calculations of $[\eta]$ and s_0 for some tetrameric models of phycocyanin aggregate eliminated this possibility.

TABLE 1. CALCULATED VALUES OF INTRINSIC VISCOSITY AND SEDIMENTATION COEFFICIENT FOR THE ASSUMED MODEL OF THE PHYCOCYANIN TRIMER

At pH 6.8 the experimental value of $[\eta]$ is 3.92 ml/g and s_0 is 6.4s.

Model	$[\eta]$ (ml/g)	s_0 (S)
Fig. 5-a	4.47	7.16
Fig. 5-b	3.65	7.74

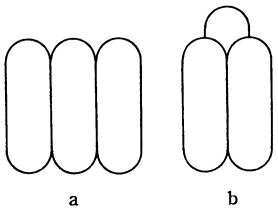

Fig. 5. Schematic models of phycocyanin trimer.

Table 1 shows the results of the calculations for some trimer models depicted in Figs. 5-a and 5-b. As is evident from Table 1, the calculated value of $[\eta]$ for the assumed structure of trimer, shows a remarkable deviation from the experimental value although it satisfactorily explains the sedimentation behavior.

From these results, it seems to be impossible to represent the trimer by a self-consistent model for both the sedimentation constant and the intrinsic viscosity. However, it should be remembered that the sedimentation constant measurements were carried out at concentrations below 0.5 g/dl. On the other hand, both the intrinsic viscosity and the osmotic pressure were measured at higher concentration. The existence of higher order aggregate cannot be neglected in the higher concentration regions at pH 6.8. It seems that the values of intrinsic viscosity and number-average molecular weight obtained in this study are averages for a mixture of trimer and higher order aggregates (probably hexamers).

The weight fraction for each species in the mixture can be calculated from the number-average molecular weight, assuming a hexamer⇄trimer equilibrium for the mixture. The results indicate the weight fraction of trimer is 0.46 and of hexamer, 0.54. By considering the intrinsic viscosity of the mixture as the weight average value, the value of $[\eta]$ for the mixture was calculated from the intrinsic viscosity estimated for trimer and hexamer. The calculated value (4.26 ml/g) of $[\eta]$ for the mixture agrees well with the experimental value (4.32 ml/g). Agreement between calculated and exprimental values suggests that the coexistence of higher order aggregates in higher concentration regions cannot be neglected.

Scheraga and Mandelkern[12] derived the following equation for a revolutional ellipsoid:

$$s_0[\eta]^{1/3} = \frac{M^{2/3}(1-\bar{v}\rho)\beta}{N_A\eta_0} \tag{4}$$

where η_0 is the viscosity of the solvent. They indicated that the quantity β is a function of the axial ratio of the ellipsoid, and has a value of $2.12—2.20 \times 10^6$ for the prolate ellipsoild when the axial ratio is less than 5.

The β values for the various aggregates of phycocyanin were calculated using Eq. (4). In the calculation of β for the monomer, an intrinsic viscosity value of 4.20 ml/g was used, which was obtained by computation with the shell model as shown in Fig. 3. The β values for the monomer, the trimer and the hexamer of phycocyanin are 2.00×10^6, 1.95×10^6 and 2.05×10^6, respectively. The results agree with the theoretical value for a prolate ellipsoid having an axial ratio lower than 5.

From the β-values obtained, the geometrical structures for phycocyanin aggregates used in this study seem to be consistent; that is, the monomer model is that as shown in Fig. 3, the trimer model that is Fig. 5-a or 5-b, and the hexamer model that in Fig. 1.

Conclusion

We conclude that the aggregate of phycocyanin at pH 5.4 is a hexamer. From an analysis of the sedimentation constant and intrinsic viscosity by the shell model, we proposed that the hexamer structurally consists of an aggregate of six juxtaposed monomers, whose major axes are parallel to each other forming a closed ring structure. Each monomer is represented by a prolate ellipsoid with axial lengths of 35 Å and 105 Å. This structure for the phycocyanin hexamer is identical to that proposed by Jennings.

The phycocyanin aggregates at pH 6.8 in higher concentration regions are considered to be composed of various aggregates with different structures. Therefore, a definite structural description of the phycocyanin aggregates at pH 6.8 cannot be given.

It has shown from the values of β that the aggregates of phycocyanin, that is, monomer, trimer and hexamer, are prolate ellipsoids with an axial ratio less than 5.

The authors wish to express their gratitude to Dr. K. Tsuda and Dr. T. Sakai, of the Research Institute for Polymers and Textiles, for their interest and helpful discussions of the problems. They also wish to express their gratitude to Dr. Y. Matsumoto, of the Industrial Research Institute of Kanagawa Prefecture, for providing facilities for the osmotic pressure measurements and for his valuable assistance in the osmometry.

References

1) T. Saito, N. Iso, and H. Mizuno, This Bulletin, **47**, 1375 (1974).
2) D. S. Berns and M. R. Edwards, *Arch. Biochem. Biophys.*, **110**, 511 (1965).
3) E. Scott and D. S. Berns, *Biochemistry*, **4**, 2597 (1965).
4) B. R. Jennings, *Biopolymers*, **6**, 1177 (1965).
5) D. S. Berns, H. L. Crespi, and J. J. Katz, *J. Amer. Chem. Soc.*, **85**, 8 (1963).
6) V. A. Bloomfield, W. O. Dalton, and K. E. van Holde, *Biopolymers*, **5**, 135 (1967).
7) V. A. Bloomfield, K. E. van Holde, and W. O. Dalton, *ibid.*, **5**, 149 (1967).
8) K. Tsuda, *Rheol. Acta*, **9**, 509 (1970).
9) K. Tsuda, *Polymer J.*, **1**, 616 (1970).
10) J. G. Kirkwood, *J. Polymer Sci.*, **12**, 1 (1954).
11) A. Hattori, H. L. Crespi, and J. J. Katz, *Biochemistry*, **4**, 1225 (1965).
12) H. A. Scheraga and L. Mandelkern, *J. Amer. Chem. Soc.*, **75**, 179 (1953).

Effects of Anionic and Cationic Surfactants on the Ion Flotation of Cu^{2+}

Koichi KOBAYASHI

Department of Chemistry, Faculty of Science, Tokyo Metropolitan University, Tokyo 158

(Received October 16, 1974)

The effects of several anionic surfactants—sodium α-sulfolaurate, sodium laurate, sodium dodecylsulfate, and cationic surfactants, dodecylpyridinium chloride, and dodecyltrimethylammonium chloride—on the bubble flotation of Cu^{2+} ions were studied. Sodium α-sulfolaurate was found to be most effective for the flotation of Cu^{2+} ions. The flotation rate (percent removed) increased sharply from zero at about pH 6, and a rate larger than 95% was attained in the pH region of about 7 to 11. Cationic surfactants alone could float Cu^{2+} ions only slightly. They floated most of the Cu^{2+} ions upon the addition of bentonite, however. A flotation rate of about 90% was attained in the pH region larger than about 6. This was explained by the Cu^{2+} ions being removed as polynuclear species, which combined directly with an anionic surfactant or a cationic surfactant with the aid of bentonite.

The foam separations of soluble and suspended matters in water have drawn increasing attention in connection with industrial waste water,[1,2] sewage treatment,[1,2] the removal of trace amounts of radioactive substance from solutions[3] and the concentration of rare elements from sea water.[4,5] The techniques of ion flotation involve the removal of surface inactive ions from aqueous solutions with the aid of bubbles and can be divided into several processes differing in detail, such as adsorption flotation, precipitation flotation, and adsorbing-particle flotation.[6] The adsorption flotation consists of the flotation of ions in a solution by adsorption on ascending bubbles. In the precipitation flotation, ions in the solution are precipitated by the addition of proper substances or by controling the pH, and the precipitates formed are floated by adding a surfactant. The adsorbing-particle flotation consists of the adsorption of ions from a solution on adsorbent particles like bentonite or a synthetic ion-exchanger; the ions are subsequently floated by the addition of a suitable surfactant. The adsorption flotation requires a stoichiometric or greater concentration of surfactants, while in the case of precipitation flotation relatively small amounts of surfactants are sufficient. A preliminary experiment showed that the adsorbing-particle flotation was the most efficient among these methods of flotation.[7]

The ion-adsorption flotation was first introduced by Sebba,[8] and the ion-precipitation flotation, by Baarson and Ray.[9] Rubin *et al.*[10] compared the effects of several variables on these processes. Recently a number of studies of ion adsorption and precipitation flotations from theoretical points of view have been reported,[11,12] but much remains unsolved.

The present work has been undertaken in order to study the flotation of Cu^{2+} ions by a number of surfactants from the surface-chemical point of view, under varying conditions of pH, gas-flow rate, time, and concentrations of the surfactants and Cu^{2+} ions.

Experimental

Materials. The cupric sulfate used was a reagent-grade $CuSO_4 \cdot 5H_2O$; it was recrystallized from distilled water, and stock solutions of 2×10^{-3} and 1×10^{-3} mol/l concentrations were prepared.

The surfactants used included sodium *n*-dodecylsulfate (SDS), sodium *n*-dodecylbenzenesulfate (DBS), sodium laurate (LNa), and sodium α-sulfolaurate (α-SLNa) as anionic surfactants, and *n*-dodecylpyridinium chloride (DPC) and *n*-dodecyltrimethylammonium chloride (DTAC) as cationic surfactants.

The SDS was synthesized from dodecanol and chlorosulfonic acid, and the product was purified by extraction with ethyl ether and recrystallization from ethanol.[13] Pure-grade DBS was supplied by the Kao Soap Co., Ltd., and was dried over phosphorus pentoxide. A reagent-grade LNa, a product of the Tokyo Kasei Industrial Co., Ltd., was recrystallized from ethanol with water. The α-SLNa, a product of the Kao Soap Co., Ltd., was recrystallized from ethanol with a little water. The DPC and DTAC, products of the Tokyo Kasei Industrial Co., Ltd., were recrystallized from acetone and ethanol respectively; the latter was washed with ether and dried. These surfactants were kept in a desiccator. The aqueous solutions were prepared before use.

The bentonite powders used as ion-exchange adsorbents were obtained from the Wako Pure Chemical Co., Ltd.; the fraction passing through a 350-mesh sieve was collected, and a suspension of 0.01 g/l concentration was made and used after shaking before each experiment. The pH of the solution was controlled by using sulfuric acid and sodium hydroxide of an extra pure grade. The water used was triply distilled; it was found to be free from Cu^{2+} ions by the use of an atomic absorption spectrometer.

Apparatus and Procedure. The apparatus used is shown in Fig. 1. Nitrogen gas from a nitrogen cylinder, A; successively passing through a gas filter, B; a manostat, C; an empty chamber, D, and a humidifier, E, saturated with water, was introduced into a flotation cell, G, at a constant rate of flow controlled with a calibrated capillary flow meter, F. The flow rate of the nitrogen gas was measured by

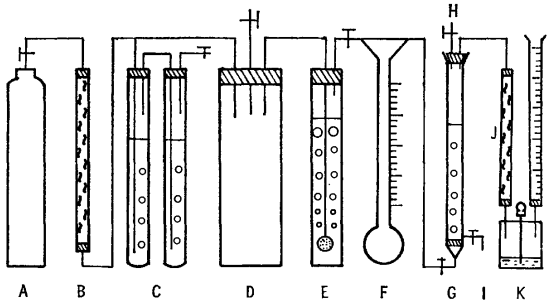

Fig. 1. Apparatus for ion flotation.
A: N_2 gas cylinder, B: glass filter, C: manostat, D: empty chamber, E: humidifier, F: capillary flow meter, G: flotation cell (No. 4), H: inlet, I: outlet J: glass filter, K: soap film flow meter.

means of a soap-film flow meter, K; after the gas has been filtered through a glass wool filter, J. The flotation cell used was a glass column, 32.0 cm long and 1.0 cm in inner diameter, equipped with a sintered glass plate with a porosity of No. 4.

The sample liquid was introduced into the cell from an inlet, H, and the residual solution after flotation was withdrawn from an outlet, I, for the measurements of the Cu^{2+}-ion concentration and the pH. The concentration of the Cu^{2+} ions was measured by using an atomic absorption spectrometer (Techtron Pty., Ltd., Model-AA-100). The absorbance was measured at 3248 Å. A glass electrode pH meter (Toadenpa Co., Ltd., HM-5A) was used to measure the pH. For the measurement of the flotation, 2 ml of a stock solution of 1×10^{-3} or 2×10^{-3} mol/l Cu^{2+} ions, a small amount of a sodium hydroxide or sulfuric acid solution to adjust the pH to a desired value, 2 ml of a bentonite suspension in the case of a cationic surfactant, and 2 ml of a surfactant solution were introduced successively into a 20-ml measuring flask; the total volume was then made 20 ml with water. About 10 ml of the sample solution thus prepared was used to measure the initial pH (pH_i). Ten ml of the remaining solution was transferred to the flotation cell, the gas flow was started, and flotation was carried out as has been described above. The gas-flow rate was kept at 10 ml/min for all the experiments except for the study of the effect of the gas-flow rate. The gas-flow time was kept at 2 or 7 min unless otherwise stated. After the flotation, about 7 ml of the solution was taken out of the flotation cell for the measurements of the final pH (pH_f) and the Cu^{2+}-ion concentration (C_f). The measurements of the flotation were carried out at a room temperature of about 25 °C.

Results and Discussion

The flotation rate, $F(\%)$, of Cu^{2+} ions is conventionally expressed by:

$$F = (1-C_f/C_i)\times100$$

where C_i denotes the initial concentration of Cu^{2+} ions.

All the experiments were run under the conditions of bubble flotation—namely, flotation using only ascending bubbles, without the aid of foam formation. Since the solution was made uniform in concentration by bubbling, and since most of the solution after flotation was used for the determination of the Cu^{2+}-ion concentration, the F measured substantially expresses the total percentage of Cu^{2+} ions removed from the solution.

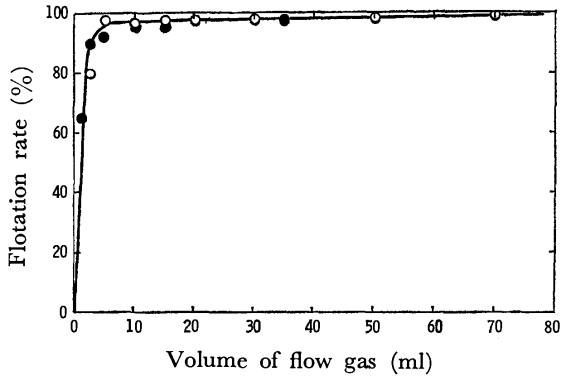

Fig. 2. Flotation rate *vs.* volume of flow gas for Cu^{2+}-α-SLNa system.
Cu^{2+}: 2×10^{-4} mol/l, α-SLNa: 4×10^{-4} mol/l, pH_i: 9.3, gas-flow rate: ○; 10 ml/min, ●; 5 ml/min.

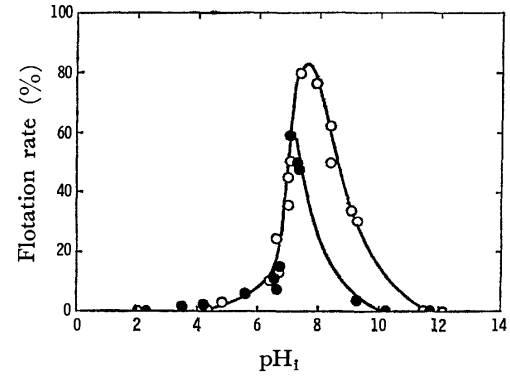

Fig. 3. Flotation rate *vs.* initial pH for Cu^{2+}-SDS system.
Cu^{2+}: 2×10^{-4} mol/l, SDS: 1×10^{-5} mol/l, gas-flow time: ●; 2 min, ○; 7 min.

(1) *Flotation of Cu^{2+} Ions by Anionic Surfactants. Relation between the Volume of the Flow Gas and the Flotation Rate*: Figure 2 shows the flotation rate as a function of the total volume of the gas flow at various rates for the Cu^{2+}-α-SLNa system. The figure shows that the flotation rate is simply a function of the volume of the gas flow and is independent of the flow rate. This is in accord with Rubin's view[14] that the flotation rate depends only on the volume of the gas flow. In the present case, F of nearly 100% is obtained, at least after 10 ml of nitrogen gas has flowed. Accordingly, all subsequent experiments were run at a gas-flow rate of 10 ml/min and a gas-flow time of 2 or 7 min.

Relation between the pH and the Flotation Rate. Figure 3 shows the effect of the pH on the flotation rate for the 2×10^{-4} mol/l Cu^{2+} and 1×10^{-5} mol/l SDS systems. As may be seen in this figure, the flotation rate increases sharply at about pH 6 and reaches its maximum at a pH value from 7 to 8 for the gas-flow times of both 2 and 7 min. An F of about 80% is obtained at the gas-flow time of 7 min. Beyond a 1×10^{-5} mol/l SDS concentration, the condition of bubble flotation changes to that of froth flotation, which was not studied since excessive foaming results in a large hold-up of the solution, thus preventing effective bubble flotation.

Figures 4 and 5 show the F *vs.* the gas-flow time and the F *vs.* surfactant concentration curves respectively for the Cu^{2+}-α-SLNa system. It may be seen in Fig. 3 that, at a 1×10^{-5}mol/l SDS concentration, the flotation rate increases with the gas-flow time. A similar effect may be expected for the Cu^{2+}-α-SLNa system, considering the same rate of flotation for the 1×10^{-5} mol/l α-SLNa concentration and the gas-flow time of 7 min. At a 4×10^{-4} mol/l α-SLNa concentration, the rate increases and shows a flat maximum of F of 98% extending from pH 7 to 11, independent of the gas-flow time, while for the SDS system the increase in the SDS concentration from 1×10^{-5} to 1×10^{-4} mol/l results in both an excessive foaming and hold-up of the solution, as has been mentioned above.

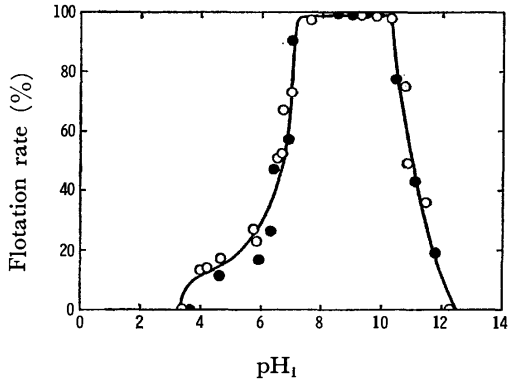

Fig. 4. Flotation rate *vs.* initial pH for Cu^{2+}–α-SLNa system.
Cu^{2+}: 2×10^{-4} mol/l, α-SLNa: 4×10^{-4} mol/l, gas-flow time: ●; 2 min, ○; 7 min.

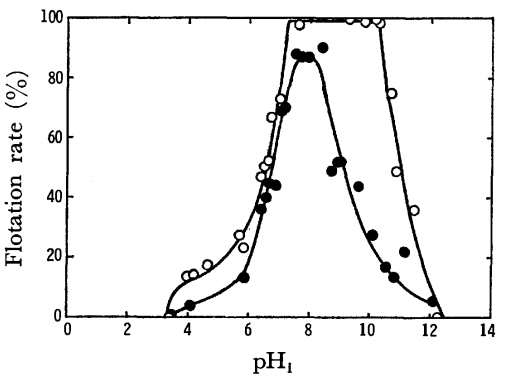

Fig. 5. Flotation rate *vs.* initial pH for Cu^{2+}–α-SLNa system.
Cu^{2+}: 2×10^{-4} mol/l, α-SLNa: ○; 4×10^{-4} mol/l, ●; 1×10^{-5} mol/l, gas-flow time: 7 min.

This may indicate that α-SLNa is superior to SDS as the additive for Cu^{2+} flotation, and confirms the view that the introduction of a carboxylic group into alkylsulfate increases the flotation efficiency.[15]

Figure 6 shows the pH dependence of the flotation rate for the Cu^{2+}–LNa system. The behavior is similar to that of the Cu^{2+}–α-SLNa system, showing a broad maximum, but a somewhat lower *F* value than that of the Cu^{2+}–α-SLNa system. Figure 7 shows the *F vs.* pH curve for the Cu^{2+}–DBS system. The rate of flotation, like that of Cu^{2+}–LNa system, shows a sharp increase at pH 6. On a further increase in the pH, a plateau or a minimum appears after a slight maximum, and then marked maxima at pH 10 appear, showing an *F* of 96% for DBS at the concentration of 2×10^{-5} mol/l. The system of 1×10^{-4} mol/l DBS exhibits stable foam formation, and so it was not studied. The Cu^{2+}–DBS system is seen to be intermediate in behavior between the Cu^{2+}–SDS and Cu^{2+}–α-SLNa systems.

Mechanism of Flotation of Cu^{2+} Ions by Means of an Anionic Surfactant. When we compare Figs. 3, 4 and 6, the cooperative effect of sulfate and carboxylic groups is evident. It may be explained by the fact that the presence of carboxylic groups is effective for the bubble flotation by combining with Cu^{2+} ions, while the coexistence of sulfonic groups enhances the

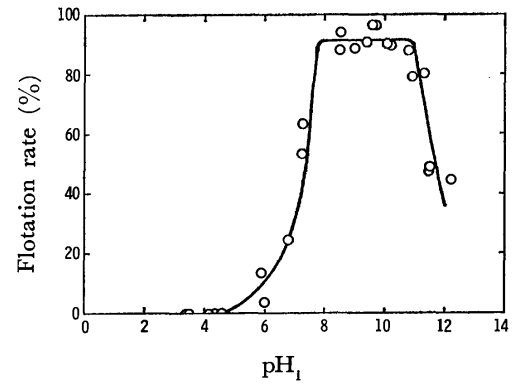

Fig. 6. Flotation rate *vs.* initial pH for Cu^{2+}–LNa system.
Cu^{2+}: 1×10^{-4} mol/l, LNa: 2×10^{-4} mol/l, gas-flow time: 7 min.

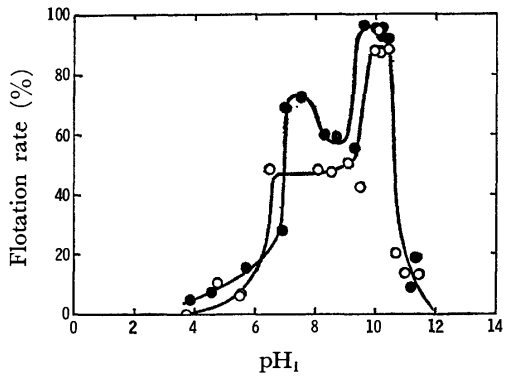

Fig. 7. Flotation rate *vs.* initial pH for Cu^{2+}–DBS system.
Cu^{2+}: 1×10^{-4} mol/l, DBS: ○; 1×10^{-5} mol/l, ●; 2×10^{-5} mol/l, gas-flow time: 7 min.

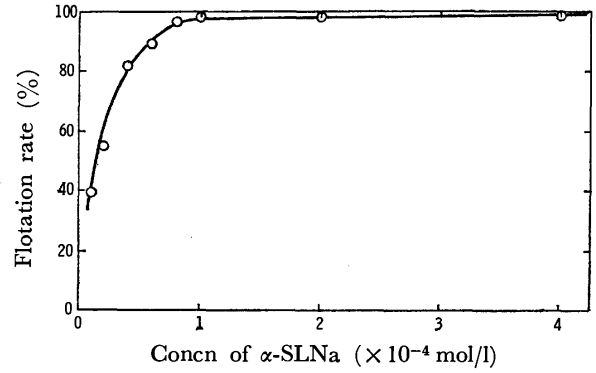

Fig. 8. Flotation rate *vs.* concentration of α-SLNa for Cu^{2+}–α-SLNa system.
Cu^{2+}: 2×10^{-4} mol/l, pH_i: 9.30—9.50, gas-flow time: 7 min.

flotation rate by increasing the solubility of the collector, as has previously been reported.[11]

As has been mentioned above, Figs. 3—7 show sharp rises in the *F vs.* pH curves at pH 6, which correspond to the beginning of copper-hydroxide precipitation. This might indicate that the sublate consists mainly of a polynuclear hydroxide-surfactant complex, the process being called the precipitation flotation of the first type.[16] Figure 8 shows the effect of the concentration of α-SLNa on the rate of the

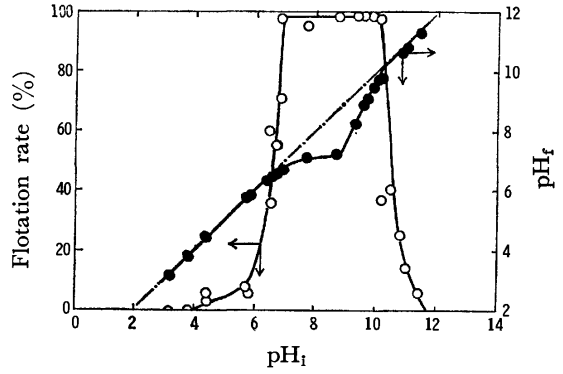

Fig. 9. Initial pH *vs.* final pH and flotation rate for Cu^{2+}-α-SLNa system.
Cu^{2+}: 1×10^{-4} mol/l, α-SLNa: 2×10^{-4} mol/l, gas-flow time: 7 min.

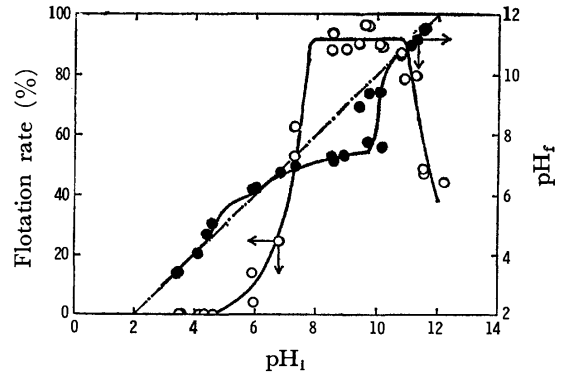

Fig. 10. Initial pH *vs.* final pH and flotation rate for Cu^{2+}-LNa system.
Cu^{2+}: 1×10^{-4} mol/l, LNa: 2×10^{-4} mol/l, gas-flow time: 7 min.

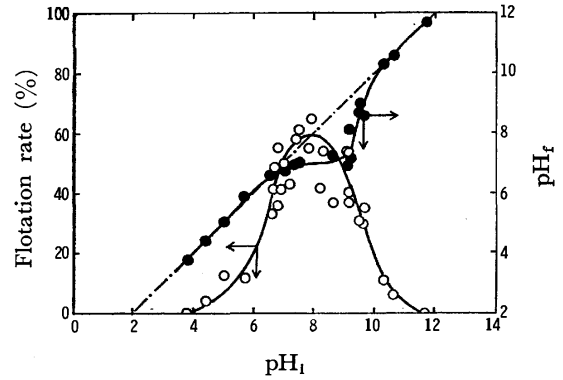

Fig. 11. Initial pH *vs.* final pH and flotation rate for Cu^{2+}-SDS system.
Cu^{2+}: 1×10^{-4} mol/l, SDS: 1×10^{-5} mol/l, gas-flow time: 7 min.

flotation of the 2×10^{-4} mol/l Cu^{2+} solution. It may be seen in this figure that F of nearly 100% is obtained at the surfactant concentration of about 1×10^{-4} mol/l, which is equivalent to one-fourth of the Cu^{2+} ion concentration of this solution. It may be suggested that one surfactant molecule combines with at least four Cu^{2+} ions for a 100% flotation. It may similarly be estimated that the SDS/Cu^{2+} ratio is lower than 1/40 for the Cu^{2+}–SDS system. These

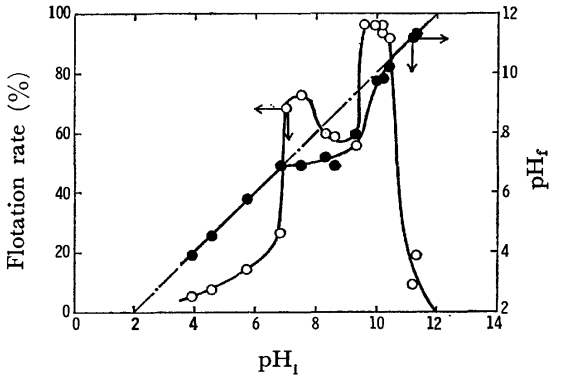

Fig. 12. Initial pH *vs.* final pH and flotation rate for Cu^{2+}-DBS system.
Cu^{2+}: 1×10^{-4} mol/l, DBS: 2×10^{-5} mol/l, gas-flow time: 7 min.

small collector/colligend ratios may be considered to be specific for the precipitation flotation of the first type as compared with the case of ion-adsorption flotation, where the surfactants combine with Cu^{2+} ions at a stoichiometric or greater ratio.[17] This also confirms that the precipitation flotation is the dominant factor in the present case.

In Figs. 9, 10, 11 and 12, the values of pH$_f$ and F are plotted against the pH$_i$ for the flotation of Cu^{2+} by α-SLNa, LNa, SDS, and DBS respectively. As may be seen in these figures, the plateau appears in the pH$_f$ *vs.* pH$_i$ curve in the vicinity of pH 8. This may be explained by the liberation of hydrogen ions due to the formation of polynuclear species,[11,18] according, for instance, to

$$n\mathrm{Cu^{2+}} + (n-1)\mathrm{H_2O} \rightarrow {}^{+}\mathrm{Cu(OCu)}_{n-2}\mathrm{OCu^{+}} + 2(n-1)\mathrm{H^{+}}$$

This may also explain the fact that large amounts of Cu^{2+} ions are removed by a small amount of a surfactant. The decrease in the flotation rate on the alkaline side is due to the competition between OH^- and surfactant anions for polynuclear Cu^{2+} ions; therefore, the pH region of the decreasing branch and the shape of the maximum of the F *vs.* pH curve depend on the nature of the acid groups.

It is also confirmed that the plateau region of the pH$_f$ *vs.* pH$_i$ curve and the maximum region of the F *vs.* pH$_i$ curve coincide with each other as a whole; this again indicates the formation of a polynuclear Cu^{2+}-surfactant complex, as has been mentioned above. The decrease in the flotation rate of Cu^{2+} ions below pH 6 can be explained by the competition between H^+ and Cu^{2+} ions for the anionic surfactant.

Now, in the case of α-SLNa system, the question arises as to whether the polynuclear Cu^{2+} ion attaches to the carboxylic or the sulfonic group of the surfactant molecule. It may be expected, from the similarity of the F *vs.* pH$_i$ curve of α-SLNa to that of the LNa curve (Fig. 6), and from a consideration of the solubility product, that the combination between the Cu^{2+} ion and the carboxylic-acid group is preferred, although Davis and Sebba have reported that the Sr^{2+} ions reacted preferentially with sulfonic groups.[15] The exact determination requires further study.

(2) *Flotation of Cu^{2+} Ions by Means of a Cationic Surfactant.* *Results Obtained*: Figure 13 indicates

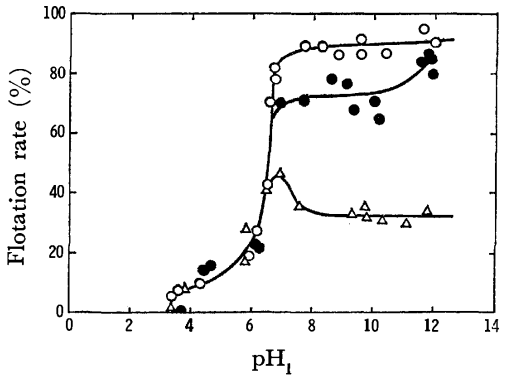

Fig. 13. Flotation rate *vs.* initial pH for Cu^{2+}-DTAC system.
Cu^{2+}: 1×10^{-4} mol/l, DTAC: 2×10^{-4} mol/l, bentonite: △; 0.001%, ●; 0.005%, ○; 0.01%, gas-flow time: 7 min.

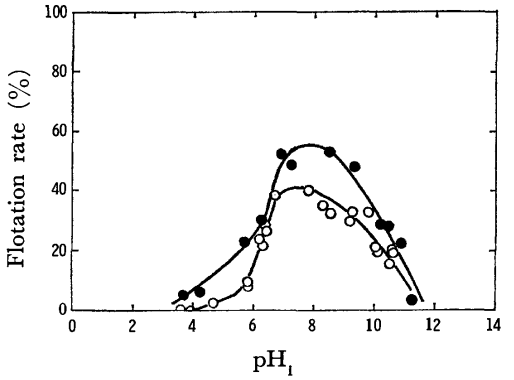

Fig. 14. Flotation rate *vs.* initial pH for Cu^{2+}-DPC system.
Cu^{2+}: 1×10^{-4} mol/l, DPC: 1×10^{-5} mol/l, bentonite: ○; 0%, ●; 0.01%, gas-flow time: 7 min.

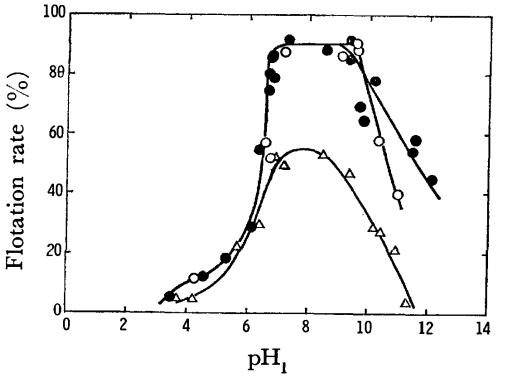

Fig. 15. Flotation rate *vs.* initial pH for Cu^{2+}-DPC system.
Cu^{2+}: 1×10^{-4} mol/l, bentonite: 0.01%, DPC: △; 1×10^{-5} mol/l, ○; 1×10^{-4} mol/l, ●; 2×10^{-4} mol/l, gas-flow time: 7 min.

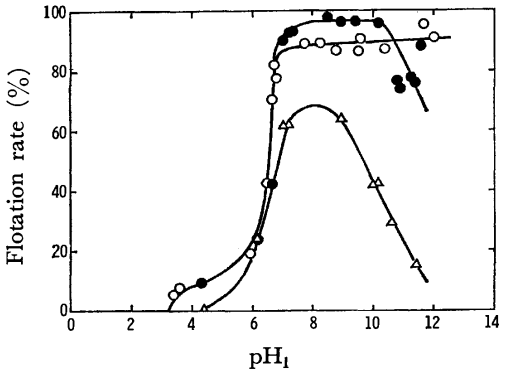

Fig. 16. Flotation rate *vs.* initial pH for Cu^{2+}-DTAC system.
Cu^{2+}: 1×10^{-4} mol/l, bentonite: 0.01%, DTAC: △; 1×10^{-5} mol/l, ●; 1×10^{-4} mol/l, ○; 2×10^{-4} mol/l, gas-flow time: 7 min.

the plots of the flotation rate *vs.* the amount of bentonite for DTAC at various pH values. Figure 14 shows the flotation rate *vs.* the pH curve for DPC with and without the addition of bentonite. Figures 15 and 16 show the relationship between the flotation rate and the surfactant concentration for DPC and DTAC respectively at various pH values.

Relation between the pH and the Flotation Rate. As may be seen in Figs. 13 to 16, the flotation rate remains almost zero for the systems of both DPC and DTAC up to pH 6, above which point it increases much as in the cases of anionic surfactants; a maximum appears in the pH region from 7 to 10 or more. The flotation rate generally decreases in a sufficiently high pH region. In the case of Cu^{2+}-ion flotation by bentonite and a cationic surfactant, bentonite enhances the flotation by the adsorption of Cu^{2+} ions, followed by coagulation and flotation, since a system lacking bentonite markedly decreases the flotation rate, as will be discussed later. Thus, this flotation is classified as an ion-adsorbing particle flotation.[6] Bentonite, being considered as an macromolecular anion, acts as a bridge between the cationic Cu^{2+} ions and the cationic surfactant. The region of large F extends to a higher pH region for the Cu^{2+}–bentonite–cationic surfactant system (Fig. 16) than for the Cu^{2+}–anionic surfactant system (Fig. 5) because, in the former system, the multiple points of attachment are supplied by bentonite for the polynuclear Cu^{2+} ions and the cationic surfactant, while in the latter system the anionic surfactant offers for less site for the polynuclear Cu^{2+} ions. This results is not only an extension of the pH region to a higher value, but also a larger flotation rate of the Cu^{2+}–bentonite–cationic surfactant complex than that of the Cu^{2+}–anionic surfactant. At a sufficiently high pH, OH^- ions compete with bentonite for both cationic surfactant and Cu^{2+} ions in the case of a dilute surfactant or a surfactant of a relatively weak base, and a general tendency for F to decrease is expected, as can be seen for DPC in Figs. 14 and 15 and for DTAC in Fig. 16. A marked decrease in F above pH 10 in the case of the Cu^{2+}–bentonite–DPC system was found to be a result of the weaker basic nature of DPC than of DTAC, as confirmed by the potentiometric titration. At pH values lower than 6, the flotation rate is practically zero for Cu^{2+}–bentonite–cationic surfactant systems; this is a result of the strong adsorption of H^+ on bentonite, which prevents the adsorption of the cationic surfactant and Cu^{2+} ions.

Effect of Bentonite. As may be seen in Fig. 13, an increase in the bentonite concentration from 0.001

to 0.01% increases the flotation rate for the DTAC system. This is a result of the decrease in liquid hold-up by the suppression of foaming and the maintenance of the condition of bubble flotation. The system lacking bentonite strongly foams, so it could not be studied by the bubble-flotation system. Therefore, bentonite acts not only as a bridge between Cu^{2+} ions and bubbles, but also as an inhibitor of foaming caused by the surfactant, thus making effective bubble flotation possible. The complete removal of bentonite, however, exhibited some residual flotation rate, as is shown in Fig. 14 for the Cu^{2+}–DPC system. This may be due to some Cu^{2+} ions being adsorbed on the cationic foam, even in the absence of bentonite, perhaps by a nonspecific interaction between the polynuclear Cu^{2+} ions and the cationic surfactant.

Effect of the Concentration of the Surfactant. As may be seen in Figs. 15 and 16, the flotation rate increases with an increase in the concentration of the surfactant, and reaches a maximum, showing F values of 90% for the 1×10^{-4} mol/l DPC system and 98% for the 1×10^{-4} mol/l DTAC system. Under these conditions, the solutions after flotation look quite transparent and seem free from suspended matter. Therefore, the concentration of the 1×10^{-4} mol/l cationic surfactant is just sufficient for the flotation of both 1×10^{-4} mol/l Cu^{2+} and 001% of bentonite under the present conditions of measurement. The incomplete flotation shown in Figs. 15 and 16 can also be interpreted as resulting from the surfactant being insufficient to float the bentonite. It shoud be noted, however, that the decrease in the surfactant to 1/10 of the optimum concentration only reduces the flotation rate to more than half the optimum value.

It has been reported that the base-exchange capacity of clay mineral ranges from 70 to 150 m eq./100 g.[19] Using the values of 70 m eq./100 g clay, 1×10^{-4} mol/l Cu^{2+}, 0.01% bentonite, and 2×10^{-4} mol/l surfactant, 1000 g of a solution contains 0.07 meq. of exchange sites due to bentonite, 0.2 m eq. of Cu^{2+}, and 0.2 meq. of the surfactant. Therefore, a nearly complete flotation of Cu^{2+} requires a Cu^{2+} polynuclear structure of far less effective equivalence and only a partial adsorption of the surfactant on a limited area on the bentonite surface. The details of such a structure will be reported elsewhere.

The author wishes to thank Professor Tsunetaka Sasaki for his valuable advice and continual encouragement, and also the Ministry of Education for the financial support given to Professor Sasaki.

References

1) R. Lemlich, "Adsorptive Bubble Separation Techniques," Academic Press, New York and London (1972), p. 219.
2) F. Sebba, "Ion Flotation," Elsevier Publisher, London and New York (1962), p. 137.
3) R. Lemlich, "Adsorptive Bubble Separation Techniques," Academic Press, New York and London (1972), p. 71, 85, 285—290.
4) F. Sebba, "Ion Flotation," Elsevier Publisher, London and New York (1962), p. 142.
5) T. Yamabe and N. Takai, *Seisan Kenkyu*, **21**, 530 (1969).
6) R. Lemlich, "Adsorptive Bubble Separation Techniques," Academic Press, New York and London (1972), p. 273.
7) R. Lemlich, *ibid.*, p. 275.
8) F. Sebba, *Nature*, **184**, 1062 (1959).
9) R. E. Baarson and C. L. Ray, "Precipitate Flotation—A New Metal Extraction and Concentration Technique," Amer. Inst. of Mining, Metallurgical and Petroleum Engineers Symposium, Dallas, Texas, 1963.
10) A. J. Rubin, J. D. Jonson, and J. C. Lamb, *Ind. Eng. Chem., Process Design Develop.*, **5**, 368 (1966).
11) F. Sebba, "Ion Flotation," Elsevier Publisher, London and New York (1962).
12) R. Lemlich, "Adsorptive Bubble Separation Techniques," Academic Press, New York and London, (1972).
13) E. E. Dreger, *Ind. Eng. Chem.*, **36**, 610 (1944).
14) A. J. Rubin, J. D. Johnson, and J. Lamb, "Ion and Precipitate Flotation". A paper presented to the American Chemical Society, Atlantic City, N. J., September (1965).
15) B. M. Davis, and F. Sebba, *J. Appl. Chem.* **16**, 293 (1966).
16) R. Lemlich, "Adsorptive Bubble Separation Techniques," Academic Press, New York and London (1972), p. 78.
17) R. Lemlich, *ibid.*, p. 200.
18) D. D. Perrin, *J. Chem. Soc.*, **1960**, 3189.
19) H. Van Olphen, "An Introduction to Clay Colloid Chemistry," Interscience, New York and London (1963), pp. 71, 81.

The Role of the Promoting Mode in Nonradiative Transitions in Large Molecules

Yuichi FUJIMURA and Takeshi NAKAJIMA
Department of Chemistry, Tohoku University, Sendai 980
(Received November 26, 1973)

A rate expression for the intramolecular nonradiative transition where a promoting mode acts also as an accepting mode at the same time has been derived within the statistical limit. The dependence of the nonradiative transition rate on the shift of the equilibrium point of the promoting mode in the relevant electronic states, Δ_p, has been examined for two cases, i) excited ⇝ ground states and ii) excited ⇝ excited states, in aromatic hydrocarbons which satisfy the above condition.

In recent years, there have been many theoretical and experimental discussions[1-18] regarding the nature of the intramolecular nonradiative transitions in large molecules. Many theoretical discussions have been made of electronic relaxation processes in which vibrational modes are explicitly classified as promoting, accepting, and irrelevant modes for the nonradiative transitions: further, the promoting modes have been distinguished from the accepting modes.

The promoting modes for the internal conversions are determined from the symmetry consideration in the coupling matrix element between the relevant electronic states.[19] On the other hand, for the intersystem crossings where two kinds of perturbing operators, *i.e.*, the spin-orbit and nuclear kinetic energy operators, may act, the identification of the promoting modes is dependent on the coupling mechanism; when the zero order spin-orbit interaction does not vanish by symmetry, the rate for the intersystem crossing is irrelevent to the promoting modes, while when the higher order spin-orbit vibronic interaction has to be included, the promoting modes will play an essential role in the intersystem crossing. Various mechanisms have been proposed,[20-24] but no one has been able to uniquely identify the promoting mode for the intersystem crossing. We shall confine our investigation to the role of the promoting mode for the internal conversion of large molecules.

Considering the simple model of the non-displaced and non-distorted harmonic potential-energy surfaces for the promoting mode, Lin[1] and Freed and Jortner[7] have demonstrated the propensity rule for the promoting mode—that is, it must gain or lose one quantum of the vibrational energy in the electronic transition. The propensity rule for the promoting mode leads to the concept of an effective energy gap which differs, as a result of increase or decrease by one quantum of the vibrational energy of the promoting mode, from the electronic energy gap between the relevant electronic states. The applicability of the propensity rule is, however, restricted to the electronic relaxation between electronic states with different irreducible representations of the point groups of a molecule in the weak coupling cases. When we consider the nonradiative transitions between the electronic states with the same irreducible representation of the point group of a molecule, the propensity rule should be altered because the promoting mode will act as an accepting mode at the same time. The physical situation in this category will involve, for example, the internal conversion from the first excited singlet state ($^1A_1$) to the ground state of phenanthrene.[25,26]

A similar problem was considered by Fong and Wassam.[27] Their formalism was based on the time-correlation function proposed by Kubo.[28] They thought that the situation will be encountered in the nonradiative transition, S_1 ⇝ T_1, of benzene in the solid state, where the D_{6h} symmetry is retained in the first excited singlet state and where, on the other hand, the symmetry in the lowest triplet state has a lower value than D_{6h}. However, the application of the formalism of Fong and Wassam to the S_1 ⇝ T_1 transition of benzene in the solid state was criticized by Nitzan and Jortner[29] because the symmetry reduction in the lowest triplet state might be due to the crystal-field effect.

In the present paper, we will derive a rate expression for the nonradiative transition, considering that the promoting mode acts also as an accepting mode in the weak coupling case; the results will be compared with those of the case in which the promoting and accepting modes act independently. The present formalism will be primarily based on the treatment by Lin[1] and Englman and Jortner[6] in the framework of the weak coupling case in large molecules. The interference effect between promoting modes will be neglected. As a simple case in which there is no displacement for the promoting mode between the relevant electronic states, the expression contains the same results as those derived by Freed and Jortner.[7] The steepest-descent method will be used to determine the most probable path for the nonradiative transition (the highest frequency mode belonging to the displaced potential surfaces) and to examine the contribution of the second-highest frequency mode to the partitioning of the excess energy. Nonradiative transitions between the excited states of such aromatic hydrocarbons as naphthalene having dimensions larger than benzene will be treated, where the shift of the origin of the highest mode ($\hbar\omega_{C-H}\approx 3000\ cm^{-1}$) may be considered to be smaller than that of the second-highest ($\hbar\omega_{C-C}\approx 1500\ cm^{-1}$) by about one order.

Theory

The nonradiative transition rate from an electronic state, s, to a lower electronic state, t, with a quasicontinuum vibronic manifold is given by the time-dependent perturbation theory as:

$$W(\mathrm{s} \rightsquigarrow \mathrm{t}) = \frac{2\pi}{\hbar}\sum_{lm} P_{sl}|\langle tm|V|sl\rangle|^2\delta(E_{tm}-E_{sl}) \quad (1)$$

where l and m refer to vibrational states belonging to s and t electronic states respectively and where E_{sl} and E_{tm} refer to the energies of the initial and final states respectively. P_{sl} is the Boltzmann weighting factor for the initial vibronic states:

$$P_{sl} = \exp(-\beta E_{sl})/\sum_{l}\exp(-\beta E_{sl}) \tag{2}$$

where $\beta = 1/k_B T$.

There has been a fair amount of discussion concerning the choice of the zero-order basis set for describing the nonradiative transition in an isolated molecule.[30-35] We shall take Born-Oppenheimer states as the zero-order set in the present treatment. In the adiabatic representation, the electronic wave function, Φ_s, and the vibrational wave function, Ξ_{sl}, satisfy the following equations:

$$H_0(r, Q)\Phi_s(r, Q) = E_s(Q)\Phi_s(r, Q), \tag{3}$$

and:

$$[T(Q)+E_s(Q)]\Xi_{sl}(Q) = E_{sl}\Xi_{sl}(Q) \tag{4}$$

where

$$H_0(r, Q) = T(r) + U(r, Q), \tag{5}$$

and where r and Q denote the coordinate of the electrons and the vibrational coordinates respectively. $T(r)$, $T(Q)$, and $U(r,Q)$ denote the kinetic energy of the electrons, the kinetic energy of the nuclei, and the electrostatic potential energy respectively. The adiabatic wave function, $\Psi_{sl}(r,Q)$, is given by the product of the electronic wavefunction, $\Phi_s(r,Q)$, and the vibrational wave function, $\Xi_{sl}(Q)$:

$$\Psi_{sl}(r, Q) = \Phi_s(r, Q)\Xi_{sl}(Q). \tag{6}$$

The perturbation, V, for the nonradiative transition is the nuclear kinetic energy, $T(Q)$. Then, the matrix element in Eq. (1) can be expressed in the following way:

$$\langle tm|V|sl\rangle = -\hbar^2\sum_p\frac{1}{M_p}\left\langle\Phi_t(r, Q)\Xi_{tm}(Q)\left|\frac{\partial\Phi_s(r, Q)}{\partial Q_p}\frac{\partial}{\partial Q_p}\Xi_{sl}(Q)\right.\right\rangle - \frac{\hbar^2}{2}\sum_p\frac{1}{M_p}\left\langle\Phi_t(r, Q)\Xi_{tm}(Q)\left|\frac{\partial^2\Phi_s(r, Q)}{\partial Q_p{}^2}\Xi_{sl}(Q)\right.\right\rangle \tag{7}$$

where the subscript, p, denotes the promoting mode which induces the nonradiative transition between relevant electronic states. We assume the potential energy surfaces to be harmonic and displaced.

In the present treatment, Eq. (1) will be evaluated within the so-called Condon approximation, which is based on the assumption that the first derivative of the initial electronic state varies slowly with the nuclear coordinates. We assume that the nonradiative transition is induced by a promoting mode, q_p.[36] We utilize the time-integral representation of the δ-function in Eq. (1). Performing the summation over the vibrational quanta, m_i and l_i, for the i-th mode in Eq. (1) by the aid of the Slater sum rule, and integrating Eq. (1) over the normal coordinates, we obtain:

$$W(s \rightsquigarrow t) = \omega_p{}^2|V_{st}{}^p|^2\int_{-\infty}^{\infty}dt\exp\left[-\frac{i\Delta Et}{\hbar}\right]\Delta_p\prod_i^{N'}\Omega_i \tag{8}$$

where:

$$V_{st}{}^p = \frac{\left\langle\Phi_t\left|\left(\frac{\partial U}{\partial q_p}\right)\right|\Phi_s\right\rangle}{\Delta E_{st}} \tag{9}$$

$$\Omega_i = \exp\left[-\frac{2n_i+1}{2}\Delta_i{}^2+\frac{n_i+1}{2}\Delta_i{}^2\exp(i\omega_i t) + \frac{n_i}{2}\Delta_i{}^2\exp(-i\omega_i t)\right] \tag{10}$$

and:

$$\Delta_p = \frac{\Omega_p}{2}\left[(n_p+1)\exp(i\omega_p t)+n_p\exp(-i\omega_p t) + \frac{\Delta_p{}^2}{2}\{2n_p+1-(n_p+1)\exp(i\omega_p t)-n_p\exp(-i\omega_p t)\}^2\right] \tag{11}$$

ΔE_{st} in Eq. (9) is the virtual energy-separation between zero-order electronic states, s and t. The n_i notation, in Eqs. (10) and (11) represents the average number of the excited vibrations with the frequency of ω_i at thermal equilibrium: that is,

$$n_i = [\exp(\beta\hbar\omega_i)-1]^{-1} \tag{12}$$

and $\Delta_i = (\mu_i\omega_i/\hbar)^{1/2}(Q_i{}^{t(0)} - Q_i{}^{s(0)})$, the reduced displacement of the equilibrium position of the i-th normal coordinate in the two electronic states. In deriving Eq. (8), the Herzberg-Teller expansion was utilized in order to obtain the approximate adiabatic electronic wave functions. The prime in Eq. (8) means the exclusion of the promoting mode in the Ω_i product. The inclusion of the Ω_p appearing in Δ_p in the Ω_i product leads to the following equation:

$$W(s \rightsquigarrow t) = \frac{\omega_p{}^2}{2}|V_{st}{}^p|^2\exp(-\eta)\int_{-\infty}^{\infty}dt\left[(n_p+1)\exp(i\omega_p t) + n_p\exp(-i\omega_p t)+\frac{\Delta_p{}^2}{2}\{2n_p+1-(n_p+1)\exp(i\omega_p t) - n_p\exp(-i\omega_p t)\}^2\right]\exp\left[-\frac{i\Delta Et}{\hbar}+\eta_+(t)+\eta_-(t)\right] \tag{13}$$

where

$$\eta = \eta_+(0)+\eta_-(0) = \sum_i\left(n_i+\frac{1}{2}\right)\Delta_i{}^2 \tag{14}$$

$$\eta_+(t) = \frac{1}{2}\sum_i(n_i+1)\Delta_i{}^2\exp(i\omega_i t) \tag{15}$$

and

$$\eta_-(t) = \frac{1}{2}\sum_i n_i\Delta_i{}^2\exp(-i\omega_i t) \tag{16}$$

We have derived the rate expression for the nonradiative transition using the harmonic displaced potential-surface model in the form of the Fourier transformation. Let us, for the sake of simplicity, consider the nonradiative transitions within the low-temperature limit; then we have

$$W(s \rightsquigarrow t) = \frac{\omega_p{}^2}{2}|V_{st}{}^p|^2\exp\left(-\sum_i\frac{\Delta_i{}^2}{2}\right)\int_{-\infty}^{\infty}dt\left[\exp\left\{-\frac{i(\Delta E-\hbar\omega_p)t}{\hbar} + \sum_i\frac{\Delta_i{}^2}{2}\exp(i\omega_i t)\right\}+\frac{\Delta_p{}^2}{2}\{1-\exp(i\omega_p t)\}^2 \times\exp\left\{-\frac{i\Delta Et}{\hbar}+\sum_i\frac{\Delta_i{}^2}{2}\exp(i\omega_i t)\right\}\right] \tag{17}$$

We are interested in the nonradiative transitions of large molecules within the statistical limit. The time integration of the nonradiative transition rate in Eq. (13) can be carried out by the steepest-descent method, which has frequently been applied to the evaluation of the nonradiative transition rates in large molecules on the assumption that the highest frequency mode with the displaced potential acts as an accepting mode. The modes with the displaced potential surface between relevant electronic states in the case of the weak coupling of large molecules such as aromatic hydrocarbons are identified as follows: (1) totally symmetric C–H stretching modes, and (2) totally symmetric C–C skeletal stretching modes. The other vibrational modes do not lead to the shifts of the adiabatic potentials when the vibronic coupling, such as the Jahn-Teller coupling and the pseudo-Jahn-Teller coupling, may be neglected. This assumption may be justified in benzene, which has a relatively low second-high frequency mode (the C–C skeletal stretching mode with $\sim$1000 cm^{-1}) compared with the highest frequency mode (the C–H stretching mode with $\sim$3000 cm^{-1}), and in the case of the nonradiative transitions between the excited and ground states of other aromatic hydrocarbons, where the reduced displacements of the accepting modes are considered to be of the same order. In this case, we have $\exp(i\omega_{C-H}t)=X^3$ if $X=\exp(i\omega_{C-C}t)$ and the coefficients of X and X^3 are of the same order in the time integration of the nonradiative transition rate; therefore the highest frequency terms, $\exp(i\omega_{C-H}t)$, makes the main contribution to the determination of the saddle point. However, this assumption may lead to a drastic error in evaluating the rates of the nonradiative transitions between the excited states of the aromatic hydrocarbons larger than benzene, where the frequency of the highest-frequency mode remains constant (3000 cm^{-1}); on the other hand, that of the next highest frequency mode increases (the C–C stretching: $\sim$1500 cm^{-1}) compared with that of benzene, and the reduced displacement of the latter may be considered to be larger than that of the former by about one order. From the above point of view, we shall use the steepest-descent method, taking into account the fact that both the C–H stretching (3000 cm^{-1}) and C–C stretching (1500 cm^{-1}) modes act as accepting modes. Utilizing the steepest-descent method, we obtain this final expression for W(s ⇝ t) at low temperature:

$$W(\mathrm{s} \rightsquigarrow \mathrm{t}) = \frac{\omega_p^2}{2}|V_{st}^p|^2 \exp\left(-\sum_i \frac{\Delta_i^2}{2}\right)\left[(1-\Delta_p^2)I(\hbar\omega_p) + \frac{\Delta_p^2}{2}\{I(0)+I(2\hbar\omega_p)\}\right] \quad (18)$$

where

$$I(\varepsilon) = \hbar(2\pi)^{1/2} \times \exp\left\{-\frac{(\Delta E-\varepsilon)}{\hbar\omega_p}\log A(\varepsilon) + \frac{\Delta_H^2}{2}A^2(\varepsilon) + \frac{\Delta_p^2}{2}A(\varepsilon)\right\} \times \left\{2(\hbar\omega_p)^2\Delta_H^2A^2(\varepsilon) + \frac{1}{2}(\hbar\omega_p)^2\Delta_p^2A(\varepsilon)\right\}^{-1/2} \quad (19)$$

and where

$$A(\varepsilon) = \frac{\Delta_p^2}{4\Delta_H^2}\left[-1+\left\{1+\frac{16\Delta_H^4(\Delta E-\varepsilon)}{\hbar\omega_p\Delta_p^4}\right\}^{1/2}\right] \quad (20)$$

The Δ_p and Δ_H which appear in Eqs. (18), (19), and (20) denote the reduced displacements of the C–C stretching mode with the ω_p frequency and the C–H stretching mode with the ω_H frequency respectively.

Discussion

Assuming that the promoting mode is independent of the accepting modes, Englman and Jortner[6] and Freed and Jortner[7] have derived the rate expression for the nonradiative transitions in large molecules using the displaced potential-surface model for the accepting modes. Their results imply that in the case of weak coupling, the nonradiative decay is characterized by the exponential dependence on the effective gap, $\Delta E-\hbar\omega_p$, in the low-temperature range (energy-gap law). It should be noted that Eq. (18) reduces to the expression derived by Freed and Jortner when there is no displacement for the promoting mode. Equation (18) reveals that, when $\Delta_p \neq 0$, the nonradiative decay occurs through Processes 1, 2, and 3, whose energy gaps are ΔE, $\Delta E-\hbar\omega_p$, and $\Delta E-2\hbar\omega_p$ respectively.

Considering the simple model systems for the nonradiative transitions, we have examined the dependence of the nonradiative transition rate, W(s ⇝ t), on the reduced displacement for the promoting mode, Δ_p, in the low-temperature range. Regrettably, the exact electronic wave function is not known at present, so we cannot obtain a reliable value of V_{st}^p by direct computation. We will instead calculate the $R=W(\Delta_p \neq 0)/W(\Delta_p=0)$ ratio, since by using it V_{st}^p need not be determined. The present information concerning the potential surfaces of aromatic hydrocarbons is insufficient for us to determine the magnitude of displacement required to evaluate the nonradiative transition rates, but at least it can be seen that the modes with the nonvanishing reduced displacements belong to the totally symmetric C–C skeletal stretching and the totally symmetric C–H stretching modes in the case of weak coupling, the magnitudes of the reduced displacements for the C–C stretching modes being of the same order between any electronic states considered. Recently, we proposed a semi-empirical method for evaluating the reduced displacements of the skeletal stretching modes in aromatic hydrocarbons; we found that the magnitudes of the reduced displacements for the C–C stretching modes are of the same order between any π–π^* electronic states considered.[37] For the reduced displacements of the C–H stretching modes in aromatic hydrocarbons, we expect the Δ_H between π–π^* excited states to be smaller than the Δ_H between π–π^* excited and ground states, as the change in the C–H bonds is considered to be smaller between π–π^* excited states, especially when lower π–π^* excited states are involved. In fact, Burland and Robinson[3] have reported that the Δ_H between the first excited-singlet and the lowest-triplet states in benzene is smaller by about one order than the Δ_H between the first excited singlet and ground states. In the absence of more detailed information concerning the value of Δ_H for other molecular systems, we suppose that the Δ_H between the excited states is also smaller

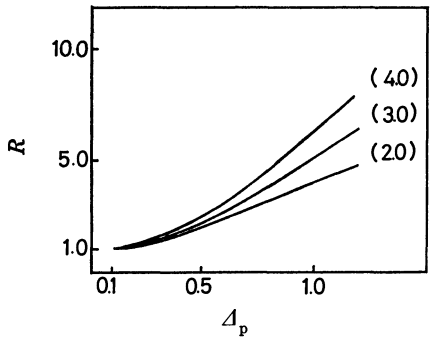

Fig. 1. Variation of R as a function of Δ_p in the excited ⟿ ground state nonradiative transition. Numbers in parentheses denote the energy gap, ΔE in eV.

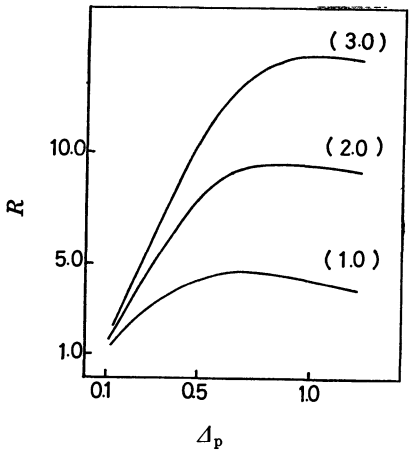

Fig. 2. Variation of R as a function of Δ_p in the excited ⟿ excited state nonradiative transition.

by one order than the Δ_H between excited and ground states in the present calculations. For the present models, two cases will be examined: i) excited ⟿ ground states, and ii) excited ⟿ excited states.

i) *Excited ⟿ Ground States.* From the analysis of the absorption spectra of aromatic hydrocarbons, Byrne *et al.*[38] have concluded that the values of Δ_H are in the range of 0.18—0.42 and that Δ_H is independent of the dimensions of the molecules. For the present calculations, the value of $\Delta_H=0.3$ will be taken. In Fig. 1, R is plotted as a function of Δ_p in the range of 0.1—1.2. Figure 1 shows that the ratio, R, of the nonradiative transition between the excited and ground states within the statistical limit increases only by a factor of 2 in the vicinity of $\Delta_p=0.5$. Using the steepest-descent condition, $\partial F(t)/\partial(it)|_{it=\tau}=0$, where $F(t)$ and $it=\tau$ are the exponent in the time integration of the nonradiative transition rate and the saddle point obtained respectively, we can then determine the partitioning of the excess electronic energy into the vibrational modes involved. Considering the nonradiative transition, whose energy gap is 24000 cm^{-1} and whose reduced displacement Δ_p is 0.5, 90% of the excess energy goes into the C–H stretching mode through Process 2 with $\Delta E-\hbar\omega_p$. From the above results it seems that the existence of an effective accepting mode (the C–H stretching mode) will be enough to explain the characteristics of nonradiative transition rates when the Δ_p and Δ_H are of the same order. In this case, the ratio, R, of the nonradiative transition rates in the low-temperature limit is expressed as a function of Δ_p as following:

$$R = K\Delta_p^2 + 1,$$

where

$$K = \frac{1}{2}\left(1-\frac{\hbar\omega_p}{\Delta E}\right)^{1/2}(\zeta\Delta E)^{-\frac{\Delta E}{\hbar\omega_H}}\{\zeta(\Delta E-\hbar\omega_p)\}^{\frac{\Delta E-\hbar\omega_p}{\hbar\omega_H}} \times \exp\left(\frac{\hbar\omega_p}{\hbar\omega_H}\right)+\frac{1}{2}\left(\frac{\Delta E-\hbar\omega_p}{\Delta E-2\hbar\omega_p}\right)^{1/2} \times \{\zeta(\Delta E-2\hbar\omega_p)\}^{-\frac{\Delta E-2\hbar\omega_p}{\hbar\omega_H}}\{\zeta(\Delta E-\hbar\omega_p)\}^{\frac{\Delta E-\hbar\omega_p}{\hbar\omega_H}} \times \exp\left(-\frac{\hbar\omega_p}{\hbar\omega_H}\right)-1. \quad (21)$$

K is independent of Δ_p, since $\zeta=\left(\sum_i\frac{\hbar\omega_i\Delta_i^2}{2}\right)^{-1}$ includes the parameters of the C–H stretching mode only. The role of the promoting mode is only to reduce the excess energy by zero, one, and two quanta of vibrations for Processes 1, 2, and 3 respectively.

ii) *Excited ⟿ Excited States.* As has been stated above, we suppose that the Δ_H between lower π–π^* excited states is smaller by one order than the Δ_H between the excited and ground states. A variation in Δ_H by a numerical factor does not contribute significantly to the present results. Then, for the sake of simplicity, the $\Delta_H=3\times10^{-2}$ value is taken regardless of the relevant π–π^* excited states. Figure 2 indicates that the ratio of the nonradiative transition rates increases from a factor of 3 to one order in the Δ_p range of 0.3—0.5; this may be considered to be a case of weak coupling, and the magnitude of the ratio may be dependent on the energy gap. Let us consider the distribution of the excess electronic energy into the vibrational modes. The distribution is strongly dependent on the Δ_p: a rough estimation shows that, contrary to the nonradiative transition to the ground state, 60, 70, and 90% of the excess energy, $\Delta E=$ 16000 cm^{-1}, go into the C–C stretching modes through Process 2 when $\Delta_p=0.3$, 0.5, and 0.8 respectively. The promoting mode may, then, act as the accepting mode in this case. This fact also indicates that we cannot exclude the second-highest frequency mode with a displaced potential from the accepting modes when we study the nature of the nonradiative transition between excited states in such large molecules as aromatic hydrocarbons.

Fong and Wassam[27] suggested that, as a consequence of the removal of the zero displacement for the promoting modes, the most important point is the effective diminution of the energy gap by the $\Delta v=2$ process in the event of a small configuration change corresponding to a case of weak coupling. The present result obtained by numerical analysis indicates that the above suggestion by Fong and Wassam is justified in the case of nonradiative transitions between excited states in the aromatic hydrocarbons.

In the present treatment we have derived the nonradiative transition rate, neglecting the interference effect between promoting modes. As has been stated

by Freed and Jortner[7], the interference effect can be expected between two modes, p and p', if the following conditions are satisfied: $\Delta_p \neq 0$, $\Delta_{p'} \neq 0$, $V_{st}^{p} \neq 0$ and $V_{st}^{p'} \neq 0$. In a subsequent paper, the interference effect between promoting modes will be described in detail.

References

1) S. H. Lin, *J. Chem. Phys.*, **44**, 3759 (1966).
2) M. Bixon and J. Jortner, *ibid.*, **48**, 715 (1968).
3) D. M. Burland and G. W. Robinson, *ibid.*, **51**, 4548 (1969).
4) B. Sharf and R. Silbey, *Chem. Phys. Lett.*, **4**, 423 (1969).
5) B. Sharf and R. Silbey, *ibid.*, **4**, 561 (1970).
6) R. Englman and J. Jortner, *Mol. Phys.*, **18**, 145 (1970).
7) K. F. Freed and J. Jortner, *J. Chem. Phys.*, **52**, 6272 (1970).
8) S. Fischer, *ibid.*, **53**, 3195 (1970).
9) A. Nitzan and J. Jortner, *ibid.*, **55**, 1355 (1971).
10) A. Nitzan and J. Jortner, *ibid.*, **56**, 2076 (1972).
11) B. Katz and M. Brith, B. Sharf, and J. Jortner, *ibid.*, **52**, 88 (1970).
12) C. S. Parmenter and M. W. Schuyler, *ibid.*, **52**, 5366 (1970).
13) C. S. Parmenter and M. W. Schuyler, *Chem. Phys. Lett.*, **6**, 339 (1970).
14) W. R. Ware, B. K. Selinger, C. S. Parmenter, and M. W. Schuyler, *ibid.*, **6**, 342 (1970).
15) J. L. Richard and S. A. Rice, *ibid.*, **9**, 444 (1971).
16) J. P. Byrne and I. G. Ross, *Aust. J. Chem.*, **24**, 1107 (1971).
17) K. G. Spears and S. A. Rice, *J. Chem. Phys.*, **55**, 5561 (1971).
18) R. Scheps, D. Florida, and S. A. Rice, *ibid.*, **56**, 295 (1972).
19) It is true that the zero-order molecular eigenstates represented by the Born-Oppenheimer adiabatic basis cannot be specified in terms of the symmetry classification (A. Nitzan and J. Jortner, *Mol. Phys.*, **24**, 109 (1972)). Then, strictly speaking, the classification of the vibrational modes into the promoting and accepting modes will be invalid in the adiabatic basis. However, it seems reasonable to consider the symmetry restriction in the coupling matrix element between the electronic states in the weak coupling case where the harmonic approximation may be applicable to the multidimensional potential surfaces.
20) M. A. El-Sayed, *J. Chem. Phys.*, **38**, 2834 (1963).
21) B. R. Henry and W. Seibrand, *ibid.*, **54**, 1072 (1971).
22) V. Lawetz, G. Orlandi, and W. Siebrand, *ibid.*, **56**, 4058 (1972).
23) T. Azumi, *Chem. Phys. Lett.*, **17**, 211 (1973).
24) B. Shaif, *ibid.*, **19**, 351 (1973).
25) D. P. Craig and R. D. Gorden, *Proc. Roy. Soc.* (*London*), **A288**, 69 (1965).
26) R. M. Hochstrasser and G. J. Small, *J. Chem. Phys.*, **35**, 2270 (1966).
27) F. K. Fong and W. A. Wassam, *ibid.*, **58**, 2667 (1973).
28) R. Kubo, *J. Phys. Soc. Japan*, **12**, 570 (1957).
29) A. Nitzan and J. Jortner, *J. Chem. Phys.*, **58**, 2669 (1973).
30) D. M. Burland and G. W. Robinson, *Proc. Nat. Acad. Sci. U.S.* **66**, 257 (1970).
31) G. Orlandi and W. Siebrand, *Chem. Phys. Lett.*, **8**, 473 (1971).
32) B. Sharf and R. Silbey, *ibid.*, **9**, 125 (1971).
33) K. F. Freed and W. M. Gelbart, *ibid.*, **10**, 187 (1971).
34) A. Nitzan and J. Jortner, *ibid.*, **11**, 458 (1971).
35) B. Sharf, *ibid.*, **14**, 315 (1972).
36) The small letter q denotes dimensionless normal coordinate. The relation between the dimensionless normal coordinate and normal coordinate is given by $q=(\mu\omega/\hbar^{1/2}(Q^s-Q^{s(0)})$, where μ and $Q^{s(0)}$ are the reduced mass and the equilibrium position of the s-th electronic state, respectively.
37) Y. Fujimura and T. Nakajima, *Chem. Phys. Lett.*, **14**, 108 (1972).
38) J. P. Byrne, E. F. McCoy, and I. G. Ross, *Aust. J. Chem.*, **18**, 1859 (1965).

Substitution and Hydrogen Bonding Effects on Fluorescence and Intersystem Crossing in Naphthaldehydes and Their Derivatives

Michio KITAMURA and Hiroaki BABA

Division of Chemistry, Research Institute of Applied Electricity, Hokkaido University, Sapporo 060

(Received December 20, 1974)

Absorption and fluorescence spectra, fluorescence and phosphorescence quantum yields and lifetimes of 1- and 2-naphthaldehyde and their derivatives have been measured in rigid glass solution at 77 K. Naphthaldehydes and acetonaphthones are non-fluorescent, whereas naphthoyl chlorides and methyl naphthoates are fluorescent. Upon formation of a hydrogen bond with ethyl alcohol, 2-naphthaldehyde and 2-acetonaphthone become fluorescent, and 1-naphthoyl chloride increases in fluorescence quantum yield by a factor of about 65. The rate constants for intersystem crossing in these three molecules decrease by about two orders of magnitudes as a result of hydrogen bonding. The decrease of the rate constants is attributed to elevation of the (n, π^*) level and the resulting change in its position relative to the (π, π^*) level. The experimental results are discussed in relation to the current theories of radiationless transition, and are found to conform to the theory in which both spin-orbit coupling and nuclear kinetic-energy operators are treated as the perturbation causing intersystem crossing.

Molecules possessing low-lying (n, π^*) states, such as aromatic carbonyls and nitrogen heterocyclics, are in general non-fluorescent or only very weakly fluorescent but strongly phosphorescent.[1,2] These phenomena have been extensively discussed by taking into account the relative positions of (n, π^*) and (π, π^*) levels and their role in intersystem crossing.[3-9]

Recently, Henry and Siebrand formulated a general rate expression for intersystem crossing by treating both spin-orbit coupling and nuclear kinetic-energy operators as the perturbation which causes the nonradiative transition.[10] The rate expression of these authors is very different from that of Lin[11] and Bixon and Jortner.[12] As has been noted by Azumi,[13] these two types of theories may predict different fluorescence characteristics for molecules with (n, π^*) states. At the present stage of the theory of intersystem crossing, therefore, a systematic study on the fluorescence characteristics of molecules of this kind is desirable to clarify the nature of the perturbation for the intersystem crossing.

In the present study, the absorption spectra and fluorescence characteristics of the simplest carbonyl substituted naphthalenes, 1- and 2-naphthaldehyde (1-, 2-NA), and their respective three derivatives have been examined in detail at 77 K with particular regard to substitution and hydrogen bonding effects. The derivatives used are as follows: acetonaphthones (1-, 2-AN), naphthoyl chlorides (1-, 2-NC), and methyl naphthoates (1-, 2-MN). On the basis of rate constants estimated for intersystem crossing and other pertinent results obtained, the mechanism of the intersystem crossing in these molecules is discussed in relation to the current theories mentioned above.

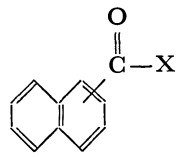

1-, 2-NA: X=H
1-, 2-AN: X=CH_3
1-, 2-NC: X=Cl
1-, 2-MN: X=OCH_3

Experimental

1-Substituted compounds were purified by distillation under reduced pressure, and 2-substituted compounds were recrystallized twice from *n*-hexane. Isopentane and methylcyclohexane were purified by chromatography using a column of silica gel. Spectro-grade ethyl alcohol (EtOH) was refluxed for five hours over calcium oxide and distilled. A mixture of isopentane and methylcyclohexane (4 : 1 by volume, abbreviated to PM hereafter) was used as solvent.

Absorption and fluorescence spectra, quantum yields and lifetimes were obtained at 77 K by the same methods as described in previous papers.[7,14] The correction of fluorescence and excitation spectra was made by the relative method.[7]

Sample solutions for quantum yield and lifetime measurements were degassed by freeze-thaw cycles. Unusual absorption and emission bands, probably due to aggregated species, appeared at concentrations higher than $(6—7)\times10^{-5}$ M. For this reason, concentrations of the sample solutions were chosen as $\sim5\times10^{-5}$ M for 1-substituted compounds and $\sim3\times10^{-5}$ M for 2-substituted compounds.

Results and Discussion

Substitution Effects on Fluorescence Characteristics and Positions of (n, π^*) Levels. The fluorescence quantum yields (Φ_F) and observed fluorescence lifetimes (τ_F) of 1- and 2-NA and their derivatives in PM at 77 K are shown in column (a) of Table 1. NA and AN do not fluoresce. The chloro or methoxy

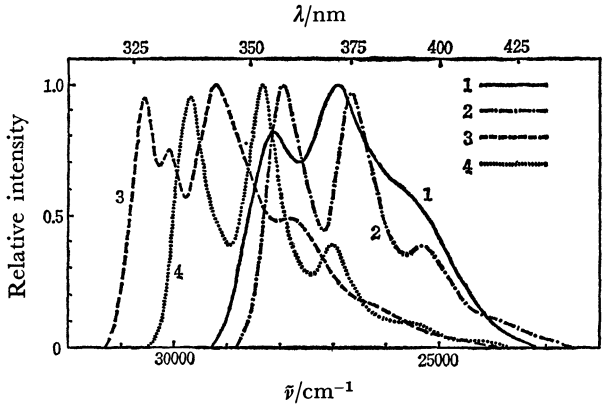

Fig. 1. Fluorescence spectra of naphthoyl chlorides and methyl naphthoates in PM at 77 K. The relative intensity represents relative quanta per unit frequency interval. (1) 1-NC; (2) 2-NC; (3) 1-MN; (4) 2-MN.

Table 1. Fluorescence data on naphthaldehyde series at 77 K

Compound	(a) Free molecule				(b) H-bonded molecule			
	Φ_F	τ_F (ns)	k_F (s^{-1})	k_{ISC}[e] (s^{-1})	Φ_F	τ_F (ns)	k_F (s^{-1})	k_{ISC}[e] (s^{-1})
1-Naphthaldehyde	~0[a]	—	$\sim5\times10^{5}$[c]	$>5\times10^{10}$	~0[a]	—	$\sim5\times10^{5}$[c]	$>5\times10^{10}$
1-Acetonaphthone	0[a]	—	$\sim5\times10^{5}$[c]	$>5\times10^{10}$	~0[a]	—	$\sim5\times10^{5}$[c]	$>5\times10^{10}$
1-Naphthoyl chloride	0.002	—	$\sim4\times10^{7}$[c]	$\sim2\times10^{10}$	0.13	(~3)[b]	4.3×10^{7}[d]	2.9×10^{8}
Methyl 1-naphthoate	0.08	~2	4.0×10^{7}[d]	4.6×10^{8}	0.08	~2	4.0×10^{7}[d]	4.6×10^{8}
2-Naphthaldehyde	~0[a]	—	$\sim5\times10^{5}$[c]	$>5\times10^{10}$	$\sim10^{-2}$	—	$\sim10^{7}$[c]	$\sim10^{9}$
2-Acetonaphthone	~0[a]	—	$\sim5\times10^{5}$[c]	$>5\times10^{10}$	0.05	—	$\sim10^{7}$[c]	$\sim2\times10^{8}$
2-Naphthoyl chloride	0.19	17.4 (16.1)[b]	1.1×10^{7}[d]	4.7×10^{7}	0.37	(17.8)[b]	2.1×10^{7}[d]	3.6×10^{7}
Methyl 2-naphthoate	0.32	38.4	0.8×10^{7}[d]	1.7×10^{7}	0.29	32.5	0.9×10^{7}[d]	2.2×10^{7}

a) Fluorescence emission could not be detected by the spectrofluorometer used in this study; Φ_F is estimated to be $<10^{-5}$. b) Obtained for a sample solution without degassing. (1- and 2-NC react with EtOH during degassing.) c) Calculated from absorption spectra. d) Calculated by the relation, $k_F=\Phi_F/\tau_F$. e) Calculated by the relation, $k_{ISC}=k_F\times(1-\Phi_F)/\Phi_F$.

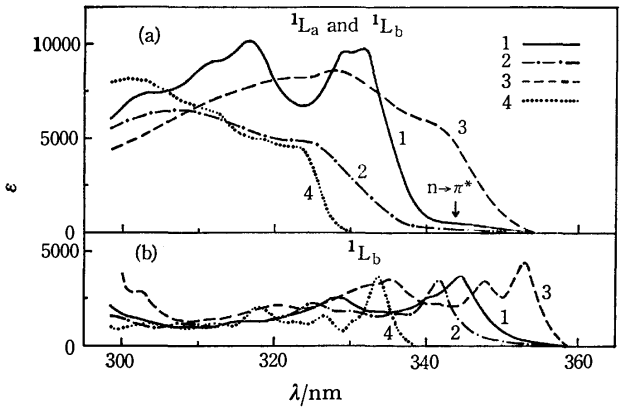

Fig. 2. Absorption spectra of 1-naphthaldehyde series (a) and 2-naphthaldehyde series (b) in PM at 77 K. The Platt notation is used for designation of electronic transitions. (1) NA; (2) AN; (3) NC; (4) MN.

substitution increases the fluorescence yield in that order in both 1- and 2-compounds. The fluorescence spectra of NC and MN in PM at 77 K are shown in Fig. 1. The fluorescence spectra of 1-MN and 2-MN are very similar to those of 1- and 2-naphthoic acid monomers, respectively.[14]

As is well known, the n→π* absorption band of saturated carbonyl compounds such as acetaldehyde is shifted to the blue by an electron-donating substituent.[15,16] The magnitude of the blue shift increases with increasing electron-donating power of the substituent, *i.e.*, in the order CH_3, Cl, and OCH_3. Roughly speaking, the fluorescence quantum yield of the molecules in Table 1 increases in the same order.

Absorption spectra of 1- and 2-NA and their derivatives in PM at 77 K are shown in Figs. 2(a) and (b). The n→π* bands of these molecules cannot easily be distinguished from π→π* bands. Absorption spectra of 1-NA and 1-AN in Fig. 2(a) show a weak band as a long tail in the region from 340 to 350 nm. It was found that this band was shifted to the blue on addition of a small amount of EtOH (~0.1%, v/v). The weak band is therefore most likely an n→π* band, which is known to be blue-shifted by hydrogen

Table 2. Phosphorescence lifetimes and yields and energies of $T_1(\pi,\pi^*)$ levels for naphthaldehyde series in PM at 77 K

Compound	τ_P (s)	Φ_P	$\nu_P(0\text{-}0)$ (cm^{-1})
1-Naphthaldehyde	0.048	0.01	19610
1-Acetonaphthone	0.093	0.01	19610
1-Naphthoyl chloride	0.25	0.04	19490
Methyl 1-naphthoate	1.05	0.02	19960
2-Naphthaldehyde	0.34	0.02	20700
2-Acetonaphthone	0.84	0.03	20700
2-Naphthoyl chloride	0.94	0.07	20410
Methyl 2-naphthoate	2.18	0.02	20660

bond formation.[17,18] The S_1 state in these molecules is then an (n, π*) state at 77 K, as well as at 20 °C.[19] On the other hand, absorption spectra of 1-NC and 1-MN do not show such an n→π* band. For 2-NA and 2-AN in Fig. 2(b), the π→π* (^1L_b) band is situated at longer wavelengths than that of the corresponding 1-substituted compounds, and consequently the n→π* band is not clearly resolved. However, an n→π* transition is likely to contribute to the tail which appears at the longest wavelength portion of the absorption spectra of these molecules. On close inspection, it is found that such a tail is absent in 2-NC and 2-MN. On the assumption that the location of the (n, π*) level is not greatly affected by the position of the substituent (1- or 2-position of the naphthalene nucleus), and on the basis of the spectral shape described above, the S_1 state at 77 K of 2-NA and 2-AN can be assigned to an (n, π*) state, in agreement with the assignment at 20 °C.[19] The S_1 state at 77 K of 1-, 2-NC and 1-, 2-MN can be assigned to a (π, π*) state from the substitution effect and spectral shape mentioned above.

When the phosphorescent triplet state (T_1) in a molecule possessing (n, π*) states is of the (π, π*) type, the radiative lifetime of T_1 is known to increase with the elevation of the (n, π*) levels.[20] Accordingly, the position of a ^{1}(n, π*) level relative to the T_1 (π, π*)

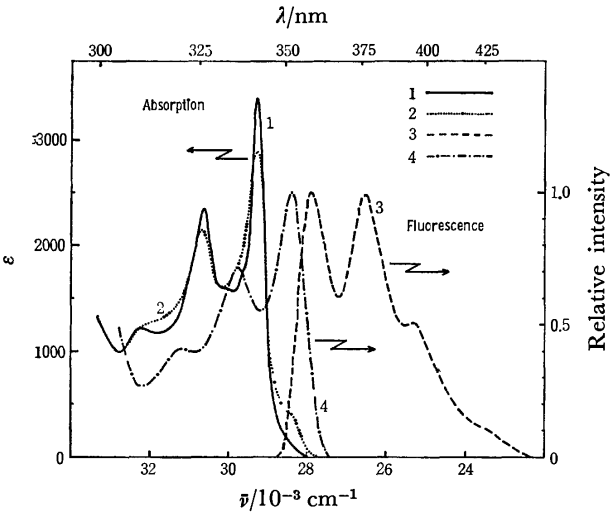

Fig. 3. Absorption, fluorescence, and excitation spectra of 2-acetonaphthone at 77 K. (1) absorption spectrum, [EtOH]=0; (2) absorption spectrum, [EtOH]= 0.05% (v/v); (3) fluorescence spectrum, [EtOH]= 0.05% (v/v); (4) excitation spectrum, [EtOH]=0.05 % (v/v).

level may be inferred from the data on the phosphorescence lifetimes. Observed phosphorescence lifetimes (τ_P) and quantum yields (Φ_P) are shown in Table 2, together with the energies of the $T_1(\pi, \pi^*)$ levels expressed by the frequency of the 0—0 band of phosphorescence ν_p (0—0). For 1- or 2-substituted compounds, the T_1 energies and the phosphorescence quantum yields are fairly constant regardless of the substituent, so that the lifetime data would reflect to some extent the differences in position of the $^1(n, \pi^*)$ levels. It may then be said from Table 2 that the $^1(n, \pi^*)$ levels are located at higher energies in the order NA, AN, NC, and MN. This is consistent with the results obtained from the absorption-spectral data.

Hydrogen Bonding Effects on Fluorescence and Intersystem Crossing. Figure 3 shows changes in the absorption spectrum of 2-AN in PM due to addition of a very small amount of EtOH (0.05%, v/v). The band intensity at 341.5 nm slightly decreases with the addition of EtOH, and at the same time a new, weak band grows at about 350 nm. These spectral changes may safely be attributed to the formation of a hydrogen bond between 2-AN and EtOH.

Although 2-AN in PM is not fluorescent, the addition of EtOH drastically changes its emission characteristics, making 2-AN fluorescent owing to the hydrogen bond. The fluorescence and excitation spectra of the hydrogen(H)-bonded 2-AN are also shown in Fig. 3. The longest wavelength band at 351 nm in the fluorescence excitation spectrum corresponds to the absorption band at about 350 nm of the H-bonded 2-AN.

As described before, the S_1 state of 2-AN in PM is of an (n, π^*) type. Since in general an $n\rightarrow\pi^*$ transition shifts to the blue by about 1000—2000 cm^{-1} as a result of hydrogen bond formation,[18] the 350 nm absorption band of the H-bonded 2-AN cannot be assigned to the $n\rightarrow\pi^*$ transition. The overall shape of the excitation spectrum resembles that of the absorption spectrum due to the ^1L_b transition in the free molecule. From these facts, the excitation spectrum, or the corresponding absorption spectrum including the 350 nm band, can be assigned to the ^1L_b transition in the H-bonded 2-AN. Thus, when 2-AN forms a hydrogen bond with EtOH, the S_1 state must change from an (n, π^*) to a (π, π^*) state.

Changes in absorption and fluorescence characteristics of 2-NA by hydrogen bond formation are similar to those of 2-AN described above. On the other hand, hydrogen bonding does not induce fluorescence in 1-NA and 1-AN. The fluorescence quantum yields and observed fluorescence lifetimes of the molecules forming hydrogen bonds with EtOH at 77 K are shown in column (b) of Table 1. It can be seen that the fluorescence quantum yields of the H-bonded 2-NA and 2-AN are at least 1000 times higher than those of the corresponding free molecules, whereas the yields of 2-NC, 1-MN, and 2-MN, which show relatively strong fluorescence in PM, are not affected significantly by hydrogen bonding. The fluorescence quantum yield of 1-NC increases by a factor of about 65 on hydrogen bond formation. Changes in fluorescence characteristics similar to those observed in 2-NA, 2-AN, and 1-NC have been reported for other molecules possessing (n, π^*) states such as pyrene-3-aldehyde,[21] acridine, quinoline, and isoquinoline.[22,23]

To explain the changes in fluorescence characteristics by hydrogen bonding, radiative rate constants for fluorescence (k_F) and rate constants for intersystem crossing (k_{ISC}) were estimated from the intensities of $S_0\rightarrow S_1$ absorption transitions and the fluorescence quantum yields and lifetimes; the results are shown in Table 1. The values of k_F for molecules with the S_1 state of (n, π^*) type were tentatively estimated from the intensity of the $n\rightarrow\pi^*$ absorption of benzaldehyde, since the $n\rightarrow\pi^*$ transition in these molecules is hardly separated from the neighboring transition (see Fig. 2).

In the estimates of k_{ISC} values the rate constants for the internal conversion $S_1 \rightsquigarrow S_0$ processes (k_{FQ}) were tentatively neglected, as usually done.[24] This procedure is supported by the fact that efficient intersystem crossing is considered to take place in non-fluorescent carbonyls.[1,2] For example, the quantum yield of intersystem crossing (Φ_{ISC}) of 2-AN, which gives no fluorescence in PM, has been reported to be 0.84 in benzene at room temperature.[25] However, even in the non-fluorescent molecules such as NA and AN the phosphorescence emission was relatively weak ($\Phi_P \approx 10^{-2}$). To confirm the validity of our procedure, we measured triplet–triplet absorption at 77 K. All the molecules showed at least the same absorption intensity as naphthalene. The Φ_{ISC} value for naphthalene has been reported to be 0.25[26] in a mixture of 30% *n*-butanol and 70% isopentane at 77 K, and 0.40[25] in benzene at room temperature. Thus, in the naphthaldehyde series studied, even if internal conversion from S_1 to S_0 should occur, k_{FQ} would be of comparable magnitude to k_{ISC} at the greatest. We may therefore reasonably neglect k_{FQ} in the following discussion, where we are concerned with the order of magnitude of k_{ISC}. As the detection limit of the

spectrofluorometer used in this study was 10^{-5} in quantum yield, the k_{ISC} values for non-fluorescent molecules were estimated by assuming Φ_F to be smaller than 10^{-5}.

To begin with, 2-NA and 2-AN will be discussed in comparison with 1-NA and 1-AN. As is seen in Table 1, the k_{ISC} values for 2-NA and 2-AN decrease with hydrogen bonding by about two orders of magnitude, while those for 1-NA and 1-AN remain unchanged. For the 2-substituted compounds, the energy separation between $S_1(n, \pi^*)$ and $S_2(\pi, \pi^*)$ (^1L_b) states is $\sim$400 cm^{-1} (see Fig. 2(b)). The (n, π^*) states in aromatic carbonyls have singlet–triplet intervals of about 2000 cm^{-1}.[27,28] This implies that the $S_2(\pi, \pi^*)$—$T_j(n, \pi^*)$ energy gaps in 2-NA and 2-AN are $\sim$2400 cm^{-1}. The $^1A \rightarrow {}^1L_b$ transition shifts to the red by about 800 cm^{-1} with hydrogen bond formation (see Fig. 3), while the $n \rightarrow \pi^*$ transition to the blue, as described before. The estimated k_{ISC} values and relatively small $S_2(\pi, \pi^*)$—$T_j(n, \pi^*)$ energy gaps suggest that in 2-NA and 2-AN a reversal of the S_1 state from the (n, π^*) to the (π, π^*) type and elevation of the $T_j(n, \pi^*)$ level above the resulting $S_1(\pi, \pi^*)$ level are likely to occur simultaneously as a result of hydrogen bonding. On the other hand, in 1-NA and 1-AN the energy separation between $S_1(n, \pi^*)$ and $S_2(\pi, \pi^*)$ (^1L_b) states is $\sim$1500 cm^{-1} (see Fig. 2(a)), and hence the $S_2(\pi, \pi^*)$—$T_j(n, \pi^*)$ energy gaps are $\sim$3500 cm^{-1}. In this case, the magnitude of the red shift due to hydrogen bonding of the ^1L_b transition is difficult to obtain because of the broadness of absorption bands. It is generally known that the red shifts of the $^1A \rightarrow {}^1L_b$ transitions due to hydrogen bonding are smaller in 1-substituted naphthalenes such as 1-naphthol than in the corresponding 2-substituted ones.[29,30] Thus, the elevation of the $T_j(n, \pi^*)$ level above the ^1L_b level is not likely to occur in the case of 1-NA and 1-AN.

The relative positions of the energy levels for both the free and H-bonded molecules of 1-NA and 1-AN and for the free molecules of 2-NA and 2-AN are schematically represented by Fig. 4(a), while those for the H-bonded 2-NA and 2-AN by Fig. 4(b). In the former group of molecules, the efficient spin-orbit coupling between $^1(n, \pi^*)$ and $^3(\pi, \pi^*)$ states should result in the fast rate of intersystem crossing.[3]

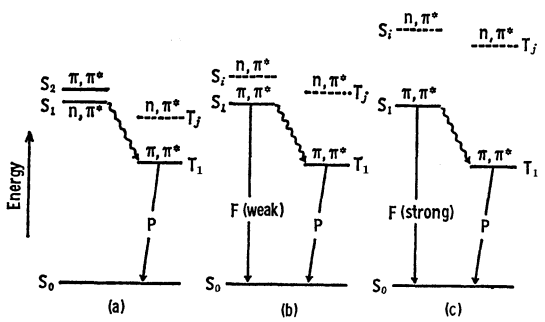

Fig. 4. Electronic energy level diagrams showing differences in fluorescence and intersystem-crossing characteristics among naphthaldehyde series. Broken lines represent the energy levels which are assumed to exist.

However, in the H-bonded 2-NA and 2-AN, the spin-orbit interaction between the singlet and triplet (π, π^*) states is vanishingly small,[3] so that the rate of the direct intersystem crossing $^1(\pi, \pi^*) \rightsquigarrow {}^3(\pi, \pi^*)$ would be low enough for fluorescence emission to compete with the intersystem crossing.

Next, the case of 1- and 2-MN will be discussed. According to the substitution effects described before, the $^1(n, \pi^*)$ state of these molecules is probably situated at a relatively high level, as shown in Fig. 4(c). Further elevation of the (n, π^*) level by hydrogen bonding will not greatly affect the intersystem crossing, and leave the fluorescence characteristics essentially unchanged.

Finally, the case of 1-NC and 2-NC will be considered. The fluorescence characteristics of 1-NC are changed by hydrogen bonding as in the case of 2-NA and 2-AN, while those of 2-NC are not changed significantly as in the case of MN. The S_1 states of the free and H-bonded NC are of (π, π^*) type, as previously mentioned. Although the definite positions of (n, π^*) levels are not known, the experimental data for 1-NC and 2-NC suggest that the $T_j(n, \pi^*)$ level should be higher than the $S_1(\pi, \pi^*)$ level. It follows from Fig. 2 that the $S_1(\pi, \pi^*)$ level of 1-NC is higher than that of 2-NC. This implies that the magnitudes of energy separations between $T_j(n, \pi^*)$ and $S_1(\pi, \pi^*)$ levels for 1- and 2-NC are different from each other, provided the (n, π^*) levels of these molecules are situated at approximately the same position. We assume that the $T_j(n, \pi^*)$ level of 1-NC in PM lies closely above the $S_1(\pi, \pi^*)$ level, as shown in Fig. 4(b). The free molecule of 1-NC will then show weak fluorescence. When 1-NC forms a hydrogen bond with EtOH, the $^3(n, \pi^*)$ level rises and the fluorescence intensity increases. From the fact that the energy separation between $T_j(n, \pi^*)$ and $S_1(\pi, \pi^*)$ levels is larger in 2-NC than in 1-NC, the relative positions of the energy levels for 2-NC are thought to be similar to Fig. 4(c). Further elevation of the (n, π^*) level of 2-NC by hydrogen bonding would not change greatly the fluorescence characteristics, as has been shown for MN.

On the Mechanism of Intersystem Crossing. Three different rate expressions have been theoretically derived so far for intersystem crossing. El-Sayed[3] first obtained a rate expression, based on the theory of Robinson and Frosch,[31] by considering the spin-orbit coupling operator (H_{SO}) as the perturbation (H') which causes the non-radiative transition. Lin[11] and Bixon and Jortner[12] independently formulated an expression by treating the nuclear kinetic-energy operator (T_N) alone as the perturbation. On the other hand, Henry and Siebrand[10] and Lawetz, Orlandi, and Siebrand[32] recently formulated a rate expression by including both H_{SO} and T_N in the perturbation.

The matrix element, H'_{mn}, in the expressions by El-Sayed and Siebrand *et al.* involves the first-order term $\langle {}^3\Psi_m | H_{SO} | {}^1\Psi_n \rangle$. Here, $^1\Psi_n$ and $^3\Psi_m$ stand for pure-spin Born-Oppenheimer wave functions of singlet and triplet states, respectively; they are written as products of an electronic wavefunction (Φ) and

a vibrational wavefunction (Λ), *i.e.*, ${}^1\Phi_n \cdot \Lambda_n$ and ${}^3\Phi_m \cdot \Lambda_m$ respectively. Such a first-order term does not appear in the formulation by Lin *et al.* As is well known, the electronic matrix element of H_{SO} between ${}^{1,3}(n, \pi^*)$ and ${}^{3,1}(\pi, \pi^*)$ states, *e.g.*, $\langle {}^3\Phi(\pi, \pi^*)|H_{SO}|{}^1\Phi(n, \pi^*)\rangle$, is far larger than that between ${}^1(\pi, \pi^*)$ and ${}^3(\pi, \pi^*)$ states, $\langle {}^3\Phi(\pi, \pi^*)|H_{SO}|{}^1\Phi(\pi, \pi^*)\rangle$. According to the theory of El-Sayed or Siebrand *et al.*, therefore, in molecules possessing (n, π^*) states, the rate of intersystem crossing depends strongly on whether or not ${}^3(\pi, \pi^*)$ and ${}^3(n, \pi^*)$ levels are located below $S_1(n, \pi^*)$ and $S_1(\pi, \pi^*)$, respectively, and the fluorescence characteristics are expected to be changed drastically by a reversal of the relative positions of (n, π^*) and (π, π^*) levels. On the other hand, the theory by Lin *et al.* does not predict such changes in fluorescence, as noted recently by Azumi.[13,33]

As has been mentioned, the fluorescence characteristics and intersystem crossing rates in the naphthaldehyde series, particularly in 2-NA and 2-AN, vary markedly, depending upon the relative positions of (n, π^*) and (π, π^*) levels. In other words, the experimental results suggest that the intersystem crossing is caused by the perturbation including H_{SO}.

The experimental results show also that there is a distinct difference in fluorescent behavior between molecules related to Fig. 4(b) and those to 4(c) (cf. Table 1). In either case the $S_1(\pi, \pi^*)$ and $T_j(n, \pi^*)$ states are arranged in the same order of energy, so that the above-mentioned difference cannot be explained in terms of the theory including only H_{SO} in the perturbation.

The matrix element H'_{mn} in the rate expression by Siebrand *et al.* involves second-order terms such as

$$\sum_i [\langle {}^3\Psi_m|H_{SO}|{}^1\Psi_i\rangle\langle {}^1\Psi_i|T_N|{}^1\Psi_n\rangle/(E_i - E_n)]$$

and

$$\sum_i [\langle {}^3\Psi_m|T_N|{}^3\Psi_i\rangle\langle {}^3\Psi_i|H_{SO}|{}^1\Psi_n\rangle/(E_i - E_n)]$$

where the subscript i refers to intermediate states, and E_i and E_n represent the energies of ${}^{1,3}\Psi_j$ and ${}^1\Psi_n$, respectively. Similar terms appear also in the rate expression by Lin *et al.* From these second-order terms it follows that an increase in energy difference between initial and intermediate states (see Figs. 4(b) and (c)) may lead to a distinct change in the intersystem crossing rate and hence in the fluorescence characteristics, in agreement with the experiment.

Thus, the present experimental results are best explained in terms of the theory in which both H_{SO} and T_N are treated as the perturbation causing intersystem crossing.

We wish to thank Professor Pill-Soon Song for his valuable discussions. We are also indebted to Mr. Masahisa Fujita for carrying out the lifetime measurement and to Mr. Yohji Achiba for obtaining triplet-triplet absorption spectra.

References

1) S. P. McGlynn, T. Azumi, and M. Kinoshita, "Molecular Spectroscopy of the Triplet State," Prentice-Hall, Englewood Cliffs, New Jersey (1969), Chapter 6.
2) R. S. Becker, "Theory and Interpretation of Fluorescence and Phosphorescence," John Wiley and Sons, New York (1969), Chapter 12.
3) M. A. El-Sayed, *J. Chem. Phys.*, **38**, 2834 (1963).
4) V. G. Plotnikov, *Opt. Spectrosc.*, **23**, 20 (1967).
5) H. Baba, *J. Chem. Phys.*, **49**, 1763 (1968).
6) H. Dewey and S. G. Hadley, *Chem. Phys. Lett.*, **12**, 57 (1971).
7) H. Baba and M. Kitamura, *J. Mol. Spectrosc.*, **41**, 302 (1972).
8) T. Matsumoto, M. Sato, and S. Hirayama, *Chem. Phys. Lett.*, **13**, 13 (1972).
9) R. O. Loutfy and J. M. Morris, *ibid.*, **19**, 377 (1973).
10) B. R. Henry and W. Siebrand, *J. Chem. Phys.*, **54**, 1072 (1971).
11) S. H. Lin, *ibid.*, **44**, 3759 (1966).
12) M. Bixon and J. Jortner, *ibid.*, **48**, 715 (1968).
13) T. Azumi, *Chem. Phys. Lett.*, **17**, 211 (1972).
14) M. Kitamura and H. Baba, This Bulletin, **46**, 3056 (1973).
15) H. H. Jaffé and M. Orchin, "Theory and Applications of Ultraviolet Spectroscopy," John Wiley and Sons, New York (1962), p. 178.
16) K. Higasi, H. Baba, and A. Rembaum, "Quantum Organic Chemistry," Interscience, New York (1965), p. 200.
17) G. J. Brealey and M. Kasha, *J. Amer. Chem. Soc.*, **77**, 4462 (1955).
18) G. C. Pimentel and A. L. McClellan, "The Hydrogen Bond," W. H. Freeman and Company, San Francisco (1960).
19) R. N. Nurmukhametov, *Opt. Spectrosc.*, **23**, 209 (1967).
20) H. Baba and T. Takemura, This Bulletin, **40**, 2215 (1967).
21) K. Bredereck, Th. Förster, and H.-G. Oesterlin, "Luminescence of Organic and Inorganic Materials," ed. by H. P. Kallmann and G. M. Spruch, John Wiley and Sons, New York (1962), p. 161.
22) N. Mataga and S. Tsuno, This Bulletin, **30**, 368 (1967).
23) E. C. Lim and J. M. H. Yu, *J. Chem. Phys.*, **47**, 3270 (1967).
24) Ref. 1, p. 10.
25) A. A. Lamola and G. S. Hammond, *J. Chem. Phys.*, **43**, 2129 (1965).
26) S. G. Hadley and R. A. Keller, *J. Phys. Chem.*, **73**, 4356 (1969).
27) R. Shimada and L. Goodman, *J. Chem. Phys.*, **43**, 2027 (1965).
28) T. Takemura and H. Baba, This Bulletin, **42**, 2756 (1969).
29) S. Nagakura and M. Gouterman, *J. Chem. Phys.*, **26**, 881 (1957).
30) H. Baba and S. Suzuki, *ibid.*, **35**, 1118 (1961).
31) G. W. Robinson and R. P. Frosch, *ibid.*, **37**, 1962 (1962).
32) V. Lawetz, G. Orlandi, and W. Siebrand, *ibid.*, **56**, 4058 (1972).
33) T. Azumi, *Chem. Phys. Lett.*, **25**, 135 (1974).

Diffusion and Adsorption of a Model Cationic Dye, *m*-Nitrobenzylamine, in Polyacrylonitrile

Zenzo MORITA,* T. M. Abul HOSSAIN, and Toshiro IIJIMA

Department of Polymer Science, Faculty of Engineering, Tokyo Institute of Technology, Ookayama, Meguro-ku, Tokyo 152

(Received January 8, 1975)

A model cationic dye, *m*-nitrobenzylamine (NBA), was synthesized, and the diffusion and adsorption behavior in polyacrylonitrile was investigated by the cylindrical film roll method. pK_a of NBA was determined spectroscopically to be 9.2 at 25 °C. The diffusion was concentration dependent and was described by the chemical potential gradient model. The temperature dependence of the diffusion coefficients above T_g, which was found to be 65 °C from the inflection point of Arrhenius plot, could be described by WLF equation, where C_1^g and C_2^g are 1.64 and 17.09 (deg.) at pH 4.2, and 2.41 and 33.11 (deg.) at pH 6.8, respectively. Adsorption isotherm of NBA was obtained at 95 °C and pH 1.5, 4.2 and 6.8. The adsorption of NBA, bis(*m*-nitrobenzyl)amine and Malachite Green at pH 4.2 and those of NBA and bis(*m*-nitrobenzyl)amine at pH 6.8 were more or less the same. It is concluded that the adsorption of cationic compounds on polyacrylonitrile is virtually dependent upon the ion exchange mechanism. But the presence of sodium chloride in the dye bath did not change the adsorption of NBA at pH 4.2 and 95 °C. The surface concentration of NBA was gradually increased with rise of temperature at pH 1.5, 4.2 and 6.8.

In previous papers, the diffusions of Malachite Green, a model cationic dye, *i.e.*, bis(*m*-nitrobenzyl)-amine and some model disperse dyes in polyacrylonitrile were investigated in detail.[1–4] The model cationic penetrant was synthesized to give a general view of dyeing of polyacrylonitrile. A comparison was made between the diffusion behavior of Malachite Green and bis(*m*-nitrobenzyl)amine. In both the cases the profiles as cationic penetrants were shown to be non-Fickian. It should be noted that the experimental concentration profiles of Malachite Green at pH 4.2 was described by chemical potential gradient model without any modification. But in the case of bis(*m*-nitrobenzyl)amine, the Fickian and non-Fickian diffusions were observed because it behaved simultaneously as both ionic and non-ionic penetrants. In this connection, a cationic compound having higher pK_a value than that of bis(*m*-nitrobenzyl)amine may be much better model penetrant.

Temperature dependence of diffusion and surface concentration was investigated with Malachite Green but no experiment with the variation of pH except at pH 4.2 was possible. On the other hand, diffusion and surface concentration experiments with variation of pH were carried out with bis(*m*-nitrobenzyl)amine only at 95 °C. The results obtained in both the cases of Malachite Green and bis(*m*-nitrobenzyl)amine differed in some aspects from those of the former workers in this field.[5–9] Besides different opinion and experimental data, new aspects of kinetics and equilibria in polyacrylonitrile were also revealed which need further verification and confirmation by experiments and discussion. Thermal properties, *i.e.*, glass transition temperature and the value of constants in the WLF equation were found to vary widely from the value of original WLF equation and that of Rosenbaum.[7] Again surface concentration, instead of decreasing, increased with rise of temperature. Different assumptions were made to explain the data. It is therefore desirable that in order to establish the generality of the conclusions, confirmatory experiments should be done with a better model compound, which may provide a comprehensive description of dyeing of polyacrylonitrile. With this purpose the present paper is aimed at synthesizing a suitable compound, *m*-nitrobenzylamine, to carry out the experiments of diffusion and equilibrium adsorption. Wide range of temperature and pH are taken to study the diffusion and thermal properties of polymer.

Experimental

Polymer: The polymer was the same polyacrylonitrile film that was prepared in the previous papers.[3] *Penetrant:* The penetrant, *m*-nitrobenzylamine hydrochloride, was synthesized by Gabriel method[10] with some modifications. The *m*-nitrobenzylamine produced was extracted by ether, dry potassium hydroxide was added to the extracted solution and kept overnight to absorb water in solution. It was then filtered. The ether was removed by distillation and finally completely by vacuum. Yellowish *m*-nitrobenzylamine was obtained in liquid state which was dissolved in benzene and then dry HCl gas was passed through, white precipitate of *m*-nitrobenzylamine hydrochloride was obtained instantaneously, which on crystallization from water gave the product (mp 228.5–229.0 °C). Found: N, 15.0; Cl, 18.8%. Calcd for $C_7H_9N_2O_2Cl$: N, 14.9; Cl, 18.8%. pK_a was determined spectroscopically and found to be 9.2 in water at 25 °C. pH of the solution was adjusted by HCl and CH_3COONa keeping ionic strength constant (I=0.1). *Diffusion and Adsorption:* The diffusion experiments were carried out with the concentration of 0.05 g/50 ml bath at pH 1.5, 4.2 and 6.8 with HCl–CH_3COONa buffer (I=0.1) over the temperature range between 55 and 95 °C. The equilibrium adsorption experiments were carried out at 95 °C and pH 1.5, 4.2 and 6.8 in 50 ml diffusion bath. Three different concentrations of 0.05 g/50 ml, 0.1 g/50 ml and 0.2 g/50 ml were taken. The values of equilibrium adsorption C_s were obtained from the surface concentration of respective diffusion experiment. The absorption spectra of solution and dyed film were measured by a Shimadzu SV-50A recording spectrophotometer.

* Present address: Department of Textiles and Polymer Science, Faculty of Engineering, Tokyo University of Agriculture and Technology, Koganei, Tokyo 184.

Results and Discussion

Diffusion. At pH 1.5 due to the low surface concentration the suitable concentration/distance curve for calculation of diffusion coefficient was not obtained. The distribution profiles C/C_s *vs.* $x/2\sqrt{t}$ of *m*-nitrobenzylamine in polyacrylonitrile at 95 °C and pH 4.2 is shown in Fig. 1, where C is the concentration, C_s, the surface concentration, x, the distance, and t, the diffusion time. Diffusion coefficients in respective cases were calculated by Matano's method. D *vs.* C/C_s $(=\theta)$ plots were shown in Fig. 2. The concentration dependence of diffusion coefficients in both the cases was well described by the chemical potential gradient model as in the case of Malachite Green.[1]

The diffusion coefficients and surface concentrations for different temperatures from 55 to 95 °C were shown in Arrhenius plots of log D_0 *vs.* $1/T$ (Fig. 3). The results shown the inflection points in both pH 4.2 and 6.8 at 65 °C which may be assigned as the glass transition temperature of polyacrylonitrile during diffusion with *m*-nitrobenzylamine just as in the case of Malachite Green and model disperse dye penetrants.[1-4] The transition point during diffusion with Malachite Green in the same polymer was 80 °C. The difference may be explained by the larger size of the penetrant, which requires much energy than that required for a small size molecule like *m*-nitrobenzylamine. The occurence of the transition point at the same temperature for pH 4.2 and 6.8 was shown in Fig. 3. The ionic character of the penetrant is not changed at pH 4.2 and 6.8 due to high pK_a $(=9.2)$ but the ionic character of the polymer is changed. At pH 4.2 sulfonate end group completely and weak acidic groups, carboxyl end group, partly are ionized in polyacrylonitrile, while at pH 6.8 the weak acidic groups including strong sulfonate end groups are all completely ionized. It was already shown in previous paper with bis(*m*-nitrobenzyl)amine, from the dependence of the surface concentrations on the pH of the dye bath.[4] Thus pH of dye bath was found to be meant for the availability of the acidic groups in polymer to cationic penetrant. The appearence of the transition point in both the cases of pH 4.2 and 6.8 at the same temperature may be explained in the

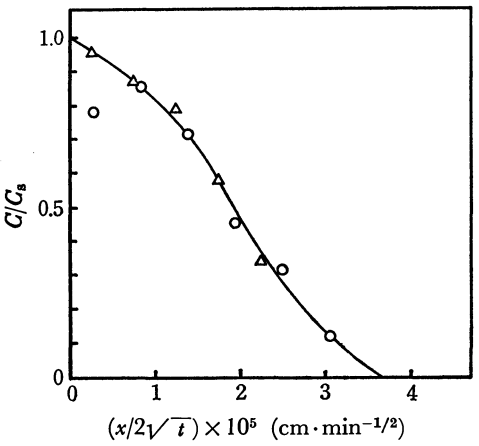

Fig. 1. Diffusion profile of *m*-nitrobenzylamine.
95 °C; pH 4.2; concentration 1.0 g/l; ○: 39 hr, △: 48 hr

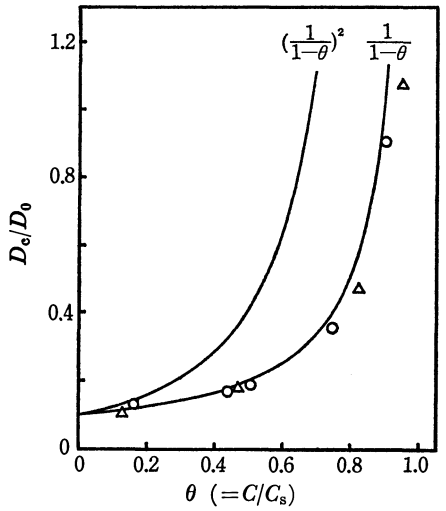

Fig. 2. Relative diffusion coefficients of *m*-nitrobenzylamine at 95 °C.
○: pH 6.8, △: pH 4.2

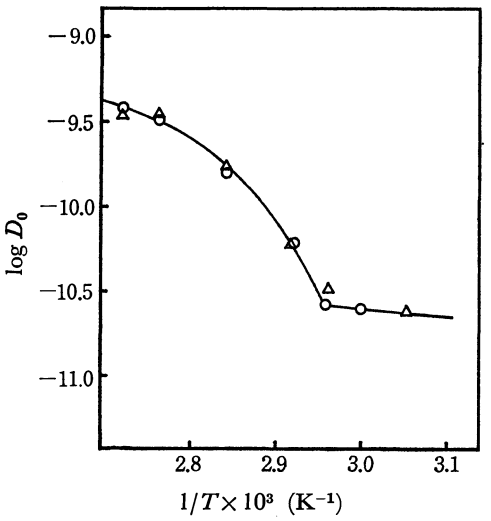

Fig. 3. Arrhenius plot of diffusion coefficients D_0 of *m*-nitrobenzylamine into polyacrylonitrile at pH 4.2 and 6.8.
○: pH 6.8, △: pH 4.2

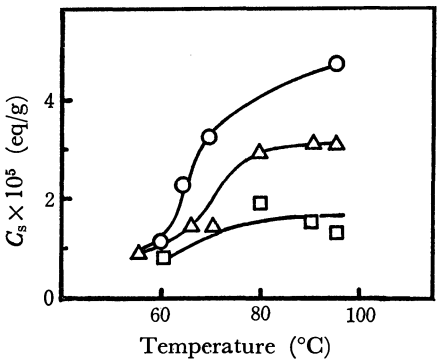

Fig. 4. Surface concentration of *m*-nitrobenzylamine at various temperatures.
○: pH 6.8, △: pH 4.2, □: pH 1.5

way that below T_g in both pH 4.2 and 6.8 only sulfonate end groups of polymer are concerned in diffusion. In Fig. 4 the variation of surface concentration with temperature is found to be of same pattern as in the case of Malachite Green above T_g.[1] A little difference is observed in the pattern below T_g where in the case of Malachite Green, the surface concentrations are almost constant, but in the case of *m*-nitrobenzylamine gradual increase with rise of temperature which is similar in shape as in the case of *m*-nitroaniline.[3]

As in the case of Malachite Green the diffusion behavior above T_g was applied to the general form of WLF equation. The constants C_1^g and C_2^g were calculated by least square method and found to be 1.64, 17.09 (deg.) for pH 4.2 and 2.41, 33.11 (deg) for pH 6.8, respectively.

The good fit of WLF equation with diffusion behavior above T_g in both pH 4.2 and 6.8, confirms the fact that the diffusion in polyacrylonitrile is governed by the segmental motion of the polymer, which sets in at T_g. The result is in agreement with those of Rosenbaum[7-9] and in previous papers.[1-4] The physical significance of the constants C_1^g and C_2^g of WLF equation from diffusion experiments with those of Malachite Green and *m*-nitrobenzylamine is not yet clear. As mentioned in the previous papers that the constant C_1^g is directly related with fractional free volume f_g at T_g, and C_2^g with f_g as well as $\Delta\alpha$, the difference of thermal expansion coefficient above and below T_g.[3] The different values of C_1^g and C_2^g for different penetrants in the same polymer may be reasonable, but the proper explanation and theoretical treatment has not yet been made.

Equilibrium. Surface concentration from the diffusion experiments carried out at 95 °C and pH 1.5, 4.2 and 6.8, were used for adsorption isotherm plot. The plot of C_s *vs.* dye bath concentration was shown in Fig. 5. The reciprocal plots, by Eq. (1), which were all straight lines were in Fig. 6.

$$\frac{[D]_\phi}{[D]_o} = K_L([S]_\phi - [D]_\phi) \qquad (1)$$

In Eq. (1), $[D]_\phi$ and $[D]_o$ denote the dye concentration on fiber and that in the dyebath, K_L, Langmuir constant, and $[S]_\phi$, the site content in the fiber.

It was found that same results were obtained for different cationic penetrants. So it may be concluded that the adsorption of cationic penetrants is adequately described by Langmuir isotherm, which may be superimposed by constant partition isotherm or Freundlich isotherm dependent upon penetrant as in the case of bis(*m*-nitrobenzyl)amine. It is found from the results of Malachite Green, bis(*m*-nitrobenzyl)amine and *m*-nitrobenzylamine at pH 4.2 and 6.8 that the uptake of these three compounds at pH 4.2 and those of bis(*m*-nitrobenzyl)amine and *m*-nitrobenzylamine at pH 6.8 are more or less the same.[1-4] As regards to the dyeing of polyacrylonitrile especially with cationic dye, important aspect is the ion exchange phenomenon. Rosenbaum showed the increase of equilibrium uptake which shows virtually no ion exhange mechanism in polyacrylonitrile dyeing.[11]

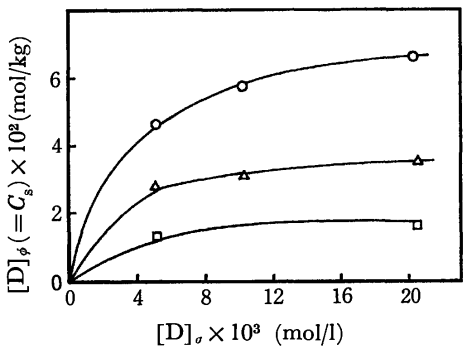

Fig. 5. Adsorption isotherms of *m*-nitrobenzylamine at 95 °C.
○: pH 6.8, △: pH 4.2, □: pH 1.5

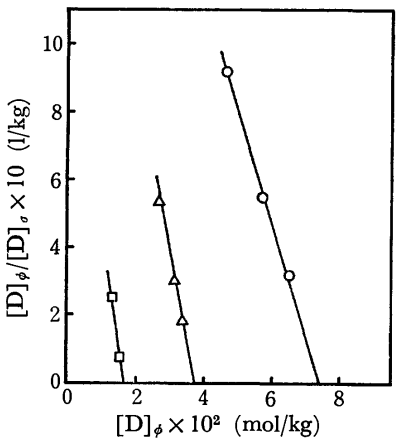

Fig. 6. Reciprocal plots of Fig. 5 by Eq. (1).
○: pH 6.8, △: pH 4.2, □: pH 1.5

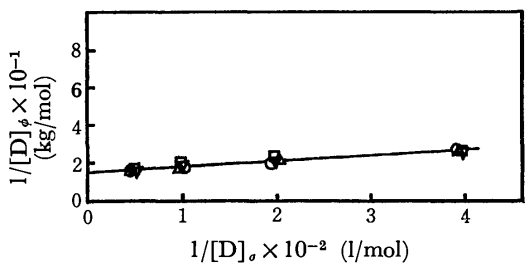

Fig. 7. Adsorption isotherm of *m*-nitrobenzylamine at 95 °C and pH 4.2 in the presence of NaCl.
○: 0 g, △: 0.4 g/l, ▽: 2.5 g/l, □: 4.0 g/l

In the series of these experiments, however, it is concluded that the adsorption of cationic compounds on polyacrylonitrile is nearly equal to the anionic site in the polymer available at that pH. No adsorption more than the anionic site in the polymer could be observed except the case such as bis(*m*-nitrobenzyl)-amine where the non-ionic species coexisted in the dyebath and were also adsorbed by the substrate.

On the other hand Sand, Glenz *et al.*, and Harwood *et al.* showed the decrease of the uptake by the addition of salt in the dye bath.[5,12,13] In this paper, an attempt was made to study the problem by the addition of sodium chloride in the bath. As is shown in Fig. 7, no change of equilibrium was detected. The adsorption of cationic compounds will be due to the salt formation or ion exchange and non-ionic

interaction of ionic species also due to the non-ionic adsorption of non-ionic species. The addition of salt will influence the salt formation and increase the non-ionic interaction and the formation of non-ionic species in the dyebath. In the series of these experiments, the salt addition was considered to bring about no influence on the salt formation and no change of the non-ionic species.

References

1) T. M. A. Hossain, H. Maeda, T. Iijima, and Z. Morita, *Kogyo Kagaku Zasshi*, **71**, 872 (1968).
2) Idem, *J. Polymer Sci., Part B*, **5**, 1069 (1967).
3) Idem, *J. Appl. Polym. Sci.*, **13**, 541 (1969).
4) Z. Morita, T. M. A. Hossain, and T. Iijima, *Nippon Kagaku Kaishi*, **1972**, 958.
5) W. Beckmann and O. Glenz, *Melliand Textilber.*, **38**, 296, 783 (1957).
6) D. Balmforth, C. A. Bowers, and T. H. Guion, *J. Soc. Dyers Colour.*, **80**, 577 (1964).
7) S. Rosenbaum, *J. Polym. Sci.*, **A-3**, 1949 (1956).
8) S. Rosenbaum, *J. Appl. Polym. Sci.*, **7**, 1225 (1963).
9) S. Rosenbaum, *Text. Res. J.*, **34**, 52, 159, 291 (1964).
10) S. Gabriel and H. Hendess, *Chem. Ber.*, **20**, 2869 (1887).
11) S. Rosenbaum, *Text. Res. J.*, **33**, 899 (1963).
12) H. Sand, *Kolloid-Z. Z. Polym.*, **218**, 30 (1966).
13) R. J. Harwood, R. McGregor, and R. H. Peters, *J. Soc. Dyers Colour.*, **88**, 216 (1972).

Laser Photochemistry. II.* Determination of the ORD and CD Spectra of Some Chromium(III) β-Diketonates

Hayami YONEDA, Ushio SAKAGUCHI, and Yoshiaki NAKASHIMA

Department of Chemistry, Faculty of Science, Hiroshima University, Higashisenda-machi, Hiroshima 730

(Received October 17, 1974)

An argon ion laser has been used to partially photoresolve the following tris(β-diketonato)chromium(III) complexes; $Cr(acac)_3$, $Cr(3\text{-X-acac})_3$ (X=Cl^-, Br^-, I^-, and NO_2^-), $Cr(tfac)_3$, and $Cr(bzac)_3$, where the abbreviations are acac=acetylacetonate ion, 3-X-acac=γ-substituted acetylacetonate ion, tfac=trifluoroacetylacetonate ion, and bzac=benzoylacetonate ion. From the wavelength dependence of the steady state resolution yield, the method of photoresolution has been confirmed to allow the determination of the ORD and CD spectra of optically pure enantiomers. The ORD and CD spectra of the above-mentioned compounds are given.

Induction of optical activity into chemical systems without resort to any asymmetric chemical agent is a rather interesting but less investigated phenomenon. Only scattered examples have been known to date in which the effect of circularly polarized light (CPL) on chemical systems or reactions has been studied. The photochemistry with CPL has recently been reviewed by Buchardt.[1] We may tentatively classify this field of research into three categories; "asymmetric photodecomposition" where the optical activity is introduced transiently by irradiating the light of circular polarization but is lost on long illumination due to photodecomposition, "total asymmetric synthesis" wherein optically inactive materials are allowed to react under the influence of CPL to produce optically active material(s), followed by the fading out of optical activity because of photodecomposition, and "partial photoresolution" which is similar in nature to the first category but different in that the material photoresolved does not lose its optical activity, except due to thermal racemization, even on long illumination. If we limit ourselves to metal compounds, a reported example of the first category may be, to our knowledge, only on potassium tris(oxalato)cobaltate(III).[2] No example of asymmetric synthesis appears to be reported for metal complexes. Partial photoresolution has been effected successfully on $[Cr(ox)_3]^{3-}$,**[4,3] $Cr(acac)_3$,[5] and $[Cr(ox)(phen)_2]^+$, $[Cr(ox)_2(phen)]^-$, $[Cr(bipy)_3]^{3+}$[6] and several other cobalt(III) and chromium(III) complexes.[7,8] A slight modification of this method has been utilized by Kane-Maguire *et al.*[9] to achieve a partial resolution of $[Cr(phen)_3]^{3+}$ using an analogue of the Pfeiffer effect.

It is reported here that partial photoresolution of tris(β-diketonate)chromium(III) complexes can be made successfully by using the beam of an argon ion laser. This method of resolution is quite important in that it allows the otherwise impossible determination of the optical rotatory dispersion (ORD) and circular dichroism (CD) spectra of optically pure enantiomers.

* Part I: H. Yoneda, Y. Nakashima, and U. Sakaguchi, *Chem. Lett.*, **1973**, 1343.

** The following abbreviations are used in this paper; ox=oxalate ion, phen=phenanthroline, bipy=bipyridyl, oxine=8-hydroxyquinolinate ion, dbzm=dibenzoylmethanate ion, TTA=thenoyltrifluoroacetonate ion, FTA=furoyltrifluoroacetonate ion, and DTC=diethyldithiocarbamate ion.

Experimental

Material. $Cr(acac)_3$, $Cr(tfac)_3$, and $Cr(bzac)_3$ have been prepared by well established methods.[10-12] The identity of the complexes has been confirmed by chemical analysis. $Cr(tfac)_3$, Found: C, 35.22; H, 2.42%. Calcd for $CrC_{15}H_{12}O_6F_9$: C, 35.24; H, 2.37%. $Cr(bzac)_3$, Found: C, 67.81; H, 5.19%. Calcd for $CrC_{30}H_{27}O_6$: C, 67.28; H, 5.08%. The γ-substituted acetylacetonates have been prepared from chromium acetylacetonate after the method of Collman and coworkers.[13] $Cr(3\text{-I-acac})_3$, Found: C, 25.43; H, 2.67%. Calcd for $CrC_{15}H_{18}O_6I_3$: C, 24.78; H, 2.50%. $Cr(3\text{-Br-acac})_3$ has been obtained as chloroform solvate. Found: C, 27.77; H, 2.66%. Calcd for $CrC_{16}H_{19}O_6Br_3Cl_3$: C, 27.24; H, 2.71%. $Cr(3\text{-NO}_2\text{-acac})_3$, Found: C, 36.74; H, 3.79; N, 8.34%. Calcd for $CrC_{15}H_{18}O_{12}N_3$: C, 37.20; H, 3.79; N, 8.68%.

Solvents are of special grade, purchased from Katayama Chemical Co., and used without further purification.

Apparatus and Measurements. The experimental arrangement used in this work is essentially similar to that reported in the literature.[3] The light source is a NEC GLG-2023 argon ion laser operating at either 514.5, 501.7, 496.5, 488.0, 476.5, or 457.9 nm(in single mode). The light of linear polarization emitted from the laser is passed through a quartz quarter-wave plate matched for the wavelength of the irradiating light to produce CPL. The light of circular polarization is then incident on a 1 cm quartz cell containing the solution to be illuminated. The diameter of the beam is approximately 8 mm. The ellipticity of CPL has been confirmed to be small enough to be neglected from measurement of the light intensity passing through a linear polarizer situated beyond the quarter-wave plate. An approximate value of the light intensity incident on the sample solution is monitored by measuring the current induced in a photovoltaic CdS cell, which is precalibrated.

The ORD and CD spectra have been recorded on a JASCO Model ORD/UV-5 spectrometer with a CD attachment. Some CD spectra have been measured also on a JASCO Model J-2 spectrometer. The process of photoresolution has been traced by checking at suitable time intervals the optical rotation of the sample solution with the aid of a Union Giken PM-71 digital polarimeter. Absorption spectra are taken on a Shimadzu double beam spectrophotometer Model UV-200.

Unless otherwise stated, all solutions have been made to 5.0×10^{-3} mol/l in benzene and irradiated at room temperature.

Principles

The principle of photoresolution is the preferential isomerization of one enantiomer over the other, which

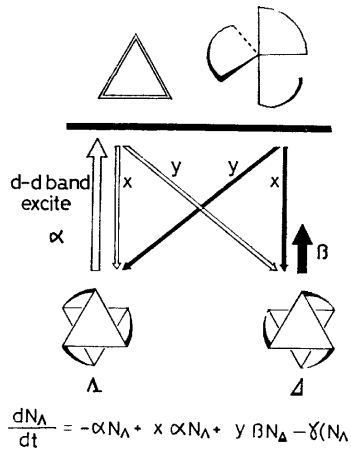

Fig. 1. Schematic illustration of a possible mechanism of photoresolution.

is a mere consequence of the differential absorptivities of the two enantiomers in a CPL (circular dichroism). Thus, the efficiency of photoresolution is expected to be a function of the asymmetric factor g.

We consider a racemic mixture of some metal complex. If right-CPL, whose intensity is I_0, is incident on the system, the complex absorbs the power ΔI. According to the Lambert-Beer's law

$$\Delta I = I_0[1-10^{-(\varepsilon_\Delta c_\Delta + \varepsilon_\Lambda c_\Lambda)d}] \tag{1}$$

where ε_Δ and c_Δ are the absorption coefficient and the concentration of the Δ-isomer and d the length of the optical path.

Note that the wavelength of the CPL corresponds to the electronic excitation of the metal compounds. Thus, absorption of the light by metal racemate induces some form of electronic excitation; metal d–d transition and/or charge transfer excitation, *etc.* (see Fig. 1). In Fig. 1 the horizontal bar is assumed to represent some excited state wherein the structure of the complex may be trigonally twisted or bond-ruptured. The transition probabilities from the excited Δ-isomer to the ground state Δ- and Λ-isomers are denoted by x and y, respectively. By symmetry the probabilities from the excited Λ-isomer to the ground state Λ- and Δ-molecules should be x and y. The values of x and y are related to the quantum yield for photoresolution and may be determined by the mechanisms of electronic relaxation and/or vibrational relaxation. Irrespective of these relaxation mechanisms, the following identity holds.

$$x + y = 1 \tag{2}$$

The change with time in the number of Λ-molecule will be governed by the kinetic equation.

$$\frac{dN_\Lambda}{dt} = -\alpha N_\Lambda + x\alpha N_\Lambda + y\beta N_\Delta \tag{3}$$

Similarly, for Δ-molecules

$$\frac{dN_\Delta}{dt} = -\beta N_\Delta + x\beta N_\Delta + y\alpha N_\Lambda \tag{4}$$

αN_Λ and βN_Δ are the numbers of Λ and Δ isomers excited by the CPL and are defined by

$$\alpha N_\Lambda = \frac{\Delta I}{h\nu}\frac{\varepsilon_\Lambda c_\Lambda}{\varepsilon_\Delta c_\Delta + \varepsilon_\Lambda c_\Lambda} \tag{5}$$

$$\beta N_\Delta = \frac{\Delta I}{h\nu}\frac{\varepsilon_\Delta c_\Delta}{\varepsilon_\Delta c_\Delta + \varepsilon_\Lambda c_\Lambda} \tag{6}$$

Since the difference between ε_Δ and ε_Λ are small as compared with ε and the best yield attainable by this method is rather low (see below), we can safely regard the coefficients α and β as the time-independent constants. To this approximation the rate of photoresolution is given by $y(\alpha+\beta)$. The photostationary state (PSS) is defined by the condition $dN_\Delta/dt=0$ and $dN_\Lambda/dt=0$. This condition leads us to the ratio of N_Λ to N_Δ as given by

$$\frac{N_\Lambda}{N_\Delta} = \frac{\beta}{\alpha} \tag{7}$$

From Eqs. (5) and (6), we obtain

$$\frac{N_\Lambda}{N_\Delta} = \frac{\varepsilon_\Delta}{\varepsilon_\Lambda} \tag{8}$$

Equation (8) holds exactly irrespective of the approximation made above. Therefore the yield of partial photoresolution is expressed in terms of the asymmetric factor g as follows.

$$\frac{N^\Lambda - N^\Delta}{N_\Lambda + N_\Delta} = \frac{g}{2} \tag{9}$$

where $g=(\varepsilon_\Delta-\varepsilon_\Lambda)/\varepsilon$. Thus, it is readily seen that the sample solution partially photoresolved will show the optical rotation at PSS

$$\theta_{PSS} = (g/2)\,\theta \tag{10}$$

and the CD proportional to

$$(g/2)\ (g\varepsilon c_0 d) \tag{11}$$

Here, θ and $(g\varepsilon c_0 d)$ are the optical rotation and the CD values, both at the wavelength used for the resolution, and expected for the optically pure enantiomer whose concentration is c_0. Note that the yield does not depend on the individual values of x and y and is determined only by the asymmetric factor g. Equations (10) and (11) hold also for the irradiation of the left-CPL, if we replace $(g/2)$ by $-(g/2)$ in both equations.

The effect of thermal racemization can be taken into account by introducing a term $-\gamma(N_\Delta - N_\Lambda)$, γ being the rate of thermal racemization. In this situation, the PSS should render the (N_Λ/N_Δ) value as given by

$$\frac{N_\Lambda}{N_\Delta} = \frac{\beta+2\gamma}{\alpha+2\gamma} \tag{12}$$

This equation indicates that as thermal racemization becomes faster, the optical activity of the sample solution at PSS are expected to decrease. The effect has really been observed and reported in some cases.[3,4]

Results and Discussion

Wavelength Dependence. Stevenson[5] has investigated the wavelength dependence of the kinetic behavior of the photoresolution process of $Cr(acac)_3$ but the effect of wavelength on the PSS yield has not been stated explicitly. Norden[4] and Stevenson and Ver-

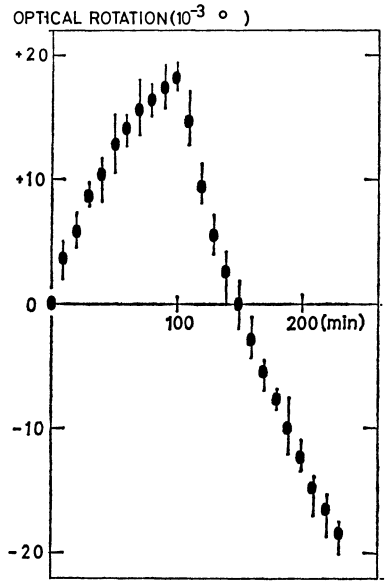

Fig. 2. The time-evolution of the optical rotation of $Cr(acac)_3$ accompanying the photoresolution.

dieck[3] have attained an apparent PSS for $[Cr(ox)_3]^{3-}$. However, it can readily be seen that the process of photoresolution is competitive with thermal or dark racemization, resulting in the optical activity much lower than that expected from Eqs. (10) and (11).

Fay *et al.*[14] have separated $Cr(acac)_3$ partially into its optical antipodes by passing through a chromatographic column containing D(+)-lactose. The first- and the second-eluted fractions have been slowly recrystallized from benzene–hexane, which gave rise to racemic crystals and resulted in an approximately tenfold enhancement in the optical rotation of the solution left uncrystallized. Molecular rotations after this partial recrystallization treatment are reported to amount to +3600° and −5240° for the first- and the second-elutions, respectively. These methods cannot, however, lead to a complete resolution and the ORD and CD curves given by them do not correspond to the optically pure enantiomers.

To ascertain whether or not the optical activity at PSS is in actuality coincident with that given by Eqs. (10) and (11), we examined the wavelength dependence of the PSS yield using $Cr(acac)_3$ as an example. A necessary prerequisite to this experiment is that the rate of thermal racemization is much smaller than that of photoresolution. For this compound, the thermal racemization rate is reported at $k=0.134\times10^{-5}$ s^{-1} (96.1 °C) so that we can neglect its effect completely. Figure 2 shows the time-evolution of the optical rotation of $Cr(acac)_3$ accompanying the photoresoution. Irradiating wavelength is 514.5 nm and the incident power is approximately 150 mW. At time $t=100$ min, the sense of the circular polarization is inverted by rotating the quarter-wave plate through 90 °. The fact that no measurable photodecomposition has occured is confirmed spectrophotometrically. This plot clearly shows that the process of photoresolution is reversible. When the light intensity incident on the sample solution is approximately 200 mW, the PSS can be reached in 3 to 4 hr. In this experiment, $Cr(acac)_3$ has been partially resolved by irradiating

Table 1. The $\Delta\varepsilon$ values of the optically pure $Cr(acac)_3$ photoresolved at four different wavelengths

λ (nm) irrad.	$\Delta\varepsilon$ at 530 nm
514.5	4.49
501.7	4.37
496.5	4.30
488.0	4.49

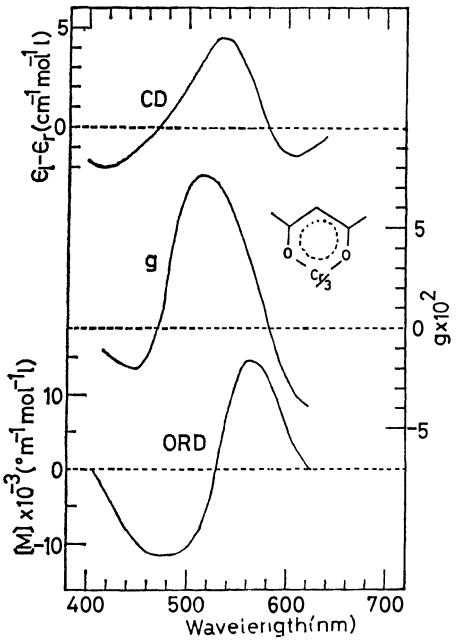

Fig. 3. The ORD, CD, and g curves of the optically pure $(+)_{589}$-$Cr(acac)_3$ in benzene solution.

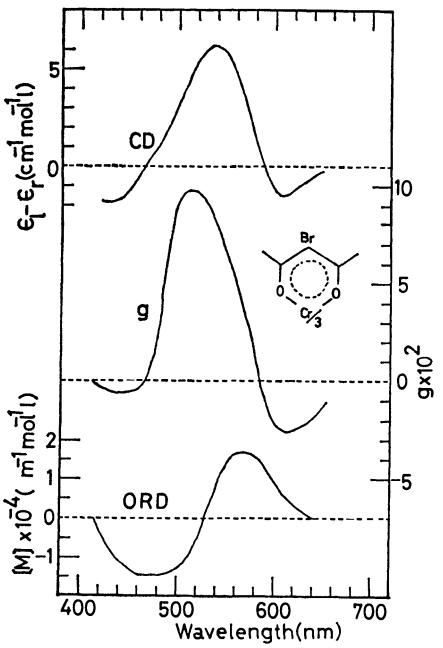

Fig. 4. The ORD, CD, and g curves of $(+)_{589}$-Cr-(3-Br-acac)$_3$.

Table 2. Summary of data obtained in this work
[M] in units of $^{\circ}\,m^{-1}M^{-1}$ and $\Delta\varepsilon$ in $cm^{-1}M^{-1}$

Complex	ORD		CD		g	
	λ_{max}	$[M]\times10^{-3}$	λ_{max}	$\Delta\varepsilon$	λ_{max}	$g\times10^{2}$
$(+)_{589}$-Cr(acac)$_3$	480	−11.24	415	−2.00	450	−1.90
	562	+14.18	535	+4.50	515	+7.60
			610	−1.44	650	−4.40
$(-)_{589}$-Cr(3-Cl-acac)$_3$	480	+16.95	540	−5.64	530	−9.00
	570	−17.82	610	+1.96		
$(+)_{589}$-Cr(3-Br-acac)$_3$	470	−15.0	430	−1.82	440	−0.64
	570	+17.0	538	+6.20	515	+9.70
			610	−1.44	614	−2.60
$(-)_{589}$-Cr(3-I-acac)$_3$	485	+27.5	540	−8.67	542	−8.10
	575	−25.5	620	+2.48		
$(+)_{589}$-Cr(3-NO_2-acac)$_3$	475	−13.94	534	+5.60	450	−2.20
	560	+16.83	610	−1.83	518	+8.00
$(+)_{589}$-Cr(tfac)$_3$	470	−12.0	420	−2.52	460	−2.40
	560	+10.0	540	+3.65	530	+6.80
	650	−5.0	610	−2.14		
$(-)_{589}$-Cr(bzac)$_3$	495	+10.48	535	−4.40	520	−5.72
	565	−16.46	605	+1.65		

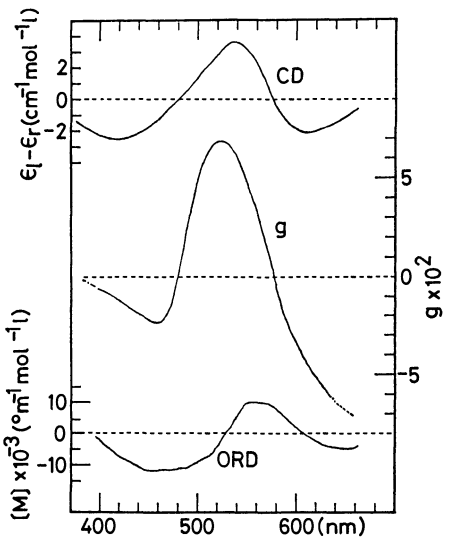

Fig. 5. $(+)_{589}$-Cr(tfac)$_3$.

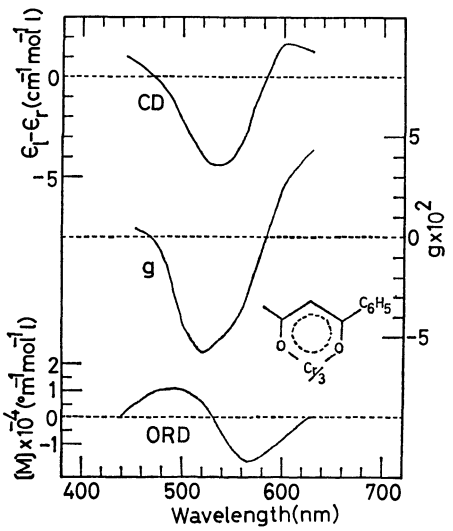

Fig. 6. $(-)_{589}$-Cr(bzac)$_3$ in 5×10^{-3} M chlorobenzene solution. Photoresolved at about 70 °C.

CPL at four different wavelengths, 514.5, 501.7, 496.5, and 488.0 nm. The ORD and CD spectra of the optically pure enantiomer have been calculated by using Eqs. (10) and (11). If these equations are correct, these four CD spectra should coincide with each other. As seen from Table 1, the $\Delta\varepsilon$ values at the CD peak position (530 nm) are equal well within experimental uncertainties. This method of justification appears to be somewhat round-about indeed but inevitable since no other method for determining ORD and CD curves has been available at present.[15]

ORD and CD Spectra. As mentioned previously, the optical resolution with CPL has one distinctive advantage over other chemical methods of resolution in that it enables one to determine the ORD and CD spectra of the optically pure enantiomers. This is especially the case with those complexes which have no formal charge. The ORD and CD spectra and the asymmetric factor g of the optically pure $(-)_{589}$-Cr(acac)$_3$ are depicted in Fig. 3. Spectra of the other complexes are given in Figs. 4—6. Numerical values for all the compounds investigated in this work are summarized in Table 2. Cr(acac)$_3$ has been partially resolved by Stevenson[5] using a high pressure mercury lamp in more than 200 hr. Our results for this complex are in good agreement with those given by him. All the asymmetric factors listed in Table 2 fall in the range from 5.7 to 9.7×10^{-2} around the wavelength of 514.5 nm. These values correspond to the photoresolution efficiency of 2.85 to 4.85%.

Interesting is the case with Cr(bzac)$_3$, where the compound has been dissolved in chlorobenzene and

photoresolution examined. However, no optical activity was detected at room temperature even on long irradiation (5 to 8 hr at 514.5 nm). Thus, experiments have been made at elevated temperatures and the PSS has been achieved in less than 3 hr at about 70 °C. This result, along with the fact that all the complexes photoresolved in this work and so far racemize thermally, suggests that photoresolution can be effected, if possible at all, on those compounds which racemize thermally and in addition at some adequate rates.

We have tried in vain to photoresolve some complexes of chromium(III). These include $Cr(dbzm)_3$, $Cr(TTA)_3$, $Cr(FTA)_3$, $Cr(oxine)_3$, and $Cr(DTC)_3$. The first three compounds seem to have precluded the resolution for kinetic reasons mentioned just above because it is unrealistic that the asymmetric factors for these compounds differ greatly from that of $Cr(acac)_3$.

References

1) O. Buchardt, *Angew. Chem. Internat. Ed.*, **13**, 180 (1974).
2) R. Tsuchida, A. Nakamura, and M. Kobayashi, *J. Chem. Soc. Japan*, **56**, 1335(1935).
3) K. L. Stevenson and J. F. Verdieck, *J. Amer. Chem. Soc.*, **90**, 2974(1968); *Mol. Photochem.*, **1**, 271 (1969).
4) B. Norden, *Acta Chem. Scand.*, **24**, 349 (1970).
5) K. L. Stevenson, *J. Amer. Chem. Soc.*, **94**, 6652 (1972).
6) N. A. P. Kane-Maguire and C. H. Langford, *Can. J. Chem.*, **50**, 3381 (1972).
7) V. S. Sastri, *Inorg. Chim. Acta*, **7**, 381 (1973).
8) H. Yoneda, Y. Nakashima, and U. Sakaguchi, *Chem. Lett.*, **1973**, 1343.
9) N. A. P. Kane-Maguire, B. Dunlop, and C. H. Langford, *J. Amer. Chem. Soc.*, **93**, 6293 (1971).
10) *Inorg. Syntheses*, **5**, 130 (1957).
11) R. C. Fay and T. S. Piper, *J. Amer. Chem. Soc.*, **85**, 500 (1963).
12) R. C. Fay and T. S. Piper, *ibid.*, **84**, 2303 (1962).
13) (a) J. P. Collman, R. A. Moss, H. Maltz, and C. C. Heindel, *ibid.*, **83**, 531 (1961).
(b) J. P. Collman, R. L. Marshall, W. L. Young, III, and S. D. Goldby, *Inorg. Chem.*, **1**, 704 (1962);
(c) R. W. Kluiber, *J. Amer. Chem. Soc.*, **82**, 4839 (1960).
14) R. C. Fay, A. Y. Girgis, and U. Klabunde, *ibid.*, **92**, 7056 (1970).
15) See, however, (a) W. C. M. C. Kokke, *ibid.*, **96**, 2627 (1974); (b) H. P. J. M. Dekkers, C. A. Emeis, and L. J. Oosterhoff, *ibid.*, **91**, 4589 (1969).

Metal Complexes Containing Six-membered Chelate Rings. IV. The Preparation and Structure of Dichlorocobalt(III) Complexes with Tetramines Derived from 2,4-Pentanediamine[1)]

Fujio MIZUKAMI*

Department of Chemistry, Faculty of Science, Tohoku University, Aoba, Aramaki, Sendai 980

(Received May 7, 1974)

The tetramine ligands, 4,6-dimethyl-3,7-diaza-1,9-nonanediamine (2,3″, 2-tet), 6,8-dimethyl-2,5,9,12-tetraazatridecane (*N,N′*-Me_2-2,3″, 2-tet), and 4,9-dimethyl-5,8-diaza-2,11-dodecanediamine (3″,2,3″-tet), were prepared by using *RR*- and *RS*-2,4-pentanediamine as the starting material. Six kinds of *trans*-dichloro cobalt(III) complexes with these ligands were prepared and characterized. Among these complexes, three kinds of optically active complexes were obtained. The *RR*-2,4-pentanediamine and *RS*-2,4-pentanediamine parts in these complexes were considered to take a λ-skew-boat and a chair conformation respectively on the basis of molecular models, PMR, and the absorption and CD spectra.

Many cobalt(III) complexes with tetramine containing one or two β-diamine parts have been prepared in recent years.[2-9)] In these complexes, the most probable conformations for the β-diamine part have been considered to be the chair and skew-boat (or twist) conformations. Actually, two isomers in the *trans*-dichloro (3, 7-diaza-1,9-nonanediamine) cobalt(III) complex, *trans*-$[CoCl_2(2,3,2\text{-tet})]^+$, have been isolated.[2-4)] One has been assigned to the *meso* structure, in which the six-membered chelate ring takes a chair form. The other has been assigned to the racemic structure, giving a skew-boat conformation. It is considered that the *meso* isomer is thermodynamically more stable than the racemic isomer, since the latter isomerizes to the former in a methanolic solution.

On the other hand, the *trans*-dichloro(4,7-diaza-1, 10-decanediamine)cobalt(III) complex, *trans*-$[CoCl_2(3, 2, 3\text{-tet})]^+$, which has also previously been isolated, is of only one kind and has been assigned a structure in which both the six-membered chelate rings take the chair conformation and both the secondary nitrogen atoms give the same configuration.[5-8)]

Previously, we have reported that, in the cobalt(III) complexes containing 2,4-pentanediamine (2,4-ptn), *RR*-, *SS*- and *RS*-2,4-pentanediamine give the λ- and δ-skew-boat and chair conformations respectively in six-membered chelate rings.[10,11)] Accordingly, it seemed that it would be interesting to prepare cobalt(III) complexes containing tetramines derived from 2,4-pentanediamines. Thus, in the present study, seven tetramines, *R*(4),*R*(6)- and *R*(4),*S*(6)-4,6-dimethyl-3,7-diaza-1,9-nonanediamine (*RR*-2,3″,2-tet and *RS*-2,3″, 2-tet), *R*(6),*S*(8)-6,8-dimethyl-2,5,9,12-tetraazatridecane (*N,N′*-Me_2-*RS*-2,3″,2-tet) and *R*(2),*R*(4),*R*(9), *R*(11), *R*(2),*S*(4),*S*(9),*R*(11)-, *S*(2),*R*(4),*R*(9),*S*(11)-, and *R*(2),*S*(4),*R*(9),*S*(11)-4,9-dimethyl-5,8-diaza-2,11-dodecanediamine (*RRRR*-, *RSSR*-, *SRRS*-, and *RSRS*-3″,2,3″-tet), were prepared.

This paper will deal with the preparation and structure of cobalt(III) complexes containing these tetramines on the basis of molecular models, PMR, and the absorption and CD spectra.

* Present Address: National Chemical Laboratory for Industry (Tokyo Kogyo Shikensho), 1-1-5, Honmachi, Shibuya-ku, Tokyo 151.

Experimental

Preparation of Ligands. The 4,6-dimethyl-3,7-diaza-1,9-nonanediamine (2,3″,2-tet) and 6,8-dimethyl-2,5,9,12-tetraazatridecane (*N,N′*-Me_2-2,3″,2-tet) were synthesized by a method similar to that used for *C*-substituted triethylenetetramine by Goto, Saburi and Yoshikawa.[12)] The 4,9-dimethyl-5,8-diaza-2,11-dodecanediamine (3″,2,3″-tet) was synthesized according to a method similar to that used for 4,7-diaza-1,10-decanediamine (3,2,3-tet) by Hamilton and Alexander.[2)] Thus, these ligands were prepared from 2,4-pentanediamines as shown in Schemes I, II, and III.

Scheme I (Method I)

$$2ClCH_2COCl + NH_2CH(CH_3)CH_2CH(CH_3)NH_2 \xrightarrow{NaOH}$$
$$ClCH_2CONHCH(CH_3)CH_2CH(CH_3)NHCOCH_2Cl \xrightarrow{NH_3\ aq.}$$
$$NH_2CH_2CONHCH(CH_3)CH_2CH(CH_3)NHCONH_2\cdot 2HCl \xrightarrow{LiAlH_4}$$
$$NH_2CH_2CH_2NHCH(CH_3)CH_2CH(CH_3)NHCH_2CH_2NH_2$$
(2,3″,2-tet)

Scheme II (Method II)

$$2ClCH_2COCl + NH_2CH(CH_3)CH_2CH(CH_3)NH_2 \xrightarrow{NaOH}$$
$$ClCH_2CONHCH(CH_3)CH_2CH(CH_3)NHCOCH_2Cl \xrightarrow{CH_3NH_2\ aq.}$$
$$CH_3NHCH_2CONHCH(CH_3)CH_2CH(CH_3)NHCOCH_2\text{-}NHCH_3\cdot 2HCl \xrightarrow{LiAlH_4}$$
$$CH_3NHCH_2CH_2NHCH(CH_3)CH_2CH(CH_3)\text{-}NHCH_2CH_2NHCH_3$$
(*N,N′*-Me_2-2,3″,2-tet)

Scheme III (Method III)

$$2NH_2CH(CH_3)CH_2CH(CH_3)NH_2 + BrCH_2CH_2Br \xrightarrow{C_2H_5ONa}$$
$$NH_2CH(CH_3)CH_2CH(CH_3)NHCH_2CH_2NHCH(CH_3)\text{-}CH_2CH(CH_3)NH_2$$
(3″,2,3″-tet)

The optically active (*RR* and *SS*) and *meso* (*RS*) 2,4-pentanediamine (2,4-ptn) used as the starting materials in the preparation of the tetramines were synthesized according to a method reported previously.[10,13-15)]

R(4),R(6)-*4,6-Dimethyl-3,7-diaza-1,9-nonanediamine* (RR-*2, 3″,2-tet*): To 120 ml of a vigorously stirred aqueous

sodium hydroxide solution (5 M NaOH), cooled in an ice-salt bath, was added 13.7 g of *RR*-2,4-pentanediamine (0.135 mol). A solution of chloroacetyl chloride (32 g, 0.28 mol) in 100 ml of benzene was then added dropwise over a period of 30 min. The solution was stirred and cooled throughout the addition. The reaction mixture was then allowed to stand at room temperature for another 3 hr. The resulting precipitate, *N,N'*-bis(chloroacetyl)-*RR*-2,4-pentanediamine, was filtered, washed with cold water, and dried under a vacuum. The product was purified by recrystallization from ethanol; yield, 25.3 g (74%); $[\alpha]_D^{28}$ +6.11. Found: C, 42.05; H, 6.46; N, 11.01%. Calcd for $C_9H_{16}N_2O_2Cl_2$: C, 42.37; H, 6.32; N, 10.98%.

The *N,N'*-bis(chloroacetyl)-*RR*-2,4-pentanediamine (11.2 g) and 100 g of ammonium carbonate were dissolved in 500 ml of a 28% ammonium hydroxyide solution. The solution was allowed to stand for 10 days and then evaporated to dryness at 60 °C on a rotary evaporator. The product, 4,6-dimethyl-3,7-diaza-1,9-diaminononane-2,8-dione dihydrochloride, which was a pale yellow oil, was dried in a vacumm desiccator over phosphorous pentoxide and used in the next step without further purification.

The product obtained above (14 g) was dissolved in 200 ml of dry tetrahydrofuran (THF). The solution was then placed into a 500-ml, four-necked, round-bottomed flask equipped with a mechanical stirrer, a dropping funnel, and a reflux condenser with a soda lime tube. To the vigorously stirred solution was added 11 g of lithium aluminum hydride in small portions while the vessel was kept in an ice-cold bath. After the addition was complete, the mixture was allowed to stand at room temperature for another 30 min and then refluxed overnight. The reaction mixture was cooled in an ice-cold bath and carefully quenched by the dropwise addition of 30 ml of water. The white precipitate was filtered off. The filtered solid was then washed twice with 200 ml of boiling THF. The combined filtrate and washing were evaporated on a rotary evaporator. The oily residue, the crude *R*(4),*R*(6)-dimethyl-3,7-diaza-1,9-nonanediamine (*RR*-2,3″,2-tet), was used in the synthesis of the cobalt(III) complex without further purification. However, the cobalt(III) complex of this tetramine gave very satisfactory analytical results as stated in the preparation of complexes. Therefore, the oily residue is the desired product (*RR*-2,3″,2-tet).

R(4),S(6)-*Dimethyl-3,7-diaza-1,9-nonanediamine* (RS-*2,3″,2-tet*): *N,N'*-Bis(chloroacetyl)-*RS*-2,4-pentanediamine was prepared from *RS*-2,4-pentanediamine and chloroacetyl chloride by a method similar to that used for the corresponding *RR*-2,3″,2-tet described above. Found: C, 42.46; H, 6.34; N, 10.98%. Calcd for $C_9H_{16}N_2O_2Cl$: C, 42.37; H, 6.32; N, 10.98%.

The remainder of the procedure used to obtain *RS*-2,3″,2-tet is identical with the method for the corresponding *RR*-2,3″,2-tet described above. The elemental analysis of *RS*-2,3″,2-tet was achieved by the formation of the cobalt(III) complex as well as the *RR*-2,3″,2-tet described above.

R(6), S(8)-*6,8-Dimethyl-2,5,9,12-tetraazatridecane* (N,N'-Me_2-RS-*2,3″,2*-tet): According to Method II, *N,N'*-bis-(chloroacetyl)-*RS*-2,4-pentanediamine (11.2 g) wasdissolved in an aqueous solution of 30% methylamine. The solution was allowed to stand for 10 days and then evaporated to dryness on a rotary evaporator. The product, *R*(6), *S*(8)-6,8-dimethyl-2,5,9,12-tetraazatridecane-4,10-dione, was used in the next step without further purification. The remainder of the procedure was identical with that of the method for the corresponding *RR*-2,3″,2-tet described above. The elemental analysis of *N,N'*-Me_2-*RS*-2,3″,2-tet was achieved by the formation of the cobalt(III) complex as well as the *RR*-2,3″,2-tet described above.

R(2),S(4),S(9),R(11)-, S(2),R(4),R(9),S(11)-, *and* R-(2), S(4),R(9),S(11)-*4,9-Dimethyl-5,8-diaza-2,11-dodecanediamine* (RSSR-, SRRS-, *and* RSRS-*3″,2,3″-tet*): The procedure reported by Hamilton and Alexander[3] was modified. To a vigorously stirred solution of *RS*-2,4-pentanediamine (26.7 g) in 100 ml of ethanol was added 10 g of 1,2-dibromoethane in small portions. The solution was stirred and the temperature kept at about 50 °C in a water bath throughout the addition. The reaction mixture was stirred at 50 °C for another 1.5 hr and then refluxed for 12 hr. The reaction mixture was subsequently cooled to room temperature. To the vigorously stirred solution was added 2.5 g of metallic sodium in small portions. The reaction mixture was stirred at 50 °C for another 2 hr and cooled to 0 °C. After filtration, the ethanol was removed by distillation. The product, a mixture of *RSSR*-, *SRRS*- and *RSRS*-3″,2,3″-tet, was then collected by vacuum distillation at 140—160 °C (3 mmHg). Found: C, 63.15; H, 13.18; N, 23.71%. Calcd for $C_{12}H_{30}N_4$: C, 62.56; H, 13.13; N, 24.32%. A mixture of *RSSR*-, *SRRS*-, and *RSRS*-3″,2,3″-tet was separated by complexing with cobalt(III) ions as described below.

R(2),R(4),R(9),R(11)-*4,9-Dimethyl-5,8-diaza-2,11-dodecanediamine* (RRRR-*3″,2,3″-tet*): This was prepared from *RR*-2,4-pentanediamine and 1,2-dibromoethane by a method similar to that used for the corresponding *RSSR*-, *SRRS*-, and *RSRS*-3″,2,3″-tet described above. The rotation of *RRRR*-3″,2,3″-tet in water showed a plus sign at the Na D line. This tetramine gave only an approximate coincidence between the found and calculated analytical results, but its cobalt(III) complex gave very satisfactory analytical results.

Preparation of Cobalt(III) Complexes. $(+)_{600}$-trans-[$CoCl_2$(RR-*2,3″,2-tet*)]ClO_4: The ligand, *RR*-2,3″,2-tet (1 g), was added to 60 ml of an aqueous solution containing 1.2 g of cobalt(II) chloride hexahydrate and the solution was aerated with carbon dioxide-free air for 10 hr at room temperature. The solution was then filtered off, and the insoluble material was washed with a small amount of water. The filtrate and the washing were combined. To the solution was added 20 ml of concd HCl. The solution was warmed at 60 °C for 30 min to give a green solution. This solution was concentrated to 50 ml at 50 °C on a water bath and cooled to room temperature. To the solution was added 15 ml of 60% perchloric acid. The solution was allowed to stand overnight in a refrigerator. The green crystals were then filtered off, washed with a small amount of cold ethanol and ether, and air-dried. Yield: 60%. Found: C, 25.87; H, 5.92; N, 13.09%. Calcd for $C_9H_{24}N_4Cl_3CoO_4$: C, 25.89; H, 5.79; N, 13.42%.

trans-[$CoCl_2$(RS-*2,3″,2-tet*)]ClO_4, trans-[$CoCl_2$(*N,N'*-Me_2-RS-*2,3″,2-tet*)]ClO_4: These complexes were prepared from $CoCl_2 \cdot 6H_2O$ and *RS*-2,3″,2-tet or *N,N'*-Me_2-*RS*-2,3″,2-tet by a method similar to that used for the corresponding *RR*-2,3″,2-tet complex described above. *trans*-[$CoCl_2$(*RS*-2,3″,2-tet)]ClO_4 is soluble in water, but *trans*-[$CoCl_2$(*N,N'*-Me_2-*RS*-2,3″,2-tet)]ClO_4 is only slightly soluble. The yields of the former and the latter: 50% and 80% respectively. Found: C, 25.92 H, 6.03; N, 13.15%. Calcd for $C_9H_{24}N_4Cl_3CoO_4$: C, 25.89; H, 5.79; N, 13.42%. Found: C, 29.48; H, 6.70; N, 12.52%. Calcd for $C_{11}H_{28}N_4Cl_3CoO_4$: C, 29.64; H, 6.33; N, 12.57%.

trans-[$CoCl_2$(RSSR- *and* SRRS-3″,2,3″-*tet*)]$Cl \cdot H_2O$: A mixed tetramine containing a racemic pair (*RSSR* and *SRRS*) and *meso* (*RSRS*) 3″,2,3″-tet (11 g) was dissolved in 120 ml of water. To the solution was added 11.4 g of $CoCl_2 \cdot 6H_2O$. The solution was aerated with carbon dioxide-free air for

14 hr at room temperature. The deposited green powder was filtered off and washed with a small amount of water. The filtrate and the washing were then combined. To this solution was added 100 ml of concd HCl. The resulting green precipitate was filtered off and washed with a small amount of cold water. The powder and the precipitate were combined and recrystallized from water by adding concd HCl. Yield: 7.6 g. Found: C, 34.50; H, 7.96; N, 13.55%. Calcd for $C_{12}H_{32}N_4Cl_3CoO$: C, 34.84; H, 7.80; N, 13.54%.

trans-[*CoCl*$_2$(RSRS-*3″,2,3″-tet*)]*ClO*$_4$: To the blue filtrate from which the green crystals of *trans*-[$CoCl_2$(*RSSR*- and *SRRS*-3″,2,3″-tet)]Cl·H_2O had been removed, was added 60 ml of 60% perchloric acid. The solution was then concentrated on a water bath at 60 °C to yield green crystals, though the color of the solution remained blue. The green crystals were recrystallized from hot methanol. Yield 8 g. Found C, 31.58; H, 6.56; N, 11.89%. Calcd for $C_{12}H_{30}N_4Cl_3CoO_4$: C, 31.35; H, 6.58; N, 12.19%.

This complex showed a green color in the methanol solution, but a blue-violet in a concd HCl solution. This shows that the complex takes the *trans* (Cl–Cl) configuration in the methanol and the *cis* (Cl–Cl) configuration in the concd HCl solution.

cis-[*CoCl*$_2$(RSRS-*3″,2,3″-tet*)]*Cl*: The blue filtrate from which the green crystals of *trans*-[$CoCl_2$(*RSSR*- and *SRRS*-3″,2,3″-tet)]Cl·H_2O had been removed was concentrated on a water bath at 60 °C. The deposited blue-violet powder was filtered off and dried over sodium hydroxide under reduced pressure. The complex was recrystallized from concd HCl by evaporating on a water bath at 60 °C. Found: C, 36.00; H, 7.85; N, 13.84%. Calcd for $C_{12}H_{30}N_4Cl_3Co$: C, 36.43; H, 7.64; N, 14.16%.

This complex showed a blue-violet color (*cis* (Cl–Cl)) in a concd HCl solution, but a green color (*trans* (Cl–Cl)) in the methanol solution.

$(+)_{600}$-trans-[*CoCl*$_2$(RSSR-*3″,2,3″-tet*)]*Cl*·*H*$_2$*O*: The *trans*-[$CoCl_2$(*RSSR*- and *SRRS*-3″,2,3″-tet)]Cl·H_2O complex (5 g) was dissolved in 100 ml of water. To the solution was added 2.4 g of potassium oxalate monohydrate, and the solution was warmed at 70 °C for 4 hr. The reaction mixture was evaporated to dryness at 60 °C under reduced pressure. The residue was dissolved in 95% ethanol, and the potassium chloride was removed by filtration. The product was crystallized by gradually evaporating the filtrate. This product was assigned to *cisβ*-[Co(ox)(*RSSR*- and *SRRS*-3″,2,3″-tet)]Cl·H_2O, because its PMR spectrum showed four kinds of methyl signals.

The *cisβ*-[Co(ox)(*RSSR*- and *SRRS*-3″,2,3″-tet)]Cl·H_2O complex (3.1 g) was dissolved in 200 ml of water at 60 °C. To the solution was added a solution of sodium hydrogen dibenzoyl-*d*-tartrate (3.3 g) in 200 ml of hot water. The solution was stirred at 60 °C for 6 hr. The solution was subsequently cooled to room temperature, and the deposited powder was filtered off. The filtrate was concentrated to 250 ml, and the precipitated second powder was filtered off. To the second filtrate was added an appropriate amount of concd HCl slowly. The solution was stirred throughout the addition. The deposited white precipitate was filtered off. The third filtrate was evaporated in a vacuum desiccator over potassium hydroxide, and the resulting red crystals were filtered off. Red crystals were recrystallized fractionally from water until the CD spectra exhibited a constant curve.

This optically pure complex of oxalatotetramine was dissolved in concd HCl and warmed at 70 °C for 3 hr. The resulting green crystals were filtered off, washed with a small amount of cold water and ethanol, and air-dried. It was found that the optically active complex of oxalatotetramine was almost quantitatively converted to the $(+)_{600}$-*trans*-dichloro complex by this procedure. Found: C, 34.84; H, 7.62; N, 13.14%. Calcd for $C_{12}H_{32}N_4Cl_3CoO$: C, 34.84; H, 7.80; N, 13.54%.

The $(+)_{600}$-*trans*[$CoCl_2$(*RSSR*-3″,2,3″-tet)]Cl·H_2O complex was also obtained by the optical resolution of *trans*-[$CoCl_2$(*RSSR*- and *SRRS*-3″,2,3″-tet)]Cl·H_2O in water using sodium hydrogen dibenzoyl-*d*-tartrate as the resolving agent. This procedure was not very good, however, because the *trans*-[$CoCl_2$(*RSSR*- and *SRRS*-3″,2,3″-tet)]$^+$ aquated slowly in water.

$(-)_{600}$-trans-[*CoCl*$_2$(*RRRR-3″,2,3″-tet*)]*ClO*$_4$·*H*$_2$*O*: This complex was prepared from $CoCl_2$·$6H_2O$ and *RRRR*-3″,2,3″-tet by a method similar to that used for the corresponding *RR*-2,3″,2-tet described above. *trans*-[$CoCl_2$(*RRRR*-3″,2,3″-tet)]ClO_4·H_2O aquated slowly in water at room temperature, as did the other *trans*-2,3″,2-tet and 3″,2,3″-tet complexes of cobalt(III) except for *trans*-[($CoCl_2$(*RSRS*-3″,2,3″-tet)]ClO_4. Found: C, 30.61; H, 6.78; N, 12.15%. Calcd for $C_{12}H_{32}N_4Cl_3CoO_5$: C, 30.17, H, 6.75; N, 11.73%.

Measurements. The visible and ultraviolet absorption spectra were recorded with a Hitachi 124 recording spectrophotometer. The CD curves were recorded with Model ORD/UV-5 spectrophotometer of the Japan Spectroscopic Co., with a CD attachment. The spectra of the *trans*-dichloro complexes were recorded in a methanol solution, while the spectrum of the *cis*-dichloro complex was recorded in a concd HCl solution. The PMR spectra were obtained with Varian T-60 and HA-100 spectrophotometers, using Na-TMS as the internal standard. The perchlorate salts of three *trans*-dichloro complexes, *trans*-[$CoCl_2$(*RR*-2,3″,2-tet)]ClO_4, *trans*-[$CoCl_2$(*RS*-2,3″,2-tet)]ClO_4, and *trans*-[$CoCl_2$(*N,N′*-Me_2-*RS*-2,3″,2-tet)]ClO_4, were converted into chloride salts by the use of an anion exchanger, Dowex 1-X4, because the perchlorate salts were not sufficiently soluble in D_2O. The PMR spectra of the corresponding *RSSR*-, *SRRS*-, and *RSRS*-3″,2,3″-tet complexes could not be obtained, because these complexes were not sufficiently soluble in D_2O. All the measurements were made at room temperature.

Results and Discussion

Geometrical Isomers of Complexes and Configurations of Ligands. Three topological isomers are possible for the dichlorotetramine complexes of cobalt(III). However, it is rare that all three isomers are prepared by the usual air-oxidation procedure. In fact, the *trans* isomer is preferentially produced in the 2,3,2-tet and 3,2,3-tet complexes of cobalt(III).[2,3] While, on the contrary, the main products are *cis*-dichloro isomers (*cisα*, *cisβ*) in the triethylenetetramine complexes of cobalt(III).[18–20] This difference may be roughly attributed to the reaction rate, the solubility, and the steric factor of the complexes.

In the present study, dichlorotetramine cobalt(III) complexes were prepared by using the usual air-oxidation procedure. The green dichloro isomers only could be isolated from the reaction solution when any of the five tetramines (*RR*-2,3″,2-tet, *RS*-2,3″,2-tet, *N,N′*-Me_2-*RS*-2,3″,2-tet, *RRRR*-3″,2,3″-tet, and a racemic pair of *RSSR*- and *SRRS*-3″,2,3″-tet) was employed as a ligand. In the case of the [$CoCl_2$-(*RSRS*-3″,2,3″-tet)]$^+$ complexes, however, the blue-violet salt of [$CoCl_2$(*RSRS*-3″,2,3″-tet)]Cl and the green salt of [$CoCl_2$(*RSRS*-3″,2,3″-tet)]ClO_4 could be

Table 1. Numerical data of absorption (AB) and circular dichroism (CD) $\bar{\nu}$ in $10^3\,cm^{-1}$, ($\log\varepsilon$) and (ε_l-ε_r)

Complex	AB		CD	
trans-[$CoCl_2$(*RS*-2,3″,2-tet)]ClO_4	16.16	(1.64)		
	21.83	(1.57)		
	25.45	(1.76)		
	32.26	(3.17)		
	39.53	(4.40)		
trans-[$CoCl_2$(*RR*-2,3″,2-tet)]ClO_4	16.16	(1.70)	15.27	(−0.42)
			16.95	(+0.36)
	ca. 21.80	(*ca.* 1.45)	21.51	(−0.60)
	26.11	(1.75)	25.32	(+0.26)
	32.57	(3.15)	30.58	(−1.21)
	39.52	(4.35)	40.32	(+7.66)
trans-[$CoCl_2$(*N*,*N*′-Me_2-*RS*-2,3″,2-tet)]ClO_4	15.77	(1.57)		
	20.83	(1.48)		
	24.88	(1.84)		
	ca. 31.80	(*ca.* 3.23)		
	39.06	(4.39)		
trans-[$CoCl_2$(*RRRR*-3″,2,3″-tet)]$ClO_4\cdot H_2O$	15.90	(1.64)	15.87	(+0.59)
	21.74	(1.56)	21.05	(−1.04)
	25.45	(1.81)	26.32	(+0.57)
	32.26	(3.33)	33.33	(−1.65)
	39.06	(4.37)	39.37	(+16.49)
trans-[$CoCl_2$(*RSSR*-3″,2,3″-tet)]$Cl\cdot H_2O$	15.87	(1.60)	15.15	(−0.23)
			16.81	(+0.07)
	21.41	(1.53)	21.28	(+0.07)
	25.19	(1.81)	26.04	(−0.29)
	31.95	(3.25)	30.30	(−0.39)
			34.01	(+2.68)
	39.06	(4.41)	37.04	(−5.39)
trans-[$CoCl_2$(*RSRS*-3″,2,3″-tet)]ClO_4	15.77	(1.66)		
	21.28	(1.53)		
	25.19	(1.86)		
	31.95	(3.23)		
	38.91	(4.34)		

isolated from the reaction solution as described in detail in Experimental. The six green complexes and the blue-violet complex prepared here were assigned to the *trans*(Cl–Cl) and *cis*(Cl–Cl) structures respectively from their characteristic color and absorption spectra, as shown in Figs. 5—7 and Table 1.

The configurational assignments of the asymmetric carbon atoms in the ligands of *RR*-2,3″,2-tet, *RS*-2,3″, 2-tet, *N*,*N*′-Me_2-*RS*-2,3″,2-tet, and *RRRR*-3″,2,3″-tet were confirmed unequivocally from the preparative processes of these tetramines described in Experimental.

However, when *RS*-2,4-pentanediamine was employed as the starting material in Method III, the products of the reaction contained three isomers of 3″,2,3″-tet, *meso* (*RSRS*), and a pair of racemic (*RSSR* and *SRRS*) tetramines. These three isomers were separated, resolved, and characterized on the basis of the following considerations. The molecular models indicate that *RSRS*-3″,2,3″-tet and racemic (*RSSR* and *SRRS*) 3″,2,3″-tet tend to form *cis*-[$CoCl_2$(*RSRS*-3″, 2,3″-tet)]$^+$ and *trans*-[$CoCl_2$(*RSSR*- and *SRRS*-3″,2,3″-tet)]$^+$ complexes respectively by the steric regulation of the ligands. In the first stage, a mixture of *meso* and racemic tetramine was separated by complexing with the cobalt(III) ion as follows (see Experimental). The green chloride salt was obtained in the step of air-oxidation, and then from its filtrate blue-violet chloride and green perchlorate salts were obtained. The first green chloride could be resolved into the optically active form ($(+)_{600}$-*trans*-isomer). This complex may be assigned to *trans*-[$CoCl_2$(*RSSR*- and *SRRS*-3″,2,3″-tet)]$Cl\cdot H_2O$. The blue-violet chloride salt may be assigned to *cis*-[$CoCl_2$(*RSRS*-3″,2,3″-tet)]Cl on the basis of a molecular-model study. This *cis*-dichloro complex was converted to *trans*-dichloro complex in the methanolic solution. The absorption spectrum of this *trans*-dichloro complex is in accord with that of the secondarily obtained green perchlorate salt, which was converted to the *cis*-dichloro form in concentrated hydrochloric acid. The green perchlorate salt may be *trans*-[$CoCl_2$(*RSRS*-3″,2,3″-tet)]ClO_4.

In the second stage, the configuration of the tetramine ligand in $(+)_{600}$-*trans*-dichloro complex was determined. The molecular models indicate that the most stable forms among the possible isomers in [Co (ox) (*RSSR*-3″,2,3″-tet)]$^+$ and [Co(ox) (*SRRS*-3″,2,3″-tet)]$^+$ are the *Λ-cisβ* and *Λ-cisβ* isomer respectively. The oxalatotetramine complex prepared from the

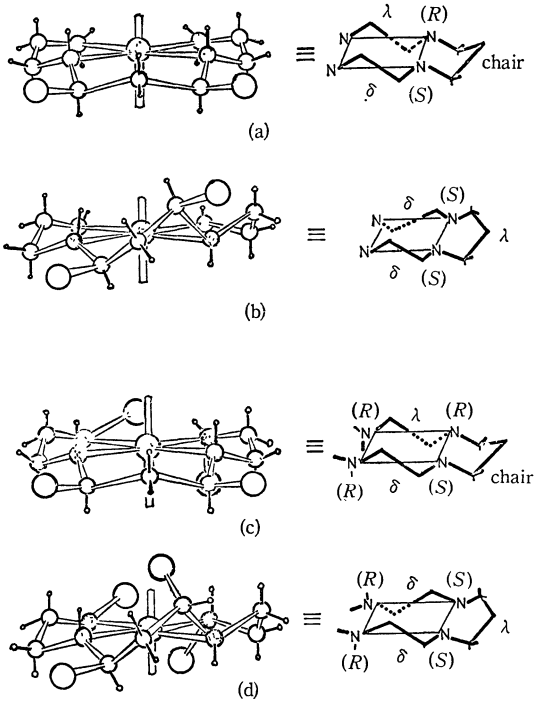

Fig. 1. Schematic structures of *trans*-$[CoCl_2(2,3'',2\text{-tet})]^+$.
(a) *trans*-$[CoCl_2(RS\text{-}2,3'',2\text{-tet})]^+$
(b) *trans*-$[CoCl_2(RR\text{-}2,3'',2\text{-tet})]^+$
(c) *trans*-$[CoCl_2(N,N'\text{-}Me_2\text{-}RS\text{-}2,3'',2\text{-tet})]^+$
(d) *trans*-$[CoCl_2(N,N'\text{-}Me_2\text{-}RS\text{-}2,3'',2\text{-tet})]^+$.

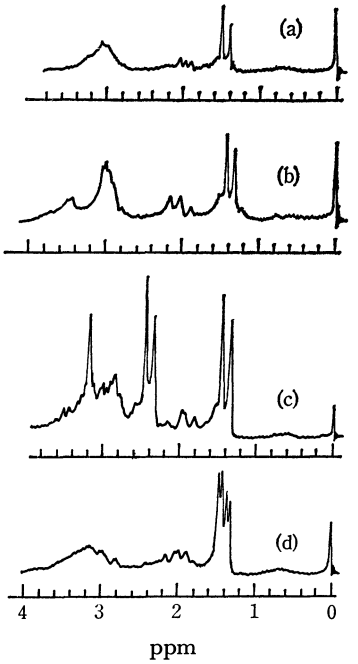

Fig. 2. PMR spectra (60 MHz) of
(a) *trans*-$[CoCl_2(RS\text{-}2,3'',2\text{-tet})]Cl$,
(b) *trans*-$[CoCl_2(RR\text{-}2,3'',2\text{-tet})]Cl$,
(c) *trans*-$[CoCl_2(N,N'\text{-}Me_2\text{-}RS\text{-}2,3'',2\text{-tet})]Cl$,
(d) *trans*-$[CoCl_2(RRRR\text{-}3'',2,3''\text{-tet})]Cl$, in diluted DCl.

$(+)_{600}$-*trans*-dichloro complex was optically active ($\Delta\varepsilon=+0.53$ at 17730 cm^{-1} and $\Delta\varepsilon=-2.09$ at 19920 cm^{-1}) and gave more than three kinds of methyl signals in the PMR spectrum in D_2O. These facts seem to indicate that the oxalatotetramine complex takes *Δ-cisβ* configuration.[16] The details of this compound will be reported later.[17] This oxalatotetramine complex of cobalt(III) was almost quantitatively coverted to the *trans*-dichlorotetramine complex of cobalt(III) by warming in a concd HCl solution. The absorption and CD spectra of the resulting *trans*-dichloro complex was cosistent with those of the $(+)_{600}$-*trans*-isomer used as the starting material. Therefore, it seems that the $(+)_{600}$-$[CoCl_2(3'',2,3''\text{-tet})]^+$ complex can be assigned to *trans*-$[CoCl_2(RSSR\text{-}3'',2,3''\text{-tet})]^+$.

Conformation and Structure. As stated previously,[1,10,11] *RR*-, *SS*-, and *RS*-2,4-pentanediamine are expected to give *λ*- and *δ*-skew-boat and chair conformations respectively in six-membered chelate rings. Also, it is generally understood that substituting groups on carbon atoms in puckered chelate rings always tend to take equatorial positions. When the tetramines prepared here coordinate to the cobalt(III) ion, each of the three chelate rings in the tetramine complexes of cobalt(III) can be expected to have a specific conformation because of the steric regulation coming from the methyl groups on the α-carbon atoms as *C*-substituted triethylenetetramine cobalt(III) complexes.[12,20–22]

For the above reasons, the pentanediamine part of *RR*-2,3″,2-tet is expected to give a *λ*-skew-boat conformation in the complex of *trans*-$[CoCl_2(RR\text{-}2,3'',2\text{-tet})]^+$. Then, both of the five-membered chelate rings seem to take the *δ-gauche* conformation, and both of secondary nitrogen atoms seem to take the *S*-configuration as shown in Fig. 1-b. Accordingly, the two methyl groups are equivalent to each other, because this presumed structure has the C_2 symmetry. The molecular models indicate that the structure shown in Fig. 1-b (C_2) is formed without any great steric hindrance and involves a smaller steric interaction among the chelate rings than the other possible structure. This most probable structure was confirmed by the fact that the PMR spectrum of *trans*-$[CoCl_2(RR\text{-}2,3'',2\text{-tet})]^+$ gave only one sharp doublet of the methyl signal at 1.4 ppm as shown in Fig. 2-b.

From a similar consideration, *trans*-$[CoCl_2(RS\text{-}2,3'',2\text{-tet})]^+$ seems to take the *trans-N(S),N(R)*-[(*δ-gauche*) (chair) (*λ-gauche*)] structure as shown in Fig. 1-a. As shown in Fig. 2-a, the PMR spectrum of *trans*-$[CoCl_2(RS\text{-}2,3'',2\text{-tet})]^+$ gave a doublet of the methyl signal at 1.5 ppm, in accord with the above assignment.

The structural consideration of *trans*-$[CoCl_2(N,N'\text{-}Me_2\text{-}RS\text{-}2,3'',2\text{-tet})]^+$ gives three probable structure. In the first structure, all the methyl groups take equatorial positions and the six-membered chelate ring gives a chair conformation. In the second (an enantiomeric pair of Fig. 1-c), one *N*-methyl and two *C*-methyl groups exist in equatorial positions, while the other *N*-methyl group exists in an axial position. In this structure, the six-membered chelate ring gives a chair conformation. In the third structure (an enantiomeric pair of Fig. 1-b), the six-membered chelate ring forms a skew-boat conformation in which one *C*-methyl group takes an equatorial position and

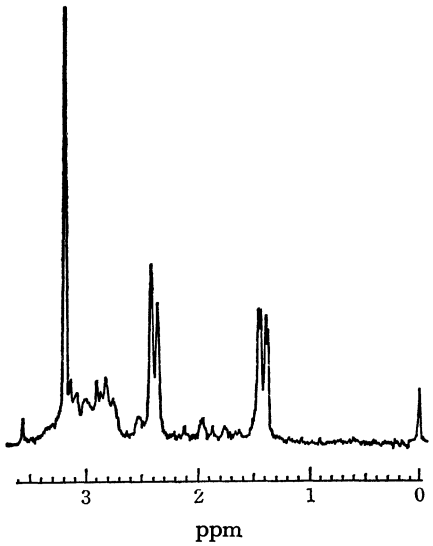

Fig. 3. PMR spectrum (100 MHz) of *trans*-[$CoCl_2$-(*N*,*N'*-Me_2-*RS*-2,3″,2-tet)]Cl in 3—4 M DCl.

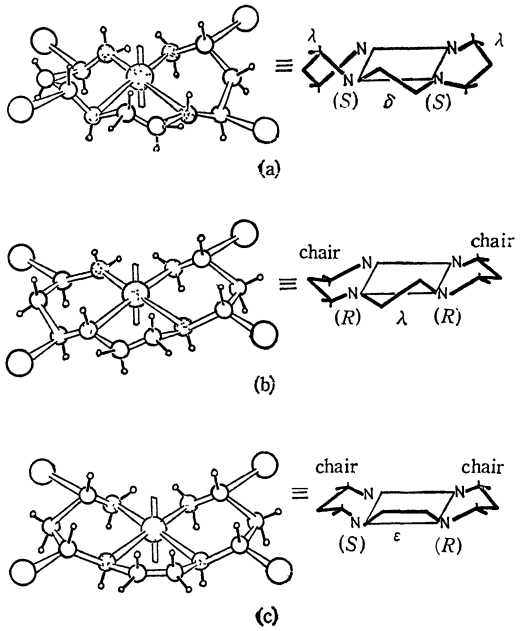

Fig. 4. Schematic structures of *trans*-[$CoCl_2$(3″,2,3″-tet)]$^+$.
(a) *trans*-[$CoCl_2$(*RRRR*-3″,2,3″-tet)]$^+$
(b) *trans*-[$CoCl_2$(*RSSR*-3″,2,3″-tet)]$^+$
(c) *trans*-[$CoCl_2$(*RSRS*-3″,2,3″-tet)]$^+$

the other *C*-methyl group is orientated in an axial position. In addition, two *N*-methyl groups take equatorial positions in this third structure. The first structure does not seem to be formed because of the great steric hindrance among the two *N*-methyl groups in equatorial positions. The structure of *trans*-[$CoCl_2$-(*N*,*N'*-Me_2-*RS*-2,3″,2-tet)]$^+$ is probably the second or the third.

The PMR spectra of the *trans*-[$CoCl_2$(*N*,*N'*-Me_2-*RS*-2,3″,2-tet)]$^+$ complex are shown in Fig. 2-c (60 MHz) and Fig. 3 (100 MHz). The two kinds of doublets at 1.4 ppm can probably be assigned to the two *C*-methyl groups. The broad doublet at 2.4 ppm, in which two kinds of doublets seem to overlap, is probably to be assigned to the *N*-methyl groups. The sharp singlet at 3.2 ppm may be assigned to the signal of amino protons, because the intensity of the signal depends upon the concentration of DCl. However, it is difficult to assign the detailed structure of *trans*-[$CoCl_2$(*N*,*N'*-Me_2-*RS*-2,3″,2-tet)]$^+$, because all four methyl groups are nonequivalent to each other in such a structure as shown in Fig. 1-c or Fig. 1-d. All attempts at the optical resolution of *trans*-[$CoCl_2$ (*N*,*N'*-Me_2-*RS*-2,3″,2-tet)]$^+$ have been unsuccessful so far.

Both six-membered chelate rings in *trans*-[$CoCl_2$-(*RRRR*-3″,2,3″-tet)]$^+$ seem to take a λ-skew-boat conformation in which each of the two α-carbon atoms has an equatorial methyl group. In this case, the central five-membered chelate ring and both secondary nitrogen atoms unequivocally take the *δ-gauche* and *S*-configurations respectively. In this presumed structure (C_2 symmetry), the two methyl groups near the five-membered chelate ring are equivalent to one another, and the two methyl groups far away are also equivalent to one another as shown in Fig. 4-a. Actually, the PMR spectrum of *trans*-[$CoCl_2$(*RRRR*-3″,2,3″-tet)]$^+$ gave two doublets of a methyl signal at 1.40 ppm and 1.45 ppm respectively as shown in Fig. 2-d. Accordingly, it seems that the structure of *trans*-[$CoCl_2$(*RRRR*-3″,2,3″-tet)]$^+$ can be assigned to *trans*-*N*(*S*), *N*(*S*)-[(λ-skew-boat) (*δ-gauche*) (λ-skew-boat)] as shown in Fig. 4-a.

The most probable structrue for *trans*-[$CoCl_2$(*RSSR*-3″,2,3″-tet)]$^+$ seems to be the *trans*-*N*(*R*), *N*(*R*)-[(chair) (*λ-gauche*) (chair)] structure as shown in Fig. 4-b. Studies with molecular models disclose that this assumed structure has a more strain-free and complete puckered conformation than the other possible structure. Also, it has been considered that the skeletal structure shown in Fig. 4-b is the most stable form in *trans*-[CoX_2(3,2,3-tet)]$^+$ (X=Cl, Br, NO_2)[5–9] and its analogs.[23,24] The PMR spectrum of *trans*-[$CoCl_2$-(*RSSR*-3″,2,3″-tet)]Cl·H_2O could not be obtained, because this complex was not sufficiently soluble in D_2O.

As the *RS*-2,4-pentanediamine parts of *RSRS*-3″,2,3″-tet tend to take chair conformations in a six-membered chelate ring, the most probable structure for the complex of *trans*-[$CoCl_2$(*RSRS*-3″,2,3″-tet)]$^+$ may be the form shown in Fig. 4-c. This structure, in which the central five-membered chelate ring takes an envelope conformation, has great strain in the bond angles of the two secondary nitrogen atoms, and it seems to be quite unstable compared with the structures of the other *trans*-dichlorotetramine complexes prepared here. Also, it was clear from the change in the absorption spectra that *trans*-[$CoCl_2$-(*RSRS*-3″,2,3″-tet)]ClO_4 rapidly aquated with a steric change in water and dilute hydrochloric acid, whereas the other *trans*-dichlorotetramine complexes prepared here aquated very slowly, retaining their configurations, and did not aquate in dilute hydrochloric acid. This may be related to the structural considerations presented above.

It is difficult to assign the structure of *cis*-[$CoCl_2$-

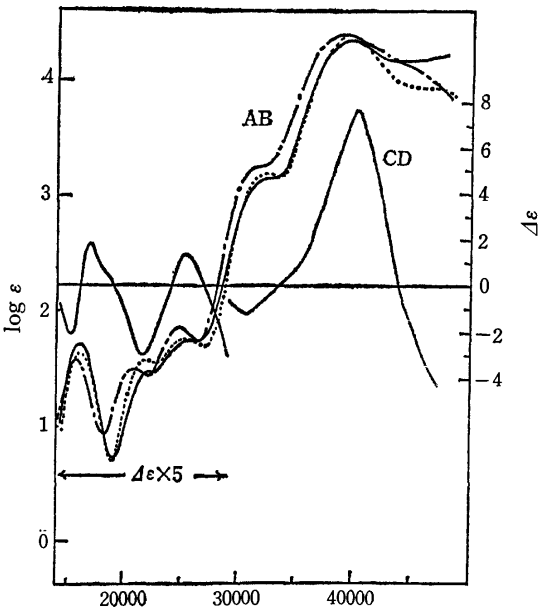

Fig. 5. Absorption (AB) and CD spectra of
(——) *trans*-[$CoCl_2$(*RR*-2,3″,2-tet)]ClO_4,
(·····) *trans*-[$CoCl_2$(*RS*-2,3″,2-tet)]ClO_4,
(—·—) *trans*-[$CoCl_2$(*N*,*N*′-Me_2-*RS*-2,3″,2-tet)]ClO_4 in CH_3OH.

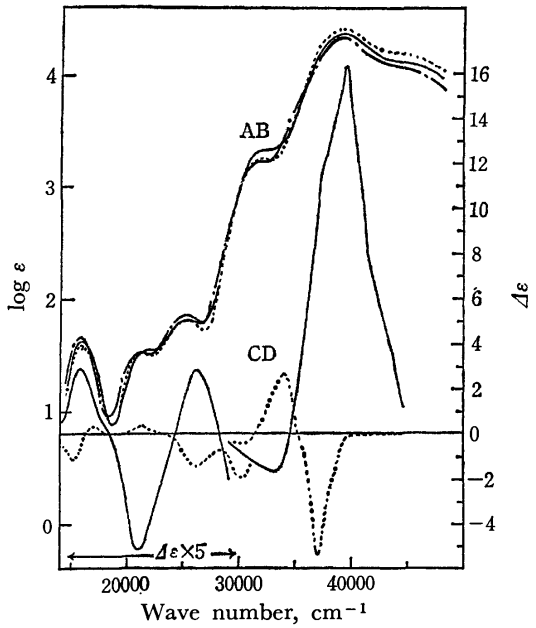

Fig. 6. Absorption (AB) and CD spectra of
(——) *trans*-[$CoCl_2$(*RRRR*-3″,2,3″-tet)]$ClO_4 \cdot H_2O$,
(·····) *trans*-[$CoCl_2$(*RSSR*-3″,2,3″-tet)]$Cl \cdot H_2O$,
(—·—) *trans*-[$CoCl_2$(*RSRS*-3″,2,3″-tet)]ClO_4 in CH_3OH.

(*RSRS*-3″,2,3″-tet)]$^+$ in detail at present. This complex readily aquated in water and smoothly isomerized to the *trans*-dichloro form in methanol. In addition, the complex of *cis*-[$CoCl_2$(*RSRS*-3″,2,3″-tet)]Cl was not sufficiently soluble in water and hydrochloric acid. Because of the above facts, the PMR spectrum of this complex could not be obtained.

Absorption Spectra. The absorption spectra of the complexes prepared here are shown in Figs. 5—7 and Table 1. The absorption spectra of *trans*-[$CoCl_2$(*RR*-2,3″,2-tet)]$^+$ and *trans*-[$CoCl_2$(*RS*-2,3″,2-tet)]$^+$ are almost identical with each other. However, the first, the second, and the charge-transfer bands of *trans*-[$CoCl_2$(*N*,*N*′-Me_2-RS-2,3″,2-tet)]$^+$ are shifted to longer wavelength than those of *trans*-[$CoCl_2$(*RR*-2,3″,2-tet)]$^+$ and *trans*-[$CoCl_2$(*RS*-2,3″,2-tet)]$^+$ (Fig. 5 and Table 1). Such a relationship is in accord with the phenomenon that the absorption bands of *trans*-[$CoCl_2$(*N*,*N*′-Me_2-en)$_2$]$^+$,[25] *trans*-[$CoCl_2$(*N*-Me-pn)$_2$]$^+$,[26] and *trans*-[$CoCl_2$(*N*,*N*′-Me_2-pn)$_2$]$^+$,[27] are shifted to longer wavelength than those of *trans*-[$CoCl_2en_2$]$^+$ and *trans*-[$CoCl_2pn_2$]$^+$ respectively.

As shown in Fig. 6, the absorption bands of *trans*-[$CoCl_2$(*RSRS*-3″,2,3″-tet)]$^+$ are shifted to longer wavelength than those of *trans*-[$CoCl_2$(*RRRR*-3″,2,3″-tet)]$^+$ and *trans*-[$CoCl_2$(*RSSR*-3″,2,3″-tet)]$^+$, which are almost identical with each other. It is difficult to discuss this result in detail at present. However, it seems to be related to the steric interaction among chelate rings and to strain in the bond angles of the secondary nitrogen atoms.

Figure 7 shows the absorption spectrum of *cis*-[$CoCl_2$(*RSRS*-3″,2,3″-tet)]$^+$ in a 12 M HCl solution. It is apparent from this spectrum that the blue-violet complex of [$CoCl_2$(*RSRS*-3″,2,3″-tet)]$^+$ takes the *cis*-

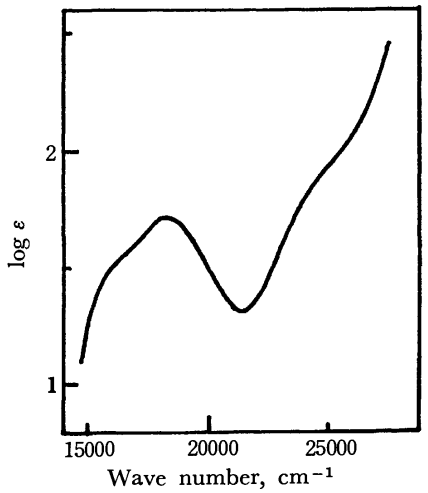

Fig. 7. Absorption spectrum of *cis*-[$CoCl_2$(*RSRS*-3″,2,3″-tet)]Cl in 12 M HCl.

dichloro configuration.

As shown in Figs. 5, and 6 and Table 1, the absorption bands of six *trans*-dichloro complexes are shifted from lower to higher wave numbers with a decrease in the number of the six-membered chelate ring or the secondary nitrogen atom, *i.e.*, in this order: *trans*-[$CoCl_2$(*N*,*N*′-Me_2-*RS*-2,3″,2-tet)]$^+$ ≃ *trans*-[$CoCl_2$(*RSRS*-3″,2,3″-tet)]$^+$ < *trans*-[$CoCl_2$(*RSSR*-3″,2,3″-tet)]$^+$ ≃ *trans*-[$CoCl_2$(*RRRR*-3″,2,3″-tet)]$^+$ < *trans*-[$CoCl_2$(*RR*-2,3″,2-tet)]$^+$ ≃ *trans*-[$CoCl_2$(*RS*-2,3″,2-tet)]$^+$. Also, a similar relationship holds between the *trans*-dichloro bisdiamine complexes of cobalt(III). The absorption bands of *trans*-[$CoCl_2$(diamine)$_2$]$^+$ are shifted to higher wave numbers in this sequence: *trans*-[$CoCl_2$(*N*,*N*′-Me_2-en)$_2$]$^+$ [25] ≃ *trans*-[$CoCl_2$(*N*,*N*′-Me_2-pn)$_2$]$^+$ [27] < *trans*-

$[CoCl_2tn_2]^+$[28] $\simeq$ *trans*-$[CoCl_2(2,4\text{-ptn})_2]^+$[11] $<$ *trans*-$[CoCl_2en_2]^+ \simeq$ *trans*-$[CoCl_2pn_2]^+$.

The above results show that the absorption bands are shifted to lower wave numbers in the order of *N*-nonsubstituted α-diamine, *N*-nonsubstituted β-diamine, and *N*-substituted α-diamine chelate in such *trans*-dichloro complexes of cobalt(III).

CD Spectra. The CD spectrum of *trans*-$[CoCl_2(RR\text{-}2,3'',2\text{-tet})]^+$ is shown in Fig. 5 and Table 1. The CD spectrum of *trans*-$[CoCl_2(RR\text{-}2,3'',2\text{-tet})]^+$ is very similar to the spectra of *trans*-*N*(*R*),*N*(*R*)-$[CoCl_2(2,3,2\text{-tet})]^+$[5-7] and *trans*-$[CoCl_2(SS\text{-diMe-}2,3,2\text{-tet})]^+$[29], which are assigned to the trans-[(*δ-gauche*)(λ-skew-boat)(*δ-gauche*)] structure. Such a similarity between the CD spectra of the three complexes strongly suggests that *trans*-$[CoCl_2(RR\text{-}2,3'',2\text{-tet})]^+$ should be assigned to the *trans*-*N*(*S*),*N*(*S*)-[(*δ-gauche*)(λ-skew-boat)(*δ-gauche*)] structure shown in Fig. 1-b.

As shown in Fig. 6 and Table 1, *trans*-$[CoCl_2(RRRR\text{-}3'',2,3''\text{-tet})]^+$ gives a CD curve very similar to that of *trans*-$[CoCl_2(RR\text{-}2,4\text{-ptn})_2]^+$.[11] Also, the spectrum of *trans*-$[CoCl_2(RR\text{-}2,3'',2\text{-tet})]^+$ in the region of about 16000 to 45000 cm^{-1} resembles that of *trans*-$[CoCl_2(RRRR\text{-}3'',2,3''\text{-tet})]^+$.

Figure 6 shows the CD spectrum of *trans*-$[CoCl_2(RSSR\text{-}3'',2,3''\text{-tet})]^+$, which is assigned to the *trans*-*N*(*R*), *N*(*R*)-[(chair)(λ-*gauche*)(chair)] structure (Fig. 4-b). This spectrum is appreciably different from the CD spectra of $(-)_{589}$-*trans*-$[CoCl_2(3,2,3\text{-tet})]^+$,[5-8] and *trans*-$[CoCl_2(R\text{-appn})]^+$,[23,24] which are very similar to each other. However, the backbones of 3,2,3-tet and *R*-appn[30] in these two complexes are identified as taking the same configuration as the backbone of *RSSR*-3″,2,3″-tet in *trans*-$[CoCl_2(RSSR\text{-}3'',2,3''\text{-tet})]^+$. Such a difference in CD spectra may be elucidated as follows: the two terminal, six-membered chelate rings in $(-)_{589}$-*trans*-$[CoCl_2(3,2,3\text{-tet})]^+$ and *trans*-$[CoCl_2(R\text{-appn})]^+$ are flexible, and it is conceivable that a conformational equilibrium exists where the terminal rings flip from the nonchiral to the chiral, skew-boat conformations. On the other hand, such a flipping in *trans*-$[CoCl_2(RSSR\text{-}3'',2,3''\text{-tet})]^+$ is not likely because of the preference of the methyl groups for an equatorial orientation.

The author wishes to thank Drs. Shigenobu Yano and Masahiko Saburi for their helpful suggestions. He also wishes to thank the Ministry of Education for a Grant-in-Aid.

References

1) Part III of this series: F. Mizukami, H. Ito, J. Fujita, and K. Saito, This Bulletin, **46**, 2410 (1973).
2) H. G. Hamilton, Jr. and M. D. Alexander, *Inorg. Chem.*, **5**, 2060 (1966).
3) B. Boshich, R. D. Gillard, E. D. Mckenzie, and G.A. Webb, *J. Chem. Soc., A*, **1966**, 1331.
4) H. G. Hamilton and M. D. Alexander, *J. Amer. Chem. Soc.*, **89**, 5066 (1967).
5) G. R. Brubaker and D. P. Schaefer, *Inorg. Chem.*, **9**, 2373 (1970).
6) G. R. Brubaker and D. P. Schaefer, *ibid.*, **10**, 811 (1971).
7) G. R. Brubaker and D. P. Schaefer, *ibid.*, **10**, 986 (1971).
8) M. D. Alexander and H. G. Hamilton, Jr., *ibid.*, **8**, 2131 (1969).
9) N. C. Payne, *ibid.*, **11**, 1376 (1972).
10) F. Mizukami, H. Ito, J. Fujita, and K. Saito, This Bulletin, **44**, 3051 (1971).
11) F. Mizukami, H. Ito, J. Fujita, and K. Saito, *ibid.*, **45**, 2129 (1972)
12) M. Goto, M. Saburi, and S. Yoshikawa, *Inorg. Chem.*, **8**, 358 (1969).
13) T. G. Appleton and J. R. Hall, *ibid.*, **9**, 1807 (1970).
14) C. Harries and T. Haga, *Ber.*, **32**, 1191 (1899).
15) C. J. Dippel, *Rec. Trav. Chim.*, **50**, 525 (1931).
16) It is generally known that the complex of cobalt (III) with minus main CD sign in the region of the first absorption band has Δ-configuration. A. J. McCaffery, S. F. Mason, and R. E. Ballard, *J. Chem. Soc.*, **1965**, 2882. G. R. Brubaker and D. P. Schaefer, *Inorg. Chem.*, **10**, 968 (1971).
17) F. Mizukami, presented at the 22 nd Symposium on Coordination Chemistry, Osaka, Japan (1972); Ph. D. Thesis, Tohoku University, 1972.
18) A. M. Sargeson and G. H. Searle, *Inorg. Chem.*, **6**, 787 (1967).
19) F. Basolo, *J. Amer. Chem. Soc.*, **70**, 2634 (1948).
20) R. G. Asperger and C. F. Liu, *Inorg. Chem.*, **4**, 1395 (1965).
21) M. Saburi and S. Yoshikawa, This Bulletin, **45**, 806 (1972).
22) M. Saburi, T. Sawai, and S. Yoshikawa, *ibid.*, **45**, 1086 (1972).
23) L. J. Dehayes, M. Parris, and D. H. Busch, *Chem. Commun.*, **1971**, 1398.
24) M. Saburi, C. Hattori, and S. Yoshikawa, *Inorg. Chim. Acta*, **6**, 427 (1972).
25) J. A. Tiethof and D. W. Cooke, *Inorg. Chem.*, **11**, 315 (1972).
26) M. Saburi, Y. Tsujito, and S. Yoshikawa, *ibid.*, **9**, 1476 (1970).
27) S. Yano, Ph. D. Thesis, Tohoku University, **1971**.
28) H. Kawaguchi, N. Yano, and S. Kawaguchi, This Bulletin, **42**, 136 (1969).
29) R. C. Harrington, S. Linke, and M. D. Alexander, *Inorg. Chem.*, **12**, 168 (1973).
SS-diMe-2,3,2-tet: $NH_2CH(CH_3)CH_2NHCH_2CH_2CH_2NHCH_2CH(CH_3)NH_2$.
30) *R*-appn: $NH_2CH_2CH_2CH_2NHCH_2CH(CH_3)NHCH_2CH_2CH_2NH_2$.

Valence States of Arsenic and Antimony in Sea Water

Shiro GOHDA

Department of Nuclear Reactor Engineering, Faculty of Science and Technology, Kinki University, Kowakae, Higashiosaka 577

(Received June 14, 1974)

A simple and convenient chemical procedure for the determination of As(III), As(V), Sb(III) and Sb(V) by thermal neutron activation analysis is proposed and applied to the study of the valence state of As and Sb in sea water. Immediately after sampling, As(III) and Sb(III) were separated from As(V) and Sb(V) by extracting their diethyldithiocarbamates with chloroform, and then back-extracted into diluted nitric acid. As(V) and Sb(V) in the aqueous phase were collected by thionalide cocrystallization. They were then irradiated for 30 min at a neutron flux of 2×10^{13} n/(cm^2·s), and treated in the same manner as described in the previous report.[6] The As and Sb were determined by gamma-ray spectrometry. Sea water has been found to contain 1.56—2.45 μg As/l and 0.37—0.60 μg Sb/l. 80—97% of arsenic and 70—94% of antimony existed as the pentavelent species, only 5—20% as the trivalent species, and the remainder was probably included in suspended matter.

Because arsenic and antimony exist in aqueous solution in two chemical forms, a trivalent and a pentavalent species, it is an interesting problem to investigate the valence state of these elements in sea water. A few reports have been published on the state of arsenic in sea water. Arsenate seems to be much more stable,[1] and Armstrong and Harvey,[2] Gorgy and his cowarkers,[3] Sugawara and Kanamori,[4] Johnson and Pilson[5] studied on the valence state of arsenic in sea water. These studies were useful for the separation and the determination of trivalent and pentavalent arsenic, although their procedures were very complicated. The valence state depends strongly upon the condition of the aqueous solution, and it changes considerably as aqueous conditions change. Accordingly the separation of trivalent and pentavalent species must be done as quickly as possible, because the valence state may be changed during the storage of the sea water sample.

There is no report on the valence state of antimony in sea water.

In a previous report,[6] we proposed a procedure for the neutron activation analysis of arsenic, copper, and antimony in sea water, but the valence states of arsenic and antimony cannot be determined by that method. In the present research, a rapid, simple and convenient procedure for the determination of valence states of arsenic and antimony in sea water was developed. This procedure was based on solvent extraction followed by the neutron activation. Trivalent species were separated from pentavalent species by extraction into chloroform as the diethyldithiocarbamate chelates, and arsenic and antimony in both states were separately collected by thionalide cocrystallization. After neutron irradiation, antimony was precipitated as oxinate and arsenic was coprecipitated with ferric hydroxide, and then the ^{76}As and ^{122}Sb activities were measured. By this procedure, the valence states of micro amounts of arsenic and antimony in aqueous solution can be precisely determined. Some coastal sea water samples were analyzed by this method.

Experimental

Materials. Sodium diethyldithiocarbamate (Na-DDTC): Reagent grade Na-DDTC was used without further purification. To 1 l of sea water 0.3 g of this reagent was added directly.

Thionalide solution, 2% (w/v): 2 g of thionalide (thioglycollic-β-aminonaphthalide) was dissolved in acetone and diluted to 100 ml with acetone. The solution was freshly prepared before use.

Oxine solution, 2% (w/v): 2 g of 8-quinolinol was dissolved in 7 ml of glacial acetic acid and diluted to 100 ml with water.

Sulfuric acid, 3M : Arsenic free sulfuric acid was diluted with water.

Radioisotopes, ^{74}As and ^{124}Sb, were purchased from the Radiochemical Centre, Amersham, England. It was confirmed that the isotopes could not be extracted with DDTC-chloroform, that is, they were the pentavalent species. The trivalent species were obtained by reduction with ascorbic acid.

Apparatus. Gamma-ray spectra were obtained with a well-type 3″×3″ NaI(Tl) scintillation detector connected to a Hitachi RAH-403 400 channel pulse-height analyzer. The activities measurements were measured with a 2″×2″ NaI(Tl) detector and a Hitachi RC-2 scaler.

Extraction Procedure of Arsenic and Antimony Diethyldithiocarbamates. For separation of trivalent species of arsenic and antimony from pentavalent species in sea water, the extraction of arsenic-DDTC and antimony-DDTC chelates using radioactive tracers was studied. Na-DDTC was added to the sea water containing ^{76}As, ^{122}Sb, and ^{124}Sb in trivalent or pentavalent states and 2 μg of the carrier. After the pH was adjusted, the resulting solution was shaken with chloroform. Two milliliters of samples were pipetted from the organic and the aqueous layers, and the activities were measured.

Analytical Procedure. From the experimental results presented below, the following analytical procedure is recommended.

Immediately after the collection of sea water samples, 1 l of sea water was filtered through a 0.45 μm pore-size Millipore filter. After 0.3 g of Na-DDTC was added to the filtered sample, trivalent arsenic and trivalent antimony were extracted as DDTC chelates at pH 2.5—4.0 by shaking successively with 200 ml and 50 ml of chloroform, and then stripped by shaking the organic phase with 50 ml of 3 M nitric acid. After the solution was heated to boil out the dissolved chloroform and diluted to 1 l with redistilled water, the trivalent species were collected by thionalide cocrystallization: after 8 ml of 2% thionalide acetone solution was added to the cooled solution with vigorous stirring, the solutions were boiled for about 30 minutes and then allowed to stand overnight at room temperature. The precipitates were filtered with Millipore filters (pore-size: 0.45 μm) and

washed with redistilled water.

After the extraction the aqueous phase was acidified to 0.15 M with sulfuric acid, and pentavalent species remaining in the solution were also collected by the thionalide cocrystallization.

Millipore filters employed for the filtration of sea water samples, the filters including the thionalide precipitates, and the standards were separately packed in polyethylene capsules (8 mm long × 12 mm in diameter), which were placed in a polyethylene rabbit tube, and irradiated for 30 minutes at a thermal neutron flux of 2×10^{13} n/(cm^2·s) in the Kyoto University Reactor.

After cooling for a few hours, the irradiated samples were treated as reported previously.[6]

The oxinates and the ferric hydroxide precipitates were used for the gamma-ray spectrometry of ^{76}As and ^{122}Sb. For the hydroxide precipitate, the 0.55 MeV gamma-ray photopeak following the decay of ^{76}As was counted. For the oxinates precipitate, the decay of the 0.57 MeV photopeak of ^{122}Sb was followed, after ^{64}Cu (0.51 MeV annihilation gamma-rays) had decayed.

Results and Discussion

Redox Behavior of Arsenic in Salt Solution and Sea Water. Oxidation of arsenic(III) was measured by determining arsenic(V) by the molybdenum blue method, and reduction of arsenic(V) was followed by DDTC extraction using the radioactive isotope, ^{74}As(V). The rate of oxidation of arsenic(III) in 0.1 M sodium perchlorate, 0.1 M sodium chloride, and 0.025 M sodium sulfate solutions is shown in Fig. 1. When sodium arsenite (containing 5 mg of arsenic(III)) was dissolved in 1 l of these solutions, the pH of which had been previously adjusted to 8.0—8.5 with sodium hydroxide solution, 20—30% of arsenic(III) was immediately oxidized to arsenic(V). Then the oxidation proceeded slowly and 50—60% of arsenic existed as the pentavalent species after 400 hours standing. Aeration accelerated oxidation.

The oxidation-reduction of arsenic in sea water and artificial sea water are shown in Fig. 2. In artificial sea water, the effect of aeration was not appreciable, and after 400 hours, about 50% of arsenic(III) was oxidized to arsenic(V). The effect of aeration was significant in sea water; about 50% of the arsenic(III), which was added as sodium arsenite (containing 5 mg of arsenic) to sea water (1 l), was oxidized after 400 hours of aeration, but only about 20% was oxidized without aeration.

Curves 3—6 in Fig. 2 show the behavior of arsenic(V) added to sea water. The reduction of arsenic(V) to arsenic(III) may be caused by the decomposition of organic matter in the samples. In sea water which contains very small amounts of organic substances, reduction was not observed even after standing for 400 hrs (as shown by curve 6), and the same result was obtained in artificial sea water or the salt solutions described above.

In the case of antimony, decisive results could not be obtained because of hydrolysis of the element.

As the above results show, the trivalent species and pentavalent species must be separated immediately after the collection of the water samples.

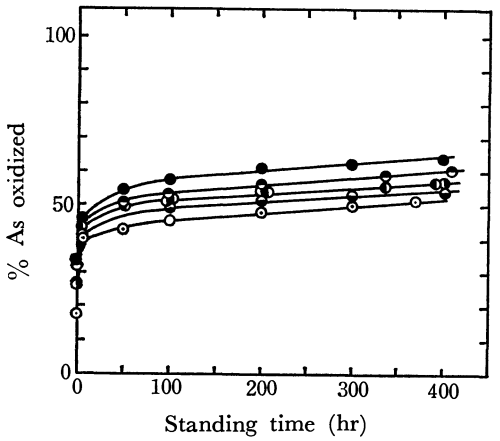

Fig. 1. Oxidation of arsenic(III) on standing in various salt solutions.
Without aeration; ⊙: 0.1 M $NaClO_4$, ◑: 0.025 M Na_2SO_4, ◐: 0.1 M NaCl
With aeration; ◒: 0.1 M $NaClO_4$, ◓: 0.025 M Na_2SO_4, ●: 0.1 M NaCl.

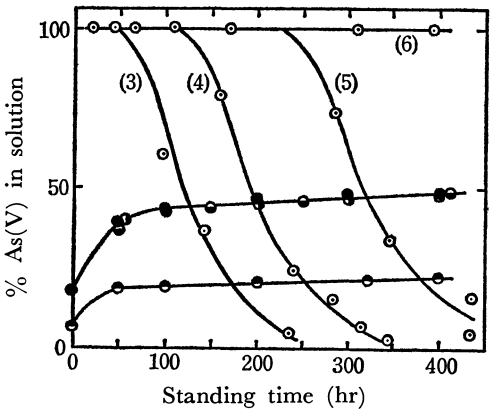

Fig. 2. Redox behavior of arsenic in sea water and artificial sea water.
●: sea water, As(III)→As(V), with aeration
◑: artificial sea water, As(III)→As(V), with aeration
◒: artificial sea water, As(III)→As(V), without aeration
◓: sea water, As(III)→As(V), without aeration
Curve (3): sea water, As(V)→As(III), without aeration, at 25 °C
Curve (4): sea water, As(V)→As(III), without aeration, at 10 °C
Curve (5): sea water, As(V)→As(III), with aeration, at 10 °C
Curve (6): sea water As(V)→As(III), with aeration, at 25 °C

Extraction Conditions for Arsenic and Antimony Diethyldithiocarbamates. The extraction conditions for arsenic and antimony diethyldithiocarbamates were studied, and following results were obtained.

1) Effect of pH Value: The effect of pH was investigated, using 1 ml of 1% Na-DDTC solution per 20 ml of sea water. Figure 3 shows that the optimum pH region is 2.5—5.0 for the separation of the trivalent species from the pentavalent species. Because the pH value shifts to a higher value during the extraction, the initial pH must be controlled in the range between 2.5 and 4.0.

Table 1. Arsenic and antimony concentrations in sea water

Sampling date and station	Sample No.	Depth m	As(III) μg/l	As(V) μg/l	Particulate μg/l	Total μg/l
Shirahama, Wakayama Pref. 30 Oct. 1970	1	0	0.22	1.49	0.02	1.73
	2	0	0.35	1.41	0.02	1.78
	3	0	0.17	1.38	0.01	1.56
Uragami, Wakayama Pref. 4 Nov. 1971	4[a]	0	0.14	1.56	0.04	1.74
	5[a]	0	0.14	1.44	0.08	1.66
	6[a]	0	0.15	1.24	0.04	1.43
	7[b]	0	0.22	1.45		1.67
	8[b]	40	0.36	1.50		1.86
Kojima, Osaka Pref. 1 Dec. 1970	9	0	0.22	2.20	0.03	2.45
	10	0	0.16	2.20	0.03	2.39
	11	0	0.17	1.66	0.01	1.84
	12	0	0.28	2.07	0.01	2.36

Sampling date and station	Sample No.	Depth m	Sb(III) μg/l	Sb(V) μg/l	Particulate μg/l	Total μg/l
Shirahama, Wakayama Pref. 30 Oct. 1970	1	0	0.06	0.38	0.01	0.45
	2	0	0.09	0.35	0.01	0.45
	3	0	0.05	0.31	0.01	0.37
Uragami, Wakayama Pref. 4 Nov. 1971	4[a]	0	0.03	0.19	0.02	0.24
	5[a]	0	0.03	0.16	0.02	0.21
	6[a]	0	0.06	0.12	0.02	0.20
	7[b]	0	0.03	0.13		0.16
	8[b]	40	0.05	0.18		0.23
Kojima, Osaka Pref. 1 Dec. 1970	9	0	0.06	0.41	0.02	0.49
	10	0	0.03	0.44	0.02	0.49
	11	0	0.10	0.47	0.03	0.60
	12	0	0.05	0.49	0.03	0.57

a) The Bay of Uragami. b) Outside the Bay.

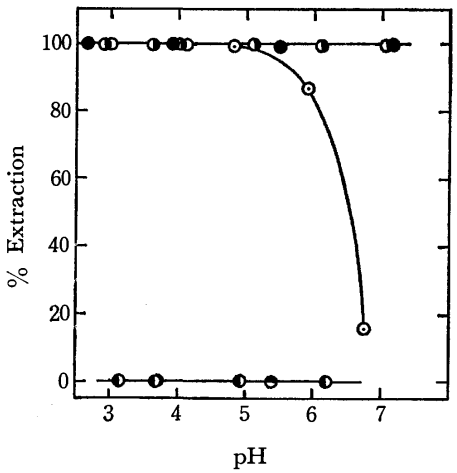

Fig. 3. Effect of pH on the extraction of arsenic and antimony diethyldithiocarbamates.
⊙: ^{74}As(III), ●: ^{122}Sb(III), ◑: Cu(II), ◐: ^{74}As(V)
◓: ^{124}Sb(V)

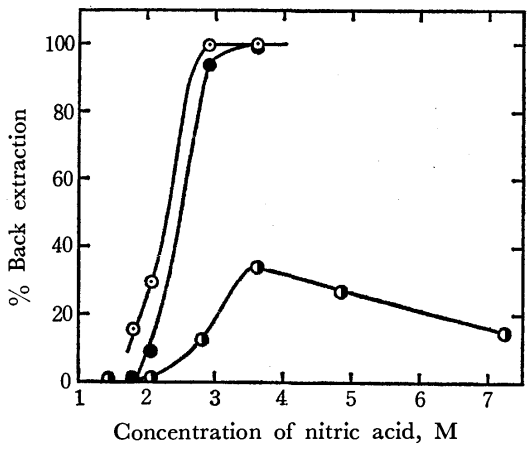

Fig. 4. Back extraction curves of arsenic(III), antimony(III), and copper(II).
⊙: As(III), ●: Sb(III), ◑: Cu(II).

2) *Effect of Na–DDTC Concentration*: The effect of the amount of Na–DDTC was also studied by adding various amount of the reagent to 1 l of sea water containing the tracers and 2 μg of the carriers. More than 99% of the trivalent species could be extracted by adding 0.1 g or more of Na–DDTC per 1 l, and therefore, in subsequent experiments, 0.3 g of Na–DDTC was employed per 1 l of sea water.

3) *Effect of Nitric Acid Concentration on Back Extraction*: The back extraction of trivalent arsenic and antimony was effected by shaking the organic phase with an equal volume of nitric acid. As shown in Fig. 4, trivalent arsenic and antimony could be readily stripped into 3 M nitric acid. Sulfuric and hydrochloric acids were less effective.

In the practical procedure, 250 ml of chloroform was used for the extraction from 1 l of sea water sample, and at least 50 ml of 3 M nitric acid was needed for the back extraction. The more than 98.8% recovery could be attained.

Under these extracting and stripping conditions, copper, which is cocrystallized with thionalide, was quantitatively extracted, but incompletely stripped (see Fig. 4).

TABLE 2. RESULTS OF ARSENIC AND ANTIMONY DETERMINATIONS ON SPIKED SAMPLES

Sea water sample taken (litter)	As and Sb added (μg)	As(III) found (μg)	As(V) found (μg)	Sb(III) found (μg)	Sb(V) found (μg)
1	0	0.22[a)]	1.49[a)]	0.06[a)]	0.38[a)]
1	As(III) 0.5 + As(V) 1.0 + Sb(III) 0.5 + Sb(V) 0.5	0.74 (0.24)	2.51 (1.51)	0.55 (0.05)	0.90 (0.40)
1	As(III) 0.5 + Sb(III) 0.3	0.76 (0.26)	1.53	0.39 (0.09)	0.35
1	As(V) 1.0 + Sb(V) 0.5	0.20	2.45 (1.45)	0.08	0.85 (0.35)

a) The values are the amounts of the elements in the original samples of sea water (μg/l). The values in brackets are differences between the value in original sample of sea water and the analytical value.

4) *Effect of the Amount of Thionalide*: In previous research, arsenic and antimony could be quantitatively cocrystallized with thionalide from diluted sulfuric acid solution.[6] Since nitric acid was used for the back extraction of the trivalent arsenic and antimony, in the present experiments, the thionalide was cocrystallized from diluted nitric acid solution. Recovery of more than 98% was attained by adding 8 ml or more of 2% thionalide acetone solution to 1 l of 0.03—0.2 M nitric acid solution.

Analysis of As(III), As(V), Sb(III), and Sb(V) in Sea Water. The above procedure was recommended and applied to the determination of arsenic(III), arsenic(V), antimony(III), and antimony(V) in sea water samples. Surface sea water samples were collected from 5 stations, offshore from Shirahama and Uragami, Wakayama Prefecture, and from Kojima, Osaka Prefecture.

The analytical results are shown in Table 1. As shown in Table 1, the total contents of arsenic and antimony were in the range of 1.43—2.45 μg As/l and 0.16—0.60 μg Sb/l, and these values were in good agreement with the values found in previous studies[6] and with the data recently reported,[4,7,8-11] From 80 to 93% of the dissolved arsenic and from 74 to 94% of the dissolved antimony existed as arsenate and antimonate. This result also agrees with the results of Sugawara *et al.*[4,7] The result for antimony cannot be compared with others, because no report has been published on the valence state. Overall recovery in the pre- and post-irradiation procedure was over 98%.

In order to examine the accuracy of the proposed procedure for the determination of arsenic (III), (V) and antimony(III), (V), definite amounts of arsenic (III), (V) and antimony(III), (V) ions were added to sea water samples and the entire procedure for the determination of these elements was applied to the samples. The results of this spiking analysis are shown in Table 2. From these results, the relative error for the trivalent and pentavalent species of these elements was estimated to be less than ±10 percent and ±5 percent respectively. In this case, the concentrations of trivalent species were about one tenth of the concentrations of pentavalent species, and the analytical result for the former includes a comparatively large relative error. The blank value for arsenic was 0.01—0.03 μg and for antimony 0.005—0.01 μg.

The author wishes to express his sincere thanks to Professor Tsunenobu Shigematsu, Institute for Chemical Research, Kyoto University, Professor Yasuharu Nishikawa, Faculty of Science and Technology, Kinki University, and Professor Masayuki Tabushi, Tōhoku Women's college, for their kind advice and suggestions throughout this work. The author is deeply indebted to the Hot Laboratory groups of Kyoto University for their help in the irradiation operation, and is also indebted to Professor Shiro Okabe, Faculty of Oceanography, Tokai University, for his kind help in the sampling of sea water.

References

1) L. G. Sillén, "Oceanography," ed. by M. Sears, Am. Assoc. Adv. Sci., Washington, D. C. (1961), p. 654.
2) F. A. J. Armstrong and H. W. Harvey, *J. Marine Biol. Assoc. U. K.*, **29**, 145 (1950).
3) S. Gorgy, N. W. Rakestraw, and D. L. Fox, *J. Marine Res.*, **7**, 22 (1948).
4) K. Sugawara and S. Kanamori, This Bulletin, **37**, 1358 (1964).
5) D. L. Johnson and M. E. Q. Pilson, *Anal. Chim. Acta*, **58**, 289 (1972).
6) S. Gohda, This Bulletin, **45**, 1704 (1972).
7) K. Sugawara, K. Terada, S. Kanamori, N. Kanamori, and S. Okabe, *J. Earth Sci., Nagoya Univ.*, **10**, 34 (1962).
8) J. E. Portmann and J. P. Riley, *Anal. Chim. Acta*, **31**, 509 (1964).
9) J. E. Portmann and J. P. Riley, *ibid.*, **35**, 35 (1966).
10) I. Noddack and W. Noddack, *Ark. Zool.*, **1**, 32 (1940).
11) D. F. Schutz and K. K. Turekian, *Geochim. Cosmochim. Acta*, **29**, 259 (1969).

Analysis of a Magnesium-containing β-Eucryptite Solid Solution by the Lattice Constant Method and Its Application[1,2]

Masaaki IWATSUKI, Norio TSUKADA, and Tsutomu FUKASAWA

Department of Applied Chemistry, Faculty of Engineering, Yamanashi University, Takeda, Kofu 400

(Received August 30, 1974)

An X-ray diffraction method has been developed for the determination of the composition of a magnesium-containing β-eucryptite solid solution which consists of a pseudo-ternary system, SiO_2–$Mg_{1/2}AlO_2$–$LiAlO_2$. Standard samples of the solid solution within the range of 60—75 mol% SiO_2 and 0—15 mol% $Mg_{1/2}AlO_2$ were prepared from high-purity materials by the "glass-crystallization" technique. The diffraction angles of the (206) and (212) planes were measured from the center of gravity of the profile recorded on a chart by a counter diffractometer. After having been corrected for various systematic errors, both angles were used for the calculation of the lattice constants. It was found that $Mg_{1/2}AlO_2$ and $LiAlO_2$ contributed similarly to a_0, but in a different way to c_0. The composition of the solid solution in a commercial glass-ceramic could be determined from the correlation between the composition and the lattice constants. The standard deviation of the determination from one measurement was about 0.2—0.4 mol%, and the time required for analysis was about 30 min.

Low-thermal-expansion glass-ceramics contain a β-spodumene solid solution ($Li_2O \cdot Al_2O_3 \cdot nSiO_2$, $n>3$) or a β-eucryptite solid solution ($Li_2O \cdot Al_2O_3 \cdot nSiO_2$, $n \geq 2$), and their properties, such as the thermal expansion, depend not only on the content, but also on the composition of the solid solution. Therefore, the determination of the composition of the solid solution in the glass-ceramics is very important for the quality control and the study of the glass-ceramics; it is possible, however, only by the X-ray diffration method, as has been described in our previous papers.[1,3] The application of this method to a β-spodumene solid solution and a β-eucryptite solid solution has already been reported by us.[1,3] A magnesium-containing β-eucryptite solid solution consists of Li_2O, MgO, Al_2O_3, and SiO_2, and the number of moles of Li_2O plus that of MgO is equal to that of Al_2O_3. Therefore, the solid solution can be expressed as a pseudo-ternary system, SiO_2–$Mg_{1/2}AlO_2$–$LiAlO_2$. Since the solid solution is a hexagonal crystal, it is expected that the composition can be determined by measurements of the lattice constants, a_0 and c_0, if the three components contribute to a_0 and c_0 in any different manner. In the present paper, the analysis of a magnesium-containing β-eucryptite solid solution in glass-ceramics will be described on the basis of measurements of the two lattice constants.

Experimental

Apparatus. A Rigaku X-ray diffractometer with a proportional counter was used for this study. The glass samples were prepared by the use of an electric furnace with a silicon carbide heating element. A nichrome wire furnace was used for the crystallization of the glass. A Nippon Jarrell-Ash atomic-absorption and flame-emission spectrophotometer, AA-500, was used to check the lithium contents in the prepared samples.

Preparation of Standard Samples. Standard samples of the magnesium-containing β-eucryptite solid solution were prepared from lithium carbonate of a guaranteed reagent grade (min. 99.0%, Kanto Chemicals) and high-purity magnesium oxide (99.9% nominal, High Purity Chemical Laboratory), aluminum oxide (99.9—99.99% nominal, Iwatani & Co.), and silicon dioxide (min. 99.8%, Nissan Rare Elements). The magnesium oxide was heated in a platinum dish for 1.5 hr by means of a Mecker burner to dehydrate it. The aluminum oxide and silicon dioxide were similarly heated for 1 hr. The raw materials were weighed out by the amounts calculated for the intended compositions of the solid solution within the range of 60—75 mol% SiO_2 and 0—15 mol% $Mg_{1/2}AlO_2$ (the residual was $LiAlO_2$). The lithium carbonate was weighed out by the 3% excess of the calculated amount, considering a partial loss of lithium due to evaporation.[1] The materials weighed were mixed in an agate mortar for about 30 min, loaded into a platinum crucible, and heated at 1430 °C for 3 hr in the electric furnace. The melt was quenched in water, together with the crucible. The resultant glass was dried in an electric drying oven and subsequently powdered in an alumina mortar. The glass powder (48—200 mesh) was placed in a platinum crucible and then kept at a constant temperature in the range of 670 to 900 °C for 2—96 hr. When a glass or β-spodumene solid solution which is stable at higher temperatures was found by means of the X-ray diffraction method, a different condition of heat-treatment was used to obtain a sample containing the β-eucryptite solid solution only. In order to check the lithium content of the prepared sample, the sample was decomposed with hydrofluoric acid, perchloric acid, and nitric acid, and the lithium content was determined by flame photometry.

Measurement of Interplanar Spacings. Since the concentrations of any two components of the solid solution vary independently, at least two diffraction lines must be measured. The lines must not overlap with any other line. In addition, it is preferable for the lines to satisfy the following requirements: (1) one of these lines be that from a plane nearly perpendicular to the c axis, and the other be that from a plain nearly parallel to the c axis, because the analysis is based on the different contributions of the three components of the solid solution to a_0 and c_0 ; (2) the diffraction angles of the lines shift as much as possible with the change in the composition; (3) the intensities of lines be as high as possible. From these requirements, the (212) and (206) lines were selected as the best lines; and each line was measured three times under the conditions shown in Table 1. In order to compensate for any slight misalignment of the goniometer, (311) and (400) lines of a high-purity, sintered silicon plate (an external standard) were measured under the same conditions before and after the measurements of the lines of the solid solution. The internal standard technique was not adopted, because the diffraction lines of any internal standard and those of the solid solution were liable to overlap.

The diffraction profiles obtained by the use of the Cu$K\alpha_1$ ($\lambda=1.54051$Å) and $K\alpha_2$ ($\lambda=1.54433$Å) radiations overlapped in part. The profiles of thirteen samples of the solid solution

were separated into α_1- and α_2-components on the charts on the basis of the intensity ratio and the degree of the α_1-α_2 angular separation. The diffraction angle obtained from the center of gravity of the triangle approximating the α_1-component was compared with the $K\bar{\alpha}$-diffraction angle obtained in a similar way from the intact profile. The difference agreed, within the limits of experimental error, with the angular separation calculated from the wavelengths of Cu$K\alpha_1$ and $K\bar{\alpha}$ (λ=1.54178 Å). For economy of time, therefore, the interplanar spacings of the other samples of the solid solution were obtained by the latter method, *i.e.*, by $K\bar{\alpha}$ angle measurements. Each profile of the (400) and (311) lines of the silicon standard was measured about ten times, and separated into α_1- and α_2-components. The difference was calculated between the angle obtained from the center of gravity of the triangle approximating the α_1-component and that obtained from the midpoint of the width at two-thirds of the maximum intensity of the intact profile. The reproducibility of the difference was good. Consequently, the diffraction angles of the silicon standard were obtained from the midpoint of the two-thirds-width of the intact profile, and corrected for the above difference.

The diffraction angles thus obtained still include the systematic errors due to the diffraction at the inner parts of specimens, the use of flat specimens, and the divergence of the primary beam perpendicular to the plane of Bragg

Table 1. Experimental condition

X-ray tube	Cu
Filter	Ni
Tube voltage (kV)	35
Tube current (mA)	15
Divergence and scatter slit (°)	2
Receiving slit (mm)	0.3
Time constant (s)	4
Scanning speed (°/min)	1/4
Chart speed (mm/min)	40
Silicon standard	
For (212) Line	(311)
For (212) 2θ (°)[a]	56.122
For (206) Line	(400)
For (206) 2θ (°)[a]	69.130

a) Diffraction angle of Cu$K\alpha_1$ corrected for systematic errors.

Table 2. Results of analysis of lithium and conditions of crystallization of glasses

Sample no.	Intended composition (mol%) SiO_2	$Mg_{1/2}AlO_2$	$LiAlO_2$	Intended Li_2O (wt%)	Analyzed Li_2O (wt%)	Crystalliz. cond. Temp. (°C)	Time (hr)
M60- 0[a]	60.0	0.0	40.0	—	—	—	—
2.5	60.0	2.5	37.5	9.0	9.0	750	24
5	60.0	5.0	35.0	8.3	8.3	750	24
10	60.0	10.0	30.0	7.1	6.9	750	24
15	60.0	15.0	25.0	5.9	6.0	750	24
M62.5- 0[a]	62.5	0.0	37.5	—	—	—	—
2.5	62.5	2.5	35.0	8.4	8.5	750	24
5	62.5	5.0	32.5	7.8	7.8	750	24
7.5	62.5	7.5	30.0	7.2	7.2	750	24
12.5	62.5	12.5	25.0	5.9	6.0	750	24
M65- 0[a]	65.0	0.0	35.0	—	—	—	—
5	65.0	5.0	30.0	7.2	7.2	750	6
10	65.0	10.0	25.0	6.0	6.0	750	24
15	65.0	15.0	20.0	4.8	4.8	750	72
M67.5- 0[a]	67.5	0.0	32.5	—	—	—	—
2.5	67.5	2.5	30.0	7.2	7.3	750	24
7.5	67.5	7.5	25.0	6.0	6.0	750	24
12.5	67.5	12.5	20.0	4.8	4.6	800	24
M70- 0[a]	70.0	0.0	30.0	—	—	—	—
5	70.0	5.0	25.0	6.0	6.0	750	48
7.5	70.0	7.5	22.5	5.4	5.3	800	24
10	70.0	10.0	20.0	4.8	5.0	800	24
15	70.0	15.0	15.0	3.6	3.6	800	48
M72.5- 0[a]	72.5	0.0	27.5	—	—	—	—
2.5	72.5	2.5	25.0	6.0	6.2	850	24
7.5	72.5	7.5	20.0	4.8	4.8	850	24
12.5	72.5	12.5	15.0	3.6	3.6	900	36
M75- 0	75.0	0.0	25.0	6.1	5.9	700	4
5	75.0	5.0	20.0	4.8	4.7	850	24
10	75.0	10.0	15.0	3.6	3.5	850	24
15	75.0	15.0	10.0	2.4	2.4	900	48

a) Although the samples of these compositions were not prepared, these samples will be also discussed in the study by the use of the diffraction data from the preceding paper.[1]

focusing. These errors were compensated for on the basis of the equation given by Willson and Pike.[4]

Results and Discussion

Magnesium-containing β-Eucryptite Solid Solution. Table 2 shows the conditions of crystallization and the results of the analysis of lithium. The intended and analyzed Li_2O contents agreed well, and no impurity was detected by the X-ray diffraction method. These results indicate that the prepared samples were pure enough for this study. The crystallization required higher temperatures as the content of SiO_2 or $Mg_{1/2}AlO_2$ increased.

Correlation between the Composition and the Lattice Constants. The interplanar spacings and lattice constants of the solid solution are shown in Table 3. The relation between the composition and lattice constants is shown in Fig. 1. The results can be summarized as follows: (1) when $LiAlO_2$ or $Mg_{1/2}AlO_2$ was substituted for SiO_2, a_0 increased markedly; (2) when $LiAlO_2$ was substituted for SiO_2, c_0 hardly changed at all, or even decreased somewhat, in the low-lithium region, and increased in the high-lithium region; (3) when $Mg_{1/2}AlO_2$ was substituted for SiO_2, c_0 decreased markedly except in the high-lithium region.

Table 3. Interplanar spacings (d) and lattice constants of magnesium-containing β-eucryptite solid solution

Sample no.		d (Å)		Lattice const. (Å)	
		(212)	(206)	a_0	c_0
M60-	0[a]	1.6370	1.4218	5.241	10.945
	2.5	1.6371	1.4204	5.242	10.925
	5	1.6369	1.4187	5.243	10.904
	10	1.6348	1.4147	5.237	10.860
	15	1.6326	1.4111	5.232	10.822
M62.5-	0[a]	1.6345	1.4192	5.233	10.923
	2.5	1.6350	1.4182	5.236	10.907
	5	1.6333	1.4162	5.231	10.887
	7.5	1.6319	1.4142	5.227	10.868
	12.5	1.6298	1.4108	5.221	10.833
M65-	0[a]	1.6315	1.4173	5.223	10.912
	5	1.6303	1.4143	5.221	10.877
	10	1.6270	1.4108	5.210	10.847
	15	1.6227	1.4065	5.197	10.810
M67.5-	0[a]	1.6283	1.4157	5.212	10.907
	2.5	1.6281	1.4148	5.212	10.895
	7.5	1.6239	1.4105	5.199	10.860
	12.5	1.6214	1.4073	5.192	10.827
M70-	0[a]	1.6250	1.4144	5.201	10.906
	5	1.6225	1.4113	5.193	10.876
	7.5	1.6199	1.4088	5.185	10.856
	10	1.6189	1.4072	5.182	10.839
	15	1.6155	1.4038	5.172	10.810
M72.5-	0[a]	1.6211	1.4129	5.187	10.906
	2.5	1.6200	1.4112	5.184	10.888
	7.5	1.6155	1.4073	5.170	10.858
	12.5	1.6127	1.4042	5.161	10.830
M75-	0	1.6155	1.4109	5.167	10.907
	5	1.6135	1.4077	5.162	10.874
	10	1.6106	1.4044	5.153	10.844
	15	1.6068	1.4012	5.141	10.821

a) The data obtained from the preceding paper.[1]

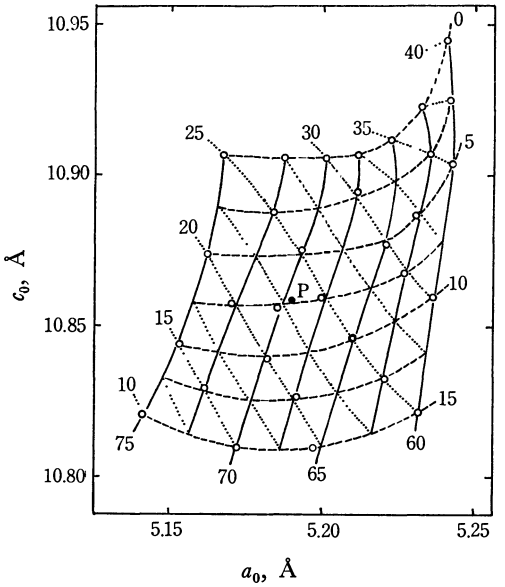

Fig. 1. Correlation between composition and lattice constants of the solid solution.
——: Line on which mol% of SiO_2 is equal.
----: Line on which mol% of $Mg_{1/2}AlO_2$ is equal.
·····: Line on which mol% of $LiAlO_2$ is equal.
Numbers in the figure indicate mol% of each component.
P: The solid solution in the glass-ceramic described in the text.

These facts may be explained as follows on the basis of the crystal structure of the solid solution. The crystal structure was determined by Chi-Tang Li[5] for the composition of 66.7 mol% SiO_2 and 33.3 mol% $LiAlO_2$. The solid solution consists of the SiO_4 and AlO_4 tetrahedra arranged along a hexagonal screw axis parallel to the c axis in double helical fashon, and of the lithium and magnesium ions on the interstitial sites along the hexagonal screw axis. The lithium or magnesium ion compensates for the deficiency in the positive charge due to the substitution of an aluminum ion for a silicon ion, and is coordinated by four oxygen ions. This LiO_4 or MgO_4 tetrahedron shares two edges with the two opposite $Al(Si)O_4$ tetrahedra. The shared edges are the shortest for both the $Li(Mg)O_4$ and $Al(Si)O_4$ tetrahedra; they have a slope of about 45° to the c axis. Two of the unshared edges of the $Al(Si)O_4$ tetrahedron lie on the $(00l)$ planes, while the others have a slope of about 45° to the c axis.[5] When $LiAlO_2$ or $Mg_{1/2}AlO_2$ is substituted for SiO_2, the lithium or magnesium ion wedges itself in the hexagonal screw. The shortest distance between a lithium (or magnesium) ion and an aluminum (or silicon) ion lies on a $(00l)$ plane and is very short (about 2.58 Å for the composition of 75 mol% SiO_2 and 25 mol% $LiAlO_2$). Therefore, the screw may be compelled to widen by the repulsive force between

Table 4. Comparison of lattice constants of magnesium-containing β-eucryptite solid solution with data of several other authors

Author	Composition (mol%)			Lattice const. (Å)		Lattice const. (Å) in this work[a]	
	SiO_2	$Mg_{1/2}AlO_2$	$LiAlO_2$	a_0	c_0	c_0	a_0
Ray and Muchow	60.0	8.0	32.0	5.240	10.876	5.240	10.877
	66.7	6.7	26.6	5.210	10.868	5.209	10.866
	71.4	5.7	22.9	5.172	10.824	5.183	10.868
Petzoldt	66.1	15.0	18.9	5.18	10.85	5.193	10.810
	70.2	4.4	25.4	5.19	10.90	5.199	10.894

a) Obtained from Fig. 1 for the composition.

the lithium (or magnesium) ion and the aluminum (or silicon) ion, and hence a_0 increases. On the contrary, the effect of the Li(Mg)–Al(Si) repulsive force on c_0 may be small, because the shortest Li(Mg)–Al(Si) distance lies on a (00l) plane, and the next shortest distance is relatively long and has a large slope to the c axis. Since the Li–Li distance along the c axis is long in the low-lithium region, the Li–Li repulsive force may be weak. In the high-lithium region, the distance is short; hence, the repulsive force may be strong enough to increase the c_0. Since the magnesium ion has a stronger polarizing power than the lithium ion, the Mg–O bond is stronger and more covalent than the Li–O bond. Therefore, the edges of the $Al(Si)O_4$ tetrahedra shared by the MgO_4 tetrahedra may be shorter than those of the $Al(Si)O_4$ tetrahedra shared by the LiO_4 tetrahedra. As can be seen from the orientation of the $Al(Si)O_4$ tetrahedra described above, this effect may decrease c_0 of the magnesium-containing solid solution. However, it may not decrease a_0, because the unshared edges may be elongated and counteract the contraction of the shared edges. Since the Mg–O bond is more covalent than the Li–O bond, the effective charge of the magnesium ion may be relatively small. Moreover, the number of the magnesium ions introduced is half of that of the lithium ions. Therefore, the Mg–Mg repulsive force along the c axis may be smaller than the Li–Li repulsive force. Consequently, the c_0-decreasing effect may overcome the c_0-increasing effect; hence, c_0 may be decreased by introducing magnesium ions. In the high-lithium region, though, c_0 is hardly decreased at all by introducing magnesium ions, because the Li–Li repulsive force may increase considerably.

In any case, the data indicate that the composition of the solid solution can be determined by the measurements of a_0 and c_0, because the contributions of the three components to a_0 and c_0 were markedly different.

Application to a Glass-Ceramic Sample. In the preceding paper, it was found that slightly different values of the SiO_2 content of a β-eucryptite solid solution in a glass-ceramic were obtained depending on the diffraction line used. This phenomenon was presumed to result from the partial substitution of the magnesium ion for the lithium ion. Therefore, the present method was applied to this glass-ceramic sample. The P point (a_0=5.190 Å, c_0=10.858 Å) in Fig. 1 shows the solid solution in the sample. The concentration between adjacent lines of Fig. 1 can be considered to be approximately proportional to the distance from each line. Therefore, the composition could be obtained as follows: 69.5 mol% SiO_2, 7.3 mol% $Mg_{1/2}AlO_2$, and 23.2 mol% $LiAlO_2$.

Comparison with the Data of Several Other Authors. Table 4 compares the lattice constants of the solid solution with the data reported by several other authors.[6,7] Two of Ray and Muchow's data agreed well with ours, but one disagreed. When we compare the disagreeing datum with the tendency of the composition *vs.* lattice constant curves of their paper,[6] it seems that their value is too low. Petzoldt used lower diffraction angles for the measurement of the lattice constants, and so that precision of his measurement was only ±0.005 Å for a_0.[7] In addition, the authors of both papers did not consider the possibility of the evaporation of lithium during the sample preparation. In this study, the evaporation of lithium was taken into account, and higher diffraction angles were used and corrected for the systematic errors. The standard deviation of the data was 0.0005 Å for a_0. Moreover, a large number of data were accumulated. Therefore, it seems that the data of the present paper are more reliable.

Error in the Determination. The precision of the present method was as follows. The standard deviations of 2θ, a_0, and c_0 on one measurement were about 0.01°, 0.0008 Å, and 0.0025 Å respectively. The corresponding standard deviations of the analytical values of each component varied somewhat depending on the composition region. For example, in the neighborhood of the composition of 70 mol% SiO_2, 7.5 mol% $Mg_{1/2}AlO_2$, and 22.5 mol% $LiAlO_2$, the standard deviations of SiO_2, $Mg_{1/2}AlO_2$, and $LiAlO_2$ were 0.20, 0.39, and 0.28 mol% respectively. For the weight percentage, the standard deviations of SiO_2, MgO, Li_2O, and Al_2O_3 were 0.19, 0.13, 0.07, and 0.39 wt% respectively. For the purpose of obtaining the absolute composition by the use of Fig. 1, the errors of the equi-concentration lines in the figure must also be taken into account. These errors consist of the deviations of the compositions and the errors of the lattice constants of the standard samples. Since the lattice constants were obtained from the average of three measurements, the variances of the lattice constants were one-third of those described above.

The systematic errors of the lattice constants were compensated for; hence, they are negligible here. The deviation of the composition in Fig. 1 could be estimated as follows from the errors of weighing in sample preparation, the variations of impurities of the raw materials, and the permitted differences between the intended and determined lithium contents: SiO_2 0.3 mol% or less, $Mg_{1/2}AlO_2$ 0.1 mol% or less, and $LiAlO_2$ 0.4 mol% or less as the standard deviations. Then the errors of the equi-concentration lines were calculated: SiO_2 0.32 mol% or less, $Mg_{1/2}AlO_2$ 0.25 mol% or less, and $LiAlO_2$ 0.43 mol% or less as the standard deviations. Consequently, the absolute composition of the solid solution can be obtained by the use of Fig. 1 with the following maximum errors from one measurement in the neighborhood of the above composition: SiO_2 0.38 mol%, $Mg_{1/2}AlO_2$ 0.46 mol%, $LiAlO_2$ 0.51 mol%; SiO_2 0.37 wt%, MgO 0.15 wt%, Li_2O 0.12 wt%, and Al_2O_3 0.56 wt%.

The correlation between the lattice constants and the composition has been exclusively discussed for general use. The correlation between the composition and interplanar spacings or diffraction angles of (206) and (212), however, can also be used; its use is recommended for routine work because of the simplicity of calculation. The time required for analysis was about 30 min by the use of a desk electronic computer.

We wish to thank Mr. Masanao Arakawa for supplying us with high-purity aluminum oxide and silicon dioxide, and Mr. Hiroyuki Watanabe for carrying out some of the experiments.

References

1) Study on Application of Lattice Constant Measurement by X-ray Diffraction Method to the Analysis of Industrial Materials. IV. Preceding paper: M. Iwatsuki, M. Tanaka, and T. Fukasawa, *Nippon Kagaku Kaishi*, **1974**, 505.
2) Presented at the 35th Symposium on Analytical Chemistry, Yonezawa, Japan, June, 1974.
3) T. Fukasawa, M. Iwatsuki, and K. Yamaguchi, *Bunseki Kagaku*, **22**, 745 (1973).
4) T. Fukasawa, M. Iwatsuki, and K. Ota, "Ekkususen Bunseki no Shimpo," Vol. 4, ed. by Ekkususen Bunseki Kenkyu Kondan-Kai, Kagaku Gijutsu-Sha, Tokyo (1972), p. 138.
5) Chi-Tang Li, *Z. Kristallogr.*, **127**, 327 (1968).
6) S. Ray and G. M. Muchow, *J. Amer. Ceram. Soc.*, **51**, 678 (1968).
7) J. Petzoldt, *Glastechn. Ber.*, **40**, 385 (1967).

Molecular Complexes of Arenetricarbonylchromium, -molybdenum and -wolfram

Hiroshi KOBAYASHI, Mitaka KOBAYASHI, and Youkoh KAIZU

Department of Chemistry, Tokyo Institute of Technology, Ookayama, Meguro-ku, Tokyo 152

(Received December 9, 1974)

Arenetricarbonylchromium forms a charge-transfer complex with 1,3,5-trinitrobenzene (1,3,5-TNB), while arenetricarbonylmolybdenum and -wolfram do not form a charge-transfer complex with 1,3,5-TNB. On the other hand, arenetricarbonylchromium, -molybdenum and -wolfram form a charge-transfer complex with tetracyanoethylene (TCNE). Since the intramolecular charge transfer from coordinated arene to carbonyls increases in the molybdenum and wolfram derivatives, 1,3,5-trinitrobenzene cannot form a molecular complex accepting an electronic charge of the coordinated arene. In the case of TCNE, however, a molecular complex is formed by an inner-sphere charge-transfer interaction between the acceptor and the central metal atom. Thus the stability of the TCNE molecular complexes is dependent upon the charge density of the central metal atom and also the steric effects due to the functional groups in coordinated arenes. The ionization potentials of the molybdenum and wolfram derivatives observed for their TCNE molecular complexes are almost equal but higher than those of the corresponding chromium derivatives, whereas the highest stability is obtained for the molybdenum derivatives.

Arenetricarbonylchromium forms charge-transfer complexes with electron acceptors such as 1,3,5-trinitrobenzene (1,3,5-TNB) and tetracyanoethylene (TCNE) rather than with electron donors.[1] Nevertheless, the effects of tricarbonylchromium group to the chemical properties of π-coordinated benzene ring are more likely those of an electron-withdrawing group. In fact, benzoic acid tricarbonylchromium is a stronger acid than benzoic acid and anilinetricarbonylchromium is a weaker base than aniline.[2,3] Furthermore arenetricarbonylchromium exhibits a higher susceptibility to nucleophilic substitutions while it is less susceptible to electrophilic substitutions.[2,4,5]

The ionization potential of arenetricarbonylchromium was determined from the charge-transfer transition energies in the molecular complexes with 1,3,5-TNB[1,6] and with TCNE.[1]

1,3,5-TNB forms a molecular complex with arenetricarbonylchromium by a charge-transfer interaction toward the π-coordinated benzene ring in "face-to-face" stack of the counter benzene rings as revealed by an X-ray study on the molecular complex of anisoletricarbonylchromium and 1,3,5-TNB.[7] The ionization potentials of arenetricarbonylchromium obtained from the charge-transfer transition energies in the 1,3,5-TNB molecular complexes can well reproduce the ionization potentials measured directly by electron impact technique.[8] The ionization potentials of arenetricarbonylchromium obtained from the charge-transfer transition energies in the TCNE molecular complexes increase with a decrease in the ionization potential of coordinated arene. This is opposite to the corresponding shift of the ionization potentials observed for the 1,3,5-TNB molecular complexes. The stability of the TCNE complexes increases with a decrease in the ionization potential of arenetricarbonylchromium obtained for the TCNE complexes. This indicates that TCNE forms a charge-transfer molecular complex with arenetricarbonylchromium in a structure different from the 1,3,5-TNB molecular complex. In a previous paper,[1] an inner-sphere charge-transfer interaction of TCNE with the central chromium atom of arenetricarbonylchromium was proposed. In this paper, we present further evidences of the inner-sphere charge-transfer interaction of TCNE with arenetricarbonylchromium, -molybdenum and -wolfram.

Experimental

Materials. Arenetricarbonylchromium,[2] -molybdenum,[9,10] and -wolfram[9,11] were prepared according to the methods described in the literature by refluxing hexacarbonylchromium (High Pressure Chem. Co., Pennsylvania, U.S.A.), hexacarbonylmolybdenum (High Pressure Chem. Co., Pennsylvania, U.S.A.), or hexacarbonylwolfram (Research Organic/Inorganic Chem. Corp., California, U.S.A.) with the corresponding benzene derivatives under dry nitrogen atmosphere. For the preparation of arenetricarbonylwolfram, diglyme was used as solvent. For the preparation of arenetricarbonylmolybdenum, however, the use of diglyme usually results in poor yield and thus hexacarbonylmolybdenum was refluxed directly in the corresponding arenes. The refluxed mixtures were filtered, and then the filtrate was condensed by vacuum distillation. In the case of arenetricarbonylmolybdenum, the condensed solution was filtered and the complex was precipitated by adding *n*-pentane, the precipitate being then washed with isopentane. Arenetricarbonylchromium and -wolfram were obtained as residue by condensation of the filtrates of the refluxed mixtures. Arenetricarbonylchromium was purified by recrystallization of the residue from petroleum ether. Raw arenetricarbonylwolfram was dissolved in a small amount of benzene and then filtered. By adding *n*-pentane to the filtrate, arenetricarbonylwolfram was precipitated, and then the precipitate was washed with isopentane. The complexes were identified by elemental analysis (Table 1).

Diglyme, petroleum ether, *n*-pentane, isopentane and benzene derivatives used for the preparations were dried and distilled by the usual methods.[12]

N,N,N',N'-Tetramethyl-*p*-phenylenediamine (TMPD) dihydrochloride (Tokyo Kasei Co.) was neutralized with NaOH and the free amine thus obtained was purified by vacuum distillation. 1,3,5-TNB (Tokyo Kasei Co.) was recrystallized from dil HNO_3 and then from ethanol. TCNE (Tokyo Kasei Co.) was recrystallized from chlorobenzene.

Measurements of Absorption Spectra and Determinations of the Complex Formation Constants. Absorption spectra were recorded on a Shimadzu automatic recording spectrophotometer Model MPS-50. The cell compartment was thermostatted at a constant temperature (25 °C).

Table 1. Analyses of the arenetricarbonylchromium, -molybdenum, and -wolfram

Arene metal tricarbonyls	Found (%)			Calcd (%)		
	C	H	Cr	C	H	Cr
$C_6H_5CH_3Cr(CO)_3$	52.2	3.3	22.5	52.6	3.5	22.8
o-$C_6H_4(CH_3)_2Cr(CO)_3$	55.3	4.6	21.2	54.5	4.2	21.5
m-$C_6H_4(CH_3)_2Cr(CO)_3$	55.5	4.3	21.5	54.5	4.2	21.5
p-$C_6H_4(CH_3)_2Cr(CO)_3$	54.8	4.2	21.5	54.5	4.2	21.5
1,3,5-$C_6H_3(CH_3)_3Cr(CO)_3$	55.9	4.7	20.4	56.2	4.7	20.3
$C_6H_5CH_3Mo(CO)_3$	44.5	3.1		44.1	3.0	
o-$C_6H_4(CH_3)_2Mo(CO)_3$	46.4	3.4		46.2	3.5	
m-$C_6H_4(CH_3)_2Mo(CO)_3$	45.7	3.7		46.2	3.5	
p-$C_6H_4(CH_3)_2Mo(CO)_3$	46.3	3.4		46.2	3.5	
1,3,5-$C_6H_3(CH_3)_3Mo(CO)_3$	48.5	4.0		48.0	4.0	
$C_6H_5CH_3W(CO)_3$	33.4	2.3		33.4	2.2	
p-$C_6H_4(CH_3)_2W(CO)_3$	35.3	2.6		35.3	2.7	
1,3,5-$C_6H_3(CH_3)_3W(CO)_3$	36.8	3.2		37.1	3.1	

The solvent 1,2-dichloroethane (Wako Pure Chem. Co.) was dried and purified by the usual procedure.[12]

The equilibrium constant K of a 1 : 1 molecular-complex formation between electron donor D and electron acceptor A is given by

$$K = \frac{[D\cdot A]}{([D]_0-[D\cdot A])([A]_0-[D\cdot A])},$$

where $[\ ]_0$ denotes the initial concentrations, and $[D\cdot A]$ is the concentration of molecular complex D·A. Measurements were carried out at a wave number in the charge-transfer band of D·A where the molar absorption coefficients of D and A (ε_D and ε_A) are negligibly small. Assuming Beer's law, $[D\cdot A]$ is rewritten in terms of the observed absorbance $E=\varepsilon_C\cdot[D\cdot A]\cdot l$, where ε_C is the molar absorption coefficient of D·A and l is the optical path length. Thus it follows that

$$[D]_0[A]_0\, l/E = \{[D]_0+[A]_0-E/\varepsilon_c\cdot l\}\cdot 1/\varepsilon_c+1/K\varepsilon_c .$$

Measurements were carried out at 25 °C for various sets of the initial concentrations of D and A. K and ε_C were then evaluated according to the method described by Rose and Drago,[13] and Lang.[14] Plots of $[D]_0[A]_0 l/E$ against $\{[D]_0+[A]_0-E/\varepsilon_C\cdot l\}$ give a straight line for a self-consistent value of ε_C obtained by iterative calculations.

Infrared Absorption Spectra. Infrared absorption spectra of arenetricarbonylchromium, -molybdenum, and -wolfram in 1,2-dichloroethane were taken on a Hitachi spectrophotometer Model EPI-G3.

NMR spectra. NMR spectra of arene metal tricarbonyls in 1,2-dichloroethane were recorded on a 100 MHz Japan Electron Optics Laboratory spectrometer Model JNM 4H-100. Tetramethylsilane was used as an internal standard.

He Photoelectron Spectra. He (584 Å) photoelectron spectra were measured on a JASCO PE-1 photoelectron spectrometer.

Results and Discussion

Arenetricarbonylchromium, -molybdenum and -wolfram do not form a molecular complex with electron donors such as TMPD. On the other hand arenetricarbonylchromium forms molecular complexes with electron acceptors such as TCNE and 1,3,5-TNB. In fact the molecular complexes of 1,3,5-TNB have been isolated.[1,15,16] Although we have not succeeded so far in the isolation of the molecular complexes of TCNE, the charge-transfer absorption band indicates the molecular-complex formation between TCNE and arenetricarbonylchromium.

Arenetricarbonylmolybdenum and -wolfram do not form a molecular complex with 1,3,5-TNB. Neither a complex could be isolated nor a significant spectroscopic evidence of molecular-complex formation was detected. However, arenetricarbonylmolybdenum and -wolfram evidently form a charge-transfer molecular complex with TCNE. Figures 1, 2 and 3 present the charge-transfer absorption bands of toluenetricarbonylchromium (toluene $Cr(CO)_3$)–TCNE, toluene $Mo(CO)_3$–TCNE and toluene $W(CO)_3$–TCNE systems in 1,2-dichloroethane.

The absorption measurements were carried out at 25 °C in the charge-transfer band for various sets of the initial concentrations of TCNE and arenetricarbonylchromium, -molybdenum or -wolfram. From the values thus obtained, K and ε_C were evaluated. Table 2 shows K and ε_C obtained in the present work for various 1 : 1 molecular complexes of arenetricarbonylchromium, -molybdenum, and -wolfram with TCNE.

The ionization potentials of arenetricarbonylchromium, -molybdenum and -wolfram were evaluated from the charge-transfer transition energies in the molecular complexes with TCNE using an empirical relationship[17]

$$h\nu_{CT} = (I_p-6.10) + 0.54/(I_p-6.10),$$

where $h\nu_{CT}$ is the charge-transfer transition energy in eV and I_p is the ionization potential in eV of arenetricarbonylchromium, -molybdenum or -wolfram. The results are summarized in Table 3.

The ionization potentials determined by using the empirical relationship are in good agreement with the values directly observed for some chromium derivatives by photoelectron spectroscopy as shown in Fig. 5. The spectra are discussed later. The ionization potential of toluene is 8.90 eV[18] while the ionization potentials of toluene $Cr(CO)_3$, toluene $Mo(CO)_3$ and toluene $W(CO)_3$ are 7.40 eV, 8.13 eV and 8.14 eV,

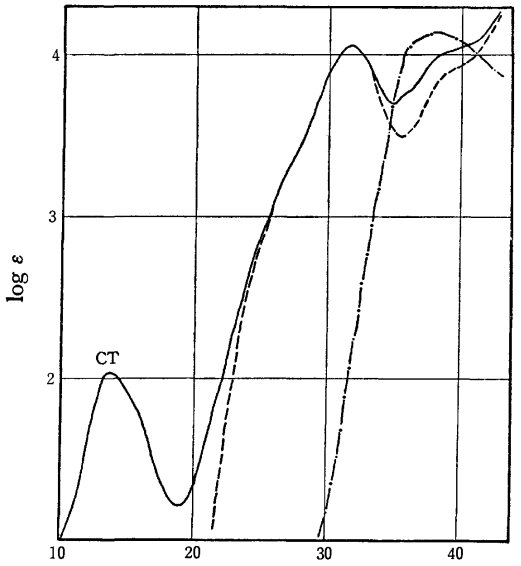

Fig. 1. The charge-transfer band (CT) of toluene Cr-$(CO)_3$-TCNE system in 1,2-dichloroethane at 25 °C.
[toluene $Cr(CO)_3]_0 = 4.51 \times 10^{-3}$ mol l^{-1}; $[TCNE]_0 = 1.06 \times 10^{-3}$ mol l^{-1}.
——: toluene $Cr(CO)_3$-TCNE
----: toluene $Cr(CO)_3$
—·—: TCNE

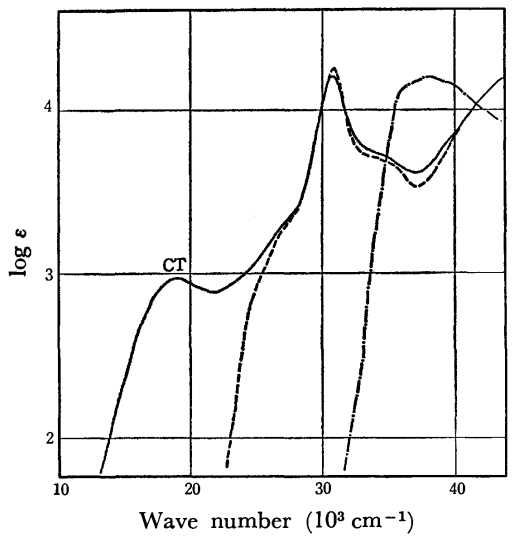

Fig. 2. The charge-transfer band (CT) of toluene $Mo(CO)_3$-TCNE system in 1,2-dichloroethane at 25 °C.
[toluene $Mo(CO)_3]_0 = 4.92 \times 10^{-4}$ mol l^{-1}; $[TCNE]_0 = 9.22 \times 10^{-5}$ mol l^{-1}.
——: toluene $Mo(CO)_3$-TCNE
----: toluene $Mo(CO)_3$
—·—: TCNE

respectively. The ionization potential of arenes varies with their substituents, while the ionization potential of arene metal tricarbonyls is rather independent of the substituents. The ionization potentials of the molybdenum and wolfram derivatives are almost equal but higher than those of the corresponding chromium derivatives.

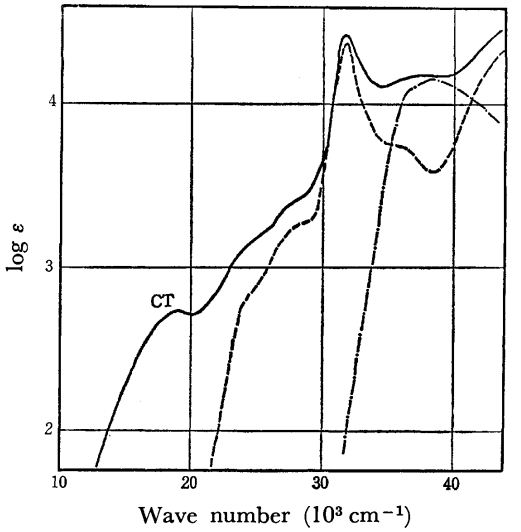

Fig. 3. The charge-transfer band (CT) of toluene $W(CO)_3$-TCNE system in 1,2-dichloroethane at 25 °C.
[toluene $W(CO)_3]_0 = 1.70 \times 10^{-3}$ mol l^{-1}; $[TCNE]_0 = 4.68 \times 10^{-4}$ mol l^{-1}.
——: toluene $W(CO)_3$-TCNE
----: toluene $W(CO)_3$
—·—: TCNE

TABLE 2. MOLAR ABSORPTION COEFFICIENTS AND COMPLEX FORMATION CONSTANTS OF THE 1 : 1 MOLECULAR COMPLEXES OF ARENETRICARBONYLCHROMIUM, -MOLYBDENUM, AND -WOLFRAM WITH TCNE[a)]

Donors	K at 25 °C (l·mol^{-1})	ε_c(max) (l·mol^{-1}·cm^{-1})
$C_6H_5CH_3Cr(CO)_3$	661	520
o-$C_6H_4(CH_3)_2Cr(CO)_3$	952	667
m-$C_6H_4(CH_3)_2Cr(CO)_3$	504	482
p-$C_6H_4(CH_3)_2Cr(CO)_3$	240	616
1,3,5-$C_6H_3(CH_3)_3Cr(CO)_3$	686	703
$C_6H_5CH_3Mo(CO)_3$	20400	5220
o-$C_6H_4(CH_3)_2Mo(CO)_3$	20100	5070
m-$C_6H_4(CH_3)_2Mo(CO)_3$	6810	5250
p-$C_6H_4(CH_3)_2Mo(CO)_3$	11200	5120
1,3,5-$C_6H_3(CH_3)_3Mo(CO)_3$	1110	4740
$C_6H_5CH_3W(CO)_3$	657	3960
p-$C_6H_4(CH_3)_2W(CO)_3$	468	3510

a) Quantitative values were not obtained for 1,3,5-$C_6H_3(CH_3)_3W(CO)_3$.

The stretching frequencies of coordinated carbonyl ($\tilde{\nu}_{CO}$) of arenetricarbonylchromium, -molybdenum and -wolfram in 1,2-$C_2H_4Cl_2$ are also presented in Table 3. An increase in the number of methyl groups in the coordinated arene gives rise to a decrease in the CO-stretching frequency, which indicates an enhancement of the back-donation of metal $d\pi$ electron toward coordinated carbonyl groups. For the same arene, the CO-stretching frequency shows a shift toward lower frequency in the order W>Mo>Cr. The NMR signals of methyl-proton presented in Table 4 also support an enhanced charge-transfer from coordinated arene to carbonyl groups in the order W>Mo>Cr.

Table 3. The charge-transfer excitation energies ($h\nu_{CT}$) in the TCNE molecular complexes, and the ionization potentials (I_p) and CO-stretching frequencies ($\bar{\nu}_{CO}$) of the arenetricarbonyl-chromium, -molybdenum and -wolfram

Arene metal tricarbonyls	$h\nu_{CT}$ (kK)	I_p (eV)	$\bar{\nu}_{CO}$ in 1,2-$C_2H_4Cl_2$ (cm^{-1})
$C_6H_5CH_3Cr(CO)_3$	13.9	7.40	1965
o-$C_6H_4(CH_3)_2Cr(CO)_3$	13.9	7.42	1962
m-$C_6H_4(CH_3)_2Cr(CO)_3$	14.0	7.43	1962
p-$C_6H_4(CH_3)_2Cr(CO)_3$	14.2	7.46	1960
1,3,5-$C_6H_3(CH_3)_3Cr(CO)_3$	14.0	7.43	1958
$C_6H_5CH_3Mo(CO)_3$	18.5	8.13	1964
o-$C_6H_4(CH_3)_2Mo(CO)_3$	18.6	8.14	1960
m-$C_6H_4(CH_3)_2Mo(CO)_3$	18.6	8.14	1961
p-$C_6H_4(CH_3)_2Mo(CO)_3$	18.7	8.15	1959
1,3,5-$C_6H_3(CH_3)_3Mo(CO)_3$	18.7	8.15	1957
$C_6H_5CH_3W(CO)_3$	18.6	8.14	1962
p-$C_6H_4(CH_3)_2W(CO)_3$	18.5	8.13	1959
1,3,5-$C_6H_3(CH_3)_3W(CO)_3$	18.6	8.14	1955

Arenes	I_p[a] (eV)
$C_6H_5CH_3$	8.90
o-$C_6H_4(CH_3)_2$	8.70
m-$C_6H_4(CH_3)_2$	8.69
p-$C_6H_4(CH_3)_2$	8.52
1,3,5-$C_6H_3(CH_3)_3$	8.52

a) Ref. 18.

Table 4. The ^{1}H-chemical shifts of arenetricarbonylchromium, -molybdenum, and -wolfram in 1,2-dichloroethane

	Phenyl-H (ppm)	Methyl-H (ppm)	Ref.
$C_6H_5CH_3$	7.18	2.33	b)
$C_6H_5CH_3Cr(CO)_3$	5.21[a]	2.18	b)
$C_6H_5CH_3Mo(CO)_3$	5.48[a]	2.24	c)
$C_6H_5CH_3W(CO)_3$	5.31[a]	2.42	c)
p-$C_6H_4(CH_3)_2$	7.07	2.28	b)
p-$C_6H_4(CH_3)_2Cr(CO)_3$	5.23	2.12	b)
p-$C_6H_4(CH_3)_2Mo(CO)_3$	5.58	2.17	c)
p-$C_6H_4(CH_3)_2W(CO)_3$	5.42	2.32	c)
1,3,5-$C_6H_3(CH_3)_3$	6.77	2.25	b)
1,3,5-$C_6H_3(CH_3)_3Cr(CO)_3$	4.90	2.20	b)
1,3,5-$C_6H_3(CH_3)_3Mo(CO)_3$	5.23	2.25	c)
1,3,5-$C_6H_3(CH_3)_3W(CO)_3$	5.10	2.45	c)

a) Center of gravity of the multiplet. b) Ref. 19. In Ref. 19, the NMR peaks in deuterochloroform were given. c) Ref. 20. In Ref. 20, no details of the observation were presented. However the plots given in a graph of the chemical shifts of protons in the complexes are in good agreement with those observed in the present work.

An upfield shift of phenyl-proton observed in the coordinated arenes arises from a quenching of the ring current upon the formation of molecular orbitals between the central metal atom and its coordinated arene. This effect is enhanced in the order Cr> W>Mo. Such an upfield shift has been observed also in the ^{13}C NMR of ring carbons of the corresponding mesitylene metal tricarbonyls.[21]

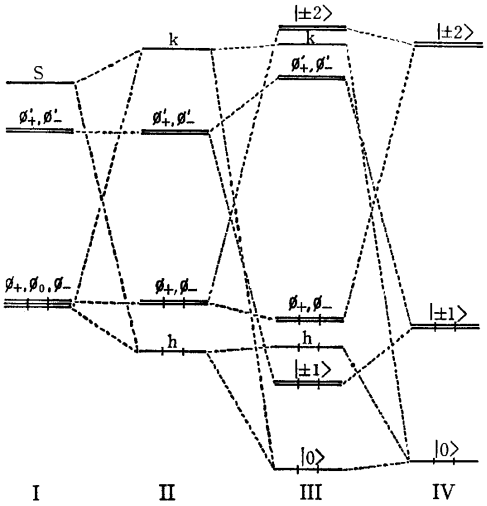

Fig. 4. The energy levels of the arene metal tricarbonyls (schematic).
I: The outer orbitals of the central metal.
II: The ϕ_0 and s orbitals are hybridized.
III: The molecular orbitals formed (Each molecular orbital is characterized by its predominant component).
IV: The π-orbitals of arene.

Since an increase in the charge density on carbonyl groups in arenetricarbonylmolybdenum and -wolfram causes no enhancement of the molecular-complex formation with electron acceptor, the molecular-complex formation cannot be attributed to a charge-transfer interaction between the carbonyl groups and the acceptor. Arenetricarbonylchromium forms a molecular complex with 1,3,5-TNB in "face-to-face" stack of the counter benzene rings, and thus an increase in the intramolecular charge migration from arene to carbonyl groups in arenetricarbonylmolybdenum and -wolfram inhibits the formation of the 1,3,5-TNB molecular complexes.

An increase in the number of methyl groups in coordinated arene promotes the intramolecular charge migration. However, the ionization potential of arene metal tricarbonyls in the TCNE molecular complexes is almost independent of the methyl substitutions. This indicates that the molecular orbital involved in an intermolecular charge transfer arising from the formation of TCNE molecular complexes is different from the molecular orbital participating in the intramolecular charge migration from coordinated arene to carbonyl groups.

The antibonding molecular orbitals predominantly localized on metal d orbitals are given by

$$\phi_+ = -\frac{1}{\sqrt{3}}\{\sqrt{2}|d_{-2}> + |d_{+1}>\}$$

$$\phi_- = \frac{1}{\sqrt{3}}\{\sqrt{2}|d_{+2}> - |d_{-1}>\}$$

$$\phi_0 = |d_0>$$

$$\phi_+' = -\frac{1}{\sqrt{3}}\{|d_{-2}> - \sqrt{2}|d_{+1}>\}$$

$$\phi_-' = \frac{1}{\sqrt{3}}\{|d_{+2}> + \sqrt{2}|d_{-1}>\},$$

where $|d_0>$, $|d_{\pm1}>$ and $|d_{\pm2}>$ are the basis set for C_3 symmetry axis. By the ligand field of carbonyl groups, ϕ_+, ϕ_- and ϕ_0 are stabilized by $2\varepsilon_\pi$ for π back-donation while ϕ_+' and ϕ_-' are destabilized by $\varepsilon_\sigma 3/2$ for σ donation. Thus a splitting between (ϕ_+, ϕ_-, ϕ_0) and (ϕ_+', ϕ_-') is $(3/2\varepsilon_\sigma + 2\varepsilon_\pi)$, which is approximately a half of the ligand field splitting in the corresponding metal hexacarbonyl. The molecular orbitals formed in the arene metal tricarbonyl are shown in a schematic fashion as in Fig. 4.

The top filled degenerate molecularo rbital pair of benzene is $|\pm1>$ and the lowest vacant degenerate molecular orbital pair is $|\pm2>$. Thus $|d_{\pm1}>$ can accept an electronic charge from $|\pm1>$, and $|d_{\pm2}>$ can donate an electronic charge into $|\pm2>$. Since the overlap $<d_{\pm1}|\pm1>$ is greater than $<d_{\pm2}|\pm2>$, a charge transfer from $|\pm1>$ toward $|d_{\pm1}>$ is predominant. 1,3,5-TNB can accept a $d\pi$-electronic charge in the $|\pm2>$ orbital of the coordinated arene

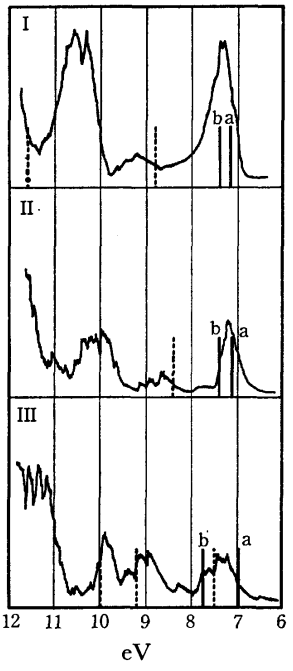

Fig. 5. The He(584 Å) photoelectron spectra of toluene $Cr(CO)_3$, mesitylene $Cr(CO)_3$ and dimethylaniline $Cr(CO)_3$.
I: toluene $Cr(CO)_3$
II: mesitylene $Cr(CO)_3$
III: dimethylaniline $Cr(CO)_3$
——: the ionization potentials of the metal complex determined by the charge-transfer excitation energies in the molcular complexes with 1,3,5-TNB (a) and TCNE (b).
……: the ionization potentials of the corresponding free arenes.
(The values for toluene and dimethylaniline were directly observed by Turner and his coworkers[25] and the value for mesitylene was determined by Watanabe.[26])

in the chromium derivatives. The methyl-proton signal exhibits an upfield shift in the chromium and molybdenum derivatives while it shows a downfield shift in the wolfram derivatives. This indicates that a charge transfer from $|\pm1>$ to $|d_{\pm1}>$ is exclusive in the wolfram derivatives while the charge transfer from $|d_{\pm2}>$ to $|\pm2>$ cannot be eliminated in the chromium and molybdenum derivatives. The resultant intramolecular charge migration from coordinated arene to carbonyl groups is enhanced in the order W>Mo>Cr as revealed by the CO-stretching frequency. Since an electronic charge in $|\pm1>$ of the coordinated arene is transferred into $|d_{\pm1}>$ of the central metal, the coordinated arene displays chemical properties which the corresponding free arene can exhibit only when substituted by more electron-withdrawing groups. The orbital ϕ_0 is not directly participating in the intramolecular charge migration, and thus less depends upon methyl substitutions in the coordinated arene. The energy of ϕ_0, however, is stabilized as a result of the countercurrent intramolecular charge transfers in the case of the chromium and molybdenum derivatives while destabilized for a one-way intramolecular charge transfer from arene to metal in the case of the wolfram derivatives. In fact, the observed ionization potentials of arene metal tricarbonyls in their TCNE molecular complexes were 7.4 eV, 8.1 eV and 8.1 eV for chromium, molybdenum and wolfram, respectively (Table 3), while the $d\pi$-ionization potentials of CrI and MoI are estimated as 3.97 eV and 4.92 eV and are lower than 8.46 eV of WI.[22]

The oxidation state of the central metal atom in the arene metal tricarbonyls is zero, and thus the energy of 4s orbital should be comparable to that of 3d orbital.[23] Although the σ bond formation between metal and carbonyl groups raises the energy of 4s orbital, a participation of 4s orbital in the outer-shell electronic structure of arene metal tricarbonyl could be sizable.[24] A mixing between ϕ_0 and 4s gives rise to an extra stabilization of the occupied counterpart orbital, which extends in a space between coordinated arene and carbonyl groups. TCNE accepts an electronic charge of this occupied hybrid orbital upon molecular-complex formation.

Figure 5 shows the He (584 Å) photoelectron spectra of toluene $Cr(CO)_3$, mesitylene $Cr(CO)_3$, and dimethylaniline $Cr(CO)_3$. The lowest ionization is attributed to an electron detachment from the filled molecular orbital predominantly localized on the metal d orbitals. A splitting of d orbitals $\phi_\pm$ and ϕ_0 was observed, although a more resolved splitting of d orbitals in some other transition-metal sandwich complexes was recently reported.[27,28] The spectrum also indicates that the top filled orbitals of the coordinated arene are more stabilized than those of the corresponding free arene.

Methyl substitutions in the coordinated arenes do not change the ionization potentials of arene metal tricarbonyls, whereas the substitutions reduce the stability of the molecular complexes with TCNE. This might be due to a steric hindrance of the methyl groups introduced to the coordinated arene. The

molecular complexes with TCNE are the most stabilized in the molybdenum derivatives, although the intramolecular charge migration increases in the order W>Mo>Cr and the ionization potentials of the molybdenum and wolfram derivatives are almost equal. This should arise from a high charge density on the molybdenum occupied hybrid orbital.

The authors would like to thank Mr. Yoshio Niwa, National Chemical Laboratory for Industry, for the measurements of He (584 Å) photoelectron spectra.

References

1) H. Kobayashi, M. Kobayashi, and Y. Kaizu, This Bulletin, **46**, 3109 (1973).
2) B. Nicholls and M. C. Whiting, *J. Chem. Soc.*, **1959**, 551.
3) E. O. Fischer, K. Öfele, H. Essler, W. Fröhlich, J. P. Mortensen, and W. Semmlinger, *Chem. Ber.*, **91**, 2763 (1958).
4) D. A. Brown and J. R. Raju, *J. Chem. Soc., A*, **1966**, 40.
5) R. Riemschneider, O. Becker, and K. Franz, *Monatsh. Chem.*, **90**, 571 (1959).
6) G. Huttner and E. O. Fischer, *J. Organometal. Chem.*, **8**, 299 (1967).
7) O. L. Carter, A. T. McPhail, and G. A. Sim, *J. Chem. Soc., A*, **1966**, 822.
8) J. Müller, *J. Organometal. Chem.*, **18**, 321 (1969).
9) E. O. Fischer and K. Öfele, *Z. Naturforsch.*, **13b**, 458 (1958).
10) W. Strohmeier, *Chem. Ber.*, **94**, 3337 (1961).
11) W. Strohmeier, *Z. Naturforsch.*, **17b**, 566 (1962).
12) D. D. Perrin, W. L. F. Armarego, and D. R. Perrin, "Purification of Laboratory Chemicals," Pergamon Press, Oxford (1966).
13) N. J. Rose and R. S. Drago, *J. Amer. Chem. Soc.*, **81**, 6138 (1959).
14) R. P. Lang, *ibid.*, **84**, 1185 (1962).
15) J. W. Fitch, III, and J. J. Lagowski, *J. Organometal. Chem.*, **5**, 480 (1966).
16) G. Huttner, E. O. Fischer, R. D. Fischer, O. L. Carter, A. T. McPhail, and G. A. Sim, *ibid.*, **6**, 288 (1966).
17) G. Briegleb, J. Czekalla, and G. Reuss, *Z. Phys. Chem. N.F.*, **30**, 333 (1961).
18) P. G. Farrell and J. Newton, *J. Phys. Chem.*, **69**, 3506 (1965).
19) R. V. Emanuel and E. W. Randall, *J. Chem. Soc., A*, **1969**, 3002.
20) J. T. Price and T. S. Sorensen, *Can. J. Chem.*, **46**, 515 (1968).
21) B. E. Mann, *Chem. Commun.*, **1971**, 976.
22) J. S. Griffith, "The Theory of Transiton-Metal Ions," Cambridge University Press (1961), p. 100.
23) C. E. Moore, "Atomic Energy Levels," Vol. 1, 2 and 3, National Bureau of Standards, Washington (1949, 1952, 1958).
24) W. Moffitt, *J. Amer. Chem. Soc.*, **76**, 3386 (1954).
25) D. W. Turner, C. Baker, A. D. Baker and C. R. Brundle, "Molecular Photoelectron Spectroscopy," John-Wiley & Sons, London (1970), p. 297 and p. 300.
26) K. Watanabe, *J. Chem. Phys.*, **26**, 542 (1957).
27) S. Evans, J. C. Green, and S. E. Jackson, *J. Chem. Soc., Faraday II*, **68**, 249 (1972).
28) S. Evans, J. C. Green, and S. E. Jackson, *J. Chem. Soc., Dalton*, **1974**, 304.

Mechanism of Racemization of Octahedral Silicon(IV) Complexes with Various β-Diketones in Organic Solvents

Tomoaki INOUE,* Junnosuke FUJITA,** and Kazuo SAITO

Chemistry Department, Faculty of Science, Tohoku University, Aoba, Aramaki, Sendai 980

(Received December 10, 1974)

Silicon(IV) complexes of 4 kinds of β-diketonate have been resolved and their racemization has been kinetically studied in 1,1,2,2-tetrachloroethane (TCE) and acetonitrile (AN) at 30 to 80 °C. Ultra-violet absorption spectroscopy and isotopic exchange studies with labelled ligands verified intra-molecular mechanism. A similar rate formula to that for the tris(acetylacetonato)silicon(IV)[1] was obtained: $k_0=k_1+k_2$[acid or base]. Increase in basicity of the ligand decreases the rate. Introduction of methyl group on the central carbon of the six-membered chelate ring markedly enhanced the racemization. It seems as if the intermediate species with a unidentate ligand tends to take *trans* form around the C=C axis and retards the recombination, giving rise to bigger k values. Mechanism of acid and base catalysis was also discussed.

In a previous paper we gave the results of kinetics of racemization of tris(acetylacetonato)silicon(IV) [Si(acac)$_3$]$^+$ in 1,1,2,2-tetrachloroethane (TCE) and acetonitrile (AN), and postulated an intra-molecular mechanism through an intermediate with a unidentate ligand.[1] This paper deals with further results of kinetic studies of racemization of some tris(β-diketonato)silicon(IV), with aims of examining the influence of substituents on the chelate rings upon the rate, and of verifying the proposed reaction mechanism.

The ligands are acetylacetone homologues with ethyl and phenyl on α-carbon and methyl on the central carbon. The names and abbreviated symbols are given in Table 1.

Experimental

Materials. *The ligands*: Hdprm, Hdbm and Hmedprm were obtained by the Claisen condensation of the corresponding ketones and esters.[2] Hacac was methylated with methyl iodide in the presence of potassium carbonate and acetone to give Hmeacac.[3] All the products were identified by boiling point measurement, elementary analysis and UV and PMR spectrometry.

The complexes: Dilthey's method was employed for the synthesis of the tris-type complexes. They were obtained in the form of hydrogendichlorides (2 g), which were dissolved in water (30 ml) and converted into perchlorates by adding sodium perchlorate monohydrate (*e.g.* 2 g). The product was dried, dissolved in chloroform (*e.g.* 5 ml) and treated with diethyl ether (60 ml) to precipitate the anhydrous perchlorate, which was filtered off and dried. The conversion yield was *ca.* 80%. The dprm$^-$ and medprm$^-$ complexes are new compounds. Anal. [Si(dprm)$_3$]ClO$_4$: Found: C, 49.6 and H, 6.53; Calcd for $C_{21}H_{33}O_{10}ClSi$, C, 49.6 and H, 6.53%. [Si(medprm)$_3$]ClO$_4$: Found: C, 51.7 and H, 7.07%; Calcd for $C_{24}H_{39}O_{10}ClSi$: C, 52.6 and H, 7.16%.

Resolution: All the tris-type complexes were resolved for the first time. Dibenzoyl-*d*-tartrate used for [Si(acac)$_3$]$^+$[4] is the best agent. The racemic hydrogendichloride (2 g) in a mixture of 80 ml of water and 160 ml of AN was treated with the reagent (0.6 g) in 20 ml of water and 0.1 M soldium hydroxide solution (3.8 ml). Gradual addition of water (200 to 250 ml) gave colorless precipitate of the diastereoisomer (or jelly precipitate for meacac$^-$ and medprm$^-$ complexes). Addition of sodium perchlorate monohydrate (*ca.* 3 g) to the filtrate gave crystalline (+)$_D$-enantiomer of the complex (1 g), which was dissolved in AN (35 ml) and recrystallized by adding diethyl ether (25 ml), to give anhydrous perchlorate.

All the (+)$_D$-enantiomers gave plus and minus CD peaks from longer to shorter wavelength in the π–π^* transition region and assigned to Λ configuration.[5] The CD peaks are at 306, 400, 324 and 325 nm and the $\Delta\varepsilon$ values of the perchlorates were 30 to 70, 50 to 70, 20 to 30 and 5 to 10, for dprm$^-$, dbm$^-$, meacac$^-$ and medprm$^-$ complexes respectively. The percentage of resolution seems to be *ca.* 10%.

Other reagents: The Hdbm-^{14}C was prepared by Mr. Matsuzawa.[6] Labelled Hmeacac was synthesized from Hacac and methyl iodide-^{14}C similarly to the unlabelled ligand. Acetonitrile (AN) was dehydrated with diphosphoruspentoxide and distilled with potassium carbonate. The water content was *ca.* 3×10^{-3} M. TCE was dehydrated with calcium sulfate and distilled. The water content was 5×10^{-3} M. Mono- and trichloroacetic acid were sublimed *in vacuo*. Pyridine was dehydrated with calcium sulfate and distilled *in vacuo*. The water content was less than 0.01 M.

Procedure for kinetic runs and the measurements are the same as those in Ref. 1.

Results and Discussion

All the complexes are stable in TCE and AN under the given conditions. The absorption spectrum did not change during the measurements, regardless of the concentration of dissolved water and the excessive ligand, and of the presence of acid or base. Hence the change in CD strength or the rotatory power is exclusively due to the racemization of the resolved species. The rate of decrease in rotatory power obeys first order rate law and is expressed by first order rate constant, k_0 which is expressed by Eq. (1)

$$k_0 = 1/2t(\ln[\alpha_0/\alpha_t]) \quad (1)$$

where t is the lapse of time in seconds, and α_0 and α_t are the rotations at Na-D line or 405 nm or CD strength at the plus CD peak in near UV region at time zero and t, respectively. The k_0 values were independent of the complex concentration for 0.001 to 0.02 M in TCE and AN.

The ligand isotopic exchange rate was studied with [Si(dbm)$_3$]$^+$ and Hdbm-^{14}C, and [Si(meacac)$_3$]$^+$ and

* Present address: Chemistry Department, Wayne State University, Detroit, Michigan, U.S.A.

** Present Address: Chemistry Department, Faculty of Science, Nagoya University, Chikusa, Nagoya.

Table 1. The ligands used in this study

Name	R	R′	Abbreviation	pK_a[a]	pK_e[b]
2,4-pentanedione	CH_3	H	Hacac	12.75	8.23
3,5-heptanedione	C_2H_5	H	Hdprm	13.40	8.76
1,3-diphenyl-1,3-propanedione	C_6H_5	H	Hdbm	13.75	[9.1]
3-methyl-2,4-pentanedione	CH_3	CH_3	Hmeacac	—	9.2
4-methyl-3,5-heptanedione	C_2H_5	CH_3	Hmedprm	—	—

a) pK values for the diketone in 75% aqueous dioxane at 30 °C; b) pK values for the enol from of the diketones in water at 20 °C.[7] [The pK_e of Hdbm is an estimated value.]

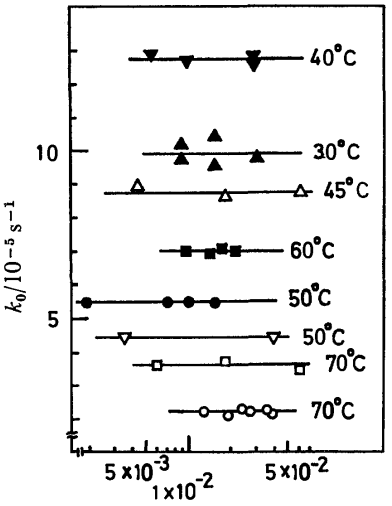

Fig. 1. Relationship between the racemization rate and the concentration of water.
Open marks in TCE, full marks in AN.
□: $[Si(dprm)_3]^+$, ○: $[Si(dbm)_3]^+$,
△: $[Si(meacac)_3]^+$, ▽: $[Si(medprm)_3]^+$.

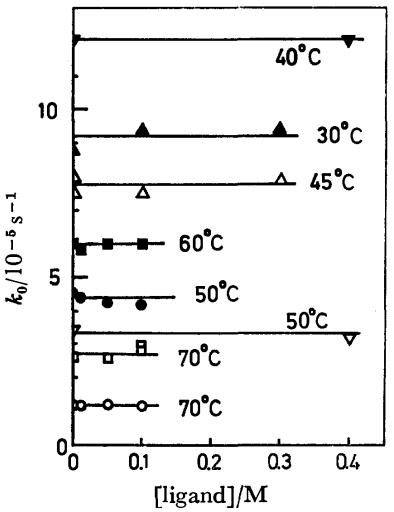

Fig. 2. Influence of the concentration of free ligands on the racemization constants.
Open marks in TCE, full marks in AN.
□: $[Si(dprm)_3]^+$, ○: $[Si(dbm)_3]^+$,
△: $[Si(meacac)_3]^+$, ▽: $[Si(medprm)_3]^+$.

Hmeacac-^{14}C in TCE and AN, both in presence and absence of acid and base. No appreciable isotopic exchange was observed in all the systems within 2—5 half life time of racemization at 70 °C. It is thus concluded that the racemization takes place intramolecularly.

Table 2. Rate constants and activation parameters for the racemization in TCE and AN at 50 °C

Complex	Solvent	k_1 / s^{-1}	$\Delta H^{\neq}$ / kcal·mol^{-1}	$\Delta S^{\neq}$ / cal·mol^{-1} K^{-1}
$[Si(acac)_3]^+$	TCE	4.8×10^{-6}	32±1	15
	AN	3.9×10^{-5}	26±1	0.5
$[Si(dprm)_3]^+$	TCE	1.8×10^{-6}	33±1	16
	AN	2.4×10^{-5}	24±1	−7
$[Si(dbm)_3]^+$	TCE	1.1×10^{-6}	32±1	14
	AN	5.5×10^{-5}	25±1	−1
$[Si(meacac)_3]^+$	TCE	2.0×10^{-4}	34±1	30
	AN	1.8×10^{-3}	28±1	14
$[Si(medprm)_3]^+$	TCE	4.4×10^{-5}	28±1	9
	AN	4.9×10^{-4}	25±1	3

Figs. 1 and 2 show the dependence of the rate constants upon the concentrations of water and free ligand in TCE and AN. It is clear that these concentrations do not affect the rate.

The racemization rate increases in the presence of mono- and trichloroacetic acid in TCE and of pyridine in AN. The influence is exemplified in Figs. 3 and 4. The diagrams are straight lines with intercepts, and k_0 is expressed by Eq. (2).

$$k_0 = k_1 + k_2[\text{acid or base}] \quad (2)$$

The k_1 *path.* Table 2 summerizes the rate constants k_1 and the activation parameters obtained from the experiments at 30 to 80 °C. The basic feature of the kinetics of racemization of the present Si(IV) complexes is very similar to that of previously reported $[Si(acac)_3]^+$ [1]. We postulated an intramolecular mechanism involving an intermediate with a unidentate acetylacetonate ligand and considered the break of the first Si–O bond as the rate-determining step. The present data in Table 2 seem to give support for the proposed mechanism.

If the break of the Si–O bond were the rate-determining step, the k values would decrease and the $\Delta H^{\neq}$ values increase as basicity of the ligand increases. The basicity of the ligands is best indicated by the pK values of their enol forms in the given solvents. However, only limited information is available concerning the pK values of various β-diketones in enol form. These values (pK_e) in water at 20 °C[7] are given in Table 1.

So far as the complexes with acac$^-$, dprm$^-$ and dbm$^-$ (hydrogen atom on the R′ position) are concerned, the k_1 values in TCE decrease slightly with increase in pK_e values, and the activation parameters

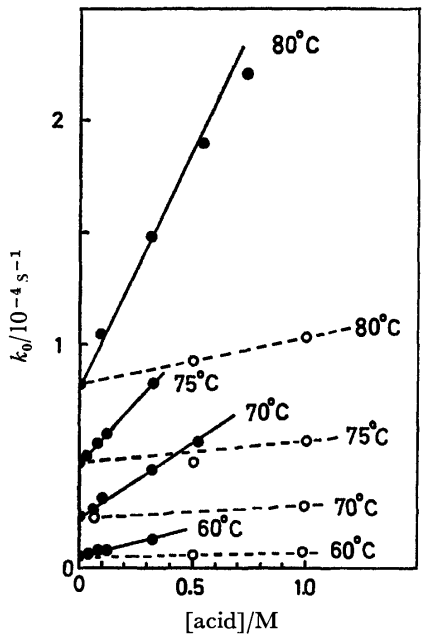

Fig. 3. Influence of acid concentration upon the racemization rate of [Si(dbm)$_3$]$^+$ in TCE.
Open marks with broken lines, $CH_2ClCOOH$; full marks with solid lines, CCl_3COOH.

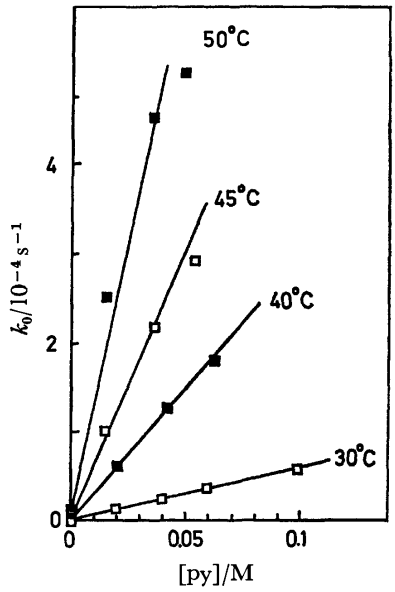

Fig. 4. Influence of concentration of pyridine on the racemization rate of [Si(dprm)$_3$]$^+$ in AN.

are similar to one another. On the other hand, the complexes with meacac$^-$ and medprm$^-$ (methyl on the R′ position) give much greater k_1 values than the corresponding complexes with hydrogen on R′. The pK_e value of Hmeacac is significantly larger than that of Hacac, and the big k_1 value should be interpreted otherwise.

Whenever alkyl groups are introduced on the R′ position of β-diketones, the keto-enol tautomeric equilibrium is shifted in favor of the keto form,[7] and the enol tautomer tends to take *trans* form around the C=C double bond axis.[8] This fact was also observed by PMR spectroscopy for Hmeacac,[9] and the conversion rate from *cis* to *trans* was reckoned to be very big.[10]

If the β-diketonate anion in the form of unidentate ligand in the intermediate state could be compared to the enol tautomer of the protonated ligand, the unidentate meacac$^-$ and medprm$^-$ ligand would tend to take *trans* form as shown in Fig. 5. Such a rearrangement would decrease the probability of the recombination of the ligand, to facilitate the racemization. When the k_1 value is written as Eq. (3) on the assumption of a stationary state,

$$k_1 = k_a(k_b/[k_{-a}+k_b])(k_c/[k_{-b}+k_c]) \quad (3)$$

the ligands with methyl on R′ would decrease the k_{-a} value to increase k_1. Comparison of $\Delta H^{\neq}$ and $\Delta S^{\neq}$ values between Hacac and Hmeacac complexes clearly shows that the labilization comes from the entropy contribution. The latter has bigger $\Delta H^{\neq}$ than the former, reflecting the bigger pK_e value of the ligand. (Comparison between dprm$^-$ and medprm$^-$ complexes is not useful, because pK_e value of the latter ligand is not known.) Thus we conclude that the present data gave concrete support for the reaction mechanism proposed before.

Either Si–O or C–O bond can be broken at the rate-determining step. Pinnavaia, Collins and Howe studied the NMR spectra of various alkyldimethylsilyl ether of Hacac in enol form and found a very rapid intramolecular rearrangement in *cis*-R(CH$_3$)$_2$Si(acac), which interchanges the allylic and acetyl methyl groups on the acac moiety.[11] The Arrhenius activation energy for the interchange was measured at −36 to +38 °C to be 13.8±0.5 kcal per mol. These are tetrahedral silicon(IV) compounds and the results may reflect the ease of homolytic cleavage of Si–O bond. Hence they should not be directly applied to our octahedral silicon(IV). Nevertheless we tend to consider that Si–O bond would be broken at the rate-determining step, although nothing decisive could be stated at the present stage.

In AN the racemization is faster than in TCE, and

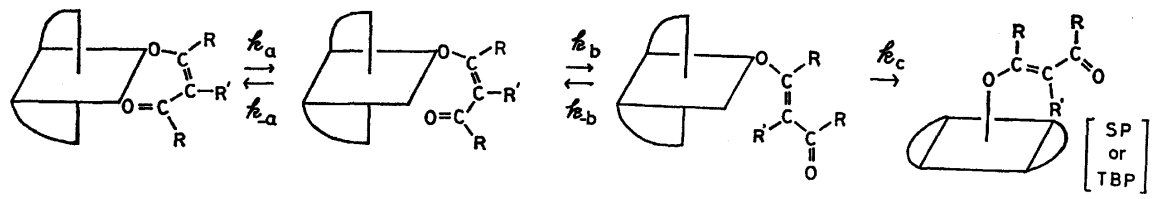

Fig. 5. Plausible racemization mechanism.

TABLE 3. SECOND ORDER RATE CONSTANT AND ACTIVATION PARAMETERS FOR THE RACEMIZATION IN THE PRESENCE OF ACID AND BASE AT 50 °C

Complex	Acid (Base)	k_2 / $M^{-1}\,s^{-1}$	$\Delta H^{\neq}$ / kcal·mol^{-1}	$\Delta S^{\neq}$ / cal·mol^{-1} K^{-1}
Acid catalysis in TCE				
$[Si(acac)_3]^+$	CCl_3COOH	1.4×10^{-4}	30±2	14
$[Si(dprm)_3]^+$	CCl_3COOH	2.2×10^{-5}	25±1	−3
	$CH_2ClCOOH$	2.0×10^{-6}	22±1	−17
$[Si(dbm)_3]^+$	CCl_3COOH	7.1×10^{-6}	25±1	−5
	$CH_2ClCOOH$	5.0×10^{-7}	27±2	−4
$[Si(meacac)_3]^+$	CCl_3COOH	2.0×10^{-3}	28±1	−5
$[Si(medprm)_3]^+$	CCl_3COOH	2.5×10^{-4}	28±1	11
	$CH_2ClCOOH$	1.5×10^{-5}	28±2	6
Base catalysis in AN				
$[Si(acac)_3]^+$	pyridine	1.5×10^{-1}	26±2	11
$[Si(dprm)_3]^+$	pyridine	1.3×10^{-1}	29±1	21
$[Si(meacac)_3]^+$	pyridine	3.0×10^{-2}	27±1	19
$[Si(medprm)_3]^+$	pyridine	3.7×10^{-2}	27±1	19

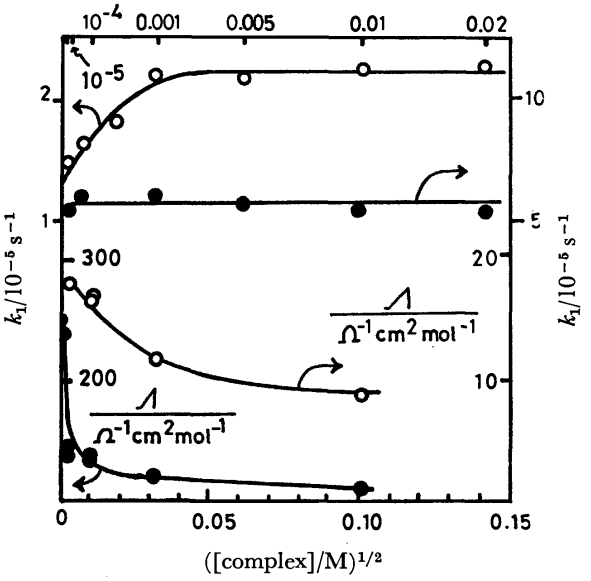

Fig. 6. Dependence of the molar conductivity and the racemization rate constant on the complex concentration of $[Si(dbm)_3]ClO_4$.
Upper: Rate constant k_1 in TCE(○) at 70° and in AN(●) at 50 °C. Lower: conductivity in TCE(○) and in AN(●) at 20 °C.

the $\Delta H^{\neq}$ values are smaller by *ca.* 6 kcal per mole. This fact indicates that the break of Si–O bond is facilitated in AN with dielectric constant 37.5. In a similar racemization of $[Ge(acac)_3]^+$ in various organic solvents,[12] we have proposed solvent-assisted dissociation of Ge–O bond, on the basis of a good correlation between Gutmann's donor number and the rate constant. Such a contribution cannot be excluded in the present racemization. However, silicon(IV) has a smaller octahedral ionic radius (0.47 Å) than germanium(IV) (0.53 Å), and the approach of a solvent molecule to Si(IV) would be more difficult than to Ge(IV). Hence solvent-assisted bond break seems less feasible for the present silicon(IV) complexes. Increase in racemization rate accompanied by the introduction of methyl on R′ could be similarly interpreted to that in TCE.

When the complex concentration was less than 0.001 M, the k_1 value decreased with decrease in concentration, as exemplified in Fig. 6. The decrease in molar conductivity with increase in complex concentration in TCE and AN is also illustrated in Fig. 6. The complexes seem to be present almost perfectly as ion pairs in more than 10^{-4} and 10^{-3} M solution in TCE and AN, respectively. The change in k_1 must reflect the state of the complexes. The constant values in more than 10^{-3} M solutions must be those of ion pairs. (The data in Tables 2 and 3 are so, too.) The racemization must proceed mostly in the form of ion pairs.

The k_2 *path.* The second order rate constants and activation parameters are shown in Table 3. Increase in racemization rate in the presence of acid was seen only in TCE. This effect must be due to the proton catalysis.[1] The absence of acid catalysis in AN may be due to hydrogen bond formation between the acid and AN.[13] Difference in $\Delta H^{\neq}$ values between k_1 and k_2 path is larger in most complexes in Table 2 than that in $[Si(acac)_3]^+$. We postulated in our previous paper that the protons are attached to the coordinated oxygen atom and facilitate the break of Si–O bond at the rate-determining step.[1] Ligands of the complexes in Table 2 are more basic than $acac^-$ and are subject to proton catalysis more remarkably. The stronger acid, trichloroacetic gives bigger influence than the weaker acid monochloroacetic does. Introduction of methyl on R′ increases the rate, and this fact can be interpreted by Eq. (3). Since the complexes are almost entirely in the form of ion pairs in the solutions used for the present study, interaction of protons with the complexes is not electrostatically implausible.

Base catalysis is only seen in AN. The absence of such an effect in TCE would be due to the hydrogen bond formation between pyridine and TCE.[14] The dbm^- complex did not give k_2 path up to 0.05 M pyridine for 0.001 to 0.02 M complex. Pyridine can

attack the Si(IV) ion as well as the ligand as a nucleophile. However, the $\Delta H^{\ddagger}$ values for the k_1 and k_2 paths in AN do not differ much. Hence pyridine seems to occupy the vacant coordination site of the intermediate with a unidentate ligand, to decrease the k_{-a} of Eq. (3). The dbm^- ligand is bulky and may hinder the approach of pyridine to the vacant site.

The authors thank the Ministry of Education for Grand-in-aid.

References

1) T. Inoue and K. Saito, This Bulletin, **46**, 2417 (1973).
2) F. W. Swamer and C. R. Hauser, *J. Amer. Chem. Soc.*, **72**, 1352 (1950).
3) A. W. Johnson, E. Markham, and R. Prince, "Organic Synthesis," Coll. Vol. 5, p. 785 (1973).
4) S. K. Dhar, V. Dorn, and S. Kirschner, *J. Amer. Chem. Soc.*, **80**, 753 (1958).
5) E. Larsen, S. F. Mason, and G. H. Searle, *Acta Chem. Scand.*, **20**, 191 (1966).
6) K. Matsuzawa and K. Saito, This Bulletin, **46**, 2777 (1973).
7) M. P. Rumpf and R. L. Riviere, *C. R. Acad. Sci. Paris*, **244**, 902 (1957).
8) M. I. Kabachnik, S. T. Ioffe, E. M. Popov, and K. Vatsuro, *Tetrahedron*, **12**, 76 (1961).
9) M. T. Rogers, *Can. J. Chem.*, **43**, 1516 (1965); G. Allen, *J. Chem. Soc., Phys. Org.* **1966**, 161.
10) B. Eistert, F. Arudt, L. Löuve, and E. Ayca, *Ber.*, **80**, 156 (1951).
11) T. J. Pinnavaia, W. T. Collins, and J. J. Howe, *J. Amer. Chem. Soc.*, **92**, 4544 (1970).
12) A. Nagasawa and K. Saito, This Bulletin, **47**, 131 (1974).
13) I. M. Kolthoff, J. F. Coetzee, and M. K. Chantooni, *J. Amer. Chem. Soc.*, **95**, 4768 (1973).
14) H. Gotz, E. Heilbronner, A. R. Katritzky, and R. A. Jones, *Helv. Chim. Acta*, **44**, 387 (1961); G. R. Wiley and S. I. Mitler, *J. Amer. Chem. Soc.*, **94**, 3287 (1972).

Kinetics and Steric Course of the Substitution of Various Olefins for the Asymmetric Olefin in *trans*(*N*,olefin)-Chloro-L-prolinato-*trans*-2-buteneplatinum(II)

Yoshiro TERAI, Hiroaki KIDO, Junnosuke FUJITA,* and Kazuo SAITO

Chemistry Department, Faculty of Science, Tohoku University, Aoba, Aramaki, Sendai 980

(Received December 25, 1974)

Replacement of the coordinated *trans*-2-butene in *trans*(*N*,olefin)[PtCl(L-pro)(*S,S-trans*-2-butene)] (L-pro= L-prolinate anion) by various olefins in acetone has been studied at −20 to +23 °C. The rate is proportional to concentrations of the complex and the olefin nucleophile. No solvent path is observed. The second order rate constant k_2 (10^{-4} to 10^{-1} M^{-1} s^{-1} at 8.0 °C) can be the measure of each substitution. The $\Delta H^{\neq}$ is around 10 kcal/mol, and $\Delta S^{\neq}$ ranges from −25 to −46 cal/mol K. Substitution of *cis*-2-butene for the asymmetrically coordinated *trans*-2-butene-^{3}H gives equal k_2's on the measurement of CD strength and on that of isotopic exchange. Similar substitution of *trans*-2-butene gives significantly larger k_2 on isotopic exchange than that on CD measurement, indicating sterically selective substitution with retention of configuration. Substitution of ethylene derivatives with various groups on the carbon atoms gives different k_2's depending on the kind of substituents. The steric interaction between the olefin nucleophile and the coordinated ligands seems to be a very important factor in determining the ease of substitution.

In a previous paper we reported the inversion of coordinated olefins in the diastereoisomer *trans*(*N*, olefin) [PtCl(L-pro)(*S,S-trans*-2-butene)] (L-pro=L-prolinate anion) and its 2-methyl-2-butene analogue, and proposed an S_N2 mechanism involving nucleophilic attack of added olefin molecules.[1] We have attempted to verify the mechanism by use of various olefin nucleophiles including *cis*- and *trans*-substituted ethylene derivatives. On comparing the rates of olefin exchange measured by CD spectroscopy and by isotopic exchange technique with *trans*-2-butene-^{3}H, a novel stereoselectivity was detected in the substitution of *trans*-2-butene for the coordinated *S,S*- and *R,R-trans*-2-butene-^{3}H in the complex in acetone. This paper deals with the verification, and the discussion on mechanism of stereoselectivity with reference to the steric interaction between the incoming olefin molecule and the coordinated ligands.

Experimental

Materials. *trans*(*N*,olefin)[(L-pro)(*S,S-trans*-2-butene)] was prepared as in Ref. 2. *trans*-(*N*,olefin)[PtCl(L-pro)(*S,S*- or *R,R-trans*-2-butene-^{3}H)]: *trans*-2-Buene-^{3}H was synthesized by the known method,[3] slightly modified to suit for a radiochemical synthesis. Lithium aluminum hydride (1.08 g) containing lithium aluminum tritide (5 mCi, 1.66 mg, New England Nuclear Co.) suspended in diethyleneglycoldiethyl ether was added to a slight excess of *trans*-1,4-dibromo-2-butene in the same solvent in a current of nitrogen. The product, *trans*-2-butene-^{3}H was trapped in dry ice-acetone (Chemical yield 0.8 g, radiochemical yield 16%). The ligand was added to *trans*(*N*,olefin)[PtCl(L-pro)(ethylene)] in acetone. The product was resolved[2] to give *trans*(N,olefin)-[PtCl(L-pro)(*S,S*- or *R,R-trans*-2-butene-^{3}H)]. The purity of the final product (*ca.* 2×10^{-2} μCi/mg) was examined by UV absorption spectrum.

Other Reagents: Extra pure grade *trans*-2-butene and *cis*-2-butene were used without further purification. The purity was checked by gas chromatography. Chemical grade *trans*-1,4-dichloro-2-butene, *cis*-2-butene-1,4-diol, and *cis*- and *trans*-1,2-dichloroethylene were distilled under a reduced pressure. Maleic and fumaric acid were recrystallized from acetone. *cis*-1,4-Dichloro-2-butene[4] and *trans*-1,4-dibromo-2-butene[5] were synthesized by the ordinary method.

Procedure. *Kinetic Runs for Loss of Optical Activity*: The complex solution in acetone was cooled, and a certain amount of cooled olefin solution in acetone added with a pipet. The solution was transferred into the cell box of the spectrometer which had been thermostated at the reaction temperatures (8.0, 17.0 and 23.6±0.3 °C). The $\Delta\varepsilon$ value at 370 nm was continuously recorded. The concentrations of the complex and the olefins at the measured temperature were calculated by taking the density of acetone at the given temperatures into consideration.

Kinetic Runs for Isotopic Exchange and Accompanied Loss of Optical Activity: The reaction mixture was similarly prepared and dispensed into 5—9 small glass-stoppered test tubes. They were kept in a thermostat at 8.0 or −20.0 (±0.3) °C, and taken out one by one at appropriate time intervals. The reaction was quenched by immersing the tubes in liquid nitrogen. Free olefin and acetone were evaporated off *in*

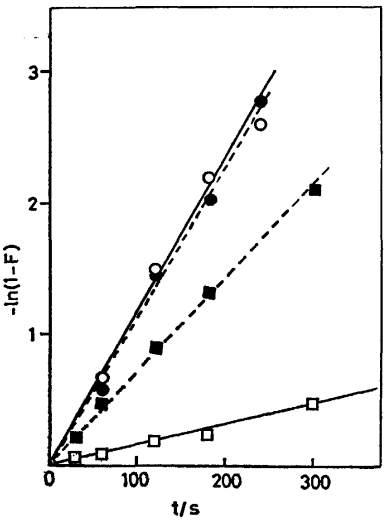

Fig. 1. Decrease in CD strength and in specific counting rate of the complex *trans*(*N*,olefin)[PtCl(L-pro)-(*S,S-trans*-2-butene-^{3}H)] in acetone with reaction time.
Open marks with solid lines by CD measurement and full marks with broken lines by isotopic exchange.
Circles, with *cis*-2-butene (0.17 M) at −20 °C; squares, with *trans*-2-butene (0.19 M) at 8.0 °C.

* Present address: Chemistry Department, Faculty of Science, Nagoya University, Chikusa, Nagoya 464.

vacuo at dry ice-acetone temperature and room temperature, respectively. The residue was dissolved in ethanol and its absorption spectrum, CD strength and β-activity were measured. The decrease in CD strength with time obeyed first order rate law as shown in Fig. 1.

Calculation of the Exchange Constant: In our experiments the complex concentration was very small as compared with the olefin solution. Hence McKay formula can be simplified, and the isotopic exchange constant was approximated by the first order kinetic formula Eq. (1) (Fig. 1)

$$k_{0(\mathrm{iso})} = -\ln(1-F)/t \qquad (1)$$

where F is the fraction of reaction expressed by $(x_t-x_\infty)/(x_0-x_\infty)$, x's being the specific counting rate of the recovered complex.

Apparatus. Circular dichroism was measured with a JASCO Model ORD/UV-5 Spectrometer with CD attachment. Absorption spectra were recorded with a Hitachi 323 Spectrometer. β-Activity of ^3H was recorded with a Nuclear-Chicago Unilux II-A liquid scintillation counter. A Komatsu-Yamato Coolnics and Haake KT 33 thermostat were used.

Results

Isotopic Exchange. The reaction mixtures gave equal absorption spectra throughout given kinetic runs, and the recovered complexes gave almost identical absorption spectrum with the original complex in ethanol. The CD strength at 370 nm in ethanol and the β-activity of the recovered complexes decreased as the reaction vessels were kept longer in the thermostat. All the data of isotopic exchange obeyed the kinetic law of Eq. (1). Hence the $k_{0(\mathrm{iso})}$ is the first order rate constant with respect to the complex concentration. The k_0 values are proportional to the concentration of added olefins (Fig. 2) and Eq. (2) is given in the range 0.05 to 0.3 M.

$$k_{0(\mathrm{iso})} = k_{2(\mathrm{iso})}[\mathrm{olefin}] \qquad (2)$$

The CD strength of the recovered complex also obeyed first order rate law with respect to the complex concentration and the rate constant $k_{0(\mathrm{cd})}$ is the first order rate constant. When the olefin concentration of the reaction mixture was changed, Eq. (3) was substantiated.

$$k_{0(\mathrm{cd})} = k_{2(\mathrm{cd})}[\mathrm{olefin}] \qquad (3)$$

The k_2's are second order rate constants, and tabulated in Table 1.

Table 1. Second order rate constants of the substitution of 2-butene for the coordinated *trans*-2-butene in [PtCl(L-pro)(*S,S-* or *R,R-trans*-2-butene)] in acetone

Added olefin[a]	*cis*-2-butene		*trans*-2-butene[c]	
T/°C	8.0	−20.0	8.0	−20.0
$k_{2(\mathrm{cd})SS}/10^{-3}\mathrm{M}^{-1}\mathrm{s}^{-1}$ [b]	347	70.9±7.6	6.2	0.9
$k_{2(\mathrm{iso})SS}/10^{-3}\mathrm{M}^{-1}\mathrm{s}^{-1}$	—	70.2±4.1	32.3	5.6
$k_{2(\mathrm{cd})RR}/10^{-3}\mathrm{M}^{-1}\mathrm{s}^{-1}$ [b]	—	—	5.5	(0.9)[d]
$k_{2(\mathrm{iso})RR}/10^{-3}\mathrm{M}^{-1}\mathrm{s}^{-1}$	—	—	16.6	(2.1)[d]

a) Concn range: [2-butene], 0.05—0.3 M; [complex], 0.0015 M. b) *SS* and *RR* in the suffices denote the configuration of coordinated *trans*-2-butene in the original complex. cd and iso in parentheses denote that the k_2's were obtained by the measurement of CD strength and isotopic exchange, respectively. c) See the legend of Fig. 2. d) Calcd from only one run.

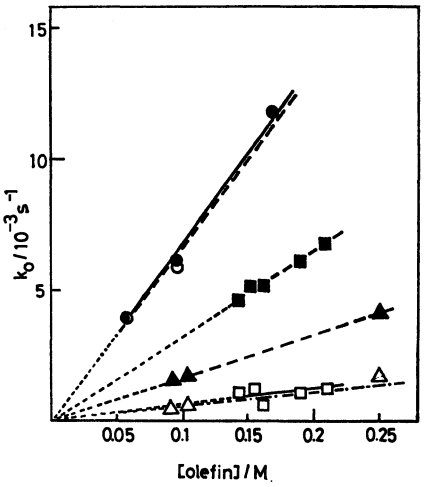

Fig. 2. Dependence of the rate constant k_0 upon the olefin concentration in acetone.
Open marks by CD measurement ($k_{0(\mathrm{cd})}$) and full marks by isotopic exchange ($k_{0(\mathrm{iso})}$). —○— and --●-- substitution of *cis*-2-butene for *S,S-trans*-2-butene at −20 °C; —□— and --■-- substitution of *trans*-2-butene for *S,S-trans*-2-butene at 8.0 °C; —△— and —▲— substitution for *R,R-trans*-2-butene at 8.0 °C. (The free *trans*-2-butene contained 1.0% *cis*-2-butene, and the individual plots were corrected for the contribution of the *cis*-isomer.)

Substitution. When those olefins in Table 3 were added to the *trans*(*N*,olefin)[PtCl(L-pro)(*S,S-trans*-2-butene)] in acetone, the UV absorption changed little, whereas the CD strength at 370 nm decreased. The final CD pattern was almost equal to that of *trans*(*N*,olefin)[PtCl(L-pro)(ethylene)], which gives only the vicinal effect of coordinated L-prolinate. The rate of decrease in CD strength obeyed first order rate law with respect to the complex concentration, and the rate constant $k_{0(\mathrm{cd})}$ was proportional to the olefin concentration. Second order rate constants $k_{2(\mathrm{cd})}$ can be calculated as in Eq. (3). They are listed in Table 3 together with the activation parameters obtained by the measurements at 8.0, 17.0 and 23.6 (±0.3 °C).

Discussion

Replacement of olefins in *trans*(*N*,olefin)[PtCl(L-pro)(olefin)] complexes by other olefins gave little change in the visible and UV absorption spectrum. Throughout the present isotopic exchange and CD measurements, the absorption spectra of the reaction mixtures and the recovered species gave little change. The geometrical isomers *trans*(*O*,olefin)[PtCl(L-pro)(olefin)] give different absorption patterns in UV region. Hence we can conclude that the essential structure of the complex remained unchanged throughout the present experiments, and only substitution of olefins for the coordinated olefin has taken place.

Nature of the decrease in CD strength. The substitution reaction of Eq. (4) with *cis*-2-butene

[PtCl(L-pro)(*S,S-trans*-2-butene)] + *cis*-2-butene
$\rightleftharpoons$ [PtCl(L-pro)(*cis*-2-butene)] + *trans*-2-butene (4)

gave equal $k_{2(\mathrm{iso})}$ and $k_{2(\mathrm{cd})}$ (Table 1). Hence the

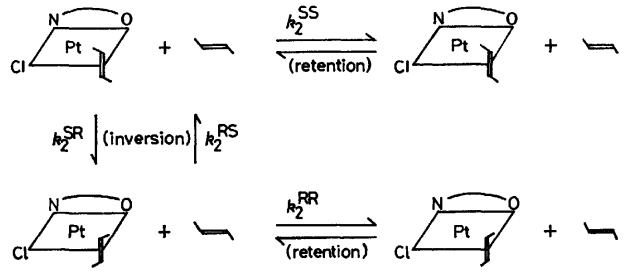

Fig. 3. Individual routes of the substitution of *trans*-2-butene for *S,S*- and *R,R-trans*-2-butene in the complex. Arcs represent L-prolinate. (*cf.* the note for Fig. 4).

decrease in CD strength at 370 nm should be exclusively due to the intermolecular substitution. Our proposal in Ref. 1 is thus verified. It is also made clear that there is no local proton exchange between free and coordinated olefin molecules.

Stereoselectivity. In the reaction between *trans*-2-butene and *trans*(*N*,olefin)[PtCl(L-pro)(*S,S-trans*-2-butene)], $k_{2(\mathrm{iso})}$ is significantly bigger than $k_{2(\mathrm{cd})}$. The former includes substitutions both with retention and with inversion of configuration of coordinated olefin, and the latter does only substitution with inversion of configuration. The same is true for the replacement of coordinated *R,R-trans*-2-butene. Hence the reactions are summerized as shown in Fig. 3. When the second order rate constants of individual routes of substitution between free *trans*-2-butene and coordinated *S,S*- and *R,R-trans*-2-butene are named as in Fig. 3, the following relationships are given between the individual k_2's and the observed k_2's. (The subscripts *SS* and *RR* denote the configuration of *trans*-2-butene in the original complexes.)

$$k_{2(\mathrm{iso})SS} = k_2{}^{SS} + k_2{}^{SR} \quad (5)$$

$$k_{2(\mathrm{iso})RR} = k_2{}^{RR} + k_2{}^{RS} \quad (6)$$

$$k_{2(\mathrm{cd})SS} = k_2{}^{SR} + k_2{}^{RS} \quad (7)$$

$$k_{2(\mathrm{cd})RR} = k_2{}^{RS} + k_2{}^{SR} \quad (8)$$

When the ratio of $k_2{}^{SR}$ and $k_2{}^{RS}$ is defined as Eq. (9),

$$K_{(SR)} = k_2{}^{SR}/k_2{}^{RS} \quad (9)$$

the $K_{(SR)}$ should be related to the CD strength due to the coordinated olefin in the equilibrated solution. The CD pattern of the reaction mixtures at infinite time is practically identical with that of non-prochiral olefin complexes such as *trans*(*N*,olefin)[PtCl(L-pro)(ethylene)], and $K_{(SR)}$ can be approximated to be unity. Hence Eq. (10) is substantiated.

$$k_{2(\mathrm{cd})SS} = 2k_2{}^{SR} = 2k_2{}^{RS} = k_{2(\mathrm{cd})RR} \quad (10)$$

Table 2 gives the rate constants calculated in accordance with Eqs. (5) to (8). The $k_2{}^{SR}$ and $k_2{}^{RS}$ values obtained by use of diastereoisomers of *trans*(*N*,olefin)[PtCl(L-pro)(*S,S*- or *R,R-trans*-2-butene)] as substrate coincide with each other, indicating equal probability of inversion. The ease of substitution reaction with retention of configuration seems to differ from each other so that $k_2{}^{SS}$ is *ca.* twice as big as $k_2{}^{RR}$. The ratio of second order rate constants with retention and with inversion of configuration are *ca.* 10 and 5, respectively for the complexes with *S,S*- and *R,R*- *trans*-2-butene ligand.

This fact indicates that both diastereoisomers are

Table 2. Calculated rate constants for individual routes of substitution and their ratios (*cf.* Fig. 3)

T/°C	+8.0	−20.0
$k_2/10^{-3}\mathrm{M}^{-1}\,\mathrm{s}^{-1}$		
$k_2{}^{SS}$	29	5.1
$k_2{}^{RR}$	14	(1.7) c)
$k_2{}^{SR}$ a)	3.1	0.45
$k_2{}^{SR}$ b)	2.8	(0.46) c)
$k_2{}^{SS}/k_2{}^{RR}$	2.1	(3) c)
$k_2{}^{SS}/k_2{}^{SR}$ a)	9.4	11
$k_2{}^{RR}/k_2{}^{SR}$ b)	5.0	(3.7) c)

a) The original complex contained *S,S-trans*-2-butene (Eqs. (7) and (9)). b) The original complex contained *R,R-trans*-2-butene (Eqs. (8) and (9)). c) Calcd from only one run.

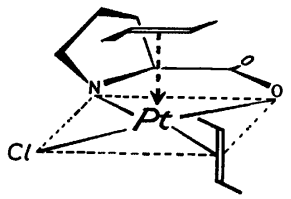

Fig. 4. Probable nucleophilic attack of *trans*-2-butene towards the complex.
The coordinated *trans*-2-butene was claimed to be rotating around the bond axis between Pt(II) and C=C[6]; the ligand is so illustrated as to make the configuration clear.

subject to olefin exchange more easily with retention of configuration than with inversion of configuration. Such a stereoselectivity is of a novel kind, and the present result is the first example. The reason why such a stereoselectivity is observed cannot be made clear at the present stage. The kinetic formulae have no term for the solvent path, and solvent molecules do not seem to give significant contribution. Difference in affinities between *trans*-2-butene nucleophile and the diastereoisomers is quite unlikely, and some kind of steric effect between the nucleophile and the coordinated ligands should be responsible. The $\Delta H^{\ddagger}$ values for $k_2{}^{SS}$ and $k_2{}^{SR}$ are 8.2 and 9.1 kcal mol^{-1} and the $\Delta S^{\ddagger}$ values are −38 and −40 cal mol^{-1} K^{-1}, respectively. These figures are only approximate, because measurements were made at two temperatures.

Figure 4 shows the possible mode of approach of the olefin nucleophile to the complex. (It was claimed that the coordinated olefin is rotating at a high rate around the metal–(C=C) axis[6]; the figure was so drawn as to make the configuration of the ligand clearer.)

Substitution. Whenever a large excess of olefin is added to the *trans*(*N*,olefin)[PtCl(L-pro)(*S,S-trans*-2-butene)] solution in acetone, the coordinated olefin is replaced by the added olefin and only a negligible amount of the original complex remains after a certain lapse of time. The CD pattern of the reaction mixture at infinite time is almost identical with that of [PtCl(L-pro)(ethylene)], and no other reaction than substitution of the olefin is feasible. The substitution

Table 3. Second order rate constants and activation parameters for the substitution of various olefins for the *S,S-trans*-2-butene in [PtCl(L-pro)(*S,S-trans*-2-butene)] in acetone measured by CD strength

Added olefin	R[b]	$k_{2(cd)}/10^{-3}M^{-1}s^{-1}$			$\Delta H^{\ddagger}$	$\Delta S^{\ddagger}$
		8.0 °C	17.0 °C	23.6 °C	kcal·mol^{-1}	cal K^{-1} mol^{-1}
cis-2-Butene	CH_3	347	480	621	9.6	−26
trans-2-Butene	CH_3	4.1	6.3	9.7	8.4	−39
cis-1,2-Dichloroethylene	Cl	0.63		1.08	(8)	(−44)
trans-1,2-Dichloroethylene	Cl	0.081		0.22	(10)	(−40)
Maleic acid	COOH	18.5		47	(10)	(−32)
Fumaric acid	COOH	1				
cis-1,4-Dichloro-2-butene	CH_2Cl	150		310	(7)	(−36)
trans-1,4-Dichloro-2-butene	CH_2Cl	8.8		19.2	(8)	(−40)
cis-2-Butene-1,4-diol	CH_2OH	335		775	(9)	(−29)
trans-1,4-Dibromo-2-butene	CH_2Br	8.05		22	(10)	(−31)
2-Methyl-2-butene[a]	CH_3	3.41	5.35	7.29	8.0	−41
2,3-Dimethyl-2-butene[a,c]	CH_3			0.22	8.0	−46
Styrene[a]	C_6H_5	303	480	621	7.6	−34

a) Data from Ref. 1. b) Substituents on ethylene. c) Activation papmeters from data at 23.6, 31.5 and 39.5 °C.

of the olefins listed in Table 3 obeyed Eq. (3) and the $k_{2(cd)}$ and the activation parameters are given there.

Electronic Effect: When the k_2 values are compared with one another for either the *cis* or the *trans* olefins with one substituent on each of ethylenic carbon, an overall decrease in rate is seen in the following squence.

$-CH_3 \simeq -CH_2Cl \simeq -CH_2OH \simeq -CH_2Br > -COOH > -Cl$

Introduction of electro-nagative substituents on ethylenic carbon decreases the rate significantly. More electro-negative chlorine (3.25) decreases the rate to a greater extent than less electro-negative carboxyl[7] (2.60)(*cf.* methyl 2.50) does. Increase in electronegativity of the substituent should bring about decrease of electron density in the bonding orbital of the ethylene moiety, and thus decrease of the σ-bond strength between platinum(II) and olefin. Our previous proposal that strength of the σ-metal–ligand bond would be responsible in determining the substitution rate of olefins[1], has thus found further experimental support.

Substitution of chlorine, bromine and hydroxyl for the methyl protons of 2-butene does not give big change in k_2's. The order of k_2 change is different for the *cis*-olefins and the *trans*-olefins. The significance of k_2 can be different for the two kinds of geometrically isomeric olefin nucleophiles (see below), and no further discussion will be made at the present stage.

Steric Effect: An overall trend is seen in Table 3 that the *cis*-isomers give larger k_2 values than the *trans*-isomers do. It is also seen that increase in number of methyl groups on ethylenic carbons decreases the k_2 quite remarkably. These factors should be ascribed to some kind of steric effect at the rate-determining step.

Since the *trans*-isomers and 2-methyl-2-butene are prochiral and can bring forward stereo-selectivity as mentioned above, the $k_{2(cd)}$ value of their substitution reckons the rate of substitution with inversion of configuration. On the other hand, the *cis*-isomers, styrene and 2,3-dimethyl-2-butene are not prochiral and their k_2 values represent the real rate of substitution. Hence the k_2 values for these two series of olefins should not be directly compared. However, the ratio of k_2's for substitution with retention and those with inversion of configuration is not extremely big; *i.e.* it is *ca.* 10 for *trans*-2-butene (Table 2). Hence such comparisons should not be very unfair so far as the discussion remains qualitative.

The olefin nucleophiles in Table 3 (except those with very electro-negative groups on ethylenic carbons) could be classified into three groups according to the k_2 values. The *cis*-isomers and styrene give the biggest k_2's, 2,3-dimethyl-2-butene gives the smallest k_2, and others, *i.e.* the *trans*-isomers and 2-methyl-2-butene, give intermediate values. Members of each group seem to have common feature in their structures. The first group has substituent only on one side of the C=C bond axis and has two protons on the other side. The third group has at least one proton on one side of the axis, and 2,3-dimethyl-2-butene has no proton on either side. If the nucleophilic attack of the olefin molecule were visualized as shown in Fig. 4, the assemblage around the C=C bond axis would be responsible in determining the ease of approach to the substrate. It seems as if the number of vacant site (*i.e.* with proton) on one side of the C=C bond axis were an important factor in determining the ease of approach.

The $\Delta H^{\ddagger}$ values in Table 3 do not give useful information, because they are more or less similar to one other, when experimental errors are taken into consideration. The $\Delta S^{\ddagger}$ values do not differ very significantly from one another but could be reckoned to reflect the steric factor to some extent.

References

1) K. Konya, J. Fujita, H. Kido, and K. Saito, This Bulletin, **45**, 2161 (1972).

2) J. Fujita, K. Konya, and K. Nakamoto, *Inorg. Chem.*, **9**, 2794 (1970).

3) L. W. Trevoy and W. G. Brown, *J. Amer. Chem. Soc.*, **71**, 1675 (1949).

4) L. H. Amundsen, R. H. Mayer, L. S. Pitts, and L. A. Malentacchi, *ibid.*, **73**, 2118 (1951).

5) A. Valett, *Ann. Chim.*, **3**, 644 (1948).

6) C. E. Holloway, G. Hulley, B. F. G. Johnson, and J. Lewis, *J. Chem. Soc., A*, **1969**, 53; **1970**, 1653; J. Ashley-Smith, I. Douek, B. F. G. Johnson, and J. Lewis, *J. Chem. Soc., Dalton*, **1972**, 1776; J. Ashley-Smith, Z. Douek, B. F. G. Johnson, and J. Lewis, *ibid*, **1974**, 128.

7) J. R. Cavanaugh and B. P. Bailey, *J. Chem. Phys.*, **34**, 1099 (1961).

Sugars Containing a Carbon-phosphorus Bond. VI.[1,2] 5-(Alkylphosphinyl)-5-deoxy-D-xylopyranose

Kuniaki SEO and Saburo INOKAWA*

Department of Industrial Chemistry, Numazu Technical College, Ooka, Numazu 410

**Department of Synthetic Chemistry, Faculty of Engineering, Shizuoka University, Johoku, Hamamatsu 432*

(Received February 22, 1974)

The reactions of diethyl ethylphosphonite with 3-*O*-acetyl-5-deoxy-5-iodo-1,2-*O*-isorpopylidine-α-D-xylofuranose (Ia) or 3-*O*-benzoyl-5-deoxy-5-iodo-1,2-*O*-isopropylidene-α-D-xylofuranose(Ib) afforded IIa or IIc, respectively. Similarly, using diethyl butylphosphonite in place of diethyl ethylphosphonite, IIb and IId were obtained. Treatment of IIb with methanolic sodium methoxide gave 5-deoxy-1,2-*O*-isopropylidene-5-(methoxybutylphosphinyl)-α-D-xylofuranose together with a small amount of 5-(3-*O*-cyclo-butylphosphinate)-5-deoxy-1,2-*O*-isopropylidene-α-D-xylofuranose(VII). Compound VII was also obtained from the reaction of 5-deoxy-5-iodo-1,2-*O*-isopropylidene-α-D-xylofuranose(VIII) and diethyl butylphosphonite. The reaction of IIa or IIc with sodium dihydrobis(2-methoxyethoxy)aluminate gave 5-deoxy-5-(ethylphosphinyl)-1,2-*O*-isopropylidene-α-D-xylofuranose(IIIa). Similarly, 5-(butylphosphinyl)-5-deoxy-1,2-*O*-isopropylidene-α-D-xylofuranose(IIIb) was obtained from IIb, IId, VI, and VII. Hydrolysis of IIIa and IIIb with sulfuric acid gave 5-deoxy-5-(ethylphosphinyl)-(IVa) and 5-(butylphosphinyl)-5-deoxy-D-xylopyranose(IVb), respectively. Acetylation of IVa and IVb with acetic anhydride in pyridine gave the corresponding *O*-acetates Va and Vb.

Recently, we reported the synthesis of 3-*O*-benzyl-5-deoxy-5-(ethylphosphinyl)-D-xylopyranose,[3] 5-(alkylphosphinyl)-5-deoxy-3-*O*-methyl-D-xylopyranose (alkyl; ethyl, butyl)[4] and 5-deoxy-5-(ethylphosphinyl)-D-ribopyranose,[1] sugar analoges having a phosphorus atom in the hemiacetal ring. In this paper we wish to report the syntheses of 5-deoxy-5-(ethylphosphinyl)-D-xylopyranose(IVa) and 5-(butylphosphinyl)-5-deoxy-D-xylopyranose(IVb).

Results and Discussion

In the present experiments, 3-*O*-acety-5-deoxy-5-iodo-1,2-*O*-isopropylidene-α-D-xylofuranose(Ia) and 3-*O*-benzoyl-5-deoxy-5-iodo-1,2-*O*-isopropylidene-α-D-xylofuranose(Ib) were used as the starting materials. The Michaelis-Arbuzov reaction[5] of Ia or Ib with diethyl ethylphosphonite gave, almost quantitatively, 3-*O*-acetyl-(IIa) or 3-*O*-benzoyl-5-deoxy-5-(ethoxyethylphosphinyl)-1,2-*O*-isopropylidene-α-D-xylofuranose(IIc), respectively. Similarly, the reaction of Ia or Ib with diethyl butylphosphonite gave 3-*O*-acetyl-(IIb) or 3-*O*-benzoyl-5-deoxy-5-(ethoxybutylphosphinyl)-1,2-*O*-isopropylidene-α-D-xylofuranose (IId), respectively. Reduction of IIa(IIc) or IIb(IId) with 3.3 molar equivalents of sodium dihydrobis(2-methoxyethoxy)aluminate(SDMA) in tetrahydrofuran (THF) gave, almost quantitatively,** syrupy 5-deoxy-5-(ethylphosphinyl)-(IIIa)or5-(butylphosphinyl)-5-deoxy-1,2-*O*-isopropylidene-α-D-xylofuranose(IIIb), respectively. The PMR spectrum of IIIa(IIIb) in chloroform-*d* showed a characteristic J_{P-H} value[6] of 469 Hz at δ 6.90 (470 Hz at δ 5.90); the signal disappeared on deuteration. The IR spectrum (KBr) of IIIa(IIIb) showed absorption due to a P–H group at 2350 cm^{-1} (2350 cm^{-1})[7] and absorption due to a P=O group at 1220 cm^{-1} (1220 cm^{-1}).[8] Compound IIIb was also obtained by hydrolysis of IIb and subsequent reduction. Treatment of IIb with sodium methoxide in methanol gave, in good yield, syrupy 5-deoxy-1,2-*O*-isopropylidene-5-(methoxybutylphosphinyl)-α-D-xylofuranose(VI) together with a small amount of crystalline 5-(3-*O*-cyclo-butylphosphinate)-5-deoxy-1,2-*O*-isopropylidne-α-D-xylofuranose(VII). The PMR spectrum of VI on chloroform-*d* showed P–OCH_3 (J_{P-H} = 10.5 Hz) at δ 3.56 and OH at δ 4.79 (disappearing on deuteration). The PMR spectrum of VII showed an H-3 proton signal at δ 5.18 which was at lower field than that of VI (δ 4.00). No P–OCH_3 (or P–OC_2H_5) and OH signals were found. On reduction with SDMA, VI and VII both gave IIIb in good yield. Compound VII was also obtained, almost quantitatively, by heating 5-deoxy-5-iodo-1,2-*O*-

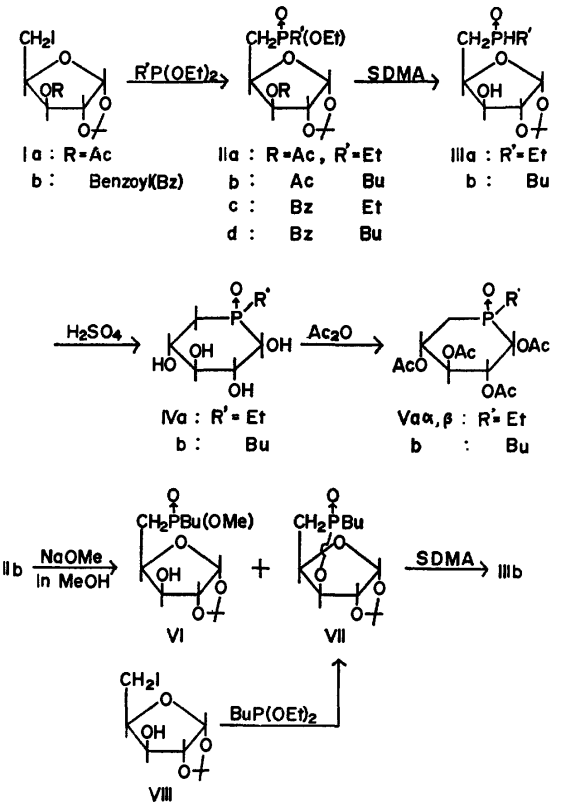

* To whom correspondence should be addressed.

** Treatment of IId with lithium aluminum hydride[3] gave IIIb in lower yield.

isopropylidene-α-D-xylofuranose(VIII) in diethyl butylphosphonite.

Hydrolysis of IIIa or IIIb with dilute sulfuric acid (1—2%) for two hr at 80—100 °C afforded, in good yield, a hygroscopic solid, 5-deoxy-5-(ethylphosphinyl)-(IVa) or 5-(butylphosphinyl)-5-deoxy-D-xylopyranose (IVb), respectively. Study of their PMR (DMSO-d_6) and IR(KBr) spectra showed that IVa(IVb) had four OH groups and no P–H group. Acetylation of IVa with acetic anhydride in pyridine gave two kinds of crystalline 1,2,3,4-tetra-*O*-acetyl-5-deoxy-(ethylphosphinyl)-D-xylopyranose: one(Vaβ) had mp 232—234.5 °C, $[\alpha]_D^{18}$ −22° and the other(Vaα) had mp 176—178 °C, $[\alpha]_D^{18}$ +26°. The PMR spectra of Vaα and Vaβ showed four acetyl groups and no P–H group. Acetylation of IVb gave only one crystalline tetra-*O*-acetate(Vb), mp 156.5—158.5 °C, $[\alpha]_D^{19}$ +28°. The PMR spectrum of Vb showed four acetyl groups and no P–H group. Attempts to analyze the conformations of Vaα and Vaβ by 100 MHz PMR have been so faru nsuccessful.

Experimental

Melting points were determined by a Yanagimoto micro melting point apparatus. Infrared spectra were measured on a Hitachi EPI-G2 grating spectrophotometer. Proton magnetic resonance spectra were taken at 60 MHz on a Hitachi-Perkin-Elmer R-20 spectrometer, with tetramethylsilane as an internal standard. Optical rotations (sodium D line) were measured with a Hitachi PO-B polarimeter using a 0.5-dm cell. Thin-layer chromatography (tlc) was carried out on microscope slides coated with silica gel[9] in ethyl acetate–petroleum ether (A) (1 : 1 v/v), (B) (1 : 2 v/v), and (C) (1 : 4 v/v): the spots were visualized with sulfuric acid–ethanol solution.

Materials. *3-O-Acetyl-5-deoxy-5-iodo-1,2-O-isopropylidene-α-D-xylofuranose(Ia)* was prepared in 91% yield by conventional acetylation of 5-deoxy-5-iodo-1,2-*O*-isopropylidene-α-D-xylofuranose(IX)[10]. Mp 65—66 °C, $[\alpha]_D^{16.5}$ −49° (*c* 2.3, $CHCl_3$);

Found: C, 35.11; H, 4.46%. Calcd for $C_{10}H_{15}IO_5$: C, 35.11, H, 4.42%.

3-O-Benxoyl-5-deoxy-5-iodo-1,2-O-isopropylidene-α-D-xylofuranose(Ib) was prepared in 86% yield by conventional benzoylation of IX. Mp 46—48 °C, $[\alpha]_D^{16}$ −40° (*c* 10, CH_3OH);

Found: C, 44.53; H, 4.20%. Calcd for $C_{15}H_{17}IO_5$: C, 44.68; H, 4.25%.

3-O-Acetyl-5-(ethoxyethylphosphinyl)-1,2-O-isopropylidene-α-D-xylofuranose(IIa). A solution of Ia(5 g) in diethyl ethylphosphonite (10 ml) was heated under a nitrogen atmosphere for 10 hr at 140—150 °C, while the phosphonite (2 ml) was added several times. The excess phosphonite was distilled off *in vacuo* and the residue was dissolved in chloroform; the solution was washed with water, dried (sodium sulfate), and evaporated *in vacuo* to give a syrup of IIa (4.8 g, 98%); R_f: 0.25 (Solvent B); $[\alpha]_D^{20}$ −9.1° (*c* 1.3, $CHCl_3$); IR (KBr): 124 cm^{-1} (P=O); PMR ($CDCl_3$): δ 0.80—2.16 (16H, m, H-5,5′, P-C_2H_5, O-C-CH_3, $C(CH_3)_2$), 2.19 (3H, s, $COCH_3$), 4.01 (2H, q, $POCH_2$–), 4.47 (1H, d, overlapping with H-4, H-2), 5.10 (1H, d, $J_{3,4}$=3.0 Hz, H-3), 5.81(1H, d, $J_{1,2}$=4.0 Hz, H-1).

*3-O-Acetyl-5-(ethoxybutylphosphinyl)-1,2-O-isopropylidene-α-D-xylofuranose(IIb).**** 98%; R_f 0.20 (solvent B); $[\alpha]_D^{20}$ −9.1° (*c* 13, $CHCl_3$); IR (KBr) 1240 cm^{-1} (P=O); PMR ($CDCl_3$): δ 0.69—2.65 (20H, m, H-5,5′, P-C_4H_9, O-C-CH_3, $C(CH_3)_2$, 2.04 (3H, s, $COCH_3$), 3.99 (2H, m, $POCH_2$–), 4.42 (1H, d, overlapping with H-4, H-2), 5.04 (1H, d, $J_{3,4}$=3.0 Hz, H-3), 5.75 (1H, d, $J_{1,2}$=4.0 Hz, H-1).

*3-O-Benzoyl-5-deoxy-5-(ethoxyethylphosphinyl)-1,2-O-isopropylidene-α-D-xylofuranose(IIc).**** 96%; R_f: 0.20 (Solvent B); $[\alpha]_D^{21}$ −13° (*c* 4.3, $CHCl_3$); IR (KBr): 1240 cm^{-1} (P=O); PMR ($CDCl_3$): δ 0.74—2.40 (16H, m, H-5,5′, P-C_2H_5, O-C-CH_3, $C(CH_3)_2$), 4.00 (2H, m, $POCH_2$–), 4.64 (1H, d, overlapping with H-4, H-2), 5.41 (1H, d, $J_{3,4}$=3.0 Hz, H-3), 5.96 (1H, $J_{1,2}$=4.0 Hz, H-1), 7.22–8.20 (5H, *m*, COC_6H_5).

*3-O-Benzoyl-5-deoxy-5-(ethoxybutylphosphinyl)-1,2-O-isopropylidene-α-D-xylofuranose(IId).**** 98%; R_f: 0.20 (Solvent B); $[\alpha]_D^{13}$ −7.5° (*c* 14, $CHCl_3$); IR (KBr): 1240 cm^{-1} (P=O); PMR ($CDCl_3$): δ 0.63—2.23 (20H, m, H-5,5′, P-C_4H_9, O-C-CH_3, $C(CH_3)_2$, 3.94 (2H, m, $POCH_2$–), 4.54 (1H, d, overlapping with H-4, H-2), 5.28 (1H, d, $J_{3,4}$=3.0 Hz, H-3), 5.80 (1H, d, $J_{1,2}$=4.0 Hz, H-1), 7.20—8.10 (5H, m, COC_6H_5).

5-Deoxy-5-(ethylphosphinyl)-1,2-O-isopropylidene-α-D-xylofuranose (IIIa). To a solution of IIa (0.2 g) (IIb) in tetrahydrofuran (THF) (200 ml) was added THF (100 ml) containing a 70% benzene solution (6.0 g) of sodium dihydrobis(2-methoxyethoxy)alminate (SDMA) under a nitrogen atmosphere in an ice-salt bath. After stirring for 1 hr at room temperature, the reaction mixture was neutralized with THF containing hydrochloric acid and filtered; the filtrate was dried (sodium sulfate) and evaporated, to give a syrup of IIIa (1.4 g, 94%). An analytical crystalline sample was obtained by silica-gel column chromatography (Solvent A and methanol); R_f: 0.1 (Solvent A); mp 120—121 °C, $[\alpha]_D^{17}$ −12.4° (*c* 2.6, $CHCl_3$); IR (KBr): 2350 cm^{-1} (P–H), 1220 cm^{-1} (P=O); PMR ($CDCl_3$): δ 0.73—2.58 (13H, m, H-5,5′, P-C_2H_5), $C(CH_3)_2$, 4.12 (1H, d, H-3), 4.53 (1H, d, overlapping with H-4, H-2), 5.15 (1H, broad s, disappearing on deuteration, OH), 5.86 (1H, d, $J_{1,2}$=4.0 Hz, H-1), 6.90 (1H, m, disappearing on deuteration, J_{P-H}=468 Hz, P–H).

Found: C, 47.67; H, 8.04%. Calcd for $C_{10}H_{19}O_5P$: C, 47.98; H, 8.00%.

5-(Butylphosphinyl)-5-deoxy-1,2-O-isopropylidene-α-D-xylofuranose(IIIb). Compound IIb (2.5 g) was treated as described above to give a syrup of IIIb (1.8 g, 94%). R_f: 0.10 (Solvent A); $[\alpha]_D^{16.5}$ −17.3° (*c* 4.4, $CHCl_3$), IR (KBr): 2350 cm^{-1} (P–H), 1220 cm^{-1} (P=O); PMR ($CDCl_3$): δ 0.70—2.55 (17H, m, H-5,5′, P-C_4H_9, $C(CH_3)_2$), 4.18 (1H, d, H-3), 4.56 (1H, d, overlapping with H-4, H-2), 4.95 (1H, broad s, disappearing on deuteration, OH), 5.90 (1H, d, $J_{1,2}$=4.0 Hz, H-1), 6.90 (1H, m, diasppearing on deuteration, J_{P-H}=470 Hz, P–H).

5-Deoxy-1,2-O-isopropylidene-5-(methoxybutylphosphinyl)-α-D-xylofuranose(VI) and 5-(3-O-cyclo-butylphosphinate)-5-deoxy-1,2-O-isopropylidene-α-D-xylofuranose(VII). To a solution of IIb (2.1 g) in methanol (20 ml) was added a small amount of sodium methoxide and the solution stood for two days at room temperature. The solution was neutralized with Amberlite IRC-50 (H^+) ion-exchange resin and evaporated *in vacuo* to give a syrup (VI) containing a solid (VII) (1.5 g, 94% as VI) (VI : VII=5 : 1 from the PMR spectrum). The solid (VII) was collected and recrystallized from ethyl acetate. (VI), R_f: 0.30 (Solvent A), $[\alpha]_D^{16}$ −20° (*c* 2.5, $CHCl_3$); PMR ($CDCl_3$): δ 0.61—2.30 (17H, m, H-5,5′, P-C_4H_9, $C(CH_3)_2$), 3.56 (3H, d, J_{P-H}=10.5 Hz, P-OCH_3), 4.00 (1H,

*** These compounds were prepared by treatment of the corresponding sugars with the phosphonites.

d, H-3), 4.40 (1H, d, overlapping with H-4, H-2), 4.75 (1H, broad s, disappearing on deuteration, OH), 5.73 (1H, d, $J_{1,2}$=4.0 Hz, H-1). (VII), R_f, 0.35 (Solvent A); mp 221.5—222 °C; $[\alpha]_D^{14}$ +32° (*c* 2.3, CH_3OH); PMR ($CDCl_3$): δ 0.80—2.63 (17H, m, H-5,5′, P-C_4H_9, $C(CH_3)_2$); 4.58 (1H, m, H-4), 4.79 (1H, d, H-2), 5.18 (1H, *m*, 1H, m, H-3), 6.02 (1H, d, $J_{1,2}$=4.0 Hz, H-1).

Found: C, 52.19; H, 7.71%. Calcd for $C_{12}H_{21}O_5P$: C, 52.17; H, 7.66%.

The reduction of VI and VII with 1.2 molar equivalents of SDMA gave, almost quantitatively, IIIb.

Compound VII from 5-deoxy-5-iodo-1,2-O-isopropylidene-α-D-xylofuranose (VIII). A solution of VIII (1.4 g) in diethyl butylphosphonite (3 ml) was heated under a nitrogen atmosphere for 2 hr at 130—140 °C; the resulting precipitates were collected by filtration and the filtrate was evaporated *in vacuo*. The conbined precipitates were recrystallized from ethyl acetate to give pure crystalline VII (1.2 g, 93%).

5-Deoxy-5-(ethylphosphinyl)-D-xylopyranose (IVa). A solution of IIIa (1.0 g) and concentrated sulfuric acid (0.5 ml) in water (50 ml) containing a small amount of THF was heated under a stream of nitrogen for 2 hr at 100 °C. The hot solution was neutralized with barium carbonate, followed by filtration and evaporation to give a hygroscopic solid of IVa (0.8 g, 95%); R_f: 0.10 (Solvent C); $[\alpha]_D^{16.5}$ +5.8° (*c* 6.8, H_2O); IR (KBr): 1240 cm^{-1} (P=O); PMR (DMSO-d_6): δ 0.5—2.4 (7H, m, H-5,5′, P-C_2H_5), 3.0—4.5 (7H, m, four of them disappearing on deuteration).

5-(Butylphosphinyl)-5-deoxy-D-xylopyranose (IVb). Compound IIIb (0.9 g) was treated as described above to give a hygroscopic solid, IVb (0.7 g, 91%; R_f: 0.10 (Solvent C); $[\alpha]_D^{16.5}$ +11° (*c* 5.5, CH_3OH); IR (KBr): 1240 cm^{-1} (P=O); PMR (DMSO-d_6): δ 0.5—2.0 (11H, m, H-5,5′, P-C_4H_9), 4.6—5.3 (5H, m, four of them disappearing on deuteration).

1,2,3,4-Tetra-O-acetyl-5-deoxy-5-(ethylphosphinyl)-D-xylopyranose (Va). Treatment of IVa (1.4 g) with acetic anhydride (4.5 ml) in pyridine (20 ml) in the usual way gave a syrupy mixture of Vaα and Vaβ (2.2 g, 88%, $[\alpha]_D^{14.5}$ +20.9° (*c* 2.2, $CHCl_3$)). The syrup was crystallized by standing for several days in a refrigerator. Recrystallization from ethanol gave colorless crystals (Vaβ, 0.06 g), mp 232—234.5 °C, $[\alpha]_D^{18}$ −22° (*c* 1.6, $CHCl_3$). The ethanolic mother solution was evaporated *in vacuo*: recrystallization of the precipitates from ethanol-*n*-hexane gave colorless crystals (Vaα, 0.21 g), mp 176—178 °C, $[\alpha]_D^{18}$ +26° (*c* 1.4, $CHCl_3$).

Vaβ; PMR ($CDCl_3$): δ 0.80—2.82 (7H, m, H-5,5′, P-C_2H_5), 1.95, 1.98, 2.10 (12H, s, 1,2,3,4-$COCH_3$), 5.00-5.75 (4H, m, H-1,2,3,4).

Found: C, 47.32; H, 6.53%. Calcd for $C_{15}H_{23}O_9P$: C, 47.62; H, 6.13%.

Vaβ; PMR ($CDCl_3$): δ 1.00—2.76 (7H, m, H-5,5′, P-C_2H_5), 1.95, 2.00, 2.06 (12H, s, 1,2,3,4-$COCH_3$), 5.04—5.76 (4H, m, H-1,2,3,4).

1,2,3,4-Tetra-O-acetyl-5-(butylphosphinyl)-5-deoxy-D-xylopyranose (Vb). Compound IVb (0.7 g) was treated as described above to give a syrup of Vb (1.0 g, 84%, $[\alpha]_D^{14.5}$ +20.3 ° (*c* 3.5, $CHCl_3$)). Crystals were obtained from the syrup by standing for several days in a refrigerator. Recrystallization from ethanol-*n*-hexane gave colorless crystals (Vb, 0.2 g); mp 156.5—158.5 °C; $[\alpha]_D^{19}$ +28° (*c* 1.4, $CHCl_3$); PMR ($CDCl_3$): δ 1.00—2.76 (11H, m, H-5,5′, P-C_4H_9), 1.96, 2.02, 2.17 (12H, s, 1,2,3,4-$COCH_3$), 5.17—5.93 (4H, m, H-1,2,3,4).

Found: C, 49.80; 6.85%. Calcd for $C_{17}H_{27}O_9P$: C, 50.25; H, 6.70%.

References

1) Part V: S. Inokawa, H. Kitagawa, K. Seo, H. Yoshida, and T. Ogata, *Carbohyd. Res.*, **30**, 127 (1973).

2) This paper was reported in part at the 26th (Hiratsuka, April, 1972) and 30th (Higashi-osaka, April, 1974) Annual Meetings of the Chemical Society of Japan.

3) S. Inokawa, Y. Tsuchiya, K. Seo, H. Yoshida, and T. Ogata, This Bulletin, **44**, 2279 (1971).

4) K. Seo and S. Inokawa, *ibid.* **46**, 3301 (1973).

5) See, for example, G. M. Kosolapoff, "Organic Reactions," Vol. 6, John Wiley & Sons, New York (1951), p. 273.

6) H. R. Hays, *J. Org. Chem.*, **33**, 3690 (1968).

7) R. A. Chittenden and L. C. Thomas, *Spectrochim. Acta*, **20**, 861 (1964).

8) L. C. Thomas and R. A. Chittenden, *ibid.*, **20**, 467 (1964).

9) Silica-Layer G-10, Nakarai Chemicals.

Conformations of Sequential Polypeptides of L-Leucine and Glycine in Solution

Takayoshi Iio and Sho Takahashi*

Department of Physics, Faculty of Science, Nagoya University, Chikusa-ku, Nagoya 464

**Institute for Chemical Research, Kyoto University, Uji, Kyoto-fu 611*

(Received May 7, 1974)

With the aid of optical rotatory dispersion, circular dichroism, and infrared spectra, the conformations of the sequential polypeptides of L-leucine and glycine, $(Leu_3Gly)_n$, $(Leu_2Gly)_n$, $(LeuGly)_n$, and $(LeuGly_2)_n$, were studied and compared with the conformation of poly-L-leucine. It was shown that the polymers $(Leu)_n$, $(Leu_3Gly)_n$, $(Leu_2Gly)_n$, and $(LeuGly)_n$ could be α-helical in solution, but $(LeuGly_2)_n$ was not. The order of the stability of the α-helix of these polymers was found to be: $(Leu)_n > (Leu_3Gly)_n \sim (Leu_2Gly)_n > (LeuGly)_n > (LeuGly_2)_n$. This was attributed to interactions between side chains of L-leucines which were regularly arranged on the α-helix.

Poly-L-alanine is known to assume the very stable α-helix conformation in solution[1], on the other hand, glycine destabilizes the α-helix when it is incorporated in a polypeptide chain which otherwise might be α-helical[2]. By studying the sequential polypeptides of L-alanine and glycine we concluded that, although the short range interactions between a side chain and the atoms of the backbone of the same amino acid residue were important, the interactions between the neighboring residues could not be neglected in explaining the stability of the α-helix of the polymers, which was in the order: Ala > $(Ala_2Gly)_n$ > $(Ala_3Gly)_n$ > $(AlaGly_2)_n$ and was not proportional to the alanine content.

Poly-L-leucine also forms the very stable α-helix in water.[4] Because the side chain of leucine is much larger than that of alanine, it is desirable to study the conformational stability of sequential polypeptides of L-leucine and glycine. In this paper we report a conformational study of sequential polypeptides of L-leucine and glycine in solution.

Experimental

Polymers. The sequential polypeptides, poly(L-leucyl$_3$-glycine) (intrinsic viscosity in dichloroacetic acid at 25 °C, $[\eta]=0.158$ dl/g), poly(L-leucyl$_2$glycine)($[\eta]=0.191$), poly(L-leucylglycine) ($[\eta]=0.151$), and poly(L-leucylglycylglycine) ($[\eta]=0.262$), were obtained from the *p*-nitrophenylesters of L-leucyl$_3$glycine, L-leucyl$_2$glycine, (L-leucylglycyl)$_2$, and L-leucylglycylglycine, respectively.[5] Poly-L-leucine ($[\eta]=1.86$ in 80% trifluoroacetic acid/20% chloroform) was prepared via the usual N-carboxyanhydride method by Dr. A. Warashina of the Faculty of Science, Nagoya University. These polymers are abbreviated: $(L_3G)_n$, $(L_2G)_n$, $(LG)_n$, and $(L)_n$, respectively. The fairly large values of the intrinsic viscosity in solvents favoring the random coil conformation should be noted as they indicated that the degrees of polymerization of these polymers were high enough for conformational studies.[6]

Solution Studies. The plymers could only be dissolved in dichloroacetic acid (DCA) or in trifluoroacetic acid (TFA), so their solutions were prepared by dissolving vacuum-dried polymer in TFA and then adding TFA and chloroform or 2,2,2-trifluoroethanol (TFE) to give a solution of the required solvent ratio.

Optical rotatory dispersion (ORD) spectra over the 280—500 nm wavelength range were measured with a JASCO ORD/UV 5 spectrometer using a 1 cm cell. The solution concentrations were in the range 0.8—1.1 g/100 ml.

Circular dichroism (CD) spectra below 250 nm were measured with the same apparatus using a 0.2 cm cell. The concentration of the solution was 0.035 g/100 ml. All measurements were performed at 24 °C. To calculate [m'], the reduced mean residue rotation in degree cm^2/dmol, and [θ], molar ellipticity in the same units, from the observed rotation angle, χ^{ORD} and χ^{CD}, Eqs. (1) and (2) were used.

$$[m'] = \frac{n^2+2}{3} \cdot \frac{M}{c} \cdot \frac{\chi^{ORD}}{l} \quad (1)$$

$$[\theta] = \frac{45 \ln 10}{\pi} \cdot \frac{M}{c} \cdot \frac{\chi^{CD}}{l} \quad (2)$$

where the refractive index of the composite solvent, n, was calculated from the Lorentz-Lorenz equation using the refractive index of each pure solvent, c is the concentration of a polymer in grams per 100 ml, l is the path length in decimeters, and M is the mean residue molecular weight of polymer. ORD parameters, a_0 and b_0, were obtained by plotting the values of the optical rotation in terms of the Moffitt-Yang equation (3)[7] with a value of $\lambda_0=212$ nm.

$$[m'] = \frac{a_0\lambda_0^2}{\lambda^2-\lambda_0^2} + \frac{b_0\lambda_0^4}{(\lambda^2-\lambda_0^2)^2} \quad (3)$$

Infrared (IR) spectra were recorded with a JASCO IR-G spectrophotometer. The concentration of the solution ranged from 3 to 5 g/100 ml. Films of each polymer were prepared from TFA solution by casting the solution (polymer concentration about 5 g/100 ml) on a KBr plate and by drying the film under a vacuum at 40 °C.

Results

ORD Measurements. a_0 and b_0 values as a function of solvent composition were obtained from ORD spectra measured in a TFA–$CHCl_3$ system. These values are plotted in Fig. 1, which shows that $(L)_n$ had a random coil conformation in TFA, a random coil favoring solvent, and changed to an α-helix when the content of $CHCl_3$, a helix favoring solvent, increased.[1] The values of b_0 for $(LG)_n$ and $(LG_2)_n$ were low and did not change appreciably with solvent composition, indicating that the glycyl residues in these polymers inhibited the transition from the random coil to the helix. Polymers $(L_3G)_n$ and $(L_2G)_n$ showed a transition, but in these cases the helical content, which was considered to reflect the stability of the helix, was reduced. The magnitude of b_0 is slightly larger for $(L_2G)_n$ than for $(L_3G)_n$ throughout the whole range of TFA concentration. The

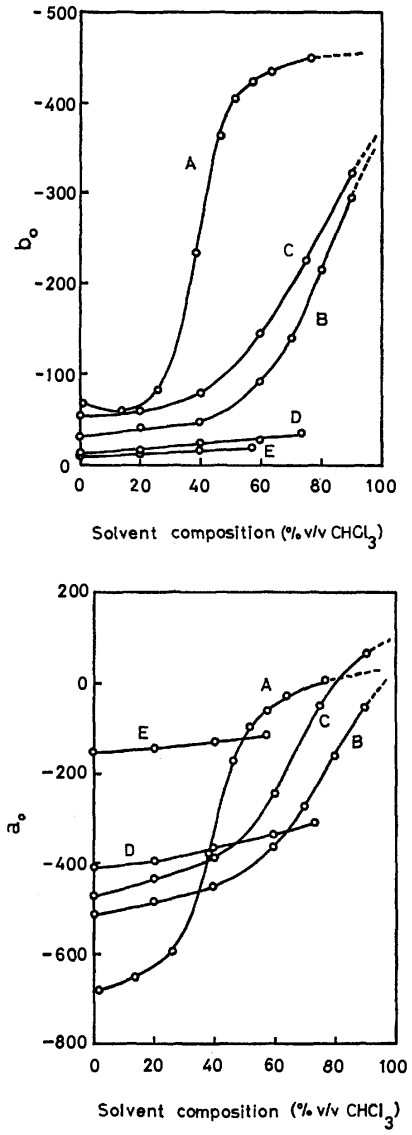

Fig. 1. Variation of the ORD parameters, a_0 and b_0, with solvent composition. A: $(L)_n$, B: $(L_3G)_n$, C: $(L_2G)_n$, D: $(LG)_n$, E: $(LG_2)_n$. Data on $(L)_n$ were obtained by A. Warashina in Ref. 8.

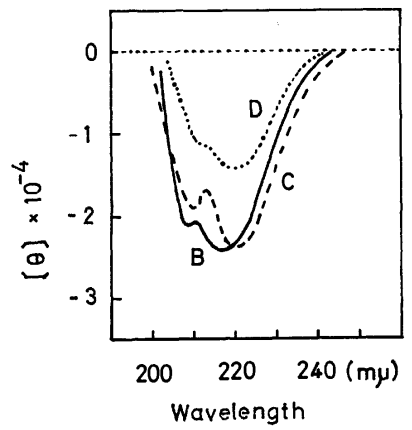

Fig. 2. CD spectra of the polymers in 96.8%TFE/3.2% TFA (v/v).
Letter symbols are the same as used in Fig. 1.

increase in b_0 in each case is accompanied by the corresponding increase in the value of a_0.

CD Measurements. The CD spectra in the far ultraviolet region for $(L_3G)_n$, $(L_2G)_n$, and $(LG)_n$ in 96.8% TFE/3.2% TFA are shown in Fig. 2. The polymers $(L)_n$ and $(LG_2)_n$ did not dissolve in such a solvent having such a large amount of TFE which was required if the solution was to be transparent in the far-ultraviolet region.

The polymer $(L_3G)_n$ exhibited two minima at 209 and 218 nm in the CD spectrum, and $(L_2G)_n$ exhibited minima at 210 and 222 nm. These bands are characteristic of the α-helix.[9] Though the magnitude of the molar ellipticity was reduced, polymer $(LG)_n$ also exhibited a spectrum characteristic of an α-helix. The value of the molar ellipticity of the band near 220 nm was −24000 for $(L_3G)_n$, −23000 for $(L_2G)_n$, and −14000 for $(LG)_n$ (a molar ellipticity of −32000 was reported for a complete α-helix in the 220 nm region[9]). From these observations, we can conclude that an α-helix exists in the polymers $(L_3G)_n$, $(L_2G)_n$, and also exists in $(LG)_n$ in solutions which contain a large amount of a helix-favoring solvent.

IR Measurements. IR spectra of the polymers in 70% $CHCl_3$/30% TFA solutions are shown in Fig. 3. All the polymers exhibited the amide I band at 1650 cm^{-1} and the amide II band around 1540 cm^{-1}, these were considered to originate from either the α-helical or the randomly coiled conformation of the polypeptide chain.[10] In addition to these bands, we observed a strong band around 1620 cm^{-1}. The peak of this band shifted from 1610 cm^{-1} as the glycine content of the polymer increased from $(L)_n$ to $(LG_2)_n$. Although the absorption band near 1630 cm^{-1} had been generally attributed to the β-structure,[10] however, in this case, the band at 1610—1635 cm^{-1} was not ascribed to the β-structure for the following reasons:

(i) The IR spectra of $(L)_n$ in TFA–$CHCl_3$ systems containing different amounts of TFA are shown in Fig. 4. As may be seen in Fig. 1, the b_0 value of $(L)_n$ showed that $(L)_n$ changed from the random coil to the α-helix as the TFA content decreased from 80% to 40%. The randomly coiled conformation of $(L)_n$ in 80% TFA has also been confirmed by NMR spectra.[8] In contrast, in the IR spectra, $(L)_n$ exhibited a band at 1610 cm^{-1} in addition to the amide

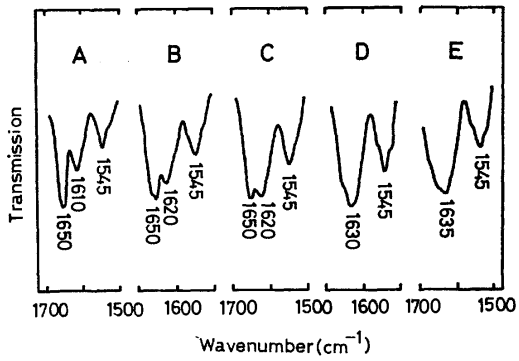

Fig. 3. IR spectra of the polymers in 70% $CHCl_3$/30% TFA (v/v).
Letter symbols, see Fig. 1.

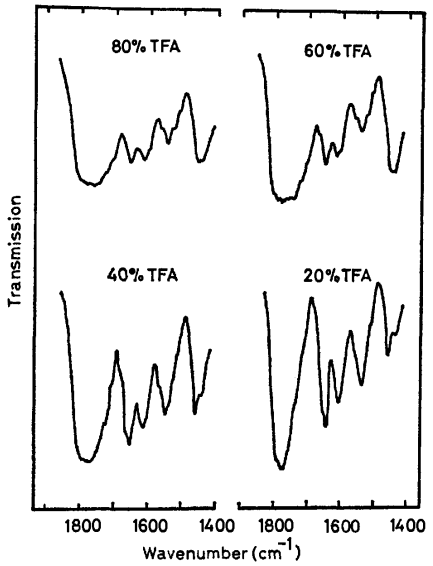

Fig. 4. IR spectra of $(L)_n$ in TFA-$CHCl_3$.

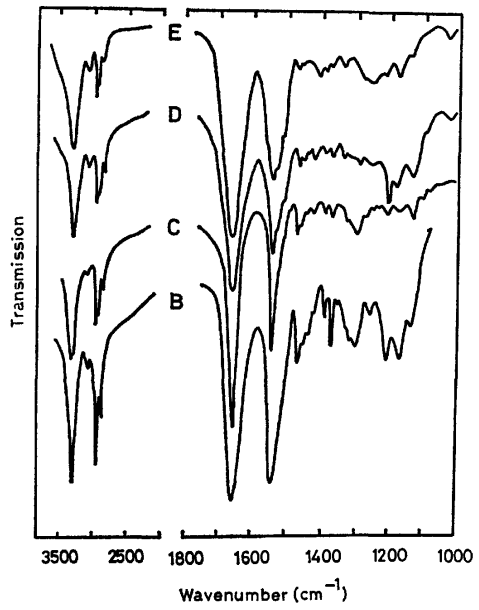

Fig. 5. IR spectra of films of the sequential polypeptides. All films were prepared from TFA solutions. Letter symbols, see Fig. 1.

I band at 1650 cm^{-1} and the amide II band at 1545 cm^{-1} for all TFA concentrations between 80 and 20%.

(ii) As was pointed out in the previous section, $(L_2G)_n$ and $(L_3G)_n$ exhibited CD spectra characteristic of the α-helix in a TFA–TFE system. However, IR spectra of the polymers in 50% TFA/50% TFE were the same as those in 70% TFA/30% $CHCl_3$: they showed the band at 1620 cm^{-1} in addition to the usual amide I band at 1650 cm^{-1} and the amide II band at 1545 cm^{-1}.

(iii) In general, the polypeptide chains cast in film have been considered to have the same conformation as they might be assumed to have in a solvent such as $CHCl_3$. IR spectra of the sequential polypeptides cast in films from TFA solutions did not exhibit the band near 1620 cm^{-1}, they exhibited only the amide I band at 1650—1660 cm^{-1} and the amide II band at 1545 cm^{-1} (Fig. 5). The 1610 cm^{-1} band was observed in a film of $(L)_n$ if the film was incompletely dried: this band disappeared as TFA was completely removed (Fig. 6).

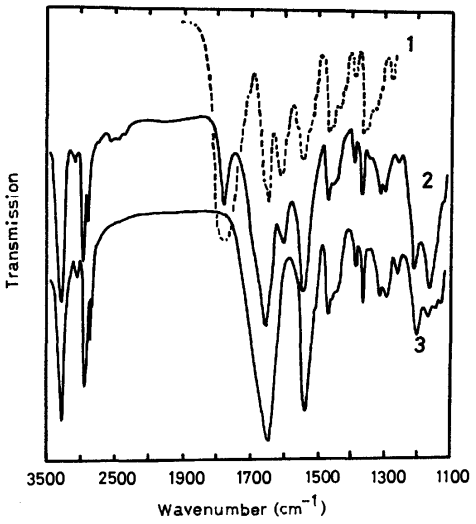

Fig. 6. IR spectra of $(L)_n$. 1: solution (80% $CHCl_3$/20% TFA (v/v)), 2: film from TFA solution (incompletely dried), 3: film from TFA solution (completely dried).

All these results strongly suggest that the band near 1620 cm^{-1} which was observed in solutions containing TFA should not be attributed to the β-structure of the polypeptide chain but to interactions between the polymer and the solvent TFA. Recently, Nagayama[11a] attributed the band at 1610 cm^{-1} to solvation of TFA with the polypeptide chain, and Combelas *et al.*[11b] also gave the same conclusion.

Discussion

Our experimental results showed that the sequential polypeptides except for $(LG_2)_n$ were α-helical in solution, although each polymer had a different helicity. The helical content, f_α, was calculated from Eq. (4) for each of the polymers,

$$f_\alpha = \frac{(-455)-(-60)}{b_0 - b_0^{TFA}}, \quad (4)$$

where we assumed that the b_0 values of $(L)_n$ were −455 at 100% helix and −60 at 100% random coil, and that all the sequential polypeptides had random coils in 100% TFA, although the b_0 value obtained with 100% TFA solution for each sequential polypeptide (b_0^{TFA}) was not zero. The results are shown in Fig. 7.

$(L)_n$ changed from a random coil to an α-helix when the $CHCl_3$ content increased from 25% to 55%, the midpoint of the transition was at 40% $CHCl_3$. On the other hand, polymers $(L_2G)_n$ and $(L_3G)_n$ showed a transition at a $CHCl_3$ content higher than 40%. For $CHCl_3$ contents between 40% and 90%, the helicity of $(L_2G)_n$ was slightly higher than that of $(L_3G)_n$. When the $CHCl_3$ content reached 90%, the helix content of $(L_2G)_n$ was the same as that of

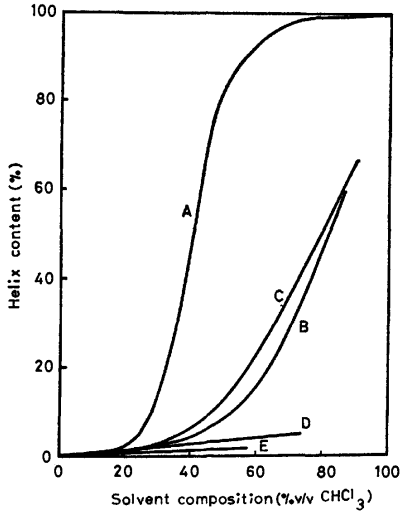

Fig. 7. Variation of the helix content (in %) of the polymers with solvent compositions. Helix content is calculated from equation (4). Letter symbols, see Fig. 1.

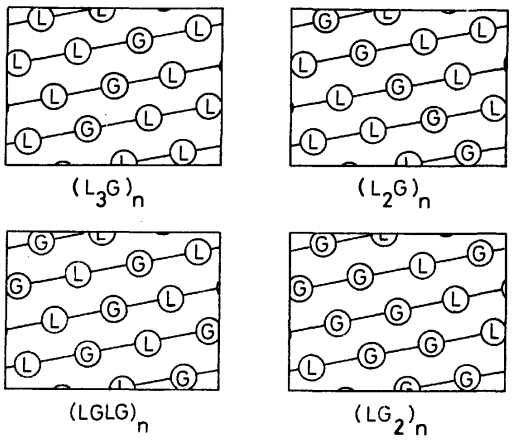

Fig. 8. Radial projection showing the distribution of the residues on the α-helix. L: leucine, G: glycine.

$(L_3G)_n$, 67%. The helix content of $(L_3G)_n$ may be higher than that of $(L_2G)_n$ when the $CHCl_3$ content is higher than 90%: this expectation was supported by CD spectra although the solvent system (TFA–TFE) was different from that used in the ORD studies (TFA–$CHCl_3$). Analysis of the CD spectra (Fig. 2) gave helical contents of 75% for $(L_3G)_n$ and 72% for $(L_2G)_n$. On the other hand $(LG)_n$ and $(LG_2)_n$ were hardly α-helical in TFA–$CHCl_3$, although $(LG)_n$ was partially α-helical in 96.8% TFE/3.2% TFA as shown by CD spectra.

These observations show us that the presence of a glycyl residue in an amino acid sequence has an important effect on the conformation of these polypeptides, causing a marked reduction in the stability of the α-helix. The magnitude of this reduction depends not only on the glycine content but also on the residue sequence, as the stability of the α-helix decreased in the order: $(L)_n > (L_3G)_n \sim (L_2G)_n > (LG)_n > (LG_2)_n$. In spite of the helicity of (L_2G) being slightly higher than that of $(L_3G)_n$, $(L_3G)_n$ and $(L_2G)_n$ were conservatively considered to have nearly equal helical stability, noting that the degree of polymerization of $(L_2G)_n$ might be slightly higher than that of $(L_3G)_n$ since the former polymer had a higher intrinsic viscosity in DCA than the latter and that the stability of the α-helix might depend on chain length.[12]

A schematic representation of α-helices, showing the radial projection of the distribution of amino acid residues onto the surface of the α-helix, is presented in Fig. 8 for each of the polymers. Each residue position corresponds to the location of an α-carbon of an amino acid, not of a side chain. The successive residues were numbered 1, 2, 3, *etc.* in the $-CO-C_\alpha-NH-$ direction from the C-terminal of the chain.

The α-helix is stabilized by the hydrogen bond between the NH group of the i-th residue and the CO group of the $(i+4)$th residue.[13] In addition to the hydrogen bond, non-covalent interaction between aliphatic side chains is the other important factor stabilizing the α-helix in solution.[14] For instance, non-covalent interaction between the i-th and the $(i+3)$th residues has been taken into account to explain the remarkable stability of the α-helix of poly-L-alanine in water.[15] In $(L)_n$, the interaction becomes more larger than in poly-L-alanine since leucine has a large aliphatic side chain. This has been actually confirmed in conformational studies on $(L)_n$ in water by Ostroy *et al.*[4a]

By considering a molecular model, we can see that two types of non-covalent interaction, one between the i-th and the $(i+3)$th residues and the other between the i-th and the $(i+4)$th residues, are possible in $(L)_n$. The magnitude of the energy of the non-covalent interaction should depend on the distance between the residues—the shorter distance would produce the larger interaction energy. We estimated the interatomic distances between the atoms of L-leucyl residues in the α-helix with the aid of a molecular model and deduced the following conclusion: the interaction between the i-th and the $(i+3)$th residues was the most effective, followed by the one between the i-th and the $(i+4)$th residues. Such interactions are not expected with polyglycine. The energy of the hydrogen bond would not be affected so much with a change in the side chain of an amino acid, provided that only amino acids which could form the α-helix were considered. However, the energy associated with the interaction between lyophobic side chains would depend significantly on the nature of side chains, and the larger the energy of the interaction, the more stable the α-helix would be. In this respect, eight kinds of side chain–side chain interaction are conceivable in the sequential polypeptides of L-leucine (L) and glycine (G) (see Fig. 8): $L(i)-L(i+3)$, $L(i)-G(i+3)$, $G(i)-G(i+3)$, $G(i)-L(i+3)$, $L(i)-L(i+4)$, $L(i)-G(i+4)$, $G(i)-G(i+4)$, $G(i)-L(i+4)$. It was concluded from examination of a molecular model that only three kinds of interaction were significant with the order of the interaction energy being $L(i)-L(i+3) > L(i)-G(i+3) > L(i)-L(i+4)$. If we assume a value of 1.0 for the energy of interaction for $L(i)-L(i+3)$, 0.4 for $L(i)-G(i+3)$, and 0.1 for $L(i)-L(i+4)$, then we could

calculate the average interaction energy per residue for each of the polymers to be 1.1 for $(L)_n$, 0.7 for $(L_3G)_n$, 0.7 for $(L_2G)_n$, 0.3 for $(LG)_n$, and 0.3 for $(LG_2)_n$. This order of the interaction energies is in good agreement with the experimentally observed stabilities of the α-helix in the polymers.

Similar studies on the influence of glycine on the stability of the α-helix of other sequential polypeptides have been reported by us[3] and by Fraser *et al.*[2] Our previous study showed that the stabilities of the α-helix of sequential polypeptides containing L-alanine (A) and glycine were in the order: $(A)_n > (A_2G)_n > (A_3G)_n > (AG_2)_n$. In this case a small amount of the α-helix was observed for $(AG_2)_n$. Fraser *et al.* reported that the stabilities of the α-helix of their sequential polypeptides of γ-ethyl-L-glutamic acid (E) and glycine were in the order: $(E)_n > (E_5G)_n > (E_4G)_n > (E_3G)_n > (E_2G)_n > (EG)_n$.[2] These two results and our present results on $(L_xG_y)_n$ apparently contradict each other. The contradiction may, however, be eliminated if we consider that the nature and magnitudes of interaction between side chains of polypeptides are different in three series of sequential polypeptides. As discussed in the previous paper[3], the order of the α-helical stability of the polymers $(A_xG_y)_n$ was explained by interactions between the i-th L-alanyl residue and $(i+3)$th residue. Recently, Brack and Spach reported that the α-helical stability of their sequential polypeptides of L-alanine and glycine in solution were in the order: $(A)_n > (A_2G)_n > (A_2G_2)_n > (AG)_n > (A_3G_3)_n > (A_2G_3)_n > (AG_2)_n > (AG_3)_n$.[16] This order can be explained by our calculation with the exception of $(AG_2)_n$. For the polymers $(E_xG_y)_n$, interactions between the i-th and the $(i+3)$th residues and between the i-th and the $(i+4)$th residues are equally important because the γ-ethyl-L-glutamic acid side chain is long enough to make the contribution of the $(i+3)$th and the $(i+4)$th residues on the i-th residue equal. If we assumed a value of 1.0 for the interaction energy for $E(i)-E(i+3)$ and $E(i)-E(i+4)$, and 0.4 for $E(i)-G(i+3)$ and for $E(i)-G(i+4)$, we could calculate the average energy of the interaction to be 2.0 for $(E)_n$, 1.5 for $(E_5G)_n$, 1.4 for $(E_4G)_n$, 1.35 for $(E_3G)_n$, 1.1 for $(E_2G)_n$, and 0.7 for $(EG)_n$. This order of the interaction energy is in good agreement with their experimental results.

We wish to thank Professor F. Oosawa of Nagoya University and Professor T. Ooi of Kyoto University for their encouragement and discussions. We are greatly indebted to Dr. A. Warashina for his kind gift of poly-L-leucine. Thanks are also due to Professor K. Yamasaki of Nagoya University who kindly made available an ORD–CD spectrometer for the experiment.

References

1) P. Doty and W. B. Gratzer, "Polyamino Acids, Polypeptides, and Proteins," ed. by M. A. Stahman, University of Wisconsin Press, Madison, Wis. (1962), p. 111.
2) R. D. B. Fraser, B. S. Harrap, T.P. MacRae, F. H. C. Stewart, and E. Suzuki, *Biopolymers*, **5**, 251 (1967).
3) T. Iio and S. Takahashi, This Bulletin, **43**, 515 (1970); T. Iio, *Biopolymers*, **10**, 1583 (1971).
4) a) S. E. Ostroy, N. Lotan, R. T. Ingwall, and H. A. Scheraga, *Biopolymers*, **9**, 749 (1970). b) C. R. Snell and G. D. Fasman, *ibid.*, **11**, 1723 (1972). c) P. Y. Chou, M. Wells, and G. D. Fasman, *Biochemistry*, **11**, 3028 (1972).
5) T. Iio and S. Takahashi, This Bulletin, **47**, 2720 (1974).
6) J. H. Bradbury and M. D. Fenn, *J. Mol. Biol.*, **36**, 231 (1968).
7) W. Moffitt and J. T. Yang, *Proc. Nat. Acad. Sci. U.S.A.*, **42**, 596 (1956).
8) A. Warashina, T. Iio, and T. Isemura, *Biopolymers*, **9**, 1445 (1970).
9) G. Holzwarth and P. Doty, *J. Amer. Chem. Soc.*, **87**, 218 (1965).
10) T. Miyazawa and E. R. Blout, *ibid.*, **83**, 712 (1961).
11) a) K. Nagayama, *Tanpakushitsu Kakusan Koso*, **17**, 653 (1972). b) P. Combelas, G. Garrigou-Lagrange, and J. Lascombe, *Biopolymers*, **12**, 611 (1973).
12) A. Yaron, E. Katchalski, A. Berger, G. D. Fasman, and H. A. Sober, *Biopolymers*, **10**, 1107 (1971).
13) L. Pauling, R. Corey, and H. Branson, *Proc. Nat. Acad. Sci. U.S.A.*, **37**, 205 (1951).
14) G. Nemethy and H. A. Scheraga, *J. Phys. Chem.*, **66**, 1773 (1962).
15) M. Bixon, H. A. Scheraga, and S. Lifson, *Biopolymers*, **1**, 419 (1963).
16) A. Brack and G. Spach, *ibid.*, **11**, 563 (1972).

Liquid-phase Oxidation Catalyzed by Cu(II)-Cl. II. Chloride Ion Transfer during the Oxidation of Cyclohexene

Sei-ichiro IMAMURA, Takafumi OTANI, and Hiroshi TERANISHI

Department of Chemistry, Kyoto Institute of Technology, Sakyoku, Matsugasaki, Kyoto 606

(Received June 11, 1974)

Cyclohexene was oxidized in glacial acetic acid with a Cu(II)-Cl catalyst. In addition to the main oxidation products, 3-cyclohexenyl chloride, 3-cyclohexenyl acetate, 2-chlorocyclohexanol-(1), cyclohexene oxide, and hydrogen chloride were produced. The mechanism of the formation of these compounds was investigated in detail: the deactivation of the catalyst was explained by chloride ion transfer.

Previously it has been reported that, in the liquid-phase oxidation of cyclohexene in glacial acetic acid, the catalytic activity of cupric chloride was greatly increased by the addition of various alkali chlorides which formed complexes with copper.[1] As the reaction proceeded, however, the catalyst was deactivated owing to the consumption of chloride ion, but the mechanism of this deactivation could not be elucidated fully.

In this work, we have attempted to analyze the reaction products in detail in order to explain the consumption of chloride ion during the reaction.

Experimental

3-Cyclohexenyl acetate was obtained from cyclohexenol and acetyl chloride.[2] 2-Chlorocyclohexanol-(1) was prepared by the reaction of cyclohexene with hypochloric acid[3] and trans-dichlorocyclohexane by the reaction of cyclohexene with molecular chlorine.[4] Anhydrous cupric acetate was obtained by dehydration of cupric acetate monohydrate. G. R. grade commercial *t*-butyl hydroperoxide (*t*-butyl HPO) and cyclohexene oxide were used without further purification. Other reagents were obtained and purified as described previously.[1]

The oxidation apparatus used was the same as in the previous work.[1] It was confirmed that the reactions were not controlled by the diffusion of oxygen into the liquid phase. *t*-Butyl HPO was decomposed under a nitrogen atmosphere.

The reaction products were analyzed with a Hitachi 063 Gas Chromatograph equipped with a flame ionization detector, a Hitachi 215 Infrared Spectrophotometer, and a Hitachi RMU-6L Mass Spectrometer. The conditions for the operation of the gas chromatograph were as follows: (1) Column packing—Ethylhexyl sebacate/Chromosorb 101 (5 : 1); Carrier gas–N_2 (30 ml/min); Column temperature—80~100 °C, and (2) Column packing—Ethylhexyl sebacate (2 m); Carrier gas–N_2 (30 ml/min); Column temperature—115 °C.

Results and Discussion

Accumulation of By-products during the Oxidation of Cyclohexene. The main products were cyclohexenyl hydroperoxide (cyclohexenyl HPO), cyclohexenol, and cyclohexenone, which were analyzed as described previously.[1] In addition, 3-cyclohexenyl chloride, 3-cyclohexenyl acetate, 2-chlorocyclohexanol-(1), cyclohexene oxide, and a trace amount of trans-dichlorocyclohexane were detected in this work. However, cyclohexene oxide was detected only in the later stages of the oxidation. Fig. 1 shows the amounts of 2-chlorocyclohexanol-(1), 3-cyclohexenyl acetate, and 3-cyclohexenyl chloride formed together with the amount of oxygen absorbed. These curves all show a maximum when the rate of oxidation begins to decrease.[5] The amounts of main products formed after twenty minutes were 0.037 mol/l of cyclohexenyl HPO, 0.071 mol/l of cyclohexenone, and 0.015 mol/l of cyclohexenol. Table 1 shows the yield of 3-cyclohexenyl chloride plus 2-chlorocyclohexanol-(1) after various reaction times. From the table it may be seen that almost all the chloride ion added was transferred to organic chlorine compounds after forty to sixty minutes. Chloride ion forms complexes with cupric acetate in glacial acetic acid and increases its

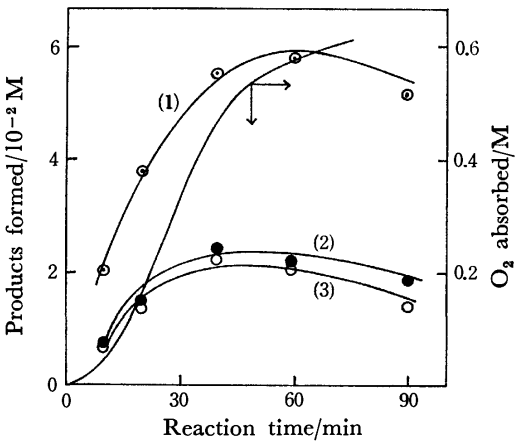

Fig. 1. Production of by-products in the oxidation of cyclohexene in glacial acetic acid at 60 °C.
$[Cu(OAc)_2]=8.1\times10^{-3}$ M; $[LiCl]=8.0\times10^{-2}$ M; [Cyclohexene] = 4.94 M
(1) 2-Chlorocyclohexanol-(1)
(2) 3-Cyclohexenyl acetate
(3) 3-Cyclohexenyl chloride

TABLE 1. YIELD OF CHLORINATED PRODUCTS IN THE OXIDATION OF CYCLOHEXENE AT 60 °C

Reaction time/min	[3-Cyclohexenyl chloride + 2-chlorocyclohexanol-(1)]/%[a]
10	32.8
20	63.8
40	97.6
60	98.3
90	80.0

$[Cu(OAc)_2]=8.1\times10^{-3}$ M, $[LiCl]=8.0\times10^{-2}$ M, [Cyclohexene] = 4.94 M, Solvent: AcOH, a) Based on LiCl.

TABLE 2. REACTION OF THE OXIDATION PRODUCTS WITH Cu(II)-Cl-*t*-butyl HPO IN GLACIAL ACETIC ACID AT 60 °C

Reactant (0.1 M)	[Cu(II)-Cl]/10^{-3} M[a]	*t*-Butyl HPO/M	H_2O/M	2-Chlorocyclohexanol-(1)/%
Cyclohexenol	8.0	0.10	0	0
Cyclohexenone	8.0	0.10	0	0
Cyclohexenyl HPO	8.0	0	0	trace
3-Cyclohexenyl chloride	8.0	0.10	0	0
3-Cyclohexenyl chloride	8.0	0.10	2.5	0
Cyclohexene	8.0	0.10	2.5	trace
trans-Dichlorocyclohexane	8.0	0.10	2.5	0

a) $Cl^-/Cu=10$

activity in the oxidation of hydrocarbons.[1,6]

$$Cu(OAc)_2 \xrightarrow{Cl^-} Cu(OAc)Cl \xrightarrow{Cl^-} CuCl_2 \xrightarrow{Cl^-} \cdots\cdots$$

From this and the results shown in Fig. 1 and Table 1, we concluded that chloride ion transfer occurred to form these organic chlorine compounds and an inactive cupric acetate. This is the reverse of the reaction shown above. In the following sections we discuss the mechanisms of the formation of these by-products.

Formation of 3-Cyclohexenyl Acetate 3-Cyclohexenyl acetate may be formed in one of the following three possible ways. The first is an esterification of cyclohexenol, one of the oxidation products, with acetic acid.

$$ROH + AcOH \rightarrow ROAc \quad (1)$$

R: cyclohexenyl-

The second is a chloride ion transfer oxidation of cyclohexenyl radical, an intermediate radical in the oxidation of cyclohexene, by the catalyst. This is followed by acetolysis of the resulting 3-cyclohexenyl cyloride. The chloride ion transfer to cyclohexenyl radical would occur and compete with attack by oxygen, the rate constant of which is close to the diffusion controlled limit.[7]

$$R\cdot + Cu(II)Cl_x(OAc)_y \rightarrow RCl + Cu(I)_{x-1}(OAc)_y \quad (2)$$

$$RCl + AcOH \rightarrow ROAc \quad (3)$$

The third is a direct acetate ion transfer oxidation of cyclohexenyl radical.

$$R\cdot + Cu(II)Cl_x(OAc)_y \rightarrow ROAc + Cu(I)_x(OAc)_{y-1} \quad (4)$$

To investigate the possibility of the first two mechanisms, cyclohexenol and 3-cyclohexenyl chloride were refluxed in glacial acetic acid at 60 °C. For cyclohexenol (initial concentration of 0.29 mol/l), only about 2% of 3-cyclohexenyl acetate was produced after sixty minutes. The yield of cyclohexenol in the oxidation after a reaction time of twenty minutes was about 0.014 mol/l, therefore the quantity of 3-cyclohexenyl acetate formed by esterification of cyclohexenol would be calculated to be less than $0.014\times 0.02=0.00028$ mol/l. Actually the yield of 3-cyclohexenyl acetate was 0.015 mol/l after twenty minutes (see Fig. 1), so the esterification of 3-cyclohexenol can be excluded. The result for 3-cyclohexenyl chloride is shown in Fig. 2. This figure shows that the yield of 3-cyclohexenyl acetate reaches about 20% after sixty minutes. However, as shown in Fig. 1, 3-cyclohexenyl acetate accumulated from the beginning of the reaction and in almost the same amount as 3-cyclohexenyl chloride. From the results shown in Figs. 1 and 2, it seems that the formation of 3-cyclohexenyl acetate by the acetolysis of 3-cyclohexenyl chloride, although it does occur, is not the main but

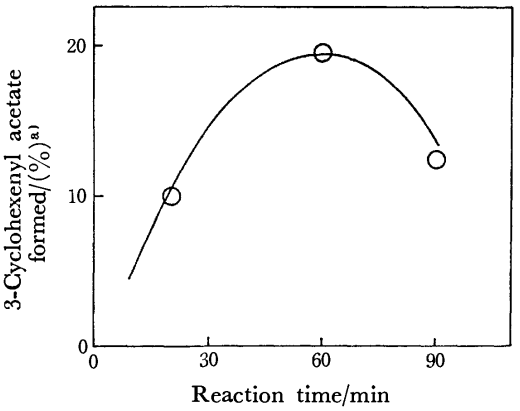

Fig. 2. Formation of 3-cyclohexenyl acetate from 3-cyclohexenyl chloride in glacial acetic acid at 60 °C.
[3-Cyclohexenyl chloride]=0.40 M
a) Based on 3-cyclohexenyl chloride

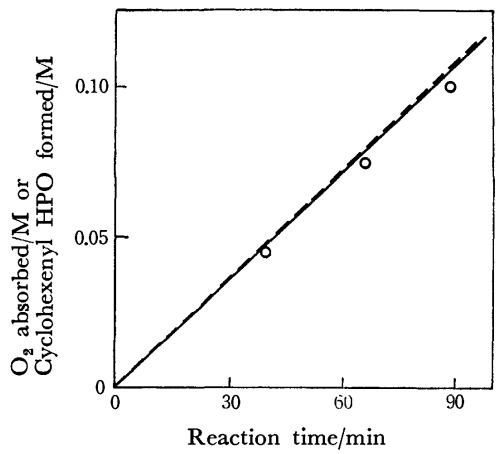

Fig. 3. Oxidation of cyclohexene initiated by azobisisobutyronitrile in glacial acetic acid at 60 °C.
--- In the absence of cupric acetate
—— In the presence of cupric acetate
○ Cyclohexenyl HPO formed
$[Cu(OAc)_2]=8.0\times10^{-3}$ M; [Azobisisobutyronitrile]$=6.0\times10^{-2}$ M; [Cyclohexene]=4.94 M

the side route.

Next the effect of cupric acetate on the cyclohexenyl radical in the oxidation of cyclohexene was investigated. As cupric acetate in the absence of lithium chloride was inactive in initiating the oxidation, azobisisobutyronitrile was added. Figure 3 shows that the shapes of the two oxidation curves which correspond to the reaction with and without cupric acetate are almost the same. Moreover, in the presence of cupric acetate, more than 95% of cyclohexenyl HPO was obtained, showing an inactivity of cupric acetate in decomposing the HPO. Though a trace amount of 3-cyclohexenyl acetate (less than 1.4% based on oxygen absorbed) was produced after a reaction time of ninety minutes, the yield was too low compared with that obtained in the oxidation. From these results, it appears that cupric acetate itself is inactive and does not interact with cyclohexenyl radical. However, it does not mean that the active cupric acetate-chloride ion complex, $Cu(II)Cl_x(OAc)_y$, does not transfer acetate ion. As stated earlier, because 3-cyclohexenyl acetate and 3-cyclohexenyl chloride seem to be formed in a competitive process, it is preferable to assume that 3-cyclohexenyl acetate is formed by the acetate ion transfer oxidation of cyclohexenyl radical by the active catalyst system (Eq. (4)). However, this cannot be proved using the present experimental technique.

Formation of 2-Chlorocyclohexanol-(1). We assumed that 2-cyclohexanol-(1) was formed by the chlorination of the olefinic bond of cyclohexenol or cyclohexenone with Cu(II)–Cl–HPO.[8] So these compounds were treated with cupric acetate-lithium chloride-*t*-butyl HPO and the results are shown in Table 2. Other oxidation products, together with cyclohexene, were also treated in a similar manner. As water was assumed to be produced in the oxidation, the effect of addition of it was also discussed. From the table it may be seen that chlorination of cyclohexenol or cyclohexenone did not occur. It is also seen that other compounds are not intermediates for 2-chlorocyclohexanol-(1).

Next we investigated the reaction of cyclohexene oxide, which was formed in a later stage of the oxidation, with the catalyst. From Fig. 4, we can see that cyclohexene oxide reacted rapidly with the catalyst to produce 2-chlorocyclohexanol-(1) almost quantitatively (based on lithium chloride added) after twenty minutes. This indicates that chloride ion transfer from the catalyst to cyclohexene oxide is the main route leading to 2-chlorocyclohexanol-(1). As the chlorination shown above proceeded rapidly, cyclohexene oxide could not be detected in the early stages of the oxidation when the catalyst still had active chloride ion.

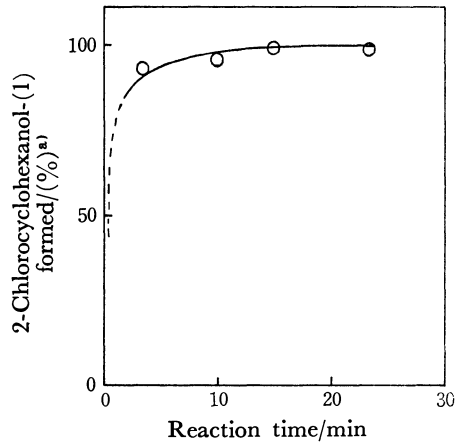

Fig. 4. Reaction of cyclohexene oxide with Cu(II)-Cl in glacial acetic acid at 60 °C.
$[Cu(OAc)_2]=8.6\times10^{-3}$ M; $[LiCl]=8.2\times10^{-2}$ M;
[Cyclohexene oxide]=0.11 M
a) Based on LiCl

Formation of Hydrogen Chloride. As shown in Fig. 1 and Table 1, the total quantity of chloride ion in the chlorinated products had a maximum value during the reaction, that is, in the later stages of the reaction it became less than that added initially as lithium chloride. As no other chlorinated products were detected, it was assumed that chloride ion was transferred to hydrogen chloride. Therefore cyclohexene was oxidized by Cu(II)–Cl (Cu : Cl=1 : 50) and the gaseous products were analyzed. As was expected, a considerable amount of hydrogen chloride, which was not measured, was detected by the gas chromatograph in the later stages of the oxidation.[9]

Mechanism of Chloride Ion Transfer. From the results obtained so far, the mechanism of the chloride ion transfer from the catalyst can be summarized as follows.

$$Cu(OAc)_2 + Cl^- \rightarrow CuCl_x(OAc)_y \quad (5)$$

$$RH \rightarrow R\cdot \xrightarrow{O_2} ROO\cdot \quad (6)$$

$$ROO\cdot + RH \rightarrow ROOH + R\cdot \quad (7)$$

$$ROOH + CuCl_x(OAc)_y \rightarrow \text{radicals} \quad (8)$$

$$ROO\cdot + RH \rightarrow \text{Cyclohexene oxide} + RO\cdot \quad (9)$$

$$\text{Cyclohexene oxide} + CuCl_x(OAc)_y \xrightarrow{H^+} \text{2-Chlorocyclohexanol-(1)} + CuCl_{x-1}(OAc)_y \quad (10)$$

$$R\cdot + CuCl_x(OAc)_y \rightarrow RCl + CuCl_{x-1}(OAc)_y \quad (2)$$

$$RCl + AcOH \rightarrow ROAc + HCl \quad (3)$$

$$R\cdot + CuCl_x(OAc)_y \rightarrow ROAc + CuCl_x(OAc)_{y-1} \quad (4)$$

In the first step cupric acetate forms complexes with chloride ion. (Eq. (5)) Equations (6) and (7) are the propagation steps. In Eq. (8) cyclohexenyl HPO is decomposed by the catalyst and the active radicals are formed. Cyclohexene oxide would be produced by the reaction of cyclohexenylperoxy radical with cyclohexene (Eq. (9)),followed by chloride ion transfer to give 2-chlorocyclohexanol-(1). (Eq. (10)) In Eq. (2) the ligand transfer oxidation of cyclohexenyl radical occurs and 3-cyclohexenyl chloride is formed. A part of the 3-cyclohexenyl chloride formed suffers an acetolysis by acetic acid to give 3-cyclohexenyl acetate. (Eq. (3)) Hydrogen chloride produced in this process partly diffuses into the gas phase and partly remains in the liquid phase to form complexes with copper again. The acetate ion transfer oxidation of cyclohexenyl radical (Eq. (4)) should occur as the main route for the formation of 3-cyclohexenyl acetate, although this could not be confirmed in this work.

The deactivation of the catalyst occurs by the chloride ion transfer as shown by Eqs. (2) and (10) to form inactive cupric acetate. The direct chlorination of the olefinic bonds of cyclohexene or its oxidation products[8] does not proceed owing to the presence of cyclohexene oxide or cyclohexenyl radical which reacts with the catalyst more rapidly than those compounds.

The authors wish to thank Dr. Masaaki Teramoto for his helpful advice and discussions. 3-Cyclohexenyl chloride was kindly provided by Dr. Akira Oku of our department of the Kyoto Institute of Technology.

References

1) S. I. Imamura, T. Banba, and Y. Takegami, This Bulletin, **46**, 856 (1973)
2) K. Richter, *J. Prakt. Chem.*, **111**, 385 (1925).
3) H. Gilman, "Organic Syntheses", Coll. Vol. I, p. 158 (1956).
4) B. Carroll, D. G. Kubler, H. W. Davis and A. M. Whaley, *J. Amer. Chem. Soc.*, **73**, 5382 (1951).
5) It was found that 3-cyclohexenyl acetate was unstable toward Cu(II)–Cl–HPO and decomposed to some unknown compounds with lower boiling points. This seems to lower its yield in the later stages of the reaction.
6) S. I. Imamura, T. Sumi, M. Teramoto, and Y. Takegami, Proceedings of the sixth Symposium on Oxidation, Tokyo, p. 54 (1972).
7) C. L. Jenkins and J. K. Kochi, *J. Amer. Chem. Soc.*, **94**, 856 (1972).
8) Chlorination of olefins by Cu(II)–Cl was found to be markedly accelerated in the presence of HPO. For example, cyclohexene was chlorinated almost quantitatively to produce trans-dichlorocyclohexane by Cu(II)–Cl–*t*-butyl HPO under a nitrogen atmosphere at 30 °C. A detailed investigation of this phenomenon is under way.
9) A Hitachi 063 Gas Chromatograph equipped with a thermal conductivity detector was used.

Furan Derivatives. I. On the Methods of Synthesizing Some Naphtho[1,8-*bc*]furans

Takaaki HORAGUCHI, Takahachi SHIMIZU, and Tsuneo SUZUKI

Department of Chemistry, Faculty of Science, Niigata University, Igarashi, Niigata 950-21

(Received June 14, 1974)

Two kinds of methods of synthesizing naphtho[1,8-*bc*]furans (VIa–VId) are described. In the first method, naphtho[1,8-*bc*]furans (VIa–VId) were obtained by the decarboxylation of IIa–IId, which had previously been prepared from Ia–Id and ethyl bromoacetate. The yields of IIa–IId from Ia–Id were 45, 43, 49, and 46% respectively. In the second method, VIa–VId were obtained by heating Va–Vd with acetic anhydride and sodium acetate. The yields of VIa–VId were 34, 46, 46, and 70% respectively.

In previous papers,[1-3] we have reported on the syntheses of phenanthro[4,5-*bcd*]furans. In the course of the syntheses, naphtho[1,8-*bc*]furan derivatives (Xa–Xc) played an important part as the intermediate products, and the syntheses of the compounds Xa–Xc were attempted in the ways of A and B.

Attempts using Method B were all unsuccessful, however, resulting, for example, in the formation of the lactone (IX) rather than the expected naphtho-[1,8-*bc*]furan (Xb). However, the syntheses of simple naphtho[1,8-*bc*]furans such as VI, which have no propionic acid residues, may be possible by this method. By Method A, naphtho[1,8-*bc*]furans (IIe—IIg) were obtained in relatively low yields (*ca.* 40%). One of the causes of the low yields may be the steric hindrance of the propionic acid residues, and it seems that Compounds Ia—Id, which have no propionic acid residues, are converted to IIa—IId in better yields. For these reasons, syntheses of naphtho[1,8-*bc*]furans (IIa—IId and VIa—VId) were attempted from Ia—Id and Va—Vd respectively using Methods A and B. Only a few articles[4-6] on naphtho[1,8-*bc*]furan derivatives have been published: for example, Royer *et al.* obtained naphtho[1,8-*bc*]furans in very poor yields by a method similar to A.

Results and Discussion

The syntheses of naphtho[1,8-*bc*]furans (IIa—IId and VIa—VId) were attempted from 8-hydroxy-1-tetralone derivatives (Ia—Id) by two kinds of methods. The first method is the same (A) as those used in the syntheses of IIe—IIg. Naphtho[1,8-*bc*]furans (IIa—IId) were obtained by the heating of Ia—Id, ethyl bromoacetate, and potassium carbonate at 120°C, followed by hydrolyses. From the reaction mixture before the hydrolyses, Compounds IIIa—IIId were also isolated. The carboxylic acids, IIa—IId, were decarboxylated with quinoline and copper to the expected naphto[1,8-*bc*]furans (VIa—VId). The yields of the reactions from tetralones (Ia—Id) to naphtho-[1,8-*bc*]furans (IIa—IId) are shown in Table 1, along with those of IIe—IIg from Ie—Ig.

Table 1 shows that the yields of IIa—IId were comparable to one another and similar to those of IIe—IIg; the effects of the substituents (R_1, R_2, and R_3) on the yields did not appear, but in the presence of the propionic acid residues a higher reaction temperature (170—180 °C) was required to prepare IIe—IIg from Ie—Ig compared with that needed in the syntheses (120 °C) of IIa—IId. The yields of IIa—IId from Ia—Id did not vary at the reaction temperature of 150 °C. In the same way (150 °C), a benzofuran derivative (XII) was obtained in a yield of 76% from 2-acetyl-*p*-cresol (XI) and ethyl bromoacetate. It seems that the low yields of IIa—IId are a result of the inhibition of the free rotations of the carbonyl groups in Ia—Id, that is, to the difficult access of the

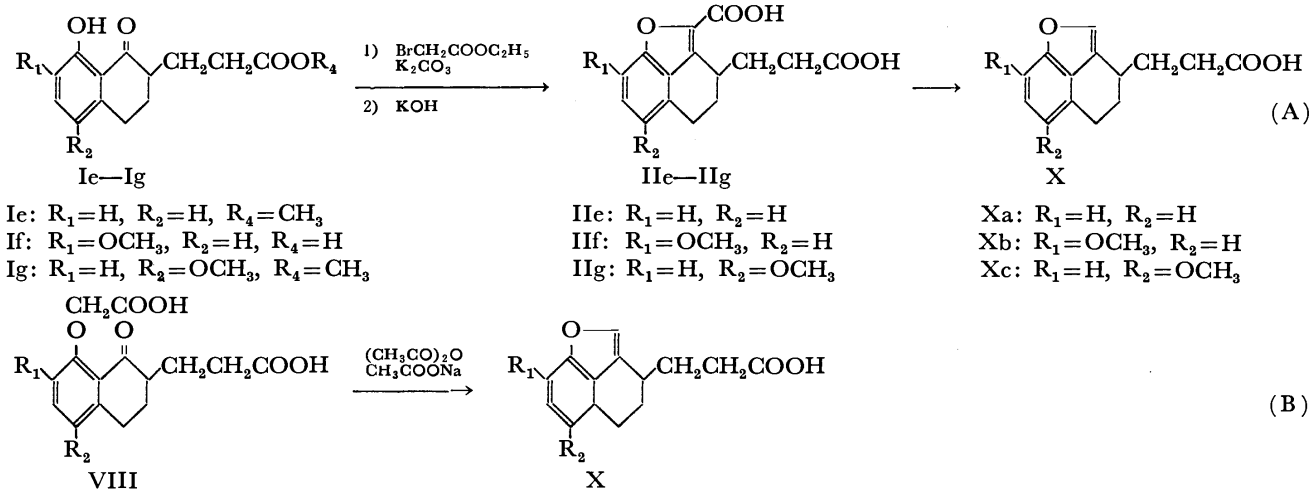

Fig. 1.

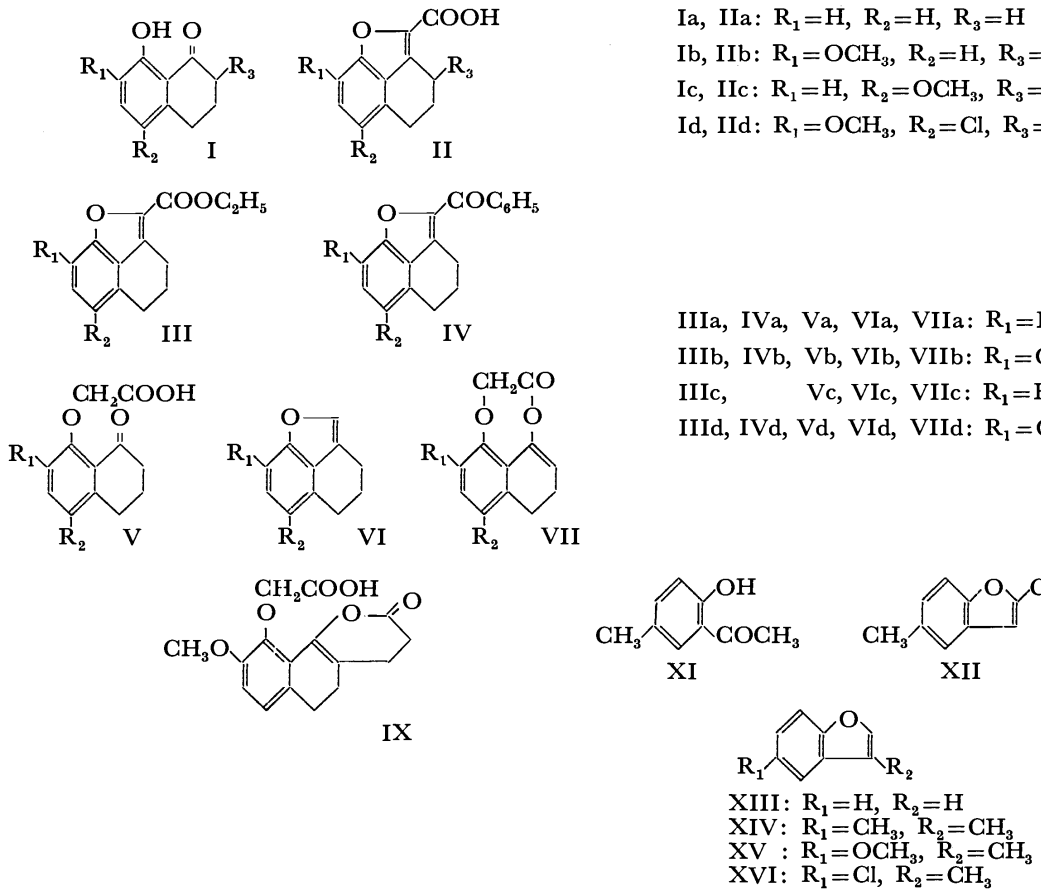

Ia, IIa: $R_1=H$, $R_2=H$, $R_3=H$
Ib, IIb: $R_1=OCH_3$, $R_2=H$, $R_3=H$
Ic, IIc: $R_1=H$, $R_2=OCH_3$, $R_3=H$
Id, IId: $R_1=OCH_3$, $R_2=Cl$, $R_3=H$

IIIa, IVa, Va, VIa, VIIa: $R_1=H$, $R_2=H$
IIIb, IVb, Vb, VIb, VIIb: $R_1=OCH_3$, $R_2=H$
IIIc, Vc, VIc, VIIc: $R_1=H$, $R_2=OCH_3$
IIId, IVd, Vd, VId, VIId: $R_1=OCH_3$, $R_2=Cl$

Fig. 2.

Table 1. The yields (%) of naphtho[1,8-*bc*]furans

Starting material	Product (%)	Starting material	Product (%)	Starting material	Product (%)
Ia	IIa (45)	Ie	IIe (41)	Ia	IVa (41)
Ib	IIb (43)	If[a)]	IIf (39)	Ib	IVb (65)
Ic	IIc (49)	Ig	IIg (43)	—	—
Id	IId (46)	—	—	Id	IVd (71)

a) The corresponding acid was used as the starting material in place of ester.

active methylene to the carbonyl groups or, perhaps more likely, to ring strains in IIa—IId.

The acids IIa—IId showed absorptions corresponding to those of conjugated-carboxyl groups near 1680 cm^{-1} in the IR spectra and near 276 nm (ε 16000—20000) in the UV spectra. The naphtho[1,8-*bc*]furans (VIa—VId) exhibited signals due to hydrogens of the furan ring near δ 7.15 in the NMR spectra and absorptions characteristic of benzofurans near 253 nm in the UV spectra.

When phenacyl bromide was used in place of ethyl bromoacetate in the reactions from I to II, Compounds IV were obtained (Table 1). The yield (41%) of IVa was not good because of the difficulty of isolating IVa from the reaction mixture.

The second method of synthesizing naphtho[1,8-*bc*]-furans (VIa—VId) is a way (B) by which benzofurans are usually obtained.[7-10] 8-Hydroxy-1-tetralone derivatives (Ia—Id) reacted with ethyl bromoacetate to give the corresponding acids, Va—Vd, after hydrolyses.

Table 2. The yields (%) of naphtho[1,8-*bc*]furans and lactones

Starting material	Products (%)	
Va	VIa (34)	Va[a)] (37)
Vb	VIb (46)	VIIb (32)
Vc	VIc (46)	VIIc (32)
Vd	VId (70)	VIIb (19)

a) Starting material (Va) recovered in place of a lactone (VIIa) because of hydrolysis during the working up.

When the Va—Vd acids were treated with acetic anhydride and sodium acetate, two kinds of products, VIa—VId and VIIb—VIId, were obtained. The results are shown in Table 2.

The yields of VIa—VIc were low because of the formation of lactones, but the total yields of the naphtho-[1,8-*bc*]furans and lactones were good. The better

Table 3. The ultraviolet absorption maxima of naphtho[1,8-*bc*]furans (solvent: ethanol)

Compound	λ nm (ε)				
VIa	283 (1100)	272 (1600)		250 (9800)	212 (26300)
VIb	290 (1600)	280 (1800)	255 (9200)	248 (9800)	216 (28500)
VIc	302 (2700)	290 (3200)		253 (10000)	213 (25500)
VId	294 (1600)	283 (1700)	255 (7700)	248 (8200)	217 (29200)

Table 4. The ultraviolet absorption maxima of benzofurans (solvent: ethanol).

Compound	λ nm (ε)			
XIII[13]	281 (2800)	274 (2400)	243 (9800)	205 (21100)
XIV[12]	289 (3100)	282 (2600)	249 (9200)	209 (25000)
XV[14]	302 (3500)	293 (3900)	251 (9100)	211 (24800)
XVI[15]	292 (2800)	284 (1700)	251 (7800)	214 (30000)

yield (70%) of VId suggests that the inductive effect of the chlorine atom in Vd played an important role in the formation of the furan ring. As benzofurans are usually obtained from phenoxyacetic acid derivatives in good yields (*ca.* 80%)[7,8,10] by the same method, the generally low yields of naphtho[1,8-*bc*]furans may be due to the inhibition of the free rotations of the carbonyl groups in Va—Vd or, more likely, to ring strains in VIa—VId. For these reasons, the formation of seven-membered lactones is comparable to that of five-membered furan rings.

The VIa—VId products were identical with the compounds obtained by the decarboxylation of IIa—IId respectively. The VIIb—VIId products showed absorptions corresponding to those of lactone rings near 1765 cm^{-1} and to those of carbon-carbon double bonds near 1646 cm^{-1} in the IR spectra.

The UV absorption maxima of the naphtho[1,8-*bc*]-furans (VIa—VId) and similar benzofurans (XIII—XVI) are shown in Table 3 and Table 4 respectively. The molecular extinction coefficients (ε) and wavelengths (λ) of naphtho[1,8-*bc*]furans and benzofurans are similar to one another except that the values of ε near 280 nm of the naphtho[1,8-*bc*]furans are lower than those of benzofurans. The differences in spectra may be due to the greater strain in the naphto[1,8-*bc*]-furan rings.

The other synthetic methods and reactivities of the naphtho[1,8-*bc*]furans will be further investigated.

Experimental

All the melting points are uncorrected. The column chromatography was performed on silica gel (WACOGEL C-200). Unless otherwise stated, anhydrous sodium sulfate was employed as the drying agent. The infrared absorption spectra were determined with a JASCO Model DS 402G infrared spectrophotometer. The ultraviolet absorption spectra were determined with a Shimadzu Model UV-200 spectrophotometer. The nuclear magnetic resonance spectra were determined at 100 MHz with a JEOL Model 4H-100 NMR spectrometer, using tetramethylsilane as the internal standard.

*4,5-Dihidro-3H-naphtho[1,8-*bc*]furan-2-carboxylic Acid (IIa).* A mixture of 8-hydroxy-1-tetralone (Ia; 5.0 g),[11] ethyl bromoacetate (18.5 g), potassium carbonate (30.7 g), and ethyl methyl ketone (10 ml) was refluxed for 6 hr at 120 °C. The reaction mixture was then extracted with acetone, and the acetone was evaporated. The residue was dissolved in a small amount of ethanol and hydrolized with a 3 M potassium hydroxide solution. The alkaline solution was acidified with 6 M hydrochloric acid, and the resulting precipitates were extracted with ether. The ethereal layer was washed with water and dried, and then evaporated. When the residue was then washed with benzene, 2.8 g (45%) of IIa were obtained; mp 238 °C (decompn.). Recrystallization from tetrahydrofuran gave colorless prisms; mp 240 °C (decompn.). IR (KBr): 1675 (COOH), 778 cm^{-1} (three adjacent aromatic hydrogen atoms). UV (EtOH): λ_{max} 282^{sh} (ε 18200), 275 (20100), 229^{sh} (13700), 224 nm (14800).

Found: C, 71.04; H, 5.06%. Calcd for $C_{12}H_{10}O_3$: C, 71.28; H, 4.99%.

*8-Methoxy-4,5-dihydro-3H-naphtho[1,8-*bc*]furan-2-carboxylic Acid (IIb).* Colorless needles (from tetrahydrofuran; 43%): mp 229 °C (decompn.). IR (KBr): 1680 (COOH), 795 cm^{-1} (two adjacent aromatic hydrogen atoms). UV (EtOH): λ_{max} 305^{sh} (ε 3300), 276 (16100), 234 nm (22000).

Found: C, 67.26; H, 5.31%. Calcd for $C_{13}H_{12}O_4$: C, 67.24; H, 5.21%.

*6-Methoxy-4,5-dihydro-3H-naphtho[1,8-*bc*]furan-2-carboxylic Acid (IIc).* Colorless needles (from dioxane; 49%), mp 240—241 °C (decompn.). IR (KBr): 1675 (COOH), 802 cm^{-1} (two adjacent aromatic hydrogen atoms). UV (EtOH): λ_{max} 275 (ε 20000), 218 nm (17100).

Found: C, 66.95; H, 5.23%. Calcd for $C_{13}H_{12}O_4$: C, 67.24; H, 5.21%.

*6-Chloro-8-methoxy-4,5-dihydro-3H-naphtho[1,8-*bc*]furan-2-carboxylic Acid (IId).* Colorless needles (from tetrahydrofuran; 46%): mp 249 °C (decompn.). IR (KBr): 1687 (COOH), 817 cm^{-1} (C-Cl). UV (EtOH): λ_{max} 310^{sh} (ε 2400), 276 (16400), 269^{sh} (15800), 235 nm (24700).

Found: C, 58.35; H, 4.25%. Calcd for $C_{13}H_{11}O_4Cl$: C, 58.55; H, 4.16%.

*Ethyl 4,5-Dihydro-3H-naphtho[1,8-*bc*]furan-2-carboxylate (IIIa).* A mixture of Ia (3.0 g), ethyl bromoacetate (11.1 g), potassium carbonate (18.4 g), and ethyl methyl ketone (10 ml was refluxed for 6 hr at 120 °C. The reaction mixture was then extracted with ether; the ethereal layer was washed with water and dried, and then evaporated. The residue was recrystallized from ethanol to give 1.5 g (35%) of IIIa as colorless needles; mp 85—86 °C. IR (KBr): 1720 (ester), 786 cm^{-1} (three adjacent aromatic hydrogen atoms). NMR (CCl_4): δ 7.30 (d, 1H, J=8 Hz, Ar-H), 7.20 (d, 1H, J= 8 Hz, Ar-H), 6.85—6.98 (m, 1H, Ar-H), 4.32 (q, 2H, J=

6 Hz, $-OCH_2-$), 3.03 (t, 2H, J=6 Hz, $-CH_2-$), 2.86 (t, 2H, J=6 Hz, $-CH_2-$), 1.91—2.17 (m, 2H, $-CH_2-$), 1.40 (t, 3H, J=6 Hz, CH_3). UV (EtOH): λ_{max} 281 (ε 23000), 231 (13600), 226 nm (13200).

Found: C, 72.77; H, 6.05%. Calcd. for $C_{14}H_{14}O_3$: C, 73.03; H, 6.13%.

*Ethyl 8-Methoxy-4,5-dihydro-3*H*-naphtho[1,8-*bc*]furan-2-carboxylate (IIIb).* Colorless needles (from ethanol; 34%); mp 100—101 °C. IR (KBr): 1722 (ester), 809 cm^{-1} (two adjacent aromatic hydrogen atoms). NMR (CD_3COCD_3): δ 6.93 (s, 2H, Ar–H), 4.38 (q, 2H, J=6 Hz, $-OCH_2-$), 3.99 (s, 3H, OCH_3), 3.03 (t, 2H, J=6 Hz, $-CH_2-$), 2.83 (t, 2H, J=6 Hz, $-CH_2-$), 1.40 (t, 2H, J=6 Hz, CH_3). UV (EtOH): λ_{max} 305 (ε 4400), 283 (19200), 237 nm (23400).

Found: C, 68.96; H, 6.07%. Calcd for $C_{15}H_{16}O_4$: C, 69.22; H, 6.20%.

*Ethyl 6-Methoxy-4,5-dihydro-3*H*-naphtho[1,8-*bc*]furan-3-carboxylate (IIIc).* Colorless needles (from ethanol; 44%); mp 95—96 °C. IR (KBr): 1702 (ester), 796 cm^{-1} (two adjacent aromatic hydrogen atoms). NMR (CD_3COCD_3): δ 6.99 (d, 1H, J=9 Hz, Ar–H), 6.72 (d, 1H, J=9 Hz, Ar–H), 4.38 (q, 2H, J=8 Hz, $-OCH_2-$), 3.88 (s, 3H, OCH_3), 3.02 (t, 2H, J=6 Hz, $-CH_2-$), 2.81 (t, 2H, J=6 Hz, $-CH_2-$), 1.40 (t, 3H, J=8 Hz, CH_3). UV (EtOH): λ_{max} 315 (ε 3400), 287 (21600), 279 (22000), 221 nm (14900).

Found: C, 69.28; H, 6.19%. Calcd for $C_{15}H_{16}O_4$: C, 69.22; H, 6.20%.

*Ethyl 6-Chloro-8-methoxy-4,5-dihydro-3*H*-naphtho[1,8-*bc*]furan-2-carboxylate (IIId).* Colorless needles (from ethanol; 36%); mp 117.5—119.5 °C. IR (KBr): 1704 (ester), 808 cm^{-1} (C–Cl). NMR (CD_3COCD_3): δ 6.93 (s, 1H, Ar–H), 4.40 (q, 2H, J=8 Hz, $-OCH_2-$), 4.02 (s, 3H, OCH_3), 3.00 (t, 2H, J=6 Hz, $-CH_2-$), 2.80 (t, 2H, J=6 Hz, $-CH_2-$), 1.40 (t, 3H, J=6 Hz, CH_3). UV (EtOH): λ_{max} 305 (ε 3300), 283 (19000), 276 (17800), 239 cm (25300).

Found: C, 60.88; H, 5.04%. Calcd for $C_{15}H_{15}O_4Cl$: C, 61.13; H, 5.13%.

*2-Benzoyl-8-methoxy-4,5-dihydro-3*H*-naphto[1,8-*bc*]furan (IVb).* A mixture of Ib (3.0 g), phenacyl bromide (4.6 g), potassium carbonate (7.0 g), and dioxane (10 ml) was refluxed for 8 hr at 120 °C. The reaction mixture was then extracted with ether; the ethereal layer was washed with water and dried, and then evaporated. The residue was recrystallized from ethanol to give 3.0 g (66%) of IVb as colorless needles; mp 80.5—81.5 °C. IR(KBr): 1625 (C=O), 815 (two adjacent aromatic hydrogen atoms), 702 cm^{-1} (five adjacent aromatic hydrogen atoms). UV(EtOH): λ_{max}313 (ε17000), 254 (16500), 205 nm (28700).

Found: C, 77.80; H, 5.35%. Calcd for $C_{19}H_{16}O_3$: C, 78.06; H, 5.52%.

*2-Benzoyl-3,4-dihydro-3*H*-naphtho[1,8-*bc*]furan (IVa).* Colorless needles (from ethanol; 41%); mp 51—52° C. IR (KBr): 1629 (C=O), 773 (three adjacent aromatic hydrogen atoms), 718 cm^{-1} (five adjacent aromatic hydrogen atoms). UV (EtOH): λ_{max} 320 (ε 19100), 256^{sh} (8600), 240 (11000), 205 nm (29100).

Found: C, 82.18; H, 5.20%. Calcd for $C_{18}H_{14}O_2$: C, 82.42; H, 5.38%

*2-Benzoyl-6-chloro-8-methoxy-4,5-dihydro-3*H*-naphtho[1,8-*bc*]-furan (IVd).* Colorless needles (from acetone; 71%); mp 114—115 °C. IR (KBr): 1628 (C=O), 810 (C–Cl), 720 cm^{-1} (five adjacent aromatic hydrogen atoms). UV (EtOH): λ_{max} 314 (ε19800), 257 (16500), 210 nm (32700).

Found: C, 69.73; H, 4.66%. Calcd for $C_{19}H_{15}O_3Cl$: C, 69.89; H, 4.63%.

(2-Methoxy-8-oxo-5,6,7,8-tetrahydro-1-naphthoxy) acetic Acid (Vb). A mixture of Ib (5.0 g), ethyl bromoacetate (18.5 g), potassium carbonate (30.0 g), and acetone (40 ml) was refluxed for 6 hr at 70 °C. The reaction mixture was subsequently extracted with acetone, and the acetone was evaporated. The residue was dissolved in a small amount of ethanol and hydrolyzed with a 3 M potassium hydroxide solution. The alkaline solution was acidified with 6 M hydrochloric acid, and the resulting precipitates were collected by filtration. Recrystallization from acetone gave 4.8 g (73%) of Vb as colorless needles; mp 176—178 °C. IR (KBr): 1750 (CO-OH), 1650 (C=O), 822 cm^{-1} (two adjacent aromatic hydrogen atoms). UV (EtOH): λ_{max} 325 (ε 3200), 256 (8200), 216 nm (21600).

Found: C, 62.63; H, 5.65%. Calcd for $C_{13}H_{14}O_5$: C, 62.40; H, 5.64%.

(8-Oxo-5,6,7,8-tetrahydro-1-naphthoxy) acetic Acid (Va). Colorless plates (from acetone-*n*-hexane; 22%); mp 100—102 °C. IR (KBr): 1775, 1757 (COOH), 1645 (C=O), 798 cm^{-1} (three adjacent aromatic hydrogen atoms). UV (EtOH): λ_{max} 313 (ε 3700), 254 (9000), 216 nm (18600).

Found: C, 65.35; H, 5.51%. Calcd for $C_{12}H_{12}O_4$: C, 65.45, H, 5.49%.

(4-Methoxy-8-oxo-5,6,7,8-tetrahydro-1-naphthoxy) acetic Acid (Vc). Colorless plates (from acetone; 30%); mp 152—153 °C. IR (KBr): 1776, 1758 (COOH), 1650 (C=O), 827 cm^{-1} (two adjacent aromatic hydrogen atoms). UV (EtOH): λ_{max} 348 (ε 3500), 252 (6300), 229 nm (18200).

Found: C, 62.42; H, 5.68%. Calcd for $C_{13}H_{14}O_5$: C, 62.40; H, 5.64%.

(4-Chloro-2-methoxy-8-oxo-5,6,7,8-tetrahydro-1-naphthoxy) acetic Acid (Vd). Colorless needles (from acetone; 71%); mp 148—150 °C. IR (KBr): 1755 (COOH), 1657 (C=O), 802 cm^{-1} (C–Cl). UV (EtOH): λ_{max} 325 (ε 3300), 257 (5600), 220 nm (23100).

Found: C, 55.00; H, 4.75%. Calcd for $C_{13}H_{13}O_5Cl$: C, 54.85; H, 4.60%.

Decarboxylation of IIa–IId. A mixture of IIa (1.0 g), copper powder (1.0 g), and quinoline (10 g) was heated for 45 min at 160 °C. The reaction mixture was then extracted with ether; the etheral layer was acidified with 2 M hydrochloric acid and washed with 2 M hydrochloric acid, a 1 M potassium carbonate solution, and water, dried, and then evaporated. The residue was chromatographed on silica gel and eluted with benzene. A pale yellow fraction was collected to give 650 mg (83%) of VIa as a colorless oil. Bp 68 °C at 1.5 mmHg. IR (neat): 1627 (furan), 772 (three adjacent aromatic hydrogen atoms), 750 cm^{-1} (furan H). NMR (CCl_4): δ 6.80—7.20 (m, 3H, Ar–H), 7.13 (s, 1H, furan H), 2.82 (q, 4H, J=6 Hz, $-CH_2-+-CH_2-$), 2.00 (q, 2H, J=6 Hz, $-CH_2-$).

Found: C, 83.31; H, 6.19%. Calcd for $C_{11}H_{10}O$: C, 83.52; H, 6.37%.

VIb. Colorless oil (86%); bp 102 °C at 0.7 mmHg. IR (neat): 1638 (furan), 794 cm^{-1} (two adjacent aromatic hydrogen atoms, furan H). NMR (CCl_4): δ 7.18 (s, 1H, furan H), 6.73 (d, 1H, J=8 Hz, Ar–H), 6.55, (d, 1H, J=8 Hz, Ar–H), 5.96 (s, 3H, OCH_3), 2.75 (q, 4H, J=5 Hz, $-CH_2-+-CH_2-$), 1.98 (q, 2H, J=5 Hz, $-CH_2-$).

Found: C, 76.68; H, 6.29%. Calcd for $C_{12}H_{12}O_2$: C, 76.57; H, 6.43%.

VIc. Colorless oil (80%); bp 105 °C at 1.8 mmHg. IR (neat): 775, 765 cm^{-1} (two adjacent aromatic hydrogen atoms, furan H). NMR (CCl_4): δ 7.16 (s, 1H, furan H), 7.05 (d, 1H, J=9 Hz, Ar–H), 6.64 (d, 1H, J=9 Hz, Ar—H), 5.77 (s, 3H, OCH_3), 2.75 (q, 4H, J=8 Hz, $-CH_2-+-CH_2-$), 1.98 (q, 2H, J=5 Hz, $-CH_2-$).

Found: C, 76.44; H, 6.33%. Calcd for $C_{12}H_{12}O_2$: C, 76.57; H, 6.43%.

VId. Colorless oil (78%); bp 110 °C at 0.6 mmHg. IR (neat): 1638 (furan), 805 cm^{-1} (C–Cl). NMR (CCl_4): δ 7.21 (s, 1H, furan H), 6.60 (s, 1H, Ar–H), 3.95 (s, 3H, OCH_3), 2.73 (q, 4H, J=6 Hz, $-CH_2-+-CH_2-$), 1.90 (q, 2H, J=6 Hz, $-CH_2-$).

Found: C, 64.45; H, 4.94%. Calcd for $C_{12}H_{11}O_2Cl$: C, 64.73; H, 4.98%.

*8-Methoxy-4,5-dihydro-3*H-*naphtho*[*1,8*-bc]*furan (VIb) and Lactone (VIIb).* *VIb*: A mixture of Vb (1.0 g), sodium acetate (4.6 g), and acetic anhydride (15 ml) was heated for 1 hr at 145 °C and then for 10 min at 160 °C. The reaction mixture was poured into water, and the solution was extracted with ether. The ethereal layer was washed with a 1 M potassium carbonate solution and water, dried, and then evaporated. The residue was chromatographed on silica gel and eluted with benzene. The first fraction gave 350 mg (46%) of IVb as a colorless oil.

VIIb: A latter fraction gave 250 mg (32%) of colorless crystals. Recrystallization from benzene-*n*-hexane gave VIIb as colorless needles; mp 112—114 °C. IR (KBr): 1764 (lactone), 1642 (C=C), 810 cm^{-1} (two adjacent aromatic hydrogen atoms).

Found: C, 67.14; H, 5.35%. Calcd for $C_{13}H_{12}O_4$: C, 67.24; H, 5.21%.

*6-Methoxy-4,5-dihydro-3*H-*naphto*[*1,8*-bc]*furan (VIc) and Lactone (VIIc).* *VIc*: Colorless oil (46%).

VIIc: Colorless needles from benzene-*n*-hexane (32%); mp 102—103 °C. IR (KBr): 1759 (lactone), 1650 (C=O), 804 cm^{-1} (two adjacent aromatic hydrogen atoms).

Found: C, 67.13; H, 5.11%. Calcd for $C_{13}H_{12}O_4$: C, 67.24; H, 5.21%.

*6-Chloro-8-methoxy-4,5-dihydro-3*H-*naphtho*[*1,8*-bc]*furan (VId) and Lactone (VIId).* *VId*: Colorless oil (70%).

VIId: Colorless needles from benzene-*n*-hexane (19%); mp 153.5—155 °C. IR (KBr): 1771 (lactone), 1642 (C=C), 837 cm^{-1} (C–Cl).

Found: C, 58.33; H, 3.96%. Calcd for $C_{13}H_{13}O_5Cl$: C, 58.55; H, 4.16%.

*4,5-Dihydro-3*H-*naphtho*[*1,8*-bc]*furan (VIa).* *VIa*: Colorless oil (34%).

Va: A latter fraction gave 450 mg (37%) of crystals; mp 96—98 °C. The compound was identical with Va in its infrared spectra. This suggests that the corresponding lactone should be hydrolyzed during the working-up.

3,5-Dimethylbenzofuran-2-carboxylic Acid (XII). A mixture of XI, ethyl bromoacetate (15.2 g), and potassium carbonate (12.3 g) was heated for 6 hr at 150 °C. The following procedures were done in the same way as the synthesis of IIa to give 1.9 g (76%) of XII; mp 220—222 °C (dec.). Recrystallization from acetone-tetrahydrofuran gave colorless prisms; mp 222—223 °C (decompn.) (lit,[12] mp 224—225 °C). IR (KBr): 1670 (COOH), 815 cm^{-1} (two adjacent aromatic hydrogen atoms). UV (EtOH): λ_{max} 300[sh] (ε 5600), 273 (18700), 214 nm (17600).

The authors wish to Mr. Hideo Saisu for the infrared analyses and Mr. Takao Ono for the nuclear magnetic resonance analyses.

References

1) T. Shimizu, T. Horaguchi, and A. Watanabe, This Bulletin, **46**, 1772 (1973).
2) T. Horaguchi, and T. Shimizu, *ibid.*, **47**, 485 (1974).
3) T. Horaguchi, and T. Shimizu, *ibid.*, **48**, 488 (1975).
4) R. Royer, E. Bisagni, and G. Menichi, *Bull. Soc. Chim. Fr.*, **1964** (9), 2112 (*Chem. Abstr.*, **62**, 1619[d]).
5) S. Swaminathan, R. K. Natharajan, S. Ramachandran, and S. K. Sankarappa, *J. Org. Chem.*, **31**, 656 (1966).
6) D. Berry and D. C. C. Smith, *J. Chem. Soc., Perkin I*, **1972**, 699.
7) G. H. Phillips, A. Robertson, and W. B. Whalley, *J. Chem. Soc.*, **1952**, 4951.
8) A. Müller, M. Mészàros, and K. Körmendy, *J. Org. Chem.*, **19**, 472 (1954).
9) D. C. Johnson and A. Robertson, *J. Chem. Soc.*, **1950**, 2381.
10) T. Abe and T. Shimizu, *Nippon Kagaku Zasshi*, **91**, 753 (1970).
11) I. A. Kaye, R. S. Mattews, and A. A. Scals, *J. Chem. Soc.*, **1964**, 2816.
12) A. Hantzsch and E. Lang, *Ber.*, **19**, 1298 (1886).
13) A. W. Burgstahler and L. R. Worden, "Organic Syntheses," Vol. 46, p. 28 (1966).
14) W. B. Whalley, *J. Chem. Soc.*, **1953**, 3479.
15) D. S. Deohra and P. Gapta, *Indian J. Chem.*, **2**, (11), 459 (1964).

Stereospecific Synthesis of Natural (+)Blastmycinone and Its Three (2*R*)-Diastereomers

Shinpei ABURAKI, Norio KONISHI, and Mitsuhiro KINOSHITA

Department of Applied Chemistry, Faculty of Engineering, Keio University, Hiyoshi, Kohoku-ku, Yokohama 223

(Received June 29, 1974)

Natural (+)blastmycinone [(+)**1a**] and its three (2*R*)-diastereomers [(+)**1b**, (−)**1c**, and (−)**1d**] were synthesized through stereospecific routes *via* the corresponding (−)blastmycinolactol [(−)**2a**] and its diastereomeric hydroxylactones [(+)**2b**, (−)**2c**, and (−)**2d**] from methyl 4,6-*O*-benzylidene-3-*C*-butyl-3-deoxy-α-D-altropyranoside (**4**) prepared by the Grignard reaction of methyl 2,3-anhydro-4,6-*O*-benzylidene-α-D-mannopyranoside (**3**) with butylmagnesium chloride. By the synthesis the relative configurations of natural type of racemic blastmycinone and its all diastereomers were completely established.

Natural (+)blastmycinone[1] [(+)**1a**], obtained by saponification of antimycin A_3 (blastmycin) under mild conditions, has recently been synthesized[2] from the synthetic (−)hydroxylactone [(−)**2a**] identical with natural (−)blastmycinolactol.[1] Hydroxylactone [(−)**2a**] was prepared by lithium aluminum hydride-reduction of the optically active (+)diastereomer (**A**) of *t*-butyl 4-(*N*-benzyloxycarbonyl-*O*-*t*-butyl-L-threonyloxy)-2-butyl-3-(isovaleryloxy)pentanoate; only this is adequate for the total synthesis of natural antimycin

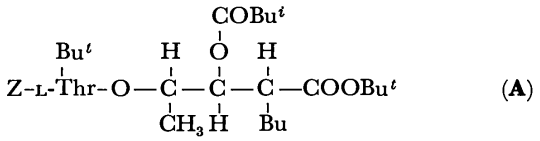

(**A**)

A_3.[2] The absolute configuration(2*R*,3*R*,4*S*) of the natural (+)blastmycinone [(+)**1a**] has been established on the basis of the absolute configuration of (−)blastmycinolactol [(−)**2a**] which was determined through a stereospecific synthesis of the enantiomeric blastmycinolactol [(+) **2a**].[3] The natural type of racemic blastmycinone and its diastereomers have also been synthesized and characterized by tlc and PMR.[2]* An optically active diastereomer (−)**1b** has been obtained together with the enantiomeric blastmycinone [(−)**1a**] as a byproduct in the lactonization reaction** of (2*S*,3*S*,4*R*)-4-(*N*-benzyloxycarbonyl-L-threonyloxy)-2-butyl-3-(isovaleryloxy)pentanoic acid (**B**) with trifluoroacetic anhydride in benzene.

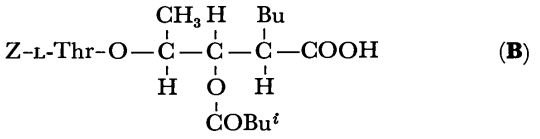

(**B**)

A recent study by Koyama *et al.*[4] on stereoselective synthesis and relative configurations of the racemic diastereomers of blastmycinone indicates that the configuration of the diastereomer **1b** is 2,3-*cis*: 3,4-*cis*. The diastereomer (−)**1b** appears to be the 3-epimer of the enantiomeric blastmycinone (−)**1a**. However, the possibility of 4-epimerization, which may partly occur on the C-4 of compound **B** under the reaction conditions of lactonization, cannot be excluded. Confirmation of the configuration of **1b** was thus undertaken by an unambiguous method. For this purpose, we attempted a stereospecific synthesis of four optically active diastereomeric blastmycinones [(+)**1a**, (+)**1b**, (−)**1c**, and (−)**1d**], all of which have "2*R*" configuration, similar to that in the natural blastmycinone (+)**1a**, as shown in Fig. 1.

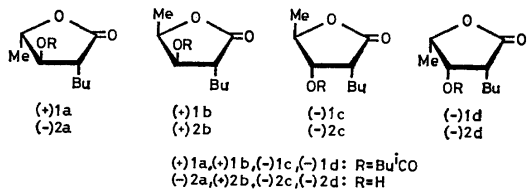

Fig. 1. Absolute configurations of diastereomeric (2*R*)blastmycinones and blastmycinolactols.

Methyl 2,3-anhydro-4,6-*O*-benzylidene-α-D-mannopyranoside[5] (**3**) was treated with excess butylmagnesium chloride in ether according to the procedure of Inch and Lewis[6] to afford methyl 4,6-*O*-benzylidene-3-*C*-butyl-3-deoxy-α-D-altropyranoside (**4**) in a 64% yield. Acetylation of **4** with acetic anhydride in pyridine gave the 2-acetate (**5**). The structures of **4** and **5** were confirmed by PMR analysis. Compounds **4** and **5** were treated with *N*-bromosuccinimide[7] in boiling carbon tetrachloride to yield methyl 4-*O*-benzoyl-6-bromo-3-*C*-butyl-3,6-dideoxy-α-D-altropyranoside (**6**) and its 2-acetate (**7**), respectively, in excellent yields.

Lithium aluminum hydride-reduction of **6** in tetrahydrofuran gave methyl 3-*C*-butyl-3,6-dideoxy-α-D-altropyranoside (**8**) in a 76% yield. Acetolysis of **8** with acetic anhydride–sulfuric acid afforded 1,2,4-tri-*O*-acetyl-3-*C*-butyl-3,6-dideoxy-D-altropyranose (**9**) as a syrupy anomeric mixture. Hydrolysis of **9** with methanolic sodium hydroxide gave a free sugar **10**, which was subjected to periodate oxidation to yield 2-*C*-butyl-2,5-dideoxy-3-*O*-formyl-D-ribofuranose (**11**) in an excellent yield. The structure of **11** was supported by its PMR spectral data ($J_{1,2}$=4.7 Hz, $J_{2,3}$=10.0 Hz, $J_{3,4}$=5.8 Hz, and δ($CDCl_3$) 8.23(s, OCHO)]. De-O-formylation of **11** with 2% hydrochloric acid in aqueous dioxane followed by oxidation with bromine–water afforded (−)(2*R*,3*S*,4*R*)-2-butyl-3,4-dihydroxypentanoic acid-1,4-lactone[(−)**2c**] in a 68% yield. Isovalerylation of (−)**2c** with isovaleric anhydride in

* Racemic blastmycinone and its diastereomers were previously designated in order of decreasing R_f-value of tlc with the solvent G (see Experimental) as **1a**, **1b**, **1c**, and **1d**.

** This reaction mainly gave the nine-membered dilactone derivative, from which the diastereomeric antimycin A_3 was synthesized.[2]

Table 1. PMR-spectra data of synthetic (2*R*)blastmycinolactols (in CD_3OD) and blastmycinones (in $CDCl_3$). Chemical shifts (δ values) and coupling constants (Hz)

Compounds:	(2*R*)Blastmycinolactols				(2*R*)Blastmycinones			
	(−)**2a**	(+)**2b**	(−)**2c**	(−)**2d**	(+)**1a**	(+)**1b**	(−)**1c**	(−)**1d**
H-3(dd)	3.76	4.18	4.18	4.31	4.95	5.24	5.20	5.68
H-4(dq)	4.20	4.73	4.52	4.56	4.37	4.82	4.51	4.63
4-CH_3(d)	1.41	1.36	1.33	1.38	1.45	1.36	1.40	1.32
$J_{2,3}$	8.2	3.4	5.6	4.7	5.8	3.0	6.0	5.5
$J_{3,4}$	7.5	5.0	1.1	3.3	4.5	5.0	0.7	3.4
J_{4,CH_3}	6.0	6.7	6.8	6.3	6.5	6.5	6.5	6.5

pyridine gave (−)blastmycinone-c [(−)**1c**] in an 86% yield. The synthetic sample showed on tlc (solvent G) a single spot having the same R_f-value as that of the racemic blastmycinone-c (**1c**). The PMR spectrum of (−)**1c** was identical with that of **1c**. (Table 1)

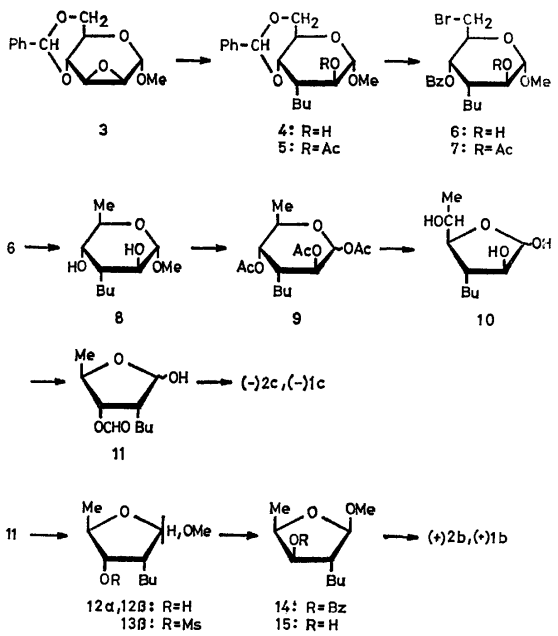

Chart 1.

The periodate-oxidation product **11** was treated with 0.5% methanolic hydrogen chloride to afford an anomeric mixture of the methyl glycoside, which was fractionated on silica gel to give α-anomer (**12**α, 30%) and β-anomer (**12**β, 50%). Treatment of the major product **12**β with methanesulfonyl chloride in pyridine gave 3-mesylate (**13**β), which was subsequently treated with sodium benzoate in dimethylsulfoxide (DMSO) at 140—145 °C for 3 hr to afford the 3-inverted-benzoate (**14**) in a 41% yield. De-O-benzoylated glycoside **15**, obtained by hydrolysis of **14** with 0.1 M methanolic sodium hydroxide, was easily converted into free sugar by treatment with 0.1 M hydrochloric acid in aqueous dioxane at room temperature. The product was then oxidized with bromine-water to afford (+)(2*R*,3*R*,4*R*)-2-butyl-3,4-dihydroxypentanoic acid-1,4-lactone [(+)**2b**] in a 62% yield based on **14**. Isovalerylation of (+)**2b** gave (+)blastmycinone-b [(+)**1b**] in an 88% yield. This showed the same R_f-value as that of the racemic blastmycinone-b (**1b**) on tlc (solvent G), its PMR spectrum also being identical with that of **1b**. (Table 1)

Compound **7** was treated with silver fluoride[8a,8b] in pyridine at room temperature to afford 5-enopyranoside (**16**, 91%) as a syrup, whose PMR spectrum showed overlapping narrow multiplets at δ 4.77—4.88 attributed to the terminal methylene protons (H-6, H-6′). Since **16** did not crystallize and showed an R_f-value close to that of **7** on tlc with all solvent systems employed, it was used without further purification for the subsequent synthesis. Hydrogenation of **16** on palladium black followed by removal of some impurities through a silica gel column gave exclusively methyl 2-*O*-acetyl-4-*O*-benzoyl-3-*C*-butyl-3,6-dideoxy-β-L-galactopyranoside (**17**) in a 70% yield. First-order analysis of the PMR spectrum of **17** revealed large ring proton coupling constants ($J_{1,2}$=8.0 and $J_{2,3}$=11.1 Hz), which suggest the preferred conformation of **17** to be 1*C* chair. Acetolysis of **17** with acetic anhydride–sulfuric acid yielded 1,2-di-*O*-acetyl-4-*O*-benzoyl-3-*C*-butyl-3,6-dideoxy-α-L-galactopyranose (**18**) which was contaminated by a small amount of its β-anomer. The protecting groups of **18** were removed with methanolic sodium hydroxide to give **19**, which was then subjected to periodate-oxidation to afford 2-*C*-butyl-2,5-dideoxy-3-*O*-formyl-L-lyxofuranose (**20**) as a semicrystalline anomeric mixture in a 98% yield based on **17**. De-O-formylation of **20** followed by oxidation with bromine–water gave the crystalline diastereomeric hydroxylactone[(−)**2d**, mp 99.0—100.5 °C] in a 51% yield. Isovalerylation of (−)**2d** afforded (−)blastmycinone-d [(−)**1d**, mp 47–48 °C] in an 86% yield, which could be characterized as blastmycinone-d by tlc and PMR.

Subsequently, the natural (+)blastmycinone [(+)**1a**] was synthesized *via* the natural (−)blastmycinolactol [(−)**2a**] as follows. Free sugar **20** was treated with 0.1 M methanolic hydrogen chloride to afford methyl 2-*C*-butyl-2,5-dideoxy-β-L-lxyofuranoside (**21**) as a major product in a 60% yield. The β-glycoside **21** was mesylated and the resulting crystalline mesylate **22** was treated with sodium benzoate in DMSO to give methyl 3-*O*-benzoyl-2-*C*-butyl-2,5-dideoxy-β-L-arabinofuranoside (**23**) in a 42% yield based on **21**, which was proved to be structurally homogeneous by PMR analysis. Debenzoylated product **24** obtained from **23** was hydrolyzed with 0.1 M hydrochloric acid and the resulting free sugar was treated with bromine-water to afford (−)**2a** (mp 49.5—50.5 °C) in an 84% yield.

This product was identical with the authentic sample of natural (−)blastmycinolactol,[2] from which the natural (+)blastmycinone [(+)**1a**] had been derived in an excellent yield.[2]

The configuration of the diastereomer **1b** was unambiguously determined from the above results, the relative configurations of all diastereomeric blastmycinones (**1a**, **1b**, **1c**, and **1d**) being completely established. Configurations [2,3-*cis*:3,4-*cis* for **1b** and 2,3-*trans*:3,4-*cis* for **1d**] proposed by Koyama *et al.*[4] should be revised to 2,3-*trans*:3,4-*cis* for **1b** and 2,3-*cis*:3,4-*cis* for **1d**. Consequently, the byproduct (−)**1b** formed during the lactonization of **B** was proved to be the 4-epimer of the enantiomeric blastmycinone [(−)**1a**].

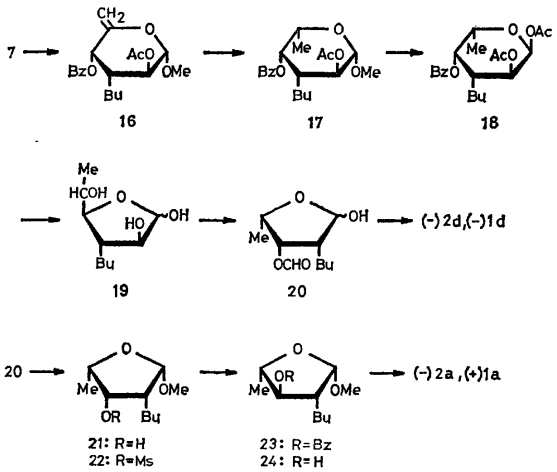

Chart 2.

Finally, we wish to describe the preferred conformations of the optically pure hydroxylactones, (−)**2a**, (+)**2b**, (−)**2c**, and (−)**2d**, in various solvents, which may closely be related to those of the corresponding diastereomeric blastmycinones, (+)**1a**, (+)**1b**, (−)**1c**, and (−)**1d**. The observed ring proton coupling constants ($J_{2,3}$, $J_{3,4}$) of these hydroxylactones in deuteromethanol (Table 1), benzene, pyridine, and deuterochloroform were approximately equal and their CD spectra in methanol measured at room temperature showed no double-humped CD curve[9] but single negative Gaussian curves corresponding to a negative Cotton effect. These evidences indicate that the hydroxylactones in solution may predominantly exist in either nonplaner E_3 or E^3 conformation which is considered to be stable conformation[10] of 1,4-lactone under the preference of co-planarity of the five atoms of lactone group (C–CO–O–C).

Legrand and Bucourt rules[11] on ring chirality allow the negative sign of the Cotton effect to be predicted for the E_3 conformations (Fig. 2) without any conflict with the established correlation between the negative sign of the Cotton effect and the absolute configuration (2*R*) at C_2 of the 1,4-lactone, which has been proposed for the aldono-1,4-lactone by Okuda *et al.*[12] and discussed by Beecham.[13] The prediction was confirmed by PMR data (Table 1) in the following way.

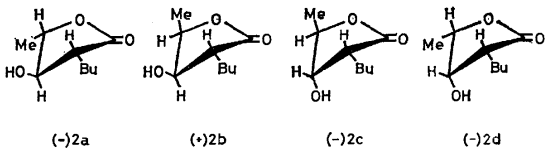

Fig. 2. Preferred conformations of diastereomeric (2*R*)blastmycinolactols.

Coupling constants ($J_{2,3}$, $J_{3,4}$) of (−)**2a** and (−)**2c** could be explained most satisfactorily on the assumption of E_3 conformation (Fig. 2) for the hydroxylactones, (−)**2a** and (−)**2c**. Calculation of the dihedral angles ($\phi_{2,3}$, $\phi_{3,4}$) of (+)**2b** carried out according to the method of Karplus[14] with the coupling constants ($J_{2,3}$, $J_{3,4}$) of (+)**2b** indicates that two conformers, (E^3 $\phi_{2,3}=128°28'$, $\phi_{3,4}=37°54'$) and E^3 ($\phi_{2,3}=48°51'$, $\phi_{3,4}=37°54'$), are possible for (+)**2b**. From a consideration of the Dreiding models, it appears that, in the E_3 conformer, the observed angle (θ *ca.* 20°) of the buckle*** of the lactone ring forces the C-4 methyl group and the C-2 hydrogen atom into a non-parallel axial orientation by which they are kept at a distance, a small 1,3-diaxial interaction between them thus being expected, while is in the E^3 conformation ($\theta \leq 65°$) the bulky C-2 butyl group closely located to the C-4 hydrogen atom which is oriented in an almost parallel axial position to the butyl group, and thus a larger 1,3-diaxial interaction should be expected. In conclusion, the E_3 conformer appears to be more favorable.

On the last hydroxylactone (−)**2d**, the calculated dihedral angles ($\phi_{2,3}=40°00'$ and $\phi_{3,4}=49°32'$) could be applied to both E_3 and E^3 conformers of the lactone. Consideration by means of the model suggests the E^3 conformer (θ *ca.* 45°) to be unfavorable, since a larger 1,3-diaxial interaction between the bulky butyl group in quasi axial position at C-2 and the quasi axial methyl group at C-4 is expected, and the interaction between the hydrogen atoms at C-2 and C-4 in the E_3 conformer might be smaller.

Experimental

Melting points were determined on a micro hot stage and are uncorrected. IR spectra were taken on a Hitachi 225 Spectrophotometer, and PMR spectra on a Varian A-60D Spectrometer using TMS as an internal standard. Optical rotations were measured with a Zeiss Photoelectric Precision Polarimeter. CD spectra were taken on a JASCO J-20 Spectropolarimeter. Tlc was carried out on Wakogel B-5 (Wako Pure Chemical Industries, Ltd.) and silica gel column chromatography on Wakogel C-200 which was activated at 110 °C for 1 hr. The following solvent systems were used: A [hexane-acetone(5 : 1)], B [*ditto*(10 : 1)], C [benzene-ethyl acetate(12 : 1)], D [*ditto*(1 : 1)], E [*ditto*(6 : 1)], F [*ditto*(50 : 1)], and G [petroleum ether-diisopropyl ether (7 : 4)]. In general, all concentrations were carried out at reduced pressure below 40 °C.

*** Extent of the buckle is represented in the angle (θ) between planes $C_{(2)}-\underset{\underset{O}{\|}}{C}_{(1)}-O-C_{(4)}$ and $C_{(2)}-C_{(3)}-C_{(4)}$.[15]

1. *Methyl 4,6-O-Benzylidene-3-C-butyl-3-deoxy-α-D-altropyranoside (4).*[3] Fresh magnesium shavings (11.1 g, 0.457 mol) were covered with dry ether (160 ml) and activated by addition of a piece of iodine. After the activation reaction had started, butyl chloride (47.9 ml, 0.460 mol) was added under stirring at room temperature for 1 hr to form butylmagnesium chloride. After standing for 12 hr, a solution of methyl 2,3-anhydro-4,6-*O*-benzylidene-α-D-mannopyranoside (**3**)[5] (8.00 g, 30.3 mmol) in dry ether (400 ml) was added to the viscous suspension. The mixture was refluxed for 9 hr under vigorous stirring, then cooled in an ice-bath, and carefully decomposed with ice-water (200 ml). The ether layer was washed with saturated aqueous NaCl, dried and evaporated to give a syrup (11.3 g), which was chromatographed on a silica gel column (1.7 kg) with solvent A to afford a homogeneous sample of **4** as a colorless oil (6.25 g, 64%): $[\alpha]_D^{18}$ +135° (*c* 1.80, chloroform); δ ($CDCl_3$) 3.41 (s, OCH_3), 4.58 (dd, H-1, $J_{1,2}=J_{1,3}=1.0$ Hz), and 5.67 (s, PhC<u>H</u>).

Found: C, 67.36; H, 7.82%. Calcd for $C_{18}H_6O_5$: C, 67.06; H, 8.13%.

2. *Methyl 2-O-Acetyl-4,6-O-benzylidene-3-C-butyl-3-deoxy-α-D-altropyranoside (5).* Acetic anhydride (1.29 ml, 13.6 mmol) was added to a solution of **4** (2.20 g, 6.82 mmol) in dry pyridine (20 ml). After standing overnight at 40 °C, the mixture was poured into cold water (45 ml) and then extracted with chloroform (30 ml×4). The combined organic layers were washed with saturated aqueous $KHSO_4$, $NaHCO_3$, and NaCl, successively. The dried solution was evaporated to give the 2-acetate **5** (2.49 g, 100%) as a pale yellow syrup. A part of this was purified through a silica gel column with solvent B to afford an analytical sample of **5**: $[\alpha]_D^{23}$ +78° (*c* 1.4, chloroform); δ ($CDCl_3$) 2.11 (s, OAc), 3.41 (s, OCH_3), 4.56 (dd, H-1, $J_{1,2}=J_{1,3}=1.0$ Hz), 5.04 (dd, H-2, $J_{2,3}=2.0$ Hz), and 5.68 (s, PhC<u>H</u>).

Found: C, 66.14; H, 7.63%. Calcd for $C_{20}H_{28}O_6$: C, 65.91; H, 7.74%.

3. *Methyl 4-O-Benzoyl-6-bromo-3-C-butyl-3,6-dideoxy-α-D-altropyranoside (6).* A mixture of **4** (2.80 g, 8.70 mmol), and *N*-bromosuccinimide (NBS) (1.86 g, 10.4 mmol) in carbon tetrachloride (100 ml) containing barium carbonate (2.42 g, 12.3 mmol) was heated for 2.5 hr under stirring at 80 °C. Solids were filtered off, and the filtrate was washed with saturated aqueous $Na_2S_2O_3$, $NaHCO_3$, and NaCl, successively. The dried solution was evaporated to give 6-bromo-4-benzoate **6** (3.49 g, 100%) as a syrup which was suitable for the next synthesis. A part of this was chromatographed on silica gel with solvent C to afford a pure sample of **6**: $[\alpha]_D^{20}$ +19° (*c* 2.02, chloroform); δ ($CDCl_3$) 3.56 (s, OCH_3), 4.66 (d, H-I, $J_{1,2}=4.7$ Hz), and 5.45 (dd, H-4, $J_{3,4}=4.0$, $J_{4,5}=5.2$ Hz).

Found: C, 53.86; H, 6.24; Br, 20.03%. Calcd for $C_{18}H_{25}O_5Br$: C, 53.87; H, 6.28; Br, 19.91%.

4. *Methyl 2-O-Acetyl-4-O-benzoyl-6-bromo-3-C-butyl-3,6-dideoxy-α-D-altropyranoside (7).* A solution of **5** (2.30 g, 6.32 mmol) in dry carbon tetrachloride (100 ml) was treated with NBS (1.35 g, 7.58 mmol) and barium carbonate (1.77 g, 8.95 mmol) in the manner described in the Expt. 3 to afford a practically pure sample of **7** (2.80 g, 100%). A part of this was purified through a silica gel column with solvent C to give a pure sample of **7** as a colorless syrup: $[\alpha]_D^{23}$ +46° (*c* 1.62, chloroform); δ ($CDCl_3$) 2.16 (s, OAc), 4.73 (d, H-1, $J_{1,2}=1.8$ Hz), 5.09 (dd, H-2, $J_{2,3}=4.4$ Hz), and 5.40 (dd, H-4, $J_{3,4}=5.1$, $J_{4,5}=8.6$ Hz)

Found: C, 54.48; H, 6.11; Br, 18.33%. Calcd for $C_{20}H_{27}O_6Br$: C, 54.18; H, 6.14; Br, 18.03%.

5. *Methyl 3-C-Butyl-3,6-dideoxy-α-D-altropyranoside (8).* A suspension of $LiAlH_4$ (2.65 g, 69.6 mmol) in dry tetrahydrofuran (THF) (100 ml) was added in one portion to a stirred and cooled solution of **6** (3.45 g, 8.60 mmol) in dry THF (140 ml). The mixture was refluxed for 1 hr under stirring. To the cooled reaction mixture was slowly added ethyl acetate and water under stirring and solids were then filtered off. The filtrate was washed with water and saturated aqueous NaCl. The dried solution was evaporated and the residue (3.0 g) was purified through a silica gel column (200 g) with solvent D to afford a homogeneous sample of **8** (1.43 g, 76%) as a colorless oil: $[\alpha]_D^{19}$ +24° (*c* 1.31, chloroform); δ ($CDCl_3$) 1.31 (d, 5-CH_3, $J=6.7$ Hz), 3.49 (s, OCH_3), 4.13 (dq, H-5, $J_{4,5}=4.2$ Hz), and 4.51 (d, H-1, $J_{1,2}=6.0$ Hz).

Found: C, 60.64; H, 10.20%. Calcd for $C_{11}H_{21}O_4$: C, 60.52; H, 10.16%.

6. *1,2,4-Tri-O-acetyl-3-C-butyl-3,6-dideoxy-D-altropyranose (9).* To a solution of **8** (1.05 g, 4.82 mmol) in acetic anhydride (25.6 ml, 270 mmol) was added concd sulfuric acid (0.226 ml, 4.24 mmol) under ice-cooling. After being kept for 30 min at room temperature, the reaction mixture was poured into cold water (150 ml) and the solution was neutralized with solid $NaHCO_3$ and then extracted with chloroform (60 ml× 3). The combined extracts were washed with saturated aqueous NaCl, dried and evaporated to give a sample of **9** (1.59 g, 100%) as a yellow syrup: δ ($CDCl_3$) 1.31 (d, 5-CH_3, $J=6.8$ Hz) and 2.1—2.2 (three OAc).

7. *3-C-Butyl-3,6-dideoxy-D-altrofuranose (10).* To a solution of **9** (1.59 g, 4.82 mmol) in methanol (15 ml) was added aqueous 1M NaOH (14 ml) under ice-cooling. After being kept standing for 50 min at room temperature, the solution was neutralized with carbon dioxide and evaporated. To the residue was added acetone. The insoluble matter was filtered off and the filtrate was evaporated to afford the syrupy free sugar **10** (980 mg, 100%) as an anomeric mixture: δ ($CDCl_3$) 1.11 (d, 5-CH_3, $J=6.8$ Hz), 5.29 (d, $J_{1,2}=3.8$ Hz) and 5.40 (s) (each anomeric H-1).

8. *2-C-Butyl-2,5-dideoxy-3-O-formyl-D-ribofuranose (11).* To a solution of **10** (948 mg, 4.64 mmol) in acetone (28 ml) was added a solution of sodium metaperiodate (3.08 g, 14.4 mmol) in water (30 ml). The mixture was stirred for 4 hr at room temperature and the precipitates formed were filtered off and washed with acetone. The combined filtrate and washings were evaporated and the residue was dissolved in chloroform. The solution was washed with saturated aqueous NaCl, dried and evaporated to afford a sample of **11** (940 mg, 100%) as a colorless syrup, which was used for the subsequent synthesis without further purification: δ ($CDCl_3$) 1.28 (d, 4-CH_3, $J=6.8$ Hz), 5.22 (dd, H-3, $J_{2,3}=10.0$ Hz, $J_{3,4}=5.8$ Hz), 5.44 (d, H-1, $J_{1,2}=4.7$ Hz), and 8.23 (s, OC<u>H</u>O).

9. *(−)(2R,3S,4R)-2-Butyl-3,4-dihydroxypentanoic Acid-1,4-Lactone[(−)2c].* A sample of **11** (50 mg, 0.25 mmol) was de-O-formylated with 2% HCl (W/V) in 50% dioxane-water (v/v) (8.8 ml) for 2 hr at room temperature. The reaction mixture was then neutralized with solid $NaHCO_3$. To the mixture containing the de-O-formylated product was added bromine (0.016 ml, 0.32 mmol) and the mixture was stirred at room temperature for 2.5 hr. The oxidation product was extracted with ethyl acetate. The extract was washed with saturated aqueous $Na_2S_2O_3$ and saturated aqueous NaCl, successively, dried and evaporated. The residue (60 mg) was purified through silica gel (6 g) with solvent E to afford a homogeneous sample of (−)**2c** (29.1 mg, 68%) as a colorless syrup: $[\alpha]_D^{17}$ −69° (*c* 0.28, methanol); $[\theta]_{215}^{MeOH}$ −6400; $\nu_{max}^{CCl_4}$ (0.002 M) 3620 (OH) and 1780 cm^{-1} (1,4-lactone).

Found: C, 62.56; H, 9.18%. Calcd for $C_9H_{16}O_3$: C, 62.76; H, 9.36%.

10. *(−)(2R,3S,4R)-2-Butyl-4-hydroxy-3-(isovaleryloxy)-pentanoic Acid-1,4-lactone [(−)blastmycinone-c][(−)**1c**].* Isovaleric anhydride (0.042 ml, 0.20 mmol) was added to a solution of (−)**2c** (18.2 mg, 0.106 mmol) in dry pyridine (0.7 ml). After being kept for 40 hr at room temperature, the reaction mixture was poured into cold water and extracted with ether. The ethereal extracts were washed with saturated aqueous NaCl, dried and evaporated. The residue (31 mg) was chromatographed on silica gel (3 g) with solvent G to afford a pure sample of (−)**1c** (23.1 mg, 86%) as a colorless oil: $[\alpha]_D^{18}$ −88° (*c* 0.97, chloroform); $\nu_{max}^{CCl_4}$ (0.1 M) 1790 (1,4-lactone) and 1742 cm^{-1} (ester); R_f 0.48 (solvent G).

Found: C, 65.66; H, 9.39%. Calcd for $C_{14}H_{24}O_4$: C, 65.59; H, 9.44%.

11. *Methyl 2-C-Butyl-2,5-dideoxy-β-D-ribofuranoside (**12β**) and Its α-Anomer (**12α**).* Periodate-oxidation product **11** (646 mg, 3.19 mmol) was treated with 0.5% methanolic HCl (32.3 ml) for 1.5 hr at room temperature. The reaction mixture was neutralized with solid $NaHCO_3$ and the insoluble matter was removed by filtration. The filtrate was evaporated and the residue (561 mg) was chromatographed on silica gel (70 g) with solvent E to fractionate α-anomer (**12α**) as a faster-moving component and the β-anomer (**12β**) as a slower migration component. α-Anomer (**12α**): colorless oil, 180 mg (30%); $[\alpha]_D^{18}$ +95° (*c* 0.86, chloroform); δ ($CDCl_3$) 1.19 (d, 4-CH_3, J=6.7 Hz), 3.39 (s, OCH_3), 3.74 (dd, H-3, $J_{2,3}$=5.2 Hz, $J_{3,4}$=0.4 Hz), 4.29 (dq, H-4), and 4.91 (d, H-1, $J_{1,2}$=3.8 Hz).

Found: C, 64.06; H, 10.50%. Calcd for $C_{10}H_{20}O_3$: C, 63.79; H, 10.71%.

β-Anomer (**12β**): colorless oil, 295 mg (50%); $[\alpha]_D^{18}$ −79° (*c* 1.26, chloroform); δ ($CDCl_3$) 1.30 (d, 4-CH_3, J=6.3 Hz), 3.45 (s, OCH_3), 4.11 (dd, H-3, $J_{2,3}$=5.7 Hz, $J_{3,4}$=2.3 Hz), 4.14 (dq, H-4), and 4.80 (d, H-1, $J_{1,2}$=4.1 Hz).

Found: C, 64.07; H, 10.50%. Calcd for $C_{10}H_{20}O_3$: C, 63.79; H, 10.71%.

12. *Methyl 2-C-Butyl-2,5-dideoxy-3-O-methanesulfonyl-β-D-ribofuranoside (**13β**).* To a solution of **12β** (120 mg, 0.64 mmol) in dry pyridine (1.2 ml) was added methanesulfonyl chloride (0.06 ml, 0.77 mmol) and the solution was kept for 2 hr at room temperature. After addition of water (15 ml), the mixture was extracted with chloroform and the extract was washed with saturated aqueous NaCl, dried and evaporated to afford 3-mesylate (**13β**) (157 mg, 93%) as a pale yellow syrup, which was used for the subsequent synthesis without further purifications, because of its instability. **13β**: δ ($CDCl_3$) 1.34 (d, 4-CH_3, J=6.7 Hz), 3.06 (s, OMs), 3.44 (s, OCH_3), 4.42 (dq, H-4, $J_{3,4}$=2.3 Hz), 4.83 (d, H-1, $J_{1,2}$=4.4 Hz), and 5.01 (dd, H-3, $J_{2,3}$=5.7 Hz).

13. *Methyl 3-O-Benzoyl-2-C-butyl-2,5-dideoxy-β-D-xylofuranoside (**14**).* A mixture of **13β** (157 mg, 0.59 mmol) and sodium benzoate (255 mg, 1.77 mmol) in dry DMSO (3.1 ml) was heated at 140—145 °C for 3 hr. After being cooled to room temperature, the solids were filtered and washed with ethyl acetate. The combined filtrate and washings were washed with water and saturated aqueous NaCl. The dried solution was evaporated and the residue (210 mg) was chromatographed on silica gel (20 g) with solvent F to afford a homogeneous sample of **14** (70 mg, 41%) as a colorless syrup: $[\alpha]_D^{18}$ −15° (*c* 0.45, chloroform); δ ($CDCl_3$) 1.32 (d, 4-CH_3, J=6.4 Hz), 3.45 (s, OCH_3), 4.52 (dq, H-4, $J_{3,4}$=5.8 Hz), 4.76 (d, H-1, $J_{1,2}$=2.3 Hz), and 5.25 (dd, H-3, $J_{2,3}$=2.7 Hz).

Found: C, 69.61; H, 8.22%. Calcd for $C_{17}H_{24}O_4$: C, 69.83; H, 8.27%.

14. *Methyl 2-C-Butyl-2,5-dideoxy-β-D-xylofuranoside (**15**).* A solution of **14** (70 mg, 0.24 mmol) in dry methanol (0.29 ml) was treated with 1M methanolic sodium methoxide (0.288 ml) for 1 hr at room temperature. The solution was neutralized with 1M HCl and evaporated to give a sample of **15** (45 mg, 100%) as a pale yellow oil: δ ($CDCl_3$) 1.34 (d, 4-CH_3, J=6.7 Hz), 3.40 (s, OCH_3), and 4.78 (s, H-1).

15. *(+)(2R,3R,4R)-2-Butyl-3,4-dihydroxypentanoic Acid-1,4-Lactone [(+)**2b**].* A sample of **15** (45 mg, 0.24 mmol) was treated with 1M HCl/50% aqueous dioxane (0.45 ml) for 1 hr at room temperature. The reaction mixture containing the free sugar was neutralized with solid $NaHCO_3$, and then treated with bromine (0.015 ml, 0.30 mmol) for 3 hr at room temperature. The reaction mixture was worked up and purified by the procedure described in Expt. 9 to afford a homogeneous sample of (+)**2b** (25.3 mg, 62%) as a colorless oil: $[\alpha]_D^{18}$ +71° (*c* 0.53, methanol); $[\theta]_{216}^{MeOH}$ −3500; $\nu_{max}^{CCl_4}$ (0.002M) 3625 (OH) and 1783 cm^{-1} (lactone).

Found: C, 62.45; H, 9.10%. Calcd for $C_9H_{16}O_3$: C, 62.76; H, 9.36%.

16. *(+)(2R,3R,4R)-2-Butyl-4-hydroxy-3-(isovaleryloxy)-pentanoic Acid-1,4-Lactone [(+)Blastmycinone-b] [(+)**1b**].* By the same procedure as in the preparation of (−)**1c**, the hydroxylactone (+)**2b** (18.5 mg) was isovalerylated to afford (+)**1b** (24.3 mg, 88%) as a colorless oil: $[\alpha]_D^{17}$ +57° (*c* 1.01, chloroform); $\nu_{max}^{CCl_4}$ (0.1 M) 1790 (1,4-lactone) and 1743 cm^{-1} (ester); R_f 0.60 (solvent G).

Found: C, 65.82; H, 9.40%. Calcd for $C_{14}H_{24}O_4$: C, 65.59; H, 9.44%.

17. *Methyl 2-O-Acetyl-4-O-benzoyl-3-C-butyl-3,6-dideoxy-α-D-arabino-hex-5-enopyranoside (**16**).* Anhydrous silver fluoride (3.40 g, 26.8 mmol) was added to a solution of **7** (2.00 g, 4.52 mmol) in dry pyridine (30 ml), and the mixture was stirred for 1.5 hr at room temperature in the dark. Addition of ether (100 ml) to the reaction mixture gave precipitates, which were filtered and washed with ether. The combined filtrate and washings were washed with saturated aqueous $KHSO_4$, $NaHCO_3$, and NaCl, successively. The dried solution was evaporated to afford a sample of **16** (1.48 g, 91%) as a yellow syrup which was used for the subsequent synthesis without further purification: δ ($CDCl_3$) 2.16 (s, OAc), 3.54 (s, OCH_3), 4.68 (d, H-1, $J_{1,2}$=4.7 Hz), 4.77–4.88 (m, 2H, H-6 and H-6'), 5.24 (dd, H-2, $J_{2,3}$=7.8 Hz), and 5.89 (d, H-4, $J_{3,4}$=3.2 Hz).

18. *Methyl 2-O-Acetyl-4-O-benzoyl-3-C-butyl-3,6-dideoxy-β-L-galactopyranoside (**17**).* To a solution of **16** (1.48 g, 4.08 mmol) in dioxane (50 ml) was added freshly prepared palladium black (*ca.* 300 mg) and the mixture was stirred vigorously for 2 hr under bubbling with hydrogen. The filtered solution was evaporated and the residue (1.60 g) was chromatographed on silica gel (160 g) with solvent B to afford a homogeneous sample of **17** (1.03 g, 70%) as a colorless syrup: $[\alpha]_D^{23}$ −89° (*c* 1.52, chloroform); δ ($CDCl_3$) 1.24 (d, 5-CH_3, J=6.4 Hz), 2.13 (s, OAc), 3.55 (s, OCH_3), 3.91 (dq, H-5, $J_{4,5}$=1.0 Hz), 4.43 (d, H-1, $J_{1,2}$=8.0 Hz), 5.11 (dd, H-2, $J_{2,3}$=11.1 Hz), and 5.44 (dd, H-4, $J_{3,4}$=2.8 Hz).

Found: C, 66.13; H, 7.66%. Calcd for $C_{20}H_{28}O_6$: C, 65.91; H, 7.74%.

19. *1,2,-Di-O-acetyl-4-O-benzoyl-3-C-butyl-3,6-dideoxy-α-L-galactopyranose (**18**).* A sample of **17** (1.00 g, 2.74 mmol) was treated with acetic anhydride (30 ml, 313 mmol) and concd. sulfuric acid (0.29 ml, 5.46 mmol) for 1 hr at room temperature. The solution was worked up by the procedure described in Expt. 6 to give a sample of **18** (1.08 g, 100%) contaminated by a small amount of its β-anomer, as a yellow syrup: δ ($CDCl_3$) 1.17 (d, 5-CH_3, J=6.6 Hz), 2.07 and

2.18 (each s, OAc), 4.37 (dq, H-5, $J_{4,5}$=0.8 Hz), 5.29 (dd, H-2, $J_{2,3}$=11.8 Hz), 5.57 (dd, H-4, $J_{3,4}$=2.3 Hz), and 6.46 (d, H-1, $J_{1,2}$=3.4 Hz) [β-anomer contaminated, 5.83 (d, H-1, $J_{1,2}$=8.2 Hz)].

20. *2-C-Butyl-2,5-dideoxy-3-O-formyl-L-lyxofuranose (**20**).* A solution of product **18** (1.00 g, 2.55 mmol) in methanol (25 ml) was treated with 1 M NaOH (16.5 ml) for 4 hr at room temperature. The solution was worked up by the procedure described in Expt. 7 to afford 3-*C*-butyl-3,6-dideoxy-L-galactofuranose (**19**) (520 mg, 100%) as a pale yellow syrup. A solution of **19** (500 mg, 2.45 mmol) in acetone (35 ml) was treated with a solution of sodium metaperiodate (1.57 g, 7.35 mmol) in water (40 ml) for 2 hr at room temperature in the dark. The reaction mixture was worked up by the procedure described in Expt. 8 to afford a semicrystalline anomeric mixture of **20** (485 mg, 98%) which was used for the subsequent synthesis without further purification: δ ($CDCl_3$) 1.28 (d, 4-CH_3, J=6.3 Hz), 4.53 (dq, H-4, $J_{3,4}$=3.0 Hz), 5.35 (dd, H-3, $J_{2,3}$=3.0 Hz), *ca.* 5.6 (1H, H-1 in α- and β-anomer), and 8.28 (s, 1H, OCHO).

21. *(−)(2R,3S,4S)-2-Butyl-3,4-dihydroxypentanoic Acid-1,4-lactone [(−)**2d**].* A crystalline sample of (−)**2d** (41.9 mg, 51%) was obtained from **20** (97 mg) by the method described in Expt. 9. Recrystallization of the sample from ethyl acetate-petroleum ether afforded an analytical sample of (−)**2d**: mp 99.5–100.5 °C; $[\alpha]_D^{17}$ −96° (*c* 0.34, methanol); $[\theta]_{214}^{MeOH}$ −5230; $\nu_{max}^{CCl_4}$ (0.002M) 3625 (OH) and 1780 cm^{-1} (lactone).

Found: C, 62.56; H, 9.24%. Calcd for $C_9H_{16}O_3$: C, 62.76; H, 9.36%.

22. *(−)(2R,3S,4S)-2-Butyl-4-hydroxy-3-(isovaleryloxy)-pentanoic Acid-1,4-Lactone [(−)Blastmycinone-d] [(−)**1d**].* The hydroxylactone (−)**2d** (14.5 mg) was isovalerylated by the procedure described in Expt. 10 to afford a crystalline (−)**1d** (18.5 mg, 86%) which was recrystallized from ethyl acetate-petroleum ether: mp 47.0—48.0 °C; $[\alpha]_D^{18}$ −89° (*c* 0.90, chloroform); $\nu_{max}^{CCl_4}$ (0.1 M) 1792 (lactone) and 1748 cm^{-1} (ester); R_f 0.33 (solvent G).

Found: C, 65.82; H, 9.42%. Calcd for $C_{14}H_{24}O_4$: C, 65.59; H, 9.44%.

23. *Methyl 2-C-butyl-2,5-dideoxy-β-L-lyxofuranoside (**21**).* The periodate oxidation product **20** (300 mg, 1.48 mmol) was treated with 0.5% methanolic hydrogen chloride (15 ml, 2.06 mmol) for 3 hr at room temperature. The solution was worked up by the same procedure as described in Expt. 11 and the product (415 mg) was fractionated on silica gel (40 g) with solvent E. The faster-moving fraction gave the α-anomer showing a positive rotation and the slower-moving fraction afforded β-anomer **21** with a negative rotation as a major product. Since both anomers separated were very unstable, no analytical samples could be obtained. (+)α-Anomer: 15.2 mg (5.5%); δ ($CDCl_3$) 1.32 (d, 4-CH_3, J=6.3 Hz), 3.39 (s, OCH_3), 4.19 (dq, H-4, $J_{3,4}$=3.7 Hz), and 4.85 (d, H-1, $J_{1,2}$=4.0 Hz). (−)β-Anomer (**21**): 167 mg (60%); δ ($CDCl_3$) 1.24 (d, 4-CH_3, J=6.5 Hz), 3.40 (s, OCH_3), 3.98 (dd, H-3, $J_{2,3}$=4.5, $J_{3,4}$=2.5 Hz), 4.19 (dq, H-4), and 4.71 (d, H-1, $J_{1,2}$=5.0 Hz).

24. *Methyl 2-C-Butyl-2,5-dideoxy-3-O-methanesulfonyl-β-L-lyxofuranoside (**22**).* A crystalline sample of **22** (219 mg) was prepared from freshly prepared **21** (155 mg) by the procedure in Expt. 12. It was recrystallized from ether-petroleum ether to afford fine needles which were also very unstable: mp 56—58 °C; δ ($CDCl_3$) 1.37 (d, 4-CH_3, J=6.3 Hz), 3.09 (s, OMs), 3.45 (s, OCH_3), 4.39 (dq, H-4, $J_{3,4}$=2.8 Hz), 4.82 (d, H-1, $J_{1,2}$=4.9 Hz), and 5.17 (dd, H-3, $J_{2,3}$=5.2 Hz).

25. *Methyl 3-O-Benzoyl-2-C-butyl-2,5-dideoxy-β-L-arabinofuranoside (**23**).* A solution of **22** (200 mg, 0.753 mmol) in DMSO (4 ml) was heated with sodium benzoate (326 mg, 2.26 mmol) at 140 °C for 1 hr and the reaction mixture was worked up by the procedure in Expt. 13 to afford a homogeneous sample of **23** (91 mg, 42%) as a colorless syrup: $[\alpha]_D^{22}$ −48° (*c* 1.67, chloroform); δ ($CDCl_3$) 1.42 (d, 4-CH_3, J=6.3 Hz), 3.44 (s, OCH_3), 4.28 (dq, H-4, $J_{3,4}$=5.9 Hz), 4.81 (d, H-1, $J_{1,2}$=1.2 Hz), and 4.88 (dd, H-3, $J_{2,3}$=3.8 Hz).

Found: C, 69.50; H, 8.13%. Calcd for $C_{17}H_{24}O_4$: C, 69.83; H, 8.27%.

26. *Methyl 2-C-Butyl-2,5-dideoxy-β-L-arabinofuranoside (**24**).* A sample of **24** (29 mg, 100%) was obtained from **23** (45 mg) by the procedure in Expt. 14: δ ($CDCl_3$) 1.32 (d, 4-CH_3, J=6.5 Hz), 3.41 (s, OCH_3), 4.06 (dq, H-4, $J_{3,4}$=5.8 Hz), and 4.74 (d, H-1, $J_{1,2}$=1.5 Hz).

27. *Natural (−)Blastmycinolactol [(−)**2a**].* A crystalline sample of (−)**2a** (22.3 mg, 84%) was obtained by treatment of **24** (29 mg) with 1 M HCl followed by bromine-oxidation by the same procedure as described in Expt. 15. Recrystallization from ether-petroleum ether afforded a pure sample of (−)**2a**: mp 49.5—50.5 °C; $[\alpha]_D^{18}$ −18° (*c* 1.09, methanol); $[\theta]_{217}^{MeOH}$ −5500; $\nu_{max}^{CCl_4}$ (0.002 M) 3635 (OH) and 1785 cm^{-1} (lactone).

Found: C, 62.60; H, 9.22%. Calcd for $C_9H_{16}O_3$: C, 62.76; H, 9.36%.

28. *Natural (+)Blastmycinone [(+)**1a**].* Isovalerylation of (−)**2a** (16.5 mg) in the same manner as described in Expt. 10 afforded (+)**1a** (21.3 mg, 86%) as a colorless oil: $[\alpha]_D^{17}$ +10° (*c* 1.20, chloroform); $\nu_{max}^{CCl_4}$ (0.1 M) 1788 (lactone) and 1745 cm^{-1} (ester); R_f 0.66 (solvent G).

Found: C, 65.72; H, 9.31%. Calcd for $C_{14}H_{24}O_4$: C, 65.59; H, 9.44%.

The authors wish to thank Prof. Sumio Umezawa, Keio University, for his interest and kind advice. Thanks are also due to Prof. Shonosuke Zen, Kitasato University, for the measurment of CD spectra and to Mr. Saburo Nakada, Keio University, for elemental analyses. Financial support by the Asahi Glass Foundation for Contribution to Industrial Technology is acknowledged.

References

1) H. Yonehara and S. Takeuchi, *J. Antibiot., Ser. A*, **11**, 254 (1958).
2) M. Kinoshita, S. Aburaki, M. Wada, and S. Umezawa, This Bulletin, **46**, 1279 (1973).
3) M. Kinoshita, S. Aburaki, and S. Umezawa, *J. Antibiot.* (Tokyo), **25**, 373 (1972).
4) H. Koyama, K. Kogure, K. Mori, and M. Matsui, *Agr. Biol. Chem.*, **37**, 915 (1973).
5) L. F. Wiggins, *Methods Carbohyd. Chem.*, **2**, 188 (1963).
6) T. D. Inch and J. Lewis, *Carbohyd. Res.*, **15**, 1 (1970).
7) S. Hanessian, *ibid.*, **2**, 86 (1966); J. S. Brimacombe, O. A. Ching, and M. Stacey, *J. Chem. Soc., C*, **1969**, 197.
8) (a) B. Helferich and E. Himmen, *Ber.*, **61**, 1825 (1928); B. Helferich and E. Himmen, *ibid.*, **62**, 2136 (1929). (b) D. Ikeda, T. Tsuchiya, and S. Umezawa, This Bulletin, **44**, 2529 (1971).
9) K. M. Wellman, P. H. A. Laur, W. S. Brigs, A. Moscowitz, and C. Djerassi, *J. Amer. Chem. Soc.*, **87**, 66 (1965).
10) A. Mcl. Mathieson, *Tetrahedron Lett.*, **1963**, 81.
11) M. Legrand and R. Bucourt, *Bull. Soc. Chim. Fr.*, **1967**, 2241.
12) T. Okuda, S. Harigaya, and A. Kiyomoto, *Chem. Pharm. Bull.*, **12**, 504 (1964).
13) A. F. Beecham, *Tetrahedron Lett.*, **1968**, 2355.
14) M. Karplus, *J. Chem. Phys.*, **30**, 11 (1959).
15) R. J. Abraham and K. A. McLauchlan, *Molecular Phys.*, **5**, 513 (1962).

Crystallographic Studies of Interaction between Nucleotides and Metal Ions. I. Crystal Structures of the 1 : 1 Complexes of Cobalt and Nickel with Inosine 5′-Phosphate

Katsuyuki Aoki

The Institute of Physical and Chemical Research, Wako-shi, Saitama 351

(Received July 6, 1974)

The crystal structures of the 1 : 1 complexes of inosine 5′-phosphate with cobalt ($C_{10}H_{11}O_8N_4PCo,7H_2O$) and inosine 5′-phosphate with nickel($C_{10}H_{11}O_8N_4PNi,7H_2O$) have been determined from single-crystal X-ray data collected on an automated diffractometer. The both isomorphous crystals belong to orthorhombic system, space group $P2_12_12_1$ with four formula units in the unit cell of dimensions $a=10.859$, $b=25.987$, $c=6.845$ Å for the cobalt complex and $a=10.812$, $b=25.898$, $c=6.845$ Å for the nickel complex respectively. The structure of the cobalt complex was determined by three-dimensional Patterson and Fourier methods and that of the nickel complex was elucidated from that of the cobalt complex. Both were refined by the block-diagonal least-squares method including anisotropic temperature factors. The final R values were 0.051 and 0.075 for the cobalt and nickel complexes, respectively. All of the 25 hydrogen atoms in the case of the cobalt complex and 22 hydrogen atoms in the case of the nickel complex were found. The hypoxanthine bases related by the two-fold screw axis parallel to c are extensively overlapped at a distance of 3.42 Å for both complexes. The nucleotides have the preferred *anti* conformation about the glycoside linkage with the ribose ring showing the C(3′)-*endo* pucker. The torsion angles around the C(5′)−O(5′) bond are 161.6° (cobalt complex) and 162.0° (nickel complex). In the both complexes, therefore, the phosphate group has the extended conformation. The metals are not directly bonded to the phosphate oxygen atoms but are bonded to the nitrogen atom N(7) of the base and to five water oxygen atoms. There is extensive hydrogen bonding involving the hypoxanthine ring, the phosphate anion, the hydroxyl groups of the furanose ring and seven water molecules in the crystal.

It has now been widely recognized that metal ions have profound effects on the structure and function of nucleic acids and their constituents. They stabilize or destabilize the manifold structure of nucleic acid[1,2] and alter the coding specificity in protein synthesis.[3]

The other interesting area of metallonucleic acid chemistry includes the use of heavy metals to determine the sequence of nucleic acid biopolymers by electron microscope techniques[4,5] and to determine the structure of tRNA by X-ray method.[6] We have investigated the crystal structures of 1 : 1 metal complexes of inosine 5′-phosphate(5′-IMP) in order to obtain the fundamental and precise informations regarding interaction of transition metals with the component of nucleic acid, where inosine is present as minor base in the triplet anticodon of yeast tRNAs such as alanine tRNA, serine tRNA1, serine tRNA2 and valine tRNA.

The crystal structures of 5′-IMP containing alkali metals such as barium and sodium have been investigated by Nagashima and Iitaka,[7] and Rao and Sundaralingam.[8]

After we had completed those structure determinations it came to our attention that Clark and Orbell had reported the brief communication on the same crystal structure of the inosine 5′-phosphate–nickel complex.[9] Their data are in agreement with those obtained from our X-ray crystallographic studies.

Experimental

Violet crystals of ($C_{10}H_{11}O_8N_4PCo$, $7H_2O$) and light green crystals of ($C_{10}H_{11}O_8N_4PNi$, $7H_2O$) were prepared by adding aqueous solution of cobalt nitrate hexahydrate and nickel nitrate hexahydrate to that of disodium inosine 5′-phosphate in an equivalent mole ratio, adjusting to pH 4.5 with dilute nitric acid. They were grown from an aqueous solution by slow evaporation. The elementary analysis revealed that the ratio of inosine 5′-phosphate to metal is 1 : 1 for both complexes.

The unit-cell dimensions were determined from high-order reflexions on a Rigaku four-circle automated diffractometer.

	Crystal data	
	$C_{10}H_{11}O_8N_4PCo$, $7H_2O$(5′-IMP-Co)	$C_{10}H_{11}O_8N_4PNi$, $7H_2O$(5′-IMP-Ni)
System	Orthorhombic	Orthorhombic
a	10.859±0.005 Å	10.812±0.005 Å
b	25.987	25.898
c	6.845	6.845
U	1931.6 Å^3	1916.1 Å^3
F(000)	1100	1104
Space group	$P2_12_12_1$	$P2_12_12_1$
Number of independent non-zero reflexions used for the structure determination	1424	1500

Three-dimensional intensity data in the 2θ-range from 0 to 50° for the cobalt complex with Zr-filtered Mo$K\alpha$ radiation and 130° for the nickel complex with Ni-filtered Cu$K\alpha$ radiation were collected on a Rigaku four-circle automated diffractometer. A 2θ-ω scan technique at a rate of 2°/min for the cobalt complex and 4°/min for the nickel complex was employed for the data collection. Background counts of 10 s were measured at each beginning and end of the scan. Three standard reflections were checked at an interval of every 52 reflections and they showed fluctuations in intensity of only ±2.0% for the cobalt complex and ±2.8% for the nickel complex. The data were corrected for Lorentz and polarization effects, but no absorption corrections were made ($\mu=10.8$ cm^{-1} (Co complex for Mo $K\alpha$ radiation) and 20.9 cm^{-1} (Ni complex for Cu $K\alpha$ radiation) and approximate crystal dimensions of $0.1\times0.2\times0.3$ mm (Co complex) and $0.1\times0.1\times0.2$ mm (Ni complex)). A reflection was considered unobserved if the intensity was smaller than 3.0 times its standard deviation. On this basis, 1424 reflections out of the total of 2067 reflections (Co complex) and 1500 out of the total of 1986 reflections (Ni complex) were adopted in the subsequent refinement of the structure.

TABLE 1. FINAL ATOMIC PARAMETERS AND STANDARD DEVIATIONS FOR $C_{10}H_{11}O_8N_4PCo$, $7H_2O$

Atom	X	Y	Z	β_{11} or B(Å^2)	β_{22}	β_{33}	β_{12}	β_{13}	β_{23}
Co	0.0783(2)	0.3547(1)	0.2756(2)	0.0032(1)	0.0008(0)	0.0111(3)	−0.0002(1)	−0.0000(2)	−0.0001(1)
P	0.4204(3)	0.2436(1)	0.2287(5)	0.0034(2)	0.0008(0)	0.0073(6)	0.0000(1)	−0.0007(5)	−0.0000(1)
O(5′)	0.5000(8)	0.2921(3)	0.3027(13)	0.0046(8)	0.0010(1)	0.0130(22)	−0.0002(3)	0.0015(12)	−0.0001(5)
O(7)	0.5081(7)	0.1974(3)	0.2238(12)	0.0038(7)	0.0009(1)	0.0068(17)	0.0006(2)	0.0007(11)	−0.0002(4)
O(8)	0.3685(8)	0.2574(4)	0.0296(12)	0.0052(9)	0.0017(2)	0.0048(18)	0.0010(3)	−0.0005(10)	−0.0000(5)
O(9)	0.3225(7)	0.2377(3)	0.3872(12)	0.0025(7)	0.0011(2)	0.0105(19)	0.0004(3)	0.0012(10)	−0.0002(5)
N(1)	0.1837(9)	0.5530(4)	0.2995(16)	0.0056(10)	0.0008(2)	0.0159(26)	0.0006(3)	0.0004(16)	−0.0000(6)
C(2)	0.3060(12)	0.5645(4)	0.2913(23)	0.0069(13)	0.0006(2)	0.0206(36)	−0.0005(4)	−0.0026(22)	0.0004(8)
N(3)	0.3930(9)	0.5299(3)	0.2885(17)	0.0044(10)	0.0008(2)	0.0159(25)	0.0000(3)	0.0012(15)	0.0012(6)
C(4)	0.3479(11)	0.4815(4)	0.2911(18)	0.0047(11)	0.0009(2)	0.0083(25)	−0.0002(4)	−0.0017(18)	0.0001(6)
C(5)	0.2274(10)	0.4652(4)	0.2891(20)	0.0030(10)	0.0008(2)	0.0146(28)	0.0002(3)	0.0001(18)	−0.0002(7)
C(6)	0.1332(12)	0.5036(5)	0.3027(18)	0.0050(11)	0.0013(2)	0.0081(27)	0.0005(4)	−0.0000(17)	0.0005(7)
O(6)	0.0212(8)	0.4982(4)	0.3154(14)	0.0052(8)	0.0011(2)	0.0225(28)	0.0010(3)	0.0006(13)	0.0015(6)
N(7)	0.2230(9)	0.4118(3)	0.2859(16)	0.0053(9)	0.0007(1)	0.0107(22)	0.0002(3)	0.0018(15)	0.0004(5)
C(8)	0.3371(10)	0.3971(5)	0.2726(22)	0.0033(10)	0.0011(2)	0.0191(35)	0.0006(4)	0.0011(21)	−0.0015(8)
N(9)	0.4159(9)	0.4374(3)	0.2752(16)	0.0032(7)	0.0007(1)	0.0157(24)	−0.0001(3)	−0.0032(18)	0.0012(5)
C(1′)	0.5530(9)	0.4364(4)	0.2480(21)	0.0033(10)	0.0009(2)	0.0167(34)	−0.0003(3)	−0.0030(19)	−0.0007(7)
C(2′)	0.6249(12)	0.4326(5)	0.4465(24)	0.0027(11)	0.0010(2)	0.0283(46)	0.0004(4)	−0.0037(20)	0.0005(8)
C(3′)	0.6391(11)	0.3741(5)	0.4631(19)	0.0031(11)	0.0010(2)	0.0142(31)	0.0004(4)	−0.0023(16)	−0.0023(7)
C(4′)	0.6570(10)	0.3559(4)	0.2502(19)	0.0056(11)	0.0007(2)	0.0147(31)	0.0008(4)	0.0012(19)	0.0010(8)
C(5′)	0.6193(11)	0.3015(4)	0.2097(20)	0.0063(12)	0.0008(2)	0.0114(29)	−0.0006(4)	0.0030(18)	0.0000(7)
O(1′)	0.5800(9)	0.3921(3)	0.1372(12)	0.0049(8)	0.0011(1)	0.0130(19)	0.0005(3)	−0.0001(14)	0.0004(4)
O(2′)	0.7458(9)	0.4530(3)	0.4099(18)	0.0057(9)	0.0006(1)	0.0430(37)	0.0001(3)	−0.0033(17)	−0.0011(6)
O(3′)	0.7425(8)	0.3628(3)	0.5819(12)	0.0047(8)	0.0011(2)	0.0137(21)	−0.0003(3)	−0.0016(12)	−0.0003(5)
W(1)	−0.0207(9)	0.3841(4)	0.0331(15)	0.0075(10)	0.0016(2)	0.0165(25)	−0.0005(4)	−0.0033(14)	0.0011(6)
W(2)	−0.0236(8)	0.3966(3)	0.4766(15)	0.0046(9)	0.0011(2)	0.0233(28)	0.0001(3)	0.0031(14)	−0.0020(6)
W(3)	0.1729(8)	0.3155(4)	0.0568(12)	0.0028(8)	0.0017(2)	0.0098(20)	0.0009(3)	−0.0018(11)	−0.0014(5)
W(4)	0.1788(8)	0.3175(3)	0.4993(12)	0.0055(9)	0.0010(1)	0.0094(20)	−0.0001(3)	0.0035(12)	0.0006(5)
W(5)	−0.0529(8)	0.2966(3)	0.2850(13)	0.0068(9)	0.0014(2)	0.0097(19)	−0.0015(3)	0.0034(13)	−0.0004(5)
W(6)	0.8993(9)	0.1557(3)	0.2383(17)	0.0108(12)	0.0011(2)	0.0252(28)	−0.0005(3)	−0.0056(19)	0.0010(6)
W(7)	0.7265(11)	0·5578(4)	0.3873(16)	0.0110(14)	0.0020(2)	0.0218(29)	0.0006(5)	0.0013(18)	0.0013(7)
H(N1)	0.125(12)	0.592(5)	0.321(19)	4.7(3.4)					
H(C2)	0.325(10)	0.603(4)	0.306(17)	2.4(2.8)					
H(C8)	0.369(11)	0.361(5)	0.276(22)	4.8(3.4)					
H(C1′)	0.575(12)	0.470(4)	0.152(17)	3.5(2.9)					
H(C2′)	0.576(13)	0.454(5)	0.578(19)	4.7(3.3)					
H(C3′)	0.547(9)	0.363(4)	0.517(15)	1.1(2.4)					
H(C4′)	0.764(14)	0.364(6)	0.207(23)	7.0(4.2)					
H(C5′)	0.612(12)	0.290(4)	0.047(19)	3.6(3.1)					
H′(C5′)	0.685(12)	0.273(5)	0.270(24)	5.5(3.7)					
H(O2′)	0.727(12)	0.491(5)	0.441(17)	2.8(3.1)					
H(O3′)	0.732(10)	0.324(4)	0.613(14)	0.8(2.2)					
H(W1)	−0.061(10)	0.352(4)	−0.095(15)	2.2(2.5)					
H′(W1)	−0.019(11)	0.422(4)	0.040(17)	2.5(2.8)					
H(W2)	−0.085	0.380	0.490	3.0					
H′(W2)	−0.066(12)	0.422(5)	0.463(19)	4.3(3.2)					
H(W3)	0.096(13)	0.303(5)	−0.039(20)	4.5(3.4)					
H′(W3)	0.226(13)	0.294(5)	0.053(20)	4.1(3.6)					
H(W4)	0.119(9)	0.310(3)	0.562(14)	0.4(2.0)					
H′(W4)	0.224(15)	0.290(5)	0.489(24)	7.0(4.5)					
H(W5)	−0.112(15)	0.292(5)	0.131(23)	7.0(4.3)					
H′(W5)	−0.097(10)	0.280(4)	0.385(15)	1.1(2.3)					
H(W6)	0.817	0.169	0.365	3.0					
H′(W6)	0.913(16)	0.190(6)	0.138(24)	8.9(4.5)					
H(W7)	0.776(13)	0.581(5)	0.344(19)	4.9(3.6)					
H′(W7)	0.644(14)	0.553(5)	0.331(23)	7.3(4.4)					

The temperature factors for the heavier atoms are of the form, $T=\exp[-(\beta_{11}h^2+\beta_{22}k^2+\beta_{33}l^2+2\beta_{12}hk+2\beta_{13}hl+2\beta_{23}kl)]$, and those for the hydrogen atoms are, $T=\exp[-B(\sin\theta/\lambda)^2]$. The hydrogen atoms H(W2) and H(W6) were found on the final difference electron density map and their atomic parameters were not refined.

Table 2. Final atomic parameters and standard deviations for $C_{10}H_{11}O_8N_4PNi$, $7H_2O$

Atom	X	Y	Z	β_{11} or B(Å^2)	β_{22}	β_{33}	β_{12}	β_{13}	β_{23}
Ni	0.0812(2)	0.3547(1)	0.2740(4)	0.0047(1)	0.0010(0)	0.0239(5)	−0.0001(1)	0.0003(3)	−0.0001(1)
P	0.4211(3)	0.2423(1)	0.2288(5)	0.0021(2)	0.0004(0)	0.0135(8)	0.0001(1)	0.0001(5)	−0.0001(2)
O(5′)	0.5005(7)	0.2914(3)	0.3020(16)	0.0029(7)	0.0004(1)	0.0237(29)	−0.0003(2)	0.0017(13)	−0.0010(5)
O(7)	0.5084(7)	0.1967(3)	0.2218(16)	0.0030(7)	0.0005(1)	0.0181(26)	0.0001(2)	0.0009(13)	−0.0006(5)
O(8)	0.3689(8)	0.2554(4)	0.0346(14)	0.0032(2)	0.0011(2)	0.0123(24)	0.0009(3)	0.0022(12)	−0.0003(5)
O(9)	0.3231(8)	0.2374(3)	0.3896(15)	0.0037(8)	0.0006(1)	0.0158(24)	−0.0002(3)	0.0030(12)	0.0003(5)
N(1)	0.1827(10)	0.5525(4)	0.2916(20)	0.0045(9)	0.0005(1)	0.0196(32)	0.0006(3)	−0.0013(17)	0.0001(7)
C(2)	0.3071(13)	0.5639(5)	0.2844(28)	0.0053(12)	0.0006(2)	0.0247(44)	−0.0005(4)	−0.0004(23)	0.0014(9)
N(3)	0.3936(9)	0.5295(4)	0.2790(20)	0.0038(9)	0.0008(2)	0.0206(33)	−0.0003(3)	0.0016(17)	0.0018(7)
C(4)	0.3487(11)	0.4807(5)	0.2770(24)	0.0029(10)	0.0006(2)	0.0189(37)	0.0001(3)	−0.0010(20)	0.0010(8)
C(5)	0.2254(10)	0.4642(5)	0.2828(22)	0.0023(9)	0.0008(2)	0.0121(30)	0.0002(4)	0.0001(17)	0.0002(7)
C(6)	0.1323(12)	0.5033(5)	0.2942(24)	0.0036(10)	0.0006(2)	0.0209(39)	0.0003(4)	0.0023(20)	0.0008(8)
O(6)	0.0181(8)	0.4964(3)	0.3077(17)	0.0027(7)	0.0008(1)	0.0275(33)	0.0007(3)	−0.0006(14)	0.0004(6)
N(7)	0.2210(9)	0.4113(4)	0.2773(20)	0.0020(8)	0.0006(1)	0.0209(32)	−0.0001(3)	−0.0020(16)	0.0009(7)
C(8)	0.3379(10)	0.3965(4)	0.2708(27)	0.0026(9)	0.0004(2)	0.0270(44)	0.0001(3)	−0.0000(22)	−0.0008(8)
N(9)	0.4182(8)	0.4369(3)	0.2707(18)	0.0014(7)	0.0006(1)	0.0196(29)	−0.0003(3)	0.0005(17)	0.0002(6)
C(1′)	0.5546(10)	0.4354(4)	0.2387(23)	0.0021(9)	0.0004(2)	0.0200(37)	−0.0003(3)	0.0034(19)	0.0012(8)
C(2′)	0.6279(12)	0.4329(6)	0.4334(26)	0.0022(10)	0.0010(2)	0.0236(45)	−0.0004(4)	−0.0012(20)	0.0002(9)
C(3′)	0.6417(11)	0.3749(5)	0.4551(24)	0.0019(10)	0.0006(2)	0.0211(39)	−0.0003(4)	−0.0004(18)	−0.0002(7)
C(4′)	0.6586(10)	0.3561(4)	0.2439(25)	0.0025(9)	0.0005(2)	0.0254(43)	0.0003(3)	0.0050(20)	0.0012(9)
C(5′)	0.6201(11)	0.3016(5)	0.2032(26)	0.0027(10)	0.0007(2)	0.0233(43)	0.0002(4)	−0.0041(19)	0.0001(8)
O(1′)	0.5828(8)	0.3910(3)	0.1319(15)	0.0035(7)	0.0006(1)	0.0199(25)	0.0003(3)	−0.0003(14)	−0.0001(5)
O(2′)	0.7484(8)	0.4524(4)	0.3956(22)	0.0021(8)	0.0008(2)	0.0493(46)	−0.0005(3)	−0.0039(17)	0.0002(7)
O(3′)	0.7450(9)	0.3631(3)	0.5829(18)	0.0043(8)	0.0004(1)	0.0296(32)	0.0000(3)	−0.0029(16)	−0.0010(6)
W(1)	−0.0187(9)	0.3850(4)	0.0415(18)	0.0040(8)	0.0011(2)	0.0251(32)	0.0003(3)	−0.0023(15)	0.0012(6)
W(2)	−0.0179(8)	0.3970(3)	0.4728(17)	0.0029(8)	0.0009(2)	0.0235(30)	−0.0004(3)	0.0015(14)	−0.0010(6)
W(3)	0.1721(8)	0.3169(4)	0.0568(15)	0.0027(7)	0.0009(1)	0.0180(26)	0.0001(3)	−0.0027(13)	−0.0004(6)
W(4)	0.1791(8)	0.3179(3)	0.4954(14)	0.0038(7)	0.0008(1)	0.0128(22)	0.0003(3)	0.0006(12)	0.0002(5)
W(5)	−0.0519(8)	0.2971(3)	0.2804(16)	0.0050(8)	0.0009(1)	0.0156(24)	−0.0014(3)	0.0008(14)	−0.0008(6)
W(6)	0.8991(11)	0.1542(3)	0.2426(21)	0.0108(12)	0.0008(1)	0.0315(36)	0.0004(4)	−0.0017(23)	0.0004(7)
W(7)	0.7231(12)	0.5571(4)	0.3817(21)	0.0106(13)	0.0011(2)	0.0316(39)	0.0004(4)	−0.0005(21)	0.0006(8)
H(N1)	0.141(10)	0.574(4)	0.257(19)	1.0(2.3)					
H(C2)	0.324(9)	0.603(4)	0.301(16)	2.4(2.0)					
H(C8)	0.368(13)	0.368(5)	0.222(25)	3.9(3.7)					
H(C1′)	0.563(9)	0.460(4)	0.140(15)	1.3(2.0)					
H(C2′)	0.592(11)	0.441(4)	0.550(16)	1.0(2.2)					
H(C3′)	0.584(10)	0.360(4)	0.465(16)	0.5(2.2)					
H(C4′)	0.737(11)	0.370(4)	0.200(19)	1.9(2.6)					
H(C5′)	0.594(9)	0.299(4)	0.081(15)	2.0(2.0)					
H′(C5′)	0.675(9)	0.277(4)	0.227(17)	0.1(2.0)					
H(O2′)	0.741(12)	0.477(5)	0.367(20)	1.9(2.8)					
H(O3′)	0.768(14)	0.327(6)	0.589(23)	3.0(3.6)					
H(W1)	−0.078(11)	0.380(5)	−0.088(19)	1.1(2.6)					
H′(W1)	−0.068(11)	0.417(5)	0.034(18)	1.0(2.4)					
H(W3)	0.125(10)	0.308(4)	−0.092(17)	0.8(2.3)					
H′(W3)	0.233	0.293	0.030	3.0					
H(W4)	0.154(17)	0.311(7)	0.594(28)	3.3(5.0)					
H′(W4)	0.197(13)	0.297(5)	0.406(22)	3.7(3.2)					
H(W5)	−0.036(13)	0.292(5)	0.163(22)	3.5(3.5)					
H′(W5)	−0.080(14)	0.265(5)	0.362(21)	2.5(3.3)					
H(W6)	0.841	0.149	0.410	3.0					
H′(W6)	0.874	0.187	0.140	3.0					
H′(W7)	0.697(15)	0.569(6)	0.262(29)	5.1(4.6)					

The temperature factors for the heavier atoms are of the form, $T=\exp[-(\beta_{11}h^2+\beta_{22}k^2+\beta_{33}l^2+2\beta_{12}hk+2\beta_{13}hl+2\beta_{23}kl)]$, and those for the hydrogen atoms are, $T=\exp[-B(\sin\theta/\lambda)^2]$. The hydrogen atoms H′(W3), H(W6) and H′(W6) were found on the final difference electron density map and their atomic parameters were not refined. Three hydrogen atoms bonded to W(2) and W(7) were not clearly found on the difference map.

TABLE 3. COMPARISON OF BOND LENGTHS AND ANGLES OF DIFFERENT COMPOUNDS INVOLVING INOSINE MOIETY

Compound	5′-IMP-Co	5′-IMP-Ni	5′-IMP-Na	Inosine, $2H_2O$		Inosine
Space group	$P2_12_12_1$	$P2_12_12_1$	$C222_1$	$P2_1$		$P2_1$
No. of molecules in the unit cell	4	4	8	4		2
				Molecule I	Molecule II	
Bond lengths						
N (1) - C (2)	1.362 (16) Å	1.377 (17) Å	1.38 (2) Å	1.360 (6) Å	1.351 (6) Å	1.355 (5) Å
C (2) - N (3)	1.305 (15)	1.292 (17)	1.27	1.307	1.308	1.308
N (3) - C (4)	1.351 (14)	1.356 (16)	1.30	1.362	1.364	1.365
C (4) - C (5)	1.375 (16)	1.399 (16)	1.33	1.382	1.367	1.374
C (5) - C (6)	1.432 (17)	1.430 (17)	1.44	1.429	1.436	1.433
C (6) - O (6)	1.227 (15)	1.251 (15)	1.22	1.221	1.235	1.233
C (6) - N (1)	1.397 (16)	1.386 (16)	1.36	1.401	1.390	1.397
C (5) - N (7)	1.388 (14)	1.373 (16)	1.40	1.371	1.379	1.371
N (7) - C (8)	1.300 (15)	1.321 (15)	1.43	1.311	1.301	1.307
C (8) - N (9)	1.353 (15)	1.358 (14)	1.33	1.359	1.369	1.372
N (9) - C (4)	1.369 (14)	1.361 (15)	1.39	1.372	1.370	1.372
N (9) - C (1′)	1.500 (14)	1.491 (14)	1.46	1.460	1.452	1.477
C (1′) - C (2′)	1.571 (20)	1.552 (22)	1.54	1.525	1.516	1.530
C (2′) - C (3′)	1.532 (18)	1.518 (19)	1.52	1.517	1.529	1.525
C (3′) - C (4′)	1.545 (18)	1.536 (23)	1.56	1.526	1.525	1.522
C (4′) - O (1′)	1.478 (15)	1.441 (16)	1.44	1.452	1.450	1.459
O (1′) - C (1′)	1.409 (14)	1.396 (15)	1.43	1.416	1.410	1.417
C (2′) - O (2′)	1.437 (16)	1.422 (16)	1.41	1.417	1.407	1.420
C (3′) - O (3′)	1.417 (15)	1.451 (17)	1.41	1.418	1.412	1.413
C (4′) - C (5′)	1.496 (17)	1.498 (17)	1.48	1.513	1.503	1.506
C (5′) - O (5′)	1.465 (15)	1.483 (16)	1.45	1.437	1.418	1.428
P - O (5′)	1.610 (9)	1.614 (9)	1.62 (1)			
P - O (7)	1.533 (8)	1.515 (8)	1.53			
P - O (8)	1.518 (9)	1.483 (10)	1.53			
P - O (9)	1.527 (9)	1.533 (10)	1.52			
N (1) - H	1.22 (12)	0.75 (11)		1.00 (5)	1.06 (5)	0.84 (5)
C (2) - H	1.04 (10)	1.05 (9)		0.93	1.07	0.98
C (8) - H	1.00 (13)	0.88 (15)		0.92	0.94	0.99
C (1′) - H	1.12 (11)	0.94 (10)		1.01	1.01	1.04
C (2′) - H	1.19 (13)	0.91 (11)		1.05	0.96	1.01
C (3′) - H	1.11 (10)	0.74 (11)		0.94	0.99	0.95
C (4′) - H	1.22 (15)	0.97 (12)		1.02	0.97	0.96
C (5′) - H	1.16 (13)	0.88 (11)		1.00	0.90	0.97
C (5′) - H′	1.11 (14)	0.88 (10)		1.01	1.06	0.99
O (2′) - H	1.02 (12)	0.67 (10)		0.78	0.84	0.88
O (3′) - H	1.05 (9)	0.97 (14)		0.83	0.79	0.90
Bond angles						
N (1) - C (2) - N (3)	123.7 (12)°	124.0 (14)°	123 (1)°	126.2 (5)°	126.7 (5)°	124.6 (3)°
C (2) - N (3) - C (4)	112.3 (11)	112.6 (12)	114	111.2	110.7	111.9
N (3) - C (4) - C (5)	129.2 (11)	128.7 (12)	127	127.7	128.0	128.5
C (4) - C (5) - C (6)	117.7 (11)	117.2 (12)	122	119.7	119.5	118.3
C (5) - C (6) - N (1)	111.0 (11)	111.9 (12)	107	110.6	110.7	111.0
C (6) - N (1) - C (2)	125.9 (11)	125.5 (12)	126	124.5	124.4	125.4
C (4) - C (5) - N (7)	110.0 (10)	109.6 (11)	111	110.6	111.6	111.6
C (5) - N (7) - C (8)	105.2 (10)	104.9 (11)	103	104.3	103.4	103.8
N (7) - C (8) - N (9)	112.0 (11)	112.9 (12)	108	113.5	113.8	113.6
C (8) - N (9) - C (4)	107.9 (10)	106.7 (11)	110	106.0	105.8	105.7
N (9) - C (4) - C (5)	104.8 (10)	105.9 (11)	107	105.6	105.3	105.4
N (3) - C (4) - N (9)	125.7 (11)	125.5 (12)	127	126.7	126.7	126.1
C (5) - C (6) - O (6)	129.3 (12)	126.7 (13)	132	128.1	128.6	128.4
N (1) - C (6) - O (6)	119.7 (11)	121.4 (12)	121	121.2	120.6	120.6
C (6) - C (5) - N (7)	132.2 (11)	133.2 (12)	126	129.7	128.8	130.1
C (8) - N (9) - C (1′)	127.8 (10)	127.7 (11)	126	128.9	125.9	128.1

Table 3. Continued

Compound	5′-IMP-Co	5′-IMP-Ni	5′-IMP-Na	Inosine, $2H_2O$		Inosine
Space group	$P2_12_12_1$	$P2_12_12_1$	$C222_1$	$P2_1$		$P2_1$
No. of molecules in the unit cell	4	4	8	4		2
				Molecule I	Molecule II	
C (4) - N (9) - C (1′)	124.1 (10)	124.9 (11)	124	125.1	128.3	126.0
O (1′) - C (1′) - C (2′)	108.1 (10)	107.7 (11)	104	105.1	105.1	106.8
C (1′) - C (2′) - C (3′)	100.1 (10)	100.1 (11)	102	101.4	100.6	100.6
C (2′) - C (3′) - C (4′)	104.3 (10)	103.5 (11)	102	102.7	102.5	101.5
C (3′) - C (4′) - O (1′)	103.1 (9)	103.6 (10)	105	105.8	106.9	104.0
C (4′) - O (1′) - C (1′)	110.9 (9)	111.2 (10)	111	109.9	108.1	109.6
N (9) - C (1′) - O (1′)	106.7 (9)	108.3 (10)	107	107.6	107.3	108.4
N (9) - C (1′) - C (2′)	112.8 (10)	112.3 (11)	114	113.4	114.4	111.5
C (1′) - C (2′) - O (2′)	106.3 (11)	107.3 (12)	111	113.9	114.4	109.6
O (2′) - C (2′) - C (3′)	106.7 (11)	106.3 (12)	112	115.6	112.2	107·5
C (2′) - C (3′) - O (3′)	109.1 (10)	110.0 (11)	107	112.0	111.2	115.9
O (3′) - C (3′) - C (4′)	112.2 (10)	114.1 (11)	111	107.8	109.1	114.2
C (3′) - C (4′) - C (5′)	115.5 (10)	116.1 (12)	119	117.4	115.8	114.1
C (5′) - C (4′) - O (1′)	110.4 (10)	109.6 (11)	112	107.8	108.8	110.0
C (4′) - C (5′) - O (5′)	108.7 (10)	108.9 (11)	109	111.2	112.5	112.0
C (5′) - O (5′) - P	118.0 (7)	117.6 (8)	114			
O (5′) - P - O (7)	106.7 (5)	107.1 (5)	107			
O (5′) - P - O (8)	107·3 (5)	107.6 (5)	104			
O (5′) - P - O (9)	103.2 (5)	103.1 (8)	107			
O (7) - P - O (8)	113.4 (5)	113.7 (9)	113			
O (7) - P - O (9)	111.7 (5)	112.9 (5)	112			
O (8) - P - O (9)	113.8 (5)	113.5 (5)	112			
H - N (1) - C (6)	124 (6)	116 (9)		119.5 (5)	118.2 (5)	112 (3)
H - N (1) - C (2)	109 (6)	115 (9)		115.8	117.4	122
H - C (2) - N (1)	114 (6)	112 (6)		109.9	115.2	120
H - C (2) - N (3)	122 (6)	123 (6)		123.8	118.1	115
H - C (8) - N (7)	127 (8)	128 (10)		119.9	125.0	123
H - C (8) - N (9)	120 (8)	115 (10)		126.6	121.2	123
H - C (1′) - N (9)	106 (6)	101 (6)		109.1	104.0	113
H - C (1′) - O (1′)	106 (6)	99 (6)		107.2	112.7	105
H - C (1′) - C (2′)	117 (6)	127 (6)		114.0	113.4	111
H - C (2′) - C (1′)	114 (6)	121 (7)		106.9	108.4	109
H - C (2′) - C (3′)	117 (6)	101 (7)		112.9	105.3	115
H - C (2′) - O (2′)	111 (6)	118 (7)		106.2	114.6	114
H - C (3′) - C (2′)	101 (5)	117 (8)		112.2	111.6	110
H - C (3′) - C (4′)	111 (5)	91 (8)		112.8	110.6	108
H - C (3′) - O (3′)	118 (5)	119 (8)		109.1	111.3	107
H - C (4′) - C (3′)	107 (7)	106 (7)		112.9	107.9	109
H - C (4′) - C (5′)	112 (7)	122 (7)		108.5	109.6	111
H - C (4′) - O (1′)	108 (7)	96 (7)		103.2	107.5	108
H - C (5′) - C (4′)	117 (6)	109 (7)		109.3	104.2	113
H - C (5′) - O (5′)	108 (6)	98 (7)		109.0	115.4	110
H - C (5′) - H′	103 (10)	110 (9)		104.6	106.9	113
H′ - C (5′) - C (4′)	113 (7)	117 (7)		108.5	105.6	104
H′ - C (5′) - O (5′)	107 (7)	112 (7)		113.9	111.5	104
H - O (2′) - C (2′)	98 (7)	106 (11)		113.3	111.4	111
H - O (3′) - C (3′)	103 (5)	115 (9)		107.9	117.8	106
	Present study	Present study	Rao and Sundaralingam (1969)	Thewalt, Bugg, and Marsh (1970)		Munns and Tollin (1970)

Determination and Refinement of the Structure

The structure was established by heavy atom method. Approximate positional parameters of the cobalt atom were determined from (1/2, v, w), (u, 1/2, w) and (u, v, 1/2) Harker sections. The Fourier synthesis based on the phases of the cobalt atom revealed the complete molecular structure and seven water oxygen atoms. The refinement was carried out using the block-diagonal least-squares method. Five cycles of isotropic and five cycles of anisotropic refinement reduced R value to 0.08. The least-squares weighting was that similar to Hugehes,[10] where $\sqrt{w}=50/|F_o|$ for $|F_o|>50$, $\sqrt{w}=1.0$ for $|F_o|\leq 50$. At this stage a difference Fourier synthesis could locate 23 hydrogen atoms out of 25. Three more cycles of refinement including hydrogen atoms with isotropic thermal parameters gave final R value of 0.051. Finally, two remaining hydrogen atoms could be found from the subsequent difference Fourier synthesis. The final atomic parameters are given in Table 1 together with their standard deviations.

The structure of the nickel complex was elucidated from that of the cobalt complex. Five cycles of isotropic block-diagonal least-squares refinement using the atomic parameters of the cobalt complex as starting parameters reduced the R value to 0.134. Subsequent five cycles of anisotropic refinement decreased R to 0.088. In a difference Fourier synthesis calculated at this stage, 19 hydrogen atoms in the asymmetric unit were actually located and their positions were in accord with the stereochemistry of the molecule, and they were included in the refinement with isotropic temperature factors. Three cycles of refinement, including all atoms brought R to 0.075; an additional final cycle gave no significant changes in positional or thermal parameters. Finally, a difference Fourier synthesis was computed in order to locate the six remaining hydrogen atoms, three of which were actually located. The weighting scheme was; $\sqrt{w}=25/|F_o|$ for $|F_o|>25$, $\sqrt{w}=1.0$ for $|F_o|\leq 25$. The refined atomic parameters are given in Table 2. Complete lists of the observed and calculated structure factors are preserved by the Chemical Society of Japan.[11]

The atomic scattering factors used in the present structure determination were; for hydrogen atoms those cited as Q–1 in International Tables for X-ray Crystallography,[12] for carbon SX–6, for nitrogen SX–7, for oxygen SX–8, for phosphorus SX–70, for cobalt SX–27 and for nickel SX–28.

Discussion of the Structure

The bond lengths and bond angles of the inosine 5′-phosphate molecules along with their estimated standard deviations are listed in Table 3. In this table the values are compared with those of the inosine molecules in monosodium inosine 5′-phosphate (5′-IMP–Na),[8] inosine dihydrate (Inosine, $2H_2O$)[13] and inosine.[14] Figure 1 is a perspective view of the molecule in the cobalt complex showing the numbering

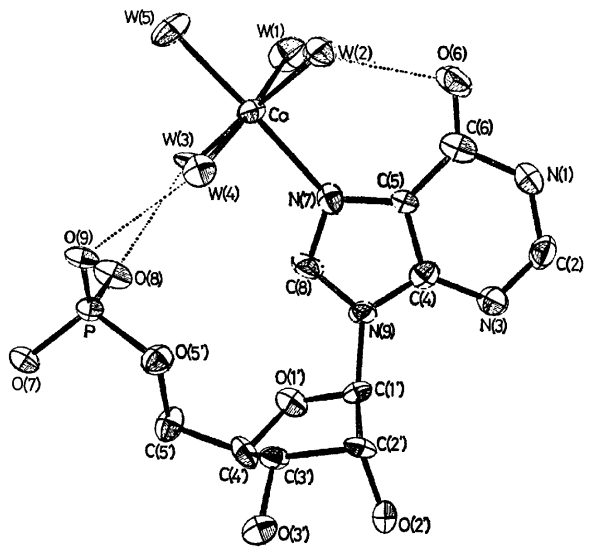

Fig. 1. Perspective view of the molecule in the cobalt complex showing the numbering system and the anisotropic thermal motion of the non-hydrogen atoms represented by 50% probability ellipsoids.

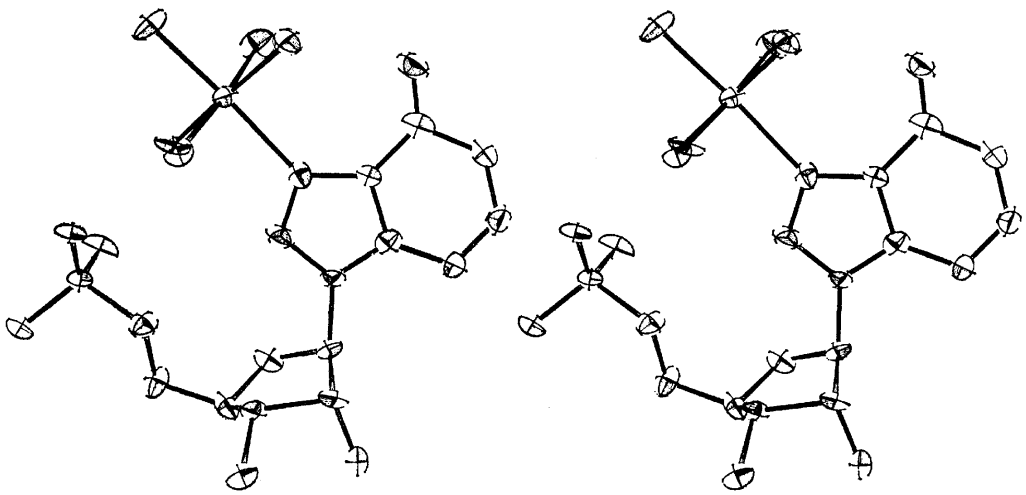

Fig. 2. Stereoscopic view of the structure of the molecule in the cobalt complex.

Table 4. Least-squares planes through the base and sugar

	5′-IMP-Co	5′-IMP-Ni	5′-IMP-Na	Inosine, $2H_2O$		Inosine
				Molecule I	Molecule II	
(1) Plane through the hypoxanthine ring						
N(1)	−0.015* Å	−0.006* Å	0.002* Å	−0.009* Å	0.008* Å	0.020* Å
C(2)	−0.028*	−0.011*	−0.002*	−0.001*	−0.009*	0.020*
N(3)	0.013*	0.005*	0.004*	0.037*	0.005*	−0.010*
C(4)	0.045*	0.000*	−0.020*	0.023*	0.011*	−0.008*
C(5)	−0.007*	−0.001*	0.060*	0.030*	−0.001*	−0.010*
C(6)	0.020*	0.018*	−0.024*	−0.010*	−0.001*	−0.045*
N(7)	0.006*	−0.012*	−0.018*	0.023*	−0.001*	0.023*
C(8)	−0.028*	−0.002*	0.003*	0.012*	0.004*	0.004*
N(9)	−0.005*	0.008*	−0.005*	−0.002*	0.012*	−0.014*
O(6)	0.064	0.069	−0.091	−0.042	−0.010	−0.161
C(1′)	−0.134	−0.155	−0.072	−0.061	−0.018	−0.149
A	0.0383	0.0371	0.875	0.0533	0.0319	0.7237
B	−0.0265	−0.0207	0.118	0.0577	0.0124	−0.4684
C	0.9989	0.9991	−0·446	0.9790	0.9845	−0.5068
D	1.7586	1.7759	0.741	4.0891	6.9433	−1.2786
(2) Plane through the ribose ring						
C(1′)	−0.025*	−0.030*	0.012*	−0.004*	0.028*	0.042*
O(1′)	0.026*	0.032*	−0.020*	0.007*	0.045*	−0.043*
C(2′)	0.014*	0.017*	0.610	−0.589	−0.605	−0.025*
C(3′)	−0.560	−0.566	−0.011*	0.004*	−0.026*	0.626
C(4′)	−0.015*	−0.019*	0.018*	−0.007*	0.043*	0.026*
O(2′)	1.402	1.386	0.232	−0.319	−0.287	−1.379
O(3′)	−0.108	−0.168	−1.334	1.353	1.279	0.440
C(5′)	−0.839	−0.836	1.105	−1.178	−1.025	0.845
	C(3′)-*endo*	C(3′)-*endo*	C(2′)-*endo*	C(2′)-*endo*	C(2′)-*endo*	C(3′)-*endo*
A	0.8074	0.8013	0.666	−0.6207	−0.4733	0.7363
B	0.4288	0.4259	−0.728	−0.4972	0.7752	−0.2892
C	−0.4051	−0.4202	−0.166	0.6887	0.4816	0.6329
D	9.0486	8.9507	−5.188	−4.3651	5.3742	0.9278
(3) The dihedral angle between planes, (1) and (2)						
	67.3°	66.5°	55.2°	52.2°	62.0°	69.7°
	Present study	Present study	Rao and Sundaralingam (1969)	Thewalt, Bugg and Marsh (1970)		Munns and Tollin (1970)

The atoms marked * were included in the calculations of the least-squares planes. The equation of the least-squares plane is defined by $AX+BY+CZ=D$, where X, Y and Z are the orthogonal coordinates measured in Å units along the crystallographic a, b and c axes, respectively.

Table 5. Comparison of the conformations of 5′-IMP molecules

	ϕ_{OO}	ϕ_{OC}	Conformation about the C(4′)-C(5′) bond	ϕ_{CN}	ϕ_{OP}	Displaced suger atom
5′-IMP-Co	−71.7°	44.7°	*gg*	25.4°	161.6°	C(3′)-*endo*
5′-IMP-Ni	−73.7	43.1	*gg*	24.0	162.0	C(3′)-*endo*
5′-IMP-Ba						
molecule I	58	49	*gg*	−46	170	C(2′)-*endo*
molecule II	57	51	*gg*	−34	160	C(2′)-*endo*
5′-IMP2-Na	61	56	*gg*	−43	172	C(2′)-*endo*
5′-IMP-Na	−63	59	*gg*	41	176	C(2′)-*endo*

ϕ_{OO}: torsion angle O(1′)-C(4′)-C(5′)-O(5′), defined by Shefter and Trueblood (1965).
ϕ_{OC}: torsion angle C(3′)-C(4′)-C(5′)-O(5′), defined by Shefter and Trueblood (1965).
ϕ_{CN}: torsion angle C(8)-N(9)-C(1′)-O(1′), defined by Sundaralingam and Jensen (1965).
ϕ_{OP}: torsion angle C(4′)-C(5′)-O(5′)-P.

system. A stereoscopic view of the structure of the molecule in the cobalt complex is also shown in Fig. 2. Aspects of the coordination and the conformation of the inosine 5′-phosphate molecule in the cobalt and nickel complexes are similar to each other.

The Hypoxanthine Ring. The bond lengths and bond angles in the both hypoxanthine rings are in over all agreement with those found in the compounds mentioned above. A common and characteristic feature of the hypoxanthine moieties is regarding angles around the C(6)–O(6) bond; the C(5)–C(6)–O(6) angle is apparently larger than the N(1)–C(6)–O(6), differences of which are distributed in the range of 6—11°. This may be due to the effect of the steric interaction between the oxygen atom O(6) and the nitrogen atom N(7).

The least-squares plane through the nine atoms of the base, excluding the substituent atom O(6), and the deviations of atoms from this plane are given in Table 4, comparing with those of the compounds mentioned above. The atoms composing the purine ring show a significant degree of puckering, which has been often found in purine and pyrimidine derivatives.

The binding of the metal to N(7) has little effect on the base geometry as shown in Tables 3 and 4.

The Ribose Ring. The bond lengths and bond angles in the ribose ring have their usual values.[15] The conformational parameters of the ribose ring for the inosine 5′-phosphate molecule are listed in Table 5, comparing with those of monosodium inosine 5′-phosphate,[8] disodium inosine 5′-phosphate (5′-IMP–2Na)[7] and barium inosine 5′-phosphate (5′-IMP–Ba).[7] An important stereochemical parameter in nucleosides and nucleotides is the glycosyl torsion angle ϕ_{CN},[15] C(8)–N(9)–C(1′)–O(1′), which describes the relative orientation of the base with respect to the sugar. Those angles are 25.4° (Co complex) and 24.0° (Ni complex), therefore, the conformation about the glycosyl bond is *anti* in both complexes.

The ribose carbon atom C(1′) is out of the base plane by 0.134 Å (Co complex) and 0.155 Å (Ni complex) and the glycosidic C(1′)–N(9) bond makes an angle of about 5.0° (Co complex) and 6.0° (Ni complex) with the base plane. As shown in Table 4, the ribose ring is puckered with C(3′) displaced by the best four-atom plane of the furanose ring by 0.560 Å (Co complex) and 0.566 Å (Ni complex) on the same side as C(5′), the conformation of the ribose ring is, therefore, C(3′)-*endo*. When refered to the three-atom plane C(1′), O(1′) and C(4′), the conformation is C(3′)-*endo*-C(2′)-*exo* for both complexes, where C(3′) and C(2′) are displaced by 0.465 and 0.122 Å (Co complex) and 0.477 and 0.151 Å (Ni complex).

Dihedral angles between the base and the ribose planes are 67.3° (Co complex) and 66.5° (Ni complex) (Table 4).

The ribose ring conformation can also be described in terms of torsion angles around the ring bonds. The conformation around the C(4′)–C(5′) bond, described by the angles ϕ_{OO},[16] O(1′)–C(4′)–C(5′)–O(5′) and ϕ_{OC},[16] C(3′)–C(4′)–C(5′)–O(5′), is *gauche-gauche* for both complexes.

The Phosphate Group. The ester linkage, C(5′)–O(5′), shows the elongated conformation as usual, the torsion angle ϕ_{OP}, C(4′)–C(5′)–O(5′)–P, being 161.6° (Co complex) and 162.0° (Ni complex).

It may be noted that both phosphorus atoms in the cobalt and nickel complexes lie approximately in the base plane; only 0.188 Å (Co complex) and 0.173 Å (Ni complex) off the base plane.

Coordination Geometry about the Metal Atom. The coordination geometries about (a) the cobalt and (b) nickel atoms are shown in Fig. 3, together with the bond lengths and bond angles within the metal coordination spheres. They are approximately octahedral with the six coordination sites occupied by the five oxygen atoms of the water molecules and the nitrogen atom N(7) of the hypoxanthine moiety, a site which is accessible and presumedly favorable in the biopolymer, and are similar to that found in the cobalt-theophylline complex.[5] Other two cases of the transition metal binding to N(7) of the purine base have been reported in the zinc–adenine[17] and the copper–9-methylhypoxanthine[18] complexes. Although in the vitamine B_{12} derivatives,[19] the analogous N(7) site of the dimethylbenzimidazole base is coordinated to the cobalt atom which is chelated to the corrine nucleus in a manner similar to that of the present complexes, it is to our knowledge the first case in the crystal structure of nucleotides that the transition metal directly bonds to the base. Bond lengths and bond angles of the cobalt complex agree in general

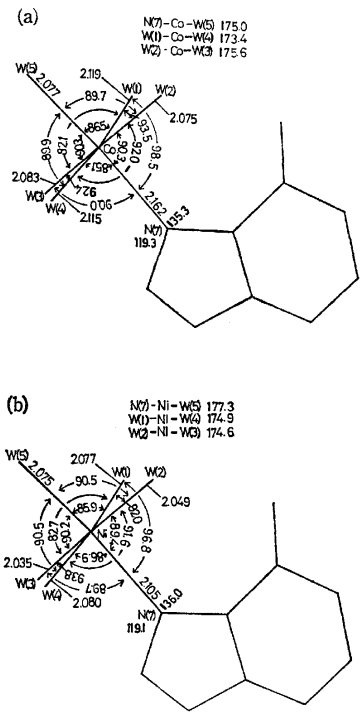

Fig. 3. The coordination geometries around (a) the cobalt atom and (b) the nickel atom. The bond lengths and angles within the metal coordination spheres are shown. The average estimated standard deviations are 0.009 Å for Metal-W bonds and 0.010 Å for Metal-N bonds and 0.4° for W-Metal-W and W-Metal-N angles and 0.8° for C-N-Metal angles.

Table 6. Deviations of the atoms from the least-squares planes (Å)

Atom	5′-IMP-Co	5′-IMP-Ni
(1) Plane through the hypoxanthine ring[a]		
Metal	−0.086	−0.060
W(1)	−1.805	−1.706
W(2)	1.218	1.237
W(3)	−1.516	−1.489
W(4)	1.511	1.513
W(5)	−0.036	−0.039
(2) Plane through the four water oxygen atoms, W(1), W(2), W(3) and W(4)		
W(1)	−0.036*	−0.043*
W(2)	0.033*	0.040*
W(3)	0.037*	0.043*
W(4)	−0.034*	−0.039*
Metal	0.033	0.026
N(7)	2.180	2.122
W(5)	−2.044	−2.047
A	0.6681	0.6745
B	0.7414	0.7365
C	−0.0499	−0.0512
D	7.2853	7.2365
(3) The dihedral angle between the planes, (1) and (2)	87.5°	87.6°

The atoms marked * were included in the calculations of the least-squares planes. The equation of the least-squares plane is defined by $AX+BY+CZ=D$, where X, Y and Z are the orthogonal coordinates measured in Å units along the crystallographic a, b and c axes, respectively.

a) This plane is identical with that in Table 4.

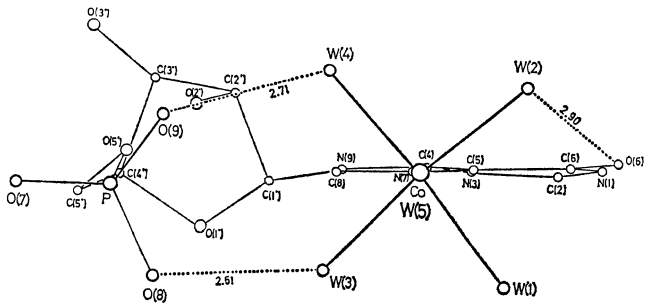

Fig. 4. A view of the cobalts complex down the W(5)–Co bond. Note the dispositions of the hypoxanthine ring system, and in particular the intramolecular hydrogen bonds from W(3) and W(4) to O(8) and O(9) of the phosphate group respectively.

with those of the nickel complex. However, each bond length in the nickel complex is smaller than the corresponding one in the cobalt complex. The metal–oxygen coordination distances range from 2.075 to 2.119 Å with an average value of 2.094 Å for the cobalt complex and from 2.035 to 2.080 Å with that of 2.063 Å for the nickel complex. The metal–nitrogen coordination distances are 2.162 Å for the cobalt complex and 2.105 Å for the nickel complex. These values of the nickel complex in the present study are in good agreement with those of the same nickel complex reported by Clark and Orbell[9]; (Ni–H_2O)average= 2.06 Å and Ni–N(7)=2.11 Å. As shown in Table 6, the cobalt and nickel atoms involving the water oxygen W(5) lie in the base plane. The cobalt and nickel atoms are also in the least-squares plane through four water oxygen atoms, W(1), W(2), W(3) and W(4), which is approximately perpendicular to the base plane.

Table 7. Bond lengths and angles involving hydrogen atoms in water molecules

Bond length	5′-IMP-Co	5′-IMP-Ni
W(1)-H	1.28(11) Å	1.10(13) Å
W(1)-H′	0.98(11)	0.98(12)
W(2)-H	0.80	—
W(2)-H′	0.80(12)	—
W(3)-H	1.14(14)	1.16(12)
W(3)-H′	0.81(13)	0.92
W(4)-H	0.80(10)	0.75(19)
W(4)-H′	0.88(15)	0.85(14)
W(5)-H	1.24(16)	0.83(15)
W(5)-H′	0.94(10)	1.05(14)
W(6)-H	1.29	1.31
W(6)-H′	1.13(16)	1.14
W(7)-H	0.86(13)	—
W(7)-H′	0.98(15)	0.92(19)
Bond angle		
H-W(1)-H′	133(8)°	75(9)°
H-W(2)-H′	88	—
H-W(3)-H′	108(12)	90
H-W(4)-H′	108(12)	125(17)
H-W(5)-H′	109(11)	117(13)
H-W(6)-H′	107	120
H-W(7)-H′	121(12)	—

A notable feature of the metal coordination is that metals are not directly attached to the phosphate oxygen atoms, as is found for sodium ion in the crystal structures of disodium inosine 5′-phosphate[7] and monosodium inosine 5′-phosphate[8] and for barium ion in those of barium inosine 5′-phosphate,[7] barium uridine 5′-phosphate[16] and barium 5′-ribophosphate,[20] whereas in the structures of calcium thymidylate[21] and disodium adenosine triphosphate,[22] metal ions bond directly to the phosphate oxygen atoms.

Figure 4 is a view of the cobalt complex down to W(5)–Co bond. The hypoxanthine ring has positioned itself nearly symmetrically between the bonds Co–W(3) and Co–W(4), but asymmetrically between the bonds Co–W(1) and Co–W(2). This may be due to the intramolecular hydrogen bond from the water W(2) to the carbonyl oxygen O(6) of the base. Figure 5 is the arrangement of the molecules in the unit cell in projection down the c axis for the cobalt complex. Cobalt atom interacts indirectly with phosphate oxygens through the water molecules.

Molecular Packing and Hydrogen Bonds. In Fig. 5, the close contacts are shown by broken lines, which may represent hydrogen bonds. The positions of the molecules are denoted as following: I at x, y, z; II at

Table 8. Hydrogen bond distances and angles

Donor (D)	Acceptor (A)	Of molecule	Distance (D)·····(A) 5′-IMP-Co	Distance (D)·····(A) 5′-IMP-Ni	Distance H·····(A) 5′-IMP-Co	Distance H·····(A) 5′-IMP-Ni	Angle H–(D)·····(A) 5′-IMP-Co	Angle H–(D)·····(A) 5′-IMP-Ni
N(1)	W(6)	IV(000)	2.830(13) Å	2.788(14) Å	1.72(12) Å	2.13(10) Å	18(6)°	24(9)°
O(2′)	W(7)	I(000)	2.734(14)	2.726(14)	1.78(12)	2.09(12)	17(7)	15(11)
O(3′)	O(9)	III(000)	2.761(12)	2.744(12)	1.87(10)	1.78(14)	26(5)	4(9)
W(1)	O(7)	III($\bar{1}0\bar{1}$)	2.769(13)	2.795(14)	1.74(11)	2.37(12)	27(5)	56(6)
W(1)	W(7)	II(00$\bar{1}$)	2.876(15)	2.885(16)	2.54(12)	2.09(12)	60(7)	29(7)
W(2)	O(6)	I(000)	2.901(13)	2.838(13)	2.43(12)	—	7(9)	—
W(2)	O(2′)	I($\bar{1}$00)	2.938(13)	2.953(13)	2.23(13)	—	24(9)	—
W(2)	O(3′)	I($\bar{1}$00)	2.783(13)	2.812(13)	2.03	—	16	—
W(3)	O(7)	III($\bar{1}0\bar{1}$)	2.646(11)	2.625(14)	1.58(14)	1.54(11)	13(7)	16(5)
W(3)	O(8)	I(000)	2.613(12)	2.662(13)	1.82(14)	1.76	9(10)	10
W(4)	O(7)	III($\bar{1}$00)	2.679(12)	2.701(13)	1.91(10)	2.03(19)	13(7)	22(14)
W(4)	O(9)	I(000)	2.707(12)	2.701(12)	1.86(15)	2.05(13)	12(10)	34(9)
W(5)	O(8)	III($\bar{1}0\bar{1}$)	2.708(12)	2.688(14)	1.71(15)	2.10(14)	27(7)	38(10)
W(5)	O(9)	III($\bar{1}$00)	2.767(12)	2.780(14)	1.85(10)	1.99(15)	9(6)	34(8)
W(6)	O(8)	III(00$\bar{1}$)	2.927(13)	3.031(15)	1.86(16)	1.91	14(8)	8
W(6)	W(4)	III(000)	3.074(13)	3.065(15)	1.80	2.05	7	31
W(7)	O(3′)	II(10$\bar{1}$)	2.956(14)	2.928(16)	2.32(13)	—	36(9)	—

Table 9. Hydrogen bond directions around the donor atom

Hydrogen bond from	to Atom	to Of molecule	to Code No.	Angles subtended at the donor atom[a]	5′-IMP-Co	5′-IMP-Ni
N(1)	W(6)	IV(000)	1	C(2)-N(1)···1	95.7(8)°	96.0(9)°
				C(2)-N(1)···1	138.0(8)	131.1(9)
O(2′)	W(7)	I(000)	2	C(2′)-O(2′)···2	107.9(8)	105.6(9)
O(3′)	O(9)	III(000)	3	C(3′)-O(3′)···3	119.3(7)	118.5(8)
W(1)	O(7)	III($\bar{1}0\bar{1}$)	4	4···W(1)···5	105.6(4)	103.2(5)
W(1)	W(7)	II(00$\bar{1}$)	5	Metal-W(1)···4	99.0(4)	98.8(4)
				Metal-W(1)···5	148.7(5)	152.2(6)
W(2)	O(6)	I(000)	6	6···W(2)···7	68.3(3)	66.8(4)
W(2)	O(2′)	I($\bar{1}$00)	7	7···W(2)···8	54.5(3)	54.6(4)
W(2)	O(3′)	I($\bar{1}$00)	8	6···W(2)···8	122.6(4)	121.0(5)
				Metal-W(2)···6	97.8(4)	98.5(4)
				Metal-W(2)···7	127.8(5)	126.0(5)
				Metal-W(2)···8	119.5(4)	119.2(5)
W(3)	O(7)	III($\bar{1}0\bar{1}$)	9	9···W(3)···8	115.2(4)	114.7(4)
	O(8)	I(000)	10	Metal-W(3)···9	104.5(4)	105.6(4)
				Metal-W(3)···10	137.3(4)	135.8(5)
W(4)	O(7)	III($\bar{1}$00)	11	11···W(4)···12	119.3(4)	118.6(4)
W(4)	O(9)	I(000)	12	Metal-W(4)···11	102.8(4)	103.8(4)
				Metal-W(4)···12	116.3(4)	116.9(4)
W(5)	O(8)	III($\bar{1}0\bar{1}$)	13	13···W(5)···14	108.9(4)	109.5(4)
W(5)	O(9)	III($\bar{1}$00)	14	Metal-W(5)···13	124.6(4)	124.6(5)
				Metal-W(5)···14	126.5(4)	125.9(5)
W(6)	O(8)	III(00$\bar{1}$)	15	15···W(6)···16	95.9(4)	95.8(4)
W(6)	W(4)	III(000)	16	W(6)···16-Metal	136.2(4)	135.5(5)

a) Some of the atoms are designated by Code No.

1/2−x, 1−y, 1/2+z; III at 1/2+x, 1/2−y, 1−z and IV at 1−x, 1/2+y, 1/2−z, with the x, y and z coordinates as given in Tables 1 and 2. The translations along the three edges of the unit cell are indicated in parentheses.

The packing of the molecules seems to be governed by the base stacking and intermolecular hydrogen bonds. Further stabilization of the structure is provided by hydrogen bonding of the complex to two water molecules of crystallization. The bond lengths and bond angles involving hydrogen atoms in water molecules are listed in Table 7. The lengths and the

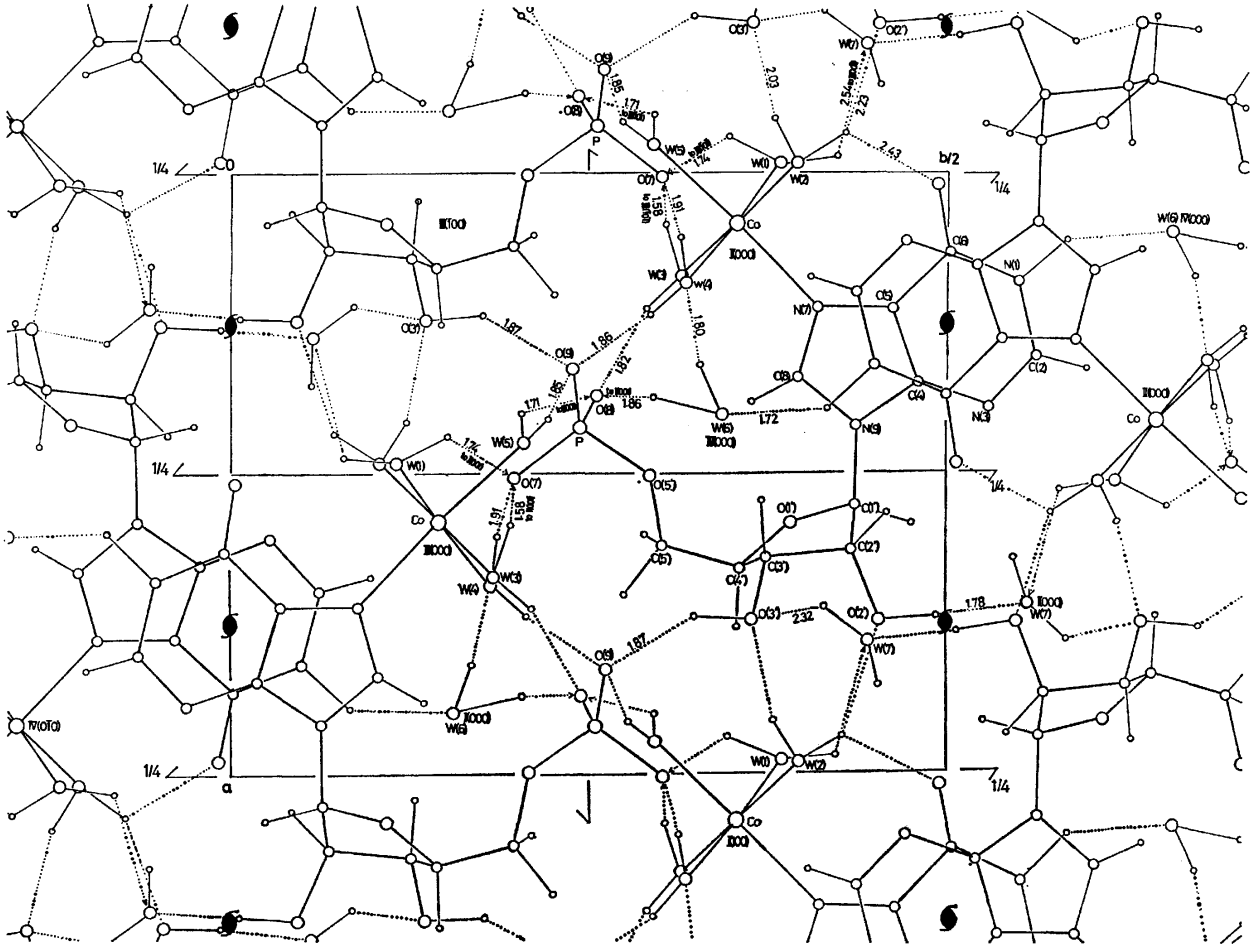

Fig. 5. Projection of the crystal structure of the cobalt complex along the c axis. Hydrogen bonds are shown by broken lines.

directions of the hydrogen bonds are summarized in Tables 8 and 9.

There is an infinite stack of relatively extensive overlapping bases about a two-fold screw axis along the c axis. Adjacent bases are rotated by 180° from each other, which favours dipole-dipole interactions. It is well known that this type of purine superposition may be an important stabilizing force in the inosine and guanosine structures.[23] The hypoxanthine rings lie in the ab plane so that they are stacked with a separation of 3.42 Å along the c axis in both complexes, this value is normal for the perpendicular distance between the base planes.

As expected, the highest concentrations of water molecules are seen around the metal and the anionic phosphate group of the nucleotide. The base, sugar and phosphate moieties are all hydrogen bonded to different degrees with the water molecules, but there is only one hydrogen bond which does not involve a water molecule, that from O(3′) to the phosphate oxygen O(9) (III(000)), and there are no interbase hydrogen bonds. The phosphate groups are running parallel to the a axis about the two-fold screw axis (at x, 1/4, 0) forming hydrogen-bonded ribons, $-(-\text{P}-\text{O}(7)\cdots\text{W}(3)\cdots\text{O}(8)-)-_n$.

The author wishes to thank Professor Y. Iitaka, the University of Tokyo, for his valuable discussion and suggestions.

References

1) J. R. Fresco, A. Adams, R. Ascione, D. Henry, and T. Lindahl, *Cold Spring Harbor Sym. Quant. Biol.*, **31**, 527 (1966).

2) G. L. Eichhorn, N. A. Berger, J. J. Butzow, P. Clark, J. M. Rifkind, Y. A. Shin, and E. Tarien, *Advan. Chem. Ser.*, **No. 100**, 135 (1971).

3) W. Szer and S. Ochoa, *J. Mol. Biol.*, **8**, 823 (1964).

4) D. W. Gibson, M. Beer, and R. J. Barrnett, *Biochemistry*, **10**, 3669 (1971).

5) L. G. Marzilli, T. J. Kistenmacher, and C. H. Chang, *J. Amer. Chem. Soc.*, **95**, 7507 (1973).

6) S. H. Kim, G. J. Quigley, F. L. Suddath, A. McPherson, D. Snedon, J. J. Kim, J. Weinzierl, and A. Rich, *Science*, **179**, 285 (1973).

7) N. Nagashima and Y. Iitaka, *Acta Crystallogr.*, **B24**, 1136 (1968).

8) S. T. Rao and M. Sundaralingam, *J. Amer. Chem. Soc.*, **91**, 1210 (1969).

9) G. R. Clark and J. D. Orbell, *Chem. Commun.*, **1974**, 139.

10) E. W. Hughes, *J. Amer. Chem. Soc.*, **63**, 1737 (1941).

11) The complete data of the F_o-F_c tables are kept as Document No. 7510 at the office of the Chemical Society

of Japan. (Document No. 7510A for the cobalt complex and No. 7510B for the nickel complex).
12) "International Tables for X-ray Crystallography," Vol. III, Knoch Press, Birmingham, (1962).
13) U. Thewalt, C. E. Bugg, and R. E. Marsh, *Acta Crystallogr.*, **B26**, 1089 (1970).
14) A. R. I. Munns and P. Tollin, *ibid.*, **B26**, 1101 (1970).
15) M. Sundaralingam and L. H. Jensen, *J. Mol. Biol.*, **13**, 930 (1965).
16) E. Shefter and K. N. Trueblood, *Acta Crystallogr.*, **18**, 1067 (1965).
17) L. Srinivasan and M. R. Taylor, *Chem. Commun.*, **1970**, 1668.
18) E. Sletten, *ibid.*, **1971**, 558.
19) D. C. Hodgkin, J. Lindsey, R. A. Sparks, K. N. Trueblood, and J. G. White, *Proc. Roy. Soc., A*, **266**, 494 (1962).
20) S. Furburg and A. Mostad, *Acta Chem. Scand.*, **16**, 1627 (1962).
21) K. N. Trueblood, P. Horn, and V. Luzzati, *Acta Crystallogr.*, **14**, 965 (1961).
22) O. Kennerd, N. W. Isaacs, J. C. Coppola, A. J. Kirby, S. Warren, W. D. S. Motherwell, D. G. Watson, D. L. Wampler, D. H. Chenery, A. C. Larson, K. Ann Kerr, and L. Riva Di Sanseverino, *Nature*, **225**, 333 (1970).
23) C. E. Bugg, J. M. Thomas, and M. Sundaralingam, *Biopolymers*, **10**, 175 (1971).

Selective Dimerization of Propene to 4-Methyl-1-pentene by Potassium–Copper based Catalysts

Junzo YAMASHITA, Kiyoshi SASAKI, Takao KAWAMURA, Koichi HIGUCHI, Shotaro MIURA, and Harukichi HASHIMOTO

Department of Applied Chemistry, Faculty of Engineering, Tohoku University, Sendai 980

(Received July 9, 1974)

The dimerization of propene by potassium catalyst was carried out at 180 °C in *n*-heptane to give 4-methyl-1-pentene as a major product. The effects of the addition of metal powders, potassium alkoxides and tertiary amines were investigated. The selective production of 4-methyl-1-pentene on adding metal powders increased in the order of Cu, Ag>Mg, Co>Al, Fe, Ni, Zn. When long-chain alkoxides were added to the potassium-copper catalyst system, potassium catalyst was observed to be dispersed, the relative reaction rates increased, and the isomerization of 4-methyl-1-pentene formed was retarded. Thus, the selectivity increased more than 90% after 40% conversion of propene. The potassium-copper-aliphatic tertiary amine-catalyst system caused the yield of 4-methyl-1-pentene to increase in a similar manner to the potassium-copper-alkoxide-catalyst system and inhibited the formation of the carbonaceous substance covering the surface of the catalyst, and the selectivity was not lowered after a higher conversion of propene.

The dimerization of propene by heavier alkali metal- or alkylalkali-catalysts has been reported to give 4-methyl-1-pentene,[1] from which a stereoregular polymer with a low density and a higher melting point than polyethylene and polypropylene is obtained, whereas the dimerization catalyzed by an acid[2] or a transition metal complex[3] gives a mixture of *n*-hexenes, methylpentenes and 2,3-dimethylbutenes. In the alkali metal- or alkylalkali-catalyzed dimerization, the catalyst system is heterogeneous so that the surface area of the catalyst may have a significant effect upon the reaction. Therefore, the effect of the addition of powdered metals (inert carriers) has been studied. It has been proposed by Wilkes[1c] that organoalkali intermediates were the active species in this reaction. So we have investigated the effect of the addition of bases such as potassium alkoxides and tertiary amines upon the reaction. These bases may coordinate with the counter cation of carbanions to dissociate the insoluble organoalkali intermediates. These effects of bases have been reported in Grignard reactions in hydrocarbon solvents,[4] in reactions of organolithium compounds,[5] and in polymerization of butadiene by alfin catalyst.[6] A highly selective catalyst system which affords 4-methyl-1-pentene in more than 90% after a higher conversion of propene has been found.[7]

Results and Discussion

The Effect of Powdered Metals. Potassium was chosen as a catalyst because it is easier to handle:

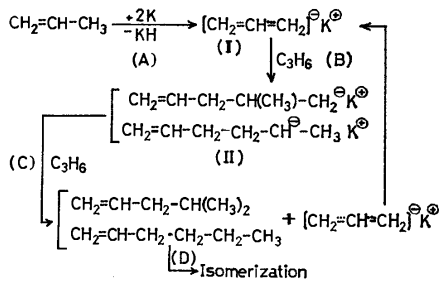

Fig. 1. Reaction scheme for propene-dimerization catalyzed by potassium.

both cesium and potassium have been reported to be effective in the formation of 4-methyl-1-pentene from propene.[1] The reaction was carried out at 180 °C under pressure with vigorous stirring (*ca.* 1000 rpm) in an autoclave equipped with a magnetic stirrer. *n*-Heptane was used as a solvent. Aromatics such as benzene, used in other reports,[1] were found to inhibit the reaction.

The scheme of the reaction has been considered to be as in Fig. 1,[1] *i.e.* allylpotassium (I) was formed in step A, followed by the addition step B and the exchange step C to yield the products. The organopotassium intermediates (I) and (II) are insoluble in the reaction medium, and probably aggregate in the course of the reaction. Since the condition of the catalyst surface may influence the reaction, the effect of adding powdered metals was investigated (Table 1). These powdered metals were expected to function as inert carriers and to increase the surface area of the molten potassium.

The selectivity was increased by added metals in the order of Cu, Ag>Mg, Co>Al, Fe, Ni, Zn. The potassium catalyst was observed to be finely dispersed when the powdered metals were added.

Curtin and Koehl reported that coating of lithium with powdered copper was effective in preparing organolithium compounds.[8] They indicated that it covered the surface of the lithium and inhibited the oxidation of the lithium. They also suggested that the chemical interaction between lithium and copper might be involved. However there has been no report which implies the formation of an alloy or other compounds between potassium and copper. No appropriate explanation for the difference of the effect of the metals can be offered at present.

The Effect of the Addition of Potassium Alkoxides. The reaction step A occurs on the surface of potassium metal. As described above, the reactivity of the catalyst could be increased by an increase in the surface area due to the added powdered metals. In addition, the dissociation of aggregated organopotassium may promote the reaction rate.[5,6] Thus, the effect of the addition of various potassium alkoxides to the potassium–copper catalyst system was investigated.

Table 1. Effect of added metal powders on the potassium catalyzed dimerization of propene[a]

Metal[b] powder	Propene (g)	Reaction time (hr)	Conv. (%)	Yields (%)[c] (1)	(2)	(3)	(4)	(5)
None	61	5	5	60.8	26.5	4.5	8.2	
Mg	40	5	32	77.7	13.0	4.3	3.9	1.1
Al	38	5.2	7	71.5	17.8	5.9	4.8	
Fe	34	5	8	67.5	22.0	4.9	4.6	1.2
Co	38	5	41	76.5	14.4	4.9	4.4	
Ni	36	5	18	59.4	25.5	4.8	9.0	1.1
Cu	51	3	29	86.7	6.9	4.3	1.8	t
Zn	35	5.2	1	62.6	15.2	6.5	15.7	
Ag	37	5	15	84.2	7.5	4.7	3.6	

a) Reaction conditions: K 2.0 g (0.05 g atom), *n*-heptane 70 ml, 180 °C, 1000 rpm. b) 0.05 g atom of powdered metal (*ca.* 100 mesh). c) Yields on the basis of propene converted. (1) 4-Methyl-1-pentene, (2) *cis*- and *trans*-4-methyl-2-pentene, (3) 1-hexene and 2-methyl-1-pentene, (4) *trans*-2-hexene and 2-methyl-2-pentene, (5) *cis*-2-hexene.

Table 2. Isomerization of the reaction products[a]

Additive (0.05 mol)	Propene (g)	Reaction time (hr)	Conv. (%)	Yields (%)[c] (1)	(2)	(1)[b]	(2)[b]
None	70	3.0	28.2	88.8	4.5	54.2	28.2
n-BuOK	77	3.0	25.0	95.2	2.0	61.5	27.1
n-Bu_3N	43	3.0	21.0	90.4	2.8	73.0	16.3

a) Reaction conditions: K 2.0 g (0.05 g atom), *n*-heptane 70 ml, powdered copper 3.2 g (0.05 g atom), 180 °C, 1000 rpm. b) Yields obtained upon heating for 6 hr after the removal of unreacted propene. c) See Table 1.

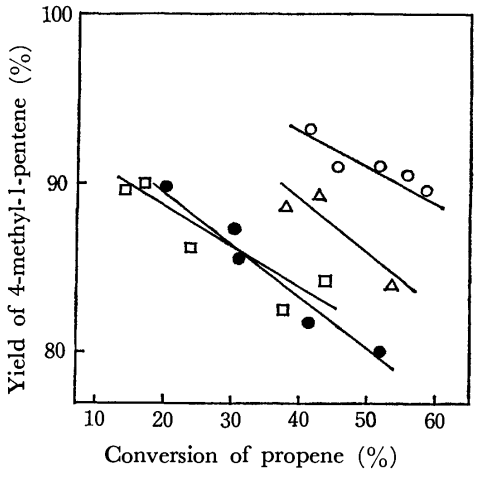

Fig. 2. Variation of the yield of 4-methyl-1-pentene *versus* propene conversion.
●: no additive △: isopropoxide
○: *n*-octyloxide □: *sec*-butoxide
See Table 3 for the other reaction conditions

Figure 2 shows the yields of 4-methyl-1-pentene against the propene conversion for this catalyst system, where the selectivity decreased as the conversion of propene increased. Intermediate organopotassium (I) or (II) in Fig. 1 can also react with primary products resulting in isomerization. So the isomerization of the terminal olefins may become significant as the reaction proceeds. It is compatible with the decreasing selectivity at a higher conversion shown in Fig. 2. Base catalyzed isomerization of methylpentenes and other olefins[9] are known to occur under milder reaction conditions.

Table 3. Effect of the addition of ROK[a]

R	Yields (%)[b] (1)	(1) + (2)	Relative[c] rate
None	85	94	11
Methyl	88	94	16
n-Propyl	93	95	14
iso-Propyl	88	95	36
n-Butyl	97	97	22
iso-Butyl	91	94	23
sec-Butyl	84	94	22
tert-Butyl	79	89	15
n-Octyl	93	94	40
Benzyl	no reaction		

a) Reaction conditions: K 2.0 g, *n*-heptane 70 ml, powdered copper 3.2 g (0.05 g atom), ROK 0.05 mol, propene 40—60 g, 180 °C, 1000 rpm. b) Yields were calculated at 40% conversion of propene, referred to Fig. 2. See Table 1 for (1) and (2). Isomerization of (1) to the other isomers than (2) is very small. c) (Maximum pressure − minimum pressure) (atm) × 100/maximum pressure/reaction time (hr).

Without propene, isomerization of 4-methyl-1-pentene was also significant in our catalyst systems as shown in Table 2. The yields of 4-methyl-1-pentene at 40% conversion of propene and the relative reaction rates in potassium–copper–potassium alkoxide catalyst systems are shown in Table 3, where added alkoxides in the range 0.5—2.0 mol per mol of potassium produced no significant differences in the results. The long chain alkoxides, such as *n*-butoxide, *n*-octyloxide and

n-propoxide, were the most effective additives. More branched, short chain, secondary or tertiary alkoxides were less effective. It was noticed that the addition of tertiary butoxide promoted the isomerization of 4-methyl-1-pentene and that the byproducts(carbonaceous substances) covering the catalyst surface served to gradually slow down the reaction rate. This unexpected observation may be due to the instability of the butoxide under the reaction conditions or the pronounced proton transfer from the products on increase of the catalytic activity. Benzyloxide inhibited the reaction as efficiently as aromatic solvents due to the presence of the aromatic nucleus. Since the isomerization of the olefins occurs without any detectable rearrangement of the carbon skeleton in this catalyst system, the ratio of methylpentenes to *n*-hexenes should be determined at step B in Fig. 1. The total yields of methylpentenes shown in the column (1)+(2) in Table 3 were constant. This indicates that the addition of alkoxides does not affect the course of the addition reaction in step B. The added alkoxides suppressed the isomerization of 4-methyl-1-pentene formed as shown in Table 2. When longer chain alkoxides were added, the catalysts were finely dispersed. The observation suggested that the dispersing effect of the alkoxides has a significant role in the nature of the catalyst systems. When the alkoxides were added, the relative rates became considerably larger, but had no direct correlation with the selectivity. More precise studies of the role of the alkoxides are now in progress.

The Effect of the Addition of Tertiary Amines. Tertiary amines are known to coordinate to counter ions in carbanion reactions where the reactivity of carbanions increases.[5a] Thus, the effect of the addition of various tertiary amines was investigated with the results shown in Table 4 and Fig. 3. The added aliphatic tertiary amines inhibited the formation of the carbonaceous substance covering the surface of the catalyst and did not lower the selectivity at a higher conversion of propene (Fig. 3). The result has a practical importance in the preparation of 4-methyl-1-pentene. The difference between the effect of the alkoxides and tertiary amines is not yet explained. The other effects of the amines were similar to those of the alkoxides.

TABLE 4. EFFECT OF THE ADDITION OF R_3N[a]

R	Yields (%)[b] (1)	Yields (%)[b] (1)+(2)	Relative[c] rate
None	85	94	11
Ethyl[d]	87	93	21
n-Propyl[d]	86	92	15
n-Butyl[d]	90	93	15
n-Hexyl[e]	90	92	14
n-Octyl[e]	90	92	11
N-Methylpiperidine[f]	91	95	25
Pyridine[f]	no reaction		

a) See Table 3 for reaction conditions. b) Yields were the averages of 3 or 5 sets of data in the 25—75% conversion range for propene. See text. c) See Table 3. d) 0.03 mol. e) 0.01 mol. f) 0.06 mol.

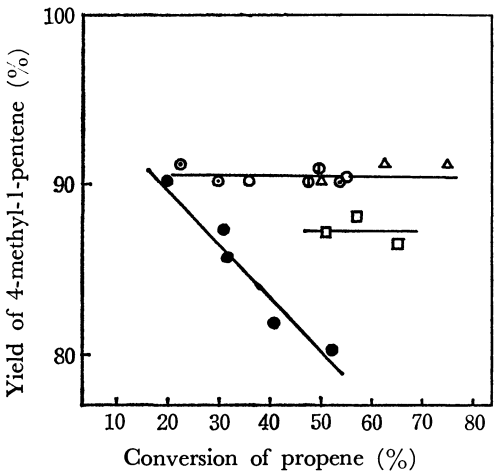

Fig. 3. Variation of the yield of 4-methyl-1-pentene *versus* propene conversion.
●: no additive
△: *N*-methylpiperidine 0.06 mol
□: triethylamine 0.03 mol
○: tri-*n*-octylamine 0.005 mol
⊙: tri-*n*-octylamine 0.01 mol
◐: tri-*n*-octylamine 0.02 mol
See Table 1 for the other reaction conditions.

Experimental

Materials. Propene of polymerization grade was dried on a column of molecular sieve 3A. *n*-Heptane of guaranteed reagent grade was washed several times with concentrated sulfuric acid and then with water, refluxed over sodium for 20 hr., distilled and stored over sodium. Reagent grade alcohols were dried with magnesium or sodium and distilled. Reagent grade amines were dried with calcium hydride or naphthylisocyanide and distilled. Powdered Mg, Al, Fe, Co, Ni, Cu, Zn and Ag of reagent grade (*ca.* 100 mesh) were dried under vacuum and stored in a desiccator. The oxide coating of reagent grade potassium was removed under *n*-heptane and the potassium was immediately used for the reaction.

Analyses. The reaction products were analyzed at 50 °C on a Hitachi-Perkin-Elmer Model 6DH gas chromatograph using a 2 m column packed with squalane 20 wt% on Diasolid M. Their NMR spectra and relative retention times in glc analyses agreed with those of authentic samples.

Standard Procedure. *n*-Heptane (70 ml), potassium (3.9 g, 0.1 mol), powdered copper (3.2 g, 0.05 mol) and *n*-butanol (3.7 g, 0.05 mol) were placed in a 300 ml autoclave (SUS 32) equipped with a magnetic stirrer and heated at 100 °C under a nitrogen atmosphere for 3 hr to form potassium *n*-butoxide *in situ*. After purging hydrogrn gas formed during the reaction with nitrogn, propene (*ca.* 50 g) was introduced and allowed to react at 180 °C while stirring at 1000 rpm. for several hours. The autoclave was then cooled rapidly. When powdered metals alone or copper plus tertiary amines were used, potassium (2.0 g, 0.05 mol) was used without the above pretreatment.

The authors wish to thank Dr. S. Miyano for his valuable comments on the problem and to acknowledge the assistance of Mr. Y. Morimoto, S. Kushiyama and S. Omiya in obtaining some of the data. This work

was supported in part by a Grant for Scientific Research from the Ministry of Education, and was presented in part at the 20th (Tokyo 1964) and 30th (Osaka 1974) Annual Meetings of the Chemical Society of Japan.

References

1) a) J. K. Hambling, *Chem. Brit.*, **5**, 354 (1969); b) A. W. Shaw, C. W. Bittner, W. V. Bush, and G. Holzman, *J. Org. Chem.*, **30**, 3286 (1965); c) J. B. Wilkes, 7th International Petroleum Congress Preprints, Mexico (1967).

2) J. P. Hogan, R. L. Banks, and W. C. Lanning, *Ind. Eng. Chem.*, **47**, 752 (1955).

3) G. Wilke, B. Bogdanović, H. Hardt, P. Heimbach, W. Keim, M. Kroener, W. Oberkirch, K. Tanaka, E. Steinrücke, D. Walter, and H. Zimmermann, *Angew. Chem.*, **78**, 157 (1966).

4) E. C. Ashby and R. Reed, *J. Org. Chem.*, **31**, 971 (1966).

5) a) G. B. Trimitsis, A. Tuncay, R. D. Beyer, and K. J. Ketterman, *J. Org. Chem.*, **38**, 1491 (1973); b) M. Schlosser, *J. Organometal. Chem.*, **8**, 9 (1967); c) R. A. Benkeser, T. F. Crimmins, and Wen-hong Tong, *J. Amer. Chem. Soc.*, **90**, 4366 (1968).

6) a) A. A. Morton, M. L. Brown, and E. Magat, *J. Amer. Chem. Soc.*, **69**, 161 (1947); b) A. A. Morton, F. H. Bolton, F. W. Collins, and E. F. Cluff, *Ind. Eng. Chem.*, **44**, 2876 (1952).

7) a) H. Hashimoto and Y. Morimoto, Jap. 645565 (1971); b) H. Hashimoto, Jap. 656359 (1972); c) H. Hashimoto, U. S. 3755491 (1973); d) H. Hashimoto, Brit. 1338190 (1972).

8) D. Y. Curtin and W. J. Koehl, Jr., *J. Amer. Chem. Soc.*, **84**, 1967 (1962).

9) a) A. Schriesheim and C. A. Rowe, Jr., *ibid.*, **84**, 3161 (1962); b) A. Schriesheim, C. A. Rowe, Jr., and L. Naslund, *ibid.*, **85**, 2111 (1963).

The Reaction of Cycloalkanones with Copper(II) Halides. I. The Reaction of Cyclohexanones with Copper(II) Chloride

Kyoko NISHIZAWA* and J. Yasuo SATOH

Department of Chemistry, St. Paul's (Rikkyo) University, Nishi-Ikebukuro, Toshima-ku, Tokyo 171

(Received July 18, 1974)

The reaction of cyclohexanones with copper(II) chloride gave polychlorinated cyclohexanediones directly in fairly good yields. With methylcyclohexanones, in general the type of product depends on the number of methylene groups between the carbonyl group and the methyl-substituted carbon in the starting material. A possible mechanism for the reaction is discussed.

The reactions of organic compounds with copper(II) halides have been known to involve addition reactions with olefins[1] and substitution reactions with aromatic[2] or carbonyl compounds. Although substitution reactions with copper(II) chloride have also been reported for saturated or unsaturated ketones[3,4] and aldehydes,[5] monochloro-derivatives were obtained in all cases. Recently, the γ-chlorination of unsaturated ketones and aldehydes was reported by Dietl *et al.*[6] A report by Castro *et al.*[7] on both addition and substitution reactions has also appeared. In the above works, however, the reactions were carried out using only 3—5-fold molar amounts of copper(II) chloride, hence, they proceeded only to the stage of mono- or di-chlorination.

Previously, in synthesizing diosphenol from menthone with a 3-fold molar amount of iron(III) chloride according to the method of Asahina,[8] we found that a quinone derivative, which seemed to be a product of a further reaction, was obtained as a minor product, together with diosphenol.[9] It was also found that the reaction in a dioxane medium proceeded more slowly than in the case of an acetic acid medium; the reaction with copper(II) chloride also proceeded more slowly than in the case of iron(III) chloride. On the basis of these preliminary results, the reaction of cyclohexanones with excess copper(II) chloride in 50% dioxane was carried out in order to investigate the formation of the quinone derivative mentioned above. We reported[10] in a previous communication that, in this reaction, the corresponding polychlorinated cyclohexanediones were obtained in fairly good yields. In the present paper, we wish to describe the details of this reaction.

Experimental

All the melting points are uncorrected. Thin-layer chromatography was carried out on silica gel (Wakogel B-5), with detection done by means of iodine or an *o*-phenylenediamine-ethanol solution. Column chromatography was carried out on silica gel (Wakogel C-100). The IR spectra were measured with a Hitachi 215 grating infrared spectrophotometer by the KBr disk method, and the UV spectra, with a JASCO ORD/UV-5 spectrometer and a Hitachi 323 recording spectrophotometer in an ethanol solution. The NMR spectra were recorded in $CDCl_3$, unless otherwise noted, with TMS as the internal standard and using a Hitachi R-20A nuclear magnetic resonance spectrometer. The chemical shifts are presented in terms of the δ value. The mass spectra were obtained with a Hitachi RMU-7M mass spectrometer at 70 eV.

Materials. The 2-, 3-, and 4-methylcyclohexanone and 3,4- and 3,5-dimethylcyclohexanone were prepared from the corresponding alcohols by oxidation with sodium dichromate.[10]

Reaction of Cyclohexanones with Copper(II) Chloride. A typical procedure was as follows: the cyclohexanone (2 g) with 20—30 times as much $CuCl_2 \cdot 2H_2O$ in 50% dioxane (v/v, 200 ml) was reacted under reflux conditions for 1—4 hr. The reaction mixture was then extracted with ether, and the extract, after being washed and dried (sodium sulfate), was evaporated under reduced pressure. The residue was purified by column chromatography.

Reaction of 2-Chlorocyclohexanone with Copper(II) Chloride. In the general manner described for the cyclohexanones, 2-chlorocyclohexanone (2 g) with $CuCl_2 \cdot 2H_2O$ (77 g) was treated under reflux for 4 hr; the usual work-up subsequently gave 1.1 g (34%) of 3,6,6-trichloro-2-hydroxycyclohex-2-en-1-one (**3**); mp 119—120 °C (lit,[12] 115—116 °C).

*Reaction of 2-Hydroxy-3-methylcyclohex-2-en-1-one (**11**) with Copper(II) Chloride.* 2-Hydroxy-3-methylcyclohex-2-en-1-one (**11**) was prepared from 2-methylcyclohexanone (10 g) according to the method of Wallach.[11a] The recrystallization of the resultant product from water containing a small amount of methanol gave needles (**11**, 2.8 g; overall yield, 22%); mp 59—60 °C (lit,[11] 62—63 °C), IR; ν_{OH} 3407 cm^{-1}, $\nu_{C=O}$ 1670 cm^{-1}, and $\nu_{C=C}$ 1640 cm^{-1}, NMR; 1.92 ppm (s, 3H), 2.03—2.85 ppm (m, 6H), and 6.22 ppm (s, 1H). By the general procedure described for the cyclohexanones, 1 g of (**11**) was refluxed with $CuCl_2 \cdot 2H_2O$ (26.8 g) for 2 hr; the reaction mixture was subsequently worked up in the usual way to give 1.1 g (70%) of 6,6-dichloro-2-hydroxy-3-methylcyclohex-2-en-1-one (**4**); mp 115—116 °C.

*Reduction of 3,6,6-Trichloro-2-hydroxy-4-methylcyclohex-2-en-1-one (**7**) with $LiAlH_4$.* The trichlorocyclohexanedione (0.5 g) in ether (15 ml) was treated with $LiAlH_4$ (0.17 g) under reflux for 1.5 hr. After the usual work-up, 0.095 g (22%) of 3,6-dichloro-2-hydroxy-4-methylcyclohex-2-en-1-one (**6**) [mp 150—153 °C (subl.)] was obtained by recrystallization from CCl_4.

Results and Discussion

The products resulting from the reaction of cyclohexanone and of its methyl derivatives with a 20-fold molar amount of copper(II) chloride are shown in Table 1, and their physical constants (Table 2). The product obtained from cyclohexanone itself showed peaks due to a diosphenolic hydroxyl group (3363 cm^{-1}) and an α,β-unsaturated ketone (1678 cm^{-1} and 1640 cm^{-1}) in the IR spectrum, and the K band (λ_{max}^{EtOH} 281 nm, ε=10900) due to an α,β-unsaturated

* Present address: Meiji College of Pharmacy, 1-22-1 Yato-machi, Tanashi, Tokyo 188.

Table 1. Reaction of cyclohexanones with copper(II) chloride

Starting material	Mole ratio per ketone	Time (hr)	Product		Yield (%)
Cyclohexanone	20	1	3-Chloro-2-hydroxycyclohex-2-en-1-one	(**1**)	88
	20	2	3,6-Dichloro-2-hydroxycyclohex-2-en-1-one	(**2**)	72
	30	4	3,6,6-Trichloro-2-hydroxycyclohex-2-en-1-one	(**3**)	53
2-Methylcyclohexanone	20	2	6,6-Dichloro-2-hydroxy-3-methylcyclohex-2-en-1-one	(**4**)	70
3-Methylcyclohexanone	20	2	6,6-Dichloro-2-hydroxy-3-methylcyclohex-2-en-1-one	(**4**)	68
4-Methylcyclohexanone	20	2	3,6-Dichloro-2-hydroxy-5-methylcyclohex-2-en-1-one	(**5**)	23
			3,6-Dichloro-2-hydroxy-4-methylcyclohex-2-en-1-one	(**6**)	25
	30	4	3,6,6-Trichloro-2-hydroxy-4-methylcyclohex-2-en-1-one	(**7**)	65
3,4-Dimethylcyclohexanone	20	2	6,6-Dichloro-2-hydroxy-3,4-dimethylcyclohex-2-en-1-one	(**8**)	61
3,5-Dimethylcyclohexanone	20	2	6,6-Dichloro-2-hydroxy-3,5-dimethylcyclohex-2-en-1-one	(**9**)	58

Table 2. Physical properties and elemental analyses of products

Product	Mp (°C) (lit.)	IR (cm^{-1})	UV (nm)	NMR (ppm)	C (%) Found (Calcd) [Mol. formula]	H (%) Found (Calcd)
(**1**)	118—119 (119, 122)[12]	3290 1681 1648	271 (ε=12800)	1.94—2.28 (m, 2H) 2.43—2.84 (m, 4H) 6.34 (s, 1H)	48.95 (49.17) [$C_6H_7O_2Cl$]	4.88 (4.81)
(**2**)	98—100 (96— 98)[12]	3363 1678 1640	281 (ε=10900)	2.31—2.58 (m, 2H) 2.75—3.06 (m, 2H) 4.51 (t, J=6Hz, 1H), 6.18 (s, 1H)	39.71 (39.81) [$C_6H_6O_2Cl_2$]	3.37 (3.34)
(**3**)	119—120 (115—116)[12]	3394 1698 1638	290 (ε=10500)	2.91 (bs, 4H) 6.14 (s, 1H)	33.24 (33.44) [$C_6H_5O_2Cl_3$]	2.34 (2.34)
(**4**)	115—116	3402 1678 1641	286 (ε=6800)	1.77 (s, 3H) 2.18—2.40 (m, 2H) 2.64—3.45 (m, 2H), 6.21 (s, 1H)	43.12 (43.11) [$C_7H_8O_2Cl_2$]	4.32 (4.13)
(**5**)	78— 80	3545 1678 1634	285 (ε=7500)	1.20 (d, J=6Hz, 3H) 2.13—3.19 (m, 3H) 4.34 (d, J=2.5Hz, 1H), 6.17 (b, 1H)	43.00 (43.11) [$C_7H_8O_2Cl_2$]	4.05 (4.13)
(**6**)	150—153 (subl.)	3356 1688 1648	280 (ε=7500)	1.28 (d, J=6Hz, 3H), 2.20—3.25 (m, 3H) 4.25 (dd, J=10.5 and 1.5Hz, 1H) 6.18 (s, 1H)	43.08 (43.11) [$C_7H_8O_2Cl_2$]	4.16 (4.13)
(**7**)	119—121	3398 1696 1643	290 (ε=8300)	1.39 (d, J=7Hz, 3H) 2.74 (m, 3H) 6.12 (s, 1H)	36.88 (36.63) [$C_7H_7O_2Cl_3$]	3.22 (3.07)
(**8**)	142—143	3356 1690 1655	285 (ε=10900)	1.18 (d, J=6Hz, 3H), 1.71 (s, 3H) 1.94—2.50 (m, 2H) 2.43 (dd, J=4.5 and 18.5Hz, 1H) 6.18 (s, 1H)	Found[a] 208.0070 [$C_8H_{10}O_2Cl_2$]	Calcd 208.0058
(**9**)	107—109	3399 1667 1626	289 (ε=10200)	1.30 (d, J=7Hz, 3H), 1.75 (s, 1H) 1.87 (dd, J=9.7 and 14Hz, 1H) 2.48 (dd, J=4 and 14Hz, 1H) 2.80—3.35 (m, 1H), 6.37 (s, 1H)	45.91 (45.96) [$C_8H_{10}O_2Cl_2$]	5.09 (4.81)

a) Analyzed by high resolution mass spectrometry.

ketone in the UV spectrum. In the NMR spectrum, the peaks appeared at 4.51 ppm (triplet, J=6 Hz) due to $-CH(Cl)-$ and at 6.18 ppm (singlet) due to a phenolic hydroxyl group. From these data, the mp, and analysis, the product was identified as Compound **2**.

In the cases of 2- and 3-methylcyclohexanone, the same product was obtained. The IR and UV spectra had peaks due to an α-hydroxy-α,β-unsaturated ketone. In the NMR spectrum, a peak at 1.77 ppm (singlet) attributable to methyl protons was observed, but the peak due to $-CH(Cl)-$ was not observed. From

these data, the resulting product was identified as Compound **4**.

In the reaction of 4-methylcyclohexanone with copper(II) chloride, two products were obtained. One of these was obtained as crystals from the reaction mixture; the other was obtained from the mother liquor by column chromatography with hexane/ether (9/1). The IR and UV spectra of the former definitely indicated the presence of an α-hydroxy-α,β-unsaturated ketone, and the NMR spectrum showed a peak at 1.20 ppm (doublet, $J=6$ Hz) due to methyl protons and a peak at 4.34 ppm (doublet, $J=2.5$ Hz) due to -CH(Cl)-. This product was concluded to be Compound **5** on the basis of the above data. The other product also showed the presence of an α-hydroxy-α,β-unsaturated ketone in the IR and UV spectra. The NMR spectrum had a peak at 1.28 ppm (doublet, $J=6$ Hz) due to methyl protons and a peak at 4.25 ppm (double-doublet, $J=10.5$ and 1.5 Hz) due to -CH(Cl)-. Hence, this product must have the structure of **6**.

In the reaction with a 20-fold molar amount of the reagent, 2- and 3-methylcyclohexanone gave a *gem*-dichloro derivative, while cyclohexanone and 4-methylcyclohexanone did not give such a product with a *gem*-dichloro-function. It was considered that, in the cases of cyclohexanone and 4-methylcyclohexanone, their reactive carbon in the α-position with respect to the carbonyl group should make them capable of yielding the products mentioned above, just as in the cases of 2- and 3-methylcyclohexanone. Therefore, the reaction was attempted using a 30-fold molar amount of copper(II) chloride. The product resulting from cyclohexanone was identified as Compound **3**, with the *gem*-dichloro-function, from the facts that it did not show a peak due to -CH(Cl)- in the NMR spectrum and that the IR and UV spectra had peaks attributable to an α-hydroxy-α,β-unsaturated ketone. Furthermore, the product from 4-methylcyclohexanone was found to be Compound **7** inasmuch as its IR and UV spectra indicated an α-hydroxy-α,β-unsaturated ketone, while its NMR spectrum showed a peak at 1.39 ppm (doublet, $J=7$ Hz) due to methyl protons and another peak at 6.12 ppm (singlet due to a phenolic hydroxyl group.

These results indicate that, in the reaction of monomethylcyclohexanone with copper(II) chloride, in general the type of product depends on the number of methylene groups between the carbonyl group and methyl-substituted carbon in the starting material. In the case of no or only one methylene group—that is, 2- or 3-methylcyclohexanone—the product obtained in either case was a *gem*-dichloroderivative—that is, of Type B, with a vinyl methyl group. In the case of two methylene groups—that is, 4-methylcyclohexanone—the product obtained was a trichloro-derivative—that is, of Type A, with a methyl group at the 4-position.

Therefore, in order to find out whether this reaction could occur in the cases of dimethylcyclohexanones, the reactions of 3,4- and 3,5-dimethylcyclohexanone with a 20-fold molar amount of the reagent were carried out under the same conditions. Compounds **8** and **9** were thus obtained from the 3,4- and 3,5-dimethyl derivatives respectively. Consequently, it was found that a reaction like that in the case of the monomethyl derivatives also occurred in the case of such dimethylcyclohexanones. Moreover, from the fact that the product obtained was Type B in the case of 3,4-dimethylcyclohexanone, it was found that the generality that the oxygen group enters the 2-position, not the 6-position, is also applicable in this case.

Now, on the basis of these results, let us consider the pathway for the formation of Type A. It has previously been reported[3] that an α-chlorination occurs easily *via* the enol complex in the reactions of saturated ketones with copper(II) chloride. It was found that, in steroidal ketone, a *gem*-dichloro derivative was obtained together with an α-chloro derivative.** Hence, the present reaction would be initiated by an attack on the α-carbon in cyclohexanone with copper(II) chloride, followed by α,α- and/or α,α'-dichlorination.

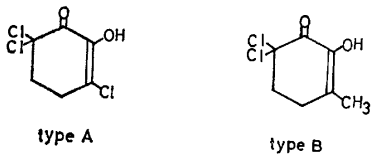

Fig. 1.

Therefore, the α-chlorination product (**a**)—namely, 2-chlorocyclohexanone—, was treated under the same conditions. It was found that oxidative chlorination occurred to give Compound **3**, just as in the case of cyclohexanone. To ascertain the intermediate product in the oxidative chlorination of cyclohexanone, the reaction with a 20-fold molar amount of the reagent was stopped after the mixture had been refluxed for only 1 hr under the same conditions. The product was isolated from the reaction mixture in the usual way and identified as Compound **1** from its spectroscopic data and from its melting point. Moreover, Compounds **2** and **3** were obtained in fairly good yields from the reaction of cyclohexanone with 20-fold molar and 30-fold molar amounts of reagents respectively, as has been mentioned before.

The foregoing results suggest that, after the α-monochlorination product (**a**) is chlorinated to give α,α,α'-trichlorinated cyclohexanone (**c**) through α,α- and/or α,α'-dichlorinated derivatives (**b**), the resulting product (**c**) is hydrolyzed to give 3-chloro-2-hydroxycyclohex-2-en-1-one (**1**). In the later stages, **1** is further chlorinated at the α-position with respect to the carbonyl group to give **3** through **2**. In the case of 4-methylcyclohexanone, the reaction proceeds according to the pathway described above, not being affected by the methyl group, for the methyl group in the methylcyclohexanone is located in a γ-position with respect to the carbonyl group. Hence, this is the pathway proposed for the formation of Type A (Fig. 2):

Next, let us consider the pathway for the formation

** Unpublished data: in the reaction of 5α-cholestan-3-one with copper(II) chloride under the same condentions, 2α-chloro- and 2,2-dichloro-5α-cholestan-3-one were obtained.

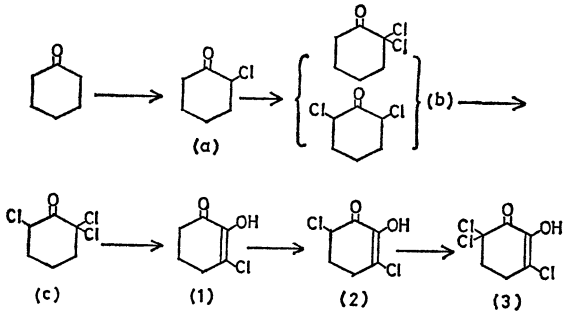

Fig. 2.

of Type B. In the cases of 2- and 3-methylcyclohexanone, the same product (**4**) was obtained. In these cases, the reaction also proceeds *via* Type (**1**), according to Fig. 2. Hence, Type (**1**) —namely, 2-hydroxy-3-methylcyclohex-2-en-1-one (**11**)—was prepared by the method of Wallach,[11a] and the product (**11**) was reacted with copper(II) chloride under the same conditions to give Compound **4**. Also, the reaction of 2-methylcyclohexanone with a 20-fold molar amount of copper(II) chloride was stopped after 15 min under the same conditions. The NMR spectrum of the reaction mixture showed that Compounds **4** and **11** had already been produced. Consequently, 2- and 3-methylcyclohexanone were each refluxed with a 10-fold molar amount of the reagent for 7 hr under the same conditions. The NMR spectra of the reaction mixtures suggested that Compound **11** was quantitatively produced in both cases. Therefore, it was found that Compound **11** was an intermediate of the reaction for the formation of Type B.

It was considered that, in these cases, the reaction also proceeded *via* the enol complex in the earlier stage. Then, in the case of 2-methylcyclohexanone, α-chlorination occurs preferentially at C_6 in the methylcyclohexanone, in contrast with the case of halogenation with molecular halogen,[11a] because the steric hindrance at C_6 is smaller than that at C_2 in the formation of the enol complex. This assumption is supported by the findings that Compound **4**, derived from the C_6-chlorination product, not from the C_2 product, was isolated in a 70% yield, and that no phenol derivative, such as would be derived from the C_2-chlorination product, could be isolated. The α-chlorinated product (**a'**) is dichlorinated at C_6, followed by hydrolysis to give **10**. The dione (**10**) is enolized in the direction of the methyl group to give Compound **11** because of the stabilization by hyperconjugation of the methyl group.

In the case of 3-methylcyclohexanone, the methyl group should have no influence on the earlier stage of the reaction, just as in the case of 4-methylcyclohexanone, because the methyl group was located in the β-position with respect to the carbonyl group in the starting material, in contrast with the 2-methylcyclohexanone. Therefore, it was considered that the pathway were: (**a''**)→(**b''**)→(**10**)→(**11**)→(**2''**)→(**4**) and/or (**a''**)→(**b''**)→(**c''**)→(**2''**)→(**4**). The former pathway, however, is more reasonable because Compound **11**, as an intermediate, was obtained from the reaction of 3-methylcyclohexanone with a 10-fold molar amount of copper(II) chloride, as has been mentioned above. Hence, the pathway for the formation of Type B may be described as follows:

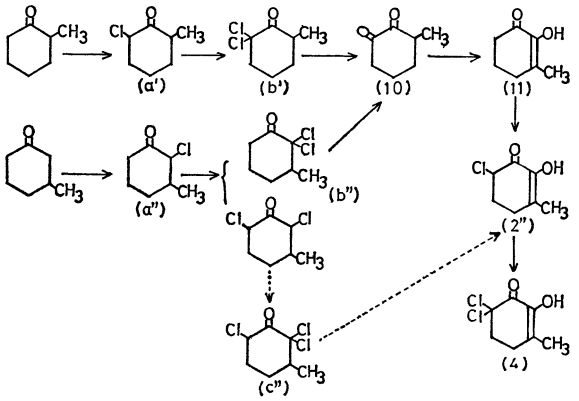

Fig. 3.

On the synthesis of the compounds obtained from the present work, there have been only a few reports. One of these is by Sucrow and Wanzlick,[12] in which 3,6,6-trichloro-2-hydroxycyclohex-2-en-1-one (**3**) was synthesized *via* Compounds **1** and **2** from cyclohexane-1,2-dione in several steps. The present work, however, has demonstrated that Compound **3** can be synthesized in one step from readily available cyclohexanone and copper(II) chloride. Thus, it can be concluded that this reaction constitutes an improved method for the synthesis of polychlorinated cyclohexanediones.

The authors wish to thank Professor A. Hagitani of Rikkyo University for his kind guidance and helpful suggestions in this work. Thanks are also due to Dr. S. Hishida, Naka Works, Hitachi Ltd., for his measurement of the high resolution mass spectra.

References

1) W. C. Baird, JR., J. H. Surridge, and M. Buga, *J. Org. Chem.*, **36**, 3324 (1971).
2) H. P. Crocker and R. Walser, *J. Chem. Soc.*, **1970**, 1982.
3) J. K. Kochi, *J. Amer. Chem. Soc.*, **77**, 5274 (1955).
4) E. M. Kosower, W. J. Cole, G.-S. Wu, D. E. Cardy, and G. Meisters, *J. Org. Chem.*, **28**, 630 (1963); E. M. Kosower and G.-S. Wu, *ibid.*, **28**, 633 (1963).
5) A. Lorenzini and C. Walling, *ibid.*, **32**, 4008 (1967).
6) H. K. Dietl, J. R. Normark, D. A. Payne, J. G. Thweat, and D. A. Young, *Tetrahedron Lett.*, **1973**, 1719.
7) C. E. Castro, E. J. Gaughan, and D. C. Owsley, *J. Org. Chem.*, **30**, 587 (1965).
8) Y. Asahina and S. Mitsuhori, *Yakugaku Zasshi*, **482**, 255 (1922).
9) M. Hirose, K. Nishizawa, S. Yamamoto, A. Hagitani, and J. Y. Satoh, Abstract of 15th Symposium on the Chemistry of Terpens, Essential Oils and Aromatics, Osaka, Japan, November, 1971, p. 173.
10) J. Y. Satoh and K. Nishizawa, *Chem. Commun.*, **1973**, 83.
11) (a) O. Wallach, *Ann. Chem.*, **414**, 314 (1918). (b) K. Sato, S. Inoue, and M. Ōhashi, This Bulletin, **47**, 2519 (1974).
12) W. Sucrow and H.-W. Wanzlick, *Chem. Ber.*, **92**, 2516 (1959).

Vinyl Polymerization. 327.[1] Determination of the Initiating Radical Species in Polymerization with a Dimethylmercury and Copper(II)-Ion System

Minoru IMOTO, Yoshiaki NAKAMURA, and Tatsuro OUCHI

Department of Applied Chemistry, Faculty of Engineering, Kansai University, Suita-shi, Osaka 564

(Received July 31, 1974)

Dimethylmercury was found to give a methyl radical ($\cdot CH_3$) by the reaction with Cu(II)-ion in the presence of water. Generation of $\cdot CH_3$ was proved by scavenging with 1,3,5,-triphenylverdazyl. Radical polymerization of methyl methacrylate and acrylonitrile was carried out with the system dimethylmercury/water/Cu(II)- or Fe(III)-ion.

Koton[2] found that dialkylmercury could initiated the polymerization of vinyl monomer and that the stronger the bond strength of C–Hg of dialkylmercury, the slower the rate of polymerization, *i.e.* dimethylmercury(DM-Hg) was the weakest promoter. Inoue[3] *et al.* and Razubaev[4] *et al.* carried out vinyl polymerization initiated by dibutylmercury or diisopropylmercury in the presence of various metallic salts, using appropriate organic solvents. However, the initiating mechanism remains unclarified.

We have carried out the polymerization using DM–Hg as an initiator in the presence of metallic salts, water being used instead of organic solvent. The initiating species for the polymerization was determined by reaction of DM–Hg with 1,3,5-triphenylverdazyl(TPV) and cupric chloride in benzene.

Experimental

Materials: All metallic salts, DM–Hg and methylmercury chloride (MC–Hg) of special grade were used without further purification. TPV was synthesized by Kuhn's method.[5] Methyl methacrylate(MMA), styrene(St), acrylonitrile(AN) and solvents were purified, according to the usual method.

Procedure: Polymerization was carried out in a 30 cm^3 tube. Monomer, mercury compound, metallic salt and solvent were placed in the tube which was cooled to −78 °C and thawed thrice with nitrogen and sealed under vacuum. After the tube had been shaken in a thermostat at 85 °C for 6 hr, the contents of the tube were poured into a large amount of methanol to precipitate the polymer.

TABLE 1. POLYMERIZATION OF VINYL MONOMERS INITIATED WITH DM-Hg
(metallic salt 1.5×10^{-5} mol, DM-Hg 0.1 ml, monomer 5 ml; 85 °C, 6 hr)

Group	Salts	H_2O (ml)	Conversion (%) MMA	AN	St
1[a]	0	0	0.7	trace	4.6
	0	3	1.0	trace	4.2
2	$CuCl_2\cdot2H_2O$	0	2.4	1.2	5.3
	$CuCl_2\cdot2H_2O$	3	7.3	7.1	6.7
3	$FeCl_3\cdot6H_2O$	0	0	1.4	0.5
	$FeCl_3\cdot6H_2O$	3	11.3	7.6	7.1
4	NaCl	3	4.2	trace	4.4
	$NiCl_2\cdot6H_2O$	0	1.0	trace	4.8
	$NiCl_2\cdot6H_2O$	3	1.2	trace	4.8
	CuCl	3	1.9	trace	5.3
	$FeCl_2\cdot nH_2O$	3	0.6	trace	5.2
	$SnCl_4\cdot nH_2O$	3	4.5	trace	4.5
	$CrCl_3\cdot6H_2O$	3	0.4	0.2	5.0
	$HgCl_2$	3	2.0	3.5	4.8

a) Blank experiments

Results and Discussion

Polymerization in the Presence of Metallic Salt and Water. The effects of metallic salt and water on the polymerization of MMA, AN and St are given in Table 1. It can be seen that cupric chloride and ferric chloride in groups 2 and 3 are active promoters for the polymerization of MMA and AN, the presence of water being necessary. NaCl, $NiCl_2$, $SnCl_4$, $CrCl_3$, $HgCl_2$ and the lower valency salts of iron and copper(group 4) can not be regarded as promoters in such small amount as 1.5×10^{-5} mol.

Effect of Amount of Water on Polymerization. In order to confirm the effect of water on the polymerization of MMA initiated with DM–Hg and Cu(II)-ion, polymerization was carried out, varying the amount of water and keeping the amounts of DM–Hg and MMA constant. The results are shown in Fig. 1. It was confirmed that the presence of water is indispensable.

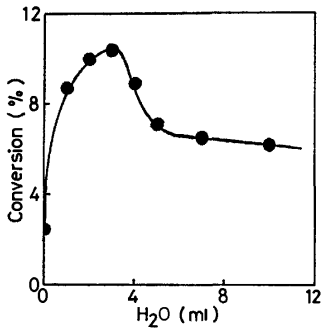

Fig. 1. Effect of the amount of water on the polymerization of MMA.
MMA 5 ml, DM-Hg 0.1 ml, Cu(II)-ion 1.5×10^{-5} mol; 85 °C, 6 hr

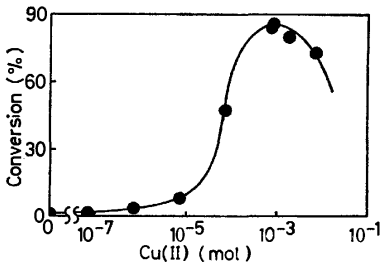

Fig. 2. Effect of the amount of Cu(II)-ion on the polymerization of MMA.
MMA 5 ml, DM-Hg 0.1 ml, H_2O 3 ml; 85 °C, 6 hr

Effect of Amount of Metallic Salt on Polymerization. Keeping the amounts of water and monomer constant and varying the amount of cupric chloride, the polymerization of MMA was carried out at 85 °C for 6 hr (Fig. 2).

Maximum conversion was attained at 1.3×10^{-3} mol of Cu(II)-ion. 0.1 ml of DM–Hg corresponds to 1.28×10^{-3} mol, *viz.*, maximum conversion was obtained when the molar quantity of DM–Hg was equal to that of Cu(II)-ion. This suggests that the initiation proceeds through the bimolecular reaction of DM–Hg with Cu(II)-ion. No formation of a complex of DM–Hg with Cu(II)-ion could be observed from its electronic spectrum.

Excess Cu(II)-ion might act as an inhibitor of the propagation by the following reaction:

$$\cdots\cdots M\cdot + CuCl_2 \rightarrow \cdots\cdots M\text{-}Cl + CuCl$$

Proof of the Radical Mechanism. In order to confirm the radical mechanism of the polymerization, the copolymerization of St and MMA was carried out (Fig. 3).

Determination of Initiating Radical Species. We have assumed that the initiating species is the methyl radical from DM–Hg. If this is the case, the methyl radical should be captured TPV and become colorless methyl-TPV.

2.56×10^{-3} mol (2 ml) of DM–Hg, 1.4×10^{-3} mol (2.16 g) of $CuCl_2\cdot2H_2O$, 9.57×10^{-4} mol (0.300 g) of TPV and 8 ml of benzene were placed in a tube, evacuated, sealed and warmed at 85 °C for 2 hr under shaking. The content turned almost colorless from a deep green. The reacted system was fractionated into three portions: Residue, Fractions I and II (Fig. 4).

Fraction I: Recrystallization of Fraction I from methanol gave pale yellow powder-like crystals (0.21 g). mp 138—139 °C, mol wt 328.6 (by VPO-method, using benzene as a solvent at 37 °C); *cf.* the values by Kuhn and Trischmarm,[5] mp of methyl-TPV 138—139 °C, mol wt of methyl-TPV 328.4.

Found: C, 76.89; H, 6.12; N, 16.99%.

Calcd for $C_{21}H_{20}N_4$: C, 76.80; H, 6.14; N, 17.06%.

The yield (0.21 g) corresponds to 6.39×10^{-4} mol of methyl-TPV, corresponding to 67% of the theoretical value. IR-spectrum of TPV showed no definite absorption of C=N at 1660 cm^{-1} by resonance of π-electrons. Fraction I had a strong absorption of νC=N at 1660 cm^{-1}.

Fraction II: Fraction II gave white plate crystals. By successive recrystallization from methanol and water. Yield 2.41 g; mp 170—171 °C; mol wt 251.4 (VPO). The reported melting point of chloromethylmercury (MC–Hg) is 170 °C[6] and its mol wt 251.5. The mixed melting point of the crystals with an authentic sample was also 170—171 °C. Thus Fraction II was found to be consistent with MC–Hg.

Residue: The residue, yellow green, was washed thoroughly with benzene, methanol and water, yield 1.23 g. Its solution in dilute aqueous nitric acid gave a white precipitate of AgCl with $AgNO_3$ solution. The washed residue contained 76.36% copper.

Calcd for CuCl: Cu, 79.88%; calcd for $CuCl_2$: Cu, 41.68% Thus the residue mainly consists of cuprous chloride.

The reaction was thus concluded to proceed as follows:

$$(CH_3)_2Hg + CuCl_2 \longrightarrow \underset{\text{(MC-Hg)}}{CH_3HgCl} + CuCl + \cdot CH_3$$
$$\text{(DM-Hg)}$$

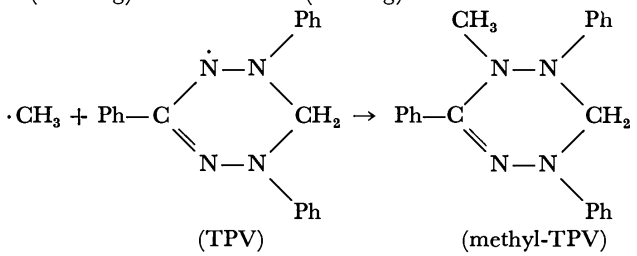

It can be concluded that the initiating species is the methyl radical.

Polymerization of MMA with MC–Hg and Cu(II)-ion. 5 ml of MMA, 1.5×10^{-5} mol of $CuCl_2\cdot2H_2O$, 0.2 g of MC–Hg and 3 ml of water were shaken under vacuum at 85 °C for 6 hr to obtain a trace of poly-MMA. MC–Hg is thus found to be unable to initiate the polymerization of MMA, even in the presence of cupric chloride and water.

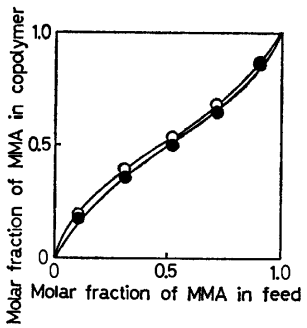

Fig. 3. Composition curves in the copolymerization of MMA with St.
Monomer 5 ml, DM-Hg 0.1 ml, H_2O 3 ml; 85 °C, 3 hr
○: Cu(II)-ion 1.5×10^{-5} mol
●: Fe(III)-ion 1.5×10^{-5} mol

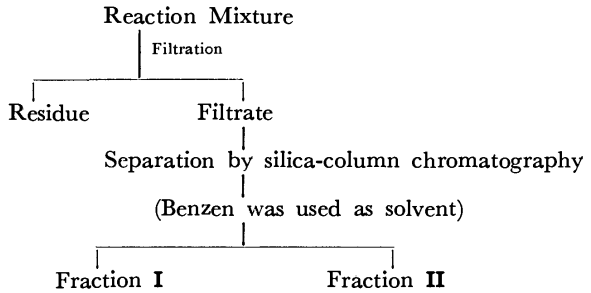

Fig. 4. Separation of products obtained from the reaction of DM-Hg with Cu(II) and TPV.

References

1) Part 326: T. Ouchi, T. Nishimura, M. Imoto *Kobunshi Ronbunshi*, Subimitted.
2) M. M. Koton, *Dokl. Akad. Nauk. SSSR*, **88**, 991 (1953).
3) S. Inoue, J. Furukawa, T. Tsuruta, *Kogaku Kagaku Zasshi*, **63**, 2046 (1960).
4) G. A. Razubaev, A. V. Ryabov, V. A. Solova, G. A. Voskoboink, *Tr. Khim. Khim Tekhnol.*, **1962**, 78.
5) R. Kuhn, H. Trischmann, *Monatsh. Chem.*, **95**, 457 (1964).
6) Kinkikagaku Kogyo Kai Yukikinzoku Bukai, "Yukikinzoku Handbook", Asakura Shoten (1967), p. 796.

A-Substituted 5β-Steroids. VII. The Polyhalogenation of 5β-Cholestan-2-one

J. Yasuo SATOH, C. Akira HORIUCHI, and Akira HAGITANI

Department of Chemistry, St. Paul's (Rikkyo) University, Nishi-Ikebukuro, Toshima-ku, Tokyo 171

(Received September 5, 1974)

The polyhalogenation of 5β-cholestan-2-one (I) in acetic acid containing hydrogen halide occurs in this positional order: $C_1 \rightarrow C_3 \rightarrow C_3$ and finally at C_1, which has the largest steric hindrance. The tetrahalogenation of the ketone (I) yields 1,1,3,3-tetrachloro-5β-cholestan-2-one (IXb), but fails to give the tetrabromo derivative; rather, it yields 1β,3,3-tribromo-5β-cholestan-2-one (Va), 1,1,3-tribromo-5β-cholest-3-en-2-one (VIIIa), and 1β,3-dibromo-5β-cholest-3-en-2-one (VIa). The conformations of the dihalo-, the trihalo-, and the tetrachloroketone derivatives are discussed in connection with the ORD, CD, IR, and NMR spectra.

Although the halogenation of most 5α-steroids[1] which possess an oxo group on each position in Ring A has been thoroughly investigated, only very little information on 5β-steroids is found in the literature, and even this concerns only the bromination of 3-oxo-5β-steroids.[2] We reported earlier that the monohalogenation of 2-oxo-5β-steroids affords the 1β-halo-2-oxo-5β-steroids[3] in good yields.

In this paper, we would like to discuss the positional order of the halogens introduced, and the conformation of the haloketones produced by the polyhalogenation of 5β-cholestan-2-one.

Results and Discussion

The dibromination of 5β-cholestan-2-one (I) in acetic acid in the presence of hydrogen bromide gave the dibromo Compound A (mp 182—185 °C) and, from the filtrate, the dibromo Compound B (mp 155—156 °C). Compound A was epimerized by treatment with hydrogen bromide in acetic acid at room temperature to the stable Compound B. These dibromo derivatives showed shifts of the carbonyl absorption (+3 and +18 cm^{-1} respectively) compared with that of the parent ketone (I) in their IR spectra. The NMR spectra also showed a multiplet at τ 5.6—5.8, with a small half-band width ($W/2$= 12 Hz) with an equatorial character, and at τ 4.20, with a large half-band width ($W/2$=20 Hz) of an axial character due to the C_3HBr. From these facts, the structures of the two dibromoketones were confirmed to be 1β,3β-dibromo-(IIIa) and 1β,3α-dibromo-5β-cholestan-2-one (IVa) respectively.

On the other hand, the dichlorination of 5β-cholestan-2-one (I) gave the dichloroketone (IVb) (mp 128—129 °C). This product was presumed to be 1β,3α-dichloro-5β-cholestan-2-one from the sign of the Cotton effect, Δ[A]*-, and the $\Delta\lambda_1$**-values (+192 and +12 nm respectively compared with 5β-cholestan-2-one) in the ORD spectrum, the shift of the C=O stretching band (1745 cm^{-1}) in the IR spectrum, and the signal (τ 4.70, $W/2$=20 Hz) due to the C_3HCl in the NMR spectrum.

Also, by tlc, it was confirmed that, when a solution of bromine was slowly added to the ketone (I) in acetic acid containing hydrogen bromide to effect dibromination, 1β-bromoketone (IIa) was formed first, and then the dibromoketones.

Thus, these results show that, as was previously reported for the monohalogenation[3] of the ketone (I), in the case of dihalogenation also the halogen enters first at the C_1β-bond, and then at the C_3β-bond. The 1β,3β-dibromo derivative thus produced is epimerized to a more stable 1β,3α-dibromo derivative.

On the basis of these data, we shall now discuss the conformation of the dihaloketones. It is considered, from the shifts in the C=O absorption (+18 for IVa and +33 cm^{-1} for IVb) compared with the ketone (I) in the IR spectra and from the pattern of the NMR spectra, that 1β,3α-dihaloketones (IV) exists as a chair conformation. This is supported by the signs of the Cotton effect, Δ[A]*-(+248 for IVa and +192 for IVb) and the $\Delta\lambda_1$**-values (+13 and +12 nm respectively) in ORD. Further, it is generally presumed that, if the A ring assumes a chair conformation, the ORD curve of 1β,3β-dibromoketone (IIIa) exhibits a negative sign of the Cotton effect, in accordance with the Octant rule.[4] However, the ORD data (Δ[A]*: +93 compared with 5β-cholestan-2-one) of this compound are unusual in view of this presumption. Hence, it is considered that this compound (IIIa) prefers a deformed conformation because of the 1 : 3-interaction between the C_1β-Br and the C_3β-Br. This was supported by showing the half-band width ($W/2$=12 Hz) due to the C_3–H and also by the shift of C=O ($\Delta\nu$: +2 cm^{-1}) compared with that of 5β-cholestan-2-one in the IR spectrum.

In order to determine the position of the third halogen in the trihalogenation of 5β-cholestan-2-one (I), the ketone (I) was treated with 3 M bromine in acetic acid. The reaction mixture was then chromatographed on silica gel. Elution with *n*-hexane–benzene (10 : 1) gave the tribromoketone (Va) (mp 157—158 °C). It was determined to be 1β,3,3-tribromo-5β-cholestan-2-one by means of its NMR spectrum, which shows a singlet at τ 4.47 and no proton signal due to the C_3HX. The second fraction, eluted with the same solvent, gave the 1β,3α-dibromo derivative (IVa), while the last fraction, eluted with the same solvent, gave the unsaturated dibromoketone (VIa), which shows absorptions at 1708 (C=O) and 1611 cm^{-1} (C=C) in its IR spectrum, as the main product. The NMR spectrum of VIa showed a singlet at τ 5.31 due to the proton at C_1, and a doublet at τ 3.12 due to the vinyl proton. Therefore, the derivative (VIa) was presumed to be 1β,3-dibromo-5β-cholest-3-en-2-one, which is formed by the elimination of hydrogen bromide from the 1β,3,3-tribromo derivative (Va). It was then demonstrated that the trichlorination of 5β-

* Molar dispersion contribution of the substituent.

** The difference (nm) between the first extremum of the derivative and that of the parent ketone.

cholestan-2-one gave 1β,3,3-trichloro-5β-cholestan-2-one (Vb).

From these results, it was concluded that the trihalogenation occurs at the C_3 position.

On the basis of the CD, ORD, and IR spectral data for Va and Vb (Δ[A]*: −57, Δ[θ]: −98, $\Delta\lambda_1$**: +14 nm, $\Delta\nu$: +42 cm^{-1} and Δ[A]*: −62, Δ[θ]: −37, $\Delta\lambda_1$**: +14 nm, $\Delta\nu$: +31 cm^{-1}), it is considered that the conformation in the A ring of the trihaloketone is a considerably distorted boat form.

In a previous paper[5], we reported that 1β-halo-5β-cholestan-2-one (II) can not change to the 1α-isomer, probably because of the 1 : 3-interaction between the C_1-equatorial bond and the C_9–C_{11} bond. Also, the steric hindrance at the C_3-position is considerably less than that at C_1, and its position has mobility. Consequently, the halogen in the 1β-haloketone rearranges to the allylic position.

In order to study the introduction of the fourth halogen at the position, which has a large steric hindrance, the ketone (I) was allowed to react with 4 M bromine in acetic acid containing hydrogen bromide at 20 °C for 48 hr. The reaction product did not give the tetrabromo derivative; rather, it yielded 1β,3,3-tribromoketone (Va) as the main product. This reaction at 85 °C for 1 hr gave 1β,3,3-tribromoketone (Va) and the unsaturated tribromoketone (VIIIa), showing absorptions at 1708 (C=O) and 1602 cm^{-1} (C=C) in its IR spectrum. The NMR spectrum of VIIIa also showed a doublet (J=3.0 Hz) due to the vinyl proton. From these data, the unsaturated ketone (VIIIa) was presumed to be 1,1,3-tribromo-5β-cholest-3-en-2-one (VIIIa).

Under the same conditions, the chlorination of the ketone(I) yielded 1,1,3,3-tetrachloro-5β-cholestan-2-one (IXb). This structure was determined from the fact that no signal due to the CHX appeared in the NMR spectrum.

From the ORD, CD, and IR spectral data, it can be considered that the conformation of IXb in the A ring preferred a form that was considerably distorted and had no eclipsed conformation between the C_1β-X bond and the C_{10}–Me bond, as in the case of the trihaloketone, no 1 : 3-interaction between the C_1α-X bond and the C_9–C_{11} bond, and no 1 : 3-interaction between the C_1–X bond and the C_3–X bond.

It is considered that this difference in the bromination and the chlorination has the following causes: in the case of the tetrabromo derivative, a possible explanation is that there is a large steric hindrance between the axial bromines at the C_1 and C_3 positions, and between the C_9–C_{11} bond and C_1–α bond, than those in the case of tetrachloro derivative. This consideration is supported by the experimental fact that the bromination of 1β,3-dibromo-5β-cholest-3-en-2-one which no longer has the 1 : 3-interaction between the axial bromine at the C_1 and C_3 positions, occurs at the C_1 position.

On the basis of these results, it was concluded that the polyhalogenation of 5β-cholestan-2-one (I) in acetic acid containing hydrogen halide occurs in this positional order: $C_1 \rightarrow C_3 \rightarrow C_3$, and finally at C_1, with the largest steric hindrance in the A ring.

Experimental

All the melting points are uncorrected. The IR, ORD, and CD spectra were measured using a Hitachi model 215 grating infrared spectrophotometer and two JASCO spectropolarimeters, models ORD/UV-5 and J-20, respectively. The NMR spectra were measured in carbon tetrachloride, with TMS as the internal standard, using a nuclear magnetic resonance spectrometer, Hitachi-Perkin Elmer R-20A.

Dibromination of 5β-Chlestan-2-one (I). I (1.0 g) in acetic acid (50 ml) was treated with bromine (0.91 g) in acetic acid (5 ml) containing a few drops of 48% hydrobromic acid at room temperature for 40 min. The reaction mixture was then taken up in ether, and the ether extracts were washed with a sodium hydrogen carbonate solution and water, dried, and evaporated. The crystallization of the residue from ethanol gave plates of IIIa (40 mg); mp 182—185 °C; IR (KBr): 1715 cm^{-1}; IR (CCl_4): 1716 cm^{-1}; ORD (c, 0.207, Di) at 21 °C: $[\alpha]_D$ +14°, $[\alpha]_{400}$ +125°, $[\alpha]_{356}$ +405° (peak), $[\alpha]_{325}$ 0° and $[\alpha]_{250}$ −935° (trough); CD (c, 0.207, Di) at 21 °C: $[\theta]_{325}$ +3465° (peak); NMR (CCl_4) τ: 5.67 (1H, s, C_1α-H) and *ca.* 5.6—5.8 (1H, m, $W/2$=12 Hz, C_3α-H). Found: C, 59.49; H, 7.93%. Calcd for $C_{27}H_{44}OBr_2$: C, 59.56; H, 8.14%.

From the mother liquor, recrystallization gave plates of IVa (360 mg); mp 155—156 °C; IR (KBr): 1730 cm^{-1}; IR (CCl_4): 1736 cm^{-1}; ORD (c, 0.190, Di) at 21 °C: $[\alpha]_D$ +105°, $[\alpha]_{400}$ +434°, $[\alpha]_{329}$ +2237° (peak), $[\alpha]_{300}$ +1868° (shoulder), $[\alpha]_{305}$ 0° and $[\alpha]_{283}$ −1947° (trough); CD (c, 0.169, Di) at 21 °C: $[\theta]_{308}$ +20610° (shoulder) and $[\theta]_{303}$ +21040° (peak); NMR (CCl_4) τ: 5.64 (1H, s, C_1α-H) and 4.20 (1H, m, $W/2$=20 Hz, C_3β-H). Found: C, 59.34; H, 8.08%. Calcd for $C_{27}H_{44}OBr_2$: C, 59.56; H, 8.14%.

Isomerization of 1β,3β-Dibromo-5β-cholestan-2-one (IIIa). IIIa (10 mg) in acetic acid (5 ml) was stirred with a few drops of 48% hydrobromic acid at room temperature for 15 hr. After the usual work-up, crystallization from ethanol afforded plates of IVa (6 mg); mp 155—156 °C.

Tribromination of 5β-Cholestan-2-one (I). I (800 mg) in acetic acid (40 ml) was treated with bromine (1.09 g) in acetic acid (4 ml) at room temperature. After 17 hr, decolorization was complete; the reaction mixture was then taken up in ether, and the ether extracts were washed with a sodium hydrogen carbonate solution and water, dried, and evaporated. The resultant oil (1.225 g) was chromatographed on silica gel (100 g). Elution with *n*-hexane-benzene (10 : 1) (400 ml) gave needles of Va (41 mg) from ethanol; mp 157—158 °C; IR (KBr): 1747 cm^{-1}; IR (CCl_4): 1756 cm^{-1}; ORD (c, 0.150, Di) at 19.5 °C: $[\alpha]_D$ +33°, $[\alpha]_{400}$ +87°, $[\alpha]_{373}$ 0°, $[\alpha]_{370}$ −6.7° (trough), $[\alpha]_{367}$ 0°, $[\alpha]_{324}$ +1223° (peak), $[\alpha]_{299}$ 0° and $[\alpha]_{281}$ −588° (trough); CD (c, 0.111, Di) at 22 °C: $[\theta]_{347}$ −2328° (trough), $[\theta]_{330}$ 0° and $[\theta]_{303}$ +5611° (peak); NMR (CCl_4) τ: 5.68 (1H, s, C_1α-H). Found: C, 52.03; H, 6.90%. Calcd for $C_{27}H_{43}OBr_3$: C, 52.03; H, 6.95%.

The next fraction, eluted by the same solvent (300 ml), on crystallization from ethanol gave needles of IVa (134 mg), while the last fraction, eluted with the same solvent (370 ml) and with benzene (400 ml), on crystallization from ethanol gave needles of VIa (287 mg); mp 186—189 °C; IR (KBr): 1695 and 1610 cm^{-1}; ORD (c, 0.220, Di) at 25 °C: $[\alpha]_D$ −20°, $[\alpha]_{400}$ −89°, $[\alpha]_{360}$ −282° (shoulder), $[\alpha]_{350}$ −341° (trough), $[\alpha]_{335}$ −150° (shoulder), $[\alpha]_{329}$ 0° and $[\alpha]_{280}$ +1592° (peak); CD (c, 0.164, Di) at 25 °C: $[\theta]_{338}$ −2330° (shoulder), $[\theta]_{328}$ −3174° (trough), $[\theta]_{320}$ −2667° (peak), $[\theta]_{316}$ −2755° (trough), $[\theta]_{290}$ 0° and $[\theta]_{264}$ +13070° (peak); λ^{D1}_{max} 260 nm (ε 4,900); NMR (CCl_4) τ: 5.31 (1H, s, C_1α-H) and 3.12

(1H, d, J=3.0 Hz, C_4-H). Found: C, 60.08; H, 7.77%. Calcd for $C_{27}H_{42}OBr_2$: C, 59.79; H, 7.80%.

Tetrabromination of 5β-Cholestan-2-one (I) at Room Temperature. A solution of I (800 mg) in acetic acid (40 ml) was treated with bromine (1.452 g) according to the procedure described for the tribromination of I. After the usual work-up, the resultant oil, on crystallization from ethanol, gave needles of Va (451 mg); mp 157—159 °C. After the crystallization filtrate had been evaporated *in vacuo*, the resultant oil (602 mg) was chromatographed on silica gel (80 g). Elution with *n*-hexane-benzene (9 : 1) (1350 ml) gave needles of Va (81 mg) from ethanol; mp 154—157 °C. The second fraction, eluted with the same solvent (800 ml), on crystallization from ethanol gave IVa (42 mg); the third fraction, eluted with *n*-hexane-benzene (5 : 1) (1750 ml), on crystallization from ethanol gave VIa (124 mg) (mp 186—189 °C).

Bromination of 1β,3-Dibromo-5β-cholest-3-en-2-one (VIa). The bromination of VIa was carried out using the technique described for the synthesis of the 1β-bromoketone.[3] After the usual work-up, the resultant oil was chromatographed on silica gel (10 g). Elution with *n*-hexane-benzene (1 : 10) (330 ml) and with benzene (300 ml) gave needles of VIIIa (19 mg) from ethanol; mp 84—86 °C; IR (KBr): 1708 and 1605 cm^{-1}; ORD (*c*, 0.169 Di) at 25 °C: $[\alpha]_D$ −44°, $[\alpha]_{400}$ −288°, $[\alpha]_{340}$ −616° (shoulder), $[\alpha]_{294}$ −2272° (trough), $[\alpha]_{284}$ 0° and $[\alpha]_{250}$ +7558° (peak); CD (c, 0.182, Di) at 25 °C: $[\theta]_{443}$ +469° (peak), $[\theta]_{394}$ 0°, $[\theta]_{347}$ −2203° (trough), $[\theta]_{320}$ 0°, $[\theta]_{303}$ +2711° (peak), $[\theta]_{294}$ 0° and $[\theta]_{269}$ −12200° (trough); λ_{max}^{Di} 266 nm (ε 3,800); NMR (CCl_4) τ: 3.22 (1H, d, J=3.0 Hz, C_4-H). Found: C, 52.43; H, 6.76 %. Calcd for $C_{27}H_{41}OBr_3$: C, 52.19; H, 6.65%.

Tetrabromination of 5β-Chlestan-2-one (I) at 85 °C. I (500 mg) in acetic acid (25 ml) was treated with bromine (908 mg) in the presence of 48% hydrobromic acid at 85 °C for 1 hr. After the usual work-up, the resultant oil (532 mg) was chromatographed on silica gel (100 g). Elution with *n*-hexane-benzene (10 : 1) (550 ml) gave needles of Va (77 mg) from ethanol (mp 154—157 °C). The next fraction, eluted with *n*-hexane-benzene (5 : 1) (600 ml), on crystallization from ethanol gave needles of VIIIa (98 mg) (mp 84—86 °C); the last fraction, eluted with *n*-hexane-benzene (3 : 1) (3200 ml), on crystallization from ethanol gave VIa (147 mg) (mp 186—189 °C).

Dichlorination of 5β-Cholestan-2-one (I). A mixture of I (2.0 g), chlorine gas (855 mg) in chloroform (10 ml), and acetic acid was carried out according to the procedure described for the synthesis of the 1β-chloroketone.[3] After the usual work-up, the resultant oil was chromatographed on silica gel (100 g). Elution with *n*-hexane gave plates of IVb (343 mg) from ethanol; mp 128—129 °C; IR (KBr): 1740 cm^{-1}; IR (CCl_4): 1737 cm^{-1}; ORD (*c*, 0.203, Di) at 26 °C: $[\alpha]_D$ +103°, $[\alpha]_{400}$ +370°, $[\alpha]_{328}$ +2069° (peak), $[\alpha]_{318}$ +1601° (shoulder), $[\alpha]_{304}$ 0°, $[\alpha]_{280}$ −1675° (trough); CD (*c*, 0.203, Di) at 26 °C: $[\theta]_{309}$ +12070° (peak), $[\theta]_{305}$ +11850° (trough) and $[\theta]_{302}$ +12070° (peak); NMR (CCl_4) τ: 5.65 (1H, s, $C_1\alpha$-H) and 4.20 (1H, m, $W/2$=20 Hz, $C_3\beta$-H). Found: C, 71.04; H, 9.36%. Calcd for $C_{27}H_{44}OCl_2$: C, 71.19; H, 9.73%. The next fraction, eluted with the same solvent (1300 ml), on crystallization from ethanol-acetone gave 1β-chloro-5β-cholestan-2-one (IIb) (253 mg) (mp 116—118 °C).[3]

Trichlorination of 5β-Chlestan-2-one (I). The trichlorination of I (800 mg) was carried out using the technique described for the synthesis of the 1β-chloroketone.[3] The resultant oil (1.01 g) was chromatographed on silica gel (100 g). From the first elution with *n*-hexane (2450 ml) and with *n*-hexane-benzene (5 : 1) (450 ml), Vb was obtained as needles (389 mg); mp 142—145 °C; IR (KBr): 1745 cm^{-1}; IR (CCl_4): 1745 cm^{-1}; ORD (*c*, 0.219, Di) at 19.5 °C: $[\alpha]_D$ −9.1°, $[\alpha]_{400}$ −37°, $[\alpha]_{330}$ −624° (trough), $[\alpha]_{322}$ −452° (peak), $[\alpha]_{318}$ −485° (trough), $[\alpha]_{310}$ 0° and $[\alpha]_{275}$ +1050° (peak); CD (*c*, 0.219, Di) at 19.5 °C: $[\theta]_{324}$ −2769° (trough), $[\theta]_{312}$ −5021° (trough), $[\theta]_{308}$ −4762° (peak) and $[\theta]_{302}$ −5242° (trough); NMR (CCl_4) τ: 5.68 (1H, s, $C_1\alpha$-H). Found: C, 66.02; H, 8.56%. Calcd for $C_{27}H_{43}OCl_3$: C, 66.18; H, 8.84%. The second fraction, eluted with *n*-hexane-benzene (1 : 1) (200 ml), on crystallization from ethanol gave plates of IVb (57 mg) (mp 128—129 °C).

Tetrachlorination of 5β-Cholestan-2-one (I). I (2.5 g) and concd hydrochloric acid (0.3 ml) in acetic acid (100 ml) were treated with chlorine gas in chloroform (10 ml) at 85 °C for 20 hr. After the usual work-up, the resultant oil (3.0 g) was chromatographed on silica gel (100 g); further treatment with *n*-hexane (500 ml) eluted a yellow oil, which, on crystallization from ethanol, gave needles of IXb (810 mg); mp 104—105 °C; IR (KBr): 1766 cm^{-1}; IR (CCl_4): 1765 cm^{-1}: ORD (*c*, 0.242, Di) at 19.5 °C: $[\alpha]_D$ +87°, $[\alpha]_{400}$ +253°, $[\alpha]_{332}$ +636° (peak), $[\alpha]_{304}$ 0° and $[\alpha]_{289}$ −178° (trough); CD (*c*, 0.242, Di) at 19.5 °C: $[\theta]_{311}$ 3537° (peak). Found: C, 61.66; H, 7.99%. Calcd for $C_{27}H_{42}OCl_4$: C, 61.84; H, 8.07%. The next fraction, eluted with the same solvent (2500 ml) and with *n*-hexane-benzene (7 : 3) (350 ml), on crystallization from ethanol gave needles of 1β,3-dichloro-5β-cholest-3-en-2-one (VIb) (56 mg); mp 147—149 °C; IR (KBr): 1700 and 1615 cm^{-1}; ORD (*c*, 0.096, Di) at 19.5 °C: $[\alpha]_D$ +41°, $[\alpha]_{460}$ 0°, $[\alpha]_{400}$ −131°, $[\alpha]_{364}$ −386° (shoulder), $[\alpha]_{360}$ −438° (trough), $[\alpha]_{353}$ −399° (peak), $[\alpha]_{345}$ −522° (trough), $[\alpha]_{335}$ −256° (peak), $[\alpha]_{322}$ −282° (trough), $[\alpha]_{324}$ 0°, $[\alpha]_{307}$ +418° (shoulder) and $[\alpha]_{274}$ +522° (peak); CD (*c*, 0.096, Di) at 19.5 °C: $[\theta]_{335}$ −2625° (shoulder), $[\theta]_{324}$ −3515° (trough), $[\theta]_{317}$ −2929° (peak) and $[\theta]_{313}$ −3046° (trough); λ_{max}^{Di} 251 nm (ε 6,700); NMR (CCl_4) τ: 5.48 (1H, s, $C_1\alpha$-H) and 3.40 (1H, d, J=2.5 Hz, C_4-H). Found: C, 70.63; H, 9.33%. Calcd for $C_{27}H_{42}OCl_2$: C, 71.50; H, 9.33%.

The authors are indebted to Mr. Takashi Takakuwa, Applied Research Laboratory of the Japan Spectroscopic Co., Ltd., for the measurement of the ORD and CD spectra, and to Mr. Tohru Miyasaka for collaboration in the experimental work.

References

1) a) H. P. Sigg and Ch. Tamm, *Helv. Chim. Acta*, **43**, 1402 (1960). b) C. W. Shoppee and S. C. Sharma, *J. Chem. Soc.*, **1968**, 245. c) C. W. Shoppee and T. E. Bellas, *ibid.*, **1963**, 3366. d) C. W. Shoppee and S. C. Sharma, *ibid.*, **1967**, 2385. e) C. W. Shoppee, R. E. Lack, and J. Scott, *ibid.*, **1962**, 2233. f) B. Ellis and V. Petrow, *ibid.*, **1953**, 3869. g) C. W. Shoppee and R. E. Lack, *ibid.*, **1961**, 3271.

2) C. W. Shoppee, A. B. Devine, and R. E. Lack, *ibid.*, **1965**, 6458.

3) a) J. Y. Satoh, C. A. Horiuchi, T. Matsukura, and A. Hagitani, This Bulletin, **41**, 3032 (1968). b) J. Y. Satoh, C. A. Horiuchi, and A. Hagitani, *ibid.*, **43**, 491 (1970).

4) W. Moffitt, R. B. Woodward, A. Moscowitz, W. Klyne and C. Djerassi, *J. Amer. Chem. Soc.*, **83**, 4013 (1961).

5) a) J. Y. Satoh, C. A. Horiuchi, and A Hagitani, *Chem. Lett.*, **1972**, 995. b) C. A. Horiuchi, *St. Paul's Rev. Sci.*, **3**, 73 (1973).

The Effects of Substituents and Solvents on the Structure of Fluorenyl and Cyclopentadienyl Salts

Masao TOMOI, Toshio YONEYAMA, and Hiroshi KAKIUCHI

Department of Applied Chemistry, Faculty of Engineering, Yokohama National University, Yokohama 233

(Received September 14, 1974)

The electronic spectra of 9-(ω-methoxyalkyl) and 9-(ω-dimethylaminoalkyl)fluorenyl salts of alkali cations were measured in ethereal solvents. The relative amounts of the contract ion pairs connected with the 9-substituents (R) decreased in this order: $R=(CH_3)_2N-(CH_2)_2->CH_3O-(CH_2)_2->CH_3O-(CH_2)_3->(CH_3)_2N-(CH_2)_3-\gg CH_3O-(CH_2)_4-\approx n\text{-}C_4H_9-$. This behavior was explained in terms of the formation of an intramolecular association between the hetero atoms in the substituents and the counter ions; such an association favored the formation of the contact ion pair. The interaction of magnesium fluorenide and cyclopentadienide with hexamethylphosphoramide (HMPA) was studied by means of NMR spectroscopy in ether or tetrahydrofuran. The fluorenide changed from a covalent type to a solvent-separated ion pair by the coordination of three HMPA with the magnesium. The cyclopentadienide was proposed to change from a contact ion pair to a solvent-separated ion pair by means of two-step process in which the cyclopentadienyl ions became successively separated from the magnesium ion.

It is well-known that donor solvents interact with organometallic compounds of alkali or alkaline earth metals and affect the structure or reactivity of the compounds.[1] For example, Hogen-Esch and Smid have reported that alkali fluorenides exist as two kinds of ion pairs—contact and solvent-separated ion pairs in ethereal solvents.[2] In previous papers,[3–5] it was shown that the reactivity of organo-magnesium compounds increased markedly in the presence of hexamethylphosphoramide (HMPA). Such phenomena can be explained in terms of the coordination of donor solvents with the metals of organometallic compounds. In this paper, the electronic spectra of 9-substituted fluorenyl salts of alkali cations, in which the substituents can interact with the cations, were measured in ethereal solvents in order to investigate the nature of the intramolecular association. The interaction of magnesium fluorenide and cyclopentadienide with HMPA was also studied by NMR spectroscopy.

The study of such interaction will be useful in accounting for the behavior of the anionic polymerization initiated with organometallic compounds of alkali or alkaline earth metals.

Experimental

Reagents. Six 9-substituted fluorenes were prepared by the reaction of fluorenylsodium with the corresponding alkyl halides[6,9] or by the base-catalyzed alkylation of fluorene with alcohols[7,8]: *n*-butyl-[8] (bp 127 °C/0.6 mmHg), 2-methoxyethyl-(bp 143 °C/0.5 mmHg. Found: C, 85.08; H, 7.44%. Calcd for $C_{16}H_{16}O$: C, 85.71; H, 7.14%), 3-methoxypropyl- (bp 135 °C/0.2 mmHg. Found: C, 84.90; H, 7.62%. Calcd for $C_{17}H_{18}O$: C, 85.71; H, 7.56%), 4-methoxybutyl- (bp 169 °C/1.5 mmHg. Found: C,85.00; H, 7.99%. Calcd for $C_{18}H_{20}O$: C, 85.71; H, 7.94%), 2-dimethylaminoethyl-[9] (bp 137 °C/0.5 mmHg), 3-dimethylaminopropyl-fluorene[9] (bp 154 °C/0.5 mmHg). The structure of these fluorenes was also confirmed by means of NMR spectroscopy. The tetrahydrofuran (THF), dimethoxyethane (DME), and *n*-hexane were refluxed and distilled over metallic sodium under a nitrogen atomosphere. The HMPA was refluxed and distilled over calcium hydride *in vacuo*.

The substituted fluorenyl salts of lithium, sodium, and potassium ions were prepared by the reaction of the corresponding fluorenes with *n*-butyllithium, sodium hydride or amide, and metallic potassium respectively. The magnesium fluorenide was prepared by the reaction of fluorene with diethylmagnesium in the presence of HMPA.[4] The dicyclopentadienylmagnesium was prepared from magnesium turnings and cyclopentadiene at about 500 °C.[10]

Spectroscopic Measurements. The samples for spectral measurements were prepared under a nitrogen atmosphere. The electronic spectra of the fluorenyl salts were recorded at room temperature by means of a Shimadzu UV-200 spectrophotometer, using 0.2-cm optical cells provided with a 0.18-cm spacer. The NMR spectra of the organo-magnesium-HMPA systems were taken on a JNM C-60H spectrometer, using benzene or tetramethylsilane as the internal standard.

Results and Discussion

Electronic Spectra of 9-Substituted Fluorenyl Salts of Alkali Cations. Figures 1 and 2 show the spectra of 9-substituted fluorenyllithiums in THF at room temperature. The peaks near 360 and 380 nm could be assigned to contact and solvent-separated ion pairs

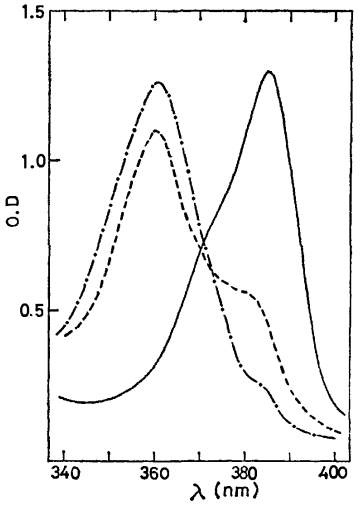

Fig. 1. Electronic spectra of 9-substituted fluorenyllithiums in THF at room temperature.
(——): 9-(*n*-butyl)fluorenyllithium,
(----): 9-(2-methoxyethyl)fluorenyllithium,
(·—·): 9-(2-dimethylaminoethyl)fluorenyllithium.

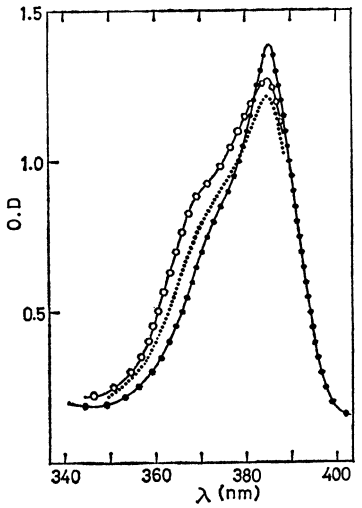

Fig. 2. Electronic spectra of 9-substituted fluorenyllithiums in THF at room temperature.
(-●-): 9-(4-methoxybutyl)fluorenyllithium,
(-○-): 9-(3-methoxypropyl)fluorenyllithium,
(·····): 9-(3-dimethylaminopropyl)fluorenyllithium.

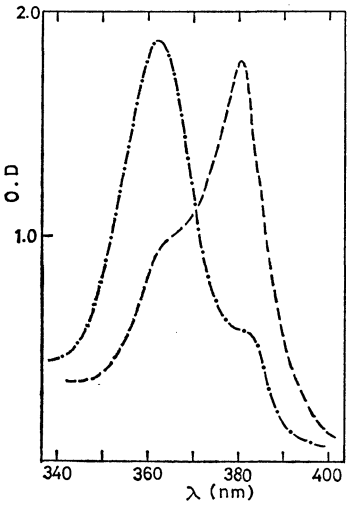

Fig. 3. Electronic spectra of 9-substituted fluorenyllithiums in DME at room temperature.
(----): 9-(2-methoxyethyl)fluorenyllithium,
(·—·): 9-(2-dimethylaminoethyl)fluorenyllithium.

respectively, by analogy with the results obtained by Chan and Smid.[11] The methoxyethyl and dimethylaminoethyl derivatives were found to yield higher fractions of contact ion pairs, while the other derivatives gave much higher fractions of solvent-separated ion pairs. Figure 3 shows the spectra of the methoxyethyl and dimethylaminoethyl derivatives with the lithium counter-ion in DME at room temperature. The former was predominantly present as a solvent-separated ion pair, while the latter was predominantly present as a contact ion pair. In a *n*-hexane–THF (1 : 1) mixture, the methoxypropyl derivative gave a higher fraction of a contact ion pair, while the *n*-butyl, methoxybutyl, and dimethylaminopropyl derivatives gave higher fractions of solvent-separated ion pairs. Consequently, the relative amounts of the contact ion pairs of the lithium salts due to the 9-substituents (R) decreased in the following order: R= $(CH_3)_2N-(CH_2)_2- > CH_3O-(CH_2)_2- > CH_3O-(CH_2)_3- > (CH_3)_2N-(CH_2)_3- \gg CH_3O-(CH_2)_4- \approx n\text{-}C_4H_9-$. A similar order was observed for the sodium and potassium salts.

Such an effect of substituents suggests that a special interaction between the counter ions and the oxygen or nitrogen of the substituents may take place because of the favorable position of the hetero atoms with respect to the cations. In the case of the methoxyethyl and dimethylaminoethyl derivatives, the hetero atom exists at a position where a five-membered ring can be formed by the intramolecular coordination of the atom with the counter ion. For example, the structure of a contact ion pair for the methoxyethyl derivative could be represented as in Formula (I): In this

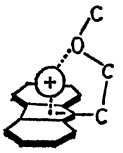

(I)

formula, the counter ion was assumed to be located over the aromatic ring, by analogy with the results on fluorenyllithium in THF.[12] In contrast, the X-ray analysis of fluorenyllithium as a tertiary amine complex has shown the lithium ion to be located above the plane, but outside the perimeter of the ring.[13] The intramolecular association as is shown in Formula (I) is, in any event, considered to take place easily and to favor the formation of a contact ion pair.

The observed order also shows that the formation of a contact ion pair becomes easier with a decrease in the size (n) of a ring, which is formed by intramolecular association— *i.e.*, in the order of $n=5>6>7$. Kuhn and Wires[14] have measured the equilibrium constant for the equilibrium between intramolecularly hydrogen bonded conformations and nonbonded conformations in the monomethyl ethers of ethylene glycol, propane-1,3-diol, and butane-1,4-diol: the constant became smaller with an increase in the number of carbon atoms between two oxygen atoms. The observed order for the fluorenyl salts is in good agreement with this order. This finding supports the presence of an intramolecular association such as has been described above.

The coordinating power of aliphatic nitrogen donors is generally stronger than that of aliphatic oxygen donors.[15] The difference between the dimethylaminoethyl and methoxyethyl derivatives, therefore, can be explained in terms of that in the coordinating power of the hetero atoms. However, the dimethylaminopropyl derivative gave fewer contact ion pairs than the methoxypropyl one. The formation of an intramolecular bonding must result in conformational changes, and thereby increase the repulsive interactions among atoms, groups, and bonds in the ring formed. Such interactions, which reduce the formation of a contact ion pair, may be stronger in the former derivative, which has two methyl groups, than in the latter, which has only one.

All the salts yielded higher fractions of solvent-separated ion pairs in ethereal solvents containing a small amount of HMPA. This fact suggests that the solvating power of HMPA is stronger than the intramolecular coordinating power of the hetero atoms.

Such an intramolecular solvation has also been proposed to account for the behavior of the anionic polymerizations of 2-vinylpyridine[16] and ω-methoxyalkyl methacrylate.[17]

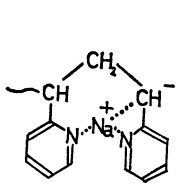

(II)

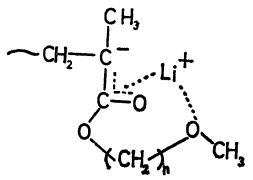

(III)

In the case of 2-vinylpyridine, (II), the nitrogens of both the ultimate and penultimate units have been considered to contribute to the coordination of the counter cation. Such a penultimate unit effect seems reasonable in view of the similarity of structure between (II) and 9-(3-dimethylaminopropyl)fluorenyl salt, in which six-membered rings formed by intramolecular coordination.

Ito *et al.*[17] have proposed that, in the case of the methacrylate, (III), the interaction of the methoxy oxygen in the substituent (R′) with the counter ion decreases with an increase in the number of carbon atoms between the oxygen and ester oxygen, so that the syndiotacticities of the polymers obtained in toluene increase in this order: $R'=CH_3O-(CH_2)_2- > CH_3O(CH_2)_3- > CH_3O-(CH_2)_4-$. This order is in agreement with that of the ease of formation of contact ion pairs for 9-(ω-methoxyalkyl)fluorenyl salts. Therefore, it is reasonable that the intramolecular association shown as Formula (III) is present in the propagation step of the anionic polymerization of these methacrylates.

Intraction of Magnesium Fluorenide with HMPA. Figure 4 shows the NMR spectrum of the magnesium fluorenide prepared by the reaction of fluorene with equimolar quantities of diethylmagnesium (Et_2Mg) at $[HMPA]/[Et_2Mg]=3$. This spectrum indicates that the fluorenide consists of equimolar amounts of fluorenyl and ethyl groups. The chemical shift of methylene protons, δ_{CH_2}, in the fluorenide was −1.10, while the δ_{CH_2} for Et_2Mg was −0.88 at $[HMPA]/[Et_2Mg]=3$.[4] This fact indicates that the diamagnetic anisotropy induced by the aromatic ring strongly shields the ethyl protones. The fluorenyl part of the NMR spectrum of the fluorenide was similar to that of fluorenyllithium in THF.[18,19] Consequently, the metalation results in the formation of ethylfluorenylmagnesium (Fl^-Mg^+Et) as follows:

$$\text{Fluorene}+Et_2Mg \xrightarrow{\text{HMPA}} Fl^-Mg^+Et+\text{Ethane}$$

The chemical shifts of the ethyl and fluorenyl ring protons for Fl^-Mg^+Et changed as is shown in Fig. 5 on the addition of Et_2Mg to the fluorenide solution. The chemical shift of the 9-proton for the fluorenide, δ_9, changed markedly with the molar ratio of HMPA to magnesium, [HMPA]/[Mg]. This fact indicates that the nature of the carbon–magnesium bond of the fluorenide is highly dependent on the [HMPA]/[Mg] ratio. The chemical shifts of the 9-proton for alkali fluorenides are between ~5.8 and ~6.0, and they are not appreciably affected by the variation in the counter ion and the solvent.[18,19] This behavior must correspond to the fact that the carbon–alkali bonds of alkali fluorenides are essentially ionic.[1d] On the other hand, the large shift in δ_9 (from ~4.9 to ~5.8) suggests that the carbon–magnesium bond of the magnesium fluorenide is essentially covalent in the absence of HMPA (see below) and that the bond changes to an ionic type in the presence of HMPA. The charge formed on the 9-carbon delocalizes over the aromatic ring; hence, the peaks due to the ring protons and 9-proton must shift upfield and downfield respectively. The fact that the values of δ_9 become approximately constant at $[HMPA]/[Mg] \geq \sim 3$ suggests that the ionic species are formed by the coordination of three HMPA molecules to the magnesium. Figure 6 shows the variation in the chemical shift of the methyl protons for HMPA with the [HMPA]/[Mg] ratio. The chemical shift was approximately constant (~2.0) at $[HMPA]/[Mg] < \sim 3$, and then it

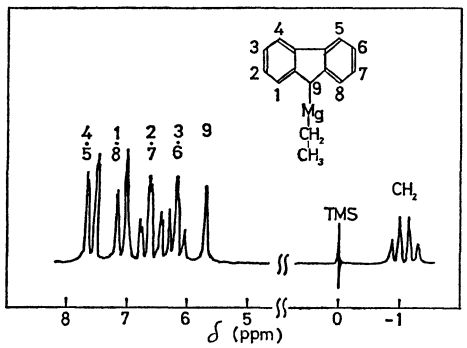

Fig. 4. NMR spectrum of magnesium fluorenide.
Solvent: ether, [HMPA]/[Mg]=3.
Peaks of ether, HMPA, and methyl group in Fl^-Mg^+-Et are not written in the figure.

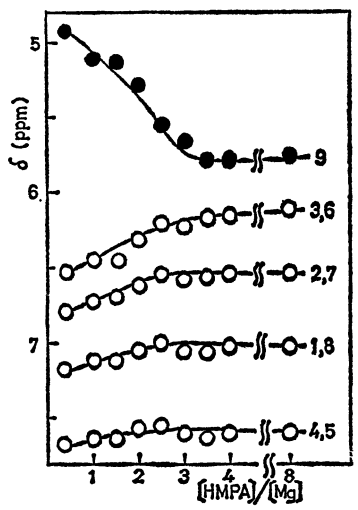

Fig. 5. Variation of chemical shifts for fluorenyl ring protons with [HMPA]/[Mg] ratio.
Numbers in the figure denote positions of the protons.

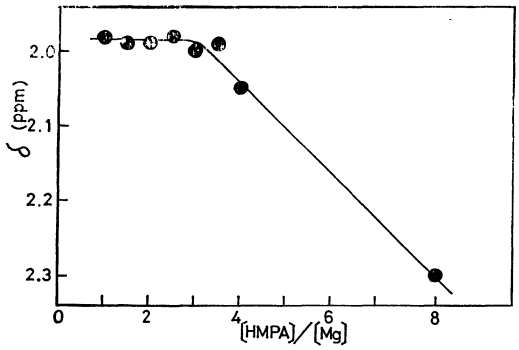

Fig. 6. Variation of chemical shift for HMPA with [HMPA]/[Mg] ratio.

shifted downfield with a further increase in the [HMPA]/[Mg] ratio, while the chemical shift for free HMPA was ~2.5. Those facts indicate that the diamagnetic anisotropy induced by the aromatic ring strongly shields the methyl protons of the HMPA coordinated with the magnesium; they also support the above concept of the formation of the ionic species.

This ionic species was confirmed to be a solvent-separated ion pair by a study of its electronic spectrum. However, the spectra of the magnesium fluorenide–HMPA systems, even at [HMPA]/[Mg]<3, had no peak near 340 nm, where the contact ion pair of the fluorenide is considered to have a characteristic peak by analogy with the results of barium and strontium fluorenides (347 and 344 nm respectively).[20,21] This finding suggests that magnesium fluorenide of a covalent type may change to a solvent-separated ion pair directly, not *via* a contact ion pair.

In the case of the interaction of HMPA with Et_2Mg, the species coordinated by two HMPA molecules was predominantly formed at [HMPA]/[Mg]>2, and the ionic species with the coordination of three HMPA was considered to be formed only slightly.[4] This behavior is in contrast to that in the case of the fluorenide. Such a difference can be explained in terms of that in the stabilities of the carbanions formed. That is to say, the fluorenyl anion, in which there is a resonance stabilization, must be formed more easily than the ethyl anion, in which there is no resonance stabilization.

Interaction of Dicyclopentadienylmagnesium with HMPA. The NMR spectrum of dicyclopentadienylmagnesium (Cp_2Mg) had a singlet peak in THF. The shape of the spectrum, however, varied upon the addition of HMPA to the Cp_2Mg solution (Fig. 7). The signal due to Cp_2Mg shifted upfield with an increase in the [HMPA]/[Mg] ratio when the ratio was less than ~1.5. A second peak began to appear at a lower field at [HMPA]/[Mg]=~2. The upfield peak shifted upfield with a further increase in the [HMPA]/[Mg] ratio, while the intensity of the peak decreased at the same time. In contrast, the intensity of the downfield peak increased and came to be almost equal to that of the upfield peak at [HMPA]/[Mg]=~3. The peaks gradually overlapped with a further increase in the HMPA concentration, and broadened at [HMPA]/[Mg]=~6. At [HMPA]/[Mg]>6, the spectrum had again a singlet peak, one between the previous peaks. The width of this peak decreased with an increase in the [HMPA]/[Mg] ratio. A similar phenomenon was observed for the variation in the spectrum with an increase in the temperature at a constant [HMPA]/[Mg] ratio. Figure 8 shows the variation in the spectrum at [HMPA]/[Mg]=3.3. These results indicate that, in the Cp_2Mg–HMPA system, several species coexist at equilibrium, one which is dependent on the [HMPA]/[Mg] ratio and the temperature.

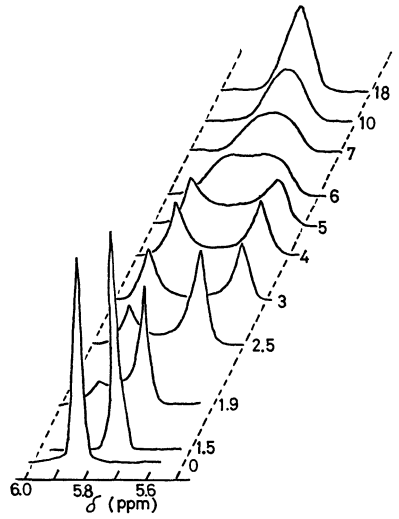

Fig. 7. Variation of NMR spectrum of Cp_2Mg with [HMPA]/[Mg] ratio.
Solvent: THF, Temp.: 22 °C.
Numbers in the figure denote values of [HMPA]/[Mg] ratio.

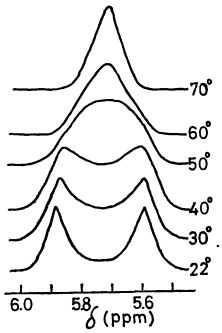

Fig. 8. Dependence of NMR spectrum of Cp_2Mg on temperature.
Solvent: THF, [HMPA]/[Mg]=3.3.

When Cp_2Mg and HMPA were mixed in ether at [HMPA]/[Mg]<~2.5, the solution separated into two layers. The spectrum of the lower portion of the solution had peaks for ether and two kinds of peaks for Cp_2Mg and HMPA (Fig. 9). The downfield peaks were assigned to free species of Cp_2Mg and HMPA, in comparison with the spectra of separate solutions of Cp_2Mg and HMPA. The upfield peaks of Cp_2Mg was found to shift upfield gradually with an increase in the HMPA concentration. The upfield peaks, therefore, were assigned to coordinated species

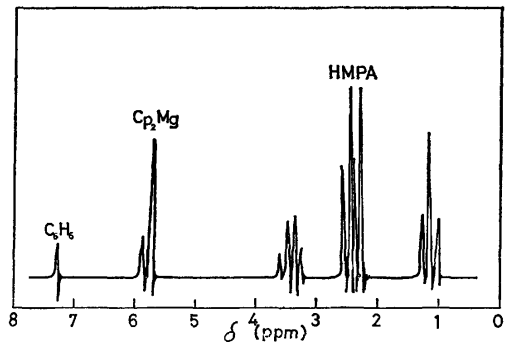

Fig. 9. NMR spectrum of Cp_2Mg in the presence of HMPA in ether.

of Cp_2Mg and HMPA. The unmber of HMPA molecules coordinated with magnesium was estimated from the intensity ratio of the upfield peaks of Cp_2Mg and HMPA; the number was ~1.6 when Cp_2Mg and HMPA were mixed at [HMPA]/[Mg]=2. This fact indicates that the upfield peak of Cp_2Mg is due to the Cp_2Mg coordinated with one or two HMPA molecules. When Cp_2Mg and HMPA were mixed in ether at 5>[HMPA]/[Hg]>~2.5, an ether-insoluble product was obtained. The precipitate, which was filtered, washed with ether, and dried under a vacuum, was found by acid-base titration to be a complex with the formula of $Cp_2Mg\cdot(HMPA)_{3.0-3.1}$. The NMR spectrum of this precipitate (THF-soluble) in THF had two kinds of peaks for Cp_2Mg, and the intensities were almost equal. This spectrum, moreover, was almost the same as that of the Cp_2Mg–HMPA mixture prepared directly in THF at [HMPA]/[Mg]=~3 (see Fig. 7). This finding suggests that the evolution of two peaks for Cp_2Mg in a THF–HMPA mixture is also due to the coordination of three HMPA molecules with the magnesium.

Consequently, the spectral change in the presence of HMPA is most likely to be due to the structural change in the Cp_2Mg ion pair, since Cp_2Mg has been considered to be an ion triplet in THF.[22] The change in the contact ion pair to the solvent-separated ion pair could be accounted for by the following scheme:

$$\underset{\text{(I)}}{\overset{\text{THF}}{\overset{\downarrow}{Cp^-, Mg^{2+}, Cp^-}\overset{\uparrow}{\text{THF}}}} + \text{HMPA} \rightleftharpoons \underset{\text{(II)}}{\overset{\text{THF}}{\overset{\downarrow}{Cp^-, Mg^{2+}, Cp^-}\overset{\uparrow}{\text{HMPA}}}} + \text{THF}$$

$$\text{(II)} + \text{HMPA} \rightleftharpoons \underset{\text{(III)}}{\overset{\text{HMPA}}{\overset{\downarrow}{Cp^-, Mg^{2+}, Cp^-}\overset{\uparrow}{\text{HMPA}}}} + \text{THF}$$

$$\text{(III)} + \text{HMPA} \rightleftharpoons Cp^-//\text{HMPA} \rightarrow \underset{\text{(IV)}}{\overset{\text{HMPA}}{\overset{\downarrow}{Mg^{2+}, Cp^-}\overset{\uparrow}{\text{HMPA}}}}$$

$$\text{(IV)} + m\text{HMPA} \rightleftharpoons \underset{\text{(V)}}{Cp^-//Mg^{2+} \leftarrow (3+m)\text{HMPA}//Cp^-}$$

It is reasonable to assume that Cp_2Mg exists as monomeric Species (I) coordinated with two THF molecules in THF, since other Grignard reagents and dialkylmagnesium compounds have been found to be monomeric in THF, even at concentrations>1 M.[23] Species (I) and also Species (II), which is coordinated by one HMPA and one THF, coexist at equilibrium at [HMPA]/[Mg]<1. When the [HMPA]/[Mg] ratio is between about unity and about two, Species (III), which is coordinated by two HMPA molecules, coexists with Species (II). The spectrum of Species (II) must have a singlet peak, since the two cyclopentadienyl rings of the species are equivalent. In the same manner, the spectrum of Species (III) must have a singlet peak different from that of Species (II) if the exchange between these species is slow. However, the fact that the chemical shift of Cp_2Mg changes continuously at [HMPA]/[Mg]<~2 suggests that the exchanges among Species (I), (II), and (III) are rapid at room temperature.

When the [HMPA]/[Mg] ratio is more than about two, Species (IV) coexists with Species (III), and the former becomes a predominant species at [HMPA]/[Mg]=~3. Species (IV), which is coordinated with three HMPA molecules, was concluded, by a comparison with the results for the magnesium fluorenide–HMPA complex (see the above section), to be an asymmetrically solvent-separated ion pair in which one of the cyclopentadienyl rings is separated from the magnesium ion. The two rings of Species (IV) are nonidentical; hence, the spectrum must have two singlet peaks if the exchange between the two rings is slow. Actually the spectral behavior at [HMPA]/[Mg]≥3 indicates that the exchange between the distinct rings is slow at room temperature on the NMR time scale, but becomes rapid with an increase in the temperature. On the basis of the spectral change with the [HMPA]/[Mg] ratio, the upfield and downfield peaks of Cp_2Mg at [HMPA]/[Mg]=~3 were assigned to the contact and the separated cyclopentadienyl rings respectively.

When the [HMPA]/[Mg] ratio is more than three, Species (IV) changes gradually to Species (V) by interaction with *m* molecules of HMPA. Species (V) is a symmetrically separated ion pair, in which two of the cyclopentadienyl rings are separated from the magnesium. This species has two identical rings; hence, the NMR spectrum must give a singlet peak. The spectral change at [HMPA]/[Mg]>3 can be explained by assuming that Species (V) is formed by the interaction of Species (IV) with three HMPA molecules; that is, the *m* in the equation is three. That is to say, the symmetrically separated ion pair of Cp_2Mg is formed by the interaction of Cp_2Mg with six HMPA molecules. Cp_2Mg was found to form a THF-insoluble complex with three octamethylpyrophosphoramide (OMPA) molecules. The coordination number of the magnesium ion is six since OMPA is a bidentate ligand. Magnesium perchlorate has also been reported to form a complex with three OMPA.[24] These results support the above concept. Such a two-step separation process has already reported in the case of fluorenylstrontium in THF when studied

by electronic spectroscopy.[21]

References

1) For leads into this field see: a) G. E. Coates, M. L. H. Green, P. Powell, and K. Wade, "Principles of Organometallic Chemistry", Methuen & Co. Ltd., London, (1968), Chapter III; b) M. Szwarc, "Carbanions, Living Polymers, and Electron-Transfer Processes", Interscience Publishers, New York, N.Y. (1968), Chapters V and VI; c) C. Agami, *Bull. Soc. Chim. Fr.*, **1970**, 1619; d) J. Smid, *Angew, Chem.*, **84**, 127 (1972).
2) T. E. Hogen-Esch and J. Smid, *J. Amer. Chem. Soc.*, **88**, 307 (1966).
3) M. Tomoi and H. Kakiuchi, *Kogyo Kagaku Zasshi*, **73**, 2367 (1970).
4) M. Tomoi and H. Kakiuchi, This Bulletin, **46**, 3233 (1973).
5) M. Tomoi and H. Kakiuchi, *Polym. J.*, **5**, 195 (1973).
6) E. J. Greenhow, E. N. White, and D. McNeil, *J. Chem. Soc.*, **1951**, 2848.
7) S. S. Hirsch, D. H. Lorenz, and E. I. Becker, *J. Org. Chem.*, **23**, 1829 (1958).
8) K. L. Schoen and E. I. Becker, *J. Amer. Chem. Soc.*, **77**, 6030 (1955).
9) J. A. King, R. I. Meltzer, and J. Doczi, *ibid.*, **77**, 2217 (1955).
10) W. A. Barber, "Inorganic Syntheses", Vol. VI, p. 11 (1960).
11) L. L. Chan and J. Smid, *J. Amer. Chem. Soc.*, **90**, 4654 (1968).
12) a) J. A. Dixon, P. A. Gwinner, and D. C. Lini, *ibid.*, **87**, 1379 (1965); b) R. H. Cox, H. W. Terry, Jr., and L. W. Harrison, *ibid.*, **93**, 3297 (1971).
13) J. J. Brooks, W. Rhine, and G. D. Stucky, *ibid.*, **94**, 7339 (1972).
14) L. P. Kuhn and R. A. Wires, *ibid.*, **86**, 2161 (1964).
15) a) H. H. Freedmann, *ibid.*, **83**, 2900 (1961); b) T. Kagiya, Y. Sumida, and T. Inoue, This Bulletin, **41**, 767 (1968).
16) M. Fischer and M. Szwarc, *Macromolecules*, **3**, 23 (1970).
17) T. Ito, K. Aoshima, F. Toda, K. Uno, and Y. Ikawara, *Polym. J.*, **1**, 278 (1970).
18) R. H. Cox, *J. Phys. Chem.*, **73**, 2649 (1969).
19) J. B. Grutzner, J. M. Lawlor, and L. M. Jackman, *J. Amer. Chem. Soc.*, **94**, 2306 (1972).
20) T. E. Hogen-Esch and J. Smid, *ibid.*, **91**, 4580 (1969).
21) T. E. Hogen-Esch and J. Smid, *ibid.*, **94**, 9240 (1972).
22) W. T. Ford, *J. Organometal, Chem.*, **32**, 27 (1971) and references therein.
23) F. W. Walker and E. C. Ashby, *J. Amer. Chem. Soc.*, **91**, 3845 (1969) and references therein.
24) M. D. Joesten, M. S. Hussain and P. G. Lenhert, *Inorg. Chem.*, **9**, 151 (1970).

Syntheses and Properties of Crosslinked Ferrocene Polymers

Mamoru OMORI, Masayasu KURONO* and Seishi YAJIMA

The Oarai Branch, The Research Institute for Iron, Steel and Other Metals, Tohoku University, Oarai, Ibaraki-ken, 311-13

**Ono Research Institute, 3-1-1 Sakurai, Simamoto-Cho, Mishima-Gun, Osaka, 618*

(Received September 19, 1974)

The polycondensation reaction of acetylferrocene and furfural was investigated in the presence of concentrated H_2SO_4 as a catalyst without solvent. Stoichiometric reaction took place with 2 mol of acetylferrocene and 5 mol of furfural. Polycondensation afforded satisfactory results when 1 mol of acetylferrocene was treated with 2—7 mol of furfural. The structural evidence for these products was derived from chemical and infrared analyses. Density, micro Vickers hardness, magnetic susceptibility, and thermal behavior of these products were measured in comparison with those of other resins.

In recent years efforts have been made to obtain polymers with properties differing from those of conventional organic polymers, the ultimate objective being polymers with better electrical and magnetic properties with abrasion resistance, thermal stability and opaqueness to certain types of radiation. Organometallic compounds have been suggested as starting materials for the synthesis of these polymers; they have been polymerized by means of various procedures.[1] The organometallic polymer is expected to have properties characteristic of both organic compounds and metals, since it contains a metal as the organometallic complex. Ferrocene ($C_{10}H_{10}Fe$) is stable against acid and base, and easily undergoes aromatic substitution reactions.[2] Synthetic studies of ferrocene polymers have been carried out in the past two decades.[3] Emphasis was placed on soluble products possessing linear chain structures. However, very few attempts have been made to synthesize crosslinked ferrocene polymers (resins).[4-7]

From ferrocene, iron atoms are released by heat treatment above 400°C and then coagulate to metallic iron.[8] In the case of ferrocene resins, iron atoms would be also released from ferrocene skeletons by heat treatment. It appears that the released iron atoms do not coagulate and are isolated in the form of atoms or ultra-fine particles above room temperature due to networks of the resins. The preparation of metal atoms was reported by Barrett *et al.*[9,10] An inert gas and vapourized metal were condensed on a Be disk at liquid helium temperature, iron atoms being frozen into an inert gas matrix. The isolated iron atoms could only be present near liquid helium temperature. Preparation of ultra-fine particles of metals and their compounds has been sought by Mulay *et al.*[11,12]

Our studies deal with the synthesis of resins containing ferrocene. Reports were given on the preparation of free iron atoms or ultra-fine particles of an iron metal by pyrolysis of the ferrocene resin.[13,14] The resin used was synthesized by polymerization of furfural (II) and a ferrocene derivative. Furfural (II) was polycondensed with acetone.[15] Acetylferrocene (I) is considered to serve as a ketone derivative of ferrocene for the polycondensation. Acetylferrocene (I) was polycondensed with various proportions of furfural (II) in the presence of concentrated sulfuric acid. The structure of the synthetic resin was elucidated by chemical and infrared spectroscopic analyses. Density, micro Vickers hardness and magnetic susceptibility were measured and thermal behavior was observed.

Experimental

Materials. Polycondensation was carried out with acetylferrocene, furfural and concentrated sulfuric acid. Ferrocene was synthesized according to the method given by Hata *et al.*[16] Acetylferrocene was prepared by reacting ferrocene with acetic anhydride in anhydrous dichloromethane.[17] It was then purified by recrystallization from *n*-hexane and sublimation *in vacuo*; mp 85—86 °C (Ref. 17, 85—86 °C). Furfural was redistilled prior to use; bp 67—68 °C/20 mmHg. Concentrated sulfuric acid (reagent grade) was used.

Preparation of Resins. Concentrated sulfuric acid which was used for the preparation of furfural-acetone resins was used as the catalyst of polycondensation.[15] Polycondensation temperature was fixed at 45 °C, since low temperature is preferable for preventing the decomposition of ferrocene skeletons by acid. Acetylferrocene was dissolved in furfural in a test tube. Concentrated sulfuric acid was added to this solution at certain wt% of acetylferrocene and furfural. The reaction mixtures were stirred and then heated at 45 °C for a certain period of time. After polycondensation, synthetic resins were dried *in vacuo* at room temperature and then heated up to 100 °C for 24 hr in order to remove volatile materials.

Elemental Analysis and Measurement of Properties. Iron determination was carried out with a Hitachi-207 atomic absorption spectrophotometer. IR spectra were measured with a Nihonbunko Jasco IR-S grating IR spectrometer using potassium bromide disks. Apparent densities were calculated from the weight and size of resins. Micro Vickers hardness was measured with an Akashi Model MVK Type D instrument with a load of 200 g. Magnetic susceptibility was recorded on a Shimadzu MB-10A magnetic balance. A helical spring microbalance was used for thermogravimetric analysis (TGA), the heating rate being 2 °C/min. Powdered samples with initial weight of 100 mg were used, the determination being performed *in vacuo* (1×10^{-3} mmHg).

Results and Discussion

Polycondensation Reaction and Resin Structure. The results are summarized in Tables 1—3. Polycondensation seems to be affected by experimental conditions. Effects of (a) amount of a catalyst and (b) the length of reaction time were investigated using a mixture of 1 mol of acetylferrocene and 5 mol of furfural. Forty-hour polycondensation data are given in Table 1 for (a),

Table 1. Effect of amounts of H_2SO_4 on polycondensation[a)]

Amounts of Concd H_2SO_4 (wt%)	Yield (wt%)	Density (g/cm³)	Elemental analysis (wt%)			Furfural (mol) / Acetylferrocene (mol)
			Fe	C	H	
2	58.5	1.42	11.7	65.52	4.03	2.81
3	81.6	1.41	9.55	65.02	4.13	3.93
4	83.9	1.43	9.08	64.01	3.77	4.16
5	82.7	1.40	8.71	64.24	3.75	4.46
6	85.2	1.40	8.64	63.96	3.81	4.48

a) Acetylferrocene; 1 mol, furfural; 5 mol, time; 40 hr, temperature; 45 °C.

Table 2. Effect of reaction time on polycondensation[a)]

Reaction time (hr)	Yield (wt%)	Density (g/cm³)	Elemental analysis (wt%)			Furfural (mol) / Acetylferrocene (mol)
			Fe	C	H	
6	71.7	1.45	10.8	62.62	4.10	2.99
11	72.4	1.44	10.2	63.19	4.15	3.36
20	76.9	1.43	9.97	63.27	3.97	3.50
40	83.9	1.43	9.08	64.01	3.77	4.16
72	82.2	1.40	9.05	64.84	3.83	4.26
96	85.0	1.43	8.80	63.82	3.82	4.34
137	83.4	1.40	8.28	64.31	3.95	4.71

a) Acetylferrocene; 1 mol, furfural; 5 mol, concd H_2SO_4; 4 wt%, temperature; 45 °C.

Table 3. Effect of different ratios of acetylferrocene and furfural on polycondensation[a)]

Samples	Acetyl-ferrocene (mol)	Furfural (mol)	Yield (wt%)	Density (g/cm³)	Elemental analysis (wt%)			Furfural (mol) / Acetylferrocene (mol)
					Fe	C	H	
2-Resin	1	2	93.1	1.43	12.2	64.98	4.29	2.55
3-Resin	1	3	89.3	1.43	11.6	64.50	4.29	2.77
5-Resin	1	5	83.9	1.43	9.08	64.01	3.77	4.16
7-Resin	1	7	74.5	1.43	7.85	63.12	4.02	5.08
10-Resin	1	10	61.6	1.02	7.51	62.50	3.95	5.34
12-Resin	1	12	55.4	0.878	6.87	60.72	3.32	5.82
15-Resin	1	15	52.2	0.758	6.28	60.18	3.35	6.51

a) Concd H_2SO_4; 4 wt%, time; 40 hr, temperature; 45 °C.

The yields of resins were constant when more than 3% of the catalyst was used, their density being independent of the amount of the catalyst. Molar ratios of furfural to acetylferrocene (F/A) in resins could be calculated from elemental analyses of carbon, hydrogen and iron contents. The molar ratios of F/A increased with the amount of catalyst. The effects of the reaction time were investigated with 4% catalyst (Table 2). Yields of resins were approximately constant when polycondensation was continued for 40 hr or longer. The density of resins was independent of the reaction time. The molar ratios of F/A in resins increased with an increase in the reaction time. The behavior of polycondensation was considered to be influenced by the molar ratios of F/A in starting materials. The influence was investigated under experimental conditions where the catalyst was 4% and reaction time was 40 hr. In Table 3, the notation of resins shows the number of moles of furfural per mole of acetylferrocene in the starting materials. No resins were formed when the concentration of the acetylferrocene component was reduced to below 15 of F/A. Yield of resins decreased in proportion to the decrease in acetylferrocene. The density of resins was invariable for 2- to 7-Resins, but reduced rapidly for 10- to 15-Resins. The molar ratio of F/A in the resin of the 2-Resin was greater than that in the starting material. For other resins, the relation between the molar ratios of the starting material and the resin was reversed. The stoichiometry of polycondensation was thus considered to be as follows. In the case of the 2-Resin, excess acetylferrocene not capable of reacting with furfural was removed. On the other hand, furfural in the starting material of the 3-Resin was more than enough to react with acetylferrocene. The excess furfural was removed, but what remained might have become partially incorporated into resins according to the progress of polycondensation. Thus, the stoichiometry of polycondensation was decided to be a reaction of 2 mol of acetylferrocene and 5 mol of furfural (2-Resin). The mechanism of the stoichiometric reaction was estimated on the chemical reactivities of acetylferrocene and furfural. Furfural could not be subject to polycondensation without the

presence of other compounds.[15] Furfuryl alcohol has been established to be a versatile polymer precursor.[18] Thus, if furfural is converted into the form of furfuryl alcohol in the course of polycondensation process, the polycondensation reaction would successfully proceed to give resin. The initial step in polycondensation involves 1 mol of acetylferrocene and 2 mol of furfural to undergo aldol condensation and Friedel-Crafts reactions to yield oligomer (III). The oligomer was in the form of furfuryl alcohol containing four reaction points (1, 2, 3, 4); with further reactions with each other and 1 mol of furfural, it produces polymers (IV), as shown in Fig. 1. The polymer was reactive with

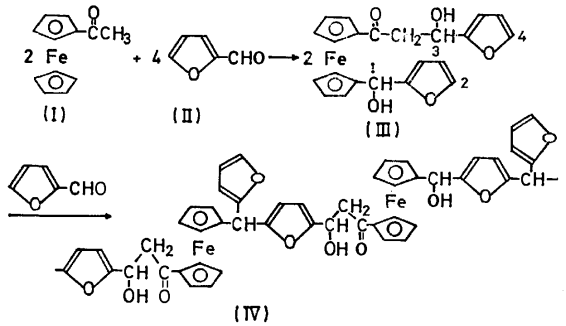

Fig. 1.

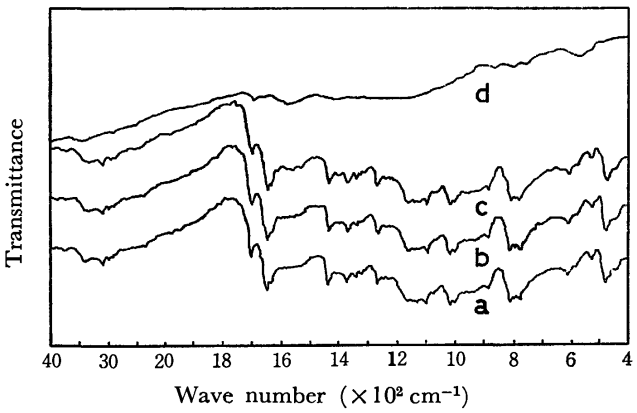

Fig. 2. IR spectra of 2-Resin, the heat-treated at various temperatures; (a) 2-Resin, (b) 200 °C, (c) 300 °C, (d) 400 °C.

TABLE 4. IR BANDS OF 2-RESIN AND THEIR ASSIGNMENTS

Absorption band (cm^{-1})	Assignment	Reference
3080	Ferrocene C-H stretching	19
2930 2850	Aliphatic C-H stretching	20
1655	νC=O of ferrocenyl ketone	21
1445	δCH of methylene or methyl	20
1375	δCH of methyl	20
1160	Furan	22
1103	In-plane bending of ferrocene C-H	23
1017	C-O-C Vibration	22
818	Out-of-plane bending of ferrocene C-H	23
780	Out-of-plane bending of furan C-H	22
478	Ring metal stretching of ferrocene	19

furfural or became crosslinked with each other, after removal of hydroxy groups.

The IR spectrum of the 2-Resin, shown in Fig. 2, exhibited absorption bands at 3080, 2930, 2850, 1700, 1655, 1445, 1375, 1273, 1160, 1103, 1017, 818, 780, and 478 cm^{-1}. Assignments of all bands except for those at 1700 and 1273 cm^{-1} were referred to those of ferrocene polymers available in literature (Table 4). The 1700 cm^{-1} band corresponded to one of the absorption bands in the IR spectrum of furfural.[24] It is therefore considered to be due to a ketone conjugated with a furan ring (furyl ketone). The 1273 cm^{-1} band would be assigned to the acetylated cyclopentadienyl ring since this absorption band was observed in the IR spectrum of acetylferrocene[25] but not in that of ferrocene.[19] Rosenblum and Woodward reported that two bands near 1000 and 1100 cm^{-1} indicated the presence of unsubstituted cyclopentadienyl rings.[26] In the case of the 2-Resin, unsubstituted cyclopentadienyl rings were not contained in its structure because of the lack of the 1000 cm^{-1} band of those bands in the resin. Results of IR spectrum studies are in accord with the structure (IV) of the 2-Resin predicted here. However, its actual structure might partially deviate from structure (IV) owing to the effect of the furyl ketones and the acetylated cyclopentadienyl rings remaining in the structure. For 3-Resin to 15-Resin, the excess furfural which exceeded the stoichiometric composition in the starting material would be expected to lead to a Diels-Alder addition reaction in furyl side-groups of the polymer structure (IV)[22] and a substitution reaction with the hydroxyl groups. Thus, structures of these resins were considered to decrease in crosslinkages. Holliday suggested that the connection number is useful in describing crosslinkages and it can be derived from the density of the polymer.[27] From the relationship between density and connection number, 1.43 density was found to correspond to 2.3 (connection number). Since the maximum connection number is 2.5 for CH polymer, 2.3 shows a considerably high value of crosslinkages. Low density of 10- to 15-Resins as compared to other resins corresponded to the decrease in crosslinkages. The densities of 2- to 7-Resins were higher than those of phenolic novolac resins.[28]

Micro Vickers Hardness. Micro Vickers hardness measurements were carried out for the mechanical properties of resins. The values of hardness were approximately the same for 2-Resin to 7-Resin. The hardness of 10-Resin to 15-Resin decreased with the decrease in density. A linear relationship was obtained between hardness and density (Fig. 3). Close packed resins (2- to 7-Resins) are assumed to have high hardness characteristics. Hardness of these resins was similar to that of phenolic novolac and melamine resins.[29]

Magnetic Properties. Magnetic susceptibilities of 2-Resin, 5-Resin and 15-Resin are given in Table 5. The observed values of magnetic susceptibility were all positive and of the order of 10^{-6} irrespective of iron content. The paramagnetism should be discussed in connection with the structure of resins since the magnetic susceptibility of ferrocene has been reported

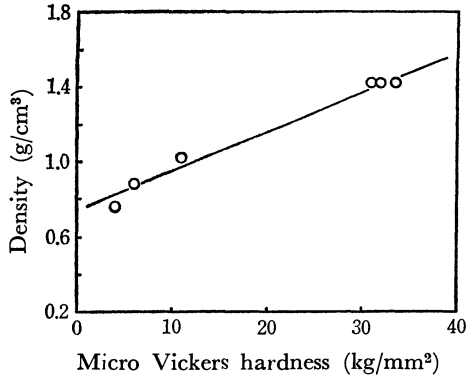

Fig. 3. Relation between density and micro Vickers hardness of resins.

Table 5. Magnetic susceptibility of the resins at 20 °C

Samples	χ_g cgs units
2-Resin	2.91×10^{-6}
5-Resin	2.74×10^{-6}
15-Resin	2.88×10^{-6}

to be $\chi_a=-99.0\times10^{-6}$ cgs units.[30] Kalimov and Shchegolev demonstrated that the products can be converted from paramagnetic into diamagnetic with the use of paramagnetic ferrocene polymers[31] described by Nesmeyanov *et al.*[32] Since the present specimens could not be purified because of insolubility, the paramagnetism does not seem to arise from the structure of the resins; instead, it might be related to magnetic contaminants. However, it is evident that no ferromagnetic iron compounds are contained in the resins.

Thermal Behavior. Structural changes of resins were investigated by means of IR spectroscopy. IR spectra of heat-treated 2-Resin (200 and 300 °C) do not differ from those of 2-Resin (Fig. 2). From the IR spectrum of 2-Resin heat-treated at 400 °C, we see that the structure was decomposed on heating at 400 °C. This structural change corresponded to carbonization of resins, since carbonization of organic compounds starts near 400 °C.[33] Thermal behavior was investigated by means of a thermobalance. The thermograms of resins, heated up to 800 °C, are shown in Fig. 4. The weight losses were remarkable above 300 °C for 2- to 7-Resins and above 100 °C for 10- to 15-Resins. Residues at the end of thermogravimetric analysis are given in Table 6. The reduced residues are derived by subtraction of the amounts of iron from the residues. The residues of 2- to 7-Resins differ from each other, but no difference is seen in their reduced residues. In the case of 10- to 15-Resins, no such difference was observed in the reduced residue. Thermograms and reduced residues of 2- to 7-Resins are similar to those of phenolic novolac resins.[34] We see that the thermal behavior of the resins was not affected by the presence of iron. It is known that the residues of organic polymers heat-treated above 600 °C increase with the formation of crosslinkages.[35] A decrease in reduced residues of 10- to 15-Resins as

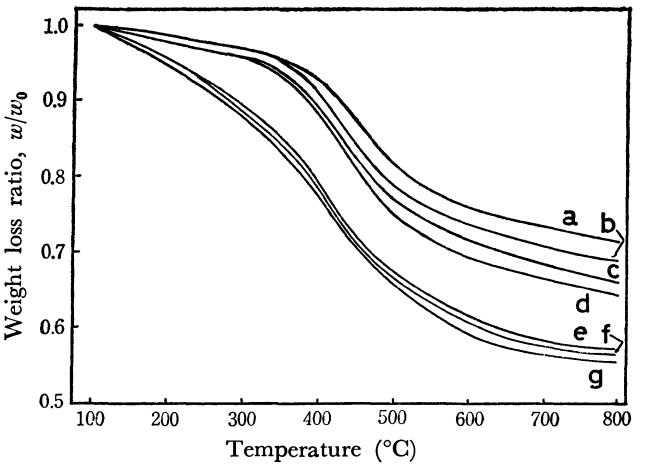

Fig. 4. Thermograms for resins; (a) 2-Resin, (b) 3-Resin, (c) 5-Resin, (d) 7-Resin, (e) 10-Resin, (f) 12-Resin, (g) 15-Resin.

Table 6. Residue and reduced residue of the resins heat-treated at 800 °C

Samples	Residue (wt%)	Fe in residue (wt%)	Reduced residue[a] (wt%)
2-Resin	71.4	19.1	52.3
3-Resin	69.0	16.9	52.1
5-Resin	66.0	13.8	52.2
7-Resin	64.3	13.0	51.3
10-Resin	57.3	12.1	45.2
12-Resin	56.4	11.5	44.9
15-Resin	55.4	9.40	46.0

a) Reduced residue=Residue-Amounts of Fe.

compared with 2- to 7-Resins is considered to correspond to the decrease in crosslinkages. Thermograms of 10- to 15-Resins show that the decrease of their reduced residues mainly results from the weight loss at low temperatures (100—300 °C).

The authors would like to thank Dr. T. Hirai, Tohoku University, for valuable suggestions. Thanks are also due to Mr. T. Shoji and Mrs. H. Arai, Tohoku University, for their assistance in iron and CH analyses.

References

1) Ed. by F. G. R. Gimblett and K. A. Hodd, *Inorg. Macromol. Rev.*, **1**, Nos. 1 and 2 (1970), No. 3 (1971), No. 4 (1972).

2) M. Rosenblum, "Chemistry of Iron Group Metallocenes", Part 1, ed. by D. Seyferth, John Wiley & Sons Inc., New York (1965).

3) E. W. Neuse, "Advances in Macromolecular Chemistry", Vol. 1, ed. by W. M. Pasika, Academic Press, London (1968), p. 1.

4) N. Bilow and H. Rosenberg, *J. Polym. Sci., Part A-1*, **7**, 2689 (1969).

5) N. Bilow, A. L. Landis, and H. Rosenberg, *ibid*, **7**, 2719 (1969).

6) A. Gal, M. Cais, and D. H. Kohn, *J. Appl. Polym. Sci.*, **15**, 1571 (1971).

7) E. W. Neuse, *J. Mater. Sci.*, **7**, 708 (1972).

8) B. Ya. Andreev, L. M. Dyagileva, and G. I. Feklisov, *Dokl. Akad. Nauk SSSR*, **158**,, 1348 (1964).
9) T. K. McNab, H. Micklitz, and P. H. Barrett, *Phys. Rev. B*, **4**, 3787 (1971).
10) H. Micklitz and P. H. Barrett, *Appl. Phys. Lett.*, **20**, 387 (1972).
11) D. W. Collins and L. N. Mulay, *J. Amer. Ceram. Soc.*, **54**, 69 (1971).
12) A. W. Thompson, P. L. Walker, Jr., and L. N. Mulay, "Amorphous Magnetism", Proceedings of the international symposium on amorphous magnetism, ed. by H. O. Hooper and A. M. de Graaf, Plenum Press, New York-London (1973), p. 111.
13) S. Yajima and M. Omori, *Chem. Lett.*, **1972**, 843.
14) S. Yajima and M. Omori, *ibid.*, **1974**, 277.
15) K. J. Siegfried, "Encyclopedia Polymer Science and Technology", Vol. 7, ed. by H. F. Mark, N. G. Gaylord and N. M. Bikales, John Wiley & Sons, Inc., New York (1967), p. 432.
16) K. Hata, I. Motoyama, and H. Watanabe, This Bulletin, **38**, 853 (1965).
17) C. R. Hauser and J. K. Lindsay, *J. Org. Chem.*, **22**, 482 (1957).
18) J. B. Barr and S. B. Wallon, *J. Appl. Polym. Sci.*, **15**, 1079 (1971).
19) E. R. Lippincott and R. D. Nelson, *Spectrochim. Acta*, **10**, 307 (1958).
20) K. Nakanishi, "Infrared Absorption Spectroscopy", Nankodo Co., Tokyo (1962).
21) T. Asahara, M. Seno, K. Mitsuhashi, and Y. Ichikawa, This Bulletin, **44**, 207 (1971).
22) E. W. Neuse, K. Koda, and E. Carter, *Makromol. Chem.*, **84**, 213 (1965).
23) C. U. Pittman, Jr., *J. Polym. Sci., Part A-1*, **5**, 2927 (1967).
24) IRDC Card, No. 5408, Nankodo Co., Tokyo.
25) H. Imai, *Kagaku*, **25**, 430 (1970).
26) M. Rosenblum and R. B. Woodward, *J. Amer. Chem. Soc.*, **80**, 5443 (1958).
27) L. Holliday, *J. Appl. Polym. Sci.*, **12**, 333 (1968).
28) "Goseijushi Binran", ed. by S. Iwai, Sangyotosho Co., Tokyo (1973).
29) S. Yamaguchi and F. Masuda, *Zairyoshiken*, **11**, 18 (1962).
30) L. N. Mulay and M. E. Fox, *J. Chem. Phys.*, **38**, 760 (1973).
31) A. N. Nesmeyanov, V. V. Korshak, V. V. Voevodskii, N. S. Kochetkova, S. L. Sosin, R. B. Materikova, T. N. Bolotnikova, V. M. Chibrikin, and N. M. Bazhin, *Dokl. Akad. Nauk SSSR*, **137**, 1370 (1961).
32) Yu. S. Karimov and I. F. Shchegolev. *ibid.*, **146**, 1370 (1962).
33) J. D. Brooks and G. H. Taylor, "Chemistry and Physics of Carbon", Vol. 4, ed. by P. L. Walker, Jr., Marcel Deckker, Inc., New York (1968), p. 243.
34) J. B. Nelson, "Nasa Technical Note", NASA TN D-3919 (1967).
35) E. L. Winkler and J. A. Parker, "Reviews in Macromolecular Chemistry", Vol. 6, ed. by G. B. Butler, K. F. O'Driscoll, and M. Shen, Marcel Deckker, Inc., New York (1971), p. 245.

Photosensitized Polar Addition of Acetic Acid to 4-Homoadamantene: The Behavior of the 4-Homoadamantyl Cation*

Ryohei YAMAGUCHI and Mituyosi KAWANISI

Department of Industrial Chemistry, Faculty of Engineering, Kyoto University, Yoshida, Sakyo-ku, Kyoto 606

(Received October 3, 1974)

The photosensitized polar addition of acetic acid to 4-homoadamantene (I) gave 2,4-dehydrohomoadamantene (II), 2-adamantylmethyl acetate (IIIa), and 4-homoadamantyl acetate (IVa). The same treatment of I in pivalic acid gave analogous products, II, 2-adamantylmethyl pivalate (IIIb), and 4-homoadamantyl pivalate (IVb). It was shown that II and III were derived from the 4-homoadamantyl cation (V). On the other hand, the diazotization of 4-homoadamantylamine (XV) in the presence of acetic acid gave I, II, and IVa, whereas it has been reported that a buffered acetolysis of 4-homoadamantyl tosylate (XIV) gave I and IVa, but not II. The formation of II may be explained by assuming a different energy state of V of different origin; it proves a vibrationally excited nature of V generated in the photosensitized polar addition reaction.

The photochemical incorporation of protic solvents into 6- and 7-membered cycloalkenes in the presence of BTX (aromatic hydrocarbon sensitizer) has been extensively investigated.[1] We ourselves have reported that the chemically reactive species in the reaction of photosensitized polar addition to *cis*-cyclooctene was *trans*-cyclooctane[2] and that a carbocation was the intermediate in the photosensitized polar addition to bicyclo[3.3.1]non-2-ene system, a bridged cyclooctene, since a novel intramolecular hydride shift was observed.[3]

On the other hand, the behavior of carbocations of cage compounds has attracted considerable attention in the field of carbocation chemistry.[4] The behavior of the 4-homoadamantyl cation (V) has been studied in three different ways—solvolysis of 4-homoadamantyl tosylate (XIV),[5,6] the treatment of 4-homoadamantene (I) with Lewis acid,[7] and the treatment of I or 4-homoadamantanol (VIII) with concentrated sulfuric acid in the presence of pentane.[8] In this paper, we wish to report on the behavior of V, which is generated by the photosensitized polar addition of acetic acid to I[9] and by diazotization of 4-homoadamantylamine (XV).

Results and Discussion

A solution of I in acetic acid containing benzene or xylene as a sensitizer was irradiated in a quartz vessel by means of a medium-pressure mercury arc; three products were detected by glc analysis: 2,4-dehydrohomoadamantane(II), 2-adamantylmethyl acetate (IIIa), and 4-homoadamantyl acetate (IVa).[10] A similar reaction of I in pivalic acid gave II, 2-adamantylmethyl pivalate (IIIb), and 4-homoadamantyl pivalate (IVb). The results are summarized in Table 1.

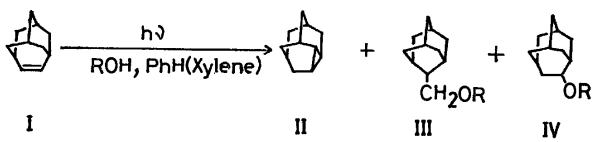

Formula 1.

Table 1. Irradiation of I in protic solvents[a]

	R	Conversion[b] (%)	Products ratio[b] II(%)	III(%)	IV(%)
a	Ac	62	40	8	52
b	*t*-BuCO	46	63	9	28

a) Irradiated at room temperature for 7 day.
b) Determined by glc (PEG 20 M, 160 °C).

The structures of the products were confirmed by comparison with the corresponding authentic samples. No product other than II, III, and IV was detected by glc or NMR analyses. The ratio of II in the reaction with pivalic acid was larger than that in the reaction with acetic acid, probably because of the bulkiness of pivalic acid.

The following observations confirm that the presence of a proton source is indispensable for the isomerization of I into II. (a) When the irradiation of I in an xylene or benzene solution was effected without a proton source—*i.e.*, acetic acid or pivalic acid, no isomerization of I into II was observed. (b) The irradiation of I in xylene containing a small amount of methanesulfonic acid as a proton source did induce the isomerization of I into II. (c) When I was irradiated in AcOD containing xylene, the resulting II contained one deuterium (41% d_1 by mass spectroscopic analysis). The above observations, as well as the diazotization of XV (*vide infra*), prove that II is produced *via* 4-homoadamantyl cation (V).

In order to ascertain that III was produced from V by rearrangement, the photochemical reaction was effected in AcOD. The resulting deuterated compound (III-d_1) was reduced by lithium aluminum hydride to give deuterated 2-adamantylmethanol (IX-d_1). The mass spectra of IX-d_1 and an authentic

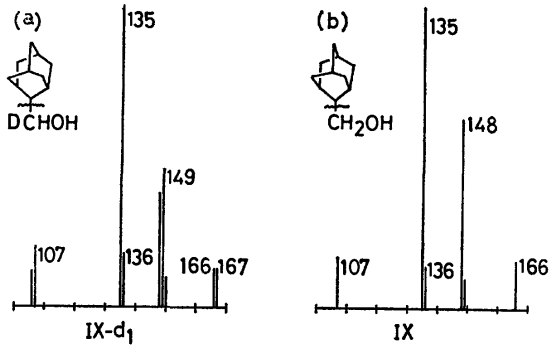

Fig. 1. Mass spectra of IX-d_1 and IX

2-adamantylmethanol (IX) are depicted in Fig. 1.

As is shown in Fig. 1a, IX-d_1 contains one deuterium (49% d_1). The base peak at *m/e* 135 in Fig. 1b is characteristic of the adamantyl skeleton. The fact that the intensity of the peak at *m/e* 136 in Fig. 1a is almost the same as that in Fig. 1b implies that deuterium is not located on the adamantyl skeleton, but on the α-carbon atom. These results shows that V must rearrange into the 2-adamantylmethyl cation (VI) through a simple Wagner-Meerwein rearrangement (Path A) or into a non-classical cation (VII) (Path B), which subsequently gives III due to the nucleophilic trapping of the solvent (Scheme 1). In our experiments it is still not clear which pathway (A or B) the rearrangement proceeds through, although we feel that Path B is more likely because a simple primary carbocation appears to be energetically inaccessible under usual reaction conditions.[7,11,18b]

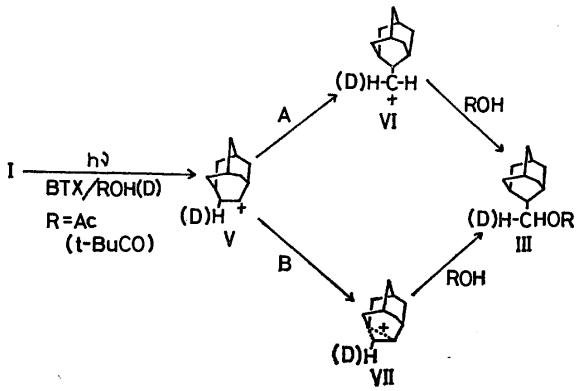

Scheme 1.

It has been proposed that a photosensitized polar addition of protic solvents to 6—8 membered cycloalkenes proceeds through the following sequences:[1-3] (i) the BTX sensitized photo-induced *cis-trans* isomerization of olefins,[12] (ii) protonation to the strained *trans*-olefins producing cycloalkyl cations, and (iii) nucleophilic trapping by the protic solvents, deprotonation to other olefins (*i.e.*, exocyclic olefins), and the regeneration of the starting olefins. Since I is regarded as a bridged cycloheptane, it is highly probable that the present reaction proceeds through the same sequences.[13] Consequently, the corresponding cycloalkyl cation is the 4-homoadamantyl cation (V).

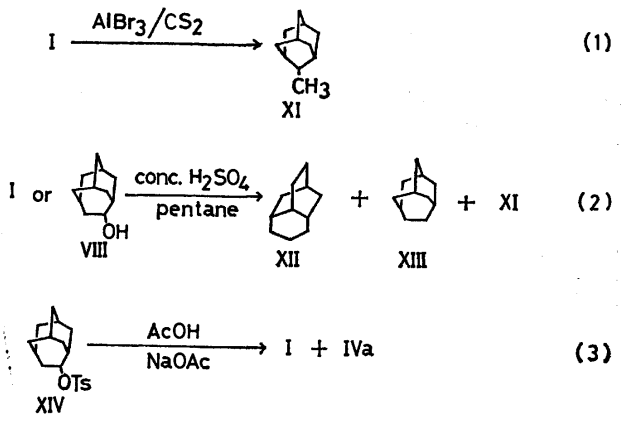

Scheme 2.

As to the behavior of V, there have been several reports, as has been mentioned above. The treatment of I with Lewis acid gave a single product, 2-methyladamantane (XI)[7] (Scheme 2, Eq. 1), while the reaction of I or 4-homoadamantanol (VIII) with concentrated sulfuric acid in the presence of pentane gave 4-homoisotwistane (XII), homoadamantane (XIII), and XI[8] (Scheme 2, Eq. 2). Furthermore, the buffered acetolysis of 4-homoadamantyl tosylate (XIV) gave I and IVa[5,6] (Scheme 2, Eq. 3).

The photochemical reaction and the buffered acetolysis are kinetically controlled,[15] while the adamantane rearrangement (Scheme 2, Eqs. 1 and 2) is thermodynamically controlled. However, differences were observed in the reaction products between the photochemical reaction and the acetolysis. These differences can be explained by assuming a vibrationally excited nature of V generated in the photosensitized polar addition reaction.[16] In order to support this assumption, we have examined the diazotization of 4-homoadamantylamine (XV), since it has been suggested that a "hot" ("highly energetic" or "poorly solvated") carbocation is formed from the diazonium ion and that it is different from the "normal carbocation" formed during solvolysis.[17]

The diazotization of XV was effected in two different ways. A compound, 3-(4-homoadamantyl)-1-phenyltriazene (XVI), was prepared from XV by a conventional method and decomposed with acetic acid (Method A), and isopentyl nitrite was used in the direct diazotization of XV (Method B). The results are summarized in Table 2.

The products, I, II, and IVa, were identical with the respective authentic samples in glc retention time, mass, and IR spectra. Every reaction mixture contained I, II, and IVa, but IIIa could not be detected by glc analysis. On the other hand, as has been mentioned above, it has been reported that no II was

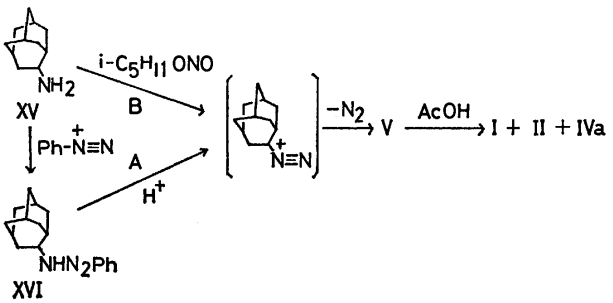

Formula 2.

Table 2. Diazotizations of XV

Method	Sovent	AcOH	Temp.	Time (hr)	Products ratio (%)[a]		
					I	II	IVa
A	AcOH	excess	room temp.	1	31	20	49
A	PhH	1 eq.	room temp.	12	35	37	28
B	AcOH	excess	room temp.	72	7	14	79
B	PhH	1 eq.	reflux	12	26	39	35

a) Determined by glc (PEG 20 M, 160 °C).

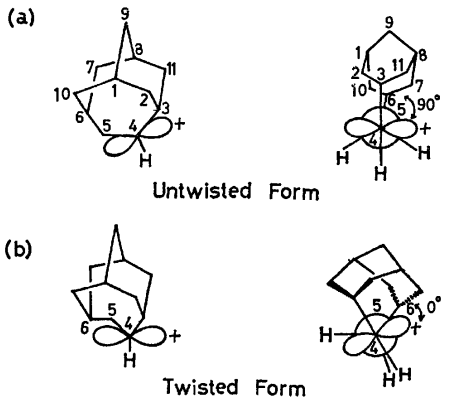

Fig. 2. Conformations of V.

produced in the solvolysis.[5,6] The possibility that II would be formed in the acetolysis and would subsequently react with acetic acid, thus giving I and IVa, can be ruled out, since II was stable under the acetolysis conditions (70 °C for 3 hr[6]). Thus, the formation of II should be due to the "hot," *i.e.*, vibrationally excited, nature of V. Therefore, V must have the enhanced nature of the non-classical cation (XVII), which is nicely deprotonated to give II (Scheme 3).

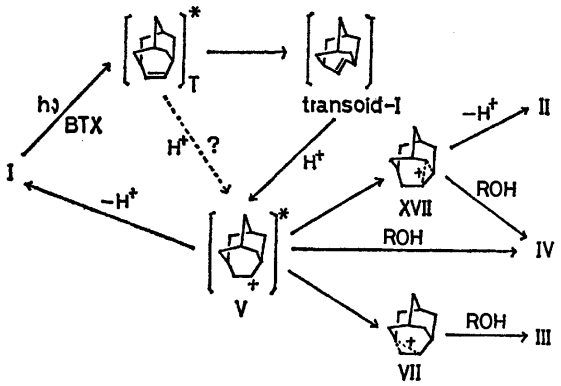

Scheme 3.

Although III was produced in the photochemical reaction, no III was detected in the diazotization or in the acetolysis[5,6] (Scheme 2, Eq. 3). Under thermodynamic controlled conditions, as are shown in Scheme 2, Eqs. 1 and 2,[7,8] the formation of XI is not surprising, because the homoadamantyl skeleton is known to be about 10 kcal/mol more strained than the adamantyl skeleton.[18] Therefore, III should be thermodynamically more stable than IV.[19] However, the photochemical reaction, the diazotization, and the buffered acetolysis[5,6] should be kinetically controlled. The cation (V) generated in the solvolysis must be in the ground state and, therefore, would not have enough energy to produce II. On the other hand, the cation (V) generated in the diazotization as well as the photochemical reaction would have enough energy to produce II. Although the reason why III is produced only in the case of the photochemical reaction is still not clear, in this rearrangement not only a energetic factor but also a stereochemical one would be operative.[20]

In summary, the total pathway of the photosensitized polar addition of protic solvents to I can be depicted as is shown in Scheme 3. Additionally, it should be noted that no 1,2-hydride shift in V forming a 3-homoadamantyl cation is observed in any of the three different ways so far as the product analysis is concerned.

Experimental

All the temperatures are uncorrected. The IR spectra were obtained on a Shimadzu IR-27 spectrometer. The mass spectra were taken by using a Hitachi RMS-4 mass spectrometer. The NMR spectra were obtained on a Varian EM-360 spectrometer, TMS being chosen as the internal standard. The microanalyses were performed in the Kyoto University Elemental Analysis Center.

Photosensitized Polar Addition of Acetic Acid to I. In an analytical-scale experiment, a solution of I (50 mg, 0.34 mmol) in 5 ml of glacial acetic acid containing 1 ml of benzene (xylene) was irradiated by means of a 300 W medium-pressure mercury lamp under nitrogen for 7 days. The reaction mixture was then poured onto water, neutralized by sodium hydrogen carbonate, and extracted by CH_2Cl_2. The organic layer was washed with aq. $NaHCO_3$ and water, and dried (Na_2SO_4). The solvent was removed, and the residue was analyzed by glc (PEG 20 M, 160 °C). Each product was isolated by preparative glc and was identical with the corresponding authentic sample (II, IIIa, and IVa) in glc retention time and in IR and NMR spectra.

In a preparative-scale run, a solution of I (1.00 g, 6.75 mmol) in 45 ml of glacial acetic acid containing 5 ml of xylene was irradiated by means of a 300 W medium-pressure mercury lamp under nitrogen for 30 days. The usual work-up (see above) gave a crude oil, from which xylene was quickly removed under reduced pressure, but the high subliming property of II prevented the complete removal of the xylene. The glc analysis showed the complete disappearance of I. The residue (2.0 g) was chromatographed on silica gel (200 g). The eluting solvent was gradually changed from *n*-hexane to a mixture of *n*-hexane and ether (95 : 5). The eluent of *n*-hexane gave pure II (216 mg, 21.6%). The eluent of *n*-hexane with ether gave pure IIIa (25 mg, 1.8%), a mixture of IIIa and IVa (303 mg, 21.6%), and pure IVa (360 mg, 25.7%).

A solution of I (500 mg; 3.4 mmol) in 10 ml of AcOD containing 3 ml of xylene was irradiated for 14 days. The usual work-up and chromatography on silica gel gave a mixture of I and II (185 mg, I : II=1 : 2.5 by glc analysis) and a mixture of III-d_1 and IV-d_1 (278 mg, 6 : 1 by glc analysis). The preparative glc gave pure I and pure II, which contained 12% d_1 and 41% d_1 respectively, as determined by mass spectrometry. The mixture of III-d_1 and IV-d_1 (150 mg) was treated with $LiAlH_4$ (75 mg) in refluxed ether for 10 hr, the subsequent usual work-up gave a crude solid (140 mg) which contained IX-d_1 and VIII-d_1 (*ca.* 1 : 6 by glc analysis). The preparative glc gave pure VIII-d_1 and pure IX-d_1, which contained 45% d_1 and 49% d_1 respectively, as determined by mass spectrometry.

The products, II, IIIa, and IVa, were shown by control experiments to be stable under the present photochemical reaction conditions.

Photosensitized Polar Addition of Pivalic Acid to I. A mixture of I (50 mg; 0.34 mmol), 2.5 ml of pivalic acid, and 2.5 ml of benzene was irradiated by means of a 300 W medium-pressure mercury lamp under nitrogen for 7 days.

The usual work-up gave a crude oil, which was then analyzed by glc (PEG 20 M, 160 °C). Each product, when isolated by preparative glc, was found to be identical with the corresponding authentic sample (II, IIIb, and IVb) in glc retention time and in IR and NMR spectra.

The authentic samples were prepared as follows:

2,4-Dehydrohomoadamantane (II)[21] and 4-homoadamantyl acetate (IVa)[5] were synthesized by the reported method.

4-Homoadamantyl Pivalate (IVb). To a solution of 4-homoadamantanol (VIII) (166 mg; 1.0 mmol) in 1 ml of pyridine, we added pivaloyl chloride[22] (180 mg; 1.5 mmol) in an ice-water bath. The reaction mixture was stirred at room temperature for 24 hr and then poured onto aq. HCl (5%) and extracted with CH_2Cl_2. The CH_2Cl_2 solution was washed successively with 5% aqueous HCl, aqueous $NaHCO_3$, and water, and then dried (Na_2SO_4). The subsequent removal of the solvent gave a crude oil, which was chromatographed on silica gel. The eluent of *n*-hexane with ether (5%) gave pure IVb (204 mg, 81.6%); bp 140 °C/40 mmHg (bath temp.); IR (neat) 2980, 1750, 1160, cm^{-1}; NMR δ (CCl_4) 1.13 (s, 9H), 1.30—2.30 (complex m, 16H), 4.93 (m, 1H). Found: C, 76.49; H, 10.55%. Calcd for $C_{16}H_{26}O_2$: C, 76.75; H, 10.14%.

2-Adamantylmethanol (IX).[23] This compound was prepared by the reported methods. Adamantane-2-carboaldehyde[24] was synthesized by the treatment of adamantyleneoxirane[25,26] with BF_3-etherate.[26] The aldehyde was oxidized by Jones' reagent to give adamantane-2-carboxylic acid,[24,26] which was then reduced with $LiAlH_4$ to furnish IX.[23]

2-Adamantylmethyl Acetate (IIIa). To a solution of IX (50 mg; 0.30 mmol) in 1 ml of pyridine, we added 0.5 ml of acetic anhydride, after which the reaction mixture was stirred for 19 hr at room temperature. The usual work-up gave crude IIIa (60 mg, 96%); bp 135 °C/40 mmHg (bath temp.); IR (neat) 2930, 1750, 1455, 1370, 1220, 1035 cm^{-1}; NMR δ(CCl_4) 1.87 (broad s, 15H), 2.00 (s, 3H), 4.17 (d, 2H, J=7.5 Hz). Found: C, 75.09; H, 9.75%. Calcd for $C_{13}H_{20}O_2$: C, 74.96; H, 9.68%.

2-Adamantylmethyl Pivalate (IIIb). To a solution of IX (50 mg; 0.30 mmol) in 0.5 ml of pyridine, we added pivaloyl chloride (60 mg; 0.5 mmol) in an ice-water bath. The reaction mixture was then stirred at room temperature for 19 hr, after which the usual work-up gave a crude oil, which was subsequently chromatographed on silica gel. The eluent of *n*-hexane with ether (5%) gave pure IIIb (64 mg, 85%); bp 135 °C/30 mmHg (bath temp.); IR (neat) 2940, 1745, 1480, 1460, 1290, 1150 cm^{-1}; NMR δ (CCl_4) 1.17 (s, 9H), 1.83 (broad s, 15H), 4.14 (d, 2H, J= 7.5 Hz). Found: C, 77.02; H, 10.85%. Calcd for $C_{16}H_{26}O_2$: C, 76.75; H, 1047%.

Diazotization of 4-Homoadamantylamine (XV). The amine was synthesized by a previously reported method.[27] Some typical examples will be described.

Diazotization by Isopentyl Nitrite: A solution of XV (80 mg; 0.48 mmol) and isopentyl nitrite (65 mg; 0.55 mmol) in 5 ml of glacial acetic acid was stirred at room temperature for 72 hr. The reaction mixture was then poured onto water, neutralized with $NaHCO_3$, and extracted with CH_2Cl_2. The CH_2Cl_2 solution was washed with aq. $NaHCO_3$ and water, and dried (Na_2SO_4). After the removal of the solvent, the residue was analyzed by glc (PEG 20 M, 160 °C). Each product, when isolated by preparative glc, was found to be identical with the corresponding authentic sample (I, II, and IVa) in glc retention time and in mass and IR spectra.

Diazotization via XVI: The triazene (XVI) was synthesized by the usual method.[28] Since XVI could not be isolated, the crude XVI was used immediately after its preparation. To the crude XVI (100 mg) we added glacial acetic acid (4.5 ml); nitrogen evolved. The reaction mixture was then stirred at room temperature for 1 hr and poured onto water. The solution was neutralized with $NaHCO_3$ and extracted with CH_2Cl_2. The extract was washed with aqueous $NaHCO_3$ and water, and dried (Na_2SO_4). After the removal of the solvent the residue was analyzed by glc (PEG 20 M, 160 °C). Each product, when isolated by preparative glc, was found to be identical with the corresponding authentic sample (I, II, and IVa) in glc retention time and in mass and IR spectra.

Stability of II under the Buffered Solvolysis Conditions. A mixture of II (50 mg; 0.34 mmol), NaOAc (60 mg; 0.73 mmol), and 1 ml of glacial acetic acid was heated at 70 °C for 3 hr.[6] No change was observed by glc analysis.

The authors are indebted to Mr. S. Arimatsu for the preliminary studies.

References and Footnotes

1) a) P. J. Kropp, *J. Amer. Chem. Soc.*, **91**, 5783 (1969) and the references cited therein; *Pure Appl. Chem.*, **24**, 585 (1970). b) J. A. Marshall, *Accounts Chem. Res.*, **2**, 33 (1969); *Science*, **170**, 130 (1970).

2) H. Kato and M. Kawanisi, *Tetrahedron Lett.*, **1970**, 865.

3) M. Kawanisi and H. Kato, *ibid.*, **1970**, 721.

4) For pertinent data as to the chemistry of carbocation, *cf.* G. A. Olah and P. v. R. Schleyer, eds., "Carbonium Ions," Vols. 1—4, Wiley-Interscience, New York, N.Y. (1968, 1970, 1972, 1973).

5) J. E. Nordlander, F. Y-H. Wu, S. P. Jindal, and J. B. Hamilton, *J. Amer. Chem. Soc.*, **91**, 3962 (1969).

6) P. v. R. Schleyer, E. Funke, and S. H. Liggero, *ibid.*, **91**, 3965 (1969).

7) Z. Majerski and K. Milinarić, *Chem. Commun.*, **1972**, 1030

8) K. M. Majerski and Z. Majerski, *Tetrahedron Lett.*, **1972**, 4915

9) A preliminary account on this subject has been reported: R. Yamaguchi, S. Arimatsu, and M. Kawanisi, *Chem. Lett.*, **1973**, 121.

10) In a preliminary report[9] we assigned an incorrect structure, 3-homoadamantyl acetate, to the second product. Subsequent detailed studies confirmed the structure of the product to be IIIa instead of 3-homoadamantyl acetate. It is exactly the same as the structure of IIIb.

11) Another reason why Path B would be favored is as follows: The classical cation (VI) would be likely deprotonated to give methyleneadamantane,[29] which would be stable under the present photochemical reaction conditions. However, this compound was not detected by either glc or NMR analyses.

12) Recently evidence has been presented for the ground state *trans*-isomers as chemically reactive intermediates in the photo-induced polar addition of protic solvents to 7- and 8-membered cycloalkenones; R. Noyori and M. Kato, This Bulletin, **47**, 1460 (1974).

13) Scheleyer *et al.* have suggested that the C_4–C_5 ethylene bridge in homoadamantane system is so flexible that the dihedral angle can change from 0 to *ca.* 30°.[14] Therefore, it is not improbable to assume for geometrical reasons that considerably twisted *transoid*-4-homoadamantene is a chemically reactive intermediate.

14) E. M. Engler, L. Chang, and P. v. R. Schleyer, *Tetrahedron Lett.*, **1972**, 2525; T. M. Corrie, E. M. Engler, R. C. Bingham, and P. v. R. Schleyer, *ibid.*, **1972**, 3039.

15) Control experiments showed that the products, II, III, and IV, are stable under the present photochemical reaction conditions.

16) As to the nature of the carbocation generated in a photosensitized polar addition reaction, Kropp and Krauss described as follows: Caution must be urged against carrying the analogy too close to ground state chemistry, since the carbonium ion will, at least initially, have much more vibrational energy and probably a different geometry than an analogous carbonium ion generated by the simple protonation of a ground state *cis*-olefin; P. J. Kropp and H. J. Krauss, *J. Amer. Chem. Soc.*, **89**, 5199 (1967).

17) L. Friedman, "Carbonium Ions," Vol. II, G. A. Olah and P. v. R. Schleyer, ed., Wiley-Interscience, New York (1970), p. 655.

18) a) R. C. Fort, Jr. and P. v. R. Schleyer, *Advan. Alicycl. Chem.*, **1**, 283 (1966). b) J. Janjatovic, D. Skare, and Z. Majerski, *J. Org. Chem.*, **39**, 651 (1974).

19) It has been reported that 3-homoadamantyl acetate was converted into 1-adamantylmethyl acetate by treatment with *p*-toluenesulfonic acid in refluxed acetic acid (J. E. Nordlander, S. P. Jindal, P. v. R. Schleyer, R. C. Fort, Jr., J. J. Harper, and R. D. Nicholas, *J. Amer. Chem. Soc.*, **88**, 4475 (1966)). We have examined the similar treatment of IVa; we thus obtained IIIa and an additional acetate, the structure of which has not yet been determined. However, this result does not contradict our present discussion.

20) An important factor in skeletal rearrangement, especially under kinetically controlled conditions, may be the degree of overlap of the vacant orbital of the carbocation center and the C–C bond, which migrates. At this point, for the anticipated most stable geometry of V, which has an untwisted ethylene bridge (C_4–C_5), it would be unfavorable for V to being converted into VII (or VI), because the sp^2-vacant orbital at C_4 is orthogonal to the C_5–C_6 bond, which migrates (Fig. 2a). The more twisted the ethylene bridge is (Fig. 2b), the more favorable would be the rearrangement, because the overlap of the sp^2-vacant orbital at C_4 and C_5–C_6 bond increases. Since the geometry of V generated in the photochemical reaction would probably be a twisted one (Fig. 2b), at least initially,[16] the conversion of V into VII (or VI) would occur, while the geometry of the V generated in the solvolysis as well as in the diazotization would be an untwisted one (Fig. 2a).
Cf. R. Yamaguchi, T. Katsushima, and M. Kawanishi, This Bulletin, **47**, 2830 (1974).

21) Z. Majerski, S. H. Liggero, and P. v. R. Schleyer, *Chem. Commun.*, **1970**, 949.

22) F. L. Greenwood, F. C. Whitmore, and H. M. Crooks, *J. Amer. Chem. Soc.*, **60**, 2028 (1938).

23) J. Burkhard, J. Vais, and S. Landa, *Z. Chem.*, **9**, 29 (1969).

24) J. Scharp, H. Wynberg, and J. Strating, *Rec. Trav. Chim. Pays-Bas*, **89**, 18 (1970).

25) E. Bernaert, D. Danneels, M. Anteunis, and G. Verhegge, *Tetrahedron*, **29**, 4127 (1973).

26) D. Fărcaşiu, *Synthesis*, **1972**, 615.

27) J. L. M. A. Schlatmann, J. G. Korsloot, and J. Schut, *Tetrahedron*, **26**, 949 (1970).

28) C. Süling, Houben-Weyl, "Methoden der organischen Chemie," Georg Thieme Verlag, Stuttgart, Bd. X/3, p. 731 (1965).

29) P. v. R. Schleyer and R. D. Nicholas, *J. Amer. Chem. Soc.*, **83**, 182 (1961).

* Throughout this paper we have adopted trivial nomenclature for simplicity. The IUPAC names for I, II, and IV are tricyclo[4.3.1.$1^{3,8}$]undec-4-ene, tetracyclo[5.3.1.$0^{3,5}$-$0^{4,9}$]undecane, and tricyclo[4.3.1.$1^{3,8}$]undec-4-yl acetate (pivalate), respectively.

Formation of 9,9′:9′,9″-Terfluorenyl Isomers Using Metalated Fluorenes as Synthetic Intermediates

Masahiro MINABE and Kazuo SUZUKI

Department of Industrial Chemistry, Faculty of Technology, Utsunomiya University, Ishii-cho, Utsunomiya 321–31

(Received October 7, 1974)

Rotational isomers of 9,9′: 9′,9″-terfluorenyl were obtained by the addition of 9-lithiofluorene to 9,9′-bifluorenylidene (III). 2,7-Dibromo- (VI) and 2,7,2″,7″-tetrabromo-9,9′: 9′,9″-terfluorenyl (VIII) resulted from similar reactions of the corresponding bromo-derivatives. 9-Lithio-9,9′-bifluorenyl was treated with 9-bromo-9,9′-bifluorenyl to give 9,9′-bis(9,9′-bifluorenyl) (X), 9,9′: 9′,9″-terfluorenyl isomers (mp 293 °C (dec) (I) and mp 257 °C (dec) (II)), 9,9′-bifluorenyl (IX), III, and fluorenone. The isomerization of I by metallic potassium gave the other rotamer II, which decomposed into its components, IX, III, and fluorene (IV).

The formation of the stereoisomeric 9,9′: 9′,9″-terfluorenyl, mp 293 °C (dec) (I) and mp 257 °C (dec) (II), has been reported in the previous paper of this series.[1] The conformations of I and II were proposed to be *s-cis,s-cis* and *s-cis,s-trans*, respectively.[2] Both rotamers were produced simultaneously by the Michael reaction[3] of 9,9′-bifluorenylidene (III)[4] with fluorene (IV), by the reaction[5] of 9-bromofluorene with methanolic potassium hydroxide in acetone, and by the reaction[6] of 9-lithiofluorene with 9-bromo-9,9′-bifluorenyl.[7]

The present investigation was undertaken in order to discover additional synthetic routes which gave 9,9′: 9′,9″-terfluorenyls through 9-lithiofluorenyl derivatives or other alkali metal compounds as active intermediates.

Results and Discussion

A possible route for the formation of both I and II was achieved by addition of 9-lithiofluorene to III in dry benzene. Similarly, 9-lithiofluorene was treated with 2,7-dibromo-9,9′-bifluorenylidene (V)[8] to yield 2,7-dibromo-9,9′: 9′,9″-terfluorenyl (VI)[8] as the main product, accompanied by a trace amount of 2′,7′-dibromo-9,9′: 9′,9″-terfluorenyl (VII).[8] 2,7,2″7″-Tetrabromo-9,9′: 9′,9″-terfluorenyl (VIII)[8] was obtained by the reaction of 2,7-dibromo-9-lithiofluorene with V.

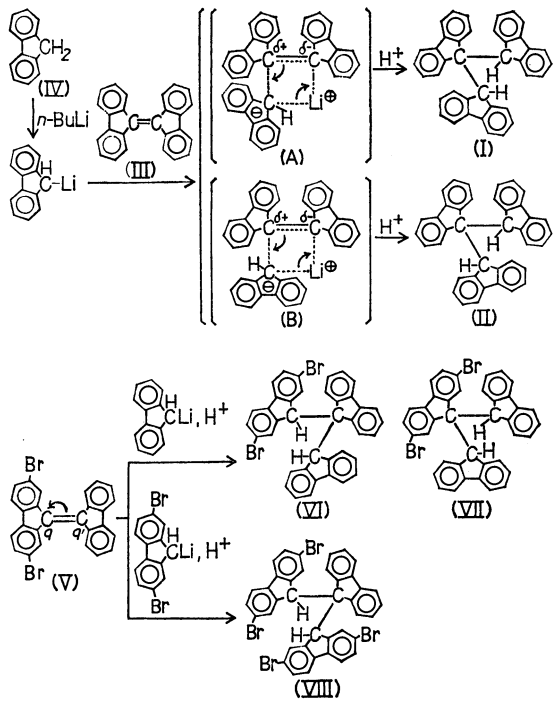

Fig. 1.

The formation of I and II by the reaction of 9-lithiofluorene with III could be expected to proceed through the four-center transition states (A) and (B), as shown in Fig. 1. The 9′-carbon is more electropositive than the 9-carbon in such a highly-polarized unsymmetrical ethylenic linkage as V owing to the electro-withdrawing effect of the two bromine atoms. This effect is brought out in the reaction of 9-lithiofluorene with V which gives a major product VI and a trace amount of VII.

The reaction of 9-lithio-9,9′-bifluorenyl with 9-bromo-9,9′-bifluorenyl yielded I, II, III, 9,9′-bifluorenyl (IX), 9,9′-bis(9,9′-bifluorenyl) (X),[9] and fluorenone. When 9-bromo-9,9′-bifluorenyl was treated with a half mole equivalent of *n*-butyl lithium and the reaction mixture was immediately refluxed in xylene, 9-*n*-butyl-9,9′: 9′,9″-terfluorenyl (XI) was also isolated.

The formation of I and II can be attributed to the reaction of 9-bromo-9,9′-bifluorenyl with 9-lithiofluorene which may be generated by the metal-halogen interconversion reaction between 9-bromo-9,9′-bifluorenyl and *n*-butyl lithium.

It has been reported by Nasielski *et al.*[9] that X was obtained by photo-reduction of III, however, no data on melting point, elementary analysis, molecular weight, *etc.*, were reported.

The structures of X and XI were confirmed from their mass spectral fragmentation patterns. The parent peak of X is small at *m/e* 658. The fragmentary ions *m/e* 493 (9,9′: 9′,9″-terfluorenyl cation, strong), 329 (9,9′-bifluorenyl cation, base peak), 328 (9,9′-bifluorenylidene ion, strong), and 165 (9-fluorenyl cation) originate from the simple cleavage of $C_{9-9'}$, $C_{9''-9'''}$, and/or $C_{9'-9''}$ bonds of the parent ion, X.

The mass spectrum of XI was as follows: the parent peak was small at *m/e* 550, and the fragment peaks were at *m/e* 493, 385 (9-*n*-butyl-9,9′-bifluorenyl cation, weak), 329, 328 (strong), 221 (9-*n*-butyl-9-fluorenyl cation, base peak), 191 (9-vinyl-9-fluorenyl cation), 179 (9-methyl-9-fluorenyl cation and/or 9,10-dihydrophenanthryl cation, strong), and 165 (very strong). The peaks at *m/e* 493, 329, 328, and 165 were identical with those of X.

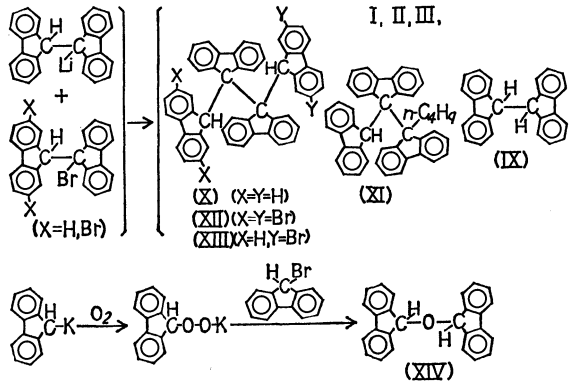

Fig. 2.

The IR spectrum of X closely resembled those of I and II.

An analogous reaction between 9-lithio-9,9′-bifluorenyl with 2,7,9′-tribromo-9,9′-bifluorenyl[10] yielded 9,9′-bis(2′,7′-dibromo-9,9′-bifluorenyl)(XII), 9-(2,7-dibromo-9-fluorenyl)-9,9′: 9′,9″-terfluorenyl (XIII), X, II, V, IX, III, 2,7-dibromofluorenone, and fluorenone. The IR spectra of XII and XIII were very similar to those of I, II, VIII, and X.

An attempt to synthesize X by the reaction of I, metallic potassium, and 9-bromofluorene was unsuccessful; however, isomeric II, IX, III, and di(9-fluorenyl) ether (XIV)[11] were isolated. Compound XIV was obtained by the reaction between 9-bromofluorene and metallic potassium, accompanied by II, IX, and III. The formation of II may result from the reaction of intermediate 9-potassio-9,9′-bifluorenyl with 9-bromofluorene.[6] The occurrence of XIV can be explained by the reaction of 9-bromofluorene with 9-fluorenylpotassium peroxide which could be formed by action of metallic potassium and 9-bromofluorene in the presence of contaminating oxygen in the nitrogen, as Fig. 2 shows.

I isomerized into II by reaction with metallic potassium; II was broken down into its components, IX, IV, and III by the same reaction.

These findings are analogous to the reaction[12] of I (or II) with lithium aluminum hydride, therefore, the isomerization presumably proceeds *via* intermediary 9-potassio-9,9′: 9′,9″-terfluorenyl.

Experimental

All the melting points are uncorrected.

The compounds were confirmed by mixed-melting-point determinations and by comparison of their IR spectra with those of authentic samples.

Mass, NMR, and IR spectra were recorded using Hitachi RMU-6E, JEOL JNM-C60-HL, and JASCO IR-G spectrometers.

All reactions were carried out under an atmosphere of dry nitrogen.

Reaction of 9-Lithiofluorene with 9,9-Bifluorenylidene (III): 9-Lithiofluorene was prepared in the usual way[13] by the reactions of *n*-butyl bromide (3.3 g in 20 ml of ether) with lithium chips (0.31 g) in ether (20 ml), and of the resulting mixture with IV (5.0 g) in benzene (45 ml). A solution of 6.56 g of III in 60 ml of benzene was added dropwise into the 9-lithiofluorene solution at 0 °C for 20 min, and the mixture was boiled.

After standing at room temperature, the reaction mixture was treated with 5% aqueous ammonium chloride, and the organic layer was dried over calcium chloride, and evaporated to dryness under reduced pressure.

The residue was purified by means of fractional recrystallization, alumina column chromatography, and vacuum sublimation: 1.25 g (13%) of I, mp 291—293 °C (dec) (benzene), 1.05 g (11%) of II, mp 255—257 °C (dec) (ethyl acetate), 0.20 g (2%) of fluorenone, mp 82—83 °C (ethanol), 2.13 g (32%) of III, mp 181—183 °C (cyclohexane), and 1.85 g (37%) of IV, mp 111—113 °C (ethanol), were isolated.

Reaction of 9-Lithiofluorene with 2,7-Dibromo-9,9′-bifluorenylidene (V): To the 9-lithiofluorene solution obtained from 2.3 g of IV in 25 ml of benzene, 6.7 g of V in benzene was added during a period of 35 min below 10 °C.

The reaction mixture was then worked-up as usual, the crude product afforded 6.55 g (73%) of VI, mp 285—286 °C (dec) (ethyl acetate), a trace amount of VII, mp 302—303 °C (dec) (benzene), and 0.12 g (2%) of V, mp 244—245 °C (ethyl acetate).

Reaction of 2,7-Dibromo-9-lithiofluorene[14] *with V*: 2,7-Dibromofluorene (4.5 g) was metalated to the corresponding 9-lithio-compound in the usual way, and then allowed to react with V (6.7 g) in benzene.

After the usual treatment, 2.34 g (21%) of VIII, mp 313—314 °C (dec) (benzene), a trace amount of 2,7-dibromofluorenone, mp 201—202 °C, 1.46 g (32%) of 2,7-dibromofluorene, mp 162—163 °C, and 3.29 g (49%) of V, mp 244—245 °C, were obtained.

Reaction of 9-Lithio-9,9′-bifluorenyl with 9-Bromo-9,9′-bifluorenyl. a): A solution of 4.1 g (10 mmol) of 9-bromo-9,9′-bifluorenyl in 70 ml of xylene was added dropwise to the *n*-butyl lithium solution obtained from 12.5 mmol of *n*-butyl bromide and 0.025 g. atom of lithium chips, while being stirred at 0—2 °C for 45 min, and the mixture was heated gradually to 135 °C. After cooling, 3.3 g (8 mmol) of 9-bromo-9,9′-bifluorenyl in 60 ml of xylene was added dropwise to the resulting solution at 5—10 °C for 30 min. The mixture was stirred for 24 hr at room temperature, and then was maintained at a boil for 30 min.

The resulting mixture was treated in the usual manner, and the residual part was chromatographed on alumina in benzene. Further elution and subsequent evaporation gave 0.016 g of X, mp 313—314 °C (dec) (pyridine). Found: C, 94.92; H, 5.06%. Calcd for $C_{52}H_{34}$: C, 94.80; H, 5.20%. Mass: *m/e* 658 (M^+), 493, 329, 328, and 165.

In addition, 0.13 g of I, mp 292—293 °C (dec) (ethyl acetate), 0.42 g of II, mp 256—257 °C (dec) (ethyl acetate), 0.10 g of IX, mp 244—245 °C (ethyl acetate), and 0.36 g of III, mp 182—183.5 °C (ethanol), were obtained from the benzene mother liquor.

By extraction with ethanol from the lower band on the column, 1.05 g of 9-hydroxy-9,9′-bifluorenyl, mp 193—195 °C (benzene), was isolated. Fluorenone (0.65 g), mp 82—83 °C (ethanol), was obtained from the upper yellow band.

b): To an *n*-butyl lithium solution (prepared from 0.08 g of lithium chips and 0.78 g (5.7 m mol) of *n*-butyl bromide in ether) was added slowly 4.1 g (10 m mol) of 9-bromo-9,9′-bifluorenyl in 45 ml of xylene at 3—7 °C, and then refluxed at 135 °C for 1 hr.

The solution was treated in the usual way, affording 0.43 g of X, mp 313—314 °C (dec) (pyridine), 0.08 g of XI, mp 280—281 °C (dec) (benzene), 0.01 g of I, mp 292—293 °C (dec) (benzene), 0.022 g of II, mp 256—257 °C (dec) (benzene), 0.86 g of III, mp 184—186 °C (cyclohexane), 0.01 g

of IX, mp 244—245 °C (ethyl acetate), and 0.45 g of 9-hydroxy-9,9′-bifluorenyl, mp 193—195 °C (benzene). Found for XI: C, 93.85; H, 6.04%. Calcd for $C_{43}H_{34}$: C, 93.82; H, 6.18%. Mass: *m/e* 550 (M^+), 493, 385, 329, 328, 221, 191, 179, and 165.

The mother liquor was concentrated to dryness under reduced pressure, and the residue was steam distilled to give 0.021 g of oily products. The oil was confirmed to consist of fluorenone and a small amount (*ca.* 1%) of IV by comparing of their retention times on a gas chromatogram with those of authentic samples.

Reaction of 9-Lithio-9,9′-bifluorenyl with 2,7,9′-Tribromo-9,9′-bifluorenyl: A xylene (200 ml) solution containing 4.54 g of 2,7,9′-tribromo-9,9′-bifluorenyl was added to 9-lithio-9,9′-bifluorenyl (prepared from 4.09 g of 9-bromo-9,9′-bifluorenyl) solution while being stirred for 45 min at room temperature. The mixture was then continuously stirred for a period of 23 hr, and followed by refluxing for another 1 hr.

The reaction mixture was worked-up as usual and the following compounds were obtained: 0.70 g of XII, mp 295—296 °C (dec) (pyridine), 0.08 g of XIII, mp 292—294 °C (dec) (pyridine), 0.04 g of X, mp 313—314 °C (dec) (pyridine), 0.24 g of II, mp 254—256 °C (dec) (ethyl acetate), 1.36 g of V, mp 241—242 °C (ethyl acetate), 0.16 g of IX, mp 242—244 °C (ethyl acetate), 0.31 g of III, mp 183—185 °C (ethyl acetate), 0.03 g of 2,7-dibromofluorenone, mp 198—200 °C (ethanol), 0.23 g of fluorenone, mp 80—83 °C (ethanol), and 0.03 g of 9-hydroxy-9,9′-bifluorenyl, mp 193—194 °C (benzene). Found for XII: C, 64.29; H, 3.17%. Calcd for $C_{52}H_{30}Br_4$: C, 64.10; H, 3.10%. Found for XIII: C, 76.11; H, 3.89%. Calcd for $C_{52}H_{32}Br_2$: C, 76.48; H, 3.95%.

Reaction of 9,9′: 9′,9″-Terfluorenyls with Potassium Metal and 9-Bromofluorene. a): A solution of 1.0 g of I and 0.1 g of potassium chips in 60 ml of tetrahydrofuran (THF) was refluxed for 3 hr. 9-Bromofluorene (1.25 g) in THF (20 ml) was added dropwise to the resulting mixture while it was stirred for 50 min at 5—10 °C. Then the reaction mixture was stirred for 13 hr at room temperature and refluxed briefly.

The mixture was decomposed with 10 ml of ethanol, then with dilute hydrochloric acid, and extracted with benzene. The organic layer was concentrated to give 0.66 g of I, mp 291—293 °C (dec) (ethyl acetate), 0.17 g of II, mp 255—257 °C (dec) (ethyl acetate), 0.04 g of IX, mp 243—245 °C (ethyl acetate), and 0.03 g of XIV, mp 227—228 °C (benzene).

Found for XIV: C, 90.24; H, 5.41%. Calcd for $C_{26}H_{18}O$: C, 90.15; H, 5.24%. Mass: *m/e* 346 (M^+), 181, 165, and 152. NMR (in 99% C_6D_6): δ 5.74 (2H, s) and 6.97—7.49 (16H, m) ppm.

The benzene mother liquor was chromatographed on an alumina column: 0.06 g of III, mp 183—184 °C (ethanol), and 0.03 g of fluorenone, mp 82—84 °C (ethanol), were separated.

b): II (1.0 g) was treated as in (a) to give 0.74 g of II, mp 255—257 °C (dec) (ethyl acetate), 0.03 g of IX, mp 243—245 °C (ethyl acetate), 0.06 g of XIV, mp 227—228 °C (benzene), 0.014 g of III, mp 181—183 °C (ethanol) and 0.15 g of fluorenone, mp 82—85 °C (ethanol).

Reaction of 9-Bromofluorene with Metallic Potassium: A mixture of 4.9 g of 9-bromofluorene and 0.78 g of potassium chips in 50 ml of THF was stirred at room temperature for 20 hr.

The reaction mixture was treated as usual and 0.57 g of II, mp 255—257 °C (dec) (ethyl acetate), 0.22 g of IX, mp 242—244 °C (ethyl acetate), 0.20 g of XIV, mp 226—228 °C (benzene), and 0.47 g of III, mp 184—186 °C (ethyl acetate), were isolated.

Reaction of I with Potassium: A solution of 1.0 g of I and 0.2 g of potassium chips in 70 ml of THF was refluxed for 3.5 hr.

After cooling, the resulting mixture was then worked-up as usual, and afforded 0.32 g of II, mp 256—257 °C (dec) (ethyl acetate). The mother liquor was evaporated to dryness under reduced pressure and sublimed *in vacuo* at 120 °C to give 0.10 g of IV, mp 111—113 °C (ethanol).

The residue from the sublimation gave 0.32 g of IX, mp 242—243 °C (ethyl acetate), and 0.03 g of III, mp 183—185 °C (ethyl acetate).

Reaction of II with Potassium: A solution of 1.0 g of II and 0.2 g of potassium chips in 70 ml of THF was refluxed for 20 hr and the mixture was treated as usual: 0.24 g of II, mp 256—257 °C (dec) (ethyl acetate), 0.35 g of IX, mp 242—243 °C (ethyl acetate), 0.02 g of III, mp 183—185 °C (ethanol), and 0.24 g of IV, mp 111—112.5 °C (ethanol), were obtained.

This work was partially supported by a Grant-in-Aid for Scientific Research from the Ministry of Education, which is acknowledged. The authors are grateful to Dr. Elizabeth K. Weisburger of the National Institutes of Health, U.S.A., for reading their manuscript.

References

1) K. Suzuki, *Technol. Rept. Tohoku Univ.*, **19**, 63 (1955).
2) K. Suzuki and M. Minabe, *Tetrahedron Lett.*, **1974**, 1541.
3) M. Minabe and K. Suzuki, *J. Org. Chem.*, **40**, (May, 1975), to be published, entitled "Stable Rotamers of 9,9′: 9′,9″-Terfluorenyls at Room Temperature".
4) J. Thiele and S. Wansheidt, *Ann.*, **376**, 278 (1910).
5) K. Suzuki and S. Kajigaeshi, This Bulletin, **35**, 408 (1962).
6) S. Kajigaeshi, *Nippon Kagaku Zasshi*, **83**, 191 (1962).
7) S. Kajigaeshi, *ibid.*, **82**, 1712 (1961).
8) K. Suzuki, M. Minabe, M. Fujimoto, and N. Nohara, This Bulletin, **42**, 1609 (1969).
9) J. Nasielski, M. Jauquet, E. V. Donckt, and A. V. Sinoy, *Tetrahedron Lett.*, **1969**, 4859.
10) K. Suzuki and M. Fujimoto, This Bulletin, **36**, 1654 (1963).
11) A. Kliegel, *Ber.*, **43**, 2488 (1910).
12) M. Minabe and K. Suzuki, This Bulletin, to be published, entitled "Isomerization of the Stable Rotamers of 9,9′: 9′,9″-Terfluorenyls".
13) M. Minabe, A. Tanaka, M. Wakui, and K. Suzuki, *ibid.*, **44**, 1614 (1971).
14) As we have already reported[8], the formation of 2,7-dibromo-9-lithiofluorene was confirmed as 2,7-dibromofluorene-9-carboxylic acid. However a misprint shows the melting point of the carboxylic acid as 208—209 °C instead of the correct value, 258—259 °C (dec).

Multifunctional Hydrolytic Catalyses. III. Catalytic Hydrolysis of *p*-Nitrophenyl Acetate by Imidazole-4-carbohydroxamic Acids[1)]

Toyoki KUNITAKE and Seiji HORIE

Department of Organic Synthesis, Faculty of Engineering, Kyushu University, Fukuoka 812

(Received November 5, 1974)

Imidazole-4-carbohydroxamic acids (I) and its *N*-methylhydroxamic acid derivative (II) were synthesized from imidazolecarboxylic acid and hydroxylamines, and the catalytic hydrolysis of *p*-nitrophenyl acetate was studied. The reaction was analyzed by the pseudo-first-order kinetics and the burst kinetics. The hydrolysis proceeds *via* the formation and the subsequent decomposition of the acetyl hydroxamate intermediate. The acylation rate with these catalysts were comparable to those observed with other simple hydroxamic acids. On the other hand, the deacylation of the acetyl intermediate of II was greater than expected and increased with pH. This suggests that the intramolecular imidazole group (neutral and/or anionic species) assists deacylation, thus increasing the overall efficiency of catalysis.

Multifunctional catalysis is one of the major characteristics of the enzyme reaction. A typical example is the charge relay system which is present at the active site of several serine proteases.[2)] This system is composed of a series of hydrogen bonding connecting the aspartyl carboxylate, histidyl imidazole and seryl hydroxyl groups, and acylation by specific ester and amide substrates occurs at the seryl hydroxyl group. Therefore, a combination of the imidazole function and a good oxygen nucleophile like the hydroxamate anion would be considered as a model charge relay system.

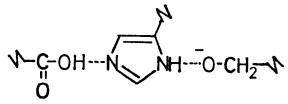

charge relay system

The present paper is an account of our initial efforts toward preparations of such catalysts in small-molecule systems. The catalyst compounds employed are imidazole-4-carbohydroxamic acid (I) and its *N*-methyl derivative (II). Similar attempts by using polymer catalysts have been described elsewhere.[3,4)]

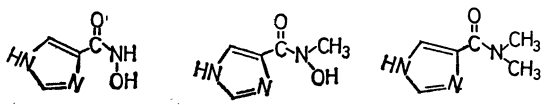

I II III

Experimental

Melting points are uncorrected. UV-visible spectroscopic measurements were made with a Hitachi 124 spectrophotometer. NMR spectra were obtained with a Varian A 60 instrument.

Materials. *p*-Nitrophenyl acetate was prepared by reaction of *p*-nitrophenol with acetic anhydride and recrystallized from cyclohexane, mp 78 °C (lit[5)], 81—82 °C).

Imidazole-4-carboxylic acid was prepared essentially by the procedure of Pyman[6)] by oxidation of 4-hydroxymethylimidazole[7)] with concentrated nitric acid ($d=1.38$) at 80 °C for 3 hr. After the reaction was over, solvent was removed *in vacuo*. Water was removed completely as an azeotrope with benzene. The remaining colorless granules were dissolved in a smallest amount of water, and the solution was neutralized to pH 6 by slow addition of a cold saturated aqueous solution of Na_2CO_3. Colorless precipitates were recrystallized repeatedly from hot water. Mp 285—287 °C (dec) (lit[6)] mp 281 °C (dec)).

According to the procedure of Wegner and Weidenhagen,[8)] imidazole-4-carboxylic acid was converted by PCl_5 to the corresponding acid chloride. The pale yellow, hygroscopic solid was used as such for the subsequent experiment.

N,N-*Dimethylimidazole-4-carboxamide (III).* The acid chloride was prepared from 1.0 g (0.0089 mol) of imidazolecarboxylic acid and 1.78 g (0.0089 mol) of PCl_5. Dimethylamine hydrochloride (1.4 g, 0.0178 mol) was mixed with 3.6 g (0.036 mol) of triethylamine in 30 m*l* of DMF. Triethylamine hydrochloride was filtered and the solution was added to the solid acid chloride with cooling. After standing overnight, precipitates were filtered and the solvent removed *in vacuo*. The dark brown, viscous residue was carefully dissolved in concentrated hydrochloric acid and, then solvent was removed *in vacuo* from the resulting solution. The white solid formed was recrystallized from a mixture of ethanol and ethyl acetate and from ethanol to give pale yellow needles: yield 30—40%, mp 196—198 °C. IR and NMR spectra were consistent with the structure. Found: C, 39.05; H, 5.98; N, 22.81%. Calcd for $C_6H_9N_3O\cdot 1/2H_2O$: C, 39.12; H, 5.96; N, 22.76%.

Imidazole-4-carbohydroxamic Acid (I). Hydroxylamine hydrochloride (10.0 g, 0.144 mol) was reacted with 29 g (0.287 mol) of triethylamine in DMF, and triethylamine hydrochloride was filtered. The solution was added to the solid acid chloride which had been prepared from 2.8 g (0.025 mol) of imidazolecarboxylic acid. After standing overnight, triethylamine hydrochloride was filtered and the solvent removed *in vacuo*. The pale red residue was dissolved in hydrochloric acid and the solvent evaporated to dryness. Recrystallization from 1 : 2 H_2O-CH_3OH gave 1.5 g (40% yield) of colorless needles. Mp 202—206 °C. IR: 3420 cm^{-1} (ν_{NH}, hydroxamic acid), 1650 cm^{-1} ($\nu_{C=O}$, hydroxamic acid). Found: C, 26.57; H, 4.35; N, 23.18%. Calcd for $C_4H_5N_3O_2\cdot HCl\cdot H_2O$; C, 26.44; H, 4.41; N, 23.14%.

N-*Methylimidazole-4-carbohydroxamic Acid (II).* *N*-Methylhydroxylamine hydrochloride (4.0 g, 0.042 mol) which was obtained by zinc reduction of nitromethane was mixed with 8.0 g (0.080 mol) of triethylamine in dry DMF, and triethylamine hydrochloride formed was filtered. The DMF solution was added to the acid chloride which had been prepared from 2.24 g (0.020 mol) of imidazolecarboxylic acid. The work-up was the same as that described above. Pale yellow crystals were obtained as the hydrochloride in 40% yield and recrystallized from methanol or from methanol-acetonitrile: mp 196—197 °C (dec). IR: hydroxamic acid, 3220 cm^{-1} (ν_{OH}), 1640 cm^{-1} ($\nu_{C=O}$); imidazole, 3080, 2800, 860 cm^{-1}. Found: C, 33.85; H, 4.50; N, 23.58%. Calcd for $C_5H_7N_3O_2\cdot HCl$: C, 33.80; H, 4.51; N, 23.66%.

Rate Measurements. The rate of reaction of hydroxamic acids with PNPA was determined by following the formation of the *p*-nitrophenolate anion at 401 nm. A 1-cm cell was employed for the hydrolysis of PNPA at low concentrations. On the other hand, when high PNPA concentrations were used in order to observe the burst kinetics, a 0.9-cm spacer was inserted into the 1-cm cell.

Results

pK_a *Determination.* Imidazolecarbohydroxamic acids I and II possess the following three dissociation processes:

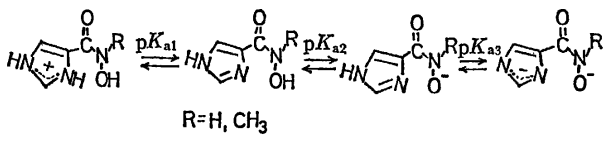

(1)

The pK_a values for the first two processes can be readily determined by the potentiometric titration. The titration was carried out by using a Toa pH stat system, using a jacketed titration vessel. Water was circulated from a constant temperature bath and 0.1 N alkali was added in 0.05-m*l* portions from an autoburet. The pK_{a3} value was difficult to determine by this method.

Two dissociation processes are present for imidazole derivative III, and its pK_{a1} was determined by the potentiometric titration.

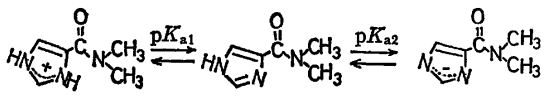

(2)

The pK_a values for the dissociation of the imidazole proton were difficult to determine by the potentiometric titration, because they are above 10.

The UV titration can be employed for the pK_a determination by using the characteristic absorption of each species.[9]

$$pK_a = pH + \log\frac{OD_I - OD}{OD - OD_M} \quad (3)$$

where OD_I: absorbance of the ionic species at a given wavelength, OD_M: absorbance of the neutral species and OD: absorbance of species mixtures. The above equation is transformed to

$$OD = OD_I - \frac{1}{K_a}[H^+](OD - OD_M) \quad (4)$$

The hydroxamate anion possesses a characteristic UV absorption maximum at *ca.* 270 nm. In the case of hydroxamic acid I, UV spectra showed a complex variation with pH and an attempt to determine pK_a was unsuccessful. An anionic species in which proton on the hydroxamic acid nitrogen is dissociated may exist at higher pH's, in addition to those shown in Eq. (1).

The dissociation behavior of hydroxamic acid II is simpler than that of I. Assuming that only the monoanionic species exist at pH 12, OD_I (300 nm) = 0.740 and OD_M (300 nm) = 0.009 were obtained at pH 12 and pH 2, respectively (30 °C, 28.9 v/v% EtOH–H_2O, [I] = 1.13×10^{-4} M). The OD values were determined in the pH range of 8.3 to 9.3, and pK_{a2} was obtained from those data, using Eq. (3). The pK_{a3} value was not obtainable by this method.

The determination of the pK_{a2} value of III from Eq. (3) was not possible, because the accurate determination of OD_I was difficult. Eq. (4) is useful in this case. Thus, OD (280 nm) was measured at pH 10 to 13, and plotted against $[H^+](OD - OD_M)$ (OD_M = 0.005, [III] = 2.06×10^{-4} M). A good linear relationship was obtained (correlation coefficient = 0.9998), and OD_I and pK_a were determined to be 0.300 and 12.09, respectively. These results are summarized in Table 1.

Reaction of I with PNPA. The hydroxamate anion reacts with PNPA quite readily to yield acetyl hydroxamate and *p*-nitrophenol.[10-13]

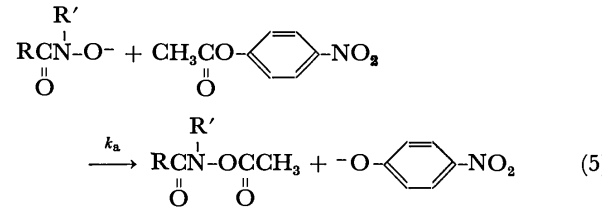

(5)

The reaction can be followed very readily by the release of the *p*-nitrophenolate anion. Since PNPA hydrolyzes spontaneously, the overall rate v is composed of the catalytic and spontaneous terms.

$$v_{total} = v_{cat} + v_{spont} \quad (6)$$

When hydroxamic acid I (1.98×10^{-4} M) was reacted with an excess of PNPA (3.86×10^{-3} M) at 30 °C, pH 8.92, *p*-nitrophenol (2.28×10^{-4} M) was released within one minute and further release was not observed, apart from the spontaneous hydrolysis. The amount of *p*-nitrophenol released approximately corresponded to that of the hydroxamic acid. This means that the acetyl transfer occurred quantitatively according to Eq. (1), and that the acetyl hydroxamate formed is too stable to regenerate hydroxamic acid.

The acetylation reaction was further investigated under the pseudo-first-order condition ([HA] ≫ [PNPA]), and $k_{a,obs}$ was determined by

$$k_{total} = k_{a,obs}[HA]_0 + k_{spont} \quad (7)$$

$$\log\frac{OD_\infty}{OD_\infty - OD_t} = \frac{k_{total}\cdot t}{2.303} \quad (8)$$

Table 1. pK_a values[a]

Compound	pK_{a1}	pK_{a2}	pK_{a3}
I	3.52	9.43	>12[c]
II	4.50	8.90, 8.81[b]	>12[c]
III	4.30	12.1[b]	—
Benzohydroxamic acid	9.36	—	—

a) Determined by the potentiometric titration. 30 °C, aqueous ethanol (ethanol content: 20—30 v/v%). b) Determined by UV titration. The pK_{a2} value of II from the UV titration is less reliable than that obtained by the potentiometric titration and, therefore, not used for the calculation of rate data. c) Estimated from potentiometric titration.

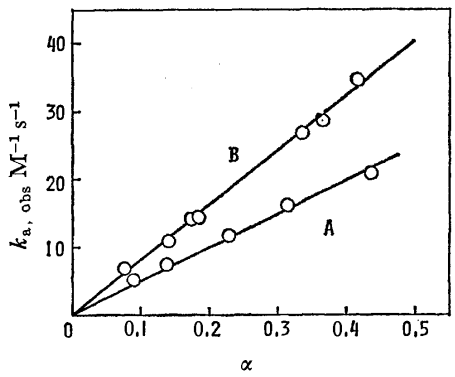

Fig. 1. Dependence of the rate constant of reaction between PNPA and hydroxamic acid upon the degree of dissociation of hydroxamic acids (α).
Reaction conditions: 30 °C, 28.9 vol% EtOH-H_2O, 0.1 M KCl, 0.15 M Barbital buffer.
A: benzohydroxamic acid, 1.88×10^{-3} M. PNPA, 4.07×10^{-5} M.
B: I, 4.44×10^{-4} M, 13.9×10^{-4} M or 17.3×10^{-4} M. PNPA, 3.85×10^{-5} M.

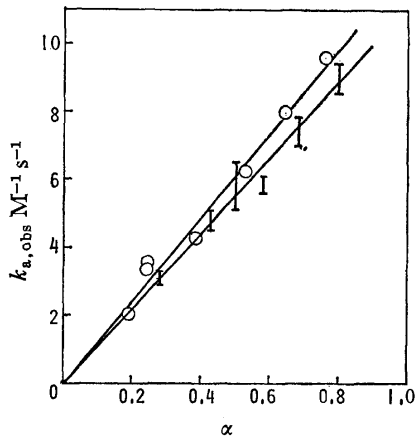

Fig. 2. Dependence of the rate constant of acylation of II by PNPA upon the degree of dissociation of the hydroxamic acid group (α).
Reaction condition: 30 °C, 28.9 vol%EtOH-H_2O, 0.1 M KCl, 0.15 M Barbital buffer.
The circle is the rate constant determined under the pseudo first-order condition. The vertical line indicates the range of $k_{a,obs}$ estimated from the burst kinetics (see Table 2).

where OD_∞ is the absorbance of *p*-nitrophenol at the infinite reaction time and OD_t is the absorbance at time *t*.

The reaction was carried out in the pH range of 8.3 to 9.3, and $k_{a,obs}$ was determined by using Eqs. (7) and (8). Figure 1 shows the relationship of $k_{a,obs}$ thus obtained and α (degree of dissociation of hydroxamic acid). A linear relationship was obtained (correlation coefficient=0.9987). Similar results were obtained for the reaction of benzohydroxamic acid and PNPA.

The k_a values (true second-order rate constant) determined from the slope of Fig. 1 were 80.4 and 50.0 M^{-1} s^{-1} for I and benzohydroxamic acid, respectively.

Reaction of II with PNPA. In the first place, the reaction of PNPA was carried out with large excesses of hydroxamic acid II: *i.e.*, under the pseudo-first-order condition. And $k_{a,obs}$ was determined by the use of Eqs. (7) and (8). The $k_{a,obs}$ value showed a linear dependence on α, as shown in Fig. 2. The true second-order rate constant k_a was determined to be 12.1 M^{-1} s^{-1} from the slope by the least squares method (correlation coefficient=0.9996).

Subsequently, when the reaction was carried out in the presence of large excesses of PNPA relative to II, typical burst reactions were observed: the initial rapid release of *p*-nitrophenol followed by the slower, steady release. This result suggests that the acetyl hydroxamate formed is hydrolyzed to a measurable degree and that the hydroxamate anion is regenerated.

The burst kinetics were analyzed according to the procedure of Bender *et al.*[14] The nucleophilic catalysis of the ester hydrolysis is expressed by

$$\begin{array}{c} C + S \xrightarrow{k_a} CS' \xrightarrow{k_d} C + P_2 \\ + \\ P_1 \end{array} \qquad (9)$$

where C, S and CS′ denote catalyst, ester substrate and acyl intermediate, respectively.

The formation of *p*-nitrophenol (P_1) is given by

$$[P_1] = At + B(1-e^{-bt}) \qquad (10)$$

where $A=a-(a/b)k_a[S]_0$, $B=(a/b^2)\cdot k_a\cdot[S]_0$, $a=k_a[C]_0-[S]_0$, and $b=k_a[S]_0+k_d$.

The rate constants may be determined by more than one method. However, the slope of the linear portion was rather small in the present system, and the following equations were employed for calculating rate constants in order to minimize the arithmetic erorr.

$$k_a = \frac{b}{[S]_0}\sqrt{\frac{B}{[C]_0}} \qquad (11)$$

$$k_d = b - k_a[S]_0 \qquad (12)$$

Since determination of the k_a and k_d values can sometimes involve large errors, the reaction was carried out many times at a given pH, and the undoubtedly erroneous data were discarded. The approximate agreement of the k_a values thus determined with those determined under the pseudo-first-order condition was a measure of the reliability of data. The resulting k_a and k_d values are summarized in Table 2. The k_a value for the hydroxamate anion was determined from the slope of $k_{a,obs}$ *vs.* α (Fig. 2) by the least-squares method to be 11.1 M^{-1} s^{-1}.

Reaction of III with PNPA. The hydrolysis of PNPA is catalyzed by imidazole compound III.

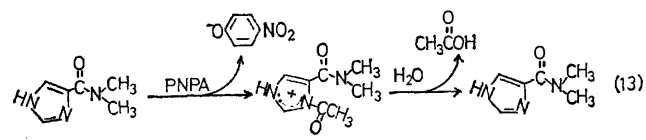

Supposedly, the formation of the acetylimidazole intermediate is rate-limiting, and the decomposition of acetylimidazoles is fast. The reaction was conducted under the pseudo-first-order condition ([III]≫

Table 2. Hydrolysis of PNPA catalyzed by II[a]

pH	Degree of dissociation of hydroxamic acid (α)	$k_{a,obs}$ $M^{-1}s^{-1}$	$10^4 \cdot k_{d,obs}$ s^{-1}
8.48	0.275	3.24, 3.11 3.35, (3.08)	5.55, 5.04 5.38, (5.92)
8.77	0.426	(5.48), 5.06, 5.09, 4.95, 4.64	(9.08), 7.06, 6.58, 8.75, 6.98
8.93	0.503	5.56, 5.17, 6.30, 6.45, 6.48	8.07, 8.74, 8.29, 7.51, (9.17)
9.04	0.580	5.60, 6.05, 5.80, 5.78	10.43, 10.53, 10.56, 10.00
9.24	0.686	7.05, 7.35, 7.64, 7.80, (8.57)	13.53, (8.87), 12.81, 13.98, 15.31, 16.08
9.50	0.799	9.02, 8.71, 8.56, 9.38, 9.25	17.72, 19.66, 18.14, (23.79), 17.96

a) 30 °C, 0.1 M KCl, 0.15 M Barbital, 28.9 vol% EtOH-H_2O, $[HA]_0=(6-8)\times10^{-4}$M, $[PNPA]=(5-14)\times10^{-3}$ M. The data in parenthesis are less reliable.

Table 3. Reaction of III with PNPA[a]

Reaction pH	$10^5 \cdot k_{total}$ s^{-1}	$10^5 \cdot k_{spont}$ s^{-1}	$10^2 \cdot k_{a,obs}$ $M^{-1}s^{-1}$
7.06	2.76	0.86	0.43[b]
7.84	3.11	1.92	0.26
8.43	7.40	4.82	0.58
9.08	22.0	15.2[c]	1.51
9.68	82.0	55.7	5.89

a) 30 °C, 0.1 M KCl, 0.15 M Barbital, 28.9 v/v% EtOH-H_2O, $[III]=4.46\times10^{-3}$ M, $[PNPA]=1.20\times10^{-4}$ M. b) Phosphate buffer, 0.15 M. c) Obtained at pH 9.04.

[PNPA]). The release of *p*-nitrophenol was quite slow, and, therefore, the rate constants (k_{total} and k_{spont}) were determined from the initial portion of the first-order plot. The results are summarized in Table 3. The $k_{a,obs}$ value increases rapidly above pH 9.

Hydrolysis of O-Acetyl Benzohydroxamate. O-acetyl benzohydroxamate was dissolved in aqueous alkali (pH 12) and the solution kept at 30 °C. Figure 3 shows the change of the UV spectra with time. An isosbetic point is found at 265 nm. After 24 hr, the spectrum became identical with that of the benzohydroxamate anion. The final concentration of the anion was calculated to be 3.38×10^{-5} M by using $\varepsilon=5150$ at $\lambda_{max}=268$ nm. The initial concentration of *O*-acetyl benzohydroxamate was 3.16×10^{-5} M.

These UV results imply that the following hydrolysis occurred.

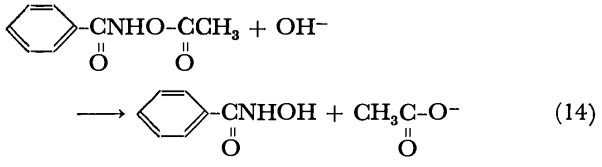

(14)

The half-life of the hydrolysis was estimated to be approximately 4 hr from the UV spectral change. The corresponding rate constant was *ca.* 10^{-5} s^{-1} at pH 12. The k_a value of acetyl isobutyro-*N*-methylhydroxamate is estimated to be 0.24 s^{-1} at pH 12.[13] The difference amounts to more than 10^4 fold.

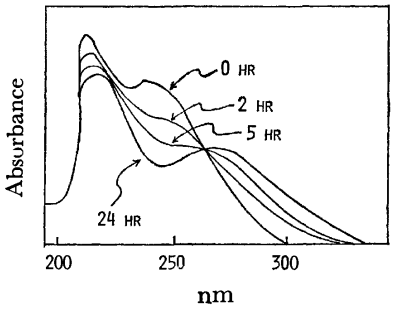

Fig. 3. Spectral change of aqueous acetyl benzohydroxamate.
pH 12, 30 °C.
Acetyl benzohydroxamate; 3.16×10^{-5} M.

The smooth hydrolysis observed for *O*-acetyl benzohydroxamate is not necessarily consistent with the literature. Dougherty and Jones[15] reported the occurrence of the Lossen rearrangement along with hydrolysis, and Hauser *et al.*[16,17] made a kinetic study for potassium *N,O*-dibenzoylhydroxylamine derivatives in 0.1 N aqueous ammonia.

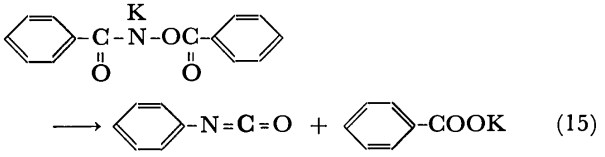

(15)

In contrast, the exclusive hydrolysis was observed in the present study. It is possible that the *O*-acetyl derivative is less prone to rearrange than the *O*-benzoyl counterpart.

Discussion

The object of the present study is two-fold. The hydroxamate anion is a very good nucleophile toward esters. However, the hydrolysis of acyl hydroxamate intermediates is very slow under ordinary reaction conditions, and the use of hydroxamic acids as catalyst for ester hydrolysis is limited. It was hoped that introduction of the neighboring imidazole group would facilitate the deacylation process. Secondly, the combination of a good oxygen nucleophile and the

Table 4. Rate constants of acetylation[a]

Hydroxamic acid	pK_a of hydroxamic acid group	k_a $M^{-1}s^{-1}$
I	9.43	80.4
II	8.90	12.1[b], 11.1[c]
Benzhydroxamic acid	9.36	50.0
Imidazole	6.70[d]	0.47

a) 30 °C, 28.9 vol% EtOH-H_2O, 0.1 M KCl, (0.15 M Barbital). b) Determined under the pseudo-first-order condition. c) Estimated from the burst kinetics. d) pK_a of imidazole.

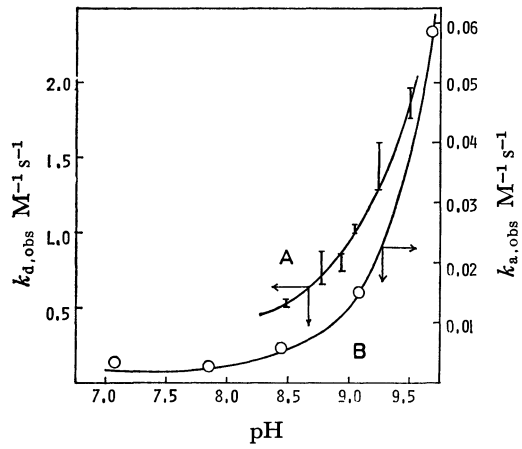

Fig. 4. pH Dependences of deacylation of the acetyl derivative of II(A) and acylation of III with PNPA (B).
Reaction condition: 30 °C, 28.9 vol%EtOH-H_2O, 0.1 M KCl, 0.15 M Barbital buffer.
The vertical line indicate the range of $k_{d,obs}$ estimated from the burst kinetics (see Table 2).

imidazole function resembles the charge relay system found at the active site of serine esterases, and an examination of this combination as a model enzyme system is important.

The powerful nucleophilicity of the hydroxamic acids employed are readily seen from the rate data of Table 4. The k_a value of hydroxamic acid I is greater than that of benzohydroxamic acid by 60%. This may be a reflection of the pK_a difference between the two hydroxamic acids (ΔpK_a=0.07), in consistence with a good Brønsted relationship (β=0.72) found by Dessolin *et al.*[11] for ring-substituted benzohydroxamic acids.

The smaller k_a value for II relative to that of I is not unexpected. The nucleophilic reactivity of *N*-alkylhydroxamic acids is several times lower than that of the corresponding *N*-unsubstituted hydroxamic acids, and the reason for this difference has been discussed previously.[12,18] The observed difference in nucleophilicity between I and II is a reasonable one, when compared with other examples.

The deacylation reaction of the acetyl derivative of I was very slow. In fact, the occurrence of deacylation could not be detected in the burst kinetics at pH 8 to 9. On the other hand, the deacylation step was clearly observed in the burst kinetics of the *N*-methylhydroxamic acid II.

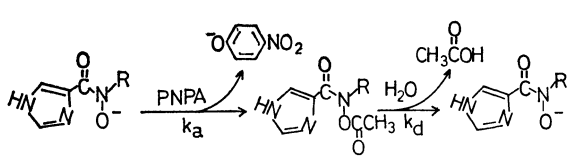

(16)

Figure 4 shows the pH dependence of the apparent rate constant of deacylation. The observed rate of deacylation is estimated to be much greater than those of simple hydroxamic acids. For example, $k_{d,obs}$ was 2.8×10^{-5} s^{-1} at pH 9 for acetyl *N*-phenylisobutyrohydroxamic acid.[13] The corresponding rate constant for acetylated II is 1×10^{-3} s^{-1}. This difference of almost 40 fold may suggest that deacylation is assisted by the intramolecular imidazole group, as we had conceived.

The intramolecular imidazole group can assist the hydrolysis of the acetyl intermediate by nucleophillic catalysis (A) and/or by general-base catalysis (B).

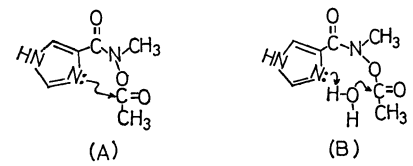
(A) (B)

In general, the general-base mechanism will be of greater significance compared with the nucleophilic mechanism in the hydrolysis of esters whose leaving groups are stronger bases than the imidazole catalyst.[19] The pK_a values of II are 8.9 for the hydroxamic acid group and 4.5 for the imidazole group. Therefore, the pK_a difference is 4.4, and the general-base mechanism B may be the preferred course of deacylation in the pH region where the neutral imidazole species plays a greater role. However, the anionic imidazole species (p$K_a\cong$12.5) is more important above pH 8 (see below) and the intramolecular attack of this species appears to be difinitely nucleophilic.

Bruice and Schmir found in the hydrolysis of PNPA with a large number of imidazole derivatives that imidazoles with values of pK_{a1} of 4.0 or lower owed their catalytic activity partially or primarily to the presence of their anionic species.[20] The increase of $k_{d,obs}$ at higher pH's (Figure 4) suggests the increasing involvement of the anionic imidazole group in the deacylation process. Unfortunately, the pK_{a3} value of II was not possible to determine by titration, and the efficiencies of intramolecular catalysis of the neutral and anionic imidazole species cannot be compared directly. However, pK_{a3} for II in 28.9% EtOH-H_2O may be estimated to be *ca.* 12.5 on the basis of the pK_a data shown in Table 1, by considering the difference of pK_a of the first and second deprotonations of III and the solvent change.

The following Brønsted rules have been reported for the nucleophilic attack of the neutral and anionic imidazole species.[20]

$$\log k_N = 0.8\ pK_{a1} - 4.30 \quad (17)$$

$$\log k_A = 0.15\ pK_{a2} + 1.35 \quad (18)$$

where k_N and k_A are rate constants for neutral and anionic imidazoles, respectively.

By substituting pK_a values (pK_{a1}=4.50, pK_{a2}=12.5), the relative rate constant (k_A/k_N) becomes *ca.* 10^4. The fraction of the anionic imidazole is about 10^{-3} at pH 9.5, the rest being the neutral species. Therefore, the anionic imidazole species is ten times more effective than the neutral species in the deacylation at pH 9.5. On the other hand, the anionic imidazole fraction is 4×10^{-5} at pH 8, and the contribution of the anionic imidazole species toward deacylation can be considered negligible below pH 8.

Quite the same conclusion is obtained for the reaction of PNPA with imidazole-4-carboxamide (III).

This reaction is a model reaction of deacylation of the acyl intermediate (compare Eqs. (13) and (16)).

As shown in Fig. 4, the $k_{a,obs}$ value does not change from pH 7 to 8.5 and then increases with pH rather rapidly. This increase is again considered to be a reflection of the involvement of the anionic imidazole species. The parallel tendency observed in Fig. 4 is not unexpected, since the pK_a values for the imidazole proton are very close in these imidazole compounds.

In conclusion, it was shown that a bifunctional catalyst containing the hydroxamate and imidazole functions, II, was effective in the hydrolysis of PNPA. The neighboring imidazole group appears to assist the decomposition of the acetyl hydroxamate intermediate. Unfortunately, the acceleration of deacylation is not remarkable. This may be attributed to the lower nucleophilicity of the imidazole group and/or to the possibly unfavorable arrangement of the two functional groups. Hopefully, superior hydrolytic catalyst systems will evolve from the study of compounds possessing various arrangements of the hydroxamate and imidazole functions.

The authors wish to express their appreciation to Mr. Y. Okahata and Miss R. Ando for their cooperation during the course of this study.

References

1) Contribution No. 328 from this department. Presented in part at the 29th meeting of the Chemical Society of Japan, Oct 1973, Hiroshima.
2) D. M. Blow, J. J. Birktoft, and B. S. Hartley, *Nature*, **221**, 337 (1969).
3) T. Kunitake, Y. Okahata, and R. Ando, *Macromolecules*, **7**, 140 (1974).
4) T. Kunitake and Y. Okahata, *Chem. Lett.*, **1974**, 1059.
5) I. Heilbron and H. M. Bunbury, "Dictionary of Organic Compounds," Oxford Univ. Press, New York, N.Y. (1953).
6) F. L. Pyman, *J. Chem. Soc.*, **109**, 186 (1916).
7) J. R. Tolter and W. D. Darby, "Organic Syntheses," Coll. Vol. 3, p. 460 (1955).
8) H. Wegner and R. Weidenhagen, *Ber.*, **70**, 7309 (1937).
9) A. Albert and E. P. Serjeant, "Ionization Constants of Acids and Bases. A Laboratory Manual," Methuen & Co. (1962), Chapt. 4.
10) M. Dessolin and M. Laloi-Diard, *Bull. Soc. Chem. Fr.*, **1971**, 2946.
11) M. Dessolin, M. Laloi-Diard, and M. Vilkas, *ibid.*, **1970**, 2573.
12) M. Dessolin, *Tetrahedron Lett.*, **1972**, 4585.
13) T. Kunitake, Y. Okahata, and R. Ando, This Bulletin, **47**, 1509 (1974).
14) M. L. Bender and T. H. Marshall, *J. Amer. Chem. Soc.*, **90**, 201 (1968).
15) G. Dougherty and L. W. Jones, *ibid.*, **46**, 1535 (1924).
16) W. B. Renfrow and C. R. Hauser, *ibid.*, **59**, 2308 (1937).
17) R. D. Bright and C. R. Hauser, *ibid.*, **61**, 618 (1939).
18) J. D. Aubort and R. F. Hudson, *Chem. Commun.*, **1970**, 938.
19) T. C. Bruice and S. J. Benkovic, "Bioorganic Mechanisms," Vol. 1., Benjamin, N.Y. (1966), p. 58.
20) T. C. Bruice and G. L. Schmir, *J. Amer. Chem. Soc.*, **80**, 148 (1958).

Infrared Spectra and Structure of Substituted Unsaturated Carbonyl Compounds. XIX. Four Component Conformational Equilibria in β-Ketoaldehyde *Trans* Enol Ethers

Janusz DABROWSKI and Michal TENCER
Institute of Organic Chemistry, Polish Academy of Sciences, 00-961 Warsaw, Poland

(Received January 7, 1974)

Acylic aliphatic *trans* β-alkoxy-α,β-unsaturated ketones, $R^1COCR^2{=}CHOR^3$, have been shown to exhibit restricted rotation around both the C_{sp^2}–C_{sp^2} and C_{sp^2}–O single bonds. The conformational equilibria between the *EZZ*, *EEZ*, *EZE* and *EEE* rotamers, estimated from comparison of the IR band intensities, are dependent on the steric requirements of the alkyl substituents. The sequence of the $\nu_{C=O}$ and $\nu_{C=C}$ vibrational frequences is $\nu_{C=O}$(*s-cis/O-s-trans*)>$\nu_{C=O}$(*s-cis/O-s-cis*)>$\nu_{C=O}$(*s-trans/O-s-trans*)>$\nu_{C=O}$(*s-trans/O-s-cis*)>$\nu_{C=C}$(*s-trans/O-s-trans*)>$\nu_{C=C}$(*s-trans/O-s-cis*)>$\nu_{C=C}$(*s-cis/O-s-trans*)>$\nu_{C=C}$(*s-cis/O-s-cis*). The wave number differences $\Delta\nu_{C=C}^{C=O}=\nu_{C=O}-\nu_{C=C}$ enable to classify the particular compounds according to their conformation in that $\Delta\nu_{C=C}^{C=O}$(*s-cis/O-s-trans*)=75—85 cm^{-1}, $\Delta\nu_{C=C}^{C=O}$(*s-cis/O-s-cis*)=80—100 cm^{-1}, $\Delta\nu_{C=C}^{C=O}$(*s-trans/O-s-trans*)=20—30 cm^{-1} and $\Delta\nu_{C=C}^{C=O}$(*s-trans/O-s-cis*)=35—50 cm^{-1}.

In studies on the rotational isomerism in α,β-unsaturated carbonyl compounds comparatively little attention has been paid to their β-alkoxy derivatives. Eistert *et al.*[1] were able to isolate the *cis* and *trans* methyl enol ethers of acetyloacetone. Their structure was subsequently confirmed by Awang[2] in his nuclear Overhauser effect and solvent shift ("ASIS") studies. In the same paper[2] a choice was made between the possible conformers resulting from restricted rotation around the C_{sp^2}–C_{sp^2} single bond, *i.e. s-cis* and *s-trans* rotational isomers. In many cases because of its unfavourable time scale NMR spectroscopy is unsuitable for detecting the individual rotamers and Awang's results must be considered only as an approximation. Therefore, it was of interest to us to study by means of IR spectroscopy a series of β-ketoaldehyde enol ethers capable of existing in these rotational forms. This technique has proved helpful in numerous investigations on rapid rotational equilibria.[3-9] In the dissertation by Giza[10] several spectra of β-alkoxy-α,β-unsaturated ketones were published but the resolution was obviously too low to reveal the band splittings observed in our work.

A further reason for the present study was the possibility of the simultaneous occurence of another restricted rotation, *viz.* that around the C_{sp^2}–O bond; the latter type of isomerism has been observed[11-13] in simple vinyl ethers.

Results and Discussion

As follows from the Introduction, in general, eight stereoisomeric forms are to be expected for β-alkoxy-α,β-unsaturated ketones having formula $R^1COCR^2{=}CHOR^3$. In our study their number is reduced to four however, as in all cases, due to thermodynamic considerations, only the *trans* (*E*) geometrical isomers were obtained. Four isomers are possible because of restricted rotation around the C_{sp^2}–C_{sp^2} and C_{sp^2}–O single bonds:

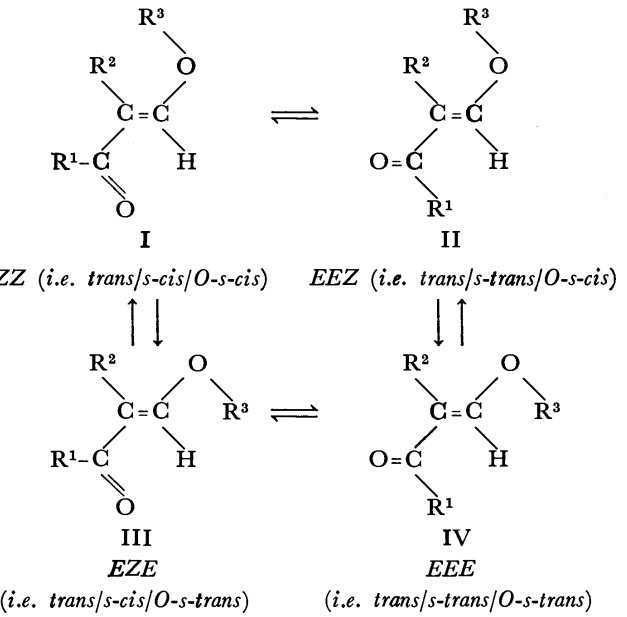

Since two IR bands, *viz.*, $\nu_{C=O}$ and $\nu_{C=C}$* are to be expected in the double bond stretching region for each of the isomers, their total number should amount to eight if all the isomers I—IV were present at equilibrium. Such is the case in the spectra of the methyl ketones (R^1=Me) **1**, **5**, and **6**. However, in all other cases investigated the number of bands was less, which can be explained either by the absence of some of these isomers or by coincidence of some of their bands.

The experimental data for the solutions in tetrachloroethylene are presented in Table 1.

In order to illustrate the relationship between band intensities and the bulkiness of the substituents R^1, R^2 and R^3 the IR spectra of the appropriate compounds are compared in Figures 1, 2, 4, and 5. The estimation of the populations of the rotamers are based on the reasonable assumption of approximately constant absorbances of the given absorptions for all the compounds investigated.

Let us consider first, for simplicity, the ketones for which the $\nu_{C=O}$ band is split into two components only, *i.e.* those other than **1**, **5**, and **6**. As can be seen from Fig. 1 presenting compounds with constant R^3=Me one band in the $\nu_{C=O}$ region (band B) and two bands

* Although it is obvious that the vibrations of the C=O and C=C groups are strongly coupled, nevertheless the bands, for simplicity, will be called $\nu_{C=O}$ and $\nu_{C=C}$.

TABLE 1. WAVE NUMBERS (cm^{-1}) OF ABSORPTION BANDS AND PROBABLE CONFORMATIONAL PREFERENCES OF *trans* β-ALKOXY-α,β-UNSATURATED KETONES $R^1COCR^2{=}CHOR^3$ (IN TETRACHLOROETHYLENE)

Compound	R_1	R_2	R_3	Concentration M	Absorption bands[a] $\nu_{C=O}$ *s-cis* *O-s-trans* A¹	*O-s-cis* A²	$\nu_{C=O}$ *s-trans* *O-s-trans* B¹	*O-s-cis* B²	$\nu_{C=C}$ *s-trans* *O-s-trans* C¹	*O-s-cis* C²	$\nu_{C=C}$ *s-cis* *O-s-trans* D¹	*O-s-cis* D²	Preferred conformation C_{sp^2}–C_{sp^2}	C_{sp^2}–O[b]
1	CH_3	H	CH_3	0.22	1697	1686	1675	1662	1648	1626	1615	1601	*s-cis*~*s-trans*[c]	*O-s-cis*>*O-s-trans*[d]
2	CH_3CH_2	H	CH_3	0.18	1697		1673		1645	1626	1617	1603	*s-cis*~*s-trans*	*O-s-cis*>*O-s-trans*
3	$(CH_3)_2CH$	H	CH_3	0.17	1693		1669		1642	1622	1611	1597	*s-cis*>*s-trans*	*O-s-cis*>*O-s-trans*
4	$(CH_3)_3C$	H	CH_3	0.14	1689		~1660[e]		—		1611	1596	*s-cis*	*O-s-cis*>*O-s-trans*[d]
5	CH_3	H	CH_3CH_2	0.18	1696	1679	1672	1660	1645	1622	1612	1598	*s-cis*~*s-trans*	*O-s-cis*~*O-s-trans*
6	CH_3	H	$(CH_3)_2CH$	0.13	1694	~1686 sh	1668	~1664 sh	1637	1617	1609	1592	*s-cis*~*s-trans*	*O-s-trans*>*O-s-cis*
7	$(CH_3)_2CH$	H	$(CH_3)_2CH$	0.13	1690		1665		1641	~1625 sh	1610	1591	*s-cis*>*s-trans*	*O-s-trans*>*O-s-cis*
8	$(CH_3)_3C$	H	$(CH_3)_2CH$	0.12	1686		~1660[e]		—		1607	1591	*s-cis*	*O-s-trans*>*O-s-cis*
9	$(CH_3)_3C$	H	$(CH_3)_3C$	0.11	1683		~1660[e]		~1635[e]		1602	~1588 sh	*s-cis*	*O-s-trans*
10	CH_3	CH_3	CH_3	0.17	1693		1667		1646	1625	1615	1604	*s-trans*>*s-cis*	*O-s-trans*~*O-s-cis* for the *s-cis* isomer *O-s-trans*>*O-s-cis* for the *s-trans* isomer
11	CH_3CH_2	CH_3	CH_3	0.17	1693		1667		1645	—	1617	—	*s-trans*>*s-cis*	*O-s-trans*

a) The spectra of all solutions were obtained in a standard cell of thickness 0.1 mm. b) In both the *s-cis* and *s-trans* isomers, if present, except for compound **10**. c) The variable temperature measurements showed some preference of the *s-trans* rotamer. d) Checked by the variable temperature study. e) Weak absorption of a probably non-planar form.

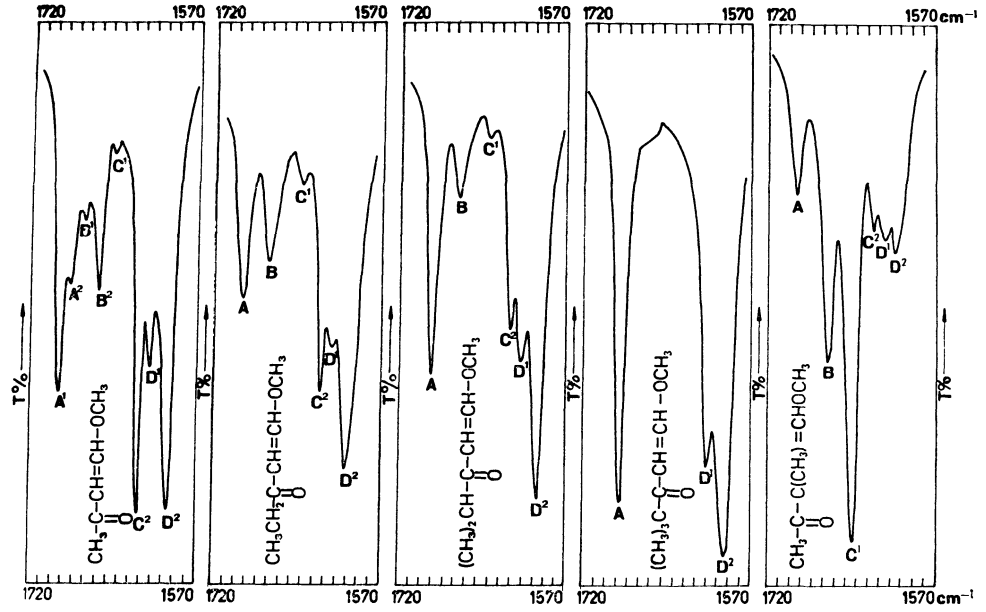

Fig. 1. Infrared spectra of compounds **1**, **2**, **3**, **4**, and **10** in tetrachloroethylene. Cell thicknesses and concentrations are given in Table 1.

in the $\nu_{C=C}$ region (bands C^1 and C^2) decrease in intensity with increasing size of the substituent R^1 in going from compound **2** to **3** and **4** while another $\nu_{C=O}$ band (band A) and two $\nu_{C=C}$ bands (D^1 and D^2) increase in the same sequence. On the basis of published data concerning other α,β-unsaturated systems[3–9] these intensity changes can be attributed to the shift of the equilibrium towards the *s-cis* rotamer due to growing steric interactions between R^1 and the β-hydrogen atom in the *s-trans* rotamer. Therefore, the decreasing bands B, C^1 and C^2 are assigned here to the $\nu_{C=O}$ and $\nu_{C=C}$ vibrations of the *s-trans* rotamers II and/or IV, and the increasing bands A, D^1 and D^2 are ascribed to the *s-cis* rotamers I and/or III. As shown further in the text (see the next page) the splittings of the bands C and D result from restricted rotation around the C_{sp^2}–O bond. This rotation is also responsible for the splitting of the bands A and B in the spectrum of the methyl ketone **1**.** Taking this splitting into account the band intensities of **1** fit very well to the sequence **1**, **2**, **3** and **4**.

A similar regularity occurs when comparing compounds **6**, **7** and **8**.

Solvent-induced intensity changes are in agreement with these assignments: when passing from hexane to tetrachloroethylene and particularly to the more polar tetrahydrofuran solutions an enhancement of the bands

** The IR spectrum of **1** has been published,[14] but no splitting of bands A, B, C and D was reported.

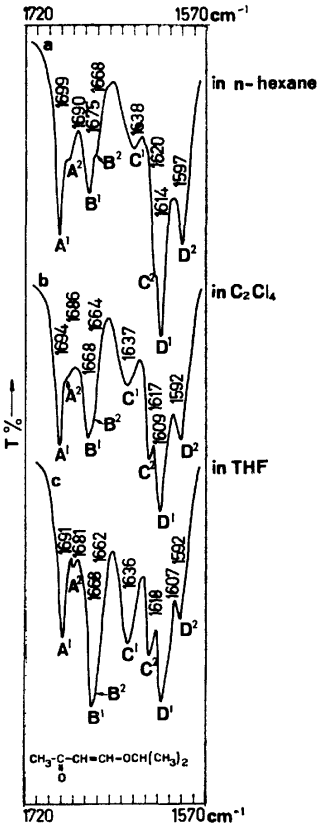

Fig. 2. Infrared spectra of compound **6**. (a) in *n*-hexane (b) in tetrachloroethylene (c) in tetrahydrofuran. Concentrations 0.13 M, cell thicknesses 0.1 mm.

B and C of the more polar *s-trans* form is observed (*e. g.* for **6**; Fig. 2).

The results concerning the *t*-butyl ketones **4**, **8** and **9** are remarkable in that a residual absorption near wave number characteristic of the *s-trans* form is still observed in spite of extremely high strain energy in this form. It seems likely that a twisted form is involved.

If R^2 is larger than hydrogen its non-bonded interactions with R^1 in the *s-cis* rotamers I and III increase dramatically[15] resulting in an equilibrium shift towards the *s-trans* rotamers II and IV as clearly seen from the relative intensities of the bands B and C^1+C^2 *vs.* A and D^1+D^2 (*e.g.* for compound **10**, see Fig. 1).

As already mentioned on the foregoing page, we believe that the splitting of bands A, B, C and D into two components is a consequence of the restricted rotation around the C_{sp^2}–O bond. This assumption finds convincing support in the intensity changes occuring on varying the steric requirements of the substituent R^3 and, in part, of R^2 and R^1. Like other rotational equilibria, the *O-s-cis*⇌*O-s-trans* equilibrium is dependent on electronic and steric factors. The latter can be estimated by comparing the corresponding interatomic distances in these two rotamers. Although it is virtually impossible to exactly calculate these distances, the approximation sufficient for the present purposes can be made by adopting the parameters obtained experimentally by Cahill, Gold and Owen[11b] for the *O-s-cis* isomer of the methyl vinyl

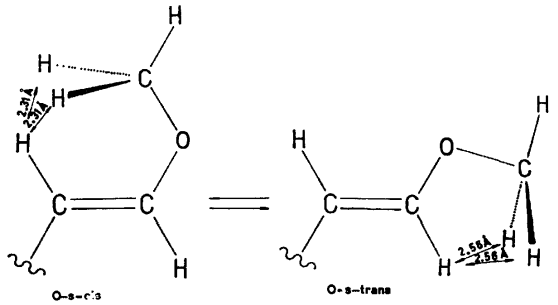

Fig. 3. H–H interatomic distances in *O-s-cis* and *O-s-trans* conformers of methyl enol ethers.

ether. In our analysis equal bond lengths and angles were taken for both the *O-s-cis* and *O-s-trans* conformations and no allowance was made for their distortion (*i.e.* optimalization was not attempted). The interatomic H–H distances were calculated for the most probable orientation of the methyl group. The strain differences thus deduced are undoubtedly even more pronounced for larger R^3 groups.

As can be seen from Fig. 3, the interatomic distance between the methyl hydrogens and the nearest vinylic hydrogen is considerably less in the *O-s-cis* rotamer. Nevertheless, this rotamer prevails in the methyl vinyl ether,[11] obviously due to electronic factors.[12]

Let us consider now the splitting of band D in compounds **4**, **8** and **9** having invariable R^1=*t*-Bu (see Fig. 4).

In the spectrum of the *O*-methyl derivative **4** the much more intense $\nu_{C=C}$ band D^2 can safely be ascribed to the energetically favoured rotamer, as proved by its diminution on raising the temperature. As follows from the above scheme, replacing of R=Me by a bulkier group should shift the equilibrium towards the *O-s-*

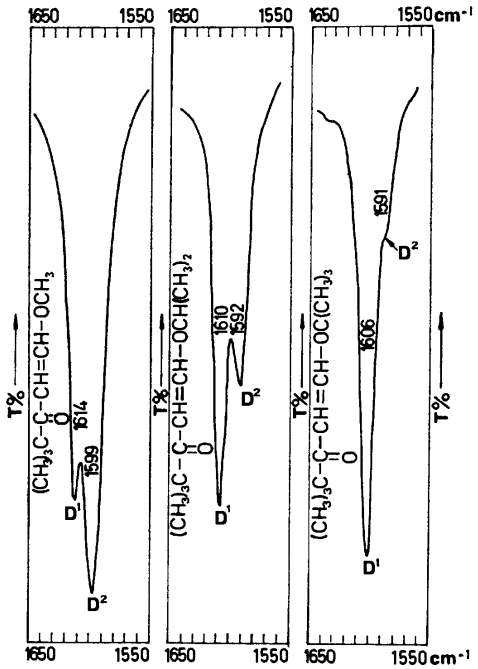

Fig. 4. Infrared spectra of compounds: **4** (concn 0.14 M) **8** (concn 0.12 M) and **9** (concn 0.11 M) in *n*-hexane. Cell thicknesses 0.1 mm.

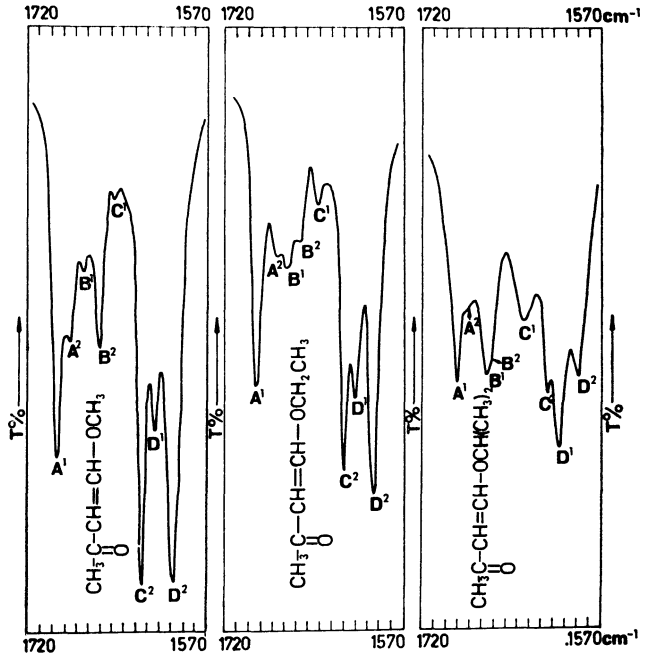

Fig. 5. Infrared spectra of compounds **1**, **5** and **6** in tetrachloroethylene. Concentrations and cell thicknesses are given in Table 1.

trans rotamer, assuming the electronic factor to be constant. Accordingly, the D^1 band which dramatically increases in the series **4**, **8**, **9** is ascribed here to this rotamer. Band D^2 which corresponds thus to the *O-s-cis* rotamer disappears almost completely when R^3=*t*-Bu, due to extremely high strain in this form.

Similar splittings and intensity changes due to the restricted rotation around the C_{sp^2}–O bond are always observed with band C (if present) and also with bands A and B, provided R^1=Me. In the latter case, the high frequency components of all the bands under consideration, *i.e.* A^1, B^1, C^1, and D^1, increase on the expense of the A^2, B^2, C^2, and D^2 ones along with increasing steric requirements of the R^3 group (see Fig. 5). Therefore, the index "1" is assigned to all bands of the *O-s-trans* rotamers and the bands of the *O-s-cis* ones are indexed "2". It should be noted that band A^1 of the *O-s-trans* rotamer has a very high absorbance as seen from its higher intensity *vs.* that of band A^2 in cases of prevailing *O-s-cis* conformation in **1**. The assignment of bands A^1 and A^2 is conclusively supported here by the enhancement of the former on the expense of the latter on going to higher temperature.

Substitution of R^2=H by a methyl group enhances the steric interactions not only with the substituent R^1, which was already discussed above, but also with R^3 in the *O-s-cis* isomers I and II. The resulting *O-s-cis*→*O-s-trans* equilibrium shift manifests itself in the increase of the intensities of bands C^1 and D^1 on the expense of C^2 and D^2 if the spectrum of **10** is compared with that of **1**. With the ethyl ketone **11**, the complete disappearance of band D^2 is readily explainable by the buttressing effect in the *s-cis* rotamer but no simple explanation can be offered for the simultaneous disappearance of band C^2. This point seems to deserve a separate investigation.

The sequence of the $\nu_{C=O}$ and $\nu_{C=C}$ vibrational frequencies proposed here follows that known for other types of unsaturated ketones[3-9] but is further differentiated by taking into consideration the *O-s-cis* and *O-s-trans* rotamers. Thus, $\nu_{C=O}$(*s-cis*/*O-s-trans*) > $\nu_{C=O}$(*s-cis*/*O-s-cis*) > $\nu_{C=O}$(*s-trans*/*O-s-trans*) > $\nu_{C=O}$(*s-trans*/*O-s-cis*) > $\nu_{C=C}$(*s-trans*/*O-s-trans*) > $\nu_{C=C}$(*s-trans-O-s-cis*) > $\nu_{C=C}$(*s-cis*/*O-s-trans*) > $\nu_{C=C}$(*s-cis*/*O-s-cis*). Moreover, the wave number differences $\Delta\nu_{C=C}^{C=O}=\nu_{C=O}-\nu_{C=C}$ corroborate the regularities established by Braude and Timmons[4] and Mecke and Noack[5] enabling at the same time to more precisely classify the particular compounds according to their conformation, especially for the *s-trans* conformation. As can easily be derived from Table 1, $\Delta\nu_{C=C}^{C=O}$(*s-cis*/*O-s-trans*) = 75—85 cm^{-1}, $\Delta\nu_{C=C}^{C=O}$(*s-cis*/*O-s-cis*) = 80—100 cm^{-1}, $\Delta\nu_{C=C}^{C=O}$(*s-trans*/*O-s-trans*) = 20—30 cm^{-1} and $\Delta\nu_{C=C}^{C=O}$(*s-trans*/*O-s-cis*) = 35—50 cm^{-1}.

Experimental

4-Methoxy-3-buten-2-one (**1**), bp 53—54 °C/7 mmHg, lit,[16a] 52—53 °C/4—5 mmHg, *1-methoxy-4-methyl-1-penten-3-one* (**3**), bp 74—75 °C/7 mmHg, lit,[16a] 61—62 °C/3.5 mmHg, *1-methoxy-4,4-dimethyl-1-penten-3-one* (**4**) bp 69—70 °C/5 mmHg, lit,[16a] 61 °C/3 mmHg and *1-methoxy-2-methyl-1-penten-3-one* (**11**), bp 80—81 °C/8 mmHg, lit,[16a] 70°C/4.5 mmHg were obtained according to standard procedure described by Royals and Brannock,[16a] *viz.*, by pyrolysis of the corresponding β-ketoaldehyde dimethylacetals[16b,17] in the presence of catalytic amount of sodium methoxide. These reactions, however, were carried out under more vigorous conditions than described in order to obtain products free of starting material. This modification resulted in considerable lowering of the yield.

The same method was applied for obtaining of *1-methoxy-1-penten-3-one* (**2**), bp 65 °C/7 mmHg, lit,[18] 94 °C/15 mmHg from *1,1-dimethoxypentan-3-one*[18] and of *4-methoxy-3-methyl-3-buten-2-one* (**10**), bp 84—85 °C/10 mmHg, lit,[19b] 62—64 °C/4 mmHg, lit,[20] 83—86°C/10 mmHg from *4,4-dimethoxy-3-methylbutan-2-one*.

4-Ethoxy-3-buten-2-one(**5**): *1-Diethoxybutan-3-one*[19b] was heated with solid sodium ethoxide (3 per cent by weight) in an oil bath at 190°C while ethanol was removed by distillation at atmospheric pressure. After the distillation of ethanol has been finished (approx. 3 hr), the vacuum distillation was carried out yielding **5**, bp 87—89 °C/17 mmHg, lit,[21] 91—93° C/20 mmHg.

4-Isopropoxy-3-buten-2-one (**6**) and *1-isopropoxy-4-methyl-1-penten-3-one* (**7**) were prepared as follows:
To a solution of corresponding chlorovinylketone[22] in 2-propanol cooled to −15 °C an excess of a solution of potassium hydroxide in 2-propanol was dropped. The mixture was then allowed to reach the room temperature, stirred for 4 hr, poured out into water and extracted with ether. The ethereal layer was worked up in usual manner. The distillation *in vacuo* afforded a mixture of **6** or **7** and corresponding diisopropyl β-ketoacetal. The mixture thus obtained was heated in a distillation flask with 3 per cent by weight of solid potassium isopropoxide in an oil bath at 190—200 °C, while isopropanol distilled. After loss of 2-propanol had stopped (approx. 4 hr) the product was distilled *in vacuo*, affording **6**, bp 88 °C/15 mmHg lit,[18] 98—102 °C/12 mmHg, lit,[21] 112—118 °C/65 mmHg or **7**.

1-Isopropoxy-4,4-dimethyl-1-penten-3-one (**8**): An excess of saturated isopropanolic solution of hydrogen chloride was added to a solution of sodium salt of hydroxymethylenepinacoline (obtained from pinacoline, ethyl formate and

sodium) in 2-propanol. The mixture was then stirred for 3 hrs alkalized with 2-propanolic potassium hydroxide, poured out into water and extracted with ether. The ethereal layer was worked up in usual manner. The distillation *in vacuo* afforded a mixture of **8** and corresponding diisopropyl β-ketoacetal. The mixture was pyrolized in the same manner as described above.

1-t-Butoxy-4,4-dimethylpenten-1-one-3 (**9**) was obtained by the method analogous to that of Seifert and Schinz[23]: In a flask fitted with a reflux condenser and a water separator was placed hydroxymethylenpinacoline, equimolar amount of *t*-butyl alcohol, catalytic amount of *p*-toluenesulphonic acid and a large excess of benzene. The mixture was boiled for 16 hours while water was removed by azeotropic distillation. The mixture was then washed with aqueous sodium bicarbonate and water and benzene was removed. Vacuum distillation gave an oil which solidified immediately. Twofold sublimation of the resulting solid at 0.8 mmHg gave pure **9**.

Physical properties and analytical data for the three new compounds are given below.

Compound	Bp (°C/mmHg)	Mp (°C)	%C Calcd (Found)	%H Calcd (Found)
7	75—76/3 mmHg	—	69.19 (69.00)	10.32 (10.60)
8	71—72/2.5 mmHg	—	70.54 (70.55)	10.66 (10.63)
9	—	72	71.69 (71.74)	10.94 (11.08)

Bp and mp were not corrected.

Structures of all the compounds **1**—**11** were confirmed by NMR spectra (Table 2).

Infrared spectra were recorded on a Perkin-Elmer 325 spectrometer with a spectral slit width of 0.7—0.9 cm^{-1} and a scanning speed of 0.8 $cm^{-1} \cdot s^{-1}$. Better spectral parameters gave no better resolution. Commercial "for spectroscopy" solvents were used. The substances investigated were freshly distilled or sublimed before the measurements. Preparative thin layer chromatography was used where necessary. The spectra were calibrated with polystyrene.

NMR spectra were recorded on Varian HA-60/IL and JEOL JNM-4H-100 instruments.

TABLE 2. ^{1}H-NMR CHEMICAL SHIFTS OF β-KETOALDEHYDE *trans* ENOL ETHERS (ppm; in CCl_4)

$$C^{1}-C^{2}-C^{3}=C^{4}-O-C^{5}-C^{6}$$
$$\underset{O}{\overset{\|}{}} \quad \underset{H}{\overset{|}{}} \text{ (or } C^{7})$$

Compound[a]	1	2	3[b]	4[b]	5	6	7
1	—	2.09	5.47 d	7.47 d	3.70	—	—
2	1.03 t	2.39 q	5.49 d	7.49 d	3.70	—	—
3	1.08 d	2.57 spt	5.54 d	7.48 d	3.72	—	—
4	1.07	—	5.72 d	7.36 d	3.62	—	—
5	—	2.11	5.51 d	7.50 d	3.96 q	1.36	—
6	—	2.03	5.42 d	7.30 d	4.20 spt	1.23 d	—
7	1.00 d	2.47 spt	5.49 d	7.31 d	4.17 spt	1.25 d	—
8	1.13	—	5.82 d	7.34 d	4.21 spt	1.32 d	—
9	1.12	—	5.87 d	7.55 d	—	1.40	—
10	—	2.10	—	7.10	3.83	—	1.61
11	1.04 t	2.47 q	—	7.26	3.84	—	1.63

a) See Table 1. b) The coupling constant J_{34} in compounds 1—9 equals 12—13 Hz.

The authors are indebted to Dr. K. Kamieńska-Trela for helpful discussions and to Dr. U. Dabrowska, Dr. I. Ratajczyk and Mrs. E. Lewandowska for assistance in obtaining the IR spectra.

This work is a part of the Polish Academy of Sciences Programme for Structural Research (PAN-3).

References

1) B. Eistert, F. Arndt, L. Loewe, and E. Ayca, *Chem. Ber.*, **84**, 156 (1951).
2) D. V. C. Awang, *Can. J. Chem.* **49**, 2672 (1971).
3) J. Kossanyi, *Bull. Soc. Chim. Fr.*, (**1965**), 704.
4) E. A. Braude and C. J. Timmons, *J. Chem. Soc.*, **1955**, 3766.
5) R. Mecke and K. Noack, *Chem. Ber.*, **93**, 210 (1960).
6) (a) R. L. Erskine and E. S. Waight, *J. Chem. Soc.*, **1960**, 3425; (b) E. S. Waight and R. L. Erskine, "Steric Effects in Conjugated Systems," Butterworths (1958), p. 73.
7) (a) J. Dabrowski and K. Kamieńska-Trela, *Spectrochim. Acta*, **22**, 211 (1966); (b) J. Dabrowski and U. Dabrowska, *Chem. Ber.*, **101**, 3392 (1968); (c) J. Dabrowski and K. Kamieńska-Trela, This Bulletin, **39**, 2565 (1966); (d) J. Dabrowski and J. Terpiński, *J. Org. Chem.*, **31**, 2159 (1966); (e) J. Dabrowski, K. Kamienska-Trela, and A. J. Sadlej, *J. Mol. Struct.*, **12**, 185 (1972) and refernces cited in these papers.
8) R. Barlet, M. Montagne and P. Arnaud, *Spectrochim. Acta*, **25A**, 1081 (1969).
9) A. Bienvenüe, *J. Amer. Chem. Soc.*, **95**, 7345 (1973).
10) Y. C. Giza, Dissertation, Univ. of Massachusetts, Amherst Univ. Microfilms, Order No. 64-7123.
11) (a) N. L. Owen and N. Sheppard, *Trans. Faraday Soc.*, **60**, 634 (1964); (b) P. Cahiel, L. P. Gold, and N. L. Owen, *J. Chem. Phys.*, **48**, 1629 (1968) (c) N. L. Owen and V. M. Seip, *Chem. Phys. Lett.*, **5**, 162 (1970).
12) B. Cadioli and M. Pinceli, *J. Chem. Soc., Faraday II*, **1972**, 991.
13) F. Marsault-Herail, G. S. Chiglien, J. P. Dorie, and M. L. Martin, *Spectrochim. Acta*, **29A**, 151 (1973).
14) S. Hoffmann and E. Mühle, *Z. Chem.*, **9**, 65 (1969).
15) J. Dabrowski and Z. Świstun, *Tetrahedron*, **29**, 2261 (1973).
16) (a) E. E. Royals and K. C. Brannock, *J. Amer. Chem. Soc.*, **76**, 3041 (1954); (b) E. E. Royals and K. C. Brannock, *ibid.*, **75**, 2050 (1953).
17) (a) A. N. Nesmeyanov, N. K. Kochetkov, and M. I. Rybinskaya, *Izv. AN SSR, Otd. Khim. Nauk*, **1951**, 395; (b) C. C. Price and J. A. Pappalardo, *J. Amer. Chem. Soc.*, **72**, 2631 (1950); (c) J. Nelles, U.S. Patent 8091373 (1937).
18) P.R. Hills and F. J. McQuillin, *J. Chem. Soc.*, **1953**, 4060.
19) (a) S. Sugasawa, S. Yamada and M. Narahashi, *J. Pharm. Soc. Japan*, **71**, 1345 (1951); (b) S. Sugasawa, Y. Ban and R. Mochizuki, *ibid.*, **69**, 82 (1949).
20) L. R. Fedor, N. C. De, and S. K. Gurwara, *J. Amer. Chem. Soc.*, **95**, 2905 (1973).
21) A. Spassky-Pasteur and H. Rivière, *Bull. Soc. Chim. Fr.*, **1969**, 811.
22) A. N. Nesmeyanov, N. K. Kochetkov, and M. I. Rybinskaya, *Izv. AN SSSR, Otd. Khim. Nauk*, **1951**, 350.
23) P. Seifert and H. Schinz, *Helv. Chim. Acta*, **84**, 728 (1951).

NOTES

BULLETIN OF THE CHEMICAL SOCIETY OF JAPAN, VOL. 48(4), 1315—1316 (1975)

The Formation of Crystalline Complexes between Inosine and Several Hydroxybenzoic Acids

Yoshihisa SUZUKI and Kentaro HARA

Central Research Laboratories, Ajinomoto Co., Inc., Suzuki-cho, Kawasaki 210

(Received June 15, 1974)

Synopsis. Inosine was found to form 1 : 1 crystalline complexes with 2,4-, 2,5-, 2,6-, 3,4-, 3,5-dihydroxybenzoic acids, and with 3,4,5-trihydroxybenzoic acid, but was found to give no crystalline complex with benzoic acid, *o*-, *m*-, *p*-hydroxybenzoic acids, 2,3-dihydroxybenzoic acid, or 2,3,4-trihydroxybenzoic acid.

Several nucleic acid bases, such as adenine and cytosine, have been known to form crystalline intermolecular complexes with benzoic acid or monohydroxybenzoic acids.[1] One of the ribonucleotides, 5′-guanylic acid, has also been known to form crystalline complexes with several hydroxybenzoic acids.[2] On the basis of these facts, ribonucleosides have also been interested to form crystalline intermolecular complexes with benzoic acid or hydroxybenzoic acids.

The present paper will deal with a study of the complex-formation of inosine or guanosine with several hydroxybenzoic acids. Inosine has been known to be a good counterpart for complex-formation with other organic substances, since only inosine, from among several ribonucleosides, has been demonstrated to form a 1 : 1 stable crystalline intermolecular complex with L-tryptophan[3,4] or with D-tryptophan.[3] On the other hand, no crystalline complex has ever been known between guanosine and other organic compounds, whereas interaction in the solution has been reported.[4]

An equimolar aqueous solution of the benzoic acid and the nucleoside was evaporated to dryness, and the resultant solid was examined by means of the X-ray powder diffraction method.

The results obtained are shown in Table 1. They are of interest, but not fully convincing. No acid—benzoic acid, *o*-, *m*-, or *p*-monohydroxybenzoic acid—showed any evidence of the complex-formation in the crystalline solid with inosine giving a mixture of the two components, whereas all of these benzoic acids are known to give crystalline complexes with adenine or cytosine.[1] The five dihydroxybenzoic acids (2,4-, 2,5-, 2,6-, 3,4-, and 3,5-), but not the 2,3-isomer and 3,4,5-trihydroxybenzoic acid, have been associated with inosine to give the corresponding crystalline complexes as is summarized in Tables 2 and 3, while 2,3,4-trihydroxybenzoic acid has not.

TABLE 1. THE FORMATION OF THE CRYSTALLINE INTERMOLECULAR COMPLEXES BETWEEN INOSINE AND SEVERAL HYDROXYBENZOIC ACIDS

Benzoic acid	−
o-Monohydroxybenzoic acid	−
m-Monohydroxybenzoic acid	−
p-Monohydroxybenzoic acid	−
2,3-Dihydroxybenzoic acid	−
2,4-Dihydroxybenzoic acid	+
2,5-Dihydroxybenzoic acid	+
2,6-Dihydroxybenzoic acid	+
3,4-Dihydroxybenzoic acid	+
3,5-Dihydroxybenzoic acid	+
2,3,4-Trihydroxybenzoic acid	−
3,4,5-Trihydroxybenzoic acid	+

The ionization constants of the benzoic acids are not available to aid in interpreting the specific capability of complex-formation between inosine and the selected benzoic acids. For example, the ionization constant of 2,3-dihydroxybenzoic acid (1.14×10^{-3})[5] exhibits no significant difference from those of the 2,4-isomer (5.16×10^{-4}),[5] the 2,5-isomer (1.3×10^{-3}),[5] and the 2,6-isomer (6×10^{-2}).[5] The information obtained in this study was that the phenolic hydroxyl groups of more than two in the benzoic acid may be important in forming crystalline complexes, and that such an arrangement in the structure as 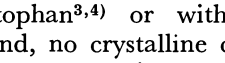 may prevent the complex-formation with inosine. This information suggests that the hydrogen bonding may play an important role in the formation of the present crystalline molecular complexes.

The large crystals of the complexes were obtained from a dilute equimolar aqueous solution of the two components. The stoichiometry in the complexes was 1 : 1 without exception, while the number of the water of crystallization varied case by case between zero and three moles per mole of inosine (Table 2). Table 3 shows the X-ray powder diffraction data of the new complexes obtained in the present study.

Guanosine failed to form any crystalline molecular complex with any of those benzoic acids to give a mixtures of the two components. The characteristic properties of inosine to form a crystalline complex with several hydroxybenzoic acids were thus demonstrated in this study.

Experimental

Materials. The nucleosides and the benzoic acids were obtained from the Ajinomoto Co., Inc., and the Tokyo Kasei Co., respectively.

Examination of the Complex-Formation. An equimolar amount of inosine (or guanosine) and one of the benzoic acids were dissolved together in water, and the solution was evaporated to dryness in a desiccator. The resultant

Table 2. The analytical results of the crystalline intermolecular complexes between inosine and several hydroxybenzoic acids

Complex	Mp (°C)	Component (%)			Elementary analysis (%)		
		I[1]	HBA[2]	W[3]	C	H	N
Found Inosine·2,4-DihydroxyBA[4]	187—189	65.4	36.6	0.2	47.93	4.33	13.34
Calcd for $C_{10}H_{12}N_4O_5 \cdot C_7H_6O_4$		63.5	36.5	0.0	48.34	4.30	13.27
Found Inosine·2,5-DihydroxyBA	86—90	57.9	35.0	8.2	44.61	4.92	12.19
Calcd for $C_{10}H_{12}N_4O_5 \cdot C_7H_6O_4 \cdot 2H_2O$		58.5	33.6	7.9	44.54	4.84	12.22
Found Inosine·2,6-DihydroxyBA	81—83	57.3	34.5	10.0	44.02	5.32	11.85
Calcd for $C_{10}H_{12}N_4O_5 \cdot C_7H_6O_4 \cdot 2.5H_2O$		57.5	32.9	9.6	43.68	4.96	11.98
Found Inosine·3,4-DihydroxyBA	189—193	58.8	33.2	8.3	44.46	4.83	11.80
Calcd for $C_{10}H_{12}N_4O_5 \cdot C_7H_6O_4 \cdot 2H_2O$		58.5	33.6	7.9	44.54	4.84	12.22
Found Inosine·3,5-DihydroxyBA	110—113	56.6	31.6	11.4	42.92	5.22	11.49
Calcd for $C_{10}H_{12}N_4O_5 \cdot C_7H_6O_4 \cdot 3H_2O$		56.3	32.4	11.3	42.86	5.08	11.76
Found Inosine·3,4,5-TrihydroxyBA	163—165	58.1	34.7	7.4	42.98	5.02	11.94
Calcd for $C_{10}H_{12}N_4O_5 \cdot C_7H_6O_5 \cdot 2H_2O$		56.5	35.9	7.6	43.04	4.67	11.81

1) I: Inosine. 2) HBA: Hydroxybenzoic acid. 3) W: Water. 4) BA: Benzoic acid.

Table 3. The x-ray powder diffraction data of several inosine-hydroxybenzoic acid complexes

1[a]		2[b]		3[c]		4[d]		5[e]		6[f]	
d (Å)	I/I_0	d (Å)	I/I_0	d (Å)	I/I_0	d (Å)	I/I_0	d (Å)	I/I_0	d (Å)	I/I_0
5.83	70	13.00	15	10.53	80	8.59	15	10.78	50	10.05	40
5.87	30	10.53	60	8.67	70	8.04	20	9.72	40	9.61	30
5.34	20	8.67	80	6.56	30	7.44	20	6.46	100	6.81	20
4.77	100	6.97	40	6.46	30	7.95	50	4.65	20	6.37	40
4.17	20	6.51	30	5.79	50	5.72	50	3.97	20	5.40	30
3.87	30	5.68	100	5.64	90	4.98	30	3.43	20	4.77	50
3.62	30	5.28	30	4.87	30	4.72	40	3.34	20	4.48	30
3.53	50	4.87	30	4.82	30	4.23	40	3.23	20	4.40	50
		4.80	30	3.27	100	4.13	40	3.19	15	3.63	100
		4.35	40	3.23	70	3.44	100	3.15	15	3.49	70
		3.27	70								
		3.21	70								

The scale of intensity (I/I_0) is so chosen as to make the most intense line have the value 100.
a) Inosine—2,4-Dihydroxybenzoic acid Complex (anhydrate). b) Inosine—2,5-Dihydroxybenzoic acid Complex (2 hydrate). c) Inosine—2,6-Dihydroxybenzoic acid Complex (2.5 hydrate). d) Inosine—3,4-Dihydroxybenzoic acid Complex (2 hydrate). e) Inosine—3,5-Dihydroxybenzoic acid Complex (3 hydrate). f) Inosine—3,4,5-Trihydroxybenzoic acid Complex (2 hydrate).

solids were examined by means of the X-ray powder diffraction method, and their data were compared with those of mechanical mixtures of the two components.

The Crystallization of the Complexes. Inosine (13.4 g) was dissolved in water (160 ml) with heating, and then one of the hydroxybenzoic acids (0.05 M) was stirred, drop by drop, into this solution at 40 °C over a 2-hr period. After the mixture had then been cooled to 0—5 °C for 3 hr, the crystals precipitated were filtered and analyzed.

Analysis. Paper chromatography was carried out on Toyo-Roshi No. 51A, with the *n*-butanol—acetic acid—water (4 : 1 : 1) solvent system, and the components of the crystals were determined by comparing the UV absorption at the maximum wavelength with the standard references. The water of crystallization was determined by Karl-Fischer titration.

References

1) C. Tamura, N. Sakurai, and S. Sato, This Bulletin, **44**, 1473 (1971).
2) Y. Suzuki, T. Toki, A. Fukuda, and T. Hirahara, Japan. Pat. 46-4380 (1971).
3) Y. Suzuki, T. Hirahara, T. Akashi, and T. Nakamura, U. S. Pat. 3532684 (1970); Brit. 1180635 (1970); Fr. 1601066 (1970); West Ger. Offen. 1645977 (1970).
4) I. Ibáñez, M. Pieber, and J. C. Tohá, *Z. Naturforsh. C*, **28**, 385 (1973).
5) "Encyclopedia Chimica", Kyoritsu Publishers, Tokyo (1960).

BULLETIN OF THE CHEMICAL SOCIETY OF JAPAN, VOL. 48(4), 1317—1318 (1975)

Dielectric Relaxation and Molecular Structure. XIV. The Dielectric Behavior of Six Isomeric Pentyl Alcohols

Hiroshi SATO, Taro KOSHII, Hiroaki TAKAHASHI, and Keniti HIGASI

Department of Chemistry, Waseda University, Shinjuku, Tokyo 160

(Received October 17, 1974)

Synopsis. The dielectric constants and losses of six isomeric pentyl alcohols have been measured in the frequency range of 1—0.35 GHz at 25 °C. The relaxation times of these alcohols decrease with an increase in the steric hindrance of the hydroxyl group.

Low-frequency measurements at room temperature showed that both the dielectric constants, ε_0, and the Kirkwood correlation factors, g, decrease with an increase in the steric hindrance of the hydroxyl groups of butanol,[1,2] heptanol,[3,4] and octanol.[5] Few repotrs are available, however, regarding the dependence of the relaxation times upon the isomeric configuration, especially in the liquid state at room temperature.[5-7] Emphasis will be placed in this report on the dielectric relaxation of six isomeric pentyl alcohols at 25 °C.

Experimental

Commercial chemicals were dehydrated by the usual methods and were fractionally distilled prior to their use. In order to check the purity of the samples, the refractive indices for the Na D line were measured with a Pulfrich refractometer. Both the boiling points and the refractive indices of the purified samples were in good agreement with the literature values[8,9]; 1-pentanol, bp=138.2—140.0 °C, n_D=1.408; 3-methyl-1-butanol, bp=131.0—131.2 °C, n_D=1.406; 2-pentanol, bp=118.8—119.2 °C, n_D=1.405; 3-pentanol, bp=113.6—115.0 °C, n_D=1.408; 3-methyl-2-butanol, bp=112.2 °C, n_D=1.407; and 2-methyl-2-butanol, bp=102.8—103.2 °C, n_D=1.403.

The dielectric constants and losses were measured at the frequencies of 0.356, 0.515, 0.601, 0.697, 0.807, and 1.00 GHz by the use of an UHF apparatus of the coaxial-slotted-line type.[10] The relaxation time, τ, and the limiting low- and high-frequency dielectric constants, ε_0 and ε_∞ respectively, were calculated on the basis of the Debye equation.[11] This is because the Debye equation has been found to be valid for the principal, low-frequency dispersion of any mono-alcohol[5,10,12,13] ever studied in the liquid state. The Kirkwood correlation factor, g,[14] was calculated by the use of ε_0 and ε_∞ in the following equation:

$$g = \frac{9kT(\varepsilon_0-\varepsilon_\infty)(2\varepsilon_0+\varepsilon_\infty)}{4\pi N\varepsilon_0(\varepsilon_\infty+2)^2\mu_0^2}$$

The g values thus obtained are denoted by $g(\varepsilon_0,\varepsilon_\infty)$, which are also compared with the $g(\varepsilon_0,n_D^2)$ values obtained by substituting n_D^2 for ε_∞. Since the exact value of the dipole moment, μ_0, in the liquid state is still unknown, we tentatively assumed the value of μ_0=1.66 D obtained by the dilute-solution method.[15]

Results and Discussion

Debye semicircles are plotted from the dielectric data obtained for six isomers of pentyl alcohols (Fig. 1). The relaxation time, τ, and the limiting low- and high-frequency dielectric constants, ε_0 and ε_∞ respectively, in the Debye equation are listed in Table 1, together with the Kirkwood correlation factor, g. The static dielectric constants, ε_0, from the literature for 1-pentanol are 13.9[16] and 14.6,[13]* for 3-methyl-1-butanol, 14.7,[16] and for 2-methyl-2-butanol, 5.82.[16] It should be noted that these values compare fairly well with the observed limiting values, which are not entirely free from error because of the large extrapolation. The relaxation time, τ, for 1-pentanol is also in fair agreement with the literature values, 7.5×10^2 ps[13]* and 7.6×10^2 ps.[17]* The differences between ε_∞ and n_D^2 are 1.1—1.3 for all the isomeric alcohols, which seems to reveal that there exists no essential difference in the high-frequency absorption.

1-Pentanol, which has the least sterically hindered OH group, has the largest ε_0, while the smallest ε_0 is found for 2-methyl-2-butanol, with the most sterically hindered OH group. The static dielectric constants decrease with an increase in the degree of steric hindrance. Of the two g values, $g(\varepsilon_0,n_D^2)$ is larger than $g(\varepsilon_0,\varepsilon_\infty)$; both $g(\varepsilon_0,n_D^2)$ and ε_0 decrease with an increase in the amount of steric hindrance of the hydroxyl group; similar trends have been observed by other workers[1-4] for other mono-alcohols.

The dielectric relaxation time, τ, decreases in the

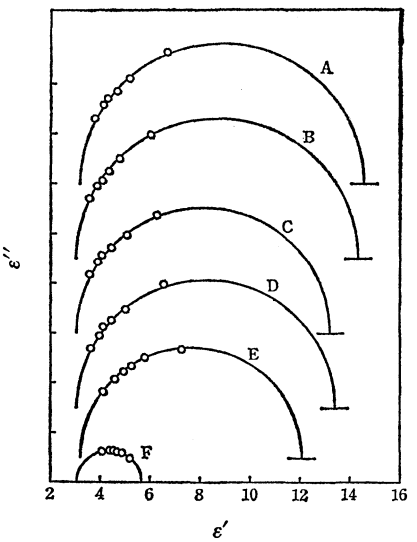

Fig. 1. Semi-circle plots for liquid isomeric pentanols at 25 °C.
A: 1-pentanol, B: 3-methyl-1-butanol, C: 2-pentanol, D: 3-pentanol, E: 3-methyl-2-butanol, F: 2-methyl-2-butanol.

* These values were obtained by the interpolation or extrpolation of the literature values given at different temperatures.

TABLE 1. THE RELAXATION TIMES, τ, THE LIMITING LOW- AND HIGH-FREQUENCY DIELECTRIC CONSTANTS, ε_0 AND ε_∞ RESPECTIVELY, THE DIFFERENCES, $\varepsilon_\infty - n_D^2$, AND TWO KIRKWOOD CORRELATION FACTORS, g, FOR SIX ISOMERIC PENTYL ALCOHOLS AT 25 °C

	1-Pentanol	3-Methyl-1-butanol	2-Pentanol	3-Pentanol	3-Methyl-2-butanol	2-Methyl-2-butanol
	C-C-C-C-C OH	C C-C-C-C OH	C-C-C-C-C OH	C-C-C-C-C OH	C C-C-C-C OH	C C-C-C-C OH
$\tau(\times 10^{-2}$ ps)	6.7	7.4	6.5	6.5	4.8	2.0
ε_0	14.6	14.3	13.2	13.4	12.1	5.7
ε_∞	3.2	3.0	3.0	3.1	3.3	3.1
$\varepsilon_\infty - n_D^2$	1.2	1.1	1.1	1.1	1.3	1.1
$g(\varepsilon_0, \varepsilon_\infty)$	1.8	1.9	1.7	1.7	1.4	0.5
$g(\varepsilon_0, n_D^2)$	3.3	3.2	3.0	3.0	2.7	1.1

order of: the primary pentyl alcohols (1-pentanol $\tau=6.7\times10^2$ ps, 3-methyl-1-butanol $\tau=7.4\times10^2$ ps)> secondary pentyl alcohols (2-pentanol $\tau=6.5\times10^2$ ps, 3-pentanol $\tau=6.5\times10^2$ ps, 3-methyl-2-butanol $\tau=4.8\times10^2$ ps)> tertiary pentyl alcohol (2-methyl-2-butanol $\tau=2.0\times10^2$ ps). In a preceding paper[18] we found, in contrast to this, that the relaxation time for tertiary butyl alcohol ($\tau=5.3\times10^2$ ps) is longer than that for normal butyl alcohol ($\tau=5.1\times10^2$ ps) at 25 °C. The longer relaxation time of the former than that of the latter may be associated with the considerable viscosity of the former. If we take the reduced relaxation time, τ/η, instead of τ, it will be found that τ/η decreases in the order of: primary butyl alcohols (1-butanol $\tau/\eta=2.0\times10^2$ ps/cP,** 2-methyl-1-propanol $\tau/\eta=1.9\times10^2$ ps/cP**)>secondary butyl alcohol (2-butanol $\tau/\eta=1.4\times10^2$ ps/cP***)> tertiary butyl alcohol (2-methyl-2-propanol $\tau/\eta=1.1\times10^2$ ps/cP**). For isomeric pentyl alcohols, a similar trend exists in the reduced relaxation time; *e.g.*, primary pentyl alcohol (3-methyl-1-butanol $\tau/\eta=2.0\times10^2$ ps/cP**)>secondary pentyl alcohol (3-methyl-2-butanol $\tau/\eta=1.4\times10^2$ ps/cP**)>tertiary pentyl alcohol (2-methyl-2-butanol $\tau/\eta=0.6\times10^2$ ps/cp**).

References

1) W. Dannhauser and R. H. Cole, *J. Chem. Phys.*, **23**, 1762 (1955).
2) W. Dannhauser and L. W. Bohe, *ibid.*, **40**, 3058 (1964).
3) J. Middelhoek and C. J. F. Böttcher, "Molecular Relaxation Processes," Chem. Soc., Spec. Publ., 20, p. 69 (1966).
4) P. Bordewijk, F. Gransch, and C. J. F. Böttcher, *Trans. Faraday Soc.*, **66**, 293 (1970).
5) W. Dannhauser and A. F. Flueckinger, *Phys. Chem. Liquids*, **2**, 37 (1970).
6) W. Dannhauser, *J. Chem. Phys.*, **48**, 1918 (1968).
7) J. Crossley, L. Glasser, and C. P. Smyth, *ibid.*, **55**, 2197 (1971).
8) Landolt-Börnstein, "Zahlenwerte und Funktionen aus Physik, Chemie, Astronomie, Geophysik und Technik," 2 Band, 8 Teil, Optische Konstanten (1962).
9) E. W. Washburn, "International Critical Tables of Numerical Data, Physics, Chemistry and Technology," NRC McGraw-Hill Book Co., Inc., New York and London (1926).
10) T. Koshii, E. Arie, M. Nakamura, H. Takahashi, and K. Higasi, This Bulletin, **47**, 618 (1974).
11) C. P. Smyth, "Dielectric Behavior and Structure," McGraw-Hill Book Co., Inc., New York, Toronto, and London (1955), p. 56.
12) *ibid.*, p. 105.
13) S. K. Garg and C. P. Smyth, *J. Phys. Chem.*, **69**, 1294 (1965).
14) J. G. Kirkwood, *J. Chem. Phys.*, **7**, 911 (1939).
15) A. L. McClellan, "Tables of Experimental Dipole Moments," W. H. Freeman and Co., San Francisco and London (1963).
16) A. A. Maryott and E. R. Smith, "Table of Dielectric Constants of Pure Liquids," NBS Circular 514 (1951).
17) F. F. Hanna and I. K. Hakim, *Z. Naturforsch.*, **26a**, 1194 (1971).
18) H. Sato, T. Koshii, H. Takahashi, and K. Higasi, *Chem. Lett.*, **1974**, 579.
19) J. Timmermans, "Physico-Chemical Constants of Pure Organic Compounds," Elsevier Pub. Co., Inc. (1950).

** η from the Critical Table.[9]
*** η from Timmermans.[19]

BULLETIN OF THE CHEMICAL SOCIETY OF JAPAN, VOL. 48(4), 1319—1320 (1975)

On the Melting Point of *N*-Methylacetamide–Silver Nitrate Adduct

Takaharu MATSUBARA and Toshio TANAKA*

Department of Chemistry, College of Liberal Arts and Science, Kyoto University, Yoshida-Nihommatsu-cho, Sakyo-ku, Kyoto 606

** Department of Photographic Technology, Kyoto Technical University, Matsugasaki, Sakyo-ku, Kyoto 606*

(Received December 17, 1974)

Synopsis. The melting point of *N*-methylacetamide-silver nitrate adduct $AgNO_3 \cdot 2NMA$ was found to be 46—47 °C which is in large disagreement with that reported by Paul and Chadha. The discrepancy was interpreted to result from the tendency of the adduct to lose NMA at high temperatures or at low partial pressures of NMA.

Formation of stable solid adducts of silver nitrate with some oxygen donor ligands was reported by Paul and Chadha.[1] Of the adducts $AgNO_3 \cdot 2NMA$ (NMA: *N*-methylacetamide) was reported to have melting point (or the temperature of decomposition) at 148 °C. We also prepared[2] the adduct in an infrared absorption spectroscopic study of the interaction between photographic gelatin and silver nitrate, and found its melting point to be 46—47 °C (in sealed tubes) and not 148 °C. The purpose of the present note is to point out and discuss the discrepancy.

Our method of preparation is as follows: solid silver nitrate was dissolved in an excess (2—3 times the equivalent) of molten NMA. The solution was cooled down to room temperature to crystallize out the adduct. This method of crystallization differs from that of Paul and Chadha who added excess benzene to the solution for the purpose of crystallization, the former taking more time and giving larger and probably purer crystals. The crystal was then ground, washed several times with benzene or carbon tetrachloride to remove excess NMA and freed from the solvent in dry streaming nitrogen. The adduct was kept in a closed vessel filled with dry nitrogen because of its high deliquescence. Drying and storing in a vacuum or in the presence of desiccating agents were avoided since the adduct tended to lose NMA (effloresce) under such conditions.

The composition of the adduct thus obtained was examined by dissolving the weighed adduct in water and measuring the absorption of nitrate ions at 300 nm. The molar ratio of NMA to $AgNO_3$ was found to be 2.00 which is in very good agreement with the expected value.

Combined thermogravimetry (TG) and differential thermal analysis (DTA) were carried out at several pressures and heating rates to find out what would happen when the $AgNO_3 \cdot 2NMA$ was heated up from room temperature to the melting point of pure silver nitrate. A Chyo Balance Corporation Type $TRDA_1$–L DTA Instrument was used. The results are given in Figs. 1 and 2. Neither NMA nor silver nitrate itself decomposed, nor did they react to each other, to a significant extent within the temperature range studied, except for an eventual slight darkening of silver nitrate near its melting point.

The endothermic peak of the DTA curve around 47 °C is distinct and reproducible. The fact that there is no change in weight at this temperature shows that this is the genuine melting point of the adduct.

Between 60 and 190 °C no definite transition was observed except for an abrupt fall of the DTA curve and a knick on the TG curve at the same time. Visual observation showed that these anomalies correspond to re-solidification of the melt due to the loss of a fraction of the initial amount of NMA. The temperature at which the anomalies appeared and the composition of the solid at that stage depended considerably on

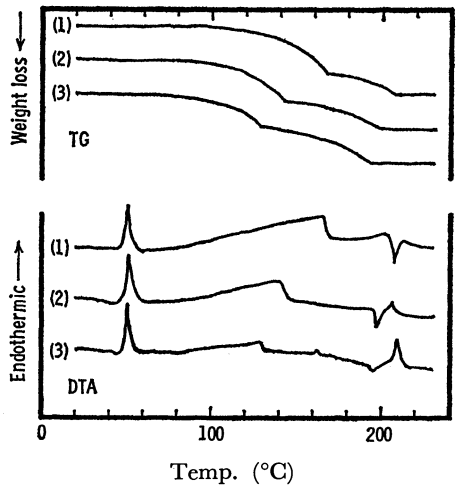

Fig. 1. TG and DTA curves of $AgNO_3$–NMA adduct at different heating rates.
Pressure: 760 mmHg. Heating rate: (1) 3.3 °C/min, (2) 1.8 °C/min, (3) 1.1 °C/min.

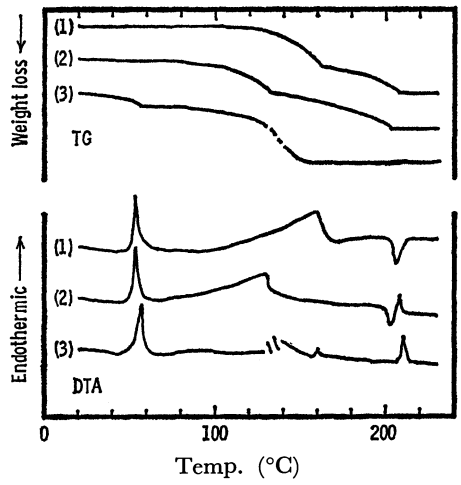

Fig. 2. TG and DTA curves of $AgNO_3$–NMA adduct at different pressures.
Heating rate: 2.6 °C/min. Pressure: (1) 760 mmHg, (2) 200 mmHg, (3) 8 mmHg.

experimental conditions. No evidence was found for the existence of another stable homogeneous phase richer in silver nitrate than the initial adduct. The cause of the knick on the TG curve would be merely the difference in the rate of vaporization of NMA from the liquid and the solid surfaces. Some DTA curves showed that the solid might contain a pure silver nitrate phase even in the presence of NMA. Traces of endothermic transition of normal silver nitrate from orthorhombic to rhombohedral structure were seen at 160 °C. (See, for example, the bottom curve in Fig. 1.)

Since we could find no "melting (or decomposition) point" at the temperature indicated by Paul and Chadha, it seems that their specimen might have lost a part of NMA during the course of drying and preservation, in particular, if the procedures had been carried out at a high temperature or at a low partial pressure of NMA, *e.g.*, in a vacuum or in the presence of desiccating agents.[3~5] On rapid heating, their specimen apparently melted at a temperature higher than the actual melting point of the adduct but lower than that of pure silver nitrate.

Attempts were made to prepare solids with NMA-content less than the adduct, by mixing powdered silver nitrate with a small amount of hot NMA and cooling the mixture rapidly in order to determine the apparent melting point of the solids in sealed tubes. Even on rapid heating, however, they melted first partly at around 50 °C, and solids coexisted with the melt. At *ca.* 140 °C generation of bubbles began to take place. This seems to correspond to the "decomposition of the adduct" mentioned by Paul and Chadha, but we consider it to be mere vaporization of NMA from the viscous melt-solid mixture.

We conclude that the actual melting point of the adduct $AgNO_3 \cdot 2NMA$ is 46—47 °C, and that the adduct is stable only at temperatures lower than this and in the presence of sufficient NMA vapor.

We are grateful to Prof. H. Hada, Kyoto University, for his kind discussions.

References

1) R. C. Paul and S. L. Chadha, *Indian J. Chem.*, **9**, 175 (1971).
2) T. Matsubara and T. Tanaka, *Nippon Shashin Gakkaishi*, **37**, 78 (1974).
3) R. C. Paul and S. L. Chadha, *Spectrochim. Acta*, **23A**, 1243, 1249 (1967).
4) R. C. Paul, H. R. Singal and S. L. Chadha, *J. Chem. Soc., A*, **1969**, 1849.
5) R. C. Paul and S. L. Chadha, *J. Inorg. Nucl. Chem.*, **31**, 2753 (1969).

BULLETIN OF THE CHEMICAL SOCIETY OF JAPAN, VOL. 48(4), 1321—1322 (1975)

α,β-Unsaturated Carboxylic Acid Derivatives. VII. Reaction of Ethyl α,β-Unsaturated α-Cyanocarboxylates with Triethyl or Diethyl Phosphonate[1]

Chung-gi SHIN, Yasuchika YONEZAWA, Yasuo SEKINE, and Juji YOSHIMURA*

Laboratory of Organic Chemistry, Faculty of Technology, Kanagawa University, Rokkakubashi, Kanagawa-ku, Yokohama 221

** Laboratory of Chemistry for Natural Products, Faculty of Science, Tokyo Institute of Technology, Ōkayama, Meguro-ku, Tokyo 152*

(Received April 16, 1974)

Synopsis. The reaction of ethyl α,β-unsaturated α-cyanocarboxylates with triethyl phosphonate gave ethyl α-cyano-β-diethoxyphosphinyl-carboxylates in about 50% yields.

In a previous paper,[2] we reported that the reaction of ethyl α,β-unsaturated α-nitrocarboxylates with triethyl phosphonate gave ethyl α,β-unsaturated β-diethoxyphosphinyl-carboxylates *via* unstable 3-ethoxycarbonyl-1,2,5-oxazaphospholine derivatives.

In this paper, we wish to report the reaction of ethyl α,β-unsaturated α-cyanocarboxylates (**1**) with triethyl or diethyl phosphonate.

Results and Discussion

When compound **1a**—**d** (**a**; R=methyl, **b**; R=ethyl, **c**; R=*n*-propyl, **d**; R=*i*-propyl) was treated with triethyl phosphonate at room temperature for 30 min and then the mixture was heated at *ca.* 120 °C for 2 hr with continuous stirring, ethyl α-cyano-β-diethoxyphosphinyl-carboxylate (**3a**—**d**) was obtained in about 50% yield as a colorless oil. In the reaction of ethyl 2-cyanocinnamate (**1e**) with triethyl phosphonate, an adduct (**2e**) was obtained in a good yield. The IR spectrum of **2e** showed a strong absorption of C=C=N⁻ at 2050 cm^{-1} (Fig. 1). The compound **2e** can be repeatedly distilled (bp 152—155 °C/0.25 mmHg), but it changed gradually into **3e** at room temperature over 6 months. The stability of the intermediate, **2e**, is probably due to the resonance stabilization between its intramolecular phosphonium salt and phenyl group attached to the carbon atom at the 3-position. However, when a solution of **2e** in cyclohexane was irradiated at room temperature for 24 hr by using an external high-pressure mercury lamp, ethyl 2-cyano-3-diethoxyphosphinyl-3-phenylpropanoate (**3e**) was obtained in a good yield and ethylene was liberated. The reaction seems to proceed through the compound **2** which in turn decomposes to the compound **3** and ethylene as shown in Scheme 1. The structure of **3** was confirmed by IR spectra and an independent preparation from diethyl phosphonate and **1**. The physical properties of **3** were summarized in Table 1.

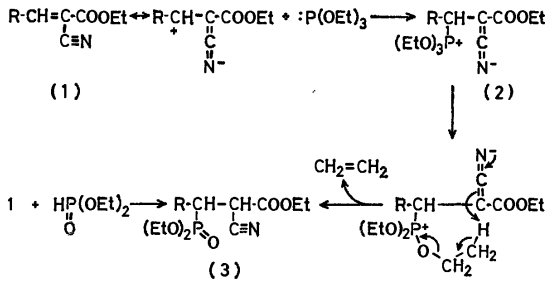

a:R=CH_3 b:R=C_2H_5 c:R=n-C_3H_7 d:R=i-C_3H_7 e:R=C_6H_5

Scheme 1.

Table 1. Ethyl 2-cyano-3-diethoxyphosphinyl-alkanoates (3) $\left(\text{R-CH(P(O)(OEt)}_2\text{)-CH(C}\equiv\text{N)-COOEt}\right)$

Compound	R	Yield (%) A[a]	Yield (%) B[b]	bp °C/mmHg	Formula	Found (Calcd), % C	H	N	cm⁻¹, IR in KBr -C≡N (w)[c]	-COOEt (s)[d]	P=O (s)	P-O-C (s)	¹H (δ) NMR[e] α-H	β-H
3a	CH_3	49	65	118—120/0.25	$C_{11}H_{20}NO_5P$	47.83 (47.69)	7.75 (7.22)	5.39 (5.05)	2200	1745	1240	1020	3.77	2.65
3b	C_2H_5	35	—	118—120/0.18	$C_{12}H_{22}NO_5P$	49.19 (49.14)	7.75 (7.76)	4.64 (4.81)	2200	1745	1245	1020	3.76	2.63
3c	*n*-C_3H_7	36	58	120—125/0.18	$C_{13}H_{24}NO_5P$	51.08 (51.12)	7.77 (7.87)	4.50 (4.54)	2200	1745	1245	1020	3.76	2.60
3d	*i*-C_3H_7	58	—	124—127/0.18	$C_{13}H_{24}NO_5P$	51.08 (51.12)	7.75 (7.87)	4.49 (4.54)	2200	1740	1240	1020	3.75	2.62
3e	C_6H_5	66	—	148—152/0.25	$C_{15}H_{22}NO_5P$	54.92 (55.05)	6.95 (6.73)	4.11 (4.28)	2250	1750	1240	1020	3.55	2.39

a) From the reaction of **1** with triethyl phosphonate. b) From the reaction of **1** with diethyl phosphonate.
c) w=Weak. d) s=Strong. e) Measured in $CDCl_3$.

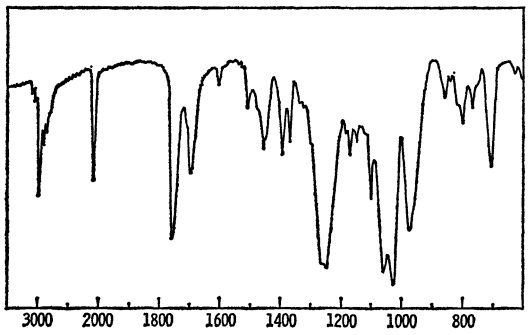

Wave number (cm^{-1})

Fig. 1. IR absorption spectrum of **2e**.

Experimental

All boiling points are uncorrected. The IR spectra were recorded with a Hitachi EPI-S2 Spectrometer. The NMR spectra were measured with a JNM-4H-100 Spectrometer using tetramethylsilane as an internal standard.

Material. Compound **1** was prepared by the reaction of appropriate aldehyde with ethyl cyanoacetate.[3,4]

*Reaction of **1a–d** with Triethyl Phosphonate.* A mixture of **1a–d** (0.05 mol) and triethyl phosphonate (0.06 mol) was stirred at room temperature for 30 min and then heated at 120—130 °C for 2 hr. The corresponding ethyl α-cyano-β-diethoxyphosphinyl-β-alkylpropanoate was obtained by distillation under reduced pressure. The physical properties are listed in Table 1.

*Reaction of **1e** with Triethyl Phosphonate.* A mixture of **1e** (0.05 mol) and triethyl phosphonate (0.1 mol) was refluxed for 5 hr. After removal of excess triethyl phosphonate, the residual syrup was distilled under reduced pressure to give an adduct (**2e**) (70.5%) as a colorless oil, bp 152—155 °C/0.25 mmHg. IR (KBr disk); 2050 (–C=C=N–), 1740 (–COOEt) and 1020 (⩾P–O–C⩽)cm^{-1}. NMR ($CDCl_3$); δ 2.40 (1H, s, C_6H_5–CH–C–).

Found: C, 58.47; H, 7.67; N, 4.12%. Calcd for $C_{18}H_{26}NO_5P$: C, 58.85; H, 7.08; N, 3.81%.

*Irradiation of **2e**.* A solution of **2e** (7 g) in dry cyclohexane (90 ml) was irradiated at room temperature for 24 hr by an external high-pressure mercury lamp. After removal of cyclohexane, the residue was purified on a silica gel column using benzene-acetone (10 : 1 V/V). After removal of the solvent, the residual oil was distilled under reduced pressure to give a colorless oil (**3e**).

*Reaction of **1a** or **1c** with Diethyl Phosphonate.* A mixture of **1a** (0.05 ml) and diethyl phosphonate (0.1 mol) was refluxed for about 5 hr. After removal of the excess diethyl phosphonate, the residual oil was distilled under reduced pressure to give a colorless oil (**3a**).

In a similar manner, **3c** was obtained as a colorless oil starting from **1c** with diethyl phosphonate.

References

1) Part VI. C. Shin, K. Nanjo, E. Ando, and J. Yoshimura, This Bulletin, **47**, 3109 (1974).

2) C. Shin, Y. Yonezawa, and J. Yoshimura, This Bulletin, **46**, 1727 (1973).

3) F. D. Popp and A. Catala, *J. Org. Chem.*, **26**, 2738 (1961).

4) F. D. Popp, *ibid.*, **25**, 646 (1960).

BULLETIN OF THE CHEMICAL SOCIETY OF JAPAN, VOL. 48(4), 1323—1324 (1975)

Normal and Reverse Photochromism of 1-(β-carboxyethyl)-3,3-dimethyl-6′-nitrospiro[indoline-2,2′-2*H*-benzopyran] in Water–Dioxane

Kenryo NAMBA and Shuichi SUZUKI

Research Laboratory of Resources Utilization, Tokyo Institute of Technology, Ookayama, Meguro-ku, Tokyo 152

(Received May 18, 1974)

Synopsis. The photochromism of 1-(β-carboxyethyl)-3,3-dimethyl-6′-nitrospiro[indoline-2,2′-2*H*-benzopyran] (I) was studied in water-dioxane. It was found that (I) exhibits normal photochromism in dioxane and reverse photochromism on addition of water to the solution.

A number of derivatives of 1-alkyl-3,3′-dimethylspiro [indoline-2,2′-2*H*-benzopyran] show photoreversible color change in organic solvents. Most of them are converted from a colorless stable state into a colored metastable state by irradiation with ultraviolet light. We have found that a photochromic compound, 1-(β-carboxyethyl)-3-3-dimethyl-6′-nitrospiro[indoline-2,2′-2*H*-benzopyran] (I), synthesized for chemical modification of enzymes, showed reverse photochromism in a water–dioxane mixture.

Experimental

Compound (I) was prepared by the reaction of 1-(β-carboxyethyl)-3,3-dimethylindolenium iodide and 5-nitrosalicylaldehyde in methyl ethyl ketone in the presence of piperidine, mp. 109.5—110.5 °C.

Absorption spectra were obtained with a Hitachi Rapidscan RSP-2 Spectrophotometer, the absorbances at λ_{max} being determined with a Shimazu Spectrophotometer UV-200 equipped with a thermostated cell compartment.

Results and Discussion

Variations of the absorption spectrum in the mixed solvents are shown in Fig. 1.

A colorless dioxane solution of (I) became violet after ultraviolet irradiation. The color faded very rapidly after the cessation of irradiation. In water–dioxane (water mole fraction of 0.34), compound (I) showed a weak absorption band at 566 nm before the ultraviolet irradiation (solid line 2), the absorbance increasing after the irradiation. At mole fraction 0.88, the solution of (I) showed an absorption band at 528 nm in the dark (solid line 3), the absorbance being reduced with the ultraviolet irradiation (dotted line 3). The absorption band reappeared spontaneously in the dark.

The difference in absorbance after and before the ultraviolet irradiation was determined in various water–dioxane mixtures. The results are given in Table 1.

It is clear that the difference in absorbance after ($O.D._L$) and before ($O.D._D$) the irradiation decreased with increasing mole fraction of water. Absorption maxima shifted toward shorter wavelengths with increasing solvent polarity.

Compound (I) exhibited reverse photochromism in formamide (Dimroth's solvent polarity value : E_t, 56.6),

Table 1. Effect of water on absorbance of (I)
After 24 hr in the dark at 25 °C after preparation of the solutions (10^{-4} M)

Mole fraction of water	λ_{max} (nm)	$O.D._L$[a] $-O.D._D$[b]
0	600	+0.95
0.34	566	+0.965
0.54	552	+0.30
0.67	546	+0.22
0.76	540	+0.07
0.83	532	−0.09
0.88	528	−0.25

a) 10 s after UV irradiation. b) Before UV irradiation.

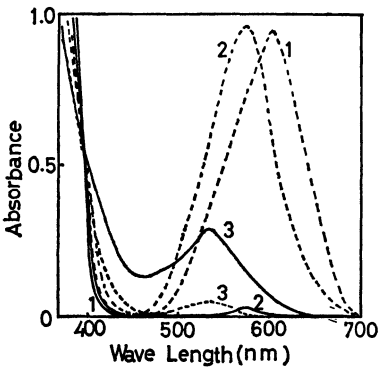

Fig. 1. Absorption spectra of (I) in water-dioxane (10^{-4} M).
—— before UV irradiation. ---- 10 s after UV irradiation. Mole fraction of water
1: 0, 2; 0.34, 3; 0.88.

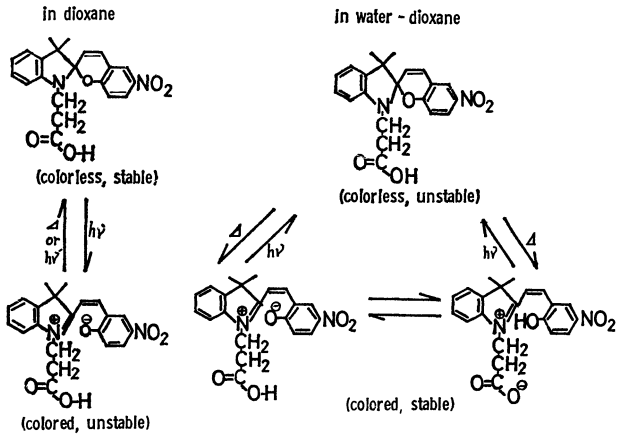

Fig. 2. Reaction Scheme of 1-(β-carboxyethyl)-3,3-dimethyl-6′-nitorospiro[indoline-2,2′-2*H*-benzopyran].

ethylene glycol (E_t, 56.3) and methanol (E_t, 55.5), but normal photochromism in other organic solvents having lower polarity such as ethanol (E_t, 51.9) and *n*-propanol (E_t, 50.7).

The results are attributed to the stabilization of ground state of the colored form due to the interaction with solvent.[1] At low mole fraction *ca.* 0.8, the ground state of the colored species was more unstable than that of the colorless species. Above 0.8, the increase of stabilization energy with the solvent might make the ground state of the colored species more stable than that of the colorless species, giving rise to reverse photochromism. The carboxyl group of (I) might play an important role in the reverse photochromism since 1,3,3-trimethyl-6′-nitrospiro[indoline-2,2′-2*H*-benzopyran] shows no remarkable effect in water–dioxane. The schemes are considered in Fig. 2.

Reference

1) I. Shimizu, H. Kokado, and E. Inoue, This Bulletin, **42**, 1726, 1730 (1969).

BULLETIN OF THE CHEMICAL SOCIETY OF JAPAN, VOL. 48(4), 1325—1326 (1975)

Electronic Structures and Spectra of Quinarene Molecules

Hiroyuki YAMAGUCHI* and Takeshi NAKAJIMA
Department of Chemistry, Tohoku University, Sendai 980

(Received June 10, 1974)

Synopsis. The electronic structures and spectra of fundamental quinarene molecules, **1**—**9** (Fig. 1) and some of their diphenyl derivatives (Fig. 2) have been studied by using the variable bond-length SCF LCAO-π-MO CI method.

Although syntheses of the quinarene molecules have been attempted by many investigators, and although some derivatives have been synthesized,[1-6] the parent hydrocarbons, **1**—**9** (Fig. 1), have so far not been synthesized. Very recently, Takahashi *et al.* attempted to synthesize the 9,9-diphenyl derivative of **3**, (**3'**),[7] and the 10, 11-diphenyl derivative of **8**, (**8'**)[8] (Fig. 2).

The present note will report the results of calculations of the electronic structures and spectra of the quinarene molecules by the semiempirical LCAO MO method. Further, by comparing the calculated electronic spectra with the experimental ones, we will examine whether or not the unknown compound obtained recently by Takahashi *et al.* in an attempt to synthesize **8'** is really the **8'** molecule.

The method of calculation used is the variable bond-length SCF LCAO-π-MO CI method,[9] in which the bond lengths and, consequently, the resonance and Coulomb repulsion integrals are allowed to vary with the bond order at each iteration until self-consistency is reached. In order to discuss the electronic spectra, a configuration mixing of all the singly excited states is included.

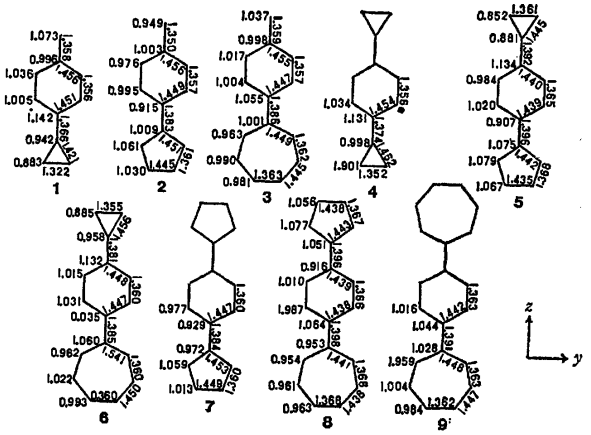

Fig. 1. Electron densities (in units of one electron) and bond lengths (in units of Å) of quinarenes.

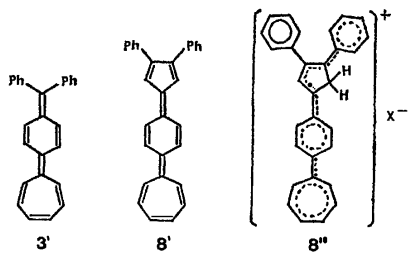

Fig. 2.

The calculated charge densities and bond lengths are shown in Fig. 1. The dipole moments of **1**, **2**, **3**, **5**, **6**, and **8** were predicted to be 5.44, 3.87, 2.94, 12.85, 4.56, and 11.08 D respectively. The dipole moments of **1** and **5** turn out to be larger than those of **3** and **8**. This means that the electron-releasing power of the 3-membered ring should be appreciably greater than that of the 7-membered ring. This fact is reflected in the appreciable dipole moment calculated for **6**, the dipolar structure of this molecule being such that the negative pole is directed toward the 7-membered ring.

The calculated transition energies and oscillator

TABLE 1. TRANSITION ENERGIES (ΔE) AND INTENSITIES (f) OF QUINARENES

Molecule	ΔE (eV)	f (cgs)
1	3.22	0.026 (y)
	3.56	1.56 (z)
	4.05	0.015 (y)
2	2.43	0.008 (y)
	3.13	1.84 (z)
	4.06	0.012 (y)
3	2.21	0.010 (y)
	2.86	1.90 (z)
	4.06	0.010 (y)
4	2.87	0
	2.88	0.044 (y)
	3.35	1.77 (z)
5	2.54	0.013 (y)
	2.70	1.93 (z)
	3.16	0.030 (y)
6	1.90	0.004 (y)
	2.69	2.18 (z)
	2.90	0.030 (y)
7	2.13	0
	2.14	0.013 (y)
	2.64	2.45 (z)
8	2.12	0.011 (y)
	2.25	0.008 (y)
	2.26	2.45 (z)
9	1.88	0.011 (y)
	1.89	0
	2.24	2.76 (z)

* Present address: Department of Chemistry, Kumamoto University, Kumamoto 860.

Table 2. Transition energies (ΔE) and intensities (f) of **8′**, **8″**, and the unknown compound

Calc.				Exp.[a]
Molecnle **8′**		Molecule **8″**		Unknown compound
ΔE(eV)	f	ΔE(eV)	f	ΔE(eV)
2.00	0.004(y)	2.02	0.79	2.02 ($\log\varepsilon$=4.2)
2.08	0.008(y)	2.52	0.008	
2.09	2.96 (z)	3.10	0.57	3.40 ($\log\varepsilon$=4.0)
3.33	0.06 (z)	3.45	0.27	
3.81	0.000(y)	3.60	0.003	

a) Ref. 8, in chloroform.

strengths, f, for the lowest three singlet transitions are presented in Table 1. The gross spectral features of **1**—**9** should be similar to those of triafulvene, pentafulvene, heptafulvene, triafulvalene, calicene, heptatriafulvalene,[9] pentafulvalene, sesquifulvalene, and heptafulvalene[10] respectively, except for the fact that the absorption maxima for the former are predicted to shift to wavelengths longer than those for the latter.

We have also calculated the electronic spectra of **3′**. The observed electronic spectra of the pigment formed on the attempted preparation of **3′** show absorption maxima at 2.05 ($\log\varepsilon$=4.28) and 2.92 eV ($\log\varepsilon$=4.27).[7] The calculated transition energies for **3′** are 2.05 (f=0.012), 2.25 (f=2.46), 3.69 (f=0.004), and 3.84 eV (f=0.001). The pigment obtained is not expected to be **3′**, since the observed second absorption maximum is not found in the predicted spectra.

The unknown compound obtained recently by Takahashi *et al.*[8] in an attempt to synthesize **8′** seems to be either the aimed-molecule (**8′**) or the quinarenium ion of **8′** (the **8″** molecule Fig. 2). The calculated results for **8′** and **8″** are summarized in Table 2*, and compared with the observed results for the unknown compound. The experimental values for the unknown compound are in better agreement with the calculated values for **8″** than with those calculated for **8′**. From this fact, it may be concluded that the unknown compound is likely to be **8″**, not **8′**.

References

1) A. S. Kende, *J. Amer. Chem. Soc.*, **85**, 1882 (1963).
2) R. von Helden, A. P. ter Borg, and A. F. Bickel, *Rev. Trav. Chim. Pays-Bas*, **81**, 599 (1962).
3) C. Jutz and F. Voithenleitner, *Chem. Ber.*, **97**, 29 (1964).
4) T. Nozoe, Japan 17674 (1964), *Chem. Abst.*, **62**, 5234 (1965).
5) P. Bladon, P. L. Pauson, G. P. Proctor, and W. J. Rodger, *J. Chem. Soc. C*, **1966**, 926.
6) K. Takahashi, N. Hirata, and K. Takase, *Tetrahedron Lett.*, **1970**, 1285.
7) K. Takahashi, S. Takenaka, and T. Nozoe, *Tetrahedron*, **30**, 2191 (1974).
8) K. Takahashi, S. Takenaka, J. Kikuchi, K. Takase, and T. Nozoe, This Bulletin, **47**, 2272 (1974).
9) H. Yamaguchi, T. Nakajima, and T. L. Kunii, *Theor. Chim. Acta*, **12**, 349 (1968).
10) T. Nakajima, *Topics in Current Chem.*, **32**, 1 (1972).

* In calculating the electronic spectra of **8″**, we have neglected the hyperconjugation effect due to the methylenic group.

BULLETIN OF THE CHEMICAL SOCIETY OF JAPAN, VOL. 48(4), 1327—1328 (1975)

Abnormal Grignard Reaction of 2,4,6-Trimethylbenzophenone: An Electron-transfer Mechanism

Masao Ōkubo

Department of Chemistry, Faculty of Science and Engineering, Saga University, Honshō-chō, Saga 840

(Received June 24, 1974)

Synopsis. The reaction of 2,4,6-trimethylbenzophenone with phenyl-MgBr in tetrahydrofuran was examined by ESR technique. A high amount of the ketyl radical was detected. An electron-transfer mechanism was proposed to explain the formation of *o*-biphenylyl mesityl ketone.

2,4,6-Trimethylbenzophenone(I) undergoes nuclear phenylation in the reaction with phenyl-MgBr as reported by Fuson *et al.*[1] They explained the formation of *o*-biphenylyl mesityl ketone(III) in terms of 1,4-addition followed by air-oxidation.

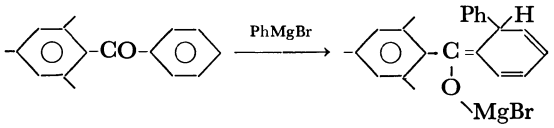

(I) (II)

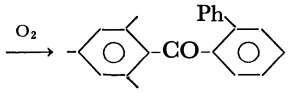

(III)

However, aeration of the ether extract of the hydrolyzed reaction mixture did not improved the yield of III. Intense red-coloration of the reaction solution seemed to indicate the presence of the ketyl radical derived from I. These results led the author to re-examine the reaction by means of ESR spectroscopy.

When ketone I was treated with five moles of phenyl-MgBr in tetrahydrofuran (THF) under vacuum at room temperature, the colorless solution turned to wine-red. A radical species was detected, its concentration increasing gradually and becoming *ca.* 30 mol% of the original ketone after four days. When the colored solution was sufficiently diluted, ESR spectrum A (Fig. 1) consisting of ninety lines evenly spaced at an interval of 0.23 gauss (total width 20.9 gauss) was obtained. When the dilution was not sufficient, the spectrum turned to one consisting of four broad lines (splitting constant 4.87 gauss, relative strength 1 : 3 : 3 : 1). Spectrum A was observed even after the solution had been allowed to stand for thirty days at room temperature.

The magnesium-ketyl prepared by the treatment of I with Mg-amalgum in THF gave a spectrum consisting of four broad lines, ascribable to the equivalent coupling of *o*- and *p*-hydrogen atoms of phenyl group with free spin.[2] However, when the treatment with amalgum was not sufficient, a spectrum identical with A was obtained. Since insufficient treatment left the original ketone mostly unchanged, spectrum A can be ascribed to a particular form of the ketyl radical existing as a dimeric or an oligomeric "aggregate" in which other neutral ketone molecules coordinate to the "monomeric" ketyl. The result of a recent work on the Grignard-ketyl of *o*-methylbenzophenone[3] suggests that "aggregate-formation" suppresses the twisting vibration of mesityl group out of the plane of benzoyl group, making it possible to observe the hyperfine splittings. The Grignard-ketyl of d_5-phenyl mesityl ketone gave a spectrum with the very small total width of 3.45 gauss, which indicates that almost all the free spin of Grignard-ketyl of I is delocalized on the phenyl group.[4] This can be explained in terms of the inhibition of conjugation due to the large twisting angle between the plane of the mesityl group and that of the benzoyl group.

As the observed radical concentration is high, most part of the original ketone may be involved in the "aggregate-formation." The main reaction should proceed in the agregate *via* an electron-transfer mechanism. The following processes can elucidate the formation of the identified products: the 1,4-adduct (II, AdH),[1] III(Ad)[1] and 2,4,6-trimethylbenzhydrol (KH).[5]

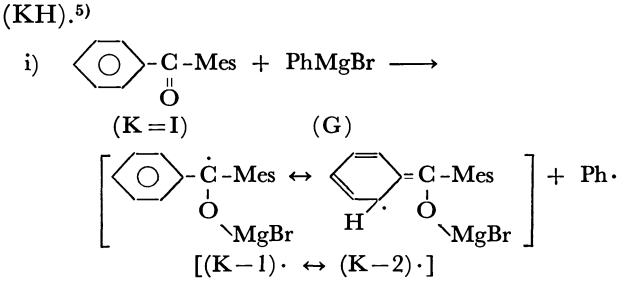

[(K−1)· ↔ (K−2)·]

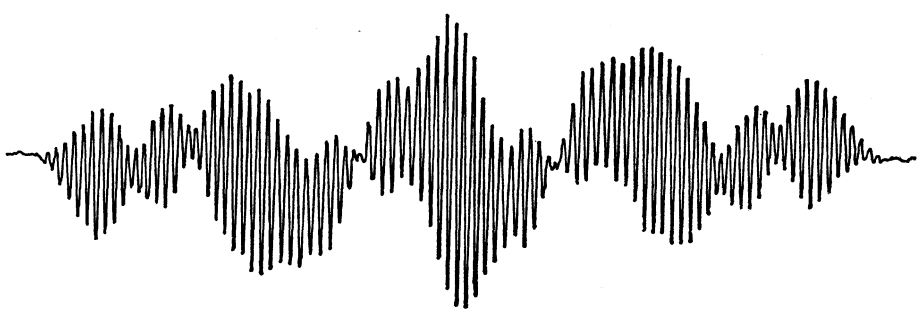

Fig. 1. ESR spectrum A obtained from the reaction of 2,4,6-trimethylbenzophenone and phenyl-MgBr.

ii) $(K-2)\cdot + (G) \rightarrow$ 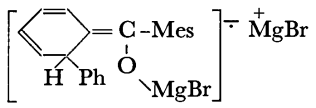

$(AdH)^{\overline{\cdot}}$

iii) $(AdH)^{\overline{\cdot}}{}^{+}MgBr + (K) \rightarrow$ 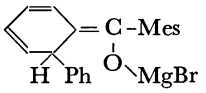

(AdH=II)

$+ [(K-1)\cdot \leftrightarrow (K-2)\cdot]$

iv) $(AdH) + (K-2)\cdot \rightarrow$ 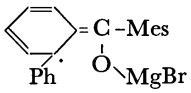

(Ad)·

$+$ 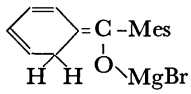

(KH-enol)

v) $(Ad)\cdot + (K) \rightarrow$ 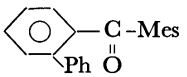

(Ad=III)

$+ [(K-1)\cdot \leftrightarrow (K-2)\cdot]$

(Mes=mesityl)

The five processes can explain the fact that product III(Ad) was obtained in a fair yield even if the reaction was carried out in the absence of air. Processes i), iii) and v) can also explain the presence of the high amount of ketyl radical throughout the course of reaction. The ketyl radical can be represented mainly by formula (K–2)· on the basis of the extremely high spin density on the phenyl group. The phenyl radical produced in process i) probably abstracts hydrogen from the solvent molecule.[6] Radical (K–2)·, which can be regarded as a neutral radical because of covalency of the O–Mg linkage, might reveal affinity towards another molecule of phenyl-MgBr, a nucleophile[7] (process ii). No *para*-phenylated product (*p*-biphenylyl mesityl ketone) was detected. Thus the attack of the carbanion on the *ortho*-position is favored because the position is nearer to the carbonyl-oxygen coordinating to the Mg-atom. The benzpinacol[8] was absent possibly due to the steric hindrance of the mesityl group.

Experimental

2,4,6-Trimethylbenzophenone was prepared from mesitylene and benzoyl chloride by the Friedel-Crafts method. d_5-Phenyl mesityl ketone was prepared by the same method with the use of d_5-benzoyl chloride. *o*-Biphenylyl mesityl ketone was prepared according to the reported method,[1] and *p*-biphenylyl mesityl ketone by the Friedel-Crafts method. 2,4,6-Trimethylbenzhydrol was obtained by reduction of the corresponding ketone.[5] *sym*-Diphenyldimesitylpinacol was prepared according to the method of Kharasch, Morrison and Urry.[8] The reaction products were compared with authentic samples by means of column- and thin-layer-chromatography.

The evacuated samples for ESR measurements were prepared according to the method previously reported.[9] The radical concentration was determined by the over-modulation technique with a THF solution of galvinoxyl as a standard in the same sample tube.

References

1) R. C. Fuson, M. D. Armstrong, and S. B. Speck, *J. Org. Chem.*, **7**, 297 (1942).
2) K. Maruyama, R. Tanikaga, and R. Gotō, This Bulletin, **36**, 1141 (1963).
3) M. Ōkubo, *ibid.*, **48**, 1057 (1975).
4) H. M. McConnell, *J. Chem. Phys.*, **24**, 632, 764 (1956).
5) K. Elbs, *J. Prakt. Chem.*, [ii] **35**, 472 (1887).
6) In the reaction of benzophenone with mesityl-MgBr, evidence was obtained for hydrogen-abstraction from THF molecule by the mesityl radical.
7) R. A. Rossi and J. F. Bunnett, *J. Org. Chem.*, **38**, 3020 (1973).
8) M. S. Kharasch, R. Morrison, and W. H. Urry, *J. Amer. Chem. Soc.*, **66**, 368 (1944).
9) K. Maruyama, This Bulletin, **37**, 1013 (1964).

BULLETIN OF THE CHEMICAL SOCIETY OF JAPAN, VOL. 48(4), 1329—1330 (1975)

Photolysis of *p*-Benzoquinone in Aqueous Solution. Possibility of a Polar Mechanism in the Primary Process

Masamitsu SHIRAI, Toshio AWATSUJI, and Makoto TANAKA

Department of Applied Chemistry, Faculty of Engineering, University of Osaka Prefecture, Sakai, Osaka 591

(Received August 1, 1974)

Synopsis. The photochemistry of *p*-benzoquinone in water was investigated spectrophotometrically. The effect of *p*-nitroso-*N*,*N*-dimethylaniline as an additive confirmed a non-radical mechanism. The small positive deuterium isotopic effect suggests an electrophilic attack of the excited *p*-benzoquinone on water.

The photochemical reactions of *p*-benzoquinone (BQ) have been extensively studied in alcoholic solutions but less in aqueous solutions. In the photolysis of aqueous solutions of BQ, hydroquinone (HQ) has been isolated as the sole stable product in addition to the transient formation of benzene-1,2,4-triol (BTO) and 2-hydroxy-1,4-benzoquinone (HOBQ).[1] From the results it was suggested that the photolysis of BQ in aqueous solutions consists of a two stage process; formation of BTO from the reaction of the excited BQ with water molecule in the primary process, and dark reaction of BTO with BQ to yield HQ and HOBQ which is unstable in water in the secondary process. Kurien and Robins[2a] and Joschek and Miller[2b] proposed a radical mechanism for the primary process: the excited BQ abstracts a hydrogen atom from a water molecule forming semiquinone and a hydroxyl radical, the hydroxyl radical reacting with either the semiquinone radical or another BQ, ultimately resulting in the formation of BTO. Kano and Matsuo[3] suggested the possibility of an ionic mechanism including a cationic intermediate from the effect of micellar system on the photolysis of BQ in aqueous solutions. This paper presents some evidences supporting a polar mechanism in the primary process.

p-Nitroso-*N*,*N*-dimethylaniline(NDA), an effective hydroxyl radical scavenger,[4] was dissolved in an aqueous solution of BQ and an aqueous solution of sodium 9,10-anthraquinone-2-sulfonate(AQS), respectively. Absorption peaks of BQ and AQS were not affected by the added NDA. No direct photolysis of NDA occurred under our experimental conditions. Variation in absorbance during the course of irradiation with 313 nm light was followed at 247 nm, 255 nm, and 440 nm for BQ, AQS, and NDA, respectively. The results are shown in Fig. 1. No detectable change in the absorbance of NDA was observed in the photolysis of BQ in the BQ–NDA mixed system, while an appreciable decrease was observed in that of AQS in the AQS–NDA mixed system. The former result indicates that the photolysis of BQ takes place *via* a non-radical process. The latter result reflects a radical intermediate formation in the photolysis of aqueous AQS.[5]

The only basis for the radical mechanism[2a] was the halogen ion effect. Decrease in the quantum yield by the addition of halogen ion was ascribed to its function as radical scavenger. However, the effect

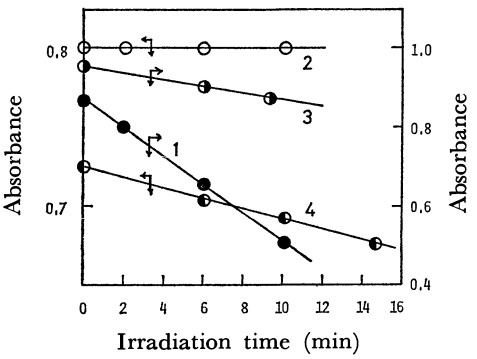

Fig. 1. Variations in the absorbance of BQ, AQS, and NDA with irradiation time.
a) BQ–NDA mixed system. $[BQ]=3.80\times10^{-5}$ M, $[NDA]=2.34\times10^{-5}$ M. Change in the absorbance; 1) at 247 nm for BQ, 2) at 440 nm for NDA.
b) AQS–NDA mixed system. $[AQS]=1.80\times10^{-5}$ M, $[NDA]=2.12\times10^{-5}$ M. Change in the absorbance; 3) at 255 nm for AQS, 4) at 440 nm for NDA.

of halogen ion should result from the quenching function as well as in the photolysis of aqueous AQS.[6] The Stern-Volmer plot for Cl^- as quencher gave a straight line.

The photochemistry of pyrimidine base in water has been investigated widely because of its significance in photobiology.[7] The photohydration of pyrimidine was suggested to occur *via* an electrophilic attack of the excited base on water. The small positive value ($k_H/k_D=1.18$) of the deuterium isotopic effect for uracil in acetonitrile–D_2O was ascribed to a secondary isotopic effect and provided strong evidence for the confirmation of an electrophilic attack mechanism.[8] The rate of photolysis of BQ in water (Fig. 2) was somewhat lower in D_2O than in H_2O. This small isotopic effect ($k_H/k_D=1.15$) suggests that the rate-determining step of the photolysis of BQ in water is

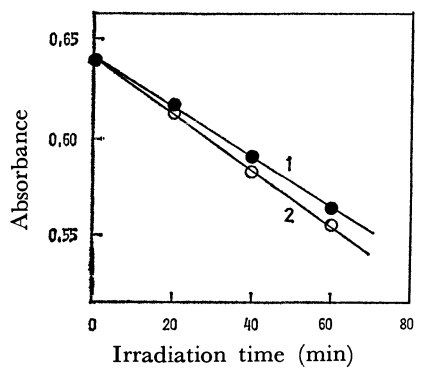

Fig. 2. Photolysis of BQ in H_2O and in D_2O.
1) in D_2O, 2) in H_2O. $[BQ]=3.0\times10^{-5}$ M.

not a direct hydrogen abstraction from water but an electrophilic attack of the excited BQ on water, as well as uracil. There are several reports on the photo-induced polar reactions of cyclic enones[9] and dienones.[10] These polar reactions are explicable in terms of the contribution of polar state in the product controlling step.[11] The primary process of the photochemical reaction of BQ in water seems to pass through a polar intermediate as shown in Scheme 1.

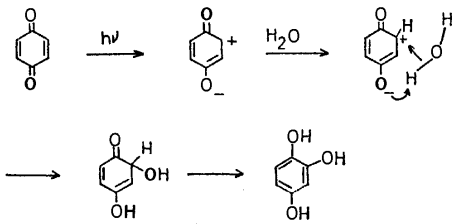

Scheme 1.

Experimental

A Toshiba SHL-100 UV high-pressure mercury lamp was used as a light source. A combination filter, a Toshiba UV-D 25 filter, an aqueous nickel sulfate solution and a Pyrex filter were employed to obtain the light of 313 nm. The light intensity determined with aqueous potassium ferrioxalate as an actinometer was 7.1×10^{18} quanta$\cdot l^{-1} \cdot$ min.$^{-1}$ The photolysis in the presence of NDA was carried out with a light of wave length below 350 nm. The samples were irradiated in spectrophotometer cells at room temperature. The rate of photolysis for BQ was followed by the change in absorbance at 247 nm. HQ was isolated as the sole stable product but separation of HOBQ which is unstable in the dark was unsuccessful. The formation of BTO was confirmed by UV spectrum (λ_{max} 289 nm, $\varepsilon = 3300$). Spectra were measured on a Shimadzu UV-200 recording spectrophotometer. BQ was sublimed (mp 116°). NDA was recrystallized from ligroin (mp 86—87°). Water was purified by the usual method.

References

1) P. A. Leighton and G. S. Forbes, *J. Amer. Chem. Soc.*, **51**, 3549 (1929). S. Hashimoto, K. Kano, and H. Okamoto, This Bulletin, **45**, 966 (1972). F. Poupe, *Collect. Czech. Chem. Cimmun.*, **12**, 225 (1949).

2) a) K. C. Kurien and P. A. Robins, *J. Chem. Soc., B*, **1970**, 855.

b) H. I. Joschek and S. I. Miller, *J. Amer. Chem. Soc.*, **81**, 3273 (1966).

3) K. Kano and T. Matsuo, *Chem. Lett.*, **1973**, 1127.

4) I. Kraljic and C. N. Trumbore, *J. Amer. Chem. Soc.*, **87**, 2547 (1965).

5) G. O. Phillips, N. W. Worthington, J. F. McKellar, and R. R. Sharpe, *J. Chem. Soc., A*, **1969**, 767.

K. P. Clark and H. I. Stonehill, *J. Chem. Soc. Faraday*, **1972**, 577, 1676.

6) H. R. Cooper, *Trans. Faraday Soc.*, **62**, 2865 (1966).

7) J. G. Burr, "Advances in photochemistry", Vol. 6, ed. by W. A. Noyes, Jr, G. S. Hammond and J. N. Pitts, Jr., John Wiley & Sons, New York (1968), p. 193.

8) J. G. Burr, B. R. Gordon, and E. H. Park, *Photochem. Photobiol.*, **8**, 73 (1968).

9) R. Noyori, A. Watanabe, and M. Kato, *Tetrahedron Lett.*, **1968**, 5443.

T. Matsuura and K. Ogura, *J. Amer. Chem. Soc.*, **88**, 2602 (1966).

10) H. Nozaki and M. Kurita, *Tetrahedron Lett.*, **1968**, 3635.

11) O. L. Chapman, "Advances in Photochemistry", Vol. 1, ed. by W. A. Noyes, Jr, G. S. Hammond and J. N. Pitts, Jr., John Wiley and Sons, New York (1968), p. 323.

BULLETIN OF THE CHEMICAL SOCIETY OF JAPAN, VOL. 48(4), 1331—1332 (1975)

The Allylic Rearrangement. IV.[1] New Synthesis of 4-Hexenoic Acid

Sadao TSUBOI and Akira TAKEDA

Department of Synthetic Chemistry, School of Engineering, Okayama University, Tsushima, Okayama 700

(Received August 12, 1974)

Synopsis. *trans*-4-Hexenoic acid, a useful starting material for the synthesis of racemic 4*R* : 5*S* and 4*S* : 5*R* 4,5-dihydroxyhexanoic acid γ-lactone, one component of the aroma extracts from one Californian and two Spanish flor sherries, has been conveniently prepared by the Favorskii-type rearrangement of 5-chloro-3-hexen-2-one.

The investigation of two samples of Spanish fino sherry and one sample of a California palomino flor sherry has been reported by Webb *et al.*[2] They were unable to identify two of the major high boiling components completely. Muller *et al.*[3] have isolated these components from the aroma extracts of the California palomino flor sherry, using the techniques described by Webb *et al.* and identified as (−) 4*R* : 5*R* or 4*S* : 5*S* 4,5-dihydroxyhexanoic acid γ-lactone and (+) 4*R* : 5*S* or 4*S* : 5*R* 4,5-dihydroxyhexanoic acid γ-lactone, which are diastereomeric forms of 5-(1′-hydroxyethyl)dihydro-2(3*H*)-furanone (**1**).

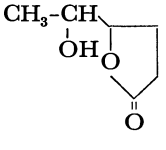

1

They have synthesized lactone **1** by the hydroxylation of *trans*-4-hexenoic acid (**2**), which was obtained from cyclopropyl methyl ketone *via* four steps by adaptation of the procedure reported by Julia *et al.*[4] This synthetic method of **2** seems to us less profitable for the purpose of a large scale preparation because only a mixture (approximately 1 : 1) of *trans* and *cis* isomers was obtained and gas-chromatographical fractionation was needed to isolate *trans*-**2**. We wish to report here a simple and more convenient synthesis of acid **2**, by means of the vinylogous Favorskii rearrangement[1] previously reported by us. The starting material, 5-chloro-3-hexen-2-one (**3**) was prepared by the Wittig-type reaction of 2-chloropropanal and diethylphosphonoacetone. Ketone **3** is thought to be of *trans* configuration because a large coupling constant (J=15.8 Hz) has been observed in its NMR spectrum. The treatment of ketone **3** with 15% aqueous NaOH afforded 4-hexenoic acid (**2**) in a 47% yield, with a small amount of 3-hexenoic acid (**4**). The formation of **2** can be well explained by the following mechanism involving a Favorskii-type rearrangement[1] of ketone **3**, the vinylogue of methyl α-chloroethyl ketone.

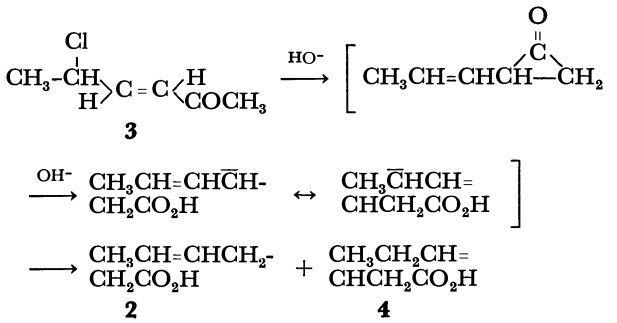

3 **2** **4**

The NMR spectrum of the product **2** exhibited a complicated pattern due to the existence of acid **4**, but its IR spectrum was identical with that of *trans*-acid **2** reported by Muller *et al.* Therefore, it is suspected that the *trans*-acid **2** obtained by Muller *at al.* also may be a mixture of the acid **2** and **4**.

trans Hydroxylation of the acid **2** with peracetic acid was done according to the Muller's procedure to give a racemic mixture of 4*R* : 5*S* and 4*S* : 5*R* 4,5-dihydroxyhexanoic acid γ-lactone (**1**) in a total yield of 29%.

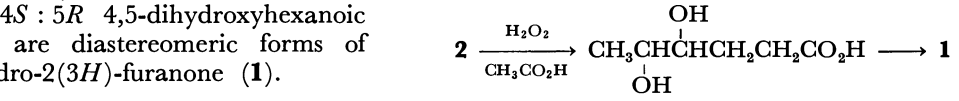

Experimental

Materials. 2-Chloropropanal was prepared by the method described by us previously.[5] Diethyl phosphonoacetone was obtained by the procedure described in the literature,[6] yield 68%: bp 101—106 °C/4 mmHg (lit.[6] bp 126 °C/9 mmHg).

trans-*5-Chloro-3-hexen-2-one (**3**).* To a stirred solution of 0.96 g (0.04 mol) of sodium hydride in 60 ml of dry ether was added 7.7 g (0.04 mol) of diethyl phosphonoacetone at 0 °C. After evolution of hydrogen gas ceased, 3.7 g (0.04 mol) of freshly distilled 2-chloropropanal was added dropwise. The mixture was stirred for 30 min and then poured into a large amount of water. The ethereal extract of the organic layer was washed with water and dried over $MgSO_4$. After removal of the solvent, the residue was distilled to give 1.7 g (32%) of **3**: bp 65—70 °C/5 mmHg; IR (neat) 1695 (cisoid C=O), 1670 (transoid C=O), 1625 (C=C), 980 cm^{-1} ($\left(\text{H}\right)\text{C}=\text{C}\left(\text{H}\right)$); NMR ($CCl_4$) δ 1.65 (d, 3H, J=7 Hz, CH_3CHCl–), 2.20 (s, 3H, CH_3CO), 4.60 (doublet of quartet, 1H, J=7 Hz, CH_3CHCl–), 6.08 (d, 1H, J=15.8 Hz, –CH=CHCO–), 6.68 ppm (double d, 1H, J=7 and 15.8 Hz, –CH=CHCO–); MS (70 eV) *m/e* (rel. intensity) 132 (40, M^+, 1Cl), 117 (100, M^+-CH_3), 97 (84, M^+-Cl), 89 (75, M^+-COCH_3), 53 (75), 43 (84, $COCH_3$).

Found: C, 54.05; H, 6.81%. Calcd for C_6H_9ClO: C, 54.36; H, 6.84%.

trans-*4-Hexenoic Acid (**2**).* Ketone **3** (1.5 g, 0.011 mol) was added slowly to 15 ml of 15% aqueous NaOH with stirring at 50—55 °C. The mixture was stirred for 15 min, and washed with ether to remove neutral materials. The aqueous layer was treated with active charcoal, and then acidified with dilute hydrochloric acid. After the organic layer was extracted several times with ether, the combined etheral extract was dried over $MgSO_4$. Removal of the solvent left 0.59 g (crude yield 47%) of crude **2**. Tlc analysis[7] showed one clean spot at R_f value of 0.58: IR (neat)[8]

3500—2500 (COOH), 1710 (C=O), 1411, 1210, 1172, 968 cm^{-1} $\left(\begin{matrix}H\\ \\ H\end{matrix}\!\!>C=C<\!\!\begin{matrix}\\ \\ H\end{matrix}\right)$; NMR ($CDCl_3$)[9] δ 1.00 (t, 0.6H, $C\underline{H}_3CH_2$- of **4**), 1.63 (broad d, 3H, $C\underline{H}_3CH$=), 2.09 (m, 0.4H, $CH_3C\underline{H}_2$- of **4**), 2.37 (m, 4H, $-C\underline{H}_2C\underline{H}_2-$), 3.10 (m, 0.4H, $-C\underline{H}_2CO_2H$ of **4**), 5.50 (m, 2H, -CH=CH-), 9.57 ppm (broad s, 1.2H, CO_2H of **2** and **4**); MS (70 eV) *m/e* (rel. intensity) 114 (68, M^+), 99 (13, M^+-CH_3), 96 (13, M^+-H_2O), 68 (71), 55 (100).

*Racemic Mixture of 4R : 5S and 4S : 5R 4,5-Dihydroxyhexanoic Acid γ-Lactone (**1**).* Trans hydroxylation of **2** was carried out by the modification of the procedure of Muller *et al.*[3] A solution of 0.28 g of 30% H_2O_2 in 0.50 g of glacial acetic acid was heated for 30 min at 75 °C, and then cooled. The peracid solution was added dropwise to 0.21 g (0.0018 mol) of **2** with stirring. The solution was then heated at 40 °C for 30 min, cooled, and extracted with ether. The etheral solution was dried over $MgSO_4$, and then the solvent was removed. The residue (clean oil, 0.18 g) was analyzed by glpc.[10] The peaks, retention times (min), and integrated percentages are as follows: 1, 1.3, 11%; 2, 3.7, 37%; 3, 4.8, 12%; 4, 9.7, 40%. Component 2 was identified as the starting material **2** by comparison of the retention time. Component 4 was collected by preparative glpc and identified as **1** (yield 29%): IR (neat) 3440 (OH), 1760 (lactone C=O), 1415, 1190 cm^{-1}; NMR ($CDCl_3$) δ 1.20 (d, 3H, J=7 Hz, $-CH_3$), 2.0—3.0 (m, 4H, α- and β-H), 3.42 (s, 1H, OH), 4.10 (m, 1H, $CH_3C\underline{H}(OH)$-), 4.42 ppm (m, 1H, γ-H). Its IR and NMR spectra were identical with those of the lactone **1** reported by Muller[3]: IR (neat) 3436, 1762, 1415, 1192 cm^{-1}; NMR ($CDCl_3$) δ 1.20 (m, 3H), 2.0—3.0 (m, 4H), 3.00 (s, 1H), 4.10 (m, 1H), 4.42 ppm (m, 1H). Components 1 and 3 were not further investigated.

References

1) Preceding paper: A. Takeda and S. Tsuboi, *J. Org. Chem.*, **38**, 1709 (1973).

2) A. D. Webb, R. E. Kepner, and L. Maggiora, *Amer. J. Enol. Viticult.*, **18**, 190 (1967).

3) C. J. Muller, L. Maggiora, R. E. Kepner, and A. D. Webb, *J. Agr. Food Chem.*, **17**, 1373 (1969).

4) M. Julia, S. Julia, and S. Y. Tchen, *Bull. Soc. Chim. France*, **1961**, 1849.

5) A. Takeda, S. Tsuboi, S. Wada, and H. Kato, This Bulletin, **45**, 1217 (1972).

6) A. N. Pudovik, *Zhur. Obschei. Khim.*, **25**, 2173 (1955).

7) Condition of tlc: support, silica gel GF_{254}, 0.1 mm thickness; developer, benzene-methanol-acetic acid (10 : 1 : 1, v/v).

8) IR spectrum was identical with that of an authentic sample.[2]

9) Spectral intensity shows the existence of **2** and **4** in a ratio of 5 : 1.

10) Condition of glpc: column, 10% polyneopentyl glycol succinate on Chromosorb W, 190 °C; carrier gas, He, 20 ml/min; detector, TCD.

BULLETIN OF THE CHEMICAL SOCIETY OF JAPAN, VOL. 48(4), 1333—1334 (1975)

Potential Antitumor *N*-Carbamoyl-*N'*-methyl-*N'*-nitroso Derivatives of Amino Acids

Tomoya MACHINAMI and Tetsuo SUAMI

Department of Applied Chemistry, Faculty of Engineering, Keio University, Hiyoshi, Yokohama 223

(Received October 16, 1974)

Synopsis. *N*-Carbamoyl-*N'*-methyl-*N'*-nitroso derivatives of amino acids have been prepared by treating the amino acids with methyl isocyanate followed by nitrosation with sodium nitrite in dilute acetic acid solution.

An *N*-alkyl-*N*-nitrosoureido group seems to be an essential functional group for the appearance of biological activity in streptozotocin[1] and its analogues.[2-4] In all the compounds studied so far in our laboratory, the functional group was attached to a carbohydrate residue, which does not seem to have an inconvertible role in their biological activity. Therefore, it might be possible to replace the carbohydrate moiety by other groups without losing the antitumor activity.

In the present paper, we wish to report a preparation of *N*-carbamoyl-*N'*-methyl-*N'*-nitroso derivatives of amino acids.

Potassium cyanate[5] or aryl isocyanate[6,7] have been used to prepare carbamoyl derivatives of amino acids. Under similar reaction conditions, methyl isocyanate was used to prepare *N*-carbamoyl-*N'*-methyl derivatives of glycine, alanine, aspragine, phenylalanine and methionine in the present study. The *N*-carbamoyl-*N'*-methyl derivatives of phenylalanine and methionine were obtained only as the potassium salts. Acidification of the salts resulted in an intramolecular cyclization giving hydantoin derivatives, which had large negative optical rotations.[8] Formation of hydantoin from a carbamoyl derivative under more drastic conditions has been described in a literature.[5,9-11]

Nitrosation of the *N*-carbamoyl-*N'*-methyl derivatives was performed in aqueous acetic acid solution with sodium nitrite at 0 °C, and the structure of the product was determined by PMR. The spectrum of the product had a singlet at τ 6.8—6.9 corresponding to N–CH_3 protons, clearly indicating the absence of a proton on the nitrogen atom attached to the methyl group.

The antitumor activities will be reported in the near future in an appropriate journal.

Experimental

Glycine, L-alanine, L-asparagine, L-phenylalanine and L-methionine were purchased from Asahi Kasei. Melting points were determined in capillary tubes and are uncorrected. PMR spectra were measured at 60 and 100 MHz on a Varian A-60D and a JEOL JMN-MH 100 spectrometers with reference to tetramethylsilane as an internal standard and the peak positions are given in τ values.

General Procedure for N-*Carbamoyl*-N'-*methyl Amino Acids.* The amino acid was dissolved in an equivalent molar amount of 10% potassium hydroxide solution and methyl isocyanate was added to the solution under ice cooling. The mixture was agitated overnight at room temperature and the pH was brought to 2—3 with Amberlite IR-120 (H^+ type). The solution was evaporated under reduced pressure below 30 °C to give a crude product.

N-*Carbamoyl*-N'-*methyl-glycine* (**1**). The crude crystalline product was recrystallized from methanol to give **1**, mp 147—148 °C, in 81% yield.

Found: C, 36.44; H, 6.07; N, 21.53%. Calcd for $C_4H_8N_2O_3$: C, 36.36; H, 6.10; N, 21.20%.

N-*Carbamoyl*-N'-*methyl*-L-*alanine* (**3**). The crude product was crystallized from ethanol and recrystallized from the same solvent to give **3**, mp 137—138 °C, $[\alpha]_D^{15}$ +3.0° (*c* 1.0, water), in 56% yield.

Found: C, 40.79; H, 6.74; N, 19.07%. Calcd for $C_5H_{10}N_2O_3$: C, 41.09; H, 6.90; N, 19.17%.

N-*Carbamoyl*-N'-*methyl*-L-*asparagine* (**5**). The crude product was crystallized from ethanol to give **5**, mp 142—143 °C, $[\alpha]_D^{15}$ +7.5° (*c* 1.0, water), in 66% yield.

Found: C, 38.32; H, 5.95; N, 22.44%. Calcd for $C_6H_{11}N_3O_4$: C, 38.09; H, 5.86; N, 22.21%.

Potassium Salt of N-*Carbamoyl*-N'-*methyl*-L-*phenylalanine* (**7**). The reaction mixture was evaporated without the treatment with Amberlite IR-120. The residue was crystallized from ethanol and the crystalline product was recrystallized from the same solvent to give **7** as hygroscopic needles, mp 179 °C (dec.), $[\alpha]_D^{24}$ +34.2° (*c* 1.0, water), in 69% yield.

Found: C, 47.28; H, 5.14; N, 9.67%. Calcd for $C_{11}H_{13}N_2O_3K \cdot H_2O$: C, 47.47; H, 5.43; N, 10.06%.

Potassium Salt of N-*Carbamoyl*-N'-*methyl*-L-*methionine* (**9**). The mixture was evaporated without the treatment with Amberlite IR-120. The residue was crystallized from isopropyl alcohol and the product was recrystallized from the same solvent to give **9**, mp 162—164 °C, $[\alpha]_D^{22}$ +4.7° (*c* 1.0, water), in 91% yield.

Found: C, 34.19; H, 5.46; N, 11.46%. Calcd for $C_7H_{13}N_2O_3SK$: C, 34.41; H, 5.36; N, 11.46%.

5-Benzyl-3-methyl-hydantoin (L-*Phenylalanine hydantoin*) (**11**). A 2.3 g portion of **7** was dissolved in water (20 ml) and the solution was adjusted to pH 3 with Amberlite IR-120 (H^+ type) to give an oily precipitate. Ethanol was added to the mixture until the precipitate was dissolved. The ion exchange resin was removed by filtration and the filtrate was evaporated to give a crystalline residue. The residue was recrystallized from methanol to give 1.6 g (93%) of **11**, mp 164—166 °C, $[\alpha]_D^{21}$ −103° (*c* 1.0, ethanol). PMR ($CDCl_3$): τ 7.12 (s, 3H, NCH_3).

Found: C, 64.58; H, 5.94; N, 13.79%. Calcd for $C_{11}H_{12}N_2O_2$: C, 64.69; H, 5.92; N, 13.71%.

3-Methyl-5-(methylmercapto)ethyl-hydantoin (L-*Methionine hydantoin*) (**12**). Compound **9** (6.0 g) was dissolved in water (50 ml) and the solution was adjusted to pH 3 with Amberlite IR-120 (H^+ type). The solution was evaporated under reduced pressure to give a syrup, which yielded crystals in 2-methoxyethanol at −20 °C. Recrystallization from the same solvent afforded 0.7 g (13%) of **12**, mp 88—89 °C, $[\alpha]_D^{17}$ −56.1° (*c* 1.0, ethanol). PMR ($CDCl_3$): τ 7.02 (s, 3H, NCH_3).

Found: C, 45.00; H, 6.36; N, 14.59; S, 17.33%. Calcd for $C_7H_{12}N_2O_2S$: C, 44.66; H, 6.43; N, 14.88; S, 17.03%.

General Procedure for Nitrosation. The *N*-carbamoyl-*N'*-methyl amino acid or its potassium salt was dissolved in aqueous acetic acid and sodium nitrite was added to the solution under ice cooling with agitation. The solution was settled overnight and afterwards treated with Amberlite IR-120 (H^+ type), the solution was lyophylized to give a crude product.

N-*Carbamoyl*-N'-*methyl*-N'-*nitroso-glycine (2).* The crude product was crystallized from chloroform to give **2**, mp 116—117 °C in 63% yield. PMR (C_5D_5N): τ 5.46 (d, 2H, CH_2), 6.86 (s, 3H, NCH_3); (C_5D_5N–D_2O): τ 5.32 (s, 2H, CH_2).

Found: C, 30.12; H, 4.43; N, 25.91%. Calcd for $C_4H_7N_3O_4$: C, 29.82; H, 4.38; N, 26.08%.

N-*Carbamoyl*-N'-*methyl*-N'-*nitroso*-L-*alanine (4).* The residue was crystallized from ether to give **4**, mp 85—87 °C, $[\alpha]_D^{15}$ +71° (*c* 1.0, chloroform) in 62% yield. PMR (C_5D_5N): τ 4.7—5.1 (m, 1H, CH), 6.84 (s, 3H, NCH_3); (C_5D_5N–D_2O): τ 5.08 (q, 1H, CH).

Found: C, 34.07; H, 5.16; N, 24.21%. Calcd for $C_5H_9N_3O_4$: C, 34.29; H, 5.18; N, 23.99%.

N-*Carbamoyl*-N'-*methyl*-N'-*nitroso*-L-*asparagine (6).* The crude product was crystallized from ethanol to give **6**, mp 139 °C, $[\alpha]_D^{26}$ +12°‖ (*c* 0.5, water), in 61% yield. PMR (C_5D_5N): τ 4.2—4.5 (m, 1H, CH), 6.84 (s, 3H, NCH_3); (C_5D_5N–D_2O): τ 4.49 (t, 1H, CH).

Found: C, 33.25; H, 4.70; N, 25.52%. Calcd for $C_6H_{10}N_4O_5$: C, 33.03; H, 4.62; N, 25.68%.

N-*Carbamoyl*-N'-*methyl*-N'-*nitroso*-L-*phenlalanine (8).* A 0.5 g portion of **11** and sodium nitrite (0.21 g) were dissolved in cold water (10 ml) and a mixture of glacial acetic acid (0.2 ml) and ether (10 ml) was added to the solution cooled by ice with gentle agitation. After the mixture was stirred overnight at room temperature, the etheral layer was washed with water, dried over anhydrous sodium sulfate and evaporated. The residue was crystallized from ethyl acetate–*n*-pentane to give 0.23 g (51%) of **8**, mp 97—98 °C, $[\alpha]_D^{28}$ −18° (*c* 0.2, ethanol). PMR ($CDCl_3$): τ 4.7—5.1 (m, 1H, CH), 6.82 (s, 3H, NCH_3); ($CDCl_3$–D_2O): 4.92 (t, 1H, CH)

Found: C, 52.53; H, 5.21; N, 16.71%. Calcd for $C_{11}H_{13}N_3O_4$: C, 52.59; H, 5.21; N, 16.73%.

N-*Carbamoyl*-N'-*methyl*-N'-*nitroso*-L-*methionine (10).* **9** (1.0 g) was dissolved in water (6 ml), and the solution was added to a mixture of sodium nitrite (0.48 g), glacial acetic acid (0.4 ml) and water (3 ml) under ice cooling with agitation. After standing at room temperature overnight, the solution was treated with Amberlite IR-120 (H^+ type) and extracted with chloroform. The chloroform solution was dried over anhydrous sodium sulfate and evaporated. The residue was crystallized from acetone to give 780 mg (75%) of **10**, mp 103—104 °C, $[\alpha]_D^{22}$ +17° (*c* 1.0, chloroform). PMR ($CDCl_3$): τ 4.8—5.3 (m, 1H, CH), 6.81 (s, 3H, NCH_3); ($CDCl_3$–D_2O): τ 5.19 (t, 1H, CH).

Found: C, 35.97; H, 5.63; N, 18.12; S, 13.35%. Calcd for $C_7H_{13}N_3O_4S$: C, 35.74, H, 5.57; N, 17.86; S, 13.63%.

Our thanks are due to Mr. Saburo Nakada who performed the elemental analyses and to Mr. Hitoshi Kimura who assisted in the preparations.

References

1) J. J. Vavra, C. Deboer, A. Dietz, L. J. Hanka, and W. T. Sokolski, *Antibiot. Ann.*, **1959—1960**, 230 (1960); W. T. Sokolski, J. J. Vavra, and L. J. Hanka, *ibid.*, **1959—1960**, 241 (1960); C. Lewis and A. R. Barbiers, *ibid.*, **1959—1960**, 247 (1960); R. R. Herr, T. E. Ebler, M. E. Bergy, and H. K. Janke, *ibid.*, **1959—1960**, 236 (1960).

2) T. Suami and T. Machinami, This Bulletin, **43**, 2953 (1970); *ditto*, *ibid.*, **43**, 3013 (1970).

3) T. Machinami and T. Suami, *ibid.*, **46**, 1013 (1973).

4) B. Bannister, *J. Antibiot.*, **25**, 377 (1972).

5) J. P. Greenstein and M. Winitz, "Chemistry of the Amino Acids", Vol. 3, John Wiley & Sons, Inc., New York (1961) p 2497; J. F. Nyc and H. K. Mitchell, *J. Amer. Chem. Soc.*, **69**, 1382 (1947).

6) H. P. Kaufmann, E. Gindsberg, W. Rottig, and R. Salchow, *Ber.*, **70**, 2519 (1937).

7) C. Paal, *Ber.*, **27**, 974 (1894).

8) A. Neuberger, "Advances in Protein Chemistry", Vol. 4, 297 (1948); J. P. Greenstein and M. Winitz, "Chemistry of the Amino Acids", Vol. 1, John Wiley & Sons, Inc., New York (1961), p. 94.

9) C. Neuberg, H. Wolf, and W. Neimann, *Ber.*, **35**, 4009 (1902).

10) F. Urech, *Ann.*, **165**, 99 (1873).

11) P. Schwebel, *Ber.*, **10**, 2045 (1877).

BULLETIN OF THE CHEMICAL SOCIETY OF JAPAN, VOL. 48(4), 1335—1336 (1975)

Syntheses of Fluorine-Containing Chromans: A Radical Cycloaddition of Phenyl Alkyl Ethers with Hexafluoropropene

Hiroshi KIMOTO, Hiroshige MURAMATSU, and Kan INUKAI

Government Industrial Research Institute, Nagoya, Hirate-machi, Kita-ku, Nagoya 462

(Received October 22, 1974)

Synopsis. Four 2-substituted 4-trifluoromethyl-3,3,4-trifluorochromans were synthesized in one step by the radical cycloaddition of phenyl alkyl ethers and hexafluoropropene in the presence of di-*t*-butyl peroxide.

Although the syntheses of compounds containing a five or six membered ring fused to an aromatic ring are established in the ionic process, such as the Friedel-Crafts ring closure and various condensation reactions, only a few investigations have been reported on the radical process, such as the radical cycloaddition reaction of aromatic compounds with olefins.

In a previous communication[1] we reported on the syntheses of 1-trifluoromethyl-1,2,2-trifluoroindanes by the radical cycloaddition reaction of alkylbenzenes with hexafluoropropene.

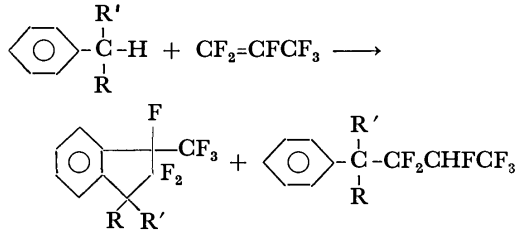

(R, R′ : H, CH_3)

The present work was undertaken with the aim of extending this type of cycloaddition to phenyl alkyl ethers(I), and preparing the fluorine-containing chromans(III).

Four 4-trifluoromethyl-3,3,4-trifluorochromans(III) were synthesized in one step from I and hexafluoropropene(II) in the presence of di-*t*-butyl peroxide.

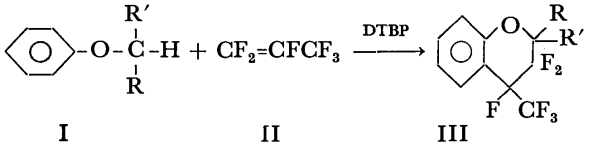

I II III

(Ia, IIIa: R=R′=H; Ib, IIIb[2]: R=H, R′=CH_3; Ic, IIIc: R=R′=CH_3)

To investigate the effect of dilution with a solvent, two kinds of experimental procedure were employed: method A in which no solvent was used, and method B in which inert solvent was used. The reaction conditions and product yields are given in Table 1.

TABLE 1. THE RADICAL CYCLOADDITION REACTION OF PHENYL ALKYL ETHERS AND HEXAFLUOROPROPENE

	Phenyl alkyl ether (mol)	HFP (mol)	DTBP (mol)	Method[a]	Conversion (%)	Yield[b] (%)	Higher boiling products (g)
Ia	0.400	0.660	0.410	A	39.9	44.1	59
Ia	0.400	0.579	0.410	B	33.0	66.7	44
Ib	0.400	0.641	0.410	A	38.7	36.0	83
Ib	0.400	0.561	0.410	B	31.9	85.9	41
Ic	0.400	0.683	0.410	A	37.6	56.1	49
Ic	0.400	0.608	0.410	B	17.5	74.3	49

a) Method A: no solvent; Method B: CCl_2FCClF_2 (1.00 mol) as a solvent.
b) Yields are calculated from the amounts of the consumed phenyl alkyl ether.

As compared with the case of cycloaddition reactions of alkylbenzenes,[1] less reactive phenyl alkyl ethers afford the cycloadducts in a lower conversion, no 1 : 1 adduct, $C_6H_5OCRR'CF_2CHFCF_3$ being formed. Lack of 1 : 1 adduct formation might be due to the incapability of the intermediate radical ($C_6H_5OCRR'CF_2\dot{C}FCF_3$) to abstract a hydrogen from less reactive phenyl alkyl ethers.

Of the two methods A and B, the former is slightly better in total conversion, although a larger quantity of higher boiling products is produced. Higher yields of III were eventually obtained by method B. The yield of III was almost the same with each of the three kinds of phenyl alkyl ethers. Two stereoisomers, IIIb-1 and IIIb-2, were obtained from Ib in the ratio 1 : 3.

In order to prepare the corresponding chromen, dehydrofluorination of IIIa was attempted by treating it with an alcoholic potassium hydroxide solution, but no reaction occurred even in a reflux condition.

The structures of III were elucidated by IR, NMR and mass spectra.

In the mass spectrum, the large molecular ion peak was observed in each chroman(III). Another large ion peak of IIIa, IIIb-1 and IIIb-2 was generated by the loss of CF_3 group from the molecule, IIIc being cleaved to two fragments, *m/e* : 92 C_6H_4O and *m/e* : 192 $(CH_3)_2CCF_2CFCF_3$. Two stereoisomers, IIIb-1 and IIIb-2, gave an identical pattern of fragmentation.

The effect of temperature on the proton NMR spectra was studied in the region from −80 °C to 35 °C. No variation of the spectra was observed. Since no temperature variation was observed in ^1H NMR spectrum, it seems that most of the molecules have a fixed conformation at room temperature.[3] The predominant conformation of the dihydropyrane ring of III may be that of the half-chair form in the same manner as for cyclohexene.[4] Since the CF_3 group is bulky, the molecules are fixed in a position having the CF_3 group in the *quasi*-equatorial position. Non-equivalent *quasi*-axial and equatorial fluorines of each CF_2 group of all the chromans and protons of the CH_2 group of IIIa produced separate AB patterns, methyl groups of IIIc being also non-equivalent. Two isomers, IIIb-1 and IIIb-2, could be observed between the methyl group having a *quasi*-axial position and that having a *quasi*-equatorial one. These configurations were estimated by means of the vicinal H–F coupling constants. By irradiation on methyl protons, quartet splitting was removed from complex multiplet of their tertiary proton spectrum, leaving doublets of doublets (J=7.2 Hz, 18.4 Hz for lower

boiling isomer, IIIb-1 and $J=5.2$ Hz, 23.7 Hz for higher boiling isomer, IIIb-2). The largest doublet splitting (23.7 Hz) might be due to the vicinal coupling of *quasi*-axial hydrogen with *quasi*-axial fluorine.[5] Thus higher boiling isomer (IIIb-2), which was predominant, seems to have its methyl group in the *quasi*-equatorial position.

Characterization of the NMR spectra was made on the basis of the following rules;

(1) chemical shifts of fluorine
$\delta CF > \delta CF_2 > \delta CF_3$

(2) coupling type in the fragment H-C-C-F[5]
$J_{H^{ax}-F^{ax}} > J_{H^{eq}-F^{eq}} > J_{H^{ax}-F^{eq}}$, $J_{H^{eq}-F^{ax}}$

(3) coupling type in the fragment F-C-C-F[6]
$J_{F^{ax}-F^{eq}} > J_{F^{ax}-F^{ax}}$

(4) coupling type in the fragment F-C-C-CF_3[7]
$J_{F^{ax}-CF_3{}^{eq}} > J_{F^{eq}-CF_3{}^{eq}}$

Since signals of CH_2 and CF_2 appeared in a complex ABXY pattern in the spectrum of IIIa, it is not certain to which fluorine nuclei the CH_2 proton couples by first-order analysis. Many sets of heteronuclear and fluorine-fluorine decoupling experiments were needed in order to characterize the spectrum completely. Very weak long-range proton–fluorine couplings were indicated by the signal width.

Mass and NMR spectral data are shown in Table 2 and physical properties and analytical data in Table 3.

TABLE 2. MASS AND NMR SPECTRAL DATA OF CHROMANS

Compounds 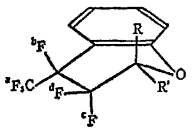

R R′	H H IIIa		CH_3 H IIIb-1		H CH_3 IIIb-2		CH_3 CH_3 IIIc	
Chemical shift[a] (ppm)								
τCH_2	5.8	AB m	—		—		—	
τCH	—		5.38	d-d-q	5.80	d-d-q	—	
$\tau CH_3{}^{ax}$	—		8.55	d	—		8.48	s
$\tau CH_3{}^{eq}$	—		—		8.56	d-d	8.67	d
δCF_3	−4.7	d-d-d	−3.0	d-d-d	−7.0	d-d-d	−6.5	d-d-d
$\delta CF_2{}^{ax}$ $\delta CF_2{}^{eq}$	46.3} 42.6}	AB m m	49.6} 50.0}	AB m m	57.4} 50.2}	AB m m	46.1} 50.2}	AB m m
δCF	85.6	m	100.7	m	67.8	m	73.5	m
Coupling constant[b] (Hz)								
J^aF-^bF	9.3		9.1		9.3		8.5	
J^aF-^cF	13.0		13.1		13.4		15.2	
J^aF-^dF	9.0		8.5		11.8		11.0	
J^bF-^cF					5.1		6.2	
J^bF-^dF			8.5		8.5		7.3	
J^cF-^dF	272		270		272		269	
J^cF-H			7.2		23.7		—	
J^dF-H			18.4		5.2		—	
JH-H	—		6.5		6.4		—	
Mass spectra *m/e* (relative abundance)								
	256 (58.2)		270 (93.9)		280 (67.1)		284 (44.2)	
	187 (100)		201 (100)		201 (100)		192 (100)	
	139 (26.3)		139 (29.0)		139 (26.0)		145 (19.5)	
	109 (51.9)		65 (31.8)		65 (31.5)		92 (27.4)	

a) Neat liquid, using TMS as an internal standard for ^1H and CF_3COOH as an external standard for ^{19}F; the signals being denoted by s(singlet), d(doublet), q(quartet), m(multiplet) and AB(AB pattern). b) Values are of first-order.

TABLE 3. PHYSICAL PROPERTIES AND ANALYTICAL DATA OF CHROMANS

Compound	Bp (°C)	n_D^{20}	d_4^{20}	Formula	Elemental analysis (%) C Found (Calcd)	H Found (Calcd)
IIIa	187	1.4458	1.446	$C_{10}H_8OF_6$	47.06 (46.89)	2.38 (2.36)
IIIb-1	203	1.4358	1.386	$C_{11}H_8OF_6$	49.08 (48.90)	3.22 (2.98)
IIIb-2	205	1.4385	1.421	$C_{11}H_8OF_6$	48.66 (48.90)	3.12 (2.98)
IIIc	210	1.4453	1.361	$C_{12}H_{10}OF_6$	51.07 (50.71)	3.66 (3.55)

Experimental

Phenyl isopropyl ether (Ic) was prepared (yield 69%) from phenol and isopropyl bromide in the presence of sodium hydroxide, according to the method of Marvel and Tanenbaum.[8]

General Procedures Used in the Cycloaddition Reactions of Phenyl Alkyl Ethers(I) with Hexafluoropropene(II). *Method A*: A mixture of I (0.40 mol), II (0.64—0.68 mol) and DTBP (60 g, 0.41 mol) was heated in a 300 ml stainless steel autoclave at temperature gradually rising from 130 °C to 160 °C for about 6 hr. The products were separated by vacuum distillation.

Method B: A solution of I (0.40 mol), II (0.56—0.61 mol) and DTBP (60 g, 0.41 mol) in 1,1,2-trichloro-1,2,2-trifluoroethane (187 g, 1.00 mol) was heated in a 500 ml stainless steel autoclave, under the same conditions as used for method A. After removal of the solvent, the residue was distilled *in vacuo*.

The stereoisomers IIIb-1 and IIIb-2 were separated on preparative glc (with an aluminum column, length 6 m, dia. 10 mm, packed with 20% Silicone DC550–Celite 545).

References

1) H. Kimoto, H. Muramatsu, and K. Inukai, *Chem. Lett.*, **1974**, 791.

2) IIIb consists of two stereoisomers.

3) Some comparable compounds, perfluoromethylcyclohexane and perfluoro(*N*-fluoro-methylpiperidines), were reported to have a conformationally rigid structure at room temperature. J. Feeney and L. H. Sutcliffe, *Trans. Faraday Soc.*, **56**, 1559 (1960); J. Lee and K. G. Orrell, *ibid.*, **63**, 16 (1967).

4) E. J. Corey and R. A. Sneen, *J. Amer. Chem. Soc.*, **77**, 2505 (1955); R. Bucourt, *Bull. Chim. Soc. Fr.*, **1963**, 1262.

5) It was proposed that the dihedral angle (θ) dependence of vicinal proton–fluorine coupling constants (J^{vic}_{H-F}) is similar to vicinal J_{H-H}— a maximum at 0°, a minimum at 90° and a maximum at 180°—and can be expressed as follows.

$$J^{vic}_{H-F} = A\cos^2\theta$$

K. L. Williamson, Y. F. Hsu, F. H. Hall, and S. Swager, *J. Amer. Chem. Soc.*, **90**, 6717 (1968); A. M. Ihrig and S. L. Smith, *ibid.*, **92**, 759 (1970).
The calculated dihedral angles between substituent of 4 and 5 carbon of the cyclohexene by using the Bucourt model[4] are axial-axial : 169°; axial-equatorial : 58°; and equatorial-equatorial : 53°

6) The vicinal axial fluorine–equatorial fluorine coupling constant has the largest value for 1,2,4-trichloroheptafluorocyclohexene.
J. Feeney, L. H. Sutcliffe and S. M. Walker, *Trans. Faraday Soc.*, **62**, 2650 (1966).

7) From a consideration of the through space contribution of fluorine-fluorine coupling, the nearest fluorine-fluorine distance of F^{ax}—$CF_3{}^{eq}$ is shorter than that of F^{eq}—$CF_3{}^{eq}$.

8) C. S. Marvel and A. L. Tanenbaum, "Organic Syntheses", Coll. Vol. I, p. 435 (1956).

BULLETIN OF THE CHEMICAL SOCIETY OF JAPAN, VOL. 48(4), 1337—1338 (1975)

Catalytic Transformation of Cyclohexene Hydroperoxides to Epoxy Alcohols with Vanadyl Acetylacetonate

Takashi ITOH, Kiyotomi KANEDA, and Shiichiro TERANISHI

Department of Chemical Engineering, Faculty of Engineering Science, Osaka University, Toyonaka, Osaka 560

(Received November 5, 1974)

Synopsis. Cyclohexene hydroperoxide and its methyl derivatives undergo rearrangement in the presence of the vanadyl acetylacetonate catalyst to the corresponding epoxy-alcohols with high *cis*-stereoselectivity in high yields.

Hydroperoxide decomposition with transition metals can be classified mainly into homolytic decomposition (Fe, Co, Cu catalysts)[1] and heterolytic decomposition (Mo, V, W catalysts).[2] Rhodium complexes catalyze the homolytic decomposition of cyclohex-2-enyl hydroperoxide (I) to cyclohex-2-en-1-one (II) and cyclohex-2-en-1-ol (III).[3] Little information is available on the heterolytic decomposition of cyclohexene hydroperoxides.

We wish to report the selective transformation of cyclohexene hydroperoxides with the $VO(acac)_2$ catalyst into *cis*-epoxy-alcohols.

The reaction of cyclohex-2-enyl hydroperoxide (I) with $VO(acac)_2$ was carried out in benzene with stirring under nitrogen atmosphere at 40 °C. After 4 hr, glc analysis of the resulting solution revealed that the main product was 2,3-epoxy-cyclohexanol (IV) (79% yield based on consumed peroxide) accompanied by a small amount of the usual decomposition products (II (8%) and III (5%)). The stereochemistry of this epoxy-alcohol was assigned to *cis*-configuration by IR and NMR spectra.[4] The presence of *trans*-isomer could not be detected by glc analysis.

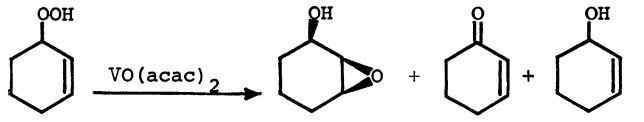

In order to ascertain the generality of this reaction and to clarify the stereochemistry of the rearrangement, hydroperoxides from an unsymmetric olefin were also investigated. Thus, a mixture of three hydroperoxides from 1-methylcyclohexene, containing 3-methylcyclohex-2-enyl hydroperoxide (Va) (51%), 2-methylcyclohex-2-enyl hydroperoxide (Vb) (34%) and 1-methylcyclohex-2-enyl hydroperoxide (Vc) (15%), was treated with $VO(acac)_2$ under the same conditions. The main products were three epoxy-alcohols, 3-methyl-*cis*-2,3-epoxycyclohexanol (VI) (46%), 2-methyl-*cis*-2,3-epoxycyclohexanol (VII) (24%) and 1-methyl-*cis*-2,3-epoxycyclohexanol (VIII) (1%).

The structures of the three epoxy-alcohols were assigned by comparison of their NMR and IR spectra and retention times with those of authentic samples prepared by the $VO(acac)_2$ catalyzed epoxidations of the corresponding methylcyclohexenols with *t*-butyl hydroperoxide.[5] *cis*-Configurations of these epoxy-alcohols were further confirmed by the reductive opening of epoxide rings with $LiAlH_4$ to the corresponding *cis*-diols.[6]

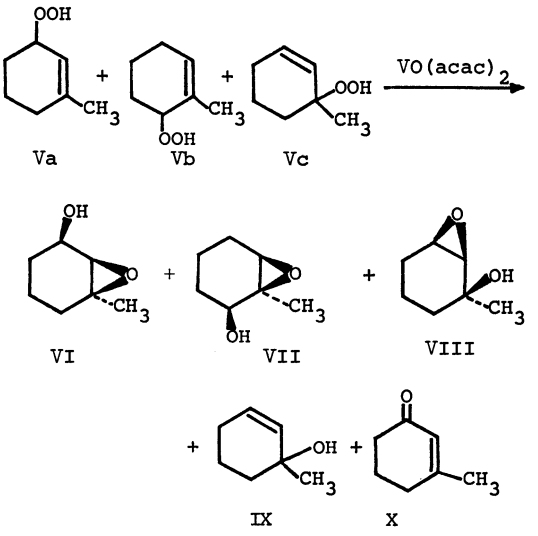

The product distribution of the above reaction showed that peroxides Va, Vb and Vc were transformed into epoxy-alcohols VI, VII and VIII, respectively. This indicates that the transformation follows reaction pattern b rather than pattern a.[7]

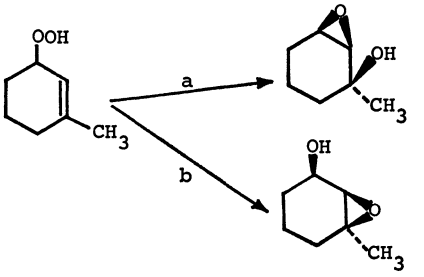

Scheme 1.

Thus, $VO(acac)_2$ catalyst can transform cyclohexene hydroperoxides selectively into epoxy-alcohols with a high *cis*-stereoselectivity (*cis*-isomer>99%). $V(acac)_3$ gave lower yields and selectivity. The molybdenum analogue $MoO_2(acac)_2$ was found to be a poor catalyst.

Equimolar reaction of cyclohexene hydroperoxide and $VO(acac)_2$ gave II (25%), III (63%) and a trace amount of IV. ESR study showed that the addition of hydroperoxide (I) to the benzene solution of $VO(acac)_2$ (molar ratio 1 : 1—5 : 1) causes a large reduction (85—90%) in the strength of the V^{IV} signal and no new other signals appeared. Thus, it seems that $VO(acac)_2$ can be oxidized with hydroperoxide

to higher valence species (V^v), which might act as an actual catalyst for the formation of epoxy-alcohols.

Experimental

Materials. Cyclohexene hydroperoxides, I and V, were prepared as reported previously.[3] The purity was determined by iodometric titration;[8] I (86%) and V (87%). Impurities found were the corresponding cyclohexenols and cyclohexenones. The isomer distribution of hydroperoxides (V) was determined by the area ratios of signals of vinylic protons and hydroperoxy protons in NMR spectrum.

Reaction of I. Peroxide I (10 mmol) in 5 ml dry benzene solution was added dropwise to a 25 ml dry benzene solution of $VO(acac)_2$ (0.1 mmol) at 40 °C under nitrogen atmosphere with stirring. After 4 hr, 98% of I was consumed. Three products were found by glc analysis (OV 17 at 80 °C); IV (7.7 mmol), II (0.8 mmol) and III (0.5 mmol). These compounds were identified by comparison of their NMR and IR spectra and retention times with those of authentic samples.[3,4]

Fractional distillation under reduced pressure gave IV (0.65 g); bp 86 °C/6 mmHg (Ref.,[4] 100—102 °C/12 mmHg).

Reaction of V. The same procedure as for I was used. Three epoxy-alcohols were obtained as the main products by glc analysis (PEG 6000 at 120 °C); VI (4.5 mmol), VII (2.4 mmol) and VIII (0.1 mmol). VI; IR (neat) 3400, 1092, 1034, 888 and 839 cm^{-1}. NMR (CCl_4) τ 6.13 (m, 1H), 7.00 (d, 1H), 7.9—8.8 (m, 6H) and 8.69 (s, 3H). VII; IR (neat) 3400, 1041 and 835 cm^{-1}. NMR (CCl_4): τ 6.32 (m, 1H), 6.96 (t, 1H), 7.8—8.7 (m, 6H) and 8.62 (s, 3H). VIII; IR (neat) 3400, 1143, 1100, 1087, 930, 857 and 820 cm^{-1}. NMR (CCl_4): τ 6.70 (m, 1H), 7.09 (d, 1H), 7.7—8.8 (m, 6H) and 8.66 (s, 3H). The usual decomposition products, methylcyclohexenols and methylcyclohexenones, *e.g.*, IX (0.8 mmol) and X (0.5 mmol), were minor products.

$LiAlH_4$ Reduction of Epoxy-alcohol to cis*-Diol.* VII was separated by preparative glc and then 1.0 mmol of VII was treated with 2.5 mmol of $LiAlH_4$ in 10 ml dry ether. From ethyl acetate extract of the reaction mixture, white crystals of 1-methylcyclohexane-*cis*-1,2-diol (0.08 g, 0.6 mmol) were obtained; mp 68.0—68.5 °C (Ref.,[9] 68.5 °C). NMR (C_2D_5OD): τ 5.60 (m, 1H), 8.1—8.8 (m, 8H) and 8.84 (s, 3H).

References

1) For a recent review see, G. Sosnovsky and D. J. Rawlinson, in "Organic Peroxides" D. Swern, ed., Vol. 2, Wiley-Interscience, New York, N.Y. (1971), pp. 157—191.

2) R. A. Sheldon and J. A. Van Doorn, *J. Catal.*, **31**, 427 (1973) and references cited therein.

3) K. Kaneda, T. Itoh, Y. Fujiwara, and S. Teranish, This Bulletin, **46**, 3810 (1973).

4) P. Chamberlain, M. L. Roberts, and G. H. Whitham, *J. Chem. Soc., B*, **1970**, 1374.

5) K. B. Sharpless and R. C. Michaelson, *J. Amer. Chem. Soc.*, **95**, 6136 (1973).

6) H. B. Henbest and R. A. L. Wilson, *J. Chem. Soc.*, **1957**, 1958.

7) Detailed mechanism, in particular the discrimination between intramolecular rearrangement and intermolecular epoxidation, is not clear at present but it can be said that the epoxidation takes place at olefinic double bonds of the starting hydroperoxides.

8) V. R. Kokatnur and M. Jelling, *J. Amer. Chem. Soc.*, **63**, 1432 (1941).

9) C. A. Bunton and M. D. Carr, *J. Chem. Soc.*, **1963**, 770.

BULLETIN OF THE CHEMICAL SOCIETY OF JAPAN, VOL. 48(4), 1339—1340 (1975)

The Preparation of Aryl Heptafluoroisopropyl Ketones from Aroyl Chlorides and Hexafluoropropene in the Presence of Fluoride Ions

Nobuo ISHIKAWA and Seiji SHIN-YA

Department of Chemical Engineering, Tokyo Institute of Technology, Meguro-ku, Tokyo 152

(Received November 25, 1974)

Synopsis. Aroyl chlorides and hexafluoropropene in the KF/DMF system gave aryl heptafluoroisopropyl ketones. The substituent effect on the yield was discussed.

The hexafluoroisopropyl anion prepared from hexafluoropropene (HFP) and the fluoride ion in an aprotic polar solvent is known as a useful nucleophile for heptafluoroisopropylation.[1] As for the preparation of perfluoroisopropyl ketons, $(CF_3)_2CF-CO-R_f$, Smith *et al.*[2] have obtained perfluoroalkyl heptafluoroisopropyl ketones by the reaction of this nucleophile with various perfluoroacyl fluorides. In the aromatic series, Chambers *et al.*[3] have reported on the similar formation of perfluoro(isopropyl phenyl ketone) and perfluoro-(isopropyl 4-pyridyl ketone) from pentafluorobenzoyl or tetrafluoroisonicotinoyl fluorides respectively. However, they mentioned that pentafluorobenzoyl chloride did not react with HFP under the same conditions.

We wish now to report a convenient method for the preparation of aryl heptafluoroisopropyl ketones in which aryl groups are the general substituted or unsubstituted phenyls. In this case, satisfactory yields were obtained by the reaction of aroyl chlorides with hexafluoropropene in the presence of the fluoride ion and it was not necessary to use aroyl fluorides as the starting material. The reactions were carried out in the potassium fluoride–dimethylformamide system at 120—130 °C under an autogeneous pressure. The amount of potassium fluoride must be present in excess, probably to convert the aroyl chloride into fluoride.

$$CF_3CF{=}CF_2 + F^- \rightleftharpoons (CF_3)_2CF^- \quad (1)$$

$$Ar\text{-}\underset{\underset{O}{\|}}{C}\text{-}Cl + F^- \rightleftharpoons Ar\text{-}\underset{\underset{O}{\|}}{C}\text{-}F + Cl^- \quad (2)$$

$$Ar\text{-}\underset{\underset{O}{\|}}{C}\text{-}F + (CF_3)_2CF^- \rightleftharpoons Ar\text{-}\underset{\underset{O}{\|}}{C}\text{-}CF(CF_3)_2 + F^- \quad (3)$$

For the purpose of checking the scope of this reaction, we also examined a similar reaction between substituted aroyl chlorides and HFP.

The effects of the substituents of the aroyl halides upon the yields of the heptafluoroisopropyl ketones were noteworthy. The strong electron-attractive *p*-nitro group and the strong electron-donative *p*-methoxy group both served to produce poor yields (Table 1). In the former case, it was assumed that the *p*-nitrophenyl heptafluoroisopropyl ketone formed must be very unstable thermodynamically, because the carbon atom of the carbonyl group is linked on both sides to the strong electron-attractive groups. Then the equilibrium of Eq. (3) becomes unfavorable for the formation of the ketone.

On the other hand, in the case of *p*-methoxybenzoyl halide, the electron-donative mesomeric effect of the methoxyl group increases the electron density on the carbon atom of the carbonyl group, thus making the nucleophilic attack of the heptafluoroisopropyl anion difficult. Consequently, the reaction of the *p*-nitrobenzoyl halide is controlled thermodynamically, whereas that of the *p*-methoxybenzoyl halide is controlled kinetically.

In order to improve our knowledge about the electronic effect of the $COCF(CF_3)_2$ group as a benzene substituent, we calculated the σ values for this group from ^{19}F NMR according to Taft's equation.[4] Since the chemical shifts for the aromatic fluorine atoms of *m*- and *p*-fluorophenyl heptafluorisopropyl ketones in CCl_4 from fluorobenzene were observed to be $\delta_m = -2.50$ and $\delta_P = -12.13$ ppm, the σ_R^0 and σ_I values for the heptafluoroisobutyryl group were determined to be 0.326 and 0.437 respectively. These figures suggest that the inductive and conjugative effects for the $COCF(CF_3)_2$ group are almost the same as those for the $COCF_3$ group ($\sigma_R^0 = 0.329$, and $\sigma_I = 0.455$).[4]

TABLE 1. PREPARATION AND SPECTRAL DATA FOR Ar-CO-CF$(CF_3)_2$

Subst. or Ar	Preparation					Spectral data			
	KF/ArCOCl	Bp °C/mmHg	Yield %	F-Anal (%) Obsd	F-Anal (%) Calcd	IR (cm^{-1}) C=O	^{19}F NMR[a] CF_3	^{19}F NMR[a] CF	^{19}F NMR[a] Ar-F
H	2	80—81/39	47	48.7	48.5	1700	−39.0(d)	64.5(m)	—
H	4	80—81/39	66	—	—	—	—	—	—
p-Me	4	76—78/14	63	46.3	46.2	1700	−37.8(d)	66.0(m)	—
p-OMe	4	84/5	14	43.4	43.8	1695	−38.6(d)	64.8(m)	—
m-F	4	65/18	48	52.2	52.1	1700	−38.5(d)	66.4(m)	−1.4
p-F	4	68/19	48	51.9	52.1	1700	−37.7(d)	66·0(m)	−10.7
p-Cl	4	87—88/19	50	42.9	43.1	1700	−38.9(d)	65.8(m)	--
p-NO_2	4	103/8	3	41.3	41.7	1720	−39.1(d)	66.1(m)	—

a) The chemical shifs are given in δ ppm from ext. PhF in CCl_4 or in neat.

Experimental

Phenyl Heptafluoroisopropyl Ketone. A mixture of benzoyl chloride (2.81 g, 0.02 mol), dimethylformamide (10 ml), and finely ground potassium fluoride (4.64 g, 0.08 mol) was put into a glass tube vessel equipped with a mechanical stirrer. At −70 °C liquefied hexafluoropropene (0.045 mol) was added, and after having been sealed the vessel was brought to room temperature. The whole was then heated for 6 hr in an oil bath kept at 120—130 °C under mechanical stirring. The reaction mixture was then poured into water and the separated oily material was extracted with diethyl ether. The extract was washed with a dilute aqueous solution of potassium hydroxide and water successively, and then dried over magnesium sulfate. After the solvent had been removed, the residual oil was subjected to a vacuum distillation. Phenyl heptafluoroisopropyl ketone (bp 80—81 °C/39 mmHg) was thus obtained in a yield of 66%.

Other substituted aryl heptafluoroisopropyl ketones were prepared in a similar manner.

References

1) J. A. Young, "Fluorine Chemistry Reviews", **1**, 359 (1967).

2) R. D. Smith, F. S. Fawcett, and D. D. Coffman, *J. Amer. Chem. Soc.*, **84**, 4285 (1962).

3) R. D. Chambers, C. A. Heaton, and W. K. R. Musgrave, *J. Chem. Soc. C*, **1968**, 1933.

4a) R. W. Taft, E. Price, I. R. Fox, I. C. Lewis, K. K. Anderson, and G. T. Davis, *J. Amer. Chem. Soc.*, **85**, 709 (1963). b) *ibid*, **85**, 3146 (1963).

BULLETIN OF THE CHEMICAL SOCIETY OF JAPAN, VOL. 48 (4), 1341—1342 (1975)

A Novel Synthesis of L-Pipecolic Acid

Toshiyuki FUJII and Muneji MIYOSHI

Research Laboratory of Applied Biochemistry, Tanabe Seiyaku Co. Ltd., 16-89, Kashima-3-chome, Yodogawa-ku, Osaka, 532

(Received December, 1974)

Synopsis. A novel synthesis of L-pipecolic acid from L-lysine is described. Bromination of ε-NH_2 group on N^{α}-tosyl-L-lysine, followed by cyclization with NaH in DMF gave *N*-tosyl-L-pipecolic acid in 45% yield.

Pipecolic acid, a non-proteinogenic amino acid, was first prepared in DL form by Ladenburg in 1891,[1] then it was resolved into optically active components by Mende.[2] Later, Morrison[3] isolated the amino acid having levo rotation from *trifolium repens* (white clover). Since then, the widespread occurrence of L-pipecolic acid in plant kingdom has attracted an interest in the metabolism of the amino acid, and several possible biosynthetic routes have also been suggested.[4] Although the full role of pipecolic acid in metabolism still remains obscure, several experiments reported so far give support that lysine may be a precursor in the biosynthesis of pipecolic acid.[5-8]

Up to date, L-pipecolic acid has been usually synthesized by reduction of 2-picolinic acid,[9] followed by resolution of the racemate. Attempts to obtain the L-form by the conversion of naturally occuring six-membered ring compounds were carried out *via* the oxidation of L-conhydrine[10] or *via* the reduction of L-baikiain.[11] The preparation of D-pipecolic acid from L-lysine by the use of Walden inversion has also been reported,[12] however, a synthetic route of L-pipecolic acid from L-lysine has not been established as yet.

In a series of our studies[13] on the conversion of L-amino acid to the optically active one, we have found a new synthesis of L-pipecolic acid from L-lysine, as shown in the scheme.

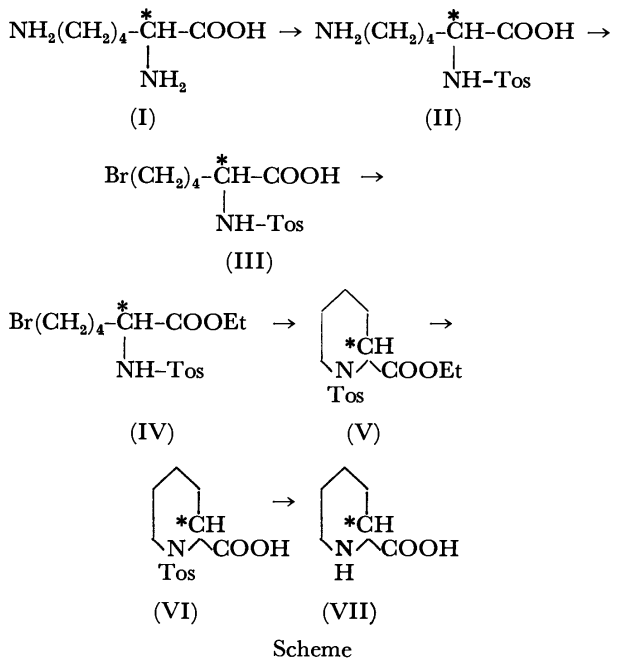

Scheme

Ring closure was performed *via* dehydrobromination by the abstraction of the NH proton at the α-position of L-lysine. Since this new route does not involve any substitution reaction on the asymmetric carbon of the starting material, full optical activity may be retained throughout the reaction.

Diazotization of N^{α}-tosyl-L-lysine (II) was investigated under several conditions: reaction temperature (0—80 °C) and the concentration of bromine ion (5—20 equivalents). Bromination of II took place with difficulty as compared with that of N^{α}-tosyl-diaminopropionic acid.[13a] It seems that the rate of substitution of the amino group with bromine at the ω-position would be decreased in proportion to the length of the alkyl chain. III was obtained as an oil, however, the esterification gave crystalline product (IV): the over-all yield of IV from II was about 45% after recrystallization.

Cyclization of IV with sodium hydride in DMF quantitatively proceeded as expected. It is noted that the ester moiety was unaffected during the cyclization reaction (IV→V) under the same condition reported previously on the synthesis of *N*-tosyl-L-azetidine-2-carboxylic acid;[13b] in that case the ester was completely saponified to the corresponding acid.

The detosylation was carried out successfully either by the treatment of V with 47% hydrobromic acid in acetic acid or by the reduction of VI with metallic sodium (4—5 equivalents) in liquid ammonia.

L-Pipecolic acid thus obtained was proved to be identical with an authentic specimen by the physical and the spectral data.

Experimental

The melting points are uncorrected. IR spectra were recorded on Shimadzu IR-27G. NMR spectra were taken at 60 MHz with tetramethylsilane as the internal standard using Hitachi R-20A.

ε-Bromo-N$^{\alpha}$-tosylamide-L-caproic acid (III). N^{α}-Tosyl-L-lysine* (60.0 g) and potasium bromide (60.0 g) were dissolved in 16% hydrobromic acid (500 ml). To the solution was added dropwise a solution of sodium nitrite (42.0 g) in water (100 ml) at 50—55 °C with vigorous stirring for 1 hr. Then, the reaction mixture was stirred for additional 1 hr at the same temperature, and the resulting oil was extracted with ether (200 ml × 3). The ether solution was washed with saturated sodium chloride solution and dried over magnesium sulfate. The dried solution was concentrated *in vacuo* to obtain an oily residue (III, 77.4 g), which was used to the following reaction without further purification.

Ethyl ε-Bromo-N$^{\alpha}$-tosylamido-L-caproate (IV). A solution

* This was prepared from L-lysine by Barrass and Elmore; mp 272—273 °C (dec.), $[\alpha]_D^{20}$ +13.9 °C (*c* 1, AcOH). [lit.[14] mp 263—264 °C (dec.)]

of III (77.4 g) in absolute ethanol (300 ml) was treated with hydrogen chloride under bubbling at 60—70 °C for 1 hr. After standing overnight at room temperature, the reaction mixture was concentrated, and the resulting oil was dissolved in ether (600 ml). The ether solution was washed with aqueous solution of 5% sodium carbonate and of saturated sodium chloride, successively. The solution was dried over magnesium sulfate and was evaporated *in vacuo*. The residual oil was crystallized from ether-petroleum ether to afford IV, which was positive to Beilstein test, 35.3 g (45% from II), mp 65—66 °C, $[\alpha]_D^{20}$ −2.3° (*c* 1, EtOH). IR (Nujol) ν_{NH}: 3280, $\nu_{C=O}$ 1740, ν_{SO_2} 1375, 1160 cm^{-1}; NMR (CCl_4, δ): 7.75—7.15 (4H, arom), 5.58—5.44 (1H, NH), 4.1—3.64 (3H, CH–CH_2), 3.39—3.18 (2H, CH_2–Br), 2.41 (3H, CH_3– 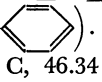).

Found: C, 46.34; H, 5.69; N, 3.49%. Calcd for $C_{15}H_{22}NO_4SBr$: C, 45.91; H, 5.65; N, 3.57%.

Ethyl N-*tosyl*-L-*pipecolinate (V).* To a solution of IV (13.7 g) in DMF (250 ml) was added sodium hydride (1.84 g, 50% oil dispersion) at 10—15 °C, and the reaction mixture was stirred at the same temperature for 45 min. The reaction mixture was neutralized with a few drops of AcOH, and the insoluble materials were filtered. The filtrate was evaporated *in vacuo* below 40 °C, then the residue was extracted with ether and water. The ether solution was washed well with water and dried over magnesium sulfate. The dried solution was evaporated *in vacuo* to afford an oily residue (V, 11.5 g), which was negative to Beilstein test. IR (Film): $\nu_{C=O}$ 1740, ν_{SO_2} 1350, 1155 cm^{-1}.

N-*Tosyl*-L-*pipecolic Acid Dicyclohexylamine Salt (VI·DCHA).* To a solution of V (11.5 g) in methanol (100 ml) was added dropwise 2M sodium hydroxide solution (70 ml) at 15—17 °C under stirring. After 4 hr, the reaction mixture was neutralized and methanol was evaporated *in vacuo*. The residue was dissolved in sodium carbonate solution (100 ml) and the solution was washed with ether. Aqueous phase was acidified with 6M hydrochloric acid, and the resulted oil was extracted with ether. The ether solution was washed with saturated sodium chloride solution and dried over anhydrous magnesium sulfate. The dried solution was evaporated *in vacuo* to afford VI, 9.8 g. To a solution of the oily compound VI in ethyl acetate (70 ml), dicyclohexylamine (6.3 g) was added to obtain VI·DCHA salt, 13.3 g (82%), mp 166—168 °C, $[\alpha]_D^{20}$ −20.3° (*c* 1, MeOH), IR (Nujol): $\nu_{NH_2}{}^+$ 2300—2700, $\nu_{C=O}$ 1625, 1560, ν_{SO_2} 1375, 1155 cm^{-1}; NMR (DMSO-d_6, δ): 7.8—7.2 (4H, arom), 6.4—5.6 (2H, $NH_2{}^+$) 4.1—4.4 (1H, α-CH), 3.6—0.6 (30H, complex, other protons). Found: C, 64.26; H, 8.68; N, 5.97; S, 6.90%. Calcd for $C_{25}H_{40}N_2O_4S$: C, 64.63; H, 8.68; N, 6.03; S, 6.88%.

L-*Pipecolic Acid (VII).* A suspension of VI·DCHA (11.13 g) in 0.5 M sulfuric acid was vigorously shaken with ethyl acetate and the extract was concentrated *in vacuo*. The residue was detosylated with metallic sodium (2.2 g) in liquid ammonia (200 ml). After evaporation of excess ammonia, the residue was dissolved in 0.5M sulfuric acid solution, and the solution was washed with ether. The aqueous phase was treated with ion-exchange resin, Dowex 50 (H^+ form). The resin was eluted with 5% ammonium hydroxide solution, and the eluate was evaporated *in vacuo* to afford VII. Crude VII was recrystallized from methanol-ether, 2.33 g (76%), mp 259—260 °C, $[\alpha]_D^{20}$ −30.6° (*c* 1, water) [lit,[3] mp 271 °C (dec.), $[\alpha]_D^{18}$ −25.4° (*c* 5, water)]. IR (Nujol): $\nu_{NH_2}{}^+$ 2380—2500, $\nu_{C=O}$ 1615 cm^{-1}. Found: C, 55.30; H, 8.50; N, 11.02%. Calcd for $C_6H_{11}NO_2$: C, 55.77; H, 8.38; N, 10.84%.

References

1) A. Ladenburg, *Ber.*, **24**, 640 (1891).
2) F. Mende, *ibid.*, **29**, 2887 (1896).
3) R. I. Morrison, *Biochem. J.*, **53**, 574 (1953).
4) M. Guggenheim, "Die Biogenen Amine", J. Springer, Berline, 1940.
5) N. Grobbelaar and F. C. Steward, *J. Amer. Chem. Soc.*, **75**, 4341 (1953).
6) M. Rothstein and L. L. Miller, *ibid.*, **75**, 4371 (1953).
7) F. P. Guengerich and H. P. Broquist, *Biochemistry*, **12**, 4270 (1973).
8) E. Leistner, R. N. Gupta, and I. D. Spenser, *J. Amer. Chem. Soc.*, **95**, 4040 (1973).
9) A. Harris and J. R. A. Pollock, *Chem. Ind.* (London), 462 (1953). C. M. Stevens, and P. B. Ellman, *J. Biol. Chem.*, **182**, 75 (1950).
10) R. Willstätter, *Ber.*, **34**, 3166 (1901).
11) F. E. King, T. J. King, and A. J. Warwick, *J. Chem. Soc.*, 3590 (1950).
12) U. Schiedt and H. G. Höss, *Z. Physiol. Chem.*, **308**, 179 (1957).
13) a) N. Yoneda, T. Fujii, M. Umeda, H. Yasuo, Y. Taguchi, and K. Okumura, *Yakugaku Zasshi*, **89**, 98 (1969). b) M. Miyoshi, H. Sugano, T. Fujii, T. Ishihara, and N. Yoneda, *Chem. Lett.*, **1973**, 5.
14) B. C. Barrass and D. T. Elmore, *J. Chem. Soc.*, 4830 (1957).

BULLETIN OF THE CHEMICAL SOCIETY OF JAPAN, VOL. 48 (4), 1343—1344 (1975)

Deoxygenation of Sulfoxides to Sulfides in an Iodine–Pyridine–Sulfur Dioxide System

Masatomo NOJIMA, Tsuyoshi NAGATA, and Niichiro TOKURA

Department of Applied Chemistry, Faculty of Engineering, Osaka University, Suita, Osaka, 565

(Received December 5, 1974)

Synopsis. Sulfoxides were deoxygenated quantitatively in an iodine-pyridine-sulfur dioxide system under mild reaction conditions. The same reaction also occurred with bromine.

An iodine–pyridine–sulfur dioxide system was found to be effective for the dehydration reaction between carboxylic acid and amine.[1] Deoxygenation of sulfoxides to sulfides was examined in this system in order to find a convenient and selective reduction method for sulfoxides.[2]

Sulfoxides were allowed to react with 1 equiv. mole of iodine in the presence of excess pyridine–sulfur dioxide complex (1 : 1 molar ratio) using acetonitrile as a solvent at 80 °C for 2 hr. The products were isolated and characterized by comparing the physical data with those of authentic samples.

$$\mathrm{RS(O)R} \xrightarrow[\text{in acetonitrile, 80°C, 2 hr.}]{\mathrm{I_2}\ (1),\ \mathrm{SO_2}\text{-Pyridine}\ (10)} \mathrm{RSR}$$

The results obtained are summarized in Table 1. All the sulfoxides were selectively deoxygenated to give the corresponding sulfides in excellent yields. Although diphenyl sulfoxide was reduced slowly, diphenyl sulfide was obtained quantitatively when the reaction was continued for 18 hr.

TABLE 1. REDUCTION OF SULFOXIDES

Sulfoxide	Yield of Sulfide (%)	
	Reaction with Iodine[a]	Reaction with Bromine[b]
Diphenyl	20 95[c]	38
Dibenzyl	93	95
Di-*n*-butyl	84	73
Dimethyl	96	85
Tetramethylene	95	19

a) A solution of 1×10^{-3} mol of sulfoxide, 1×10^{-3} mol of iodine, 1×10^{-2} mol of sulfur dioxide-pyridine complex in 50 ml of acetonitrile was allowed to react at 80 °C for 2 hr. b) The reaction was carried out by keeping a mixture of 1×10^{-3} mol of sulfoxide, 1×10^{-3} mol of bromine and 1×10^{-2} mol of sulfur dioxide in 50 ml of acetonitrile at 80 °C for 2 hr. c) The reaction was carried out for 18 hr.

The reaction with bromine was carried out in the absence of pyridine, since in its presence α-bromination of the sulfoxide[3] competes with reduction. The reaction proceeded well, but in the case of tetramethylene sulfoxide a complex side-reaction took place.

In order to investigate the behavior of iodine we examined the UV spectra of iodine and tetraethylammonium iodide in the pyridine–sulfur dioxide–acetonitrile system.[4] No absorption of iodine was detected. An absorption considered to be that of iodosulfinate ion[5] was observed at 362 nm (ε, 7400 $\mathrm{l\cdot mol^{-1}\,cm^{-1}}$). The value is consistent with that of iodosulfinate ion in this system (ε, 8900 $\mathrm{l\cdot mol^{-1}\,cm^{-1}}$). It is reasonable to consider that iodine is dissociated into iodonium ion and iodosulfinate ion quantitatively. In the system of bromine–pyridine–sulfur dioxide, the absorption of bromosulfinate ion was also observed at 322 nm.[5]

In order to clarify the mechanism of the reaction, the following reactions were examined. When *N*-iodosuccinimide[6] or tetraethylammonium iodide was used instead of iodine, no reaction occurred suggesting the necessity of both iodonium and iodide ions for the reduction of sulfoxides. The reaction did not proceed either in the absence of sulfur dioxide. By the reaction of di-*n*-butyl sulfoxide with one third molar equiv. of iodine sulfide was obtained in 54% yield indicating that iodine works as a catalyst. No reversible reaction seems to occur in this system, since diphenyl sulfoxide was not obtained by the reaction of diphenyl sulfide with iodine in the presence of sulfur trioxide–pyridine complex.

The following scheme is considered to be the most plausible one for this novel deoxygenation reaction.

$$\mathrm{I_2} \xrightarrow{\mathrm{SO_2}} \mathrm{I^+} + {}^-\mathrm{SO_2I}$$

$$\mathrm{RS(O)R} \xrightarrow{\mathrm{I^+}} \mathrm{RS^+(O)R} \quad (\mathrm{I}) \xrightarrow{-\mathrm{SO_2I}} \mathrm{RS^{\delta+}R} \quad (\mathrm{OSO_2I^{\delta-}})$$

A

$$\mathrm{A} \longrightarrow \mathrm{RS^+R} + {}^-\mathrm{SO_3I} \quad (\mathrm{I})$$

$$-\mathrm{SO_3I} + \mathrm{SO_2\cdot Py} \longrightarrow -\mathrm{SO_2I} + \mathrm{SO_3\cdot Py}$$

Iodine ionizes to iodonium ion and iodosulfinate ion. Iodonium ion attacks sulfoxide first,[7] and then iodosulfinate ion may add to form intermediate A. Elimination of iodosulfonate ion and iodonium ion probably occurs from A to produce sulfide. Iodosulfonate ion formed would react with sulfur dioxide–pyridine complex generating again iodosulfinate ion with sulfur trioxide–pyridine complex.

Experimental

Reaction of Diphenyl Sulfoxide in the Iodine–Pyridine–Sulfur Dioxide System. In a round-bottomed flask fitted with a dry ice condenser was placed 2.52 g (0.01 mol) of iodine and 10 ml of pyridine–sulfur dioxide complex in 30 ml of acetonitrile. To this was added diphenyl sulfoxide (2.02 g,

0.01 mol) in 20 ml of acetonitrile over a period of 10 min at room temperature. The reaction mixture was kept at 80 °C for 2 hr, and then treated in the usual way. The product was analyzed with a Hitachi K-53 vpc apparatus equipped with a flame ionization detector.

Reaction of Diphenyl Sulfoxide in the Bromine-Sulfur Dioxide System. To a mixture of diphenyl sulfoxide (2.52 g, 0.01 mol) and bromine (1.6 g, 0.01 mol) in 50 ml of acetonitrile was added 5.0 ml of sulfur dioxide. The reaction mixture was kept at 80 °C for 2 hr and then extracted with ether and dried over anhydrous sodium sulfate. After removal of the solvent the product was analyzed by vpc. Diphenyl sulfide was obtained as the sole product.

References

1) M. Nojima, S. Hasegawa, and N. Tokura, This Bulletin, **46**, 1254 (1953).
2) H. C. Brown and N. Ravindran, *Synthesis*, **1973**, 42.
3) S. Iriuchijima and G. Tsuchihashi, *ibid.*, 588 (1970).
4) Iodine dissociates into iodonium and iodide ions in pyridine. O. Hassel and H. Hope, *Acta Chem. Scand.*, **15**, 407 (1961).
5) D. F. Burow, *Inorg. Chem.*, **11**, 574 (1972).
6) *N*-Iodosuccinimide is known to generate iodonium ion under certain conditions. G. A. Olah, M. Nojima, and I. Kerekes, *Synthesis*, **1973**, 780.
7) E. J. Corey and C. U. Kim, *Tetrahedron Lett.*, **1973**, 919.

The Catalytic Hydrogenation of Ethylene over Calcium Hydride and the Role of the Hydrogen of the Hydride

Masaru YAMAGUCHI, Yozaburo HIRAKI, Masatada WADA,* and Kimio TARAMA*

Faculty of Living Science, Kyoto Prefectural University, Sakyo-ku, Kyoto 606

* *Department of Hydrocarbon Chemistry, Faculty of Engineering, Kyoto University, Sakyo-ku, Kyoto 606*

(Received July 20, 1974)

The catalytic hydrogenation of ethylene over the non-stoichiometric calcium hydride ($CaH_{2-\delta}$) prepared by means of high-temperature evacuation was studied. The order of introducing gases had no effect on the rate of ethylene hydrogenation. The rate expressions for the initial stage were $v=k\,P_H^{0.8-1.0}\,P_E$ and $v'=k'\,P_H^{0.8-1.0}\,P_E^0$ in the lower and higher pressure ranges of ethylene respectively. The amount of hydrogen bound initially to $CaH_{2-\delta}$ and participating in the reaction was estimated from the results of the D_2–$CaH_{2-\delta}$ exchange and H_2–D_2 equilibration reactions. From these results, the mechanism of ethylene hydrogenation over calcium hydride and the role of the hydrogen of the hydride were discussed. The poisoning caused by water and acetylene was also studied. Furthermore, the catalytic activity of calcium hydride was compared with that of three metallic hydrides.

It has been established that the non-stoichiometric calcium hydride prepared by means of high-temperature evacuation has an remarkable catalytic activity for hydrogenation,[1–3] whereas metallic calcium and stoichiometric calcium hydride are far less active as catalysts of the hydrogenation of olefins. Though it has been pointed out[4] that the electrons in s-, p-, and d-bands are overlapped with each other in metallic calcium, its electronic structure is remarkably different from that of the transition metals of the 8th group, known to be excellent catalysts for hydrogenation. The distance between calcium atoms in the hydride is unusually longer (minimum distance: about 3.4 Å) in comparison with that of the transition metals of the 8th group. Also, the hydride has a highly ionic character. Therefore, it may be said that the non-stoichiometric calcium hydride is a peculiar catalyst for hydrogenation.

When the catalytic activities of calcium hydride have been studied thus far,[1–3] the investigations have been limited to the qualitative aspect of hydrogenation, the detailed mechanism has been left unsurveyed. The present investigation was undertaken in order to obtain more detailed kinetic information concerning the mechanism of the ethylene hydrogenation on this catalyst and in order to determine the role of the hydrogen bound initially to the hydride during the catalytic reaction. The experimental results will also be compared with those of the previous works on palladium black,[5] tantalum powder,[6] and titanium hydride.[7]

Experimental

Materials. The calcium hydride was obtained from the Metal Hydride Co. (purity: 98—99 %). The major impurities in this specimen were nitrogen and oxygen. It was also contaminated with trace amounts of magnesium, manganese, sodium, strontium, and iron. Noble metals, which are known as excellent hydrogenation catalysts, were not detected by emission spectrographic analysis. The hydrogen was prepared by the thermal decomposition of titanium hydride.[6,7] The deuterium (purity: D_2 97.8 %, HD 2.2 %) and the acetylene (99.6 %) in a glass ampoule were obtained from the Takachiho Trading Co.; they were used without further purification. The ethylene was purified by the conventional procedure, followed by repeated fractionations at the temperature of liquid nitrogen.

Procedure. All of the experimental runs were conducted in a closed circulating system at a constant pressure or within a constant volume. The apparatus used in these experiments was similar to that reported in a previous paper.[6] Since calcium hydride is very sensitive to the moisture, each sampling manipulation was carried out carefully in a dry box. About two grams of the powdered catalyst was placed in the reaction vessel; as a standard pretreatment, it was evacuated at 200 °C for 1 hr and finally at 450 °C under 1×10^{-5} Torr for 1 hr. After the vessel has then been cooled to the predetermined temperature, all the runs were carried out. The rate of ethylene hydrogenation was measured in the temperature range between −78 and 450 °C and in the range of total pressure between 50 and 500 Torr. The relative concentrations of ethylene and ethane in the product were estimated by a micro gas-absorption method similar to that of a previous paper;[7] these concentrations agreed with the value calculated from the volume change, thus excluding any possibility of reactions other than ethylene hydrogenation occurring. The adsorption of reactant gases to the catalyst was negligible in the rate measurements. The hydrogen isotopes were analyzed by using a CEC-21-401 mass spectrometer. The spectrum of hydrogen isotopes was taken at an ionization energy of 70 eV and at an ion-accelerating voltage of 500 V. A Shimadzu GX-3B X-ray diffractometer with copper $K\alpha$ radiation was used to obtain the diffraction diagrams of calcium hydride.

Results and Discussion

Effect of the Pretreatments of Stoichiometric Calcium Hydride on Surface Area, the Amount of Hydrogen Evolved, and the Initial Rate of Ethylene Hydrogenation. As is shown in Fig. 1, evacuation at temperatures below 200°C evolved only a slight amount of hydrogen, and the increase in the surface area was minor. No catalytic activity was observed for ethylene hydrogenation. As the temperature was raised above 250°C, the amount of hydrogen evolved and the surface area increased remarkably. The catalytic activity was considerably raised when more than ten percent of hydrogen was removed from the stoichiometric calcium hydride. Though an evaporated film of metallic calcium was formed on the wall of the evacuated reaction vessel above 450 °C,

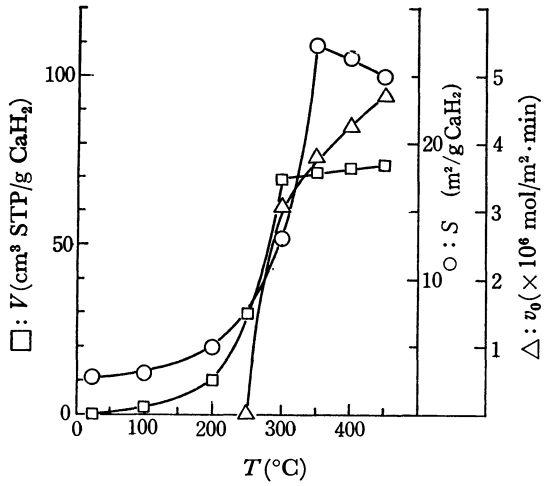

Fig. 1. Effects of the evacuation temperature (T) on the amount of hydrogen evolved (V), B.E.T. surface area (S) and the initial rate of ethylene hydrogenation (v_0).

the film revealed no catalytic activity.

It is thought that the increase in the surface area is caused by the loss of hydrogen from the crystal lattice, thus bringing about a higher porosity. Such a surface may contain many lattice defects, basic or base-like sites, metallic or metal like sites, and their interfaces.

Hydrogenation of Ethylene. Although the order of introducing gases significantly affects the rate of ethylene hydrogenation using palladium-, tantalum- and titanium hydride,[5-7] no significant differences were observed with the non-stoichiometric calcium hydride, $CaH_{2-\delta}$,* as is shown in Fig. 2. The reaction proceeds even at −40 °C; the maximum initial rate was observed at about 250 °C.

Figure 3 shows the dependence of the initial rate upon the hydrogen or ethylene pressure. From this figure, the initial rate of the ethane formation is expressed by:

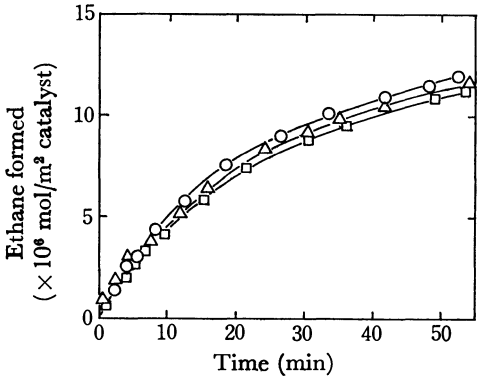

Fig. 2. Ethane formed—time plots at 0 °C (Effect of the order of introducing gases).

Each initial rate (v_0) was evaluated as follows:

Order of introduction	P_H Torr	P_E Torr	v_0 ×10⁷·mol/m²·min
○: H+E	44.1	42.7	4.88
△: H→E	41.8	44.3	5.00
□: E→H	44.7	41.1	4.68

* δ=0.35 after the standard pretreatment.

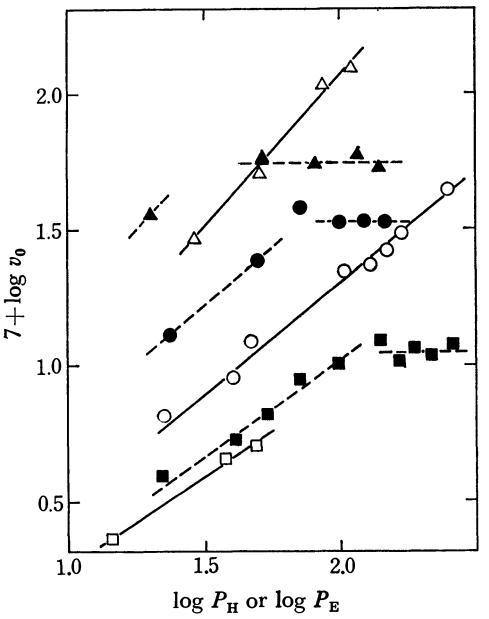

Fig. 3. Dependence of the initial rate of ethylene hydrogenation upon the pressures of ethylene and hydrogen. closed mark: dependencies upon ethylene (P_H= 48 Torr), open mark: dependencies upon hydrogen (P_E= 45 Torr), □, ■: 0°C, ○, ●: 50 °C, △, ▲: 100 °C.

$$v = kP_H^{0.8-1.0}P_E \text{ and } v' = k'P_H^{0.8-1.0}P_E^0$$

in the regions of lower and higher pressures of ethylene respectively. The apparent activation energies between 0 and 100°C were estimated to be 4.6 and 3.3 kcal/mol for k and k' respectively.

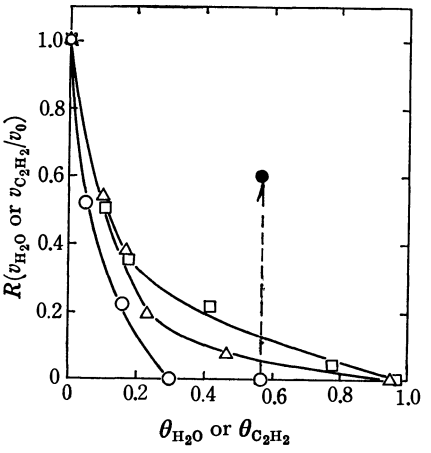

Fig. 4. Effects of the surface coverage, $\theta^{a)}$, by water or acetylene on the relative activity (R).

Pretreated substances	Reaction temperature	P_H Torr	P_E Torr
○: H_2O	100 °C	47.5	48.0
□: C_2H_2	100	52.5	49.3
△: C_2H_2	200	51.8	48.3

Closed circle shows restored relative activity after high temperature evacuation.

a) θ_{H_2O} (or $\theta_{C_2H_2}$) was estimated on the basis of the assumption that two molecules (or one molecule) of water (or acetylene) react with one atom of surface-exposed calcium: number of calcium atoms exposed on the surface was calculated from B.E.T. nitrogen surface area.

The effect of the pretreatment by water or acetylene on the catalytic activity is shown in Fig. 4. The relative catalytic activity (R), which is defined as the ratio of the initial rate of hydrogenation with the catalysts after and before the pretreatment, decreased sharply, along with the surface coverage (θ_{H_2O}) by water, falling to zero at $\theta_{H_2O}=0.3$. When this deactivated catalyst was evacuated at 650°C and when the standard pretreatment was carried out after treating it with 300 Torr hydrogen at 400°C for 1 hr, the activity was restored to some extent. The poisoning by acetylene was similar to that of water up to about $\theta_{C_2H_2}=0.1$, though the relative activity fell to zero in the vicinity of $\theta_{C_2H_2}=1$. Contrary to the case of water, the poisoning by acetylene was perfectly irreversible, regardless of the kind of treatment thereafter. When a mixture of acetylene and hydrogen was introduced into the catalyst vessel, a considerable decrease in the pressure was observed. The analysis of the remaining gas, however, revealed that the pressure decrease was caused by the adsorption or by the reaction of the acetylene with the catalyst; it was not caused by the hydrogenation.

Table 1. H_2–D_2 equilibration on $CaH_{2-\delta}$ and D_2–$CaH_{2-\delta}$ exchange reaction[a)]

(a) H_2–D_2 equilibration on $CaH_{2-\delta}$ (at 200 °C).
Initial gas composition (%) D_2: 51.6, HD: 1.2, H_2: 47.2
Total amount: 39.90 cm³ STP

	V_{ph}[c)] cm³ STP	Final gas composition (%)[b)] H_2	HD	D_2
Calcd	5.0	29.6	48.0	22.4
	6.0	30.6	48.1	21.3
	6.5	31.1	48.1	20.8
Obsd		28.9	49.5	21.6

(b) D_2–$CaH_{2-\delta}$ exchange (at 200 °C).
Initial gas composition (%) D_2: 97.8, HD: 2.2
Total amount: 38.29 cm³ STP

Calcd	6.0	2.4	24.2	73.4
	6.5	2.4	26.1	71.5
Obsd		2.8	25.4	71.8

(c) H_2–D_2 equilibration on $CaH_{2-\delta}$ (at 100 °C).
Initial gas composition (%) D_2: 49.7, HD: 1.1, H_2: 49.2
Total amount: 41.28 cm³ STP

Calcd	0	25.7	48.1	26.2
	0.2_5	26.0	48.1	25.9
	0.5	26.3	48.1	25.6
Obsd		24.1	49.9	26.0

(d) D_2–$CaH_{2-\delta}$ exchange (at 100 °C).
Initial gas composition (%) D_2: 97.8, HD: 2.2
Total amount: 39.91 cm³ STP

Calcd	0	~0	2.2	97.8
	0.2_5	0.0_3	3.4_2	96.5_5
	0.5	0.0_5	4.6_2	95.3_3
Obsd		0.4	3.3	96.3

a) $CaH_{2-\delta}$: *ca.* 2.2 g, reaction time: 30 min. The conversion of ethylene hydrogenation was about 95 % under the same condition. b) On the equilibrium constants K for $H_2+D_2 \rightleftarrows 2HD$, the values of 3.59 and 3.43 were used for 200 and 100 °C, respectively.[9)] c) The amount of hydrogen bound initially to $CaH_{2-\delta}$ and participated to the reaction.

$CaH_{2-\delta}$–D_2 Exchange and $CaH_{2-\delta}$–(H_2+D_2) Equilibration Reactions. In order to ascertain the role of the hydrogen of calcium hydride during the catalytic reaction, these two reactions were studied. The experiments were carried out when the equilibration reaction had almost been completed. The equilibrium compositions of the hydrogen isotopes, which must be composed of the hydrogen initially bound to $CaH_{2-\delta}$ and which participate in the reaction (V_{ph}), and the gas-phase hydrogen were calculated with respect to the temporal figure of V_{ph}. As is shown in Table 1 [(a) and (b), at 200°C], the observed equilibrium compositions are in good agreement with the calculated ones, in which 6.0—6.5 cm³ STP of V_{ph} was assumed. This V_{ph} value corresponds to about 0.6% of the amount of the hydrogen initially bound to $CaH_{2-\delta}$, and it roughly corresponds to half of the hydrogen in the surface monolayer (12 cm³ STP). The amount of hydrogen in the surface monolayer was estimated on the basis of the assumption that one molecule of hydrogen is attached to one atom of calcium. The V_{ph} value was very low at 100 °C compared with the values at 200 °C; it was estimated to be 0.1—0.3 cm³ STP [Table 1, (c) and (d)]. These results suggest that only a minor amount of the hydrogen of calcium hydride participates in both reactions, contrary to the results by Wright and Weller.[2)]

X-Ray Measurements. When calcium hydride of a stoichiometric composition is heated under a vacuum, the specimen is gradually changed with the rise in the heating temperature from greyish white to grey (400 °C) and to greyish black (500 °C), and a calcium mirror is formed above 450 °C at the cold parts of the vessel. These observations indicate that a part of the hydride is converted into metallic calcium. However, the X-ray diffraction analysis conducted on the powdered specimens which had been placed in a vacuum at 100, 250, 450 and 510 °C for 1 hr showed only the pattern of the stoichiometric hydride; that of metallic calcium was not detected. These results may suggest that metallic calcium is formed after the high-temperature evacuation, but it can not be detected

Table 2. Initial rate of ethylene hydrogenation on Pd-,[5)] Ta-,[6)] Ti-[7)] and Ca-hydride

Hydride	Reaction temp. °C	P_H Torr	P_E Torr	Initial rate of hydrogenation mol/g-cat·min	mol/m²-cat·min
Pd (β-phase)	75	198	82	8.27×10^{-4}	6.3×10^{-5}
Ta	300	200	100	12.5×10^{-6}	12.5×10^{-5}
Ti	300	191	109	2.46×10^{-6}	0.3×10^{-5}
Ca	50	203	45	7.81×10^{-5}	0.3×10^{-5}
Ca	100	109	46	34.3×10^{-5}	1.35×10^{-5}

by X-ray measurements because of its extremely fine particle size.

Comparison with the Catalytic Activity of Other Metal Hydrides. The initial rates of ethylene hydrogenation on the non-stoichiometric calcium hydride are, in Table 2, compared with those of three metallic hydrides.[5-7] The catalytic activity of non-stoichiometric calcium hydride is slightly lower than that of palladium hydride (β-phase) under similar experimental conditions. It might be higher than that of tantalum- and titanium-hydride, however, because the rates of ethylene hydrogenation at 50—100 °C on non-stoichiometric calcium hydride are of the same magnitude as the rates at 300 °C on the two hydrides mentioned above.

The Mechanism of the Hydrogenation of Ethylene and the Role of Hydrogen Bound to $CaH_{2-\delta}$. From the results of the effect of the order of introducing gases and of the dependence of the initial rate upon the pressure, it was presumed that the rate-determining step of the ethylene hydrogenation on $CaH_{2-\delta}$ is the surface reaction between adsorbed ethylene and adsorbed hydrogen on different sites. The formation of HD during the H_2–D_2 equilibration reaction strongly suggests the dissociative adsorption of hydrogen and deuterium on the catalyst surface.

From the V_{ph} values at lower temperatures ($<$ 100 °C) shown in Table 1, it can be said that the hydrogen which is initially bound to $CaH_{2-\delta}$ does not participate in the hydrogenation—only the hydrogen adsorbed from the gas phase does. At higher temperatures ($>$100 °C), on the other hand, both the hydrogen adsorbed from the gas phase and a part of the hydrogen loosely bound to calcium on the surface monolayer of $CaH_{2-\delta}$ participate in the hydrogenation. In both cases, the hydrogen in the bulk $CaH_{2-\delta}$ dose not participate. These interpretation are also supported by the results of the isomerization of butene over $CaD_{2-\delta}$.[8]

Although it is not yet certain what kind of site is catalytically active, the following suggestion may be made: the carbanion-type ethylene adsorbed on the basic or base-like sites may be able to associate with the hydrogen adsorbed on the neighboring metallic sites and may thus be converted to ethane.

The authors are grateful to Professor Shiichiro Teranishi of Osaka University and Professor Makoto Kumada of Kyoto University for their valuable suggestions. They are also thankful to Mr. Masataka Nakanishi of the Daiseru Co., Ltd., for his assistance. Thanks are further extended to Dr. Tsutomu Makita of Kyoto University for the mass spectrometric measurements.

References

1) R. N. Pease and L. Stewart, *J. Amer. Chem. Soc.*, **47**, 2763 (1925).
2) L. Wright and Sol Weller, *ibid.*, **76**, 5302, 5305, 5948 (1954).
3) E. Wiberg and E. Amberger, "Hydrides of the Elements of Main Group I—IV," Elsevier Publishing Co., Amsterdam (1971), p.69.
4) M. F. Manning and H. M. Krutter, *Phys. Rev.*, **51**, 76 (1937).
5) M. Yamaguchi, S. Teranishi, and K. Tarama, *Nippon Kagaku Zasshi*, **78**, 759 (1957).
6) M. Yamaguchi, *Sci. Rep. Kyoto Pref. Univ., No.* 20, *Ser. A*, 5 (1969).
7) M. Yamaguchi, *ibid., No.* 19, *Ser. A*, 11 (1968).
8) To be published.
9) S. Z. Roginsky, "Theoretical Principles of Isotope Methods for Investigating Chemical Reaction," U.S.A. A.E. C. tr-2873 (1956), p.155.

A Study on Electronic Spectra of Organic Compounds with S-Cl Group

Tokio YAMABE, Shinichi NAGATA, Yasuo KIKUZONO, and Kenichi FUKUI

Department of Hydrocarbon Chemistry, Faculty of Engineering, Kyoto University, Kyoto 606

(Received August 30, 1974)

MO calculations were carried out for CH_3SCl, C_6H_5SCl, and related compounds with the S–Cl group by the CNDO/2 or the ASMO-SCF method. The absorption bands in the 300—400 nm region observed were assigned to the $\sigma^*_{S\text{-}Cl} \leftarrow n_S$ transition in view of transition energy and oscillator strength. Such characteristic bands are attributed to the extraordinarily low energy level of the $\sigma^*_{S\text{-}Cl}$ orbital.

Various organic compounds containing the sulfenyl group (S–Cl) are generally known to be highly reactive ones, often with characteristic colors (orange-red) irrespective of whether they are arylsulfenyl or alkanesulfenyl.

The first discussion on the color of such compounds was given by Kharasch *et al.*,[1] for *o*-nitrobenzenesulfenyl chloride and its derivatives which have an intensely red color, especially in sulfuric acid. They attributed this to the intramolecular π resonance formed between the sulfenium cation and the nitro group adjoining, as shown below.

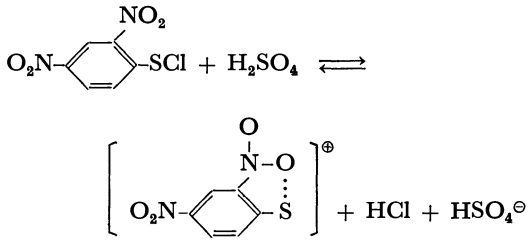

The characteristic color, however, is common to *o*-nitrobenzene-sulfenyl chloride and such compounds as benzenesulfenyl chloride and methanesulfenyl chloride which have no nitro group adjacent to the S–Cl group. Studies[2,3] concerning the electronic absorption spectra of organic compounds with the S–Cl group were reported without theoretical investigation on the absorption bands of 300—400 nm common to such compounds. It seemed to be of interest to study the characteristic bands which may be closely related to formation of the S–Cl bond.

In the present study, MO calculation by the CNDO/2[4] or ASMO-SCF method[5] using the zero-differential overlap approximation were carried out for CH_3SCl, C_6H_5SCl and some related compounds containing the S–Cl bond, in order to investigate the character of the S–Cl bond. For the sake of comparison, electronic absorption spectra of methanesulfenyl and *p*-toluenesulfenyl chlorides were measured in various solvents.

Method of Calculation

Calculations of σ-electron systems such as alkanesulfenyl chlorides were carried out by the CNDO/2 method, developed by Pople *et al.*,[4] and the singlet excitation energies and oscillator strengths were calculated using the virtual orbital approximation. The atomic orbitals of sulfur atom were employed up to its 3p orbitals.* For calculations of $SOCl_2$, SO_2Cl_2, and CH_3SO_2Cl we tried to include 3d orbitals of sulfur atom having the same exponent ζ_{3d} as ζ_{3s}.[6]

In the case of benzenesulfenyl chloride, the singlet excitation energies and oscillator strengths were calculated by the ASMO-SCF method with the zero-defferential overlap approximation,[5] in order to avoid defects of the CNDO/2 method when applied to the π electron systems.** In the present calculation, the configurational interaction is not taken into account, because the transition energies of CH_3SCl and C_6H_5SCl are not changed so remarkably by the consideration of CI.

Table 1. Molecular structures of CH_3SCl, CF_3SCl, and C_6H_5SCl

Compound	Bond distance (Å)		Bond angle (deg.)
	C–S	S–Cl	∠CSCl
CH_3SCl[a]	1.815	2.014	100.39
CF_3SCl	1.829		105.4
C_6H_5SCl	1.805		103.2

a) See Ref. 7.

The assumed molecular structures of the compounds with the S–Cl group are given in Table 1. Microwave spectral analysis[7] was used for methanesulfenyl chloride, while CF_3SCl and C_6H_5SCl were estimated from both calculations and the molecular structures of $(CF_3)_2S_2$[8] and $(C_6H_5)_2S_2$,[9] respectively. For the molecular structures of all the other compounds, the observed structures were employed.[10-13]

Experimental

Methanesulfenyl chloride and *p*-toluenesulfenyl chloride were prepared by the previously reported methods[14,15] from dimethyl disulfide in 1,1,2,2-tetrachloroethane and chlorine, and from *p*-thiocresol in carbon tetrachloride and chlorine,

* Preliminary calculations including those of 3d orbitals of the sulfur atom were carried out to estimate their contribution. The results predict the unacceptable polarization of $S(\delta-)$-$Cl(\delta+)$ and the larger bond energy of E_{S-Cl} than E_{C-S} in contrast with the results obtained by restricting up to the 3p orbitals. These results are unreasonable from experimental aspects and the 3d orbitals for sulfur have thus been excluded from this study.

** For example, the π-MO of ethylene is not calculated as the highest occupied molecular orbital (HOMO) but as the next highest occupied molecular orbital (NHOMO). Furthermore, our preliminary calculation on C_6H_5SCl by the CNDO/2 gave a too large $\pi^* \leftarrow \pi$ excitation energy, *i.e.*, 12.5eV.

respectively. The products were isolated by vacuum distillation, and their electronic absorption spectra in the region 210—700 nm were measured in various solvents.

Results and Discussion

The observed electronic spectra of methanesulfenyl chloride and *p*-toluenesulfenyl chloride are shown in Fig. 1. The most stable conformation of CH_3SCl in its ground state was calculated by means of the CNDO/2 method to optimize the total energy by changing the bond distance R(S–Cl) between sulfur and chlorine atom. The optimized bond length, $R=2.064$ Å, is in good agreement with the experimental value (2.014 Å) in the gas phase. With this bond length, the transition energies were calculated to be 301.1 nm (the first band) and 203.0 nm (the second band) in the ultraviolet region. The predicted wavelength for the first band seems a little shorter than the observed one (355.0 nm). The calculated wavelengths for both bands, however, are sensitive to the change of the bond distance R(S–Cl) and shift toward the longer wavelengths by a slight elongation of the bond (Table 3).

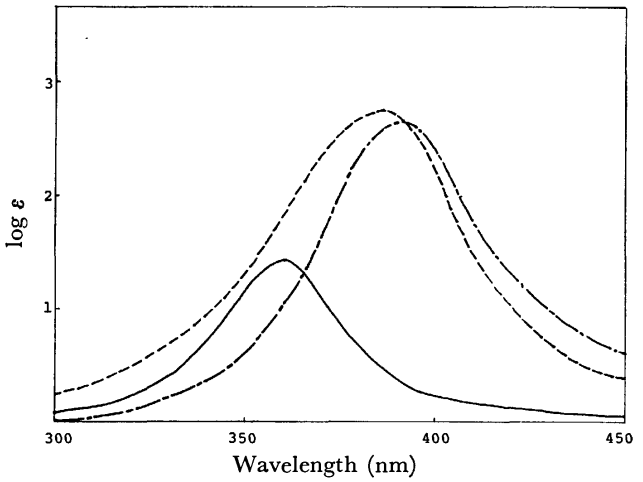

Fig. 1. Electronic absorption spectra of CH_3SCl (——), C_6H_5SCl (------), and *p*-$CH_3C_6H_4SCl$ (-·-·-) in the region of 300—450 nm.

Table 2. Observed electronic transitions of compounds with the S–Cl group

Compound	Solvent	λ_{max}(nm)	ε_{max}	Reference
CH_3SCl	(Gas phase)	355.0	24.5	3
		205.0	671	
	Cyclohexane	360.0	27.2	This work
		275.6	542	
	CCl_4	361.0	29.7	This work
		276.3	503	
CF_3SCl	(Gas phase)	333.0	25	2
		214.0	235	
CCl_3SCl	Light petroleum	322.0	10.0	2
	CCl_4	324.0	12.0	
p-$CH_3C_6H_4SCl$	Cyclohexane	391.2	424	This work
		243.0	10240	
	Ethyl ether	391.0	254	This work
		241.0	9325	
	Methylene chloride	391.5	451	This work
C_6H_5SCl	CCl_4	386	589	This work

Table 3. Dependence of the singlet excitation energies of CH_3SCl on the bond distance R(S–Cl)

R(S–Cl) (Å)	$\sigma^*_{S\text{-}Cl}\leftarrow n_S$ Transition energy (nm)	$\sigma^*_{S\text{-}Cl}\leftarrow n_S$ Oscillator strength	$\sigma^*_{S\text{-}Cl}\leftarrow n_{Cl}$ Transition energy (nm)	$\sigma^*_{S\text{-}Cl}\leftarrow n_{Cl}$ Oscillator strength
2.014	288.1	3.77×10^{-5}	196.9	8.07×10^{-3}
2.064	301.1	4.36×10^{-5}	203.0	3.21×10^{-3}
2.114	316.0	4.15×10^{-5}	206.7	2.90×10^{-2}
2.314	379.4	3.93×10^{-5}	239.2	5.21×10^{-2}

From the calculated results, the first band is assigned to the excitation of the lone pair electron on the sulfur atom to the lowest unoccupied orbital (LUMO), which is mainly localized in the anti-bonding MO of the S–Cl bond (σ^*_{S-Cl}). The band is thus closely related to the presence of the S–Cl bond. In fact, atom to the lowest unoccupied orbital (LUMO), which is mainly localized in the anti-bonding MO of the S–Cl

Table 4. Observed and calculated excitation energies of compounds with the S–Cl bond

Compound	Solvent	Observed λ_{max} (nm)	Observed ε_{max}	Calculated Excitation energy (nm)	Calculated Oscillator strength	Assignment
SCl_2	*n*-hexane[a]	263	520	286.4[b]	4.56×10^{-5}	$\sigma^*_{S\text{-}Cl}\leftarrow n_S$
		246	417	250.2	4.18×10^{-5}	$\sigma^{*'}_{S\text{-}Cl}\leftarrow n_S$
$SOCl_2$	*n*-hexane	253†	2240	205.2[b]	2.15×10^{-4}	$\sigma^*_{S\text{-}Cl}\leftarrow n_S$
				201.1[c]	2.81×10^{-4}	
SO_2Cl_2	cyclohexane	<210[d]		218.2[b]	3.74×10^{-2}	
				196.9[c]	3.92×10^{-2}	
CH_3SO_2Cl	ethyl ether	<210[d]		221.0[b]	4.51×10^{-2}	
				197.4[c]	5.03×10^{-2}	

† Absorption shoulder.

a) H. P. Koch, *J. Chem. Soc.*, **1949**, 394, C. C. Price and S. Oae, "Sulfur Bonding," Ronald Press Company (1962). b) Calculated by the CNDO/2 method excluding the 3d orbitals of sulfur atom. c) Calculated by the CNDO/2 method including the 3d orbitals of sulfur atom. d) No absorption band exists in the region 210—700 nm.

bond (σ^*_{S-Cl}). The band is thus closely related to the presence of the S–Cl bond. In fact, CH_3SH and $(CH_3)_2S$ have no absorption band above 300 nm.[16] Other possibilities of excitation of either the lone pair electron on chlorine atom or the σ-electron of the S–Cl bond might be considered. The former is assigned to the second band, but the latter is hardly acceptable since the excitation energy of the $\sigma^*\leftarrow\sigma$ transition is much larger than that of the $\sigma^*\leftarrow$n transition (*e.g.*, for $(CH_3)_2S$ $\Delta E^*_{\sigma-\sigma}$=6.2 eV $\Delta E^*_{\sigma-n}$=5.2 eV). This may be supported by the fact that methanesulfonyl chloride (CH_3SO_2Cl) without lone pairs on the sulfur atom has no absorption band in the ultraviolet and visible regions (Table 4). Moreover, the molar extinction coefficient of the $\sigma^*\leftarrow\sigma$ transition is, in general, of the order of 10^2—10^3 as ε_{max} whereas the observed one is less by one order, implying that the assignment ($\sigma^*\leftarrow\sigma$) is not reasonable for the first band.

The second band is assigned from the present calculation to be the excitation of the lone pair electron (n′) of chlorine atom to the $\sigma^*_{S\text{-}Cl}$ orbital ($\sigma^*\leftarrow$n′). The wavelength, however, is considerably longer than that of the usual alkyl chloride, *e.g.*, CH_3Cl (154–161 nm);[17] in addition the wavelength of the first band is greater than that of usual alkyl sulfides. The main reason for such large shifts toward the longer wavelength of these two bands in comparison with those of the related compounds, $(CH_3)_2S$ and CH_3Cl, may be attributed to the extraordinarily low orbital level of $\sigma^*_{S\text{-}Cl}$ in CH_3SCl. Moreover, it is seen from the increase of the S–Cl bond length that the energy level of $\sigma^*_{S\text{-}Cl}$ is greatly lowered in comparison with that of the lone pairs of sulfur and chlorine atoms (Fig. 2). Such a tendency may be connected with the color of the sulfenyl compounds. Furthermore the ratio between the calculated oscillator strengths of the two bands is in good agreement with that between the observed ε_{max}'s. Thus, it may be concluded that the first band is assigned to the σ^* (S–Cl)←n(S) transition and the second one to the σ^* (S–Cl)←n′ (Cl).

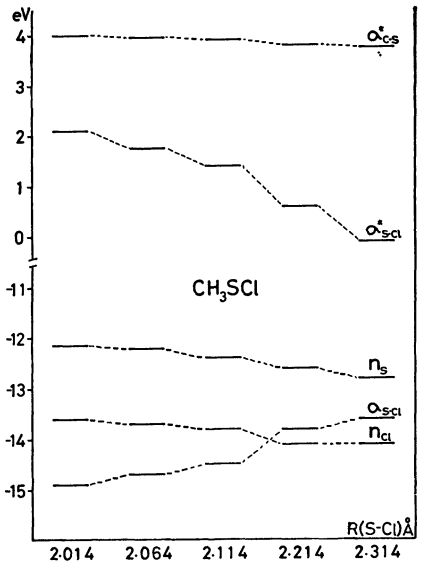

Fig. 2. The relation between the bond distance R(S–Cl) and the molecular orbital levels in CH_3SCl.

As a related compound, sulfur dichloride (SCl_2) was also studied. The results are given in Table 4. The observed absorption bands at 263 and 246 nm which have almost the same intensities as and shorter wavelengths than the $\sigma^*_{S\text{-}Cl}\leftarrow n_S$ transition of CH_3SCl were predicted to be due to the excitations of $\sigma^*_{S\text{-}Cl}\leftarrow n_S$ and $\sigma^{*\prime}_{S\text{-}Cl}\leftarrow n_S$, respectively. These assignments may be reasonable since the two σ^* orbitals of the S–Cl bond are nearly degenerate and therefore the calculated oscillator strengths for the transitions give almost the same values. For $SOCl_2$, where one oxygen atom combines with the lone pair electron of sulfur atom, its absorption band further shifts toward a shorter wavelength in comparison with that of SCl_2. This may be attributed to the stabilization of the S–Cl bond by the formation of S–O bond. The σ_{S-Cl} orbital level of $SOCl_2$ is lower than that of SCl_2 by *ca.* 1.2 eV and the corresponding σ^* orbital becomes higher accordingly. Furthermore, the absorption bands of SO_2Cl_2 and CH_3SO_2Cl, which have a sulfur atom combining with two oxygen atoms and hence no lone pair electrons, have not yet been found in the ultraviolet region. From these experimental and theoretical investigations it is demonstrated that compounds with the S–Cl group have, in general, weak absorption bands in the 350—400 nm region due to the transition between the lone pair orbital of sulfur (n_S) with small ionization potential and the low-energy anti-bonding orbital, $\sigma^*_{S\text{-}Cl}$.

Table 5. Singlet excitation energies of CF_3SCl and C_6H_5SCl

Compound	Excitation energy (nm)	Oscillator strength	Assignment
CF_3SCl[a]	290.0	4.68×10^{-6}	$\sigma^*_{S\text{-}Cl}\leftarrow n_S$
	194.0	2.40×10^{-2}	$\sigma^*_{S\text{-}Cl}\leftarrow n_{Cl}$
C_6H_5SCl[b]	372.2	5.40×10^{-3}	$\sigma^*_{S\text{-}Cl}\leftarrow n_S$

a) Calculation carried out with R(S–Cl) of 2.060 Å by the CNDO/2 method. b) Calculation carried out with R(S–Cl) of 2.070 Å by the ASMO-SCF method.

For further investigation of alkanesulfenyl chloride, CF_3SCl was studied by the same method as mentioned above and the optimized molecular structure was obtained to give a potential energy minimum at 2.060 Å of R(S–Cl). The singlet excitation energies for the optimized structure are given in Table 5. The first and second absorption bands are attributed to the excitations of $\sigma^*_{S\text{-}Cl}\leftarrow n_S$ and $\sigma^*_{S\text{-}Cl}\leftarrow n_{Cl}'$, respectively, in a manner similar to the case of CH_3SCl. These calculated results are also in fair agreement with the observed values (Table 2) not only in the wavelengths but also the intensities. The first and second absorption bands of CF_3SCl, however, shift toward shorter and longer wavelength, respectively, in comparison with those of CH_3SCl. This is also realized from a comparison of the energy levels of CH_3SCl and CF_3SCl shown in Fig. 3; in particular, the n_S orbital of CF_3SCl is largely stabilized in comparison with the $\sigma^*_{S\text{-}Cl}$ orbital.

In order to clarify such a trend, we compared the bond energy E_{AB} of CF_3SCl with that of CH_3SCl

TABLE 6. BOND ENERGIES E_{AB} (a.u.) IN CH_3SCl AND CF_3SCl CALCULATED BY THE CNDO/2 METHOD

Compound	R(S–Cl) (Å)	C–S	S–Cl
CH_3SCl	2.064	−0.612	−0.476
CF_3SCl	2.060	−0.588	−0.484

(Table 6).*** CF_3SCl has a larger S–Cl bond energy and a smaller C–S bond energy than those in CH_3SCl. This might be due to the inductive effect of fluorine atom which attracts electron on carbon atom. As a consequence, the C–S bond is weakened but the S–Cl bond undergoes no such remarkable inductive effect. From these results, it may be expected that CF_3SCl has two reactive bonds, C–S and S–Cl, which may lead to interesting chemical reactions. The shifts observed in the absorption bands of CF_3SCl in comparison with those of CH_3SCl seem to be consistent with the change of bond energies of S–Cl and C–S bonds.

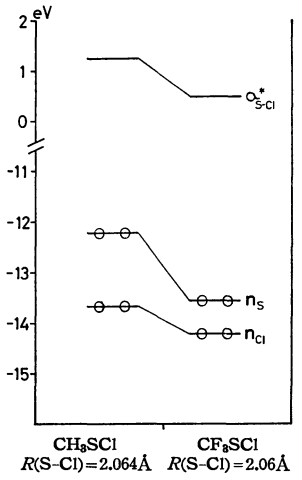

Fig. 3. The molecular orbital levels in CH_3SCl and CF_3SCl.

In the case of the arylsulfenyl chlorides, *o*-nitrobenzenesulfenyl chloride and its derivatives studied previously,[1] there may be interaction between the *ortho*-substituted nitro group and the sulfur atom to give rise to the sulfenium cation. These molecules are therefore not suitable for an investigation of the cause of the reddish color which many arylsulfenyl chlorides bear. Accordingly, benzenesulfenyl chloride which can not have such an interaction was taken as the simplest arylsulfenyl chloride.

For the calculations, the molecular structure was determined by using the CNDO/2 method; two conformations of the chlorine atom (Fig. 4, A and B) were compared. Conformation A, where the chlorine atom is on the same plane as the benzene ring, is more stable than B, where it is out of plane. The stabilization of A may be attributed to the π-conjugation effect between

*** In the CNDO/2 approximation, the total energy E_T can be expressed by the following equation, $E_T=\sum_A E_A+\sum_{A<B} E_{AB}$, where E_A and E_{AB} denote the monatomic and diatomic terms, respectively.

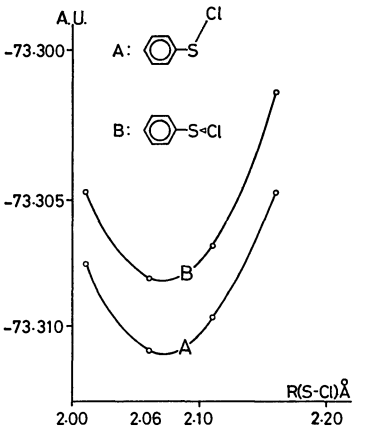

Fig. 4. Dependence of the total energies of benzenesulfenyl chloride on the parameter R(S–Cl).

the lone pair electrons on the sulfur atom and the π-electrons on the benzene ring; there is no such conjugation effect in B since the lone pair orbital is perpendicular to the π-orbitals.

Using the resulting bond distance R(S–Cl)=2.070 Å *i.e.*, the optimized bond distance of conformation A, the singlet excitation energies and oscillator strengths were calculated by the ASMO-SCF method (Table 5). It is seen that the calculated location of the absorption band of the longest wavelength (372.2 nm) is in accord with the observed one (386 nm), and that it is also due to the excitation of $\sigma^*_{S\text{-}Cl}\leftarrow n_S$ is accord with the assignment for the alkanesulfenyl chlorides.

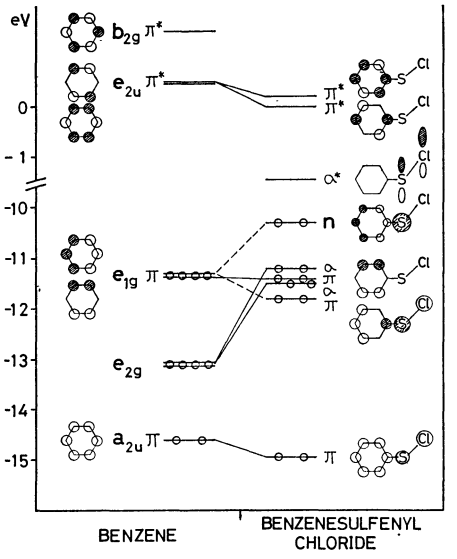

Fig. 5. The relation between the molecular orbital levels of benzene and benzenesulfenyl chloride.

In molecules having π and lone pair electrons such as carbonyl compounds, the absorption bands of the longest wavelength are generally known to be $\pi^*\leftarrow$n transitions.[18] However, the energy level of the $\sigma^*_{S\text{-}Cl}$ orbital is lower than that of the π^* orbital in this molecule, which may lead the $\sigma^*\leftarrow$n transition to be the lowest energy excitation (Fig. 5). Furthermore, the $\sigma^*\leftarrow$n transition in C_6H_5SCl is smaller than that of the alkane sulfenyl chlorides. This may be attributed to

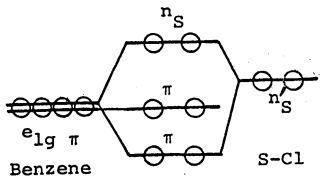

Fig. 6. Energy level of benzenesulfenyl chloride.

the participation of the lone pair orbital in the π-conjugation as follows; the n_S orbital in C_6H_5SCl is constructed from the interaction between the n_S' orbital (lone pair orbital on the sulfur atom) and degenerate π orbitals (e_{1g}) of benzene, and hence the lone pair orbital as shown in Fig. 6. This result suggests that the $\sigma^*\leftarrow$n transition in C_6H_5SCl gives a smaller excitation energy than that of alkanesulfenyl chlorides which can not have such interactions. Moreover, there is no absorption band in the region above 300 nm in $C_6H_5SC_6H_5$.[19] The calculated oscillator strength (of the order of 10^{-3}) is larger than that of CH_3SCl (of the order of 10^{-5}), and such a tendency is also found in the observed values of ε_{max} (Table 2). Thus, as in the case of the alkanesulfenyl chlorides, the observed absorption band at the longest wavelength in C_6H_5SCl is assigned to be the transition of $\sigma^*_{S\text{-}Cl}\leftarrow$n.

Conclusion

The characteristic absorption band in the ultraviolet region of organic compounds with the S–Cl group, commonly appearing at 300—400 nm, was assigned to the excitation of the lone pair electron of sulfur atom to the $\sigma^*_{S\text{-}Cl}$ orbital; the present calculation reveals that such a band at a fairly long wavelength which induces an intensely red color may be mainly due to the extraordinarily low energy level of the $\sigma^*_{S\text{-}Cl}$ orbital and the small ionization potential of 3p electron of the sulfur atom. From the present theoretical study, the high reactivity of S–Cl bond is attributed to the weakness of this bond, probably caused by the large electron repulsion between 3p electrons of sulfur and chlorine atoms.

The authors are grateful to Professor Hiroshi Kato and Mr. Katsumi Nakai for their helpful discussions.

References

1) N. Kharasch, C. M. Buess, and W. King, *J. Amer. Chem. Soc.*, **75**, 6035 (1953), and the references cited therein.
2) R. N. Naszeldine and J. M. Kidd, *J. Chem. Soc.*, **1953**, 3219.
3) J. M. White, *Spectrosc. Lett.*, **2**, 301 (1969).
4) J. A. Pople and D. L. Beveridge, "Approximate Molecular Orbital Theory," McGraw-Hill (1970).
5) T. Yonezawa, H. Konishi, and H. Kato, This Bulletin, **42**, 933 (1969).
6) D. P. Santry and G. A. Segal, *J. Chem. Phys.*, **47**, 158 (1967).
7) A. Guarnieri, *Z. Naturforsch.*, **25a**, 18 (1970).
8) H. J. M. Bowen, *Trans. Faraday Soc.*, **50**, 452 (1954).
9) A. Senning, "Sulfur in Organic and Inorganic Chemistry," Vol. 3, pp. 99—112, Marcel Dekker, Inc. (1972).
10) For sulfur dichloride, Y. Morino, T. Ito, and J. Nakamura, *J. Phys. Soc. Japan*, **17**, Supple. B-2, 37 (1962).
11) For thionyl chloride, I. Hargittai, *Magy. Kem. Foly.*, **74** 596 (1968); *Acta Chim.*, (Budapest), **59**, 351 (1969).
12) For sulfuryl chloride, M. Hargittai, *ibid.*, **60**, 231 (1969).
13) For methanesulfonyl chloride, M. Hargittai and I. Hargittai, *J. Chem. Phys.*, **59**, 3251 (1973).
14) H. Brintzinger, K. Phannsteil, H. Koddebusch, and K. E. Kling, *Chem. Ber.*, **83**, 87 (1950).
15) H. Lecher, *ibid.*, **58**, 409 (1925).
16) O. H. Wheeler and L. A. Kaplan, "Organic Spectral Data," Vol. 3, p. 1, Interscience (1966); C. C. Price and S. Oae, "Sulfur Bonding," p. 171, Ronald Press Company, New York (1962).
17) M. J. Kamlet, "Organic Spectral Data," Vol. 1, Interscience (1960).
18) H. Suzuki, "Electronic Absorption Spectra and Geometry of Organic Molecules," Academic Press Inc., New York (1967).
19) N. A. Valyashko and F. F. Cheshko, *Sbornik Statei Obshchei Khim.*, **1**, 584 (1953); L. Horner and H. Nickel, *Ann. Chem.*, **597**, 20 (1955).

Polarographic Reduction of Ubiquinone-10 Solubilized in Micelles

Tatsuo ERABI, Hisahide HIURA, and Masaya TANAKA
The Department of Industrial Chemistry, Faculty of Engineering, Tottori University, Tottori 680
(Received October 9, 1974)

Ubiquinone-10 solubilized in an aqueous solution containing sodium dodecyl sulfate as an anionic surfactant was polarographically investigated. Ubiquinone-10 solubilized in micelles shows a well-defined, diffusion-controlled, pH-dependent wave. Diffusion coefficient and apparent particles radii were calculated. The surfactant concentration dependence of the diffusion coefficient and of the apparent particle radii was also determined.

The electron transport system in respiratory chains and in the photosynthetic system, in which electron transfer takes place very smoothly, consists of various combinations of redox reaction. Electrochemical techniques are being developed for the analysis of the mechanism of electron transfer.

Underwood and his co-workers[1-3] investigated the electrode kinetics of NAD and its analogues by cyclic voltammetry. Takahashi *et al.*[4,5] reported that NADH produced from NAD by an enzymatic process can be anodically oxidized to NAD. Most of these studies were usually carried out in aqueous or nonaqueous media, and the difference from actual physiological conditions must be accounted for. Erabi *et al.*[6] investigated the polalographic behavior of redox components bound with chromatophores from photosynthetic bacterium, *Rhodospirillum rubrum*, under the physiological conditions, although reactions involved were not completely elucidated because of the difficulty of mass transfer.

In the photosynthetic organ, chromatophores, redox components have been arranged in good order. In such membrane systems, the usual electrochemical theory developed for homogeneous solution systems cannot be applied directly. No such development of electrochemical theory for the membrane systems have been carried out.

Hayano and Shinozuka[7-9] explained the polarographic behavior of the disperse-dyes solubilized in aqueous surfactant solutions. Westmoreland *et al.*[10] studied the polarography of *trans*-azobenzene in aqueous surfactant solutions, and discussed the boundary region between the properties of an aqueous system and those of a nonaqueous system. Micelle represents a good model for individual macromolecules and for a hydrophobic region within subcellular membrane systems. The electrochemical treatment of disperse systems is of interest not only in electrochemistry but also in biology. By accumulating the data for such disperse systems, we might obtain information on the membrane structure.

Experiments were carried out for ubiquinone-10 (UQ_{10}) solubilized in micelles, which plays an important role in the photosynthetic electron transport system.

Experimental

Materials. Pure UQ_{10} was extracted from chromatophores from photosynthetic bacterium, *R. rubrum*, by the usual method.[11] Sodium dodecyl sulfate (SDS, Marubishi Oil Co., Osaka) was washed with ether, and then recrystallized twice from ethanol. Tris(hydroxymethyl)aminomethane (Tris, Sigma Chemical Co., St. Louis) was used without further purification. Isooctane (Nakarai Chemicals Ltd., Kyoto) and other reagents (Wako Pure Chemical Industries Ltd., Osaka) were used.

Buffer solutions of various pH values were prepared with 0.12 M GTA (containing 0.04 M β-β-dimethylglutamic acid, 0.04 M Tris, and 0.04 M 2-amino-2-methyl-1,3-propandiol)–HCl and 0.12 M GTA–Tris, respectively. Water was used after five times distillation.

Apparatus. A solution containing a surfactant, 0.12 M GTA buffer solution, and UQ_{10} was irradiated with a 29kHz supersonic wave for 10 min. The solution was then stored for a day at room temperature. The equilibrium of the solution was thus attained. Excess UQ_{10} was removed by filtration through a G4 glass filter. The solid UQ_{10} remaining on the filter was dissolved with isooctane, and its quantity was determined by means of absorption spectrum at 271 nm[12] using a Hitachi Model 101 spectrophotometer. Polarographic measurements were carried out at room temperature for the filtrate, and UQ_{10} concentration in the filtrate was rechecked by the solid content on the filter. Polarograms were recorded with a high sensitive polarograph PA-202 (Yanagimoto Mfg. Co., Ltd., Kyoto).

Dissolved oxygen was removed from solutions by bubbling oxygen-free nitrogen for 2 hr.

A dropping mercury electrode (DME) was used as the working electrode, and a saturated calomel electrode (SCE) as the reference and counter electrode. The DME had the following characteristics; $m=0.93$ mg/s (in pure water at zero applied potential) and $t=3.0$ s. The height of mercury head was usually 75 cm.

The viscosity of the basic solution was measured with an Ostwald viscometer.

Results and Discussion

UQ_{10} in an Aqueous Ethanol Solution. The polarogram of UQ_{10} in an 80% (v/v) ethanolic solution showed pH-dependent wave. In the pH region pH 4.7—8.7,

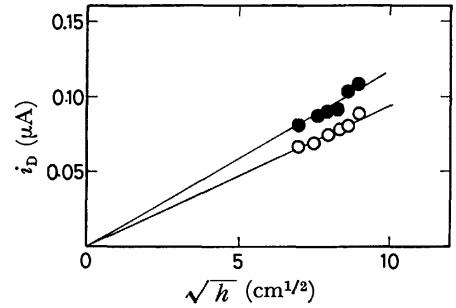

Fig. 1. Dependence of current on mercury height at pH 7.5.
●, and ○ represent the data in 80% ethanolic solution and in 4×10^{-2} M SDS solution, respectively.

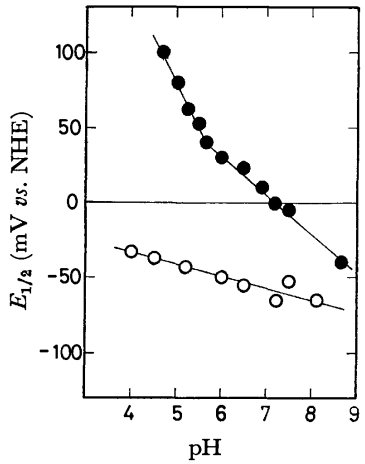

Fig. 2. Plots showing the pH dependence of the half-wave potentials for UQ_{10} reduction.
●, and ○ represent the data in 80% ethanolic solution and in 4×10^{-2} M SDS solution, respectively.

a typical well-defined cathodic wave was observed, and the limiting current was proportional to the square root of the mercury-column height as shown in Fig. 1.

The half-wave potential ($E_{1/2}$) was plotted against the solution pH (Fig. 2). The slope of the straight line for UQ_{10} was 60 mV/pH in the more acidic region than pH 5.7 and 27 mV/pH in the more basic region. When the Tafel plots and Heyrovskii-Ilkovic plots were made for the polarogram obtained, a value of $\alpha n=1.0$ (α being the transfer coefficient) was obtained, the number of electrons exchanged being presumed to be 2. The α values was thus calculated to be 0.5. The number of proton transfer was therefore estimated to be 2 in the more acidic region than pH 5.7 and 1 in the more basic region. The proportionality of the limiting current to the square root of the mercury height and to UQ_{10} concentration indicates the wave to be diffusion-controlled. The Ilkovic equation was applied to calculate the diffusion coefficient, and the value was 1.04×10^{-6} cm^2/s at pH 7.5.

UQ_{10} Solubilized in SDS Solution. The polarogram of UQ_{10} solubilized in SDS solution also showed a pH-dependent wave. A typical well-defined cathodic wave was observed and the current was also proportional to the square root of the mercury-column height (Fig. 1).

The slope of straight line for UQ_{10} solubilized in a SDS solution was 8 mV/pH in the pH region 4.0—8.2

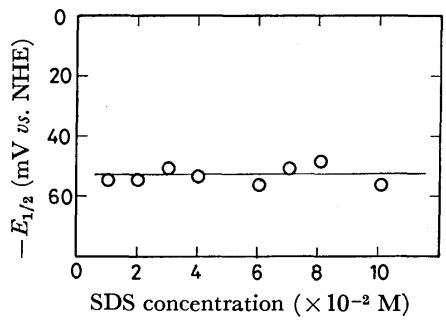

Fig. 3. Effect of surfactant concentration upon half-wave potential at pH 7.5.

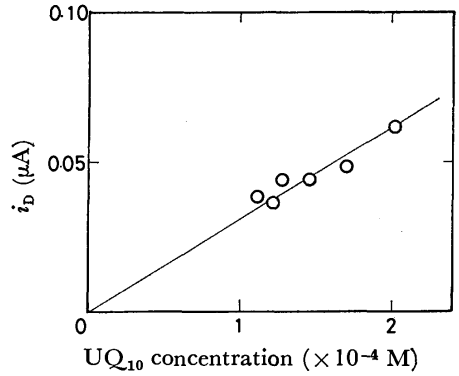

Fig. 4. Relationship of limiting current to UQ_{10} concentration at pH 7.5.

(Fig. 2). In Fig. 3 the half-wave potential for UQ_{10} reduction is shown as a function of SDS concentration. The half-wave potential was not affected by SDS concentration ($1—10\times10^{-2}$ M), that is, the solvent effect discussed by Mairanovskii[13] was not observed. Thus, UQ_{10} seems to be merely solubilized in micelles.

The dependence of the limiting current on UQ_{10} concentration is shown in Fig. 4, where a linear relationship is indicated. From the above results, it is evident that the observed waves are due to the reduction of UQ_{10} itself, and indicated to be diffusion-controlled.

The Tafel plots were drawn for the polarograms obtained at each SDS concentration, and αn values calculated from these results were plotted against the SDS concentration (Fig. 5). The αn value was not

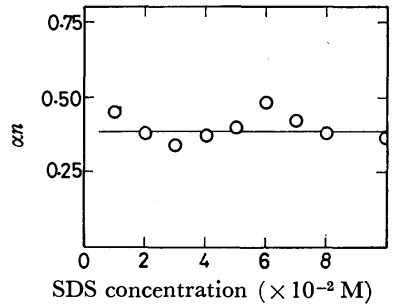

Fig. 5. Relationship of αn value to surfactant concentration at pH 7.5.

strongly affected by SDS concentration, being about 0.4 throughout the measurements in this study. Since the number of electrons exchanged for UQ_{10} in SDS solution was presumed to be 2 as well as in ethanolic medium, the α value was estimated to be 0.2. It is clear from experimental results that the diffusion particle is the micelle with UQ_{10}; this causes the diffusion current. On the one hand, adsorption and re-orientation of the surfactant molecules and micelles on the electrode were also considered to occur,[14] and micelles containing no UQ_{10} might exist in the neighborhood of the electrode. Futhermore, it was indicated by Kuta and Smoler[15] that the α value was lowered in the presence of a surface-active substance. As in the above case, the α value for UQ_{10} reduction is lowered to a greater extent in an aqueous surfactant solution than in an ethanolic one.

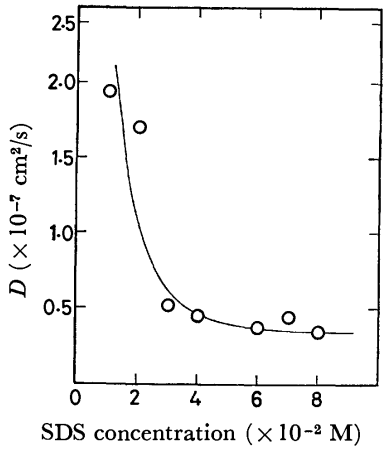

Fig. 6. Dependence of diffusion coefficient on surfactant concentration at pH 7.5.

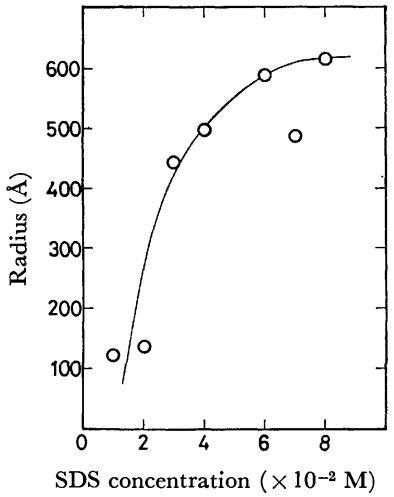

Fig. 7. Dependence of apparent mean particle radii on surfactant concentration at pH 7.5.

Since the limiting current of solubilized UQ_{10} was thought to be diffusion-controlled, the Ilkovic equation was applied to calculate the diffusion coefficient at each SDS concentration. Figure 6 shows the dependence of diffusion coefficient on SDS concentration. The apparent diffusion coefficient of solubilized UQ_{10} was about one-tenth compared with that in the ethanolic solution. Applying Stokes-Einstein's law for the diffusion coefficient (Fig. 6), the apparent mean radii of micelles were evaluated at various SDS concentrations, assuming that the micelles were perfectly spherical. The results are shown in Fig. 7. The obtained diffusion coefficients of solubilized UQ_{10} were more or less smaller than those of disperse-dyes reported by Hayano and Shinozuka.[9] However, in view of the size of a micelle which solubilized UQ_{10} containing a very long side-chain, these values seem to be appropriate. Tartar[16] and Tanford[17] reported that the theoretical micelle's radius for SDS is 16.68 Å and the aggregation number of molecules is 56. However, the radius and aggregation number of a micelle increase with increasing concentration of the electrolytes and, if a distortion in the micelle shape arises, the aggregation number of micelle increases still further. Therefore, the values for the particle radii (Fig. 7) do not seem too large if we take both existence of the electrolytes and situation of solubilized UQ_{10} into consideration.

The authors wish to express their thanks to Prof. Takekazu Horio, the Institute for Protein Research, Osaka University, for helpful assistance in the culture of photosynthetic bacterium, *R. rubrum*, and in the extraction of ubiquinone-10.

References

1) J. N. Burnett and A. L. Underwood, *Biochem.*, **4**, 2060 (1965).
2) A. J. Cunningham and A. L. Underwood, *Arch. Biochem. Biophys.*, **117**, 88 (1966).
3) A. J. Cunningham and A. L. Underwood, *Biochem.*, **6**, 266 (1967).
4) F. Takahashi, M. Aizawa, J. Mizuguchi, and S. Suzuki, *Kogyo Kagaku Zasshi*, **73**, 62 (1970).
5) F. Takahashi, M. Aizawa, J. Mizuguchi, and S. Suzuki, *ibid.*, **73**, 66 (1970).
6) T. Erabi, T. Higuti, T. Kakuno, M. Tanaka, and T. Horio, *J. Biochem.*, in press.
7) S. Hayano and N. Shinozuka, This Bulletin, **42**, 1469 (1969).
8) S. Hayano and N. Shinozuka, *ibid.*, **43**, 2083 (1970).
9) S. Hayano and N. Shinozuka, *ibid.*, **44**, 1503 (1971).
10) P. G. Westmoreland, R. A. Day, Jr., and A. L. Underwood, *Anal. Chem.*, **44**, 737 (1972).
11) S. Okayama, N. Yamamoto, K. Nishikawa, and T. Horio, *J. Biol. Chem.*, **243**, 2995 (1972).
12) R. A. Morton, U. Gloor, O. Shindler, G. M. Wilson, L. H. Choparddit-Jean, F. W. Hemming, O. Isler, W. M. F. Leat, J. F. Pennock, R. Ruegg, U. Schwieter, and O. Wiss, *Helv. Chim. Acta*, **41**, 2343 (1958).
13) S. G. Mairanovskii, "Catalytic and Kinetic Waves in Polarography," Plenum Press, New York, N. Y. (1968), Chap. X.
14) K. Eda, *Nippon Kagaku Zasshi*, **80**, 349 (1959).
15) J. Kuta and I. Smoler, *Z. Elektrochem.*, **64**, 285 (1960).
16) H. V. Tartar, *J. Phys. Chem.*, **59**, 1195 (1955).
17) C. Tanford, *ibid.*, **76**, 3020 (1972).

Polarography of Dialkylthallium(III) Compounds. I. Polarography of Dibutylthallium(III) Compounds

Teisuke MURAYAMA and Kenji KIKUCHI

Department of Industrial Chemistry, Faculty of Engineering, Shizuoka University, Johoku, Hamamatsu 432

(Received October 14, 1974)

Electrochemical reduction of three dibutylthallium(III) cations has been studied through the use of polarographic methods. Reduction at a dropping mercury electrode occurs in two steps for the di-*n*-butylthallium (DNBT) and diisobutylthallium (DIBT) cations in alkaline solutions, and for the di-*sec*-butylthallium (DSBT) cation in all pH ranges examined. The first and second waves of the DSBT cation in alkaline solutions correspond to, respectively, no-proton one-electron and two-proton two-electron processes. The DNBT and DIBT cations produce a single wave in acid solutions, consuming two protons and three electrons. On polarograms recorded with Kalousek's switching circuit a product and two kinds of intermediates were observed for the reduction of the DNBT and DIBT cations, and a product and one kind of intermediate for the reduction of the DSBT cation. A reaction scheme is proposed for the polarographic reduction of dibutylthallium cations.

Several authors have reported on the polarographic reduction of dialkyl- and diarylthallium(III) compounds. Costa studied di-*n*-alkylthallium bromides in an aqueous propanol solution,[1] and observed three waves of approximately equal heights for dipropyl- and dibutylthallium bromides. He attributed the first wave to Reaction (1) or (2), and the third to a reaction leading to the production of metallic thallium.

$$R_2Tl^+ + e \longrightarrow R_2Tl\cdot \quad (1)$$

$$2R_2Tl^+ + 2e \longrightarrow R_2Tl\text{-}TlR_2 \quad (2)$$

DiGregorio and Morris observed three waves for the diphenylthallium cation in aqueous solutions, and proposed a reduction mechanism including transmetallation with the electrode mercury.[2] Issleib *et al.* investigated five di-*n*-alkylthallium bromides in aqueous buffer solutions and dimethylformamide.[3] They obtained single waves in aqueous solutions with pH values below 7, and double waves in solutions with pH values above 7. The single step reduction was interpreted by them as follows.

$$R_2Tl^+ + e \longrightarrow R_2Tl\cdot \quad (1)$$

$$3R_2Tl\cdot \longrightarrow 2R_3Tl + Tl(Hg) \quad (3)$$

$$R_3Tl + H^+ \longrightarrow R_2Tl^+ + RH \quad (4)$$

Results of our investigation on dialkylthallium compounds indicate that the real electrode process should be more complex than any of the above-mentioned mechanisms. The present paper reports polarographic behavior of di-*n*-butyl-, diisobutyl-, and di-*sec*-butylthallium compounds. (Hereafter these are denoted as DNBT, DIBT, and DSBT compounds, respectively.) Molar conductivity data show that dimethyl, diethyl-, and diphenylthallium hydroxides are strong electrolytes.[4] By analogy dibutyl compounds may be regarded as strong electrolytes. Hence, this paper deals with the polarography of DNBT, DIBT, and DSBT cations.

Experimental

Dibutylthallium(III) chlorides were prepared by the reaction of organomagnesium compounds with thallium trichloride as described in the literature.[5] Diethyl ether was used as alkylation solvent in the preparation of DNBT chloride, but was replaced with tetrahydrofuran in the preparation of DIBT and DSBT chlorides. Nitrates were prepared from the chlorides and silver nitrate, and recrystallized three times from aqueous methanol solution. The thallium content of the products was assayed by Goddard's method.[6] Tl %: DNBT nitrate, 52.9; DIBT nitrate, 53.1; DSBT nitrate, 53.0; Calcd., 53.7. Stock solutions of dibutylthallium nitrates were made by dissolving weighed amounts.

Supporting electrolytes used were a mixture of 0.02 M sulfuric acid and 0.15 M sodium sulfate (pH 2.01), acetate buffers (pH 3.94—5.95), phosphate buffers (pH 6.34—7.64), and ammonia buffers (pH 8.71—10.16). The ionic strength of the test solutions was controlled to 0.5 with sodium sulfate by reason of solubility of dibutylthallium salts. Gelatin was used as maximum suppressor.

All solutions were prepared with redistilled water.

Test solutions were degassed with nitrogen and thermostated at 25.0±0.1 °C.

The dropping mercury electrode (DME) had the following characteristics (in 0.17 M sodium sulfate solution at zero applied potential *vs.* SCE and at mercury pressure of 800 mm): rate of flow of mercury (m), 1.401 mg/s; drop time (τ), 4.96 s; $m^{2/3}\,\tau^{1/6} = 1.64$.

The cell used was of a beaker type with a Hume and Harris type salt bridge.[7] The original design of the bridge uses an intermediate agar plug saturated with potassium chloride, of which contamination causes precipitation of dibutylthallium chloride from the test solution. To avoid this difficulty the agar plug was prepared with 1 M potassium nitrate, and its nitrate ions were replaced by sulfate ions by standing the plug in a saturated potassium sulfate solution.

DC polarograms were obtained with a Yanagimoto PB-105 polarograph operated manually. The bridge of the instrument was calibrated by a precise potentiometer. All potentials were corrected for the internal resistance (iR drop) across the cell. A simple switching circuit was used in place of Kalousek's commutator.[8] AC polarograms were recorded with a Yanagimoto PA-102 polarograph. To minimize cell impedance, the AC voltage was applied through an auxiliary platinum electrode which connected with an SCE and the positive terminal of the polarograph through a 300 μF capacitor. Coulometry was accomplished according to the method proposed by De Vries and Kroon.[9]

Results and Discussion

DC polarograms of dibutylthallium compounds exhibit slight but persistent maxima. It needed 0.05%

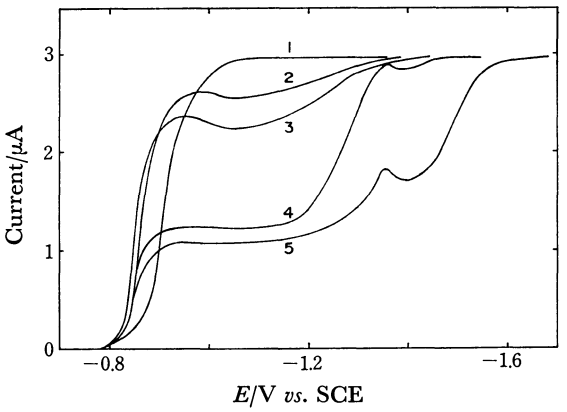

Fig. 1. Polarograms of DNBT nitrate. Concentration of DNBT nitrate, 0.410 mM. pH: 1, 5.20; 2, 6.99; 3, 7.64; 4, 8.71; 5, 10.16.

TABLE 1. VARIATION OF THE HALF-WAVE POTENTIAL OF DNBT NITRATE WITH CONCENTRATION AND MERCURY PRESSURE

pH	C[a] (mM)	h_{Hg}[b] (mm)	$-E_{1/2}$[c] *vs.* SCE (V)
5.20	0.205	800	0.925
	0.307	800	0.917
	0.410	400	0.909
	0.410	500	0.911
	0.410	600	0.912
	0.410	700	0.913
	0.410	800	0.914
	0.410	900	0.917
	0.614	800	0.903
9.58	0.102	800	0.880
	0.205	800	0.860
	0.307	800	0.852
	0.410	800	0.844
	0.614	800	0.837

a) Concentration of DNBT nitrate. b) Height of mercury column. c) Since the second wave was accompanied by a maximum, only the half-wave potential of the first wave is shown.

gelatin to suppress them. Accordingly all polarograms shown in the present paper were measured in the presence of 0.05% gelatin. The polarographic behavior of DNBT nitrate is illustrated in Fig. 1. The compound shows a reduction wave with the half-wave potential of *ca.* −0.91 V *vs.* SCE in the range of pH 3—6. The half-wave potential changes by varying concentration of DNBT nitrate as shown in Table 1. This indicates that the reversible electron transfer step is followed by a multimolecular reaction. When the pH increases above 6, the half-wave potential shifts to positive and the rising part of the wave becomes steeper. This behavior is unlike that observed for other organic compounds. It implies that a species of which existence is favorable in acid solutions hinders the easiest reaction route, and that the reduction takes place through a route with higher energy as the pH is lowered below the optimum value.

The wave splits into two at about pH 7 when the pH is increased. Although the total height of waves remains unchanged the height of the first wave decreases with increasing pH, and at pH 10 it becomes almost a third of the wave height in acid solutions. The second wave is accompanied by a maximum, even in the presence of 0.05% gelatin. The wave height in acid solutions and the total wave height in neutral and alkaline solutions increase in proportion to the concentration of DNBT nitrate and to the square root of the height of mercury column. This indicates that the limiting currents are controlled by diffusion. The variation of the half-wave potential with the mercury pressure is included in Table 1.

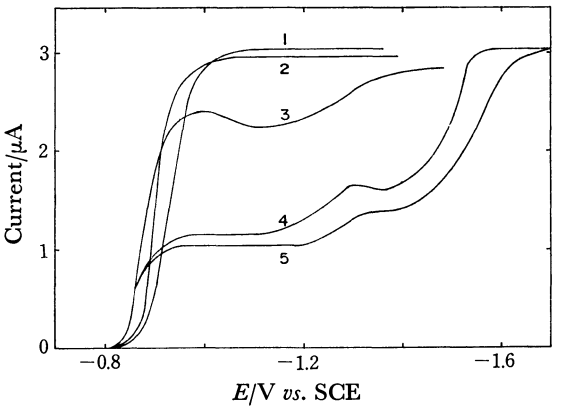

Fig. 2. Polarograms of DIBT nitrate. Concentration of DIBT nitrate, 0.421 mM. pH: 1, 4.56; 2, 6.34; 3, 7.64; 4, 8.71; 5, 10.16.

TABLE 2. VARIATION OF THE HALF-WAVE POTENTIAL OF DIBT NITRATE WITH CONCENTRATION AND MERCURY PRESSURE

pH	C[a] (mM)	h_{Hg}[b] (mm)	$-E_{1/2}$[c] *vs.* SCE (V)
5.20	0.103	800	0.983
	0.206	800	0.966
	0.309	800	0.945
	0.412	400	0.917
	0.412	500	0.918
	0.412	600	0.919
	0.412	700	0.920
	0.412	800	0.921
	0.412	900	0.923
9.58	0.103	800	0.902
	0.206	800	0.880
	0.309	800	0.870
	0.412	800	0.864
	0.618	800	0.846

a) Concentration of DIBT nitrate. b) Height of mercury column. c) Since the second wave was accompanied by a maximum, only the half-wave potential of the first wave is shown.

The behavior of DIBT nitrate is much the same as that of DNBT nitrate. Figure 2 shows typical polarograms of the compound, and Table 2 the variation of the half-wave potential.

Figure 3 shows polarograms of DSBT nitrate, which undergoes a two-step reduction in all pH ranges examined. While the half-wave potential of the first

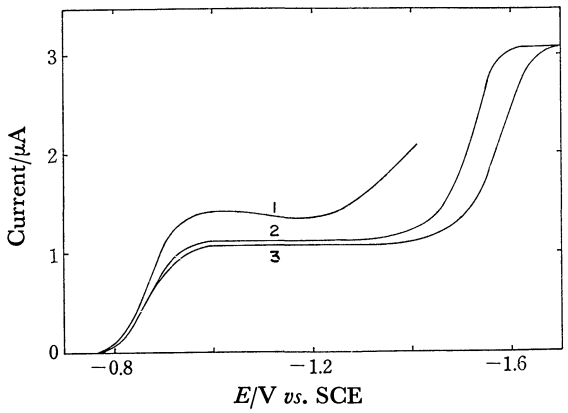

Fig. 3. Polarograms of DSBT nitrate. Concentration of DSBT nitrate, 0.424 mM. pH: 1, 3.94 (the second wave is overlapped by the hydrogen wave); 2, 8.71; 3, 10.16.

wave does not change to any noticeable extent, its limiting current decreases as much as a fifth of the wave height at pH 4 as the pH increases from 4 to 8.7. Further increase of pH, however, does not produce any appreciable change on the wave height. The limiting current of the first wave and the total wave height in alkaline solutions are in proportion to the concentration of DSBT nitrate and to the square root of the height of mercury column. This implies that the limiting currents of the first and second waves are diffusion currents. Table 3 shows the variation of the half-wave potential.

Table 3. Variation of the half-wave potential of DSBT nitrate with concentration

pH	C[a] (mM)	$-E_{1/2}$[b] *vs.* SCE (V)
5.20	0.106	0.878
	0.212	0.878
	0.318	0.874
	0.424	0.870
	0.636	0.874
9.58	0.106	0.872
	0.212	0.866
	0.318	0.865
	0.424	0.860
	0.636	0.858

a) Concentration of DSBT nitrate. b) Since the second wave was not well-defined, only the half-wave potential of the first wave is shown. The height of mercury column was 800 mm.

Electrocapillary curves of DNBT, DIBT, and DSBT nitrates indicate that these compounds are not adsorbed to any appreciable extent on the surface of DME.

The pH dependency of the polarograms suggests that hydrogen ions participate in the electrode processes. Amperometric titrations were carried out to establish the relation between the number of hydrogen ions and the number of electrons consumed in the electrode reaction. Figure 4 shows the change of the polarogram of DNBT nitrate during the titration with 2.02 mM sulfuric acid. The supporting electrolyte is 0.167 M sodium sulfate. The current at potentials corresponding to the limiting current region of the second wave remains unchanged until the concentration of hydrogen ions reaches a certain value, then increases from there on. The titration curve is shown in Fig. 5, where the current is measured at a potential of the limiting current region of the second wave. A similar change in the polarogram was observed for DIBT nitrate.

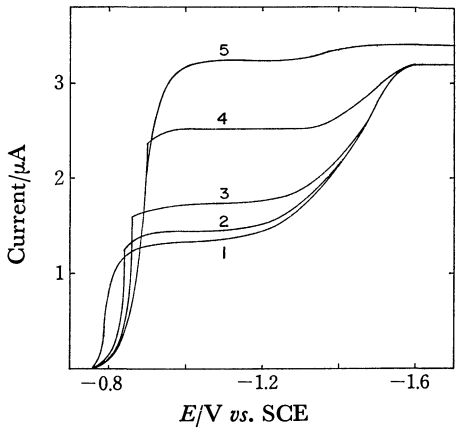

Fig. 4. Variation of the polarogram of DNBT nitrate during the titration with 2.02 mM sulfuric acid. The current was corrected for volume change. Original concentration of DNBT nitrate, 0.410 mM. Original volume of the solution, 25 ml. Supporting electrolyte, 0.167 M sodium sulfate. Volume of sulfuric acid, added: 1, 0 ml; 2, 0.5 ml; 3, 1.0 ml; 4, 2.0 ml; 5, 3.1 ml.

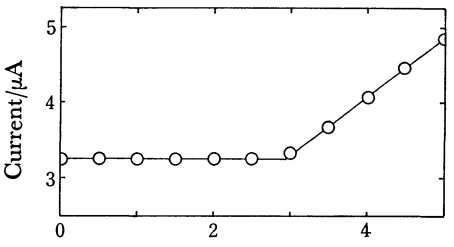

Fig. 5. Amperometric titration curve of 25 ml of 0.410 mM DNBT nitrate with 2.02 mM sulfuric acid. Titrated at −1.60 V *vs.* SCE.

When DSBT nitrate was titrated by the acid, the height of the first wave increased a little (by about a fourth of the initial height) at first and then remained unchanged, unlike that of the first wave of DNBT and DIBT nitrates. The hydrogen wave appeared at potentials between the first and second waves, and grew with increasing concentration of hydrogen ions, consuming the second wave. The titration curve is given in Fig. 6, where the current is measured at a potential of the limiting current region of the second wave.

The concentration of hydrogen ions at the end point, C_h, is related with the concentration of the dibutylthallium compound, C, by

$$I_h C_h = \frac{n_h}{n} IC \qquad (5)$$

where I is the diffusion current constant of the dibutylthallium compound, I_h the diffusion current constant of hydrogen ions, n the number of electrons involved in the electrode process, and n_h the number of hydrogen

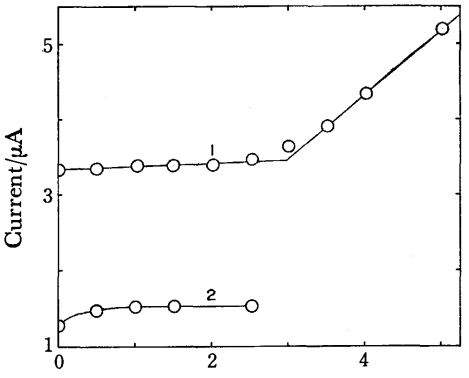

Fig. 6. Amperometric titration curves of 25 ml of 0.424 mM DSBT nitrate with 2.02 mM sulfuric acid. Curve 1, titrated at −1.80 V *vs.* SCE, of which potential lies in the limiting current region of the second wave. Curve 2, titrated at −1.10 V *vs.* SCE, of which potential lies in the limiting current region of the first wave.

ions consumed.[10] Values of the ratio n_h/n, calculated with Eq. (5) from observed values, are: 0.6_9 for DNBT nitrate, 0.6_9 for DIBT nitrate, and 0.7_2 for DSBT nitrate.

Coulometry was used for determination of the n value of DNBT nitrate reduction. The supporting electrolyte used is a mixture of 0.09 M sodium chloride and 0.01 M hydrochloric acid, where DNBT nitrate undergoes the single step reduction. A value of $n=3.0_2$ was obtained for the reduction. The n values of other reduction waves were estimated by comparison of the respective diffusion currents with the limiting current of DNBT nitrate in acid solutions.

Based on values of n and n_h/n, it was concluded that single step reductions of DNBT and DIBT nitrates in acid solutions are two-proton three-electron processes. The same reasoning was applied to the two-step reduction of DSBT nitrate. Besides, the inspection of the behavior of the first and second waves during the titration with sulfuric acid revealed that in unbuffered solutions all hydrogen ions are consumed by the electrode reaction of the second wave except a quite small fraction to be consumed by that of the first wave. Taking this and the change of height of the first wave with pH into consideration, it was concluded that the first and second waves of DSBT nitrate in alkaline solutions correspond to, respectively, no-proton one-electron and two-proton two-electron processes. In acid and neutral solutions a proton-consuming reaction proceeds to some extent at potentials of the first wave.

Figure 7 shows polarograms of DNBT nitrate recorded with Kalousek's circuit. This compound in acid solutions gives an only anodic wave at −0.4 V *vs.* SCE, of which the potential coincides with that of the anodic wave of thallium amalgam. Hence, thallium amalgam is one of the reduction products of DNBT nitrate in acid solutions where the single wave is observed on the DC polarogram. The DC polarographic wave splits into two at about pH 7 as the pH increases. Three anodic waves appear in the solution of pH 6.99 when the constant auxiliary potential (CAP) is controlled to be equal to a potential in the limiting current region

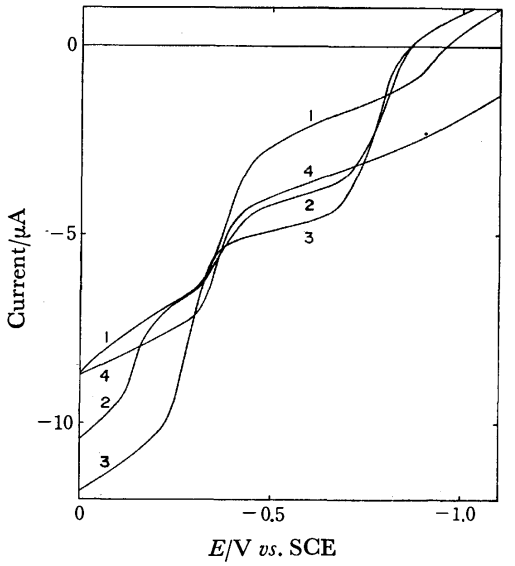

Fig. 7. Polarograms of DNBT nitrate recorded with Kalousek's circuit. Concentration of DNBT nitrate, 0.410 mM. pH and CAP (V *vs.* SCE), respectively: 1, 5.20 and −1.25; 2, 6.99 and −1.05; 3, 9.58 and −1.05; 4, 9.58 and −1.65.

of the first wave on the DC polarogram. The first and third anodic waves (counting from negative potentials to positive) decrease in height and disappear as the CAP successively becomes more negative. The second anodic wave is the dissolution wave of thallium amalgam. At pH 9.58 DNBT nitrate produces two anodic waves, namely, the first and second waves, the former disappearing with negative shift of the CAP to a potential corresponding to the limiting current region of the second wave on the DC polarogram.

DIBT nitrate produced similar polarograms when they were recorded with Kalousek's circuit.

Figure 8 shows polarograms of DSBT nitrate recorded

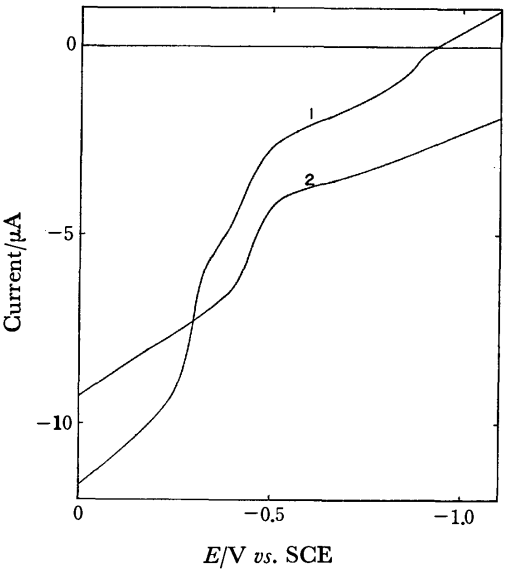

Fig. 8. Polarograms of DSBT nitrate recorded with Kalousek's circiut. Concentration of DSBT nitrate, 0.424 mM. pH and CAP (V *vs.* SCE), respectively: 1, 9.58 and −1.00; 2, 9.58 and −1.70.

with Kalousek's circuit. This compound gives two waves on the DC polarogram in all pH ranges examined. When the CAP is controlled to be equal to a potential in the limiting current region of the first wave on the DC polarogram, the compound produces two anodic waves: the dissolution wave of thallium amalgam and a wave which appears at more positive potentials and disappears with negative shift of the CAP.

The behavior of the anodic waves clearly indicates that at least two kinds of intermediates are involved in the reduction of DNBT and DIBT nitrates: one which produces the first anodic wave and of which formation does not require hydrogen ions, and the other which produces the third anodic wave and of which formation requires hydrogen ions. While the former also takes part in the reduction of DSBT nitrate (and produces the second anodic wave of this compound), participation of the latter was not proved experimentally. These conclusions were confirmed by comparison of the polarograms, recorded with Kalousek's circuit, of the three dibutylthallium nitrates in 0.167 M sodium sulfate with and without addition of sulfuric acid.

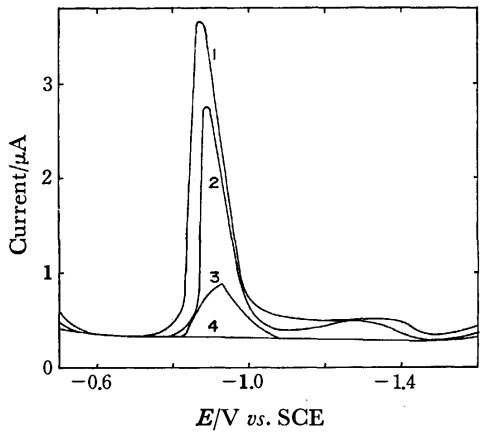

Fig. 9. AC polarograms of dibutylthallium nitrates in 0.1 M sodium hydroxide. Ionic strength was controlled to 0.5 with sodium sulfate. Curve 1, 0.410 mM DNBT nitrate; Curve 2, 0.421 mM DIBT nitrate; Curve 3, 0.424 mM DSBT nitrate; Curve 4, supporting electrolyte only.

Figure 9 shows AC polarograms of dibutylthallium nitrates in 0.1 M sodium hydroxide. It indicates that the electrode process of the first wave is most reversible for DNBT nitrate and least for DSBT nitrate. The peak heights decrease with increasing concentration of hydrogen ions, except that the peak height of DSBT nitrate does not change to any noticeable extent.

Mechanisms so far presented are not adequate enough to explain the results described above.[1-3] The following reaction scheme, accordingly, is proposed tentatively for the polarographic reduction of dibutylthallium compounds:

$$Bu_2Tl^+ + e \rightleftarrows Bu_2Tl \quad (6)$$

$$Bu_2Tl + H^+ \rightleftarrows Bu_2TlH^+ \quad (7)$$

$$2Bu_2TlH^+ \longrightarrow Bu_2Tl^+ + Tl^+ + 2BuH \quad (8)$$

$$Tl^+ + e \rightleftarrows Tl(Hg) \quad (9)$$

$$Bu_2TlH^+ + Bu_2Tl \rightleftarrows Bu_2Tl^+ + Bu_2TlH \quad (10)$$

$$Bu_2TlH + H^+ + e \longrightarrow Tl(Hg) + 2BuH \quad (11)$$

$$Bu_2Tl + Hg \longrightarrow Tl(Hg) + Bu_2Hg \quad (12)$$

$$Bu_2Tl + 2e \longrightarrow Tl(Hg) + 2Bu^- \quad (13)$$

$$Bu^- + H_2O \rightleftarrows BuH + OH^- \quad (14)$$

In the above scheme a sequence of Reactions (6)-(7)-(8)-(9) explains the single wave of DNBT and DIBT nitrates in solutions having pH values below 6. The regenerated ion Bu_2Tl^+ in Reaction (8) again enters the sequence at Reaction (6). For the species Bu_2TlH^+ it should be noted that the Tl-H^+ bond is a one-electron bond. With increase of pH another sequence of Reactions (6)-(7)-(10)-(11) becomes favorable, and is responsible for the positive shift of the wave with increase of pH in neutral solutions. Further increase of pH, however, decreases the height of the wave by making Reaction (7) difficult to proceed. The Bu_2Tl molecules that are not consumed by the reaction with Bu_2TlH^+ ions undergo transmetallation with the electrode mercury as given in Reaction (12). A two-electron reduction of the molecule is also possible by negative increase of the potential of DME. This results in a sequence Reaction (13)-(14), which corresponds to the second wave. The species Bu_2Tl and Bu_2TlH (or Bu_2TlH^+) are responsible for, respectively, the first and third anodic waves on the polarogram recorded with Kalousek's circuit.

The equilibrium constant of Reaction (7) in the reduction of DSBT nitrate does not seem to be as large as that in the reduction of DNBT and DIBT nitrates, since DSBT nitrate gives the double wave in all pH ranges examined.

References

1) G. Costa, *Ann. Chim.* (Rome), **40**, 559 (1950).
2) J. S. DiGregorio and M. D. Morris, *Anal. Chem.*, **40**, 1286 (1968).
3) K. Issleib, S. Naumann, H. Matschiner, and B. Walther, *Z. Anorg. Allg. Chem.*, **381**, 226 (1971).
4) F. Hein and H. Meininger, *ibid.*, **145**, 95 (1925).
5) A. N. Nesmeyanov and R. A. Sokolik, "Methods of Elemento-Organic Chemistry," Vol. 1, North-Holland Publishing Co., Amsterdam (1967), p. 553.
6) A. N. Nesmeyanov and R. A. Sokolik, *ibid.*, p. 594.
7) D. N. Hume and W. E. Harris, *Ind. Eng. Chem., Anal. Ed.*, **15**, 465 (1943).
8) N. Tanaka, R. Tamamushi, and M. Kodama, This Bulletin, **33**, 14 (1960).
9) T. De Vries and J. L. Kroon, *J. Amer. Chem. Soc.*, **75**, 2484 (1953).
10) I. M. Kolthoff and S. E. Khalafalla, *Inorg. Chem.*, **2**, 133 (1963).

Charge-transfer Complexes of Vinyl Polymers with Large Pendant π-electron Systems. I. Poly(*N*-vinylcarbazole) and Related Compounds

Ken-ichi OKAMOTO, Miyuki OZEKI, Akira ITAYA, Shigekazu KUSABAYASHI, and Hiroshi MIKAWA*

Department of Chemical Engineering, Faculty of Engineering, Yamaguchi University, Ube 755
** Department of Applied Chemistry, Faculty of Engineering, Osaka University, Suita 565*

(Received October 18, 1974)

The absorption spectra and the thermodynamic constants (K_{CT}, ΔH, and ΔS of formation) of the charge-transfer (CT) complexes of poly-*N*-vinylcarbazole (PVCz), the oligomers of *N*-vinylcarbazole (VCzOlig I and II, $\overline{DP}=5$ and 10 respectively), poly-*N*-carbazolylethylvinylether (PCzEVE), and the monomeric model compounds were examined in solution in order to clarify the characteristics of the complexes of polymeric donors with large pendant π-electron systems. The apparent spectra were resolved into two CT bands. The complexes of PVCz and VCzOlig II showed a lower frequency shift in the absorption maximum of the first CT band and an increase in the intensity ratio of the first to the second CT bands as compared with those of the monomeric complexes. This behavior, regarded as a kind of so-called polymer effect, seems to arise from some electronic interaction between neighboring carbazolyl groups in one polymer chain; it can be explained by variation both in the electron-donating character and in the distribution of the orientational isomers between the PVCz complexes and the others. A comparison of the observed values of K_{CT}, ΔH, and ΔS among the donors suggested that a dominant factor in determining these values is the steric hindrance rather than the small difference in the electron-donating character in the case of the structurally related polymeric complexes. The steric hindrance is important in the complexes of PCzEVE and VCzOlig I, where the electronic interaction is hardly present.

There have been many spectrophotometric investigations concerning a charge-transfer (CT) complex in which the donor consists of a polymeric species. The characteristics of CT complexes of polymeric donors can be clarified by a detailed comparison of both the absorption spectra and the thermodynamic constants (equilibrium constant (K_{CT}), and enthalpy (ΔH), and entropy (ΔS) of formation) of polymeric CT complexes with those of the corresponding monomeric ones. However, such a comparison has been made for only a few polymers.[1-6] Iwatsuki and Arai have studied the CT complexes formed between either poly-*N*-dimethylaminostyrene, copolymers of *N*,*N*-dimethylaminostyrene with styrene, or *N*,*N*-dimethyltoluidine and maleic anhydride; they have found a bathochromic shift in the CT absorption maximum and increases both in K_{CT} and in ΔH with an increase in the mean sequence length of the *N*,*N*-dimethylaminostyrene units. They have concluded that the electron-donating character of the dimethylaniline group increases with an increase in the number of groups attached to one polymer chain. This may be regarded as a kind of "polymer effect."

On the other hand, of the vinylpolymers with large pendant π-electron systems, poly-*N*-vinylcarbazole (PVCz) has been studied by two groups of investigators. Rembaum and his co-workers[4] have reported that K_{CT} values determined by the Benesi-Hildebrand method[7] were higher for the monomeric model, *N*-ethylcarbazole (ECz), than for the polymer, while Boudevska[5] have reported the opposite result for K_{CT} values determined by a modification of the successive dilution. Furthermore, the CT absorption maxima, ΔH, and ΔS have never been compared in detail between PVCz and ECz. Thus, no information about the "polymer effect" has been obtained in the case of CT complexes of the vinylpolymers with large pendant π-electron systems.

Recently, the present authors[8] have found, from the absorption spectra of the vinylpolymers, that there is some electronic interaction between pendant π-electron systems in one polymer chain in solution only for the vinylpolymers with large pendant π-electron systems connected directly to the skeletal chain. It seemed that it would be very interesting to see how the interaction affects the properties of the polymeric CT complexes. In the present series of papers, the authors have examined systematically the CT complexes of the vinylpolymers with large pendant π-electron systems and their monomeric compounds. This paper will deal with the CT complexes of PVCz and related compounds.

Experimental

Materials. The donor compounds studied were the following seven compounds containing carbazolyl (Cz) groups.

The ECz, 1,4-bis(*N*-carbazolyl)butane (DCzB), and 1,3-bis(*N*-carbazolyl)propane (DCzP) were used as monomeric model compounds of PVCz. They were prepared from purified carbazole[9] according to the literature.[10]

The oligomers of *N*-vinylcarbazole (VCz) were prepared by the HCl-initiated polymerization of VCz in acetonitrile. A 10-ml portion of acetonitrile containing 5×10^{-5} mol of dry HCl was stirred into 150 ml of acetonitrile containing 5 g of purified VCz and 2 ml of methanol at 10 °C in the dark. After half an hour, the solution was poured into 500 ml of a methanol–water (1:1) mixture. The oligomer was then filtered off, reprecipitated twice from the acetone solution with a methanol–water (7:3) mixture, and dried in a vacuum. The oligomer thus prepared (VCzOlig I) melts at 119—123 °C and has a degree of polymerization ($\overline{DP}$) of about 5. When no methanol was present in the polymerization solution, the oligomer (VCzOlig II) with a $\overline{DP}$ of about 10 and a mp of 175—185 °C was obtained.

The PVCz was prepared by the polymerization of a 0.5 M benzene solution of VCz in the presence of 1 mol % azobis-

isobutyronitrile in an evacuated sealed tube at 60 °C for 5 hr and was reprecipitated three times from the benzene solution with methanol. The polymer has $\overline{DP}$ of about 600.

The poly-*N*-carbazolylethylvinylether (PCzEVE) was used as a high molecular compound related to PVCz, in which the Cz groups are connected to the skeletal chain at a distance of about 4 Å by $-O-CH_2-CH_2-$ bonds. The polymer was prepared by the polymerization of a 0.2 M toluene solution of *N*-carbazolylethylvinylether in the presence of 3 mol % $BF_3O(C_2H_5)_2$ under a nitrogen atmosphere at −25 °C for 9 hr[11] and was reprecipitated three times from the benzene solution with methanol. The polymer has a $\overline{DP}$ of 33 and melts at 137—148 °C.

Tetracyanoethylene (TCNE), tetracyanoquinodimethane (TCNQ), *p*-chloranil (CA), 2,3-dichloro-5,6-dicyano-*p*-benzoquinone (DDQ), and 2,3,7-trinitrofluorenone (TNF) were used as acceptor compounds. The TCNE was recrystallized twice from monochlorobenzene and was subsequently sublimed in *vacuo*. The TCNQ, CA, and DDQ were recrystallized twice from acetonitrile, benzene, and methylene chloride respectively. The TNF was prepared from fluorenone according to the literature.[12]

The ethylene chloride used as a solvent was purified by the ordinary method.

Method. The absorption spectra and optical density were measured by means of two Shimadzu spectrophotometers, UV-200 and MPS-50 L, using 1-cm quartz cells and a temperature-regulated cell holder.

The K_{CT} was determined by the use of the Benesi-Hildebrand equation (1):[7]

$$[A]_0(l/A_\lambda) = (1/\varepsilon K_{CT}[D]_0) + (1/\varepsilon) \quad (1)$$

where $[A]_0$ and $[D]_0$ are the initial concentrations of the acceptor and the donor respectively; l is the path length; A_λ is the absorbance at λ due only to the complex, and ε is the molar extinction coefficient of the complex at λ. This equation is valid for a 1:1 complex when $[D]_0 \gg [A]_0$.

The K_{CT} was determined at six different temperatures from 2 °C to 30 °C. The ΔH and ΔS of formation of a CT complex were calculated by using Eq. (2),

$$\ln K_{CT}\varepsilon = (-\Delta H/RT) + (\Delta S/R) + \ln \varepsilon \quad (2)$$

Results and Discussion

The complexes with DDQ were unstable, and the CT spectra changed slowly with the time. Especially, the complexes with PCzEVE and VCzOlig I were more unstable and changes of the spectra began in a few minutes after the mixing. The other complexes were stable, and no change in absorbance with time was observed even after 12 hr. The 1:1 stoichiometry of all the complexes studied was confirmed by the continuous-variation method.

CT Absorption Spectra. The absorption spectra of the complexes with TCNE, TCNQ, CA, and DDQ are shown in Figs. 1—3. The apparent CT absorption maxima (ν_{max}) and the shifts in ν_{max} ($\Delta\nu_{max}$) as compared with that of the ECz complex are listed in Table 1.

The apparent ν_{max} appears at lower frequencies for the polymeric donors than for the monomeric ones. This is especially clear in the case of the complexes with CA or DDQ. It is well-known that there is a linear relationship between the energy of the CT transition ($h\nu_{CT}$) and the ionization potential of the donor (I_p) for a series of complexes consisting of like donors and

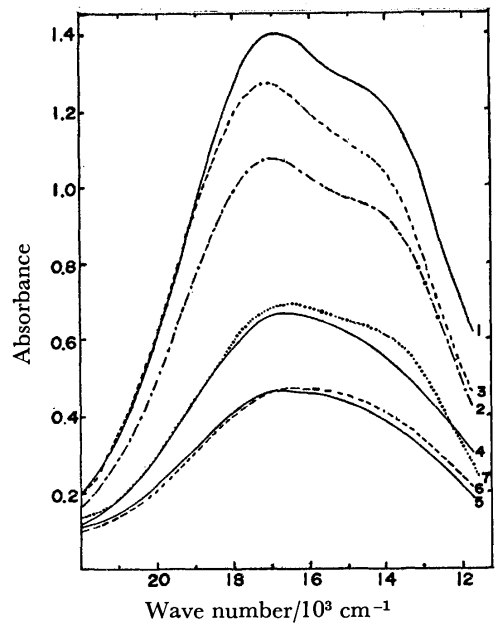

Fig. 1. CT spectra of TCNE complexes in ethylene chloride at 10 °C.

Donor	$[D]_0$	$[A]_0$
(1) ECz	0.0135 M	0.019 M
(2) DCzB	0.0135	0.019
(3) DCzP	0.016	0.023
(4) VCzOlig I	0.0185	0.023
(5) VCzOlig II	0.015	0.023
(6) PVCz	0.015	0.023
(7) PCzEVE	0.0134	0.007

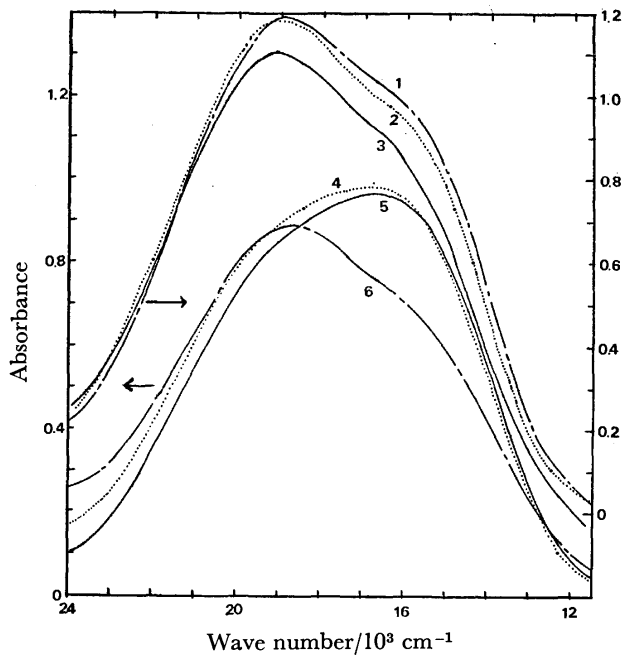

Fig. 2. CT spectra of CA complexes in ethylene chloride at 10 °C.

Donor	$[D]_0$	$[A]_0$
(1) ECz	0.050 M	0.011 M
(2) DCzB	0.050	0.011
(3) DCzP	0.050	0.011
(4) VCzOlig II	0.054	0.011
(5) PVCz	0.056	0.011
(6) PCzEVE	0.043	0.011

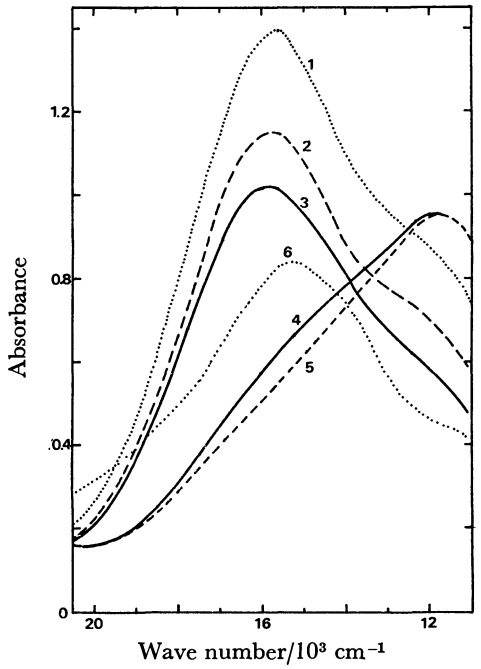

Fig. 3. CT spectra of DDQ complexes in ethylene chloride at 10 °C.

Donor	$[D]_0$	$[A]_0$
(1) ECz	0.015 M	0.006 M
(2) DCzB	0.015	0.006
(3) DCzP	0.015	0.006
(4) VCzOlig II	0.030	0.006
(5) PVCz	0.030	0.006
(6) PCzEVE	0.008	0.003

Table 1. Apparent CT absorption maxima (ν_{max}) and the shifts in ν_{max} ($\Delta\nu_{max}$) as compared with that of the ECz complex[a)]

Donor	Acceptor	ν_{max}/cm^{-1}	$\Delta\nu_{max}/cm^{-1}$
ECz	TCNE	16810	—
DCzB		16950	140
DCzP		17090	280
VCzOlig I		16530	−280
VCzOlig II		16530	−280
PVCz		16260	−550
PCzEVE		16530	−280
ECz	TCNQ	17120	—
DCzB		17120	0
DCzP		17330	210
VCzOlig II		17010	−110
PVCz		16860	−260
PCzEVE		16640	−480
ECz	CA	18830	—
DCzB		18980	150
DCzP		19120	290
VCzOlig I		17550	−1280
VCzOlig II		17040	−1790
PVCz		16840	−1990
PCzEVE		18690	−140
ECz	DDQ	15720	—
DCzB		15800	80
DCzP		15820	100
VCzOlig II		11790	−3930
PVCz		11770	−3950
PCzEVE		(15270)	(−550)

a) at 10 °C in ethylene chloride; errors in ν_{max} and $\Delta\nu_{max}$ are $\pm 20\ cm^{-1}$.

a common acceptor. However, in the present case, the lower frequency shift in the apparent ν_{max} should be considered not to correspond directly to a decrease in the I_p of the polymeric donors. This is because it is considered, for the following reasons that the spectra of all the complexes studied are composed of multiple overlapping bands: 1) in the spectra of the monomeric complexes, the absorption shoulders are apparently observed at frequencies lower than the apparent ν_{max}, and Klopffer has satisfactorily resolved the spectra of the complexes between *N*-isopropylcarbazole, one of the monomeric donors, and either TCNE or CA into two CT bands[13)]: 2) in the case of the polymeric donors, although the shoulders are hardly observed at all, the spectra have asymmetric bands with exceptionally large half bandwidths: 3) in the cases of CA and DDQ, although considerably shifted, the apparent absorption peaks for PVCz and VCzOlig II appear near the absorption shoulder for the monomeric donors.

Therefore, the spectra were resolved into two CT

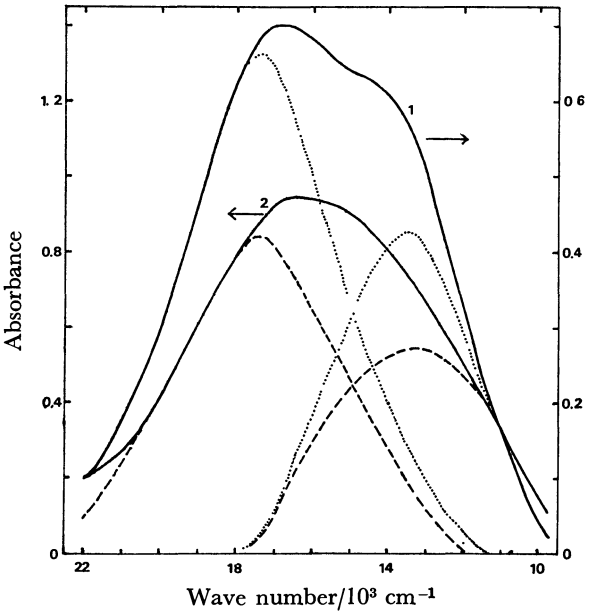

Fig. 4. Resolution spectra of TCNE complexes of ECz (1) and PVCz (2).

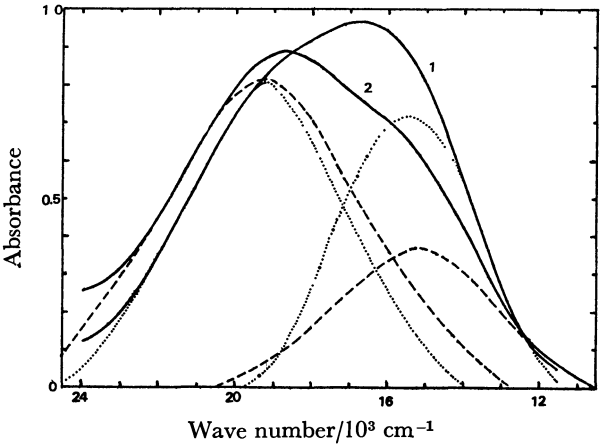

Fig. 5. Resolution spectra of CA complexes of PVCz (1) and PCzEVE (2).

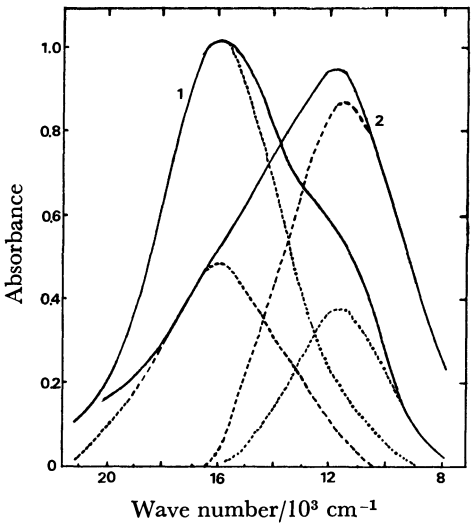

Fig. 6. Resolution spectra of DDQ complexes of DCzP (1) and PVCz (2).

Table 2. First and second CT band maxima (ν_1 and ν_2), the differences $\Delta\nu_{12}$ ($=\nu_2-\nu_1$) and $\Delta\nu_1$ ($\nu_1-\nu_{1\cdot EC_2}$), and intensity ratios of the first to the second CT bands (f_1/f_2)[a]

Donor	Acceptor	ν_1 cm^{-1}	ν_2 cm^{-1}	$\Delta\nu_{12}$ cm^{-1}	$\Delta\nu_1$ cm^{-1}	f_1/f_2
ECz	TCNE	13580	17400	3820	—	0.52
DCzB		13550	17400	3850	30	0.48
DCzP		13650	17400	3750	−70	0.40
VCzOlig I		13650	17400	3750	−70	0.45
VCzOlig II		13500	17400	3900	80	0.58
PVCz		13350	17400	4050	230	0.64
PCzEVE		13650	17400	3750	−70	0.54
ECz	TCNQ	12800	17100	4300	—	0.20
DCzB		12800	17100	4300	0	0.17
DCzP		12900	17300	4350	−100	0.17
VCzOlig II		12750	17100	4350	50	0.25
PVCz		12750	17100	4350	50	0.29
PCzEVE		12700	17200	4500	100	0.11
ECz	CA	15350	19250	3900	—	0.34
DCzB		15350	19250	3900	0	0.20
DCzP		15450	19250	3800	−100	0.25
VCzOlig I		15500	19250	3750	−150	0.42
VCzOlig II		15400	19250	3850	−50	0.63
PVCz		15500	19250	3750	−150	0.76
PCzEVE		15350	19250	3900	0	0.34
ECz	DDQ	11700	15900	4200	—	0.32
DCzB		11700	15900	4200	0	0.30
DCzP		11650	15900	4250	50	0.27
VCzOlig II		11500	15900	4400	200	1.4
PVCz		11400	15900	4500	300	1.7
PCzEVE		(11000)	(15300)	(4300)	(700)	(0.27)
ECz	TNF	18750	22900	4150		0.43
DCzP		(18750)	(23000)	(4250)		(0.41)
PVCz		(18750)	(23000)	(4250)		(0.49)

a) Errors in ν_1, ν_2, $\Delta\nu_{12}$ and $\Delta\nu_1$ are ±100 cm^{-1} for the CA complexes of VCzOlig I, II and PVCz and ±50 cm^{-1} for the other complexes. Errors in f_1/f_2 are $\pm15\%$ for the former complexes and $\pm10\%$ for the latter ones. The parenthesized numerical values are less reliable because of either decomposition of the complex or overlapping of absorption of TNF with that of the complexes.

bands by the use of a curve-analyzer, based on the assumptions that the individual resolved CT bands were symmetrical and that the location of the second CT band was almost the same for the complexes between a series of donors and a common acceptor. These assumptions seem reasonable judging from the spectra of the complexes with poly-1-vinylpyrene and related compounds.[14] The results were satisfactory, as is shown by the examples in Figs. 4—6. The absorption maxima of the first and the second CT bands (ν_1 and ν_2), the differences ($\Delta\nu_{12}$ and $\Delta\nu_1$ ($\Delta\nu_{12}=\nu_2-\nu_1$, and $\Delta\nu_1=\nu_1-\nu_{1\cdot EC_2}$)), and the intensity ratios (f_1/f_2) of the first to the second CT bands are listed in Table 2.

As the $\Delta\nu_{12}$ values are regarded to be constant at 4100 ± 400 cm^{-1} for all the complexes studied, irrespective of the acceptors, the first and the second CT bands are considered to be due to the CT from the highest occupied and the second highest occupied levels of the donor, respectively, to the lowest vacant level of the acceptor.

There is no appreciable difference in either ν_1 or f_1/f_2 among the monomeric donors, with the exception of ν_1 for DCzP. DCzP shows a little higher frequency shift in ν_1 as compared with the ν_1 values for the other monomeric donors. This is mainly due to the weakness of the electron-donating character of the substituent group per Cz ring as compared with that of an ethyl group, and not to some interactions between the two Cz rings connected at 1,3-positions, as was found in the study concerning the UV spectra.[8] PVCz and VCzOlig II show a lower frequency shift in ν_1 (50—300 cm^{-1}), with the exception of the ν_1 values for the CA complexes, and a considerable increase in f_1/f_2, especially in the cases of CA and DDQ, as compared with those for the monomeric donors. The changes are larger for PVCz than for VCzOlig II. VCzOlig I shows no clear shift in ν_1, but a small increase in f_1/f_2 only in the case of CA. On the other hand, PCzEVE shows no appreciable change in either ν_1 or f_1/f_2 as compared with those for the monomeric donors, in spite of the high value of $\overline{DP}$.

It was thus clarified that the apparent complicated variation in the shape of the CT spectra between the monomeric and the polymeric donors results from the phenomena regarded as a kind of so-called polymer effect—namely, a lower frequency shift in ν_1 and a considerable increase in f_1/f_2 of the polymeric CT complexes as compared with those of the monomeric ones. It should be noted that the phenomena become clear with an increase in the $\overline{DP}$, although they are unobservable for the pentamer, in a series of the polymers of VCz, and that they are not observed for PCzEVE, which has Cz groups apart from the skeletal chain in spite of the high value of $\overline{DP}$ ($\overline{DP}=33$). It is interesting that the $\overline{DP}$ dependency of the shift in ν_1 mentioned above is quite different from that of the maleic anhydride complexes of poly-*N*,*N*-dimethylaminostyrene and related copolymers,[3] where the bathochromic shift results from the aminostyrene unit with a $\overline{DP}$ value of only two.

The results mentioned above are closely related to the results obtained from the UV absorption spectra concerning the electronic interaction between pendant

π-electron systems in one polymer chain.[8] The phenomena mentioned above, therefore, seem to arise from some electronic interaction between neighboring Cz groups in one polymer chain.

The increase in f_1/f_2 upon a replacement of the monomeric donors by the polymeric ones is an interesting phenomenon which has hitherto never been reported, to the knowledge of the authors. It has been suggested that the complexes between either naphthalene or substituted benzenes and TCNE in solution have isomers differing in the mutual orientations of the symmetry axes of the donor and acceptor.[15] Kuroda and his co-workers[16] have made a theoretical treatment of the CT interaction in the TCNE complexes of naphthalene and pyrene, considering the effect of the interaction of higher CT states, and have concluded that the binding energy varies little with the angle between the symmetry axes of the donor and acceptor and that the energy barrier hindering the rotation of one molecule relative to its partner is less than 1 kcal/mol. Therefore, in some complexes, the orientational isomers are considered to coexist in solution with an almost equal probability because of the ease of the rotational interconversion among them. They have also suggested that f_1/f_2 is a parameter which offers information on the orientation of the donor molecule to the acceptor one.[16] The variation in f_1/f_2 in the present case may be a result of the orientational isomers, the distribution of which is affected by a perturbation effect of neighboring Cz groups to the complex. No detailed explanation can be offered at present.

Table 3. Temperature dependence of apparent CT absorption maxima of the CA complexes of PVCz and VCzOlig II

	λ_{max} [nm][a]					
	2 °C	5 °C	10 °C	20 °C	35 °C	60 °C
VCzOlig II	590	586	585	573	556	—
PVCz	597	595	593	588	585	567

a) $[D]_0=0.156$ M (VCz unit), $[A]_0=0.007$ M in ethylene chloride.

In the complexes between either PVCz or VCzOlig II and CA, the apparent absorption maxima shifted reversibly to higher frequencies with an increase in the temperature, as is shown in Table 3. The shift was apparently due to a decrease in f_1/f_2 with an increase in the temperature and was larger for VCzOlig II than for PVCz. This suggests that the perturbation effect of neighboring Cz groups on the complex weakens according to the gradual disappearance of the local helical structure and/or the gradual ease of the internal rotation of a polymer chain with an increase in the temperature. The NMR measurements[17] have suggested that the internal rotation of the polymer chain, being restricted by neighboring bulky Cz groups, is sensitive to the temperature. In the PVCz (or VCzOlig II) complexes of TCNE and TCNQ, such a shift could not be observed, probably because of the small variation in f_1/f_2 between the PVCz and the ECz complexes.

The $h\nu_{CT}$ for a series of complexes with a common acceptor can be described by the following expressions:

$$h\nu_{CT} = (I_p - C_1) + C_2/(I_p - C_1) \quad (3)$$

$$h\nu_{CT} = aI_p + b \quad (4)$$

where C_1, C_2, a, and b are constants for a given acceptor. The first and the second ionization potentials of ECz are determined to be 7.43 ± 0.03 eV and 8.02 ± 0.04 eV respectively by the use of sets of the constants for TCNE, TCNQ, CA, and TNF.[18] These values are in agreement with those reported by Klopffer,[13] and the first ionization potential (I_{p1}) is much smaller than the previously reported values, determined from the apparent absorption maxima.[4,19,20]

The lower frequency shift in ν_1 of the PVCz complexes as compared with the ν_1 of the monomeric complexes cannot be explained by supposing an effect of insufficient solvation due to both the polymer backbone and adjacent Cz groups, because such an effect would tend to cause a higher frequency shift, if it is present at all. The lower frequency shift in ν_1 may, therefore, be attributed to a decrease in the I_{p1} value of PVCz as compared with those of ECz due to some electronic interaction between neighboring Cz groups, assuming that the ν_1 varies little with a variation in the distribution of the orientational isomers. A decrease in the I_{p1} value of PVCz is evaluated to be about 0.03 eV from the variation in the ν_1 of the TCNE complexes, which is most reliable. This value seems reasonable, because it is comparable to the value of 0.04 eV for poly-1-vinylpyrene, the CT complexes of which show no variation in f_1/f_2 as compared with that of the monomeric CT complex.[14]

Thermodynamic Constants of the Formation of CT Complexes. For all the complexes studied, fairly good straight lines of Benesi-Hildebrand plots were obtained. The thermodynamic constants are listed in Table 4. Although Livina and his co-workers[20] have reported that the values of ε in the PVCz complexes have decreased with an increase in the temperature, ε was independent of the temperature in the region from 2 °C to 30 °C with the exception of the values of the complexes between either PVCz or VCzOlig II and CA. The data for the CA complexes are less reliable because of a little variation in the spectra with the temperature.

In a series of complexes with a common acceptor, the ε_{max} values are almost constant, contrary to the results reported by Boudevska.[5] The values of K_{CT}, $-\Delta H$, and $-\Delta S$ are in the following orders: ECz$>$DCzP$\sim$PCzEVE$>$VCzOlig$\sim$PVCz for K_{CT}; ECz$\sim$PCzEVE$>$PVCz$\gtrsim$VCzOlig$\gtrsim$DCzP for $-\Delta H$, and PVCz$>$VCzOlig$\sim$PCzEVE$>$ECz$>$DCzP for $-\Delta S$.

In general, there is a near-linear correlation between K_{CT} and $-\Delta H$ as well as between $-\Delta H$ and $-\Delta S$ for a set of complexes of a common acceptor with a series of structurally related donors.[21] In the present case, this correlation holds roughly only for the complexes with ECz and DCzP, where a dominant factor in determining K_{CT}, ΔH, and ΔS is the electron-donating character rather than the steric hindrance. The steric hindrance in a series of donors is considered to be in the order of: PVCz$>$VCzOlig$>$PCzEVE$>$DCzP$>$ECz. The values of K_{CT} and $-\Delta H$ of the complexes with PVCz and VCzOlig I and II are smaller than

Table 4. Thermodynamic constants of formation of CT complexes[a)]

Donor	$[D]_0$ M	Acceptor	$[A]_0$ 10^3 M	ε_{max}[b)] (cm/M)	K_{CT} (M^{-1}) at 15 °C	$-\Delta H$ kcal/mol	$-\Delta S$ e.u.
ECz	0.02—0.2	TCNE	1.5	2500±150	2.8±0.2	3.2±0.2	8.9±0.5
DCzP	0.04—0.18		1.5	2500±150	1.9±0.2	2.5±0.2	7.0±1.0
VCzOlig I	0.08—0.3		3.0	2600±200	0.7±0.1	2.5±0.2	9.4±0.8
PVCz	0.06—0.3		3.0	2400±250	0.6±0.1	2.8±0.2	10.8±1.0
PCzEVE	0.04—0.2		3.0	2400±200	1.9±0.2	3.1±0.2	9.6±0.8
ECz	0.04—0.13	TCNQ	1.0	2600±200	3.5±0.3	3.8±0.2	10.8±0.7
DCzP	0.04—0.16		1.0	2600±200	2.0±0.2	3.1±0.2	10.2±1.0
PVCz	0.08—0.30		3.0	2300±300	0.9±0.2	3.2±0.2	11.4±1.0
ECz	0.06—0.2	CA	3.0	1720±150	1.3±0.2	3.0±0.2	9.4±0.6
DCzP	0.06—0.2		5.0	1800±200	1.0±0.2	2.7±0.2	10.2±0.8
VCzOlig II	0.06—0.2		6.0	1430±300[c)]	0.6±0.2	2.9±0.5	10.7±1.7
PVCz	0.05—0.2		6.0	830±120[c)]	1.0±0.2	3.4±0.4	12.0±1.5
ECz	0.02—0.1	TNF	2.0	2000±100	4.3±0.2	2.6±0.1	6.2±0.3
DCzP	0.03—0.18		2.0	2080±100	3.7±0.2	1.8±0.1	3.7±0.3
PVCz	0.05—0.2		3.0	1200±150	2.1±0.2	2.3±0.2	6.8±0.4

a) Solvent: methylene chloride for TNF and ethylene chloride for the other acceptors. b) at an apparent absorption maximum. c) at 15 °C.

those of ECz, in spite of a small enhancement in the electron-donating character of PVCz as compared with that of ECz. Futhermore, the value of K_{CT} of the PCzEVE complex is smaller than that of the ECz complex, in spite of no difference in the spectral properties (ν_1, ν_2, and f_1/f_2) between the former and the latter complexes. Therefore, it is clear that a dominant factor in determining K_{CT}, ΔH, and ΔS is the steric hindrance rather than a small difference in the electron-donating character in the case of the structurally related polymeric complexes. It should be noted that the situation is the same even in the case of VCzOlig I ($\overline{DP}=5$), as in the case of PVCz. This is quite different from the situation of the variation in both ν_1 and f_1/f_2 resulting from some electronic interaction between neighboring Cz groups.

The results presented above are in contrast to the results for the maleic anhydride complexes of poly-*N*,*N*-dimethylaminostyrene and related copolymers, where both K_{CT} and $-\Delta H$ increase with an increase in the $\overline{DP}$. This may be explained as follows. Poly-*N*,*N*-dimethylaminostyrene is one of the vinylpolymers with small pendant π-electron systems, although it is a fairly strong electron donor, and its electron-donating charater is to a considerable extent localized on the dimethylamino group. Therefore, the steric hindrance in forming a CT complex may not be serious in this polymer.

It is important to examine whether the interesting results for the PVCz complexes can be applied generally to the complexes of the other vinylpolymers with large pendant π-electron systems. A further study concerning the other polymeric complexes is now in progress.

This work was supported in part by a Scientific Research Grant of the Ministry of Education.

Reference

1) H. Sugiyama and H. Kamogawa, *J. Polym. Sci. A*-1, **4**, 2281 (1966).
2) W. Klopffer and W. Willicks, *Makromol. Chem.*, **115**, 156 (1968).
3) S. Iwatsuki and K. Arai, *J. Polym. Sci. A*-1, **10**, 3329 (1972).
4) A. Rembaum, A. M. Hermann, and R. Haack, *ibid.*, **6**, 1955 (1968).
5) H. Boudevska, *Makromol. Chem.*, **143**, 11 (1971). *ibid.*, **151**, 147 (1972).
6) M. H. Litt and J. W. Summers, *J. Polym. Sci. A*-1, **11**, 1359 (1973).
7) H. A. Benesi and J. H. Hildebrand, *J. Amer. Chem. Soc.*, **71**, 2703 (1949).
8) K. Okamoto, A. Itaya, and S. Kusabayashi, *Chem. Lett.*, **1974**, 1167.
9) K. Kihara, Y. Ishii, Y. Suzuki, and T. Takeuchi, *Kogyo Kagaku Zasshi*, **73**, 2630 (1970).
10) I. K. Lewis, G. B. Russell, R. D. Topson, and J. Vaughan, *J. Org. Chem.*, **29**, 1183 (1964).
11) K. Okamoto, M. Yamada, A. Itaya, S. Kusabayashi, and T. Kimura, 29th annual Meeting of Chem. Soc. of Japan (Hiroshima) 2J18, October, 1973. To be published elsewhere.
12) E. O. Woolfolk and M. Orchin, "Organic Synthesis," Coll. Vol. III, p. 837.
13) W. Klopffer, *Z. Naturforsch.*, **24a**, 1923 (1969)
14) To be published by us in the near furture.
15) J. R. Gott and W. G. Maish, *J. Chem. Phys.*, **39**, 2229 (1963). A. Zwing, *Tetrahedron Lett.*, **1964**, 89
16) H. Kuroda, I. Ikemoto, and H. Akamatu, This Bulletin, **39**, 1842 (1966). H. Kuroda, T. Amano, I. Ikemoto, and H. Akamatu, *J. Amer. Chem. Soc.*, **89**, 6056 (1967)
17) D. J. Williams, *Macromolecules*, **3**, 602 (1970); S. Yoshimoto, Y. Akana, A. Kimura, H. Hirata, S. Kusabayashi, and H. Mikawa, *Chem. Commun.*, **1969**, 987.
18) a) H. Kuroda, M. Kobayashi, M. Kinoshita, and S. Takemoto, *J. Chem. Phys.*, **36**, 457 (1962); b) E. M. Voigt and C. Reid, *J. Amer. Chem. Soc.*, **86**, 3930 (1964); c) G. Briegleb, J. Czekalla, and G. Reuss, *Z. Phys. Chem.*, **30**, 333 (1961); *idem.*, *Z. Elektrochem.*, **63**, 6 (1959); d) R. S. Becker and E. Chen, *J. Chem. Phys.*, **45**, 2403 (1966).
19) J. H. Sharp, *J. Phys. Chem.*, **70**, 584 (1966)
20) F. A. Levina, I. Sidravicius, S. I. Peredereeva, I. G. Orlov, G. E. Zaikov, and M. I. Cherhashin, *Izv. Akad. Nauk SSSR, Ser. Khim*, **1971**, 57.
21) R. Foster,"Organic Charge-Transfer Complexes," Academic Press, New York (1969), p. 205.

Simple and Complex Anion-radical Salts Derived from 2,3-Dicyano-1,4-naphthoquinone

Izumi MAKI, Yoshio MATSUNAGA,* Mitsuru NAKAKURA, and Akihiko NONAKA

Department of Chemistry, Faculty of Science, Hokkaido University, Sapporo 060

(Received November 8, 1974)

Simple and complex anion-radical salts were prepared by the reduction of 2,3-dicyano-1,4-naphthoquinone with a number of onium iodides. The simple salts are green-colored, and the complex salts, with a composition of 1 : 2, are dark green or brown. The latter salts show electronic absorptions extending into the near-infrared region. The electrical resistivities are rather high—— 10^7—10^{12} ohm cm in the simple salts and 10^3—10^7 ohm cm in the complex salts. The ESR spectra characteristic of triplet excitons were observed with polycrystalline samples, and the zero-field splitting parameters and the singlet-triplet separation energies were estimated for most of the salts. The anion-radicals appeared to be in strong pair-by-pair interactions in these salts.

Extensive studies have been carried out on the synthesis and physical properties of the anion-radical salts derived from 7,7,8,8-tetracyanoquinodimethane (TCNQ); however, little attention has been paid to the possibility of finding new series derived from compounds other than TCNQ. So far, only the following compounds have been reported to form series of the onium salts: 9-dicyanomethylene-2,4,7-trinitrofluorene and -2,4,5,7-tetranitrofluorene,[1,2] 3,3′,5,5′-tetrachloro-4,4′-diphenoquinone (TCDQ), its bromo analogue (TBDQ),[3] and 2,3-dichloro-5,6-dicyano-1,4-benzoquinone (DDQ).[4] Continuing our search for highly-conducting anion-radical salts,[3] we worked on the preparation of a new series based on 2,3-dicyano-1,4-naphthoquinone, hereafter abbreviated as DCNQ. This quinone has an electron-acceptor strength comparable with that of *o*-bromanil in terms of their complexing properties,[5,6] and it is readily reduced to the semiquinone anion by the use of the iodide ion. The solid-state spectra of some alkali salts have been described by Iida of our laboratory.[7] The anion-radical salts formed with most of the onium ions were of a 1 : 1 composition, and the complex salts, when available, were not always well-defined. Moreover, the electrical resistivities of this series were found to be discouragingly high. Nevertheless, the recent report by Gordon and Hove on triplet excitons in the four tetraalkylammonium salts of the DDQ anion-radical, which is the only other anion-radical after TCNQ which exhibits this behavior, prompted us to do a little more work and to publish the results.

Experimental

Materials. 2,3-Dicyano-1,4-naphthoquinone was prepared by the procedures reported by Reynolds and VanAllan or by Wallenfels *et al.* starting from 2,3-dichloro-1,4-naphthoquinone,[8,9] Eastman yellow label. The crude product was purified by recrystallization from toluene and then by sublimation *in vacuo*. The anion-radical salts were obtained by the reduction of the quinone dissolved in acetone with an appropriate onium iodide. All the cations employed were diamagnetic, and their iodides were taken from the stock prepared for our earlier work.[3] The precipitated salt was filtered and washed with a small amount of acetone. The salts are fairly soluble in this solvent. The composition was determined by microanalysis.

Measurements. The electrical resistivities of compressed polycrystalline samples were examined by means of a Wheatstone bridge (Yokogawa Electric Works, Type 2768) employing a cell similar to that designed by LaFlamme.[10] The electronic spectra of the solid salts in the region from 325 to 25000 nm were measured with a Beckman DK-2A spectro-reflectometer. The pulverized sample was diluted with sodium chloride in concentrations of the order of 1 weight percent in order to obtain a reasonable reflectance. The spectra were recorded as the difference in reflectance between the mixture and pure sodium chloride and were plotted using the Kubelka-Munk function $f(R)=(1-R)^2/2R$, where R is the reflectance. The ESR measurements were carried out by means of a JEOL model JES-ME-3X spectrometer in the temperature range from room temperature to 100 °C. The magnetic field scan was calibrated with Mn^{2+}-doped MgO powder (86.9 G).

Results and Discussion

The twenty-five DCNQ anion-radical salts for which the compositions could be established by microanalysis are listed in Table 1. They are of a 1 : 1 composition unless otherwise stated. The onium cations employed in the present series include ammonium, phosphonium, arsonium, quinolinium, and acridinium. The resistivities of the simple salts range from 10^7 to 10^{12} ohm cm, and those of the complex salts, from 10^3 to 10^7 ohm cm. Thus, complex salts are apparently more conducting than the simple salts, in agreement with the tendency well-established for TCNQ anion-radical salts.[11,12] However, the resistivity values, especially those of the complex salts, are appreciably greater than those of TCNQ salts and also those of the TCDQ and TBDQ salts prepared by us.

All the simple DCNQ salts are dark green, and the solid-state spectra are similar to each other. For example, Fig. 1 presents the spectra of the morpholinium and methyltriphenylphosphonium salts. They consist of three bands, located at 12.9, 20.4, and 26.3×10^3 cm^{-1}, and at 14.8, 20.0, and 27.6×10^3 cm^{-1}, respectively. Although the locations are somewhat different, the other salts including the sodium salt show essentially the same pattern. The band maxima are listed in Table 1. The low-energy bands are found in the region from 12.9 to 15.1×10^3 cm^{-1}; the middle bands, in the

* To whom inquiries may be addressed.

Table 1. Electrical resistivities and electronic absorption bands of the anion-radical salts derived from dicyanonaphthoquinone

Cation	Resistivity (ohm cm)	Band maxima (10^3 cm^{-1})
Sodium	7×10^{7}	13.3, 22.8, 26.3
Dibenzylammonium	3×10^{11}	13.3, 21.1, 25.7
Ethyldibenzylammonium	1×10^{10}	13.2, 22.2, 25.3
n-Propyl-dibenzylammonium	1×10^{10}	13.5, 21.5, 25.0
Morpholinium	1×10^{9}	12.9, 20.4, 26.3
N-Methylmorpholinium	4×10^{9}	13.1, 21.1, 25.3
N-Ethylmorpholinium	4×10^{9}	13.2, 20.8, 26.3
N-*n*-Propylmorpholinium	4×10^{9}	13.1, 20.8, 26.3
Methyltriphenyl-phosphonium	1×10^{10}	14.8, 20.0, 27.6
Ethyltriphenylphosphonium	1×10^{10}	14.8, 20.0, 27.5
n-Propyltriphenyl-phosphonium	3×10^{10}	14.8, 20.0, 26.3
Methyltriphenylarsonium	2×10^{12}	14.7, 19.8, 27.0
Ethyltriphenylarsonium	1×10^{10}	15.1, 19.5, 27.0
4-Methylquinolinium	2×10^{10}	13.7, 20.4, 27.4
N-Ethyl-4-methyl-quinolinium	4×10^{10}	12.9, 21.0, 26.0
N-*n*-Propyl-4-methyl-quinolinium	1×10^{8}	13.5, 20.0, 26.7
N-*n*-Propylisoquinolinium	6×10^{8}	13.8, 20.5, 29.3
Acridinium	4×10^{9}	12.9, 22.2, 28.6
N-Ethylacridinium	8×10^{8}	14.0, ——, 28.2
Di-*n*-propylammonium (1:2)	5×10^{7}	8.9, 14.1, 20.7, 24.4
Methyldi-*n*-propyl-ammonium (1:2)	2×10^{7}	8.7, 14.1, 22.2, 25.0
Ethyldi-*n*-propyl-ammonium (1:2)	1×10^{7}	8.8, 13.5, 22.0, 24.1
Tri-*n*-propylammonium (1:2)	1×10^{7}	9.1, 13.8, ——, ——
N-Ethylquinolinium (1:2)	7×10^{3}	<4.0, —, 21.1, >30.0
Isoquinolinium (1:2)	1×10^{4}	4.8, 14.3, 20.5, 29.0

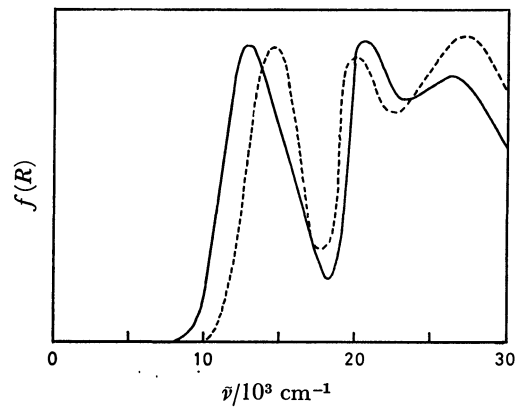

Fig. 1. Diffuse reflection spectra of the simple DCNQ salts containing morpholinium ion (——) and methyltriphenylphosphonium ion (------).

region from 19.5 to 22.8×10^3 cm^{-1}, and the high-energy bands, in the region from 25.0 to 29.3×10^3 cm^{-1}. The last location may be affected by the absorption due to the counter ion. In the case of the *N*-ethylacridinium salt, the middle band could not be determined clearly because of its breadth. These radical salts are supposed to contain columns of the semiquinone ions, which may be in an essentially pair-by-pair or more-than-by-pairs interaction. Although Iida did not identify the type of interaction in the alkali salts,[7] the observation of the triplet exciton ESR to be described later indicates that the pattern in Fig. 1 arises from the former interaction.

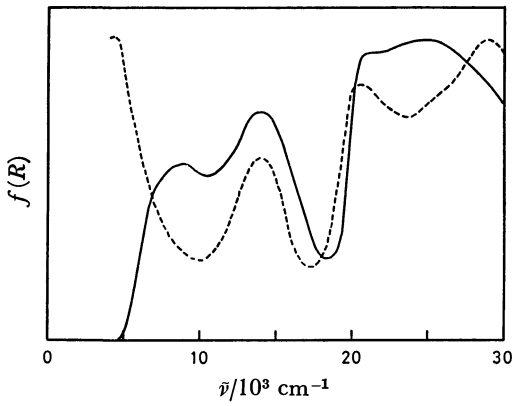

Fig. 2. Diffuse reflection spectra of the complex DCNQ salts containing tri-*n*-propylammonium ion (——) and isoquinolinium ion (------).

The complex ammonium salts are dark green, and the quinolinium salts are brown. As is shown in Fig. 2, the spectra of the complex tri-*n*-propylammonium and isoquinolinium salts consist of four bands; therefore, the whole pattern looks like the pattern of the simple salts, with an "additional" band in the near-infrared region. The location of this band depends greatly upon the kind of the onium ion. The bands in the four ammonium salts are located at energy values nearly twice as high as those in the *N*-ethylquinolinium and isoquinolinium salts. In accordance with LeBlanc's postulate that aromatic counter ions with large polarizabilities are effective in producing low resistivities of anion-radical salts,[13] the latter two may be said to be about one thousand times more conducting than the former four. The tendency for the energy of the lowest-energy band to be less as the resistivity is lower is also roughly observed in the TCDQ and TBDQ anion-radical salts studied earlier.[3] When the band shifts to a lower energy, the intensity becomes relatively higher than that of the second low-energy band. Thus, the maximum of the latter band in the most conducting *N*-ethylquinolinium salt is not observed in the spectrum. The lowest-energy absorption may be ascribed to the interaction between the DCNQ anion-radical and the neighboring DCNQ molecule, which are possibly stacked together to form a column. However, the correlation between the location of the absorption band and the resistivity suggests that the interaction is not strictly limited within such a pair.

Although the results of microanalysis were far from the values calculated for any composition, the DCNQ salts with the following cations appeared to be not simple: methyldibenzylammonium, isopropyltriphenylphosphonium, *N*-methylquinolinium, *N*-methyl-4-methylquinolinium, *N*-methylisoquinolinium, *N*-ethyl-

isoquinolinium, and *N*-methylacridinium. The resistivity values of the first two are of the orders of 10^6 and 10^4 ohm cm respectively, while those of the rest of the order of 10^3 ohm cm. These values are too low to be considered as those of the simple salts, but they fit into the range shown by the six complex salts given in Table 1. All the salts except the methyldibenzylammonium salt are dark brown in color. The spectral patterns are also characteristic of the complex salts mentioned above. The lowest-energy band in the ammonium salt is located at 7.7×10^3 cm^{-1}, and that of the phosphonium salt, at 5.8×10^3 cm^{-1}. The absorption maxima in the other salts are beyond the limits of the spectrophotometer employed—namely, below 4×10^3 cm^{-1}.

Würster's blue perchlorate and various TCNQ anion-radical salts have been known to exhibit ESR spectra from triplet spin excitons.[14-19] When a polycrystalline sample is employed for the measurement, the triplet character of the paramagnetic excitations is best manifested by the appearance of three pairs of resonance lines.[4,19] They correspond to the three principal axis splittings, which result from an anisotropic zero-field splitting of the triplet levels caused by the dipole-dipole interaction of the two electrons. All the above-mentioned salts are apparently of the class in which each radical interacts strongly with only one other free radical,[20] and they are known to exhibit rather high electrical resistivities.[16] It seems very likely that the DCNQ anion-radical salts belong mostly to such a class also. Indeed, the ESR spectra characteristic of triplet excitons could be observed with all the salts having resistivity values of 10^7 ohm cm or higher.

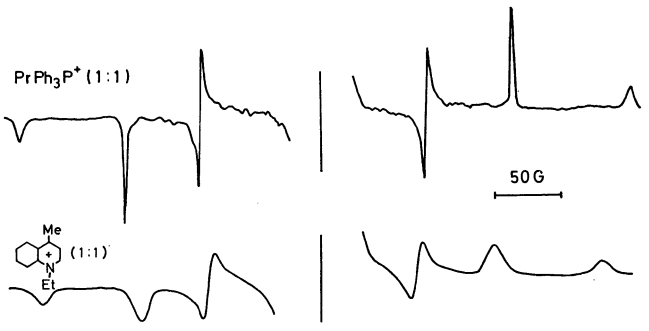

Fig. 3. First derivatives of ESR absorption spectra of the simple *n*-propyltriphenylphosphonium and *N*-ethyl-4-methylquinolinium DCNQ salts.

The triplet spectrum, particularly the outermost pair, is very weak at room temperature, and the salt starts to decompose between 80 and 110 °C; therefore, the measurements could be made only in a limited temperature range. No change in the shape and separation of the pair was detected in such a narrow range. For example, Fig. 3 shows the polycrystalline powder spectra of the *n*-propyltriphenylphosphonium and *N*-ethyl-4-methylquinolinium salts. The former spectrum was recorded at 80 °C, and the latter, at 70 °C. The central line, which may be attributed to impurities or lattice imperfections, is several orders of magnitude stronger than the triplet spectrum and becomes broader as the temperature is raised. Assuming, for the sake of simplicity, an isotropic *g* value equal to the free electron value, the principal axis splittings are related to the zero-field splitting parameters, *D* and *E*, by the following equations:[20]

$$d_1 = 2|D|$$
$$d_2 = |D| + 3|E|$$
$$d_3 = |D| - 3|E|,$$

where d_i is the measured separation. The numbering is given starting from the outermost pair of resonance lines. The parameters may be expressed in terms of the spatial distribution of the correlated spins of the triplet excitons. The values of *D* and *E* for seventeen salts, including four complex ones, are summarized in Table 2. Among the salts here, the outermost pairs in the ethyl- and *n*-propyl-dibenzylammonium salts were too weak to be accurately located, even at the highest temperature examined, 90 °C. Consequently, only the values of d_2 and d_3 were used to estimate the parameters. In addition to the salts given in Table 2, we observed the triplet spectra with the *N*-methyl- and *N*-propylmorpholinium and acridinium salts; however, these spectra were so poor that no assignment of the resonance lines could be made with confidence.

Table 2. Zero-field splitting parameters and singlet-triplet separation energies of the anion-radical salts derived from dicyanonaphthoquinone

Cation	$\lvert D\rvert$ (gauss)	$\lvert E\rvert$ (gauss)	ΔE (eV)
Sodium	111	8	0.20
Dibenzylammonium	236	19	0.35
Ethyldibenzylammonium	222	23	0.41
n-Propyldibenzylammonium	225	21	0.33
Morpholinium	238	20	0.44
N-Ethylmorpholinium	232	20	0.43
Methyltriphenylphosphonium	239	22	0.41
Ethyltriphenylphosphonium	234	19	0.45
n-Propyltriphenylphosphonium	231	21	0.41
Methyltriphenylarsonium	238	23	0.47
N-Ethyl-4-methylquinolinium	211	18	0.33
N-*n*-Propyl-4-methylquinolinium	241	25	0.37
N-Ethylacridinium	226	20	0.41
Di-*n*-propylammonium (1 : 2)	206	18	0.43
Methyldi-*n*-propylammonium (1 : 2)	165	13	0.14
Ethyldi-*n*-propylammonium (1 : 2)	203	17	0.47
Tri-*n*-propylammonium (1 : 2)	207	18	0.38

The spectra of the complex salts are exemplified by the methyldi-*n*-propylammonium and tri-*n*-propylammonium salts presented in Fig. 4. They were recorded at 30 and 80 °C respectively. The magnitude of the parameters depends on the size of exciton, which in turn may be expected to depend on the composition of the salt. As a matter of fact, both the zero-field splitting parameters in the simple TCNQ salts are about twice as large as those of the complex salts of a 1 : 2 composition, while those of a 2 : 3 composition come between them.[19] Nevertheless, the difference found with the DCNQ salts is not appreciable at all. We can see that the parameters in the complex salts are

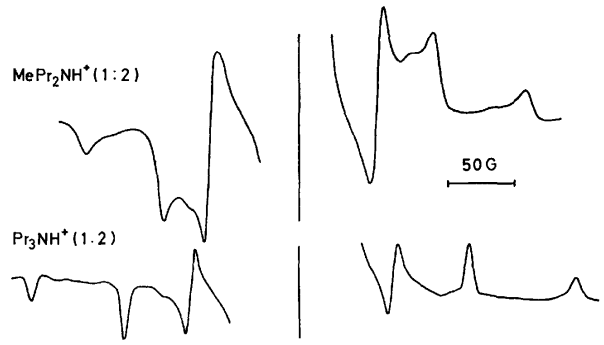

Fig. 4. First derivatives of ESR absorption spectra of the complex methyl di-*n*-propylammonium and tri-*n*-propylammonium DCNQ salts.

only slightly less than those in the simple salts. This observation may imply that the DCNQ anion-radicals in a column do not alternate with the molecules. The repeating unit might be approximated by $(DCNQ)^0$-$(DCNQ)^-$-$(DCNQ)^-$-$(DCNQ)^0$, which is analogous to a tetrad of TCNQ established by the structural analysis of triethylammonium $(TCNQ)_2$.[21] Except for the sodium and methyldi-*n*-propylammonium salts, all the salts have D values over 200 gauss and E values of about 20 gauss. Gordon and Hove have reported that the D parameter of their tetrapropylammonium DDQ salt, 231 gauss, exceeds the largest value ever recorded for the linear-chain radical salts, that is, 215 gauss for $[TMPD^+]_2[Ni(nmt)_2]^{2-}$, where TMPD is *N,N,N',N'*-tetramethyl-*p*-phenylenediamine and where nmt is the dinegative *cis*-1,2-dicyanoethylene-1,2-dithiolate anion, studied earlier by the same author.[20] The D parameter in many of the DCNQ salts matches the value in the DDQ salts or is even larger. Both the simple and complex DCNQ salts undoubtedly belong to the class of ion-radical salts with strong pair-by-pair interactions.

The integrated intensity of the ESR absorption for a triplet state is given by:

$$I \propto T^{-1}[\exp(\Delta E/kT)+3]^{-1},$$

where ΔE is the energy for the singlet-triplet separation. As the shape remains the same through the measured temperature range, the peak-to-peak intensity on the first derivative curve was taken as a measure of I. Because the separation energy was expected to be larger than kT, the following approximation was employed in the present work:

$$I \times T \propto \exp(-\Delta E/kT).$$

Plots of log IT in arbitrary unit *versus* $1/T$ give straight lines, as is demonstrated by the five salts shown in Fig. 5. The open and shaded circles represent the data taken from different pairs. The separation energies of the DCNQ salts also listed in Table 2 are generally larger than those observed with the four DDQ salts (0.19—0.30 eV) and are comparable with the value for the simple morpholinium TCNQ salt reported by Jones and Chesnut (0.41 eV) and also with that reported by Bailey and Chesnut (0.36 eV).[17,18] In this TCNQ salt, the exciton creation energy is so high that, at accessible temperatures, the exciton concentration is too low to enable one to observe any appreciable exciton-exciton

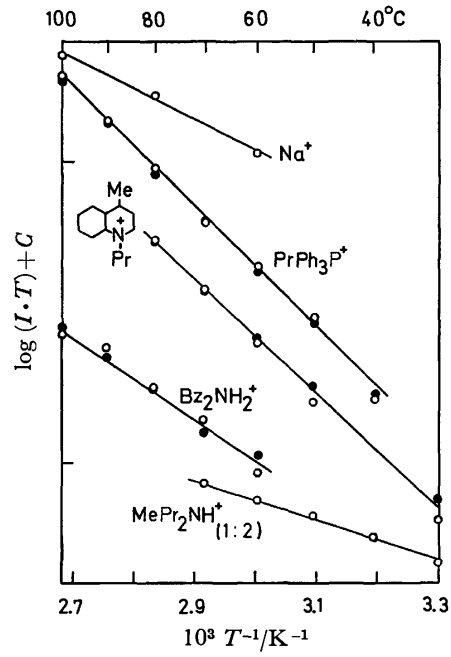

Fig. 5. Temperature dependence of ESR absorption characteristic of triplet excitons in the simple sodium, *n*-propyltriphenylphosphonium, *N*-propyl-4-methyl quinolinium, and dibenzylammonium DCNQ salts and in the complex methyldi-*n*-propylammonium DCNQ salt.

exchange.[15,17] Moreover, the resistivity at room temperature has been reported to be as high as 10^9 ohm cm.[11,12] This feature is quite similar to that of most of the DCNQ salts.

In conclusion, all the properties studied here seem to indicate that 2,3-dicyano-1,4-naphthoquinone was not a good choice for our original purpose of finding a new series of highly-conducting anion-radical salts. However, the salts may be worthwhile for a detailed study of the behavior of the triplet exciton.

References

1) T. Mukherjee and L. A. Levasseur, *J. Org. Chem.*, **30**, 644 (1965).
2) P. Dupuis and J. Néel, *C. R. Acad. Sci. Paris. Sér. C*, **268**, 557 (1969).
3) Y. Matsunaga and Y. Narita, This Bulletin, **45**, 408 (1972).
4) D. Gordon and M. J. Hove, *J. Chem. Phys.*, **59**, 3419 (1973).
5) G. Saito and Y. Matsunaga, This Bulletin, **44**, 1788 (1971).
6) S. Chatterjee, *J. Chem. Soc., B*, **1971**, 2194.
7) Y. Iida, This Bulletin, **45**, 624 (1972).
8) G. A. Reynolds and J. A. VanAllen, *J. Org. Chem.*, **29**, 3591 (1964).
9) K. Wallenfels, G. Bachmann, D. Hofmann, and R. Kern, *Tetrahedron*, **21**, 2239 (1965).
10) P. M. LaFlamme, *Rev. Sci. Instrum.*, **35**, 1193 (1964).
11) L. R. Melby, R. J. Harder, W. R. Hertler, W. Mahler, R. E. Benson, and W. E. Mochel, *J. Amer. Chem. Soc.*, **84**, 3374 (1962).
12) W. J. Siemons, P. E. Bierstedt, and R. G. Kepler, *J. Chem. Phys.*, **39**, 3523 (1963).

13) O. H. LeBlanc, Jr., *J. Chem. Phys.*, **42**, 4307 (1965).
14) D. D. Thomas, H. Keller, and H. M. McConnell, *ibid.*, **39**, 2321 (1963).
15) D. B. Chesnut and W. D. Phillips, *ibid.*, **35**, 1002 (1961).
16) D. B. Chesnut and P. Arthur, Jr., *ibid.*, **36**, 2969 (1962).
17) M. T. Jones and D. B. Chesnut, *ibid.*, **38**, 1311 (1963).
18) J. C. Bailey and D. B. Chesnut, *ibid.*, **51**, 5118 (1969).
19) T. Hibma, P. Dupuis, and J. Kommandeur, *Chem. Phys. Lett.*, **15**, 17 (1972).
20) M. J. Hove, B. M. Hoffman, and J. A. Ibers, *J. Chem. Phys.*, **56**, 3490 (1972).
21) H. Kobayashi, Y. Ohashi, F. Marumo, and Y. Saito, *Acta Crystallogr.*, **B26**, 459 (1970).

An X-Ray Analysis of the Orientational Disorder of *N*-Methylphenazinium-TCNQ

Hayao KOBAYASHI

Department of Chemistry, Faculty of Science, Toho University, Funabashi, Chiba 274

(Received September 4, 1974)

The X-ray diffraction patterns of NMP-TCNQ show diffuse streaks along the c* direction. The analysis of the intensities of these streaks revealed that the orientation of NMP is one-dimensionally disordered along the c axis. The structure obtained indicates that the potential exerting on an electron moving in a column of TCNQ is not random, but can be expressed by a periodic function; this implies that NMP-TCNQ can not be regarded as a disordered one-dimensional conductor. The periodicity of the potential means that the one-dimensional energy band must be filled.

N-Methylphenazinium-7,7,8,8-tetracyanoquinodimethanide (NMP-TCNQ) is one of the highly conducting TCNQ salts. The physical properties of the salt have been intensively investigated.[1] Based on the theorem that the electronic states in any disordered one-dimensional structure are localized, Bloch, Weisman, and Varma (BWV) have explained the temperature dependence of the electrical conductivity of NMP-TCNQ.[2] Their interpretation depends on Fritchie's average structure of NMP-TCNQ[3] and the published electrical conductivity of Shchegolev *et al.*[4] NMP is located at the position of (1/2, 1/2, 1/2), whose site symmetry is $\bar{1}(C_i)$, taking either of the two possible orientations as equally probable (Fig. 1). This disorder seems to be

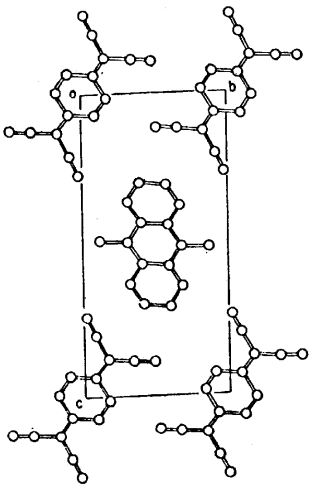

Fig. 1. The avarage structure of NMP-TCNQ.[3]

able to produce a potential which varies randomly along a TCNQ column. The low-temperature conductivity can be approximately fitted by $\ln \sigma \sim (T_0/T)^{1/2}$, derived for a disordered one-dimensional system by the application of the theories of Mott and Ambergaakar, Halperin, and Langer.[2] On the other hand, Heeger *et al.*[1,5,6] regarded NMP-TCNQ as a realization of the one-dimensional Mott-Hubbard model, with the disorder playing only a peripheral role. Their experimental study and analysis of the low-temperature conductivity of high-purity single crystals of NMP-TCNQ revealed that the plot of $\log_{10}(\sigma/\sigma_0)$ *vs.* $1/T$ shows straight-line behavior; this is not consistent with the analysis of BWV. Because of the electron-electron Coulomb repulsion, the electron localizes to from a magnetic insulator at low temperatures. The magnitude of the Hubbard gap goes smoothly to zero at *ca.* 200 K.[6] In this paper, the details of the orientational disorder will be reported in order to contribute to a better knowledge of one-dimensional conductors.

Experimental

The specimens of *N*-methylphenazinium-7,7,8,8-tetracyanoquinodimethanide(NMP–TCNQ: $C_{13}H_{11}N_2 \cdot C_{12}H_4N_4$) was kindly supplied by Ichimin Shirotani, who has paid particular

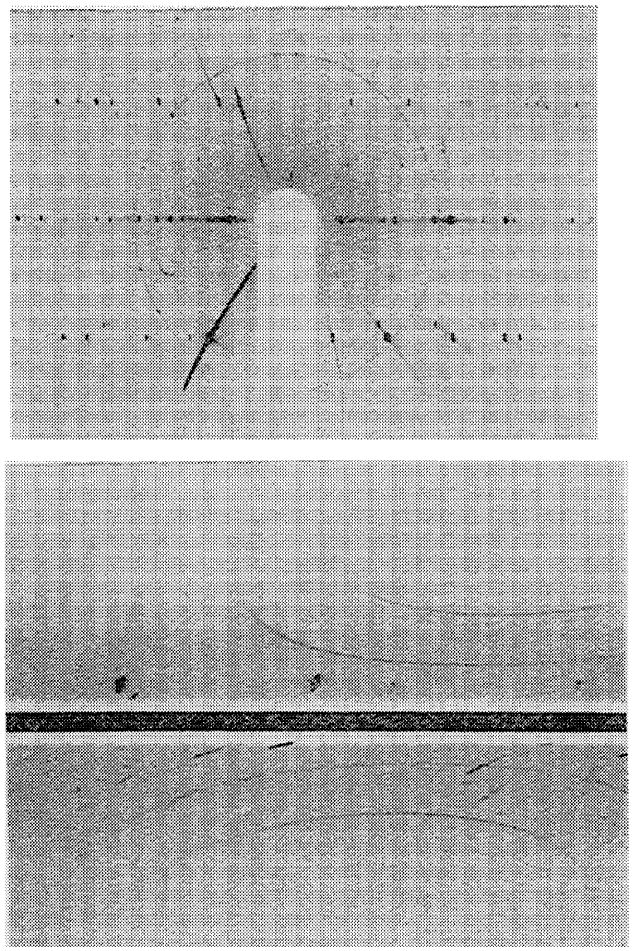

Fig. 2. (a) Oscillation photograph: weak reflections observable in the middle of the strong layer lines
(b) Weissenberg photograph (1/2, η, ζ)

attention to the purification of the samples.[7] The single crystals are black needles, with long axes parallel to the crystallographic a axis. The lattice constants has been reported to be[3]: $a=3.8682$, $b=7.7807$, $c=15.735$ Å, $\alpha=91.67$, $\beta=92.67$, $\gamma=95.38°$ (at 23 °C); space group: $P\bar{1}$. TCNQ and NMP are stacked separately along the a axis to form modadic columns.

Although oscillation and Weissenberg photographs indicated that the intensity distribution of Bragg reflections is the same as that given in Fritchie's paper,[3] a closer examination revealed that diffuse streaks occur along the c* direction in the middle of the strong layer lines around the a axis (Fig. 2). These faint X-ray scatterings were overlooked in an earlier analysis by Fritchie.[3] The streaks appear at the $(h+1/2, k, \zeta)$ position of the reciprocal space, where h and k are integers and where $(h+1/2)\boldsymbol{a}^*+k\boldsymbol{b}^*+\zeta\boldsymbol{c}^*$ is the scattering vector, $\boldsymbol{k}$. The intesities along the streaks vary slowly, and no sharp maxima were observed. Similar streaks were also observed in a Weissenberg photograph of 3/2 layer line around the a axis. All the experiments were performed at room temperature.

Analysis of the Diffuse Streaks and Discussion

The extra reflections indicate: (1) the arrangement of NMP and TCNQ is regular in each a-b layer, but each layer has no correlation to the adjacent layers, and (2) in each a-b layer, the lattice period along the a direction is twice the reported value. Thus, the Fritchie's structure must be regarded as the average structure of the one-dimensionally disordered lattice.

The probable models of the disordered structure could then be easily deduced.

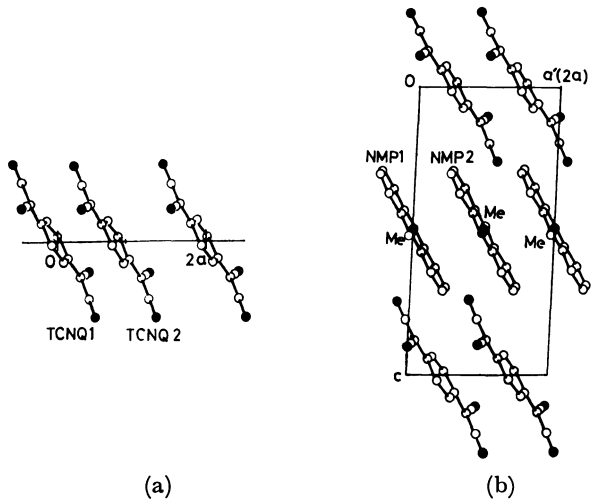

Fig. 3. The models of the molecular arrangement
(a) Model I (rejected) (b) Model II (true)

Model I: TCNQ are not stacked with an equal intermolecular spacing; rather, two different spacings appear alternately, as is found in simple salts of TCNQ[8,9] (Fig. 3a). Each TCNQ is shifted from its position in the average structure by $\varepsilon\boldsymbol{a}$ or $-\varepsilon\boldsymbol{a}$, while the orientation of NMP is disordered in the same way as in the average structure.

Model II: Two possible orientations of NMP alternate along the a axis (Fig. 2). On the other hand, the arrangement of TCNQ is the same as that given by Fritchie.

The important role of the dimeric arrangement of $TCNQ^-$ anions has been previously discussed in connection with the monomer-dimer transition of the simple salts of TCNQ[9] and a Peierls transition of one-dimensional conductors.[10,11] However, Model I can not explain the features of the X-ray diffraction patterns. Based on Model I, the intensities of the streaks are expressed as:

$$I_D(\boldsymbol{k}) = \sum_{ij}\chi_{ij}(f_1-f_2)^2 \exp(i\boldsymbol{k}\boldsymbol{R}_{ij})$$

where $\boldsymbol{R}_{ij}=\boldsymbol{R}_i-\boldsymbol{R}_j$ ($\boldsymbol{R}_i$ is the lattice vector of the i-th lattice point), $\boldsymbol{k}$ is the scattering vector $(\xi\boldsymbol{a}^*+\eta\boldsymbol{b}^*+\zeta\boldsymbol{c}^*)$, χ_{ij} is the correlation function representing the mode of the disorder of the arrangement of TCNQ, and f_1 and f_2 are the scattering factors of TCNQ shifted by $\varepsilon\boldsymbol{a}$ and $-\varepsilon\boldsymbol{a}$ respectively. $I_D(\boldsymbol{k})$ is closely related to the molecular structure factor of TCNQ, because f_1-f_2 can be written as:

$$f_1-f_2 = 2\{\sum_j f_j \cos 2\pi(\xi x_j+\eta y_j+\zeta z_j)\}\sin 2\pi\xi\varepsilon$$

where f_j is the atomic scattering factor of the j-th atom and where (x_j,y_j,z_j) is the atomic coordinate. The general features of the calculated intensity curves do not resemble those of the observed curves. Especially, according to this intensity formula, a very strong streak must be observed at the reciprocal point $(1/2,0,\zeta)$; however, the intensities were, in fact, too weak to be observed. Thus, Model I was rejected.

Using Model II, the structure factors of the disordered lattice can be written as:

$$F(\boldsymbol{k}) = \sum_j\{f_{TCNQ}+(n_j f_{NMP\uparrow}+(1-n_j)f_{NMP\downarrow})\}\exp(i\boldsymbol{k}\boldsymbol{R}_j)$$

where f is a molecular scattering factor; NMP↑ and NMP↓ indicate two types of the orientations of NMP, and n_j is the probability that the orientation of NMP in the j-th cell is that of NMP↑. The corresponding intensity is given by[12]:

$$I(\boldsymbol{k}) = |\langle F(\boldsymbol{k})\rangle|^2 + I_B + I_D$$

where

$$I_B(\boldsymbol{k}) = |\sum_j(f_{TCNQ}+f_{NMP})\exp(i\boldsymbol{k}\boldsymbol{R}_j)|^2$$

and by:

$$I_D(\boldsymbol{k}) = \sum_{jj'}\chi_{jj'}(f_{NMP\uparrow}-f_{NMP\downarrow})^2\exp(i\boldsymbol{k}\boldsymbol{R}_{jj'})$$

where $f_{NMP}=(f_{NMP\uparrow}+f_{NMP\downarrow})/2$, $\langle\ \rangle$ indicates the statistical average and where the correlation function, $\chi_{jj'}$, is expressed as

$$\chi_{jj'} = \langle(n_j-\langle n\rangle)(n_{j'}-\langle n\rangle)\rangle$$

I_B represents the reflections from the lattice with the average structure, which is the same as that derived by Fritchie[3], while I_D is due to the disorder of the crystal. Besides the methyl group, NMP is centrosymmetric. By the use of the atomic parameters of the methyl carbon given by Fritchie, $(f_{NMP\uparrow}-f_{NMP\downarrow})$ may be written simply as:

$$f_{NMP\uparrow}-f_{NMP\downarrow} = 2f_C \sin 2\pi(-0.0328\xi+0.3750\eta+0.0141\zeta),$$

where f_C is the scattering factor of a carbon atom. The correlation function of the orientation of NMP between

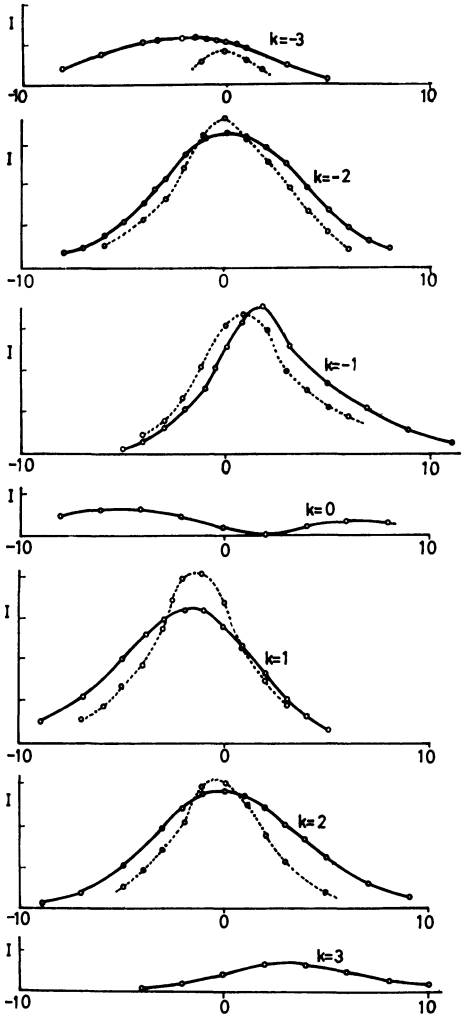

Fig. 4. The observed (broken lines) and calculated (solid lines) intensities of the streaks. The streaks were not observed ($I_{obs}=0$) for $k=0$ and 3. The intensities are plotted as ordinate and the values of ζ as abscissa. Scattering vector $\boldsymbol{k}$ is $\boldsymbol{a}^*/2+k\boldsymbol{b}^*+\zeta\boldsymbol{c}^*$.

i-th and j-th sites ($\boldsymbol{R}_{ij}=n_1\boldsymbol{a}+n_2\boldsymbol{b}+n_3\boldsymbol{c}$) is

$$\chi_{ij}=\begin{cases} 1/4 \cdots n_1=2m \text{ and } n_3=0 \\ -1/4 \cdots n_1=2m+1 \text{ and } n_3=0 \\ 0 \cdots n_3 \neq 0 \end{cases}$$

Because of the orientational disorder, the observed temperature factor of the methyl carbon is very large[3]; it was, therefore, replaced by that of the nitrogen atom of NMP in the calculation of I_D. The observed and calculated intensities of the streaks of the 1/2-layer line ($\xi=1/2$) are compared in Fig. 4. The scale of the observed intensities was adjusted so as to give the best fit to the calculated ones. The comparison was not attempted for the streaks of the 3/2-layer line because of the weakness of the intensities. Considering the roughness of the estimation of the temperature factor, the agreement is satisfactory. Therefore, we may conclude that Model II represents the real structure of NMP-TCNQ.

The molecular arrangement of NMP-TCNQ thus obtained is shown in Figs. 3b and 5. Two orientations of NMP alternate along the a axis, while one fixed orientation is repeated along the b direction. The

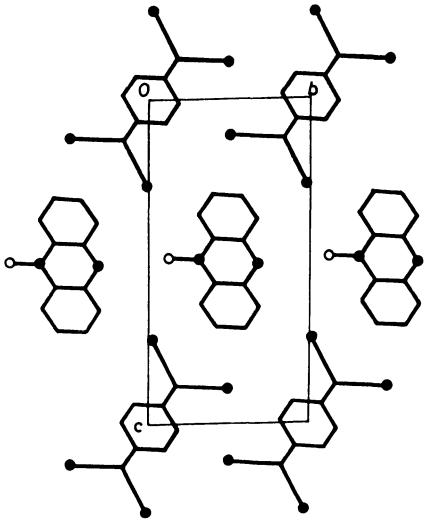

Fig. 5. A regular sequence of NMP along the b axis. This and the other arrangements of NMP with opposite orientations alternate along the a axis to form a regular *a–b* layer. Such regular layers of NMP are randomly correlated with each other along the c axis.

correlation of the orientation dose not exist between NMP, which belong to different *a–b* layers. The unusually short contact of 2.01 Å between two neighbouring methyl carbons which occur randomly in the average structure dose not exist in the real structure. The two-dimensionally ordered molecular arrangement in each *a–b* layer seems to be natural in view of the dipole-dipole interaction between NMP(Fig. 6). There is no direct intermolecular contact of NMP along the c direction. Thus, this type of one-dimensional disorder is very likely to occur in this crystal.

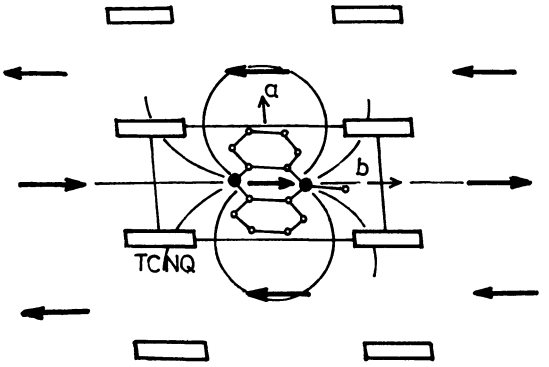

Fig. 6. Schematic drawing of the two-dimensionally ordered arrangement of NMP and TCNQ and an electric field due to a dipole moment of an NMP.

The localized model of BWV has been criticized by Heeger *et al.*,[5,6] Kurkijarvi,[13] and Suezaki.[14] Suezaki suggested the possibility that the randomness in NMP-TCNQ is insufficient to adopt the localized model, since the possible orientations of NMP are restricted in two directions, as has been shown in an earlier crystal structure analysis.[3] From the structural viewpoint, we can show evidence that the localized model of BWV is not suited for the interpretation of the electrical properties of NMP-TCNQ. Let us consider an electric potential being exerted on an electron moving along

a column of TCNQ. Within a simple noninteracting-electron approximation, the Hamiltonian can be written as

$$H(x) = -\frac{\hbar^2}{2m}\frac{\partial^2}{\partial x^2} + \sum_j V_j(x)$$

where V_j is the potential due to the ions in the j-th layer and where x is the coordinate of the electron in this column. Since all ions in each a–b layer are arranged regularly with a period of $2a$(7.736 Å), $V_j(x)$ must be a periodic function:

$$V_j(x+2a) = V_j(x).$$

Therefore, the total potential, $V(x)(=\sum V_j(x))$, is also periodic along the TCNQ column parallel to the a axis. Thus, the localized model of BWV which is based on the assumption of the random potential along the column of TCNQ can not be adopted in the interpretation of the electrical properties of NMP-TCNQ. In addition, based on this periodicity of the potential function $V(x)$, it is easy to see that there are some difficulties in the application of the one-dimensional half-filled-band Hubbard model proposed by Heeger *et al.*[1,6] Because the periodic unit is $2a$, the Bloch function $\phi(x)$ can be given as:

$$\phi(x) = \exp(ikx)u_k(x)$$
$$-\pi/2a < k \leqq \pi/2a$$

The corresponding energy band is shown schematically in Fig. 7a. There are two excess electrons in each periodic unit, so the band must be filled. Therefore, NMP-TCNQ must be semiconductive, even if the electron-electron Coulomb repulsion is small (the electron-electron Coulomb repulsion produces a Hubbard gap in a half-filled-band Hubbard model (Fig. 7b)[15]). This conclusion is qualitatively consistent with the observed low-temperature conductivities of this salt.[1]

The orientational disorder of cations has also been found in the crystals of ARD-$TCNQ_2$[11] and Q-$TCNQ_2$[16], which are also highly conducting salts. However, no X-ray diffuse streaks have been observed. The modes of the arrangement of cations in these crystals are similar to each other, but they do not resemble that of NMP-TCNQ. According to BWV, the electronic properties of these salts can also be interpreted by means of the localized model. In the crystals of ARD-$TCNQ_2$ and Q-$TCNQ_2$, the cations are stacked to form monadic columns of ARD and Q respectively. As is shown in Fig. 8, however, these columns of cations are surrounded by six TCNQ columns and have no direct contact between them. Therefore, the features of the orientational disorder in these complex salts are probably different from those in the simple NMP-TCNQ salt described above.

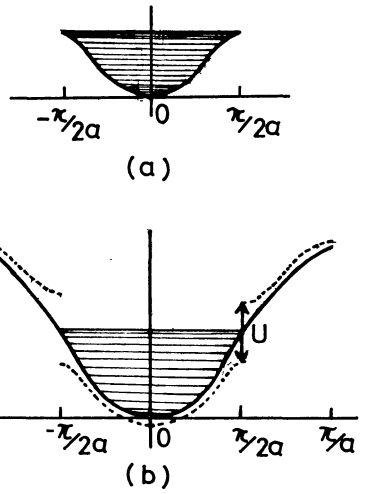

Fig. 7. Schematic drawing of the band structure of NMP-TCNQ.
(a) A filled band of one dimensionally disordered structure of NMP-TCMQ.
(b) A half-filled band of the average structure of NMP-TCNQ. Broken lines indicate the band structure in the presence of the electronic correlation and U is the magnitude of a Hubbard gap.

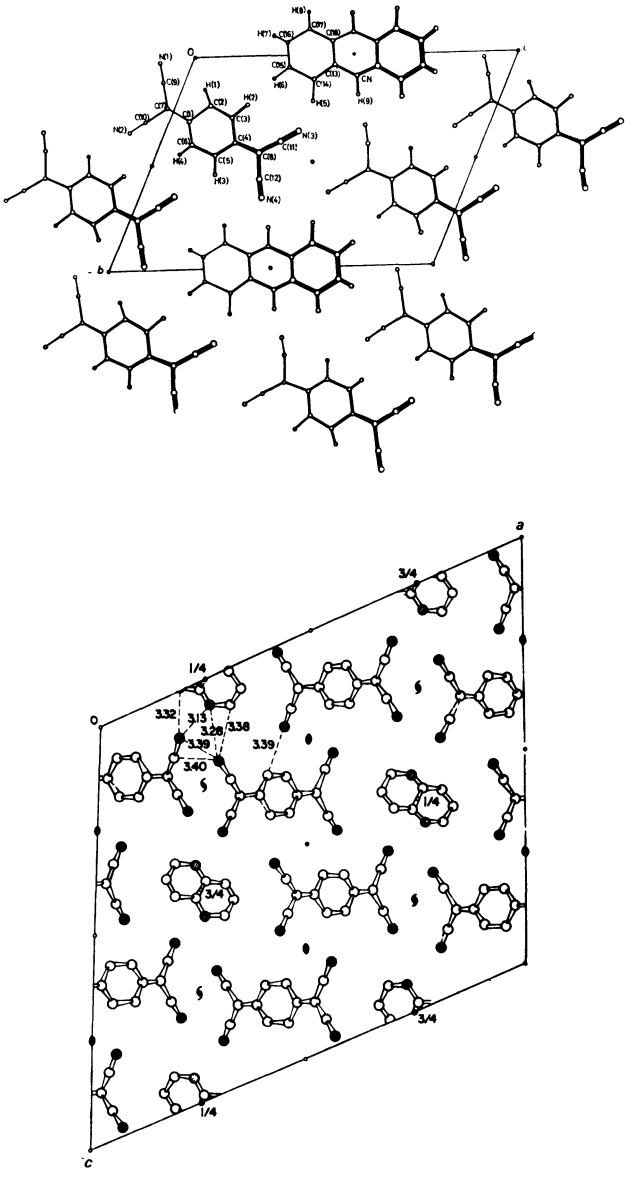

Fig. 8. The structures of ARD-$TCNQ_2$ and Q-$TCNQ_2$.
(a) ARD-$TCNQ_2$[10] (b) Q-$TCNQ_2$[15]

The author wishes to express his thanks to Dr. Ichimin Shirotani for kindly supplying the specimens and also much valuable information.

References

1) A. J. Epstein, S. Etemad, A. F. Garito, and A. J. Heeger, *Phys. Rev.*, **B5**, 952 (1971).
2) A. N. Bloch, R. B. Weisman, and C. M. Varma, *Phys. Rev. Lett.*, **28**, 753 (1972).
3) C. J. Fritchie, *Acta Crystallogr.*, **20**, 892 (1966).
4) I. F. Shchegolve, L. I. Buravov, A. V. Zvarykina, and R. B. Lyubovskii, *JETP Lett.*, **8**, 218 (1968).
5) E. Ehrenfreund, S. Etemad, L. B. Coleman, E. F. Rybaczewski, A. F. Garito, and A. J. Heeger, *Phys. Rev. Lett.*, **29**, 269 (1972).
6) L. B. Coleman, J. A. Cohen, A. F. Garito, and A. J. Heeger, *Phys. Rev.*, **B7**, 2122 (1973).
7) Preparation of NMP-TCNQ will be reported elswhere by I. Shirotani, A. Onodera, H. Anzai, S. Hashimoto, Y. Kamura, and H. Inokuchi.
8) A. Hoekstra, T. Spoelder, and A. Vos, *Acta Crystallogr.*, **B28**, 14 (1972).
9) H. Kobayashi, This Bulletin, to be published
10) R. A. Craven, M. B. Salamon, G. DePasquali, R. M. Herman, G. Stucky, and A. Schultz, *Phys. Rev. Lett.*, **32**, 769 (1974); M. J. Rice, and S. Strassler, *Solid State Commun.*, **13**, 125 (1973).
11) H. Kobayashi, This Bulletin, **47**, 1346 (1974).
12) H. Kobayashi, *ibid.*, **46**, 2675 (1973).
13) J. Kurkijarvi, *Phys. Rev.*, **B8**, 922 (1973).
14) Y. Suezaki, *Butsuri*, **29**, 404 (1974).
15) H. Shiba, *Bussei*, **13**, 615 (1972).
16) H. Kobayashi, F. Marumo, and Y. Saito, *Acta Crystallogr.*, **B27**, 373 (1971).

Electron Transfer Reaction in the Triplet State. Role of Ferrocene as an Electron Donor

Koichi KIKUCHI, Hiroshi KOKUBUN, and Masae KIKUCHI*

Department of Chemistry, Faculty of Science, Tohoku University, Aoba, Aramaki, Sendai 980

* *The Research Institute for Iron, Steel and other Metals, Tohoku University, Katahira, Sendai 980*

(Received November 20, 1974)

Quenching of the triplet state of methylene blue by ferrocene and *p*-phenylenediamine in ethanol has been investigated by an emission-absorption flash technique. The triplet dye is quenched by ferrocene and *p*-phenylenediamine at a diffusion-controlled rate, yielding the semi-reduced dye. Efficiency of the semi-reduced dye formation is 0.09 and 1.0 for ferrocene and *p*-phenylenediamine, respectively. Since the triplet level of the dye is lower than that of ferrocene, quenching of the triplet dye by ferrocene seems to occur through the charge (electron) transfer interaction.

Many triplets of aromatic compounds are quenched by ferrocence (F) at a diffusion-controlled rate.[1-3] However, the quenching mechanism has not been elucidated because the triplet level of F[4-6] remained obscure.

Fry *et al.*[1] studied the quenching rate of some triplets by F with a conventional flash technique, and presumed that quenching is due to the formation of a short-lived charge transfer complex, because they could not observe any transient absorption attributable to the addition of F.

We measured quenching rate constants by F for several triplets with levels located in the range 8000—23800 cm^{-1},[7] and studied the triplet energy transfer for the eosin-tetracene-ferrocene mixed system. It was concluded that the triplet level of F is 15000 ± 1000 cm^{-1} and the lifetime of triplet F shorter than 1 μs. Thus, it is obvious that the triplet with level higher than 15000 cm^{-1} is mainly quenched by triplet energy transfer to F and that with level lower than 15000 cm^{-1} is quenched by some other mechanism. Since the oxidation potential of F is low,[8] it is anticipated that charge transfer interaction plays an important role.

In order to show this role, quenching of the lowest triplet state of methylene blue ($^3D^+$) by F has been studied by an emission-absorption flash technique.[9] Since the dye (D^+) has a low reduction potential[10] and a triplet level lower than that of F, it is considered to be the most appropriate for the purpose. Quenching by *p*-phenylenediamine (P) has been also studied for comparison.

Experimental

Materials. Ferrocene (G. R. grade, Tokyo Kasei) was recrystallized from benzene, zone refined, and sublimated. Methylene blue (G. R. grade, Merck) was recrystallized from *n*-butanol. *p*-Phenylenediamine (E. P. grade, Tokyo Kasei) was recrystallized twice from ethanol and used immediately after sublimation. Ethanol (G. R. grade, Wako Jun-yaku) was used without further purification.

Apparatus and Procedure. Flash energy was controlled in the range 56—130 J its half duration being about 10 μs. A Toshiba V-O51 filter was used for exciting the dye only. A Q-switched ruby laser provides a 15 ns pulse of about 0.15 J. All measurements were made at room temperature. Ethanol solutions were degassed by repeating bulb-to-trap-distillation in vacuum.

Results and Discussion

Two transient absorption spectra obtained when the deaerated solution of the dye was flashed are shown in

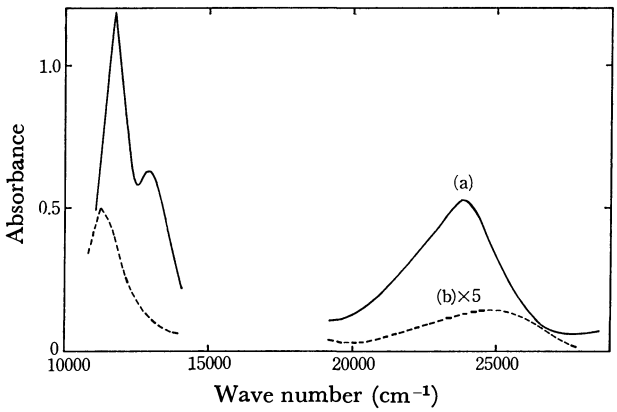

Fig. 1. Transient absorption spectra of methylene blue in deaerated ethanol (10^{-5} M). (a) triplet, (b) long-lived intermediate (5 ms after flashing).

Fig. 1. Spectrum (a) is attributed to the T–T absorption of the dye because of its close resemblance to the spectrum in literature.[11,12] The decay is nearly

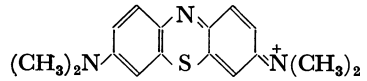

methylene blue (D^+)

of first order, but its rate increases with increasing dye concentration. This is apparently due to the D–D mechanism given by Koizumi *et al.*[13] The result is consistent with that of steady light illumination.[14] The observed rate constant is linear with respect to dye concentration (Fig. 2).

$$k_{obsd} = k_t = k_0 + k[D]$$

From the intercept and the slope we obtain

$$k_0 = 2.2 \times 10^3\ s^{-1}$$

$$k = 4.5 \times 10^8\ M^{-1} \cdot s^{-1}.$$

Spectrum (b) (Fig. 1) was observed after the disappearance of the T–T absorption spectrum (a) and seems to be that of the protonated semireduced dye ($DH^{\ddagger}$), since the spectral shape accords substantially with the

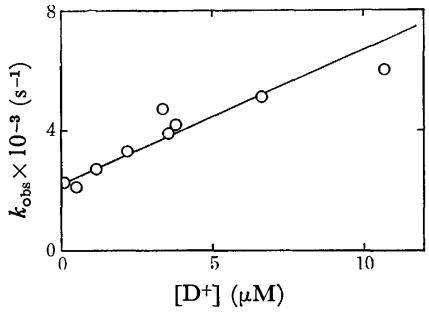

Fig. 2. The dependence of the observed first order decay constant of the triplet methylene blue on dye concentration.

reported one.[15] The decay of DH‡ is not reproducible, and the lifetime is much longer than 1 ms. The absorption spectrum of the dye changes slightly with repeated flashing.

The decay rate constant of the triplet dye increases linearly with F concentration.

$$k_{obsd} = k_t + k_F[F]$$

From the slope we obtain

$$k_F = 4.5 \times 10^9\ M^{-1} \cdot s^{-1}.$$

For F concentrations higher than 10^{-4} M (Fig. 3), quite a different spectrum (a) completely replaces the T–T absorption spectrum. The spectrum decays as a first order process to produce a long-lived absorption spectrum (b), but the decay rate is not reproducible.

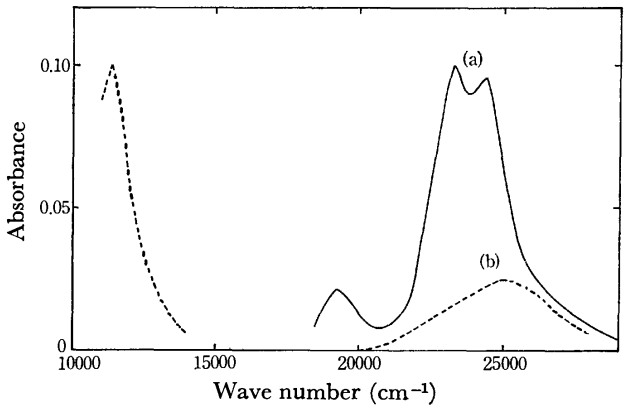

Fig. 3. Transient absorption spectra of methylene blue (5×10^{-6} M) in ethanol containing 10^{-4} M ferrocene. (a) immediately after flashing, (b) 1 ms after flashing.

With the addition of an efficient electron donor, P, the decay of the triplet dye also increases. For P concentrations higher than 10^{-4} M (Fig. 4), spectrum (a) was observed instead of the T–T absorption spectrum. The spectrum decays in first order, giving a long-lived absorption spectrum (b). The decay of the long-lived absorption is not reproducible.

The transient absorption spectrum (a) in Fig. 3 is similar to the spectrum of the semireduced dye (D·) in a basic solution.[11,15] The transient absorption spectra (a) shown in Figs. 3 and 4 resemble each other, the latter having an additional absorption peak at *ca.* 500 nm. The absorption spectrum of P cation radical (P‡)[16] was obtained by flashing the aerated ethanol

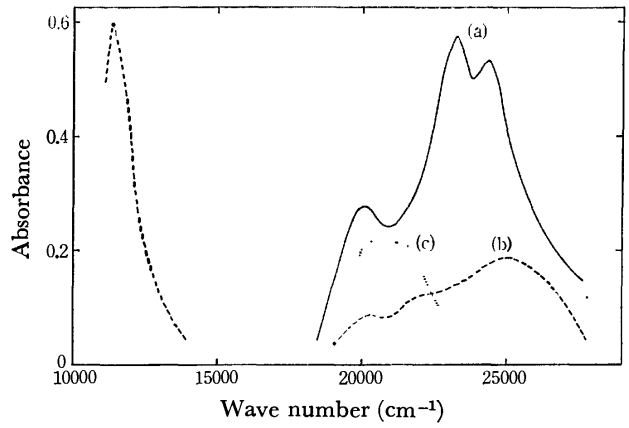

Fig. 4. Transient absorption spectra of methylene blue (5×10^{-6} M) in ethanol containing 10^{-4} M *p*-phenylenediamine. (a) immediately after flashing, (b) 1 ms after flashing. (c) The spectrum of *p*-phenylenediamine cation radical in ethanol is drawn for comparison.

solution of P (Fig. 4(c)). It is obvious that the spectrum (Fig. 4(a)) consists of the superposition of D· and P‡.

The spectra (b) shown in Figs. 1, 3, and 4 are similar to the spectrum of DH‡. Since pK_a of D· is 9.0,[15] it might be protonated in ethanol as in other basic compounds such as proflavine.[17] Thus, spectra (a) and (b) in Fig. 3 can be assigned respectively to D· and DH‡, since the contribution of F added to absorbance in this wavelength region is negligible owing to the small molar extinction coefficients of F and its cation radical (F‡).[18] The absorbance of DH‡ increases at the expense of that of D·, implying that the protonation is the main decay process of D·. The fact that the decay rate of D· is not reproducible can be interpreted as a result of unregulated proton concentration. No transient absorption was observed by flashing the aerated solution of the dye. However, the transient absorption spectra (a) in Figs. 3 and 4 were observed in the aerated solution containing F and P, respectively. These spectra decay as a second order process to reproduce the dye. The spectrum of DH$^+$ was not observed in either case. The results suggest that D· is stable against oxygen, and that DH‡ may react with oxygen as follows,

$$DH^\ddagger + O_2 \longrightarrow D^+ + HO_2\cdot$$

The absorption and fluorescence spectra are not affected by the addition of F or P. Hence, the reaction state of the dye is the lowest triplet state alone. The scheme can thus be summarized as follows.

$$\begin{aligned}
&(1)\ D^+ \xrightarrow{I_{ab}\phi_{ST}} {}^3D^+ \\
&(2)\ {}^3D^+ \longrightarrow D^+ \\
&(3)\ {}^3D^+ + D^+ \longrightarrow D\cdot + D^{\ddagger +} \quad k_t \\
&(4)\ {}^3D^+ + O_2 \longrightarrow D^+ + {}^1O_2{}^* \quad k_0[O_2] \qquad \Big\} k_{dt} \\
&(5)\ {}^3D^+ + F \longrightarrow D\cdot + F^\ddagger \quad k_F{}^r \\
&(6)\ {}^3D^+ + F \longrightarrow D^+ + F \qquad \Big\} k_F \\
&(7)\ {}^3D^+ + P \longrightarrow D\cdot + P^\ddagger \quad k_P{}^r \\
&(8)\ {}^3D^+ + P \longrightarrow D^+ + P \qquad \Big\} k_P
\end{aligned}$$

The semi-oxidized dye ($D^{\ddagger+}$) produced by process (3) has an absorption peak at *ca.* 520 nm.[11] This may interpret the fact that spectrum (b) in Fig. 1 is significantly swelled at about 500 nm compared with spectrum (b) in Fig. 3.

The yield of D· at the end of a flash is related with the total quantity of light absorbed during one flash by

$$\int d[D] \equiv [D\cdot]_0 = \phi_{ST}\cdot\frac{k_Q{}^r[Q]}{k_{dt}+k_Q[Q]}\cdot\int I_{ab}dt \qquad (1)$$

where Q indicates F or P and the subscript "0" stands for the quantity immediately after flashing. The time integrated fluorescence intensity measured at λ' during a flash is given by

$$\int I_f(\lambda')dt = \alpha\phi_f\int I_{ab}dt \qquad (2)$$

When Q is F, the transient absorption spectrum (a) in Fig. 3 is entirely attributable to D·. Thus, from Eqs. (1), (2), and the relation

$$D_0(\lambda) = \varepsilon(\lambda)[D\cdot]_0 d \qquad (3)$$

we obtain

$$\frac{\int I_f(\lambda')dt}{D_0(\lambda)} = \frac{\alpha\phi_f}{\varepsilon(\lambda)d\cdot\phi_{ST}}\cdot\frac{k_F}{k_F{}^r}\left(1+\frac{k_{dt}}{k_F}\cdot\frac{1}{[F]}\right) \qquad (4)$$

where $D(\lambda)$ and $\varepsilon(\lambda)$ are the absorbance and the molar extinction coefficient of D· at wavelength λ, respectively, and d=10 cm. When Q is P, the transient absorption is composed of D· and $P^{\ddagger}$. As the concentration of $P^{\ddagger}$ is equal to that of D·, the following relation holds instead of Eq. (3).

$$\begin{aligned} D_0(\lambda) &= \{\varepsilon(\lambda)[D\cdot]_0+\varepsilon'(\lambda)[P^{\ddagger}]_0\}d \\ &= \{\varepsilon(\lambda)+\varepsilon'(\lambda)\}[D\cdot]_0 d \end{aligned} \qquad (5)$$

where $\varepsilon'(\lambda)$ is the molar extinction coefficient of $P^{\ddagger}$ at λ. $\int I_f(720)dt$ and $D_0(420)$ were measured at various F and P concentrations. The results are given in Table 1. $\int I_f(\lambda')dt/D_0(\lambda)$ is plotted against the reciprocals of F and P concentration in Fig. 5. From the plots we have

$$k_{dt}/k_F = 7.4\times10^{-4}\,M \qquad (6)$$

$$k_{dt}/k_P = 7.3\times10^{-4}\,M \qquad (7)$$

TABLE 1. YIELDS OF THE SEMIREDUCED DYE AND TIME INTEGRATED FLUORESCENCE INTENSITY

	$D_0(420)$	$\int I_f(720)dt$	$\int I_f(720)dt/D_0(420)$
[F]			
1.02×10^{-4}M	0.013_8	5.7	41_3
2.0×10^{-4}	0.023_4	5.7	24_4
3.06×10^{-4}	0.030_0	5.7	19_0
4.0×10^{-4}	0.041_6	5.6	13_4
5.1×10^{-4}	0.043_5	5.5	12_6
6.0×10^{-4}	0.048_1	5.4	11_2
[P]			
8.87×10^{-5}	0.096	5.5	$57._3$
1.43×10^{-4}	0.15_4	5.5	$35._7$
2.21×10^{-4}	0.20_8	5.4	$25._9$
4.44×10^{-4}	0.29_4	5.0	$17._0$
9.53×10^{-4}	0.41_6	4.5	$10._8$
1.33×10^{-3}	0.47_6	4.3	$9._0$

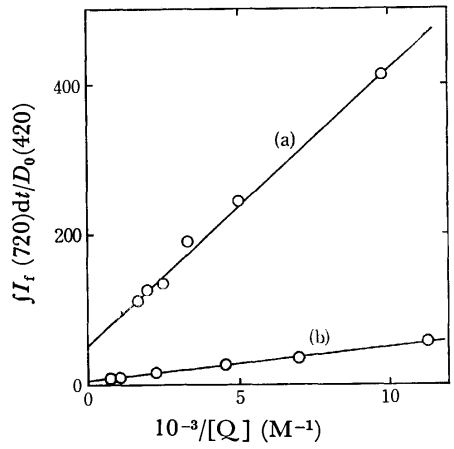

Fig. 5. The plot of $\int I_f(\lambda')dt/D_0$ (λ) *vs.* 1/[Q].
(a) Q: ferrocene, (b) Q: *p*-phenylenediamine.

The decay rate of the triplet dye in the aerated solution was measured by using a Q-switched ruby laser.

$$k_{dt} = k_t + k_0[O_2] = 3.7\times10^6\,s^{-1} \qquad (8)$$

From Eqs. (6), (7), and (8), we have

$$k_F = 5.0\times10^9\,M^{-1}\cdot s^{-1}$$

$$k_P = 5.1\times10^9\,M^{-1}\cdot s^{-1}$$

The value of k_F agrees with that (k_F=$4.5\times10^9\,M^{-1}\,s^{-1}$) obtained from the effect of F concentration on the triplet decay.

It should be noted that the yield of D· is larger for P than for F (Table 1). This indicates that the rate constant of the formation of D·, $k_P{}^r$, is larger than $k_F{}^r$, because the rate constants of the triplet quenching by P and F are nearly equal.

The efficiency of D· formation, $k_P{}^r/k_P$ and $k_F{}^r/k_F$, was estimated as follows. In the deaerated solution, the absorbance of the T–T absorption immediately after flashing is expressed by

$$\left[\frac{D_0{}^T(\lambda)}{\int I_f(\lambda')dt}\right] = \varepsilon^T(\lambda)d\cdot\frac{\phi_{ST}}{\alpha\phi_f} \qquad (9)$$

where $D^r(\lambda)$ and $\varepsilon^T(\lambda)$ are the absorbance and the molar extinction coefficient of the T-T absorption, respectively. For F concentration higher than 10^{-4} M, the T–T absorption spectrum is replaced by the spectra of D·, because the triplet dye reacts rapidly with F ($k_F[P]\gg k_{dt}$). The following relation is then obtained from Eqs. (4) and (9).

$$\frac{k_F{}^r}{k_F} = \frac{[D_0(\lambda)/\int I_f(\lambda')dt]_F}{[D_0{}^T(\lambda)/\int I_f(\lambda')dt]}\cdot\frac{\varepsilon^T(\lambda)}{\varepsilon(\lambda)} \qquad (10)$$

For P concentration higher than 10^{-4} M, we have also

$$\frac{k_P{}^r}{k_P} = \frac{[D_0(\lambda)/\int I_f(\lambda')dt]_P}{[D_0{}^T(\lambda)/\int I_f(\lambda')dt]}\cdot\frac{\varepsilon^T(\lambda)}{\varepsilon(\lambda)+\varepsilon'(\lambda)} \qquad (11)$$

The molar extinction coefficients were obtained by completely converting the dye into the triplet state or D·.

$$\varepsilon^T(825) = 1.6_5\times10^4\,M^{-1}\cdot cm^{-1}$$

$$\varepsilon(420)+\varepsilon'(420) = 1.1\times10^4\,M^{-1}\cdot cm^{-1}$$

The molar extinction coefficient of D· was estimated by correcting the absorption of P^{+}.

$$\varepsilon(420) = 9.4 \times 10^3\ M^{-1}\cdot cm^{-1}$$

$D_0(420)$ and $D_0^T(825)$ are plotted against $\int I_f(720)dt$ in Fig. 6. From the slope of the plots, we have

$$[D_0(420)/\int I_f(720)dt]_F = 0.009$$

$$[D_0(420)/\int I_f(720)dt]_P = 0.12$$

$$[D_0^T(825)/\int I_f(720)dt] = 0.18$$

From these values and the molar extinction coefficients obtained above and with the aid of Eqs. (10) and (11), we obtain

$$k_P^r/k_P = 1.0$$

$$k_F^r/k_F = 0.09$$

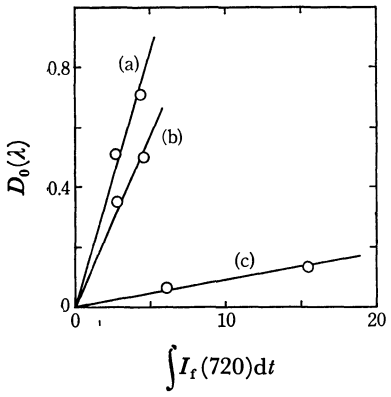

Fig. 6. The plot of $D_0(\lambda)$ and $D_0^T(\lambda)$ *vs.* $\int I_f(\lambda')d\lambda'$.
(a) $D_0^T(825)$, (b) $D_0(420)$: *p*-phenylenediamine, (c) $D_0(420)$: ferrocene.

It was suggested[7] that quenching of the triplet whose level is lower than 15000 cm^{-1} by F is due to the charge transfer interaction. However, we could not directly demonstrate quenching by the charge transfer interaction, since all the triplets studied did not give any new transient absorption in the case of quenching by F. The triplet level of the dye is 11650 cm^{-1} [19] and its reduction potential 0.008 V (*vs.* S.C.E.)[10] in aqueous solution at pH=7. The oxidation potentials of F and P in acetonitrile are 0.30[8] and 0.185 V (*vs.* S.C.E.),[20] respectively. According to the method of Rehm and Weller,[21] the changes of free enthalpy (ΔG) involved in the electron transfer reaction from F and P to the triplet dye were estimated both as $\Delta G < -20$ kcal/mol. The result suggests that the triplet dye must be quenched by F and P at a diffusion-controlled rate, which agrees well with the experimental results described above. In addition, the electron transfer reaction from F to the triplet dye, though its efficiency is small, has been confirmed. It can thus be shown that the charge (electron) transfer interaction plays an important role on the triplet quenching by F. The fact that the efficiency of electron transfer reaction from F to the triplet dye is small suggests that the lifetime of encounter complex of the triplet dye and F is too short to react. It can therefore be supposed that the triplet quenching of an aromatic compound whose triplet level is lower than 15000 cm^{-1} by F is ascribed to the instantaneous formation of the charge transfer complex.

Consequently, F can act as an electron donor for the triplet quenching by charge transfer interaction, but the efficiency of the electron transfer reaction is generally very small.

M. K. wishes to express her thanks to Professor Masao Honma for his kind guidance and encouragement in the course of the work.

References

1) A. J. Fry, R. S. H. Liu, and G. S. Hammond, *J. Amer. Chem. Soc.*, **88**, 4781 (1966).
2) M. L. Bhaumik and M. A. El-Sayed, *J. Phys. Chem.*, **69**, 275 (1965).
3) R. B. Cundall, G. B. Evans, and E. J. Land, *ibid.*, **73**, 3982 (1969).
4) D. R. Scott and R. S. Becker, *J. Amer. Chem. Soc.*, **35**, 516 (1961).
5) A. T. Armstrong, F. Smith, E. Elder, and S. P. McGlynn, *J. Chem. Phys.*, **46**, 4321 (1967).
6) J. J. Smith and B. Meyer, *ibid.*, **48**, 5436 (1968).
7) M. Kikuchi, K. Kikuchi, and H. Kokubun, This Bulletin, **47**, 1339 (1974).
8) T. Kuwata, D. E. Bublitz, and G. Hoh, *J. Amer. Chem. Soc.*, **82**, 5811 (1960).
9) K. Kikuchi, H. Kokubun, and M. Koizumi, This Bulletin, **41**, 1545 (1968), *Photochem. Photobiol.*, **7**, 499 (1968).
10) H. W. Meyer and W. D. Treadwell, *Helv. Chim. Acta*, **35**, 1444 (1952).
11) S. Kato, M. Morita, and M. Koizumi, This Bulletin, **37**, 117 (1964).
12) J. Faure, R. Bonneau, and J. Joussot-Dubien, *Photochem. Photobiol.*, **6**, 331 (1967).
13) Y. Usui, K. Itoh, and M. Koizumi, This Bulletin, **38**, 1015 (1965), N. Kosui, K. Uchida, and M. Koizumi, *ibid.*, **38**, 1958 (1965).
14) Y. Usui, *ibid.*, **38**, 206 (1965).
15) R. Bonneau, J. Faure, and J. Joussot-Dubien, *Ber. Bunsenges. Physik. Chem.*, **72**, 263 (1968).
16) K. Kimura, K. Yoshinaga, and H. Tsubomura, *J. Phys. Chem.*, **71**, 4485 (1967).
17) J. Ferguson and A. W. H. Mau, *Chem. Phys. Lett.*, **17**, 543 (1972).
18) G. Wilkinson, M. Rosenblum, M. C. Whiting, and R. B. Woodward, *J. Amer. Chem. Soc.*, **74**, 2125 (1952).
19) K. Gollnick, *Ann. N. Y. Acad. Sci.*, **171**, 89 (1970).
20) V. Dvorak, I. Nemec, and J. Zyka, *Microchem. J.*, **12**, 324 (1967).
21) D. Rehm and A. Weller, *Ber. Bunsenges. Phys. Chem.*, **73**, 834 (1969).

The Quenching of the Cadmium Resonance Radiation at 326.1 nm by Some Aliphatic Amines and the Cadmium-sensitized Luminescence of These Amines

Shunzo YAMAMOTO and Shin SATO*

Department of Chemistry, Faculty of Sciences, Okayama University, Tsushima, Okayama 700
** Department of Applied Physics, Tokyo Institute of Technology, Ookayama, Meguro-ku, Tokyo 152*

(Received November 21, 1974)

From the pressure dependence of the intensity of the 326.1 nm resonance line, the efficiencies of the quenching of the resonance line by methylamine, ethylamine, *n*-propylamine, *n*-butylamine, *sec*-butylamine, *tert*-butylamine, diethylamine, and triethylamine were estimated to be 14.2, 36.0, 58.6, 71.2, 116.7, 434.5, 69.6, and 66.0 respectively, the efficiency of ammonia being assumed to be unity. The relative values of rate constants for the formation of excited complexes between the excited cadmium atoms and the amines, and the wavelengths at the peaks of the emission bands from the complexes, were measured. The quantum yields of luminescence were also measured by comparing the integrated intensities of the emission bands with the decrease in the intensities of the resonance line at 326.1 nm upon the addition of amines. From the relationship between these values and the structure of the amines, it is concluded that the complexes are of the charge-transfer type.

In a previous study[1] of the cadmium-sensitized reaction of rare gases and nitrogen, we indicated that the $Cd(^3P_0)$ state is produced by collisions between $Cd(^3P_1)$ atoms and rare gases or nitrogen, and that, at pressures higher than a few Torr of foreign gases, an equilibrium is established between the 5 $^3P_1$ and 5 $^3P_0$ states. Therefore, in spite of the fact that Morten *et al.*[2] described the emitting species in the cadmium-sensitized luminescence of ammonia as being produced by the reaction between $Cd(^3P_0)$ atoms and ammonia, it is impossible to distinguish between $Cd(^3P_1)$ and $Cd(^3P_0)$ atoms as precursors of the emitting species.

In an earlier study of the quenching of the resonance radiation at 326.1 nm by ammonia,[3] we proposed a mechanism by which an unstabilized complex, produced from the excited cadmium atoms ($Cd(^3P_1)$ or $Cd(^3P_0)$) and ammonia, is partly decomposed to the original excited cadmium atoms and ammonia and is partly stabilized by collisions with third bodies. Since a back reaction exists, the Stern-Volmer plots for the quenching of the 326.1 nm resonance line deviate from a straight line in the low-pressure region. If other molecules more complex than ammonia can form the emitting species, and if the back reaction is not so important, we shall not be able to observe the second-order pressure dependence of the Stern-Volmer plots in the low-pressure region, as in the case of ammonia. The present paper will report the results of a study of the cadmium-sensitized luminescence of some aliphatic amines and their quenching for the 326.1 nm resonance line.

Experimental

The apparatus and procedure were the same as those previously described.[3-5] The reaction cell and the cadmium resonance lamp were kept in an electric furnace at 220 ± 1 °C. The vapor pressure of cadmium at 220 °C is 1.04×10^{-3} Torr. The lamp was operated by an alternating current (50 Hz).[1]

The cadmium metal used was high-purity cadmium (99.9999%) manufactured by the Osaka Asahi Metal Co. Pure-grade methylamine and ethylamine were used after degassing at the temperature of liquid nitrogen. Other amines (G.R. grade) were used after drying by calcium hydride and repeated trap-to-trap distillation. Pure-grade argon was used after repeated adsorption and desorption on a molecular sieve at the temperature of liquid nitrogen. In order to minimize the pressure dependence of the absorption intensity, the amines were diluted with argon, and the total pressure in the reaction cell was kept constant.

In order to estimate the quantum yields of the luminescence, the dependence of the sensitivity on the wavelength for the monochromator/photomultiplier combination was determined by using a tungsten lamp operated at 2307 K, using the emissivity data of tungsten presented by de Vos.[6]

Results

In order to estimate the efficiency of the quenching of the 326.1 nm resonance line by amines, the emission intensity at 326.1 nm was measured as a function of the pressure of amines. The Stern-Volmer plots are shown in Fig. 1, where $I_{326.1}{}^0$ and $I_{326.1}$ are the emission intensities at 326.1 nm in the absence and in the presence of amines respectively. On the assumption that 100 Torr carbon dioxide quenches the 326.1 nm resonance line completely,[1] the scattered-light intensity at 326.1 nm was estimated to be less than 0.2% of the $I_{326.1}{}^0$ and thereafter it was neglected. As the intensity, $I_{326.1}$, decreased with the increase in the irradiation time because of the influence of reaction products (one of them may be hydrogen[4]), the intensities shown in Fig. 1 were obtained by extrapolation to zero irradiation time. As has been described previously,[3] the plots obtained with ammonia do not lie on a straight line. However, the plots for the other amines from typical Stern-Volmer plots (straight lines, the intercepts of which

TABLE 1. HALF-QUENCHING PRESSURE FOR THE QUENCHING OF 326.1 nm RESONANCE LINE

Amine	Torr	Amine	Torr
Ammonia	12.6	*sec*-Butylamine	0.108
Methylamine	0.885	*tert*-Butylamine	0.029
Ethylamine	0.350	Diethylamine	0.181
n-Propylamine	0.215	Triethylamine	0.191
n-Butylamine	0.177		

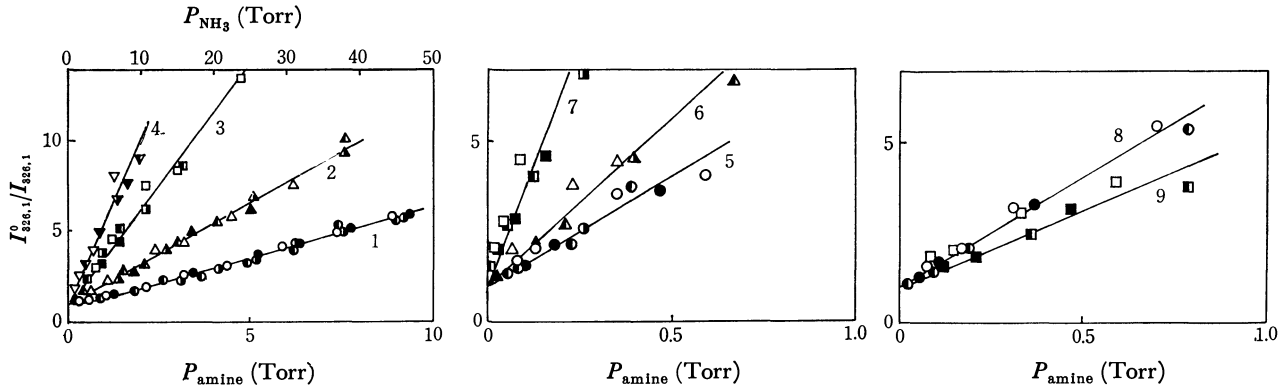

Fig. 1. Stern-Volmer plots for the quenching of the resonance radiation at 326.1 nm by amines diluted with argon. 1) ammonia; Total pressures are 208 (○), 175 (◐), 147 (◑), and 123 (●) in Torr. 2) methylamine; 106 (△), 70 (▲), 48 (▲), and 32 (▲). 3) ethylamine; 106 (□), 70 (■), 48 (■), and 32 (■). 4) *n*-propylamine; 106 (▽), 70 (▼), 48 (▼), and 32 (▼). 5) *n*-butylamine; 106 (○), 70 (◐), 48 (◑), and 32 (●). 6) *sec*-butyl-amine; 106 (△), 70 (▲), 48 (▲), and 32 (▲). 7) *tert*-butylamine; 106 (□), 70 (■), 48 (■), and 32 (■). 8) diethylamine; 80 (○), 48 (◑), and 28 (●). 9) tri-ethylamine; 80 (□), 48 (■), and 28 (■).

are equal to unity). As is shown in Fig. 1, the plots for each amine at various total pressures all lie on one straight line, and no total pressure dependence can be seen. The half-quenching pressures obtained from Fig. 1 are listed in Table 1. The efficiency of the quenching by primary amines increases with an increase in the molecular complexity.

Table 2. Wavelength at the peak of the emission band and quantum yield of the luminescence

Amine	λ (nm)	Quantum yield
Ammonia	432±2	0.67±0.10
Methylamine	449±5	0.58±0.10
Ethylamine	452±5	0.26±0.09
n-Propylamine	452±5	0.20±0.09
n-Butylamine	453±5	0.18±0.05
sec-Butylamine	453±5	0.12±0.05
tert-Butylamine	454±5	0.04±0.02
Diethylamine	longer than 460 nm	
Triethylamine	longer than 460 nm	

The emission band for ammonia was shown previously.[4] The band for the primary amines studied had the same basic shape and so will not be given here. The wavelengths at the peak of the emission band are listed in Table 2. Since the emission intensity changes with the irradiation time, the position of the peak is somewhat obscure. The wavelength at the peak for diethylamine and triethylamine could not be measured because of the interference of the scattered light of the line at 468 nm from the lamp.

According to the method of Newman *et al.*,[7] the quantum yield of the luminescence for ammonia was calculated. The ratios of the intensity of the luminescence at 432 nm to the decrease in the fluorescence intensity of the 326.1 nm line were measured at various ammonia pressures (5—50 Torr), the total pressure being kept constant. The intensity of the 326.1 nm line should be corrected for the absorption of the line on its way out of the cell. The transmission was calculated for the pure Doppler-broadening case,[8] using the known dimensions of the cell. Some typical data for

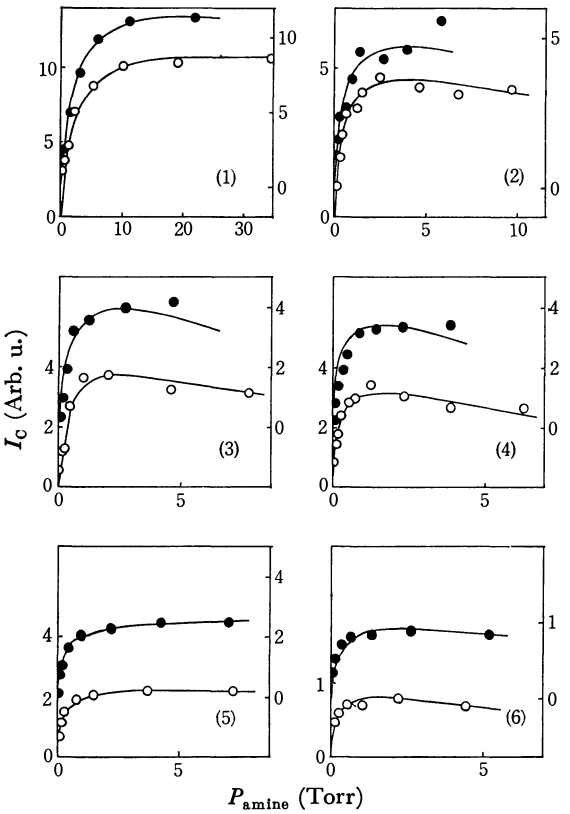

Fig. 2. The intensity at the peak of the emission band from the complex as a function of the partial pressure of amines. The total pressures are 80 (○) and 48 (●) in Torr. The plots for 48 Torr are displaced upwards for clarity. 1) methylamine; 2) ethylamine; 3) *n*-propylamine; 4) *n*-butylamine; 5) *sec*-butylamine; 6) *tert*-butylamine.

ammonia are as follows:

$$\frac{I_{432}}{\Delta I_{326.1}} = \frac{2.15}{19.31}$$

$$\frac{\text{sensitivity at 326.1 nm}}{\text{sensitivity at 432 nm}} = 0.42$$

$$\frac{\text{area under emission band}}{\text{instrumental bandwidth}} = \frac{53.4}{2.74}$$

$$\text{cell transmission at } 326.1 \text{ nm} = 0.685$$

$$\text{quantum yield} = \frac{2.15\times0.42\times53.5\times0.685}{19.31\times2.74} = 0.63$$

The mean of 25 determinations was 0.67 ± 0.10. The quantum yields for the other amines were determined by a comparison of the integrated intensity of the emission band for the amine in question with that for ammonia under the same conditions. The results are listed in Table 2.

The pressure dependence of the intensity at the peak of the emission band is shown in Fig. 2. The intensities were obtained by extrapolation to zero irradiation time. The maximum intensity is reached at a lower pressure in this order: *tert*-butylamine, *n*-butylamine, *n*-propylamine, ethylamine, *sec*-butylamine, methylamine, and ammonia. This order (except for *sec*-butylamine) is in agreement with the order of molecular complexity.

Discussion

As was described in the previous paper,[5] in the presence of foreign gases—for example, 5 Torr of Ar or 0.1 Torr of ammonia, the equilibrium between the 5 $^3P_1$ and 5 $^3P_0$ states of cadmium is readily established. Consequently, we cannot specify which state is the precursor of the emitting species. In the following treatment, therefore, we will use the symbol Cd* to express either Cd($^3P_1$) or Cd($^3P_0$).

In a manner similar to that described in a previous paper,[3] the following reaction mechanism was considered:

$$\mathrm{Cd} + h\nu \longrightarrow \mathrm{Cd}(^3P_1) \qquad I_a$$
$$\mathrm{Cd}(^3P_1) \longrightarrow \mathrm{Cd} + h\nu \qquad k_0$$
$$\mathrm{Cd}(^3P_1) + \mathrm{M} \rightleftarrows \mathrm{Cd}(^3P_0) + \mathrm{M} \qquad k_1, k_{-1}$$
$$\mathrm{Cd}(^3P_1) + \mathrm{A} \longrightarrow \text{products} \qquad k_2$$
$$\mathrm{Cd}(^3P_0) + \mathrm{A} \longrightarrow \text{products} \qquad k_3$$
$$\mathrm{Cd}^* + \mathrm{A} \rightleftarrows \mathrm{CdA_v}^* \qquad k_4, k_{-4}$$
$$\mathrm{CdA_v}^* + \mathrm{A} \longrightarrow \mathrm{CdA}^* + \mathrm{A} \qquad k_5$$
$$\mathrm{CdA_v}^* + \mathrm{Ar} \longrightarrow \mathrm{CdA}^* + \mathrm{Ar} \qquad k_5'$$
$$\mathrm{CdA}^* \longrightarrow \mathrm{Cd} + \mathrm{A} + h\nu' \qquad k_6$$
$$\mathrm{CdA}^* + \mathrm{A} \longrightarrow \mathrm{Cd} + 2\mathrm{A} \qquad k_7$$
$$\mathrm{CdA}^* + \mathrm{Ar} \longrightarrow \mathrm{Cd} + \mathrm{A} + \mathrm{Ar} \qquad k_7'$$

Here, M stands for Ar or amine, while A represents amine. CdA_v* and CdA* represent, respectively, an unstabilized and a stabilized complex between the triplet cadmium atoms and amines. In this mechanism, it is assumed that the unstabilized complex does not fluoresce.

The steady-state treatment on the assumption that the equilibration reaction between $^3P_1$ and $^3P_0$ states is very fast gives the following relation with respect to the quenching of the resonance radiation:

$$\frac{I_{326.1}}{I^0_{326.1}} = 1 + a[\mathrm{A}] + \frac{b[\mathrm{A}]}{1+c[\mathrm{M}]+d[\mathrm{A}]} \qquad (1)$$

Here, $I_{326.1}{}^0$ and $I_{326.1}$ are the emission intensities at 326.1 nm in the absence and in the presence of amines respectively. a, b, c, and d are constants; they are expressed as follows: when Cd* = Cd($^3P_1$),

$$a = \frac{1}{k_0}\left(k_2+\frac{k_1}{k_{-1}}k_3\right),\quad b = \frac{k_4}{k_0},\quad c = \frac{k_5'}{k_{-4}},$$

and $$d = \frac{k_5-k_5'}{k_{-4}}.$$

In the case of Cd*=Cd($^3P_0$), k_4 should be replaced by $(k_1/k_{-1})k_4$. If c and/or d are sufficiently large, Eq. (1) can be approximated to:

$$\frac{I^0_{326.1}}{I_{326.1}} = 1 + (a+b)[\mathrm{A}] \qquad (2)$$

The Stern-Volmer plots for amines other than ammonia in Fig. 1 are expressed by Eq. (2). The constants, $(a+b)$, were evaluated by the least-squares method; they are listed in Table 3.

The steady-state treatment of the above mechanism gives the following relation for the intensity of the emission from the complex:

$$\frac{I_{326.1}[\mathrm{A}]}{I_c} = \alpha(e+f[\mathrm{A}])\left(1+\frac{g}{h+[\mathrm{A}]}\right) \qquad (3)$$

TABLE 3. CONSTANTS INVOLVED IN EQS. (2) AND (3)

Amine	[M] (Torr)	$a+b$ (Torr^{-1})	αe(Torr)	αf	g (Torr)	h/[M]
Ammonia	208	0.113±0.04	2.17	0	3.20	0.0072
	175	0.113±0.04	1.99	0	3.23	0.0072
	147	0.113±0.04	1.87	0	2.78	0.0072
	123	0.113±0.04	1.74	0	2.52	0.0072
Methylamine	80	1.13 ±0.02	0.155	0.0005	1.23	0.0073
	48	1.13 ±0.02	0.135	0.0005	1.23	0.0073
Ethylamine	80	2.86 ±0.06	0.126	0.0048	0.239	0.0073
	48	2.86 ±0.06	0.104	0.0048	0.287	0.0073
n-Propylamine	80	4.65 ±0.09	0.090	0.0065	0.287	0.0073
	48	4.65 ±0.09	0.072	0.0065	0.287	0.0073
n-Butylamine	80	5.65 ±0.20	0.090	0.0097	0.112	0.0073
	48	5.65 ±0.20	0.070	0.0097	0.112	0.0073
sec-Butylamine	80	9.30 ±0.38	0.098	0	0.128	0.0025
	48	9.30 ±0.38	0.084	0	0.128	0.0025
tert-Butylamine	80	34.7 ±2.1	0.049	0.0073	0.434	0.0025
	48	34.7 ±2.1	0.038	0.0073	0.434	0.0025

Here, I_c represents the observed emission intensity from the complex at the peak. α is a proportional factor between the total emission intensity and the observed one; it depends on the geometry of the apparatus, the slit width, and the sensitivity of the photomultiplier used. e, f, g, and h are constants depending only on the total pressure:
when $Cd^* = Cd(^3P_1)$,

$$e = \frac{k_0}{k_4} + \frac{k_0 k_7'}{k_4 k_6}[M], \quad f = \frac{k_0(k_7 - k_7')}{k_4 k_6},$$

$$g = \frac{k_{-4}}{k_5 - k_5'}, \text{ and } h = \frac{k_5'}{k_5 - k_5'}[M].$$

In the case of $Cd^* = Cd(^3P_1)$, k_4 should be replaced by $(k_1/k_{-1})k_4$. These constants have been evaluated by the method described in the previous paper[3] and are listed in Table 3. The solid lines in Fig. 2 were drawn by substituting the values in Table 3 into Eq. (3).

From the relationships between the constants, $(a+b)$, αe, αf, g, and h and [M], several ratios of the rate constants can be evaluated. The results are summarized in Table 4. The lifetime (τ_0) of $Cd(^3P_1)$ has been reported to be 2.39×10^{-6} s.[9] As was mentioned in the previous paper,[1] the effective lifetime is independent of the pressure of foreign gases. Therefore, k_0 may be set equal to $1/\tau_0$ (4.19×10^5 s^{-1}). By using this value, some rate constants can be calculated. The relative values of k_4 can also be calculated by assuming that α does not depend on the kind of amine. This assumption seems reasonable, because the profile of the emission band is almost independent of the amines. These values are also listed in Table 4.

The rate constants, k_4, for the primary amines increase in this order: ammonia<methylamine<ethylamine<*sec*-butylamine<*n*-propylamine<*n*-butylamine<*tert*-butylamine. This order is in agreement with the order of the decrease in the ionization potential of amines, except for *sec*-butylamine. Figure 3 shows the correlation between the relative values of k_4 and the ionization potential of amines. Relationship of this type have also been reported in the cases of the quenching of $I(5^2P_{1/2})$[10] and $P(3^2D_j)$ and $P(3^2P_j)$.[11] This relationship indicates that the complex has the characteristics of a charge-transfer type. The tendency of the efficiency of the quenching of the resonance radiation by amines shown in Table 1 is almost the same as that of k_4. This suggests that the quenching occurs mainly through the formation of the complex (Reaction (k_4)).

The k_5/k_{-4} and k_5'/k_{-4} ratios increase generally with an increase in the molecular complexity. Thus,

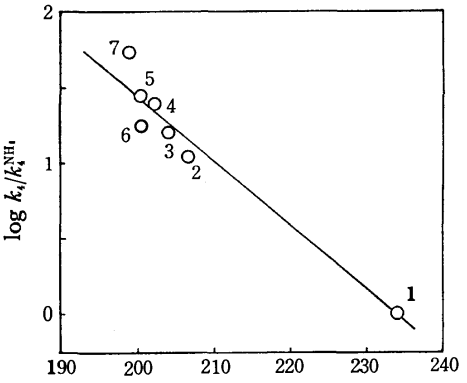

Fig. 3. Relationship between the relative values of the rate constant for the formation of complex and the ionization potential of amines.
1) ammonia; 2) methylamine; 3) ethylamine; 4) *n*-propylamine; 5) *n*-butylamine; 6) *sec*-butylamine; 7) *tert*-butylamine.

it can be said that, for the complex amines, the back reaction (Reaction (k_{-4})) is not important (c and d in Eq. (1) are large); therefore, the Stern-Volmer plots lie on a straight line.

As is shown in Table 2, the peak wavelength shifts to longer wavelengths as the ionization potentials of the amines decrease. Most of the wavelength shift occurs upon methyl substitution. These tendencies agree with the observations in the mercury-sensitized luminescence of alcohols[12] and amines.[13] These findings indicate that the complex formed between the excited cadmium atoms and amines is of the charge-transfer type, by analogy with the mercury-amines and mercury-alcohols systems. This explains why the emission band has no fine structure.

The quantum yield of the luminescence for ammonia given in Table 2 is approximately equal to that of the mercury-sensitized luminescence of ammonia. As is shown in Table 2, the quantum yield for amines decrease steadily with the increase in the molecular complexity. This tendency differs from that observed in the mercury-amines system.[13]

In the mercury-sensitized reaction, it was shown that the quenching process of $Hg(^3P_1)$ with all alcohols and amines except methylamine yields mainly Hg $(^3P_0)$.[12,13] However, in the cadmium-sensitized reaction an equilibrium between the $^3P_1$ and $^3P_0$ states is established; the quenching of the resonance radiation by amines occurs mainly through the formation of

Table 4. Rate constants and ratios between rate constants

Amine	$k_2+1.68k_3+k_4$ (or $k_2+1.68(k_3+k_4)$) (cm^3 molecule^{-1} s^{-1})	$k_4/k_4^{NH_3}$	k_5'/k_{-4} (Torr^{-1})	k_5/k_{-4} (Torr^{-1})	$10^3k_7/k_6$ (Torr^{-1})	k_7/k_7'
Ammonia	$(2.4\pm0.4)\times10^{-12}$	1.0	0.0024	0.336	4.9	1.0
Methylamine	$(2.4\pm0.2)\times10^{-11}$	10.7	0.0059	0.813	10.8	1.8
Ethylamine	$(6.1\pm0.1)\times10^{-11}$	15.8	0.0275	3.80	77.6	8.0
n-Propylamine	$(9.9\pm0.2)\times10^{-11}$	24.9	0.0253	3.48	153.7	12.2
n-Butylamine	$(1.2\pm0.1)\times10^{-10}$	28.0	0.0649	8.93	259.0	16.4
sec-Butylamine	$(2.0\pm0.1)\times10^{-10}$	17.8	0.0195	7.81	7.0	1.0
tert-butylamine	$(7.4\pm0.4)\times10^{-10}$	53.3	0.0058	2.30	347.9	20.8

the complex, as has been mentioned above. It has been reported that, in the mercury-sensitized reaction of methylamine, the abstraction of an α-hydrogen by $Hg(^3P_1)$ atoms is important; this reaction competes with the luminescence. Therefore, in spite of the large efficiency of the quenching of $Hg(^3P_1)$ by methylamine, the quantum yield of the luminescence is very small. This explanation is supported by the fact that the quantum yield with *tert*-butylamine, which has no α-hydrogen, is large.[12] On the other hand, in the cadmium-sensitized reaction of amines the relative values of k_4 vary steadily with the decrease in the ionization potential of amines; this was taken as an indication that the relative efficiency of the formation of complex did not change markedly on going from one amine to the next. That is to say, the efficiency of the quenching can be interpreted in terms of the electron-donating ability of the nitrogen atom of amines alone.

As is seen in Table 4, the k_7/k_6 ratio increases with an increase in the molecular complexity of the amines with the exception of the case of *sec*-butylamine. If it is assumed that $1/k_6$, or the lifetime of the complex, dose not depend appreciably on the kind of amines, the above order indicates the order of the efficiency of the quenching of the complex luminescence by amines. As is shown in Table 2, therefore, the quantum yields of the luminescence decrease in this order, though the rate constants of the complex formation increase in the same order. The efficiency of the quenching of the luminescence by ammonia is very small. On the other hand, the efficiency by *tert*-butylamine is about two orders of magnitude larger than that by ammonia. This large efficiency of the quenching by *tert*-butylamine cannot be explained by the increase in the cross section of collision alone. Morten *et al.*[2] described how, at high pressures of ammonia, complexes with two or more ammonia molecules may be formed, and how the possibility of the formation of the higher complexes, which radiate at almost the same wavelength, probably provides a good explanation of the small efficiency of the quenching of the complex luminescence by ammonia. Such complexes were indeed found in the mercury–ammonia system.[14] If this explanation is correct, it can be said that the increase in the efficiency of the quenching by amines with an increase in the molecular complexity results from the difficulty in the formation of the higher complexes because of the steric hindrance of alkyl group.

The financial support for part of this work by a grant from the Ministry of Education is gratefully acknowledged.

References

1) S. Yamamoto, M. Takaoka, S. Tsunashima, and S. Sato, This Bulletin, **48**, 130 (1975).
2) P. D. Morten, C. G. Freeman, M. J. McEwan, R. F. C. Claridge, and L. F. Philips, *Chem. Phys. Lett.*, **16**, 148 (1972).
3) S. Yamamoto, S. Tsunashima, and S. Sato, This Bulletin, **48**, 1172 (1975).
4) S. Tsunashima, T. Toyono, and S. Sato, *ibid.*, **46**, 2654 (1973).
5) M. Takaoka, S. Yamamoto, S. Tsunashima, and S. Sato, *Chem. Lett.*, **1974**, 343.
6) J. C. de Vos, *Physica*, **20**, 715 (1954).
7) R. H. Newman, C. G. Freeman, M. J. McEwan, R. F. C. Claridge, and L. F. Phillips, *Trans. Faraday Soc.*, **66**, 2827 (1970).
8) A. C. G. Mitchell and M. W. Zemansky, "Resonance Radiation and Excited Atoms," Cambridge University Press, Cambridge, (1934).
9) F. W. Byron, Jr., M. N. McDermott, and R. Novick, *Phys. Rev.*, **134**, A615 (1964).
10) R. J. Donovan, D. Husain, and C. D. Stevenson, *Trans. Faraday Soc.*, **65**, 2941 (1969).
11) A. U. Acuna and D. Husain, *J. Chem. Soc., Faraday*, **69**, 585 (1973).
12) C. G. Freeman, M. J. McEwan, R. F. C. Claridge, and L. F. Phillips, *Trans. Faraday Soc.*, **67**, 2565 (1971).
13) R. H. Newman, C. G. Freeman, M. J. McEwan, R. F. C. Claridge, and F. L. Phillips, *ibid.*, **67**, 1360 (1971).
14) A. B. Callear and J. H. Connor, *Chem. Phys. Lett.*, **13**, 245 (1972).

The Micelle Formation of Mixtures of Polyoxyethylene Type Nonionic Surfactants in Aqueous Solutions

Nagamune NISHIKIDO, Yoshikiyo MOROI, and Ryohei MATUURA
Department of Chemistry, Faculty of Science, Kyushu University, Fukuoka 812
(Received November 28, 1974)

The critical micelle concentrations (CMC) of mixtures of nonionic surfactants with the same hydrocarbon, *i.e.* dodecyl group, and with various chain lengths of ethylene oxide, were determined. The observed values were compared with the values calculated by means of the equation derived from the pseudo-phase separation model on the assumption that the mixed micelle is a perfect solution. A good agreement between observed and calculated values was obtained in the mixtures of the surfactants with six or more ethylene-oxide units. However, the observed values of the two-component mixture, one component with five ethylene-oxide units, showed a small deviation from the calculated values. The difference between the above two cases was explained from the viewpoint of the most suitable packing of the first six or fewer ethylene-oxide units near the micelle core in the micelle state.

It is well known that mixtures of surfactants, either ionic-ionic, ionic-nonionic, or nonionic-nonionic, form mixed micelles in an aqueous solution. Especially, the mixed micelle formation of ionic surfactants has been widely investigated.[1,5] Also, in the work of mixed systems of ionic-nonionic surfactants, useful information has been obtained.[2,5] However, only a few studies have been made of the critical micelle concentrations (CMC) of mixture of nonionic surfactants.[3-5] Recently, using polyoxyethylene type nonionic surfactants with almost the same oxyethylene chain length, but with different hydrocarbon chain lengths, Shinoda-Nakagawa[4] and Lange[5] predicted the CMC of their mixtures by the use of a pseudo-phase separation approach, treating the mixed micelle as a perfect solution. For practical purposes, it is important to be able to predict the CMC of surfactant mixtures from the CMC of each component.

In the present work, by determining the CMC of two-, three-, and four-component mixtures of nonionic surfactants with various oxyethylene chain lengths and the same hydrocarbon chain length, we examined the CMC equation derived on the assumption that the mixed micelle behaves as a perfect solution in the pseudo-phase separation model.

Experimental

Materials. The nonionic surfactants, polyoxyethylene lauryl ethers ($C_{12}H_{25}O(CH_2CH_2O)_{\bar{n}}H$, $\bar{n}$=5, 6, 10, 15, 20, 29, 49, $\bar{n}$: the average number of ethylene oxide groups) were the same materials, supplied by the Kao Soap Co., Ltd., as those used in our previous paper.[6] The sharp distribution of the oxyethylene chain lengths could be assessed by means of the sharp breaks and the lack of, or small, minimum in the surface tension *vs.* logarithm of the surfactant concentration plots. Throughout this work, the difference in the number of oxyethylene groups between the components in mixtures was more than five units, so each component was regarded as a single species in making a good approximation for the purposes of the present work.

Method. The CMC was determined at 20 °C by the use of both the surface tension and the dye-color-change methods.[7] The details of the procedures of the former were described in a previous paper.[6] The dye used was pinacyanol chloride (Eastman Kodak Co.), and its concentration was 1×10^{-5} mol/l throughout this work. The shift of the absorption spectrum was measured with a DSB-70 spectrophotometer manufactured by the Beckman-Toshiba Co., Ltd. The procedure of direct calorimetry used to determine the standard entropy of micelle formation, ΔS_m°, was described in the previous paper.[6]

Results and Discussion

With an increase in the content of the component with a higher CMC, the extent of the minimum in the surface tension-logarithm of the concentration curve gets larger; however, we could detect distinct breaks in the curve even for four-component mixtures. These distinct breaks agreed with the CMC determined by the dye-color-change method. The CMC's of single surfactants with various lengths of ethylene-oxide chains in the aqueous solution at 20 °C are tabulated in Table 1. The CMC's of mixtures are shown in Figs. 1, 2, and Tables 2, 3, with the composition.

TABLE 1. CMC AND THE STANDARD FREE ENERGY OF MICELLE FORMATION ΔG_m^0 OF THE SULFACTANTS WITH VARIOUS ETHYLENE OXIDE CHAIN LENGTHS IN THE AQUEOUS SOLUTION AT 20 °C

Ethylene oxide chain length, $\bar{n}$	CMC (10^{-5} mol/l)	ΔG_m^0 (kcal/mol)
5	4.5	−8.15
6	6.0	−7.99
10	9.0	−7.75
15	12.0	−7.58
20	15.5	−7.43
29	26.0	−7.14
49	63.0	−6.62

Using the same pseudo-phase separation treatment as that of Lange *et al.* for two-component mixtures,[5] the equation of the CMC for multi-component mixtures of nonionic surfactants can be easily derived as follows.

In a sufficiently low concentration range, the CMC can be expressed by the mole fraction instead of by the activity in the chemical potential of the monomer. Recently, nuclear magnetic resonance studies have shown that the micelle contains some water molecules,[8] but their solubility can be neglected in a good approxi-

mation. In addition, assuming that the mixed micellar phase behaves as a perfect solution, the following equation holds for the ith-component:

$$x_i C_M = x_i^m C_i \quad (1)$$

where x_i, x_i^m: mole fraction of the ith-component in a mixture in the bulk solution and in the micellar phase respectively, C_M, C_i: the CMC (molar concentration) of a mixture and of a single system of the ith-component respectively.

The sum of the mole fractions of components in the micelle phase is unity; that is, $\sum x_i^m = 1$. Thus, Eq. (1) leads to:

$$C_M = \frac{1}{\sum_i (x_i/C_i)}. \quad (2)$$

The CMC values calculated from Eq. (2) are shown in Figs. 1 and 2 for two-component mixtures, and in Tables 2 and 3 for three- and four-component systems respectively, together with the observed values. Within the limits of experimental error, a good agreement between calculated and observed CMC's is usually obtained. However, in the case of one two-component system, $\bar{n}=5$—$\bar{n}=49$ (Fig. 2), a small disagreement is observed. The difference between the system containing $\bar{n}=5$ and the system containing $\bar{n}\geqq 6$ may be connected with the assumption made in the course of the derivation of Eq. (2). The assumption that the mixed micelle can be regarded as a perfect solution must be checked, since the other assumption, an ideal dilution in bulk solution, is sufficiently acceptable.

In order to clarify the situation, let us consider the following equation by Shinoda:[9]

TABLE 2. COMPARISON OF CALCULATED WITH OBSERVED CMC FOR THREE-COMPONENT MIXTURES AT 20 °C

Mole fraction of surfactants			CMC (10^{-5} mol/l)	
$\bar{n}=10$	29	49	Obsd	Calcd
0.333	0.333	0.333	18.7	18.2
0.125	0.25	0.625	29.0	29.9
0.125	0.625	0.25	23.0	23.9
0.625	0.125	0.25	12.3	12.8
0.222	0.222	0.555	24.5	23.8

$\bar{n}=10$	20	29	Obsd	Calcd
0.333	0.333	0.333	13.2	14.0

TABLE 3. COMPARISON OF CALCULATED WITH OBSERVED CMC FOR FOUR-COMPONENT MIXTURES AT 20 °C

Mole fraction of surfactants				CMC (10^{-5} mol/l)	
$\bar{n}=6$	15	29	49	Obsd	Calcd
0.25	0.25	0.25	0.25	13.5	13.1
0.125	0.5	0.25	0.125	12.5	13.5
0.25	0.125	0.5	0.125	13.0	13.6
0.125	0.125	0.125	0.625	21.5	21.7

$\bar{n}=10$	15	20	29	Obsd	Calcd
0.25	0.25	0.25	0.25	13.7	13.4

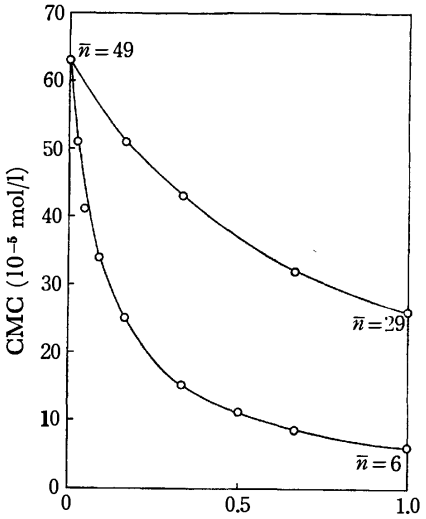

Fig. 1. Calculated and observed CMC for two-component mixtures at 20 °C ($\bar{n}=6$—$\bar{n}=49$, $\bar{n}=29$—$\bar{n}=49$)
○: observed, ——: calculated CMC from Eq. (2)

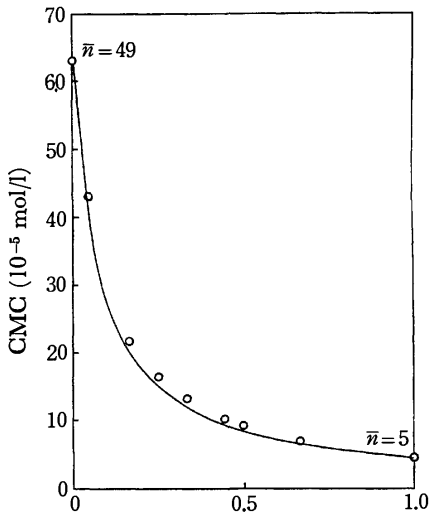

Fig. 2. Calculated and observed CMC for $\bar{n}=5$—$\bar{n}=49$ mixture at 20 °C
○: observed, ——: calculated CMC from Eq. (2)

$$\ln C = -\frac{\chi-\chi'}{kT} + \ln\frac{1000}{Nv} - 1, \quad (3)$$

where C: CMC in molarity, $\chi-\chi'$: the free energy difference of a surfactant between micellar and monomer states, N: the Avogadro number, v: the free volume of a surfactant molecule in a micelle.

In the case of nonionic surfactants,

$$\chi - \chi' = mw - \Delta,$$

where m: the number of methylene groups in a hydrocarbon chain, w: the free energy change per methylene group transferred from water into the micelle (constant value of *ca.* 1.1 kT), Δ: the free energy change of a polyoxyethylene chain between micelle and monomer states,

containing the terms of dehydration energy, configuration entropy, and oxyethylene-oxyethylene interaction energy. It is possible to evaluate this term experimentally from the ln C *vs.* ethylene-oxide chain length plots. However, it is not necessary to evaluate it experimentally or mathematically in the discussion below, so we will treat it as a parameter.

We have obtained the following equation for nonionic surfactants with the same hydrocarbon chain in the most simple form:

$$\ln C_i = -\frac{mw}{kT} + \frac{\Delta_i}{kT} + \ln\frac{1000}{Nv_i} - 1. \quad (4)$$

As each component has the same hydrocarbon chain, the assumption that the mixed micelle is a perfect solution needs an ideal mixing term, ln x_i^m, in Eq. (4):

$$\ln (x_i C_M) = -\frac{mw}{kT} + \frac{\Delta_i}{kT} + \ln\frac{1000}{Nv_i} - 1 + \ln x_i^m \quad (5)$$

Of course, we obtain Eq. (2) from Eqs. (4) and (5). In other words, in the concept of a perfect solution, the free energy difference, $mw-\Delta_i$, is not altered by mixing in a micelle. That is, the free energy difference in a mixed system is the same as that in a single system.

If the mixing process brings a small variation in mw or Δ_i in Eq. (5),

$$\ln (x_i C_M) = -\frac{mw}{kT} + \frac{\Delta_i}{kT} + \frac{\delta_i}{kT} + \ln\frac{1000}{Nv_i} - 1 + \ln x_i^m, \quad (6)$$

where δ_i is the quantity of deviation from mw or Δ_i in Eq. (5), neglecting the variation in v_i. In Eq. (6), δ_i corresponds to the heat of mixing term in the regular solution approximation, in analogy with a macroscopic solution. In Fig. 2, it may be seen that the deviation in the observed CMC's from the calculated values, *i.e.*, the ideal values, is small. Thus, Eq. (6) can be expected to be valid in this case. Alternatively and generally, by adding the excess term, ln γ_i^m, in Eq. (5), we obtain:

$$\ln (x_i C_M) = -\frac{mw}{kT} + \frac{\Delta_i}{kT} + \ln\frac{1000}{Nv_i} - 1 + \ln x_i^m \gamma_i^m \quad (7)$$

where γ_i^m is the activity coefficient of the ith-component in a mixed micelle. From Eqs. (4), (6), and (7), we obtain:

$$C_M = \frac{1}{\sum_i (x_i/C_i\gamma_i^m)} = \frac{1}{\sum_i (x_i/C_i \exp(\delta_i/kT))} \quad (8)$$

It may be seen in Fig. 2 that the observed CMC deviates positively from the ideal CMC. Then, at least, judging from Eq. (8), the activity coefficient of one component in a mixed micelle must be greater than unity. In a non-ideal macroscopic solution composed of two components, the deviation from ideality occurs in the same direction for both components. Therefore, we may conclude that the activity coefficients of both components in the mixed micelle are greater than unity. The free energy difference, $mw-\Delta_i-\delta_i$, in a mixed system is smaller than the $mw-\Delta_i$ in a single system. Thus, the micelle environments of both components are less stable than those in a single system. This conclusion is only the sufficient condition for the validity of positive deviation from the ideal CMC shown in Fig. 2. This point will be explained further in the subsequent discussions.

In the present work, the plots of the standard free energy of micelle formation, ΔG_m° ($\Delta G_m^\circ = RT \ln X_c$, where X_c represents the CMC in mole fraction) against $\bar{n}$, the number of ethylene-oxide (EO) units, yield two lines and cross around $\bar{n}=6$, *i.e.*, around the sixth unit (Table 1). In addition, the standard entropy of micelle formation, ΔS_m°, for the surfactant with 5 EO units is 41 ± 6 e.u./mol, while the values of ΔS_m° for the surfactants with 6 to 31 units are almost constant, *ca.* 52 e.u./mol in aqueous solutions at 20 °C.[6] Crook *et al.* found the similar trend for *p,t*-octylphenoxyethoxyethanol in the aqueous solution below 50 °C.[10] From the break at the sixth EO unit in the plots of the thermodymanic quantities of micelle formation against EO units, Ray and Nemethy assumed as follows:[11] in the micelle state, the first six or less EO units, near the nonpolar core of the micelle, pack together and lose some of their hydration water because of the need for close packing of the nonpolar tails, while in longer chains, the EO units beyond the sixth are located sufficiently far from each other so that their local environment is changed very little compared to that for the monomer. This picture can be applied to the present CMC data in order to explain why the deviation from the ideal mixing in the mixed micelle occurs only in the $\bar{n}=5$—$\bar{n}=49$ system.

As the steric interaction among the EO units beyond the sixth in the micelle state is not very strong, the mixing of the surfactants with six or more EO units brings little difference in the micelle environment of EO units between mixed and single micelles. In addition, as each component has the same hydrocarbon chain, the free energy difference in the hydrocarbon chain and EO units between the micelle and monomer states, $mw-\Delta_i$ in Eq. (5), is independent of the number of components in a micelle, as has already been described. Thus, the above situation leads to the concept that the mixed micelle is a perfect solution.

On the other hand, in Fig. 2, the surfactant of $\bar{n}=49$ only needs the packing of the first six EO units, while the other component has five EO units. Therefore, the positive deviation from the ideal mixing may be expected to occur only for the surfactant of $\bar{n}=49$. In this case, the activity coefficient of $\bar{n}=5$ in the mixed micelle must be unity, and that of $\bar{n}=49$ must be *ca.* 10 at 0.5 of the mole fraction in a bulk solution, in order to satisfy the experimental results in Fig. 2. However, the value of the activity coefficient, $\gamma^m=10$, corresponds to the heat of mixing term, $\delta=2.3\,kT$, which is too large to explain the small deviation from the ideal CMC. Thus, the micelle state of the surfactant of $\bar{n}=5$ in a mixed system may be also be obliged to deviate from the most suitable packing in a single system by the surfactant of $\bar{n}=49$. This deviation brings about the decrease in the free energy difference of each surfactant in a mixed system between micelle and monomer states compared to each single-component system; that is, $\delta_i>0$ in Eq. (6). Then, the surfactant with five EO units brings about the positive deviation from the ideal CMC shown in Fig. 2.

From the viewpoint of predicting the CMC, it may be concluded that the CMC's of multi-component mixtures, in which each component has six or more EO units, can be determined by means of Eq. (2).

We wish to express our hearty thanks to the Kao Soap Co., Ltd., for the supply of nonionic surfactants.

References

1) H. Lange, *Kolloid-Z.*, **131**, 96 (1953); K. J. Mysels and R. J. Otter, *J. Colloid Sci.*, **16**, 462, 472 (1961); Y. Iwadare, This Bulletin, **43**, 3364 (1970); F. Tokiwa, K. Ohki, and I. Kokubo, *ibid.*, **41**, 2845 (1968); L. Shedlovsky, C. W. Jacob, and M. B. Epstein, *J. Phys. Chem.*, **67**, 2075 (1963); Y. Moroi, K. Motomura, and R. Matuura, *J. Colloid Interface Sci.*, **47**, 111 (1974); Y. Moroi, N. Nishikido, and R. Matsuura, *ibid.*, in press, "The Critical Micelle Concentration of Multicomponent Mixtures of Metal Alkyl Sulfates in Aqueous Solution. II"; *etc.*

2) M. J. Schick and F. M. Fowkes, *J. Phys. Chem.*, **61**, 1062 (1957); A. K. Biswas and B. K. Mukherji, *ibid.*, **64**, 1 (1960); F. Tokiwa and K. Tsujii, *ibid.*, **75**, 3560 (1971); M. J. Schick and D. J. Manning, *J. Amer. Oil. Chemists' Soc.*, **43**, 133 (1966); A. M. Mankowich, *ibid.*, **41**, 449 (1964); M. J. Shick, *ibid.*, **43**, 681 (1966); *etc.*

3) K. Onoda, *Oil Chem.*, **10**, 612 (1961).

4) K. Shinoda, T. Nakagawa, B. Tamamushi, and T. Isemura, "Colloidal Surfactants," Academic Press, New York (1963), p. 68.

5) H. Lange and K.-H. Beck, *Kolloid-Z. Z. Polym.*, **251**, 424 (1973).

6) N. Nishikido, Y. Moroi, H. Uehara, and R. Matuura, This Bulletin, **47**, 2634 (1974).

7) T. Nakagawa, K. Tori, and K. Kuriyama, *Nippon Kagaku Zasshi*, **77**, 52 (1956).

8) T. Waiker, *J. Colloid Interface Sci.*, **45**, 372 (1973).

9) K. Shinoda, "Colloidal Surfactants," p. 41.

10) E. H. Crook, G. F. Trebbi, and D. B. Fordyce, *J. Phys. Chem.*, **68**, 3592 (1964).

11) A. Ray and G. Nemethy, *ibid.*, **75**, 809 (1971).

Basic Properties of Metal Phosphates and Their Catalytic Activity in the Decomposition of Diacetone Alcohol

Akio TADA

Department of Industrial Chemistry, Kitami Institute of Technology, Koen-cho, Kitami 090

(Received December 2, 1974)

The basic properties of alkali and alkaline earth metal phosphates calcined at various temperatures were investigated. The strength of the surface base was determined by the adsorption of acidic indicators from benzene solution. It was found that K_3PO_4 shows a fairly high basic strength of $H_0 \geqq 17.2$. The surface basicity was evaluated by the catalytic activity for the decomposition of diacetone alcohol, which is known to be catalyzed only by basic catalysts. Comparison of the result of the activity measurement with that of TGA indicated that the basicity of a metal phosphate reaches a maximum when dehydrated completely. The nature of the basic sites on metal phosphates is also discussed.

The surface basicities of metal phosphates have not been extensively studied as compared to the surface acidities of those. Scheidt[1] has reported that lithium phosphate, sodium orthophosphate, and calcium orthophosphate catalyze aldol condensations which are typically base-catalyzed. On the other hand, the condensation of acetaldehyde in low yield by passing the feed in the vapor phase over magnesium, zinc, strontium, cadmium, or barium phosphates has been reported by Ivanov *et al.*[2] In our preceding paper,[3] the surface of sodium and calcium orthophosphates was found to have a basic character, but that of others such as magnesium, zinc, or nickel salts an acidic character. These observations seem to be in agreement with the above results. Recently, Imanaka *et al.*[4] have reported that Li_3PO_4 has only acidic character, but Li_2MPO_4- and LiM_2PO_4- type phosphates (M=Na or K) and $Ca_3(PO_4)_2$ have both basic and acidic properties. The basic properties of metal phosphates are considered to be closely related to their structures, and it is important to clarify the relations between them. Very little work, however, has been made on such relationships. From these point of view, an attempt was made to clarify the nature or structure of the basic sites on metal phosphates calcined at various temperatures.

Experimental

Samples. The following chemicals were reagent grade, and were used without further treatment: $Ca_3(PO_4)_2$, $Na_3PO_4 \cdot 12H_2O$, K_3PO_4, Li_3PO_4, $Na_2HPO_4 \cdot 12H_2O$, $NaH_2PO_4 \cdot 2H_2O$, $Ca(H_2PO_4)_2 \cdot H_2O$, K_2HPO_4, KH_2PO_4, and $Na_4P_2O_7 \cdot 10H_2O$. $Na_2HPO_4 \cdot 12H_2O$ and $Na_3PO_4 \cdot 12H_2O$ were first calcined at about 130 °C for 6—7 hr, sieved below 100 mesh after grinding to powder and then calcined at various temperatures for 3 hr in air. The other phosphates were calcined immediately after sieving.

Measurement of Basic Property. The basicities and basic strengths of samples were measured by titrating the powder suspended in benzene with 0.1 N benzoic acid benzene solution, using bromothymol blue ($pK_a=7.1$), phenolphthalein (9.3), 2,4-dinitroaniline (15.0), and 4-chloro-2-nitroaniline (17.2) as indicators.

Measurement of Catalytic Activity. Decomposition of diacetone alcohol, which was selected as a model reaction, was carried out in the temperature range 30—55 °C, by stirring the reaction mixture in a reaction vessel containing 1.0 g of catalysts, 23.0 g of diacetone alcohol, and 2.5 g of benzene (internal standard). At an appropriate time interval, stirring was stopped and 0.15 ml of the solution was taken up through sampling rubber and analyzed by gas chromatography, after the catalyst had been removed by centrifuging. Diacetone alcohol was purified by drying with Drierite and distilling two times under 10 Torrr.

TGA and DTA. The rate of heating was maintained at 5 °C/min. The sample holder was a platinum vessel.

Results and Discussion

Basic Property. The basic color of the indicator adsorbed on the solids changes to acidic color on addition of benzoic acid but the acidic color changes again gradually to the basic color after several minutes. The results of the basic strength measurements, given in Table 1, suggests that the tertiary phosphates of sodium, potassium, and calcium as well as the secondary phosphates of sodium and potassium may be used as solid base catalysts. The basic strength of tertiary potassium phosphate is comparable to that of an alkaline earth metal oxide.[5] Although secondary potassium phosphate might show catalytic activity, its effectiveness is probably limited. Lithium phosphate is known to be a catalyst for aldol condendsation reaction,[1] but Li_3PO_4 shows no solid basicity in agreement with the result of Imanaka *et al.*[4] This fact suggests that the lithium phosphate used by Scheidt is not Li_3PO_4 but

Table 1. Basic strength of alkali and alkaline earth metal phosphates

Original metal phosphate	Calcination temp., °C	Basic strength (H_0)[a]			
		7.1	9.3	15.0	17.2
Li_3PO_4	22—400	−	−	−	−
$Na_3PO_4 \cdot 12H_2O$	22—700	+	+	−	−
$Na_2HPO_4 \cdot 12H_2O$	22— 60	−	−	−	−
	150—500	+	+	−	−
$NaH_2PO_4 \cdot 2H_2O$	22—400	−	−	−	−
$Na_4P_2O_7 \cdot 10H_2O$	22—500	−	−	−	−
K_3PO_4	22—800	+	+	+	+
K_2HPO_4	22—500	+	−	−	−
KH_2PO_4	22—400	−	−	−	−
$Ca_3(PO_4)_2$	22—600	+	+	−	−
$Ca(H_2PO_4)_2 \cdot H_2O$	22—400	−	−	−	−

a) + or − denotes yes or no.

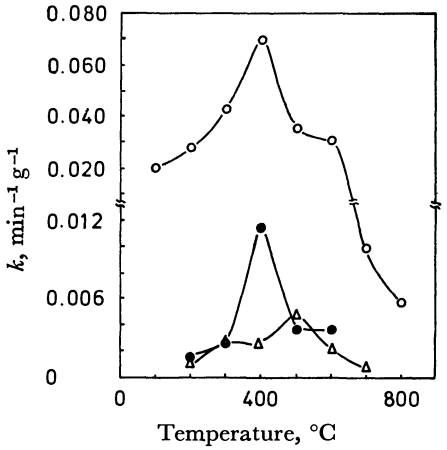

Fig. 1. The reaction rate constants over phosphates at 40 °C as a function of the calcination tempetraure.
○: K_3PO_4, ●: $Ca_3(PO_4)_2$, △: Na_3PO_4

a substituted phosphate such as $NaLi_2PO_4$. $Ca_3(PO_4)_2$ has been found to have both acidity (H_0=4.8) and basicity (7.1).[4] According to Table 1, this salt has only basicity (9.3). This inconsistency may be due to a difference in the samples.

Decomposition of Diacetone Alcohol. The only reaction product was acetone. It has been observed that the rate of decomposition of diacetone alcohol catalyzed by MgO–Al_2O_3[6] and alkaline earth metal oxides[7] is of the first order. Similarly the rate on the metal phosphates was found to be of the first order with respect to diacetone alcohol concentration. Fukuda *et al.*[7] have reported that a long induction period is observed on SrO and BaO, while it disappears by the removal of CO_2. However, no induction period was observed on the metal phosphates. The reaction rate constants over the tertiary phosphates of potassium, sodium, and calcium at 40 °C as a function of the calcination temperature are shown in Fig. 1. The catalytic activity of secondary sodium phosphate was much lower under similar conditions. Since the decomposition of diacetone alcohol is known to be catalyzed only by basic catalyst,[7] the catalytic activity is considered to be proportional to the amount of effective basic sites. Only tertiary potassium phosphate showed the catalytic activity at 30 °C. At 40 °C tertiary sodium phosphate, secondary sodium phosphate, and tertiary calcium phosphate were also found to be active, but secondary potassium phosphate inactive. These observations show that the effective basic sites at 40 °C are those having a basic strength of $H_0 \geqq 9.3$.

Arrhenius activation energies in the temperature range from 30 to 55 °C are compared to the literature values in Table 2. The activation energy for tertiary sodium phosphate is comparable with those for CaO and MgO, while the activation energies for other phosphates are comparable with those for SrO, BaO, and NaOH solution. The activation energy for tertiary potassium phosphate is considered to be rather high in view of its basic strength of $H_0 \geqq 17.2$. This may be related to the formation of light brown, unknown substance on the catalyst during the reaction.

Table 2. Activation energies of decomposition of diacetone alcohol with various catalysts

Catalyst	Calcination temp., °C	Activation energy[a] (kcal/mol)
Na_3PO_4	500	10.8
K_3PO_4	400	21.7
$Ca_3(PO_4)_2$	400	18.0
MgO	500	11.1
CaO	500	11.5
SrO	500	20.3
BaO	no heat treatment	20.3
NaOH (aq. soln.)		18.4

a) Activation energies for catalysts from MgO to NaOH are cited from Ref. 7.

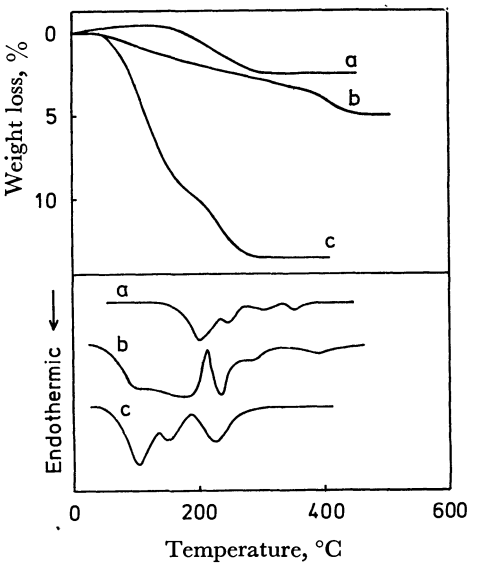

Fig. 2. TGA and DTA of K_3PO_4 (a), $Ca_3(PO_4)_2$ (b), and $Na_3PO_4 \cdot xH_2O$ (c).

Change in Structure with Calcining. TGA and DTA curves are shown in Fig. 2. The amount of crystal water contained in metal phosphates were calculated from the TGA data by assuming the formation of anhydrides at the stage of no further detectable loss in weight. The dehydrating experiments show that tertiary sodium phosphate predried at 130 °C contains about 1.5 mol of water. The anhydride formation is detected at about 250 °C in agreement with the literature value.[8] The initial increase in weight of tertiary potassium phosphate may be attributable to the absorption of moisture during weighing, because this substance is highly hygroscopic. The water is lost at 280 °C in agreement with the result of Ben-Dor and Felner.[9] According to Fig. 2, it is obvious that $Ca_3(PO_4)_2$ contains about 1 mol of water and reaches complete dehydration at 400 °C. $Na_2HPO_4 \cdot 12H_2O$ has been reported to lose its water of hydration when heated up to 110 °C, and at 300 °C condensation to the pyrophosphate occurs.[9]

Basic Sites on Metal Phosphates. The structures of metal phosphates have been studied by many workers.[10] In hydrated metal orthophosphates, the phosphorus atoms are tetrahedrally surrounded by oxygen atoms, and the metal atoms (M) are surrounded by the oxygens

of the PO_4 groups and of the water molecules, while in anhydrous metal phosphates, the metal atoms are surrounded only by the oxygens of the PO_4 groups. Thus, the following structures I and II are considered

I II

to be a part of the structure of the hydrates and anhydrides, respectively. If the electron donating power of the metal atoms is adequate, the oxygen atoms in M–O linkages may be basified. Comparison of Fig. 1 with Fig. 2 indicates that the catalytic activities (basicities) of metal phosphates reach their maxima when dehydrated completely. These results are reasonably explained as follows. Since the negative charge on the oxygen of II is higher than that of I, the basicities of the anhydrides are larger than those of the hydrates, and hence the activities of the former are higher than those of the latter. In view of the valency and radius, the order of the electron donating power of alkali metal atoms is K>Na>Li and corresponds to the order of the basic strengths of tertiary phosphates: K_3PO_4>Na_3PO_4 >Li_3PO_4. A portion of the structure of an acidic phosphate is probably as given below. Since the negative charge on the oxygen of II is higher compared to that of III, the basicity of a tertiary phosphate is expected

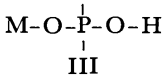

III

to be superior to that of an acidic phosphate. Indeed, this prediction is confirmed by the results from basic property measurements and activity measurements. Ivanov *et al.*[2] have also reported that the activity of the neutral phosphates is greater than that of the disubstituted phosphates. No basicity or the very low activity[1] of a pyrophosphate can be attributed to the poorer negative charge on the oxygen atom in M–O linkages of IV, because the electron-withdrawing power

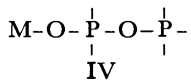

IV

of pyrophosphate ion is considered to be stronger than that of orthophosphate ion.

According to Tillmanns and Baur,[11] NaOH is built into the crystal structure of $Na_3PO_4 \cdot 12H_2O$ and its amount (0—0.25 mol) depends on the conditions under which the crystal was formed. If this is the case, it seems to deserve examination how NaOH contributes to the basicity of tertiary sodium phosphate. It was found that both NaOH and KOH initially show little basicity, but the basic colors of bromothymol blue and phenolphthalein adsorbed on the solids gradually deepen as the suspensions take up moisture. Moreover, neither dry nor wet salts converted 2,4-dinitroaniline and 4-chloro-2-nitroaniline to their conjugate bases. These results indicate that a caustic alkali is not a so-called solid base, and its concentrated solution has not so high basic strength as the surface of K_3PO_4 has. Therefore, the basic properties of metal phosphates are considered to be predominantly attributable to negatively charged oxygens on structures I—III.

References

1) F. M. Scheidt, *J. Catal.*, **3**, 372 (1964).

2) V. Ivanov, V. K. Smirnova, A. P. Kleptsova, V. I. Barabash, N. E. Trarevskii, Yu. D. Emelin, N. A. Shirokov, and V. M. Zavalei, *Vestn. Leningr. Univ. Ser. Fiz. Khim.*, No. 4, **16**, 1939 (1961); *Chem. Abstr.*, **56**, 9465d (1962).

3) A. Tada, Y. Yamamoto, M. Itoh, and A. Suzuki, *Kogyo Kagaku Zasshi*, **73**, 1069 (1970).

4) T. Imanaka, Y. Okamoto, and S. Teranishi, This Bulletin, **45**, 1353 (1972).

5) J. Take, N. Kikuchi, and Y. Yoneda, *J. Catal.*, **21**, 164 (1971).

6) Y. Fukuda, T. Nishizaki, and K. Tanabe, *Nippon Kagaku Zasshi*, **1972**, 1756.

7) Y. Fukuda, K. Tanabe, and S. Okazaki, *ibid.*, **1972**, 513.

8) C. Duval, "Inorganic Thermal Gravimetric Analysis," Elsevier Publ. Co., New York (1963).

9) L. Ben-Dor and I. Felner, *Inorg. Chim. Acta*, **4**, 49 (1970).

10) J. R. van Wazer, "Phosphorus and its Compounds," Interscience Publishers, New York, London (1958).

11) E. Tillmanns and W. H. Baur, *Inorg. Chem.*, **9**, 1957 (1970).

Resonance Raman Spectra of Methylorange Bound to Proteins and Cationic Surfactants

Bak-Kwang Kim, Akira Kagayama, Yutaka Saito, Katsunosuke Machida, and Toyozo Uno
Faculty of Pharmaceutical Sciences, Kyoto University, Sakyo-ku, Kyoto 606
(Received December 9, 1974)

Resonance Raman spectra of methylorange were recorded for aqueous solutions containing various proteins and cationic surfactants. The base form of methylorange was found to retain its trans-azo structure on the interaction with human serum albumin and with cetyltrimethylammonium bromide. The relative intensities of the Raman bands at 1420 cm^{-1} and at 1155 cm^{-1} of methylorange change appreciably along with the shift of the absorption maximum in the visible and ultraviolet region on addition of proteins and surfactants.

Proteins and surface active agents give rise often to the anomaly in visible and ultraviolet absorption spectra and the deviation of the color-change interval of various acid-base indicators.[1-4] This phenomenon has long been the subject of extensive studies with special attention on the intermolecular interaction involved. Structure changes of indicator molecules associated with this color change may be reflected, if any, in resonance Raman spectra of the indicators in aqueous solutions in the presence of proteins and surfactants.

The absorption maximum, λ_{max}, in the visible absorption spectrum of methylorange (MO) in neutral aqueous solutions undergoes a blue shift by 20—30 nm on addition of bovine serum albumin (BSA).[2,3] Various postulates such as the change in the molecular environment[5] or the twisting around the N=N bond[6] have been forwarded to account for this shift. Carey *et al.* have recently found, based on rather small changes in the resonance Raman spectrum, that no appreciable twisting around the N=N bond occurs for MO bound to BSA.[7] Change of the λ_{max} in the visible and ultraviolet absorption spectra of MO is also known for the solutions containing human serum albumin (HSA),[5] poly-L-lysine hydrobromide (PLL)[8] and cetyltrimethylammonium bromide (CTB).[4,8] We have investigated the effects of these substances on the resonance Raman spectrum of MO with particular interest in the change of the relative band intensities.

Experimental

Reagent grade methylorange (Tokyo Kasei Co.) was recrystallized several times from water. Crystallized and lyophilized bovine serum albumin (Sigma Chem. Corp.), poly-L-lysine hydrobromide (Protein Research Foundation, Osaka) and crystallized human serum albumin (Miles Lab.) were used without further purification. Cetyltrimethylammonium bromide (Tokyo Kasei Co.) was recrystallized from ethanolic solution. The concentration of MO in the sample solutions was 1×10^{-4} M and those of proteins and surfactants were between 5% and 0.5%. The pH of these solutions was controlled by using 0.1 M HCl and the phosphate buffers, and was determined by Radiometer titrator TTT2 and combined electrode GK 2302C.

Resonance Raman spectra were recorded on a JEOL S-1 laser Raman spectrophotometer with the spectral slitwidth 12 to 15 cm^{-1}. The excitation lines at 514.5 nm, 488.0 nm and 476.5 nm were obtained from a Coherent 52G Ar^+ laser. The sample solutions were sealed in 1 mm glass capillary tubes. Band intensities were measured as the peak heights on appropriate base lines. The visible and ultraviolet spectra were recorded on a Shimadzu W-40 spectrophotometer.

Results and Discussion

In the previous work,[9] we could not detect any noticeable change in relative intensities of resonance Raman bands of the base form of MO on changing the excitation wavelength from 488.0 nm to 514.5 nm. The 1420 cm^{-1} band due to the N=N stretching vibration is always much stronger than the other bands. We found in this work, however, that the intensity ratio of the two bands at 1420 and 1155 cm^{-1}, I_{1420}/I_{1155}, in the spectra excited by the 514.5 nm line decreases appreciably on addition of BSA. It has been known that the λ_{max} of the base form of MO is at 464 nm in the neutral aqueous solution and shifts to 440—430 nm on addition of BSA up to 0.2%.[2,3] In the case of the presently used 3% BSA solution (pH 3.9—5.5), the λ_{max} of MO appears at 430 nm. Thus the change in I_{1420}/I_{1155} may be attributed to the different sensitivities of the band intensities I_{1420} and I_{1155} on the separation between the λ_{max} and the excitation wavelength. According to Ito *et al.*, the intensity of the N=N stretching band of *p*-aminoazobenzene at 1422 cm^{-1} increases much more quickly than those of two bands around 1150 cm^{-1} on changing the excitation wavelength from 632.8 to 337.1 nm.[10] In this work, a similar dependence of the relative band intensities on the excitation wavelength was observed for MO bound to BSA. As shown in Fig. 1, the ratio I_{1420}/I_{1155} increases when the excitation wavelength is

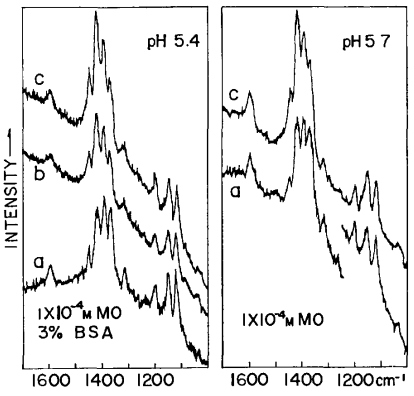

Fig. 1. Resonance Raman spectra of MO and MO–BSA solutions. Excitation wavelength: a, 514.5 nm; b, 488.0 nm; c, 476.5 nm.

shortened in the order 514.5, 488.0, and 476.5 nm. The BSA-bound molecules of MO excited by these Ar^+ lines seem therefore to be in the state of preresonance, during which the resonance effect on the stretching vibration of the N=N bond increases as the excitation line approaches the λ_{max} 430 nm. On the other hand, the unbound MO with the λ_{max} 464 nm shows no appreciable change in I_{1420}/I_{1155} on the change of the excitation line from 476.5 to 514.5 nm, probably because the band intensity I_{1420} is saturated under a rigorous resonance and is almost insensitive to the change of the excitation wavelength within the visible absorption band.

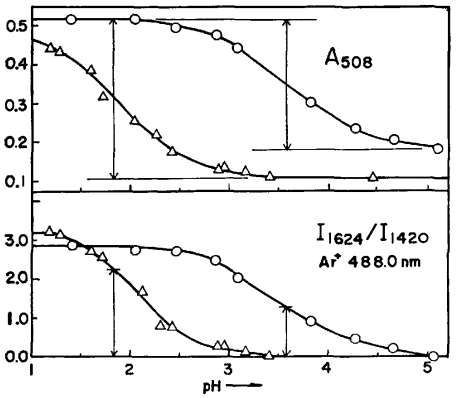

Fig. 2. The pH dependence of the absorbance (A_{508}) and the Raman intensity ratio (I_{1624}/I_{1420}): circle, 1×10^{-4} M MO; triangle, 1×10^{-4} M MO+3% BSA. The arrows indicate the pH at which the concentrations of the acid and the base forms become equal to each other.

The decrease of I_{1420} on the shift of λ_{max} from 464 nm to 430 nm is manifested in the change of the resonance Raman spectra of the bound MO and the unbound MO on the change of pH across the color-change interval. In the acidic solutions, MO is not bound to BSA, and the absorption spectrum of the acid form of MO (λ_{max}= 508 nm) dose not change on addition of BSA. The Raman band at 1624 cm^{-1} of the acid form of MO may thus be used, in the middle of the color change interval, as an internal standard to estimate the difference in I_{1420} between the bound MO and the unbound MO in the base form. In Fig. 2, the pH dependence of the ratio I_{1624}/I_{1420} is compared with that of the absorbance A_{508} for both the MO and the MO–BSA solutions. The pH's at which the concentrations of the base and the acid forms in these solutions become equal are easily determined from the sigmoid curves for A_{508}. Comparing the ratio I_{1624}/I_{1420} at these pH's, we can conclude that I_{1420} of MO bound to BSA is about 3/5 of that of the unbound MO.

Klotz *et al.* have found that the solution of MO containing HSA shows a complicated shift of the λ_{max} on the change of pH.[5] Figure 3 shows the resonance Raman spectra of the MO-HSA solution excited by the 488.0 nm and the 514.5 nm lines. The shifts of the λ_{max} on the addition of HSA and on the subsequent change of pH are not accompanied by the shift of the Raman bands, and the resonance Raman spectra of the MO–HSA solutions are entirely different from the previously reported spectrum of the acidic solution of MO.[9] This

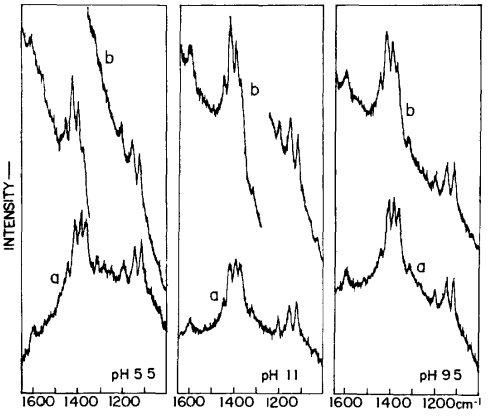

Fig. 3. Resonance Raman spectra of MO–HSA solutions (1×10^{-4} M MO+1.5% HSA) at various pH. Excitation wavelength: a, 514.5 nm; b, 488.0 nm.

result indicates that there is no proton donation from protein residues to MO bound to HSA. In the resonance Raman spectra of the MO-BSA solutions excited by the 514.5 nm line, the ratio I_{1420}/I_{1155} increases appreciably as the approach of the λ_{max} to the excitation wavelength. On the contrary, there seems to be no appreciable change in I_{1420}/I_{1155} on the change of the λ_{max} for the spectra recorded for the 488.0 nm excitation.

According to Quadrifoglio and Crescenzi, the λ_{max} of MO in the visible region undergoes a marked blue-shift to 370 nm on addition of poly-L-lysine hydrobromide (PLL).[8] These authors obtained, by using the 1×10^{-5}M solution, the absorption spectra in which no peaks were observed above 400 nm. Unfortunately, the limitation in the Raman sensitivity compelled us to use the solution 10 times as concentrated as these authors' solution, and with this concentration, we could not find the condition for eliminating a peak around 450 nm. The resonance Raman spectrum of this solution (Fig. 4) taken by the 488.0 nm excitation is the same as that of MO bound to HSA, and is thought to arise from the species responsible for the absorption at 450 nm.

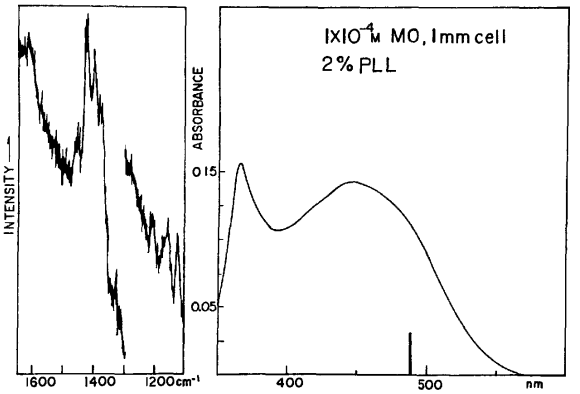

Fig. 4. Resonance Raman and visible absorption spectra of MO–PLL solution. The bar indicates the excitation wavelength (488.0 nm).

The absorption spectrum of the base form of MO changes in two steps on addition of the cationic surfactant cetyltrimethylammonium bromide (CTB). When the concentration of this surfactant is slightly lower than

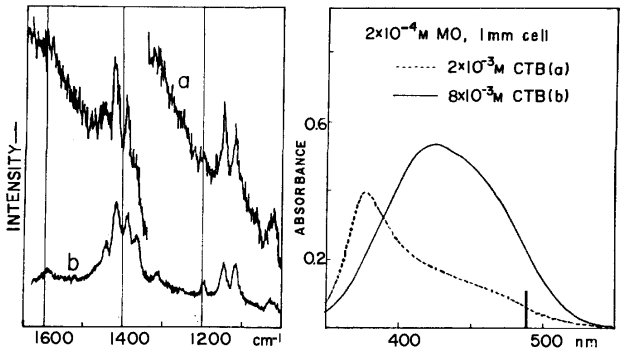

Fig. 5. Resonance Raman and visible absorption spectra of MO–CTB solutions. The bar indicates the excitation wavelength (488.0 nm).

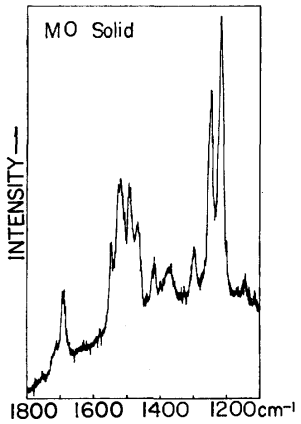

Fig. 6. Raman spectrum of solid MO excited by the He–Ne 632.8 nm line.

the critical micelle concentration (3×10^{-3} M), a peak appears at 370 nm as in case of MO bound to PLL.[8] As shown in Fig. 5a, the noise level of the resonance Raman spectrum of the MO solution containing 2×10^{-3} M of CTB is very high because the resonance effect is diminished according to the large separation between the λ_{max} and the excitation wavelength. It is recognized, however, that the intensity ratio I_{1420}/I_{1155} in Fig. 5a is appreciably smaller than that in the spectrum of the solution containing 8×10^{-3} M of CTB (Fig. 5b). In contrast to the case of the MO–PLL solution, the Raman bands shown in Fig. 5a and the λ_{max} at 370 nm are due certainly to the same species. A conformational change of the azo group from the *trans* form to the *cis* form has been postulated in order to explain the large blue-shift of the λ_{max} of MO on being bound to PLL and CTB.[8] However, the resonance Raman spectrum shows clearly that there is no possibility for such a conformational change; the *cis*-azo group is known to give the stretching frequency around 1500 cm^{-1}, about 100 cm^{-1} higher than that of the *trans*-azo group.[11] This conclusion has been drawn by Carey *et al.* for the BSA-bound MO showing the λ_{max} 430 nm.[7] When the concentration of CTB is much higher than the critical micelle concentration, the absorption spectrum of MO is similar to the case when BSA is added.[4] The corresponding Raman spectrum is identical to that of MO bound to BSA.

The difference in the sensitivities of the Raman band intensities to the excitation wavelength is reflected also on the spectra of MO in the crystalline state. As shown in Fig. 6, the Raman spectrum of the crystalline MO excited by the He–Ne 632.8 nm line gives the ratio I_{1420}/I_{1155} less than unity. According to the spectrum reported by Carey *et al.*, this ratio is much larger than unity when excited by the Ar^+ 488.0 nm line.[7] Presumably, the λ_{max} of the crystalline MO is at the shorter wavelength side of the 488.0 nm line, giving rise to the above difference in I_{1420}/I_{1155} between the 488.0 nm and the 632.8 nm excitations.

We wish to thank Professor Hisashi Tanaka for the use of the W-40 spectrophotometer in his laboraroty.

References

1) G. S. Hartley, *Trans. Faraday Soc.*, **30**, 444 (1934).
2) I. M. Klotz, *J. Am. Chem. Soc.*, **68**, 2299 (1946).
3) J. R. Colvin, *Can. J. Chem.*, **31**, 734 (1953).
4) C. F. Hiskey and T. A. Downey, *J. Phys. Chem.*, **58**, 835 (1954).
5) I. M. Klotz, R. K. Burkhard, and J. M. Urquhart, *J. Phys. Chem.*, **56**, 77 (1952).
6) W. F. Forbes and B. Milligan, *Australian J. Chem.*, **15**, 841 (1962).
7) P. R. Carey, H. Schneider, and H. J. Bernstein, *Biochem. Biophys. Res. Commun.*, **47**, 588 (1972).
8) F. Quadrifoglio and V. Crescenzi, *J. Colloid Interface Sci.*, **35**, 447 (1971).
9) K. Machida, B.-K. Kim, Y. Saito, K. Igarashi, and T. Uno, This Bulletin, **47**, 78 (1974).
10) S. Koide, Y. Udagawa, N. Mikami, K. Kaya, and M. Ito, This Bulletin, **45**, 3542 (1972).
11) R. Kübler, W. Lüttke, and S. Weckherlin, *Z. Elektrochem.*, **64**, 650 (1960).

Studies of Aqueous Sodium Dodecyl Sulfate Solutions by Activity Measurements

Tsunetaka SASAKI, Michihiro HATTORI,*1 Jun SASAKI,*2 and Kenji NUKINA*3

Department of Chemistry, Faculty of Science, Tokyo Metropolitan University, Setagaya, Tokyo 158

(Received December 12, 1974)

The activities of surfactant ions (a_D) and counterions (a_{Na}) were directly obtained by the EMF measurement of a concentration cell with an ion-exchange membrane and by pNa measurements respectively for aqueous solutions of sodium dodecyl sulfate (NaDS) below and above the CMC. The mean activity and activity coefficient were also calculated. From these data, together with the surface tension (γ) measured by the Wilhelmy method and the amount of adsorption (Γ) measured by the radiotracer method, the following results were obtained: (1) Mean activity was not constant, but increased with the concentration above the CMC. (2) The Gibbs adsorption isotherm was directly verified from the a_D and a_{Na} *vs.* concentration relations. (3) The decrease in γ observed above the CMC was in agreement with that calculated from the activity data. (4) The log a_D *vs.* log a_{Na} plots above the CMC showed a linear relation, indicating the validity of the charged phase separation model as the mechanism of micelle formation. The degree of the counterion attachment of the micelles was found to be 0.73 up to about 80 mmol/l. (5) The intermicellar concentrations of Na^+ and DS^- ions were calculated; the former increases, while the latter decreases with the concentration. (6) The product of the concentration with an osmotic coefficient was linear with the concentration above the CMC, tangent of the slope being about 0.7.

A number of problems remain unconfirmed as regards the properies of aqueous solutions of surface active substances, in spite of their theoretical and practical importance. For instance: 1) Surface tension of an aqueous surfactant solution usually shows aging, and empirical equations to give a correct surface tension by extrapolating it to the sufficiently long time have been proposed.[1-4] On the other hand, some are of the opinion that such aging is due to the presence of impurities and that purification largely eliminates the time effect.[5-7] 2) The formation of dimers or premicelles below the CMC and the second- and higher-order CMC's have been suggested,[8-11] but the absence of such aggregates has also been insisted on.[12,13] 3) The constancies of the activity,[14] the intermicellar concentration,[15-17] and the surface tension above the CMC have often been stated or assumed,[14] whereas a gradual decrease in the surface tension,[5,6] in the intermicellar surfactant concentration,[18,19] and an increase in the activity[6,20] have also been reported. 4) As to the micelle formation, theories based upon the mass action law[6,21,22] and the phase separation mechanism[14,23-25] have been proposed and discussed. Also, a theory covering both mechanisms has been stated.[14] The degrees of the counterion attachment of the ionic micelle thus far reported widely differ from each other according to the method of measurement.[26-28] 6) The equation for the calculation of the activity coefficient of large organic ions has been proposed,[29] but a large deviation from the calculated value has also been experimentally confirmed.[11] 7) A number of studies of the experimental confirmation of the Gibbs adsorption isotherm for an aqueous solution of the surfactant have been reported,[30-34] but no confirmation based upon the direct measurements of all the quantities involved in the isotherm, *i.e.*, the surface tension of the solution, the amount of adsorption and the activity of the surfactant, has yet been attempted as far as the present authors are aware.

The measurement of the activity of a surfactant, together with measurements of the amounts of the adsorption and surface tension of the surfactant solution, enables us not only to make a direct confirmation of the Gibbs adsorption isotherm, but also to solve most of the other problems listed above without any assumptions. The present paper will deal with these studies of an aqueous solution of sodium dodecyl sulfate.

Experimental

Materials. The surfactant used was sodium dodecyl sulfate (NaDS), which has been prepared by the sulfation of dodecanol free from its homologues with chlorosulfonic acid,[35] followed by purification by solvent extraction using ethyl ether and recrystallization from ethanol. The purity was confirmed by the absence of a minimum in the surface tension *vs.* concentration curve. The ammonium nitrate used for the agar bridges was recrystallized from a pure commercial product.

Activity Measurement. The activity of sodium ions, a_{Na} was measured by using a Hitachi-Horiba N-5 pNa meter as a sodium responsive electrode. The cell used was

pNa electrode | NaDS (a_{Na}) | NH_4NO_3 (1M) | KCl (saturate) | calomel electrode (saturate)

Sodium chloride of a known activity was used to confirm that the electrode was acting correctly according to the Nernst equation. The activity of sodium ions, a_{Na}, was then calculated according to the following equation:

$$\log a_{Na} = \frac{0.4343F}{RT}(E_{Na} - E_{Na,0}) \quad (1)$$

where E_{Na} is the EMF of the cell; F, the Faraday constant; T, the absolute temperature; R, the gas constant, and $E_{Na,0}$, a constant depending on the calomel and the glass electrodes. The $E_{Na,0}$ value was determined by extrapolating an extrapolation function;[36]

*1 Present address: Household Good Research Laboratory Kao Soap Co. Ltd., Sumida, Tokyo.

*2 Present address: Fuji Photo-Film Co. Ltd., Nakanuma 210, Minami-Ashigara.

*3 Present adress: Kawamura Institute of Chemical Research, Kamikizaki 2-7-8, Urawa.

$$\Delta_{Na} = \frac{0.4343F}{RT}E_{Na} - \log C$$

to $C=0$; namely,

$$E_{Na,0} = \frac{RT}{0.4343F}\lim_{C\to 0}\Delta_{Na} \qquad (2)$$

where C is the concentration of sodium dodecyl sulfate.

As for the measurement of the activity of dodecyl sulfate ions, a_D, methods using the Hg/HgDS electrode[37] and a concentration cell using an ion-exchange membrane[28,38] or an oil-phase as a semipermeable septum[39] have been reported. However, the Hg electrode liberates Hg ions, which may influence the dissolved state of DS^- ions in an unpredictable way, and the oil-phase cell is unfavorable because of the possibility of the solubilization of the oil by the surfactant micelles. Thus, the concentration cell using an ion-exchange membrane is preferable. A cell of the following type was used in the present experiment:

calomel electd. (sat)	KCl (sat)	NH_4NO_3 (1M)	NaDS (a_D)	NaDS ($a_{D,10}$)	KCl (sat)	NH_4NO_3 (1M)	calomel electd. (sat)

Here, || indicates the anion-exchange membrane, NEOSEPTA AV-4T, the product of the Tokuyama Soda Co., Ltd.; NaDS ($a_{D,10}$), the reference solution of 10 mmol/l NaDS, and (sat), a saturated solution. A 1 M NH_4NO_3 solution was used for the agar bridges.

The ion-exchange membrane used was 0.16 cm thick. It was cut in 1.5 cm square piece and was made permeable only to dodecyl sulfate ions by soaking it in a 10 mmol/l NaDS solution for two days. Immediately before use, it was rinsed with as little water as possible and firmly supported by pressing it between two franged tubes, 5 mm in inner diameter, containing the sample and referenee solutions. The reference solution of 10 mmol/l NaDS was chosen since the electrode potential was confirmed to be almost constant near this concentration. A steady EMF value, E_D', was exhibited after 30 to 60 min, and the equilibrium value, E_D, was obtained by subtracting from E_D', the asymmetry potential measured, after each measurement of E_D', for the cell prepared by filling both sides of the membrane with the 10 mmol/l NaDS solution. To obtain reproducible results, the membrane was renewed after three successive measurements. The calculation of the activity, a_D, will be described later.

Surface Tension Measurement. The surface tension was measured by the Wilhelmy method using a Shimadzu Surface Tensiometer, ST-1. The vassel containing the solution was doubly covered with glass plates, each having a small hole at its center for the passage of a rod attached to a vertical hanging plate. Contamination from the surrounding atmosphere and the evaporation of water during the measurement were practically avoided by this device. The surface tension was automatically recorded with the time, In cases in which the surface tension decreased with the time, the steady values finally obtained or extrapolated were used for the calculation.*

The EMF and surface tension measurements were carried out at 25 °C.

Results and Discussion

Surface Tension. The surface tension *vs.* concentration relation is shown in Fig. 1. As may be seen, the surface tension decreases with an increase in the concentration and a sharp break point appears at about 7.6 mmol/l, contrary to the curve without a sharp break near the CMC reported by Mysels.[6] Above the CMC, the surface tension stays nearly constant up to about 20 mmol/l, beyond which it decreases slowly with the concentration. Since, above CMC, the surface tension does not change with the time, a gradual though slight decrease is certain, as Mysels indicated.[6] It should be noted that the constancy of the surface tension of the surfactant solution above the CMC often cited[14,17] is not always valid.

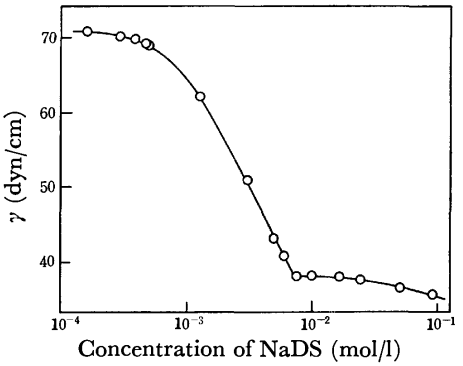

Fig. 1. Surface tension of aqueous NaDS solution.
γ: Surface tension of NaDS soln.

Activity and Activity Coefficient. The activity of Na^+ ions was calculated according to

$$\log a_{Na} = \frac{0.4343F}{RT}E_{Na} + 0.01 \quad (a_{Na} \text{ in mol/l}) \qquad (3)$$

which was obtained by putting the observed value of Eq. (2) into Eq. (1). The calculation of a_D is similar to that of a_{Na}, but it is somewhat complicated.

The EMF of the DS^- ion-concentration cell is expressed as

$$E_D = \frac{\lambda RT}{0.4343F}\log\frac{a_D}{a_{D,10}} \qquad (4)$$

where $\lambda = u_- - u_+$, and u_- and u_+ are the transport numbers of DS^- and Na^+ ions respectively in the membrane. Then the extrapolation function takes the following form:

$$\Delta_D = \frac{0.4343F}{\lambda RT}E_D - \log C \qquad (5)$$

By putting $\lambda = 1$ in Eq. (5), we obtain, similarly to Eq. (2),

$$\log a_{D,10} = -\lim_{C\to 0}\Delta_D$$

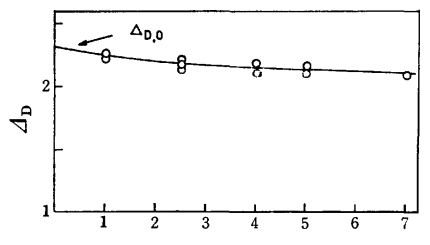

Fig. 2. Extrapolation of Δ_D function.
Δ_D: Extrapolation function (see text)
$\Delta_{D,0}$: Δ_D extrapolated to $C=0$

* As to the aging of an aqueous surfactant solution, we should like to discuss it in detail elsewhere.

The plot of Δ_D *vs.* C is shown in Fig. 2; extrapolation gave $\log a_{D\cdot 10} = -2.30$. Then, a_D was calculated, according to Eq. (4), by

$$\log a_D = \frac{0.4343F}{RT}E_D - 2.30 \quad (a_D \text{ in mol/l}) \qquad (6)$$

Here the assumption of $\lambda=1$ might be valid, considering that the value of $dE_D/d \log C$ observed is equal to the value of $RT/0.4343F$ and that Δ_D *vs.* C is linear as a whole down to a low concentration of NaDS, where the plots are expected to deviate markedly from linearity if λ is slightly less than unity.* A rough estimation shows that λ is larger than 0.99. Also, the agreement between the calculated and observed values of the amount of adsorption below the CMC, to be discussed later, indicates λ as unity.

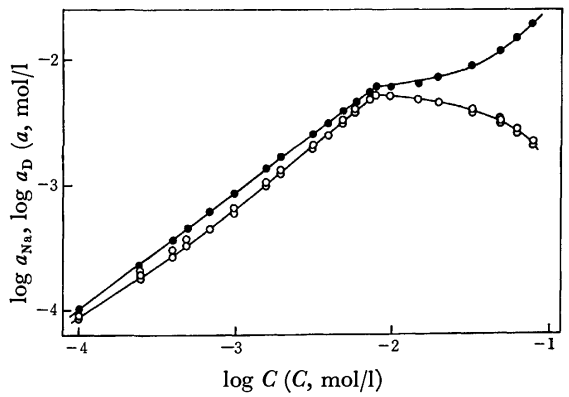

Fig. 3. Activities of Na^+ and DS^- *vs.* NaDS concentration.
a_{Na}, a_D: Activies of Na^+ and DS^- ions, respectively

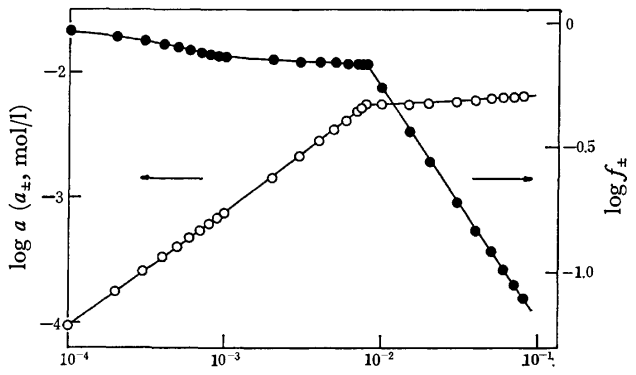

Fig. 4. Mean activity and activity coefficient of NaDS.
$a_\pm$, $f_\pm$: Mean activity and activity coefficient, respectively

The values of a_{Na} and a_D calculated according to Eqs. (3) and (6) are plotted against log C in Fig. 3. The mean activity, $a_\pm$, and the mean activity coefficient, $f_\pm$, are shown in Fig. 4. It is found that

$$\log f_\pm = -(0.033 \log C + 0.240) \quad (C \text{ in mol/l}) \qquad (7)$$

holds for the concentration region from 1×10^{-3} mol/l up to the CMC and that

$$\log f_\pm = -(0.930 \log C + 2.125) \quad (C \text{ in mol/l}) \qquad (8)$$

holds above the CMC up to about 80×10^{-3} mol/l. The coefficient of 0.033 of Eq. (7) is in accord with the estimation of Mysels.[6] However, rather unexpectedly, $f_\pm=0.68$ was obtained at the CMC. This is considerably smaller than the value of about 0.9 calculated by the modified Debye-Hückel equation, taking account of the molecular size.[29] In this connection, it is noticable that a similar value of $f_\pm=0.7$ was recently reported for cetyltrimethylammonium bromide near the CMC.[11] Whether or not this low $f_\pm$ value is due to the dimerization or premicelle formation of surfactant molecules, as has been suggested in the report, requires further study. However, it is necessary at least to check experimentally the validity of the conventional formula used for the calculation of the activity coefficients of the large organic ions mentioned above.[29]

Adsorption Isotherm below the CMC. The Gibbs adsorption isotherm is written in its general form as:

$$-d\gamma = RT\sum_i \Gamma_i \ln a_i \qquad (8)$$

where γ is the surface tension of a solution, and Γ_i and a_i, the amounts of adsorption and the activity of the i'th component of the solutes in the solution respectively. For the 1—1 electrolyte, Eq. (8) takes the form:

$$\Gamma = -\frac{d\gamma}{2RTd \ln a_\pm} = -\frac{d\gamma}{2RTd \ln f_\pm C} \qquad (9)$$

A number of studies of the verification of the Gibbs adsorption isotherm have been reported, in which the activity coefficient has been properly calculated by, for instance, using a modified Debye-Hückel equation,[29,40] or has been assumed to be unity.[41] However, in the present experiment, it is possible to confirm Eq. (8) by a direct measurement of the activity change with the concentration of NaDS without reference to the activity coefficient.

For this purpose, Eq. (8) is rewritten for an aqueous solution of NaDS as

$$\Gamma = \frac{0.4343d\gamma/d \log C}{RT(d \log a_{Na}/d \log C + d \log a_D/d \log C)} \qquad (10)$$

According to Eq. (10), the amount of adsorption can be calculated from $d\gamma/d \log C$, $d \log a_{Na}/d \log C$ and $d \log a_D/d \log C$, which are obtained from the tangents to the curves of Figs. 1 and 3. The calculated values of

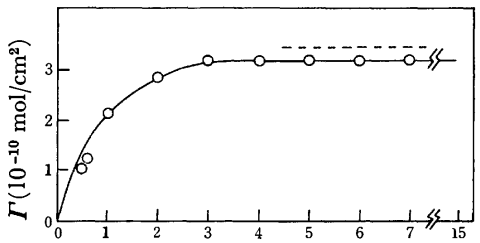

Fig. 5. Direct confirmation of Gibbs adsorption isotherm for NaDS soln.
Γ: Amount of adsorption
○: Γ calculated from steady γ value
——: Γ calculated from γ extrapolated to time zero
——: Γ observed

* A detailed discussion of λ will be made in a following paper.

Γ are plotted against C in Fig. 5 as a solid line, together with the observed amount of adsorption (open circles) obtained by the radiotracer method using tritiated NaDS.[42] The agreement is seen to be satisfactory, except for a slight deviation for dilute solutions. This is the most direct confirmation of the Gibbs adsorption isotherm in that the calculation is solely based on the observed data, without any assumptions.

It may also be pointed out that, as was mentioned above, the surface tension used for the calculation is the steady value attained after a sufficient time. The value of Γ calculated by using the surface tension extrapolated to time zero is also shown as a broken line, but it does not agree with the observed value . This is an indication that the steady value of the surface tension is better taken as an equilibrium, and the attribution of the surface aging to impurities is not valid, at least in the present case.

The agreement of the calculated and observed Γ's also indicates that λ is unity, since the introduction of a λ value of less than unity reduces the calculated Γ to $\lambda\Gamma$, resulting in a disagreement of the observed and calculated Γ's. The argument is the same for Eq. (11).

Surface Tension above the CMC. As is shown in Fig. 1, the surface tension remains nearly constant above the CMC up to about 20 mmol/l, and then it decreases with the concentration of NaDS. Since it is often stated that the surface tension above the CMC is constant and that the constancy is an indication of the micelle formation being the phase separation,[14] it is worthwhile to confirm the observed decrease in the surface tension by an independent calculation. In this connection, Mysels has made an elaborate computer calculation of the surface tension of an aqueous NaDS solution above the CMC, assuming that the micelle formation obeys the mass action law and that the activity coefficient is independent of the concentration.[6] In the present study, however, the observed $a_{\pm}$ *vs.* C relation shown in Fig. 4 makes possible a simple and direct calculation of the surface tension above the CMC without such assumptions.

Since Γ is confirmed to be constant, 3.19×10^{-10} mol/cm^2,[42] the integration of Eq. (9) above the CMC gives

$$\gamma = \gamma_8 - \frac{2RT}{0.4343}\Gamma_8[\log a_{\pm} - a_{\pm,8}] \qquad (11)$$

where γ_8, Γ_8 and $a_{\pm,8}$ denote the γ, Γ and $a_{\pm}$ values of NaDS respectively, at the concentration of 8×10^{-3}mol/l. From the observed relations of $a_{\pm}$ *vs.* C, the surface tension above the CMC was calculated according to Eq. (11). The values of γ calculated are plotted against C in Fig. 6 as open circles, together with the observed surface tension, shown by a solid line. An agreement between the observed and calculated values is seen. Here, the constancy of Γ has been confirmed experimentally up to about 15 mmol/l,[42] but the agreement seen in Fig. 5 may suggest a further constancy of Γ up to about 80 mmol/l NaDS.

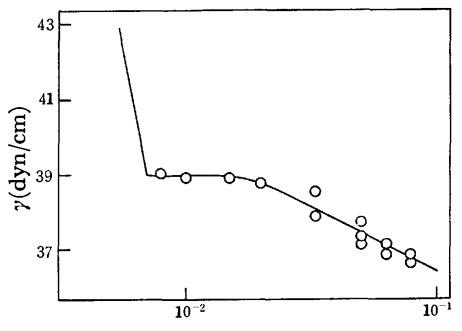

Fig. 6. Observed and calculated surface tension above CMC.
γ: Surface tension of NaDS soln
——: Observed γ
○: Calculated γ

TABLE 1. COUNTERION ATTACHMENT OF NaDS MICELLES

Degree of counterion attachment (r)	Method of measurement	Reference[a]
0.86	EMF (a_{Na})	26
0.85	Light scattering	43
0.84	EMF (a_{Na})	15, 37
0.82	Mass action law	22
0.82	Equil. dialysis	44
0.80	Osmotic coef.	45
0.78	EMF (a_{Na})	46
0.75	Mass action law	6, 47
0.74	Osmotic coef.	45
0.73	EMF (a_{Na}, a_D)	Present exp.
0.72	Electrophoresis	48
0.63	EMF (E_{Na}, E_D)	28
0.50	Zeta-potential	27
0.46	Mass action law	49

a) For further references see, E. W. Anacker, "Cationic Surfactants," edited by E. Jungermann, Marcel Dekker, Inc., New York (1970), p. 272.

Micelle Formation and Counterion Attachment. As has been mentioned, various mechanisms of micelle formation have been proposed,[14,23-25] but no satisfactory understanding has yet been obtained, at least experimentally. A similar situation prevails as to the degree of counterion attachment, r, of an ionic micelle. Various methods have been employed to estimate r; values ranging from 0.46 to 0.86 have been reported for NaDS, as shown in Table 1. The wide scattering of the data comes from the differences in the methods of measurement and in the assumptions necessary for the calculation. Also, in this case, the activity measurement enables us to give convincing answers to the questions of both the mechanism of micelle formation and the degree of counterion attachment.

According to the mass action law, the micelle formation of NaDS is expressed as a homogeneous equilibrium by[21,22]

$$p\mathrm{DS}^- + q\mathrm{Na}^+ \rightleftarrows \mathrm{Na}_q\mathrm{DS}_p^{-(p-q)}$$

and the condition of equilibrium by

$$a_M/(a_D^q \cdot a_{Na}^p) = \text{constant} \qquad (12)$$

where a_M is the activity of micelles, and p and q, the numbers of DS^- and Na^+ ions respectively forming a

micelle.

On the other hand, according to the phase separation theory,[23-25] micelles are considered as a separate microphase or pseudophase, and the micelle formation is expressed:

1) in the case of an unchanged phase separation, by

$$p\mathrm{DS}^- + p\mathrm{Na}^+ \rightleftarrows \mathrm{Na}_p\mathrm{DS}_p \quad \text{(separate phase)}$$

and the equlibrium condition by

$$a_{\mathrm{Na}} \cdot a_{\mathrm{D}} = \text{constant} \tag{13}$$

2) in the case of a charged phase separation, by

$$p\mathrm{DS}^- + q\mathrm{Na}^+ \rightleftarrows \mathrm{Na}_q\mathrm{DS}_p^{-(p-q)} \quad \text{(separate phase)}$$

and the equilibrium condition by

$$a_{\mathrm{Na}}{}^q \cdot a_{\mathrm{D}}{}^p = \text{constant}, \quad p \neq q \tag{14}$$

Eqs. (12), (13), and (14) may be summarized as

$$\left.\begin{aligned} &\log a_{\mathrm{D}} + r \log a_{\mathrm{Na}} \neq \text{constant} \qquad \text{mass action law} \\ &\log a_{\mathrm{D}} + r \log a_{\mathrm{Na}} = \text{constant} \\ &\qquad r = 1, \text{ uncharged phase separation model} \\ &\qquad r \neq 1, \text{ charged phase separation model} \end{aligned}\right\} \tag{15}$$

where $r = q/p$.

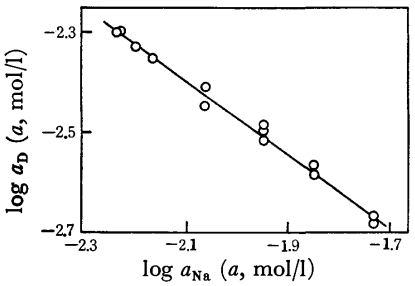

Fig. 7. Log a_{D} *vs.* log a_{Na} above CMC.
a_{D},a_{Na}: Activities of Na^+ and DS^- ions, respectively observed above CMC

As is shown in Fig. 7, the plot of log a_{D} *vs.* log a_{Na} gives a straight line expressed by

$$\log a_{\mathrm{D}} + r \log a_{\mathrm{Na}} = \text{constant} \tag{16}$$

with $r=0.73$ and the constant $=-3.94$. According to Eq. (15), Eq. (16) clearly indicates that the charged phase separation is the most probable mechanism of micelle formation; the charged micelles with the degree of counterion attachment of 0.73 are considered to form up to a concentration of about 80 mmol/l. The value of $r=0.73$ is also listed in Table 1. It may be noted that, among the widely scattered values of r, that obtained in the present study is sufficiently reliable, since it is almost free from any assumptions or approximations. It should be noticed in connection with Eq. (16) that it is the product of $a_{\mathrm{D}}{}^p \cdot a_{\mathrm{Na}}{}^q$ that becomes constant above the CMC. Since $p \neq q$ has been confirmed, $a_\pm = (a_{\mathrm{D}} \cdot a_{\mathrm{Na}})^{1/2}$ is not constant, but slowly increases with the concentration, as is shown in Fig. 4. This is not in agreement with the constancy of $a_\pm$ often stated in connection with the phase separation theory.[14,25] However, it is also contrary to the opinion that the phase separation requires a constancy of $a_\pm$ above the CMC,[20] since the charged phase separation model explains the change of $a_\pm$ above the CMC as has been described above.

The only question remaining is whether or not the aggregates bearing the net electrical charge can be separated as a phase. It may be possible only when the aggregates are separated as such a microphase as the form of micelles. For this reason, it is better called microphase separation or pseudophase separation, as has been proposed by Shinoda.[14,25] The increase in $a_\pm$ above the CMC also corresponds to the decrease in the surface tension in this region, as is shown in Fig. 1.

Equation (16) bears another implication. It is known[21,22,49] that the CMC of an ionic surfactant, C_{M}, decreases with the concentration of added salt, C_{S}, as

$$\log C_{\mathrm{M}} = -k \log (C_{\mathrm{M}} + C_{\mathrm{S}}) - m \tag{17}$$

where $C_{\mathrm{M}}+C_{\mathrm{S}}$ expresses the total counterion concentration, and k and m are constant. Here, if we replace C_{M} by a_{D} and $C_{\mathrm{M}}+C_{\mathrm{S}}$ by a_{Na}, we obtain an equation similar to Eq. (16), with k corresponding to r. This means that the application of Eq. (17) is not restricted to the solution at the CMC, but is extended above the CMC to the relation between the intermicellar activities (concentration) of single surfactant ions and counterions.

The numerical values of k and m of Eq. (17) have been reported to be 0.88 and 3.89[21] or 0.679 and 3.508[50] respectively. The constant of Eq. (16) is in close agreement with the former m value with an opposite sign, while the r value of Eq. (16) lies between the above two k's. The disagreement comes from the differences in the activity and concentration involved respectively in Eqs. (16) and (17). It is interesting to notice that the slope of Eq. (17) can be interpreted as the degree of counterion attachment from the viewpoint of mass action theory also, provided the aggregation number of the micelle (p in Eq. (12)) is large.[21,22]

The second- and higher-order CMC's could not be confirmed up to 80 mmol/l for an aqueous NaDS solution as far as the counterion attachment and activity measurements are concerned.

Intermicellar Ion Concentration. Although sugestions have been made referring the decrease in the intermicellar concentration of surfactant ions,[18,19] the constancy of the intermiceller concentration is practically assumed to be equal to C_{M} in most studies,[15-17] and its actual measurement has not been attempted.

Considering the electrical neutrality of the ions in the solution of NaDS as a whole, and the excess number of DS^- ions compared with that of the Na^+ ions in Na DS micelles, the intermicellar concentration of the DS^- ions is expected to be smaller than that of the Na^+ ions. In addition, the increase and decrease in the activities of the Na^+ and DS^- ions respectively with concentrations above the CMC may suggest an increase and a decrease in the concentration of the respective ions. The intermicellar concentration of the DS^- and Na^+ ions can be estimated from the a_{D} and a_{Na} measurenents as follows.

The activities of Na^+ and DS^- ions above the CMC are expressed by

$$a_{\mathrm{Na}} = f_{\mathrm{Na}} C_{\mathrm{Na}} \quad \text{and} \quad a_{\mathrm{D}} = f_{\mathrm{D}} C_{\mathrm{D}} \tag{18}$$

where f_{Na} and f_{D} are the true activity coefficients, and C_{Na} and C_{D}, the intermicellar concentrations of the Na^+ and DS^- ions respectively. Then we obtain from Eq.

(18)

$$a_{\pm} = f_{\pm}C_{\pm} \tag{19}$$

where

$$C_{\pm} = C_{Na}C_D \tag{20}$$

Further, we obtain from the condition of the electrical neutrality,

$$C_{Na} = (C-C_D)(1-r) + C_D \tag{21}$$

Now, if we neglect the effect of micelles on the activity coefficient above the CMC, Eq. (7) can be considered to hold above the CMC,[6] with C being replaced by $C_{\pm}$, and the following relation is obtained:

$$\log f_{\pm} = -(0.033 \log C_{\pm} + 0.240) \tag{22}$$

From Eqs. (19) to (22) with r=0.73, we obtain

$$C_D = -0.185 + 0.685[0.0729C^2 + 2.92 \times 10^{0.496+2.068 \log a_{\pm}}]^{1/2} \tag{23}$$

According to Eq. (23), the intermicellar concentration, C_D, can be calculated from the $a_{\pm}$ *vs.* C relation above the CMC as is shown in Fig. 4. The values of C_{Na} can be calculated by putting the value of C_D thus obtained into Eq. (21). The C_D and C_{Na} values thus calculated are plotted against C in Fig. 8, together with $C_{\pm}$.

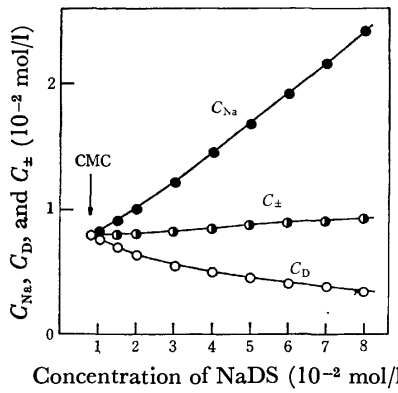

Fig. 8. Intermicellar concentrations of Na^+ and DS^- ions and $C_{\pm}$.
C_{Na},C_D: Intermicellar concentrations of Na^+ and DS^- ions, respectively
$C_{\pm}$: $(C_{Na} \cdot C_D)^{1/2}$

It may be seen that C_{Na} increases, while C_D decreases, with the increase in the NaDS concentration. The mean intermicellar concentration, $C_{\pm}$, is seen to be nearly constant or to increase only slightly with the concentration. Here, it should be noted that the actual micellar concentration, $C-C_D$, is larger than the usually assumed concentration, $C-C_M$.[15,16,21,22] However, the problem of the influence of micelles on the activity coefficient of NaDS remains unsolved; it may affect the calculation of the intermicellar concentration of the surfactant.

Osmotic Coefficient above the CMC. Brady reported that, for some surfactants, the product of the concentration, C, and the osmotic coefficient, g, plotted against C consists of two straight lines, with a break point at the CMC, and that the slope of the straight line:

$$d(gC)/dC = \beta \tag{24}$$

is proper to each substance.[51]

Applying the Gibbs-Duhem relation to Eq. (24), we obtain

$$\frac{d(gC)}{dC} = \frac{d \ln a_{\pm}}{d \ln C} = 1 + \frac{d \log f_{\pm}}{d \log C} = \beta \tag{25}$$

Eqs. (8) and (25) give β=0.07 above the CMC, which is comparable with the value of 0.06 for dodecylsulfonic acid.[52]

References

1) A. Boutaric and P. Berthier, *J. Chim. Phys.*, **36**, 1 (1939); S. Ross, *J. Phys. Chem.*, **49**, 377 (1945).
2) H. Lange, *Proc. 3rd. Int Congr. Surface Active Substances*, **1**, 279 (1960).
3) M. Nakamura and T. Sasaki, This Bulletin, **43**, 3667 (1970).
4) A. W. Adamson, "Physical Chemistry of Surfaces," 2nd ed., Interscience Publishers, New York (1967), p. 31.
5) A. P. Brady, *J. Phys. Chem.*, **53**, 56 (1949).
6) H. Elworthy and K. J. Mysels, *J. Colloid Interfac. Sci.*, **21**, 331 (1966).
7) K. J. Mysels and A. T. Florence, *ibid.*, **43**, 577 (1973).
8) P. Ekwall, *Proc. 4th Int. Congr. Surface Active Substances*, **2**, B 651 (1964); P. Mukerjee, K. J. Mysels, and C. I. Dulin, *J. Phys. Chem.*, **62**, 1390 (1958).
9) D. Eagland and F. Franks, *Trans. Faraday Soc.*, **61**, 2468 (1965).
10) P. Mukerjee, *J. Phys. Chem.*, **69**, 2821 (1965).
11) A. I. Rusanov and V. V. Krotov, *Proc. 6th Int. Congr. Surface Active Subsrtances*, **2**, Part 2, 795 (1973).
12) F. van Voorst Vader, *Trans. Faraday Soc.*, **57**, 110 (1961).
13) G. D. Parfit and A. L. Smith, *J. Phys. Chem.*, **66**, 942 (1962).
14) K. Shinoda and E. Hutchinson, *ibid.*, **66**, 577 (1962); F. M. Fowkes, *ibid.*, **66**, 1843 (1962).
15) C. Botré, V. L. Crescenzi, and A. Mele, *ibid.*, **63**, 650 (1959).
16) K. J. Mysels, *J. Colloid Sci.*, **10**, 507 (1955).
17) A. W. Adamson, *loc. cit.*, p. 75.
18) P. H. Elworthy, A. T. Florence, and C. B. Macfarlane, "Solubilization by Surface-active Agents," Chapman and Hall Ltd., London (1968), pp. 49, 50.
19) R. C. Murray, *General Discussion of Faraday Soc.*, January, 206 (1935).
20) K. J. Mysels, P. Mukerjee, and Abu-Hamdiyyah, *J. Phys. Chem.*, **67**, 1943 (1963); P. Ekwall, H. Eikrem, and P. Stenius, *Acta Chem. Scand.*, **21**, 1639 (1967).
21) E. Matijević and B. A. Pethica, *Trans. Faraday Soc.*, **54**, 587 (1958).
22) J. N. Phillips, *ibid.*, **51**, 561 (1955).
23) G. Stainsby and A. E. Alexander, *ibid.*, **46**, 527 (1950).
24) K. Shinoda, This Bulletin, **26**, 101 (1953).
25) K. Shinoda, *Proc. 4th Int. Congr. Surface Active Substances*, **2**, 527 (1964).
26) M. E. Feinstein and H. L. Rosano, *J. Colloid Interfac. Sci.*, **24**, 73 (1967).
27) D. Stigter, *ibid.*, **23**, 379 (1967).
28) K. Shirahama, *Kolloid-Z. Z. Polym.*, **250**, 620 (1972).
29) J. Kielland, *J. Amer. Chem. Soc.*, **59**, 1675 (1937).
30) F. G. Donnan and J. T. Barker, *Proc. Roy. Soc.*, (London) **A 55**, 557 (1911).
31) J. W. McBain and R. C. Swain, *ibid.*, **A 154**, 608 (1936).
32) G. Aniansson, *J. Phys. Colloid Chem.*, **55**, 1286 (1951).
33) G. Nilsson, *J. Phys. Chem.*, **61**, 1135 (1957).

34) M. Muramatsu, K. Tajima, M. Iwahashi, and K. Nukina, *J. Colloid Interfac. Sci.*, **43**, 499 (1973).
35) E. E. Dreger, *Ind. Eng. Chem.*, **36**, 610 (1944).
36) R. A. Robinson and R. H. Stokes, "Electrolyte Solutions," 2nd ed., Butterworths Scientific Pub., London (1959), p. 190.
37) C. Botré, V. Crescenzi, and A. M. Liquori, *Proc. 3rd Int. Congr. Surface Active Substances*, **A II 3**, Nr 49, 302 (1960).
38) C. Botré, D. G. Hall, and R. V. Scowen, *Kolloid-Z. Z. Polym.*, **250**, 900 (1972).
39) C. Gavach, *Proc. 5th Int. Congr. Surface Active Substances*, **2**, 859 (1968).
40) E. Günterberg, *Z. Phys. Chem.*, **123**, 199 (1926).
41) S. N. Flengas and E. Rideal, *Trans. Faraday Soc.*, **55**, 339 (1959).
42) K. Tajima, M. Muramatsu, and T. Sasaki, This Bulletin, **43**, 1991 (1970).
43) J. N. Phillips and K. J. Mysels, *J. Phys. Chem.*, **59**, 325 (1955).
44) M. L. Fishman and E. R. Eirich, *ibid.*, **75**, 3135 (1971).
45) H. Huff, J. W. McBain, and A. P. Brady, *J. Phys. Colloid Chem.*, **55**, 311 (1951).
46) L. Shedlovsky, C. W. Jakob, and M. B. Epstein, *J. Phys. Chem.*, **67**, 2075 (1963).
47) I. Satake, T. Tahara, and R. Matsuura, This Bulletin, **42**, 319 (1969).
48) D. Stigter and K. J. Mysels, *J. Phys. Chem.*, **59**, 45 (1955); K. J. Mysels and C. I. Dulin, *J. Colloid Sci.*, **10**, 461 (1955).
49) M. L. Corrin, *ibid.*, **3**, 333 (1948); M. L. Corrin and W. D. Harikns, *J. Amer. Chem. Soc.*, **69**, 683 (1947).
50) R. J. Williams, J. N. Phillips, and K. J. Mysels, *Trans. Faraday Soc.*, **51**, 728 (1955).
51) A. P. Brady and D. J. Salley, *J. Amer. Chem. Soc.*, **70**, 914 (1948).
52) A. P. Brady, *J. Phys. Colloid Chem.*, **53**, 56 (1949).

The Heating-rate Dependence of the Mechanical Properties of Several Polymers at Higher Temperatures

Noboru FURUSHO, Tsuyoshi KOMATSU, and Tsurutaro NAKAGAWA
Department of Polymer Science, Faculty of Science, Hokkaido University, Sapporo 060
(Received December 23, 1974)

Measurements of the mechanical properties of various polymers at higher temperatures under the conditions of several heating rates were carried out in the air using the torsional braid analysis (TBA) method. It has become apparent that the examples of the dependence of the mechanical properties upon the heating rate at higher temperatures are classified into two groups. The first is characterized by the fact that the temperature of the maximum in the logarithmic decrement remains unchanged, irrespective of any changes in the heating rate. This situation is related to the physical process. On the other hand, in the case of the second group, the TBA curves are shifted to higher temperatures with an increase in the heating rate; this is the results of chemical processes. A kinetic treatment of thermal analysis, in which kinetic parameters can be calculated from the heating-rate dependence of the characteristic point in the observed curves, was used in the present study. From this analysis, the apparent activation energies of the thermal degradation of polymers were obtained, and comparisons of these values with those from the isothermal measurements were made.

Previously, we measured the chemorheological properties of a series of polymers during thermal degradation using the torsional braid analysis (TBA) method and discussed the relationship between the mechanical behavior and the chemical processes with the aid of the results of IR spectroscopy, thermogravimetry, and calorimetric measurements. From these studies, it has become apparent that the TBA method can be used for the studies of the thermal degradation of polymers and can also be used as a convenient kinetic tool, and that the shapes of the TBA curves of the polymers can be classified into three groups according to their degradation mechanisms. Moreover, it was found that the isothermal TBA curves were superposed into one composite curve by shifting them along the axis of the logarithms of time and that activation energies were obtained from the shift factor which agree well with those estimated from the slopes of the curves of the moduli *versus* the time.[1,2]

Furthermore, from the study of the heating-rate dependence of the TBA curves of poly(acrylic acid), we found that the mechanical behavior due to the glass transition is scarcely affected at all by the heating rate and that the chemorheological behavior is shifted to higher-temperature region with an increase in the heating rate. Using the kinetic treatment in thermal analysis, in which the kinetic parameters can be derived from the plots of the logarithmic heating rate *versus* the reciprocal temperature at the characteristic point in the curves observed, the apparent activation energies of the thermal degradation of polymers were obtained. These values agree well with those obtained from the isothermal measurements.[3]

In the present study, we will report the results of studies of the heating-rate dependence of the TBA curves of several polymers at higher temperatures. For these polymers, the isothermal mechanical measurements had previously been carried out.

The purpose of this work is to examine the possibility and the validity of the classification of the mechanical properties into one group resulting from chemical processes and another resulting from physical processes on the basis of measurements of the heating-rate dependence. It was also intended to examine the general applicability of the kinetic treatment in thermal analysis, in which the kinetic parameters can be obtained from the heating-rate dependence of the characteristic point in the curves observed, and to compare the activation energies obtained from this non-isothermal analysis with those obtained from the isothermal measurements.

Experimental

The poly(methyl methacrylate) (PMMA), the poly(vinyl fluoride) (PVF), the poly(vinyl chloride) (PVC), the vinylidene chloride–vinyl chloride copolymer(PVdC-VC) with the weight ratio of 82: 18, the poly(vinyl acetate) (PVAc), the poly(methyl acrylate) (PMA), the polyacrylonitrile(PAN), and the polyacrylamide(PAAm) were all commercial materials. The polystyrene(PSt), the poly(α-methyl styrene) (PMSt), and the poly(methacrylic acid) (PMAA) were, on the other hand, synthesized in our laboratory.

The procedure of the torsional braid analysis (TBA) has been described in previous papers.[1-3] Measurements of the mechanical properties were carried out in the air using a modified TBA apparatus made by the addition of a Shinku Riko model HPC-5000 programed temperature controller. The relative shear moduli, $(1/P)^2$, were calculated from the periods, P, of damped oscillations. The logarithmic decrement $[\lambda=(1/n)\ln(A_{2n+1}/A_1)]$ is calculated from the amplitudes of the damped oscillations, where n is the number of oscillations and A_1, A_{2n+1} are amplitudes of the first and n-th oscillations respectively.

Results and Discussion

Heating-rate Dependence of the Mechanical Properties. The results of the dependence of the TBA curves of several polymers upon the heating rate are shown in Figs. 1—6. As is shown in the figures, the heating-rate dependences of the mechanical properties can be classified into two types. The first type is characterized by the fact that little change occurs in the temperature of the maximum in λ, which is accompanied by an abrupt or slight drop in the modulus. In the second type, the TBA curves are shifted to higher temperatures as the heating rate increases.

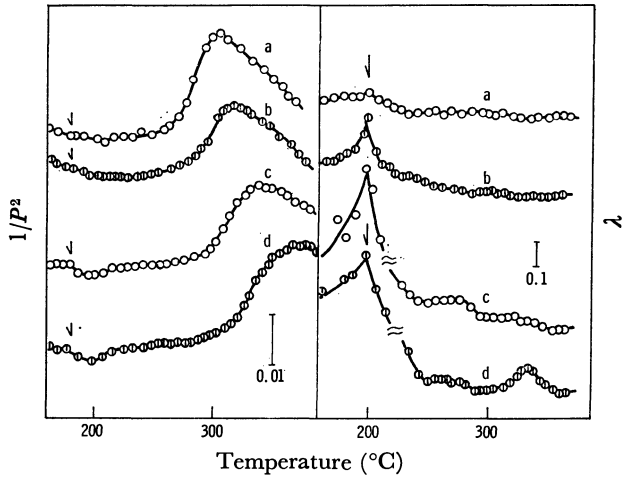

Fig. 1. The plots of $(1/P)^2$, λ *vs.* T of PVF under the several heating rates.
The arrows indicate the mechanical changes due to the melting. (a): 0.5 °C/min, (b): 1 °C/min, (c): 2 °C/min, (d): 5 °C/min.

First, the mechanism of the mechanical changes classified as the first type will be discussed. In the case of PVF, as is shown in Fig. 1, the temperature at which a slight drop in the moduli and the corresponding maximum in λ were found does not alter, irrespective of the change in the heating rate. Situations similar to that in PVF were found in the cases of PMSt and PMMA. That is, in PMSt (Fig. 2), the maximum in λ and the abrupt drop in the moduli at about 180 °C remain unaltered, and also in PMMA, an intense peak of λ and the slight drop in the moduli at about 230 °C are not shifted. Such phenomena, which have been discussed in our previous papers, too, may be interpreted as follows by the aid of the results of the calorimetric and other results reported by us and by other workers. First, the mechanical change at about 200 °C in PVF may be assigned to the melting.[2,4,5] Second, that at about 180 °C in PMSt is attributed to the glass transition.[6,7] Lastly, that at about 230 °C in PMMA is due to the melting.[1,8]

Wunderlich *et al.* have studied the heating-rate dependence of the glass-transition temperature (T_g) of polystyrene by means of dynamic differential thermal analysis.[9] In their results, the increase in T_g is only a few degrees in the heating-rate region from 1 to 7.6 K/min in a system in which the sample has been cooled slowly above 400 K. They compared their experimental data with the results of the theoretical considerations derived from the hole theory of liquids and calculated the activation energy at 160 kcal/mol (669 kJ/mol) from the plots of the logarithmic heating rate against the reciprocal glass-transition temperature. In PMSt, assuming that the value of the activation energy is analogous to that in PSt (probably larger than

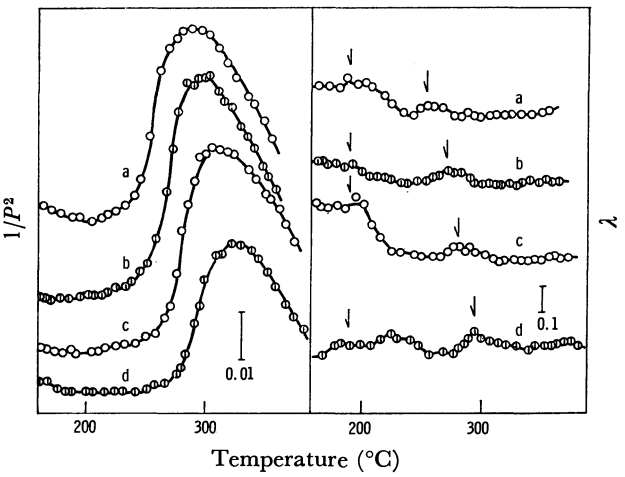

Fig. 3. The plots of $(1/P)^2$, λ *vs.* T of PVC under the several heating rates. The arrows at about 200 °C indicate the mechanical changes due to the physical process and those at higher temperatures indicate the maximum in λ due to the chemical process.
(a): 0.5 °C/min, (b): 1 °C/min, (c): 2 °C/min, (d): 5 °C/min.

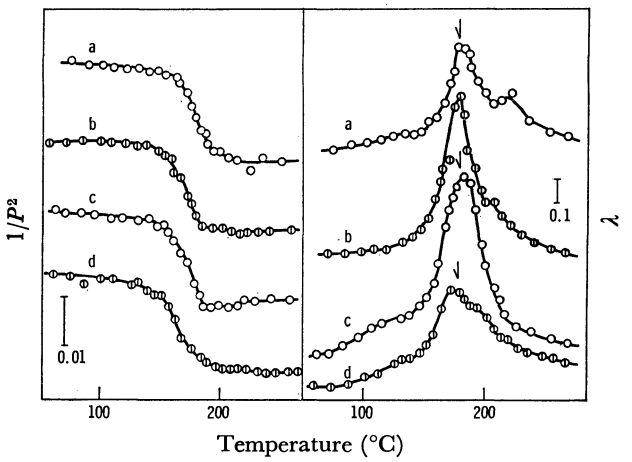

Fig. 2. The plots of $(1/P)^2$, λ *vs.* T of PMSt under the several heating rates. The arrows indicate the maximum in λ due to the glass transition.
(a): 0.5 °C/min, (b): 1 °C/min, (c): 2 °C/min, (d): 5 °C/min.

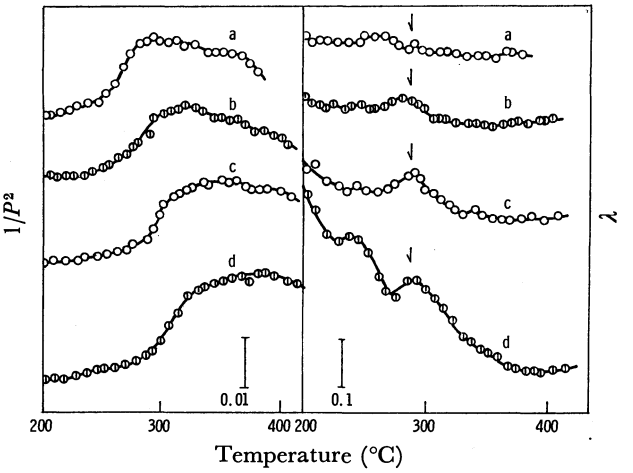

Fig. 4. The plots of $(1/P)^2$, λ *vs.* T of PAN under the several heating rates. The arrows indicate the maxima in λ due to the physical process.
(a): 0.5 °C/min, (b): 1 °C/min, (c): 2 °C/min, (d): 5 °C/min.

that in PSt), the change in T_g is calculated at a few degrees from the analysis described just above. Therefore, our experimental data in PMSt are reasonable.

The above discussions have demonstrated that the slight dependence of the TBA curves upon the heating rate is a characteristic feature in the physical processes: glass transition, melting, *etc.* In order to make clear the mechanical changes in polymers in the higher-temperature region, an inspection of the heating-rate dependence of the TBA curves of PAN, PVC, PAAm, PMAA, and PSt will be made on the basis of this consideration. The nature of the processes (physical or chemical) has not yet been fully elucidated.[1-3]

In PVC, as is shown in Fig. 3, it was found that the increase in the moduli begins at about 200 °C and that the broad maximum in the λ curve at around 200 °C does not shift. In the previous paper, the origin of this change in λ (the fusion or the result of the formation of conjugated carbon–carbon double bonds) was not determined. From its slight dependence upon the heating rate in the present study, it may be concluded that this broad maximum in the λ curve is due to a physical process, presumably the fusion. This consideration agrees with the results of the measurements in the fusion of PVC by other workers.[9-11] We found, in PVC (Fig. 3), that both the increase in the moduli and the corresponding maximum in λ in the region of temperatures higher than those discussed above are shifted to higher temperatures with an increase in the heating rate. In PAN (Fig. 4), in contrast to this, slight dependence of λ at about 290 °C upon the heating rate was observed irrespective of the existence of a considerable increase in the moduli. Gillham and Schwenker have mentioned that these mechanical changes (the considerable increase in the moduli and the maximum in λ at about 290 °C) coincide in position with a exothermic peak in the differential thermal analysis.[12] This exothermic peak is assigned by Thompson to the formation of the ladder structure.[13] However, in view of the slight dependence of this maximum in λ upon the heating rate in this study, it may be concluded that the change in λ at about 290 °C is attributed to a physical process. This conclusion is supported by our finding that this exothermic peak shifts to higher temperatures with an increase in the heating rate. However, considering that this exothermic peak temperature moves below or just above the temperature of the maximum in λ according to the heating rate, it is not clear whether this change in λ is a characteristic feature in the original PAN or in the so-formed ladder polymer from PAN.

In a similar manner, the mechanism of the mechanical change above 200 °C in PAAm and PMAA is determined by the aid of the calorimetric analysis to be due to the following physical processes. First, in PAAm, the maximum of λ at about 200 °C is due to the glass transition, and that of λ at about 240 °C is due to some physical process, the details being not yet clear. Second, in PMAA, the maximum in λ at about 220 °C is attributable to the glass transition, while the peak in λ at about 270 °C is presumably due to the melting.

In the case of PSt (Fig. 5), in contrast to the cases of

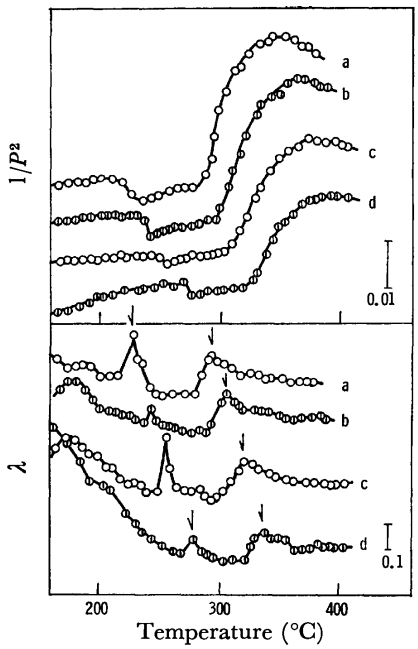

Fig. 5. The plots of $(1/P)^2$, λ *vs.* T of PSt under the several heating rates.
The arrows in left-hand side and right-hand side indicate the maxima in λ due to the chemical processes.
(a): 0.5 °C/min, (b): 1 °C/min, (c): 2 °C/min, (d): 5 °C/min.

PVC, PAN, PAAm, and PMAA, it was found that the small maximum in λ and the corresponding drop in the moduli shift from 220 °C to 280 °C with an increase in the heating rate. On the basis of the above discussions of the heating-rate dependence of the TBA curves, this mechanical change is considered to be attributable to the chemical process, not to the physical process. Considering that the weight loss during heating is slight in this temperature region, as has been reported in a previous paper,[1] and that the abrupt drop in the molecular weight at an early stage of the thermal

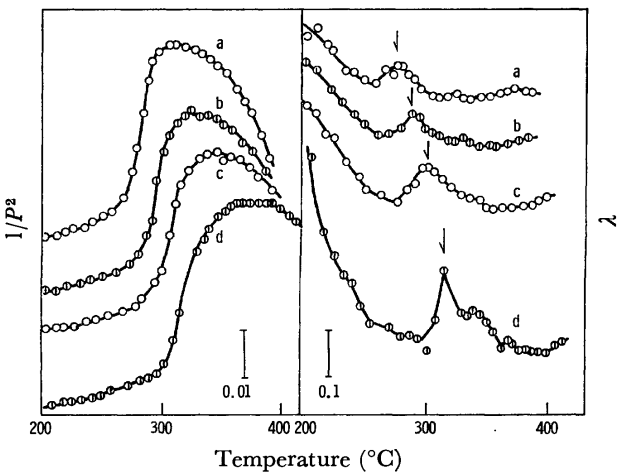

Fig. 6. The plots of $(1/P)^2$, λ *vs.* T of PVAc under the several heating rates.
The arrows indicate the maxima in λ due to the chemical process. (a): 0.5 °C/min, (b): 1 °C/min, (c): 2 °C/min, (d): 5 °C/min.

degradation of PSt was observed by Jellinek,[14] the mechanism of this mechanical change seems to be related to the abrupt drop in the molecular weight.

Here, turning the viewpoint to the mechanical changes grouped into the second type, in which the increase or decrease in the moduli and the corresponding change in the λ are shifted to higher temperatures with an increase in the heating rate (a typical example is shown in Fig. 6, the case of PVAc), the mechanism of these mechanical changes will be discussed. For PVC, it was found that the IR absorption peak of the carbon-carbon double bond becomes more intense with the progress of the reaction and that the temperature at which the weight loss occurs is near to that at which the moduli begin to increase. From these findings, it has been concluded that the increase in the moduli is attributable to the formation of the C–C double bond resulting from dehydrochlorination and the cross-linking through the double bond, while the decrease in the moduli is due to the chain scission.[2] In a similar way, in PAN, it has been shown that the formation of the ladder structures leads to an increase in the moduli.[1] For other polymers, the relationship between the mechanical change and the chemical process was demonstrated in the previous works by the aid of the results of IR spectroscopy, thermogravimetry, calorimetric study, and the results of other workers. From the above discussions, it may be concluded that a distinct dependence of the mechanical behavior upon the heating rate in these polymers is a peculiar feature of the chemorheological processes.

The considerations in this section suggest that the inspection of the heating-rate dependence of the mechanical properties can be used as a convenient tool for the identification of the nature of mechanical changes in higher-temperature regions in which not only physical processes but also chemical reaction can simultaneously occur.

Kinetic Analysis of Chemorheological Properties during Thermal Degradation. In the preceding sections, it has become clear that the heating-rate dependence of the mechanical properties can be classified into two groups. In the second group, the observed chemorheological curves shift to higher temperatures with an increase in the heating rate. A similar heating-rate dependence has been found in several kinds of thermal analysis: the thermogravimetry,[15] the mass spectrometric thermal analysis,[16] the electric thermal analysis,[17] *etc.* In these measurements, the procedures derived from the isothermal kinetic equation were used to obtain the kinetic parameters. In these procedures, the following assumptions are made. That is, the observed quantity characterizing some properties, y, is a function of a structural quantity, x; $y=f(x)$, and the change in the structural quantity obeys the Arrhenius equation; $dx/dt=A\cdot\exp(-E/RT)\cdot g(x)$, where A, E, and R are the frequency factor, the activation energy, and the gas constant respectively. Also, the same degree of change in the structural quantity leads to an equal degree of change in the properties observed. Here, a linear temperature change is also assumed; $T=T_0+ht$, where T_0 and h are the initial temperature and the heating rate respectively, and then x is integrated. The details of this calculation have been shown in the works by Ozawa and other workers.[18,19]

From the final solution of this calculation, a linear relationship between the logarithmic heating rate and the reciprocal of the temperature at the characteristic point in the observed curves is derived, and then the activation energies can be estimated from the slope of their plots. Also, it has been concluded that the superposition of the TBA curves into one composite curve is possible by their shift along the axis of the reciprocal temperatures. This kinetic treatment is extended to the systems in which the exact quantitative correlation between the observed properties and the structural quantities is not clear, assuming that conditions similar to those presented above are satisfied in such systems.[20]

In the previous paper, we attempted to apply this kinetic treatment to the chemorheological behavior in PAA and obtained reasonable activation energies, which agree well with those from the isothermal measurements. Moreover, the superposition of the isothermal TBA curves into one composite curve was successfully carried out by shifting them along the axis of the logarithmic time in all the polymers studied. In both procedures, it was assumed that the mechanical properties depend only upon their chemical structure and that the same extent of reaction leads to an equal degree of mechanical change. These assumptions are the same as those used in the kinetic procedure in thermal analysis. The success of the application of the non-isothermal kinetic treatment to the chemorheological behavior in PAA and the superposition procedure of the isothermal curves suggest that the TBA method can be used as a convenient kinetic tool in thermal analysis, despite a lack of information about the exact quantitative relationship between the mechanical properties and the chemical structures.

Below, the results of the examination of the application of this non-isothermal kinetic procedure to the chemorheological behavior during the thermal degradation of various polymers will be discussed. This was

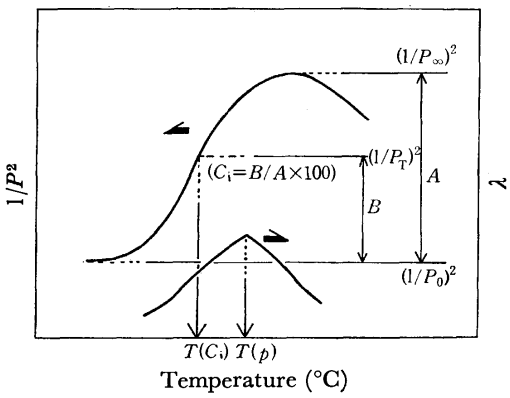

Fig. 7. The schema of the kinetic procedure.
The $(1/P_T)^2$, $(1/P_0)^2$, and $(1/P_\infty)^2$ are the values at temperature T, at minimum point, and at the maximum point in moduli, respectively.
The $T(C_1)$, $T(p)$ are the temperatures at conversion C_1 and of maximum in λ.

made by noting whether or not the following conditions are satisfied. (1) The plot of the logarithmic heating rate *versus* the reciprocal of the temperature of the maximum in λ, $T(p)$, is linear. (2) The plot of the logarithmic heating rate *versus* the reciprocal of the temperature to the same degree of conversion in the chemorheological change, $T(C_i)$, is linear. (3) The superposition of the curves of the chemorheological properties, plotted as a function of the reciprocal temperature, is possible. A schema of this procedure is shown in Fig.7.

The obvious maxima in λ which correspond to the increase or decrease in the moduli were found in PSt, PVC, PVdC–VC, PVAc, and PMA. The plots of the logarithmic heating rate against the reciprocal of the temperature of the maximum in λ are shown in Fig. 8. As is clear in the figure, these plots are linear in all the polymers mentioned above. From the slopes of these plots, the activation energies were obtained as listed in Table 1. Here, these values will be compared with those calculated from the isothermal measurements. In general, the values from these two procedures roughly agree with each other for the individual polymer.

In PMA, a good agreement similar to that in PAA reported previously[3] was found. However, in PSt, in which the increase in the moduli was controlled by the cross-linking, as in PAA and PMA, the agreement is not so satisfactory as in the above two polymers. Also, in the cases of PVC, PVdC–VC, and PVAc, in which the cross-linking is undeniable but is not the main factor affecting the chemorheological properties, as was discussed in the preceding paper, the situation is not simple. That is, a good agreement was found in PVdC–VC, but the agreement in PVC and PVAc is not so good as in PVdC-VC. This suggests that these discrepancies can not be explained by only the difference in the degradation mechanisms. In order to make clear the nature of these facts, further work is necessary.

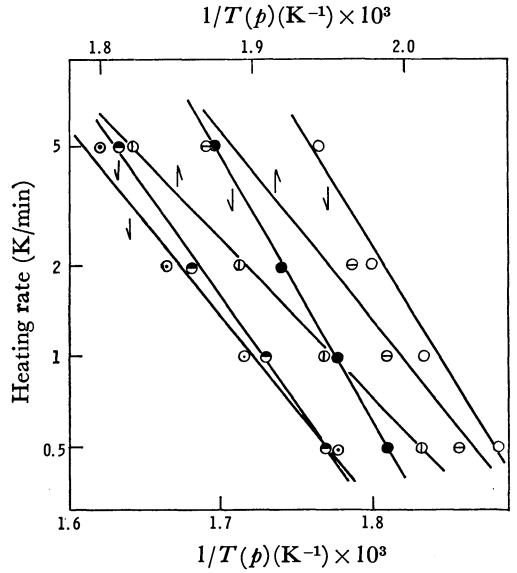

Fig. 8. The plots of the logarithmic heating rates *versus* the reciprocal of the temperatures of the maximum in λ of several polymers. ○: PVC, ⊖: PVdC–VC, ●: PVAc, ◑: PSt(L) (the maximum in λ at lower temperatures), ◓: PSt (H) (the maximum in λ at higher temperatures), ⊙: PMA.

Table 1. The apparent activation energies estimated from the various procedures of analysis

Sample	The apparent activation energy (kJ/mol)[a]					
	From this work[b]	From isothermal measurements				
		initial slope[c]			shift factor $(1/P)^2$	time of max. λ
		G_r *vs.* t	log G_r *vs.* t	A_r *vs.* t		
PVC	151	103	124	110	124	—
PVdC–VC	113	109	111	115	111	—
PSt(H)[d]	140	102	102	—	129	104
PVAc	168	118	118	—	103	—
PMA	101	92	90	—	77	67
PSt(L)[e]	96	—	—	—	—	—

a) 1J=1/4.184 cal. b) The value is estimated from the slope of the plot of the logarithmic heating rate *versus* the reciprocal of the temperature of maximum in λ. c) Assuming $dG_r/dt=k_0$, $dA_r/dt=k'_0$, and $d(\log G_r)/dt=k_{1st}$, where k_0, k'_0, and k_{1st} are the apparent rate constants of the zero order and first order reactions, respectively. The value of A_r are the relative absorbance ratio for C–C double bond and C–H group in IR spectra. d, e) In PSt(H) and PSt(L), the maxima in λ were found in the relatively higher temperature side and relatively lower temperature side, respectively.

The examination of the second point—that the plot of the logarithmic heating rate *versus* the reciprocal of the temperature to the same degree of conversion in the chemorheological change is linear—was carried out in the following manner. The degree of conversion in the chemorheological change was defined as follows:

$$C = [(1/P_T)^2 - (1/P_0)^2]/[(1/P_{00})^2 - (1/P_0)^2]$$

where $(1/P_T)^2$ is the value at a cetain temperature, T, and where $(1/P_0)^2$ and $(1/P_\infty)^2$ are the values of the minimum and maximum in the moduli respectively. Then the temperature in the degree of the conversion C_i was determined from the figure. The schema of this treatment is shown in Fig. 7. Finally, the plot of the logarithmic heating rate *versus* the reciprocal of the temperature at C_i was made. It should be added here that the determination of the value of $(1/P_0)^2$ is approximative because of the lack of a wide and flat base line of the modulus.

Some typical plots of log h *vs.* $1/T(C_i)$ are shown in Fig. 9. As is clear in the figure, in PVC the plots are linear. In the other polymers, also, similar straight lines were obtained. By means of the analysis described above, the activation energies are also obtained, as is listed in Table 2.

In PVC, the values are scarcely affected by the degree of conversion. On the other hand, in PVAc, it was found that the activation energies below C=70 % are analogous to each other, while above C=80 % the values become smaller. This fact suggests that some reaction which probably leads to the decrease in the moduli occurs simultaneously at a high degree of conversion. Similar situations have been found in

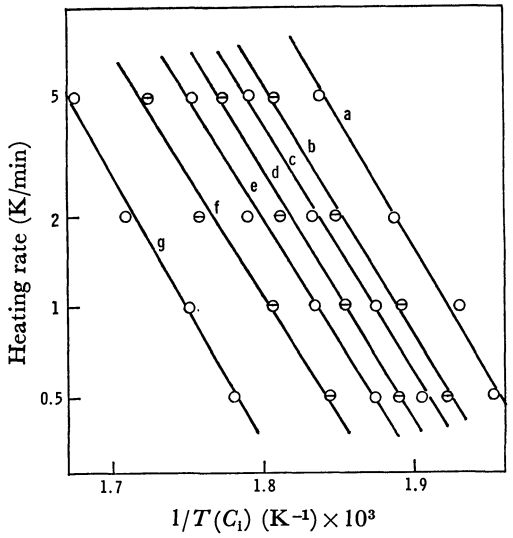

Fig. 9. The plots of the logarithmic heating rates versus the reciprocal temperatures at conversion C_i of PVC. (a): 10%, (b): 20%, (c): 30%, (d): 50%, (e): 70%, (f): 90%, (g): 100%.

TABLE 2. THE APPARENT ACTIVATION ENERGIES ESTIMATED FROM THE SLOPE OF THE PLOT OF THE LOGARITHMIC HEATING RATE VERSUS THE RECIPROCAL TEMPERATURE AT THE SAME DEGREE OF CONVERSION

Sample	The apparent activation energy (kJ/mol)[a] Degree of conversion (%)									
	10	20	30	40	50	60	70	80	90	100
PVC	161	158	158	161	160	159	156	155	156	176
PVdC-VC	126	125	143	140	149	151	141	139	139	120
PSt	152	156	156	147	146	140	132	131	159	159
PMA	—	109	93	86	83	78	75	73	71	37
PVAc	—	168	173	169	173	170	157	142	134	116
PVF	147	137	135	135	139	137	124	123	114	105
PAN	93	87	112	112	114	116	116	111	104	76
PAAm	169	153	146	136	133	124	118	111	103	100
PMAA	209	190	178	168	155	151	141	133	127	114

a) 1J=1/4.184 cal.

some other polymers. However, the nature of the decrease in the activation energies at an early stage in PAAm and PMAA is not yet clear. The values at the relatively lower degrees of conversions estimated by this analysis also roughly agree with those from the isothermal kinetic treatment and agree well those from the first non-isothermal kinetic treatment described above.

Furthermore, we attempted to superpose the TBA curves plotted against the reciprocal temperature for all the polymers studied. As is shown in Fig. 10, the procedure in PVAc was carried out successfully. In the other polymers, composite curves were also obtained. The quantities of the shift along the axis of the reciprocal temperature in the two temperature regions, where the moduli increase, or decrease, do not always coincide. This situation corresponds to the fact that the relationships of a shift factor to the reciprocal temperature in the two regions, where the moduli increase or decrease, are different in the superposition procedures of the isothermal TBA curves. The quantity of the shift in this procedure was not analyzed further in the present study.

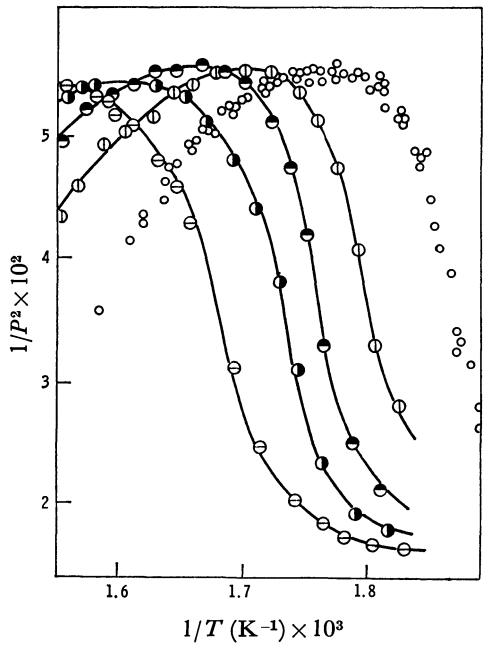

Fig. 10. The composite curve and the plots of $(1/P)^2$ *vs.* $1/T$ of PVAc under the several heating rates. ○: composite curve, ⓘ: 0.5 °C/min, ◓: 1 °C/min, ◑: 5 °C/min, ⓘ: 2 °C/min.

In the preceding sections, it has been demonstrated that the plots of the logarithmic heating rate *versus* the reciprocal of the temperature of the maximum in λ or at the conversion, C_i, are linear, and that the TBA curves observed under several heating rates can be superposed into one composite curve by means of their shift along the axis of the reciprocal temperature. These facts suggest that this kinetic treatment, in which the assumption that the same degree of change in the structural quantity leads to an equal degree of change in the observed properties was made, can be used in the kinetic studies of chemorheological behavior. However, the problem of the nature of the discrepancies between the activation energies obtained from this non-isothermal analysis and those obtained from the isothermal methods remains unsolved.

References

1) N. Furusho, T. Komatsu, and T. Nakagawa, *Nippon Kagaku Kaishi*, **1973**, 1166.
2) N. Furusho, T. Komatsu, and T. Nakagawa, This Bulletin, **47**, 1573 (1974).
3) N. Furusho, T. Komatsu, and T. Nakagawa, *ibid.*, **48**, 396 (1975).
4) N. Kawasaki and T. Hashimoto, *J. Polym. Sci., Part A-2*, **9**, 2095 (1971).
5) D. I. Sapper, *J. Polym. Sci.*, **43**, 383 (1960).
6) R. F. Boyer, *Rubber Chem. Technol.*, **36**, 1303 (1963).
7) W. G. Barb, *J. Polym. Sci.*, **37**, 515 (1959).
8) L. E. Nielsen, "Mechanical Properties of Polymers," Reinhold Publishing Co., New York (1953), p. 34, 35.
9) B. Wunderlich and D. M. Bodily, *J. Polym. Sci., Part C*, **6**, 137 (1964).
10) J. A. Juijn, J. H. Gisolf, and W. A. de Jong, *Kolloid-Z.*

Z. Polym., **235**, 1157 (1969).
11) C. E. Anagnostopoulus, A. Y. Coran, and H. R. Gamrath, *J. Appl. Polym. Sci.*, **4**, 181 (1960).
12) J. K. Gillham and R. F. Schwenker, Jr., *Appl. Polym. Symposia*, **2**, 59 (1966).
13) E. V. Thompson, *J. Polym. Sci., Part B*, **4**, 361 (1966).
14) H. H. G. Jellinek, *J. Polym. Sci.*, **3**, 850 (1948).
15) T. Ozawa, This Bulletin, **38**, 1881 (1965).
16) R. Sakamoto, Y. Takahashi, and T. Ozawa, *J. Appl. Polym. Sci.*, **16**, 1047 (1972).
17) T. Takamatsu and E. Fukada, *Bussei*, **12**, 513 (1971).
18) T. Ozawa, *J. Thermal Analysis*, **2**, 301 (1970).
19) L. Reich and S. S. Stivala, "Elements of Polymer Degradation," McGraw-Hill Book Co., New York (1971), Chapter 2.
20) T. W. Dakin, *AIEE Trans.*, **67**, 113 (1948).

The Contribution of the Double Collision Occurring in an Atom to the Yield of the Ionization and Excitations of Noble Gases Irradiated by 100 keV Electrons

Kiyoshi OKAZAKI, Shin SATO, and Shin-ichi OHNO*

Department of Applied Physics, Tokyo Institute of Technology, Ookayama, Meguro-ku, Tokyo 152

* *Japan Atomic Energy Research Institute, Tokai-mura, Ibaragi 319-11*

(Received December 24, 1974)

Gryzinski's classical treatment of the double ionization has been used to estimate the contribution of the double-collision process to the *G*-values of the ionizations and excitations of noble gases irradiated by 100 keV electrons. Except for helium, the double collision accounted for 5—15% of the yield of electrons. The total *G*-values calculated are ultimately as follows (in the order of He, Ne, Ar, Kr, and Xe): 2.28, 2.53, 3.09, 3.41, 3.67 for *G*(electrons); 0.84, 1.37, 1.78, 1.54, 1.41 for *G*(excited singlet states); 0.17, 0.07, 0.13, 0.23, 0.39 for *G*(triplet states).

The cross sections for the formation of multiply-charged ions of atoms and diatomic molecules in collision with high-energy electrons have been measured by many investigators over the past forty years.[1-6] Recently more reliable values of the cross sections in a wide energy range of the incident electrons have been reported.[7-10] On the other hand, the theoretical treatment of the formation of the multiply-charged ions has not been developed remarkably since Gryzinski proposed the classical treatment of double ionization.[11] Although a quantum mechanical estimation of the double ionization has been proposed by Mittleman,[12] his method is at present limited in its field of application. Gryzinski's classical method has recently been modified and used by Tripathi and Rai[13] to estimate the cross section for the double ionization of He and Li^+. Their results agreed reasonably well with the experimental ones.

In a previous paper,[14] we ourselves have calculated the *G*-values of the ionizations and excitations of noble gases irradiated by 100 keV electron, using the classical binary encounter collision theory. Although the *G*-values calculated were roughly consistent with those expected from the experiment, there were a few defects in the results. One of the most serious was that the calculated *W*-value of Ne was larger than that of He. It is experimentally known that these values are reversed in magnitude. This discrepancy might result from the assumption on the basis of which the calculation was carried out. In the previous calculation, we ignored the contributions of the double ionization and the excitation from the inner shells. This might have affected the *W*-values obtained. In the present paper, we calculated the amount of the double ionization by using Gryzinski's classical method and also estimated the contributions of the double excitation and the excitations from the inner shells.

Method of Calculation

Approximations. Since the probability of the double collision of high-energy electrons in an atom is much smaller than that of the single collision, we used the following three approximations: 1) When the stopping power, $S(T)$, of a gas and the degradation spectrum, $y(T)$, of electron are calculated, the contributions of the double collision and the excitations from the inner shells are ignored; that is, the $S(T)$ and $y(T)$ previously obtained are used as they were. 2) The cross section of the double collision is formulated by Gryzinski's method.[11] The differential cross sections involved in the formulation of the double collision are, however, evaluated by the method previously used.[14] The details of the formulation will be shown later. 3) The double collision is calculated only on the electrons in the outermost shell of the atom. In order to calculate the double collision in which the electrons in the inner shells are involved, we need more parameters than are available at present. According to the estimation of Roy *et al.*,[15] the contribution of the inner shells to the double collision is much smaller than that of the outermost shell.

Formulation. Even within the treatment of the single collision we had to consider various types of collisions, such as the ionizations from all of the shells, the ionization accompanied by the exchange of electrons, and the singlet and triplet excitations. Moreover, the energy range of the incident electrons, higher or lower than the ionization potential or the energies of the excited states, had to be taken into account.[14] In the treatment of the double collision, we have to consider all of the combinations of these collisions.

Double Ionization: After the occurrence of the first ionizing collision with an incident electron, there are two types of second ionizations; one is Case A, in which the second ionization is induced by the incident electron, while the other is Case B, in which the second ionization is induced by the electron which recoiled in the first collision. According to the treatment of Gryzinski,[11] the total ionization cross section in Case A is expressed in this form:

$$Q_{ii}^{A}(T) = \frac{1}{2}\int_{I_i}^{T-I_{ii}} [\sigma_{E,\mathrm{dir}} + \sigma_{E,\mathrm{exc}}] \frac{n_e(n_e-1)}{4\pi\bar{r}^2} \times \int_{I_{ii}}^{T-E} [\sigma_{E',\mathrm{dir}}(T-E) + \sigma_{E',\mathrm{exc}}(T-E)]\mathrm{d}E'\mathrm{d}E \quad (1)$$

for $T \geq I_i + I_{ii}$. Here, n_e is the number of electrons in the outermost shell of the target atom; $\bar{r}$, the mean distance between atomic electrons; T, the initial energy of the incident electron; E, the energy loss of the incident electron in the first collision—therefore, $T-E$ is the energy of the scattered electron and $E-I_i$ is the energy

of the electron ejected from the atom in the first collision; I_i, the ionization potential of the target atom; I_{ii}, the second ionization potential of the atom; E', the energy loss in the second collision—therefore, $T-E-E'$ is the energy of the doubly scattered electron and $E'-I_{ii}$ is the energy of the electron ejected from the atom in the second collision.

As has been stated above, the differential cross sections, $\sigma_{E,\mathrm{dir}}$ and $\sigma_{E,\mathrm{exc}}$, are the same as those used in the previous paper:[14]

$$\sigma_{E,\mathrm{dir}} = \frac{\pi e^4}{T+I_i+E_i}\left(\frac{1}{E^2}+\frac{4E_i}{3E^3}\right) \tag{2}$$

$$\sigma_{E,\mathrm{exc}} = \frac{\pi e^4}{T+I_i+E_i}\left\{\frac{1}{(T+I_i-E)^2}+\frac{4E_i}{3(T+I_i-E)^3}\right\} \tag{3}$$ [16]

In a similar manner, the differential cross sections for the second ionizations are expressed as follows:

$$\sigma_{E',\mathrm{dir}}(T-E) = \frac{\pi e^4}{T-E+E_i+I_{ii}}\left(\frac{1}{E'^2}+\frac{4E_i}{3E'^3}\right) \tag{4}$$

$$\sigma_{E',\mathrm{exc}}(T-E) = \frac{\pi e^4}{T-E+E_i+I_{ii}}\left\{\frac{1}{(T-E+I_{ii}-E')^2} + \frac{4E_i}{3(T-E+I_{ii}-E')^3}\right\} \tag{5}$$

When $T<I_i+I_{ii}$, $Q_{ii}^{A}(T)$ is set equal to zero.

Similarly, the total double-ionization cross section in Case B may be expressed by:

$$Q_{ii}^{B}(T) = \frac{1}{2}\int_{I_i+I_{ii}}^{T}[\sigma_{E,\mathrm{dir}}+\sigma_{E,\mathrm{exc}}]\frac{n_e(n_e-1)}{4\pi\bar{r}^2} \times\int_{I_{ii}}^{E-I_i}[\sigma_{E',\mathrm{dir}}(E-I_i)+\sigma_{E',\mathrm{exc}}(E-I_i)]\mathrm{d}E'\mathrm{d}E \tag{6}$$

for $T\geq I_i+I_{ii}$. When $T<I_i+I_{ii}$, $Q_{ii}^{B}(T)$ is set equal to zero. A simple calculation can show that $Q_{ii}^{A}(T)=Q_{ii}^{B}(T)$.

Although, in the above treatment, Cases A and B have been formulated separately, the final states obtained through the two processes cannot be distinguished. Since we cannot specify the origin of the electron inducing the second ionization—cannot determine whether it is an incident electron or the atomic one, the total cross section of the double ionization should be a half of the sum of $Q_{ii}^{A}(T)$ and $Q_{ii}^{B}(T)$:

$$Q_{ii}(T) = \frac{1}{2}[Q_{ii}^{A}(T)+Q_{ii}^{B}(T)] = Q_{ii}^{A}(T) \tag{7}$$

Double Excitation: The above treatment of double ionization can be extended to the double excitation. In the case of excitation, we have two types; one is accompanied by a change in the spin state (SC), while the other is not accompanied by such a change (SNC). In the formulation of the double excitation, therefore, we have to consider the combination of these two types of excitations.

By referring to the formulation of the excitation shown in the previous paper, the total cross sections of all kinds of double excitations can easily be formulated. Here, only the formulation for the case of SNC-SNC will be shown. This case leads to the formation of an excited singlet state. The total cross section for this process may be described as follows:

$$Q_{ee}(\mathrm{SNC\text{-}SNC}) = \int_{E_s}^{I_i}[\sigma_{E,\mathrm{dir}}+\frac{1}{2}\sigma_{E,\mathrm{exc}}]\frac{n_e(n_e-1)}{4\pi\bar{r}^2} \times\int_{E_{s2}}^{I_{ii}}[\sigma_{E',\mathrm{dir}}(T-E)+\frac{1}{2}\sigma_{E',\mathrm{exc}}(T-E)]\mathrm{d}E'\mathrm{d}E \tag{8}$$

for $T\geq I_i+I_{ii}$. Here, E_s is the energy of the lowest excited singlet state and E_{s2} is the energy necessary for the excitation in the second collision; that is, $E_{s2}=E^{**}-E_s$, where E^{**} is the energy of the double excitation state. When $E_s+I_{ii}\leq T<I_i+I_{ii}$,

$$Q_{ee}(\mathrm{SNC\text{-}SNC}) = \int_{T-I_{ii}}^{I_i}[\sigma_{E,\mathrm{dir}}+\frac{1}{2}\sigma_{E,\mathrm{exc}}]\frac{n_e(n_e-1)}{4\pi\bar{r}^2} \times\int_{E_{s2}}^{T-E}[\sigma_{E',\mathrm{dir}}(T-E)+\frac{1}{2}\sigma_{E',\mathrm{exc}}(T-E)]\mathrm{d}E'\mathrm{d}E + \int_{E_s}^{T-I_{ii}}[\sigma_{E,\mathrm{dir}}+\frac{1}{2}\sigma_{E,\mathrm{exc}}]\frac{n_e(n_e-1)}{4\pi\bar{r}^2} \times\int_{E_{s2}}^{I_{ii}}[\sigma_{E',\mathrm{dir}}(T-E)+\frac{1}{2}\sigma_{E',\mathrm{exc}}(T-E)]\mathrm{d}E'\mathrm{d}E \tag{9}$$

When $I_i+E_{s2}\leq T<E_s+I_{ii}$, the upper limit of the second integral of Eq. (8) should be replaced by $T-E$. When $E_s+E_{s2}\leq T<I_i+E_{s2}$, the upper limit of the first integral of Eq. (8) has to be replaced by $T-E_s$, in addition to the replacement of the upper limit of the second integral by $T-E$. When $T<E_s+E_{s2}$, Q_{ee}(SNC-SNC) is set equal to zero.

Other combinations, SC–SC, SNC–SC, and SC–SNC, of the double excitation can be formulated in a similar manner by using the energies of the first triplet state (E_t) and the energy necessary for the excitation from the first excited-triplet state to the double-excitation state (E_{t2}). In the case of SC–SC, we obtain a singlet or a quintet state as the final state. However, the G-value for this process is so small that we assume that the obtained state is always a singlet state.

Ionization and Successive Excitation: This process leads to the formation of a hot ion. As in the case of the double ionization, the second collisions in this case are of two types; one is induced by the electrons scattered in the first collision, while the other is induced by the recoiled electron. The total cross sections of these two processes have the same value. Again, as in the case of the double ionization, we cannot distinguish these two processes. The total cross section, therefore, is equal to that of either of the two processes.

The following shows the case of the ionization and successive excitation without any spin change (I–SNC). A similar formulation can easily be made for the case of I–SC, which is not shown here.

$$Q_{ie}(\mathrm{I\text{-}SNC}) = \int_{I_i}^{T-I_{ii}}[\sigma_{E,\mathrm{dir}}+\sigma_{E,\mathrm{exc}}]\frac{n_e(n_e-1)}{4\pi\bar{r}^2} \times\int_{E_{s1}}^{I_{ii}}[\sigma_{E',\mathrm{dir}}(T-E)+\frac{1}{2}\sigma_{E',\mathrm{exc}}(T-E)]\mathrm{d}E'\mathrm{d}E + \int_{T-I_{ii}}^{T-E_{s1}}[\sigma_{E,\mathrm{dir}}+\sigma_{E,\mathrm{exc}}]\frac{n_e(n_e-1)}{4\pi\bar{r}^2} \times\int_{E_{s1}}^{T-E}[\sigma_{E',\mathrm{dir}}(T-E)+\frac{1}{2}\sigma_{E',\mathrm{exc}}(T-E)]\mathrm{d}E'\mathrm{d}E \tag{10}$$

for $T\geq I_i+I_{ii}$. When $I_i+E_{s2}\leq T<I_i+I_{ii}$,

$$Q_{ie}(\text{I-SNC}) = \int_{I_i}^{T-E_{s2}} [\sigma_{E,dir}+\sigma_{E,exc}]\frac{n_e(n_e-1)}{4\pi\bar{r}^2} \times \int_{E_{s2}}^{T-E} [\sigma_{E',dir}(T-E)+\frac{1}{2}\sigma_{E',exc}(T-E)]dE'dE \quad (11)$$

When $T<I_i+E_{s2}$, Q_{ie}(I–SNC) is set equal to zero.

Excitation and Successive Ionization: This process also leads to the formation of a hot ion. The formulations of Q_{ei}(SNC–I) and Q_{ei}(SC–I) can easily be made by referring to the treatments described above. Only the latter case is shown here:

$$Q_{ei}(\text{SC-I}) = \frac{1}{2}\int_{E_{t_i}}^{I_i}\left[\frac{1}{2}\sigma_{E,exc}\right]\frac{n_e(n_e-1)}{4\pi\bar{r}^2} \times \int_{E_{t_i}}^{T-E} [\sigma_{E',dir}(T-E)+\sigma_{E',exc}(T-E)]dE'dE \quad (12)$$

for $T\geq I_i+E_{ti}$, where E_{ti} is the energy necessary for the ionization from the lowest excited-triplet state to the lowest excited ion. When $E_t+E_{ti}\leq T<I_i+E_{ti}$, the I_i in the first integral should be replaced by $T-E_{ti}$. When $T<E_t+E_{ti}$, Q_{ei}(SC–I) is set equal to zero.

Inner-shell Excitation: The formulation is exactly the same as that of the single excitation described in a previous paper,[14] except that the parameters, I_i, E_i, E_s, and E_t, have to be replaced by the values corresponding to those of the inner shells. In the present calculation, the contributions of the shells more inner than 3s in Ar, 3d in Kr, and 4p in Xe are ignored.

Constants Used for Calculation

The values of E_s, E_t, I_i, and E_i are the same as those used in the previous paper.[14] Table 1 summarizes the I_i, E_s, and E_t values of the inner shells, where the last two values are assumed to be the same. Table 2 shows the mean distance between electrons in the outermost shell of each atom and the second ionization potential (I_{ii}). The mean distance was calculated by placing the electrons uniformly on a sphere the radius of which had been estimated by Slater.[17]

Table 3 shows the double-excitation energy (E^{**}) and the energy of the lowest excited state of the singly charged ion (E^{+*}). Some of these values have been experimentally obtained;[18–24] from them we can calculate E_{s2} and E_{t2}. In the case of the double excitation, we can assume that $E_{s2}=E^{**}-E_s$ and $E_{t2}=E^{**}-E_t$.

Table 1. Ionization potential (I_i) and the excitation energies to the fierst excited singlet (E_s) and the lowest triplet (E_t) states with respect to the inner shells

Atom (shell)	I_i	E_s, E_t	Reference
Ne(2s)	48.42	43.65	23)
(1s)	867	865[a]	
Ar(3s)	29.3	25.22	24)
Kr(4s)	27.4	23.73	19)
(3d)	93.7	91.24	18, 24)
Xe(5s)	23.3	20.95	19)
(4d)	67.5	65.2	18)
(4p)	145.5	142	22, 24)

a) Assumed.

Table 2. The mean distance between electrons ($\bar{r}$) and the second ionization potential (I_{ii})

Atom (shell)	$\bar{r}$ (A)	I_{ii} (eV)
He (1s)	0.60	54.40
Ne (2p)	0.45	41.07
Ar (3p)	0.95	27.62
Kr (4p)	1.22	24.56
Xe (5p)	1.41	21.20

Table 3. The double excitation energy (E^{**}) and the energy of the excited state of the singly charged ion (E^{+*})

Atom	E^{**} (eV)	E^{+*} (eV)
He	57.82 (^{1}S)	65.4
	58.34 (^{3}P)	
Ne	45.0	57.6[a]
Ar	30[b]	36[c]
Kr	27[b]	33[c]
Xe	23[b]	28[c]

a) Assumed. b) Calculated on the assumption that $E^{**}=I_i+I_{ii}/2$. c) Calculated on the assumption that $E^{+*}=I_i+3I_{ii}/4$.

In the case of the ionization and successive excitation, we assumed $E_{s2}=E_{t2}=E^{+*}-I_i$.

Results

Figure 1 shows the $T\cdot y(T)\cdot Q_s(T)$ for the double collision in Ne as a function of ln T. Similar curves were also obtained in other cases —He, Ar, Kr, and Xe. All the curves for the double ionization have maxima at about twice the threshold energy of each atom and rise again as the T increases over 10^4 eV. A similar tendency was observed for the cases of the ionization and successive excitation. On the other hand, the cases of the double excitation and the excitation and successive ionization have maxima near the threshould energies and decrease rapidly as the T increases.

Tables 4 and 5 summarize, respectively, the G-values obtained for all of the double collisions and for the inner-shell excitations.

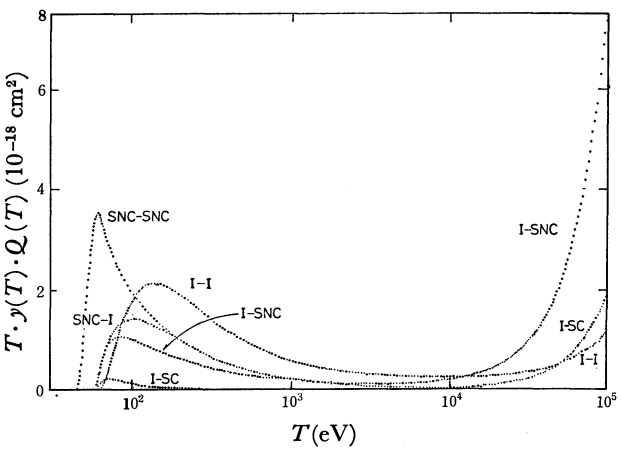

Fig. 1. Contribution of different portions of the electron degradation spectrum to the double collision in Ne.

Table 4. The G-values for each double collision

Process	He	Ne	Ar	Kr	Xe
Double ionization	0.0076	0.146	0.079	0.053	0.057
Double excitation	0.0031	0.112	0.081	0.059	0.060
SNC–SNC	0.0028	0.105	0.075	0.054	0.055
SC–SC	0.0000050	0.000097	0.00011	0.000099	0.00013
SNC–SC	0.00022	0.0062	0.0049	0.0041	0.0041
SC–SNC	0.000037	0.00081	0.00086	0.00075	0.00095
Ionization excitation	0.017	0.192	0.231	0.097	0.120
I–SNC	0.015	0.160	0.202	0.085	0.105
I–SC	0.0022	0.032	0.029	0.012	0.015
Excitation ionization	0.0029	0.068	0.060	0.038	0.037
SNC–I	0.0029	0.068	0.060	0.038	0.037
SC–I	0.000021	0.00018	0.00032	0.00026	0.00034

Table 5. The G-values for the inner shell excitations

Shell	Ne	Ar	Kr	Xe
1s singlet	0.000014			
triplet	0.00000015			
2s singlet	0.0164			
triplet	0.00062			
3s singlet		0.0540		
triplet		0.0025		
3d singlet			0.0176	
triplet			0.00039	
4s singlet			0.0418	
triplet			0.0028	
4p singlet				0.0016
triplet				0.000062
4d singlet				0.0244
triplet				0.00079
5s singlet				0.0365
triplet				0.0027
Total	0.0170	0.0565	0.0626	0.0661
singlet	0.0164	0.0540	0.0594	0.0625
triplet	0.00062	0.0025	0.0032	0.0036

Discussion

Experimentally, the formation of the doubly charged ions is due not only to the double ionization, which we have just calculated, but also to the Auger effect. Therefore, the comparison of the calculated values with the experimental values is somewhat complicated. In the case of He, however, there is no Auger effect, so a direct comparison is possible.

Figure 2 compares the experimentally obtained total cross sections of the double ionization[6–10] with those calculated by the method described above. A serious discrepancy appears near its maximum value and at very high energies of the incident electrons. Figure 3 summarizes the He^+/He^{2+} ratios obtained both experimentally[4,6–10] and theoretically. The a curve is the present calculation, while the b and c curves are the results obtained by means of Mittleman's procedure[12] and a modification of it[25] respectively. The d curve is the result obtained by Roy and Rai.[26] Their treatment seems to be very similar to ours except for a modification which is not clear for us. Judging from the semi-quantitative agreement of the present calculation with the observed data, it may be concluded that

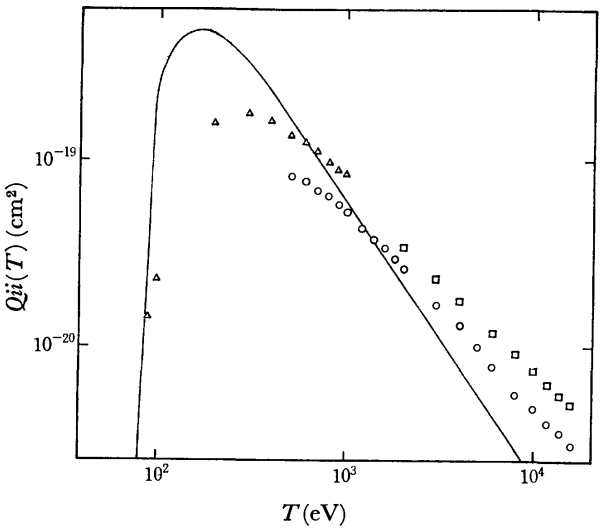

Fig. 2. The total cross section of the double ionization in He. ——, calculated; ○, Ref. 7; □, Ref. 9; △, Ref. 6.

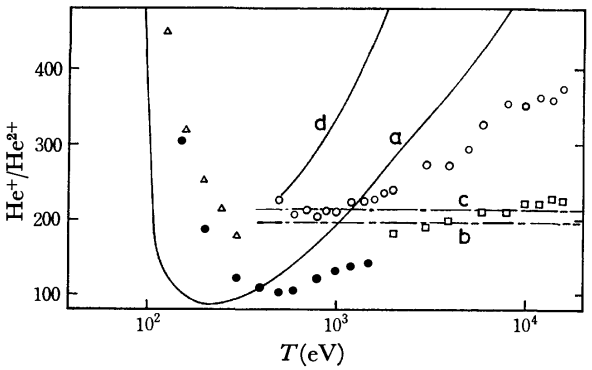

Fig. 3. The He^+/He^{2+} ratios as a function of ln T. ○, Ref. 7; □, Ref. 9; ●, Ref. 4; △, Ref. 6.

Gryzinski's treatment of the double ionization is generally correct when the yield of the doubly charged ions formed through the double collision is estimated.

Figures 4 and 5 show the ratios of M^+/M^{2+} as a function of the energy of the incident electron, where M stands for Ne, Ar, Kr, or Xe.[1–10] In the case of Ne, only the double-ionization process seems to explain the experimental data. Probably the Auger effect does not play an important role in the formation of doubly charged ions in Ne. In the cases of Ar, Kr, and Xe, on

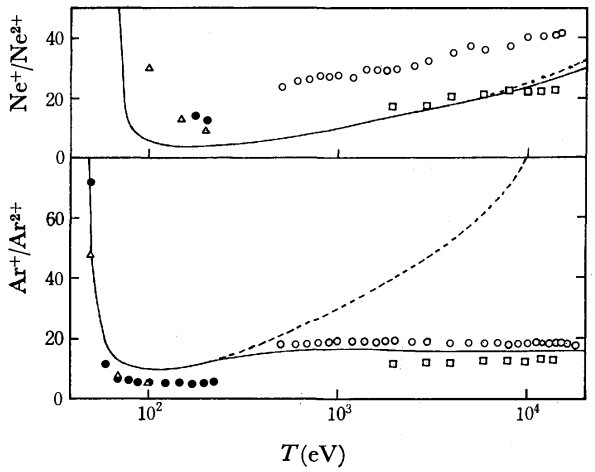

Fig. 4. The Ne^+/Ne^{2+} and Ar^+/Ar^{2+} ratios as a function of ln T. ----, calculated only on the double ionization; ——, calculated by including the Auger effect; ○, Ref. 7, 8; □, Ref. 9; ●, Ref. 1; △, Ref. 3.

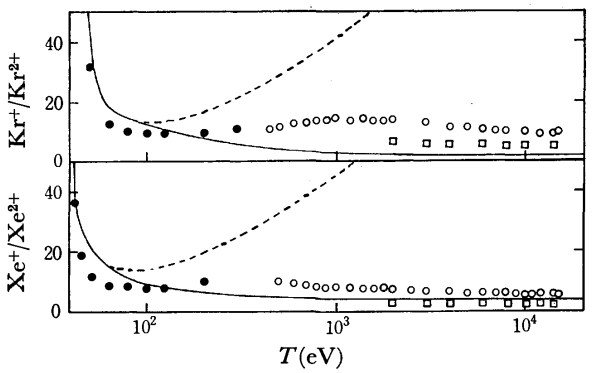

Fig. 5. The Kr^+/Kr^{2+} and Xe^+/Xe^{2+} ratios as a function of ln T. ----, calculated only on the double ionization; ——, calculated by including the Auger effect; ○, Ref. 8; □, Ref. 10; ●, Ref. 6.

the other hand, the Auger effect seems to play a principal role in the formation of the doubly charged ions at the higher energies of the incident electrons. Since the distribution of the multiply charged ions produced through the Auger effect has been reported for all of the rare gases,[27] and since the fluorescence yields have also been reported in the literature,[28] we can estimate the relative amounts of the doubly charged ions formed through the Auger effect by using the cross sections of ionizations from the inner shells.[14] Tables 6 and 7 show, respectively, the values used of the relative yields of the doubly charged ions and the fluorescence yields. The corrected M^+/M^{2+} ratios obtained by using these values are also shown in Figs. 4 and 5. The agreement with the experimental plots is satisfactory.

Table 6. The fluorescence yield of M^+ ion with a vacancy in the inner shell

Shell	He	Ne	Ar	Kr	Xe
K		0	0.1	0.6	0.87
L			0	0.04	0.15
M				0	0
N					0

Table 7. The fraction of M^{2+} ion produced through the Auger effect

Shell	He	Ne	Ar	Kr	Xe
1s		0.736	0.105	0.015	0.003
2s			0.02	0.001	0.01
2p			0.74	0.01	0.02
3s				0.13	0.02
3p				0.09	0.04
3d				0.60	0.03
4s					0.4
4p					
4d					

Table 8. The G-values of electrons and W-values

	He	Ne	Ar	Kr	Xe
G-value	2.28	2.53	3.09	3.41	3.67
single collision	2.27	2.19	2.81	3.20	3.45
double collision	0.014	0.326	0.220	0.150	0.154
inner shell excitation		0.017	0.057	0.063	0.066
W-value					
present	43.9	39.5	32.4	29.3	27.2
experimental	42.3	36.3	26.4	24.2	22.0

Table 9. The ratio of the G-value for excitation to that of electrons

	He	Ne	Ar	Kr	Xe
G_{exc}	1.01	1.44	1.91	1.77	1.80
singlet	0.84	1.37	1.78	1.54	1.41
triplet	0.17	0.07	0.13	0.23	0.39
G_{exc}/G_e	0.44	0.57	0.62	0.52	0.49

The Calculation of the G-values. When the G-values of electrons are calculated, the contribution of the double ionization, G_{ii}, should be added to the total, because the first ionization in the double ionization has already been counted as a single ionization. In the case of the ionization and successive excitation, the G-value of this process does not contribute to the increase in the G-value of the electrons, while in the case of the excitation and successive ionization, its G-value should be added to the G-value of the electrons and the same amount has to be subtracted from the G-value of the excitations.

The sum of the G-value of the double excitation and the inner-shell excitation corresponds to the G-value of the autoionization state of each atom. Some species in this state may autoionize into multiply charged ions; however, in the present calculation, we assumed that all of the autoionization states produce only singly charged ions.

Table 8 summarizes the G-values of electrons and the W-values both calculated and observed.[29] The results appear to be better than those reported in the previous paper,[14] where the double collision and the inner-shell excitation were ignored. Table 9 shows the G-values of the excitations and the ratios of the excitation and ionization. There are no remarkable differences between the values calculated here and those obtained previously.

The authors are indebted to Professor Kazuo Hisatake for estimating the fluorescence yields.

References

1) W. Bleakney, *Phys. Rev.*, **36**, 1303 (1930).
2) J. T. Tate and P. T. Smith, *ibid.*, **46**, 773 (1934).
3) D. P. Stevenson and J. A. Hipple, *ibid.*, **62**, 237 (1942).
4) H. E. Stanton and J. E. Monahan, *ibid.*, **119**, 711 (1960).
5) F. A. Stuber, *J. Chem. Phys.*, **42**, 2639 (1965).
6) L. J. Kieffer and G. H. Dunn, *Rev. Mod. Phys.*, **38**, 1 (1966).
7) B. L. Schram, A. J. H. Boerboom, and J. Kistemaker, *Physica*, **32**, 185 (1966).
8) B. L. Schram, *ibid.*, **32**, 197 (1966).
9) M. J. Van der Wiel, Th. M. El-Sherbini, and L. Vriens, *ibid.*, **42**, 411 (1969).
10) Th. M. El-Sherbini, M. J. Van der Wiel, and F. J. de Heer, *ibid.*, **48**, 157 (1970).
11) M. Gryzinski, *Phys. Rev.*, **A138**, 305, 322, 336 (1965).
12) M. H. Mittleman, *Phys. Rev. Lett.*, **16**, 498 (1966).
13) D. N. Tripathi and D. K. Rai, *J. Chem. Phys.*, **55**, 1268 (1971).
14) S. Sato, K. Okazaki, and S. Ohno, This Bulletin, **47**, 2174 (1974).
15) B. N. Roy, D. N. Tripathi, and D. K. Rai, *Can. J. Phys.*, **50**, 2961 (1972).
16) $4E_i$ in the second term of Eq. (3) is missing in Eq. (1) of Ref. 14).
17) J. C. Slater, "Quantum Theory of Matter," McGraw-Hill Book Co., New York (1951), p. 146.
18) K. Codling and R. P. Madden, *Phys. Rev. Lett.*, **12**, 106 (1964).
19) R. P. Madden and Codling, *J. Opt. Soc. Amer.*, **54**, 268 (1964).
20) J. A. Simpson, S. R. Mielczarek, and J. Cooper, *ibid.*, **54**, 269 (1964).
21) R. P. Madden and K. Codling, *Astrophys. J.*, **141**, 364 (1965).
22) K. Codling and R. P. Madden, *Appl. Opt.*, **4**, 1431 (1965).
23) K. Codling, R. P. Madden, and D. L. Ederer, *Phys. Rev.*, **155**, 26 (1967).
24) K. Siegbahn *et al.*, "ESCA Atomic, Molecular and Solid State Structure Studied by Means of Electron Spectroscopy," Ser. IV, Vol. 20, Nova Acta Regiae Societatis Scientarum Upsaliensis (1967).
25) F. W. Byron, Jr. and C. J. Joachain, *Phys. Rev. Lett.*, **16**, 1139 (1966).
26) B. N. Roy and D. K. Rai, *J. Phys., B*, **6**, 816 (1973).
27) T. A. Carlson, W. E. Hunt, and M. O. Krause, *Phys. Rev.*, **151**, 41 (1966).
28) I. Bergstrom and C. Nordling, "The Auger Effect" in the "Alpha-, Beta-, Gamma-Ray Spectroscopy," Vol. 2, ed. by K. Siegbahn, North-Holland Publishing Co., Amsterdam (1965), p. 1532.
29) R. L. Platzman, *Int. J. Radiation Isotopes*, **10**, 116 (1961).

The Specific Refractive Index Increment and the Partial Specific Volume of Atactic Poly(2-vinylpyridine)

Shizuo ARICHI, Masafumi YOSHIDA, and Yoshihiro OGAWA

Chemical Laboratory, Department of General Education, Kumamoto University, Kurokami-2-chome, Kumamoto 860

(Received January 6, 1975)

The specific refractive index increment, dn/dc, of atactic poly(2-vinylpyridine) was measured in 18 solvents with 436 nm light at 25 °C. Using these data, the partial specific volume, $\bar{v}_2$, of the polymer in these solvents was then evaluated by means of the method proposed by Heller. A sufficient agreement was found between the values of $\bar{v}_2$ thus obtained optically and those determined directly by the density measurement of solutions in several solvents. It was found that $\bar{v}_2$ varies considerably with the kind of solvent and that, in some solvents, such as methanol and ethanol, it takes an extremely lower value than that of bulk crystalline isotactic poly(2-vinylpyridine). The results were discussed in terms of thermodynamic interactions between the polymer and the solvent, the molar volume, and the compressibility of the solvent molecule. The relationship between dn/dc and the refractive index of a solvent, n_1, for 436 nm light is expressed by $dn/dc = 0.900 \times (1.628 - n_1)$.

The specific refractive index increment, dn/dc, of a dilute solution of a polymer is indispensable for an investigation of the polymer in solution by light scattering. Besides, the partial specific volume of a polymer, $\bar{v}_2$, is not only a very important value, often appearing in various parameters representing thermodynamic and hydrodynamic interactions between polymer and solvent, for example, the second virial coefficient, A_2, but also $\bar{v}_2$ itself is a useful quantity, showing polymer-solvent interactions. On the other hand, the very intimate relationships between the dn/dc and the $\bar{v}_2$ of a polymer in solution have been intensively studied by many investigators.

In spite of the ever-increasing number of related papers[1-3] on the solution properties of poly(2-vinylpyridine), there has been no systematic investigation of the dn/dc and the $\bar{v}_2$ of this polymer. Because of the very strong interactions between this polymer and certain solvents,[3-5] some specific characteristics can be expected to exist in the $\bar{v}_2$ of this polymer in those solvents which may be absent in a non-polar polymer such as polystyrene dissolved in a non-polar solvent.

The objects of this work are, first, to perform the direct measurement of the dn/dc of atactic poly(2-vinylpyridine) in as many solvents as possible; the results will enable us to make a broader choice of the solvent in light-scattering measurements of this polymer, and second, to evaluate the value of $\bar{v}_2$ according to the method proposed by Heller,[6] using the dn/dc data. The values of $\bar{v}_2$ thus obtained will be compared with those measured densitometrically in several solvents, and the relationship between the $\bar{v}_2$ and various properties of the solvents will be discussed.

Experimental

Specific Refractive Index Increment. The specific refractive index increments were measured photometrically with a Shimadzu DR-3-type differential refractometer.[7] All the measurements were carried out using the blue light of Hg (436 nm). The temperature in the cell was controlled at 25±0.01 °C. The instrumental constant was carefully calibrated with the standard aqueous solutions of KCl[8] and sucrose;[9] it was agreed within the range of 1.5%. The specific refractive index increment of the standard polystyrene, obtained from the Pressure Chemicals Co., in benzene at 25 °C for the 436 nm light gave experimental values ranging from 0.109 to 0.111, within the range of values reported in the most recent literature.[7]

Refractive Index of the Solvent. The refractive index of the solvent was measured with a Pulfrich refractometer manufactured by the Shimadzu Co. with 436 nm light of Hg at 25± 0.05 °C. The calibration of the instrument was done as usual.[10]

Refractive Index of Bulk Atactic Poly(2-vinylpyridine). The refractive index of bulk atactic poly(2-vinylpyridine) was measured with an Abbe-type refractometer manufactured by the Atago Kogakukikai Co. at 25±0.05 °C with 436 nm light of Hg. A thin film of the atactic poly(2-vinylpyridine) made from a benzene solution on mercury was placed on the major prism demounted from the instrument and carefully warmed to 115 °C in a nitrogen atmosphere. That temperature was then maintained for 15 hr. As the glass-transition temperature of this polymer is 104 °C,[11] a close adherence of the film to the surface of the prism was attained, and the border line between light and shade could be recognized. After the measurements had been completed and the film on the prism had been removed by dissolving with methanol, the calibration of the instrument was done as usual.[10]

Density of Solution. Measurements of the density of the polymer solution in several solvents were made with a usual Ostwald-Sprengel-type pycnometer. For solutions in benzene and dioxane, the density was measured by means of a graduated pycnometer. The concentrations of the polymer ranged from 1×10^{-2} to 6×10^{-2} in the weight fraction of the polymer. The temperature of the bath was maintained at 25±0.002 °C.

Density of Bulk Atactic Poly(2-vinylpyridine). The density of bulk atactic poly(2-vinylpyridine) was measured with the Weld-type pycnometer, immersing the thin film in decahydronaphthalene at 20±0.002 °C. The temperature coefficient of the volume expansion of the polymer was measured with a dilatometer manufactured by Shibayama Kagakukikai Co.; thus the value of the density of the polymer at 25 °C was determined. The density of the bulk isotactic crystalline poly(2-vinylpyridine) was measured in the same way, but directly at 25 °C.

Viscosity. The limiting viscosity number, $[\eta]$, of poly(2-vinylpyridine) in a number of solvents was determined in a Ubbelohde-type viscometer at 25±0.01 °C. The values of $[\eta]$ were obtained by plotting η_{sp}/c against the concentration, c, and by extrapolating to a zero concentration.

Polymers. The polymerizations and fractionations of atactic and isotactic poly(2-vinylpyridine) were all the same

as those previously reported.[12,13] The crystallization of a fraction of isotactic poly(2-vinylpyridine) was performed by heating it at 150 °C for a night in a nitrogen atmosphere; its crystallinity was checked by the X-ray diffraction method.[13,14]

Solvents. All the solvents used in this experiment were of a reagent grade; some of them had been dried and fractionally distilled.

Results and Discussion

Recent advances in both the theory and practice of the influence of a solvent on the specific refractive index increment, dn/dc, including the proposals of Heller,[6] Bodmann,[15] and Mächtle and Fischer,[16] have been summarized in the monograph by Huglin.[7] These theories are based on the concept of the specific refraction, R, which is a constant value and is a function of the specific volume, v, and the refractive index, n, of the component. The expressions for R proposed by Gladstone-Dale, Lorenz-Lorentz, and Eykman are:[7]

$$\text{Gladstone-Dale (GD)} : R = (n-1)v \quad (1)$$

$$\text{Lorenz-Lorentz (LL)} : R = [(n^2-1)/(n^2+2)]v \quad (2)$$

$$\text{Eykman (Ey)} : R = [(n^2-1)/(n+0.4)]v \quad (3)$$

According to the theory of the mixing rule,[17] the specific refraction of a binary solution can be expressed by:

$$R_{12} = R_1 w_1 + R_2 w_2 \quad (4)$$

where R_i and w_i are the specific refraction and the weight fraction of the component, i, respectively, and where $i=1$, 2, and 12 refer to the solvent, the solute, and the solution respectively. Equation (4) is correct only when there is no volume change upon mixing in the component, when the polarizability of the components is the same before and after mixing and when the solute is spherically symmetrical isotropic.[6]

For the polymer-solvent system where the volume change of mixing cannot be neglected, Heller[6] derived an expression of the relationship between dn/dc and the partial specific volume of a polymer, $\bar{v}_2$, in solution at an infinite dilution, assuming Lorenz-Lorentz expression, Eq. (2), for the specific refraction of each component. The final expression of Heller is:

$$[dn/dc]_{c=0} = 3\bar{v}_2(B-A)/2n_1(1-A)^2 \quad (5)$$

$$A = (n_1^2-1)/(n_1^2+2)$$

$$B = (n_2^{*2}-2)/(n_2^{*2}+2)$$

where n_1 is the same as above and where n_2^* is the refractive index of the polymer in solution. Heller assumed further that the Lorenz-Lorentz relation for a single component system:

$$(\varepsilon-1)/(\varepsilon+2) = 4\pi N\alpha/3 \quad (6)$$

where ε is the optical dielectric constant; α, the polarizability, and N, the number of molecules in a unit of volume, is valid for not only a bulk polymer but also for polymer in a very dilute solution if the polarizability of the polymer does not change measurably before and after mixing, even if the volume change can not be neglected. Then the following relationship must hold:

$$R_{2,\mathrm{He}} = (n_2^2-1)/(n_2^2+2)\rho_2$$

$$= [(n_2^{*2}-1)/(n_2^{*2}+2)]\bar{v}_{2,\mathrm{op}} = \text{constant} = k \quad (7)$$

where ρ_2 is the density of the bulk polymer.

If we can obtain the values of n_2 and ρ_2 of the bulk polymer, the value of k in Eq. (7) can be determined. Then, using Eqs. (5) and (7), a series of tentative pairs of $\bar{v}_{2,\mathrm{op}}$ and dn/dc can be obtained. Thus, the true value of $\bar{v}_{2,\mathrm{op}}$ can be evaluated graphically using the experimental value of dn/dc.

Another analytical method for obtaining $\bar{v}_{2,\mathrm{op}}$ was reported by Heller[18] in his second series concerned with the optical determination of the partial specific volume of macromolecules in solution. From Eq. (5) we can obtain:

$$\bar{v}_{2,\mathrm{op}} = k/A - f(dn/dc) = R_{2,\mathrm{He}}/A - f(dn/dc) \quad (8)$$

$$f = (2/3)n_1(1-A)^2/A \quad (9)$$

From Eq. (8), $\bar{v}_{2,\mathrm{op}}$ can then be readily calculated by using our knowledge of $R_{2,\mathrm{He}}$, dn/dc, and n_1 and/or A.

The usefulness of Heller's method for the evaluation of $\bar{v}_2$ from the dn/dc data has been confirmed recently;[19] also, Scholte[20] obtained an equation identical with Eq. (5) on the same assumption as Heller's but with a rather different approach.

Another approach made by Bodmann[15] concerning the relationship between dn/dc and the $\bar{v}_2$ of the polymer at an infinite dilution established that the R_{12} should be expressed by the partial specific refractions, $\bar{R}_1$ and $\bar{R}_2$, instead of R_1 and R_2 in Eq. (4); Bodmann's final expressions for $\bar{R}_2$ for the three functions, Eqs. (1), (2), and (3) were as follows:

$$\bar{R}_{2,\mathrm{GD}} = [(n_1-1)\bar{v}_2] + (dn/dc) \quad (10)$$

$$\bar{R}_{2,\mathrm{LL}} = [(n_1^2-1)/(n_1^2+2)]\bar{v}_2 + [6n_1/(n_1^2+2)](dn/dc) \quad (11)$$

$$\bar{R}_{2,\mathrm{Ey}} = [(n_1^2-1)/(n_1+0.4)]\bar{v}_2 + [(n_1+0.84)/(n_1+0.4)^2](dn/dc) \quad (12)$$

Equations (5) and (11) are equivalent when the specific refraction, $R_{2,\mathrm{He}}$ (Eq. (7)), is equal to the partial specific refraction, $\bar{R}_{2,\mathrm{LL}}$ (Eq. (11)), because only under this condition can Eq. (5) be derived from Eq. (11).

Examinations were made into the $\bar{R}_2$ values for the three functions calculated from the data of the densitometrically determined values of n_1, dn/dc, and $\bar{v}_{2,\mathrm{d}}$ in seven solvents; the results will be discussed later.

The results of the measurement of the refractive index of a pure solvent at 25 °C with 436 nm light, all of which were used for the dn/dc measurements, are shown in the third column of Table 1.

The refractive index increment for a fraction of atactic poly(2-vinylpyridine) ($M_w = 5.5\times10^4$) in several solvents is plotted against the concentration in Fig. 1. The linearity is satisfactory in all the solvents measured. The resultant values of dn/dc in all the solvents obtained by the least-squares method are shown in the fourth column of Table 1.

The value of the refractive index of a fraction of atactic poly(2-vinylpyridine) ($M_w = 34.7\times10^4$) in bulk for 436 nm light at 25 °C was 1.622. The specific volumes of three fractions of the same polymer ($M_w = 44.7\times10^4$, 34.7×10^4, and 19.0×10^4) at 20 °C were, on the average, 0.895, 0.896, and 0.895 cm³/g respectively.

TABLE 1. PARTIAL SPECIFIC VOLUME $\bar{v}_{2,op}$ OF ATACTIC POLY(2-VINYLPYRIDINE) OBTAINED OPTICALLY

No.	Solvent	n_1	dn/dc	$\bar{v}_{2,op}$ [a]	Δ [b]	δ [c]	$[\eta]$	$(0.5-\chi_1)/V_1\times10^4$	V_1	κ_s [d]
1	1,1,2,2-Tetrachloroethane	1.5040	0.109	0.884	1.4	4.4	1.06	3.96	105.7	45.8
2	Aniline	1.6168	0.023	0.874	2.6	3.2	1.05	3.93	91.5	35.6
3	2-Butanol	1.4022	0.216	0.845	5.8	−0.2	0.99	3.66	92.9	81
4	Chloroform	1.4536	0.168	0.848	5.5	0.1	0.99	3.58	80.7	67.1
5	*n*-Propanol	1.3912	0.215	0.842	6.1	−0.6	0.96	3.30	75.1	82.8
6	Methanol	1.3334	0.270	0.798	11.0	−5.8	0.90	3.06	40.7	100.1
7	*n*-Butanol	1.4021	0.209	0.838	6.6	−1.1	0.87	2.61	92.0	76.9
8	Ethanol	1.3671	0.245	0.809	9.8	−4.5	0.81	2.26	58.7	92.5
9	1,2-Dichloroethane	1.4539	0.148	0.885	1.3	4.5	0.73	1.66	79.4	55
10	Cyclohexanone	1.4591	0.144	0.885	1.3	4.5	0.71	1.50	97.2	50.2
11	Dimethylformamide	1.4411	0.165	0.872	2.8	3.0	0.58	0.74	77.4	
12	2-Propanol	1.3832	0.221	0.841	6.2	−0.7	0.54	0.57	75.1	93.2
13	1,1,1-Trichloroethane	1.4484	0.162	0.866	3.5	2.2	0.52	0.38	100.4	
14	Tetrahydrofuran	1.4135	0.195	0.851	5.1	0.5	0.51	0.37	81.7	
15	Nitroethane	1.4043	0.197	0.860	4.1	1.5	0.48	0.20	71.9	
16	Benzene	1.5192	0.107	0.868	3.2	2.5	0.48	0.19	89.5	64.9
17	Dioxane	1.4296	0.175	0.869	3.1	2.6	0.42	−0.02	85.7	50.1
18	Methylethylketone	1.3869	0.215	0.849	5.4	0.2	0.31	−0.37	91.5	83.8

a) $\bar{v}_{2,op}$=the values obtained with Eq. (5) in combination with Eq. (7). b) Δ=per cent deviation of $\bar{v}_{2,op}$ relative to the specific volume of bulk atactic poly(2-vinylpyridine) $v_{2,a}$. c) δ=per cent deviation of $\bar{v}_{2,op}$ relative to the specific volume of bulk isotactic crystalline poly(2-vinylpyridine) $v_{2,c}$. d) κ_s=adiabatic compressibility of solvent at 25 °C and 1 atmosphere. Ref.: "Chemical Hand Books, Part II", ed. by Chem. Soc. Japan, Maruzen, Tokyo (1966), p. 485

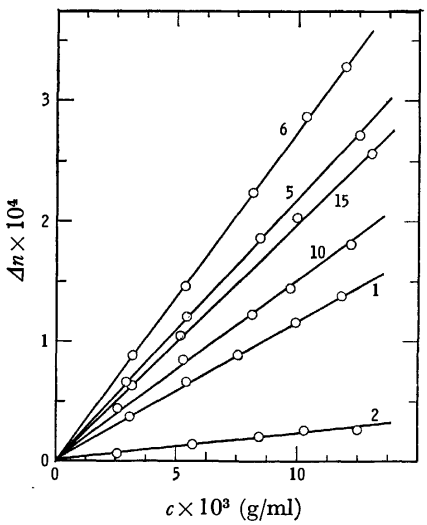

Fig. 1. Plots of the refractive index increment Δn *vs.* concentration c for atactic poly(2-vinylpyridine) at 25 °C. λ=436 nm. The numbers on the lines correspond to those in Table 1.

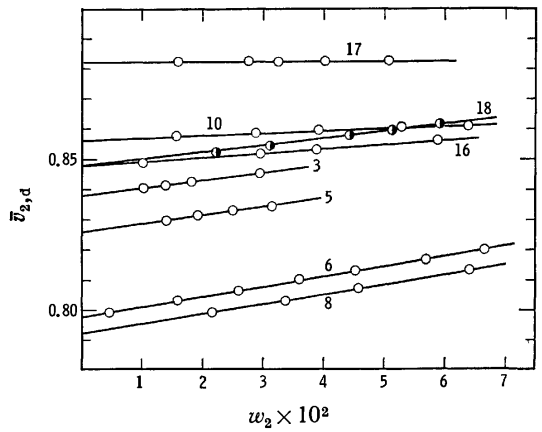

Fig. 2. Plots of the partial specific volume $\bar{v}_{2,d}$ of atactic poly(2-vinylpyridine) evaluated by densitometrically *vs.* concentration w in weight fraction at 25 °C. The numbers on the lines correspond to those in Table 2.

The mean value of these three values is 0.895 cm³/g. The volume-expansion coefficient of this polymer, as determined by dilatometry, was 3.0×10^{-4} cm³/g °C, so that the specific volume of this polymer at 25 °C was 0.897 cm³/g.

In Fig. 2 the values of the partial specific volume, $\bar{v}_{2,d}$ of the polymer at 25 °C, obtained by densitometric measurements of the solution in seven solvents, are plotted against the weight fraction of the polymer. The $\bar{v}_{2,d}$ value at each concentration was calculated, using the data of the density of a solution, with Kraemer's equation:[21,22]

$$\bar{v}_{2,d} = 1/\rho_{12}\{1-[(1-w_2)/\rho_{12}](d\rho_{12}/dw_2)\}$$

where ρ_{12} is the density of the solution, and w_2, the concentration of the polymer expressed by the weight fraction. The extrapolated values of $\bar{v}_{2,d}$ at w_2=0, which are the main interest in this investigation, are summarized in the sixth column of Table 2.

The values of the partial specific refraction, $\bar{R}_{2,GD}$, $\bar{R}_{2,LL}$, and $\bar{R}_{2,Ey}$, were calculated by fitting Eqs. (10), (11), and (12) to the data of n_1, dn/dc, and $\bar{v}_{2,d}$. The results are shown in Table 2.

As may be seen in Table 2, the deviation of the partial specific refraction from the mean value in any particular solvent is smallest in the case of $\bar{R}_{2,LL}$, and the specific refraction, $R_{2,He}$ (=0.316, Eq. (7)) of bulk atactic poly(2-vinylpyridine) is in fair agreement with the averaged value of the partial specific refraction, $\bar{R}_{2,LL}$ (=0.314, Eq. (11)). On the other hand, larger deviations are found with the corresponding specific refrac-

Table 2. Partial specific refraction and partial specific volume of atactic poly(2-vinylpyridine) at 25 °C

No.	Solvent	$R_{2,GD}$ Eq. (10)	$R_{2,LL}$ Eq. (11)	$R_{2,Ey}$ Eq. (12)	$\bar{v}_{2,}$ a)	$\bar{v}_{2,op}$ b)	$\frac{(\bar{v}_{2,op}-\bar{v}_{2,d})}{\bar{v}_{2,d}}\times 100$
5	*n*-Propanol	0.538	0.312	0.702	0.826	0.842	+1.9
6	Methanol	0.536	0.316	0.702	0.798	0.798	0
7	*n*-Buthanol	0.546	0.316	0.712	0.838	0.838	0
8	Ethanol	0.536	0.312	0.700	0.792	0.809	+2.1
10	Cyclohexanone	0.537	0.308	0.699	0.856	0.885	+3.4
16	Benzene	0.537	0.310	0.709	0.848	0.868	+2.4
17	Dioxane	0.553	0.319	0.721	0.882	0.869	−1.5
18	Methylethylketone	0.543	0.316	0.710	0.848	0.849	+0.1
	Mean	0.542	0.314	0.707			
		±0.011	±0.006	±0.015			
		$R_{2,HD}$ Eq. (1)	$R_{2,He}$ Eq. (2)	$R_{2,Ey}$ Eq. (3)			
	Bulk a-P2VP	0.558	0.316	0.724			

a) $\bar{v}_{2,d}$=the values obtained densitometrically. b) $\bar{v}_{2,op}$=the values obtained optically.

tions of the bulk polymer, $R_{2,GD}$ (=0.558, Eq. (1)) and $R_{2,Ey}$ (=0.724, Eq. (3)), in comparison with the mean values of the partial specific refractions, $\bar{R}_{2,op}$ (=0.542, Eq. (10)) and $\bar{R}_{2,Hy}$(=0.707, Eq. (12)).

Of course, the specific refraction, R_2, is not necessarily the same as the partial specific refraction, $\bar{R}_2$; however, the agreement between $\bar{R}_{2,LL}$ and $R_{2,He}$ is a satisfactory indication of the applicability of the Heller's method in this polymer-solvent system.

The partial specific volume of the polymer, $\bar{v}_{2,op}$, in all the solvents used in this experiment was evaluated according to the graphical scheme described previously using the value of 0.316 for $R_{2,He}$ (=k). Examples in several solvents are illustrated in Fig. 3. The $\bar{v}_{2,op}$ values in all the solvents were also evaluated from Eq. (8); they agreed very closely with those obtained graphically.

The values of $\bar{v}_{2,op}$ thus obtained are summarized in the fifth and seventh columns of Tables 1 and 2 respectively. In the eighth column of Table 2 the percent deviation of $\bar{v}_{2,op}$ from $\bar{v}_{2,d}$ defined by $[(\bar{v}_{2,op}-\bar{v}_{2,d})/\bar{v}_{2,d}]\times 100$ is shown. Except for the solution in cyclohexanone, the percentage of deviation is less than 2.4; this is almost

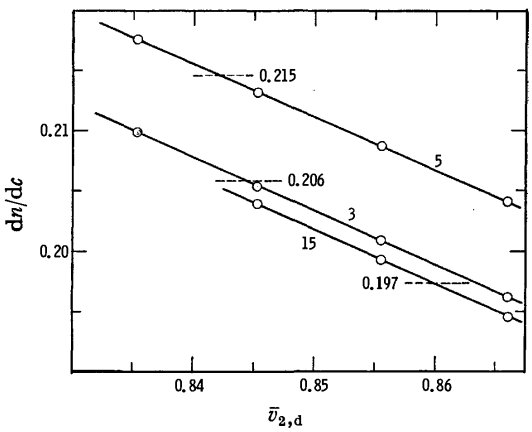

Fig. 3. Heller's plots for the tentative pairs of $\bar{v}_{2,op}$ and dn/dc obtained from Eqs. (5) and (7). The intersection of horizontal dashed lines with main plot gives $\bar{v}_{2,op}$ corresponding to experimentally obtained dn/dc. The numbers on the lines correspond to those in Table 1.

the same as the results for polystyrene reported by Heller,[6] and this is also an indication of the validity of the application of the method of Heller to this polymer-solvent system.

The values of Δ cited in the sixth column of Table 1 show the difference in $\bar{v}_{2,op}$ and the specific volume of bulk atactic poly(2-vinylpyridine), $v_{2,a}$ (=0.897 cm³/g), defined by $\Delta=[(v_{2,a}-\bar{v}_{2,op})/v_{2,a}]\times 100$. As a whole, they are larger than those reported for polystyrene.[6]

The specific volume, $v_{2,c}$ of the bulk crystalline isotactic poly(2-vinylpyridine) was 0.847 cm³/g at 25 °C for a fraction ($M_W=8.7\times 10^4$). The difference in $v_{2,a}$ and $v_{2,c}$ may be attributed to the increase in the free volume of the amorphous polymer. The apparent absolute free volume of bulk poly(2-vinylpyridine), as defined by $[(v_{2,a}-v_{2,c})/v_{2,c}]\times 100$, is 5.90%, which is comparable to the value for polystyrene:[6] 6.00—6.06%.

In the seventh column of Table 1 the apparent absolute free volumes of dissolved atactic poly(2-vinylpyridine), as defined by $\delta=[(\bar{v}_{2,op}-v_{,c})/v_{2,c}]\times 100$, are shown. Since the crystalline state is considered to be the most compact in the arrangement of the polymer segments, the negative values found in several solvents seem peculiar. The solvents which show negative values are 2-butanol, 1-propanol, 2-propanol, *n*-butanol, ethanol, and methanol, arranged in descending order of negative values. Even for a non-polar polymer such as polystyrene, a very small or slightly negative value of the apparent free volume in solution was pointed out by Heller,[6] therefore, the extremely large negative values found for this polymer in ethanol and methanol are remarkable.

In order to explain the effect of the change in the values of $\bar{v}_{2,op}$ with the nature of the solvents, we considered first the thermodynamic interactions between the polymer and the solvent. For such a thermodynamic parameter,[22] we used the values of $[(1/2-\chi_1)/V_1]$, where χ_1 is Flory's interaction parameter, and V_1, the molar volume of the solvent, as listed in the tenth column of Table 1. These values were obtained from the data of the limiting viscosity number for a fraction of atactic poly(2-vinylpyridine) ($M_W=28.7\times 10^4$) at 25 °C, assuming Flory's well-known expressions:[23]

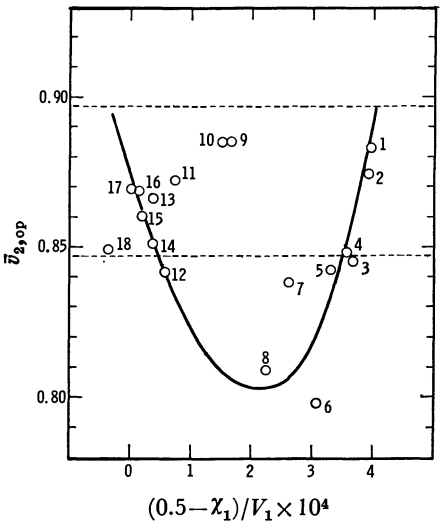

Fig. 4. Plots of the partial specific volume $\bar{v}_{2,op}$ *vs.* thermodynamic parameter $(1/2-\chi_1)/\bar{V}_1$ at 25 °C. The numbers on the points correspond to those in Table 1. The upper and lower dashed lines correspond to the specific volumes, $v_{2,a}$ and $v_{2,c}$ of bulk atactic and bulk crystalline poly(2-vinylpyridine), respectively.

$$\alpha^5 - \alpha^3 = 2C_m'(1/2-\chi_1)M^{1/2}$$

$$\alpha^3 = [\eta]/[\eta]_\theta \qquad [\eta]_\theta = KM^{1/2}$$

They are cited in the ninth column of Table 1, while $\bar{v}_{2,op}$ is plotted against them in Fig. 4. The points are rather scattered, some U-type relationship seems to exist between them. The shape of the curve is similar to that for the polystyrene-solvent system reported by Streeter and Boyer.[22] The decrease in the $\bar{v}_{2,op}$ with an increase in the solvent power may be attributed to the increase in the packing effect of the solvent molecules into the interior of the polymer coil because of the attraction between segments and solvent molecules.

As we have already shown, the interactions of poly(2-vinylpyridine) and alcohols, especially ethanol and methanol, are very strong because of the hydrogen-bonding formation.[1,4,5] The anomalous light-scattering behavior of poly(2-vinylpyridine) in methanol has been explained in terms of the extremely strong solvation of methanol to the segment-forming wire netting.[3] The peculiarity that the value of $\bar{v}_{2,op}$ is smaller than that of $v_{2,c}$ for isotactic crystalline poly(2-vinylpyridine) can also be attributed to this strong attraction between segments and solvents, which may result in a decrease in the partial specific volume of the solvent in addition to making for a closer packing of the solvent in the polymer coil.

The compressibility of the solvent molecule must also play an important role in such a case. In Fig. 5, $\bar{v}_{2,op}$ is plotted against the values of the adiabatic compressibility, κ_s, at 25 °C and one atmosphere as cited in the eleventh column of Table 1. As may be seen in this figure, there is some tendency for the value of $\bar{v}_{2,op}$ to decrease with an increase in the compressibility of the solvent. The compatibility of the large compressibility of methanol and ethanol and the large negative values of the apparent free volume of the polymer in these solvents are particularly remarkable.

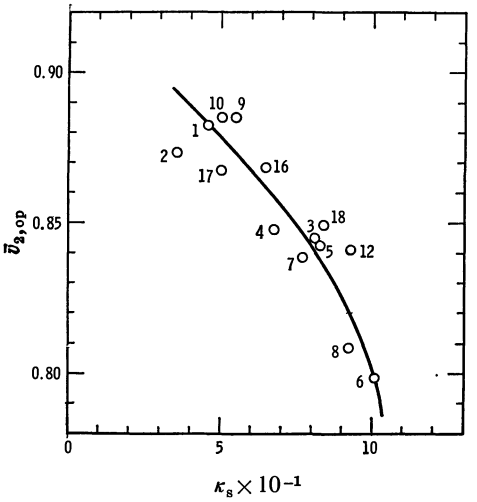

Fig. 5. Plots of the partial specific volume $\bar{v}_{2,op}$ *vs.* adiabatic compressibility of solvent κ_s at 25 °C and 1 atomsphere. The numbers on the points correspond to those in Table 1.

The tendency for them to be a rapid increase in $\bar{v}_{2,op}$ with an increase in $[(1/2-\chi_1)/\bar{V}_1]$ on the right-hand side of Fig. 4 is difficult to explain, but, it may be attributable to the crowding of the segments of different molecules in such a good solvent and to a decrease in the packing efficiency of solvent molecules. In addition, there may be some effects of the size and shape of the solvent molecule in their packing process. In Fig. 6, the values of $\bar{v}_{2,op}$ are plotted against the value of the molar volume of the solvent molecule. Although there is no definite reciprocity between $\bar{v}_{2,op}$ and V_1, some tendency for $\bar{v}_{2,op}$ to increase with V_1 is shown by the line in Fig. 6. Here again, methanol and ethanol seem to be favorable for the packing in the polymer coil because of their small volume.

Finally, for the purposes of practical use in light-scattering measurements[24,25] the empirical relation between dn/dc and n_1 for this polymer-solvent system was

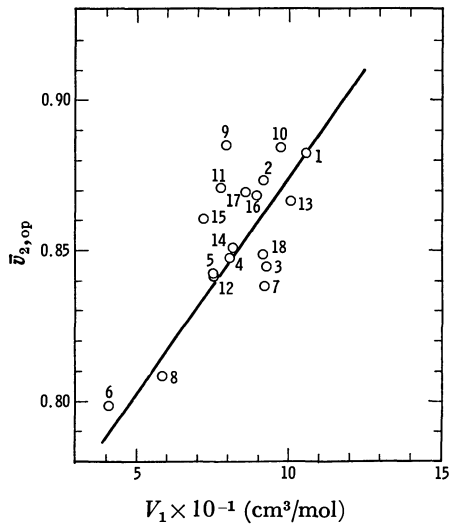

Fig. 6. Plots of the partial specific volume $\bar{v}_{2,op}$ *vs.* molar volume of solvent V_1 at 25 °C. The numbers on the points correspond to those in Table 1.

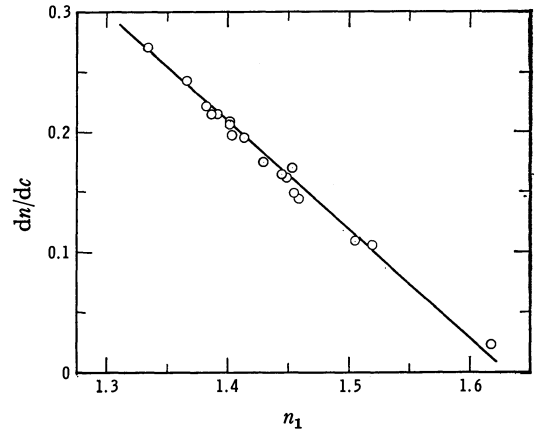

Fig. 7. Plots of specific refractive index increment dn/dc of atactic poly(2-vinylpyridine) *vs.* refractive index n_1 of solvent for 436 nm light at 25 °C.

evaluated. In Fig. 7 the values of dn/dc are plotted against the value of n_1 for 436 nm light. Their relation is represented by a linear line whose equation, as obtained by the least-squares method, is:

$$dn/dc = 0.900 \times (1.628 - n_1) \quad (13)$$

When volume additivity is assumed on the Gladstone-Dale expression for the specific refraction, Eq. (1) leads to this well-known equation:[26]

$$dn/dc = v_2(n_2 - n_1) \quad (14)$$

where each suffix is the same as before. The constants in Eq. (13), 0.900 and 1.628, agree well with the experimental values of $v_{2,a}$ (=0.897 cm^3/g) and n_2 (=1.622) presented previously.

Because the volume change on mixing the components in this polymer-solvent system is very remarkable, as has already been shown, the agreement between these values is clearly fortuitous; however, Eq. (13) can be used for predicting the value of dn/dc of atactic poly(2-vinylpyridine) within ± 0.002 in a given solvent possessing the value of n_1.

References

1) A. Dondos, *Makromol. Chem.*, **135**, 181 (1970).
2) A. Dondos and H. Benoit, *Macromolecules*, **4**, 279 (1971).
3) N. Sakamoto, M. Yoshida, and S. Arichi, This Bulletin, **47**, 1363 (1974).
4) S. Arichi, *ibid.*, **41**, 548 (1968).
5) S. Arichi, *ibid.*, **41**, 1296 (1968).
6) W. Heller, *J. Polym. Sci., Part A*-2, **4**, 209 (1966).
7) M. B. Huglin, "Light Scattering from Polymer Solutions," Academic Press, London and New York (1972).
8) A. Kruis, *Z. Physik. Chem., B.* **34**, 13 (1936).
9) L. J. Gosting and M. S. Morris, *J. Amer. Chem. Soc.*, **71**, 1998 (1949).
10) G. M. Kline, "Analytical Chemistry of Polymers, Part II, Analysis of Molecular Structure and Chemical Groups," Interscience Publishers, New York and London (1962).
11) C. Nöel, *C. R. Acad. Sci. Paris*, **258**, 3702 (1964).
12) S. Arichi, S. Mitsuta, N. Sakamoto, and H. Murata, This Bulletin, **39**, 428 (1966).
13) S. Arichi, *ibid.*, **41**, 244 (1968).
14) G. Natta, G. Mazzanti, P. Longi, G. Dall'asta, and F. Bernardini, *J. Polym. Sci.*, **51**, 487 (1961).
15) O. Bodmann, *Makromol. Chem.*, **122**, 196 (1969).
16) W. Mächtle and H. Fischer, *Angew. Makromol. Chem.*, **7**, 147 (1969).
17) W. Heller, *J. Phys. Chem.*, **69**. 1123 (1965).
18) W. Heller and E. S. E. Schwartz, *J. Polym. Sci.*, Polymer Phys. Ed., **10**, 1903 (1972).
19) B. J. Rietveld, *ibid.*, *A*-2, **8**, 1837 (1970).
20) Th. G. Scholte, *ibid.*, *A*-2, **10**, 519 (1972).
21) T. Svedberg and K. Pedersen, "The Ultracentrifuge," Oxford University Press, Oxford (1940).
22) D. J. Streeter and R. F. Boyer, *Ind. Eng. Chem.*, **43**, 1790 (1951).
23) P. J. Flory and T. G. Fox, *J. Amer. Chem. Soc.*, **73**, 1904 (1951).
24) H. Inagaki, H. Suzuki, M. Fujii, and T. Matsuo, *J. Phys. Chem.*, **70**, 1718 (1966).
25) J. M. G. Cowie, *J. Polym. Sci., Part C*-**23**, 267 (1968).
26) M. B. Huglin, *J. Appl. Polym. Sci.*, **9**, 4003 (1965).

Dielectric Relaxation and Molecular Structure. XV. A Further Study of the Benzene Effect of 1,2-Dichloroethane and Related Molecules

Naoyuki SHIRATORI, Hiroaki TAKAHASHI, and Keniti HIGASI
Department of Chemistry, Waseda University, Shinjuku, Tokyo 160

(Received January 23, 1975)

The dielectric relaxation times, τ, and dipole moments, μ, of 1,2-dichloroethane (A), *cis*-1,2-dichloroethylene(B), 1,3-dichloropropane(C), *o*-dichlorobenzene(D), and 1-chloro-2-propanone(E) have been measured in two aromatic and two aliphatic nonpolar solvents. The results are as follows: both the τ and μ of (A) and (E) are exceptionally large in aromatic solvents, showing the benzene effect; (B) and (C) have large τ but normal μ values in aromatic solvents, while (D) shows normal effects of the solvent upon both τ and μ in two different sets of solvents. Finally, the intetmolecular interaction between the solute and the solvent is discussed with special regard to the origin of the benzene effect.

A previous dielectric study[1] of the solvent effects of 1,2-dichloroethane was based on the measurements on the frequencies, 1 MHz and 9.33, 24.15, and 48.00 GHz. A further investigation of the same subject by the use of millimeter waves with the frequencies of 96.3—96.6 GHz will be reported here. In addition, the results of new dielectric measurements will be discussed with regard to three dichloro-compounds (one aromatic and two aliphatic) and one ketone (1-chloro-2-propanone), which exhibits the benzene effect in dipole moments.[2]

Experimental

The samples employed were all commercially available. They were carefully purified before use. The boiling points and the refractive indices were checked against the literature values. The apparatus and the experimental technique for the dielectric measurements at 96.3—96.6 GHz were described in a preceding paper.[3] The static dielectric constants were measured by the heterodyne beat method, while the refractive indices for the Na D line were measured by the use of a Pulfrich refractometer.

Results

The values of the slopes a_0, a', a'', a_D, and b obtained in this experiments for five compounds, (A), (B), (C), (D), and (E), in four solvents are collected in Table 1. The slopes a' and a'' were obtained on the assumption that the linear relationship of the dielectric constant, ε', and loss, ε'', with the concentration (weight fraction), w_2, is valid in dilute solutions:

$$\begin{aligned} \varepsilon' &= \varepsilon_1' + a'w_2 \\ \varepsilon'' &= \varepsilon_1'' + a''w_2 \end{aligned} \qquad (1)$$

Further, a_0, a_D, and b represent the slopes for the static dielectric constant, ε_0, the square of the refractive index, n_D^2, and the specific volume, v, against the weight fraction respectively. (Regarding the symbols and equations in detail, see the preceding papers.[1,4,5])

Table 2 records the molecular polarization, ${}_\infty P_2$, at an infinitely dilute concentration; it was obtained from a_0 and b by the use of the following equation:[5,6]

$${}_\infty P_2 = M_2\left\{\frac{3a_0v_1}{(\varepsilon_{10}+2)^2} + (v_1+b)\frac{\varepsilon_{10}-1}{\varepsilon_{10}+2}\right\} \qquad (2)$$

Table 1. THE SLOPES a_0(STATIC), a', a'' (96 GHz), a_D(OPTICAL), AND b(VOLUME) AT 20 °C

Solvent	a_0	a'	a''	a_D	b
(A) 1,2-Dichloroethane[a]					
Benzene	3.585	0.899	1.062	−0.143	−0.331
p-Xylene	2.941	0.770	0.692	−0.133	−0.351
Carbon tetrachloride	4.074	1.353	1.432	−0.091	0.187
Cyclohexane	1.797	0.895	0.647	−0.017	−0.435
(B) *cis*-1,2-Dichloroethylene[b]					
Benzene	3.611	0.936	1.138	−0.118	−0.358
p-Xylene	3.609	0.970	0.998	−0.095	−0.387
Carbon tetrachloride	6.420	2.058	2.313	−0.053	0.154
Cyclohexane	2.991	1.408	1.122	0.013	−0.487
(C) 1,3-Dichloropropane[b]					
Benzene	4.121	0.894	1.154	−0.129	−0.292
p-Xylene	4.027	0.884	1.035	−0.102	−0.321
Carbon tetrachloride	7.460	1.814	2.228	−0.034	0.212
Cyclohexane	3.386	1.271	1.148	0.007	−0.408
(D) *o*-Dichlorobenzene[c]					
Benzene	3.565	0.285	0.567	0.102	−0.363
p-Xylene	3.467	0.322	0.519	0.118	−0.403
Carbon tetrachloride	5.972	0.534	0.843	0.353	0.148
Cyclohexane	2.919	0.414	0.512	0.213	−0.506
(E) 1-Chloro-2-propanone[c]					
Benzene	9.646	2.115	2.536	−0.184	−0.264
p-Xylene	8.538	2.017	1.967	−0.166	−0.286
Carbon tetrachloride	12.187	4.141	3.449	−0.174	0.265
Cyclohexane	5.046	2.439	1.712	−0.056	−0.344

Frequencies of measurements: a) 96.31 GHz; b) 96.46 GHz; c) 96.59 GHz.

The molar refraction, R_D, of Table 2 is given by:[5]

$$R_D = M_2\left\{\frac{3a_Dv_1}{(n_{1D}^2+2)^2} + (v_1+b)\frac{n_{1D}^2-1}{n_{1D}^2+2}\right\} \qquad (3)$$

The symbols M_2, ε_{10}, and n_{1D} have their usual significance.[4,5] The dipole moment, μ(D), in Table 2 is calculated from Eq. (4):

$$\mu = 0.0128\{({}_\infty P_2 - R_D)T\}^{1/2} \qquad (4)$$

TABLE 2. POLARIZATIONS, REFRACTIONS, AND DIPOLE MOMEMTS (20 °C)

Solvent	$_{\infty}P_2$ (cm^3)	R_D (cm^3)	μ (D)	μ(lit.) (D)
(A) 1,2-Dichloroethane				
Benzene	89.9	20.9	1.82	1.78,[a] 1.85[a]
p-Xylene	79.4	20.9	1.68	1.63,[b] 1.58[c]
Carbon tetrachloride	65.8	21.1	1.47	1.38,[b] 1.56[d]
Cyclohexane	63.7	21.1	1.43	1.46[c]
(B) *cis*-1,2-Dichloroethylene				
Benzene	87.7	20.1	1.80	1.76[a] (25 °C)
p-Xylene	89.2	20.2	1.82	—
Carbon tetrachloride	87.3	20.2	1.80	1.80[a] (25 °C)
Cyclohexane	88.7	20.1	1.82	—
(C) 1,3-Dichloropropane				
Benzene	115.2	25.4	2.08	2.09[a]
p-Xylene	115.2	25.5	2.08	—
Carbon tetrachloride	116.0	25.6	2.09	—
Cyclohexane	116.3	25.6	2.09	—
(D) *o*-Dichlorobenzene				
Benzene	131.6	36.4	2.14	2.26[e]
p-Xylene	130.5	35.9	2.13	—
Carbon tetrachloride	125.3	36.9	2.06	—
Cyclohexane	131.2	36.7	2.13	2.27[f] (25 °C)
(E) 1-Chloro-2-propanone				
Benzene	190.2	20.6	2.86	2.89[g] (25 °C)
p-Xylene	175.1	20.7	2.73	—
Carbon tetrachloride	142.3	20.9	2.42	2.38[a] (25 °C)
Cyclohexane	133.3	21.1	2.32	2.36[g] (25 °C)

a) A. L. McClellan, "Tables of Experimental Dipole Moments," W. H. Freeman and Co., San Francisco and London (1963). b) Ref. 1. c) Ref. 22. d) J. Crossley and S. Walker, *J. Chem. Phys.*, **45**, 4733 (1966). e) B. Krishna and K. K. Srivastava, *ibid.*, **32**, 663 (1960). f) J. Crossley and W. H. Hassell, *ibid.*, **48**, 1261 (1968). g) Ref. 2.

where T is the absolute temperature. It may be seen from Table 2 that both benzene and *p*-xylene give higher dipole moments for two solutes, (A) and (E), while they provide the remaining three molecules, (B), (C), and (D), with almost the same dipole moments as those in aliphatic solvents.

Discussion

The Cole-Cole equation[7] for a dilute solution is expressed in the following form:[8]

$$\frac{(a'-ia'')-a_{\infty}}{a_0-a_{\infty}}=\frac{1}{1+(i\omega\tau_0)^{1-\alpha}} \qquad (5)$$

where τ_0 is the most probable relaxation time, α is the distribution parameter, and ω is the angular frequency. Using the a' and a'' values obtained for 1,2-dichloroethane at five frequencies, 1 MHz and 9, 24, 48, and 96 GHz, three parameters, τ_0, α, and a_{∞}, of Eq. (5) were calculated for various solutions by the use of a computer. The results are shown in Table 3.

We find the distribution parameter, α, to be almost zero in non-aromatic solvents. We also find that α values are also small, but differ from zero in aromatic solvents. Using Budo's equation,[9] we are able to

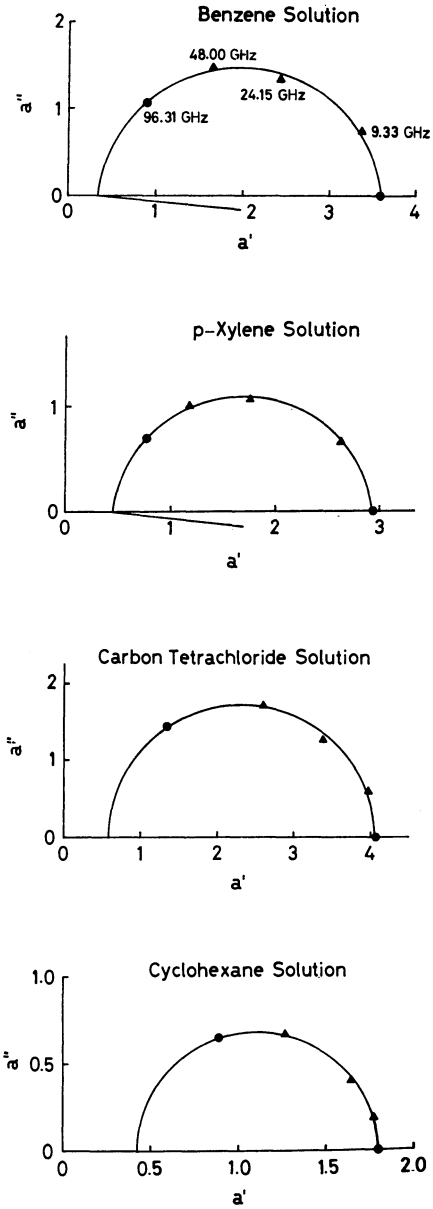

Fig. 1. The Cole-Cole plots for 1,2-dichloroethane in various solvents at 20 °C.
●: This work, ▲: A previous work (Ref. 1).

TABLE 3. THREE COLE-COLE PARAMETERS FOR 1,2-DICHLOROETHANE AT 20 °C

Solvent	a_{∞}	τ_0(ps)	α
Benzene	0.339	4.28	0.07
p-Xylene	0.450	5.67	0.08
Carbon tetrachloride	0.587	2.96	0.00
Cyclohexane	0.422	2.38	0.01

obtain, for aromatic solvents, two reasonable relaxation times (τ_1 and τ_2) and also the weight factors, C_2 and C_1 ($=1-C_2$) *viz.*, τ_1=6.81 ps, τ_2=2.75 ps, C_2=0.502 (for benzene) and τ_1=7.22 ps, τ_2=2.00 ps, C_2=0.233 (for *p*-xylene)*, but we failed to obtain any sensible results for other solvents. However, this cannot be regarded

* This means that the number of *free gauche* isomers becomes smaller in *p*-xylene than in benzene.

TABLE 4. THE RELAXATION TIMES τ(ps) CALCULATED FROM MEASUREMENTS AT 100 GHz (20 °C)

Substance	Benzene	*p*-Xylene	Carbon tetrachloride	Cyclohexane
(A) 1,2-Dichloroethane	4.18±0.12	5.18±0.12	3.14±0.06	2.30±0.11
(B) *cis*-1,2-Dichloroethylene	3.88±0.11	4.36±0.17	3.11±0.07	2.33±0.05
(C) 1,3-Dichloropropane	4.61±0.09	5.01±0.10	4.18±0.05	3.04±0.10
(D) *o*-Dichlorobenzene	9.52±0.22	9.99±0.16	10.62±0.08	8.06±0.12
(E) 1-Chloro-2-propanone	4.89±0.05	5.46±0.08	3.84±0.07	2.51±0.17

as good evidence for complex formation[10] in the aromatic medium, since the observed α values are too small to make such an analysis reliable.

Another point of interest is that the slopes, a_∞, for the extremely high frequency were found to be unusually large.** In fact, the present work gives much higher values of a_∞ than those estimated roughly in the preceding paper.[1] Possibly this indicates some appreciable absorption in the submillimeter region; however, this point is not yet clear.

As has been reported in the preceding paper[1] the relaxation times of 1,2-dichloroethane are of a considerable magnitude in both benzene and *p*-xylene. That is, the τ_0 values in the aromatic solvent, 4.28 ps (benzene) and 5.67 ps (*p*-xylene), are about twice the τ_0 values in non-aromatic solvents, *viz.*, 2.96 ps (carbon tetrachloride) and 2.38 ps (cyclohexane), while the viscosities of the aromatic solvents are even smaller than those of the non-aromatic solvents (cyclohexane and carbon tetrachloride) by 32.4% (benzene) and 33.9% (*p*-xylene).

Two different approaches have been made to the benzene effect of 1,2-dichloroethane. One was made by Wada and Morino,[11] who showed that the *gauche* isomers are stabilized in the medium of benzene for an unspecified reason, resulting in a higher dipole moment. The other, by Kubo,[12] is that 1,2-dichloroethane forms a 1:1 complex with benzene, from which an increase in the relaxation time can be predicted. Morita *et al.*[10] reached Kubo's conclusion by repeating the same experiment and further confirmed that the 1:1 complex of 1,2-dichloroethane has the dipole moment of the *gauche* isomer, 2.55 D.[13]

However, there are some difficulties with the Kubo-Morita's conclusion, First. thermodynamical studies have failed in producing any evidence for the complex formation.[14] Secondly, the equilibrium constant for the complex formation has been found to depend upon the inert solvent,*** K_c (ml/mol) is 30.0 in carbon tetrachloride, 90.7 in *n*-hexane, and 139 in cyclohexane; further, the dipole moment of the complex is affected also by the solvent, μ(D)=2.54 in carbon tetrachloride, 2.11 in *n*-hexane, and 1.99 in cyclohexane.[10,15] Probably, benzene interacts with 1,2-dichloroethane in such a way that the configuration of the *gauche* isomer is more favored; however, this interaction is not strong enough to produce an aggregate with a structure rigid enough at room temperature to be unaffected by the surrounding molecules of the inert solvent.

The interaction between 1,2-dichloroethane and *p*-xylene is somewhat similar to, but stronger than, that of 1,2-dichloroethane and benzene, since the τ_0 value (5.67 ps) in *p*-xylene is larger than that (4.28 ps) in benzene—compare this change with the change in the weight factor, C_2, and its related footnote. The above findings are in accord with the changes in the equilibrium constants—*e.g.*, K_c=30.0 ml/mol in benzene and 51.0 ml/mol in *p*-xylene (in the inert solvent CCl_4).[10,15] On the other hand, the dipole moment, or the configuration itself, of the *gauche* isomer might be changed in the 1:1 complex. In fact, the polarity of the complex becomes smaller upon a change in solvent from benzene to *p*-xylene, *e.g.*, μ=2.54 D in benzene and 2.04 D in *p*-xylene (in the inert solvent CCl_4).

In Table 4 the relaxation times, τ, for five molecules, (A), (B), (C), (D), and (E), are collected. The values were all obtained by the use of the following Debye equation:

$$\tau = \frac{1}{w}\frac{a_0 - a'}{a''} \tag{6}$$

in which a' and a'' at 96 GHz are employed for the calculation.[8] In Table 4 we find the relaxation times of all the five solutes in carbon tetrachloride to be larger by 32—53% than the corresponding ones in cyclohexane. This is surprising because the two solvents have practically the same viscosity at room temperature; the two τ values should, then, be equal to each other for any solute if the usual Debye equation[18] were valid. The unusual rise in the relaxation time in carbon tetrachloride indicates, therefore, that the Debye approach is wrong. The alternative interpretation[19] after Eyring would indicate that particularly strong forces exist between all the solutes and carbon tetrachloride, by which the rotation of the solute molecules is hindered.

The skeleton of *cis*-1,2-dichloroethylene (B) is flat, and its C=C bond is slightly shorter than the C–C bond in 1,2-dichloroethane (A); the dipole moment, 1.80—1.82 D, for (B) is smaller than the *gauche* isomer of (A) 2.55 D. In other respects, however, the configuration of (B) may well compare with that the *gauche* isomer of (A). The relaxation times in the last two solvents are almost the same for the two molecules, (A) and (B). Although they differ in magnitude, the relaxation times of (B) are similarly high in aromatic solvents in spite of the fact that (A) has rotational isomers, while (B) has none. Perphaps this suggests that the relaxation

** If a_D is used instead of a_∞, we obtain a skewed arc, as has been pointed out by some Indian workers. For instance, see, for the benzene solutions, S. Chandra and R. A. Yadav, This Bulletin, **46**, 1900 (1973), and for a liquid, S. Chandra and R. A. Yadav, *J. Chim. Phys.*, **69**, 1018 (1972).

*** Similar variations in K with inert solvents were observed on charge-transfer complexes.[16,17] Possibly, the inert solvent is not ideal, but it interacts with either the solute or the solvent, or with both.

time is affected mostly by forces acting between the solute and the solvents in the first approximation.

The solvent interaction of 1,3-dichloropropane (C) with aromatic solvents is similar to, but somewhat weaker than, that of *cis*-1,2-dichloroethylene (B), while the corresponding interactions of (D) in aromatic solvents are the least pronounced of all. On the other hand, the interactions of 1-chloro-2-propanone (E) may well compare with those of 1,2-dichloroethane (A); both molecules have two rotational isomers, one strongly polar and the other nonpolar or at least less polar.

Next, we shall turn to the problem of the nature of the interaction between aromatic solvents and 1,2-dichloroethane. The mechanism of complex formation through hydrogen bonds was first proposed by Neckel and Volk[20] and later examined by Crossley and Walker[21] and Smyth.[22] However, this hypothesis of hydrogen bonding is not supported by the fact that the benzene effect in the dipole moment exists[23] even when all the hydrogen atoms of 1,2-dichloroethane are replaced by methyl groups. The alternative hypothesis is that the interaction originates from the chlorine atoms of 1,2-dichloroethane or, rather, from the C–Cl bonds. In other words, because of the large dipole moments of the C–Cl bonds and the large hyperpolarizability[24] of the aromatic solvent, the dipole-polarizability effect is possibly the origin of the benzene effect. The second explanation, however, has not yet been provided with any definitive proof.

Concluding Remarks on the Benzene Effect

The following conclusions are reached on the basis of the present investigation, together with the three preceding ones:[1,10,15]

1) 1,2-Dichloroethane and aromatic hydrocarbon molecules seem to interact in such a way as to form a loosely bound 1:1 complex in which 1,2-dichloroethane maintains its *gauche* configuration without much distortion.

2) Extra stabilization energy which cannot be explained by a simple electrostatic model[11] is gained by the *gauche* isomers in the medium of an aromatic solvent as a result of the above complex formation. Also, the Raman lines for the *gauche* isomer become stronger[11,25] in the presence of aromatic hydrocarbon molecules.

3) The apparent dipole moment of (A) becomes larger, since the number of the *gauche* isomers increases in the aromatic medium.[1] The dielectric relaxation time of (A) becomes high in the medium of an aromatic solvent because the rotation of the polar solute molecules becomes hindered in this medium.

4) The benzene effect for 1,2-dichloroethane (A) described above will be found even when another aromatic solvent is used instead of benzene. The benzene effect will also be found for some other polar molecules, *e.g.*, 1-chloro-2-propanone (E).

5) The dielectroric-relaxation-time method is useful for detecting the weakest intermolecular interaction. The dipole-polarization and other forces in the solute-solvent intraction are important in this effect.

We wish to thank the Science and Engineering Research Laboratory of Waseda University for its financial aid. We also indebted to Dr. Yoshinori Koga and Mr. Ryuichi Minami for providing us with unpublished data on the benzene effect of 1,2-dichloroethane and also for their helpful discussions.

References

1) K. Chitoku and K. Higasi, This Bulletin, **40**, 773 (1967).
2) A. Abadie, C. Michel, and P. Mauret, *C. R. Acad. Sci. Paris*, **264C**, 1433 (1967).
3) K. Chitoku, K. Higasi, M. Nakamura, Y. Koga, and H. Takahashi, This Bulletin, **44**, 992 (1971).
4) Y. Koga, H. Takahashi, and K. Higasi, *ibid.*, **46**, 3359 (1973).
5) Y. Koga, H. Takahashi, and K. Higasi, *ibid.*, **47**, 84 (1974).
6) I. F. Halverstadt and W. D. Kumler, *J. Amer. Chem. Soc.*, **64**, 2988 (1942).
7) K. S. Cole and R. H. Cole, *J. Chem. Phys.*, **9**, 341 (1941).
8) K. Higasi, This Bulletin, **39**, 2157 (1966).
9) A. Budo, *Phys. Z.*, **39**, 706 (1938).
10) A. Morita, H. Takahashi, and K. Higasi, This Bulletin, **45**, 1045 (1972).
11) A. Wada, and Y. Morino, *J. Chem. Phys.*, **22**, 1276 (1954).
12) M. Kubo, *Bull. Inst. Phys. Chem. Res. Tokyo*, **13**, 1221 (1934).
13) S. Mizushima, "Structure of Molecules and Internal Rotation," Academic Press, New York (1954), p. 35.
14) O. Kiyohara and K. Arakawa, This Bulletin, **43**, 3037 (1970).
15) K. Higasi, H. Takahashi, K. Chitoku, and A. Morita, *Memo. Sch. Sci. Eng., Waseda Univ.*, **35**, 75 (1971).
16) C. C. Thompson, Jr., and P. A. D. de Maine, *J. Phys. Chem.*, **69**, 2766 (1965).
17) R. Foster, *J. Chem. Soc.*, **1960**, 1075.
18) P. Debye, "Polare Molekeln," S. Hirzel, Leipzig (1929), Eqs. (50) and (52), pp. 96—97.
19) K. Chitoku and K. Higasi, This Bulletin, **39**, 2160 (1966).
20) A. Neckel and H. Volk, *Z. Electrochem.*, **62**, 1104 (1958).
21) J. Crossley and S. Walker, *J. Chem. Phys.*, **48**, 4742 (1968).
22) J. Crossley and C. P. Smyth, *J. Amer. Chem. Soc.*, **91**, 2482 (1969).
23) Y. Morino, I. Miyagawa, Y. Haga, and S. Mizushima, This Bulletin, **28**, 165 (1955).
24) C. A. Coulson, A. Maccoll, and L. E. Sutton, *Trans. Faraday Soc.*, **48**, 106 (1952).
25) S. Mizushima, Y. Morino, and K. Higasi, *Sci. Pap. Inst. Phys. Chem. Res. Tokyo*, **25**, 159 (1934).

Chemical Equilibria between a Lanthanide Shift Reagent and *n*-Hexylamine in Chloroform

Fuyuhiko INAGAKI, Mitsuo TASUMI, and Tatsuo MIYAZAWA

Department of Biophysics and Biochemistry, Faculty of Science, The University of Tokyo, Bunkyo-ku, Tokyo 113

(Received February 18, 1975)

The $Eu(fod)_3$-induced ^1H NMR shifts of *n*-hexylamine were observed using two kinds of dilution methods. The results are analyzed in terms of the chemical equilibria among the shift reagent (L), substrate (S), 1 : 1 (LS), and 1 : 2 (LS_2) complexes. The association constants and the induced shifts intrinsic to the LS and LS_2 complexes are evaluated accurately by fitting the theoretical curves to the observed data. The values obtained are utilized to confirm the validity and usefulness of the extrapolation method proposed previously to determine the shift ratios for the LS complex.

It has been pointed out that, in order to determine the molecular structure in solution by means of the lanthanide-induced NMR shift (LIS), the ratios of shifts intrinsic to the lanthanide–substrate 1 : 1 complex (LS complex) should be used.[1-4] In a previous paper[4] we proposed an experimental method to derive the shift ratios for the LS complex and applied it to the Eu(III)–L-azetidine-2-carboxylic acid system in D_2O solution. A lanthanide chelate compound such as $Eu(fod)_3$ (fod = 1,1,1,2,2,3,3-heptafluoro-7,7-dimethyl-4,6-octanedione) induces much larger shifts to a substrate dissolved in an organic solvent than a lanthanide ion does in aqueous solution. The stoichiometric analysis can therefore be made more precisely for the system of a lanthanide chelate and a substrate in an organic solvent. In the present paper we analyze the chemical equilibria of $Eu(fod)_3$ and *n*-hexylamine in chloroform, taking into account the formation of not only the LS complex but also the LS_2 (1 : 2) complex. The results are utilized to show that the experimental method of obtaining the shift ratios for the LS complex[4] is an appropriate and useful one.

Experimental

All the NMR spectra were run on a Hitachi R-22 NMR spectrometer (90 MHz) in the frequency-sweep mode at a probe temperature of 37 °C. The shifts were measured using a frequency counter with estimated accuracy of ± 1 Hz or less.

n-Hexylamine, $Eu(fod)_3$, and deuterated chloroform containing 1% tetramethylsilane were purchased, respectively, from Tokyo Chemical Industry Co., Dojin Chemicals, and E. Merck. As a trace amount of water in the reagents was found to have a serious effect on the results of LIS mesurements, it was eliminated with special caution. *n*-Hexylamine was distilled over sodium hydroxide in the dry nitrogen atmosphere and was stored with synthetic zeolite A-4. $Eu(fod)_3$, was dried over phosphorus pentoxide in an evacuated desiccator (10^{-3}—10^{-4} mmHg) for a week.[5,6] Deuterated chloroform was mixed with active alumina which was then removed by filtration. The samples for NMR measurements were prepared in a dry box flushed with nitrogen gas. The LIS values obtained in this way were reproducible and considerably larger than those obtained without these procedures.

The LIS's of *n*-hexylamine were observed for a series of solutions prepared by the following two methods.[4] In the successive dilution method an original solution containing approximately equimolar substrate and shift reagent was diluted stepwise with the solvent. The original concentrations of *n*-hexylamine and $Eu(fod)_3$ were 0.286 and 0.272 M, respectively. On the other hand, in the incremental dilution method an original solution was diluted stepwise with the substrate solution of the same concentration as in the original solution, so that only the $Eu(fod)_3$ concentration was lowered. The original concentrations of *n*-hexylamine and $Eu(fod)_3$ were 0.097 and 0.248 M, respectively.

Method of Analysis

Chemical equilibria among a lanthanide shift reagent (L), a substrate (S), and the complexes are described by the following schemes under the assumption that the formation of complexes LS_x ($x \geqq 3$) may be neglected.

$$L + S \overset{K_1}{\rightleftharpoons} LS \quad (1)$$

$$LS + S \overset{K_2}{\rightleftharpoons} LS_2 \quad (2)$$

where K_1 and K_2 are the association constants given as

$$K_1 = [LS]/[L][S] \quad (3)$$

$$K_2 = [LS_2]/[LS][S] \quad (4)$$

If the LIS (of the ith nucleus, $i = 1$—n) intrinsic to the LS and LS_2 complexes are expressed as $\Delta_1{}^i$ and $\Delta_2{}^i$, respectively, the observed shift ($\Delta\delta^i_{obsd}$) may be given on the fast-exchange condition as

$$\Delta\delta^i_{obsd} = ([LS]/[S_0])\Delta_1{}^i + 2([LS_2]/[S_0])\Delta_2{}^i \quad (5)$$

where $[S_0]$ is the total concentration of the substrate.

The purpose of the present analysis is to obtain the most probable values of K_1, K_2, $\Delta_1{}^1$—$\Delta_1{}^n$, and $\Delta_2{}^1$—$\Delta_2{}^n$ which reproduce both sets of observed LIS data derived from the successive dilution and the incremental dilution methods. This can be done according to the following steps. (a) The values of K_1 and K_2 are assumed. (b) Equations (3) and (4) are solved for [LS] and $[LS_2]$ using the Newton-Raphson method. (c) The expected LIS value ($\Delta\delta^i_{calcd}$) is calculated by Eq. (5) with assumed values of $\Delta_1{}^i$ and $\Delta_2{}^i$. The best values of $\Delta_1{}^i$ and $\Delta_2{}^i$ can then be obtained by minimizing the sum (S) given as

$$S = \sum_{i=1}^{n} \sum_{j=1}^{N_i} w_j \{\delta^i_{obsd}(j) - \delta^i_{calc}(j)\}^2 \quad (6)$$

where N_i is the total number of observed data for the ith nucleus and w_j is the weight for the jth observed LIS value. All the values of w_j were set equal to unity. (d) The steps (a) to (c) are repeated for various sets of K_1 and K_2 until the parameters which minimize S

are finally found.

The computation outlined above was performed with the program SHIFT using a HITAC 8800/8700 system at the Computer Centre of the University of Tokyo.

Results and Discussion

By the addition of $Eu(fod)_3$ the NMR spectrum of *n*-hexylamine becomes first-order and all the resonances due to the α—ε methylene protons and the ω methyl protons are easily assigned. The results of the successive dilution and the incremental dilution methods are shown with open circles in Figs. 1 and 2, respectively. In the former method the molar ratio $\rho([L_0]/[S_0]$, the ratio of total concentrations) is kept constant (0.951), whereas

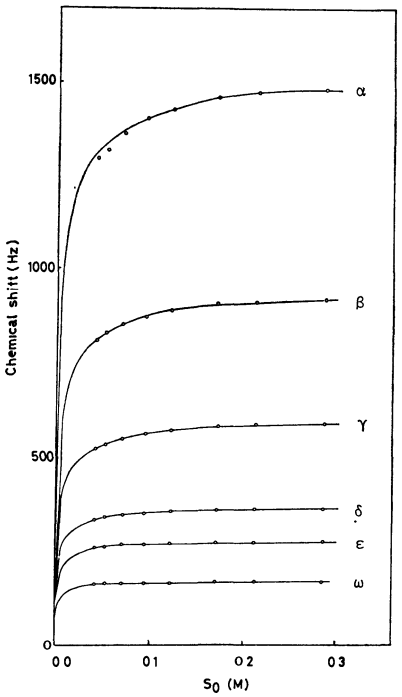

Fig. 1. $Eu(fod)_3$-induced shifts $\Delta\delta_{obsd}$ of *n*-hexylamine *vs.* total substrate concentration $[S_0]$ obtained by the successive dilution method. $CDCl_3$ solution, 37 °C, $\rho=0.95$. The observed data for α—ε methylene and ω methyl protons are shown with open circles. The curves were obtained by the calculation (see text).

TABLE 1. THE ASSOCIATION CONSTANTS (K_1 AND K_2) AND THE SHIFTS INTRINSIC TO THE LS AND LS_2 COMPLEXES (Δ_1 AND Δ_2) FOR THE $Eu(fod)_3$–*n*-HEXYLAMINE SYSTEM

Proton	Δ_1,[a] Hz	Δ_2,[a] Hz
α	1264.5 (6.8)	1373.6 (14.8)
β	793.2 (1.9)	936.7 (6.2)
γ	473.2 (1.6)	528.0 (5.3)
δ	245.5 (1.9)	304.4 (6.3)
ε	152.3 (1.5)	219.2 (4.9)
ω	89.7 (1.1)	124.4 (3.6)
	$K_1=535.5$[b]	$K_2=13.9$[b]

a) The calculated standard deviation is shown in parentheses. b) In the unit of M^{-1}.

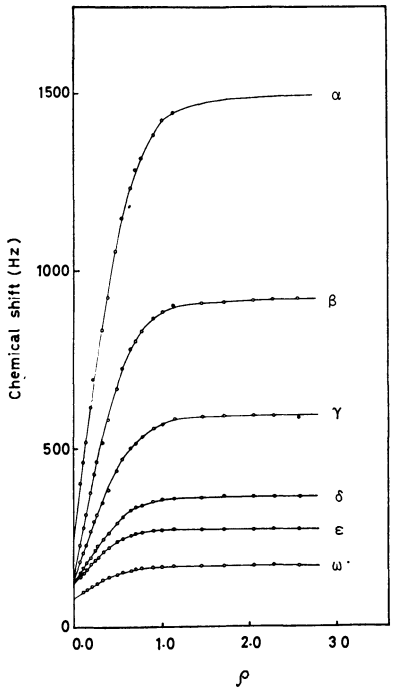

Fig. 2. $Eu(fod)_3$-induced shifts $\Delta\delta_{obsd}$ of *n*-hexylamine *vs.* ρ ($\equiv[L_0]/[S_0]$) obtained by the incremental dilution method. $CDCl_3$ solution, 37 °C, $[S_0]=0.097$ M. The observed data for α—ε methylene and ω methyl protons are shown with open circles. The curves were obtained by the calculation (see text).

in the latter method $[S_0]$ is maintained at 0.097 M. In Table 1 are given the best values of K_1, K_2, Δ_1^i's, and Δ_2^i's which were obtained by the analysis described above. The LIS values calculated using these parameters are shown by the curves in Figs. 1 and 2. The agreement between the calculated curves and the observed data is quite satisfactory.

In Figs. 3 and 4 the calculated concentration ratios $[LS]/[S_0]$, $[LS_2]/[S_0]$, and $[LS_2]/[LS]$ are shown for the successive dilution and the incremental dilution processes, respectively. As is clearly seen in these figures, the ratio $[LS_2]/[LS]$ increases rapidly to $K_2[S_0]$ as ρ approaches zero in the incremental dilution method,

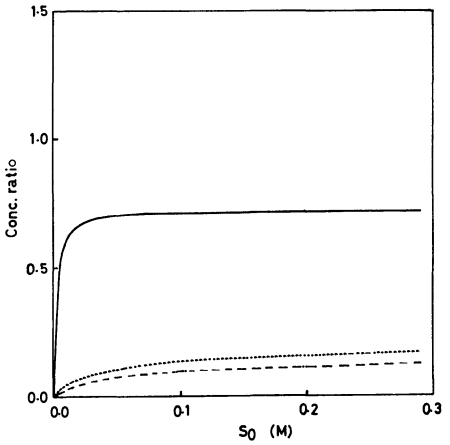

Fig. 3. The calculated concentration ratios $[LS]/[S_0]$ (——), $[LS_2]/[S_0]$ (– – –), and $[LS_2]/[LS]$ (– – – –) *vs.* $[S_0]$.

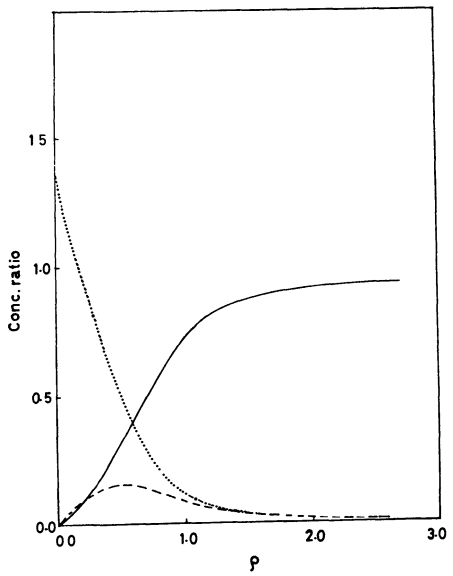

Fig. 4. The calculated concentration ratios [LS]/[S_0] (——), [LS_2]/[S_0] (— —), and [LS_2]/[LS] (– – –), *vs.* ρ.

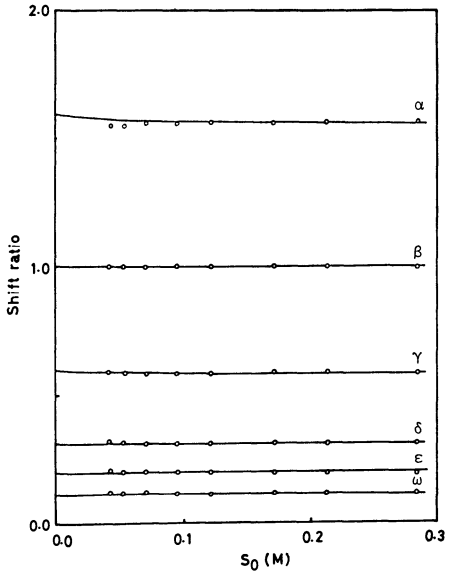

Fig. 5. The ratios of Eu(fod)$_3$-induced shifts of *n*-hexylamine *vs.* [S_0] obtained by the successive dilution method. The shift of β proton is taken as reference. The observed data are shown with open circles. The curves were obtained by the calculation (see text).

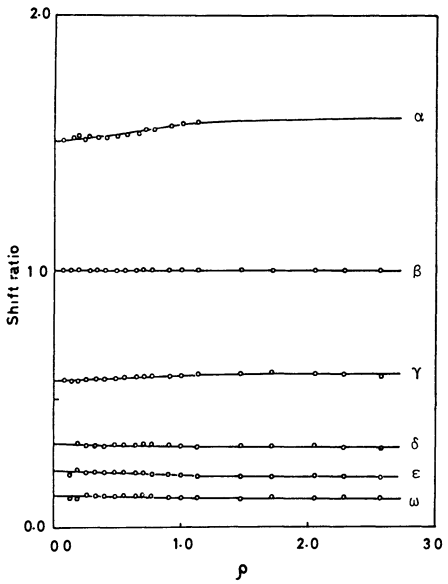

Fig. 6. The ratios of Eu(fod)$_3$-induced shifts of *n*-hexylamine *vs.* ρ obtained by the incremental dilution method. The shift of β proton is taken as reference. The observed data are shown with open circles. The curves were obtained by the calculation (see text).

whereas the ratio decreases gradually to zero as [S_0] is lowered in the successive dilution method. This point should be borne in mind in deriving the shift ratios for the LS complex. Since the successive dilution and the incremental dilution methods have quite different patterns with respect to the complex formation, a combined analysis of LIS values of the two methods enhances the reliability of the parameters listed in Table 1.

In a previous paper[4] a method of obtaining the shift ratio for the LS complex was proposed. It is interesting to apply this method to the present system. The ratio of the LIS of the ith nucleus and that of the sth nucleus is derived from Eqs. (3)—(5) as

$$\frac{\Delta\delta^i_{\mathrm{obsd}}}{\Delta\delta^s_{\mathrm{obsd}}} = \frac{\Delta_1{}^i + 2K_2[S_0]\Delta_2{}^i + 2K_2(\Delta_1{}^i - \Delta_2{}^i)[LS]}{\Delta_1{}^s + 2K_2[S_0]\Delta_2{}^s + 2K_2(\Delta_1{}^s - \Delta_2{}^s)[LS]} \quad (7)$$

The extrapolations of the shift ratio to [S_0]=0 and to ρ=0 give the following relations.

$$\lim_{[S_0]\to 0}\left(\frac{\Delta\delta^i_{\mathrm{obsd}}}{\Delta\delta^s_{\mathrm{obsd}}}\right) = \frac{\Delta_1{}^i}{\Delta_1{}^s} \quad (8)$$

$$\lim_{\rho\to 0}\left(\frac{\Delta\delta^i_{\mathrm{obsd}}}{\Delta\delta^s_{\mathrm{obsd}}}\right) = \frac{\Delta_1{}^i + 2K_2[S_0]\Delta_2{}^i}{\Delta_1{}^s + 2K_2[S_0]\Delta_2{}^s} \quad (9)$$

These equations indicate that the ratio of shifts intrinsic to the LS complex can be obtained only by extrapolating the shift ratio derived from the successive dilution method to [S_0]=0. The extrapolation of the shift ratio derived from the incremental dilution method to ρ=0 leads to a value which has also the contribution of LS_2 properties.

In Figs. 5 and 6 are shown the shift ratios obtained by the successive dilution and the incremental dilution methods, respectively. The LIS of the β proton is taken as reference. The curves in these figures indicate the shift ratios calculated using the parameters listed in Table 1. In Table 2 the observed and calculated shift ratios extrapolated to [S_0]=0 and to ρ=0 are compared. It is noted that the shift ratios extrapolated to [S_0]=0 differ significantly (*ca.* 10% for the ε proton) from those extrapolated to ρ=0 and these differences are also confirmed by the calculation. These results indicate that all the theoretical analysis and experimental procedures described above are self-consistent and useful.

It may be worthwhile to mention about the so-called "*S* value". This is often used to represent the magnitude of LIS in the conventional method of adding a

Table 2. The shift ratios extrapolated to $[S_0]=0$ and $\rho=0$

Proton	$[S_0]=0$		$\rho=0$	
	Obsd[a]	Calcd	Obsd[b]	Calcd
α	1.56_0	1.59_4	1.50_1	1.49_7
β[c]	1.000	1.000	1.000	1.000
γ	0.58_7	0.59_6	0.57_1	0.57_2
δ	0.31_5	0.31_0	0.32_0	0.32_1
ε	0.20_5	0.19_2	0.22_0	0.22_4
ω	0.12_0	0.11_3	0.12_2	0.12_8

a) Observed by the successive dilution method.
b) Observed by the incremental dilution method.
c) Chosen as reference.

solid shift reagent to a substrate solution or in the incremental dilution method. Like the shift ratio extrapolated to $\rho=0$ given in Eq. (9), the S value contains the contribution of LS_2 properties. Therefore, its use may lead to some erroneous results in the structure determinations.

References

1) B. Bleaney, C. M. Dobson, B. A. Levine, R. B. Martin, R. J. P. Williams, and A. V. Xavier, *Chem. Commun.*, **1972**, 791.
2) C. D. Barry, J. A. Glasel, R. J. P. Williams, and A. V. Xavier, *J. Mol. Biol.*, **84**, 471 (1974).
3) C. D. Barry, D. R. Martin, R. J. P. Williams, and A. V. Xavier, *ibid.*, **84**, 491 (1974).
4) F. Inagaki, S. Takahashi, M. Tasumi, and T. Miyazawa, This Bulletin, **48**, 853 (1975).
5) D. S. Dyer, J. A. Cunningham, J. J. Brooks, R. E. Sievers, and R. E. Roudeau, "Nuclear Magnetic Resonance Shift Reagents," ed. by R. E. Sievers, Academic Press, New York, N. Y. (1973), p. 21.
6) C. S. Springer, A. H. Bruder, S. R. Tanny, M. Pickering, and H. A. Rockefeller, *ibid.*, p. 283

The Chemistry of Americium. III. The Coprecipitation of Am(III), Am(V), and Am(VI) by Some Fluorides and Phosphates

Mitsuo HARA and Shin SUZUKI

The Research Institute for Iron, Steel and Other Metals, Tohoku University, Katahira 2-chome, Sendai 980

(Received May 8, 1974)

The radiochemical behavior of americium in the coprecipitation process involving a precipitate such as lanthanum, thorium, and ceric fluorides, zirconium, and bismuth phosphates was investigated at the tracer concentrations of americium. All the precipitates except zirconium phosphate completely carried the Am(III), leaving the Am(VI) in the supernatant. The lanthanum and thorium fluorides carried portions of the Am(V) in proportion to the amounts of the metal ion of the carrier added under any given conditions. Then, the analytical conditions were established for determining the distributions of the oxidation states of americium.

The recognized oxidation states of americium in an ordinary aqueous solution are the tri-, penta-, and hexavalent states. They can usually be identified by means of spectrophotometry.[1] However, this method is not sensitive enough here because of the low molar extinction coefficients of both Am(V) and Am(VI) ions. The development of an oxidation-state separation scheme at low americium concentrations is often beset by certain inherent difficulties. The properties of a trace amount of an element (tracer) can often be observed by means only of its chemical behavior, which in most cases closely resembles the chemical behavior of the element at a macro concentration. In some cases, however, it is necessary to pay attention to such peculiarities of the tracer behavior as the radiocolloid formation, the adsorption on the container walls, and the oxidation-state perturbation caused by small amounts of impurities.

A few workers have reported methods for the separation of Am(III) and the higher oxidation states of americium at low concentrations utilizing these differences in the chemical properties: the solubility in the lanthanum-fluoride[2] and calcium-fluoride systems,[3] the adsorbability on a chromatographic column consisting of bis(2-ethylhexyl)phosphoric acid[4,5] or on a column consisting of zirconium phosphate,[6] and the extractability in liquid-liquid extraction using 2-thenoyltrifluoroacetone as the extractant.[7,8]

The methods involving the organic agents substantially perturb the oxidation states of americium in the course of the separation process, and the column operations take much time. The coprecipitation technique involving the lanthanum fluoride is based on the facts that the actinoid(III,IV) ions are carried, while the actinoid(VI) ions are not carried, by the lanthanum fluoride.[2,9] However, the behavior of the actinoid(V) ions in this system has not yet been confirmed.

In a previous work the present authors investigated the instability of Am(V) in several media and found that Am(V) at tracer concentrations was stable within a few hours after preparation in a nitric acid solution, *etc.* at 0—5 °C.[8] In order to develop the solution chemistry of the higher oxidation states of americium, it is necessary to establish a method for determining the oxidation-state distributions of americium. For this purpose, the coprecipitation technique was chosen because of its rapidity and convenience. In this work, the coprecipitation of americium by lanthanum, thorium, and ceric fluorides and by zirconium and bismuth phosphates was investigated under various conditions. The results will be discussed from the standpoints of the coprecipitation process and the oxidation-state analysis.

Experimental

Reagents. The independent solutions of Am(III), Am(V), and Am(VI) were prepared by the methods reported previously;[5,8] in some cases, they were arbitrarily mixed in order to prepare the multi-component solutions. The initial concentration of ^{241}Am was of the order of 10^{-6} M. Solutions of lanthanum, thorium, cerium(IV), bismuth, and zirconium nitrates were used as the metal ion of the carrier. The precipitants were solutions of ammonium fluoride and phosphoric acid and also, if necessary, hydrofluoric acid and ammonium dihydrogenphosphate solutions. These and other chemicals were all of a G. R. grade.

Apparatus. The experiments prior to centrifuging were carried out in an Onishi Netsu-Kagaku thermostated box at 0—5 °C. For the centrifugation, a Sakuma Model SMC 30-1 centrifuge was used. The γ-ray assay was performed by the use of a Kobe Kogyo Model PS-500 flat-type NaI(Tl) scintillation probe connected with a Kobe Kogyo Model SA-400 scaler.

Procedure. Suitable aliquots of the americium, the metal ion of the carrier, and nitric acid solutions were transferred into a polyethylene test tube; a precipitant was then added, and the volume and the acidity were adjusted to the desired values. The mixture was then shaken mechanically for enough time to obtain an apparently constant fraction of americium carried. The recommended shaking time was 10 and 30 min for the fluoride and phosphate systems respectively. The final concentration of ^{241}Am in the mixture was $(0.5-5)\times 10^{-6}$ M. By measureing the ^{241}Am activity in both the mixture and the supernatant obtained by centrifuging the mixture at about 6000 rpm for 5 min, the fraction of americium carried was determined. When thorium was used, the correction for the γ-activity from the daughters of ^{232}Th was performed, but the interference from them was negligibly small in most cases. The acidity of the supernatant was stoichiometrically calculated. In the preliminary experiments it was confirmed that no oxidation state of americium was centrifuged under the conditions examined when neither the metal ion of carrier nor the precipitant was added.

Results

The fraction of americium carried generally depended on the volume and composition of the mixture, the

amounts of the metal ion of the carrier, and the molar ratio of the precipitant to the metal ion of the carrier added. For instance, under the same conditions except for the volume, 14, 65, and 95 % of Am(III) were carried by the thorium fluoride by the use of 0.1 mg Th^{4+} per 3.5, 3.0, and 2.5 ml respectively of the mixture at an acidity of 0.1 M. Therefore, the volume of the mixture was adjusted to 2.5 ml except when otherwise noted.

Coprecipitation by the Insoluble Fluorides. The relation between the fraction of americium carried and the amounts of a metal ion of the carrier was investigated at the acidity of 0.2 M, as is shown in Fig. 1. In the range of the amounts of the thorium ion examined, more than 95 % of the Am(III) and less than 12 % of the Am(VI) were carried, but the fraction of Am(V) carried increased from 1 to 100 % with an increase in the amount of the thorium ion from 0.15 to 75 mg per 2.5 ml of the mixture. The coprecipitation behavior with the lanthanum fluoride showed a tendency similar to that with the thorium fluoride. On the other hand, in the ceric-fluoride system the fractions of Am(V) and Am(VI) carried were both very small, irrespective of the amounts of the ceric ion, while the coprecipitation of Am(III) was complete when more than 0.2 mg Ce^{4+}/ml was used.

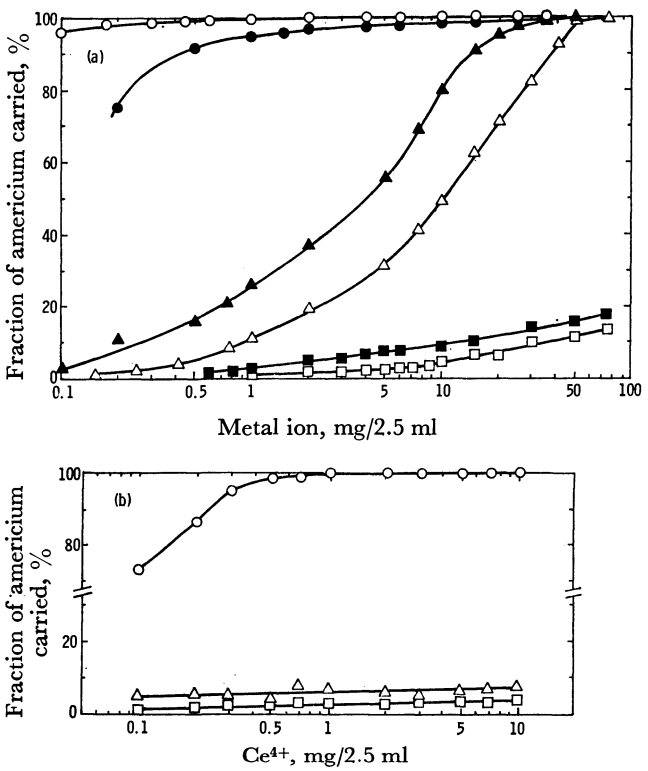

Fig. 1. The dependence of the coprecipitation of americium on the amounts of metal ion of carrier in the lanthanum, thorium, and ceric fluoride systems.
(a) Thorium fluoride system: ○, Am(III); △, Am(V); □, Am(VI). Lanthanum fluorides system: ●, Am(III); ▲, Am(V); ■, Am(VI).
(b) Ceric fluoride system: ○, Am(III); △, Am(V); □, Am(VI).
In each system, the acidity of the mixture is 0.2 M and F/M>10.

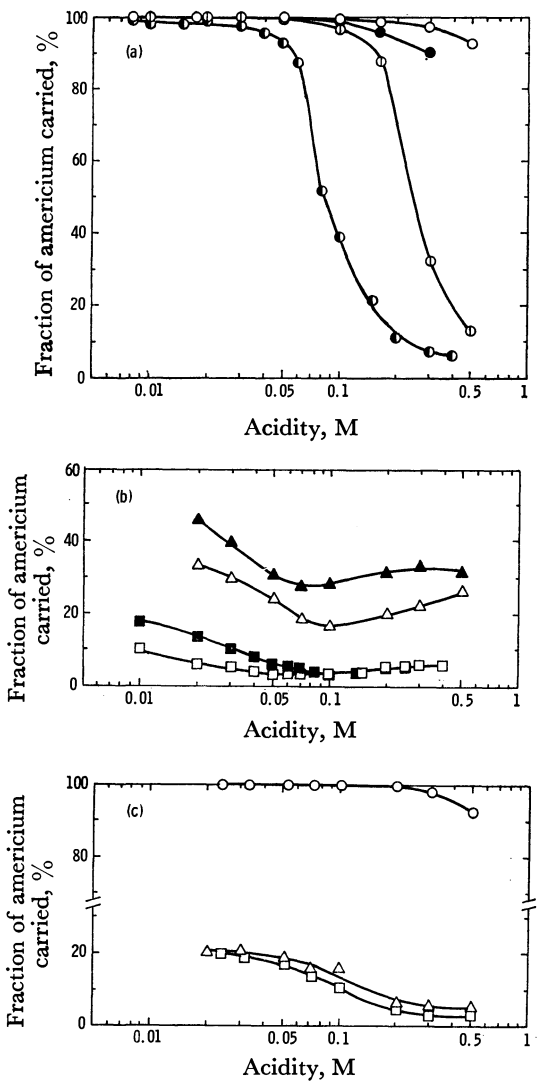

Fig. 2. The acidity-dependence of the coprecipitation of americium by the lanthanum, thorium, and ceric fluorides.
(a) Am(III): ○, F/Th=115; ◑, F/Th=23; ●, F/La=70; ◐, F/La=14.
(b) Am(V): △, F/Th=115; ▲, F/La=70. Am(VI): ■, F/Th=115; □, F/La=70.
(c) F/Ce=14: ○, Am(III); △, Am(V); □, Am(VI).
In each system, 1 mg of metal ion per 2.5 ml of the mixture was used.

The acidity dependence of the coprecipitation of americium was also studied at a constant amounts of the carrier-metal ion and at a constant molar ratio of the precipitant to the metal ion of the carrier added (F/M). The results are shown in Fig. 2. The larger fractions of americium were carried at the lower acidities, and the coprecipitation of Am(III) was less complete at the higher acidities, especially at smaller F/M values. The fractions of Am(III), Am(V), and Am(VI) carried by the insoluble fluoride under the given conditions are summarized in Table 1.

Coprecipitation by the Insoluble Phosphates. The acidity dependence of the coprecipitation of americium by the zirconium and bismuth phosphates was also investigated. The experiments with the latter were per-

Table 1. Summary of the coprecipitation of americium

Run	Experimental condition[a]			Fraction carried, %		
	Precipitate	Metal ion, mg[b]	Precipitant, mM[b]	Am(III)	Am(V)	Am(VI)
1	Thorium fluoride	1	0.5	99±1	11±2	1±1
2	Thorium fluoride	50	2.5	99±1	99±1	11±1
3	Lanthanum fluoride	1	0.5	94±2	26±3	3±2
4	Lanthanum fluoride	50	2.5	98±2	98±3	16±2
5	Ceric fluoride	1	0.5	99±1	5±2	4±2
6	Bismuth phosphate	10	2.5	99±1	0[c]	1±1

a) Acidity of the mixture is 0.2 M. b) Amounts per 2.5 ml of the mixture. c) Not investigated.

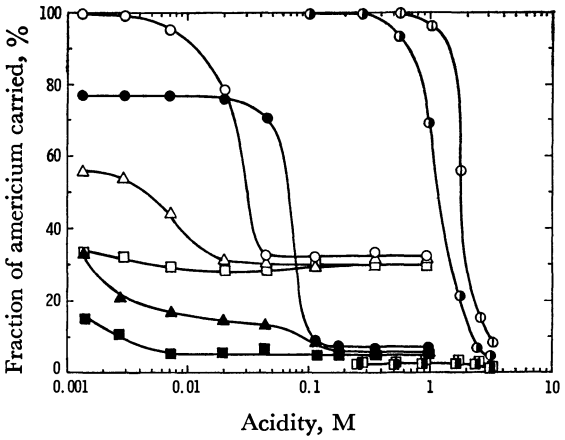

Fig. 3. The acidity-dependence of the coprecipitation of americium by the zirconium and bismuth phosphates at PO_4/M 20.
1 mg Zr^{4+}/3.5 ml: ●, Am(III); ▲, Am(V); ■, Am(VI).
10 mg Zr^{4+}/3.5 ml: ○, Am(III); △, Am(V); □, Am(VI).
1 mg Bi^{3+}/2.5 ml: ◑, Am(III); ◨, Am(VI).
10 mg Bi^{3+}/2.5 ml: ⊕, Am(III); [], Am(VI).

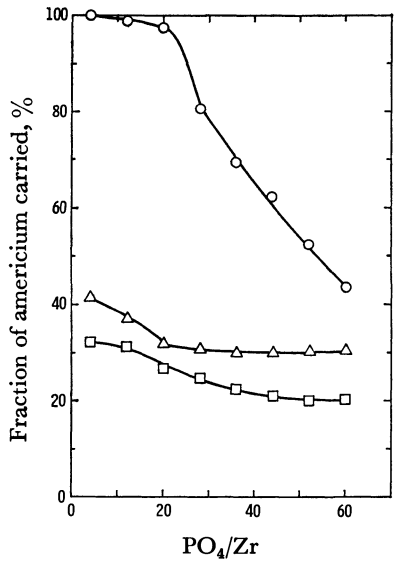

Fig. 4. The variation of the coprecipitation of americium by zirconium phosphate with the molar ratio PO_4/Zr by using 10 mg Zr^{4+} per 3.5 ml of the mixture at the acidity 0.01 M.
○, Am(III); △, Am(V); □, Am(VI).

formed at acidities above 0.1 M because the hydrolysis products of a bismuth ion were precipitated at lower acidities without the addition of any precipitant. Significant coprecipitation of americium took place with amounts of zirconium and bismuth ions of more than 0.3 and 0.5 mg/ml respectively. Some typical results with a constant amount of the carrier-metal ion are shown in Fig. 3. The fractions of Am(III) and Am(V) carried by the zirconium phosphate increased with a decrease in the acidity below 0.1 M, while the acidity dependence of the fraction of Am(VI) carried was small. The complete coprecipitation of Am(III) by bismuth phosphate took place at the higher acidities, at which not so much Am(III) was carried by the zirconium phosphate, while the fraction of Am(VI) carried remained constant at lower levels. The behavior of Am(V) in the bismuth-phosphate system was not investigated, since the method of preparation and the stability of the Am(V) ion have not been established at higher acidities.

The molar ratio, PO_4/M, had a remarkable effect on the coprecipitation of americium, especially in the zirconium-phosphate system. As is shown in Fig. 4, 97—100 % of the Am(III) was carried at ratios less than 20, using a constant amount of zirconium ions, but the fraction of Am(III) carried decreased strikingly when the ratio increased to more than 20. On the other hand, the variations in the fractions of Am(V) and Am(VI) carried were very small, even at ratios more than 20. The separation of the precipitate and the supernatant by centrifuging was not complete at ratios less than 2, since the fine suspension of the zirconium phosphate could hardly be centrifuged at all. The fraction of americium carried by the bismuth phosphate under the given conditions is also postulated in Table 1.

Analysis of the Multi-component Solutions. The multi-component solutions, which were prepared by mixing independent solutions of Am(III), Am(V), and Am(VI), had the following compositions with respect to the oxidation state of americium: Sample 1: Am(III) 55.4±0.3 % and Am(V) 44.6±0.2 %; sample 2: Am(III) 48.5±0.3 % and Am(VI) 51.5±0.3 %, and Sample 3: Am(III) 34.1±0.2 %, Am(V) 30.7± 0.2 %, and Am(VI) 35.2±0.2 %.

Suitable aliquots of a sample solution were simultaneously taken for the six kinds of coprecipitation experiments under the conditions presented in Table 1; the results are shown in Table 2. If the Am(III), Am(V),

TABLE 2. ANALYSIS OF THE MULTI-COMPONENT SOLUTIONS OF AMERICIUM

Run i[a]	Y^i, %					
	Sample 1		Sample 2		Sample 3	
	Obsd	Calcd	Obsd	Calcd	Obsd	Calcd
1	59.3±0.7	59.8±1.1	48.8±0.7	48.5±0.8	37.4±0.6	37.5±0.8
2	98.9±0.6	99.0±0.8	55.5±0.7	53.7±1.2	66.6±0.8	68.0±0.9
3	63.3±1.5	63.7±1.8	46.6±1.7	47.1±1.4	37.9±1.5	41.1±1.4
4	96.2±1.7	98.0±1.5	60.4±1.5	55.8±1.4	66.6±1.5	69.1±1.2
5	57.6±0.8	57.1±1.1	53.1±0.7	50.1±1.2	40.9±0.7	36.7±1.0
6	56.6±0.3	54.9±0.6	48.0±0.4	48.5±0.8	34.6±0.5	34.1±0.5

a) Experimental conditions are given in Table 1.

and Am(VI) in the multi-component solution all behave independently in the course of the coprecipitation process, the fraction of americium carried under the i condition may be given as:

$$Y^i = f_{III}Y^i_{III} + f_V Y^i_V + f_{VI}Y^i_{VI}, \quad (1)$$

where Y^i_x is the fraction of Am(x) carried which is obtained in the independent system, and where f_x is the mole fraction of Am(x) in the multi-component solution. Then, the fraction of americium carried from the multi-component solution was calculated according to Eq.(1) by the use of the Y^i_x given in Table 1 and the f_x described previously; it is also presented in Table 2. The calculated values nearly agree with the observed values in all cases. Therefore, the assumption that Y^i_V in the bismuth-phosphate system is very small is reasonable.

By the way, Eq.(1) can also be written as Eq.(2), for instance, because $f_{III}+f_V+f_{VI}=1$:

$$Y^i = f_{III}(Y^i_{III}-Y^i_{VI}) + f_V(Y^i_V-Y^i_{VI}) + Y^i_{VI} \quad (2)$$

Therefore, if the Y^i_x is reproducibly established under the given condition, i, the mole fraction, f_x, in the multi-component solution can be deduced by solving two simultaneous equations like Eq.(2) with two unknowns. For instance, when two pairs of data obtained for the same sample solution in both lanthanum- and thorium-fluoride systems were analyzed, it was found that the calculated mole fractions satisfactorily agreed with those known previously, especially in the thorium-fluoride system (*cf.* Table 3).

TABLE 3. DISTRIBUTION OF THE OXIDATION STATE OF AMERICIUM IN THE MULTI-COMPONENT SOLUTIONS

Sample	State	Percentage of the oxidation state		
		Taken	Calcd[a]	Calcd[b]
1	Am(III)	55.4±0.3	54.9±4.4	55.6±9.9
	Am(V)	44.6±0.2	45.0±4.4	42.2±9.5
	Am(VI)	0	0.1±0.1	2.2±2.2
2	Am(III)	48.5±0.3	48.6±3.4	47.0±7.0
	Am(V)	0	2.0±2.0	3.5±3.5
	Am(VI)	51.5±0.3	49.4±4.5	49.5±11.4
3	Am(III)	34.1±0.2	34.2±3.1	30.4±7.2
	Am(V)	30.7±0.2	29.0±3.8	31.3±7.9
	Am(VI)	35.2±0.2	36.8±4.3	38.3±10.4

a) Values calculated by using the couple of data with runs 1 and 2. b) Values calculated by using the couple of data with runs 3 and 4.

Discussion

It has been found that the coprecipitation behavior of Am(III) and Am(VI) with lanthanum fluoride agree essentially with that reported previously.[2] On the other hand, the present work revealed the chemical behavior of Am(V) in the lanthanum-fluoride system for the first time. Portions of the Am(V) were carried by the lanthanum fluoride in proportion to the amounts of lanthanum ions of more than 0.04 mg/ml. Nearly the same results have been obtained in the thorium-fluoride system.

The processes by which the tracer is carried by a precipitate formed in the presence of the tracer have been discussed by many workers-for instance, by Bonner and Kahn[10] and by Starik.[11] The coprecipitation processes can be classified as follows:

(a) Isomorphous replacement.

(b) Adsorption. Chemical adsorption and ion-exchange adsorption.

(c) Anomalous-mixed-crystal formation.

(d) Internal adsorption.

The available information concerning the fluoro-complex formation of americium[12] or those elements whose chemical properties closely resemble those of americium, such as neptunium and plutonium,[13] suggests that the predominant species of Am(III), Am(V), and Am(VI) in the floride solutions investigated are the insoluble AmF_3, insoluble AmO_2F (or $NH_4AmO_2F_2$), and soluble $AmO_2F_4^{2-}$(and/or $AmO_2F_3^-$) respectively. The observation that both the amorphous lanthanum and thorium fluorides carried more of the insoluble and neutral species of Am(III) and Am(V) than the ionic species of Am(VI) may be explained by the adsorption process, especially by the chemical adsorption process. This mechanism is based on the phenomenon that a tracer is carried well when it forms an insoluble compound at macro concentrations. In this sense, the fluoride species of Am(V) may not be so insoluble as AmF_3, for Am(V) is less carried than Am(III). The findings obtained in the present studies with regard to the dependence of the coprecipitation of americium on the several parameters can be easily correlated to the extent to which the complex formation of americium occurs.

The coprecipitation behavior of americium in the ceric-fluoride system was considerably different from that in the other fluoride systems, and it could not be

explained by the argument presented above. Evidently the precipitate of ceric fluoride was not amorphous, but crystalline. It is known that Am(III) and Ce(IV) fluorides have a hexagonal structure.[14,15] On the other hand, if an $NH_4AmO_2F_2$ crystal is isostructural to $KAmO_2F_2$, it may be rhombohedral.[16] Therefore, it is reasonable that the ceric fluoride carries the isomorphous AmF_3 better than either the heteromorphous $NH_4AmO_2F_2$ or the ionic species of Am(VI), according to the isomorphous replacement process.

On the other hand, the behavior of americium in the zirconium-phosphate system is rather complex. All of the experiments were performed at low temperatures and within a short time, taking into account the instabilities of the higher oxidation states of americium. Such experimental conditions resulted in an ununiform and less reproducible precipitation of the zirconium phosphate. The available information concerning the phosphato-complex formation of americium,[17] neptunium,[18] and plutonium,[19] and the behavior of americium in a phosphoric acid,[20] suggests that the predominant species of Am(III), Am(V), and Am(VI) in the phosphate solutions examined are the Am^{3+} (and/or $AmH_2PO_4^{2+}$), AmO_2^+(and/or $AmO_2H_2PO_4$), and $AmO_2H_2PO_4^+$ ions respectively. It is well known that a crystal of the preliminarily-prepared zirconium phosphate has ability of ion-exchange adsorption.[6] Therefore, the coprecipitation of the ionic species of americium by zirconium phosphate must result mainly from the ion-exchange adsorption. The results obtained in the zirconium-phosphate system suggest that the adsorbability of the species decrease in this order: $Am^{3+} > AmH_2PO_4^{2+} > AmO_2^+ > AmO_2H_2PO_4^+ \gg AmO_2H_2PO_4$. The decrease in the coprecipitation of Am(III) with an increase in PO_4/Zr, as is shown in Fig. 4, can be explained by the formation of less adsorbable phosphate species.

By the way, the fine crystalline bismuth phosphate carried Am(III) completely even at higher acidities at which the zirconium phosphate did not so carry it. It seems that this finding cannot be explained simply by the ion-exchange adsorption process, but can de explained by the argument used in the case of the crystalline ceric fluoride. If this is true, Am(III) may form a phosphate compound which is isostructural to a hexagonal bismuth phosphate[21] as well as lanthanoid(III) ions.[22]

The analytical results obtained for the multi-component solutions demonstrate that the perturbation of the oxidation state in the course of the coprecipitation process was negligible, and that the fraction of americium carried by the precipitates studied was additive and constitutive. Equation (1) or Eq. (2) guarantees that the coprecipitation behavior of each oxidation state of americium must be established under the given conditions. In the lanthanum- and thorium-fluoride systems, two sets of analytical conditions have been established; they are shown in Table 1. Therefore, the distribution of the oxidation state of americium in the multi-component solutions can be approximately deduced by investigating the coprecipitation of americium by the lanthanum or thorium fluoride under the recommended conditions, followed by solving two simultaneous equations like Eq. (2). However, the sets of such conditions could not be established in the ceric-fluoride and bismuth-phosphate systems alone.

References

1) R. A. Penneman and L. B. Asprey, Proceedings of the International Coference on the Peaceful Uses of Atomic Energy, **7**, Geneva (1955), p. 355. United Nations(1956).
2) F. L. Moore, *Anal. Chem.*, **35**, 715 (1963).
3) H. P. Holcomb, *ibid.*, **36**, 2329 (1964).
4) F. L. Moore, *ibid.*, **40**, 2130 (1968).
5) M. Hara and S. Suzuki, This Bulletin, **47**, 635 (1974).
6) F. L. Moore, *Anal. Chem.*, **43**, 487 (1971); A. I. Shafiew, Yu. V. Efremov, V. M. Nikolaev, and G. N. Yakovlev, *Radiokhimiya*, **13**, 129 (1971).
7) J. R. Stokely, Jr. and F. L. Moore, *Anal. Chem.*, **39**, 994 (1967).
8) M. Hara, This Bulletin, **43**, 89 (1971).
9) S. C. Foti and E. C. Freiling, *Talanta*, **11**, 385 (1964).
10) N. A. Bonner and M. Kahn, "Radioactivity Applied to Chemistry," ed. by A. C. Wahl and N. A. Bonner, John Wiley & Sons, Inc., New York N. Y. (1951), p. 102.
11) I. E. Starik, "Osnovy Radiokhimii," Izdatel. Akad. Nauk SSSR, Leningrad (1960), Chapters 2 and 3. (Translated in Japanese by H. Ichikawa, *et al.*, Nankodo, Tokyo (1962).
12) D. C. Feay, Thesis, Berkeley, 1954. UCRL-2547.
13) V. N. Krylov, E. V. Komarov, and M. F. Pushlenkov, *Radiokhimiya*, **10**, 717, 719, 723 (1968).
14) W. H. Zachariasen, *Phys. Rev.*, **73**, 1104 (1948).
15) R. Hoppe, *Angew. Chem.*, **71**, 45 (1959).
16) L. B. Asprey, F. H. Effinger, and W. H. Zachariasen, *J. Amer. Chem. Soc.*, **76**, 5235 (1954).
17) R. Bury, *J. Chim. Phys.*, **65**, 1494 (1968).
18) A. I. Moskvin and V. F. Peretrukhin, *Radiokhimiya*, **6**, 206 (1964).
19) R. G. Denotkina and U. B. Shevelenko, *Zhur. Neorg. Khim.*, **12**, 2345 (1967).
20) B. F. Myasoedov, V. M. Mikhailov, I. A. Lebedov, O. E. Koiro, and V. Ya. Frankel, *Radiochem. Radioanal. Lett.*, **14**, 17 (1973).
21) G. R. Leader, U. S. Atom. Energy Commun. CN-1863 (1957).
22) R. C. L. Mooney, *Acta Crystallogr.*, **3**, 337 (1950).

Studies on Mass Spectrometry of Metal Chelates. IV. Synthesis and Mass Spectrometry of Cobalt(III) Mixed Ligand Chelates

Yoshinori KIDANI, Shinobu NAGA, and Hisashi KOIKE*

Faculty of Pharmaceutical Sciences, Nagoya City University, Tanabe-dori, Mizuho-ku, Nagoya 467

** School of Medical Technology and Nursing, Fujita Gakuen University, Toyoake City, Aichi Prefecture 470-11*

(Received July 11, 1974)

The ligand substitution reaction of $Co(acac)_3$ proceeded with other ligands L (L=oxine, 2-Me-oxine, 4-Me-oxine, 5-Me-oxine, and 7-Me-oxine), to afford mixed ligand chelates, $Co(acac)_2(L)$ and $Co(acac)(L)_2$. Their mass spectra gave the following fragmentation patterns. The $Co(acac)_2(L)$ type chelate gave a fragment ion Co(acac)(L), produced by the loss of one molecule of acac from the molecular ion. At the same time it produced another fragment ion, $Co(acac)_2$, by the loss of L from the molecular ion. From this fragmentation pattern it was confirmed that the compound is a mixed ligand chelate having the binding ratio Co: acac: L=1: 2: 1. The $Co(acac)(L)_2$ type chelate produced a fragment ion, Co(acac)(L), by the loss of one molecule of L from the molecular ion, and another fragment ion of $Co(L)_2$ by the loss of acac from the molecular ion. From this fragmentation pattern it was confirmed that the compound is another mixed ligand chelate having the binding ratio Co: acac: L= 1: 1: 2.

In order to apply mass spectrometry to the investigation of metal chelates, the authors reported on the mass spectrometric studies of the divalent metal chelates of 8-quinolinol (oxine),[1] 8-quinolinethiol (thiooxine),[2] 2-methyl-8-quinolinol (2-Me-oxine), 4-methyl-8-quinolinol (4-Me-oxine), 5-methyl-8-quinolinol (5-Me-oxine), 7-methyl-8-quinolinol (7-Me-oxine), and 5-chloro-8-quinolinol (5-Cl-oxine).[3] As a part of this study, the authors attempted to apply mass spectrometry to the mixed ligand chelates. Cobalt(III) mixed ligand chelates with 2,4-pentanedione (acac) and oxine,[4] 2-, 4-, 5-, and 7-Me-oxine were newly synthesized, and analyses of their mass spectra, thin layer chromatogram and infrared absorption spectra were made. In this paper, syntheses of two types of Co(III) mixed ligand chelate with acac and oxine and its mono-methyl derivatives are described. From identification of the mixed ligand chelate formation by thin layer chromatography, infrared absorption spectral analyses and elementary analyses, mass spectrometry has been carried out, the fragmentations mainly being discussed. No investigation of the application of mass spectrometry to mixed ligand chelates seems to have been reported yet. The present studies suggest that mass spectrometry could well be applied to the identification of mixed ligand chelate formation and also to the determination of a binding ratio of ligand to metal.

Results and Discussion

Syntheses of Mixed Ligand Chelates. Various mixed ligand chelates were newly synthesized by means of ligand substitution reactions of tris(acetylacetonato) cobalt(III), $Co(acac)_3$, with oxine, 2-, 4-, 5-, and 7-Me-oxine. The reaction products were separated by means of column chromatography into four fractions a, b, c, and d as follows: Ia—Id for oxine, IIa—IId for 2-Me-oxine, IIIa—IIId for 4-Me-oxine, IVa—IVd for 5-Me-oxine, and Va—Vd for 7-Me-oxine.

Thin Layer Chromatography. Four fractions of five oxine derivatives. The twenty fractions separated by column chromatography were identified in comparison with thin layer chromatography of the parent metal chelates, $Co(acac)_3$, $Co(oxine)_3$, and $Co(mono\text{-}Me\text{-}oxine)_3$ (Table 1). It was confirmed that Ia, IIa, IIIa, IVa, and Va have the same R_f value as $Co(acac)_3$; Id, IId, IIId, IVd, and Vd have the same R_f value as $Co(oxine)_3$, $Co(2\text{-}Me\text{-}oxine)_3$, $Co(4\text{-}Me\text{-}oxine)_3$, $Co(5\text{-}Me\text{-}oxine)_3$, and $Co(7\text{-}Me\text{-}oxine)_3$, respectively. On the other hand, b and c fractions of I—V show characteristic R_f values, quite different from the corresponding parent metal chelates, suggesting the production of mixed ligand chelates.

Infrared Absorption Spectra. Infrared (IR) absorption spectra were measured (4000—400 cm^{-1}) by means of the KBr disc method. Infrared absorption spectra of fraction a of I—V coincided with the spectrum of $Co(acac)_3$, while fraction d of I—V gave the same IR spectra as those of $Co(oxine)_3$, $Co(2\text{-}Me\text{-}oxine)_3$, $Co(4\text{-}Me\text{-}oxine)_3$, $Co(5\text{-}Me\text{-}oxine)_3$, and $Co(7\text{-}Me\text{-}oxine)_3$, respectively. On the other hand, similar spectra were shown for Ib and Ic, IIb and IIc, IIIb and IIIc, IVb and IVc, and Vb and Vc. In addition they have characteristic absorption bands of the corresponding parent metal chelates. It thus appears that fractions b and c of I—V possess acetylacetone and either oxine or mono-Me-oxine. From a detailed investigation of the spectra between fractions Ib and Ic, it was found that in the IR spectrum of Ib the intensity of the absorption band at 1513 cm^{-1} (assignable to the C=O stretch-

TABLE 1. R_f VALUES OF MIXED LIGAND CHELATES ON THIN LAYER CHROMATOGRAM

Oxine	Ia (0.63)	Ib (0.25)	Ic (0.30)	Id (0.12)
2-Me-oxine	IIa (0.65)	IIb (0.21)	IIc (0.18)	IId (0.10)
4-Me-oxine	IIIa (0.63)	IIIb (0.29)	IIIc (0.35)	IIId (0.16)
5-Me-oxine	IVa (0.64)	IVb (0.25)	IVc (0.28)	IVd (0.16)
7-Me-oxine	Va (0.65)	Vb (0.31)	Vc (0.36)	Vd (0.30)

R_f values of parental metal chelates

$Co(acac)_3=0.64$ $Co(oxine)_3=0.12$

$Co(2\text{-}Me\text{-}oxine)_3=0.11$ $Co(4\text{-}Me\text{-}oxine)_3=0.17$

$Co(5\text{-}Me\text{-}oxine)_3=0.16$ $Co(7\text{-}Me\text{-}oxine)_3=0.31$

adsorbent; Kieselgel H nach Stahl, 0.25 mm.

developer; benzene: methanol=95: 5 v/v.

ing vibration of $Co(acac)_3$[5]) is stronger than that at 1496 cm^{-1} (assignable to the quinoline ring vibration[6]), but in that of Ic the intensity of the absorption band at 1497 cm^{-1} is stronger than that at 1520 cm^{-1} (Fig. 1-a). In the IR spectra of IIc, IIIb, IVb, and Vb, absorption bands at 1505 cm^{-1} assignable to the quinoline ring vibration are observed as a shoulder, while in those of IIb, IIIc, IVc, and Vc absorption bands with medium strength are observed (Fig. 1-b, c, d, and e). The fractions can be classified into two groups, (1) in which the quinoline ring vibration band is of low intensity (Ib, IIc, IIIb, IVb, and Vb), and (2) in which it is

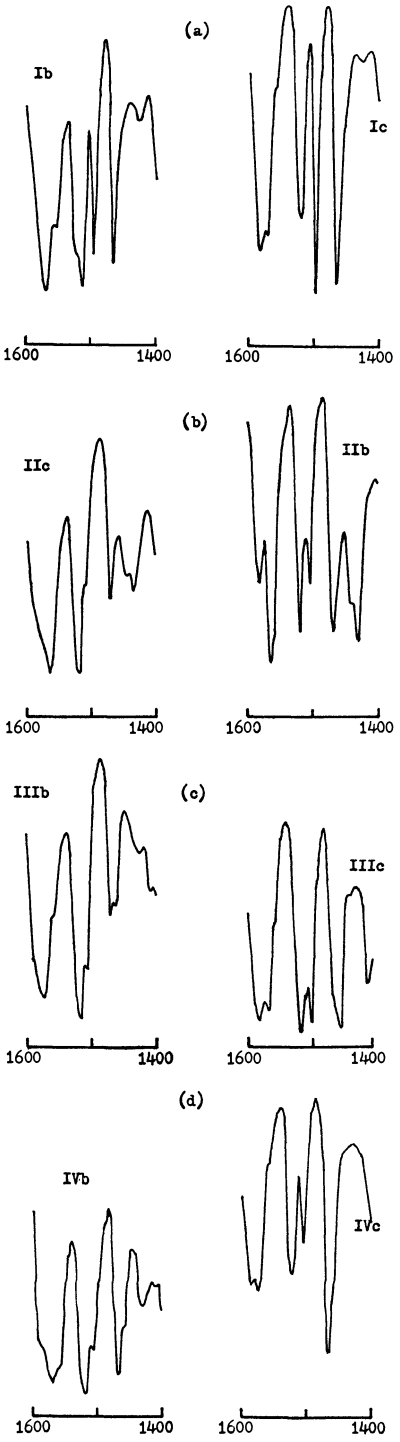

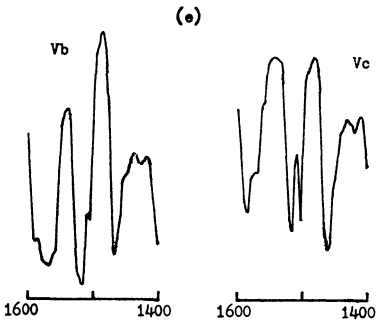

Fig. 1. IR spectra of mixed ligand chelates.
Ib; $Co(acac)_2(oxine)$, Ic; $Co(acac)(oxine)_2$, IIb; $Co(acac)(2\text{-Me-oxine})_2$ IIc; $Co(acac)_2(2\text{-Me-oxine})$, IIIb; $Co(acac)_2(4\text{-Me-oxine})$, IIIc; $Co(acac)(4\text{-Me-oxine})_2$, IVb; $Co(acac)_2(5\text{-Me-oxine})$, IVc; $Co(acac)(5\text{-Me-oxine})_2$, Vb; $Co(acac)_2(7\text{-Me-oxine})$, Vc; $Co(acac)(7\text{-Me-oxine})_2$.

of high intensity (Ic, IIb, IIIc, IVc, and Vc). It appears that the ligand substitution reaction of $Co(acac)_3$ takes place with the stepwise substitution of the acac ion in $Co(acac)_3$ with the other ligand. It is thus presumed that group (1) includes the mixed ligand chelates produced by the substitution of one acac ion in $Co(acac)_3$ with the other ligand, and group (2) the chelate produced by the substitution of two acac ions in $Co(acac)_3$ with the other ligands.

Elementary analyses of these mixed ligand chelates coincided well with the theoretical values as shown in Table 2.

Mass Spectra. Mass spectra of compounds Ib and Ic, inferred from their IR spectra, are shown in Fig. 2. They are seen to have compositions $Co(acac)_2$-(oxine) and $Co(acac)(oxine)_2$, respectively. In the

Table 2. Elementary analyses of mixed ligand chelates

Compound	Analyses (%) Calcd (Found)		
	C	H	N
Ib; $Co(acac)_2(oxine)$	56.87 (57.08	5.02 5.17	3.49 3.48)
Ic; $Co(acac)(oxine)_2$	61.88 (61.49	4.26 4.55	6.28 6.16)
IIb; $Co(acac)(2\text{-Me-oxine})_2$	63.30 (63.40	4.89 5.05	5.90 6.35)
IIc; $Co(acac)_2(2\text{-Me-oxine})$	57.84 (58.01	5.34 5.31	3.37 3.31)
IIIb; $Co(acac)_2(4\text{-Me-oxine})$	57.84 (57.78	5.34 5.61	3.37 3.53)
IIIc; $Co(acac)(4\text{-Me-oxine})_2$	63.30 (63.32	4.89 5.01	5.90 5.50)
IVb; $Co(acac)_2(5\text{-Me-oxine})$	57.84 (57.81	5.34 5.30	3.37 3.29)
IVc; $Co(acac)(5\text{-Me-oxine})_2$	63.30 (63.57	4.89 5.15	5.90 5.70)
Vb; $Co(acac)_2(7\text{-Me-oxine})$	57.84 (57.89	5.34 5.47	3.37 3.35)
Vc; $Co(acac)(7\text{-Me-oxine})_2$	63.30 (63.30	4.89 4.99	5.90 5.85)

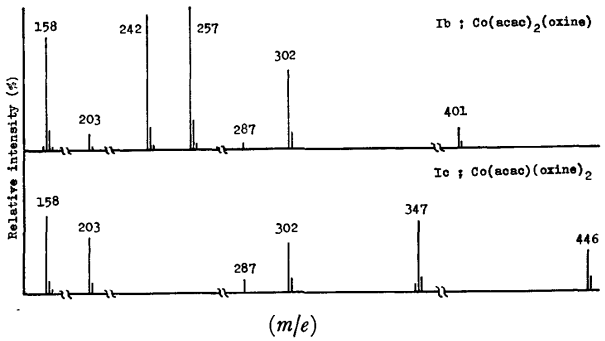

Fig. 2. Mass spectra of $Co(acac)_2(oxine)$ and $Co(acac)(oxine)_2$.

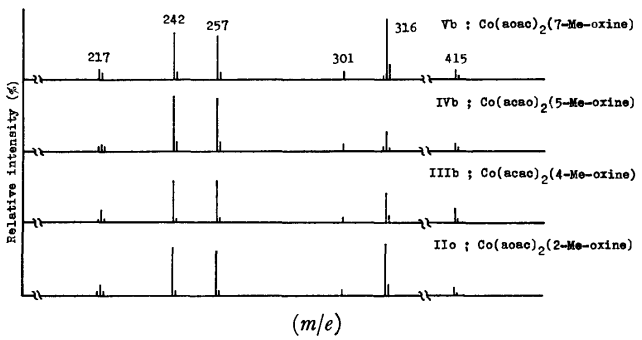

Fig. 3. Mass spectra of $Co(acac)_2$(2-Me-oxine), $Co(acac)_2$(4-Me-oxine), $Co(acac)_2$(5-Me-oxine), and $Co(acac)_2$(7-Me-oxine).

highest mass region of their spectra, the peak appears at *m/e* 401 and 446, respectively, which correspond to the respective molecular weight of the inferred mixed ligand chelates. Peaks at *m/e* 302, 287, 203, and 158 are commonly observed in both spectra. The peak at *m/e* 302 appears with a difference of 99 amu from *m/e* 401 and 144 amu from *m/e* 446. The peak at *m/e* 203 appears with a difference of 99 amu from the peak at *m/e* 302, and that at *m/e* 158 with a difference of 144 amu from the peak at *m/e* 302. The 99 amu corresponds to one molecule of acac, while the 144 amu corresponds to one molecule of oxine. Consequently, it appears that the fragment ion of *m/e* 302 has a 1: 1: 1 ratio of Co: acac: oxine, and the fragment ions of *m/e* 203 and 158 have a 1: 1 ratio of Co: oxine and Co: acac, respectively. It seems that the ion of *m/e* 287 is produced by the loss of $CH_3\cdot$ from the ion of *m/e* 302. Two peaks at *m/e* 257 and 242 are observed only in the spectrum of $Co(acac)_2(oxine)$, and they correspond to the difference between the molecular ion peak (*m/e* 401) and 144 or 144+15 amu. Accordingly, the ion of *m/e* 257 has the composition $Co(acac)_2$, while that of *m/e* 242 is produced by the loss of $CH_3\cdot$ from the ion of *m/e* 257. Since the peak at *m/e* 347 observed only in the spectrum of $Co(acac)(oxine)_2$ corresponds to the molecular ion peak (*m/e* 446) minus 99 amu, it appears that the ion has the composition $Co(oxine)_2$. The fragmentation pathways of these mixed ligand chelates are shown in Scheme 1. Based on these fragmentation patterns, the compounds were identified as the mixed ligand chelates having a 1: 2: 1 and 1: 1: 2 binding ratio of Co: acac: oxine.

Figure 3 shows mass spectra of the compounds inferred to have respective compositions $Co(acac)_2$(2-Me-oxine), $Co(acac)_2$(4-Me-oxine), $Co(acac)_2$(5-Me-oxine), and $Co(acac)_2$(7-Me-oxine). Each has a peak in the highest mass region at *m/e* 415, which corresponds to the molecular weight of the assumed compound. In the mass range lower than *m/e* 415, major peaks were observed at *m/e* 316, 301, 257, 242, 217, and 158. It appears that these peaks originate in the ion produced according to the fragmentation pathway shown in Scheme 2. The fragment ion of *m/e* 316 with the composition Co(acac)(mono-Me-oxine) is produced by the loss of one molecule of acac from the molecular ion (*m/e* 415). On the other hand, the fragment ion of *m/e* 257 with the composition $Co(acac)_2$ is produced by the loss of mono-Me-oxine (158 amu) from the molecular ion. Other fragment ions of *m/e* 158 and 217 are produced by the loss of acac and mono-Me-oxine from the ion of *m/e* 316, respectively. It seems that the ion of *m/e* 301 is produced by the loss of $CH_3\cdot$ from the ion of *m/e* 316. Based on this fragmentation pattern, it has been confirmed that these mixed ligand chelates have a 1: 2: 1 binding ratio of Co: acac: mono-Me-oxine.

Fugure 4 shows mass spectra of the compounds assumed to have respective compositions Co(acac)(2-Me-oxine)$_2$, Co(acac)(4-Me-oxine)$_2$, Co(acac)(5-Me-oxine)$_2$, and Co(acac)(7-Me-oxine)$_2$. The spectra of

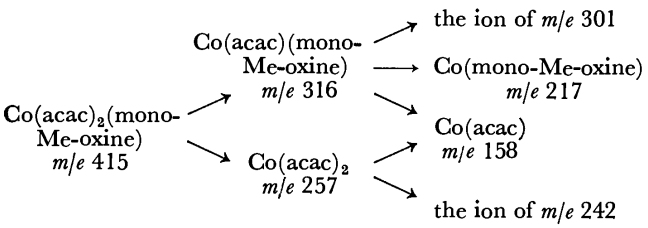

Scheme 2. Fragmentation of $Co(acac)_2$(mono-Me-oxine) type mixed ligand chelate.

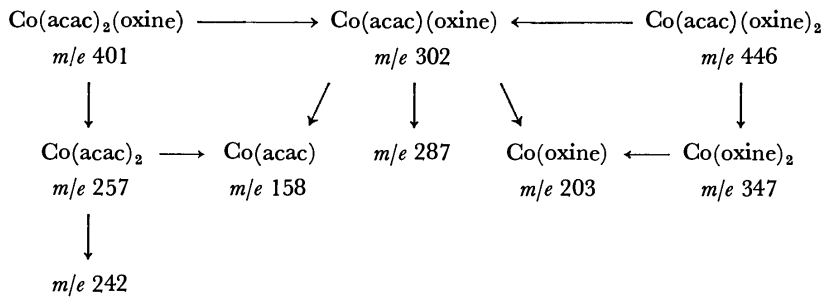

Scheme 1. Fragmentation of mixed ligand chelates, $Co(acac)_2(oxine)$ and $Co(acac)(oxine)_2$.

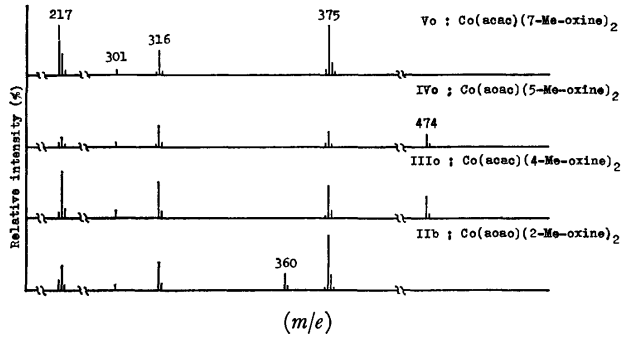

Fig. 4. Mass spectra of Co(acac)(2-Me-oxine)$_2$, Co(acac)-(4-Me-oxine)$_2$, Co(acac)(5-Me-oxine)$_2$, and Co(acac)-(7-Me-oxine)$_2$.

both Co(acac)(4-Me-oxine)$_2$ and Co(acac)(5-Me-oxine)$_2$ have a peak at *m/e* 474 in the highest mass region, corresponding to the molecular weight of the assumed compound, but the spectra of Co(acac)(2-Me-oxine)$_2$ and Co(acac)(7-Me-oxine)$_2$ do not give a molecular ion peak at *m/e* 474. The reason for its absence is explained by the fact that the two mixed ligand chelates have two molecules of 2-Me-oxine or 7-Me-oxine and therefore the chelates are liable to undergo steric hindrance. Thus, it may be difficult for the molecular ion produced by electron impact to exist stably. Since the peak at *m/e* 375 observed in each spectrum corresponds to the fragment ion with a difference of 99 amu (one molecule of acac) from the molecular ion peak, it appears that the peak at *m/e* 375 is a fragment ion having the composition Co(mono-Me-oxine)$_2$. The peak at *m/e* 360 can only be observed in the spectrum of Co(acac)(2-Me-oxine)$_2$. This corresponds to the ion produced by the loss of $CH_3\cdot$ from the ion of *m/e* 375, and the fragmentation pattern coincides with that of Co(2-Me-oxine)$_2$ already described by the authors.[3] The peak at *m/e* 316 appears with a difference of 158 amu (corresponding to one molecule of mono-Me-oxine) and is also observed in the spectrum of Co(acac)$_2$(mono-Me-oxine). Thus it is the peak corresponding to the fragment ion having the composition Co(acac)(mono-Me-oxine). The fragmentation pattern is shown in Scheme 3. Based on this fragmentation pattern, it has been confirmed that these mixed ligand chelates have a 1 : 1 : 2 binding ratio in Co : acac : mono-Me-oxine.

It may be suspected that each of these chelates containing either 2- or 7-Me-oxine is a mixture of Co(acac)-(mono-Me-oxine) and Co(mono-Me-oxine)$_2$, since no molecular ion peak was observed at *m/e* 474. However, the authors confirmed that all the compounds synthesized and used for the measurement of mass spectra are completely pure single substance by identification

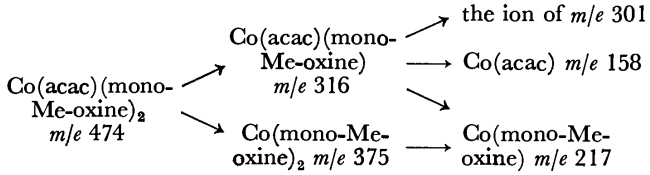

Scheme 3. Fragmentation of Co(acac)(mono-Me-oxine)$_2$ type mixed ligand chelate.

of thin layer chromatography and elementary analyses as is shown in Table 2. Based on these facts, it seems that the spectra are not those of a mixture of Co(acac)-(mono-Me-oxine) and Co(mono-Me-oxine)$_2$.

Experimental

Reagents. Co(acac)$_3$, oxine, and 2-Me-oxine of special grade regents were used without further purification. 4-Me-oxine,[7] 5-Me-oxine,[8] and 7-Me-oxine[8] were synthesized by the reported methods. Kieselgel 60, Merck Co., and Activated Alumina, Wako Pure Chemicals Co., were used as adsorbent for column chromatography. Kieselgel H nach Stahl, Merck Co., was used as adsorbent for thin layer chromatography.

Apparatus. IR spectra were measured with a Nihon Bunko JASCO IRA-2 by means of the KBr disc method. Mass spectra were measured with a Hitachi RMU-7 mass spectrometer by introducing the samples through a direct inlet system. The other conditions were as follows; ionizing voltage 70 eV, ion accelerating voltage 1800 V, total emission current 80 μA, ion source temperature 250 °C, and sample evaporating temperature 110—240 °C.

Thin Layer Chromatography. Thin layer chromatography was carried out on plates of 0.25 mm thickness, which were activated at 110 °C for 1 hr. The solvent mixture used was benzene: methanol=95:5 v/v.

Synthesis. Tris(acetylacetonato) cobalt (III) and oxine or its methyl derivatives are dissolved in either water, methanol, or a mixed solvent of acetone and methanol and this solution in the presence of active charcoal is refluxed on a water bath. After a few minutes, the charcoal is filtered off while hot and the residue is washed well with chloroform. This washing is combined to the preceding filtrate and the solution is concentrated under reduced pressure. The concentrate thus obtained was separated by column chromatography with silica gel or alumina (eluent; chloroform or benzene).

The authors' thanks are due to Professor Akira Tatematsu, the Faculty of Pharmacy, Meijo University, for permission to use the apparatus.

References

1) Y. Kidani, S. Naga, and H. Koike, *Chem. Lett.*, **1972**, 507; This Bulletin, **46**, 2105 (1973).
2) Y. Kidani, S. Naga, and H. Koike, to be published in *Chem. Pharm. Bull.* (Tokyo).
3) S. Naga, Y. Kidani, and H. Koike, This Bulletin, **48**, 863 (1975).
4) Y. Kidani, S. Naga, and H. Koike, *Chem. Lett.*, **1974**, 781.
5) K. Nakamoto, "Infrared Spectra of Inorganic and Coordination Compounds," 2nd ed., John-Wiley & Sons, Inc., New York, N. Y. (1970), p. 247.
6) T. Shimanouchi, "Analysis of Infrared Spectra," Nankodo, Tokyo (1960), p. 95.
7) J. P. Phillips, R. L. Elbinger, and L. L. Merritt, Jr., *J. Amer. Chem. Soc.*, **71**, 3986 (1949).
8) E. Noelting and E. Trautmann, *Ber.*, **23**, 3654 (1890).

Synthesis and Proton Magnetic Resonance Spectra of Some Dichloro-(picolinaldimine*)palladium(II) and -platinum(II) Complexes

Katsuhiko KAWAKAMI, Takeshi OHARA, Gen-etsu MATSUBAYASHI, and Toshio TANAKA

Department of Applied Chemistry, Faculty of Engineering, Osaka University, Yamada-kami, Suita, Osaka 565

(Received October 22, 1974)

A series of dichloro(picolinaldimine)palladium(II) and -platinum(II) complexes was prepared. The PMR parameters, the chemical shifts of the ligand protons and the coupling constants between the platinum-195 nucleus and protons attached to carbons adjacent to donor nitrogens of the ligands, are discussed in the light of the metal-to-ligand bonds.

Recently we have reported that some picolinaldimines (**A**) form stable complexes with dimethyltin dichloride (**B**, M=$(CH_3)_2Sn$(IV)).[1] The ligands of this kind are interesting in that (1) the coordinating ability of the imine nitrogen atom can be altered by varying the substituent on it, (2) their configurational change from *trans* to *cis* on complex formation (**A** and **B**) is accompanied by remarkable changes in the chemical shifts of the various protons, and (3) information on the coordination bonds can be obtained through the observation of spin-spin couplings between the H_a and H_6 protons and the acceptor metal nucleus, if any, as was found in their dimethyltin dichloride complexes.[1]

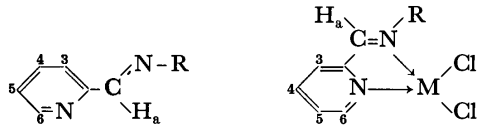

(**A**) (**B**)

M=$(CH_3)_2Sn$ (IV), Pd (II), Pt (II)

This paper will report on the synthesis of a series of dichloro(picolinaldimine)palladium(II) and -platinum-(II) complexes (**B**, M=Pd(II) and Pt(II)) and on their PMR parameters in relation to the nature of the metal-to-ligand bonds.

Experimental

Materials. Na_2PdCl_4 and K_2PtCl_4 were reagent grade and were used as supplied. The picolinaldimines[1] and dichlorobis(benzonitrile)platinum(II)[2] were prepared by the literature methods.

Dichloro(picolinaldimine)palladium(II) Complexes. To a solution of Na_2PdCl_4 (0.50 g, 1.44 mmol) in C_2H_5OH (40 ml) was added dropwise a solution of *p*-tolylpicolinaldimine (0.34 g, 1.72 mmol) in C_2H_5OH (5 ml). Microcrystals were precipitated immediately. The mixture was then stirred for 1 hr at the ambient temperature. The resulting product was filtered and recrystallized from CH_2Cl_2/CH_3CN to give orange crystals of dichloro(*p*-tolylpicolinaldimine)palladium(II) (0.46 g, 85%).

Other Pd complexes were similarly obtained with the exception of the *n*-butyl derivative, which was recrystallized from CH_2Cl_2/petroleum ether.

Dichloro(picolinaldimine)platinum(II) Complexes. To a solution of $(C_6H_5CN)_2PtCl_2$[2] (0.30 g, 0.63 mmol) in 1,2-$C_2H_4Cl_2$ (30 ml) was added a solution of *p*-tolylpicolinaldimine (0.13 g, 0.64 mmol) in the same solvent (5 ml). The solution was refluxed for 4 hrs and then concentrated under reduced pressure to give an oily product, which was stirred in ether for 1 hr. The resultant precipitate was recrystallized from hot methanol to yield orange crystals of dichloro(*p*-tolylpicolinaldimine)-platinum(II) (0.17 g, 58%).

The *p*-chloro and *p*-nitro-phenyl analogs were precipitated as orange solids, which were subsequently recrystallized from hot acetonitrile.

Table 1 shows the melting points, analytical data, and molecular weights of the complexes, together with their ν(M–Cl) frequencies.

Instrumentation. The molecular weights and IR and PMR spectra were obtained as has been described elsewhere.[1] The PMR spectra were usually recorded in CH_3CN at 50 °C because of the limited solubility of the complexes at 25 °C. Little temperature effect on the PMR parameters was observed in the *n*-butylpicolinaldimine complexes of Pd(II) and Pt(II); this was assumed to be true for the other as well. The *p*-substituted picolinaldimine complexes of Pt(II) showed a limited solubility in most organic solvents, and so their spectra were obtained in *N,N*-dimethylacetamide. The solvent effect on PMR parameters in the two solvents was checked by using dichloro(*n*-butylpicolinaldimine)platinum(II) and was found to be small. Tetramethylsilane was used as the internal reference.

Results and Discussion

The analytical data (Table 1) confirm that a series of picolinaldimines forms 1:1 complexes with palladium-(II) and platinum(II) dichlorides. The molecular-weight determinations of some representative complexes showed that they were monomeric in solution. Both Pd(II) and Pt(II) complexes exhibit two ν(M-Cl) bands in the region of 360—325 cm^{-1} (Table 1). These facts indicate that the complexes adopt a square-planar configuration with the chelating ligand, as has been illustrated above in (**B**) (M=Pd(II) and Pt(II)). The chelation of the ligand is further verified in the Pt complexes from the observation of spin-spin couplings between the ^{195}Pt nucleus and the H_6, H_a, and the α-CH protons of the alkyl group on the imine nitrogen.

Table 2 shows the relevant PMR data of the picolinald imine complexes of Pd(II) and Pt(II). The H_3 and H_6 signals of these ligands occur at low fields; this is taken to be evidence for the *trans* structure (**A**), the reasons having been discussed previously in the case of *p*-anisylpicolinaldimine.[1]

On complex formation, the chemical shift of each proton may be influenced by some of the following three effects; (1) a low-field shift caused by the electron-

* Chem. Abstr. name: 2-formimidoylpyridine

Table 1. Melting points, analytical data, molecular weights, and metal–chlorine stretching frequencies of the complexes $MCl_2 \cdot (NC_5H_4\text{–}CH{=}N\text{–}R)$

M	R	Mp (°C)	Analyses C% Found	C% Calcd	H% Found	H% Calcd	N% Found	N% Calcd	Mol. wt.[a] Found	Mol. wt.[a] Calcd	ν(M–Cl)[b] cm^{-1}	
Pd	n-C_4H_9	173—175	35.40	35.39	4.13	4.13	8.35	8.25	332	340	356	343
	i-C_3H_7	>250	33.28	33.20	3.77	3.72	8.85	8.61	302	326	356	340
	C_2H_5	221 (dec)	30.93	30.84	3.36	3.24	9.03	9.00	c)	312	358	345
	$C_6H_5CH_2$	220 (dec)	41.30	41.79	3.14	3.24	7.36	7.50	c)	374	352	337
	p-$CH_3C_6H_4$	267 (dec)	41.61	41.79	3.36	3.24	7.79	7.50	c)	374	358	348
Pt	t-C_4H_9	>250	27.76	28.04	3.44	3.30	6.34	6.54	c)	428	351	325
	n-C_4H_9	159—163	28.40	28.04	3.26	3.30	6.61	6.54	c)	428	352	337
	i-C_3H_7	>250	26.14	26.09	2.97	2.93	6.66	6.77	417	414	354	337
	C_2H_5	247 (dec)	24.28	24.01	2.67	2.52	7.02	7.00	387	400	348	331
	$C_6H_5CH_2$	220 (dec)	33.78	33.78	2.53	2.62	6.25	6.06	c)	463	353	338
	p-$CH_3C_6H_4$	>250	33.61	33.78	2.64	2.62	6.35	6.06	c)	463	357	339
	p-ClC_6H_4	>250	30.02	29.86	1.88	1.88	6.00	5.81	c)	483	354	338
	p-$NO_2C_6H_4$	>250	29.19	29.22	1.85	1.84	8.56	8.52	c)	493	357	345

a) Measured in CH_3CN at 37 °C by a Mechrolab vapor pressure osmometer. b) Nujol mulls. c) Insufficiently soluble.

Table 2. Relevant PMR data[a] of the complexes $MCl_2 \cdot (NC_5H_4\text{–}CH{=}N\text{–}R)$

M	R	Chemical shifts, δ(ppm)[c] H_3	H_4	H_5	H_6	H_a	α-CH-	Coupling constants J(Pt–H_6)	J(Pt–H_a)	^3J(^{195}Pt–H), Hz J(Pt–N–CH–)
Pd	n-C_4H_9	7.94	8.23	7.74	9.12	8.29	3.83			
		(−0.02)	(+0.44)	(+0.36)	(+0.52)	(−0.04)	(+0.16)			
	i-C_3H_7	7.93	8.22	7.72	9.15	8.30	4.67			
		(−0.01)	(+0.44)	(+0.36)	(+0.55)	(−0.03)	(+1.03)			
	C_2H_5	7.90	8.20	7.73	9.14	8.29	3.89			
		(−0.06)	(+0.42)	(+0.36)	(+0.55)	(−0.04)	(+0.20)			
	$C_6H_5CH_2$	7.90	8.20	7.74	9.12	8.27	5.30			
		(−0.12)	(+0.42)	d)	(+0.50)	(−0.20)	(+0.44)			
	p-$CH_3C_6H_4$	8.02	8.27	7.78	9.23	8.23	—			
		(−0.12)	(+0.41)	(+0.35)	(+0.57)	(−0.18)	—			
Pt	t-C_4H_9	7.94	8.22	7.67	9.67	8.72	—	39.9	101.7	—
		(−0.01)	(+0.46)	(+0.34)	(+1.09)	(+0.42)	—			
	n-C_4H_9	7.97	8.26	7.77	9.52	8.86	4.10	39.6	99.5	38.7
		(+0.01)	(+0.47)	(+0.39)	(+0.92)	(+0.53)	(+0.43)			
	i-C_3H_7	7.96	8.27	7.76	9.60	8.90	5.03	39.1	99.6	e)
		(+0.02)	(+0.49)	(+0.40)	(+1.00)	(+0.57)	(+1.39)			
	C_2H_5	7.87	8.19	7.71	9.48	8.80	4.14	38.3	99.1	e)
		(−0.09)	(+0.41)	(+0.34)	(+0.89)	(+0.47)	(+0.45)			
	$C_6H_5CH_2$	7.93	8.23	7.76	9.51	8.85	5.43	39.9	97.3	33.3
		(−0.09)	(+0.45)	d)	(+0.89)	(+0.38)	(+0.57)			
	p-$CH_3C_6H_4$[b]	8.24	8.02	7.57	8.78	9.53	—	39.5	94.3	—
		(+0.20)	(+0.61)	(+0.58)	(+0.92)	(+0.88)	—			
	p-ClC_6H_4[b,f]				9.69	9.61	—	38.9	93.5	—
					(+0.88)	(+0.94)				
	p-$NO_2C_6H_4$[b,f]				9.64	9.78	—	37.6	93.5	—
					(+0.77)	(+1.09)	—			

a) Measured in CH_3CN at 50 °C, unless otherwise noted. b) Measured in *N*,*N*-dimethylacetamide at 25 °C. c) The values in parentheses are $\Delta\delta$ ($\delta_{complexed}-\delta_{free}$). d) Could not be obtained since the signal of the ligand was obscured by other signals. e) Could not be measured because of too weak intensity. f) Assignments for the H_3, H_4, and H_5 protons are ambiguous because of too weak intensity of the signals.

withdrawal, (2) a high-field shift caused by the disappearance of the paramagnetic effect of the imine nitrogen (to H_3)[1] and that of the ring nitrogen (to H_6 and H_a), and (3) a low-field shift caused by the paramagnetic effect of the halogen atoms[1] and/or certain d orbitals of the central metal atom[3] because of their proximity to the H_6 and α-CH protons, as has been suggested in the case of the complexes of pyridine and its derivatives with metal halides. The almost unchanged chemical shifts of the H_3 proton in all the complexes

(Table 2) are due to the two mutually opposite effects, (1) and (2), when the ligand takes the *cis* configuration (**B**) with respect to the nitrogen atom. The coordination shifts, $\Delta\delta$ ($\delta_{complex}-\delta_{free}$), of the H_4 and H_5 protons are not significantly different in the Pt and Pd complexes. The $\Delta\delta$ values of these protons are influenced only by the (1) effect, which, in turn, is a measure of the $M-N_{ring}$ bond strength if the effect of the substituent on the imine nitrogen through the azomethine group is assumed to be negligible. Thus, it may be suggested that the $Pd-N_{ring}$ bond is nearly as strong as the Pt counterpart.

On the other hand, the $\Delta\delta$ values of the H_6 proton are much larger in the Pt than in the Pd complexes; this is a result of the predominance of the (3) effect in the Pt complexes, since the (1) and (2) effects seem to be similar in the Pd and Pt complexes, as has been discussed above.

The $\Delta\delta$ values of the H_a proton in the Pt complexes are also large, whereas those of the Pd complexes are close to zero except for those of the benzyl and *p*-tolyl complexes. The $\Delta\delta$ values of the H_a proton can be explained in a manner similar to that used to explain those of the H_3 proton. Thus, in the case of the Pd complexes the (1) effect and the (2) effect of the ring nitrogen upon $Pd-N_{imine}$ coordination appear to cancel out each other. However, the large $\Delta\delta$ values of the H_a proton in the Pt complexes indicate the predominance of the former; this may be explained by assuming a stronger coordination in the $Pt-N_{imine}$ than in the $Pd-N_{imine}$ bond. In fact, the values of the α-CH protons are larger in the Pt than in the Pd complexes, although the difference in the (3) effect may be another factor.

The large values of the coupling constants, $^3J(Pt-H_a)$, $^3J(Pt-H_6)$, and $^3J(Pt-N-CH-)$, given in Table 2 confirm the presence of solid Pt–N bonds in the Pt complexes. The first value is overwhelmingly larger than the latter two. This must be due to the *trans* arrangement of the H_a proton and the ^{195}Pt nucleus with respect to the C=N bond.[4] The observation of $^3J(Pt-H_6)$ in our complexes may be the first example in the $PtCl_2$ complexes with pyridine and its derivatives; it stems from the chelation of the ligands.

References

1) G. Matsubayashi, M. Okunaka, and T. Tanaka, *J. Organometal. Chem.*, **56**, 215 (1973).
2) R. A. Walter, *Spectrochim. Acta*, **21**, 1795 (1965).
3) J. Chatt and A. D. Westland, *J. Chem. Soc. A*, **1968**, 88.
4) J. W. Emsley, J. Feeney, and L. H. Sutcliffe, "High Resolution Nuclear Magnetic Resonance Spectroscopy", Vol. 2, Pergamon Press, New York, N. Y. (1966), p. 712.

Ruthenium Complexes with Coordinated Hydroxyiminoacetylacetonato or Bridging Nitrosyl Groups Formed by the Reactions of Nitrosylruthenium(III) with Acetylacetone

Masao MUKAIDA, Terunosuke NOMURA, and Tatsujiro ISHIMORI*

Department of Chemistry, Sophia University, Chiyoda, Tokyo 102

**Department of Chemistry, Rikkyo (St. Paul's) University, Ikebukuro, Tokyo 171*

(Received October 29, 1974)

Complexes formed by the reactions of nitrosylruthenium(III) with acetylacetone were investigated. The following products: $[Ru(acac)_2(hia)]$, **1**; *cis*-$[RuCl(NO)(acac)_2]$, **2**; and $[\{Ru(NO)(acac)_2\}_4]$, **3**; (acac= $C_5H_7O_2^-$ and hia=$C_5H_6NO_3^-$), were isolated as crystals and were characterized. On the basis of chemical and thermal analyses, and on the basis of observations of the magnetic properties, the conductivities, the molecular weights, the infrared spectra, and the NMR spectra, it was concluded that **1** contains the hydroxyiminoacetyl acetonato ligand, which is formed by the reaction of the coordinated nitrosyl group with acetylacetone, and that **2** contains a terminal nitrosyl group, and **3**, bridging nitrosyl groups.

The reactivity of coordinated nitrosyl has received much attention recently. The reactions of a variety of nitrosylruthenium(III) complexes with nucleophiles, such as ammonia, hydrazins, hydroxylamine, potassium azide, and potassium hydroxide, have recently been investigated.[1-7] The reactions of nitrosylruthenium-(III) halides with reducing reagents, such as tin(II) chloride and formaldehyde, have also been reported.[8,9] This paper will describe the preparation and characterization of the ruthenium complexes with the coordinated hydroxyiminoacetylacetonato or bridging nitrosyl groups obtained by the reactions of nitrosylruthenium(III) with acetylacetone.

Experimental

Preparation. Bis(acetylacetonato)hydroxyiminoacetylacetonatoruthenium(III), $[Ru(acac)_2(hia)]$, 1: To a hydrochloric-acid solution of nitrosylruthenium(III) (100 mg as Ru/10 ml) were added methanol (2 ml) and acetylacetone (2 ml). Then, the pH of the mixed solution was adjusted to 6.5 with an aqueous solution of potassium hydroxide. When the mixed solution was allowed to stand at room temperature for about a week, dark brown crystals appeared. The crystals were recrystallized from ethanol. Yield, 40 mg. Found: Ru, 23.9; C, 42.3; H, 4.75; N, 3.37%. Calcd for $[Ru(C_5H_7O_2)_2(C_5H_6NO_3)]$: Ru, 23.6; C, 42.1; H, 4.68; N, 3.28%.

Bis(acetylacetonato)chloronitrosylruthenium(III), $[RuCl(NO)(acac)_2]$, 2: To a hydrochloric-acid solution of nitrosylruthenium(III) (100 mg as Ru/10 ml) were added methanol (2 ml) and acetylacetone (2 ml). Then, the pH of the mixed solution was adjusted to 3.5 with an aqueous solution of potassium hydroxide. The solution was refluxed for 2 hr and was then allowed to stand at room temperature for several days, until dark brown crystals were separated out. The crystals were recrystallized from ethanol. Yield, 35 mg. This complex was also obtained from the filtrate of **3** when the filtrate was allowed to stand at room temperature for a long period. Found Ru, 27.4; C, 32.6; H, 3.80; N, 3.81; Cl, 9.57%. Calcd for $[RuCl(NO)(C_5H_7O_2)_2]$: Ru, 27.7; C, 32.9; H, 3.87; N, 3.84; Cl, 9.73%.

Cyclo-tetra-μ-nitrosyl-tetrakis(diacetylacetonato)ruthenium(II), $[\{Ru(NO)(acac)_2\}_4]$, 3: To a hydrochloric-acid solution of nitrosylruthenium(III) (135 mg as Ru/10 ml) were added acetylacetone (2 ml), and the pH of the solution was adjusted to 3.5 with an aqueous solution of potassium hydroxide. To this mixed solution, an equal volume of ethanol was added. The solution was refluxed for 50 min and was then allowed to stand at room temperature for about ten days, until dark green crystals were separated out. The crystals were recrystallized from a mixed solution of ethanol and benzene three times. Yield, 35 mg. Found: C, 36.2; H, 4.35; N, 4.18%. Calcd for $Ru(NO)(C_5H_7O_2)_2$: C, 36.5; H, 4.25; N, 4.25%.

Materials. Nitrosylruthenium(III) in a hydrochloric acid solution was prepared by a conventional method.[10] The nitrosylruthenium(III) chloride [^{15}N] was prepared by the method reported by Miki *et al.*[11] The palladium complexes, $[Pd(acac)_2]$ and [Pd(acac)(hia)], were prepared according to the method in the literature.[12] $[Pd(hia)_2]$ was obtained by the reaction of Pd(II) chloride with hia, which had been purchased from the Dojin Lab. (Kumamoto, Japan).

Measurements. The infrared spectra of these complexes were recorded on Leitz 221, JASCO DS-301, or Hitachi EPI-L spectrophotometers, using the KBr-pellet or Nujol-mull method. The NMR spectra were taken on a Hitachi R-22 instrument, with tetramethylsilane as the internal standard. The visible absorption spectra were recorded on a Hitachi-Perkin-Elmer 139 spectrophotometer. The conductivity and the molecular weight were measured with a Metrohm Konduktoskop E356 and with a Mecrolab Osmometer 302 respectively. The DTA and TG measurements were carried out by the use of a Rigaku TG-DTA standard-type apparatus. The measurments were made at a heating rate of 10 °C/min in atmosphere. The magnetic susceptibilities were measured by the Gouy method.

Results and Discussion

From the reactions between nitrosylruthenium(III) and acetylacetone, Complexes **1**, **2** and **3** were newly isolated. The chemical formulae of these complexes and some of their properties are shown in Table 1. The molecular weights of **1** and **3**, which were obtained in benzene by a vapor-pressure osmometry, corresponded to those of the monomeric and of the tetrameric species respectively. The molecular weight of **2** could not be measured because of an insufficient solubility in benzene, but the monomeric form of the complex can be expected from the observations of its IR and NMR spectra. All these complexes were non-electrolyte in benzene and DMF. The thermal properties of the complexes were examined by DTA and TG methods. **1**, **2**, and **3** decomposed at about 149 °C, 126 °C and 265 °C respectively, without showing any endothermic

TABLE 1. SOME PROPERTIES OF RUTHENIUM COMPLEXES FORMED BY THE REACTIONS OF RuNO(III) WITH ACETYLACETONE

Complex	Chemical Formula	χ_g 10^6 c.g.s., e.m.u.	μ_{eff} (B.M.)	Type of[a] electrolyte	Molecular[b] weight	Visible[b] Absorption spectra nm (ε)
1	$[Ru(acac)_2(hia)]$	2.94 (296 K)	1.87	nonelectrolyte	435	460 (4.43×10^3) 395 (3.28×10^3)
2	*cis*-$[RuCl(NO)(acac)_2]$	−0.32 (293 K)	dia	nonelectrolyte		505 (1.84×10^2)
3	$[\{Ru(NO)(acac)_2\}_4]$	−0.28 (293 K)	dia	nonelectrolyte	1324	635 (2.83×10^3) 420sh (7.2×10^3)

a) In MeOH and in DMF. b) in MeOH.

peaks due to the deaquation of crystalline or coordinating water.

The structures of these complexes will now be discussed on the basis of their IR and NMR spectra and their magnetic properties.

$[Ru(acac)_2(hia)]$ (**1**): The composition of **1** is consistent with either of the following two formulae; $[Ru(acac)_2(hia)]$ and $[Ru(NO)(acac)_3]$. However, tris(acetylacetonato)nitrosylruthenium(III) was clearly excluded by the paramagnetism observed, since nitrosylruthenium(III) complexes are essentially diamagnetic. The observed magnetic moment (1.87 B.M.) is fairly close to the value, 1.73 B.M., estimated by the spin-only equation.

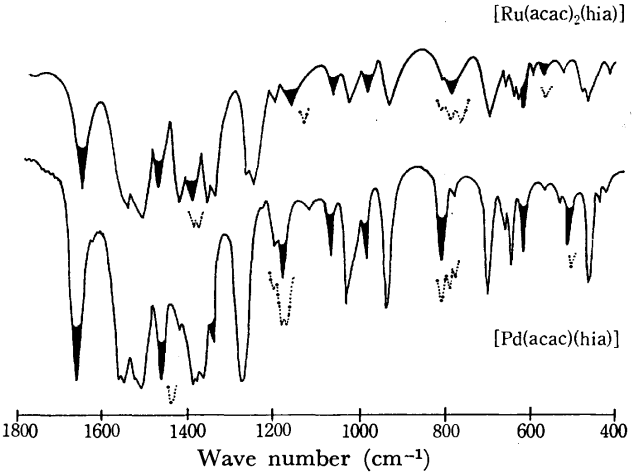

Fig. 1. Infrared spectra of $[Ru(acac)_2(hia)]$ and [Pd(acac)(hia)] (KBr disk). Painted peaks were assigned to the bands which were caused by the hia ligand. Identity of the ligand was established by a comparison of the infrared spectra of $[Ru(acac)_2(hia)]$ (**1**), $[RuCl(NO)(acac)_2]$ (**2**), $[Pd(acac)_2]$, [Pd(acac)(hia)] and $[Pd(hia)_2]$.
^{14}NO-complex, ——; ^{15}NO-complex, ·····.

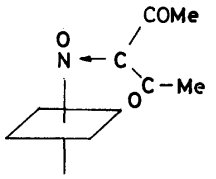

Fig. 2. Proposed structure for Complex **1**.

The infrared spectra of **1** and relevant compounds are shown in Fig. 1. The characteristic vibrations in **1** [^{14}N] and **1** [^{15}N] are summarized in Table 2. Recently, several complexes containing hia and analogous ligands were identified, by Masuda *et al.* and by White on the basis of their infrared spectra.[12,13] The spectral features observed here can be understood on the basis of the idea that one of the acetylacetonato ligands and the coordinated nitrosyl combine through the γ-carbon atom to produce the hia ligand, as is shown in Fig. 2. Evidence for the presence of the hia ligand in **1** may be found in the similarity between the infrared spectrum of **1** and that of [Pd(acac)(hia)], including their ^{15}N isotopic effects. As is shown in

Table 2. CHARACTERISTIC INFEARED SPECTRA (cm^{-1}) OF COMPLEXES **1**, **2**, AND **3**

$[Ru(acac)_2(hia)]$		*cis*-$[RuCl(NO)(acac)_2]$		$[\{Ru(NO)(acac)_2\}_4]$		Tentative assignments
1 [^{14}N]	**1** [^{15}N]	**2** [^{14}N]	**2** [^{15}N]	**3** [^{14}N]	**3** [^{15}N]	
		1884 vs	1883 w 1849 vs			νNO(terminal)
1662 vs	1660 vs					νCO (uncoordinated)
1564 vs 1549 s	1565 vs 1553 s	1571 vs	1573 vs	1573 vs	1571 vs	νCO+νCC
					1543 sp	νNO(bridging)
1520 vs	1526 vs	1526 vs	1529 vs	1518 vs	1516 vs	νCO+νCC
1403 s	1400 s 1387 sp					νCN(hia)
1162 m	1148 m					νNO(hia)
807 w	796 w			795 m	795 m	
782 s	782 s 771 s	787 m	787 m	780 m 769 m	780 m 769 m 760 sh	πCH
587 w	582 w	601 w 587 w	591 w 575 w	553 w	544 w	νRuN σRuNO

Fig. 1, the bands due to the hia in both complexes were found in almost the same regions and intensities. By comparing the infrared spectrum of **1** with those of analogous complexes,[12-14] the bands at 1387, 1148, and 1660 cm^{-1} in **1** [^{15}N] can be assigned tentatively to the stretching vibrations of the C=N, N–O, and uncoordinated C=O groups of the hia ligand respectively. These bands seem to be most diagnostic for the characterization of this ligand.

cis-[RuCl(NO)(acac)$_2$] (**2**): **2** is diamagnetic. The infrared spectra of **2** [^{14}N] and **2** [^{15}N] are compared in the 200—4000 cm^{-1} region. The characteristic vibrations of both complexes are summarized in Table 2. By comparing these bands with the spectra of pentachloronitrosylruthenium(III) complexes and acetylacetonato metal chelate complexes,[15-19] the presence of the terminal nitrosyl ligand in **2** was easily verified.

Table 3. Proton magnetic resonance data (ppm) for complexes **2** and **3**

Complex	Solvent	Resonance	
		$-CH_3$	$-CH$
2, *cis*-[RuCl(NO)(acac)$_2$]	$CDCl_3$	2.05 2.14 2.24 2.29	5.47 5.73
3, [{Ru(NO)(acac)$_2$}$_4$]	$CDCl_3$	1.73 2.21	5.31

The NMR spectrum of **2** listed in Table 3 was measured in $CDCl_3$. The assignments are based on those for *cis*- and *trans*-β-diketonato complexes, which have been investigated extensively by Boucher *et al.*[20] The observed chemical shifts for the methyl and the methine protons provide proof that the complex has a *cis* arrangement of the chloride and the nitrosyl.

[{Ru(NO)(acac)$_2$}$_4$] (**3**): The molecular weight of **3** corresponded to that of a tetrameric species. X-Ray single crystal photographs of **3** showed that the cell volume of this complex was about 2598×10^{-24} cm^3 (uncalibrated film). The calculated density for two molecules per cell is 1.68 g/cm^3, and the observed density was 1.70 g/cm^3 (by floatation in CH_3Br and CCl_4). The possibility of **3** being a tri- or pentanuclear complex may thus be excluded.

The infrared spectrum of **3** is shown in Table 2. The absorption bands of the acetylacetonato moiety in **3** were identical with those of **2**, showing a chelate coordination of the ligand. No absorption band due to the nitrosyl stretching frequency of the linear or near-linear RuNO(III) group was found in the 1700—2000 cm^{-1} region. It has recently been revealed by structural investigations that a marked lowering of the nitrosyl stretching frequency reflects the presence of the NO^- ligand or the bridging nitrosyl ligand.[21-23] One of the present authors (M.M.) has reported that the infrared spectrum of a nitrosyl complex, which is believed to contain bridging nitrosyl, shows frequency shifts for the bands in the 1500, 800 and 550 cm^{-1} regions with the replacement of ^{14}N by ^{15}N.[9] ^{15}N substitution effects for **3** were observed, as is shown in Table 2. The strong band at 1573 cm^{-1} in **3** [^{14}N] was

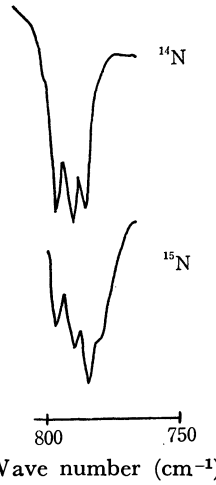

Fig. 3. IR spectra of Complex **3** at 800 cm^{-1} region (KBr).

partially split into two bands, at 1571 and 1543 cm^{-1}, in **3** [^{15}N]. The weak band at 553 cm^{-1} in **3** [^{14}N] was shifted to the lower-frequency side. As is shown in Fig. 3, a splitting of the bands was observed in the near 800 cm^{-1} region. These findings are quite similar to those found for the complex bridged with nitrosyl mentioned above,[9] suggesting that **3** contains the bridged nitrosyl group.

The NMR spectroscopy provides additional evidence for the bridged structure assumed. As is shown in Table 3, the NMR spectrum of the complex in $CDCl_3$ shows three peaks, with an area ratio of 1: 3: 3. It has been established that two methine protons in monomeric *cis*-bis(acetylacetonato)cobaltate(III), $[Co(acac)_2X_2]^-$ (X=N_3^- or OH^-), are equivalent, while the methyl protons are divided into two sets of methyl groups[20,24] A similar spectrum has also been found for di-μ-hydroxo-bis[bis(acetylacetonato)cobalt(III)],[25] $[Co_2(acac)_4(OH)_2]$. In the latter, however, quite a large methyl resonance splitting (0.48 ppm), which is thought to arise because of the hydroxo bridge and the dimeric structure,[25] has been found. The NMR spectrum observed here is identical with that of the dimeric acetylacetonato complex referred to above.

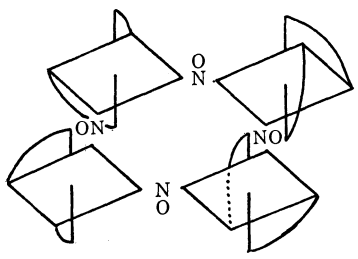

Fig. 4. Probable structure for Complex **3**

On the basis of the spectral observations, the most probable structure of **3** is thought to be the tetrameric structure bridged with nitrosyls, depicted in Fig. 4. This structure consists of four monomeric octahedral unit, Ru(NO)(acac)$_2$, containing both equivalent acetylacetonate anions and the bridged nitrosyl group.

3 is diamagnetic. The majority of nitrosylruthe-

nium(III) complexes which have a linear terminal Ru–N–O group have been considered to contain NO^+.[26] The nitrosylruthenium group in **3**, however, may be considered to be Ru(II)NO or Ru(III)NO^-. The diamagnetism of **3** may be explained using the bonding scheme applied to a complex bridged with nitrosyls, $(Me_4N)_4[Ru_2(NO)_2(SnCl_3)_2Cl_6]\cdot H_2O$, which has an analogous bridged structure.[9]

Reactions. The reactions of the nitrosylruthenium-(III) described above are summarized in the following scheme.

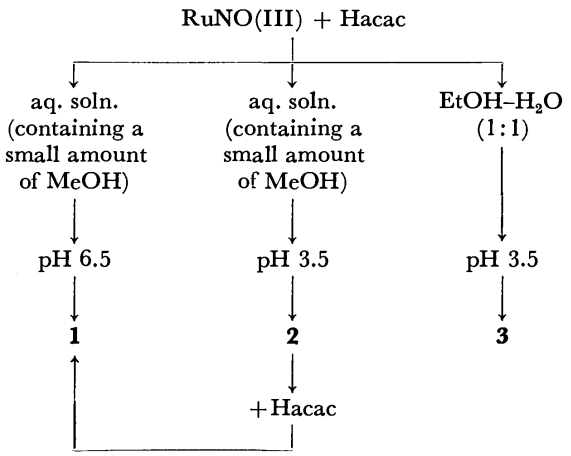

In a neutral solution, the coordinated nitrosyl is converted into the hia ligand under mild reaction conditions. On the other hand, **2** is formed in an acid aqueous or methanolic solution, whereas **3** is produced in an acid ethanolic solution. It should be noted that the isolation of these complexes depends on the pH of the reaction mixture and the kind of alcohol used as a solvent. **1** could also be derived by the reaction of **2** with acetylacetone in a methanolic solution. However, the formation of **1** was not observed in the reaction between RuNO(III) chloride and acetylacetone at pH 8.5—9.0. In an aqueous solution of this pH, dark brown materials were obtained in place of **1**. This is thought to be an acetylacetonato complex containing a terminal nitrosyl group([Ru(OH)(NO)$(acac)_2$]) on the basis of its composition and infrared spectrum.

The reaction of coordinated β-diketonato and analogous ligands with nitric oxide to give an oxime-type bonding has recently been reported.[12,13] However, no reaction between coordinated nitrosyl and β-diketone has yet been reported. The isolation of **1** reported here appears to be the first example of the latter reaction. The mechanism of this reaction is not clear. However, it is thought to differ from the acid-catalyzed mechanism which has been presumed for the formation of [Pd(acac)(hia)] by means of the reaction of NO on [Pd$(acac)_2$],[12] since it appears unlikely that the cleavage of Ru–NO bonding occurs under the conditions specified above. This discrepancy seems to be responsible for the difference in reactivity between coordinated nitrosyl and free nitric oxide.

The authors wish to express their thanks to Dr. Eiichi Miki of St. Paul's (Rikkyo) University for the measurement of the IR spectra. Thanks are also due to Mr. Masaaki Sakamoto and Mr. Akira Hoshi for their technical assistance. This investigation was supported in part by a grant from the Ministry of Education.

References

1) E. J. Baran and A. Muller, *Chem. Ber.*, **102**, 3915 (1969).
2) P. G. Douglas, R. D. Feltham, and H. G. Metzger, *J. Amer. Chem. Soc.*, **93**, 84 (1971).
3) P. G. Douglas and R. D. Feltham, *ibid.*, **94**, 5254 (1972).
4) F. J. Miller and T. J. Meyer, *ibid.*, **93**, 1294 (1971).
5) S. A. Adeyemi, F. J. Miller, and T. J. Meyer, *Inorg. Chem.*, **11**, 994 (1972).
6) J. B. Godwin and T. J. Meyer, *ibid.*, a) **10**, 471(1971); b) **10**, 2150 (1971).
7) F. Bottomley and J. R. Crawford, a) *J. Chem. Soc., Dalton.*, **1972**, 2145; b) *J. Amer. Chem. Soc.*, **94**, 9092 (1972).
8) M. J. Cleare and W. P. Griffith, *J. Chem. Soc., A*, **1970**, 1117.
9) M. Mukaida, This Bulletin, **43**, 3805 (1970).
10) J. M. Fletcher, I. L. Jenkins, F. M. Lever, F. S. Martin, A. R. Powell, and R. Todd, *J. Inorg. Nucl. Chem.*, **1**, 378 (1955).
11) E. Miki, T. Ishimori, H. Yamatera, and H. Okuno, *Nippon Kagaku Zasshi*, **87**, 703 (1966).
12) D. A. White, *J. Chem. Soc., A*, **1971**, 233.
13) I. Masuda, M. Tamaki, and K. Shinra, This Bulletin, **42**, 157 (1969).
14) a) K. S. Bose, B. C. Sharma, and C. C. Patel, *Inorg. Chem.*, **12**, 120 (1973). b) M. J. Lacey, C. G. Macdonald, J. S. Shannon and P. J. Collin, *Aust. J. Chem.*, **23**, 2279 (1970) and references cited therein.
15) J. Lewis, R. J. Irving, and G. Wilkinson, *J. Inorg. Nucl. Chem.*, **7**, 32 (1958).
16) P. Gans, A. Sabatini, and L. Sacconi, *Inorg. Chem.*, **5**. 1877 (1966).
17) M. J. Cleare and W. P. Griffith, *J. Chem. Soc., A*, **1967**, 1144.
18) E. Miki, This Bulletin, **41**, 1835 (1968).
19) K. Nakamoto, "Infrared spectra of Inorganic and Coordination Compounds," 2nd Ed., Wiley-Interscience, New York (1970), p. 247.
20) L. J. Boucher and D. R. Herrington, *Inorg. Chem.*, **11**, 1772 (1972).
21) C. G. Pierpont and R. Eisenberg, a) *J. Amer. Chem. Soc.*, **92**, 4760 (1970); b) *Inorg. Chem.*, **11**, 1088 (1972).
22) J. R. Norton, J. P. Collman, G. Dolcetti and W. T. Robinson, *ibid.*, **11**, 382 (1972).
23) R. C. Elder, *ibid.*, **13**, 1037 (1974).
24) B. P. Cotsoradis and R. D. Archer, *ibid.*, **6**, 800 (1967).
25) L. J. Boucher and D. R. Herrington, *J. Inorg. Nucl. Chem.*, **33**, 4349 (1971).
26) F. A. Cotton and G. Wilkinson, "Advanced Inorganic Chemistry," 3rd Ed., Interscience, New York (1972), p. 713, p. 1012.

The Complexing of the Lithium Ion in Acetonitrile with Other Solvents. Investigation by the Use of a Cation-sensitive Glass Electrode

Toshio NAKAMURA

Chemistry Department, Faculty of Science, Shinshu University, Asahi, Matsumoto 390

(Received November 5, 1974)

The complexing of the lithium ion with other popular solvents has been studied in acetonitrile (AN) using a monovalent cation-sensitive glass electrode. A method similar to that developed to study the complexing of the sodium ion was employed.[1] Mono- and di-solvated species were formed for methanol, pyridine, formamide, methylfomamide, and HMPA. Tri-solvated species were also formed for DMF, DMA, and DMSO. In general, the complexing of the lithium ion with these solvents was more pronounced than that of the sodium ion. The formation constants for the mono-solvated lithium ion were 4.5 for methanol, 5.2 for pyridine, 16 for DMF, 20 for formamide, 25 for methylformamide, 49 for DMSO, 62 for DMA, and 2.1×10^3 for HMPA. When water was the complexing solvent, the equilibrium potential could not be obtained, probably because of the hydrolysis of the hydrated lithium ion. Prior to these experiments, the cation-sensitive glass electrode was confirmed to respond to the lithium-ion activity in different solvents by comparing its behavior with that of a lithium-amalgam electrode.

In the previous paper,[1] the author and his collaborators reported a potentiometric method which used a monovalent cation-sensitive glass electrode to obtain the formation constants of the complexing of the sodium ion in acetonitrile (AN) with several popular solvents. In this experiment, a similar method has been used to determine the formation constants (the so-called hybrid formation constants), β_x, of the complexing of the lithium ion in AN with other solvents (Eqs. (1) and (2)):

$$Li_s^+ + xD = Li_{xD}^+ \quad (1)$$

$$\beta_x = \frac{(Li_{xD}^+)}{(Li_s^+)[D]^x} \quad (2)$$

In Eqs. (1) and (2), Li_s^+ shows the lithium ion solvated only by AN, and Li_{xD}^+, that complexed by x molecules of the D solvent. (Li_s^+) and (Li_{xD}^+) are the activities of Li_s^+ and Li_{xD}^+ respectively, and [D], the concentration of the free (uncomplexed) solvent, D.

Prior to the determination of the formation constants, the glass electrode was verified to respond with a Nernstian slope to the activity of the lithium ion in different solvents. This was done by comparing the response of the glass electrode, immersed in solutions of the 10^{-3}M lithium ion in different solvents, with the response of a lithium amalgam electrode immersed in the same solutions. The formation constants were determined by the emf measurement of Cell I, in the compartment (C) of which the D solvent was titrated to a solution of 10^{-3}M $LiClO_4$+10^{-2}M Et_4NClO_4, originally in pure AN:

Ag|0.005M $AgNO_3$(AN)‖0.1M Et_4NPic(AN)‖
(A) (B)
10^{-3}M $LiClO_4$ + 0.01M Et_4NClO_4(AN-D)|glass electrode
(C)
Cell I

(D denotes the solvents added)
The following relations were used:

$$R \equiv \left\{\frac{(Li_s^+)_{AN}}{(Li_s^+)_{AN-D}} - 1\right\}/[D] = \beta_1 + \beta_2[D] + \beta_3[D]^2 + \cdots \quad (3)$$

$$(R-\beta_1)/[D] = \beta_2 + \beta_3[D] + \cdots \quad (4)$$

$$(Li_s^+)_{AN}/(Li_s^+)_{AN-D} = 10^{(E_{AN}-E_{AN-D})/59} \quad (5)$$

where $(Li_s^+)_{AN}$ and $(Li_s^+)_{AN-D}$ are the activities of Li_s^+ in pure AN and in the mixture of AN and D respectively. E_{AN} and E_{AN-D} show the potentials of the glass electrode in mV obtained in pure AN and in the AN–D mixture respectively. Assumptions similar to those in the previous paper[1] were made: (i) the (D) solvent in AN–D mixtures is monomeric; (ii) the activity of AN does not change upon the addition of D and is equal to unity; (iii) the salt-effect activity coefficient of the lithium ion, as calculated by the Debye-Hückel equation, is equal in pure AN and in AN–D mixtures; (iv) the amount of (D) solvent consumed by the solvation of the ions of an indifferent electrolyte is negligible and (v) the liquid-junction potential between the solutions in the salt bridge (B) and the compartment (C) in Cell I does not change upon the addition of D.

By this method, such formation constants for D as methanol, pyridine, DMF, formamide, methylformamide, DMSO, DMA, and HMPA were obtained. In general, the complexing of the lithium ion occurs to a fairly greater extent than that of the sodium ion. The formation constants for the hydration of the lithium ion in AN, however, could not be determined because of a peculiar behavior of the electrode potential which is probably due to the hydrolysis of the lithium ion, as will be described later.

Apparatus and Reagents

Apparatus. Most of the apparatus and experimental techniques for the determination of formation constants are the same as those in the previous report.[1] The assembly of Cell I is that Shown in Fig. 1 of Ref. (1), except that in the compartment (C) 10^{-3}M $LiClO_4$ was used instead of 10^{-3}M $NaClO_4$. The lithium-amalgam electrode was constructed by modifying the one used by Matsuura *et al.*[2]; the lithium amalgam was prepared by electrolyzing 10^{-2}M $LiClO_4$ in AN, and the concentration of lithium in the amalgam was determined to be 6.58×10^{-2}M by titration with perchloric acid. The potential of the amalgam electrode was measured with a voltameter equipped with a voltage follower with an input impedance of $10^{11}\Omega$. For the acid-base titration in AN containing a small amount

of water, a pH glass electrode, Hitachi-Horiba 1026, was used.

Reagents. Unhydrated lithium perchlorate was dried before use at 250 °C under a vacuum. The tetraethylammonium picrate, tetraethylammonium perchlorate, acetonitrile, and pyridine were the same as those in the previous work.[1] The DMF, DMSO, PC, and HMPA were purified by the conventional methods. The methylformamide was used after the purification of an analytical reagent-grade substance by fractional crystallization. The formamide was a chromatographic product. The lithium tetraphenylborate was prepared by passing an aqueous solution of sodium tetraphenylborate through a column of amberlite IR 120 exchange resin in the Li^+-form. It was dried at 50 °C under a high vacuum. The tetrabutylammonium tetraphenylborate was prepared by the method of Accascina *et al.*[3] The procedure of Cundiff and Markunas[4] was used to prepare the tetrabutylammonium hydroxide solution in a benzene–methanol (3:2) mixture. The other solvents and reagents were of an analytical reagent grade and were used without further purification.

Results

Response of the Glass Electrode to the Activity of the Lithium Ion in Different Solvents. The glass electrode used in the present study showed a slope of 57 mV to the lithium ion between 10^{-4}M and 10^{-2}M in AN–0.01M Et_4NClO_4. If corrected for the change in the salt-effect activity coefficient, the response towards pa_{Li}^+ is very near the Nernstian slope of 59 mV.

In order to confirm that the glass electrode can respond to the difference in the activity of the lithium ion in different solvents, the emf of Cell II was compared with that of Cell III. Because the reference electrode and the salt bridge in both cells are the same as each other (and as those used in Cell I), a comparison of the emf's of Cells II and III is equivalent to a comparison of the potentials of the glass electrode and the amalgam electrode.

$$\text{Ag}|0.005\text{M } AgNO_3(\text{AN})\|0.1\text{M } Et_4NPi(\text{AN})\|$$
$$10^{-3}\text{M } LiClO_4 + 0.01\text{M } Et_4NClO_4(\text{D})|\text{Glass Electrode}$$
Cell II

$$\text{Ag}|0.005\text{M } AgNO_3(\text{AN})\|0.1\text{M } Et_4NPi(\text{AN})\|$$
$$10^{-3}\text{M } LiClO_4 + 0.01\text{M } Et_4NClO_4(\text{D})|\text{Li(Hg)}$$
Cell III

(D denotes AN, methanol, DMF, and DMSO)

The results are shown in Fig. 1. From these results, it may be considered that the glass electrode used in the present experiment responds to the activity of the lithium ion in those different solvents.

Complexing of the Lithium Ion in AN with Other Solvents. From the emf measurement of Cell I, the values of the formation constants (β_x) were calculated by using Eqs. (3) to (5). The results are summarized in Table 1. Figures 2 to 6 show some examples of the R–[D] and $(R-\beta_1)/[D]$–[D] relations used to obtain the formation constants.

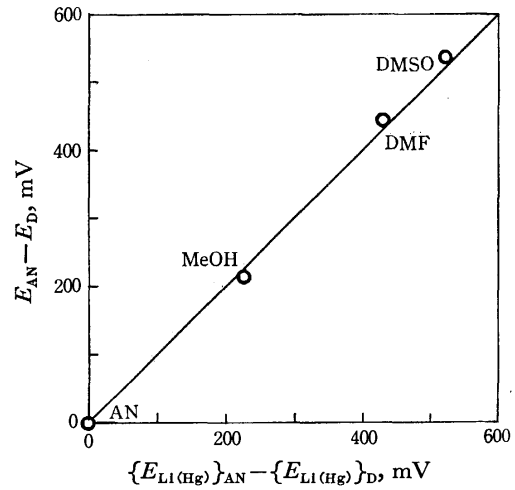

Fig. 1. Relations between potentials of the ion-sensitive glass electrode and those of the lithium amalgam electrode in various solvents, both referred to the values in AN.

When water was the complexing solvent, the equilibrium potential could not be obtained. As is shown in Fig. 7, Curve A, when water was added to the AN solution of the lithium ion, the potential shifted first to the more negative direction, but then back to the less negative direction, and it did not attain a constant value even after 60 min. (When the other solvents in Table 1 were the complexing solvents, equilibrium potentials were usually obtained soon after their addi-

Table 1. Complex formation constants of lithium ion with other solvents in AN

Solvent	Upper mol added (M)	β_1	β_2	β_3
PC	0.4	<0.3		
H_2O		?	?	?
		[1.8]	[1.8]	
Methanol	1.0	4.3	6.4	
		4.6	7.0	
		[1.1]	[0.4]	
Pyridine	0.2	5.1	2.7	
		5.3	2.7	
		[0.7]	[0.5]	
DMF	0.4	16	1.0×10^2	61
		16	1.1×10^2	71
		[2.5]	[2.1]	[1.2]
Formamide	0.2	19	91	
		20	89	
Methyl-formamide	0.25	25	2.4×10^2	
		25	2.6×10^2	
DMSO	0.3	49	9.6×10^2	3.1×10^3
		49	9.8×10^2	3.2×10^3
		[6.0]	[11]	[14]
DMA	0.4	60	8.8×10^2	2.1×10^3
		63	8.5×10^2	1.6×10^3
		[5.3]	[11]	[6.4]
HMPA	0.04	2.0×10^3	3.0×10^5	
		2.2×10^3	3.1×10^5	
		[29]	$[3.1\times10^2]$	$[1.2\times10^3]$

Values in brackets are those in the case of the sodium ion. Abbreviation: PC = propylene carbonate; DMF = dimethylformamide; DMSO = dimethyl sulfoxide; DMA = dimethylacetoamide; HMPA = hexamethylphosphoramide. (at 25 ±0.1 °C)

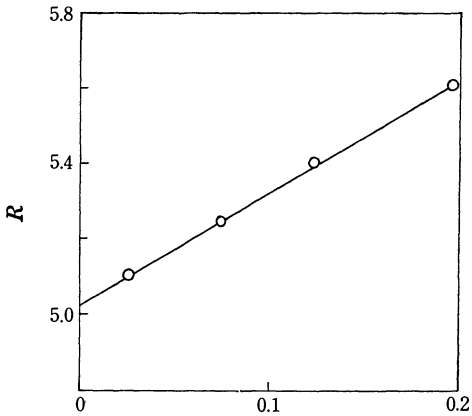

Fig. 2. R-[Pyridine] relation.

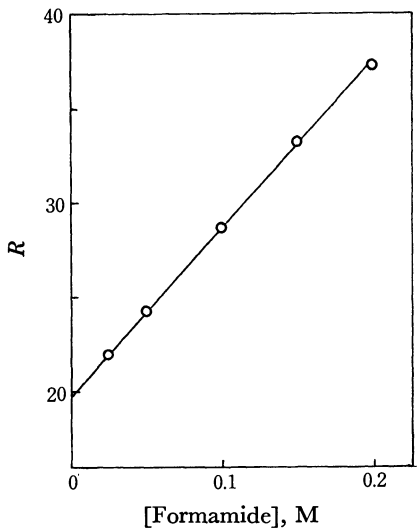

Fig. 3. R-[Formamide] relation.

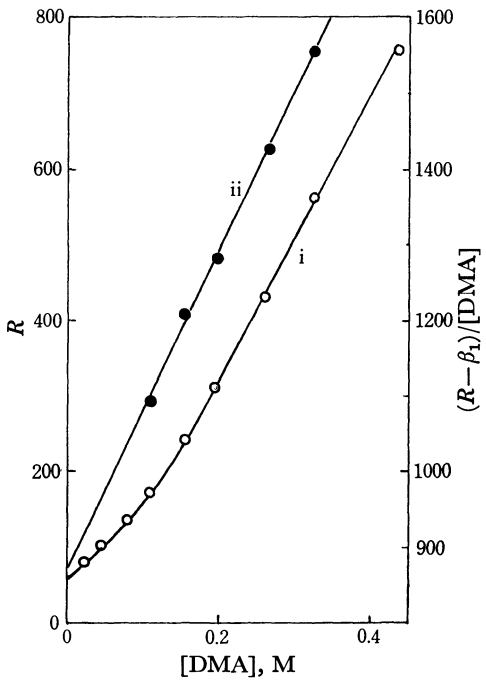

Fig. 4. R-[DMA] (Curve i) and $(R-\beta_1)$/[DMA]-[DMA] (Curve ii) relations.

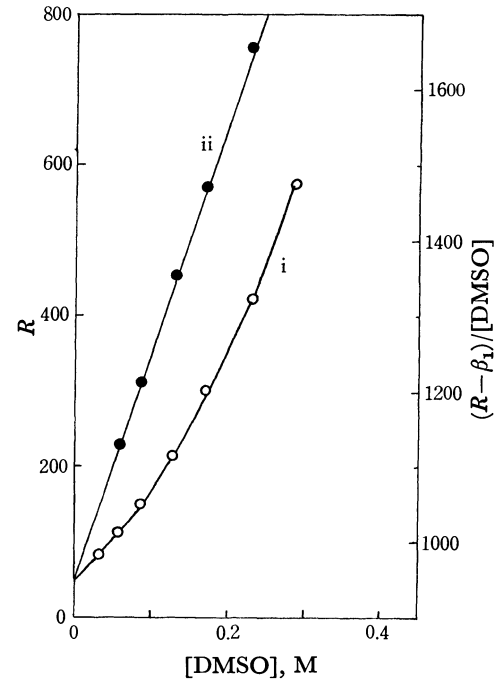

Fig. 5. R-[DMSO] (Curve i) and $(R-\beta_1)$/[DMSO]-[DMSO] (Curve ii) relations.

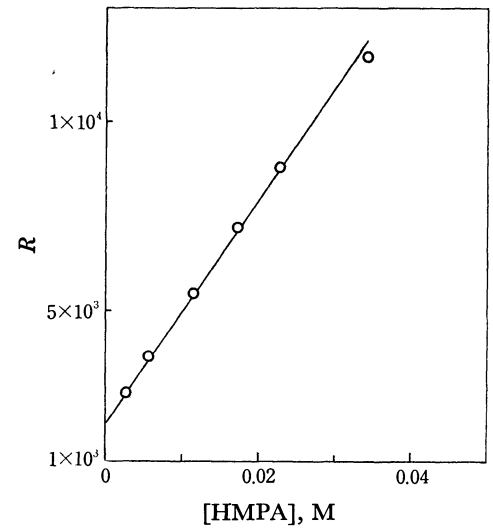

Fig. 6. R-[HMPA] relation.

tion. As example is shown in Fig. 7, Curve B, for DMSO.) Because of this behavior, hydration constants could not be obtained by the present experiment.

Discussion

From the results in Fig. 1, it seems reasonable to consider that the glass electrode can respond to the activity of the lithium ion in solvents of different species or compositions.

The formation constants in Table 1 show that the complexing of the lithium ion in AN with other solvents is generally more extensive than in the case of the sodium ion. For DMF, DMA, and DMSO, a complexing up to three solvent molecules was observed. For HMPA, however, no tri-solvated complex was formed in spite of the quite large values of β_1 and β_2. This may be

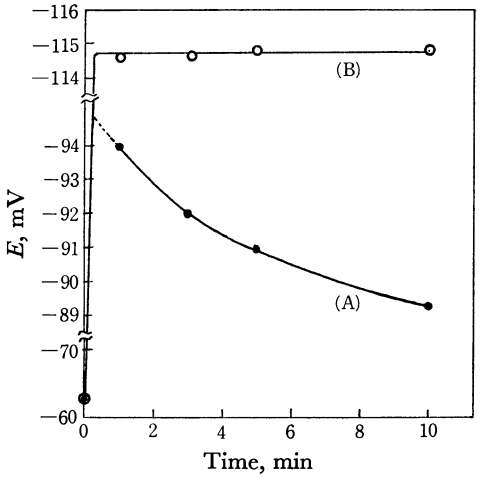

Fig. 7. Potential curves of the ion-sensitive glass electrode after the addition of complexing solvent to the AN solution of 10^{-3} M $LiClO_4$ and 10^{-2} M Et_4NClO_4. (A) H_2O, 200 μl/50 ml, (B) DMSO, 200 μl/50 ml.

because of the steric effect in the reactions between large HMPA molecules and the small lithium ion. The solvation of PC, which has a weak basic character but a large dielectric constant, occurred only weakly. From these results, it can be said that, except for the case of pyridine, the complexing of the lithium ion in AN with other solvents is more pronounced when the solvent basicity increases. The solvation of pyridine, which has a strong basic character but a small dielectric constant, occurred to only a small extent, as in the case of the sodium ion.

The values of β_1 in Table 1 seem to be reliable enough within ±10% for pyridine, DMF, DMSO, and HMPA. For protic solvents, such as methanol, formamide, and methylformamide, the reliability might be somewhat less because the junction potentials between the compartments (B) and (C) of Cell I may change during titration to a somewhat larger extent than in the case of the dipolar aprotic solvents, in which the change of the junction potential is quite small.[5]

In order to elucidate the peculiar potential change observed when water was the complexing solvent, some experiments were carried out:

(1) The lithium ion in AN has been found conductometrically to associate with the perchlorate ion, though to an extent somewhat smaller than that of the ion association between the sodium ion and the perchlorate ion.[6,7] The addition of water to the AN solution may cause the dissociation of the ion association (though the possibility of this is very small, considering the small change in the dielectric constant by the addition of water[8]) and the increase in the lithium-ion activity (the shift of the potential to a less negative direction). In order to investigate the influence of this reaction, measurements were carried out by changing the concentration of the indifferent electrolyte, Et_4NClO_4, from 0 M to 0.1 M. However, the phenomena shown in the Curve A, Fig. 7, were observed in all concentrations. The tetraphenylborate may be completely dissociated in AN, considering the case of the sodium ion.[7] Therefore, instead of the $LiClO_4$ and Et_4NClO_4 in the above experiments, $LiBPh_4$ and Bu_4NBPh_4 were used, and similar measurments were carried out. However the results did not change. From these experiments, the peculiar phenomena in Fig. 7 do not seem to be due to the effect of ion association.

(2) The hydrolysis of the lithium ion may cause behavior such as is shown in Fig. 7 if the hydrogen ion liberated by hydrolysis shifts the potential of the glass electrode to a less negative direction. Curve 1 in Fig. 8 is a acid-base titration curve obtained by titrating 10^{-3}M $LiClO_4$ in 1.2 v/v % aqueous AN–0.01M Et_4NClO_4 with Bu_4NOH (0.176M in benzene–methanol (3:2)). The pH glass electrode was a Hitachi-Horiba 1026 electrode. The titration curve of the lithium ion indicates the possibility of the lithium ion being hydrolyzed considerably in AN containing a small amount of water. The hydrolysis of the sodium ion also occurs, but to a much smaller extent; Curve 2 is the titration curve of 10^{-3} M $NaClO_4$ under the same conditions, while Curve 3 is that of the blank solution. Curve 4 in Fig. 8 is the titration curve of acetic acid with Bu_4NOH in the same solution as that of Curve 3. From Curves 1 and 4, the lithium ion can be considered as an acid, the strength of which is roughly of the same order of magnitude as that of acetic acid. When a similar titration of acetic acid was carried out by using a mono-valent cation sensitive glass electrode, Beckman 39047, Curve 5 was obtained. In this curve, the potential is almost constant before the equivalent point, but the potential change to a negative direction occurs near the equivalent; after the equivalent point, the potential changes slowly to a less negative direction.

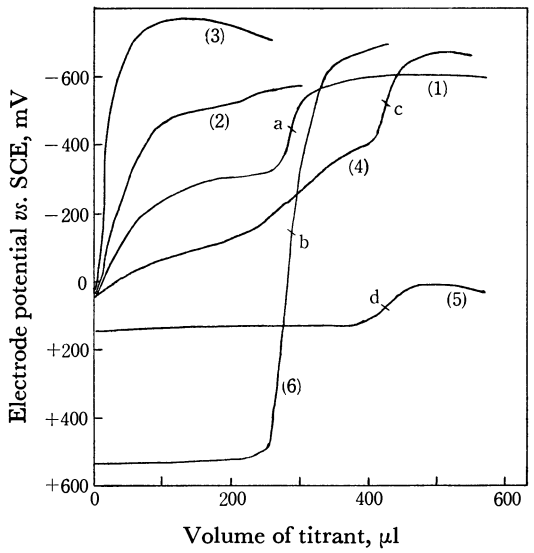

Fig. 8. Titration curves with benzene–methanol (3:2) solution of tetrabutylammoniumhydroxide (0.18 M). Curves (1) 10^{-3} M $LiClO_4$+10^{-2} M Et_4NClO_4+667 mM H_2O in 50 ml AN solution, (2) 10^{-3} M $NaClO_4$+10^{-2} M Et_4ClO_4+667 mM H_2O in 50 ml AN solution, (3) 10^{-2} M Et_4NClO_4+667 mM H_2O in 50 ml AN solution (blank), (4), (5) 10^{-2} M Et_4NClO_4+1.44 mM CH_3COOH+667 mM H_2O in 50 ml AN solution, and (6) 10^{-3} M $HClO_4$+667 mM H_2O in AN solution. The letters a,b, c, and d are the equivalent end point, respectively. For the glass electrodes used, see text.

From this, it seems reasonable to conclude that the cation-sensitive glass electrode can respond to the hydrogen ion liberated by the hydrolysis of the lithium ion in AN containing a small amount of water. Curve 6 was obtained by titrating 10^{-3} M $HClO_4$ in 1.2 v/v % aqueous AN with Bu_4NOH. From these experimental results, the peculiar behavior observed when water is the complexing solvent seems to be caused by the hydrolysis of the lithium ion and the response of the cation-sensitive glass electrode to the hydrogen ion liberated.

The author wishes to express his hearty thanks to Dr. Kosuke Izutsu of this department for his kind discussions and to Mr. Shigeo Nakajima for his experimental support.

This work was supported in part by a Grant-in-aid for Scientific Research from the Ministry of Education.

References

1) K. Izustu, T. Nomura, T. Nakamura, H. Kazama, and S. Nakajima, This Bulletin, **47**, 1657 (1974).
2) N. Matsuura, K. Umemoto, and Z. Takeuchi, *ibid.*, **47**, 813 (1974).
3) F. Accascina, S. Petrucci, and R. M. Fuoss, *J. Amer. Chem. Soc.*, **81**, 1301 (1959).
4) R. H. Cundiff and P. C. Markunas, *Anal. Chem.*, **28**, 792 (1956).
5) B. G. Cox, A. J. Parker, and W. E. Waghorne, *J. Amer. Chem. Soc.*, **95**, 1010 (1973); K. Izutsu, T. Nakamura, unpublished results.
6) F. Accascina, *Ric. Sci. Rend.*, **7**, 556 (1966).
7) R. L. Kay, B. J. Hales, and G. P. Cunningham, *J. Phys. Chem.*, **71**, 3925 (1967).
8) A. D'Aprano and R. M. Fuoss, *ibid.*, **73**, 400 (1969).

Viscosity Behavior of Coacervates of Magnesium and Calcium Highpolyphosphates[1]

Takao UMEGAKI and Takafumi KANAZAWA

Department of Industrial Chemistry, Faculty of Technology, Tokyo Metropolitan University, Fukazawa, Setagaya-ku, Tokyo 158

(Received December 6, 1974)

The viscosities of magnesium and calcium highpolyphosphate coacervates were measured in the temperature range of 20 to 90 °C. The Andrade's Equation was an approximate representation for the temperature dependence of viscosities of the coacervates. The activation energies of flow for the highpolyphosphate coacervates of magnesium and calcium were calculated to be about 7 kcal/mol and about 15 kcal/mol, respectively. The extension of the phosphate chains in coacervates was considered to be restricted, and the spinnability of the coacervates was probably originated, not by an elastic network structure, but by high viscosity of the coacervates. The viscosities of the magnesium coacervates decreased with an increase in water content and no remarkable effect of ethyl alcohol on the preparation of the coacervates was found.

Viscometric studies of dilute solutions of alkaline highpolyphosphates were carried out by Strauss, Smith, and Wineman[2] for the determination of the molecular dimensions. In the previous paper[3] viscosities of magnesium, calcium and aluminum highpolyphosphate coacervate solutions were measured in order to examine their conformational features during the dissolution into acid solvents. The viscoelasticity of the composite specimen of the magnesium highpolyphosphate coacervate and glass cloth was also determined by torsional braid analysis.[4] However, there has been no quantitative study on the viscosity behavior of the coacervates themselves.

The present paper deals with temperature dependence of viscosity at temperatures, from 20 to 90 °C, for magnesium highpolyphosphate coacervate (MPC). Moreover, the viscosities for MPC and CPC prepared according to the new methods without addition of ethyl alcohol were compared with those of the coacervates obtained by the procedures already reported,[4,5] and the viscosity change of MPC with water content was studied.

On the basis of the results on the viscometric experiments, the extension of phosphate anion chains and the complex formation in the coacervates were discussed, and viscosity behaviors of MPC and CPC were compared.

Experimental

Materials. According to the methods for synthesizing MPC and CPC[4,5] both coacervates were obtained by adding ethyl alcohol to the mixture of a 15% sodium metaphosphate solution and a 20% solution of magnesium or calcium chloride. MPC and CPC were also prepared by direct addition of $MgCl_2 \cdot 6H_2O$ (167 g) and $CaCl_2 \cdot 2H_2O$ (73.5 g), respectively, to a 20% sodium metaphosphate solution (500 g). Then all the coacervates separated became transparent in a week at room temperature.

Analysis. The coacervates were analyzed for calcium by ETA titration and for phosphorous by the vanadomolybdate colorimetry.[6] Sodium was determined by titrating a standardized HCl, which was partially neutralized by the liberated sodium ion in advance adsorbed on Amberlite IR-120 from a coacervate solution.[7] Paper chromatography of the polyphosphate ions in MPC and CPC was carried out according to the method by Kolloff.[8]

Viscosity Measurement. Shearing stresses of MPC and CPC at shear rates, from 10 to 600 s^{-1} and temperatures, from 20 to 90 °C, were measured with a rotational viscometer of cone-and-plate type (Shibayama Kagaku Co., Ltd.). The viscometer was calibrated at 20 °C by using JS 200 (1.78 P), JS 1000 (8.918 P), JS 2000 (18.14 P), 60H (497.3 P) and 200H (1683 P) as standard liquids for viscosity manufactured by Showa Oil Co., Ltd. All the above oils were assumed to be Newtonian fluid whose shearing stress is proportional to shear rate. A strain gauge was used for the measurement of torque of the cone evolved by the rotation of viscous fluid on the plate. The viscometer was so designed that the electromotive force of the strain gauge was proportional to shearing stress in the fluid. Consequently, the shearing stress was calculated from the electromotive force of the strain gauge.

Results and Discussion

From the linearity of flow curves for MPC and CPC (Figs. 1 and 2), most coacervates were recognized to be Newtonian, although the curve for MPC at 20 °C was concave upward very slightly. The non-Newtonian flow of MPC at 20 °C might be attributed to the heterogeneity of vicosity in the coacervate, which formed on coacervation and remained on viscosity measurement

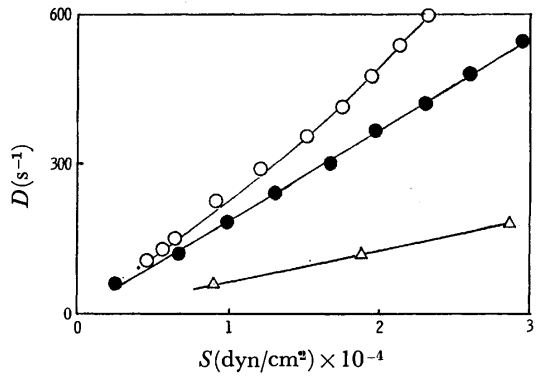

Fig. 1. Flow curves of MPC samples.
○: coacervated by $MgCl_2 \cdot 6H_2O$ powder, settled for 240 hr at 20 °C (P_2O_5 20%), ●: coacervated by $MgCl_2 \cdot 6H_2O$ powder, settled for 240 hr at 30 °C (P_2O_5 25%), △: coacervated by ethyl alcohol, settled for 912 hr at 30 °C (P_2O_5 45%)

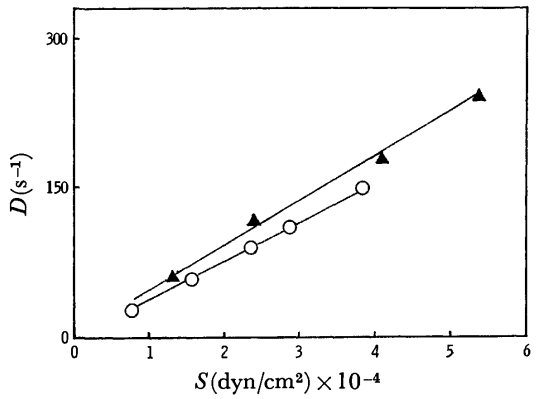

Fig. 2. Flow curves of CPC samples at 30 °C.
▲: coacervated by $MgCl_2 \cdot 6H_2O$ powder, ○: coacervated by ethyl alcohol

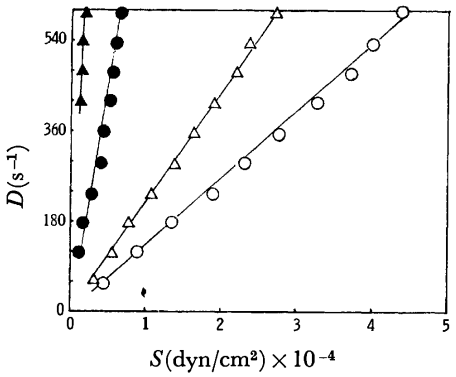

Fig. 3. Effect of the addition of distilled water to MPC on flow curve of MPC.
The ratios of MPC to water by weight are as follows: 85:15 (○), 80:20 (△), 75:25 (●), and 70:30 (▲).

at 20 °C. The viscous part remaining locally in the coacervate might act like the so-called scaffolding structure formed suspended particles in solutions.[9]

Figure 3 shows the viscosity change with water content. These samples in Fig. 3 were prepared by the mere addition of water to MPC (P_2O_5 31.8%), being settled in a week. The viscosity of MPC decreased remarkably with decrease in P_2O_5 content. For example, the addition of distilled water to MPC (P_2O_5 31.8%), in a ratio of 1:1 in weight changed the viscosity of the coacervate from 10^2 to about 2 P. Then, no degradation of highpolyphosphates upon the water addition was recognized by the paper chromatography. This viscosity change was attributed to the easily weakened interaction of various electrolytes with each other in the coacervates.

Figures 4 and 5 show the temperature dependence of viscosity for MPC and CPC, respectively. Although some flow curves of coacervates showed non-Newtonian behavior, the apparent viscosity (η) was calculated by assuming a linear relationship between shearing stress and shear rate concerning the coacervates used here. According to the Andrade's Equation ($\eta = Ae^{B/T}$, where A and B are quantities independent of temperature), a plot of the logarithmic viscosity against the reciprocal of absolute temperature should be a straight line. The apparent activation energy of flow (E) was obtained

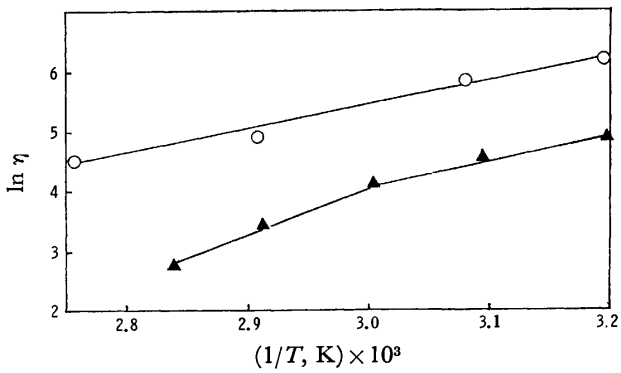

Fig. 4. Temperature dependence of viscosity of MPC.
○: coacervated by ethyl alcohol, ▲: coacervated by $MgCl \cdot 6H_2O$

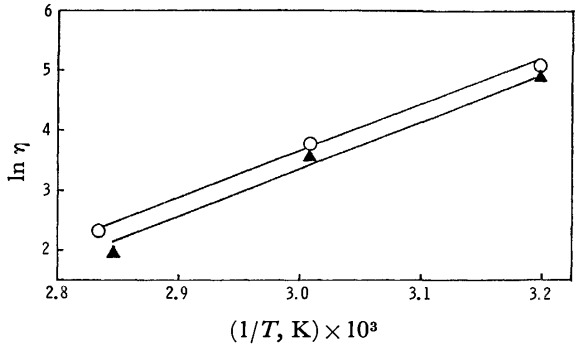

Fig. 5. Temperature dependence of viscosity of CPC.
▲: coacervated by ethyl alcohol, ○: coacervated by $MgCl_2 \cdot 6H_2O$

from the slope of the line (B) and gas constant (R) as follows: $E = B \times R = 1.986B$ (cal/mol).

The values of E for MPC and CPC calculated from the slopes in Figs. 4 and 5 are given in Table 1. The values of E for MPC were found to be 6—8 kcal/mol. This value is probably interpreted in terms of the presence of the cross-linking due to the weak bonding like a hydrogen bond in MPC, both values for MPC and water having the same order of magnitude.[10] However, the values of E for two MPC were somewhat larger than those for water. From the comparison of E for MPC with that for water, it is concluded that hydrogen bond in coacervates has a considerable effect on the viscosity of the coacervates and that the difference of the potential barriers on flow process between MPC and water is brought about by the difference in both dimension and mutual interaction of solute molecules.

Table 1. Activation energies of flow (E) of coacervates

Sample	P_2O_5 content (%)	Temperature range (°C)	E (kcal/mol)
MPC	60.1[a]	40— 90	6.4
	36.0	40— 60	8.1
CPC	63.9[a]	40— 79	16.4
	51.8	40— 80	13.9
H_2O	—	0— 20	4.61[b]
	—	50—100	3.10[b]

a) Coacervated by the addition of ethyl alcohol. b) Cited from Ref. 9.

Although MPC prepared by the addition of ethyl alcohol might contain the alcohol, the slope of $\ln\eta_i$ plot against 1/T was recognized to be almost the same as that of MPC obtained by the direct addition of $MgCl_2 \cdot 6H_2O$. Then, probably, no essential change in the configuration of highpolyphosphate ion in MPC was induced by the addition of alcohol, but in the course of the synthesis of MPC ethyl alcohol was effective only for the depression in the ionic dissociation in the mixture of sodium highpolyphosphate and magnesium chloride solutions, the dielectric constant of the mixture being reduced by the addition of alcohol.

The linearity of flow curves for most MPC indicates no remarkable conformational change of highpolyphosphate chains with an increase in shear rate. Since the values of E for MPC and water are comparable, the extension of the highpolyphosphate chains is considered to be small and the chains might be coiled spherically and somewhat tightly.

The values of E for CPC are larger than those for MPC, although the apparent viscosities for CPC are smaller or the same compared with those for MPC. Therefore, the interaction among highpolyphosphate chains in CPC is considered to be stronger than that in MPC, and the phosphate coils are extended more widely in CPC than in MPC.

The complex formation between highpolyphosphate and metal ion is well-known and sodium highpolyphosphate has been industrially utilized as a masking agent for Ca^{2+}, Mg^{2+} and other metal ions.[11] Moreover, the stability constants of some complexes were calculated from the pH lowering during the titration of highpolyphosphate ion with hydrogen ion.[11,12] It was reported that the treatment of some calcium highpolyphosphate coacervates with ammonium fluoride solution yielded no calcium fluoride, indicating that the calcium ions were strongly masked by the highpolyphosphate.[13] Then, there is no doubt about the presence of a certain stable complex between calcium and polyphosphate, even in CPC. The activation energies of flow for CPC (14—16 kcal/mol) may indicate the slight extension of the highpolyphosphate chains, and some part of the calcium-polyphosphate complex may be expected to form a network structure with the cross-linkage of the chains by calcium ions.

Erbring[14] and Nakagawa[15] found that some liquids having an elastic network structure are spinnable and some highly viscous substances (40—50 poise or more) with no anomalous structure also possess a thread-forming property. The origin of the spinnability for MPC and CPC reported in the previous paper[3] might be explained on the basis of the results on the viscosity measurement described above. The viscosity measurement of dilute solutions of the coacervates suggested the presence of the tightly coiled highpolyphosphate chains in the acid solvents.[3] On the other hand, in the coacervates themselves the extension of the highpolyphosphate chains is also supposed to be restricted from a consideration of the low activation energies of flow for coacervates compared with those for ordinary linear high molecular organic polymers. The linearity of flow curves for the coacervates used here indicates no anomalous structure, while the electron micrographs by Danno[16] and the observation with an optical microscope by Yamaguchi and Kashiwase[17] showed the network structure in such thread-forming liquids as mercury sulfosalicylate solution and potassium highpolyphosphate solution, respectively. It is concluded that the spinnability of the coacervates in this work was originated, not by an elastic network structure, but by high viscosity of the coacervates as well as that of sodium silicate solution or sugar solution with high concentration.

Conclusion

From the results of the viscometric studies on MPC and CPC, the following facts were obtained.

(1) The coacervates used here were mostly Newtonian.

(2) The Andrade's Equation was an approximate representation for the temperature dependence of the viscosities of MPC and CPC, from which the activation energies for flow process of MPC and CPC were calculated to be about 7 kcal/mol and about 15 kcal/mol, respectively.

(3) The addition of water to MPC caused the viscocity lowering, but no degradation of polyphosphate chains occurred.

(4) No essential change in the configuration of highpolyphosphate ion in MPC was induced by the addition of ethyl alcohol.

(5) The extension of the phosphate chains was restricted and the spinnability of MPC and CPC were originated, not by an elastic network structure, but by high viscosity of the coacervates.

References

1) This paper was read at the Autumn Meeting of the Union of Chubu Branches of the Chemical Societies and Associations, Nagoya, October, 1973.

2) U. P. Strauss, E. W. Smith, and P. Wineman, *J. Amer. Chem. Soc.*, **75**, 3935 (1953).

3) T. Kanazawa, T. Umegaki, Y. Kitajima, and T. Ogawa, This Bulletin, **47**, 1419 (1974).

4) T. Umegaki and T. Kanazawa, *ibid.*, **46**, 3587 (1973).

5) T. Kanazawa, T. Umegaki, and H. Kawazoe, *Asahi Garasu Kogyo Gijutsu Shorei-Kai Kenkyu Hokoku*, **21**, 81 (1972).

6) "Official Methods of Analysis of Fertilizers," ed. by the National Institute of Agricultural Sciences, Tokyo, (1972), p. 24.

7) H. Kakihana, *Nippon Kagaku Zasshi*, **72**, 203 (1951).

8) R. H. Kolloff, *Anal. Chem.*, **33**, 373 (1961).

9) T. Nakagawa, "Rheology," Iwanami Publishing Co., Tokyo, (1968), p. 142.

10) T. Nakagawa, *ibid.*, (1968), p. 112.

11) E. Kobayashi, "Chemistry of Phosphates and their Utilization," ed. by S. Hori, Kagakukogyo-sya Co., Ltd., Tokyo, (1971), p. 185.

12) T. Sugano and K. Kubo, *Nippon Kagaku Kaishi*, **1974**, 1068.

13) E. H. Brown and J. R. Lehr, *J. Agr. Food. Chem*, **12**, 201 (1964).

14) H. Erbring, *Kolloid. Z.*, **98**, 164 (1942).

15) T. Nakagawa, This Bulletin, **25**, 88, 93 (1952).

16) T. Danno, *ibid.*, **32**, 1033 (1959).

17) T. Yamaguchi and H. Kashiwase, *Kogyo Kagaku Zasshi*, **66**, 576 (1963).

The Coprecipitation of Strontium with Hydroxyapatite.

Osamu FUJINO

Institute for Chemical Research, Kyoto University, Uji, Kyoto 611

(Received December 16, 1974)

The distribution behavior of the strontium ion between hydroxyapatite and the parent solution was investigated. The hydroxyapatite was formed by the extremely slow addition of diammonium hydrogenphosphate to solutions of calcium and strontium nitrate buffered with ethylenediamine at 80 °C. The precipitate yielded a typical X-ray diffraction pattern of hydroxyapatite and had a composition in which the Ca/P molar ratio was 1.67 at pH 6.80. The strontium ion was coprecipitated in the apatite, obeying the Doerner and Hoskins logarithnmic distribution law. The distribution coefficient was scarcely affected by the strontium concentration on the pH value in the parent solution, and had a value of 0.26 ± 0.02 at 80 °C. On the other hand, the apparent distribution coefficient was a little affected by such organic anions as acetate, citrate, lactate, glycinate, and glutamate ions. The lattice constants of the precipitates prepared in the research were measured in order to confirm the formation of the solid solutions.

There is a considerably extensive literature[1] dealing with the abundance of trace elements in such geochemical samples as phosphate minerals and sediments, and in such biological samples as human bones and teeth. However, there are still very scant experimental data on the coprecipitation of trace elements with the hydroxyapatite, which is the pricipal inorganic constituent of these samples.

In previous papers we have ourselves reported data on the coprecipitation of copper[2] and zinc[3] with hydroxyapatite. The coprecipitation of strontium with the apatite is also of great interest because strontium-90 has such a long biological half life as 18000 days in bone and is well known as one of the most dangerous radioisotopes for the human body.

Experimental

Apparatus. The radioactivity countings were made with a Packard Tri-carb Liquid Scintillation Spectrometer, Model 3320. A Hitachi-Horiba pH Meter, Model F-5, was used for the pH measurements. The X-ray patterns of the hydroxyapatite samples were measured by using a Shimadzu X-ray Diffractometer, Model AZ-2A, with nickel-filtered copper radiation.

Reagents. The strontium-89 was supplied as chloride in hydrochloric acid by the Oak Ridge National Laboratory, Oak Ridge, Tennessee, U.S.A., and was diluted with 0.1 M nitric acid to make a solution of $\simeq 1$ μCi/ml. The strontium and calcium solutions were prepared from their respective reagent-grade nitrates and were standardized by EDTA titration. A standard EDTA solution containing EDTA-magnesium complex was standardized with a calcium solution which had been prepared from dry calcium oxide. A liquid scintillator for the measurement of the strontium activity was prepared by dissolving 100 mg of 1,4-bis(5-phenyloxazolyl)-benzene (POPOP), 4 g of 2,5-diphenyloxazole (DPO), and 75 g of naphthalene with dioxane and by then diluting them to 1 l with the solvent.

The other chemicals were reagent-grade materials.

Preparation of Hydroxyapatite. The following procedure was used to prepare the hydroxyapatite precipitates. Twenty milliliters of a 0.5 M calcium nitrate solution and 25 ml of 5 M ethylenediamine were placed in a one-liter Erlenmeyer flask, and the mixture was diluted to around 400 ml with water. The solution, after pH adjustment, was diluted to 500 ml. The flask equipped with a reflux condenser was placed in a thermostat, and nitrogen gas was passed through to prevent the formation of calcium carbonate. The diammonium hydrogenphosphate solution (0.1 M) was then pumped, drop by drop into the calcium solution, which was being stirred by a magnetic stirrer. The supernatent solution was pulled off by an aspirator working through a sintered glass filter, and the precipitate was washed with water repeatedly. The precipitate was then filtered and dried at 110 °C.

Chemical Analysis of Hydroxyapatite. The calcium and phosphate ions in the hydroxyapatite precipitate were determined by the EDTA titration method as follows. *Determination of calcium*: EDTA and buffer (pH 10) solutions were added to a sample solution which had been prepared by dissolving the dry sample in hydrochloric acid, and the calcium ions were determined by titrating an excess of EDTA with a magnesium standard solution, using Eriochrome Black T as the indicator. *Determination of phosphate ions*: The phosphate ions in the sample solution above were precipitated as magnesium ammonium phosphate. The precipitate was filtered and dissolved with hydrochloric acid. The phosphate ions could then be determined by titrating the magnesium with the EDTA solution.

Coprecipitation Procedure. The procedure of the coprecipitation was essentially the same as those of the hydroxyapatite preparation. The carrier and the radiotracer of strontium were added to the calcium solution in the thermostat described above. At appropriate intervals of time, an aliquot of the supernatent solution was pipetted out through a sintered glass filter. The calcium ions in the solution phase were determined by EDTA titration. The strontium ions were counted with a liquid scintillation spectrometer after the supernatent had been ashed with a mixture of perchloric, nitric and hydrochloric acids and after 4 ml of 0.1 M hydrochloric acid and 13 ml of liquid scintillator had been added to it.

The homogeneous[4,5] and logarithmic[6] distribution coefficients, K_D and K_λ, were calculated by means of the following equations:

$$\left(\frac{\text{micro-component}}{\text{macro-component}}\right)_{\text{cryst.}} = K_D \left(\frac{\text{micro-component}}{\text{macro-component}}\right)_{\text{soln.}} \quad (1)$$

$$\log\left(\frac{\text{initial quantity}}{\text{quantity left in soln.}}\right)_{\text{micro-component}} = K_\lambda \log\left(\frac{\text{initial quantity}}{\text{quantity left in soln.}}\right)_{\text{macro-component}} \quad (2)$$

Lattice Constant. Hydroxyapatite is hexagonal, with

two lattice constants, A_0 and C_0. These were determined by measuring the diffraction angles, 2θ, of the three planes—(312), (213), and (321).

Results and Discussion

Composition of Apatite Precipitate. On the apatite precipitates formed from an aqueous solution, it is well known that solid phases may be precipitated which yield X-ray diffraction patterns typical of hydroxyapatite, $Ca_{10}(PO_4)_6(OH)_2$, while deviating considerably from it in composition.[7,8] Figure 1 shows the influence of the precipitation rate on the Ca/P ratio of the apatites, which were prepared by precipitating 50 per cent of calcium with a phosphate solution at pH 6.80 and 8.60. The Ca/P ratio became constant in the range of addition rates slower than 10 ml/hr. The apatite prepared at pH 6.80 gave X-ray diffraction patterns typical of hydroxyapatite, although that produced by the rapid addition of phosphate had diffraction patterns with poorly crystallized materials.

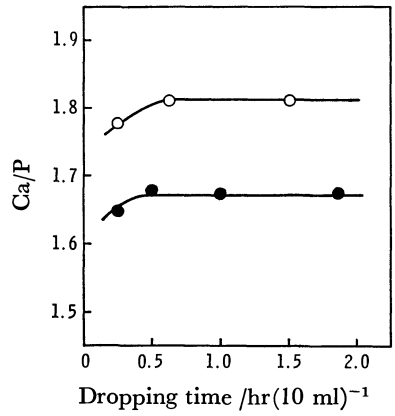

Fig. 1. The Ca/P ratio in the precipitates formed at various precipitation rates.
$Ca(NO_3)_2$, 0.02 M; ethylenediamine, 0.25 M; $(NH_4)_2HPO_4$, 0.1 M; ●, pH 6.80; ○, pH 8.60; initial volume, 500 ml; temperature, 80 °C.

In order to examine the effect of the percentage of calcium precipitation on the Ca/P ratio, the composition of the precipitates was determined; they had been prepared by changing the addition volume of phosphate. As is shown in Fig. 2, the Ca/P ratio was constant throughout the precipitation process of calcium. These precipitates showed X-ray patterns typical of hydroxyapatite.

The pH value affected the Ca/P ratio in the synthesized apatite (50% precipitation), as may be seen in Fig. 3; the Ca/P ratio decreased as the pH decreased. The Ca/P ratio in mineral bone when organic matter has been removed is between 1.57 and 1.61,[9] which implies that the apatite is a little calcium-deficient. As the value of pH 6.80 at 80 °C corresponds to about 8.0 at room temperature, the results in Fig. 3 may not be inconsistent with the fact that the accretion and resorption in bone occur around the neutral pH range.

At pH 6.80, the Ca/P ratio was 1.67; this corresponded to the composition of hydroxyapatite, $Ca_{10}(PO_4)_6(OH)_2$. This pH value was, therefore adopted throughout the experiments.

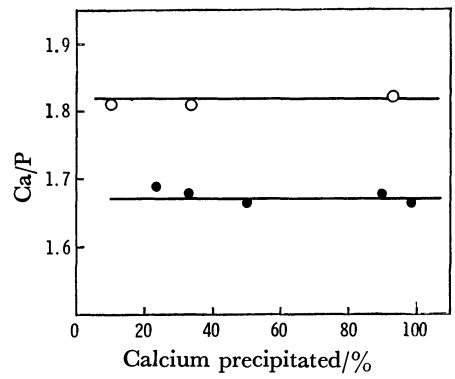

Fig. 2. The Ca/P ratio in the precipitation process.
●, pH 6.80; ○, pH 8.60; dropping velocity, 10 ml/hr. Other are the same as in Fig. 1.

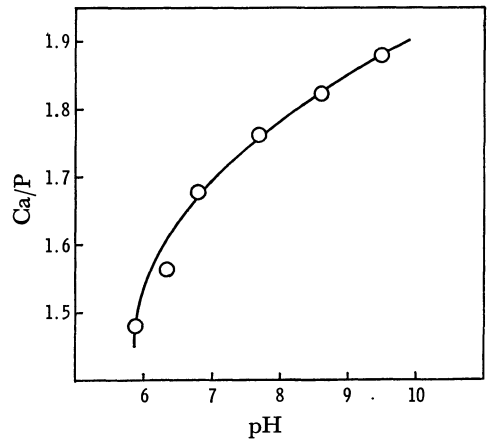

Fig. 3. The pH effect on Ca/P ratio.
Dropping velocity of phosphate, 10 ml/hr. Others are the same as in Fig. 1.

Coprecipitation of Strontium. In order to examine the influence of the precipitation rate on the coprecipitation behavior of strontium, the precipitation reaction was performed at the pumping velocities of 7, 12.2, and 65.8 ml of phosphate solutions per hour; the

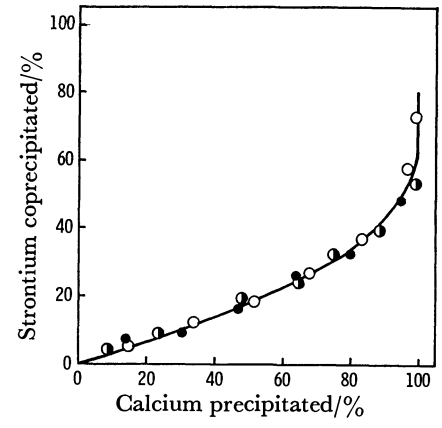

Fig. 4. The coprecipitation of strontium with hydroxyapatite formed at various precipitation rates.
Ca^{2+}, 0.02 M; Sr^{2+}, 10^{-6} M; ethylenediamine, 0.25 M; HPO_4^{2-}, 0.1 M; dropping velocity, ●, 7.0 ml/hr; ○, 12.2 ml/hr; ◑, 65.8 ml/hr; pH 6.80; initial volume, 500 ml; temperature, 80 °C.

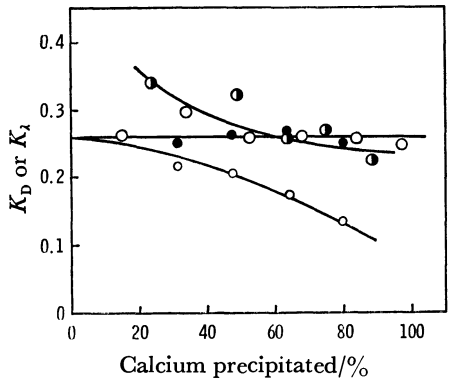

Fig. 5. The distribution manner of strontium.
◑, K_λ at 65.8 ml/hr of the dropping velocity;
○, K_λ at 12.2 ml/hr; ●, K_λ at 7.0 ml/hr;
○, K_D at 7.0 ml/hr, respectively.
Others are the same as indicated in Fig. 4.

concentrations of calcium, strontium and ethylenediamine were 2×10^{-2} M, 1×10^{-6} M, and 0.25 M respectively; the thermostat was regulated at 80 °C. The results are shown in Fig. 4, in which the percentages of the coprecipitated strontium are plotted against the fractions of precipitated calcium. The strontium ion was enriched in the solution phase, as is shown in Fig. 4. The homogeneous and logarithmic distribution coefficients are plotted in Fig. 5 against the percentage of calcium precipitated. In the case of the slower addition of phosphate ions, the strontium ions were coprecipitated obeying the logarithmic law (the coefficient, $K_\lambda=0.26\pm0.02$), while in the more rapid addition the distribution coefficient decreased as the amount of precipitated calcium increased. The X-ray diffraction pattern of the latter solid phase denoted that the material was a poorly crystallized one. The coprecipitation behavior of strontium at pH 6.80, 7.70, and 8.60 is shown in Figs. 6 and 7. The Ca/P ratio of the apatite was affected by the pH, as has been mentioned above, while the logarithmic distribution coefficient did not change with the pH ($K_\lambda=0.26$).

The hydroxyapatite was precipitated at pH 6.80 from solutions containing strontium ranging from 10^{-8} M to 2.5×10^{-2} M, with the other circumstances kept identical. The results are shown in Fig. 8; no significant change in the coprecipitation behavior of strontium was observed between 10^{-8} M and 5×10^{-4} M. However, the distribution coefficient in the calcium-strontium apatite system tended to decrease at higher concentrations of strontium. It was observed from the X-ray diffraction pattern that this precipitate crystallized somewhat poorly; this tendency became clearer as the strontium content increased. Calcium-strontium apatite may crystallize more slowly than the pure calcium apatite.

The effect of the concentration of ethylenediamine used as a buffering agent was examined at pH 6.80 with regard to solutions of 0.10, 0.25, 0.50, and 1.0 M ethylenediamine; the effect was found not to be

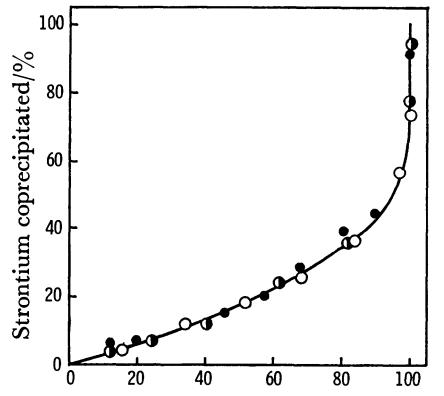

Fig. 6. The coprecipitation of strontium at different pH values.
○, pH 6.80; ◑, pH 7.70; ●, pH 8.60.

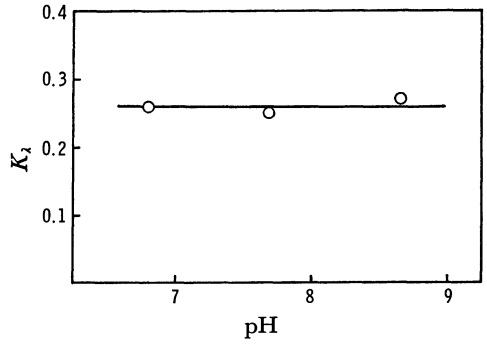

Fig. 7. The effect of pH on the logarithmic distribution coefficient.

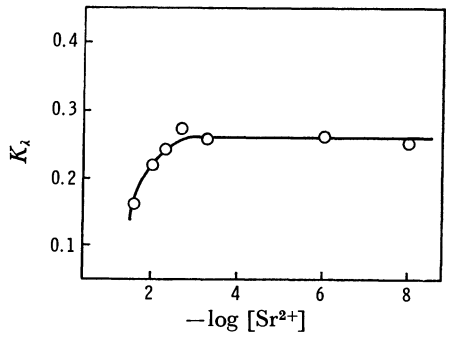

Fig. 8. The effect of strontium concentration.

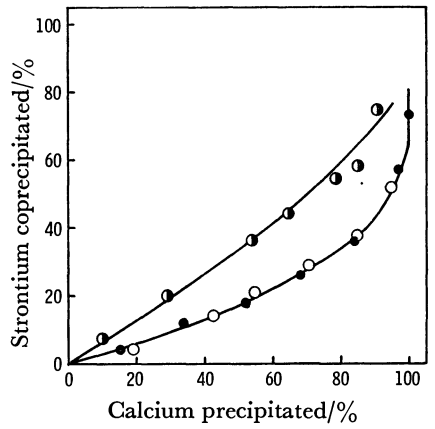

Fig. 9. The temperature effect on the coprecipitation of strontium.
●, 80 °C $K_\lambda=0.27$; ○, 55 °C $K_\lambda=0.26$;
◑, 25 °C $K_\lambda=0.56$; dropping velocity, 10 ml/hr.

noticeable in the range investigated. This may be caused by the fact that calcium and strontium ions do not form complexes with ethylenediamine so stable as to influence the distribution coefficient.

Calcium-strontium apatite was precipitated at 20, 55, and 80 °C. As is shown in Fig. 9, the coprecipitation behavior of strontium was identical at both 55 and 80 °C, while at 20 °C the behavior was different. The precipitate prepared at 20 °C had broad peaks in its X-ray diffraction pattern. The Ca/P mole ratio of the precipitate was 1.36 at the beginning of precipitation and decreased to 1.07 at 90 per cent precipitation. The abnormal distribution of strontium was probably caused by an incompleteness of apatite crystallization such as was observed above.

Collin prepared homogeneous solid solutions of strontium and calcium hydroxyapatite by heating precipitates formed from an aqueous solution to 950 °C,[10] and the lattice constants of these solid solutions were measured accurately. In the present apatites, the lattice constants were also measured in order to confirm the formation of the solid solutions (Table 1); the values were found to be close enough to those in Collin's paper, though there was a little error caused by the imcompleteness of crystallization.

Table 1. Lattice constants of calcium and strontium apatites

Sr/(Sr+Ca), %	A_0	C_0
0	9.417 Å	6.870 Å
14.5	9.479	6.924
20.0	9.494	6.966
42.3	9.559	7.039

It is also interesting to investigate the influence of chelating agents on the present coprecipitation system, because considerably strong chelate-forming substances should exist in the calcium-metabolism system. Acetate, citrate, lactate, glycinate, and L-glutamate ions were used as the organic anions. The results are summarized in Table 2. As is shown in the table, the apparent distribution coefficient, K_d, increases as the concentration of these organic anions increases.

Solid solutions were formed between calcium and strontium apatite by slow precipitation from a neutral or weakly basic solution at 80 °C, and the distribution coefficient of the strontium ions was about 0.26. A direct extension of these results to the processes occurring in biological systems may be difficult. However, it is possible that the very long biological half-life of strontium is caused by the formation of solid solutions.

Table 2. The effect of organic acids on the distribution coefficient

Organic acid	Concn of acid, M	K_d
Acetic acid	0	0.24_5
	0.1	0.26
	0.3	0.27_3
	0.4	0.29_3
	0.5	0.33_7
	0.7	0.35_7
Citric acid	2×10^{-4}	0.28_4
	1×10^{-3}	0.41_8
Lactic acid	3×10^{-3}	0.27_9
	5×10^{-2}	0.31_7
	0.1	0.35_2
Glycine	0.1	0.24_2
	0.4	0.31_5
Glutamic acid	0.04	0.27_8
	0.1	0.31_6

pH 6.80, Ca 0.02 M, ethylenediamine 0.25 M, Sr 10^{-6} M, temperature 80 °C

The author would like to express his thanks to Professor Eiji Suito for his helpful discussions and to Mr. Tsunoru Yoshida for his X-ray mesurements. The author would also like to thank Professor Tsunenobu Shigematsu, Professor Masayuki Tabushi, and Dr. Masakazu Matsui for their helpful discussions and comments during the preparation of this paper.

References

1) F. W. Spiers, "Radioisotopes in the Human Body," Academic Press, New York (1968).
2) T. Shigematsu, O. Fujino, and M. Matsui, *Bull. Inst. Chem. Res., Kyoto Univ.*, **50**, 645 (1972).
3) O. Fujino, M. Matsui, M. Tabushi, and T. Shigematsu, *Radioisotopes*, **24**, 7 (1975).
4) W. Chlopin, *Z. Anorg. Allg. Chem.*, **143**, 97 (1925).
5) L. M. Henderson and F. C. Kracek, *J. Amer. Chem. Soc.*, **49**, 738 (1927).
6) H. A. Doerner and W. M. Hoskins, *ibid.*, **47**, 662 (1925).
7) A. S. Posner, J. M. Stutman, and E. R. Lippincott, *Nature*, **188**, 486 (1960).
8) E. E. Berry, *J. Inorg. Nucl. Chem.*, **29**, 317 (1967).
9) F. C. McLean and M. R. Urist, "Bone," the University of Chicago Press, Chicago (1961), p. 53.
10) R. L. Collin, *J. Amer. Chem. Soc.*, **81**, 5275 (1959).

Studies on Electrode Processes of Oxovanadium(IV). I. Polarographic Behaviors and Photochemical Reaction in Potassium Oxalate Solution

Mitsutaka KITAMURA and Hideo IMAI

Faculty of Integrated Arts and Sciences, Hiroshima University, Hiroshima 730

(Received December 19, 1974)

Oxovanadium(IV) was found to develop a fairly stable oxidation wave as well as a reduction wave at the dropping mercury electrode in an aqueous solution containing M potassium oxalate. The predominant entity in the solution was $[VO(ox)_2]^{2-}$, and both the oxidation wave with one-electron transfer, and the reduction wave with two-electron transfer were irreversible. The anodic transfer coefficient evaluated from the logarithmic plot and Tafel plot was 0.60—0.63, and the exchange current density estimated tentatively from the Tafel plot was 1.8×10^{-6} A/cm^2. The effect of aerial oxidation of V(IV) to V(V) and the photochemical reduction of V(V) to V(IV) were investigated through the controlled potential electrolysis, absorption spectroscopy and ESR studies. The polarographic kinetic current of the oxidation process was observed under ultra-violet light irradiation. The apparent rate constant of the photochemical reduction evaluated from the kinetic current was $(0.02—0.04)/\varepsilon\phi I_0$ s^{-1}, where ε is the molecular extinction coefficient, ϕ the quantum yield and I_0 the intensity of the incident light.

Since vanadium shows various oxidation states from −1 to 5, numerous electrochemical investigations on its oxidation and reduction processes have been reported. However, only a limited number of papers refers to the oxidation process of oxovanadium (IV).

Lingane[1] has investigated the polarographic behaviors of vanadyl ion in various media, and has found the oxidation wave in a strongly alkaline medium. He has observed both the oxidation and reduction waves in an ammoniacal solution. However, the solution is very unstable and form a precipitate even in the presence of sodium sulfite added in order to avoid the oxidation. Bishop and Hitchcock[2] reported the oxidation of V(IV) in an acetate buffer of pH=4 at a platinum electrode, and suggested the possible chemical step coupled with the electrochemical oxidation. On the other hand, Dean and Herringshaw[3] have studied the oxidation of vanadyl ion by aerial oxygen. In relation to the photochemical reaction Setapathy *et al.*[4] have studied the photolysis of the aqueous suspension of V_2O_5 in oxalic acid. In general, the electrode processes of oxovanadium (IV) involve complications due to the aerial oxidation and coupled chemical and photochemical reactions.[5,6]

Our findings are that a stable polarographic oxidation wave as well as the reduction wave of oxovanadium (IV) can be observed in the solution containing M potassium oxalate, and that the oxidized entity is easily reduced by the irradiation of ultra-violet light. The kinetics of the polarographic oxidation process of oxovanadium (IV) and that of the photochemical reduction of V(V) are presented in this paper.

Experimental

The test solution was prepared by mixing the deaerated stock solution of vanadyl sulfate and M potassium oxalate solution unless otherwise noted. All reagents were of an analytical grade.

The electrochemical experiments were carried out by using a Shimadzu Model RP-50 polarograph and a Model PS-2 potentiostat. A quartz cell with a dropping mercury electrode (DME) and a saturated calomel electrode (SCE) were used for the measurement. The characteristics of the DME were as follows; the rate of flow of mercury=0.72 mg/s, the life-time=9.1 s under the head of mercury=40 cm at the applied potential of +0.15 V *vs.* SCE.

A xenon lamp (500 W) and Toshiba UV-D25 filter to pass 250—350 nm light were used for the photochemical study.

The spectrophotometric measurements were carried out by using a Shimadzu Model UV-200 dual beam spectrometer. For the ESR studies a Nihon Denki Model JES-ME ESR spectrometer was used under the following conditions; X-band microwave, modulation frequency of 100 kHz, modulation width of 6.3 gauss, the sample tubing of 1 mm diameter with 6 μl test solution.

The temperature was 28±1 °C.

Results and Discussion

Polarographic Behaviors of Oxovanadium(IV) in M Potassium Oxalate. The predominant entity of oxovanadium(IV) in M potassium oxalate solution (pH=8.4) is considered to be $[VO(ox)_2]^{2-}$.[6] It develops the polarographic oxidation wave as well as the reduction wave as shown in Fig. 1.

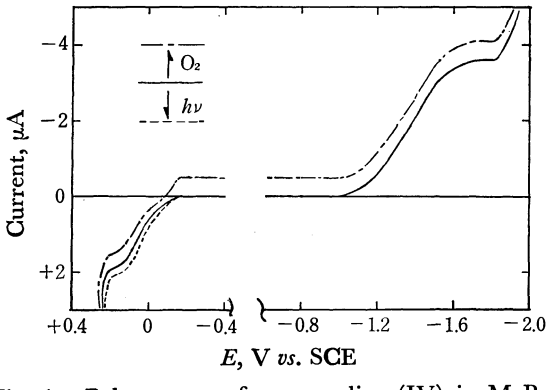

Fig. 1. Polarograms of oxovanadium(IV) in M Potassium oxalate.
—— polarogram of deaerated solution, ----- polarogram of oxidized solution, ------ polarogram of irradiated solution

The oxidation wave appeared at +0.025 V *vs.* SCE. The wave form was rather extended along with the potential axis than the well-defined reversible wave. The wave-height was approximately one half of the

reduction wave. The electrode process can be expressed as follows:

$$V(IV) - e = V(V) \quad (1)$$

Bishop and Hitchcock[2] have suggested the kinetic complication due to the coupled chemical reaction. However, no evidence could be observed so far as the effect of the mercury head on the wave-height was concerned as shown in Fig. 7.

The reduction wave of the two-electron transfer process appeared at −1.35 V *vs.* SCE. The wave form was also extended along with the potential axis, and the process was irreversible. It is noteworthy that the reduction wave showed the trend to split into two steps when the concentration of vanadyl ion was higher than 4 mM.

The dependence of the wave-height on the concentration of the vanadyl ion is illustrated in Fig. 2. Both the oxidation and reduction wave-heights showed good linear relationship with the vanadyl ion concentration. However, the linearity was no longer observed when the concentration exceeded 2 mM. The value of the diffusion coefficient estimated from the Ilkovic equation was 6.6×10^{-6} cm²/s.

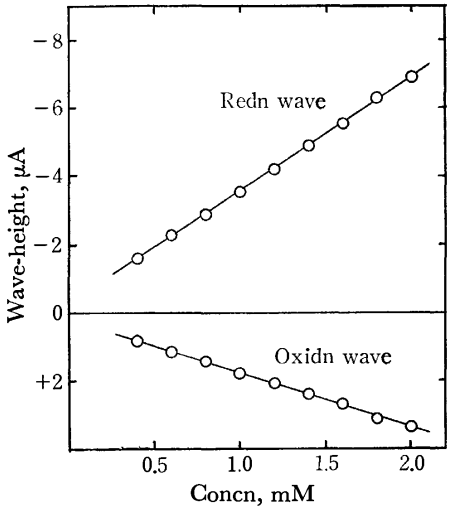

Fig. 2. Dependence of polarographic wave-height on concentration of oxovanadium(IV).

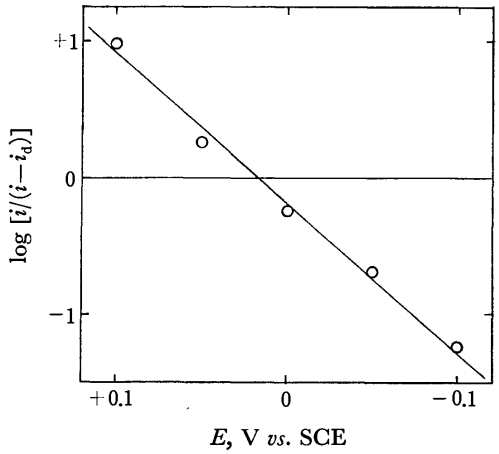

Fig. 3. Logarithmic plot of oxidation process of oxovanadium(IV).

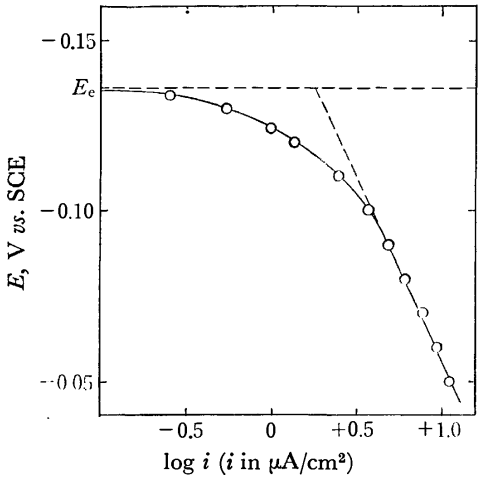

Fig. 4. Tafel plot of oxidation process of oxovanadium-(IV). E_e: equilibrium potential

Electrode Kinetics of Oxidation Process of Oxovanadium(IV). The polarographic oxidation current was recorded at each potential controlled by the potentiostat, and the $\log[i/(i_d-i)]$ *versus* the potential plot was obtained as shown in Fig. 3. From the inclination of this linear plot the anodic transfer coefficient of 0.63 was estimated.[7] On the other hand, the Tafel plot was obtained from the foot of this oxidation wave as shown in Fig. 4. The inclination of this Tafel plot gave the value of the anodic transfer coefficient as great as 0.60. Both data showed a fairly good agreement.

The value of the equilibrium potential for V(V)—V(IV) couple was tentatively evaluated assuming that the Tafel plot will be an asymptote along with the potential coordinate at the equilibrium potential as shown in Fig. 4. The exchange current density estimated from the intercept was 1.8×10^{-6} A/cm².

Oxidation of Oxovanadium(IV) by Aerial Oxygen, Electrolytic Oxidation of V(IV) and Photochemical Reduction of V(V). When dissolved oxygen was contained in the oxovanadium(IV) solution, the wave-height of the polarographic oxidation decreased and a new reduction wave appeared at −0.13 V *vs.* SCE as shown in Fig. 1. The height of the new wave was exactly equal to the decrement of the oxidation wave. The oxidation process of V(IV) by aerial oxygen in an alkaline solution was studied by Dean and Herringshaw[3] as formulated in the following;

$$O_2 + 2VO_3^{2-} + H_2O = 2VO_3^{-} + 2OH' + H_2O_2 \quad (2)$$

followed by

$$H_2O_2 + 2VO_3^{2-} = 2VO_3^{-} + 2OH' \quad (3)$$

In view of their results, the new reduction wave appeared at −0.13 V *vs.* SCE seems to be the reduction of V(V) to V(IV).

The solution color changed from light blue to light yellowish green by the aerial oxidation. A similar color change was observed by the electrolytic oxidation at the controlled potential of +0.15 V *vs.* SCE. The absorption band at λ_{max}=600 nm disappeared completely by the oxidation and the band at λ_{max}=310 nm decreased simultaneously in its intensity as shown in Fig. 5.[8,9] The ESR spectra of oxovanadium(IV) in

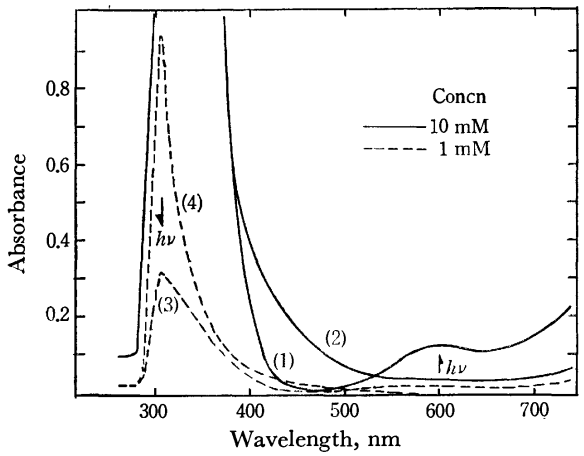

Fig. 5. Absorption spectra of oxovanadium(IV) and (V). Curves 1 and 2: 10 mM, Curves 3 and 4: 1 mM, Curves 1 and 3: deaerated or irradiated solution, Curves 2 and and 4: oxidized solution

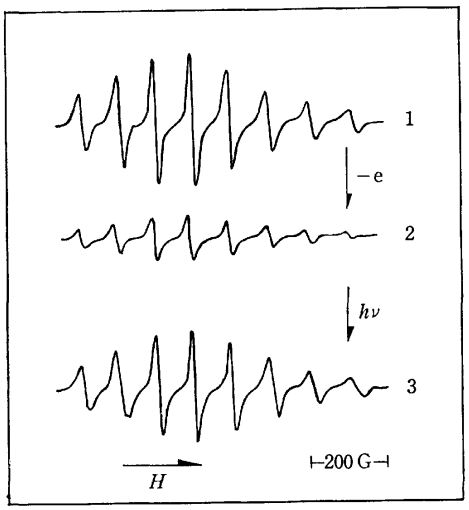

Fig. 6. ESR spectra of oxovanadium(IV). Curve 1: deaerated solution, Curve 2: oxidized solution, Curve 3: irradiated solution

M potassium oxalate solution showed eight components corresponding to the nuclear spin of 7/2 as shown in Fig. 6.[9] The ESR spectrum also decreased and disappeared in its intensity as the oxidation proceeded. It is noteworthy that vanadium of +5 oxidation state has no more spin in its d-shell. These changes in color, electronic absorption and ESR spectra were restored to the original state by the irradiation of ultra-violet light as shown in Figs. 5 and 6. The increase of the oxidation wave-height and disappearance of the new reduction wave were observed by the ultra-violet light irradiation as shown in Fig. 1. The photochemical reaction can be expressed as follows;

$$V(V) + h\nu = V(IV) - e \qquad (4)$$

and the oxidation of oxalate to form carbon dioxide seems to be coupled with Reaction (4), *i.e.*, $1/2C_2O_4^{2-} - e = CO_2$.

Kinetics of Photochemical Reduction of V(V) in M Potassium Oxalate Solution. The effect of the mercury head of the DME on the polarographic oxidation and reduction wave-heights is illustrated in Fig. 7. Both waves showed the linear increase with the square root of the mercury head. This characteristic corresponds well to the polarographic diffusion-controlled current. However, when the solution was irradiated by the ultra-violet light in the course of the polarographic oxidation, the inclination of the plot decreased slightly as shown in Fig. 7. This reveals the characteristic of the polarographic kinetic current, namely, the oxidation process of oxovanadium(IV) is coupled with the regeneration of V(IV) by the photochemical reduction of V(V), which is the product of the electrolytic oxidation. The reaction scheme is expressed by the combination of Reactions (1) and (4).

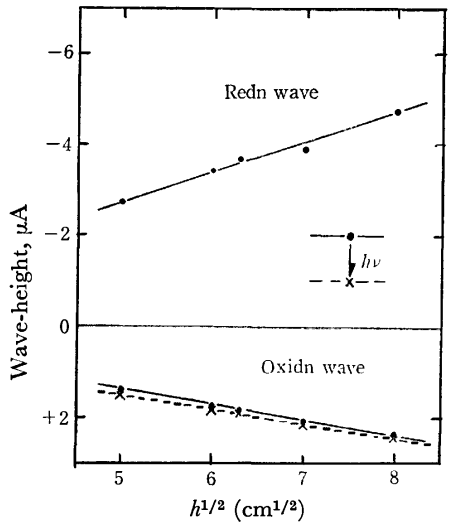

Fig. 7. Dependence of polarographic wave-height on DME mercury head.
Broken line: oxidation wave under ultra-violet light irradiation

Assuming that the Lambert-Beer's law holds for the light absorption of the V(V) species, the differential equation relating to the semi-infinite diffusion at the vicinity of the electrode-solution interface can be expressed as follows;

$$\frac{\partial C_{IV}}{\partial t} = D_{IV}\frac{\partial^2 C_{IV}}{\partial x^2} + \frac{2x}{3t}\frac{\partial C_{IV}}{\partial x} + \frac{k\phi I_0}{l}(1-e^{-\varepsilon C_V l}) \qquad (5)$$

$$\frac{\partial C_V}{\partial t} = D_V\frac{\partial^2 C_V}{\partial x^2} + \frac{2x}{3t}\frac{\partial C_V}{\partial x} - \frac{k\phi I_0}{l}(1-e^{-\varepsilon C_V l}) \qquad (6)$$

where C's are the concentration of respective species, k the rate constant of the photochemical reduction, ϕ the quantum yield, ε the molecular extinction coefficient, I_0 the intensity of the incident light, the thickness of the reaction layer and the other symbols are of the usual significance. Eqs. (5) and (6) can be simplified by the approximation that $\exp[-\varepsilon C_V l] \approx 1-\varepsilon C_V l$ and that $D_{IV} \approx D_V$.[10] The explicit equation for this case has been derived by Henke and Hans.[11] The numerical data of i_c/i_d were in the range from 1.04 to 1.10, where i_c is the mean limiting current under ultra-violet light irradiation and i_d the mean diffusion-controlled current. From the data the rate constant of the photochemical reduction, k, was evaluated as $(0.02—0.04)/\varepsilon\phi I_0\ s^{-1}$. The evaluation of the molecular extinction coefficient,

ε, the quantum yield, ϕ, and the intensity of the incident light, I_0, involves complication in this case so that it will be remained for the future.

References

1) J. J. Lingane, *J. Amer. Chem. Soc.*, **67**, 182 (1945).
2) E. Bishop and P. H. Hitchcock, *Analyst*, **98**, 553 (1973).
3) G. A. Dean and J. F. Herringshaw, *Talanta*, **10**, 797 (1963).
4) K. C. Satapathy, R. Palmer, and B. Sahoo, *Indian J. Chem.*, **1**, 402 (1963).
5) Y. Israel and L. Meites, *J. Electroanal. Chem.*, **8**, 99 (1964).
6) For a review see, J. Selbin, *Chem. Rev.*, **65**, 153 (1965).
7) H. Matsuda and Y. Ayabe, This Bulletin, **28**, 422 (1955).
8) J. Selbin and T. R. Ortolano, *J. Inorg. Nucl. Chem.*, **26**, 37 (1964).
9) R. N. Rogers and G. E. Pake, *J. Chem. Phys.*, **33**, 1107 (1960), Y. Ujihira, Y. Suzuki, and H. Takami, *Bunseki Kagaku*, **23**, 987 (1974), T. R. Ortolano, J. Selbin, and S. P. McGlynn, *J. Chem. Phys.*, **41**, 262 (1964).
10) K. Yamashita and H. Imai, *Rev. Polarog. Kyoto*, **18**, 10 (1972).
11) Karl-Heinz Henke and W. Hans, *Z. Elektrochem.*, **59**, 676 (1955).

Chemical Vapor Deposition of Tetraboron Silicide Whiskers

Seizi MOTOZIMA, Kozoh SUGIYAMA, and Yasutaka TAKAHASHI

Department of Synthetic Chemistry, Faculty of Egineering, Gifu University, Kakamigahara, Gifu 504

(Received January 6, 1975)

Growth conditions of B_4Si whiskers were investigated at the temperature range of 1000—1100 °C. Optimum composition of halides was determined as $BCl_3/SiCl_4=2$—0.5, and $BCl_3=1$—6 vol%, $SiCl_4=1$—7 vol%. Gold had an excellent impurity effect with optimum concentration of 20—50 μg/cm² on whisker growth, and gave wool like whiskers of 0.1—1 μm in thickness and 0.5—2 mm in length. B_4Si whisker growth was explained in terms of a tip VLS mechanism, for a drop-like deposit of impurity was observed on each tip.

Boron silicides are well known to have useful properties of high stability in oxygen, high elastic modulus, high mechanical strength, and so on. In the system of B–Si, a number of stoichiometric compounds, BSi, B_3Si, B_4Si, B_6Si, $B_nSi(n=10-14)$,[1] $B_{16}Si$,[2] $B_nSi(n=20-30)$,[2] and a few of nonstoichiometric compounds[3] have been prepared. Of these silicides, tetraboron silicide is the most stable and inert for oxygen up to its decomposition temperature (above 1400 °C).[4] Therefore, it is frequentry used as one of refractories[5] or coating materials of graphite to improve its oxidation resistivity.[6] On the other hand, the semiconducting properties of tetraboron silicide have been extensively studied, and are of much interest in its anisotropy.

Up to date, B_4Si has been prepared by various methods as follows: 1) solid-phase reactions between the elements,[7-10] 2) solid-vapor reactions of boron metal with silicon halides [11] and of silicon metal with boron trichloride or borane,[11] 3) vapor phase reactions in systems: $SiCl_4+BBr_3+H_2$,[12] $SiH_4+BCl_3+H_2$,[13] and $BCl_3+SiCl_4(SiHCl_3)$.[14] In these reactions, however, has never been reported the formation of B_4Si whiskers, which are expected as an excellent composite material.

In present work, B_4Si whiskers are found to grow from a vapor phase of BCl_3, $SiCl_4$, H_2, and Ar onto a quartz substrate at 1000—1100 °C and effects of various factors including gas concentration, temperature, and impurity in particular on whisker growth are examined.

Experimental

Materials. Commercial guaranteed reagent grade silicon tetrachloride, boron carbide, and chlorine gas were used without further purification. Argon was purified by passing over titanium sponge kept at 800 °C, and hydrogen was also refined by passing through active copper nets heated about 400 °C, conc sulfuric acid and phosphorus pentoxide, successively. Boron trichloride was prepared *in situ* (*vide infra*).

Preparation of B_4Si. The equipment used in this study is shown schematically in Fig. 1. The quartz tube(1) (7 mm in outside diameter and 100 mm in length), in which a SiC heater was inserted, was placed as a substrate in the center of reaction tube (quartz of 24 mm in inside diameter). The substrate was heated at 950—1200 °C dually from outside and inside. Boron trichloride (bp 12.5 °C) was prepared by chlorination of boron carbide at 800 °C, and supplied into the reaction tube. Silicon tetrachloride (bp 57.6 °C) was carried into the reactor by argon or hydrogen which was bubbled through its saturator(3) maintained at a given temperature. Hydrogen was also introduced through an upper

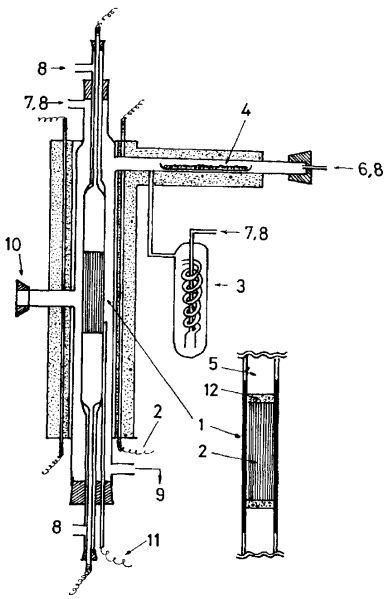

Fig. 1. Schematic diagram of the experimental apparatus.
1) Quartz substrate, 2) SiC heater, 3) $SiCl_4$ saturater, 4) B_4Si, 5) carbon electrode, 6) Cl_2, 7) H_2, 8) Ar. 9) outlet, 10) observation window, 11) alumel-chromel thermocouple, 12) carbon powder.

inlet (7) and allowed to be mixed with the streams of boron trichloride and silicon tetrachloride in the reaction zone. After the reactions had been quenched by stopping the supply of all reagent gases except argon, the furnace was allowed to cool below 200 °C to take out the substrate. The surface temperature of the substrate was measured by an optical pyrometer through a window(10), and the atmospheric temperature by an alumel–chromel thermocouple. The flow rates of each gas at room temperature were measured by an orifice type flow meter. The products formed on the surface of substrate were examined thoroughly by X-ray diffraction and an optical or electron microscope.

Whisker growth was found to be affected only when and where the substrate was painted with one of impurities such as gold, cobalt and nickel which were obtained by painting on the substrate in the form of aqueous solution of their salts: $HAuCl_4$, $CoCl_2$, and $NiCl_2$, followed by decomposition or reduction in the reactor below the reaction temperature.

Results and Discussion

When a mixture of boron trichloride, silicon tetrachloride, hydrogen and argon was introduced on a substrate(quartz) heated around 1100 °C, no deposition

was observed except formation of microcrystallites of boron metal at a condition of higher concentration of boron chloride. However, a large quantity of grayish wool-like crystals were obtained, only when the substrate was coated with gold. The X-ray diffraction profile of the crystals (Fig. 2) is consistent with that of ASTM data of tetraboron silicide,[15] and no peaks due to other products but gold were detected, even if a highly sensitive measurement was performed. In order to achieve the formation of well-formed and long crystals, the reaction conditions and impurity effects were thoroughly examined, and the results are discussed in the following sections in relation to the growth mechanism.

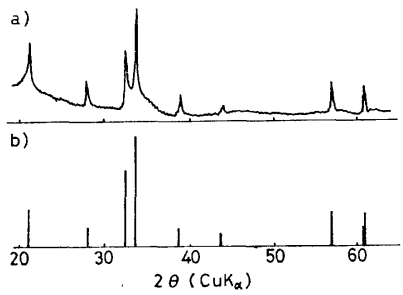

Fig. 2. X-Ray diffraction patterns.
a) B_4Si whiskers as grown, b) ASTM powder data of B_4Si

Growth conditions. In this work, composition and concentration of reaction gas, which is considered to be the most impotant factors for whisker growth, were mainly studied.

The influences of $SiCl_4$ and BCl_3 flow rates on the whisker growth are shown in Fig. 3, where gold was used as an impurity. In this figure, it is found that optimum gas flow rates of BCl_3 and $SiCl_4$ are 0.02—0.14 cm^3/s and 0.02—0.15 cm^3/s, respectively; in other words, the growth of tetraboron silicide whisker takes place in the narrow range of molar ratio $BCl_3/SiCl_4$ of 2—0.5. In condition of an excess of boron trichloride ($BCl_3/SiCl_4 > 2$) or silicon tetrachloride ($SiCl_4/BCl_3 > 3$), whiskers of boron or silicon metal were obtained, respectively,

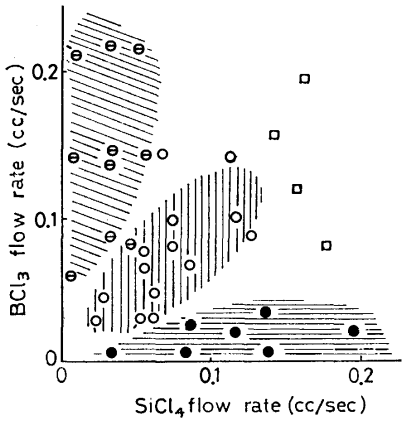

Fig. 3. Influence of $SiCl_4$ and BCl_3 flow rates on whisker growth.
(□): No-deposition; (⊖): boron whiskers; (○): B_4Si whiskers: (●): silicon whiskers.
Temperature: 1050 °C; total gas flow rate: 2.3 ml/s.

but tetraboron silicide was not formed. The increase of concentration of both halides could not result in deposition of the silicide, perhaps due to insufficiency of reducing agent. Although the stoichimetric ratio of chlorides in the reaction $4BCl_3+SiCl_4+8H_2=B_4Si+16HCl$, $BCl_3/SiCl_4=4$, growth experiments show the ratio to be near unity. Such a tendency that boron compound whiskers grow from a gaseous mixture of poorer boron trichloride content than that expected from stoichiometry has been found also in the case of TiB_2[16] and ZrB_2[17] whisker growth. It is supposed that such a tendency came from the difference in reactivity of halides with hydrogen on the one hand, and from the lower activity of metals such as Ti, Si, and Zr in a impurity liquid phase from which whiskers grow on the other hand.

Morphology. Figure 4 is a micrograph of B_4Si whisker typical in present experiments, where gold was used as an impurity. The appearance of whiskers was woolly and curled with dimensions of 0.5—2 mm in length and of 0.1—1 μm in diameter. The side surface of whisker was very smooth. Silicon or boron whiskers also have been obtained generally in the woolly form in contrast to a needle form of ZrB_2 or TiB_2.

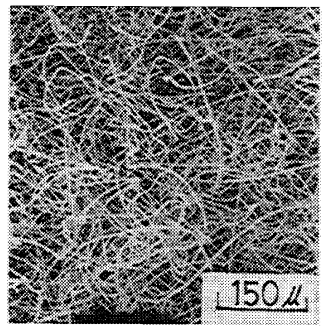

Fig. 4. Micrograph of typical B_4Si whiskers.
Temperature: 1050 °C; reaction time: 30 min; $SiCl_4$: 0.05 ml/s; BCl_3: 0.05 ml/s; H_2: 2.1 ml/s.

Table 1. Impurity effect on whisker growth and eutectic temperature of binary alloys[18-20]

	Impurity effect[a]			Eutectic temperature (°C)[b]	
	B_4Si	Boron	Silicon	Boron-impurity	Silicon-impurity
Cu	−	++	−	1060 (10.7)	802 (30)
Ag	−	−	−		840 (10.6)
Au	++	++	++		370 (31)
Fe	−	+	−	1149 (~17)	1200 (34)
Co	+	++	+	1095 (18.5)	1195 (23)
Ni	+	++	+	1080 (18.4)	964 (46)
Rh	−	++	++		1438 (10)
Pd	−	++	++	845 (27)	800 (15.5)
Pt	−	++	++	830 (40)	830 (25)
Nd	−	−	+		
Tl	−	−	−		
Al	−	−	−		577 (11.3)
Cr	−	−		1570 (13)	1335 (85)

a) (−): no or negative effects, (+): weak positive effects, (++): positive effects. b) Atomic percents of boron or silicon in corresponding binary systems are shown in the parentheses, respectively.

Impurity effect. In Table 1, impurity effects of various metals on whisker growth at 1050 °C are shown qualitatively together with the eutectic temperature of corresponding binary system.[18-20] Although many kinds of impurities affected whisker growth of boron and silicon, for B_4Si gold alone showed an excellent effect, and Co and Ni weak effect. If vapor-liquid-solid(VLS) mechanism proposed by Wagner and Ellis[21] can be applied to B_4Si whisker growth, the impurity metal must fulfil at least following requirements: 1) the binary or ternary system among the impurity, boron and silicon has eutectic temperature lower than growth temperature, and 2) the impurity metal is stable in the corrosive atmosphere of BCl_3, $SiCl_4$, H_2, HCl, *etc.* The reason why excellent impurities such as Pd, Rh, or Pt metals for boron or silicon whisker growth are ineffective in B_4Si whisker growth is difficult to explain. However, it seems plausible that they have so strong affinity with both boron and silicon that the activities of both or one of elements in their ternary liquid may be lowered below the limit of B_4Si growth. Though the system Si–B–Au has not been reported, it may be considered from the two binary systems, that is, soluble Au–Si system and insoluble Au–B system, that the ternary system contains trace of boron in homogeneity. Therefore, growth kinetic requires fast diffusion of boron.

Whisker growth was very slow below 1000 °C, but was fast at the temperature above 1100 °C, where radial growth or branchings became striking. At the higher temperature, no deposition was observed, probably due to the following reasons: 1) activity of relevant species in Au drops is low, 2) Au disappears due to the reaction with quartz, 3) etching temperature may be attained.

In Figs. 5 and 6, the influence of Au impurity concen-

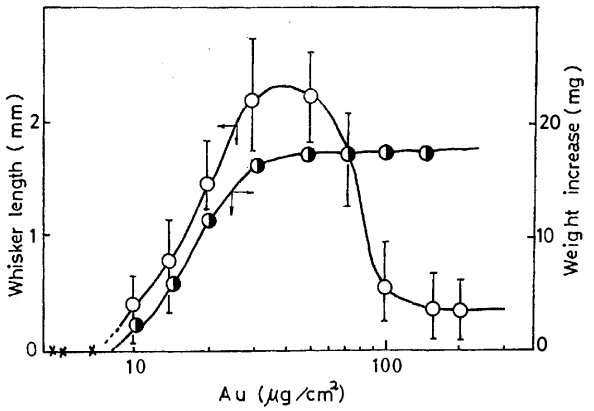

Fig. 5. Influence of impurity (Au) concentration on the growth.
Temperature: 1050 °C; total gas flow rate: 1.7 ml/s; reaction time: 1 hr.

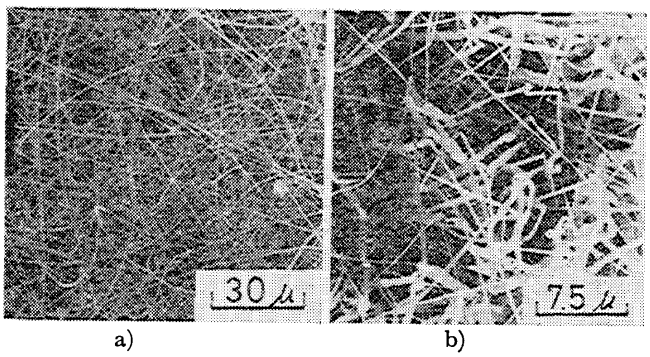

Fig. 6. Whiskers grown in different Au concentration.
Temperature: 1050 °C; reaction time: 30 min; impurity (Au) concentration, (a): 0.03 mg/cm²; (b): 0.2 mg/cm².

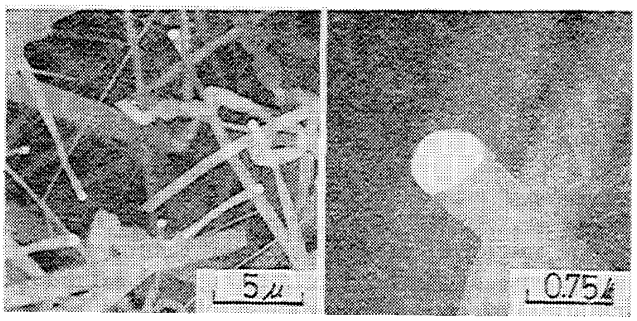

Fig. 7. The typical tip of whiskers.
Growth temperature: 1050 °C.

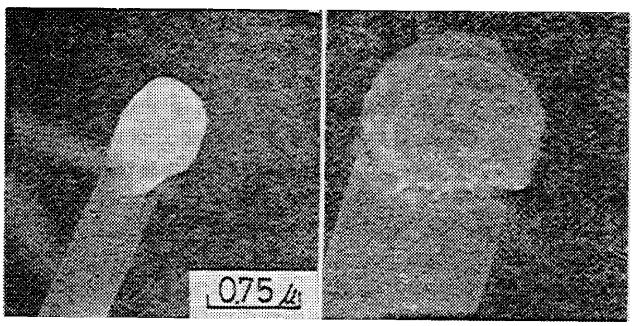

Fig. 8. Whiskers with unique tips.
Growth temperature: 1050 °C; (a) hollow: (b): rough cap.

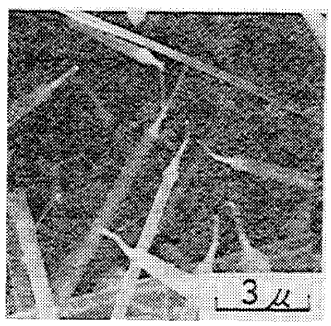

Fig. 9. The tip of whiskers (secondary growth).
Growth temperature: 1080 °C.

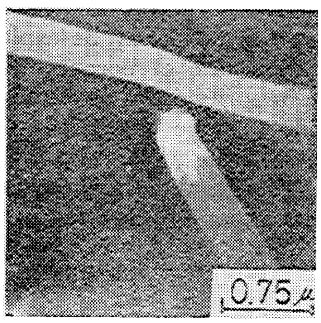

Fig. 10. The tip of whisker (tailing of liquid).

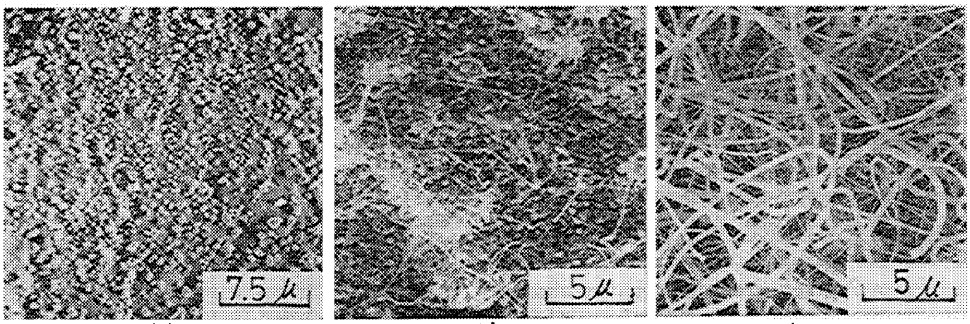

(a) (b) (c)

Fig. 11. Growth process of whiskers.
Au concentration: 0.05 mg/cm², reaction time (a): 0 min; (b) 5 min; (c) 30 min.

tration on growth rate of whiskers and their morphology are shown. It can be seen from Fig. 6 that the lower impurity concentration (the range of 20 to 50 μg/cm²) results in the more smooth whiskers and irregular whiskers are grown at the Au concentration of above 100 μg/cm². The lowest Au concentration for whisker growth is found to be 5 μg/cm² as seen in Fig. 5. Micrograph of the tip of typical whiskers obtained is shown in Fig. 7. There can be seen "cap" on each whisker which has a smooth surface with an apparent boundary with whisker. Rarely a hollow at the interface between the cap and crystal, and rough surface were observed (Fig. 8). The caps on the tips of whiskers look like Au or Au alloy. Accordingly, it is reasonable to consider that the wisker was grown by a tip VLS mechanism. Sometimes, whiskers with secondary growth of more thin crystals were found, too (Fig. 9), which may be attributed to a sudden fluctuation of reaction conditions such as temperature, or to precipitation during the cooling process. As shown in Figs. 7 and 9, a bright part which might be regarded as a residue of drop is frequentry observed to remain in side of the whiskers. Moreover, Fig. 10 indicates the creeping of cap material from tip to shoulder. The growing process of whiskers is shown in Fig. 11. When the quartz substrate which was painted with 2% aqueous $HAuCl_4$ solution was heated at 1050 °C in H_2 and cooled to room temperature, fine gold drops were found to be dispersed uniformly on the substrate and its size was about 0.5 μm (Fig. 11a) in diameter. This dimension is consistent with the diameter of whiskers, suggesting that the thickness of whiskers can be determined with the drop size of impurity. The number of drops per unit area quite agreed with that of whiskers (10^{7-8} per square centimeter of the substrate). Whisker growth was observed 5 minutes later after the reactant gas mixture had been introduced. This "induction time" for whisker growth may be explained in terms of a slow diffusion rate of boron, silicon and other species into the impurity drops or of the time necessary to nucleation. It can be concluded therefore that a whisker is grown from a Au-drop by the tip VLS mechanism. Although the thermodynamic data tell the gross concentrations of species in vapor phase, whiskers are grown from an impurity drop as mentioned above in which each component must be ballanced for the sake of whisker growth. Therefore, the solubility of the components to the impurity (liquid) and/or the diffusions to crystallizing sites must be more impotant factors for the growth than the concentration in vapor phase.

References

1) L. K. Lamikhov, *Izv. Akad. Nauk., SSSR, Neorg. Mater.*, **4**, 1076 (1968).
2) W. Dietze, M. Miller, and E. Amberger, *Electron Technol.*, **3**, 73 (1970).
3) M. Bergt and B. Cyrill, *Acta Chem. Scand.*, **16**, 449 (1962).
4) R. S. Fergelson and W. D. Kingery, *Spec. Ceram., Proc. Symp. Brit. Ceram. Res. Assoc.*, **1962**, 27.
5) K. Aktiebolag, Swed. 201850 (1967).
6) C. Ervin, U. S. 3275467 (1966).
7) V. I. Matkovich and C. Ervin, U.S. 3138468 (1964).
8) G. V. Samsonov and V. M. Sleptsov, *Poroshkovaya Met., Akad. Nauk Ukr., SSSR*, **4**, 58 (1964).
9) V. I. Matkovich and C. Ervin, U.S. 3427131 (1969).
10) G. V. Samsonov and V. P. Latysheva, *Doklady Akad. Nauk, SSSR*, **105**, 499 (1955).
11) E. L. Kern and G. A. Jerone, Fr. 1538423 (1968).
12) I. V. Petrusvich, L. A. Niselson, A. I. Belyaev, and M. A. Gurevich. *Izv. Akad. Nauk., SSSR, Neorg. Mater.*, **3**, 1389 (1967).
13) L. C. McCandless and J. C. Withers, U.S. 3607367 (1971).
14) L. C. McCandless, J. C. Withers, and C. R. Brummett, U.S. 3549413 (1970).
15) V. I. Matkovich, *Acta Crystallogr.*, **13**, 679 (1960).
16) K. Sugiyama, Y. Takahashi, F. Sugimori, and S. Motozima, in preparation for publication
17) S. Motozima, F. Sugimori, Y. Takahashi, and K. Sugiyama, in preparation for publication
18) M. Hansen, "Constitution of Binary Alloys," McGraw-Hill, London (1958).
19) R. P. Elliot, *ibid.*, First Supplement (1964).
20) F. A. Shunk, *ibid.*, Second Supplement (1969).
21) R. S. Wagner and W. C. Ellis, *Appl. Phys. Lett.*, **4**, 89 (1964). R. S. Wagner and W. C. Ellis, *Trans. AIME*, **233**, 1053 (1965).

The Reactions of Tetrafluorobenzyne with Carboxylic Acids in Cyclic Ethers

Sei-ichi HAYASHI and Nobuo ISHIKAWA

Department of Chemical Engineering, Tokyo Institute of Technology, Meguro-ku, Tokyo 152

(Received May 2, 1974)

The reactions between tetrafluorobenzyne generated from tetrafluorobenzenediazonium-2-carboxylate and several carboxylic acids in cyclic ethers, such as THF and dioxane, were carried out. During these reactions, the cyclic ethers were cleaved and participated in the reactions to give acetate, benzoate, and salicylate esters of 4-(2′,3′,4′,5′-tetrafluorophenoxy)butanol and 2-[2′-(2″,3″,4″,5″-tetrafluorophenoxy)ethoxy]ethanol.

A number of cases have been reported of the reactions of unsubstituted or tetrahalogeno-substituted benzynes with ethers.[1,2] As for the ring cleavage of cyclic ethers during the reactions, Wolthuis *et al.* reported that tetrahydrofuran (THF) was cleaved by benzyne, thus affording a betaine intermediate, which was intercepted with water to give 23% 4-phenoxybutanol and 8% 1,4-diphenoxybutane.[3] In our own previous paper, we reported that dioxane was cleaved by tetrafluorobenzyne generated from tetrafluorobenzenediazonium-2-carboxylate and that the resulting betaine intermediate (**6**) was intercepted with bromine to give 28% 1-[2′-(2″-bromoethoxy) ethoxy]-2-bromo-3, 4, 5, 6-tetrafluorobenzene.[4]

We shall now describe further examples of this type of reaction, *i.e.*, those between tetrafluorobenzyne and carboxylic acids in the cyclic ethers, such as THF and dioxane, in which the solvents participate through their cleavage.

Results and Discussion

It is known that benzynes generated from benzenediazonium-2-carboxylate[5] or its tetrahalogeno derivatives[6–8] sometimes yield acridones by reactions with anthranilic or tetrahalogenoanthranilic acid. By analogy with these, we attempted to have tetrafluorobenzyne react with salicylic acid, expecting to obtain 2-(2′,3′,4′,5′-tetrafluorophenoxy)benzoic acid or its dehydrocyclized product, tetrafluoroxanthenone.

The reaction was carried out in THF by diazotizing tetrafluoroanthranilic acid with *n*-butyl nitrite in the presence of salicylic acid, and by subsequent refluxing for several hours. The main products were crystals with a melting point of 84—85 °C; unexpectedly, the compound contained four methylene groups. The structure of this compound was established, by means of the NMR and the mass spectra, as 4-(2′,3′,4′,5′-tetrafluorophenoxy)butyl salicylate (**4c**).

In the NMR spectrum three signals appeared at τ 5.58, 5.95, and 8.03 in a 1 : 1 : 2 ratio of strength; they are due to two $-OCH_2-$ groups and one $-CH_2CH_2-$ group. Other signals due to four protons appeared in the non-fluorinated benzene ring at τ 2.25—3.25, while signals due to a proton appeared in the fluorinated ring at τ 3.23—3.67. The signal of the OH proton appeared at an unusually lower magnetic field, τ −0.73; this may be supposed to have resulted from a strong intramolecular hydrogen bonding. The ^{19}F NMR spectrum showed the presence of four unequivalent aromatic fluorine atoms.

In the mass spectrum, the molecular ion, M^+ 358, is in agreement with the calculated value and the fragmentation is as is shown in Fig. 1. The base peak, *m/e* 149, corresponded to the tetrafluorophenyl fragment; another characteristic fragment peak, *m/e* 120, probably resulted from the elimination of 4-tetrafluorophenoxybutanol from the molecular ion. The **4c** structure was adequately

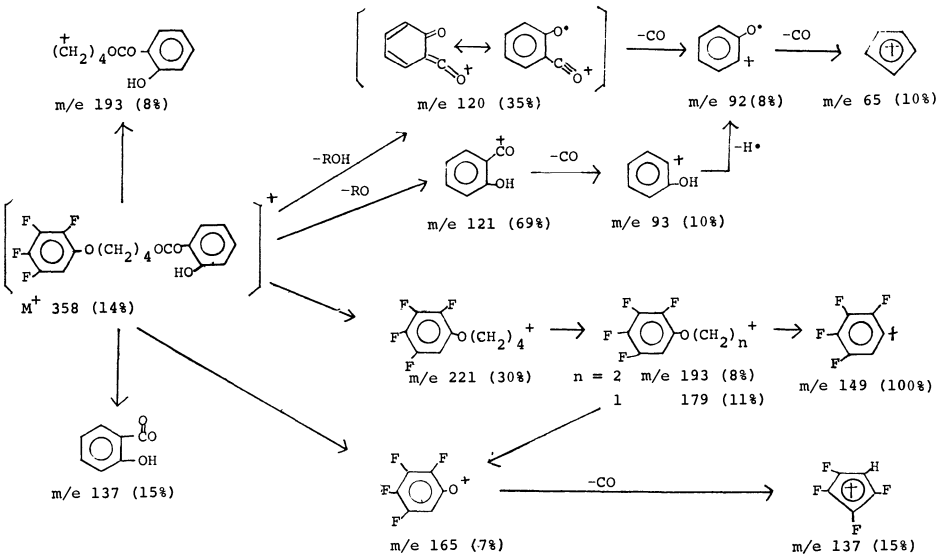

Fig. 1. MS fragmentation for **4c**.

supported by this degradation, which can be explained by the so-called ortho-effect.[9]

In this reaction it is evident that the strong electrophilic tetrafluorobenzyne initially attacked the abundant THF, prior to dilute carboxylic acid, to give **2**, followed by the ring cleavage to a betaine intermediate, **3**, which then electrophilically attacked the oxygen of carboxylic acid to give **4c**. The last two steps, **2** to **3** and **4c**, might have occurred simultaneously.

Other carboxylic acids, such as acetic and benzoic acids, were also subjected to the reaction with tetrafluorobenzyne in THF. In these cases, too, we could obtain the analogous compounds, *i.e.*, 4-(tetrafluorophenoxy)butyl acetate (**4a**) and benzoate (**4b**) respectively. The NMR spectra of these products revealed patterns similar to that of **4c** (Table 1).

The **4b** benzoate was alternately prepared by the benzoylation of 4-(2′,3′,4′,5′-tetrafluorophenoxy)butanol which had been obtained by a direct reaction between tetrafluorobenzyne and 1,4-butanediol.

Other hydroxy compounds, such as water and 3-trifluoromethylphenol, when reacted with tetrafluorobenzyne in THF gave similar results. Water yielded 4-(2′,3′,4′,5′-tetrafluorophenoxy)butanol and 2,3,4,5-tetrafluorophenol in yields of 50 and 13% respectively. The latter compound must result from the direct reaction of tetrafluorobenzyne with water, without the participation of THF.

m-Trifluoromethylphenol was chosen as the phenol to be examined, avoiding the diazo-coupling reaction

TABLE 1. PHYSICAL DATA OF

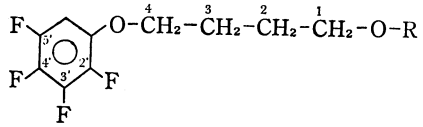

Compd. No.	R	Yield %	Bp °C/mmHg (Mp °C)	NMR chemical shift: ^{1}H (τ) 1-CH_2	2,3-$(CH_2)_2$	4-CH_2	6-H	R	^{19}F (δ ppm)[a] 2′-F	3′-F	4′-F	5′-F	F-Anal (%) Found	Calcd
4a	CH_3CO	40	120/4	5.93	8.14	5.93	3.12—3.56	8.00 (CH_3)	83.0	78.5	90.7	62.5	27.0	27.1
4b	C_6H_5CO	29	(41—42)	6.04	8.08	5.70	3.30—3.72	2.14—2.56 (C_6H_5)	81.9	77.8	89.4	62.0	22.1	22.2
4c	2-HO-C_6H_4CO	51	(84—85)	5.95	8.03	5.58	3.23—3.67	2.25—3.25 (C_6H_4) −0.73 (OH)	82.2	77.8	89.4	61.8	21.4	21.2
	H	50	110—111/3	6.02	8.21	6.34	3.23—3.65	5.78 (OH)	83.0	78.6	90.1	62.1	31.4	31.9
4d	3-CF_3-C_6H_4-	29	146—148/3	6.01	8.04	6.01	3.32—3.64	2.62—3.25 (C_6H_4)	82.2	77.8	89.4	61.8	34.9	34.8

a) The ^{19}F NMR chemical shifts are given in δ ppm from ext. CF_3CO_2H, in CCl_4.

TABLE 2. PHYSICAL DATA OF

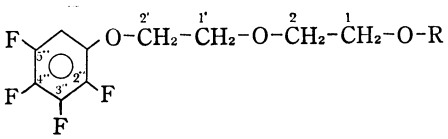

Compd. No.	R	Yield %	Bp °C/mmHg (Mp °C)	NMR chemical shift: ^{1}H (τ) 1-CH_2	2-CH_2 / 1′-CH_2	2′-CH_2	6″-H	R	^{19}F (δ ppm)[a] 2″-F	3″-F	4″-F	5″-F	F Anal (%) Found	Calcd
7a	CH_3CO	39	129/3	5.90	6.28	5.90	3.08—3.52	8.02 (CH_3)	81.4	77.8	89.1	61.9	25.3	25.7
7b	C_6H_5CO	29	(70.5—71.5)	5.60	6.21	5.92	3.23—3.66	2.0 —2.8 (C_6H_5)	81.8	78.1	89.1	61.9	21.8	21.2
7c	2-HOC_6H_4CO	28	(48—49)	5.52	6.16	5.88	3.20—3.62	2.24—3.14 (C_6H_4) −0.55 (OH)	81.5	77.7	88.8	61.7	19.9	20.3
	H	17	156—157/15	6.36	6.20 / 6.36	5.81	3.04—3.40	6.37 (OH)	82.0	78.2	89.5	61.9	30.2	29.2

a) Similar to that of Table 1.

with tetrafluorobenzenediazonium-2-carboxylate. The phenol also gave the expected product, 4-(2′,3′;4′,5′-tetrafluorophenoxy)butyl *m*-trifluoromethylphenolate (**4d**), but in a low yield.

Since analogous reactions could be expected when using dioxane instead of THF, we reacted the carboxylic acids, such as acetic, benzoic and salicylic with tetrafluorobenzyne in this solvent. In these cases, the reaction proceeded through the betaine intermediate **6**, and the resulting products were 2-[2′-(2″,3″,4″,5″-tetrafluorophenoxy)ethoxy]ethyl acetate (**7a**), benzoate (**7b**) and salicylate (**7c**).

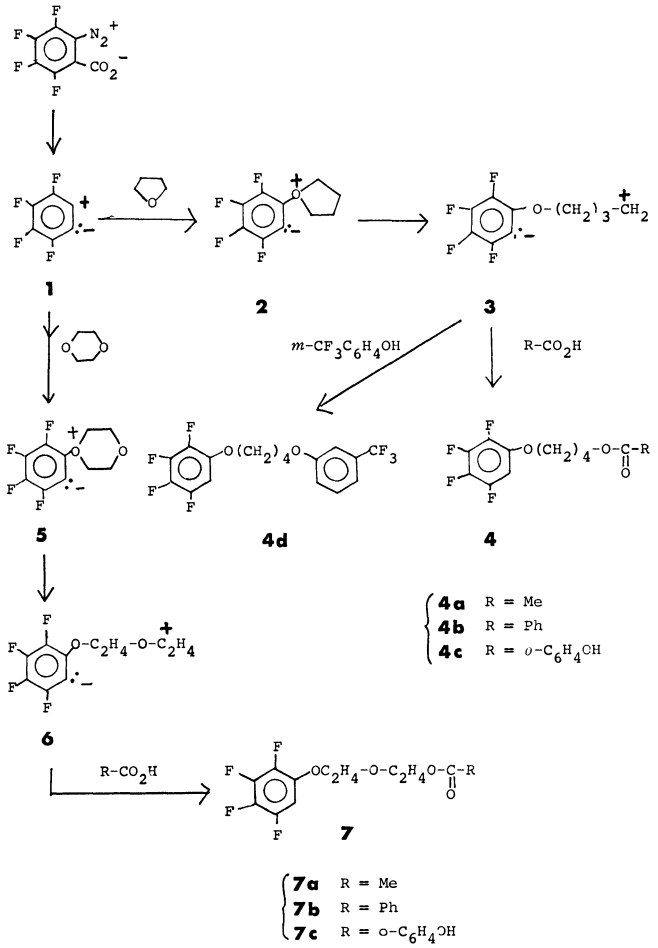

Compound **7b** was also obtained by the benzoylation of 2-[2′-(2″,3″,4″,5″-tetrafluorophenoxy)ethoxy]ethanol, which had been prepared from tetrafluorobenzyne and diethyleneglycol.

Experimental

4-(2′,3′,4′,5′-Tetrafluorophenoxy)butyl Salicylate (4c). A solution of tetrafluoroanthranilic acid (4.18 g, 20 mmol) in THF (40 ml) was added dropwise into a mixture of *n*-butyl nitrite (2.6 g, 25 mmol), salicylic acid (13.8 g, 100 mmol), and THF (10 ml) at 55—56 °C with stirring. After refluxing for 5 hours, the solvent was distilled out under reduced pressure and the residue was dissolved in diethyl ether. The solution was then treated with a dilute aqueous sodium hydroxide solution to remove the excess salicylic acid, washed with dilute hydrochloric acid and water successively, and dried over magnesium sulfate. After the solvent had been removed, the residue was recrystallized from methanol to give crude **4c**. Sublimation gave pure crystals; mp 84—85 °C.

IR (KBr): 3388 (OH, intramolecularly H-bonded), 1661 (C=O), 1136, 1091 cm^{-1} (C–F).

4-(2′,3′,4′,5′-Tetrafluorophenoxy)butyl Acetate (4a), Benzoate (4b) and m-*Trifluoromethylphenolate (4d).* Instead of salicylic acid in the above reaction, acetic acid, benzoic acid and *m*-trifluoromethylphenol were used. When the reactions were carried out and worked-up in the same way, they gave **4a**, **4b**, and **4d** respectively (Table 1).

The benzoate (**4b**) was also obtained by the benzoylation of (2′,3′,4′,5′-tetrafluorophenoxy)butanol. Thus, a mixture of the alcohol (2.00 g), benzoyl chloride (1.18 g), and two drops of concentrated sulfuric acid was heated until the evolution of gas ceased. Upon cooling, the reaction mixture was poured onto ice water; the precipitate was separated by filtration and washed with a dilute aqueous solution of sodium bicarbonate to remove benzoic acid, thus giving crude benzoate (2.42 g). After recrystallization from petroleum ether, a pure material (mp 42—44 °C) was obtained. No depression in mp was observed on admixture with the product described above.

4-(2′,3′,4′,5′-Tetrafluorophenoxy)butanol. A solution of anthranilic acid (2.09 g) in THF (10 ml) was dropped into a mixture of *n*-butyl nitrite (1.3 g), deionized water (10 ml), and THF (10 ml) at 60 °C, and then the mixture was refluxed for 5 hr. The reaction mixture was then worked-up as usual. In addition to the main product (1.20 g, bp 110—111 °C/3 mmHg), a small amount (0.21 g) of an alkaline-soluble material was obtained. This compound was identified as 2,3,4,5-tetrafluorophenol by means of its IR spectrum.

4-(2′,3′,4′,5′-Tetrafluorophenoxy)butanol was also alternatively obtained as follows. Into a mixture of tetrafluoroanthranilic acid (10.45 g) and 1,4-butanol (50 ml), a solution of *n*-butyl nitrite (6.5 g) in dichloroethane (10 ml) was added at 50 °C. After having been refluxed for 3 hr, the reaction mixture was worked-up as usual to give the alcohol (7.50 g, 64%).

2-[2′-(2″,3″,4″,5″-Tetrafluorophenoxy)ethoxy]ethanol. Into a mixture of *n*-butyl nitrile (2.6 g), dioxane (10 ml), and deionized water (15 ml), a solution of tetrafluoroanthranilic acid (4.18 g) in dioxane (20 ml) was added at 50 °C, and then the mixture was worked-up as usual. In addition to the alcohol (0.85 g, 17%; bp 156—157 °C/15 mmHg), 2,3,4,5-tetrafluorophenol (0.37 g, 11%; bp 143—145 °C (lit. bp 145 °C[10])) was obtained as an alkaline-soluble material.

The alcohol was also prepared by the diazotization of tetrafluoroanthranilic acid (4.18 g) in diethyleneglycol (20 ml) with *n*-butyl nitrile (2.6 g). The product (2.90 g) was identified by means of its IR spectrum.

2-[2′-(2″,3″,4″,5″-Tetrafluorophenoxy)ethoxy]ethyl Acetate (7a), Benzoate (7b), and Salicylate (7c). Instead of THF in the procedure for the preparation of **4a**—**4c** described above, dioxane was used. The results are shown in Table 2. The **7b** benzoate was also prepared by the benzoylation of the alcohol with benzoyl chloride.

References

1) R. W. Hoffmann, "Dehydrobenzene and Cycloalkynes," Academic Press, New York (1967), p. 177.

2) J. P. N. Brewer, H. Heaney, and J. M. Jablonski, *Tetrahedron Lett.*, **1968**, 4455.

3) E. Wolthuis, B. Bouna, J. Modderman, and L. Sytsma, *ibid.*, **1970**, 407.

4) S. Hayashi and N. Ishikawa, This Bulletin, **45**, 642 (1972).

5) S. F. Dyke, A. R. Marshall, and J. P. Watson, *Tetrahedron*, **22**, 2515 (1966).
6) H. Heaney and J. M. Jablonski, *J. Chem. Soc., C*, **1968**, 1895.
7) H. Heaney, K. G. Mason, and J. M. Sketchley, *ibid.*, **1971**, 567.
8) S. Hayashi and N. Ishikawa, *Chem. Lett.*, **1972**, 99; *Nippon Kagaku Kaishi*, **1973**, 1319.
9) H. Budzikiewicz, C. Djerassi, and D. H. Williams, "Mass Spectrometry of Organic Compounds," Holden-Day (1971), p. 199.
10) G. M. Brooke, and B. S. Furniss, *J. Chem. Soc., C*, **1967**, 869.

Reactivity of Electrogenerated Superoxide Ion. I. Autoxidation of 9,10-Dihydroanthracene

Meguru TEZUKA, Yasukazu OHKATSU, and Tetsuo OSA

Department of Industrial Chemistry, Faculty of Engineering, The University of Tokyo, Bunkyo-ku, Tokyo 113

(Received June 18, 1974)

The superoxide ion, which was generated by means of electroreduction of the oxygen molecule dissolved in pyridine, abstracted the labile hydrogen from 9,10-dihydroanthracene and yielded anthraquinone and anthracene as the final products. From the products and their kinetics, the reaction was proposed to be a radical-chain autoxidation. Reactions with some other hydrocarbons were also carried out. The addition of ferrous or cobaltous phthalocyanine to the reaction system resulted in the increase of the reaction rate. A discussion of the effects led to the postulation of the intermediate formation of the superoxide ion-metal phthalocyanine complex.

Electrochemically an oxygen molecule is reduced by a reversible one-electron transfer to form a fairly stable species, namely a superoxide ion in common solvents such as dimethylformamide, dimethylsulfoxide and pyridine.[1-3]

$$O_2 + e \longrightarrow O_2^-$$

The superoxide ion might be a kind of an extreme form of activated oxygen molecule, which is usually observed in the adsorption on metal oxide[4,5] and in the coordination with transition metal complexes, due to the electron transfer from a low-valent metal atom.[6,7] Hence, it is interesting to investigate the reactivity of the superoxide ion, since it leads to a clearer understanding of the chemical nature of the activated oxygen.

The superoxide ion is expected to possess various reactivities to extensive organic compounds, because of its basic, nucleophilic and other properties.[8,9]

In this paper we report on the reactions of the superoxide ion with some hydrocarbons having labile hydrogens. In the case of 9,10-dihydroanthracene as a substrate, the rate equation was determined and the mechanism was proposed to be a radical-chain autoxidation. The catalytic effect of metal phthalocyanine added to this reaction system was also discussed.

Experimental

Materials. Pyridine was dried over potassium hydroxide for several days, then distilled and stored under nitrogen atmosphere. Tetraethylammonium perchlorate (TEAP) was synthesized and purified by the ordinary method.[10] 9,10-Dihydroanthracene, fluorene and diphenylmethane of reagent grade were used without any further purification. Cumene and cyclohexane were used after distillation. Ferrous and cobaltous phthalocyanines were synthesized and purified according to the method given in literature.[11]

Cyclic Voltammetry. In the solvent of pyridine, cyclic voltammograms were recorded using TEAP as a supporting electrolyte on a platinum plate of 0.40 cm^2. Potential was referred to saturated calomel electrode (SCE).

Macro-electrolysis. For controlled potential electrolysis, an H-type cell was employed in which cathodic and anodic chambers were separated from each other by a glass filter and a reference electrode was connected to the cathodic chamber with a double salt bridge. Platinum gauze of 50 cm^2 was used as a cathode. 20 ml each of the electrolytic solution containing 0.1 M TEAP was put in each chamber and vigorously stirred. The cathode potential was controlled with a Yanagimoto Type VE-3 controlled potential electrolyzer.

The consumed amount of oxygen during electrolysis was measured by means of a gas burette connected to the cell in a closed oxidation system. The temperature of the solution was kept at 20±1 °C.

Spectrometry. In the ESR study, the solution was charged into the quartz tube immediately aftet electrolysis, and then the spectra were recorded at room temperature or −196 °C with a JEOL Model JS-3BS-X spectrometer. Otherwise, the spectra were measured while electrolysis was being carried out in the cavity. The *g*-factors were determined in comparison with Mn^{2+} marker. The electronic spectra of the solution after electrolysis were recorded with a Shimadzu MPS-50L spectrophotometer.

Results and Discussion

Electrogenerated Superoxide Ion. An oxygen molecule dissolved in 0.1 M TEAP–pyridine solution was reduced on platinum to form the superoxide ion (Fig. 1). This species was re-oxidized in the reverse sweep of the potential. The peak potentials of reduction and re-oxidation were respectively −0.91 and −0.77 V. The value of 140 mV as ΔE_p shows that the electrode process is quasi-reversible.[12] In addition, the fact that the ratio of anodic current to cathodic one is substantially unity even at slow sweep rate such as 0.02 V/s means that the superoxide ion remains fairly stable in a pyridine solution.[13]

In the ESR measurement, the superoxide ion gave no signal at room temperature, but the spectrum, which possessed marked anisotropy of $g_{//}=2.069$ and $g_{\perp}=2.006$, was obtained at −196 °C (Fig. 2). These

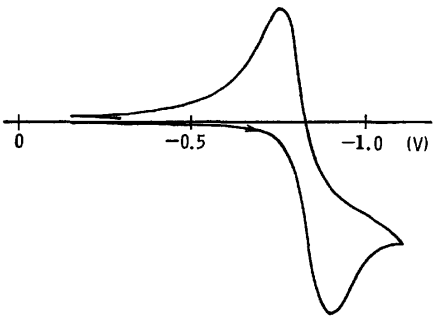

Fig. 1. Cyclic voltammogram of oxygen molecule in 0.1 M TEAP–pyridine solution, scan rate; 0.02 V/s, V *vs.* SCE.

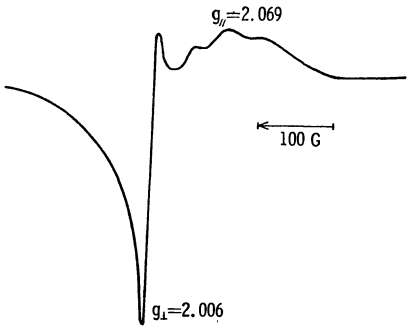

Fig. 2. ESR spectrum of the superoxide ion in 0.1 M TEAP–pyridine solution, measured at −196 °C.

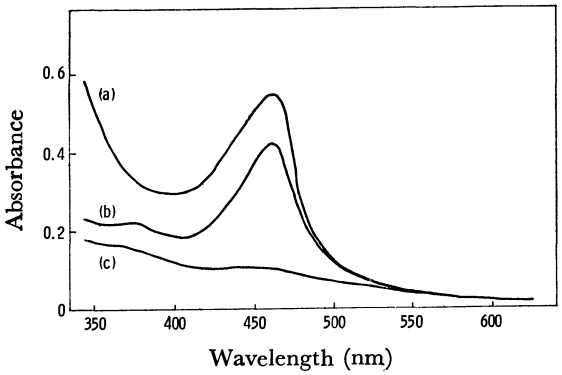

Fig. 3. Electronic spectra of the superoxide ion in 0.1 M TEAP–pyridine solution. After electrolysis, (a); 20 min, (b); 3 hr, (c); 20 hr.

results were identical with those reported previously.[1,3]

The superoxide ion in pyridine gave electronic spectra which had an absorption band of λ_{max}=462 nm (Fig. 3). This band became reduced in intensity as the anion radical decayed. After 20 hours at room temperature, it almost disappeared and a small absorption band at λ_{max}=375 nm appeared, due probably to the absorption of the products from the reaction of the superoxide ion with pyridine or other possible substances in the system. The band at 462 nm seems to be due not to the electronic transition in the free superoxide ion but to the charge-transfer complex, where the superoxide ion behaves as a donor and pyridine as an acceptor.[14]

Effect of Metal Phthalocyanine. In the voltammetric study, ferrous or cobaltous phthalocyanine added into the electrolytic solution gave the catalytic current to the reduction wave of oxygen and shifted the reduction potential to the positive direction (Table 1). These results suggest the intermediate formation of superoxide ion-metal phthalocyanine complex (**1**), which was concluded by Beyer *et al.* with respect to a phthalocyanine electrode.[15]

TABLE 1. EFFECT OF METAL PHTHALOCYANINE ON VOLTAMMETRIC REDUCTION OF OXYGEN

M–Pc	E_p (V *vs.* SCE)	I_p (mA)
None	−0.90	0.105
Fe–Pc	−0.86	0.124
Co–Pc	−0.82	0.148

M–Pc; metal phthalocyanine, 1 mM in 0.1 M TEAP–pyridine solution. E_p: peak potential. I_p: peak current. potential sweep rate; 0.02 V/s.

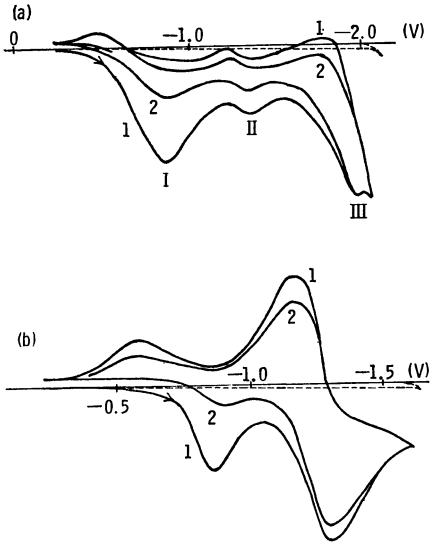

Fig. 4. Cyclic voltammograms of 9,10-dihydroanthracene (a) and fluorene (b), respectively 10 mM in 0.1 M TEAP–pyridine solution. Scan rate; 0.02 V/s. ——; under nitrogen atmosphere, ——; aerated. 1; the first sweep, 2; the second sweep. V *vs.* SCE.

$$O_2 + e \longrightarrow O_2^-$$

$$O_2^- + \text{M-Pc} \rightleftharpoons [O_2^- \cdots \text{M-PC}]$$

complex **1**

$$\longrightarrow O_2 + [\text{M-Pc}]^- \qquad (1)$$

Reactions of Superoxide Ion with Hydrocarbons Having Labile Hydrogens. 9,10-Dihydroanthracene or fluorene were oxidized easily by the seperoxide ion. Figure 4a is the cyclic voltammogram of 9,10-dihydroanthracene in 0.1 M TEAP–pyridine solution with or without oxygen. In the presence of oxygen, some new reduction peaks, which were not observed in the absence of oxygen, appeared. These peaks I, II and III corresponded respectively to the reduction of oxygen, anthraquinone monoanion radical and anthracene. But the re-oxidation peak of the superoxide ion disappeared. In the second sweep the reduction peak of oxygen was remarkably diminished. In the case of fluorene, the similar phenomena were observed (Fig. 4b). The new reduction peak differed from that of oxygen was due to fluorenone. These results show that the electrogenerated superoxide ion reacted easily with 9,10-dihydroanthracene or fluorene, the species resulting from which subsequently took up oxygen molecule in the vicinity of electrode to yield anthraquinone and anthracene or fluorenone.

In order to elucidate the reaction mechanism, the consumption of oxygen during the reaction of the superoxide ion and 9,10-dihydroanthracene was pursued. The reactions were carried out by the controlled potential electrolysis of oxygen-saturated electrolytic sloution containing a certain amount of the substrate at −0.8 V which was approximately the minimum potential for the generation of the superoxide ion and at which the substrate was not reduced. When electrolysis was commenced, the absorption of oxygen

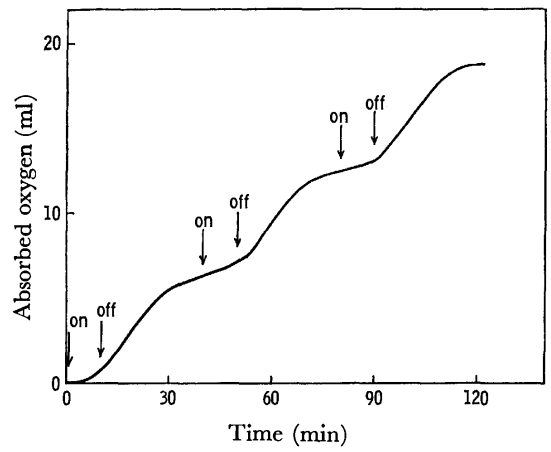

Fig. 5. Oxidation of 9,10-dihydroanthracene in 0.1 M TEAP–pyridine solution, oxygen-saturated at 20 °C, on; cathode (−0.8 V *vs.* SCE), concentration of 9,10-dihydroanthracene; 50 mM.

was observed after several minutes of induction period. Almost simultaneously the electrolytic current increased and the solution gradually became deep wine-red which seemed to be derived from anthraquinone monoanion radical since the ESR spectra of this solution gave the same signal as that of anthraquinone monoanion radical.[16] After long electrolysis, anthraquinone precipitated.

As shown in Fig. 5, when the electric circuit was opened (off) just after the beginning of oxygen absorption, the absorption went on constantly for a while and then gradually ceased. The subsequent closing of the circuit (on) recovered the absorption, preceded by the same induction period as ever.

Zinc isopropyl dithioxantate, which is a peroxy radical-trapping agent in ordinary autoxidations and is reduced at a much more negative potential than −0.8 V,[17] was added to solution, causing a remarkable prolongation of the induction period, followed by the absorption of oxygen at the same rate as that in the absence of the antioxidant. Use of 2,6-di-*tert*-butyl-4-methyphenol as another antioxidant was unsuccess, for the phenol itself was reduced and evolved hydrogen gas.

The reaction orders on substrate and oxygen partial pressure concerning the rate of oxygen absorption were determined experimentally, and the following rate equation was given in lower concentration than 2×10^{-2} M of substrate.

$$-d[O_2]/dt = k_1[RH]^{3/2}[O_2]^{1/2} \quad (2)$$

When a considerable chain length and sufficient oxygen pressure in the general elementary steps of autoxidation are present, the rate of oxygen absorption is expressed as follows, where R_i represents the rate of initiation reaction.[18]

$$-d[O_2]/dt = k_2[RH](R_i)^{1/2} \quad (3)$$

Comparison of Eqs. (2) and (3) gives the rate equation of the initiation of this reaction as

$$R_i = k_3[RH][O_2] \quad (4)$$

From the products and their kinetics mentioned above, the following mechanism seems to be acceptable for the initiation;

$$O_2 + e \rightleftharpoons O_2^- \quad (5)$$

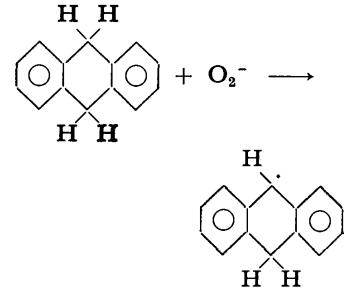

(6)

The electrogenerated superoxide ion abstracts hydrogen from 9,10-dihydroanthracene to yield radical **A**. The subsequent process may be illustrated as follows.

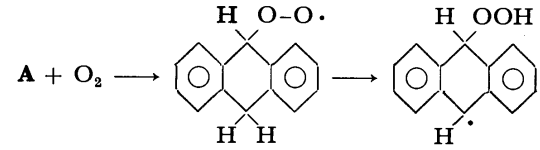

(7)

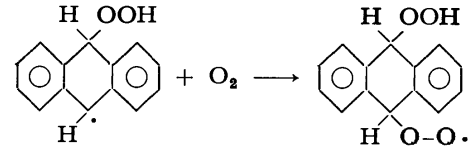

(8)

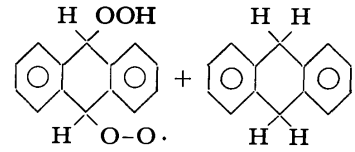

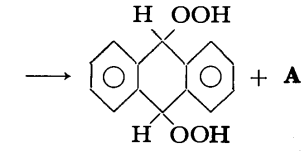

(9)

The addition of oxygen to radical **A** is followed by intramolecular hydrogen abstraction, as proposed by Hawthorne *et al.* in their study of base-catalyzed autoxidation.[19] Dihydroperoxide, one of the products in mechanism (9), is decomposed to give anthraquinone.

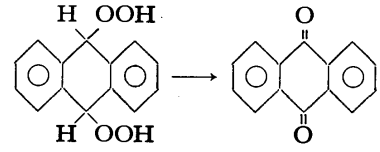

(10)

On the other hand, the production mechanism of anthracene seems to be as follows.

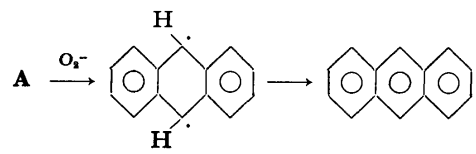

(11)

Some other compounds were also used as substrate. The results are shown in Table 2. The superoxide ion oxidized the compounds with the secondary hydrogen such as fluorene or diphenylmethane to yield ketones, that is fluorenone or benzophenone. It also oxidized cumene to yield the hydroperoxide. Moreover,

TABLE 2. OXIDATION BY ELECTROGENERATED SUPEROXIDE ION

Compounds	$-d[O_2]/dt$ ($\times 10^6$ M/s)	Main products
9,10-Dihydroanthracene	4.37	Anthraquinone: Anthracene (3: 1)
Fluorene	1.17	Fluorenone
Diphenylmethane	3.53	Benzophenone
Cumene	3.27	Cumene hydroperoxide
Cyclohexane	0.35	Unidentified

Concentration of hydrocarbons; 50 mM in oxygen-saturated 0.1 M TEAP–pyridine solution, 20 °C.

it could abstract the hydrogen of cyclohexane although its bond energy of C–H is considerably higher than those of the other substrates.[20] However, the final product could not be detected because of the slow rate of oxidation. Differing from the case of 9,10-dihydroanthracene, the oxidations of these compounds do not proceed according to the usual autoxidation, for these chain lengths were very short.

TABLE 3. EFFECT OF METAL PHTHALOCYANINE ON THE OXIDATION RATE OF 9,10-DIHYDROANTHRACENE

M–Pc	$-d[O_2]/dt$ ($\times 10^6$ M/s)
None	4.37
Fe–Pc	10.2
Co–Pc	10.4

Concentrations of M–Pc and 9,10-DHA; repectively, 1 mM and 50 mM in oxygen-saturated 0.1 M TEAP–pyridine solution, 20 °C.

It is well known that metal phthalocyanine activates oxygen molecule to initiate the autoxidation of various organic compounds such as cumene and α-methylstyrene.[21,22] In our study, ferrous or cobaltous phthalocyanine added to the macro-electrolytic solution acted as a positive catalyst and increased the reaction rate (Table 3). In the presence of ferrous phthalocyanine under 0.2 mM concentration, the rate equation was determined as follows.

$$-d[O_2]/dt = k_4[RH]^{3/2}[O_2]^{1/2}[Cat.]^{1/2} \quad (12)$$

The initiation rate is then expressed as

$$R_i = k_5[RH][O_2][Cat.] \quad (13)$$

This means that the catalyst is involved in the initiation step of Eq. 6. Addition of the catalyst gave no substantial change to the macro-electrolytic current. Therefore, it is inferred that the catalyst makes the superoxide ion more powerful in the hydrogen abstraction by the formation of complex **1** described in Eq. (1) and consequently increases the reaction rate. In the absence of a compound having labile hydrogen, complex **1** regenerates oxygen and gives the catalytic current (Table 1). However, the role of metal phthalocyanine might be more complicated, since it will deactivate the peroxy radical and decompose hydroperoxide.[23,24]

References

1) D. L. Maricle and W. G. Hodgson, *Anal. Chem.*, **37**, 1562 (1965).
2) D. T. Sawyer and J. L. Roberts, Jr., *J. Electroanal. Chem.*, **12**, 90 (1966).
3) M. E. Peover and B. S. White, *Elecrtochimica Acta*, **11**, 1061 (1966).
4) C. Naccache, P. Meriaudeau, M. Che, and A. J. Tench, *Trans. Faraday Soc.*, **67**, 506 (1971).
5) Y. Doi, *Kogyo Kagaku Zasshi*, **74**, 803 (1971).
6) K. Yamamoto and T. Kwan, *J. Catal.*, **18**, 354 (1970).
7) J. J. Weiss, *Nature*, **203**, 183 (1964).
8) R. Dietz, M. E. Peover, and P. Rothbaum, *Chem. Ing. Techn.*, **42**, 185 (1970).
9) R. Dietz, A. E. J. Forno, B. E. Lascombe, and M. E. Peover, *J. Chem. Soc., B*, **1970**, 816.
10) S. Yamaguchi, Y. Yamakawa, and T. Tsukamoto, *Rev. Polarography*, **17**, 145 (1971).
11) F. H. Moser and A. L. Thomas, "Phthalocyanine Compounds," ACS Monograph 157, Reinhold Pub. Corp., New York (1963).
12) C. K. Mann and K. K. Barnes, "Electrochemical Reactions in Nonaqueous Systems," Marcel Dekker, Inc., New York (1970), p. 9.
13) R. N. Adams, "Electrochemistry at Solid Electrode," Marcel Dekker, Inc., New York (1969), p. 143.
14) W. Slough, *Chem. Commun.*, **1965**, 184.
15) W. Beyer and F. Sturm, *Angew. Chem.*, **84**, 154 (1972).
16) B. H. J. Bielski and J. M. Gebicki, "Atlas of Electron Spin Resonance Spectra," Academic Press, New York (1967), p. 554.
17) J. A. Howard, Y. Ohkatsu, J. H. B. Chenier, and K. U. Ingold, *Can. J. Chem.*, **51**, 1543 (1973).
18) N. M. Emanuel, E. T. Denisov, and Z. K. Maizus, "Liquid-Phase Oxidation of Hydrocarbons," Plenum Press, New York (1967), p. 10.
19) J. O. Hawthorne, K. A. Showalter, A. W. Simon, M. H. Wilt, and M. S. Morgan, "Oxidation of Organic Compounds," Vol. 1, ACS, Washington, D. C. (1968), p. 203.
20) S. Korcek, J. H. B. Chenier, J. A. Howard, and K. U. Ingold, *Can. J. Chem.*, **50**, 2285 (1972).
21) H. Hock and H. Kropf, *J. Pract. Chem.*, **9**, 193 (1959).
22) Y. Kamiya, *Tetrahedron Lett.*, **1968**, 4965.
23) A. A. Balanine, Vikt. I. Spitsyn, A. P. Rudenko, and N. P. Dobrosel'skaya, *Kinet. Katal.*, **8**, 808 (1967).
24) A. P. Rudenko and N. P. Dobrosel'skaya, *ibid.*, **9**, 635 (1968).

The PMR Study of the *cis-trans* Isomerization of the Dimethylaluminum Methylphenylamide Dimer, $[(CH_3)_2AlN(CH_3)(C_6H_5)]_2$

Kizuku WAKATSUKI and Toshio TANAKA

Department of Applied Chemistry, Faculty of Engineering, Osaka University, Yamada-kami, Suita, Osaka 565

(Received October 3, 1974)

The dimethylaluminum methylphenylamide dimer exists as an equilibrium mixture of *trans*- (I) and *cis*-isomers (II) with respect to the four-membered Al_2N_2 skeleton, and the latter involves the magnetic non-equivalence of the Al–CH_3 groups. Thermodynamic parameters for the *cis* to *trans* isomerization are obtained from the variable-temperature PMR spectra; $\Delta H = 4.47 \pm 0.09$ kJ·mol^{-1} and $\Delta S = 1.74 \pm 0.48$ J·deg^{-1}·mol^{-1}. The isomerization is markedly accelerated by adding 4-methylpyridine or tetrahydrofuran. A possible mechanism of the isomerization is proposed.

Structural studies of organoaluminum compounds have been widely undertaken by means of X-ray analysis and the PMR spectra in connection with stereospecific catalysis and the bridge-bond character in dimeric or oligomeric aluminum derivatives.[1-12]

In the course of our studies of the reaction of aluminum amides with carbon disulfide,[13] we have found that the dimethylaluminum methylphenylamide dimer $[(CH_3)_2AlN(CH_3)(C_6H_5)]_2$ exists as an equilibrium mixture of *trans*- (I) and *cis*-isomers (II) with respect to the four-membered Al_2N_2 skeleton. This paper will report the PMR study of the equilibrium between the two isomers, of which the *cis*-isomer involves a magnetic non-equivalence of the terminal Al–CH_3 groups. The isomerization between the *cis*- and *trans*-isomers upon the addition of Lewis bases will also be described.

Experimental

The preparation of dimethylaluminum methylphenylamide has been described elsewhere.[13] The PMR spectra were obtained at 100 MHz on a JEOL JNM-PS-100 spectrometer equipped with a variable-temperature probe. Toluene or cyclohexane was used as the internal reference. The sampling was carried out under dry nitrogen. The materials were dried over appropriate desiccants and were distilled under dry nitrogen.

Results and Discussion

The molecular-weight determination indicates the association degree of 1.96 for $(CH_3)_2AlN(CH_3)(C_6H_5)$ (Found: 319 at the 1.96 wt% solution in benzene by the cryoscopic method. Calcd for $C_9H_{14}NAl$: 163). The PMR spectrum of this compound in benzene at room temperature shows two N–CH_3 proton signals (δ 2.68 (relative intensity 4.4) and 2.64 (1.0) ppm) and three Al–CH_3 proton signals (δ −0.21 (4.4), −0.36 (2.0), and −0.54 (4.4) ppm) (Fig. 1a). The relative intensities of these signals change reversibly with the temperature. These results confirm that dimethylaluminum methylphenylamide exists essentially as an equilibrium mixture of dimeric *trans*- (I) and *cis*-isomers (II), with the mole ratio of *ca.* 1.0: 4.4 in benzene at room temperature. The mole ratio is a little solvent-dependent, such as *ca.* 1.0: 5.0 in dichloromethane at room temperature. The existence of analogous isomers has been reported for $[(C_2H_5)XAlN(H)(tert\text{-}C_4H_9)]_2$ (X = C_2H_5, Cl, Br, I) in the course of preparing this paper.[14]

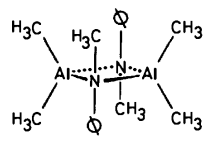

I

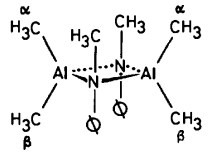

II

The *cis*-isomer involves two kinds of Al–CH_3 groups located in magnetically different environments: α and β, while the four Al–CH_3 groups of the *trans*-isomer are equivalent. The signals at δ 2.64 and −0.36 ppm are assigned to the *trans*-isomer, while the others are assigned to the *cis*-isomer on the basis of their relative intensities. A similar non-equivalence of terminal Al–CH_3 groups has only been reported in the low-temperature PMR spectra of the dimethylcyclopropylaluminum dimer in toluene, in which the two bridging cyclopropyl groups are both bent toward the same side of the four-membered ring.[5]

Table 1. The equilibrium constants between *trans*- and *cis*-$[(CH_3)_2AlN(CH_3)(C_6H_5)]_2$ at various temperatures in dichloromethane

T(K)	296	279	268	257	244	229	216	205
K([*cis*-]/[*trans*-])	5.00	5.76	5.82	6.40	7.59	8.34	10.17	10.94

Equilibrium constants (K) measured in dichloromethane at various temperatures (T) are given in Table 1. A plot of log K *versus* $1/T$ gives $\Delta H = 4.47 \pm 0.09$ kJ·mol^{-1} and $\Delta S = 1.74 \pm 0.48$ J·deg^{-1}·mol^{-1} in the *cis*-to-*trans* isomerization. Both the enthalpy and entropy changes are fairly small compared with those in the interconversion of trimeric $[(CH_3)_2AlN(CH_2)_3]_3$ to the dimer ($\Delta H = 57.8$ kJ·mol^{-1}, $\Delta S = 168$ J·deg^{-1}·mol^{-1}).[10] This may imply that the steric effects and valence-angle strains are not very different between the two isomers of the present compound.

Figure 1 displays the PMR spectra of dimethylaluminum methylphenylamide in benzene containing varying amounts of 4-methylpyridine. When a small amount of 4-methylpyridine (4.32×10^{-2} M) was added to a benzene solution of the aluminum amide (3.93×10^{-1} M as monomer), the Al–CH_3 signals of both the *trans*- and *cis*-isomers broadened and new Al–CH_3 and N–CH_3

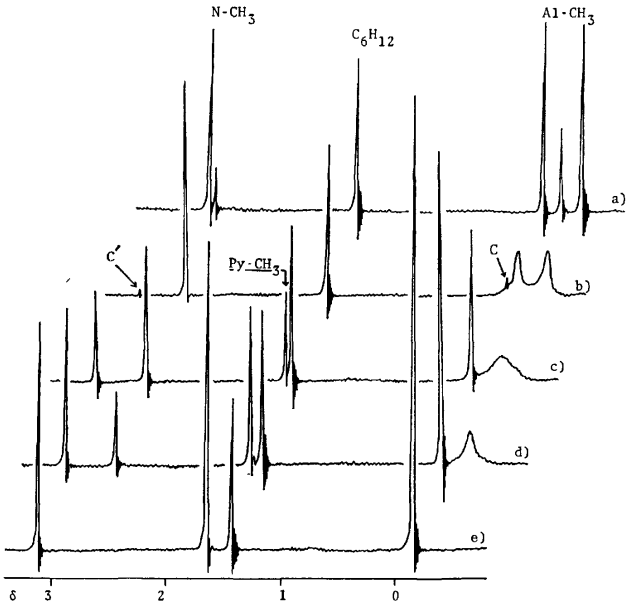

Fig. 1. The PMR spectra of $(CH_3)_2AlN(CH_3)(C_6H_5)$ (3.93×10^{-1} M) in benzene containing varying amounts of 4-methylpyridine; mole ratios of a) 1.00: 0.00, b) 1.00: 0.11, c) 1.00: 0.41, d) 1.00: 0.70, and e) 1.00: 1.37, measured at 100 MHz at 23 °C.

signals (denoted C and C′) occurred at δ −0.12 and 3.13 ppm respectively (Fig. 1b). The pyridine–CH_3 signal, however, was obscured by the proton signal of cyclohexane used as the internal reference in this case, probably because of their almost identical chemical shifts. This is supported by the fact that the pyridine–CH_3 signal gradually moves to a low field and is intensified as the amount of 4-methylpyridine added increases (Figs. 1c, d). The C and C′ signals were similarly strengthened when increasing amounts of 4-methylpyridine were added, and the intensity ratios of the C, C′ and pyridine–CH_3 signals were almost 2: 1: 1 up to the addition of an equimolar amount of 4-methylpyridine to the aluminum amide as a monomer. All the signals of the aluminum amide dimer disappeared in the presence of excess 4-methylpyridine (Fig. 1e). These observations suggest the formation of the 1: 1 adduct between the aluminum amide monomer and 4-methylpyridine; therefore, the C and C′ signals are assigned to the Al–CH_3 and N–CH_3 protons of the adduct respectively. In addition, the sharp and broad Al–CH_3 signals observed in Fig. 1c coalesced at about 50 °C, while the two N–CH_3 signals also merged at the same time. The spectrum was reversibly changed with the temperature. Thus, for the dimethylaluminum methylphenylamide–4-methylpyridine system the following equilibria are suggested:

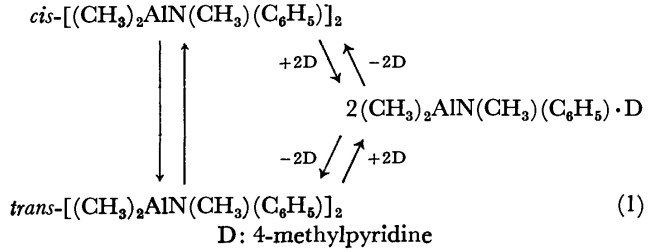

(1)

The broadening of the Al–CH_3 signals of the *cis*- and *trans*-isomers (Figs. 1b—d) suggests that the *cis-trans* isomerization and the site-exchange between α- and β-CH_3 of the *cis*-isomer (shown as Eq. (2)) could be accelerated by the presence of 4-methylpyridine. It

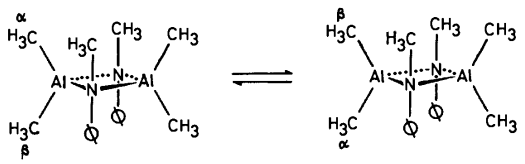

(2)

is noted that the adduct invariably exhibits sharp Al–CH_3 and N–CH_3 signals at room temperature, irrespective of the amount of 4-methylpyridine added. This fact seems to indicate that neither the isomerization nor the site-exchange proceeds *via* the adduct formation at room temperature. At high temperatures, however, both the isomerization and site-exchange possibly occur *via* the adduct formation, since the signals of the 1: 1 adduct and the non-complexed aluminum amide coalesce at about 50 °C.

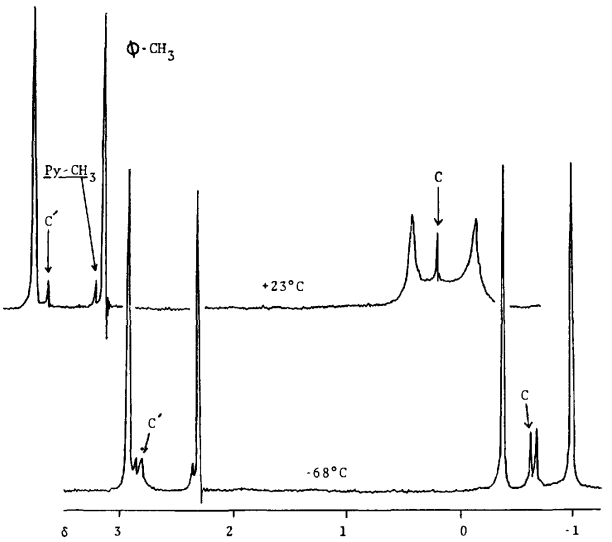

Fig. 2. The temperature-dependent PMR spectra of a mixture of $(CH_3)_2AlN(CH_3)(C_6H_5)$ (5.80×10^{-1} M) and 4-methylpyridine (7.10×10^{-2} M) measured at 100 MHz in dichloromethane.

Figure 2 shows the temperature-dependent PMR spectra of the aluminum amide (5.80×10^{-1} M as monomer) in dichloromethane containing a small amount of 4-methylpyridine (7.0×10^{-2} M). The spectral pattern observed at room temperature was similar to that in benzene, except that the Al–CH_3 and N–CH_3 signals (C, C′) of the adduct occurred very close to those of the respective *trans*-isomer. Each signal becomes sharp with a lowering of the temperature, and the spectrum at −65 °C indicates that the rates of the *cis-trans* isomerization and of the site-exchange are much slower than the NMR time scale. Tetrahydrofuran can also accelerate the *cis-trans* isomerization and the site-exchange. In the presence of less than one mol of tetrahydrofuran per mol of Al, the Al–CH_3 signals were seemingly coalesced into a broad one at room

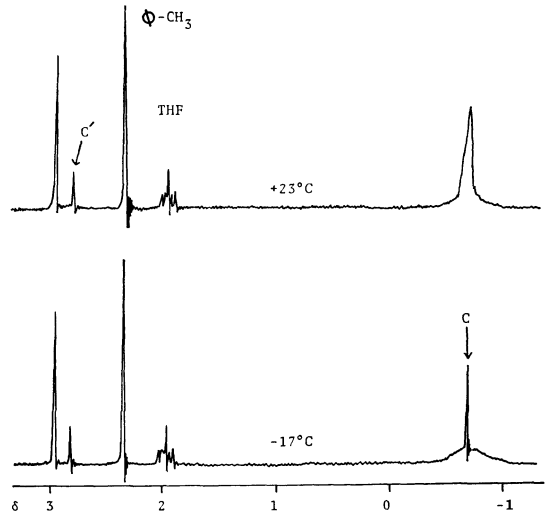

Fig. 3. The temperature-dependent PMR spectra of a mixture of $(CH_3)_2AlN(CH_3)(C_6H_5)$ (6.20×10^{-1} M) and tetrahydrofuran (1.85×10^{-1} M) measured at 100 MHz in dichloromethane.

temperature, while at −17 °C the Al–CH_3 protons of the 1:1 adduct occurred as a sharp signal, as is shown in Fig. 3. The appearance of the Al–CH_3 signal at room temperature is, rather, probably due to the overlap of a sharp signal of the 1:1 adduct and a broadened signal resulting from the isomerization and site-exchange, because the N–CH_3 signal of the 1:1 adduct was observed as a sharp signal even at room temperature. Thus, the isomerization and the site-exchange in the presence of tetrahydrofuran also do not proceed *via* the adduct formation.

There are two possible mechanisms for the *cis-trans* isomerization or the site-exchange; one involves the breaking of an Al–N bond in the $(Al–N)_2$ ring, followed by the rotation-inversion of the non-bridged nitrogen atom or by the rotation of the bridged Al–N bond. The other involves simply the dissociation of the dimeric unit, followed by recombination. The former mechanism is more probable, since the breaking of two Al–N bonds requires a high energy barrier. In the presence of less than one mol of Lewis base per mol of Al, the formation of an intermediate such as III, where L is either the 1:1 adduct of the aluminum amide with a base or the base itself, may be considered to lower the

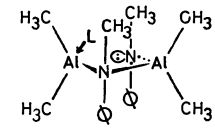

III

barrier of the isomerization and the site-exchange. The formation of such an intermediate is supported by a similar dimeric structure for $C_5H_5N\cdot Al_2(OC_3H_7\text{-}iso)_6$ tentatively proposed by Oliver and Worrall.[15]

References

1) J. F. Malone and W. S. McDonald, *Chem. Commun.*, **1967**, 444.
2) V. R. Magnuson and G. D. Stucky, *J. Amer. Chem. Soc.*, **90**, 3269 (1968).
3) J. L. Atwood and G. D. Stucky, *ibid.*, **92**, 285 (1970).
4) J. C. Huffman and W. E. Streib, *J. Chem. Soc., D*, **1971**, 911.
5) J. W. Moore, D. A. Sanders, P. A. Scherr, M. D. Glick, and J. P. Oliver, *J. Amer. Chem. Soc.*, **93**, 1035 (1971).
6) H. Yasuda, T. Araki, and H. Tani, *J. Organometal. Chem.*, **49**, 103 (1973).
7) M. Kawai, T. Ogawa, and K. Hirota, This Bulletin, **37**, 1302 (1964).
8) K. C. Williams and T. L. Brown, *J. Amer. Chem. Soc.*, **88**, 5460 (1966).
9) E. A. Jeffery, T. Mole, and J. K. Saunders, *Australian J. Chem.*, **21**, 137 (1968).
10) A. Storr and B. S. Thomas, *J. Chem. Soc., A*, **1971**, 3850.
11) J. Müller, K. Margiolis, and K. Dehnicke, *J. Organometal. Chem.*, **46**, 218 (1972).
12) K. J. Alford, K. Gosling, and J. D. Smith, *J. Chem. Soc., Dalton*, **1972**, 2203.
13) K. Wakatsuki, Y. Takeda, and T. Tanaka, *Inorg. Nucl. Chem. Lett.*, **10**, 383 (1974).
14) R. E. Bowen and K. Gosling, *J. Chem. Soc., Dalton*, **1974**, 964.
15) J. G. Oliver and I. J. Worrall, *J. Inorg. Nucl. Chem.*, **33**, 1281 (1971).

Reduction of Nitro and Nitroso Compounds with Tetracarbonylhydridoferrate

Yoshihisa WATANABE, Take-aki MITSUDO, Masakazu YAMASHITA, and Yoshinobu TAKEGAMI

Department of Hydrocarbon Chemistry, Faculty of Engineering, Kyoto University, Sakyo-ku, Kyoto 606

(Received October 22, 1974)

An applicability of potassium tetracarbonylhydridoferrate as a reducing reagent to synthesis of primary amines from a wide variety of nitro and nitroso compounds has been examined. The reaction proceeds vigorously and exothermally at room temperature to give the corresponding amines in excellent yields. For nitroaryls, some substituents have interfering effect on the formation of amines. *o*-Nitrocinnamic aldehyde gives quinoline.

The reduction of nitro compounds using carbon monoxide, hydrogen, and/or metal carbonyls, and their derivatives has long been of interest. Transition metal carbonyls ($Fe(CO)_5$, $Fe_3(CO)_{12}$, $Ru_3(CO)_{12}$, $Co_2(CO)_8$, $[Rh(CO)_2Cl]_2$, $Ni(CO)_4$, and Cu compounds) and their derivatives have been used as reducing catalysts or reagents.[1-12] These compounds have different activities for the reduction of nitro compounds which are converted into a variety of products with groups such as –NO, –N=N–, $-NH_2$, –NCO, $\gtrless NC(=O)N\lessgtr$, and $\gtrless NOH$. Carbonylferrates, $[Fe(CO)_4]^{2-}$ and $[Fe_3(CO)_{11}]^{2-}$, are active for the formation of primary amines from nitro compounds.[1,11] Although tetracarbonylhydridoferrate among the metal carbonyls and their derivatives appears to be effective for the reduction of nitro compounds under mildest conditions, detailed reactivity of this reagent has not been clear.

The present study deals in some detail with the applicability of potassium tetracarbonylhydridoferrate to synthesis of primary amines from nitro and nitroso compounds, mainly substituted nitrobenzenes.

Experimental

Potassium tetracarbonylhydridoferrate was prepared according to the method described in a previous paper:[13] 1.8—3.7 mmol of the ferrate was used in each run. Iron pentacarbonyl, nitrobenzenes, and the other compounds employed were all commercial products.

Reaction Procedure. To the alcoholic ferrate, a certain amount of nitrobenzene or related compounds were stirred in at room temperature under argon or carbon monoxide. After a certain reaction time the reaction mixture was submitted to analysis.

Analytical Procedure. Aniline, cyclohexylamine, and quinoline were analyzed by glpc using internal standards: a column (0.3 cmϕ, 3 m) packed with 10% Versamid on Neopak 60—80 mesh. Other reaction products were isolated as amines or their salts and identified by means of infrared spectra which were recorded on a 215 Hitachi grating spectrophotometer. The products were isolated by evaporating a filtered solution exposed to air for about two days to dryness. For example, the filtered reaction mixture of *o*-nitrobiphenyl (0.95 g, 1.4 mol/mol-$KHFe(CO)_4$) was concentrated to *ca.* 2 ml, IR spectra of which had bands characteristic of *o*-aminobiphenyl, and then the solution was treated with hydrochloric acid and evaporated to dryness to give a white solid, 1.05 g (140%), IR spectra of which had bands characteristic of *o*-aminobiphenyl hydrochloride. *m*-Nitroaniline (0.70 g) gave 1,3-diaminobenzene dihydrochloride as an orange solid, 0.61 g (94%). *o*-Nitrocinnamic acid (1.0 g) gave *o*-aminocinnamic acid as a pale yellow solid, 0.45 g (65%). Carbon dioxide produced in the reaction was volumetrically determined.

Results and Discussion

The ferrate reacted with nitrobenzene to give aniline selectively. The reaction proceeded vigorously and exothermally at room temperature with an evolution of carbon dioxide (about 0.5 mol/mol-$KHFe(CO)_4$) and appeared to complete in several minutes with rapid color change from pale yellow to brown. The results are summarized in Table 1.

TABLE 1. REDUCTION OF NITROBENZENE AND RELATED COMPOUNDS WITH FERRATE[a]

Substrate[b]		Reaction time hr	Aniline[c] %
Nitrobenzene	1.6	0.5	160
Nitrobenzene	2.5	0.5	180
Nitrobenzene	4.0	0.5	180
Nitrosobenzene	4.0	0.5	210
Azobenzene	2.0	10	260
Nitrocyclohexane	2.0	1.5	140[d]

a) Room temperature under argon. b) mol/mol-$KHFe(CO)_4$. c) Based on an amount of the ferrate used. d) Cyclohexylamine.

The reducing power of one mol of the ferrate corresponds to *ca.* 1.8 mol of nitrobenzene which is selectively converted to an equimolar aniline. At this time about 2.0 mol/mol-$KHFe(CO)_4$ of carbonate, $KHCO_3$, are produced and the ferrate is oxidized to di- or trivalent. This consideration is supported by the fact that nitromethane oxidizes the ferrate in alcohol to ferric hydroxide in 12 hr.[14] Ethanol and water, and the hydrido species are hydrogen sources in this reaction but a mechanism of the hydrogen transfer is not clear.

The reaction proceeds without an absorption of carbon monoxide under carbon monoxide and is not affected by reaction atmospheres, argon and carbon monoxide. On the other hand, the reduction of olefin oxides, isoprene, and enamines with the ferrate is highly affected by the carbon monoxide atmosphere:[15] the reaction is generally accelerated under carbon monoxide with an absorption of the gas and the ferrate in the course of the reaction is converted to polynuclear ferrates, $[Fe_2(CO)_8]^{2-}$ and $[Fe_3(CO)_{11}]^{2-}$, and finally to iron pentacarbonyl. In the reduction of nitrobenzene with the ferrate, nitrobenzene acts as a powerful

oxidizing agent and then the ferrate is converted finally to higher valent states inactive to carbon monoxide.

The ferrate had also high reactivity for nitrosobenzene and moderate one for azobenzene. From these, aniline was obtained in excellent yields. Nitrocyclohexane reacted more slowly than nitrobenzene.

Although the reaction is not catalytic, this reagent appears to have a wide applicability to the reduction of nitro and nitroso compounds to primary amines.

Table 2. Reduction of substituted nitrobenzenes with ferrate[a)]

Substituted nitrobenzene	Substituted aniline (%)	Substituted nitrobenzene	Substituted aniline (%)
o-Cl	125	*o*-OH	Black solid
m-Cl	105	*m*-OH	85
p-Cl	105	*p*-OH	63
o-CH_3	120	*o*-OCH_3	85
m-CH_3	125	*o*-NH_2	Black solid
p-CH_3	120	*m*-NH_2	95
o-C_6H_5	140	*p*-NH_2	Black solid
o-COOH[b)]	70	*o*-NO_2[c)]	*o*-NH_2 10
m-COOH[b)]	60	*m*-NO_2[c)]	*m*-NH_2 45
p-COOH[b)]	30	*p*-NO_2[c)]	Black solid

a) Room temperature under argon for 30 min. Nitrobenzenes, 1.4 mol/mol-$KHFe(CO)_4$. Dinitrobenzenes, 0.7 mol/mol-$KHFe(CO)_4$. b) $K_2Fe(CO)_4$ was used. c) The ferrate was enough for the reduction of two nitro groups.

The results of the reduction of substituted nitrobenzenes are listed in Table 2. Nitrobenzenes having a variety of functional groups were readily reduced to the corresponding amines. Conditions were not optimized for these compounds. *o*-Nitrobiphenyl gave *o*-aminobiphenyl, but carbazole, which is taken as evidence for nitrene intermediate,[4,10)] was not obtained. Some functional groups can block the formation of amines and positions of the substituents in a benzene ring have a remarkable effect on the reduction. Nitrobenzenes with groups, *o*-OH, *o*-NH_2, *o*-NO_2, and *p*-NO_2 gave intractable black solids, some of which seem to be iron carbonyl-amine complexes,[16)] although further analysis of the solids was not done. These groups, however, have no interfering effect on the formation of amines when located at the *meta* position. Such substituents as –Cl, –CH_3, and –COOH have no interfering effect.

α-Nitronaphthalene and *o*-nitroacetophenone were reduced to the corresponding amines. The ferrate selectively attacked the more reactive nitro group of *o*-nitrocinnamic acid and the olefinic group remained unchanged when an amount of the ferrate used was enough only for the reduction of the nitro group. *o*-Nitrocinnamic aldehyde gave quinoline in an excellent yield, which appears to be derived *via* *o*-aminocinnamaldehyde by an intramolecular condensation.

An *N*-nitroso group had a poor reactivity for the ferrate. *N*-Nitrosodiphenylamine slowly reacted with the ferrate to give diphenylamine which seemed to be derived *via* *N,N*-diphenylhydrazine by a N–N bond cleavage. *N*-Nitrosodicyclohexylamine was recovered unchanged under the condition used. ω-Nitrostyrene had a high reactivity for the ferrate but gave an intractable, tarry material.

References

1) German Patent 441179 (1925).
2) S. Murahashi and S. Horiie, This Bulletin, **33**, 78 (1960).
3) G. D. Buckey and N. H. Ray, *J. Chem. Soc.*, **1949**, 1154.
4) J. E. Kmiecik, *J. Org. Chem.*, **30**, 2014 (1965).
5) E. K. von Gustorf, M. C. Henry, R. E. Sacher, and C. DiPietro, *Z. Naturforsch.*, **21b**, 1152 (1966).
6) Brit. Patent (*Chem. Abstr.*, **64**, 11126h (1966)).
7) W. B. Hardy and R. P. Bennett, *Tetrahedron Lett.*, **1967**, 961.
8) T. Kajimoto and J. Tsuji, This Bulletin, **42**, 827 (1969).
9) F. L'Eplattenier, P. Matthys, and F. Calderazzo, *Inorg. Chem.*, **9**, 342 (1970).
10) H. Alper and J. T. Edward, *Can. J. Chem.*, **48**, 1543 (1970).
11) J. M. Landesberg, L. Katz, and C. Olsen, *J. Org. Chem.*, **37**, 930 (1970), and references cited therein.
12) J. F. Knifton, *ibid.*, **38**, 3296 (1973).
13) Y. Takegami, Y. Watanabe, H. Masada, and I. Kanaya, This Bulletin, **40**, 1456 (1967).
14) J. C. Case and M. C. Whiting, *J. Chem. Soc.*, **1960**, 4632.
15) Y. Takegami, Y. Watanabe, T. Mitsudo, I. Kanaya, and H. Masada, This Bulletin, **41**, 158 (1968); Y. Takegami, Y. Watanabe, T. Mitsudo, and H. Masada, *ibid.*, **42**, 202 (1969); T. Mitsudo, Ph. D. Thesis, Kyoto University (1972).
16) A. J. Carty, *Organomet. Chem. Rev.* A, **7**, 191 (1972), and references cited therein.

The Isomerization of the Stable Rotamers of 9,9′: 9′,9″-Terfluorenyls

Masahiro MINABE and Kazuo SUZUKI

Department of Industrial Chemistry, Faculty of Technology, Utsunomiya University, Ishii-cho, Utsunomiya 321–31

(Received October 24, 1974)

The conformational change of the *s-cis*, *s-trans*-9,9′: 9′,9″-terfluorenyl to the *s-cis*, *s-cis* form *via* the radical process was performed by means of a reaction with *N*-bromosuccinimide and with various oxidizing agents. A reverse change occurred on treatment with lithium aluminum hydride and with sodium bis(2-methoxyethoxy)-aluminum hydride.

Two stereoisomers (mp 293 °C (dec) and mp 257 °C (dec)) have hitherto been obtained by various reactions.[1] The conformational isomers of 9,9′: 9′,9″-terfluorenyls were inferred[2] from the results of restricted rotation around the $C_{9-9'-9''}$ single bonds: *s-cis*, *s-cis* (mp 293 °C (dec)) (**1**) and *s-cis*, *s-trans* (mp 257 °C (dec)) (**2**), both of which were stable at room temperature in solution.

1 was converted to **2** by a pyrolytic reaction[3] and by treatment with Raney nickel[2]; however, no isomer was obtained by the reverse change.

The present paper will deal with the isomerization from **1** to **2** or *vice versa*. The **2** rotamer was converted into **1** by reactions with molecular oxygen-benzyltrimethylammonium hydroxide (Triton B), with *N*-bromosuccinimide (NBS), and with such oxidants as manganese dioxide, selenium dioxide, and potassium permanganate.

Conversely, **1** was isomerized to **2** by treatment with lithium aluminum hydride. Both conformers were interconverted by refluxing with sodium bis(2-methoxyethoxy)aluminum hydride (SMAH) in benzene.

Results and Discussion

The hydrogen atoms on the 1,8, 1′,8′,1″,8″, 9, and 9″ positions are close in the overcrowded molecules, **1** and **2**. The conformation of the 9-hydrogen atom in **2** corresponds to that of *s-trans*-9,9′-bifluorenyl, and the other hydrogen on 9″-carbon is located on entering the back of the 9-fluorenyl plane, as the models indicate.[2] Therefore, the bulky 9-fluorenyl plane would tend to shield the 9″-carbon atom from an attack of approaching reagents, and it could be expected to facilitate the formation of a free radical at the less hindered 9-carbon atom.

Table 1 shows the results of the isomerization of **2** to **1** (maximum yield, 56%) by means of a reaction with NBS. 9,9′-Dibromo-9,9′-bifluorenyl,[4] 9-bromo-9,9′-bifluorenyl,[1a] fluorenone (**3**), and 9,9′-bifluorenylidene (**4**) were isolated as by-products.

The reaction is initiated by the abstraction of the hydrogen atom from the tertiary 9-carbon of **2** by a bromine atom; 9,9′: 9′,9″-terfluorenyl 9-radical (R) and hydrogen bromide are formed in the main reaction. The radical (R) may abstract a hydrogen atom of hydrogen bromide to form the six-membered hydrogen-bonded intermediate (A), without any homolytic cleavage of the $C_{9-9'}$ or $C_{9'-9''}$ bond, as Scheme 1 shows. Moreover, the radical reaction can be conducted so as to form the *s-cis*, *s-cis* conformer **1**, with the loss of a bromine atom from (A).

This finding may be explained in terms of the bond energies of C-H and C-Br in the crowded molecule.

TABLE 1. THE REACTION OF 9,9′: 9′,9″-TERFLUORENYLS WITH NBS

Reaction conditions					Products g(%)				Recovered g(%)
Substrate (g)	NBS g	Benzene ml	Temp. °C	Time hr	**1**	9,9′-Dibromo-9,9′-bifluorenyl	9-Bromo-9,9′ bifluorenyl[a]	**4**	
2 (1.24)	0.49	150	Room Temp.	40 (days)	0.70 (56)	0.08 (4)	(25)	0.02 (2)	0.01 (1)
2 (1.24)	0.49	120	50	5	0.54 (44)	0.05 (3)	(35)	trace	
2[b] (1.24)	0.49	50	Refl.	3	0.58 (47)	0.09 (5)	(14)	0.11 (9)	
2[c] (1.24)	0.49	310 (CCl_4)	50	5	0.17 (14)		(8)	0.01 (1)	0.85 (69)
2 (1.24)	0.38 (NBA)	120	50	5	0.62 (50)	0.20 (11)	(15)	0.09 (7)	
1 (1.24)	0.49	120	50	5		trace			1.19 (96)
1[b,c] (1.24)	0.49	50	Refl.	3		0.01 (1)		0.02 (2)	1.12 (90)
1 (1.24)	0.38 (NBA)	120	50	5					1.20 (97)

a) Yield of 9-bromo-9,9′-bifluorenyl shows the total amounts of 9-bromo-9,9′-bifluorenyl and 9-hydroxy-9,9′-bifluorenyl.
b) A trace of benzoyl peroxide was used. c) A trace amount of **3** was additionally obtained. d) NBA = *N*-bromoacetamide.

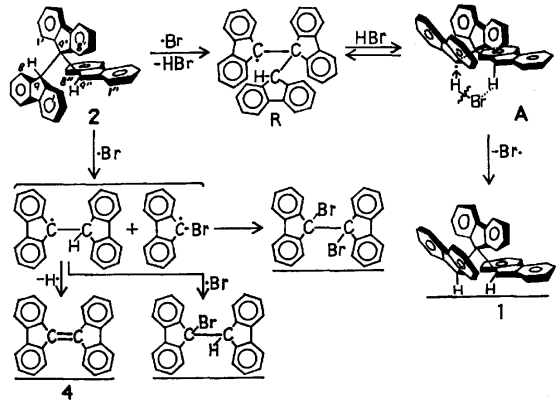

Scheme 1. (Underscored compounds were isolated.)

The molecular strain can be relieved when the radical is formed on the 9-position in **2**. Conversely, the steric compression may be increased when the crowed 9-position is occupied by a bulky bromine atom or when radical coupling takes place. Therefore, (A) is converted to **1**, or the $C_{9-9'}$ linkage in **2** dissociates partially into 9-bromofluorenyl and 9,9′-bifluorenyl radicals by an attack of the bromine atom to form stable dimerization and disproportionation products, without the formation of 9-bromoterfluorenyl.

The **2** isomerized to **1** (maximum yield, 42%) in pyridine upon treatment with molecular oxygen in the presence of a basic catalyst such as Triton B, as is shown in Table 2.

The initial radical (R) is formed along with hydroperoxide, and both species may recombine to form 9,9′:9′,9″-terfluorenyl-9-hydroperoxide (B). The **1** isomer is formed by the dissociation of the 9,9′:9′,9″-terfluorenyl-9-peroxide radical ($\cdot O_2R$) from the hydrogen-bonded intermediate (C) which is attributable to the reaction of (R) and (B), as Scheme 2 shows. The (R) and (B) intermediates can be reproduced by an attack of the radical ($\cdot O_2R$) on **2**.

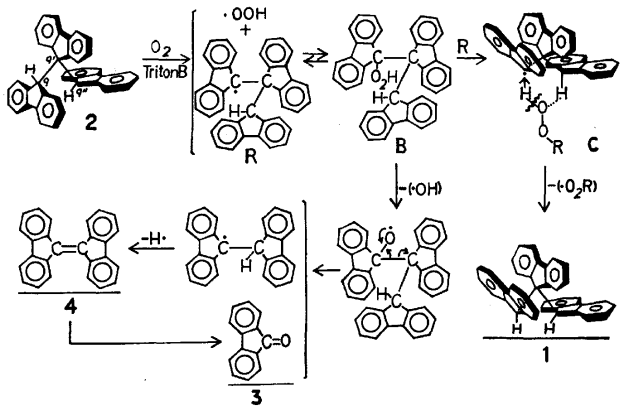

Scheme 2. (Underscored compounds were isolated.)

The 9,9′-bifluorenyl radical and **3** may be formed from a part of (B) by the cleavage of the hydroxy radical. The 9,9′-bifluorenyl radical is converted into **4** by the splitting of the hydrogen atom, and **4** is oxidized finally to **3**.

The isomerization of **2** with bromine was performed under ultraviolet irradiation at room temperature; the **1** rotamer (29% yield) and 2-bromo-9,9′:9′,9″-terfluorenyl[1b] (16% yield) were thus isolated. Compound **2** was isomerized to **1** by treatment with selenium dioxide (22% yield) and with potassium permanganate (61% yield). However, no reverse isomerization occurred under the same conditions. The formation of **1** is explicable in the same way as in the reaction using NBS.

Table 2. The reaction of 9,9′:9′,9″-terfluorenyls with Triton B

Substrate (g)	Reaction conditions: Triton B ml	Temp. °C	Time hr	Products g(%): 1	4	3	Recovered g(%)
2 (1.24)	0.05	−2	1	0.08 (7)	0.01 (1)	0.01 (1)	0.97 (77)
		−2→10	1				
2 (1.24)	0.25	2→10	2	0.44 (36)	0.02 (2)	0.16 (11)	0.52 (42)
2 (1.24)	0.25	23	2	0.52 (42)	0.04 (3)	0.28 (19)	0.32 (26)
2[a] (1.24)	0.25	25	2	0.06 (5)	0.02 (2)	0.01 (1)	0.96 (77)
2 (1.24)	None	115	4				1.21 (98)
1 (1.24)	0.25	22	2		0.05 (4)	0.10 (7)	1.00 (81)
1 (1.24)	1.00	23	2		0.24 (19)	0.27 (19)	0.46 (37)
1 (1.24)	12.0	115	2			1.13 (84)	
4[b] (0.82)	1.00	20	2			0.33 (37)	0.48 (59)
Fluorenol (1.82)	8.00	25	2			1.70 (94)	
Fluorene (1.66)	8.00	24	2			1.29 (72)	0.25 (15)

a) The reaction was carried out under nitrogen atmosphere. b) A 20 ml of pyridine was used as solvent.

The conformer **2**-9,9″-d_2[5] (or *s-cis*, *s-trans*-9,9′: 9′,9″-terfluorenyl-9,9″-dideuteride) was treated with suspended manganese(IV) dioxide in benzene to give **1**-9,9″-d_2[5] (58% yield). The deuterium contents of **1**-9,9″-d_2 and the recovered **2**-9,9″-d_2 are of the same order with that of the starting material.

It may be proposed that, under these conditions, the abstraction of 9-hydrogen in **2** by manganese dioxide may form a radical (R) and manganic oxyhydrate ($HO-Mn^{III}=O$). These are then converted to **1** and manganese dioxide through a six-membered hydrogen-bonded intermediate such as (A).

Conversely, **1** was isomerized to **2** by treatment with lithium aluminum hydride in dry tetrahydrofuran: **1**-9,9″-d_2 gave **2**-9-d[5] (36% yield) by being decomposed with ethanol and water. Moreover, **1** was allowed to react with the same reagent; subsequently it was decomposed with heavy water to give **2**-9″-d (50% yield). The **2** rotamer afforded only 9,9′-bifluorenyl (**5**) (0.3% yield) by the same reaction.

This isomerization presumably proceeds *via* 9-lithio-9,9′: 9′,9″-terfluorenyl (D), not through an intermediate such as (A) or (C), as Scheme 3 shows. Therefore, the conformation of (D) is considered to be *s-cis*, *s-trans* rather than *s-cis*, *s-cis*; (D) is then converted into **2**.

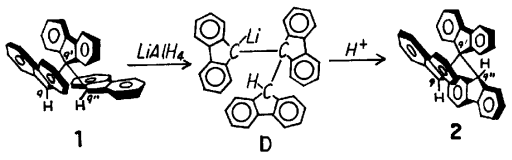

Scheme 3.

Furthermore, both rotamers were interconverted by means of a reaction with SMAH:[6] **1** into **2** (23% yield) and **2** into **1** (13% yield). The isomerization of **1** to **2** by a reducing agent may occur through 9-sodio-9,9′: 9′,9″-terfluorenyl in a way similar to that found for lithium aluminum hydride. The reverse change of **2** to **1** may be attributed to the strong basicity of SMAH, and the reaction may be proceed in analogy with the case of Triton B.

Experimental

All the melting points are uncorrected.

The compounds were confirmed by mixed-melting-point determinations and by a comparison of their IR spectra with those of authentic samples. The IR spectra were recorded as KBr-pellets using a IR-G spectrophotometer (Japan Spectroscopic Co., Ltd.).

The NMR data were obtained in a C_6D_6 solution with a JNM-C60HL spectrometer (Japan Electron Optics Lab. Co., Ltd.).

The deuterium content was confirmed from the average value of five mass spectra recorded on a RMU-6E apparatus (Hitachi, Ltd.).

Isomerization of **2** *to* **1** *by Treatment with NBS. Typical Procedure*: A solution of 1.24 g (2.5 mmol) of **2** and 0.49 g (2.7 mmol) of NBS in 120 ml of dry benzene was maintained at 50 °C for 5 hr while being stirred. The dark-red benzene solution was then evaporated to dryness under reduced pressure, and the residue was washed with hot water, dried, and recrystallized from benzene (50 ml) to give 0.34 g of **1** (mp 290—292 °C (dec)).

When the benzene mother liquor was chromatographed on alumina, the elute gave the following compounds by recrystallization from cyclohexane, cyclohexane–benzene, or benzene–ligroin: 0.20 g (total 0.54 g, 44%) of **1** (mp 292—293 °C (dec)), 0.05 g (3%) of 9,9′-dibromo-9,9′-bifluorenyl (mp 239—240 °C (dec)), and a trace amount of **4** (mp 182—184 °C).

A 0.45-g portion (35%) of 9-hydroxy-9,9′-bifluorenyl (mp 193—194 °C) was isolated from the column.[7]

Isomerization of **2** *by Treatment with Triton B and Oxygen. Typical Procedure*: To a solution of 1.24 g of **2** and 0.25 g of Triton B (10% aqueous solution) in 50 ml of pyridine, oxygen was passed gently at 23 °C for 2 hr (the color changed to black).

The reaction mixture was then diluted with 500 ml of water, and the precipitate was sublimed *in vacuo* at 140 °C to give 0.28 g (19%) of **3** (mp 82—83 °C (ethanol)). The residue after sublimation afforded 0.52 g (42%) of **1** (mp 292.5—293 °C (dec)), 0.32 g (26%) of recovered **2** (mp 256—257 °C (dec)), and 0.04 g (3%) of **4** (mp 183—184.5 °C) by recrystallization from benzene.

With Manganese Dioxide. a): A solution of 0.5 g (1 mmol) of **2**-9,9″-d_2 in 25 ml of dry benzene was refluxed with 2.5 g of manganese dioxide (E. Merck, for synthesis) for 2 hr.

Upon cooling, the reaction mixture was filtered, and the manganese dioxide was extraced with a 150-ml portion of benzene. All of the benzene solution was chromatographed on alumina; 0.29 g (58%) of **1**-9,9″-d_2 (mp 292—293 °C (dec)), 0.02 g (4%) of **5** (mp 243—244 °C), 0.11 g (20%) of **3** (mp 81—83 °C), and 0.03 g (6%) of **2**-9,9″-d_2 (mp 255-257 °C (dec)) were thus obtained.

The deuterium contents in **1**-9,9″-d_2 and the recovered **2**-9,9″-d_2 were of the same order with that of the starting **2**-9,9″-d_2, as is shown by their mass spectra: *m/e* 494 (d_0, 1%), 495 (d_1, 12%), and 496 (d_2, 87%).

b): In a similar treatment, **1** gave only **3** (2%) and recovered **1** (90%).

With Potassium Permanganate. a): Compound **2** (1.0 g, 2 mmol) was refluxed with 3.5 g of potassium permanganate in 50 ml of dry pyridine for 5 hr. After cooling, the reaction mixture was decomposed with aqueous sodium bisulfite and hydrochloric acid, and the precipitate was sublimed *in vacuo* at 120 °C.

The sublimate gave 0.28 g (26%) of **3** (mp 83—84 °C), and the residue after sublimation yielded 0.61 g (61%) of **1** (mp 292—293 °C (dec)).

When **1** was treated in a similar manner, 97% of the starting material was recovered.

b): A mixture of **2** (1.0 g), potassium permanganate (6.5 g), and aluminum sulfate (6.8 g) in dry acetone (300 ml) was refluxed for 5 hr. The reaction mixture was then treated as has been described above to afford 0.58 g (58%) of **1** (mp 292—293 °C (dec)) and 0.41 g (38%) of **3** (mp 80—82 °C).

With Selenium Dioxide. a): A mixture of 1.0 g (2 mmol) of **2**, 0.5 g of selenium oxide, and 200 ml of dry acetic acid was refluxed for 10 hr. Upon cooling, the precipitate was filtered and then recrystallized from benzene to give 0.22 g (22%) of **1** (mp 292—293 °C (dec)).

The acetic acid solution was evaporated *in vacuo*, and the residue was extracted with a 50-ml portion of benzene to give 0.62 g (62%) of **2** (mp 255—257 °C (dec)). The benzene mother liquor was chromatographed on alumina to yield 0.01 g (1%) of **3** (mp 83—85 °C).

b): The **1** isomer (1.0 g) was treated with selenium oxide (0.5 g) in dry acetic acid (200 ml) for 5 hr. 98% of the **1** (mp 292—293 °C (dec)) was recovered, accompanied by a trace

amount of **3**.

With Bromine. a): A solution of 1.0 g of **2** and 0.32 g of bromine in 130 ml of chloroform was irradiated with a 100-W high-pressure mercury lamp for 4 hr at room temperature in an atmosphere of nitrogen. The reaction mixture was then washed with a 2% sodium hydroxide solution and with water and evaporated to dryness; the residue was recrystallized from ethyl acetate: 0.19 g (16%) of 2-bromo-9,9′:9′,9″-terfluorenyl (mp 255—257 °C (dec)) and 0.29 g (29%) of **1** (mp 291—293 °C (dec)) were isolated.

b): To a solution of 1.0 g (2 mmol) of **1** and 0.01 g of anhydrous ferric chloride in 90 ml of chloroform, a 0.32-g portion (2 mmol) of bromine in 10 ml of chloroform was added, drop by drop, over a period of 1 hr at room temperature under a nitrogen atmosphere in the dark, after which stirring was continued for an additional 23 hr.

Upon treatment as above, 0.63 g (54%) of 2-bromo-9,9′:9′,9″-terfluorenyl (mp 256—257 °C (dec)) and 0.30 g (30%) of **1** (mp 292—293 °C (dec)) were obtained.

*Isomerization of **1** to **2** by Treatment with Lithium Aluminum Hydride. a)*: The **1**-9,9″-d_2 rotamer (1.0 g, 2 mmol) was refluxed with 0.76 g (20 mmol) of lithium aluminum hydride in 70 ml of dry tetrahydrofuran for 5 hr. The reaction mixture was then evaporated to dryness under reduced pressure and decomposed with a 20-ml portion of ethanol and with a 100-ml portion of 1 M hydrochloric acid. The precipitate was filtered off, dried, and recrystallized from ethyl acetate; this afforded 0.36 g (36%) of **2**-9-*d* (mp 256—257 °C (dec)), 0.03 g of **5** (mp 242—243 °C), and 0.46 g (46%) of **1**-9,9″-d_2 (mp 291—293 °C (dec)).

The deuterium content of the recovered **1** was of the same order with that of the starting material. The NMR spectrum of **2**-9-*d* showed no peak at 5.36 ppm assigned to the 9-position.

Mass spectrum for recovered **1**-9,9″-d_2: *m/e* 494 (d_0, 1%), 495 (d_1, 8%), and 496 (d_2, 91%). For **2**-9-*d*: *m/e* 494 (d_0. 25%), 495 (d_1, 74%), and 496 (d_2, 1%).

b): A solution of 1.0 g of **1** in 70 ml of dry tetrahydrofuran was refluxed with 0.76 g lithium aluminum hydride for 5 hr, Upon cooling, 14 ml of deuterium oxide containing 4% of deuterium chloride was slowly added to the resulting mixture. The precipitate was recrystallized from ethyl acetate to give 0.50 g (50%) of **2**-9″-*d* (mp 256—257 °C (dec)) and 0.15 g of **5** (mp 242—243.5 °C). The mother liquor was then evaporated to dryness, and the residue was sublimed *in vacuo* at 120 °C; the sublimate gave 0.02 g of fluorene (mp 113—114.5 °C (recrystallized from *n*-hexane)).

The signal at 4.61 ppm (9″-position) was confirmed to decrease in the NMR spectrum of **2**-9″-*d*.

Deuterium content for **2**-9″-*d*: *m/e* 494 (d_0, 81%), 495 (d_1, 16%), and 496 (d_2, 3%).

c): Compound **2** (1.5 g) was treated with 1.1 g of lithium aluminum hydride in 100 ml of dry tetrahydrofuran for 9 hr. The reaction mixture was then worked-up as has been described above to yield 1.36 g (91%) of **2** (mp 255—257 °C (dec)) and 0.004 g of **5** (mp 242—244 °C).

*Interconvertion Reactions of **1** and **2** by Treatment with SMAH. a)*: A solution of 1.0 g (2 mmol) of **1** and 8 ml of SMAH (70% benzene solution) in 50 ml of dry benzene was refluxed for 15 hr (it turned dark).

Upon cooling, the reaction mixture was washed successively with a 100-ml portion of 10% hydrochloric acid and with two 100-ml portions of water and dried over calcium chloride to yield, after the removal of the solvent, 0.23 g (23%) of **2** (mp 254—256 °C (dec)) and 0.38 g (38%) of **1** (mp 291—293 °C (dec)). Additionally, 0.17 g of **4** (mp 183—185 °C), 0.05 g of fluorene (mp 112—114 °C), and 0.04 g of **3** (mp 82—83.5 °C) were obtained.

b): The **2** isomer (1.0 g) was treated with 4 ml of SMAH in 50 ml of dry benzene for 15 hr; 0.13 g (13%) of **1** (mp 292—293 °C (dec)), 0.68 g (68%) of **2** (mp 256—257 °C (dec)), 0.18 g of **4** (mp 182—184 °C), 0.01 g of fluorene (mp 112—115 °C), and 0.07 g of **3** (mp 81—83 °C) were thus isolated.

References

1) a) S. Kajigaeshi, *Nippon Kagaku Zasshi*, **82**, 1712 (1961); b) K. Suzuki, *ibid.*, **75**, 711 (1954); c) K. Suzuki, *ibid.*, **72**, 825, 827 (1951); S. Kajigaeshi, *ibid.*, **82**, 1397 (1961); K. Suzuki and S. Kajigaeshi, This Bulletin, **35**, 408 (1962); N. Filipescu and J. R. DeMember, *Tetrahedron*, **24**, 5181 (1968).

2) K. Suzuki and M. Minabe, *Tetrahedron Lett.*, **1974**, 1541.

3) K. Suzuki, M. Minabe, S. Kubota, and T. Isobe, This Bulletin, **43**, 2217 (1970).

4) A. Hantzsch and W. H. Glover, *Ber.*, **39**, 4153 (1906); C. Graebe and B. Mantz, *Ann.*, **290**, 238 (1896).

5) M. Minabe and K. Suzuki, *J. Org. Chem.*, **40**, (May, 1975).

6) Fluorenol was treated with SMAH and gave **3** (20%), **5** (0.7%), fluorene (0.06%), and recovered fluorenol (73%). This indicates that SMAH acts as oxidizing and reducing agent.

7) It is already known that 9-bromo-9,9′-bifluorenyl was converted to 9-hydroxy-9,9′-bifluorenyl by percolating through alumina. See Ref. la.

The Thermolysis and Photolysis of 6-(Benzylidenehydrazino)uracils. New Syntheses of Pyrazolo[3,4-*d*]pyrimidines. A Method to Convert Aldehydes to Nitriles

Fumio YONEDA and Tomohisa NAGAMATSU

Faculty of Pharmaceutical Sciences, Kumamoto University, Oe-honmachi, Kumamoto 862

(Received November 1, 1974)

The thermolysis of 6-(benzylidenehydrazino)uracil derivatives generally involves their oxidative cyclization to give the corresponding pyrazolo[3,4-*d*]pyrimidine derivatives. However, the thermolysis of fully methylated 6-(benzylidenehydrazino)uracils gave no pyrazolo[3,4-*d*]pyrimidines, but mixtures of the respective nitriles and 1,3-dimethyl-6-methylaminouracil. The photolysis of the fully methylated 6-(benzylidenehydrazino)uracils give the desired pyrazolo[3,4-*d*]pyrimidines.

Our interest in the pyrazolo[3,4-*d*]pyrimidine ring system,[1] bolstered by the fact that derivatives of pyrazolo[3,4-*d*]pyrimidine possess many kinds of biological activities prompted us to investigate the systematic syntheses of this ring system. Our initial efforts have been directed toward the exploration of a convenient synthesis of derivatives of pyrazolo[3,4-*d*]-pyrimidine-4,6(5*H*,7*H*)-dione, which is isomeric with xanthine. The known synthetic methods for the preparation of pyrazolo[3,4-*d*]pyrimidines have involved the construction of suitably substituted pyrazole precursors, followed by the subsequent annelation of the condensed pyrimidine ring[2,3] and the condensation cyclization of 6-hydrazinopyrimidine derivatives.[4,5] This paper will describe a new, convenient method of synthesizing pyrazolo[3,4-*d*]pyrimidine-4,6(5*H*,7*H*)-dione derivatives, a method which consists of the thermal and photochemical cyclizations of the 6-(benzylidenehydrazino)-uracils, followed by dehydrogenation.[6]

The key intermediates, the 6-(benzylidenehydrazino)-uracil derivatives (**1a**—**w**), were prepared by the treatment of the appropriate 6-hydrazinouracils with several aldehydes in ethanol at room temperature (Table 1).

TABLE 1. 6-(BENZYLIDENEHYDRAZINO)URACILS (**1a**—**w**)

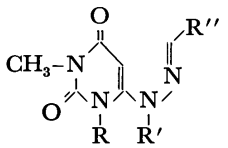

Compd.	R	R′	R″	Mp[a] (°C)	Yield (%)	Analyses % Found (Calcd) C	H	N
1a	CH_3	H	C_6H_5	261[11]	94	60.52 (60.45)	5.78 (5.46)	21.65 (21.70)
1b	CH_3	H	*p*-Cl-C_6H_4	258	100	53.30 (53.34)	4.45 (4.48)	19.08 (19.14)
1c	CH_3	H	3,4-Cl_2-C_6H_3	282	92	47.75 (47.72)	3.72 (3.70)	16.89 (17.13)
1d	CH_3	H	*p*-CH_3O-C_6H_4	261	95	58.43 (58.32)	5.55 (5.59)	19.26 (19.44)
1e	CH_3	H	*p*-$(CH_3)_2N$-C_6H_4	256[11]	95	59.69 (59.78)	6.31 (6.36)	23.05 (23.24)
1f	H	CH_3	C_6H_5	245	96	60.33 (60.45)	5.39 (5.46)	21.42 (21.70)
1g	H	CH_3	*p*-Cl-C_6H_4	194	97	53.42 (53.34)	4.42 (4.48)	19.01 (19.14)
1h	H	CH_3	3,4-Cl_2-C_6H_3	261	71	47.68 (47.72)	3.66 (3.70)	16.92 (17.13)
1i	H	CH_3	*p*-CH_3O-C_6H_4	223	92	58.29 (58.32)	5.40 (5.59)	19.44 (19.44)
1j	H	CH_3	*p*-$(CH_3)_2N$-C_6H_4	244	88	59.64 (59.78)	6.28 (6.36)	23.19 (23.24)
1k	H	H	C_6H_5	298	83	58.74 (59.01)	4.94 (4.95)	22.75 (22.94)
1l	H	H	*p*-Cl-C_6H_4	260	86	51.99 (51.71)	3.78 (3.98)	19.93 (20.15)
1m	H	H	3,4-Cl_2-C_6H_3	262	91	46.30 (46.02)	3.21 (3.22)	17.68 (17.89)
1n	H	H	*p*-CH_3O-C_6H_4	233	76	56.78 (56.93)	5.14 (5.15)	20.26 (20.43)
1o	H	H	*p*-$(CH_3)_2N$-C_6H_4	262	99	58.32 (58.52)	5.93 (5.96)	24.07 (24.38)
1p	CH_3	CH_3	CH_3	131	88	51.55 (51.42)	6.92 (6.71)	26.61 (26.65)
1q	CH_3	CH_3	CH_3CH=CH	151	78	56.23 (55.91)	6.75 (6.83)	23.40 (23.72)
1r	CH_3	CH_3	C_6H_5	151	86	61.90 (61.75)	5.93 (5.92)	20.28 (20.58)
1s	CH_3	CH_3	*p*-Cl-C_6H_4	231	100	55.16 (54.81)	4.85 (4.93)	18.60 (18.27)
1t	CH_3	CH_3	3,4-Cl_2-C_6H_3	225	100	49.51 (49.28)	4.05 (4.14)	16.62 (16.42)
1u	CH_3	CH_3	*p*-CH_3O-C_6H_4	164	90	59.73 (59.59)	6.08 (6.00)	18.60 (18.53)
1v	CH_3	CH_3	*p*-$(CH_3)_2N$-C_6H_4	150	87	60.99 (60.93)	6.90 (6.71)	22.21 (22.21)
1w	CH_3	CH_3	3-Pyridyl	203	94	57.08 (57.13)	5.52 (5.53)	25.34 (25.63)

a) All products were recrystallized from ethanol.

Results and Discussion

*Pyrolysis of 6-(Benzylidenehydrazino)uracils (**1a—o**).* The fusion of Compounds **1a—o** at temeratures slightly higher than their melting points for 5 to 30 min, followed by dilution with ethanol, caused a separation of the corresponding pyrazolo[3,4-*d*]pyrimidines (**2a—o**) (Table 2). The fusion of fully methylated 6-(benzylidenehydrazino)uracils (**1p—w**) took a completely different route and gave no detectable amount of pyrazolo[3,4-*d*]-pyrimidines, as will be described below. In the cases of the cyclization of **1a—d** (R=CH_3, R′=H), the

TABLE 2. PYRAZOLO[3,4-*d*]PYRIMIDINE-4,6(5*H*,7*H*)-DIONES (**2a—o**)

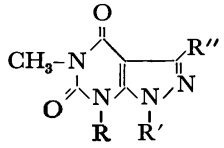

Compd.	R	R′	R″	Reaction condition Temp. (°C)	Time (min)	Mp[a] (°C)	Yield (%)	Analyses % Found (Calcd) C	H	N	IR cm^{-1} (KBr)		
2a	CH_3	H	C_6H_5	280	15	242[5]	35	60.90 (60.93)	4.68 (4.72)	21.59 (21.87)	1703s, 1593s,	1660s, 1572m,	1608m, 1523m
2b	CH_3	H	*p*-Cl-C_6H_4	260	20	>270(sublim.)	45	53.83 (53.71)	3.90 (3.81)	19.04 (19.27)	1706s, 1592s,	1650s, 1520m	1610s,
2c	CH_3	H	3,4-Cl_2-C_6H_3	300	20	>340(sublim.)	42	48.31 (48.02)	3.11 (3.10)	17.20 (17.23)	1707s, 1585s,	1645s, 1516m	1608s,
2d	CH_3	H	*p*-CH_3O-C_6H_4	270	20	267	45	58.79 (58.73)	4.75 (4.93)	19.29 (19.57)	1702s, 1598s,	1660s, 1556m,	1608sh, 1530m
2e	CH_3	H	*p*-$(CH_3)_2N$-C_6H_4	270	20	273	28	60.22 (60.19)	5.66 (5.72)	23.23 (23.40)	1702s, 1610s, 1530m	1668s, 1595s,	1650s, 1560m,
2f	H	CH_3	C_6H_5	300	30	>300(sublim.)	40	60.72 (60.93)	4.76 (4.72)	21.91 (21.87)	1712s, 1600m,	1643s, 1572m	1622s,
2g	H	CH_3	*p*-Cl-C_6H_4	260	5	>320(sublim.)	55	53.88 (53.71)	3.77 (3.81)	19.06 (19.27)	1713s, 1582m,	1645s, 1560m	1619s,
2h	H	CH_3	3,4-Cl_2-C_6H_3	260	5	>320(sublim.)	56	48.22 (48.01)	3.15 (3.10)	17.14 (17.23)	1715s, 1580m,	1643s, 1560m	1619s,
2i	H	CH_3	*p*-CH_3O-C_6H_4	260	20	>330(sublim.)	30	58.66 (58.73)	4.92 (4.93)	19.33 (19.57)	1708s, 1550m,	1650s, 1510w	1610s,
2j	H	CH_3	*p*-$(CH_3)_2N$-C_6H_4	260	20	>350(sublim.)	43	60.24 (60.19)	5.78 (5.72)	23.19 (23.40)	1707s, 1550w,	1650s, 1534m	1605s,
2k	H	H	C_6H_5	300	5	>330(sublim.)	55	59.63 (59.50)	4.09 (4.16)	23.24 (23.13)	1700s, 1530m	1662s,	1620s,
2l	H	H	*p*-Cl-C_6H_4	300	5	>290(sublim.)	51	52.22 (52.09)	3.27 (3.28)	20.11 (20.25)	1706s, 1530m	1669s,	1620m,
2m	H	H	3,4-Cl_2-C_6H_3	300	5	>285(sublim.)	52	46.22 (46.32)	2.58 (2.59)	17.86 (18.01)	1706s, 1527m	1665s,	1622m,
2n	H	H	*p*-CH_3O-C_6H_4	300	5	>295(sublim.)	45	57.22 (57.35)	4.39 (4.44)	20.37 (20.58)	1700s, 1532w,	1664s, 1500s	1611s,
2o	H	H	*p*-$(CH_3)_2N$-C_6H_4	300	5	>360(sublim.)	60	58.79 (58.93)	5.27 (5.30)	24.63 (24.55)	1712s, 1570m,	1664s, 1515m	1613s,

a) All products were recrystallized from ethanol.

TABLE 3. 3-ARYL-2-BENZYLPYRAZOLO[3,4-*d*]PYRIMIDINES (**3a—d**)

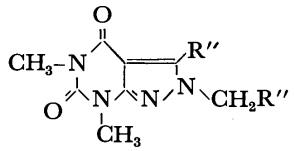

Compd.	R″	Mp[a] (°C)	Yield (%)	Analyses % Found (Calcd) C	H	N
3a	C_6H_5	193	37	69.44 (69.35)	5.30 (5.24)	16.18 (16.18)
3b	*p*-Cl-C_6H_4	177	57	57.75 (57.84)	3.89 (3.88)	13.19 (13.49)
3c	3,4-Cl_2-C_6H_3	194	40	49.70 (49.61)	2.97 (2.91)	11.33 (11.57)
3d	*p*-CH_3O-C_6H_4	160	21	65.00 (65.01)	5.38 (5.46)	13.83 (13.79)

a) All products were recrystallized from ethanol.

formation of 3-aryl-2-benzylpyrazolo[3,4-*d*]pyrimidine derivatives (**3a—d**) in addition to **2a—d** (see Table 3) was observed; their structures were established by unequivocal synthesis by the benzylation of **2a—d** with the corresponding benzyl halides. The mechanism of the formation of these compounds is currently under investigation.

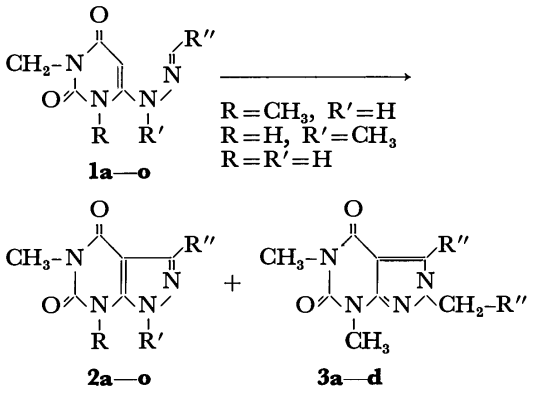

Scheme 1.

Structural Elucidation of (2a—o) Products. The structures of **2a—o** were established by microanalyses and by the use of mass and other spectral data. Furthermore, representatives of these compounds were identified by comparison with authentic samples prepared by the following alternative routes. Some of the **2a—o** compounds were identified with the products prepared by the cyclization of the corresponding 6-benzylidenehydrazino-1,3-dimethyl-5-nitrouracils[5] in dimethylformamide. Compound **2f** was alternatively synthesized as follows: the treatment of 6-chloro-3-methyl-5-nitrouracil (**4**)[7] with benzaldehyde methylhydrazone gave 6-(benzylidene-1'-methylhydrazino)-3-methyl-5-nitrouracil (**5**); it was then converted into **2f** in 40 and 42% yields by fusion and by refluxing in dimethylformamide respectively.

The nitration of **1k** with potassium nitrate in acetic acid in the presence of sulfuric acid gave a mixture of **2k** (32%) and 5,7-dioxo-6-methyl-8-nitro-3-phenyl-1,5,6,7-tetrahydro-*s*-triazolo[4,3-*c*]pyrimidine (**6**) (15.3 %). The latter belongs to a type of compound observed previously.[7-9]

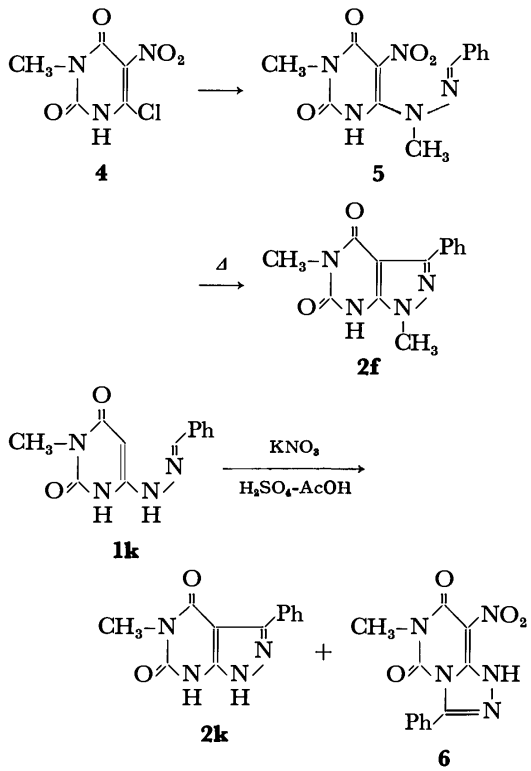

Scheme 2.

Pyrolysis of 6-(Benzylidene-1'-methylhydrazino)-1,3-dimethyluracils (1p—w). Formation of Nitriles (7p—w): As has been stated above, the thermolysis of 6-(benzylidenehydrazino)uracils constituted a convenient synthetic route to pyrazolo[3,4-*d*]pyrimidines. The reaction, however, appeared to be dependent on the presence of protons at the 1-position and/or the 1'-position of the 6-substituent. The thermolysis of fully substituted 6-benzylidenehydrazinouracils (**1p—w**) gave no pyrazolo[3,4-*d*]pyrimidines, but mixtures of the respective

TABLE 4. PYROLYSIS OF 6-(BENZYLIDENE-1'-METHYLHYDRAZINO)-1,3-DIMETHYLURACILS (**1p—w**)

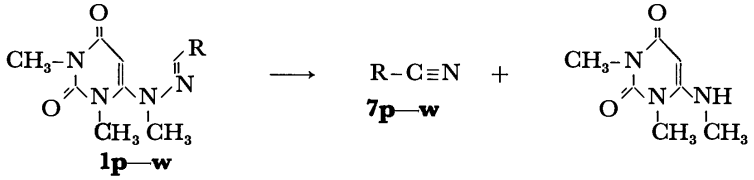

Starting materials No.	Reaction condition		No.	Products		
	Temp. (°C)	Time (min)		Nitriles R	Yield (%)	1,3-Dimethyl-6-methylaminouracil Yield (%)
1p	200	10	**7p**	CH_3	59	85
1q	190	30	**7q**	CH_3–CH=CH	not identified	70
1r	250	30	**7r**	C_6H_5	83	85
1s	260	30	**7s**	*p*-Cl-C_6H_4	87	91
1t	280	15	**7t**	3,4-Cl_2-C_6H_3	86	90
1u	220	30	**7u**	*p*-CH_3O-C_6H_4	75	82
1v	220	40	**7v**	*p*-$(CH_3)_2N$-C_6H_4	73	80
1w	240	30	**7w**	3-Pyridyl	69	75

TABLE 5. 1,5,7-TRIMETHYLPYRAZOLO[3,4-*d*]PYRIMIDINE-4,6(5*H*,7*H*)-DIONES (**2p—w**)

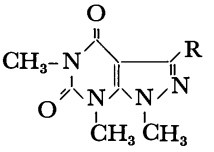

Compd.	R	Irradiation time hr	Mp (°C)	Yield (%)	Recrystn solvent	Analyses % Found (Calcd) C	H	N	IR cm^{-1} (KBr)
2p	CH_3	35	251	78	ethanol	51.61 (51.91)	5.92 (5.81)	26.87 (26.91)	1693s, 1651s, 1583s, 1555s
2q	CH_3–CH=CH	35	215	81	ethanol	56.69 (56.40)	6.10 (6.02)	23.90 (23.92)	1693s, 1645s, 1581s, 1550s
2r	C_6H_5	43	192[5]	82	ethanol	62.40 (62.21)	5.12 (5.22)	20.60 (20.73)	1690s, 1659s, 1640sh, 1578s, 1538s
2s	*p*-Cl–C_6H_4	26	257	78	dioxane	55.13 (55.18)	4.14 (4.30)	18.27 (18.39)	1695s, 1645s, 1578s, 1527m
2t	3,4-Cl_2–C_6H_3	30	242	82	dioxane	49.42 (49.57)	3.57 (3.57)	16.37 (16.52)	1698s, 1650s, 1576s, 1527m
2u	*p*-CH_3O–C_6H_4	34	214	90	ethanol	60.01 (59.99)	5.07 (5.37)	18.69 (18.66)	1695s, 1647s, 1575s, 1534m 1515m
2v	*p*-$(CH_3)_2N$–C_6H_4	35	193	85	ethanol	61.21 (61.32)	6.00 (6.11)	22.75 (22.35)	1689s, 1648s, 1601m, 1578s, 1558s, 1527s
2w	3-Pyridyl	38	211	75	ethanol	57.26 (57.56)	4.49 (4.83)	25.65 (25.82)	1691s, 1645s, 1572s, 1532s

nitriles (**7p—w**) and 1,3-dimethyl-6-methylaminouracil[4] in high yields and in a state of high purity. The reaction can be performed merely by heating the starting materials at temperatures slightly higher than their melting points for 10—40 min, followed by distillation, sublimation, or extraction using the ether of the reaction mixtures to give the respective nitriles (**7p—w**). The residue includes 1,3-dimethyl-6-methylaminouracil[4] exclusively (Table 4). We consider this nitrile formation as possessing a potential synthetic utility because of the good yields obtained and the neutral condition employed.

Photolysis of Compounds ***1p—w***. For the purpose of exploiting the preparative method of fully substituted pyrazolo[3,4-*d*]pyrimidine-4,6(5*H*,7*H*)-diones, photolysis of Compounds **1p—w** was carried out. The irradiation of solution of **1p—w** in benzene under aerobic condition, with a 100 W high-pressure mercury lamp at room temperature resulted in the formation of the respective pyrazolo[3,4-*d*]pyrimidines (**2p—w**) as the sole products in excellent yields (Table 5). Thus, the photolysis of fully methylated 6-(benzylidenehydrazino)uracils (**1p—w**) has been proved to offer a new method of synthesizing 1,5,7-trimethylpyrazolo[3,4-*d*]pyrimidine-4,6(5*H*,7*H*)diones (**2p—w**).

On the other hand, the photolysis of **1a—o** under the same conditions did not give **2a—o**; rather the starting materials were completely recovered.

Structural Elucidation of (2p—w) Products. The structures of **2p—w** were established by microanalyses, by molecular-weight determination by means of mass spectrometry, and by comparison with authentic samples prepared by the methylation of the corresponding 1,5-dimethylpyrazolo[3,4-*d*]pyrimidine-4,6(5*H*,7*H*)-diones (**2f—j**). The methylation of **2k** with methyl iodide gave **2r** (15.4%) and its isomeric 2,5,7-trimethylpyrazolo[3,4-*d*]pyrimidine-4,6(5*H*,7*H*)-dione (**8**) (51.3 %). Table 6 gives the ultraviolet absorption data for a series of 3-phenylpyrazolo[3,4-*d*]pyrimidine-4,6-

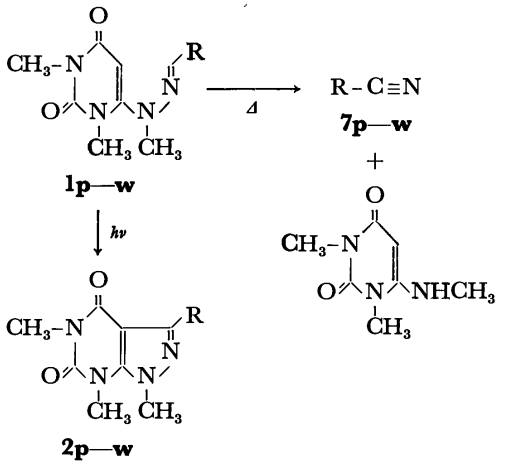

Scheme 3.

TABLE 6. UV ABSORPTIONS OF PYRAZOLO-[3,4-*d*]PYRIMIDINES

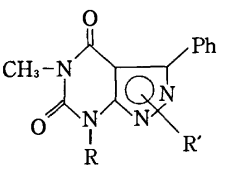

Compd.	R	R′	λ_{max}^{EtOH} nm	log ε
2a	CH_3	2-H	267.5	4.10
2k	H	2-H	267	4.13
8	CH_3	2-CH_3	261	4.12
2f	H	1-CH_3	231.5, 244(sh), 263(sh)	4.26, 4.21 4.09
2r	CH_3	1-CH_3	232, 261	4.32, 4.13

TABLE 7. 5-BENZYLIDENE-1,3-DIMETHYLBARBITURIC ACIDS (**9r—v**)

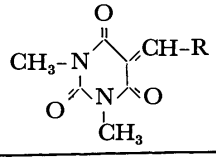

Compd.	R	Mp[a] (°C)	Yield (%)	Analyses % Found (Calcd) C	H	N
9r	C_6H_5	164	53	63.81 (63.92)	4.77 (4.95)	11.27 (11.47)
9s	p-Cl-C_6H_4	155	82	55.79 (56.00)	3.83 (3.98)	9.92 (10.05)
9t	3,4-Cl_2-C_6H_3	200	81	49.73 (49.86)	3.07 (3.22)	9.09 (9.27)
9u	p-CH_3O-C_6H_4	151	84	61.82 (61.31)	5.02 (5.15)	10.55 (10.21)
9v	p-$(CH_3)_2N$-C_6H_4	242	77	63.01 (62.70)	5.80 (5.96)	14.14 (14.63)

a) All products were recrystallized from ethanol.

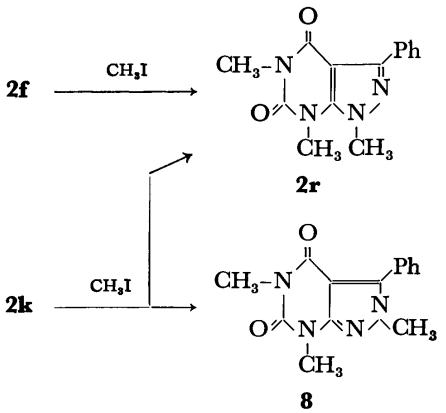

Scheme 4.

(5*H*,7*H*)-diones. The 1,5,7-trimethyl derivative (**2r**) exhibited spectra with two intense peaks at *ca.* 230 and 260 nm, while the 2,5,7-trimethyl derivative (**8**) exhibited spectra with only one peak in the 260-nm region. It is noticeable that both **2a** and **2k** have the 2*H*-pyrazole tautomeric form in alcoholic solutions.

Reaction of ***1r—v*** *with Sulfuric Acid in Acetic Acid.* In order to find another method of cyclizing Compounds **1r—v**, we tried the reaction of **1r—v** with sulfuric acid in acetic acid. However, the products obtained were 5-benzylidene-1,3-dimethylbarbituric acid (**9r—v**) (Table 7), whose structures were established by comparison with authentic samples prepared by the condensation of 1,3-dimethylbarbituric acid with the corresponding aryl aldehydes.

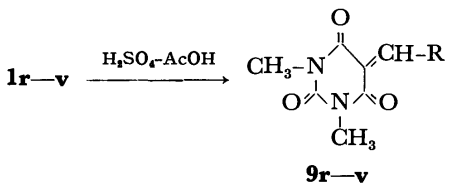

Scheme 5.

Experimental

All the melting points are corrected and were determined on a Mettler FP-1 apparatus.

1,3-Dimethyl-6-hydrazinouracil,[4] *3-methyl-6-(1'-methylhydrazino)uracil,*[10] and *3-methyl-6-hydrazinouracil.*[7] These were prepared by the known procedures.

1,3-Dimethyl-6-(1'-methylhydrazino)uracil. To a solution of 6-chloro-1,3-dimethyluracil (5 g, 0.029 mol) in EtOH (60 ml), we added methylhydrazine (5.25 g, 0.114 mol), after which the mixture was stirred for 2 hr at room temperature. The crystals which separated were collected by filtration. The filtrate was evaporated *in vacuo* to give more crystals. The combined crystals were recrystallized from EtOH to give 4.47 g (84.7%) of colorless needles; mp 135—137 °C. Found: C, 45.50; H, 6.59; N, 30.23%. Calcd. for $C_7H_{12}N_4O_2$: C, 45.64; H, 6.57; N, 30.42%.

*6-(Benzylidenehydrazino)uracils (**1a—w**): General Procedure.* To a stirred solution or suspension of a 6-hydrazinouracil (0.01 mol) in 50—200 ml of EtOH, we added an aldehyde (0.015—0.02 mol) at room temperature. After stirring had been continued for 2 hr at room temperature, the product which separated was collected by filtration and recrystallized from EtOH.

*Pyrazolo[3,4-d]pyrimidine-4,6(5H,7H)-dione Derivatives (**2a—o**): General Procedure.* A 6-(benzylidenehydrazino)uracil (**1a—o**) (0.005 mol) was fused as has been described in Table 2. The reaction mixture was then dissolved in 100—200 ml of EtOH with warming. After cooling, the precipitated crystals were collected by filtration and recrystallized from EtOH.

*2-Benzyl Derivatives of **2a—d** (**3a—d**).* When Compounds **1a—d** were used as the starting materials in the above reaction, the 2-benzyl derivatives of **2a—d** (**3a—d**) were obtained by the evaporation of the filtrate, followed by the recrystallization of the residue from EtOH.

*6-(Benzylidene-1'-methylhydrazino)-3-methyl-5-nitrouracil (**5**).* To a stirred solution of 6-chloro-3-methyl-5-nitrouracil (**4**) (5 g, 0.024 mol) in EtOH (70 ml), we added methylhydrazine (1.12 g, 0.024 mol) and benzaldehyde (2.58 g, 0.024 mol) at room temperature. After stirring for 2 hr, the crystals thus precipitated were collected by filtration and recrystallized from EtOH to give 6.53 g (85.8%) of **5** as yellow prisms; mp 226—227 °C. Found: C, 51.32; H, 4.29; N, 22.84%. Calcd for $C_{13}H_{13}N_5O_4$: C, 51.48; H, 4.32; N, 23.09%.

*5-Mehtyl-3-phenylpyrazolo[3,4-d]pyrimidine-4,6(5H,7H)-dione (**2k**)* and *5,7-Dioxo-6-methyl-8-nitro-3-phenyl-1,5,6,7-tetrahydro-s-triazolo[4,3-c]pyrimidine (**6**).* A mixture of **1k** (0.5 g, 0.002 mol), potassium nitrate (0.415 g, 0.0041 mol), and sulfuric acid (0.3 g) in acetic acid (20 ml) was heated at 90—95 °C for 2 hr. After removing the undissolved inorganic substances by filtration, the filtrate was evaporated to dryness and the residue was diluted with water to precipitate crystals, which were then collected by filtration and recrystallized from

EtOH to give 0.16 g (32%) of **2k**. After the filtrate had been kept in the refrigerator, the crystals separated were collected by filtration and recrystallized from EtOH to give 0.09 g (15.3%) of **6** as pale yellow plates; mp 148—149 °C. Mass: 287 (M^+). UV λ_{max}^{EtOH} nm (log ε): 219sh (4.21), 264.5 (4.05), and 356 (3.87). IR cm^{-1} (KBr): 3470, 3375, 1733s, 1659s, 1608s, and 1340 (NO_2). Found: C, 50.08; H, 3.12; N, 24.07%. Calcd for $C_{12}H_9N_5O_4$: C, 50.18; H, 3.16; N, 24.38%.

*Pyrolysis of 6-(Benzylidene-1'-methylhydrazino)-1,3-dimethyluracils (**1p—w**). Formation of Nitriles (**7p—w**): General Procedure.* One gram of Compound **1p—w** was fused under the conditions indicated in Table 4. During the reaction, the respective nitriles (**8p—w**) were sublimed or distilled; they were then collected. After the reaction, the mixtures were extracted with ether, and the ether extracts were evaporated to give more nitriles. The residue was almost pure 1,3-dimethyl-6-methylaminouracil.[4]

*Photolysis of **1p—w**. Synthesis of 1,5,7-Trimethylpyrazolo[3,4-d]pyrimidine-4,6(5H,7H)-diones (**2p—w**).* A solution of **1p—w** (0.5 g) in benzene (600 ml) was irradiated with a 100 W high-pressure mercury lamp surrounded by a water-cooled Pyrex filter, as is shown in Table 5. The completion of the reaction was judged by tlc, using silica gel G and the appropriate mixtures of benzene, acetone, EtOH, and chloroform as the developing solvents. The removal of the solvent, followed by recrystallization from EtOH or dioxane, gave the respective pyrazolo[3,4-*d*]pyrimidines (**2p—w**).

*Methylation of 3-Substituted 1,5-Dimethylpyrazolo[3,4-d]pyrimidine-4,6(5H,7H)-diones (**2f—j**): General Procedure.* To a solution of **2f—j** (0.001 mol) in dimethylformamide (5 ml), we added methyl iodide (0.21 g, 0.015 mol) and potassium carbonate (0.2 g), after which the mixture was refluxed for 3 hr. After the reaction mixture had then been evaporated *in vacuo*, the residue was diluted with water to precipitate crystals; these crystals were collected by filtration and recrystallized from EtOH to afford **2r—v** in 50—65% yields.

*Methylation of 5-Methyl-3-phenylpyrazolo[3,4-d]pyrimidine-4,6(5H,7H)-dione (**2k**). 3-Phenyl-1,5,7-trimethylpyrazolo[3,4-d]pyrimidine-4,6(5H,7H)-dione (**2r**) and 3-Phenyl-2,5,7-trimethylpyrazolo[3,4-d]pyrimidine-4,6(5H,7H)-dione (**8**).* To a solution of **2k** (0.35 g, 0.0015 mol) in dimethylformamide (10 ml), we added methyl iodide (2.1 g, 0.015 mol) and potassium carbonate (0.7 g), after which the mixture was refluxed for 1 hr. After the reaction mixture had then been evaporated under reduced pressure, the residue was recrystallized from EtOH to give 0.2 g (51.3%) of **8** as colorless prisms; mp 204—206 °C. Mass: 270 (M^+). IR cm^{-1} (KBr): 1699s, 1662s, 1600m, 1580s, 1539m, and 1512m. Found: C, 62.01; H, 5.40; N, 20.78%. Calcd for $C_{14}H_{14}N_4O_2$: C, 62.21; H, 5.22; N, 20.73%.

The filtrate was evaporated to dryness, and the residue was diluted with H_2O to separate 0.06 g (15.4%) of **2r**.

*5-Benzylidene-1,3-dimethylbarbituric Acids (**9r—v**): General Procedure.* *A)* To a solution of **1r—v** (0.5 g) in acetic acid (10 ml), sulfuric acid (0.25 g) was added. After the mixture had been heated under stirring at 90—95 °C for 2 hr, the reaction mixture was diluted with H_2O to precipitate crystals; these crystals were then collected by filtration and recrystallized from EtOH.

B) A mixture of 1,3-dimethylbarbituric acid (1.5 g, 0.0096 mol) and aryl aldehyde (0.014 mol) in EtOH (40 ml) was refluxed for 1 hr. After cooling, the crystals which separated were collected by filtration. The filtrate was evaporated to dryness to give more crystals. The combined crystals were recrystallized from EtOH to give **9r—v**.

References

1) R. K. Robins in "Heterocyclic Compounds," ed. by R. C. Elderfield, Vol. 8, Wiley, New York (1967), p. 406—421, and references therein.

2) S. M. Mecht and D. Werner, *J. Chem. Soc., Perkin I*, **1973**, 1903.

3) S. Senda, K. Hirota, and G.-N. Yang, *Chem. Pharm. Bull.* (Tokyo), **20**, 391, 399 (1972).

4) W. Pfleiderer and K. H. Schündehütte, *Ann.*, **712**, 158 (1958).

5) Y. Maki, K. Izuta, and M. Suzuki, *Chem. Commun.*, **1971**, 1442.

6) A part of this paper has been reported in preliminary form: see F. Yoneda and T. Nagamatsu, *Synthesis*, **1973**, 300; F. Yoneda and T. Nagamatsu, *Heterocycles*, **2**, 153 (1974).

7) T. K. Liao, F. Baiochi, and C. C. Cheng, *J. Org. Chem.*, **31**, 900 (1966).

8) M. E. C. Biffin, D. J. Brown, and T. Sugimoto, *J. Chem. Soc., C*, **1970**, 139.

9) D. J. Brown and J. R. Kershaw, *J. Chem. Soc., Perkin I*, **1972**, 2316.

10) G. D. Daves, R. K. Robins, and C. C. Cheng, *J. Amer. Chem. Soc.*, **84**, 1724 (1962).

11) G. Blankenhorn and W. Pfleiderer, *Chem. Ber.*, **105**, 3334 (1972).

The Intramolecular Participation of Sulfide Linkage on the Reactivity of Carbenes and Diazoalkanes. II. Alkylcarbenes and Diazoalkanes Bearing Arylthio and Allylthio Groups on β-Carbon

Kiyosi KONDO and Iwao OJIMA

Sagami Chemical Research Center, Nishi-Ohnuma 4-4-1, Sagamihara, Kanagawa 229

(Received November 20, 1974)

β-Arylthio- and β-allylthioalkylcarbenes were generated from the corresponding ketones by a modification of the Bamford–Stevens method. Chemical evidence for the formation of novel cyclic ylides, *i.e.*, thietanonium ylides, by an intramolecular electrophilic addition of the carbene to the sulfur atom was obtained. The resulting ylides underwent various types of rearrangements to afford cyclopropyl sulfides, thiaazulenes, thietanes, and/or tetrahydrothiophenes. The mechanisms and the relative amounts of the transition energies for these rearrangements are discussed. An intramolecular cycloaddition of β-allyl- and β-crotylthioalkyldiazoalkanes is also described. The final products of the reaction were 3-thiabicyclo[4.1.0]heptanes. A thiabicyclic pyrazoline, which is presumed to be an intermediate of the cycloaddition, could be isolated in the case of the thermal decomposition of 4-allylthio-4-methylpentan-2-one tosylhydrazone.

Many reports on the formation of ylides by the intermolecular electrophilic addition of carbenes to the lone-pair electrons of hetero atoms can be found in the literature.[1] The most representative patterns of these "*intermolecular reactions*" might be summarized as: i) insertion into carbon–hydrogen bonds,[1a] ii) allylic [2,3]sigmatropic rearrangement,[1b] and iii) the formation of stable ylides.[1c] On the contrary, relatively little is known about the *intramolecular* counterpart of this addition, especially in view of the ylide formation.[2,3] When a sulfide linkage is introduced into the same molecule of the carbene, it can be expected that the carbene carbon will be transformed into the ylide carbon by an intramolecular ylide formation.

In the first paper of this series,[4] we reported on the characteristic behavior of the episulfonium ylides produced by the intramolecular addition of α-alkyl and α-arylthioalkylcarbenes. The introduction of the sulfide linkage at the γ-position of the carbene may also cause the cyclization to form four-membered ring ylide. Herein we will describe the behavior of β-aryl-, β-alkyl-, and β-allylthioalkylcarbenes and will present definite evidence for the intramolecular formation of their ylides.[5]

During the course of our study of this subject, we have also found that certain diazoalkanes bearing an allylthio group on β-carbon, a precursor of the carbenes described above, underwent a facile intramolecular cycloaddition to produce bicyclic pyrazolines, which were then transformed into cyclopropanes under the present reaction conditions.[6] As the reaction may open a novel route to thiabicyclic systems, we will also touch briefly on the characteristic behavior of these diazoalkanes.

Results

β-Phenylthioalkylcarbenes. The starting materials were prepared by the Michael addition of thiophenol to the appropriate α,β-unsaturated ketones, followed by treatment with *p*-toluenesulfonylhydrazide. The desired carbenes were generated by the thermal decomposition of the sodium salts of the resulting tosylhydrazones

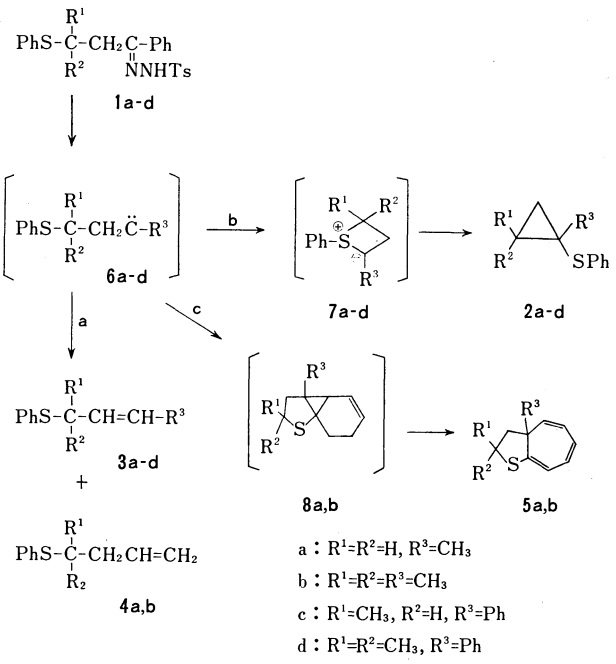

Scheme 1.

(**1a—d**) in diglyme at 150—160 °C. The products were separated by column chromatography on silica gel and/or by preparative vpc. The structural assignments were based on the spectra and on the results of elemental analyses. The products caused by intramolecular reactions were olefins (**3** and **4**), cyclopropyl sulfides (**2**), and thiaazulenes (**5**). The patterns for these intramolecular carbene reactions are shown in Scheme 1. The first path, **a**, of these reactions is a usual 1,2-shift of hydrogen, and the second path, **b**, is the intramolecular ylide formation, followed by a novel rearrangement of the phenylthio group. The third path, **c**, is the addition of these carbenes to the benzene nucleus. Thiaazulene might be formed through a valence-bond isomerization of the intermediary-formed norcaradiene, **8**. This is a rare example of the cycloaddition of an alkylcarbene to a benzene nucleus. The finding that no thiaazulenes were obtained in the cases of two

carbenes, **6c** and **6d**, must be due to an inherent difference in reactivity between the arylcarbenes and the alkylcarbenes. Accordingly, **3**, **4**, and **5** are supposed to be the products from the carbene process, and **2**, from the ylide process. In order to compare the effect of the phenylthio group with that of the alkylthio group on these two competitive processes, β-ethylthio-β-methylbutyrophenone tosylhydrazone (**1e**) was decomposed under the same conditions. The product was also found to be a mixture of cyclopropylsulfide (**2e**) and olefins (**3e**) (Scheme 2).

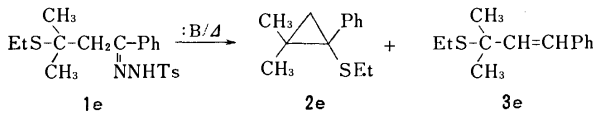

1e 2e 3e

Scheme 2.

Though the photolysis of tosylhydrazone, **1d**, afforded cyclopropyl sulfide, **2d**, in a 37% yield, the olefin, **3d**, was obtained in only 18% yield; the residue was a high-boiling intractable oil. The photolyses of other tosylhydrazones were, therefore, not attempted.

The configuration of the cyclopropyl sulfide, **2c**, was identified as *cis* with respect to the methyl and phenyl groups, based on its NMR spectrum; the methyl of this cyclopropyl sulfide was highly shielded by the *cis* phenyl group and was thus observed at τ 9.17 as a doublet. The discussion of the shielding effect of the *cis* phenyl group in cyclopropane systems advanced by Closs and Moss[7] was also found to be applicable to our systems. In the case of the cyclopropyl sulfide, **2b**, which has no *cis* phenyl group, the methyl absorption

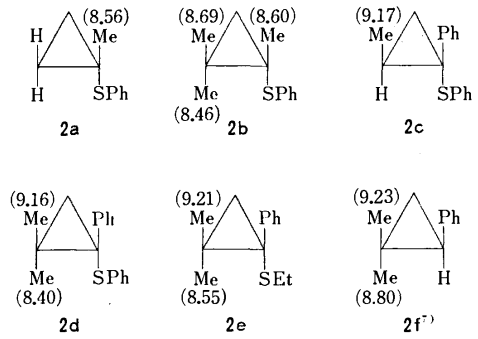

Scheme 3.

Table 1. Intramolecular reactions of β-phenylthio- and β-alkylthioalkylcarbenes in diglyme

Carbene 6	Total yield (%)[a]	Product ratios (%)[a] 2	3	4	5
6a	81.2	5.4	77.3[c]	10.6	6.8
6b	90.0	17.4	66.0[d]	7.2	9.4
6c	93.5[b]	31.8	68.2[e]		
6d	94.0	45.5	54.5[d]		
6e	89.5	56.8	43.2[d]		

a) Yields were calculated by comparing the vpc peak area of crude products with that of pure samples using a column (1 m) packed with 20% SE-30 or 10% QF-1 on chromosorb W at 140—220 °C. b) There are also obtained 1-methyl-1-phenylthio-2-phenylcyclopropane as an insertion product of the carbene **6c** to a carbon-hydrogen bond. c) *cis*/*trans*=17/83. d) *cis*/*trans*=0/100. e) The olefin **3** (*cis*/*trans*=4/96) contained 1-methyl-3-phenylpropen-1-yl phenyl sulfide (38%), which was proved to be an isomerization product of **3c** by a controlled experiment.[8]

was observed at τ 8.69, while the cyclopropyl sulfide, **2d**, displayed an absorption at τ 9.16 which could be assigned to the *cis* methyl, as is shown in Scheme 3.

β-Allylthioalkylcarbenes Generated by the Photolyses. In order to obtain more definite evidence for the intervention of thietanonium ylide, the thermolysis and photolysis of the tosylhydrazone, **1f**, derived from β-allylthioalkylphenylketone were performed. We chose **1f** as the substrate because, once the allyl sulfonium ylide is produced, the ylide may undergo a smooth [2,3]sigmatropic rearrangement.

The photolysis of the sodium salt of β-allylthio-β-methylbutyrophenone tosylhydrazone (**1f**) in monoglyme at 10 °C afforded three products in a total yield of 68.5%. Each of the components was roughly separated by column chromatography on silica and was finally purified by preparative vpc. The identified products were 2-allyl-2-phenyl-4,4-dimethylthietane (**10a**), 2-vinyl-3-phenyl-5,5-dimethyltetrahydrothiophene (**11a**), and 1-phenyl-3-allylthio-3-methyl-1-butene (**12a**). The formation of thietane **10a** demonstrates that a definite chemical bond is formed between the carbene carbon and the sulfur; that is, there is an intervention of thietanonium ylide, **13a**. The succeeding

Table 2. Intramolecular reactions of β-allylthio- and β-benzylthioalkylcarbenes

Carbene 9 R	Method of generation	Total yields[a] (%)	Product ratios[a] 10	11	12	15
9a	*hν*	68.5	20.7	32.3[b]	47.0[c]	
9a	*Δ*	47.7	7.2	—	2.9	89.9
9b	*hν*	55.8	25.3[d]	33.2[e]	41.5[f]	
9b	*Δ*	49.8	2.7	3.2	6.2	87.9[g]
9c $PhCH_2$	*hν*	57.2	17.0[h]	33.0[h]	50.0[i]	
9c $PhCH_2$	*Δ*	57.8	20.0	27.3[j]	52.7[k]	

a) See footnote a) in Table 1. b) *cis*/*trans*=58/42. c) *cis*/*trans*=40/60. d) mixture of diastereoisomers in the ratio of 56: 44. e) *cis*/*trans*=58/42. f) *cis*/*trans*=49.5/50.5. g) *exo*/*endo*=74.5/25.5. h) *cis*/*trans*=50/50. i) *cis*/*trans*=0/100. j) *cis*/*trans*=58/42. k) *cis*/*trans*=27/73.

[2,3]sigmatropic rearrangement of the allylsulfonium ylide affords the thietane, **10a**, as the final product. In order to establish the [2,3]sigmatropic rearrangement and to exclude the possibility of a Stevens-type 1,2-shift of the allylic substituent, 3-crotylthio-3-methylbutyrophenone tosylhydrazone (**1g**) was photolyzed under the same conditions. The identified products were 2-(1-methylallyl)-2-phenyl-4,4-dimethylthietane (**10b**), 2-(1-propenyl)-3-phenyl-5,5-dimethyltetrahydrothiophene (**11b**), and 1-phenyl-3-crotylthio-3-methyl-1-butene (**12b**). The thietane, **10b**, was obtained as a mixture of diastereoisomers (56:44); the tetrahydrothiophene, **11b**, was also a mixture of *cis* and *trans* isomers. The facts that no 2-crotyl-2-phenyl-4,4-dimethylthietane was obtained, but **10b** was, clearly indicate the exclusive occurrence of [2,3]sigmatropic rearrangement.

The relatively high yield production of the tetrahydrothiophenes, **11a** and **11b**, deserves to be mentioned. The formation of these five-membered ring products can also be explained by assuming the intervention of the ylide, **13**. Thus, an ylide exchange reaction of **13** to the exocyclic ylide, **14**, followed by a Stevens-type rearrangement, may constitute the ring-enlargement process. The total yield and the products ratio are listed in Table 2. In the thermolyses of the tosylhydrazones, **1f** and **1g**, an intramolecular 1,3-cycload-

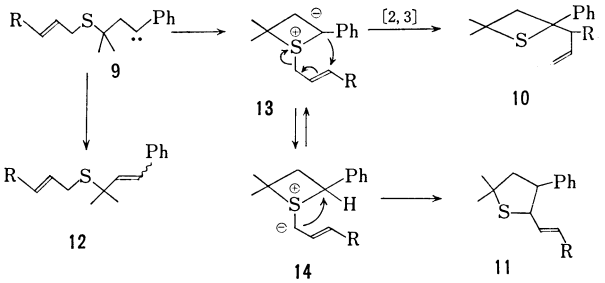

Scheme 4.

dition of a generated diazoalkane to the double bond of the allyl group was found to be the major process of the reaction; two 4-thiabicyclo[4.1.0]heptanes, **15** and **16**, were thus obtained. The details of this reaction will be discussed later.

β-Benzylthioalkylcarbenes. The ylide-exchange reaction observed in the case of β-allylthioalkylcarbene is expected to be characteristic of systems in which the intermediate cyclic ylide has an acidic hydrogen on the exocyclic α-carbon of the sulfonium function. Thus, an intramolecular reaction of the carbene-bearing benzylthio group on β-carbon was further investigated. The carbene was generated by the thermolysis or photolysis of the corresponding tosylhydrazone (**1h**). Besides the olefin, **12c**, caused by the carbenic process, two products were isolated from the reaction mixture. One was identified as the tetrahydrothiophene, **11c**, by means of its spectra and by elemental analysis; it is the expected product from the ylide-exchange reaction. The other was proved to be the thietane, **10c**, which must be formed through a Stevens-type rearrangement of the intermediate ylide, **13c**.

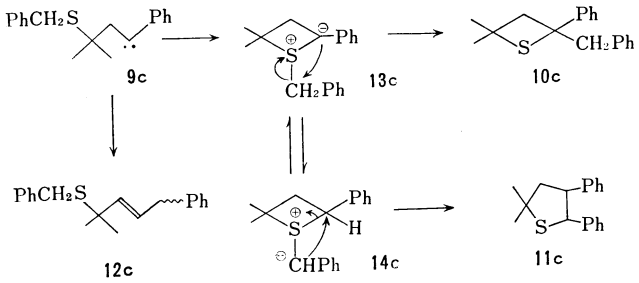

Scheme 5.

β-Allylthioalkyl Diazoalkanes Generated by the Thermolyses. β-Allylthio-β-methylbutyrophenone tosylhydrazone (**1f**) was thermally decomposed in diglyme in the presence of sodium methoxide at 150 °C. When the reaction mixture was chromatographed on silica, 4,4-dimethyl-6-phenyl-3-thiabicyclo[4.1.0]heptane (**15**) was obtained as the predominant product (Scheme 6). The analysis of the reaction mixture revealed that small amounts of thietane, **10a**, and the **12a** olefin were also present in the product (Table 2). Similarly, the thermolysis of β-crotylthio-β-methylbutyrophenone tosylhydrazone (**1g**) afforded 6-phenyl-4,4,7-trimethyl-3-thiabicyclo-[4.1.0]heptane (**16**) in a 44% yield, accompanied by small amounts of thietane, **10b**, tetrahydrothiophene, **11b**, and the **12b** olefin. The photolyses of these β-allylthio compounds at 10 °C underwent a completely different process, *i.e.*, a carbenic process, as has been described in the previous section. Thus, the formation of the two 3-thiabicyclo[4.1.0]heptanes, **15** and **16**, may mean that an intramolecular cycloaddition of the diazoalkane moiety to the double bond of the allylthio group and a subsequent elimination of the molecular nitrogen really do occur under the thermolysis conditions.

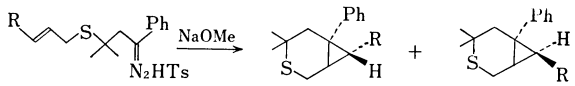

Scheme 6.

The NMR spectrum and vpc analysis of the product indicated that **16** is a mixture of *exo-* and *endo*-isomers (**16a** and **16b**) in the ratio of 74.5:25.5. The product isomer ratio was found to be constant even when the *cis-trans* mixing ratios of the starting **1g** were changed from 28/72 to 9/91. This fact indicates that the isomer ratio directly reflects the thermodynamic stabilities of the products.

Conclusive evidence for the intramolecular thermal cycloaddition of these diazoalkanes was obtained when 4-allylthio-4-methyl-2-pentanone tosylhydrazone (**1i**) was used as a substrate. That is, the thermal decomposition of **1i** in the presence of sodium methoxide at 150 °C afforded the bicyclic pyrazoline, **17**, in a 33% yield. On the other hand, the photolysis of the sodium salts of **1i** at 10 °C for two hours yielded 4,4,6-trimethyl-3-thiabicyclo[4.1.0]heptane (**18**) in a 48% yield. Furthermore, the irradiation of the bicyclic pyrazoline,

17, under the same conditions produced the same product, **18**, in a good yield.

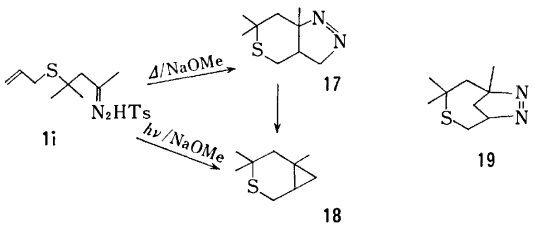

Scheme 7.

Two orientations are possible in considering the intramolecular cycloaddition. The one possible product is **17**, and the other is **19**. The structure of the obtained product was deduced to be **17** on the basis of its NMR spectrum: the chemical shift of the C-3 methylene of the pyrazoline ring was observed at 4.31 ppm (2H) from TMS. This value is in accordance with that reported for vicinal methylenes of the azo function in a usual pyrazoline system.[9] On the other hand, the C-9 methylene of the diazabicyclononene, **19**, is expected to absorb in a much higher field.[9]

The photochemical *in-situ* generation of carbenes from tosylhydrazones has been reported to proceed through diazo precursors.[10] Therefore, it can be concluded that the intramolecular thermal cycloaddition of the diazo compound derived from **1i** is a facile process, even at 10 °C, and that the succeeding elimination of nitrogen is an effective process under photolytic conditions.

Discussion

In all the cases examined, the carbene with sulfide functions on β-carbon underwent two types of reaction: i) a normal carbene reaction, and ii) an intramolecular formation of the cyclic ylide. The relative dominance of these two processes, however, seems to be markedly affected by the nature of the substituents. The relative ratios of these two processes, along with the variation in the substituents, are summarized in Table 3.

The data on the reaction of the carbenes, **6a—6d**, clearly indicate that the ylide process is dramatically favored when the substituent on the carbene carbon is changed from methyl to phenyl and when the number of substituents on the β-carbon is increased. These phenomena can be explained as follows. The phenyl on the ylide carbon may stabilize the ylide by its inductive effect, and the methyl(s) on the β-carbon may favor the formation of the four-membered ring by their steric repulsion. From the steric and electronic points of view, it seems plausible that an alkylthio group on the β-carbon of the carbene would favor the intramolecular formation of the ylide, as compared with the phenylthio group. However, the data on the reactivities of the **6d** and **6e** carbenes tell us that there is no significant difference between these two groups. The results indicate that the basicity of the sulfur atom, as well as the steric bulk of the substituent on the sulfur, may not be at all important in determining the ratio of these two processes. On the other hand, a comparison of the data on the reactivities of the **6e** carbene with those on **9a—9c** suggests that the efficiency of the product-forming steps, *i.e.*, the rearrangement of the intermediate ylide, seems to have influence on the relative dominance of these two processes. That is, the results indicate that the ylide process gains an advantage over the carbene process when the thietanonium ylide thus formed can undergo a rearrangement with a lower transition energy (*vide infra*).

Table 3. The percentage ratios of the carbene process *vs.* ylide process

No.	R^1	R^2	R^3	R^4	Carbene (%)	Ylide (%)
6a	Ph	H	H	Me	94.6	5.4
6b	Ph	Me	Me	Me	82.6	17.4
6c	Ph	Me	H	Ph	68.2	31.8
6d	Ph	Me	Me	Ph	54.5	45.5
6e	Et	Me	Me	Ph	56.8	43.2
9a	C_3H_5	Me	Me	Ph	47.0	53.0
9b	C_4H_7	Me	Me	Ph	41.5	58.5
9c	$PhCH_2$	Me	Me	Ph	50.0	50.0

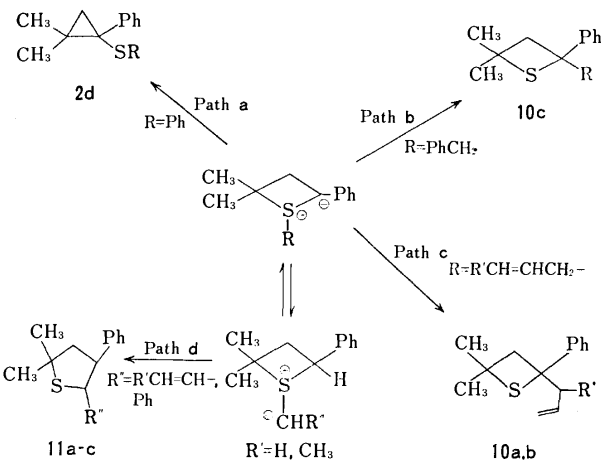

Scheme 8.

On the basis of the results collected in Tables 1 and 2, a discussion of the relative heights of the transition energies in the rearrangements of the thietanonium ylides can now be undertaken. Four different pathways of the rearrangements observed are summarized in Scheme 8. Path **a** is the rearrangement process which affords cyclopropyl sulfides. Path **b** is the Stevens-type rearrangement of the benzyl group on sulfur to give the thietane. Path **c** is the [2,3]sigmatropic rearrangement observed in the β-allylthio system, and Path **d** is the ring-enlargement process *via* the ylide-exchange reaction. In the β-allylthio and β-crotylthio systems, all four pathways are, in principle, possible. However, only two products through Paths **c** and **d** could be observed in the reaction mixture. Accordingly, the thietane formation by [2,3]sigmatropic rearrangement and tetrahydrothiophene formation by ylide-exchange reaction may have lower transition energies than those

of Paths **a** and **b**. Furthermore, the product ratios listed in Table 2 reveal that Path **d** predominates over Path **c**. In the β-benzylthio system, only Paths **b** and **d** were observed, though Path **a** was also a possible candidate for this system. Thus, it can be said that Path **a** has the highest transition energy. In conclusion, the order of the transition energies in these four processes may be as follows: Path **a**>Path **b**>Path **c**>Path **d**.

The next discussion will concern the stereospecificity of the reaction which affords the only isomer of the cyclopropyl sulfide (**2c**). An inspection of the Dreiding model indicated that the most stable conformation of the ylide might be the one that minimizes the steric repulsion between substituents and the electronic repulsion between lone pairs; this conformation has two phenyl groups and a methyl group in *pseudo-equatorial* positions, and two lone paris in *pseudo-axial* positions, as is shown in Scheme 9. Therefore, in order to accommodate the observed stereospecificity, an inversion of the configuration at C^1 or C^2 must occur during the ring contraction.

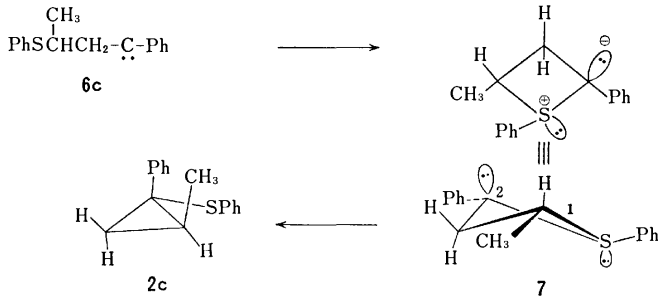

Scheme 9.

Three mechanisms (Scheme 10) can be considered for this stereospecific reaction. The first one is a concerted mechanism with an inversion of the configuration at C^1; the ylide lone pair attacks from the back side of the cleaving carbon–sulfur bond (Mechanism 1.).

Mechanism 1. Concerted process (inversion at C^1)

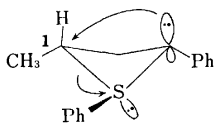

Mechanism 2. Concerted process (inversion at C^2)

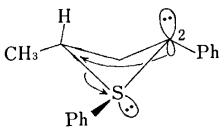

Mechanism 3. Radical pair process (inversion at C^2)

Scheme 10.

The second one is also a concerted mechanism, but with an inversion at C^2; a partially developed back lobe of the carbanion attacks C^1 from the front side, with a retention of the configuration at C^1. This mechanism has some similarity to the so-called "*double inversion mechanism*" proposed by Bordwell *et al.* in the case of the 1,3-elimination of α-halosulfones.[11] The third one is a radical-pair mechanism. This mechanism has been confirmed for the Stevens rearrangements of certain ylides[12] and is known to proceed with a retention of the configuration at the migrating carbon, C^1.[13] This means that the inversion must occur at C^2. As far as we know, however, there has never been observed such a stereospecificity at the migrating terminus in a Stevens rearrangement. On the other hand, a stereospecific rearrangement of 2,4-diphenylthietane-1-oxide to the anion of cyclopropylsulfenic acid in the presence of a base has recently been reported by Dodson *et al.*[14] They proposed that the stereospecific reaction proceeded through the most stable conformation of the anion produced and that, therefore, an inversion of the configuration should occur at the carbanion carbon.

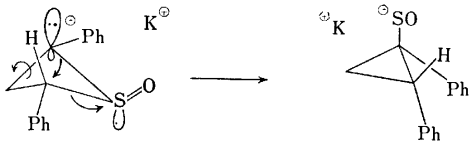

Their observation corresponds well to the results obtained in our system and supports the concerted Mechanism 2 for the rearrangement of the thietanonium ylide, **7**.

In connection with the mechanism of the formation of the 3-thiabicyclo[4.1.0]heptanes, **15** and **16**, it is worth-while to discuss the stereochemistry of the reaction. The cycloaddition of a diazoalkane to carbon–carbon double bonds is assumed to be a stereospecific concerted process.[15] Therefore, the formation of *exo*-methylpyrazoline (A) from the tosylhydrazone bearing *trans*-crotyl group is an allowed process, while the formation of the corresponding *endo*-isomer from the same precursor is strongly forbidden.

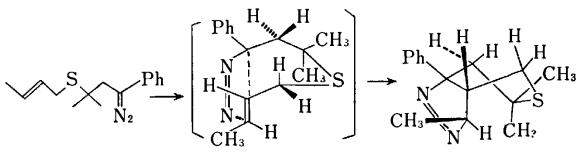

A: exo-methyl

Fig. 2.

The final product, **16**, which is produced by the nitrogen elimination of the intermediary-formed pyrazoline, dose not retain the stereochemical integrity of the starting materials. Thus, the stereochemical crossover should occur at the stage of radical recombination, as is shown in the following scheme.

The high efficiency of the *intramolecular* cycloaddition observed in the β-allylthio system is probably due chiefly to the intramolecular nature of the reaction. Another factor, however, must be considered in order to explain the results, because the addition of a diazoalkane to nonconjugated olefins is usually a very slow and difficult process.[15,16] One possible interpretation is that some kind of activating effect of the

allylic sulfur atom on the double bond is operating in these systems.[17]

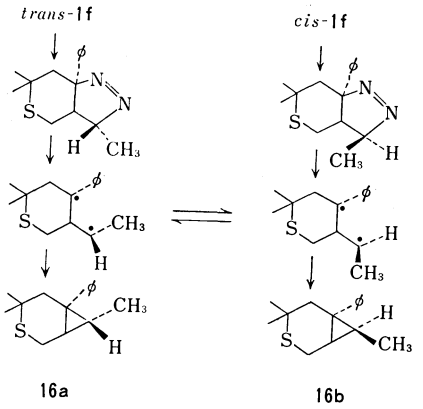

Scheme 11.

Experimental

Measurements. The melting points and boiling points were uncorrected. The infrared spectra were recorded on a Hitachi-Perkin-Elmer Model 337 Infracord or a Hitachi EPI-G3 spectrophotometer, using as samples neat liquids, KBr disks, or Nujol mulls. The nuclear magnetic resonance spectra were obtained by the use of a Varian HA-100 or a Hitachi R20-B spectrometer, using TMS as the internal standard. The mass spectra were measured using a Hitachi RMU-6E spectrometer at 70 eV. Analytical gas chromatography (vpc) was carried out on a Hitachi K-53 equipped with a flame-ionization detector. The total yield and product ratios were determined by the vpc using a column packed with 20% SE-30 or 10% QF-1 on Chromosorb W. Preparative gas chromatography was performed with an Aerograph A-700 instrument or a Hitachi KGL-2B instrument using a 4 mm×1 m column packed with 3% SE-30 or 20% XF-1150 on Chromosorb W. The photolyses were carried out with the use of a 450-W high-pressure mercury lamp (Ushio Electric, Inc.).

Preparation of Tosylhydrazones. The Bamford-Stevens method[18,19] was employed for the *in-situ* generation of carbenes and diazoalkanes. Thus, the required tosylhydrazones were prepared by the condensation of the corresponding ketones with *p*-toluenesulfonylhydrazide.

*4-Phenylthio-2-butanone Tosylhydrazone (**1a**).* 4-Phenylthio-2-butanone was prepared by the addition of thiophenol to methyl vinyl ketone.[20] 4-Phenylthio-2-butanone (5 g, 0.0278 mol) and *p*-toluenesulfonylhydrazide (6 g, 0.0322 mol) were dissolved in 100 ml of ethanol, after which the solution was heated to reflux for an hour. The reaction mixture was cooled with dry ice and gradually warmed to room temperature. The precipitated colorless needles of the corresponding tosylhydrazone (**1a**) were collected by filtration. Yield: 8.24 g; 85%; mp 100—101 °C. Found: C, 58.38; H, 5.84; N, 8.15; S, 18.53%. Calcd for $C_{17}H_{21}N_2O_2S_2$: C, 58.59; H, 5.78; N, 8.04; S, 18.40%.

*4-Phenylthio-4-methyl-2-pentanone Tosylhydrazone (**1b**).* To a mixture of mesityl oxide (25 g, 0.255 mol) and thiophenol (28 g, 0.255 mol), we added a few drops of piperidine. After an initial exothermic reaction had subsided, the reaction mixture was further stirred with a magnetic stirrer overnight at room temperature. 4-Phenylthio-4-methyl-2-pentanone[21] was obtained by the distillation of the reaction mixture under reduced pressure. Yield: 42.5 g; 80%; bp 109 °C/0.35 mmHg. NMR (CCl_4): τ 8.65 (s, 6H), 7.97 (s, 3H), 7.44 (s, 2H), and 2.90—2.40 (m, 5H). The corresponding tosylhydrazone (**1b**) was prepared by a method similar to that described above. Mp 109—110 °C (colorless needles). Found: C, 60.38; H, 6.59; N, 7.37; S, 16.88%. Calcd for $C_{19}H_{25}N_2O_2S_2$: C, 60.61; H, 6.42; N, 7.44; S, 17.03%.

*3-Phenylthiobutyrophenone Tosylhydrazone (**1c**).* Phenyl propenyl ketone was prepared from crotonyl chloride and benzene employing the Friedel-Crafts method.[22] The base-catalyzed addition of thiophenol to the ketone, as has been described in the previous section, produced 3-phenylthiobutyrophenone; 86%; bp 167 °C/0.25 mmHg. Tosylhydrazone **1c**: mp 128—129 °C (colorless needles). Found: C, 64.65; H, 5.95; N, 6.43; S, 15.09%. Calcd for $C_{23}H_{25}N_2O_2S_2$: C, 64.86; H, 5.70; N, 6.60; S, 15.10%.

*3-Phenylthio-3-methylbutyrophenone Tosylhydrazone (**1d**).* Isopropylideneacetophenone was prepared from 3-methylcrotonyl chloride and benzene by the method of Smith and Engelhardt,[23] with some modifications. 3-Phenylthio-3-methylbutyrophenone was synthesized by the base-catalyzed addition of thiophenol to the ketone; 88%; bp 178—181 °C/1.0 mmHg, NMR (CCl_4): τ 8.57 (s, 6H), 6.90 (s, 2H) and 2.95—2.20 (m, 10H). Tosylhydrazone **1d**: mp 110—111 °C (colorless needles). Found: C, 65.74; H, 5.97; N, 6.45; S, 14.51%. Calcd for $C_{24}H_{26}N_2O_2S_2$: C, 65.72; H, 5.97; N, 6.39; S, 14.62%.

*3-Ethylthio-3-methylbutyrophenone Tosylhydrazone (**1e**).* The base-catalyzed addition of ethanethiol to isopropylideneacetophenone afforded 3-ethylthio-3-methylbutyrophenone: bp 127 °C/0.4 mmHg. NMR (CCl_4): τ 8.80 (t, J=7 Hz, 3H), 8.52 (s, 6H), 7.43 (quartet, J=7 Hz, 2H), 6.81 (s, 2H,) and 2.80—1.90 (m, 5H). Tosylhydrazone **1e**: mp 160—161 °C (colorless needles). Found: C, 61.55; H, 6.65; N, 7.45; S, 16.42%. Calcd for $C_{20}H_{26}O_2S_2N_2$: C, 61.51; H, 6.71; N, 7.17; S, 16.65%.

*3-Allylthio-3-methylbutyrophenone Tosylhydrazone (**1f**).* 3-Allylthio-3-methylbutyrophenone was prepared by the addition reaction of 2-propenethiol to isopropylideneacetophenone: bp 122 °C/0.3 mmHg. NMR (CCl_4): τ 8.52 (s, 6H), 6.80 (s, 2H), 6.78 (d, J=7 Hz, 2H), 5.10—4.65 (m, 2H), 4.50—3.90 (m, 1H) and 2.70—2.00 (m, 5H). The ketone was converted to the corresponding tosylhydrazone by treatment with an equimolar amount of tosylhydrazide in the presence of a catalytic amount of sulfuric acid. The use of an excess of tosylhydrazide should be avoided, as it was found that the existing allylic double bond was partially hydrogenated under such circumstances. Tosylhydrazone **1e**: mp 135—136 °C (colorless prisms). Found: C, 62.60; H, 6.26; N, 7.13; S, 15.66%. Calcd for $C_{21}H_{26}N_2O_2S_2$: C, 62.65; H, 6.51; N, 6.96; S, 15.93%.

*3-Crotylthio-3-methylbutyrophenone Tosylhydrazone (**1g**).* 2-Butenethiol was prepared from crotyl alcohol according to the standard procedure.[24] The *cis*/*trans* isomer ratio of crotyl alcohol was determined on the basis of the NMR spectrum, employing $Eu(DPM)_3$ as a shift reagent, and by vpc analysis, using a column packed with 20% XF-1150. According to the spectrum, a commercial-grade crotyl alcohol has a *trans*/*cis* ratio of 72/28. An alcohol with a *trans*/*cis* ratio of 91/9 was obtained by fractional distillation through a spinning-band column.

3-Crotylthio-3-methylbutyrophenone was synthesized from the 2-butanethiol and isopropylideneacetophenone in a manner similar to that described before: bp 142 °C/0.2 mmHg. NMR (CCl_4): τ 8.54 (s, 6H), 8.32 (d, J=4 Hz, 3H), 6.84 (d, J=7 Hz, 2H), 6.82 (s, 2H), 4.64—4.20 (m, 2H), and 2.70—2.00 (m, 5H).

The condensation of the ketone with tosylhydrazide afforded

the corresponding tosylhydrazone (**1g**): mp 97—98 °C (colorless prisms). Found: C, 63.88; H, 6.67; N, 6.55; S, 15.77%. Calcd for $C_{22}H_{28}N_2O_2S_2$: C, 63.63; H, 6.77; N, 6.72; S, 15.39%.

*3-Benzylthio-3-methylbutyrophenone Tosylhydrazone (**1h**).* The desired tosylhydrazone was prepared from tosylhydrazide and 3-benzylthio-3-methylbutyrophenone. The latter was obtained by the addition of phenylmethanethiol to isopropylideneacetophenone in a manner similar to that described previously. 3-Benzylthio-3-methylbutyrophenone: NMR (CCl_4): τ 8.52 (s, 6H), 6.90 (s, 2H), 6.27 (s, 2H) and 2.90—2.10 (m, 10H). Tosylhydrazone **1h**: mp 93—94 °C (colorless prisms). Found: C, 65.88; H, 6.27; N, 6.24; S, 14.14%. Calcd for $C_{25}H_{28}N_2O_2S_2$: C, 66.04; H, 6.24; N, 6.19; S, 14.17%.

*4-Allylthio-4-methyl-2-pentanone Tosylhydrazone (**1i**).* The base-catalyzed addition of 2-propenethiol to mesityl oxide produced 4-allylthio-4-methyl-2-pentanone, which was then further converted to the corresponding tosylhydrazone (**1i**). 4-Allylthio-4-methyl-2-pentanone: bp 67 °C/1.0 mmHg. NMR (CCl_4): τ 8.60 (s, 6H), 7.80 (s, 3H), 7.37 (s, 2H), 6.82 (d, J=7 Hz, 2H), 5.10—4.65 (m, 2H) and 4.50—3.80 (m, 1H). Tosylhydrazone **1i**: mp 75—76 °C (colorless prisms). Found: C, 56.41; H, 6.99; N, 8.36; S, 18.84%. Calcd for $C_{16}H_{24}N_2O_2S_2$: C, 56.44; H, 7.10; N, 8.23; S, 18.83%.

*Thermal Decomposition of **1a**.* In a flask equipped with a reflux condenser a 1.04 g portion (3.0 mmol) of the **1a** tosylhydrazone was dissolved in 40 ml of diglyme, and then a 180 mg portion (*ca.* 0.35 mmol) of sodium hydride (50% suspension in mineral oil) was stirred in. After the gas evolution had ceased, the reaction flask was immersed in an oil bath heated at 180 °C. Thermolysis was monitored by nitrogen evolution, which was completed in the temperature range of 130—150 °C. The reaction mixture was heated to reflux for 15 minutes and was then left to cool at room temperature. The sodium *p*-toluenesulfinate thus precipitated was filtered off, and the filtrate was distilled under reduced pressure to remove the solvent. The residue was then submitted to column chromatography on silica (WAKO C-200), using *n*-hexane as the eluent. 1-Methylcyclopropyl phenyl sulfide (**2a**), 3a-methyl-1,2,3,3a-tetrahydro-1-thiaazulene (**5a**), and a mixture of 2-butenyl phenyl sulfide (**3a**) and 3-butenyl phenyl sulfide (**4a**) were eluted, in this order. Although the **3a** and **4a** olefins could not be completely separated by either column chromatography on silica or gas chromatography, the NMR spectrum of the mixture supported the structures. The ratio of these olefins could be calculated from the spectrum. When sodium methoxide was used as the base, cyclopropyl sulfide, **2a**, could not be detected in the product; furthermore, the total yield of the isolable product decreased. **2a**: NMR (CCl_4): τ 9.14 (H^b and H^c: ABq, J=7 Hz, 4H), 8.56 (H^a: s, 3H) and 3.00—2.70 (Ph: m, 5H).

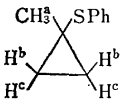

3a: NMR (CCl_4): *cis* and *trans* τ 8.43 (*cis*-H^a: d, Jad=7 Hz) and 8.35 (*trans*-H^a: d, Jad=7 Hz) (3H), 6.65—6.45 (H^b: m, 2H), 4.62—4.44 (H^c and H^d: m, 2H), and 3.00—2.65 (Ph: m, 5H). IR (neat): 958 cm^{-1} ($\delta_{HC=CH}$). Mass: 164 (M^+), 149 (M^+-CH_3), 110 ($PhSH^+$), 109 (PhS^+), 77 (Ph^+), and 55 (M^+-PhS).

$$PhSCH_2^bCH{=}^cCH{-}^dCH_3^a$$

4a: NMR (CCl_4): τ 7.66 (H^b: q, Jab=Jbc=7 Hz, 2H), 7.10 (H^a: t, Jab=7 Hz), 5.10—4.65 (H^c and H^d: m, 3H), and 3.00—2.65 (Ph: m, 5H).

$$PhSCH_2^aCH_2^bCH{=}^cCH_2^d$$

5a: NMR (CCl_4): τ 9.15 (H^a: s, 3H), 7.65 (H^b: octet, 2H), 7.20 (H^c: octet, 2H), 5.01 (H^d: d, Jde=10 Hz, 1H), and 4.20—3.80 (H^e: m, 4H). Found: (a mixture of products, **2a**—**5a**): C, 73.00; H, 7.15; S, 19.25%. Calcd for $C_{10}H_{12}S$: C, 73.12; H, 7.36; S, 19.52%.

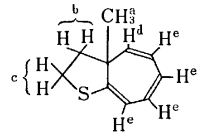

*Thermal Decomposition of **1b**.* The sodium salt of **1b** was prepared and decomposed in diglyme under the conditions described above. The crude products were chromatographed on silica, and 1,3,3-trimethylcyclopropyl phenyl sulfide (**2b**), 2,2,3a-trimethyl-1,2,3,3a-tetrahydro-1-thiaazulene (**5b**), 4-phenylthio-4-methyl-2-pentene (**3b**), and 4-phenylthio-4-methyl-1-pentene (**4b**) were eluted by *n*-hexane. The pure **3b** olefin was obtained by column chromatography, but the **4b** olefin could not be separated from the **3b** olefin. The pure sample of the **4b** olefin was, however, obtained from the reaction performed in a protic solvent. Although cyclopropyl sulfide, **2b**, and thiaazulene, **5b**, were obtained as a mixture by column chromatography on silica, further purification by preparative vpc afforded pure samples. In this case, the use of sodium methoxide as a base resulted in similar products. **2b**: NMR (CCl_4): τ 9.29 (H^a: ABq, J=5.0 Hz, 2H), 8.69 (H^b: s, 3H), 8.60 (H^d: s, 3H), 8.46 (H^c: s, 3H), and 3.20—2.80 (Ph: m, 5H). Mass: 192 (M^+, base peak), 177 (M^+-CH_3). 110 ($PhSH^+$), 109 (PhS^+), 83 (M^+-PhS), and 77 (Ph^+). Found: C, 74.78; H, 8.16; S, 16.89%. Calcd for $C_{12}H_{16}S$: C, 74.94; H, 8.39; S, 16.67%.

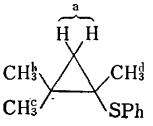

3b: NMR (CCl_4): *trans* τ 8.70 (H^a: s, 6H), 8.39 (H^b: d, Jbd=6 Hz, 3H), 5.00 (H^d: octet, Jcd=16 Hz, 1H), 4.52 (H^c: d, Jcd=16 Hz, 1H), and 2.95—2.50 (Ph: m, 5H). IR (neat): 963 cm^{-1} ($\delta_{HC=CH}$).

$$PhS{-}\overset{\overset{CH_3^a}{|}}{\underset{\underset{CH_3^a}{|}}{C}}{-}CH{=}^cCH{-}^dCH_3^b$$

4b: NMR (CCl_4): τ 8.82 (H^a: s, 6H), 7.83 (H^b: d, Jbc=6 Hz, 2H), 4.40—3.75 (H^c and H^d: m, 3H), and 2.95—2.50 (Ph: m, 5H). Found (a mixture of **3b** and **4b**): C, 74.82; H, 8.35; S, 16.66%. Calcd for $C_{12}H_{16}S$: C, 74.94; H, 8.39; S, 16.67%.

$$PhS{-}\overset{\overset{CH_3^a}{|}}{\underset{\underset{CH_3^a}{|}}{C}}{-}CH_2^bCH{=}^cCH_2^d$$

5b: NMR (CCl_4): τ 9.07 (H^a: s, 3H), 8.53 (H^b: s, 3H), 8.40 (H^c: s, 3H), 7.70 (H^d: s, 2H), 4.94 (H^e: d, Jef=10 Hz, 1H), and 4.20—3.70 (H^f: m, 4H). Found: C, 74.68; H, 8.40; S, 16.94%. Calcd for $C_{12}H_{16}S$: C, 74.94; H, 8.39; S, 16.69%.

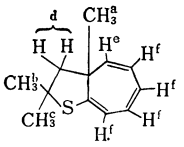

Thermal Decomposition of **1c**. The **1c** tosylhydrazone (1.49 g, 4.0 mmol) was decomposed in the presence of 220 mg of sodium methoxide in diglyme under the conditions described above. The crude products were submitted to column chromatography on silica, and 3-methyl-1-phenylcyclopropyl phenyl sulfide (**2c**), 3-phenyl-1-methylcyclopropyl phenyl sulfide (**20**), and 1-phenyl-3-phenylthio-1-butene, **3c**, (*cis* and *trans*) were eluted by *n*-hexane. Although cyclopropyl sulfide, **20**, could not be separated from cyclopropyl sulfide, **2c**, by the column chromatography, purification by preparative vpc gave a pure sample. Both *cis* and *trans* **3c** olefins were successfully isolated by column chromatography.

When sodium hydride was used as a base instead of sodium methoxide, 1-phenyl-3-phenylthio-2-butene (*cis*/*trans*=50/50) (**3c'**) was obtained, together with the **3c** olefin in the ratio of 38/62. Pure samples of *cis* and *trans* isomers of the **3c'** olefin were obtained by column chromatography on silica.

In a control experiment, the **3c** olefin (100 mg) was treated with 20 mg of sodium hydride in 50 ml of diglyme under reflux for 15 min.[8] The reaction mixture was concentrated under reduced pressure, dissolved in chloroform, washed with water, dried over anhydrous magnesium sulfate, and then concentrated again. A study of the NMR spectrum of the reaction mixture revealed the formation of a mixture of the **3c** and **3c'** olefins in the ratio of 60/40.

2c: NMR (CCl_4): τ 9.17 (H^a: d, Jab=6 Hz, 3H), 9.00—8.20 (H^b and H^c: m, 3H), and 3.10—2.75 (Ph: m, 10H). Mass: 240 (M^+). 225 (M^+-CH_3), 163 (M^+-Ph), 131 (M^+-PhS, base peak), 110 ($PhSH^+$), 109 (PhS^+), and 77 (Ph^+). Found: C, 79.72; H, 6.49; S, 13.60%. Calcd for $C_{16}H_{16}S$: C, 79.95; H, 6.71; S, 13.34%.

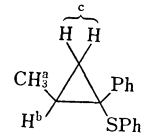

20: NMR (CCl_4): τ 9.10—8.10 (H^b and H^c: m, 3H), 8.57 (H^a: s, 3H), and 3.10—2.70 (Ph: m, 10H). Mass: 240 (M^+-CH_3), 131 (M^+-PhS, base peak), 109 (PhS^+), 91 ($C_7H_7^+$),

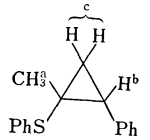

and 77 (Ph^+). Found: S, 13.44%. Calcd: S, 13.34%.

3c: NMR (CCl_4): *trans* τ 8.55 (H^a: d, Jab=7 Hz, 3H), 6.40—6.10 (H^b: m, 1H), 4.05—3.95 (H^c and H^d: m, 2H), and 3.00—2.60 (Ph: m, 10H). IR (neat): 960 cm^{-1} ($\delta_{HC=CH}$). Mass: 240 (M^+), 131 (M^+-PhS, base peak), 110 ($PhSH^+$), 109 (PhS^+), 91 ($C_7H_7^+$), and 77 (Ph^+). NMR (CCl_4): *cis* τ 8.62 (H^a: d, Jab=7 Hz, 3H), 5.82 (H^b: octet, Jbc=11 Hz, Jab=7 Hz, 1H), 4.56 (H^c: t, Jbc=11 Hz, 1H), 3.71 (H^d: d, Jcd=11 Hz, 1H), and 3.10—2.70 (Ph: m, 10H). Found: C, 79.75; H, 6.75; S, 13.46%. Calcd for $C_{16}H_{16}S$: C, 79.95; H, 6.71; S, 13.34%.

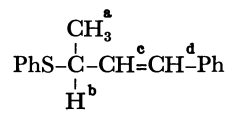

3c': NMR (CCl_4): *trans* τ 8.07 (H^a: s, 3H), 6.61 (H^b: d, Jbc=8 Hz, 2H), 4.12 (H^c: t, Jbc=8 Hz, 1H), and 3.10—2.70 (Ph: m, 10H). *cis* τ 8.11 (H^a: s, 3H), 6.40 (H^b: d, Jbc=8 Hz, 2H), 4.17 (H^c: t, Jbc=8 Hz, 1H), and 3.10—2.70 (Ph: m, 10H). Mass: 240 (M^+), 225 (M^+-CH_3), 131 (M^+-PhS, base peak), 110 ($PhSH^+$), 109 (PhS^+), 105 ($PhCH_2CH_2^+$), 91 ($PhCH_2^+$), and 77 (Ph^+).

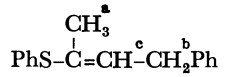

Thermolysis and Photolysis of **1d**. The sodium salt of **1d** was prepared and themally decomposed in diglyme under the conditions described above. When the crude products were chromatographed on silica, 3,3-dimethyl-1-phenylcyclopropyl phenyl sulfide (**2d**) and 3-methyl-3-phenylthio-1-phenyl-1-butene (**3d**) were obtained. The same products were obtained in similar yields when sodium methoxide was used as the base.

The photolysis of the sodium salt of **1d** (219 mg, 0.5 mmol) was carried out in 50 ml of monoglyme, using a Pyrex cell cooled with water and employing a 450 W high-pressure Hg lamp. The same treatment of the crude products described above afforded cyclopropyl sulfide, **2d** (37%), and the **3d** olefin (18%). It seems that the **3d** olefin was polymerized or decomposed under the photolytic conditions.

2d: NMR (CCl_4): τ 9.16 (H^a: s, 3H), 8.80 (H^c: ABq, J=5 Hz, 2H), 8.40 (H^b: s, 3H), and 3.10—2.85 (Ph: m, 10H). Mass: 254 (M^+, base peak), 239 (M^+-CH_3), 177 (M^+-Ph), 145 (M^+-PhS), 110 ($PhSH^+$), 109 (PhS^+), and 77 (Ph^+). Found: C, 80.50; H, 7.18; S, 12.64%. Calcd for $C_{17}H_{18}S$: C, 80.26; H, 7.18; S, 12.64%.

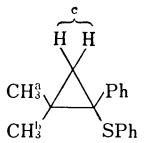

3d: NMR (CCl_4): *trans* τ 8.56 (H^a: s, 6H), 4.00 (H^b and H^c: ABq, J=16 Hz, 2H), and 3.10—2.60 (Ph: m, 10H). IR (neat): 958 cm^{-1} ($\delta_{HC=CH}$). Mass: 254 (M^+), 145 (M^+-PhS), 110 ($PhSH^+$), 109 (PhS^+), 91 ($C_7H_7^+$), and 77 (Ph^+). Found: C, 80.00; H, 7.22; S, 12.36%. Calcd. for $C_{17}H_{18}S$: C, 80.26; H, 7.14; S, 12.60%.

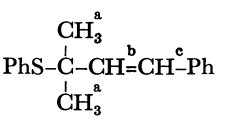

Thermal Decomposition of **1e**. The sodium salt of the **1e** tosylhydrazone was prepared from 1.56 g (4.0 mmol) of the tosylhydrazone and 240 mg of sodium hydride in mineral oil (50%), and was decomposed in diglyme under the conditions described above. When the crude products were chromatographed on silica gel, 3,3-dimethyl-1-phenylcyclopropyl ethyl sulfide (**2e**) and 3-ethylthio-3-methyl-1-phenyl-1-butene (**3e**) were obtained.

2e: NMR (CCl_4): τ 9.21 (H^a: s, 3H), 8.96 (H^c: ABq, J=5 Hz, 2H), 8.92 (H^d: t, J=7 Hz, 3H), 8.55 (H^b: s, 3H), 7.72 (H^e:

quartet, J=7 Hz, 2H), and 2.88 (Ph: 2, 5H), Found: C, 75.52; H, 8.88; S, 15.49%. Calcd for $C_{13}H_{18}S$: C, 75.67; H, 8.79; S, 15.54%.

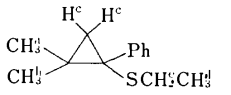

3e: NMR (CCl_4): *trans* τ 8.83 (H^a: t, J=7 Hz, 3H), 8.56 (H^c: s, 6H), 7.60 (H^b: quartet, J=7 Hz, 2H), 3.76 (H^d, H^e: s, 2H) and 3.00—2.40 (Ph: m, 5H). IR (neat): 960 cm^{-1} ($\delta_{HC=CH}$). Found: C, 75.60; H, 8.86; S, 15.52%. Calcd for $C_{13}H_{18}S$: C, 75.67; H, 8.79; S, 15.54%.

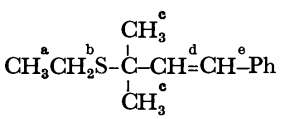

Photolysis of ***1f***. The **1f** tosylhydrazone (1.07 g, 4.0 mmol) and sodium methoxide (280 mg) were dissolved in 80 ml of monoglyme in a Pyrex photolysis vessel. After a stream of nitrogen had been bubbled into the photolysis vessel, the mixture was irradiated with a 450 W high-pressure Hg lamp for 4 hr under stirring and cooling by water. The sodium *p*-toluenesulfinate thus precipitated was filtered off. The filtrate was concentrated under reduced pressure, dissolved in chloroform, washed with water, and dried over anhydrous magnesium sulfate. The crude products were submitted to column chromatography on silica, using *n*-hexane as the eluent. 2-Allyl-4,4-dimethyl-1-phenylthietane (**10a**), 3-allylthio-3-methyl-1-phenyl-1-butene (**12a**) (*cis* and *trans*), and 2-vinyl-5,5-dimethyl-3-phenyltetrahydrothiophene (**11a**) were eluted in this order. Although the diastereoisomers of tetrahydrothiophene (**11a**) could not be separated from each other, purification by preparative vpc (20% SE-30 at 180 °C) afforded each component in the pure form. The use of sodium hydride as a base resulted in the hydrogenation of the allylic double bond.

10a: NMR (CCl_4): τ 8.62 (H^a: s, 3H), 8.44 (H^b: s, 3H), 7.30 (H^d: d, J=7 Hz, 2H), 7.06 (H^c: ABq, J=12 Hz, 2H), 5.40—5.00 (H^f: m, 2H), 4.80—4.20 (H^e: m, 1H), and 3.00—2.65 (Ph: m, 5H).

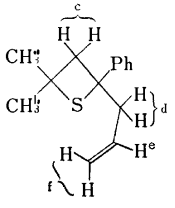

11a: NMR (CCl_4): *cis* (as for phenyl and vinyl) τ 8.53 (H^a: s, 3H), 8.50 (H^b: s, 3H), 7.87 (H^c: octet, Jcc=16 Hz, Jcd=2 Hz, 6 Hz, 2H), 6.80 (H^d: octet, 1H), 6.01 (H^e: q, Jde=10 Hz, Jef=8 Hz, 1H), 5.30—5.00 (H^g: m, 2H), 4.55—4.15 (H^f: m, 1H), and 2.90—2.65 (Ph: m, 5H). *trans* τ 8.51 (H^a: s, 3H), 8.44 (H^b: s, 3H), 7.88 (H^c: octet, Jcc=12 Hz, Jcd=4 Hz, 12 Hz, 2H), 6.05 (H^e: d, Jef=7 Hz, Jde=0, 1H), 6.05 (H^d: octet, 1H), 5.30—4.95 (H^g: m, 2H), 4.75—4.20 (H^f: m, 1H), and 2.95—2.65 (Ph: m, 5H).

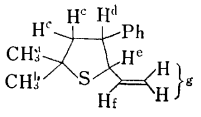

12a: *cis*: NMR (CCl_4): τ 8.76 (H^a: s, 6H), 6.85 (H^b: d, Jbc=7 Hz, 2H), 5.10—4.75 (H^d: m, 2H), 4.50—4.05 (H^c: m, 1H), 4.40 (H^e: d, Jef=12 Hz, 1H), 3.54 (H^f: d, Jef=12 Hz, 1H), and 2.90—2.70 (Ph: m, 5H). IR (neat): 1640 ($\nu_{C=C}$), 980, 910 ($\delta_{HC=CH_2}$), and 780 cm^{-1} ($\delta_{HC=CH}$). *trans* NMR (CCl_4): τ 8.56 (H^a: s, 6H), 7.01 (H^b: d, Jbc=7 Hz, 2H), 5.20—4.80 (H^d: m, 2H), 4.50—4.05 (H^c: m, 1H), 3.83 (H^e, H^f: m, 2H), and 2.90—2.60 (Ph: m, 5H). IR (neat): 1640 ($\nu_{C=C}$), 978, 910 ($\delta_{HC=CH_2}$), and 960 cm^{-1} ($\delta_{HC=CH}$) Found (a mixture of **10a**, **11a**, and **12a**): C, 76.99; H, 8.10; S, 14.43%. Calcd for $C_{14}H_{18}S$: C, 77.01; H, 8.31; S, 14.68%.

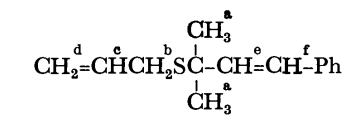

Photolysis of ***1g***. The **1g** tosylhydrazone was photolyzed in a manner similar to that described above, and the crude products were chromatographed on silica. 4,4-Dimethyl-2-(1-methylallyl)-2-phenylthietane (**10b**), 5,5-dimethyl-3-phenyl-2-(1-propenyl)tetrahydrothiophene (**11b**), and 3-crotylthio-3-methyl-1-phenylbutene (**12b**) (*cis* and *trans*) were eluted by *n*-hexane, in this order.

10b: NMR (CCl_4): diastereoisomer-(A) τ 9.34 (H^c: d, Jce=7 Hz, 3H), 8.72 (H^a: s, 3H), 8.57 (H^b: s, 3H), 7.44 (H^e: quintet, 1H), 7.04 (H^d: ABq, J=12 Hz, 2H), 5.20—4.90 (H^g: m, 2H), 4.40—4.00 (H^f: m, 1H), and 3.00—2.60 (Ph: m, 5H).

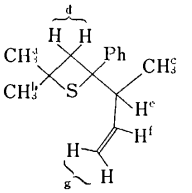

diastereoisomer-(B) τ 9.21 (H^c: d, Jce=7 Hz, 3H), 8.70 (H^a: s, 3H), 8.49 (H^b: s, 3H), 7.25—6.90 (H^e: m, 1H), 7.03 (H^d: ABq, J=12 Hz, 2H), 5.25—4.60 (H^f and H^g: m, 3H), and 3.00—2.70 (Ph: m, 5H).

11b: NMR (CCl_4): τ 8.60—8.30 (H^a, H^b, and H^c: m, 9H), 8.15—7.50 (H^d: m, 2H), 7.05—6.50 (H^e: m, 1H), 6.50—5.85 (H^f: m, 1H), 5.10—4.40 (H^g: m, 2H), and 3.00—2.60 (Ph: m, 5H).

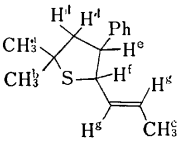

12b: NMR (CCl_4): *cis* τ 8.76 (H^a: s, 6H), 8.35 (H^b: d, Jbc=5 Hz, 3H), 6.91 (H^d: d, Jcd=6 Hz, 2H), 4.70—4.40 (H^c: m, 2H), 4.40 (H^e: d, Jef=12 Hz, 1H), 3.54 (H^f: d, Jef=12 Hz, 1H), 2.95—2.70 (Ph: m, 5H). IR (neat): 955 (δ *trans* -CH=CH-), 775 cm^{-1} (*cis* -CH=CH-). NMR (CCl_4): *trans* τ 8.58 (H^a: s, 6H), 8.40 (H^b: d, Jbc=5 Hz, 3H), 7.07 (H^d: d, Jcd=6 Hz, 2H), 4.80—4.50 (H^c: m, 2H), 3.84 (H^e and H^f: s, 2H), 2.90—2.60 (Ph: m, 5H). IR (neat): 970 (δ *trans* -CH=CH-), 955 cm^{-1} (δ *trans* -CH=CH-).

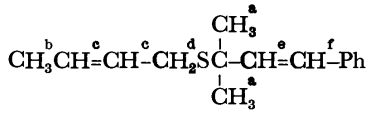

Found (a mixture of **10b**, **11b**, and **12b**): C, 77.85; H, 9.03; S, 13.88%. Calcd for $C_{15}H_{20}S$: C, 77.53; H, 8.67; S, 13.80%.

Thermal Decomposition of ***1f***. The **1f** tosylhydrazone (804 mg, 2.0 mmol) was dissolved in 50 ml of diglyme, and then we added 130 mg of sodium methoxide. Thermolysis was performed in accordance with the procedure described previously. The products were purified by column chromatography on silica. 6-Phenyl-4,4-dimethyl-3-thiabicyclo[4.1.0]-heptane (**15**) was obtained from the eluate of *n*-hexane. Yield, 196 mg (45%). The analytical vpc (20% SE-30, 200 °C) of the crude products, however, showed the formation of small amounts of thietane, **10a**, and the **12a** olefin, as is shown in Table 2.

15: NMR (CCl_4): τ 9.20—8.40 (H^d and H^e: m, 3H), 8.84 (H^a: s, 3H), 8.62 (H^b: s, 3H), 8.01 (H^c: s, 2H), 7.01 (H^f: octet, Jef=2 Hz, 4 Hz, 2H), and 3.10—2.80 (Ph: m, 5H). Found: C, 77.14; H, 8.20; S, 14.40%. Calcd for $C_{14}H_{18}S$: C, 77.01; H, 8.31; S, 14.68%.

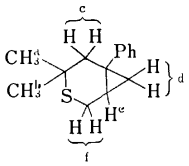

Thermal Decomposition of ***1g***. The **1g** tosylhydrazone was decomposed at 150 °C in the presence of a slight excess of sodium methoxide, as has been described previously. Two products were observed in the analytical vpc (20% SE-30, 220 °C) of the crude product. Separation by column chromatography on silica afforded 1-phenyl-4,4-dimethyl-7-(*exo*)-methyl-3-thiabicyclo[4.1.0]heptane (**16a**) and its *endo* isomer (**16b**) in the pure form. Their structures were assigned based on the NMR spectra; the absorption peak of the methyl in the *exo*-isomer appeared at τ 9.29, while that of the *endo*-isomer was at τ 8.68.

16: NMR (CCl_4): *exo* τ 9.29 (H^c: d, Jce=5.5 Hz, 3H), 9.00—8.60 (H^e and H^f: m, 2H), 8.89 (H^a: s, 3H), 8.78 (H^b: s, 3H), 8.03 (H^d: s, 2H), 6.98 (H^g: octet, Jgg=14 Hz, Jfg=1.5 Hz, 4 Hz, 2H), and 3.00—2.70 (Ph: m, 5H). *endo* τ 8.95—8.40 (H^e and H^f: m, 2H), 8.81 (H^a: s, 3H), 8.73 (H^b: s, 3H), 8.68 (H^c: d, Jce=6 Hz, 3H), 8.09 (H^d: ABq, J=14 Hz, 2H), 7.06 (H^g: octet, Jgg=13 Hz, Jfg=2 Hz, 4 Hz, 2H), and 3.10—2.70 (Ph: m, 5H). Found: C, 77.39; H, 8.87; S, 13.90%. Calcd for $C_{15}H_{20}S$: C, 77.53; H, 8.67; S, 13.80%.

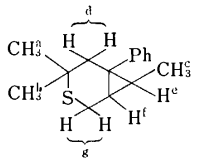

Thermolysis and Photolysis of ***1h***. The **1h** tosylhydrazone (904 mg, 2.0 mmol) was thermally decomposed in the presence of 130 mg of sodium methoxide in diglyme under the conditions described previously. The crude products were then chromatographed on silica, and 2-benzyl-2-phenyl-4,4-dimethylthietane (**10c**), 2,3-diphenyl-5,5-dimethyltetrahydrothiophene (**11c**), and 3-benzylthio-3-methyl-1-phenylbut-1-ene (**12c**, *trans*) were eluted by *n*-hexane. The tetrahydrothiophene, **11c**, was a mixture of diastereoisomers, and each component was sufficiently separated by column chromatography on silica. The isomer ratio was determined to be 50:50, based on the NMR spectrum.

The photolysis of the **1h** tosylhydrazone was performed in a manner similar to that described previously. Thietane, **10c**, tetrahydrothiophene, **11c**, and the **12c** olefin were also obtained, but the **12c** olefin was a mixture of *cis* and *trans* isomers (*cis*/*trans*=27/73).

10c: NMR (CCl_4): τ 8.69 (H^a: s, 3H), 8.50 (H^b: s, 3H), 6.96 (H^c: ABq, J=12 Hz, 2H), 6.79 (H^d: ABq, J=13 Hz, 2H), and 3.40—2.80 (Ph: m, 10H). Found: C, 80.58; H, 7.26; S, 11.79%. Calcd for $C_{18}H_{20}S$: C, 80.54; H, 7.51; S, 11.95%.

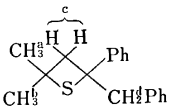

11c: NMR (CCl_4) *cis* τ 8.45 (H^a: s, 3H), 8.34 (H^b: s, 3H), 7.95—7.65 (H^c: m, 2H), 6.20—5.80 (H^d: m, 1H), 5.48 (H^e: d, Jde=10 Hz, 1H), and 3.40—2.75 (Ph: m, 10H). *trans* τ 8.40 (H^a: s, 3H), 8.29 (H^b: s, 3H), 7.80—7.40 (H^c: m, 2H), 6.30—5.80 (H^d: m, 1H), 5.42 (H^e: d, Jde=7.5 Hz, 1H), and 3.40—2.75 (Ph: m, 10H). Found: C, 80.31; H, 7.24; S, 11.93%. Calcd for $C_{18}H_{20}S$: C, 80.54; H, 7.51; S, 11.95%.

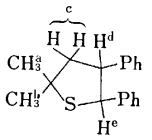

12c: NMR (CCl_4): *trans* τ 8.58 (H^a: s, 6H), 6.46 (H^b: s, 2H), 3.80 (H^c and H^d: s, 2H), and 3.00—2.65 (Ph: m, 10H). *cis* τ 8.49 (H^a: s, 6H), 6.34 (H^b: s, 2H), 3.96 (H^c and H^d: ABq, Jcd=12 Hz, 2H), and 3.10—2.65 (Ph: m, 10H). Found: C, 80.26; H, 7.25; S, 12.21%. Calcd for $C_{18}H_{20}S$: C, 80.54; H, 7.51; S, 11.95%.

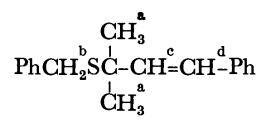

Thermolysis and Photolysis of ***1i***. The **1i** tosylhydrazone (1.70 g, 5.0 mmol) was thermally decomposed in the presence of 300 mg of sodium methoxide in diglyme. The subsequent purification of the crude products by column chromatography on silica gave 4,4,6-trimethyl-3,7,8-thiadiazabicyclo[4.3.0]-nonene (**17**), 303 mg (33%). The Δ^1-pyrazoline, **17**, is thermally stable, but sensitive to light.

The photolysis of the **1i** tosylhydrazone was performed in monoglyme in a manner similar to that described previously. The identifiable product obtained by column chromatography (silica/*n*-hexane) was found to be 4,4,6-trimethyl-3-thiabicyclo[4.1.0]heptane (**18**) (48%).

The Δ^1-pyrazoline (**17**) was irradiated in monoglyme with a 450 W high-pressure Hg lamp at room temperature, using a Pyrex filter. The solvent was evacuated off, and the residue was dissolved in carbon tetrachloride. The NMR spectrum of the reaction mixture showed the formation of 3-thiabicyclo[4.1.0]heptane **18**. The analytical vpc (20% SE-30, 140 °C) also supported the formation of the isomeric mixture of **18**.

17: NMR (CCl_4): τ 8.92 (H^a: s, 3H,) 8.85 (H^b: s, 3H), 8.67 (H^c: s, 3H), 7.88 (H^d: ABq, J=14 Hz, 2H), 7.69 (H^e: octet, Jee=14 Hz, Jef=5.5 Hz, 8 Hz, 2H), 8.35—7.80 (H^f: m, 1H), and 5.69 (H^g: octet, Jgg=17 Hz, Jfg=4 Hz, 6 Hz, 2H). Mass: 184 (M^+), 156 (M^+-N_2), 141 (156−CH_3), 123, 115,

107 (base peak). Found: C, 58.65; H, 8.90; S, 17.69%. Calcd for $C_{19}H_{16}N_2S$: C, 58.65; H, 8.75; S, 17.40%.

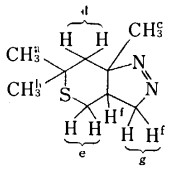

18: NMR (CCl_4) τ 9.75—9.10 (H^e and H^f: m, 3H), 8.95 (H^c: s, 3H), 8.87 (H^a: s, 3H), 8.72 (H^b: s, 3H), 8.35 (H^d: ABq, J=14 Hz, 2H), and 7.11 (H^g: octet, Jgg=14 Hz, Jfg=1 Hz, 2H). Found: C, 68.89; H, 10.21; S, 20.81%. Calcd for $C_9H_{16}S$: C, 69.17; H, 10.32; S, 20.52%.

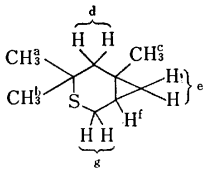

The authors wish to express their thanks to the Kawakami Memorial Foundation for its partial support of this research.

References

1) For example, G. Wittig and M. Schlosser, *Tetrahedron* **18**, 1023 (1962); W. E. Parham and S. H. Groen, *J. Org. Chem.*, **29**, 2214 (1964); V. Franzen and L. Finketcher, *Ann. Chem.*, **617**, 1 (1958); J. Dieckmann, *J. Org. Chem.*, **28**, 2933 (1963); M. Saunders and R. W. Murray, *Tetrahedron*, **6**, 88 (1959); H. Nozaki, R. Noyori, and K. Sisido, *ibid.*, **20**, 1125 (1964); a) W. E. Parham and R. Koncos, *J. Amer. Chem. Soc.*, **83**, 4034 (1961); b) W. Kirmse and M. Kapps, *Chem. Ber.*, **101**, 994, 1004 (1968); W. Ando, K. Nakayama, K. Ichibori, and T. Migita, *J. Amer. Chem. Soc.*, **91**. 5164 (1969); c) W. Ando, T. Yagihara, S. Tozune, and T. Migita, *ibid.*, **91**, 2786 (1969).

2) W. Kirmse and M. Buschhoff, *Chem. Ber.*, **100**, 1491 (1969).

3) J. H. Robson and H. Shechter, *J. Amer. Chem. Soc.*, **89**, 7112 (1969).

4) K. Kondo and I. Ojima, *Chem. Commun.*, **1972**, 62; I. Ojima and K. Kondo, This Bulletin, **46**, 1539 (1973).

5) K. Kondo and I. Ojima, *Chem. Lett.*, **1972**, 119.

6) K. Kondo and I. Ojima, *Chem. Commun.*, **1972**, 63.

7) G. L. Closs and R. A. Moss, *J. Amer. Chem. Soc.*, **86**, 4042 (1964).

8) For an isomerization of allyl sulfides by base, see D. S. Tarbell and M. A. McCall, *J. Amer. Chem. Soc.*, **74**, 48 (1952).

9) R. J. Crawford, A. Mishra, and R. J. Dummel, *ibid.*, **88**, 3959 (1966).

10) W. M. Jones and C. L. Ennis, *ibid.*, **91**, 6391 (1969).

11) L. A. Paquette, *Accounts Chem. Res.*, **1**, 209 (1968); F. G. Bordwell, B. B. Jarvis, and D. W. R. Corfield, *ibid.*, **90**, 5298 (1968); L. A. Paquette and L. S. Wittenbrook, *ibid.*, **90**, 6783 (1968).

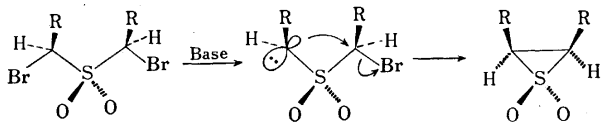

12) U. Schöllkopf, G. Ostermann, and J. Schossig, *Tetrahedron Lett.*, **1969**, 2619; J. E. Baldwin and J. E. Brown, *J. Amer. Chem. Soc.*, **91**, 3647 (1969).

13) J. H. Brewster and M. W. Kline, *ibid.*, **74**, 5179 (1952); B. J. Millard and T. S. Stevens, *J. Chem. Soc.*, **1963**, 3397; E. F. Jenny and J. Druey, *Angew. Chem.*, **74**, 152 (1962).

14) R. M. Dodson, P. D. Hammen, and J. Yu Fan, *J. Org. Chem.*, **36**, 2703 (1971).

15) R. Hiusgen, R. Grashey, and J. Sauer in "The Chemistry of Alkenes," ed. by S. Patai, Interscience Publishers, New York, N.Y. (1964).

16) H. Paul, I. Lange, and A. Kausmann, *Chem. Ber.*, **98**, 1789 (1965).

17) K. Kondo and I. Ojima, *Chem. Lett.*, **1972**, 771; I. Ojima and K. Kondo, This Bulletin, **46**, 2571 (1973).

18) W. R. Bamford and T. S. Stevens, *J. Chem. Soc.*, **1952**, 4735.

19) D. G. Farnum, *J. Org. Chem.*, **28**, 870 (1963).

20) K. Yamagishi, *Nippon Kagaku Zasshi*, **80**, 76 (1956).

21) B. D. Tilak and V. M. Vaidya, *Tetrahedron Lett.*, **1963**, 487.

22) R. C. Fuson, R. E. Christ, and G. M. Whitman, *J. Amer. Chem. Soc.*, **58**, 2450 (1936).

23) L. I. Smith and V. A. Engelhardt, *ibid.*, **71**, 2671 (1949).

24) C. G. Moore and B. R. Trego, *Tetrahedron*, **18**, 205 (1962).

A General Method for Evaluating the Resonance Energies of Monocyclic Conjugated Systems and Its Application to Heteroannulenes and Annulenones

Jun-ichi AIHARA

Department of Chemistry, Faculty of Science, Hokkaido University, Sapporo 060

(Received November 20, 1974)

The unit binding energy of a monocyclic conjugated system with an infinite number of the same unit structures can be employed as the reference energy in evaluating the resonance energy of a monocyclic conjugated system with a single unit structure. The latter system may be totally asymmetric in geometry. The resonance energy is then given as the difference between the π-energy of the system with the one-unit structure and the unit binding energy of the infinitely large system. This approach is justified by the proper prediction of the resonance energies for heteroannulenes and annulenones. The HMO theory was used in its simplest form.

Almost all compounds, even those which are obviously unstable, are known to have a significant HMO delocalization energy.[1,2] The lack of correlation between the calculated delocalization energy and the observed aromatic behavior has, though, been widely pointed out as a failure of the HMO method. Recently, Dewar, using the more elaborate PPP method, has for the first time obtained calculated resonance energies which correlate well with the experimental aromaticity for a wide range of conjugated hydrocarbons.[1] However, the important point turned out to be that he changed the reference structure relative to which aromatic stabilization was calculated. With the original HMO method, on the other hand, Hess *et al.* obtained resonance energies which correlate as well as Dewar's with the experimental properties for a wide variety of both conjugated hydrocarbons and heterocycles.[3-7]

In the calculation of the delocalization energy, the π-energy of a compound with n double bonds was compared to the π-energy of n isolated double bonds (ethylene). In the method of Hess *et al.*, modeled after Dewar's, the π-energy of a compound was compared to the π-energy of a reference structure with contributions from both single and double bonds. It is noteworthy that a considerable double-bond character was attached to the single bonds in the resonance structure of the conjugated system.[1,3] Hence, the π-energy of an acyclic compound was generally represented as an additive function of the individual π-bond energies. This fact indicates that any acyclic compound has essentially zero resonance energy, whereas cyclic compounds have been found to have a wide and continuous variation in resonance energies, from positive (aromatic) to negative (antiaromatic).[1-7] In this article, we attempted to refine this kind of resonance energies simply on the basis of the additivity of π-bond energies for nonaromatic species, and examined the aromaticity of less symmetric monocyclic compounds, such as heteroannulenes and annulenones, without referring to the individual π-bond energies. We used the HMO theory in its simplest form.

When HMO calculations are performed on conjugated compounds containing heteroatoms, appropriate corrections must be made of the Coulomb integral for each heteroatom and of the resonance integral for each carbon-heteroatom bond. A considerable amount of effort has been devoted to the determination of heteroatom parameters for such compounds.[8] Recently, Hess *et al.* evaluated the heteroatom parameters for the amine nitrogen, the ether oxygen, the thioether sulfur, and the carbonyl oxygen strictly on the basis of an experimental ground-state property, the heat of atomization.[5-7] We adopted their values, as they can be expected to be most suited to the estimation of another ground-state property, the resonance energy. They are listed in Table 1.

TABLE 1. HETEROATOM PARAMETERS

X	h_x	k_{c-x}
Amine nitrogen[5]	1.50	0.90
Ether oxygen[5]	2.00	0.34
Thioether sulfur[6]	1.00	0.68
Carbonyl oxygen[7]	0.22	0.99
sp^2-carbon	0.00	1.00

Theoretical

The reference energy relative to which the resonance energy of a monocyclic system is calculated is defined as follows. First, consider four hypothetical compounds of Type I-IV, in each of which n heteroatoms are periodically inserted in the cyclic chain of carbon atoms. X may be NH, O, or S. The π-energies for such systems can easily be obtained within the framework of the HMO theory.

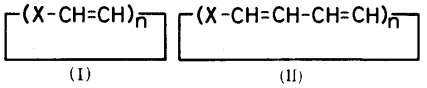

(I) (II)

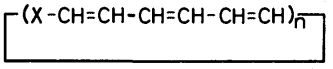

(III)

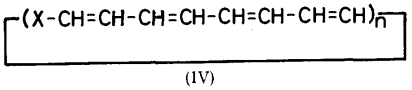

(IV)

For example, the π-energy of a compound of Type II can be obtained by solving the following secular equations:

$$a_i(\chi+h) + ke_{i-1} + kb_i = 0$$
$$b_i\chi + ka_i + c_i = 0$$
$$c_i\chi + b_i + d_i = 0$$
$$d_i\chi + c_i + e_i = 0$$
$$e_i\chi + d_i + ka_{i+1} = 0 \quad i = 1, 2, \cdots, n \tag{1}$$

where $\chi=(\alpha-E)/\beta$ and where a_i, b_i, c_i, d_i, and e_i are the Hückel coefficients of the atomic orbitals concerned on the atoms arranged in this manner:

$$\underset{d_{i-1}}{\text{—CH=CH—}}\underset{e_{i-1}}{\text{X—}}\underset{a_i}{\text{CH=CH—}}\underset{b_i}{\text{CH=CH—}}\underset{c_i}{\text{CH=CH—}}\underset{d_i}{\text{X—}}\underset{e_i}{\text{CH=CH—}}$$

These equations must be solved together with the boundary conditions:[3]

$$a_{n+1} = a_1, \quad b_{n+1} = b_1, \quad c_{n+1} = c_1, \quad d_{n+1} = d_1,$$
$$\text{and} \quad e_{n+1} = e_1 \tag{2}$$

The function

$$a_i = \sin i\lambda \tag{3}$$

automatically satisfies Eq. (2) for $i=n+1$ if

$$\lambda = \lambda_{nm} = \frac{2m\pi}{n} \qquad m = 0, 1, \cdots, (n-1) \tag{4}$$

The elimination of b_i, c_i, d_i, e_i, and e_{i-1} in Eq. (1), followed by the substitution of Eqs. (3) and (4), gives n algebraic equations of degree five:

$$\chi^5 + h\chi^4 - (2k^2+3)\chi^3 - 3h\chi^2 + (1+4k^2)\chi + (h+2k^2\cos\lambda_{nm}) = 0 \quad m = 0, 1, \cdots, (n-1) \tag{5}$$

Each of these equations possesses five real roots:

$$\chi = \chi_1(\lambda_{nm}) \leq \chi_2(\lambda_{nm}) \leq \chi_3(\lambda_{nm}) \leq \chi_4(\lambda_{nm}) \leq \chi_5(\lambda_{nm}) \tag{6}$$

Among them, the smaller three roots correspond to the π-energies of the occupied orbitals in the heterocycle in quetion. Accordingly, the π-energy of a compound of Type II can be obtained by summing the smaller three roots for every λ_{nm} over all the m's.

As may easily be seen, the unit structure of the periodic compound of Type II is composed of the two CH=CH, one CH–CH, and two CH–X bonds when the classical resonance structure is written for it. The unit binding energy corresponding to the unit structure is obtained by dividing the π-energy of the whole system by the number of the unit structures (n). It is a function of the number of the unit structures, as the π-energy might be influenced by the possible aromatic character of the smaller systems. When the n is large enough, the system can, however, be considered without difficulty as a nonaromatic species, regardless of the X. The unit binding energy of any infinitely large system should, therefore, be free from aromaticity. The unit binding energy (E_u) of an infinitely large system of Type II can be expressed in units of β as:

$$E_u(X) = -\lim_{n\to\infty}\frac{2}{n}\sum_{m=0}^{n-1}\left\{\chi_1(\lambda_{nm}) + \chi_2(\lambda_{nm}) + \chi_3(\lambda_{nm})\right\} - 2h_x$$
$$= -2\int_0^1\{\chi_1(2\pi x) + \chi_2(2\pi x) + \chi_3(2\pi x)\}dx - 2h_x \tag{7}$$

Note that it is not difficult to regard such unit binding energy as the reference energy in evaluating the aromaticity of a five-membered heterocycle of Type VI. The five-membered ring of Type VI is a special case of the compound of Type II, in which only one unit

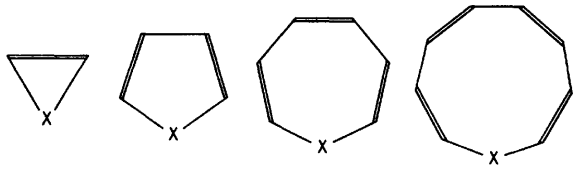

(V) (VI) (VII) (VIII)

structure is present. If any compound of Type II is assumed to be absolutely nonaromatic, it should possess the same unit binding energy as the compound of Type II with $n=\infty$. Therefore, as long as the additivity of π-bond energies is assumed for the like nonaromatic systems, the unit binding energy derived from Eq. (7) can be considered as the reference energy of the five-membered heterocycle of Type VI.

In other words, the five-membered heterocycle of Type VI has the same numbers of the CH=CH, CH–CH, and CH–X bonds as the unit structure of the compound of Type II containing the same heteroatom. Furthermore, the positions of the carbon atoms relative to the position of the heteroatom in the five-membered heterocycle are exactly equivalent to those in the unit structure. The effect of the electronegative heteroatom on the nearby π-bonds in the heterocycle of Type VI is necessarily taken into account in the unit binding energy derived from Eq. (7). This explain well how that the unit binding energy of an infinitely large system represents the reference energy of the corresponding five-membered heterocycle. The resonance energy of a given heterocycle of Type VI is, then, the difference between the π-energy of the compound and the unit binding energy of the infinitely large system of Type II.

The resonance energies of the three-, seven-, and nine-membered heteroannulenes containing single heteroatoms (V, VII, and VIII) are calculated in the same manner by comparing their π-energies with the unit binding energies of the infinitely large systems of Type I, III, and IV respectively. The secular equations for these systems are analogously reduced to the following algebraic equations:

$$\chi^3 + h\chi^2 - (2k^2+1)\chi + (2k^2\cos\lambda_{nm} - h) = 0 \quad \text{for I} \tag{8}$$
$$\chi^7 + h\chi^6 - (2k^2+5)\chi^5 - 5h\chi^4 + (8k^2+6)\chi^3 + 6h\chi^2 - (6k^2+1)\chi + (2k^2\cos\lambda_{nm} - h) = 0 \quad \text{for III} \tag{9}$$
$$\chi^9 + h\chi^8 - (2k^2+7)\chi^7 - 7h\chi^6 + (12k^2+15)\chi^5 + 15\chi^4 - (20k^2+10)\chi^3 - 10h\chi^2 + (8k^2+1)\chi + (2k^2\cos\lambda_{nm} + h) = 0 \quad \text{for IV} \tag{10}$$

The unit binding energies are numerically computed

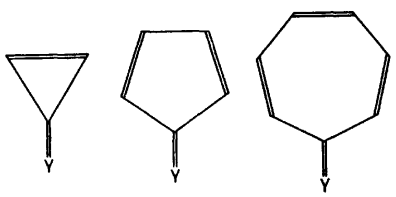

(IX) (X) (XI)

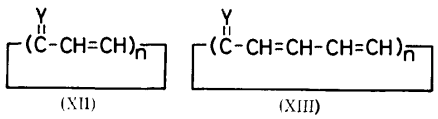
(XII)

(XIII)

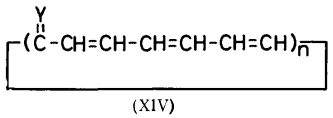
(XIV)

with these equations as in Eq. (7) for the five-membered heteroannulenes.

On the other hand, the reference energies of the first three members of annulenones (IX, X, and XI; Y=O) and fulvenes (IX, X, and XI; Y=CH_2) are obtained on the basis of the following equations, which are the algebraic versions of the secular equations for the systems of Types XII, XIII, and XIV:

$$\chi^4 + h\chi^3 - (k^2+3)\chi^2 - (3h-2\cos\lambda_{nm})\chi + (k^2+2h\cos\lambda_{nm}) = 0 \quad \text{for XII} \tag{11}$$

$$\chi^6 + h\chi^5 - (k^2+5)\chi^4 - 5h\chi^3 + (3k^2+5)\chi^2 + (5h+2\cos\lambda_{nm})\chi - (k^2-2h\cos\lambda_{nm}) = 0 \quad \text{for XIII} \tag{12}$$

$$\chi^8 + h\chi^7 - (k^2+7)\chi^6 - 7h\chi^5 + (5k^2+14)\chi^4 + 14h\chi^3 - (6k^2+7)\chi^2 - (7h-2\cos\lambda_{nm})\chi + (k^2+2h\cos\lambda_{nm}) = 0 \quad \text{for XIV} \tag{13}$$

The resonance energy of a given annulenone or fulvene is the difference between the π-energy of the compound and the unit binding energy of an infinitely large system composed of like unit structures.

Results and Discussion

The resonance energies of the heteroannulenes calculated according to the above-mentioned procedure are all listed in Table 2. The most striking aspect of these resonance energies is the strong alternation between aromaticity and antiaromaticity. The alternation decreases as the ring size increases. When the heteroannulenes are $(4r+2)\pi$-electron systems, they are predicted to be aromatic, with positive resonance energies. Conversely, when they are $4r$ π-electron systems, they are predicted to be antiaromatic, with negative resonance energies. Here, r is an integer. Such a trend in the aromatic character is clearly common to all the heteroannulenes containing single heteroatoms. This fact indicates that the Hückel $(4r+2)\pi$ rule of aromaticity can still be applied to such heterocyclic systems as heteroannulenes.

It should, then, be emphasized that their chemistry is in good accord with these predictions. The three-membered rings are predicted to be strongly antiaromatic, probably because of their four π-electron systems. These compounds are correspondingly unknown as yet. On the other hand, the five-membered rings, each of which forms an aromatic sextet, are predicted to be aromatic, in line with their well-known properties.[9,10] Among them, furan is predicted to be only slightly aromatic, as is indicated by its chemistry. Furan undergoes Diels-Alder reactions readily, while pyrrole and thiophene do not.

Table 2. Calculated resonance energies of heteroannulenes

Species	n	Hückel MO π-energy (β)	Reference energy (β)	Resonance energy (β)	Resonance energy (kcal/mol)
			Aza[n]annulenes		
C_2H_2NH	3	2.0000	2.6590	−0.6590 (−0.666)	−20.224
C_4H_4NH	5	5.4351	5.1557	0.2794 (0.233)	8.574
C_6H_6NH	7	7.4469	7.7077	−0.2607 (−0.291)	−8.003
C_8H_8NH	9	10.4126	10.2573	0.1552 (0.139)	4.764
			Oxa[n]annulenes		
C_2H_2O	3	2.0000	2.2210	−0.2210 (−0.018)	−6.783
C_4H_4O	5	4.5982	4.5539	0.0443 (0.044)	1.361
C_6H_6O	7	7.0385	7.0714	−0.0329 (−0.051)	−1.009
C_8H_8O	9	9.6266	9.6018	0.0247 (0.001)	0.759
			Thia[n]annulenes		
C_2H_2S	3	2.0000	2.6052	−0.6052 (−0.457)	−18.575
C_4H_4S	5	5.1855	4.9607	0.2248 (0.193)	6.900
C_6H_6S	7	7.2959	7.5044	−0.2085 (−0.232)	−6.400
C_8H_8S	9	10.1819	10.0497	0.1322 (0.118)	4.057

Resonance energies given in kcal/mol were calculated with $\beta=-1.33077$ eV.[5]

The seven-membered ring systems, azepine, oxepin, and thiepin, are characterized by a cyclic array of eight π-electrons, and are predicted to be antiaromatic. Though planarity is feasible in such compounds, the maintenance of such a conformation would not be energetically preferable. X-ray studies suggest that 1H-azepines are nonplanar in the crystalline state and also, probably, in solution, so as to be liberated from antiaromaticity.[11] Azepine and oxepin are very reactive, in agreement with their calculated resonance energies.[11] Unsubstituted thiepin and the higher members of the thiaannulenes have not been reported on.

One of the nine-membered ring systems, azonine, has a positive resonance energy, which suggests that it is probably aromatic, while oxonin has a negligible resonance energy, and therefore is probably olefinic in nature. According to the experimental studies by Anastassiou *et al.*,[12] these nine-membered heterocycles are characterized in an analogous way, as azonine is considerably more stable than oxonin.

The calculated resonance energies for some annulenones and fulvenes are given in Table 3. Cyclopropenone and tropone are predicted to be aromatic, with positive resonance energies, whereas cyclopentadienone is predicted to be antiaromatic, with a negative resonance energy. The fulvenes are all predicted to be substantially

TABLE 3. CALCULATED RESONANCE ENERGIES OF SOME ANNULENONES AND FULVENES

Species	Hückel MO π-energy (β)	Reference energy (β)	Resonance energy (β)	Resonance energy (kcal/mol)
Cyclopropenone	5.0648	4.9292	0.1356 (0.126)	4.161
Cyclopentadienone	7.3811	7.4578	−0.0767 (−0.094)	−2.355
Tropone	10.0638	9.9941	0.0696 (0.053)	2.137
Methylenecyclopropene	4.9624	4.9312	0.0312	0.956
Fulvene	7.4659	7.4560	0.0099	0.304
Heptafulvene	9.9944	9.9898	0.0045	0.139

Resonance energies given in kcal/mol were calculated with $\beta = -1.33077$ eV.[5]

nonaromatic, with slight resonance energies. As was stated by Hess *et al.*,[7] their chemistry also appears to be in good accord with these predictions.

Recently, Machiguchi *et al.*[13] reported on the aromaticity of tropothione (cycloheptatrienethione), suggesting, from the carbon-13 chemical shifts, that this compound is considerably less aromatic than tropone. As the electronegativity of sulfur is presumably close to that of carbon,[8] the Coulomb integral on the thionyl sulfur might be approximated by that on the carbon atom—that is, $h \sim 0$. Consequently, the electronic structure of tropothione is likely to resemble that of heptafulvene rather than that of tropone.

On the other hand, chemical evidence of aromatic character is much easier to find in the case of tropolone (2-hydroxytropone).[14] Interaction between the neighboring hydroxy and ketone groups due to the intramolecular hydrogen bonding has been seen as a source of difference between tropone and tropolone, since the isomers of tropolone, 3- and 4-hydroxytropones, resemble tropone in their chemical properties. One of the most prominent effects arising from the intramolecular hydrogen bonding is probably that the attached proton tends to increase the effective Coulomb integral on the carbonyl oxygen within the Hückel approximation. Chemically speaking, the hydrogen bonding may be said to stabilize the classical ionic structure of tropone.

According to this scheme, we tentatively increased the Coulomb integral on the carbonyl oxygen as an effect of hydrogen bonding; we thus found that the resonance energy of tropone is a function of the Coulomb integral on the carbonyl oxygen—it increases rapidly with an increase in the h-value for the carbonyl oxygen. For example, the resonance energy amounts to 0.2108β or 6.471 kcal/mol with this set of parameters; $h=1.00$ and $k=1.00$. Such a trend in aromaticity strongly suggests that, as has long been expected, the aromatic character of troponoid compounds is attributable to the formation of an aromatic sextet in the tropenylium structure. At present, we can not determine the amount of change in the effective Coulomb integral due to the hydrogen bonding. Nevertheless, the above idea appears to give quite a possible explanation of the enhanced aromaticity of tropolone within the HMO theory.

The resonance energies presented in Tables 2 and 3 parallel fairly well those determined by Hess *et al.*,[3-7] which are placed within parentheses in the tables. In estimating these resonance energies, they classified the π-bonds according to the number of attached hydrogens, and assigned a π-energy to every π-bond type. The reference energy of a given conjugated compound is a combination of such π-bond energy terms. Therefore, the slight differences between the resonance energies determined by Hess *et al.* and those determined by us are probably due to the fact that they applied the fixed π-bond energies of carbon-carbon bonds to the conjugated hydrocarbons and to the heterocycles as well.

If the π-bond energies are universally additive in the nonaromatic compounds, the increase in the reference energy on going from a given heteroannulene to the next member of the same series must be the same as the unit binding energy of an infinitely large annulene. Both should correspond to the sum of the π-energies of the CH=CH bond and the CH–CH bond in the classical resonance structure. However, the actual increases in the reference energies, for example, for the azaannulene series (2.4967β, 2.5520β, and 2.5496β) are somewhat different from the unit binding energy of an infinitely large annulene (2.5465β).[15] The situation is the same for the other cyclic systems considered. As was suggested before, such a discrepancy should be ascribed to the electronegativity of the heteroatom or to the polarity of the carbon-heteroatom bonds. It is, hence, noteworthy that the present approach skillfully avoids this kind of difficulty by evaluating the π-energy of a group of π-bonds.

As may be seen from the above discussion, the present approach assumes, for the sake of simplicity, the planarity of the compound, and it does not take into consideration the effects of the bond alternation and the ring strain on the π-energy of the compound. Since the geometry of the reference structure is necessarily assumed to be the same as that of the compound under consideration, the rsonance energy defined by us should be regarded as a kind of vertical resonance energy. Such assumptions are analogous to those made in calculating the delocalization energy. As far as the vertical resonance energy is concerned, the distortion energy brought about in the flattened molecule is retained in the reference structure.

When there is a bond alternation in the actual conjugated compound, the same bond alternation must be present in the reference structure for the vertical resonance energy to be evaluated. Though the introduction of bond alternation is often preferable,[16-18] it can not easily be carried out, and it might cause a considerable amount of ambiguity in the obtained resonance energy. In general, the resonance energy is a very small quantity as compared to the total π-energy of the compound. To make matters worse, when the

bond alternation is considered, some other comparable terms, such as the strain energy and the σ-compression energy, must be considered at the same time.

However, the good correlation found between the calculated resonance energies and the experimental properties for various monocyclic systems definitely shows that these resonance energies are still excellent indices, much better than the delocalization energies, in predicting the stability of the compounds in the ground state.

With this aspect of the present results in mind, the stability of the actual compounds should be understood in the following manner. If the calculated resonance energy is large enough, a large portion of it will be preserved in the actual compound. On the other hand, if the calculated resonance energy is small or negative, the bond alternation will be significant in the actual system and will lower the π-energy of the compound. Especially, when the compound is predicted to be markedly antiaromatic, the bond alternation is assuredly introduced in the system, and even the planarity of the compound might be broken so as to be relieved from antiaromaticity, as in the case of azepines. The bond alternation is thus necessary to lower the absolute value of the resonance energy as well as the π-energy of the antiaromatic system. However, the sign of the resonance energy always remains unchanged upon the introduction of bond alternation. The resonance energy obtained on the assumption of constant resonance integrals hence denotes the upper limit of the absolute value of the resonance energy.

In this connection, it must be noticed that the experimental resonance energies so far published are all related to the delocalization energies; they should rather be called the "conjugation energies" in the sense that any conjugation among the formal double bonds contributes to the increase in the delocalization energy. In general, the delocalization energy is large for the large conjugated compounds, as they contain many formal single bonds. Therefore, the experimental conjugation energies should not be correlated with the present results.

In a previous paper,[15] we examined the aromaticity of some monocyclic systems, such as annulenes and radialenes, for which analytical solutions of the HMO secular equations are available. The present approach is an extension of the same procedure to less symmetric systems. In general, the unit binding energy of a monocyclic conjugated system with an infinite number of unit structures can be employed as the reference energy in evaluating the resonance energy of a monocyclic conjugated system with a single-unit structure. It should be emphasized that this approach is applicable to almost all kinds of monocyclic conjugated systems, even to those totally asymmetric in geometry. As for heteroannulenes and annulenones, the present approach gives proper values for the resonance energies which are consistent with their chemical properties. It goes without saying that the estimation of these resonance energies was made possible by the accurate heteroatom parameters determined by Hess *et al.* All the simplicity and elegance of the HMO theory remain in the present approach.

We are grateful to the Hokkaido University Computing Center for the use of their FACOM 230-60, on which all the calculations were performed.

References

1) M. J. S. Dewar, "The Molecular Orbital Theory of Organic Chemistry," McGraw-Hill, New York, N. Y. (1969), Ch. 5.
2) L. J. Schaad and B. A. Hess, Jr., *J. Amer. Chem. Soc.*, **94**, 3068 (1972).
3) B. A. Hess, Jr. and L. J. Schaad, *ibid.*, **93**, 305 (1971).
4) B. A. Hess, Jr. and L. J. Schaad, *ibid.*, **93**, 2413 (1971).
5) B. A. Hess, Jr., L. J. Schaad, and C. W. Holyoke, Jr., *Tetrahedron*, **28**, 3657 (1972).
6) B. A. Hess, Jr. and L. J. Schaad, *J. Amer. Chem. Soc.*, **95**, 3907 (1973).
7) B. A. Hess, Jr., L. J. Schaad, and C. W. Holyoke, Jr., *Tetrahedron*, **28**, 5299 (1972).
8) A. Streitwieser, Jr., "Molecular Orbital Theory for Organic Chemists," John Wiley & Sons, New York, N. Y. (1961), Ch. 4.
9) G. Marino, "Advances in Heterocyclic Chemistry," Vol. XIII, edited by A. R. Katritzky and A. J. Boulton, Academic Press, New York, N. Y. (1971), pp. 235—314.
10) L. A. Paquette, "Principles of Modern Heterocyclic Chemistry," Benjamin, New York, N. Y. (1968).
11) L. A. Paquette, "Nonbenzenoid Aromatics," Vol. I, edited by J. P. Snyder, Academic Press, New York, N. Y. (1969), Ch. 5.
12) A. G. Anastassiou, S. W. Eachus, R. P. Cellura, and J. H. Gebrian, *Chem. Commun.*, **1970**, 1133.
13) T. Machiguchi, Y. Inagaki, M. Hoshino, and Y. Kitahara, *Chem. Lett.*, **1974**, 497.
14) D. Lloyd, "Carbocyclic Non-Benzenoid Aromatic Compounds," Elsevier, Amsterdam (1966), Ch. 6.
15) J. Aihara, This Bulletin, **48**, 517 (1975).
16) T. Nakajima and S. Katagiri, *Mol. Phys.*, **6**, 149 (1963).
17) M. J. S. Dewar and C. de Llano, *J. Amer. Chem. Soc.*, **91**, 789 (1969).
18) G. J. Gleicher, D. D. Newkirk, and J. C. Arnold, *ibid.*, **95**, 2526 (1973).

The Reduction of Enamines with Carbonylhydridoferrates

Take-aki MITSUDO, Yoshihisa WATANABE, Masato TANAKA, Shoji ATSUTA, Kazuo YAMAMOTO, and Yoshinobu TAKEGAMI

Department of Hydrocarbon Chemistry, Faculty of Engineering, Kyoto University, Sakyo-ku, Kyoto 606

(Received December 11, 1974)

Enamines react with an alcoholic solution of $[FeH(CO)_4]^-$ (**1**), $[Fe_2H(CO)_8]^-$ (**2**), and $[Fe_3H(CO)_{11}]^-$ (**3**), with the absorption of carbon monoxide at room temperature, to give the corresponding saturated tertiary amines. The reduction of the pyrrolidine enamine of 2-methylcyclohexanone with **1**, **2**, and **3** gave *cis* and *trans* *N*-(2-methyl-1-cyclohexyl)pyrrolidine. The *cis*/*trans* ratio of the products were characteristic of **1**, **2**, and **3**; the values, 0.67, 1.2, and 2.1 respectively, represent the bulkiness of the hydrides. The mechanism of the reduction was discussed.

Enamines are known to be very useful starting materials for various organic syntheses, particularly for the formation of α-substituted carbonyl compounds and cyclic ones.[1] This reactivity of enamine is mainly due to the polarized carbon-carbon double bond.

On the other hand, only a few reactions of enamines with transition-metal complexes have been reported.[2] Moreover, little attention has been paid to the reaction of enamines with hydridotransition metal complexes. Previously, we briefly mentioned the reduction of enamines with $[FeH(CO)_4]^-$ (**1**).[3] This paper will deal in detail with the reduction of enamines with **1**, $[Fe_2H(CO)_8]^-$ (**2**), and $[Fe_3H(CO)_{11}]^-$ (**3**).

Experimental

The PMR spectra were obtained on a JOEL Model 3H60 NMR spectrometer. The infrared spectra were measured on a Hitachi Model 215 grating infrared spectrometer. The mass spectra were obtained with a JMS-OISG mass spectrometer.

Materials. The *N*-(1-cyclohexenyl)morpholine (**4**),[4] *N*-(2-methyl-1-propenyl) piperidine (**6**),[5] *N*-(1-phenyl-1-vinyl)-morpholine (**5**),[6] and the pyrrolidine enamine of 2-methylcyclohexanone (**7**)[7] were prepared according to the methods described in the literature and were stored in ampoules under an argon atmosphere in a refrigerator. The pentacarbonyliron, morpholine, cyclohexanone, ethyl alcohol, and other compounds employed in this study were all commercial products; their purity were checked and found to be satisfactory for the reaction. The tetrahydrofuran was dried over lithium aluminum hydride.

Preparation of Carbonylferrates. All the reactions were carried out in a 300 ml, three-necked flask equipped with a gas buret and a magnetic stirrer under an carbon monoxide or nitrogen atmosphere. $K[FeH(CO)_4]$ (**1**) and $K_2[Fe(CO)_4]$ (**1'**) were prepared according to the methods described in a previous paper.[8] Eleven mmol of each complex in 50 ml of a solvent was used in each run. The preparation of $K[FeH(CO)_4]$ is accompanied by the formation of an equivalent mole of water:[9]

$$Fe(CO)_5 + 3KOH \longrightarrow K[FeH(CO)_4] + K_2CO_3 + H_2O \quad (a)$$
(**1**)

Therefore, when a dry solution of **1** was required, the solvent of the **1** was once distilled off under a vacuum, and then 50 ml of a new dry solvent was added.

$K_2[Fe_2(CO)_8]$ (**2'**) was prepared by the method described in the literature.[10] $Fe_2(CO)_9$ (2.0 g, 5.5 mmol=11 mg-atom-Fe) was treated with 22 mmol of KOH in 50 ml of ethanol at 30 °C for 2 hr.

$[Et_3NH][Fe_3H(CO)_{11}]$ (**3**) was prepared according to the published method.[11] In each run, a 2.1 g portion of **3** (3.7 mmol=11 mg-atom-Fe) in 50 ml of ethanol was used.

General Reaction Procedures and Analysis. To the solution of the carbonylferrates described above, 33 mmol of the enamine or an equimolar mixture of a ketone and a secondary amine and an internal standard for gc analysis were added, and the mixture was agitated. After a certain reaction time, a 0.2 ml sample of the solution was taken out, oxidized with air or with an equivalent mole of iodine in ethanol for 20 s to terminate the reaction, and then submitted to gc analysis; column: SE-30 on chromosorb(I), 3 mmφ×1.5 m; Diethylene Glycol Adipate Polyester on chromosorb(II), 3 mmφ×3 m. *N*-Isobutylpiperidine(**10**), tri(*n*-butyl) amine(**13**), and *N*-propylmorpholine(**14**) were identified by gc analysis by the use of the authentic samples. The amount of $Fe(CO)_5$ was analyzed by TCD-type gas chromatography, using the latter column(II) and with benzene as the internal standard.

The amount of CO_3^{2-} was analyzed as follows. The gas evolved by the acidification of the reaction solution was collected in a gas buret; after standing for 1 hr, the gas was bubbled in aqueous KOH. The volume of the absorbed gas was regarded as the amount of CO_2. This method was verified by gc analysis; column: active carbon(III), 3 mmφ×3 m.

Reaction of Enamine (4) with 1. Enamine (**4**) (5.5 g, 33 mmol) was added to an ethanolic solution of (**1**) (11 mmol) under a carbon monoxide atmosphere, and the mixture was agitated for 4 hr at 30 °C, during which time 1.6-mol portion of carbon monoxide was absorbed. The reaction mixture was filtered in a hood and 2.6 g of *N*-cyclohexylmorpholine (**8**) was obtained by distillation (bp 100 °C/6 mmHg; Yield, 1.4 mol/g-atom-Fe). Found: C, 70.99; H, 11.21%; mol wt (Mass) 169. Calcd for $C_{10}H_{17}NO$: C, 70.96; H, 11.32% mol wt 169.26. PMR(acetone-d_6): δ 3.3(m, 4H), 2.3(m, 4H), 1.6(m, 6H), 1.1(m, 5H) ppm.

Reaction of Enamine (5) with 1. Enamine (**5**) (6.2 g, 33 mmol) was treated with an ethanolic solution of **1** (11 mmol) at 30 °C for 24 hr, during which time a 1.6 mol portion of carbon monoxide was absorbed and 3.1 g of *N*-(1-phenylethyl)-morpholine (**9**) was obtained by distillation (bp 80 °C/0.3 mmHg; Yield, 1.6 mol/g-atom-Fe). Found: C, 75.28; H, 8.89%; mol wt (Mass) 191. Calcd for $C_{12}H_{17}NO$: C, 75.35; H, 8.96%; mol wt 191.27. PMR($CDCl_3$): δ 7.0(m, 5H), 3.5 (m, 4H), 3.2(q, 1H, J=6Hz), 2.4(m, 4H), 1.3(d, 3H, J=6Hz) ppm.

Reaction of Enamine (7) with 1. This reaction was carried out in a manner similar to that described above. Gc analysis showed that two products, (A) and (B), were formed at the retention time of 8.3 and 9.9 min, respectively (Column temperature, 120 °C; carrier gas: N_2, 40 ml/min). The products, (A) and (B), were identified as *N*-(*trans*-2-methyl-1-cyclohexyl)pyrrolidine (**12**) and *N*-(*cis*-2-methyl-1-cyclohexyl)-

pyrrolidine (**11**) respectively by the use of authentic samples prepared by the reduction of enamine (**7**) with atmospheric hydrogen.[12]

Reduction of Enamine (7) with Raney Nickel.[12] Enamine (**7**) (7.6 ml) was reduced catalytically with Raney nickel (1.0 g) in dry ethyl alcohol at 30 °C under 1 atm. of hydrogen. After 2 hr, the reaction mixture was analyzes by gas chromatography. Two peaks, (A′) and (B′), were found at the same retention time of (A) and (B). The ratio of (A′) to (B′) was 27:73, the same ratio as Mitsui has reported. Five grams of the mixture of (A′) and (B′) was separated from the reaction mixture by distillation (bp 82—85 °C/9 mmHg; Yield, 63%; Found: C, 79.00; H, 12.65; N, 8.37%; mol wt (Mass) 167). The separation of (A′) and (B′) by column chromatography (Silica gel) was attempted. Pure (A′) or (B′) could not be obtained, but two mixtures, 1) (A′)/(B′)=90/10 and 2) (A′)/(B′)=14/86, were obtained. The PMR spectra of these mixtures showed that (A′) and (B′) are *trans* and *cis* *N*-(2-methyl-1-cyclohexyl)pyrrolidine, respectively.[13] PMR (CCl_4): (A′) δ 0.94(d, J=6.0 Hz, 3H), 1.4—1.1(m, 5H), 1.9—1.5(m, 8H), 2.0—2.4(m,1H), 2.8—2.4(m, 4H) ppm, (B′) 0.89(d, J=6.8 Hz, 3H), 1.4—1.2(m, 1H), 2.6—2.3(m, 4H) ppm.

Results and Discussion

Reaction of Enamines with 1. Enamines such as *N*-(1-cyclohexenyl)morpholine (**4**), *N*-(1-phenyl-1-vinyl)morpholine (**5**), and *N*-(2-methyl-1-propenyl)-piperidine (**6**) reacted with an alcoholic solution of $[FeH(CO)_4]^-$ (**1**) at 30 °C, with a rapid absorption of carbon monoxide after a certain induction period. However, no carbonylated products were detected; rather the corresponding saturated tertiary amines, *N*-cyclohexylmorpholine (**8**), *N*-(1-phenylethyl)-

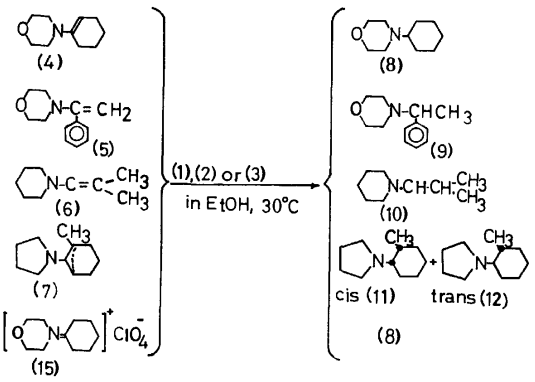

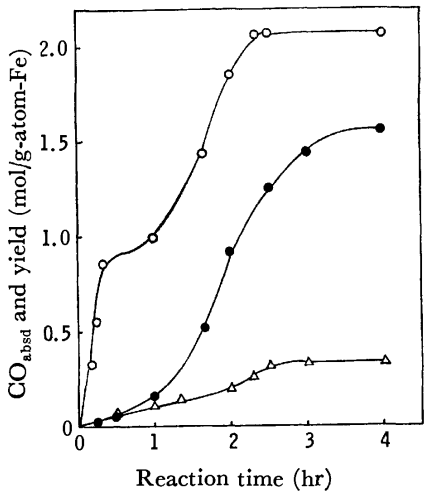

Fig. 1. Reaction of enamine (**4**) with $K[FeH(CO)_4]$ in ethanol at 30 °C. ○: *N*-Cyclohexylmorpholine, ●: CO absorbed, △: $Fe(CO)_5$.

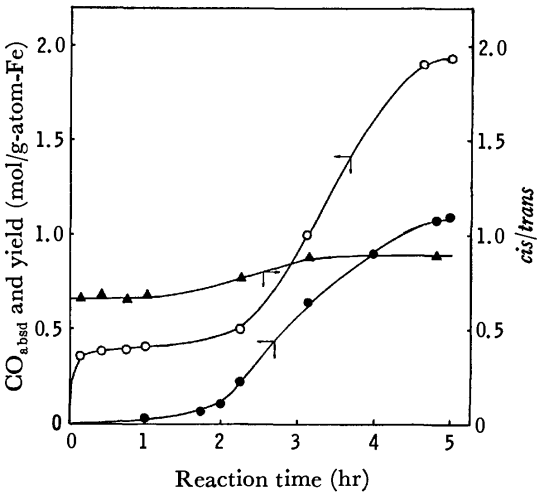

Fig. 2. Reaction of enamine (**7**) with $K[FeH(CO)_4]$ in ethanol at 30 °C. ○: Total yield of *cis* and *trans* N-(2-methylcyclohexyl)pyrrolidine. ●: CO absorbed, ▲: *cis*/*trans*.

Table 1. The reaction of enamines with mononuclear carbonylferrates in ethanol

Exp. No.	Enamine (33 mmol)	Carbonyl Ferrate (11 mmol)	Reaction conditions		CO absd[a]	Product	Yield[a]	*cis*/*trans*
			Temp °C	Time hr				
1	**4**	$KFeH(CO)_4$	30	4	1.6	**8**	2.1	
2	**4**	$KFeH(CO)_4$	30	1.5	N_2	**8**	0.9	
3	**4**	$KFeH(CO)_4$	30	216	N_2	**8**	1.0	
4	**5**	$KFeH(CO)_4$	30	48	1.7	**9**	1.6	
5	**6**	$KFeH(CO)_4$	30	48	1.9	**10**	1.5	
6	**7**	$KFeH(CO)_4$	30	5(min)	0	**11**+**12**	0.4	0.67
7	**7**	$KFeH(CO)_4$	30	5	1.1	**11**+**12**	1.9	0.88
8	**7**	$KFeH(CO)_4$	−60	0.5	0	**11**+**12**	0.16	0.65
9	**4**	$K_2Fe(CO)_4$	30	29	2.0	**8**	2.4	
10	**4**	$KFeH(CO)_4$+5KOH	30	192	4.9	**8**	1.0	
11	**4**	$KFeH(CO)_4$+$5H_2O$	30	120	1.3	**8**	0.9	
12	**15**	$KFeH(CO)_4$	30	24	1.0	**8**	1.0	

a) mol/g-atom-Fe

Table 2. The reaction of enamines with $K_2Fe_2(CO)_8$[a] in ethanol

Exp. No.	Enamine (33m mol)	Reaction conditions		CO absd[b]	Product	Yield[b]	*cis/trans*
		Temp (°C)	Time (hr)				
13	**4**	30	4	2.1	**8**	2.2	
14	**4**	45	24	2.1	**8**	1.9	
15	**7**	30	10(min)	0.65	**11**+**12**	0.88	1.2
16	**7**	30	5	1.45	**11**+**12**	1.88	0.94

a) 5.5 mmol of $K_2Fe_2(CO)_8$ was used. b) mol/g-atom-Fe

morpholine (**9**), and *N*-isobutylpiperidine (**10**), were produced in high yields.

The pyrrolidine enamine of 2-methylcyclohexanone (**7**) was also reduced to *cis* (**11**) and *trans* (**12**) *N*-(2-methyl-1-cyclohexyl)pyrrolidine. The results are summarized in Table 1. The periodical change in the yields of the saturated tertiary amines and the absorption of carbon monixide in a typical reaction of **4** and **7** are shown in Figs. 1 and 2. Time plots of the *cis/trans* ratio of the isomers of the products are also shown in Fig. 2. In both cases, the plots of the yields of the products *vs.* the reaction time are very characteristic. They clearly have two steps. At first, the yield of the product increases rapidly, with a very slow absorption of carbon monoxide, and the yield amounts to 0.4—0.9 mol* in 30 min. Then the rate of the formation of the product becomes very slow for about 0.5—2 hr, after which it becomes very fast again, with a rapid absorption of carbon monoxide, and the yield of the product amounts to about 2 mol.

As the reaction proceeded, the color of the reaction solution changed from pale brown to dark red, and $[Fe_3H(CO)_{11}]^-$** and CO_3^{2-}, as well as $Fe(CO)_5$, were detected in the reaction mixture. The amount of $Fe(CO)_5$ formed is also shown in Fig. 1.

The reaction also proceeded under a nitrogen atmosphere, but the yield did not exceed 1.0 mol (Exps. 2, 3).

In the reduction of enamine (**7**), the *cis/trans* ratio of the products was 0.67 at the beginning, and it stayed constant for about 1.5 hr. Then it became large with the progress of the reduction, with a rapid absorption of carbon monoxide, reaching 0.88 at the end of the reaction. The *cis/trans* ratio of the products newly formed with the absorption of cabon monoxide was 1.1, which was easily calculated from the data at 60 min and at 190 min. These results apparently show that there are at least two different ways for the reduction of enamines; the first may be the reduction with **1** itself, while the second is that with the newly produced active species, with an absorption of carbon monoxide.

The Reaction of $K_2[Fe(CO)_4]$ with Enamine (4). When $K_2[Fe(CO)_4]$ is used instead of **1**, the rate of the reduction is slower than that in the reaction of **1**. However, the total amount of gas absorbed and the yield of the product were larger than those in the reaction of **1** (Exp. 9). In this system, $K_2[Fe(CO)_4]$ may be hydrolyzed[14] to **1**, which is active in the reduction of enamine, and a 1 mol excess of potassium hydroxide is considered to be effective for the reformation of the new hydride species.

$$K_2Fe(CO)_4 + H_2O \rightleftarrows K[FeH(CO)_4] + KOH \quad (b)$$
(1)

However, a large exess of potassium hydroxide disturbed the reduction (Exp. 10). In this case, the concentration of the active hydride (**1**) is low, and the reaction may be highly inhibited.

The Reaction of $K_2[Fe_2(CO)_8]$ with Enamines. The enamines **4** and **7** also reacted with an alcoholic solution

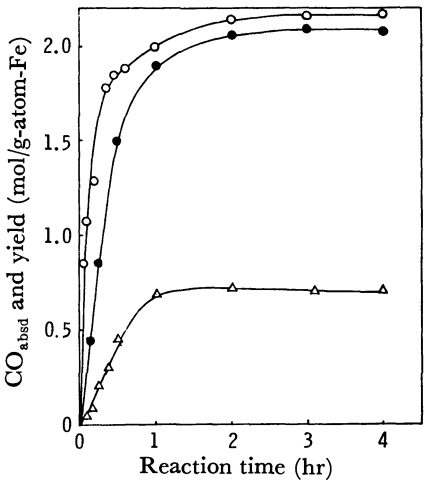

Fig. 3. Reaction of enamine (**4**) with $K_2[Fe_2(CO)_8]$ in ethanol at 30 °C. ○: *N*-Cyclohexylmorpholine, ●: CO absorbed, △: $Fe(CO)_5$.

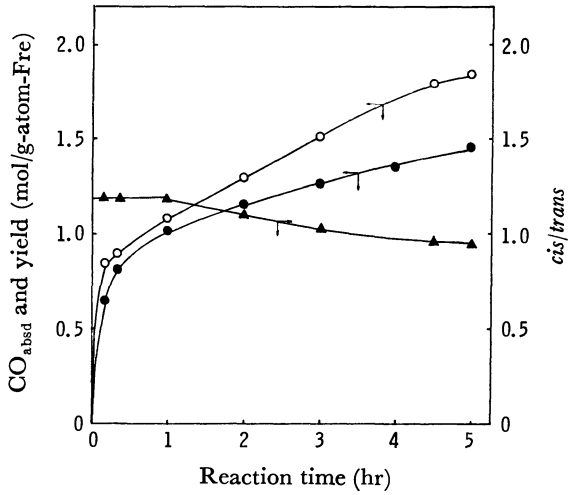

Fig. 4. Reaction of enamine (**7**) with $K_2[Fe_2(CO)_8]$ in ethanol at 30 °C. ○: Total yield of *cis* and *trans N*-(2-methylcyclohexyl)pyrrolidine, ●: CO absorbed, ▲: *cis/trans*.

* "mol" means mol/g-atom-Fe hereafter.

** ~0.06 mol/g-atom-Fe of $[Fe_3H(CO)_{11}]^-$ was detected by means of UV spectra in the reaction mixture of Exp. 1.

Table 3. The reaction of enamines with $[Fe_3H(CO)_{11}]^-$ [a] in ethanol

Exp. No.	Enamine (33 mmol)	Reaction conditions		CO_{absd}[b]	Product	Yield[b]	*cis/trans*
		Temp (°C)	Time (hr)				
17	**4**	30	120	1.3	(**8**)	0.46	
18	**4**+KOH (50 mmol)	30	24	1.7	(**8**)	1.2	
19	**7**	30	0.5	0.1	(**11**) + (**12**)	0.11	2.1
20[c]	**7**	30	5	0.6	(**11**) + (**12**)	0.17	1.9
21	**7**+H_2O (11 mmol)	30	5	0.6	(**11**) + (**12**)	0.08	1.9
22	**7**+H_2O (11 mmol)	−60	0.25	0	(**11**) + (**12**)	0.05	1.8

a) 3.7 mmol of $[Fe_3H(CO)_{11}]^-$ was used. b) mol/g-atom-Fe. c) 11 mmol of $[Fe_3H(CO)_{11}]^-$ was used.

of dinuclear carbonylferrate, $K_2[Fe_2(CO)_8]$, with an absorption of carbon monoxide, to give saturated amines. The results are shown in Table 2 and Figs. 3 and 4. The mode of the reaction of $K_2[Fe_2(CO)_8]$ was, however, different from that of **1**. The yield of the product increased smoothly without the step which was observed in the reaction of **1**, and it amounted to 1.9—2.2 mol, *i.e.*, 3.8—4.4 mol/mol-$[Fe_2(CO)_8]^{2-}$. The induction period of the carbon-monoxide absorption was not observed; the rate of the absorption was very rapid in spite of the half concentration of the carbonylferrate complex as compared with the case of **1**, and a large amount of $Fe(CO)_5$ was formed.

The *cis/trans* ratio of the product in the reaction of enamine **7** was 1.2 at the beginning of the reaction, and it stayed constant for 1 hr, during which period 2 mol/mol-$[Fe_2(CO)_8]^{2-}$ of the product was formed; thereafter it became smaller, reaching 0.94 in 5 hr. Apparently, an active species is also reproduced during the reaction. The active species formed during the first 1 hr gave the ratio of ~1.2, which is almost the same as that observed in the reduction with the newly formed active species in the reaction of **1**.

Considering the results of the reaction of $K[FeH(CO)_4]$ and $K_2[Fe(CO)_4]$, the dinuclear hydride species, $K[Fe_2H(CO)_8]$ (**2**), which exists in the reaction system in the equilibrium:

$$K_2[Fe_2(CO)_8] + H_2O \rightleftharpoons K[Fe_2H(CO)_8] + KOH \quad (c)$$
(**2**)

may be the active species at the beginning of the reaction.

Reaction of $[Fe_3H(CO)_{11}]^-$ (3) with Enamines. An alcoholic solution of $[Fe_3H(CO)_{11}]^-$ (**3**) also reduce enamines. The results are summarized in Table 3. The mode of the reduction of the enamine (**7**) is shown in Fig. 5. The reduction of the enamine proceeded rapidly and ceased in ten min. The yield of the product was small (0.11 mol, *i. e.*, 0.33 mol/mol.$[Fe_3H(CO)_{11}]^-$), and the *cis/trans* ratio of the isomers was 2.1. The ratio stayed constant for more than 4 hr. The addition of 11 mmol of a 1M-ethanolic potassium hydroxide solution to this reaction mixture caused a dramatic change of the mode of the reaction. The yield of the product increased rapidly, with an absorption of carbon monoxide. The *cis/trans* ratio of the isomers decreased rapidly to the value of 1.0, and then it reached 0.9 by the end of the reaction. It is calculated that the *cis/trans* ratio of the isomers of the newly formed

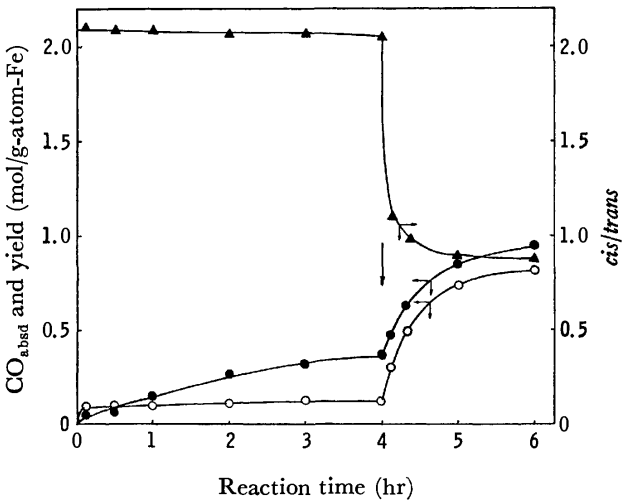

Fig. 5. Reaction of enamine (**7**) with $[Et_3NH][Fe_3H(CO)_{11}]$ in ethanol at 30 °C. ○: Total yield of *cis* and *trans* *N*-(2-methylcyclohexyl)pyrrolidine, ●: CO absorbed, ▲: *cis/trans*, ↓: 11 ml of 1 M-KOH–EtOH was added.

product is about 0.88. The effect of the mole ratio of **3** to the enamine on the *cis/trans* ratio of the products which were observed in the reduction with $LiAlH_4$[15] was small (Exp. 20). The effects of the addition of water or of the reaction temperature on the *cis/trans* ratio were also small.

Reaction of Enamine (4) with 1 in Dry THF and the Effect of the Addition of Water. In order to investigate the source of the hydrogen, the enamine (**4**) was treated with **1** in dry THF. As is shown in Fig. 6, no carbon monoxide absorption occurred, and even after a prolonged reaction time only a small amount of the product was formed. The addition of water to this reaction solution caused a rapid carbon monoxide uptake and an increase in the quantity of the product, the yield of which amounted to more than 2 mol. This result shows that the hydrogen source in the reduction of enamines is water and that carbon monoxide and water are indispensable for the reproduction of the active species of the reduction. However, a large excess of water disturbed the reduction (Exp. 11).

The Fate of the Carbon Monoxide Absorbed. The fate of the carbon monoxide absorbed was investigated. The amounts of $Fe(CO)_5$ and carbonate formed in the

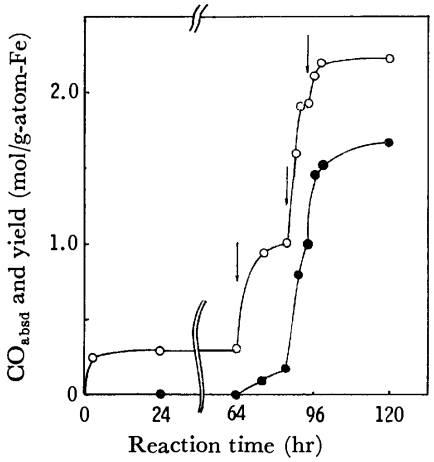

Fig. 6. Reaction of enamine (**4**) with $K[FeH(CO)_4]$ in dry THF and the effect of the addition of water. ○: *N*-Cyclohexylmorpholine, ●: CO absorbed, ↓: 1.0 mol of water was added.

Table 4. Material balance of carbon monoxide absorbed

Exp. No.	Carbonylferrate	CO_{absd}	$Fe(CO)_5$ (mol/g-atom-Fe)	CO_3^{2-}
1	$KFeH(CO)_4$	1.6	0.32	1.30
13	$K_2Fe_2(CO)_8$	2.1	0.70	1.42
17	$[Fe_3H(CO)_{11}]^-$	1.3	1.05	0.11
18	$[Fe_3H(CO)_{11}]^-$+KOH	1.7	0.41	1.31

reaction solution are summarized in Table 4. These results show that the carbon monoxide absorbed ultimately goes into $Fe(CO)_5$ and carbonate:

$$[\text{CO absorbed}] = [Fe(CO)_5] + [CO_3^{3-}] \quad \text{(d)}$$

Mechanism of the Reduction of Enamines. The mechanism of the reduction of enamines with formic acid[16] and sodium borohydride,[17] and that of the hydrolysis of enamines,[18] have been studied. The first step of both the reaction is shown to be the rapid protonation of the β-carbon atom of enamines to form the iminium salts:

$$\text{>N-CH=CHR} + H^+ \longrightarrow \text{>}\overset{+}{\text{N}}\text{=CH-CH}_2\text{R} \quad \text{(e)}$$

In our reaction, carried out in moist ethanol, it is reasonable to consider that the first step of the reduction is also the formation of iminium salt. In fact, enamine could not be detected in the reaction solution, even 10 min after the beginning of the reaction by means of gas chromatography, but iminium salt was detected by means of the IR spectra. On the other hand, enamine was detected in the reaction solution when the reduction was carried out in a dry solvent.

The fact that the iminium salt, *N*-cyclohexylidenemorpholinium perchlorate (**15**), reacts with **1**, with absorption of carbon monoxide, to give *N*-cyclohexylmorpholine (**8**) (Table 1. Exp. 12) shows that the second step is surely the nucleophilic attack of carbonylhydridoferrates on the iminium cation and the abstraction of a hydride ion from the complex.

$$\text{>}\overset{+}{\text{N}}\text{=CHCH}_2\text{R} + [HFe_m(CO)_n]^- \longrightarrow \text{>N-CH}_2\text{CH}_2\text{R} + Fe_m(CO)_n \quad \text{(f)}$$

In the reduction of iminium salts with $LiAlH_4$,[19] $NaBH_4$,[17] and formic acid,[1,16] a similar abstraction of a hydride ion has been observed.

Reproduction of Active Species. Alcoholic solutions of **1** and **2** have been known to reduce isoprene[20] and the Shiff base[21] to the corresponding monoolefins and saturated amines respectively, with absorption of carbon monoxide. The yields of the products often exceeded 1.0 mol, and the reproduction of the active species was observed. However, little has been studied on the mechanism of the reformation of the active species. The infrared spectra of the reaction solution showed too complicated absorption to resolve at 2100—1750 cm^{-1}.

In the reduction of enamines with **1** and **2**, the active species is also reproduced, with an absorption of cabon monoxide. The reduction of the enamine (**7**) with **1**, **2**, and **3** gives us some information on the reproduction of the active species. The results show that **1**, **2**, and **3** have their own ability in the reduction of enamine and have characteristic values of the *cis/trans* ratio of the products, 0.67, 1.2, and 2.1, respectively. The fact that the *cis/trans* ratios of the products stay constant for more than 1 hr in each reaction system shows that the isomerization between these isomers is negligible.

In the reduction with **1**, the *cis/trans* ratio of the newly formed product, with a rapid absorption of carbon monoxide, was 1.1, this value shows that the active species mainly reproduced is not **1**, but another active species. Considering the results of the reduction with **2**, we may suppose that the newly formed active species in the reaction of **1** is **2**. Once **2** is formed it may reduce the iminium salt catalytically, with a rapid absorption of carbon monoxide in the presence of the hydroxide ion, which is necessary for the formation of hydride species by the base reaction.[10] In this process, the formation of the carbonate may also occur. The catalytic cycle may be terminated by a lack of hydroxide ion and the formation of some such stable iron carbonyl complexes as $Fe(CO)_5$, which can not reduce the iminium salt by itself. However, to elucidate the mechanism of these reactions further studies will be required.

The Factors Which Determine the cis/trans *Ratio in the Reduction of the Enamine (7).* Considering the mechanism of the reduction of enamines with carbonylhydridoferrates discussed above the factors which determine the *cis/trans* ratio in the reduction of the

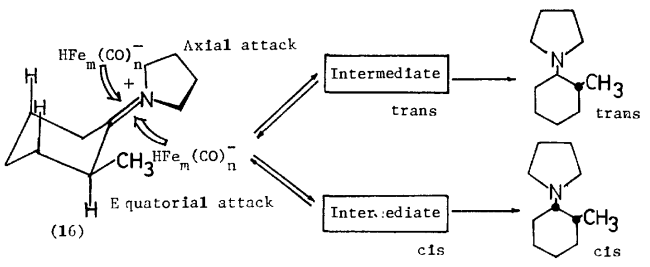

Scheme 1.

Table 5. Reductive alkylation of *sec*-amines with $[FeH(CO)_4]^-$ [a]

Exp. No.	Amine (33 mmol)	Carbonyl compounds (33 mmol)	Temp (°C)	Time (hr)	CO absd[b]	Product	Yield[b]
23	Morpholine	Cyclohexanone	30	48	1.7	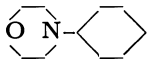	1.4
24	Dibutylamine	Butyraldehyde	30	24	1.4	$(n\text{-Bu})_3N$	0.50
25	Pyrrolidine	Acetophenone	30	48	1.5	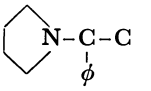	1.1
26	Morpholine	Propionaldehyde	30	24	1.4	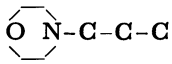	0.41
27	Morpholine	Acetophenone	65	48	—	No reaction	
28	Diisopropylamine	Acetone	30	24	—	No reaction	

a) Solvent: EtOH: $[FeH(CO)_4]^-$: 11 mmol. b) mol/mol-$[FeH(CO)_4]^-$

enamine (**7**) are 1) the direction of the attack of the hydride complexes on the iminium salt (**16**); the axial and equatorial attack of the hydrides may give *trans* and *cis* isomers respectively, and 2) the stability of the reaction intermediates (Scheme 1). The ratios of 1.2 and 2.1 for **2** and **3** may be reasonably explained by the direction of the attack of the hydrides. The axial attack of the bulky polynuclear hydrides may be retarded by the axial hydrogens at the 3 and 5 positions, and an equatorial attack may precede. However, to explain the ratio 0.65 for **1**, another factor must be considered. It may be the stability of the intermediates. One of the possible models is a four-centered model, **16** or **17**. As **17**, in which all the axial positions are occupied by hydrogen atom, is considered to be more stable than **16**, the *cis*/*trans* ratio may become less than 1.0.

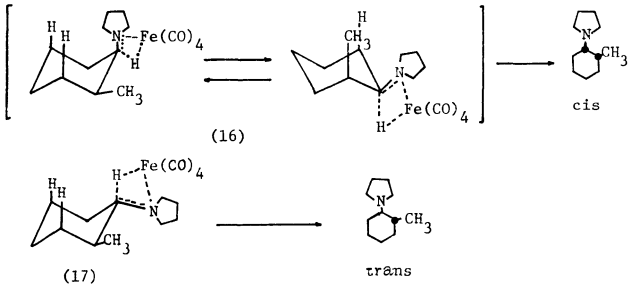

The Reductive Alkylation of sec*-Amines with* **1**. In the course of this investigation, it was found that an equimolar mixture of a secondary amine and ketone or aldehyde reacts with an alcoholic solution of **1** at room temperature, with an absorption of carbon monoxide, to give the corresponding tertiary amine:

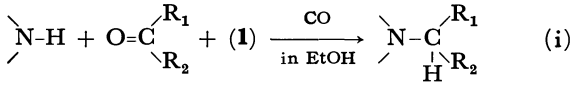

(i)

The results are summarized in Table 5. Morpholine and cyclohexanone gave 1.4 mol of *N*-cyclohexylmorpholine, with an absorption of 1.7 mol of carbon monoxide. Acetophenone and pyrrolidine gave *N*-(1-phenylethyl)pyrrolidine. This reaction should be compared with the Leuckart-Wallach reaction.[22] The mechanism of the Leuckart-Wallach reaction of a ketone and a secondary amine has been considered to be as follows.[1] In the first step, the ketone and the secondary amine form a 1:1 adduct and then an iminium salt (**18**) is formed, which abstracts a hydride ion from formic acid or its derivatives:

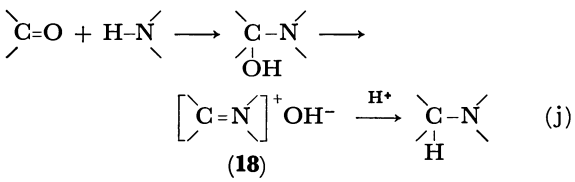

(j)

In our reaction, neither ketone nor secondary amine reacts separately with **1**, and the boundary of the reaction is almost the same as that of the Leuckart-Wallach reaction. These facts strongly suggest that, in our reductive alkylation, the iminium salt (**18**) formed by the (j) equation abstracts a hydride ion from **1**; they support the mechanism of the reduction of enamines with **1** presented above.

The reductive alkylation using **1** is characterized by a low reaction temperature and the successful mono-[21] and dimethylation[23] of anilines. A full report on these reactions will be published soon.

References

1) For a review of enamines, see, for example, A. G. Cook, "Enamines: Synthesis, Structure and Reaction," Marcel Dekker, New York (1969).

2) R. Noyori, K. Yokoyama, S. Makino, and Y. Hayakawa, *J. Amer. Chem. Soc.*, **94**, 1772 (1972); J. Tsuji, *Tetrahedron Lett.*, **1965**, 4387.

3) T. Mitsudo, Y. Watanabe, M. Tanaka, K. Yamamoto, and Y. Takegami, This Bulletin, **44**, 302 (1971); Presented in part at the Annual Meeting of the Chemical Society of Japan, Osaka, April, 1971.

4) H. E. Lücke and W. Brenninger, "Organic Syntheses," Coll. Vol. V (1973), p. 808.

5) E. Benzing, *Angew. Chem.*, **71**, 521 (1959).

6) M. E. Munk and Y. K. Kim, *J. Amer. Chem. Soc.*, **86**, 2213 (1964).

7) The pyrrolidine enamine of 2-methylcyclohexanone is a 9:1 mixture of *N*-(2-methyl-1-cyclohexenyl)pyrrolidine and *N*-(6-methyl-1-cyclohexenyl)pyrrolidine; W. D. Gurowitz and M. A. Joseph, *Tetrahedron Lett.*, **1965**, 4433.

8) Y. Takegami, Y. Watanabe, H. Masada, and I. Kanaya, This Bulletin, **40**, 1456 (1967).

9) P. Krumholz and H. M. A. Stettiner, *J. Amer. Chem. Soc.*, **71**, 3035 (1949).
10) K. Farmery, M. Kilner, R. Greatex, and N. N. Greenwood, *J. Chem. Soc., A*, **1969**, 2339; W. Hieber and N. Kahlen, *Chem. Ber.*, **91**, 2234 (1958).
11) W. McFarlane and G. Wilkinson, "Inorganic. Syntheses," **8**, 181 (1966).
12) Y. Yamashita and S. Mitsui, Annual Meeting of the Chem. Soc. Japan, Osaka, April, 1971.
13) I. J. Borowitz and G. J. Williams, *J. Chem. Soc.*, **1967**, 4157.
14) The basicity of $[Fe(CO)_4]^{2-}$ is estimated to be about that of $[OH]^-$ ion; W. Hieber and W. Hubel, *Z. Electrochem.*, **57**, 235 (1953).
15) D. Cabaret, G. Chauviere, and Z. Welvart, *Tetrahedron Lett.*, **1966**, 4109.
16) N. J. Leonald and R. R. Sauer, *J. Amer. Chem. Soc.*, **79**, 6210 (1957).
17) J. A. Marshall and W. S. Johnson, *J. Org. Chem.*, **28**, 421 (1963); J. Shmitt, J. J. Panouse, A. Hallot, P. J. Cornu, P. Comoy, and H. Pluche, *Bull. Soc. Chim. France*, **1963**, 798.
18) G. Stork, A. Brizzolara, H. Landesman, J. Szmuszkvicz, and R. Terrell, *J. Amer. Chem. Soc.*, **85**, 207 (1963).
19) J. A. Marshall and W. S. Johnson, *ibid.*, **84**, 1485 (1962).
20) Y. Takegami, Y. Watanabe, T. Mitsudo, I. Kanaya, and H. Masada, This Bulletin, **41**, 158 (1968).
21) Y. Watanabe, M. Yamashita, T. Mitsudo, M. Tanaka, and Y. Takegami, *Tetrahedron Lett.*, **1974**, 1879.
22) W. S. Emerson, "Organic Reactions," **4**, 174 (1949).
23) Y. Watanabe, T. Mitsudo, M. Yamashita, S. C. Shim, and Y. Takegami, *Chem. Lett.*, **1974**, 1265.

Synthesis of Arylethylenesulfonamides and Intramolecular Rearrangement of *N*-(Arylethylenesulfonyl)thioureas

Kiyoshi HASEGAWA, Syuzi HIROOKA and Tadashi SASAKI*

Department of Industrial Chemistry, Faculty of Engineering, Toyama University, Takaoka-shi, Toyama 933

** Institute of Applied Organic Chemistry, Faculty of Engineering, Nagoya University, Furo-cho, Chigusa-ku, Nagoya 464*

(Received December 13, 1974)

The reactions of *p*- and *p'*- substituted *N*-(2,2-diarylethylenesulfonyl)- (**8**), *N*-[2-phenyl-2-(α-naphthyl)ethylenesulfonyl]- (**9**), and *N*-(*p*-nitrostyrene-1-sulfonyl)-*N'*-alkylthioureas (**12**) with bases afforded new intramolecularly rearranged *N*-alkyl-*S*-(2,2-diarylvinyl)- (**13**), *N*-alkyl-*S*-[2-phenyl-2-(α-naphthyl)vinyl]- (**14**), and *N*-alkyl-*S*-(*p*-nitrostyryl)isothioureas (**15**), respectively. *p*- and *p'*-Substituted 2,2-diarylethylene-*N*-methylsulfonamides (**6**) were treated with carbon disulfide and alkyl halides in the presence of a base to give alkyl 2,2-diarylvinyl trithiocarbonates (**17**). The order of reactivity of the sulfonylthioureas and -amides indicates that the rearrangement is retarded by electron-releasing *p*-substituents on benzene rings (Cl>H>CH_3>OCH_3).

Waldan and Pütter reported that *N*-arylnitrostyrenesulfonamide undergoes intramolecular rearrangement on C-1 to afford a sulfur free compound, stilbene derivatives.[1] The reaction requires the presence of an electron-withdrawing nitro group in the *ortho* or *para* position. In continuation of our studies on α,β-unsaturated sulfonamides,[2a-d] we have recently proposed[3] a five-membered Sn mechanism for the formation of trithiocarbonates ($(C_6H_5)_2C{=}CHSC(=S)SR$ (**17**) from 2,2-diphenylethylenesulfonamide (**5a**) ($R^1{=}R^2{=}H$) in the presence of carbon disulfide, and concluded that this rearrangement on C-1 is characteristic of **5a**, in which C-2 has two phenyl groups. However, the effect of *p*- and *p'*-substituents on the formation of **17** was not investigated. We have now studied the base treatment of thioureas **8**, **9** and **12** which were prepared as model compounds to confirm the proposed mechanism. This paper describes the mechanism for a Smiles-type reaction of the thioureas and for the formation of **17** from **6**, carbon disulfide and alkyl halides, and also describes the effect of *p*-substituents on the yield of the rearranged products.

Results and Discussion

Syntheses of α,β-Unsaturated Sulfonamides and Thioureas. The convenient sulfochlorination method of styrene[4] gave generally low yields (<10%) when applied to *p*- and *p'*-substituted 1,1-diarylethylenes (**1**). Scheme 1 shows the synthetic pathways of sulfonamides and thioureas. Compound **1** and dioxane–sulfur trioxide gave 2,2-diarylethylenesulfonates (**3**) (Table 1), which were converted into 2,2-diarylethylenesulfonyl chlorides (**4**) (Table 2). Sulfonamides **5** and **6** were pre-

Table 1. Sodium sulfonates[a]

Compd.	R^1	R^2	*n*	Yield[b] (%)	Mp (°C)	Calcd (%)			Found (%)		
						C	H	S	C	H	S
3a	H	H	1	85	174—176	55.99	4.36	10.68	55.75	4.07	10.51
3b	H	Cl	1	64	177—179	50.23	3.61	9.58	50.00	3.87	9.81
3c	Cl	Cl	2	86	170—171	43.42	3.38	8.28	43.16	3.22	8.36
3d	H	CH_3	2	70	167—168	54.21	5.16	9.65	53.92	5.05	9.58
3e	CH_3	CH_3	2	78	140—142	55.48	5.53	9.26	55.42	5.32	9.37
3f	H	OCH_3	1	54	115—116	54.53	4.58	9.71	54.31	4.40	9.87
3g	OCH_3	OCH_3	1	56	122—124	53.32	4.76	8.90	53.42	4.77	8.89

a) They have water of crystallization (n=1—2). b) Sulfonates **3a-e** were slightly soluble in cold water. Sulfonates **3f** and **3g** were moderately soluble in cold water, and several crops of crystals were taken by evaporating the aqueous filtrate.

Table 2. Sulfonyl chlorides

Compd	R^1	R^2	Yield (%)	Mp (°C)	Recrystn solvent	Calcd (%)			Found (%)		
						C	H	S	C	H	S
4a	H	H	71	81— 82[a]	b	60.32	3.98	11.50	60.16	3.72	11.42
4b	H	Cl	56	94— 95	b	53.69	3.22	10.24	53.46	2.94	10.22
4c	Cl	Cl	49	89— 91	c	48.36	2.61	9.22	48.54	2.47	9.39
4d	H	CH_3	33	119—120	b	61.53	4.48	10.95	61.40	4.58	10.83
4e	CH_3	CH_3	10	56— 58	c	62.63	4.93	10.45	62.87	4.78	10.22
4f	H	OCH_3	17	88— 90	c	58.34	4.24	10.83	58.63	4.04	10.77
4g	OCH_3	OCH_3	42	109—111	d	56.71	4.46	9.46	56.46	4.68	9.46

a) Lit.[5] mp 65 °C. b) $CHCl_3$–petroleum ether. c) Benzene–petroleum ether. d) Ether–petroleum ether.

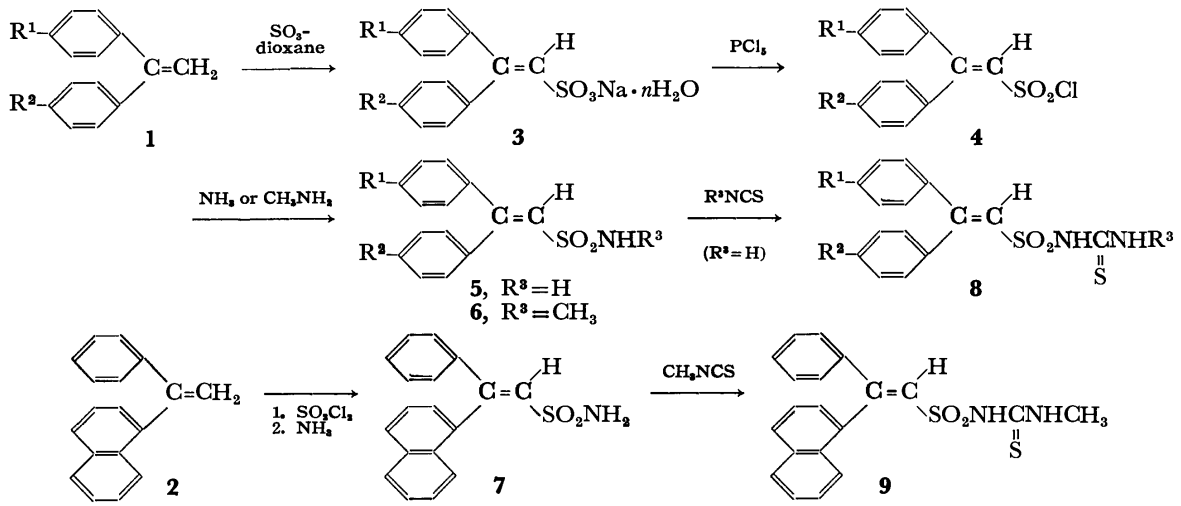

Scheme 1.

Table 3. Sulfonamides

Compd	R^1	R^2	R^3	Yield (%)	Mp (°C)	Calcd (%) C	H	N	S	Found (%) C	H	N	S
5b	H	Cl	H	94	116—117	57.24	4.12	4.77	10.91	56.98	4.02	4.98	10.98
5c	Cl	Cl	H	95	152—153	51.22	3.38	4.27	9.77	51.48	3.36	4.00	9.41
5d	H	CH_3	H	97	151—152	65.92	5.53	5.13	11.72	66.20	5.65	5.22	11.68
5e	CH_3	CH_3	H	95	146—147	66.88	5.96	4.88	11.14	67.04	5.93	4.61	11.15
5f	H	OCH_3	H	97	92— 94	62.28	5.23	4.84	11.06	62.25	5.10	4.84	11.12
5g	OCH_3	OCH_3	H	95	149—150	60.18	5.37	4.39	10.12	60.16	5.29	4.12	10.12
6a	H	H	CH_3	93	119—120	65.92	5.53	5.13	11.72	66.11	5.59	5.27	11.77
6b	H	Cl	CH_3	92	96— 98	58.53	4.58	4.55	10.42	58.77	4.62	4.65	10.30
6c	Cl	Cl	CH_3	93	132—134	52.64	3.83	4.09	9.37	52.84	3.69	4.35	9.56
6d	H	CH_3	CH_3	91	145—146	66.88	5.96	4.88	11.14	67.01	6.16	4.87	11.04
6e	CH_3	CH_3	CH_3	90	118—119	67.76	6.36	4.65	10.62	67.51	6.60	4.74	10.52
6f	H	OCH_3	CH_3	98	107—109	63.36	5.65	4.62	10.55	63.25	5.86	4.37	10.71
6g	OCH_3	OCH_3	CH_3	94	78— 79	61.25	5.75	4.20	9.40	61.46	5.48	3.95	9.17
7	1-Phenyl-1-(α-naphthyl)ethylene-sulfonamide			6[a]	78— 80	69.89	4.89	4.53	10.15	69.64	4.78	4.24	9.86

a) Overall yield from **2**.

Table 4. Thioureas

Compd	R^1	R^2	R^3	Yield (%)	Mp (°C)	Calcd (%) C	H	N	S	Found (%) C	H	N	S
8a	H	H	CH_3	95	158—159	57.83	4.85	8.43	19.26	57.97	4.77	8.37	19.33
8b	H	H	C_2H_5	72	142—144	58.95	5.24	8.09	18.48	58.73	5.21	7.95	18.26
8c	H	H	n-C_3H_7	77	154—156	59.99	5.59	7.77	17.76	59.80	5.47	7.70	17.68
8d	H	H	n-C_4H_9	67	151—153	60.95	5.92	7.48	17.09	61.00	5.82	7.77	16.96
8e	H	H	C_6H_5	89	142—143	63.95	4.60	7.10	16.23	63.85	4.78	7.03	16.33
8f	H	H	p-ClC_6H_4	95[a]	137—139	54.01	3.45	6.00	13.73	54.08	3.75	5.77	13.35
8g	H	H	p-$CH_3C_6H_4$	95[a]	190—191	59.17	4.29	6.27	14.33	58.89	4.37	6.28	14.09
8h	H	Cl	CH_3	58	136—138	52.38	4.12	7.64	17.48	52.20	3.98	7.68	17.30
8i	Cl	Cl	CH_3	49	133—134	47.88	3.52	6.98	15.98	48.17	3.51	6.80	15.91
8j	H	CH_3	CH_3	95	151—152	58.95	5.24	8.09	18.48	58.95	5.32	7.89	18.44
8k	CH_3	CH_3	CH_3	91	168—170	59.99	5.59	7.77	17.76	60.27	5.52	8.00	17.67
8l	H	OCH_3	CH_3	53	132—134	56.35	5.01	7.73	17.66	56.28	4.84	7.91	18.07
8m	OCH_3	OCH_3	CH_3	91	145—146	55.10	5.14	7.14	16.31	54.85	5.05	7.13	16.18
9	2-Phenyl-2-(α-naphthyl)-ethylenesulfonyl		CH_3	68	164—166	62.82	4.75	7.33	16.74	62.89	4.48	7.31	16.94
12	p-Nitrostyrene-1-sulfonyl		CH_3	18	234—236	39.87	3.68	13.95	21.25	40.12	3.55	13.73	21.01

a) Purified as potassium salts.

Table 5. Isothioureas

Compd	R^1	X[a]	R^3	Yield(%) Method A[b]	Yield(%) Method B[c]	Mp (°C)	Calcd (%) C	Calcd (%) H	Calcd (%) N	Calcd (%) S	Found (%) C	Found (%) H	Found (%) N	Found (%) S
13a	H	C_6H_5	CH_3	70	93	146—147	71.62	6.06	10.44	11.93	71.90	6.16	10.34	11.75
13b	H	C_6H_5	C_2H_5	56	92	164—166	72.32	6.43	9.92	11.33	72.26	6.47	9.90	11.20
13c	H	C_6H_5	n-C_3H_7	31[d]		141—143	72.95	6.80	9.45	10.80	72.84	6.76	9.21	10.83
13d	H	C_6H_5	C_6H_5	75	78	195—196	76.34	5.49	8.48	9.69	76.24	5.25	8.27	9.63
13e	H	ClC_6H_4	CH_3	89	97	64— 66	63.46	4.99	9.25	10.59	63.64	4.73	9.14	10.58
13f	Cl	ClC_6H_4	CH_3	92	98	217—218	56.98	4.18	8.31	9.51	56.88	4.08	8.22	9.25
13g	H	$H_3CC_6H_4$	CH_3	41	90	159—161	72.32	6.43	9.92	11.33	72.54	6.43	9.72	11.05
13h	CH_3	$H_3CC_6H_4$	CH_3	30	89	160—162	72.95	6.80	9.45	10.40	72.70	6.64	9.23	10.18
13i	H	$H_3COC_6H_4$	CH_3	27	81	130—132	68.44	6.08	9.39	10.73	68.25	6.21	9.20	10.37
13j	OCH_3	$H_3COC_6H_4$	CH_3	5	51	172—173	65.84	6.14	8.53	9.75	65.83	6.41	8.29	9.68
14	H	α-naphthyl	CH_3		80	82— 84	75.45	5.70	8.80		75.65	5.90	9.07	
15	NO_2	H	CH_3	79		181—182	50.63	4.67	17.72	13.49	50.73	4.52	17.75	13.69

a) X=*p*-$R^2C_6H_4$. b) 80 °C, 2 hr in DMF. c) 80 °C, 15 hr in DMF. d) Purified by chromatography on silicagel using $CHCl_3$ as the eluent.

pared from them with aqueous ammonia or methylamine (Table 3). A 2-α-naphthyl derivative (**7**) was obtained by a procedure similar to that described by Culbortson and Dietz.[4] A mixture of **5**, potassium carbonate and isothiocyanates in acetone was refluxed to yield thioureas **8**. Similar treatment of **7** afforded **9** (Table 4). As a nitrated derivative, **12**, could not be formed from *p*-nitrostyrenesulfonamide and methyl isothiocyanate, it was prepared by nitration of 3-methylamino-5-phenyl-1,1-dioxo-5,6-dihydro-1,4,2-dithiazine[2a] (**10**) followed by hydrolytic cleavage of the ring C-S bond. Thiourea **12** was recyclized under weakly alkaline conditions and also by heating at 145 °C. The structures of **8**, **9**, **11** and **12** were determined on the basis of analytical and spectral data. The NMR spectrum of **11** shows that **11** consists of about a 3:2 mixture of 3-methylamino and 3-methylimino tautomers in DMSO-d_6.

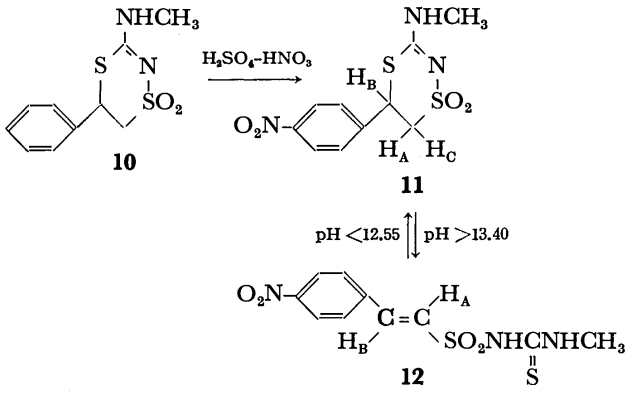

A New Intramolecular Rearrangement of Thioureas to Isothioureas. Thioureas **8** and **9** were treated with ten molar equivalents of aqueous 5 M NaOH in DMF for 2 hr at 80 °C (Method A) or for 15 hr at 80 °C (Method B) to afford rearranged isothioureas **13** and **14** respectively (Table 5).

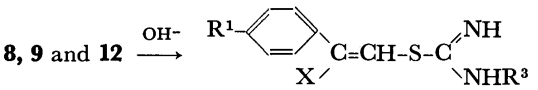

13, X=*p*-$R^2C_6H_4$ **15**, X=H
14, X=α-naphthyl

The rearrangement was carried out with variations of the *p*- and *p'*-substituents from electron-withdrawing to -releasing groups. All of the isothioureas were resistant to hydrolytic decomposition in aqueous 10 M NaOH even for 15 hr at 80 °C. The structures of **13** and **14** were determined on the basis of analytical and spectral data. The IR spectra of **13** and **14** displayed no SO_2 bands. The formation of isothioureas has a tendency to be favored by polar solvents. For example, **13a** was obtained by Method A (2 hr, 80 °C) in the following yields: ethanol 86%, DMSO 85%, no solvent 72%, DMF 70%, diglyme 31% and dioxane 26%. More concentrated aqueous NaOH than 2 M was necessary to effect rearrangement. The yield increased with concentration of base and with aqueous 10 M NaOH **13a** was obtained in 92% yield even at room temperature after 3 days. The results of Method A shown in Table 5 indicate that the rate of rearrangement is

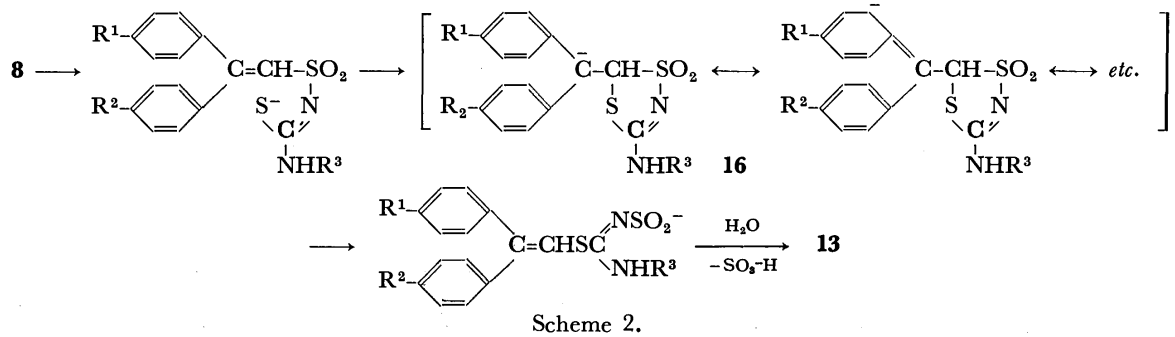

Scheme 2.

Table 6. 2,2-Diarylvinyl trithiocarbonates[a)]

Compd	R^1	R^2	R^3	Yield (%) path A	Yield (%) path B	Mp (°C)	Calcd (%) C	Calcd (%) H	Calcd (%) S	Found (%) C	Found (%) H	Found (%) S
17a	H	H	CH_3	55	54	110—111						
17b	H	H	C_2H_5	52	45	87— 88						
17c	H	H	n-C_3H_7	44	42	40— 41						
17d	H	H	n-C_4H_9	39	38	36— 37						
17e	H	Cl	CH_3	58	60	84— 85	57.04	3.89	26.55	57.28	3.96	26.84
17f	Cl	Cl	CH_3	66	74	70— 71	51.74	3.26	25.20	51.51	3.05	26.90
17g	H	CH_3	CH_3	46	50	75— 77	64.55	5.10	30.35	64.84	4.87	29.80
17h	CH_3	CH_3	CH_3	43	41	67— 68	65.44	5.49	29.06	65.65	5.25	28.86
17i	H	OCH_3	CH_3	39	28	76— 78	61.44	4.85	28.89	61.58	4.58	28.84
17j	OCH_3	OCH_3	CH_3	27	5	oil	59.66	5.01	26.50	59.76	4.86	26.62

a) Purified by chromatography on silica gel using benzene–n-hexane (**17a—e** 1: 1, **17f—h** 1: 5, and **17i—j** 1: 1 v/v) as the eluent.

increased by electron-withdrawing p,p'-substituents (Cl $>$H$>$$CH_3$$>$$OCH_3$). The probable interpretation may involve the formation of a five-membered cyclic intermediate such as **16** and subsequent removal of sulfite moiety (Scheme 2). An electron-withdrawing chlorine substituent may enhance the stabilization of **16** and electron-releasing methyl and methoxy substituents would have opposite effects. In this connection, **12**, a p-nitrated derivative of N-(2-phenylethene-1-sulfonyl)-N'-methylthiourea[2a)] underwent a rearrangement in aqueous 5 M NaOH under even more moderate conditions (60 °C, 10 min) than those used with **8** to afford N-methyl-S-(p-nitrostyryl)isothiourea (**15**) in 79% yield.

Reaction of Sulfonamides with Carbon Disulfide. In the same way as reported in the formation of trithiocarbonate **17** from **5a**[3)] methylsulfonamides **6** also gave **17** from two molar equivalents of carbon disulfide and alkyl halides in the presence of base (Table 6). The

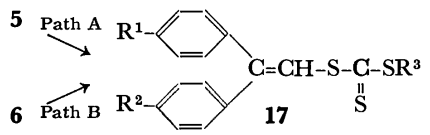

yield from **5** (Path A) or **6** (Path B) was increased by electron-withdrawing p,p'-substituents (Cl$>$H$>$$CH_3$$>$$OCH_3$). The order is in accord with that obtained in the rearrangement of thioureas. The structures of **17a—d** were characterized by comparison of their IR spectra and melting points with those of authentic samples[3)] and **17e—j** by their analytical and spectral data. The proposed mechanism for the formation of **17** from **6** is shown in Scheme 3. The mechanism is similar to that[3)] described in the formation of **17** from **5a** except that base-catalyzed hydrolysis of dithiocarbamate (**19**) is followed by degradation to diphenylvinylthiol (**20**) and N-methylthiocarbamate (**21**). Acid-catalyzed decomposition[6)] of **21** or **22** gave carbonyl sulfide and methylammonium chloride. In addition to the resonance stabilization of **18** by two phenyl groups, the stabilization of **18** by the electron-withdrawing groups, R^1 and R^2, would provide an important driving force for the thiolate anion to attack on C-1. It is a novel case[7)]

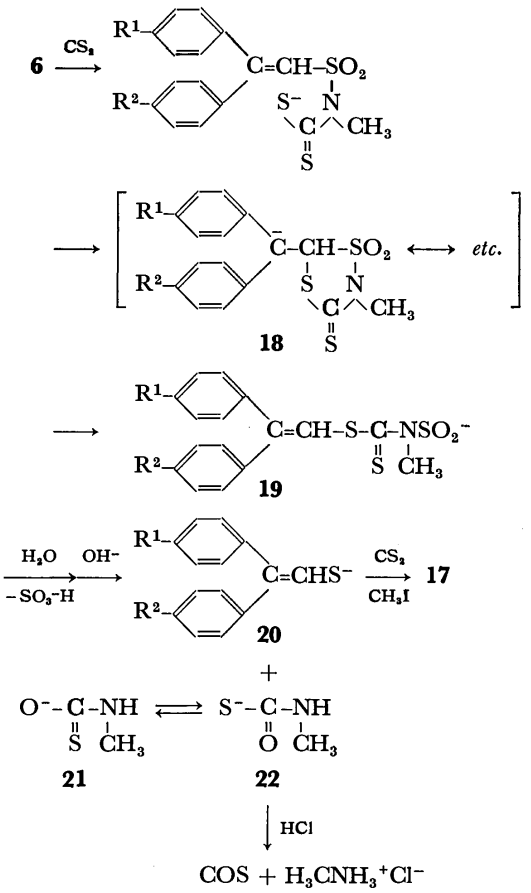

Scheme 3.

that the rearrangement could occur under moderate conditions even when R^1 and R^2 are electron-releasing groups.

Experimental

All melting points were determined on a Yanagimoto micro-melting point measuring apparatus, MP-S2, and are uncorrected. The IR spectra were recorded on a JASCO IRA-1 spectrometer. The NMR spectra were determined with a JEOL JNM-MH-100 spectrometer, using tetramethylsilane as the internal standard, and the mass spectra were recorded at

75 eV on a JEOL-O1SG-2 spectrometer. Column chromatography was performed with Wakogel C-200.

Reagents. *p*-Substituted diphenylethylenes were prepared by dehydration of the corresponding carbinols obtained from *p*-substituted acetophenone or α-acetonaphtone and phenylmagnesium bromide: 1-*p*-Chlorophenyl-1-phenylethylene, bp 136—140 °C/3 mmHg (lit,[8] 134—136 °C/1.5 mmHg); 1-*p*-tolyl-1-phenylethylene, bp 126—129 °C/3 mmHg (lit,[9] 278—294 °C); 1-*p*-anisyl-1-phenylethylene, bp 140—150 °C/2 mmHg, mp 74—75 °C (lit,[10] bp 155—170 °C/2 mmHg, mp 75 °C); 1-phenyl-1-(α-naphthyl)ethylene, mp 58—59 °C (lit,[9] 60 °C). *p,p'*-Disubstituted diphenylethylenes were prepared by dehydration of the corresponding carbinols obtained from *p*-substituted phenylmagnesium bromide (2 mol) and ethyl acetate (1 mol): 1,1-Diphenylethylene, bp 127—132 °C/10 mmHg (lit,[11] 113 °C/2 mmHg); 1,1-bis(*p*-chlorophenyl)ethylene, bp 150—158 °C/3 mmHg, mp 84—85 °C (lit,[12] mp 84—85 °C); 1,1-bis(*p*-tolyl)ethylene, bp 132—136 °C/4 mmHg, mp 61—62 °C (lit,[10] mp 62.5—63.0 °C), 1,1-bis(*p*-anisyl)ethylene, mp 141—143 °C (lit,[10] 144—145 °C).

*Sodium 2,2-Diphenylethylenesulfonate (**3a**).* Diphenylethylene was sulfonated with dioxane–sulfur trioxide by a procedure similar to that used for the sulfonation of styrene.[4] The resulting brown solution was neutralized with aqueous NaOH to give **3a**. Recrystallization from water gave monohydrate of **3a** as colorless thin plates. IR (KBr): 3050 (=CH), 1600 (C=C), and 1200 (SO_2) cm^{-1}. NMR (DMSO-d_6) δ: 6.84 (s, 1, CH), 7.33 (s, 10, $2C_6H_5$).

*2,2-Diphenylethylenesulfonyl Chloride (**4a**).* Dry **4a** (28.20 g, 0.100 mol) was treated with PCl_5 (24.99 g, 0.120 mol) similar to the procedure of chlorination of sodium 2-phenylethylene-1-sulfonate[13] to give a yellow brown oil. Recrystallization from $CHCl_3$–petroleum ether gave 19.70 g (71%) of **4a**. IR (KBr): 3060 (=CH), 1600 (C=C), 1330 and 1160 (SO_2) cm^{-1}. NMR ($CDCl_3$) δ: 7.09 (s, a, CH), 7.28±0.06 (m, 10, $2C_6H_5$). MS *m/e*: 89, 102, 152, 165, 178, 179 (base peak), 214, 243 and 278 (M^+).

Crude **4c**, **4e**, and **4f—g** were chromatographed on silica gel using benzene–*n*-hexane (**4c** and **4e** 1 : 1, **4f—g** 5 : 1 v/v) as the eluene and recrystallized from the solvents shown in Table 2.

2,2-Diphenylethylene-N-*methylsulfonamide (**6a**).* To a stirred solution of **4a** (2.78 g, 0.100 mol) in benzene (10 ml) was added dropwise a 30% aqueous methylamine (4.14 g, 0.040 mol). After stirring was continued for 1 hr at 40—50 °C the mixture was cooled and resultant precipitates were filtered to give 2.54 g (93%) of **6a**. Recrystallization from benzene gave colorless crystals. IR (KBr): 3340 (NH), 3060 (=CH), 1600 (C=C), 1315, 1150, and 1120 (SO_2) cm^{-1}. NMR ($CDCl_3$) δ: 2.42 (d, J_{NH-CH_3} = 5.0 Hz, 3, CH_3), 3.58 (broad, 1, NH), 6.64 (s, 1, CH), 7.20±0.06 (m, 10, $2C_6H_5$). MS *m/e*: 89, 102, 152, 165, 167, 178, 179 (base peak), 209 243 and 273 (M^+).

N-*(2,2-Diphenylethylenesulfonyl)*-N'-*methylthiourea (**8a**).* To a solution of **5a** (7.79 g, 0.030 mol) in acetone (20 ml) was added methyl isothiocyanate (2.63 g, 0.036 mol) and anhydrous K_2CO_3 (6.21 g, 0.045 mol), and the reaction mixture was refluxed for 10 hr with stirring. The resulting potassium salt of **8a** was filtered and washed with acetone to remove unreacted **6a**. The salt was dissolved in water (300 ml), and the solution was acidified with concd HCl to give 9.50 g (95%) of **8a**. Recrystallization from methanol gave colorless crystals. IR (KBr): 3320 (NH), 3060 (=CH), 1600 (C=C), 1570 (NH), 1380, 1180, and 1130 (SO_2) cm^{-1}. NMR (MDSO-d_6) δ: 3.00 (s, 3, CH_3), 3.40 (broad, 1, $NHCH_3$), 7.12 (s, 1, CH), 7.32±0.10 (m, 10, $2C_6H_5$), 7.80 (broad, 1, SO_2NH). MS *m/e*: 89, 102, 121, 134, 152, 165, 167, 178, 179, 195, 211, 212 (base peak), 243, 268, and 298. M^+ was not observed.

Thioureas, **8b**, **8c**, and **8d**, were obtained by evaporation of acetone from the filtrate and subsequent recrystallization of the residual oils from methanol.

*3-Methylamino-5-(*p*-nitrophenyl)-5,6-dihydro-1,4,2-dithiazine-1,1-dioxide (**11**).* To a stirred mixture of concd HNO_3 (*d*= 1.42, 40 ml) and concd H_2SO_4 (40 ml) was added 3-methylamino-5-phenyl-5,6-dihydro-1,4,2-dithiazine-1,1-dioxide (4.17 g, 0.0163 mol) portionwise at 0—5 °C. After stirring was continued for 3 hr at 5 °C, the solution was poured onto ice water (400 ml), and the solid was filtered to give 4.78 g (98%) of the crude product which was most likely contaminated with *ortho* and *meta* isomers. Repeated fractional recrystallization from methanol gave a *para* isomer (**11**) as pale-yellow crystals. IR (KBr): 3240 (NH), 1560 (N=C), 1520 (NO_2), 1340 (NO_2) and 1115 (SO_2) cm^{-1}. NMR (DMSO-d_6) δ: 2.78 (d, J_{NH-CH_3} = 4.5 Hz, 1.7H, $NHCH_3$), 2.78 (s, 1.3H, $=NCH_3$), 3.57 (q, 1, H_A), 3.83 (q, 1, H_C), 5.25 (q, 1, H_B), J_{AB} = 6.0 Hz, J_{AC} = 13.5 Hz, J_{BC} = 4.5 Hz, 7.60—8.50 (m, 4, C_6H_4), a NH proton was ambiguous. MS *m/e*: 57 (base peak), 91, 103, 120, 135, 149, 164, 166, 181, 191, 236, 255, and 301 (M^+).

N-*(*p*-Nitrostyrene-1-sulfonyl)*-N'-*methylthiourea (**12**).* When aqueous 1 M NaOH (21.0 ml, 0.0214 mol) was added to a stirred suspension of **11** (3.23 g, 0.0107 mol) in acetone (42 ml), a deep brown solution was formed. After stirring was continued for 10 min, acetone was removed *in vacuo* and the residual solution was acidified with concd HCl to give **12** (1.50 g) as brown crystals. Recrystallization from acetone gave 0.57 g (18%) of **12** as pale-yellow crystals. IR (KBr): 3330 (NH), 3040 (=CH), 1615 (C=C), 1560 (NH), 1520, 1490 and 1350 (NO_2), 1150 and 1130 (SO_2) cm^{-1}. NMR DMSO-d_6) δ: 2.74 (d, J_{NH-CH_3} = 4.0 Hz, 3, CH_3), 7.40 (d, 1, H_A), 7.94 (d, 1, H_B), J_{AB} = 15.0 Hz, 7.40—8.20 (m, 4, C_6H_4), two NH protons were ambiguous. Mass spectrum was identical with that of **11** because of ready cyclization of **12** to **11** on heating.

N-*Methyl*-S-*(2,2-diphenylvinyl)isothiourea (**13a**).* To a stirred solution of **8a** (0.40 g, 0.0012 mol) in DMF (6 ml) was added aqueous 5M NaOH (2.4 ml, 0.012 mol) and the mixture was stirred for 2 hr at 80 °C. The mixture was poured onto ice water (100 ml). The precipitates were filtered to give 0.224 g (70%) of **13a**. Recrystallization from methanol gave colorless crystals. IR (KBr): 3400, 3260 and 3180 (NH), 1605 (C=N), 1470, 1450, 1360, 1040, 770 and 695 cm^{-1}. NMR ($CDCl_3$) δ: 3.05 (s, 3, CH_3), 6.50—5.30 (broad, 2, 2NH), 6.74 (s, 1, CH), 7.24 (s, 10, $2C_6H_5$). MS *m/e*: 42, 44, 57, 77, 165, 178, 193, 212, 219, 234 (base peak) and 268 (M^+).

N-*Methyl*-S-*(*p*-nitrostyryl)isothiourea (**15**).* Similar to the synthesis of **13a**, **12** (0.36 g, 0.0012 mol) was treated with aqueous 5M NaOH (2.40 ml, 0.012 mol) in DMF (3 ml) for 10 min at 60 °C to give 0.22 g (79%) of **15**. Recrystallization from acetone gave yellow crystals. IR (KBr): 3400, 3260, and 3170 (NH), 1620 (C=N), 1510, 1470, 1370, and 1350 (NO_2), 1255, 1050, 940, 825, 800, 750, and 730 cm^{-1}. NMR ($CDCl_3$) δ: 3.30 (d, J_{NH-CH_3} = 5.0 Hz, 3, CH_3), 6.60 (d, 1, H_A), 8.18 (d, 1, H_B), J_{AB} = 15.0 Hz, 7.20—7.80 (broad, 1, NH), 8.50 (broad, 1, $NHCH_3$), 7.28—8.10 (m, 4, C_6H_4). MS *m/e*: 42, 57, 76, 89, 102, 115, 131, 136, 178, 180, 203, and 237 (M^+).

*Methyl 2,2-bis(*p*-chlorophenyl)vinyl trithiocarbonate (**17f**).* *Path A*: A solution of **5c** (0.295 g, 0.00090 mol) in DMF (3 ml) was treated with aqueous 5M NaOH (0.54 ml, 0.0027 mol), carbon disulfide (0.21 g, 0.0027 mol), and then methyl iodide (0.16 g, 0.0011 mol) by the way described by us[3] to give yellow crystals. Chromatography on silica gel to remove **5c** gave 0.220 g (66%) of pure **17f** as yellow crystals.

Path B: By using the way described in Path A, 0.241 g

(74%) of **17f** was obtained from **6c** (0.30 g, 0.00088 mol), aqueous 5M NaOH (0.52 ml, 0.0026 mol), carbon disulfide (0.17 g, 0.0022 mol) and methyl iodide (0.16 g, 0.0011 mol). Materials which were contained in the filtrate of **17f** were examined. Sulfite anion, SO_3^{-2}, in the filtrate was oxidized with H_2O_2 and detected by $BaSO_4$ precipitation. Carbonyl sulfide was confirmed with lead paper. Methylammonium chloride was converted into a red rhodamine dye exhibiting yellow green fluorescence.[14]

The authors wish to thank Mr. S. Ikeda, Mr. H. Annaka, Mr. Y. Mizukami and Mr. T. Yamamoto for assistance in preparing some of the compounds.

References

1) E. Waldan and R. Pütter, *Angew. Chem.*, **84**, 822 (1972).
2) a) K. Hasegawa and S. Hirooka, This Bulletin, **45**, 525 (1972); b) K. Hasegawa and S. Hirooka, *ibid.*, **45**, 1567 (1972); c) K. Nakahashi, S. Hirooka, and K. Hasegawa, *ibid.*, **45**, 3217 (1972); d) K. Hasegawa, T. Sasaki, and S. Hirooka, *ibid.*, **46**, 696 (1973).
3) K. Hasegawa, T. Sasaki, and S. Hirooka, *ibid.*, **46**, 2894 (1973).
4) B. M. Culbortson and S. Dietz, *J. Chem. Soc., C*, **1968**, 992.
5) A. P. Terentév and R. A. Gracheva, *Zhur Obshchei Khim.*, **30**, 3663 (1960). *Chem. Abstr.*, **55**, 18659f (1961).
6) E. Müller, Houben-Weyl, "Methoden der Organishen Chemie," George Thieme Verlag, Stuttgart (1955). Vol. XI/2, p. 782 and 823.
7) W. E. Truce, E. M. Kreider, and W. W. Brand, "Organic Reactions," Vol. 18, Wiley, New York, N. Y., 1970, p. 103.
8) S. N. Ege and K. W. Sherk, *J. Amer. Chem. Soc.*, **75**, 354 (1953).
9) C. D. Hurd and C. N. Webb, *ibid.*, **49**, 549 (1927).
10) A. G. Evans, N. Jones, P. M. S. Jones, and J. H. Thomas, *J. Chem. Soc.*, **1956**, 2757.
11) C. F. H. Allen, "Organic Syntheses," Coll. Vol. I, (1956), p. 226.
12) W. L. Beneze and M. J. Allen, *J. Org. Chem.*, **22**, 352 (1957).
13) C. S. Rodestvedt Jr., and F. G. Bordwell, "Organic Syntheses," Coll. Vol. IV, (1963), p. 846.
14) F. Feigl, "Spot Tests in Organic Analysis," Elsevier, Maruzen Asian Edition, Tokyo, (1960), p. 275.

Charge-Transfer Complexes of Thiopyrylium Cation with Aromatic Hydrocarbons and Olefins

Zen-ichi YOSHIDA,* Toyonari SUGIMOTO, and Shigeo YONEDA

Department of Synthetic Chemistry, Faculty of Engineering, Kyoto University, Yoshida, Kyoto 606

(Received December 17, 1974)

Charge-transfer (CT) interaction of the thiopyrylium cation (**1**) with aromatic hydrocarbons and olefins has been investigated by electronic spectroscopy. It is noteworthy that **1** formed a CT complex with a monoolefin. The observed CT spectra in the **1**–olefin system showed the following remarkable contrasts compared with those in the **1**–aromatic system. 1) Although one CT absorption band was observed for the **1**–aromatic hydrocarbon CT complex, while two CT absorption bands for the 1–olefin CT complex, and 2) the value of a in the equation of $\Delta E_{CT}=aIP_D+b$ was 1.04 for the former complex and 0.27 for the latter complex. A detailed discussion on the difference between the two CT complexes is presented.

Thiopyrylium cation (**1**)[1] belongs to a novel class of heterocyclic system. The question whether this system is represented by the dominant cyclic 6π aromatic structure (**1a**) or it is more accurately represented as a hybrid structure principally composed of sulfur-bridged carbonium ion structure (**1b**) is intriguing from organic as well as physicochemical view points.

1a **1b**

Our studies on the interpretation of its electronic spectrum[2] by the SCF-MO method and on its reactions with nucleophiles[3] indicated that **1** can be regarded as the carbonium ion stabilized by the (2p-3p)π conjugation with the sulfur atom. In the reactions of **1** with carbanions and amines, we expected that the reaction might proceed *via* a CT complex between **1** and the nucleophile. However, for both **1**-carbanion and **1**-amine systems such CT complex formation has not been observed by spectroscopic means because the reaction between **1** and the nucleophile with low ionization potential occurs very rapidly. This situation prompted us to investigate the CT complex formation between **1** and aromatic hydrocarbons or olefins which have higher ionization potentials than carbanions and amines. Interestingly, we observed the **1**-monoolefin CT complexes[4] as well as the **1**-aromatic hydrocarbon CT complexes, and found that **1** behaves as a strikingly different π electron acceptor from tetracyanoethylene[5] and 1,3,5-trinitrobenzene[6] in the CT complex formation with aromatic hydrocarbons and olefins. In this paper we report investigation on such an interesting CT interaction of **1** with aromatic hydrocarbon and monoolefin, and discuss difference between the two CT complexes.

Experimental

Thiopyrylium perchlorate was prepared according to the method of Degani *et al.*[1c] and purified by reprecipitation from acetonitrile–ether.

Aromatic hydrocarbons and olefins used were purified before use in the following manners. *m*-Xylene, mesitylene, 1-methylnaphthalene and 2-methylnaphthalene were purified by distillation *in vacuo*. Naphthalene, pyrene and anthracene were purified by sublimation under reduced pressure. Cyclohexene, 1-methylcyclohexene, 3-methylcyclohexene, 4-methylcyclohexene, 1-pentene, ethyl vinyl ether and *n*-butyl vinyl ether were purified by distillation *in vacuo*. Acetonitrile was dried over phosphorus pentoxide, repeatedly distilled, treated with anhydrous potassium carbonate and finally distilled without a drying agent.

The electronic spectra were recorded on a Hitachi EPS-3T type spectrophotometer at room temperature.

The pK_{R^+} value for the 1-ethylpyridinium cation was estimated from a determination of the pH of aqueous solutions of the perchlorate salt.

Results and Discussion

CT Complexes between the Thiopyrylium Cation **1** *and Aromatic Hydrocarbons.* A new absorption band was observed in the ultraviolet or visible region for the mixed solution of **1** and an aromatic hydrocarbon in acetonitrile, which is due to neither **1** nor an aromatic hydrocarbon. For example, the absorption spectrum of the **1**-mesitylene system reveals a new band at 345 nm as shown in Fig. 1. The maximum wavelengths of new bands observed for the **1**-aromatic hydrocarbon system are listed in Table 1. When the maximum

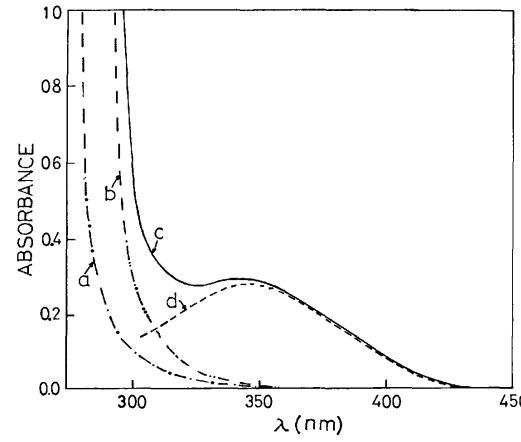

Fig. 1. Absorption spectra in acetonitrile: (a) Thiopyrylium perchlorate (1.3×10^{-3} mol/l) (b) Mesitylene (0.3 mol/l) (c) Thiopyrylium perchlorate (1.3×10^{-3} mol/l) and mesitylene (0.3 mol/l) (d) The calculated absorption for the thiopyrylium perchlorate–mesitylene CT complex.

TABLE 1. CT ABSORPTION BANDS OF THE **1**[a] -AROMATIC HYDROCARBON COMPLEXES IN ACETONITRILE

Donor[b]	λ_{max} (nm)	*IP* (eV)
m-Xylene	319	8.56[c]
Mesitylene	345	8.39[c]
Naphthalene	383	8.12[c]
2-Methylnaphthalene	396	8.03[c]
1-Methylnaphthalene	405	7.96[c]
Pyrene	462	7.55[d]
Anthracene	467	7.37[d]

a) A concentration of 1.3×10^{-3} mol/l. b) A concentration in the 0.1—0.5 mol/l range. c) K. Watanabe, *J. Chem. Phys.*, **26**,, 542 (1957). d) J. B. Birks and M. A. Slifkin, *Nature*, **191**, 761 (1961).

transition energies (ΔE_{CT}) of the new bands are plotted against the ionization potentials (IP_D) of aromatic hydrocarbons, a straight line with slope close to unity is obtained (Fig. 2). This demonstrates that the new bands are due to the CT complexes between **1** and aromatic hydrocarbons.

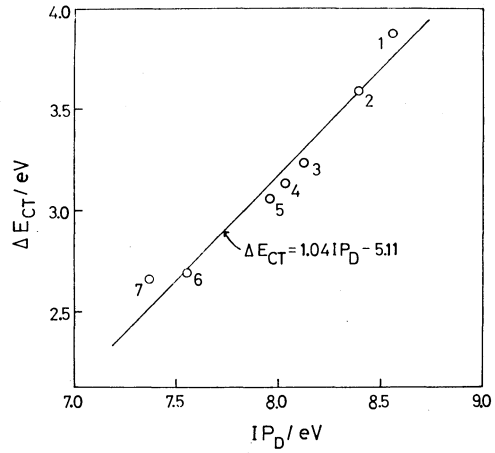

Fig. 2. Plot of the CT transition energies (ΔE_{CT}) *vs.* the ionization potentials (IP_D) of aromatic hydrocarbons: (1) *m*-Xylene, (2) Mesitylene, (3) Naphthalene, (4) 2-Methylnaphthalene, (5) 1-Methylnaphthalene, (6) Pyrene, and (7) Anthracene.

The equilibrium constant and the extinction coefficient for the **1**-mesitylene CT complex were determined to be 0.16 $l\cdot mol^{-1}$ and 2900 at 20.0°C, respectively, by the Benesi-Hildebrand equation.[7] Feldman and Winstein have observed the similar phenomenon for the tropylium perchlorate (**2**)-aromatic hydrocarbon system in acetonitrile and obtained the equilibrium constant of 0.67 $l\cdot mol^{-1}$ (25.0°C) and the extinction coefficient of 1850 for the 1:1 CT complex between **2** and mesitylene.[2,8] The value of the equilibrium constant obtained for the **1**-mesitylene CT complex is much smaller than that for the **2**-mesitylene CT complex. In contrast with these cations, the 1-ethylpyridinium cation (**3**) did not exhibit CT absorptions with aromatic hydrocarbons. This clearly indicates that abilities of their cations as electron acceptors in the CT complex formation decrease in the order of tropylium>thiopyrylium>pyridinium cations. This tendency is coincident with the reverse order of the pK_{R^+} values for their cations (**2**, +4.7;[9] **1**, +8.7;[10] **3**, +11.5). The contribution of the carbonium ion structure to the cations is closely related to their electron accepting ability in the CT complex formation.

CT Complexes between 1 and Olefins. When olefins are employed in place of aromatic hydrocarbons as an electron donor, two CT bands are observed in the ultraviolet and visible regions.[11] As one example the CT absorption spectrum of the **1**-cyclohexene system is shown in Fig. 3. The maximum wavelength of the two CT bands observed for the **1**-olefin system are listed in Table 2. Figure 4 shows that the plots of the transition energies (ΔE_{CT}) of the first (I) and the second (II) CT bands *vs.* the ionization potentials (IP_D) of olefins give straight lines with the same slope (0.27) whose value is significantly small compared with that (1.04) for the **1**-aromatic hydrocarbon CT complexes (see Fig. 2). The two absorption bands observed for the **1**-olefin system are attributed to those due to the CT complex formation between **1** and olefin.

The equilibrium constant and the extinction coefficient for the **1**-cyclohexene CT complex were determined to be 2.00 $l\cdot mol^{-1}$ and 185, respectively.

Multiple CT bands in donor-acceptor complexes

TABLE 2. CT ABSORPTION BANDS OF THE **1**[a] -OLEFIN COMPLEXES IN ACETONITRILE

Donor[b]	λ_{max} (nm)		*IP* (eV)
	Second CT band[c] (II)	First CT band (I)	
1-Pentene	—[d]	406	9.67[f]
Isobutene	310	420	9.26[f]
Cyclohexene	311	422	9.18[f]
1-Methylcyclohexene	311	422	
3-Methylcyclohexene	311	422	
4-Methylcyclohexene	311	—[e]	
Ethyl vinyl ether	315 (sh)	434	8.93[f]
n-Butyl vinyl ether	315 (sh)	434	

a) A concentration of 1.3×10^{-3} mol/l. b) A concentration in the 0.1—0.3 mol range. c) Thiopyrylium perchlorate itself has the absorptions at 246 nm (log ε=3.74) and 284 (3.55) in acetonitrile. The second CT bands are found by the usual procedure dissolving the component molecules. d) Exact analysis between 284 nm band of thiopyrylium perchlorate and the second CT band is difficult. e) The spectrum in this region can not be analyzed, because the absorption band of the reaction product overlaps with the first CT band of the system. f) J. Collins and F. P. Lossing, *J. Amer. Chem. Soc.*, **81**, 2064 (1959).

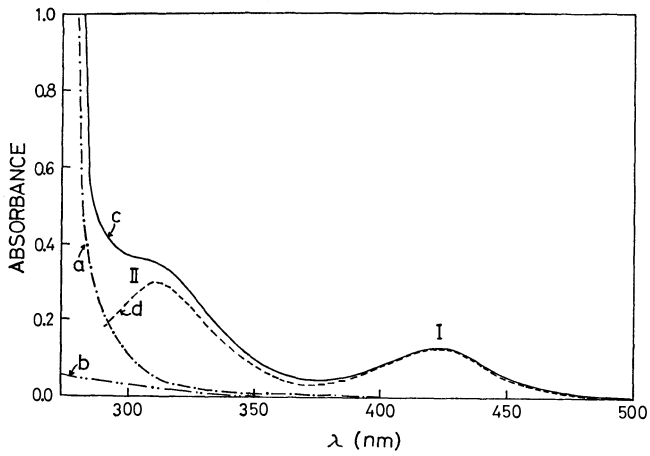

Fig. 3. Absorption spectra in acetonitrile: (a) Thiopyrylium perchlorate (1.3×10^{-3} mol/l) (b) Cyclohexene (0.3 mol/l) (c) Thiopyrylium perchlorate (1.3×10^{-3} mol/l) and cyclohexene (0.3 mol/l) (d) The calculated absorption for the thiopyrylium perchlorate–cyclohexene CT complex. The bands, I and II, correspond to the first and the second CT absorption bands, respectively.

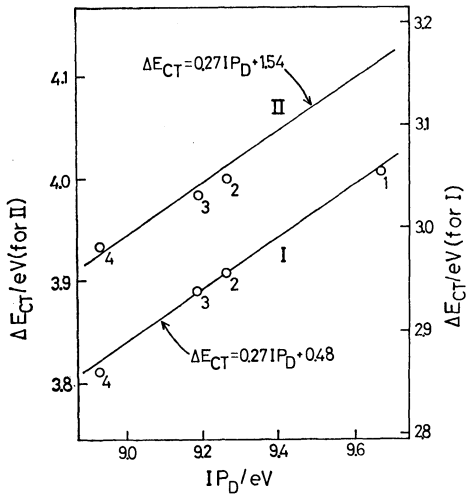

Fig. 4. Plots of the CT transition energies (ΔE_{CT}) of the first (I) and the second (II) CT absorption bands *vs.* the ionization potentials (IP_D) of olefins: (1) 1-Pentene, (2) Isobutene, (3) Cyclohexene and (4) Ethyl vinyl ether.

have been assigned to electronic transitions from two upper occupied levels in the donor[12] or to two lower unoccupied levels in the acceptor.[1,13] In the case of 1-methylpyridinium iodide[14] and 2,4,6-trimethylpyrylium iodide[15] two CT bands were once assigned to the formation of $^2P_{3/2}$ and $^2P_{1/2}$ iodine atoms in the excited state, on the basis that the separation between the two bands corresponded nearly to that expected for the formation of iodine atom in two states.[16] However, recent experimental results have indicated that the two CT bands observed in 1-methylpyridinium iodide are in fact due to the electronic transitions from the highest occupied MO of the iodide anion to the lowest and the second unoccupied π-MO's of the pyridinium cation.[17–19] Verhoeven, Dirkx and de Boer have investigated the CT interaction between the *N*-methyl-4-cyanopyridinium ions and aromatic hydrocarbons, and also observed the two CT bands which are caused by the presence of two closely located unoccupied MO's in the pyridinium cation.[20] In the case of the **1**–olefin CT complexes, the two CT bands should be assigned to the electronic transitions from the highest occupied π-MO of olefin to the lowest and the second unoccupied π-MO's of **1** as visualized in Fig. 5,

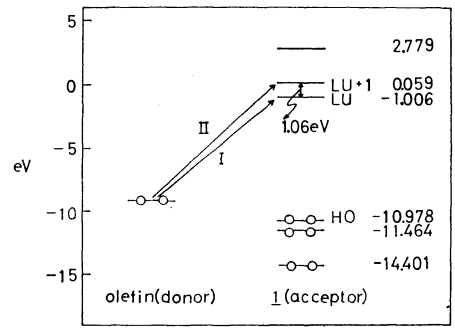

Fig. 5. Energy diagram for the **1**–olefin CT complex. I and II correspond to the first and the second CT absorption bands, respectively.

since olefin has only one occupied π-MO. From Fig. 4, the energy difference between the first and the second CT bands is almost constant independent of olefins employed and 1.06 eV. Furthermore, the observed energy difference is very close to the calculated energy difference between the lowest and the second unoccupied π-MO's of **1** by the SCF-MO method;[2] *i.e.*, 1.065 eV. The above mentioned facts lead to the conclusion that the two closely located unoccupied π-MO's of **1** play an important role in the appearance of the two CT bands for the case of the olefin complexes.

We can suggest the geometry of the **1**–olefin CT complex considering the "overlap and orientation principle."[21] The overlap between the orbitals of two component molecules will determine the resonance capability of the CT-bond and the nobond structures; that is, the relative positions of **1** and olefin molecules in the CT complex will be such as to make possible overlaps of the highest occupied π-MO of olefin with the lowest and the second unoccupied π-MO's of **1**

Fig. 6. The lowest unoccupied (LU) and the second unoccupied (LU+1) MO's of **1** calculated by the SCF-MO method.

(see Fig. 6). From Fig. 6 we can immediately illustrate only one possible configuration shown in Fig. 7 as the geometrical structure of the **1**–olefin CT complex, where olefin is located on the α-carbons of **1**. The SCF-MO calculation indicates that in this configuration the highest occupied MO of olefin overlaps more effectively with the (LU+1)MO than with the LUMO of **1**, consistent with the observation that the higher energy

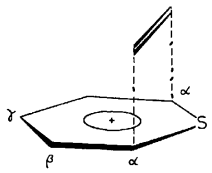

Fig. 7. Geometrical configuration for **1**-olefin CT complex.

CT band is more intense than the lower energy one (see Fig. 3).

Comparison between the 1-Aromatic Hydrocarbon and the 1-Olefin CT Complexes. The **1**-aromatic hydrocarbon and the **1**-olefin CT complexes have the folowing marked differences: (1) only one CT band is observed for the former,[22] while two CT bands for the later, and (2) the slope obtained by the plot of the CT transition energies *vs.* the ionization potentials of donors is 1.04 for the aromatic hydrocarbon complexes and 0.27 for the olefin complexes.

According to Mulliken's CT treatment of the electron donor-acceptor complexes,[23] their CT transition energy (ΔE_{CT}) depends upon the donor ionization potential (IP_D) and the acceptor electron affinity (EA_A) as expressed in Eq. (1):

$$\Delta E_{CT} = IP_D - EA_A + C_1 + \frac{C_2}{IP_D - EA_A + C_1} \quad (1)$$

The energy term C_1 mainly comprises the difference between the Coulomb attraction D^+-A^- after excitation and the van der Waals bonding energy D···A before excitation; C_2 reflects intermolecular resonance. If CT interaction is weak, the fourth term in Eq. (1) will vanish because C_2 is considered to be nearly zero. Actually, the following equation (Eq. (2))* was obtained in the **1**-aromatic hydrocarbon ($IP_D = 7.37$—8.56 eV) complexes as shown in Fig. (2). On the other hand, in the case of **1**-olefin ($IP_D = 8.93$—9.67 eV) CT

$$\Delta E_{CT} = 1.04 IP_D - 5.11 \quad (2)$$

complexes, Eqs. (3) and (4) were empirically obtained from Fig. 4 for the first and second CT absorption bands, respectively, since the C_2 term is considerably large, indicating that olefins more strongly interact with **1**.

$$\Delta E_{CT} = 0.27 IP_D + 0.48 \quad (3)$$

$$\Delta E_{CT} = 0.27 IP_D + 1.54 \quad (4)$$

This is also supported by the fact that the **1**-cyclohexene CT complex has a large equilibrium constant (2.00) compared with the **1**-mesitylene CT complex (0.16). Thus appearance of two CT bands in the **1**-olefin CT complexes is considered to be due to strong interaction between them.

* Under the assumption that C_1, C_2 and EA_A are constants for comparable CT complexes between the same electron acceptor and different electron donors of high ionization potentials,[24] Eq. (1) canbe replaced by linear expression as follows:[25]

$$\Delta E_{CT} = aIP_D + b$$

In a weak CT interaction, the value of a is nearly equal to unity because the C_2 term is nearly zero. Whereas, in a stronger CT interaction the values of a becomes smaller than unity because C_2 is not zero.

It is well known that generally π electron acceptors such as tetracyanoethylene[5] and 1,3,5-trinitrobenzene[6] form stronger CT complexes with aromatic hydrocarbons than with olefins. In marked contrast with the usual case, it is interesting that **1** forms stronger CT complex with olefin than with aromatic hydrocarbon. This is the first case in π-π type CT complexes.

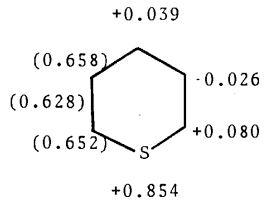

Fig. 8. Positive charge distribution and π-bond orders of **1** calculated by the SCF-MO method.

The strong CT interaction of **1** with olefin is due to the characteristic nature of **1**. It has already been suggested that the possible geometry for the **1**-olefin CT complex is one of olefin locating itself on the α-carbons of **1** (see Fig. 7), on which the positive charge localizes most as seen in the positive charge distribution calculated by the SCF-MO method[2] (Fig. 8). This geometry supplies a condition for the strong CT interaction between **1** and olefin, in which the unoccupied α-carbon 2p π-MO's of **1** overlap effectively with the occupied 2p π-MO's of olefin.

References

1) (a) R. Pettit, *Tetrahedron Lett.*, **1960**, 11; (b) A. Lüttringhaus and N. Engelhard, *Angew. Chem.*, **73**, 218 (1961); (c) I. Degani, R. Fochi, and C. Vincenzi, *Tetrahedron Lett.*, **1963**, 1167; (d) I. Degani, R. Fochi, and C. Vincenzi, *Gazz. Chim. Ital.*, **94**, 203 (1964); (e) E. Molenaar and J. Strating, *Tetrahedron Lett.*, **1965**, 2941.

2) Z. Yoshida, H. Sugimoto, and S. Yoneda, *Tetrahedron*, **28**, 5873 (1972).

3) (a) Z. Yoshida, S. Yoneda, H. Sugimoto, and T. Sugimoto, *Tetrahedron*, **27**, 6083 (1971); (b) Z. Yoshida, H. Sugimoto, T. Sugimoto and S. Yoneda, *J. Org. Chem.*, **38**, 3990 (1973).

4) Z. Yoshida, S. Yoneda, and T. Sugimoto, *Chem. Lett.*, **1972**, 17.

5) R. E. Merrifield and W. D. Phillips, *J. Amer. Chem. Soc.*, **80**, 2778 (1958).

6) G. Briegleb and J. Czekalla, *Z. Elektrochem.*, **59**, 184 (1955).

7) H. A. Benesi and J. H. Hildebrand, *J. Amer. Chem. Soc.*, **71**, 2703 (1949).

8) (a) M. Feldman and S. Winstein, *ibid.*, **83**, 3338 (1961); (b) M. Feldman and S. Winstein, *Theoret. Chim. Acta*, **10**, 86 (1968).

9) W. von E. Doering and M. H. Knox, *J. Amer. Chem. Soc.*, **76**, 3203 (1954).

10) R. G. Turnbo, D. M. Sullivan, and R. Pettit, *ibid.*, **86**, 5630 (1964).

11) Immediate color formation from **1** and dienes or trienes was observed, but it disappeared gradually.

12) E. M. Voigt and C. Reid, *J. Amer. Chem. Soc.*, **86**, 3930 (1964).

13) S. Iwata, J. Tanaka, and S. Nagakura, *ibid.*, **88**, 894 (1966).

14) E. M. Kosower, J. A. Skorcz, W. M. Schwarz, Jr., and J. W. Patton, *ibid.*, **82**, 2188 (1960).
15) A.T. Balaban, M. Mocanu, and Z. Simon, *Tetrahedron*, **20**, 119 (1964).
16) E. Lederle, *Z. Phys. Chem.*, **B10**, 121 (1930).
17) R. A. Mackay, J. R. Landolph, and E. J. Poziomek, *J. Amer. Chem. Soc.*, **93**, 5026 (1971).
18) R. A. Mackay and E. J. Pozimek, *ibid.*, **94**, 4167 (1972).
19) E.M. Kosower, E. J. Land, and A. J. Swallow, *ibid.*, **94**, 986 (1972).
20) J.W. Verhoeven, I. P. Dirkx, and Th. J. de Boer, *Tetrahedron*, **25**, 3395 (1969).
21) S. P. McGlynn, *Chem. Rev.*, **58**, 1113 (1958).
22) The second CT band for **1**–aromatic hydrocarbon CT complex may be obscured by the absorption of aromatic hydrocarbon. Generally, in the case of the aromatic hydrocarbon complexes, appearance of multiple CT bands due to electronic transitions from two upper occupied levels in aromatic hydrocarbons or to two lower unoccupied levels in **1** might be possible. However, the second and higher energy CT bands have not been observed in our aromatic hydrocarbon complexes.
23) R. S. Mulliken, *J. Amer. Chem. Soc.*, **72**, 600 (1950); **74**, 811 (1952).
24) G. Briegleb, "Elektronen-Donator-Akzeptor-Komplexe," Springer, Berlin (1961).
25) H. McConnel, J. S. Ham, and J. F. Platt, *J. Chem. Phys.*, **21**, 66 (1953).

Synthetic Studies on Phosphorylating Reagent. I. The Phosphorylation of Alcohols by Means of *N*-[2-(Dihydrogen phosphoroxy)-5-nitrobenzyl]pyridinium Hydroxide

Yoshihiko TAGUCHI, Yoshitaka MUSHIKA, and Naoto YONEDA

Research Laboratory of Applied Biochemistry, Tanabe Seiyaku Co., Ltd., 16–89, Kashima-3-chome, Yodogawa-ku, Osaka 532

(Received December 28, 1974)

The phosphorylation of alcohols by means of *N*-[2-(dihydrogen phosphoroxy)-5-nitrobenzyl]pyridinium hydroxide (**3**), which was prepared from 2-(chloromethyl)-4-nitrophenyl phosphorodichloridate (**1**) through two steps, was demonstrated. Alcohol with a tertiary amino group in its alkyl moiety was readily phosphorylated with **3** to afford the aminoalkyl dihydrogen phosphate in good yield. On the other hand, the phosphorylation of the usual neutral alcohol proceeded only in the presence of a strong base such as triethylamine to give the corresponding alkyl dihydrogen phosphate (**9**). Thus, several alkyl dihydrogen phosphates **9** were prepared. In this phosphorylation, the formation of alkyl 2-hydroxy-5-nitrobenzyl ether (**10**) was also observed.

In our previous papers,[1–5] we reported on the preparation of various phosphoric esters by means of 2-(chloromethyl)-4-nitrophenyl phosphorodichloridate (**1**), a phosphorylating reagent with an activatable protecting group, and demonstrated that the reagent is very useful for the preparation of alkyl dihydrogen phosphate and dialkyl hydrogen phosphate. However, the reagent could not be utilized in the phosphorylation of amino alcohol because of the complicated reaction with the basic part of the reactant.

The present study was undertaken with an aim to explore a more versatile reagent which could be used in the phosphorylation of amino alcohol. An inner salt of *N*-[2-(dihydrogen phosphoroxy)-5-nitrobenzyl]-pyridinium hydroxide (**3**), which has no active chlorine atom, was chosen as a candidate for this purpose, since, in our earlier study,[4] the inner salt of *N*-[2-(alkyl hydrogen phosphoroxy)-5-nitrobenzyl]pyridinium hydroxide was shown to retain its reactivity toward alcohol.

The inner salt **3** was obtained quantitatively by the reaction of pyridine with 2-(chloromethyl)-4-nitrophenyl dihydrogen phosphate (**2**) which was prepared by the hydrolysis of **1**. The isolation of pure crystals of **3** was somewhat difficult because of the instability upon recrystallization from aqueous ethanol. The reaction of a stoichiometric amount of 2-(*N*,*N*-diethylamino)ethanol (**4**) with **3** in pyridine at 90—95 °C afforded a mixture of the resinous compounds, which were characterized on paper chromatography (PPC) as a phenolic polymer and an inorganic polyphosphoric acid. However, when a 10-equivalent amount of **4** was used, 2-(*N*,*N*-diethyl-

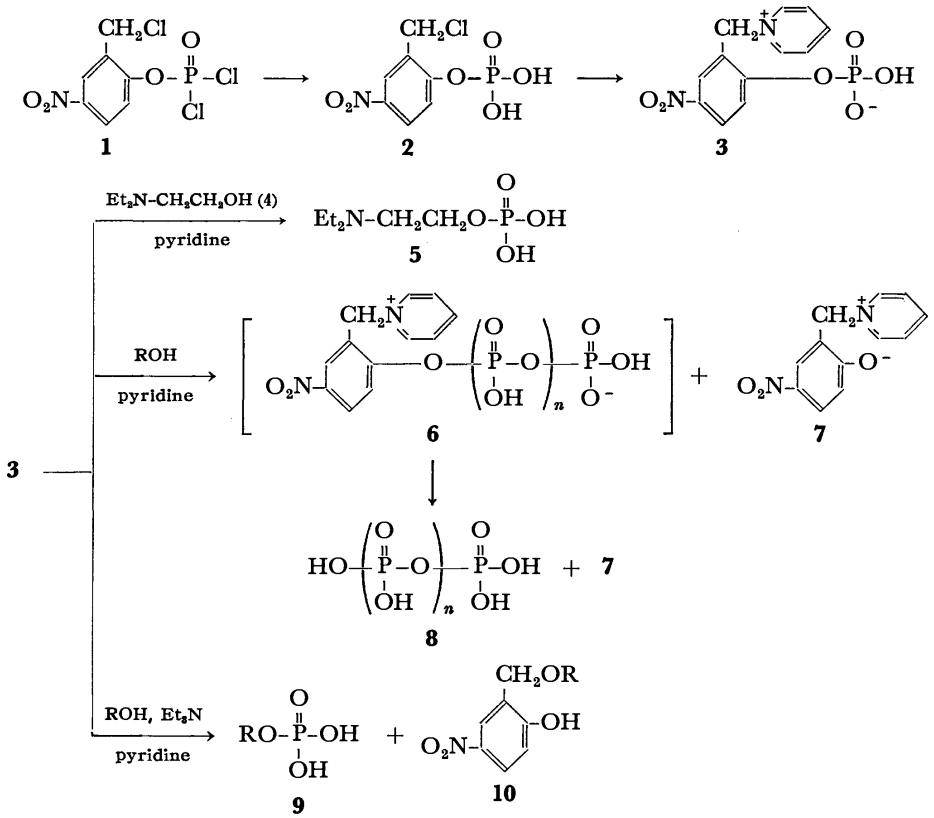

Scheme 1.

Table 1. Reaction of alcohol with **3** in the presence of triethylamine

R	Alkyl dihydrogen phosphate (**9**)[a]				Ethereal derivative (**10**)			
	Compd No.	Yield[b] (%)	Mp (°C)	R_f[c]	Compd No.	Yield[b] (%)	Mp (°C)	R_f[c]
Ethyl	**9a**	46	163—164	0.24	**10a**	36	83—85	0.85
n-Butyl	**9b**	40	138—140	0.36	**10b**	31	54—55	0.85
s-Butyl	**9c**	39	159—160	0.36	**10c**	44	54—55	0.85
n-Amyl	**9d**	31	137—139	0.49	**10d**	46	51—52	0.82
n-Dodecyl	**9e**	45	131—133	0.67	**10e**	30	49—50	0.85
Cyclohexyl	**9f**	55	169—170	0.40	**10f**	56	62—63	0.82
Benzyl	**9g**	53	168—169	0.35	**10g**	58	89—91	0.77

a) Alkyl dihydrogen phosphates were isolated as monoanilinium salt. b) Yields of **9** and **10** were based on 2-(chloromethyl)-4-nitrophenyl dihydrogen phosphate (**2**). c) Solvent A was used.

amino)ethyl dihydrogen phosphate (**5**) was obtained in 71% yield.

The elemental analysis and the downfield shift of the methylene protons adjacent to the phosphate group[6] in the nuclear magnetic resonance (NMR) spectrum supported the structure of the product. On the other hand, the phosphorylation of 2-aminoethanol resulted in the multiformation of intractable compounds. The reaction of an alcohol which does not contain a *tert*-amino residue, such as ethanol and benzyl alcohol, did not proceed at all under similar conditions, however, inorganic polyphosphoric acid and *N*-(2-hydroxy-5-nitrobenzyl)pyridinium hydroxide (**7**) were produced as the main products. This unexpected result could be explained by the self-condensation reaction of **3**, since the nucleophilicity of the second dissociable hydroxyl group in the phosphate group is larger than that of alcohol. An inner salt of *N*-[2-(polyhydrogen polyphosphoroxy)-5-nitrobenzyl]pyridinium hydroxide (**6**) formed would then be hydrolysed to give inorganic polyphosphoric acid (**8**) and **7** during work-up. Therefore, triethylamine was added to the reaction system in order to prevent the self-condensation.

First, the reaction with two equivalent amounts of ethanol was carried out in pyridine in the presence of three equivalents of triethylamine at 90—95 °C, however, ethyl dihydrogen phosphate (**9a**) was obtained in only 11% yield, followed by a considerable amount of the resinous phenolic polymer and inorganic polyphosphoric acid. Therefore, the reaction with ten equivalents of ethanol and three equivalents of triethylamine was attempted under the same conditions. The phosphorylation of ethanol occurred readily; ethyl dihydrogen phosphate (**9a**) was isolated in an improved yield as its monoanilinium salt, which was identified with an authentic sample on infrared (IR) spectrum. Similar results (Table 1) were obtained in the cases of other primary and secondary alcohols, such as *n*-butyl, *s*-butyl, *n*-dodecyl, cyclohexyl, and benzyl alcohol.

In these reactions, nearly equal amounts of alkyl 2-hydroxy-5-nitrobenzyl ethers (**10a-g**) to **9a-g** were isolated. The products were identified by a direct comparison with each authentic specimen, which was prepared by an alternate method.[2,7-8] It was considered that the formation of **10** is closely related to the mechanism of the phosphorylation. One conceivable mechanism (Path A) is the S_N2-type phosphorylation

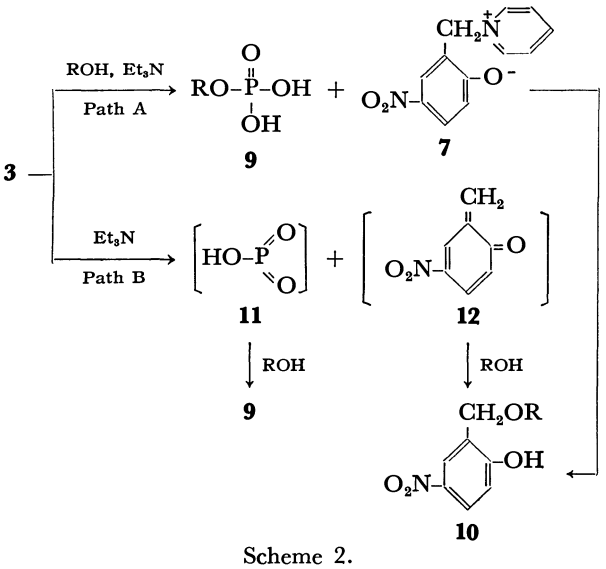

Scheme 2.

with alcohol, followed by the formation of alkyl 2-hydroxy-5-nitrobenzyl ether (**10**) *via* pyridinium compound **7** formed.

However, this seemed not to be the case in view of the following results: the phosphorylation with **3** required a large excess of alcohol in order to improve the yield of the phosphate **9a-g**, whereas the same type of phosphorylation[1-3] with *N*-[2-(alkyl hydrogen phosphoroxy)-5-nitrobenzyl]pyridinium hydroxide, which probably proceeded through S_N2 mechanism, has been shown to proceed satisfactorily with a stoichiometric amount of alcohol; the formations of large amounts of inorganic polyphosphoric acid and the phenolic polymer were observed when the reaction was run with a stoichiometric amount of alcohol. Another mechanism (Path B) involves the decomposition of the reagent **3** to the quinomethide (**12**) and methaphosphoric acid (**11**) under the present reaction conditions and subsequent condensations with alcohol giving alkyl ether **10** and alkyl dihydrogen phosphate **9**, respectively. This mechanism is supported not only by the above results, but also by the formation of **9** and **10** in nearly equal amounts in all cases. The quinomethide **12** has been proposed by Horton and Koshland[9] as an active species in the reaction of 2-(bromomethyl)-4-nitrophenol with tryptophan. In view of the equivalence of the requisite structure, it seems likely that the same intermediate is generated also in the present reaction.

From these considerations, Path B is a plausible mechanism of this phosphorylation.

In conclusion, it has been shown that a new compound, *N*-[2-(dihydrogen phosphoroxy)-5-nitrobenzyl]-pyridinium hydroxide **3** has phosphorylating ability toward the alcohol in the presence of triethylamine and toward the *tert*-amino alcohol in the absence of the base. Further modification of the reagent would be necessary to improve its efficiency as a phosphorylating reagent.

Experimental

Paper chromatography was carried out by ascending technique using Toyo Roshi No. 51 paper. Solvent systems used were: isopropyl alcohol-concd NH_4OH–H_2O (7:1:2 v/v) (Solvent A) and *n*-butanol–AcOH–H_2O (5:1:4 v/v, upper layer) (Solvent B). UV lamp (254 nm) and Hanes–Isherwood reagent[10] were used for the detection of spots on paper chromatogram. Melting points are uncorrected and were determined on a Yamato apparatus MP-21. NMR spectra were determined on Hitachi Perkin-Elmer R-20A instrument (Me_4Si). IR spectra were determined on a Shimadzu IR-27G spectrometer.

Materials. Alcohols, amines, and solvents were purified and dried by the ordinary procedures.

2-(Chloromethyl)-4-nitrophenyl phosphorodichloridate (**1**) was prepared as described in the previous paper.[2]

2-(Chloromethyl)-4-nitrophenyl Dihydrogen Phosphate (2) (Improved Procedure).[2] To a solution of 3.04 g, (0.01 mol) of 2-(chloromethyl)-4-nitrophenyl phosphorodichloridate (**1**) in 15 ml of acetone was added 15 ml of cold water in one portion with stirring under ice-cooling and the stirring was continued at a temperature below 15 °C for 30 min. After concentration of the reaction mixture to dryness under reduced pressure, the residue was crystallized with $CHCl_3$ to afford 2.28 g (85%) of the phosphate **2** as a white powder; mp 137—139 °C. The product was identified with an authentic sample by the criteria of PPC and NMR spectroscopy.

Inner Salt of N-[*2-(Dihydrogen phosphoroxy)-5-nitrobenzyl*]*pyridinium Hydroxide (3).* To 16 ml (0.20 mol) of anhydrous pyridine was added 5.35 g (0.02 mol) of 2-chloromethyl-4-nitrophenyl dihydrogen phosphate (**2**) with stirring at room temperature. After being allowed to stand at room temperature overnight, the reaction mixture was diluted with 30 ml of acetone, the precipitate was then collected by filtration. The precipitate was recrystallized from 50% ethanol to afford 3.94 g (64%) of analytically pure **3** as white needles; mp 204—205 °C (decomp.); R_f 0.28 (Solvent A) and 0.61 (Solvent B); UV (H_2O, nm): 261.5 (log ε 3.90), 267.5 (3.90) and 303 (3.96); IR (Nujol, cm^{-1}): 2700—2300 (>$\overset{+}{N}$<), 1630 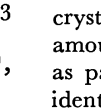 , 1515, 1348 (NO_2), 1280 (P=O), and 1040 (P–O–C). Found: C, 46.39; H, 3.86; N, 8.97%. Calcd for $C_{12}H_{11}N_2O_6P$: C, 46.46; H, 3.57; N, 9.03%.

2-(N,N-Diethylamino)ethyl Dihydrogen Phosphate (5).[11] To a reaction mixture containing 0.01 mol of **3**, which was prepared from 2.67 g (0.01 mol) of **2** and 20 ml of anhydrous pyridine, was added 11.7 g (0.10 mol) of 2-(*N,N*-diethylamino)ethanol (**4**), and then the mixture was heated at 90—100 °C for 7 hr with stirring. After concentration of the reaction mixture to dryness under reduced pressure, water (60 ml) was added to the residue. A water-insoluble, gummy compound was removed by filtration, and the filtrate was passed through a column (1.5 cm×60 cm) of Amberlite IR 120 resin (H^+ form). The column was washed with water until the washings became neutral to litmus. The column was eluted with 5% ammonia. The eluent was concentrated to dryness under reduced pressure, and an aqueous solution of the residue was applied to a column (1.5 cm×50 cm) of Amberlite IRC 50 resin (H^+ form). The column was sufficiently washed with water. The combined original eluent and washings were evaporated to dryness under reduced pressure, and the colorless viscous residue was crystallized with acetone to afford 1.40 g (71%) of 2-(*N,N*-diethylamino)ethyl dihydrogen phosphate (**5**) as white powder; mp 155—159 °C. Recrystallization from ethanol afforded analytically pure **5** as hygroscopic white powder; mp 159—160 °C; R_f 0.23 (Sovlent A); IR (Nujol, cm^{-1}): 2600—2330 (=$\overset{+}{N}$H–), 1270 (P=O), 1180 and 1085 (P–O–C alkyl and organic phosphoric salt); NMR (D_2O, ppm): 1.54 (t, 6H, CH_3×2), 3.36—3.73 [m, 6H, $(CH_3-C\underline{H}_2)_2N-C\underline{H}_2-$], 4.42 (m, 2H, $-CH_2O-$). Found: C, 36.20; H, 8.32; N, 7.05%. Calcd for $C_6H_{16}NO_4P$: C, 36.55; H, 8.18; N, 7.10%.

Reaction of Alcohol with 3. Typical Procedure; Reaction with Benzyl Alcohol: To a reaction mixture containing 0.01 mol of **3**, which was prepared from 2.67 g (0.01 mol) of **2** and 20 ml of anhydrous pyridine, was added 10.81 g (0.10 mol) of benzyl alcohol and 2.8 ml (0.02 mol) of triethylamine, then the reaction mixture was heated at 90—100 °C for 10 hr. After concentration of the reaction mixture to dryness under reduced pressure, an aqueous solution of the residue (H_2O, 50 ml) was extracted with three 20 ml portions of ether. The aqueous layer was passed through a column (1.0cm×50cm) of Amberlite IR 120 resin (pyridinium form), and the column was washed with water. The combined original eluent and washings were neutralized with a small amount of pyridine and were evaporated to dryness under reduced pressure. To the acetone solution of the residue was added 1.6 ml of aniline, and the precipitate was collected by filtration. The precipitate was washed with a small amount of water to remove the salt of inorganic phosphoric acid, and then the insoluble precipitate was recrystallized from 95% ethanol to afford 1.49 g (53%) of monoanilinium salt of **9 g** as white needles; mp 168—169 °C. The product was identified with an authentic specimen by a comparison of its R_f-value of PPC and the IR spectrum and by the mixed melting point test.

The combined ethereal extracts were again extracted with three 20 ml portions of 2M-NaOH. After acidification of the alkaline layer with 10% HCl, the aqueous layer was extracted with three 20 ml portions of ether. The combined ethereal extracts was evaporated to dryness, and the residue was extracted with 100 ml of a boiling mixture of benzene and *n*-hexane (1:3 v/v). After removal of an insoluble gummy substance by decantation, the solution was decolorized with charcoal and concentrated to dryness. The residue was crystallized from boiling *n*-hexane which contained a small amount of benzene to afford 1.58 g (58%) of the ether **10g** as pale yellow prisms; mp 89—91 °C. The ether **10g** was identified with an authentic specimen which was prepared by the established procedure.[8]

In a similar manner, alcohols, such as ethyl, *n*-butyl, *s*-butyl, *n*-amyl, *n*-dodecyl, and cyclohexyl alcohol, were treated with **3** in the presence of triethylamine to afford the corresponding alkyl dihydrogen phosphates **9a—f** and alkyl 2-hydroxy-5-nitrobenzyl ethers **10a—f**.

We wish to express our thanks to Professors Teruaki Mukaiyama and Tsujiaki Hata, and Drs. Takashi Takayanagi, Ichiro Chibata, Muneji Miyoshi and Ichizo Inoue for their valuable discussions and suggestions.

References

1) Y. Mushika and N. Yoneda, *Chem. Pharm. Bull.* (Tokyo), **19**, 696 (1971).
2) T. Hata, Y. Mushika, and T. Mukaiyama, *J. Amer. Chem. Soc.*, **91**, 4532 (1969).
3) T. Hata, Y. Mushika, and T. Mukaiyama, *Tetrahedron Lett.*, **1970**, 3505.
4) Y. Mushika, T. Hata, and T. Mukaiyama, This Bulletin, **44**, 232 (1971).
5) Y. Mushika and N. Yoneda, *Chem. Pharm. Bull.* (Tokyo), **19**, 687 (1971).
6) I. Feldman and R. P. Agarwal, *J. Amer. Chem. Soc.*, **90**, 7329 (1968).
7) T. Obata and T. Mukaiyama, *J. Org. Chem.*, **32**, 1063 (1967).
8) V. I. Starrovskaya, *Zh. Obshch. Khim.*, **24**, 2068 (1954). We obtained **10** by the reaction of 2-(chloromethyl)-4-nitrophenol with alcohols in the presence of triethylamine, and its details will be reported elsewhere.
9) H. T. Horton and D. E. Koshland, Jr., *J. Amer. Chem. Soc.*, **87**, 1126 (1966).
10) C. S. Hanes and F. A. Isherwood, *Nature*, **164**, 1107 (1949).
11) E. Cherbuliez and J. Robinowitz, *Helv. Chim. Acta*, **41**, 1168 (1958). They have described that the phosphate **5** was a white crystal having a melting point of 118—123 °C and its crystallization was difficult. However, by improving this purification, authers obtained a hygroscopic white crystal, mp 159—160 °C, as an authentic sample.

Synthetic Studies on Phosphorylating Reagent. IV. A Novel Synthesis of Nucleoside-3′,5′ Cyclic Phosphates by the Use of 2-(*N*,*N*-Dimethylamino)-4-nitrophenyl Phosphate

Yoshihiko TAGUCHI and Yoshitaka MUSHIKA

Research Laboratory of Applied Biochemistry, Tanabe Seiyaku Co., Ltd., 16–89, Kashima-3-chome, Yodogawa-ku, Osaka 532

(Received December 28. 1974)

A novel method for the synthesis of nucleoside-3′,5′ cyclic phosphate has been investigated. The intermediates, nucleoside-5′ 2-(*N*,*N*-dimethylamino)-4-nitrophenyl phosphates (**3a—d**), were prepared in good yields by the condensation of unprotected nucleosides with 2-(*N*,*N*-dimethylamino)-4-nitrophenyl phosphate (**2**), using dicyclohexylcarbodiimide (DCC) in dimethylformamide (DMF). Treatment of the intermediates **3a—d** with acetic acid in boiling pyridine under high dilution condition gave nucleoside-3′,5′ cyclic phosphates in fairly good yields and small amount of other nucleotides, whereas nucleoside-2′,3′ cyclic phosphate was obtained by the reaction in DMF at 100 °C. An attempt at the direct synthesis of the cyclic nucleotide by refluxing the reaction mixture of unprotected nucleoside with DCC and **2** in pyridine was also successful to afford the similar results as in the stepwise procedure.

Adenosine-3′,5′ cyclic phosphate has been recognized as an intracellular second messenger of hormone action, and some of the various biological properties attributed to adenosine-3′,5′ cyclic phosphate can be explained by the stimulation of these protein kinases.

A number of procedures[1–4] have been applied to the synthesis of nucleoside-3′,5′ cyclic phosphates. Lipkin *et al.*[1] obtained adenosine-3′,5′ cyclic phosphate by the barium hydroxide-catalyzed degradation of adenosine-5′ triphosphate. Intramolecular cyclization of nucleoside-5′ phosphate was carried out by Smith *et al.*[2] using dicyclohexylcarbodiimide (DCC) in pyridine under high dilution condition. Borden and Smith[3] reported the synthesis of nucleoside-3′,5′ cyclic phosphate from nucleoside-5′ 4-nitrophenyl phosphates with potassium *t*-butoxide in dimethyl sulfoxide. Recently, Mukaiyama and Hashimoto[4] obtained nucleoside-3′,5′ cyclic phosphate in a similar manner to the method of Smith *et al.* except using triphenylphosphine and 2,2′-dipyridyl disulfide as condensation reagents.

In previous papers,[5–7] we reported that a new phosphorylating reagent, 2-(*N*,*N*-dimethylamino)-4-nitrophenyl phosphate (**2**), which has an activatable protecting group, reacted with various alcohols and amino alcohols to afford the corresponding alkyl dihydrogen phosphates and amino alkyl dihydrogen phosphates, respectively. The acid catalyzed phosphorylations of unprotected nucleosides with just one equiv. of this reagent **2** gave the corresponding nucleoside-5′ phosphates selectively.

In view of our success in the direct synthesis of nucleoside-5′ phosphate from unprotected nucleoside, it was considered that the DCC coupling reaction of unprotected nucleoside with one molar equivalent of **2** would give nucloside-5′ 2-(*N*,*N*-dimethylamino)-4-nitrophenyl phosphate (**3a—d**) selectively, probably because of the bulkiness of the reagent, and subsequently its intramolecular phosphorylation would afford nucleoside-3′,5′ cyclic phosphate. In this communication, we describe a new synthetic method of nucleoside-3′,5′ cyclic phosphate by the use of **2**.

Initial attempt was carried out with adenosine. One mmole of adenosine in dimethylformamide (DMF) was allowed to react with the pyridinium salt of **2** (1.5 mmol) and DCC (2 mmol) at room temperature. After the usual work-up, the column chromatography of the reaction products using DEAE Sephadex afforded adenosine-5′ 2-(*N*,*N*-dimethylamino)-4-nitrophenyl phosphate (**3a**) in 79% yield and adenosine-2′,3′ cyclic phosphate-5′ 2-(*N*,*N*-dimethylamino)-4-nitrophenyl phosphate (**4a**) in 12% yield. The former product could be crystallized as calcium salt, though a good elemental analysis was not obtained. The NMR spectrum in D_2O showed the presence of the 2-(*N*,*N*-dimethylamino)-4-nitrophenyl group and the 5′-methylene protons at 4.32 ppm, which usually appears at lower field than those of the original nucleoside upon 5′-*O*-phosphorylation.[8] Comparison of the mobility in paper electrophoresis (PEP) with those of the analogous nucleotides (Table 4) also supported the assigned structure. The latter product was crystallized as lithium salt pentahydrate, mp 242—243 °C. The NMR spectrum in D_2O exhibited the 2′,3′-protons at 5.16—5.65 ppm and the 4′,5′-protons at 4.23—4.67, showing again downfield shift upon phosphorylation. In addition, the structures of both compounds were ascertained by the consideration of the following chemical reactions. Treatment of 2′,3′-*O*-isopropyl-

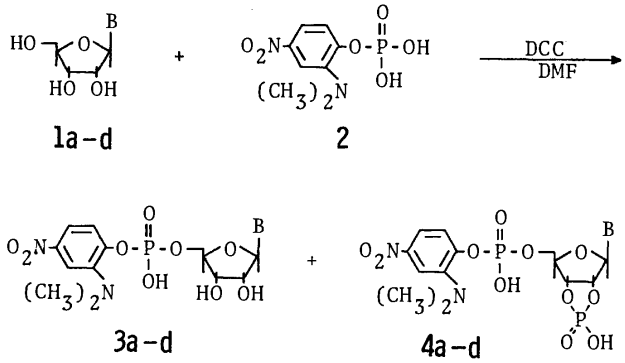

a, B=adenine, **b**, B=guanine
c, B=uracil, **d**, B=cytosine

Scheme 1.

ideneadenosine (**5**) with the triethylammonium salt of **2** and DCC under the same conditions gave a sole nucleotide, 2′,3′-*O*-isopropylideneadenosine-5′ 2-(*N*,*N*-dimethylamino)-4-nitrophenyl phosphate (**6**), having R_f value of 0.81 in Solvent A on paper partition chromatography (PPC). Subsequent deblocking with 1M-hydrochloric acid afforded a mixture of **3a** and adenosine-5′ phosphate (**7**), which were characterized by PPC and PEP. On the other hand, when 5′-monomethoxytrityladenosine (**8**) was allowed to react with the triethylammonium salt of **2** and DCC under the same conditions, the liberation of a significant amount of 2-(*N*,*N*-dimethylamino)-4-nitrophenol (**10**) was observed, showing the occurrence of intramolecular cyclization after the phosphorylation of **8** at either the 2′- or 3′-hydroxyl group. In fact, usual work-up and DEAE Sephadex column chromatography afforded 5′-monomethoxytrityladenosine-2′,3′ cyclic phosphate

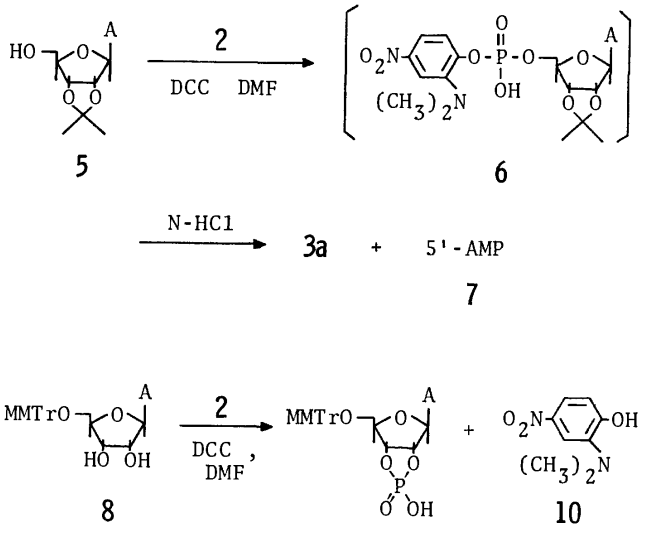

Scheme 2.

(**9**) quantitatively. This ready formation of the 2′,3′-cyclic phosphate linkage under mild conditions contrasts with the conversion of nucleoside-2′(3′) 4-nitrophenyl phosphate into the corresponding 2′,3′-cyclic nucleotide under rather vigorous conditions,[3,9] and also with the studies of Agarwal and Dhar.[10] Condensation reactions of other nucleosides underwent similarly to give the corresponding nucleotides, **3b—d** and **4b—d** (Table 1).

Table 1. Products in the reaction of nucleosides with **2**

Nucleoside	Products (Yield %)[a]		
	3	**4**	Recovered nucleoside
Adenosine	79	12	9
Guanosine	99	0[b]	1
Uridine	49	7[b]	44
Cytidine	62	6[b]	32

a) Yields were estimated from the total optical densities at their absorption maxima corresponding to the each products. b) The yields of these products were calculated from the additive optical densities of corresponding **1** and **2**.

DMF was found to be a suitable solvent for this reaction, whereas the use of pyridine resulted in the recovery of the unreacted nucleoside. Next, the intramolecular phosphorylation of **3** to nucleoside-3′,5′ cyclic phosphate was attempted in pyridine under high dilution condition. The triethylammonium salt of **3** was so soluble in anhydrous pyridine that the use of 4-morpholine-*N*,*N*′-dicyclohexylcarboxamidine was unnecessary. The cyclization was carried out by the dropwise addition of a solution of **3** and acetic acid in anhydrous pyridine to a large amount of boiling pyridine that is enough to make high dilution condition. In this reaction, acetic acid would serve as a proton catalyst, converting the dimethylamino group to the electron-withdrawing group. Thus, when **3a** was treated under these conditions, adenosine-3′,5′ cyclic phosphate (**12a**) was obtained in 61% yield, the other porducts being adenosine-5′ phosphate, adenylyl-(5′→5′)-adenosine, and dephosphorylated adenosine. These products were separated by linear gradient chromatography with DEAE Sephadex and identified with the authentic samples by the criteria of PPC and PEP. Similar result was obtained in the cyclization reaction with guanosine-5′ 2-(*N*,*N*-dimethylamino)-4-nitrophenyl phosphate (**3b**) (Table 2). Further attempt was made to improve this method

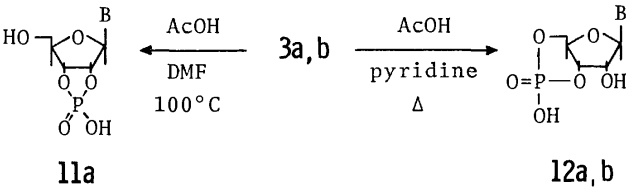

Scheme. 3.

Table 2. Products composition in the cyclization of **3a,b** in pyridine

Products from **3a**	Yield %[a]	Products from **3b**	Yield %[a]
12a	61	**12b**	52
5′-AMP (**7**)	8	5′-GMP	3
A_pA (5′→5′)	13	G_pG (5′→5′)	22
1a	12	**1b**	21

a) Yields were estimated from the total optical densities at their absorption maxima corresponding to those of the authentic samples.

without isolation of the intermediate **3**. In a typical run, the reaction of one equivalent amount of **2** and two equivalents of adenosine with DCC was carried out in DMF at room temperature. Treatment of this reaction mixture in DMF at 100 °C under high dilution condition afforded a major product with the same PEP mobility as adenosine-(2′,3′ and 3′,5′) cyclic phosphates (**11a** and **12a**). The yield of this material was estimated spectrophotometrically to be 75%. On mechanistic consideration, it seemed likely that this product was adenosine-3′,5′ cyclic phosphate (**12a**). However, this proved not to be the case: that the product was indeed adenosine-2′,3′ cyclic phosphate (**11a**) followed from its hydrolysis properties. When the product was treated with Dowex-50 (H^+ form) in water, it was readily converted into a mixture of adenosine-(2′ and

Table 3. Products composition in the direct synthesis of **12a—d**

Compd from **1a**	Yield %[a]	Compd from **1b**	Yield %[a]	Compd from **1c**	Yield %[a]	Compd from **1d**	Yield %[a]
12a	64	**12b**	51	**12c**	58	**12d**	32
5′-AMP	12	5′-GMP	6	5′-UMP	17	5′-CMP	11
A_pA (5′→5′)	12	G_pG (5′→5′)	11	U_pU (5′→5′)	2	C_pC (5′→5′)	2
1a	111	**1b**	128	**1c**	120	**1d**	128

a) Yields were based on the phosphorylating agent **2**, and estimated from the total optical densities at the absorption maxima corresponding to those of the authentic samples.

3′) phosphates. No adenosine-5′ phosphate could be detected in the products. Reese and Khwaja[11] have observed the same phenomenon in the intramolecular phosphorylation of adenosine-5′ 2-hydroxyphenyl phosphate in pyridine, and proposed the pyridine-promoted dephosphorylation, followed by the phosphorylation of the nucleoside thus produced, as a possible mechanism. However, this would not be the case with ours, because the present reaction was run in DMF and the reagent has no participating *O*-hydroxyl group. The mechanism of this reaction remains as a matter of further investigation.

Finally, the cyclization reaction proceeded in the desired direction by high dilution treatment in boiling pyridine. Thus, after concentration of the reaction mixture, the original solvent was replaced by pyridine, and the solution was added dropwise to the boiling pyridine in the presence of acetic acid under high dilution condition. The reaction mixture was worked up as described in the Experimental section and subjected to DEAE Sephadex column chromatography with a linear gradient of triethylammonium bicarbonate to give product compositions similar to those in the stepwise procedure. All the compounds listed in the Table 3 were identified with authentic samples by PPC and PEP, and the yields were estimated spectrophotomotrically.

This reagent **2** with its high solubility and selectivity would provide a useful tool for the preparations of nucleoside-3′,5′ cyclic phosphate and nucleoside-2′,3′ cyclic phosphate.

Experimental

General Methods. Reagent grade pyridine was used after being dried over calcium hydride or Linde 4-A Molecular Sieves for several days. Solutions were concentrated to dryness at 30 to 40 °C using either a rotary evaporator or, when anhydrous conditions were required, an oil pump equipped with Dry Ice trap.

Paper chromatography was carried out using the descending technique on Toyo Roshi No. 51A paper. The solvent systems used were: isopropyl alchohol–concentrated ammonia–water (7:1:2) (Solvent A); *n*-butyl alcohol–acetic acid–water (5:2:3) (Solvent B). Paper electrophoresis was performed at pH 7.5 (0.05 M triethylammonium bicarbonate, 900 V/40 cm). Chromatographic and electrophoretic mobilities are recorded in Table 4. Melting points are uncorrected and were determined on a Yamato apparatus MP-21. The NMR spectra were determined on a Hitachi Perkin-Elmer R-20A instrument (DSS). IR spectra were determined on a Shimadzu IR-27G spectrometer, and UV spectra, on a Hitachi EPS-3T spectrometer.

*Adenosine-5′ 2-(*N,N*-Dimethylamino)-4-nitrophenyl phosphate (3a)* Adenosine (0.27 g, 1 mmol) and the pyridinium salt of **2** (1.5 mmol) were treated with DCC (0.41 g, 2 mmol) in DMF (50 ml) for 24 hr at room temperature. The reaction mixture was concentrated to dryness and water (500 ml) was added. After the precipitate was removed by filtration, the filtrate was applied to a 1.8×60 cm column of DEAE Sephadex (HCO_3^-) which was eluted with a linear gradient of triethylammonium bicarbonate (4 l., 0.0005—0.1 M), and the elution was followed spectrophotometrically at 260 nm. A major peak (22460 OD units, 79%) of electrophoretically and chromatographically homogeneous adenosine-5′ 2-(*N,N*-dimethylamino)-4-nitrophenyl phosphate (**3a**) was first eluted and a small peak of adenosine-2′,3′ cyclic phosphate-5′ 2-(*N,N*-dimethylamino)-4-nitrophenyl phosphate (**4a**) (3410 OD units, 12%) was followed. The pooled peak of **3a** was evaporated to dryness and coevaporated several times with methanol. The residue was dissolved in water (10 ml), and a stoichiometric amount of calcium hydroxide was added. The solution was concentrated to dryness and the residue was crystallized from aqueous ethanol to give **3a** calcium salt, in pale yellow powder; mp 187—190 °C (decomp.); $\lambda_{max}^{H_2O}$ (pH 6.85 and 12.3) 259 nm, 292 (sh); (pH 1.55) 259; NMR (D_2O) 2.73 (s, 6, N-Me_2), 4.15—5.07 (m, 5, $C_2'H+C_3'H+C_4'H+C_5'H_2$), 5.97 (d, J=5 Hz, 1, $C_1'H$), 7.10—7.64 (m, 3, Ph), 8.03 and 8.16 ppm (2 s, 2, C_2H and C_8H). The fractions containing **4a** were evaporated to dryness and the residue was dissolved with methanol. The solution was treated with lithium chloride, and precipitation with acetone gave pale yellow powder; mp 242—243 °C (decomp.); $\lambda_{max}^{H_2O}$ (pH 6.85 and 12.3) 259 (28400) nm, 292 (sh) (10800); (pH 1.55) 259 (24200); NMR (D_2O) 2.74 (s, 6, N-Me_2), 4.23—4.68 (m, 3, $C_4'H+C_5'H_2$), 5.16—5.65 (m, 2, $C_2'H+C_3'H$), 6.27 (d, J=3.2 Hz, 1, $C_1'H$), 7.06—7.71 (m, 3, Ph), 8.09 and 8.23 ppm (2 s, 2, C_2H and C_8H). Found: C, 32.07; H, 4.43; N, 14.52%. Calcd for $C_{18}H_{19}N_7O_{11}P_2Li_2 \cdot 5H_2O$: C, 32.30; H, 4.52; N, 14.63%.

*Guanosine-5′ 2-(*N,N*-Dimethylamino)-4-nitrophenyl Phosphate (3b).* Guanosine (0.28 g, 1 mmol) and the pyridinium salt of **2** (1.5 mmol) were treated with DCC (0.41 g, 2 mmol) in DMF (50 ml) at room temperature for 24 hr. The reaction mixture was concentrated to dryness and water (500 ml) was added. After the precipitates was removed by filtration, the filtrate was applied to a 1.8×60 cm column of DEAE Sephadex (HCO_3^-), which was eluted with linear gradient of triethylammonium bicarbonate (4 l., 0.005—0.1 M). A major peak (27580 OD units, 99%) of electrophoretically and chromatographically homogeneous guanosine-5′ 2-(*N,N*-dimethylamino)-4-nitrophenyl phosphate (**3b**) was eluted. The by-product **4b** was not detected in the products. The pooled peak of **3b** was evaporated to dryness and coevaporated several times with methanol. The residue was dissolved in water (10 ml) and a stoichiometric amount of calcium hydroxide was added. The solution was concentrated to dryness and the residue was crystallized from aqueous ethanol to give **3b** calcium salt, in pale yellow powder; mp 193—196 °C (decomp.); $\lambda_{max}^{H_2O}$ (pH 6.85) 254.5 nm; (pH 1.55) 258.5, 269 (sh); (pH 12.3)

Table 4. Paper chromatography and paper electrophoresis of nucleotides

Compound	R_f values		Electrophoretic mobility[a]
	Sovlent A	Solvent B	
Adenosine-5′ phosphate	0.07	0.16	1.00
Adenosine-2′(3′)phosphate	0.13		1.00
Adenosine-3′,5′ cyclic phosphate	0.35	0.31	0.66
Adenosine-2′,3′ cyclic phosphate	0.41		0.66
Adenosine-5′ 2-(*N*,*N*-dimethylamino)-4-nitrophenyl phosphate	0.62		0.49
Adenosine-2′,3′ cyclic phosphate-5′ 2-(*N*,*N*-dimethylamino)-4-nitrophenyl phosphate	0.50		0.83
P^1,P^2-Diadenosine-5′-pyrophosphate	0.10	0.07	0.79
Adenylyl-(5′→5′)-adenosine	0.18		0.51
Adenylyl-(3′→5′)-adenosine	0.14		0.51
Adenosine	0.52		0.09
5′-Monomethoxytrityladenosine	0.74		0
5′-Monomethoxytrityladenosine-2′,3′ cyclic phosphate	0.72		0.63
2′,3′-*O*-isopropylideneadenosine	0.88		0
2′,3′-*O*-isopropylideneadenosine-5′ 2-(*N*,*N*-dimethylamino)-4-nitrophenyl phosphate	0.81		0.48
Guanosine-5′ phosphate	0.03	0.20	1.00
Guanosine-2′(3′) phosphate	0.07		1.00
Guanosine-3′,5′ cyclic phosphate	0.25	0.26	0.68
Guanosine-2′,3′ cyclic phosphate	0.24		0.68
Guanosine-5′ 2-(*N*,*N*-dimethylamino)-4-nitrophenyl phosphate	0.52		0.42
Guanosine-2′,3′ cyclic phosphate-5′ 2-(*N*,*N*-dimethylamino)-dimethylamino)-4-nitrophenyl phosphate	0.27		0.70
Guanylyl-(5′→5′)-guanosine	0.04		0.53
Guanosine	0.28		0.15
Uridine-5′ phosphate	0.07	0.24	1.00
Uridine-2′(3′) phosphate	0.12		1.00
Uridine-3′,5′ cyclic phosphate	0.35	0.31	0.65
Uridine-2′,3′ cyclic phosphate	0.34		0.67
Uridine-5′ 2-(*N*,*N*-dimethylamino)-4-nitrophenyl phosphate	0.65		0.46
Uridine-2′,3′ cyclic phosphate-5′ 2-(*N*,*N*-dimethylamino)-4-nitrophenyl phosphate	0.44		0.72
Uridylyl-(5′→5′)-uridine	0.14		0.64
Uridine	0.49		0.17
Cytidine-5′ phosphate	0.09	0.08	1.00
Cytidine-2′(3′) phosphate	0.14	0.04	1.00
Cytidine-3′,5′ cyclic phosphate	0.38	0.32	0.63
Cytidine-2′,3′ cyclic phosphate	0.41		0.63
Cytidine-5′ 2-(*N*,*N*-dimethylamino)-4-nitrophenyl phosphate	0.64		0.44
Cytidine-2′,3′ cyclic phosphate-5′ 2-(*N*,*N*-dimethylamino)-4-nitrophenyl phosphate	0.52		0.71
Cytidylyl-(5′→5′)-cytidine	0.18		0.56
Cytidine	0.56		0.09
2-(*N*,*N*-Dimethylamino)-4-nitrophenol	0.80		0.70[b]
2-(*N*,*N*-Dimethylamino)-4-nitrophenyl phosphate	0.39		1.37[b]

a) The mobilities are relative to those of the parent nucleoside-5′ phosphate. b) The mobilities are relative to adenosine-5′ phosphate.

257; NMR (D_2O) 2.68 (s, 6, N-Me_2), 4.05—4.48 (m, 5, $C_2'H+C_3'H+C_4'H+C_5'H_2$), 5.74 (d, J=4.5 Hz, 1, $C_1'H$), 7.02—7.66 (m, 3, Ph), and 7.76 ppm (s, 1, C_8H).

*Uridine-5′ 2-(N,N-Dimethylamino)-4-nitrophenyl Phosphate (**3c**).* The procedure described for the preparation of guanosine-5′ 2-(*N*,*N*-dimethylamino)-4-nitrophenyl phosphate was applied. Uridine-5′ 2-(*N*,*N*-dimethylamino)-4-nitrophenyl phosphate (**3c**) calcium salt (11900 OD units, 49%) was obtained by crystallization from aqueous ethanol; mp> 260 °C; $\lambda_{max}^{H_2O}$ (pH 6.85) 258.5 nm; (pH 1.55) 268; (pH 12.3) 257; NMR (D_2O) 2.82 (s, 6, N-Me_2), 4.19—4.40 (m, 5, $C_2'H+C_3'H+C_4'H+C_5'H_2$), 5.70 (d, J=8.2 Hz, 1, C_5H), 5.88. (d, J=3 Hz, 1, $C_1'H$) and 7.35—7.93 ppm (m, 4, Ph+C_6H).

*Cytidine-5′ 2-(N,N-Dimethylamino)-4-nitrophenyl Phosphate (**3d**).* The procedure described for the preparation of guanosine-5′ 2-(*N*,*N*-dimethylamino)-4-nitrophenyl phosphate was applied. Cytidine-5′ 2-(*N*,*N*-dimethylamino)-4-nitrophenyl phosphate (**3d**) calcium salt (16300 OD units, 62%) was obtained by the crystallization from aqueous ethanol; mp>260 °C; $\lambda_{max}^{H_2O}$ (pH 6.85) 261 nm; (pH 1.55) 280; (pH 12.3) 253; NMR (D_2O) 2.87 (s, 6, N-Me_2), 4.14—4.35 (m, 5, $C_2'H+C_3'H+C_4'H+C_5'H_2$), 5.86 (d, J=7.5 Hz, 1, C_5H), 5.91 (d, J=3 Hz, 1, $C_1'H$), and 7.73—7.98 ppm (m, 4, Ph+C_6H).

Adenosine-3′,5′ Cyclic Phosphate (12a) from 3a. The triethylammonium salt of **3a** (0.2 mmol) was dissolved in pyridine (20 ml) containing acetic acid (12 mg, 0.2 mmol), and the solution was added dropwise to a boiling solution of pyridine (20 ml) over a 3-hr period. Heating was continued for further 3 hr and then the solution was concentrated to dryness. The residue was suspended in a mixture of water (10 ml) and ethyl acetate (20 ml). The aqueous layer was adjusted to pH 2 with 1M-hydrochloric acid. The solution was applied to a column of DEAE Sephadex (1.2×20 cm, HCO_3^-), which was eluted with a linear gradient of triethylammonium bicarbonate (4 l., 0.005—0.1 M) (fraction size, 20 g). Fractions containing **12a** (fractions 68—85) were concentrated to dryness. The residue was dissolved in 50% aqueous ethanol and adjusted to pH 2 with 10% hydrochloric acid. The precipitate was collected by filtration and washed with ethanol to give adenosine-3′,5′ cyclic phosphate monohydrate (43 mg, 61%), in white powder; $\lambda_{max}^{H_2O}$ (pH 2.0) 256 nm (ε 14500); (pH 7.0) 258 (14650); NMR [$D_2O+(NH_4)_2CO_3$] 4.23—5.25 (m, 5, $C_2'H+C_3'H+C_4'H+C_5'H_2$), 6.08 (s, 1, $C_1'H$), 8.09 and 8.15 ppm (2s, 2, C_2H and C_8H); ν_{max}^{nujol} 1690 (C=N), 1233 (P=O), 1202, 1081 cm^{-1} (P–O–C). This product was identified with an authentic specimen.

Guanosine-3′,5′ Cyclic Phosphate (12b) from 3b. The reaction was carried out as described for the preparation of **12a**. Guanosine-3′,5′ cyclic phosphate (1420 OD units, 55%) was isolated after the ion-exchange chromatography. This product was identified with an authentic specimen on PPC, PEP, and UV spectra; $\lambda_{max}^{H_2O}$ (pH 1.0) 256.5 nm (ε 11350); (pH 7.0) 254 (12950).

Adenosine-3′,5′ Cyclic Phosphate (12a) from Adenosine. Adenosine (2.7 g, 10 mmol) and the monotriethylammonium salt of **2** (5 mmol) were treated with DCC (2.05 g, 10 mmol) in DMF at room temperature for 24 hr. The reaction mixture was then concentrated to dryness. The residue was dissolved in pyridine (1 l) containing acetic acid (0.3 g, 5 mmol), and the insoluble dicyclohexylurea was removed by filtration. The solution was added dropwise to a boiling solution of pyridine (1 l) over a 3-hr period. Heating was continued for further 3 hr and then the solution was concentrated to dryness. The residue was suspended in a mixture of water (1 l) and ethyl acetate (500 ml). The aqueous layer was adjusted to pH 2 with 1M-hydrochloric acid. The solution was applied to a column of DEAE Sephadex (HCO_3^-, 1.5×60 cm). Elution was carried out using linear gradient with 0.005 M triethylammonium bicarbonate (2 l) in the mixing chamber and 0.1 M triethylammonium bicarbonate (2 l) in the reservoir. Fractions (20 g) were collected; adenosine-3′,5′ cyclic phosphate appeared in fractions 74—108. The combined fractions was concentrated to dryness and the solid residue was taken up in water (50 ml). The aqueous solution was evaporated to dryness to remove any residual triethylammonium bicarbonate. The residue was dissolved in 50% aqueous ethanol (10 ml) and adjusted to pH 2 with 1M-hydrochloric acid. The precipitates were filtered and washed with ethanol to give adenosine-3′,5′ cyclic phosphate (**12a**) monohydrate (1.11 g, 64%) as white powder. This product was identified with an authentic specimen.

Guanosine-3′,5′ Cyclic Phosphate (12b) from Guanosine. Guanosine (2.83 g, 10 mmol) and the monotriethylammonium salt of **2** (5 mmol) were treated with DCC (2.05 g, 10 mmol) in DMF as in the preparation of adenosine-3′,5′ cyclic phosphate. After usual work-up and ion-exchange chromatography, guanosine-3′,5′ cyclic phosphate (**12b**) (35400 OD units, 55%) was obtained in fractions 68 to 95. The product was homogeneous and identical with authentic guanosine-3′,5′ cyclic phosphate on PPC in Solvents A and B and on PEP.

Uridine-3′,5′ Cyclic Phosphate (12c) from Uridine. Uridine (2.44 g, 10 mmol) and the monotriethylammonium salt of **2** (5 mmol) were treated with DCC (2.05 g, 10 mmol) in DMF as in the preparation of adenosine-3′,5′ cyclic phosphate. After usual work-up and ion-exchange chromatography, uridine-3′,5′ cyclic phosphate (28600 OD units, 58%) was obtained in fractions 45 to 68. The nucleotide was homogeneous on PPC in Solvents A and B and on PEP.

Cytidine-3′,5′ Cyclic Phosphate (12d) from Cytidine. The procedure described for the preparation of adenosine-3′,5′ cyclic phosphate was applied. Cytidine-3′,5′ cyclic phosphate (**12d**) (14900 OD units, 32%) was obtained in fractions 45 to 72. The product was identified with an authentic specimen.

Adenosine-2′,3′ Cyclic Phosphate (11a) from Adenosine. Adenosine (5.4 g, 20mmol) and the monotriethylammonium salt of **2** (10 mmol) were treated with DCC (4.1 g, 20 mmol) in DMF (300 ml) at room temperature for 40 hr. To the reaction mixture, acetic acid 0.6 g (10 mmol) was added. The solution was added dropwise to a solution of DMF (30 ml) at 100 °C over a 3-hr period. Heating was continued for further 1 hr and the solution was concentrated to dryness. The residue was suspended in a mixture of water (1 l) and ethyl acetate (500 ml). The aqueous layer was applied to a column of DEAE Sephadex (HCO_3^-, 3.8×60 cm). Elution was carried out using linear gradient with 0.005 M triethylammonium bicarbonate (4 l) in the mixing chamber and 0.1 M triethylammonium bicarbonate (4 l) in the reservoir. The elution of nucleotides was followed spectrophotometrically at 260 nm. The fractions containing the major peak were combined and concentrated to dryness to give adenosine-2′,3′ cyclic phosphate (**11a**) monotriethylammonium salt (105140 OD units, 75.1%). This product was identified with an authentic specimen on PPC, PEP, and UV spectra.

We wish to express our thanks to Professor Yasumitsu Tamura, Drs. Takashi Takayanagi, Ichiro Chibata, Muneji Miyoshi and Ichizo Inoue for their valuable discussions and suggestions.

References

1) D. Lipkin, W. H. Cook, and R. Markham, *J. Amer. Chem. Soc.*, **81**, 6198 (1959).
2) M. Smith, G. I. Drummond, and H. G. Khorana, *ibid.*, **83**, 698 (1961).
3) R. K. Borden and M. Smith, *J. Org. Chem.*, **31**, 3247 (1966).
4) T. Mukaiyama and M. Hashimoto, *J. Amer. Chem. Soc.*, **94**, 8528 (1972).
5) Y. Taguchi and Y. Mushika, *Tetrahedron Lett.*, in press.
6) Y. Taguchi and Y. Mushika, *J. Org. Chem.*, in press.
7) Y. Taguchi and Y. Mushika, *Chem. Pharm. Bull.* (Tokyo), in press.
8) I. Feldman and R. P. Agarwal, *J. Amer. Chem. Soc.*, **90**, 7329 (1968).
9) K. Tanaka, *J. Biochem.* (Tokyo), **47**, 398 (1960).
10) K. L. Agarwal and M. M. Dhar, *Indian J. Chem.*, **2**, 493 (1962).
11) T. A. Khwaja and C. B. Reese, *Tetrahedron*, **27**, 6189 (1971).

Intramolecular Oxypalladation. Cyclization Reaction of 2-Allylphenols with Palladium Salts

Takahiro HOSOKAWA,* Hisao OHKATA, and Ichiro MORITANI

Department of Chemistry, Faculty of Engineering Science, Osaka University, Toyonaka, Osaka 560

(Received May 24, 1974)

The stoichiometric reaction of sodium salts of 2-allylphenols **1** with dichlorobis(benzonitrile)palladium(II) gives generally 2-substituted benzofurans **2** in moderate yields. The formation of cyclized products is explained by intramolecular oxypalladation followed by elimination of a palladium hydride species. The cyclization can be made catalytic by using palladium(II) acetate, cupric acetate, and oxygen.

Recently we found the intramolecular cyclization of 2-allylphenols into 2-substituted benzofurans by means of dichlorobis(benzonitrile)palladium(II).[1] The synthetic usefulness of the reaction is, however, limited by the expence of palladium salt since a stoichiometric amount of palladium salt is utilized. Accordingly, we have investigated to make the cyclization catalytic with respect to the metal salt.

The present paper describes a study of the stoichiometric and catalytic reactions of 2-allylphenols induced by palladium salts. It is also indicated that intramolecular oxypalladation intermediate plays an important role in the reaction.

Results and Discussion

Stoichiometric Cyclization Using Palladium Salts. (a) Dichlorobis(benzonitrile)palladium(II): Sodium salts of 2-allylphenols **1** were employed in the stoichiometric reaction in order to form a Pd–O bond easily *in situ*. An equimolecular amount of dichlorobis(benzonitrile)-palladium(II) was allowed to react with the sodium salts as reported previously.[1]

In general, the reaction gave 2-subsituted benzofurans **2** in moderate yields as shown in Table 1. 2,3-Dihydro-2-methyl-2-ethylbenzofuran (**3**), hydrogenated product of 2,3-dihydro-2-methyl-2-vinylbenzofuran (**2f**), was formed as a by-product in the reaction of 2-(β,γ-dimethylallyl)phenol (**1f**). The structures of products were deduced from elemental analyses and spectral data which are summarized in Tables 2. and 3. In these reactions no starting material was recovered, but polymeric residue was formed.

It was reported that the treatment of 2-allylphenol (**1a**) with palladium on charcol at 500—800 °C gave 2-methylbenzofuran (**2a**).[2] Compared with this, the present method provides a very convenient synthetic method of 2-substituted benzofurans.

The formation of 2-substituted benzofurans **2** is elucidated by the following Scheme 1** involving intramolecular oxypalladation to give the intermediate **6** followed by β-elimination of PdHCl species.[3]

In the oxypalladation intermediate **6**, where R = H or Ph, the hydrogen on the C-2 carbon is an only β-hydrogen to be eliminated with palladium. The elimination gives *exo*-methylenebenzofuran which even-

TABLE 1. STOICHIOMETRIC CYCLIZATION OF SODIUM SALTS OF ALLYLPHENOL **1** WITH $PdCl_2(PhCN)_2$

Allylphenol **1**	Product (Yield, %)
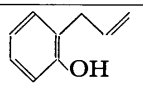 **1a**	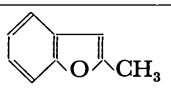 **2a** (31%)
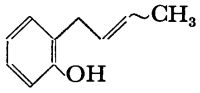 **1b**	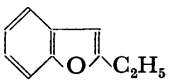 **2b** (26%)
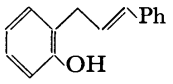 **1c**	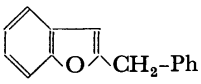 **2c** (53%)
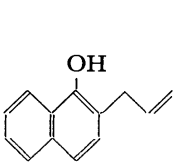 **1d**	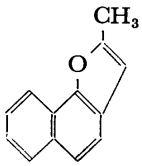 **2d** (22%)
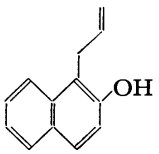 **1e**	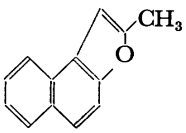 **2e** (42%)
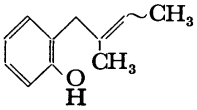 **1f**	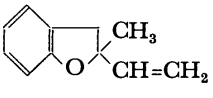 **2f** (41%) 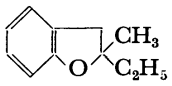 **3** (13%)
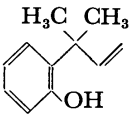 **1g**	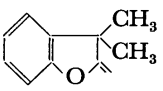 **2g** (40%)
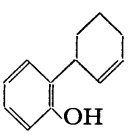 **1h**	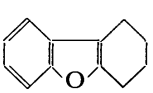 **2h** (19%) 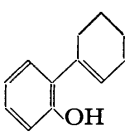 **4** (43%)

* To whom correspondence should be addressed.

** Although the complex **5** was not isolated, similar complexes are known to be formed by the treatment of 2-allylphenyldimethylarsine or 2-allylphenyldiphenylphosphine with dichlorobis(benzonitrile) palladium(II) (M. A. Bennet, W. R. Keen, and R. S. Nyholm, *Inorg. Chem.*, **7**, 556 (1968).).

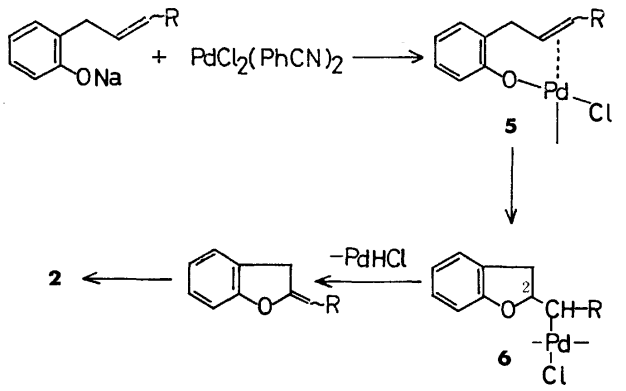

Scheme 1.

Table 2. Elemental analyses and mass spectra of products

Compd No.	Formula	Calcd (%) C	Calcd (%) H	Found (%) C	Found (%) H	m/e (M^+)
2a	C_9H_8O	81.79	6.10	81.79	5.95	132
2b	$C_{10}H_{10}O$	81.26	6.90	82.13	6.84	146
2c	$C_{15}H_{12}O$	86.51	5.81	86.63	5.91	208
2d	$C_{13}H_{10}O$	85.69	5.53	86.26	5.41	182
2e	$C_{13}H_{10}O$	85.69	5.53	85.47	5.48	182
2f	$C_{11}H_{12}O$	82.64	7.55	82.59	7.69	160
3	$C_{11}H_{14}O$	81.44	8.70	81.28	8.59	162
2g	$C_{11}H_{12}O$	82.46	7.55	81.98	7.54	160
2h	$C_{12}H_{12}O$	83.69	7.02	83.45	7.05	172
4	$C_{12}H_{14}O$	82.72	8.10	82.26	7.92	174

tually isomerizes to the thermodynamically stable 2-substituted benzofuran (**2a**—**2e**). However, exo-methylenebenzofuran **2g** is isolated in the reaction of **1g**.

In the case of **1f**, β-hydrogen elimination is only possible from the methyl group attached to α-carbon. The elimination gives **2f** as shown below.

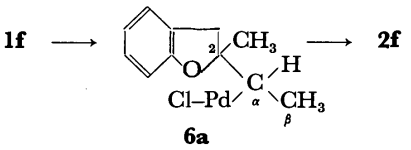

The product **3** can be considered to arise from hydrogenolysis of the Pd–C bond in **6a**.

In the case of **1b** (or **1h**), there are two possibilities for β-elimination of a palladium hydride in the intermediate **6** (R=CH_3). One is from the C-2 carbon leading to 2-ethylbenzofuran (**2b**), and the other from the methyl group to give 2,3-dihydro-2-vinylbenzofuran (**8a**) (*vide infra*). Similarly, dihydrobenzofuran **8b** is expected from **1h**. However, **8a** (or **8b**) would be isomerized to the thermodynamically more stable isomer **2b** (or **2h**) by the generated PdHCl species.[4] The species is known to prompt double bond isomerization.[5]

It was also found that 2-(1'propenyl)phenol (**7a**) and 2-hydroxystilbene (**7b**) gave 2-substituted benzofurans

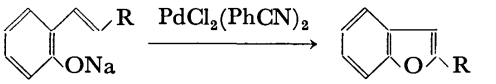

7a, R=CH_3 **2a**, R=CH_3 17%
7b, R=Ph **2i**, R=Ph 20%

Table 3. Spectral data of products

Compd No	C-3-H	NMR (δ, in CCl_4)[a] Side chain-H	Phenyl-H	IR (ν_{max}, cm^{-1})
2a	6.02(m, 1H)	2.36(d, 1H, J=1)	7.07(m, 4H)	1610, 1590, 1450, 1252, 1180, 1010
2b	6.17—6.30 (m, 1H)	1.34(t, 3H, J=8) 2.78(q, 2H, J=8)	6.8—7.4(m, 4H)	1604, 1590, 1250, 1050
2c	6.10(m, 1H)	3.91(broad s, 2H)	7.08(m, 6H)	1640, 1584, 1453, 1257, 940
2d	6.41(m, 1H)	2.48(d, 3H, J=1)	7.1—8.3(m, 6H)	1602, 1580, 1386, 1318, 1175, 1084
2e	6.55(m, 1H)	2.40(d, 3H, J=1)	7.2—7.9(m, 6H)	1601, 1580, 1464, 1443, 1386, 1269, 1184, 940
2f	3.04(broad s, 2H)	1.49(s, 3H) 4.98(dd, 1H, J=11, 2) 5.21(dd, 1H, J=16, 2) 6.00(dd, 1H, J=11, 16)	6.48—7.14(m, 4H)	1640, 1608, 1598, 1250, 1070
3	2.85—3.05 (m, 2H)	0.98(t, 3H, J=8) 1.42(s, 3H) 1.74(q, 2H, J=8)	6.46—7.15(m, 4H)	1602, 1250, 1020
2g		1.45(s, 6H) 4.76(s, 1H) 5.29(s, 1H)	6.81(dd, 2H, J=2) 7.24(dd, 2H, J=2)	1640, 1608, 1598, 1275, 1080, 1010, 880,
2h		1.68—2.2(m, 4H) 2.4—3.0(m, 4H)	6.85—7.55(m, 4H)	1640, 1615, 1585, 1280 1260, 1225, 1010
4		1.56—2.40(m, 6H) 5.22—5.50(m, 1H) 5.80—5.94(m, 1H)	6.65—7.16(m, 4H)	3500, 1640

a) Coupling constants, J, have the unite of Hz.

2a and **2i**, respectively, but in low yields.[6]

(b) Palladium(II) Acetate: Palladium(II) acetate was found to cause the cyclization of 2-allyl phenols **1** themselves. The treatment of **1b** with an equimolecular amount of palladium(II)acetate gave **2b**(20%) and **8a** (21%). In this case, however, these two isomers were primary products because the isomerization of **8a** to the stable isomer **2b** was eliminated by the following results. 1) The amounts of both products **2b** and **8a** increased with reaction time, and the product ratio of **2b** and **8a** did not change with time. 2) The treatment of **8a** under the same conditions resulted in the recovery of **8a**. 3) Even when **8a** was added to the starting substrate in advance, the amount of **2b** did not increase under the corresponding conditions. The difference of product composition between two stoichiometric cyclizations of **1b** would be due to the difference of palladium salts used.

Moreover, the composition of products **2b** and **8a** was found to vary with the relative amount of **1b** to palladium(II) acetate. As indicated in Table 4, the ratio of **8a** to **2b** increased with increase in the relative amount of **1b** to palladium(II) acetate. Further study is required to understand the result.

Table 4. Product composition in the reaction of **1b** with palladium(II) acertate[a]

Mole ratio **1b**/$Pd(OAc)_2$	Yield on $Pd(OAc)_2$		Product ratio **8a**/**2b**
	2b, %	**8a**, %	
1	19.5	20.8	1.1
2	19.0	46.4	2.4
5	17.4	85.6	4.9
10	13.6	92.5	6.8

a) The reaction was carried out at 55°C for 30 min in methanol-water. Yields were determined by glc with biphenyl as an internal standard.

Catalytic Cyclization Using Palladium(II) Acetate.

Palladium(II) acetate was found to be a convenient reagent for the reaction because it caused the cyclization of 2-allylphenols directly without using the sodium salts. Hence, the catalytic reaction was performed by use of the reagent.

Table 5. Catalytic cyclization of allylphenols with palladium(II) acetate in the presence of cupric acetate[a]

Allylphenol **1**	Product	Yield on $Pd(OAc)_2$, % (Yield on **1** used, %)	Conversion of **1**, %
1a	**2a**	1960 (34)	99
1b	**8a**	2720 (54)	99
	2b	trace	
1c	**2c**	1170 (23)	63
1d	—	—	—
1e	**2e**	786 (16)	53.5
1h	**8b**	1000 (20)	46

a) All reactions were carried out at ~55 °C for 24 hr in methanol (25 ml)-water (2 ml). Allylphenol **1** (10 mmol), $Pd(OAc)_2$ (0.2 mmol), and $Cu(OAc)_2 \cdot H_2O$ (5 mmol) were used. Yields and conversions were determined by glc and/or NMR analyses.

By considering the fact that reduced palladium metal is readily reoxidized with cupric salt and molecular oxygen as is well known in the Wacker process,[7] the reaction of 2-allylphenols **1** (10 mmol) was carried out in methanol–water solvent in the presence of a catalytic amount of palladium(II) acetate (0.2 mmol) and cupric acetate (5 mmol) under oxygen atomosphere. As indicated in Table 5, the reaction gave 2-substituted benzofurans catalytically with palladium(II) acetate, but 2-allyl-1-naphthol (**1d**) afforded polymeric material probably because of its oxidation with oxygen. In the catalytic reaction it should be noted that 2-(2′-butenyl) phenol (**1b**) gave 2,3-dihydro-2-vinylbenzofuran (**8a**) exclusively with a trace amount of 2-ethylbenzofuran (**2b**). Furthermore, 2-(2′-cyclohexenyl)phenol (**1h**) gave **8b** exclusively. (Scheme 2).

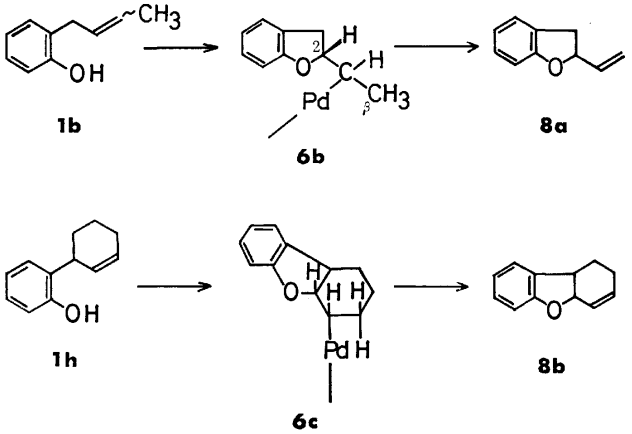

Scheme 2.

The exclusive formation of **8a** is probably due to the excess amount of **1b** to palladium(II) acetate as already shown in Table 4, although the influence of cupric salt cannot be neglected.[8] Mechanistic detail is not yet clear at present, but exclusive formation of **8a** in *the catalytic reaction* indicates that the β-hydrogen elimination occurs preferentially from the methyl group in **6b** as shown in Scheme 2. Thus, it is reasonable to suppose that the hydrogen on the C-2 carbon in **6b** is to take *trans*-configuration to palladium, since *cis*-palladium hydride eliminations are generally accepted.[9] In other words, the present catalytic reaction conceivably proceeds *via* a *cis*-oxypalladation step.

Exclusive formation of **8b** in the catalytic reaction of **1h** is also explained by the *cis*-oxypalladation followed by *cis*-elimination of a hydridopalladium species. *cis*-Oxypalladation of **1h** leads to the intermediate **6c** which bears only one *cis*-β-hydrogen to palladium as shown in Scheme 2. The elimination of the hydrogen gives only **8b**.

Experimental

2-Allylphenols 1. 2-Allylphenol (**1a**) and 2-cinnamylphenol (**1c**) were prepared by the method described in the literature.[10] 2-Allyl-1-naphthol (**1d**) and 1-allyl-2-naphthol (**1e**) were prepared by heating the corresponding allyloxynaphthalenes at 210—230 °C for 1 hr according to the method of Claisen.[11,12] 2-(2′-Cyclohexenyl)phenol (**1h**) was prepared by heating cyclohex-2-enyl phenyl ether in *N*,*N*-diethyl aniline

at 200—215 °C for 30 min.[13] 2-(α,α-Dimethylallyl)phenol (**1g**) was prepared from 3-methylbut-2-enyl phenyl ether according to the method of Vdovtsova[14] and purified by preparative glc.

2-(2′-Butenyl)phenol (**1b**) and 2-(2′-methyl-2′-butenyl)phenol (**1f**) were synthesized by C-alkylation of sodium phenoxide with crotylbromide and 1-bromo-2-methylbut-2-ene[15], respectively, according to the procedure of Hurd and Hoffman.[16] (2′-Butenyl)phenol (**1b**) was obtained in a mixture of *trans* and *cis*-isomers on a ratio of 1.9:1. 2-(2′-Methyl-2′-butenyl)phenol (**1f**) was obtained in a mixture of *trans* and *cis*-isomers on the ratio of 4.5:1. **1f** *trans-dimethyl*, NMR, δ 1.59 (broad s, 3H), 1.63 (nearly dd, $J=7$ and 1 Hz, 3H), 3.30 (broad s, 2H), 5.13 (broad s, 1H), 5.15—5.56 (m, 1H), and 6.53—7.20 (m, 4H). (Found: C, 81.04; H, 8.93%. Calcd for $C_{11}H_{14}O$: C, 81.44; H, 8.70%). **1f** *cis-dimethyl*, NMR, δ 1.62 (nearly dd, $J=1.5$ and 2.0 Hz, 3H), 1.74 (broad d, $J=7$ Hz, 3H), 3.38 (broad s, 2H), 4.82—5.10 (m, 1H), 5.48 (nearly q, $J=7$ Hz, 1H), and 6.50—7.18 (m, 4H). (Found: C, 81.00; H, 8.78%. Calcd for $C_{11}H_{14}O$: C, 81.44; H, 8.70%).

General Procedure for Stoichiometric Cyclization. A suspension of allylphenol **1** (5 mmol) and sodium methoxide (5 mmol) in dry benzene (50 ml) was stirred at room temperature under argon atmosphere. Dark green or blue coloration developed after 1—2 day's stirring. Dichlorobis(benzonitrile) palladium (5 mmol) was added into the suspension. The mixture was slowly heated to reflux for 3 hr. Palladium black gradually precipitated. After filtration of palladium black, the filtrate was concentrated *in vacuo* to leave reddish oil which was distilled under reduced pressure. Generally, distillation gave a mixture of benzonitrile and cyclized product, but the following products were separated from benzonitrile by distillation; bp **2c**, 94—95 °C/4 mmHg, **2d**, 70—72 °C/6 mmHg, and **2e**, 90 °C/8 mmHg. Analytically pure samples were obtained by preparative glc using 10% PEG 20 M–Celite or Apiezon L–Celite column. Elemental analyses and spectral data of the products are listed in Tables 2 and 3.

Cyclization of 2-(1′-Propenyl)phenol (7a) and 2-Styrylphenol (7b). 2-1′-Propenyl)phenol was prepared by isomerization of 2-allylphenol.[10] 2-Hydroxystilbene was synthesized by the procedure of Kauffman.[17]

The cyclization reaction was carried out by the same procedure described above. The yield of the product **2a** (17%) was determined by glc and NMR analyses. Sodium salt of **7b** (0.50 g, 2.5 mmol) was treated by the same procedure. The product was separated by column chromatography on alumina. Elution with benzene gave colorless crystals of **2i** (0.10 g, 20%) which was recrystallized from petroleum ether, mp 120—121 °C (lit,[18] 120 °C). (Found: C, 86.55; H, 5.10%. Calcd. for $C_{14}H_{10}O$: C, 86.57; H, 5.19%). From a fraction eluted by ether and methanol, 2-styrylphenol (0.24 g) was recovered.

General Procedure for Catalytic Cyclization. A suspension of allylphenol **1** (10 mmol) in methanol (25 ml) and water (2 ml) was stirred at ~55 °C for 24 hr in the presence of $Pd(OAc)_2$ (0.2 mmol) and $Cu(OAc)_2 \cdot H_2O$ (5 mmol) under slow stream of oxygen. After filtration, the solution was diluted with water, extracted with ether, and dried over magnesium sulfate and the solvent was removed. The cyclized product was separated by distillation under reduced pressure and was analyzed by glc and NMR analyses. In some cases, the starting phenol was removed by washing the distillate with Claisen's alkali. Analytically pure samples were obtained by preparative glc. The yields of the products and the conversions of the starting materials are given in Table 5. Specific results were described below.

Reaction of 1b. **1b** (*trans*/*cis*=1.9/1) was treated by the general procedure. The product **8a** was separated by distillation (bp 75 °C/4 mmHg). The NMR spectrum of **8a** was identical with the reported data.[19]

Reaction of 1h. **1h** was treated by the general procedure. The distillate was washed four times with Claisen's alkali, extracted with ether, washed with water, and dried over magnesium sulfate. Evaporation of ether gave a colorless oil which was only **8b** by glc analysis. Distillation gave pure **8b**, bp 109—110 °C/3 mmHg. **8b**, NMR, δ 1.4—2.4 (m, 4H), 3.28 (m, 1H), 4.85 (dd, $J=8$ and 2 Hz, 1H), 5.90 (m $J=2$ Hz, olefinic H), 6.69 (phenyl, 2H), and 6.98 (phenyl, 2H); IR, 1650 cm^{-1} (C=C); Mass *m/e* 172; Found: C, 83.44; H, 7.00%. Calcd for $C_{12}H_{12}O$: C, 83.67; H, 7.02%. The assignment of the structure **8b** was supported by double irradiation experiment in NMR. The signal of the tertiary proton (H_a) adjacent to oxygen atom (δ 4.85) was simplified by double irradiation at the signal of the other tertiary proton (H_b) to show a doublet ($J=2$ Hz). Also, the irradiation of olefinic proton (δ 5.90) simplified the signal of H_a to show clearly a doublet ($J=8$ Hz). Double irradiation of H_a proton transformed the signal of H_b from a multiplet to nearly double doublet ($J=4$ and 8 Hz). The irradiation at δ 1.99 (one of protons on cyclohexene ring) simplified the multiplet of H_b proton to show nearly triplet ($J=8$ Hz).

Reaction of 2-γ-Methylallylphenol (1b) with Palladium(II) Acetate. Palladium(II) acetate was allowed to react with various amounts of **1b** in methanol–water at 55 °C for 30 min. In each run the crude reaction mixture was analyzed by glc (flame ionization detector, 5% PEG-20M on Gas Chrom Q, lm) with biphenyl as an internal standard.

References

1) T. Hosokawa, K. Maeda, K. Koga, and I. Moritani, *Tetrahedron Lett.*, **1973**, 739.

2) C. Hansch, W. Saltonstall, and J. Settle, *J. Amer. Chem. Soc.*, **71**, 943 (1949).

3) The elimination of PdHCl species from a similar system has been observed to occure, see, T. Hosokawa and P. M. Maitlis, *J. Amer. Chem. Soc.*, **95**, 4924 (1973).

4) Although the detailed mechanism of double bond isomerization by palladium salt is still the subject of considerable studies, it is known that precipitated metallic palladium is virtually inactive for the isomerization, see, Ref. 7) p. 136.

5) R. F. Heck, *J. Amer. Chem. Soc.*, **91**, 6707 (1969).

6) In the previous paper[1] we described that 2-prop-1′-enylphenol (**7a**) did not undergo the cyclization under the same consitions. Although at that time **2a** could not be detected because of its low yield, repeated experiments have confirmed that the cyclization occurs with reproducibility.

7) P. M. Maitlis, "The Organic Chemistry of Palladium," Vol. 2, Academic Press, New York (1971), pp. 77—126.

8) In some palladium-catalyzed reactions, product distributions are affected by the presence of copper(II) salts, see, Ref. 9b.

9) a) Ref. 5 and R. F. Heck, *J. Amer. Chem. Soc.*, **93**, 6896 (1971). b) P. M. Henry, *ibid.*, **94**, 7305 (1972).

10) D. S. Tarbell, "Organic Reactions," Vol. 2, ed. by R. Adams, Wiley, New York (1944), pp. 27—28.

11) L. Claisen, *Ber.*, **45**, 3157 (1912).

12) L. Claisen and O. Eisleb, *Ann. Chem.*, **401**, 79 (1913).

13) Gy. Fráter and H. Schmid, *Helv. Chim. Acta*, **50**, 255 (1967).

14) E. A. Vdovtsova, *J. Org. Chem. USSR. Int. Ed.*, **5**, 486 (1969).

15) A. Lauchenauer and H. Schmiz, *Helv. Chim. Acta*, **34**, 1514 (1951).

16) C. D. Hurd and W. A. Hoffman, *J. Org. Chem.*, **5**, 212 (1940).

17) H. Kauffmann, *Ann. Chem.*, **433**, 241 (1923).

18) K. Nogami and K. Kurosawa, This Bulletin, **47**, 505 (1974).

19) K. Kirmse and H. Dietrich, *Ber.*, **100**, 2710 (1967).

A Macrocyclic Enzyme Model System. Substrate Specificity for the Inclusion into Paracyclophane Oxime and the Subsequent Acyl Transfer Reaction

Yukito MURAKAMI, Junzo SUNAMOTO,* Hiroshi OKAMOTO,* and Kiyomiki KAWANAMI

Department of Organic Synthesis, Faculty of Engineering, Kyushu University, Hakozaki, Higashi-ku, Fukuoka 812

** Department of Industrial Chemistry, Faculty of Engineering, Nagasaki University, Nagasaki 852*

(Received July 8, 1974)

In order to characterize the intrinsic nature of 10-hydroxy-11-hydroxyimino[20]paracyclophane (Oxime-I) as being an enzyme model, the acylation reactions of Oxime-I with *p*-nitrophenyl carboxylates have been investigated in an alkaline aqueous acetone. The usual saturation-type kinetics has been observed for the reactions of *p*-nitrophenyl decanoate (PNPD), laurate (PNPL), and palmitate (PNPP) with Oxime-I. The acyl transfer reaction was consistent with the following two sequences: (1a) pre-equilibrium formation of the inclusion complex between Oxime-I and a substrate, (1b) pre-equilibrium acid dissociation of the inclusion complex, and (1c) rate-determining acyl transfer from a substrate to Oximate-I in the inclusion state; and (2a) pre-equilibrium acid dissociation of Oxime-I, (2b) pre-equilibrium formation of the inclusion complex between Oximate-I and a substrate, and (2c) rate-determining acyl transfer from a substrate to Oximate-I in the inclusion state. On the basis of the compensation correlation between enthalpy and entropy for binding process, the inclusion of a long chain carboxylate into the cavity of Oxime-I is controlled by entropy. It is interesting to note that the binding constants for the present inclusion complexes are considerably larger ($K \simeq 10^4 - 10^5\ M^{-1}$) than those for the complexes formed between phenyl esters or azo dyes and cycloamyloses ($K \simeq 10^2 - 10^3\ M^{-1}$). Thus, the paracyclophane skeleton provides an effective binding site due to the hydrophobic cavity. Since the most stable inclusion complex was formed with PNPD, the inclusion of the present esters may be not exclusively due to the hydrophobicity provided by an apolar hydrocarbon tail, but significantly due to the molecular geometry or bulkiness characterized by the folded ester molecule. This effect approves the presence of substrate specificity due to the molecular geometry for Oxime-I. In reference to the activation parameters, the acyl transfer process is controlled by entropy in a manner similar to the alkaline hydrolysis in the bulk phase and the complex formation as well. PNPP is least stabilized in the binding process due to the most unfavorable entropy effect, whereas most favorably deacylated in the acyl transfer due to the entropy factor. Consequently, the net change in the free energy is largely reflected on the entropy term. The deceleration effect observed in the reaction of PNPD with Oxime-I at a higher acetone content and the kinetic behavior of alkaline hydrolysis of the three carboxylate esters have also been discussed.

Micellar surfactants,[1] synthetic water-soluble polymers carrying various functional groups,[2] and macrocyclic compounds[3] are the three major types of enzyme models recently developed. Of these three model systems, macrocyclic compounds may exhibit several unique characters which can never be expected for other two systems: 1) a steady binding site provided by a characteristic ring conformation of hydrophobic nature; 2) a high substrate specificity brought about by the geometric requirements for binding of substrates into these macrocyclic cavities as well as by spatial geometries of substrate molecules incorporated into these cavities; and 3) a high possibility of introducing a charge relay system or a polyfunctional catalytic one, which is provided by the spatial arrangement of appropriate functional groups. Consequently, a well-designed macrocyclic compound may exhibit a catalytic ability more favorably than other types of enzyme models, providing one binding site and one catalytic function for each substrate.

From these view points, we have previously prepared two macrocyclic oximes, 10-hydroxy-11-hydroxyimino-[20]paracyclophane (Oxime-I) and 2-hydroxycyclodecanone oxime (sebacoin oxime, Oxime-II), and investigated their catalytic efficiencies for the deacylation reaction of *p*-nitrophenyl carboxylates.[4,5] The sizable cyclic cavity of Oxime-I provided an appropriate binding site as expected owing to the restricted ring conformation as well as to the hydrophobicity of paracyclophane skeleton. Oxime-I was, thus, acylated by *p*-nitrophenyl laurate (PNPL) and decanoate (PNPD), which were suitably incorporated into the Oxime-I cavity because of their relatively large molecular volume in a folded form. On the contrary, the oxime did not show any catalytic activity toward smaller esters such as *p*-nitrophenyl acetate (PNPA) or hexanoate (PNPH). Oxime-II did not undergo any reaction with all of these esters under the same conditions. In order to characterize the intrinsic nature of Oxime-I as being an enzyme model, we have employed an additional substrate having a longer alkyl chain, *p*-nitrophenyl palmitate (PNPP). On the basis of thorough thermodynamic and kinetic analyses for binding and acyl transfer processes, respectively, the substrate specificity has been elucidated for the inclusion into Oxime-I and for the subsequent acyl transfer reaction.

Experimental

Materials. Cyclic oximes, Oxime-I and -II, and two *p*-nitrophenyl carboxylates, PNPD and PNPL, were the same as those used in our previous investigations.[5] *p*-Nitrophenyl palmitate (PNPP) was commercially obtained from E. Merck, Darmstadt and used after the inspection of its purity (Found: C, 70.06; H, 9.08; N, 3.90%; mp 64.0 °C).

Kinetic Measurements. The rate of liberation of *p*-nitrophenoxide ion was measured at 400 nm either on a Hitachi 124 recording spectrometer or on a Shimadzu-Bausch & Lomb Spectronic 88 equipped with a Riken Denshi SP-G3 recorder. Reactions were initiated by the addition of a substrate dis-

solved in acetone to a reaction solution which was pre-incubated at an appropriate temperature in the thermostatted cell set in the spectrometer. The preparation of stock and reaction solutions, and the measurement procedures were essentially the same as those described previously.[5] The rate constants were checked by duplicate runs and observed to retain an accuracy within ±1%.

pH Measurements. pH-Values of the reaction solutions, which were prepared with 10.9% (v/v) aqueous acetone as the solvent, were measured and calibrated by using two separate buffer solutions in the same solvent, the pH values of which were referred to those measured in the aqueous system. The measurements were carried out either with a TOA HM-9A recording pH meter or a TOA HM-5A pH meter equipped with an attachment for expandomatic reading. Both pH meters were connected with a Metrohm EA-125 combined electrode or a set of Metrome EA-107H glass electrode and Beckman 39402 saturated calomel electrode.

Results and Discussion

As shown in Scheme 1, the present reaction system may be roughly classified into two competitive reactions: the alkaline hydrolysis of a free substrate in the bulk solution and the acyl transfer reaction occurring in the inclusion complex formed between Oxime-I and a substrate.[5] For the reactions of PNPD, PNPL,[5] and PNPP with Oxime-I, the usual saturation-type kinetics has been observed. The rate constant of alkaline hydrolysis k_{hyd} can be separately obtained from the rate measurements in the absence of Oxime-I. Kinetic results obtained for PNPD and PNPP are summarized in Tables 1 and 2, respectively.

$$\begin{array}{ccc} S + \text{Oxime-I} & \overset{K}{\rightleftharpoons} & (S\text{—Oxime-I}) \\ \downarrow k_{hyd} & & \downarrow k_{acyl} \\ P_1 & & P_2 \end{array}$$

Scheme 1.

Alkaline Hydrolysis of p-*Nitrophenyl Carboxylates.* In the absence of cyclic oximes, *p*-nitrophenyl carboxylates undergo usual hydrolytic decomposition through the hydroxide ion catalysis. The rate of alkaline hydrolysis of carboxylates having a long hydrocarbon chain was largely inhibited with increasing the chain length as previously indicated by Menger and Portnoy:[6] $k_{hyd}=4.47\times10^{-3}$ s^{-1} at pH 10.71 for PNPD, 1.41×10^{-4} s^{-1} at pH 10.31 for PNPL,[5] and 7.24×10^{-5} s^{-1} at pH 10.71 for PNPP (at 43.1 °C), respectively, among which the values for PNPD and PNPP were estimated by the aid of activation energies. A large decrease in the hydrolysis rate along with the extension of hydrocarbon chain is readily explained by the self-aggregation effect due to hydrophobic interaction. The ester carbonyl group, as being the reaction center, is presumably shielded from the attack of a nucleophile by the hydrophobic aggregation. The hydrolysis rate of these esters was retarded also with increasing the initial concentration[6] due to the similar reason. In this work, therefore, we have maintained the initial ester concentration at about 1.0×10^{-5} M, where a small change in the ester concentration gives off a

Table 1. First-order rate constants for the *p*-nitrophenol release from *p*-nitrophenyl palmitate in the presence of Oxime-I in 10.9% (v/v) aqueous acetone at $\mu=0.10$ (KCl)

Temp. °C	[Oxime-I] $\times10^6$ M	$k_{obs}\times10^4$ s^{-1}
[PNPP]$_0=9.65\times10^{-6}$ M and pH 10.71[a]		
49.8±0.1	20.1	52.9
	11.2	40.2
	10.1	35.8
	4.02	20.3
	2.01	10.3
	1.31	7.91
	1.01	6.75
	None	0.82
39.9±0.1	20.9	24.2
	10.4	16.5
	4.17	9.17
	2.07	4.96
	1.04	3.00
	None	0.62
30.1±0.1	20.9	9.64
	13.6	9.11
	10.4	8.17
	4.17	4.30
	2.07	3.13
	1.36	1.95
	None	0.35
20.2±0.1	20.1	3.08
	11.2	3.03
	10.1	2.68
	4.02	2.10
	2.01	1.33
	1.01	0.82
	None	0.18[c]
[PNPP]$_0=9.65\times10^{-6}$ M and pH 11.78[b]		
49.8±0.1	20.1	257
	10.4	178
	4.02	75.2
	2.01	29.2
	1.31	22.4
	1.01	17.3
	None	2.24
39.9±0.1	20.9	101
	13.6	86.7
	4.17	40.8
	2.07	18.8
	1.36	13.0
	None	1.29
20.2±0.1	20.1	22.3
	13.1	18.9
	4.02	11.7
	2.01	7.85
	1.31	6.00
	1.01	3.17
	None	0.28

a) Buffer, 9.64×10^{-3} M Na_2CO_3—0.03×10^{-3} M $Na_2B_4O_7$. b) Buffer, 1.15×10^{-2} M NaOH. c) Estimated from the data obtained at other temperatures using the activation energy, because of the extremely slow rate under the present kinetic conditions.

Table 2. First-order rate constants for the *p*-nitrophenol release from *p*-nitrophenyl decanoate in the presence of Oxime-I in 10.9% (v/v) aqueous acetone at μ=0.10 (KCl)

Temp. °C	[Oxime-I]×10^6 M	$k_{obs}\times10^4$ s^{-1}
[PNPD]$_0$=10.3×10^{-6} M and pH 10.12[a]		
35.4±0.1	20.5	19.6
	10.3	16.0
	6.18	13.1
	4.10	9.92
	1.03	6.92
	None	4.13
25.5±.01	20.5	8.00
	10.3	6.67
	6.18	4.60
	4.10	3.93
	2.05	3.03
	None	1.55
15.5±0.1	20.5	2.65
	10.3	2.23
	6.18	1.83
	4.10	1.47
	None	0.50
[PNPD]$_0$=10.3×10^{-6} M and pH 10.71[b]		
35.6±0.1	20.5	34.3
	10.3	33.9
	4.10	28.8
	2.05	24.2
	1.03	22.0
	None	20.6
24.8±0.1	20.5	12.3
	10.3	11.1
	4.10	9.33
	2.05	7.53
	None	7.03
14.3±0.1	20.5	3.05
	10.3	2.80
	4.10	2.37
	2.05	2.13
	None	1.83

a) Buffer, 7.53×10^{-3} M Na_2CO_3–2.46×10^{-3} M $Na_2B_4O_7$
b) Buffer, 9.64×10^{-3} M Na_2CO_3–0.03×10^{-3} M $Na_2B_4O_7$

relatively minor effect on the hydrolysis rate[6] and the linearity of first-order plot is good at least for the first half-life (rate data given in Table 3).

The base-catalyzed hydrolysis rate is in general subjected to the second-order kinetics. In the present cases, however, the overall rate was not observed to depend on hydroxide ion concentration linearly as seen in Fig. 1. The rate becomes less dependent on hydroxide concentration either by decreasing the reaction temperature or by increasing the length of hydrocarbon chain of substrates. Though convincing evidence is not available at present, the self-aggregation would be favored with decreasing temperature and increasing hydrocarbon chain length, and subsequently the reaction center would be more completely encased and protected from the attack of nucleophile. As a result, the simple bimolecular mechanism with participation of hydroxide ion may be no longer observed. These effects must be reflected on the entropy of activation in terms of solvation and molecular mobility. As is clear from the apparent activation parameters listed in Table 4 for the hydrolysis of PNPD and PNPP obtained at pH 10.71, the reaction is more effectively controlled by the entropy term along with the extension

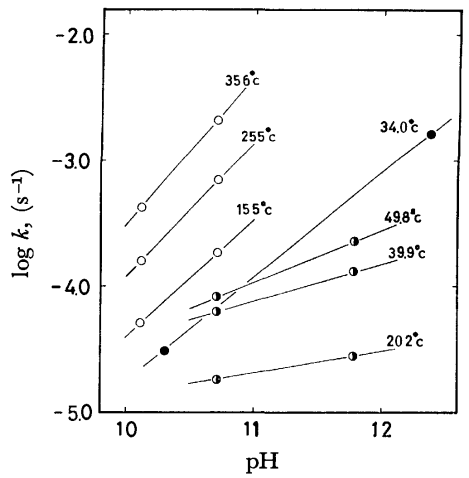

Fig. 1. pH-rate correlations for alkaline hydrolysis of PNPD (○), PNPL (●), and PNPP (◑) at various temperatures: solvent, 10.9% (v/v) aqueous acetone; μ=0.10 (KCl) (refer to Tables 1 and 2).

Table 3. Kinetic parameters for the reactions of *p*-nitrophenyl decanoate, laurate, and palmitate with Oxime-I at μ=0.10 (KCl)

Substrate	pH	Temp. °C	$10^4\times k_{hyd}$ s^{-1}	$10^4\cdot 1/\gamma\cdot k'_{acyl}$ s^{-1}	$10^{-4}\times K_b$[c] M^{-1}
PNPD[a]	10.12	35.4	4.13	32.7	41.5
	10.12	25.5	1.55	11.6	100
	10.12	15.1	0.50	4.17	(167)
	10.71	35.6	20.6	46.9	40.0
	10.71	24.8	7.03	16.1	93.5
	10.71	14.3	1.83	6.61	(167)
PNPL[b]	10.31	43.1	1.4	12.0	20.2
	10.31	33.9	0.3	6.28	43.7
	12.37	42.1	37.1	162	10.6
	12.37	34.1	16.1	71.6	18.1
	12.37	24.5	5.1	52.7	38.5
	12.37	15.2	2.1	19.1	(105)
PNPP[a]	10.71	49.8	0.82	112	5.82
	10.71	39.9	0.62	44.1	15.0
	10.71	30.1	0.35	11.5	38.5
	10.71	20.2	0.18	3.55	(940)
	11.78	49.8	2.24	627	3.59
	11.78	39.9	1.29	251	8.16
	11.78	20.2	0.28	29.7	51.3

a) Parameters were calculated from the data listed in Table 1 or 2 by the aid of Eq. (1). b) Data were quoted from Ref. 5. pH-Values have been reevaluated according to the present procedure. c) Values in parentheses may involve a sizable error due to computational means.

Table 4. Apparent activation parameters for alkaline hydrolysis of *p*-nitrophenyl carboxylates[a)]

Substrate	pH	$\Delta H^{\ddagger}_{hyd}$ kcal/mol	$\Delta S^{\ddagger}_{hyd}$ e.u.	$\Delta G^{\ddagger}_{hyd}$ (303 K) kcal/mol
PNPD	10.12	18.0	−14.9	22.5
	10.71	21.2	−1.7	21.7
PNPP	10.71	10.6	−44.0	24.0
	11.78	11.5	−39.7	23.6

a) Solvent, 10.9% (v/v) aqueous acetone; μ=0.10 (KCl). These apparent activation parameters were evaluated directly from the overall rate constants listed in Tables 1 and 2. The true second-order rate constants were not evaluated due to some difficulty in estimating hydroxide-ion effect (see Fig. 1).

of alkyl chain. The loss of free energy of activation ($\Delta\Delta G^{\ddagger}_{hyd}$) per methylene unit (see Fig. 3) is estimated approximately as 370 cal mole^{-1}. This value, which is due to the contribution from hydrophobic interaction,[7)] is very close to that observed for the aminolysis of phthalic anhydride with amines of long alkyl chain,[8)] where the rate enhancement was observed with increasing hydrophobic character of nucleophiles. Thus, it is clear that the hydrophobicity of an apolar hydrocarbon tail of esters gives out a large effect on their hydrolytic reactivities.

Formation of Inclusion Complex and Subsequent Acyl Transfer Reaction. In the presence of Oxime-I, the inclusion of a *p*-nitrophenyl ester of carboxylate with a long alkyl chain into the cyclic cavity takes place prior to the acyl transfer from the carboxylate to Oxime-I[5)] as represented in Scheme 1. The driving force for the inclusion of a substrate was primarily attributed to the hydrophobic interaction between the alkyl chain of a substrate and the paracyclophane skeleton of Oxime-I, which has been verified by the effects of organic solvent and added urea on the kinetic behavior.[5)]

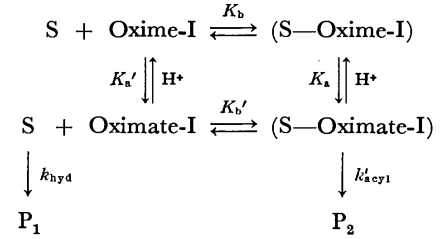

P_1: carboxylate and *p*-nitrophenolate ions
P_2: acylated Oxime-I and *p*-nitrophenolate ion

Scheme 2.

As pointed out in our previous paper,[5)] the acyl transferring rate is dependent on pH of the medium. Thus, it seems reasonable to establish the whole reaction sequences in more critical manner as shown in Scheme 2. This means that the real nucleophile is not the neutral oxime but the oximate group of Oxime-I in the inclusion complex. As a consequence, the equilibrium constants and the specific rate constant for acyl transfer defined in Scheme 2 can be evaluated by the aid of Eq. (1), the derivation of which is given in Appendix.

$$\frac{1}{k_{obs}-k_{hyd}} = \frac{\left(\frac{1+\beta}{1+\alpha}\right)+K_b[S]_T}{\left(\frac{1}{\gamma}k'_{acyl}-k_{hyd}\right)K_b[C]_T} + \frac{1}{\left(\frac{1}{\gamma}k'_{acyl}-k_{hyd}\right)} \quad (1)$$

and $\alpha = \frac{K_a}{[H^+]}$, $\beta = \frac{K_a'}{[H^+]}$, and $\gamma = \frac{[H^+]}{K_a} + 1$,

where k_{obs} is the observed pseudo-first-order rate constant, and $[S]_T$ and $[C]_T$ stand for the total concentrations of substrate and Oxime-I, respectively. Thus, a good linear relationship must be obtained by plotting the left-hand side of Eq. (1) against the reciprocal initial concentration of Oxime-I, when the initial concentration of substrate and pH of the reaction medium are maintained constant. Since $(1/\gamma)k'_{acyl}$ is obtained as a constant value from Eq. (1), K_a and k'_{acyl} can be evaluated by Eq. (2).

$$k = \frac{\gamma}{k'_{acyl}} = \frac{[H^+]}{K_a k'_{acyl}} + \frac{1}{k'_{acyl}} \quad (2)$$

In fact, all the kinetic data were satisfactorily analyzed by the aid of Eqs. (1) and (2). This seems to validate the reaction sequences given in Scheme 2.

Table 5. Thermodynamic parameters for binding of *p*-nitrophenyl carboxylates with Oxime-I[a)]

Substrate	pH	$\Delta G^{\circ}_{303\,K}$ kcal/mol	ΔH° kcal/mol	ΔS° e.u.
PNPD	10.12	−8.01	−11.97	−13.06
	10.71	−7.96	−12.07	−13.55
PNPL	12.37	−7.50	−14.4	−22.8
PNPP	10.71	−7.65	−16.2	−28.2
	11.78	−7.32	−16.1	−28.9

a) Solvent, 10.9% (v/v) aqueous acetone; μ=0.10 (KCl).

Binding constants and the corresponding thermodynamic parameters for the combination of Oxime-I either with *p*-nitrophenyl decanoate or palmitate are listed in Tables 3 and 5, respectively, along with those for the combination of the oxime with *p*-nitrophenyl laurate previously investigated[5)] upon re-evaluation by Eqs. (1) and (2). The binding constants for these inclusion complexes are considerably larger ($K \simeq 10^4 - 10^5$ M^{-1}) than those for the complexes formed between phenyl esters[9-11)] or azo dyes[12)] and cycloamyloses ($K \simeq 10^2 - 10^3$ M^{-1}). The difference is also reflected on the respective reaction conditions: only equimolar or twice molar amount of Oxime-I relative to the substrate was used to gain a significant catalytic effect, while the cycloamyloses were required in a large excess (about 10^3 fold).[9,10)] The free energy change due to binding is in a range of −3——5 kcal mol^{-1} for the cyaloamylose system,[9,11)] while −7——8 kcal mol^{-1} for the Oxime-I system. This means that the paracyclophane skeleton provides a more favorable binding site due to the hydrophobic cavity.

The inclusion of the esters into Oxime-I is considerably dependent on the temperature: the binding constant becomes larger with decreasing the reaction temperature (negative enthalpy change). Such a negative temperature dependency of binding has also

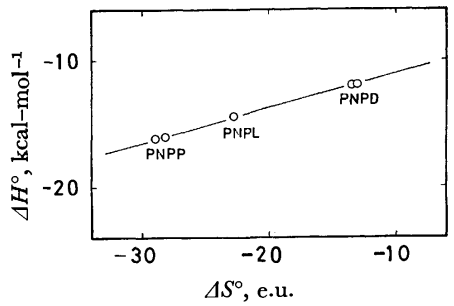

Fig. 2. Isoequilibrium relationship for binding of *p*-nitrophenyl carboxylates with Oxime-I (refer to Table 5).

been noticed for the systems of cycloamyloses[9-12] and of chymotrypsin.[13,14] A different state of affairs has been observed previously:[15,16] the hydrophobic binding increases with increasing temperature. Thus, the positive enthalpy change reported in those studies is not an intrinsic nature of hydrophobic interaction, and the binding behavior is apparently much affected by the nature of host molecules.

There exists a good linear compensation effect between enthalpy and entropy for binding as shown in Table 5 and Fig. 2. Also for the binding process, a considerably low isoequilibrium temperature (β=265 °K) was obtained. This β-value suggests that the inclusion of a long chain carboxylate into the cavity of Oxime-I is certainly controlled by entropy at ordinary temperatures[17] (see Table 5). We can see an analogous compensation effect between enthalpy and entropy in binding process of cycloamyloses with various pseudo-substrates.[18]

We have to notice that the binding stability in terms of free energy change is indicative of the strength of hydrophobic interaction and/or of the structural specificity existing between host and guest molecules. Table 5 indicates that the decanoate ester shows the largest binding stability among three carboxylates (PNPD, PNPL, and PNPP); *i.e.*, the most stable inclusion complex is formed with PNPD. If the binding force is due only to the hydrophobicity, the palmitate ester having the longest apolar tail would be expected to be most strongly bound judging from their reactivities in alkaline hydrolysis. The release of bound water from the catalyst may cause the entropy gain. A substrate molecule, which is more tightly bound with a host molecule, is expected to release more water molecules than those loosely bound, giving off the larger entropy gain. However, this is not the case for the complex formation between PNPD and Oxime-I. The relatively large enthalpy change given out in the binding process seems, therefore, not to be due to the release of bound water in the cavity of Oxime-I. These explanations lead to a conclusion that the inclusion of the present esters may be not exclusively due to the hydrophobicity provided by an apolar hydrocarbon tail, but significantly due to the molecular geometry or bulkiness characterized by the folded ester molecule[5] which is tightly fitted into the cavity. This effect approves the presence of substrate specificity due to the molecular geometry for Oxime-I. Moreover, the enthalpy of binding is evidently insensitive to the pH-value of bulk phase. This fact implies that the intrinsic binding force may be not due to electrostatic interactions such as hydrogen bonding (>C=N-OH··· O=C<) or dipole-ion interaction (>C=N-O$^-$···>C=O).

Investigations dealing with the acyl transfer *via* complex formation between acyl-substrate and nucleophilic catalyst have been recently carried out: *e.g.*, aminolysis of *p*-nitrophenyl decanoate with *n*-decylamine,[16,17] and of phthalic anhydride with various amines having a long alkyl chain.[8] The acyl transfer from a carboxylate ester to cycloamyloses involves the nucleophilic participation of an alkoxide ion derived from the secondary hydroxyl groups of the cycloamyloses.[9-11] A similar mechanistic behavior is considered to take place in the present acyl transfer reaction between a *p*-nitrophenyl carboxylate and an oxime nucleophile. However, in the case of cycloamyloses the subsequent deacylation proceeds at a significantly large rate, while hardly detected in the case of Oxime-I because of the inertness of the acylated oxime to deacylation reaction.[5] Therefore, the present acyl transfer assumes a pseudo-intramolecular mechanism as observed in some aminolysis reactions.[8,16,19]

Kinetic parameters obtained are listed in Table 6 along with their activation parameters calculated from the true rate constants for ac l transfer. Acid dissociation constants for the complexed Oxime-I, which were kinetically estimated (pK_a 10—12), are reasonable in magnitude in reference to that for acetoxime (pK_a 12.4[20]) since an additional substituent effect due to the neighboring hydroxyl group may act in favor

Table 6. Kinetic, thermodynamic, and activation parameters for acyl transfer occurring in the inclusion complexes between Oxime-I and *p*-nitrophenyl carboxylates[a]

	Temp. °C	K_a M^{-1}	pK_a	k'_{acyl} s^{-1}	$\Delta H^{\neq}$ kcal/mol	$\Delta S^{\neq}$ e.u.	$\Delta G^{\neq}$ (303 K) kcal/mol
PNPD	35.6	11.03×10^{-11}	9.99	5.52×10^{-3}			
	25.5	12.57×10^{-11}	9.90	1.86×10^{-3}	17.7	−11.5	21.2
	15.1	7.68×10^{-11}	10.11	0.82×10^{-3}			
PNPL	43	3.46×10^{-12}	11.5	18.2×10^{-3}	17.7	−10.6	20.9
	34	4.29×10^{-12}	11.4	7.80×10^{-3}			
PNPP	49.8	2.25×10^{-12}	11.7	108×10^{-3}			
	39.9	2.14×10^{-12}	11.7	44.5×10^{-3}	17.6	−8.6	20.2
	20.2	7.62×10^{-13}	12.1	9.44×10^{-3}			

a) Kinetic and thermodynamic parameters were obtained from the data listed in Table 3 by the aid of Eq. (2).

of the liberation of oxime proton. The acid dissociation of the PNPD–Oxime-I complex is favored relative to the other, two substrate–Oxime-I system. Since the PNPD–Oxime-I complex is formed by the entropically favored inclusion process (see Table 5), this complex is presumably solvated by water molecules in a more feasible manner for the proton transfer without much destruction of the ice-berg.

On the other hand, their activation parameters show characteristic behavior: the enthalpy of activation is equal to each other among all the substrates while the entropy of activation varies in an decreasing sequence of PNPP, PNPL, and PNPD. These results suggest that the acyl transfer process in the inclusion complexes is controlled by entropy in a manner similar to the alkaline hydrolysis in the bulk phase and the complex formation as well. The palmitate ester, which is least stabilized in the binding process due to the most unfavorable entropy effect, is most favorably deacylated in the acyl transfer process due to the entropy factor.

Catalytic Effect and Substrate Specificity. Clearly from Scheme 1, the catalytic effect of Oxime-I on the acyl transfer reaction can not be simply discussed in terms of the rate ratio k_{obs}/k_{hyd}, because the acyl transfer and the alkaline hydrolysis are rather competitive reactions mutually. Therefore, the reactivity of Oxime-I is compared with that of a smaller cyclic oxime (Oxime-II), which has the same catalysis site as Oxime-I, as previously suggested.[5] The catalytic specificity of Oxime-I for the acyl transfer is defined in terms of $k_{c(Oxime-I)}/k_{c(Oxime-II)}$, where k_c is the apparent catalytic rate constant given by Eq. (3).

$$k_c = \frac{k_{obs} - k_{hyd}}{[\text{Oxime-I or -II}]} \qquad (3)$$

The catalytic specificity obtained under the controlled reaction conditions for the different carboxylate esters of *p*-nitrophenol is shown in Table 7.

Table 7. Catalytic effects of Oxime-I and -II on the *p*-nitrophenyl carboxylates[a]

[Subtrate] $\times 10^5$ M	[Oxime] $\times 10^5$ M	$k_{obs}\times 10^4$ s^{-1}	k_c $s^{-1}M^{-1}$	Rate[b] ratio
PNPA: 1.09	II: 17.5	22.8	0.86	
	II: 1.90	22.6	6.83	1.4
	I: 1.96	23.1	9.20	
PNPD: 1.03	II: 17.5	4.30	0.02	
	II: 1.90	4.30	0.15	420
	I: 1.96	16.8	62.8	
PNPL: 1.00	II: 17.5	0.77	0.05	
	II: 1.90	0.70	0.05	1420
	I: 1.96	15.3	73.2	
PNPP: 1.02	II: 17.5	0.11	0.07	
	II: 1.90	0.11	0.04	1520
	I: 1.96	12.6	62.6	

a) All runs were carried out at 23.5 °C and pH 9.23 (0.03 M $Na_2B_4O_7$) in 10.9% (v/v) aqueous acetone. The rate constants for alkaline hydrolysis of these esters were 21.3×10^{-4}, 4.27×10^{-4}, 0.69×10^{-4}, and 0.10×10^{-4} s^{-1} for PNPA, PNPD, PNPL, and PNPP, respectively, under the present reaction conditions. b) $k_{c(Oxime-I)}/k_{c(Oxime-II)}$, see text.

For a small substrate, *p*-nitrophenyl acetate, both Oxime-I and -II did not show any significant rate enhancement. On the other hand, for larger three esters, PNPD, PNPL, and PNPP, the large rate acceleration in acyl transfer has been observed with Oxime-I, particularly for the latter two esters. These rate accelerations by $1.4—1.5\times 10^3$ fold must be brought about by incorporation of the substrate into the Oxime-I cavity, which results in a pseudo-intramolecular reaction. In other words, the rate enhancement is due neither to a simple hydrophobic entanglement nor to a bimolecular reaction between the substrate and the paracyclophane oxime. Since little effect has been observed on the reaction rate even in the presence of 10 fold excess amount of Oxime-II, there is apparently no significant interaction between the substrates and the smaller cyclic oxime. Consequently, the difference in reactivity between these two cyclic oximes needs to be explained in terms of the correlations between the cavity size of a host molecule and the molecular volume of a substrate in the included state, and of their hydrophobic nature as well. When the folded substrate[5] is effectively incorporated into the cavity, the spatial orientation of the nucleophilic site in the oxime against the carbonyl carbon of the substrate is certainly an important factor to control the subsequent acyl transfer process. This orientation effect seems to be subjected to variation due to the molecular size of an incorporated substrate.

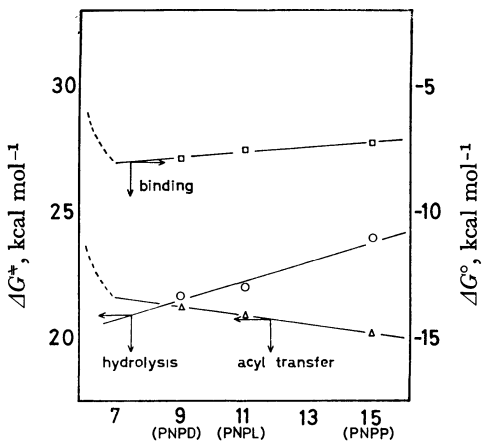

Fig. 3. Correlations between the structure of substrates and free energy changes: binding process of *p*-nitrophenyl carboxylates with Oxime-I (refer to Table 5); acyl transfer process of carboxylates to Oxime-I in the inclusion state on the basis of Scheme 2 (refer to Table 6); alkaline hydrolysis of carboxylates in the bulk solution at pH 10.71 for PNPD and PNPP and 12.37 for PNPL[5] (refer to Table 4).

It is interesting to examine the differences in reactivity in terms of thermodynamic parameters. Figure 3 shows that there are no large differences in free energies of binding among three esters examined, but that the free energy of activation for alkaline hydrolysis increases while that for acyl transfer somewhat decreases with increasing the chain length of acyl residues. A schematic representation for the correlations between relative potential energy due to free energy change and reaction

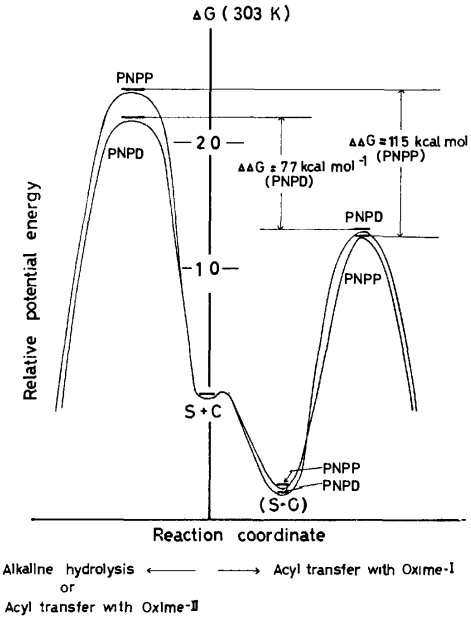

Fig. 4. Reaction coordinate diagram for alkaline hydrolysis and acyl transfer reactions of PNPD and PNPP at 303 K: relative potential energy is represented in free energy change.

coordinate for the two competitive reactions is illustrated in Fig. 4. The activation free energy values for the two carboxylate esters adopted in Fig. 4 in alkaline hydrolysis and acyl transfer reaction are based on Scheme 2 (refer to Tables 4 through 6) so that both reactions can be compared on the equal basis: the difference in $\Delta\Delta G$ between PNPP and PNPD is about 3.8 kcal mol^{-1} at 303 K and pH 10.71.

Deceleration in the Reaction of p-*Nitrophenyl Decanoate with Oxime-I.* Different from the reactions of PNPL and PNPP with Oxime-I, the liberation of *p*-nitrophnoxide ion in the case of PNPD and Oxime-I was somewhat inhibited at a higher acetone content (20.8% (v/v)) with increasing the reaction temperature as illustrated in Fig. 5. An increase in acetone content may cause the decrease in hydrophobicity of the substrate itself, which results in a rate acceleration of the alkaline hydrolysis in the bulk solution.[6] Of course, the decrease in hydrophobicity of the substrate may somehow tend to decrease the binding constant.[5] However, the effect on the binding process is not necessarily large and even some compensation effect comes into play in the subsequent acyl transfer process. As a result, the large rate enhancement for the alkaline hydrolysis in the bulk phase seems to exceed the deacylation in the Oxime-I complex. Therefore, under these circumstances substrate specificity for acyl transfer seems to be more distinctly observed. A similar inhibition phenomenon has been observed in the hydrolysis of ethyl *p*-aminobenzoate in the presence of *β*-cycloamylose.[21]

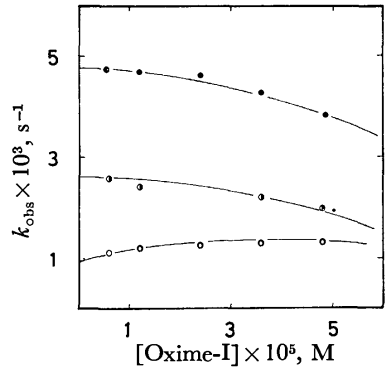

Fig. 5. Correlations between Oxime-I concentration and rate of liberation of *p*-nitrophenoxide ion from PNPD at various temperatures; ● 30.3 °C, ◑ 25.3 °C, and ○ 20.4 °C.

Appendix

Determination of Kinetic and Thermodynamic Parameters for Saturation-type Kinetics. The kinetic and thermodynamic parameters given in Scheme 2 have been evaluated by the aid of Eq. (1). The derivation of this equation is given below.

At the beginning, the abbreviations are made as follows:

S: a substrate species.

C: all the Oxime-I species.

CH: Oxime-I with a undissociated oxime proton.

C$^-$: Oxime-I with an anionic oximate group (Oximate-I in Scheme 2).

S–CH: a substrate–Oxime-I inclusion complex with a undissociated oxime proton (S–Oxime-I in Scheme 2).

S–C$^-$: a substrate–Oxime-I inclusion complex with an anionic oximate group (S–Oximate-I in Scheme 2).

Mass balances in consistent with Scheme 2 are established as follows.

$$[S]_T = [S] + [S\text{–}CH] + [S\text{–}C^-] \quad (4)$$

$$[C]_T = [CH] + [C^-] + [S\text{–}CH] + [S\text{–}C^-] \quad (5)$$

Relevant equilibrium constants are also given.

$$K_a = \frac{[S\text{–}C^-][H^+]}{[S\text{–}CH]} \quad (6); \qquad K_a' = \frac{[C^-][H^+]}{[CH]} \quad (7)$$

$$K_b = \frac{[S\text{–}CH]}{[S][CH]} \quad (8); \qquad K_b' = \frac{[S\text{–}C^-]}{[S][C^-]} \quad (9)$$

Through combination of Eqs. (4), (5), (6), and (8), the following relation is derived.

$$\begin{aligned}[S\text{–}C^-] &= \frac{K_a}{[H^+]}[S\text{–}CH] = \frac{K_a}{[H^+]}K_b[S][CH] \\ &= \frac{K_a}{[H^+]}K_b\{[S]_T - [S\text{–}CH] - [S\text{–}C^-]\} \\ &\quad \times\{[C]_T - [S\text{–}CH] - [S\text{–}C^-] - [C^-]\} \\ &= \frac{K_a}{[H^+]}K_b\left\{[S]_T - \left(\frac{[H^+]}{K_a}+1\right)[S\text{–}C^-]\right\} \\ &\quad \times\left\{[C]_T - \left(\frac{[H^+]}{K_a}+1\right)[S\text{–}C^-] - [C^-]\right\}\end{aligned}$$

Thus, this leads to the following expression.

$$\begin{aligned}[S\text{–}C^-] &= \alpha K_b\{[S]_T - \gamma[S\text{–}C^-]\} \\ &\quad \times\{[C]_T - \gamma[S\text{–}C^-] - [C^-]\}\end{aligned} \quad (10)$$

where $\alpha = K_a/[H^+]$ and $\gamma = ([H^+]/K_a)+1$.

On the other hand, Eqs. (5) and (7) give

$$[C^-] = \frac{K_a'}{[H^+]}[CH] = \frac{K_a'}{[H^+]}\{[C]_T - [S\text{–}CH] - [S\text{–}C^-] - [C^-]\}$$

Thus,

$$[C^-] = \beta\{[C]_T - \gamma[S\text{-}C^-]\} - \beta[C^-]$$

where $\beta = K'_a/[H^+]$.

Rearrangement results in the following relation.

$$[C^-] = \frac{\{[C]_T - \gamma[S\text{-}C^-]\}\beta}{1+\beta} \quad (11)$$

Combining Eqs. (10) and (11),

$$[S\text{-}C^-] = \alpha K_b\{[S]_T - \gamma[S\text{-}C^-]\} \times \left\{[C]_T - \gamma[S\text{-}C^-] - \frac{\beta\{[C]_T - \gamma[S\text{-}C^-]\}}{1+\beta}\right\}$$

Then,

$$(1+\beta)[S\text{-}C^-] = \alpha K_b\{[S]_T[C]_T - \gamma[S\text{-}C^-][S]_T - \gamma[S\text{-}C^-][C]_T + \gamma^2[S\text{-}C^-]^2\} \quad (12)$$

Since $[S]_T[C]_T \gg \gamma^2[S\text{-}C^-]^2$ is valid, under present experimental conditions,[22] Eq. (12) is simplified as

$$(1+\beta)[S\text{-}C^-] = \alpha K_b[S]_T[C]_T - \alpha K_b\gamma\{[S]_T + [C]_T\}[S\text{-}C^-]$$

This gives the relation as follows.

$$[S\text{-}C^-] = \frac{\alpha K_b[S]_T[C]_T}{1+\beta+\alpha\gamma K_b\{[S]_T+[C]_T\}} \quad (13)$$

The overall rate can be expressed as follows.

$$\begin{aligned} k_{obs}[S]_T &= k_{hyd}[S] + k'_{acyl}[S\text{-}C^-] \\ &= k_{hyd}\{[S]_T - \gamma[S\text{-}C^-]\} + k'_{acyl}[S\text{-}C^-] \\ &= k_{hyd}[S]_T - (k_{hyd}\gamma - k'_{acyl})[S\text{-}C^-] \end{aligned}$$

Upon rearrangement after introduction of Eq. (13) into the above equation,

$$\begin{aligned} k_{obs} - k_{hyd} &= (k'_{acyl} - k_{hyd}\gamma)\frac{\alpha K_b[C]_T}{1+\beta+\alpha\gamma K_b\{[S]_T+[C]_T\}} \\ &= \left(\frac{1}{\gamma}k'_{acyl} - k_{hyd}\right)\frac{K_b[C]_T}{\left(\frac{1+\beta}{1+\alpha}\right)+K_b[S]_T+K_b[C]_T} \end{aligned}$$

Thus, the following equation can be derived from the above reletionship.

$$\frac{1}{k_{obs}-k_{hyd}} = \frac{\left(\frac{1+\beta}{1+\alpha}\right)+K_b[S]_T}{\left(\frac{1}{\gamma}k'_{acyl}-k_{hyd}\right)K_b[C]_T} + \frac{1}{\left(\frac{1}{\gamma}k'_{acyl}-k_{hyd}\right)} \quad (14)$$

References

1) (a) E. J. Fendler and J. H. Fendler, "Advances in Physical Organic Chemistry," Vol. 8, ed. by V. Gold, Academic Press, New York, N. Y. (1970), p. 271. (b) E. Cordes, ed., "Reaction Kinetics in Micelles," Plenum Press, New York, N. Y. (1973).

2) (a) M. L. Bender, "Mechanisms of Homogeneous Catalysis from Protons to Proteins," Wiley-Interscience of John Wiley & Sons, Inc., New York, N. Y. (1971), pp. 382—390. (b) H. C. Kiefer, W. I. Congdon, I. S. Scarpa, and I. M. Klotz, *Proc. Nat. Acad. Sci. U.S.A.*, **69**, 2155 (1972) and references cited therein. (c) T. Kunitake and S. Shinkai, *J. Amer. Chem. Soc.*, **93**, 4247 (1971) and references cited therein.

3) (a) Ref. 2a, pp. 373—382. (b) R. Hershfield and M. L. Bender, *J. Amer. Chem. Soc.*, **94**, 1376 (1972).

4) Y. Murakami, J. Sunamoto, and K. Kano, *Chem. Lett.*, **1973**, 223.

5) Y. Murakami, J. Sunamoto, and K. Kano, This Bulletin, **47**, 1238 (1974).

6) F. M. Menger and C. E. Portnoy, *J. Amer. Chem. Soc.*, **90**, 1875 (1968).

7) G. Némethy and H. Scheraga, *J. Phys. Chem.*, **66**, 1773 (1962).

8) I. H. Pitman, K. Uekama, T. Higuchi, and W. E. Hall, *J. Amer. Chem. Soc.*, **94**, 8147 (1972).

9) R. L. VanEtten, J. F. Sebastian, G. A. Clowes, and M. L. Bender, *ibid.*, **89**, 3242 (1967).

10) R. L. VanEtten, G. A. Clowes, J. F. Sebastian, and M. L. Bender, *ibid.*, **89**, 3253 (1967).

11) D. L. VanderJagt, F. L. Killian, and M. L. Bender, *ibid.*, **92**, 1016 (1970).

12) F. Cramer, W. Saenger, and H.-Ch. Spatz, *ibid.*, **89**, 14 (1967).

13) D. G. Doherty and F. Vaslow, *ibid.*, **74**, 931 (1952).

14) F. Vaslow and D. G. Doherty, *ibid.*, **75**, 928 (1953).

15) A. Ben-Naim, *J. Chem. Phys.*, **54**, 3696 (1971).

16) D. Oakenfull, *J. Chem. Soc., Perkin II*, **1973**, 1006.

17) R. D. Gilliom, "Introduction to Physical Organic Chemistry," Addison-Wesley Publishing Co., Inc., Reading, Mass. (1970), p. 168.

18) E. A. Lewis and L. D. Hansen, *J. Chem. Soc., Perkin II*, **1973**, 2081.

19) C. A. Blyth and J. R. Knowles, *J. Amer. Chem. Soc.*, **93**, 3017 and 3021 (1971).

20) J. O. Edwards and R. G. Pearson, *ibid.*, **84**, 16 (1962).

21) J. L. Lach and T. F. Chin, *J. Pharm. Sci.*, **53**, 924 (1964).

22) The first-order rate constants for the overall reaction were recalculated by the use of those evaluated kinetic parameters (K_a, K_b, and k'_{acyl}) on the basis of Eqs. (1) and (2). These calculated rate constants satisfactorily reproduced the experimental correlation between rate constant and total Oxime-I concentration.

Inositol Derivatives. 9. Lithium Aluminum Hydride Reduction of Inositol Epoxides and Their Sulfonates[1]

Tetsuo SUAMI, Seiichiro OGAWA, and Yuji FUNAKI

Department of Applied Chemistry, Faculty of Engineering, Keio University, Hiyoshi, Yokohama 223

(Received September 5, 1974)

The reduction of two dianhydroinositols: 1,2:3,4-dianhydro-5,6-*O*-cyclohexylidene-*allo*-inositol (**1**) and 1,2: 5,6-dianhydro-3,4-*O*-cyclohexylidene-*allo*-inositol (**2**), and four sulfonylated anhydroinositols: 1,2-anhydro-5,6-*O*-cyclohexylidene-3,4-di-*O*-mesyl-*chiro*-inositol (**5b**), 1,2-anhydro-5,6-*O*-cyclohexylidene-3,4-di-*O*-tosyl-*chiro*-inositol (**5c**), 1,2-anhydro-5,6-*O*-cyclohexylidene-4-*O*-tosyl-*neo*-inositol (**6**) and 2,3-anhydro-4,5-*O*-cyclohexylidene-1,6-di-*O*-mesyl-*epi*-inositol (**8**), with lithium aluminum hydride has been investigated.

During a course of synthetic studies on deoxy- and dideoxy-inosadiamines,[2] it became necessary to prepare deoxy- and dideoxy-inositol derivatives. The reductive ring opening of an epoxide in sugars with lithium aluminum hydride ($LiAlH_4$) is an extensively studied reaction[3] which has been often used in a synthesis of deoxy-sugars.[4] However, few works have been done on the $LiAlH_4$ reduction of inositol epoxides.

$LiAlH_4$ reduction of 1,2-anhydro-5,6-*O*-cyclohexylidene-*chiro*-inositol (**5a**)[5] has been described to proceed regioselectively to give the 2-deoxy derivative in 87% yield,[6] and it has been suggested that the remote position in the epoxide from the *O*-cyclohexylidene group was preferentially attacked by the hydride. In the present study, the $LiAlH_4$ reduction of dianhydroinositol and sulfonyl derivatives of anhydroinositols have been attempted.

1,2: 3,4-Dianhydro-5,6-*O*-cyclohexylidene-*allo*-inositol (**1**)[5] was treated with $LiAlH_4$ in refluxing tetrahydrofuran (THF) to give a product (**3a**) in 54% yield, whose structure was established as 2,3-*O*-cyclohexylidene-1,4/2,3-cyclohexanetetrol on the basis of the following results.

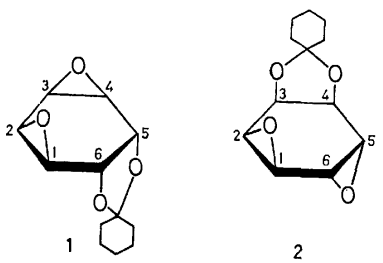

Scheme 1.

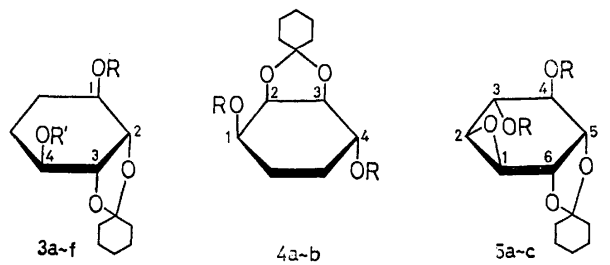

	R	R′
a	H	H
b	Ms	H
c	Ms	Ac
d	Ms	Ms
e	Ts	H
f	Ts	

a	R=H
b	R=Ms

a	R=H
b	R=Ms
c	R=Ts

Scheme 2.

Reduction of 1,2: 5,6-dianhydro-3,4-*O*-cyclohexylidene-*allo*-inositol (**2**)[5] with $LiAlH_4$ at room temperature gave predominantly 2,3-*O*-cyclohexylidene-1,2,3/4-cyclohexanetetrol (**4a**) in 66% yield. Compound **4a** was characterized by converting it into the dimesyl derivative (**4b**), which revealed two sets of quartets at τ 5.43 and 5.79 in its PMR spectrum. These signals are attributed to the H-2 and H-3 protons and the stereochemistry between C-1 and C-4 has been established as *trans*.

In general, $LiAlH_4$ reduction of a secondary sulfonyloxy group of pyranose causes desulfonylation or desulfonyloxylation to give rise to a corresponding hydroxyl or deoxy derivative. Therefore, 1,2-anhydro-5,6-*O*-cyclohexylidene-3,4-di-*O*-sulfonyl-*chiro*-inositol (**5b**: dimesylate[7] and **5c**: ditosylate[5]) were subjected to the $LiAlH_4$ reduction.

Reduction of **5b** at room temperature gave exclusively 2,3-*O*-cyclohexylidene-1-*O*-mesyl-1,4/2,3-cyclohexanetetrol (**3b**) in 70% yield, which was further converted to the acetyl (**3c**) and dimesyl derivatives (**3d**). The PMR spectrum of **3d** revealed a symmetrical multiplet (the A_2 part of the A_2X_2 system) due to the H-2 and H-3 protons at τ 5.62, which indicated a 1,4-*cis* arrangement of two mesyloxy groups, and thus the structure of **3d** was established. When the reduction was carried out at reflux temperature, **3a** was obtained predominantly in 50% yield. It was observed by tlc analysis that **3b** was formed initially in an earlier stage of the reaction and **3b** was subsequently converted into **3a** by further desulfonylation. The structure of **3a** was tentatively established by this fact.

Under the similar condition at reflux temperature, **5c** gave a monotosyl compound (**3e**) in 64% yield. It was shown that the tosyl group was less susceptible to the reduction than the mesyl group.

The reaction mechanism of these reductions might be explained as follows: Initially the hydride attacks exclusively on C-2 as in the case of **5a**, leading to the 2-deoxy compound. Then, a neighboring group participation of the hydroxyl group at C-1, probably by way of alumino hydride complex,[3b,8] results in a removal of the sulfonyloxy group on C-3 by a rear-side attack of the hydride giving rise to the dideoxy compounds.

In the above four compounds, the reduction occurred at the remote points from the *O*-cyclohexylidene group and this might be a reflection of the steric effect of the *O*-cyclohexylidene group.[4c,9]

The reduction of 1,2-anhydro-5,6-*O*-cyclohexylidene-4-*O*-tosyl-*neo*-inositol (**6**)[5] and that of 2,3-anhydro-4,5-*O*-cyclohexylidene-1,6-di-*O*-mesyl-*epi*-inositol (**8**)[7] afforded 1,4-anhydro-5,6-*O*-cyclohexylidene-2-deoxy-*allo*-inositol (**7a**) and -*cis*-inositol (**9a**) in 53 and 17% yield respectively.

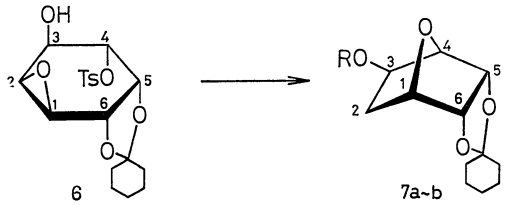

Scheme 3.

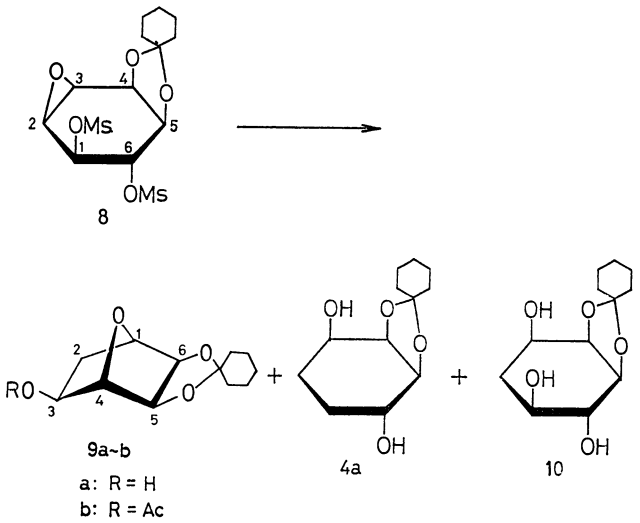

Scheme 4.

The structure of **7a** was deduced from the elementary analysis and PMR spectrum. The C-2 *endo* proton appeared as a quartet at τ 7.29, which was remarkably deshielded by the 5,6-*endo* cyclohexylidene group. Acetylation of **7a** gave the acetyl derivative (**7b**), whose PMR spectrum showed the double doublet due to C-3 *endo* proton at τ 4.56. The formation of **7a** is reasonably explained by a mechanism involving reductive opening of the 1,2-epoxide ring at C-2 in the initial step followed by a transannular nucleophilic substitution by the C-1 hydroxyl group on the C-4 tosyloxy group.[5,10]

The structure of **9a** was also established by the elementary analysis and the well resolved PMR spectrum along with that of its acetyl derivative (**9b**) (Table 1). The coupling constants were shown to be in accordance with those reported for the related compound, *i.e.*, 2,3,5-tri-*O*-acetyl-1,4-anhydro-(2*S*)-2-hydroxyquinate.[11] In the case of **9b**, the double doublet due to the C-3 *endo* proton was upshifted by 0.76 ppm in comparison with that of **7b**, suggesting the presence of the cyclohexylidene group in the *exo* orientation.

Table 1. PMR spectral data of 1,4-anhydro-5,6-*O*-cyclohexylidene-2-deoxy-*cis*-inositol (**9a**) and its acetyl derivative (**9b**) in $CDCl_3$ at 100 MHz

Compd	Chemical shifts[a]	
	9a	**9c**
H_1	5.53 d	5.53 dt
H_{2endo}	—	8.18 qd
H_{2exo}	—	—
H_3	6.15 dd	5.32 dd
H_4	5.73 s	5.62 s
H_5	5.88 d	5.82 d
H_6	5.82 d	5.73 d

Compd	Coupling constants[b]	
	9a	**9b**
$J_{1,2endo}$	0	1
$J_{1,2exo}$	5.5	5.2
$J_{2endo,3}$	6.3	6.8
$J_{2exo,3}$	2.8	3.2
$J_{3,4}$	0	0
$J_{4,5}$	0	0
$J_{5,6}$	5.5	5.5
$J_{1,6}$	0	1
J_{2gem}	—	−13.5

a) Measured on Varian HA-100D (100 MHz) spectrometer. Chemical shifts are given in terms of τ-values, the signals being denoted by s (singlet), d (doublet), dd (double doublet), dt (double triplet), and qd (quartet of doublet). b) Values given for coupling constants are of first-order.

In the case of the reduction of **8**, **9a**, **4a** and 4,5-*O*-cyclohexylidene-2-deoxy-*epi*-inositol (**10**) were obtained in 17, 4.5 and 11% yields, respectively, after fractionation by a column chromatography. The structure of **10** was confirmed by converting it to the known 2-deoxy-*epi*-inositol (**11a**) and its derivative (**11b**).[12] The hydride might attack predominantly on C-2 of **8** to give an intermediary 2-deoxy derivative, from which the three crystalline compounds thus identified are obtained without a big contradiction in a reaction mechanism. That is, desulfonylations of the intermediate afford **10**, and desulfonylation along with desulfonyloxylation gives **4a**. Desulfonylation on the C-1 mesyloxy group and transannular displacement of the C-6 mesyloxy group by the C-3 hydroxyl group yield **9a**.

Experimental

Melting points were determined on a Mitamura Riken micro hot stage and are uncorrected. IR spectra were measured on a JASCO IR-E spectrophotometer in KBr disks. PMR spectra were obtained on a Varian A-60D (60 MHz) spectrometer in deuteriochloroform solution with tetramethylsilane as an internal standard. Chemical shifts are given in terms of τ-values and signals are denoted by s (singlet), d (doublet), dd (double doublet), t (triplet), or m (complex multiplet). All the solutions were concentrated under reduced pressure at 40—50 °C. Tlc was performed on a silica gel plate (Wako-gel B-10, Wako Pure Chemical Industries, Ltd.).

$LiAlH_4$ Reduction of 1,2: 3,4-Dianhydro-5,6-O-cyclohexylidene-allo-inositol (1).[5] To a stirred slurry of $LiAlH_4$ (0.16 g, 3 mol equiv.) in THF (20 ml), was added slowly a solution of **1** (0.30 g) in THF (5 ml), and the reaction mixture was heated under reflux for 30 min. The aluminum complex was then decomposed by addition of water (1 ml). The precipitates were removed by filtration and the filtrate was evaporated to give a crystalline residue which was pulverized with ethanol–*n*-hexane (1: 1, v/v) yielding 0.17 g (54%) of 2,3-*O*-cyclohexylidene-1,4/2,3-cyclohexanetetrol (**3a**): mp 138—139 °C. A part of the product was recrystallized from chloroform–ethanol to give an analytically pure sample, mp 140 °C.

Found: C, 63.12; H, 8.62%. Calcd for $C_{12}H_{20}O_4$: C, 63.13; H, 8.83%.

$LiAlH_4$ Reduction of 1,2: 5,6-Dianhydro-3,4-O-cyclohexylidene-allo-inositol (2).[5] To a stirred slurry of $LiAlH_4$ (80 mg, 3 mol equiv.) in THF (10 ml), a solution of **2** (150 mg) in THF (5 ml) was added, and the agitation was continued for 21 hr at room temperature. The mixture was worked up as described for **1** to give 101 mg (66%) of 2,3-*O*-cyclohexylidene-1,2,3/4-cyclohexanetetrol (**4a**), mp 98—101 °C. A part of **4a** was recrystallized from ethyl acetate–*n*-hexane (1: 2, v/v) to give an analytically pure sample, mp 101—103 °C.

Found: C, 62.91; H, 8.71%. Calcd for $C_{12}H_{20}O_4$: C, 63.12; H, 8.83%.

2,3-O-Cyclohexylidene-1,4-di-O-mesyl-1,2,3,4-cyclohexanetetrol (4b). a) Compound **2** (0.50 g) was treated with $LiAlH_4$ (0.50 g) in THF (12 ml) as described above to give a crude product of **4a**, which was, without any purification, treated with mesyl chloride (0.80 g) in pyridine (5 ml) for 4 hr at room temperature. The reaction mixture was poured into ice-water to give a crystalline product. The product was recrystallized from ethanol to give 0.56 g (65%) of **4b**, mp 151.5—153.5 °C. PMR data: τ 5.43 (dd, 1, H-2, $J_{1,2}$ 3.5 Hz, $J_{2,3}$ 5.5 Hz), 5.79 (dd, 1, H-3, $J_{3,4}$ 6.5 Hz), 6.85 (s, 3, OMs) and 6.89 (s, 3, OMs).

Found: C, 43.62; H, 6.13; S, 16.82%. Calcd for $C_{14}H_{24}O_8S_2$: C, 43.73; H, 6.30; S, 16.68%.

b) A solution of **2** (1.0 g) in ethanol (40 ml) was hydrogenated in the presence of Raney nickel T-4[13] in a Parr shaker apparatus under 3.4 kg/cm^2 of hydrogen pressure for 43 hr at room temperature. The catalyst was filtered off and the filtrate was evaporated to dryness. The residue was treated with mesyl chloride as described in a) to give 1.05 g (61%) of **4b**, mp 152—153 °C. This compound was identical with that obtained in a).

1,2-Anhydro-5,6-O-cyclohexylidene-3,4-di-O-mesyl-chiro-inositol (5b). 1,2-Anhydro-5,6-*O*-cyclohexylidene-*chiro*-inositol (**5a**)[5] (1.5 g) was treated with mesyl chloride (2.9 ml) in pyridine (30 ml) in a refrigerator for 2 days, and then at room temperature for 2 days. The mixture was poured into ice-water and the resulting crystals were recrystallized from chloroform–ethanol (1: 1, v/v) to give 1.97 g (80%) of **5b**, mp 150—152 °C.

Found: C, 42.51; H, 5.54; S, 15.84%. Calcd for $C_{14}H_{22}O_9S_2$: C, 42.20; H, 5.57; S, 16.09%.

$LiAlH_4$ Reduction of 5b. A solution of **5b** (6.0 g) in THF (50 ml) was added dropwise to a stirred slurry of $LiAlH_4$ (1.8 g, 3 mol equiv.) in THF (250 ml), and the mixture was stirred at room temperature for 2.5 hr. The mixture was worked up as described in the reduction of **1** to give, after recrystallization from ethanol, 3.18 g (70%) of 2,3-*O*-cyclohexylidene-1-*O*-mesyl-1,4/2,3-cyclohexanetetrol (**3b**), mp 135—139 °C. A part of the product was recrystallized from ethanol to give an analytically pure sample, mp 139—141 °C.

Found: C, 51.10; H, 7.16; S, 10.28%. Calcd for $C_{13}H_{22}O_6S$: C, 50.96; H, 7.24; S, 10.46%.

Compound **3b** (0.20 g) was treated with acetic anhydride (5 ml) and pyridine (5 ml) overnight at room temperature. The solution was evaporated to give a syrup which was crystallized from ethanol to give 0.15 g (65%) of the acetyl derivative (**3c**), mp 90—93 °C. PMR data: τ 5.80 (the A_2 part of A_2X_2 system, 2, H-2 and H-3), 6.86 (s, 3, OMs) and 7.91 (s, 3, OAc).

Found: C, 52.08; H, 6.95; S, 9.35%. Calcd for $C_{15}H_{24}O_7S$: C, 51.71; H, 6.94; S, 9.20%.

Compound **3b** (2.6 g) was mesylated as described in **4b** to give, after recrystallization from chloroform–ethanol (1: 2, v/v), 2.8 g (86%) of the dimesyl derivative (**3d**), mp 169—170 °C. PMR data: τ 5.03 (m, 2, H-1 an H-4), 5.62 (the A_2 part of A_2X_2 system, 2, H-2 and H-3), 6.82 (s, 6, 2OMs), and 7.94 (t, 4, methylene protons on C-5 and C-6, J 3 Hz).

Found: C, 43.45; H, 6.27; S, 16.66%. Calcd for $C_{14}H_{24}O_8S_2$: C, 43.73; H, 6.30; S, 16.68%.

$LiAlH_4$ Reduction of 5a at Elevated Temperature. A solution of **5b** (1.0 g) in THF (40 ml) was treated with $LiAlH_4$ (0.70 g, 7 mol equiv.) at reflux temperature for 2.5 hr. The reaction mixture was worked up in the usual way to give 0.31 g (55%) of **3a**, mp 124—130 °C. A part of the product was recrystallized as described in **1** to give crystals of mp 140 °C which was identical with the compound **3a** obtained by the reduction of **1**.

$LiAlH_4$ Reduction of 1,2-Anhydro-5,6-O-cyclohexylidene-3,4-di-O-tosyl-chiro-inositol (5c).[5] A mixture of **5c** (8.0 g), $LiAlH_4$ (3.5 g, 6 mol equiv.) and THF (350 ml) was treated at reflux temperature for 1 hr. The reaction mixture was worked up as described in the preparation of **3b** to give, after recrystallization from ethanol, 3.54 g (64%) of 2,3-*O*-cyclohexylidene-1-*O*-tosyl-1,4/2,3-cyclohexanetetrol (**3e**), mp 136—139 °C. Recrystallization from ethanol afforded an analytically pure sample, mp 138—139 °C.

Found: C, 59.86; H, 6.82; S, 8.35%. Calcd for $C_{19}H_{27}O_6S$: C, 59.51; H, 7.09; S, 8.38%.

Conventional acetylation of **3e** (0.15 g) gave 0.12 g (70%) of the acetyl derivative (**3f**), mp 91—92 °C. PMR data: τ 5.88 (m, 2, H-2 and H-3), 7.54 (s, 3, aryl-CH_3) and 7.95 (s, 3, OAc).

Found: C, 59.29; H, 6.68; S, 7.72%. Calcd for $C_{21}H_{28}O_7S$: C, 59.42; H, 6.65; S, 7.55%.

$LiAlH_4$ Reduction of 1,2-Anhydro-5,6-O-cyclohexylidene-4-O-tosyl-neo-inositol (6).[5] To a slurry of $LiAlH_4$ (0.23 g, 3 mol equiv.) in THF (38 ml) was added a solution of **6** (0.80 g) in THF (6 ml), and the mixture was stirred for 6 hr at room temperature. The reaction mixture was worked up as described above to give a product, which showed in tlc (2-butanone–toluene 1: 1, v/v) a presence of one major component (R_f 0.51) and two minor components (R_f 0.33 and 0.29). The crude product was recrystallized from methanol to give 0.24 g (53%) of the major product: 1,4-anhydro-5,6-*O*-cyclohexylidene-2-deoxy-*allo*-inositol (**7a**), mp 77—80 °C. PMR data: τ 7.29 (dd, 1, H-2 *endo*, $J_{1.2endo}$ 0 Hz, J_{2gem} −13 Hz, $J_{2endo,3}$ 7.5 Hz).

Found: C, 63.85; H, 7.97%. Calcd for $C_{12}H_{18}O_4$: C, 63.70; H, 8.02%.

Conventional acetylation of **7a** (0.10 g) gave the acetyl derivative (**7b**), which was recrystallized from ethanol to give an analytically pure sample (70 mg, 59%), mp 88—89 °C. PMR data: τ 4.56 (dd, 1, H-3, $J_{2endo,3}$ 7.5 Hz, $J_{2exo,3}$ 2.5 Hz, $J_{3,4}$ 0 Hz), 7.21 (dd, 1, H-2endo, $J_{1,2endo}$ 0 Hz, J_{2gem} −13 Hz) and 7.94 (s, 3, OAc).

Found: C, 62.42; H, 7.37%. Calcd for $C_{14}H_{20}O_5$: C, 62.67; H, 7.51%.

The mother liquor from **7a** was concentrated to give a syrup which was chromatographed on a silica gel column (50 g) and eluted by 2-butanone–toluene (1: 1, v/v). From the fraction

of the two minor components, 4 mg of crystals, mp 130—131 °C were obtained by recrystallization from ethanol–*n*-hexane (1:2, v/v). This product was indistinguishable from **3a** on tlc, but the IR spectrum was somewhat different from that of **3a** to suggest that the product was probably an isomer of *O*-cyclohexylidene-cyclohexanetetrol.

*$LiAlH_4$ Reduction of 2,3-Anhydro-4,5-O-cyclohexylidene-1,6-di-O-mesyl-*epi*-inositol (8).*[7] Compound **8** (4.0 g) was treated with $LiAlH_4$ (1.52 g) in THF (150 ml) at reflux temperature for 2 hr. The mixture was worked up in the usual manner to give a syrupy product (1.8 g), whose tlc showed the presence of four components: R_f 0.46, 0.38, 0.32, and 0.18 (2-butanone–toluene 2:1, v/v). The product was chromatographed on a silica gel column (100 g) with 2-butanone–toluene (2:5, v/v) as an eluent.

First fraction gave 391 mg (17%) of 1,4-anhydro-5,6-*O*-cyclohexylidene-2-deoxy-*cis*-inositol (**9a**), mp 100 °C. Recrystallization from ethanol–*n*-hexane (1:2, v/v) gave an analytically pure sample, mp 98—101 °C.

Found: C, 63.60; H, 8.00%. Calcd for $C_{12}H_{18}O_4$: C, 63.70; H, 8.02%.

Compound **9a** was acetylated in the usual manner to give the acetyl derivative (**9b**), mp 88—90 °C. Recrystallization from ethanol–*n*-hexane (1:2, v/v) gave an analytical sample, mp 90—91 °C.

Found: C, 62.36; H, 7.40%. Calcd for $C_{14}H_{20}O_5$: C, 62.67; H, 7.51%.

Second fraction gave 103 mg (4.5%) of **4a**, mp 98—100 °C, which was identified with the compound obtained from **2**.

Third fraction gave a homogeneous syrup (0.20 g, 8.7%) which was shown by tlc and IR spectrum to be an isomer of *O*-cyclohexylidene-cyclohexanetetrol. But a further structural elucidation was not attempted.

Fourth fraction gave 283 mg (11%) of 4,5-*O*-cyclohexylidene-2-deoxy-*epi*-inositol (**10**), mp 129—133 °C. Recrystallization from ethyl acetate gave an analytically pure sample, mp 133—135 °C.

Found: C, 59.02; H, 8.42%. Calcd for $C_{12}H_{20}O_5$: C, 59.00; H, 8.25%.

Compound **10** (0.20 g) was hydrolyzed in 80% aqueous acetic acid to give, after recrystallization from aqueous methanol, 33 mg of 2-deoxy-*epi*-inositol (**11a**), mp 205—215 °C (lit.[12a] mp 208 °C). (Found: C, 43.66; H, 7.36%).

Conventional acetylation of **11a** (70 mg) gave, after recrystallization from chloroform–ethanol, 140 mg (88%) of the pentaacetyl derivative (**11b**), mp 124—125 °C (lit.[12] mp 113—114 °C, 123—124 °C). PMR data: τ 7.79 (s, 3, axial OAc), 7.94 (s, 3, equatorial OAc), 7.95 (s, 3, equatorial OAc), 7.98 (s, 3, equatorial OAc) and 7.99 (s, 3, equatorial OAc). (Found: C, 51.55; H, 6.02%).

References

1) A part of this experiment was presented at the 30th Annual Meeting of the Chemical Society of Japan, Osaka, April 4, 1974 (Abstract of papers of the meeting, Vol. 3, p.1888). In this paper, all the compounds except for *meso*-compounds are racemic and the formulas depict one enantiomer of the racemate.

2) T. Suami, S. Ogawa, H. Uchino, and Y. Funaki, *J. Org. Chem.*, **40**, 456 (1975).

3) a) N. R. Williams, *Advans. Carbohyd. Chem. Biochem.*, **25**, 109 (1970); b) J. G. Buchanan and H. Z. Sable, "Selective Organic Transformation," Vol. 2, ed. by B. C. Thyagarajan, Wiley Interscience, New York, N. Y. (1972), pp. 40—43.

4) a) S. Umezawa, T. Tsuchiya, and H. Hineno, This Bulletin, **43**, 1212 (1970); b) A. Zobacova, V. Hermankova, and J. Jary, *Coll. Czech. Chem. Commun.*, **36**, 1860 (1971) and references cited therein; c) U. P. Singh and R. K. Brown, *Can. J. Chem.*, **49**, 3342 (1971) and references cited therein; d) T. Trnka and M. Cerny, *Coll. Czech. Chem. Commun.*, **37**, 3632 (1972).

5) T. Suami, S. Ogawa, S. Oki, and K. Ohashi, This Bulletin, **45**, 2597 (1972).

6) T. Suami, S. Ogawa, T. Ueda, and H. Uchino, *ibid.*, **45**, 3226 (1972).

7) T. Suami, S. Ogawa, K. Ohashi, and S. Oki, *ibid.*, **45**, 3660 (1972).

8) a) E. J. Hedgley, O. Merez, and W. G. Overend, *J. Chem. Soc., C*, **1967**, 888; b) F. Sweet and R. K. Brown, *Can. J. Chem.*, **46**, 707 (1968).

9) J. Halbych, T. Trnka, and M. Cerny, *Coll. Czech. Chem. Commun.*, **38**, 2151 (1973).

10) J. S. Brimacombe, J. Minshall, and L. C. N. Tucker, *J. Chem. Soc., Perkin I*, **1973**, 2691 and references cited therein.

11) M. Adlersberg, W. E. Bondinell, and D. B. Sprinson, *J. Amer. Chem. Soc.*, **95**, 887 (1973).

12) a) E. L. May and E. Mosetting, *J. Org. Chem.*, **14**, 1137 (1949); b) B. Magasanik, R. E. Franzl, and E. Chargaff, *J. Amer. Chem. Soc.*, **74**, 2618 (1952).

13) S. Nishimura, This Bulletin, **32**, 61 (1959).

N-Alkylideneanilines. IV.[1] Kinetics and Mechanism for Site-Exchange of the Methyl Groups in *N*-Isopropylideneanilines

Hiizu IWAMURA, Michiko TSUCHIMOTO,* and Shigeo NISHIMURA*

Department of Chemistry, Faculty of Science, The University of Tokyo, Hongo, Tokyo 113
**Department of Industrial Chemistry, Tokyo University of Agriculture and Technology, Koganei, Tokyo 184*

(Received October 26, 1974)

The kinetics of the site-exchange of the methyl groups in twelve *N*-isopropylideneanilines have been studied by the coalescence point analysis of their proton NMR spectra. The free energies of activation at the coalescence temperature were found to be in the range 16.5 (at 53.5 °C for *p*-nitro) ~22.4 (at 161 °C for *p*-amino derivative) kcal/mol. They give a Hammett σ^- ρ plot with ρ=2.83 (r=0.976). The results are interpreted in terms of an in-plane inversion about the imine nitrogen for the site-exchange. Noticeable deviation of the points representing *p*-chloro and *p*-bromo compounds from the linearity indicates the destabilization of the transition state by the electron-releasing resonance effect of the substituents and is consistent with the inversion mechanism.

Of recent years the mechanism of interconversion of (*Z*)- and (*E*)-*N*-arylimines has been the subject of considerable debate, and has been considered in terms of either an in-plane inversion (1) or a torsional mechanism (2).[2,3] The rate of isomerization is characteristically dependent on substituents at either side of the carbon-nitrogen bond of *N*-arylimines. The application of the Hammett linear free energy relationship to the process has shown that the rate is generally less sensitive to the nature of the *C*-aryl substituents. In *N*-benzylideneanilines, for example, substituents on the phenyl rings bound to nitrogen have a much larger effect on the isomerization rate, being correlated by ρ=2.0, while the ρ-value for substitution on the aldehyde ring is only+0.4 (at 30 °C).[2c] Since the torsional mechanism is favored by contribution of a dipolar transition state (I), there should be appreciable substituent effects at both the carbon and nitrogen rings as in the rotation of amide groups. On the other hand, an inversion transition state (II) should be stabilized by resonance interaction with the electron-withdrawing *N*-substituents as in amine inversion, but may be affected to a lesser extent by the *C*-aryl substituents. Thus an inversion mechanism appears in many cases to be preferred.[3] In hexafluoroacetone *N*-arylimines, however, a Hammett plot gives the ρ value of −0.98.[2n] The result is interpreted as being the consequence of a torsional mechanism, in which the single bond character of the imine bond is considered to be favored by contribution of electron-releasing substituents (III). All of these studies concern with *N*-arylimines which carry at the imine carbon atom groups with strong inductive and/or resonance interaction with the imine moiety.

As only limited information is available for the

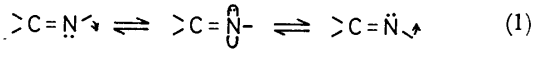

(1)

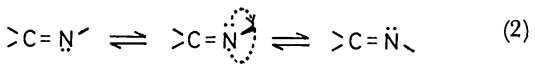

(2)

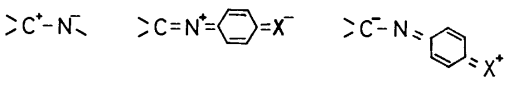

(I) (II) (III)

imines with the *C*-substituents of only moderate electronic effects, we wish to report here the kinetic study on the *N*-isopropylideneanilines.

Results

The temperature-dependent NMR spectra of a series of acetone *N*-arylimines[4] as dilute solutions in bromobenzene were examined. The two characteristic signals due to the (*Z*)- and (*E*)-methyl groups which are separated by 22 (for the *p*-NH_2) to 28.5 Hz (for the *m*-CF_3 derivative) were taken into account. The chemical shift differences between these two methyl signals for each imine change very little in the temperature range of −40 °C to +20 °C (in the case of *N*-isopropylidene-*p*-nitroaniline the range is −40 °C to −10 °C). As the temperature is raised, the two lines first start to broaden and then coalesce to a singlet. The coalescence temperature depends heavily on the nature of ring substituents. In a lower extreme of *N*-*p*-nitrophenylimine, it is only at 54 °C. In the other extreme it is as high as 161 °C for the *p*-amino derivative. One-point interconversion rate constants, k_c, at the coalescence temperature were obtained from the spectra using the relationship in Eq. (3) where ν_{ab} refers to the chemical shift difference of the two methyl singlets.[5] From the values of k_c and T_c thus determined, the free energy of activation at T_c, denoted $\Delta G_c^{\ddagger}$, was calculated using the Eyring equation and assuming as usual a value of unity for the transmission coefficient (Eq. (4)).

$$k_c = \pi \cdot \nu_{ab}/\sqrt{2} = 2.22\nu_{ab} \quad (3)$$

$$\ln(k/T) = \ln(k/h) - \Delta G^{\ddagger}/RT = \ln(k/h) + \Delta S^{\ddagger}/R - (\Delta H^{\ddagger}/RT) \quad (4)$$

The pertinent NMR and kinetic data are summarized in Table 1. Although it is difficult to estimate the error in such one-point rate constants, it can be shown that the value of $\Delta G_c^{\ddagger}$ is rather insensitive to the exact choice of k_c.[2e] It is desirable for the following discussion to compare the rates of interconversion at the same temperature. Strictly speaking, this can be done only with a knowledge of $\Delta S^{\ddagger}$ for each compound as seen in Eq. (4). Therefore the $\Delta G_c^{\ddagger}$ values are compared to show the substituent effects.

Table 1. NMR and kinetic data of *N*-isopropylideneanilines

X	T_c, °C	$\Delta\nu_{ab}$, Hz	k_c, s^{-1}	ΔG_c^*, kcal/mol	k_{25}, s^{-1} [a]
p-NH_2	161.1	22.0	48.9	22.4	2.36×10^{-4}
p-OCH_3	138.8	23.5	52.2	21.1	1.98×10^{-3}
p-CH_3	133.8	24.0	53.3	20.9	3.92×10^{-3}
H	127.1	25.5	56.7	20.5	6.06×10^{-3}
	126			20.3 [2b]	
p-F	124.4	25.0	55.5	20.3	7.68×10^{-3}
p-I	122.3	26.0	57.5	20.2	9.70×10^{-3}
p-Cl	130.8	26.5	58.9	20.6	4.71×10^{-3}
p-Br	128.3	26.5	58.9	20.5	5.92×10^{-3}
m-CF_3	110.2	28.5	63.2	19.5	3.22×10^{-2}
p-$COOCH_3$	99.7	27.0	59.9	19.0	7.76×10^{-2}
p-$COCH_3$	87.7	26.5	58.8	18.3	2.21×10^{-1}
p-NO_2	53.5	27.5	61.1	16.5	4.78×10^{-1}

a) The rate constants at 25 °C estimated on assuming a similar entropy of activation.

Discussion

The site-exchange of the methyl groups in *N*-isopropylideneanilines can be achieved either by an in-plane inversion at the nitrogen center or by rotation of the carbon-nitrogen bond (Eqs. (1) and (2), respectively). Both mechanisms are found to be actually operative in lower analogues; typical examples are the inversion in methyleneimine CH_2=NH and the rotation in carbodiimide HN=C=NH.[6] Attempts to choose between these mechanisms have been made by the application of the Hammett free energy relationship to the ΔG_c^* data in Table 1. On assuming a similar entropy of activation for the series of *N*-isopropylideneanilines, we note the results correspond to 10^3-fold enhancement of the rates at 25 °C on going from the *p*-amino to *p*-nitro derivatives. The increased facility of isomerization with electron-withdrawing groups on *N*-phenyl rings, as indicated by the positive slope, is consistent with a transition state of type II. A better linear correlation (ρ=2.83, r=0.976) is found when σ^- values are used in place of σ. The result suggests that the para-substituents capable of stabilizing a negative charge by resonance are especially favorable, thus providing further support for the transition state structure II. It may be argued that the same trend of $\sigma^-\rho$ correlation could also have been predicated for a rotational transition state I.[2k] However, two methyl groups are considered not to be strong enough to stabilize the positive charge on the imine carbon. In contrast to the groups such as dimethylamino, methoxy and methylthio which have unshared electron pairs on the heteroatoms that permit resonance stabilization of I, hyperconjugative effect of methyl groups are limited. The ΔG^* values for a series of *N*-phenylimines summarized in the first column of Table 2 afford an excellent insight into the effect of *C*-substituents. We note that the trasition state for the site-exchange in the acetone *N*-phenylimine under discussion is among the least stabilized. The lower free energies of activation for other *N*-phenylimines might suggest contribution of torsional character in the transition state which is stabilized as in IV, especially when the *C*-substituents X_1 and X_2 are Me_2N, MeO, and MeS. Since analyses of the *C*-aryl substituent effects,[2c,7] MO calculations,[8] and other arguments[9] have favored an inversion mechanism for the site-exchange process in these *N*-phenylimines, a torsional mechanism finds the remotest possibility in *N*-isopropylideneanilines.

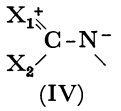

(IV)

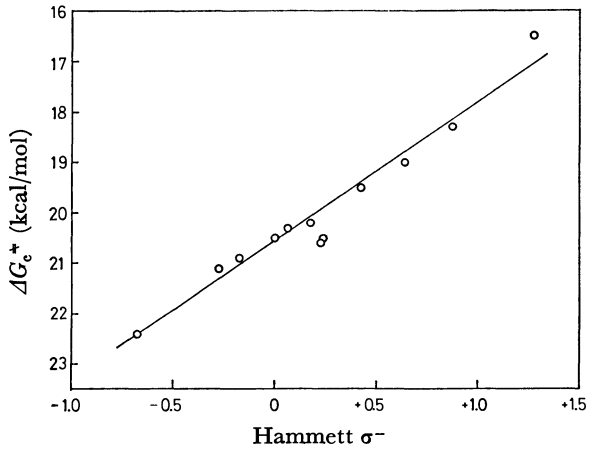

Fig. 1. The Hammett σ^- plots of $-\Delta G_c^*$ values for the site-exchange reaction.

Further inspection of the Hammett plot reveals that the points for the *p*-chloro and *p*-bromo substituents deviate considerably from the linear correlation (see Fig. 1). The errors involved in the approximation used in the coalescence point method can be a responsible factor. However, they are expected to be systematic and may not be a reason for deviation of a particular point or two. It has been shown by the results of more elaborate procedure, *e.g.*, a total line shape analysis, on the similar quinoneanils and ketimines that the relative rates of interconversion are not a sensitive function of the choice of ΔS^* which is furthermore found not to be much different from zero.[2g,2j] It is well-documented that the increase in resonance release of electron density and in inductive electron withdrawal is effective in raising the barrier to inversion of amines.[3] The observed deviation suggests that

Table 2. Hammett correlations in *N*-arylimines $X_1X_2C=NAr$

X_1	X_2	$\Delta G^{\ddagger}$ (T °C)	$\rho_{25°}$	Reference
Me_2N	Me_2N	12.1 (−35)	2.11	2h, 2l, 2m
Ph	H	16.5 (30)	2.04	2c, 2l
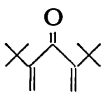		22.2 (140)	1.90	2g, 2l
p-Me-OC_6H_4	*p*-Me-OC_6H_4	18.1 (62)	1.88	2e, 2l
CH_3	CH_3	20.5 (127)	1.71[a]	this work
MeO	MeO	14.3 (0)	1.44	2h
CF_3	CF_3	15.5 (25)	−0.98	2n
CH_3S	CH_3S	13.7 (−22)		2f

a) The rate constants at 25 °C estimated on assuming a similar entropy of activation.

both electronic substituent effects are not adequately represented by the Hammett σ^- constants. The standard Hammett σ values of 0.227 and 0.232 for the *p*-Cl and *p*-Br substituents, respectively, reflect the interplay of the electron-withdrawing inductive (σ_I; 0.348 and 0.337, respectively) and electron-donating resonance effects (σ_π; −0.070 and −0.054, respectively).[10] The fact that the rates of interconversion in *p*-Cl and *p*-Br compounds are slower than in the parent *N*-isopropylideneanilines, *i.e.*, $k_{Cl}/k_H=0.78$ and $k_{Br}/k_H=0.98$,[11] means that resonance substituent effect dominates the stability of the transition state. Precedent for the prevalence of the resonance substituent effect can be found in the pyramidal inversion of aryl *p*-tolyl sulfoxides.[12] Electronic effects on the inversion process for both series of compounds, namely, acetone *N*-arylimines and aryl *p*-tolyl sulfoxides, are quite similar.

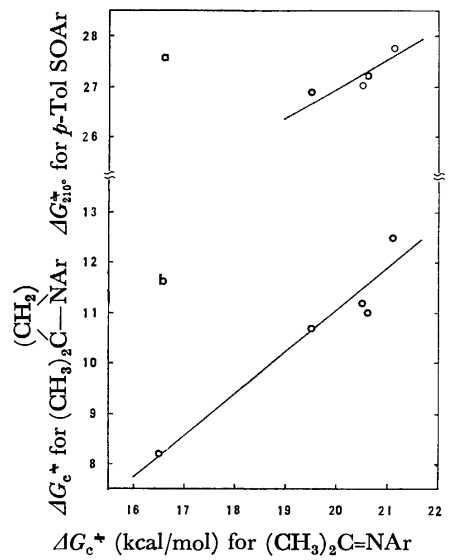

Fig. 2. Correlation of $\Delta G_c^{\ddagger}$ values for inversion of (a) aryl *p*-tolyl sulfoxides and (b) 2,2-dimethyl-1-arylaziridines *vs.* *N*-isopropylideneanilines.

While the Hammett plots against σ^- give positive slopes as a whole, the relative rates k_{Cl}/k_H are equally less than unity (0.78, at 25 °C in the former and 0.81 at 210 °C in the latter). As a result, the $\Delta G^{\ddagger}$ values correlate very nicely between the two series as shown in Fig. 2a.

Of related interest to the inversion of *N*-arylimine nitrogen is the pyramidal inversion of 1-aryl-2,2-dimethylaziridines (V).[13] When we consider the structural similarity with respect to the unit Me_2C–N–Ar between *N*-isopropylideneanilines and V, it is not unexpected that plots of $\Delta G^{\ddagger}$ values of V *vs.* those of the former show good linear correlation (Fig. 2b). This is taken as another support for an inversion mechanism in the *N*-arylimines. The slope of the line, 0.84, may be regarded as a measure of the sensitivity of the *N*-isopropylideneanilines relative to the aziridines to electronic substituent effects. Furthermore the point for the *N*-*p*-chlorophenylaziridine conforms to the Hammett correlation defined by the other aziridines V; $k_{Cl}/k_H=1.7$ at −60 °C.[13] Thus resonance substituent effects appear not to be dominant in V. These two points, slightly diminished sensitivity to ring substituents and reduced resonance substituent effects in V, indicate that the structural analogy between *N*-arylimines and *N*-arylaziridines for inversion at the

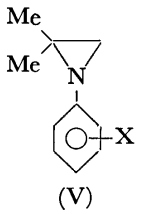

(V)

nitrogen center is only superficial. We propose as one of a number of possible origins of the more effective transmission of substituent effects in the *N*-arylimines relative to *N*-arylaziridines the difference in the nitrogen hybridization in the transition state for inversion, In the *N*-arylimines, the nitrogen center is sp hybridized and the lone pair of electrons reside in a purely *p*-charactered AO which is most favorably situated to conjugate with the benzene ring (VI). The carbon-nitrogen bonds of aziridine rings are rich in *p*-character as approximated by $sp^{4.1}$ hybridization for the cyclopropane ring orbitals in the Coulson-Moffit model.[14] As a result, the hybridized orbital in which lone pair of electrons reside has some s character to effect reluctance to delocalize into the aromatic ring (VII).

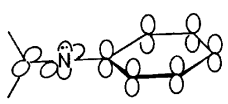

VI

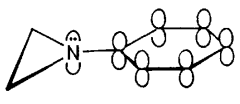

VII

Recently a third mechanism in which tautomerization to the enamine (Eq. 5) has been proposed for the imines which contain a *C*-alkyl-substituent with at least

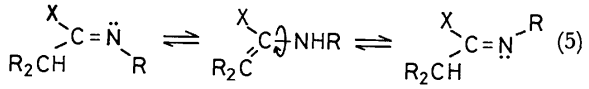

(5)

one α-hydrogen atom.[7] The mechanism has been

shown to be operative in some *N*-alkylimines in which barriers to inversion can often be high ($\Delta G^{\ddagger}\sim25$ kcal/mol).[7] The tautomerism has been shown by the deuterium incorporation experiments in methanol-d_4 to be considerably slower(10^{-5}—10^{-6} s^{-1})[1] than inversion (10^{-1}—10^{-4} s^{-1})[11] in *N*-isopropylideneanilines. Therefore the site-exchange of the methyl groups *via* imine-enamine tautomerism can be ruled out in the case of *N*-isopropylideneanilines.

Experimental

General procedure for the preparation of *N*-isopropylideneanilines:[4] 30 g of Molecular Sieve 4A were added to a solution of 0.1 mol of acetone and 0.05 mol of aniline in anhydrous ether. The mixture was kept at 10 °C for 2 to 3 days, by renewing the Molecular Sieve 2—3 times. After removing the Molecular Sieve by filtration and the solvent by application of a rotary evaporator, the residue was fractionaly distilled.

NMR spectra were obtained on a JEOL C-60HL (Japan Electron Optics Lab. Co., Ltd.) spectrometer (60 MHz), equipped with a variable temperature probe. Solutions of 0.25 mmol of *N*-isopropylideneanilines in 0.5 ml bromobenzene (25 °C——40 °C) containing TMS as internal references were employed. Temperature were calibrated by 1,3-propanediol in the region of 25 °C—160 °C, and by methanol in the region 25 °C——40 °C, and are believed to be accurate to ±1 °C. In the recording of spectra, care was taken to avoid saturation of the signal especially when the height intensity is weak near the coalescence point. Three or more spectra were recorded in the vicinity of each coalescence temperature.

References

1) For part III see: H. Iwamura, M. Tsuchimoto, and S. Nishimura, This Bulletin, **47**, 193 (1974).

2) a) D. Y. Curtin and J. W. Hausser, *J. Amer. Chem. Soc.*, **83**, 3473 (1961); b) H. A. Staab and F. Vögtle, *Tetrahedron Lett.*, **1965**, 51; c) G. Wettermark, J. Weinstein, J. Sousa, and L. Dogliotti, *J. Phys. Chem.*, **69**, 1584 (1965); d) N. P. Marullo and E. H. Wagener, *J. Amer. Chem. Soc.*, **88**, 5034 (1966); e) D. Y. Curtin, E. J. Grubbs, and C. G. McCarty, *ibid.*, **88**, 2775 (1966); f) D. Warmb-Gerlich, F. Vögtle, A. Mammschreck, and H. A. Staab, *Ann.*, **708**, 36, 51, (1967); g) A. Rieker and H. Kessler, *Tetrahedron*, **23**, 3727 (1967); h) H. Kessler, *Tetrahedron Lett.*, **1968**, 2041; i) C. G. McCarty and D. M. Wieland, *ibid.*, **1969**, 1787; j) E. Carlson, F. B. Jones Jr., and M. Raban, *Chem. Commun.*, **1969**, 1235; k) N. P. Marullo and E. H. Wagener, *Tetrahedron Lett.*, **1969**, 2555; l) D. Leibfritz and H. Kessler, *Chem. Commun.*, **1970**, 655; m) H. Kessler and D. Leibfritz, *Tetrahedron*, **26**, 1805 (1970); n) G. E. Hall, W. J. Middleton, and J. D. Roberts, *J. Amer. Chem. Soc.*, **93**, 4778 (1971).

3) For recent reviews see (a) J. M. Lehn, *Fortschr. Chem. Forsch.*, **15**, 311 (1970); Pure and Appl. Chem., Supplement, Special Lectures presented at the XXIIIrd International Congress of Pure and Applied Chemistry, Boston, Vol. 1 (1971), p. 91; (b) I. O. Sutherland, *Ann. Rep. Nucl. Magn. Resonance Spectrosc.*, **4**, 71 (1971); (c) C. G. McCarty in "The Chemistry of the Carbon-Nitrogen Double Bond," S. Patai, Ed., Interscience, London (1969), p. 363.

4) M. Tsuchimoto, S. Nishimura, and H. Iwamura, This Bulletin, **46**, 675 (1973).

5) J. A. Pople, W. G. Schneider, and H. J. Bernstein, "High-resolution Nuclear Magnetic Resonance," McGraw-Hill, New York, N. Y. (1959), p. 223; G. Binsch, *Topics Stereochem.*, **3**, 97 (1968).

6) J. M. Lehn, B. Munsch, and Ph. Millié, *Theor. Chim. Acta*, **10**, 351 (1970); F. A. L. Anet, J. C. Jochins, and C. H. Bradley, *J. Amer. Chem. Soc.*, **92**, 2557 (1970).

7) W. B. Jennings and D. R. Boyd, *ibid.*, **94**, 7187 (1972).

8) C. H. Warren, G. Wettermark, and K. Weiss, *ibid.*, **93**, 4658 (1971), and papers cited therein.

9) The ρ values in the range of 1.4—2.2 in a Hammett $\sigma^{-}\rho$ plot (see Table 2) are often taken as a proof of an inversion mechanism.[21]

10) Y. Yukawa and Y. Tsuno, *Nippon Kagaku Zasshi*, **86**, 887 (1965).

11) See footnote a) in Table 2.

12) D. R. Rayner, A. J. Gordon, and K. Mislow, *J. Amer. Chem. Soc.*, **90**, 4854 (1968); D. R. Rayner, E. G. Miller, P. Brickart, A. J. Gordon, and K. Mislow, *ibid.*, **88**, 3138 (1966).

13) J. D. Andose, J. M. Lehn, K. Mislow, and J. Wagner, *ibid.*, **92**, 4050 (1970).

14) C. A. Coulson and W. E. Moffitt, *J. Chem. Phys.*, **15**, 151 (1947).

Photo-addition Reaction of 1,4-Naphthoquinone with Olefins.[1] Formation of 2:1 Addition Compounds

Kazuhiro MARUYAMA, Yoshinori NARUTA, and Tetsuo OTSUKI*

Department of Chemistry, Faculty of Science, Kyoto University, Kyoto 606

** Department of Chemistry, Faculty of Home Economics, Kyoto Women's University, Kyoto 605*

(Received November 18, 1974)

A novel type of the photo-addition compound, 5,8,13,14-tetraoxo-5,5a,6, 7,7a,8,13,13a,13b,14-decahydropentaphene derivatives (**3**), consisting of two molecules of 1,4-naphthoquinone and one molecule of an olefin was obtained in the photochemical reaction of 1,4-naphthoquinone with olefins. Its structure was determined from spectral data as well as results obtained from the chemical reactions. Olefins which give this type of photo-addition compound are characterized by their bicyclo-ring systems containing considerable ring strains. The reaction mechanism for formation of the compound was discussed in terms of the ring strains of olefins and the nature of the photo-excited 1,4-naphthoquinone.

Photochemistry has provided versatile routes to many elegant compounds which otherwise are difficult to prepare.[2] From synthetic and theoretical viewpoints, elucidation of the photochemical behaviour of quinones would be fruitful since quinones and related compounds play an important role in natural environments. Several workers[3,4] have investigated the photochemical reaction of 1,4-naphthoquinone with olefins. 1,4-Naphthoquinone has been found to give 1:1 photo-addition compounds with olefins, besides the photo-reduction products of 1,4-naphthoquinone such as 1,4-naphthohydroquinone and 1,4-naphthoquinhydrones. The photo-addition compounds reported

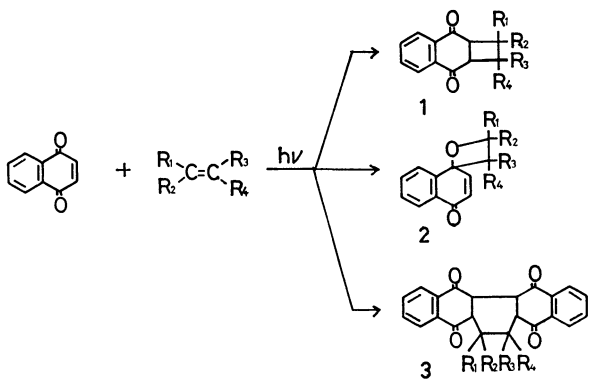

so far were classified into structural types **1** and **2**.[3,4] We have now been able to isolate a novel type of 2:1 photo-addition compound **3** in the photochemical reaction of 1,4-naphthoquinone with olefins characterized by their bicyclo-ring systems containing considerable ring strains. The photo-addition compound was confirmed to consist of two molecules of 1,4-naphthoquinone and one molecule of an olefin and to have the structure **3** by inspection of the spectral data and from the Baeyer-Villiger oxidation of the addition compound.[1] In this report the reaction mechanism for the formation of this novel photo-addition compound **3** is discussed on the basis of product analyses and quenching experiments.

Results and Discussion

Photo-addition Compounds Obtained in the Photochemical Reaction of 1,4-Naphthoquinone with Olefins. A benzene solution of 1,4-naphthoquinone was subjected to photochemical reaction of olefins on irradiation with a high pressure Hg arc lamp. Olefins examined here were all characterized by their strained bicyclo-ring systems, such as bicyclo[4.2.0]oct-7-ene **4a**,[5] bicyclo[2.2.1]hept-2-ene **4b**, *endo*-2-acetoxybicyclo[2.2.1]hept-5-ene **4c**,[6] bicyclo[2.2.2]oct-2-ene **4d**, *trans*-2,3-dicyanobicylo[2.2.2]oct-5-ene **4e**,[7] 2,2,3,3-tetracyanobicyclo[2.2.2]oct-5-ene **4f**[8] and 4-oxatricyclo[2.2.5^{2,6}]undec-8-ene **4g**.

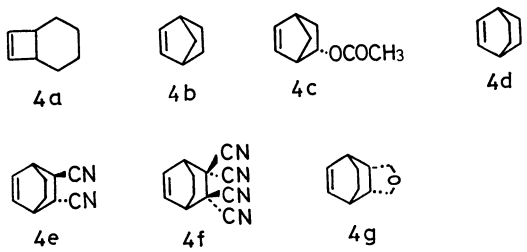

With olefins **4a**, **4b** and **4d**, the photochemical reaction of 1,4-naphthoquinone was found to produce the photo-addition compounds without the formation of 1,4-naphthohydroquinone or 1,4-naphthoquinhydrones. The photo-addition compounds isolated were subjected to further examination for determination of their structures. From the results the photo-addition compounds could be classified into three structural types **1**, **2** and **3**. Structure **3** was determined by the isolation of methyl ester of cyclohexane tetracarboxylic acid derivatives **5** when the photo-addition compound **3b** was subjected to oxidative degradation by perfluoroacetic acid and subsequent esterification with diazomethane.[1] The photo-addition compound **3** is outstanding, being constructed from two molecules of 1,4-naphthoquinone and one molecule of an olefin, while **1** and **2** are each composed of one moelcule of 1,4-naphthoquinone and an olefin. Compound **3** was

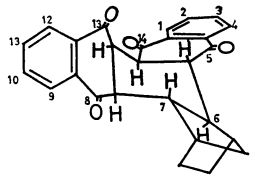

3b

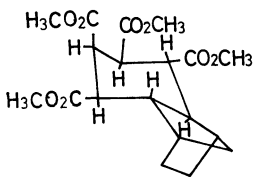

5

Table 1. Yields of the photo-addition compounds[a)]

Olefin	The photo-addition compounds %)[c)]		
	1	2	3
4a	—(**1a**)	—(**2a**)	1(**3a**)
4b	[b)](**1b**)	6(**2b**)	10(**3b**)
4d	9(**1d**)	trace(**2d**)	4(**3d**)

a) The yields were estimated on the basis of the amount of quinones consumed (30 °C). b) **1b** was identified only in the presence of fumaronitrile in the reaction system. c) The other products were unidentified resionous matters.

first isolated in this work. The distributions and the yields of these photo-addition products are summarized in Table 1.

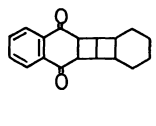

1a

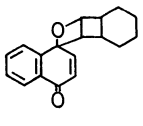

2a

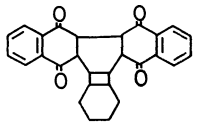

3a

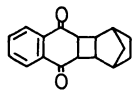

1b

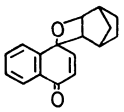

2b

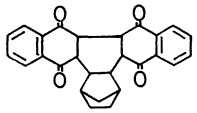

3b

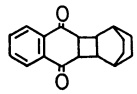

1d

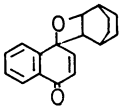

2d

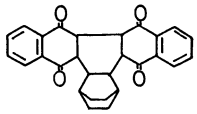

3d

Olefin **4g** was found to react as a reducing agent due to its active hydrogen atoms to yield 1,4-naphthoquinhydrones, no photo-addition products being isolated. With olefins characterized by having electron withdrawing substituents such as **4c**, **4e** and **4f**, 1,4-naphthoquinone could not undergo the photo-addition reaction, but the photo-dimerization of 1,4-naphthoquinone proceeded to yield its dimer **6**[9)] as a sole reaction product. For elucidation of the mechanism for formation of the photo-addition compounds **1**, **2** and especially **3**, the behaviour of photo-excited 1,4-naphthoquinone was investigated.

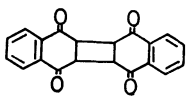

6

Quantum Yields and Relation to Their Ring Strains in Olefins. Quantum yields of the cycloaddition were measured in the reaction of 1,4-naphthoquinone with **4b** and **4d** on irradiating (λ>300 nm) the degassed solution of 1,4-naphthoquinone and an olefin at room temperature using potassium ferrioxalate as a chemical actinometer. The results are summarized in Table 2. Although the quantum yields for the formation of **3b** and **3d** are comparable, it should be noted that the quantum yield for the formation of **1d**+**2d** is about five times greater than that of **1b**+**2b**, and the quantum yield for the formation of **2b** is about ten times greater than that of **2d**. Taking into account the fact that olefin **4a** gives none of **1a** or **2a**, we find that the formation of **1** or **2** is much influenced by the nature of olefins subjected to the reaction, particularly by the ring strains in olefins. Coupling constants of olefinic protons with ^{13}C ($J_{^{13}C-H}$) are the direct measure of the ring strains of the double bonds in olefins. They are given in Table 3 together with the % *s*-character

Table 2. Quantum yields for the formation of photo-addition compounds[a,b)]

Olefin	The photo-addition compounds		
	1	2	3
4b	~0 (**1b**)	5.6×10^{-3}(**2b**)	8.8×10^{-3}(**3b**)
4d	26.0×10^{-3}(**1d**)	0.5×10^{-3}(**2d**)	9.0×10^{-3}(**3d**)

a) The quantum yields were extrapolated to zero hours of the reaction. b) The quantum yields were measured at 30 °C.

Table 3. Coupling constants of ^{13}C–H and its % *s*-character

Olefin	$J_{^{13}C-H}$	% *s*-character
4a	170 Hz	34
4b	165 Hz[a)]	33
4d	158 Hz	32

a) K. Tori, R. Muneyuki, H. Tanida, *Can. J. Chem.*, **14**, 3142 (1963).

of the C–H bonds estimated therefrom. The $J_{^{13}C-H}$ in **4d** (158 Hz) is comparable to that in cyclohexane ($J_{^{13}C-H}$=157 Hz),[10)] which is estimated to have no ring strains. It was deduced that the formation of the cyclobutane or oxetane type of compound **1** or **2** becomes less favorable as the ring strains in olefins increase; that is, none of **1a** or **2a** could be identified in the photochemical reaction of 1,4-naphthoquinone with **4a**, which has the greatest value of $J_{^{13}C-H}$ and is consequently of the greatest ring strain among the olefins examined here. On the other hand, no further chemical change could be observed on irradiating the benzene solution of **1b** in the presence of excess 1,4-naphthoquinone nor on irradiating the benzene solution of the dimer **6** in the presence of excess bicyclo[2.2.1]-hept-2-ene **4b**. From these results neither **1b** nor **6** could be the precursor of **3b**. Dependence of the yields of the photo-addition compounds **2b** and **3b** on the concentration of bicyclo[2.2.1]hept-2-ene **4b** was measured (Fig. 1). As the concentration of bicyclo-[2.2.1]hept-2-ene increases, the yields of both **2b** and **3b** increase, while the amount of the dimer **6** is depressed. Moreover, it is seen that the ratio **3b**/**2b** is nearly constant irrespective of the concentration of bicyclo-[2.2.1]hept-2-ene. The results exclude the possibility of simultaneous formation of **3b** from two molecules of 1,4-naphthoquinone and one molecule of bicyclo-[2.2.1]hept-2-ene, and suggest that the similar types of

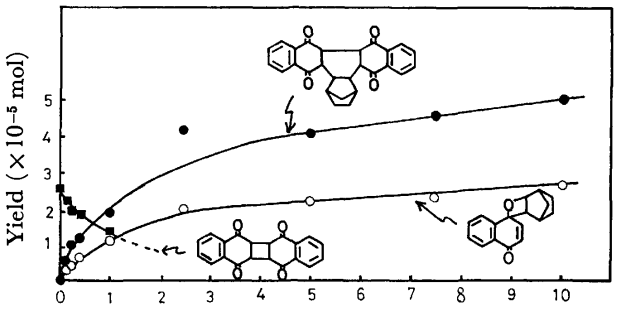

Fig. 1. Dependence of the yields of the photo-addition compounds on the concentration of bicyclo[2.2.1]hept-2-ene.
The 0.100 M-benzene solution of 1,4-naphthoquinone is submitted to the photochemical reaction (30 °C).

reaction intermediates are concerned with the formation of **2b** and **3b**. Consequently it can be deduced that the reaction intermediates for the formation of **2b** and **3b** are each composed of one molecule of 1,4-naphthoquinone and bicyclo[2.2.1]hept-2-ene as illustrated by **7** and **8**, respectively. The effects of higher

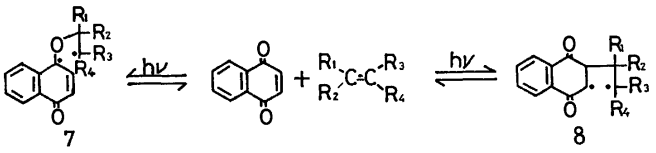

ring strains in olefin **4** on the formation of **2** might be explained, if we assume that compound **2** is produced *via* the ring closure of diradical **7** (see Tables 1 and 2), and compounds **1** and **3** *via* diradical **8**. The larger ring strains in olefins would be less favourable for the ring closure to yield **1** and **2**, because of the lack of the energy relaxation mode to bonding vibration or ring fluctuation. This would result in the longer life-time of the diradicals to meet other molecules or to decompose to the starting quinone and olefin. The fairly large steric repulsion for the ring closure may be another factor to lead to the longer life-time of the diradicals. Thus, **3** may be formed. Actually, the relative yield of **3** in each reaction is high in the order of the higher ring strain of olefins, and the cyclobutane type of **1** could be isolated only in the reaction of 1,4-naphthoquinone with **4d**, which would contain the least ring strains of the three olefins examined. The unidentified resinous matter, *i.e.* polymers produced in the highest yield of the products, may be formed on the same basis as described above. The smaller yield of **2d** compared with **2b** could result from the larger steric hindrance against the ring closure due to bulkier bicyclo[2.2.2]-oct-2-ene moiety. In the presence of fumaronitrile, however, the excess energy in **8b** would transfer to fumaronitrile to produced **1b** even if the minor portion of **8b** is concerned. Details of the photo-excited states

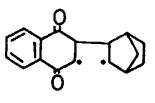
8b

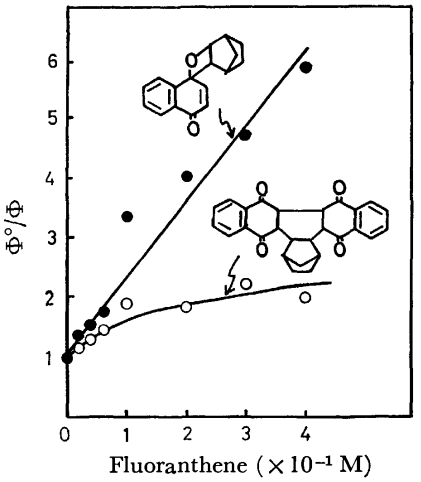

Fig. 2. Stern-Volmer plots quenched by fluoranthene in the photochemical reaction of 1,4-naphthoquinone with bicyclo[2.2.1]hept-2-ene (30 °C).

of 1,4-naphthoquinone to produce the diradical intermediates such as **7** or **8**, and subsequently to yield the photo-addition compounds are discussed in the following.

Correlation between the Reactivity and the Multiplicity of the Photo-excited 1,4-Naphthoquinone. The triplet energy of 1,4-naphthoquinone has been estimated to be 58 kcal/mol.[11] Fluoranthene could quench the triplet excited state of 1,4-naphthoquinone since E_T-value for fluoranthene has been estimated to be 54 kcal/mol.[12a] Dependence of the quantum yields for the formation of **2b** and **3b** on the concentration of fluoranthene as a quencher was estimated. The Stern-Volmer plots are shown in Fig. 2, in which the straight line for the formation of **2b** indicates that **2b** is formed through the triplet excited state of 1,4-naphthoquinone. This agrees with the findings that the oxetanes are formed *via* the triplet excited states in the photochemical reaction of benzophenone[12b] or *p*-benzoquinone[16] with olefins. Scheme 1 shows the reaction paths for the formation of oxetanes *via* diradical **7**, involving unimolecular deactivation of the excited state of 1,4-

$$D \xrightarrow{h\nu} {}^1D^*$$

$$^1D^* \xrightarrow{k_f,\ k_d^S} D$$

$$^1D^* \xrightarrow{k_{ST}} {}^3D^*$$

$$^3D^* \xrightarrow{k_d^T} D$$

$$^3D^* + A \xrightarrow{k_a} D\text{-}A$$

$$D\text{-}A \xrightarrow{k_r} Ox$$

$$D\text{-}A \xrightarrow{k_d'} D + A$$

$$^3D^* + Q \xrightarrow{k_q} D + {}^3Q^*$$

D : 1,4-Naphthoquinone
A : Bicyclo[2.2.1]hept-2-ene (**4b**)
Q : Fluoranthene
Ox: Spiro-oxetane (**2b**)

Scheme 1.

naphthoquinone (k_f, k_d^S, k_p^T), intersystem crossing (k_{ST}), formation of diradical intermediate **7** (k_a), formation of oxetane (k_r) and dissociation of diradical intermediate **7** (k_d') and the triplet quenching of 1,4-naphthoquinone by fluoranthene (k_q). The quantum yields for the formation of oxetanes are expressed as Φ_{ox} and/or Φ_{ox}°, corresponding to whether in the presence and/or absence of quencher, respectively (Eqs. (1) and/or (2)).

$$\frac{1}{\Phi_{ox}} = \frac{1}{\Phi_{ST}}\left(1+\frac{k_d'}{k_r}\right)\left(1+\frac{k_d^T+k_q[Q]}{k_a[A]}\right) \quad (1)$$

$$\frac{1}{\Phi_{ox}^{\circ}} = \frac{1}{\Phi_{ST}}\left(1+\frac{k_d'}{k_r}\right)\left(1+\frac{k_d^T}{k_a[A]}\right) \quad (2)$$

The relative ratio $\Phi_{ox}^{\circ}/\Phi_{ox}$ can be derived from Eqs. (1) and (2) as follows.

$$\frac{\Phi_{ox}^{\circ}}{\Phi_{ox}} = 1 + \frac{k_q[Q]}{k_a[A]+k_d^T} = 1 + k_q\tau[Q] \quad (3)$$

τ: the life-time of the tripelt state of 1,4-naphthoquinone in the absence of a quencher.

From the slope and the intercept of the plots shown in Fig. 2 and $\Phi_{ox}^{\circ}=0.0056$, the following rate constants and the ratio can be evaluated; $k_a=2.0\times10^6$ $M^{-1}s^{-1}$, $k_d^T=3.0\times10^7$ s^{-1}, $k_d'/k_r=100$, assuming $\Phi_{ST}\simeq1$[13] and $k_q=5.0\times10^9$ $M^{-1}s^{-1}$ for the benzene solution at 25 °C[14]. These values are compatible to those obtained in the photochemical reaction of benzophenone with furan.[15] The state diagram estimated for the formation of oxetanes is given in Fig. 3.

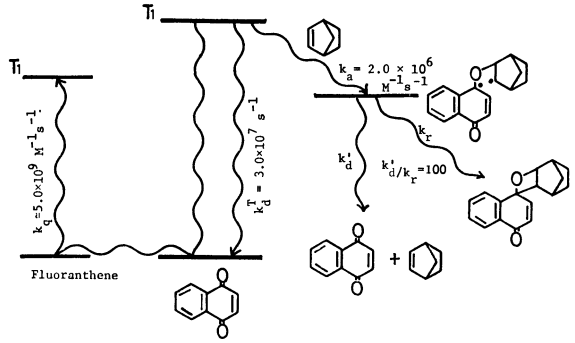

Fig. 3. The state diagram for the formation of spiro-oxetane (30 °C).

The formation of **3b**, on the other hand, is expected to proceed through both the singlet excited state and the triplet excited state of 1,4-naphthoquinone since the Stern-Volmer plots for the formation of **3b** does not give a straight line; it can be estimated that about 60% of the reaction proceeds through the singlet excited state of 1,4-naphthoquinone and the residual 40% through the triplet state since the ratio of quantum yields approaches a constant value (2.5) with increasing concentration of the quencher. It could be assumed that the singlet excited state of 1,4-naphthoquinone reacts also with olefins to give the photo-addition compound and this could be substantiated further by the following results.

Quenching of the Fluorescene of 1,4-Naphthoquinone by Olefins. The fluorescene of 1,4-naphthoquinone at 77 K and at room temperature was observed when

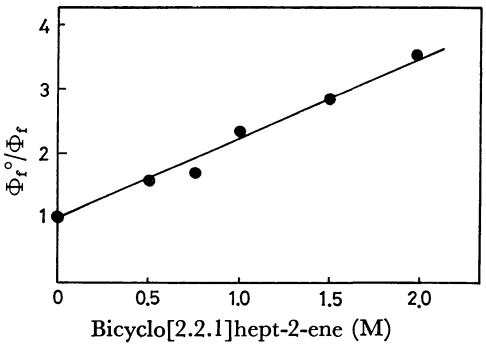

Fig. 4. Quenching of the fluorescene of 1,4-naphthoquinone by bicyclo[2.2.1]hept-2-ene (20 °C).

degassed solution of 1,4-naphthoquinone of ether–ethyl alcohol (vol/vol=1/1) was irradiated by light at 333 nm. The intensity of fluorescene was measured at λ_{max}=400 nm in the absence and in the presence of bicyclo[2.2.2]-hept-2-ene (Fig. 4). From the linear relationship observed, it is concluded that the singlet excited state of 1,4-naphthoquinone can be quenched by bicyclo[2.2.1]-hept-2-ene. This is consistent with the findings that the formation of **3b** proceeds partly through the singlet excited state of 1,4-naphthoquinone.

TABLE 4. QUANTUM YIELDS FOR THE FORMATION OF **2b** AND **3b** THROUGH THE EXCITATION OF n–π^* AND π–π^* TRANSITIONS (measured at 30 °C)

Photo-addition compound	Φ_{total} [a]	Φ_{333} [b]	Φ_{420} [c]
2b	8.8×10^{-3}	8.1×10^{-3}	7.0×10^{-3}
3b	5.6×10^{-3}	4.4×10^{-3}	4.4×10^{-3}

a) Excited through both n-π^* and π-π^* transitions. b) Excited through π-π^* transition with use of a Corning CS-7-54 filter. c) Excited through n-π^* transition with use of a Toshiba VY-42 filter.

Mixing between the π-π^* Excited States of 1,4-Naphthoquinone. The benzene solution of 1,4-naphthoquinone shows two characteristic absorption bands in the region of wavelength greater than 300 nm. The bands, λ_{max}=333 nm and 420 nm, can be assigned to π-π^* and n-π^* transitions, respectively. The quantum yields for the formation of **2b** and **3b** were measured in each case when 1,4-naphthoquinone was excited through π-π^* and n-π^* transitions to react with bicyclo-[2.2.1]hept-2-ene (Table 4). The π-π^* excitation of 1,4-naphthoquinone was as equally effective as the n-π^* excitation for the formation of **2b** and **3b**. These results suggest that the lower excited singlet or triplet state would be responsible to the formation of **3b**, irrespective of the bands used for the excitation. However, the lower triplet excited state would contribute predominantly to the formation of **2b**. From the results the mixting between the π-π^* and n-π^* excited states of 1,4-naphthoquinone seems to exist to a considerable extent. This is not the case in the photo-excited states of *p*-benzoquinone. The suggestion was supported further by the following facts: in the photochemical reaction of 1,4-naphthoquinone with 2-methylbut-2-ene the oxetanes isolated are found to be a non-stereo-

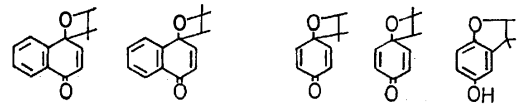

9a 9b 10a 10b 11

selective mixture of **9a** and **9b** (**9a**/**9b**=1.3); in the photochemical reaction of *p*-benzoquinone with 2-methylbut-2-ene, only one isomer **10a** of the possible two isomers and its further rearrangement product **11** could be isolated stereoselectively from the reaction mixture, but none of the other isomer **10b**.[16] The lack of stereoselectivity in the photochemical reaction of 1,4-naphthoquinone with 2-methylbut-2-ene is attributable solely to the smaller degree of electron defficiency of oxygen atom in the n-π^* excited state of 1,4-naphthoquinone, *i.e.*, indication of larger mixing of the n-π^* state with π-π^* state than in the case of *p*-benzoquinone, since the stability of the diradical intermediates **7** to form **9a** and **9b**, or **10a** and **10b** could be estimated in the same order.

We can thus formulate the reaction of 1,4-naphthoquinone with bicyclo[2.2.1]hept-2-ene as shown in Scheme 2. A novel type of photo-addition compound **3** derived from the other higher strained olefins would be formed following a similar reaction scheme.

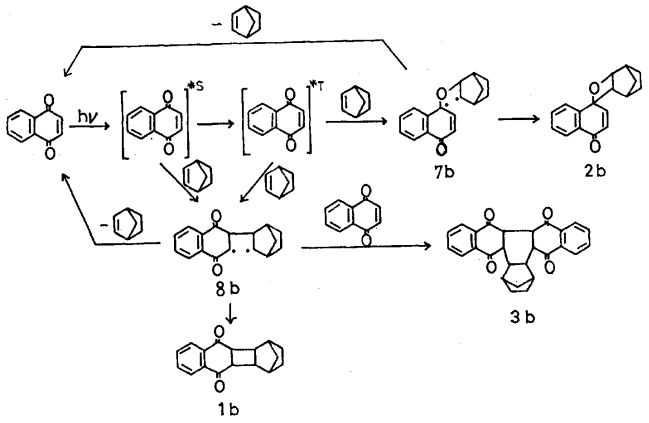

Scheme 2.

Experimental

Materials. 1,4-Naphthoquinone, *p*-benzoquinone, bicyclo[2.2.1]hept-2-ene (**4b**) and fluoranthene were used after sublimation of commercial reagents of guaranteed grade. Bicyclo[2.2.2]oct-2-ene (**4d**) and 2-methylbut-2-ene were subjected to the reaction without further purification. Bicyclo-[4.2.0]oct-7-ene (**4a**), *endo*-2-acetoxybicylo[2.2.1]hept-5-ene (**4c**), *trans*-2,3-dicyanobicyclo[2.2.2]oct-5-ene (**4e**) and 2,2,3,3-tetracyanobicyclo[2.2.2]oct-5-ene (**4f**) were synthesized according to reported method.[5-8]

*4-Oxatricyclo[2.2.5^{2,6}]undec-8-ene (**4g**)*; *endo-cis*-Bicyclo[2.2.2]-oct-5-ene-2,3-dicarboxylic anhydride[17] was treated with lithium aluminum hydride in dry ether for conversion into *endo-cis*-2,3-bis(hydroxymethyl)bicyclo[2.2.2]oct-5-ene. *p*-Toluenesulfonyl chloride (29.5 g) was added to 100 ml of pyridine solution containing 6.5 g of *endo-cis*-2,3-bis(hydroxymethyl)-bicyclo[2.2.2]oct-5-ene in an ice-cooled bath with stirring, then allowed to stand for two days at room temperature. The pyridine solution was poured into ice water (200 ml) and extracted twice with 75 ml of ether. The extract was washed twice with cold dilute hydrochloric acid solution, once with water and then dried over anhydrous sodium sulfate. Oily ditosylate was obtained after ether had been evaporated. The crude ditosylate was reduced with lithium aluminum hydride. After the work-up, the cyclic ether (**4g**) was distilled under a reduced pressure, yield: 4.0 g (76%): bp 134.5—135.6 °C (80 mmHg); mp 51—52 °C; Mass; *m/e*=149 (M^+). IR (liq. film); 3040, 2930, 1377 (C–H), 1010 cm^{-1} (C–O). PMR (CCl_4); δ: 1.34 (4H, C-10 and C-11 CH_2' s, m), 2.32 (4H, C-1, C-2, C-6, and C-7 CH's, m), 3.16 (2H, C-3 and C-5 CH's, m), 3.70 (2H, C-3 and C-5 CH's, m), 6.12 ppm (2H, C-8 and C-9 CH's, m). Found: C, 79.34; H, 9.32%. Calcd for $C_{10}H_{14}O$: C, 79.95; H, 9.39%.

General Procedures. 1,4-Naphthoquinone (1 mmol) and an olefin (2 mmol) were dissolved in dry benzene (25 ml) and irradiated in a glass tube with a high pressure Hg arc lamp (300 W) through a water layer 5 cm thick (10 °C). After the reaction was completed the photo-addition compounds were isolated by the usual work-up from the reaction mixture and subjected to further examination for structure determination.

Identification of the Photo-addition Compounds. Bicyclo-[4.2.0]octano[2',3'-h]-*5,8,13,14-tetraoxo-5,5a,6,7,7a,8,13,13a,13b,14-decahydropentaphene (**3a**)*: white needles, mp 235 °C. Found: C, 79.08; H, 5.35%. Calcd for $C_{28}H_{24}O_4$: C, 79.23; H, 5.70%. Mass: *m/e*=424 (M^+). IR (KBr disk): 1675 cm^{-1} (C=O). PMR ($CDCl_3$); δ 1.00—2.40 (12H, aliphatic protons, m), 3.43 (1H, C-7a CH, dd, J=6.0 and 11.0 Hz), 3.53 (1H, C-5a CH, dd, J=6.0 and 12.0 Hz), 4.50 (2H, C-13a and C-13 CH's, m), 7.85 (4H, aromatic protons, m), 8.16 ppm (4H, aromatic protons, m).

*Bicyclo[2.2.1]heptano[2',3': 4,5]tricyclo[6.4.0.0^{3,6}]dodeca-8,10,12-triene-2,7-dione (**1b**)*: colorless cubes from *n*-hexane, mp 113.0—114.0 °C. Found: C, 81.15; H, 6.35%. Calcd for $C_{17}H_{16}O_2$: 80.92; H, 6.39%. Mass: *m/e*=252 (M^+). IR (KBr disk); 1670 cm^{-1} (C=O). PMR ($CDCl_3$): δ; 0.80—2.00 (8H, aliphatic protons, m), 2.40 (2H, C-4 and C-5 CH's, s), 3.18 (2H, C-3 and C-4 CH's, d, J=3.0 Hz), 7.80—8.30 ppm (4H, aromatic protons, m).

4-Oxo-1,4-dihydronaphthalene-1-spiro-*2'-bicyclo[2.2.1]heptano-[2'',3'': 3',4']oxetane (**2b**)*: colorless cubes from petroleum ether, mp 101.0—102.0 °C. Found: C, 80.76; H, 6.25. Calcd for $C_{17}H_{16}O_2$: C, 80.92; H, 6.39%. Mass; *m/e*=252 (M^+). IR (KBr disk); 1668 (C=O), 977 cm^{-1} (oxetane ring). UV max ($CHCl_3$); 248 nm (ε: 1.20×10^5), 281 (5.43×10^4). PMR (CCl_4): δ: 0.80—2.90 (9H, aliphatic protons, m), 5.05 (1H, C-3' CH, dd, J=5.0 and 6.0 Hz), 6.16 (1H, C-2 CH, d, J=10.0 Hz), 7.70 (1H, C-3 CH, d, J=10.0 Hz), 7.20—8.10 ppm (4H, aromatic protons, m).

Bicyclo[2.2.1]heptano[2',3'-h]-*5,8,13,14-tetraoxo-5,5a,6,7,7a,8,13,13a,13b,14-decahydropentaphene (**3b**)*: white needles from chloroform, mp 227.5—228.5 °C. Found: C, 78.84; H, 5.39. Calcd for $C_{27}H_{22}O_4$: C, 79.00; H, 5.40%. Mass *m/e*=410; (M^+). IR (KBr disk); 1670 cm^{-1} (C=O). UV max ($CHCl_3$): 256 nm (ε: 2.35×10^4), 304 (5.40×10^3). PMR ($CDCl_3$); δ: 0.60—1.70 (8H, aliphatic protons, m). 2.03 (2H, C-6 and C-7 CH's, m), 3.13 (1H, C-7a CH, dd, J=5.0 and 12.0 Hz), 3.27 (1H, C-5a CH, dd, J=5.0 and 14.0 Hz), 4.56 (2H, C-13a and C-13b CH's, d, J=5.0 Hz), 7.70—8.24 ppm (8H, aromatic protons, m).

*Bicyclo[2.2.2]octano[2',3': 4,5]tricyclo[6.4.0.0^{3,6}]dodeca-8,10,12-triene-2,7-dione (**1d**)*: colorless cubes from benzene–petroleum ether, mp 141.5—142.3 °C. Found: C, 81.24; H, 6.76%. Calcd for $C_{18}H_{18}O_2$: C, 81.17; H, 6.81%. Mass: *m/e*=266 (M^+). IR (KBr disk); 1674 cm^{-1} (C=O). UV max ($CHCl_3$); 254 nm (ε: 1.18×10^4), 302 (1.90×10^3), 309 (2.08×10^3), 348 (1.64×10^2). PMR ($CDCl_3$); δ: 1.40—2.30 (10H, aliphatic protons, m), 2.61 (2H, C-4 and C-5 CH's, broad s), 3.37 (2H,

C-3 and C-6 CH's, d, J=6.0 Hz), 7.70—8.30 ppm (4H, aromatic protons, m).

4-Oxo-1,4-dihydronaphthalene-1-spiro-*2'-bicyclo*[*2.2.2*]*octano*[*2'', 3'': 3',4'*]*oxetane* (**2d**): assignment of the structure was confirmed by IR and UV spectra which were in good agreement with those of **2b**: IR (CCl_4 solution); 1670 (C=O), 980 cm^{-1} (oxetane ring). UV max ($CHCl_3$); 253, 281 nm.

Bicyclo[*2.2.2*]*octano*[*2',3'*-h]-*5,8,13,14-tetraoxo-5,5a,6,7,7a,8, 13,13a,13b,14-decahydropentaphene* (**3d**): white needles from benzene–petroleum ether, mp 245 °C (decomp.). Found: C, 79.15; H, 5.58%. Calcd for $C_{28}H_{24}O_4$: C, 79.21; H, 5.70%. Mass; m/e=424 (M^+). IR (KBr disk); 1675 cm^{-1} (C=O). UV max ($CHCl_3$); 258 nm (ε: 2.31×10^4), 300 (4.13×10^3), 308 (4.56×10^3). PMR ($CDCl_3$); δ: 1.35 (12H, aliphatic protons, m), 3.30 (2H, C-5a and C-7a CH's, m), 4.50 (2H, C-13a and C-13b CH's d, J=4.0 Hz), 7.77 (4H, aromatic protons, m), 8.08 ppm (4H, aromatic protons, m).

4-Oxo-1,4-dihydronaphthalene-1-spiro-*2'-3',3',4'-trimethyloxetane* (**9a**) *and 4-Oxo-1,4-dihydronaphthalene-1*-spiro-*2'-3',4',4'-trimethyloxetane* (**9b**): these two isomers were isolated as a mixture. The relative ratio of the isomer content (**9a**/**9b**) was estimated to be 1.3/1.0 through integration of the PMR signals due to the methine protons of the oxetane ring. They appeared at δ=4.74 ppm (C-4' CH, q, J=6.0 Hz) for **9a** and 2.86 ppm (C-3' CH, q, J=6.0 Hz) for **9b**, respectively; colorless oil. Mass; m/e=228 (M^+). IR (liq. film); 1670 (C=O), 960 cm^{-1} (oxetane ring).

Measurement of the Quantum Yields. Light of wavelengths in the range 300—400 nm (filters, Corning CS 7–54 and usual glass, 2 mm thick) was used. The quanta absorbed by the reaction mixture were calibrated using potassium ferrioxalate as a chemical actinometer.[18] The benzene solution of 1,4-naphthoquinone (0.100 M) and an olefin (0.200 M) in a quartz cell was degassed and subjected to measurement. After the reaction was over the reaction mixture was purified by thin layer chromatography on silica gel, the amount of photoaddition compounds produced being estimated by their absorptions in the UV region.

Part of the work was carried out with research funds of the Ministry of Education (No. 943019) and the Takeda Science Fundation.

References

1) A preliminary report: K. Maruyama, T. Otsuki, and Y. Naruta, *Chem. Lett.*, **1973**, 641.
2) J. M. Bruce, *Quart. Revs.*, **21**, 405 (1967).
3) C. H. Krauch and S. Farid, *Tetrahedron Lett.*, **1966**, 4733.
4) K. Maruyama, T. Otsuki, A. Takuwa, and S. Kako, *Bull. Inst. Chem. Res., Kyoto Univ.*, **50**, 344 (1972).
5) R. S. Liu, *J. Amer. Chem. Soc.*, **89**, 112 (1968).
6) H. V. Anderson, E. R. Garret, F. H. Lincoln, Jr., A. N. Nathan, and J. A. Hogg, *ibid.*, **79**, 743 (1958).
7) P. Scheiner and W. R. Vaugham, *J. Org. Chem.*, **26**, 1923 (1961).
8) W. J. Middleton, R. E. Heckert, E. J. Little, and C. G. Krespan, *J. Amer. Chem. Soc.*, **80**, 2783 (1958).
9) J. M. Bruce, *J. Chem. Soc.*, **1962**, 2782; J. Dekker, P. J. Vuuren, and D. P. Venter, *J. Org. Chem.*, **33**, 464 (1968); J. Rennert, S. Japar, and M. Guttman, *Photochem. Photobiol.*, **6**, 485 (1967).
10) P. Lazolo and P. R. Schleyer, *J. Amer. Chem. Soc.*, **85**, 2017 (1963).
11) N. A. Schglova and D. N. Shigorin, *Zh. Fiz. Khim.*, **38**, 1261 (1964); *Chem. Abstr.*, **61**, 9063e (1964); W. Herre and P. Weis, *Spectrochim. Acta, A*, **29**, 205 (1973); A. Kuboyama, This Bulletin, **35**, 295 (1962).
12) N. J. Turro, "Molecular Photochemistry," W. A. Benjamin, Inc., New York (1965), a) p. 117, b) p. 208.
13) A. A. Lamola and N. J. Turro, "Energy Transfer and Organic Photochemistry," (Technique of Organic Photochemistry, Vol. XIV, A. Weissberger ed.), Interscience, New York (1969), p. 239.
14) P. J. Wagner and I. Kocherer, *J. Amer. Chem. Soc.*, **90**, 2232 (1968); W. R. K. Clark, A. T. Litt, and C. Steel, *ibid.*, **91**, 5413 (1969); G. Porter, and M. R. Topp, *Proc. Roy. Soc., Ser. A*, **315**, 163 (1970).
15) H. Sakurai, K. Shima, and S. Toki, *Nippon Kagaku Zasshi*, **89**, 935 (1968); S. Toki and H. Sakurai, This Bulletin, **40**, 2885 (1967).
16) D. Bryce-Smith and A. Gilbert, *Chem. Commun.*, **1964**, 87; D. Bryce-Smith, A. Gilbert, and M. G. Johnson, *J. Chem. Soc., C*, **1967**, 383.
17) E. H. Farmer and F. L. Warren, *J. Chem. Soc.*, **1929**, 897.
18) C. A. Parker, *Proc. Roy. Soc., Ser. A*, **220**, 104 (1952); D. A. Hatchard and C. A. Parker, *ibid.*, **235**, 518 (1956).

The Thermal Reaction of 3-Formylguaiazulene

Shinji KUROKAWA, Teruyo SAFO, Toru NOGUCHI, and Katsumi YANO*

Department of Chemistry, Faculty of Education, Saga University, Honjo-machi, Saga 840

**Department of Chemistry, Fukuoka University of Education, Munakata-machi, Munakata-gun, Fukuoka 811-41*

(Received November 25, 1974)

When 3-formxlguaiazulene was heated at 200 °C for 1 hr, three new compounds were isolated in addition to *S*-guaiazulene (formed by loss of the formyl group). They were shown to be 2-formylguaiazulene, produced by migration of the formyl group, and dimers produced from two molecules of the starting material through dehydration between the formyl and the aromatic methyl groups. The observed elimination or migration of the formyl group was analogous to the behavior of 3-acylguaiazulenes which had been studied earlier. On the other hand, the extent of the loss of the acyl group and the formation of the dimers was peculiar to this substance. Moreover, migration of the formyl group was not reversible at 200 °C, but was at 250 °C.

In the previous papers[1-3] dealing with the thermal reaction of 3-acylguaiazulene at 200—260 °C, it was shown that *S*-guaiazulene, 2-acylguaiazulene and 1-acyl-7-isopropyl-3,4-dimethylazulene were formed by the loss of the acyl group, migration of the acyl group, or by the interchange of the acyl and methyl groups in the five-membered ring of the azulene nucleus, respectively. On the other hand, a discrepancy among the reactions due to differences of the carbonyl components was also noted:[3] the main reaction in such a ketone as acetylguaiazulene or benzoylguaiazulene is migration of the acyl group, while that in a methyl ester is interchange of the ester and the methyl groups in the five-membered ring, and reduction of an acyl group is observed only in the benzoyl compound.

In an effort to determine the effect of a formyl substituent on the thermal reaction of 3-acylguaiazulene, the behavior of 3-formylguaiazulene was studied.

Results and Discussion

3-Formylguaiazulene (I) was heated at 200 °C for 1 hr or 2 hr, and compounds III—V were isolated in addition to *S*-guaiazulene (II), the main product, formed by loss of the formyl group.

a) 2-Formylguaiazulene (III): A dark red crystalline product (mp 80—81 °C) isolated in the next highest yield had the same molecular formula, $C_{16}H_{18}O$, as I. The existence of a formyl group was indicated by the appearance of a $\nu_{C=O}$ band at 1666 cm^{-1} and ν_{C-H} bands at 2710 and 2795 cm^{-1} in the IR spectrum, and by presence of a singlet at 10.58 ppm attributable to the formyl proton in the NMR spectrum.

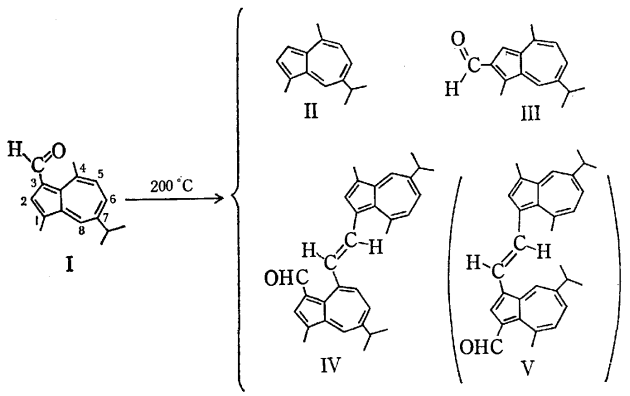

Chart 1.

Moreover, the NMR spectrum (*cf.* Experimental section) showed, besides the formyl-proton signal, signals due to one isopropyl-, two aromatic methyl-, and four aromatic ring hydrogens, a pattern of which is quite similar to that of I. The compound is, therefore, thought to be a positional isomer of I.

The visible absorption spectrum of this compound had two maxima of nearly equal intensities at 660 and 705 nm, and bore a marked resemblance to that of 2-acetylguaiazulene (VI).[1]

These facts lead us to conclude the present compound to be 2-formylguaiazulene (III). In agreement with this deduction, this compound gave VI when treated with diazomethane.[4,5]

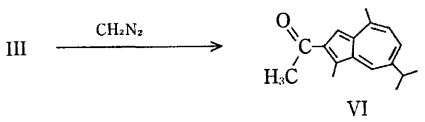

Chart 2.

b) trans-1,2-(1,4-Diazulyl)ethene Derivative (IV). A purple crystalline substance (mp 160—161 °C), the third reaction product, was also an aldehyde, since it exhibited a $\nu_{C=O}$ band at 1620 cm^{-1} in its IR spectrum and a formyl signal at 10.68 ppm in its NMR spectrum. It also gave semicarbazone (mp 192—194 °C). The visible absorption maximum of the compound (513 nm) exhibited, however, an ε value larger than that of I or III by a factor of about twenty, and this is not consistent with the structure of an ordinary formylguaiazulene.

Based on the molecular ion of the mass spectrum, this compound is thought to have a composition, $C_{32}H_{34}O$ (MW, 434), made up through dehydration from two molecules of I ($C_{16}H_{18}O$, 226). This deduction was supported by the observation in the NMR spectrum (*cf.* Experimental section) that the signals ascribed to 34H were recognized.

In the methyl region of the NMR spectrum there were three aromatic methyl signals in addition to two isopropyl ones. Among them, two aromatic methyl signals (2.58 and 2.62 ppm) adjacent to one another

corresponded to Me_1 of I, and a down-field signal (3.08 ppm), to Me_4 of I (*cf.* Experimental section). The appearance of only one signal (3H) corresponding to Me_4 indicates that the formyl group of one molecule of I was condensed with methyl group at 4-position of a second molecule. Consequently, the present compound was postulated to be a diazulylethene derivative (IV).

On the other hand, this compound could possibly be a condensation product of I and III or of III and III, since III was also found in the reaction mixture. This possibility was, however, excluded because IV was isolated as a by-product in preparing I through formylation of II, where no III was obtained.

As to geometrical isomerism, IV was determined to have a *trans* configuration on the basis of the following three reasons: i) According to the NMR spectrum, the coupling constant for the olefinic protons was found to be 15.5 Hz, the value of which fits with a *trans* configuration.[6] ii) From a model examination, a fully conjugated system of two azulene rings and an olefinic bond may hardly be attainable in the *cis* form of IV. Thus, the configuration cannot explain the extremely large ε value in the visible spectrum of IV. iii) IV is expected to take a thermally stable configuration, since it is a thermal reaction product.

c) 1,2-(1,3-Diazulyl)ethene Derivative (V). This substance was isolated as a purple oil, but was not well characterized because of its poor yield and instability. On the basis of the observation in the NMR spectrum that the signals from two isopropyl and three aromatic methyl groups existed and that the pattern of an aromatic proton region was close to that for IV, this compound is thought to be another dimer V formed from two molecules of I through dehydration of the formyl group and the methyl group at 1-position.

Sequence of the Reaction. As is obvious from the above arguments, the heating of 3-formylguaiazulene (I) yielded two monomers, which were formed by elimination or migration of a formyl group, and two dimers, generated by condensation of two molecules of I.

In Table 1 are listed the yields (%) of the products obtained by a reaction time of 1 hr. The yield of IV was found to increase almost linearly with increasing reaction time, while no change in the yield of II and a decrease in that of III were observed. This kind of dehydration is well known in the presence of an appropriate dehydrating reagent,[7] and is apparently characteristic of formyl compounds.

With regard to the acyl migration 2-formylguaiazulene (III) afforded no appreciable product when heated at 200 °C for 1 hr but gave II and I by heating at 250 °C for 1 hr. Thus the acyl migration is concluded to be reversible at the higher temperature, the same as alkyl- and phenyl-migration[8,9] which were investigated at a temperature above 250 °C.

Table 1 also includes the yields (%) of the reaction products formed from the three 3-acylguaiazulenes studied before.[1-3] As is obvious from the Table 1, the thermal exchange between the acyl and the methyl groups was not observed in the case of 3-formylguaiazulene, while it was common to the other acylguaiazulenes. Another feature of the thermal reaction of the 3-formyl compound is that elimination of the acyl group, less important in the other acylguaiazulene, is a major reaction.

In order to clarify the reasons for the observed differences in the reactions, further work is in progress in our laboratory on the reactions of phenyl esters having a variety of electron releasing- or withdrawing-groups at the *p*-position.

Experimental

All melting points are uncorrected. The UV and the visible absorption spectra (VS) were taken in a cyclohexane solution. The IR spectra were obtained as KBr disks, and the mass spectra (MS), at 70 eV. Unless otherwise stated, the NMR spectra were measured at 60 MHz using deuteriochloroform as the solvent: the chemical shifts are given in ppm using TMS as an internal standard, and the coupling constants in Hz. The thin-layer chromatography (tlc) was conducted by the use of silica gel-G (Merck), and the gas chromatography (vpc), using a column (1 m in length) of Chromosorb W impregnated with Silicone SE-30 (1.5%) under a 20 ml/min flow of helium.

3-Formylguaiazulene (I). This compound was synthesized by a Vilsmeier-Haack formylation of *S*-guaiazulene (II).[10] The recrystallization of the product from *n*-hexane gave dark reddish-brown needles [mp 86.0—86.1 °C (mp 85—86 °C[10])], which showed a single brown spot (R_f, 0.16) in tlc (benzene). VS: nm (ε), 573 (539), 600 sh (453), 618 sh (404), 678 (297) [571 (501), 680 (118)[10]]. UV: nm (log ε), 247.5 (4.35), 277.5 (4.05), 310.5 (4.50), 316.5 (4.58), 366 sh (3.71), 385 (3.98), 400 (4.07). IR: 1608 cm^{-1} (C=O). NMR: 1.37/3.05 (d, 6H/m, 1H, J=6.8; *i*-Pr), 2.58 (s, 3H; Me_1), 3.12 (s, 3H; Me_4), 7.40 (d, 1H, J=12.0; H_5), 7.65 (dd, 1H, J=2.0 and 12.0; H_6), 8.25 (s, 1H; H_2), 8.32 (d, 1H, J=2.0; H_8), 10.63 (s, 1H; CHO). NMR (CF_3COOH)[11]: 1.52/3.47 (d, 6H/m, 1H, J=7.2; *i*-Pr), 2.60 (s, 3H; Me_1), 3.23 (s, 3H; Me_4), 8.25 (s, 1H; H_2), 8.35 (s, 2H; $H_{5,6}$), 8.73 (s, 1H; H_8), 9.12 (s, 1H; $=C<^{O}_{H}$).

Table 1. Yields (%) of the thermal reaction products

Products	Carbonyl components			
	HCO	CH_3CO[1,2]	C_6H_5CO[3]	CH_3OCO[3]
S-Guaiazulene	9.1	1.4	1.8	0.8
2-Acylgauaiazulene	6.1	16.4	11.3	0.08
1-Acyl-7-isopropyl-3,4-dimethylazulene	—	7.0	5.7	5.3
2-Benzylguaiazulene	—	—	2.5	—
Diazulylethene derivatives	0.3	—	—	—

Thermal Reaction of 3-Formylguaiazulene (I). *a) Determination of the Reaction Temperature*: Three glass tubes, each containing 50 mg of I, were sealed under a nitrogen atmosphere and heated at 150 °C, 200 °C and 250 °C for 1 hr, respectively. The reaction mixture was, after being dissolved in a small amount of benzene, investigated by tlc (benzene) and vpc (200 °C). The ratio of the reaction products relative to the recovery of I was of 0.8, 15.7 and 108% corresponding to the temperatures of 150, 200 and 250 °C, respectively, on the basis of the vpc. Contrary to these data, in the case of 250 °C we observed tlc spots of degradation products which were spread out over a whole region or did not move from the original point, while those were scarcely apparent in the other cases.

b) The Case of 1 hr Heating. I (1.0255 g) was heated in a sealed tube at 200 °C for 1 hr. The reaction mixture was eluted through a silica-gel column with petroleum ether, subsequently with benzene, and separated into the following three fractions.[12]

petroleum ether:

Fr. 1 blue oil (106.9 mg)···*S*-guaiazulene (II) (93.5 mg)

benzene:

Fr. 2 greenish-brown oil (140.9 mg)···
- 1,2-(1,3-diazulyl)ethene derivative (V) (0.15 mg)
- 2-formylguaiazulene (III) (62.25 mg)

Fr. 3 violet crystals (301.1 mg)···
- *trans*-1,2-(1,4-diazulyl)ethane derivative (IV) (2.74 mg)
- 3-formylguaizulene (I) (277.4 mg) (recovered)

c) The Case of 2 hr Heating. I (3.36 mg) was heated at 200 °C for 2 hr. By treating the reaction mixture as described for (b), each product was obtained in the following yield:

II (262.4 mg), V (0.6 mg), III (58.6 mg), IV (21.0 mg).

S-Guaiazulene (II). This compound was obtained as a blue oil which showed a single blue spot (R_f, 0.46 in tlc (petroleum ether)). It was identical with an authentic specimen[13] in tlc and vpc (180 °C).

1,2-(1,3-Diazulyl)ethene Derivative (V). The greenish brown oil from Fr. 2 exhibited violet and blue spots (R_f, 0.37 and 0.34) overlapping each other in tlc (benzene). By means of repeated benzene–silica-gel elution chromatography, it was roughly separated into a red oil (V portion) and a blue oil (III portion), corresponding to each spot in tlc. The red oil, still containing some of the III portion, was then chromatographed on an aluminum oxide column with a mixed solvent of petroleum ether–benzene (7:3); R_f, 0.29]. NMR (90 MHz, accumulated 34 times): 1.28 (d, 6H, J=6.8; *i*-Pr), 2.57, 2.80 and 3.02 (each s, 3H; Me), 6.90—8.43 (10H; aromatic- and vinyl protons), 10.23 (s, 1H; CHO).

2-Formylguaiazulene (III). The blue oily portion described above was purified by repeated benzene–silica-gel elution chromatography to give III as dark red needles, which showed a single blue spot (R_f, 0.34) in tlc (benzene). After being recrystallized from ethanol, it showed a mp of 80.0—81.0 °C. IR: 1666 cm^{-1} (C=O), 2710 and 2795 cm^{-1} (CH: aldehyde). UV: nm (log ε), 251.2 (4.37), 286.5 (4.47), 304.5 (4.58), 312 sh (4.47), 347 (3.74), 361.5 (3.78), 374 (3.41). VS: nm (ε), 392 (223), 416 (70), 570 sh (277), 616 sh (495), 660 (675), 705 (697). NMR: 1.38/3.07 (d, 6H/m, 1H, J=6.9; *i*-Pr), 2.83 (s, 3H; Me_1), 2.90 (s, 3H; Me_4), 7.00 (d, 1H, J= 2.1 and 10.4; H_5), 7.46 (dd, 1H, J=2.1 and 10.4; H_6), 7.60 (s, 1H; H_3, 8.35 (d, 1H, J=2.1; H_8), 10.58 (s, 1H; CHO). MS: *m/e* 226 (M, $C_{16}H_{18}O$; 96.4%), m/e 225 (M−H; 11.1%), *m/e* 211 (M−CH_3; base peak), *m/e* 197 (M−CHO: 13.1%).

Reaction of 2-Formylguaiazulene (III) with Diazomethane. To a solution of III (32.00 mg) in ether (1 ml), was added an ethereal solution (2 ml) of diazomethane prepared from nitrosomethylurea (0.4 g); the solution was then kept at room temperature for 25 days. After the remaining reagent was decomposed by adding a few drops of formic acid, the reaction mixture was submitted to benzene–silica gel elution chromatography to afford VI (3.90 mg) as green crystals and the recovery of III (11.56 mg) as dark red crystals. VI, thus obtained, was idetical with an authentic specimen[1] in tlc (benzene) and vpc (195 °C).

Thermal Reaction of 2-Formylguaiazulene (III). III was sealed in three glass tubes (*ca.* 50 mg in each ampoule), and heated at 150, 200 and 250 °C for 1 hr, respectively. The reaction mixture, dissolved in a small amount of benzene, was investigated by tlc (benzene) and vpc (195 °C). The formations of II, I and an unknown substance were observed in the case of 250 °C, while only unchanged III was detected in the cases of 150 °C and 200 °C. The yield of each compound at 250 °C (III; 46.2 mg) was estimated on vpc (195 °C) to be 7.5 (II), 2.5 (I), 13.7 (unknown) and 76.4% (III; recovered). Successively the reaction mixture was subjected to benzene–silica-gel elution chromatography to be separated into II (15.78 mg), I (1.15 mg) and unchanged III (12.71 mg). These compounds were identical with the authentic specimens in tlc and vpc.

trans-*1,2-(1,4-Diazulyl)ethene Derivative (IV).* *a) By Thermal Reaction of 3-Formylguaiazulene (I).* The violet crystals from Fr. 3 were chromatographed on a silica-gel column with a mixed solvent of benzene–ether (49:1), and separated into purple crystals of IV and reddish-brown crystals of I (recovered). The former showed a single violet spot (R_f, 0.19) in tlc (benzene), and had a mp of 160.0—160.1 °C after being recrystallized from *n*-hexane. IR: 1620 cm^{-1} (C=O). UV: nm (log ε), 256 (4.40). 262 (4.40), 310 (4.44). VS: nm (log ε), 403 (4.00), 513 (4.21). NMR (90 MHz, accumulated 41 times): 1.36 and 1.42 (each d, 6H, J=7.0; 2*i*-Pr), 2.58 and 2.62 (each s, 3H; $2Me_1$), 3.08 (s, 3H; Me_4), 6.97—8.20 (8H; aromatic protons), 7.88 and 8.32 (each d, 1H, J=15.5; vinyl protons), 10.68 (s, 1H; CHO). MS: *m/e* 434 (M, 16.5%), *m/e* 211 (M−CH=CH; base peak).

The semicarbazone of this compound was obtained as a dark brown powder in a usual manner. After being recrystallized from ethanol, it showed a mp of 192.0—194.0 °C.

b) As a By-product in the Preparation of 3-Formylguaiazulene (I). *S*-Guaiazulene (II) (10.0 g) was formylated with a mixed reagent of dimethylformamide (65 ml) and phosphorous oxychloride (8.7 g).[10] The reaction mixture was submitted to benzene–silica-gel elution chromatography giving I (3.05 g) and IV (13.32 mg). The IV obtained thereby was identical with that from (a) (thermal reaction product) in tlc and in IR spectrum.

The authors wish to thank Professor Shûichi Hayashi of Hiroshima University for the mass spectral measurements, Professor Yûho Tsuno of Kyushu University for the measurements of the accumulated NMR spectra, and to Professor Arthur G. Anderson, Jr., University of Washington, U.S.A., for assistance in preparing the manuscript. Thanks are also due to the Ministry of Education, Japanese Government, for a Scientific Research Grant-in-Aid.

References

1) S. Kurokawa, This Bulletin, **43**, 509 (1970).

2) *Idem.*, *Tetrahedron Lett.*, **1969**, 3567.
3) S. Kurokawa, M. Hashimoto, and S. Hayashi, This Bulletin, **45**, 3559 (1972).
4) C. D. Gutsche, *Organic Reactions*, **8**, 364 (1954).
5) F. Schlotterbeck, *Ber.*, **40**, 479 (1907).
6) S. A. Barker, A. B. Foster, D. C. Lamb, and L. M. Jackman, *Tetrahedron*, **18**, 177 (1962).
7) Z. Horii, "Jikken Kagaku Koza," Vol. 18, ed. by M. Kotake, Maruzen, Tokyo, Japan (1966), p. 237.
8) Pl. A. Plattner, A. Furst, M. Gordon, and K. Zimmerman, *Helv. Chim. Acta*, **33**, 1910 (1950).
9) K. Yano, T. Hashizume, and S. Kurokawa, *Flavour Industry*, **1974**, 186.
10) K. Hafner and C. Bernhard, *Ann.*, **625**, 108 (1959).
11) The conjugate acid is represented as follows, according to D. Meuche, D. Dreyer, K. Hafner, and E. Heilbronner, *Helv. Chim. Acta*, **50**, 1178 (1967).

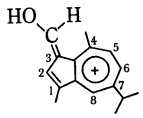

12) Next to the dotted lines are shown the compounds obtained finally from each fraction after it had been further purified.
13) S. Hayashi, S. Kurokawa, and T. Matsuura, This Bulletin, **41**, 2182 (1968).

Autoxidation of Toluic Acids Catalyzed by Cobalt and Bromide Ions in Acetic Acid

Yoshio KAMIYA and Toshisuke USHIBA

Department of Reaction Chemistry, Faculty of Engineering, University of Tokyo, Hongo 113

(Received December 25, 1974)

The effect of toluic acid concentration on the rate of autoxidation of toluic acids catalyzed by cobalt acetate and sodium bromide was elucidated. *p*-Toluic acid has shown a similar reactivity against oxidation to *m*-toluic acid, but a much different one from *o*-toluic acid. Although the rate of oxidation of *p*-toluic acid at 0.023 M cobalt increased with increasing *p*-toluic acid concentration and appeared to reach a limiting value, it was of first order with respect to the substrate concentration over wide range of concentration in the presence of 0.058 M cobalt. While, the rate of oxidation of *o*-toluic acid has shown higher values than the other toluic acids at substrate concentrations below 1.5 M and a maximum value at substrate concentration 0.75 M, suggesting that *o*-toluic acid can be oxidized easily but retards the catalysis by cobalt bromide. It was found that benzenecarboxylic acids remarkably retard the catalysis by cobalt and bromide ions, and the rate of oxidation of toluic acids is higher than that of toluene at such a low substrate concentrations as 0.34 M. The ease of oxidation of toluic acids can be attributed to the smaller rate constant of termination of carboxy benzyl peroxy radicals according to the polar and steric effects.

Although the rate of oxidation of alkylbenzenes[1-3] in acetic acid catalyzed by cobalt and bromide ions is of first order with respect to substrate concentration as in the cases of ordinary autoxidation reaction, that of *p*-toluic acid was reported to be independent of toluic acid concentration according to Ravens,[4] Bawn and Wright.[5] There has never been presented any successful explanations for this interesting result on *p*-toluic acid. Previously,[6] we have shown that the relative reactivity of substituted toluenes in this catalysis can be correlated by the polar effect of the substituent and is largely different from the relative rate of oxidation of single component. We intended to clarify the effect of benzenecarboxylic acids on the catalysis by cobalt and bromide ions and also to make clear the substituent effect on the rate of oxidation of substituted toluenes.

Experimental

Acetic acid, sodium bromide, cobaltous acetate $Co(OAc)_2 \cdot 4H_2O$, benzoic acid, phthalic acid, and three isomers of toluic acids were of reagent grade and used as received.

The oxygen absorption apparatus has been described elsewhere.[6]

Results and Discussion

The oxygen absorption curves in Fig. 1 shows that the rate of oxidation of toluic acids catalyzed by cobalt and bromide ions in acetic acid reaches a maximum and steady value within ten minutes of reaction.

In the cases of *m*- and *p*-toluic acids, the rate of oxidation slowly decreased after the absorption of considerable amount of oxygen and the solution became turbid indicating the formation of insoluble dibasic acids. The decrease in the rate of oxidation can be attributed to the decrease in the concentration of bromide ion, since it has been accepted[3,8,9] that bromide ion is slowly converted to an inactive form of organic bromide in the autoxidation of alkylbenzenes catalyzed by cobalt bromide.

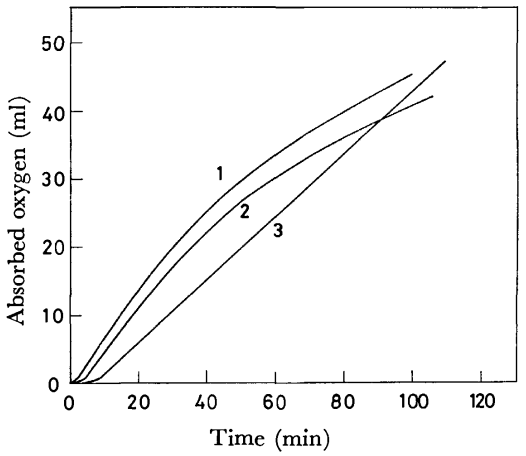

Fig. 1. Oxygen absorption curves of 2.4 M toluic acids in the autoxidation catalyzed by 0.023 M $Co(OAc)_2$ and 0.046 M NaBr in acetic acid at 85 °C.
1: *p*-Toluic, 2: *m*-Toluic, 3: *o*-Toluic acids.

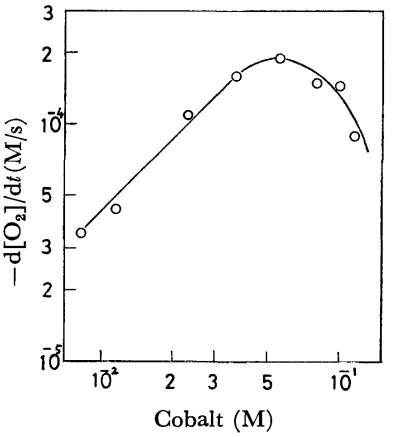

Fig. 2. The rate of oxidation of 0.65 M *p*-toluic acid catalyzed by cobaltous acetate and sodium bromide in acetic acid as a function of the concentration of cobalt acetate at the molar ratio of cobalt to bromide ion 2 and 85 °C.

However, in the case of *o*-toluic acid the oxygen absorption curve has shown a complete straight line for a long time. This might be due to the slower formation of organic bromides from the bromide ion than the other toluic acids, since Nakayama[7] observed a very small amounts of organic bromides in the oxidation of *o*-xylene to *o*-phthalic acid.

The steady rate of oxidation of *p*-toluic acid was nearly of first order with respect to cobalt concentration below 0.05 M in the presence of twice concentration of sodium bromide, as shown in Fig. 2. And the rate of oxidation was increased with increasing bromide ion until the ratio of cobalt to bromide ion became two. Hence, the oxidation was carried out at cobalt concentrations below 0.058 M and at the ratio of cobalt to bromide ions 2.

The steady rate of oxidation of three toluic acids as a function of substrate concentration is shown in Figs. 3, 4

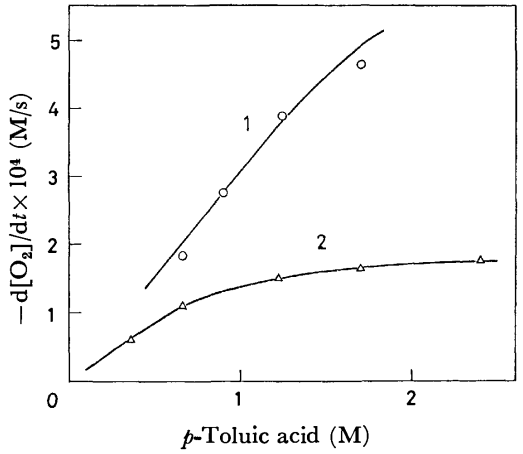

Fig. 3. The rate of oxidation of *p*-toluic acid catalyzed by cobaltous acetate and sodium bromide in acetic acid as a function of the concentration of *p*-toluic acid at 85 °C.
1: $Co(OAc)_2$ 0.058 M and NaBr 0.116 M
2: $Co(OAc)_2$ 0.023 M and NaBr 0.046 M

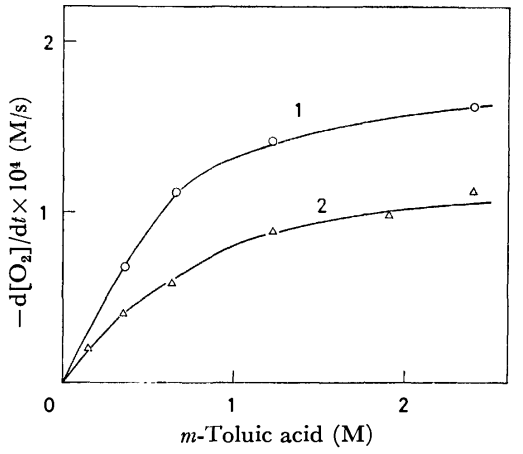

Fig. 4. The rate of oxidation of *m*-toluic acid catalyzed by cobaltous acetate and sodium bromide in acetic acid as a function of the concentration of *m*-toluic acid at 85 °C.
1: $Co(OAc)_2$ 0.023 M and NaBr 0.046 M
2: $Co(OAc)_2$ 0.023 M and NaBr 0.023 M

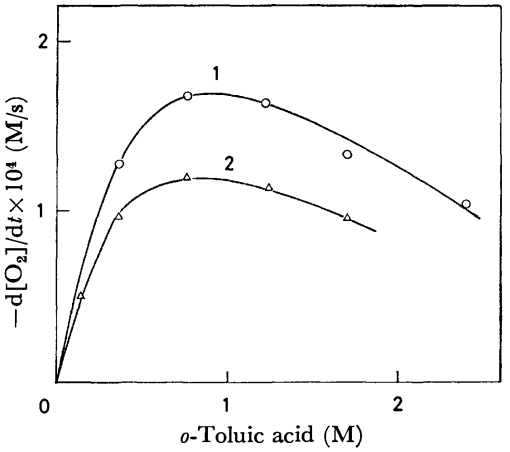

Fig. 5. The rate of oxidation of *o*-toluic acid catalyzed by cobaltous acetate and sodium bromide in acetic acid as a function of the concentration of *o*-toluic acid at 85 °C.
1: $Co(OAc)_2$ 0.023 M and NaBr 0.046 M
2: $Co(OAc)_2$ 0.023 M and NaBr 0.023 M

and 5. When 0.023 M of cobalt acetate was used, the rates of oxidation of *p*- and *m*-toluic acids increased with increasing toluic acid concentration at concentrations below 1.0 M, and approached to a limiting value. The reactivity of *p*-toluic acid seems entirely the same as that of *m*-toluic acid. On the other hand, *o*-toluic acid has shown a maximum rate at 0.75 M and started to decrease as the substrate concentration was further increased.

o-Toluic acid was oxidized faster than *p*- and *m*-toluic acids by a factor of two, but it seems to deactivate the catalyst remarkably.

When the concentration of cobalt acetate was increased from 0.023 M to 0.058 M, the rate of oxidation of *p*-toluic acid showed an almost linear relation against the substrate concentration over a wide range of concentration, suggesting that *p*-toluic acid suppressed the catalytic effect due to cobalt and bromide ions. The retardation effect due to *o*-phthalic and benzoic acids on the oxidation of *o*-toluic acid was further studied as shown in Table 1. The addition of 0.54 M *o*-phthalic acid has shown a considerable retardation effect, but further addition of phthalic acid higher than 1.0 M presented no additional retardation effect according to the low solubility in acetic acid.

It was confirmed that isophthalic and terephthalic acids have no effect on the rate of oxidation of toluic acids because of very low solubility.

In contrast, benzoic acid, which was quite stable against oxidation, has shown a quite clear retardation effect on the cobalt bromide catalysis. The rate of oxidation of *o*-toluic acid decreased by factors of two and three in the presence of 1.28 and 2.44 M of benzoic acid, respectively.

Since the rate of oxidation is nearly first order with respect to cobalt, 1.28 M of benzoic acid can be considered to deactivate 0.01 M cobalt ion.

As reported previously,[6] cobaltous acetate bromide was oxidized by 2-cyano-2-propyl peroxy radical quantitatively in acetic acid solution, yielding cobaltic

Table 1. Retardation effect of benzenecarboxylic acids on the rate of oxidation of *o*-toluic acid in acetic acid solution at 85 °C

o-Toluic acid (M)	0.75	0.75	0.75	0.75	0.67	0.67	0.75
Benzoic acid (M)	0	1.28	1.86	2.44	—	—	—
o-Phthalic acid (M)	—	—	—	—	0	0.54	0.91
$Co(OAc)_2$ (M)	0.023	0.023	0.023	0.023	0.023	0.023	0.023
NaBr (M)	0.046	0.046	0.046	0.046	0.023	0.023	0.046
$-d[O_2]/dt$ (M/s) $\times 10^4$	1.70	0.84	0.83	0.58	1.20	0.89	1.39

ion. It was confirmed that the rate of formation of cobaltic ion by peroxy radical decreased by a factor of three in the presence of 2.4 M benzoic acid.

Coordinated benzoic acid to cobaltous ion may retard the reaction of cobalt with peroxy radical and the formation of cobaltic ion because of steric hindrace, and so retard the successive oxidation of toluic acid.

In order to exclude the retardation effect due to toluic acids, the relative rate of oxidation of toluic acids at concentration of 0.34 M is compared with the other rates of substituted toluenes as shown in Table 2. It is surprizing that toluic acids are apparently more reactive than toluene or methoxy toluene.

Table 2. Relative rate of oxidation of substituted toluenes catalyzed by 0.023 M $Co(OAc)_2$ and 0.046 M NaBr in acetic acid at 85 °C

Substituted toluene (0.34M)	Relative rate of oxidation
Toluene	1.00
p-Xylene[a)]	1.96
p-Methoxytoluene[a)]	0.96
p-Chlorotoluene[a)]	1.05
o-Chlorotoluene[a)]	1.03
p-Toluic acid	1.10
m-Toluic acid	1.15
o-Toluic acid	2.30

a) Ref. 6.

Apparently, the rate of oxidation of toluene was much higher than those of toluic acids at higher substrate concentration, for example, it was about 2.4 times as fast as those of *m*- and *p*-toluic acids at concentration of 2.4 M and 85 °C.

Previously,[6)] we have shown that the relative rates of autoxidation of substituted toluenes were quite different from the relative reactivities obtained by the competitive oxidation and we ascribed these results to the difference in the rate of termination reaction between substituted benzyl peroxy radical. An electron withdrawing substituent such as carboxyl group will decrease the rate of hydrogen abstraction step as in the case of ordinary free radical reaction, but it seems also to reduce considerably the rate of bimolecular reaction of benzyl peroxy radicals. Although we can not present any measured values about the termination rate constant of substituted toluenes, the polar effect seems to be a good explanation for the results given in Table 2. In addition, the bimolecular reaction of 2-carboxy benzyl peroxy radical can be expected to be slower than that of 4-carboxy benzyl peroxy radical because of steric hindrance. However, the steric effect of chlorine atom on the rate of termination seems not so large as the carboxyl group.

In order to elucidate the steric effect of carboxyl group, the mixing effect of toluic acids was studied and shown in Table 3. The rate of oxidation of an equimolar mixture of *m*- and *p*-toluic acids was nearly equal to those of twice amount of single components, because the rates of oxidation of 0.68 M and 1.22 M *p*-toluic acid were 1.10×10^{-4} and 1.50×10^{-4} M/s, respectively, and those of 0.68 M and 1.22 M *m*-toluic acid were 1.12×10^{-4} and 1.43×10^{-4} M/s.

It can be concluded that *m*- and *p*-toluic acids have similar reactivities in the autoxidation reaction. On the other hand, the rate of oxidation of 0.34 M *o*-toluic acid decreased from 1.30 to 1.21 or 1.18×10^{-4} M/s by the addition of 0.34 M *m*-toluic or *p*-toluic acids. These results can only be explained on the basis of cross termination between two different peroxy radicals as in the case of cumene and tetralin.[10)] The retardation effect due to *m*- and *p*-toluic acids should be much smaller than by *o*-toluic acid according to Figs. 3—5.

The higher rate of oxidation of *o*-toluic acid than *p*-toluic acid can be attributed to the smaller termination rate constant (k_t) of the derived peroxy radical. However, in the presence of *p*-toluic acid, the cross termination between different peroxy radicals will be predominant and the rate constant of cross termination will be larger than k_t of *o*-toluic acid and similar to k_t of *p*-toluic acid, since no more significant steric effect can be expected in the bimolecular reaction between different peroxy radicals. Thus, a mixture of *o*- and *p*-toluic acids will present a similar rate of oxidation as a mixture of *m*- and *p*-toluic acids.

Incidentally, we observed similar antagonistic effect in the oxidation of a mixture composed of *p*-toluic acid and toluene, that is, the rate of oxidation of 0.86 M toluene catalyzed by 0.023 M $Co(OAc)_2$ and 0.046 M NaBr just increased from 1.35 to 1.43×10^{-4} M/s by adding 0.34 M *p*-toluic acid.

Table 3. Mixing effect of toluic acids on the rate of oxidation at $Co(OAc)_2$ 0.023M, NaBr 0.046 M and 85 °C in acetic acid

p-Toluic acid (M)	0.34	0.68	1.22	—	—	—	—	0.34	0.34	0.61	—	—
m-Toluic acid (M)	—	—	—	0.34	0.68	1.22	—	0.34	—	0.61	0.34	0.61
o-Toluic acid (M)	—	—	—	—	—	—	0.34	—	0.34	—	0.34	0.61
$-d[O_2]/dt$(M/s) $\times 10^4$	0.62	1.10	1.50	0.66	1.12	1.43	1.30	1.13	1.21	1.43	1.18	1.48

References

1) Y. Kamiya, *Tetrahedron*, **22**, 2020 (1966).
2) Y. Kamiya, *Advan. Chem. Ser.*, **76**, 193 (1968), published by the Amer. Chem. Soc.
3) K. Sakota, Y. Kamiya, and N. Ohta, This Bulletin, **41**, 641 (1968).
4) D. A. S. Ravens, *Trans. Faraday Soc.*, **55**, 1768 (1959).
5) C. E. H. Bawn and T. K. Wright, *Discuss. Faraday Soc.*, **46**, 164 (1969).
6) Y. Kamiya, *J. Catal.*, **33**, 480 (1974).
7) T. Nakayama, Unpublished work.
8) A. S. Hay and H. S. Blanchard, *Can. J. Chem.*, **43**, 1306 (1965).
9) K. Kawamoto, T. Yoshioka, and Y. Fujita, "6th Oxidation Symposium," Japan, 1972.
10) J. A. Howard, W. J. Schwalm, and K. U. Ingold, *Advan. Chem. Ser.*, **75**, 6 (1968), published by the Amer. Chem. Soc.

Carbon-Carbon Bond Formation by Selective Coupling of Alkylthioallylcopper Reagent with Allylic Halides

Koichiro OSHIMA, Hisashi YAMAMOTO, and Hitosi NOZAKI
Department of Industrial Chemistry, Kyoto University, Yoshida, Kyoto 606
(Received January 30, 1975)

The reaction of 1-alkylthioallylcopper reagents with allylic halides affords the S_N2' type substitution product in excellent yield. The more synthetically useful reagent, 1,3-bis(methylthio)allylcopper reagent behaves in the same fashion. Attempts to hydrolyze the vinyl sulfide moiety to an aldehyde unit is successful only in the latter case. Yomogi alcohol is synthesized stereospecifically in the light of these results.

The remarkable regio- and stereospecificity of simple organocopper derivatives, *e.g.*, CuR or $LiCuR_2$, where R=alkyl, vinyl, or aryl, to form carbon-carbon bond with organic halides[2] raises the question whether the specific reactivity of more stable carbanionic intermediates could be enhanced by copper(I) ion.[3] The answer to the question is of particular interest for the 1-alkylthioallyl anions since the reaction of these systems has substantial synthetic utility. Moreover, the recent development of effective methods for converting allylic sulfides to 1-alkylthioallyllithium species[4] has made 1-alkylthioallylcopper(I) derivatives readily available for synthetic studies.

1-Alkylthioallyl anion is synthetically equivalent to either the 1-oxopropyl anion ($-COCH_2CH_3$) or 3-oxopropyl anion ($-CH_2CH_2CHO$). It was already

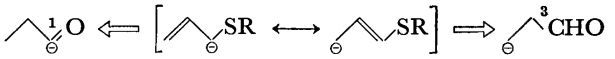

known that aryl- or alkylthioallyllithium undergoes reaction with organic halides to introduce an alkyl group specifically on the carbon α to the alkylthio group and not γ to the sulfur atom.[4] In this study we have synthesized alkylthioallylcopper(I) derivatives and have examined their behavior as potential synthon of 3-oxopropyl anion. We have also examined 1,3-bis(methylthio)allylcopper(I) as a synthon of 3-oxopropenyl anion ($-CH=CHCHO$).

A solution of 1-alkylthioallyllithium **1**—**3** in ether or tetrahydrofuran was prepared from the corresponding allyl sulfide and *sec*-butyllithium at −25 °C for 30 min. Treatment of the ethereal solution of organolithium derivative **1** or **2** with slightly excess cuprous iodide (CuI) at −78 °C for 15 min furnished a gray to white suspension which by analogy with the previous work[5] probably due to the polymeric organocopper derivatives **4** and **5**, respectively.

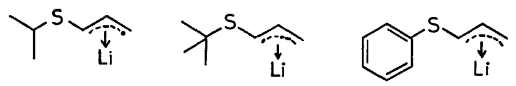

1 2 3

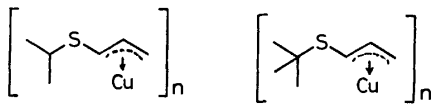

4 5

These suspensions were stable at −78 °C for 1 hr but decomposed gradually at −25 °C to form a black precipitate.[6] Although the similar complex could be formed in tetrahydrofuran, the resulting complex was found to decompose much faster. Thus, alkylthioallylcopper derivatives should be prepared in ether at −78 °C in a period of 15—30 min. It is noteworthy, however, that similar treatment of **3** with CuI failed to produce analogous monoalkylcopper derivatives but only a black tar.

Attempted preparation of lithium di(alkylthioallyl)-cuprate derivatives failed. After addition of a half equiv of CuI to the lithium derivative **1** a black precipitate formed, the behavior of which was quite similar to that of **1**. From the previous observation,[6b] it would appear that the tendency of metal cuprate species to undergo specific reaction is retarded by the presence of carbon ligand which could form reasonably stable anion.

$$R_2Cu^- \rightleftharpoons RCu + R^-$$

The reaction of 2-cyclohexylideneethyl bromide (1.0 equiv) with isopropylthioallylcopper (2.0 equiv) in ether at −78 °C for 4 hr produced the substitution product **6** in 92% yield;>96% pure by glpc and NMR assay.

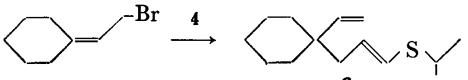

6

The reaction appears to be a pure S_N2' type displacement of bromine by isopropylthioallyl group. In addition this ambident anion undergoes alkylation exclusively γ to sulfur atom in high yield: thus, the alkylthioallylcopper reagent did behave as a synthon of 3-oxopropyl anion. Although the S_N2' type displacement of allylic or propargylic acetate by metal dialkylcuprate reagent have been shown previously,[7] the present reaction offers the advantage of high regio selectivity to a unique degree.

In a similar experiment, allyl bromide and 1-cyclohexenylmethyl bromide gave the sulfides **7** and **8** in 88% and 87% yields, respectively.

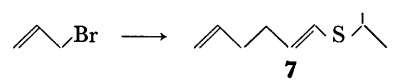

7

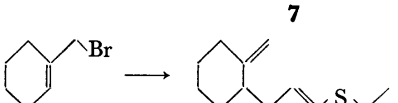

8

Further study is required before the stereochemical and mechanistic details of these reactions can be

undestood. However, we could assume the involvement of a radical type intermediate for this reaction on the basis of the following results. Treatment of benzyl bromide with the copper complex **4** at −78 °C for 2 hr produced bibenzyl in a moderate yield. Similarly benzhydryl chloride gave 1,1,2,2-tetraphenylethane as a major product. These observations are possibly indicative of the presence of benzyl radical or benzhydryl radical in the course of the reaction, since both of which are known to be dimerized easily to form the isolated coupling products.[8]

Alkylthioallylcopper also reacts with substances other than allylic halides. The isopropylthio complex **4** reacts with acetone in ether at −78 °C to yield **9** as a major product. Thus, the behavior of carbonyl compounds toward the copper derivative **4** contrasts sharply with that of allylic halides as those appearing above.

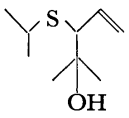

9

Finally, we examine the possibility of Michael reactions including the addition of **4** or **5** to mesityl oxide. In no case, however, did the presence of excess copper(I) derivatives in the reaction mixture have any substantial effect on the rate or product distribution of the Michael reaction.

The experimental procedure generally used for hydrolysis of vinyl sulfides with mercuric chloride[9] was applied to the product **6** without any success. Only minimal conversion to the corresponding aldehyde was observed, and the major products constitute a complex mixture, possibly as a result of acid-catalyzed cyclization followed by rearrangements. The relative difficulties associated with δ,ε-unsaturated aldehyde synthesis led us to explore the following route starting from 1,3-bis(methylthio)propene.

1,3-Bis(methylthio)allyllithium (**10**) was readily prepared by metallation of 1,3-bis(methylthio)propene with *sec*-butyllithium in ether at −25 °C, a procedure superior to previous methods[10] for our present purpose in that **10** is formed in high yield in the absence of secondary amine. Although a solution of the lithio derivative **10** was reported to be purple, a pale yellow solution was obtained in the absence of diisopropylamine. Treatment of this solution with CuI at −78 °C and stirring for 15 min produced the corresponding copper derivative **11** which behaved similarly as isopropylthioallylcopper in the following reaction with allylic halides.

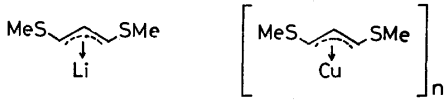

10 11

Thus, 2-cyclohexylideneethyl bromide was treated with the copper reagent **11** at −78 °C to furnish the expected S_N2' type substitution product **12** in almost quantitative yield.

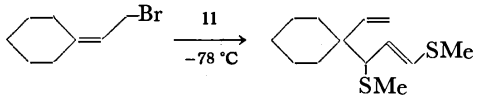

12

Previously, the hydrolysis of 1,3-bis(methylthio)-propene derivatives to α,β-unsaturated carbonyl compounds has been effected by mercury(II) ion.[10] Seeking a milder hydrolysis procedure, we investigated the use of cupric ion in ethanol[11] and found that this ion afforded very high yields of pure aldehydes. The process is devoid of the cationic cyclization of **11** as well as other side reactions.

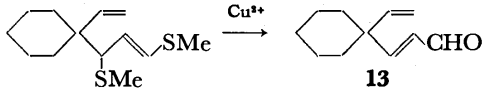

13

The δ,ε-unsaturated aldehyde **13** was obtained in 92% over-all yield from the cyclohexylideneethyl bromide. Similarly, the reaction of 1,3-bis(methylthio)-allylcopper with several allylic halides in ether as solvent, followed by cupric ion catalyzed hydrolysis, led to efficient cross coupling as indicated below.

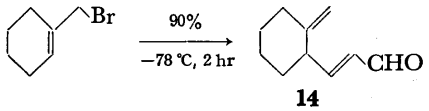

14

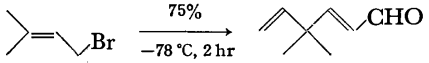

15

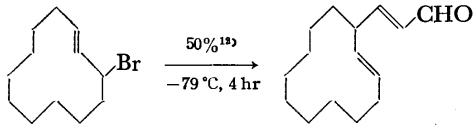

16

The observed regio- and stereoselectivity of our new reaction portends its broad synthetic application in the field of natural product chemistry. As an example, Yomogi alcohol, (*E*)-2,5,5-trimethyl-3,6-heptadien-2-ol (**17**),[13] was prepared regio- and stereoselectively when the aldehyde **15** was subjected to the following two-step sequence.

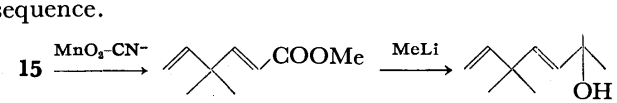

18 **17**

The aldehyde **15** was converted to the corresponding carboxylic ester **18** stereospecifically in good yield by manganese dioxide-cyanide ion method.[14] The homogeneity of the ester **18** was indicated by tlc and glpc analysis. In addition, the NMR and infrared spectra of **18** were entirely analogous to those of the corresponding ethyl ester.[13] The ester so obtained was alkylated by the treatment of excess methyllithium[13] at −25 °C for 30 min to yield Yomogi alcohol (**17**) in 75% yield. The NMR, infrared, and mass spectra of **17** were identical with those of the natural alcohol **17**.[13]

The authors acknowledge with pleasure the financial support by the Grant-in-aid administered by the Ministry

of Education, Japanese Government. We are also grateful to Dr. Y. Kato, Teijin Limited, for the exact mass spectral data.

Experimental

IR spectra were determined on a Shimadzu IR-27-G spectrometer, mass spectra on a Hitachi RMU-6L mass spectrometer, glpc analyses on a Yanagimoto GCG-550F, and NMR spectra on a JEOL-C-60-H or Varian EM-360 spectrometer; chemical shifts are given in δ with TMS as the internal standard. Analyses were carried out by Mrs. K. Fujimoto at Prof. Kawanisi's Laboratory and by the staffs at the Elemental Analyses Center of Kyoto University. High resolution mass spectra were taken on a JMS-D100 mass spectrometer operating at 75 eV. All experiments were carried out under an atmosphere of dry nitrogen, preparative thin layer chromatography (plc) on silica gel PF-254 (Merck) plates with hexane or benzene as a developing solvent, and preparative column chromatography on silica gel WAKO-gel C-100 (Wako).

Preparation of Allyl Alkyl Sulfides. A mixture of alkyl mercaptane (0.27 mol), sodium ethoxide (20 g, 0.30 mol), and ethanol (200 ml) was heated at reflux and treated with a solution of allyl bromide (37 g, 0.30 mol) in ethanol (20 ml) dropwise over 30 min. The mixture was heated at reflux for 1 hr, and allowed to cool to room temperature. The reaction was quenched by the addition of water and the separated organic layer was dried. Fractional distillation through a 20 cm Vigreux column afforded NMR-pure allyl sulfides in 60—80% yield.

Allyl isopropyl sulfide: bp 127—128 °C (760 mmHg); IR (neat) 1640, 1250, 1230, 990, 910 cm^{-1}; NMR (CCl_4) δ 1.20 (d, J=7, 6H), 2.82 (dq, J=7, 1H), 3.12 (d, J=8, 2H), 4.85—5.27 (m, 2H), 5.45—6.10 (m, 1H); mass *m/e* (%) 116 (38), 74 (80), 59 (35), 43 (42), 41 (100).

Allyl *tert*-butyl sulfide: bp 60 °C (43 mmHg); NMR (CCl_4) δ 1.29 (s, 9H), 3.0—3.3 (m, 2H), 4.8—6.3 (m, 3H); mass *m/e*: 130 (M^+).

Generation of Isopropylthioallylcopper **4** *and* tert-*Butylthioallylcopper* **5**. Allyl isopropyl sulfide or allyl *tert*-butyl siulfide (2.0 mmol) was dissolved in dry ether (15 ml). The solution was cooled to −78 °C and treated with *s*-butyllithium in pentane (2.0 ml of 1.02 M solution). After stirring for 30 min at −26 °C, the resulting organge or pale yellow solution was recooled to −78 °C. Solid cuprous iodide (2.4 mmol) was added. A white precipitate formed immediately and the mixture was stirred at the same temperature for 15 min before subsequent treatments described below.

Reaction of **4** *with Cyclohexylideneethyl Bromide.* A solution of cyclohexylideneethyl bromide (1.9 g, 10 mmol) in either (10 ml) was added at −78 °C to a solution of **4** prepared from allyl isopropyl sulfide (2.4 g, 20 mmol), ether (70 ml), *s*-butyllithium (20 ml of 1.02 M solution in pentane), and cuprous iodide (5.0 g, 26 mmol). The mixture was kept at −78 °C for 4 hr. The resulting black mixture was filtered through a pad of Celite 545 and the filter cake was washed with ether. The filtrate and washings were combined, washed with water, dried, and freed of the solvent. The residual liquid was separated through a column chromatography on silica gel (100 g) with hexane–benzene as an eluant. The less polar fraction (tlc R_f 0.50 (hexane)) provided the sulfide **6** (2.1 g, 92% yield): bp 145 °C (bath temp., 3 mmHg); IR (neat) 1640, 1242, 945, 912 cm^{-1}; NMR (CCl_4) δ 1.25 (d, J=7, 6H), 1.40 (bs, 10H), 2.03 (d, J=7, 2H), 3.00 (dq, J=7, 1H), 4.96 (dd, J=2 and 17, 1H), 5.09 (dd, J=2 and 12, 1H), 5.60 (dt, J=7 and 15, 1H), 5.70 (dd, J=12 and 17, 1H), 6.02 (d, J=15, 1H); mass *m/e* (%) 224 (5), 181 (16), 116 (20), 115 (100), 73 (70); Anal. Found: C, 75.2; H, 11.0. Calcd for $C_{14}H_{24}S$: C, 74.9; H, 10.8. The more polar fraction (tlc R_f 0.15 (hexane)) afforded the dimer of allyl isopropyl sulfide (0.48 g, *m/e* 230 (M^+)) which was not identified completely.

Reaction of **4** *with 1-Cyclohexenylmethyl Bromide.* A solution of **4** prepared from allyl isopropyl sulfide (0.23 g, 2.0 mmol) was treated with 1-cyclohexenylmethyl bromide (0.18 g, 1.0 mmol) at −78 °C and stirred at −78 °C for additional 4 hr. The orange liquid obtained on extractive work-up was submitted to preparative tlc on silica gel with hexane as an eluant. The band at R_f 0.4—0.6 provided the sulfide **8** (0.18 g, 87% yield) as a colorless liquid: bp 130 °C (bath temp., 3 mmHg); IR (neat) 1645, 1240, 945, 905, 890 cm^{-1}; NMR (CCl_4) δ 1.25 (d, J=7, 6H), 2.95 (dq, J=7, 1H), 4.58 (bd, J=7, 2H), 5.63 (dt, J=7 and 15, 1H), 5.90 (d, J=15, 1H); mass *m/e* (%) 210 (24), 167 (92), 134 (44), 116 (76), 115 (100). Found: C, 73.9; H, 10.4%. Calcd for $C_{13}H_{22}S$: C, 74.2; H, 10.5%.

Reaction of **4** *with Allyl Bromide.* A solution of **4** prepared from allyl isopropyl sulfide (0.23 g, 2.0 mmol) was treated with allyl bromide (86 μl, 1.0 mmol) at −78 °C. The resulting solution was kept at −78 °C for 4 hr, and the color of the solution was turned black at the end of the period. Tetralin (100 μl, 97 mg) was injected and the entire mixture was filtered through a pad of Celite 545 and washed with ether. The filtrate was washed with dilute hydrochloric acid, water, and dried. The resulting organic phase was submitted directly to glpc to obtain the yield of the sulfide **7** using tetralin as the internal standard: 88% yield. The analytical sample was prepared by preparative tlc and bulb to bulb distillation: bp 110 °C (bath temp., 45 mmHg); IR (neat) 1640, 1240, 990, 940, 910 cm^{-1}; NMR (CCl_4) δ 1.30 (d, J=7, 6H), 2.02—2.38 (m, 4H), 2.98 (dq, J=7, 1H), 4.75—5.16 (m, 2H), 5.40—6.05 (m, 3H); mass *m/e* (%) 156 (8), 115 (51), 113 (18), 84 (14), 73 (100); Found: C, 69.2; H, 10.2%. Calcd for $C_9H_{16}S$: C, 69.2; H, 10.3%.

Reaction of **4** *with Benzyl Bromide.* Benzyl bromide (0.17 g, 1.0 mmol) was treated with the complex **4** (2.0 mmol) in ether (13 ml) at −78 °C for 2 hr. The preparative tlc separation of the crude reaction mixture gave bibenzyl (71 mg, 78% yield) as the major product; it was identical in all respects with an authentic sample.

Reaction of **4** *with Benzhydryl Chloride.* Benzhydryl chloride (0.20 g, 1.0 mmol) was treated with the complex **4** (2.0 mmol) in ether (10 ml) at −78 °C for 2 hr. After the concentration of the dried extracts *in vacuo*, a white solid was obtained. Recrystallization from benzene-hexane (1: 1) gave pure 1,1,2,2-tetraphenylethane (0.12 g, 70%) as colorless crystals; the product was identical in all respects with an authentic sample.

Reaction of **4** *with Acetone.* A solution of **4** prepared from allyl isopropyl sulfide (0.23 g, 2.0 mmol) was treated with acetone (1.0 ml) at −78 °C and kept there for 1 hr. The mixture was filtered through a pad of Celite 545 and washed through with ether. The filtrate was washed with dilute hydrochloric acid and water, dried, and concentrated *in vacuo*. The residual liquid (0.31 g) was submitted to glpc; α-adduct/γ-adduct=20: 1 by comparison with an authentic sample.[15]

Generation of 1,3-bis(Methylthio)allylcopper **11**. *sec*-Butyllithium in pentane (1.02 M, 2.0 ml, 2.0 mmol) was added to a solution of 1,3-bis(methylthio)propene (2.0 mmol) in ether (15ml) with stirring under nitrogen at −78 °C and kept at −26 °C for 30 min. The resulting orange solution was recooled to −78 °C and treated with cuprous iodide (2.4 mmol) and stirred at that temperature for 15 min before subsequent

treatments described below.

*Reaction of **11** with Cyclohexylideneethyl Bromide.* A solution of **11** derived from 0.27 g (2.0 mmol) of 1,3-bis(methylthio)propene was treated with cyclohexylideneethyl bromide (0.19 g, 1.0 mmol) at −78 °C. The color of the solution turned brown rapidly and black after stirring for additional 2 hr. The liquid (0.35 g) obtained on extractive work-up was treated with cupric chloride (0.44 g, 3.0 mmol) and cupric oxide (0.24 g, 3.0 mmol) in ethanol (20 ml) at 25 °C for 1 hr. The mixture was filtered through a pad of Celite 545 and the filter cake was washed with ether. The ethereal solutions were washed with dilute hydrochloric acid and water and concentrated *in vacuo*. The residual liquid was submitted to preparative tlc with benzene as an eluant. The band at R_f 0.5—0.6 provided the aldehyde **13** (0.15 g, 92% yield) as a colorless liquid: bp 120 °C (bath temp., 18 mmHg); IR (neat) 1685, 1625, 1110, 980, 915, 850 cm^{-1}; NMR (CCl_4) δ 1.2—2.1 (m, 10H), 4.7—5.8 (m, 2H), 5.95 (dd, J=7 and 15, 1H), 6.6 (d, J=15, 1H), 9.45 (d, J=7, 1H); mass *m/e* (%) 164 (12), 135 (67), 121 (24), 107 (36), 81 (64), 79 (70), 67 (100); Mol wt. Found: 164.1170. Calcd for $C_{11}H_{16}O$: 164.1201.

*Reaction of **11** with 1-Cyclohexenylmethyl Bromide.* A solution of **11** derived from 1,3-bis(methylthio)propene (0.27 g, 2.0 mmol) was treated with 1-cyclohexenylmethyl bromide (0.18 g, 1.0 mmol) at −78 °C and kept there for 2 hr. After extractive work-up, a mixture of residual liquid, cupric chloride (0.40 g, 3.0 mmol), and cupric oxide (0.24 g, 3.0 mmol) in ethanol (20 ml) was stirred under nitrogen at 25 °C for 1 hr. The black suspension was filtered through a pad of Celite 545 and the filter cake was washed with ether. The ethereal solutions were washed with water, dried, and freed of the solvent. The remaining oil was submitted to preparative tlc on silica gel with benzene as an eluant. The band at R_f 0.45—0.60 provided the aldehyde **14** (0.14 g, 90% yield) as a colorless liquid: bp 100 °C (bath temp., 18 mmHg); IR (neat) 1690, 1645, 1150, 1120, 980, 890 cm^{-1}; NMR (CCl_4) δ 4.5—4.65 (bd, 2H), 6.0 (dd, J=7 and 15, 1H), 6.8 (dd, J=8 and 15, 1H), 10.1 (d, J=7, 1H); mass *m/e* (%) 150 (21), 135 (33), 121 (62), 107 (65), 93 (39), 81 (94), 79 (100); Anal. Found: C, 79.8; H, 9.65%. Calcd for $C_{10}H_{14}O$: C, 80.0; H, 9.39%.

*Reaction of **11** with 4-Bromo-2-methyl-2-butene.* A solution of **11** prepared from 1,3-bis(methylthio)propene (0.27 g, 2.0 mmol) was treated with 4-bromo-2-methyl-2-butene (0.15 g, 1.0 mmol) at −78 °C for 2 hr. Ethereal extracts were washed with water, dried, and concentrated. Powdered cupric chloride (0.40 g, 3.0 mmol) and cupric oxide (0.24 g, 3.0 mmol) were sequentially added to a solution of the remaining liquid (0.25 g) in ethanol (20 ml). The heterogeneous reaction mixture was stirred under nitrogen at 25 °C for 1 hr. Extractive workup furnished a liquid which was submitted to preparative tlc with benzene as an eluant. The band at R_f 0.5—0.65 provided the aldehyde **15** (0.18 g, 72% yield) as a colorless liquid: IR (neat) 1690, 1160, 1110, 986, 920, 785 cm^{-1}; NMR (CCl_4) δ 1.25 (s, 6H), 4.95 (dd, J=2 and 20, 1H), 5.02 (dd, J=2 and 10, 1H), 5.80 (dd, J=10 and 20, 1H), 5.95 (dd, J=7 and 16, 1H), 6.7 (d, J=16, 1H), 9.5 (d, J=7, 1H); mass *m/e* (%) 124 (13), 109 (85), 81 (90), 79 (64), 67 (100); Mol wt. Found: 124.0843. Calcd for $C_8H_{12}O$: 124.0889.

*Reaction of **11** with 2-Cyclododecenyl Bromide.* A solution of **11** prepared from 1,3-bis(methylthio)propene (0.27 g, 2.0 mmol) was treated with 2-cyclododecenyl bromide (0.24 g, 1.0 mmol) at −78 °C. The color of the solution changed very slowly to brown and then the solution was maintained at −78 °C for 4 hr. The similar procedure afforded the aldehyde **16** (0.11 g, 50% yield) as a colorless liquid: bp 140 °C (bath temp., 0.1 mmHg); IR (neat) 1690, 1630, 1130, 975 cm^{-1}; NMR (CCl_4) δ 1.2—2.2 (m, 19H), 5.1—5.7 (m, 2H), 6.95 (ddd, J=16, 7, and 1.5, 1H), 7.65 (dd, J=7 and 16, 1H), 9.41 (d, J=8, 1H); mass *m/e* (%) 220 (25), 135 (17), 121 (28), 107 (50), 95 (70), 81 (100); Mol wt. Found: 220.1862. Calcd for $C_{15}H_{24}O$: 220.1830.

*Generation of Yomogi Alcohol from the Aldehyde **15**.* The aldehyde **15** (0.26 g, 2.1 mmol) was stirred with a mixture of sodium cyanide (0.40 g), acetic acid (0.16 g), and manganese dioxide[16] (5.0 g) in methanol (25 ml) for 12 hr at 25 °C. The remaining liquid on extractive work-up after filtration was subjected to preparative tlc with benzene as an eluant. The band at R_f 0.6—0.8 provided the ester **18** (0.24 g, 76% yield) as a colorless liquid: IR (neat) 1725, 1655, 1190, 1165, 1010, 985 cm^{-1}; mass *m/e* (%) 154 (6), 139 (12), 125 (10), 123 (12), 111 (16), 95 (100), 79 (44), 67 (38); Found: C, 70.2; H, 9.23%. Calcd for $C_9H_{14}O_2$: C, 70.1; H, 9.15%.

The ester **18** (0.15 g) was treated with methyllithium (5 ml of 1.5 M solution in ether) in ether at 0 °C and kept at 25 °C for an additional 1 hr. The reaction mixture was poured into ice-cold water and the product was extracted with ether repeatedly. The combined ethereal extracts were washed with water, dried, and freed of the solvent. The remaining oil was submitted to preparative tlc on silica gel with dichloromethane as an eluant to yield the desired Yomogi alcohol as a colorless liquid, identical in all respects with the authentic sample.

References

1) A preliminary account of this work has appeared: K. Oshima, H. Yamamoto, and H. Nozaki, *J. Amer. Chem. Soc.*, **95**, 7926 (1973).

2) J. F. Normant, *Synthesis*, **2**, 63 (1972) and references cited therein.

3) E. J. Corey and M. Jautelat, *Tetrahedron Lett.*, **1968**, 5787; T. Mukaiyama, K. Narasaka, and M. Furusato, *J. Amer. Chem. Soc.*, **94**, 8641 (1972).

4) a) K. Oshima, H. Takahashi, H. Yamamoto, and H. Nozaki, *ibid.*, **95**, 2693 (1973); K. Oshima, H. Yamamoto, and H. Nozaki, *ibid.*, **95**, 4446 (1973); b) J. F. Bielmann and J. B. Ducep, *Tetrahedron Lett.*, 5629 (1968).

5) H. Gilman, R. G. Jones, and L. A. Woods, *J. Org. Chem.*, **17**, 1630 (1952); see also Ref. 2.

6) a) H. Gilman and J. M. Straley, *Rec. Trav. Chim. Pays-Bas.*, **55**, 821 (1936); b) H. O. House and W. F. Fischer, Jr., *J. Org. Chem.*, **34**, 3615 (1969).

7) Dimethylcopper and its homologs undergo the similar substitution reaction with allylic or propargylic acetate, although *n*-BuCu-LiI does not react. Allylic acetate: P. Rona, L. Tokes, J. Tremble, and P. Crabbe, *Chem. Commun.*, **1969**, 43; R. J. Anderson, C. A. Henrick, and J. B. Siddal, *J. Amer. Chem. Soc.*, **92**, 735 (1970); E. E. van Tamelen and J. P. McCormick, *ibid.*, **92**, 737 (1970); Propargyl acetate: P. Rona and P. Crabbe, *ibid.*, **90**, 4733 (1968); **91**, 3289 (1969).

8) K. Oshima, T. Shirafuji, H. Yamamoto, and H. Nozaki, This Bulletin, **46**, 1233 (1973).

9) E. J. Corey and J. I. Schulman, *J. Org. Chem.*, **35**, 777 (1970); K. Oshima, K. Shimoji, H. Takahashi, H. Yamamoto, and H. Nozaki, *J. Amer. Chem. Soc.*, **95**, 2694 (1973).

10) E. J. Corey, B. W. Erickson, and R. Noyori, *ibid.*, **93**, 1724 (1973).

11) H. Takahashi, K. Oshima, H. Yamamoto, and H. Nozaki, *ibid.*, **95**, 5803 (1973).

12) The low yield of this reaction was due to the low reactivity of the secondary halide.

13) W. Sucrow and W. Richter, *Chem. Ber.*, **103**, 3771 (1970); B. Willhalm and A. F. Thomas, *Chem. Commun.*, **1969**, 1380; H. Kwart and R. K. Miller, *J. Amer. Chem. Soc.*, **76**, 5403 (1954).
14) E. J. Corey, N. W. Gilman, and B. E. Ganem, *ibid.*, **90**, 5616 (1968).
15) Prepared from 1-isopropylthioallyllithium and acetone at 0 °C for 10 min.
16) Active manganes dioxide of E. Merck was used without further activation.

Steric Requirements in Base-Promoted Elimination Reactions

Akio ISHIZAWA

Department of Chemistry, Faculty of Science, Kyoto University, Sakyo-ku, Kyoto 606

(Received February 24, 1975)

The effect of the steric requirement of the attacking base in base-promoted elimination reactions was studied using a variety of pairs of diastereoisomeric bases. The pairs of diastereoisomeric alkoxide bases examined gave difinitely different *cis*-olefin to *trans*-olefin ratios from elimination reactions of secondary alkyl bromides and tosylates in dimethyl sulfoxide. The results indicate unambiguously that the steric requirement of the attacking base is an important controlling factor in determining the olefinic product distribution in these elimination reactions. The structural effect of the solvent molecule was also investigated using pairs of diastereoisomeric alcohols in base-promoted elimination reactions. Under a variety of conditions the effect upon the product distribution observed was rather small, as compared with those observed for the diastereoisomeric bases, to be an important contributing factor on the product distribution.

Extensive studies on the base-promoted elimination reactions have revealed that the olefinic product distribution (positional and geometrical isomers) is affected by various factors such as the structure of the substrate, the nature of the leaving group, the strength and the structure of the attacking base, and the nature of the reaction medium.[1] Since the structure of the substrate can be varied independently to the other variables such as the base, the solvent and the leaving group, the importance of this factor has easily been tested and clearly evidenced experimentally.[1] The effect of the base, on the other hand, are much more complicated because these must depend both on the structure and on the strength of the base and an ambiguity of many experimental works attempting to separate the factors arises mainly from the fact that the strength of the base is not an independent variable to the structure of the base. Moreover, since the effect of the base depends strongly on the solvent used, it is very difficult to separate the effects on the product distribution that are caused by intrinsic properties of the base from those they are the result of solvent effects. A metal alkoxide dissolved in the corresponding alcohol is the most common reagent for bringing about elimination reactions, so that much of the data available are on the results of simultaneous change in the base and the solvent.

Intramolecular non-bonded interactions such as eclipsing effects are effectively able to alter the relative stereochemical stabilities between the possible conformers at the transition state in elimination reactions, so that it is reasonably anticipated that the intermolecular interactions between reactants or between reactants and the environment (such as the solvent molecule), though lesser extent than the intramolecular by virtue of the greater freedom with the intermolecular, will constitute a contributing factor on the product distribution.

To understand the effect of the attacking base on the product distribution in base-promoted elimination reactions, it is, therefore, desired to determine the effects of the strength and of the structure of the attacking base separately. The present work was undertaken to make this point clear, and also to examine the effect of the molecular structure of the solvent as one of the effects of the environment in elimination reactions.

For the examination of the structural effect of the base it is necessary to use such bases that the variation of the structure should have little effect upon the base strength. A pair of diastereoisomeric alkoxide bases that differ only in the spatial alignment of the substituents around the basic center would satisfy the requisite, because the electronic effect of the substituents may cause little differences in the base strength between the pair. With such a pair of bases, the transition states are diastereoisomeric in each other, so that they should give different product distributions.

In a similar sense, the parent diastereoisomeric alcohols can also be utilized as solvent for the elucidation of the structural effects of the environment in elimination reactions.

Results and Discussion

Effects of Diastereoisomeric Alkoxide Bases. The effect of pairs of diastereoisomeric alkoxides, the conjugate bases of *dl-threo-* and *dl-erythro*-alcohols, **1**—**6**, was examined for the product distribution from base-promoted elimination reactions of secondary alkyl

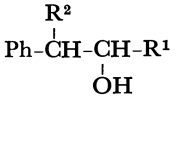

1, R^1=Me R^2=Me
2, R^1=Et R^2=Me
3, R^1=^{n}Bu R^2=Me
4, R^1=Et R^2=Et
5, R^1=Et R^2=^{n}Bu
6, R^1=Ph R^2=Me

bromides and tosylates. Since the nature of the transition state is affected by the solvent, the steric requirement of the attacking base must also be dependent on the nature of the solvent used. With changing the polarity the influence of the solvent upon the steric requirement of the base was first examined using two pairs of alkoxides, **1** and **2**, and the results are given in Table 1. The solvents used in these runs were mixtures of the solvent in question and 3-methyl-3-pentanol which was added to make all the base solutions easily homogeneous. Though the reaction temperatures were different, little differences were observed in the product distributions between a pair of the diastereosiomeric alkoxides **1** or **2** in dimethyl sulfoxide-methylpentanol system (Table 1) and in the pure dimethyl sulfoxide system (Table 3),[2] so that the equilibrium between an alkoxide

Table 1. Effects of the solvent on the product distribution from elimination reactions of 4-heptyl-X with diastereoisomeric pairs of alkoxides **1** and **2** in the dipolar aprotic solvent (75 v/v %)-3-methyl-3-pentanol (25 v/v %) mixture at 60 °C

X in subst.[a]	Base[b]	Dipolar aprotic component[c]	$\left(\frac{cis}{trans}\right)_E$[d]	$\left(\frac{cis}{trans}\right)_T$[e]	$\frac{(cis/trans)_E}{(cis/trans)_T}$
Br	**1**	DMSO	0.150	0.131	1.15
Br	**1**	DMF	0.157	0.135	1.16
Br	**1**	ACN	0.196	0.184	1.07
Br	**1**	Diglyme	0.190	0.181	1.05
Br	**2**	DMSO	0.250	0.165	1.52
Br	**2**	DMF	0.269	0.177	1.52
Br	**2**	ACN	0.281	0.229	1.23
Br	**2**	Diglyme	0.277	0.222	1.25
OTs	**1**	DMSO	0.376	0.334	1.13
OTs	**1**	DMF	0.380	0.354	1.07
OTs	**1**	ACN	0.506	0.492	1.03
OTs	**1**	Diglyme	0.558	0.560	0.996
OTs	**2**	DMSO	0.539	0.414	1.30
OTs	**2**	DMF	0.550	0.437	1.26
OTs	**2**	ACN	0.590	0.536	1.10
OTs	**2**	Diglyme	0.664	0.599	1.11

a) $[subst.]_i \doteqdot 0.1$ M. b) $[alkoxide]_i \doteqdot 0.2$ M. c) DMSO=dimethyl sulfoxide; DMF=dimethylformamide; ACN=acetonitrile; Diglyme=diethyleneglycol dimethyl ether. d) E=*erythro*-alkoxide. e) T=*threo*-alkoxide.

base and the added alcoholic component, $ROH+R'O^- \rightleftharpoons RO^-+R'OH$, seems to contribute little in the mixed solvent systems.[3] Though the factors attributable to the apparent trend in the product distribution were not clear, the results indicated that the larger the polarity of the solvent used, the larger the difference in the product distribution between a pair of the diastereoisomeric alkoxides. Hence dimethyl sulfoxide was the prefered solvent throughout the studies of the structural effect of the attacking base.

Table 2. Effects of diastereoisomeric pairs of alkoxides **1** and **2** on the product distribution from elimination reactions of 2- and 3-pentyl-X in dimethyl sulfoxide at 35 °C

Subst.[a]	Base[b]	$\frac{1\text{-ene}}{2\text{-ene}}$	$\frac{cis}{trans}$[c]	$\frac{(cis/trans)_E}{(cis/trans)_T}$
2-Br	E-**1**	0.396	0.166	1.07
2-Br	T-**1**	0.407	0.155	
2-Br	E-**2**	0.574	0.258	1.29
2-Br	T-**2**	0.584	0.200	
3-Br	E-**1**		0.182	0.978
3-Br	T-**1**		0.186	
3-Br	E-**2**		0.235	1.12
3-Br	T-**2**		0.209	
2-OTs	E-**1**	1.48	0.318	1.11
2-OTs	T-**1**	1.47	0.286	
2-OTs	E-**2**	1.82	0.457	1.29
2-OTs	T-**2**	1.85	0.353	
3-OTs	E-**1**		0.293	0.983
3-OTs	T-**1**		0.298	
3-OTs	E-**2**		0.382	1.16
3-OTs	T-**2**		0.328	

a) $[subst.]_i \doteqdot 0.1$ M. b) E=*erythro*-alkoxide, T=*threo*-alkoxide. $[alkoxide]_i \doteqdot 0.2$ M. c) 2-pentenes.

Table 3. Effects of diastereoisomeric pairs of alkoxides **1**—**6** on the product distribution from elimination reactions of 4-heptyl-X in dimethyl sulfoxide at 35 °C

X in Subst.[a]	Base[b]	$\left(\frac{cis}{trans}\right)_E$[c]	$\left(\frac{cis}{trans}\right)_T$[d]	$\frac{(cis/trans)_E}{(cis/trans)_T}$
Br	**1**	0.161	0.132	1.22
Br	**2**	0.248	0.182	1.36
Br	**3**	0.263	0.183	1.44
Br	**4**	0.273	0.186	1.47
Br	**5**	0.274	0.179	1.53
Br	**6**	0.107	0.146	0.733
OTs	**1**	0.374	0.319	1.17
OTs	**2**	0.508	0.388	1.31
OTs	**3**	0.564	0.422	1.34
OTs	**4**	0.533	0.409	1.30
OTs	**5**	0.554	0.411	1.35
OTs	**6**	0.247	0.285	0.867

a) $[subst.]_i \doteqdot 0.1$ M. b) $[alkoxide]_i \doteqdot 0.2$ M. c) E=*erythro*-alkoxide. d) T=*threo*-alkoxide.

The product distributions from elimination reactions of 2-, 3-pentyl and 4-heptyl bromides and tosylates with pairs of diastereoisomeric sodium alkoxides, **1**—**6**, in dimethyl sulfoxide are given in Tables 2 and 3. In these runs the results are much less complicated than those in Table 1, because neither an alcoholic cosolvent was present nor the polarity of the solvent varied. The remarkable feature of the results is that all the pairs of diastereoisomeric alkoxides examined gave definitely different product distributions. With 4-heptyl systems the *erythro*-alkoxides always produced larger *cis* to *trans* ratios than the *threo*-alkoxides except for the diastereoisomeric diphenylpropoxides **6** with which the ratios were just the opposite to those for the other members.[4] Generally the larger the steric bulk of the attacking base, the larger the difference in the product distribution between the pair of diastereoisomeric bases. By comparing the results of 2- and 3-pentyl systems with those of 4-heptyl system, the alkyl substituents on the α and the β' carbons of the substrate seems to play a certain role in controlling the steric interactions between the substrate and the attacking base, that is, the larger the alkyl substituents on the substrate, the larger the ratio of $(cis/trans)_E$ to $(cis/trans)_T$ with a given pair of diastereoisomeric alkoxides.

As mentioned, since the base strength should be of little difference between a pair of diastereoisomeric bases, it must contribute little to the variation of the product distribution, so that a steric factor must be the controlling one. The relationship generally observed between the reactivity and the selectivity[5] will also ascertain steric factors to be responsible for the variation of the product distribution. Though, strictly speaking, the comparison of the product distributions should be limited within a given pair of diastereoisomeric bases only where the strength of the bases is held constant, the apparent trend of the change in the product distribution with different pairs of bases is opposite

to that predicted by the change in the base strength, that is, the variation of the alkyl substituents R^1 or R^2 in the alkoxide from methyl to ethyl to *n*-butyl (from **1** to **2** to **3** or from **2** to **4** to **5**) should make the alkoxide base stronger, so that a decrease in selectivity (expressed in $(cis/trans)_E/(cis/trans)_T$) would be anticipated in this order. The selectivity observed, however, is just the opposite (Table 3).

The contribution of the parent alcohol produced during reaction to the variation of the product distribution appears to be negligible, since no effect of a pair of diastereoisomeric alcoholic solvent was observed when a large amount of dimethylformamide, as a cosolvent, was present (see below).

Recent studies on the stereochemistry of the base-promoted elimination reactions have revealed that a *syn-anti* dual mechanism of elimination prevails a wide range of conditions of the base and the solvent properties and the substrate structure.[6] In general, a *syn* mechanism appears to become important when the substrate carries large alkyl substituents on the both α positions to the leaving group and a poor leaving group such as trimethylammonio, and when the elimination is effected by a bulky and strong base in a poor ion dissociating solvent such as *tert*-butoxide in *tert*-butanol or in benzene. With the systems examined here, incursion of a *syn* mechanism seems unlikely to be a significant factor to the *cis* to *trans* ratio. A *syn* mechanism accounts for only 10 per cent of the overall reaction in the reaction of 5-decyl tosylate with *tert*-butoxide in *tert*-butanol,[6f] and even smaller contributions of the mechanism with the same substrate have been reported when a good ion dissociating solvent was used (5.2 and 4.2 per cent of the overall reaction with *tert*-butoxide in dimethylformamide[6f] and in dimethyl sulfoxide[6i] respectively). With secondary alkyl bromides the mechanism seems to contribute to the *cis* to *trans* ratio even lesser extent than with secondary alkyl tosylates.[6g]

These results confirm unambiguously that the steric requirement of the attacking base to be an important contributing factor to the product distribution in base-promoted elimination reactions.

Effects of Diastereoisomeric Solvents. Using pairs of diastereoisomeric alcohols **1**, **2** and **3** as solvent, the olefinic product distributions from elimination reactions of 4-heptyl bromide and tosylate were examined under a variety of conditions, and the results are collected in Tables 4 and 5. As anticipated, the effect of the diastereoisomeric solvent, *i.e.*, the steric requirement for solvation, upon the product distribution was less pronounced compared to that of the diastereoisomeric attacking base in Tables 2 and 3. From the Tables it is clearly seen that the effect of the steric requirement for solvation upon the product distribution changes in a complex manner by the nature of the reaction medium and by the attacking base. With the bicyclic amine base known as a very efficient dehydrohalogenating agent,[7] the difference in the product distribution, *i.e.*, the selectivity, between a given pair of diastereoisomeric solvents gradually decreased with increasing the steric bulk of the solvent molecule, whereas complex changes in the product distributions were observed with phenoxide base. In the presence of 18-Crown-6 ether which has been believed to make an alkoxide base reactive by dissociating ion paired species,[6g,6h] a maximum selectivity was observed in the diastereoisomeric phenylheptanols **3**. When 25 volume per cent of dimethylformamide was present as a cosolvent,[8] a maximum selectivity was obtained from the eliminations of the bromide in the diastereoisomeric phenylpentanols **2**. The tosylate, though only two pairs of diastereoisomeric alcohols **1** and **2** were examined, showed a similar change to that of the bromide. In the presence of 50 and 75 volume per cent of the cosolvent, no selectivity between a given pair of diastereoisomeric solvents could be observed from elimination reactions of either the bromide and the tosylate.

Neither the stereochemistry of these elimination reactions nor the details of the interactions between the reactants and the solvent molecules are known, but these results show definitely that it is necessary to take into account the structural effects of the solvent molecule as well as the polarity of the solvent,[9] when

Table 4. Product distributions from elimination reactions of 4-heptyl bromide with DBU[a] in diastereoisomeric alcoholic solvents at 50 °C[b]

Solvent	$\frac{cis}{trans}$	$\frac{(cis/trans)_{erythro}}{(cis/trans)_{threo}}$
erythro-**1**	0.0768	1.08
threo-**1**	0.0708	
erythro-**2**	0.0760	1.06
threo-**2**	0.0716	
erythro-**3**	0.0692	1.03
threo-**3**	0.0674	

a) 1,8-Diazabicyclo[5.4.0]undec-7-ene. b) $[subst.]_i$ = 0.1 M. $[DBU]_i$ = 0.5 M. Reaction period, 50 hr.

Table 5. Product distributions from elimination reactions of 4-heptyl-X with sodium phenoxide[a] in diastereoisomeric alcoholic solvents

X in Subst.[b]	Solvent[c]	$\frac{cis}{trans}$	$\frac{(cis/trans)_E}{(cis/trans)_T}$
Br	E-**1**+DMF[d]	0.153	1.02
Br	T-**1**+DMF[d]	0.150	
Br	E-**2**+DMF[d]	0.139	0.921
Br	T-**2**+DMF[d]	0.151	
Br	E-**3**+DMF[d]	0.143	0.947
Br	T-**3**+DMF[d]	0.151	
OTs	E-**1**+DMF[d]	0.405	0.998
OTs	T-**1**+DMF[d]	0.406	
OTs	E-**2**+DMF[d]	0.369	0.932
OTs	T-**2**+DMF[d]	0.396	
Br	E-**1**+Crown[e]	0.167	1.03
Br	T-**1**+Crown[e]	0.162	
Br	E-**2**+Crown[e]	0.161	1.01
Br	T-**2**+Crown[e]	0.159	
Br	E-**3**+Crown[e]	0.176	0.941
Br	T-**3**+Crown[e]	0.187	

a) $[phenoxide]_i \fallingdotseq 0.2$ M. b) $[subst.]_i \fallingdotseq 0.1$ M. c) E=*erythro*-alcohol, T=*threo*-alcohol. DMF=dimethylformamide, 25 v/v%. Crown=18-Crown-6 ether, 0.2 M. d) at 40 °C for 15 hr. e) at 50 °C for 2 hr.

the solvent effects upon the product distribution in the elimination reactions are considered.

Experimental

Materials. *2-Pentyl, 3-Pentyl, and 4-Heptyl Bromides*: The bromides were prepared by treating the corresponding alcohols with triphenyl phosphite dibromides at −10—0 °C.[10] 2-Pentyl bromide, bp 117—118 °C, n_D^{20} 1.4409 (lit.,[9a] bp 58.4—58.8 °C/100 mmHg, n_D^{20} 1.4412); 3-pentyl bromide, bp 47 °C/60 mmHg, n_D^{20} 1.4454 (lit.,[9a] bp 59—59.5 °C/100 mmHg, n_D^{20} 1.4444); 4-heptyl bromide, bp 64—65 °C/24 mmHg, n_D^{20} 1.4501 (lit.,[11] bp 75—75.5 °C/38 mmHg, n_D^{25} 1.4478).

2-Pentyl, 3-Pentyl, and 4-Heptyl Tosylates: The tosylates were prepared by the standard method.[12] 2-Pentyl tosylate, n_D^{20} 1.5008 (lit.,[9e] n_D^{20} 1.4995); 3-pentyl tosylate, mp 44.6—44.8 °C (lit.,[9a] mp 42—44 °C); 4-heptyl tosylate, n_D^{20} 1.4978. Found: C, 62.33; H, 8.44%. Calcd for $C_{14}H_{22}O_3S$: C, 62.20; H, 8.20%.

18-Crown-6 Ether: This macrocyclic polyether was prepared according to Greene.[13] mp 39.7—40.7 °C, PMR ($CDCl_3$) δ 3.7 (s) (lit.,[13] mp 39.5—40.5 °C, PMR ($CDCl_3$) δ 3.67 (s)).

1,8-Diazabicyclo[5.4.0]undec-7-ene: A commercial sample was dried over potassium hydroxide and distilled under reduced pressure. bp 96—97 °C/3 mmHg.

Diastereoisomeric Alcohols, 1—6: The alcohols **1**, **2**, **4**, and **6** were prepared and separated into the diastereomers according to Cram *et al.*[14] The alcohol **3** obtained by the action of *n*-butyl-magnesium bromide upon 2-phenylpropionaldehyde, bp 137—140 °C/14 mmHg (lit.,[15] bp 156—160 °C/30 mmHg), was separated into the diastereomers *via* their ester derivatives. 4-Phenyl-3-octanone obtained by *n*-butylation of ethyl benzyl ketone, bp 142—145 °C/14.5 mmHg, semicarbazone, mp 105—106 °C (lit.,[15] bp 147—150 °C/16 mmHg, semicarbazone, mp 104—105 °C) was reduced to **5** by sodium borohydride, bp 146.5—147.5 °C/15 mmHg. The diastereomers were separated *via* their ester derivatives. The properties of the alcohols and their derivatives are collected in Table 6.

Purification of Solvents. Dimethyl sulfoxide was distilled from calcium hydride under reduced pressure. Dimethylformamide was first dehydrated by distilling with anhydrous benzene, dried over Driereit and then redistilled under reduced pressure. Acetonitrile was distilled from phosphorus pentoxide. Diethyleneglycol dimethyl ether was distilled from lithium aluminum hydride under reduced pressure. 3-Methyl-3-pentanol was purified by distilling twice from sodium metal.

Preparation of Base Solutions. A. Sodium hydride (Ventron Co., dispersed in mineral oil) was washed three to four times with anhydrous *n*-pentane, weighed and dissolved in an appropriate amount of anhydrous dimethyl sulfoxide or a solvent mixture. The resulting solution was converted into the desired alkoxide solution by adding a slightly excess of the calculated amount of an alcohol.

B. Phenoxide solutions were prepared by dissolving sodium hydride into an appropriate solvent mixture containing a calculated amount of phenol. All the preparations were operated under dry nitrogen atmosphere.

Procedure for Elimination Reactions. An appropriate amount (2 to 5 ml) of the base solution was pipetted into an ampoule with a serum stopper under dry nitrogen atmosphere. The substrate was added by a syringe through the stopper just before the reaction. The ampoule was sealed and reacted in a thermostated bath.

Analysis of the Reaction Mixtures. The reaction mixture was poured into about 100 ml of cold water and extracted with 1 to 1.5 ml of *n*-pentane when the reaction was fast. With slow reactions 1 ml of *n*-pentane was added to the reaction mixture and the low boiling fractions were distilled into a dry ice-acetone trap under reduced pressure (about 30 mmHg) at room temperature. The pentane solutions were analyzed for the olefins produced by glpc on JEOL Model JGC 20K or JGC 1100 instruments. The pentenes were analyzed on a 3 m×3 mm column of silver nitrate in *p*-methoxybenzyl cyanide on Celite 545 at 25 °C. The heptenes were analyzed on a 2 m×3 mm column of silver nitrate in benzyl cyanide on Celite 545 at 35 °C (JGC 1100) or on 3 m×3 mm column of silver nitrate in *p*-nitrobenzyl cyanide on Celite 545 at 35 °C (JGC 20K). The *cis* to *trans* ratios obtained from the peak heights were calibrated by the standard curves prepared by analyzing the *cis-trans* mixtures of known compositions under the same conditions.

Control Experiments. Neither synthetic *cis*- nor *trans*-3-heptenes were isomerized on exposure to the reaction condition, 0.2 M of sodium 3-phenyl-2-butoxide (a mixture of *threo*- and *erythro*-isomers) in dimethyl sulfoxide at 35 °C for 60 min.

No isomerizations between the pairs of diastereoisomeric alkoxides could be detected for the recovered alcohols, **1** and **2**, from the elimination reactions carried out in dimethyl

Table 6. Properties of the alcohols 1—6 and their derivatives

Alcohol[a]	Bp (mp) (°C)	Isomeric[b] Purity (%)	Deriv.[c]	Recrystn.[d] Solvent	mp (°C)
1 T	103.5—104/15[e]	97.8	AP	AcOEt–PE	130—131.3[e]
1 E	107.8—108/16[e]	98.5	ANP	AcOEt–PE	160—161[e]
2 T	125/20[f]	97	AP	AcOEt–PE	137—138[f]
2 E	127—127.2/22[f]	98.6	ANP	AcOEt–PE	155—157[f]
3 T	136.3—137.7/13.5[g]	96	AP	E–PE	95—96
3 E	138—140/14.5[g]	99.6	PNB	EtOH	39—39.2
4 T	134—134.8/22[h]	96.1	AP	E–P	126—127[h]
4 E	(44.8—45)[h]	98.3			
5 T	112—113/3.5	99.8	AP	E–PE	122—123
5 E	110/3, (46—46.5)	99.8	DNB	MeOH	61—62
6 T	136—136.5/3[i]	—[j]	PNB	Benzene	142—143[i]
6 E	(50—51)[i]	—[j]			

a) T=*threo*, E=*erythro*. b) The purity was estimated by the relative glpc peak heights. PEG 20 M on Diasolid L 2 m. c) AP=acid phthalate, ANP=acid 3-nitrophthalate, PNB=*p*-nitrobenzoate, DNB=3,5-dinitrobenzoate. d) PE=petroleum ether, E=ether, P=*n*-pentane. e) ref. 14a. f) ref. 14b. g) ref. 15. h) ref. 14c. i) ref. 14d. j) No separation could be attained on glpc.

sulfoxide.

The author wishes to thank Professor K. Maruyama for his stimulating discussions. The author is also grateful to Dr. H. Akiyama, Sanyo Kasei Co., for providing a DBU sample.

References

1) a) W. H. Saunders, Jr. and A. F. Cockerill, "Mechanisms of Elimination Reactions," John Wiley & Sons, New York, N. Y. (1973), Chapter 2. b) C. K. Ingold, "Structure and Mechanism in Organic Chemistry," 2nd Ed., Cornell University Press (1969), Chapter 9.

2) A similar tendency was observed between the diglyme–methylpentanol and the pure diglyme systems. In diglyme, the diastereoisomeric alkoxides **2** gave the ratios, $(cis/trans)_E/(cis/trans)_T$, of 1.16 and 1.24 with 4-heptyl bromide and tosylate respectively.

3) Ref. 1a. p. 190.

4) The irregularity is only a superficial, *i.e.*, the configuration of the *threo*-alcohol **6** corresponds to those of the *erythro*-alcohols **1**—**5**.

5) J. E. Leffler and E. Grunwald, "Rates and Equilibria of Organic Reactions," John Wiley & Sons, New York, N. Y. (1963), p. 162.

6) a) J. Sicher, J. Závada, and J. Krupička, *Tetrahedron Lett.*, **1966**, 1619. b) J. Závada, M. Svoboda, and J. Sicher, *ibid.*, **1966**, 1627. c) J. Závada, J. Krupička, and J. Sicher, *Chem. Commun.*, **1967**, 66. d) M. Pánková, J. Sicher, and J. Závada, *ibid.*, **1967**, 394. e) M. Pánková, J. Závada, and J. Sicher, *ibid.*, **1968**, 1142. f) J. Závada, M. Pánková, and J. Sicher, *ibid.*, **1968**, 1145. g) M. Svoboda, H. Hapala, and J. Závada, *Tetrahedron Lett.*, **1972**, 265. h) J. Závada, M. Svoboda, and M. Pánková, *ibid.*, **1972**, 711. i) M. Pánková, M. Svoboda, and J. Závada, *ibid.*, **1972**, 2465. j) D. S. Bailey and W. H. Saunders, Jr., *Chem. Commun.*, **1968**, 1598. k) I. N. Feit and W. H. Saunders, Jr., *J. Amer. Chem. Soc.*, **92**, 5615 (1970). l) D. S. Bailey and W. H. Sanuders, Jr., *ibid.*, **92**, 6904 (1970). m) I. N. Feit, F. Schadt, J. Labinkowski, and W. H. Saunders, Jr., *ibid.*, **93**, 6606 (1971).

7) M. Fieser and L. Fieser, "Reagents for Organic Synthesis," Vol. 2, John Wiley & Sons, New York, N. Y. (1969), p. 101.

8) A homogeneous sodium phenoxide solution (0.1 M) in pure alcohol **1** or **2** could be obtained only at an elevated temperature (~100 °C).

9) a) H. C. Brown, I. Moritani, and Y. Okamoto, *J. Amer. Chem. Soc.*, **78**, 2193 (1956). b) H. C. Brown and R. L. Klimisch, *ibid.*, **87**, 5517 (1965). c) D. H. Froesdorf, M. E. McCain, and W. W. Wilkison, *ibid.*, **87**, 3984 (1965). d) D. H. Froemsdorf, W. Dowd, and K. E. Leimer, *ibid.*, **88**, 2345 (1966). e) I. N. Feit and W. H. Saunders, Jr., *ibid.*, **92**, 1630 (1970).

10) D. G. Coe, S. R. Landauer, and H. N. Rydon, *J. Chem. Soc.*, **1954**, 2281.

11) H. A. Shonle, J. H. Waldo, A. K. Keltch, and H. W. Coles, *J. Amer. Chem. Soc.*, **58**, 585 (1936).

12) L. Fieser and M. Fieser, "Reagents for Organic Synthesis," Vol. 1, John Wiley & Sons, New York, N. Y. (1967), p. 1180.

13) R. N. Greene, *Tetrahedron Lett.*, **1972**, 1793.

14) a) D. J. Cram, *J. Amer. Chem. Soc.*, **71**, 3863 (1949). b) D. J. Cram and R. Davis, *ibid.*, **71**, 3871 (1949). c) D. J. Cram, F. A. A. Elhafez, and H. Weigartner, *ibid.*, **75**, 2293 (1953). d) D. J. Cram and F. A. A. Elhafez, *ibid.*, **74**, 5828 (1952).

15) J. Lévy and P. Jullien, *Bull. Soc. Chim. France*, **45**, 941 (1929).

The Segregation of Sodium Ions in KCl Minute Crystals

Yoshihiro SENSUI and Kenji TOMURA

Institute for Atomic Energy, Rikkyo University, Yokosuka, Kanagawa 240-01

(Received February 7, 1975)

The surface accumulation of solute sodium ions in KCl crystallites was measured as a function of the annealing temperature, 250—450 °C. The minute crystals were baked out under 3×10^{-7} Torr, and their surface layers were dissolved successively with anhydrous ethyl alcohol. The contents of sodium and potassium were determined by instrumental neutron-activation analysis with the aid of a 50 cc-Ge(Li)-4K gamma spectrometer.

In a solid solution of ionic crystals with a common anion, quantitative measurements of the distribution coefficients of cations between the surface and the bulk are of interest in relation to the surface distortion[1] and the surface reactivity of the solids.[2,3] However, few experimental works have been reported even for such a simple system as alkali chloride, ACl/BCl. Kummer and his co-workers investigated the system of the Ca impurity in NaCl minute crystals[4] by the dissolution method using acetone, and that of Cs in KCl minute crystals by isotopic exchange techniques[5] using an acetone-solution/KCl-solid system. In these works, their attention was principally in the first surface layer of crystals in connection with the surface reactivity. According to the gas/solid-isotopic exchange reaction studied by the present authors[2,3] and theoretical works by Benson *et al.*,[1] the structure and properties of the surface change gradually in the range from the first layer to the fifth. With this in view, the present paper will study the accumulation of the sodium impurity in the surface layers of KCl crystals. The solubility of NaCl in KCl is rather high,[6] for they have the same type of structure. This situation differs very much from that in the previously studied systems.[4,5]

Experimental

Materials and Procedure. The KCl (Merck reagent, item No. 4933) used as a starting material contains 2.4 ppm of an Na impurity, as determined by radio-activation analysis. The precipitates of KCl, doped with Na amounting to 300—900 ppm, were prepared by a modified Marshall method.[7] The precipitates were washed twice with fresh ethanol. After the supernatant ethanol phase had been replaced completely with ethyl ether, the precipitates were transferred, together with ether, into a vessel connected to a vacuum system. Both the ethanol and ethyl ether used were dehydrated with CaO baked at 1100 °C for 12 hr and then distilled *in situ*. The precipitates were carefully dehydrated and degassed by baking then in a vacuum, 3×10^{-7} Torr. The baking temperature was raised, step by step, to 450 °C over a 140 hr period and then kept at that temperature for 48 hr. The crystallites thus obtained had a surface area of about 1.5 m^2/g, as determined by krypton adsorption at 77 K and electronmicrography showed that the faces exposed were the {100} planes as well as the crystallites used by Kummer *et al.*[5]

After pretreatment at 450 °C, the crystallites were annealed at a temperature between 250 and 450 °C for 48 hr at 3×10^{-7} Torr in order to establish the equilibrium distribution of the impurity at that temperature. Then, the surface regions of the crystals were dissolved successively with a small amount of anhydrous ethanol under atmospheric pressure. The solubility of NaCl in absolute ethanol at 20 °C is 1.149 mg/ml,[8] while that of KCl is 1.1624 mg/ml.[9] Because of these small solubilities, it is usually possible to remove several monolayers of the crystal surfaces in a batch-by-batch fractionation. The amounts of Na and K in each fraction were determined as follows. The alcoholic sample solution was irradiated with thermal neutrons, amounting to 1.08×10^{16} n/cm^2, by means of the TRIGA II reactor of Rikkyo University. The gamma rays of 1524.7 keV from ^{42}K and 1368.4 and 2753.6 keV from ^{24}Na in the samples concerned were measured by the use of a 50 cc-Ge(Li)-4K gamma spectrometer.

Results and Discussion

Figure 1 illustrates the relationship between the surface accumulation of sodium and the layer number as a function of the sodium concentration in the crystals. The sodium concentration in the surface region is very high as compared with that in the bulk, but far lower than the solubility limit, judging from the phase diagram of the NaCl/KCl solid solution.[6,10] Let us define the accumulation coefficient, $C_A(n)$, by the quantity $([Na]/[K])_n/([Na]/[K])_{bulk}$, where n designates

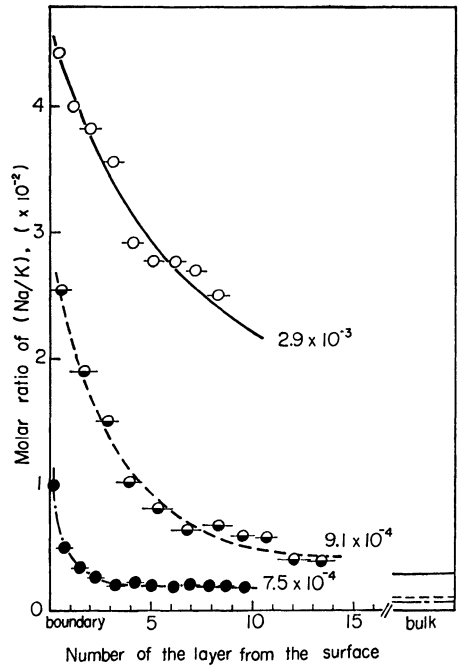

Fig. 1. The concentration dependence of the surface accumulation of sodium in potassium chloride crystallites at 300 °C.
○, ◒ and ● for the molar ratio of $(Na/K)=2.9\times10^{-3}$, 9.1×10^{-4} and 7.5×10^{-4}, respectively.

the numbering of the layer from the surface. Then, $C_A(n)$ may be independent of $([Na]/[K])_{bulk}$ as long as the impurity concentration is very low and far from the solubility limit. The present data may, then, be interpreted under these conditions. Figure 2 shows a typical profile of $C_A(n)$ as a function of the annealing temperature. The curves seem to converge to unity, but the rate of convergence is very low, *i.e.*, about 1/3—1/4 times that expected from the isotopic exchang reaction between chlorine gas and alkali chloride crystals.[2,3] This discrepancy may be attributed to the fact that the process of surface dissolution cannot be so well controlled as to remove strictly the specified n-th layer from various crystallites. The surface accumulation increases with the rise of the temperature. The value of C_A (1) is determined from the smoothed curve in Fig. 2, and its logarithms are plotted against the reciprocal of the temperature in Fig. 3. We obtain a straight line, though the figure shows some scatter of points. If an equilibrium is established, the slope of the line gives, as the enthalpy difference, ΔH, and the intercept of the coordinate at $1/T=0$ gives the entropy difference, ΔS, when sodium atoms segregate into the first layer from the bulk. We obtain $\Delta H=4.9\pm1.0$ kcal/mol and $\Delta S=13\pm1.6$ e.u. The values for both ΔH and ΔS are considerably large compared with the values predicted from the thermodynamic data of the NaCl/KCl solid solution.[6] These values cannot be explained on the basis of simple statistical thermodynamics; further detailed studies of various samples is, therefore, desired.

Next, let us discuss the rate of the eluilibriation of the impurity distribution in minute crystals of alkali

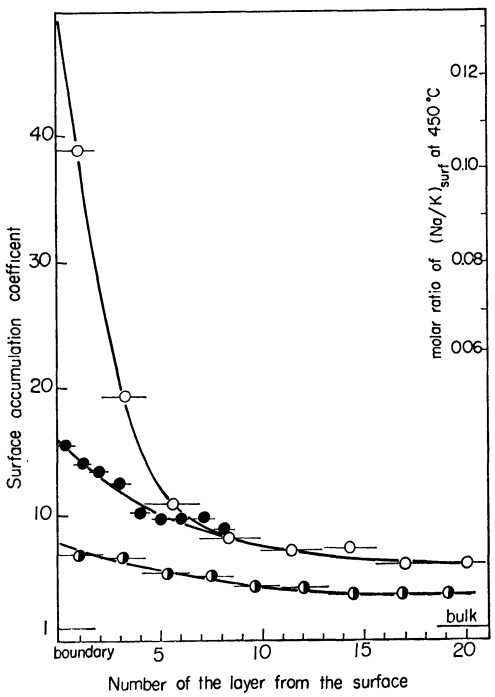

Fig. 2. The temperature dependence of the surface accumulation coefficients of sodium in potassium chloride crystallites.
○, 450 °C, 24 hr; ●, 300 °C, 24 hr and ◑, 250 °C, 48 hr.

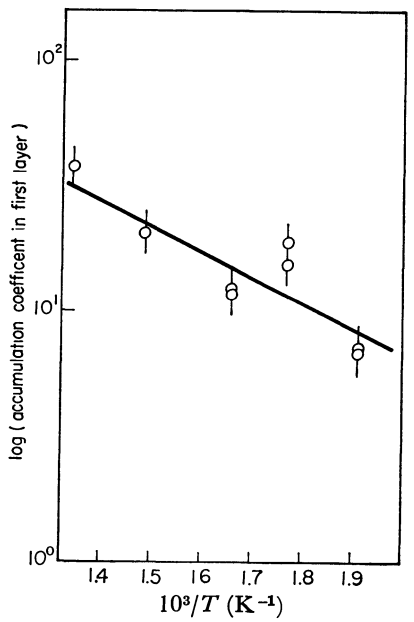

Fig. 3. Arrhenius plots of the accumulation coefficient of the surface first layer.

chloride. According to Kummer *et al.*,[4,5] it takes longer than thirty hours to eliminate step-dislocation on the surface of KCl crystallites doped with cesium at 600 °C.[5] On the other hand, Voss *et al.*[11] proposed that the equilibrium was easily established in the system of NaCl/KCl minute crystals, even while cooling the crystals from 350 °C to room temperature. The present results support the idea that it takes a long time to attain an equilibrium distribution of the Na^+ impurity. If the latter view is true, the two curves referred to 300 and 450 °C in Fig. 2 may be reduced to the same curve.

Finally, we must discuss the phase separation, fissures, and dislocation, the existence of which makes the analysis of the results complex. According to Barret *et al.*[6] and Tichelaar,[10] no macroscopic-phase separation takes place in the concentration range of sodium used at 250—450 °C. Even if a minute amount of NaCl crystals arises on the surface of KCl crystals during the preparation of the precipitates, it is considered that the NaCl phase is dissolved and removed by ethanol washing, as has been mentioned before. This results from the solubilities of the chlorides concerned in ethanol.[8,9] On the other hand, if crystals contain fissures and dislocations, the impurity accumulates along them as well as on the surface region; furthermore, these regions are selectively etched. Thus, fissures and dislocations remarkably disturb the study of the surface accumulation of impurities if their density is high. The present authors believe that the influence of fissures and dislocations in KCl minute crystals disapper upon the pre-baking treatment used in the present experiment. This view is supported by a comparison between the self-diffusion of Cl^- ions in large NaCl single crystals reported by Morrison *et al.*[12] and that in minute crystals reported earlier by the present authors.[3] Consequently, it can safely be concluded that the present results are a connected with the surface accumulation of impurities.

The authors would like to express their grateful acknowledgement to Professor Tetsuo Takaishi of Rikkyo Unviersity for his valuable suggestions.

References

1) G. C. Benson, P. I. Freeman, and E. Dempsey, *Advan. Chem. Ser.*, **33**, 26 (1961); *J. Chem. Phys.*, **39**, 302 (1963). G. C. Benson and T. A. Claxton, *ibid.*, **48**, 1356 (1968).

2) T. Takaishi and Y. Sensui, *Trans. Faraday Soc.*, **63**, 1003 (1967); *ibid.*, **65**, 131 (1969). Y. Sensui, This Bulletin, **45**, 2677 (1972); *ibid.*, **46**, 3324 (1973).

3) T. Takaishi and Y. Sensui, *Surface Science*, **19**, 339 (1970).

4) J. K. Kummer and J. D. Youngs, *J. Phys. Chem.*, **67**, 107 (1963).

5) Yung-Fang Yu Yao and J. T. Kummer, *ibid.*, **73**, 2262 (1969).

6) W. T. Barrett and W. E. Wallace, *J. Amer. Chem. Soc.*, **76**, 366 (1954).

7) F. G. Marshall, *Phys. Rev.*, **58**, 642 (1940).

8) W. F. Linke, ed., "Solubilities of Inorganic and Metal Organic Compounds." Amer. Chem. Soc. (1965), Vol. II, p. 1008.

9) *ibid.*, Vol. II, p. 166.

10) G. W. Tichelaar, Proefschrift, *Techn. Hogeschool, Deft*, (1956).

11) B. Voss, G. Santhoff, and M. Kahlweit, *Acta Met.*, **20**, 1177 (1972).

12) L. W. Barr, J. A. Morrison, and P. A. Schroeder, *J. Appl. Phys.*, **36**, 624 (1965).

Role of Chlorine in β-FeOOH on Its Thermal Change and Reactivity to Sulfur Dioxide

Tatsuo ISHIKAWA and Katsuya INOUYE

Department of Chemistry, Faculty of Science, Chiba University, Chiba 280

(Received January 8, 1975)

The state of Cl in β-ferric oxide hydroxide (β-FeOOH) was examined by X-ray diffraction, IR absorption, chemical analysis, DTA, and TGA. The adsorption of SO_2 was determined as a measure of the surface activity. No influence of Cl contained in the crystal appeared in the X-ray diffraction patterns and surface area. The absorption bands at 640 and 840 cm^{-1} in IR spectra showing the deformation vibration of OH group diminished with the decrease of Cl content. It was shown that the path for β-FeOOH to transform into α-Fe_2O_3 by heating differentiates from the sample including more than 11.5% Cl/Fe to one including less than 11.5% Cl/Fe. This critical Cl content is equal to the amount of Cl when Cl fills up the characteristic tunnels existing in the β-FeOOH crystal. Cl in β-FeOOH interferes both its transformation into α-Fe_2O_3 and the recrystallization of resultant α-Fe_2O_3. These effects were explained by the stabilization of the β-FeOOH structure by Cl in tunnels and the bonding between Cl and Fe. The amount of chemisorbed SO_2 was lowered by Cl which was adsorbed on outer surfaces.

It has been known that β-FeOOH is formed in the presence of Cl^- ions. It results in the fact, for example, that the corrosion products of steel, formed in marine environments, contain β-FeOOH amounting to 20—30 %.[1] The β-FeOOH sample prepared by the hydrolysis of an $FeCl_3$ solution also contains a certain amount of Cl and the Cl content varies with the conditions of preparation and subsequent treatments.[2] Mackay[3] asserted that β-FeOOH has the hollandite ($BaMn_8O_{16}$) or α-MnO_2 structure[4] and presumed that Cl^- ions and H_2O molecules fill the positions which in hollandite are occupied by Ba^{2+} ions and that Cl^- ions are replaced by H_2O molecules on washing, accompanied by the conversion of OH^- to O^{2-} to maintain the electrical neutrality. This structure of β-FeOOH was confirmed recently by means of neutron diffraction.[5] Chlorine in β-FeOOH is believed to affect some properties of β-FeOOH, *e.g.*, the thermal transformation into α-Fe_2O_3 and the surface activity. Hofer, Peebles, and Deiter[6] investigated the catalytic activity of various ferric oxides and oxide hydroxides in the Fisher-Tropsh synthesis but concluded that β-FeOOH is inactive. However, the present authors found that β-FeOOH shows higher reactivity to SO_2[7] and higher heat of immersion in water[8] than those of α-FeOOH and γ-FeOOH.

In the present work, β-FeOOH samples containing different amounts of Cl were examined by X-ray diffraction, infrared absorption, thermal analyses (DTA and TGA), chemical analysis, and the adsorption of SO_2 to reveal the influence of Cl on the reactivity of crystal surface.

Experimental

Materials. β-FeOOH was precipitated by heating 0.1 M $FeCl_3$ solution for 5 hr at 96—99 °C. The resultant precipitate was washed by the following method in order to change the Cl content. The sample A-1 was obtained by washing the precipitate with distilled water until no Fe^{3+} ions were detected, and A-2 by electrodialyzing the sample A-1 at 10 V/cm for 10 hr. A-3 was obtained by washing the original precipitate with 1 M NH_4Cl solution till free of Fe^{3+} ions, with 1 M NH_4OH solution to remove Cl^- ions, and finally with distilled water. The electrodialysis of A-3 at 10 V/cm for 10 hr gave A-4. A-5 was obtained by dispersing A-3 in 1 M NH_4OH for 3 day, followed by filtering and washing with distilled water. Another kind of β-FeOOH was prepared by heating 500 ml of 0.1 M $FeCl_3$ solution containing 30 g urea at 96—99 °C for 5 hr. The sample U-1 was obtained by washing the resultant precipitate with distilled water (500 ml) till free of Fe^{3+} ions and U-2 with 4 l distilled water. Each sample was dried in an air oven for 2 hr at 100 °C.

Procedure. The SO_2 adsorption was measured at 30.0 °C by use of a quartz spring balance. The samples were pretreated by outgassing under 10^{-5} Torr for 14 hr at 110 °C. The BET surface area was determined by N_2 adsorption measurement at liquid nitrogen temperature. The X-ray diffraction examination was carried out by the powder method by use of Mn-filtered FeKα at 30 kV and 10 mA. The differential thermal analysis (DTA) was done in air using α-Al_2O_3 as a reference sample at a heating rate of 10 °C/min, and the thermogravimetric analysis (TGA) by means of a quartz spring at a heating rate of 10 °C/min. Infrared absorption spectra were taken by the KBr disk method with JASCO IR-G spectrophotometer. Cl and Fe contents of the sample were determined according to the procedures described in the previous paper.[9]

Results

The Cl content expressed in atomic % Cl/Fe (Table 1) could not be reduced below 7% by the washing procedures used in this work. The X-ray diffraction patterns and the surface area were almost identical regardless of the Cl content. IR spectra (Fig. 1) changed with the Cl content; the absorption bands at 640 and 840 cm^{-1} shifted to higher frequencies and their absorbance increased with the Cl content. Müller[10] reported that β-FeOOH prepared from $FeCl_3$ solution shows IR spectra having two bands at 690 cm^{-1} and 840 cm^{-1} due to the OH deformation vibration, but the 840 cm^{-1} band disappears on treating with alkali bicarbonate or carbonate. In our spectra, the 640 cm^{-1} and 840 cm^{-1} bands diminished with the removal of Cl. It is accordingly speculated that the bands at 640 cm^{-1} and 840 cm^{-1} are due to the deformation vibration of the OH^- which become O^{2-} to maintain the electrical neutrality when Cl^- ion is replaced by H_2O molecule.

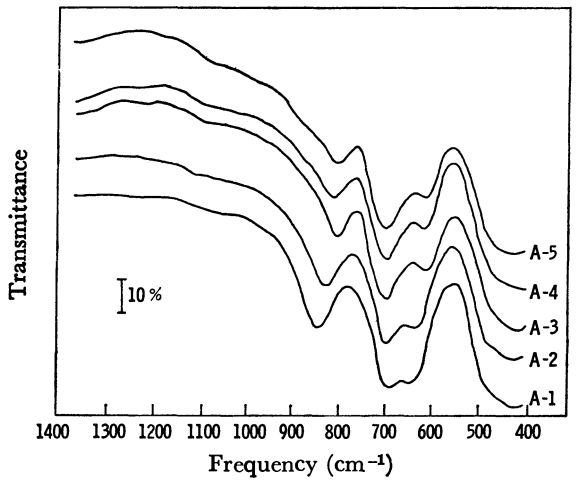

Fig. 1. Variations of IR spectrum with Cl content.

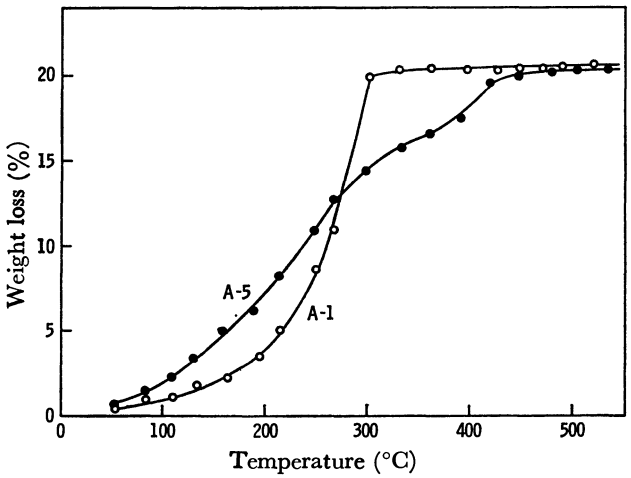

Fig. 2. TGA curves of A-1 and A-5.

TGA curves of samples A-1 and A-5 are shown in Fig. 2. The weight loss up to 270 °C of A-5 sample of 7% Cl/Fe was larger than that of A-1 of 17% Cl/Fe, but a gradual weight loss up to 420 °C was observed for A-5. The weight loss is considered to be caused by the dehydration of hydroxyl group ($2FeOOH \rightarrow Fe_2O_3 + H_2O$), the release of HCl, and the sublimation of $FeCl_3$. Then, the water content was calculated by subtracting the amount of released Cl and Fe from the weight loss between 110 and 500 °C in TGA curves. The water content thus obtained (Table 1) was still larger than the theoretical dehydration value (10.1 wt %). This result indicates that β-FeOOH embraces some more water molecules in addition to hydroxyl groups which produce

Table 1. Surface area and composition of samples

Sample	Surface area (m^2/g)	Cl (Cl/Fe, %)	Fe (mmol/g)	H_2O molecule (wt %)	(H_2O/Fe, %)
A-1	35	17	11.1	12.5	12.5
A-2	34	12	11.5	12.7	13.1
A-3	32	7.7	10.7	13.5	18.2
A-4	32	7.4	11.4	13.8	18.6
A-5	32	7.0	10.6	13.8	20.0
U-1	33	10	10.7	12.9	15.0
U-2	31	9.4	10.6	13.0	15.7

the "crystallization water" on dehydration.[11] As Mackay suggested,[3] this excess water seems to exist in tunnels parallel to the c-axis of the crystal. The amount of these water molecules, calculated by subtracting the theoretical dehydration value (10.1 wt %) from the water content, increases with the decrease of Cl content (Table 1). This result shows that Cl in β-FeOOH is replaced by H_2O molecule in the course of washing with water. The larger weight loss of A-5 below 270 °C will be due to the release of such water molecules.

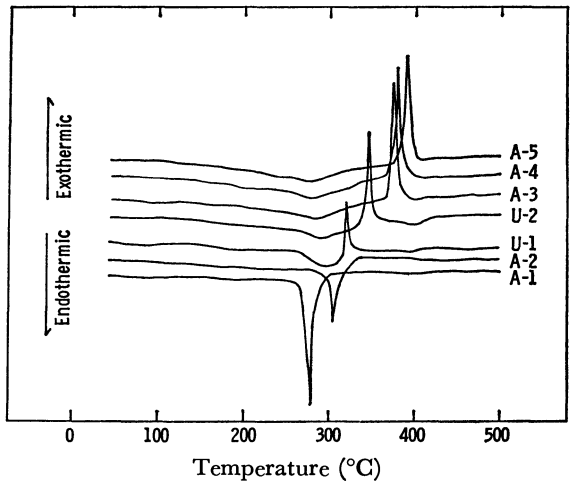

Fig. 3. Variations of DTA curve with Cl content

Variations of DTA curve with the Cl content are illustrated in Fig. 3. The sample A-1 of 17% Cl/Fe showed an endothermic peak at 280 °C, whereas A-5 of 7% Cl/Fe showed a broad endothermic peak at 275 °C and a sharp exothermic peak at 390 °C.

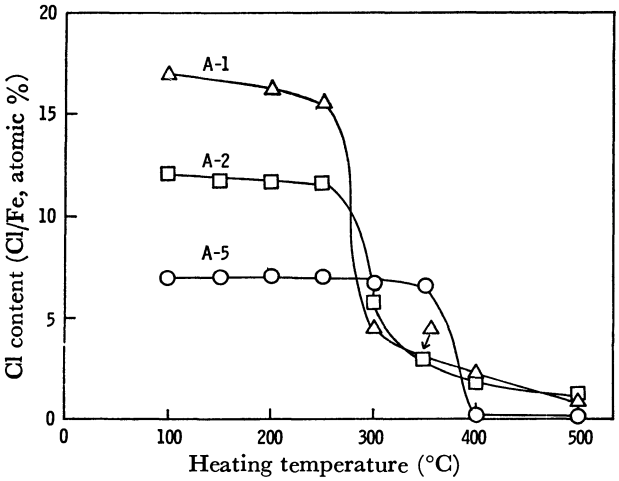

Fig. 4. Relation between Cl content and heating temperature.

The curves expressing the relationship between the Cl content and heating temperature (Fig. 4) showed the steep drop of Cl content at different temperatures. This temperature fell with the increase in the original Cl content. The sublimation of $FeCl_3$ was observed for A-3, A-4, and A-5 and the evolution of HCl was observed for A-1 and A-2 at each temperature corresponding to the sudden decrease of Cl.

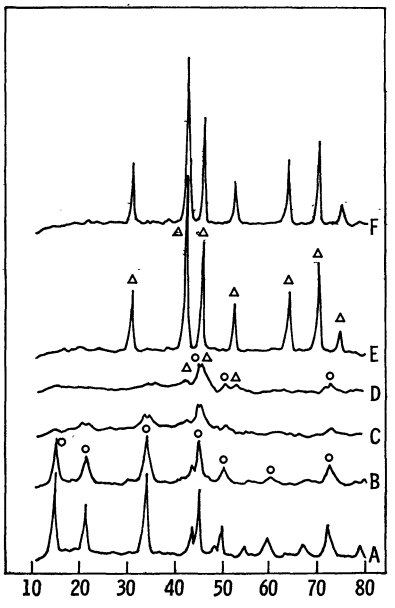

Fig. 5. X-ray diffraction patterns of A-1 at various heating temperatures: ○, β-FeOOH; △, α-Fe_2O_3; A, 100 °C; B, 200 °C; C, 300 °C; D, 350 °C; E, 400 °C; F, 500 °C.

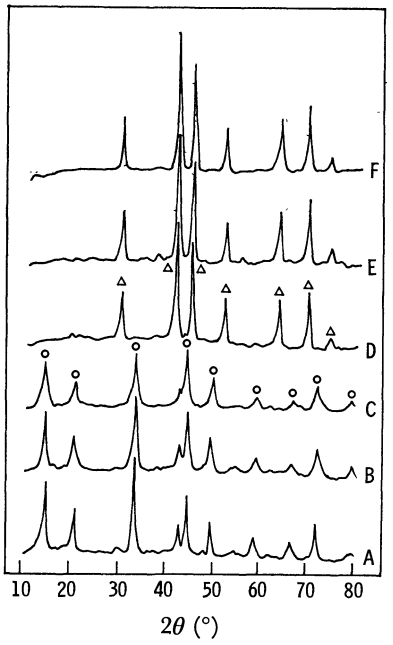

Fig. 6. X-ray diffraction patterns of A-5 at various heating temperatures: ○, β-FeOOH; △, α-Fe_2O_3; A, 100 °C; B, 200 °C; C, 250 °C; D, 300 °C; E, 400 °C; F, 500 °C.

Variations of X-ray diffraction patterns of A-1 and A-5 with heating up to various temperatures are shown in Figs. 5 and 6. A-1 was converted into an amorphous mixture of β-FeOOH and α-Fe_2O_3 at the temperature range 300—350 °C, whereas A-5 was transformed from β-FeOOH to α-Fe_2O_3 at 300 °C. Above 400 °C all the samples were completely transformed into α-Fe_2O_3. The crystallite size, calculated by the Scherrer equation for the (301) pattern of β-FeOOH at 2θ of 50.2 ° and

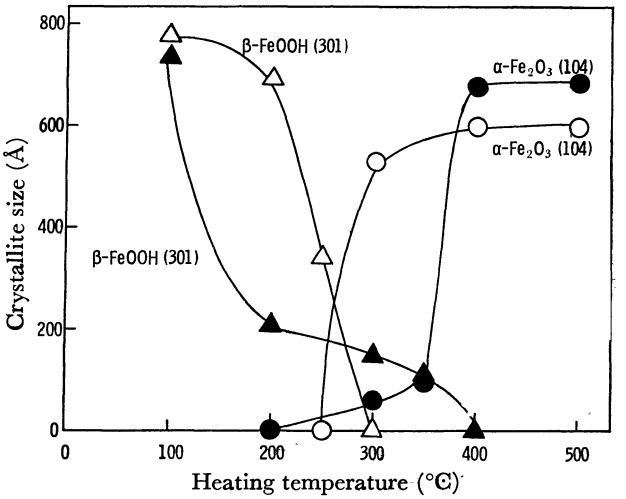

Fig. 7. Relation between crystallite size and heating temperature: △ and ○, A-1; ▲ and ●, A-5.

for the (104) pattern of α-Fe_2O_3 at 2θ of 41.9 °, is given in Fig. 7 for A-1 and A-5 as the function of heating temperature. The β-FeOOH structure of A-5 must be more liable to be destroyed on heating than that of A-1.

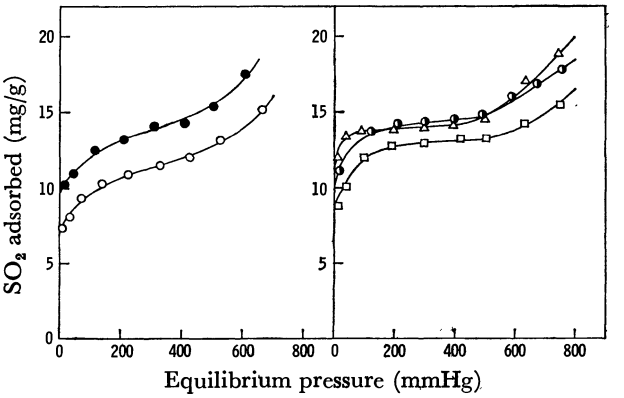

Fig. 8. SO_2 adsorption isotherms: ○, A-1; ●, A-2; △, A-3; ◑, A-4; □, A-5.

TABLE 2. AMOUNTS OF ADSORPTION (A_m and A_c) OF SO_2 ON β-FeOOH AND THE C CONSTANT OF THE BET EQUATION

Sample	Cl content (Cl/Fe, %)	A_m (mg/m²)	A_c (mg/m²)	A_c/A_m	C constant
A-1	17	0.31	0.25	0.8	390
A-2	12	0.38	0.34	0.9	390
A-3	7.7	0.40	0.40	1.0	520
A-4	7.4	0.44	0.43	1.0	720
A-5	7.0	0.45	0.46	1.0	1100

All the SO_2 adsorption isotherms are the BET-II type as shown in Fig. 8. However, the C constant of the BET equation, representing the adsorption strength in the first adsorption layer, increases with the decrease of Cl content. The monolayer adsorption capacity (A_m) calculated by the BET equation and the amount of the chemisorbed SO_2 (A_c) determined by the desorption under 10^{-5} Torr at 30.0 °C for 24 hr increased as the Cl content lowered (Table 2). The A_c/A_m ratio

also increased up to unity as the Cl content decreased. These results indicate that the adsorption force for A-3, A-4, and A-5 is stronger than that for A-1 and A-2.

Discussion

Structure of β-FeOOH and the existence of Cl. The unit cell of β-FeOOH crystal contains two tunnels parallel to the c-axis (Fig. 9), in which water molecules and Cl^- ions can be accomodated.[3] If we assume that the unit cell includes one Cl^- ion, the Cl content is 1/8=12.5% Cl/Fe, since a unit cell has eight Fe atoms. The H_2O/Fe ratio (Table 1) and the atomic ratio (Cl+H_2O)/Fe obtained by the chemical analysis and TGA are plotted against the Cl content in Figs. 10 and 11, respectively. The values of (Cl+H_2O)/Fe (Fig. 11) and H_2O/Fe (Fig. 10) amount to about 25% and 12.5%, respectively, at 12.5% Cl/Fe on each abscissa corresponding to the Cl content postulated from crystal structure as discussed above. It is therefore likely that tunnels and outer surfaces are to be filled up with Cl^- ions and H_2O molecules of equal amounts. As the crystal surfaces of β-FeOOH consist of a—c or b—c planes, the amount of Fe existing in the surface, estimated from the surface area obtained by N_2 adsorption and the unit cell area of a—c or b—c plane (31.7 Å^2), is 6.5% of the total Fe atoms. Therefore, the amount of Fe in the bulk is 93.5%. The Cl content in the crystal, which is overwhelmingly the amount of Cl in tunnels, is calculated as 11.7% Cl/Fe from the Cl/Fe ratio 12.5% and the Fe content 93.5%. The ratio (Cl+H_2O)/Fe for the samples containing more than 12 or less than 9 atomic % is over 25% as shown in Fig. 11. As the tunnels in the 17% Cl/Fe sample are filled with H_2O molecules and Cl^- ions, the Cl^- ions of 17 minus 11.7% appear to exist on the crystal

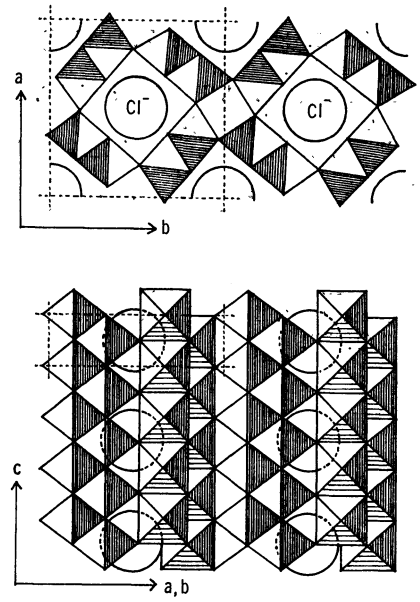

Fig. 9. Crystal structure of β-FeOOH. O^{2-} and OH^- ions are to be imagined at the corners of each octahedron and an Fe^{3+} ion at its center. β-FeOOH has a tetragonal lattice with the following unit cell dimensions: $a=b=10.48$ Å, $c=3.02$ Å.

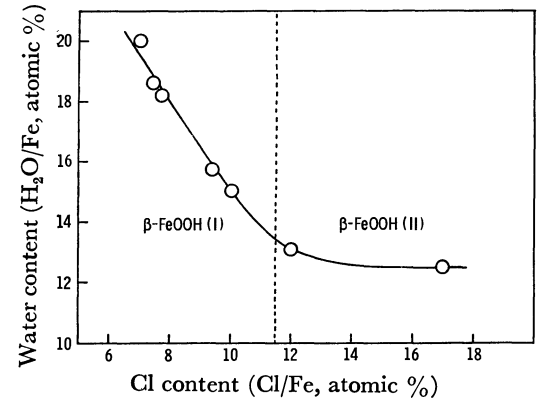

Fig. 10. Variation of H_2O content with Cl content.

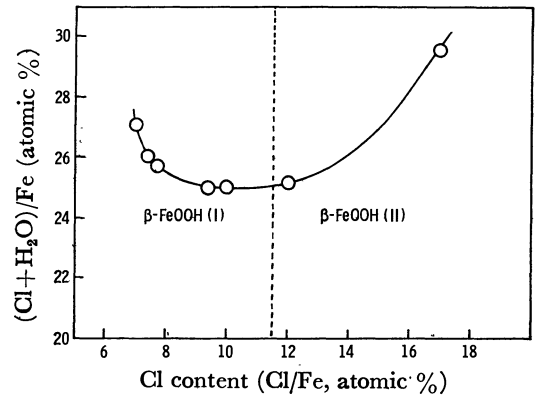

Fig. 11. Variation of (Cl+H_2O)/Fe with Cl content.

surfaces. The large value of (Cl+H_2O)/Fe for the 7% Cl/Fe sample is considered to be due to the accumulation of H_2O molecules in the tunnels by replacing Cl^- ions.

The broad endothermic DTA peaks at 275—295 °C observed for A-3, A-4, A-5, U-1, and U-2 correspond to the conversion of β-FeOOH to the mixtures of β-FeOOH and α-Fe_2O_3. The sharp exothermic peaks at 345—390 °C correspond to the recrystallization of less-crystalline α-Fe_2O_3 produced from β-FeOOH at lower temperatures. On the other hand, A-1 and A-2 show only one endothermic DTA peak in the temperature region around 300 °C. It is confirmed by the X-ray diffraction and the chemical analysis of Cl that in cases of A-1 and A-2 the transformation of β-FeOOH into α-Fe_2O_3, the crystallization of resultant α-Fe_2O_3, and the Cl elimination occur simultaneously around 300 °C. The peak temperatures in those DTA curves are plotted against the Cl content in Fig. 12, where the following three areas are defined; the region of β-FeOOH, region of a mixture of β-FeOOH and α-Fe_2O_3, and region of α-Fe_2O_3. The three lines intersect each other at a point of 11.5% Cl/Fe. The Cl content of 11.5% Cl/Fe is nearly equal to the amount of Cl filling up the tunnels (11.7%). The samples containing Cl of less than 11.5% Cl/Fe and more than 11.5% Cl/Fe are denoted in Figs. 10, 11, and 12 as β-FeOOH(I) and β-FeOOH(II), respectively. The α-Fe_2O_3(II) transformed from β-FeOOH(II) contains an appreciable amount of Cl and is less crystalline than the α-Fe_2O_3(I) transformed from β-FeOOH(I).

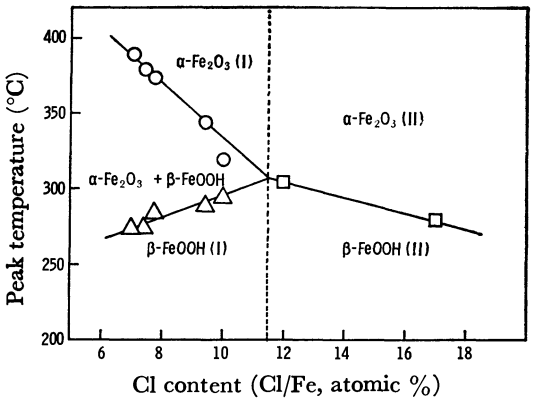

Fig. 12. Relation between peak temperature of DTA curve and Cl content in the original crystals: ○, exothermic peak; △ and □, endothermic peaks.

Cl in β-FeOOH(I). TGA curves (Fig. 2) show that H_2O molecules in the tunnels in A-5 (β-FeOOH(I)) are easily released by heating at temperature below 250 °C, so that the β-FeOOH structure of A-5 is more easily destroyed by heating than that of A-1 (β-FeOOH-(II)) as shown in Fig. 7. β-FeOOH(I) is not completely transformed into α-Fe_2O_3 until Cl is removed as $FeCl_3$, though it changed into the mixture of less-crystalline β-FeOOH and α-Fe_2O_3. This fact suggests the roles of Cl in β-FeOOH: Cl inhibits both its transformation into α-Fe_2O_3 and the recrystallization of less-crystalline α-Fe_2O_3. The inhibitory effect of Cl on the transformation into α-Fe_2O_3 will be due to the stabilization of the β-FeOOH structure by Cl. The recrystallization of α-Fe_2O_3 seems to be obstructed by the bonding between Cl and Fe.

Cl in β-FeOOH(II). Fig. 7 indicates that A-1 (β-FeOOH(II)) is thermally more stable than A-5 (β-FeOOH(I)) up to 250 °C, probably because Cl^- ions on the surface interfere the release of H_2O molecules. However, the transformation of β-FeOOH(II) into α-Fe_2O_3 occurs abruptly at the temperature of release of Cl. The evolution of HCl was observed at the transformation temperature of β-FeOOH(II) into α-Fe_2O_3. It is presumed from this fact that Cl^- ions on the surface produce HCl on heating according to the formula; $OH^- + Cl^- \rightarrow O^{2-} + HCl$. The resulting HCl may accelerate the formation of α-Fe_2O_3 by destructing β-FeOOH crystal structure.

SO_2 adsorption. The monolayer adsorption capacity (A_m) and the amount of chemisorbed SO_2 (A_c) decrease with the increase of Cl content. Furthermore, A_c/A_m value approaches unity and the C constant in the BET equation increases as the Cl content decreases. From these results, we can conceive that Cl in β-FeOOH interferes the SO_2 adsorption, especially the chemisorption of SO_2. The chemisorption sites for SO_2 are presumably the O^{2-} ions in β-FeOOH. The surface is covered with Cl^- ions as the Cl content increases, The estimation of the surface coverage with Cl^- ions. using the diameter of Cl^- ion (3.6 Å) and the surface area obtained by N_2 adsorption, shows that the surface of the 17% Cl/Fe sample is completely covered by the monolayer of Cl^- ions, and suggests that the chemisorption does not occur. However, Table 2 indicates that the sample of 17% Cl/Fe chemisorbs a considerable amount of SO_2, which is nearly equal to half A_c of 7% Cl/Fe sample adsorbing no Cl^- ions on the surface. This conflict can be understood by assuming that SO_2 binds with a half O^{2-} ions, pushing Cl^- ions aside. According to the structure of a—c or b—c plane constituting the crystal structure, there are two kinds of surface O^{2-} ions; O^{2-} ion bound with one Fe atom and O^{2-} ion bound with two Fe atoms. The former O^{2-} ions are considered to have stronger affinity with sulfur in SO_2 than the latter O^{2-} ions.

The authors wish to thank Dr. K. Sato (Fundamental Res. Inst., Nippon Steel Corp.) for IR spectra measurements.

This work was partly supported by the Science Research Fund of the Ministry of Education.

References

1) V. P. Keller, *Werkstoffe u. Korrosion*, **20**, 102 (1969).
2) H. B. Weiser and W. O. Milligan, *J. Amer. Chem. Soc.*, **57**, 238 (1934).
3) A. L. Mackay, *Miner. Mag.*, **32**, 545 (1960).
4) A. Byström and A. M. Byström, *Acta Crystallogr.*, **3**, 146 (1950).
5) A. Szytula, M. Balanda, and Z. Dimitrijević, *Phys. Stat. Sol.*, (a) **3**, 1033 (1970).
6) L. J. E. Hofer, W. C. Peebles, and W. E. Deiter, *J. Amer. Chem. Soc.*, **68**, 1953 (1946).
7) T. Ishikawa and K. Inouye, *Nippon Kagaku Zasshi*, **91**, 935 (1970).
8) T. Ishikawa and K. Inouye, This Bulletin, **46**, 2665 (1973).
9) T. Ishikawa and K. Inouye, *ibid.*, **45**, 2350 (1972).
10) A. Müller, *Arzneimittel Forsch.*, **17**, 921 (1967).
11) G. Okamoto, R. Furuichi, and N. Sato, *Electrochim. Acta*, **12**, 1287 (1967).

Transfer Hydrogenation and Transfer Hydrogenolysis VII. The Mechanism of Hydrogen Transfer from 2-Propanol to Olefins Catalyzed by Dihydridotetrakis-(triphenylphosphine)ruthenium(II)

Hideaki IMAI, Takeshi NISHIGUCHI, Masaki KOBAYASHI, and Kazuo FUKUZUMI

Department of Applied Chemistry, Faculty of Engineering, Nagoya University, Chikusa-ku, Nagoya 464

(Received January 16, 1975)

The dihydride complex, $RuH_2(PPh_3)_4$, has been found to be an excellent catalyst for the hydrogen transfer from 2-propanol to olefins. For cyclohexene in toluene solution, the rate law at 80°C was:

$$\text{Rate} = \frac{0.04[C]_0[D]}{1+24[P]}$$

where $[C]_0$, [D] and [P] are the concentration of the catalyst, 2-propanol and triphenylphosphine, respectively. It is pressumed that active intermediates of the reaction are not Ru(IV)-species but Ru(0)-species. The rate-determining step of the reaction is inferred to be the dehydrogenation of 2-propanol, that is, the hydrogen transfer from the alcohol to Ru(0)-complex to form a hydride complex by oxidative addition.

We have reported previously that cyclic ethers,[1] amines[2] and 2-propanol[3] donate hydrogen to olefins in the presence of $RhCl(PPh_3)_3$ or $RhH(PPh_3)_4$. In these transfer hydrogenations or in other homogeneous catalytic hydrogenations with molecular hydrogen, hydride complexes of transition metals have been considered as active intermediate.[4] Thus, hydride complexes may be expected to have high catalytic activity. Moreover, they seem to have good solubilities in organic solvent.

We have studied the catalytic nature of the monohydride complex, $RhH(PPh_3)_4$,[3] for the hydrogen transfer from alcohol to olefins, and now have undertaken to study that of the dihydride complex, $RuH_2(PPh_3)_4$. It has been reported that $RuH_2(PPh_3)_4$[5] and $RuH_4(PPh_3)_3$[6] have activity for hydrogenation of olefins and $RuH_2(PPh_3)_4$ gives $RuH_4(PPh_3)_3$ in the reaction with hydrogen.[7] Further, $RuClH(PPh_3)_3$ and $RuCl_2(PPh_3)_3$ are thought to catalyze the hydrogenation of olefins *via* Ru(IV)-species.[4] So, which of the Ru(0)-, Ru(II)- and/or Ru(IV)-complex is a reaction intermediate in the transfer hydrogenation is of interest.

Results and Discussion

Measurement of Initial Rates. Unless otherwise noted, the transfer hydrogenation was carried out in any instance under the standard condition that $RuH_2(PPh_3)_4$ (0.01 mol·l^{-1}), cyclohexene (0.5 mol·l^{-1}) and 2-propanol (1.0 mol·l^{-1}) were heated in toluene at 80°. The reaction proceeded stoichiometrically without side reactions, for the amount of the dehydrogenation product, acetone, was equal to that of the formed cyclohexane and the total amounts of the cyclohexene and cyclohexane were equal to the amount of the charged cyclohexene within experimental error. The conversion of the olefin to paraffin was proportional to reaction time until 30% conversion. However, the linearity did not hold at higher conversion, perhaps because the formed acetone competes with the olefin for a vacant coordination site of the catalyst though the initial rate of the reaction, which was derived from the linear part, is independent of the olefin concentration as described later.

Table 1. Effect of solvents on the initial rate[a]

Solvent	Rate×10^4 (mol·l^{-1} min^{-1})
Dimethylsulfoxide	0.0
Acetic acid	0.1
Chlorobenzene	0.1
N,N-Dimethylacetamide	1.0
Anisole	3.6
Toluene	4.0
Benzene	4.1

a) Cyclohexene (0.5 mol·l^{-1}), 2-propanol (1.0 mol·l^{-1}) and $RuH_2(PPh_3)_4$ (0.01 mol·l^{-1}) were heated at 80°C in the solvent.

Initial rates of the transfer hydrogenation in several solvents were measured and the results are summarized in Table 1. Some solvents, which have high polarity and strong coordinating power, dissolved the catalyst easily but the reaction in those solvents was slow. This may be explainable by the fact that highly polar solvents make the coordination of other reagents difficult. In a few aromatic solvents, such as toluene and benzene, the catalyst dissolved well at room temperature and the reaction proceeded rapidly. Toluene was used as a solvent in this kinetic study.

The rate of the hydrogenation of several cycloolefins is given in Table 2. The rate was not so varied by the

Table 2. Effect of olefine on the initial rate[a]

Olefin	Rate×10^4 (mol·l^{-1}·min^{-1})	Product
Cyclopentene	3.1	Cyclopentane
Cyclohexene	4.0	Cyclohexane
Cycloheptene	3.5	Cycloheptane
Cyclooctene	3.4	Cyclooctane
Norboranadiene	0.5	Norbornene
1,3-Cyclooctadiene	0.0	
1,5-Cyclooctadiene	0.0	

a) Olefin(0.5 mol·l^{-1}), 2-propanol (1.0 mol·l^{-1}) and $RuH_2(PPh_3)_4$ (0.01 mol·l^{-1}) were heated at 80°C in toluene.

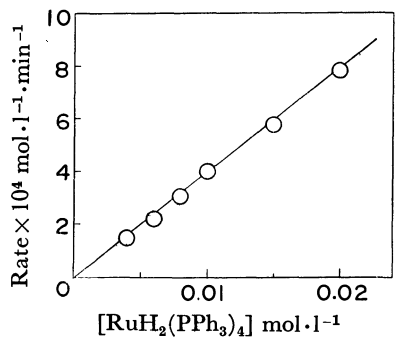

Fig. 1. Dependence of the rate of hydrogenation of cyclohexene on catalyst concentration in toluene at 80 °C, with 0.5 mol·l^{-1} cyclohexene and 1.0 mol·l^{-1} 2-propanol.

kinds of cyclomonoenes. As for dienes, norbornadiene was slowly hydrogenated to norbornene and cyclooctadienes were not reduced. Perhaps the difficulty in reduction of these dienes may be understandable by the fact that they are bidentate ligands and have strong coordinating power.

Figure 1 shows the dependence of the rate on the catalyst concentration. In the region of the catalyst concentration higher than 0.004 mol·l^{-1}, the rate was first-order in the catalyst concentration. Extrapolation of the line to lower catalyst concentration passes through the origin.

The initial rate of the hydrogenation was independent of the cyclohexene concentration in the range, examined. The zero-order dependence may be interpreted either by the assumption that the coordination of olefins to the metal occurs after the rate-determining step or by the assumption that though the olefin coordinates before the rate-determining step, the coordination occurs so completely that the intermediate olefin complex concentration is not greately changed over the range of 0.05 to 1.30 mol·l^{-1}. The former assumption seems to be more plausible on the basis of spectroscopic data described later.

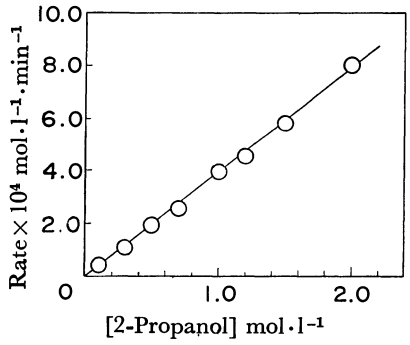

Fig. 2. Dependence of the rate of hydrogenation of cyclohexene on 2-propanol concentration in toluene at 80 °C, with 0.01 mol·l^{-1} $RuH_2(PPh_3)_4$ and 0.5 mol·l^{-1} cyclohexene.

As shown in Fig. 2, the rate of the reduction showed a good linear dependence on the concentration of 2-propanol.

Initial rates were measured at 70, 80, 90 and 100°C and a good linear plot of $\log_{10}$ (Rate) against $1/T$ was obtained, from which a value for activation energy, E_a of 31.4 kcal mol^{-1} is obtained; $\Delta H^{\ddagger}$ being 30.7 kcal mol^{-1}. The obserbed rate constant provides a value of 20 e.u. for $\Delta S^{\ddagger}$.[8]

Reaction between $RuH_2(PPh_3)_4$ and Olefins. When cyclohexene (0.5 mol·l^{-1}) and $RuH_2(PPh_3)_4$ (0.03 mol·l^{-1}) in toluene were kept at 20°C for 1 day in the absence and in the presence of 2-propanol (1.0 mol·l^{-1}), 0.01 mol·l^{-1} of cyclohexane was formed. In the reaction of 1-hexene and $RuH_2(PPh_3)_4$ (0.01 mol·l^{-1}) under the same condition, 0.33 mol·l^{-1} of internal hexenes was obtained in addition to 0.007 mol·l^{-1} of *n*-hexane. The hydrogen transfer from $RuH_2(PPh_3)_4$ to olefins at room temperature has also been reported by Komiya *et al.*[5] The transfer hydrogenation did not take place at room temperature. This fact suggests that the first step of the overall transfer hydrogenation is the transfer of hydride ligands of the metal complex to olefins. The hydrogen transfer from the catalyst to olefins is considered as Scheme 1.

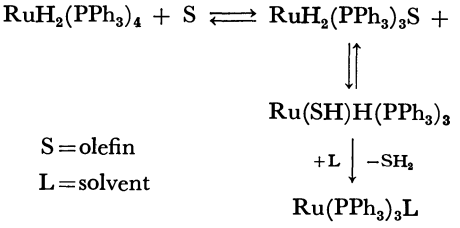

Scheme 1.

Isotopic Study. When octadeutero-2-propanol was used instead of 2-propanol at 80°C, the initial rate was 1.5×10^{-4} mol·l^{-1} min^{-1}, while in the case of 2-propanol the rate was 4.0×10^{-4} mol·l^{-1} min^{-1}. Moreover, in the reaction of octadeutero-2-propanol GC-MS spectroscopic study revealed that cyclohexane-d_1 and -d_2 were major product and cyclohexane-d_0, -d_3 and -d_4 were minor. The result proved clearly that hydrogen atoms transferred from the alcohol to cyclohexene and double bond migration of the olefin scarcely take place during the hydrogenation.

The value of the kinetic isotope effect, $R_H/R_D=2.7$, shows that a hydrogen transfer step is rate limiting.

The IR spectrum of the ether solution of $RuH_2(PPh_3)_4$ (0.03 mol·l^{-1}) and octadeutero-2-propanol (1.0 mol·l^{-1}), which had been heated at 100°C for 2 hr, showed no peaks assignable to –OH and C=O, and that of the recovered complex was identical with that of the original complex, $RuH_2(PPh_3)_4$, having no absorption attributable to Ru–D bond. As no hydrogen exchange occurred between 2-propanol and $RuH_2(PPh_3)_4$, tetrahydride species are not the reaction intermediate in this transfer hydrogenation.

Effect of Added Acetone. By the addition of 1.0 mol·l^{-1} acetone to the reaction system, the rate was decreased to one-eighth. The retarding effect is explained by the fact that acetone was hydrogenated to 2-propanol in tetralin, so it competes for the coordination sites of the metal complex with other reagents. From this point of view, when the total concentration of acetone and cyclohexene was kept constant (2.0 mol·l^{-1}) and the ratio of acetone against cyclohexene was changed, the reciprocal of the rate against [acetone]/

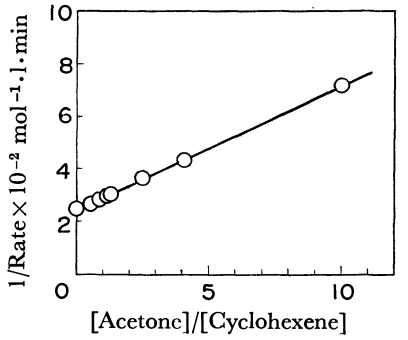

Fig. 3. Plot of the reciprocal of the rate of hydrogenation of cyclohexene *vs.* the ratio of [acetone]/[cyclohexene] in toluene at 80 °C, with 0.01 mol·l^{-1} $RuH_2(PPh_3)_4$, 0.5 mol·l^{-1} cyclohexene and 1.0 mol·l^{-1} 1-propanol.

[cyclohexene] was linear with a positive intercept on y-axis, as shown in Fig. 3.

Effect of Added Triphenylphosphine. The rate was decreased by the addition of excess triphenylphosphine to the reaction system, as in cases of the hydrogenation by molecular hydrogen catalyzed by transition metal complexes.[9-11] The plots of the reciprocal of the rate against the added triphenylphosphine concentration was linear with a positive intercept on y-axis, as shown in Fig. 4.

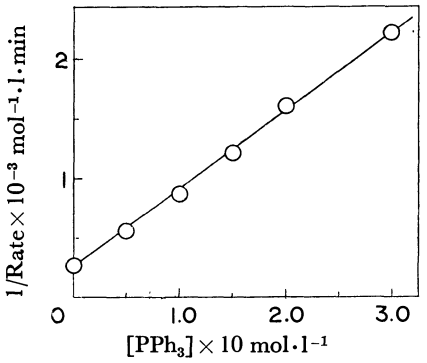

Fig. 4. Plot of the reciprocal of the rate of hydrogenation of cyclohexene *vs.* the concentration of added triphenylphosphine in toluene at 80 °C, with 0.01 mol·l^{-1} $RuH_2(PPh_3)_4$, 0.5 mol·l^{-1} cyclohexene and 1.0 mol·l^{-1} 2-propanol.

Reaction Intermediate. The infrared spectrum of a toluene solution of 0.03 mol·l^{-1} catalyst, 1.0 mol·l^{-1} 2-propanol and 0.5 mol·l^{-1} cyclohexene, which had been heated at 100 °C for 1 hr, showed no peaks assignable to the hydride ligands. The residual solid obtained from the solution had peaks at 1380 cm^{-1} and 3250 cm^{-1} (broad) in infrared spectrum (KBr). These absorption bands are attributable to 2-propanol and the ones assignable to cyclohexene or acetone were not detected. To evaluate the numbers of coordinated triphenylphosphine, diethylene glycol dimethyl ether (0.0134 g) was added as an internal standard into $CDCl_3$ solution of the residual solid (0.200 g). The NMR spectrum showed three multiplets centered at τ 2.7, τ 8.8 and τ 6.4 and a singlet at τ 6.7, with 50: 1: 38: 29 area. The peak at τ 2.7 are assignable to phenyl protons, the peaks at τ 6.4 and τ 6.7 are due to diethylene glycol dimethyl ether and the peak at τ 8.8 is due to 2-propanol, respectively. The peaks which are assignable to cyclohexene and acetone were not obserbed. Though methyl groups of free 2-propanol show a doublet, the doublet might be changed to the multiplet by the hindrance of the rotation of the methyl groups on account of the coordination on the metal. As the number of coordinated triphenylphosphine molecules, the value of 3.1 was obtained from the ratio of the area of peak at τ 2.7 to the one at τ 6.4 or at τ 6.7. This value is not contradictory to the result of elemental analysis of the residual solid. (Found: C, 73.12; H, 5.08%. Calcd for $Ru(PPh_3)_4$ C, 75.05; H, 5.21%; for $Ru(PPh_3)_3$ C, 72.89; H, 5.06%; for Ru(2-propanol)-$(PPh_3)_4$ C, 74.28; H, 5.65%; and for Ru(2-propanol)-$(PPh_3)_3$ C, 74.44; H, 5.62%;)

These result shows that $Ru(PPh_3)_3$ is the major species and $Ru(PPh_3)_4$, Ru(2-propanol)$(PPh_3)_4$ and Ru(2-propanol)$(PPh_3)_3$ are minor. When this recovered complex was used as a catalyst, the initial rate of the reaction was 3.5×10^{-4} mol·l^{-1} min^{-1}, which is roughly equal to that of the reaction in which $RuH_2(PPh_3)_4$ was used. The fact that Ru(0)-species were isolated and they had catalytic activity suggests that the Ru(0)-complex existed in the reaction process as a major intermediate and the first step of this reaction is the hydrogen transfer from catalyst to olefin to give Ru(0)-species.

Rate-determining Step. The observed kinetic isotope effect, $R_H/R_D=2.7$, distinctly shows that a hydrogen transfer step is rate limiting. There may be three hydrogen transfer steps in this transfer hydrogenation, that is; (1) hydrogen transfer from the coordinated alcohol to the Ru(0)-complex to give the Ru(II) species, (2) hydride transfer to the coordinated olefin to give the Ru(II)-alkyl complex and (3) hydrogenolysis of the Ru(II)-alkyl complex by a coordinated hydride to yield the paraffin.

The isomerization of the terminal olefin (involving step (2)) and the hydrogenation of olefins by molecular hydrogen (involving steps (2) and (3)) occurred at room temperature in the absence of 2-propanol. As the steps (2) and (3) are inferred to occur fast at the reaction temperatures of the transfer hydrogenation, these steps may not be rate limiting. Therefore, the dehydrogenation of 2-propanol to give acetone, that is step (1), is inferred be rate limiting.

Kinetic Discussion

The first step of this transfer hydrogenation was as shown in Scheme 1. So upon the results described earlier and the facts described in the literature,[1-9] we should like to propose the following reaction scheme for the catalytic cycle of transfer hydrogenation.

Based on the proposed scheme and the assumption described later, the rate (R) is expressed as follows;

$$R=\frac{k_3k_4k_5K_1[D][S][C]_0}{(k_{-3}k_{-4}[A]+k_4k_5[S])(1+K_1[D]+K_2[P])} \quad (1)$$

where K_1 and K_2 are equilibrium constants and k_3, k_{-3}, k_4, k_{-4} and k_5 are rate constants, and [D], [S], $[C]_0$, [A]

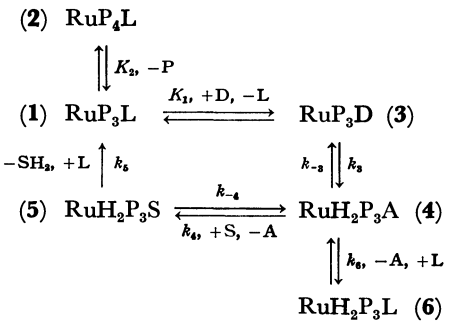

where,

P=PPh_3 S=olefin D=2-propanol
A=acetone L=solvent, PPh_3 or 2-propanol

and [P] are the concentrations of the hydrogen donor, the olefin, the added catalyst, acetone and triphenylphosphine, respectively. The assumption is that the dihydride species, **4**, **5** and **6** are so active as steady state treatment to be applied. This assumption seems not so unreasonable, because the spectroscopic study of this reaction system showed no sign of the existence of hydride species as described before.

Equation (1) accommodates the effect of the added acetone. At initial stage of the hydrogenation, the concentration of the added acetone may approximately be regarded as the total acetone concentration in the reaction system. So the dependence of the rate on [A]/[S] is derived from Eq. (1);

$$\frac{1}{R} = \frac{k_{-3}k_{-4}(1+K_1[D]+K_2[P])}{k_3k_4k_5K_1[D][C]_0}\cdot\frac{[A]}{[S]} + \frac{1+K_1[D]+K_2[P]}{k_3K_1[D][C]_0} \quad (2)$$

As free phosphine concentration is negligible compared with acetone and olefin concentration, Eq. (2) is identical in form to that obtained from Fig. 3. When acetone was not added, the initial rate was independent on the olefin concentration. Therefore, the numerator of the first term of Eq. (2) must be zero. This may be realized by the fact that at the initial stage of the reaction the amount of the formed acetone is negligible. This reasoning is supported by the fact that in the presence of added acetone the initial rate depended on the olefin concentration. Then the rate expression is reduced to;

$$R = \frac{k_3K_1[C]_0[D]}{1+K_1[D]+K_2[P]} \quad (3)$$

As described earlier, the rate had the first order dependence on the concentration of 2-propanol. This fact requires $1+K_2[P] \gg K_1[D]$, that is, $[1]+[2] \gg [3]$. This assumption seems to be not so unreasonable from the results of the isolation of reaction intermediate described previously. Therefore, Eq. (3) is reduce to;

$$R = \frac{k_3K_1[C]_0[D]}{1+K_2[P]} \quad (4)$$

This expression is found to accommodate most of the other experimental observations; (a) The dependence of the rate on the catalyst concentration should be linear, and this agrees with the experimental result shown in Fig. 1. From this figure, 4.0×10^{-4} min^{-1} was obtained as the value of $k_3K_1/(1+K_2[P])$. (b) The dependence of the rate on the donor concentration should be linear, and this agrees with Fig. 2. From this figure, 4.0×10^{-4} min^{-1} was obtained as the value of $k_3K_1/(1+K_2[P])$. (c) When triphenylphosphine was added to the reaction system, the concentration of the added triphenylphosphine may approximately equal to the total phosphine concentration in the reaction system. The dependence of the rate on the phosphine concentration is;

$$\frac{1}{R} = \frac{K_2}{k_3K_1[C]_0[D]}[P] + \frac{1}{k_3K_1[C]_0[D]} \quad (5)$$

which is in agreement with experimental observation. From Fig. 4, the value for gradient, 6.0×10^4 $mol^{-2}\cdot l$ min and the value for the intercept, 2.5×10^3 $mol^{-2}\cdot l$ min were obtained, respectively. By using these values $K_2=24$ $mol^{-1}\cdot l$ and $k_3K_1=0.04$ $mol\cdot l^{-1}\cdot min^{-1}$ were obtained, as the values at 80 °C. Then the overall rate expression at 80 °C may be formulated as;

$$R = \frac{0.04[C]_0[D]}{1+24[P]} \quad (6)$$

The intercept of Fig. 3, $(1+K_1[D]+K_2[P])/k_3K_1[D][C]_0 = 2.5\times10^{-3}$ $mol^{-1}\cdot l$ min, is in good agreement with the intercept of Fig. 4, $(1+K_2[P])/k_3K_1[D][C]_0=2.5\times10^{-3}$ $mol^{-1}\cdot l$ min. This suggests that the reduction of Eq. (3) to Eq. (4) is feasible. Moreover, both Figs. 1 and 2 gave 2.5×10^{-3} $mol^{-1}\cdot l$ min as the value of $(1+K_2[P])/k_3K_1[D][C]_0$. This value also agrees well with the one obtained from Fig. 4. (d) In Eq. (4), k_3 is the only rate constant and the most important step, so the dehydrogenation step, **3**—**4**, may be rate limiting in the transfer hydrogenation. This supposition is supported by the results of the kinetic isotope effect which has a value of 2.7 and the experimental observations described earlier.

Experimental

Materials. The experimental techniques, together with the methods of purification of the materials have been given previously.[3] Dihydridotetrakis(triphenylphosphine)-ruthenium(II) was prepared by a method given in the literature.[12] The complex was identified as follows; ν_{Ru-H} 2080 cm^{-1} (lit,[13] 2080 cm^{-1}), mp 180 °C (lit,[13] 180 °C).

An Example of Kinetic Runs. Hydrogenation were carried out in a Pyrex glass tube. The sealed tube was prepared by the following procedure. Catalysts, alcohols and olefins were put into Pyrex glass tubes which had been sealed an one end. Into the mixture, solvent was added and the total volume of the solution was made 1.0 ml. The tube was sealed under vacuum after two freeze-pump-thaw cycles at 10^{-3} Torr on a vacuum line and liquid nitrogen bath. Five samples, prepared by the method described above, were heated in the polyethylene glycol-bath kept at 80±1 °C for 15, 30, 45, 60, and 90 min. The reaction mixture were submitted to glc analysis.

Isolation of a Reaction Intermediate. Toluene was added to the mixture of $RuH_2(PPh_3)_4$ (0.0345 g, 0.03 mmol), 2-propanol (0.0600 g, 1.00 mmol) and cyclohexene (0.0410 g, 0.50 mmol), and the total volume of the solution was made 1.0 ml. This sample was heated at 100 °C for 1 hr. After cooling the solution, the volatile compounds were evaporated

from this solution *in vacuo* and the residual solid was washed with ether twice and dried *in vacuo* for 48 hr. This residual solid was submitted to IR, NMR and elemental analysis.

References

1) a) T. Nishiguchi and K. Fukuzumi, *J. Amer. Chem. Soc.*, **96**, 1893 (1974); b) T. Nishiguchi, K. Tachi, and K. Fukuzumi, *ibid.*, **94**, 8916 (1972).

2) T. Nishiguchi, K. Tachi, and K. Fukuzumi, *J. Org. Chem.*, **40**, 237 (1975); *ibid.*, **40**, 240 (1975).

3) H. Imai, T. Nishiguchi, and K. Fukuzumi, *ibid.*, **39**, 1622 (1974).

4) a) B. R. James, "Homogeneous Hydrogenation," John Wiely & Sons, New York, N. Y. (1973), p. 64; b) H. D. Kaesz and R. B. Saillant, *Chem. Rev.*, **72**, 321 (1972); c) G. N. Schrauzer, "Transition Metals in Homogeneous Catalysis," Marcel Dekker, New York, N. Y. (1971), p. 13.

5) S. Komiya, A. Yamamoto, and S. Ikeda, *J. Organometal. Chem.*, **42**, C 65 (1972).

6) F. Pennela, *ibid.*, **65**, C 17 (1974).

7) a) W. H. Knoth, *J. Amer. Chem. Soc.*, **94**, 104 (1972); b) R. O. Harris, N. K. Hata, L. Sadavoy, and J. M. C. Yuen, *J. Organometal. Chem.*, **54**, 259 (1973).

8) The activation parameters are considerably different from the values for transfer hydrogenation of cyclohexene in toluene using $RhH(PPh_3)_4$ as catalyst (ΔH^* 20.7 kcal·mol^{-1}, ΔS^* −10.8 e.u.). This suggests that the nature and the structure of the transition state of the former reaction is not so similar to those of the latter.

9) B. R. James and N. A. Memon, *Can. J. Chem.*, **46**, 217 (1968).

10) J. A. Osborn, F. H. Jardine, J. F. Young, and G. Wilkinson, *J. Chem. Soc., A*, **1966**, 1711.

11) C. O'Connor and G. Wilkinson, *ibid.*, **1968**, 2665.

12) J. J. Levison and S. D. Robinson, *ibid.*, **1970**, 2947.

13) T. Ito, S. Kitazume, A. Yamamoto, and S. Ikeda, *J. Amer. Chem. Soc.*, **92**, 3011 (1970).

Lanthanide-Induced Nuclear Magnetic Resonance Shifts and Molecular Structure of L-Azetidine-2-Carboxylic Acid. II. Determination of Molecular Conformation

Fuyuhiko INAGAKI, Seizo TAKAHASHI, Mitsuo TASUMI, and Tatsuo MIYAZAWA

Department of Biophysics and Biochemistry, Faculty of Science, The University of Tokyo, Bunkyo-ku, Tokyo 113

(Received January 30, 1975)

Lanthanide-induced shifts (LIS) in ^{1}H NMR spectra of L-azetidine-2-carboxylic acid were observed in D_2O solution using Pr(III), Nd(III), and Eu(III) nitrates as shift reagents. By taking the LIS of one of the protons as reference, the shift ratios for the other four protons were calculated. The shifts ratio obtained were nearly constant for the three lanthanide ions, except for that with respect to the α proton which is located closest to the lanthanide ion. This indicates that the contribution of the contact shift is appreciable only for the observed LIS of the α proton and is negligible for the LIS's of the β and γ protons. The constancy of shift ratios assures, in addition, that the magnetic tensor is axially symmetric. Therefore, the LIS's of the β and γ protons may be used for the structure determination. For the β and γ protons, the ratios of LIS's intrinsic to the lanthanide-substrate 1 : 1 complex were corrected for the contribution of diamagnetic shifts due to complex formation which were estimated by the use of La(III) nitrate. The line broadening induced by Gd(III) was also observed. The structure analysis based on these data shows that the four-membered ring of L-azetidine-2-carboxylic acid is puckered with the dihedral angle of 25° and the carboxylate is in the equatorial position.

In order to utilize the lanthanide-induced nuclear magnetic resonance shift (LIS) to the quantitative discussion of molecular structure in solution, it seems to be a good practice to follow the procedures outlined below.

(a) The observed LIS may be a weighted average of those intrinsic to various stoichiometric complexes. The presence of a lanthanide-substrate 1 : 2 complex (abbreviated as LS_2) in addition to a 1 : 1 complex (LS) has been established in some cases.[1-3] The LIS intrinsic to the LS complex should be evaluated for the structure determination. In a preceding paper we discussed this problem and proposed an extrapolation method useful for evaluating the ratios of LIS's intrinsic to the LS complex.[3]

(b) The position of a nucleus (i) in the substrate molecule coordinated to a lanthanide ion may be determined by the use of the following equation, provided that the observed shifts arise solely from the dipolar interaction and that the magnetic tensor is axially symmetric.

$$\Delta\nu_i/\nu_0 = K\langle(3\cos^2\theta_i - 1)/r_i^3\rangle \qquad (1)$$

where ν_0 is the probe frequency, ν_i is the observed value of LIS, r_i is the length of the vector joining the lanthanide ion with the i th nucleus, and θ_i is the angle between this vector and the unique magnetic axis. Although two different expressions have been given to K by McConnel and Robertson[4] and by Bleaney *et al.*,[5] K can be treated as a constant characteristic of a lanthanide ion in applying this equation for the structure determination. Then, the ratios of observed LIS's of different nuclei should be nearly constant for various lanthanide ions, if the observed LIS's are predominantly due to the dipolar interaction[6] and the magnetic tensor is axially symmetric. This constancy of shift ratios for various lanthanides should be checked experimentally.[5]

(c) The correction for diamagnetic shifts induced by the complex formation should be made by observing the shifts with a diamagnetic lanthanoid La(III) or Lu(III).[5]

(d) The line broadening caused by Gd(III) should also be observed to supplement the LIS data.[5,7,8]

Recently Barry *et al.* applied these procedures to the structure determination of adenosine-5'-monophosphate[9] and cyclic 3',5'-adenosine monophosphate.[10] We have applied them to L-azetidine-2-carboxylic acid (abbreviated as Az acid) in D_2O solution and have obtained satisfactory results which will be reported in this paper.

Az acid is a naturally occurring cyclic imino acid (see below) and is known to inhibit various reactions in

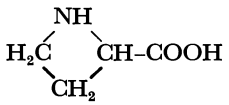

many biological systems. The inhibitory action of Az acid is related to its incorporation into some proteins, where it replaces an equivalent amount of proline. The references dealing with biological activities of Az acid may be found in the paper by Berman *et al.*[11] in which the crystal structure of this compound has been reported. The information on the molecular structure of Az acid in aqueous solution will be of use in elucidating the molecular basis of its biological activities.

Experimental

^{1}H NMR spectra were observed in a similar way as described in the previous paper.[3] For the purpose of comparing the ratios of LIS's for various lanthanide ions, the successive addition of solid lanthanide nitrates to a substrate solution was employed, because it is experimentally simpler than either the successive dilution or the incremental dilution.

The structure analysis based on the LIS data was carried out by the programs PCS-I and II prepared in our laboratory.

Results and Discussion

Shift Ratios. As described above, it is important,

before applying Eq. (1) to the structure determination, to check if the ratios of LIS's observed of different protons are constant for various lanthanide ions. For this purpose the LIS's of Az acid were observed in D_2O solution using the nitrates of praseodymium, neodymium, and europium as shift reagents.[12] Since Pr(III) and Nd(III) induced greater line broadening than Eu(III) did, the measurements with Pr(III) and Nd(III) were confined to the region of small ρ ($\equiv[L_0]/[S_0]$, where $[L_0]$ and $[S_0]$ are the total molar concentrations of the lanthanide ion and the substrate, respectively). This precluded the detailed analysis as applied previously to the results of the successive dilution and incremental dilution methods for the Az acid-Eu(III) system.[3] Therefore, in the present study, the results obtained by the successive addition method shown in Figs. 1—3 were compared. The LIS of proton A is taken as reference in these figures. It is noted that the shift ratio of proton E changes markedly for the three lanthanide ions, whereas the shift ratios for protons B, C, and D remain essentially constant.

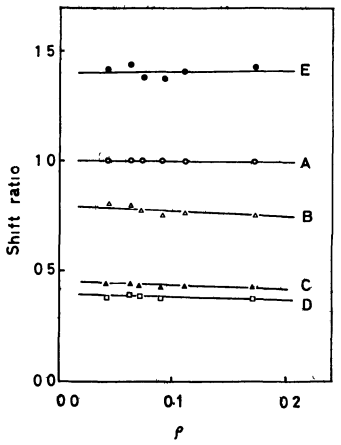

Fig. 1. The ratios of Pr(III)-induced shifts of L-azetidine-2-carboxylic acid observed by the successive addition method.
○, A; △, B; ▲, C; □, D; ●, E.

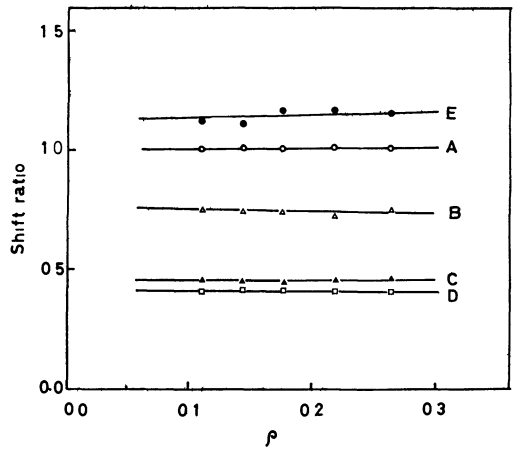

Fig. 2. The ratios of Nd(III)-induced shifts of L-azetidine-2-carboxylic acid observed by the successive addition method.
○, A; △, B; ▲, C; □, D; ●, E.

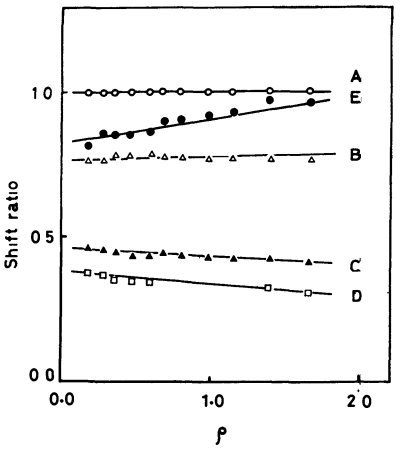

Fig. 3. The ratios of Eu(III)-induced shifts of L-azetidine-2-carboxylic acid observed by the successive addition method.
○, A; △, B; ▲, C; □, D; ●, E.

From these results it may be concluded in the first place that the contact shift makes a sizable contribution only to the observed LIS of proton E. The shift due to a contact mechanism is not expressed by Eq. (1). Accordingly, if the observed LIS's consist of contact and dipolar interaction terms, the shift ratios are not expected to be constant for various lanthanide ions. The contribution of a contact term to the shift of proton E may be explained by the fact that proton E is assigned to the α proton which is located nearest to the coordination site of the lanthanide ion;[3] the number of bonds between the α proton and the coordination site is smaller than that separating the β or γ proton from the coordination site.

In the second place the present results contain information on the axial symmetry of magnetic tensor. According to La Mar *et al.*[13] the shifts arising from the dipolar interaction may be expressed for the case with nonaxially symmetric magnetic tensor as

$$\Delta\nu/\nu_0 = k_1\langle(3\cos^2\theta-1)/r^3\rangle + k_2\langle(\sin^2\theta\cos 2\phi)/r^3\rangle \quad (2)$$

where r, θ, and ϕ are the polar coordinates of the nucleus under consideration, the Cartesian coordinates being taken along the principal magnetic axes with the lanthanide ion at the origin. If the observed LIS's are in accord with this equation, the shift ratios are expected to change their values for Pr(III), Nd(III), or Eu(III) which have different k_1 and k_2 values.[14] However, this is contrary to the results obtained for the shift ratios of protons A, B, C, and D. Therefore, it seems reasonable to conclude that the LIS's of these four protons are satisfactorily accounted for by Eq. (1) which is applicable to the axially symmetric case.

Correction for Diamagnetic Shifts Due to Complex Formation

Observed LIS's usually consist of the diamagnetic as well as paramagnetic terms. In the present case the contribution of the diamagnetic term due to complex formation was found small compared with that of the paramagnetic term. However, the diamagnetic shift should be subtracted from the observed LIS's before an accurate structure determination is attempted. The contribution of the diamagnetic shift may be estimated by measuring the shift with a diamagnetic ion such as

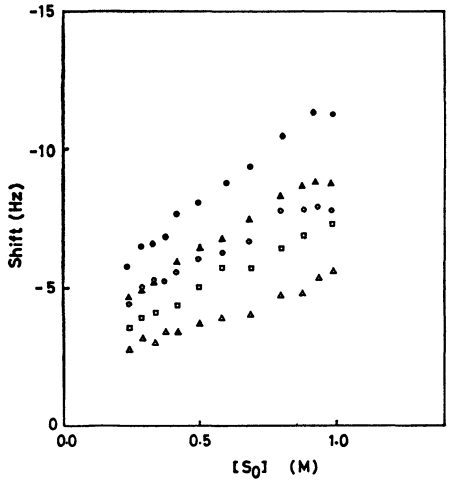

Fig. 4. La(III)-induced shifts of L-azetidine-2-carboxylic acid observed by the successive dilution method *vs.* total substrate concentration ([S_0]). D_2O solution, 37 °C, $\rho=1.01$.
○, A; △, B; ▲, C; □, D; ●, E.

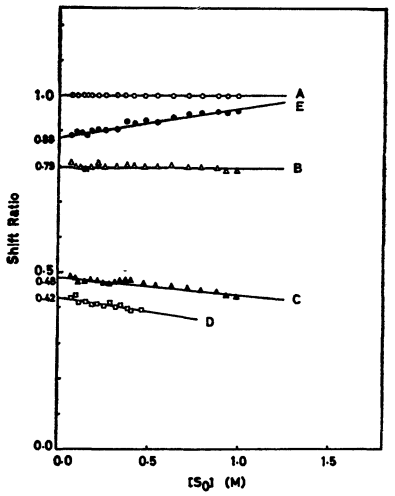

Fig. 5. The ratios of Eu(III)-induced shifts of L-azetidine-2-carboxylic acid observed by the successive dilution method and corrected for the diamagnetic shifts.
○, A; △, B; ▲, C; □, D; ●, E.

La(III). The assumption underlying this method is that the complex formed with La(III) has a structure almost identical to those formed by other lanthanide ions. The diamagnetic shifts observed by the successive dilution method for the Az acid-La(III) system are shown in Fig. 4. The low-field shifts were observed for all the protons. Using the results given in Fig. 4, the Eu(III)-induced shifts were corrected for the diamagnetic contributions. The shift ratios calculated from these corrected values for the Az acid-Eu(III) system are shown in Fig. 5. For the structure determination described below, the shift ratios of protons A, B, C, and D extrapolated to $[S_0]=0$ in this figure (1.00, 0.79, 0.48, and 0.42, respectively) will be used. These values correspond to the ratios of dipolar interaction terms in LIS's intrinsic to the LS complex.

Structure Analysis and Assignment of ^1H NMR Spectrum

As the number of observed LIS data is rather limited,

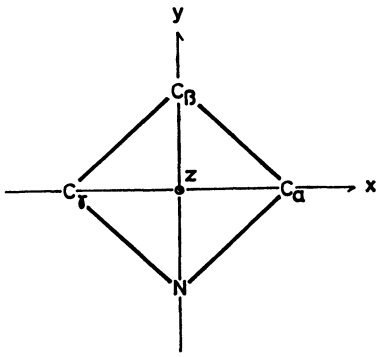

Fig. 6. The four-membered ring of L-azetidine-2-carboxylic acid and the coordinate system.

only the L-C_α distance and the ring-puckering coordinate are chosen as structural variables to be determined. The puckering mode of a four-membered ring can be best described by the coordinate (z) introduced by Chan *et al.*[15] The coordinates of atoms forming the azetidine ring (Fig. 6) are given as

$$\begin{aligned} x_\alpha &= -x_\gamma = [(x_\alpha^\circ)^2-2z^2]^{1/2} \\ y_\alpha &= y_\gamma = 0 \\ z_\alpha &= z_\gamma = z \\ x_\beta &= x_N = 0 \\ y_\beta &= [(y_\beta^\circ)^2-2z^2]^{1/2} \\ y_N &= -[(y_N^\circ)^2-2z^2]^{1/2} \\ z_\beta &= z_N = -z \end{aligned} \tag{3}$$

where α, β, γ, and N represent the α, β, and γ carbons, and the nitrogen, respectively. When the molecule is planar, the α and γ carbons are located on the x axis and the β carbon and the nitrogen on the y axis. x_α°, y_β°, and y_N° refer to the corresponding coordinates in the planar conformation. It is assumed that the four-membered ring always has a plane of symmetry (yz). The puckering mode described by Eq. (3) occurs without changing either the CC or CN bond length. The lengths of CC and CN bonds in the ring and the geometry around the α carbon and the carboxylate group are transferred from the structural parameters determined for this molecule in crystal.[11] As for the geometry around the β or γ carbons, it is assumed that the CH bond length and the HCH bond angle are 1.08 Å and 109°28′, respectively, and four CCH angles are all equal.

As for the coordination site of the lanthanide ion in the LS complex and the direction of symmetry axis of the magnetic tensor, it is most reasonable to assume that the lanthanide ion is on the bisector of the OCO angle and that the symmetry axis is collinear with the bisector.[16] This is in analogy with the lanthanide-mononucleotide complex where both the lanthanide ion and the symmetry axis are on the bisector of the OPO angle.[7,9,10] The shift ratios can now be calculated using Eq. (1).

On the other hand, four combinations (I-IV) are possible regarding the assignments of protons A, B, C, and D to *β-cis*, *β-trans*, *γ-cis*, and *γ-trans*, as given in Table 1 (*cis* and *trans* refer to the position of a proton

Table 1. Assignments of protons A, B, C, and D[a)]

Proton	Assignment			
	I	II	III	IV
A	*β-cis*	*β-cis*	*β-trans*	*β-trans*
B	*β-trans*	*β-trans*	*β-cis*	*β-cis*
C	*γ-cis*	*γ-trans*	*γ-cis*	*γ-trans*
D	*γ-trans*	*γ-cis*	*γ-trans*	*γ-cis*

a) *Cis* and *trans* refer to the positions of protons with respect to the carboxylate group.

with respect to the carboxylate group). For each one of these four assignments the agreement factor (R) defined as[17-19]

$$R=\left[\left\{\sum_i\left[\left(\frac{A_1^i}{A_1^s}\right)_{obs}-\left(\frac{A_1^i}{A_1^s}\right)_{calc}\right]^2\right\}\Big/\left\{\sum_i\left(\frac{A_1^i}{A_1^s}\right)^2_{obs}\right\}\right]^{1/2} \quad (4)$$

has been calculated for various values of the L-C_α distance and the z coordinate, so that a contour map as shown in Fig. 7 is obtained. This map shows that, for Assignment III, R is minimized only if the L–C_α distance is taken so short (2.3 Å) that the lanthanide ion partially penetrates into the carboxylate group. This indicates clearly that Assignment III should be discarded. The contour map obtained for Assignment IV is essentially the same as that shown in Fig. 7. Thus, Assignment IV is also discarded.

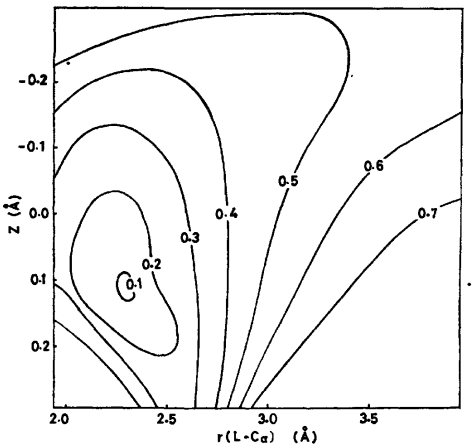

Fig. 7. The contour map of the agreement factor (R) for Assignment III.

Since only Assignments I and II remain acceptable, the assignments of β protons are now established; *i.e.*, A and B are assigned, respectively, to the *β-cis* and *β-trans* protons. The contour maps obtained for Assignments I and II are shown in Figs. 8 and 9, respectively. The minimum in the contour map in Fig. 8 corresponds to a conformation in which the ring is almost planar ($z\sim0$, Conformation I). On the other hand, the molecular structure corresponding to the minimum in the contour map in Fig. 9 has a puckered ring ($z=-0.125$ Å and the dihedral angle=25 °) with the carboxylate group in the equatorial position (Conformation II). (From the present analysis no information can be obtained about the internal-rotation angle around the C_α–CO_2^- bond.) It seems rather difficult

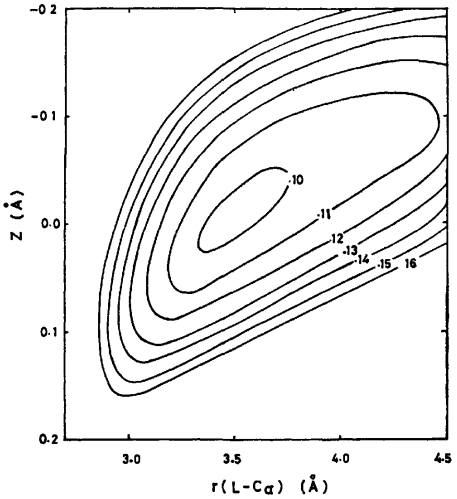

Fig. 8. The contour map of the agreement factor (R) for Assignment I.

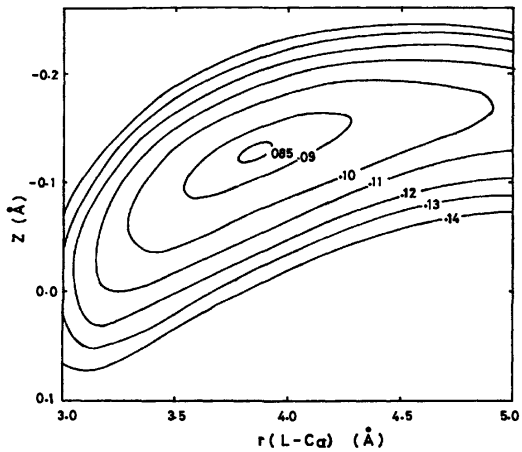

Fig. 9. The contour map of the agreement factor (R) for Assignment II.

to decide, from these results alone, which of the two conformations (therefore, which of Assignments I and II) is more probable, though the L–C_α distance in Conformation I (3.5 Å) is slightly shorter than the value (~4 Å) normally accepted.

The line broadening induced by Gd(III) has been found useful for solving the above-mentioned problem. Since the Gd(III)-induced line broadening is proportional to $1/r^6$ and independent of θ, the line-width data obtained for protons C and D are expected to be useful for determining which of these protons are closer to Gd(III). In Conformation I the distances from Gd(III) to C and D are 5.3 and 6.2 Å, respectively, whereas in Conformation II they are 6.5 and 6.3 Å, respectively. The ratios of the line broadening expected for protons, A, B, C and D in both conformations are given in Table 2. The spectra observed after adding extremely small amount of Gd(III) are shown in Fig. 10 for the lines assignable to almost pure transitions related to protons A, B, C, and D. Although the concentration of Gd(III) was not precisely determined, it was about 10^{-6} M for Fig. 10(b) and twice and three times of that for Figs. 10(c) and (d), respectively. The ratios

Table 2. The ratios of Gd(III)-induced line broadening[a)]

Proton	Calcd		Obsd
	Conformation I	Conformation II	
A	11.1	7.0	>3
B	2.8	2.5	>2
C	2.5	0.8	0.9
D	1.0	1.0	1.0

a) The broadenining of a line due to the transition of proton D is taken as reference.

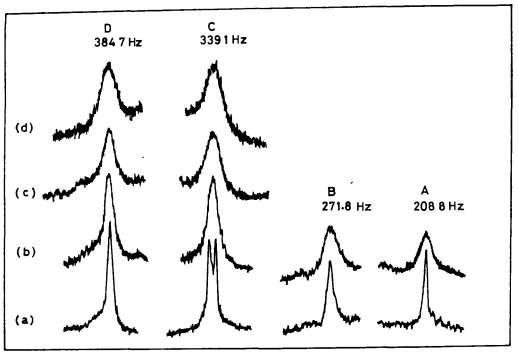

Fig. 10. Gd(III)-induced broadening of the lines assigned to the pure transitions of protons A, B, C, and D of L-azetidine-2-carboxylic acid. The concentration of Gd(III) is zero in (a), *ca.* 10^{-6} M in (b), twice and three times of *ca.* 10^{-6} M in (c) and (d), respectively.

of the line broadening thus observed are also given in Table 2. It is clear in this table that the observed ratios are in agreement with those expected for Conformation II. Thus, it may be concluded that Conformation II (therefore, Assignment II) is the real one.

It was found that the R value for Conformation II could be made as small as 0.038 by changing the bond angles N–C_α–COO^- and C_β–C_α–COO^- to 115.5 ° and 118.4 °, respectively, from the crystal data 117 ° and 113 ° with all the other parameters fixed as before. This changes the overall molecular conformation only slightly.

Conclusion

In utilizing the lanthanide-induced shifts and line broadening to the determination of molecular structure in solution, it has been shown necessary and rewarding to follow all the procedures outlined in the introductory part. In weakly acidic aqueous solution the four-membered ring of L-azetidine-2-carboxylic acid has a puckered conformation with a dihedral angle of 25 °, which compares with the angle of 11 ° as determined for this molecule in crystal.[11] The carboxylate group is in the equatorial position. This molecular structure is depicted in Fig. 2 of the preceding paper.[3]

The authors are grateful to Dr. H. Sugano of Research Laboratory of Applied Biochemistry, Tanabe Seiyaku Co., Ltd., for supplying the sample of L-azetidine-2-carboxylic acid. Thanks are also due to Dr. K. Tori of Shionogi Research Laboratory, Shionogi & Co., Ltd., and Dr. M. Kainosho of Central Research Laboratories, Ajinomoto Co., Inc., for helpful discussions.

References

1) B. L. Shapiro and M. D. Johnston, Jr., *J. Amer. Chem. Soc.*, **94**, 8185 (1972).
2) B. L. Shapiro, M. D. Johnston, Jr., R. L. R. Towns, A. D. Godwin, H. L. Pearce, T. W. Proulx, and M. J. Shapiro, in "Nuclear Magnetic Resonance Shift Reagents," ed. by R. E. Sievers, Academic Press, New York, N. Y. (1973), p. 227.
3) F. Inagaki, S. Takahashi, M. Tasumi, and T. Miyazawa, This Bulletin, **48**, 853 (1975).
4) H. M. McConnel and R. E. Robertson, *J. Chem. Phys.*, **29**, 1361 (1958).
5) B. Bleaney, C. M. Dobson, B. A. Levine, R. B. Martin, R. J. P. Williams, and A. V. Xavier, *Chem. Commun.*, **1972**, 791.
6) In some cases, contact shifts are known to make large contributions to the observed LIS's. Recently some authors proposed the methods for evaluating the dipolar and the contact parts in the observed LIS's [see the following papers: C. M. Dobson, R. J. P. Williams, and A. V. Xavier, *J. Chem. Soc. Dalton*, **1973**, 2662; D. J. Chadwick and D. H. Williams, *J. Chem. Soc. Perkin II*, **1974**, 1202; K. Ajisaka and M. Kainosho, *J. Amer. Chem. Soc.*, **97**, 330 (1975)]. In the present study, however, these methods were not tested, because contact shifts were found negligible for most protons of the molecule treated here.
7) C. D. Barry, A. C. North, J. A. Glasel, R. J. P. Williams, and A. V. Xavier, *Nature*, **232**, 236 (1971).
8) G. N. La Mar and J. W. Faller, *J. Amer. Chem. Soc.*, **95**, 3817 (1973).
9) C. D. Barry, J. A. Glasel, R. J. P. Williams, and A. V. Xavier, *J. Mol. Biol.*, **84**, 471 (1974).
10) C. D. Barry, D. R. Martin, R. J. P. Williams, and A. V. Xavier, *J. Mol. Biol.*, **84**, 491 (1974).
11) H. M. Berman, E. L. McGandy, J. W. Burgner, II, and R. L. VanEtten, *J. Amer. Chem. Soc.*, **91**, 6177 (1969).
12) All the resonance lines shifted to low fields with Pr(III) and Nd(III), whereas high-field shifts were observed with Eu(III).
13) G. N. La Mar, W. D. Horrocks, Jr., and L. C. Allen, *J. Chem. Phys.*, **42**, 2126 (1964).
14) W. D. Horrocks, Jr., and J. P. Sipe, III, *Science*, **177**, 994 (1972).
15) S. I. Chan, J. Zinn, and W. D. Gwinn, *J. Chem. Phys.*, **34**, 1319 (1961).
16) B. A. Levine, J. M. Thornton, and R. J. P. Williams, *Chem. Commun.*, **1974**, 669.
17) M. R. Willcott, III, R. E. Lenkinski, and R. E. Davis, *J. Amer. Chem. Soc.*, **94**, 1742 (1972).
18) R. E. Davis and M. R. Willcott, III, *J. Amer. Chem. Soc.*, **94**, 1744 (1972).
19) As for the definitions of Δ_1^i and Δ_1^s, see Eqs. (5) and (6) of reference 3.

Infrared Spectra and Structures of Copper(II) and Zinc(II) Complexes of Glycylglycine in Aqueous Solution

Mitsuo TASUMI, Seizo TAKAHASHI, Toshio NAKATA, and Tatsuo MIYAZAWA

Department of Biophysics and Biochemistry, Faculty of Science, The University of Tokyo, Bunkyo-ku, Tokyo 113

(Received January 21, 1975)

The infrared spectra of the Cu(II) and Zn(II) complexes of glycylglycine were observed in D_2O at various pD values. Large spectral changes in going from acidic to neutral solution were interpreted in terms of the equilibria among free and complexed forms of glycylglycine. In the Cu(II) complex formed for $3<pD<5$ the metal-ligand bonding occurs through the amino nitrogen and peptide oxygen. As pD is increased further, the structure of the Cu(II) complex changes into a form in which the metal-ligand bonding occurs through the amino nitrogen, peptide nitrogen (deprotonated), and carboxyl oxygen. In contrast to the Cu(II) complex, no change of structure is found for the Zn(II) complex. The Zn(II) complex formed for $pD>5$ is similar to the Cu(II) complex present for $3<pD<5$.

The interaction between metal ions and peptides is an important subject not only in the chemistry of coordination compounds but also from biological viewpoint. In this and subsequent papers we study the structures of metal(II) complexes of some dipeptides in aqueous (or deuterium oxide) solution of various pH (or pD) and discuss, on this basis, the role of metal ions in the hydrolysis of dipeptides.

The structure of Cu(II) complex of glycylglycine, the simplest dipeptide, has been studied by many authors in crystal[1-3] and in aqueous solution.[4-8] The most interesting feature derived from the previous studies is the change of complex structure with the increase in pH (or pD). All the authors seem to agree that the peptide group is deprotonated in going from acidic to neutral solution and that in neutral solution the metal-ligand bonding occurs through the amino nitrogen, peptide nitrogen (deprotonated), and carboxyl oxygen. As for the structure in acidic solution, two different forms have been proposed with respect to the metal-ligand bonding. We discuss this matter through the analysis of infrared spectra of this complex in deuterium oxide solution. The structure of the Zn(II) complex in aqueous solution is also examined by referring to the Cu(II) complex case.

Experimental

Materials. Glycylglycinatocopper(II) trihydrate[Cu-GG·$3H_2O$[9]], glycylglycinatocopper(II) chloride monohydrate[Cu(HGG)Cl·H_2O], bis(glycylglycinato)zinc(II) dihydrate[$Zn(HGG)_2\cdot 2H_2O$], and glycylglycinatozinc(II) hemihydrate[Zn(HGG)Cl·$0.5H_2O$] were prepared from glycylglycine and corresponding metal(II) chloride or nitrate according to the methods described in references 10—12.

Infrared Absorption Measurements. The infrared spectra were recorded for *ca.* 0.2 M D_2O solutions using a Hitachi EPI-G3 spectrophotometer and a pair of cells made of As_2Se_3 (sample layer thickness 0.05 mm). The amino and peptide protons were deuterated by conventional method before preparing the D_2O solution. The pD value was adjusted by adding suitable amount of the 1 M D_2O solution of DCl or NaOD. The pD value was determined using a Hitachi-Horiba pH-meter F-7 with a combination electrode and a set of pH test paper, and no correction for the obtained values was made.

Results and Discussion

Infrared Spectra and Structures of the Cu(II) Complexes. The spectrum of the D_2O solution of CuGG·$3D_2O$ was essentially the same as that of Cu(DGG)Cl·D_2O under common pD values. So, the structure of complexed glycylglycine in both solutions must be identical. The infrared spectra in the region between 1800 and 1200 cm^{-1} of Cu(DGG)Cl·D_2O are shown in Fig. 1. The results shown in this figure agree well with those obtained previously by Kim and Martell[5] for the mixture of the Cu(II) ion and glycylglycine in D_2O.

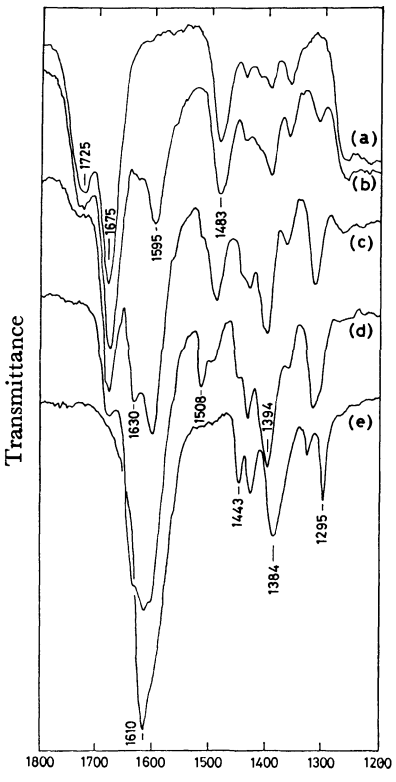

Fig. 1. Infrared spectra of the D_2O solution of the Cu(II) complex at various pD values. Concentration, *ca.* 0.2 M; sample layer thickness, 0.05 mm.
(a), pD 0.6; (b), pD 2.0; (c), pD 3.6; (d), pD 4.2; (e), pD 5.6.

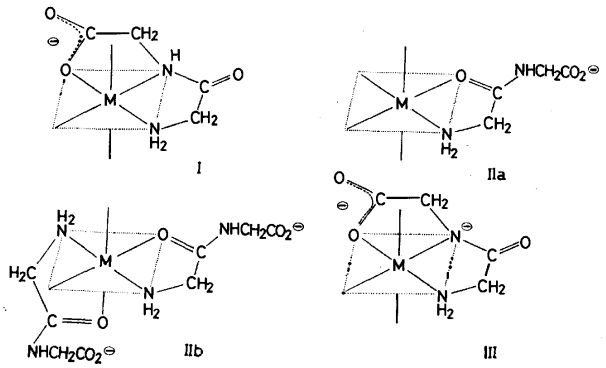

Fig. 2. Structures of the metal-glycylglycine complexes.[15]

Although Kim and Martell observed only the 1800—1500 cm^{-1} region, the region below 1500 cm^{-1} also gives useful information as will be described shortly. By comparing the spectra in Fig. 1 with pD variation of the spectra of glycylglycine itself,[13,14] it is clear that no complex is formed in the pD range below *ca.* 3. The band at 1630 cm^{-1} which appears only in the pD range between 3 and 5 was assigned by Kim and Martell[5] to the amide I vibration of Complex I shown in Fig. 2.[15] The formation of Complex I in acidic solution was later supported by a potentiometric analysis.[7] However, the present infrared results are better accounted for by assuming Complex IIa of Fig. 2 on the following grounds.

The amide II band which is located at about 1560 cm^{-1} in the spectra of simple peptides is known to shift, on deuteration, to about 1480 cm^{-1} (amide II').[16] The amide II' band is clearly seen at 1502 cm^{-1} in the spectrum of deuterated solid complex Cu(DGG)Cl·D_2O[17] (Fig. 3), whereas no corresponding band is found in the spectrum of deuterated solid complex $CuGG \cdot 3D_2O$ (Fig. 4). Since the peptide group in the latter complex is deprotonated, the normal modes would be different from those of ordinary peptide bond. So, it is reasonable that no band is found around 1500 cm^{-1} for $CuGG \cdot 3D_2O$. In D_2O the amide II' band of free glycylglycine is found at 1483 cm^{-1}. In the spectra of Cu(II) complexes in D_2O at pD 3, the presence of this band indicates, together with

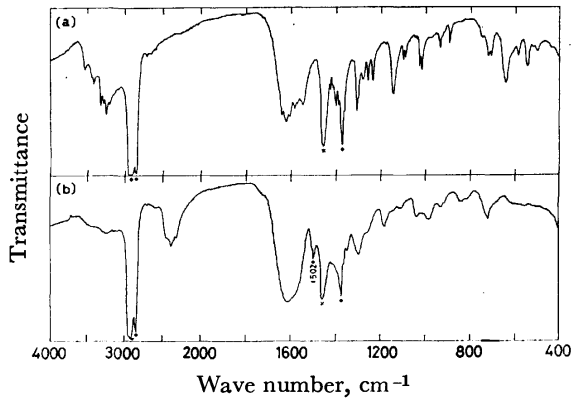

Fig. 3. Infrared spectra of solid (a) Cu(HGG)Cl·H_2O and (b) Cu(DGG)Cl·D_2O (Nujol mull).
The absorptions due to Nujol are indicated by asterisk.

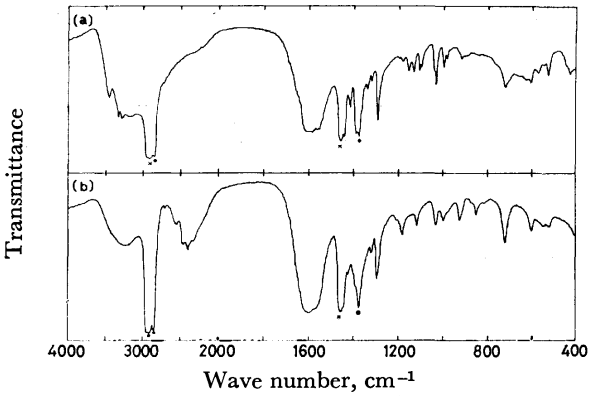

Fig. 4. Infrared spectra of solid (a) $CuGG \cdot 3H_2O$ and (b) $CuGG \cdot 3D_2O$ (Nujol mull).
The absorptions due to Nujol are indicated by asterisk.

other evidence, that the complexes are dissociated in this low pD range. In the pD range between 3 and 5 where the 1630 cm^{-1} band is observed, another band appears at 1508 cm^{-1} in addition to the 1483 cm^{-1} band. The 1508 cm^{-1} band can be assigned to the amide II' vibration of complexed glycylglycine. The shift of amide II' band to higher frequency is related to the increase in bond order of the peptide C-N linkage; in other words, the contribution of the resonance form

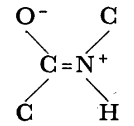

increases with the complex formation. This type of change can be expected for Complex IIa but not for Complex I (Fig. 2). In the latter the bond order of the peptide linkage would be reduced through the increased contribution of sp^3 configuration of the nitrogen atom.

The infrared analysis given above indicates that complex IIa and free glycylglycine coexist in the range $3<pD<5$. The presence of Complex IIa in acidic solution was first proposed by Rabin[4] from potentiometric studies and later supported by calorimetric[6] and kinetic[8] analyses. The X-ray diffraction analysis of Cu(HGG)Cl·H_2O crystallized from acidic solution gave a structure analogous to Complex IIa.[3]

In neutral solution with $pD>5$ new bands are observed at 1610, 1443, and 1295 cm^{-1}, whereas the bands at 1630 and 1508 cm^{-1} disappear. The spectra measured at pD values between 5 and 11 were essentially the same as that of Fig. 1(e). The new bands are undoubtedly due to Complex III shown in Fig. 2. The 1610 cm^{-1} band may be assigned to the C=O stretching and the latter two bands are probably associated with the C–N^- stretching vibration. The conversion of complex structure in going from acidic to neutral solution and the presence of Complex III in neutral solution are unanimously accepted.[4-8] In this complex the terminal CO_2^- group is also coordinated to the metal. In fact, the CO_2 symmetric stretching band is shifted to 1384 cm^{-1} [Fig. 1(e)] from 1394 cm^{-1} of free CO_2^- [Fig. 1(b), (c), and (d)].

The assignments of bands observed in the region

Table 1. Assignments of the infrared bands of the D_2O solution of the Cu (II) complex in the region between 1750 and 1440 cm^{-1}.[a)]

Obs. freq., cm^{-1} [a)]	Assignment
1725 (1725)	C=O str. of terminal COOH
1675 (1675)	Amide I of free $D_3N^+CH_2CONDCH_2CO_2^-$
1630 (1640)	(1) Amide I of free $D_2NCH_2CONDCH_2CO_2^-$ (2) Amide I of Complexes IIa and IIb
1610	C=O str. of Complex III
1595 (1595)	Antisym. str. of free and complexed CO_2^-
1508 (1500)	Amide II′ of Complexes IIa and IIb
1483 (1483)	Amide II′ of free $D_3N^+CH_2CONDCH_2CO_2^-$
1443	$C-N^-$ str. of Complex III[b)]
1394 (1394)	Sym. str. of free CO_2^-
1384	Sym. str. of complexed CO_2^-

a) This table is also applicable to the D_2O solution of the Zn (II) complex. The observed frequencies for the D_2O solution of the Zn(II) complex are given in parentheses. b) The 1295 cm^{-1} band also may be assigned to a mode which has a considerable contribution of the $C-N^-$ stretching.

between 1750 and 1300 cm^{-1} are given collectively in Table 1.

Infrared Spectra and Structures of the Zn(II) Complexes. The infrared spectrum of the D_2O solution of Zn-$(DGG)_2 \cdot 2D_2O$ was not much different from that of $Zn(DGG)Cl \cdot 0.5D_2O$ under common pD values. The structure of complexed glycylglycine in both solutions must therefore be identical. The infrared spectra in the region between 1800 and 1200 cm^{-1} of $Zn(DGG)Cl \cdot 0.5D_2O$ in D_2O are shown in Fig. 5. The examination of these spectra shows that no complex is formed for pD<4. In this pD range the amide II′ band at 1483 cm^{-1} of free glycylglycine is observed similarly as in the case of the D_2O solution of the Cu(II) complexes for pD<3. The bands at 1640 and 1500 cm^{-1} begin to appear at pD about 5 and become stronger for higher pD values until the precipitation of the complex begins from alkaline solution with pD about 9. At pD 7.6 the amide II′ band of free glycylglycine is observed as a very weak shoulder. This indicates that Complex IIa and /or Complex IIb are the predominant species in this pD range. In both of these complexes the metal-ligand bonding occurs through the amino nitrogen and peptide oxygen. Complex IIb is consistent with the structure determined for the crystal of $Zn(HGG)_2 \cdot 2H_2O$ by X-ray diffraction.[2)] It is interesting to note that no conversion of complex structure takes place for the Zn(II) complex in going from acidic to neutral solution.

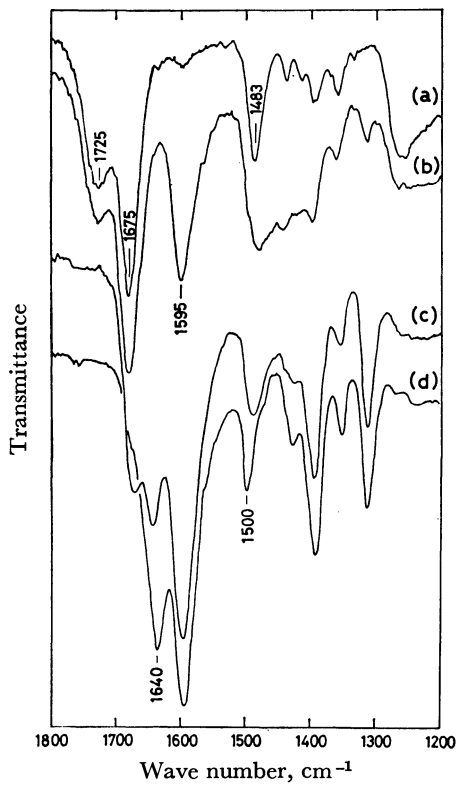

Fig. 5. Infrared spectra of the D_2O solution of the Zn(II) complex at various pD values.
Concentration, *ca.* 0.2 M; sample layer thickness, 0.05 mm. (a), pD 0.8; (b), pD 3.2; (c), pD 6.0; (d), pD 7.6.

Conclusion

The analysis of the infrared spectra of the Cu(II) complex of glycylglycine in D_2O shows that, for 3< pD<5, a complex is formed in which the metal-ligand bonding occurs through the amino nitrogen and peptide oxygen. As pD is increased, the structure of complex changes. In the complex which is present predominantly for pD>5 the metal-ligand bonding occurs through the amino nitrogen, peptide nitrogen (deprotonated), and carboxyl oxygen.

The behavior of the Zn(II) complex of glycylglycine is considerably different from that of the Cu(II) complex. No structure change of the complex is observed with increasing pD. In the complex formed for pD>5 the metal-ligand bonding is of the same type as found for the Cu(II) complex for 3<pD<5. Such structural information is useful in analysing the catalytic activities of these two metal ions in the hydrolysis of peptide bond. This point will be treated in a subsequent paper.

The authors wish to thank Miss Hideko Ito for the assistance throughout this work.

References

1) B. Strandberg, I. Lindqvist, and R. Rosenstein, *Z. Krist.*, **116**, 266 (1961).
2) H. C. Freeman, *Adv. Protein. Chem.*, **22**, 257 (1967).
3) M. Shiro, Y. Nakao, O. Yamauchi, and A. Nakahara, *Chem. Lett.*, **1972**, 123.
4) B. R. Rabin, *Trans. Faraday Soc.*, **52**, 1130 (1956).
5) M. K. Kim and A. E. Martell, *Biochemistry*, **3**, 1169 (1964).
6) A. P. Brunetti, M. C. Lim, and G. H. Nancollas, *J. Amer. Chem. Soc.*, **90**, 5120 (1968).
7) O. Yamauchi, Y. Hirano, Y. Nakao, and A. Nakahara, *Can. J. Chem.*, **47**, 344 (1969).
8) R. F. Pasternack, M. Angwin, and E. Gibbs, *J. Amer. Chem. Soc.*, **92**, 5878 (1970).
9) The abbreviation GG stands for doubly deprotonated

glycylglycine. Free glycylglycine is therefore represented as H_2GG.

10) A. R. Manyak, C. B. Murphy, and A. E. Martell, *Arch. Biochem. Biophys.*, **59**, 373 (1955).

11) A. Rosenberg, *Acta. Chem. Scand.*, **11**, 1390 (1957).

12) M. L. Bair and E. M. Larsen, *J. Amer. Chem. Soc.*, **93**, 1140 (1971).

13) M. K. Kim and A. E. Martell, *J. Amer. Chem. Soc.*, **85**, 3080 (1963).

14) The results of our measurements for glycylglycine itself were in agreement with those of Kim and Martell.[13]

15) In this figure only the metal-glycylglycine bonding is shown and other ligands such as OH^-, Cl^-, and H_2O are neglected, since no information about the latter ligands is available from the infrared spectra.

16) T. Miyazawa, T. Shimanouchi, and S. Mizushima, *J. Chem. Phys.*, **24**, 408 (1956).

17) In the spectra of solid complexes $Zn(DGG)_2 \cdot 2D_2O$ and $Zn(DGG)Cl \cdot 0.5D_2O$ the amide II′ bands are observed at 1490 and 1496 cm^{-1}, respectively.

Metal(II)-Ion Promoted Hydrolysis of Glycylglycine

Toshio NAKATA, Mitsuo TASUMI, and Tatsuo MIYAZAWA

Department of Biophysics and Biochemistry, Faculty of Science, The University of Tokyo, Bunkyo-ku, Tokyo 113

(Received January 31, 1975)

The hydrolysis of glycylglycine was studied in the presence of Cu(II) and Zn(II) at various pH values between 3.4 and 6.3. Glycine produced by the hydrolysis and remaining glycylglycine were trimethylsilylated and their relative quantities were determined by gas-liquid chromatography. The reaction is promoted by both metal ions. In the presence of Cu(II) the pH-rate profile has a maximum at pH *ca.* 4.4, whereas in the presence of Zn(II) the rate increases as pH becomes higher. These kinetic results are discussed in terms of the structures of metal(II)-glycylglycine complexes in aqueous solution.

Some metal ions are known to have catalytic activities in the hydrolysis of peptide bond.[1,2] Grant and Hay[2] have studied the hydrolysis of glycylglycine in the presence of Cu(II) and have found that the reaction rate is clearly dependent upon pH, showing a maximum at pH 4.2. The purpose of the present study is to examine more quantitatively the pH dependence of catalytic activities of Cu(II) and Zn(II) in the hydrolysis of glycylglycine and to discuss the relationship between the reactivity and structure of the metal(II)-glycylglycine complex. The structures of Cu(II) and Zn(II) complexes of glycylglycine in aqueous solution have been reported in a previous paper.[3]

Experimental

Materials. Glycylglycinatocopper(II) chloride monohydrate [Cu(HGG)Cl·H_2O][4] and glycylglycinatozinc(II) chloride hemihydrate [Zn(HGG)Cl·0.5H_2O] were prepared from glycylglycine and corresponding metal(II) chloride according to the method of Bair and Larsen.[5]

Bis(trimethylsilyl)trifluoroacetamide (BSTFA) was synthesized by adding trimethylsilyl chloride to a mixture of trifluoroacetamide and trimethylamine. The product was purified by distillation.[6] Bp 52.5 °C (30 mmHg).

Reaction. The hydrolysis of glycylglycine was studied for 0.01 and 0.1 M solutions of Cu(HGG)Cl·H_2O and Zn(HGG)Cl·0.5H_2O. The samples were dissolved in sodium acetate–acetic acid buffer solution. The total concentrations of acetate ion plus acetic acid were 0.2 and 1 M, respectively, for the sample concentrations of 0.01 and 0.1 M. Sealed reaction tubes containing 5 ml solutions were kept in an oil bath at 85 °C for 100 hr. After the reaction each solution was diluted with several ml of water, treated with hydrogen sulfide, and then freed of hydrogen sulfide with a stream of nitrogen. The precipitate (CuS or ZnS) was removed after centrifugation (2000 g, 10 min).

Thin-layer Chromatography. The solution thus obtained was analysed qualitatively by thin-layer chromatography, using phenol–water–ammonium hydroxide (3:1:trace) mixture as solvent and a 20×20 cm TLC plate covered with microcrystalline cellulose. Glycine produced by the hydrolysis and glycylglycine were both identified by the coloration with ninhydrin, R_f values being 0.37 and 0.57, respectively.

Trimethylsilylation. Trimethylsilylation of glycine and glycylglycine was carried out in order to obtain volatile derivatives which could be analysed by gas–liquid chromatography. By adjusting the pH value of the solution (from which metal sulfide was already separated) to about 2.5 with 1 M hydrochloric acid, sodium acetate was converted to acetic acid, which was then removed by freeze-drying. After dissolving the remaining solid substance in a small amount of water (1 ml), an aliquot (100—200 μl) was put into a vial for trimethylsilylation (purchased from Pierce Co., Ltd. in Rockford, Illinois, U.S.A.). The solution in the vial was frozen and evaporated completely to dryness in a vacuum desiccator over phosphorus pentoxide. To this dry sample were added 150 μl of dry acetonitrile and 150 μl of BSTFA. The vial was sealed with a silicon-lined cap and heated for 15 min at 125—130 °C. Under such a condition both glycine and glycylglycine were trimethylsilylated to a satisfactory degree. However, two kinds of trimethylsilylated derivatives were obtained as described later.

Gas-liquid Chromatography. Gas-liquid chromatographic analysis was carried out with a Shimadzu gas chromatograph GC-4BM equipped with a flame ionization detector. Glass columns of 2.0 m×4 mm i.d. containing 5.0% w/w SE-30 coated on 80/100 mesh AW-DMCS Chromosorb W were used. The flow rate of carrier gas (nitrogen) was 60 ml/min and the temperature was elevated from 100 °C to 220 °C at a programmed rate of 5 °C/min.

Mass Spectrometry. The characterization of trimethylsilylated derivatives was carried out by mass spectrometry. A Hitachi RM 50 (combined GLC-MS instrument) was used with the temperature of ion source and manifold 220 °C, accelerating voltage 3 kV, and ionizing energy 70 eV.

Results

Analysis of Trimethylsilylated Glycine and Glycylglycine by Gas-liquid Chromatography. By the reaction with BSTFA both glycine and glycylglycine gave two kinds of trimethylsilylated (TMS) derivatives as shown below.

(1) $H_2NCH_2COOH + CF_3CON[Si(CH_3)_3]_2 \longrightarrow$ TMS-$NHCH_2COO$-TMS (Di-TMS-glycine, TG-1) + $(TMS)_2NCH_2COO$-TMS (Tri-TMS-glycine, TG-2)

(2) $H_2NCH_2CONHCH_2COOH + CF_3CON[Si(CH_3)_3]_2 \longrightarrow$ TMS-$NHCH_2CONHCH_2COO$-TMS (Di-TMS-glycylglycine, TGG-1) + $(TMS)_2NCH_2CONHCH_2COO$-TMS (Tri-TMS-glycylglycine, TGG-2)

This was proved by GLC-MS analysis. The results of our GLC-MS analysis for trimethylsilylated glycine were in agreement with those reported by Bergström *et al.*[7] Both di-TMS- and tri-TMS-glycylglycine have fragmentation patterns very similar to di-TMS- and tri-TMS-glycine, respectively. Tri-TMS-glycine(M=348) gave the following fragment ions: *m/e* 333, $[(M-CH_3)^+]$; *m/e* 174, $[(TMS)_2N^+=CH_2]$; *m/e* 147, $[TMS-O^+=Si(CH_3)_2]$; *m/e* 102, $[TMS-N^+H=CH_2]$; *m/e* 86, $[(CH_3)_2Si=N^+=CH_2]$; *m/e* 73, $[TMS^+]$; *m/e* 59,

$[HSi^+(CH_3)_2]$; *m/e* 45, $[H_2Si^+CH_3]$.

It was found that trimethylsilylation of glycine at 100 °C for 15 min gave TG-1 alone, whereas the addition of trimethylsilyl chloride besides BSTFA yielded only TG-2 under the same reaction condition. Using fluorene as internal standard, the relative molar sensitivity of TG-1 and TG-2 for the flame ionization detector used in this experiment was determined to be 1.00: 1.39. In a similar manner the relative molar sensitivity of TGG-1 and TGG-2 was determined to be 1.00: 1.40. Various mixtures of glycine and glycylglycine were trimethylsilylated at 125 °C for 15 min, and the ratios of peak areas of TG-1 and TGG-1 were plotted against the molar ratio of glycine and glycylglycine. A linear relationship was obtained and from the slope the relative molar sensitivity of TG-1 and TGG-1 was determined to be 1.87: 1.00. Consequently, the relative molar sensitivity of TG-1, TG-2, TGG-1, and TGG-2 was 1.87: 2.60: 1.00: 1.40.

Hydrolysis of Glycylglycine. The solutions (0.01 and 0.1 M) of glycylglycine, $Cu(HGG)Cl\cdot H_2O$, and $Zn(HGG)Cl\cdot 0.5H_2O$ having various pH values were kept at 85 °C for 100 hr. The percentage of hydrolysis (ρ) was calculated by the following equations and the results are given in Tables 1 and 2 and Fig. 1.

$$\rho(\%) = \left\{1-\frac{[\text{Glygly}]_{100}}{[\text{Glygly}]_0}\right\}\times 100 = \left\{1-\frac{[\text{Glygly}]_{100}}{[\text{Glygly}]_{100}+(1/2)[\text{Gly}]_{100}}\right\}\times 100 = \left\{\frac{1}{2([\text{Glygly}]_{100}/[\text{Gly}]_{100})+1}\right\}\times 100 \quad (1)$$

where [Glygly] and [Gly] denote the concentrations of glycylglycine and glycine, respectively, and suffix indicates the reaction time (hr). The ratio $[\text{Glygly}]_{100}/[\text{Gly}]_{100}$ can be obtained from the gas-liquid chromatographic analysis as follows.

$$\frac{[\text{Glygly}]_{100}}{[\text{Gly}]_{100}} = \frac{A_{\text{TGG-1}}+(1/1.40)A_{\text{TGG-2}}}{(1/1.87)A_{\text{TG-1}}+(1/2.60)A_{\text{TG-2}}} \quad (2)$$

where $A_{\text{TG-1}}$, $A_{\text{TG-2}}$, $A_{\text{TGG-1}}$, and $A_{\text{TGG-2}}$ denote the peak areas of TG-1, TG-2, TGG-1, and TGG-2, respectively.

Table 1. Hydrolysis of glycylglycine in aqueous solutions (0.01 M) of glycylglycine, glycylglycinatocopper(II) chloride monohydrate, and glycylglycinatozinc (II) chloride hemihydrate.[a]

pH	Percent hydrolysis (ρ)[b]		
	Glygly	Cu(HGG)Cl-·H_2O	Zn(HGG)Cl-·0.5 H_2O
3.52	1.6	—	1.9
3.83	—	28.7	—
4.00	0.4	30.9	1.6
4.27	—	40.1	—
4.48	0.6	42.0	4.3
5.00	0.0	17.3	7.8
5.51	0.7	8.3	20.0
6.01	0.6	5.0	57.7

a) In 0.2 M CH_3COONa–CH_3COOH buffer solutions, heated at 85 °C for 100 hr. b) Defined in Eq. (1).

Table 2. Hydrolysis of glycylglycine in aqueous solutions (0.1 M) of glycylglycinatocopper (II) chloride monohydrate and glycylglycinatozinc(II) chloride hemihydrate[a]

pH	Percent hydrolysis (ρ)[b]	
	Cu(HGG)Cl-·H_2O	Zn(HGG)Cl-·0.5 H_2O
3.41	72.7	5.3
3.74	77.3	—
3.96	78.3	5.9
4.25	87.3	—
4.47	85.9	9.3
5.00	69.5	15.3
5.51	44.1	40.0
6.01	29.0	59.5
6.32	—	70.0

a) In 1M CH_3COONa–CH_3COOH buffer solutions, heated at 85 °C for 100 hr. b) Defined in Eq. (1).

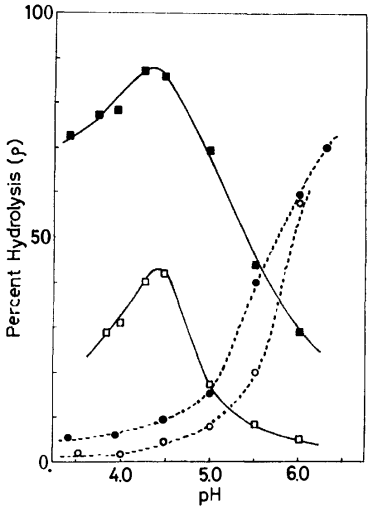

Fig. 1. The pH-rate profiles for the hydrolysis of glycylglycine in the presence of Cu(II) and Zn(II). (□), $Cu(HGG)Cl\cdot H_2O$ (0.01 M); (■), $Cu(HGG)Cl\cdot H_2O$ (0.1 M); (○), $Zn(HGG)Cl\cdot 0.5H_2O$ (0.01 M); (●), $Zn(HGG)Cl\cdot 0.5H_2O$ (0.1 M).

Discussion

The kinetic results obtained above may be summarized as follows.

(1) In the absence of the metal ion, glycylglycine is hardly hydrolysed under the present experimental conditions (Table 1).

(2) Both the Cu(II) and Zn(II) ions promote the hydrolysis of glycylglycine (Tables 1 and 2).

(3) In the presence of Cu(II) the pH-rate profile is a "bell-shape" having maximum at pH *ca.* 4.4. In contrast to this, the rate increases as pH becomes higher in the presence of Zn(II) (Fig. 1). The pH-rate profile in this case may be called "half bell-shape." (The pH range beyond 6.3 was not examined due to the lack of suitable buffer solution.)

(4) The rate of hydrolysis is greater for the solution having higher initial concentration (0.1 M *vs.* 0.01 M).

The bell-shaped pH-rate profile for the Cu(II)-glycylglycine system is in good agreement with the results reported previously by Grant and Hay[2] using an analytical method (ninhydrin technique) quite different from ours.

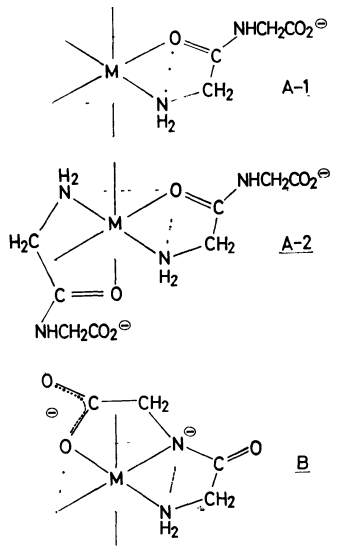

Fig. 2. Structures of metal(II)-glycylglycine complex.

An interesting aspect of the results obtained above is the correlation between the rate of hydrolysis and the structure of metal(II)-glycylglycine complex in aqueous solution. Previously we have studied the infrared spectra of D_2O solutions of the Cu(II) and Zn(II) complexes of glycylglycine and have derived the following conclusions on their structures.[3] (a) In the Cu(II) complex formed in the pD range between 3 and 5 the metal-ligand bonding occurs through the amino nitrogen and peptide oxygen (Structure A-1 of Fig. 2). (b) As pD is increased further, the structure of the Cu(II) complex changes into a form in which the metal-ligand bonding occurs through the amino nitrogen, peptide nitrogen (deprotonated), and carboxyl oxygen (Structure B of Fig. 2). (c) In contrast to the Cu(II) complex, the Zn(II) complex is formed for pD>5. Its structure is similar to the Cu(II) complex formed for 3<pD<5, the metal-ligand bonding ocurring through the amino nitrogen and peptide oxygen (Structure A-1 and/or A-2 of Fig. 2). A correlation between the rate and the complex structure is then obvious; *i.e.*, the hydrolysis occurs through the complex in which the peptide oxygen is coordinated to the metal ion (Structure A-1 and/or A-2). This suggests that the mechanism of hydrolysis might be described as follows. Due to the coordination of peptide oxygen to the metal ion, the double bond character of peptide C=O decreases. Although the bond order of peptide C–N increases somewhat at the same time,[3] the net effect of coordination results in the decrease of electron density around the peptide carbon atom. The electron-deficient carbon atom is susceptible to nucleophilic attack of the water molecule which will induce the scission of peptide bond. On the contrary, the electron density around the peptide carbon atom of Structure B would not be reduced (in comparison with free glycylglycine) due to the presence of negative charge on the nitrogen atom. Accordingly, the complex with Structure B is not as susceptible to nucleophilic attack of the water molecule.

It is interesting to compare our results with the peptidase activity of carboxypeptidase A (CPA).[8] Native CPA which has Zn(II) at its active site shows a bell-shaped pH-rate profile with maximum at pH 7.5. It is established that the peptide oxygen of the substrate molecule is coordinated to Zn(II) in the enzyme-substrate complex. If Zn(II) is replaced by Cu(II) (CuCPA), the enzymatic activities are lost. Our present results seem to suggest that a complex analogous to Structure B is formed between CuCPA and the substrate peptide. It is not surprising that this type of complex is inactive to hydrolysis. Although much more studies are needed, the investigation of the properties of metal-substrate complexes may supply useful information in delineating fundamental aspects of metalloenzyme activities.

References

1) L. Meriwether and F. H. Westheimer, *J. Amer. Chem. Soc.*, **78**, 5119 (1956).

2) I. J. Grant and R. W. Hay, *Aust. J. Chem.*, **18**, 1189 (1965).

3) M. Tasumi, S. Takahashi, T. Nakata, and T. Miyazawa, This Bulletin, **48**, 1595 (1975).

4) Doubly deprotonated glycylglycine is abbreviated as GG.

5) M. L. Bair and E. M. Larsen, *J. Amer. Chem. Soc.*, **93**, 1140 (1971).

6) D. L. Stalling, C. W. Gehrke, and R. W. Zumwalt, *Biochem. Biophys. Res. Commun.*, **31**, 616 (1968).

7) K. Bergström, J. Gurtler, and R. Blomstrand, *Anal. Biochem.*, **34**, 74 (1970).

8) F. A. Quiocho and W. N. Lipscomb, *Advan. Protein Chem.*, **25**, 1 (1971).

Sum Rule Consideration of Molecular Photoelectron Spectra. Substituted Ethylenes

Tomoko YAMAZAKI and Katsumi KIMURA

Physical Chemistry Laboratory, Institute of Applied Electricity, Hokkaido University, Sapporo 060

(Received February 24, 1975)

The ionization-energy sum rule previously proposed has been applied to photoelectron spectra of three series of chloro-, bromo-, and methyl-substituted ethylenes $C_2H_{4-m}X_m$ ($m=1$ and 2; X=Cl, Br, and CH_3) in the He(I) region. The total sums of ionization energies were obtained in the p-type region and the partial sums of ionization energies were interpreted in terms of in-plane and out-of-plane molecular orbitals. The following conclusions have been deduced: (1) The experimental total and partial sums are almost constant in the *cis*-, *trans*-, and *iso*-di-substituted ethylenes. (2) The experimental total and partial sums linearly increase with increasing number of the substituents, the slopes leading to useful informations about orbital energies. (3) Such linear relationships are supported by CNDO/2 and MINDO/2 calculations. (4) The experimental total and partial sums are approximately reproduced in terms of several appropriate localized-molecular-orbital energies based on the photoelectron data of simplest molecules.

Molecular photoelectron spectroscopy provides a variety of vertical ionization energies associated with valence molecular orbitals.[1] Total and partial sums of vertical ionization energies in the He(I) region in various alkyl halides,[2-4] alcohols and amines[5] have previously been interpreted by Kimura *et al.* in terms of empirical energy values of appropriate p-type localized molecular orbitals (LO's) under Koopmans' theorem. A similar sum rule consideration has also been applied to ionization energies associated with out-of-plane orbitals in many planar skeletal unsaturated compounds,[6] and further extended to the He(II) region including all the valence molecular orbitals in mono-, di-, and tri-methylamine.[7] These sum rule considerations of ionization energies have been found to be very helpful for interpreting molecular photoelectron spectra.[2-8]

In the present paper we wish to report an application of the sum rule to chloro-, bromo-, and methyl-substituted ethylenes in the He(I) region, placing special emphasis on the total sum of ionization energies over all the p-type LO's and on the partial sums of ionization energies corresponding to the in-plane and out-of-plane LO's.

Photoelectron spectroscopy studies of substituted ethylenes have so far been carried out by many other workers.[1,9-16] The resulting photoelectron spectra, vertical ionization energies, and orbital assignments have been published in considerable detail. In the present sum rule consideration therefore we use the available complete sets of ionization energies.

Sum Rule Consideration

In the present work we consider all the p-type LO's in the substituted ethylenes $C_2H_{4-m}X_m$ ($m=1$ and 2; X=Cl, Br, and CH_3). As previously done,[2-8] the p-type LO's used are: (1) nonbonding orbitals, n_{Cl} and n_{Br}; (2) bonding orbitals, $\pi_{C=C}$, σ_{C-Cl}, σ_{C-Br}, σ_{C-C}, and $\sigma_{C=C}$; and (3) the pseudo π orbitals of the methyl and methylene groups, π_{CH_3} and π_{CH_2}. The numbers of p-type LO's in the substituted ethylenes studied are

Table 1. Numbers of *p*-type LO's in $C_2H_{4-m}X_m$

Number of subst. (m)	In-plane (a′)				Out-of-plane (a″)		Total number of LO's
	$\sigma_{C=C}$	π_{CH_2}	n_X[a]	σ_{C-X}[a]	$\pi_{C=C}$	n_X[a]	
0	1	2			1		4
1	1	1	1	1	1	1	6
2 {*cis*, *trans*}	1		2	2	1	2	8

a) When X is the methyl group, n_X and σ_{C-X} represent π_{CH_3} and σ_{C-C} respectively.

Table 2. Vertical ionization energies (I_l) in the p-type region

	I_1	I_2	I_3	I_4	I_5	I_6	I_7	I_8
C_2H_4[a]	10.51	12.85	14.66	15.87				
C_2H_3Cl[b]	10.18	11.87	13.14	(13.6)	15.39	16.31		
cis-$C_2H_2Cl_2$[b]	9.83	11.85	12.09	12.51	13.72	(14.1)	15.66	16.72
trans-$C_2H_2Cl_2$[b]	9.81	11.86	11.93	12.61	13.85	14.20	16.23	16.23
iso-$C_2H_2Cl_2$[b]	10.00	11.67	12.17	12.51	(13.7)	14.24	16.27	16.27
C_2H_3Br[c]	9.87	10.87	12.30	12.93	15.05	16.07		
cis-$C_2H_2Br_2$[c]	9.63	10.74	11.23	11.53	12.86	(13.2)	14.83	16.35
trans-$C_2H_2Br_2$[c]	9.55	11.04	11.04	11.57	12.90	(13.3)	15.50	15.50
iso-$C_2H_2Br_2$[c]	9.78	10.73	11.23	11.60	(13.0)	(13.0)	15.20	15.90
$C_2H_3(CH_3)$[d]	10.03	12.31	13.23	14.48	(14.8)	15.90		
cis-$C_2H_2(CH_3)_2$[d]	9.36	11.65	12.76	(13.7)	14.15	(14.4)	(15.2)	16.20
trans-$C_2H_2(CH_3)_2$[d]	9.37	11.96	12.79	(13.2)	(14.5)	15.17	15.17	(15.6)
iso-$C_2H_2(CH_3)_2$[d]	9.45	11.81	12.90	(13.2)	(13.8)	15.03	(15.3)	(15.7)

a) Ref. 11. b) Ref. 9. c) Ref. 14. d) Ref. 6.

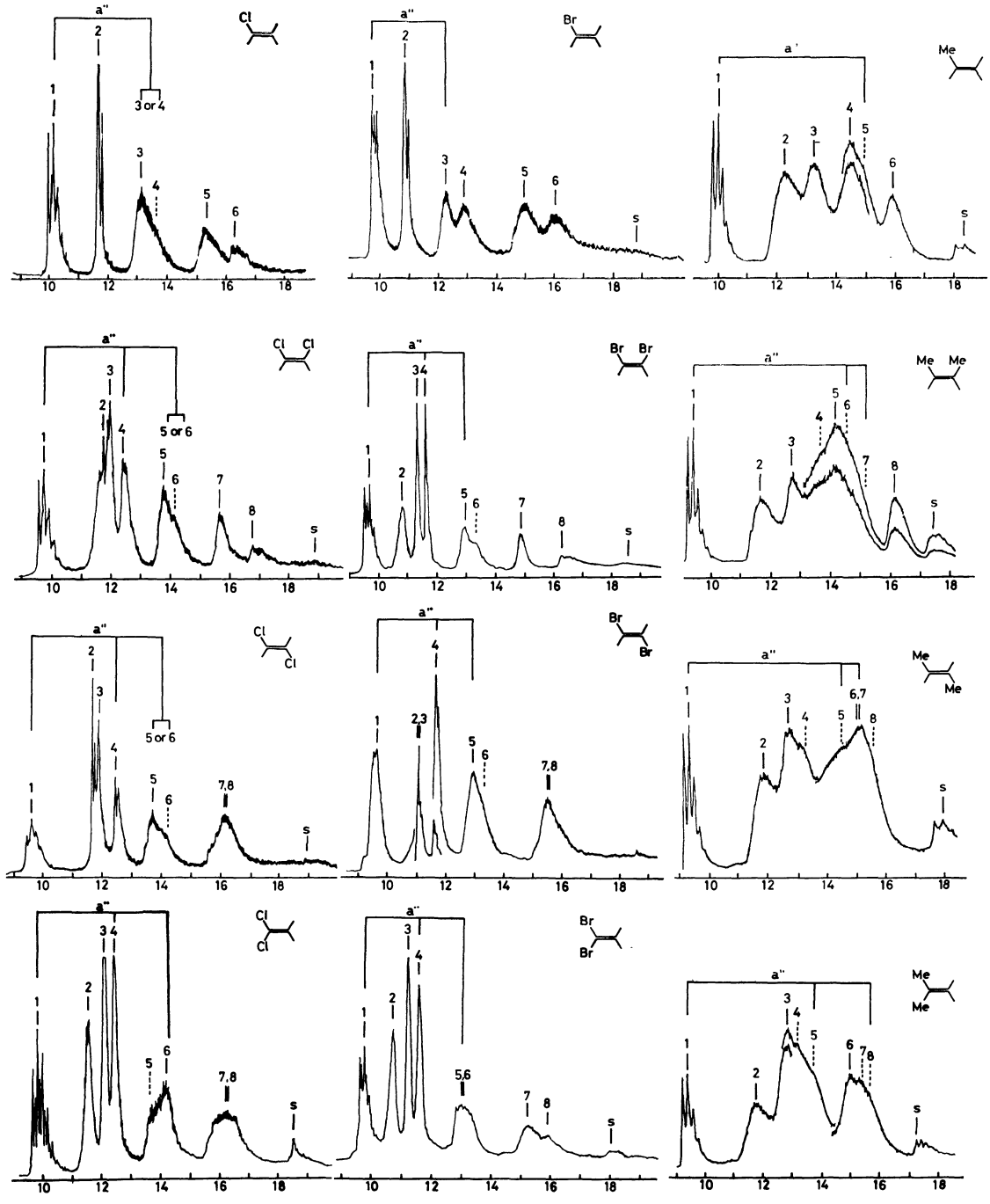

Fig. 1. Numbering of *p*-type ionization bands in He(I) photoelectron spectra of chloro-, bromo-, and methyl-substituted ethylenes.
The spectra of the chloro- and bromo-ethylenes are those reported by Wittel and Bock (Ref. 14) and the spectra of the methyl-substituted ethylenes are those reported previously by Kimura *et al.* (Ref. 6).
Out-of-plane bands are represented by a″ and s-type bands are by letters.

summarized in Table 1, indicating four, six, and eight p-type LO's in the un-, mono-, and di-substituted ethylenes, respectively. The present authors have previously indicated from several studies of alkyl compounds that all the photoelectron bands associated with p-type LO's lie below about 17—18 eV.[2-8] In order to show the numbering of the individual ionization bands, we illustrate the photoelectron spectra taken from the literatures in Fig. 1. The spectra of the series of chloro- and bromo-ethylenes in Fig. 1 are those from the paper of Wittel and Bock,[14] slightly modified in the numbering of the bands. The Wittel-Bock I_7 bands in *trans*- and *iso*-dichloroethylene and *trans*-dibromoethylene are designated as I_7 and I_8 in Fig. 1. The same numbers of ionization bands as those of p-type LO's can be recognized in the available photoelectron spectra in the region below about 17 eV in Fig. 1.

The vertical ionization energies used in the sum rule treatments are summarized in Table 2, in which the data for the chloro-, bromo-, and methyl-substituted ethylenes are those reported by Lake and Thompson,[9] by Wittel and Bock,[14] and by the present authors,[6] respectively. The values for I_8 in *trans*- and *iso*-dichloroethylene are set equal to those for I_7. The values in parentheses correspond to the shoulders which are indicated by vertical broken lines in Fig. 1.

Experimental Total and Partial Sums. The total sums of vertical ionization energies are taken over all the p-type region by

TABLE 3. EXPERIMENTAL TOTAL AND PARTIAL SUMS, COMPARED WITH CALCULATED ONES
(Values are shown in eV units and rounded to the next nearest 0.1 eV except for ethylene.)

(LO's) → (Corresponding I_1's)	Calcd.	Expt.
CH_2=CH_2	T = −53.89	−53.89[a]
a′ ($2\pi_{CH_2}$, $\sigma_{C=C}$)→(I_2,I_3,I_4)	P' = −43.38	−43.38[a]
a″(π_{CC})→(I_1)	P''= −10.51	−10.51[a]
CHCl=CH_2	T = −80.3	−80.5
a′ (n_{Cl}, π_{CH_2}, σ_{CCl}, $\sigma_{C=C}$)→(I_2,I_3,I_5,I_6)[b]	P' = −56.8	−56.7
→(I_2,I_4,I_5,I_6)[c,d]		−57.2
a″(π_{CC}, n_{Cl})→(I_1,I_4)[b]	P''= −23.6	−23.8
→(I_1,I_3)[c,d]		−23.3
cis-CHCl=CHCl	T = −106.8	−106.5
a′ ($2n_{Cl}$, $2\sigma_{CCl}$, $\sigma_{C=C}$)→(I_2,I_3,I_5,I_7,I_8)[b,d]	P' = −70.2	−70.0
→(I_2,I_3,I_6,I_7,I_8)[c]		−70.4
a″(π_{CC}, $2n_{Cl}$)→(I_1,I_4,I_6)[b,d]	P''= −36.6	−36.4
→(I_1,I_4,I_5)[c]		−36.1
trans-CHCl=CHCl	T = −106.8	−106.7
a′ ($2n_{Cl}$, $2\sigma_{CCl}$, $\sigma_{C=C}$)→(I_2,I_3,I_5,I_7,I_8)[b,d]	P' = −70.2	−70.1
→(I_2,I_3,I_6,I_7,I_8)[c]		−70.5
a″(π_{CC}, $2n_{Cl}$)→(I_1,I_4,I_6)[b,d]	P''= −36.6	−36.6
→(I_1,I_4,I_5)[c]		−36.3
CCl_2=CH_2	T = −106.4	−106.8
a′ ($2n_{Cl}$, π_{CH_2}, σ_{CCl}, $\sigma_{C=C}$)→(I_2,I_3,I_5,I_7,I_8)[b,c,d]	P' = −69.8	−70.1
a″(π_{CC}, $2n_{Cl}$)→(I_1,I_4,I_6)[b,c,d]	P''= −36.6	−36.8
CHBr=CH_2	T = −77.1	−77.1
a′ (n_{Br}, σ_{CBr}, π_{CH_2}, $\sigma_{C=C}$)→(I_2,I_4,I_5,I_6)[c,e]	P' = −54.7	−54.9
a″(π_{CC}, n_{Br})→(I_1,I_3)[c,e]	P''= −22.4	−22.2
cis-CHBr=CHBr	T = −100.4	−100.4
a′ ($2n_{Br}$, $2\sigma_{CBr}$, $\sigma_{C=C}$)→(I_2,I_3,I_6,I_7,I_8)[c]	P' = −66.1	−66.4
→(I_2,I_4,I_5,I_7,I_8)[e]		−66.3
a″(π_{CC}, $2n_{Br}$)→(I_1,I_4,I_5)[c]	P''= −34.3	−34.0
→(I_1,I_3,I_6)[e]		−34.1
trans-CHBr=CHBr	T = −100.4	−100.4
a′ ($2n_{Br}$, $2\sigma_{CBr}$, $\sigma_{C=C}$)→(I_2,I_3,I_6,I_7,I_8)[c]	P' = −66.1	−66.4
→(I_2,I_4,I_5,I_7,I_8)[e]		−66.5
a″(π_{CC}, $2n_{Br}$)→(I_1,I_4,I_5)[c]	P''= −34.3	−34.0
→(I_1,I_3,I_6)[e]		−33.9
CBr_2=CH_2	T = −100.1	−100.4
a′ ($2n_{Br}$, π_{CH_2}, $2\sigma_{CBr}$)→(I_2,I_3,I_6,I_7,I_8)[c]	P' = −65.8	−66.1
a″(π_{CC}, $2n_{Br}$)→(I_1,I_4,I_5)[c]	P''= −34.3	−34.4
CH(CH_3)=CH_2	T = −80.7	−80.8
a′ (σ_{C-C}, π_{CH_3}, π_{CH_2}, $\sigma_{C=C}$)→(I_2,I_3,I_4,I_6)[f,g,h]	P' = −55.9	−55.9
a″(π_{CC}, π_{CH_3})→(I_1,I_5)[f,g,h]	P''= −24.8	−24.8
cis-CH(CH_3)=CH(CH_3)	T = −107.5	−107.4
a′ ($2\sigma_{C-C}$, $2\pi_{CH_3}$ $\sigma_{C=C}$)→(I_2,I_3,I_4,I_5,I_8)[f,g,h]	P' = −68.4	−68.5
a″(π_{CC}, $2\pi_{CH_3}$)→(I_1,I_6,I_7)[f,g,h]	P''= −39.1	−39.0
trans-CH(CH_3)=CH(CH_3)	T = −107.5	−107.8
a′ ($2\sigma_{C-C}$, $2\pi_{CH_3}$, $\sigma_{C=C}$)→(I_2,I_3,I_4,$I_{7(6)}$,I_8)[g,h]	P' = −68.4	−68.7
a″(π_{CC}, $2\pi_{CH_3}$)→(I_1,I_5,$I_{6(7)}$)[g,h]	P''= −39.1	−39.0
$C(CH_3)_2$=CH_2	T = −107.2	−107.2
a′ ($2\sigma_{C-C}$, $2\pi_{CH_3}$, π_{CH_2})→(I_2,I_3,I_4,I_6,I_7)[f,g,h]	P' = −68.1	−68.2
a″(π_{CC}, $2\pi_{CH_3}$)→(I_1,I_5,I_8)[f,g,h]	P''= −39.1	−39.0

a) Data in Ref. 11 were used. b) Klasson and Manne (Ref. 18). c) Wittel and Bock (Ref. 14). d) Kato *et al.* (Ref. 17). e) Chadwick *et al.* (Ref. 12). f) The present MINDO/2 calculations. g) Katrib and Rabalais (Ref. 13). h) White *et al.* (Ref. 16).

Table 4. Average α values (in eV) obtained with the experimental total and partial sums

Series		α	α'	α''
$C_2H_{4-m}Cl_m$	(m=0—2)	−26.44±0.07	−13.34±0.01	−13.11±0.06
$C_2H_{4-m}Br_m$	(m=0—2)	−23.24±0.01	−11.48±0.04	−11.78±0.06
$C_2H_{4-m}(CH_3)_m$	(m=0—2)	−26.82±0.06	−12.54±0.05	−14.26±0.01

$$T_{expt} = -\sum_{i}^{all} I_i \quad (1)$$

and the experimental partial sums associated with the in-plane and out-of-plane LO's, P' and P'', respectively, are obtained by

$$P'_{expt} = -\sum_{i}^{a'} I_i \text{ and } P''_{expt} = -\sum_{i}^{a''} I_i \quad (2)$$

which are based on the available symmetry assignments. The results of the experimetal total and partial sums obtained by Eqs. (1) and (2) are summarized in Table 3. Since different kinds of orbital assignments have been proposed for the chloro- and bromo-ethylenes,[12,14,17,18] we took two kinds of possible combinations of I_i into account in the partial sums as shown in Table 3.

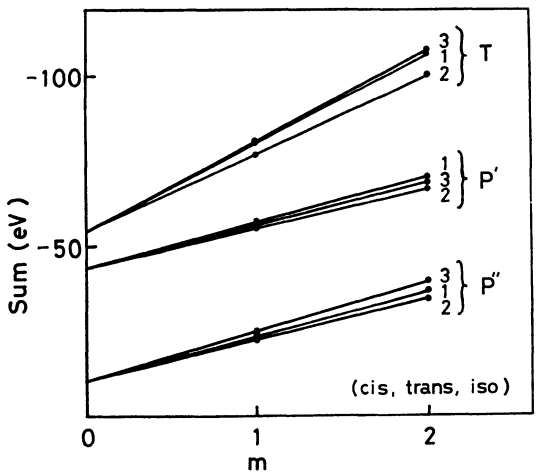

Fig. 2. Plot of the experimental total and partial sums of vertical ionization energies against the number of substituents in series of (1) chloro-, (2) bromo-, and (3) methyl-substituted ethylenes.

In Fig. 2 the experimental values for T, P', and P'' are plotted against the number (m) of substituents, indicating excellent linear relationships. The straight lines (solid lines) in Fig. 2 are drawn so as to fit the experimental data. The slope of the straight lines represents the variation of the total and partial sums with increasing number of substituents.

Calculated Total and Partial Sums. As shown previously,[2-8] the total and partial sums in the substituted ethylenes may be expressed in terms of empirical LO energies as follows,

$$T_{calc} = P'_{calc} + P''_{calc} \quad (3)$$

$$P'_{calc} = m\varepsilon_{n(X)} + m\varepsilon_{\sigma(C-X)} + (2-m)\varepsilon_{\pi(CH_2)} + \varepsilon_{\sigma(C=C)} \quad (4)$$

$$P''_{calc} = m\varepsilon_{n(X)} + \varepsilon_{\pi(C=C)} \quad (5)$$

When X is the methyl group, n(X) and σ(C-X) in Eqs. (4) and (5) represent $\pi(CH_3)$ and σ(C–C), respectively. From Eqs. (4) and (5), therefore the successive differences α' and α'' in the partial sums may be expressed as follows

$$\alpha' = \varepsilon_{n(X)} + \varepsilon_{\sigma(C-X)} - \varepsilon_{\pi(CH_2)} \quad (6)$$

$$\alpha'' = \varepsilon_{n(X)} \quad (7)$$

On the other hand, the successive differences in T, P', and P'' may be experimentally obtained from the slopes of the straight lines shown in Fig. 2. The resulting average values for α, α', and α'' are summarized in Table 4, the upper combination of I_i being used in the case in which two possible combinations of I_i are shown in Table 3.

Table 5. Empirical energies of p-type LO's (in eV)

a′ (in-plane)			
n_{Cl}= −13.05	n_{Br}= −11.89	π_{CH_3}= −14.30	π_{CH_2}= −14.36
σ_{C-Cl}= −14.70	σ_{C-Br}= −13.82	σ_{C-C}= −12.58	$\sigma_{C=C}$= −14.66
a″ (out-of-plane)			
n_{Cl}= −13.05	n_{Br}= −11.89	π_{CH_3}= −14.30	$\pi_{C=C}$= −10.51

The values for ε's used in the sum rule treatments are summarized in Table 5, which were selected on the basis of the vertical ionization energies of simple molecules as follows. The energies of n(Cl) and n(Br) were taken from the mean values of the first and second ionization energies of molecular chlorine and bromine, respectively.[19] The energies of π(C=C) and σ(C=C) were taken from the first and third ionization energies of ethylene, respectively.[11] The energy of $\pi(CH_2)$ was taken from the mean value of the second and fourth ionization energies of ethylene.[11] The energy of $\pi(CH_3)$ was determined from the ionization energies of methyl halides as described previously.[2] The energies of σ(C–Cl), σ(C–Br), and σ(C–C) were deduced by Eq. (6) from the experimental α' values shown in Table 4.

With all these energy parameters the total sums (T) and the in-plane and out-of-plane partial sums (P' and P'') were calculated by Eqs. (3)—(5), the results being compared with the experimental results in Table 3.

Discussion

The following three points may be pointed out on the experimental total and partial sums. (1) Good linear relationships can be seen between the sums (T, P', and P'') and the number of substituents. (2) The total and partial sums of the *cis*-, *trans*-, and *iso*-isomers in each series are very close to one another. (3) The effects of the chloro-, bromo-, and methyl-substitutions on the total and partial sums are very similar, as seen from Fig. 2.

Previously,[8] a good linearity was indicated between such total sums and the number of chlorine atoms in a

series of chloroethanes $C_2H_{6-m}Cl_m$ ($m=0$—6), and a value of -14.90 eV was deduced for σ(C–Cl), differing slightly from the value of -14.70 eV found here in the chloroethylenes. In the present work, the linearities have been found not only for the total sums but also for the partial sums.

From Eq. (7) it is seen that the successive difference α'' is equivalent to $\varepsilon_{n(X)}$, so that the α'' values of -13.11, -11.78 and -14.26 eV in Table 4 may be regarded as the orbital energies for n(Cl), n(Br), and $\pi(CH_3)$, respectively. It is interesting to note that these values are very close to those given in Table 5 which were determined from the photoelectron data of the simple molecules.

In the previous study of alkyl alcohols and amines (ROH and RNH_2; R = methyl to *n*-butyl),[5] we obtained an average difference of -26.04 eV in the total sums for the successive substitution of the CH_3 group. A similar value $\alpha_{av.}=-26.07$ eV was obtained in a series of alkyl halides (RX: R=methyl to *n*-butyl; X=Cl, Br, and I).[2] Furthermore, using available ionization energies of several alkanes (methane, ethane, propane, isobutane, and neopentane),[20] we may obtain a value of $\alpha_{av.}=-26.0$ eV. In these saturated alkyl compounds, therefore, the differences in T by the successive CH_3 substitutions are found to be -26.0——-26.1 eV, close to the sum of -11.75 eV and -14.30 eV which have previously been proposed for σ_{C-C} (in alkyl compounds) and π_{CH_2}, respectively.[2-5] For the methyl-substituted ethylenes studied here, however, we obtained a value of $\alpha_{av.}=-26.82$ eV which leads to a value of -12.58 eV for σ_{C-C} involving the sp^2 carbon as given in Table 5.

The α value of -26.44 eV in the series of chloroethylenes is fairly close to that (-26.69 eV) previously obtained in a series of chloroethanes.[8] The energies of -14.70 and -13.82 eV deduced for σ_{C-Cl} and σ_{C-Br}, respectively, in the present work are fairly close to those (-14.45 and -13.52 eV, respectively) previously estimated from the second ionization energies of methyl chloride and bromide, respectively.[2] As seen from Eq. (7), the α'' values of -13.11, -11.78, and -14.26 eV in Table 4 are equivalent to $\varepsilon_{n(Cl)}$, $\varepsilon_{n(Br)}$, and $\varepsilon_{\pi(CH_3)}$, respectively, in excellent agreement with those (-13.05, -11.89, and -14.30 eV, respectively) determined from the simple molecules.

From the present study it has been found that the experimental total and partial sums of the *iso*-isomers are almost the same as those of the *cis*- and *trans*-isomers. Equation (4) however does not hold for the *iso*-compounds. One of three LO's associated with the carbon sp^2 orbitals in the CCl_2 group in 1,1-dichloroethylene should be of s-type. In calculating P', therefore, one of the three in-plane p-type LO's (two σ(C–Cl) and one σ(C=C)) should be removed as an s-type LO. It is not unambiguous however to decide which one is of s-type. As shown in the combinations of LO's in Table 3, we removed one σ(C–Cl) in 1,1-dichloroethylene and σ(C=C) in 1,1-dibromoethylene and isobutene. The numbers of in-plane p-type LO's in the *iso*-isomers are of course the same as those in the *cis*- and *trans*-isomers.

Only the ionization energy data shown in Table 2 were used in the present sum rule considerations. Other complete sets of ionization energies reported for the chloroethylenes by Jonathan *et al.*[10] and Wittel and Bock[14] and for the bromoethylenes by Chadwick *et al.*[12] were also employed, and it was found that essentially the same results as above on the total and partial sums may be obtained.

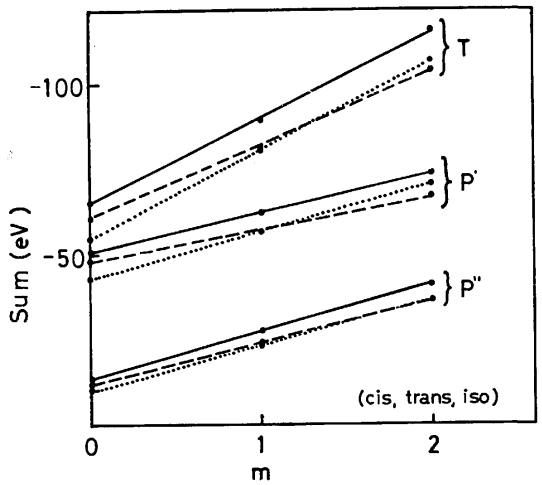

Fig. 3. Plot of theoretical total and partial sums obtained by CNDO/2 method against the number of chlorine atoms in a series of chloroethylenes.
The results multiplied by 0.85 (solid lines) and the results of the 4-eV correction (broken lines) are compared with the experimental ones (dotted lines).

In the present work we also investigated the relationship between the total (and partial) sums and the number of substituents using CNDO/2 method[21] and MINDO/2 method[22] under the Koopmans' theorem. The CNDO/2 results of T, P', and P'' for the series of chloroethylenes are plotted against the number of chlorine atoms in Fig. 3, the solid lines indicating the results multiplied by 0.85. The broken lines in Fig. 3 show the results reduced by 4 eV in each orbital. It is interesting to note in Fig. 3 that good linear relationships between the sum and the number of chlorine

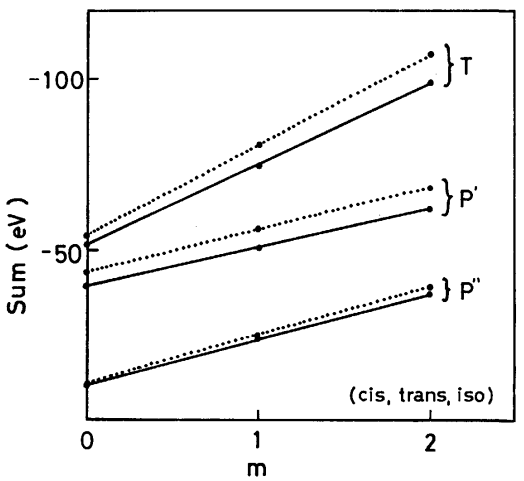

Fig. 4. Plot of theoretical total and partial sums obtained by MINDO/2 method against the number of CH_3 groups in a series of methyl-substituted ethylenes.
Dotted lines represent the experimental results.

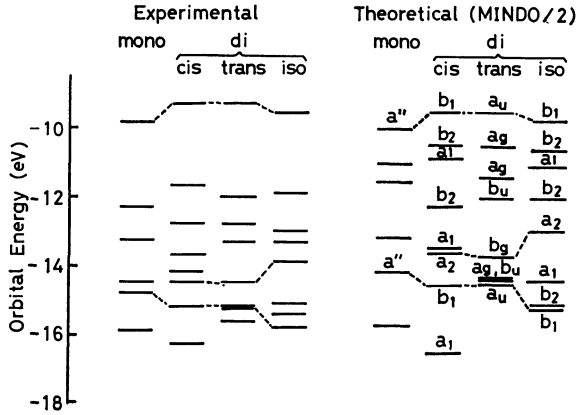

Fig. 5. Experimental and theoretical orbital level diagrams of the methyl-substituted ethylenes.

atoms can be seen and that the calculated results multiplied by 0.85 are approximately parallel to the experimental lines (dotted lines). The MINDO/2 results of T, P', and P'' for the methyl-substituted ethylenes are shown in Fig. 4, again indicating good linearities and parallelisms between calculation and experiment. The linearities between the partial sums and the number of substituents have been found for the first time in the present work.

Theoretical orbital energy diagrams obtained by the MINDO/2 method for the methyl-substituted ethylenes are shown in Fig. 5, compared with those of the experimental diagrams. The out-of-plane levels in Fig. 5 are connected by broken lines. As can be seen from Fig. 5, it may be pointed out that the variation of the out-of-plane levels in going from ethylene to *iso*-butylene is well reproduced by the MINDO/2 calculations.

Finally, the following point should be mentioned in connection with Koopmans' theorem. Koopmans' theorem has been assumed in the present orbital energy considerations using the experimental ionization energies. However, if we consider each empirical value in Table 5 (without the negative sign) as a hypothetical ionization energy of an electron from the original unperturbed p-type LO, the present sum rule consideration may be thought as an "additivity rule of ionization energy." In such a standpoint, Koopmans' theorem is unnecessary. Potts *et al.*[23] have indicated that the total sums of ionization energies associated with s- and p-type photoelectron bands in many aliphatic compounds may be reproduced in terms of atomic energy parameters on the basis of an idea of additivity rule. Most striking difference between the present sum rule consideration and the additivity rule consideration of Potts *et al.*[23] is that the former depends on the LO's whose energies are based on the molecular photoelectron spectra of simplest molecules, whereas the latter depends on the atomic parameters.

References

1) D. W. Turner, A. D. Baker, C. Baker, and C. R. Brundle, "Molecular Photoelectron Spectroscopy," Wiley-Intersciences, London, 1970.
2) K. Kimura, S. Katsumata, Y. Achiba, H. Matsumoto, and S. Nagakura, This Bulletin, **46**, 373 (1973). This study is briefly described in *Disc. Faraday Soc.*, **54**, 140 (1972).
3) T. Yamazaki, S. Katsumata, and K. Kimura, *J. Electron Spectrosc.*, **2**, 335 (1973).
4) S. Katsumata and K. Kimura, This Bulletin, **46**, 1342 (1973).
5) S. Katsumata, T. Iwai, and K. Kimura, *ibid.*, **46**, 3391 (1973).
6) K. Kimura, S. Katsumata, T. Yamazaki, and H. Wakabayashi, *J. Electron Spectrosc.*, **6**, 41 (1975).
7) K. Kimura and K. Osafune, *Mol. Phys.*, **29**, 1073 (1975).
8) S. Katsumata and K. Kimura, *J. Electron Spectrosc.*, **6**, 309 (1975).
9) R. F. Lake and H. Thompson, *Proc. Roy. Soc. Ser. A*, **315**, 323 (1970).
10) N. Jonathan, K. Ross, and V. Tomlinson, *Int. J. Mass Spectrom. Ion Phys.*, **4**, 41 (1970).
11) C. R. Brundle, M. B. Robin, N. A. Kuebler, and H. Basch, *J. Amer. Chem. Soc.*, **94**, 1451 (1972).
12) D. Chadwick, D. C. Frost, A. Katrib, C. A. McDowell, and R. A. N. McLean, *Can. J. Chem.*, **50**, 2642 (1972).
13) A. Katrib and J. W. Rabalais, *J. Phys. Chem.*, **77**, 2358 (1973).
14) K. Wittel and H. Bock, *Chem. Ber.*, **107**, 317 (1974).
15) E. Haselbach and E. Heilbronner, *Helv. Chim. Acta*, **53**, 684 (1970); U. Weidner and A. Schweig, *J. Organometal. Chem.*, **39**, 261 (1972).
16) R. M. White, T. A. Carlson, and D. P. Spears, *J. Electron Spectrosc.*, **3**, 59 (1974).
17) H. Kato, K. Hirao, H. Konishi, and T. Yonezawa, This Bulletin, **44**, 2062 (1971).
18) M. Klasson and R. Manne, "Electron Spectroscopy," ed. by D. A. Shirley, North-Holland Publishing Company, Amsterdam and London (1972), p. 471.
19) A. B. Cornford, D. C. Frost, C. A. McDowell, J. L. Ragle, and I. A. Stenhouse, *J. Chem. Phys.*, **54**, 2651 (1971).
20) J. N. Murrell and W. Schmidt, *J. Chem. Soc., Faraday Trans.* II, **68**, 1709 (1972).
21) J. A. Pople, D. P. Santry, and G. A. Segal, *J. Chem. Phys.*, **43**, S129 (1965).
22) M. J. S. Dewar and D. H. Lo, *J. Amer. Chem. Soc.*, **94**, 5296 (1972).
23) A. W. Potts, T. A. Williams, and W. C. Price, *Discuss. Faraday Soc.*, **54**, 104 (1972).

The Thermal Changes in Gels of the SiO_2–Al_2O_3–In_2O_3–H_2O System

Mitsuhiro KASAI, Yoshiyuki KUDO, and Shuichi HAMADA

Department of Chemistry, Faculty of Science, Science University of Tokyo, Kagurazaka, Shinjuku-ku, Tokyo 162

(Received March 7, 1974)

The synthesized coprecipitated gels in the SiO_2–Al_2O_3–In_2O_3–H_2O system showed an allophane-like pattern in the DTA except for the indium-rich gels. The exothermic peak temperature in the DTA was lowered from 980 to 940 °C with an increase in the indium content, while that on mixed gels was scarcely lowered at all. A new small exothermic peak around 880 °C in the DTA was observed in the coprecipitated gels with more than 11.93 wt% of In_2O_3; it was considered to be due to the structural change in the gels which arose from the formation of the indium (III) oxide. The firing products of the coprecipitated gels were identified as mullite, indium (III) oxide, and indium (III) silicate. The mullite formed in the coprecipitated gels included indium ions at 900 °C, accompanied by an increase in its unit cell volume, while the indium ions were almost entirely removed from the mullite lattice at 1200 °C.

The thermal properties of coprecipitated gels, the SiO_2–Al_2O_3–Fe_2O_3–H_2O[1] and the SiO_2–Al_2O_3–Ga_2O_3–H_2O[2] systems, have been studied. It has been found that aluminum ions are replaced by iron (III) or gallium ions in the allophane structure of the coprecipitated gels. The thermal properties of the gels in the SiO_2–Al_2O_3–In_2O_3–H_2O system have not been studied, while phase diagrams of the In_2O_3–Al_2O_3[3] and the In_2O_3–Ga_2O_3[4] systems have been reported.

In this work, the thermal properties of the coprecipitated gels in the SiO_2–Al_2O_3–In_2O_3–H_2O system were studied in order to determine the role of trivalent cations in a silicoalumina-gel structure.

Experimental

Materials. The samples were prepared by means of a method similar to that described in previous papers:[1,2] indium-coprecipitated gels were obtained by boiling mixed solutions of aluminum sulfate, indium(III) sulfate, and sodium silicate at a pH of about 4.5, a pH value obtained by adding hexamethylenetetramine. The $In_2O_3/(Al_2O_3+In_2O_3)$ molar ratio in the mixed solutions was varied from zero to 1.0 at a constant molar ratio of 2.0 as $SiO_2/(Al_2O_3+In_2O_3)$. The gels thus coprecipitated were washed by decantation and then air-dried for three weeks. They were identified as amorphous from their X-ray powder diffractograms. The indium-mixed gels were prepared by mixing a synthesized allophane, free from indium, and an amorphous hydrated indium(III) oxide in order to compare the properties of the coprecipitated gels. The hydrated indium(III) oxide was prepared by using ammonia water at pH 4.0. The gel thus obtained was identified as amorphous from its X-ray powder diffractogram, though the gels obtained at pH 5.3 and 7.0 contained crystalline InOOH.[5-7]

Procedure. The contents of SiO_2, Al_2O_3, and $H_2O(\pm)$[8] in the samples were estimated gravimetrically, and that of In_2O_3,[9] polarographically.

The differential thermal analysis for the sample was carried out at the heating rate of 10 °C/min in the temperature range from room temperature to 1000 °C with a Rigaku Denki Thermoflex, model 8002, differential thermal analyzer.

The X-ray powder diffractogram of the sample was taken by using an X-ray diffractometer, model JDX-5P, from the Japan Electron Optics Laboratory Co. The sample, in a quartz tube, was heated at 800, 900, 1000, 1100, and 1200 °C for 5 hr, and at 1300 °C for 1 hr, in an electric furnace. The firing products were identified, and their relative amounts were estimated by using the diffraction peaks at (120) and (210) of the mullite, that at (101) of the cristobalite, and those at (222) and (400) of the indium (III) oxide. The unit-cell dimensions of the mullite and the indium (III) oxide, the firing products of the samples, were calculated by using the peaks at (121), (230), (400), (041), (331), and (002) of the mullite and those at (222), (400), and (440) of the indium (III) oxide. The diffraction angles were calibrated with those of silicon.

Results and Discussion

The chemical compositions of the indium-bearing gels are shown in Table 1. The molar ratios of $SiO_2/(Al_2O_3+In_2O_3)$ in the coprecipitated gels were smaller than those of $SiO_2/(Al_2O_3+Ga_2O_3)$ in the gallium-coprecipitated gels[2] obtained from the mixed solutions with the same molar ratio of 2.0, except for the In-12C sample. These small values of the molar ratios were considered to arise from the condition of a higher acidity for precipitation than that for the gallium-coprecipitated gels, or from the nature of the indium (III) ion.

The Differential Thermal Analysis of the Samples. The DTA patterns of the gels are shown in Fig. 1. The In-0 sample, free from indium, was identified as an allophane from its DTA pattern, attributable to allophane. The exothermic peak temperature was lowered from 980 to 940 °C as the indium content increased, except for the In-8C and -9C samples, in contrast to the small shift in the mixed gels. This peak was not observed in the gels with more than 38.22 wt% of In_2O_3 (the In-10C and -11C samples). The tendency of the peak temperature in the indium-coprecipitated gels to lower was considerably less than that in the gallium-coprecipitated gels.[2]

The apparent activation energy, E_a, for the exothermic change around 980 °C was estimated by means of the Kissinger equation.[10] The E_a values of the exothermic change in the coprecipitated gels decreased with an increase in the indium content, while those in the mixed gels were nearly equal to that in the In-0 sample, as is shown in Table 2.

A new, small, broad exothermic peak around 880 °C in the DTA was observed in only the coprecipitated gels with more than 11.93 wt% of In_2O_3 (from the In-3C to -12C samples); the mixed gels did not show it.

TABLE 1. CHEMICAL COMPOSITIONS OF INDIUM-BEARING SAMPLES

Samples	Chemical composition, wt%					Molar ratio	
	SiO_2	Al_2O_3	In_2O_3	H_2O (±)	Total	$\frac{SiO_2}{R_2O_3}$ [a]	$\frac{H_2O\ (\pm)}{R_2O_3}$ [a]
In-0[b]	25.75	29.73	0	45.28	100.76	1.47	8.63
In-1C[c]	25.30	28.41	3.82	42.88	100.41	1.44	8.14
In-2C	22.63	29.04	6.93	41.84	100.44	1.22	7.47
In-3C	23.09	23.77	11.93	40.84	99.63	1.38	8.18
In-4C	23.11	22.52	15.67	39.20	100.50	1.38	8.20
In-5C	21.89	21.44	19.46	37.61	100.40	1.29	7.38
In-6C	22.52	19.63	22.56	35.40	100.11	1.35	7.11
In-7C	19.61	20.36	24.93	34.63	99.53	1.11	6.57
In-8C	21.23	18.25	27.53	32.49	99.50	1.25	6.41
In-9C	21.03	14.13	34.03	30.38	99.57	1.32	6.35
In-10C	20.96	13.41	38.22	26.84	99.43	1.27	5.44
In-11C	16.82	6.91	50.85	24.91	99.49	1.09	4.41
In-12C	26.14	0	50.45	23.99	100.58	2.31	7.07
In-13M[c]	24.79	28.62	1.64	44.95	100.00[d]	1.44	8.71
In-14M	24.18	27.92	3.29	44.62	100.00[d]	1.41	8.67
In-15M	23.31	26.92	5.62	44.15	100.00[d]	1.36	8.61
In-16M	22.30	25.75	8.34	43.61	100.00[d]	1.31	8.54
In-17M	19.00	21.95	17.24	41.82	100.00[d]	1.13	8.31
In-18M	16.10	18.60	25.04	40.26	100.00[d]	0.97	8.10
In-19M	32.70	0	8.00	59.30	100.00[d]	4.09	7.41

a) $Al_2O_3+In_2O_3$. b) Allophane, free from indium. c) The postscripts "C" and "M" denote the coprecipitated and the mixed samples, respectively. d) Calculated.

TABLE 2. APPARENT ACTIVATION ENERGY FOR EXOTHERMIC CHANGE AROUND 980 °C

Sample	E_a, kcal/mol
In-0	250
In-1C	237
In-5C	196
In-14M	245

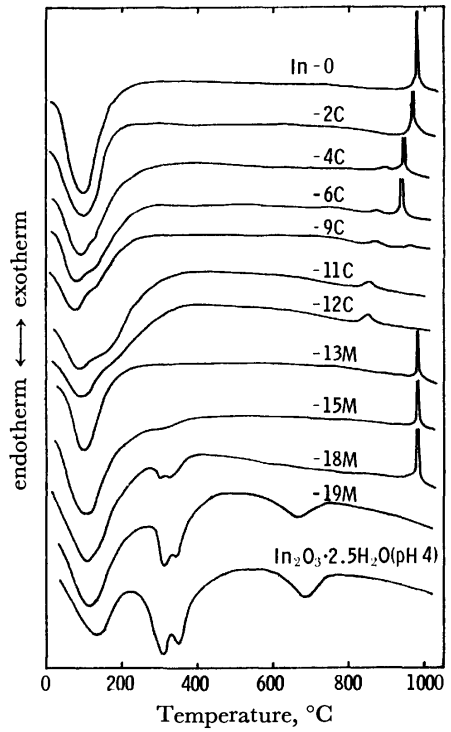

Fig. 1. DTA curves of indium-bearing samples.

This exothermic peak temperature was also lowered continuously with an increase in the indium content.

In the indium-rich mixed gels, the endothermic peaks based on the amorphous hydrated indium (III) oxide were observed besides the endo- and the exothermic peaks around 100 and 980 °C.

The Variation in the Firing Products in the Samples during the Heat Treatment. The crystalline phases formed

TABLE 3. FIRING PRODUCTS IN INDIUM-BEARING SAMPLES

Sample	Temperature, °C					
	800	900	1000	1100	1200	1300
In-0	A	M	M	M	M	M
In-1C	A	M	M	M, I	M, I, C, IS	
In-2C	A	M, I	M, I	M, I	M, I, IS	M, IS
In-3C	A	M, I	M, I	M, I	M, I, IS	M, IS
In-4C	A	M, I	M, I	M, I	M, I, IS	
In-5C	A	M, I	M, I	M, I	M, I, IS	
In-6C	I	M, I	M, I	M, I	M, I, IS	M, IS
In-7C	I	M, I	M, I	M, I, IS	M, I, IS	
In-8C	I	M, I	M, I	M, I, IS	M, I, IS	
In-9C	I	I	I	M, I, IS	M, I, IS	
In-10C	I	I	I	M, I, IS	M, I, IS	M, IS
In-11C	I	I	I	I, IS	I, IS	
In-12C	I	I	I	I	I	I
In-13M	I	M, I	M, I	M, I	M, I, IS	
In-14M	I	M, I	M, I	M, I	M, I, IS	
In-15M	I	M, I	M, I	M, I	M, I, IS	
In-16M	I	M, I	M, I	M, I	M, I, IS	
In-17M	I	M, I	M, I	M, I	M, I	
In-18M	I	M, I	M, I	M, I	M, I	
In-19M	I	I	I	I	I	

A: amorphous, M: mullite, I: indium (III) oxide, IS: indium (III) silicate (new phase), C: cristobalite.

in the samples heat-treated at 800, 900, 1000, 1100, and 1200 °C for 5 hr, and at 1300 °C for 1 hr were identified by X-ray powder diffractometry as mullite, indium (III) oxide, and a new phase, as Table 3 shows.

The indium (III) oxide formed below 1000 °C in the coprecipitated gels with more than 11.93 wt% of In_2O_3 (from the In-3C to -11C samples) showed broad X-ray powder diffraction peaks; their spacings were smaller than those of the indium (III) oxide with the usual unit-cell dimensions.[11] This contraction of the crystal lattice was considered to arise from the replacement with aluminum ions.

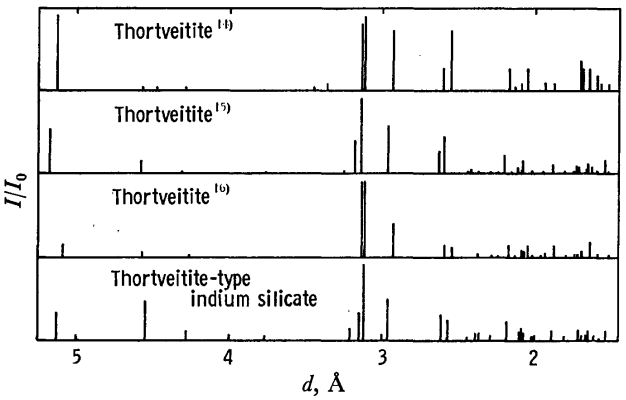

Fig. 2. X-ray powder diffraction patterns of thortveitite and thortveitite-type indium silicate.

New X-ray diffraction peaks were observed in the firing products above 1100 or 1200 °C of the indium-bearing gels, except for those of the In-17M and -18M samples, and the aluminum-free samples. This X-ray diffraction pattern, without the diffraction peaks of the known materials, was found to resemble closely that of thortveitite, $Sc_2Si_2O_7$, as is shown in Fig. 2. In the coprecipitated gels of the SiO_2–Al_2O_3–Sc_2O_3–H_2O system, a large portion of their scandium component was confirmed to separate out as thortveitite upon heating.[12] In this system, cristobalite was not found as a firing product, except in the In-1C sample, just as in the system of SiO_2–Al_2O_3–Sc_2O_3–H_2O. In the iron (III)- and the gallium-bearing systems,[1,2] excess amounts of such trivalent cations as iron (III) and gallium ions separated out as hematite and β-gallia with the formation of cristobalite at higher temperatures. Judging from the above facts and a similarity in their ionic radii (In^{3+}: 0.81 and Sc^{3+}: 0.73 Å[13]), the new phase was considered to be a thortveitite-type indium (III) silicate; it has not been found in nature, but only as a synthesized mineral. It is assumed that the crystal structure of the new phase is the same as that of thortveitite (monoclinic); the unit-cell dimensions were calculated by means of the least-squares method, using all the observed spacings (27 spacings up to 1.58 Å), as is shown in Table 4. The spacings and their Miller indices of the indium (III) silicate are shown in Table 5. It can be concluded from the results presented in Tables 4 and 5 that the new phase found in this work is thortveitite-type indium (III) silicate; however, it could not be identified chemically because it could not be isolated. The SiO_2/In_2O_3 molar ratio in the indium-rich mixed gels and the aluminum-free gels in this system were considered not to be effective in the formation of indium (III) silicate upon heating.

Table 4. UNIT-CELL DIMENSIONS OF THORTVEITITE AND THORTVEITITE-TYPE INDIUM SILICATE

Specimen	a_0, Å	b_0, Å	c_0, Å	β, °	Remarks
Thortveitite	6.57	8.60	4.57	103.1	Native[14]
Thortveitite	6.65	8.62	4.68	102.2	Native[15]
Thortveitite	6.508	8.506	4.677	102.72	Synthesized[16]
Indium silicate	6.58	8.58	4.70	102.9	This work

Table 5. SPACINGS AND THEIR MILLER INDICES OF INDIUM SILICATE

h k l	d, Å Calcd	d, Å Obsd	I/I_0	h k l	d, Å Calcd	d, Å Obsd	I/I_0
1 1 0	5.14	5.13	38	$\bar{2}$ 0 2	2.10	2.10	12
0 0 1	4.58	4.55	53	2 2 1	2.09	2.09	16
0 2 0	4.29	4.28	14	3 1 0	2.07	2.07	11
$\bar{1}$ 1 1	3.77	3.77	7	0 2 2	2.02	2.02	6
2 0 0	3.21	3.21	16	$\bar{2}$ 2 2	1.89	1.89	14
1 1 1	3.15	3.15	37	$\bar{1}$ 3 2	1.81	1.81	6
0 2 1	3.13	3.12	100	3 3 0	1.71	1.71	14
$\bar{2}$ 0 1	2.96	2.96	55	2 0 2	1.69	1.69	7
1 3 0	2.61	2.61	34	1 5 0	1.66	1.66	8
2 2 0	2.57	2.57	27	1 3 2	1.65	1.65	13
$\bar{2}$ 2 1	2.43	2.44	6	4 0 0	1.60	1.61	6
2 0 1	2.39	2.39	11	2 2 2	1.57	1.58	3
$\bar{1}$ 3 1	2.36	2.36	11	1 5 1 }	1.53	1.53	13
0 0 2	2.29	2.28	7	0 0 3 }			
1 3 1	2.19	2.18	26				

The cause of the exothermic peaks around 980 and 880 °C in the DTA was examined as follows: the In-0, -1C, -9C, -12C, and -15M samples were preheated in the DTA equipment up to temperatures just below and above their peak temperatures. The phases of the preheated samples were found by X-ray powder diffractometry to be as are shown in Table 6. While the exothermic changes around 980 and 880 °C were found to be related to the formations of the mullite and the indium (III) oxide, it could not be confirmed whether or not both the exothermic peaks themselves depended on the formations of the mullite and the indium (III) oxide. They might be caused by the same structural changes[2] in the coprecipitated gels which brought about the formations of the mullite and the indium (III) oxide.

Table 6. PHASES OF PREHEATED SAMPLES

Sample	Peak temp. of original state, °C	Phases after heat treatment: below peak temp.	Phases after heat treatment: above peak temp.
In-0	980	A (950 °C)	M (990 °C)
In-1C	965	A (945 °C)	M (975 °C)
In-9C	866	A (852 °C)	I (876 °C)
In-12C	852	A (830 °C)	I (860 °C)
In-15M	980	I (950 °C)	I, M (990 °C)

A: amorphous, M: mullite, I: indium (III) oxide.

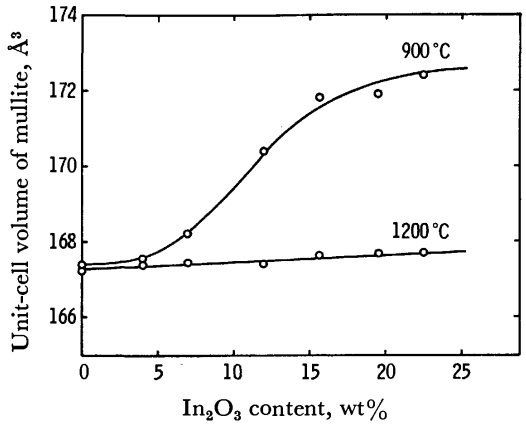

Fig. 3. Plot of unit-cell volume of mullite formed in coprecipitated gels against indium content.

The Unit-cell Volume of the Mullite Formed in the Heat-treated Samples. The unit-cell volumes of the mullite formed in the coprecipitated gels at 900 and 1200 °C for 5 hr were estimated to be as are shown in Fig. 3; those in the gels with more than 25 wt% of In_2O_3 could not be estimated because of the weak intensity of their diffraction peaks. The unit-cell volume of the mullite formed at 900 °C increased with the increase in the indium content when the indium (III) ions were included, while those in the mixed gels scarcely changed at all.

On the contrary, the unit-cell volume of the mullite decreased at 1200 °C as the crystallization proceeded with the removal of the indium (III) ions; then it became nearly equal to that in the indium-free coprecipitated gels. The exclusion of the indium (III) ions at 1200 °C from the mullite lattice was considered to arise from its large ionic radius, though the gallium ions were included in the mullite in fairly large quantities, even at 1200 °C.[2)]

References

1) J. Ossaka, S. Iwai, M. Kasai, T. Shirai, and S. Hamada, This Bulletin, **44**, 716 (1971).
2) M. Kasai, Y. Kudo, and S. Hamada, *ibid.*, **46**, 3091 (1973).
3) M. L. Keith and R. Roy, *Amer. Mineralogist.*, **39**, 1 (1954).
4) R. D. Shannon and C. T. Prewitt, *J. Inorg. Nucl. Chem.*, **30**, 1389 (1968).
5) K. Schubert and A. Seitz, *Z. Anorg. Allg. Chem.*, **256**, 226 (1948).
6) A. N. Christensen and N. C. Broch, *Acta Chem. Scand.*, **18**, 1261 (1964).
7) R. Roy and M. W. Shafer, *J. Phys. Chem.*, **58**, 372 (1954).
8) The values were estimated from the ignition loss.
9) C. W. Frank and C. E. Meloan, *Anal. Chem.*, **39**, 379 (1967).
10) H. E. Kissinger, *ibid.*, **29**, 1702 (1957).
11) The crystal system and the reported value for the a_0 of the indium (III) oxide are cubic and 1.541 Å respectively: H. E. Swanson, N. T. Gilfrich, and M. I. Cook, "NBS Circular 539, Standard X-ray Powder Diffraction Patterns," Vol. 5, National Bureau of Standards (1955), p. 26.
12) M. Kasai and S. Hamada, to be pullished in This Bulletin.
13) "Handbook of Chemistry and Physics," ed. by R. C. Weast, CRC Press, Clevelend (1974), p. F-194.
14) K. Sakurai, K. Nagashima, and A. Kato, This Bulletin, **35**, 1776 (1962).
15) J. E. T. Horne, *Bull. Geol. Surv. Gt. Britain*, **25**, 97 (1966).
16) National Bureau of Standards, Mono. 25, Sec. 7, 58 (1969).

The Structures and Thermal Behaviors of Bivalent Metal Succinates in the Solid State

Kenzo NAGASE, Hiroko YOKOBAYASHI, Kazuo MURAISHI,* and Kozo SONE**

College of General Education, Tohoku University, Kawauchi, Sendai 980

* *Department of Chemistry, Faculty of Science, Yamagata University, Koshirokawa, Yamagata 990*

** *Department of Chemistry, Faculty of Science, Ochanomizu University, Bunkyo-ku, Tokyo 112*

(Received January 6, 1975)

The relations between the structures and thermal behaviors of the succinates of Mg(II), Co(II), Ni(II), Cu(II), Zn(II), Cd(II), and Pb(II) were studied. In the case of the copper salt, the dehydration of its dihydrate began easily at room temperature. However, the tetrahydrates of Mg, Co, and Ni held their waters more tightly, and changed from crystalline to amorphous state in the course of dehydration which began at 50—60 °C. The anhydrous salts of Mg and Co recrystallized at 306 and 272 °C, respectively, with a sharp exotherm on each DTA curve. The cobalt salt showed stepwise color changes, pink $\xrightarrow{\text{dehydration}}$ bluish violet $\xrightarrow{\text{recrystallization}}$ pink. $PbC_4H_4O_4$ exhibited a phase transition from tetragonal to cubic at 160 °C with $\Delta H=2.5$ kJ/mol and $\Delta S=5.9$ J/deg·mol. The phase transition was reversible and seems to be accompanied with a conformational change of the succinate ion.

The structures of the copper salts of α,ω-dicarboxylic acids, $HOOC(CH_2)_{n-2}COOH$ with $n=2-10$ have been investigated by means of magnetic[1] and infrared measurements,[2] and it was found that, when n is even, the carbon chain assumes the *trans* conformation.[2] The structures of α,ω-dicarboxylates of other metals, on the other hand, have been determined in the case of the oxalates of Mg(II), Mn(II), Fe(II), Co(II) and Ni(II) by X-ray analyses, and it was found that two water molecules contained in the salts coordinate to the metals and the oxalate ion acts as a quadridentate ligand.[3]

This work was undertaken to obtain detailed information on the compositions and structures of the various bivalent metal succinates by means of infrared and diffuse reflectance spectroscopies and thermal analysis.

In the course of the TG-DTA measurements, heat changes without any weight-loss were found for magnesium, cobalt and lead succinates. It was considered to be worthwhile to investigate the nature of the heat changes, since a conformational change of succinate ion or a change of coordination structure is expected to occur.

Experimental

Materials. The metal succinates were prepared by the reaction of the corresponding metal carbonates with succinic acid. The results of the elemental analyses for C and H agreed with those calculated within $\pm 0.3\%$ (Table 1).

Apparatus and Procedure. Infrared absorption spectra were measured from 4000 to 250 cm^{-1} by KBr disk method with a Hitachi 215 spectrophotometer. The spectra at elevated temperatures were recorded with the apparatus equipped with a standard heating cell. Diffuse reflectance spectra were measured with a Hitachi EPS-3T spectrophotometer using a standard integrating sphere attachment; in the case of heated samples, they were cooled to room temperature and brought to measurements.

Powder X-ray diffraction diagrams at room temperature and those at elevated temperatures were obtained with a Toshiba diffractometer ADG-101 equipped with a standard high temperature sample holder. Fe Kα radiation and a manganese filter were used for cobalt salts, and Cu Kα radiation and a nickel filter for all other salts.

Thermogravimetric (TG) and differential thermal analytical (DTA) curves were obtained with a Shinku Riko TGD-3000 apparatus at a heating rate of 10 °C/min in an atmosphere of nitrogen flowing at 50 ml/min. About twenty milligrams of powdered sample in a platinum crucible were used in each measurement. Calorimetric measurements were carried out with a Rigaku Denki 8002 CS differential scanning calorimeter at a heating rate of 5 °C/min in an atmosphere of nitrogen flowing at 40 ml/min. The apparatus was calibrated against the transition heat of KNO_3.

Results and Discussion

In general, water molecules in inorganic salts gives symmetric and antisymmetric O–H stretching bands at 3500—3000 $cm,^{-1}$ and it is well known that ν(O–H) of crystal water appears at a higher frequency than that of coordinated water. The values of ν(O–H) of the hydrated succinates of Mg, Co, Ni and Cu are given in Table 1. The value of the copper salt is considerably higher (by *ca.* 300 cm^{-1}) than those of the other salts which are similar with each other. This result seems to suggest that the water in the copper salt is crystal water (or very weakly coordinated water), while that in the other salts is commonly coordinated water.

Table 1. Stretching frequencies of water (ν(O–H)), initial dehydration temperatures (T_{H_2O}) and weight-losses (ΔW) for various metal succinates

Formulas	ν(O–H)/ cm^{-1}	T_{H_2O}/ °C	ΔW_{obsd}/ %	ΔW_{calcd}/ %
$MgC_4H_4O_4\cdot 4H_2O$	3100	62	31.2	33.9
$CoC_4H_4O_4\cdot 4H_2O$	3075	53	27.8	29.2
$NiC_4H_4O_4\cdot 4H_2O$	3050	61	28.8	29.2
$CuC_4H_4O_4\cdot 2H_2O$	3370	25	14.8	16.7
$ZnC_4H_4O_4$	—	—	—	—
$CdC_4H_4O_4$	—	—	—	—
$PdC_4H_4O_4$	—	—	—	—

Dehydration temperature gives information about the

dissociation energy of the metal-coordinated water bonding. Assuming an electrostatic model, it is expected that the bond energy increases with the increase of $1/r$, where r means ionic radius of metal. The initial dehydration temperatures (T_{H_2O}) of the hydrated succinates are also given in Table 1, together with the corresponding weight-loss. For the salts of Mg, Co and Ni, the change of T_{H_2O} with $1/r$ is reasonable, but T_{H_2O} of the copper salt is too much lower than the value expected from the ionic radius of copper. Thus, the thermal data also support the view obtained from the IR study.

In the frequency region of 4000—250 cm^{-1}, the infrared absorption patterns of the salts of Mg, Co and Ni were very similar with each other, suggesting that the bonding structures of these salts are identical. The diffuse reflectance spectra of the cobalt and nickel salts indicated that the metals are surrounded octahedrally by six oxygen atoms. Since all of four water molecules contained were found to be the same kind of coordinated water, the structure represented by [**A**] seems to be most probable for these salts, although other possibilities can not be ruled out. According to Kuroda and Kubo,[2]

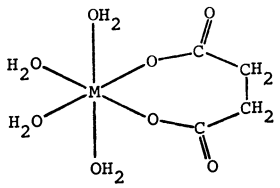

[**A**]

the succinate ion in the copper salt assumes the zigzag chain form resulting from the *trans* conformation about the $-CH_2-CH_2-$ bond. It is expected that the succinate ion forming the chelate ring in [**A**] will give more complicated spectral pattern in the frequency region of methylene group than that of the *trans* conformation. The comparison of the spectral pattern of the cobalt salt (Curve 1 in Fig. 2) with that of the copper salt (Curve 3 in Fig. 6) seems to support this expectation. The spectral pattern of succinic anhydride in the frequency region of methylene group was also found to resemble that of the cobalt salt.

Except for the copper salt, the anhydrous salts obtained by heating the corresponding hydrates at 170 °C, gave no X-ray diffraction lines, and their infrared absorption bands were broad, compared with those of their hydrates. In the case of the copper salt, on the other hand, the X-ray diffraction and infrared absorption patterns remain almost unchanged by dehydration. This difference is probably due to the fact that, in the former case, the removal of coordinated water will alter not only the crystal lattice but also the coordination structure. In fact, striking color changes, pink→bluish violet for the cobalt salt and bluish green→yellow for the nickel salt, were observed in the course of the dehydration.

The anhydrous salts of Mg and Co gave a sharp exotherm at 306 and 272 °C, respectively, on the DTA curves which are shown in Fig. 1, together with the TG curves. The X-ray diffraction, infrared absorption and diffuse reflectance data of the cobalt salts before and after the exothermic process are shown in Figs. 2, 3 and 4, respectively, together with those of its hydrate. The X-ray results indicate that the anhydrous salt is

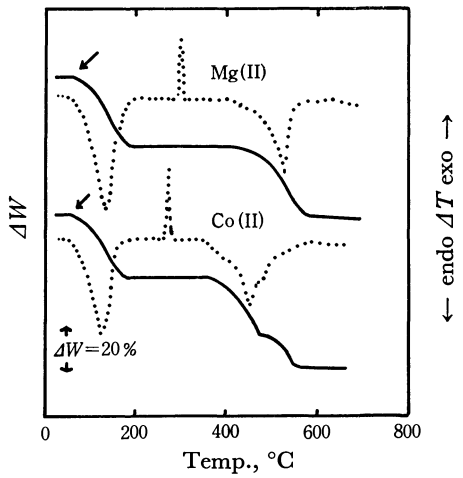

Fig. 1. TG-DTA curves of $MgC_4H_4O_4 \cdot 4H_2O$ and $CoC_4H_4O_4 \cdot 4H_2O$ in a flowing nitrogen atmosphere:
—— indicates TG; ····· DTA.
Points corresponding to T_{H_2O} are indicated with arrows.

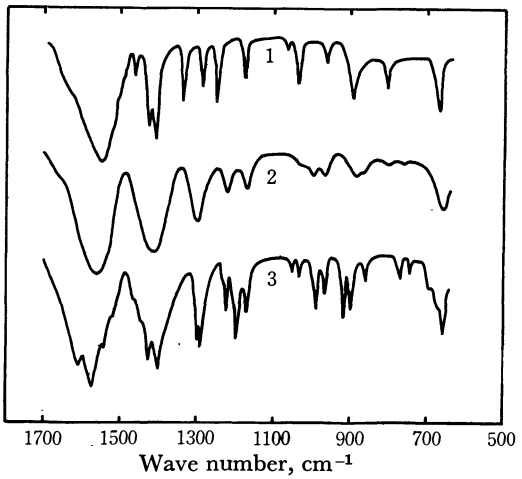

Fig. 2. Infrared absorption spectra of cobalt salts:
(1) $CoC_4H_4O_4 \cdot 4H_2O$, (2) and (3) $CoC_4H_4O_4$ heated up to 170 and 300 °C, respectively.

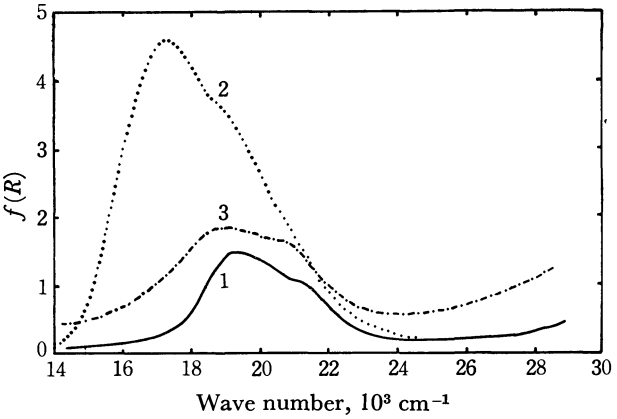

Fig. 3. Reflectance spectra of cobalt salts:
(1) $CoC_4H_4O_4 \cdot 4H_2O$, (2) and (3) $CoC_4H_4O_4$ heated up to 170 and 300 °C, respectively.

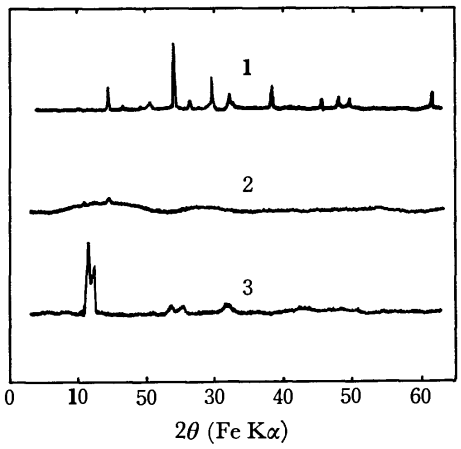

Fig. 4. X-ray diffraction patterns of cobalt salts: (1) $CoC_4H_4O_4 \cdot 4H_2O$, (2) and (3) $CoC_4H_4O_4$ heated up to 170 and 300 °C, respectively.

converted from amorphous to crystalline state through the exothermic process.[4] The infrared absorption bands become thereby remarkably sharper, showing that the crystallized salt has a rigid bonding structure. Along with these changes, the salt becomes pink again, and its reflectance spectrum shows that it has an essentially octahedral coordination structure, just as in the case of the hydrate, so that the formation of weak Co–O bonds between the coordinated oxygen atoms and adjacent Co ions must be postulated. Except for the absence of color change, the magnesium salt gave data which are similar to those of the cobalt salt. Therefore, the nature of the exotherm of the magnesium salt seems to be identical with that of the cobalt salt. By the DSC measurements, the enthalpy changes corresponding to the exothermic processes were obtained: $\Delta H = -10.0$ kJ/mol (cobalt) and -10.9 kJ/mol (magnesium). The entropy changes calculated were -18.3 J/deg·mol (cobalt) and -18.8 J/deg·mol (magnesium), respectively.

The succinates of Zn, Cd and Pb which were crystallized from the corresponding aqueous solution, were anhydrous. The infrared absorption patterns of the salts of Zn and Cd were similar to that of the copper salt in the frequency region of the methylene group, while that of the lead salt was similar to that of the hydrated cobalt salt. The TG-DTA curves of the salts of Zn, Cd and Pb were also measured, and only

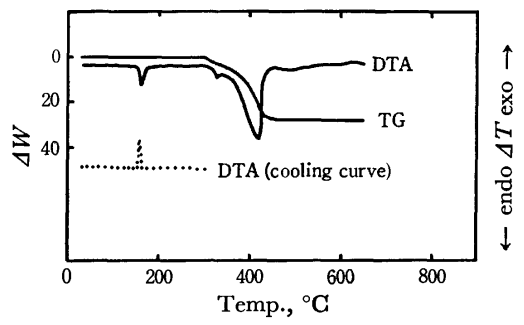

Fig. 5. TG-DTA curves of $PbC_4H_4O_4$: ……indicates cooling curve.

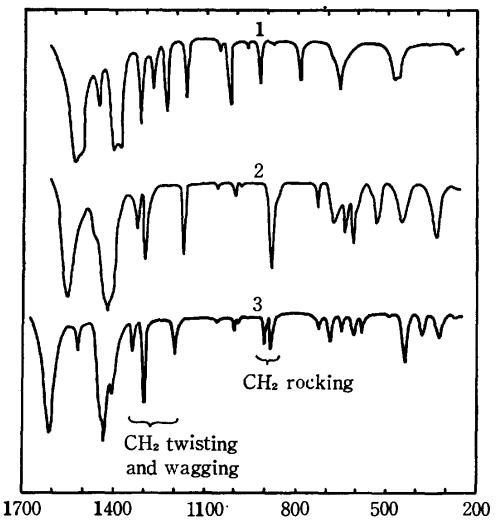

Fig. 6. Infrared absorption spectra of (1) $PbC_4H_4O_4$ at room temperature, (2) $PbC_4H_4O_4$ at 200 °C, and (3) $CuC_4H_4O_4$.

the lead salt gave an endotherm at 160 °C on the DTA curve without any weight-loss. The curves of the lead salt are given in Fig. 5, together with the cooling curve. An exotherm is observed at 153 °C on the cooling curve, and so the heat change is reversible. ΔH and ΔS of the endothermic process were 2.5kJ/mol and 5.9J/deg·mol, respectively. The analyses of the X-ray diffraction lines before and after the heat change indicated that the crystals of the lead salt changed from tetragonal to cubic at about 160 °C. The lattice constants calculated were $a=b=15.2$ and $c=14.6$ Å for the tetragonal (low temperature) form, and $a=b=c=15.2$ Å for the cubic (high temperature) form.

The phase transition of the lead salt was accompanied with a considerable change of the infrared spectrum. In Fig. 6, the infrared spectra at room temperature and at 200 °C are given. The spectral change is also reversible, *i.e.* the spectrum at 200 °C reverts to its original shape when the sample is cooled to room temperature. The spectrum at 200 °C is simpler than that at room temperature in the frequency region of the methylene group; while the latter is similar to that of the cobalt salt hydrate, the former is similar to that of the copper salt. Thus the phase transition seems to be accompanied with a conformational change of the succinate ion, and its possible structures below and above 160 °C can be represented by **[C]** and **[B]**, which can be changed into each other by rotating the chain around the $-CH_2-CH_2-$ bond.

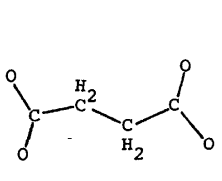

[B]

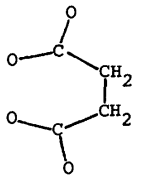

[C]

References

1) O. Asai, M. Kishita, and M. Kubo, *Naturwissenschaften*, **46**, 12 (1959).
2) Y. Kuroda and M. Kubo, *J. Phys. Chem.*, **64**, 759 (1960).
3) J. P. Lagier, H. Pezernat, and J. Dubernat, *Rev. Chim. Miner.*, **6**, 1081 (1969).
4) This peculiar change of the cobalt salt was already observed by Le V. My, G. Perinet, and R. Lafont, *C. R. Acad. Sci., Paris, Ser. C*, **268**, 406 (1969).

Crystal and Molecular Structure of $(\pi\text{-}C_5H_5)Fe_3(CO)_7C_2C_6H_5$ Obtained from $(\pi\text{-}C_5H_5)Fe(CO)_2C{\equiv}CC_6H_5$ with $Fe_2(CO)_9$[1)]

Katsutoshi YASUFUKU, Katsuyuki AOKI, and Hiroshi YAMAZAKI
The Institute of Physical and Chemical Research, Wako-shi, Saitama 351
(Received March 7, 1975)

The crystal structure of $\pi\text{-}C_5H_5Fe_3(CO)_2(C_2C_6H_5)$ obtained from the reaction of $\pi\text{-}C_5H_5Fe(CO)_2C_2C_6H_5$ with $Fe_2(CO)_9$ has been determined from single crystal X-ray diffraction data. The space group is $P\bar{1}$ and the cell constants are $a=12.635$, $b=9.457$, $c=9.033$ Å, $\alpha=94.64$, $\beta=109.10$, and $\gamma=99.60$ °, and $Z=2$. The refinement was carried out using block-diagonal least-squares calculation including anisotropic thermal factors for the non-hydrogen atoms and isotropic thermal factors for the hydrogens. The final R value for 2488 reflections is 0.035. The molecular configuration consists of an isosceles triangle of the three iron atoms, each two of which bonds to three terminal carbonyl groups and one bonds to the cyclopentadienyl ring. The phenylethynyl group is disposed above the iron plane and is σ-bonded to one iron atom with three carbonyls and π-bonded symmetrically to the other two iron atoms. The seventh carbonyl group is bridged asymmetrically between these two iron atoms, below the iron plane. The characteristic shortening in the Fe-C σ-bond and in the acetylenic C–C bond was observed.

Some interesting reactions of transition metal acetylides with organic reagents are known.[2)] However, reactions of these acetylides with organometallics have been little studied. Recently, the acetylides with organometallics have attracted attention from a viewpoint of metal cluster preparation. We have briefly reported[3)] the reactions of some transition metal acetylides with metal carbonyls giving new mixed transition metal complexes. Also, Bruce *et al.*[4)] have reported the reactions of cupper acetylides with halometal complexes to be an expedient route to clusters.

In a previous paper,[3)] we reported the reaction of ethynyldicarbonyl-π-cyclopentadienyliron (**1**), $\pi\text{-}C_5H_5Fe(CO)_2C{\equiv}CR$, with octacarbonyldicobalt which gave $\pi\text{-}C_5H_5Fe(CO)_2(C_2R)Co_2(CO)_6$ (**2a**), when $R=CH_3$, but gave $\pi\text{-}C_5H_5Fe(C_2C_6H_5)Co_2(CO)_6$, when $R=C_6H_5$. A speculative structure **2b** was presented for the product, however later remeasurement of the mass spectra of the product with various conditions revealed that the composition was incorrect but should have been **2a**($R=C_6H_5$). Thus, the reaction of **1** with $Co_2(CO)_8$ gave unequivocally **2a** irrespective of the nature of R($R=CH_3$, CO_2CH_3, and C_6H_5).

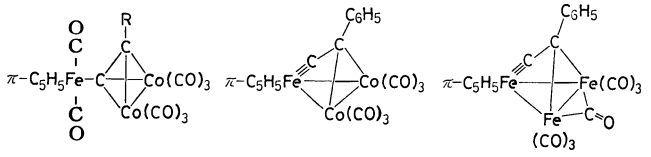

2a **2b** **3a**

It is interesting to determine the structure of $\pi\text{-}C_5H_5Fe_3(CO)_7C_2C_6H_5$ (**3**) [which was obtained by us[3)] from the reaction of **1** with $Fe_2(CO)_9$ and later also by Bruce[5)] from the reaction of $[\pi\text{-}C_5H_5Fe(CO)_2C_2Ph\cdot CuCl]_2$ with $Fe_2(CO)_9$], because the structure **3a** proposed on the basis of an analogy with **2b** is now somewhat doubtful, although metal carbine complexes, $X(CO)_4M{\equiv}CR$, have been obtained by Fischer *et al.*,[6)] recently.

Here we report the X-ray determination of the structure of **3**.

Experimental

Monoclinic and triclinic brown crystals were obtained from hexane solution. Preliminary examination of Weissenberg photographs showed that the triclinic crystals were more suitable for further examination than the monocilinic crystals because of large cell constant of the latter, $b\sim55$ Å. (The IR spectrum of the triclinic crystal was identical to that of **3** before growing the crystals.) The diffraction data for the triclinic crystal were collected on automated Phillips PW-100 Single Crystal Diffractometer using monochromatic Mo Kα radiation. The cell constants and the orientation matrix of the triclinic crystal were determined from least-squares refinements of the setting angles for high-angle reflections. These dimensions and other crystal data are given in Table 1. For collection of intensity data, the ω-2θ scan technique with a scan rate of 4.0 °/min was used and 2685 independent reflections up to a maximum 2θ value of 50 ° were measured.

TABLE 1. CRYSTAL DATA FOR $\pi\text{-}C_5H_5Fe_3(CO)_7C_2C_6H_5$

Formula wt 529.8	Triclinic $P\bar{1}$
$a=12.635$ Å	$\alpha=94.64°$
$b=9.457$ Å	$\beta=109.10°$
$c=9.033$ Å	$\gamma=99.60°$
$V=994.98$ Å^3	$Z=2$
Mo Kα radiation	$\mu=22.56$ cm^{-1}
$d_x=1.77$ g/cm^3	d_m[a)] $=1.75$ g/cm^3

a) Measured by floatation in an aqueous zinc bromide solution

The intensities of three reflections were measured every 123 reflections as a check on crystal and electronic stability. A correction for Lorentz and polarization factors but no correction for absorption was applied to the data. In the structural refinement the 2488 reflections with $Fo>3\sigma(Fo)$ were used.

The approximate positions of the three Fe atoms were determined from a sharpened Patterson function. From a three-dimensional Fourier synthesis calculated with all terms phased by the Fe atoms, all non-hydrogen atoms of the molecule were located. At this stage, the value of R was 0.353. After five cycles of block-diagonal least-squares refinement with isotropic thermal parameters and five further cycles with anisotropic thermal parameters, (minimizing the function $[\sum w||F_o|-|F_c||^2/\sum w|F_o|^2]^{1/2}$) the R value decreased to 0.045. A weighting scheme, $w=1$, was used. Scattering factors were

Table 2. Positional and anisotropic thermal parameters of the non-hydrogen atoms ($\times 10^4$) with their standard deviations in parantheses

	X	Y	Z	β_{11}	β_{22}	β_{33}	β_{12}	β_{13}	β_{23}
Fe(1)	1406(1)	2208(1)	1197(1)	53(1)	95(1)	119(1)	17(1)	38(1)	−4(1)
Fe(2)	3420(1)	1827(1)	1162(1)	47(1)	96(1)	95(1)	16(1)	21(1)	8(1)
Fe(3)	2296(1)	3206(1)	−865(1)	50(1)	83(1)	115(1)	16(1)	23(1)	15(1)
C(1)	1762(6)	3896(7)	2467(8)	86(6)	131(10)	185(14)	28(7)	59(8)	−15(9)
C(2)	−36(5)	2330(7)	161(8)	72(6)	146(10)	186(14)	35(6)	52(7)	4(10)
C(3)	1124(5)	994(7)	2513(7)	60(5)	126(9)	140(11)	19(6)	37(6)	11(8)
C(4)	3891(6)	2667(7)	3216(7)	85(6)	141(10)	114(11)	23(7)	28(7)	6(8)
C(5)	4763(5)	1931(6)	823(7)	59(5)	113(9)	115(10)	16(5)	22(6)	28(8)
C(6)	3411(4)	35(6)	1679(6)	47(5)	121(9)	105(10)	20(5)	25(6)	9(7)
C(7)	3532(5)	4174(6)	735(7)	74(6)	95(8)	138(11)	14(5)	28(7)	1(8)
C(8)	1767(4)	1247(5)	−352(6)	42(4)	85(7)	98(9)	9(4)	16(5)	0(6)
C(9)	2410(4)	1095(5)	−1195(6)	51(4)	81(7)	93(9)	17(5)	23(5)	1(6)
C(10)	2583(4)	138(6)	−2412(6)	48(4)	100(8)	75(8)	26(5)	15(5)	11(6)
C(11)	1889(5)	−1236(6)	−2961(7)	62(5)	110(8)	109(9)	27(5)	36(6)	18(7)
C(12)	2066(5)	−2166(6)	−4095(7)	84(6)	100(9)	110(10)	24(6)	21(6)	−5(8)
C(13)	2927(6)	−1723(7)	−4676(7)	99(7)	144(10)	118(11)	59(7)	44(7)	−2(9)
C(14)	3612(5)	−372(7)	−4150(7)	69(6)	178(11)	118(11)	34(6)	50(7)	20(9)
C(15)	3445(5)	557(6)	−3016(7)	58(5)	124(10)	109(10)	16(6)	34(6)	−1(8)
C(16)	2689(6)	4590(7)	−2414(8)	92(7)	148(11)	187(14)	32(7)	47(8)	83(10)
C(17)	2125(6)	5259(7)	−1524(9)	101(7)	96(10)	215(15)	28(7)	38(8)	46(10)
C(18)	1063(6)	4433(8)	−1856(9)	89(7)	153(11)	261(17)	57(7)	64(9)	109(12)
C(19)	937(6)	3207(8)	−2927(9)	88(7)	146(12)	194(15)	−7(7)	−42(8)	80(11)
C(20)	1944(7)	3307(8)	−3277(8)	169(10)	175(13)	114(13)	90(10)	32(9)	49(10)
O(1)	1973(5)	4983(6)	3252(7)	170(7)	151(9)	307(15)	26(7)	80(9)	−88(9)
O(2)	−947(4)	2409(6)	−522(7)	63(4)	219(10)	280(13)	46(5)	42(6)	31(9)
O(3)	920(4)	222(5)	3330(6)	103(5)	188(9)	186(10)	23(5)	55(6)	64(8)
O(4)	4238(5)	3146(6)	4504(6)	141(6)	220(10)	118(9)	29(6)	16(6)	−31(8)
O(5)	5587(4)	1971(5)	568(6)	60(4)	202(9)	202(10)	32(5)	52(5)	52(7)
O(6)	3426(4)	−1104(5)	1991(5)	92(4)	119(7)	188(9)	29(4)	54(5)	42(6)
O(7)	4242(4)	5150(5)	1472(6)	102(5)	114(7)	209(11)	−15(5)	−4(6)	−3(7)

The β_{ij}'s are defined by: $\exp[-(h^2\beta_{11}+k^2\beta_{33}+l^2{}_{33}\beta+2hk\beta_{12}+2hl\beta_{13}+2kl\beta_{23})]$

Table 3. Positional ($\times 10^3$) and isotropic thermal parameters for the hydrogen atoms

	X	Y	Z	B
HC(11)	132(4)	−154(5)	−266(6)	3.60(1.04)
HC(12)	163(5)	−308(6)	−442(6)	4.16(1.04)
HC(13)	307(4)	−232(6)	−533(6)	3.71(1.04)
HC(14)	416(5)	−38(6)	−456(7)	4.34(1.04)
HC(15)	387(4)	154(6)	−263(6)	3.67(1.04)
HC(16)	339(6)	503(7)	−247(8)	7.14(1.04)
HC(17)	248(5)	618(7)	−88(7)	6.06(1.04)
HC(18)	57(6)	470(7)	−122(8)	6.47(1.04)
HC(19)	35(5)	241(7)	−321(8)	6.31(1.04)
HC(20)	211(5)	272(7)	−385(8)	6.43(1.04)

The B is defined by: $\exp[-B(\sin\theta/\lambda)^2]$.

taken from the International Tables.[7] The anomalous dispersion effect was included in the calculated structure factors for iron using $\Delta f'=0.4$ and $\Delta f''=1.0$.[8]

A difference Fourier map then revealed the positions of all the hydrogen atoms. Four cycles of refinement with isotropic thermal parameters for hydrogen and anisotropic thermal parameters for non-hydrogen atoms were carried out, giving a final R of 0.038. The atomic coordinates and anisotropic thermal parameters with estimated standard deviations (esd's) for the non-hydrogen atoms are given in Table 2. The coordinates and isothermal parameters for the hydrogens are given in Table 3.

Description of the Structure and Discussion

The bond distances (with esd's) are shown in Table 4 and the bond angles (with esd's) are listed in Table 5. Important least-squares planes and dihedral angles are shown in Table 6. Fig. 1 shows the packing of the two molecules of **3** in the unit cell. The shortest intermolecular contacts are 2.970(6) Å between O(2) and O(6) at (−x, −y, −z) and 3.082(6) Å between O(5)

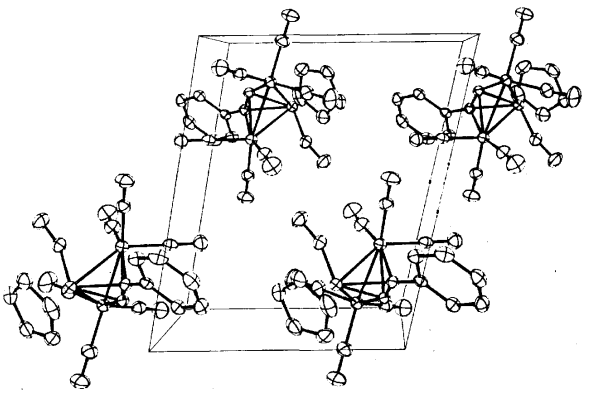

Fig. 1. View of the structure along the c axis showing crystal packing.

TABLE 4. SELECTED BOND LENGTHS (Å)

[Fe_3 Ring and Acetylene moiety]		[Fe–C≡O]	
Fe(1)–Fe(2)	2.639 (1)	Fe(1)–C(1)	1.787 (6)
Fe(1)–Fe(3)	2.632 (1)	Fe(1)–C(2)	1.783 (6)
Fe(2)–Fe(3)	2.524 (1)	Fe(1)–C(3)	1.829 (6)
Fe(1)–C(8)	1.829 (6)	Fe(2)–C(4)	1.819 (6)
Fe(2)–C(8)	2.040 (4)	Fe(2)–C(5)	1.810 (7)
Fe(3)–C(8)	2.006 (5)	Fe(2)–C(6)	1.793 (6)
Fe(2)–C(9)	2.081 (5)	Fe(2)–C(7)	2.273 (6)
Fe(3)–C(9)	2.031 (5)	Fe(3)–C(7)	1.788 (5)
C(8)–C(9)	1.299 (9)	C(1)–O(1)	1.138 (8)
[C_6H_5]		C(2)–O(2)	1.132 (8)
C(9)–C(10)	1.461 (8)	C(3)–O(3)	1.137 (9)
C(10)–C(11)	1.391 (7)	C(4)–O(4)	1.125 (7)
C(11)–C(12)	1.393 (9)	C(5)–O(5)	1.133 (8)
C(12)–C(13)	1.375 (10)	C(6)–O(6)	1.137 (7)
C(13)–C(14)	1.368 (8)	C(7)–O(7)	1.155 (6)
C(14)–C(15)	1.386 (9)		
C(15)–C(10)	1.387 (9)		
[C_5H_5]			
C(16)–C(17)	1.414 (12)		
C(17)–C(18)	1.360 (9)		
C(18)–C(19)	1.400 (11)		
C(19)–C(20)	1.399 (13)		
C(20)–C(16)	1.397 (9)		

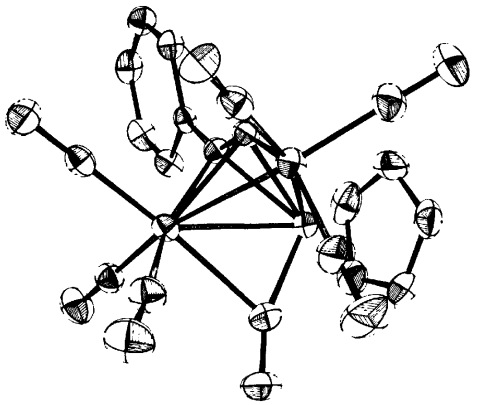

Fig. 2. Perspective view of π-$C_5H_5Fe_3(CO)_7C_2C_6H_5$ molecule.

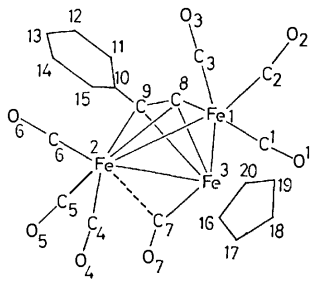

Fig. 3. Numbering scheme for the molecule.

and O(6) at (1−x, −y, −z). All other intermolecular contacts between non-hydrogen atoms are >3.34Å.

The perspective view of **3** without the hydrogens showing thermal vibration with 20% electron density is shown in Fig. 2 and the numbering scheme for the atoms in Fig. 3. The three iron atoms form a triangle in which the distance, Fe(2)–Fe(3)=2.524(1) Å, is slightly shorter than the other two Fe–Fe distances, Fe(1)–Fe(2)=2.639(1) and Fe(1)–Fe(3)=2.632(1) Å. The six carbonyls bond to the Fe(1) and Fe(2) atoms as terminal carbonyls: Two of the three carbonyls on Fe(1) and one of the three on Fe(2) are nearly in the plane of the iron atoms. The terminal carbonyl Fe–C bonds range from 1.738 to 1.829 Å (average 1.801 Å). The seventh carbonyl group is located between the Fe(2) and Fe(3) atoms as an asymmetric bridge[9] [Fe(2)–C(7)=2.273(6) Å and Fe(3)–C(7)=1.788(5) Å, ∠Fe(2)–C(7)–O(7)=126.35(46)° and ∠Fe(3)–C(7)–O(7)=157.63(56)°] below the iron plane. The dihedral angle between the iron plane and the Fe(2)C(7)Fe(3) plane is 106.95°. An IR band, $\nu_{C\equiv O}$= 1870 cm^{-1}, corresponds to this asymmetrically bridged CO. The cyclopentadienyl ring attached to Fe(3) is almost perpendicular to the iron plane: Fe(3) is 1.730 Å from the ring.

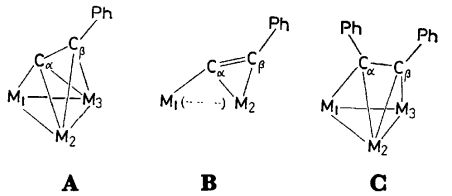

Fig. 4. Schematic geometry of the related σ,π-coordinated ethynyl complexes.

The phenylethynyl group is located above the iron plane: Fe(1)–C(8)=1.829(6), C(8)–C(9)=1.299(9), Fe(2)–C(8)=2.040(4), Fe(3)–C(8)=2.006(9), Fe(2)–C(9)=2.081(5), Fe(3)–C(9)=2.031(5) Å. The dihedral angle between the iron plane and the Fe(2)C(8)Fe(3) plane is 51.97° and that between the iron plane and the Fe(2)C(9)Fe(3) plane is 99.28°. These distances and angles show that the phenylethynyl group, originally σ-bonded to the Fe(3) atom, is now σ-bonded to the Fe(1) atom and π-bonded symmetrically to both the Fe(2) and Fe(3) atoms through the C(8)–C(9) triple bond. The configuration about the three iron atoms and the phenylethynyl group is shown in Fig. 4 (Type **A**) (in which C(α) and C(β) correspond to C(8) and C(9)). $Ru_3(CO)_9H(C_2Bu^t)$ (**4**) has been reported[10] to have a very similar configuration to **3**. Some complexes in which a σ-bonded acetylide is π-bonded to one metal (type **B**) have also been reported.[11,12] The geometries of these related complexes are summarized in Table 7.

A similarity around the C(α)–C(β) moiety in both **3** and **4** is evident when the difference (~0.1 Å) in the M–C distances for the terminal carbonyls (the average Fe–C in **3** is 1.801 and Ru–C in **4** is 1.91 Å), and in the M(1)–C(α) distances in [π-$C_5H_5Fe(CO)_2C_2Ph$·CuCl]$_2$[12] and π-$C_5H_5Ru(PPh_3)_2C_2Ph$·CuCl[5a] is assumed also to be due solely to the difference between Fe and Ru covalent radii.

The distance C(α)–C(β) in **3** is markedly shorter than the acetylenic C–C distances found in the usual dinuclear monoacetylene complexes, *e.g.* (π-$C_5H_5)_2Ni_2$-(PhC_2Ph)[13] 1.35(3), $Co_2(CO)_6(PhC_2Ph)$[14] 1.46, and (π-C_5H_5)$NiFe(CO)_3(Ph_3PC_2H)$[15] 1.37(3) Å. The C(α)–C(β) distance in the type **B** complexes are a little shorter than that in **3**, whereas the Fe(1)–C(α) distance

TABLE 5. SELECTED BOND ANGLES (deg)

Fe(2)–Fe(1)–Fe(3)	57.23 (3)	Fe(3)–Fe(1)–C(1)	96.00 (23)
Fe(1)–Fe(2)–Fe(3)	61.24 (3)	Fe(3)–Fe(1)–C(2)	97.47 (23)
Fe(1)–Fe(3)–Fe(2)	61.52 (3)	Fe(3)–Fe(1)–C(3)	156.94 (20)
C(8)–Fe(1)–Fe(2)	50.45 (17)	C(8)–Fe(1)–C(1)	142.88 (29)
C(8)–Fe(1)–Fe(3)	49.52 (17)	C(8)–Fe(1)–C(2)	101.71 (28)
C(8)–Fe(2)–Fe(1)	43.72 (15)	C(8)–Fe(1)–C(3)	110.18 (26)
C(8)–Fe(2)–Fe(3)	50.79 (15)	C(1)–Fe(1)–C(2)	95.43 (32)
C(8)–Fe(2)–C(9)	36.73 (21)	C(1)–Fe(1)–C(3)	99.61 (31)
C(8)–Fe(3)–Fe(1)	43.92 (15)	C(2)–Fe(1)–C(3)	97.83 (30)
C(8)–Fe(3)–Fe(2)	52.01 (15)		
C(8)–Fe(3)–C(9)	37.55 (21)	Fe(1)–Fe(2)–C(4)	82.66 (21)
C(9)–Fe(2)–Fe(3)	51.22 (15)	Fe(1)–Fe(2)–C(5)	165.26 (19)
C(9)–Fe(3)–Fe(2)	53.04 (15)	Fe(1)–Fe(2)–C(6)	101.05 (19)
C(9)–Fe(2)–C(7)	91.32 (22)	Fe(3)–Fe(2)–C(4)	115.95 (21)
C(9)–Fe(3)–C(7)	109.24 (25)	Fe(3)–Fe(2)–C(5)	104.52 (19)
		Fe(3)–Fe(2)–C(6)	141.39 (19)
Fe(1)–C(8)–Fe(2)	85.83 (22)	C(8)–Fe(2)–C(4)	126.02 (26)
Fe(1)–C(8)–Fe(3)	86.56 (22)	C(8)–Fe(2)–C(5)	131.43 (24)
Fe(2)–C(8)–Fe(3)	77.21 (19)	C(8)–Fe(2)–C(6)	92.01 (24)
C(9)–C(8)–Fe(1)	152.91 (45)	C(4)–Fe(2)–C(5)	101.93 (28)
C(9)–C(8)–Fe(2)	73.36 (33)	C(4)–Fe(2)–C(6)	93.10 (28)
C(9)–C(8)–Fe(3)	72.27 (33)	C(5)–Fe(2)–C(6)	92.74 (26)
Fe(2)–C(9)–Fe(3)	75.73 (18)	C(7)–Fe(2)–C(4)	82.05 (26)
C(8)–C(9)–Fe(2)	69.91 (33)	C(7)–Fe(2)–C(5)	86.57 (25)
C(8)–C(9)–Fe(3)	70.18 (33)	C(7)–Fe(2)–C(6)	174.90 (24)
C(10)–C(9)–Fe(2)	131.07 (39)	C(7)–Fe(2)–Fe(3)	43.38 (16)
C(10)–C(9)–Fe(3)	135.97 (39)	C(7)–Fe(3)–Fe(2)	60.80 (20)
C(8)–C(9)–C(10)	144.74 (52)	Fe(2)–C(7)–Fe(3)	75.82 (22)
Fe(2)–Fe(1)–C(1)	102.61 (23)	O(7)–C(7)–Fe(2)	126.35 (49)
Fe(2)–Fe(1)–C(2)	149.96 (23)	O(7)–C(7)–Fe(3)	157.63 (56)
Fe(2)–Fe(1)–C(3)	102.52 (20)		
Fe(1)–C(1)–O(1)	178.56 (66)	C(10)–C(11)–C(12)	120.20 (54)
Fe(1)–C(2)–O(2)	178.69 (64)	C(11)–C(12)–C(13)	119.91 (58)
Fe(1)–C(3)–O(3)	178.51 (58)	C(12)–C(13)–C(14)	120.48 (62)
Fe(2)–C(4)–O(4)	175.77 (61)	C(13)–C(14)–C(15)	119.97 (60)
Fe(2)–C(5)–O(5)	177.92 (55)	C(14)–C(15)–C(10)	120.76 (55)
Fe(2)–C(6)–O(6)	178.32 (52)	C(15)–C(10)–C(11)	118.68 (51)
C(16)–C(17)–C(18)	108.73 (65)		
C(17)–C(18)–C(19)	108.43 (67)		
C(18)–C(19)–C(20)	108.00 (67)		
C(19)–C(20)–C(16)	107.62 (68)		
C(20)–C(16)–C(17)	107.21 (65)		

TABLE 6. LEAST-SQUARE PLANES AND DIHEDRAL ANGLES

Plane	Atoms defining plane	Equation of mean plane
I	Fe(1) Fe(2) Fe(3)	$0.2705x+0.8548y+0.4429z=2.2267$
II	Fe(1) C(8) C(9)	$0.6420x-0.5081y+0.5742z=-0.0416$
III	Fe(2) Fe(3) C(7)	$-0.6115x+0.1302y+0.7804z=-2.4545$
IV	C(10) C(11) C(12) C(13) C(14) C(15)	$0.7250x-0.3684y+0.5819z=0.2739$
V	C(16) C(17) C(18) C(19) C(20)	$0.4864x-0.4957y+0.7195z=-3.5856$
VI	Fe(2) C(8) Fe(3)	$-0.4018x+0.4287y+0.8092z=-1.1836$
VII	Fe(2) C(9) Fe(3)	$0.7572x+0.2680y-0.5957z=3.5761$

Displacements of atoms from mean palne (Å)

Plane I		Plane II		Plane IV		Plane V	
Fe(1)	0.0000	Fe(1)	0.0000	C(10)	−0.0001	C(16)	−0.0050
Fe(2)	0.0000	C(8)	0.0000	C(11)	−0.0015	C(17)	0.0077
Fe(3)	0.0000	C(9)	0.0000	C(12)	0.0009	C(18)	−0.0074
C(8)	−1.2449	C(10)	0.0692	C(13)	0.0013	C(19)	0.0041
C(9)	−1.5989	Fe(2)	1.2907	C(14)	−0.0028	C(20)	0.0006
C(7)	1.4932	Fe(3)	−1.2335	C(15)	0.0022	Fe(3)	1.7297

Dihedral angles between planes (deg)

I—II	I—III	I—IV	I—V	II—IV	I—VI	I—VII
100.58	106.95	82.02	91.22	9.33	51.97	99.28

The planes are in cartesian coordinates with the z axis coinciding with c and the y axis coinciding with to b*.

TABLE 7. GEOMETRIES OF THE RELATED COMPLEXES

	Type[a]	Distances (Å)						Angles (deg)	
		M(1)–C(α)	C(α)–C(β)	C(α)–M(2 or 3)	C(β)–M(2 or 3)	M(1)–M(2 or 3)	M(2)–M(3)	∠M(1)-C(α) C(β)	∠C(α)-C(β)Ph
π-$C_5H_5Fe_3(CO)_7C_2Ph$[b]	A	1.829(6)	1.299(9)	2.040(4) 2.006(5)	2.081(5) 2.031(5)	2.639(1) 2.632(1)	2.524(1)	152.91(45)	144.74(52)
$Ru_3(CO)_9H(C_2Bu^t)$[c]	A	1.99(2)	1.29(3)	2.23(2) 2.26(2)	2.25(3) 2.18(2)	2.795(2) 2.796(2)	2.790(2)	153(2)	138(2)[h]
$Fe_2(CO)_6(PPh_2)(C_2Ph)$[d]	B	1.89(6)	1.232(10)	2.125(8)	2.304(7)	2.597(2)		160.3(6)	162.3(8)
$[\pi$-$C_5H_5Fe(CO)_2C_2Ph\cdot CuCl]_2$[e]	B	1.89(2)	1.27(2)	1.99(2)	1.99(2)			162(2)[i]	162(2)
π-$C_5H_5Ru(PPh_3)_2C_2Ph\cdot CuCl$[f]	B	2.016(9)	1.25(1)	2.01(1)	2.04(1)			172.76(8)[i]	165.0(1.0)
$Fe_3(CO)_9(PhC_2Ph)$[g]	C	2.048(16)	1.492(23)	2.098(15) 2.043(15)	1.947(16) 1.945(15)	2.480(10) 2.501(9)	2.579(11)	126.9(1.0)	130.8(1.3)

a) as shown in Fig. 4. b) This work, c) Ref. 10. d) Ref. 11, e) Ref. 12, f) Ref. 5a, g) Ref. 17, h) ∠C(α) C(β) C(of Bu^t), i) These two complexes have no M_1–M_2 bond and the M_1–C=C–Ph moiety has *cis* configuration.

in **3** is a little shorter than that in the type **B** compounds. The shorter distances, M(1)–C(α) and C(α)–C(β), in **3** may reflect an additional interaction between the Fe(1) and C(α) or among Fe(1), C(α), and C(β), although the decrease in the Fe(1)–C(α) distance is not so great as the decrease between carbene and carbin complexes: $(Co)_5CrC(OCH_3)C_6H_5$ 2.04(3) and $(CO)_4ICrCCH_3$ 1.69(1) Å.[16]

The shortening of the Fe(1)–C(α) and C(α)–C(β) bonds may be emphasized also by comparison with $Fe_3(CO)_9(PhC_2Ph)$[17] (**5**) (type **C**) in which the C(α) atom has more phenyls than the C(α) atom in **3**. Another difference between **3** and **5** is that the phenyl plane in **3** is almost parallel to the Fe(1)C(α)C(β) plane (dihedral angle = 9.33°), whereas the phenyls in **5** are not.

The C(β)–(phenyl) distance and ∠C(α)–C(β)–(phenyl) are in good agreement with those in $(\pi$-$C_5H_5)_2Ni_2(PhC_2Ph)$,[13] average 1.45 Å and 140°, and in $Co_2(CO)_6(PhC_2Ph)$,[14] average 1.43 Å and 138°.

References

1) Chemistry of Mixed Transition-Metal Complexes, VI. Previous paper, K. Yasufuku and H. Yamazaki, This Bulletin, **46**, 1502 (1973).

2) Y. Tohda, K. Sonogashira, and N. Hagihara, *Chem. Commun.*, **1975**, 54; P. Hong, K. Sonogashira, and N. Hagihara, presented at Symposium on Organometallic Compounds, p. 196, Osaka, 1969; *idem.*, *Tetrahedron Lett.*, **1970**, 1633; M. H. Chisholm and D. A. Couch, *Chem. Commun.*, **1974**, 42; and L. S. Meriwether, M. F. Leto, C. E. Colthup, and G. W. Kennerly, *J. Org. Chem.*, **27**, 3930 (1962).

3) K. Yasufuku and H. Yamazaki, This Bulletin, **45**, 2664 (1972).

4) O. M. AbuSalah, M. I. Bruce, M. R. Churchill, and S. A. Bezman, *Chem. Commun.*, **1972**, 858.

5) a) M. I. Bruce, O. M. AbuSalah, R. E. Davis, and N. V. Raghavan, *J. Organometal. Chem.*, **64**, C48 (1974); b) O. M. AbuSalah and M. I. Bruce, *J. Chem. Soc. Dalton*, **1974**, 2302.

6) E. O. Fischer, *Angew. Chem.*, **86**, 651 (1974), and references therein.

7) D. T. Cromer and J. T. Waber, "International Tables for X-ray Crystallography," Vol. 3, Kynoch Press, England,

8) D. T. Cromer and D. Liberman, *J. Chem. Phys.*, **53**, 1891 (1971).

9) F. A. Cotton and J. M. Troup, *J. Amer. Chem. Soc.*, **96**, 5070 (1974).

10) G. Gervasio and G. Ferraris, *Cryst. Struct. Commun.*, **3**, 447 (1973).

11) H. A. Patel, R. G. Fischer, A. J. Carty, D. V. Naik, and G. J. Palenik, *J. Organometal. Chem.*, **60**, C49 (1973).

12) M. I. Bruce, R. Clark, J. Howard, and P. Woodward, *ibid.*, **42**, C107 (1972).

13) O. S. Mills and B. W. Shaw, *ibid.*, **11**, 595 (1968).

14) W. G. Sly, *J. Amer. Chem. Soc.*, **81**, 18 (1959).

15) K. Yasufuku, K. Aoki, and H. Yamazaki, *J. Organometal. Chem.*, **84**, C28 (1975).

16) G. Huttner, H. Lorenz, and W. Gartzke, *Angew. Chem.*, **86**, 667 (1974).

17) J. F. Blount, L. F. Dahl, C. Hoogzand, and W. Hubel, *J. Amer. Chem. Soc.*, **88**, 292 (1966).

Preparation of Reinforcing Fillers from Japanese Acid Clays with Lime and by Calcination. III. Elucidation of the Reinforcing Effects Based on the Investigation of Changes in the Structure, Physicochemical Properties and Morphology of N Hard Clay

Hideki RAI and Junkichi YAMADA*

The Institute of Industrial Science, The University of Tokyo, Minato-ku, Tokyo 106

(Received November 5, 1974)

In order to elucidate the reinforcing effects of the fillers prepared from Japanese acid clay with hydrated lime and by calcination and mechanical disintegration, **N** hard clay (CaO 3—60%; calcination 400—800 °C, 1—1.5 hr; wet ball-milling 18 hr) derived from Nakajo acid clay (**N**) were investigated on the structure, physicochemical properties and morphology in comparison with those of **N**, Dixie Clay and Silene EF. X-Ray diffraction, infrared spectroscopy and electron micrography were applied to the examination of the structural and morphological features. The physicochemical properties were determined on the surface properties such as hygroscopicity, pH and DPG adsorption together with the specific gravity and bulk density. The following results were obtained: (1) Treatment under the optimum conditions (CaO 6%, calcination 600 °C, 1.5 hr; wet milling 18 hr) caused a favorable change in the structure of the prepared filler, resulting in controlling the surface properties, reduction in the particle size and its distribution, a decrease in the specific gravity and an increase in the bulk density. (2) Deviation from the conditions, *e.g.*, calcination at 400 °C for 1.5 hr remained too much residual adsorptivity to improve the great surface activity of **N**, whereas treatment at 800 °C for 1—1.5 hr afforded sintering, collapse and/or fusion yielding too hard aggregates to be disintegrated as well as a serious breakdown or complete loss in the effective functional groups involved.

Previously we reported the studies of the availability of some Japanese acid clays such as Nakajo (**N**), Matsune (**M**) and Kuramitsu (**K**) origins for the preparation of a reinforcing filler of elastomers,[1] the optimum conditions for producing good hard clays from **M** and **N**, and their reinforcing properties.[2]

Further investigations were carried out in order to elucidate the reinforcing effects in connection with the characteristics of structure, morphology and physicochemical properties of the fillers prepared. The **N** hard clay derived from **N** were investigated on the structure and morphology by means of X-ray diffraction, infrared spectroscopy and electron micrography. The physicochemical properties such as hygroscopicity, pH, DPG adsorption, specific gravity and bulk density were determined as described before. The features of the structure, morphology and physicochemical properties were compared with those of reference fillers, Dixie Clay, Silene EF, and dried or calcined **N** without lime treatment beforehand. Valuable information elucidating the characteristics of **N** hard clay with relation to the reinforcement was obtained.

Experimental

Materials. The **N** hard clay prepared under the various conditions of treatment (CaO 3—60%; calcination 400—800 °C, 1—1.5 hr; wet ball-milling 18 hr) described in the preceding paper[2] were put to use.

Dixie Clay, Silene EF and Nakajo acid clay **N**, dried in air (24 hr), in oven (110 °C, 2 hr) or calcined (400—800 °C, 1 hr) without the lime treatment and mechanical disintegration, were used as references.

Determination of Structure, Morphology and Physicochemical Properties. The same apparatus and conditions of measurement as mentioned before[1] were followed in the investigation of changes in the structure, morphology and physicochemical properties of the fillers prepared.

* Present address: AA Chemical Co., Ltd., Shibakoen, Minato-ku, Tokyo 105.

Results and Discussion

Treatment of the original acid clay with hydrated lime follwed by calcination and mechanical disintegration caused noticeable changes in the structure, physicochemical properties and morphology of the fillers obtained.

(1) Structural Changes. (a) X-Ray Diffraction Patterns: Figures 1(a)—(c) illustrate the X-ray powder diffraction patterns of **N** hard clay showing the structural changes in comparison with those of the dried or calcined **N** without the lime treatment beforehand.

It is apparent that all the hydrated lime (4.90 and 2.63 Å)[3] added to **N** has disappeared as a result of the reaction during the treatment.

An increase in the amount of alkali and the temperature of calcination for the prepared fillers resulted in some basal shift of an irreversible contraction along the c-axis of montmorillonite lattices as well as the diminution or even disappearance of the prominent basal reflection (15.77 Å (001))[4] of the montmorillonites, normal and abnormal,[1] in the air-dried **N**.

Coincidently an almost proportional decrease in the intensity of excess silica α-cristobalite (4.04 Å (101))[5] occurred in the fillers as the amount of alkali increased.

New reflections also appeared approximately in proportion to an increase in the amount of alkali. They were ascribed to calcium silicate hydrates of tobermolite group (CSH I, II and G; 2.90—3.08, 2.78—2.85 and 1.80—1.85 Å)[6,7] and calcite (3.86, 3.04, 2.50, 2.28 and 2.09 Å).[8] The former was generated by the reaction of hydrated lime with the excess silica

covering the external and internal surfaces of the montmorillonite crystallites or existing in an isolated state, and the latter by the carbonation of the alkali liberated during the courses of mixing raw materials followed by filtration, drying, calcination and mechanical disintegration.

(i) Calcination at 400 °C for 1—1.5 hr (Fig. 1 (a)). The basal reflection (15.77 Å) of the air-dried **N** shifted

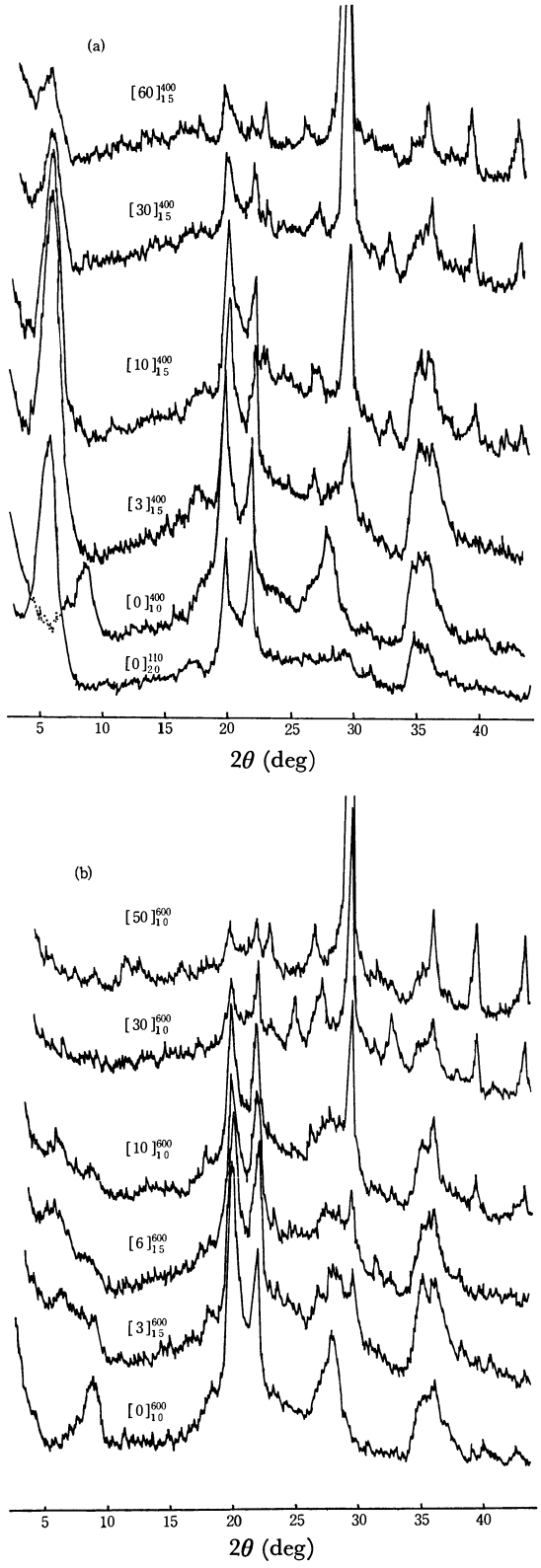

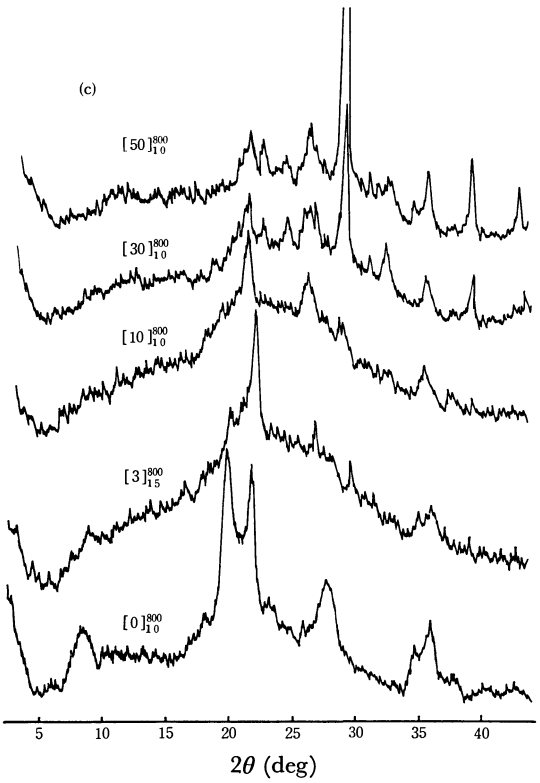

Fig. 1. X-ray diffraction patterns of **N** hard clay (CaO 3—60%; calcination 400—800 °C, 1—1.5 hr; mechanical disintegration 18 hr) in comparison with those of Nakajo acid clay **N**, dried (110 °C, 2 hr) or calcined (400—800 °C, 1 hr) without further treatment. Inscriptions are as follows. (a): CaO 3—60%; calcination 400 °C, 1—1.5 hr; wet milling 18 hr. (b) CaO 3—50%; calcination 600 °C, 1—1.5 hr; wet milling 18 hr. (c): CaO 3—50%; calcination 800 °C, 1—1.5hr; wet milling 18 hr.

* Number in brackets indicates the amount of alkali used, and the superscript and subscript numbers of the brackets denote the temperature and time of calcination, respectively.

towards 10.04 Å and decreased the intensity as much as 72.1% by the calcination at 400 °C for 1 hr without the lime treatment and mechanical disintegration.

Irrespective of the change in the amount of alkali (CaO 3—60%), the fillers prepared without the calcination showed a nearly constant shift (about 2 Å) in the basal reflections as a result of the formation of Ca-montmorillonite. The intensity of the basal reflection first increased with less than 10% CaO and then decreased with more than 30% CaO. The increase in the intensity of the basal reflection is considered to be based on the saturation of the Ca^{2+} ion interposed between the interlayers of the montmorillonites, and the decrease on the erosion initiated from the edges and outer surfaces of the crystallites with the hydrated lime. These reactions should be accelerated mechanochemically during the course of mixing raw materials, especially by the wet ball-milling.

The subsequent calcination at 400 °C for 1.5 hr and by the wet milling for 18 hr gave a considerable diminution (24.5, 39.6, 72.3 and 83.7% for 3, 10, 30 and 60%

CaO, respectively) in the basal reflection as well as a slight shift (1.97, 1.75 and 1.53 Å for 3, 10—30 and 60% CaO, respectively).

In view of the changes in the intensities and shifts of the basal reflections of the calcined **N** and the fillers prepared without such a calcination as mentioned above, the decrease in the basal shift of the fillers with an increase in the amount of alkali suggests that the formation of CSH as well as the erosion would proceed on the lamellae surfaces of the montmorillonite crystallites. The remained intensity (75.5—16.3% for 3—60% CaO) and the relatively small shift (less than 2 Å) of the basal reflection indicate that noticeable capabilities of rehydration and rehydroxylation[9-11] were still reserved in the fillers obtained. Consequently the inherent, great surface activity of the original acid clay **N** was restrained insufficiently by this procedure, which would be discussed in detail in connection with the physicochemical properties later.

(ii) Calcination at 600 °C for 1—1.5 hr (Fig. 1 (b)). The calcined **N** (600 °C, 1 hr) prepared without the lime treatment and mechanical disintegration gave an irreversible contraction (5.90 Å) in the montmorillonite lattices as well as a noticeable diminution (81.2%) in the intensity of the basal reflection, which were greater than those of the calcined **N** (400 °C, 1 hr) described above. Nevertheless, exhaustive dehydroxylation or the formation of anhydrous modification[12,13] could not be observed in the crystallites.

The treatment with hydrated lime (3—50% CaO) followed by calcination at 600 °C for 1 or 1.5 hr and the same mechanical disintegration as above afforded a further shift (2.59, 1.75 and 1.05 Å for 3, 6 and 10% CaO, respectively) and a greater diminution (91.2, 89.9 and 93.1% for 3, 6 and 10% CaO, respectively) than the corresponding values of the foregoing fillers (CaO 3—60%; 400 °C, 1.5 hr; wet milling 18 hr) or even resulted in the disappearance (for more than 30% CaO) of the basal reflection in the prepared fillers.

The intensity of α-cristobalite also decreased with an increase in the amount of alkali.

The reactions including thermal dehydration and dehydroxylation, fixation and substitution with Ca^{2+} ion, erosion by free alkali and the formation of CSH proceeded so extensively in the crystallites that the capability of rehydration and rehydroxylation during the wet milling decreased noticeably. However, the minute crystallites still persisted the montmorillonite lattices, even though they were eroded considerably.

The results obtained indicate that as the calcining temperature increased, the irreversible contraction along the c-axis of the montmorillonite lattices increased especially with a less amount of alkali, and that an increase in the amount of alkali resulted in the moderation of the thermal contraction. The moderation should be attributed mainly to the formation of CSH on the lamellae surfaces of the minute crystallites.

The treatment with alkali more than 10% CaO followed by calcination at temperatures higher than 600 °C for more than 1 hr gave the formation of calcium aluminate hydrates (CAH) (7.7 and 5.6 Å ascribable to C_4AH_{13})[6,7,14] and the appearance of some peaks of unknown significance (5.6, 4.94 and 3.36 Å for 50% CaO and 5.11, 3.57 and 3.28 Å for 30% CaO).

(iii) Calcination at 800 °C for 1—1.5 hr (Fig. 1 (c)). The calcined **N** (800 °C, 1 hr) prepared without the lime treatment and mechanical disintegration afforded an irreversible contraction (5.73 Å) of the montmorillonite lattices and a noticeable diminution (83.02%) in the intensity of the basal reflection. The basal spacing (10.04 Å) is slightly greater than those of the calcined **N** (600 °C, 1 hr; 9.87 Å) described above as well as the dehydrated layer (9.5 Å)[4] of montmorillonite, indicating the occurrence of an appreciable expansion of the crystallites.

The most serious structural changes appeared in the fillers treated with hydrated lime (3—50% CaO) followed by calcination at 800 °C for 1 or 1.5 hr and mechanical disintegration for 18 hr; all reflections of the montmorillonites disappeared completely in almost of the fillers obtained. Especially those prepared with less than 10% CaO accompanied very diffused and broadened reflections due to amorphous phases, indicating the appearance of sintering or partial fusion of the minute crystallites besides the collapse in the montmorillonite lattices. The less the amount of alkali and the higher the temperature of calcination, the greater the effect on the structural changes in the fillers prepared. In view of the appearance of relatively less intensities of CSH and calcite than in the cases of the lower-temperature calcination described above, a greater part of the alkali should be incorporated into the montmorillonite lattices.

(b) Infrared Spectra: Figures 2 (a)—(c) give the infrared spectra of the prepared fillers in comparison with those of **N**, dried or calcined without the lime treatment. The diagnostic bands[15] of montmorillonite in **N** varied with the treatment with hydrated lime followed by calcination and mechanical disintegration, and those of the new minerals appeared.

(i) Calcination at 400 °C for 1.5 hr (Fig. 2 (a)). The band at 3650 cm^{-1} (νO–H, free) observable in the dried **N** decreased with an increase in the amount of alkali added to the fillers prepared (CaO less than 10%; calcination 400 °C, 1.5 hr; wet milling 18hr), and disappeared with more than 30% CaO as a result of the formation of Ca-montmorillonite and CSH as confirmed by X-ray diffraction. Whereas the calcination without the lime treatment and mechanical disintegration remained the band up to 600 °C, although the intensity decreased with an increase in the temperature of calcination.

The bands at 914 (δAl^{3+}–O–H)[16] and 836 cm^{-1} (δFe^{3+}–O–H)[17] completely disappeared in the fillers prepared with more than 30% CaO. Whereas the calcined **N** (400 °C, 1 hr) which had excluded the lime treatment still reserved the former band slightly. The both bands were barely lost by the calcination over 600 °C for 1 hr.

Among the bands of layer silicates in the region 900—1200 cm^{-1} (νSi–O), the band at 1081 cm^{-1} related to colloidal silica[18-20] and ion saturation[21] as well as the band at 796 cm^{-1} (δSi–O) related to hydrated amorphous silica[18-20] gradually decreased the

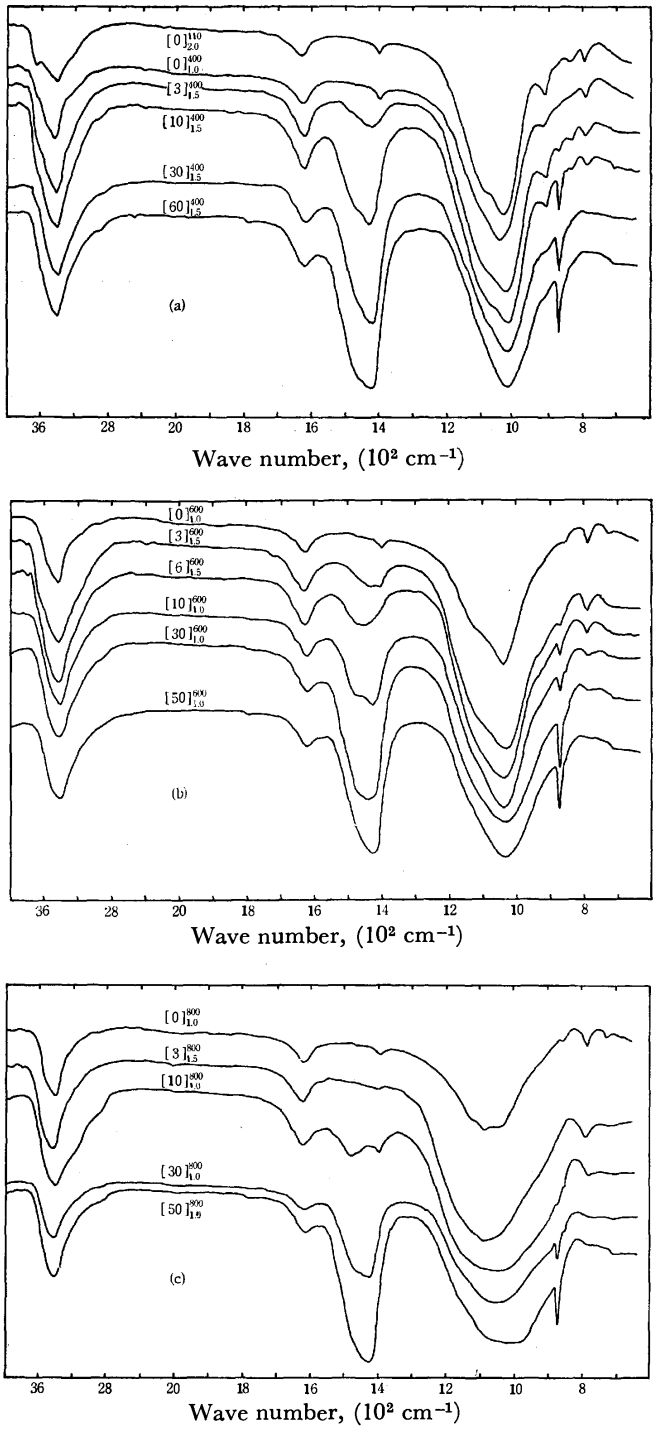

Fig. 2. Infrared spectra of **N** hard clay (CaO 3—60%; calcination 400—800 °C, 1—1.5 hr; mechanical disintegration 18 hr) in comparison with those of Nakajo acid clay **N**, dried (110 °C, 2 hr) or calcined (400—800 °C, 1 hr). The same inscriptions as in Fig. 1 are applied.

intensities as the amount of alkali increased. The latter was barely lost with more than 60% CaO in accordance with the consumption of the excess silica α-cristobalite observable in the foregoing X-ray diffraction. The abnormally great deviation in the amount of alkali required for the complete reaction with the excess silica (13%)[1] involved suggests that considerable amounts of hydrated lime were consumed by carbonation, fixation or trapping in the interior of the crystallites, substitution and some other reactions with Ca^{2+} ion in the tetrahedrons and octahedrons of the montmorillonites. The formation of calcite, CSH, CAH and some other calcium salts resulted consequently. The band at 1035 cm^{-1} related to the skeletal vibrations of the tetrahedrons of montmorillonite slightly shifted towards a lower frequency at 1025 cm^{-1} with appreciable broadening[21] with more than 30% CaO, verifying the above suggestion.

The bands ascribable to the newly formed minerals, CSH (1480 and 855 cm^{-1})[22,23] and calcite (2520, 1790, 1430, 876, and 715 cm^{-1}),[24,25] in the fillers increased with an increase in the amount of alkali.

The bands at 3410 and 1630 cm^{-1} in the calcined **N** decreased in proportion to an increase in the temperature of calcination. They are related to the waters adsorbed on the surfaces and among the interfaces of the minute crystallites and those hydrated with the exchangeable cations interposed between the interlayers of the montmorillonites. Irrespective of the calcination at 400 °C for 1.5 hr, they increased the intensities noticeably in the fillers as the amount of alkali increased. This can be explained in terms of the residual adsorptivity of the montmorillonites inducing considerable rehydration and rehydroxylation. The crystal water of CSH, remained after the calcination and rehydrated during the course of the wet milling for 18 hr, also contributed additionally.

(ii) Calcination at 600 °C for 1—1.5 hr (Fig. 2 (b)). The band at 3650 cm^{-1} was lost by degrees in the fillers treated with more than 10% CaO followed by the calcination (600 °C, 1—1.5 hr) and the same disintegration.

The bands at 914 and 836 cm^{-1} disappeared completely in those prepared with more than 3% CaO or even by the calcination (600 °C, 1 hr) alone without the lime treatment in advance.

The bands at 1081 and 796 cm^{-1} decreased more slowly with an increase in the amount of alkali than in those of the fillers calcined at 400 °C for 1.5 hr, and barely disappeared with more than 50% CaO. Diminution in the reactivity of the excess silica with alkali can be attributed mainly to more favorable polycondensation and/or the crystallization of the amorphous silica and α-cristobalite at 600 °C rather than 400 °C on the basis of a noticeable increase in the sharpness of the corresponding peaks in the X-ray diffraction patterns (Fig. 1 (a) *cf.* (b)). The phenomena of crystallization of silica gels, analogous to the natural aging of gels to hyalite and so on, are extensively studied by X-ray diffraction and other methods,[26,27] and are well known to be accelerated by thermal treatment.[28,29]

A new phase ascribable to pyrophillite dehydroxylate (864, 795, and 730 cm^{-1})[9] appeared in the fillers treated with less than 3% CaO, suggesting the occurrence of appreciable transformation as well as exhaustive dehydroxylation in the montmorillonite lattices.

As the amount of alkali increased, the band at 1035 cm^{-1} progressively shifted towards a higher frequency at 1042 cm^{-1} overlapping the adjacent band

at 1081 cm^{-1} with 6% CaO, and then towards a lower frequency at 1030 cm^{-1} with 50% CaO, giving one single, broader band. This suggests that more Ca^{2+} ions reacted with the tetrahedrons of the montmorillonites.

The bands at 3410 and 1630 cm^{-1} decreased with an increase in the amount of alkali but remained moderately, indicating the presence of preferable hygroscopicity or an appropriate surface activity as well as the formation of CSH.

For the same composition of alkali, the amount of CSH estimated from the intensities of the bands at 855 and 1480 cm^{-1} was found to be greater than in the corresponding filler calcined at 400 °C for 1.5 hr, whereas that of the calcite (1425, 875, and 715 cm^{-1}) formed fairly less. Therefore the thermal treatment (600 °C, 1—1.5 hr) is considered to be more advantageous for the production of CSH than in the lower-temperature calcination. The formation of CSH on the lamellae surfaces of the montmorillonites could restrain the excessive contraction, sintering and/or partial fusion of the minute crystallites induced by the calcination (600 °C, 1—1.5 hr). Thus the facilitation of disintegrating the calcined products resulted in the reduction of both the particle size and its distribution of the fillers prepared.

(iii) Calcination at 800 °C for 1—1.5 hr (Fig. 2 (c)). The bands at 3650, 914 and 835 cm^{-1} disappeared completely in the fillers prepared with or without alkali followed by the calcination (800 °C, 1—1.5 hr) and mechanical disintegration.

No phase attributable to the pyrophillite dehydroxylate, which was observed in the calcined **N** (600—800 °C, 1 hr), appeared in the fillers treated with hydrated lime (3—50% CaO) and by the subsequent calcination (800 °C, 1—1.5 hr) and mechanical disintegration. The restraint of forming the pyrophillite dehydroxylate might be resulted from the presence of the CSH distributed on the lamellae surfaces of the montmorillonites.

As the amount of alkali increased, the band at 796 cm^{-1} decreased with noticeable broading and still remained the intensity even with 50% CaO. Further polycondensation of the excess silica can be suggested under the conditions of preparation.

The bands at 1081, 1033 and 914 cm^{-1} overlapped each other, giving a very broad band around 1020 cm^{-1}. A considerable amount of Ca^{2+} ion might be incorporated into the octahedrons as well as the tetrahedrons of the montmorillonites by the calcination. Under such a high-temperature calcination, sintering or partial fusion of the minute crystallites should coincidently be accompanied in the fillers treated with higher composition of alkali. This should result in lowering the pulverizability of the prepared fillers due to the formation of too hard aggregates to be disintegrated.

The bands ascribable to CSH (1480 and 855 cm^{-1}) showed the intermediate intensities of the respective peaks observable in the fillers calcined at 400 and 600 °C for 1—1.5 hr, whereas the amount of calcite decreased noticeably with less than 30% CaO. A partial decomposition of calcite and the migration of CO_3^{2-} ion into the lattices of the newly formed minerals may be suggested.

The results obtained substantially agreed with those investigated by X-ray diffraction.

(2) Physicochemical Properties. (i) Hygroscopicity: Figure 3 (a) demonstrates obviously that the more the amount of alkali and the higher the temperature of calcination, the greater the effect of lowering the hygroscopicity of the fillers obtained.

A hyperbolic decrease in the hygroscopicity with an increase in the amount of alkali appeared in those treated with hydrated lime (CaO 3—60%) followed by the calcination (400—600 °C, 1—1.5 hr) and mechanical disintegration. The decreasing rate with respect to the change of the same amount of alkali was found to be greater in those calcined at the lower temperature, though the difference was relatively small.

Those prepared with more than 3% CaO and by the subsequent calcination (600 °C, 1—1.5 hr) and mechanical disintegration gave the hygroscopicity smaller than half of that (15.08%) of the dried **N**. Even those treated with more than 25% CaO followed by the calcination (400 °C, 1.5 hr) and mechanical disintegration would afford the values less than that (8.4%) of Silene EF.

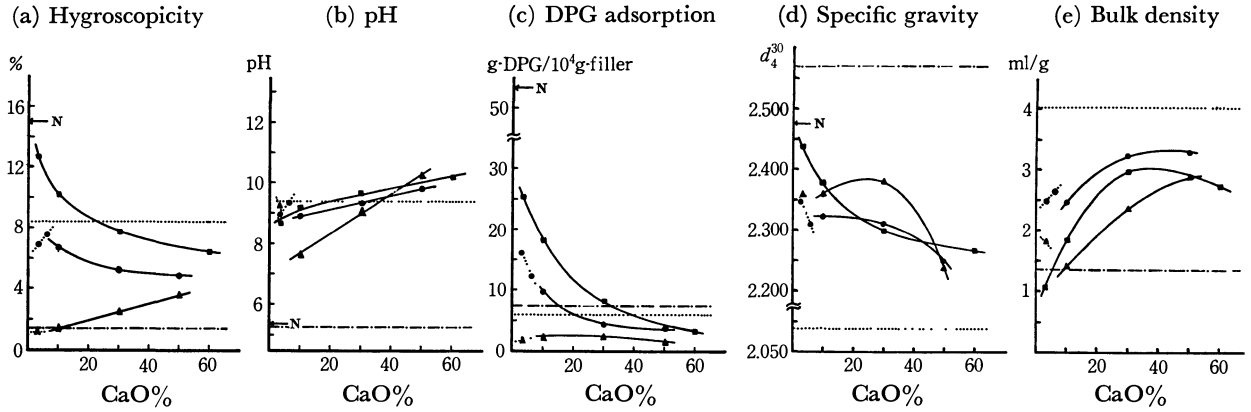

Fig. 3. Physicochemical properties of **N** hard clay (CaO 3—60%; calcination 400—800 °C, 1—1.5 hr; mechanical disintegration 18 hr) as compared with those of Dixie Clay, Silene EF and dried **N**. (a): Hygroscopicity, (b): pH, (c) DPG adsorption, (d) Specific gravity, (e): Bulk density.
▲·····▲ 800 °C, 1.5 hr; ●·····● 600 °C, 1.5 hr; ■——■ 400 °C, 1.5 hr; ▲——▲ 800 °C, 1 hr; ●——● 600 °C, 1 hr; -·-·-·- Dixie Clay; ····· Silene EF.

A noticeably-decreased hygroscopicity comparable to that (1.46%) of Dixie Clay was obtained in those prepared with less than 10% CaO and by the subsequent calcination (800 °C, 1—1.5 hr) and mechanical disintegration. Whereas the values conversely increased in proportion to an increase in the amount of alkali up to 50% CaO. The peculiar phenomenon may be attributed to the formation of some basic calcium salts (CaO/SiO_2 and/or $CaO/Al_2O_3>1$) during the course of the high-temperature calcination: A remarkable increase in pH, the lowest values in DPG adsorption and changes in the specific gravity and bulk density discussed later are considered to be the verifications in reference to the results investigated into the fillers by the X-ray diffraction and IR spectroscopy.

(ii) pH: Figure 3 (b) illustrates changes in the pH of **N** hard clay. The pH (5.40) of the dried **N**, slightly greater than that (5.30) of Dixie Clay, varied noticeably with the treatment with alkali (CaO 3—60%) followed by the calcination (400—800 °C, 1—1.5 hr) and mechanical disintegration (wet milling 18 hr), and resulted in the pH values comparable to that (9.45) of Silene EF in the fillers prepared.

Those treated with alkali (CaO 10—60%) and by the subsequent calcination (400—600 °C, 1—1.5 hr) and mechanical disintegration gave a proportional increase in the pH values with an increase in the amount of alkali. For the same composition of alkali, a high-temperature-calcined product showed a smaller value (about 0.3) than in the one treated by a lower-temperature calcination. This indicates that the higher-temperature calcination (600 °C, 1—1.5 hr) caused a further fixation of dissociative Ca^{2+} ions in the minute crystallites of the fillers.

Those prepared with alkali (CaO 10—50%) followed by the calcination (800 °C, 1 hr) and mechanical disintegration afforded an abrupt but proportional increase in the pH values as the amount of alkali increased. Formation of some basic calcium salts in the matrix can also be suggested on the basis of the followings; (1) a basic calcium salt, which generally exhibits a greater pH value than that of a normal one, is easily produced under the conditions of treatment with more alkali and by higher-temperature calcination, (2) no signal related to $Ca(OH)_2$ was observed in the fillers by means of X-ray diffraction and IR spectroscopy and (3) the results investigated on the structural changes previously described.

In the case of those produced with 3% CaO followed by the calcination (400—800 °C, 1.5 hr) and mechanical disintegration, the pH values appeared in a reverse order as compared with those treated with more than 10% CaO mentioned above. Although the difference of pH among the fillers were relatively small, they increased the values with an increase in the temperature of calcination. Presumably the formation of localized basic salts might be predominant under the conditions of preparation with such a little amount of alkali as 3% CaO followed by the calcination at a sufficiently high temperature.

(iii) DPG Adsorption: Figure 3 (c) shows changes in the DPG adsorption of **N** hard clay. A hyperbolic decrease in the DPG adsorption analogous to the hygroscopicity described above appeared in the fillers (CaO 3—60%; calcination 400—600 °C, 1—1.5 hr; wet milling 18 hr). The higher the temperature of calcination, the greater the effect of decreasing the DPG adsorption or the surface activity of the filler obtained. However, the decreasing rate with respect to the change with the same amount of alkali was found to be greater in the filler prepared with a less amount of alkali followed by calcination at a lower temperature.

The great DPG adsorption of the dried **N** (53.44 g DPG/10^4 g filler) would diminish to the degree comparable to or even less than those of Dixie Clay (6.05 g DPG/10^4 g filler) and Silene EF (5.08 g DPG/10^4 g filler) by the treatment with more than 15 (or 35)% CaO and by the subsequent calcination at 600 (or 400) °C for 1—1.5 hr and mechanical disintegration.

Those prepared with alkali (CaO 3—50%) followed by the calcination (800 °C, 1—1.5 hr) and mechanical disintegration decreased the values as low as 1/2 of that of Silene EF. They remained the values nearly unchanged irrespective of the variation in the amount of alkali. This indicates that the surface activity of the fillers disappeared almost completely.

(iv) Specific Gravity and Bulk Density: Figures 3 (d) and (e) give changes in the specific gravity and bulk density of **N** hard clay, respectively.

A hyperbolic decrease in the specific gravity and a maximum value with about 35% CaO in the bulk density appeared in the fillers (CaO 3—60%; calcination 400 °C, 1.5 hr; wet milling 18 hr).

For the same composition of alkali, however, those prepared with hydrated lime (3—50% CaO) followed by the calcination (600 °C, 1—1.5 hr) and the same mechanical disintegration as above afforded a lower specific gravity and a greater bulk density than those of the former fillers.

The higher the temperature of calcination, the greater the increase in the specific gravity and the decrease in the bulk density of the fillers prepared.

Consequently those treated with alkali (3—50% CaO) and by the subsequent calcination (800 °C, 1—1.5 hr) and mechanical disintegration showed a maximum value in the specific gravity with about 25% CaO and smaller values of the bulk density which increased almost linearly up to 50% CaO. This suggests that sintering occurred in the minute crystallites of the fillers.

The specific gravity (2.3110) and the bulk density (2.65 cc/g) of the best reinforcing filler[2] derived from **N** were found to be corresponded to the intermediates of the respective values of Dixie Clay (2.5684; 1.38 cc/g) and Silene EF (2.0989; 4.05 cc/g).

(3) Morphology. The prepared hard clays showed small, irregular flake-shaped crystallites, mostly in aggregates, which differ from those[30] of Dixie Clay and Silene EF; the former being well-formed hexagonal flakes of kaolinite[31] and the latter being spheroidal-colloid particles in clusters with some elongated lath-shaped units as given in Fig. 4 Plates 2 and 3, respectively.

Plate 1 illustrates the best **N** hard clay (CaO 6%; calcination 600 °C, 1.5 hr; wet milling 18 hr) with the

smallest average particle size and its distribution as compared with those prepared under the conditions deviated from the optima. The filler exhibited comparable tensile strength and higher elongation than those of Dixie Clay, though its modulus and hardness were found to be lower than those of the latter.[2)]

The average particle size and its distribution of the prepared fillers and the contents of newly formed minerals, CSH, CAH and calcite, were intimately related to the conditions of treatment with hydrated lime followed by calcination and mechanical disintegration besides the mineralogical composition of the original acid clay. A detailed report will be made in comparison with the morphology of **M** hard clay in the next paper.

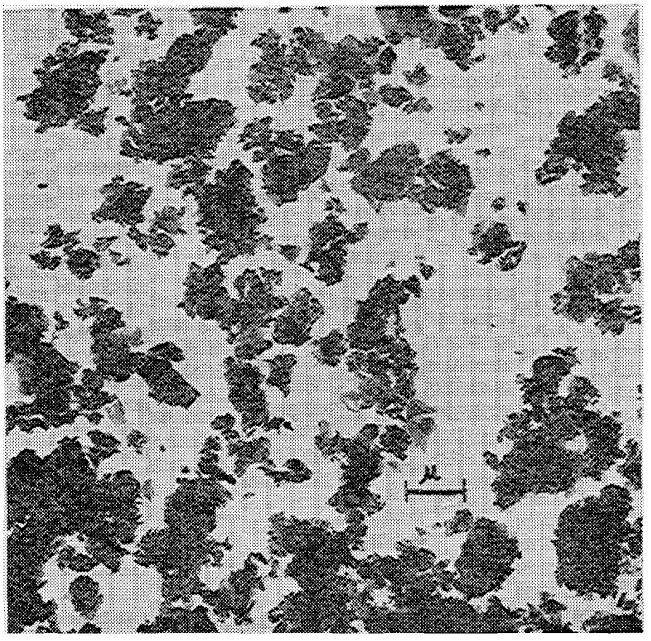

Plate 1. The best **N** hard clay ×9000

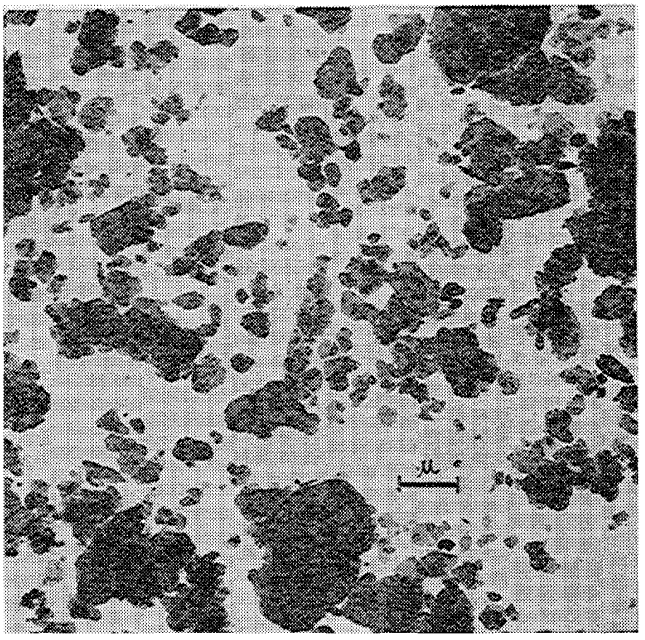

Plate 2. Dixie clay ×9000

Plate 3. Silene EF ×9000

Fig. 4. Electron micrograph of the best **N** hard clay (CaO 6%; calcination 600 °C, 1.5 hr; wet milling 18 hr) in comparsion with those of Dixie clay and Silene EF.
Plate 1: The best **N** hard clay, Plate 2: Dixie clay, Plate 3: Silene EF.

Conclusion

On the basis of the foregoing investigations on the structure, morphology and physicochemical properties of the fillers together with the results investigated on the reinforcing properties described in the previous paper,[2)] it can be unequivocally concluded that the effect on the reinforcement of SBR-1502 compounds agreed precisely with the reduction in both the particle size and its distribution of the fillers.

The treatment with an optimum amount (CaO 6%) of hydrated lime and by the subsequent calcination at an appropriate temperature (600 °C) for a proper time (1.5 hr) and sufficient mechanical disintegration (wet milling 18 hr) caused a favorable change in the structure of **N**. This resulted in an increase in the bulk density and an decrease in the specific gravity of the prepared filler. It simultaneously contributed to restrain the surface properties such as hygroscopicity, pH and DPG adsorption, which were modified to the extent closing to those of Dixie Clay and/or Silene EF.

The treatment with an appropriate amount of hydrated lime followed by proper calcination contributes not only to the formation of CSH and/or CAH on the surfaces of the montmorillonite lamellae, but also to the restraint of thermal effects inducing the excessive, irreversible contraction, unfavorable collapse, sintering and/or partial fusion of the minute crystallites due to the interposition of the newly formed minerals. The collapse, sintering and partial fusion of the calcined products resulted in the formation of too hard aggregates to be disintegrated and the occurrence of a serious breakdown or complete loss in the effective functional

groups involved. The inferior reinforcing properties[2] of the fillers treated by the calcination at 800 °C for 1—1.5 hr can be attributed to those reasons.

The authors wish to thank the late Prof. T. Kuwata for his constant interest and encouragement during this work, Prof. J. Kumanotani for his help and valuable discussion, and Mr. Y. Sugawara, the President of Mizusawa Industrial Chemicals Co., Ltd., for providing the sample of Nakajo acid clay.

References

1) H. Rai and J. Yamada, This Bulletin, **45**, 1540 (1972).
2) H. Rai and J. Yamada, *ibid.*, **46**, 3555 (1973).
3) H. E. Swanson and E. Tatge, *NBS Circular* **539**, **I**, 58 (1953); ASTM, X-Ray Powder Data File Card 4-0733.
4) D. M. C. MacEwan, "The X-ray Identification and Crystal Structures of Clay Minerals," ed. by G. Brown, Miner. Soc. London (1961), p. 143, 200.
5) H. E. Swanson and E. Tatge, *NBS Circular* **539**, **I**, 39 (1953).
6) G. R. Glenn, *J. Amer. Ceram. Soc.*, **50**, 312 (1967).
7) H. F. W. Taylor, "Progress in Ceramic Science," Vol. 1, ed. by J. E. Burke, Pergamon Press (1961), p. 89.
8) H. E. Swanson and R. K. Fuyat, *NBS Circular* **539**, **II**, 51 (1953); ASTM, X-Ray Powder Data File Card 5-0586.
9) L. Heller, V. C. Farmer, R. C. Mackenzie, B. D. Mitchell, and H. F. W. Taylor, *Clay Mineral Bull.*, **5**, 56 (1962).
10) E. C. Jonas, *Natl, Acad, Sci., Publ.*, **395**, 66 (1955).
11) R. E. Grim and W. F. Bradley, *Amer. Mineral.*, **33**, 50 (1948).
12) W. F. Bradley and R. E. Grim, *Amer. Mineral.*, **36**, 182 (1951).
13) R. E. Grim and W. F. Bradley, *J. Amer. Chem. Soc.*, **23**, 242 (1940).
14) L. S. Wells, W. F. Clarke, and H. F. McMurdie, *J. Res. Natl. Bur. Stand.*, **30**, 367 (1943).
15) I. Oinuma and H. Kodama, "Clay Science Handbook," ed. by S. Iwao, Clay Sci. Soc. Japan, Gihodo (1967), pp. 65—75.
16) V. Stubičan and R. Roy, *Amer. Mineral*, **46**, 32 (1961).
17) V. Stubičan and R. Roy, *Zeit. Krist.*, **115**, 200 (1961).
18) B. D. Mitchell, V. C. Farmer, and W. J. MacHardy, *Advan. Agr.*, **16**, 349 (1964).
19) E. R. Lippincott, A. V. Valkenburg, C. E. Weir, and E. N. Bunting, *J. Res. Natl. Bur. Stand.*, **61**, 61 (1958).
20) M. Field, I. K. Walker, and P. P. Williams, *New Zealand J. Sci. Technol.*, **38**, 31 (1956).
21) V. C. Farmer and J. D. Russel, *Spectrochim. Acta*, **20**, 1149 (1964).
22) K. Fukui, *J. Soc. Rubber Ind. Japan*, **37**, 858 (1964).
23) E. Suito and M. Arakawa, *ibid.*, **34**, 885 (1961).
24) E. E. Angino, *Amer. Mineral.*, **52**, 137 (1967).
25) C. E. Weir and E. R. Lippincott, *J. Res. Natl. Bur. Stand.*, **65A**, 175 (1961).
26) O. W. Flörke, *Neues Jahrb. Mineral. Monatsh.*, 217 (1953); Veröffentl. *Max-Planck-Inst. Silikatforsch.*, **15**, 11 (1955); *Silicates Inds.*, **26**, 424 (1961).
27) V. Z. Zabelin, *Dokl. Akad. Nauk SSSR*, **139**, 184 (1961).
28) Y. Hirata, *Kogyo Kagaku Zasshi*, **59**, 321 (1956).
29) J. A. Hockey, *Chem. Ind.*, **9**, 57 (1965).
30) E. Suito, M. Arakawa, and H. Hasegawa, *J. Soc. Rubber Ind. Japan*, **26**, 217 (1953).
31) R. E. Grim, "Clay Mineralogy," 2nd Edt., MacGraw-Hill Inc., (1968), pp. 171—174.

NOTES

BULLETIN OF THE CHEMICAL SOCIETY OF JAPAN, VOL. 48 (5), 1629—1630 (1975)

The Radical Formation of Polyethylene by Tesla Discharge

Akira YOKOHATA, Katsuyuki HARAKON, Kazuto TAKIMOTO, and Satoru TSUDA
Department of Chemistry, Faculty of Engineering, Hiroshima University, Senda-machi, Hiroshima 730
(Received March 14, 1974)

Synopsis. The ESR spectra of polyethylene discharged by a Tesla coil in an atmosphere of various gases were observed. An alkyl radical showing a six-line spectrum was formed in the Tesla discharge at 77 K, whereas a polyenyl radical was mainly produced by the discharge with an increase in the duration time; these facts showed that the effects of the Tesla discharge were similar to the γ-irradiation up to a high dose.

Many studies of the radical formation of polyethylene by γ-irradiation have been done.[1-6] The results of these works have revealed that at least three kinds of radicals are produced in polyethylene irradiated at room temperature. A radical with a short life-time gives a sextet spectrum and is identified with the alkyl radical, $-CH_2-\dot{C}H-CH_2$. A radical with a longer life-time shows a septet spectrum and is assigned to the allyl radical, $-CH_2-\dot{C}H-CH=CH-CH_2-$. The third radical has a very long life-time and gives a singlet spectrum, identified with the polyenyl radical, $-CH_2-\dot{C}H(-CH=CH)_n-CH_2-$. The alkyl and allyl radicals are the main products in γ-ray irradiation, whereas in the case of a high-dose irradiation the polyenyl radical is mainly formed.

On the contrary, the mechanism of the radical formation of polyethylene in a discharge has not been revealed. Our purpose in this work is to confirm that it is reasonable to interpret discharge chemistry from the standpoint of radiation chemistry.

H_2, N_2, and Ar gases with a high purity were used without further purification. The He gas was purified according to Polley's cold-charcoal-trap method.[7] The polyethylene used in these experiments was HZ 5000p, supplied by the Mitsui Petroleum Chemical Co. as powder. This powder sample was evacuated for 50 hr *in vacuo*. After the introduction of each gas (0.3 Torr), the sample tube was cut off. γ-Irradiation at a dose rate of 3×10^3 r/hr and a discharge by using a Tesla coil were carried out in the Pyrex-glass part of the sample tube at 77 K, while the ESR spectra were measured in the quartz-glass part at the same temperature. The ESR spectra were observed by using a Japan Electron Optics Laboratory JES-3BS-X-type spectrometer at a microwave frequency of 9400 MHz, with a 100 kHz field modulation. The gas products from irradiated and discharged polyethylene were measured by using a Hitachi-RMU-6D mass spectrometer.

It is well known that the alkyl radical formed by the γ-irradiation of unstretched polyethylene shows a six-line spectrum. It is interpreted as resulting from the abstraction of a hydrogen atom from the middle of a linear polyethylene[8] and from the apparent equal coupling of the unpaired electron to α-and β-hydrogen.[9,10]

Figure 1 shows the first derivative curve and the integrated curve of the ESR spectrum of the radical produced by Tesla discharge in an atmosphere of H_2 gas (0.3 Torr). The ESR spectrum with a hyperfine coupling constant of 30 gauss is similar to that of γ-irradiated polyethylene.[11] Furthermore, the absorption-peak intensity ratio of the sextet in the integrated curve was 1:4:11:10:4:1. This ratio is in good agreement with the theoretical ratio for the alkyl radical, 1:5:10:10:5:1. Thus, it can be concluded that, in the Tesla discharge, the alkyl radicals are mainly formed, as in radiolysis. In an atmosphere of N_2, He, and Ar gasses, the same spectra were observed, although the peaks differed in sharpness.

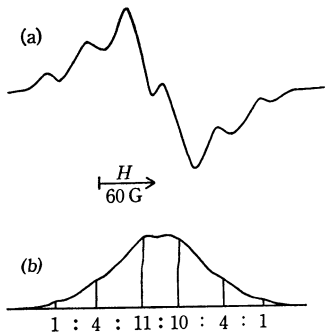

Fig. 1. ESR spectrum of radical produced by Tesla discharge at 77 K.
(a): First derivative curve, (b): Integrated curve.

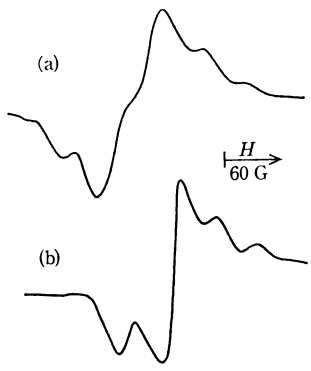

Fig. 2. Transformation of polyethylene radical generated by the dischage to peroxy radical.
(a): After the immersion into a dry-ice bath for 60 s.
(b): After exposure to air for 60 s in a dry-ice bath.

When polyethylene discharged at 77 K was exposed to air at its temperature, the ESR spectrum was almost the same as the original. Figure 2(a) shows the ESR spectrum of the discharged polyethylene after immersion into a dry-ice bath for 60 s. Although there was an appreciable loss in signal, there was little or no change in line shape. The spectrum in Fig. 2(b) represents the behavior of the alkyl radical when exposed to air for 60

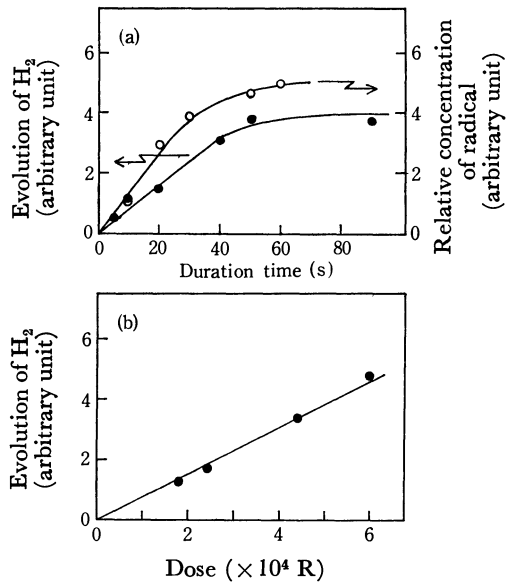

Fig. 3. Evolution of H_2 gas *vs.* duration time and dose. (a): Discharge, (b): γ-Irradiation.

s under the same conditions. It has been found that many of the polymer radicals react with oxygen to form peroxy radical.[11] Thus, the singlet line in the central part of the spectrum, which is superimposed on the spectrum attributable to the alkyl radical, represents the peroxy radical.

A relatively major quantity of H_2 gas and a trace amount of CH_4 gas were detected from the discharged polyethylene, whereas only the H_2 gas was observed from the γ-irradiated polyethylene. Lawton *et al.* have revealed the mechanism of H_2-gas evolution in γ-irradiated polyethylene.[12] Figure 3 shows the amount of H_2 gas evolved against the duration time and the irradiation dose. In the case of discharge, the amounts remained constant 50 s. The relative concentration of the alkyl radical also similarly became constant. On the contrary, in the case of γ-irradiation the amount of H_2 gas increased linearly with an increase in the irradiation dose. Figure 4 shows the ESR spectra of polyethylene with an increase in the duration time of discharge and in the irradiation dose of the γ-rays. The ESR spectrum of polyethylene discharged for 120 s ill-resolved, and the overall line-width of the spectrum of polyethylene discharged for 300 s is smaller than that in Fig. 4(b), suggesting that the alkyl radical is transformed with the dose to another radical, probably one with a singlet absorption. In the polyethylene irradiated with high dose γ-rays, the spectrum containing a six-line (4(d)) is transformed to a singlet with a smaller overall line width (4(e)). The latter spectrum is assigned to the polyenyl radical.[13] Thus, the ESR spectrum of polyethylene discharged for a long duration time is presumed to be attributable to the polyenyl radical, as in radiolysis. Although we could not find any precise correspondence between the Tesla discharge and the γ-irradiation, from these results it was semiquantitatively ascertained that their effects were similar to each other up to a high dose.

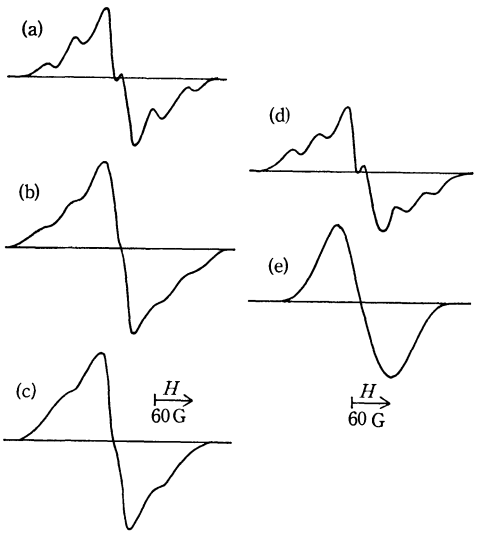

Fig. 4. ESR spectra of polyethylene discharged and irradiated with an increasing duration time and dose. (a): Discharge for 10 s, (b): 120 s, (c): 300 s, (d): γ-Irradiation with 8 MR, (e): 1000 MR.

References

1) E. J. Lawton, J. S. Balwit, and R. S. Powell, *J. Chem. Phys.*, **33**, 395 (1960); **33**, 405 (1960).
2) D. Libby, M. G. Ormerod, and A. Charlesby, *Polymer*, **2**, 212 (1960).
3) S. Ohnishi, Y. Ikeda, and M. Kashiwagi, *ibid.*, **2**, 119 (1961).
4) H. Kashiwabara, *J. Phys. Soc. Jap.*, **16**, 2494 (1961).
5) M. Kashiwagi, *J. Chem. Phys.*, **36**, 575 (1962).
6) S. Ohnishi, This Bulletin, **35**, 254 (1962).
7) M. H. Polley, W. D. Schaeffer, and W, R. Smith, *J. Phys. Chem.*, **57**, 469 (1953).
8) J. J. Windle, *J. Chem. Phys.*, **31**, 859 (1959).
9) J. F. Gibson, D. J. E. Ingram, M. C. Symons, and M. G. Townsend, *Trans. Faraday Soc.*, **53**, 914 (1957).
10) R. S. Alger, T. H. Anderson, and L. A. Webb, *J. Chem. Phys.*, **30**, 695 (1959).
11) B. R. Loy, *J. Poly, Sci.*, **44**, 341 (1960).
12) E. J. Lawton, J. S. Balwit, and R. S. Powell, *ibid.*, **32**, 257 (1958).
13) R. J. Abraham, H. W. Melville, D. W. Ovenall, and D. H. Whiffen, *Trans. Faraday Soc.*, **54**, 1133 (1958).

BULLETIN OF THE CHEMICAL SOCIETY OF JAPAN, VOL. 48 (5), 1631—1632 (1975)

The Radiation-induced Dehalogenation of Dichloromethane and Dibromomethane in Methanol Solutions

Hajime OGURA, Takashi FUJIMURA, Takaaki UNNAI,, and Masaharu KONDO
Department of Chemistry, Faculty of Science, Tokyo Metropolitan University, Setagaya-ku, Tokyo 158

(Received October 26, 1974)

Synopsis. The scheme of the radiation-induced dehalogenation of dichloromethane and dibromomethane was investigated in deaerated methanol. The relative rate constants of those solutes toward e^-_{sol} were determined by competition kinetics, using a N_2O scavenger.

Organic halides are generally radiosensitive, and the main reaction in the radiolysis is usually dehalogenation, producing readily determinable halide ions. Therefore, a number of studies concerning the radiation chemistry of organohalogen compounds and their aqueous or alcohol solutions have appeared in the literature.[1-9]

In previous work,[10-12] we ourselves have determined the reactivities of monochlorobenzene and its derivatives toward the solvated electron in alcohols. We now wish to extend those studies to simple aliphatic halogen compounds, such as dichloromethane and dibromomethane, in methanol systems and to elucidate the scheme of the radiation-induced dehalogenation of these methylene halides in methanol solutions.

Experimental

The methanol was purified according to the procedure proposed by Imamura *et al.*[13] The dichloromethane and dibromomethane were treated successively with dilute sulfric acid and a 0.1 M K_2CO_3 solution and washed repeatedly with distilled water. They were subjected to fractional distillation after being dried over $CaCl_2$. A deaerated solution (5 ml) prepared by the conventional vacuum technique with freeze and thaw cycles was sealed in a glass cell. ^{60}Co γ-irradiation was carried out at a dose rate of 1.34×10^{18} eV ml^{-1} h^{-1}. The halide ions were determined by potentiometric titration. The formaldehyde was determined spectrophotometrically by the use of chromotropic acid. The amounts of hydrogen and nitrogen were determined by gas chromatography, using a Molecular Sieve 5A column and argon as the carrier gas.

Results and Discussion

Figure 1 shows the yields of halides ions as a function of the methylene dihalide concentration in deaerated methanol solutions. $G(Cl^-)$ reaches a plateau value of 3.6 at concentrations above 0.07 M CH_2Cl_2. The significantly high yield of $G(Br^-)$, which is, for example, 54 at 0.07 M CH_2Br_2, indicates the occurrence of a chain reaction.

Figure 2 shows the yields of bromide ions and formaldehyde as a function of the absorbed dose in a 0.07 M CH_2Br_2 solution under the three following experimental conditions; (1) deaerated, (2) aerated, and (3) sealed. The experimental condition is designated as "sealed" when the irradiation ampoule is filled with an aerated solution up to a ground-glass joint stopper. Under this condition, only the oxygen initially dissolved in a solution can participate in the reaction. The condition is designated as "aerated" when the solution is equilibrated with the oxygen present in the air above a solution in a stoppered vial during irradiation. As is illustrated in Fig. 2, the yields of Br^- and H_2CO from the sealed and the aerated systems are initially the same (that is, $G(Br^-)=5.7$ and $G(H_2CO)\simeq4$), but on further irradiation, the yields from the sealed system rise very sharply at doses over 10^{22} eV l^{-1}. This might be due to a progressive depletion of the oxygen content in solutions, because the yields after the break are very close to those in deaerated solutions, that is, $G(Br^-)=54$ and $G(H_2CO)=50$, indicating that the dissolved oxygen inhibits the chain reaction.

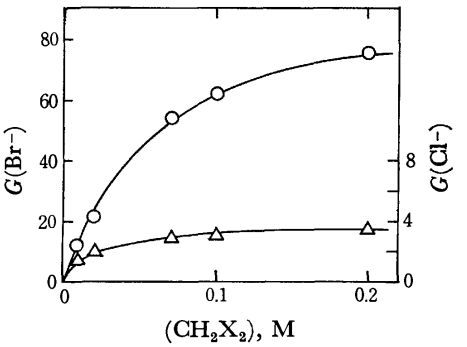

Fig. 1. Dependence of halide ion yields on the initial concentrations of methylene dihalides in methanol.
△: CH_2Cl_2 solution, ○: CH_2Br_2 solution

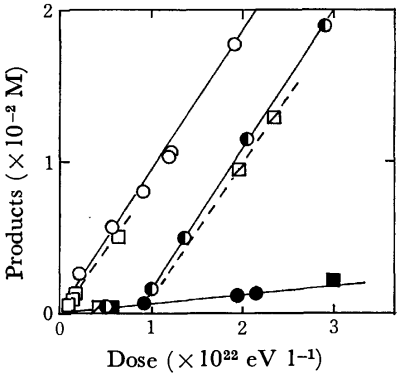

Fig. 2. Yields of bromide ion and formaldehyde as a function of absorbed dose in methanol solution of 7×10^{-2} M CH_2Br_2.
Bromide ion; ●: aerated, ○: deaerated, ◐: sealed
Formaldehyde; ■: aerated, □: deaerated, ◪: sealed

The species initially produced by the irradiation of methanol are usually presented as follows:

$CH_3OH\rightsquigarrow e^-_{sol}$, H, CH_2OH, $CH_3OH_2^+$ and molecular products (0)

The solvated electrons and H atoms are likely to react

with dihalogeno methane as follows:

$$e^-_{sol} + CH_2X_2 \longrightarrow CH_2X + X^- \quad (1)$$

$$H + CH_2X_2 \longrightarrow CH_2X + HX \quad (2)$$

$$\searrow CHX_2 + H_2 \quad (2')$$

X is Cl or Br depending on the solute. In deaerated methanol solutions of CH_2X_2 above 0.05 M, the observed $G(H_2)$ is almost equal to the molecular yield of hydrogen, $G_{H_2}=1.7$, so Reaction (2') may be excluded in the present system.[14] Our finding that, in a deaerated CH_2Cl_2 solution, $G(Cl^-)$ is 3.6 and very close to $Ge^-_{sol}+G_H$, taking $Ge^-_{sol}=2.0$ and $G_H=1.7$, indicates that all the Cl^- results from Reactions (1) and (2), while CH_2OH dose not contribute to Cl^- formation in this system. Otherwise, $G(Cl^-)$ would have to be equal to the total radical yield, $G(R)=Ge^-_{sol}+G_H+G_{CH_2OH}=6.5$. The high yields of Br^- and H_2CO from deaerated CH_2Br_2 solutions suggest that these products are formed by the following chain mechanism, similar to that proposed for the radiolysis of carbon tetrachloride in alcohols:[15]

$$CH_2OH + CH_2Br_2 \longrightarrow CH_2Br + H_2CO + HBr \quad (3)$$

$$CH_3OH + CH_2Br \longrightarrow CH_2OH + CH_3Br \quad (4)$$

Since $G(Br^-)$ and $G(H_2CO)$ are very close to each other, as is shown in Fig. 2, these products are likely to be formed by the same reactions. Although the yield of CH_3Br in Reaction (4) has been determined only qualitatively at the present time, its presence may support this view. On a thermochemical basis, Reaction (4) is exothermic ($\Delta H=-2$ kcal mol^{-1}), while it is endothermic ($\Delta H=4$ kcal mol^{-1}) when $X=Cl^-$. Moreover, in the 0.07 M CH_2Cl_2 solution, the observed $G(H_2CO)$ was only about 2,[14] close to the molecular yield of H_2CO in pure methanol, so the chain dehalogenation of CH_2Cl_2 is unlikely to occur. These considerations can explain the marked difference between $G(Cl^-)$ and $G(Br^-)$. In an aerated system, the chain breaking may be due to the reaction of dissolved oxygen with CH_2OH and CH_2Br.

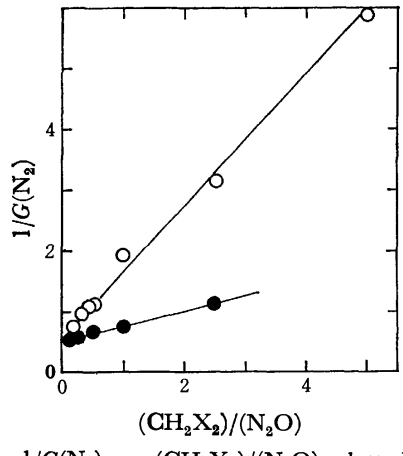

Fig. 3. $1/G(N_2)$ *vs.* $(CH_2X_2)/(N_2O)$ plotted according to Eq. (1). ●: CH_2Cl_2, ○: CH_2Br_2

When nitrous oxide is present in a deaerated system, Reaction (5) will compete with Reaction (1) for the solvated electron:

$$e^-_{sol} + N_2O \longrightarrow N_2 + O^- \quad (5)$$

On the basis of simple competition kinetics, one can formulate:

$$\frac{1}{G(N_2)} = \frac{1}{Ge^-_{sol}}\left[1+\frac{k_1(CH_2X_2)}{k_5(N_2O)}\right] \quad (I)$$

where k_1 and k_5 represent the rate constants of Reactions (1) and (5) respectively. Plots of $1/G(N_2)$ *vs.* $(CH_2X_2)/(N_2O)$ are seen to give straight lines in Fig. 3. From the slopes of the lines and the intercept, one can obtain $k_1/k_5=0.50$ for CH_2Cl_2 and $k_1/k_5=2.15$ for CH_2Br_2. Taking 1.3×10^{10} M^{-1} s^{-1} for k_5,[16] k_1 is estimated to be 6.5×10^9 M^{-1} s^{-1} for CH_2Cl_2 and 2.9×10^{10} M^{-1} s^{-1} for CH_2Br_2.

References

1) J. W. T. Spinks and R. J. Woods, "An Introduction to Radiation Chemistry," John Wiley & Sons, New York (1964).
2) M. Anbar and P. Neta, *Int. J. Appl. Radiat. Isotopes* **18**, 493 (1967).
3) W. V. Sherman, *J. Phys. Chem.*, **70**, 2872 (1966).
4) W. V. Sherman, *J. Amer. Chem. Soc.*, **88**, 1567 (1966).
5) W. V. Sherman, *J. Phys. Chem.*, **72**, 2287 (1968).
6) C. Radlowski and W. V. Sherman, *ibid.*, **74**, 3043 (1970).
7) R. Evans, E. Neyto, C. Radlowski, and W. V. Sherman *ibid.*, **75**, 2762 (1971).
8) T. Sawai and Y. Shinozaki, *Chem. Lett.*, **1972**, 865.
9) T. Sawai, T. Shimokawa, and Y. Shinozaki, This Bulletin, **47**, 1889 (1974).
10) H. Matsuoka, K. Sato, T. Masuda, and M. Kondo, *Nippon Kagaku Zasshi*, **87**, 1520 (1966).
11) H. Matsuoka, *J. Nucl. Sci. Technol.*, **8**, 23 (1971).
12) H. Matsuoka, K. Sato, Y. Asahi, T. Masuda, and M Kondo, *ibid.*, **9**, 7 (1972).
13) M. Imamura, S. U. Choi, and N. N. Lichtin, *J. Amer Chem. Soc.*, **85**, 3565 (1963).
14) H. Ogura, T. Unnai, and M. Kondo, unpublished data.
15) p. 337 in Ref. (1).
16) H. Seki and M. Imamura, *J. Phys. Chem.*, **71**, 870 (1967).

BULLETIN OF THE CHEMICAL SOCIETY OF JAPAN, VOL. 48 (5), 1633—1634 (1975)

A Study on Anode Effect in KF-2HF System. I. ESCA Spectra of Carbon and Graphite Anode Surfaces

Hiroki IMOTO, Tsuyoshi NAKAJIMA, and Nobuatsu WATANABE

Department of Industrial Chemistry, Faculty of Engineering, Kyoto University, Yoshida, Sakyoku, Kyoto 606

(Received November 7, 1974)

Synopsis. The ESCA spectra of carbon and graphite electrodes, used as an anode in the molten KF-2HF system at 100 °C, indicated that a $(CF)_n$ film was formed on the surface of the electrodes. This may give strong support to the assumption that the anode effect in molten KF-2HF is caused by the formation of $(CF)_n$ on the carbon and graphite electrodes.

Fluorine gas is produced by the electrolysis of molten KF-2HF by using a carbon anode. The electrolysis current density is in the range 0.1—0.18 A/cm^2,[1] since the anode effect takes place when the current density is higher than this, and electrolysis must be stopped. It is, therefore, necessary to study the anode effect to increase the operating current density. It has been claimed that the anode effect is caused by a decrease of the wettability of an anode surface with electrolyte, KF-2HF, owing to the formation of a $(CF)_n$ film which has very low surface energy.[2-7] The investigation confirmed this mechanism.

Experimental

Six kinds of carbon and graphite samples were prepared in the following manner. Five electrode samples were anodically polarized under various conditions and the surface of the other electrode was treated with fluorine gas.[8] Their ESCA spectra were obtained with a Du Pont 650 Electron Spectrometer. The cubic carbon and graphite electrodes which were covered with Teflon tape except for one side were fixed at the end of a brass rod coated with Teflon. A Pt rod was used as a reference electrode. The molten KF-2HF system was dehydrated by pre-electrolysis using a carbon electrode.

Results and Discussion

Figure 1 shows the ESCA spectra of the carbon 1s electron in the samples which were prepared as follows.

(A) Anodically polarized at 5 V *vs.* Pt for 30 min.

(B) Anodically polarized at 10 V *vs.* Pt for 30 min.

(C) Anodically polarized at a current density of 350 mA/cm^2, the circuit being opened immediately after onset of the anode effect.

(D) Anodically polarized at a constant current density of 350 mA/cm^2, and polarized further at 20 V *vs.* Pt for 5 min after onset of the anode effect.

(E) Conditions are the same as for (D) except for polarization of 30 min after onset of the anode effect.

(F) The carbon and graphite samples were directly treated with fluorine gas under the following conditions. (I) F_2 pressure; 200 mmHg, temp.; 450 °C, time; 2 hr. (II) F_2 pressure; 110 mmHg, temp.; 450 °C, time; 0.5 hr. $(CF)_n$ was formed on the surface of the samples.

(G) The original carbon and graphite samples.

When the carbon and graphite electrodes were polarized at various controlled potentials, the current densities

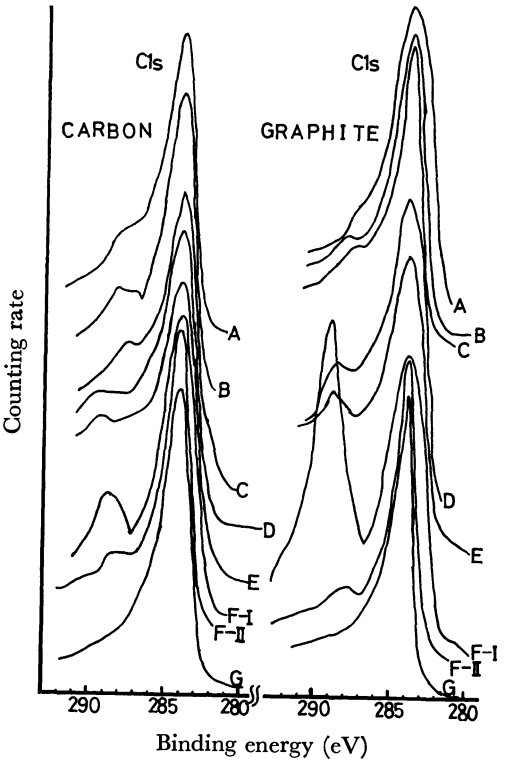

Fig. 1. ESCA spectra of carbon and graphite (C 1s).

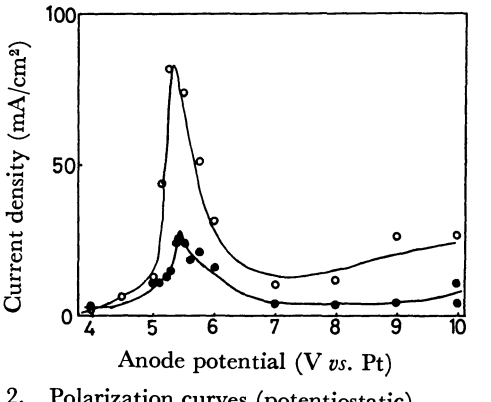

Fig. 2. Polarization curves (potentiostatic).
○: Carbon, ●: Graphite.

reached stationary values. Figure 2 shows the relation of these values against their potentials; electrode (A) was prepared under conditions of normal electrolysis, (B) under conditions of the anode effect. The latter conditions, however, are milder than those of (D) and (E). Anodic polarization of carbon and graphite electrodes with a constant current density of 350 mA/cm^2 gave rise to the anode effect within five seconds. The spectra of the original carbon and graphite samples (G) indicated

only one peak at 284 eV. This peak may correspond to the binding energy of the carbon 1s electron in cases where the carbon atom has the C–C bond. On the other hand, the spectra of samples (F) fluorinated by fluorine gas indicated two peaks at 284 and 289 eV. The peak at 289 eV may be assigned to the binding energy of the carbon 1s electron in cases where the carbon atom has the C–F bond. If the carbon atom is combined with the fluorine atom which is the most electro-negative element, the chemical shift of the binding energy of the carbon 1s electron must be large and positive. The spectra of samples (A), (B), (C), (D), and (E) indicated the same peaks as those of sample (F), that is, at 284 eV and 289 eV (the latter became a shoulder or appeared to slightly approach the peak at 284 eV as it was much smaller than this peak). Consequently, it was proved that the $(CF)_n$ film was formed on the surface of the carbon and graphite anodes not only during the anode effect but also under normal electrolysis conditions. From the results described above, it can be considered that the following reactions may occur on the anode surface, when the molten KF–2HF is electrolyzed by using the carbon or graphite anode.

$$2F^- \longrightarrow F_2 + 2e^- \quad (1)$$

$$nC + nF^- \longrightarrow (CF)_n + ne^- \quad (2)$$

When a $(CF)_n$ compound is formed on the anode surface during the evolution of fluorine, the wettability of the anode surface with the molten KF–2HF decreases markedly because of the very low surface energy of the $(CF)_n$ compound and the carbon and graphite surfaces do not come directly into contact with the electrolyte. If a large part of the anode surface is covered with the $(CF)_n$ conpound, the anode reaction does not proceed and only a small arc current flows through the interface at the anode under higher voltages. This is called the anode effect. However, since the following reaction (Eq. (3)) is considered to take place simultaneously, the net formation reaction rate of $(CF)_n$ during the fluorine evolution reaction depends upon the reaction rates of Eqs. (2) and (3).

The decomposition reaction of the $(CF)_n$ film.

$$(CF)_n \longrightarrow C + CF_4 + C_2F_6, \textit{ etc.} \quad (3)$$

In conclusion, the previous explanation that the cause of the anode effect is the formation of a compound which has a very low surface energy on the carbon and graphite electrodes has been confirmed experimentally by ESCA analysis.

Acknowledgement is due to Shimadzu Seisakusho for permission to use their electron spectrometer.

References

1) A. J. Rudge, "Industrial Electrochemical Processes," ed. by A. T. Kuhn, Elsevier Publishing Company, Amsterdam-London-New York (1971), p. 47.
2) N. Watanabe and M. Ishii, *Denki-Kagaku*, **29**, 364 (1961).
3) N. Watanabe and T. Asaue, *ibid.*, **39**, 123 (1971).
4) N. Watanabe, M. Ishii, and S. Yoshizawa, *J. Electrochem. Soc. Japan*, **29**, 177 (1961).
5) N. Watanabe, M. Ishii, and S. Yoshizawa, *ibid.*, **29**, 180 (1961).
6) N. Watanabe, M. Inoue, and S. Yoshizawa, *Denki-Kagaku*, **31**, 698 (1963).
7) M. Nishimura, A. Tasaka, K. Nakanishi, and N. Watanabe, *ibid.*, **38**, 294 (1970).
8) N. Watanabe and M. Takashima, *Kogyo Kagaku Zasshi*, **74**, 1788 (1971).

BULLETIN OF THE CHEMICAL SOCIETY OF JAPAN, VOL. 48 (5), 1635—1636 (1975)

ENDOR Studies on the Hindered Alkylbiphenyl Anion Radicals

Kazuhiko Ishizu, Fujito Nemoto, Kazuo Mukai, Masahiro Kohno,* and Hideo Hasegawa*

Department of Chemistry, Faculty of Science, Ehime University, Bunkyo-cho, Matsuyama 790

** Japan Electron Optics Laboratory, Akishima, Tokyo 196*

(Received November 8, 1974)

Synopsis. ENDOR observations were carried out for the anion radicals of 2,2′-bitolyl, 2,2′-diethylbiphenyl, and 2,2′-diisopropylbiphenyl. The spin densities obtained from the ring protons at the *ortho*-positions showed a depression in the order of the spherical bulkiness of the substituents, and the degrees of the steric hindrance of the biphenyl ring were estimated based on McLachlan's MO calculation. ENDOR experiments demonstrated that methyl groups undergo free rotation, but it is greatly hindered in each higher alkyl derivative.

Recently, ENDOR tequniques have often been applied to conformational studies of the aromatic free radicals. In particular, the multiple hyperfine components of the complex molecule have been successfully resolved, and the structures of the radicals have been discussed in detail on the basis of the accurate analysis of the spin densities.[1-3] In our previous ESR studies of the 2,2′-dialkylbiphenyl anion radicals, we have proposed that the coplanarity of the biphenyl ring would be enhanced by the delocalization of the unpaired electron and that the free rotation of the higher alkyl groups would be greatly hindered by the steric hindrance caused by the anomalous coplanarity of the biphenyl rings.[4]

In the present communication, we wish to report the ENDOR studies of the anion radicals of several hindered alkylbiphenyls, such as *o,o′*-bitolyl, 2,2′-diethylbiphenyl, and 2,2′-diisopropylbiphenyl. The validity of the ring-proton splittings assumed by ESR measurements was reconfirmed. In addition, the present ENDOR observations offered new experimental evidence to support the fact that the rotation of the ethyl and isopropyl groups at the *ortho*-position is nearly locked, while the methyl group of *o,o′*-bitolyl undergoes free rotation.

Experimental

The alkylbiphenyls used in this experiment were synthesized in the manner described in a previous paper.[5] The anion radicals were prepared by reduction with potassium metal in dimethoxyethane (DME) at the temperature of dry ice and aceton. The ENDOR spectra were recorded by a JEOL-type ES-EDX-1 spectrometer under operating conditions similar to those described elsewhere.[6] The ESR intensity began to saturate at a microwave output of about 2 mw on the dial scale of a JES-ME-3 ESR spectrometer, and the ENDOR spectra were successfully recorded in the temperature range from −65 to −85 °C.

Results and Discussion

Figure 1 shows the ENDOR spectra of the biphenyl (a), *o,o′*-bitolyl (b), 2,2′-diethylbiphenyl (c), and 2,2′-diisopropylbiphenyl (d) anion radicals. The ENDOR spectrum of the *o,o′*-bitolyl anion radical can be easily analyzed in terms of absorptions due to the *meta*-ring (14.21, 14.55 MHz), the *ortho*-ring and methyl (17.04 MHz) and the *para*-ring protons (21.26 MHz), in comparison with the ring-proton absorption of the biphenyl anion radical (*meta*: 14.37, *ortho*: 17.58 and *para*: 21.34 MHz). In the previous ESR studies of the 2,2′-diethylbiphenyl anion radical, we assumed that the methylene protons of the ethyl group reveal an equivalent splitting.[7] The ENDOR spectrum of the 2,2′-diethylbiphenyl anion radical (Fig. 1-(c)) was, however, clearly resolved into two kinds of different absorptions due to non-equivalent β-ethyl protons at 15.48 and 17.16 MHz.

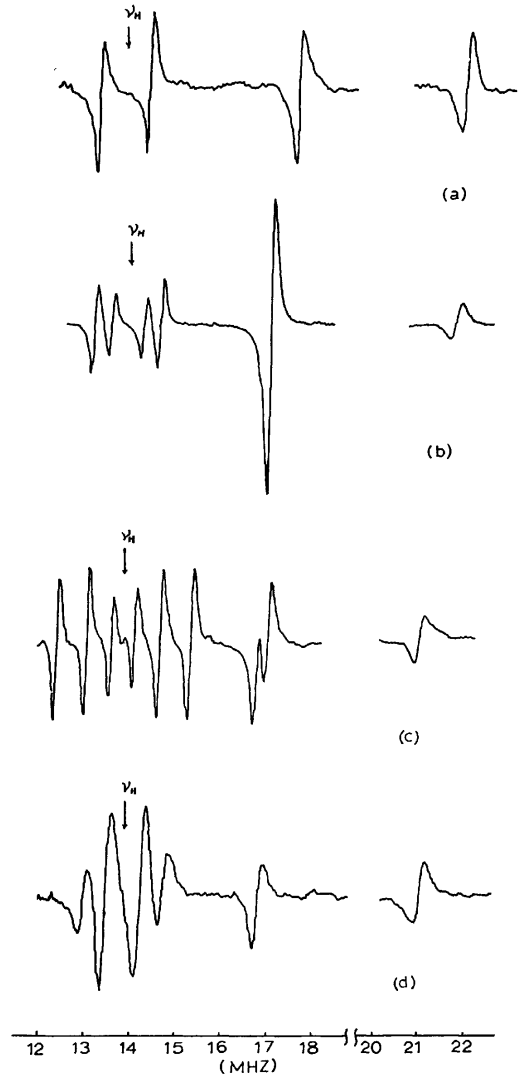

Fig. 1. The higher frequency half of the ENDOR spectra recorded at −85 °C.
(a) biphenyl, (b) *o,o′*-bitolyl, (c) 2,2′-diethylbiphenyl
(d) 2,2′-diisopropylbiphenyl, ν_H: free proton frequency

Table 1. Coupling constants of the hindered dialkylbiphenyls (G)

Position	2	3	4	5	6
Biphenyl	2.66	0.38	5.34	0.38	2.66
o,o'-Bitolyl	2.27	0.26	5.21	0.51	2.27
2,2'-Diethyl	2.29 1.07	0.19	5.20	0.59	2.11
2,2'-Diisopropyl	0.28	0.28	5.16	0.57	1.96

It is important to note here that each of the absorption frequencies of the ring protons (*meta*: 14.18, 15.40, *ortho*: 16.90 and *para*: 21.15 MHz) is nearly comparable with that of the *o,o'*-bitolyl anion radical. A similar conformational dependence of the spin-density distribution can be seen in 2,2'-diisopropylbiphenyl, but the splitting of the isopropyl-β-proton is greatly reduced and its absorption overlaps with one of the *meta* proton absorptions (14.25 MHz) in the vicinity of the free-proton frequency. The proton-coupling constants of the 2,2'-dialkylbiphenyls are summarized in Table 1. It is interesting that the experimental spin densities decrease with the order of the spherical bulkiness of the substituents.

This probably means that the higher alkyl groups bring a larger steric hindrance into the biphenyl ring than that in the methyl derivative. A quantitative estimation of the twisting angle (θ) of the phenyl rings for the higher alkyl derivatives needs elaborate MO calculations, and the hyperconjugative effect of the higher alkyl groups should be rigorously taken into account.

In a qualitative approach, however, the θ-values for higher alkyl derivatives can be estimated using the results calculated for the methyl derivative, since a perturbation of the ring-spin density due to the hyperconjugation of the higher alkyls is usually small. As is shown in Fig. 2, the θ-values of the ethyl and the isopropyl derivatives would be in the range from 40 ° to 50 °.

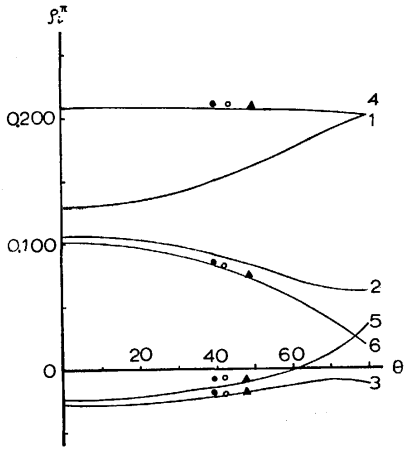

Fig. 2. Dependence of theoretical spin density of ring carbon atoms on twisting angle θ between the phenyl ring in 2,2'-bitolyl anion radical. Experimental values are shown in the figure using the following notation.
●···: *o,o'*-bitolyl, ○···: 2,2'-diethylbiphenyl, ▲···: 2,2'-diisopropylbiphenyl
Twisting angles θ of the higher alkyl derivatives were tentatively estimated based on the figure calculated for bitolyl anion radical. The Coulson and Crawford's parameters of the hyperconjugation were used in the calculation of the methyl group.[10]

In the previous paper, we proposed that the rotation of the higher alkyl groups at the *ortho*-positions may be seriously hindered and that the alkyl groups behave as torsional oscillators rather than as free rotators.[7] According to the present ENDOR experiments, this is indeed true; the *ortho*-methyl proton splitting in *o,o'*-bitolyl was found to be equivalent, while the methylene protons of the ethyl group exhibited non-equivalent splittings. Futhermore, the methine proton of the isopropyl group revealed an exceptionally small value.

The dihedral angles of the ethyl methylene-protons at the equilibrium conformation were calculated to be $\varphi_1 = 54$ ° and $\varphi_2 = 66$ ° respectively, using the McConnell-Heller equation[8] with $B_0 \approx 0$; that is, $A^H = [B_0 + B_2 \langle \cos^2\varphi \rangle] \rho_i^\pi \approx B_2 \langle \cos^2\varphi \rangle \rho_i^\pi$ (1), where $B_2 = 50$ G.

The ρ_2^π (0.0908) of *o,o'*-bitolyl, estimated from Equation (1), is in excellent agreement with the theoretical value, 0.0913 ($\theta = 40$ °), predicted by the MO calculation based on the free rotation of the methyl group, that is, $\langle \cos^2\varphi \rangle = 1/2$.

In the case of the ethyl derivative, however, the ρ_2^π·(exp) value, 0.129, obtained from Equation (1) using $\varphi_1 = 54$ ° and $\varphi_2 = 66$ ° is considerably larger than the theoretical value (0.0913). Recently, the importance of the B_0 term contributing to the β-proton splitting of the higher alkyls has been demonstrated by an ENDOR study of the *p,p',p''*-triisopropyl trityl radical.[9] The discrepancy in the experimental values between the methyl and the ethyl derivatives is probably attributable to the neglect of the B_0-term.

If $B_0/B_2 = +0.06$ is tentatively assumed, the following values of ρ_2^π, which seem to be more reliable, are obtained: ρ_2^π(methyl) = 0.081 and ρ_2^π(ethyl) = 0.094.

The large diminution in the isopropyl methine-proton splitting also indicates a tight lock of the rotation of the alkyl group. The dihedral angles of the methine proton with the twisting angle of $\theta = 50$ ° ($\rho_2^\pi = 0.0822$) are calculated to be 89 °, assuming the B_0/B_2 ratio to be +0.06. This means that the isopropyl methine-proton is fixed in a position close to one of the aromatic planes of the twisted biphenyl.

References

1) A. Lagendijk, N. F. M. Tromp, M. Glasbeek, and J. D. W. Voorst., *Chem. Phys. Lett.*, **6**, 152 (1970).
2) K. P. Dinse, R. Biehl, K. Möbius, and M. Plato., *J. Mag. Resonance.*, **6**, 444 (1972).
3) R. D. Allendoerfer, R. Change, *ibid.*, **5**, 273 (1971).
4) K. Ishizu, This Bulletin, **37**, 1093 (1964).
5) M. E. Pauline, D. M. Hall, and E. E. Turner, *J. Chem. Soc.*, **1956**, 2286.
6) T. Yamamoto, K. Sato, and T. Miyamae, *J. Appl. Phys.*, **11**, 1508 (1972).
7) K. Ishizu, K. Mukai, H. Hasegawa, K. Kubo, H. Nishiguchi, and Y. Deguchi, This Bulletin, **42**, 2808 (1969).
8) C. Heller and H. M. McConnell, *J. Chem. Phys.*, **32**, 1535 (1960).
9) N. L. Bauld, C. E. Hudson, and J. S. Hyde, *ibid.*, **54**, 1834 (1971).
10) C. A. Coulson and U. A. Crawford, *J. Chem. Soc.*, **1953**, 2052.

BULLETIN OF THE CHEMICAL SOCIETY OF JAPAN, VOL. 48 (5), 1637—1638 (1975)

A Semi-empirical Calculation of the Substituent Effect on the ^{1}H Chemical Shift of Benzene[1)]

Jun NIWA

College of General Education, Nagoya University, Chikusa, Nagoya 464

(Received November 25, 1974)

Synopsis. The applicability of a semi-empirical expression for obtaining the relative ^{1}H chemical shifts in substituted aromatic side-chains, which was presented in the preceeding paper (J. Niwa, This Bulletin, **48**, 118 (1975)), has been examined for ring protons of monosubstituted benzenes.

In the preceeding paper,[1)] we derived a semi-empirical expression for obtaining the relative chemical shifts (in ppm) of protons in substituted aromatic side-chains by considering the "ring-current" effect ($\sigma^{A,\,ring}$) in addition to the diamagnetic contribution of the hydrogen atom, A, in the C–H bond of interest (σ_{dia}^{AA}) and that from its bonded carbon, B(σ_{dia}^{AB}):

$$\delta_{calcd}(\equiv \Delta\sigma^{A}) = \Delta\sigma_{dia}^{AA} + \Delta\sigma_{dia}^{AB} + \Delta\sigma^{A,ring} \quad (1)$$

$$= a\Delta q^{A} + b\Delta q^{B} - 0.4f(\rho, z)|\sigma_{\pi}| \quad (2)$$

where the $\Delta q'$ s are the increments in electron densities on specified atoms, where a and b are, respectively, the constants particular to the hydrogen atom and the C–H bond, and where the third term is the modified Johnson and Bovey ring-current shift. We showed that Eq. (2) could correctly reproduce the relative chemical shifts of protons in substituted aromatic side-chains. In the present paper, we will examine to what degree of accuracy Eq. (2) can reproduce the relative chemical shifts observed for the ring protons of monosubstituted benzenes. In evaluating the first and second terms of Eq. (1), we have used the CNDO/2 formalism.

In order to calculate the local diamagnetic term (σ_{dia}^{AA}) of the hydrogen atom, the expression (Eq. (3)) given by Kajimoto and Fueno[2a)] was applied to the case of the ring protons:

$$\sigma_{dia}^{AA} = 17.75(-0.3q_H^2 + 1.5q_H) \quad (3)$$

The calculated value of σ_{dia}^{AA}, relative to the unsubstituted compound, is linearly correlated with the increment in the electron density on the hydrogen atom:

$$\Delta\sigma_{dia}^{AA} = 16.0\Delta q^{A} \quad (4)$$

In the preceeding paper,[1)] we showed that the diamagnetic contribution from the bonded carbon (σ_{dia}^{AB}) can be expressed as:

$$\sigma_{dia}^{AB} = (e^2/3mc^2)r_{AB}^{-1}q^{B} \quad (5)$$

where r^{-1} is the inverse distance of the A atom from the point charge on the B atom and where q is the total (2s and 2p) electron density on the B atom. In the case of benzene, too, the contribution can be calculated in the same way as in the case of the olefinic proton,[1)] because the ring proton also bonds to the sp^2-hybridized carbon atom and the C–H bond length is taken to be 1.08 Å. Thus, the σ_{dia}^{AB} term, relative to the unsubstituted compound, becomes:

$$\Delta\sigma_{dia}^{AB} = 8.70\Delta q^{B} \quad (6)$$

The paramagnetic term, σ_{para}^{AB}, calculated according to Pople's expression,[2b)] remains almost constant for the series of monosubstituted benzenes so long as we assume the same average excitation energy and the same value of the integral $\langle r_{AB}^{-3}\rangle$.

In order to calculate the contribution of the "ring-current" effect relative to the unsubstituted compound, Eq. (7) derived by Yamada, Tsuno, and Yukawa[2d)] can be applied, just as it is, to all the ring protons in the present case:

$$\Delta\sigma^{A,ring} = -0.4f(\rho, z)|\sigma_{\pi}| \quad (7)$$

where the value of $f(\rho,z)$ is -1.50 ppm.[3)]

Using Eqs. (4), (6), and (7), we obtain the following equation for the relative chemical shifts of the ring protons:

$$\delta_{calcd} = 16.0\Delta q^{A} + 8.70\Delta q^{B} + 0.6|\sigma_{\pi}| \quad (8)$$

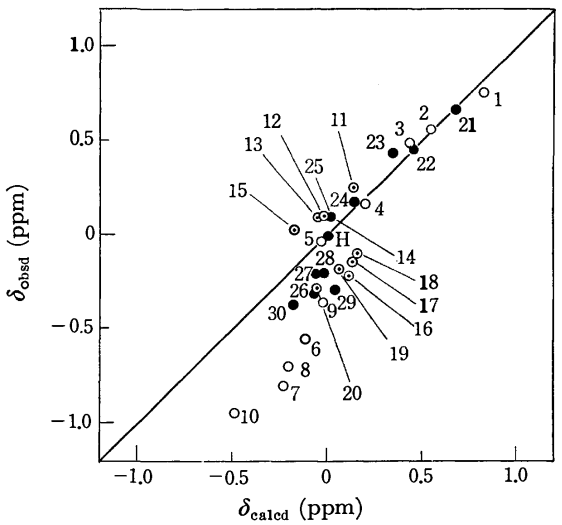

Fig. 1. Plots of δ_{obsd} against δ_{calcd} for ring protons of monosubstituted benzenes.
Numbered points correspond to entries in the Table 1.
○: *ortho*-substituent, ⊙: *meta*-substituent, ●: *para*-substituent.

The chemical shifts calculated by Eq. (8) are compared in the table with those observed for monosubstituted benzenes. In the figure, plots of the observed chemical shifts are shown against the calculated shifts. As may clearly be seen in the figure, the calculated chemical shifts can semi-quantitatively reproduce the trend of the substituent effects on the chemical shifts for protons at the position *para* to the substituents. This reveals that the three terms of Eq. (2) constitute the most important

TABLE 1. CALCULATED AND OBSERVED RELATIVE CHEMICAL SHIFTS OF RING PROTONS IN MONOSUBSTITUTED BENZENES[a)]

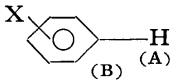

Substituent	q^{A}[b)]	q^{B}[b)]	$\Delta\sigma_{dia}^{AA}$	$\Delta\sigma_{dia}^{AB}$	$\Delta\sigma^{A,ring}$	δ_{calcd}	δ_{obsd}[c)]
1. *o*-NH_2[e)]	1.00317	4.05962	−0.054	0.576	0.288	0.81	0.746
2. *o*-OH	0.99422	4.05537	−0.197	0.539	0.192	0.53	0.558
3. *o*-OCH_3	0.99072	4.05168	−0.254	0.507	0.169	0.42	0.484
4. *o*-CH_3	1.00727	4.01035	0.011	0.147	0.047	0.21	0.17[d)]
5. *o*-Cl	0.98833	4.01909	−0.292	0.223	0.042	−0.03	−0.026
6. *o*-CHO	0.99907	3.97829	−0.120	−0.132	0.138	−0.11	−0.561
7. *o*-CO_2H	0.99485	3.97353	−0.188	−0.173	0.150	−0.21	−0.8[d)]
8. *o*-CO_2CH_3	0.99554	3.97386	−0.176	−0.170	0.168	−0.18	−0.713
9. *o*-CN	0.99888	3.98902	−0.123	−0.038	0.150	−0.01	−0.361
10. *o*-NO_2	0.97309	3.97933	−0.539	−0.123	0.204	−0.46	−0.952
11. *m*-NH_2[e)]	1.00948	3.96844	0.046	−0.217	0.288	0.12	0.249
12. *m*-OH	1.00581	3.97105	−0.012	−0.194	0.192	−0.01	0.122
13. *m*-OCH_3	1.00368	3.97210	−0.046	−0.185	0.169	−0.06	0.093
14. *m*-CH_3	1.00775	3.98830	0.019	−0.045	0.047	0.02	0.09[d)]
15. *m*-Cl	1.00067	3.98045	−0.094	−0.113	0.042	−0.17	0.022
16. *m*-CHO	1.00207	3.99905	−0.072	0.049	0.138	0.12	−0.221
17. *m*-CO_2H	1.00148	4.00019	−0.081	0.059	0.150	0.13	−0.14[d)]
18. *m*-CO_2CH_3	1.00201	4.00024	−0.073	0.059	0.168	0.16	−0.109
19. *m*-CN	1.00118	3.99280	−0.086	−0.005	0.150	0.06	−0.182
20. *m*-NO_2	0.99169	3.99228	−0.238	−0.010	0.204	−0.04	−0.257
21. *p*-NH_2[e)]	1.00880	4.03174	0.035	0.333	0.288	0.66	0.652
22. *p*-OH	1.00574	4.02194	−0.013	0.248	0.192	0.43	0.447
23. *p*-OCH_3	1.00379	4.01710	−0.045	0.206	0.169	0.33	0.439
24. *p*-CH_3	1.00740	4.00289	0.013	0.082	0.047	0.14	0.18[d)]
25. *p*-Cl	1.00166	4.00085	−0.078	0.065	0.042	0.03	0.088
26. *p*-CHO	1.00260	3.97971	−0.069	−0.119	0.138	−0.05	−0.294
27. *p*-CO_2H	1.00243	3.97786	−0.066	−0.135	0.150	−0.05	−0.2[d)]
28. *p*-CO_2CH_3	1.00288	3.97839	−0.059	−0.131	0.168	−0.02	−0.209
29. *p*-CN	1.00211	3.98908	−0.071	−0.038	0.150	0.04	−0.282
30. *p*-NO_2	0.99435	3.97395	−0.195	−0.169	0.204	−0.16	−0.378
31. H	1.00659	3.99341	0.000	0.000	0.000	0.00	0.000

a) All values are relative to the unsubstituted compound. b) All electron densities were calculated by the CNDO/2 method. c) Cited from the paper by Hayamizu *et al.*; K. Hayamizu and O. Yamamoto, *J. Mol. Spectrosc.*, **28**, 89 (1968); **28**, 422 (1968); **29**, 183 (1969). d) Cited from the monograph by Jackman *et al.* L. M. Jackman and S. Sternhell, "Applications of Nuclear Magnetic Resonance Spectroscopy in Organic Chemistry" (International Series of Monographs in Organic Chemistry, Vol. 5) ed. by D. H. R. Barton and W. Doering, Pergamon Press, Oxford (1969), p. 202. e) A planar model was used for amino groups. f) The σ_π-values necessary to calculate the $\Delta\sigma^{A,ring}$ term, which have not been established, were obtained from the correlation line between *pi*-electron densities on the carbon atoms at the position para to the substituent and the known σ_π-values of the other substituents; σ_π(*p*-CHO): 0.23, σ_π (*p*-CO_2H): 0.25, σ_π(*p*-CO_2CH_3): 0.28.

factors determining the relative chemical shifts in the case of *para*-protons remote from the substituent. In the protons at the positions *meta* and *ortho* to the substituents, however, the correlation between the observed and the calculated chemical shifts collapses appreciably. The cause of the deviations in the case of *meta*-protons may be mainly ignoring the magnetic contributions from carbon atoms neighboring the B atom. In the case of *ortho*-protons, especially in carbonyl and nitro derivatives, one reason that the calculated chemical shifts do not well reproduce the observed shifts may be ignoring the magnetic anisotropy of substituent groups which cause a low-field shift in the proton.[4)]

The CNDO/2 calculation was carried out on a FACOM-230 computer at the Nagoya University Computation Center.

References

1) J. Niwa, This Bulletin, **48**, 118 (1975).
2) a) O. Kajimoto and T. Fueno, *Chem. Lett.*, **1972**, 103; b) J. A. Pople, *J. Chem. Phys.*, **37**, 53 (1962).
3) J. W. Emsley, J. Feeney, and L. H. Sutcliffe, "Hugh Resolution Nuclear Magnetic Resonance Spectroscopy," Vol. 1, Pergamon Press, Oxford (1965), p. 595; C. E. Johnson and F. A. Bovey, *J. Chem. Phys.*, **29**, 1012 (1958).
4) For example, F. A. Bovey, "Nuclear Magnetic Resonance Spectroscopy," Academic Press, New York (1969), pp. 75, 79.

BULLETIN OF THE CHEMICAL SOCIETY OF JAPAN, VOL. 48 (5), 1639—1640 (1975)

The Crystal and Molecular Structure of Sterigmatin, A Metabolite of *Aspergillus versicolor*

Keiichi FUKUYAMA, Tomitake TSUKIHARA, Yukiteru KATSUBE, Takashi HAMASAKI,* Yuichi HATSUDA,* Nobuo TANAKA,** Tamaichi ASHIDA,** and Masao KAKUDO**

Faculty of Engineering, Tottori University, Koyama, Tottori 680

(Received December 5, 1974)

Synopsis. The crystal structure of sterigmatin has been determined by single-crystal X-ray analysis. The crystals are triclinic; space group P1, $Z=2$, with $a=14.392(4)$, $b=14.120(4)$, $c=4.256(2)$ Å, $\alpha=78.22(3)$, $\beta=100.42(3)$, $\gamma=56.90(3)$ °. The structure was refined to an R value of 0.039 for 1961 reflections. There are two intramolecular hydrogen bonds in each of the crystallographically independent molecules.

Sterigmatin was isolated as a metabolite of *Aspergillus versicolor* (Vuillemin) Tiraboschi, and its structural formula was shown to be as follows.[1]

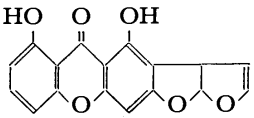

As part of a program of research on the structures of metabolites of this mold,[2,3] the structure of sterigmatin has been studied by means of the X-ray diffraction method.

Sterigmatin was crystallized from acetone in the form of pale yellow needles elongated along the c-axis. The crystals are triclinic; space group P1, $Z=2$, with $a=14.392(4)$, $b=14.120(4)$, $c=4.256(2)$ Å, $\alpha=78.22(3)$, $\beta=100.42(3)$, $\gamma=56.90(3)$ °. The intensities were collected on a Rigaku Denki computer-controlled four-circle diffractometer using Ni-filtered Cu-$K\alpha$ radiation. The ω-2θ scan technique was employed, with a scan speed of 2 ° min^{-1} in ω. The background was measured for 5 s at both the start and end points of the scan range. A total of 1968 intensities were collected, with $\sin\theta/\lambda<0.562$. The crystal used was so small (*ca.* $0.06\times0.07\times0.25$ mm) that the intensities were corrected only for the Lorentz and polarization factors.

The orientations of the xanthone skeletons of the crystallographically independent molecules were easily determined by the application of the convolution molecule method.[4] Since the origin could be arbitrarily chosen for the P1 space group, the Fourier synthesis based on the phases due to one of the xanthone skeletons revealed the other xanthone skeleton. The structure obtained by successive Fourier syntheses was refined by a block-diagonal least-squares method. Seven intense reflections with low-order indices were omitted from the refinement and difference Fourier synthesis because of the extinction effect. The difference electron density map revealed all the hydrogen atoms. The refinement was continued by including the hydrogen atoms until the R value of 0.039 for 1961 reflections. The unit weight was applied for all reflections. The final atomic parameters of the two molecules (A and B) are listed in Tables 1 and 2. The atomic scattering factors were taken from the International Tables for X-ray Crystallography.[5] The computations were performed on a TOSBAC-3400 computer at the Tottori University Computing Center and on a NEAC 2200-N700 computer at the Computation Center of Osaka University.

Since the corresponding bond lengths and angles of the two crystallographically independent molecules do not differ significantly, we may use the mean values given in Fig. 1 and Table 3 for the discussion of the

Table 1. Final atomic parameters and e.s.d.'s ($\times10^4$) for non-hydrogen atoms

The anisotropic temperature factors are of the form: $\exp(-\beta_{11}h^2-\beta_{22}k^2-\beta_{33}l^2-\beta_{12}hk-\beta_{13}hl-\beta_{23}kl)$.

	x	y	z	β_{11}	β_{22}	β_{33}	β_{12}	β_{13}	β_{23}
C(A1)	2959(3)	3202(3)	-2639(10)	46(3)	51(3)	392(27)	-57(6)	80(15)	-79(16)
C(A2)	2454(4)	4380(4)	-2987(10)	57(3)	64(4)	445(29)	-83(6)	104(16)	-95(17)
C(A3)	1454(4)	5018(4)	-2026(10)	52(3)	50(3)	442(28)	-68(6)	60(16)	-80(16)
C(A4)	910(4)	6254(4)	-2194(10)	63(4)	53(4)	426(29)	-73(7)	58(17)	-76(17)
C(A5)	-83(4)	6795(4)	-1070(10)	68(4)	56(4)	410(29)	-64(7)	61(17)	-100(17)
C(A6)	-697(4)	7991(4)	-1142(12)	89(5)	56(4)	575(34)	-71(7)	106(20)	-131(19)
C(A7)	-1675(4)	8496(4)	-146(13)	81(5)	59(4)	663(38)	-40(7)	114(22)	-182(21)
C(A8)	-2067(4)	7816(4)	867(13)	67(4)	82(5)	722(39)	-57(8)	139(21)	-225(22)
C(A9)	-1494(4)	6634(4)	985(12)	57(4)	81(5)	685(38)	-67(7)	127(20)	-210(22)
C(A10)	-507(4)	6143(4)	12(11)	53(3)	50(3)	484(30)	-47(6)	75(16)	-139(17)
C(A11)	1016(3)	4409(4)	-773(10)	45(3)	65(4)	441(28)	-65(6)	95(16)	-147(17)
C(A12)	1519(4)	3204(4)	-358(11)	57(4)	56(4)	568(31)	-77(6)	140(17)	-125(17)
C(A13)	2502(4)	2639(3)	-1295(10)	55(3)	50(3)	432(28)	-65(6)	65(16)	-95(16)
C(A14)	4113(4)	1141(4)	-2157(12)	65(4)	68(4)	640(35)	-66(7)	199(19)	-193(19)
C(A15)	5712(4)	774(5)	1479(14)	49(4)	127(6)	752(42)	-51(8)	125(21)	-270(27)
C(A16)	5186(4)	1876(5)	-577(13)	50(4)	91(5)	828(41)	-62(7)	143(20)	-287(24)
C(A17)	4067(4)	2285(4)	-3201(11)	66(4)	65(4)	588(33)	-81(7)	194(19)	-180(19)
O(A1)	2940(3)	4896(3)	-4215(8)	86(3)	76(3)	784(27)	-126(5)	248(15)	-180(15)
O(A2)	1301(3)	6816(3)	-3269(9)	97(3)	66(3)	777(26)	-118(5)	225(15)	-174(14)
O(A3)	-328(4)	8663(3)	-2139(10)	143(4)	65(3)	1066(34)	-129(7)	355(21)	-245(17)
O(A4)	44(2)	4966(2)	188(8)	59(3)	60(3)	663(23)	-77(4)	179(13)	-178(13)
O(A5)	3124(3)	1453(3)	-1020(8)	66(3)	53(3)	759(26)	-69(4)	186(14)	-183(13)
O(A6)	5177(3)	239(3)	649(10)	65(3)	71(3)	952(32)	-41(5)	126(16)	-71(16)
C(B1)	5121(4)	6264(4)	4901(10)	70(4)	51(4)	425(28)	-74(6)	145(17)	-103(17)
C(B2)	6296(4)	5596(4)	5287(10)	67(4)	65(4)	409(28)	-93(7)	115(17)	-111(17)
C(B3)	6806(3)	4561(4)	4301(10)	50(3)	51(3)	441(28)	-64(6)	113(16)	-105(16)
C(B4)	8022(4)	3847(4)	4572(11)	56(4)	65(4)	498(30)	-80(6)	123(17)	-104(17)
C(B5)	8443(4)	2831(4)	3467(10)	51(3)	49(3)	441(28)	-57(6)	83(15)	-51(16)
C(B6)	9627(4)	2049(4)	3625(11)	57(4)	79(4)	496(32)	-77(7)	108(18)	-78(19)
C(B7)	10003(4)	1081(4)	2633(13)	63(4)	67(4)	750(39)	-65(7)	201(20)	-153(21)
C(B8)	9208(4)	861(4)	1401(13)	77(5)	62(4)	825(41)	-74(8)	237(23)	-176(22)
C(B9)	8029(4)	1602(4)	1188(13)	76(4)	61(4)	768(38)	-81(7)	212(21)	-210(21)
C(B10)	7674(4)	2570(4)	2270(11)	54(3)	54(4)	525(31)	-56(6)	143(17)	-115(17)
C(B11)	6074(4)	4265(3)	3021(10)	60(3)	48(3)	485(28)	-74(6)	145(16)	-132(16)
C(B12)	4882(4)	4916(4)	2611(11)	58(3)	53(4)	578(32)	-70(6)	126(17)	-126(18)
C(B13)	4452(4)	5917(4)	3582(10)	58(4)	54(4)	512(31)	-73(6)	165(17)	-116(17)
C(B14)	3133(4)	7633(4)	4438(13)	82(4)	58(4)	780(40)	-75(7)	275(22)	-195(21)
C(B15)	2943(5)	9215(4)	961(14)	106(5)	55(4)	891(44)	-80(8)	306(26)	-182(23)
C(B16)	4051(5)	8544(4)	3030(13)	98(5)	65(4)	822(41)	-100(8)	323(23)	-228(22)
C(B17)	4331(4)	7413(4)	5531(11)	91(5)	60(4)	529(32)	-96(7)	216(20)	-177(18)
O(B1)	6965(3)	5917(3)	6594(9)	85(3)	90(3)	823(27)	-132(6)	207(15)	-294(16)
O(B2)	8702(3)	4103(3)	5732(9)	65(3)	85(3)	773(25)	-106(5)	137(13)	-224(15)
O(B3)	10427(2)	2248(3)	4826(9)	58(3)	101(3)	903(29)	-99(5)	195(14)	-256(16)
O(B4)	6510(2)	3278(2)	2011(8)	48(2)	55(3)	753(25)	-64(4)	151(12)	-207(13)
O(B5)	3295(3)	6672(3)	3301(8)	57(3)	58(3)	816(26)	-65(4)	210(13)	-188(14)
O(B6)	2330(3)	8746(3)	1602(10)	68(3)	50(3)	1103(34)	-45(5)	152(16)	-102(15)

Table 2. Final positional parameters ($\times10^3$) and isotropic temperature factors (Å^2) for hydrogen atoms

	x	y	z	B		x	y	z	B
H(A1)	262(6)	562(6)	-387(17)	5.5(1.6)	H(B1)	784(6)	537(6)	679(17)	6.2(1.8)
H(A2)	22(7)	823(7)	-302(19)	7.8(2.1)	H(B2)	1012(5)	279(5)	567(15)	4.3(1.4)
H(A3)	-217(5)	927(5)	-4(14)	3.9(1.3)	H(B3)	1089(5)	49(5)	306(13)	3.4(1.2)
H(A4)	-277(5)	817(5)	163(14)	4.2(1.4)	H(B4)	947(6)	9(6)	70(16)	5.2(1.6)
H(A5)	-170(4)	607(5)	191(13)	3.1(1.2)	H(B5)	740(5)	148(5)	-7(14)	3.7(1.3)
H(A6)	132(4)	271(4)	127(13)	3.0(1.2)	H(B6)	437(5)	469(5)	148(14)	3.4(1.2)
H(A7)	405(4)	74(4)	-391(12)	2.6(1.1)	H(B7)	271(4)	775(4)	601(12)	2.3(1.1)
H(A8)	645(5)	18(5)	350(15)	4.3(1.4)	H(B8)	240(5)	1002(5)	-110(14)	3.6(1.3)
H(A9)	550(6)	234(6)	-31(17)	5.7(1.6)	H(B9)	462(5)	856(5)	244(15)	4.9(1.5)
H(A10)	401(5)	249(5)	-570(13)	3.1(1.2)	H(B10)	466(5)	725(5)	816(14)	3.8(1.3)

* Faculty of Agriculture, Tottori University, Koyama, Tottori 680.

** Institute for Protein Research, Osaka University, Suita 565.

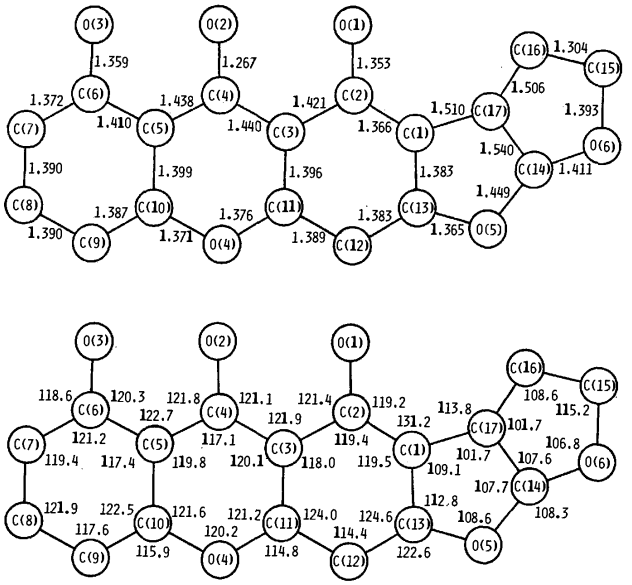

Fig. 1. Mean values of bond lengths and angles.
The e.s.d.'s of bond lengths and angles are about 0.007 Å and 0.5 °, respectively.

TABLE 3. MEAN BOND LENGTHS (Å) AND ANGLES (°) INVOLVING HYDROGEN ATOMS

Broken lines indicate hydrogen bonds.

(a) Mean bond lengths

O(1)–H(1)	0.98	O(3)–H(2)	0.87
C(7)–H(3)	0.98	C(8)–H(4)	1.03
C(9)–H(5)	1.05	C(12)–H(6)	1.05
C(14)–H(7)	1.00	C(15)–H(8)	1.01
C(16)–H(9)	0.94	C(17)–H(10)	1.03
O(2)···H(1)	1.79	O(2)···H(2)	1.83

(b) Mean bond angles

C(2)–O(1)–H(1)	112	C(6)–O(3)–H(2)	107
C(6)–C(7)–H(3)	124	C(8)–C(7)–H(3)	116
C(7)–C(8)–H(4)	121	C(9)–C(8)–H(4)	117
C(8)–C(9)–H(5)	123	C(10)–C(9)–H(5)	120
C(11)–C(12)–H(6)	120	C(13)–C(12)–H(6)	124
C(17)–C(14)–H(7)	120	O(5)–C(14)–H(7)	107
O(6)–C(14)–H(7)	105	C(16)–C(15)–H(8)	135
O(6)–C(15)–H(8)	110	C(15)–C(16)–H(9)	123
C(17)–C(16)–H(9)	125	C(1)–C(17)–H(10)	111
C(14)–C(17)–H(10)	110	C(16)–C(17)–H(10)	117
O(1)–H(1)···O(2)	139	C(4)–O(2)···H(1)	104
O(3)–H(2)···O(2)	148	C(4)–O(2)···H(2)	98
H(1)···O(2)···H(2)	158		

structure. The mean value of the C(4)–O(2) bond lengths is 1.267 Å, which is longer than the accepted value of the C–O double bond length. Such an elongation has also been found in averufin.[2] The bond lengths of C(3)–C(4) and C(4)–C(5) are 1.440 and 1.438 Å respectively; they are considerably longer than the mean

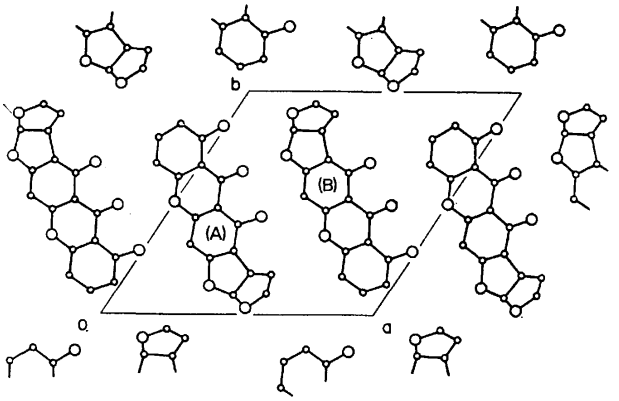

Fig. 2. The crystal structure of sterigmatin projected along the c*-axis.
The large circles indicate oxygen atoms and the small ones carbon atoms. The hydrogen atoms are omitted in the figure.

C–C bond length (1.390 Å) in the benzenoid rings. There are two intramolecular hydrogen bonds, O(1)–H(1)·····O(2) and O(3)–H(2)·····O(2). In each molecule the xanthone skeleton and terminal five-membered ring are planar within ±0.06 Å and ±0.02 Å respectively. The dihedral angles between the planes are 67.3 ° in the A molecule and 65.0 ° in the B molecule.

The crystal structure projected along the c* axis is shown in Fig. 2. Although the closest intermolecular contact (2.86 Å) of non-hydrogen atoms is found between O(A1) and O(B5), the difference electron density map calculated using the final atomic parameters showed no peak in the region between these two oxygen atoms. Therefore, there is no intermolecular hydrogen bond between the O(A1) and O(B5) atoms. The other intermolecular distances require no special comment.

The authors wish to thank Mr. Isao Tanaka of Nagoya University for his permission to use the program of the convolution molecule method.

References

1) T. Hamasaki, K. Matsui, K. Isono, and Y. Hatsuda, *Agr. Biol. Chem.*, **37** (7), 1769 (1973).
2) Y. Katsube, T. Tsukihara, N. Tanaka, K. Ando, T. Hamasaki, and Y. Hatsuda, This Bulletin, **45**, 2091 (1972).
3) N. Tanaka, Y. Katsube, Y. Hatsuda, T. Hamasaki, and M. Ishida, *ibid.*, **43**, 3635 (1970).
4) "Crystallographic Computing," ed. by F. R. Ahmed, Munksgaard, Copenhagen (1970).
5) "International Tables for X-ray Crystallography," Vol. III, Kynoch Press, Birmingham (1962), p. 202.

BULLETIN OF THE CHEMICAL SOCIETY OF JAPAN, VOL. 48 (5), 1641—1642 (1975)

Electron-transfer Kinetics of Transition-metal Complexes in Lower Oxidation States. Part III.[1] Electrochemical Rate Constants for the Fe(II)/Fe(I) Redox Systems

Tetsuo SAJI, Tamaki YAMADA, and Shigeru AOYAGUI*

Faculty of Engineering, Tokyo Institute of Technology, Ohokayama, Meguro-ku, Tokyo 152

(Received December 12, 1974)

Synopsis. The standard rate constants for the redox systems Fe(II)/Fe(I) are measured. They are about one tenth of those for the systems Fe(III)/Fe(II) and Cr(I)/Cr(0). The difference in the kind of molecular orbital occupied by the excess electron of the reductant species can account for the difference in the rate constant.

Transition-metal complexes in lower oxidation states have been widely studied from the structural chemical, magnetochemical, spectroscopic and kinetic points of view. Although electrochemical studies have also been made, they have been almost limited to polarographic ones. Eelctrode kinetic parameters have been measured so far only on two redox systems in lower oxidation states: one is the $Co(bipy)_3^{2+}/Co(bipy)_3^{+}$ system[2] and the other the $Cr(bipy)_3^{+}/Cr(bipy)_3$ system.[1] The standard rate constant of the latter system was discussed in comparison with the second order rate constant of the corresponding homogeneous homonuclear electron-transfer reaction.[3] It was pointed out that each of the electrochemical and the homogeneous electron-transfer reactions of this system fell into a class of the fastest reaction. Its electronic configuration differing by one in the number of electrons in metal t_{2g}-orbitals was considered to account for the high reaction rate.

This note treats the measurements of the standard rate constants of the redox systems $Fe(bipy)_3^{2+}/Fe(bipy)_3^{+}$ and $Fe(bipy)_2(CN)_2/Fe(bipy)_2(CN)_2^{-}$. According to our recent polarographic investigations,[4,5] the excess electron of a reductant complex of these systems occupies a ligand π^*-orbital.

Experimental

Each electrolytic solution contained a 2 mM electroactive species, *i.e.*, $Fe(bipy)_3^{2+}$, $Fe(bipy)_2(CN)_2$ or 2,2′-bipyridine in *N,N*-dimethylformamide (DMF). Supporting electrolyte was 0.2 M tetra-*n*-butylammonium perchlorate (TBAP). Either a platinum spherical electrode or a dropping mercury electrode (DME) was used as the working electrode. The standard rate constant (k°) was assumed to be identical with the rate constant at the half-wave potential ($E_{1/2}$). It was measured with the aid of the galvanostatic double-pulse method with the *in situ* generation of a reductant complex at the half-wave potential of the redox system. Measurements were made at 25±2 °C. Details of the experiments were described in a separate paper.[6]

Results and Discussion

Results obtained are listed in Table 1. They are summarized as follows: (1) a partial subtitution of a ligand bipy with a CN^- does not affect the rate constant, (2) the rate constant does not depend much on the material of the working electrode, platinum or mercury, (3) the rate constants are smaller about one order of magnitude than the rate constant for the $Cr(bipy)_3^{+}/Cr(bipy)_3$ system,[1] 1.0 cm s^{-1}, and (4) the rate constants for the Fe(II)/Fe(I) systems are nearly equal to the rate constant for the bipy/$bipy^-$ system. Feature (1) forms a striking contrast to findings obtained for Fe(III)/Fe(II) systems:[6] the apparent standard rate constants for $Fe(bipy)_3^{3+}/Fe(bipy)_3^{2+}$, $Fe(bipy)_2(CN)_2^{+}/Fe(bipy)_2(CN)_2$, $Fe(bipy)(CN)_4^{-}/Fe(bipy)(CN)_4^{2-}$ and $Fe(CN)_6^{3-}/Fe(CN)_6^{4-}$ become smaller in this order from about 1 cm s^{-1} to 0.2 cm s^{-1}. Features (3) and (4) may be consistent with the previous conclusion that the electron transferred in the course of electrochemical oxidation of Fe(I) complexes occupies a ligand π^*-orbital[4] and that of Fe(II) complexes a metal t_{2g}-orbital.[7] These facts may suggest that the electronic configuration of a redox species can be a predominant factor determining the electrochemical electron-transfer rate. It is known that the rate constant of a homogeneous electron-transfer reaction depends on the electronic configuration of the reactants. Such a dependence has been discussed on electrode reactions by Vlček[8] and later by Marcus[9] who has pointed out that when a reductant species loses a metal e_g-electron on oxidation, the rate is slower than when it loses a t_{2g}-electron. This has been interpreted on the basis of his theory[10] as follows: a t_{2g}-electron transfer, compared with an e_g-electron transfer, requires a lesser change in bond lengths or bond geometry and in its turn smaller energy of reorganization of the inner coordination shell.

Further support for the conclusion of this note will be furnished in a separate paper[11] by the same kind of experiments on more than twenty redox systems of tris-

Table 1. Standard rate constants at 25 °C for the redox systems Fe(II)/Fe(I) as compared with those for the Fe(III)/Fe(II) and BIPY/$BIPY^-$ systems

Redox system	Electrode	$E_{2/1}$(V SCE)	k°(cm s^{-1})
$Fe(bipy)_3^{3+}/Fe(bipy)_3^{2+}$	Pt	1.03[a]	1.1[a]
$Fe(bipy)_3^{2+}/Fe(bipy)_3^{+}$	Pt	−1.26	0.16
$Fe(bipy)_2(CN)_2^{+}/Fe(bipy)_2CN)_2$	Pt	0.47[a]	0.41[a]
$Fe(bipy)_2(CN)_2/Fe(bipy)_2(CN)_2^{-}$	Pt	−1.60	0.11
$bipy/bipy^-$	Pt	−2.09	0.21
$Fe(bipy)_3^{2+}/Fe(bipy)_3^{+}$	DME	−1.26	0.14
$Fe(bipy)_2(CN)_2/Fe(bipy)_2(CN)_2^{-}$	DME	−1.59	0.13
$bipy/bipy^-$	DME	−2.10	0.13

a) Ref. 6

* To whom correspondence should be addressed.

(2,2′-bipyridine) complexes of titanium, vanadium, chromium, molybdenum, iron, ruthenium, and osmium.

References

1) Part II: T. Saji and S. Aoyagui, This Bulletin, **47**, 389 (1974).
2) D. J. Macero, F. V. Lovecchio, and S. J. Pace, *Inorg. Chim. Acta*, **3**, 65 (1969).
3) T. Saji and S. Aoyagui, This Bulletin, **46**, 2101 (1973).
4) T. Saji and S. Aoyagui, *J. Electroanal. Chem.*, **58**, 401 (1975).
5) T. Saji and S. Aoyagui, to be published.
6) T. Saji, T. Yamada, and S. Aoyagui, *J. Electroanal. Chem.*, in press.
7) T. Saji and S. Aoyagui, *ibid.*, **60**, 1 (1975).
8) A. A. Vlček in F. A. Cotton (Ed.), "Progress in Inorganic Chemistry," Vol. 5, Interscience, New York (1963), p. 289.
9) R. A. Marcus, "Background Material and Lecture Note for First and Second International Summer School on Quantum Mechanical Aspects of Electrochemistry," Ohrid, Yugoslavia, (1971—1972), p. 72.
10) R. A. Marcus, *J. Chem. Phys.*, **43**, 679 (1965).
11) T. Saji and S. Aoyagui, *J. Electroanal. Chem.*, in press.

BULLETIN OF THE CHEMICAL SOCIETY OF JAPAN, VOL. 48 (5), 1643—1644 (1975)

An ESR Study of Diborane Anion Radicals in the Adsorbed State

Kunihisa SOGABE, Akinori HASEGAWA, and Masaji MIURA

Department of Chemistry, Faculty of Science, Hiroshima University, Higashisenda-machi, Hiroshima 730

(Received January 16, 1975)

Synopsis. The ESR spectra were examined for diborane anion radicals, $B_2H_6^-$, formed when diborane adsorbed on several kinds of adsorbents was irradiated with γ-rays at 77 K or diborane adsorbed at 77 K on adsorbents pre-irradiated with γ-rays at 77 K. The radicals in the adsorbed state were compared with those in an argon matrix, previously reported.

The ESR spectra of two kinds of radicals have been investigated in connection with diborane. When the solid of diborane was irradiated with γ-rays, the ESR spectrum of neutral diboranyl radicals formed by extracting one of the two bridging hydrogens of diborane was observed. The radical was investigated in detail by means of both ESR measurements with an irradiated single crystal of diborane[1] and theoretical calculations.[1,2] On the other hand, when an argon matrix containing diborane and sodium was irradiated with UV light at 4.2 K, an electron on the sodium atom was transferred to diborane and the ESR spectrum of diborane anion radicals was observed.[3] Kasai *et al.*[3] interpreted the anion radical as having a bridging structure with an unpaired electron in a b_{3g} orbital given by an antibonding combination of the 2p orbitals of the two borons perpendicular to the plane defined by the four terminal hydrogen atoms. However, Claxton *et al.*[4] recently proposed, on the basis of the results of *ab initio* UHF calculations, that the anion radical favors a staggered structure rather than the bridged D_{2h} structure of the parent molecule. They also said that the neutral diboranyl radical is presumably formed by proton loss from the cation radical of diborane, $B_2H_6^+$.

Several kinds of radicals have been revealed by ESR spectroscopy to be produced upon the irradiation of specimens adsorbed on the surfaces of solids; for example, cation radicals of benzene[5] and toluene,[6] anion radicals of O_2, CO_2, SO_2 and TCNE,[7] and neutral radicals from methane[8] and ethane[9] were observed on the surface of silica gel.

Thus, it may be of interest to investigate what kind of radical species is produced by the irradiation of diborane in such an adsorbed state.

Diborane, B_2H_6, and deuterodiborane, B_2D_6, were prepared by a method described elsewhere.[1] The silica gel, alumina, magnesium oxide, mordenite (HZ type), and zeolite (MgY type) used as the adsorbents for diborane were outgassed in a vaccum of 10^{-5} Torr at 550 °C for *ca.* 30 hr, while the adamantane was evacuated at room temperature for 1 hr. Diborane gas was introduced into ESR sample tubes containing these adsorbents through breakable seals at room temperature, except for the case of pre-irradiation, where the gas was introduced at 77 K. The irradiation with γ-rays was carried out at 77 K for 2 hr at a does rate of *ca.* 6×10^5 rad/hr from a ^{60}Co source, and the ESR spectra were measured at 77 K with an ESR spectrometer described elsewhere.[1]

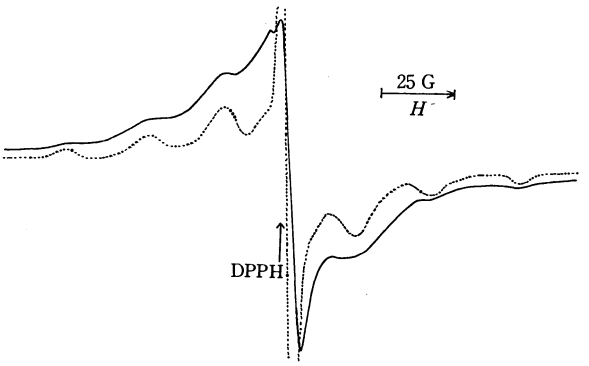

Fig. 1. ESR spectra of anion radicals of B_2H_6 (solid line) and B_2D_6 (dotted line) adsorbed on silica gel.

The ESR spectrum observed after the irradiation of diborane adsorbed on silica gel is shown in Fig. 1. The spectrum consists of a broad spectrum with seven peaks attributable to two equivalent boron atoms ($I=^3/_2$) and a spectrum of trapped electrons in the central region of the spectrum. These seven peaks could be explicitly distinguished when deuterodiborane was used, as is shown by a dotted line in Fig. 1. These observed spectra, except for that of the trapped electron, are very similar to those of the diborane anion radical, $B_2H_6^-$, and the deuterated anion radical, $B_2D_6^-$, observed in an argon matrix at 4.2 K,[3] while they are quite different from those of diboranyl radicals observed in the polycrystalline states of diborane and deuterodiborane.[1] No transformation of the observed spectrum to that of diboranyl radicals was detected during storage at 77 K under room light for several days.

In order to determine whether the cation radical or the anion radical was produced, the effect of the pre-irradiation on the radical production was investigated. The ESR spectrum of electrons trapped by defects in silica gel was observed with silica gel irradiated with γ-rays at 77 K. When diborane gas was adsorbed on the pre-irradiated silica gel, the intensity of the ESR spectral line of the trapped electrons was reduced; the same spectrum with seven peaks as that observed in the case of the post-irradiation appeared simultaneously. This observation may mean that the trapped electron on the surface silica gel is transferred to the diborane, which is well-known to be an electron-deficient molecule. The formation of the anion radical in the adsorbed state may be interpreted as arising from the electron transfer from the adsorbent to the diborane, as in the cases of the anion radicals of O_2, CO_2, SO_2, and TCNE adsorbed on silica gel.[7] Accordingly, it may be concluded that the anion radical was produced by the irradiation of diborane adsorbed on silica gel and by the adsorption of diborane

on pre-irradiated silica gel.

The ESR spectra of the anion radical of diborane in the adsorbed state were examined not only with adsorbents of metal oxides, alumina, magnesium oxide, mordenite, and zeolite, but also with the recently discovered organic adsorbent, adamantane.[10] All of the observed spectra of the anion radicals were interpreted by analogy with the analysis of the spectrum by Kasai and Mclood.[3] The parallel components of the hyperfine couling of the two boron atoms were easily determined from the spectra observed with deuterodiborane, whereas the perpendicular components for the two boron atoms and the proton coupling were not explicitly evaluated from the observed spectra. Accordingly, the parallel components for the boron atoms, $A_{//}(^{11}B)$, observed with different kinds of adsorbents were evaluated to be as follows:

Silica gel	25.0 *G*	Mordenite	25.4 *G*
Alumina	25.4 *G*	Zeolite	24.6 *G*
Magnesium oxide	24.7 *G*	Adamantane	19.0 *G*

Except for the case of adamantane, the parameters are in close agreement with that reported previously.[3] The value observed with adamantane is considerably smaller than those with the other adsorbents. For the anion radical in the argon matrix at 4.2 K, Kasai and Mclood.[3] gave these ESR parameters: $A_{//}$ (^{11}B)$=24.5\pm0.5$ *G*, $A_{\perp}$ (^{11}B)$=2.5$ *G* and $A(H)\leq 15$ *G*. Claxton *et al.*,[4] however, estimated the coupling of six hydrogens to be $A_{//}(H)=A_{\perp}(H)=7$ *G* by the use of a curve resolver. On the basis of a comparison between the estimated values of $a(^{11}B)$ and $a(H)$ and the results of their *ab initio* calculation, Claxton *et al.*[4] concluded that the anion radical of diborane has not a bridge structure, but a staggered conformation. Thus, the present authors attempted to observe the proton coupling directly by means of ENDOR.

The ENDOR spectra of the anion radical adsorbed on silica gel and adamantane were measured at 77 K with a JEOL type ES-EDX-1 spectrometer. Unfortunately, no ENDOR signal except for the ENDOR signals due to the electron trapped in the cavity of adamantane[11] was observed, in spite of careful measurements. Therefore, the attempt to check experimentally the proposed staggered conformation of the diborane anion radicals from proton couplings was unsuccessful, and the discussion of the structure of the anion radicals in the adsorbed state could not be advanced beyond the staggered conformation discussed by Claxton *et al.*[4] However, the small coupling of $A_{//}(^{11}B)$ observed with adamantane may suggest that some distortion of the staggered conformation arises from the existence of the radical in the cavity of a molecule of adamantane.

It may be mentioned that the method using an adsorbent is very much more convenient for producing the anion radicals of diborane compared with that using an inert gas matrix containing sodium at 4.2 K.[3]

The authors would like to express their gratitude to Professor Kazuhiko Ishizu of Ehime University for measuring the ENDOR spectra and to Professor Junkichi Sohma of Hokkaido University for his valuable discussions.

References

1) A. Hasegawa and J. Sohma, *Mol. Phys.*, **24**, 1177 (1972); *ibid.*, **27**, 389 (1974),
2) O. Edlund and J. Sohma, *ibid.*, **29**, in press. (1975).
3) P. H. Kasai and D. McLeod, Jr., *J. Chem. Phys.*, **51**, 1250 (1969).
4) T. A. Claxton, R. E. Overill, and M. C. R. Symons,. *Mol. Phys.*, **27**, 701 (1974).
5) T. Komatsu and A. Lund., *J. Phys. Chem.*, **76**, 1727 (1972).
6) T. Komatsu, A. Lund, and P.-O. Kinell, *ibid.*, **76**, 1721 (1972).
7) Y. Yamada, A. Hasegawa, and M. Miura, This Bulletin **42**, 1836 (1969).
8) S. Kubota, M. Iwaizumi, and T. Isobe, *ibid.*, **44**, 2684 (1971).
9) V. B. Kazanskii, G. B. Pariiskii, I. V. A. Alexandrov, and G. M. Zhidomirv, *Solid State Phys.*, **5**, 649 (1969).
10) D. E. Wood and R. V. Leoyd, *J. Chem. Phys.*, **52**, 3840 (1970).
11) K. W. Bowers, J. Nolfi, Jr., and F. D. Greene, *J. Amer. Chem. Soc.*, **85**, 3707 (1963).

BULLETIN OF THE CHEMICAL SOCIETY OF JAPAN, VOL. 48 (5), 1645—1646 (1975)

Effect of Inorganic Electrolytes on the Cloud Point of Polyoxyethylene Dodecyl Ether

Fumikatsu TOKIWA and Tadao MATSUMOTO

Research Laboratories, Kao Soap Company, 2-1-3 Bunka, Sumida-ku, Tokyo 131

(Received January 21, 1975)

Synopsis. The cloud points of polyoxyethylene dodecyl ether in the presence of different types of inorganic electrolytes have been determined. The cloud points can be expressed by the empirical equation: $(C.P.)_s/(C.P.)_0=1+A\sqrt{C_s}+BC_s$ where $(C.P.)_s$ and $(C.P.)_0$ are the cloud points with and without an electrolyte, respectively, C_s is the electrolyte concentration, and A and B are constants.

When an aqueous solution of a polyoxyethylene-type nonionic surfactant $RO(CH_2CH_2O)_pH$ with a relatively small number of p is heated, it becomes cloudy reversibly at the temperature of incipient phase separation called the cloud point. The cloud point is rather insensitive to the concentration of the surfactant itself, but is highly dependent on the kind and the concentration of an added electrolyte.[1,2] Most of inorganic electrolytes depress the cloud point of a nonionic surfactant owing to their salt-out effect, while some electrolytes such as nitrates, iodides and thiocyanates, raise the cloud point. In addition, the cloud point is in general more influenced by the anions of added electrolytes than by the cations. However, the nature of the interaction of a nonionic surfactant with an added electrolyte (or the interaction through a change in the structure of water by an added electrolyte) is not necessarily well understood.

This note describes a systematic study on the effect of various types of inorganic electrolytes on the cloud point of polyoxyethylene dodecyl ether (abbreviated to C_{12}-POE) and proposes an empirical equation to express the cloud point as a function of an added electrolyte.

Experimental

The nonionic surfactant C_{12}POE was prepared from dodecyl alcohol of high purity by addition of ethylene oxide and purified by molecular distillation. The average number of oxyethylene units per molecule for the purified sample was found to be 6.3 from its hydroxyl value. The inorganic electrolytes examined were of guaranteed reagent grade and used without further purification.

Cloud points were photometrically measured of 2.0% C_{12}POE solutions containing electrolytes in the concentration range of 0.01—0.5 m with the apparatus shown in Fig. 1a. The transmittance of light through a sample solution and the temperature of this solution were plotted on a X–Y recorder connected with the apparatus. The solution was heated or cooled at a rate of 0.4 °C per minute across the cloud point. Fig. 1b shows the transmittance *vs.* temperature curves for the 2.0% C_{12}POE solution in the absence of an electrolyte, which were obtained by heating from below the cloud point and by cooling from above; the two curves are superimposed. The cloud point was determined as a temperature at 50% transmittance. Similar curves were obtained for other sample solutions containing electrolytes. The data were reproducible within an accuracy of ±0.05 °C.

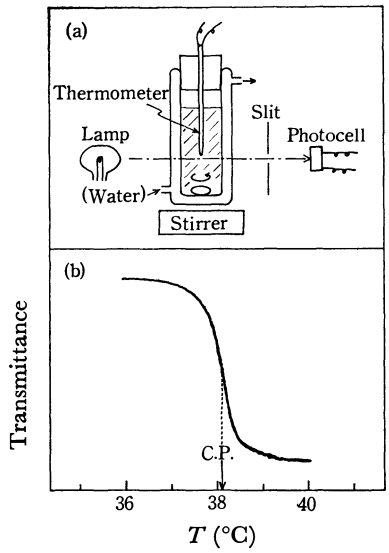

Fig. 1. (a) The apparatus used for measurement of cloud points. (b) An example of transmittance *vs.* temperature curves.

Results and Discussion

Figure 2 shows some typical examples of the effects of added electrolytes on the cloud point of the 2.0% C_{12}-POE solution. The cloud point much depends on the species of anions than on the species of cations.

Here, the present authors propose the following empirical equation, which was arrived at by analysis of the data, to describe systematically the relation of the cloud

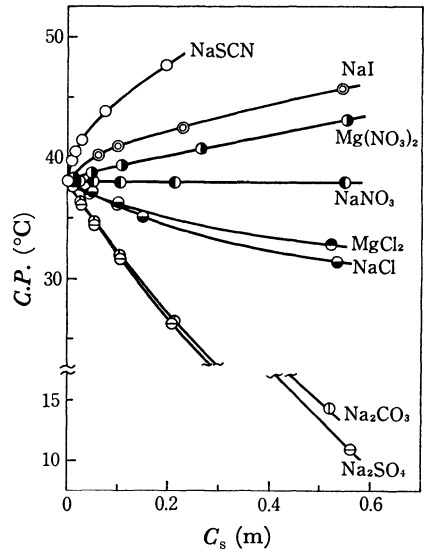

Fig. 2. Some examples of the effects of added electrolytes on the cloud point of 2.0% C_{12}POE solution.

point with the concentration of an added electrolyte.

$$(C.P.)_s/(C.P.)_0 \equiv \theta = 1 + A\sqrt{C_s} + BC_s \quad (1)$$

or $$(\theta-1)/\sqrt{C_s} = A + B\sqrt{C_s} \quad (2)$$

where $(C.P.)_s$ and $(C.P.)_0$ are the cloud points expressed, by absolute temperature with and without an electrolyte respectively, C_s is the electrolyte concentration in molality, and A and B are constants. If the quantity of $(\theta-1)/\sqrt{C_s}$ is plotted against $\sqrt{C_s}$, according to Eq. (2), a straight line is obtained for each electrolyte in the range of concentrations lower than about 0.25 m, as shown in Fig. 3. With chlorides and nitrates, linear relations are maintained up to a concentration of 0.5 m. The values of the constants A and B derived from the intercept and the slope of each straight line are summarized in Table 1.

According to the magnitudes of A and B, the electrolytes examined may be classified into the following two types. *Type I—carbonates, sulfates, and chlorides.* These electrolytes have negative values of A and B, as given in Table 1, and only small differences in A are seen among the electrolytes. The constant B varies, depending on the species of anions rather than cations. *Type II—nitrates, iodides, and thiocyanates.* The values of A for these electrolytes are positive, or negative but very close to zero. The values of B are slightly positive.

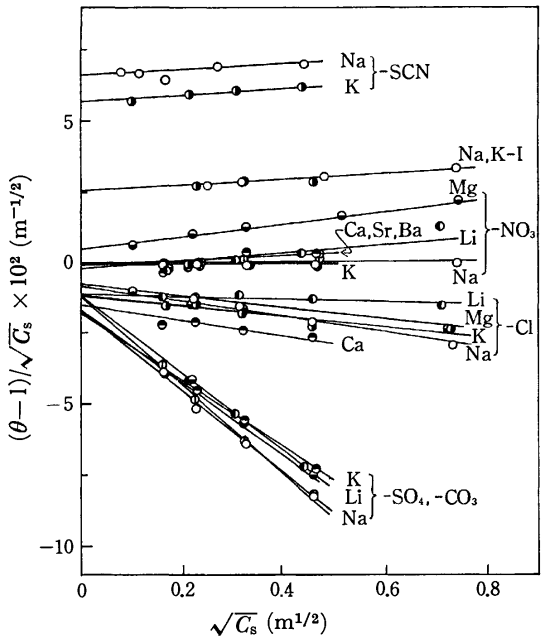

Fig. 3. Plots of $(\theta-1)/\sqrt{C_s}$ *vs.* $\sqrt{C_s}$ for various electrolytes.

Table 1. Values of A and B for various electroytes

Type I			Type II		
Electrolyte	$A\times10^2$ (m$^{-1/2}$)	$B\times10^2$ (m^{-1})	Electrolyte	$A\times10^2$ (m$^{-1/2}$)	$B\times10^2$ (m^{-1})
Na_2CO_3	−1.2	−16.2	$LiNO_3$	−0.2	1.3
K_2CO_3	−1.2	−13.5	$NaNO_3$	0	0.1
Li_2SO_4	−1.7	−12.9	KNO_3	0.1	0.1
Na_2SO_4	−1.7	−14.3	$Mg(NO_3)_2$	0.5	2.1
K_2SO_4	−1.8	−11.8	$Ca(NO_3)_2$	−0.1	0.9
LiCl	−1.1	−0.4	$Sr(NO_3)_2$	−0.1	0.9
NaCl	−0.9	−2.6	$Ba(NO_3)_2$	−0.1	0.9
KCl	−1.2	−1.7	NaI	2.6	1.0
$MgCl_2$	−0.7	−1.8	KI	2.6	1.0
$CaCl_2$	−1.5	−2.7	NaSCN	6.6	1.1
			KSCN	5.7	1.1

The solubility of nonionic surfactants in solutions of electrolytes may be discussed in terms of two factors: i) hydration of the ions, with a consequent change in the water structure nearby, which affects the affinity of the water molecules to the ether oxygens of the surfactant, and ii) binding of the ions or salts of polyvalent metals to the ether oxygens *via* cation complexation at high concentrations, resulting in an increase in solubility of the surfactant.

The structure of water in electrolyte solutions has been discussed from viscosity[3,4] and NMR[5] data with the conclusion that the effectiveness in destrusturing water around anions is in the order of $I^->NO_3^->Cl^->SO_4^{2-}>CO_3^{2-}$, in which CO_3^{2-} and SO_4^{2-} ions are rather structure-forming. Their conclusion is in accordance with the magnitude of B shown in Table 1. These results would suggest that the constant B has some close relation to the extent of destructure of water by added electrolytes, although differences in B between iodides and nitrates, and between sulfates and carbonates, are not so distinctive. Probably, added electrolytes, especially their anions, would affect the solubility of the nonionic surfactant through changes in the structure of water around them, depending on their structure-breaking or -forming ability.

The difference in A between electrolytes of the types I and II cannot be explained at the present stage: the constant A might be concerned with a factor not being related to the structure of water, presumably, with an interaction of ions (or salts) with the ether oxygens of the nonionic surfactant. Interpretation of the constant A requires additional information.

According to current views, thiocyanate ions are destructive of water,[6,7] and unassociated water hydrates nonionic surfactant molecules better than hydrogen-bonded, associated water, which results in raising the cloud point. Therefore, the positive values of B for thiocyanates could also be ascribed to their destruction of water structure. The large values of A are to be noted, which seem to be related to an increase in cloud point although the detailed mechanism is not clear.

The behavior of cations in nonionic surfactant solutions may be discussed in terms of complex formation.[8] For example, differences in A and B between $NaNO_3$ and $Mg(NO_3)_2$ could be explained in part by the complex formation of Mg^{2+} ions with the ether linkages of the surfactant.

References

1) K. Durham, "Surface Activity and Detergency," Macmillan, London (1961), p. 20.
2) M. J. Schick, *J. Colloid Sci.*, **17**, 801 (1962).
3) M. Kaminsky, *Disc. Faraday Soc.*, **24**, 171 (1957).
4) K. Miyajima, K. Inari, and M. Nakagaki, *Nippon Kagaku Kaishi*, **1974**, 2031.
5) J. N. Shoolery and B. J. Alder, *J. Phys. Chem.*, **23**, 805 (1955).
6) A. Doren and J. Goldfarb, *J. Colloid Interface Sci.*, **32**, 67 (1970).
7) G. E. Walrafen, *J. Chem. Phys.*, **55**, 768 (1971).
8) H. Schott, *J. Colloid Interface Sci.*, **43**, 150 (1973).

BULLETIN OF THE CHEMICAL SOCIETY OF JAPAN, VOL. 48 (5), 1647—1648 (1975)

A Gel-state Liquid-membrane Iodide-ion Electrode

Yoshio SHIJO

Department of Industrial Chemistry, Faculty of Engineering, University of Utsunomiya, Ishii-machi, Utsunomiya 321-31

(Received April 19, 1974)

Synopsis. A new liquid-membrane iodide-ion electrode has been developed. The liquid membrane of the electrode consists of poly vinyl chloride gel containing a nitrobenzene solution of tridodecylethylammonium iodide as an ion exchanger, a lead wire is inserted directly into the gel. The properties of the electrode, such as the response time, the effect of the temperature, the reproducibility of the preparation, and the selectivity, have been determined.

Recently, a number of studies of the simplification of the construction of liquid-membrane ion electrodes have been carried out. James *et al.*[1] developed coated-wire ion-selective electrodes with a fine platinum wire covered with poly vinyl chloride film containing an ion-association complex. Ruzicka and Rald[2] developed a simple liquid-state ion electrode, named selectrode, consisting of a graphite rod impregnated with the liquid-membrane, it was put in a Teflon tube. A stainless steel wire screwed into the graphite rod served as a lead to an electronic voltmeter. We prepared a simple liquid-membrane ion electrode consisting of a gel-state liquid-membrane and a lead wire inserted directly into the gel phase. Further, the effects of various conditions on the properties of the gel-state liquid-membrane were examined.

Experimental

A Hitachi-Horiba Model F-7 SS pH meter was used for the potential measurements. The tridodecylethylammonium bromide (TDEA) was prepared according to the method of a previous paper.[3]

The electrode body consisted of a glass tube, 8—10 mm in diameter and fitted with rubber and cork stoppers, as is shown in Fig. 1. A stainless steel wire 2 mm in diameter inserted into the gel membrane served as a lead to an electronic voltmeter. The ion-association complex solution was prepared by repeatedly shaking a nitrobenzene solution of 1×10^{-4} M TDEA with an aqueous solution of 1×10^{-3} M potassium iodide. The gel-state liquid-membrane was prepared by the following procedure. A 5 ml portion of the ion-associate solution was mixed with 0.9 g of poly vinyl chloride (PVC) in a test tube. The mixture was heated to 100 °C in an oil bath and stirred until the PVC has been completely dissolved. This solution was then poured into the B part of the electrode body and gelatinized by cooling to room temperature. The gel-state liquid-membrane electrode was preserved over nitrobenzene in a bottle fitted with a cork stopper. All the potentials were measured against a saturated calomel electrode as the reference electrode at 25.0±0.1 °C. The gel-state liquid-membrane electrode was dipped in the ion-associate solution for 1 s before use.

Results and Discussion

The variation in the potential of the gel-state liquid-membrane electrode with the concentration of the iodide ions is shown in Fig. 2. The calibration curve is linear down to 1×10^{-5} M iodide. The response of this gel-state liquid-membrane electrode was fairly fast and attained an equilibrium potential after a 2-min dipping of the electrode into the test iodide solution beyond 1×10^{-5} M. Below 1×10^{-6} M iodide, however, the equilibrium potential was attained only after 10 min. The effects of the concentration of the ion associate in nitrobenzene on the potential were examined. Four electrodes with varying concentrations of TDEA in nitrobenzene were made by the above-mentioned procedure. The variation in the potential with the concentration of iodide for each electrode is shown in Fig. 3. A better linearity of the potential variation and a higher sensitivity were obtained for the electrode with the membrane of the concentration of the ion associate of 1×10^{-4} or 7×10^{-5} M.

The surface of the gel-state liquid-membrane gradually became softer with the rise in the temperature and was

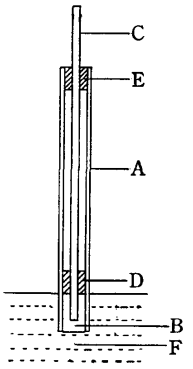

Fig. 1. Construction of the gel-state liquid-membrane electrode.
(A) glass tube, (B) gel state liquid membrane, (C) lead wire, (D) cork stopper, (E) rubber stopper, (F) test solution.

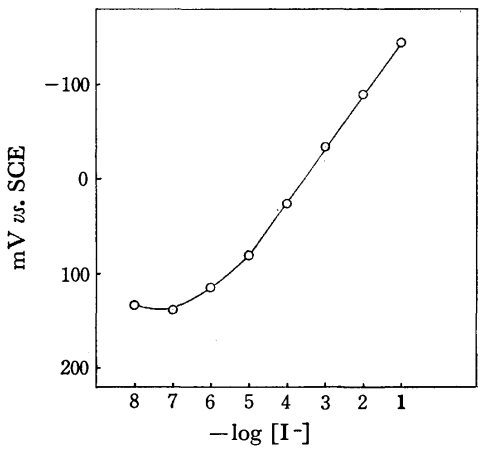

Fig. 2. Calibration curve.
Ion associate: 1×10^{-4} M

Table 1. Summary of the properties of iodide-responsive electrodes

Electrode	Ion exchanger	Slope (mV/log a)	Concn range of linear response	Selectivity ratios (NO^-_3)
Gel state liquid membrane electrode	Tridodecylethylammonium salt	56.0	10^{-1}—10^{-5}	0.058
Coarted wire[1] electrode	Tricaprylmethylammonium salt	60.0	10^{-1}—10^{-4}	0.11
Liquid membrane[5] electrode	Tricaprylmethylammonium salt	59.0	10^{-1}—10^{-3}	0.19

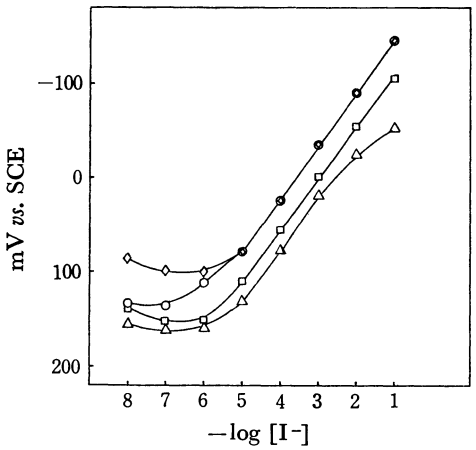

Fig. 3. Effect of concentration of the ion associate in nitrobenzene on potentials
Ion associate: △; 1×10^{-5} M, □; 7×10^{-5} M, ○; 1×10^{-4} M, ◇; 1×10^{-3} M.

deformed a little beyond 40 °C. The variation in the potential was small below 30 °C, but the potential dropped suddenly above 35 °C. Therefore, the temperature of the test solution must be kept constant below 30 °C. The pH variation in the test solution showed that the potential did not change over the pH range of 3—9. The reproducibility of the preparation of the electrode was also examined. Five pieces of electrodes were made by the above-mentioned procedure. The potentials of the electrodes for the same concentration of the iodide solution were fairly different, but the slopes of the potential variation for all the electrodes were nearly the same in the concentration range of iodide of 1×10^{-5}—1×10^{-1} M.

The gel-state liquid-membrane deteriorated on exposure to air because of the evaporation of the solvent. Therefore, the electrode should be stored over nitrobenzene in a bottle fitted with a cork stopper. If the electrode was dipped in a 1×10^{-4} M ion-associate solution before employment, the electrode could be used for two months. The influence of foreign anions on the determination of iodide was examined by adding various salts to the 1×10^{-4} M iodide solution. The selectivity ratios, as calculated by the same procedure as that of Rechnitz,[4] were 56 for perchlorate, 2.8 for thiocyanate, 0.058 for nitrate, 0.013 for cyanide, and 0.0047 for bromide.

The properties of the gel-state liquid-membrane electrode are compared with those of other, similar iodide electrodes in Table 1.

References

1) H. James, G. Carmack, and H. Freiser, *Anal. Chem.*, **44**, 856 (1972).
2) J. Ruzicka and K. Rald, *Anal. Chim. Acta*, **53**, 1 (1971).
3) Y. Shijo, *Nippon Kagaku Kaishi*, **1974**, 889.
4) K. Srinivasan and G. A. Rechnitz, *Anal. Chem.*, **41**, 1203 (1969).
5) C. J. Coetzee and H. Freiser, *ibid.*, **41**, 1128 (1969).

BULLETIN OF THE CHEMICAL SOCIETY OF JAPAN, VOL. 48 (5), 1649—1650 (1975)

The Magnetic Susceptibility of Two Coupled Dimers Consisting of S=1/2 Spins

Shuji EMORI, Tadashi TOKII, and Yoneichiro MUTO

Department of Chemistry, Faculty of Science and Engineering, Saga University, Honjo-machi, Saga 840

(Received September 2, 1974)

Synopsis. Tetramers consisting of two coupled dimers were classified as (a) linear, (b) cyclic, (c) rhombic, or (d) tetrahedral. The magnetic susceptibility for each tetramer model consisting of S=1/2 spins was obtained as an analytical equation. For the linear tetramer, the susceptibility equation was calculated numerically and compared with the observed values.

It has been found that many compounds have spin-spin interactions among their magnetic ions, so they may be regarded magnetically as composed of clusters such as a dimer and a trimer. Some of them may also have interactions among such clusters.[1-6] These interactions increasing to a certain extent, the compounds may be regarded as composed of larger complicated clusters. While such interactions are weak, the effects can be taken into consideration approximately by modifying the equation of the original cluster—for example, as the magnetic susceptibility of the modified dimer model.[7] Hatfield and Inman, Jr., tried to obtain an exact expression[5] of a tetramer consisting of two coupled dimers, the Hamiltonian of which was:

$$\mathcal{H} = -2J(S_1S_2+S_3S_4)-2J'S_2S_3 -2J''(S_1S_3+S_2S_4)-2J'''S_1S_4 \quad (1)$$

where the S_i's are spin operators, J is the exchange integral of intradimer interaction, and J', J'', and J''' are the exchange integrals of the interdimer interactions. The magnetic expression thus obtained, however, was not completely an analytical equation because of the complexity of the problem.

For a tetramer which has interaction between only the adjacent ends of two dimer units, the problem has been simplified; the Hamiltonian appropriate for this problem (Fig. 1a) is:

$$\mathcal{H} = -2J(S_1S_2+S_3S_4+\gamma S_2S_3) \quad (2)$$

Here γ is the ratio of the exchange integrals of the interdimer to the intradimer interactions. This Hamiltonian is, of course, a special case of the first (Eq. 1). Using

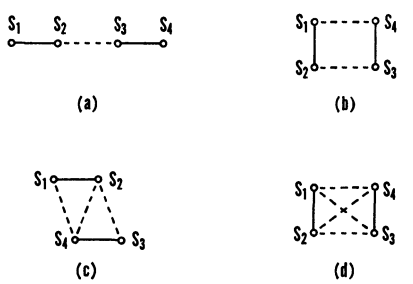

Fig. 1. Schematic representation of the two coupled dimers.
(a): Linear tetramer, (b): cyclic tetramer, (c): rhombic tetramer, (d): tetrahedral tetramer.

TABLE 1. NON-ZERO MATRIX ELEMENTS

$$(\phi_1\mathcal{H}\phi_1) = (\phi_{10}\mathcal{H}\phi_{10}) = -J\left(1+\frac{\gamma}{2}\right)$$
$$(\phi_2\mathcal{H}\phi_2) = (\phi_3\mathcal{H}\phi_3) = (\phi_7\mathcal{H}\phi_7) = (\phi_8\mathcal{H}\phi_8) = (\phi_9\mathcal{H}\phi_9) = (\phi_{12}\mathcal{H}\phi_{12}) = (\phi_{13}\mathcal{H}\phi_{13}) = (\phi_{16}\mathcal{H}\phi_{16}) = -J\gamma/2$$
$$(\phi_4\mathcal{H}\phi_4) = (\phi_5\mathcal{H}\phi_5) = J\left(1-\frac{\gamma}{2}\right)$$
$$(\phi_6\mathcal{H}\phi_6) = (\phi_{11}\mathcal{H}\phi_{11}) = (\phi_{14}\mathcal{H}\phi_{14}) = (\phi_{15}\mathcal{H}\phi_{15}) = 3J\gamma/2$$
$$(\phi_2\mathcal{H}\phi_3) = (\phi_4\mathcal{H}\phi_7) = (\phi_5\mathcal{H}\phi_7) = (\phi_6\mathcal{H}\phi_7) = (\phi_8\mathcal{H}\phi_9) = (\phi_{11}\mathcal{H}\phi_{12}) = (\phi_{13}\mathcal{H}\phi_{14}) = (\phi_{15}\mathcal{H}\phi_{16}) = -J$$
$$(\phi_4\mathcal{H}\phi_6) = (\phi_5\mathcal{H}\phi_6) = J$$

the same spin functions (products of the eigenfunctions of a dimer system consisting of S=1/2 spins) as in the literature,[5] the elements of an energy matrix are found to be as in Table 1. Diagonalizing this matrix, 6 kinds of eigenvalues (1 quintet, 3 triplets, and 2 singlets) are obtained as:

$$J\left(-1-\frac{\gamma}{2}\right) \quad \text{for S = 2}$$

$$J\left(1-\frac{\gamma}{2}\right),\ J\left(\frac{\gamma}{2}+\sqrt{1+\gamma^2}\right),\ J\left(\frac{\gamma}{2}-\sqrt{1+\gamma^2}\right) \quad \text{for S = 1}$$

$$J\left(1+\frac{\gamma}{2}+\sqrt{4-2\gamma+\gamma^2}\right),\ J\left(1+\frac{\gamma}{2}-\sqrt{4-2\gamma+\gamma^2}\right) \quad \text{for S = 0}$$

The Van Vleck susceptibility expression yields:

$$\chi = \frac{Ng^2\beta^2}{2kT}\frac{\begin{array}{l}5\exp\{J(2+\gamma)/kT\}+\exp(J\gamma/kT)\\+\exp\{J(1+\sqrt{1+\gamma^2})/kT\}\\+\exp\{J(1-\sqrt{1+\gamma^2})/kT\}\end{array}}{\begin{array}{l}5\exp\{J(2+\gamma)/kT\}+3\exp(J\gamma/kT)\\+3\exp\{J(1+\sqrt{1+\gamma^2})/kT\}\\+3\exp\{J(1-\sqrt{1+\gamma^2})/kT\}\\+2\cosh(J\sqrt{4-2\gamma+\gamma^2}/kT)\end{array}} \quad (3)$$

where differences in g-value among the 4 spins are neglected.

Figure 2 shows the results of the numerical calculations of the susceptibility for an antiferromagnetically interacting tetramer with γ=0—2. In the case of γ=0, this model represents a dimer model. If γ increases infinitely, the model tends to indicate an admixture of a dimer and two monomers. Some of the copper(II) alkanoate complexes with *N*-alkylsalicylideneimines (HSal=N–R) have been postulated to have such a linear tetramer structure.[8] The observed susceptibility for the $Cu_2(Sal{=}N{-}CH_3)(OH)(C_2H_5COO)_2$ compound does not show a maximum; perhaps it appears at lower temperatures. However, the differences among various models are already sufficiently clear in the lower part of

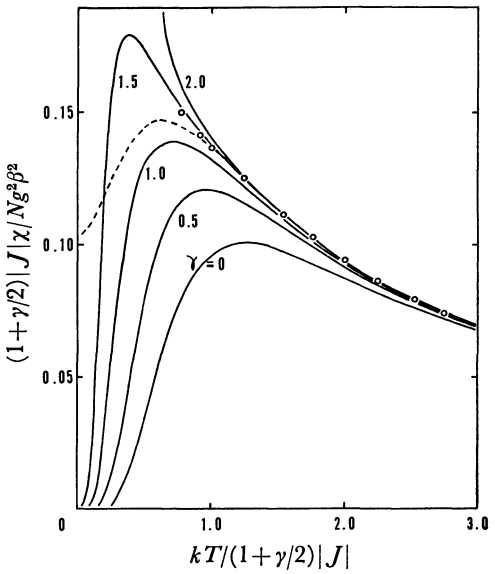

Fig. 2. Magnetic susceptibility of a linear tetramer with $\gamma=0-2$.
Broken curve is drawn for a one-dimensional Heisenberg model. The observed values of $Cu_2(Sal{=}N{-}CH_3)(OH)(C_2H_5COO)_2$ are plotted for the choice of the parameters $J(1+\gamma/2)/k=-100$ K, $g=2.17$, and $N\alpha=60\times10^{-6}$ emu/mol.

this experimental temperature range (77—300 K). The observed values agree well with the equation of a linear tetramer model, but not with that of a dimer model ($\gamma=0$) or a one-dimensional Heisenberg model, the curve of which is extrapolated to a higher temperature than in the literature.[9]

If a linear tetramer has an interaction between the remaining ends as well, a cyclic tetramer (Fig. 1b) will be formed. The Hamiltonian for this problem is:

$$\mathcal{H}=-2J\left(S_1S_2+S_3S_4+\frac{\gamma}{2}S_2S_3+\frac{\gamma}{2}S_1S_4\right) \tag{4}$$

The equation of the magnetic susceptibility can be obtained in a similar manner as for a linear tetramer:

$$\chi=\frac{Ng^2\beta^2}{2kT}\frac{\begin{array}{l}5\exp\{J(2+\gamma)/kT\}+1\\+\exp(J\gamma/kT)+\exp(2J/kT)\end{array}}{\begin{array}{l}5\exp\{J(2+\gamma)/kT\}+3\\+3\exp(J\gamma/kT)+3\exp(2J/kT)\\+2\cosh(J\sqrt{4-2\gamma+\gamma^2}/kT)\end{array}} \tag{5}$$

Considering a diagonal interaction also in a cyclic tetramer, the problem varies to that of a pseudo-rhombic tetramer (Fig. 1c), the Hamiltonian of which is:

$$\mathcal{H}=-2J\left(S_1S_2+S_3S_4+\frac{\gamma}{3}S_2S_3+\frac{\gamma}{3}S_2S_4+\frac{\gamma}{3}S_1S_4\right) \tag{6}$$

The susceptibility equation obtained in a manner similar to that above is:

$$\chi=\frac{Ng^2\beta^2}{2kT}\frac{\begin{array}{l}5\exp\{J(2+\gamma)/kT\}+\exp(J\gamma/3kT)\\+2\exp\left\{J\left(1+\frac{\gamma}{3}\right)/kT\right\}\\\times\cosh\left(J\sqrt{1-\frac{2}{3}\gamma+\frac{2}{9}\gamma^2}/kT\right)\end{array}}{\begin{array}{l}5\exp\{J(2+\gamma)/kT\}+3\exp(J\gamma/3kT)\\+6\exp\left\{J\left(1+\frac{\gamma}{3}\right)/kT\right\}\\\times\cosh\left(J\sqrt{1-\frac{2}{3}\gamma+\frac{2}{9}\gamma^2}/kT\right)\\+2\cosh\left(J\sqrt{4-2\gamma+\frac{1}{3}\gamma^2}/kT\right)\end{array}} \tag{7}$$

If the ends of a dimer unit interact with either end of the other dimer, the resulting molecule is a pseudo-tetrahedral tetramer (Fig. 1d) with this Hamiltonian:

$$\mathcal{H}=-2J\left(S_1S_2+S_3S_4+\frac{\gamma}{4}S_1S_3+\frac{\gamma}{4}S_2S_4+\frac{\gamma}{4}S_1S_4+\frac{\gamma}{4}S_2S_3\right) \tag{8}$$

The susceptibility equation thus obtained is:

$$\chi=\frac{Ng^2\beta^2}{2kT}\frac{\begin{array}{l}5\exp\left\{J\left(1+\frac{\gamma}{2}\right)/kT\right\}\\+2\exp(-J/kT)+\exp\left\{J\left(1-\frac{\gamma}{2}\right)/kT\right\}\end{array}}{\begin{array}{l}5\exp\left\{J\left(1+\frac{\gamma}{2}\right)/kT\right\}\\+6\exp(-J/kT)+3\exp\left\{J\left(1-\frac{\gamma}{2}\right)/kT\right\}\\+\exp\{J(1-\gamma)/kT\}+\exp(-3J/kT)\end{array}} \tag{9}$$

References

1) Z. G. Soos and R. G. Hughes, *J. Chem. Phys.*, **46**, 253 (1967).
2) D. D. Thomas, H. Keller, and H. M. McConnell, *ibid.*, **39**, 2321 (1963).
3) W. Duffy, Jr. and K. P. Barr, *Phys. Rev.*, **165**, 647 (1968).
4) K. Hara, M. Inoue, S. Emori, and M. Kubo, *J. Mag. Resonance*, **4**, 337 (1971).
5) W. E. Hatfield and G. W. Inman, Jr., *Inorg. Chem.*, **8**, 1376 (1969).
6) K. T. McGregor, J. A. Barnes, and W. E. Hatfield, *J. Amer. Chem. Soc.*, **95**, 7993 (1973).
7) M. Inoue, M. Kishita, and M. Kubo, *Inorg. Chem.*, **6**, 900 (1967).
8) to be published.
9) J. C. Bonner and M. E. Fisher, *Phys. Rev.*, **135**, A640 (1964).

BULLETIN OF THE CHEMICAL SOCIETY OF JAPAN, VOL. 48 (5), 1651—1652 (1975)

The Back-extraction Behavior of Chelate Compounds. II.* Some Aspects of the Secondary Dithizonate of Copper

Takaharu HONJO, Toshiyuki UNEMOTO, and Toshiyasu KIBA

Department of Chemistry, Faculty of Science, Kanazawa University, Kanazawa, Ishikawa 920

(Received November 18, 1974)

Synopsis. The behavior of secondary copper dithizonate in carbon tetrachloride, chloroform, 1,2-dichloroethane, benzene, monochlorobenzene, *o*-dichlorobenzene, and nitrobenzene has been investigated by a kinetic study of the back-extraction of the copper ion in order to clarify the extraction mechanism and to ascertain the chemical form of this chelate.

Dithizone (diphenylthiocarbazone, H_2Dz) forms an extractable, colored chelate with about twenty metals by replacing one or both hydrogen atoms, yielding the primary and the secondary dithizonate.[1,2] The primary dithizonate of copper ($Cu^{II}(HDz)_2$ type)[3] is formed in an acidic solution and appears as red-purple, while a secondary complex of a yellow-brown color ($Cu^{II}Dz$,[3] $Cu^{I}(HDz)$,[4,6] or $Cu^{II}_2(Dz)_2$[5] type) is formed in a basic solution or in the presence of a deficit of dithizone. The extraction mechanism and the structure of the secondary dithizonate of copper have not yet been fully elucidated.[1-6]

Experimental

The secondary dithizonate of copper in an organic solvent containing no free dithizone was prepared around pH 11 under the so-called substoichiometric conditions by adding an excess of copper ions over the equivalent amount of dithizone. After the phase separation, the organic phase was shaken with the same volume of an acidic aqueous solution adjusted to a desired pH with 0.1 M acetic acid. The aqueous phase was separated from the organic phase by centrifugation, and then the pH was checked again. The concentration of copper ions back-extracted into the aqueous solution was determined by atomic absorption spectrophotometry. The amount of the initial secondary complex was also determined by atomic absorption spectrophotometry after all the copper has been extracted into 6 M hydrochloric acid. All the extractions were carried out in a thermostatic room at 20 °C.

Results and Discussion

The change in the absorption spectra in the course of the back-extraction of the secondary copper dithizonate in carbon tetrachloride at pH 3.0 was determined; the results are shown in Fig. 1(a), in which No. 1 is the spectrum before the back-extraction. The spectra gradually change to No. 2, that of the primary copper dithizonate after a few hours' shaking; there are two isosbestic points—at 497 and 615 nm. The spectrum of dithizone in carbon tetrachloride is also shown in Fig. 1(a) (No. 3). Moreover, an extraction reaction between the primary complex in carbon tetrachloride and copper ions took place at pH 3.0; the change in the absorption spectrum of the secondary and primary complexes with the shaking time were determined at 450 nm and 550 nm respectively. The results are shown in Fig. 1(b). From these results, it is clear that the extraction equilibrium between the secondary copper dithizonate and the primary copper dithizonate in carbon tetrachloride is reversible under the present conditions:

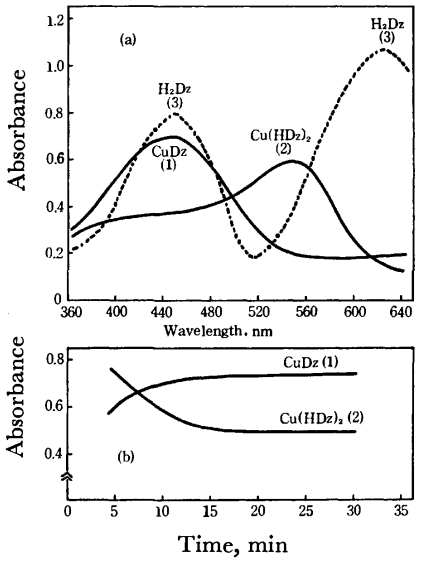

Fig. 1. (a) The change of the absorption spectra of copper dithizonate in carbon tetrachloride with the formation of $Cu(HDz)_2$ from CuDz by back-extraction at pH 3.0
(1) $(CuDz)_{initial}=3.3\times10^{-5}$ M (2) $Cu(HDz)_2=2.5\times10^{-5}$ M (3) $H_2Dz=4.0\times10^{-5}$ M
(b) The change of the absorbance of CuDz at 450 nm and $Cu(HDz)_2$ at 550 nm in carbon tetrachloride by the formation of CuDz from $Cu(HDz)_2$ and Cu^{2+} at pH 3.0
$(Cu(HDz)_2)_{initial}=5\times10^{-5}$ M, $(Cu^{2+})_{initial}=5\times10^{-5}$ M
(1) CuDz (2) $Cu(HDz)_2$

$$2CuDz + 2H^+ \rightleftarrows Cu(HDz)_2 + Cu^{2+} \quad (1)$$

Fig. 2(a) shows that the amount of copper ions increased in an aqueous phase with the shaking time in the relation of a hyperbolic curve, when the reaction was performed in carbon tetrachloride. The following two relations have been found to hold from the results after the determination of copper ions.

$$(Cu(HDz)_2)_0 = (Cu^{2+}) \quad (2)$$

For the remaining secondary dithizonate,

$$(CuDz)_0 = (CuDz)_{initial} - (Cu(HDz)_2)_0 - (Cu^{2+}) = (CuDz)_{initial} - 2(Cu^{2+}) \quad (3)$$

* T. Honjo, K. Ameno, M. Horiuchi, and T. Kiba, This Bulletin, **47**, 1799 (1974), Part I.

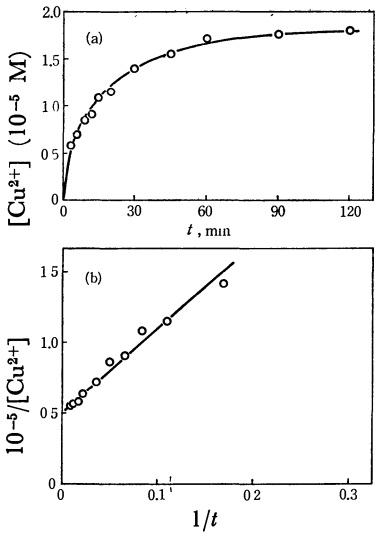

Fig. 2. The effect of the reaction time on stripping of Cu^{2+} from CuDz in carbon tetrachloride at pH 2.93. $(CuDz)_{initial}=8.6\times10^{-5}$ M

where ( ) and ( )$_0$ designate the concentration of chemical species in the aqueous and the organic phase respectively. The term of $(CuDz)_{initial}$ indicates the concentration of the secondary dithizonate at the start of the reaction. The kinetic study of the reaction shows that the increasing rate of the copper ion in the aqueous phase is the pseudo-second order reaction.

$$d(Cu^{2+})/dt = k(CuDz)_0^2 \quad (4)$$

$$d(Cu^{2+})/dt = k\{(CuDz)_{initial}-2(Cu^{2+})\}^2 \quad (5)$$

$$1/(Cu^{2+}) = 1/\{k(CuDz)_{initial}^2 t\} + 2/(CuDz)_{initial} \quad (6)$$

This equation shows that the reciprocal of the concentration of the copper ion is proportional to the reciprocal of the reaction time, that is, the shaking time, t. As is shown in Fig. 2(b), the $1/(Cu^{2+})$ *vs.* $1/t$ plot is linear at pH 2.93. This fact indicates that the treatment of the back-extraction mechanism of the secondary copper dithizonate in carbon tetrachloride is valid. The back-extraction of the secondary copper dithizonate in other solvents, such as 1,2-dichloroethane, benzene, monochlorobenzene, *o*-dichlorobenzene, and nitrobenzene, was also investigated by shaking a solution of them with an aqueous solution of pH 2.90—2.95. In the case of the complex in a chloroform solution, the back-extraction at pH 1.46 was examined because a distinct back-extraction reaction in the pH region mentioned above was observed. The wavelengths of the maximum absorptions of the secondary dithizonate in the seven solvents against the dielectric constants of the solvents are given in Table 1, together with those of dithizone. The plots of $1/Cu^{2+}$ *vs.* $1/t$ obtained with these solvents are shown in Fig. 3. This shows that the primary complex which had been formed by Reaction (1) acted with a proton to effect the following reaction:

$$Cu(HDz)_2 + 2H^+ \rightleftharpoons 2H_2Dz + Cu^{2+} \quad (7)$$

Dithizone was released as a matter of course. The solvents showing the break in the line have relatively high dielectric constants. This fact is compatible with the general rule that the polar solvents have stronger effects on the solutes than the non-polar solvents. It

Table 1. The dielectric constant, ε, of the organic solvents and the wavelength of the absorption maximum, λ_{max}, of the secondary copper dithizonate and dithizone in these solvents

Solvent	ε	λ_{max}, nm	
		CuDz	H_2Dz
Carbon tetrachloride	2.24	450	450 627
Chloroform	4.81	448	441 610
1,2-Dichloroethane	10.36	450	450 620
Benzene	2.28	454	454 627
Monochlorobenzene	5.62	454	457 629
o-Dichlorobenzene	9.93	458	457 629
Nitrobenzene	34.82	448	441 610

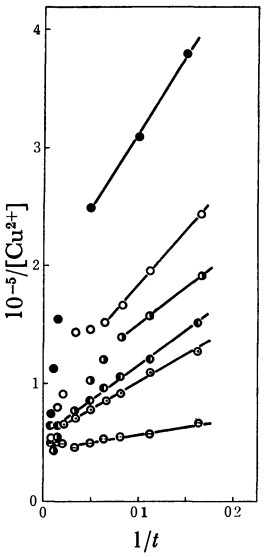

Fig. 3. The effect of the reaction time on stripping of Cu^{2+} from CuDz in various organic solvents at pH 2.90—2.95.

Solvent	$(CuDz)_{initial}$	pH
—●— chloroform	4.9×10^{-5} M	1.46
—○— 1,2-dichloroethane	9.5×10^{-5} M	2.92
—◐— benzene	7.7×10^{-5} M	2.90
—⊙— monochlorobenzene	9.7×10^{-5} M	2.90
—⊖— *o*-dichlorobenzene	8.0×10^{-5} M	2.90
—◑— nitrobenzene	5.5×10^{-5} M	2.95

is clear from these results that the extraction equilibrium between the secondary copper dithizonate and the primary dithizonate is reversible and that the secondary copper dithizonate is of the $Cu^{II}Dz$ type.

References

1) J. Stary, "The Sovent Extraction of Metal Chelate," Pergamon Press, New York, 1964.
2) Y. Marcus and A. S. Kertes, "Ion Exchange and Solvent Extraction of Metal Complexes," Wiley-Interscience, 1969.
3) H. Fischer, *Wiss. Veroeff. Siemens-Konzern*, **4**, 158 (1925).
4) B. Freiser and F. Freiser, *Anal. Chem.*, **42**, 305 (1970).
5) H. M. N. H. Irving and A. M. Kiwan, *Anal. Chim. Acta*, **56**, 435 (1971).
6) P. Brand and H. Freiser, *Anal. Chem.*, **46**, 1147 (1974).

BULLETIN OF THE CHEMICAL SOCIETY OF JAPAN, VOL. 48 (5), 1653—1654 (1975)

Circular Dichroism Spectra of (Aminocarboxylato)ammine[1,1,1-tris (aminomethyl)ethane]cobalt(III)(2+) Complexes

Kazuaki YAMANARI, Jinsai HIDAKA, and Yoichi SHIMURA

Department of Chemistry, Faculty of Science, Osaka University, Toyonaka, Osaka 560

(Received January 29, 1975)

Synopsis. Five triple mixed Co(III) complexes with one 1,1,1-tris(aminomethyl)ethane and one aminocarboxylato and one ammine ligand were prepared. The glycinato complex was optically resolved and three L-aminocarboxylato complexes were chromatographically separated into their diastereomers. The circular dichroism spectra of the complexes were discussed.

1,1,1-Tris(aminomethyl)ethane (tame) is a typical tripod ligand and coordinates facially to a Co(III) ion; then three coordination sites remain to be occupied by other ligands. A new type of chirality due to the arrangement of three different groups is expected for such tame complexes, for example, $[Co(gly)NH_3(tame)]^{2+}$ (Fig. 1). This paper deals with the preparation, optical resolution and diastereomer separation of the tame complexes, $[Co(am)NH_3(tame)]^{2+}$, where am =glycinate (gly), L-alaninate (L-ala), L-serinate (L-ser), L-valinate (L-val) and L-isoleucinate (L-ileu). The absorption and circular dichroism (CD) spectra of the complexes are reported and discussed.

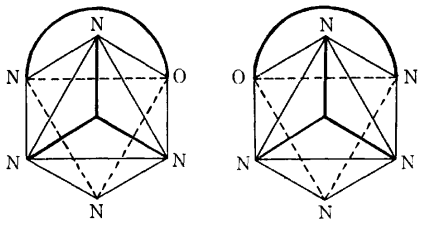

Fig. 1. Optical isomers of $[Co(gly)NH_3(tame)]^{2+}$.

Experimental

1,1,1-Tris(aminomethyl)ethane was prepared by the method of Fleischer *et al.*[1]

(−)$_{589}$-[Co(gly)NH$_3$(tame)]Cl$_2$·3H$_2$O. The mixture of *cis*-$K[Co(CO_3)_2(NH_3)_2]\cdot H_2O$[2] (10 g), tame·3HCl (8.5 g) and sodium hydroxide (4.5 g) in 100 ml of water was stirred at 70 °C for about 2 hr. The product was poured into a column containing cation exchange resin (Dowex 50W×8, Na^+ form) and eluted with 1.0 M NaCl solution. The red eluate was condensed and a crystalline complex was isolated after repeated removal of NaCl deposited out. Anal. Found: C, 22.47; H, 6.67; N, 18.01%. Calcd for $[Co(CO_3)NH_3(tame)]Cl\cdot 1.5H_2O = C_6H_{21}N_4O_{4.5}ClCo$: C, 22.83; H, 6.71; N, 17.75%. To a solution of $[Co(CO_3)NH_3(tame)]Cl\cdot 1.5H_2O$ (2 g) in 20 ml of water about 1.0 g of glycine was added and the mixture was heated at 70 °C for about 2 hr. The solution was poured into a cation exchange column of SP-Sephadex C-25 (Na^+ form) and eluted with 0.15 M NaCl solution. The orange colored eluate was concentrated in a vacuum evaporator. The crude product thus obtained, $[Co(gly)NH_3(tame)]Cl_2$, was recrystallized from as little hot water as possible.

The glycinato complex was resolved by using $K_2[Sb_2(d\text{-tart})_2]\cdot 3H_2O$ as resolving agent. The racemic glycinato complex chloride (0.5 g) was completely dissolved in 5 ml warm water (60 °C) and to the solution 0.5 g of the resolving agent was dissolved. The less soluble diastereomer gradually crystallized when the solution was kept in a refrigerator. Anal. Found: C, 20.43; H, 3.90; N, 7.88%. Calcd for (−)$_{589}$-[Co(gly)NH$_3$(tame)][Sb$_2$(*d*-tart)$_2$]·4H$_2$O = $C_{15}H_{34}N_5O_{18}CoSb_2$: C, 20.59; H, 3.92; N, 8.01%. The diastereomer was converted to optically active chloride by using an anion exchange resin (Dowex 1×8, Cl^- form). Anal. Found: C, 21.69; H, 7.15; N, 17.99%. Calcd for (−)$_{589}$-$[Co(gly)NH_3(tame)]Cl_2\cdot 3H_2O = C_7H_{28}N_5O_5Cl_2Co$: C, 21.44; H, 7.20; N, 17.86%.

The L-aminocarboxylato complexes were prepared by the method similar to that used for the racemic glycinato complex chloride, using L-alanine, L-serine, L-valine or L-isoleucine instead of glycine. Anal. Found: C, 24.56; H, 7.29; N, 18.05%. Calcd for $[Co(L\text{-ala})NH_3(tame)]Cl_2\cdot 2H_2O = C_8H_{28}N_5O_4Cl_2Co$: C, 24.75; H, 7.27; N, 18.04%. Found: C, 29.68; H, 7.48; N, 17.17%. Calcd for $[Co(L\text{-val})NH_3(tame)]Cl_2\cdot 1.5H_2O = C_{10}H_{31}N_5O_{3.5}Cl_2Co$: C, 29.57; H, 7.69; N, 17.24%. Found: C, 31.74; H, 7.68; N, 17.11%. Calcd for $[Co(L\text{-ileu})NH_3(tame)]Cl_2\cdot H_2O = C_{11}H_{32}N_5O_3Cl_2Co$: C, 32.05; H, 7.82; N, 16.99%. Found: C, 25.37; H, 6.68; N, 18.50%. Calcd for $[Co(L\text{-ser})NH_3(tame)]Cl_2\cdot 0.5H_2O = C_8H_{25}N_5O_{3.5}Cl_2Co$: C, 25.28; H, 6.68; N, 18.57%. These analytical values of each the complex are for a mixture of two diastereomers. Each the complex except L-serinato one was separated into the two diastereomers by column chromatography of SP-Sephadex C-25 (3×30 cm, Na^+ form) by using 0.075 M $Na_2[Sb_2(d\text{-tart})_2]\cdot 2H_2O$ solution as eluent. The lavels F1 and F2 denote the isomer separated earlier and later, respectively. It was confirmed that the F1 dominates over the F2 in quantity. The separation of L-serinato diastereomers was unsuccessful. The CD spectra of these diastereomers were measured with the eluates, and the concentrations were calculated from the determination of optical densities refering those of the diastereomeric mixtures (It was assumed that the two diastereomers of each the complex have identical molar absorption coefficients).

Results and Discussion

Figure 2 shows typical electronic absorption and CD spectra of the present tame complexes. These complexes can be assigned safely as $[Co^{III}(O)(N)_5]$ type[3] from their first (log ε=1.92 at 20600 cm^{-1}) and second (log ε=2.05 at 28900 cm^{-1}) absorption bands. The optical isomer of the glycinato complex, (−)$_{589}$-$[Co(gly)NH_3(tame)]^{2+}$, which was obtained from the less soluble diastereomer, shows two CD bands ($\Delta\varepsilon$=+0.016 at 18400 cm^{-1} and $\Delta\varepsilon$=−0.44 at 20500 cm^{-1}) in the first absorption band region and two weak CD bands ($\Delta\varepsilon$=−0.037 at 27500 cm^{-1} and $\Delta\varepsilon$=+0.029 at 30100 cm^{-1}) in the second absorption band region (Fig. 3). The configurational CD contribution arised from the chirality due to the arrangement of glycinate and NH_3 is considerably small

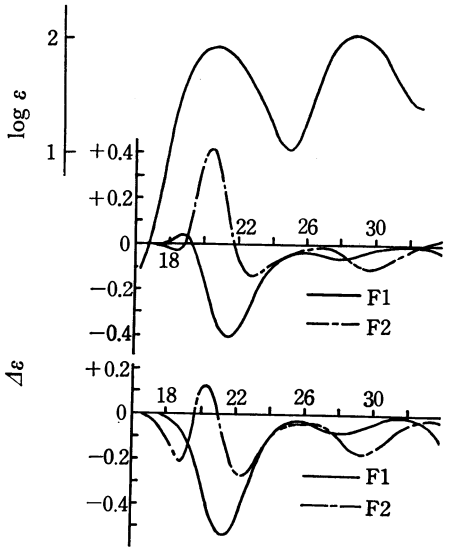

Fig. 2. Upper: Absorption and CD spectra of [Co(L-ala)-NH_3(tame)]$^{2+}$. Lower: CD spectra of [Co(L-val)NH_3-(tame)]$^{2+}$.

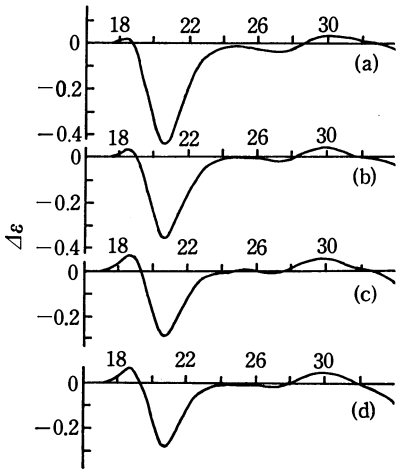

Fig. 3. CD curve of $(-)_{589}$-[Co(gly)NH_3(tame)]$Cl_2 \cdot 3H_2O$ (a), and calculated configurational effect curves, $1/2 \times \{\Delta\varepsilon(F1) - \Delta\varepsilon(F2)\}$; (b) [Co(L-ala)$NH_3$(tame)]$^{2+}$, (c) [Co(L-val)$NH_3$(tame)]$^{2+}$, and (d) [Co(L-ileu)$NH_3$-(tame)]$^{2+}$.

in comparison with those of the complexes of bis or tris chelate type.[4] The CD curves of L-alaninato, L-valinato and L-isoleucinato diastereomers deviate considerably from that of the $(-)_{589}$-glycinato isomer. However, applying the additivity rule of the configurational and vicinal contributions[5] to the CD curves of each the diastereomeric pair, a configurational CD curve similar to that of $(-)_{589}$-glycinato isomer is produced by subtracting the CD of F2 from that of F1 (Fig. 3). On the other hand, the calculated vicinal CD curves are similar to those of the corresponding [Co(L-am)$(NH_3)_4$]$^{2+}$ complexes[6] (Fig. 4). This fact points out that all three F1 isomers have the same absolute configuration and this is also the same as that of $(-)_{589}$-glycinato isomer.

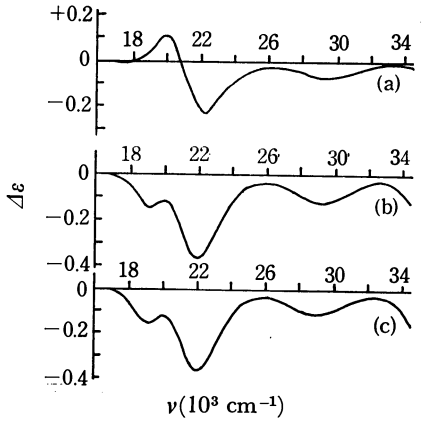

Fig. 4. Calculated vicinal effect curves: $1/2 \times \{\Delta\varepsilon(F1) + \Delta\varepsilon(F2)\}$; (a) [Co(L-ala)$NH_3$(tame)]$^{2+}$, (b) [Co(L-val)-$NH_3$(tame)]$^{2+}$, and (c) [Co(L-ileu)$NH_3$(tame)]$^{2+}$.

References

1) E. B. Fleischer, A. E. Gebala, A. Lever, and P. A. Tasker, *J. Org. Chem.*, **36**, 3042 (1971).
2) M. Mori, M. Shibata, E. Kyuno, and K. Hoshiyama, This Bulletin, **31**, 291 (1958).
3) J. Fujita, T. Yasui, and Y. Shimura, *ibid.*, **38**, 654 (1965); N. Matsuoka, J. Hidaka, and Y. Shimura, *ibid.*, **40**, 1868 (1967).
4) A. J. McCaffery, S. F. Mason, and R. E. Ballard, *J. Chem. Soc.*, **1965**, 2883; A. J. McCaffery, S. F. Mason, and B. J. Norman, *ibid.*, **1965**, 5094.
5) C. T. Liu and B. E. Douglas, *Inorg. Chem.*, **3**, 1356 (1964); N. Matsuoka, J. Hidaka, and Y. Shimura, *ibid.*, **9**, 719 (1970).
6) T. Yasui, J. Hidaka, and Y. Shimura, This Bulletin, **39**, 2417 (1966); C. J. Hawkins and P. J. Lawson, *Aust. J. Chem.*, **23**, 1735 (1970).

BULLETIN OF THE CHEMICAL SOCIETY OF JAPAN, VOL. 48 (5), 1655—1656 (1975)

Catalytic Activities of Pyridoxal Analogues. I. The Catalytic Effects of Pyridoxal, Pyridoxal Methochloride, and Pyridoxal *N*-Oxide on the Racemization of L-Glutamic Acid

Makoto ANDO and Sakae EMOTO

The Institute of Physical and Chemical Research, Wako-shi, Saitama 351

(Received July 4, 1974)

Synopsis. An improved method for the syntheses of pyridoxal methochloride (**1**) and pyridoxal *N*-oxide (**5**) was investigated. Further, the catalytic activities of pyridoxal, **1**, and **5** on the racemization of L-glutamic acid in the presence of cupric ions were studied.

In the presence of a metal ion, pyridoxal (PAL) catalyzes many reactions of amino acid, including racemization[1] and transamination.[2] Catalytic activities are also observed for the racemization with salicylaldehyde (SAL) derivatives, the benzene analogue of PAL.[3] In a previous paper, it has been reported that an electron-attracting substituent, introduced on the benzene ring of SAL derivatives, promoted the catalytic activity on the racemization of L-glutamic acid (L-Glu) in the presence of cupric ions at pH 10 and at 80 °C.[4] The catalytic activity may be expected to be more powerful when the PAL derivatives, which have a substituent on the ring nitrogen in order to increase the electron affinity of the pyridine ring, are used than when PAL itself is used.

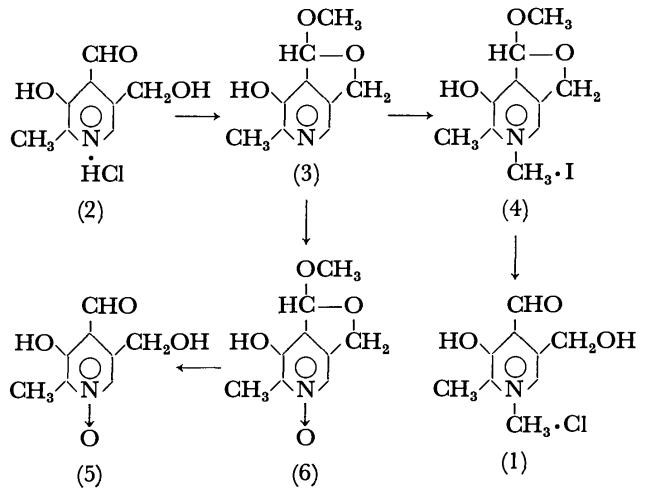

Scheme 1

Anhydrous PAL methochloride (**1**) had been synthesized from PAL hydrochloride (**2**) in a 21% yield *via* PAL monomethyl acetal (**3**) and then PAL monomethyl acetal methiodide (**4**).[5] When the synthetic conditions were improved, **1** monohydrate was prepared in a 42% yield. PAL *N*-oxide (**5**) had also been obtained from pyridoxine *via* pyridoxine *N*-oxide.[6] In tetrahydrofuran (THF), **3** was oxidized with *m*-chloroperbenzoic acid (CPA) to PAL monomethyl acetal *N*-oxide (**6**),[7] which was then easily hydrolyzed to **5**.

According to the precedents,[3,4,8] the racemization of L-Glu was carried out in the presence of cupric ions at pH 10, where it is known that side reactions, such as transamination, proceed scarcely at all. Theoretically, $(\log \alpha_t - \log \alpha_0)/t$ should be a constant, where t is the time and α_t is the observed rotation at t. Table 1 shows that the catalytic activities of **1**, **2**, and **5** were gradually lowered as the reaction proceeded at 80 °C; a similar phenomenon had been observed with **2** by Yoshikawa *et al.*[8] At 25 °C, however, the racemization catalyzed by **2** and **5** was found to obey a psudo-first-order reaction at an early stage of the reaction. Though **1** was unstable even at 25 °C, the most active catalyst was **1**, followed by **5** and **2**; this order agreed with the one expected from their molecular structures. The decrease in the catalytic activity was parallel to that in the absorption maximum of the alkaline racemization mixture at around 380 nm, attributed to the chelation of the Schiff base of Glu with **1**, **2**, or **5** and cupric ion.[9] Therefore, in these cases, the catalytic activity is seemingly lowered by the decomposition of the cayalyst. Fukui *et al.* reported that, in β-elimination and transamination, the catalytic activity of **5** was inferior to that of **2** at pH 4—5,[10] where **2** forms pyridinium salt; consequently, the electron affinity of **2** is larger than that of **5**. Although the Braunstein-Snell mechanism of the non-enzymatic reactions of amino acid catalyzed by PAL, such as racemization, transamination, and β-elimination, is generally accepted,[11] the details of the

TABLE 1. CATALYTIC ACTIVITIES

Temp. °C	Time min	$(\log \alpha_0 - \log \alpha_t) \times 10^3/t$ PMC min^{-1}	PAL min^{-1}	PNO min^{-1}
80	10	8.1	11.0	11.7
	20	5.8	9.9	11.0
	30	4.8	9.1	10.2
	40	4.4	8.5	9.5
	50	4.3	8.4	9.3
	60	4.1	8.2	8.7
	80	4.1	7.5	8.1
	100	3.8	7.1	8.1
	120	3.6	6.9	7.6
25	120	0.95	0.30	0.44
	240	0.79	0.31	0.44
	480	0.55	0.30	0.41
	960	0.50	0.29	0.39
	1440	0.47	0.29	0.40
	1920	0.47	0.27	0.36
	2400	0.46	0.27	0.37
	2880	0.42	0.27	0.37

PMC: pyridoxal methochloride; PAL: pyridoxal hydrochloride; PNO: pyridoxal *N*-oxide.

Table 2. Effect of pH on the racemization yield

pH		9	10	11	12
80 °C	PMC	45%	43%	41%	40%
1 hr	PAL	31	68	91	97
	PNO	43	70	82	89
25 °C	PMC	25	45	47	49
8 hr	PAL	7	28	58	94
	PNO	11	37	63	83

intermediates are still uncertain, and it has not been completely elucidated whether racemization, transamination, and β-elimination proceed with the same mechanism. As far as the order of the catalytic activity is concerned, the results of Fukui are consistent with those of our racemization.

No optimum pH was found for the racemization system, containing L-Glu, SAL derivatives (0.02 mole) equivalents), and cupric ions (0.02 mole equivalents) at 80 °C.[3,8] On the other hand, an optimum pH was found at around pH 10 for the racemization of L-alanine with **2** (equimolar) in the presence of cupric or aluminum ions (0.1 mole equivalents) at 100 °C for 10 min.[1] Therefore, we investigated the effect of the pH on the racemization of L-Glu under our conditions. As Table 2 shows, in a lower-pH solution, the catalytic activities decreased in the order of **1**, **5**, and **2** as was to be expected from their molecular structures, whereas, in a higher-pH solution, the order was reversed because of the unstabilities of the catalysts. In all the cases tested except the case of **1** at 80 °C, in the higher-pH solutions faster racemizations were observed. Without exception, no optimum pH was found under our conditions, in contrast to Snell's observations.[1]

It was concluded that the more powerful catalytic activities of PAL derivatives, as well as of SAL derivatives, were observed when a larger electron affinity was introduced on the aromatic ring; however, a catalyst for the racemization should be stable in an alkaline solution.

Experimental

All the mps are uncorrected. The IR spectra were recorded by means of a Shimadzu IR-27G instrument in KBr disks. The absorption spectra of the diluted alkaline racemization mixture were measured by means of a Hitachi 124 spectrophotometer.

PAL Methochloride (1). A mixture of a benzene solution of PAL monomethyl acetal (**3**), prepared from PAL hydrochloride (**2**) (8 g),[5] and CH_3I (12 ml) was refluxed for 72 hr while being stirred; during the reaction, additional 3 ml portions of CH_3I were added every 12 hr. Treating the mixture in a way similar to Heyl's method[5] gave a crude PAL monomethyl acetal methiodide (**4**) (6.1 g), which melted at 167—169 °C (decomp.) (lit,[5] mp 178—179 °C (decomp.)). Its IR spectrum showed the presence of a carbonyl group resulting from the partial hydrolysis of acetal. The crude **4** was converted to **1** as has been described in the literature.[5] Drying the final product over silica gel at room temperature under atmospheric pressure afforded 3.9 g of **1** monohydrate (42% based on **2**), which partly melted at around 100 °C and then gradually decomposed above 160 °C, as has been described in the literature.[5] IR 1660 cm^{-1} (C=O).

Found: C, 45.74; H, 5.92; N, 6.07; Cl, 15.25%. Calcd for $C_9H_{14}O_4NCl$: C, 45.86; H, 5.99; N, 5.94; Cl, 15.04%.

PAL Monomethyl Acetal N-Oxide (6). To a solution of **3** (5 g) in THF (500 ml), a solution of CPA (5.4 g; 85% purity) in THF (50 ml) was stirred at 0—5 °C over a period of 90 min; soon a precipitate resulted. The mixture was stirred for another 30 min at 0—5 °C and then left to stand overnight at room temperature. The separation of the precipitate gave 3.9 g of **6** (72%); mp>280 °C.

Found: C, 54.88; H, 5.64; N, 6.98%. Calcd for $C_9H_{11}O_4N$: C, 54.82; H, 5.62; N, 7.10%.

PAL N-Oxide (5). A solution of **6** (3.9 g) in boiling water containing a few drops of conc. HCl was cooled in an ice-water bath to precipitate 3.2 g of **5** monohydrate (80%), which melted at 120 °C (decomp.) (lit,[6] mp 120 °C (decomp.)).

Procedure of Racemization.[3] PAL was used in the form of hydrochloride; **1** and **5** monohydrates were used without drying. In a tightly stoppered test tube, a mixture of a pH-adjusted solution (2 ml) of sodium L-glutamate (2 mmol) and $CuSO_4$ (0.04 mmol) and a pH-adjusted borate buffer solution (2 ml) of the catalyst (0.04 mmol) was kept at 80 °C or 25 °C. After the required time, 6 M HCl (5 ml) was added immediately to the cooled mixture. The optical rotation of the solution was measured by means of a Perkin-Elmer 141 polarimeter; the racemization yield was calculated as follows:

$$100(\alpha_0-\alpha_t)/\alpha_0$$

The authors wish to express their thanks to Dr. Haruo Homma and his staff of this Institute for their elemental analyses and to Miss Kimiko Oguchi for her technical assistance. They also wish to acknowledge a Reaserch Grant of Life Sciences given by this Institute, which partially supported this work.

References

1) J. Olivard, D. E. Metzler, and E. E. Snell, *J. Biol. Chem.*, **199**, 669 (1952).

2) For example, see Y. Nakao, "Sakutaikagaku to Seikagaku no Kyoiki," ed. by A. Nakahara, Nankodo, Tokyo (1967), p. 192.

3) M. Ando and S. Emoto, This Biulletn, **42**, 2624 (1969), and the earlier references cited therein.

4) M. Ando and S. Emoto, *ibid.*, **42**, 2628 (1969).

5) D. Heyl, E. Luz, S. A. Harris, and K. Folkers, *J. Amer. Chem. Soc.*, **73**, 3430 (1951).

6) Y. Nakai, N. Ohishi, S. Shimidzu, and S. Fukui, *Vitamins (Japan)*, **35**, 213 (1967).

7) Independently, PAL monoethyl acetal was oxidized to *N*-oxide with CPA in EtOH, see A. Pocker, *J. Org. Chem.*, **38**, 4295 (1973).

8) S. Yoshikawa, K. Kuga, Y. Ueda, M. Goto, and H. Sugiyama, *Kogyo Kagaku Zasshi*, **70**, 331 (1967).

9) L. Davis, F. Roddy, and D. E. Metzler, *J. Amer. Chem. Soc.*, **83**, 127 (1961).

10) S. Fukui, N. Ohishi, Y. Nakai, and S. Shimizu, *Arch. Biochem. Biophys.*, **130**, 584 (1969).

11) For example, see Y. Matsushima and S. Matsumoto, "Bioinorganic Chemistry," ed. by H. Tanaka, A. Nakahara, and S. Fukui, Kagakudojin, Kyoto (1974), p. 49.

BULLETIN OF THE CHEMICAL SOCIETY OF JAPAN, VOL. 48 (5), 1657—1658 (1975)

The Reaction of Acetylenecarboxylic Acid with Amines. XVII.[1] The Addition of Dialkyl Acetylenedicarboxylates to Several Carcinogens

Yasuo IWANAMI

Department of Chemistry, Sasaki Institute, Kanda-Surugadai, Chiyoda-ku, Tokyo 101

(Received July 9, 1974)

Synopsis. Hazardous carcinogens, α-naphthylamine (I), benzidine (II), 2′,3-dimethyl-4-aminoazobenzene (*o*-aminoazotoluene) (III), 2-amino-1-naphthol (IV), and 4-methylaminoazobenzene (V), easily reacted with esters of acetylenedicarboxylic acid (VI and VII) to give addition products, whose carcinogenicity could possibly be changed.

Since Rehn noticed, in 1895, three men with bladder tumors who all worked in the same dyestuffs factory, many cases of the hazards of handling α-naphthylamine (I), benzidine (II), and other aromatic compounds have been reported.[2] 2′,3-Dimethyl-4-aminoazobenzene (III), [3] 2-amino-1-naphthol (IV),[4] and 4-methylaminoazobenzene (V)[5] have also been established as carcinogenic substances.

We have attempted the chemical modification of these hazardous compounds. It is conceivable that one can lessen or eliminate such a dangerous property by modification.

Dimethyl or diethyl acetylenedicarboxylate (VI or VII) reacted easily on admixture with these compounds. An addition reaction of an amino group onto the triple bond taking place, the primary amines, I, II, and III, gave the following fumarate-type compounds (VIII, IX, and X):

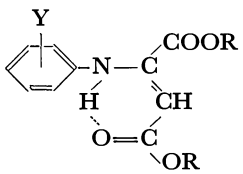

VIII: R=Methyl; Y=Benzo[*b*]
IX: R=Ethyl; *p,p′*-Linked dimer
X: R=Ethyl;
Y=*o*-Methyl-*p*-(*o′*-methylphenylazo)

In the reaction of IV, cyclocondensation followed the addition, forming a naphthoxazinone derivative (XI):

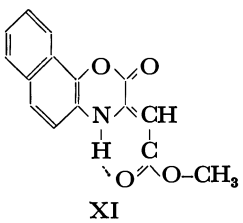

XI

Instead of the fumarate derivative, the secondary amine, V, afforded a compound of the succinate type (XII) upon the addition of two moles of V to the acetylenic bond. Except for XII, all the products are characterized by an intramolecular hydrogen bonding, as is evidenced by the IR (an absorption of ester carbonyl in the region 1674—1650 cm^{-1}) and NMR spectra.[6] Not only VIII, IX, and X, but also XI is similarly hydrogen-bonded between the ester carbonyl of the side chain and the amino group of the dihydrooxazine ring. This is one of the main structural changes as the carcinogenic amines (I, II, III, and IV) turn into the corresponding products.

All the reactions gave the adducts in high yield, proving themselves to be fit for the present purpose. These products are all new compounds; a carcinogenicity examination of them is awaited.[7]

Experimental

All the melting points are uncorrected. The IR spectra were recorded on a Nippon Bunko DS-301 or a Hitachi EPI-G3 spectrophotometer, while the NMR spectra were measured on a Hitachi H-60 spectrometer, using TMS as the external standard.

Dimethyl N-*(α-Naphthyl)aminofumarate (VIII).* Into a solution of I (0.3 g) in ethanol (10 ml), VI (0.3 g) was dropped with stirring. An exothermic reaction took place immediately, and the temperature of the reaction mixture rose to 25 °C from room temperature (21 °C). After the mixture had stood overnight, a small amount of water was added until it was turned turbid by yellow precipitates. The mixture was then left to stand in a freezer for several weeks. The crystals thus formed in an almost quantitative yield (0.6 g) were recrystallized from toluene to give pale yellow prisms; mp 69—70 °C. IR (nujol): 3242 (NH), 1736 (C=O), 1674 (chelated C=O), and 1612 (C=C) cm^{-1}. NMR (DMSO-d_6, δ): 3.57 (OCH_3), 3.72 (OCH_3), 5.41 (=CH–), and 10.17 (NH) ppm.

Found: C, 67.17; H, 5.30; N, 4.84%. Calcd for $C_{16}H_{15}O_4N$: C, 67.36; H, 5.30; N, 4.91%.

Tetraethyl Benzidine-N,N′-*difumarate (IX).* Obtained from II and VII in a similar manner. Yield, 91%. Yellow (dark) prisms from ethanol; mp 150—151 °C. IR (KBr): 3295 (NH), 1736 (C=O), 1662 (chelated C=O), and 1614 (C=C) cm^{-1}.

Found: C, 64.34; H, 6.08; N, 5.79%. Calcd for $C_{28}H_{32}N_2O_8$: C, 64.11; H, 6.15; N, 5.34%.

Diethyl 2′,3-Dimethyl-4-aminoazobenzene-N-*fumarate (X).* Obtained from III and VII. Yield, 87%. Orange prisms from methanol; mp 81—82 °C. IR(KBr): 3307 (NH), 1735 (C=O), 1662 (chelated C=O), and 1615 (C=C) cm^{-1}.

Found: C, 66.47; H, 6.40; N, 10.31%. Calcd for $C_{22}H_{25}O_4N_3$: C, 66.82; H, 6.37; N, 10.63%.

*3-(Methoxycarbonylmethylene)-3,4-dihydro-2*H-*naphtho*[*1,2*-b]-*1,4-oxazin-2-one (XI).* Obtained from IV and VI. Yield, 93%. Yellow fluorescent needles from methanol; mp 183—183.5 °C. IR (nujol): 3240 (NH), 1764 (lactone C=O), 1650 (chelated C=O), and 1623 (C=C) cm^{-1}. NMR (DMSO-d_6, δ): 3.77 (OCH_3), 5.69 (=CH–), and 10.91 (NH) ppm.

Found: C, 67.08; H, 4.36; N, 5.51%. Calcd for $C_{15}H_{11}O_4N$: C, 66.91; H, 4.12; N, 5.20%.

Dimethyl 2,3-Bis[*methyl(*p-*phenylazophenyl)amino*]*succinate*

(XII). Obtained from V and VI. Yield, 82%. Dark yellow crystals; mp 109—110 °C. IR (KBr): 1740 (C=O) cm^{-1}.

Found: C, 67.98; H, 5.82; N, 15.32%. Calcd for $C_{32}H_{32}O_4N_6$: C, 68.07; H, 5.71; N, 14.89%.

Some of the instruments used in this study were obtained by a grant-in-aid from the Ministry of Education, Japan, and a grant from the Anna Fuller Fund, U.S.A.

Thanks are due to Mr. T. Inagaki, Nitto Chemical Industry, Co., for the measurement of the NMR spectra.

References

1) Part XVI: Y. Iwanami, This Bulletin, **44**, 1314 (1971).

2) M. H. C. Williams, "Cancer," Vol. 3, ed. by R. W. Raven, Butterworth and Co., London (1958), p. 338.

3) T. Sasaki and T. Yoshida, *Virchow's Arch. Pathol. Anat. Physiol.*, **295**, 175 (1935).

4) W. C. Hueper, "Cancer," Vol. 1, ed. by R. W. Raven, Butterworth and Co., London (1957), p. 405.

5) J. A. Miller and E. C. Miller, "Carcinogenesis: A Broad Critique," The Williams and Wilkins Co., Baltimore, Ma. (1967), p. 397.

6) Y. Iwanami, This Bulletin, **44**, 1311 (1971); *Nippon Kagaku Zasshi*, **82**, 778, 780 (1961), **83**, 593 (1962).

7) Y. Iwanami and S. Odashima, *Naturwissenschaften*, **61**, 509 (1974).

BULLETIN OF THE CHEMICAL SOCIETY OF JAPAN, VOL. 48 (5), 1659—1660 (1975)

The Photolysis of α-Haloketones. II. The Intramolecular Reactions of 9-α-Bromopropionylanthracene

Tamotsu MATSUMOTO, Masanori SATO, and Satoshi HIRAYAMA[1)]

Faculty of Textile Science, Kyoto Technical University, Matsugasaki, Sakyo-ku, Kyoto 606

(Received July 18, 1974)

Synopsis. The main photolysis products of 9-α-bromopropionylanthracene were identified as 2-methyl-1-aceanthrenone and 9-vinylanthryl ketone. The yield of 9-bromoanthracene was very small. A significant solvent and temperature dependence was noted on the yields of these products. The photolysis at −196 °C resulted in the formation of almost 100% of 9-vinylanthryl ketone.

In a previous paper,[2)] we reported that 9-ω-bromoacetylanthracene (I) undergoes new intramolecular photochemical reactions, yielding mainly 1-aceanthrenone (II) and 9-bromoanthracene (III). In this note, we will describe an extension of these photochemical reactions to 9-α-bromopropionylanthracene (IV), an analogue of I. Besides the three features noted for the photochemistry of I,[2)] several new facts, including a photoelimination reaction peculiar to IV, were found and will be reported herewith.

Experimental

According to the method of May and Mosettig,[3)] IV was synthesized by brominating 9-propionylanthracene and was recrystallized from ligroin. For spectroscopic measurements, it was purified further by sublimation *in vacuo*. (UV: (ethanol), λ_{max} ($\varepsilon\times10^{-3}$), 350 nm (4.36), 366 (6.20), 384 (6.03).)

The fluorescence spectra were recorded on a Shimadzu Spectrofluorophotometer Model RF 502, and the absorption spectra were taken with a Hitachi Spectrophotometer Model 124.

To analyze the photo-products, an ethanol solution of IV (*ca.* 200 mg/250 ml) was irradiated for 2 hr in a reaction vessel previously described.[2)] The reaction vessel was kept cooled to dry ice-ethanol temperatures during irradiation. The photo-products thus obtained were separated by column chromatography on silica gel. Elution with benzene gave III, unreacted IV, 9-vinylanthryl ketone (V), 2-methyl-1-aceanthrenone (VI), and anthraquinone. V, NMR: 5.63—7.10 ppm (m, ABX type, 3H), 7.27—8.03 (m, aromatic, 8H), 8.40 (s, aromatic meso-H, 1H). Found: C, 87.44; H, 5.36%. Calcd for $C_{17}H_{12}O$: C, 87.90; H, 5.21%. IR: 1663 cm^{-1} (C=O). UV: (ethanol), λ_{max} ($\varepsilon\times10^{-3}$), 329 nm (2.65), 345 (4.72), 362 (6.53), 381 (5.92). VI, mp 88—89 °C. NMR: 1.46 ppm (d, CH_3-CH, 3H, J=7.5 Hz), 3.25 (q, CH_3-CH, 1H), 7.11—7.91 (m, aromatic, 6H), 8.31 (s, aromatic meso-H, 1H), 8.93 (m, aromatic α-H, 1H). Found: C, 88.00; H, 5.14%. Calcd for $C_{17}H_{12}O$: C, 87.90; H, 5.21%. IR: 1703 cm^{-1} (C=O). UV: (cyclohexane), λ_{max} ($\varepsilon\times10^{-3}$), 349 nm (3.86), 368 (7.83), 390 (9.71), 413 (9.97); (ethanol), λ_{max} ($\varepsilon\times10^{-3}$), 351 nm (3.71), 369 (6.80), 397 (7.67), 418 (7.16).

The irradiation source and filters used for the spectrophotometric studies of the photochemical reactions have also been described previously.[2)] The product yields were, unless otherwise stated, always determined in the photolysis of dilute solutions (*ca.* 10^{-4} M) by the use of the molar extinction coefficients reported here.

Results and Discussion

The main photolysis products of IV were identified as V and VI. Dissolved oxygen was ascertained to have no significant effect on the qualitative nature of the photochemical reactions of IV.

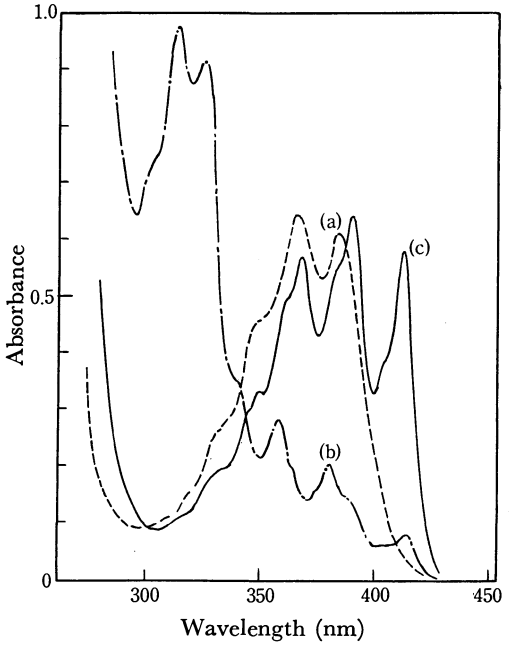

Fig. 1. Photolysis of IV in degassed *n*-hexane.
(a) ----: reactant, (b) ——: after 15 min irradiation with the filter UV-39 at room temperature, (c) ——: final products obtained by the dark reaction after irradiation (see the text).
A detailed description on the electronic spectra of VI is given in Ref. 4.

Figure 1 shows the absorption spectra of IV in degassed *n*-hexane before and after illumination. After about 15 min irradiation at room temperature through the UV-39 filter, which absorbs all light below 344 nm from a high-pressure mercury-arc lamp, a stable intermediate with the absorption band with a peak at 314 nm (Curve b) appeared. A very similar absorption band of the intermediate has been observed in the photolysis of I, indicating the formation of an analogous intermediate.[2)] The intermediate gradually underwent a thermal reaction to yield VI and finally gave the absorption spectrum represented by Curve c (two days later). When the intermediate was irradiated through the UV-DIB filter, which transmits light of 313, 334, and 366 nm, VI was formed immediately.

In ethanol the intermediate was not stable at room temperature. It was confirmed, however, that the intermediate could exist stably at dry ice-ethanol temperatures, as is shown in Fig. 2. The absorptions (Curve b) at around 314 nm and in the 340—400 nm region are due to the intermediate and to V respectively;

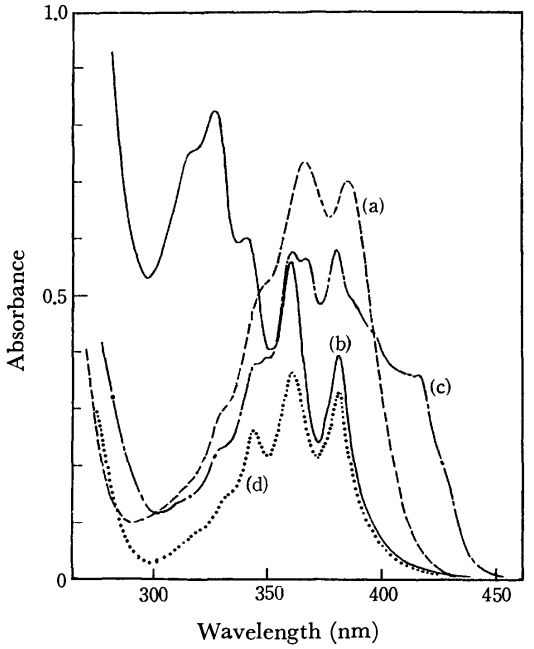

Fig. 2. Photolysis of IV in aerated ethanol.
(a) ——: reactant, (b) ——: after 30 min irradiation with the filter UV-39 at dry ice–ethanol temperatures, (c) —·—: final products obtained immediately after warming the solution in the dark (Curve b) to room temperature, (d) ·····: the absorption spectrum of V.

no absorption due to VI is seen. On the other hand, the formation of III could easily be revealed by observing the fluorescence spectrum of the solution with the absorption spectrum b.[5] When this solution was allowed to warm to room temperature in the dark, the absorption of the intermediate disappeared rapidly and the absorption due to VI built up, as is shown by Curve c. Thus, it is evident that the process to form the intermediate and those to form III and V are different and that only VI is formed from the intermediate. In this respect, the photochemistry of IV is closely similar to that of I. Thus, the reaction scheme to give III, V, and VI can be summarized as follows;

$$\text{IV} \xrightarrow{h\nu} \text{III } (ca.\ 4\%)$$
$$\text{IV} \xrightarrow{h\nu} \text{Intermediate} \xrightarrow[\text{or } \Delta]{h\nu'} \text{VI } (43\%)$$
$$\text{IV} \xrightarrow{h\nu} \text{V } (42\%).$$

Different pathways are given for the formation of III and V, because the yields of these two products show a very different temperature dependence, as will be shown below. The yields obtained in an aerated ethanol solution at dry-ice–ethanol temperatures are shown in parentheses. The value for III was determined by fluorometric measurements. In contrast to the case of the photolysis of I, the yield of III is very small.

Photolysis at Low Temperatures. The ratio of the yield of VI to that of V was found to depend significantly on the solvent and the temperature. As the temperature decreased, the ratio decreased from 4.0, 2.6, and 1.2 at 0 °C to zero at −196 °C in isopentane, EPA, and ethanol respectively.[6] The yield of V reached almost 100% at −196 °C in all these solvents. It was also confirmed by fluorometric measurements that the yield of III decreased to zero when the temperature was lowered. The retardation of the photochemical reaction of IV to give III by lowering the temperature was evidenced even more clearly by the temperature effect on the photochemical reactions of I, where the yield of III is of the order of 30% at dry ice–ethanol temperatures.[2] At first the amount of III increased against that of II as the temperature decreased (*ca.* 72% in ethanol at −145 °C), since the reaction to give II was more rapidly retarded. However, as the temperature was decreased further, the irradiation time needed to complete the reaction of I became logner and longer, and at last no photochemical reaction could be observed at −196 °C. Thus, the retardation of the reaction by lowering the temperature can be said to increase in the order of the reactions to give V, III, and VI (or II). The occurrence of the photolysis of IV at −196 °C is one of the most prominent differences in behavior between I and IV.[7]

Cause of the Great Decrease in the Yield of III. The IR absorption spectrum of a streching mode of the carbonyl group of I shows a clear splitting (1729 and 1700 cm^{-1}) characteristic of α-haloketones; this indicates the existence of two distinct conformations of the bromine atom to the carbonyl group. On the other hand, the corresponding IR absorption spectrum of IV shows no splitting (1703 cm^{-1}), suggesting that there are not two distinguishable conformations.

Since the IR and UV spectra of I and IV reveal that the plane of the carbonyl group is almost perpendicular to the anthracene ring, in one of the two conformations of I the bromine atom is expected to take a position where non-bonding electrons of the bromine atom lie just above the *p*-orbital of 9-carbon atom. If the photorearrangement mechanism proposed for 9-nitroanthracene is referred to,[8] such a conformation can be expected to be suitable for the formation of III. On the other hand, in the photolysis of IV the yield of III greatly decreased. This may, therefore, reflect either the circumstance that the allowed conformation of IV is unfavorable for such an interaction between the bromine atom and 9-carbon atom or the fact that the reaction rates to give V and VI are faster than that to give III.

References

1) To whom correspondence should be addressed.
2) T. Matsumoto, M. Sato, and S. Hirayama, This Bulletin, **47**, 358 (1974).
3) E. L. May and E. Mosettig, *J. Amer. Chem. Soc.*, **70**, 686 (1948).
4) S. Hirayama, This Bulletin, **43**, 1127 (1975).
5) The solution was immediately cooled to −196 °C in order to quench a dark reaction and to enhance the fluorescence intensity. The observed fluorescence was almost entirely due to III. Compound V is practically non-fluorescent.
6) T. Matsumoto, M. Sato, and S. Hirayama, *Chem. Phys., Lett.*, **27**, 237 (1974).
7) It is interesting to note that I comes to fluoresce near −196 °C, while IV is non-fluorescent even at −196 °C and undergoes photo-elimination at this temperature.
8) O. L. Chapman, D. C. Heckert, J. W. Reasoner, and S. P. Thackaberry, *J. Amer. Chem. Soc.*, **88**, 5550 (1966).

BULLETIN OF THE CHEMICAL SOCIETY OF JAPAN, VOL. 48 (5), 1661—1662 (1975)

The Cycloaddition Reaction of Isobenzofuran with Fulvenes: The Formation of an *endo*-(6+4)π Adduct

Hitoshi TAKESHITA, Akira MORI, Sansei SANO, and Yutaka FUJISE*

Research Institute of Industrial Science, Kyushu University, Hakozaki, Fukuoka 812

** Department of Chemistry, Tohoku University, Aramaki-Aoba, Sendai 980*

(Received July 25, 1974)

Synopsis. Isobenzofuran (I) was shown to react at 160 °C with 6,6-diphenylfulvene to give two *endo*-(2+4)π cycloadducts, an *endo*-1:1-adduct and an *endo-anti-endo*-1:2-adduct. On the other hand, I and 6,6-dimethylfulvene gave an *endo*-(6+4)π cycloadduct at room temperature.

Recently, we have reported the results on the cycloaddition reaction of isobenzofuran (I) with some typical tropones.[1] To extend the study to the reaction of I with other possible 6π-dienophiles, we have now carried out experiments with fulvenes, 6,6-diphenylfulvene (II), and 6,6-dimethylfulvene (III).

When II was placed to react with I, which has been generated at room temperature, it caused no change and resulted in the quantitative recovery of II. At higher temperatures (160—165 °C), however, a smooth reaction occurred to give two crystalline products, IV (48.1%) and V (14.9%). The structure of IV was, on the basis of the NMDR [δ: 3.77 (H_6, ddd, J=7.5, 5.5, 2.5 Hz), 4.19 (H_2, dd, J=7.5, 5.5 Hz), 4.83 (H_1, d, J=5.5 Hz), 5.38 (H_7, d, J=5.5 Hz), 5.63 (H_5, dd, J=6.0, 2.5 Hz), 5.79 (H_4, d, J=6.0 Hz) and 6.65—7.4 (14H, m)] spectral evidence, identified as an *endo*-(2+4)-π cycloadduct. The other compound, V, was shown to be a 1:2-cycloadduct, and was independently proven to be formed from I and IV, having at least one *endo*-configuration. Furthermore, its NMR [δ: 2.43 (2H, dd, J=9.0, 5.3 Hz), 2.93 (2H, dd, J=9.0, 5.3 Hz), 4.35 (2H, d, J=5.3 Hz), 5.23 (2H, d, J=5.3 Hz) and 6.8—7.4 (18H, m)] spectrum indicated the presence of an element of symmetry, ruling out two isomers of the *endo-anti-exo*- and *endo-syn-exo*-configurations. From the remaining two isomers (*endo-anti-endo*- and *endo-syn-endo*-adducts), the former must represent the structure, since it is impossible to construct the molecular frame with the latter. Accordingly, the observed chemical shifts of the methine protons are interpreted in terms of an up-field shift caused by the induced ring current from the aryl group of the other half of the molecule.[2] Obviously, the absence of the (6+4) π cycloaddition process to give a *gem*-diphenyl derivative may be a result of the steric hindrance.

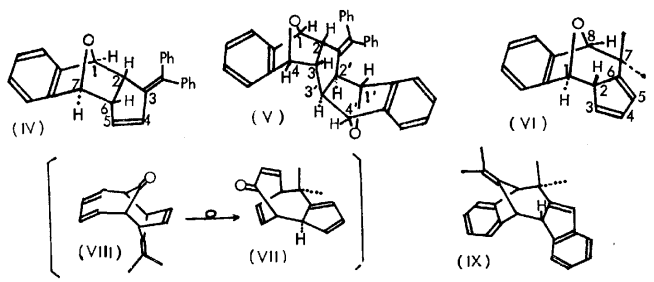

Chart

On the other hand, when III was treated with I at room temperature, a 1:1-adduct (VI), a colorles liquid, was formed in a 25.0% yield. The NMR spectrum of VI showed the presence of a *gem*-dimethyl group and three olefinic protons [δ: 1.22 (3H, s), 1.50 (3H, s), 5.56 (H_5, dddd, J=1.9, 1.4, 0.6, 0.5 Hz), 6.14 (H_3, ddd, J=5.5, 1.4, 1.0 Hz) and 6.20 (H_4, dd, J=5.5, 1.9Hz)], together with three methine protons and aromatic protons [δ: 3.46 (H_2, ddd, J=5.2, 1.0, 0.5 Hz), 4.59 (H_8, br. s), 5.48 (H_1, d, J=5.2 Hz), and 6.7—7.2 (4H, m)], indicating it to be a (6+4) π cycloadduct. Interstingly, the vicinal coupling constant between the two methine protons (H_1 and H_2), measured as 5.2 Hz, was in the range for the magnitude of the *endo*-adduct, while the *exo*-adduct was estimated to have a smaller coupling constant.[3] No other product was detected in the reaction of I with III.

The occurrence of this rather rare *endo*-(6+4)π cycloaddition is neteworthy. The cross-conjugated 6π-arrangement of the fulvene ring might be less effective in determing the stereospecificity than the linearly oriented 6π-dienophiles because of orbital overlapping, and, according to a molecular model, the *exo*- and *endo*-(6+4) π adducts show no significant difference in steric hindrance, yet the results show a throughly inverted stereospecificity. As we have shown in the cycloaddition of tropones with I,[1] the *exo*-(6+4)π adducts are derived from the *endo*-(2+4)π adduct; one should consider the possibility that VI is also formed from a thermodynamically less stable adduct, for which, only the *exo*-(2+4)π adduct can be taken into account in this case. However, (2+4)π adducts were obtained under more severe conditions, and their structures were unrelated *endo*-(2+4)π as can be seen in the formation of IV and V. Therefore, VI is probably not a secondary cycloadduct. In this regard, Paddon-Row and Warrener[4] have recently suggested that the *exo*-(6+4)π cycloadduct[5] obtained from the reaction of III with tropone could be formed afterwards by a [3,3]-sigmatropy of another initially formed *exo*-(4+6)π adduct (VIII), which was regarded as thermodynamically unstable. Thus, the stereospecificity of the formation of VII should be inherited after that of a linearly arranged (4+6)π adduct. Interestingly, dimethylisobenzofulvene has been shown to form an *endo*-(6+4)π cyclodimer (IX)[6] which, like VI, includes a non-linear 6π component; it could not be derived from a (4+2)π precursor.

Experimental

Reaction of Isobenzofuran (I) and 6,6-Diphenylfulvene (II) at a Higher Temperature. The adduct (1.24 g)[1] obtained

from tetracyclone and 7-oxabenzonorbornadiene was dissolved in cellosolv acetate (15 ml), together with II (566 mg), and the mixture was heated at 160—165 °C for 4 hr. The mixture was then poured into ice water and extracted with benzene. After the removal of the solvent, the residual mass was separated by silica gel column chromatography; from the less polar fraction eluted with benzene, recovered II (217 mg) and tetraphenylbenzene were isolated, and subsequently, from a benzene-ether (1:1) mixture, colorless crystals (IV), (mp 160—161 °C; 254 mg (Found: C, 89.16; H, 5.79%. Calcd for $C_{26}H_{22}O$: C, 89.62; H, 5.79%. λ_{max}^{MeOH}: 295 nm (ε: 27300)), and colorless crystals (V) (mp 250—251 °C, 106 mg (Found: C, 87.81; H, 5.82%. Calcd for $C_{34}H_{26}O_2$: C, 87.52; H, 5.62%)) were obtained.

Reaction of IV and I: Formation of V. IV (50 mg) was similarly allowed to react with I at 160—165 °C for 2 hr. Then, a similar work-up afforded colorless crystals (30 mg) (mp 250—251.5 °C), which were identical with the authentic V obtained from the preceeding experiment (IR and NMR spectral and mixed mp comparisons).

Reaction of I and 6,6-Dimethylfulvene (III) at Room Temperature. 3,6-Diphenyltetrazine (1.13 g) and III (500 mg) were dissolved in dichloromethane (60 ml), to which a dichloromethane (10 ml) solution of 7-oxabenzonorbornadiene (677 mg) was then added, drop by drop; the mixture was then kept 3.5 hr at room temperature with stirring. Then, the solvent was removed *in vacuo*, and the residue was fractionated by silica gel column chromatography. The first few fractions (from *n*-hexane) gave the recovered III (145 mg). The next few fractions, eluted by benzene, afforded an oily adduct VI (188 mg (*m/e*: 224 (M^+). λ_{max}^{MeOH}: 256 nm (ε: 3100), 264 (2600), 270.5 (2000). IR 1340, 1160, 755, 725 cm^{-1}). The more polar fraction gave two crystalline compounds, the *exo-exo*-adduct of 7-oxabenzonorbornadiene with I (mp 262—264 °C (lit,[7] 264—265 °C)) and the *exo-endo*-isomer (mp 174—175 °C (lit,[7] 175—176 °C)).

References and Notes

1) H. Takeshita, Y. Wada, A. Mori, and T. Hastui, *Chem. Lett.*, **1973**, 355.

2) Thus, $\Delta\delta$ (H_2 of IV and H_2 of V) is 1.76. Similarly, $\Delta\delta$ (H_6 of IV and H_3 of V) = 0.84, $\Delta\delta$ (H_1 of IV and H_1 of V) = 0.48 and $\Delta\delta$ (H_7 of IV and H_4 of V) = 0.15 are obtained.

3) The dihedral angles for *exo*- and *endo*-adducts were deduced to be *ca.* 100 and 50 °C respectively; these figures should show the *vic*-coupling constants as 0.5 Hz and 4.0 Hz according to the Williamson-Johnson modified version (*cf. J. Amer. Chem. Soc.*, **83**, 4623 (1961)), or 0.4 Hz and 5.1 Hz according to the Abraham-Holker version (*cf. J. Chem. Soc.*, **1963**, 803), of the original Karplus equation.

4) M. N. Paddon-Row and R. N. Warrenner, *Tetrahedron Lett.*, **1974**, 3797.

5) K. N. Houk, L. J. Luskus, and N. S. Bhacca, *ibid.*, **1972**, 2297.

6) H. Tanida, T. Irie, and K. Tori, This Bulletin, **45**, 1999 (1972).

7) R. N. Warrener, *J. Amer. Chem. Soc.*, **93**, 2346 (1971).

BULLETIN OF THE CHEMICAL SOCIETY OF JAPAN, VOL. 48 (5), 1663—1664 (1975)

The Catalytic Hydrogenolysis of Alkyl-substituted Aziridines

Yoshihiro SUGI,* Mitsuru NAGATA, and Sekio MITSUI

Department of Applied Science, Faculty of Engineering, Tohoku University, Aramaki aza Aoba, Sendai 980

(Received August 13, 1974)

Synopsis. Alkyl-substituted aziridines were hydrogenolysed, mainly at the less-substituted C–N bonds over Raney Ni, to yield β-amines. This hydrogenolysis occurred with the retention of the configuration. The differences in behavior between aziridines and oxiranes may be ascribed to the difference in polarisation between C–N and C–O bonds in the transition state of the hydrogenolysis.

Previous publications from our laboratory[1,2] have shown that 2-phenylaziridines undergo selective hydrogenolyses at the benzylic C–N bonds. However, there has no systematic work on the hydrogenolysis of 2-alkylaziridines. This paper will present our results for the hydrogenolysis of some 2-alkyl and 2-benzylaziridines over Raney Ni. One aspect of this investigation has been an examination of the differences in effect between alkyl and phenyl groups and in behavior between aziridine and oxirane.

Results

The results of the hydrogenolysis of 2-alkyl and 2-benzylaziridines are listed in Table 1. 2-Methyl (I), 2-ethyl (II), and 2,2-dimethyl (III) aziridines underwent rapid hydrogenolyses to yield β-amines**: *iso*-propyl, *sec*-butyl, and *t*-butylamines respectively. Karabinos and Seigen,[3] and Campbell, Sommers, and Campbell[4] have also reported the selective formation of *t*-butylamine in the hydrogenolysis of III over Raney Ni. I and II yielded small amounts of α-amines: *n*-propyl and *n*-butylamines respectively, in addition to β-amines. 1-Methyl-7-azabicyclo[4.1.0]heptane (IV) was also hydrogenolysed to a mixture of 1- and *trans*-2-methylcyclohexylamines in a ratio of 4: 1, and scarcely any *cis*-2-methylcyclohexylamine was obtained. The hydrogenolysis of 2-benzylaziridine (V) gave 1-methyl-2-phenylethylamine (82%) and 3-phenylpropylamine (18%).

Discussion

Aziridines undergo facile hydrogenolyses even under mild conditions because of their strains. 2-Alkyl and 2-benzylaziridines (I—V) were mainly hydrogenolysed at the less-substituted C–N bonds to yield β-amines. This is quite different from the hydrogenolysis of 2-phenylaziridines.[1,2] This difference may be ascribed to the fact that the latter can form π-benzyl complexes by the C–N bond fission, while the former can not.

The hydrogenolysis of IV gave *trans*-2-methylcyclohexylamine (20%) in addition to 1-methylcyclohexylamine. This suggests that the aziridine, which has no phenyl group adjacent to the ring, will be hydrogenolysed with the configurational retention over Raney Ni.

Because of the tetrahedral character of the nitrogen, the aziridine **1** will be adsorbed inclined cornerwise on the catalyst, and the nucleophilic attack to the carbon atom from the catalyst will occur to form two α,γ-diadsorbed species, **2** and **3**.[1,2] The Cα-atom*** has a

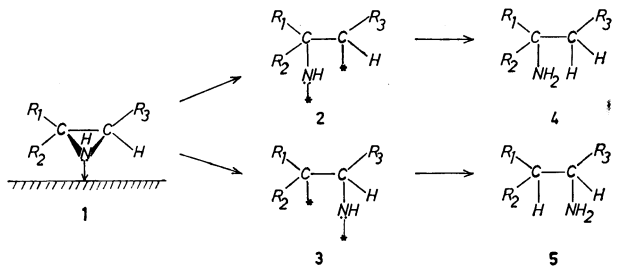

Table 1. Catalytic hydrogenolysis of 2-substituted aziridines over Raney Ni

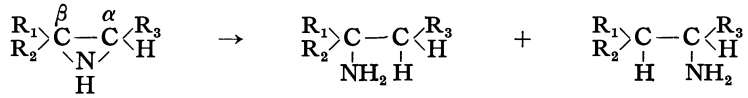

Compd (mol)	R_1	R_2	R_3	Time (hr)	Solvent (ml)	Conv (%)	Products β-amine (%)	Products α-amine (%)
I 1/200	Me	H	H	1	*n*-BuOH 10	98	87	13
II 1/200	Et	H	H	1	*n*-BuOH 10	98	87	13
III 1/200	Me	Me	H	1/2	*n*-BuOH 10	67	100	trace
IV 1/800	Me	$(CH_2)_4$		1/4	EtOH 5	80	80	20[a]
V 1/400	$PhCH_2$	H	H	1/4	EtOH 5	90	82	18

Catalyst: 500 mg (wet weight with EtOH). At 25 °C and 1 atm of H_2. a) *trans*-2-methylcyclohexylamine

* Present address: National Chemical Laboratory for Industry, 2-19-19, Mita, Meguro-ku, Tokyo 153. Any correspondence should be addressed to him.

** β-Amine is the more substituted one; the alternative is α-amine.

*** The C_α-atom is the less-substituted one; the alternative is the C_β-atom.

larger positive charge than the Cβ-atom, and it is also less hindered than the Cβ-atom because of the steric hindrance of the alkyl group. Moreover, the α,γ-diadsorbed species **2** may be more stable than the alternative **3**, because the stability of the carbon–metal bond is usually in this order: primary>secondary>tertiary.[5]† The result of these effects is that the Cα–N bond fission predominates over the Cβ–N bond fission.

2-Methyl-1,2-epoxyoctane (VI) was hydrogenolysed at the Cβ–O bond to yield an almost equimolar mixture of α-alcohol†† and 2-methyloctane, while the isomeric β-alcohol was obtained in a trace.[6] The hydrogenolysis of 1,2-epoxyoctane (VII) led to the formation of α- and β-alcohols in a ratio of 3: 2.[6] These results are in contrast with those of the aziridines (I—III). These differences we may ascribe to the difference in electronegativity between the nitrogen and oxygen atoms. The hydrogenolysis of the oxiranes VI and VII will proceed *via* carbonium ions, and the direction of the C–O bond fission will be governed by the relative stabilities of the carbonium ions: tertiary≫secondary>primary.[6] Howevev, it is unreasonably that the hydrogenolysis of the aziridines (I—V) occurs *via* the carbonium ions because more than 80% of the β-amines were obtained, in contrast with the oxiranes VI and VII. The polarisation of the C–N bond in the transition state of the hydrogenolysis may be lower than that of the C–O bond, because the nitrogen atom has a lower electronegativity than the oxygen atom. The direction of the C–N bond fission will be governed by such factors as the positive charge on the carbon, the steric hindrance of the alkyl group, and the stability of the α,γ-diadsorbed species, as has been discussed above.

† When R_1 is phenyl, **3** will be more stable than **2**, as has previously been discussed.[1,2]

†† α-Alcohol is the less-substituted one.

Experimental

Materials. The 2-methyl (I), 2-ethyl (II), and 2,2-dimethyl (III) aziridines were prepared by the procedure of Campbell *et al.*[4] The 2-benzylaziridine (V) was obtained by the Brois method[7] from 3-phenyl-1-aminopropanol-2.

1-Methyl-7-azabicyclo[4.1.0]heptane (IV). Methyl *N*-(1-methyl-*trans*-2-iodocyclohexane)carbamate was obtained by the procedure of Hassner *et al.*[8] The carbamate, without isolation, was treated with a NaOH solution in water. The usual work-up gave IV; bp 58—64 °C/25 mmHg.

Hydrogenolysis. The hydrogenolyses of I, II, and III were conducted over W-4 Raney Ni at 25 °C and 1 atm of hydrogen, using *n*-BuOH as a solvent. IV and V were hydrogenolysed in EtOH under similar conditions. The reaction mixtures were analysed by gas chromatography (liquid phase: Carbowax 4000 dispersed on firebrick†††).

References

1) Y. Sugi and S. Mitsui, This Bulletin, **42**, 2984 (1969); **43**, 1489 (1970).
2) S. Mitsui, Y. Sugi, M. Fujimoto, and K. Yokoō, *Tetrahedron*, **30**, 31 (1974).
3) J. V. Karabinos and K. T. Seigen, *J. Amer. Chem. Soc.*, **67**, 1856 (1945).
4) K. N. Campbell, A. H. Sommers, and B. K. Campbell, *ibid.*, **68**, 140 (1946); Org. Synth. Coll. Vol. III, p. 148 (1955).
5) R. P. Eischens and W. A. Pliskin, Adv. in Catal. Vol. X, Academic Press Inc., New York, N. Y. (1958), p. 1.
6) Y. Sugi, M. Hisashige, T. Nakajima, and S. Mitsui, unpublished results. *see* S. Mitsui, "Catalytic Hydrogenation," in Koza Yuki Hanno Kiko (ed. by M. Imoto) Vol. 13, Tokyo Kagaku Dojin, Tokyo, 1971, p. 295.
7) S. J. Brois, *J. Org. Chem.*, **27**, 3533 (1963).
8) A. Hassner, M. E. Lober, and C. Heathcock, *ibid.*, **32**, 540 (1967).

††† The firebrick was treated with KOH.

BULLETIN OF THE CHEMICAL SOCIETY OF JAPAN, VOL. 48 (5), 1665—1666 (1975)

Pyrolysis of 1,2-Epithiocyclohexane

Shodo INOUE and Shigeru OAE*

Department of Chemistry, Tokyo Kyoiku University, Otsuka, Bunkyo-ku, Tokyo 112

** Institute of Chemistry, The University of Tsukuba, Sakura-mura, Niihari-gun, Ibaraki 300-31*

(Received October 31, 1974)

Synopsis. Dicyclohexyl sulfide, cyclohexyl phenyl sulfide, dicyclohexyl disulfide, 2,3,5,6-bis(tetramethylene)-1,4-dithiane, cyclohexanethiol and cyclohexyl cyclohexenyl sulfide were obtained by the pyrolysis of 1,2-epithiocyclohexane apparently *via* the attack of sulfur radical species, formed by the pyrolysis of 1,2-epithiocyclohexane, on the double bond of cyclohexene.

Certain thiiranes are known to split off sulfur upon pyrolysis to give the corresponding olefins.[1] A recent report indicates that sulfur-containing products are formed by the pyrolysis of thiiranes.[2] Nevertheless, little is known about the reaction of olefins with sulfur extruded from thiiranes.[1,3]

We have carried out the liquid phase pyrolysis of 1,2-epithiocyclohexane and examined products formed in this reaction in the hope of sheding light on the reaction of cyclohexene with sulfur species[4] which would be formed by the pyrolysis of 1,2-epithiocyclohexane. The pyrolyzed products were found to consist of six gas-chromatographically separable components (A,B,C,D, E,F). From mass and NMR spectroscopic data and by comparison with authentically synthesized samples, the pyrolyzed products were identified as dicyclohexyl sulfide (A), cyclohexyl phenyl sulfide (B), dicyclohexyl disulfide (C), 2,3,5,6-bis(tetramethylene)-1,4-dithiane (D), cyclohexanethiol (E) and cyclohexyl cyclohexenyl sulfide (F).

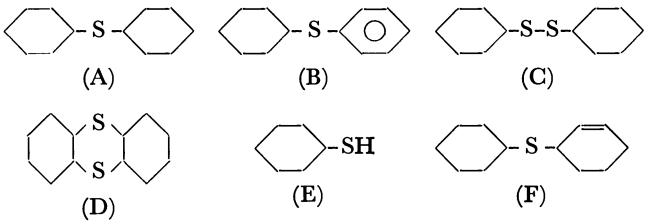

A small amount of benzene was formed apparently by the hydrogen abstraction of cyclohexene with the sulfur species formed initially.[5] The formation of hydrogen sulfide was also observed but none of elemental sulfur. When 1,2-epithiocyclohexane was heated at 210 °C for one hour in a sealed tube, compounds A,B,C,D and E were formed in 22, 4, 12, 1, and 6% yields respectively. Compound F was formed only at an early stage of the reaction but might give a compound such as B after abstraction of allylic hydrogens of F by the sulfur species. Actually, B is formed upon heating F with elemental sulfur. However, it cannot be formed by the reaction of the episulfide with benzene which is formed by the hydrogen abstraction of cyclohexene, since compound B was not formed upon heating 1,2-epithiocyclohexane in benzene. When a mixture of 1,2-epithiocyclohexane and ten equimolar amount of cyclohexene was heated at 210 °C for one hour in a sealed tube, the yield of A increased while F was also formed. This suggests that the hydrogen abstraction from F by the sulfur species is depressed by excess cyclohexene. In this case, the yields of A,C,E, and F based on the amount of episulfide used, were found to be respectively 63, 2, 2, and 7%. When a mixture of excess cyclohexene and stilbene episulfide was heated under the same conditions, compounds A,C,E, and F were similarly formed, their yields being respectively 57, 1, 2, and 8%. When a similar mixture of cyclohexene and styrene episulfide was heated, compounds A,E, and F were formed in respective yields of 26, 1, and 5%. A similar result was obtained upon heating a mixture of excess cyclohexene and 1,2-butene episulfide. These experiments suggest that a sulfur radical species produced by the pyrolysis of a certain episulfide attacks the double bond of cyclohexene as in the pyrolysis of 1,2-epithiocyclohexane.

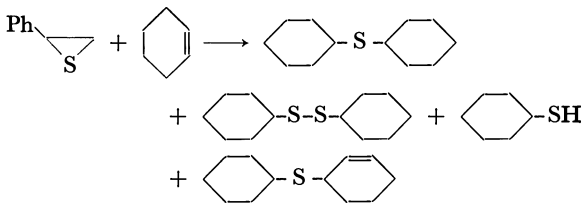

An interesting problem in the pyrolysis of episulfide is whether the two carbon-sulfur bonds of episulfide are cleaved simultaneously or consecutively, eventually yielding the corresponding olefin and sulfur. In order to clarify the mode of the C–S bond cleavage, we carried out the following experiments. An equimolar mixture of cyclohexene and 4-methylcyclohexene containing the same amount of styrene episulfide was heated in a sealed tube. Dicyclohexyl sulfide (A), cyclohexyl methylcyclohexyl sulfide (1A) and dimethyldicyclohexyl sulfide (2A) were formed in the molar ratio 1:2:1. This is the statistical ratio, since the sulfur species, formed by the pyrolysis of the styrene episulfide, will attack cyclohexene and 4-methylcyclohexene with equal ease and hence the amount of 4-methylcyclohexyl cyclohexyl sulfide formed will be twice that of dicyclohexyl or di-4-methylcyclohexyl sulfide in this reaction. The products containing one methyl group, *viz.* 3-methylcyclohexyl and 4-methylcyclohexyl sulfides, were formed nearly in the same yields. When an equimolar mixture of 1,2-epithiocyclohexane and 4-methylcyclohexene was heated in a sealed tube, compounds A, 1A, 2A, were formed in the molar ratio 1:2.3:1.2. This is similar to the results in the former case, suggesting that the sulfur species is formed by the pyrolysis of 1,2-epithiocyclohexane and attacks both the cyclohexene formed by the pyrolysis and 4-methylcyclohexene with equal ease; thus, 1,2-epithiocyclohexane seems to give sulfur and cyclohexene upon pyrolysis and not the stable thiyl

radical. When 1,2-epithiocyclohexane and 4-methylcyclohexene were heated in the molar ratio a: b, the ratio of products A, 1A, and 2A was found to be represented approximately by a^2: 2ab: b^2. However, the formation of compound A is usually slightly smaller than the calculated amount. This is because 4-methylcyclohexene, being present in the system form the beginning, will have a slightly greater chance of being attacked than cyclohexene on account of the small amount of cyclohexene formed in the early stage of the reaction.

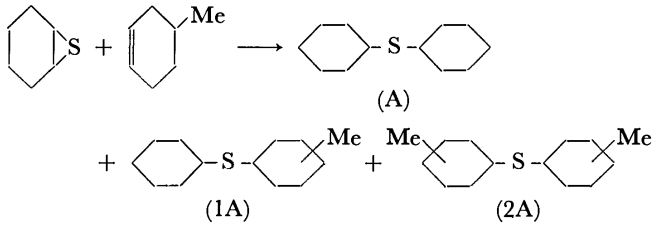

(A) (1A) (2A)

There is a possibility that compounds 1A and 2A are formed in the reaction of 4-methylcyclohexene with some other reaction products. A small amount of 1A was formed upon heating a mixture of cyclohexanethiol and 4-methylcyclohexene, but neither A nor 2A was formed. When a mixture of A and 4-methylcyclohexene was heated, 1A and 2A were obtained besides unreacted A, but the molar ratio of compounds A, 1A, and 2A was found to be 100: 9: 2. Compound 2A was not obtained in a large amount. In another experiment, a mixture of compound C and 4-methylcyclohexene was heated but no sulfide was formed. Futhermore, when an equimolar mixture of 1,2-epithiocyclohexane and 4-methylcyclohexene was heated for 4 min, the initial reaction products A, 1A, and 2A were formed in the molar ratio 1: 10: 17. Thus, 2A was formed in a large amount in the early stage of the reaction, This suggests that the sulfur species released from 1,2-epithiocyclohexane mainly attacks 4-methylcyclohexene, since there is little cyclohexene formed in the early stage of the pyrolysis. Thus it is clear that 1A and 2A are formed in the early stage of the reaction and other products such as the thiol, sulfide and disulfide which are formed in the course of the reaction would rarely undergo decomposition and recombination with 4-methylcyclohexene; therefore, the molar ratio of the products A, 1A, and 2A, 1: 2: 1, does not result from the reaction of cyclohexene and 4-methylcyclohexene with other products but from the reaction with the sulfur species. From an overall picture of the whole process, these experimental results suggest that at the relatively high temperature we employed (210 °C) the two carbon–sulfur bonds of 1,2-epithiocyclohexane may be cleaved simultaneously, resulting in the formation of cyclohexene and sulfur species. If only one of two carbon-sulfur bonds of 1,2-epithiocyclohexane were cleaved to form a highly stable biradical intermediate, compounds A and 2A would not be formed in this reaction.

Experimental

Materials. 1,2-epithiocyclohexane, styrene episulfide and 1,2-butene episulfide were prepared from the corresponding epoxy compounds with potassium thiocyanate.[6] Stilbene episulfide was obtained by reacting stilbene oxide with thiourea.[7] Dicyclohexyl sulfide, cyclohexyl phenyl sulfide and cyclohexyl cyclohexenyl sulfide were synthesized by the reaction of the corresponding bromide with the thiol in the usual way. Dicyclohexyl disulfide and cyclohexylcyclohexenyl disulfide were synthesized by heating the corresponding chloride with sodium disulfide.[8] 4-methylcyclohexyl cyclohexyl and 3-methylcyclohexyl cyclohexyl sulfides were prepared by treating 4-methylcyclohexyl and 3-methylcyclohexyl bromides with cyclohexanethiol.

Reactions. A typical run was carried out as follows. 1,2-epithiocyclohexane (0.3 g) or a mixture of 1,2-epithiocyclohexane and cyclohexene was heated at 210 °C for one hour in a vacuum sealed tube. After completion of the reaction, evolved gas was admitted into a solution of cupric sulfide and hydrogen sulfide was identified by trapping it as cupric sulfide. The liquid products of the reaction mixture were analyzed by vpc, NMR and mass spectroscopies. Their mass spectra indicate that the cracking patterns of the six compounds are similar and all of them have the cyclohexyl ring. Their parent peaks are given at *m/e* 198, 196, 192, 230, 228, 116. Since both 2,3,5,6-bis(tetramethylene)-1,4-dithiane and cyclohexyl cyclohexenyl disulfide should give the same parent peak of 228, cyclohexylcyclohexenyl disulfide was synthesized independently but was not found to be the reaction product by vpc. Compounds A, C, and E were obtained in sufficient amounts to enable their identification by NMR spectroscopy. The NMR spectrum of A gave a broad singlet at τ-value of 7.2 and a multiplet centered on a τ-value of 9.4. C and E gave similar spectra.

References

1) E. M. Lown, H. S. Sandhu, H. E. Gunning, and O. P. Strausz, *J. Amer. Chem. Soc.*, **90**, 7164 (1968).

2) K. P. C. Vollhardt and R. G. Bergman, *ibid.*, **95**, 7538 (1973).

3) P. Fowles, M. deSorgo, A. J. Yarwood, O. P. Strausz, and H. E. Gunning, *ibid.*, **89**, 1352 (1967).

4) G. W. Ross, *J. Chem. Soc.*, **1958**, 2856.

5) A. S. Broun and B. V. Ioffe, *Nauch. Byull, Leningrad Gosudarst Univ.* (1948); *C.A.*, **43**, 5376 (1949).

6) a) E. E. van Tamelen, *Org. Syn.*, Coll. Vol. 4, 232 (1963). b) C. O. Guss and D. L. Chamberlain, *J. Amer. Chem. Soc.*, **74**, 1342 (1952). c) H. R. Snyder, J. M. Stewart, and J. B. Ziegler, *ibid.*, **69**, 2672 (1947).

7) R. Ketcham and V. P. Shah, *J. Org. Chem.*, **28**, 229 (1963).

8) M. T. Bogert and A. Stull, "Organic Synthesis," Coll. Vol. 1, p. 220 (1956).

Note-20

BULLETIN OF THE CHEMICAL SOCIETY OF JAPAN, VOL. 48 (5), 1667—1668 (1975)

The Reaction of *N*-Hydroxylamino Compounds with Triphenylphosphine and CCl_4

Takehisa OHASHI[1] and Rolf APPEL

Institute of Inorganic Chemistry, University of Bonn, 53 Bonn, West Germany

(Received November 15, 1974)

Synopsis. In the reaction of triphenylphosphine with *N*-*p*-toluene-*N*-hydroxylamine and CCl_4, *p*-azotoluene and *p*-azoxytoluene were formed as the main products. On the other hand, in the reaction using *N*-*p*-toluenesulfonyl-*N*-hydroxylamine, sulfonyliminophosphorane was obtained.

In conjunction with our studies[2-8] of the ternary system phosphine/CCl_4/ammonia derivatives, we wish to report a new method of synthesizing azo and azoxy compounds by the reaction of *N*-*p*-toluene-*N*-hydroxylamine (A) with Ph_3P and CCl_4 and a new method of synthesizing sulfonyliminophosphorane by the reaction of *N*-*p*-toluenesulfonyl-*N*-hydroxylamine (B) with Ph_3P and CCl_4. It was found that *p*-azotoluene (**1**) and *p*-azoxytoluene (**2**) could easily be obtained in the reaction of (A) with Ph_3P and CCl_4 as is shown in Reaction (1).

$$\underset{\text{(A)}}{MeC_6H_4NHOH} + Ph_3P + CCl_4 \xrightarrow{(Et)_3N}$$
$$MeC_6H_4N{=}NC_6H_4Me\ (\mathbf{1}) + MeC_6H_4\overset{+}{N}{=}NC_6H_4Me\ (\mathbf{2})\ (O^-)$$
$$+ Ph_3PO\ (\mathbf{3}) + MeC_6H_4NH_2\ (\mathbf{4})$$
$$+ (Ph_3P^+CH_2Cl)Cl^-\ (\mathbf{5}) + CHCl_3 + (Et)_3NHCl \quad (1)$$

In this reaction, the formation of $CHCl_3$ was observed under several conditions (yields: 35—40%); besides the main products, two by-products, **4** and **5**, were obtained, and triphenylphosphine oxide (**3**) was isolated in high yields. However, no *N*-*p*-tolueneiminotriphenylphosphorane was found in this reaction. The results are presented in Table 1. On the other hand, *N*-*p*-toluenesulfonyliminotriphenylphosphorane (**1′**) was obtained as the main product of the reaction of (B) with Ph_3P and CCl_4 (Reaction (2)).

$$\underset{\text{(B)}}{MeC_6H_4SO_2NHOH} + Ph_3P + CCl_4 \longrightarrow$$
$$MeC_6H_4SO_2N{=}PPh_3\ (\mathbf{1'}) + (\text{Adduct of } Ph_3PO \text{ and } MeC_6H_4SO_2NHOH)\ (\mathbf{2'}) + Ph_3PO\ (\mathbf{3'}) + CHCl_3$$
$$+ (Ph_3P^+CH_2Cl)Cl^-\ (\mathbf{4'}) \quad (2)$$

Results obtained in Reaction (2) are described in Table 2.

In all the reactions described in Table 2, the formation of $CHCl_3$ was also observed, and the yield of $CHCl_3$ in the reaction using 2 mol of triphenylphosphine to (B) was higher (51.5%) than that (40.5%) observed in the reaction using an equimolar triphenylphosphine. Besides the main product (**1′**), the (**2′**) compound, triphenylphosphine oxide (**3′**) and chloromethyltriphenylphosphonium chloride (**4′**) were isolated, but no triphenylphosphine oxide was formed when triphenylphosphine equimolar to (B) was used. The new compound (**2′**) was estimated to be a hydrogen-bonded adduct, as is shown below:

Table 1. The reaction of *p*-tolyl-NHOH with Ph_3P and CCl_4

MeC_6H_4NHOH (mmol)	Ph_3P	CCl_4	Et_3N	Solvent[b]	Yields of products[a] %						
					1	**2**	**3**[c]	**4**	**5**[d]	**6**	**7**
10	10	10	10	A	39.1	27.4	88.8	15.9	8.7	61.6	—
10	10	10	10	B	28.6	39.8	92.3	15.0	6.9	65.2	—
10	5	5	5	A	20.0	35.4	89.9	12.2	4.6	58.1	—
10	5	5	5	B	11.4	47.8	97.1	16.8	3.5	72.5	—
10	10	10	—	A	28.6	19.5	79.1	7.5	15.0	—	26.4

a) **1**: Azotoluene, **2**: Azoxytoluene, **3**: Ph_3PO, **4**: *p*-Toluidine, **5**: $(Ph_3P^+CH_2Cl)Cl^-$, **6**: $(Et)_3N^+HCl^-$, **7**: *p*-Toluidine hydrochloride. b) A: 1,2-Dichloroethane, B: Acetonitrile. c) The yields of **3** were calculated based on Ph_3P used. d) The yields of **5** were calculated based on CCl_4 used.

Table 2. The reaction of *p*-tosyl NHOH with Ph_3P and CCl_4

Tosyl-NHOH (mmol)	Ph_3P	CCl_4	Solvent[b]	React. temp (°C)	React. time (min)	Yields of products[a] %			
						1′	**2′**	**3′**	**4′**
10.7	10.7	10.7	B	60	60	45.3	32.7	—	12.2
10.7	10.7	10.7	A	40	150	45.5	30.1	—	14.0
10.7	21.4	10.7	B	60	60	62.3	11.0	41.0	20.1
10.7	21.4	10.7	A	40	150	69.3	4.0	46.9	24.5

a) **1′** : $MeC_6H_4SO_2N{=}PPh_3$, **2′**: Adduct of Tosyl-NHOH and Ph_3PO, **3′**: Ph_3PO, **4′**: $(Ph_3P^+CH_2Cl)Cl.^-$ b) A: CH_2Cl_2, B: 1,2-Dichloroethane. c) Yields of **1′**, and **2′** were calculated based on Tosyl-NHOH used. Yields of **3′** were calculated based on Ph_3P used. Yields of **4′** were calculated based on CCl_4 used.

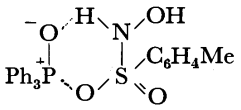

It was confirmed that the same compound can be obtained quantitatively by the reaction of triphenylphosphine oxide with (B). Similar hydrogen-bonded interactions have recently been reported[9] in the study of 1:1 adducts obtained in the reaction of triarylphosphines with *p*-toluenesulfonamide.

It is supposed that the first step in the reactions of *N*-hydroxylamino compounds with Ph_3P and CCl_4 is the formation of the intermediate phosphonium compounds (I-a) and (I-b) resulting from the reaction of (A) or (B) with the Ph_3P–CCl_4 complex,[2-8] as is shown in Reaction (3):

$$\mathrm{RNHOH\ (A) + (Ph_3P^+Cl)CCl_3^-} \longrightarrow \begin{cases} (\mathrm{Ph_3P^+Cl,\ ^-ONHR}) \\ \text{or} \\ (\mathrm{Ph_3P^+Cl,\ ^-N(OH)R}) \end{cases} + \mathrm{CHCl_3} \quad (3)$$

I-a (R; MeC_6H_4) I-b (R; $MeC_6H_4SO_2$)

In the reaction of (A) with Ph_3P and CCl_4, the nucleophilic attack of (A) on the nitrogen of the intermediate (I-a) can be assumed to be as is shown in Reaction (4):

$$\mathrm{I\text{-}a + MeC_6H_4NHOH} \xrightarrow[(A)]{} \begin{cases} \mathrm{MeC_6H_4N{=}NC_6H_4Me + Ph_3PO + HCl + H_2O} & \text{(Path a)} \\ \mathrm{MeC_6H_4NO + MeC_6H_4NH_2 + Ph_3PO + HCl} & \text{(Path b)} \end{cases} \quad (4)$$

Azotoluene was supposed to be formed *via* Path a, while azoxytoluene was estimated to be formed *via* the reaction of nitrosotoluene, which is formed *via* Path b, with Ph_3P, as has been reported by Cadagon[10] and *via* the reaction of nitrosotoluene with (A), as has been reported by Bamberger.[11] The deoxygenation of azoxytoluene[12] with Ph_3P did not occur under the mild conditions used in this investigation.

On the other hand, in the reaction of (B) with Ph_3P and CCl_4, the nucleophilicity of (B) is not so strong; therefore, the nucleophilic attack of triphenylphosphine on the nitrogen of the intermediate (I-b) was assumed to form the **1′** compound and triphenylphosphine oxide. Further, triphenylphosphine oxide reacts simultaneously with (B) to form the adduct (the **2′** compound in Reaction (2)).

Experimental

Materials. *N-p*-Toluene-*N*-hydroxylamine (A) was prepared as has been reported by Bamberger.[13] *N-p*-Toluenesulfonyl-*N*-hydroxylamine (B) was prepared as has been reported by Meyer.[14]

General Procedure of the Reaction of A with Ph_3P and CCl_4. Into a solution (solvent: acetonitrile or 1,2-dichloroethane) of A and CCl_4, a solution of Ph_3P and triethylamine was stirred, drop by drop, under an atmosphere of argon at room temperature; a slight exothermic reaction was observed. The solution was then heated at 55 °C for an additional 1 hr. The solvent was subsequently evaporated, and the semi-solid or oily residue was analysed by fractional crystallization and NMR analysis. The formation of chloroform was confirmed qualitatively and quantitatively from the NMR spectra of the distillates. The 4,4′-azotoluene, *p*-azoxytoluene, triphenylphosphine oxide, *p*-toluidine, and (chloromethyl)triphenylphosphonium chloride were identified by comparing them with the authentic compounds.

General Procedure of the Reaction of B with Ph_3P and CCl_4. A turbid dichloromethane or 1,2-dichloroethane solution of B and Ph_3P was warmed to 35—40 °C, and then CCl_4 was added to the solution. The mixture was stirred under an atmosphere of argon, keeping the temperature at 40 °C (in dichloromethane) or 60 °C (in 1,2-dichloroethane). From the reaction mixture, *N-p*-toluenesulfonyliminotriphenylphosphorane, triphenylphosphine oxide, and (chloromethyl)triphenylphosphonium chloride were isolated and identified by comparison with authentic compounds. When the reaction was carried out in the presence of triethylamine, for example, in the reaction using 2 mol of Ph_3P, CCl_4 and triethylamine equimolar to B, the same products as in the reaction without triethylamine were obtained, but the yields of the **1′** compound were low (13%).

Adduct of Triphenylphosphine Oxide and N-p-*Toluenesulfonyl*-N-*hydroxylamine.* After the removal of the **1′** compound from the reaction mixture, the residue was dissolved in benzene at 60 °C and filtered. A white precipitate obtained on cooling the filtrate was washed with ether and recrystallized from benzene. Mp 158 °C. IR: 3140, 2880, 1440, 1340, 1180. 1155, 730 and 548 cm^{-1}. NMR: (τ in CD_3OD) 2.10—2.70 (m, 19H) and 7.63 (s, 3H). ^{31}P NMR: (δ in MeOH) −31.3 ppm (relative to H_3PO_4). Found: C, 64.78; H, 5.20; N, 3.08; O, 13.42; P, 6.21; S, 7.12%. Calcd for $C_{25}H_{24}NO_4PS$: C, 64.51; H, 5.20; N, 3.01; O, 13.75; P, 6.44; S, 6.89%.

The Authors wish to thank Alexander von Humboldt-Stiftung for his help with our research.

References

1) Present adress: Central Research Laboratory, Kanegafuchi Chemical Industry Co., Ltd. 1–2, Yoshida-cho, Hyogoku, Kobe, Japan.
2) R. Appel, R. Kleinstück, and K. D. Ziehn, *Chem. Ber.*, **104**, 1030 (1971).
3) R. Appel, R. Kleinstück, and K. D. Ziehn, *Angew. Chem. Int. Ed. Engl.*, **10**, 132 (1971).
4) R. Appel, R. Kleinstück, and K. D. Ziehn, *Chem. Ber.*, **104**, 1335 (1971).
5) R. Appel, K. Warning, and K. D. Ziehn, *ibid.*, **106**, 3450 (1973).
6) R. Appel, K. D. Ziehn, and K. Warning, *ibid.*, **106**, 2093 (1973).
7) R. Appel and R. Kleinstück, *ibid.*, **107**, 5 (1974).
8) R. Appel, K. Warning, and K. D. Ziehn, *ibid.*, **107**, 698 (1974).
9) D. W. Allen, F. G. Mann, and J. C. Tebby, *J. Chem. Soc.*, **1972**, 2793.
10) P. J. Bunjan and J. I. G. Cadagon, *J. Chem. Soc.*, **1963**, 42.
11) E. Bamberger, *Ber.*, **27**, 1552 (1894).
12) T. Mukaiyama, H. Nambu, and M. Okamoto, *J. Org. Chem.*, **27**, 3651 (1962).
13) E. Bamberger and Rising, *Ann.*, **316**, 280 (1901).
14) E. V. Meyer, *J. Prakt. Chem.*, **63**, 170 (1901).

BULLETIN OF THE CHEMICAL SOCIETY OF JAPAN, VOL. 48 (5), 1669—1670 (1975)

Photochemistry of *N*-(4-Dimethylaminobenzylidene)aniline[1]

Hiroyuki OHTA and Katsumi TOKUMARU

Department of Chemistry, Faculty of Science, The University of Tokyo, Hongo, Bunkyo-ku, Tokyo 113

(Received November 30, 1974)

Synopsis. Irradiation of *N*-(4-dimethylaminobenzylidene)aniline, contrary to an earlier report, does not give *cis*-4,4′-bis(dimethylamino)stilbene and azobenzene, however, its triplet state has, exceptionally as an acyclic imine, enogh lifetime at 77 K to exhibit phosphorescence.

Recently increaseing attention has been paid to photochemistry of carbon-nitrogen double bonds.[2] For the irradiation of several imines in alcoholic solvents to give the reduced products, once the excited states of the imines were supposed to abstract hydrogen atoms from the solvents, but it is now accepted that carbonyl compounds present as impurities or as hydrolysis products are responsible for initiating the reaction on irradiation.[3] Cyclic imines, whose excited triplet states have longer lifetimes than the most acyclic imines, are still unreactive towards hydrogen atom abstraction probably on account of high π, π^* character of their triplet states.[4] Most imines are also photochemically unreactive in unimolecular cleavage except those carrying heteroatoms adjacent to carbon–nitrogen double bonds,[5] azirines[6] and acyclic imines substituted with benzyl groups.[7] The unreactive nature of the most imines in photochemical cleavage is attributable to the too short lifetimes of their excited states owing to their facile radiationless deactivation accompanid by syn-anti isomerization. Many carbonyl compounds in the n,π^* excited states and olefins in the π,π^* excited states are well known to undergo cycloaddition to unsaturated bonds.[8] On the other hand, imines have not been reported to add to unsaturated compounds except the following cases. One exception is recent finding by Koch and Rodehorst on capability of cyclic imines with conjugated carbonyl groups for addition to vinyl ether.[9] The other one, with which the present work concerns, is Searles and Clasen's report in 1965 that irradiation of *N*-(4-dimethylaminobenzylidene)aniline (I) in ether gave *cis*-4,4′-bis(dimethylamino)stilbene (II) and azobenzene (III) probably through cycloaddition between the imine to give diazetidine intermediate followed by its cleavage into the products.[10]

$$2\,\mathrm{ArCH{=}NPh} \xrightarrow{h\nu} \underset{\text{(I)}}{\mathrm{ArCH{-}NPh}\ \mathrm{ArCH{-}NPh}} \longrightarrow \underset{\text{(II)}}{\textit{cis}\text{-ArCH=CHAr}} + \underset{\text{(III)}}{\mathrm{PhN{=}NPh}}$$

(Ar: p-$Me_2NC_6H_4$)

Since most benzylideneanilines were known not to undergo this type of reaction, this report prompted us to explore the nature of the excited state of the imine (I) and the mechanism with which this excited state would be so reactive contrary to the most imines. This photochemical reaction was reinvestigated in several conditions as described below, but their results were not reproducible in our experimental conditions. However, the triplet state of this imine was found to have enough long lifetime at 77 K to phosphoresce in contrast with the most acyclic imines.

Results and Discussion

The imine (I) was irradiated in ether and in methanol with a high or a low pressure mercury lamp. The results are summarized in the Table. It indicates that after the irradiation most of the imine was recovered and a part of the imine was converted into 4-dimethylaminobenzaldehyde (IV) and aniline (V) but the reported products, II and III, were not found among the products. Thus, irradiation of I in 0.02 M ether solution with a high pressure mercury lamp or in 0.04 M ether with a low pressure mercury lamp did not afford the reported products. Use of concentrated solution (0.16 M) which would favour the bimolecular cycloaddition still failed in giving the reported products. Irradiation was also undertaken at solid carbon dioxide–ethanol temperature, but the reported products were not produced. Replacement of solvent from ether to methanol gave no effect on the reaction. A control experiment showed that II was not consumed on irradiation with the imine in ether. Therefore, we are forced to conclude that, in our experimental conditions, the imine (I) does not lead to the products earlier reported, and the reported products seem to have arisen in an adventitious or a limited condition.

Formation of IV and V in the irradiation are supposed to be due to hydrolysis of the imine by trace amount of water eventually present. Since the solution of the imine, on being kept in the dark, did not afford the hydrolysis products, the observed hydrolysis appears to be promoted by the irradiation as was reported by Furey and Kan for unsubstituted benzyldeneaniline.[11]

$$\mathrm{ArCH{=}NPh} + \mathrm{H_2O} \xrightarrow{h\nu} \mathrm{ArCHO} + \mathrm{PhNH_2}$$

To our knowledge, acyclic imines have never been reported to phosphoresce. It is therefore remarkable to have found that I exhibited phosphorescence in EPA at 77 K with maxima at 435 and 455 nm with lifetime of 0.4 sec. However, it did not fluoresce at room temperature and at 77 K. A possibility that the observed phosphorescence would result from the triplet state of IV eventually present as an impurity or as hydrolysis product of the imine is ruled out, because IV showed phosphorescence with a maximum at 465 nm in EPA and the maximum of the phosphorescence excitation spectrum of I, 345 nm, or IV, 335 nm, corresponded nearly to the respective absorption maximum, 345 or 339 nm. So, it is evident that the observed phosphorescence originates from the triplet state of I. The above result indicates that the triplet state of the imine (I) lies 63

Table 1. Products from the irradiation of *N*-(4-dimethylaminobemzylidene) aniline (I) in ether

I used (mmol)	Sovent (ml)	Lamp[b] (W)	Time (hr)	Products (%) [d,i]		
				I[e]	IV[f]	V[g]
9.15	400	H 400[c]	42	67	20	25
8.62	200	L 160[c]	42	80	13	15
4.72	30	H 100	60	*ca.* 80	h	h
3.48	30	H 100	40	*ca.* 80	h	h
7.77	400[a]	H 100[c]	68	*ca.* 80	h	h

a) methanol; b) H and L: a high or low pressure mercury lamp, respectively; c) immersion-type lamp; d) based on I used; e) recovered; f) 4-dimethylaminobenzaldehyde; g) aniline; h) present but not determined; i) IV and V were determined by vpc and I was isolated by column chromatography and weighed.

kcal mol^{-1} above the ground state and its long lifetime suggests that the triplet state is abundant in π,π^* or intramolecular charge transfer electronic configuration.[12]

Experimental

N-(4-Dimethylaminobenzylidene)aniline (I) was prepared according to literature.[13]

Irradiation was carried out for runs using 200—400 ml solution with a Riko immersion-type high or low pressure mercury lamp under nitrogen. For a concentrated ethereal solution of the imine in a Pyrex tube kept under argon atmosphere, external irradiation was done with a Riko high pressure mercury lamp. For a run at low temperature, the ethereal imine in a Pyrex tube under argon was kept in a solid carbon dioxide–ethanol in a Dewar vessel and irradiated with a high pressure lamp placed in the same bath. The irradiated mixture was analyzed by vpc with a Hitachi 063 gas chromatograph with a FID detector using a 2 m SE-30 column at 200 °C. 4-Dimethylaminobenzaldehyde (IV) and aniline (V) were determined with the use of nitrobenzene as an internal standard, however, *cis*-4,4′-bis(dimethylamino)stilbene (II) and azobenzene (III) were not detected. The mixture was concentrated under vacuum and the residue was chromatographed over well-washed silica gel to give the recovered imine together with IV and V.

The emission was measured with a Hitachi MPF 2A spectrofluorometer together with an attachment for phosphorescence observation.

The authors thank Professor O. Simamura for his stimulating discussion and the Ministry of Education for partial support of this work.

References

1) Presented at the 23rd Meeting of the Chemical Society of Japan, Tokyo, April, 1973.

2) As reviews of photochemistry of carbon–nitrogen double bonds, a) G. Wettermark, "Chemistry of Carbon–Nitrogen Double Bond," ed. by S. Patai, John Wiley, New York (1970), Chapter 12. b) H. Ohta and K. Tokumaru, *Yuki Gosei Kagaku Kyokaishi*, **30**, 1006 (1972). c) A. Padwa, M. Dharan, J. Smolanoff, and S. I. Wetmore, Jr., *Pure Appl. Chem.*, **33**, 269 (1973). d) K. Tokumaru, *Kagaku*, **29**, 68 (1974).

3) A. Padwa, W. Bergmark, and D. Pashayan, *J. Amer. Chem. Soc.*, **91**, 2653 (1969); G. Balogh and F. C. DeSchryver, *Tetrahedron Lett.*, **1969**, 1371.

4) H. Ohta and K. Tokumaru, *Tetrahedron Lett.*, **1974**, 2965.

5) T. Sato and H. Obase, *Tetrahedron Lett.*, **1967**, 1633; T. Oine and T. Mukai, *ibid.*, **1969**, 157; H. Hiraoka, *Chem. Commun.*, **1970**, 1306; T. Okada, M. Kawanisi, and H. Nozaki, This Bulletin, **42**, 2981 (1969); M. A. Fox and R. W. Binkley, *Tetrahedron Lett.*, **1970**, 5257; T. Matsuura and Y. Ito, *ibid.*, **1973**, 2283; Reference 2b and 2d.

6) A. Padwa and J. Smolanoff, *J. Amer. Chem. Soc.*, **93**, 548 (1971); A. Padwa and S. I. Wetmore, Jr., *J. Org. Chem.* **39**, 1396 (1974) and their related works.

7) H. Ohta and K. Tokumaru, *Chem. Lett.*, **1974**, 1403.

8) For example, see A. A. Lamola and N. J. Turro, "Energy Transfer and Organic Photochemistry," Interscience Publishers, New York (1969), p. 133; K. Tokumaru, "Yuki Kokagaku Hannoron," Tokyo Kagaku Dozin, Tokyo (1973), p. 151 and 193.

9) T. H. Koch and R. M. Rodehorst, *Tetrahedron Lett.*, **1972**, 4035; See also the following recent report: J. S. Swenton and J. A. Hyatt, *J. Amer. Chem. Soc.*, **96**, 4879 (1974).

10) S. Searles, Jr. and R. A. Clasen, *Tetrahedron Lett.*, **1965**, 1627.

11) R. L. Furey and R. O. Kan, *Tetrahedron*, **24**, 3085 (1968).

12) *Cf.* G. Porter and P. Suppan, *Pure Appl. Chem.*, **9**, 449 (1964).

13) F. Sachs and W. Lewin, *Ber.*, **35**, 3572 (1902).

BULLETIN OF THE CHEMICAL SOCIETY OF JAPAN, VOL. 48 (5), 1671—1672 (1975)

Photochemical Reactions of 3,3-Bis(dialkylamino)acrylophenones and 3-Dibenzylaminopropiolophenone

Hiromu AOYAMA, Tadashi HASEGAWA, Takehiko NISHIO,* and Yoshimori OMOTE*

Department of Chemistry, Tokyo Kyoiku University, Otsuka, Tokyo 112

* *Department of Chemistry, University of Tsukuba, Niihari, Ibaraki 300-31*

(Received December 4, 1974)

Synopsis. The photolysis of 3,3-bis(dialkylamino)-acrylophenones **1a**, **b**, and **c** gave the **3a**, **b**, and **c** pyrroles respectively. 3-Dibenzylaminopropiolophenone (**2**) reacted with water upon irradiation to give *N,N*-dibenzylbenzoylacetamide (**5**), whereas the addition of acetic acid to **2** proceeded without irradiation.

Recently, we reported the photochemical cyclization of 3-dialkylaminoacrylophenones.[1] This paper will be concerned with the photochemical reactions of 3,3-bis(dialkylamino)acrylophenones (**1a**, **b**, and **c**) and 3-dibenzylaminopropiolophenone (**2**).

The **1a**, **b**, and **c** ketones were prepared by the condensation of 3,3-dichloroacrylophenone (**4**) with the corresponding secondary amines according to the method in the literature.[2] On the other hand, the reaction of **4** with dibenzylamine yielded the ynaminoketone **2**.

The irradiation of **1a**, **b**, and **c** in benzene by means of a high-pressure mercury lamp gave the **3a**(trace), **3b**(25%) and **3c**(8%) pyrroles respectively. The structures of the pyrroles were confirmed by direct comparison (IR, NMR, tlc) with samples obtained in the photochemical reactions of 3-dialkylaminoacrylophenones.[1] These reactions also proceeded in *n*-hexane, but did not proceed in methanol or acetonitrile. The mechanism of these reactions is not clear at present.

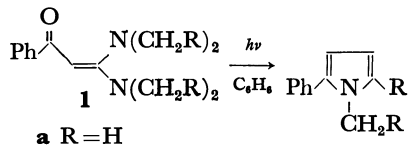

1

a R=H
b R=Et
c R=*n*-Pr

3

The ynaminoketone **2** was inert toward photolysis in dry benzene, whereas the irradiation of **2** in benzene containing water yielded *N,N*-dibenzylbenzoylacetamide (**5**). The structure of **5** was confirmed by an unequivocal synthesis from ethyl benzoylacetate and dibenzylamine. The formation of **5** can be easily explained in terms of the addition of water, followed by ketonization. The reaction did not take place in the dark. On the other hand, the addition of acetic acid to **2** proceeded without irradiation[3,4] to give an adduct **7**.

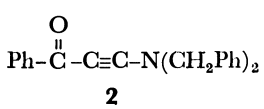

2

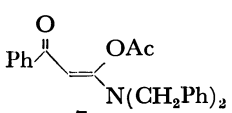

7

Experimental

All the melting points are uncorrected. An Ushio 450 W high-pressure mercury lamp was used as an irradiation source.

3-Dibenzylaminopropiolophenone (2). To dibenzylamine (25 g), 3,3-dichloroacrylophenone (3.5 g) was added, drop by drop. The temperature rose to 74 °C and then slowly fell to room temperature. After the addition of dry ether (50 ml), the mixture was refluxed for 24 hr and then stirred at room temperature for an additional 24 hr. The mixture was filtered to remove the dibenzylamine hydrochlororide, and the filtrate was evaporated *in vacuo*. On the addition of a small amount of petroleum ether to the residue, a crystalline solid was deposited; this was later recrystallized from benzene–petroleum ether to give 2.6 g of **2**; mp 109—110 °C; IR (KBr) 2300, 1610, 1570 cm^{-1}; UV λ_{max}^{EtOH} 254 (ε, 10500), 323 nm (16000); NMR ($CDCl_3$) δ 4.32 (s, 4H, CH_2), 7.20—7.45 (m, 13H, aromatic), 7.50—7.73 (m, 2H, aromatic).

Found: C, 84.83; H, 5.88; N, 4.34%. Calcd for $C_{23}H_{19}NO$: C, 84.89; H, 5.89; N, 4.30%.

General Procedure for the Photochemical Reaction of 1a, b, and c. A solution of **1** (200 mg) in benzene (70 ml) was irradiated in a Pyrex vessel under nitrogen for 30—50 hr. After the removal of the solvent, the residue was chromatographed on silica gel. Elution with benzene yielded **3**.

N,N-*Dibenzylbenzoylacetamide (5).* A solution of **2** (100 mg) in benzene (50 ml) containing a small amount of water was irradiated in a Pyrex vessel under nitrogen for 30 hr. After the removal of the solvent, the residue was chromatographed on silica gel (benzene–ethyl acetate 2: 1) to give 80 mg of **5**; mp 79—80 °C; IR (KBr) 1690, 1630, 1570 cm^{-1}.

Found: C, 80.18; H, 6.43; N, 4.08%. Calcd for $C_{23}H_{21}NO_2$: C, 80.44; H, 6.16; N, 4.08%.

The amide **5** was also prepared by heating a solution of ethyl benzoylacetate (6.1 g) and dibenzylamine (5.7 g) in xylene (7.5 ml) to 140 °C (yield, 79%).

3-Dibenzylamino-3-acetoxyacrylophenone (6). A solution of **2** (200 mg) and acetic acid (1 ml) in benzene (10 ml) was stirred for 2 hr at room temperature. After the removal of the solvent, the residue was chromatographed on silica gel (benzene–ethyl acetate 20: 1) to give 225 mg of **6**; mp 72—73 °C; IR (KBr) 1770, 1650, 1610 cm^{-1}; NMR ($CDCl_3$) δ 2.32 (s, 3H, CH_3), 4.55 (d, 4H, CH_2), 6.43 (s, 1H, olefinic), 6.80—7.80 (m, 15H, aromatic).

Found: C, 78.09; H, 5.99; N, 3.73%. Calcd for $C_{25}H_{23}NO_3$: C, 77.90; H, 6.01; N, 3.63%.

References

1) a) H. Aoyama, T. Nishio, Y. Hirabayashi, T. Hasegawa, H. Noda, and N. Sugiyama, *Chem. Commun.*, **1972**, 775; b) H. Aoyama, T. Nishio, Y. Hirabayashi, T. Hasegawa, H. Noda, and N, Sugiyama, *J. Chem. Soc. Perkin I*, **1975**, 298.

2) R. L. Soulen, Ph. D. Thesis, Kansas State University (1960).

3) The ynaminoketone **2** also reacted with ethanol (by irradiation, ~20%) and diethylamine (without irradiation, ~90%) to give the corresponding adducts. However, these adducts were viscous oils, and their complete purification was not achieved.

4) Ground-state addition reactions of ynaminoketones have been reported; A. Niederhauser, A. Frey, and M. Neuenschwander, *Helv. Chim. Acta*, **56**, 944 (1973); M. Neuenschwander and P. Bigler, *ibid.*, **56**, 959 (1973); A. Niederhauser, G. Bart, and M. Neuenschwander, *ibid.*, **56**, 2427 (1973).

BULLETIN OF THE CHEMICAL SOCIETY OF JAPAN, VOL. 48 (5), 1673—1674 (1975)

A New Synthesis of 2-Pyrones

Taeko IZUMI and Akira KASAHARA

Department of Applied Chemistry, Faculty of Engineering, Yamagata University, Yonezawa, Yamagata 992

(Received December 9, 1974)

Synopsis. The reaction of sodium salt of penta-2,4-dienoic acids with lithium chloropalladite in a polar solvent such as water led to the formation of 2-pyrone derivatives.

Numerous reports on the synthesis of 2-pyrones (**1**) have appeared in the literature.[1] However, no direct cyclization of penta-2,4-dienoic acids (**2**) into **1** has yet been reported. In this report, we wish to describe an intramolecular cyclization of **2** to **1** with lithium chloropalladite in moderate yields.

The solution of sodium salt of penta-2,4-dienoic acid (**2a**) in water was stirred with lithium chloropalladite under reflux to produce 2-pyrone (**1a**) in a 72% yield. The experiment in a mixture of dioxane and water (1:1) gave also **1a** in a 67% yield. In the conversion of **2a** to **1a** with palladium(II) salt, no formation of the five-membered-ring product [protoanemonin (**3**)] was observed.

Similarly, 6-methyl- and 6-phenyl-2-pyrone (**1b** and **1c**) were synthesized from sorbic acid (**2b**) and 5-phenylpenta-2,4-dienoic acid (**2c**) respectively. The reactions carried out are summarized in Table 1. In the presence of palladium(II) salt, the reaction of nucleophile with olefins has received considerable attention;[2] however, only a few reports are known in the field of intramolecular oxypalladation.[3] Henry and Ward.[4] have reported that the reaction of olefins with palladium(II) acetate gave products which were consistent with a *trans* acetoxypalladation, followed by a *cis* elimination of hydridopalladium. Recently, Hosokawa *et al.*[5] have reported that, in the reaction between 2-γ-methylallylphenol and palladium(II) acetate, the processes of both *cis*- and *trans*-oxypalladations are involved. However, in the reaction of **2** with palladium(II) salt, the reaction is explained only by a *trans*-oxypalladation, since a *cis*-palladium-hydride elimination is a general process.[4,6]

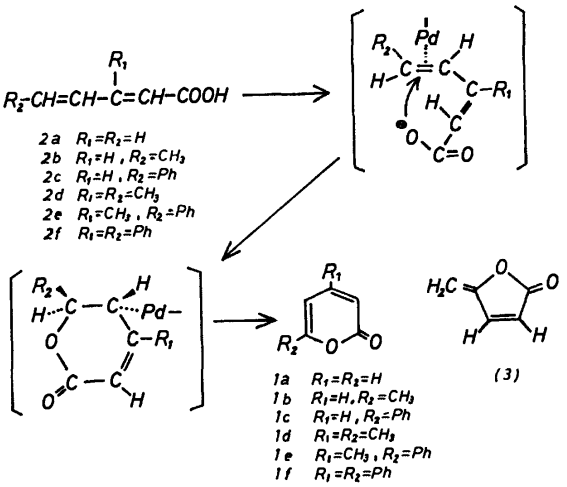

Experimental

Materials. All the melting points are uncorrected. The following compounds were synthesized by the methods described in the literature: penta-2,4-dienoic acid (**2a**),[7] 5-phenylpenta-2,4-denoic acid (**2c**)[8], 3,5-dimethylpenta-2,4-dienoic acid (**2d**),[9] 3-methyl-5-phenylpenta-2,4-dienoic acid (**2e**),[9] and 3,5-diphenylpenta-2,4-dienoic acid (**2f**).[9] Sorbic acid (**2b**) of a commercial grade was used without further purification.

General Procedure for the Preparation of 1. A solution of 10 mmol of **2** and 5 mmol of sodium carbonate in water (50 ml) or dioxane–water (1: 1, 50 ml) was stirred with 10 mmol of lithium chloropalladite under reflux for 4 hr. The reaction mixture was then extracted with ether. The ether layer was washed with water and then dried over anhydrous magnesium sulfate. After the evaporation of the solvent, the product was isolated by distillation or by column chromatogram on silica gel. The structures of the products were confirmed by a

Table 1. Reaction of penta-2,4-dienoic acid (**2**) with lithium chloropalladite

Substrate	Solvent	Product	Yield (%)[a]
2a	H_2O	2-Pyrone (**1a**)	72
2a	Dioxane–H_2O	**1a**	67
2b	H_2O	6-Methyl-2-pyrone (**1b**)[c]	75
2b	Dioxane–H_2O	**1b**	70
2c	H_2O	6-Phenyl-2-pyrone (**1c**)[d]	68
2d	H_2O	4,6-Dimethyl-2-pyrone (**1d**)[e]	65
2e	H_2O	4-Methyl-6-phenyl-2-pyrone (**1e**)[f]	65
2f	H_2O	4,6-Diphenyl-2-pyrone (**1f**)[g]	68

a) Yields are based upon the lithium chloropalladite. b) Bp 102—103 °C/18 mmHg (lit,[h] bp 110 °C/26 mmHg). c) Bp 80—82 °C/18 mm Hg (lit,[i] bp 80—85 °C/20 mm Hg). d) Mp 67—68 °C (lit,[j] mp 68 °C). e) Mp 48—49 °C (lit,[k] mp 49—50 °C). f) Mp 88—90 °C (lit,[l] mp 90 °C). g) Mp 137—139 °C (lit,[m] mp 138—139 °C). h) H. E. Zimmerman, G. L. Grunewald, and R. M. Paufler, "Organic Synthesis," Vol. 46, p. 101 (1966). i) E. Dunkelbleum, M. Rey, and A. S. Dreiding, *Helv. Chim. Acta*, **54**, 6 (1971). j) J. Kalff, *Rec. Trav. Chim. Pays-Bas*, **46**, 596 (1927). k) K. Yamada, This Bulletin, **35**, 1323 (1962). l) K. E. Schulte, J. Reisch, and O. Heine, *Arch. Pharmaz.*, **294**, 236 (1961). m) A. Arndt and B. Eistert, *Ber.*, **58**, 2318 (1925).

mixed-melting-point determination, by comparing the retention times on the gas chromatogram, and by the observation of the IR and NMR spectra. The results are summarized in Table 1.

References

1) S. Fujise, S. Hishida, S. Sasaki, H. Obara, and H. Uda, "Dai Yuki Kagaku (Comprehensive Organic Chemistry)," Vol. 14, ed. by M. Kotake, Asakura Shoten, Tokyo (1960), p. 1.

2) a) J. Tsuji "Advances in Organic Chemistry: Methods and Results," Vol. 6, ed. by E. C. Tayler and H. Wynberg, Interscience, New York (1969), p. 109. b) P. M. Maitlis, "The Organic Chemistry of Palladium," Vol. 2, Academic Press, New York (1971), p. 77.

3) a) T. Hosokawa, K. Maeda, K. Koga, and I. Moritani, *Tetrahedron Lett.*, **1973**, 739. b) A. Kasahara, T. Izumi, and M. Ooshima, This Bulletin, **47**, 2526 (1974).

4) P. M. Henry and G. A. Ward, *J. Amer. Chem. Soc.*, **93**, 1494 (1971); *ibid.*, **94**, 7305 (1972).

5) T. Hosokawa, H. Ohkata, S. Yamashita, and I. Moritani, Abstracts of 20th Symposium on Organometallic Chemistry of Japan (Kyoto), October 1974, p. 114.

6) R. F. Heck, *J. Amer. Chem. Soc.*, **91**, 6707 (1969); *ibid.*, **93**, 6896 (1971).

7) E. P. Kohler and F. R. Buther, *ibid.*, **48**, 1036 (1926).

8) O. Doebner, *Ber.*, **35**, 2129 (1902).

9) R. Kuhn and M. Hoffer, *ibid.*, **65**, 651 (1932).

BULLETIN OF THE CHEMICAL SOCIETY OF JAPAN, VOL. 48 (5), 1675—1676 (1975)

Lactone Carboxylic Acids. IX.[6] Base-Catalyzed Rearrangement of Ethyl α-Hydroxyaminoaconate Leading to the Formation of Isoxazolines

Sigeru TORII, Masasi UKIDA, and Hideo TANAKA

Department of Industrial Chemistry, School of Engineering, Okayama University, Okayama 700

(Received December 27, 1974)

Synopsis. The syntheses of 4-ethoxycarbonyl-3-methoxycarbonyl-5,5-pentamethylene-Δ^2-isoxazoline (**2b**) and its 4-hydroxy and 4-acetoxy derivatives (**3a** and **3b**) by the base-catalyzed rearrangement of ethyl γ,γ-pentamethylene-α-hydroxyaminoaconate (**1**) were described.

Several attempts have been made to find the synthetic way in obtaining appropriate Δ^2-isoxazoline-3-carboxylic acids by the reaction of hydroxamic acid with α-ketosuccinic esters,[1] by 1,3-cycloaddition of α-carbonitrile oxides[2] or nitrone esters[3] to olefins, by the condensation of nitroacetic esters,[4] and others.[5] Such compounds are of interest as potential intermediates for the preparation of useful chemicals.[2b,2d,5] We wish to report here a base-catalyzed rearrangement of ethyl γ,γ-pentamethylene-α-hydroxyaminoaconate (**1**)[6] giving the corresponding Δ^2-isoxazolines (**2b**, **3a**, and **3b**).

The reaction of ethyl α-hydroxyaminoaconate (**1**) with one equivalent of *n*-butyl lithium in THF at −78 °C afforded the isoxazoline ester **2b** in 84% yield after treating the crude acid **2a** with excess diazomethane and a small amount of **3a** (5.9%). On the other hand, the reaction of two equivalents of *n*-butyl lithium with **1** resulted in **3a** in 63% yield. The hydroxy isoxazoline **3a** could be converted into the corresponding acetate **3b** by the treatment with a mixed solution of acetic anhydride and pyridine. The structures of **2b**, **3a**, and **3b** after purifyng by column chromatography are elucidated by PMR, ^{13}C NMR, infrared, and mass spectral analyses together with elemental analyses. The ^{13}C NMR spectra of **2b**, **3a**, and **3b** (Fig. 1) provided effective evidences for their structural assignment. The ^{13}C NMR spectrum of **2b** displayed characteristic three bands at δ 149.5 (C=N), 160.7 (carbonyl attached to methoxy group), and 167.0 (carbonyl attached to ethoxy group) and, in addition, the peaks at δ 60.5 (or 61.6) and 93.1 are accounted for the C_4 and C_5 carbon atoms of **2b**. The ^{13}C NMR spectrum of **3a** was almost similar to that of **2b** except for a downfield shift of *ca.* 25 ppm for C_4 of **2b**. The structural relationship between **3a** and **3b** could be assigned reasonably, since the ^{13}C NMR spectrum of **3b** showed two new peaks at δ 21.0 and 164.8 accounted for the acetyl group.

A tentative mechanism for the formation of the isoxazolines **2a** and **3a** is outlined in Scheme 1. The mode of the base-catalyzed rearrangement of **1** is assumed to be migration of the electron on nitrogen atom as shown in (**a**) to produce (**b**), which would occur by abstraction of the hydrogen atom attached to the imino group with the

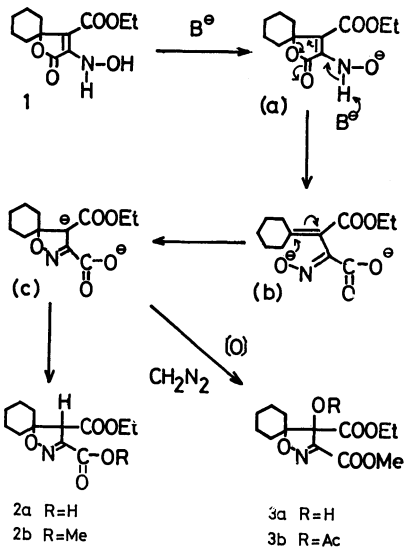

Scheme 1.

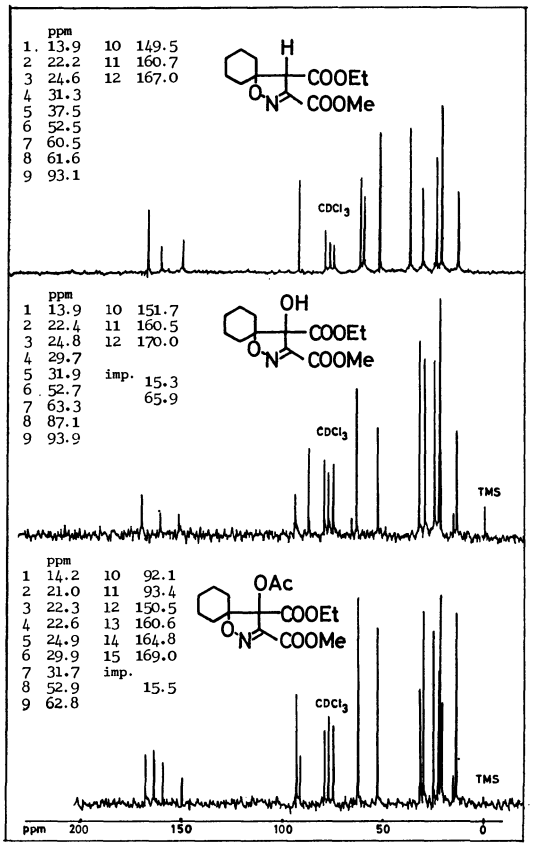

Fig. 1. The ^{13}C NMR spectra of **2b**, **3a**, and **3b** ($CDCl_3$) determined at 15.0 MHz under conditions of proton noise decoupling; scale, parts per million relative to carbons of TMS.

base. The following recyclization of the oxime anion of (**b**) would lead to a dianion (**c**), which is considered to be stable thermodynamically. Thus, the final products formed in this process seem to be similar to those produced in the acid-catalytic acyllactone rearrangement.[7]

Although the reason of the formation of **3b** is not certain, it seems likely that the formation of **3a** takes place when two equivalents of the base were used, suggesting that the dianion (**c**) may be oxidized with oxygen dissolved in the solvent.[8]

Experimental

Melting points and boiling points are uncorrected. PMR spectra were recorded on a Hitachi R-24 instrument. ^{13}C NMR spectra were recorded on a JEOL FX-60 instrument. IR spectra were determined with Hitachi EPI-S2, with only major absorptions being cited. Mass spectral analysis was carried out with a Hitachi RMS-4 spectrometer at 70 eV. Wako gel C-200 silica gel was used for elution chromatography. Elemental analysis was performed by Mr. Tsutomu Okamoto of our Laboratory.

Reaction of Ethyl γ,γ-Pentamethylene-α-hydroxyaminoaconate (1) with One Equivalent of n*-Butyl Lithium.* To a stirred solution of **1** (66.0 mg, 0.25 mmol) in THF (0.5 ml), 0.2 ml (0.25 mmol) of 1.3 M *n*-BuLi in ether was added at −78 °C. The reaction mixture was allowed to warm slowly to room temperature during 2 hr and the stirring was continued for additional 2.5 hr. The mixture was poured into ice-cold diluted HCl (0.5 ml) and extracted with $CHCl_3$. The extracts were washed with water, dried (Na_2SO_4), and concentrated *in vacuo* to give 94.5 mg of a yellow oil. Treatment of this oil with an excess amount of diazomethane and subsequent chromatography using *n*-hexane–$ClCH_2CH_2Cl$ gave 56.5 mg (84%) of **2b**: bp 105—107 °C/1.0 mmHg; IR (neat) 1726 (ester C=O), 1590 (C=N) cm^{-1}; PMR (CCl_4) δ 1.28 (t, J=7.0 Hz, 3H, CH_3), 1.20—2.10 (broad s, 10H), 3.69 (s, 1H, H_β), 3.81 (s, 3H, CH_3O), 4.16 (q, J=7.0 Hz, 2H, CH_2O); Mass *m/e* (%) 269 (M^+, 2), 253 (9), 196 (83), 154 (62), 59 (100). Found: C, 57.74; H, 7.06%. Calcd for $C_{13}H_{19}NO_5$: C, 57.98; H, 7.01%.

From the following elution with $ClCH_2CH_2Cl$ 4.0 mg (5.9%) of **3a** was obtained: bp 117—120 °C/1.0 mmHg; IR (neat) 3475 (OH), 1740 (ester C=O), 1589 (C=N) cm^{-1}; PMR (CCl_4) δ 1.30 (t, J=7.0 Hz, 3H, CH_3), 1.00—2.20 (m, 10H), 3.59 (s, 1H, HO), 3.82 (s, 3H, CH_3O), 4.26 (q, J=7.0 Hz, 2H, CH_2O); Mass *m/e* (%) 212 (28), 127 (52), 99 (100), 81 (97). Found: C, 54.99; H, 7.03%. Calcd for $C_{13}H_{19}NO_6$: C, 54.73; H, 6.71%.

Reaction of **1** *with Two Equivalents of* n*-Butyl Lithium.* To a stirred solution of **1** (66.0 mg, 0.25 mmol) in THF (1.0 ml), 0.62 ml (0.56 mmol) of 0.9 M *n*-BuLi in ether was added at −78 °C under nitrogen. The reaction mixture was allowed to warm slowly to room temperature for 2 hr and the stirring was continued for additional 2 hr. The reaction mixture was worked up as the standard manner to afford an oil. Treatment of the oil with excess diazomethane gave a yellow oil, whose tlc showed the presence of 2 spots at R_f 0.30 and 0.12 (Merck PF_{254}, benzene–EtOAc: 15/1). The column chromatography using benzene–EtOAc gave 44.8 mg (63.0%) of **3a** and 3.7 mg (3.45%) of an unknown crystal.

Preparation of the Acetate **3b** *from* **3a**. A solution of the alcohol **3a** (14.5 mg, 0.051 mmol) in Ac_2O (0.5 ml) and dry pyridine (0.5 ml) was stirred at 65 °C under nitrogen for 12 hr. The solvent was roto-evaporated to give 28.5 mg of a dull reddish material. The crude product was chromatographed using benzene and benzene–EtOAc to give 12.3 mg (74.1%) of **3b**; bp 119.5—122.5 °C/1.0 mmHg; IR (neat) 1756 (ester C=O), 1595 (C=N) cm^{-1}; PMR ($CDCl_3$) δ 1.30 (t, J=7.0 Hz, 3H, CH_3), 0.70—2.30 (broad s, 10H), 2.13 (s, 3H, CH_3CO), 3.85 (s, 3H, CH_3O), 4.28 (q, J=7.0 Hz, 2H, CH_2O); Mass *m/e* (%) 327 (M^+, 0.4), 212 (75), 127 (53), 99 (100), 81 (69). Found: C, 55.04; H, 6.54%. Calcd for $C_{15}H_{21}NO_7$: C, 55.04; H, 6.47%.

From the second elution 3.3 mg (22.8%) of **3a** was recovered.

References

1) G. Adembri and P. Tedeschi, *Boll. Sci. Fac. Chim. Ind. Bologna*, **23**, 203 (1965); *Chem. Abstr.*, **63**, 13234h (1965).

2) a) H. Dahn, B. Favre, and J.-P. Leresche, *Helv. Chim. Acta*, **56**, 457 (1973); b) Y. Kishida, T. Hiraoka, and M. Yoshimoto, Japan **70**, 40892 (1970); *Chem. Abstr.*, **75**, 5880v (1971); c) M. Gattuso, G. Lo Vecchio, and N. Uccella, *Atti Soc. Peloritana Sci. Fis. Mat. Natur.*, **14**, 393 (1968); *Chem. Abstr.*, **74**, 3545v (1971); d) H. H. Hoerhold, Ger. (East) 37461 (1965); *Chem. Abstr.*, **63**, 10062g (1965).

3) a) V. A. Tartakovskii, I. A. Savostýanova, and S. S. Novikov, *Zh. Org. Khim.*, **4**, 240 (1968); *Chem. Abstr.*, **68**, 95738n (1968); b) V. A. Tartakovskii, O. A. Lukýanov, N. I. Shlykova, and S. S. Novikov, *Zh. Org. Khim.*, **3**, 980 (1967); *Chem. Abstr.*, **67**, 100039w (1967).

4) a) Zh. A. Krasnaya, T. S. Stytsenko, E. P. Prokofév, I. P. Yakovlev, and V. F. Kucherov, *Izv. Akad. Nauk SSSR, Ser. Khim.*, 845 (1974); *Chem. Abstr.*, **81**, 49608r (1974); b) S. Zen and E. Kaji, *Chem. Pharm. Bull.* **22**, 477 (1974); *Chem. Abstr.*, **81**, 63533u (1974); c) Zh. A. Krasnaya, T. S. Stytsenko, E. P. Prokofév, I. P. Yakovlev, and V. F. Kucherov, U. S. S. R. 427,938 (1974); *Chem. Abstr.*, **81**, 77898d (1974); d) E. L. Katelkina, A. S. Sopova, V. V. Perekalin, and B. I. Ionin, *Zh. Org. Khim.*, **10**, 209 (1974); *Chem. Abstr.*, **80**, 108413c (1974); e) L. Kh. Vinograd and N. N. Suvorov, *Khim. Geterotsikl. Soedin.*, 1505 (1970); *Chem. Abstr.*, **74**, 53610h (1971).

5) N. K. Kochetkov and S. D. Sokolov, "Advances in Heterocyclic Chemistry," Vol. II, ed. by A. R. Katrilzky, Academic Press, New York, N. Y. (1963), p. 365.

6) S. Torii, M. Ukida, H. Kano, T. Furuta, and H. Tanaka, This Bulletin, in contribution.

7) F. Korte and K. H. Büchel, "New Methods of Preparative Organic Chemistry," Vol. III, ed. by W. Foerst, Academic Press, New York, N. Y. (1964), p. 199.

8) J. N. Gardner, F. E. Carlon, and O. Gnoj, *J. Org. Chem.*, **33**, 3294 (1968).

BULLETIN OF THE CHEMICAL SOCIETY OF JAPAN, VOL. 48 (5), 1677—1678 (1975)

The Photocycloaddition of 2-Cyclohexenone and Maleic Anhydride to $\Delta^{9,10}$-Octalin

Atsutaka KUNAI, Koji KIMURA, and Yoshinobu ODAIRA

Department of Petroleum Chemistry, Faculty of Engineering, Osaka University, Suita, Osaka 565

(Received December 28, 1974)

Synopsis. The photocycloaddition to $\Delta^{9,10}$-octalin (**1**) was investigated. Both 2-cyclohexenone and maleic anhydride reacted with **1** to afford the corresponding photocycloadducts, **2** and **3** respectively.

From the viewpoint of the synthesis of interesting cyclic compounds, increasing attention has been shown in the study of the photocycloaddition of cyclic enones to olefins.[1] Especially, for the synthesis of propellanones, the photocycloaddition of bicyclic enones to olefins has been generally employed as a convenient method.[2] More recently, we reported the photochemical synthesis of a new type of tetracyclic propellanone according to the above method (Path a).[3] Although the photocycloaddition of appropriate substances to bicyclic olefins, which have a central double bond, can be assumed to be an alternative method, no such study has yet been reported (Path b). In an extension of our study of the photochemical preparation of a variety of propellane derivatives, we wish to report here our preliminary finding concerning the photocycloaddition of some cyclic substrates to $\Delta^{9,10}$-octalin (**1**).

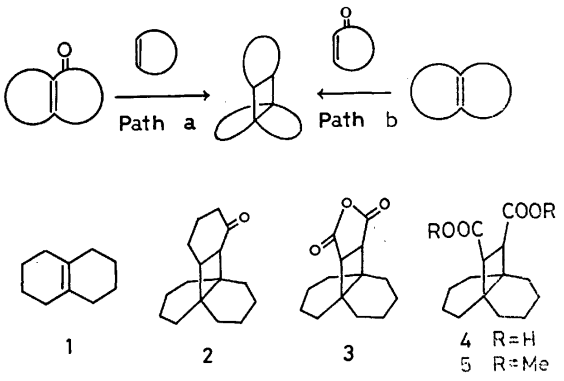

First, we examined the photocycloaddition of 2-cyclohexenone to **1**. When a neat mixture of 2-cyclohexenone and a 6-molar excess of **1** was irradiated through a Pyrex filter, a cross cycloadduct **2** was given, along with 2-cyclohexenone dimers. The yield of **2** was estimated by glpc analysis to be 13% based on the quantity of **1** reacted. The structure was determined to be **2** on the basis of the spectral data and by elemental analysis, and also, most especially, by the fact that no hydrogenation occurred when the palladium-charcoal catalyst was used.[4]

Next, we examined the photocycloaddition of maleic anhydride to **1**. When an ethereal solution of maleic anhydride and a 2-molar excess of **1** was irradiated through a Pyrex filter, a cross cycloadduct **3** was given, along with a considerable amount of the maleic anhydride dimer. When **3** was chromatographed on silica gel, spontaneous hydrolysis occurred and an acid (**4**) was isolated in a 24% yield, based on the quantity of **1** reacted. By treatment with ethereal diazomethane, **4** was changed into an ester (**5**).

As has been described above, 2-cyclohexenone and maleic anhydride easily reacted with **1** to afford the corresponding tetracyclic [4.4.2]propellanone derivatives. In connection with the above study, we have also obtained some information about the attempted photocyclodimerization of **1**. Attempts at photosensitized cyclodimerization with acetone, benzophenone, and phenanthrene were unsuccessful, but photosensitization with triphenylene gave a cyclodimer, albeit in a low yield. A detailed study of the photocyclodimerization of **1** is now in progress.

Experimental

Generals. All the melting points and boiling points are uncorrected. The IR spectra were recorded with a JASCO IR-G spectrometer. The NMR spectra were recorded for a 5% solution in carbon tetrachloride or deuterochloroform, with tetramethylsilane as the internal standard, on a JEOL JNM-3H-60 spectrometer. All the irradiations were carried out using a 500-W high-pressure mercury arc under a nitrogen atmosphere at room temperature. Analytical glpc was carried out on a Hitachi 063 gas chromatograph employing the following columns: a) 20% PEG-20M, b) 3% SE-30, c) 20% DC-550, and d) 10% FFAP.

Reagents. The $\Delta^{9,10}$-octalin (**1**) was prepared by the method of Dauben and was purified by nitrosyl-chloride treatment.[5] The maleic anhydride and the 2-cyclohexenone were purified by distillation before use. The triphenylene was recrystallized from methanol.

Photocycloaddition of 2-Cyclohexenone to 1. A neat mixture of 2-cyclohexenone (1.60 g, 16.7 mmol) and **1** (14.0 g, 103 mmol) was irradiated through a Pyrex filter for 3 hr. The photolysate was vacuum-distilled to give 13.3 g of recovered **1** (bp 60—65 °C/10 mmHg) and 2.32 g of viscous oil (bp 140—180 °C/10^{-3} mmHg). The latter was chromatographed on silica gel (200 mesh, 50 g) and was eluted initially with petroleum ether (400 ml) and then with ether (400 ml). The concentration of the latter eluate afforded 1.2 g of an oil which consisted of the cross adduct **2** and two cyclohexenone dimers.[6] The yield of **2** was estimated by glpc analysis to be 13% on the basis of **1** reacted. Preparative glpc using Column a) and d) gave an analytical sample; IR (neat) 1705 cm^{-1} (C=O); NMR (CCl_4) δ 1.00—2.80 (m); Mass *m/e* 232 (M^+); Found: C, 82.41; H, 10.39%. Calcd for $C_{16}H_{24}O$: C, 82.70; H, 10.41%; 2,4-dinitrophenylhydrazone, mp 161—163 °C. By treatment with a 5% palladium–charcoal catalyst under hydrogen, **2** was not hydrogenated (in methanol, room temp., 1 atom).[4]

Photocycloaddition of Maleic Anhydride to 1. A solution of maleic anhydride (5.4 g, 55 mmol) and **1** (15.0 g, 110 mmol) in dry ether (130 ml) was irradiated through a Pyrex

filter for 60 hr. The maleic anhydride dimer which was thus precipitated from the reaction mixture was removed by filtration, and then the ether was evaporated. The residual oil was vacuum-distilled to give 8.8 g of recovered **1** (bp 53 °C/3 mmHg) and 7.0 g of a viscous oil (bp 145—150 °C/10^{-3} mmHg) showing two characteristic IR absorptions ascribable to **3** at 1860 and 1790 cm^{-1}. The anhydride fraction was chromatographed on silica gel (200 mesh, 185 g). Elution with benzene–ether (95: 5, 10 l) brought about spontaneous hydrolysis to give 2.80 g of the acid **4** in a 24% yield, based on the quantity of **1** reacted. Recrystallization from aq. methanol provided an analytical sample; mp 181—182 °C; IR (KBr) 1700 cm^{-1} (COOH); NMR ($CDCl_3$) δ, 11.35 (s, 2H, COOH), 1.0—3.0 (m, 18H, others); Mass *m/e*, 234 (M^+-H_2O), 135; Found: C, 66.37; H, 7.99%. Calcd for $C_{14}H_{20}O_4$: C, 66.64; H, 7.99%. By treatment with ethereal diazomethane, **4** was changed into the dimethyl ester **5**, which showed an IR absorption at 1715 cm^{-1} and an NMR absorption at δ 3.70 (methyl ester).

References

1) P. E. Eaton, *Accounts Chem. Res.*, **1**, 50 (1968); P. de Mayo, *ibid.*, **4**, 41 (1971); see also D. Ginsburg, *ibid.*, **2**, 121 (1969); *ibid.*, **5**, 249 (1972).

2) R. L. Cargill, J. R. Damewood, and M. M. Cooper, *J. Amer. Chem. Soc.*, **88**, 1330 (1966); P. E. Eaton and N. Kyi, *ibid.*, **93**, 2786 (1971); P. E. Eaton and G. H. Temme, *ibid.*, **95**, 7508 (1973); see also R. L. Cargill, T. E. Jackson, N. P. Peet, and D. M. Pond, *Accounts Chem. Res.*, **7**, 106 (1974) and references cited therein.

3) A. Kunai, T. Omori, T. Miyata, K. Kimura, and Y. Odaira, *Tetrahedron Lett.*, **1974**, 2517; A. Kunai *et al.*, *Tetrahedron*, submitted for publication, "Studies on Stereoselective Photocycloaddition of Bicyclo[4.3.0]non-1(6)-en-7-one with Cyclic Olefins."

4) In order to exclude the possibility of an allylic type of adduct, we attempted the catalytic hydrogenation.

5) W. G. Dauben, E. C. Martin, and G. J. Fonken, *J. Org. Chem.*, **23**, 1205 (1958).

6) Identification was made by comparison with authentic materials.

BULLETIN OF THE CHEMICAL SOCIETY OF JAPAN, VOL. 48 (5), 1679—1680 (1975)

A New Synthesis of Pyrimido[4,5-*e*][1,2,4]triazines from 5,5-Dibromopyrimidines

Takashi SUGIMOTO and Sadao MATSUURA

College of General Education, Nagoya University, Chikusa-ku, Nagoya 464

(Received February 3, 1975)

Synopsis. A new method for the synthesis of pyrimido-[4,5-*e*][1,2,4]triazines from 5,5-dibromopyrimidines was studied. Condensation of dibromopyrimidines (**1a, b**) with aminoguanidine or its analogues gave the 6,8-dioxo series (**5**) of the pyrimidotriazine, and aminodibromopyrimidines (**2a, b**) gave the 6-amino-8-oxo series (**6**).

An approach to a pyrimido[4,5-*e*][1,2,4]triazine from a pyrimidine may usually find difficulties in introducing a hydrazino group into the 5-position of the pyrimidine nucleus. In continuing our investigation in the synthesis of pyrimido[4,5-*e*][1,2,4]triazines as a potential antiviral agent,[1] we studied a new synthetic method of the series starting from 5,5-dibromopyrimidines.

The dibromopyrimidine(**1b**)[2] condensed with 1-amino-3-methylguanidine(**3d**) to give a guanylhydrazone(**4q**); this cyclized to 3-methylamino-5,7-dimethylpyrimido[4,5-*e*][1,2,4]triazin-6,8-dione (**5q**)[1] when heated with aqueous ammonia. The analogous treatments of **1b**[2] with **3c** or **3e** gave the corresponding pyrimitriazines(**5p,r**); similarly, their 5,7-demethyl homologues(**5i,j,k**)[1] were made from **1a** and the respective aminoguanidine(**3c,d**, or **e**). The 3-ethylthio- and 3-benzyltio-pyrimidotriazines(**5s;t**) were made from **1b** and *S*-ethyl or *S*-benzyl isothiosemicarbazide(**3f,g**); the use of pyridine in stead of ammonia in the cyclization step gave better yields.

Then, we extended this method to the preparation of 6-aminopyrimidotriazin-8-ones(**6**), which could not be made by other method.[1] The required dibromopyrimidines(**2a,b**) were obtained by the action of bromine on 2-amino(or dimethylamino)-5-nitrosopyrimidin-4,6-dione in ice-cold water. The aminopyrimidine(**2a**), on condensation with **3f** or **3g** in DMF and subsequent cyclization in boiling pyridine, afforded the expected products(**6n,o**); also the dimethylaminopyrimidine(**2b**) and **3d** yielded a pyrimidotriazine (**6q**). The ethylthio ether(**6n**) readily underwent aminolysis to give the 3-amino analogues(**6i,j,k,l**) on heating with an appropriate amine. Similarly, **6o** and hydrazine gave the 3-hydrazino derivative(**6m**); the hydrazino group was easily removed from **6m** by silver oxide[3] to give the 3-unsubstituted 6-aminopyrimidotriazin-8-one(**6h**).

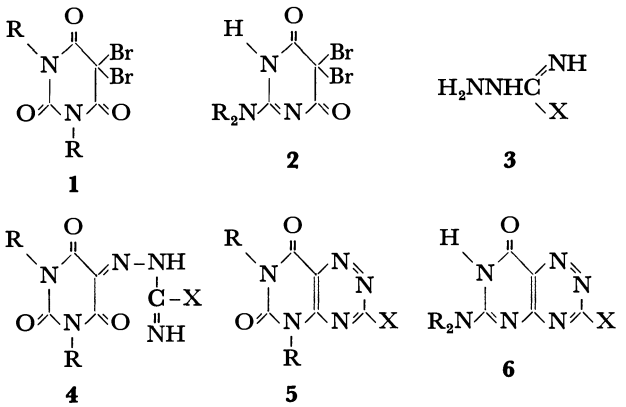

1 **2** **3** **4** **5** **6**

	R	X		R	X
a:	H	—	**k**:	H	NHEt
b:	Me	—	**l**:	H	NMe_2
c:	—	NH_2	**m**:	H	$NHNH_2$
d:	—	NHMe	**n**:	H	SEt
e:	—	NHEt	**o**:	H	SCH_2Ph
f:	—	SEt	**p**:	Me	NH_2
g:	—	SCH_2Ph	**q**:	Me	NHMe
h:	H	H	**r**:	Me	NHEt
i:	H	NH_2	**s**:	Me	SEt
j:	H	NHMe	**t**:	Me	SCH_2Ph

Experimental

The analyses were done by the Analytical Section, Meijo University, Nagoya; the UV spectra were measured with a JASCO model ORD/UV-5 spectrophotometer and the λ_{max} are given in nm with a log ε in parentheses.

*3-Methylamino-5,7-dimethylpyrimido[4,5-*e*][1,2,4]triazin-6,8-dione (5q) and its analogues (5p, r).* A solution of **1b**[2] (2.8 g) and **3d**·2HCl (1.6 g) in HOAc (50 ml) was stirred at 20 °C for 30 min, then boiled for 5 min. After cooling, the needles were collected and crystallized from 1M-HCl to give **4q**·HCl (3.5 g), mp>300 °C (Found: C, 33.6; H, 4.9; N, 29.4%. Calcd for $C_9H_{14}N_6O_3HCl \cdot 0.5H_2O$: C, 33.6; H, 4.9; N, 29.4%). Refluxing of **4q** (3.0 g) in 1% ammonia (150 ml) for 3 hr gave **5q** (1.3 g), mp 290—291 °C (from water) (lit.[1] mp 290—291 °C). The same treatments of **1b** with **3e** gave **4r** (79%), mp >300 °C (Found: C, 35.5; H, 5.6; N, 27.7%. Calcd for $C_9H_{14}N_6O_3HCl \cdot 0.5H_2O$: C, 35.6; H, 5.45; N, 27.7%); **4r** was converted to **5r** (31%), mp 267—268 °C (from MeOH) (lit,[1] mp 267—268 °C). In the analogous manner, **5p** was obtained in 37% yield, mp>300 °C (lit,[4] mp 363—365 °C dec.) (Found: C, 40.0; H, 3.2; N, 40.3%. Calcd for $C_7H_8N_6O_2$: C, 40.4; H, 3.9; N, 40.4%); λ_{max}^{MeOH}: 221 (4.57), 247 (4.14), and 329 (3.99).

*3-Aminopyrimido[4,5-*e*][1,2,4]triazin-6,8-dione (5i) and its analogues (5j, k).* These compounds were made from **1a**[2] and the respective aminoguanidines (**3c, d, e**) by an analogous method as above in 40, 55, and 34% yields respectively; all gave satisfactory elemental analyses and were identified with the authentic samples.[1]

*3-Ethylthio(and benzylthio)-5,7-dimethylpyrimido[4,5-*e*][1,2,4]-triazin-6,8-diones (5s, t).* A suspension of **1b** (0.60 g) and **3f**·HBr (0.50 g) in HOAc (20 ml) was treated as above. Evaporation under reduced pressure gave a yellow solid; this compound was heated in pyridine (40 ml) under reflux for 20 min. Evaporation and recrystallization from water gave **5s** (0.30 g), mp 146.5—147.5 °C (lit,[5] mp 146—147 °C); λ_{max}^{MeOH}: 237 (4.32), 260 (sh., 4.06), and 340 (4.00). A similar treatment of **1b** with **3g** gave **5t** (85%), mp 201—202 °C (from H_2O–EtOH) (Found: C, 53.4; H, 3.95; N, 22.5%. Calcd for $C_{14}H_{13}N_5O_2S$: C, 53.3; H, 4.15; N, 22.2%); λ_{max}^{MeOH}:

238 (4.36), 260 (sh., 4.13), and 339 (4.05).

*6-Amino-3-ethylthio(and benzylthio)pyrimido[4,5-e][1,2,4]triazin-8-ones (**6n**, **o**).* Bromine (26 g) was added dropwise to a vigorously stirred suspension of 2-amino-5-nitrosopyrimidin-4,6-dione (12 g) in ice-cold water (50 ml) during 30 min. The colorless solid (17.2 g) was collected, washed with water, and dried over P_2O_5. The product could not be purified satisfactorily for elemental analysis owing to its instabilities. A solution of the dibromopyrimidine (9.0 g) and **3f**·HBr (6.5 g) in DMF (100 ml) was stirred at 20 °C for 30 min. The solution was diluted with pyridine (100 ml) and refluxed for 2 hr, followed by filtration while hot. The filtrate, on evaporation under reduced pressure and subsequent trituration with water, gave **6n** (3.2 g), mp>300 °C (by reprecipitation)(Found: C, 37.6; H, 3.4; N, 37.75%. Calcd for $C_7H_8N_6OS$: C, 37.5; H, 3.6; N, 37.5%); pK_a 6.72±0.06; λ_{max} at pH 4.1: 261 (4.48) and 353 (3.99); at pH 10.4: 253 (4.53) and 352 (3.99).

Replacing **3f** by **3g** in the foregoing condensation gave **6o** (73%), mp >300 °C (by reprecipitation) (Found: N, 28.4%. Calcd for $C_{13}H_{10}N_6OS$: N, 28.2%); pK_a 6.72±0.03; λ_{max} at pH 4.0: 261 (4.47) and 354 (4.03); at pH 11: 255 (4.54) and 354 (4.04).

*6-Dimethylamino-3-methylaminopyrimido[4,5-e][1,2,4]triazin-8-one (**6q**).* 5,5-Dibromo-2-dimethylaminopyrimidin-4,6-dione (**2b**) was made from its 5-nitroso precursor and bromine in 70%. The dibromopyrimidine (**2b**) and **3d**, on treatments in a similar way for the 2-oxy analogue (**5j**), gave **6q** (37%), mp>300 °C (from water) (Found: C, 43.6; H, 5.0; N, 44.2%. Calcd for $C_8H_{11}N_7O$: C, 43.4; H, 5.0; N, 44.3%); pK_a 7.60±0.02; λ_{max} at pH 4.0: 247 (4.62) and 352 (4.02); at pH 10.0: 238 (4.56), 265 (sh., 4.04), and 368 (4.11).

*3,6-Diaminopyrimido[4,5-e][1,2,4]triazin-8-one (**6i**) and its 3-alkylamino analogues (**6j**, **k**, **l**).* A solution of **6n** (0.50 g) in 30% ammonia (10 ml) was heated in a sealed tube at 140 °C for 10 hr. Evaporation and subsequent trituration with dil. formic acid gave **6i** (0.30 g), mp >300 °C (from water) (Found: C, 33.5; H, 2.8%. Calcd for $C_5H_5N_7O$: C, 33.5; H, 3.2%); pK_a 8.05±0.05; λ_{max} at pH 4.0: 232 (4.54) and 346 (3.91); at pH 10.2: 227 (4.46), 245 (sh, 4.25), and 339 (4.00). The use of methylamine, ethylamine, or dimethylamine in the foregoing aminolysis gave the corresponding analogues: **6j** (93%), mp >300 °C (Found: C, 36.55; H, 3.5; N, 49.2%. Calcd for $C_6H_7N_7O\cdot0.2H_2O$: C, 36.6; H, 3.8; N, 49.8%); pK_a 7.86±0.05; λ_{max} at pH 4.1: 241 (4.59) and 345 (3.90); at pH 12: 237 (4.63) and 347 (3.99). The 3-ethylamino derivative (**6j**) was obtained in 76% yield, mp >300 °C (Found: C, 39.8; H, 4.4; N, 45.4%. Calcd for $C_7H_9N_7O\cdot0.3H_2O$: C, 39.55; H, 4.55; N, 46.1%); pK_a 8.08±0.04; λ_{max} at pH 11.0: 249 (4.60) and 346 (3.98). The 3-dimethylamino analogue (**6l**), obtained in 65% yield, had mp >300 °C (Found: C, 40.05; H, 4.3; N, 46.5%. Calcd for $C_7H_9N_7O\cdot0.2H_2O$: C, 39.9; H, 4.5; N, 46.5%); pK_a 7.94±0.02; λ_{max} at pH 4.0: 250 (4.50), 270 (sh., 4.19), 353 (3.77), and 380 (sh., 3.68); at pH 10.1: 242 (4.58) and 351 (3.87).

*6-Aminopyrimido[4,5-e][1,2,4]triazin-8-one (**6h**).* A mixture of **6o** (1.5 g), hydrazine hydrate (10 ml), and pyridine (100 ml) was refluxed for 6 hr. Chilling gave a solid (0.70 g), which was stirred with silver oxide (4 g) in water (300 ml) at 30 °C for 10 hr. Filtration and concentration to *ca.* 30 ml gave **6h** (0.18 g), mp >300 °C (from water) (Found: C, 32.7; H, 2.7; N, 45.6%. Calcd for $C_5H_4N_6O$: C, 33.0; H, 3.3; N, 46.1%); pK_a 6.37±0.03; λ_{max} at pH 4.1: 277 (3.90) and 332 (3.68); at pH 10.4: 258 (4.15) and 339 (3.73).

References

1) T. Sugimoto and S. Mastuura, This Bulletin, **48**, 725 (1975).
2) H. Biltz and T. Hamburger, *Ber.*, **49**, 635 (1916).
3) A. Albert and G. Catteral, *J. Chem. Soc. C*, **1967**, 1533.
4) L. Heinisch, *Chem. Ber.*, **100**, 893 (1967).
5) L. Heinisch, W. Ozegowski, and M. Mühlstädt, *Chem. Ber.*, **97**, 5 (1964).

BULLETIN OF THE CHEMICAL SOCIETY OF JAPAN, VOL. 48 (5), 1681—1682 (1975)

The Dipole Moments and Conformations of *cis*-2-Styrylfurans and *cis*-2-Styrylthiophenes

Salvatore GRUTTADAURIA and Giuseppe C. PAPPALARDO*
Istituto di Chimica Generale, Università di Catania, Viale A. Doria, 95125 Catania, Italy
Giuseppe SCARLATA and Michele TORRE
Istituto di Chimica Industriale, Università di Catania, Viale A. Doria, 95125 Catania, Italy

(Received November 16, 1974)

Synopsis. Electric dipole moments at 25 °C in benzene have been measured for *cis*-2-styrylfurans and -styrylthiophenes which are chloro- and nitro-substituted in 2′-, 3′-, 4′-position. Results of dipole moment analyses in conjunction with UV spectroscopic data have been discussed in terms of preferred conformations for these compounds.

Recent studies on 1,2-diarylethylenes have led to the isolation of stable *cis*-isomers of unsymmetrical derivatives bearing two distinct aryl groups.[1-5] In these works the assignment of configuration was made by means of IR, UV, and NMR spectroscopy. Information about the conformational properties of these molecular systems, however, is still lacking in the literature.

We therefore report here the results of dipole moment measurements (benzene, 25 °C) for a number of derivative compounds of the series *cis*-2-styrylfuran (**1**)—(**7**) and -styrylthiophene (**8**)—(**14**). Their preferred molecular solute conformations are discussed on the basis of comparison between the observed and calculated dipole moments.

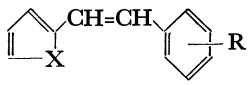

1—7 X=O; **8—14** X=S;
1, 8 R=H; **2, 9** R=2′-Cl; **3, 10** R=3′-Cl;
4, 11 R=4′-Cl; **5, 12** R=2′-NO_2; **6, 13** R=3′-NO_2;
7, 14 R=4′-NO_2

Experimental

Materials. The *cis*-2-styrylfurans (**1**)—(**7**) and -styrylthiophenes (**8**)—(**14**) were prepared as previously described.[1-3] Each compound, just before dipole moment determination, was crystallized or distilled under reduced pressure when liquid to constant mp or bp and ε_{max}. Each sample examined was at least 99% in the pure *cis* isomer, as checked by glc.

Physical Measurements. Dielectric constants of benzene solutions were measured at 25±0.01 °C using a Dipolmeter WTW DMO1 apparatus. Specific volumes and refractive indexes of solutions were determined using experimental techniques described in detail elsewhere.[6]

The total solute polarization $P_{2\infty}$ was evaluated using the Halverstadt-Kumler[7] method. The distortion polarization P_e+P_a was assumed to be 1.05 R_D, where R_D is the experimental molar refraction.

The probable error in μ was estimated not to exceed ±0.03 D for each compound examined.

Experimental results are summarized in Table 1.

TABLE 1. POLARIZATION DATA AND DIPOLE MOMENTS OF *cis*-2-STYRYLFURANS (**1**)—(**7**) AND -STYRYLTHIOPHENES (**8**)—(**14**) IN BENZENE AT 25 °C

Compound	Concentration range $100w_2$	α	ε_{12}	β	v_{12}	$P_{2\infty}$ cm³	R_D cm³	μ D
(**1**) *cis*-2-Styrylfuran	0.1882—0.8835	0.68	2.2729	−0.349	1.14283	61.99	48.00	0.75
(**2**) *cis*-2-(2′-Chlorostyryl)furan	0.1255—0.9404	2.14	2.2723	−0.325	1.14287	132.12	59.01	1.85
(**3**) *cis*-2-(3′-Chlorostyryl)furan	0.1341—1.6136	1.99	2.2728	−0.343	1.14300	125.27	58.71	1.76
(**4**) *cis*-2-(4′-Chlorostyryl)furan	0.2177—1.3438	1.91	2.2728	−0.317	1.14294	123.77	60.11	1.72
(**5**) *cis*-2-(2′-Nitrostyryl)furan	0.1802—0.4111	8.70	2.2725	−0.358	1.14296	402.01	60.44	4.06
(**6**) *cis*-2-(3′-Nitrostyryl)furan	0.2750—0.7363	9.36	2.2729	−0.599	1.14299	413.19	59.94	4.13
(**7**) *cis*-2-(4′-Nitrostyryl)furan	0.1264—0.4751	10.75	2.2723	−0.430	1.14297	480.34	60.54	4.51
(**8**) *cis*-2-Styrylthiophene	0.1594—1.0556	0.405	2.2724	−0.296	1.14303	60.83	54.00	0.45
(**9**) *cis*-2-(2′-Chlorostyryl)thiophene	0.1094—0.9897	1.60	2.2723	−0.233	1.14292	126.15	66.01	1.67
(**10**) *cis*-2-(3′-Chlorostyryl)thiophene	0.2186—0.9893	1.48	2.2723	−0.325	1.14306	115.14	66.01	1.50
(**11**) *cis*-2-(4′-Chlorostyryl)thiophene	0.1977—0.8937	1.61	2.2727	−0.284	1.14285	123.20	66.01	1.62
(**12**) *cis*-2-(2′-Nitrostyryl)thiophene	0.1681—0.8003	7.50	2.2726	−0.359	1.14301	379.85	66.53	3.89
(**13**) *cis*-2-(3′-Nitrostyryl)thiophene	0.2833—0.6764	8.68	2.2725	−0.404	1.14326	428.11	66.94	4.18
(**14**) *cis*-2-(4′-Nitrostyryl)thiophene	0.1230—0.6807	9.08	2.2727	−0.391	1.14296	446.23	67.04	4.28

Results and Discussion

In order to predict dipole moments for the various conformations of the compounds studied, the first task is estimating the direction of action of the resultant moment μ_X of the unsubstituted molecules (**1**), (**8**). The data in Table 1 show that the experimental dipole moment values for *cis*-2-styrylfuran (**1**) and -styrylthiophene (**8**) are fairly close, at less than ±0.08 D, to those of furan (0.67 D[8]) and thiophene (0.53 D[8]), respectively. On this basis we assume that: (i) the interaction moment between the phenyl and the heterocyclic ring can be neglected; (ii) the resultant μ_X can be taken as equal to the individual moment of furan or thiophene molecule; (iii) μ_X acts from the ring to the hetero-atom along the bisector of the C–X–C angle.[9]

In the calculations the following group moments were used:[10] μ_{NO_2}=3.98 D; μ_{Cl}=1.58 D.

The rotational conformations of the molecules dealt with are defined by the angles θ and ϕ described by the phenyl and furan (or thiophene) rings in clockwise and *anti*-clockwise direction, respectively, starting from the planar structure shown in Fig. 1.

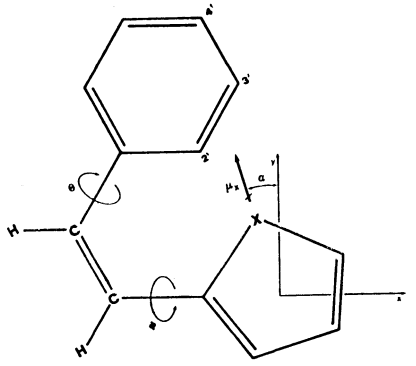

Fig. 1.

* To whom all correspondence should be addressed.

By reference to this model, the total moment was calculated using the relation (1)

$$\mu = (\mu_x^2+\mu_y^2+\mu_z^2)^{1/2}, \quad (1)$$

in which the component moments μ_x, μ_y, and μ_z along the co-ordinate axes are given as a function of θ and ϕ by Eqs. (2)—(4)

$$\mu_x = \pm\mu_R \cos 60° \cos\beta - \mu_R \sin 60° \sin\beta \cos\theta - \mu_x \sin\alpha \quad (2)$$

$$\mu_y = \mp\mu_R \cos 60° \sin\beta - \mu_R \sin 60° \cos\beta \cos\theta + \mu_x \cos\alpha \cos\phi \quad (3)$$

$$\mu_z = \mu_R \sin 60° \sin\theta + \mu_x \cos\alpha \sin\phi \quad (4)$$

In Eqs. (2)—(4) μ_x is the moment of the hetero-ring and μ_R is the group moment of the substituent; the angle α takes the values 18.5° for X=O and 11.8° for X=S, as can be calculated using the given geometries for furan[11] and thiophene.[12] The above equations are in general valid for all compounds examined by substituting β=300° and lower signs for 2′-substituted derivatives; β=300° and upper signs for 3′-substituted derivatives; β=180°, θ=0° and lower signs for 4′-substituted derivatives.

Results of computations show that for each 2′- and 3′-substituted derivative numerous combinations (ϕ,θ) are possible for which the predicted dipole moment agrees with the experimental value. Therefore the most probable conformation within the ranges (ϕ,θ) indicated cannot be decided with certainty. However, the number of possible conformations can be restricted by assuming that the ϕ angles found in the 4′-Cl derivatives **4** and **11** are preserved in all the 2′- and 3′-substituted compounds with slight distortions due to steric factors. Computations produce a value of ϕ=78° for **4** and ϕ=89° for **11**, thus indicating that non-bonded repulsive interactions, due to crowding, essentially operate to force the hetero-ring out from coplanarity with the ethylenic fragment. On the other hand, it seems highly unlikely that the angles ϕ=0° and ϕ=43° found for the 4′-NO_2 derivative compounds **7** and **14**, respectively, are retained in *cis*-2-styrylfurans and -styrylthiophenes. The powerful electron withdrawing group in 4′-position is, in fact, a factor determining a coplanarity-favoring conjugative interaction which tends to minimize ϕ in these particular derivatives.

In Table 2 are given the possible conformations (ϕ,θ) obtainable, on the basis of the above assumptions, from our calculations.

Use of scale molecular models shows that the conformations denoted by II are sterically more favorable. The general preference in both series for these conformations can be clearly understood in terms of repulsive steric interactions which determine the arrangement of the phenyl ring with the 2′- or 3′-substituent group as far as possible from the heterocyclic nucleus. A combined mesomeric effect, moreover, is the factor determining the preference for structures in which the phenyl ring is coplanar to the ethylenic fragment, *i.e.* for conformations having a ϕ value near 180°.

Table 2. Preferred conformations of *cis*-2-styryl-furanes and -styrylthiophenes

	Compound	Conformation I ϕ	I θ	II θ
2	*cis*-2-(2′-Chlorostyryl)furan	78°	36°	186°
3	*cis*-2-(3′-Chlorostyryl)furan	78°	30°	198°
5	*cis*-2-(2′-Nitrostyryl)furan	78°	26°	200°
6	*cis*-2-(3′-Nitrosrytyl)furan	78°	32°	192°
7	*cis*-2-(4′-Nitrostyryl)furan	0°	—	—
9	*cis*-2-(2′-Chlorostyryl)thiophene	89°	8°	192°
10	*cis*-2-(3′-Chlorostyryl)thiophene	89°	348°	212°
12	*cis*-2-(2′-Nitrostyryl)thiophene	89°	—	210°
13	*cis*-2-(3′-Nitrostyryl)thiophene	89°	35°	168°
14	*cis*-2-(4′-Nitrostyryl)thiophene	43°	—	—

An interesting feature of the UV spectroscopic data available[1-4] is that the conjugation band of each *cis*-2-styrylfuran derivative compound is shifted to shorter wavelengths in the corresponding derivative of thiophene series. This fact suggests that the tendence for aryl rings to be coplanar with the ethylenic group is in general more reduced in *cis*-2-styrylthiophenes. The present dipole moment results are therefore consistent with these deductions in that the twisting angle values found (see Table 2) are correspondingly greater in the derivatives of the thiophene series.

References

1) A. Arcoria, S. Fisichella, G. Scarlata, and M. Torre, *J. Heterocyclic Chem.*, **10**, 643 (1973).
2) S. Fisichella, G. Scarlata, D. Sciotto, and M. Torre, *Boll. Sedute Accad. Gioenia Sci. Nat. Catania* Serie IV, **12**, 323 (1973).
3) S. Fisichella, G. Scarlata, and M. Torre, *Gazzetta* **104**, 1237 (1974).
4) S. Fisichella, G. Scarlata, and D. Sciotto, *Ann. Chim.* (Italy), **63**, 55 (1973).
5) S. Fisichella, G. Mineri, G. Scarlata, and D. Sciotto, *ibid.*, **63**, 779 (1973).
6) G. C. Pappalardo and S. Pistarà, *J. Chem. Eng. Data*, **17**, 2 (1972).
7) I. F. Halverstadt and W. D. Kumler, *J. Amer. Chem. Soc.*, **64**, 2988 (1942).
8) A. L. McClellan, "Tables of Experimental Dipole Moments," Freeman, San Francisco (1963).
9) G. Marino, *J. Heterocyclic Chem.*, **9**, 817 (1972).
10) C. P. Smyth, "Dielectric Behaviour and Structure," McGraw-Hill, New York (1955), p. 253.
11) B. Bak, D. Christensen, W. B. Dixon, L. Hansen-Nygaard, J. Rastrup-Adersen, and M. Schottländer, *J. Mol. Spectrosc.*, **9**, 124 (1962).
12) B. Bak, D. Christensen, L. Hansen-Nygaard, and J. Rastrup-Adersen, *J. Mol. Spectrosc.*, **7**, 58 (1961).

BULLETIN OF THE CHEMICAL SOCIETY OF JAPAN, VOL. 48 (5), 1683 (1975)

Base-catalyzed Oxygenation of 2,6-Di-*t*-butylphenols. A Convenient Method for Preparation of *p*-Quinols

Akira NISHINAGA, Toshio ITAHARA, and Teruo MATSUURA

Department of Synthetic Chemistry, Faculty of Engineering, Kyoto University, Kyoto 606

(Received January 13, 1974)

Synopsis. The oxygenation of 4-alkyl-2,6-di-*t*-butylphenols in diethylamine containing sodium amide under mild conditions afforded the corresponding *p*-quinols in excellent yields.

The synthesis of *p*-quinols has been developed by the oxidation of the corresponding phenols involving Co(II)–Schiff's base complex catalyzed oxygenation[1] and thallium triperchlorate oxidation,[2] and also by the reduction of the appropriate *p*-benzoquinones with alkyllithium compounds.[3] The reduction of hydroperoxides formed from appropriate phenols by oxidation with O_2[4] or hydrogen peroxide-molybdenum complex[5] also affords *p*-quinols. No attempt has been made for a one-step synthesis of such *p*-quinols by simple oxygenation. We previously reported that the oxygenation of *t*-butylated phenols in *t*-BuOH or aprotic solvents such as DMF, DMSO, and HMPA containing *t*-BuOK leads to the exclusive formation of epoxyquinols, intramolecular decomposition products of the corresponding hydroperoxides.[6,7]

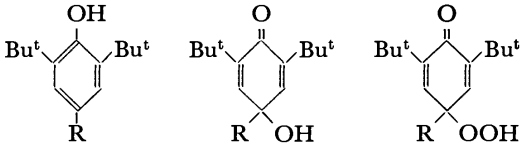

(**1**) (**2**) (**3**)

a; R=Bu^t, **b**; R=Pr^i, **c**; R=Et, **d**; R=Me

TABLE 1. THE FORMATION OF *p*-QUINOLS BY OXYGENETION OF **1**.

1	Solvent	Base	Base/1 mol/mol	Reaction time (hr)	Conversion (%)	**1** Yield (%)[a]
1a	$HNEt_2$	$NaNH_2$	5	4	100	**2a**, 86
	NEt_3	$NaNH_2$	5	6	30	90
	$HNEt_2$	*t*-BuOK	5	6	35	80
1b	$HNEt_2$	$NaNH_2$	5	6	100	**2b**, 92
1c	$HNEt_2$	$NaNH_2$	5	6	100	**2c**, 94
1d	$HNEt_2$	$NaNH_2$	5	6	100	**2d**, 95
	NEt_3	$NaNH_2$	5	6	40	90
	Me_2S	$NaNH_2$	5	6	20	90
	Me_2S	*t*-BuOK	5	6	20	90

a) Yields by isolation.

We now find that the oxygenation of 2,6-di-*t*-butylphenols in $HNEt_2$ containing $NaNH_2$ affords the corresponding *p*-quinols in excellent yields. This provides a convenient method for one-step synthesis of such *p*-quinols (**2**). The phenols (**1**) were dissolved in $HNEt_2$ containing excess $NaNH_2$ and bubbled with oxygen at room temperature. The products (**2**) could be isolated in crystalline form upon diluting the reaction mixture with ice-cooled water and were identified with authentic samples (IR and NMR). The results are summarized in the Table. Since the hydroperoxides (**3**) separately synthesized are easily reduced in $HNEt_2$ to **2**, the formation of **2** by oxygenation should proceed *via* the hydroperoxide intermediate. Replacement of the solvent with NEt_3 or of the base with *t*-BuOK reduces the reactivity (Table 1). Dimethyl sulfide is a good reducing reagent for **3** to **2** but the oxygenation of **1** in this solvent is largely inhibited (Table 1) probably due to competition of oxidation of the solvent itself.

Experimental

*Oxygenation of **1** in Diethylamine Containing Sodium Amide.* The phenols (1 mmol) were dissolved in diethyl amine (20 ml) containing sodium amide (5 mmol). Oxygen was bubbled through the solutions at room temperature for appropriate periods (see Table 1). The reaction mixtures were then poured into a large amount of ice-cooled water to give the *p*-quinols (**2**) as crystals, which were identified with authentic samples[1] (IR and NMR).

References.

1) A. Nishinaga, K. Watanabe, and T. Matsuura, *Tetrahedron Lett.*, **1974**, 1291.
2) Y. Yamada, K. Hosaka, H. Sanjoh, and M. Suzuki, *Chem. Commun.*, **1974**, 661.
3) A. Rieker, *Angew. Chem.*, **76**, 601 (1964).
4) M. S. Kharasch and B. S. Joshi, *J. Org. Chem.*, **22**, 1439 (1957); H. R. Gersmann and A. F. Bickel, *J. Chem. Soc.*, **1959**, 2711.
5) Y. Hayashi, S. Shioi, M. Togami, and T. Sakan, *Chem. Lett.*, **1973**, 651.
6) A. Nishinaga, T. Itahara, and T. Matsuura, *ibid.*, **1974**, 667.
7) A. Nishinaga, T. Itahara, and T. Matsuura, *Tetrahedron Lett.*, **1974**, 4481.

COMMENTS

BULLETIN OF THE CHEMICAL SOCIETY OF JAPAN, VOL. 48 (5), 1684 (1975)

Products of the Palladium-catalyzed Dehydrogenation of *o*-Cyclohexylphenol. A Correction

Kimiaki IMAFUKU

Department of Chemistry, Faculty of Science, Kumamoto University, Kurokami, Kumamoto 860

(Received November 18, 1974)

Previously, we reported,[1] on the basis of vpc analysis, that the dehydrogenation of *o*-cyclohexylphenol (I) over palladium-on-charcoal gave *o*-phenylphenol (II), dibenzofuran (III), and diphenyl ether (IV'). However, we have now confirmed that the structure of the compound which was previously assumed to be diphenyl ether (IV') is really diphenyl (IV); confirmation was made by its isolation and on the basis of its spectral data. It was found that the diphenyl was produced by the hydrogenolysis of *o*-phenylphenol (II) in the presence of the same catalyst.

The procedure was as follows. A mixture of *o*-cyclohexylphenol (I) (5 g) and 5% palladium-on-charcoal (1 g) was heated at 220—230 °C for 3 hr under a nitrogen atmosphere. The reaction mixture was then dissolved in benzene, and the catalyst was filtered off. The filtrate was chromatographed on a silica gel column (Wakogel C-100, 500 g) with chloroform. The resulting solid from the first fraction was recrystallized from ethanol, giving diphenyl (IV) (370 mg, 8.5%) (mp 69—70 °C (mixed mp 68.5—70 °C)). Its spectral data were also consistent with those of the authentic material.

In addition, a mixture of *o*-phenylphenol (II) (2 g) and 5% palladium-on-charcoal (0.4 g) was heated at 220—230 °C for 3 hr under a hydrogen atmosphere and treated such as above, thus giving diphenyl (IV) (260 mg, 14%).

Reference

1) H. Matsumura, K. Imafuku, I. Takano, and S. Matsuura, This Bulletin, **44**, 567 (1971).

General Anharmonic Force Constants of Carbon Disulfide

Isao SUZUKI

Educational Computer Centre, The University of Tokyo, Hongo, Bunkyo-ku, Tokyo 113

(Recieved December 27, 1974)

Twelve force constants in the general quartic force field of carbon disulfide have been determined by a least-squares method from the available spectroscopic data on four isotopic species of carbon disulfide: $^{12}C^{32}S_2$, $^{13}C^{32}S_2$, $^{12}C^{32}S^{34}S$, and $^{13}C^{32}S^{34}S$. A reasonable set of force constants is obtained together with a set of the third-order parameters λ_1, λ_2, λ_3, and δ which appear in Fermi coupling off-diagonal matrix elements. From the converged set of force constants, l-type doubling constants for a few π-vibrational states are calculated through a direct numerical diagonalization method of vibrational Hamiltonian matrix. They agree well with the observed l-type doubling constants.

In a process of extending the numerical diagonalization technique of vibrational Hamiltonian matrix[1] to the anharmonic treatment of linear symmetric triatomic molecules, it was required to obtain the most reliable set of force constants of CS_2 up to the fourth order. The general quartic force field of CS_2 has previously been studied by Smith and Overend[2] and by Giguere, Wang, Overend, and Cabana.[3] More recently, however, two high resolution infrared studies have been reported on this molecule by Maki[4] and by Blanquet and Courtoy.[5] The study of Maki covers a number of 'hot transitions' in $^{12}C^{32}S_2$ and gives the information of levels which are not directly accessible from the ground state. The study of Blanquet and Courtoy consists of the high resolution measurements of a number of $^{13}C^{32}S_2$ bands. Both studies provide very important pieces of information on the determination of anharmonic force constants of CS_2. Like CO_2, CS_2 is one of a few fundamental molecules, on which the validity of various model potential functions is tested:[6] One of the criteria for this test is whether they can reproduce the values of force constants in the general quartic force field reasonably well or not. It is, therefore, desirable to determine these force constants as precisely as possible. We have carried out such new anharmonic calculations: twelve force constants in the general quartic force field and four third-order parameters, which appear in Fermi coupling off-diagonal matrix elements of $v_1=2v_2$ type, are adjusted simultaneously to fit the presently available spectroscopic data of $^{12}C^{32}S_2$,[3,4,7-10] $^{13}C^{32}S_2$,[5] $^{12}C^{32}S^{34}S$,[11-13] and $^{13}C^{32}S^{34}S$.[11] The l-type doubling constants of $^{12}C^{32}S_2$ and $^{13}C^{32}S_2$ are also obtained from the π-π transitions.[4,5] From the refined set of force constants, the corresponding l-type doubling constants are calculated which can be compared with experimental values quite well.

Determination of Anharmonic Force Constants

A general method for the determination of force constants in the general quartic force field was described in the preceding papers[14,15] and it is not repeated here. However, our program of anharmonic calculations has been improved so as to handle 'hot transitions' directly. This is particularly useful when the spectroscopic constants associated with a given hot transition ($v_0'-v_0''$, $B'-B''$) are determined more accurately than those in the lower state (v_0'', B'').

The potential functions of linear symmetric triatomic molecules may be expanded in terms of curvilinear internal coordinates through quartic terms and

$$\begin{aligned} V = {} & K_{11}(R_1^2+R_3^2) + K_{13}R_1R_3 + K_{22}R_2^2 \\ & + K_{111}(R_1^3+R_3^3) + K_{122}(R_1+R_3)R_2^2 \\ & + K_{113}(R_1+R_3)R_1R_3 + K_{1111}(R_1^4+R_3^4) \\ & + K_{1113}(R_1^2+R_3^2)R_1R_3 + K_{1133}R_1^2R_3^2 \\ & + [K_{1122}(R_1^2+R_3^2) + K_{1223}R_1R_3 + K_{2222}R_2^2]R_2^2, \end{aligned} \quad (1)$$

where R_1 and R_3 are two stretching coordinates and R_2 is the bending coordinate.[16]

Fermi Resonance in CS_2. The vibrational levels of most non-hydride linear triatomic molecules are more or less affected by Fermi resonance through non-vanishing matrix elements $\langle v_1, v_2, l_2, v_3|v_1-1, v_2+2, l_2, v_3\rangle$. To the third order of approximation in perturbation treatment, this matrix element is expressed as

$$\begin{aligned} & (1/2)[-k_{122}/\sqrt{2}+\lambda_1 v_1+\lambda_2(v_2+2)+\lambda_3(v_3+1/2) \\ & \qquad +\delta J(J+1)][(v_2+2)^2-l_2^2]^{1/2}v_1^{1/2} \end{aligned} \quad (2)$$

The λ's and δ represent the third order vibrational and rotational effects on the matrix elements,[17] which cannot be ignored in the determination of the general quartic force field of most linear triatomic molecules.[2,3,15,18] The effect of δ on the perturbed rotational constant in each vibrational state is also taken into account. In the present calculation we are able to treat the third-order parameters of the ^{12}C- and ^{13}C-species separately,[19] thus the total number of independent parameters is twenty.

Spectroscopic Data Used in Computations. The spectroscopic data used in the refinement of twelve general quartic force constants and eight third-order parameters are listed in Table 1 along with the corresponding weights. References are also given in the last column in Table 1. The present system for the weighting is based on the fact that the band centers are usually determined within a few thousandths of a wave number and that the errors in the ΔB values are in the order of 10^{-7} cm^{-1}. The spectroscopic data associated with the transitions from the 02^20 level of $^{12}CS_2$ as well as those from the 01^10 level in $^{13}CS_2$ are used directly, since the spectroscopic constants of the lower states are known less accurately. We employed $r_e=1.5562$ Å for the equilibrium bond distance,

Table 1. Observed and calculated vibrational levels (in cm^{-1}) and rotational constants (in 10^{-4} cm^{-1}) for $^{12}C^{32}S_2$, $^{13}C^{32}S_2$, $^{12}C^{32}S^{34}S$, and $^{13}C^{32}S^{34}S$

Level	ν_{obsd}	Wt.	i	ii	(B_v-B)	Wt.	i	ii	Ref.
(a) $^{12}C^{32}S_2$									
$\begin{bmatrix}1\ 0^0\ 0\\0\ 2^0\ 0\end{bmatrix}$	658.00	1.0	1	7	−1.55	1.0	4	6	a
	801.85	1.0	7	6	3.69	1.0	1	3	b
$\begin{bmatrix}2\ 0^0\ 0\\1\ 2^0\ 0\\0\ 4^0\ 0\end{bmatrix}$	1313.70	1.0	7	11	−3.02	1.0	3	7	a
	(1446.97)	0.0			(2.59)	0.0			
	(1619.76)	0.0			(6.81)	0.0			
$0\ 0^0\ 1$	1535.35	1.0	7	7	−7.12	1.0	1	1	b
$\begin{bmatrix}1\ 0^0\ 1\\0\ 2^0\ 1\end{bmatrix}$	2185.49	1.0	3	1	−8.67	1.0	2	4	c
	2324.55	1.0	3	1	−3.43	1.0	3	1	b
$\begin{bmatrix}2\ 0^0\ 1\\1\ 2^0\ 1\\0\ 4^0\ 1\end{bmatrix}$	2833.19	1.0	4	2	−10.03	1.0	7	11	d
	2961.76	1.0	3	2	−4.57	1.0	2	2	a
	3129.98	1.0	1	2	−0.39	1.0	1	3	e
$\begin{bmatrix}3\ 0^0\ 1\\2\ 2^0\ 1\\1\ 4^0\ 1\\0\ 6^0\ 1\end{bmatrix}$	3478.39	1.0	3	4	−11.33	1.0	2	4	e
	3597.05	1.0	4	13	−5.71	1.0	10	8	a, e
	3757.45	1.0	7	15	−1.32	1.0	7	7	a
	(3948.17)	0.0			(2.41)	0.0			
$0\ 0^0\ 3$	4566.81	1.0	1	0	−21.35	1.0	4	4	b
$\begin{bmatrix}1\ 0^0\ 3\\0\ 2^0\ 3\end{bmatrix}$	5201.15	1.0	5	7	−22.91	1.0	3	1	e
	(5330.60)	0.0			(−17.79)	0.0			
$0\ 1^1\ 1$	1924.99	1.0	4	6	−5.00	0.1	2	2	b
$\begin{bmatrix}1\ 1^1\ 1\\0\ 3^1\ 1\end{bmatrix}$	2567.51	0.1	5	7	−6.15	0.1	4	2	d, c
	2723.36	0.1	4	7	−1.73	0.1	1	1	a
$\begin{bmatrix}2\ 1^1\ 1\\1\ 3^1\ 1\\0\ 5^1\ 1\end{bmatrix}$	3207.44	0.5	4	10	(−7.09)	0.0			d
	3355.18	0.5	2	6	−2.73	0.1	8	8	e, f
	(3535.69)	0.0			(1.14)	0.0			
$0\ 1^1\ 3$	4943.55	0.1	4	4	(−19.25)	0.0			
$0\ 1^1\ 0$	396.09	1.0	3	0	2.11	1.0	4	4	b, f
$\begin{bmatrix}1\ 1^1\ 0\\0\ 3^1\ 0\end{bmatrix}$	1046.58	1.0	8	8	0.98	1.0	0	2	b
	1206.98	1.0	8	12	5.39	0.1	5	7	b
$0\ 2^2\ 0$	792.52	0.01	22	15	(4.29)	0.0			b
$\begin{bmatrix}1\ 2^2\ 1\\0\ 4^2\ 1\end{bmatrix}$	(2158.20)†	0.0			(−7.94)	0.0			
	2329.03†	0.1	6	3	−4.24	0.1	3	4	a
$\begin{bmatrix}2\ 2^2\ 1\\1\ 4^2\ 1\\0\ 6^2\ 1\end{bmatrix}$	(2791.59)†	0.0			(−8.61)	0.0			
	2955.63†	0.1	10	5	−5.01	0.1	8	7	a
	(3148.05)†	0.0			(−1.50)	0.0			
(b) $^{13}C^{32}S_2$									
$\begin{bmatrix}1\ 0^0\ 0\\0\ 2^0\ 0\end{bmatrix}$	657.23	1.0	2	5	−1.57	0.01	11	11	g
	(776.46)	0.0			(3.39)	0.0			
$0\ 0^0\ 1$	1485.34	1.0	5	5	−6.87	1.0	1	0	g
$\begin{bmatrix}1\ 0^0\ 1\\0\ 2^0\ 1\end{bmatrix}$	2134.87	1.0	4	2	−8.26	1.0	2	2	g
	2250.13	1.0	1	0	−3.47	1.0	4	5	g
$\begin{bmatrix}2\ 0^0\ 1\\1\ 2^0\ 1\\0\ 4^0\ 1\end{bmatrix}$	2781.61	1.0	2	7	−9.44	1.0	5	2	g
	2886.78	1.0	3	1	−4.54	1.0	4	2	g
	(3031.24)	0.0			−0.74	0.0			
$\begin{bmatrix}3\ 0^0\ 1\\2\ 2^0\ 1\\1\ 4^0\ 1\\0\ 6^0\ 1\end{bmatrix}$	3425.29	0.1	10	18	−10.38	0.0			g
	(3521.35)	0.0			(−5.66)	0.0			
	(3658.53)	0.0			(−1.63)	0.0			
	(3824.70)	0.0			(1.78)	0.0			
$0\ 1^1\ 0$	(383.02)	0.0			1.96	0.01	9	10	g
$0\ 1^1\ 1$	1479.63*	1.0	24	25	−6.85	1.0	1	1	g
$\begin{bmatrix}1\ 1^1\ 1\\0\ 3^1\ 1\end{bmatrix}$	2120.71*	1.0	5	4	−7.82	1.0	0	3	g
	2253.60*	1.0	1	6	−3.90	1.0	7	10	g
$\begin{bmatrix}2\ 1^1\ 1\\1\ 3^1\ 1\\0\ 5^1\ 1\end{bmatrix}$	2759.23*	1.0	2	2	−8.57	1.0	1	10	g
	(2884.87)*	0.0			(−4.86)	0.0			
	(3041.52)*	0.0			(−1.39)	0.0			
(c) $^{12}C^{32}S^{34}S$									
$\begin{bmatrix}1\ 0^0\ 0\\0\ 2^0\ 0\end{bmatrix}$	648.37	1.0	17	18	(−1.57)	0.0			i
	(799.57)	0.0			(3.66)	0.0			
$\begin{bmatrix}1\ 0^0\ 1\\0\ 2^0\ 1\end{bmatrix}$	2172.77	1.0	0	2	−8.41	1.0	5	5	h
	(2318.86)	0.0			(−3.28)	0.0			

Table 1. Continued

Level	ν_{obsd}	Wt.	i	ii	(B_v-B)	Wt.	i	ii	Ref.
0 0^0 3	4556.55	1.0	1	0	−20.73	0.2	2	2	j
0 1^1 0	395.13	1.0	2	5	(2.09)	0.0			b
[1 1^1 0	1036.42	1.0	1	14	(0.86)	0.0			i
[0 3^1 0	(1203.53)	0.0			(5.38)	0.0			
0 1^1 3	4932.34	1.0	5	6	(−18.66)	0.0			j
0 2^2 0	790.72	1.0	21	13	(4.17)	0.0			b
(d) $^{13}C^{32}S^{34}S$									
[1 0^0 1	2122.18	1.0	4	4	−8.05	1.0	2	2	h
[0 2^0 1	(2244.06)	0.0			(−3.33)	0.0			

†Transitions from the 0 2^2 0 level. *Transitions from the 0 1^1 0 level.
Only differences between observed and calculated frequencies (in 10^{-2} cm^{-1}) and rotational constants (in 10^{-6} cm^{-1}) are given. Negative differences are underlined. Numbers in parenthese are calculated values from set (i). References: a) Ref. 4. b) Ref. 2. c) Ref. 9. d) Ref. 7. e) Ref. 8. f) Ref. 10. g) Ref. 5. h) Ref. 11. i) Ref. 13. j) Ref. 12.

TABLE 2. FORCE CONSTANTS OF CS_2 IN THE GENERAL QUARTIC FORCE FIELD[a,b]

	(i)		(ii)		(iii)		(iv)[d]	
K_{11}	3.9383	(16)	3.9356	(13)	3.9337	(17)	8.0089	(26)
K_{13}	0.6441	(33)	0.6388	(28)	0.6360	(34)	1.2570	(54)
K_{22}	0.2846	(2)	0.2848	(2)	0.2849	(1)	0.3928	(2)
K_{111}	−7.478	(29)	−7.478	(31)	−7.441	(14)	−18.948	(31)
K_{113}	−0.842	(93)	−0.869	(97)	−0.793	(43)	−1.886	(85)
K_{122}	−0.369	(7)	−0.365	(7)	−0.367	(4)	−0.612	(3)
K_{1111}	8.697	(190)	8.924	(172)	8.834	(149)	26.144	(157)
K_{1113}	0.643	(466)	1.390	(401)	1.382	(516)	3.329	(205)
K_{1133}	0.479	(636)	1.483	(535)	1.637	(793)	2.382	(312)
K_{1122}	0.111	(85)	0.253	(70)	0.428	(38)	0.852	(107)
K_{1223}	0.461	(185)	0.771	(146)	1.136	(97)	2.594	(221)
K_{2222}	0.044	(4)	0.037	(3)	0.032	(3)	0.035	(4)
λ_1	0.460	(120)	0.276	(100)	0.141	(112)	0.358	(111)
λ_2	0.325	(86)	0.204	(74)	0.043	(49)	0.498	(48)
λ_3	0.037	(181)	0.018	(130)	−0.041	(193)	0.281	(90)
$\delta\times10^4$	0.378	(32)	0.350	(28)	0.592	(23)	1.966	(79)
λ'_1	0.359	(106)					0.653	(111)
λ'_2	0.301	(90)					0.509	(53)
λ'_3	0.042	(174)					0.275	(91)
$\delta'\times10^4$	0.344	(31)					1.883	(77)
S[c]	0.25		0.35					

a) The units of force constants are: mdyn/Å for K_{11} and K_{13}, mdyn·Å/rad² for K_{22}, mdyn/Å² for K_{111} and K_{113}, mdyn/rad² for K_{122}, mdyn/Å³ for K_{1111}, K_{1113}, and K_{1133}, mdyn/Å rad² for K_{1122} and K_{1223}, and mdyn·Å/rad⁴ for K_{2222}. The third order parameters λ's and $\delta\times10^4$ are given in cm^{-1}. In order to retain good reproducibility of the calculated values, four or three significant numbers beyond the decimal point are given, even when the corresponding dispersions are considerably larger than that. b) Dispersions, shown in parentheses, apply to the last digits of the quantity. c) The weighted sum of squared deviations for a given set of force constants and the third order parameters. d) The corresponding force constants of CO_2 (Ref. 15).

Results and Discussion

The converged sets of the anharmonic force constants and the third-order parameters are listed in Table 2 with the corresponding previous results on CS_2 and CO_2. In preliminary calculations the differences of the third-order parameters due to isotopic substitutions were neglected, and the converged set for the sixteen parameter problem is given in column (ii). It was found, however, that the fit in frequency and rotational constant is much improved by allowing the third-order parameters vary for the ^{12}C- and ^{13}C-species, and the twenty parameter problem seems to be stable enough to give a good converged set which is listed in the column (i) of Table 2. The harmonic frequencies ω_i, the anharmonicity constants x_{ij}, the vibration-rotation constants α_i, and the cubic and quartic force constants in dimensionless normal coordinates k_{ijk} and k_{ijkl} are calculated for the four isotopic species of CS_2 from the sets (i) and (ii), their values are listed in Table 3.

Values of Force Constants. The force constants of CS_2 thus determined have the features expected for linear triatomic molecules: (1) They show a dis-

TABLE 3. HARMONIC FREQUENCIES (ω_i), ANHARMONICITY CONSTANTS (x_{ij}), VIBRATION-ROTATION CONSTANTS (α_i), AND FORCE CONSTANTS IN DIMENSIONLESS NORMAL COORDINATES (k_{ijk}, k_{iijj}) CALCULATED FROM THE GENERAL QUARTIC FORCE FIELD (in cm^{-1})

Set (i)

	$^{12}C^{32}S_2$	$^{13}C^{32}S_2$	$^{12}C^{32}S^{34}S$	$^{13}C^{32}S^{34}S$
ω_1	672.574	672.574	662.564	662.559
ω_2	398.210	358.057	397.285	385.100
ω_3	1558.849	1507.360	1555.251	1503.642
x_{11}	−1.00	−1.00	−0.97	−0.97
x_{12}	−2.49	−2.40	−2.45	−2.36
x_{22}	1.00	0.94	1.00	0.93
x_{13}	−7.66	−7.43	−7.52	−7.29
x_{23}	−6.45	−6.00	−6.43	−5.98
x_{33}	−6.57	−6.13	−6.55	−6.10
$x_{l_2l_2}$	−0.69	−0.64	−0.69	−0.64
$\alpha_1\times10^4$	2.172	2.172	2.077	2.077
$\alpha_2\times10^4$	−2.146	−2.050	−2.087	−1.993
$\alpha_3\times10^4$	7.130	6.861	6.915	6.654
k_{111}	−18.386	−18.386	−17.978†	−17.978††
k_{122}	43.153	41.728	42.729	41.311
k_{133}	−130.295	−125.992	−129.012	−124.728
k_{1111}	0.593	0.593	0.575	0.575
k_{1122}	−5.392	−5.214	−5.299	−5.123
k_{2222}	1.697	1.587	1.689	1.579
k_{1133}	8.736	8.447	8.585	8.300
k_{2233}	−15.264	−14.273	−15.196	−14.204
k_{3333}	3.826	3.578	3.809	3.561

†$k_{113}=-0.531$, $k_{223}=-1.195$, $k_{333}=1.222$
††$k_{113}=-0.567$, $k_{223}=-1.221$, $k_{333}=1.263$

Set (ii)

	$^{12}C^{32}S_2$	$^{13}C^{32}S_2$	$^{12}C^{32}S^{34}S$	$^{13}C^{32}S^{34}S$
ω_1	672.152	672.152	662.149	662.144
ω_2	398.345	385.188	397.420	384.231
ω_3	1558.838	1507.351	1555.241	1503.631
x_{11}	−0.88	−0.88	−0.85	−0.85
x_{12}	−2.16	−2.08	−2.13	−2.05
x_{22}	0.90	0.84	0.90	0.84
x_{13}	−7.63	−7.40	−7.49	−7.26
x_{23}	−6.46	−6.01	−6.44	−5.99
x_{33}	−6.57	−6.13	−6.55	−6.10
$x_{l_2l_2}$	−0.66	−0.61	−0.66	−0.61
$\alpha_1\times10^4$	2.189	2.189	2.093	2.093
$\alpha_2\times10^4$	−2.152	−2.056	−2.093	−1.999
$\alpha_3\times10^4$	7.131	6.862	6.916	6.655
k_{111}	−18.465	−18.465	−18.055†	−18.055††
k_{122}	43.218	41.790	42.792	41.371
k_{133}	−130.185	−125.885	−128.902	−124.622
k_{1111}	0.685	0.685	0.665	0.665
k_{1122}	−5.089	−4.921	−5.001	−4.835
k_{2222}	1.635	1.529	1.628	1.522
k_{1133}	8.803	8.512	8.650	8.363
k_{2233}	−15.283	−14.290	−15.215	−14.222
k_{3333}	3.818	3.570	3.801	3.553

†$k_{113}=-0.526$, $k_{223}=-1.194$, $k_{333}=1.220$
††$k_{113}=-0.562$, $k_{223}=-1.221$, $k_{333}=1.260$

Table 4. Diagonal stretching force constants associated with the CS bond

	CS_2	CS[a]	OCS[b]
K_{ii} (mdyn/Å)	3.9383	4.2445	3.7215
K_{iii} (mdyn/Å^2)	−7.478	−8.256	−6.670
K_{iiii} (mdyn/Å^3)	8.697	8.858	8.192
$-a_1$ (Å^{-1})	1.90	1.95	1.79
a_2 (Å^{-2})	2.21	2.09	2.20
a_2* (Å^{-2})	2.10	2.21	1.87
r_e (Å)	1.5526	1.5344	1.5630

a) Ref. 20. b) Ref. 21.

tinctive positive-negative-positive pattern for the quadratic, cubic and quartic force constants. (2) Off-diagonal force constants are one order of magnitude smaller than the corresponding diagonal force constants. In addition, the overall feature of the potential function is very close to that of CO_2 which is quite reasonable. In Table 4 three diagonal stretching force constants are listed and compared with the corresponding constants of CS[20] and OCS.[21] The ratios $a_1=K_{111}/K_{11}$, $a_2=K_{1111}/K_{11}$, and $a_2^*=7a_1^2/12$ are also listed in the table. Within the limits of present approximation, the Morse type potential function[22] seems to be a good model for the CS stretching mode, since the relationship $a_2=a_2^*$, which holds strictly in the Morse potential function, is nearly realized in this molecule. We may also estimate the dissociation energy of $CS_2\rightarrow CS+S$ from an assumption that the stretching potential is of Morse type. Then we have $D_e=K_{11}/a_1^2=6.8$ eV. As far as we are aware, no experimental data seem available for this process, but the value is close to that of 7.2 eV for diatomic CS.[23]

Although the least-squares dispersions for the third-order parameters λ's are relatively large, it is gratifying that the converged values are very close to those obtained on purely experimental basis. The isotopic ratios seem also reasonable. The values of harmonic frequencies, anharmonicity constants, vibration-rotation constants, and third-order parameters for $^{12}C^{32}S_2$ are collected in Table 5 from different sources: (1) calculated from the set (i) in the present work, (2) obtained by Blanquet and Courtoy[24] who made the direct least-squares fit of the experimental data to the analytical expressions of the energy levels and the rotational constants, (3) calculated from the force constants given in Ref. 3, and (4) obtained by the same authors by applying the Amat-Pimbert method to experimental data.[25] The agreements (or disagreements rather) in their values indicate, in a way, the precisions of the general quartic force constants and of some spectroscopic constants of the CS_2 molecule. As seen in Table 5, the final set of force constants yields the spectroscopic constants which are very close to those obtained experimentally. This seems to guarantee the consistency of the present anharmonic calculation.

Table 5. Spectroscopic constants of $^{12}CS_2$

	PR[a]	BC[b]	GWOC[c]	AP[d]
ω_1	672.574	672.709	671.89	672.42
ω_2	398.210	398.261	398.38	398.39
ω_3	1558.849	1558.710	1558.73	1558.70
x_{11}	−1.00	−1.021	−0.83	−1.05
x_{12}	−2.49	−2.897	−1.75	−1.13
x_{22}	1.00	1.094	0.82	0.66
x_{13}	−7.66	−7.664	−7.59	−7.62
x_{23}	−6.45	−6.446	−6.49	−6.48
x_{33}	−6.57	−6.540	−6.54	−6.54
$x_{l_2l_2}$	−0.69	−0.775	−0.74	−0.60
$\alpha_1\times10^4$	2.172	2.100	2.144	
$\alpha_2\times10^4$	−2.146	−2.130	−2.148	
$\alpha_3\times10^4$	7.130	7.142	7.130	
λ_1	0.46	0.49	0.141	
λ_2	0.33	0.42	0.043	
λ_3	0.04	0.02	−0.041	
$\delta\times10^4$	0.378	0.724	0.592	
k_{122}	43.15	42.31	43.16	44.8

a) Calculated from Set (i). b) Obtained experimentally.[24] c) Calculated from Set (iii).[3] d) Obtained by applying the Amat-Pimbert method.[3]

Unperturbed Energy Levels. Fermi resonances in CS_2 are not so strong as those in CO_2. Nevertheless, the effects are seen on most of energy levels. The unperturbed and perturbed energy levels and rotational constants are calculated from the set (i) in Table 2 and are listed in Table 6 for a few typical Fermi polyads. Shifts of 7—20 cm^{-1} are usually observed. It is also seen that Fermi resonances in $^{13}C^{32}S_2$ are stronger than those in $^{12}C^{32}S_2$, as is expected from the lowering of the ν_2 frequency on the ^{13}C-substitution.

l-Type Doubling Constants. From the analyses of the π-π transition bands, the l-type doubling constants have been determined for a few vibrational states of $^{12}C^{32}S_2$ and $^{13}C^{32}S_2$.[4,5] The dependence of l-type doubling constants on vibrational quantum numbers has previously been explored by Nakagawa and Morino who used the contact transformation method.[26] The l-type doubling in linear molecules arises essentially from the Coriolis Hamiltonian term which connects

Table 6. Unperturbed and perturbed energy levels and rotational constants (in cm^{-1})

Level	E_v^0	E_v	$B_v^0\times10^4$	$B_v\times10^4$
(i) $^{12}C^{32}S_2$				
1 0 0	664.27	657.99	1083.91	1084.50
0 2^0 0	795.50	801.78	1090.37	1089.78
1 0 1	2192.03	2185.52	1076.78	1077.40
0 2^0 1	2318.02	2324.52	1083.24	1082.62
2 0 1	2846.64	2833.23	1074.60	1075.98
1 2^0 1	2969.65	2961.73	1081.07	1081.53
0 4^0 1	3108.64	3129.97	1087.53	1085.70
1 1^1 1	2579.15	2567.46	1078.92	1079.97
0 3^1 1	2711.64	2723.32	1085.39	1084.34
(ii) $^{13}C^{32}S_2$				
1 0 0	664.47	657.21	1083.95	1084.66
0 2^0 0	769.19	776.46	1090.22	1089.51
1 0 1	2142.44	2134.91	1077.09	1077.84
0 2^0 1	2242.58	2250.12	1083.36	1082.61
2 0 1	2797.50	2781.59	1074.91	1076.63
1 2^0 1	2894.84	2886.75	1081.18	1081.54
0 4^0 1	3007.25	3031.24	1087.46	1085.38

TABLE 7. OBSERVED AND CALCULATED l-TYPE DOUBLING CONSTANTS (in 10^{-5} cm^{-1})

$^{12}C^{32}S_2$				$^{13}C^{32}S_2$			
Level	q_{obsd}[a]	q_{calcd}		Level	q_{obsd}[b]	q_{calcd}	
0 1^1 0	7.82	7.65		0 1^1 0	8.52	7.92	
1 1^1 0	9.05	8.63		0 1^1 1	8.68	7.84	
0 3^1 1	14.65	14.31		1 1^1 1	9.75	9.00	
1 3^1 1	15.78	14.96		0 3^1 1	15.19	14.53	
				2 1^1 1	11.60	10.18	

a) Ref. 4. b) Ref. 5.

with the $l=\pm 1$ levels through a common $l=0$ level. The effect of vibrational anharmonicities on l-type doubling constants may be evaluated if the perturbed vibratioanl wave functions are known. This is most easily done by solving the vibrational Hamiltonian matrix numerically. The eigenvectors indicate the mixings of the basis harmonic wave functions through the vibrational anharmonicity.[1] The l-type doubling constant for a given π-state may then be calculated numerically from the perturbed wave functions.[27] In Table 7, the l-type doubling constants calculated from the converged set (i) are listed and compared with the experimental values. In most cases the calculated constants are slightly smaller than the observed, however, differences are small and they show a remarkably similar trend in their dependence on vibrational quantum numbers as well as on isotopic substitutions.

Concluding Remarks. We believe that the general quartic force constants and the third-order parameters determined in the present work are as good as the corresponding constants in the CO_2 molecule.[15] In order to secure their reliability, however, more experimental works should be needed especially on low-lying vibrational levels of the ^{13}C- and ^{34}S-species. The measurements along this line is being planned.

The present author wishes to express his gratitude to Dr. G. Blanquet who has provided the results of the measurements for $^{13}C^{32}S_2$ prior to publication.

References

1) I. Suzuki, This Bulletin, **44**, 3277 (1971).
2) D. F. Smith, Jr. and J. Overend, *J. Chem. Phys.*, **54**, 3632 (1971).
3) J. Giguere, V. K. Wang, J. Overend, and A. Cabana, *Spectrochim. Acta*, **29A**, 1197 (1973).
4) A. G. Maki, *J. Mol. Spectrosc.*, **47**, 217 (1973).
5) G. Blanquet and C. P. Courtoy, *ibid.*, **54**, 350 (1975).
6) R. G. Parr and J. E. Brown, *J. Chem. Phys.*, **49**, 4849 (1968), D. F. Smith, Jr. and J. Overend, *ibid.*, **55**, 1157 (1971), A. B. Anderson, *ibid.*, **56**, 4228; **57**, 4143 (1972); *J. Mol. Spectrosc.*, **44**, 411 (1972).
7) D. Agar, E. K. Plyler, and E. D. Tidwell, *J. Res. Nat. Bur. Standards*, **66A**, 259 (1962).
8) G. Blanquet and C. P. Courtoy, *Ann. Soc. Sci. Bruxelles*, **84**, 293 (1970).
9) G. Blanquet, J. Warland, and C. P. Courtoy, *ibid.*, **87**, 387 (1973).
10) G. Blanquet and C. P. Courtoy, *ibid.*, **88**, 223 (1974).
11) G. Blanquet, J. Warland, and C. P. Courtoy, *ibid.*, **88**, 87 (1974).
12) A. H. Guenther, *J. Chem. Phys.*, **31**, 1095 (1959).
13) B. P. Stoicheff, *Can. J. Phys.*, **36**, 218 (1958).
14) M. A. Pariseau, I. Suzuki, and J. Overend, *J. Chem. Phys.*, **42**, 2335 (1965).
15) I. Suzuki, *J. Mol. Spectrosc.*, **25**, 479 (1968).
16) More precisely $R_2^2=R_{2x}^2+R_{2y}^2$. R_{2x} and R_{2y} are two independent bending coordinates in the xz and yz planes, respectively, the z-axis being taken as the molecular axis.
17) S. Maes, *Cahier. Phys.*, **14**, 125 (1960); *J. Mol. Spectrosc.*, **9**, 204 (1962).
18) I. Suzuki, *ibid.*, **32**, 54 (1969).
19) The isotope effect from the ^{34}S-species is ignored in the present treatment.
20) K. Kuchitsu and Y. Morino, This Bulletin, **38**, 805 (1965).
21) Y. Morino and T. Nakagawa, *J. Mol. Spectrosc.*, **26**, 497 (1968).
22) P. M. Morse, *Phys. Rev.*, **34**, 37 (1929).
23) A. G. Gaydon, "Dissociation Energies and Spectra of Diatomic Molecules," 3rd Ed., Chapman and Hall Ltd., London (1968).
24) G. Blanquet and C. P. Courtoy, *Ann. Soc. Sci. Bruxelles*, **88**, 233 (1974).
25) G. Amat and M. Pimbert, *J. Mol. Spectrosc.*, **16**, 278 (1965).
26) T. Nakagawa and Y. Morino, *J. Chem. Phys.*, **44**, 841 (1966); *J. Mol. Spectrosc.*, **31**, **208** (1969).
27) I. Suzuki, to be published.

Molecular Structure of Trimethylene Sulfide as Studied by Gas Electron Diffraction with Joint Use of Rotational Constants

Ken-ichi KARAKIDA and Kozo KUCHITSU

Department of Chemistry, Faculty of Science, The University of Tokyo, Bunkyo-ku, Tokyo 113

(Received March 5, 1975)

The molecular structure of trimethylene sulfide (thietane) has been determined by an analysis of electron diffraction intensities combined with the rotational constants determined by microwave spectroscopy by Harris *et al.*: r_g(C–S) = 1.847±0.002 Å, r_g(C–C) = 1.549±0.003Å, r_g(C_α–H) = 1.09±0.02 Å, r_g(C_β–H) = 1.12±0.04 Å, ∠C–S–C(r_{av}) = 76.8±0.3°, ∠H–C_α–H(r_{av}) = 112±4°, ∠H–C_β–H(r_{av}) = 114±5° and the dihedral angle, ∠C_2SC_4–$C_2C_3C_4$(r_{av}) = 26±2°. The uncertainties represent estimated limits of error. The definitions of the geometrical parameters have the usual physical significance except that the normal coordinate representing the large-amplitude ring-puckering motion is extrapolated to its equilibrium position. The conventional formula used in the joint analysis has been modified to account for the large-amplitude vibration.

The ring-puckering motion of trimethylene sulfide (Fig. 1) has been studied in detail by spectroscopy[1,2] by Harris *et al.*, and the potential function is found to have a double minimum with a barrier of 274 cm^{-1} at the planar configuration. The bond distances and angles in this molecule were not determined with high accuracy, however. The present study was undertaken to determine the molecular structure by electron diffraction for a quantitative comparison with those of related molecules.

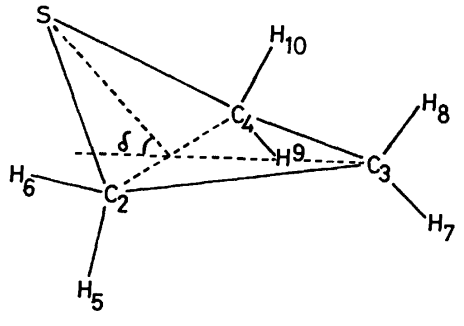

Fig. 1. Trimethylene sulfide.

The C–C, C–S and the weighted average of C–H distances were determined uniquely from electron diffraction intensities[3]. However, since the two ring diagonal distances, r(C···C) and r(C···S), are closely spaced and constitute a single peak in the radial distribution curve, it is difficult to resolve the distances with high accuracy from the electron diffraction data alone. In addition, the diffraction data has strong correlation between the hydrogen parameters in the α and β positions. Spectroscopic rotational constants A and B provide information on the r(C···C) and r(C···S) distances, respectively, and on the hydrogen parameters. Therefore, the diffraction intensities and the rotational constants have been used jointly in the present study[4]. The conventional formula used in the analysis has been modified to account for the large-amplitude ring-puckering vibration.

Experimental

The sample (bp 94 °C/752 Torr) used for the short camera length was prepared[5] in the laboratory of Professor I. Tabushi at Kyoto University. The infrared, NMR and mass spectra, and gas chromatographic analysis indicated that the sample was free from any significant impurities. The sample used for the long camera length was purchased from Tokyo Kasei Co., Ltd. (purity over 96%). Since the major impurities of the sample were solid polymers with negligible vapor pressures, it was used without further purification.

Electron diffraction photographs were taken[6] with an r^3-sector at the camera lengths of 107.73±0.02 and 243.29±0.02 mm. The electron wavelength (about 0.06 Å) was calibrated with reference to the r_a(C=O) distance of carbon dioxide (1.164_6 Å) measured under the same experimental conditions. The sample gas was maintained in thermal equilibrium with its liquid phase at room temperature. The pressure of the sample gas was about 30 Torr, and the exposure times were about 100 and 60 s for the short and long camera lengths, respectively. Other experimental details are described elsewhere.[6,7] The optical densities (0.17—0.62) were assumed to be proportional to electron intensities. The observed molecular intensity covering the range of s = 3.5—37.7 $Å^{-1}$ was used in the analysis. The data taken with the short and long camera lengths[8] were linked at s = 9.4 $Å^{-1}$. The elastic and inelastic scattering factors and the phase shifts were taken from the tables[9] prepared by

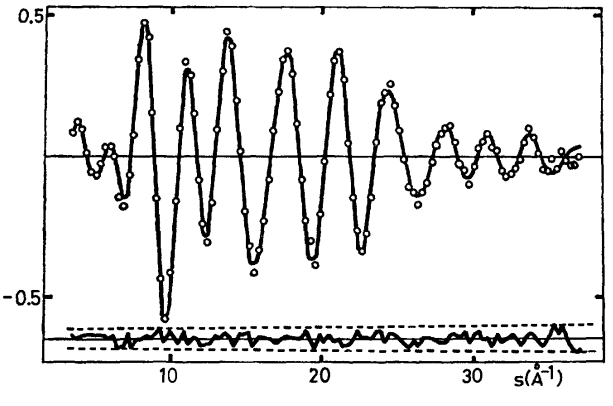

Fig. 2. Experimental and theoretical molecular intensities for trimethylene sulfide.
Typical observed $sM(s)$ values are shown in open circles, and the best-fit theoretical is shown in the solid curve. The indices of resolution are 0.84±0.03 and 0.96±0.03 for the long and short camera regions, respectively. The lower solid and broken curves represent the residuals and the error limits in the $sM(s)$ to a fractional error of 1×10^{-3} of the original photocurrent, respectively.

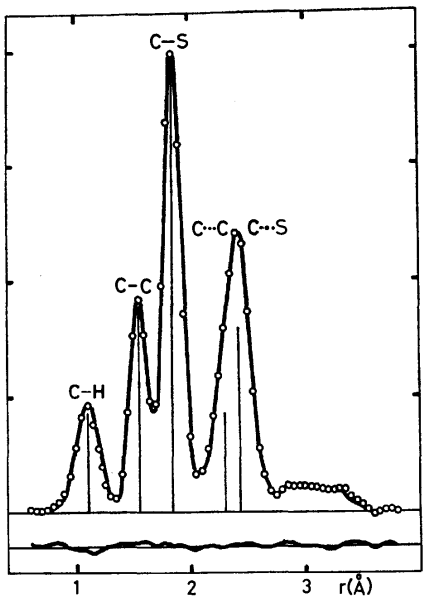

Fig. 3. Experimental (open circles) and theoretical radial distribution curves for trimethylene sulfide. The lower curve represents residuals. Vertical bars correspond to principal internuclear distances. A damping factor, $\exp(-0.0019 s^2)$, was used.

Schäfer *et al.* The molecular intensity is illustrated in Fig. 2, and the corresponding radial distribution curve is given in Fig. 3. Most of the calculations were carried out on a HITAC 8800/8700 operating system in the Computer Center of the University of Tokyo.

Analysis

Analysis of Diffraction Intensities. The C–S, C–C and the weighted average C–H distances and their mean amplitudes were determined without assumptions or constraints.[3]

In order to get further information on the rest of the structural parameters, the following assumptions were made in the analysis:

a) The average positions of the hydrogen atoms are such that the H–C–H plane is perpendicular to the plane defined by one carbon and two adjacent ring atoms, and the angle bisectors are colinear.

b) The C_α–H and C_β–H distances are equal.

c) The H–C_α–H and H–C_β–H angles in the r_α^0 structure are equal to the corresponding angles in trimethylene oxide,[10] 110.3° and 110.7°, respectively.

Since this molecule has a large-amplitude motion, the conventional formulas based on infinitesimal vibrational amplitudes have to be modified to calculate the mean amplitudes and vibrational corrections. The zero-point average structure in the present study is defined as the r_α^0 structure[11] where the normal coordinate representing the large-amplitude ring-puckering motion (Q) takes its equilibrium value (Q_e). Mean amplitudes and vibrational corrections for bonded pairs are calculated from the conventional formulas[11] but contributions from the large-amplitude vibration are not included.

The mean amplitude for a nonbonded pair is calculated by[12]

$$l^2 = (\langle r_e(Q)^2\rangle_T - \langle r_e(Q)\rangle_T^2) + \langle \Delta z^2\rangle'_T \quad (1)$$

where T denotes thermal average at T kelvin and the prime outside the bracket denotes the sum of contributions from all the small-amplitude modes, and r_e is an instantaneous distance for the nonbonded pair when all the small-amplitude coordinates take their equilibrium positions. The r_g distance for a nonbonded pair is defined as

$$r_g = \langle r_e(Q)\rangle_T + \langle \Delta r\rangle'_T \quad (2)$$

which can be rewritten by use of a diatomic approximation[13,14] as

$$r_g \cong \langle r_e(Q)\rangle_T + \frac{3}{2}a_3\langle \Delta z^2\rangle'_T \quad (3)$$

The r_g distance is assumed to satisfy the equation,

$$r_g = r_a + \frac{l^2}{r_a} \quad (4)$$

where r_a is directly derived from the diffraction intensities. Since the radial distribution of the principal nonbonded pairs in trimethylene sulfide are practically Gaussian as shown in Fig. 3, Eq. (4) appears to be a sufficient approximation. The r_α distance for a nonbonded pair is defined as

$$r_\alpha = r_e(Q_e) + \langle \Delta z\rangle'_T \quad (5)$$

where Q_e is an equilibrium value of the large-amplitude coordinate. Equation (5) can be rewritten by use of a diatomic approximation as

$$r_\alpha \cong r_e(Q_e) + \frac{3}{2}a_3\langle \Delta z^2\rangle'_T - \frac{\langle \Delta x^2\rangle'_T + \langle \Delta y^2\rangle'_T}{2r_e(Q_e)} \quad (6)$$

The r_α parameters can be extrapolated to zero kelvin (r_α^0) by using a diatomic approximation for the bonded parameters and neglecting temperature dependence of the angle parameters.[11] From Eqs. (3), (4) and (6), the vibrational correction, $d = r_a - r_\alpha$, is given by

$$d = [\langle r_e(Q)\rangle_T - r_e(Q_e)] - \frac{l^2}{r_a} + \frac{\langle \Delta x^2\rangle'_T + \langle \Delta y^2\rangle'_T}{2r_e(Q_e)} \quad (7)$$

Since neither the force constants nor the vibrational frequencies for trimethylene sulfide were available except for the puckering motion, the contributions from the small-amplitude modes to the terms in Eqs. (1) and (7) were calculated from the Urey-Bradley force constants listed in Table 1 transferred from ethylmethyl sulfide,[15] diethyl sulfide[15] and thietanone-3.[16] The contributions from the large-amplitude mode were calculated from the following molecular model: The ring-puckering motion causes a change in the dihedral angle, $\delta = \angle C_2SC_4$–$C_2C_3C_4$, and a deformation of $\alpha = \angle$C–S–C angle, but retains the C–S, C–C, C–H distances and H–C–H angles constant. The dependence of α on δ is assumed to satisfy the following relation derived from the microwave study:[1]

$$\rho = [r(C\cdots S) - r^0(C\cdots S)]/[r(C\cdots C) - r^0(C\cdots C)] = 0.54 \quad (8)$$

where r^0 is a nonbonded distance at the planar configuration ($\delta = 0°$). The potential function for the puckering motion is taken from Ref. 1.

The mean amplitudes and vibrational corrections for bonded pairs were calculated from the force constants listed in Table 1, and their uncertainties were

Table 1. Force constants for trimethylene sulfide[a]

K(C-S)	1.75	H(C-S-C)	0.24	F(C-S-C)	0.21
K(C-C)	2.10	H(S-C-C)	0.07	F(S-C-C)	0.70
K(C-H)	4.25	H(C-C-C)	0.32	F(C-C-C)	0.21
Y(C-S)	0.02	H(C-C-H)	0.21	F(C-C-H)	0.54
Y(C-C)	0.02	H(S-C-H)	0.17	F(S-C-H)	0.39
		H(H-C-H)	0.35	F(H-C-H)	0.20

a) Estimated force constants taken from ethylmetyl sulfide,[15] diethyl sulfide[15] and thietanone-3.[16] The torsional force constants (Y) are in mdyn·Å and the others are in mdyn/Å units.

Table 2. Mean amplitudes and vibrational corrections (I) (Å)

	l_{obsd}[a]	l_{calcd}[b]	$r_a - r_\alpha$[c]
C-S	0.055±0.005	0.054±0.003	−0.0010±0.0010
C-C	0.052±0.005	0.053±0.003	−0.0005±0.0001
C-H	0.080±0.008	0.078±0.004	0.0070±0.0007
C···S	0.051±0.008	0.057±0.006	0.0072±0.0025
C···C	0.057±0.015	0.068±0.007	0.0126±0.0045

a) Observed mean amplitudes derived from diffraction intensities. b) Mean amplitudes calculated from the force constants listed in Table 1 and the molecular model described in the text. The uncertainties were estimated from those in the force constants and the model. c) Vibrational corrections calculated from the force constants and the model described in the text. The uncertainties for the nonbonded pairs mainly originate from those in the model.

estimated to be ±10%. The mean amplitudes and vibrational corrections for nonbonded pairs consisted of the contributions from the small-amplitude and large-amplitude modes. The former contributions were calculated from the force constants and were estimated to have uncertainties of ±20%, while the latter contributions calculated classically and numerically from the model were estimated to have uncertainties of ±30%. The quoted errors for l_{calcd} and $r_a - r_\alpha$ in Table 2 represent these uncertainties. The asymmetry parameters[12] κ for the C–H, C–C and C–S bonds were estimated to be 1.2×10^{-5}, 2.7×10^{-6} and 2.7×10^{-6} Å^3, respectively, from the anharmonicity parameters[14] a_3 for CH, CC and CS assumed to be 1.98, 2.13 and 1.95 Å^{-1}, respectively. The κ parameters for nonbonded pairs were ignored since the observed radial distribution peaks of the nonbonded pairs were symmetric within estimated experimental error.

A least squares analysis was carried out with an empirical diagonal weight matrix.[17] The C–H, C–C and C–S distances, ∠C–S–C and dihedral angles, mean amplitudes for C–H, C–C, C–S, C···C and C···S pairs and the indices of resolution for the long and short camera regions were taken as independent variable parameters. The mean amplitudes fixed in the analysis are shown in Table 3 with vibrational corrections for the corresponding pairs. The r_α^0 parameters determined in the analysis are shown in Table 4, and the observed mean amplitudes are compared in Table 2 with the calculated values.

Systematic errors originating from slight modifications in assumptions b) and c) above had negligible effects on the structural parameters. The uncertainty in the vibrational corrections for the C···C pair caused a systematic error in the C–S–C angle, ±0.1°, and those for the other atomic pairs were unimportant compared to the random errors in the structural parameters. The uncertainty in the r_α to r_α^0 conversion was also negligible. The nonbonded mean amplitudes fixed at the calculated values (Table 3) in the analysis were estimated to have uncertainties of ±20% as mean values. Changing the value by that fraction caused a significant systematic variation only in the dihedral angle, ±2°. The fixed κ parameters caused no significant systematic errors in the distances. The error limits quoted in Table 4 include 2.5 times the

Table 3. Mean amplitudes and vibrational corrections (II)[a] (Å)

Pair	l_{calcd}	$r_a - r_\alpha$	Pair	l_{calcd}	$r_a - r_\alpha$
C_2-H_7	0.104	0.015	H_6-H_8	0.169	0.016
C_3-H_5	0.104	0.012	H_5-H_7	0.170	0.016
C_2-H_9	0.157	−0.003	H_6-H_7	0.150	0.019
C_2-H_{10}	0.105	0.002	H_5-H_8	0.134	0.017
S-H_5	0.110	0.006	H_5-H_9	0.289	−0.020
S-H_8	0.165	−0.003	H_5-H_{10}	0.151	0.001
S-H_7	0.103	0.004	H_6-H_{10}	0.183	−0.003

a) Mean amplitudes listed in this table were fixed in the least squares analysis. Uncertainties were estimated to be ±20%. See footnotes b) and c) of Table 2.

Table 4. Average structures of trimethylene sulfide[a]

	r_α^0 [b]	r_{av}[c]	r_g[d]
C-S	1.846±0.002	1.846±0.002	1.847±0.002
C-C	1.547±0.003	1.548±0.003	1.549±0.003
C-H_{av}[e]	1.085±0.006	1.086±0.006	1.100±0.006
C_α-H	—	1.08 ±0.02	1.09 ±0.02
C_β-H	—	1.11 ±0.04	1.12 ±0.04
∠C-S-C	77.0±0.5	76.8±0.3	—
δ[f]	26 ±4	26 ±2	—
∠H-C-H_{av}[e]	—	112 ±2	—
∠H-C_α-H	(110.3)[g]	112 ±4	—
∠H-C_β-H	(110.7)[g]	114 ±5	—
C···S	2.421±0.010	2.421±0.003	2.430±0.003
C···C	2.286±0.015	2.294±0.006	2.309±0.006
∠C-C-S	90.6±0.5	90.6±0.3	—
∠C-C-C	95.3±0.8	95.6±0.4	—

a) Distances in Å units, angles in degrees. b) Derived from diffraction intensities. Uncertainties are estimated limits of error. c) Derived from a joint analysis of diffraction intensities and rotational constants. Uncertainties are estimated limits of error. See text for the definition. The final structural parameters for the angles. d) Derived from the r_{av} structure. The final structural parameters for internuclear distances. e) Weighted average value. f) Dihedral angle, ∠C_2SC_4-$C_2C_3C_4$. g) Assumed value.

standard deviations plus the systematic errors estimated above.

In the next step the rotational constants determined[1] in the microwave study were combined[4] with the diffraction intensities in order to obtain more accurate angle parameters and hydrogen parameters for the α and β positions.

Joint Analysis of Diffraction Intensities and Rotational Constants. The rotational constants A, B and C for the ground and excited states (up to $v=4$) have been determined by microwave spectroscopy[1] by Harris *et al.* They expressed the rotational constants as a power series in the coordinate of the large-amplitude mode,

$$A = 10013.44 + 17.52Q^2 - 0.088Q^4 \quad (9a)$$

$$B = 6670.78 + 5.01Q^2 - 0.76Q^4 \quad (9b)$$

$$C = 4335.74 + 19.15Q^2 - 0.087Q^4 \quad (9c)$$

This procedure is based on the fact that the vibration-rotation interactions in this molecule are given simply by the quantum mechanical averaging of the rotational constant over the puckering motion, and Coriolis interactions are relatively unimportant.[1,2] The potential function for the vibration has been determined[1] by numerically fitting the experimentally determined rotational constants to the power series without assumptions on the details of the vibrational motion,

$$V(Q) = 7.0207Q^4 - 87.7581Q^2 \text{ cm}^{-1} \quad (10)$$

which has a minimum at $Q=Q_e=2.500$ (amu)$^{1/2}$ Å. Substitution of Q by Q_e in Eq. (9) leads to the rotational constants for the ground vibrational state (A'_0, B'_0 and C'_0) where the normal coordinate representing the large-amplitude motion takes its equilibrium value. A similar treatment has been applied to the rotational constants of trimethylene oxide by Chan *et al.*[10] in order to obtain a set of structural parameters corresponding to the equilibrium or nonvibrating values for the large-amplitude mode. The rotational constants A'_0, B'_0 and C'_0 were conventionally transformed into the average rotational constants[18] A_z, B_z and C_z by subtracting the vibration-rotation interactions for all the small-amplitude modes.

The uncertainties in A_z, B_z and C_z were estimated from the following sources: a) Uncertainties in the corrections for the large-amplitude mode were estimated from the deviations[1] of the observed rotational constants from the values calculated by use of Eq. (9) to be ±1, ±3 and ±1 MHz for A_z, B_z and C_z, respectively. b) Uncertainties in the corrections for all the small-amplitude modes were estimated to be $\pm10\%$ of the corrections, or ±4, ±2 and ±0.5 MHz for A_z, B_z and C_z, respectively. The A_z, B_z and C_z are compared in Table 5 with the rotational constants A^0_α, B^0_α and C^0_α calculated from the r^0_α parameters determined in the foregoing electron diffraction analy-

TABLE 5. ROTATIONAL CONSTANTS FOR TRIMETHYLENE SULFIDE[a] (MHz)

	B[b]	B_z[c]	B^0_α[d]	B_{av}[e]
A	10110.15	10096 (4)	10079 (50)	10096 (4)
B	6673.90	6660 (4)	6667 (30)	6660 (4)
C	4441.04	4450 (1)	4437 (30)	4450 (1)

a) Uncertainties attached to the last significant digits are given in parentheses. b) Effective rotational constants for the ground vibrational state determined by microwave spectroscopy. Ref. 1. c) Zero-point average rotational constants calculated from the effective rotational constants for the ground and excited vibrational states by subtracting the vibration-rotation interactions for the large-amplitude mode and the small-amplitude modes. d) Rotational constants calculated from r^0_α parameters listed in Table 4 determined in the analysis of diffraction intensities. Uncertainties are propagated from those in the r^0_α parameters. e) Best-fit rotational constants corresponding to the r_{av} structure listed in Table 4, derived from a combined analysis of electron diffraction and microwave data. Uncertainties represent 2.5 times the estimated standard deviations.

TABLE 6. ERROR MATRIX FOR TRIMETHYLENE SULFIDE[a]

	k_1	k_2	x_1	x_2	x_3	x_4	x_5	x_6	x_7	x_8	l_1	l_2	l_3	l_4
k_1	218													
k_2	55	181												
x_1	15	−7	6											
x_2	−27	15	−4	11										
x_3	27	−58	−6	−9	55									
x_4	63	74	−5	−12	−68	111								
x_5	17	−21	−3	10	16	17	21							
x_6	−86	14	−4	−10	−36	−69	−46	124						
x_7	73	−92	13	27	78	−62	65	−142	215					
x_8	125	135	15	9	−87	155	28	−149	−36	314				
l_1	12	39	−2	4	−12	15	−4	4	−19	27	10			
l_2	13	38	−2	3	−12	15	−5	5	−21	28	8	14		
l_3	27	44	0	7	−18	29	15	−26	39	−7	9	9	31	
l_4	25	50	−4	7	−24	36	17	−7	40	−60	11	10	39	62

a) k_1, k_2=indices of resolution for the long and short camera regions, respectively, $x_1=r$(C-S), $x_2=r$(C-C), $x_3=r(C_\alpha\text{-H})$, $x_4=r(C_\beta\text{-H})$, $x_5=\angle$C-S-C, $x_6=\delta$, $x_7=\angle H\text{-}C_\alpha\text{-H}$, $x_8=\angle H\text{-}C_\beta\text{-H}$, $l_1=l$(C-S), $l_2=l$(C-C), $l_3=l$(C···S) and $l_4=l$(C···C). Units ($\times10^{-4}$) for the distances and mean amplitudes are Å, those for the angles are rad, and those for the indices are dimensionless.

sis. The diffraction and spectroscopic constants agree within the experimental error of the former.

The rotational constants A_z, B_z and C_z were combined with the diffraction intensities into a joint least squares analysis, where the assumptions b) and c) made in the analysis of diffraction intensities were excluded. The mean amplitudes for C_α–H and C_β–H pairs were fixed at the calculated values. The relative weight for the rotational constants were adjusted empirically so that 2.5 times the standard errors in the rotational constants were nearly equal to their uncertainties. The weights used in the analysis were 1.5×10^6, 1.5×10^6 and 2×10^7 for A_z, B_z and C_z, respectively, where a unit weight was assigned to the molecular intensities from $s=6.3$ to 26.7 Å^{-1} taken at $\pi/10$ intervals. A typical error matrix is shown in Table 6.

The r_{a_v} structure listed in Table 4 agrees with the r_α^0 structure derived from the electron diffraction data alone except that the angle parameters are appreciably more accurate. The final r_g structure derived from the r_{a_v} structure is shown in Table 4. The structural parameters of this molecule determined earlier by the visual method of gas electron diffraction[19–21] are in good agreement with the present results to within their uncertainties: r(C–S)$=1.85_1\pm$ 0.02 Å, r(C–C)$=1.54_9\pm0.03$ Å, ∠C–S–C$=78\pm1°$ and ∠C–C–C$=97\pm5°$.

The dihedral angle determined in the present study is nearly equal to that estimated by Harris *et al.*,[1,2] 28°. The skeletal structure of trimethylene sulfide was compared[3] with those of analogous molecules. Sulfur-carbon bond lengths in 4-membered rings are clearly longer than in other environments, a trend also observed among carbon-carbon bond lengths.[22]

The authors are indebted to Professor Iwao Tabushi, Dr. Yoshinao Tamaru and Mrs. Kazumi Mizuno for preparation of the sample and to Professor Robert K. Bohn for helpful comments.

References

1) D. O. Harris, H. W. Harrington, A. C. Luntz, and W. D. Gwinn, *J. Chem. Phys.*, **44**, 3467 (1966); see also L. H. Scharpen, *ibid.*, **48**, 3552 (1968). The authors wish to thank Professr Harris for his comments on the microwave analysis of his group.

2) W. D. Gwinn and A. Luntz, *Trans. Amer. Cryst. Assoc.*, **2**, 90 (1966).

3) K. Karakida, K. Kuchitsu, and R. K. Bohn, *Chem. Lett.*, **1974**, 159.

4) K. Kuchitsu, T. Fukuyama, and Y. Morino, *J. Mol. Struct.*, **1**, 463 (1967).

5) G. M. Bennett and A. L. Hock, *J. Chem. Soc.*, **1927**, 2496.

6) Y. Murata, K. Kuchitsu, and M. Kimura, *Jap. J. Appl. Phys.*, **9**, 591 (1970).

7) M. Tanimoto, K. Kuchitsu, and Y. Morino, This Bulletin, **43**, 2766 (1970).

8) Numerical experimental data of the leveled total intensity have been deposited with the Chemical Society of Japan (Document No. 7512).

9) L. Schäfer, A. C. Yates, and R. A. Bonham, *J. Chem. Phys.*, **55**, 3055 (1971).

10) S. I. Chan, J. Zinn, and W. D. Gwinn, *ibid.*, **34**, 1319 (1961). The structure for trimethylene oxide was deduced in this literature from the rotational constants extrapolated to a hypothetical planar state.

11) K. Kuchitsu and S. J. Cyvin, "Molecular Structures and Vibrations," ed. by S. J. Cyvin, Elsevier, Amsterdam (1972), Chapter 12.

12) K. Kuchitsu, This Bulletin, **40**, 498 (1967).

13) L. S. Bartell, *J. Chem. Phys.*, **23**, 1219 (1955).

14) K. Kuchitsu and Y. Morino, This Bulletin, **38**, 805 (1965).

15) M. Ohsaku, Y. Shiro, and H. Murata, *ibid.*, **46**, 1399 (1973).

16) C. S. Blackwell, Thesis, Massachusetts Institute of Technology (1971).

17) Y. Morino, K. Kuchitsu, and Y. Murata, *Acta Crystallogr.*, **18**, 549 (1965).

18) M. Toyama, T. Oka, and Y. Morino, *J. Mol. Spectrosc.*, **13**, 193 (1964).

19) E. Goldish, Thesis, California Institute of Technology (1956).

20) E. Goldish, *J. Chem. Educ.*, **36**, 408 (1959).

21) Y. Etienne, R. Soulas, and H. Lumbroso, "Heterocyclic Compounds with Three- and Four-Membered Rings," Part II, A. Weissberger, Ed., Interscience, Chapter 5 (1964).

22) K. Kuchitsu, "Gas Electron Diffraction, HTP International Review of Science, A Biennial Series, Physical Chemistry," Vol. 2, ed. by G. Allen, Medical and Technical Publishers, Oxford (1972), Chap. 6.

The Crystal and Molecular Structure of *trans*-Bis(trimethylphosphine)propynyl-1-(4′-dicyanomethylene-cyclohexa-2′,5′-dien-1-yliden)-3,3-dicyano-2-methyl-prop-2-en-1-ylplatinum, a Reaction Product of *trans*-Bis(trimethylphosphine)bis-(propynyl)platinum and 7,7,8,8-Tetracyanoquinodimethane

Ken-ichi ONUMA, Yasushi KAI, Noritake YASUOKA, and Nobutami KASAI

Department of Applied Chemistry, Faculty of Engineering, Osaka University, Yamadakami, Suita, Osaka 565

(Received March 17, 1975)

The molecular structure of the title complex has been determined from three-dimensional X-ray diffraction data. The crystal belongs to the monoclinic system, space group $P2_1/c$, $a=14.934(2)$, $b=8.997(1)$, $c=20.221(3)$Å, $\beta=97.44(2)°$, $Z=4$. The molecular structure showed that the tetracyanoquinodimethane (TCNQ) molecule has reacted with one of the propynyl groups of *trans*-$\{(PMe_3)_2Pt(C{\equiv}CMe)_2\}$: part of the TCNQ is bonded to the α-carbon atom and the other part to the β-carbon of the propynyl ligand. The platinum atom has a square-planar geometry; Pt–P=2.302(5) and 2.290(5), Pt–C(C≡CMe$_3$)=2.009(15) and Pt–C(reacted)=2.057(15) Å.

Recently, it has been found that *trans*-bis(tertiary-phosphine)dialkynyl complexes of transition metals (Ni, Pd or Pt) react with 7,7,8,8-tetracyanoquinodimethane (TCNQ) to form stable complexes.[1] Spectroscopic studies suggested that these might be charge-transfer complexes although no other π-acceptors such as tetracyanoethylene, chloranil, bromanil or pyromellitic dianhydride show the charge-transfer interaction with the transition metal complexes mentioned above. This peculiar property of the TCNQ was explained by the possible overlapping of π system of the TCNQ and ethynyl ligands. The structure shown below has been proposed.[1]

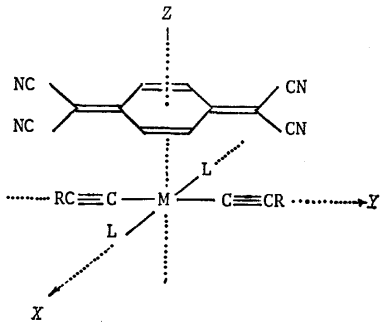

(1) M=Pt, L=PMe$_3$, R=H,
(2) M=Pt, L=PMe$_3$, R=Me,
(3) M=Pt, L=PEt$_3$, R=Me.

In order to verify this hypothesis, an X-ray crystallographic study of [*trans*-$\{(PMe_3)_2Pt(C{\equiv}CMe)_2\}\cdot$(TCNQ)] (2) has been carried out. However, as the crystal suffered from an X-ray damage, the standard deviations for all variable parameters were high and consequently the structure is not well-defined.

Experimental

Crystal Data. $C_{21}H_{28}N_4P_2Pt$, *F.W.*=629.56, monoclinic, $a=14.934(2)$, $b=8.997(1)$, $c=20.221(3)$ Å, $\beta=97.44(2)°$, $U=2694.0(7)$ Å^3, $D_m=1.56$ g·cm^{-3} (by flotation), $Z=4$, $D_c=1.55$ g·cm^{-3}, $F(000)=1232$, Space group $P2_1/c$, Mo$K\alpha$ radiation ($\lambda=0.71069$ Å), μ(Mo)=56.14 cm^{-1}.

The crystals are purple-black and long prismatic. Initially, a freshly prepared crystal (approximate dimensions 0.17×0.19×0.17 mm) was used. Accurate cell parameters were obtained by least-squares refinement of 22 high angle reflections. Intensity data were collected on a Rigaku automated, four-circle diffractometer using the θ-2θ scan technique[2] with Zr-filtered Mo$K\alpha$ radiation.

A total of 2666 (2332 non-zero) independent reflections was collected at room temperature. Intensities of three standard reflections, 060, 500, and 006, were measured every 50 reflections, and these were used to detect any crystal decay or mispositioning. The magnitudes for the structure factors of these reflections decreased at an approximately linear rate with time. At the end of the data collection ($(\sin\theta)/\lambda \leqq 0.458$) they were 85.2% of the original values and a linear decay correction was applied. Another set of 1011 (887 non-zero) higher order reflections ($0.457 \leqq (\sin\theta)/\lambda \leqq 0.527$) was collected with a second crystal (*ca.* 0.23×0.17×0.23 mm) with standard reflections decreasing by 2.7%. A linear decay correction was also applied. All these data were placed on the same scale as the first set by collecting common 1117 non-zero reflections ($(\sin\theta)/\lambda \leqq 0.350$). The interset scale factor was 1.157. No absorption correction was applied to either set of data.

Structure Solution and Refinement

The structure was solved and refined using the intensity data from the first crystal. Three-dimensional Patterson synthesis revealed the positions of platinum and phosphorous atoms. All the nonhydrogen atoms were found from subsequent Fourier and difference electron density syntheses. Block-diagonal least-aquares refinement of positional and thermal parameters was carried out using HBLS-V program[3] in three steps: three cycles of isotropic, three cycles of partial anisotropic (Pt and P), and four cycles of anisotropic parameters for nonhydrogen atoms. The second data set was then added and the refinement continued. After the final three cycles, the R was 0.060 (R_2=0.071) for non-zero reflections.

The positional and thermal parameters are given in Tables 1 and 2, respectively. The observed and calculated structure factors are listed in Table 3.[4] Throughout the refinement, neutral atomic scattering factors were taken from those given by Hanson and co-workers.[5]

TABLE 1. FRACTIONAL COORDINATES OF ATOMS ALONG WITH THEIR ESTIMATED STANDARD DEVIATIONS IN PARENTHESES

Atom	x	y	z	Atom	x	y	z
Pt	0.20891 (4)	0.30728 (6)	0.26981 (3)	C (41)	0.2863 (10)	0.3007 (17)	0.3617 (7)
P (1)	0.2919 (3)	0.1230 (5)	0.2274 (2)	C (42)	0.3560 (10)	0.4210 (18)	0.3691 (7)
P (2)	0.1126 (3)	0.4843 (5)	0.3012 (2)	C (43)	0.4164 (12)	0.4480 (23)	0.3155 (9)
N (1)	0.3833 (14)	−0.1592 (24)	0.6615 (10)	C (44)	0.2875 (9)	0.1929 (17)	0.4084 (7)
N (2)	0.1060 (12)	−0.2278 (25)	0.5781 (11)	C (45)	0.3577 (10)	0.1665 (17)	0.4638 (8)
N (3)	0.4589 (12)	0.7477 (23)	0.4296 (10)	C (46)	0.3540 (11)	0.0664 (17)	0.5109 (8)
N (4)	0.2620 (16)	0.4961 (23)	0.5159 (8)	C (47)	0.2725 (12)	−0.0172 (19)	0.5113 (7)
C (11)	0.3788 (12)	0.0232 (21)	0.2837 (9)	C (48)	0.1996 (11)	−0.0056 (19)	0.4549 (8)
C (12)	0.3518 (13)	0.1894 (24)	0.1590 (9)	C (49)	0.2093 (10)	0.0950 (18)	0.4064 (7)
C (13)	0.2213 (13)	−0.0266 (20)	0.1893 (10)	C (50)	0.2626 (12)	−0.1087 (21)	0.5634 (8)
C (21)	0.0661 (16)	0.4423 (28)	0.3756 (11)	C (51)	0.3297 (13)	−0.1329 (23)	0.6178 (10)
C (22)	0.1631 (14)	0.6671 (20)	0.3206 (12)	C (52)	0.1736 (14)	−0.1778 (21)	0.5721 (9)
C (23)	0.0153 (13)	0.5276 (23)	0.2388 (11)	C (53)	0.3592 (11)	0.5149 (19)	0.4216 (8)
C (31)	0.1409 (9)	0.3028 (17)	0.1774 (7)	C (54)	0.4135 (12)	0.6442 (23)	0.4267 (11)
C (32)	0.1026 (11)	0.2972 (20)	0.1242 (8)	C (55)	0.3030 (14)	0.5036 (21)	0.4731 (9)
C (33)	0.0581 (16)	0.2919 (31)	0.0514 (10)				

TABLE 2. THERMAL PARAMETERS ALONG WITH THEIR ESTIMATED STANDARD DEVIATIONS IN PARENTHESES

Anisotropic thermal parameters ($\times 10^4$) are expressed in the form:
$\exp\{-(\beta_{11}h^2+\beta_{22}k^2+\beta_{33}l^2+\beta_{12}hk+\beta_{13}hl+\beta_{23}kl)\}$

Atom	β_{11}	β_{22}	β_{33}	β_{12}	β_{13}	β_{23}
Pt	31.4 (3)	112.0 (8)	22.6 (2)	−4.8 (8)	0.9 (3)	1.5 (6)
P (1)	40 (2)	149 (7)	28 (1)	29 (6)	5 (3)	−14 (5)
P (2)	42 (2)	112 (6)	37 (1)	18 (6)	8 (3)	−11 (5)
N (1)	104 (14)	351 (44)	62 (8)	−134 (42)	−57 (17)	142 (31)
N (2)	68 (11)	367 (46)	90 (10)	−138 (38)	−6 (17)	155 (36)
N (3)	80 (11)	292 (38)	72 (8)	−109 (36)	10 (16)	−34 (29)
N (4)	176 (20)	290 (37)	33 (5)	−102 (47)	43 (17)	−36 (24)
C (11)	57 (10)	191 (31)	46 (7)	119 (31)	−13 (13)	13 (23)
C (12)	67 (11)	258 (38)	36 (6)	7 (35)	32 (13)	−24 (25)
C (13)	65 (11)	151 (28)	55 (7)	−1 (30)	−0 (15)	−65 (24)
C (21)	106 (16)	288 (46)	56 (8)	110 (46)	82 (20)	−24 (32)
C (22)	71 (12)	111 (26)	81 (10)	−16 (30)	−34 (18)	−43 (27)
C (23)	62 (11)	223 (36)	56 (8)	111 (34)	−48 (15)	−45 (28)
C (31)	37 (7)	150 (23)	20 (4)	−8 (22)	17 (9)	3 (16)
C (32)	48 (9)	183 (28)	33 (5)	48 (27)	23 (11)	31 (20)
C (33)	97 (16)	382 (57)	37 (7)	−87 (51)	−39 (17)	22 (32)
C (41)	47 (8)	136 (23)	19 (4)	−8 (23)	−6 (9)	−8 (15)
C (42)	44 (8)	153 (25)	29 (5)	1 (24)	−34 (10)	−12 (18)
C (43)	52 (10)	240 (36)	44 (6)	−97 (32)	35 (13)	−7 (25)
C (44)	33 (7)	155 (24)	24 (4)	−6 (22)	6 (9)	12 (17)
C (45)	40 (8)	115 (22)	35 (5)	−22 (22)	−10 (10)	−12 (17)
C (46)	50 (9)	114 (22)	34 (5)	−27 (23)	−23 (11)	21 (18)
C (47)	73 (11)	161 (27)	23 (4)	−32 (29)	−3 (11)	31 (18)
C (48)	61 (10)	156 (26)	29 (5)	−18 (27)	−8 (11)	−2 (19)
C (49)	44 (8)	149 (25)	28 (5)	−17 (24)	12 (10)	−5 (18)
C (50)	59 (10)	189 (30)	35 (5)	−66 (30)	−15 (12)	4 (21)
C (51)	75 (12)	219 (35)	48 (7)	−77 (35)	−45 (15)	82 (26)
C (52)	99 (14)	178 (31)	38 (6)	26 (35)	−31 (15)	108 (23)
C (53)	61 (10)	158 (26)	29 (5)	−65 (27)	−30 (11)	−0 (19)
C (54)	53 (10)	197 (33)	61 (8)	−40 (31)	−29 (15)	−2 (27)
C (55)	99 (14)	165 (29)	32 (5)	−32 (34)	−11 (14)	−17 (21)

Results and Discussion

A perspective view of the molecule is given in Fig. 1 with the numbering system of atoms. A stereographic drawing of the molecule is shown in Fig. 2.

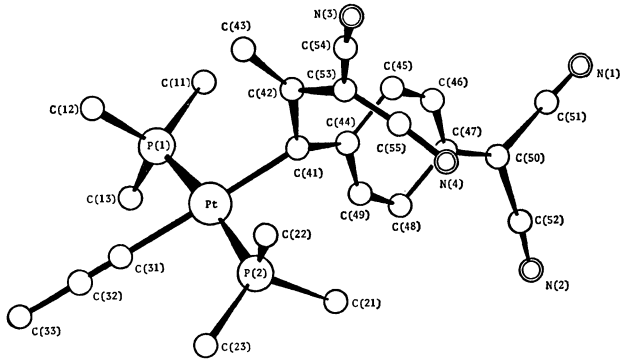

Fig. 1. Perspective view of the molecule with the numbering system of atoms.

The molecular structure determined is entirely different from that proposed[1] as no charge-transfer complex had been formed. The TCNQ molecule had reacted with one of the propynyl groups of *trans*-{$(PMe_3)_2Pt(C{\equiv}CMe)_2$} (Pt-complex), and, as a result, part of the TCNQ is bonded to the α-carbon atom (C(41)) and the remaining part to the β-carbon (C(42)) of the propynyl ligand. The product is, therefore, *trans*-bis (trimethylphosphine) propynyl-1-(4′-dicyanomethylene-cyclohexa-2′,5′-dien-1′-yliden)-3,3-dicyano-2-methyl-prop-2-en-1-ylplatinum.

Bond distances and bond angles are listed in Table 4. The environment of the platinum atom is essentially square-planar and the phosphine groups are mutually *trans*. The Pt–P distances observed [2.290(5) and 2.304(5) Å] are normal as found in the related platinum(II) complexes.[6,7] Both the Pt–C(31)(sp) and Pt–C(41)(sp^2) distances [2.009(15) and 2.057(15)Å] are equal to the respective sum of the covalent radii [Pt–C(sp)=2.00 and Pt–C(sp^2)=2.07 Å]. However, the former is longer than the Pt–C(CNR) distances in *cis*-{$PtCl_2(PEt_2Ph)(C{\equiv}NEt)$} [1.83(4) Å][8] and *cis*-{$PtCl_2(C{\equiv}NPh)_2$} [av. 1.986(16) Å],[9] and it is also longer than the Pt–C(CO) distance in *trans*-{$PtCl(CO)(PEt_3)_2$} [1.78 Å].[10] This may be caused by the reduced basicity of the σ-bonded carbon atoms. The C(31)–C(32) distance of the unreacted propynyl ligand [1.15(3) Å] is shorter than in *trans*-{$(PEt_3)_2Ni(C{\equiv}CPh)_2$}[11] [1.22(2) Å] although the difference is not fully significant.

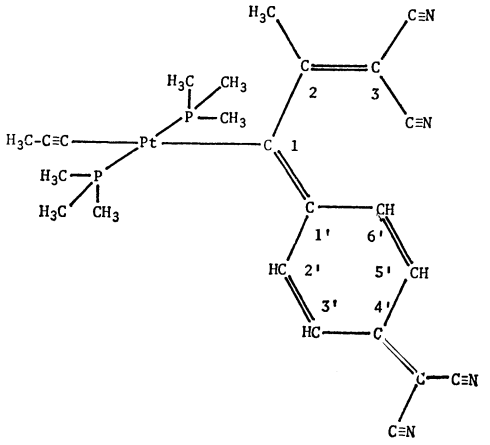

The skeleton around the resulted propyl group is shown in Fig. 3. The C(41)–C(42) and C(42)–C(43) links [1.50(2) and 1.52(3) Å] are single bonds, while the C(41)–C(44) and C(42)–C(53) [both 1.35(2) Å] are double bonds. The sum of bond angles around the C(41) and C(42) atoms are both equal to 360° within the range of experimental error. These facts suggest that both the C(41) and C(42) are sp^2 carbon atoms. The significant distortions of Pt–C(41)–C(42) and Pt–C(41)–C(44) angles from 120° [111.9(10) and 127.3(12)°] are probably due to the Pt...C(44) non-bonded interaction, and the concomitant steric strains are relieved by the distortion of the cyclohexadiene ring.

The geometry around the C(41), C(42), C(44) and C(53) atoms suggests that the C(41), C(42) and C(43) atoms are from the original propynyl ligand of the Pt-complex and the remaining C(44) to C(55) and N(1) to N(4) from the TCNQ. Of the two possibilities to arrange a triple bond of the Pt-complex and a double bond of the TCNQ approximately parallel the scheme (1) in Fig. 4 is supported from the structure determined. The charge-transfer complex proposed by Masai and co-workers[1] may be considered as an

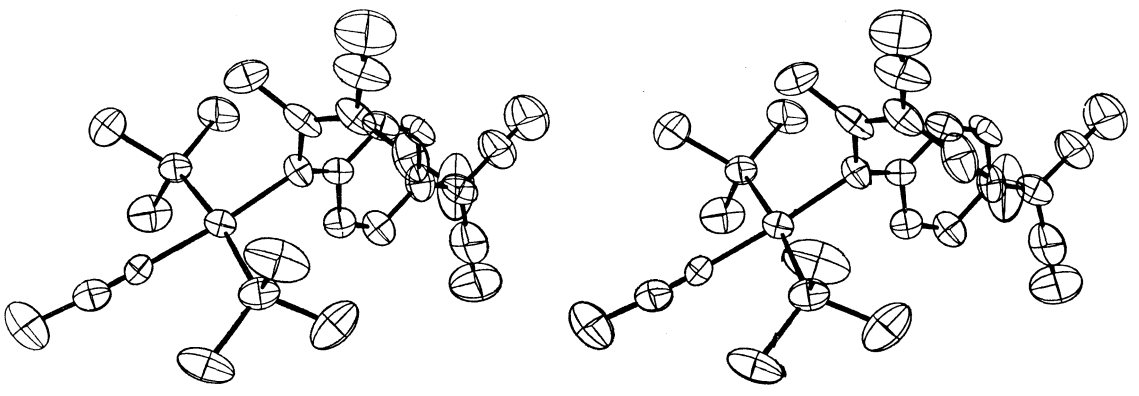

Fig. 2. Stereographic drawing of the molecule. Non-hydrogen atoms are represented by thermal ellipsoids of 50% probability.

TABLE 4. BOND DISTANCES AND BOND ANGLES ALONG WITH THEIR ESTIMATED STANDARD DEVIATIONS IN PARENTHESES

Bond distances [Å]					
Pt-P(1)	2.302 (5)	Pt-P(2)	2.290(5)	Pt-C(31)	2.009(15)
Pt-C(41)	2.057(15)	P(1)-C(11)	1.84 (2)	P(1)-C(12)	1.84 (2)
P(1)-C(13)	1.82 (2)	P(2)-C(21)	1.78 (3)	P(2)-C(22)	1.83 (3)
P(2)-C(23)	1.84 (2)	N(1)-C(51)	1.14 (3)	N(2)-C(52)	1.13 (3)
N(3)-C(54)	1.15 (3)	N(4)-C(55)	1.13 (3)	C(31)-C(32)	1.15 (3)
C(32)-C(33)	1.54 (3)	C(41)-C(42)	1.50 (2)	C(41)-C(44)	1.35 (2)
C(42)-C(43)	1.52 (3)	C(42)-C(53)	1.35 (2)	C(44)-C(45)	1.45 (2)
C(44)-C(49)	1.46 (2)	C(45)-C(46)	1.32 (2)	C(46)-C(47)	1.43 (2)
C(47)-C(48)	1.48 (2)	C(47)-C(50)	1.36 (3)	C(48)-C(49)	1.36 (3)
C(50)-C(51)	1.41 (3)	C(50)-C(52)	1.50 (3)	C(53)-C(54)	1.41 (3)
C(53)-C(55)	1.42 (3)				
Bond angles [°]					
P(1)-Pt-P(2)	172.9 (2)			P(1)-Pt-C(31)	82.6 (5)
P(1)-Pt-C(41)	92.8 (4)			P(2)-Pt-C(31)	90.7 (5)
P(2)-Pt-C(41)	93.9 (4)			C(31)-Pt-C(41)	175.3 (6)
Pt-P(1)-C(11)	119.4 (6)			Pt-P(1)-C(12)	112.6 (7)
Pt-P(1)-C(13)	112.4 (7)			C(11)-P(1)-C(12)	104.5 (9)
C(11)-P(1)-C(13)	103.0 (9)			C(12)-P(1)-C(13)	103.5(10)
Pt-P(2)-C(21)	114.5 (8)			Pt-P(2)-C(22)	115.3 (8)
Pt-P(2)-C(23)	115.2 (7)			C(21)-P(2)-C(22)	101.9(11)
C(21)-P(2)-C(23)	105.3(11)			C(22)-P(2)-C(23)	102.9(11)
Pt-C(31)-C(32)	178.5(15)			C(31)-C(32)-C(33)	175.9(20)
Pt-C(41)-C(42)	111.9(10)			Pt-C(41)-C(44)	127.3(12)
C(42)-C(41)-C(44)	120.2(14)			C(41)-C(42)-C(43)	120.9(14)
C(41)-C(42)-C(53)	119.0(15)			C(43)-C(42)-C(53)	119.8(15)
C(11)-C(44)-C(45)	126.8(15)			C(41)-C(44)-C(49)	118.4(14)
C(45)-C(44)-C(49)	114.7(14)			C(44)-C(45)-C(46)	125.2(15)
C(45)-C(46)-C(47)	118.6(15)			C(46)-C(47)-C(48)	120.1(15)
C(46)-C(47)-C(50)	120.0(16)			C(48)-C(47)-C(50)	119.9(16)
C(47)-C(48)-C(49)	117.9(15)			C(44)-C(49)-C(48)	122.9(15)
C(47)-C(50)-C(51)	124.2(18)			C(47)-C(50)-C(52)	122.0(17)
C(51)-C(50)-C(52)	113.3(17)			N(1)-C(51)-C(50)	176.9(23)
N(2)-C(52)-C(50)	178.8(23)			C(42)-C(53)-C(54)	122.3(17)
C(42)-C(53)-C(55)	124.4(17)			C(54)-C(53)-C(55)	113.0(17)
N(3)-C(54)-C(53)	178.1(23)			N(4)-C(55)-C(53)	176.8(23)

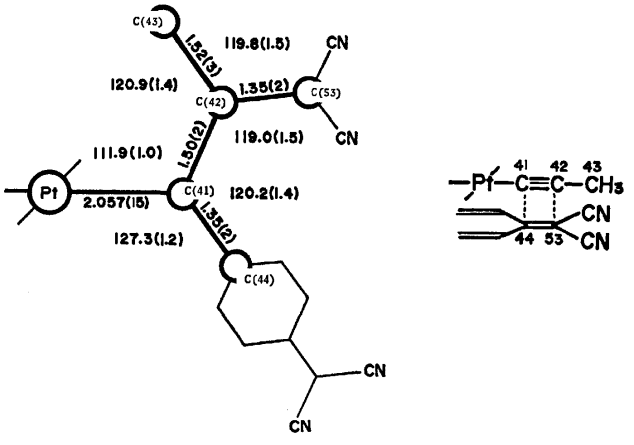

Fig. 3. Skeleton around the resulted propyl group.

intermediate. However, it is inconclusive whether both or one of the ethynyl bonds interact with a double bond of the TCNQ. The unreactivity of the other π-acceptors with the Pt-complex is supposed partly due to the steric hindrance of phosphine groups attached to the platinum atom.

Bond distances and bond angles in two dicyanomethylene groups are similar to those in TCNQ.[12]

A perspective drawing of the crystal structure along the b axis is shown in Fig. 5. No close intermolecular atomic contact less than the sum of the van der Waals radii is observed.

Computations throughout the present study were carried out on a NEAC 2200-700 computer at Osaka University. Figures 2 and 4 were drawn on a NUMMERICON 7000 system at Osaka University with a local version of ORTEP.[13]

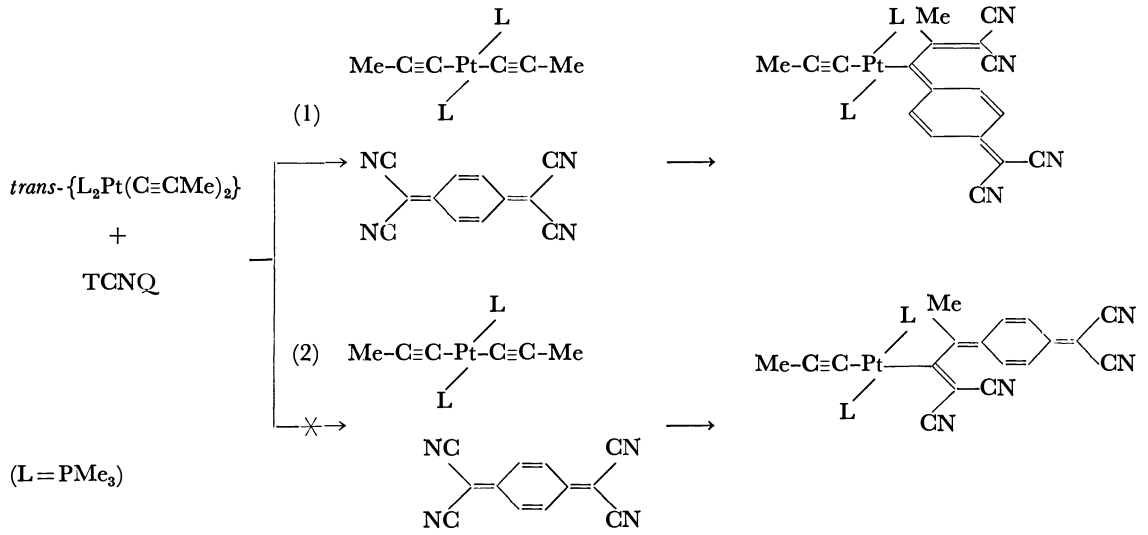

Fig. 4. Reaction scheme.

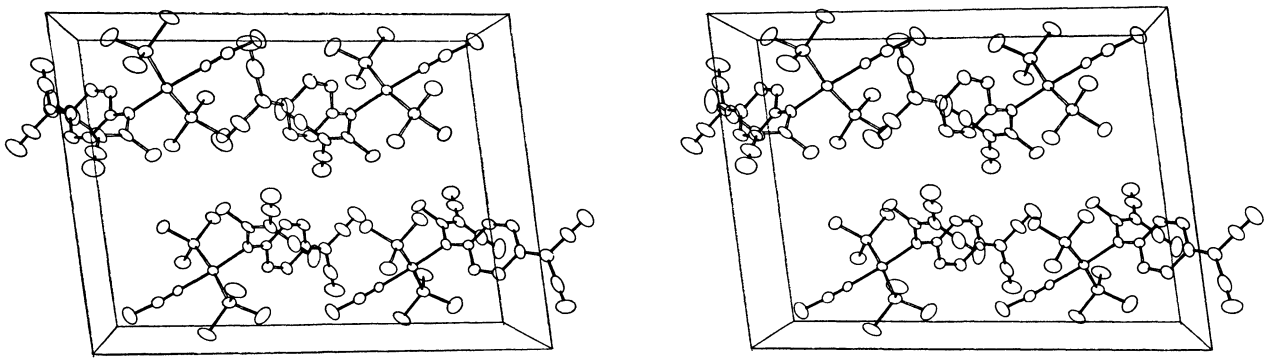

Fig. 5. Perspective drawing of the crystal structure along the b axis.

The authors wish to express their deep thanks to Professor Nobue Hagihara and his co-workers of Osaka University for their kindness in supplying crystals. Thanks are also due to Dr. C. H. L. Kennard who checked the English in the manuscript.

References

1) H. Masai, K. Sonogashira, and N. Hagihara, *J. Organometal. Chem.*, **34**, 397 (1972).
2) M. Horike, Y. Kai, N. Yasuoka, and N. Kasai, *ibid.*, **72**, 441 (1974).
3) T. Ashida, The Universal Crystallographic Computing System, Osaka, The Computation Center, Osaka University (1973), p. 55.
4) Table is filed at the Chemical Soiety of Japan, (Document No. 7513), 1—5, Kanda-Surugadai, Chiyoda-ku Tokyo, 101.
5) H. P. Hanson, F. Herman, J. D. Lea, and S. Skillman, *Acta Crystallogr.*, **17**, 1040 (1964).
6) G. G. Messmer and E. L. Amna, *Inorg. Chem.*, **5**, 1775 (1966).
7) M. R. Collier, C. Eaborn, B. Jovanovic, M. F. Lappert, Lj. Manojlovic-Muir, K. W. Muir, and M. M. Truelock, *Chem. Commun.*, **1972**, 613.
8) B. Jovanovic and Lj. Manojlovic-Muir, *J. Chem. Soc., Dalton*, **1972**, 1176.
9) B. Jovanovic and Lj. Manojlovic-Muir, *ibid.*, **1972**, 1178.
10) H. D. Clark, P. W. R. Corefield, K. R. Dixon and J. A. Ibers, *J. Amer. Chem. Soc.*, **89**, 3360 (1967).
11) W. A. Spofford, III, P. D. Carfagna, and E. L. Amma, *Inorg. Chem.*, **6**, 1553 (1967).
12) R. E. Long. R. A. Sparks, and K. N. Trueblood, *Acta Crystallogr.*, **18**, 932 (1965).
13) C. K. Johnson, ORTEP, Report ORNL-3794, Oak Ridge National Laboratory, Tennessee, 1965.

The Effect of the Hydrostatic Pressure on the Hydrogen-bond Formation between Phenol and Dioxane in Hexane*

Keizo SUZUKI and Masao TSUCHIYA**

Department of Chemistry, Faculty of Science and Engineering, Ritsumeikan University, Kita-ku, Kyoto 603

(Received September 24, 1974)

The near-UV absorption spectra of phenol-dioxane in *n*-hexane were observed under hydrostatic pressures up to 1480 atm and at 30 °C. With an increase in the pressure, the spectra shift toward the longer wavelength side and the amount of the hydrogen-bonded phenol increases. The equilibrium constant for -OH + O 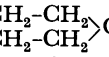 O ⇄ 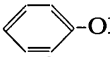 -OH···O O was obtained, and the volume change accompanying the hydrogen-bond formation was estimated to be −3.0——3.4 cm³/mol.

The effect of the hydrostatic pressure on the hydrogen-bond formation has been investigated by Shishkin and Novak,[1] Fishman and Drickamer,[2] and Osugi and Kitamura[3] on the basis of IR-absorption measurements. Shishkin and Novak[1] studied the system of phenol and some alcohols in carbon tetrachloride under pressures up to 3200 kg/cm². A pressure rise of 90—130 kg/cm² is found to have the same effect as a temperature drop of 1 °C. Using this result, Hamann[4] estimated the volume change accompanying the hydrogen-bond formation, ΔV, to be −4.5——6 cm³/mol. Fishman and Drickamer[2] investigated the association of *n*-butyl alcohol in carbon disulfide up to 11300 atm. The ΔV values estimated were −4.64 cm³/mol in the range from 1 to 5820 atm, and −2.47 cm³/mol in the range from 5820 to 11300 atm. The system of *n*-butyl alcohol in carbon disulfide was studied up to 8000 atm by Osugi and Kitamura.[3] Assuming the association numbers to be 2, 3, and 4, the ΔV was estimated to be −2.20, −4.31, and −5.74 cm³/mol respectively. The high concentration of solute used in these experiments seems to permit a higher degree of association due to hydrogen bonding. The number of solute molecules participating in the association is not necessarily certain, so that it seems difficult to estimate the ΔV value per mol H-bond exclusively from these data.[3]

Using the molecular model of hydrogen bonding, the ΔV has been calculated theoretically by Hamann.[4,5] Assuming that the distance between the α and β oxygen atoms in the hydrogen bonding ($\overset{\alpha}{O}$–H···$\overset{\beta}{O}$) is contracted by about 0.9 Å, and that this contraction occurs along the axis of a cylinder having a radius equal to the van der Waals radius of the oxygen atoms, he estimated the ΔV to be about −3.8 cm³/mol.

The purposes of the present paper are to observe the near-UV absorption spectrum of phenol–dioxane in *n*-hexane, where the concentration of phenol is very dilute and where the only hydrogen-bonded complex is 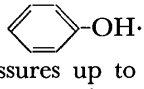 -OH···O O, under hydrostatic pressures up to 1480 atm, and to estimate the ΔV value accompanying the hydrogen-bond formation. A series of excellent studies of the same system has been performed at atmospheric pressure by Baba and Nagakura,[6,7] Nagakura and Baba,[8] and Nagakura.[9] The pressure effect on the hydrogen-bond formation, however, has never been studied on the basis of UV-absorption measurements.

Experimental

Materials. All the reagents, of an extra pure grade, were used after the following purification. The *n*-hexane was purified as has been described previously[10,11] (bp 68.9 °C) and was optically transparent to 230 nm. The phenol was purified twice by vacuum distillation (mp 40.5±0.5 °C). The dioxane was refluxed with sodium metal for two days and then fractionally distilled (bp 101.3 °C).

Apparatus. A Shimadzu model MPS-501 double-beam spectrophotometer was used to measure the absorption spectra. Figure 1 shows schematically the clamp-type optical cell used to measure the absorption spectra under high pressures. The optical cell, which was constructed from cobalt alloy (HAYNES alloy No.25, manufactured by the Mitsubishi Metal Mining Co., Ltd.), was designed so as to be set in the sample space of the spectrophotometer after the pressure had been raised. The windows of sapphire permitted measurement to wavelengths of about 230 nm. The pressure generated in the cell was calibrated against the readings of the Bourdon-tube gauge of the oil press by

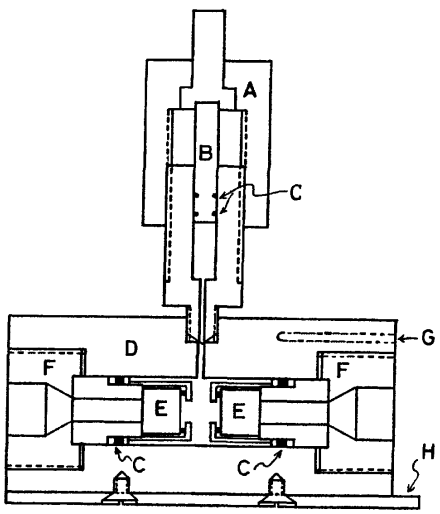

Fig. 1. Clamp type optical cell.
A: clamp nut, B: piston, C: O-ring, D: pressure bomb, E: sapphire window, F: closure of window, G: hole of thermister, H: holder.

* Presented at the 9th Symposium of High Pressure, Nagoya, October, 1967.

** Present address: Department of Chemistry, Faculty of Engineering, The College of Naval Architecture of Nagasaki, Nagasaki.

means of a manganine gauge, which was inserted in the cell instead of the window. The accuracy of the pressure was ±2.7% at 1400 atm.

Procedures. The measurement of the absorption spectra under pressure was carried out at 30 °C by the following procedures. The sample solution was admitted into the cell directly using a glass pipet before a piston was inserted into the cylinder. The piston was pushed into the cylinder by an oil press until the desired pressure was generated. Then the piston was fixed by a clamp nut to keep the pressure constant after the press load had been released. The absorption spectra were measured, with air as the reference, and the base line, which was not affected by the pressure, was subtracted. No optical contamination was observed throughout the experiment. The concentration of the solution under pressure was corrected from the compressibility data of *n*-hexane.[12]

Results and Discussion

Figure 2-1 shows the pressure effect on the absorption spectrum of phenol and dioxane (0.15 mol/l) in *n*-hexane. The a and c arrows and the b and d arrows in the figure represent the absorption bands of free phenol and hydrogen-bonded phenol respectively at atmospheric pressure.[6-9] Figures 2-2 and 2-3 show the absorption spectra corrected by the compressibility of *n*-hexane.[12] Figures 3-1 and 3-2 also show the pressure effect on the absorption spectra of the solution with a different concentration of dioxane (0.10 mol/l). Two characteristic points are noticeable from these figures: (1) the spectrum shifts toward a longer wavelength. As is shown in Fig. 4, the results of the red shift, $\Delta\lambda$, for the a-band and c-band of phenol as a function of the pressure are in good agreement with those obtained by Robertson *et al.*[13] A similar shift is found for the b-band and d-band of hydrogen-bonded phenol, though the bands are so broad that it is hard to determine $\Delta\lambda$ precisely. Many authors

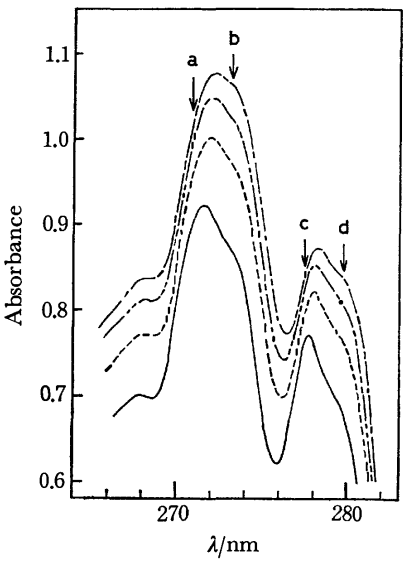

Fig. 2-1. Pressure effect on the absorption spectrum of phenol-dioxane in *n*-hexane at 30 °C.
phenol: 5.000×10^{-4} mol/l, dioxane: 0.150 mol/l
——: 1 atm, — —: 600 atm, — — —: 1160 atm, — — —: 1480 atm

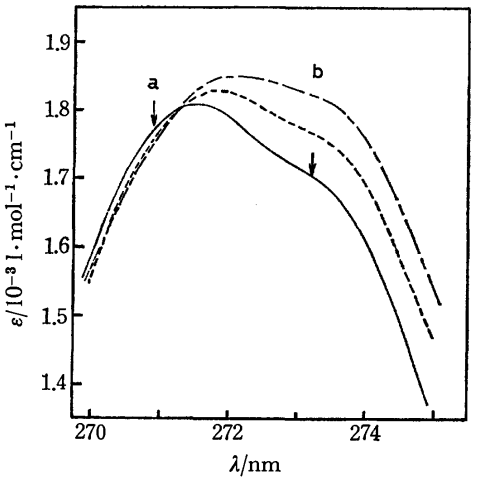

Fig. 2-2. Pressure effect on the absorption spectrum corrected by compressibility data of *n*-hexane at 30 °C.
phenol: 5.000×10^{-4} mol/l, dioxane: 0.150 mol/l
——: 1 atm, — — —: 600 atm, ——: 1480 atm

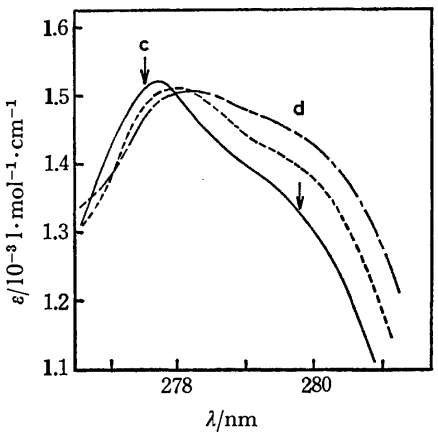

Fig. 2-3. Pressure effect on the absorption spectrum corrected by compressibility data of *n*-hexane at 30 °C.
phenol: 5.000×10^{-4} mol/l, dioxane: 0.150 mol/l
——: 1 atm, — —: 600 atm, — — —: 1480 atm

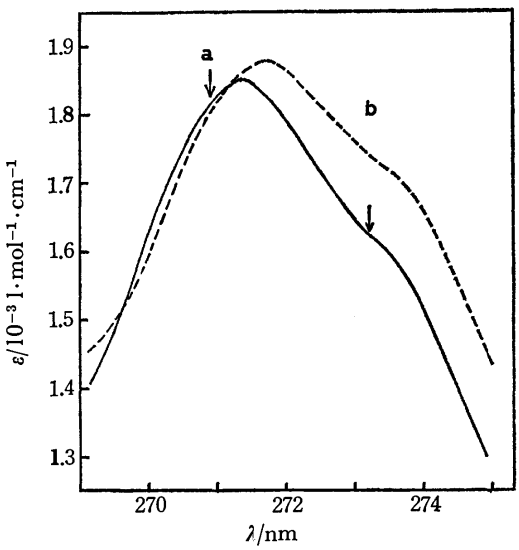

Fig. 3-1. Pressure effect on the absorption spectrum corrected by the compressibility data of *n*-hexane at 30 °C.
phenol: 5.000×10^{-4} mol/l, dioxane: 0.100 mol/l
——: 1 atm, — — —: 1160 atm

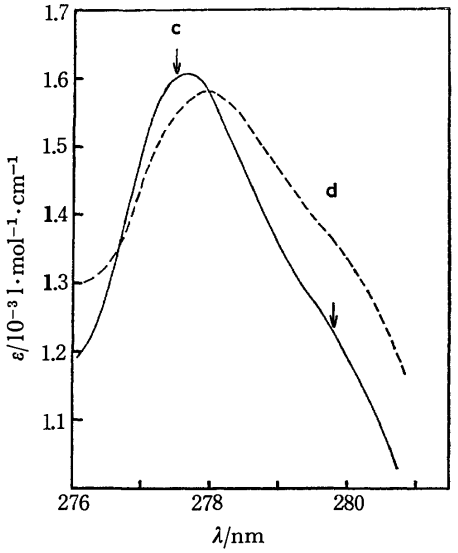

Fig. 3-2. Pressure effect on the absorption spectrum corrected by the compressibility data of *n*-hexane at 30 °C.
phenol: 5.000×10^{-4} mol/l, dioxane: 0.100 mol/l
——: 1 atm, ———: 1160 atm

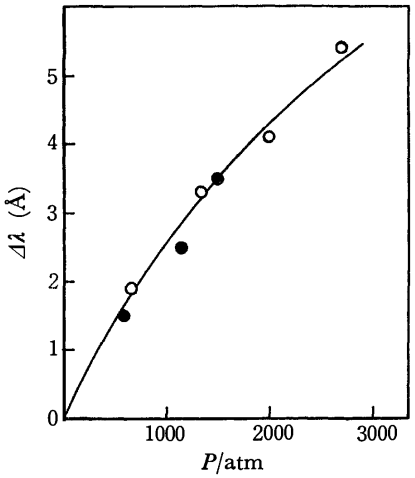

Fig. 4. Pressure effect on the amount of red shift for the a- and c-bands of phenol in *n*-hexane.
●: this work, ○: Robertson *et al.*[13]

have indicated that such a red shift is attributable to an increase in the intermolecular interaction of the London–van der Waals type between the solvent and solute molecules upon an increase in the pressure, and that the energy level of the excited state is lowered.[13,14]
(2) The ratio of the absorbance of the hydrogen-bonded-phenol band to that of the free-phenol band increases with an increase in the pressure. This shows that the hydrogen-bonded phenol increases with an increase in the pressure. From these spectral data, the equilibrium constant at each pressure and the volume change accompanying the hydrogen-bond formation can be obtained.

The following equilibrium is assumed to be established in *n*-hexane:

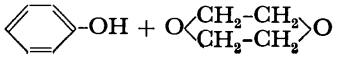

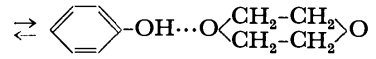

(1)

Here, the concentration of phenol is so dilute that the self-association of phenol[15,16] and the formation of 2-mol hydrogen bonds for a dioxane molecule[7]

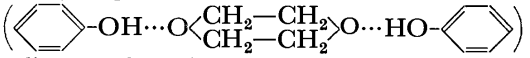

are eliminated. The equilibrium constant, K, is represented as follows:

$$K = \frac{C_H}{C_P C_D} \tag{2}$$

where C_P, C_H, and C_D are the concentrations of free phenol, hydrogen-bonded phenol, and dioxane respectively. According to Lambert–Beer's law, C_P and C_H are given as follows:

$$C_P = \frac{\beta(\alpha\varepsilon_b' - \varepsilon_a')}{(\alpha\varepsilon_b' - \varepsilon_a') + (\varepsilon_a - \alpha\varepsilon_b)} \tag{3}$$

$$C_H = \frac{\beta(\alpha\varepsilon_b - \varepsilon_a)}{(\alpha\varepsilon_b - \varepsilon_a) + (\varepsilon_a' - \alpha\varepsilon_b')} \tag{4}$$

Here, β is the total concentration of phenol, which is a sum of C_P and C_H, α is the ratio of the absorbances of the a-band and the b-band, ε and ε' are the molar absorption coefficients of free phenol and hydrogen-bonded phenol, and the subscript denotes each absorption band. When we insert Eqs. (3) and (4) in Eq. (2), K is represented as:

$$K = \frac{\varepsilon_a - \alpha\varepsilon_b}{C_D(\alpha\varepsilon_b' - \varepsilon_a')} \tag{5}$$

Similar expressions can be deduced for the c-band and the d-band. The following values were obtained in this experiment for each molar absorption coefficient ($\times10^{-3}$ l/mol): $\varepsilon_a=2.102$ and $\varepsilon_a'=1.670$ at 270.9 nm, $\varepsilon_b=1.134$ and $\varepsilon_b'=1.922$ at 273.2 nm, $\varepsilon_c=2.030$ and $\varepsilon_c'=1.318$ at 277.5 nm, $\varepsilon_d=0.650$ and $\varepsilon_d'=1.604$ at 279.8 nm. The ε' values were decided at 0.80 mol/l of dioxane, where the spectral change became to level. On the right-hand side of Eqs. (3)—(5), all the values except α are known. Therefore, C_P, C_H, and K can be calculated by using the experimental value of α. The results at atmospheric pressure are shown in Table 1, in which the K value is held approximately constant, at least in the lower concentrations cited here.[17]

Table 1. Equilibrium at atmospheric pressure (30 °C)

C_D (mol/l)	α	$C_P\times10^4$ (mol/l)	K (l/mol)
From a-band/b-band			
0.020	1.511	3.802	15.8
0.060	1.233	2.493	16.3
0.080	1.176	2.172	16.3
0.100	1.117	1.818	17.5
From c-band/d-band			
0.020	2.109	3.790	15.9
0.060	1.521	2.594	15.5
0.080	1.409	2.291	14.8
0.100	1.278	1.895	16.4

The total concentration of phenol: 5.000×10^{-4} mol/l.

Assuming that the absorbance observed under high pressures follows Lambert-Beer's law, and that the molar absorption coefficient and the optical path length do not change with the pressure, Eqs. (3)—(5) hold also under high pressure. The concentration of a solution is, of course, corrected from the compressibility data of *n*-hexane.[12] The free-energy change, ΔG°, and the volume change, ΔV, accompanying the hydrogen-bond formation are given by:

$$\Delta G^\circ = -RT \ln K \tag{6}$$

$$\Delta V = -RT\left(\frac{\partial \ln K}{\partial P}\right)_T \tag{7}$$

Table 2. Effect of pressure on the equilibrium of hydrogen-bond formation (30 °C)

Pressure (atm)	α	$C_P \times 10^4$ (mol/l)	K (l/mol)	$-\Delta G^\circ$ (kcal/mol)
a-band/b-band, dioxane: 0.15 mol/l				
1	1.036	1.286	19.3	1.78
600	1.019	1.169	20.4	1.82
1480	0.995	0.995	23.6	1.90
c-band/d-band, dioxane: 0.15 mol/l				
1	1.131	1.385	17.4	1.72
600	1.099	1.263	18.4	1.75
1480	1.053	1.080	21.3	1.84
a-band/b-band, dioxane: 0.10 mol/l				
1	1.117	1.818	17.5	1.72
1160	1.073	1.535	20.2	1.81
c-band/d-band, dioxane: 0.10 mol/l				
1	1.278	1.895	16.4	1.68
1160	1.188	1.593	19.1	1.78

Pressure (atm)	$-\Delta V$ (cm³/mol)	
	a-band/b-band	c-band/d-band
dioxane: 0.15 mol/l		
1—1480	3.4	3.4
dioxane: 0.10 mol/l		
1—1160	3.0	3.3

Where R is the gas constant, and T, the absolute temperature. The $-\Delta G^\circ$ value (1.66—1.78 kcal/mol) coincides well with the calorimetric result (1.79 kcal/mol).[18] The ΔV value obtained in this experiment is -3.0——-3.4 cm³/mol. This value is comparable with those in alcohol (-4.6——-6 cm³/mol)[2,3] and calculated theoretically (-3.8 cm³/mol).[4,5]

References

1) N. I. Shishkin and I. I. Novak, *Zhur. Tekh. Fiz.*, **23**, 1485 (1953).
2) E. Fishman and H. G. Drickamer, *J. Chem. Phys.*, **24**, 548 (1956).
3) J. Osugi and Y. Kitamura, *Rev. Phys. Chem. Japan*, **35**, 25 (1965).
4) S. D. Hamann, "High Pressure Physics and Chemistry," Vol. 2, ed. by R. S. Bradley, Academic Press, New York, N. Y. (1965), p. 131.
5) S. D. Hamann, "Physicochemical Effects of Pressure," Butterworths Scientific Publications, London (1965), p. 147.
6) H. Baba and S. Nagakura, *Nippon Kagaku Zasshi*, **71**, 610 (1950).
7) H. Baba and S. Nagakura, *ibid.*, **72**, 3 (1951).
8) S. Nagakura and H. Baba, *J. Amer. Chem. Soc.*, **74**, 5693 (1952).
9) S. Nagakura, *Nippon Kagaku Zasshi*, **74**, 153 (1953).
10) C. O. Tongberg and F. Johnston, *Ind. Eng. Chem.*, **25**, 733 (1933).
11) A. Castille and V. Henri, *Bull. Soc. Chem. Biol.*, **6**, 299 (1924).
12) P. W. Bridgman, "The Physics of High Pressure," MacMillan Co., New York, N. Y. (1931), Table II, p. 129.
13) W. W. Robertson, S. E. Babb, Jr., and F. A. Matsen, *J. Chem. Phys.*, **26**, 367 (1957).
14) H. Sponer, G. Nordheim, A. L. Sklar, and E. Teller, *ibid.*, **7**, 207 (1939).
15) E. G. Hoffman, *Z. Phys. Chem.*, **53B**, 179 (1943).
16) M. Tsuboi, *Nippon Kagaku Zasshi*, **72**, 146 (1951).
17) The K value for the higher concentration of dioxane tends to increase. We cannot explain the reason explicitly.
18) S. N. Vinogradov and R. H. Linnell, "Hydrogen Bonding," Van Nostrand Reinhold Co., New York, N. Y. (1971), Tables 6—1, p. 150.

Enthalpies of Combustion of Organic Compounds. I. 8-Quinolinol.

Minoru SAKIYAMA, Toshiro NAKANO, and Syûzô SEKI

Department of Chemistry, Faculty of Science, Osaka University, Toyonaka, Osaka 560

(Received November 1, 1974)

A rotating-oxygen-combustion bomb calorimeter equipped with a platinum lined bomb has been constructed and calibrated. The enthalpy of combustion of 8-quinolinol(c) was determined. Thermodynamic quantities obtained are as follows: $\Delta E_c^\circ = -4458.90 \pm 1.60$, $\Delta H_c^\circ = -4460.76 \pm 1.60$ and $\Delta H_f^\circ = -81.24 \pm 2.00$ kJ mol^{-1} for the crystalline state and $\Delta H_f^\circ = 27.6 \pm 2.6$ kJ mol^{-1} for the gaseous state.

Measurement of enthalpy of combustion is the standard experimental method in organic thermochemistry. It provides not only fundamental chemical-thermodynamic quantities but also the most reliable experimental means for determination of the total intramolecular energy if the enthalpy of vaporization or sublimation data are available. The usual static bomb calorimeter is sufficient for compounds containing carbon, hydrogen, oxygen and nitrogen. It is well-known that the use of a rotating bomb calorimeter is required in order to get accurate results for compounds containing halogen, sulfur or metal besides the above-mentioned elements. By rotating the bomb after the combustion reaction the internal bomb-wall is washed out thoroughly with bomb-liquid so that a thermodynamically well-defined state is established.

We have constructed an isoperibol, rotating-bomb calorimeter in order to carry out the measurement of enthalpy of combustion for various kinds of compounds with high precision and accuracy. In the present paper we report the construction, operation and calibration of the calorimeter as well as the enthalpy of combustion of 8-quinolinol. The idealized combustion reaction which the energy and enthalpy of combustion given in this paper refer to is as follows:

$$C_9H_7ON(c) + 10.25\ O_2(g) = 9\ CO_2(g) + 3.5\ H_2O(l) + 0.5\ N_2(g).$$

All the quantities refer to the reference temperature 298.15 K.

Experimental

Apparatus. The rotating-bomb calorimeter is similar in design to that used by Hubbard *et al.*[1,2] The principal calorimeter was based upon the design of the Argonne National Laboratory, U.S.A. (CAPE-432) with some modifications made by ourselves. The calorimetric apparatus consists of a calorimeter vessel surrounded by a jacket with a constant air gap of 10 mm width. The whole system is kept in a measuring-room thermostatted at 23.0±0.3 °C.

The jacket, 47 cm in diameter and 33 cm in height, is made of brass except for portions which face the calorimeter vessel and which are made of copper. The outer surface of the jacket is chromium-plated and polished. The jacket is filled with distilled water of *ca.* 46 dm^3 which is stirred by two stirrers positioned symmetrically. Two centrifugal pumps are installed at the base of the stirrers. The double walled jacket lid is divided into two parts, and a pump circulates the jacket water through each half. Each pair of stirrer and pump is driven simultaneously by an induction motor. A cold water nozzle, a manganin heater (30 V, 36 W) and a thermistor probe for temperature regulation are located at the upper, middle and lower portions, respectively, of a cylinder made of brass which surrounds the stirrer. A pipe heater (100 V, 1000 W) is attached to the bottom of the jacket for rapid heating of the jacket-water.

The calorimeter vessel is made of copper and is of a novel shape in order to minimize the heat capacity. The outer surface is chromium-plated and brightly polished to minimize heat transfer by radiation. The combustion bomb is placed in the vessel with the base upward in order to protect the bomb lid from possible damage due to the high temperature flame during combustion of the sample. The vessel is filled with 2850 g of water while the measurement is going on. The stirrer for circulation water is driven at the rate 200 rpm by a synchronous hysteresis motor attached to the lid of the jacket. The combustion bomb is driven by another synchronous hysteresis motor. The rotation motion of the combustion bomb can be stopped with a plug actuated by a solenoid if desired, after the bomb-drive-motor is switched off. The stirrer and the bomb-drive shaft are connected with each motor via Nylon couplers in the air gap space between the jacket and the vessel. The combustion bomb rotates around two axes perpendicular to each other. The modes of rotation are a spinning motion about the bomb axis at $4\,^4/_{17}$ rpm and an end-over-head motion at 10 rpm. A blade and a spring switch both made of phosphor bronze electrically connect the bomb with an outer AC power source for ignition of the sample contained. The calorimeter-water is heated up to a predetermined temperature with a cartridge heater (DC 22 V, 22 W). A quartz thermometer probe is inserted into the calorimeter can through tubing at the top of the vessel. The probe is in intimate contact with the jacket-lid by a metal-to-metal contact device. All the openings on the upper portion of the vessel are closed with rubber bushing, cork stopper and oil seals in order to minimize the possible evaporation of calorimeter-water.

A Parr 1004C stainless steel combustion bomb with platinum-lining *ca.* 0.5 mm thick was used. A platinum-10% rhodium dish (*ca.* 11.14 g in weight) is placed on a gimbal and its ring. Ignition current flows between an insulated electrode and the bomb proper *via* a platinum-ignition-wire (diam. 0.1 mm). Two needle valves are attached to the lid of the bomb, one for introduction and the other for discharge of a gas. One end of a cotton fuse is connected with the ignition wire and the other with the sample. On the outer wall of the bomb proper, miter gears and ball bearings are attached for the biaxial rotational motion mentioned above. It was found from separate experiments that rotation energy is 0.0505 J s^{-1}.

The temperature of the jacket is maintained at 25.300±0.003 °C throughout the experiment by regulating the electrical current through the jacket heater against a constant flow of cold water from outside. The electrical current is regulated in proportional mode by a vacuum tube regulator similar in principle to that used by Skinner *et al.*[3] The jacket-water is recycled with a rate of *ca.* 20 cm^3 min^{-1} by a metering pump through a spiral copper tube immersed in an ice bath. The temperature of the jacket is monitored

by a Beckmann thermometer having the finest division of 0.001 K in its scale.

A sample is ignited by heating the platinum wire to red with AC current supplied from a transformer, with output voltage 4 V and current capacity of the secondary coil 10 A. Under these conditions, ignition can be carried out without fusion of the platinum wire in most cases. The ignition energy is measured by an integrating ammeter, which is similar in principle to that used by Mackle and O'Hare[4] but designed for use of integrated circuits. It was found from calibration-experiments that the full deflection of the meter corresponds to 9.03 J. For the measurement of temperature of the calorimeter a Hewlett-Packard model 2801A quartz thermometer with a model 2850 D sensor was used. The temperature is measured with a 0.000 01 K resolution at constant intervals of *ca.* 101.5 s with the use of an option M40 and is recorded on a Hewlett-Packard model 562 A digital printer.

Experimental Procedure. In the case of solid material, the pelletted sample, cotton fuse and platinum dish are weighed separately. The pelletted sample is tied to one end of the fuse, and measurement is then made of the total weight of the sample and fuse contained in the dish. Buoyancy correction is made to the final weight. The dish with the sample and fuse is attached to the gimbal ring of the bomb, the platinum ignition wire being tied to the other of the fuse. A predetermined amount of water is then added to the bomb and finally the bomb is closed tightly. The bomb is flushed with *ca.* 3.5 dm^3 oxygen at the rate of *ca.* 400 cm^3 min^{-1}. Combustible impurities in the oxygen are removed by passing it over Deoxo M (0.5% Pt on γ-alumina) kept at 150 °C. Water and carbon dioxide formed are removed by Ascarite (NaOH on asbestos), Dehydrite ($Mg(ClO_4)_2$) and phosphorus pentoxide, contained in a train of purification-tubes. The bomb is then charged with oxygen up to 3.040 MPa at 25 °C. The bomb is weighed on a large chemical balance (measurable up to 20 kg with *ca.* 3 mg resolution). The combustion bomb is set up in an inverted position in the calorimeter vessel, 2850 g of distilled water is added to the vessel and the total weight is measured. After the outer surface is wiped clean with chamois-leather, the can is fixed on pegs in the hollow of the jacket and then the ignition and heater wires are connected. The calorimeter is heated up to 22.80 °C with the cartridge heater. It is then subjected to a gradual temperature-rise by heat exchange with the surrounding jacket wall and stirring. When it reaches 23.00 °C, the recording of the temperature is started. The temperature rise in the main period is *ca.* 1.8 °C, when the calibration experiment with the standard benzoic acid is carried out under standard bomb conditions (see next section). In combustion experiments mass of a sample is adjusted so that the temperature rise may be as equal as possible to that in the calibration experiments. The anticipated initial temperature T_i of the main period is chosen so that the final temperature of the main period is close to 25 °C. The sample is ignited around T_i and the deflection of the integrating ammeter is recorded. Twenty readings of temperature preceding the ignition compose the initial period. After forty readings following the ignition are recorded, the bomb is taken out from the calorimeter. The bomb surface and external accessories are burst with a hot blaster in open air in order to dry them completely. The bomb is then placed in a sealed-metal-tank which is evacuated ($\sim$ 0.1 Pa) by an oil rotary pump for an hour. After the gas is released, the bomb is opened and the internal wall together with the fittings are washed thoroughly with distilled water. After collecting the washings, which is adjusted to 100 cm^3, the nitric acid formed as a by-product of combustion from a nitrogen containing sample and/or the nitrogen remaining in oxygen is analyzed with 0.02 M sodium hydroxide solution.

Establishment of the Standard Calorimeter System. The energy equivalent of the calorimeter ε°(calor.) is determined by the combustion of benzoic acid (Standard Reference Material 39 i, National Bureau of Standards, U.S.A.). The certificated value for the energy of combustion of the benzoic acid is $26434 \pm 3\ Jg^{-1}$ under standard bomb conditions[9] where the uncertainty is the uncertainty interval.[11] Deviation from the standard bomb conditions is made as small as possible and correction is made for it by the expression given by Jessup.[5] The energy equivalent is defined for the total system consisting of the calorimetric vessel containing 2850.00 g of water and the bomb where the gimbal and platinum ignition wire are installed. Total weight of the calorimetric system is *ca.* 10682 g in the case of calibration.

Material: 8-Quinolinol (Kishida Chemicals Co.) was used without further purification. The sample was prepared as the organic micro-analytical standard substance. The makers assert that the sample is purified by recrystallization (three times) using two kinds of solvents or solvent mixtures. It is certificated by the subcommittee of organic micro-analysis of the Japan Society for Analytical Chemistry. The substance is known to have four crystalline modifications with melting points of 73.5, 65, 57—58, and 38—39.5 °C.[6] The present sample was examined with a Perkin-Elmer DSC-1B and no thermal anomaly was detected below 73 °C. It is therefore considered to have the most stable modification. Horton and Wendlandt[7] reported the sublimation pressure of 8-quinolinol. The maximum amount of 8-quinolinol lost by flushing with 10 dm^3 of oxygen was *ca.* 2.7×10^{-5} g at 300 K, corresponding to *ca.* 0.003% of the sample burnt. It was decided to burn the sample pellet without enclosing it in a polyester bag.

Calculations

Corrected Temperature Rise. The corrected temperature rise $\Delta T (= T_f - T_i - \Delta T_c)$, where T_i and T_f are the initial and final temperatures of the main period, respectively, and ΔT_c the temperature rise during the main period due to heat absorbed from the jacket wall and to that caused by stirring (and bomb-rotation), was calculated in the following way.

Temperature readings in the initial and the final periods are fitted to the following integrated form of Newton's cooling law: $T = T_\infty - (T_\infty - T_0)\exp[-k \cdot (t - t_0)]$, where T is the temperature at time t, T_0 the temperature at a reference time t_0, k the cooling constant (thermal leakage modulus), and T_∞ the convergence temperature. The fitting procedures were made as follows: (1) An appropriate practical value for k, a mean value ($= 3.734 \times 10^{-5}\ s^{-1}$), was first assumed from preliminary analyses. Linear least-square analysis between T and $\exp[-k(t - t_0)]$ was then carried out for the initial and final periods separately. In this case the time of onset of the initial period and that of the final period are taken as the reference time t_0. A curvature correction is applied since the temperature reading of the quartz thermometer shows a mean value during 100 s before display. The effect of rest periods (*ca.* 1.5 s) between each sample period

(100 s) is not taken into consideration in order to conform with the procedure adopted for the main period. From the values of T_∞ and T_0 thus obtained, temperatures $\bar{T}_i$ and $\bar{T}_f$ and the rates of temperature rise G_i and G_f are calculated for the time midway in the initial period and that in the final period, respectively. New values of k and T_∞ are obtained by the expressions: $k=(G_i-G_f)/(\bar{T}_f-\bar{T}_i)$ and $T_\infty=(G_i\bar{T}_f-G_f\bar{T}_i)/(G_i-G_f)$. (2) By using the newly derived values of k, the same linear least-squares analysis described above is carried out again and new values of k and T_∞ are obtained. (3) The temperatures T_i and T_f are calculated as the ending temperature of the initial period and the beginning temperature of the final period from the final set of k and T_∞ by taking the reference time midway in the initial period and that in the final period, respectively.

In each case examined, the variation in k was found to be less than 1×10^{-9} s^{-1} and that in T_∞ less than 1×10^{-5} K, after the procedure in stage (1) had been adopted.

The temperature rise ΔT_c during the main period due to heat exchange with the jacket and the heat of stirring (and rotation) is calculated by: $\Delta T_c=k\int_{t_i}^{t_f}(T_\infty-T)dt$, where t_i and t_f are the beginning and ending times, respectively, of the main period. Calculation is simple as the temperature readings are mean temperatures during 100 s before display. In the main period it is difficult to estimate the effect of the rest periods on ΔT_c. However, the effect is estimated to be negligible and is not taken into consideration for the final determination of ΔT_c.

Determination of the duration of the main period should satisfy the following requirements:[8] 1) attainment of a state in which the effect of evolution of heat due to combustion is no more detectable, and 2) minimization of heat exchange as well as heat of stirring correction which may be a cause of experimental error. The corrected temperature-rise was calculated by increasing the length of the main period from eight to twenty readings. A compromise between the two contradictory requirements has been found to be twelve readings both in calibration (using benzoic acid) and in combustion experiments. Thus, twenty readings after the main period have been assigned to the final period.

Energy Equivalent and Energy of combustion. The energy equivalent of the standard calorimetric system $\varepsilon°$(calor.) was calculated by the procedure described by Coops *et al.*[9] The mean and standard deviation of the mean for the energy equivalent was found to be 15162.8 ± 1.3 J K^{-1} from six calibration experiments interspersed between combustion experiments, where uncertainty is the standard deviation of the mean. The standard energy of combustion $\Delta E_c°$ was calculated by the method of Hubbard *et al.*,[10] the final overall precision of the $\Delta E_c°$ mean values being estimated as recommended by Rossini[11] following the scheme presented by Bjellerup.[12] All procedures in the calculation of ΔT, $\varepsilon°$(calor.) and $\Delta E_c°$ were incorporated in a Fortran program*, the computations being carried out with a NEAC 2200 computer of Osaka University.

Table 1. Auxiliary quantities used in the calculation of energy of combustion

Substance		ρ / g cm^{-3}	C_p / J K^{-1} g^{-1}	$(\partial E/\partial P)_T$ / J kPa^{-1} g^{-1}
8-Quinolinol	C_9H_7ON	1.57	(1.21) [a]	(−1.19) [a]
Fuse	$CH_{1.860}O_{0.930}$	1.50	1.70	−2.94

a) Estimated value.

The standard energy of combustion of the cotton fuse $\Delta E_c°$(fuse) was determined by separate combustion experiments and found to be -16507 J g^{-1}.

Auxiliary Quantities. Molecular weight were computed from the 1961 Table of Relative Atomic Weights. Auxiliary data necessary for calculating weights *in vacuo* from weights in air, for correcting the energy of bomb reaction to that of an isothermal reaction at 25 °C and for making the reduction to standard states are given in Table 1. The density and specific heat capacity of the dish (Pt–Rh alloy) were estimated to be respectively 20.50 g cm^{-3} and 0.1464 J K^{-1} g^{-1}.

Results and Discussion

The results of six combustion experiments on 8-quinolinol are given in Table 2. Symbols in the table are similar to those used by Hubbard *et al.*[10] except for $\Delta m(H_2O)$, ΔE_{rot}, and ΔE(std. state). $\Delta m(H_2O)$ is the mass of excess water in the calorimeter can, ΔE_{rot} the energy evolved by the rotation of the bomb and ΔE(std. state) the sum of items 81—86, 87—89, 91 and 93—94 designated by Hubbard *et al.*[10] From these results the following thermodynamic quantities were derived: $\Delta E_c°(c) = -4458.90\pm1.60$, $\Delta H_c°(c) = -4460.76\pm1.60$, $\Delta H_f°(c) = -81.24\pm2.00$ and $\Delta H_f°(g) = 27.6\pm2.6$ kJ mol^{-1}, where the uncertainties are uncertainty intervals defined by Rossini.[11] The standard enthalpy of combustion $\Delta H_c°$ has been calculated by the use of the expression: $\Delta H_c° = \Delta E_c° + \Delta n_g RT$, where Δn_g is the increase in moles of gaseous species in an idealized combustion reaction and R is the gas constant. In the calculation of the standard enthalpy of formation, CODATA key values[13] for $\Delta H_f°(CO_2,g)$ and $\Delta H_f°(H_2O, l)$ and the enthalpy of sublimation value of Horton and Wendlandt[7] for 8-quinolinol have been used. These values are as follows: $\Delta H_f°(CO_2, g) = -393.51\pm0.13$ and $\Delta H_f°(H_2O, l) = -285.830\pm0.042$ kJ mol^{-1}, where uncertainties are those at 95% confidence level and $\Delta H_{subl} = 108.8\pm1.7$ kJ mol^{-1}, where uncertainty is the uncertainty interval.

Combustion experiments were carried out with and without the rotation of the combustion bomb after ignition. No significant difference was found in $\Delta E_c°$ values for both modes. In some experiments nitric acid was analyzed separately for the solutions formed on the side wall and on the upper and lower walls of the bomb. The results in an experiment are 5.6×10^{-4} and 2.1×10^{-4} mol for the solutions on the side

* The Washburn correction portion of the program was rewritten with a slight modification from an ARGOL program supplied by courtesy of Professor S. Sunner, University of Lund, Lund, Sweden.

Table 2. Results of combustion experiments on 8-quinolinol

m^i(compd.)g	0.83862	0.85140	0.84207	0.85751	0.81135	0.82038
m^i(fuse)/g	0.00252	0.00284	0.00296	0.00306	0.00328	0.00271
m^i(H_2O tot.)/g	0.982	1.081	1.076	1.092	0.971	0.986
m(Pt)/g	11.142	11.142	11.142	11.142	11.142	11.142
Δm(H_2O cal.)/g	0.159	0.237	−0.070	0.259	0.293	−0.294
p^i(gas)/MPa	3.044	3.041	3.037	3.040	3.034	3.040
T_i/°C	23.25499	23.24191	23.25053	23.22730	23.32311	23.30232
T_f/°C	24.98287	24.99775	24.98751	24.99433	24.99748	24.99438
ΔT_{corr}/°C	0.02310	0.02467	0.02460	0.02380	0.02501	0.02455
n^f(HNO_3)/mol	0.000722	0.000798	0.000727	0.000767	0.000709	0.000709
ΔE_{ign}/J	6.14	7.77	8.13	7.86	1.86	6.86
ΔE_{rot}/J	10.61	10.33	10.59	0.0	10.60	0.0
ΔE_{diln}(HNO_3)/J	−0.12	−0.13	−0.11	−0.12	−0.11	−0.11
ΔE_{decomp}(HNO_3)/J	42.52	46.99	42.81	45.17	41.75	41.75
ΔE(std. state)/J	15.99	16.40	16.17	16.53	15.37	15.60
ε^i(cont.)/J K^{-1}	16.95	17.36	17.32	17.41	16.84	16.93
ε^f(cont.)/J K^{-1}	17.78	18.20	18.16	18.26	17.64	17.74
ΔE_c°/J g^{-1}	−30719.7	−30716.1	−30717.9	−30721.5	−30707.0	−30718.9

Mean and standard deviation of the mean = -30716.9 ± 4.4 J g^{-1}

wall and on the upper and lower walls, respectively. Judging from the relative availability of water on both portions, nitric acid is more concentrated in the solution on the side wall. The nitric acid solution on the side wall is formed by the reaction of nitrogen oxides with water from the sample. The fact that nitric acid is more concentrated on the side wall is in good agreement with the observation of Armstrong and Marantz[14] that most of nitrogen oxides from the combustion of organic nitrogen compounds not containing hydrogen may not be absorbed by bomb water effectively unless a device to vaporize the water after the combustion is made. The localization of nitric acid in the bomb, however, does not cause a significant systematic error in the determination of the standard energy of combustion because the contribution of the energy of dilution of nitric acid to the total energy is not significant and in addition the energy of dilution does not depend seriously on the concentration in the range 5—10%.

The enthalpy of combustion of 8-quinolinol was reported only briefly by Sullivan and Hunt[15] and Wood and Jones.[16] A large difference of *ca.* 12 kJ·mol^{-1} (*ca.* 0.3%) was found between their values. Our value does not agree with either of them within the assigned uncertainty intervals, but agrees fairly well with the mean of these values ($\Delta H_c^\circ = -4458.9$ kJ·mol^{-1}) cited as a selected value by Domalsky.[17]

This work was carried out with the support of a scientific research fund from the Ministry of Education.

References

1) W. N. Hubbard, C. Katz, and G. Waddington, *J. Phys. Chem.*, **58**, 142 (1954).
2) W. D. Good, D. W. Scott, and G. Waddington, *ibid.*, **60**, 1080 (1956).
3) H. A. Skinner, J. M. Sturtevant, and S. Sunner, "Experimental Thermochemistry," Vol. 2, ed. by H. A. Skinner, Interscience Publishers, London (1962), p. 209.
4) H. Mackle and P. A. G. O'Hare, *Trans. Faraday Soc.*, **54**, 353 (1958).
5) R. S. Jessup, *J. Res. Nat. Bur. Stand.* (U.S.), **29**, 247 (1942).
6) L. Kofler and E. Lindpainter, *Mikrochemie*, **24**, 43 (1938).
7) G. R. Horton and W. W. Wendlandt, *J. Inorg. Nucl. Chem.*, **25**, 241 (1963).
8) J. Coops and K. van Nes, *Rec. Trav. Chim.*, **66**, 131 (1947).
9) J. Coops, R. S. Jessup and K. van Nes, "Experimental Thermochmistry," Vol. 1, ed. by F. D. Rossini, Interscience Publishers, New York, N. Y. (1956), p. 27.
10) R. N. Hubbard, D. W. Scott, and G. Waddington, *ibid.*, p. 75.
11) F. D. Rossini, *ibid.*, p. 297.
12) L. Bjellerup, *Acta Chem. Scand.*, **15**, 121 (1961).
13) *J. Chem. Thermodynamics*, **4**, 331 (1972).
14) G. T. Armstrong and S. Marantz, *J. Phys. Chem.*, **64**, 1776 (1960).
15) H. V. Sullivan and H. Hunt, *ibid.*, **53**, 497 (1949).
16) J. L. Wood and M. M. Jones, *ibid.*, **67**, 1049 (1963).
17) E. S. Domalsky, *J. Phys. Chem. Reference Data*, **1**, 254 (1972).

Kinetic Studies of the Aggregation of Acridine Orange onto Poly-(α,L-glutamic acid)

Motoyuki TSUDA†

Department of Chemistry, Faculty of Science, Hokkaido University, Sapporo 060

(Received November 5, 1974)

The aggregation process of acridine orange (AO) onto the helical poly-α,L-glutamic acid (PLGA) was studied by means of a stopped-flow and rapid-scan spectrophotometer. After the flow stop, a rapid spectral change was observed in which the α-band and the β-band fell, and the γ-band and the polymer band rose. A mechanism of the process was proposed by which after a rapid nucleative process, AO molecules are cooperatively bound to form a dimer and that then the dimer grows to the oligomer and to the polymer of AO which has the form of a super-helix around the core of the α-helix of PLGA.

The main feature of the binding of a number of cationic dyes to polyanions is the so-called metachromasia,[1-3] an effect which has been recognized as due to different binding modes of the dye molecules exhibiting different absorption spectra in the visible region. The absorption bands show that the dye molecules bind to the polyanion in their monomeric forms, or interact with each other on the polyanion to form dimers or aggregates similar to those existing in concentrated aqueous solutions.[4-7] Various theories with regard to the phenomena have been proposed and have been rigorously tested by studying the equilibria[8-19] and the dynamic properties[20-26] of the dye-polymer interaction in aqueous solutions. So far, however, the phenomena have not been able to be interpreted in terms of a generally accepted mechanism.

The interaction of acridine orange (AO) with poly-α,L-glutamic acid (PLGA) has been extensively studied.[18-20] Since PLGA exists predominantly as the α-helix in aqueous solution below about pH 5 and as a random coil above pH 7,[27-28] the role of the structure of the polyanion in the dye-PLGA interaction can be discussed.

Hammes and Hubbard[20] reported kinetic studies of the interaction of AO and PLGA at pH 4.7 and pH 7.5. They proposed a mechanism in which an AO binds very rapidly to a site on the polymer, followed by a slower intramolecular rearrangement. Their results suggested that the same general mechanism appears to be operative for both the helical and random coil forms of PLGA. On the other band, Schwartz and his co-workers[23] proposed a cooperative binding mechanism for the association of AO with PLGA on the basis of thermodynamic and kinetic analyses. Since their measurements, however, followed only the decay of the absorbance of the α-band (monomeric form of AO), the mechanism could not interpret the processes of the formation of the other aggregates.

The associations of AO with itself and with PLGA are both very rapid processes, so the temperature-jump method has been used in most kinetic measurements.[20,23] This method, however, requires an ionic strength of about 0.1 M for the maintenance of the resistance of the solution at an appropriate value. The overall association constant for the AO and PLGA complexes has been reported to be markedly decreased as the ionic strength is increased.[11-14] Because of the above facts, the strong binding processes of the complex cannot be observed in the conventional temperature-jump method. Although the time of observation is limited by its relatively long dead time (slightly less than 1 ms), the stopped-flow method has an advantage in its applicability to a wide range of salt concentrations.[25]

A rapid-scan spectrophotometer was used for the measurement of the change in the spectral pattern after the flow stop. The fall and rise of several spectral bands of the AO and PLGA complexes could successfully be observed by means of this apparatus. In this investigation, the aggregation process of AO onto PLGA was studied in the various ionic atmosphere to clarify the mechanism.

Experimental

The AO was purified according to the following method. An aqueous solution of commercial AO (2 g) purchased from the Merck Co. was titrated with 0.1 M NaOH to pH 10.5. The suspension was then filtered, and the residue was washed with 100 ml of 3×10^{-3} M EDTA. This procedure was repeated. The residue was then dried at 100 °C and dissolved in absolute ethanol. The solution was neutralized with ethanolic HCl, refluxed for 1 hr, and filtered to remove the NaCl formed. The filtrate was passed through an 8× 40 cm acid-washed alumina column in ethanol. The elute comprising the main fraction was then filtered to remove any alumina particles present. The AO–HCl was precipitated from the filtrate by the addition of ether, collected by filtration, and dried under a vacuum. The melting point of the compound was sharp at 181 °C (Ref. 5, 180—181 °C), and the molar extinction at the absorption maximum (492 nm) extrapolated to zero concentration is 6.3×10^4 (6.1×10^4 after Zanker[5]). Generally we prepared a stock solution of 1 mM AO by weighing it in a dry polyethylene bottle. The concentration of AO was determined from the absorbance at 492 nm according to the extrapolated equation[11] for a dilute solution.

The sodium poly-α,L-glutamate was purchased from the Protein Research Foundation (Osaka); it had a weight-average molecular weight of 60,000. The poly-α,L-glutamic acid solution was made by the deionization of the salt with 0.1 M HCl and was dialyzed against frequent changes of the deionized distilled water.[27] Each solution of AO and PLGA was prepared in 2 mM sodium acetate-acetic acid (pH 4.7), adding sodium chloride to adjust the ionic strength to the chosen value. The final pH was maintained approximately

† Present address: Department of Physics, Sapporo Medical College, Sapporo 060.

at pH 4.7 throughout the experiments. In this pH region, PLGA exists predominantly as the α-helix in an aqueous solution.[27,28] All the experiments were performed at 25 °C.

The optical absorption spectra were taken with a recording spectrophotometer (Hitachi EPS-3T). The kinetics of the AO-PLGA reaction was studied using a rapid-scan spectrophotometer equipped with a stopped-flow apparatus (UNION RA-1300). After equal volumes of AO and PLGA solution had been rapidly mixed, the spectral patterns were measured by means of an image detector with a maximum speed of 300 nm/ms and were memorized by a transient recorder. The device contains five channel transient memories. Each digitizes a transient signal with an 8-bit resolution and stores it in a 512-word MOS shift-resister memory. Its sweep time can be varied between 1 ms and 10 s. An analog replica of the original can be recorded on a X-Y recorder as spectral patterns of the transmittance, absorbance, or time resolution difference spectra.

For the kinetic measurements, an absorption or fluorescence stopped-flow apparatus was used. The fluorescence was observed from the right angle to the excitation beam (492 nm), through an interference filter of 552 nm.

Results and Discussion

AO aggregates in an aqueous solution.[5] It is thought that there are at least three types of species; they may be defined as monomers, dimers, and oligomers[5-7] and their absorption bands are located at 492 nm(α-band), 464 nm(β-band), and 445 nm(γ-band), respectively. When AO is mixed with a polyanion in a dilute aqueous solution, the color of either the monomer or the aggregates may appear, depending upon the ionic strength, the pH, and the relative amounts of polymer and dye (P/D ratio).[8-18]

Figure 1 shows the visible absorption spectra of the AO (2.0×10^{-5} M) and PLGA complex at the P/D ratio of 10 while the ionic strength is changed. As the ionic strength is lowered, the shape of the spectrum is continuously changing; that is, the absorbance of the α-band decreases relative to that of β-band, and both the bands fall, while the absorbance of the γ-band and the band around 535 nm rise.

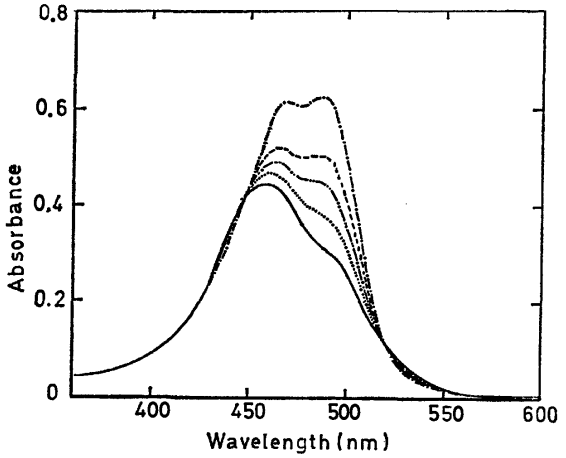

Fig. 1. Effect of ionic strength upon visible absorption spectra of AO-PLGA solutions. Solvent is 0.002 M sodium acetate-acetic acid (pH 4.7) and the ionic strength is adjusted by NaCl. The molarities of AO and PLGA are 2.0×10^{-5} M and 2.0×10^{-4} M, respectively. —— =0.005, ····· =0.01, —·—· =0.05, ---- =0.10, —·— =0.20.

The results suggest that the aggregation of dye was brought about at a low ionic strength.

The formation of these aggregates upon mixing of AO with PLGA at a low ionic strength was measured with the rapid-scan spectrophotometer. Figure 2(a) shows the results on the rapid spectral change in the reaction mixture at the times of 0, 10, 100, and 400 ms after the flow stop, the scanning speed being constant at 150 nm per 1 ms. The abrupt change in the spectra before and after the flow stop shows that almost all of the reaction occurred during the dead time (about 1 ms). After the flow stop, the α-band and the β-band fall, but the change in the other bands is not clear. To clarify the change in these absorption bands, we observed the time resolution difference spectra, which were obtained using the analog device by subtracting the absorbance at an appropriate time from the corresponding absorbance immediately after the flow stop. The results are illustrated in Fig. 2(b); they show that the α-band and β-band fall but γ-band and the band around 535 nm appear slightly. The above facts suggest that the reaction between AO and PLGA does not proceed in a single step, rather, spectrally different steps may be involved.

The mechanism of the binding processes of AO

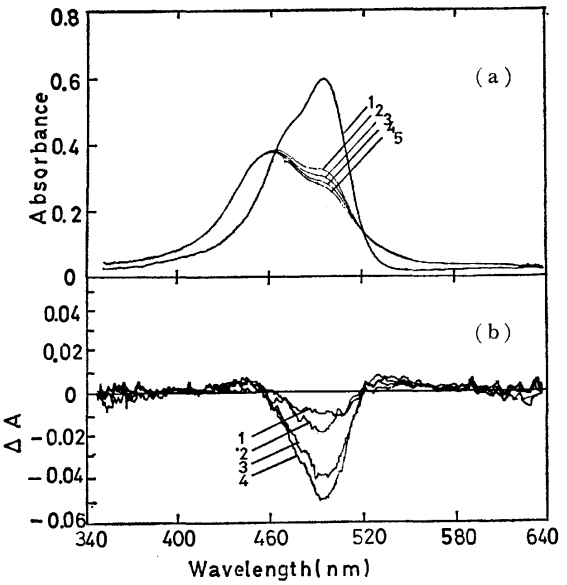

Fig. 2(a). Change of absorption spectra observed by rapid scan spectrophotometer in the reaction of AO (2.0×10^{-5} M) and PLGA (2.0×10^{-4} M) in 0.002 M acetate buffer (pH 4.7) at 25 °C. Scan speed is 150 nm/ms.
1. free AO (2.0×10^{-5} M), 2. immediately after the flow stop, 3. 10 ms after, 4. 100 ms after, 5. 400 ms after.

Fig. 2(b). Time resolution difference spectra observed by rapid scan spectrophotometer. The reaction conditions are the same as those in Fig. 2(a). ΔA is absorbance at appropriate time minus the corresponding absorbance immediately after the flow stop.
1. 4 ms after the flow stop, 2. 10 ms after, 3. 100 ms after, 4. 400 ms after.

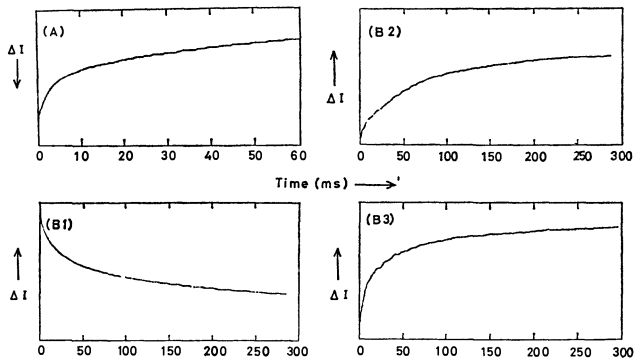

Fig. 3. The time course of AO-PLGA interaction observed by stopped-flow method. The figures are records of analogs replica from transient memories. The reaction conditions are the same as those in Fig. 2(a) and Fig. 2(b).
(A): Fluorescence emission observed at 552 nm through an interference filter (decrease upward).
(B): Change of absorbance of each absorption band. The vertical axis corresponding to the change in optical density which increase upwards.
(B1): 490 nm (α-, β-band).
(B2): 435 nm (γ-band).
(B3): 535 nm.

onto PLGA was studied by means of the stopped-flow apparatus. The decrease in the AO monomer in the species was observed by means of fluorescence quenching,[5] and the formation of the aggregates was followed by the change in the absorbance of the α-band (490 nm), the β-band (435 nm), and the band around 535 nm. Figure 3 shows a replica of the transient-memory recordings of some typical kinetic data. For each absorption band and emission band, a plot of the logarithms of the amplitude of the light intensity change *vs.* time was curved. The non-linear relaxation spectra thus obtained suggest that a cooperative binding of the dye over the polymer or some aggregation processes may take place.

The mean relaxation time (τ^*) of the non-linear relaxation spectra can be obtained in a good approximation during an initial period, with more or less appreciable deviations later on. Accordingly, τ^* was conveniently determind from the pertinent experimental curve.

To make the aggregation processes clear, the effect of the salt concentration on the relaxation time of each spectral band was studied, for the association is thought to involve electrostatic interaction between the oppositely charged dye and residue of the polymer in addition to nonelectrostatic interaction. According to the transition-state theory and the Debye-Hückel theory,[30] the relation between the rate and the ionic strength is given for dilute solutions by;

$$\log k = \log k_0 + 1.02 \cdot Z_a Z_b \sqrt{I} \qquad (1)$$

where Z_a and Z_b are the numbers of the charges on the ion and where k and k_0 are the rate constants at a finite and at an infinite dilution respectively in a given solvent. The mechanism for the overall reaction is not clear now, so we assume that the apparent

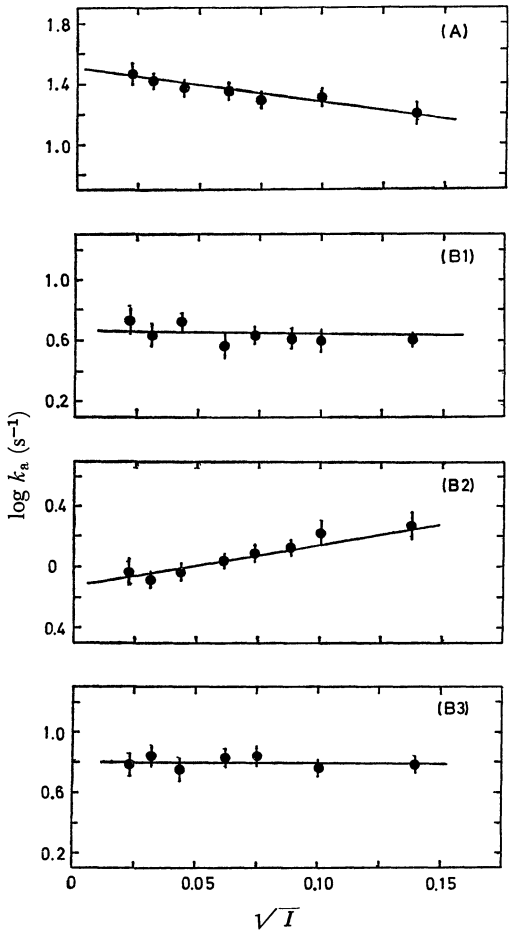

Fig. 4. Plots of $\log k_a$ against the square root of the ionic strength obtained with each spectral band as shown in Fig. 3. The curve number and the reaction conditions except ionic strength are the same as those in Fig. 3.

rate constant is approximately linear to the reciprocal relaxation time at a constant concentration. Equation (1) predicts a linear relationship if $\log k_a$ is plotted against the square root of the ionic strength with a slope proportional to the $Z_a Z_b$ product. Figure 4 shows plots of the apparent rate constants over the range of ionic strength from 5.0×10^{-4} to 2.0×10^{-2}. The results of fluorescence observation give a negative value for the $Z_a Z_b$ product. This shows that the reactants are oppositely charged. As AO is ionized to be cationic at pH 4.7, with its pK_a of 10.45,[5] the other reactant may be the negatively charged site of PLGA. The charge of the site of PLGA can be derived -1.3 ± 0.4 from the values of the product of $Z_a^* Z_b = -1.6 \pm 0.5$ and the effective charge†† of $Z_a^* = +1.2$. The result is consistent with the fact that the side-chain of PLGA is the mononegative

†† The differnce in binding affinity to the charged site of PLGA between the monomer and the dimer of the AO cation is not known. Assuming that Coulombic force may play an important role in the binding force, the effective charge, Z_a^*, of the free AO in the reaction mixture can be estimated for a given reaction. At concentration of AO used (2.0×10^{-5} M), the fraction of the dimer in free AO is estimated to be *ca.* 10%.

anion of the carboxyl group at pH 4.7.

The rate for the decrease in the absorbance of α-band was independent of the ionic strength. This suggests that two or more cationic AO molecules were associated at the occupied site of PLGA, where the negatively charged carboxyl group of the polypeptide had been neutralized by a cationic AO molecule and formed a dimer or oligomers of AO outside the complex. The close resemblance in the magnitude of the rates and the Z_aZ_b products between the rise of the band around 535 nm and the fall of the α-band and β-band indicates that the process of the decay of dimeric AO is the rate-limiting step for the rise of the band around 535 nm. Therefore, the appearance of the band around 535 nm may be due to formation of polymeric AO along the axis of the α-helix of PLGA.

The positive sign of Z_aZ_b observed at the γ-band suggests that both of the reactants are similarly charged ions. It seems reasonable to consider that the cationic AO molecules bind to the similarly charged site of PLGA, where more than two cations have been bound to a carboxylate anion of the side chain of the polypeptide. The effective charge of the Z_a* of the free AO in the reaction mixture can be estimated as $+0.9$, as the similarly charged ions associate with each other in this process. As the value of the $Z_a{}^*Z_b$ product was given as 3.2 ± 0.4 from the results, the charge of the binding site of PLGA can be estimated as 3.5 ± 0.5. These facts show that the residue of PLGA is occupied by four or five cationic AO molecules and that the oligomer bound in the outside of the helical PLGA.

Although the aggregation theory successfully explains the monomer-dimer equilibrium, the nature of the higher aggregates is not yet clear. Schwartz[7] assumed that the spectra of the γ-band is independent of the length of the oligomer. The present work shows that the γ-band appears with the association of five or six AO molecules and that the formation of the further aggregates gives rise to a polymer band around 535 nm. This polymer band of AO has also been confirmed by the CD study of Hatano *et al.*[19]

The results suggest that the primary process of the reaction mechanism is one in which the AO cation binds very rapidly to the carboxyl anion of PLGA and the charge of the binding site is neutralized. This process may be followed by the cooperative binding of a cationic AO molecule to an unoccupied site adjacent to the occupied site of PLGA and by the formation of an oligomer and polymer of AO onto the helical PLGA.

We wish to express our thanks to Dr. M. Yoneyama of Hokkaido University for reading the manuscript. This investigation was supported by the Matsunaga Science Foudation.

References

1) S. E. Sheppard, *Proc. Roy. Soc.*, (London), **A82**, 256 (1909).
2) D. F. Bradley and S. Libson, "Molecular Association (1968).
in Biology," ed. by B. Pullman Academic Press, New York
3) P. Mukerjee and A. K. Ghosh, *J. Amer. Chem. Soc.*, **92**, 6419 (1970).
4) L. Michaelis, *J. Phys. Chem.*, **54**, 1 (1950).
5) V. Zanker, *Z. Phys. Chem.*, (Leibzig), **195**, 225 (1957).
6) M. E. Lamm and D. M. Nerville, *J. Phys. Chem.*, **69**, 3872 (1965).
7) B. H. Robinson, A. Loffler, and G. Schwartz, *J. Chem. Soc. Faraday*, **1973**, 56.
8) A. R. Peacock and J. N. H. Skerrett, *Trans. Faraday Soc.*, **52**, 261 (1956).
9) R. F. Steiner and R. F. Beers, *Science*, **127**, 335 (1958).
10) D. F. Bradley and M. K. Wolf, *Proc. Nat. Acad. Sci. U.S.*, **45**, 944 (1959).
11) A. L. Stone and D. F. Bradley, *J. Amer. Chem. Soc.*, **83**, 3627 (1961).
12) A. M. Michelson, *Ann. Rev. Biochem.*, **30**, 133 (1961).
13) R. W. Armstrong, T. Kurucsev, and U. P. Strauss, *J. Amer. Chem. Soc.*, **92**, 3174 (1970).
14) R. E. Ballard and C. H. Park, *J. Chem. Soc., A*, **1970**, 1340.
15) V. Vitagliano, L. Constantino, and A. Zagari, *J. Phys. Chem.*, **70**, 204 (1966).
16) R. E. Ballard, A. J. McCaffery, and S. F. Mason, *Biopolymers*, **4**, 97 (1966).
17) G. Schwartz, S. Klose, and W. Balthasar, *Eur. J. Biochem.*, **12**, 454 (1970).
18) B. C. Myhr and J. G. Foss, *Biopolymers*, **10**, 425 (1971).
19) M. Hatano, M. Yoneyama, and Y. Sato, *ibid.*, **12**, 895 (1973); Y. Sato and M. Hatano, This Bulletin, **46**, 3339 (1973).
20) G. G. Hammes and C. D. Hubbard, *J. Phys. Chem.*, **70**, 1615 (1966).
21) G. G. Hammes and C. D. Hubbard, *ibid.*, **70**, 2889 (1966).
22) H. J. Li and D. M. Crothers, *J. Mol. Biol.*, **39**, 461 (1969).
23) G. Schwartz and W. Balthasar, *Eur. J. Biochem.*, **12**, 461 (1970).
24) V. Vilagliano, *J. Phys. Chem.*, **77**, 1922 (1973).
25) C. Steenbergen, Jr. and S. C. Mohr, *Biopolymers*, **12**, 791 (1973).
26) K. Akasaka, M. Sakoda, and K. Hiromi, *Biochem. Biophys. Res. Commun.*, **40**, 1239 (1970); M. Sakoda, K. Hiromi, and K. Akasaka, *Biopolymers*, **10**, 1003 (1971); M. Sakoda, K. Hiromi, and K. Akasaka, *J. Biochem.*, **71**, 891 (1972).
27) A. Wada, *Mol. Phys.*, **3**, 409 (1960).
28) D. S. Olander and A. Holtzer, *J. Amer. Chem. Soc.*, **90**, 4549 (1968).
29) G. Schwartz, *Biopolymers*, **6**, 837 (1968).
30) G. Schwartz, *Eur. J. Biochem.*, **12**, 442 (1970).
31) K. J. Laidler, "Chemical Kinetics," McGraw-Hill, New York (1965).

Apparent Viscosities of Ferric Oxide–Water Suspensions

Noboru MORIYAMA

Research Laboratories, Kao Soap Company, Minatoyakushubata, Wakayama 640-91

(Received July 11, 1974)

The effects of various types of anionic surfactants and inorganic phosphates on the apparent viscosities of ferric oxide–water suspensions of high pigment concentrations are examined. The additions of surfactants or inorganic phosphates to the suspensions cause depressions in their apparent viscosities from values of more than 10000 centipoise (cP) to about 10 cP. The concentration of the surfactants or the inorganic phosphates required to depress the apparent viscosity, which is designated as C_0, is highly dependent upon the alkyl-chain length of the 1-1-type surfactants, the degree of the polymerization of the surfactants of the type of the vinyl copolymers and the degree of the condensation of the surfactants of the type of the formalin condensates or inorganic phosphates. With the 1-1-type surfactants, the values of the C_0 decrease with the increases in the alkyl-chain length, and the surfactants with much shorter alkyl-chain lengths, such as Na octyl sulfate, linear-chain Na hexylbenzene sulfonate, and Na butyl-naphthalene sulfonate, have no marked viscosity depression effects. With the formalin condensates and the inorganic phosphates, the values of C_0 decrease with the degree of condensation. With the vinyl copolymers, the C_0 show smallest values at the appropriate degree of polymerization, *e.g.*, about 10—40 for the Na salt of polyacrylic acid. Both the absolute value of the zeta potential and the amount of adsorption increase remarkably in the concentration regions showing marked viscosity depressions. The viscosity depressions of the suspensions upon the additions of the surfactants or inorganic phosphates can be qualitatively explained by taking into account the contributions of the zeta potential values and concentrations to the dispersion-coagulation of the pigment particles.

It has been well known that the additions of surfactants or electrolytes to pigment–water suspensions with high pigment concentrations and with apparent viscosities of more than 10000 centipoise (cP) show the apparent viscosities to be depressed to about 10 cP.[1-9] The viscosity depressions caused by the additions of surfactants or electrolytes have been widely used as a measure of the dispersibility of surfactants.[5,10]

Many studies of the pigment–water suspensions of high pigment concentrations have been reported from the view-point of viscometric behavior,[6-9] but these few studies have been from the view point of surface chemistry, such as zeta potential and adsorption. Marked viscosity depressions have been observed in the aqueous suspensions of various sorts of inorganic pigments, such as ferric oxide, titanium dioxide, zinc oxide, and carbon black. In the present paper, ferric oxide was used as the inorganic pigment, which had no special meaning.

The present paper will describe the effects of the alkyl-chain length of 1-1-type anionic surfactants, the degree of the polymerization of vinyl copolymers, and the degree of the condensation of formalin condensates or inorganic polyphosphates on the apparent viscosities of 50 wt% ferric oxide suspensions, and will discuss these effects in relation to the zeta potential, adsorption, and the pH data.

Experimental

Materials. All the surfactants used were prepared according to a procedure described earlier.[11] Their chemical compositions, degrees of polymerization or condensation, and abbreviations are listed in Table 1. The orthophosphates (NaH_2PO_4 and Na_3PO_4), pyrophosphates ($Na_2H_2P_2O_7$ and $Na_4P_2O_7$), and tripolyphosphate ($Na_5P_3O_{10}$) were of a reagent grade. The tetrapolyphosphate ($Na_6P_4O_{13}$) was a specially prepared commercial product. The phosphates were obtained from the Wako Pure Chemicals Co. Most of the surfactants and inorganic phosphates described above are known to have dispersing power and are used widely.[10]

Pigments. Ferric Oxide (Toda Color 130R) obtained from the Toda Industries Co., which had not been treated, was washed with water until there was no change in the conductivity of the filtrate. The surface area, as determined by the B.E.T. method using nitrogen at −195 °C, was 7.0 m^2/g. The average particle radius, calculated from electron microscopic observation, was 0.2 μm. The particles have a sphere-like form. The isoelectric point of ferric oxide, determined according to the method of Parks *et al.*,[12] is 5.5.

Apparent Viscosity Measurements. Aqueous solutions of the materials, which refer to the surfactants or inorganic phosphates, were prepared by dissolving the desired quantities of the materials in distilled water of 500 ml. Into a beaker with a 750-ml capacity, a 400-ml portion of the material solutions thus prepared was poured, and maintained at 25± 0.1 °C in a water bath. The desired quantities of ferric oxide were then added to the material solutions. After the above ferric oxide–material solution suspensions had been stirred with a Homomixer, TK type (Tokushu Kiki Industries Co.), for five minutes, the apparent viscosities were determined using a Viscometer (Tokyo Kiki Manuf. Co. Type BM, rotor 60 rpm).

Sedimentation Velocity Measurements. Suspensions containing 1 wt% ferric oxide were prepared by the dilution of the desired quantities of the same suspensions used for the apparent viscosity measurements in supernatant solutions of their suspensions obtained by removing the ferric oxide particles with a refrigerated-automatic Ultracentrifuge, Serval Model RC-2B. Into graduated test cylinders with a 30-ml, capacity and 30 cm in height, 30 ml portions of the suspension thus prepared were poured, and the mixtures were maintained at 25 °C in the thermostat. The cylinders were turned end-over-end ten times and then allowed to stand. By the sedimentation of the pigment particles, a sedimentation boundary was formed between the material solution and the suspension. The positions, h, of the sedimentation boundaries were read periodically and were plotted *vs.* the standing time, t. The time (designated as the sedimenting time, $T_{1/2}$) during which h falls from a 30-cm height to a 15-cm height is calculated from the h *vs.* t curves and used as a measure of the sedimentation velocity.

Sedimentation Volume Measurements. Suspensions containing 5 wt% ferric oxide were prepared by the dilution of

Table 1. Chemical composition, average molecular weight and abbreviation of surfactants

Type	Chemical composition	Degree of condensation or polymerization	Abbreviation
1-1 type anionic surfactants	Na octyl sulfate		C_8S
	Na decyl sulfate		$C_{10}S$
	Na decyl sulfate		$C_{12}S$
	Na tetradecyl sulfate		$C_{14}S$
	linear-chain Na hexylbenzene sulfonate		C_6BS
	linear-chain Na octylbenzene sulfonate		C_8BS
	linear-chain Na decylbenzene sulfonate		$C_{10}BS$
	linear-chain Na docdecylbenzene sulfonate		$C_{12}BS$
	linear-chain Na tetradecylbenzene sulfonate		$C_{14}BS$
	Na butylnaphthalene sulfonate		C_4NS
Formalin condensate	Na salt of formalin condensate of β-naphthalene sulfonic acid	3.7	NSF-3.7
	Na salt of low formalin condensate of butylnaphthalene sulfonic acid	3.5	C_4NSF-3.5
	Na salt of high formalin condensate of butylnaphthalene sulfonic acid	5.1	C_4NSF-5.1
Vinyl copolymer	Na salt of polyacrylic acid	12	PA-12
	Na salt of polyacrylic acid	33	PA-33
	Na salt of polyacrylic acid	64	PA-64
	Na salt of polyacrylic acid	146	PA-146
	Na salt of homopolymer of maleic acid	7.5	PM
	Na salt of copolymer of vinyl acetate and maleic acid	14	VacM
	Na salt of copolymer of styrene and maleic acid	19	SM
	Na salt of copolymer of α-olefine (C_8) and maleic acid	16	OM

the desired quantities of the suspensions used for the apparent viscosity measurements into supernatant solutions of their suspensions obtained by the method described above. Into graduated test cylinders with a 30-ml capacity and 30 cm in height, 30-ml portions of the suspensions thus prepared were poured, and the mixtures were maintained at 25 °C in the thermostat. The test cylinders were turned end-over-end ten times, and then allowed to stand. The positions of the sedimentation boundary between the material solution and the suspension, formed by the sedimentation of ferric oxide particles, were lowered with the standing times. After the rates of their lowerings became almost zero, the positions of the sedimentation boundaries were measured and the sedimentation volumes of ferric oxide particles were calculated from these data.

Average Radius of the Particle Measurements. The average radius of the particle was calculated by means of microscopic observation by the dilution of a quantity of the suspensions used for apparent viscosity measurements into supernatant solutions of their suspensions.

Electrophoretic Mobility Measurements. The mobility measurements of ferric oxide particles were made using a Zeta-Meter (Zeta-Meter, Inc.) by the dilution of a quantity of the suspensions used for the apparent viscosity measurements into supernatant solutions of their suspensions.

Adsorption Measurements. The amounts of the adsorption of the materials onto ferric oxide particles were calculated from measurements of the difference in concentrations of the material solutions before and after preparing the suspensions. The material solutions after preparing the suspensions described above refer to the same supernatant solutions as those used for sedimentation velocity measurements. The concentrations of the surfactants having benzene ring or naphthalene ring in the molecule, among the surfactant solutions, were calculated by measuring the intensity of the absorption band at about 260 nm using a Shimadzu Spectrophotometer, UV-200. On the other hand, those having no benzene ring or naphthalene ring in the molecule were measured with a TOC Meter, Toshiba-Beckman Model 102, which determined the amount of carbon dioxide generated by firing the solutions at 950 °C, using CoO as the catalyst. The concentrations of orthophosphate and polyphosphate solutions were measured according to the directions of Nakahara.[13]

pH Measurements. The pH values of the suspensions used for the apparent viscosity measurements were measured with a pH meter, TOA Electronics, Ltd. The pH values of the suspensions were controlled by adding an aqueous sodium hydroxide solution or an aqueous hydrochloric acid solution to the suspensions.

Results and Discussion

In Fig. 1, the apparent viscosities of ferric oxide–water suspensions containing 30, 50, 60, and 70 wt% ferric oxide are plotted as a function of the concentration of PA-33. Figure 1 shows that the additions of PA-33 to the ferric oxide–water suspensions with apparent viscosities of more than 10000 cP have their viscosities depressed to about 10 cP, and that the concentrations of PA-33 required to depress the vis-

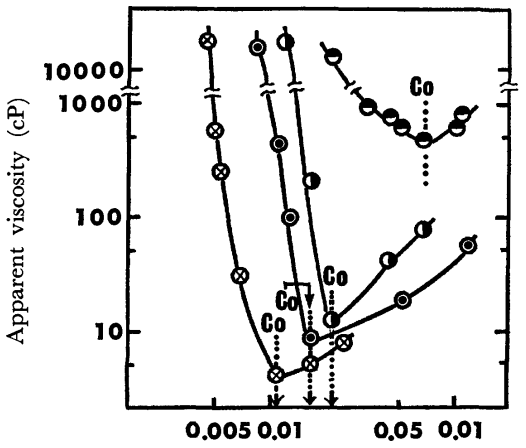

Fig. 1. The effects of the concentrations of PA-33 on the apparent viscosities of ferric oxide–water suspensions containing 30(⊗), 50(⊙), 60(◑) and 70(◓) wt% ferric oxide at 25 °C.
The initial concentrations of PA-33 refer to the mole concentrations expressed per monomer unit.

cosities up to about 10 cP, which are designated as C_0, increase with the increase in the pigment concentrations of the suspensions. As the concentrations of PA-33 approach C_0, the apparent viscosities of the suspensions decrease remarkably, but they increase gradually above C_0. These results suggest that the values of C_0 can be used as a measure of the apparent viscosity depression effects.

The values of C_0 and the apparent viscosities at C_0 for ferric oxide–aqueous-surfactant or inorganic phosphate-solution (weight ratio of 50/50) suspensions are listed in Table 2. Both the values of C_0 and the apparent viscosities at C_0 for 1-1-type anionic surfactants tend to decrease with the increases in the alkyl-chain length of the surfactants. The viscosity depression effects of the surfactants with a short alkyl-chain length, such as C_8S, $C_{10}S$, C_6BS, C_8BS, and C_4NS, are small,

Table 2. Values of the C_0 and apparent viscosities at the C_0 for ferric oxide–aqueous surfactant or inorganic phosphate solution (50/50) suspensions

Materials	Values of the C_0 (mol/l)	Apparent viscosities (cP) at the C_0
1-1 type anionic surfactants		
C_8S	—	>1000
$C_{10}S$	0.077	55
$C_{12}S$	0.035	10
$C_{14}S$	0.029	26[b]
C_6BS	—	1000
C_8BS	0.28	650
$C_{10}BS$	0.042	35
$C_{12}BS$	0.040	30
$C_{14}BS$	0.035	10
C_4NS	—	>1000
Formalin condensates		
NSF-3.7	0.023	9
C_4NSF-3.5	0.020	8
C_4NSF-5.1	0.017	8
Vinyl copolymer		
PA-12	0.018	7
PA-33	0.016	8
PA-64	0.032	25
PA-146	0.053	27
PM	0.014	10
VacM	0.020	11
SM	0.018	9
OM	0.012	10
Orthophosphate		
NaH_2PO_4	—	>1000
Na_3PO_4	—	>1000
Polyphosphate		
$Na_2H_2P_2O_7$	0.0067	10
$Na_4P_2O_7$	0.0042	7
$Na_5P_3O_{10}$	0.0041	8
$Na_6P_4O_{13}$	0.0032	7

a) Concentrations (mol/l) of vinyl copolymers and formalin condensates are expressed in those of monomer unit of them, respectively. b) Measured at 40 °C because of insolubility of $C_{14}S$ at 25 °C.

as may be seen in Table 2. These results show that the viscosity depression effects of 1-1-type anionic surfactants have a correlation with the critical micelle concentration (CMC) values of the surfactants, and that the surfactants with large CMC values have not marked viscosity depression effects. The values of C_0 for the formalin condensates decrease with the increases in the degree of condensation. The C_0 for PA series becomes smallest at a degree of polymerization of about 33. However, the changes in the degree of the polymerization from 12 to 33 have only a little influence on the values of C_0. As may be seen in Table 2, there exist only small differences in the values of C_0 among the vinyl copolymers except PA-64 and PA-146. These polymers have degrees of polymerization from 7.5 to 33, and the C_0 values are expressed in monomer units. Therefore, it can be concluded that the C_0 values undergo only a little influence by the changes in the chemical composition of the polymers, whereas they are greatly influenced by the changes in the degrees of polymerization. The C_0 values for polyphosphates are small compared with those of the surfactants described above, and tend to lower with the degree of the condensation of polyphosphates. With orthophosphates, on the other hand, no viscosity depression effects can be found.

In Fig. 2, the apparent viscosity, $T_{1/2}$, the sedimentation volume, and the average radius of pigment particles for the suspensions are plotted as functions of the concentration of PA-33, NSF-3.7, and $Na_5P_3O_{10}$ respectively. As may be seen in Fig. 2, a correlation can be found among the apparent viscosity, $T_{1/2}$, the

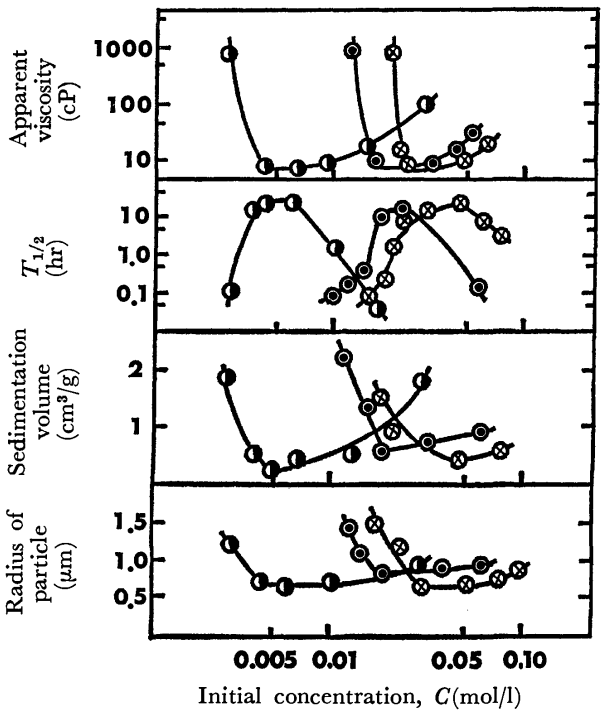

Fig. 2. Apparent viscosity, sedimenting time, $T_{1/2}$, sedimentation volume and average radius of the particle *vs.* initial concentration, C, curves for PA-33 (⊙), NSF-3.7 (⊗) and $Na_5P_3O_{10}$ (◑).
The concentrations of PA-33 and NSF-3.7 refer to the mole concentrations expressed per monomer unit of them.

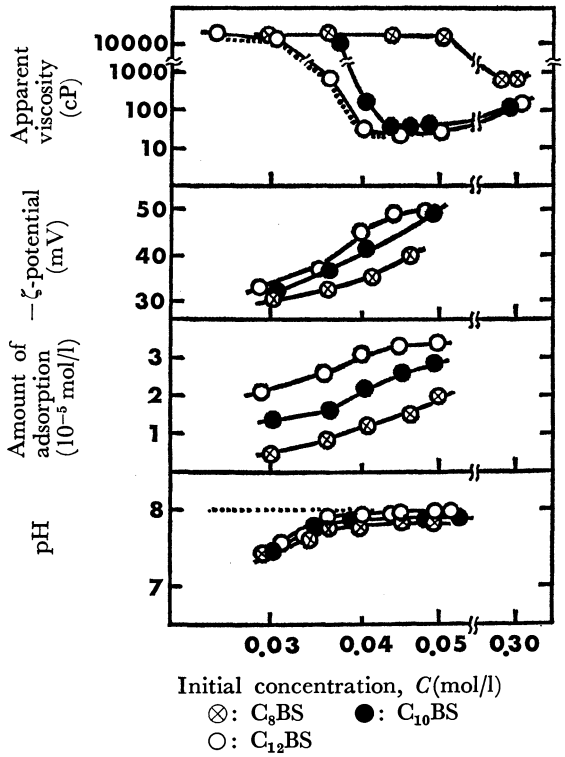

Fig. 3. The effects of the alkyl-chain length of linear-chain Na alkylbenzene sulfonates on the apparent viscosities of 50 wt% ferric oxide suspensions, and their relations with zeta potential, adsorption and pH data.
A dotted line refers to the apparent viscosity *vs.* log concentration, *C*, curve for $C_{12}BS$ at a controlled pH of 8.0.

sedimentation volume, and the average radius of the particle data. These results suggest that the viscosity changes in the suspensions are based upon the dispersion-coagulation of the ferric oxide particles.

Figure 3 shows the effects of the alkyl-chain length of linear-chain Na alkylbenzene sulfonate on the apparent viscosities, and their relations with the zeta potential, the adsorption, and the pH data. The calculation of the zeta potential, ζ, on the basis of the electrophoretic-mobility, u, measurements is done using the Helmholtz-Smoluchwski equation for the systems of $\kappa a \geq 200$,[14] where κ is the reciprocal of the thickness of the double layer, and a, the particle radius:

$$u = \frac{E\zeta\varepsilon}{4\pi\eta} \qquad (1)$$

where η and ε are the viscosity and the dielectric constant of the medium respectively, and where E is the applied electric field.

Both the absolute values of the zeta potential and the amounts of adsorption for $C_{10}BS$ and $C_{12}BS$ increase remarkably in the concentration regions showing marked viscosity depressions, as may be seen in Fig. 3. The absolute values of the zeta potential and the amounts of adsorption for C_8S are very small compared with those for $C_{10}S$ and $C_{12}S$ in all the concentrations tested.

The viscosity changes in the suspensions are due to the dispersion-coagulation of the ferric oxide particles, as has been described above. Therefore, the viscosity changes in the suspensions may be explained by taking into account the contributions of the zeta potential values and the thickness of the double layer, $1/\kappa$*), to the dispersion-coagulation of the particles, that is, by applying the DLVO theory.[16] With 1-1-type anionic surfactants, the contributions of the zeta potential and $1/\kappa$ to the dispersion-coagulation of the particles increase with the increases in the zeta potential values, and decrease with the increases in the concentrations of the surfactant ions. As may be seen in Fig. 3, the amount of adsorption is in the order of $C_{12}BS > C_{10}BS > C_8BS$ at the same initial concentration, which shows that the equilibrium concentration at the same initial concentration is in the order of $C_8BS > C_{10}BS > C_{12}BS$. Accordingly, the negative contributions of the concentrations to the viscosity depressions increase in the order $C_8BS > C_{10}BS > C_{12}BS$. The apparent viscosities for C_8BS decrease up to about 600 cP at very high concentrations, as may be seen in Fig. 3. Perhaps this viscosity depression is related to the contribution of the zeta potential. In the high concentrations, however, precise electrophoretic mobility measurements cannot be made, because electrolysis may occur between the anodic and cathodic electrodes. Therefore, the calculation of the zeta potential cannot be made at high concentrations. As may be seen in Fig. 3, the apparent viscosities for $C_{10}BS$ and $C_{12}BS$ show considerable increases at very high concentrations. This may be due to the increase in the negative contribution of the concentration to the viscosity depression.

Generally, the stabilities of lyophobic colloids and the suspensions depend upon the pH of the systems.[17,18,11] Figure 3 shows that the pH values of the suspensions dispersed with each surfactant of C_8BS, $C_{10}BS$, and $C_{12}BS$ become almost the same at the same concentration, and undergo very little changes with an increase in the concentration, except for those in the region of low concentrations. The dotted line in Fig. 3 refers to the viscosity *vs.* concentration curve for $C_{12}BS$ at a controlled pH of 8.0. The dotted line is nearly in accord with the solid line of $C_{12}BS$, for which the pH is not controlled, this shows that the pH changes of the suspensions accompanied by changes in the concentrations have no appreciable influences on the viscosities.

It can be concluded from these results that the viscosity depression data can be explained by the zeta potential and the adsorption data. The weak viscosity depression effects of 1-1-type anionic surfactants with short alkyl chain lengths, such as C_8S and C_6BS, shown in Table 2 may be due to the lack of the amounts of adsorption and their contributions to the zeta potential.

Figure 4 shows the effects of the degree of the condensation of the formalin condensates on the apparent

---

* $$1/\kappa = \left(\frac{\varepsilon KT}{4\pi e^2 \sum n_i Z_i^2}\right)^{1/2}$$

where e is the elementary charge, z_i, the valency, n_i, the number of ions of the species, i, per cubic centimeter, K, Boltzmann's constant, and T, the absolute temperature.[15]

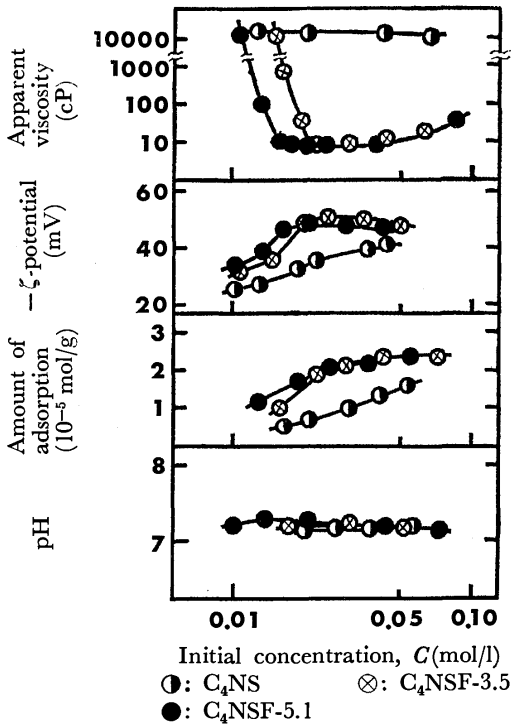

Fig. 4. The effects of the degree of the condensation of alkylnaphthalene sulfonate formalin condensates on the apparent viscosities of 50 wt% ferric oxide suspensions, and their relations with zeta potential, adsorption and pH data.

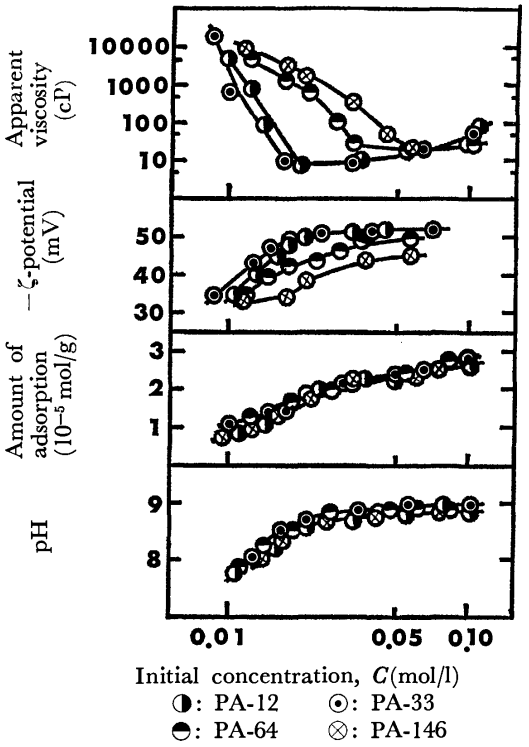

Fig. 5. The effects of the degree of the polymerization of Na salt of polyacrylic acid on the apparent viscosities of 50 wt% ferric oxide suspensions, and their relations with zeta potential, adsorption and pH data.

viscosities, and their relations with the zeta potential, the adsorption, and the pH data. With C_4NS, no marked viscosity depression effects are observed. With C_4NSF-3.5 and C_4NSF-5.1, on the other hand, marked viscosity depression effects are observed, and the value of C_0 for C_4NSF-5.1 is smaller than that for C_4NSF-3.5. That is, the viscosity depression effects are highly dependent upon the degree of condensation. As may be seen in Fig. 4, the zeta potential and the adsorption data are closely correlated with the viscosity data. The pH of the suspensions dispersed with each surfactant of C_4NS, C_4NSF-3.5, and C_4NSF-5.1 show almost the same values at the same concentration. These results suggest that the degrees of the condensation of the formalin condensates have great influences on the viscosity depression effects, and that their effects are due to the marked increases in the absolute values of the zeta potential and the amounts of adsorption with the increases in the degree of condensation.

Figure 5 shows the effects of the degree of the polymerization of the Na salt of polyacrylic acid (PA) on the viscosities, and their relations with the zeta potential, the adsorption, and the pH data. Figure 5 shows that PA with low degrees of polymerization, such as PA-12 and PA-33, show marked viscosity depressions in the region of low concentrations, whereas those with high degrees of polymerization, such as PA-64 and PA-146, show small viscosity depressions in the region of low concentrations. The absolute values of the zeta potential for the PA series increase remarkably in the concentration regions showing marked viscosity depressions, and the order of C_0 corresponds to the order of the zeta potential. Similarly, the amounts of adsorption for the PA series increase in the concentration regions showing viscosity depressions. However, no pronounced differences in the amounts of adsorption for the PA series are observed, although the amounts of adsorption may be expected to increase with the degree of polymerization. The absolute values of the zeta potential for high degrees of polymerization are small compared with those for low degrees of polymerization; this suggests that the contributions of the amounts of adsorption to the zeta potentials decrease with the increases in the degree of polymerization. In other words, the concentration of PA on the pigment surface, *i.e.*, the parts of PA which contribute to the zeta potential, decrease with an increase in the degree of polymerization. This may be attributed to the difference in the adsorption conformation among the PA on the pigment surface. Generally, the bridging action of polymers increases with an increase in the degree of polymerization,[19,20] and serves to promote coagulation. However, in the case of the PA tested the bridging action is negligible, because the degree of polymerization is not large enough to have a large bridging action.

The pH values of the suspensions dispersed with each PA show almost equal values at the same concentration; this shows that the pH's of the suspensions are not dependent upon the degrees of polymerization.

Figure 6 shows the effects of the degree of the condensation of inorganic phosphates on the viscosities, and their relations with the zeta potential, the adsorption, and the pH data. Sodium dihydrogen phosphate

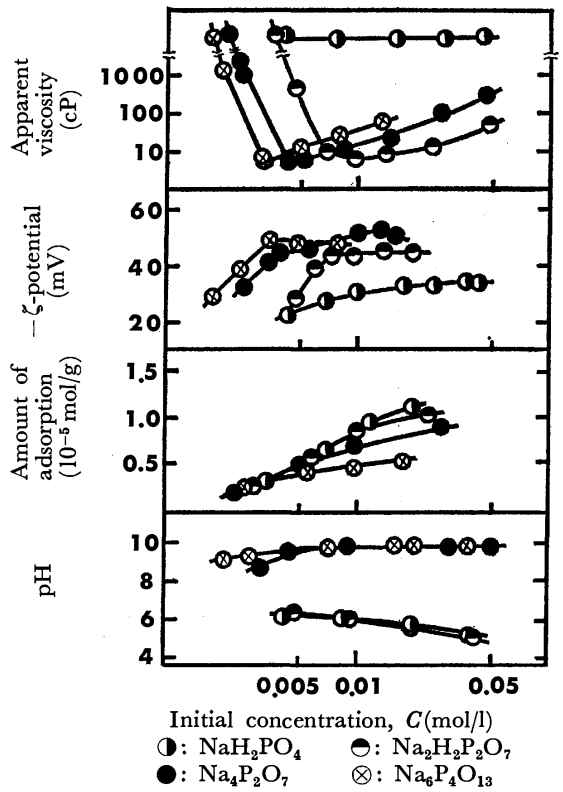

Fig. 6. The effects of the degree of the condensation of inorganic phosphates on the apparent viscosities of 50 wt% ferric oxide suspensions, and their relations with zeta potential, adsorption and pH data.

(NaH_2PO_4) has no marked viscosity depression effects, whereas acid sodium pyrophosphate ($Na_2H_2P_2O_7$), sodium pyrophosphate ($Na_4P_2O_7$), and sodium tetrapolyphosphate ($Na_6P_4O_{13}$) have such effects. The values of C_0 are in the order of $Na_6P_4O_{13}<Na_4P_2O_7,<Na_2H_2P_2O_7$. The zeta potential data are closely related with the viscosity data, whereas the adsorption data are not necessarily related with the viscosity data. The pH's of the suspensions dispersed with each phosphate of NaH_2PO_4 and $Na_2H_2P_2O_7$ show almost the same values lower than the isoelectric point (pH 5.5) of the ferric oxide particles at very high concentrations. Similarly, the pH's of the suspensions dispersed with each phosphate of $Na_4P_2O_7$ and $Na_6P_4O_{13}$ show almost the same values, much higher than the isoelectric point of the particles. In the pH range below the isoelectric point, where the pigment particle has positive charge, the anionic phosphate ion adsorbs on the particle and cancels the charge. On a further increase in adsorption, the particle comes to have a negative charge.[13] The pH's of an aqueous solution of $Na_2H_2P_2O_7$ and NaH_2PO_4** are lower than the isoelectric point of the particle. Therefore, the phosphate ion may be consumed to cancel the positive charge of the particle in the region of low concentrations. The absolute values of the zeta potential for $Na_2H_2P_2O_7$ are much smaller than those for $Na_4P_2O_7$ and $Na_6P_4O_{13}$ in the region of low concentrations, whereas the amounts of adsorption for $Na_2N_2P_2O_7$ and NaH_2PO_4 are larger than those for $Na_4P_2O_7$ and $Na_6P_4O_{13}$. These may be explained in relation to the isoelectric point of the particle described above. The zeta potential and the adsorption data show that the contributions of the amount of adsorption to the zeta-potential values increase with an increase in the valency of the phosphate ions. The pH's of the suspensions dispersed with $Na_2H_2P_2O_7$ and NaH_2PO_4 show somewhat higher values than the isoelectric point of the pigment particle in the region of low concentrations. This may be because the majority of the phosphate ions are adsorbed upon the particles.

It can be concluded from these results that the viscosity depression effects increase with the increase in the degree of the condensation of the phosphates, and have close relations with the zeta potential, the adsorption, and the pH data, especially the isoelectric point of the pigment particle.

According to the DLVO theory,[16] the total potential energy, V, between the two sphere particles (ferric oxide particles) for a system in which $\kappa a \gg 1$ and $H \ll a$ is given by:

$$V/a = \frac{\varepsilon\zeta^2}{2} \ln (1+e^{-\kappa H}) - \frac{A}{12H} \qquad (2)$$

where A is the Hamaker constant, and H, the shortest distance between the two particles.

Using the value of A (4.5×10^{-13}) calculated by Fowkes,[21] the value of V/a can be calculated from Eq. (2). The value of V/a depends upon the absolute value of the zeta potential and the value of $1/\kappa$, *i.e.*, the thickness of the double layer. The thickness of the double layer is inversely proportional to the square of the valency of the material ion and the concentration of the material ion, as has been described above. Accordingly, the value of V/a increases with the absolute value of the zeta potential and decreases with the increase in the concentration and the valency of the material ion.

The values of V/a for aqueous 50 wt% ferric oxide suspensions dispersed with 1-1-type surfactants such as $C_{12}BS$ have been calculated from Eq. (2) and plotted as a function of H in Fig. 7. In this figure, the apparent viscosity *vs.* $\log C$ curve is also shown to facilitate examination of the correlation of the V/a data with the apparent viscosity data. The abscissa in Fig. 7 is expressed in terms of the initial concentration of the surfactant. The calculation of V/a is made by using the equilibrium concentration of the surfactant, which was measured for the 50 wt% suspension. The values of V/a become positive over certain ranges of H for the concentrations of the numbers of 2 and 3, showing the suspensions with low apparent viscosity values. In other words, in the suspensions of the numbers of 2 and 3, repulsive forces enough to disturb the coagulation of the particles work between the particles. Therefore, the apparent viscosities of the suspensions may have small values. On the other hand, the values of V/a become negative in all the H values for the concentration of the number of 1, showing suspensions of very high viscosity values. In other words, in this suspension no repulsive force enough to disturb the coagula-

** The pH's of aqueous solutions of $Na_2H_2P_2O_7$ and NaH_2PO_4 change from 4.7 at 0.0045 mol/l to 4.18 at 0.45 mol/l, and from 4.98 at 0.0042 mol/l to 4.65 at 0.042 mol/l, respectively.

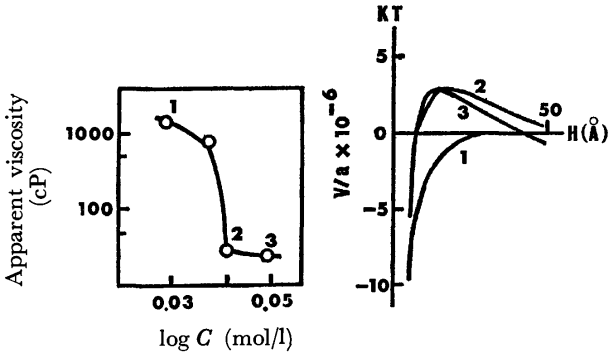

Fig. 7. The relations between V/a and apparent viscosity data for $C_{12}BS$.
1: initial concentration; 0.0287 mol/l
equilibrium concentration; 0.0084 mol/l
ζ-potential; −33 (mV)
2: initial concentration; 0.0402 mol/l
equilibrium concentration; 0.0089 mol/l
ζ-potential; −45 (mV)
3: initial concentration; 0.0489 mol/l
equilibrium concentration; 0.0152 mol/l
ζ-potential; −49 (mV)

tion of the particles works between the particles. Therefore, the particles coagulate, and the apparent viscosity of the suspension may have a large value. A relation similar to that found for the systems of $C_{12}BS$ is also found for the systems of C_8BS and $C_{10}BS$. These results show that the viscosity changes of 50 wt% ferric oxide suspensions upon the addition of surfactants can be explained by taking into account the zeta potential value, the valency, and the concentration of the surfactants, *i.e.*, the application of DLVO theory. Not only the viscosity changes in ferric oxide suspensions, but also the viscosity changes in other pigment suspensions, such as titanium dioxide and zinc oxide, can be explained qualitatively by the DLVO theory. This will be reported in a forthcoming paper.

The author wishes to express his thanks to Professor Sei Hachisu of the Institute for Optical Research, Kyoiku University for his valuable suggestions, and to Dr. Takashi Takeuchi and Dr. Kunihiko Nagase of the Research Laboratories for their encouragement and the permission to publish this paper.

References

1) H. V. Olphen, *Discuss. Faraday Soc.*, **11**, 82 (1951)
2) N. Street, *J. Colloid Sci.*, **12**, 1 (1957).
3) D. H. Declerck and G. J. Su, *J. Amer. Ceram. Soc.*, **49**, 252 (1966).
4) A. L. Johnson and F. H. Norton, *ibid.*, **24**, 189 (1941).
5) T. Takeuchi, F. Tokiwa, Y. Tanino, and K. Hattori, *Kogyo Kagaku Zasshi*, **74**, 2239 (1971).
6) H. A. Kersey, *Trans. Instin. Chem. Engrs.*, **40**, 141 (1962).
7) H. Kambe, *Zairyo*, **17**, 459 (1968).
8) H. Kambe, *ibid.*, **15**, 265 (1966).
9) J. Seto, A. Amaya, K. Umeya, *ibid.*, **16**, 537 (1967).
10) K. Hattori, and Y. Komeda., *Yushi*, **17**, 80 (1964), *ibid.*, **17**, 79 (1964).
11) N. Moriyama, *J. Colloid Interface Sci.*, **50**, 80 (1975).
12) G. A. Parks and P. L. De. Bruyn, *J. Phys. Chem.*, **66**, 967 (1962).
13) Y. Nakahara, *Nippon Kagaku Kaishi*, **1972**, 695.
14) J. Th. G. Overbeek, "Colloid Science I," ed. by H. R. Kruyt, Elsevier Co., Amsterdam-Houston-New York-London (1952), pp. 207—212.
15) J. Th. G. Overbeek, *Advan. Colloid Sci.*, **3**, 97 (1950).
16) E. J. W. Verwey, and J. Th. G., Overbeek, "Theory of the Stability of Lyophobic Colloids," Elsevier Co., Amsterdam-New York (1948).
17) E. Matijević and L. J. Stryker, *J. Colloid Interface Sci.*, **22**, 68 (1966).
18) E. Matijević and G. E. Januer, *ibid.*, **21**, 197 (1966).
19) M. Noda, *Nippon Kagaku Zasshi*, **82**, 1611 (1961).
20) Y. Toyoshima, *ibid*, **82**, 1295, 1297, 1301, (1961).
21) F. M. Fowkes, "Chemistry and Physics of Interfaces," ed. by S. Ross, American Chemical Society Publications Washington, D. C. (1965), p. 7.

The Adsorption of the Ampholytic Surfactant and the Anionic Surfactant at the Nitrogen-Solution Interface from the Mixed Aqueous Solution

Akio NAKAMURA

Department of Chemistry, Faculty of Science, Tokyo Metropolitan University, Setagaya-ku, Tokyo 158

(Received November 8, 1974)

The amounts of adsorption of an ampholytic surfactant, *N*-dodecyl-*β*-alanine(NDA), and an anionic surfactant, sodium alkylsulfate(SAS), at nitrogen–solution interface from aqueous equimolar mixtures of them were measured directly by the radiotracer method, using tritiated and non-tritiated samples of NDA and ^{35}S-labeled and non-labeled samples of SAS: sodium tetradecylsulfate(STS), sodium dodecylsulfate(SDS), and sodium decylsulfate(SDeS). The adsorption of both components of the mixed systems was observed at concentrations lower than those for the systems containing each component alone. A stronger adsorption of NDA than that of SAS was observed for all mixed systems. The overall area per alkyl chain at the maximum adsorption was about 26 Å^2 for each system, showing the adsorbed layer to be in a highly condensed state. Electrophoresis measurements, together with surface tension measurements of NDA-SDS systems and the elemental analysis of the precipitates from concentrated NDA-SDS solutions, suggested the presence of a 1 : 1-complex formed between NDA and SDS. The Gibbs adsorption isotherm for the binary system was derived. The calculated amounts of adsorption agreed with the observed values. A linear relationship was found to hold between the logarithm of the constants of complex formation and the number of carbon atoms of SAS. A free energy of the complex formation of −0.50 kcal per mole of the methylene group was found.

A number of studies have been made of the interaction between organic cations and anions in solutions, such as surfactant–surfactant[1–6] and surfactant–dye[7–11] systems, where the formation of ion pairs or association complexes may occur. Especially in an aqueous solution containing anionic and cationic surfactants, surface tension depression and micelle formation[1,6] have been observed at lower concentrations than in single-surfactant solutions, suggesting the formation of a complex with high surface activity and a mixed micelle.

Similar effects can be expected to occur in an aqueous mixture of ampholytic and ionic surfactants. However, studies of such mixtures are rather rare.[12] In the present study, the measurements of the adsorption of the ampholytic surfactant, *N*-dodecyl-*β*-ananine (NDA), and anionic surfactants including sodium tetradecylsulfate(STS), sodium dodecylsulfate(SDS), and sodium decylsulfate(SDeS) from equimolar aqueous solutions of them were made by the radiotracer method, together with measurements of the surface tension of these systems. The Gibbs adsorption isotherm for an aqueous system containing two surfactants and an equimolar complex was derived and was confirmed to be applicable to the system. The formation of a complex between two solute species was inferred, and the equilibrium constants of complex formation and the free energy of complex formation per methylene group of surfactants were estimated.

Experimental

Materials. Tritiated NDA was synthesized from tritiated dodecylamine and *β*-propiolactone and was purified as has been reported.[13] The specific activity of the sample was about 16 Ci/mol. ^{35}S-labeled sodium alkylsulfate, STS, SDS, and SDeS were synthesized by allowing them to react the corresponding alcohols with ^{35}S-labeled sulfuric acid, were purified by repeated recrystallization from ethanol, and were dried *in vacuo*. The specific activity of the samples was about 1 Ci/mol. The water used was prepared by refluxing ordinary distilled water with acid permanganate, then by distilling it from an alkaline permanganate solution, and finally by distilling twice using a Hysil flask.

Methods. The radiotracer method of adsorption measurement was similar to that reported previously.[14] Two solutions of the same composition were prepared, one containing ^{3}H-NDA and SAS, and the other, ^{35}S-SAS and NDA, in order to measure the amounts of the adsorption of both components for a given solution separately. The surface tension was measured by the Wilhelmy plate method. The time dependence of the surface tension was self-recorded, and the curve was extrapolated to an infinite time in order to obtain an equilibrium value. All the measurements were made at 30 °C in the neutral pH region, where NDA molecules have been confirmed to be in the zwitterionic state.[15]

Results and Discussion

Surface Tension. Figure 1 shows the surface tension *vs.* concentration curves of NDA and equimolar mixtures of NDA and SAS's of 4 to 14 carbon

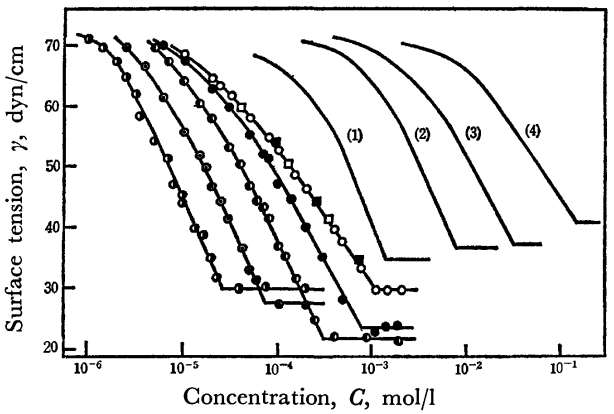

Fig. 1. Surface tension *vs.* concentration of NDA-SAS, NDA and SAS solutions.
○: NDA solution
mixed solution of NDA and
◑: STS, ⊙: SDS, ◐: SDeS, ●: sodium octylsulfate
□: sodium hexylsulfate, ■: sodium butylsulfate
SAS solution: (1) STS, (2) SDS, (3) SDeS, (4) sodium octylsulfate

atoms in a molecule. The abscissa shows the concentration of each component of the mixed solutions. The surface tension of SAS is also shown for the sake of comparison.[16] It is noticeable that DNA shows a lower critical micelle concentration and a smaller slope than those of SAS. The surface tension of NDA–SAS mixtures in an equimolar ratio is generally far lower than that expected from the surface tensions of solutions containing each component alone.

Thus, a synergistic effect of surface activity was confirmed. The effect increases with the increase in the surface activity of SAS's. This suggests some kind of interaction between NDA and SAS's, depending on the hydrocarbon chain length of the latter.

Adsorption. Figures 2, 3, and 4 show the observed amounts of the adsorption of both NDA and SAS from their equimolar mixtures for the systems of NDA–STS, NDA–SDS, and NDA–SDeS respectively. The amount of adsorption is larger for NDA than for SAS, and the amounts of the adsorption of NDA and SAS increase at a nearly constant ratio with the increase in the concentration, tending toward saturation. The amount and the molar fraction of the adsorption of SAS in the mixed systems increase with the increase in their alkyl chain length.

The adsorbed layers observed in the present study show an overall area of about 26 Å^2 per molecule and are highly condensed compared with those of each of the components, which show the values of 43 Å^2 per molecule for NDA[13] and 52 Å^2 for SDS[14] at their saturated adsorption. The value of 26 Å^2 is even smaller than that of the mixed solution containing anionic and cationic surfactants, *i.e.*, 30 Å^2.[4] These facts also suggest the interaction of NDA with SAS in the adsorbed layer.

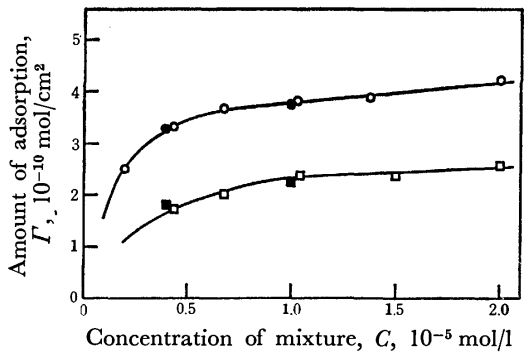

Fig. 2. Amount of adsorption of NDA and STS.
Observed value ○: NDA, □: STS
Calculated value ●: NDA, ■: STS

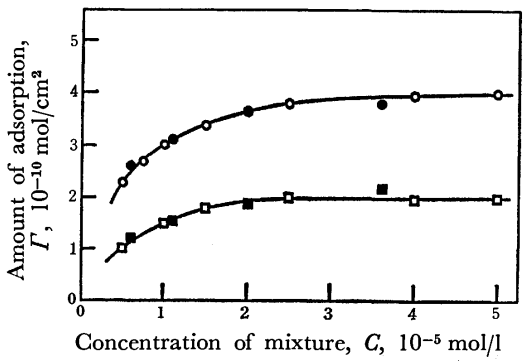

Fig. 3. Amount of adsorption of NDA and SDS.
Observed value ○: NDA, □: SDS
Calculated value ●: NDA, ■: SDS

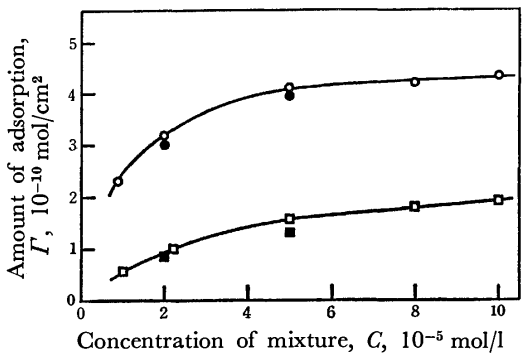

Fig. 4. Amount of adsorption of NDA and SDeS.
Observed value ○: NDA, □: SDeS
Calculated value ●: NDA, ■: SDeS

As regards the interactions between oppositely charged organic ions in a bulk solution, the formation of a complex with a 1 : 1-molar ratio has been reported for surfactant–surfactant and surfactant–dye systems by many investigators on the basis of studies of conductometry,[2,8,9] spectrophotometry,[3,11] the elemental analysis of precipitates,[3,5,8] and polarography.[10] Similar interactions of NDA with SDS in an acid solution, and with dodecyltrimethylammonium bromide in an alkaline solution, have been investigated.[12] However, the interaction between an anionic surfactant such as SAS and the zwitterionic NDA in the near neutral pH region[15] has not yet been experimentally confirmed.

In order to confirm whether or not a 1 : 1-complex forms in the present case, the electrophoresis of NDA in an aqueous SDS solution, elemental analysis of the precipitates obtained from NDA–SDS mixtures were carried out. A surface tension *vs.* composition curve was also constructed in order to examine the complex formation.

Electrophoresis. As is shown in Fig. 5, a U-tube 0.7 cm in diameter and 30 cm in length, with an opening with a rubber stopper 10 cm from a porous plate at the bottom, was used for this purpose. Platinum electrodes were put in both arms of the tube. An equimolar solution of 4×10^{-5} mol/l ^{3}H-NDA and

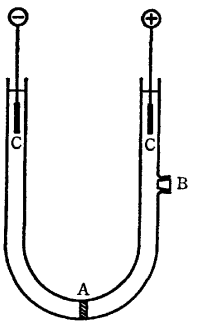

Fig. 5. Apparatus for electrophoresis.
A: porous plate, B: small opening with rubber stopper, C: platinum electrodes

SDS was introduced into the left arm while the same solution without radioactivity was introduced in the right arm. Then, a 200-volt DC current was applied between the electrodes about 30 cm apart through the solution; the migration of ^{3}H-NDA into the right arm was detected by measuring the radioactivity of a sample of about 1 μl of the solution taken out by means of a microsyringe through the rubber stopper. When the left electrode was made negative as shown, the radioactivity began to be detected several minutes after applying the DC voltage. In the absence of SDS, the migration of NDA was not detected even after a prolonged time. This indicates no net charge in the NDA, that is, the zwitterionic state of NDA in the solution without SDS and the net negative charge of NDA in the mixed solution, which would be evidence of NDA–SDS complex formation. Here, the size of the complex formed may not be so large as an ordinary micelle, since the concentration is sufficiently below the breakpoint of the surface tension *vs.* concentration curve shown in Fig. 1.

Elemental Analysis. When NDA and SDS solutions of concentrations sufficiently higher than that used for surface tension measurements were mixed at about 20 °C, a white precipitate appeared. The results of the elemental analysis of the precipitates are shown in Table 1. The molar ratio of NDA to SDS was conventionally estimated from the nitrogen-to-carbon ratio as shown in the last column. The values are found to be nearly unity for the wide range of SDS : NDA molar ratios of the solutions studied. Thus, the 1 : 1-complex formation can be confirmed, at least in the state of the precipitate, suggesting that 1 : 1-complex ions may also exist in the solution.

Surface Activity. Figure 6 shows the surface tension plotted against the molar ratio of NDA to SDS plus NDA in the solution with the total concentration kept constant at 2×10^{-5} mol/l (Curve 1), together with its deviation from the surface tension calculated assuming the additivity of the surface tension depression for each component (Curve 2). Curve 2 exhibits a distinct maximum at the molar ratio of 1 : 1. Again, this suggests a complex formation in the aqueous solution between NDA and SDS at this ratio.

TABLE 1. ELEMENTAL ANALYSIS OF PRECIPITATES FROM NDA-SDS SOLUTIONS

Composition of solution		Composition of precipitate		Molar ratio of precipitate
SDS	NDA	nitrogen	carbon	NDA/SDS
1 mM	1 mM	2.50%	54.12%	1.068
2	1	2.10	53.13	0.914
10	1	2.40	52.02	1.067

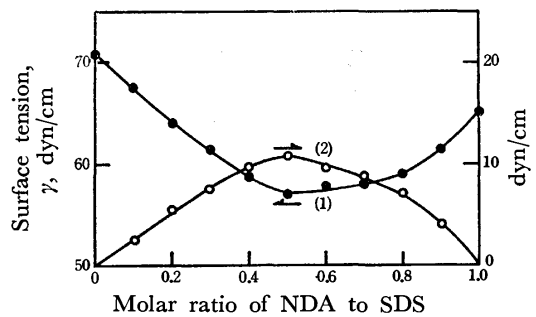

Fig. 6. Surface tension of NDA-SDS system.
(1) Surface tension of NDA-SDS system, total concentration; 2×10^{-5} mol/l.
(2) Deviation of surface tension from the additivity (see text).

The Gibbs Adsorption Isotherm for the Binary System of the Surfactants. The Gibbs adsorption isotherm giving the amount of each component adsorbed from the mixed aqueous solution of ampholytic and anionic surfactants was derived. The Gibbs adsorption isotherm is written, in its general form, as:[17]

$$-\mathrm{d}\gamma/RT = \sum_i \Gamma_i \,\mathrm{d}\ln a_i \qquad (1)$$

where γ denotes the surface tension, and Γ_i and a_i, the surface excess and the activity of the i'th solute in the solution respectively. Equation (1) is rewritten for a solution containing the ampholytic (NDA) and the anionic (SAS) surfactants as:

$$-\mathrm{d}\gamma/RT = \Gamma_\mathrm{D}\,\mathrm{d}\ln C_\mathrm{D} + \Gamma_\mathrm{Na}\,\mathrm{d}\ln C_\mathrm{Na} + \Gamma_\mathrm{A}\,\mathrm{d}\ln C_\mathrm{A} + \Gamma_\mathrm{C}\,\mathrm{d}\ln C_\mathrm{c} \qquad (2)$$

where the activities are replaced by concentrations, since the concentration of the surfactants used is of the order of magnitude of 10^{-5} mol/l; subscripts D, Na, A, and C refer to the alkylsulfate, the sodium, the ampholyte, and the complex ions respectively. Here, as has been mentioned above, we have sufficient reason to assume the 1 : 1-complex formation between NDA and SAS. Therefore, the following equation can be expected to hold:

$$C_\mathrm{C}/C_\mathrm{A}C_\mathrm{D} = K \qquad (3)$$

where K is the equilibrium constant of the complex formation. We also obtain the following equation from the condition of electrical neutrality in the adsorbed phase:

$$\Gamma_\mathrm{Na} = \Gamma^\mathrm{D} \qquad (4)$$

From Eqs. (2), (3), and (4), we obtain:

$$-\mathrm{d}\gamma/RT = \Gamma^\mathrm{D}(\mathrm{d}\ln C_\mathrm{D} + \mathrm{d}\ln C_\mathrm{Na}) + \Gamma^\mathrm{A}\,\mathrm{d}\ln C_\mathrm{A} \qquad (5)$$

where $\Gamma^\mathrm{A}=\Gamma_\mathrm{A}+\Gamma_\mathrm{C}$ and $\Gamma^\mathrm{D}=\Gamma_\mathrm{D}+\Gamma_\mathrm{C}$ are the total amounts of the adsorption of NDA and SAS respectively. In order to obtain Γ^D and Γ^A, we should derive two equations from Eq. (5). For this purpose, Eq. (5) is differentiated under two appropriate conditions. First, we differentiate Eq. (5) with respect to the logarithm of the equimolar concentration, keeping the molar ratio of NDA to SAS constant at unity:

$$-[\mathrm{d}\gamma/RT\,\mathrm{d}\ln C]_{1:1} = \Gamma^\mathrm{D}[(\mathrm{d}\ln C_\mathrm{D}/\mathrm{d}\ln C)_{1:1} + (\mathrm{d}\ln C_\mathrm{Na}/\mathrm{d}\ln C)_{1:1}] + \Gamma^\mathrm{A}(\mathrm{d}\ln C_\mathrm{A}/\mathrm{d}\ln C)_{1:1} \qquad (6)$$

where C denotes the concentration of the equimolar mixture given by:

$$C = C_\mathrm{A} + C_\mathrm{C} = C_\mathrm{D} + C_\mathrm{C} = C_\mathrm{Na} \qquad (7)$$

From Eqs. (3) and (7), we obtain, for the equimolar mixture:

$$(\mathrm{d}\ln C_D/\mathrm{d}\ln C)_{1:1} = (\mathrm{d}\ln C_A/\mathrm{d}\ln C)_{1:1}$$
$$= (C/C_A)(\mathrm{d}C_A/\mathrm{d}C)_{1:1}$$
$$= 2KC/(1+4KC-\sqrt{1+4KC}) \quad (8)$$

From Eqs. (6), (7) and (8), we obtain:

$$I_{1:1} = (p+1)\Gamma^D + p\Gamma^A \quad (9)$$

where:

$$I_{1:1} = -(\mathrm{d}\gamma/RT\,\mathrm{d}\ln C)_{1:1}$$
$$p = 2KC/(1+4KC-\sqrt{1+4KC})$$

Next, we differentiate Eq. (5) with respect to the logarithm of the total concentration of SAS, keeping the total concentration of NDA constant:

$$-[\mathrm{d}\gamma/RT\,\mathrm{d}\ln C^D]_{C^A} = \Gamma^D[(\mathrm{d}\ln C_D/\mathrm{d}\ln C^D)_{C^A}$$
$$+ (\mathrm{d}\ln C_{Na}/\mathrm{d}\ln C^D)_{C^A}]$$
$$+ \Gamma^A(\mathrm{d}\ln C_A/\mathrm{d}\ln C^D)_{C^A} \quad (10)$$

where:

$$C^A = C_A + C_C, \quad C^D = C_D + C_C = C_{Na} \quad (11)$$

By substituting Eq. (11) into Eq. (3) and differentiating with respect to C^D, while keeping C^A constant, the following equations are obtained:

$$(\mathrm{d}C_D/\mathrm{d}C^D)_{C^A} = (KC_D+1)/(2KC_D+KC^A-KC^D+1)$$
$$(\mathrm{d}C_A/\mathrm{d}C^D)_{C^A} = -KC_A/(2KC_A+KC^D-KC^A+1)$$

which, give at $C^D=C^A$:

$$(\mathrm{d}C_D/\mathrm{d}C^D)_{C^A,C^D=C^A} = (KC_D+1)/(2KC_D+1) \quad (12)$$
$$(\mathrm{d}C_A/\mathrm{d}C^D)_{C^A,C^D=C^A} = -KC_A/(2KC_A+1) \quad (13)$$

Further, we obtain from Eqs. (3) and (11), with $C^D=C^A$:

$$(C^D/C_D) = (C^D/C_A) = 2KC^D/(-1+\sqrt{1+4KC^D}) \quad (14)$$

By putting Eqs. (12), (13), (14) and $(\mathrm{d}\ln C_{Na}/\mathrm{d}\ln C^D)_{C^A}=1$ (from Eq. (11)) into Eq. (10),

$$I_{A,1:1} = (q+1)\Gamma^D - r\Gamma^A \quad (15)$$

is obtained, where:

$$I_{A,1:1} = -[\mathrm{d}\gamma/RT\,\mathrm{d}\ln C^D]_{C^A,C^D=C^A}$$
$$q = KC^D(1+\sqrt{1+4KC^D})/(1+4KC^D-\sqrt{1+4KC^D})$$
$$r = KC^D/\sqrt{1+4KC^D}$$

Equations (9) and (15) finally give:

$$\Gamma^A = [(x^2+6x+1)/2(x+1)^2]I_{1:1} - [(3x+1)/(x+1)^2]I_{A,1:1} \quad (16)$$

$$\Gamma^D = [(x-1)/2(x+1)]I_{1:1} + [1/(x+1)]I_{A,1:1} \quad (17)$$

where

$$x = \sqrt{1+4KC^D}$$

By using Eqs. (16) and (17), Γ^A and Γ^D can be calculated for each system. The values of $I_{1:1}$ in Eqs. (16) and (17) can be obtained from the slopes of the curves for the mixed systems shown in Fig. 1. The values of $I_{A,1:1}$ can be obtained from the slopes of the surface tension *vs.* C^D curves at $C^D=C^A$. The curves obtained for NDA–STS, NDA–SDS, and NDA–SDeS systems are shown in Figs. 7 and 8. The arrows in the figures indicate the equimolar concentration of $C^D=C^A$, where the slopes give the respective values of $I_{A,1:1}$ for these systems. Using these data of $I_{1:1}$ and $I_{A,1:1}$, the values of K were determined so as to obtain the best fit between the calculated and observed Γ^A's and Γ^D's.

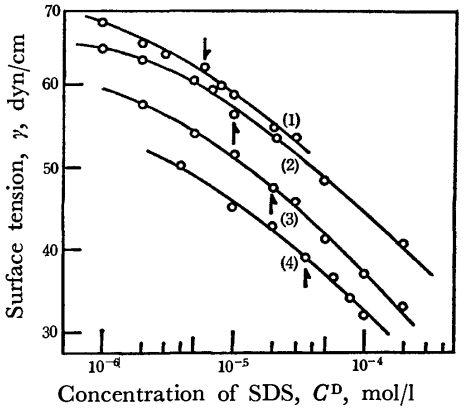

Fig. 7. Surface tension of mixed system *vs.* concentration of SDS.
concentration of NDA (10^{-5} mol/l)
(1): 0.6, (2): 1.0, (3): 2.0, (4): 3.6

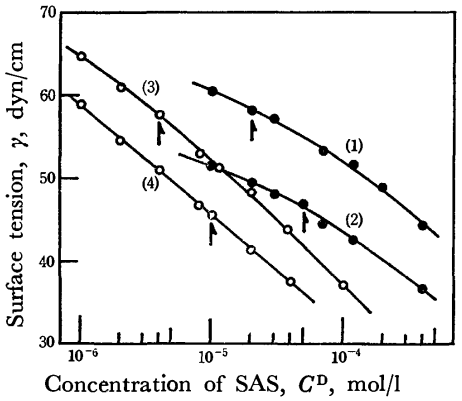

Fig. 8. Surface tension of mixed system *vs.* concentration of SAS.
(●: SDeS, ○: STS).
concentration of NDA (10^{-5} mol/l)
(1): 2.0, (2): 5.0, (3): 0.4, (4): 1.0

The best-fit Γ's thus calculated are shown, together with the observed values, in Figs. 2, 3, and 4.

The values of K were found to be 3.36×10^5, 6.54×10^4, and 1.32×10^4 mol/l for NDA–STS, NDA–SDS, and NDA–SDeS systems respectively. In the case of the interaction of SDS with a cationic surfactant(dodecyltrimethylammonium bromide) with the same hydrocarbon chain length as NDA, the equilibrium constant of complex formation has been determined by conductometry to be 1.67×10^4 mol/l.[2] The overall agreement of those results with ours suggests that the interaction between SAS and the ampholyte NDA is roughly the same in magnitude as that between SAS and the cationic surfactant. The fractions of complex formation in the solution as expressed by C_C/C^D were calculated to be 0.42, 0.55, and 0.70 for NDA–SDeS, NDA–SDS, and NDA–STS systems respectively at a concentration slightly less than the breakpoints of the curves in Fig. 1.

The Free Energy of Complex Formation. Figure 9 shows the relationship between ln K and the number of carbon atoms in the hydrocarbon chain of SAS. A linear relationship with a positive slope is found to hold. This result shows that the interaction between

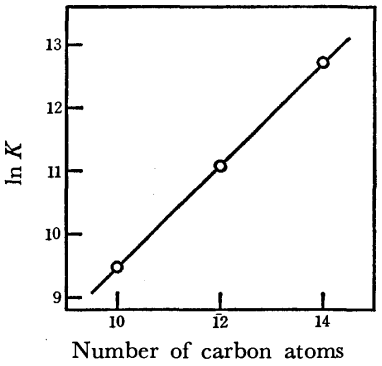

Fig. 9. ln K *vs.* number of carbon atoms in hydrocarbon chain of sodium alkylsulfate.

hydrocarbon chains affects the complex formation in addition to the electrostatic interaction. The free energy change in the complex formation calculated according to the $\Delta G^\circ = -RT \ln K$ relation is found to decrease by 0.50 kcal/mol for each increase in the methylene group of SAS. The value can be regarded as the free energy of hydrophobic interaction per mol of the methylene group of the surfactants, since the value is of the same order of magnitude as has been evaluated for amino acid side chains, *i.e.*, -0.5 to -0.6 kcal/mol for the hydrophobic bond.[18] These facts support the 1 : 1-complex formation between NDA and SAS molecules due to ionic and hydrophobic interactions.

The author expresses his hearty thanks to Professor Tsunetaka Sasaki of Tokai University for his kind discussions and suggestions.

References

1) H. Lange and M. J. Schwuger, *Kolloid-Z.*, **243**, 120 (1970); M. J. Schwuger, *ibid.*, **243**, 129 (1971).
2) M. Mitsuishi and M. Hashizume, This Bulletin, **46**, 1946 (1973).
3) R. V. Scowen and J. Leja, *Can. J. Chem.*, **45**, 2821 (1967).
4) J. M. Corkill, J. F. Goodman, S. P. Harrold, and J. R. Tate, *Trans. Faraday Soc.*, **63**, 247 (1967).
5) H. W. Hoyer and I. L. Doerr, *J. Phys. Chem.*, **68**, 3494 (1964).
6) H. W. Hoyer, A. Marno, and M. Zoellner, *ibid.*, **65**, 1804 (1961); H. W. Hoyer and A. Marno, *ibid.*, **65**, 1807 (1961).
7) W. U. Malik and S. P. Verma, *ibid.*, **70**, 26 (1966); R. Haque and W. U. Malik, *ibid.*, **67**, 2082 (1963); M. Hayashi, This Bulletin, **34**, 119 (1961); T. Kondo and K. Meguro, *ibid.*, **32**, 267 (1959); T. Kondo, K. Meguro, and H. Nito, *ibid.*, **32**, 857 (1959).
8) K. Yamaki, *Kogyo Kagaku Zasshi*, **65**, 1854 (1962).
9) K. Yamaki, *ibid.*, **65**, 1861 (1961).
10) S. Hayano, H. Kageyama, and T. Suzuki, *ibid.*, **68**, 2129 (1965).
11) T. Kondo, *Nippon Kagaku Zasshi*, **76**, 1374 (1955).
12) W. P. Evans and R. A. Hudson, *4th Int. Congr. Surface Active Substances*, 725 (1964).
13) T. Okumura, A. Nakamura, K. Tajima and T. Sasaki, This Bulletin, **47**, 2986 (1974).
14) K. Tajima, M. Muramatsu, and T. Sasaki, *ibid.*, **43**, 1991 (1970).
15) A. Nakamura, K. Tajima, and T. Sasaki, *ibid.*, **48**, 214 (1975).
16) K. Tajima, *Nippon Kagaku Kaishi*, **73**, 883.
17) E. A. Guggenheim, "Thermodynamics," North Holland Publishing Co., Amsterdam (1957), p. 50.
18) G. Nemethy and H. A. Scheraga, *J. Phys. Chem.*, **66**, 1773 (1962).

The Reflection Spectra of Complex Salts of the Tetracyanoquinodimethane Anion Radical

Yukako Oohashi and Tadayoshi Sakata*

The Institute for Solid State Physics, The University of Tokyo, Roppongi, Minato, Tokyo 106

(Received November 11, 1974)

Reflection measurements of the pressed pellets of two 2 : 3 complex salts and six 1 : 2 complex salts of the tetracyanoquinodimethane (TCNQ) anion radical were carried out over the 5000—43000 cm^{-1} range by the use of Avery's method. The polarized normal-incidence reflection was measured for the $Ph_3PCH_3(TCNQ)_2$ single crystal. The observed results were examined on the basis of the composite-system method. For 2 : 3 salts, the transition energy and the oscillator strength are interpreted by the use of the N-A-A model (N: $TCNQ^0$ and A-A: TCNQ anion dimer); it is concluded that the interaction between the two components, N and A-A, is weak. In the solid-state spectra of 1 : 2 salts, the assignments were made by the use of the polarization results of the normal-incidence reflection of the $Ph_3PCH_3(TCNQ)_2$ crystal. Besides the four transitions corresponding to those of 2 : 3 salts, two new CT bands with weak intensities were observed and assigned. Except for quinolinium$(TCNQ)_2$, a spectral change correlative to the electrical conductivity was found in the 1 : 2 salts and discussed in relation to the extent of the delocalization of the negative charge of $(TCNQ)_2^-$. The spectrum of quinolinium$(TCNQ)_2$ exhibits a remarkable intensity decrease compared with those of the other 1 : 2 salts.

It is known that anion radical salts of 7,7,8,8-tetracyanoquinodimethane (TCNQ) exhibit interesting physical properties. The 1 : 2 complex salts, $M^+(TCNQ)_2^-$, and the 2 : 3 complex salts, $(M^+)_2(TCNQ)_3^{2-}$, have been especially extensively investigated with respect to their structure[1-5] and their magnetic,[6-12] electrical,[13-16] and optical[17-22] properties. Previously, we measured the reflection intensity of the simple salts of the TCNQ anion radical, and discussed three typical types of crystalline electronic states and the correlation between the intensity of the interradical charge-transfer (CT) band and the singlet-triplet splitting of the ground state.[22] On the basis of this knowledge of the electronic structures of the simple salts, we aimed to investigate the electronic states of the complex salts containing formally-neutral TCNQ ($TCNQ^0$) besides the anion radical ($TCNQ^-$). In the present study, we measured the polarized normal-incidence reflection for a single crystal of methyltriphenylphosphonium$(TCNQ)_2$, $Ph_3PCH_3(TCNQ)_2$ and discussed the character of each electronic transition on the basis of these polarization results. Furthermore, we measured the reflection of the pressed pellets of eight complex salts of the TCNQ anion radical and obtained the oscillator strength (f) for each transition. On the basis of these experimental results (peak positions and oscillator strengths) and the knowledge of the electronic structures of the simple salts, we discuss the electronic structure of complex salts, together with its relation to the electrical and the magnetic data.

Experimental

Materials. The samples used in this experiment were prepared by the method described in the literature.[13] The eight complex salts investigated were morpholinium$_2(TCNQ)_3$ ($Mor_2(TCNQ)_3$), $Cs_2(TCNQ)_3$, $(CH_3)_3NH(TCNQ)_2$, $Ph_3PCH_3(TCNQ)_2$, $(C_2H_5)_3NH(TCNQ)_2$, *N*-ethylquinolinium $(TCNQ)_2$(EtQ$(TCNQ)_2$), bipyridinium$(TCNQ)_2$ (Bip$(TCNQ)_2$), and quinolinium$(TCNQ)_2$ (Q$(TCNQ)_2$). Large single crystals suitable for the measurement of the polarized normal-incidence reflection were obtained for $Ph_3PCH_3(TCNQ)_2$.[13]

Measurements and Analysis. The reflection intensities were usually measured with pressed pellets of the samples over the range from 5000 to 43000 cm^{-1}. The experimental details are the same as those described in a previous paper.[23] The polarized normal-incidence reflection of the single crystal was measured for $Ph_3PCH_3(TCNQ)_2$ over the range from 5000 to 37000 cm^{-1}. The analysis of these reflection data was carried out by Avery's method for the pressed pellets, and by Kramers-Kronig transformation for the single crystal. The treatment of the inaccessible spectral regions in the Kramers-Kronig analysis follows the method of Roessler.[24] The A and B values of the approximate equation of:

$$\theta(\omega_0) = A \ln\left|\frac{a+\omega_0}{a-\omega_0}\right| - \frac{1}{\pi}\int_a^b \ln\sqrt{R(\omega)}\,\frac{\mathrm{d}}{\mathrm{d}\omega} \times\left(\ln\left|\frac{\omega+\omega_0}{\omega-\omega_0}\right|\right)\mathrm{d}\omega + B\ln\left|\frac{b+\omega_0}{b-\omega_0}\right|$$

were determined from the observed reflectivities in the zero-absorbing region, the observation being carried out in the spectral region from a to b. The refractive index (n) and the extinction coefficient (k) were thus determined, and the oscillator strength (f) for each transition was calculated by means of this equation: $f = \frac{m}{e^2 n_0}\int 4n(\nu)k(\nu)\nu\mathrm{d}\nu$, where n_0 is the number of the molecules in a unit volume and where ν is the frequency of the incident light. In the figures of the present paper, the $4\pi n(\nu)k(\nu)/2.303\,\lambda C$ value (ε') will be plotted to show the wave-number dependence of the absorption intensity of the solid-state spectrum (C: molar concentration; λ: wavelength of the incident light).

Results and Discussion

In the crystal of $Ph_3PCH_3(TCNQ)_2$ at room temperature, tetrads of TCNQ molecules with the interplanar spacings of 3.22 Å, 3.24 Å and 3.22 Å compose a one-dimensional column.[5] The interplanar spacing between tetrads is 3.57 Å. In a tetrad, molecules are overlapped with a shift along the long axis of the TCNQ molecule (Y axis), and there are two crystallographycally independent molecules (II-I-I'-II'). The small difference observed between the

* Present address: Department of Chemistry, Faculty of Engineering Science, Osaka University, Toyonaka, Osaka.

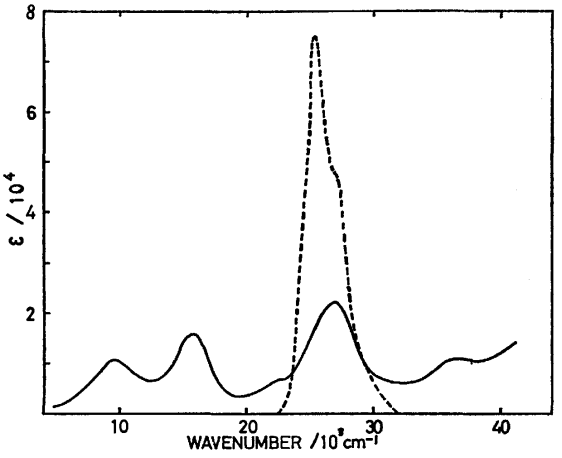

Fig. 1. The absorption spectrum of TCNQ in acetonitrile and the solid-state spectrum of NH_4TCNQ.

molecular structures of I and II suggests that the negative charge is slightly localized on the I molecule. Therefore, we will at first investigate the electronic structure of $Ph_3PCH_3(TCNQ)_2$ by the use of the simple model of N-A-A-N (A and N designate $TCNQ^-$ and $TCNQ^0$ respectively).

Figure 1 shows the absorption spectra of $TCNQ^0$ in an acetonitrile solution and of NH_4TCNQ in the solid state.[22] From the SCF-LCAO-MO-CI calculation of $TCNQ^0$ by the use of the molecular structure[25] in the TCNQ crystal, the lowest electronic transition observed at 25.3×10^3 cm^{-1} ($f=1.01$) is assigned to the 8→9 locally-excited (LE) electronic transition polarized parallel to the Y axis. The 8 and 9 molecular orbitals are the highest occupied and the lowest vacant ones respectively. In the previous paper, the peaks at 9.5×10^3, 16.0×10^3, and 26.9×10^3 cm^{-1} of NH_4TCNQ solid were assigned to the 9→9′ CT transition between $TCNQ^-$ and $TCNQ^-$, the 8→9 LE transition, and the 9→10 LE transition of $TCNQ^-$ respectively.[22] These LE transitions are polarized parallel to the Y axis. The analysis of the solid-state spectrum revealed that the NH_4TCNQ solid contains the dimer (A-A) of $TCNQ^-$. Therefore, the superposition of the two spectra in Fig. 1 gives the tentative absorption spectrum of the above-mentioned N-A-A-N model without any interaction between N and A.

Polarized Normal-Incidence Reflection of the $Ph_3PCH_3(TCNQ)_2$ Single Crystal. Figure 2 shows the normal-incidence reflections of the (100) face with the polarized lights along four directions ($b_{//}$, $b_\perp$, $c_{//}$, $c_\perp$) over the range from 5×10^3 cm^{-1} to 37.0×10^3 cm^{-1}. Table 1 shows the square of the direction cosine of the component of the molecular axis projected on (100) to the polarization direction. I and II designate the two crystallographycally independent TCNQ's. Iida suggested the assignment of the transition observed in the infrared region as a CT transition between $TCNQ^-$ and $TCNQ^0$, or as a direct transition to the electrical conduction state.[19] Since $Ph_3PCH_3(TCNQ)_2$ exhibits an intermediate conductivity, we adopted the former assignment. The transition moment of the CT transition is parallel to the I-II direction in Table 1; therefore, the former assignment sug-

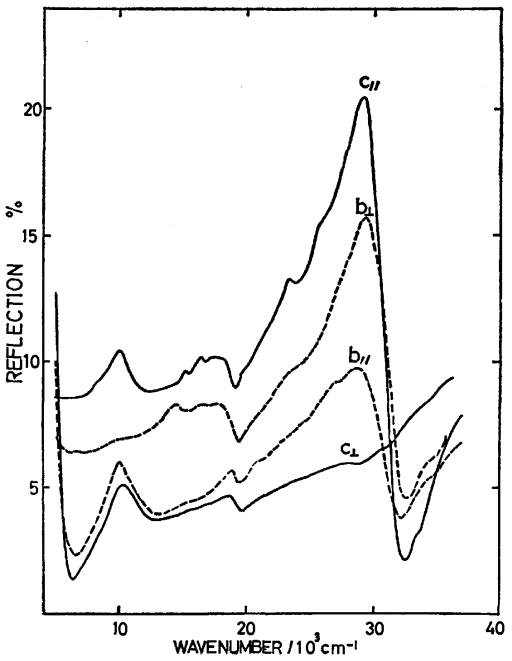

Fig. 2. The normal incidence reflection on (100) face of $Ph_3PCH_3(TCNQ)_2$ single crystal. The four spectra were obtained with the incident light polarized parallel and perpendicular to the *b* and *c* crystallographic axes.

Table 1. Square of direction cosine of the component of molecular axis projected on (100) to the polarization direction

		$b_{//}$	$b_\perp$	$c_{//}$	$c_\perp$
Long axis of TCNQ(Y)	I	0.36	0.64	0.98	0.01
	II	0.48	0.52	0.94	0.06
Short axis of TCNQ(X)	I	0.01	0.98	0.85	0.15
	II	0.03	0.96	0.88	0.12
I-II(I-I′)[a]		1.00	0.00	0.26	0.74
II-II′[a]		1.00	0.00	0.22	0.77

a) The direction connecting the molecular centers.

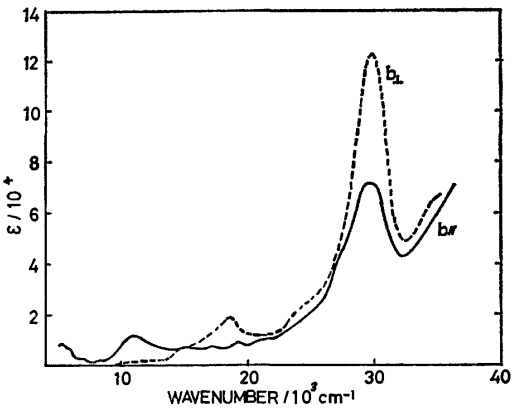

Fig. 3. The absorption spectra obtained from Kramers-Kronig analysis on (100) face of $Ph_3PCH_3(TCNQ)_2$ single crystal. The solid and the dashed curves were obtained with the incident light polarized parallel and perpendicular to the *b* axis.

gests that the infrared band is not found in the polarized spectrum perpendicular to the b axis ($b_\perp$). Therefore, the $b_\perp$ polarized reflection spectrum can be analysed by the equation of Roessler ($A=0.012$ and $B=-0.18$). The obtained spectrum is shown in Fig. 3. As may be seen from Table 1, for the other three polarization directions the infrared band has intensity and the zero-absorbing region is not found. Since the A and B values depend on the respective electronic transitions below 5×10^3 cm^{-1} and above 37.0×10^3 cm^{-1}, and since the former transition is ascribed to a CT transition between $TCNQ^-$ and $TCNQ^0$, and the latter, mainly to the LE transitions, the following relations can be estimated from Table 1:

$$B(c_{//})<B(b_\perp)<B(b_{//})<B(c_\perp)$$
$$A(b_{//})<A(c_\perp)<A(c_{//})<A(b_\perp)$$

Under these conditions, the A and B values were parametrized so as not to give the negative extinction coefficient. The obtained spectra are shown in Figs. 3 and 4. Since the absolute intensity is sensitive to the values of the parameters, no detailed discussion of the absorption intensity is carried out for the single crystal.

From the above polarization results, the I and II bands can clearly be assigned to the CT transitions, and the IV and VIII bands, to the LE transitions polarized parallel to the Y axis (LE(Y)). Although the other, weak peaks are not discussed in detail, it is noticeable that the V and VII bands were assigned with the CT polarization. In comparison with the tentative spectrum of the N-A-A-N model, the I and II bands are assigned to the 9→9′ CT transition from $TCNQ^-$ to $TCNQ^0$ and 9→9′ CT transition between $TCNQ^-$ and $TCNQ^-$. The IV and VIII bands are assigned to the 8→9 LE transition of $TCNQ^-$ and the superimposed transition of the 9→10 LE transition of $TCNQ^-$ and the 8→9 LE transition of $TCNQ^0$. Since the peak of the lowest transition (I) was reported at $2.9-3.3\times10^3$ cm^{-1} by Iida,[19] the energy separations between the I and V bands and between the II and VII bands are about 16×10^3 cm^{-1}; this value nearly coincides with the transition energy of the 8→9 LE transition of $TCNQ^-$. Therefore, the CT bands, V and VII, can possibly be assigned to 8→9′ CT transitions from $TCNQ^-$ to $TCNQ^0$ and to the 8→9′ CT transition between $TCNQ^-$ and $TCNQ^-$ (Table 2). Sakai *et al.* reported that the reversible pressure-induced absorption band was found at around 20×10^3 cm^{-1} at high pressures with respect to $(C_2H_5)_2NH(TCNQ)_2$ and $Q(TCNQ)_2$.[20] This experimental result is explained by the intensity increase of these new CT bands. The present assignments are consistent with those by Iida[19] for the I, IV, and VIII bands; also, the ambiguity of the assignment of the II band is excluded by this polarization measurement.

Table 2. Polarized absorption spectrum of $Ph_3PCH_3(TCNQ)_2$ single crystal by normal reflection analysis (in 10^3 cm^{-1})

	$b_{//}$	$b_\perp$	$c_{//}$	$c_\perp$	Assignment
I	<5	—	<5	<5	CT(A9→N9)
II	11.0	—	10.5	11.0	CT(A9→A9′)
III	15.2	15.0	15.3	—	
IV	—	18.5	18.5	—	LE(Y)(A8→9)
V	19.2	—	—	19.2	CT(A8→N9)
VI	—	24.0	24.0	—	
VII	27.0	—	—	—	CT(A8→A9′)
VIII	29.8	29.8	29.4	—	LE(Y)(A9→10, N8→9)

The Solid-state Spectra of the Pressed Pellets. The solid-state spectra and the refractive index, n, of the pressed pellets of the eight complex salts are shown in Figs. 5—8. Since four predominant transitions are observed in this spectral region, they are designated by CTI, CTII, YI, and YII in the increasing order of the transition energy; they correspond to the I,

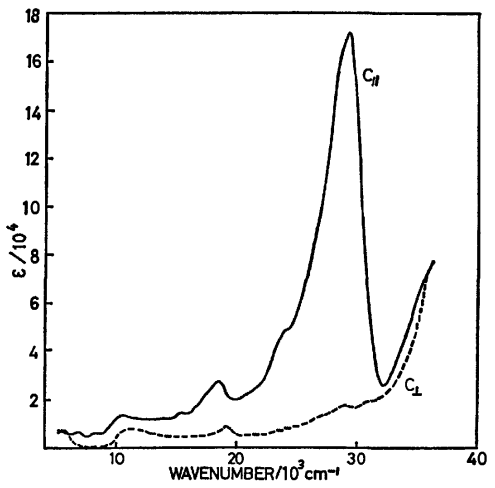

Fig. 4. The absorption spectra obtained from Kramers-Kronig analysis on (100) face of $Ph_3PCH_3(TCNQ)_2$ single crystal. The solid and the dashed curves were obtained with the incident light polarized parallel and perpendicular to the c axis.

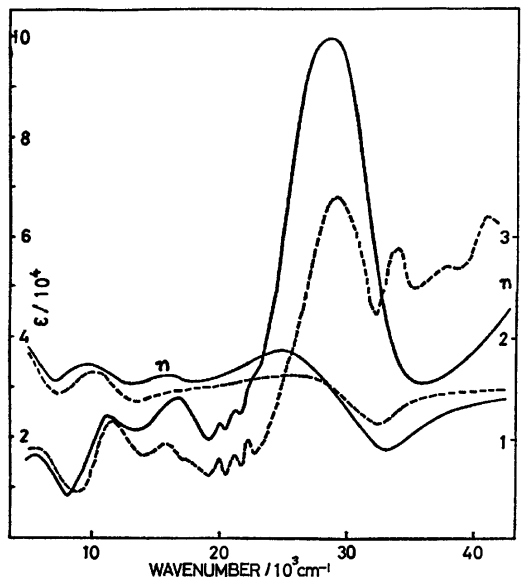

Fig. 5. The solid-state spectra and the refractive index n of $Mor_2(TCNQ)_3$ (----) and $Cs_2(TCNQ)_3$ (——).

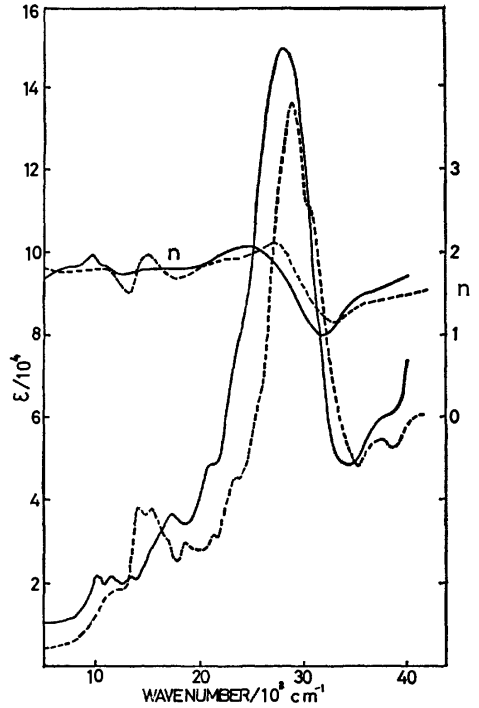

Fig. 6. The solid-state spectra and the refractive index n of $(CH_3)_3NH(TCNQ)_2$ (----) and Ph_3PCH_3-$(TCNQ)_2$ (——).

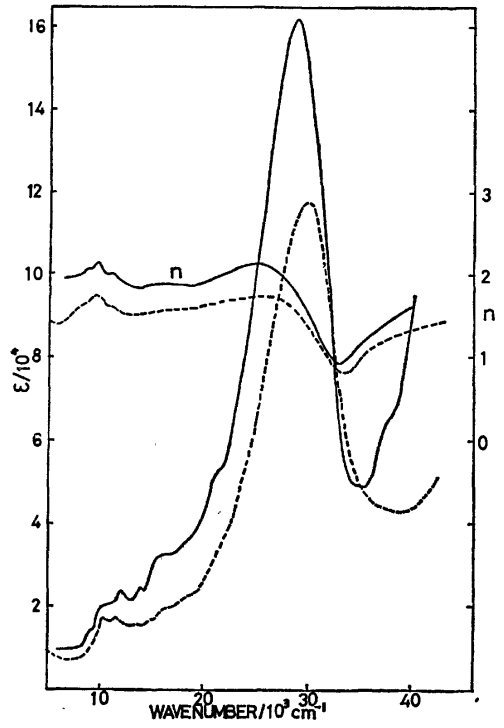

Fig. 7. The solid-state spectra and the refractive index n of $(C_2H_5)_3NH(TCNQ)_2$ (----) and $EtQ(TCNQ)_2$ (——).

II, IV, and VIII bands of the $Ph_3PCH_3(TCNQ)_2$ crystal respectively. The origin of the two or three weak peaks observed at 20—23×10^3 cm^{-1} of the 2 : 3 complex salts and some 1 : 2 complex salts is not clear, but these peaks are reproducible. For all

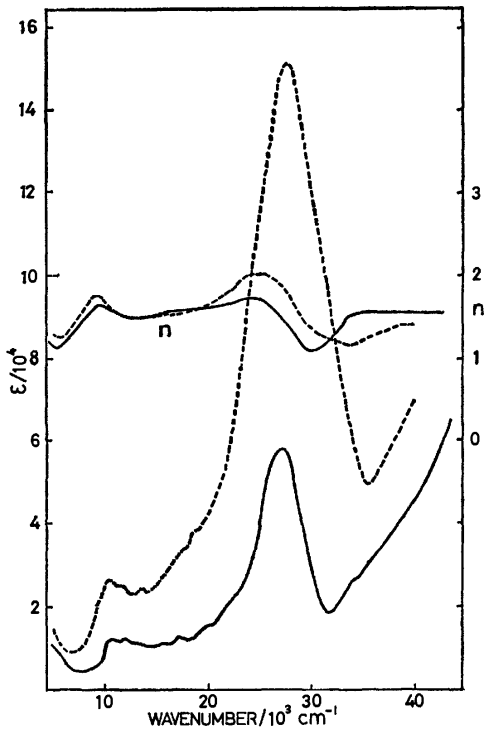

Fig. 8. The solid-state spectra and the refractive index n of $Bip(TCNQ)_2$ (----) and $Q(TCNQ)_2$ (——).

the 1 : 2 complex salts except for $Q(TCNQ)_2$, a weak peak was observed at about 14×10^3 cm^{-1}; it corresponds to the III band in the polarized crystalline spectrum of $Ph_3PCH_3(TCNQ)_2$. The III band exhibits polarization behavior a little different from that of the YI band (Figs. 3 and 4) and can be observed clearly when the YI band becomes obscure ($EtQ(TCNQ)_2$ and $Bip(TCNQ)_2$). Therefore, this peak is considered to have a different electronic origin from the YI band. The peak positions and the oscillator strengths are tabulated in Table 3, together with the solid-state results of NH_4TCNQ (Group A) and RbTCNQ-II (Group B) of the simple salt[22] and the electronic transition of $TCNQ^0$ in acetonitrile.

The crystal structures have been reported for the five complex salts investigated in this study.[1-5] In all cases, the TCNQ molecules compose a one-dimensional column. In the case of the 2 : 3 complex salts ($Mor_2(TCNQ)_3$[4]) and $Cs_2(TCNQ)_3$[1]), TCNQ molecules in a column form a triad which consists of two $TCNQ^-$ and one $TCNQ^0$. Among the 1 : 2 complex salts, $Ph_3PCH_3(TCNQ)_2$[5] and $(C_2H_5)_3NH(TCNQ)_2$[2] contain a tetrad unit which consists of two $TCNQ^-$ and two $TCNQ^0$. However, in the $Q(TCNQ)_2$ crystal,[3] the TCNQ column is composed of equally spaced TCNQ molecules and one electron per two TCNQ molecules is completely delocalized.

The 2 : 3 Complex Salts. As have been mentioned above, the TCNQ column of the 2 : 3 complex salts is represented as a repeat of N(1/2)-A-A-N(1/2). N(1/2) means that the N's on both sides half belong to this repeating unit. Therefore, we will discuss the electronic states of this repeating unit by the

Table 3. Transition energy and oscillator strength of solids of TCNQ complex salts
(σ: in 10^3 cm^{-1})

	CTI		CTII		YI		YII			R	J
	σ	f	σ	f	σ	f	σ	f	$\Delta\sigma_{1/2}$	Ω cm	eV
$Mor_2(TCQ)_3$	~5.0	0.5	11.7	0.6	{16.0 17.8}	0.5	29.2	2.5	7.8	10^5 [13]	0.31[11]
$Cs_2(TCNQ)_3$	5.5	0.3	11.1	0.5	16.8	0.7	28.5	3.7	8.0	9×10^4 [13]	0.14[9]
$(CH_3)_3NH(TCNQ)_2$			12.0	0.27	{14.1 15.4}	0.7	{29.0 30.7}	4.4	7.0	5×10^6 [14]	>0.2[9]
$Ph_3PCH_3(TCNQ)_2$	<5.0		{10.2 11.7}	0.4	17.6		28.2	5.5	7.5	50[14]	0.062[6]
$(C_2H_5)_3NH(TCNQ)_2$	<5.0		{10.2 11.7}	0.3	16.3		29.9	4.8	9.5	20[13]	0.034[6]
$EtQ(TCNQ)_2$			{10.2 11.8}	0.4	16.0		29.0	6.0	8.5	8[13]	
$Bip(TCNQ)_2$	<5.0		{10.3 11.6}	0.5	~17.0		27.8	6.2	10.0	0.5[13]	
$Q(TCNQ)_2$	<5.0		~11.0	~0.2	17.1		27.0	1.5	6.4	0.15[13]	
NH_4TCNQ			9.5	0.24	16.0	0.25	26.8	0.54	5.0	6×10^4 [13]	
RbTCNQ-II			7.4	0.39	16.7	0.33	28.1	1.5	7.0	10^2	
TCNQ in CH_3CN							{25.3 27.0}	1.0			

$\Delta\sigma_{1/2}$: half width of the YII band

method of the composite molecule, the components of which are A-A and N. In this unit, the TCNQ radicals (A-A) overlap each other with a shift along the short axis of the TCNQ radical. This packing is the same as that for the anion dimer of Group A of the simple salts. Therefore, the electronic states of the anion dimer of NH_4TCNQ (Group A)[22] and $TCNQ^0$ in acetonitrile are used as component states.

To discuss the electronic states in the energy region treated in this study, it is sufficient to take into account the following excited states of the components: the 8→9 (LEI) and the 9→10 (LEII) excited states of $TCNQ^-$, the 8→9 LE state of $TCNQ^0$ (LEN), and the CT excited state between $TCNQ^-$ (9) and $TCNQ^-$ (9′) (CTA). Furthermore, the CT configuration between two components (CTN) is considered. Therefore, the electronic configurations are as follows:

$$G = G_{AA}\cdot G_N$$
$$AYI^{\pm} = LEI^{\pm}\cdot G_N$$
$$AYII^{\pm} = LEII^{\pm}\cdot G_N$$
$$NY^{\pm} = G_{AA}\cdot LEN^{\pm}$$
$$CTA^{\pm} = CT^{\pm}\cdot G_N$$
$$CTN^{\pm} = 1/2[\{|8_A\bar{8}_A9_A8'_A\bar{8}'_A\bar{9}'_N| - |8_A\bar{8}_A\bar{9}_A8'_A\bar{8}'_A9'_N|\} \pm \{|8_A\bar{8}_A9_N8'_A\bar{8}'_A\bar{9}'_A| - |8_A\bar{8}_A\bar{9}_N8'_A\bar{8}'_A9'_A|\}]\cdot G_N$$

and

$$G_{AA} = 1/\sqrt{2}\{|8_A\bar{8}_A9_A8'_A\bar{8}'_A\bar{9}'_A| - |8_A\bar{8}_A\bar{9}_A8'_A\bar{8}'_A9'_A|\}$$
$$G_N = |8_N\bar{8}_N|$$
$$LEI^{\pm} = 1/2[\{|8_A\bar{9}_A9_A8'_A\bar{8}'_A\bar{9}'_A| - |9_A\bar{8}_A\bar{9}_A8'_A\bar{8}'_A9'_A|\} \pm \{|8_A\bar{8}_A9_A9'_A\bar{8}'_A\bar{9}'_A| - |8_A\bar{8}_A\bar{9}_A8'_A\bar{9}'_A9'_A|\}]$$
$$LEII^{\pm} = 1/2[\{|8_A\bar{8}_A10_A8'_A\bar{8}'_A\bar{9}'_A| - |8_A\bar{8}_A\overline{10}_A8'_A\bar{8}'_A9'_A|\} \pm \{|8_A\bar{8}_A9_A8'_A\bar{8}'_A\overline{10}'_A| - |8_A\bar{8}_A\bar{9}_A8'_A\bar{8}'_A10'_A|\}]$$
$$LEN^{\pm} = 1/2[\{|8_N\bar{9}_N| - |\bar{8}_N9_N|\} \pm \{|8'_N\bar{9}'_N| - |\bar{8}'_N9'_N|\}]$$
$$CT^{\pm} = 1/\sqrt{2}\{|8_A\bar{8}_A9'_A8'_A\bar{8}'_A\bar{9}'_A| \pm |8_A\bar{8}_A9_A8'_A\bar{8}'_A\bar{9}_A|\}$$

where i_N, i_A, i'_A, and i'_N designate the molecular orbitals of N, A, A′, and N′ respectively of the N(1/2)-A-A-N(1/2) model. The ± signs denote the symmetric and the antisymmetric properties with respect to the symmetric center. The doubly occupied molecular orbitals 1—7 are neglected. The configuration interactions are:

Symmetric	C	0					
	CTN^+	$\sqrt{2}\beta(9_A9_N)$	E^+_{CTN}				
	CTA^+	$2\beta(9_A9'_A)$	0	E^+_{CTA}			
	AYI^+	0	0	$-\sqrt{2}\beta(8_A9'_A)$	E^+_{AYI}		
	$AYII^+$	0	$\beta(10_A9_N)$	$\sqrt{2}\beta(9_A10'_A)$	0	E^+_{AYII}	
	NY^+	0	$-\beta(9_A8_N)$	0	0	0	E^+_{NY}
Asymmetric	CTN^-	E^-_{CTN}					
	NY^-	$\beta(9_A8_N)$	E^-_{NY}				
	CTA^-	0	0	E^-_{CTA}			
	AYI^-	0	0	$\sqrt{2}\beta(8_A9'_A)$	E^-_{AYI}		
	$AYII^-$	$-\beta(10_A9_N)$	0	$\sqrt{2}\beta(9_A10'_A)$	0	E^-_{AYII}	

where $\beta(i_A j_N) = \int i_A(1)\ H(1)\ j_N(1)\ d\tau_1$ and where H(1) is the one-electron Hamiltonian of the crystal. The asymmetric configuration matrix almost splits into two parts, and the 3×3 part is the same as the configuration matrix of the anion dimer.[22]

Really, except for a new band, CTI, based on the CT transition between two components, the observed spectra of the 2 : 3 salts are similar to the superposed spectrum of the two components, with a small blue shift caused by the stabilization of the ground state due to the interaction with CTN^+. The observed oscillator strengths of YI(0.5) and YII(2.5) of $Mor_2(TCNQ)_3$ agree with the calculated values (YI: 0.5 and YII: 2.1) for the N(1/2)-A-A-N(1/2) model without any interaction between A and N, using the solid-state spectrum of NH_4TCNQ for A-A and the acetonitrile spectrum of $TCNQ^0$ for N. These results reveal for the 2 : 3 salts that the interaction between the two components is weak in the excited states. For $Cs_2(TCNQ)_3$, a weak hyperchromism was observed.

The singlet-triplet (S-T) splittings of the ground state reported by the magnetic measurements are 0.31 eV for $Mor_2(TCNQ)_3$[11], 0.14 eV or 0.16 eV for $Cs_2(TCNQ)_3$,[6,9] and 0.16—0.29 eV for Group A of the simple salts.[6,7,12] In the present treatment of the composite system, the stabilization of the singlet ground state becomes larger by the interaction with the low-energy ^SCTN configuration for the 2 : 3 salts than for the anion dimer. However, since the triplet ground state is also stabilized by the interaction with ^TCTN for the 2 : 3 salts, it is reasonable that the S-T splitting of the 2 : 3 salts is not very different from that of the anion dimer (Group A of the simple salts).

The 1 : 2 Complex Salts. To discuss the electronic structure of the 1 : 2 salts, we can at first adopt the simple model of N-A-A-N.[26] The electronic configurations are analogous to those of the 2 : 3 complex salts. The difference in the configuration energies between the 2 : 3 and the 1 : 2 complex salts is considered to be not very large with respect to the LE and CTA configurations, because the changes in the interplanar spacings and the molecular structure are small. However, the configuration energy of CTN is lower for the 1 : 2 salts than for the 2 : 3 salts because of a difference in the electrostatic repulsion between anion radicals. This is consistent with the observed red shift of the CTI band and the small changes of three other band positions of the 1 : 2 salts compared to those of the 2 : 3 salts.

The CTII bands of the 1 : 2 salts show the vibrational structure. Since the vibrational frequency (1300—1500 cm^{-1}) agree well with that (1600 cm^{-1}) observed for the 11.8×10^3 cm^{-1} band of the $TCNQ^-$ monomer, the assignment of the CTII band to LE transition has been proposed.[19] However, as the CT character of the CTII band was determined by our polarization experiment, the vibrational structure is attributed to a small quantity of the $TCNQ^-$ monomer. The magnetic susceptibility measurement also reported the $TCNQ^-$ monomer as an intrinsic impurity.[9]

Our previous work on the simple salts[22] showed that the separations between the CTII and YI bands are larger for the salts of Group B than for the salts of Group A, as may be seen from Table 3 (6500 cm^{-1} for NH_4TCNQ and 9300 cm^{-1} for RbTCNQ-II). This was explained by the difference in the configuration interaction between the CTA and AYI configurations. A symmetry consideration of the molecular orbitals reveals that the CTA and AYI configurations interact for the A-A overlapping form of Group B (an overlap with a shift along the Y axis) and not for that of Group A (an overlap with a shift along the X axis). The overlapping form between anions of the 1 : 2 salts is the same as that of Group B, and that between anions of the 2 : 3 salts, the same as that of Group A. However, the corresponding CTII-YI separations in the spectra of the 1 : 2 salts range from 4.3 to 6.6×10^3 cm^{-1} and are not so large as those of the 2 : 3 salts (4.3 and 5.7×10^3 cm^{-1}). From the polarized reflection analysis, the CTN configuration from the 8 orbital of A to the 9 orbital of N is located just above the AYI configuration. The interaction between these two configurations based on $\beta(9_A 9_N)$ removes the YI band to the lower-energy side, so it is reasonable that the separation between the YI and CTII bands becomes not so large.

The observed transition energies and the oscillator strengths are shown in Table 3 in the decreasing order of electrical resistivity. As may be seen from Table 3 and Figs. 6—8, the solid-state spectra of the 1 : 2 salts are divided into three main groups. The first salt, $(CH_3)_3NH(TCNQ)_2$, exhibits no CTI band and a weak CTII band; this reveals the small CTN and CTA contributions in the ground state. The YI band appears at a position intermediate between those of the first LE transitions of the $TCNQ^-$ monomer and the $TCNQ^-$ dimer in the aqueous solution, and the YII band shows the same 1700 cm^{-1} shoulder as the LE band of $TCNQ^0$ in acetonitrile. These two features show weak $TCNQ^-$–$TCNQ^-$ and $TCNQ^-$–$TCNQ^0$ interactions in the excited states. The second group contains $Ph_3PCH_3(TCNQ)_2$, $(C_2H_5)_3NH(TCNQ)_2$, $EtQ(TCNQ)_2$, and $Bip(TCNQ)_2$. These salts exhibit a gradual spectral change as the electrical resistivity decreases; the dispersion of the refractive index near 5000 cm^{-1} becomes larger, which reflects the intensity increase in the CTI band: the intensity of the CTII band increases, the YI band becomes more obscure, and the oscillator strength and the half-width of the YII band increase. The increase in the absorption intensity of the two CT bands reveals the increase in the electron delocalization in the ground state; this is consistent with the tendency of the electrical property. The absolute absorption intensities of the YI and YII bands becomes nearly double the intensities calculated from the solid-state data of the simple salts and the solution data of $TCNQ^0$. In the range corresponding to these LE transitions of $TCNQ^-$ and $TCNQ^0$, several CT bands were estimated. However, the intensities of these bands are not enough large for us to interpret the remarkable hyperchromism of the YII band. Therefore, it is considered that the electron delocalization also makes an important contribution. It is noticeable that the effect of the elec-

tron delocalization is found not only in CT transitions, but also in LE transitions for the 1 : 2 salts.

The S-T splittings of the ground state have been reported for $(CH_3)_3NH(TCNQ)_2$ (>0.2 eV),[9] Ph_3PCH_3-$(TCNQ)_2$ (0.062 eV),[6] and $(C_2H_5)_3NH(TCNQ)_2$ (0.034 eV)[6] on the basis of magnetic measurements. This remarkable difference between the salts belonging to the first and second groups can be explained by the difference in the extent of delocalization of the negative charge of $(TCNQ)_2^-$. The previous discussion showed that the contribution of the CTN^+ configurations to the ground state is smallest for $(CH_3)_3$-$NH(TCNQ)_2$ in the 1 : 2 salts investigated here, therefore, the negative charge is located almost entirely on one TCNQ. However, for the two salts of the second group, the delocalization of the negative charge occurs to some extent. This delocalization makes the CT transition between A and A less important than the CT transition between A and N; therefore, the part of the S-T splitting due to the stabilization of the singlet ground state by the interaction with the ^{S}CTA configuration becomes less important.

The third group contains only $Q(TCNQ)_2$. The solid-state spectrum of $Q(TCNQ)_2$ is very different from those of the other 1 : 2 salts (Fig. 8). Its characteristics are as follows; the absorption tail near 5×10^3 cm^{-1} becomes clear, the intensity of the YII band becomes remarkably small, and the intensity as a whole becomes smaller than those of the other 1 : 2 salts. The relatively strong intensity of the absorption near 20×10^3 cm^{-1} makes the YI band obscure. The fact that $Q(TCNQ)_2$, with the highest electrical conductivity among the eight complex salts investigated here, exhibits the clearest tendency for the intensity to increase near 5×10^3 cm^{-1} is consistent with the results of the other optical study. An infrared study of $Q(TCNQ)_2$ at 1.5 K reported that the broad absorption beginning from 500 cm^{-1} with the absorption maximum near 3000 cm^{-1}, was the transition to the electrical conduction band,[21] and that the increase in the intensity of this band is accompanied by an increase in the electrical conductivity.[18] On the other hand, a study of the crystal structure reported the complete delocalization of the negative charge of $(TCNQ)_2^-$ in the ground state.[3] The delocalization of the negative charge makes the chance of the A-A pair occurrence less than that of the A-N pair occurrence. Since the CTA transition and CTN transition are based on the above pair structure, the oscillator strength ratio of CTI to CTII is expected to become larger than in the other 1 : 2 complex salts. As is seen in Fig. 8, this tendency is consistent with the experimental results. Furthermore, the charge delocalization transforms the molecular structure[3] and, as a result, changes the oscillator strengths of the LE transitions. This is considered one of the reasons for the intensity decrease in the LE transitions of $Q(TCNQ)_2$. The relatively strong intensity near 20×10^3 cm^{-1} also supports the large extent of the delocalization.

The authors would like to express their deep gratitude to Professor Saburo Nagakura of this Institute for giving them the chance to do this work and for his helpful discussions and critical reading of the manuscript. Our thanks are also due to Dr. Suehiro Iwata of the Institute of Physical and Chemical Research for his kindness in putting his computer program at our disposal and to Dr. Michiko Konno of this Institute for her X-ray determination of the crystal face of $Ph_3PCH_3(TCNQ)_2$.

References

1) C. J. Fritchie, Jr. and P. Arthur, Jr., *Acta Crystallogr.*, **21**, 139 (1966).
2) H. Kobayashi, Y. Ohashi, F. Marumo, and Y. Saito, *ibid.*, **B26**. 459 (1970).
3) H. Kobayashi, F. Marumo, and Y. Saito, *ibid.*, **B27**, 373 (1971).
4) T. Sundaresan and S. C. Wallwork, *ibid.*, **B28**, 491 (1972).
5) H. Tsuchiya, Thesis for a doctorate of Tokyo University, Tokyo, Japan, 1973.
6) D. B. Chesnut and W. D. Phillips, *J. Chem. Phys.*, **35**, 1002 (1961).
7) D. B. Chesnut and P. Arthur, Jr., *ibid.*, **36**, 2969 (1962).
8) M. T. Jones and D. B. Chesnut, *ibid.*, **38**, 1311 (1963).
9) R. G. Kepler, *ibid.*, **39**, 3528 (1963).
10) K. Siratori and T. Kondow, *J. Phys. Soc. Japan*, **27**, 301 (1969).
11) J. C. Bailey and D. B. Chesnut, *J. Chem. Phys.*, **51**, 5118 (1969).
12) T. Hibma, P. Dupuis, and J. Kommandeur, *Chem. Phys. Lett.*, **15**, 17 (1972).
13) L. R. Melby, R. J. Harder, W. R. Hertler, W. Mahler, R. E. Benson, and W. E. Mochel, *J. Amer. Chem. Soc.*, **84**, 3374 (1962).
14) W. J. Siemons, P. E. Bierstedt, and R. G. Kepler, *J. Chem. Phys.*, **39**, 3523 (1963).
15) V. Walatka and J. H. Perlstein, *Mol. Cryst. Liq. Cryst.*, **15**, 269 (1971).
16) W. Brenig, G. H. Döhler, and H. Heyszenau, *Phys. Lett.*, **39A**, 175 (1972).
17) N. Sakai, I. Shirotani, and S. Minomura, This Bulletin, **45**, 3314 (1972).
18) T. Kondow, K. Siratori, and H. Inokuchi, *J. Phys. Soc. Japan*, **23**, 98 (1967).
19) Y. Iida, This Bulletin, **42**, 637 (1969).
20) N. Sakai, I. Shirotani, and S. Minomura, *ibid.*, **43**, 57 (1970).
21) T. Kondow and T. Sakata, *Phys. Status, Solidi*, (a)**6**, 551 (1971).
22) Y. Oohashi and T. Sakata, This Bulletin, **46**, 3330 (1973).
23) Y. Oohashi and T. Sakata, *ibid.*, **46**, 765 (1973).
24) D. M. Roessler, *Brit. J. Appl. Phys.*, **16**, 1119 (1965).
25) R. E. Long, R. A. Sparks, and K. N. Trueblood, *Acta Crystallogr.*, **18**, 932 (1965).
26) For the case of $(C_2H_5)_3NH(TCNQ)_2$, the interplanar spacing in a tetrad are 3.24, 3.32 and 3.24 Å, and that between the neighbouring tetrads in 3.30 Å.[2] However, the model of N-A-A-N is also applicable to this case, because the interaction between N's is weak in comparison with that between A's.

The Intramolecular Dynamic Behavior of Tetraaryl Allyl Radicals

Kohji WATANABE

Laboratory of Solid State Chemistry, Institute for Chemical Research, Kyoto University, Uji, Kyoto 611

(Received November 29, 1974)

The electron spin resonance (ESR) and the electron nuclear double resonance (ENDOR) spectra of tetraaryl allyl radicals have been observed. A comparison of the ENDOR spectra of α,α,γ,γ-tetraphenyl allyl, α,α-diphenyl-γ,γ-dianisyl allyl, and α,α,γ,γ-tetraanisyl allyl revealed that the four aryl groups are not equivalent, but are apparently to be classified into two types with different conformations in their molecular frameworks. The molecular orbital calculations on the basis of this model have shown a fairly good agreement with the observed spectra. The temperature dependence of the ENDOR spectra at −60∼−110 °C were analyzed, assuming mutually different twisting angles for the allyl skeleton. The activation energy of the torsional vibration of the allyl skeleton is estimated to be about 2.5 kcal/mol. The ESR spectra of α,α,γ,γ-tetraphenyl allyl and α,α-diphenyl-γ,γ-diphenylene allyl change drastically with the temperature at around +115 °C and show a marked line-width alternation effect. It is concluded from the results that the torsional vibration becomes vigorous with an increase in the temperature and that the allyl skeleton begins to rotate internally at high temperatures. The activation energy of the internal rotation of the allyl skeleton has been estimated to be about 15∼20 kcal/mol. The temperature-dependent hyperfine splitting of the methine proton has also been explained by assuming a model of the internal rotation of the allyl skeleton.

Anomalously large proton hyperfine splittings have often been observed for the radicals which possess twisted π-systems in their molecular frames.[1,2] The present author and his co-workers[3] also observed similar phenomena in the ESR spectra of the tetraaryl allyl radicals. Such an extraordinarily large proton hyperfine splitting can be successfully explained by the following modified McConnell relation:

$$A_\beta^H = |Q_{CH}^H| \cdot \rho_{C\beta} + |B_{t-\pi}^H| \{\cos^2(90-\theta) \cdot \rho_{C\alpha} + \cos^2(90-\phi) \cdot \rho_{C\gamma}\} \quad (1)$$

where Q_{CH}^H is −22.5∼−29.0 G and where $\rho_{C\alpha}$, $\rho_{C\beta}$, and $\rho_{C\gamma}$ are the 2pπ spin densities on the α-carbon (Cα), β-carbon (Cβ), and γ-carbon (Cγ) atoms respectively. Here, Cα and Cγ are the carbon atoms on the two sides of Cβ in the allyl molecule, and $B_{t-\pi}^H$ is a proportionality constant for the twisted π-radical, where the magnitude of B^H for the neutral radical is usually estimated to be 50∼60 G.[4-6] The θ and φ angles are the mean values of the twisting angles of the $2p_z$-*orbitals* on Cα and Cγ respectively. From Eq. (1) and McLachlan's molecular orbital (MO) calculation assuming $\theta \approx \phi$, the twisting angles (θ, φ) of the $2p_z$-*orbitals* on both α- and γ-allyl carbons were estimated to be about 28° for α,α,γ,γ-tetraphenyl allyl (TPA).[3]

Of particular interest is the fact that the methine-proton splitting of TPA shows a marked positive temperature dependence (Fig. 1). Carter *et al.*[7] interpreted the temperature-dependent splitting of the methylene proton in terms of the restricted rotation and a simple harmonic oscillator model based on the Stone-Maki theory.[8]

In order to explain the temperature dependence of the methine-proton splitting observed here, the detailed conformational analysis of these radicals is necessary. Hence, the electron-nuclear-double-resonance (ENDOR) and electron-spin-resonance (ESR) experiments have been carried out over a wide temperature range (from −110°C to +210 °C) in order to investigate the dynamic behavior of molecular motion. The most interesting result established by the ENDOR experiments at low temperatures is that the four phenyl groups in TPA are not equivalent each other, but are apparently to be classified into two different kinds of paired groups. On the other hand, the ESR results demonstrated that, in the higher-temperature region, the torsional vibration of the allyl skeleton 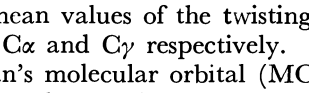 becomes vigorous and the allyl skeleton begins to rotate internally. As the result, the four phenyl rings of TPA become almost equivalent because of the averaging effect of the rapid internal rotation of the allyl skeleton. These phenomena observed in the ESR spectra can be well treated by means of the following modified Bloch equation:[9,10]

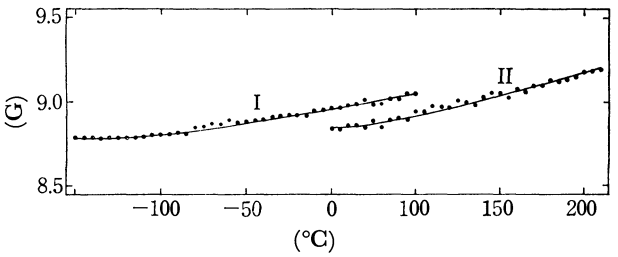

Fig. 1. Temperature dependence of the splitting constant A_β^H of TPA.
(I): in toluene, (II): in liquid paraffin.

$$G = \frac{i\omega_s M_0 \tau \sum_{s=1}^{N} f_s}{N[1 - \sum_{s=1}^{N} f_s]} \quad (2)$$

where $f_s = (N + \alpha_s \tau)$, $\alpha_s = (1/T_{2s}) - i(\omega_s - \omega)$, G: the complex transverse magnetization; ω_s: the resonance frequency for the species, s; M_0: the equilibrium value of polarization, M_z; τ: the mean life time; N: number of species; $1/T_{2s}$: transverse relaxation time, and ω: angular frequency. The results obtained from the computer simulation will be given in the following section. In this paper the author will report the results of the analyses of the temperature-dependent ESR and ENDOR spectra and will discuss in some detail the dynamic behavior of the molecular frameworks of the tetraaryl allyl radicals.

Experimental

The materials were TPA, α,α-diphenyl-γ,γ-dianisyl allyl (DPDAA), α,α,γ,γ-tetraanisyl allyl (TAA), α,α-diphenyl-γ,γ-diphenylene allyl (DDA), α,α,γ,γ-bisdiphenylene allyl (BDA), α,α,γ,γ-bisdiphenylene-β-azo allyl (BDAA), and α,α,γ,γ-bisdiphenylene-β-phenyl allyl (BDPA) (Fig. 2). They were prepared by following the process described in Refs. 11, 12, 13, 14, and 15.

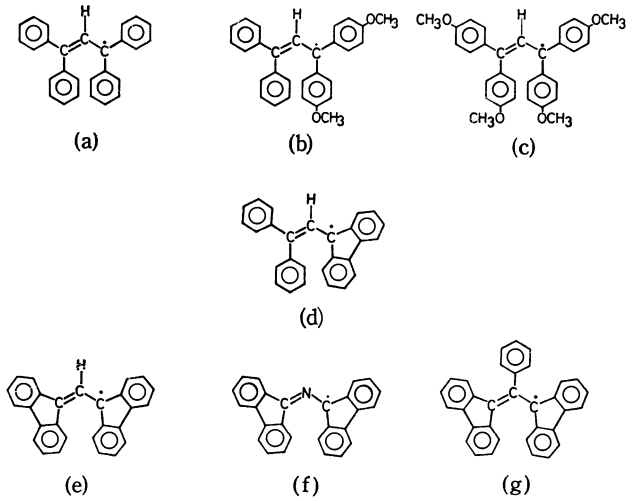

Fig. 2. Tetraaryl allyl radicals.
(a): TPA, (b): DPDAA, (c): TAA, (d): DDA, (e): BDA, f) BDAA, g): BDPA.

TPA: Found: C, 92.98; H, 5.58%. Calcd for $C_{27}H_{21}$: C, 93.86; H, 6.14%. DPDAA: Found: C, 85.56; H, 6.13%. Calcd for $C_{29}H_{25}O_2$: C, 85.89; H, 6.11%. TAA: Found: C, 79.76; H, 6.11%. Calcd for $C_{31}H_{29}O_4$: C, 79.98; H, 6.28%. DDA: mp 236.0—237.5 °C (235—237 °C).[12] BDA: mp 244.5—245.5 °C (245—246 °C).[13] BDAA: mp 270.0—271.5 °C (270—272 °C).[14] BDPA: Found: C, 94.65; H, 5.25%. Calcd for $C_{33}H_{21}$: C, 94.93; H, 5.07%.

The toluene and liquid paraffin used as solvents were well purified, dehydrated, and degassed. The ESR spectra were measured with a JEOL Model PE-3 X-band ESR spectrometer; an aqueous solution of peroxylamine disulfonate was used as standard of the magnetic field.[16] The ENDOR spectra were measured by means of a JEOL ES-EDX 1 spectrometer operating with a 80-Hz magnetic-field modulation in the temperature range from −110 to −40 °C for the toluene solutions and from 55 to 80 °C for the liquid paraffin solutions. The 150-watt CW RF field (6.5 KHz frequency modulation) was introduced into the coil inside the cavity for the NMR excitation. The hyperfine splitting constant was determined by averaging the values obtained from two or three measurements. The simulation of the spectra and the MO calculations were carried out at the Kyoto University Computer Center.

Results and Discussion

ENDOR Spectra. Tetraphenyl Allyl-type Radicals: The ENDOR spectra of TPA, DPDAA, and TAA are shown in Fig. 3. It is obvious that the absorption lines near the free-proton frequency are due to the methoxy protons. The line at around 26 MHz was undoubtedly identified as the one due to the methine proton by reference to the ESR measurements. The two

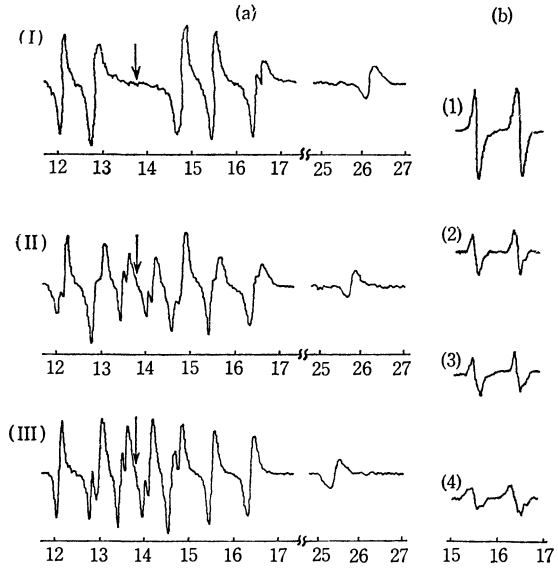

Fig. 3. ENDOR spectra of TPA-type radicals in toluene.
(a): at −80 °C: (I) TPA, (II) DPDAA, (III) TAA
(b): temperature dependence of some lines of TAA 1) at −80 °C, 2) at −90 °C, 3) at −100 °C, 4) at −110 °C. Arrows: The position of the free proton frequency.

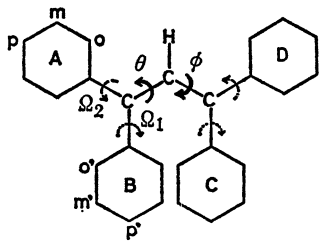

Fig. 4. Conformational model of TPA-type radicals.

lines at 15.5 MHz and 16.5 MHz for TAA are assumed to arise from the *ortho*-protons of the *interior* (**B**, **C**) and *exterior* (**A**, **D**) aryl groups respectively (see Fig. 4). From similar considerations, the absorptions at around 15.5 MHz and 16.5 MHz for TPA and DPDAA are attributed to the overlapping line arising from the *ortho*- and *para*-protons of the *interior* and *exterior* phenyl groups respectively. It should be remembered here that the *ortho*- and *para*-protons have hyperfine splitting constants of nearly the same magnitude, as is often the case with neutral aromatic free radicals.[17] The other absorptions observed at about 14.7 MHz are probably due to the *meta*-protons. The two kinds of hyperfine splitting constants observed for the methoxy protons in DPDAA and TAA imply that the methoxy-protons splitting constants on the *interior* rings are different from those on the *exterior* rings. This supports the previous assumption that the splitting of the *ortho*-proton of the *exterior* aryl groups is different from that of the *interior* groups. As has been described in a previous paper,[3] these tetraaryl allyl-type radicals have a twisted allyl skeleton, in which the distance between the rings of **B** and **C** (*interior* rings) is much closer than that between the rings of **A** and **D** (*exterior* rings) or of **A** and **B**. This model offers a reasonable theoretical basis for the present ENDOR experiments, in which a

Table 1. Observed and calculated spitting

		α	β	γ	o(A)	m(A)	p(A)
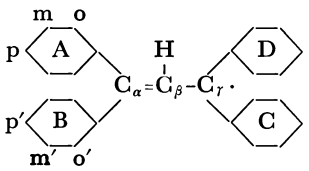	Obsd.[a] ESR		8.72		1.97	0.68	1.97
	Obsd.[a] ENDOR		8.808		1.911	0.697	2.043
	Calcd.[b]		9.142[(1)]		2.079	0.729	1.944
		+0.318	−0.099	+0.318	+0.077	−0.027	+0.072
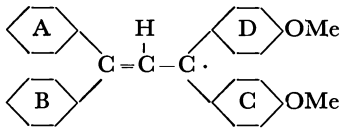	Obsd.[a] ESR		≃9		S	S	S
	Obsd.[a] ENDOR		8.496		1.917	0.732	2.005
	Calcd.[b]		8.513[(1)]		2.052	0.648	1.971
		+0.311	−0.084	+0.295	+0.076	−0.024	+0.073
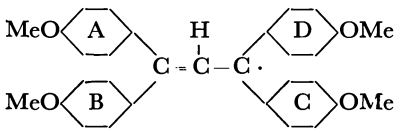	Obsd.[a] ESR		≃9		S	S	S
	Obsd.[a] ENDOR		8.234		1.876	0.731	0.247*
	Calcd.[b]		8.280[(1)]		1.836	0.567	
		+0.293	−0.083	+0.293	+0.068	−0.021	+0.056

S : Not confirmed. *: Methoxy proton. a) In toluene. b) Calculated splitting constants are obtained using the 50, $\theta=\phi=28°$, where ρ_{Ci} are spin densities obtained by McLachlan's calculation using the following param-

nonequivalent spin distribution was observed between the *exterior* and the *interior* rings. This model also gives a good agreement between the observed and the calculated hyperfine splitting constants of the ring protons if one assumes $\theta=\phi=28°$, $\Omega_1=35°$, and $\Omega_2=15°$ (see Fig. 4). Based on this model, the theoretical spin density on each carbon atom was calculated by means of McLachlan's MO method;[18] the results are given in Table 1, together with the hyperfine splitting constants calculated by the McConnell relation. The hyperfine splittings of the ring protons may be classified into three groups: the *ortho*- and *para*-protons of the *exterior* rings, those of the *interior* rings, and the *meta*-protons of all the rings. In the previous paper,[13] the four phenyl rings of TPA were assumed to be nearly equivalent. However, it is more reasonable to assume the above-mentioned molecular structure (Fig. 4) in order to account for the ENDOR and the ESR spectra on the same basis.

Bisdiphenylene Allyl-type Radicals: Since BDA and BDAA are partially dimerized in a solution at low temperatures,[19] the ENDOR spectra of these radicals were not observed in toluene solutions in the temperature region suitable for this solvent. The ENDOR spectra for BDA, BDAA, and BDPA in liquid paraffin solutions are shown in Fig. 5. The smallest hyperfine splitting group of BDPA, which has never been observed in the ESR spectra, was clearly identified as being

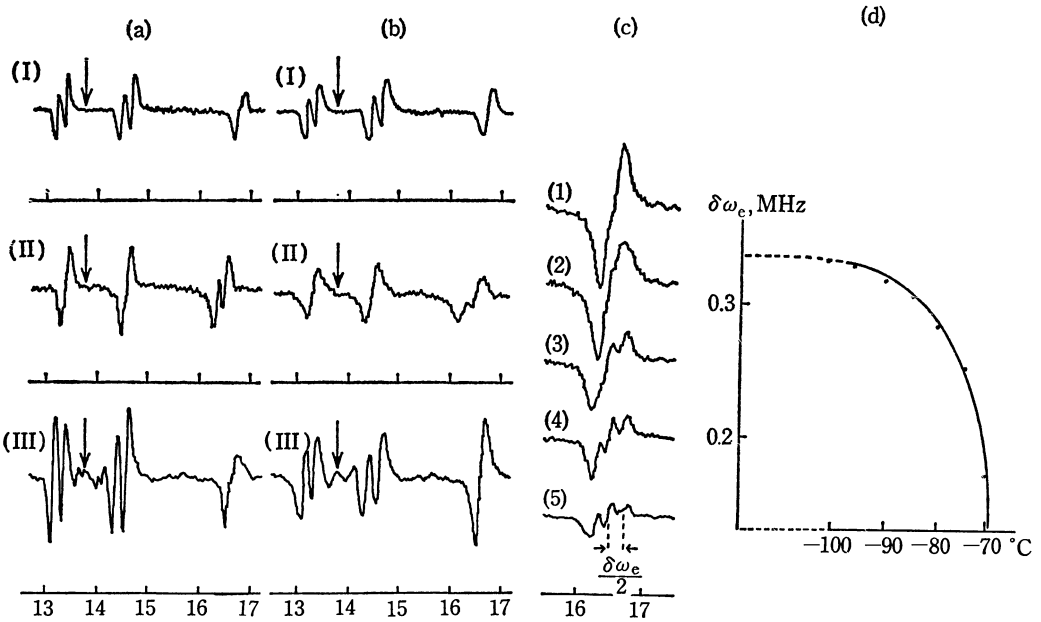

Fig. 5. ENDOR spectra of BDA-type radicals in liquid paraffin.
(a): at 55 °C, (I) BDA, (II) BDAA, (III) BDPA, (b): at 80 °C, (I) BDA, (II) BDAA, (III) BDPA, (c): temperature dependence of some lines of BDPA in toluene 1) at −75 °C, 2) at −80 °C, 3) at −85 °C, 4) at −90 °C, 5) at −95 °C, (d): line separations of spectra (c). Arrows: The position of the free proton frequency.

CONSTANTS OF THE TPA-TYPE RADICALS (IN G)

o′(B)	m′(B)	p′(B)	o′(C)	m′(C)	p′(C)	o(D)	m(D)	p(D)
1.31	0.68	1.31						
1.240	0.697	1.240						
1.458	0.513	1.377						
+0.054	−0.019	+0.051						
S	S	S	S	S	S	S	S	S
1.303	0.596	1.303	1.193	0.596	0.168*	1.917	0.732	0.256*
1.458	0.486	1.404	1.269	0.459		1.809	0.594	
+0.054	−0.018	+0.052	+0.047	−0.017	+0.038	+0.067	−0.022	+0.054
S	S	S						
1.247	0.585	0.160						
1.296	0.432							
+0.048	−0.016	+0.040						

formula $A^{H}_{Ci}=|Q^{H}_{CH}|\cdot\rho_{Ci}$ $Q^{H}_{CH}=-27.0$ (i) $A^{H}_{\beta}=|Q^{H}_{CH}|\cdot\rho_{C\beta}+|B^{H}_{t-\pi}|\{\cos^2(90-\theta)\cdot\rho_{C\alpha}+\cos^2(90-\phi)\cdot\rho_{C\gamma}\}$, $|B^{H}_{t-\pi}|=$ eters $\lambda=1.2$, $\alpha_{C-OMe}=\alpha+0.5\beta$, $\beta_{C-OMe}=0.6\beta$, $\theta=\phi=28°$, $\Omega_1=35°$, and $\Omega_2=15°$.

TABLE 2. OBSERVED AND CALCULATED SPLITTING CONSTANTS OF THE BDA-TYPE RADICALS (IN G)

		α	β	γ	1,1′	2,2′	3,3′	4,4′
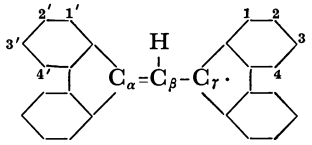	Obs.[a] ESR		13.15		1.98	0.47	1.98	0.47
	Obs.[a] ENDOR		S		2.008	0.520	1.956	0.388
	Calcd.[b]		13.29[(I)]		1.890	0.324	1.593	0.054
		+0.262	−0.091	+0.262	+0.070	−0.012	+0.059	−0.002
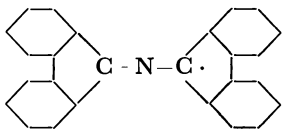	Obs.[a] ESR		3.40*		1.75	0.47	1.50	0.35
	Obs.[a] ENDOR				1.782	0.437	1.564	0.396
	Calcd.[b]		2.588[(II)]		1.809	0.324	1.539	0.054
		+0.253	−0.051	+0.253	+0.067	−0.012	+0.057	−0.002
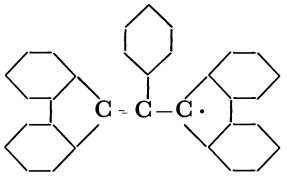	Obs.[a] ESR		S		1.96	0.67	1.96	0.67
	Obs.[a] ENDOR		0.176**		2.026	0.503	1.924	0.363
			0.095**					
	Calcd.[b]				1.890	0.324	1.620	0.054
		+0.264	−0.078	+0.264	+0.070	−0.012	+0.060	−0.002

S: Not confirmed. *: Splittings of nitrogen. **: Splittings of phenyl proton. a) In liquid paraffin. b) Calculated splitting constants are obtained using the formula $A^{H}_{Ci}=|Q^{H}_{CH}|\cdot\rho_{Ci}$, $Q^{H}_{CH}=-27.0$ (i) $A^{H}_{\beta}=|Q^{H}_{CH}|\cdot\rho_{C\beta}+|B^{H}_{t-\pi}|\{\cos^2(90-\theta)\cdot\rho_{C\alpha}+\cos^2(90-\phi)\cdot\rho_{C\gamma}\}$, $|B^{H}_{t-\pi}|=50$, $\theta=\phi=37°$ (ii) $A^{N}_{\beta}=Q_1\cdot\rho_{N\beta}+Q_2(\rho_{C\alpha}+\rho_{C\gamma})$, $Q_1=+30.9$, $Q_2=-2$, where ρ_{Ci} are spin densities obtained by McLachlan's calculation using the following parameters $\lambda=1.2$, $\alpha_N=\alpha+1.2\beta$, $\beta_{C-N}=0.9\beta$, $\theta=\phi=37°$, and in BDPA the tilted angle of the phenyl attached to the Cβ is assumed to be 30°.

due to the proton in the phenyl group attached to the β-carbon.[20,21] The multiple absorption lines at *ca.* 16.5 MHz vary as the temperature rises and collapse into a single line in the temperature region at around −65 °C, as is shown in Fig. 5-c. The proton hyperfine splitting constants thus obtained are shown in Table 2, where the assignment of the hyperfine splitting constants is based on the results of the MO calculations. From this table it may be seen that there are four kinds of equivalent protons in the biphenylene groups of each radical and that the splitting constants due to the corresponding protons in these radicals are almost equal.

In the BDA-type radicals, the two phenylene groups attached to the α- or the γ-carbon are fixed in the same plane and have no degree of free rotation, although this is not the case for the TPA-type radicals. Thus, if the two twisting angles of the allyl skeleton (θ and ϕ) were nearly equal, the spin-density distributions in the four aryl rings would be approximately equivalent. However, the temperature dependence of these ENDOR spectra (Fig. 5-c) indicates that the two twisting angles of the allyl skeleton will not be equal probably. On the other hand, the MO calculations show that if the difference in the two twisting angles ($\theta\sim\phi$) is tentatively assumed to be 10°, the difference between $A^{H}_{1,3}$ and $A^{H}_{1',3'}$ is 0.5 G, while there is no noticeable difference between $A^{H}_{2,4}$ and $A^{H}_{2',4'}$. This result implies that the spectra which reflect the difference between θ and ϕ would be observed only at quite low tem-

peratures because of the torsional vibration of the allyl skeleton ($C^{\theta}C^{\phi}C \rightleftarrows C^{\phi}C^{\theta}C$). However, this is not the case at ordinary temperatures because of the fast torsional vibration rate of the allyl skeleton. Thus, the several lines near 16.5 MHz collapse into a single line, while the two lines near 14.5 MHz remain unchanged, as is shown in Fig. 5. Similar phenomena were also observed in TPA-type radicals (Fig. 3-b). For such a temperature dependence of ENDOR spectra, Hyde *et al.*[22] used the Arrhenius equation rearranged as:

$$\log_{10} 1/\tau\delta\omega = \log_{10} 2\nu_0/\delta\omega - \Delta E/2.3RT \quad (3)$$

$$1/\tau\delta\omega = 2^{-1/2}[1-(\delta\omega_e/\delta\omega)^2]^{1/2} \quad (4)$$

where τ is the lifetime of a proton in a particular site; $\delta\omega$, the separation of the two lines within the limits of slow exchange (assumed to be 0.34 MHz); ν_0, the frequency factor; ΔE, the activation energy of the torsional vibration of the allyl skeleton; R, the gas constant; T, the absolute temperature, and $\delta\omega_e$, the experimentally observed separation (Fig. 5-d). As an example, the Arrhenius plot obtained for BDPA from Eqs. (3), (4), and from the assumed value of $\delta\omega$, is shown in Fig. 6, from which the activation energy (ΔE) of the torsional vibration of the allyl skeleton ($C^{\theta}C^{\phi}C \rightleftarrows C^{\phi}C^{\theta}C$) is estimated to be about 2.5 kcal/mol. Judging from the fairly small magnitude of ΔE for the present radicals, the torsional vibration rate of the allyl skeleton may be very sensitive to the temperature variation.

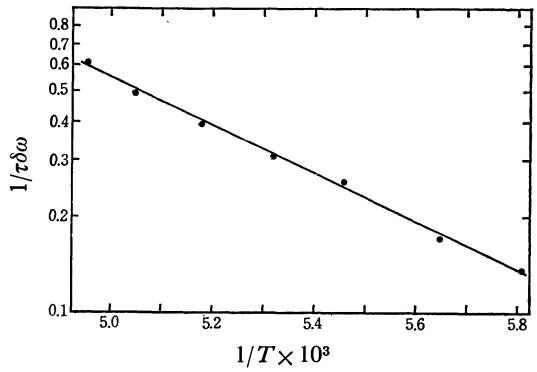

Fig. 6. Temperature dependence of the torsional vibration rate of the allyl skeleton of BDPA in toluene.

Temperature-dependent ESR Spectra and Molecular Dynamics. Tetraphenyl Allyl: As Fig. 7 shows, the hyperfine structure of the ESR spectra of TPA changes markedly with the temperature. The spectra at low temperatures (Fig. 7a-1) were analyzed assuming the three non-equivalent hyperfine components ($A^H_{o,p}$, $A^H_{o',p'}$, and $A^H_{m,m'}$), as has been established by the ENDOR measurements. The hyperfine splitting constants thus determined are listed in Table 3. As the temperature increases, the spectral pattern changes remarkably; at around 115 °C (Fig. 7a-3) it becomes a seven-line pattern with the line separation of ($A^H_{o,p}+A^H_{o',p'}$). This hyperfine pattern can be interpreted in terms of a typical line-width alternation, as has been discussed in the Introduction, and its intensity ratio coincides well with that to be expected from the theory for an extremely broadened case (the doublet of 1 : 36 : 225 : 400 : 225 : 36 : 1). The line-width alternation effect observed here may be attributed to the exchange of the *interior* and *exterior* rings due to the internal rotation of the allyl skeleton of TPA, shown in Fig. 8. At low temperatures, the rate of the internal rotation is slow, and the $A^H_{o,p}$ and $A^H_{o',p'}$

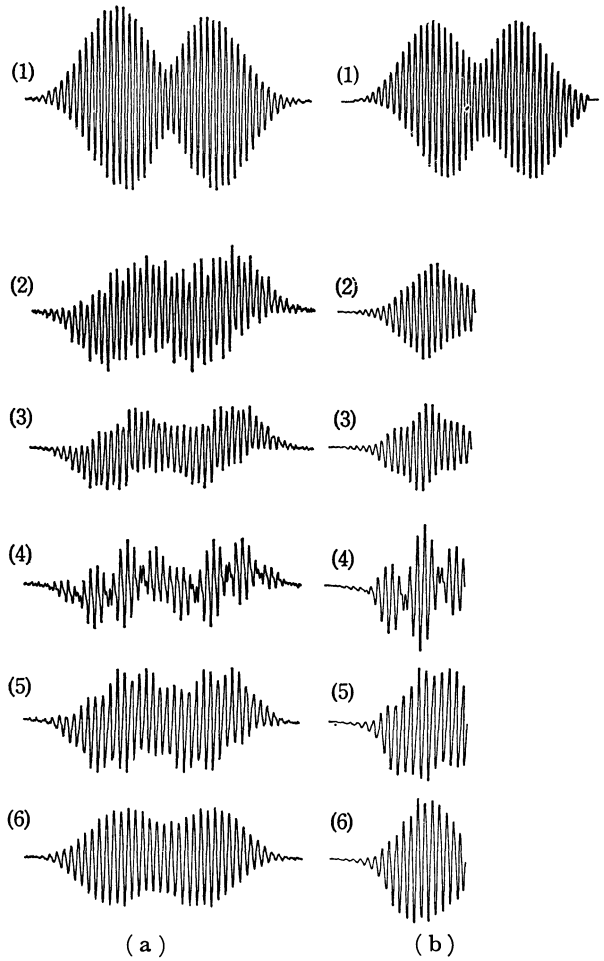

Fig. 7. Temperature-dependent ESR spectra of TPA in liquid paraffin.
(a): Observed spectra 1) at −80 °C in toluene, 2) at 55 °C, 3) at 90° C, 4) at 115 °C, 5) at 140 °C, 6) at 170 °C
(b): Simulated spectra 1) obtained by ENDOR result at −80 °C in toluene ($\tau=\infty$), 2) $\tau=1.0\times10^{-6}$, 3) $\tau=6.0\times10^{-7}$, 4) $\tau=2.0\times10^{-7}$, 5) $\tau=6.0\times10^{-8}$, 6) $\tau=4.0\times10^{-8}$

TABLE 3. HYPERFINE SPLITTING CONSTANTS OF TPA IN LIQUID PARAFFIN SOLUTION (IN G)

Temperature (°C)	method	A^H_β	$A^H_{o,p}$	$A^H_{o',p'}$	$A^H_{m,m'}$
+ 55	ENDOR	8.810	2.011 1.894	1.166	0.692
	ESR	8.86	1.95	1.22	0.67
+110	ESR	8.97	3.08/2	3.08/2	0.70
+170	ESR	9.10	1.45	1.45	0.70

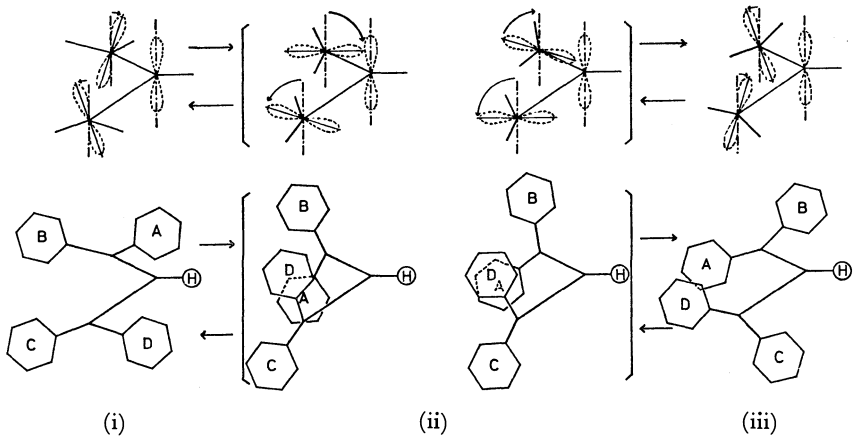

Fig. 8. Model of the internal rotation of the allyl skeleton.
Here, the interchange between the tilted angles of phenyl rings (Ω_1, Ω_2) is also considered to take place cooperative with the internal rotation of the allyl skeleton.

values are separately observed. At higher temperatures, however, the internal rotation is so rapid that it is not possible to distinguish the *interior*-phenyl protons from the *exterior*-phenyl ones because of the rapid exchange between the two states. This rate process may be analyzed by using a modified Bloch equation for the two-jump model*. The computer-simulated ESR spectra obtained on the basis of this model are compared with the observed spectra in Fig. 7. Here, the small temperature changes in the hyperfine splitting constants were ignored and the hyperfine splitting constants determined by the ENDOR measurements were used as those at the limit of the slow exchange rates. By applying the estimated lifetime (τ) to the following Arrhenius relation, the activation energy, *Ea*, of the internal rotation was evaluated:

$$k = 1/\tau = k_0 \exp(-Ea/RT), \quad (5)$$

where k is the rate constant of the internal rotation, and k_0, the frequency factor. A plot of $\log_{10} 1/\tau$ against $1/T$ is shown in Fig. 9, from which *Ea* and k_0 were calculated to be 13.4 kcal/mol and $2.3 \times 10^{14}\ s^{-1}$ respectively.

DPDAA and TAA showed merely broadened ESR spectra, as is shown in Fig. 10. The reason why these spectra do not split more clearly may owe to the unresolved small hyperfine splittings of the methoxy protons. This reasoning was confirmed by the ENDOR measurements. If these ESR spectra were well-resolved, the line-width alternation effects would be

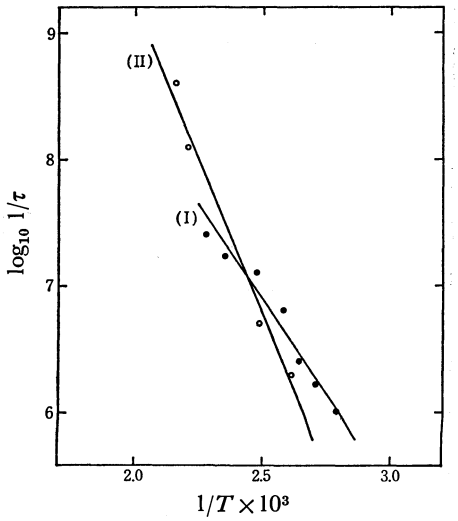

Fig. 9. Plots of $\log_{10} 1/\tau$ against $1/T$ 10^3.
(I): for TPA ●, (II) for DDA ○.

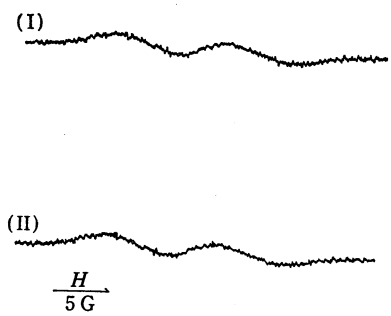

Fig. 10. ESR spectra of DPDAA (I) and TAA (II) at −85 °C in toluene.

observed as well.

Bisdiphenylene Allyl: As is shown in Fig. 11, the hyperfine patterns of the ESR spectra of BDA are not temperature-dependent. Each phenylene ring of BDA has no degree of free rotation; therefore, there may be little difference between the *interior* and *exterior* proton splittings in the biphenylene group. This was confirmed by the results of the ENDOR measurements. Because of the equivalency of the two kinds of the

* Strictly speaking, the internal rotation of the allyl skeleton must be expressed by the following four-jump model:

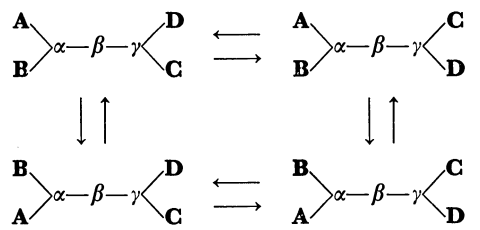

However, since only the two kinds of interconversion at the sites of α and γ are expected to be cooperative, it seems to be enough to assume merely the two-jump model.

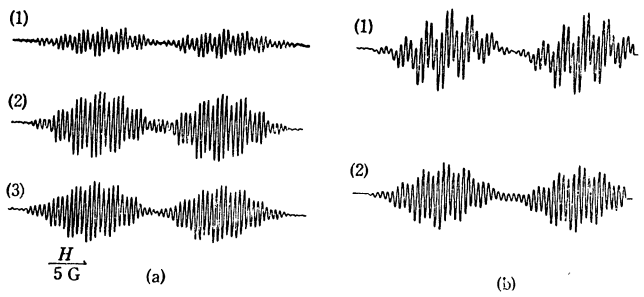

Fig. 11. ESR spectra of BDA in liquid paraffin.
(a): Observed spectra 1) at 55 °C, 2) at 115 °C, 3) at 215 °C, (b): Simulated spectra 1) obtained by ENDOR result at 55 °C, 2) obtained by ESR result at 55 °C.

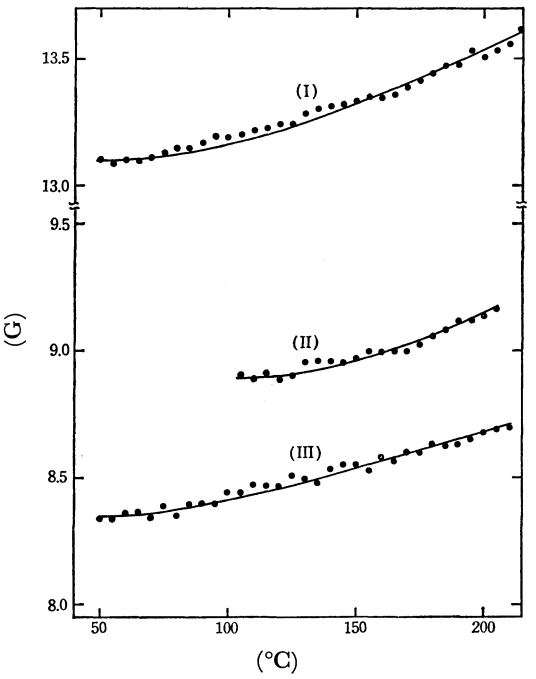

Fig. 12. Temperature dependence of the splitting constant A_β^Hs.
(I): BDA, (II): DDA, (III): TPA

aryl rings in BDA, there is no line-width alternation effect in the ESR hyperfine pattern. However, the slope of the plots of the A_β^H *vs.* temperature (Fig. 12) is similar to that for TPA. This suggests that the internal rotation of the allyl skeleton might also take place in BDA, as will be discussed later.

Diphenyl Diphenylene Allyl: The ENDOR spectrum of this radical has not been observed; therefore, its hyperfine splitting constants were analyzed with reference to the analyses of the observed ESR spectra for BDA and TPA. From the result of the computer simulation, the hyperfine splitting constants of the proton of DDA were assigned as shown in Table 4. The increase in $A_{1,3}^H$ with the temperature shows that the delocalization of an odd electron to the biphenylene group may be more favorable than that to the two phenyl rings, because with a rise in the temperature the conjugation of the biphenylene group with the allyl framework may become more favorable than that of the

Table 4. Hyperfine splitting constants of DDA in liquid paraffin solution (in G)

Temperature (°C)	A_β^H	$A_{1,3}^H$	$A_{o,p}^H$	$A_{o',p'}^H$	$A_{2,4}^H$	$A_{m,m'}^H$
+110	9.39	2.44	2.44	1.10	0.55	0.55
+150	9.46	S	S	S	0.55	0.55
+190	9.52	2.90	1.65	1.65	0.55	0.55

S not confirmed

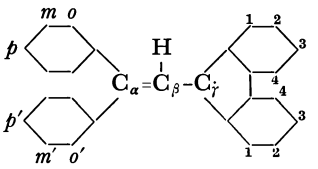

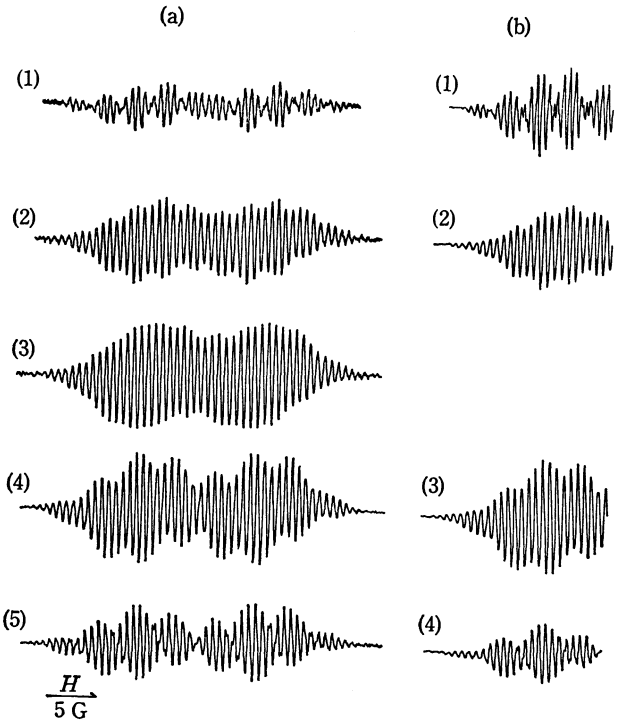

Fig. 13. Temperature-dependent ESR spectra of DDA in liquid paraffin.
(a): Observed spectra 1) at 110 °C, 2) at 130 °C, 3) at 145 °C, 4) at 180 °C, 5) at 200 °C
(b): Simulated spectra 1) $\tau=5.0\times10^{-6}$, 2) $\tau=2.5\times10^{-6}$, 3) $\tau=8.0\times10^{-8}$, 4) $\tau=5.0\times10^{-8}$

two phenyl rings, which undergo restricted rotation. Furthermore, at low temperatures evidences were obtained for inequivalent phenyl rings (*interior* and *exterior*) in DDA, while, on warming, the allyl skeleton begins to rotate internally. Hence, the interconversion between the two phenyl rings must be the origin of the complex temperature dependence of the ESR spectral pattern shown in Fig. 13. Therefore, the two-jump model was tentatively applied in the manner described for TPA. The activation energy for an interconversion of the two phenyl rings (=internal rotation of the allyl skeleton) thus estimated is about 22.3 kcal/mol, and the frequency factor (k_0), about 1.4×10^{19} s^{-1} (Fig. 9).

Temperature Dependence of A_β^H. The temperature dependence of A_β^H of TPA is shown in Fig. 1.

The slopes of the plots of the A_β^H *vs.* the temperature at high temperatures are nearly independent of the solvents. In addition, the ESR hyperfine patterns of toluene solutions at 90—100 °C are essentially the same as those of liquid paraffin solutions at 115—135 °C. This suggests that the temperature dependence of A_β^H is caused by the intramolecular dynamics of the allyl skeleton. Similar results were obtained for both BDA and DDA, as is shown in Fig. 12. The observed A_β^H at lower temperatures are likely to be constant. This is related to the fact that the torsional vibration of the allyl skeleton is very slow at very low temperatures, as was confirmed by the ENDOR analyses of the BDA-type radicals. At such temperatures, the internal rotation of the allyl skeleton does not take place; also, the two twisting angles of the allyl skeleton are different from each other. As the allyl skeleton begins to rotate internally with a rise in the temperature, the two $2p_z$-*orbitals* on both the α and γ carbon atoms tend to overlap with the ls-*orbital* of the methine proton (Fig. 8). Hence, A_β^H must reach a maximum in the state of Fig. 8-(ii)**. When the internal rotation rate is slow (that is, when the τ-values are large), the probability of finding the state of Fig. 8-(ii) may be small, resulting in a small A_β^H. On the other hand, when the internal rotation becomes faster (that is, when the τ-values are smaller), the probability of finding the state of Fig. 8-(ii) may increase, making A_β^H larger and larger.

Conclusion

1. At low temperature the allyl skeleton of the tetraaryl allyl radicals oscillates very slowly.
2. The torsional vibration becomes larger with an increase in the temperature, and the allyl skeleton begins to rotate internally at high temperatures.
3. Line-width alternation effects have been observed in TPA and DDA, the activation energies of their internal rotations being 13.4 kcal/mol and 22.3 kcal/mol respectively.
4. The temperature dependence of A_β^H is interpreted by means of the mechanism of the internal rotation of the allyl skeleton.

** Here, the author assumes that an odd electron distribution on the allyl skeleton is kept almost constant with temperature variation. (*cf.* sections of TPA and BDA)

The author wishes to thank Professor Yasuo Deguchi, Professor Kazuhiko Ishizu, Professor Saburo Kako, Dr. Hiroaki Ohya-Nishiguchi, Dr. Jun Yamauchi, and their collaborators for their helpful advices and discussions. He is also indebted to Professor Toshio Takada and Professor Hideo Takaki for their continual encouragements during this work. Thanks are also due to the attendants of the 13th ESR symposium who stimulated the author with useful discussions.

References

1) G. R. Luckhurst, *Mol. Phys.*, **11**, 205 (1966).
2) A. Berndt, *Tetrahedron*, **25**, 37 (1969).
3) K. Watanabe, J. Yamauchi, H. Ohya-Nishiguchi, Y. Deguchi, and H. Takaki, This Bulletin, **45**, 371 (1972).
4) C. Heller and H. M. McConnell, *J. Chem. Phys.*, **32**, 1535 (1960).
5) R. W. Fessenden and R. H. Shuler, *ibid.*, **39**, 2147 (1963).
6) W. A. Forbes, P. D. Sullivan, and H. M. Wang, *J. Amer. Chem. Soc.*, **89**, 2705 (1967).
7) M. K. Carter and G. Vincow, *J. Chem. Phys.*, **47**, 302 (1967).
8) E. W. Stone and A. H. Maki, *ibid.*, **37**, 1326 (1962).
9) J. H. Freed and G. K. Fraenkel, *ibid.*, **39**, 326 (1963).
10) P. D. Sullivan and J. R. Bolton, "Advances in Magnetic Resonance," Vol. 4, ed. by J. S. Wangh, Academic Press, New York, N. Y. (1970), p. 39.
11) K. Ziegler, *Ann. Chem.*, **434**, 34 (1932).
12) R. Kuhn and D. Rewicki, *ibid.*, **690**, 50 (1965).
13) R. Kuhn, H. Fischer, F. A. Neugebauer, and H. Fischer, *ibid.*, **654**, 64 (1962).
14) R. Kuhn and F. A. Neugebauer, *Monatsh. Chem.*, **94**, 16 (1963).
15) R. Kuhn and F. A. Neugebauer, *ibid.*, **95**, 3 (1964).
16) G. E. Pake, J. Townsend, and S. I. Weissman, *Phys. Rev.*, **85**, 683 (1952).
17) A. H. Maki, R. D. Allendoerfer, J. C. Danner, and R. T. Keys, *J. Amer. Chem. Soc.*, **90**, 4225 (1968).
18) A. D. McLachlan, *Mol. Phys.*, **3**, 233 (1960).
19) K. Watanabe, J. Yamauchi, H. Ohya-Nishiguchi, and Y. Deguchi, This Bulletin, **47**, 274 (1974).
20) K. Watanabe, J. Yamauchi, H. Ohya-Nishiguchi, Y. Deguchi, and K. Ishizu, *Chem. Lett.*, **1974**, 489.
21) N. S. Dalal, D. E. Kennedy, and C. A. McDowell, *J. Chem. Phys.*, **61**, 1689 (1974).
22) J. H. Hyde, R. Breslow, and C. DeBoer, *J. Amer. Chem. Soc.*, **88**, 4763 (1966).

CNDO/2 Calculations on the Configurations of the Ion-molecule Complexes. The NH_4^+–CH_4, H_3O^+–CH_4 and NH_4^+–H_2 Systems

Kazuyoshi TANAKA, Tokio YAMABE, Hiroshi KATO,* and Kenichi FUKUI

Department of Hydrocarbon Chemistry, Faculty of Engineering, Kyoto University, Sakyo-ku, Kyoto 606

**College of General Education, Nagoya University, Chikusa-ku, Nagoya 464*

(Received December 16, 1974)

The optimized configurations of several ion-non polar molecule complexes (NH_4^+–CH_4, H_3O^+–CH_4 and NH_4^+–H_2) have been discussed by the use of the CNDO/2 method. The results for NH_4^+–CH_4 and H_3O^+–CH_4 turn out to be quite different from those previously proposed by the calculations based on the classical electrostatic model. It may be demonstrated that these systems are stabilized by a kind of hydrogen bond where the charge transfer effect from a neutral molecule to a cation plays an important role, according to the configuration analysis.

In the field of intermolecular forces, there has been recent progress in the theoretical development of weak interactions, such as hydrogen bonds or ion-molecule bonds, based on *ab initio* calculations or fairly reliable semi-empirical calculations.[1,2]

Of these, ion-molecule bonds consist of interaction between ions and neutral molecules in the singlet ground state. Such bonds have usually been investigated in order to comprehend the solvation process of ions in polar solvents, such as H_2O and NH_3.[1a,1b] In contrast with the extensive studies of these ion-polar molecule complexes, there have been only a few studies of ion-non polar molecule complexes.

Recently it has become possible to obtain direct thermodynamical data on some ion-non polar molecule complexes in the gaseous state through the mass spectrometry of ion beams at low temperatures. Bennett, Field, and Beggs have obtained the equilibrium constants and thereby evaluated the ΔG_{300}, ΔH^0 and ΔS^0 values of the following reactions:[3-5]

$$CH_5^+ + CH_4 \rightleftharpoons CH_5^+\text{-}CH_4 \quad \Delta H^0 = -4.14 \text{ kcal/mol}$$

$$NH_4^+ + CH_4 \rightleftharpoons NH_4^+\text{-}CH_4 \quad \Delta H^0 = -3.59 \pm 0.11 \text{ kcal/mol}$$

$$CF_3^+ + CH_4 \rightleftharpoons CF_3^+\text{-}CH_4 \quad \Delta H^0 = -4.55 \pm 0.05 \text{ kcal/mol}$$

$$H_3O^+ + CH_4 \rightleftharpoons H_3O^+\text{-}CH_4 \quad \Delta H^0 = -8.0 \text{ kcal/mol}$$

The $-\Delta H^0$ means the interaction energy needed to stabilize such an ion-molecule complex. They have also calculated the classical electrostatic interaction energy in order to discuss the stable configurations of these complexes.

Geometries suggested by the popular semi-classical electrostatic model[6] are often consistent with the experimental results or those calculated by MO method[7] for small ion-non polar molecule complexes, such as H_5^+ and He–H_3^+. It is, however, questionable whether this method yields reliable results for larger complexes such as the NH_4^+–CH_4 system, since it quite neglects the effect of charge transfer, which seems to play an important role in stabilizing these complexes. Indeed, the models proposed by the experimentalists are far from those conjectured from the reliable geometries of the H_3O^+–H_2O and NH_3–NH_3 systems.[1a,1b]

It may, therefore, be worthwhile to discuss the geometries of some typical ion-non polar molecule systems. In this paper, we will calculate the interaction energies in order to predict the stable configurations of the NH_4^+–CH_4, H_3O^+–CH_4 and, additionally, NH_4^+–H_2 systems by means of the CNDO/2 method.** This method has yielded considerably reliable results on the interaction energies and stable configurations for neutral molecule systems and for cationic systems as well.[8] Furthermore, we will carry out the configuration analysis by expanding the MO of the optimized configuration in order to show the contribution factors which stabilize each complex.

Method of Calculation

The bond distances and angles in the isolated cations and molecules are optimized individually by the CNDO/2 calculation; they are shown in Table 1.

TABLE 1. BOND DISTANCES AND ANGLES USED FOR ISOLATED SYSTEMS

Species	Bond	Distance (Å)	Angle	Size. deg
CH_4	C-H	1.115	H-C-H	109°28′
H_2	H-H	0.741[a]	—	—
NH_4^+	N-H	1.077	H-N-H	109°28′
H_3O^+ [b]	O-H	1.045	H-O-H	114°45′

a) Assumed. b) Pyramidal form.

For the NH_4^+–CH_4 system, in which both NH_4^+ and CH_4 have the C_2 axis and the C_3 axis, ten different kinds of configurations within the probable symmetries have been selected. The optimized configuration is determined for each interacting system by changing the intermolecular distance between NH_4^+ and CH_4; subsequently, several prominent parameters are optimized in the order of their magnitudes for the interaction energy.

For the H_3O^+–CH_4 system and the NH_4^+–H_2 system, details will be described later.

The method of configuration analysis[9] is applied to the most optimized configuration of each complex. Here we will briefly outline a CI wavefunction:

$$\Psi = C_0\Psi_0 + \sum_i^{occ}\sum_l^{uno} C_{i\to l}\Psi_{i\to l} + \sum_k^{occ}\sum_j^{uno} C_{k\to j}\Psi_{k\to j} + \sum_i^{occ}\sum_j^{uno} C_{i\to j}\Psi_{i\to j} + \sum_k^{occ}\sum_l^{uno} C_{k\to l}\Psi_{k\to l} + \cdots\cdots \quad (1)$$

** As to CF_3^+–CH_4 and CH_5^+–CH_4 systems, it is doubtful whether the CNDO/2 method is suitable to treat CF_3^+ and CH_5^+ isolated systems. Thus the reliable MO calculation results of these systems are of further indices.

where i, j, k, and l represent the i-th occupied MO of an isolated system, A, the j-th unoccupied of A, the k-th occupied of B, and the l-th unoccupied of B respectively, and where the sign $i \rightarrow l$ indicates the one-electron shift from MO i to MO l and so on. We can thus make the CI wavefunction of the complexes if the coefficients are known. In order to see the contributing factors to the stabilization of the complexes, we construct a wavefunction:

$$\begin{aligned}\Psi = C_0\Psi_0 &+ [\sum_i^{occ}\sum_l^{uno}(C_{i\rightarrow l})^2]^{1/2}\Psi(A^+\cdot B^-) \\ &+ [\sum_k^{occ}\sum_j^{uno}(C_{k\rightarrow j})^2]^{1/2}\Psi(A^-\cdot B^+) \\ &+ [\sum_i^{occ}\sum_j^{uno}(C_{i\rightarrow j})^2]^{1/2}\Psi(A^*\cdot B) \\ &+ [\sum_k^{occ}\sum_l^{uno}(C_{k\rightarrow l})^2]^{1/2}\Psi(A\cdot B^*) + \cdots\cdots \quad (2)\end{aligned}$$

where, for instance, $\Psi(A^+\cdot B^-)$ and $\Psi(A^*\cdot B)$ represent all of the one-electron transferred configurations from A to B, and all of the one-electron excited configurations in A, respectively.

Results and Discussion

The NH_4^+–CH_4 System. The selected configurations are shown in Fig. 1, while the changes in the interaction energies with varying the distance between NH_4^+ and CH_4 are drawn in Fig. 2. The optimized configuration turns out to be (A). The starred hydrogen atom in (A), (B), and (C) seems to play an important role in binding the systems. The values of the net charge of the hydrogen atoms are as follows; (A)+0.300, (B)+0.296, and (C)+0.289. It can easily be seen that the (A) configuration is the most advantageous for bonding, since the positively charged hydrogen contributes to bind the system as a bridging center through Coulomb interaction with the carbon atom in CH_4. Henceforth, it may be said that the optimized configuration for the ion-molecule complex is mainly guaranteed by the existence of a positively charged hydrogen atom in the cation situated on the bonding axis of the complex as a bridging center. Furthermore, the neutral molecule retains its highest

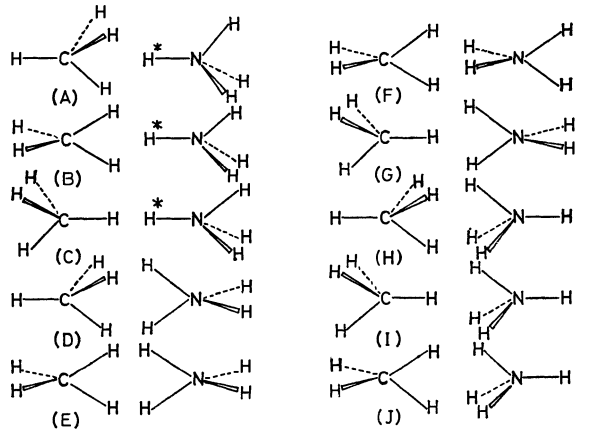

Fig. 1. The selected configurations for the NH_4^+-CH_4 system.

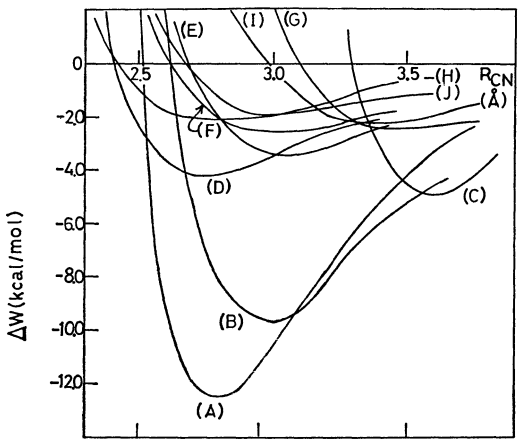

Fig. 2. Potential curves of the selected configurations for the NH_4^+-CH_4 system. The 90° rotation of either fragment along the C–N axis in (B), (D), (G), and (J) and 180° rotation in (A) yield no energy change within an error.

symmetry and avoids the form in which a hydrogen atom in the molecule confronts the positively charged hydrogen atom in the cation. Such a tendency coincides with the previous calculation results as to, for instance, the H_3O^+–H_2O and the H_2O–H_3O^+–H_2O systems.[1a]

The (A) configuration is next treated so as to be optimized with other parameters. The optimized (A) configuration in Fig. 3 shows that R_{6N7H} stretches toward 1C as far as 1.117 Å and that ∠3H1C4H *etc.* open a little to be 112°. Thus, the optimized energy of this system is 14.49 kcal/mol (experimental: 3.59 kcal/mol). We need not further optimize the (B) configuration and those following in Fig. 1, since they would not exceed the optimized (A) in Fig. 3 in interaction energy. Interestingly, the configuration in Fig. 4 proposed by Bennett and Field[5] is converse in the direction of the CH_4 and NH_4^+ from the optimized

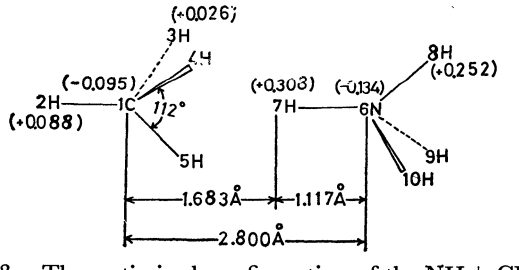

Fig. 3. The optimized configuration of the NH_4^+-CH_4 system. R_{4H7H}=1.729 Å and other bond distances remain unchanged.

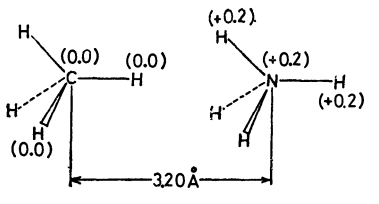

Fig. 4. Bennett and Field's model for the NH_4^+-CH_4 system.

configuration predicted here. The E_{AB} analysis in the CNDO/2 method shows that the E_{1C7H} and E_{6N7H} attractive energies have the largest effect in stabilizing the complex among the other attractive and repulsive energies. In fact, the eclipsed form yields the same $-\Delta W$ as that of the staggered form in Fig. 3. Therefore, in this configuration, CH_4 and NH_4^+ seem to rotate along their bonding axis. The values of atomic net charge are also given in Fig. 3; the quantity of the transferred charge from CH_4 to NH_4^+ is estimated to be -0.071.

The H_3O^+–CH_4 System. For this system, five kinds of configurations are treated. The (A) configuration in Fig. 5 is selected by the criterion noted above, and others that have C_{3v} geometries in both fragments are compared with (A). In Fig. 6 the optimized configuration is shown to be (A), as was expected. The other configurations are far less stable than (A) in spite of their symmetries. A further optimized form of (A) is shown in Fig. 7, where R_{6O7H} stretches toward 1C to be 1.115 Å and where ∠3H1C4H *etc.* in CH_4 open until 114°. This is also quite the same pattern as in the NH_4^+–CH_4 system in Fig. 3. The calculated interaction energy gives 31.56 kcal/mol (experimental: 8.0 kcal/mol). The configurations in Fig. 8, previously proposed by Bennett and Field,[4] are quite different from the most optimized one predicted here.

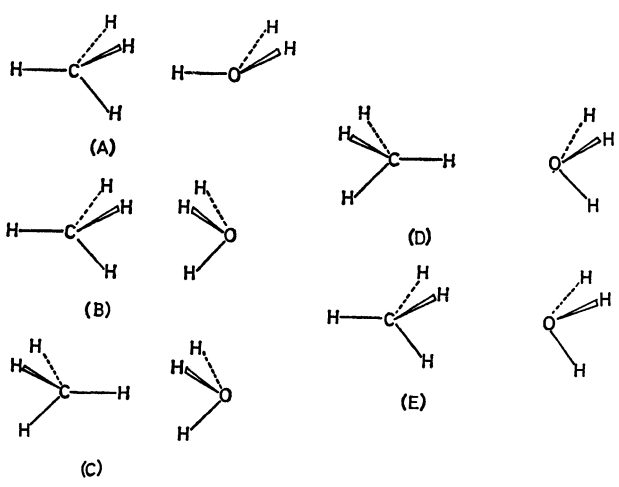

Fig. 5. The selected configurations for the H_3O^+–CH_4 system.

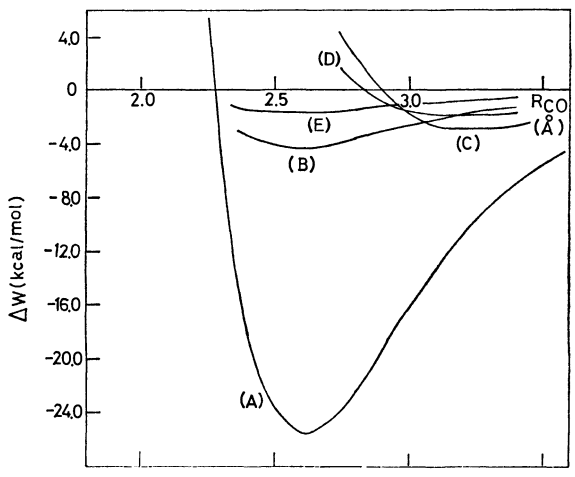

Fig. 6. Potential curves of the selected configurations for the H_3O^+–CH_4 system. The 90° and 180° rotation of either fragment along the C–O axis in (A) yields no energy change within an error.

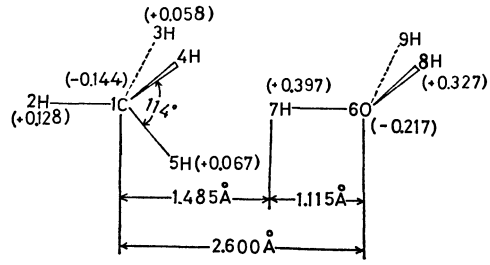

Fig. 7. The optimized configuration for the H_3O^+–CH_4 system. $R_{4H7H} = 1.619$ Å and other bond distances remain unchanged.

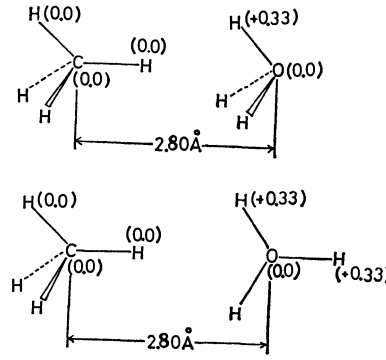

Fig. 8. Bennett and Field's model for the H_3O^+–CH_4 system.

As to the E_{AB} values, E_{1C7H} and E_{6O7H} are the dominant attractive energies, and the 90° and 180° rotations of either fragment along the C–H–O axis yield no energy change as in the NH_4^+–CH_4 system. Therefore, this system should also rotate freely along the C–H–O axis. The quantity of the transferred charge from CH_4 to H_3O^+ is -0.166, which is considerably larger than that in the NH_4^+–CH_4 system.

The NH_4^+–H_2 System. This system is considered to be a simple model of the ion-molecule complexes, although there are no previous experimental data available. Therefore, it seems that it would be

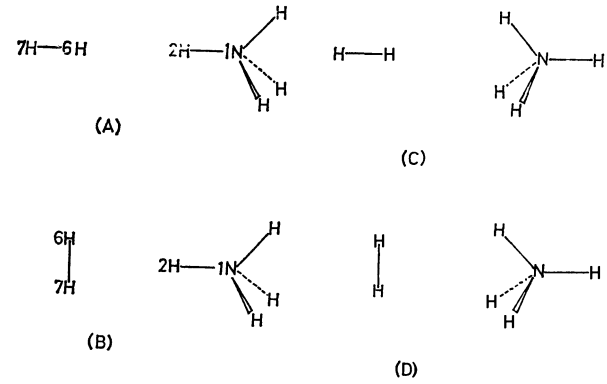

Fig. 9. The selected configurations for the NH_4^+–H_2 system.

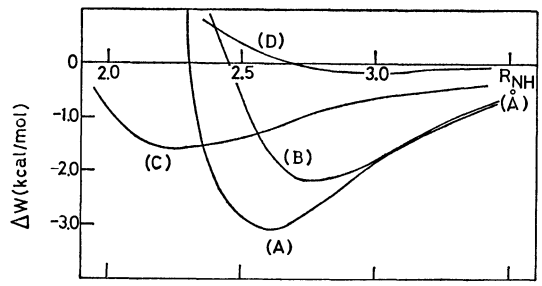

Fig. 10. Potential curves of the selected configurations for the NH_4^+-H_2 system.

TABLE 2. THE INTERACTION ENERGY OF THE NH_4^+-H_2 SYSTEM

Configuration	Parameters		Interaction energy (kcal/mol)
(A) Configuration	R_{6H7H}[a]	=0.641 Å	−7.45 (Repulsive)
		0.741 Å	3.07
		0.841 Å	2.45
	R_{1N2H}	=0.977 Å	−9.98 (Repulsive)
		1.077 Å	3.07
		1.117 Å	−3.70 (Repulsive)
(B) Configuration	R_{6H7H}	=0.721 Å	1.57
		0.741 Å	2.13
		0.761 Å	2.13
		0.781 Å	1.51
	R_{1N2H}	=1.067 Å	1.88
		1.077 Å	2.13
		1.087 Å	2.26
		1.097 Å	2.20

a) 7H is fixed.

interesting to predict the interaction energy and the optimized configuration for this system by MO theoretical treatment. In order to do so, four kinds of configurations were selected and their maximum interaction energies were calculated. The selected configurations and the potential curves are shown in Fig. 9 and Fig. 10 respectively. The interaction energy, $-\Delta W$, of the optimized (A) configuration is 3.07 kcal/mol, while that of the secondary optimized (B) configuration is 2.13 kcal/mol. Since these values are very close, both (A) and (B) should be further optimized. The results, presented in Table 2, show that the $-\Delta W$ in (A) remains unchanged, while that in (B) becomes 2.26 kcal/mol. Therefore, the (A) configuration is still most stable. In Fig. 11 the detailed form of the (A) configuration is presented. The quantity of the transferred charge from H_2 to NH_4^+ is −0.013, much less than those of the NH_4^+-CH_4 and the H_3O^+-CH_4 systems, and it produces less stabilization energy. The result that the difference in $-\Delta W$ values between (A) and (B) is only 0.81 kcal/mol, which is the same order as kT at room temperature, implies that H_2 rotates in the space near NH_4^+. Furthermore, the experimental data of $-\Delta H^0$ of this system, if any, would be about 0.5~0.75 kcal/mol, referring that the calculated $-\Delta W$ values for both the NH_4^+-CH_4 and the H_3O^+-CH_4 systems are four times the respective experimental values. If so, the $-\Delta W$ values for the (A), (B), (C), and (D) configurations will become closer, and (A) may change into (B), (C) or (D) in rapid succession, at least in the range of room temperature.

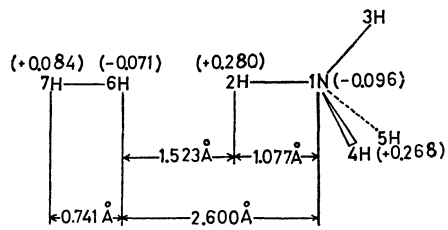

Fig. 11. The optimized configuration for the NH_4^+-H_2 system.

Thus, the NH_4^+-H_2 system is far from being a rigid complex. The two fragments, NH_4^+ and H_2, retain most of their individual integrity in the cluster. H_2 should be considered as distributed on a sphere about NH_4^+, with only a slight maximum probability at the calculated equilibrium configuration.

Configuration Analysis. Table 3 shows the results of the configuration analysis for the optimized configurations of the above systems. The values represent the weights (*i.e.*, the square of the coefficients in Eq. (2)) of the wavefunctions of various configurations. It can easily be seen that the more the weights of the charge transfer terms increase and that of the ground state decreases, the larger the stabilization energy appears, namely, the NH_4^+-H_2, the NH_4^+-CH_4, and the H_3O^+-CH_4 system, in order. The percentage contribution of the charge transfer term from the neutral molecule to the cation is particularly remarkable—that is, 1.47%, 7.22%, and 15.44% in the NH_4^+-H_2, NH_4^+-CH_4, and H_3O^+-CH_4 systems respectively, compared with the contributions from the other configurations. The weight of the polarization term of the cation is larger than that of the neutral molecule in the NH_4^+-CH_4 and H_3O^+-CH_4 system, while for the NH_4^+-H_2 system the weight in H_2 is 0.0030, surpassing that of NH_4^+.

In conclusion, it turns out that the previous results for these complexes obtained by the classical electrostatic method are deficient, since that method apparently

TABLE 3. THE WEIGHTS OF VARIOUS CONFIGURATIONS FOR EACH SYSTEM

Configurations	NH_4^+-CH_4	H_3O^+-CH_4	NH_4^+-H_2
Ground state	0.9130	0.8048	0.9797
Neutral→Cation charge transfer	0.0722	0.1544 (0.0074)[a]	0.0147
Cation→Neutral charge transfer	0.0049	0.0058	0.0022
Polarization of neutral molecule	0.0031	0.0089	0.0030
Polarization of cation	0.0044	0.0140	0.0002
Sum of the above values	0.9977	0.9964[b]	0.9999

a) Two-electron transfer configuration. b) All contributions from two-electron transfer are added.

neglects the charge transfer, which has a significant effect in stabilizing the complexes. On the contrary, the MO treatment allows us to predict the optimized configurations and display the essential factors which stabilize the complexes, as has been mentioned above. Lastly, it is interesting that the ion-molecule complexes reported here are held by a kind of hydrogen bond, X···H–Y, in which X represents a carbon atom, and Y, a nitrogen or an oxygen atom. Since the H bears most of the positive charge in the cation, this X···H–Y bond is strong enough to hold the complex, and it yields a larger interaction energy than those of the ordinary hydrogen bond systems. Either fragment of the systems treated here is able to rotate freely along the axis of the X···H–Y because of the dominance of the E_{XH} and E_{HY}-attractive energies, which are isotropic with regard to this type of rotation. Furthermore, in the NH_4^+–H_2 system H_2 would rotate three-dimensionally near NH_4^+, according to the CNDO/2 calculation. In the present calculation we have used the convenient semi-empirical MO method. An *ab initio* MO treatment for these complexes would be further expected.

One of the present authors (K.T.) is grateful to Mr. Shigeki Kato and Mr. Tsutomu Minato for their helpful advice on performing the MO calculation. We also wish to express our gratitude to the Data Processing Centre of Kyoto University for its generous permission to use the FACOM 230-60 Computer.

References

1) (a) M. D. Newton and S. Ehrenson, *J. Amer. Chem. Soc.*, **93**, 4971 (1971); (b) P. A. Kollman and L. C. Allen, *ibid.*, **93**, 4991 (1971); (c) G. Alagona, R. Cimiraglia, and U. Lamanna, *Theor. Chim. Acta* (Berl.), **29**, 93 (1973).

2) M. Losonczy, J. W. Moskowitz, and F. H. Stillinger, *J. Chem. Phys.*, **59**, 3264 (1973).

3) F. H. Field and D. P. Beggs, *J. Amer. Chem. Soc.*, **93**, 1585 (1971).

4) S. L. Bennett and F. H. Field, *ibid.*, **94**, 5188 (1972).

5) S. L. Bennett and F. H. Field, *ibid.*, **94**, 6305 (1972).

6) K. G. Spears, *J. Chem. Phys.*, **57**, 1850 (1972).

7) (a) R. D. Poshusta and V. P. Agrawal, *ibid.*, **59**, 2477 (1973); (b) W. I. Salmon and R. D. Poshusta, *ibid.*, **59**, 4867 (1973).

8) For example, see O. Sinanoğlu and K. B. Wiberg, "Sigma Molecular Orbital Theory," Yale Univ. Press (1970).

9) (a) H. Baba, S. Suzuki, and T. Takemura, *J. Chem. Phys.*, **50**, 2078 (1969); (b) H. Fujimoto, S. Kato, S. Yamabe, and K. Fukui, *ibid.*, **60**, 572 (1974); (c) S. Kato, H. Fujimoto, S. Yamabe, and K. Fukui, *J. Amer. Chem. Soc.*, **96**, 2024 (1974).

The Effects of Anionic and Cationic Surfactants on the Ion Flotation of Cd^{2+}

Koichi KOBAYASHI*

Department of Chemistry, Faculty of Science, Tokyo Metropolitan University, Setagaya, Tokyo 158

(Received November 16, 1974)

The ion flotation of Cd^{2+} ions has been investigated from the surface chemical point of view in comparison with the case of Cu^{2+} ions reported previously.[1] The effects of the change in the pH, the anionic and cationic surfactants, and bentonite on the flotation rate have also been studied. Sodium α-sulfolaurate proved to be one of the best surfactants among the anionic surfactants used for removing Cd^{2+} ions, showing as high as a 97% removal. About 97% of the Cd^{2+} ions could be floated in the region of pH 11.3 when a cationic surfactant was used with bentonite, regardless of the exact surfactant used. The addition of bentonite reduced the foam formation and liquid hold-up, resulting in effective bubble flotation. This behavior was as a whole similar to that of Cu^{2+} ions.[1] However, in all the flotation systems tested, the flotation rate increased sharply at about pH 8, and the flotation rate *vs.* pH curve for Cd^{2+} shifted towards a more alkaline region than that for Cu^{2+}, because of the stronger basic nature of the former. Also, the flotation rate of Cd^{2+} ions for the Cd^{2+}-anionic surfactant systems attained a steady value after about 7 min, longer than the 2-min gas flow required in the case of Cu^{2+} ion flotation. The adjustment of the pH using ammonia gave a lower rate of flotation than in the case of flotation using sodium hydroxide.

The importance of the process of ion flotation[2,3] is well known, as has already been mentioned in a previous paper reporting the bubble flotation of Cu^{2+} ions.[1]

The flotation of Cd^{2+} ions has become an important problem in connection with water pollution and sewage treatment.[4–6] As regards the flotation of Cd^{2+} ions, however, only a limited number of papers have been reported. Ferguson *et al.* have reported the removal of CdS using hexadecyltrimethylammonium bromide.[7] Shimoiizaka *et al.* have studied the removal of Cd^{2+} ions from mine water by using xanthates.[5] Also, this problem is of surface chemical interest, since Cd^{2+} ions are a stronger base and are fairly different chemically compared with the Cu^{2+} ions previously studied.

The present paper will report a study of the bubble flotation of cadmium ions by anionic and cationic surfactants with bentonite in order to find the condition of most efficient ion flotation, to make clear the mechanism of flotation, and to compare it with the case of Cu^{2+} ion flotation.

Experimental

Materials. A stock solution containing 1.78×10^{-4} mol l cadmium ions (Cd^{2+}) and with a pH of 2.7 was prepared by dissolving Cd metal of a 99.999% purity (obtained from the Wako Pure Chemical Co., Ltd.) in nitric acid. The surfactants used were sodium *n*-dodecylsulfate (SDS), sodium laurate (LNa), sodium *n*-dodecylbenzenesulfate (DBS), and sodium α-sulfolaurate (α-SLNa) (obtained from the Kao Soap Co., Ltd.) as anionic surfactants, and *n*-dodecyltrimethylammonium chloride (DTAC) (obtained from the Tokyo Kasei Industrial Co., Ltd.), hexadecyltrimethylammonium chloride (HTAC) and octadecyldimethylbenzylammonium chloride (OBAC) (obtained from the Kao Soap Co., Ltd.) as cationic surfactants. The bentonite powder used as an ion exchanger was obtained from the Wako Pure Chemical Co., Ltd. The methods of the purification of the materials were the same as have previously been described[1] except for the case of OBAC. The commercial product of OBAC was recrystallized twice from acetone. The surfactants were kept in a desiccator. The pH of the solution was controlled by using special-grade sodium hydroxide and ammonia.

The triply distilled water used was free from Cd^{2+} ions, as detected by means of an atomic absorption spectrometer.

Apparatus and Procedure. The flotation apparatus and method were the same as those described previously.[1] Nitrogen gas humidified with water vapor and controlled to a constant rate of gas flowing was bubbled through a glass filter of No. 4 into a flotation cell containing 10 ml of the sample solution.

To prepare a sample solution of Cd^{2+} ions, 2 ml of the stock solution of Cd^{2+} ions, a proper amount of sodium hydroxide or ammonia to adjust the pH, 2 ml of the surfactant solution, and 2 ml of bentonite solution in the case of a cationic surfactant were introduced into a 20-ml measuring flask. The total volume of the solution was made up to 20 ml with water. A part of the solution was used to measure the initial pH (pH_i) and the Cd^{2+} ion concentration (C_i mol/l). A 10-ml portion of the remaining solution was transferred into the flotation cell, and the gas flow was started. After a definite time of flotation, about a 7-ml portion of the solution was taken out in order to determine the final pH (pH_f) and Cd^{2+} ion concentration (C_f mol/l), the latter being calculated from the absorbance measured at 2288 Å and at pH 2.6 using an atomic absorption spectrometer (Techtron Pty., Ltd., Model-AA-100).

The gas-flow rate was kept constant at 10 ml/min throughout the experiments. The gas-flow time was kept at 7 min unless otherwise stated. The measurements were carried out at room temperature (about 25 °C).

Results and Discussion

In the present work, the effects of the flotation rate on the gas-flow time, the bentonite concentration, the surfactant concentration, and the pH were studied.

The flotation rate (F) of Cd^{2+} ions is conventionally given by:

$$F = (1 - C_f/C_i) \times 100\ \%$$

Experiments were mainly run under the conditions of bubble flotation, mainly flotation using only ascending bubbles, without the aid of foam formation. Since most of the solution after flotation was used for the measurement of C_f, the flotation rate calculated expresses substantially the percentage of Cd^{2+} ions removed from the total solution.

* Present address: Department of Chemistry, Musashi Institute of Technology, 1-28-1, Tamatsutsumi, Setagaya, Tokyo 158.

Flotation of Cd^{2+} Ion by Anionic Surfactants. Relation between Flotation Rate and Gas-flow Time: In order to study the optimum gas-flow time of various surfactants, flotation experiments were run at the optimum condition of flotation at around pH 11.2. Figure 1 shows the effects of the gas-flow time at the gas-flow rate of 10 ml/min on the flotation rate for the Cd^{2+}–α-SLNa, –DBS, and –SDS systems. It can be seen that the flotation rate attains a steady value after about 7 min, longer than the 2-min gas flow required in the case of Cu^{2+} ion flotation.[1]

Relation between pH and Flotation Rate. Figure 2 shows the effect of the pH on the flotation rate for the Cd^{2+}–SDS system. As may be seen, the flotation rate begins to increase from zero at around pH 8 for the 1.78×10^{-5} mol/l SDS concentration. The pH value is higher than pH 6 in the case of Cu^{2+} ions because of the stronger basic nature of Cd^{2+} ions. When the pH is adjusted using sodium hydroxide, a maximum flotation rate of about 85% was observed at pH 11.3, while the flotation rate was less in the case of the pH adjusted by using ammonia. In the former case, cadmium hydroxide, probably in the form of polynuclear Cd^{2+} ions,[8] is attracted and floated by SDS, whereas in the latter case, the formation of polynuclear Cd^{2+} ions is prevented to a certain extent by the formation of an ammine complex such as $Cd(NH_3)_4^{2+}$, which adsorbs less efficiently than the polynuclear ions. At the large SDS concentration of 8.90×10^{-5} mol/l, a stable foam layer forms and Cd^{2+} ions are floated even below pH 8, showing flotation rates of about 40% for systems with the pH adjusted by both sodium hydroxide and ammonia. This may be explained by the simple adsorption of Cd^{2+} ions on the surface of ascending bubbles, which persist as a stable foam layer and concentrate the Cd^{2+} ions. Thus, the flotation is considered to be an ion-adsorption flotation. Between pH 8 and 10, Cd^{2+} ion flotation is considered to take place either by ion adsorption and precipitation or by ion adsorption and a hindered precipitation mechanism, according to whether sodium hydroxide or ammonia is used to adjust the pH. Beyond pH 10, the curve for the system adjusted by sodium hydroxide shows a maximum and a subsequent decrease due to the competition between OH^- and DS^- ions for Cd^{2+} in the high pH region, while the curve ends before the appearance of a maximum for the system controlled with ammonia due to the weak basicity of ammonia. The flotation was carried out further for the Cd^{2+}–DBS system. A result similar as a whole to Fig. 2 was obtained except that a maximum F value of 95% was obtained at about pH 11.3 for the system containing 1.78×10^{-5} mol/l DBS and the pH adjusted using sodium hydroxide. In other pH regions, however, the flotation rates were less than those of the SDS system. Figure 3 shows the flotation rates for the Cd^{2+}–LNa system, ammonia being used to adjust the pH. In this system, the flotation rate begins to increase at about

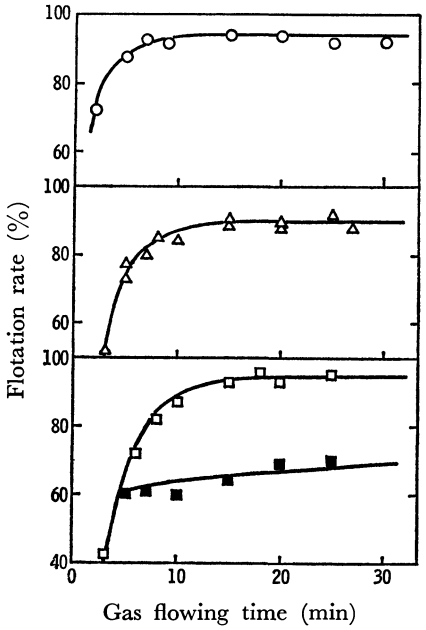

Fig. 1. Flotation rate *vs.* gas-flow time for Cd^{2+}–SDS, –DBS and –α-SLNa systems.
Cd^{2+}: 1.78×10^{-5} mol/l, gas-flow rate: 10 ml/min, α-SLNa: 1.78×10^{-4} mol/l (○: pH_i 11.2), DBS: 1.78×10^{-5} mol/l (△: pH_i 11.2), SDS: 8.90×10^{-5} mol/l (■: pH_i 10.3, □: pH_i 11.2), pH adjusted by NaOH.

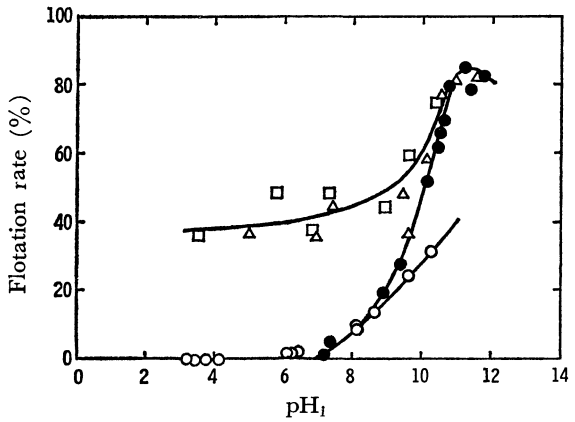

Fig. 2. Flotation rate *vs.* initial pH for Cd^{2+}–SDS system.
Cd^{2+}: 1.78×10^{-5} mol/l, SDS: 1.78×10^{-5} mol/l (○: NH_3, ●: NaOH), 8.90×10^{-5} mol/l (□: NH_3, △: NaOH).

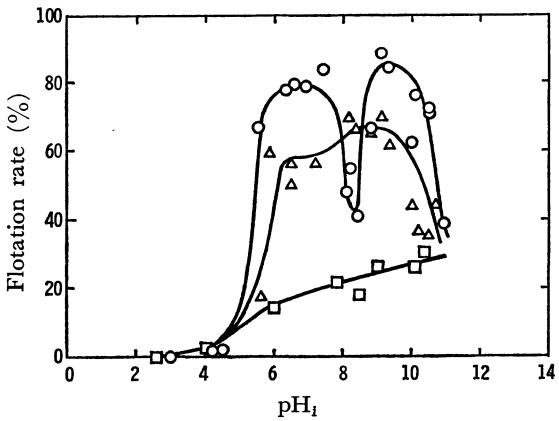

Fig. 3. Flotation rate *vs.* initial pH for Cd^{2+}–LNa system.
Cd^{2+}: 1.78×10^{-5} mol/l, LNa (□: 1.78×10^{-5} mol/l, △: 3.90×10^{-5} mol/l, ○: 1.78×10^{-4} mol/l), pH adjusted by NH_3.

pH 5.5 and sharply decreases at about pH 10.5, at least for the two systems studied. In the acid solution, LNa is hydrolyzed to form uncharged lauric acid, and the flotation may be explained by the Cd^{2+} ions being trapped in or adsorbed by the lauric acid floc. The sharp minimum or the slight step observed in the *F vs.* pH curve near pH 8 also suggests that the precipitation flotation takes place in the region of pH values larger than 8.

Figure 4 shows the *F vs.* pH_i curve for Cd^{2+}–α-SLNa systems of varying surfactant concentrations. The flotation rate increases sharply at around pH 8 and reaches a maximum at around pH 11 for all the systems observed. A maximum *F* value of 97% was observed for the 3.56×10^{-4} mol/l α-SLNa system with its pH adjusted by sodium hydroxide. The flotation rates remain far below those for the system with its pH adjusted by ammonia. The reason for this is the same as has been presented above. The decrease in *F* at higher pH values may be due, in addition to the ionic competition mentioned above, to the formation of $Cd(OH)_4^{2-}$ and $Cd(OH)_5^{3-}$.[9]

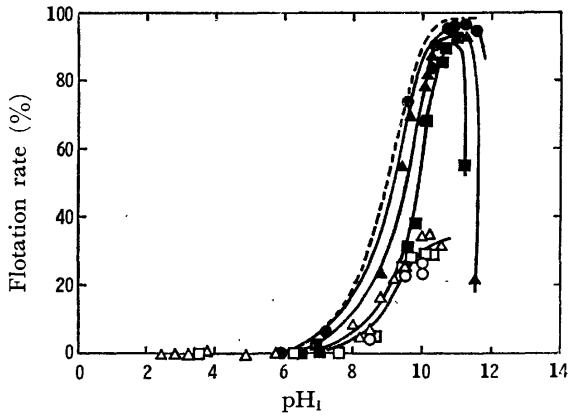

Fig. 4. Flotation rate *vs.* initial pH for Cd^{2+}–α-SLNa system.
Cd^{2+}: 1.78×10^{-5} mol/l, α-SLNa: 8.90×10^{-5} mol/l (△: NH_3, ▲: NaOH), 1.78×10^{-4} mol/l (□: NH_3, ■: NaOH), 3.58×10^{-4} mol/l (○: NH_3, ●: NaOH, ----: ultracentrifugation of cadmium solution (20000 rpm × 20 min).

Further, as may be seen in Fig. 4, the effect of the α-SLNa concentration on *F* was found to be rather small in the region of concentrations studied. It is noticeable that a larger increase in the α-SLNa concentration does not produce foam formation; only the bubble flotation of the precipitate takes place. Thus, the best condition of Cd^{2+} ion flotation is provided by the α-SLNa molecule having both carboxylic and sulfonic groups. The situation is very similar to the case of Cu^{2+} flotation.[1] These results are further evidence for the view stated previously[1] that α-SLNa forms a strongly surface-active Cd salt by the carboxylic group, while the sulfonic group protects the salt from precipitation.

It is further shown that the optimum pH of flotation roughly agrees with the pH 11 of the complete removal of Cd^{2+} as hydroxide, which is confirmed by the centrifugal separation, as is also shown in Fig. 4. It was

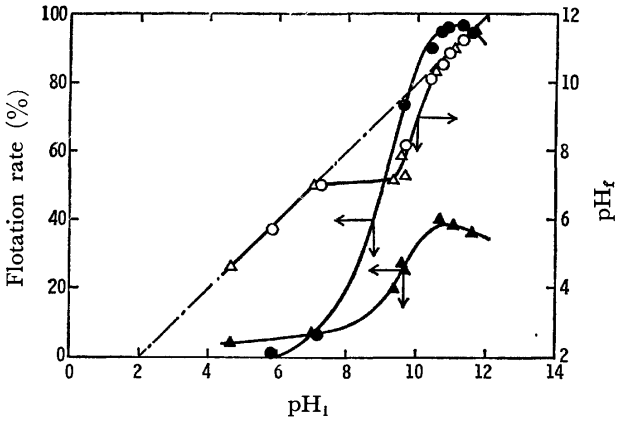

Fig. 5. Initial pH *vs.* final pH and flotation rate for Cd^{2+} and Cd^{2+}–α-SLNa systems.
Cd^{2+}: 1.78×10^{-5} mol/l, α-SLNa: 3.58×10^{-4} mol/l, ○,●: Cd^{2+} system, △,▲: Cd^{2+}–α-SLNa system, pH adjusted by NaOH.

inferred that the existence of a foam layer was not essential for precipitation flotation, although foam formation enhances the ion-adsorption flotation.

Mechanism of Flotation of Cd^{2+} Ions by Anionic Surfactant. The final pH after flotation is plotted as a function of the initial pH in Fig. 5. The *F vs.* pH curves with and without α-SLNa are also shown in Fig. 5. As may be seen in this figure, a plateau appears in the pH region from about 7 to 9 as a result of the liberation of H^+ ions by the formation of insoluble polynuclear species such as are expressed by:

$$n\mathrm{Cd^{2+}} + (n-1)\mathrm{H_2O} \rightarrow {}^{+}\mathrm{Cd(OCd)}_{n-2}\mathrm{OCd^{+}} + 2(n-1)\mathrm{H^{+}}$$

much as in a previous report.[1] Again, this is evident that large amounts of Cd^{2+} ions are removed in a polynuclear form by a small amount of a surfactant. A slight flotation was observed by the adsorption or adhesion of polynuclear species on ascending bubbles without any surfactant, but the best flotation was obtained by adding an anionic surfactant. The decrease in the flotation rate below pH 8 seems to be due to the competition between H^+ and Cd^{2+} ions for the anionic surfactant.

Flotation of Cd^{2+} Ion by Cationic Surfactants. Effect of the Time of Gas Flow: Cd^{2+} ions can be floated by a cationic surfactant through a bridge of macromolecular anions like bentonite.

The flotation was carried out for a solution containing 1.78×10^{-5} mol/l Cd^{2+} ions, 1.78×10^{-4} mol/l HTAC, and 0.01% bentonite at pH 11.3. About 98% of the *F* was obtained after a 2-min gas-flow time. It was found that the addition of bentonite markedly reduced the time of gas flow and increases the *F* compared with the case of the Cd^{2+}-anionic surfactant systems of Fig. 1. Thus, the cationic surfanctant-bentonite system is superior to the anionic surfactant system in this respect.

Relation between pH and Flotation Rate. Figure 6 shows the results of the flotation of the Cd^{2+}–bentonite–OBAC system with the gas-flow time of 7 min and with the pH being controlled with sodium hydroxide and ammonia. The flotation rate increases sharply at around pH 8 and shows a maximum of $F=93\%$ at pH 11.3 for the system of pH adjusted by sodium hydroxide,

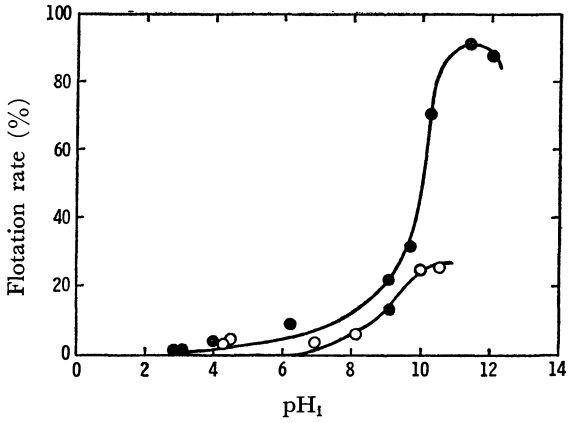

Fig. 6. Flotation rate *vs.* initial pH for Cd^{2+}-bentonite-OBAC system.
Cd^{2+}: 1.78×10^{-5} mol/l, OBAC: 3.56×10^{-5} mol/l, bentonite: 0.001%, ○: pH adjusted by NH_3, ●: pH adjusted by NaOH.

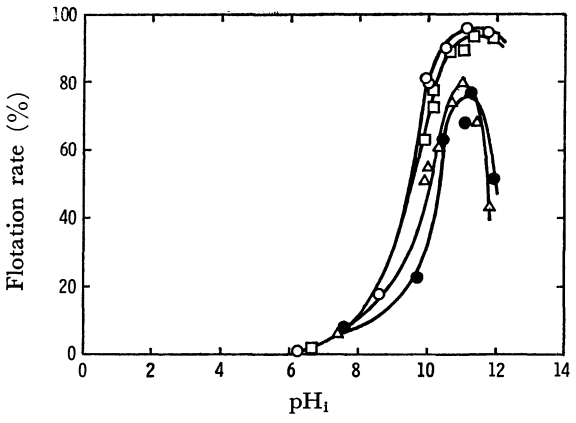

Fig. 7. Flotation rate *vs.* initial pH for Cd^{2+}-bentonite-DTAC system.
Cd^{2+}: 1.78×10^{-5} mol/l, DTAC: 1.78×10^{-4} mol/l, bentonite (●: 0%, △: 0.001%, □: 0.005%, ○: 0.01%) pH adjusted by NaOH.

while a far smaller maximum of $F=30\%$ is obtained for the system of pH controlled using ammonia in the same pH region. The difference may be caused by the reduction of the formation of polynuclear cadmium hydroxide due to ammine complex formation in the latter system mentioned above. In order to see the effect of the pH on the flotation rate, the flotation was carried out for a solution containing 1.78×10^{-5} mol/l Cd^{2+} ions, 1.78×10^{-4} mol/l surfactant, and 0.01% bentonite. No difference in the nature of the cationic surfactant on the flotation rate was observed for the surfactants used in the present study. The flotation rate remains zero up to pH 5, above which it increases gradually up to pH 8.5 and rapidly thereafter. The maximum F of 97% was observed above pH 11.3. As a whole, the F *vs.* pH curve of Cd^{2+} shifts towards a pH higher by two units than that for Cu^{2+} ions. The shift may be due to the stronger basic nature of the former. In the case of Cd^{2+} ion flotation by bentonite and cationic surfactants, Cd^{2+} ions, polynuclear cations, and complex anions such as $Cd(OH)_4^{2-}$ combined with the cationic surfactants adsorb on the bentonite particles in this order as the pH of the solution increases, and the bentonite is subsequently coagulated and floated by bubbles. Thus, the flotation may be classified as an adsorbing particle (bubble) flotation. At pH values lower than 8, the flotation rate is largely reduced by the absence of polynuclear Cd^{2+} ions and the suppression of Cd^{2+} ion adsorption of bentonite by H^+ ions.

Effect of Bentonite. To study the effect of bentonite, the F *vs.* bentonite concentration was plotted for DPC, DTAC, and HTAC. Some of the results are shown in Fig. 7 for DTAC. The flotation rates increase and the regions of the flotation range extend up to a certain point with an increase in the amount of bentonite for all the systems studied. For the cationic surfactant with the 1.78×10^{-4} mol/l concentration, the maximum F value of 97% was obtained with the addition of 0.01% bentonite and at pH 11.3, as adjusted by sodium hydroxide. Here, the addition of bentonite also favored the bubble production, without any foam

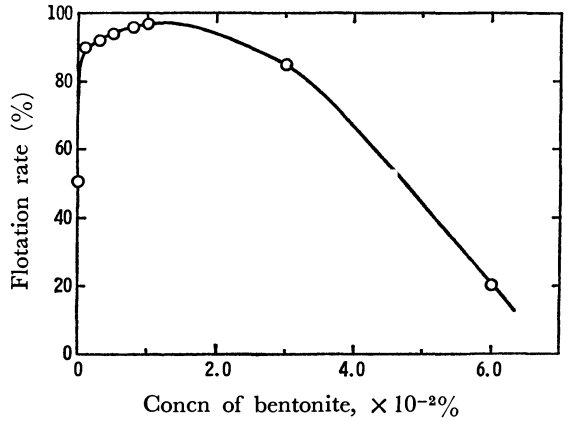

Fig. 8. Flotation rate *vs.* concn of bentonite for Cd^{2+}-bentonite-HTAC system.
Cd^{2+}: 1.78×10^{-5} mol/l, HTAC: 1.78×10^{-4} mol/l, pH adjusted by NaOH.

formation. Thus, bentonite acts not only as a bridge between Cd^{2+} ions and bubbles, but also as an inhibitor of foaming due to the surfactant, thus resulting in effective bubble flotation. The flotation was carried out further for a solution containing 1.78×10^{-4} mol/l Cd^{2+}, 2×10^{-4} mol/l HTAC, and varying amounts of bentonite at a gas-flow time of 7 min and a gas-flow rate of 10 ml/min at pH 11. The results are shown in Fig. 8. It was further confirmed that a stable foam layer was produced for the solution containing less than 0.008% bentonite. As may be seen in the figure, the flotation rate increases sharply and then decreases to zero after showing a distinct maximum. The concentration of bentonite favorable for the bubble flotation of Cd^{2+} ions is found to be 0.008—0.015%. The decrease in the flotation rate above 0.015% bentonite may be explained by the surfactant being insufficient to float the bentonite adsorbing Cd^{2+} ions evenly. About 50% of the Cd^{2+} ions are floated even in the absence of bentonite. This may be due to some Cd^{2+} ions being entrapped in or adsorbed on the cationic foam by nonspecific interaction between the cationic surfactant and polynuclear Cd^{2+} or cadmium

hydroxide.

Effect of the Concentration of the Surfactant. To study the effect of the concentration of the cationic surfactant, a *F vs.* pH_1 curve for varying concentrations of DPC, and DTAC was obtained; it is not shown in the figure, however. The flotation rate decreases from 95 to 73% with a decrease in the DPC concentration from 1.78×10^{-4} to 1.78×10^{-5} mol/l in the case of Cd^{2+} ion flotation by DPC, whereas in the case of Cd^{2+} ion flotation by DTAC the flotation rate did not change with an increase in the concentration of DTAC from 3.56×10^{-5} to 1.78×10^{-4} mol/l above pH 9. Figure 9 shows the *F vs.* surfactant concentration for HTAC at pH 11.3. As may be seen in Fig. 9, the optimum rate of bubble flotation (about 97%) was observed in the region of the HTAC concentration from 8×10^{-5} to 3.56×10^{-4} mol/l. The decrease in the flotation rate for the concentrations of HTAC larger than 3.56×10^{-4} mol/l is caused by both the excessive surfactant repelling Cd^{2+} ions from the surface of bentonite and the bimolecular layer of surfactant adsorption producing hydrophilic bentonite of a poor flotability. The decrease in the flotation rate in the low-surfactant-concentration region may be explained as resulting from the surfactant being insufficient to float the bentonite.

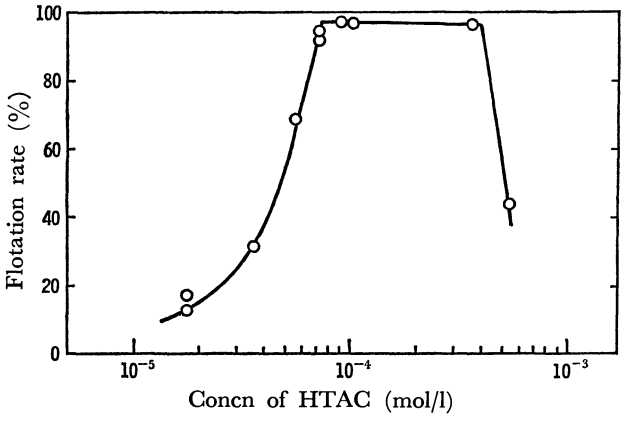

Fig. 9. Flotation rate *vs.* concn of HTAC for Cd^{2+}-bentonite-HTAC system.
Cd^{2+}: 1.78×10^{-5} mol/l, bentonite: 0.01%, pH_1: 11.2, pH adjusted by NaOH.

In conclusion, Cd^{2+} ions could be efficiently floated by using an anionic surfactant or a cationic surfactant with bentonite, and the ion-flotation method can be effectively used under such conditions for the removal of Cd^{2+} ions from sewage and waste water.

The author wishes to thank Professor Tsunetaka Sasaki of the Tokai University for his valuable discussion and suggestions.

References

1) K. Kobayashi, This Bulletin, **48**, 1180 (1975).
2) R. Lemlich, "Adsorptive Bubble Separation Techniques," Academic Press, New York and London (1972).
3) F. Sebba, "Ion Flotation," Elsevier Publisher London and New York (1962).
4) R. Lemlich, "Adsorptive Bubble Separation Techniques," Academic Press, New York and London (1972), pp. 219—245.
5) J. Shimoiizaka, S. Hasebe, I. Matsuoka, T. Takahashi, and K. Yamamoto, *J. Min. Assoc. Jap.*, **86**, 549 (1970).
6) T. Goto and G. Izumi, *Nippon Kagaku Kaishi*, **7**, 1315 (1974).
7) B. B. Ferguson, C. Hinkle, and D. J. Wilson, *Separ. Sci.*, **9**, 125 (1974).
8) F. Sebba, "Ion Flotation," Elsevier Publisher, London and New York (1962), p. 57.
9) G. Charlot, "L'analyse Qualitative et Les Réactions en Solution," Masson et Cie. Editeurs (1957).

Studies of the Removal of Cd^{2+} Ions by Adsorbing Particle Flotation

Koichi KOBAYASHI*

Department of Chemistry, Faculty of Science, Tokyo Metropolitan University, Setagaya, Tokyo 158

(Received December 20, 1974)

The conditions for the removal of Cd^{2+} ions from an aqueous solution by adsorbing particle flotation using bentonite and a cationic surfactant has been investigated. It has been found that the most suitable method was to conduct flotation in the region of the coagulation flotation of bentonite. The addition of polyacrylamide (PAA) extended not only the region of coagulation flotation towards lower and higher hexadecyltrimethylammonium chloride (HTAC) concentrations tested, but also increased the flotation efficiency (expressed as the percentage of ions removed from the total solution). The selective flotation from an aqueous solution containing two kinds of metal ions was also investigated. Each metal ion could be floated from the solution with the pH of the metal hydroxide formation. By selecting proper conditions, it was possible to remove each metal ion separately from a mixed solution.

It has been well-known that the suspended particles in an aqueous solution are coagulated and precipitated by the addition of coagulating agents.[1-5] On the other hand, the suspended particles in an aqueous solution can be floated by adhering them on bubbles by the addition of collectors or foaming agents.[6-10] It is also known that the surfactant changes the state of suspension of the particles, from coagulation precipitation through coagulation flotation to redispersion, with an increase in the amount of surfactant added.[11,14]

Since ions in solution are adsorbed on bentonite as an ion-exchanger, the flotation of bentonite is considered to have a close relation to the removal of ions. Such an ion flotation is called "adsorbing particle flotation."[11] Adsorbing particle flotation is perhaps one of the most effective methods for the ion flotation. The method consists of a simple adsorption or exchange adsorption of ions from a solution onto adsorbent particles like bentonite, which are subsequently floated by the addition of a suitable surfactant.[12]

The present paper will describe a study of the phenomena of the coagulation flotation of bentonite suspensions and the adsorbing particle flotation of Cd^{2+} ions and a Cd^{2+}–Cu^{2+} ion mixture by the addition of bentonite. The explanation of the mechanism of such an ion flotation will also be attempted.

Experimental

Materials. The bentonite powder (Bt) used as an ion-exchanger was obtained from the Wako Pure Chemical Co., Ltd.; the fraction passing through a 350-mesh sieve was collected and dried under reduced pressure. The pure-grade hexadecyltrimethylammonium chloride used as a cationic surfactant, obtained from the Kao Soap Co., Ltd., was used without further purification. A stock solution containing 1.78×10^{-4} mol/l cadmium ions (Cd^{2+}) was prepared by dissolving Cd metal of a 99.999% purity, kindly supplied by the Laboratory of General Chemistry of our department, in nitric acid. The pH of the solution was 2.7. The cupric sulfate used was a reagent-grade $CuSO_4\cdot5H_2O$, which had been recrystallized from distilled water, a stock solution of 1×10^{-3} mol/l concentration was prepared. A stock solution containing 9.3×10^{-4} mol/l ferric ions was prepared from reagent-grade ferric chloride dissolved in triply distilled water. The polyacrylamide (PAA) with an amide content of 87% used as a coagulating agent was the product of the Nitto Chemical Co., Ltd.; it was dried under reduced pressure. Special-grade sodium hydroxide and sulfuric acid supplied by the Wako Pure Chemical Co., Ltd., were used to adjust the pH.

The water used was obtained by first refluxing ordinary distilled water with an acid permanganate solution; then it was distilled from an alkaline permanganate solution and finally distilled twice with a Hysil flask.

Apparatus and Procedure. The apparatus and method used for flotation measurements were the same as have been described.[13] Nitrogen gas humidified with water vapor and controlled to a constant rate of gas flow was bubbled through a glass filter (No. 4) into a flotation cell containing 10 ml of the sample solution. The gas-flow rate and time were kept at 10 ml/min and 7 min respectively. For the measurement of the effect of HTAC on the state of Bt suspension, a 10-ml portion of a suspension containing varying amounts of Bt and HTAC was introduced into a ground test tube 1.0 cm in inner diameter and 20.0 cm in length. The tube was then shaken, and the coagulation-dispersion and precipitation-flotation behavior was judged by the naked eye.[14] The centrifugation was applied when necessary for 20 min at 3500 rpm. The concentrations of Cu^{2+} ions, Fe^{3+} ions, and Cd^{2+} ions were measured by using an atomic absorption spectrometer (Techtron Pty., Ltd., Model-AA-100). The absorbance was measured at 3248 Å for Cu^{2+} ions, 2483 Å for Fe^{3+} ions, and 2288 Å for Cd^{2+} ions. The measurements were carried out at room temperature (about 25 °C).

The flotation efficiency of Cd^{2+}, Fe^{3+}, and Cu^{2+} ions is conventionally expressed by:

$$F = (1-C_f/C_i)\times100\ \%$$

where C_i and C_f are the concentrations of ions before and after the flotation.

All the experiments were run under the conditions of bubble flotation, that is, flotation using only ascending bubbles, without the aid of foam formation. Since most of the solution after flotation was used for the measurement of C_f, the flotation efficiencies calculated substantially express the percentages of these ions removed from the total solution.

Results and Discussion

Change in the Dispersion State of Bentonite upon the Addition of HTAC. Figure 1 shows the various regions of the state of bentonite after shaking as a function of the bentonite and HTAC concentrations. As may be seen, the bentonite in an aqueous HTAC solution shows the regions of dispersion, coagulation flotation, coagulation precipitation, and redispersion, as has been reported

* Present address: Department of Chemistry, Musashi Institute of Technology, 1-28-1 Tamatsutsumi, Setagaya, Tokyo 158.

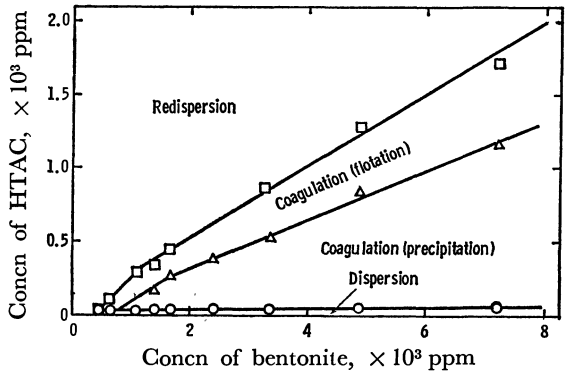

Fig. 1. Effect of HTAC on dispersion state of bentonite suspension.

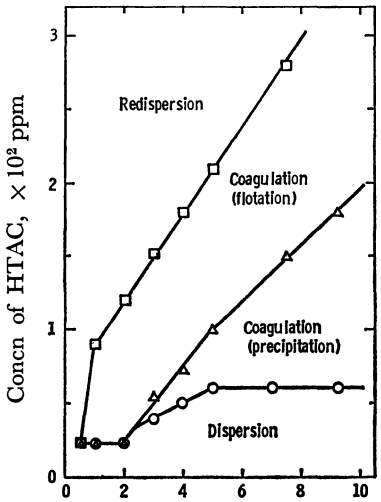

Fig. 2. Effect of HTAC on dispersion state of bentonite suspension at low concentration region.

previously.[14] In the regions of dispersion, coagulation flotation, and coagulation precipitation of Fig. 1, the layer scarecely forms on a solution, but in the region of redispersion, the stable foam layer forms with an increase in the HTAC concentration. Further, the regions of dispersion and coagulation precipitation give an opaque solution, while the region of coagulation flotation is transparent as a whole. Thus, the region of coagulation flotation seems to offer optimum conditions for bubble flotation. Also, it is noticeable that the change from coagulation precipitation to coagulation flotation is sensitive to a slight change in the HTAC concentration. Figure 2 shows the coagulation flotation region for low concentrations of Bt and HTAC especially measured in detail, which is useful for the adsorbing particle flotation.

A similar experiments was done with the addition of 10 ppm PAA as a coagulating agent. The results are shown in Fig. 3. As can be seen, the region of coagulation flotation in the Bt–HTAC–PAA system is broader with respect to the HTAC concentration and shifts towards lower concentrations with respect to the Bt concentration, compared with the Bt–HTAC system shown in Fig. 2. Therefore, the former system is more favorable for adsorbing-particle flotation than the latter.

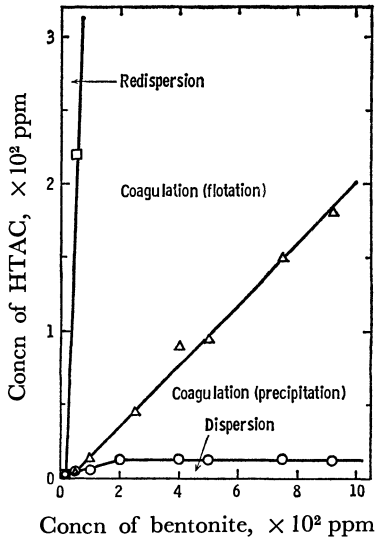

Fig. 3. Effect of HTAC on dispersion state of bentonite suspension in the presence of 10 ppm PAA.

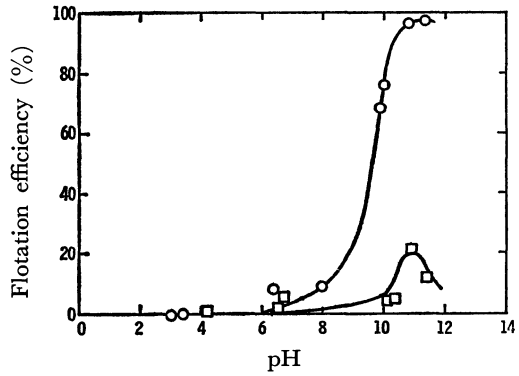

Fig. 4. Flotation rate *vs.* pH for the Cd^{2+}-Bt-HTAC system.
Cd^{2+}: 1.78×10^{-5} mol/l, HTAC: 56.8 ppm, Bt: 600 ppm (□), 100 ppm (○).

Flotation of Cd^{2+} Ions by HTAC. The adsorbing-particle flotation of Cd^{2+} was carried out under the conditions of coagulation flotation described above. The flotation was carried out for a solution containing 1.78×10^{-5} mol/l Cd^{2+}, 56.8 ppm HTAC, and 100 ppm Bt (belonging to the coagulation-flotation region) or 600 ppm bentonite (belonging to the dispersion region) under a gas flow of 7 min and a gas-flow rate of 10 ml/min. The results are shown in Fig. 4. In the case of Cd^{2+} ion flotation by 100 ppm bentonite, the flotation efficiency begins to increase at about pH 8 and a maximum F of 98% is obtained at about pH 11.3, but in the case of Cd^{2+} ion flotation by 600 ppm bentonite, the flotation efficiency is extremely low, showing a maximum of about 20% of F. In the former case, the Cd^{2+} ions are considered to float by HTAC through the bridge of bentonite, while in the latter case, the decrease in flotation efficiency may be due to the surfactants being insufficient to float the bentonite, though Cd^{2+} ions are adsorbed on the particles.

Figure 5 shows the flotation efficiency *vs.* surfactant concentration curve at an optimum pH of 11.2. The optimum efficiency of flotation was observed in the

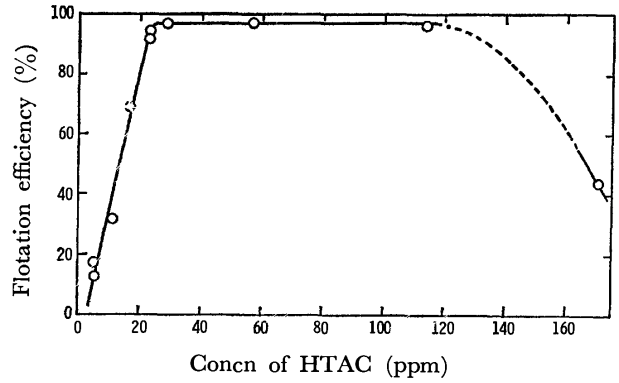

Fig. 5. Flotation rate *vs.* concentration of HTAC for the Cd^{2+}-Bt-HTAC system.
Cd^{2+}: 1.78×10^{-5} mol/l, Bt: 100 ppm, pH: 11.2.

region of HTAC concentrations from about 25 to 110 ppm. It can be seen from Fig. 2 that these ranges of the HTAC concentration coincide with those of coagulation flotation. Thus, the optimum conditions for adsorbing-particle flotation are confirmed to be the region of the optimum coagulation flotation.

Flotation of Cd^{2+} Ions by HTAC and PAA. In order to study the effect of PAA, the flotation was carried out for solutions containing 1.78×10^{-5} mol/l Cd^{2+}, 100 ppm Bt, 56.8 ppm HTAC, and 10 ppm PAA under the condition of a gas-flow time of 7 min. The results are shown in Fig. 6. A comparison of Fig. 6 with Fig. 4 shows no effect of PAA addition at the optimum Cd^{2+}-Bt-HTAC composition. Then the flotation was carried out with varying concentrations of HTAC, the other conditions being kept constant at the values mentioned above. The results are shown in Fig. 7. As may be seen, the flotation efficiency remains constant down to a lower HTAC concentration than that for the system without PAA shown in Fig. 5. Above 110 ppm HTAC, the flotation efficiency sharply decreases in the case of the system without PAA, while in the case of the system with PAA, the flotation efficiency gradually decreases with an increase in the HTAC concentration above 110 ppm. Thus, the addition of PAA increases the optimum region of Cd^{2+} ion flotation towards both the lower and higher

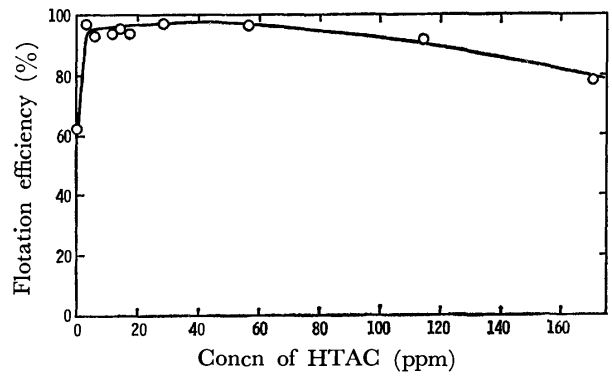

Fig. 7. Flotation rate *vs.* concentration of HTAC for the Cd^{2+}-Bt-HTAC-PAA system.
Cd^{2+}: 1.78×10^{-5} mol/l, Bt: 100 ppm, PAA: 10 ppm, pH: 11.2.

concentrations of HTAC. This increase in the region just corresponds to the increase in the region of coagulation flotation of Fig. 3 compared with that of Fig. 2. The reduction of minimum amount of 26 ppm HTAC required for the optimum flotation in the Bt-HTAC system to 3 ppm by the addition of 10 ppm PAA is particularly noticeable.

Removal of Cd^{2+} Ions by Centrifugation. To study the effects of the pH and additives on the adsorption of Cd^{2+} ions, a Bt suspension containing Cd^{2+} ions in the state of equilibrium adsorption was centrifuged and the concentration of Cd^{2+} was determined. The amount of Cd^{2+} adsorbed on Bt or the amount centrifuged was expressed by $R=(1-C_f/C_i)\times100$, which is plotted against the pH in Fig. 8. The centrifugation of Cd^{2+} ions was performed for 20 min at 3500 rpm for the Cd^{2+}-Bt-HTAC-PAA (A), Cd^{2+}-Bt-HTAC (B) and Cd^{2+}-Bt (C) systems with the compositions shown in Fig. 8. In the cases of A and B, the efficiency of the centrifugation of Cd^{2+} ions begins to increase rapidly at about pH 8 and a maximum of $R=98\%$ was obtained. In the case of C, the value of R stays rather high in the low pH region and begins to increase at pH 8, but the maximum is only 79%, attained at pH 11.3.

These facts confirm that, at an optimum pH of 11.3, the adsorption of Cd^{2+} is complete in A, B, and C, but

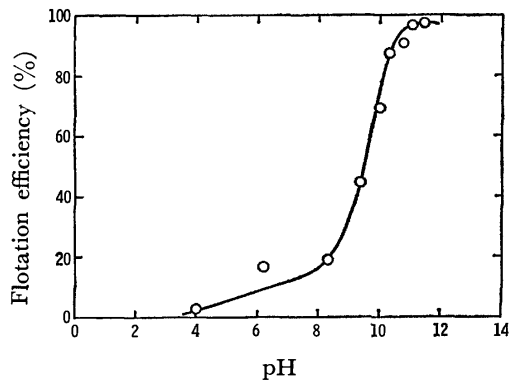

Fig. 6. Flotation rate *vs.* pH for the Cd^{2+}-Bt-HTAC-PAA system.
Cd^{2+}: 1.78×10^{-5} mol/l, Bt: 100 ppm, HTAC: 56.8 ppm, PAA: 10 ppm.

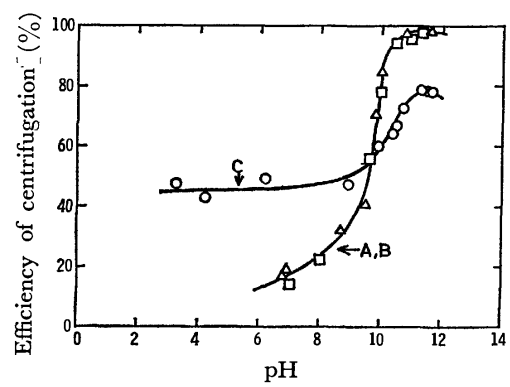

Fig. 8. Effect of pH on rate of Cd^{2+} adsorption on Bt.
Cd^{2+}: 1.78×10^{-5} mol/l, A: 100 ppm Bt, 56.8 ppm HTAC, 10 ppm PAA, B: 100 ppm Bt, 56.8 ppm HTAC, C: 100 ppm Bt.

the aggregates do not grow sufficiently large in the case of C to be centrifuged completely during 20 min, as is the case in A and B, while the removal of rather large amounts of Cd^{2+} in the pH region for C is due to a certain amount of Bt being centrifuged, upon which some Cd^{2+} ions are adsorbed, not hindered by the adsorption of HTAC which may occur in the cases of A and B. At any rate, it is confirmed that, in the cases of A and B, Cd^{2+} ion flotation is realized by the ions being adsorbed on Bt particles, which are subsequently coagulated and floated by bubbles.

Selective Ion Flotation from a Mixed System. The flotation of Cd^{2+} and Cu^{2+} ions from a solution containing 1.78×10^{-5} mol/l Cd^{2+} ions, 1×10^{-4} mol/l Cu^{2+} ions, 100 ppm Bt, and 56.8 ppm HTAC under the condition of a gas-flow rate of 10 ml/min was carried out while varying the pH. The results are shown in Fig. 9. In the mixed system, Cd^{2+} and Cu^{2+} ions are floated above pH 6 and 8 respectively, much as in the flotation of the separate system.[13] Thus, even in the mixed system the flotation begins from the point of the formation of insoluble cadmium and copper hydroxide. According to this finding, Cu^{2+} ions are exclusively floated between pH 6 and 8 and it is possible to separate Cu^{2+} ions from the mixed system by the control of the pH. From the color of the scum, it is clear that copper hydroxide has formed.

Figure 10 shows the results of the flotation of Cd^{2+}

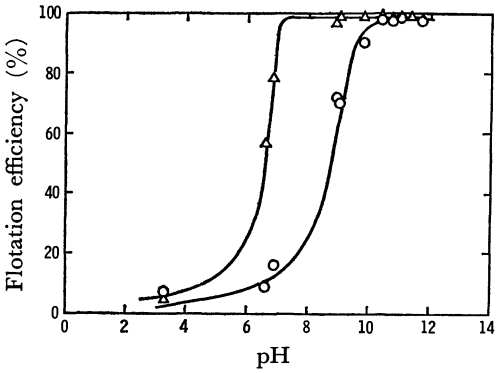

Fig. 9. Selective flotation of Cd^{2+} and Cu^{2+} ions.
Cd^{2+}: 1.78×10^{-5} mol/l (○), Cu^{2+}: 1×10^{-4} mol/l (△),
Bt: 100 ppm, HTAC: 56.8 ppm.

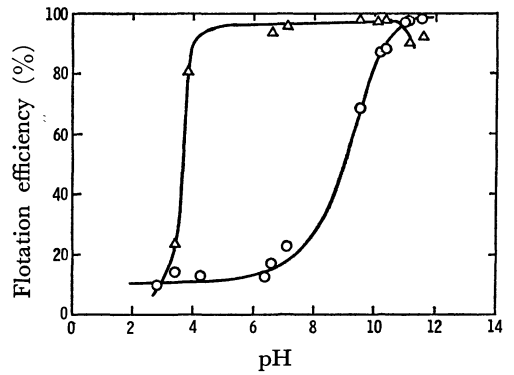

Fig. 10. Selective flotation of Cd^{2+} and Fe^{3+} ions.
Cd^{2+}: 1.78×10^{-5} mol/l (○), Fe^{3+}: 4.65×10^{-5} mol/l (△), Bt: 100 ppm, HTAC: 56.8 ppm.

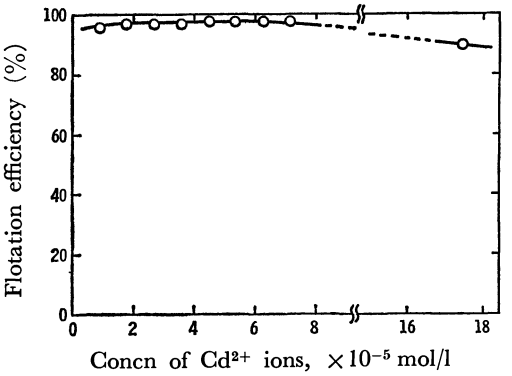

Fig. 11. Flotation rate *vs.* concentration of Cd^{2+} ions for the Cd^{2+}-Bt-HTAC system.
Bt: 100 ppm, HTAC: 56.8 ppm, pH: 11.4.

and Fe^{3+} ions from a solution containing 1.78×10^{-5} mol/l Cd^{2+} ions, 4.65×10^{-5} mol/l Fe^{3+} ions, 100 ppm Bt, and 56.8 ppm HTAC. Beyond pH 10, the complete flotation of both Cd^{2+} and Cu^{2+} is possible, showing about a 98% of flotation efficiency for both ions. In this system, as in the Cd^{2+} and Cu^{2+} systems, Fe^{3+} and Cd^{2+} ions are floated from the respective pH of the insoluble hydroxide formation, and selective flotation is possible by the method of a starvation dose, [15] although about 10% of the Cd^{2+} ions are floated even in the pH region of less than 8, which is not the case for the system containing Cd^{2+} ions alone, as is shown in Fig. 4. This may be due to some Cd^{2+} ions being adsorbed together with Fe^{3+} ions on the Bt particles. The phenomenon is preferably called coadsorption. In the case of limited amounts of cationic surfactant and Bt, it may be expected that, as the flotation of Cd^{2+} ions begins to occur above pH 8, the flotation efficiency of Fe^{3+} ions will gradually decrease with an increase in the pH above pH 10.7.

Effect of the Cd^{2+} Ion Concentration on the Flotation Efficiency. Under the optimum conditions of 100 ppm Bt, 56.8 ppm HTAC, and pH 11.5, the effect of the concentration of Cd^{2+} ions on the flotation efficiency was studied. The results are shown in Fig. 11. As may be seen, in the Cd^{2+} concentration region from about 1×10^{-5} to 7×10^{-5} mol/l, the optimum flotation efficiency of $F=98\%$ was obtained. In the more concentrated solution of 1.78×10^{-4} mol/l, the flotation efficiency decreases to about $F=90\%$. The optimum concentration of the order of magnitude of 10^{-5} mol/l is in agreement with the conditions under which ion flotation is usually carried out.

The author wishes to thank Professor Tsunetaka Sasaki of the Tokai University for his valuable discussion and suggestions.

References

1) A. S. Michael, *Ind. Eng. Chem.*, **46**, 1485 (1945).
2) M. Noda, *Kogyo Yosui*, No. 25, 60 (1960); No. 26, 26 (1960); No. 27, 34 (1960).
3) Y. Toyoshima, *ibid.*, No. 30, 34 (1961); No. 31, 50 (1961).
4) T. Oyama and S. Usui, *Nippon Kogyo Kaishi*, **73**, 551 (1957).

5) K. Meguro and T. Kondo, *Nippon Kagaku Kaishi*, **76**, 642 (1955); This Bulletin, **32**, 267 (1959).
6) T. Sasaki, In "Bunri to Seisei," Jikken Kagaku Koza, Ser. 2, Vol. 2, Section 15, Maruzen Co., (1966) pp. 565—603.
7) E. L. Gaden., Jr. and V. Kevorkin, *Chem. Eng.*, **63**, 173 (1956).
8) R. V. Shreikina and G. Morkushin, *J. Appl. Chem., (USSR)*, **31**, 933 (1958).
9) R. V. Shreikina and G. Morkushin, *ibid.*, **31**, 1099 (1958).
10) Y. Koyanaka, *Nippon Genshiryoku Gakkaishi*, **7**, 621 (1965).
11) R. Lemlich, "Adsorptive Bubble Separation Techniques," Academic Press, New York and London (1972) p. 276.
12) R. Lemlich, *ibid.*, p. 275.
13) K. Kobayashi, This Bulletin, **48**, 1180 (1975).
14) T. Inakazu, K. Kobayashi, and T. Sasaki, to be published.
15) S. Sebba, "Ion Flotation," Elsevier, Amsterdam, London and New York (1962).

Effects of the Tension and Viscosity on the Rate of Growth of Black Soap Films

Teruko YAMANAKA

Laboratory of Chemistry, Faculty of Education, Chiba University, Yayoi-cho, Chiba 280

(Received September 19, 1974)

The additional tension and the rate of growth of black films formed from aqueous solutions of polyoxyethylated nonionic surfactants and sodium dodecylsulfate, which contain inorganic electrolytes in high concentrations, were measured for the large vertical films drawn from these solutions. It was found that the rate of growth of black films was proportional to the additional tension in both systems. The reciprocal of the slope of each line was concluded to be a viscosity parameter, since the additional tension acted as the driving force for the growth of black films, and the viscosity parameter, as the resistance. The effect of added glycerol on the rate of growth of black films was compared with that of electrolytes for the films of nonionic surfactants. The former affected both the viscosity parameter and the additional tension, while the latter showed an effect on only the additional tension.

The thinning of mobile films is considered to be caused mainly by gravity and capillary suction at the border when the films are thick. As the films become thinner, they exhibit a third type of thinning behavior, namely, the spontaneous appearance and growth of a thin black film from a much thicker silver film.[1] It is generally accepted that this thinning is due to van der Waals attraction acting between the molecules in the film.[2] In such a state, additional intermolecular forces come into action and give rise to a disjoining pressure, which results in additional film tension and a macroscopic contact angle between the thin film and the bulk liquid in contact with it.[3–5]

A previous paper has dealt with the thinning of large vertical films stabilized with nonionic surfactants.[6] The addition of the inorganic electrolytes did not show any appreciable effects on the rate of movement of the position of a definite thickness in the region of interference fringes, but the specific effects of anions did appear on the blackening time, namely, the time necessary for converting the total film area completely to the black film; these effects were explained in terms of lyotropy. Such a growth of black films plays an important role in the thinning of some soap films and is, therefore, of interest in connection with foam stability, for instance.[7,8]

In this paper, studies of the additional tension and the rate of growth of black films will be reported for large vertical films drawn from aqueous solutions of anionic and of nonionic surfactants containing varying amounts of inorganic electrolytes and glycerol.

Experimental

Materials. Heptaoxyethylene dodecyl ether (N7) of the Nikko Chemicals Co., Ltd., was used. Gas chromatography proved it to be homologously pure. The polyoxyethylene nonylphenyl ether (PNE) was obtained from commercially available PNE by molecular distillation. The average number of ethylene oxide groups was 11.4 per molecule.[6] The sodium dodecylsulfate (SDS) was synthesized by the usual method and was purified by recrystallization before use. Inorganic electrolytes commercially obtained were degreased with ether in a Soxhlet extractor. The sodium sulfate used for the viscosity measurements was also purified by recrystallization from water. Pure-grade glycerol was used without further purification. The surface tension of the 39.2 wt% aqueous glycerol solution was 69.1 dyn/cm; this value did not change with time. The water used was first distilled from an alkaline potassium permanganate solution and then distilled using a fused quartz vessel. All the solutions used were freshly prepared before use.

Measurement of the Rate of Growth of Black Films. The rate of growth of black films was measured for vertical large films supported on a rectangular glass frame. The apparatus was similar to that previously reported,[6] except for the following points. The frame used was made of a glass rod about 0.6 mm in diameter and 1 cm in width. It was supported vertically from the top of the vessel through a water seal and was withdrawn in 5 s from the surfactant solution by a motor operation so that the top of the film rose 3 cm above the solution surface. All the experiments were carried out by using film of the same size except for the study of the effects of film size on the rate of growth. The cell was submerged in a thermostated water bath of 30±0.1 °C, and the whole apparatus was set in a chamber of 30±0.5 °C for about 17 hr before measurement.

The border between the black and the thicker films was photographed to plot the displacement of it against the time, from which the rate was determined. The rate gradually changed in the case of a relatively long blackening time. In such cases, the constant rate appearing in the later stage (shown in Fig. 2) was taken in PNE systems, and the overall rate, in SDS systems.

Measurement of the Additional Tension of Black Films. The additional tension, $\overline{\Delta}$, is defined by:

$$\overline{\Delta} = 2\gamma - \sigma_f \qquad (1)$$

where σ_f is the film tension, and γ, the surface tension of a solution.[9] It was measured by the microbalance technique[10,11] based on the Wilhelmy plate method. A rectangular vertical glass frame 4 cm in width was made of a glass rod about 0.4 mm in diameter. A thinner glass wire about 0.15 mm in diameter was attached horizontally across the frame at a position 1 cm below the top of frame; the wire limited the upper edge of the film formed on the frame. The frame was suspended from one arm of a recording microbalance (Cahn RG Electrobalance). The cell containing the solution and the frame were put in a glass jacket with double walls between which thermostated water was circulated to keep the temperature at 30±0.1 °C. All the apparatus was then placed in an air-thermostated chamber kept at 30± 0.5 °C.

To measure $\overline{\Delta}$, the frame was manually withdrawn from the solution up to a fixed height of 1 or 2 cm. When the

black/thicker film boundary reached the bulk liquid surface, a sudden decrease in the force exerted on the frame corresponding to the difference in tension between the black and the thicker films was recorded on a chart. The decrease divided by the width of the frame gives $\bar{A}$.

The viscosity of the solutions was measured by an Ostwald viscometer at 30±0.1 °C.

Results and Discussion

The rate of growth of black films was measured for the films formed from 0.1 wt% aqueous PNE solutions containing varying amounts of Na_2SO_4, NaF, NaCl, and NaSCN. The same measurement was made for the films formed from 0.05 wt% (1.7×10^{-3} M) aqueous SDS solutions containing varying amounts of NaCl.

Figure 1 shows the effect of the concentration of Na_2SO_4 on the growth of the black films formed from 0.1 wt% PNE solutions. The vertical length of black film is plotted against the elapsed time. The plots in Fig. 1 give the straight lines except for the final stage of the boundary approaching the bulk liquid surface. The black film formed from a 0.1 wt% aqueous PNE solution containing 0.8 N NaF gave a similar linearity and a relatively short blackening time, as in the case of Na_2SO_4. The dependence of the total height and width of the films on the growth of black films of a short blackening time drawn from aqueous solutions of 0.1 wt% PNE containing 0.7 N Na_2SO_4 was studied by using films 1.5 and 3.0 cm in height and ranging from 1 to 4 cm in width. The effects of the size were found to be negligible.

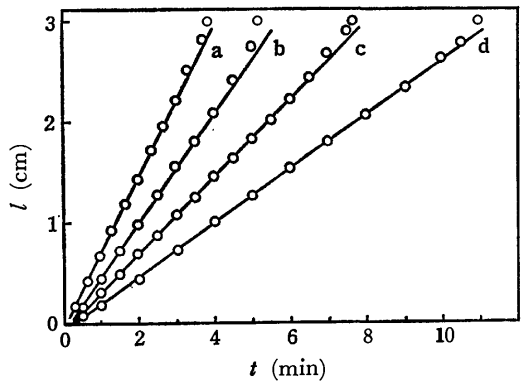

Fig. 1. Effect of the concentration of Na_2SO_4 on the rate of growth of black films formed from aqueous PNE solutions at 30 °C.
l: vertical length of black film
t: time elapsed after formation of liquid film
Composition of solutions: 0.1 wt% PNE+Na_2SO_4 (a) 0.8 N, (b) 0.7 N, (c) 0.6 N, (d) 0.5 N

Figure 2 shows the time dependence of the vertical length of the black film formed from a 0.1 wt% aqueous PNE solution containing 0.8 N NaCl. Plots a and b show the results for the films withdrawn 3.0 cm and 1.5 cm respectively above the liquid surface. As may be seen in Fig. 2, the b plot is linear, whereas the a plot exhibits a curve with a linear portion in the later stage which is nearly parallel to the b plot.[12] It is evident that the difference between the a and b plots is mainly due to the longer blackening time or the larger total height in the former film than in the latter. In the films 3 cm in total height, the black films formed from 0.1 wt% aqueous PNE solutions containing 0.5 N NaF, 0.5 N NaCl, 0.8 N NaCl, and 0.5 N NaSCN gave plots of the type of the a plot in Fig. 2. In the case of these films with a long blackening time, both the rate of film growth of the linear portion and the overall rate decreased to about four-tenths when the width of the film was changed from 1 to 4 cm, while the height was held constant at 3 cm.

Figure 3 shows the effect of the concentration of NaCl on the growth of the black films formed from 0.05 wt% SDS solutions. For the film formed from the solution containing 0.3 N NaCl, a transition from the first to the second black film was visually observed by the reflected light. A nucleation of the second black film appeared in the first black film already formed, and the former film grew rapidly at the ex-

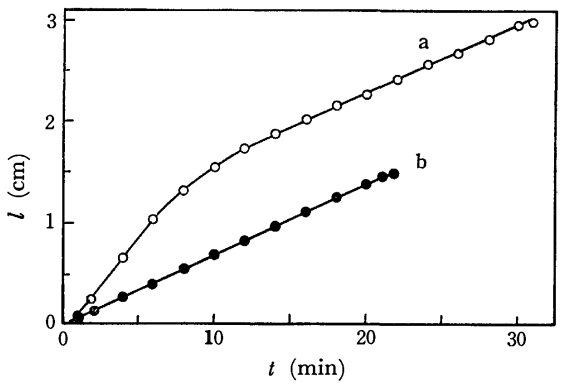

Fig. 2. Dependence of total height of film on the rate of growth of black film formed from aqueous (PNE+NaCl) solution at 30 °C.
l and t: the same as in Fig. 1
Total height of films: (a) 3 cm, (b) 1.5 cm
Width of film: (a) and (b) 1 cm
Composition of solution: 0.1 wt% PNE+0.8 N NaCl

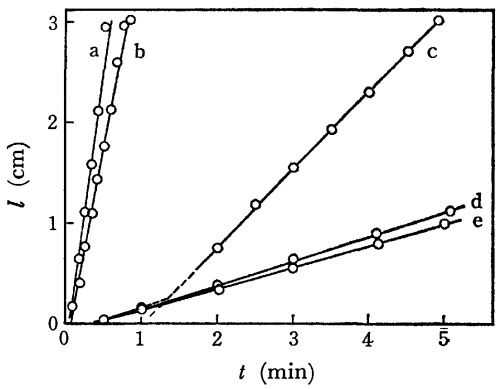

Fig. 3. Effect of the concentration of NaCl on the rate of growth of black films formed from aqueous SDS solutions at 30 °C.
l and t: the same as in Fig. 1
Composition of solutions: 0.05 wt% SDS+NaCl (a) 0.5 N, (b) 0.4 N, (c) 0.3 N, (d) 0.2 N, (e) 0.1 N

pense of the latter and any remaining thicker films. The second black film was easily distinguished from the first one because the former was darker than the latter and a sharp boundary could be observed between the two films.[13] From another study[14] it may be deduced that the first black film is exclusively formed at concentrations lower than 0.3 N, whereas above 0.3 N the second black film is exclusively formed. As is shown in Fig. 3, the second black film of SDS grows at a constant rate and faster than the first black film, which shows a gradual decrease in the rate of growth.

The values of $\overline{\Delta}$ were measured for the black films formed from the same solutions as those used for the measurements of the growth rate of black films. First, to check the reliability of the measurement, the contact angle, θ, between the black film and the bulk liquid was calculated for a 0.05 wt% aqueous SDS solution containing 0.5 N NaCl. For the calculation, the following relation was used:[5,9]

$$\overline{\Delta} = 2\gamma(1-\cos\theta) \qquad (2)$$

using the additional tension, $\overline{\Delta}$, and the surface tension, γ, separately obtained. The calculated value of 9°25′ (30.0 °C) is considered to be reasonable in comparison with the reported values of 9°54′ (28.5 °C),[11] 10°52′ (25.0 °C),[10] and 11°28′ (24.3 °C),[15] considering the temperatures.

Figures 4 and 5 show the plots of the rate of growth of black films, dl/dt, against $\overline{\Delta}$ for the black films formed from aqueous PNE and SDS solutions containing varying amounts of electrolytes. The values of $\overline{\Delta}$ and dl/dt depend strongly on the kind of surfactant, on the added electrolytes, and on the kind or the thickness of the black films. However, dl/dt is proportional to $\overline{\Delta}$, regardless of the kind and the amount

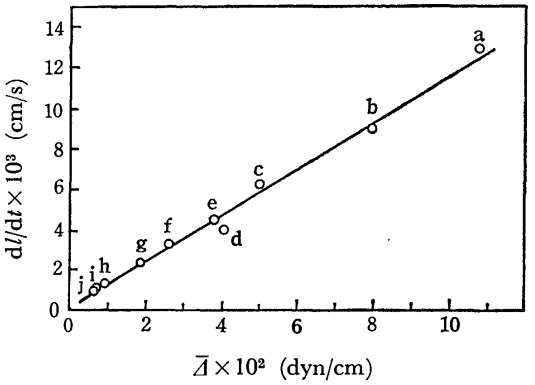

Fig. 4. Dependence of the additional tension on the rate of growth of black films formed from aqueous (PNE+electrolyte) solutions at 30 °C.
dl/dt: rate of growth of black film
$\overline{\Delta}$: additional tension of black film
Composition of solutions: 0.1 wt% PNE + (a) 0.8 N Na_2SO_4, (b) 0.7 N Na_2SO_4, (c) 0.6 N Na_2SO_4, (d) 0.8 N NaF, (e) 0.5 N Na_2SO_4, (f) 0.4 N Na_2SO_4, (g) 0.5 N NaF, (h) 0.8 N NaCl, (i) 0.5 N NaCl, (j) 0.5 N NaSCN

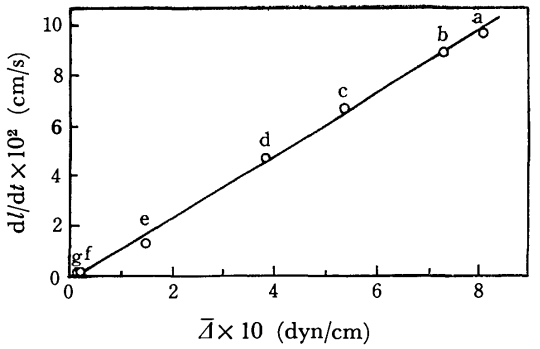

Fig. 5. Dependence of the additional tension on the rate of growth of black films formed from aqueous (SDS+NaCl) solutions at 30 °C.
dl/dt and $\overline{\Delta}$: the same as in Fig. 4
Composition of solutions: 0.05 wt% SDS+NaCl (a) 0.5 N, (b) 0.45 N, (c) 0.4 N, (d) 0.35 N, (e) 0.3 N, (f) 0.2 N, (g) 0.1 N

of added electrolytes as well as the kind of surfactants. The reciprocals of the slope of the lines in these figures, $\overline{\Delta}/(dl/dt)$, considered as a viscosity parameter, are about 8.6 and 8.3 g/(cm·s) for PNE and SDS films respectively.

Figure 6 shows the effects of the change in bulk viscosity upon the addition of glycerol on the relationship between dl/dt and the $\overline{\Delta}$ of the black films, which is formed from aqueous solutions of 5×10^{-4} M (2.5×10^{-2} wt%) N7 containing varying amounts of Na_2SO_4. The solid lines indicate the systems containing varying amounts of Na_2SO_4 while keeping the amounts of N7 and glycerol constant, and the broken lines indicate the systems in which the amounts

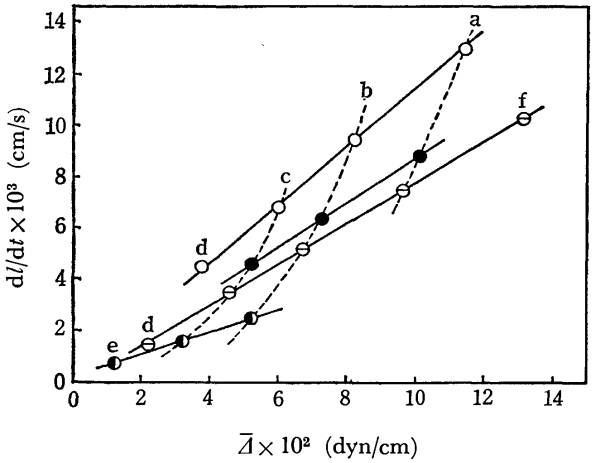

Fig. 6. Effect of glycerol on the additional tension and the rate of growth of black films formed from aqueous (N7+Na_2SO_4) solutions at 30 °C.
dl/dt and $\overline{\Delta}$: the same as in Fig. 4
Composition of solutions:
solid line, glycerol, ○ 0 wt%, ● 10 wt%, ⊖ 15wt%, ◐ 30 wt%
broken line, Na_2SO_4, (a) 0.8 N, (b) 0.7 N, (c) 0.6 N
other points, Na_2SO_4, (d) 0.5 N, (e) 0.4 N, (f) 0.9 N
N7: 5×10^{-4} M for all solutions

of glycerol are varied while N7 and Na_2SO_4 are kept constant.

The values of the bulk viscosity of 5×10^{-4} M aqueous N7 solutions containing 0.8 N Na_2SO_4 and glycerol of different concentrations, that is, 0, 10, and 15 wt%, were 0.89, 1.13, and 1.29 centipoise respectively; also, the bulk viscosity of a 5×10^{-4} M N7 solution containing 0.7 N Na_2SO_4 and 30 wt% glycerol was 1.98 centipoise. On the other hand, the bulk viscosity increased only slightly with the concentration of Na_2SO_4; that is, the bulk viscosity of the aqueous N7 solutions varying from 0.5 N to 0.8 N Na_2SO_4 increased from 0.86 to 0.89 centipoise. All the films formed from these solutions were found to be simple mobile films.[16] The reciprocals of the slope of the straight lines, $\overline{\Delta}/(dl/dt)$, shown in Fig. 6 are 8.7, 11.6, 12.4, and 21.9 g/(cm·s) for solutions of 0, 10, 15, and 30 wt% glycerol respectively. It was also found, when $\overline{\Delta}/(dl/dt)$ was plotted against the bulk viscosity from the results in Fig. 6, that $\overline{\Delta}/(dl/dt)$ was proportional to the bulk viscosity of the solution used.

As is shown in Figs. 1—3, the growth rate of the black film becomes nearly constant after arriving at the stationary state. Since the values of dl/dt in Figs. 4—6 are those in the stationary state, and since a proportionality is observed between $\overline{\Delta}$ and dl/dt, the following relation is obtained by using a proportionality constant, a_f:

$$\overline{\Delta} = a_f(dl/dt) \tag{3}$$

In this equation, it may be inferred that a_f gives a friction coefficient and that $\overline{\Delta}$ is a dominant factor in the driving force in the growing process of the black film, considering that the friction force is equal to the external force.

As Scheludko indicated,[9] $\overline{\Delta}$ is related to the disjoining pressure, π, in the expression:

$$\overline{\Delta} = -\int_h^\infty \pi dh - \pi h \tag{4}$$

where h is the film thickness. Furthermore, at a sufficiently high concentration of added electrolytes, the diffuse electrical double layer is highly compressed and $\overline{\Delta}$ is almost entirely determined by the van der Waals component of the disjoining pressure, expressed by:

$$\overline{\Delta} \approx -\int_{h_e}^\infty \pi_{vw} dh \tag{5}$$

where π_{vw} is the van der Waals component of the disjoining pressure, and h_e, the equilibrium thickness of the film. Kolarov *et al.* observed the same relationship as in this report between the growth rate of black film in the initial stage and $\overline{\Delta}$ for the micro-horizontal circular films; that is, $(dr/dt)_{t_0}=a_{t_0}\overline{\Delta}$, where r represents the radius of the black film.[17]

Here, as a_f is considered to be the friction coefficient for the growing process of black film, various kinds of factors affecting the rate of drainage, such as the bulk viscosity and the surface dilational or shear viscosity, must be included in this coefficient. However, since a_f is proportional to the bulk viscosity of the solution, as has been described above, it may be inferred that the growth rate of the black film is predominantly determined by a flow controlled by the bulk viscosity, and that the contribution of the other factors to the growth rate is negligibly small.

From this point of view, if the black film grows at an invariable thickness, its growth will be determined by the outflow of the excess liquid in the silver film. In most cases in this experiment, however, dl/dt is nearly constant, regardless of the length of the thicker film between the black/thicker film boundary and the solution surface. Therefore, if $\overline{\Delta}$ is invariable, a_f must be constant, irrespective of the length of the thicker film. It thus seems reasonable to assume that the flow of bulk solution in the whole thicker film does not determine the growth rate of the black film, but that only a certain local flow in the thicker film dominates this. It is considered that the flow of liquid between surface layers in the vicinity of the black/thicker film boundary has a high resistance to the film growth. In addition to this, the contribution of dilational surface viscosity must also be considered to some extent, but it must be small, because the relationship between a_f and the bulk viscosity of solution passes near the point of origin. In this context, it is concluded that the flow resistance resulting from the bulk viscosity in the thin film regulates the growth rate of the black film, though the precise mechanism of the growth of black films based on hydrodynamics has not yet been made clear because of its complexity.

As may be seen in Figs. 4 and 5, the effects of added electrolytes on the rate of growth of black films are mainly due to the increase in the additional tension operating as a driving force, and the magnitude of the increase of this tension depends on the nature and amounts of electrolytes, whereas glycerol is found to show the two effects shown in Fig. 6. Glycerol, as far as has been observed in the presence of the electrolytes, decreases the additional tension, as seen in the broken lines in this figure, and simultaneously reduces the slope of the straight lines. For the former, further study is still awaited.

The author wishes to express her hearty thanks to Professor Tsunetaka Sasaki of Tokyo Metropolitan University for his encouragement and guidance throughout the experiments.

References

1) K. J. Mysels, *J. Phys. Chem.*, **68**, 3441 (1964).
2) J. Th. G. Overbeek, *ibid.*, **64**, 1178 (1960).
3) J. S. Clunie, J. F. Goodman, and B. T. Ingram, "Surface and Colloid Science," Vol. 3, ed. by E. Matijević, Wiley-interscience, New York, (1971), p. 194.
4) B. V. Derjaguin and Yu. V. Gutop, *Colloid J.* (USSR), **27**, 574 (1965).
5) K. J. Mysels, H. F. Huisman, and R. I. Razouk, *J. Phys. Chem.*, **70**, 1339 (1966).
6) T. Yamanaka, This Bulletin, **43**, 633 (1970).

7) T. Yamanaka, This Bulletin, **48**, 1760 (1975).
8) A. Scheludko, *Advan. Colloid Interface Sci.*, **1**, 391 (1967).
9) A. Scheludko, B. Radoev, and T. Kolarov, *Trans. Faraday Soc.*, **64**, 2213 (1968).
10) A. Prins, *J. Colloid Interface Sci.*, **29**, 177 (1969).
11) J. H. Clint, J. S. Clunie, J. F. Goodman, and J. R. Tate, *Nature*, **223**, 292 (1969).
12) K. J. Mysels, K. Shinoda, and S. Frankel, "Soap Films, Studies of Their Thinning and a Bibliography," Pergamon Press, New York (1959), p. 41.
13) Ref. 12, p. 62.
14) M. N. Jones, K. J. Mysels, and P. C. Scholten, *Trans. Faraday Soc.*, **62**, 1336 (1966).
15) H. M. Princen, *J. Phys. Chem.*, **72**, 3342 (1968).
16) Ref. 12, p. 12.
17) T. Kolarov, A. Scheludko, and D. Exerowa, *Trans. Faraday Soc.*, **64**, 2864 (1968).

Effects of Electrolytes on Properties on Black Films and Foam Stability of Aqueous Nonionic Surfactant Solutions

Teruko YAMANAKA

Laboratory of Chemistry, Faculty of Education, Chiba University, Yayoi-cho, Chiba 280

(Received December 27, 1974)

The properties of black film, the surface tension of solution and the foam stability in the aqueous solutions of polyoxyethylene-type nonionic surfactants containing various electrolytes were studied. The additional tension $\overline{\Delta}$ of black films showed a maximum and a minimum in the concentration range of electrolytes of 1×10^{-5}—1 N. The concentration at this minimum shifted in accordance with the lyotropic series of anions. The surface tension was unaffected by the electrolyte of the concentration less than about 1×10^{-2} N, whereas $\overline{\Delta}$ exhibited a maximum in this range. The overall rate of growth of the black film was found to be proportional to $\overline{\Delta}$ over a wide range of electrolyte concentration. The effects of electrolytes on the foam stability were discussed being based upon the properties of the black films.

Single liquid film is easily formed on a frame and provides a geometrically well-defined model system for investigating the stability of foams consisting of thin liquid films. Most studies of such films have been made for ionic surfactants, while studies using nonionic surfactants have been rather few.[1,2] The films stabilized with nonionic surfactants are of particular interest in discussing the repulsive forces acting between two surfaces of the thin films consisting of non-ionic molecules.

In the previous papers, [3,4] the dependence of the rate of growth of black films formed from aqueous nonionic surfactant solutions on the added electrolytes was reported, and the phenomena were interpreted in terms of the lyotropic effect of anions. Further, a proportionality was observed between the rate of growth of the black film and the additional tension, regardless of the electrolytes used.

In the present paper, the effects of added electrolytes on the properties of black films, on the surface tension of the solutions, and on the foam stability are studied for the aqueous solutions of the polyoxyethylene-type nonionic surfactants. The effects of electrolytes on the foam stability are discussed on the basis of the properties of the black films.

Experimental

Materials. Heptaoxyethylene dodecyl ether (N7) of Nikko Chemicals Co., Ltd. was used without purification, while polyoxyethylene nonylphenyl ether (PNE) of Kao Soap Co., Ltd. was used after being purified by molecular distillation.[3,4] Inorganic reagents were recrystallized twice from water, and it was confirmed that they showed no time dependence in the surface tension of 1 M aqueous solutions. Water was first distilled from alkaline potassium permanganate solution and then distilled using fused quartz vessel. All the solutions were freshly prepared before the experiment.

Properties of Thin Liquid Films and Surface of Solutions. The additional tension, $\overline{\Delta}$, is defined by the formula:

$$\overline{\Delta} = 2\gamma - \sigma_f = 2\gamma(1-\cos\theta) \qquad (1)$$

where σ_f is the film tension, γ the surface tension of the bulk solution, and θ the contact angle formed by the black film and the bulk liquid surface.[5] The method used for $\overline{\Delta}$ measurements consists essentially of the Wilhelmy plate method, and the liquid film was formed on a rectangular vertical glass frame 4 cm in width. The difference in tension between the black and the thicker films was measured by using a electro-microbalance, details of which were described in the previous papers.[4,6] The surface tension was measured by the Wilhelmy plate method using the electro-microbalance. The contact angle was calculated from the experimental results of $\overline{\Delta}$ and γ according to Eq. (1). The overall rate, v, of growth of the black film was obtained as the reciprocal of blackening time recorded on the chart of $\overline{\Delta}$ measurement. Here the blackening time was taken as the time required for converting total film area into the black film. All the measurements were performed at 30±0.1 °C.

Foam Stability. In a cylinder of 2 cm in diameter, a foam column 30 cm in height was produced by passing nitrogen gas saturated with water vapor through the solution from a single orifice under a constant pressure. After the gas flow was cut off, the height, H, of the foam column was measured as a function of time for about an hour.

Results and Discussion

The additional tension, $\overline{\Delta}$, is of importance for the studies of thin films, since it expresses the difference of free energies, ΔF_e, between the black film and the bulk liquid, and is associated with a disjoining pressure, π, by the formula:

$$\overline{\Delta} = -\int_h^\infty \pi dh - \pi h \qquad (2)$$

where h is the film thickness.[5] Figure 1 shows $\overline{\Delta}$ of the N7 stabilized films over a wide range of concentration of the added electrolytes. It is seen that each curve gives a maximum and a minimum in $\overline{\Delta}$. The concentrations at the minimum are found to be about 2×10^{-1}, 1×10^{-1}, 5×10^{-2}, and 1×10^{-2} N for Na_2SO_4, NaCl, NaBr, and NaSCN respectively.

Recently, Clunie *et al.* and Ingram measured the thickness and the additional tension of the black films formed from aqueous solutions of nonionic surfactant *n*-decyl methyl sulfoxide (DMS) as a function of the concentration of NaCl and NaBr.[7,8] They reported that the thickness of the films formed in the lower concentrations of electrolytes was not changed, but when increased the concentration it abruptly increased, where the films were transformed from the second

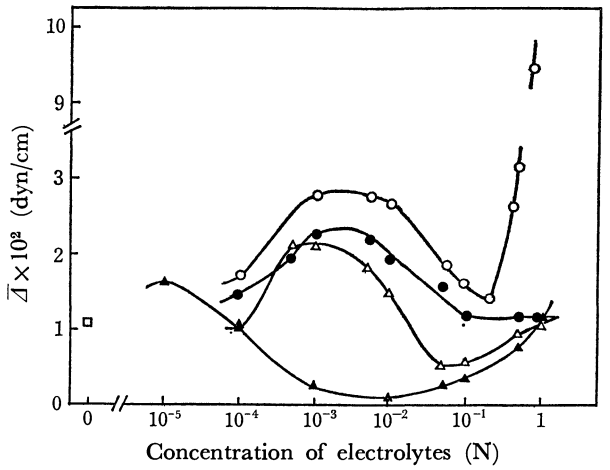

Fig. 1. Effect of electrolytes on additional tension ($\bar{\Delta}$) of black films formed from aqueous N7 solutions at 30 °C.
Concentration of N7: 5×10^{-4} M
Added electrolytes: ○ Na_2SO_4, ● NaCl, △ NaBr, ▲ NaSCN, □ None

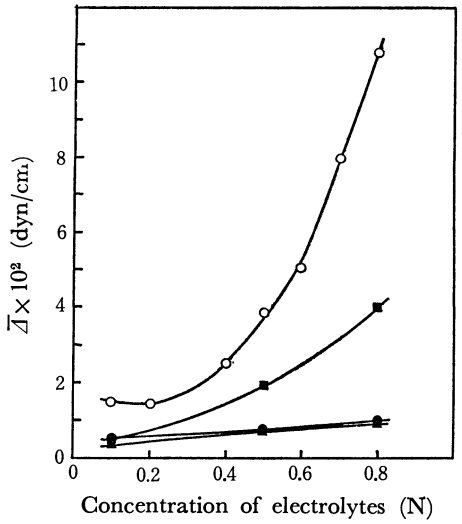

Fig. 2. Effect of electrolytes on additional tension ($\bar{\Delta}$) of black films formed from aqueous PNE solutions at 30 °C.
Concentration of PNE: 0.1 wt%
Added electrolytes: ○ Na_2SO_4, ■ NaF, ● NaCl, ▲ NaSCN

black film to the first one. They also reported that the curve of the additional tension *vs.* electrolyte concentration showed a minimum at this transition concentration. Although the thickness of the films was not measured in the present experiment, the respective minima appeared in the curves of Fig. 1 are considered to reveal the same kind of transition in the films, because of the similarity in the shape of the curves to that of DMS, despite the difference in hydrophilic groups between both systems.

The transition from the second to the first black films with increasing concentration of electrolytes was interpreted to be due to the formation of diffuse electrical double layer resulting from a specific adsorption of the respective anions at the film surfaces.[7,8] This effect is more marked for weakly hydrated ions than strongly hydrated ones. The concentrations at the minimum in the curves of Fig. 1 increase in the order of

$$NaSCN < NaBr < NaCl < 1/2Na_2SO_4.$$

Thus, the present results obtained with various anions having different adsorption tendency are in agreement with those reported[7,8] and the anions also follow the lyotropic series.

As seen in Fig. 1, the additional tensions of first black films formed from N7–Na_2SO_4 solutions remarkably increase with increasing concentration of Na_2SO_4, whereas in the other electrolytes they are all smaller than the former even at 1 M solutions. In the concentration range above the minima, that is, in the first black films, the order of $\bar{\Delta}$ for different electrolytes still obeys the lyotropic series though not so distinct. This fact is further stressed in the systems including F^- as seen in Fig. 2. It was reported that the variation of additional tension of the first black films with electrolyte concentration was in excellent agreement with the predictions of DLVO theory of colloid stability.[8] The contribution of electrical double layer to the additional tension must become much smaller than that of dispersion force, as the concentration of electrolytes increases. This effect together with the dehydration effect of electrolytes causes the formation of the thinner first black film, which leads to the significant increase of the additional tension of N7 and PNE films at high concentrations of Na_2SO_4.

It is interesting to compare the effects of electrolytes upon $\bar{\Delta}$ of the black film with those upon the surface tension of the solution. The effects of electrolytes upon the surface tension were studied for the same series of solutions used for the measurements of $\bar{\Delta}$. The results are shown in Fig. 3. The surface tension decreases with the increase in concentration of electrolytes, except for NaSCN in the concentration range above 10^{-2} N. Observed change of surface tension is in accordance with the lyotropic series of anions. This effect is analogous to that appearing on the cloud points of surfactant solutions.[9] On the other hand, in the range of electrolyte concentration less than about 1×10^{-2} N, the surface tension is unaffected by

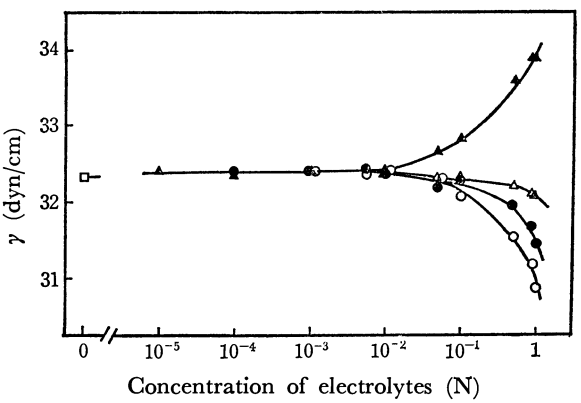

Fig. 3. Effect of electrolytes on surface tension (γ) of aqueous N7 solutions at 30 °C.
Concentration of N7 and added electrolytes: The same as in Fig. 1

TABLE 1. EFFECT OF ELECTROLYTES ON FILM CONTACT ANGLE (θ) OF BLACK FILM FOR AQUEOUS 5×10^{-4} M N7 SOLUTIONS AT 30 °C

Electrolyte	Na_2SO_4	NaCl	NaBr	NaSCN
1×10^{-4}N	1°20'	1°13'	1° 2'	1°19'
1×10^{-3}	1 42	1 30	1 28	32
1×10^{-2}	1 38	1 24	1 14	24
1×10^{-1}	1 17	1 6	46	38
5×10^{-1}		1 6	57	54
8×10^{-1}	3 24	1 6	1 7	1 4
1	4 39	1 7	1 4	1 5

the electrolytes and is equal to that of pure nonionic surfactant solution. The corresponding contact angles were calculated from the experimental results of $\bar{\Delta}$ and γ according to Eq. (1), a part of which are shown in Table 1.

As shown in Fig. 1, $\bar{\Delta}$ shows a maximum in the range of second black film for all electrolytes added, which is also observed in the DMS system.[7,8] The concentrations at maximum are 1×10^{-3}, 1×10^{-3}, 5×10^{-4}, and 1×10^{-5} N for Na_2SO_4, NaCl, NaBr, and NaSCN respectively, the values of which depend upon the kinds of anions. Since the surface tensions of the solutions are nearly constant at low electrolyte concentrations, the increase of $\bar{\Delta}$ in such a dilute electrolyte range may indicate the decrease of tension of the second black film involving a minimum. Such a behavior could be explained by the additional intermolecular forces arising from the change in the orientation of the solvent molecules and specific adsorption of ions and so on, besides the van der Waals attraction and a steric repulsion acting within the films, as appeared in the literature.[7,8]

Figure 4 shows the dependence of the blackening time on the concentration of added electrolyte, and Fig. 5 gives a plot of the overall rate of growth of the black film as a function of $\bar{\Delta}$. As seen in Fig. 5, the overall rate of growth of the black film is proportional to $\bar{\Delta}$, regardless of the amounts and kinds of added electrolytes.

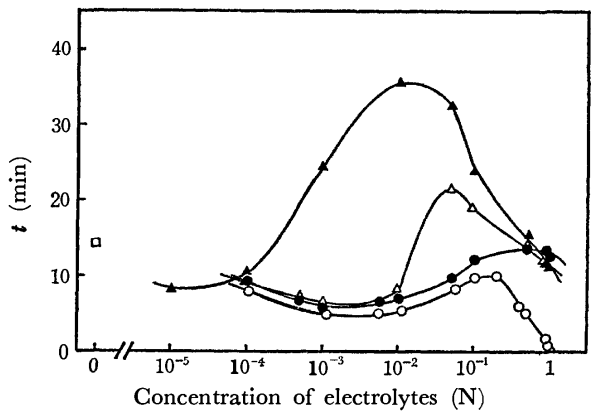

Fig. 4. Effect of electrolytes on blackening time (t) of liquid films formed from aqueous N7 solutions at 30 °C.
Concentration of N7 and added electrolytes: The same as in Fig. 1

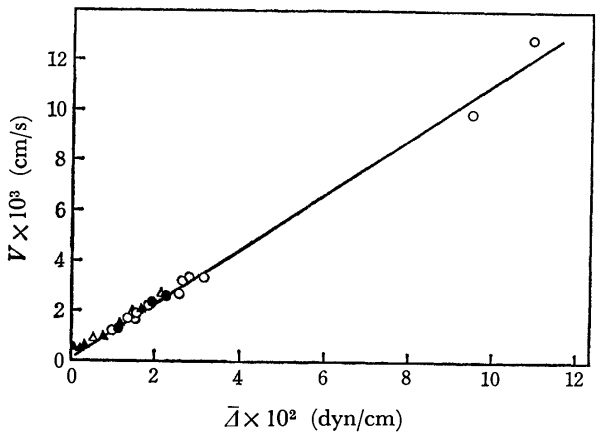

Fig. 5. Dependence of additional tension ($\bar{\Delta}$) on overall rate (v) of growth of black films formed from aqueous N7 solutions containing varying amounts of electrolytes at 30 °C.
Concentration of N7 and added electrolytes: The same as in Fig. 1

The rate of growth of the black film was previously found to be proportional to $\bar{\Delta}$ in the systems of sodium dodecylsulfate (SDS), PNE, and N7 at high concentrations of added electrolytes, and it is mentioned that a_f in the equation $\bar{\Delta}=a_f\cdot v$ may be taken as a viscosity parameter which is found to be proportional to the bulk viscosity.[4] The straight lines showing the proportionality in our preceding paper[4] fall on the same straight line together with the line of Fig. 5, except for the systems containing glycerol, irrespective of the types of the surfactants as well as the amounts and kinds of the electrolytes. This may indicate that the viscosity parameter a_f is independent of the amounts and kinds of added electrolytes, and of the types of the surfactants used at least.

Figure 6 shows the effect of electrolytes on the decay constant, k, of foams formed from 0.1 wt% aqueous PNE solutions containing varying amounts of electro-

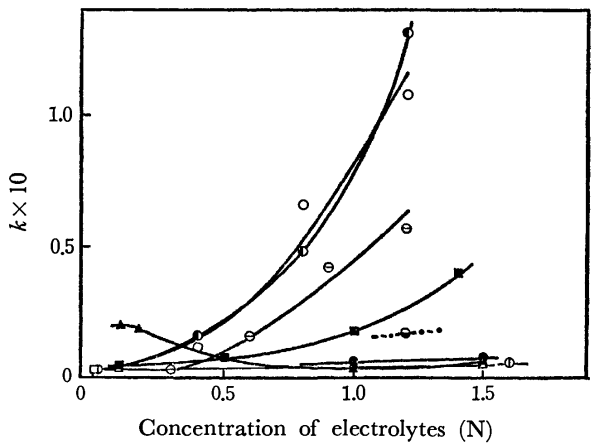

Fig. 6. Effect of electrolytes on decay constant (k) of foams formed from aqueous PNE solutions at 30 °C.
Concentration of PNE: 0.1 wt%
Added electrolytes: ◐ Na_2CO_3, ○ Na_2SO_4, ⊖ Na_3PO_4, ■ NaOH, ◒ $AlCl_3$, ● NaCl, ▲ NaSCN, ⓘ $CaCl_2$, △ HCl, □ None

lytes.[9] Foam stability was conventionally expressed by a decay constant $k=-\mathrm{d}\log H/\mathrm{d}t$, since H was found to decrease as a whole exponentially with time. Foam stability decreases with increasing concentration of electrolyte. The values of k are in the following order; $HCl \simeq 1/2\ CaCl_2 \simeq NaSCN \simeq NaCl < 1/3\ AlCl_3 < NaOH < 1/3\ Na_3PO_4 < 1/2\ Na_2SO_4 \simeq 1/2\ Na_2CO_3$.
The order for sodium salts is in agreement with the lyotropic series of anions excepting minor detail.

Figure 7 shows the plot of $\overline{\Delta}$ *vs.* k for varying concentrations of inorganic electrolytes added. It is seen that k is proportional to $\overline{\Delta}$, which indicates that the rate of collapse of foam is proportional to the additional tension and therefore to the rate of growth of the black film as seen in Fig. 5. Thus, the stability of foam is mainly determined by the rate of growth of the black film, that is, the rate of thinning or the thickness of black film, because $\overline{\Delta}$ is reported to vary with the reciprocal of the square of film thickness in the first black film.[8] This is consistent with the view proposed by de Vries.[10] No appreciable influence of the electrolytes on the thinning of films in the range of colored film was observed,[3] which indicates less influence of the drainage in the thick films on the stability of foams. Eventually, it may be concluded that the rupture of the foams under consideration does not occur until the colored foam film has given way to the black film, and the thickness and the expansion of the black of film dominates the rupture.

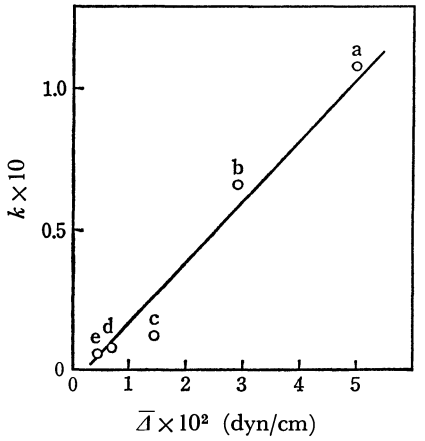

Fig. 7. Dependence of additional tension ($\overline{\Delta}$) on decay constant (k) of foams formed from aqueous PNE solutions containing varying amounts of electrolytes at 30 °C.
Composition of solutions: 0.1 wt% PNE + (a) 0.6 N Na_2SO_4, (b) 0.4 N Na_2SO_4, (c) 0.2 N Na_2SO_4, (d) 0.5 N NaSCN, (e) 0.1 N NaCl.

The author wishes to express her hearty thanks to Professor Tsunetaka Sasaki of Tokyo Metropolitan University for his encouragement and guidance throughout the experiments.

References

1) A. Scheludko, *Adv. Colloid Interface Sci.*, **1**, 391 (1967).
2) J. S. Clunie, J. F. Goodman, and B. T. Ingram, "Surface and Colloid Science," Vol. 3, ed. by E. Matijević, Wiley-interscience, New York (1971), p. 167.
3) T. Yamanaka, This Bulletin, **43**, 633 (1970).
4) T. Yamanaka, *ibid.*, **48**, 1755 (1975).
5) A. Scheludko, B. Radoev, and T. Kolarov, *Trans. Faraday Soc.*, **64**, 2213 (1968).
6) A. Prins., *J. Colloid Interface Sci.*, **29**, 177 (1969).
7) J. S. Clunie, J. M. Corkill, J. F. Goodman, and B. T. Ingram, *Spec. Disc. Faraday Soc.*, No. 1, 30 (1970).
8) B. T. Ingram, *J. Chem. Soc., Faraday 1*, **68**, 2230 (1972).
9) K. Kinoshita and T. Yamanaka, Asahi Garasu Kogyo Gijutsu Shoreikai Kenkyu Hokoku, **14**, 321 (1968).
10) A. J. de Vries, *Rec. Trav. Chim.*, **77**, 383 (1958).

Dielectric Behavior of Water Molecules Adsorbed on Iron(III) Oxide Hydroxides

Katsumi KANEKO, Mamoru SERIZAWA, Tatsuo ISHIKAWA, and Katsuya INOUYE

Department of Chemistry, Faculty of Science, Chiba University, Yayoi-cho, Chiba 280

(Received June 28, 1974)

The change in the dielectric constant of α-FeOOH, β-FeOOH, and γ-FeOOH with the amount of adsorbed water was examined at 30.0 °C in the frequency range 200 Hz—100 kHz for the purpose of clarifying the mechanism of water adsorption. The adsorption isotherms belong to the BET II type. The sample with the adsorbed water shows a particular dispersion of the dielectric constant with frequency in the low frequency range. The dispersion was ascribed to the transition between different orientational directions of the dipole moment of the adsorbed water. The change in the dielectric constant with the amount of adsorbed water for each iron(III) oxide hydroxide was interpreted in relation to the surface structure of predominant faces of crystals, in particular the number and position of hydroxyls on crystal surfaces. The following adsorption process was suggested below the monolayer adsorption coverage for each iron(III) oxide hydroxide. For α-FeOOH, water molecules are adsorbed on the (100) planes in three successive steps. For β-FeOOH, water molecules are primarily bound in the tunnels existing in the crystal along a direction parallel to the c-axis and then are adsorbed on the cracked tunnels exposing to the outer surface. For γ-FeOOH, water molecules are adsorbed on the (010) planes in two steps.

Of the four polymorphs of iron(III) oxide hydroxide (the so-called ferric oxyhydroxide) so far known, α-FeOOH, β-FeOOH, and γ-FeOOH occur naturally as minerals and as the corrosion products of iron. Each iron(III) oxide hydroxide exhibits characteristic properties, on which the authors have examined in several cases, such as the effect of Cu(II) on the crystal formation,[1-3] the activity to sulfur dioxide,[4] and the electrical conductivity.[5]

A study on the interaction between water molecules and iron(III) oxide hydroxide crystals is expected to clarify the corrosion process of iron surface in the atmospheric environments, since iron(III) oxide hydroxides are the main components in corrosion products. The dielectric measurement is used for the study of water adsorption because of the large dipole moment of the water molecule. Many dielectric studies on the water adsorption onto solids have been attempted. McCafferty *et al.*[6] reported the dielectric behavior of adsorbed water on α-Fe_2O_3. The correlation between the change in capacitance caused by applying electric field and the amount of adsorbed water appears significant to discuss the adsorption mechanism based on a structural view-point, because polar molecules adsorbed in a monolayer are too tightly connected with surface so as to orientate, whereas the molecules adsorbed in the second or higher layers are relatively free to orientate under the influence of the applied field.[7,8]

In this paper, the relationship between the dielectric behavior of water adsorbed on iron(III) oxide hydroxides and the surface structure of the oxyhydroxides is examined.

Experimental

Sample. Both α-FeOOH and β-FeOOH were synthesized by the methods described.[5] γ-FeOOH was prepared by the following procedure. After 3.6 g of $FeSO_4 \cdot 7H_2O$ was dissolved in 600 ml of oxygen-free water, air was blown for 3 hr into the solution adjusted to pH 4.3—6.5 with 10% NH_4OH solution. γ-FeOOH suspension thus obtained was aged at 30 °C for 5 days at pH 4.5. The crystals were filtered, washed with 2.5 l distilled water, and dried at 60 °C for 9 hr.

Examination of Samples. The X-ray diffraction patterns were obtained by the powder method with an automatic diffractometer (Geigerflex 2001, Rigaku Denki Co.) by use of Mn-filtered Fe*Kα* at 30 kV and 10 mA. Electron-microscopic observations were carried out by JEM 50B (Japan Electron Optics Co.). The predominant face of α-FeOOH crystals was identified by the selected-area electron diffraction with Hitachi HU-11D. The BET surface-area was determined by Shibata surface-area meter using N_2 adsorption at liquid nitrogen temperature for the samples dried at 110 °C for 1 hr in a stream of nitrogen.

The iron content in β-FeOOH crystals was determined, after the sample had been dissolved in hydrochloric acid by titration with 0.1 M $K_2Cr_2O_7$ standard solution, and the chlorine content in β-FeOOH by the Volhard method with 0.1 M $AgNO_3$ standard solution.

Adsorption of Water. The adsorption of water vapor was measured at 30.0 °C with a conventional volumetric apparatus. The water vapor was produced from $BaCl_2 \cdot 2H_2O$. Samples were outgassed at 110 °C under 10^{-5} Torr for 15 hr prior to the adsorption measurement. The adsorption reached an equilibrium within 1 hr.

Dielectric Measurements. The dielectric constant was measured in the frequency range 200 Hz—100 kHz by a substitution-type Schering bridge. The resistance-ratio bridge used consists of a precise variable air-capacitor (Yokogawa Hewlett-Packard Co., CDS-500), a low frequency oscillator and an oscilloscope in connection with a pre-amplifier as the detector. The sample cell is made of brass coaxial cylinders 5 cm long and 2 mm apart, insulated mutually by Teflon. This cell is fitted into the annular glass receptacle which can be connected with the above-mentioned adsorption apparatus. The capacitance of the cell C_0, a constant capacitance C' in parallel with C_0, and the accuracy of the apparatus, were determined and checked by the measurements with air, benzene, cyclohexane, and dichloroethane. These solvents were dried with Na wires and distilled just before the measurements. The values of C_0 and C' were 17.0 and 10.1 pF, respectively. The accuracy of the capacitance determination was ±1% in the range 40—200 pF; the capacitance was determined mostly in this range. The apparent dielectric constant is given by $(C—C')/C_0$, where C is the capacitance of the cell filled with the water-adsorbed sample.

Results

Properties of Samples. Each sample prepared gave X-ray diffraction patterns of well crystallized

Table 1. Properties of samples

	α-FeOOH	β-FeOOH	γ-FeOOH
Crystallite size by X-ray (Å)	280	550	110
Crystal length by EM (Å)	3000	2600	900
Crystal shape	Thin rectangular plate	Long square rod	Very thin rectangular plate
Predominant face	(100)	(100), (110) or (310)[9]	(010)[10]
S_{N_2} (m^2/g)	64	30	100

α-, β-, and γ-FeOOH, respectively. Table 1 gives the crystallite size calculated by the Scherrer formula from the half-value width of the principal X-ray diffraction lines, the mean crystal length by the electron microscopy (EM), the shape of crystals, and the predominant face of crystals. The predominant face of β-FeOOH crystals is cited from Mackay's results[9] and that of γ-FeOOH crystals from Oosterhout's results.[10] The specific surface area S_{N_2} by the adsorption of nitrogen is also given in Table 1. The ratio of chlorine to iron for β-FeOOH was found to be 8.2 atomic %.

Adsorption Isotherms. The adsorption isotherms at 30.0 °C for each sample are shown in Fig. 1, and are the BET II type. The monolayer-adsorption volume was determined by use of the BET plot of the adsorption data. Table 2 gives the monolayer volume V_m in milliliter of water per gram of the oxyhydroxide, the monolayer volume A_m in milliliter per S_{N_2}, and the area occupied by an adsorbed water molecule σ_w.

Dielectric Properties. Figure 2 shows the variations of apparent dielectric constant with frequency at different degrees of water adsorption for β-FeOOH. The dielectric constant of the dry sample did not exhibit any recognizable dispersion with respect to

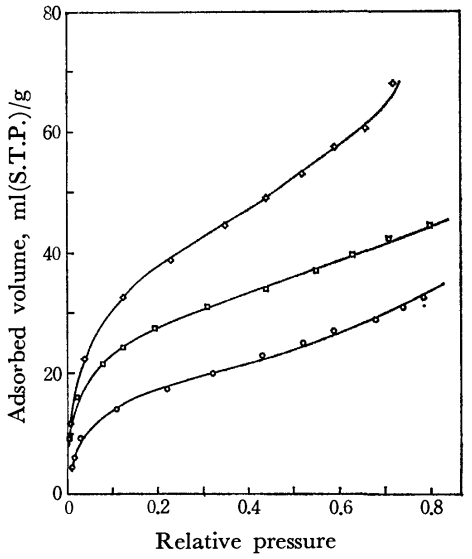

Fig. 1. Adsorption isotherms of water on α-FeOOH (□), β-FeOOH (○), and γ-FeOOH (◇).

Table 2. Monolayer volume and σ_w

	V_m (ml/g)	A_m (ml/m^2)	σ_w (Å^2)
α-FeOOH	24	0.37	10
β-FeOOH	12	0.38	9.7
γ-FeOOH	32	0.32	12

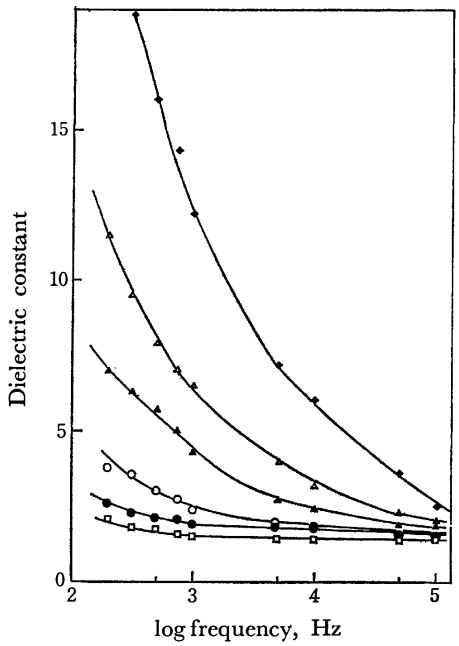

Fig. 2. Variations of dielectric constant with frequency at different degrees of water adsorption for β-FeOOH. The relative pressures are 0 for (□), 0.034 for (●), 0.067 for (○), 0.163 for (▲), 0.288 for (△), and 0.583 for (◆).

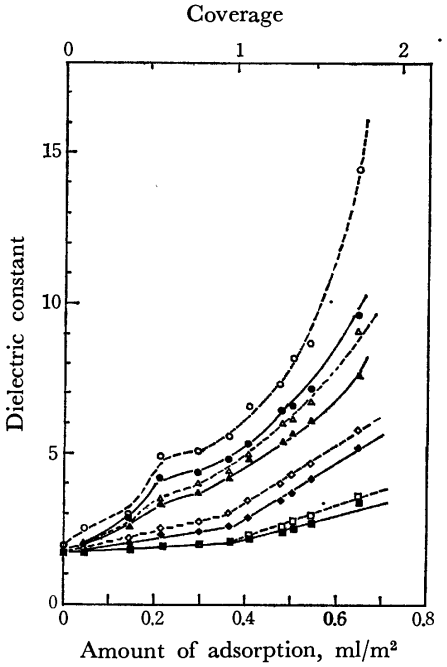

Fig. 3. Variations of dielectric constant with the amount of adsorption at various frequencies for α-FeOOH. ○: 200 Hz, ●: 500 Hz, △: 700 Hz, ▲: 1 kHz, ◇: 5 kHz, ◆: 10 kHz, □: 50 kHz, ■: 100 kHz.

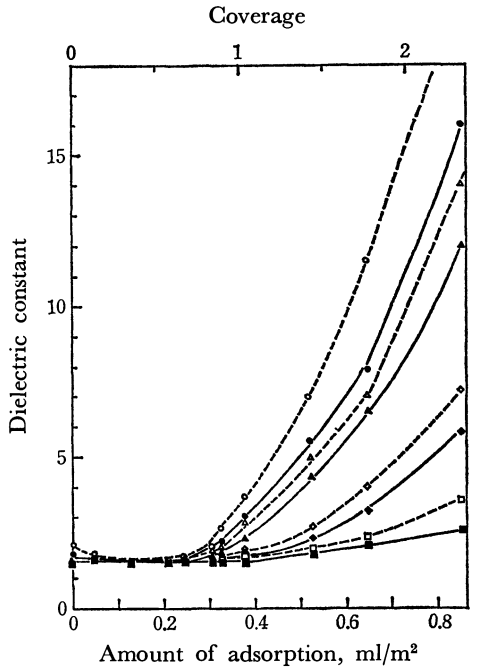

Fig. 4. Variations of dielectric constant with the amount of adsorption at various frequencies for β-FeOOH. Each symbol denotes the same frequency as that used in Fig. 3.

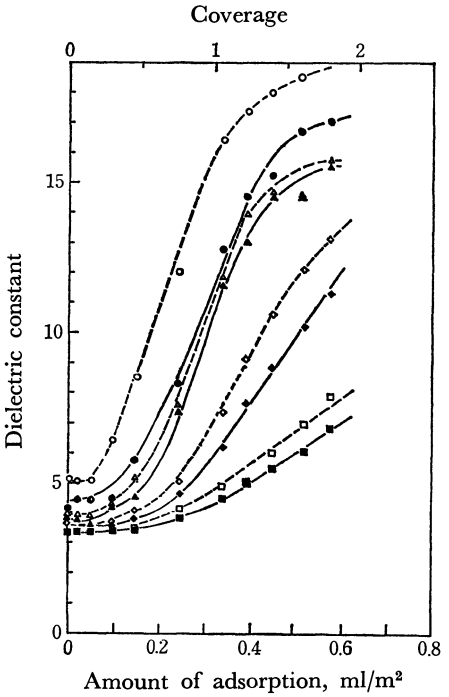

Fig. 5. Variations of dielectric constant with the amount of adsorption at various frequencies for γ-FeOOH. Each symbol denotes the same frequency as that used in Fig. 3.

frequency. The dielectric constant in lower frequency range increased considerably with the amount of adsorption, whereas that in higher frequency range increased only slightly. In Figs. 3—5, the relationship between the dielectric constant and the amount of adsorbed water in milliliter per S_{N_2} is presented at different frequencies for α-, β-, and γ-FeOOH, respectively. The coverage which indicates the number of layers of adsorbed molecules is also shown on the top abscissa of the figures. The curve at lower frequencies for α-FeOOH (Fig. 3) has a shoulder in the neighborhood of 0.6 coverage and rises steeply with adsorption at the coverage over unity. Figure 3 illustrates the fact that the dielectric constant at higher frequencies (5—100 kHz) increases with adsorption linearly and that each linear relation has a clear bend at unity of the coverage. The dielectric constant for β-FeOOH (Fig. 4) does not vary with adsorption up to 0.7 coverage (adsorbed water 0.25 ml/m²) irrespective of frequency, but it increases remarkably with adsorption above 0.7 coverage. No change in dielectric constant with the adsorption for γ-FeOOH (Fig. 5) is noticeable up to 0.5 coverage. The dielectric constant at lower frequencies with adsorption rises remarkably in the 0.5—1 range of coverage, but it increases only slightly with adsorption over unity. On the other hand, the dielectric constant at higher frequencies increases linearly with adsorption above 0.8 coverage though only slightly.

Discussion

Frequency Dependence. The dispersion of dielectric constant with frequency for the solid with adsorbed water has been explained both by the heterogeneous sturcture of the system consisting of adsorbed film, solid, and intergranular gap,[11] and by the orientation of adsorbed water under the influence of electrical field.[8] In the case of the solid with monolayer or bilayer adsorption film as in the present experiment, the dc conductance in the adsorbed film is not influenced by the dissolution of surface ions into the water film, but by the hopping of the protons in the absorbed water molecules on the solid surface. The dispersion by the latter influence may be regarded as an orientation mechanism, since the hopping of protons causes a variation in the direction of the dipole moment.

Thus the dielectric dispersion observed in the low frequency range seems to be ascribed to the transition between some different orientational directions of the dipole of adsorbed water. It is anticipated that the adsorbed water forms a structure analogous to that of ice which shows the low frequency dielectric dispersion explained by the molecular reorientaiton.[12,13] The transition of molecular orientation depends on the force on the solid surface. The low frequency dielectric constant shows sensitively the adsorption state of water molecules. On the other hand, the dielectric constant in the high frequency range, where the dipole lags behind the field, depends to a lesser extent on the adsorption state.

Dielectric Behavior and Surface Structure. Electron microscopic observation showed that the predominant face of crystals occupies more than 90% of the total surface (Table 1). The adsorption occurs therefore mainly on the predominant surfaces of each crystal. The surface structures of α-, β-, and γ-FeOOH shown in Figs. 6, 7, and 8, respectively, were illustrated from available crystallographic data (α-FeOOH,[14,15] β-

Table 3. Data on the two-dimensional unit cell of the predominant face

	Area of *TD*-unit s_u, (Å^2)	Number of H_2O per s_u, n_w	Number of OH per s_u, n_{OH}
α-FeOOH	30.3	3	2
β-FeOOH	31.7	3	2
γ-FeOOH	11.8	1	1

FeOOH,[9,16,17] and γ-FeOOH[18]). The ionic radius values of 1.40 and 1.53 Å were employed for oxygen and hydroxyl ions, respectively, in the drawing of Figs. 6—8.[19] Table 3 gives the area of the two-dimensional unit cell (TD-unit) s_u calculated from the lattice constant, the number of hydroxyls n_{OH} per s_u estimated from the structure of the predominant surfaces, and the number of water molecules n_w in the monolayer per s_u. n_w is the integer nearest to the ratio of s_u to σ_w. It is assumed that adsorption sites on α- and γ-FeOOH crystals are hydroxyls, whereas those on β-FeOOH are hydroxyls and tunnels. The dissociative adsorption of water may be ignored, since it was demonstrated that the heat of immersion in water for α- and γ-FeOOH is much less than that for α-Fe_2O_3, immersion of which in water is apparently accompanied by rehydration.[20]

The dielectric behavior of α-FeOOH with respect to the amount of adsorbed water may be explained by assuming the presence of two kinds of hydroxyl (hydroxyl-I and II) on the surface ($n_{OH}=2$). A water molecule denoted by W(I) is localized on hydroxyl-I by the triple hydrogen bonding with one OH^- and with the nearest two O^{2-}. Another water molecule W(II) is adsorbed on hydroxyl-II by the single hydrogen bond. A third water molecule W(III) assumes a position between W(I) and W(II). Figure 6 shows the state of water adsorption, where n_w equals 3. The immobile water molecules W(I) result in a slight increase in the dielectric constant up to 0.3 coverage. The freely orientating molecules W(II) exhibit a considerable increase in the dielectric constant in the 0.3—0.6 coverage range. W(III) molecules hinder the orientation of W(II); W(III) brings about a further slight increase in the dielectric constant in the 0.6—1 coverage range. Molecules in the second adsorption layer with greater freedom of movement cause a considerable increase in dielectric constant at lower frequencies.

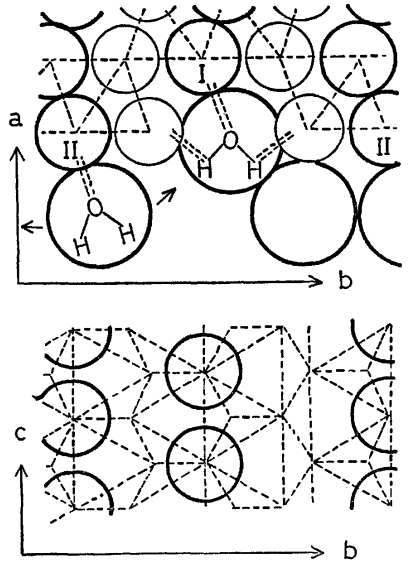

Fig. 6. Adsorption process of water molecules on the (100) plane of α-FeOOH. The smallest circle, the intermediate circle, and the largest circle denote oxygen ion, hydroxyl ion, and water molecule, respectively. The single broken line denotes the edge of the octahedron including an iron ion. The double broken line denotes hydrogen bond binding the adsorbed water molecule.

β-FeOOH is stable in the presence of F or Cl ions.[9] The Cl content in β-FeOOH can not be easily reduced below 12% by washing.[21] Mackay[9] reported that β-FeOOH has a hollandite ($BaMn_8O_{16}$) structure having tunnels parallel to the c-axis, in which Cl^- and H_2O can be occluded (Fig. 7); the extra negative charge due to Cl^- in β-FeOOH crystals must be compensated by the replacement of O^{2-} by OH^-. According to the results by Byström and Byström,[22] it is considered that in the case of hollandite a half the volume of tunnels is filled with Ba ions and the other half with water molecules; the ratio of Ba to Mn is 1/8, *viz.*, 12.5%. The chlorine in β-FeOOH plays the role of Ba ion in hollandite. The most stable composition of β-FeOOH is assumed to be $FeO_{1-1/8}(OH)_{1+1/8}Cl(t)_{1/8}H_2O(t)_{1/8}$, where (t) indicates the state bound to the tunnel. The electron-micrographs of β-FeOOH crystals obtained by several authors[9,16,23] clearly show the presence of holes, indicating that the tunnels are broken up midway. Cl ions in the neighborhood of the exits of tunnels and holes are supposedly replaced by water molecules in the course of washing. The washing process may be expressed as follows.

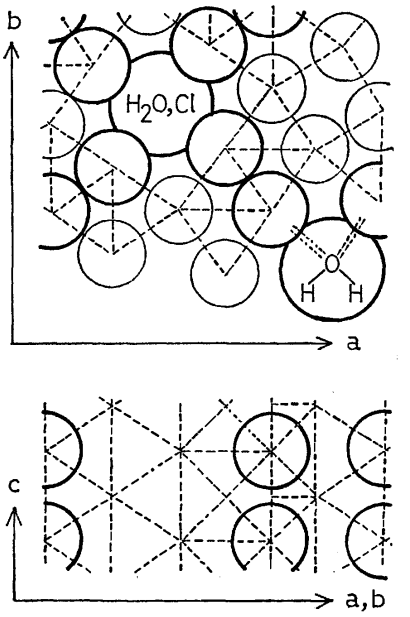

Fig. 7. Adsorption process of water molecules in the tunnels and on the cracked tunnels of β-FeOOH.

$FeO_{1-1/8}(OH)_{1+1/8}Cl(t)_{1/8}H_2O(t)_{1/8} \rightarrow FeO_{1-1/8+x}(OH)_{1+1/8-x}Cl(t)_{1/8-x}H_2O(t)_{1/8+x}$, where $1/8-x$ is equal to 8.2%. Accordingly x is equal to 4.3%. The replaced water xH_2O could be removed in the course of pretreatment. The 4.3% vacant sites thus produced can be used as the adsorption sites for water. The possible amount of water adsorbed to these sites is calculated to be 0.25 ml/m². Assuming that this amount of water is bound tightly in the tunnel, the fact that the dielectric constant is almost constant up to 0.25 ml/m² of adsorption (Fig. 4) is quite conceivable. After the tunnel is choked up, approximately 0.11 ml/m² water molecules are bound to the two hydroxyls at outer surfaces by the bifurcated hydrogen bonding (Fig. 7). The second step of adsorption corresponds to a slight increase in the dielectric constant in the range of the amount of adsorption from 0.25 to 0.4 ml/m² (A_m) (Fig. 4). The water molecules in the second layer are bound to the surface by weak forces and are mobile to orientate, when the dielectric constant increases markedly.

The dielectric behavior of γ-FeOOH with respect to the amount of adsorbed water may be explained by assuming the presence of only a kind of hydroxyl on the surface ($n_{OH}=1$). It is supposed that each water molecule is localized on two hydroxyls by the bifurcated hydrogen bonding up to the half coverage adsorption, so that only a slight increase in dielectric constant is observed in the region of coverage up to 0.5 (Fig. 5). Water molecules loosely bound to hydroxyls by single hydrogen bonds ($n_{OH}=n_w$) above the half coverage are relatively free to orientate, when the dielectric constant increases sharply. Figure 8 shows the adsorption process of water on γ-FeOOH. From the fact that the calculated density of hydroxyls on γ-FeOOH is the highest (8.4×10^{14} cm^{-2}) in comparison with 6.6×10^{14} cm^{-2} on α-FeOOH and 6.3×10^{14} cm^{-2} on β-FeOOH, it follows that even the second layer of the adsorbed water on γ-FeOOH will be comparatively ordered. The ordered adsorbed water molecule in the second layer withholds the dielectric constant from an abrupt increase in the range of coverage over unity as shown in Fig. 5.

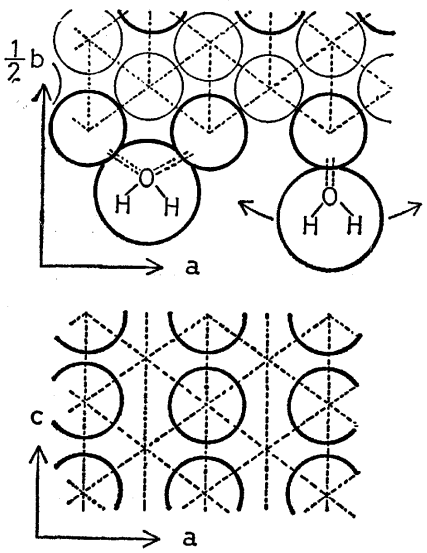

Fig. 8. Adsorption process of water molecules on the (010) plane of γ-FeOOH.

The increase in dielectric constant in a higher frequency range is due to the change in the atomic polarization, which depends on the product of the atomic polarizability and the number of molecules of adsorbed water. The atomic polarizability of the water molecule in the adsorption layer is identical, so that the dielectric constant in a higher frequency range is proportional to the number of water molecules. Therefore, the dielectric constant in higher frequency range increases linearly with the amount of adsorption. The variation in the slope of linear plots in the contiguity of monolayer capacity seems to be caused by the difference between the atomic polarizability of adsorbed water in the first layer and that in the second layer.

Conclusion

The adsorption isotherm of water on iron(III) oxide hydroxides (α-, β-, and γ-FeOOH) was found to be of the BET II type. The change in dielectric constant with the amount of adsorption of water was measured. The adsorption mechanism was discussed on a structural view-point that the relationship between the dielectric constant and the amount of adsorbed water reflects the adsorption process of coverage below unity. The structure of the predominant surface of crystals, in particular the number and position of hydroxyls, is the main determining factor in the adsorption of water; two kinds of hydroxyl on (100) plane for α-FeOOH crystal, the tunnels parallel to the c-axis and the hydroxyls on the outer surface for β-FeOOH crystal, and a kind of hydroxyls on (010) plane for γ-FeOOH crystal are the sites of adsorption. Water molecules are adsorbed on surfaces in two or three steps, which is characteristic of the surface structure of each iron(III) oxide hydroxide.

This research has been supported in part by the Government Science Research Fund of the Ministry of Education.

References

1) K. Inouye, S. Ishii, K. Kaneko, and T. Ishikawa, *Z. Anorg. Allg. Chem.*, **391**, 86 (1972).
2) K. Inouye, H. Imamura, K. Kaneko, and T. Ishikawa, This Bulletin, **47**, 727 (1974).
3) K. Inouye, K. Ichimura, S. Kono, K. Kaneko, and T. Ishikawa, Paper presented at the 30th Annual Meeting of the Chemical Society of Japan. Osaka, April, 1974.
4) T. Ishikawa and K. Inouye, *Nippon Kagaku Zasshi*, **91**, 935 (1970).
5) K. Kaneko and K. Inouye, This Bulletin, **47**, 1139 (1974).
6) E. McCafferty, V. Pravdic, and A. C. Zettlemoyer, *Trans. Faraday Soc.*, **66**, 1720 (1970).
7) D. M. Young and A. D. Crowell, "Physical Adsorption of Gases," Butterworth, London (1962), Chap. 10.
8) R. L. McIntosh, "Dielectric Behavior of Physically Adsorbed Gases," Marcel Dekker, New York (1966).
9) A. L. Mackay, *Mineral. Mag.*, **32**, 545 (1960).
10) G. W. van Oosterhout, *Acta Crystallogr.*, **13**, 932 (1960).

11) K. Kamiyoshi and T. Odake, *J. Chem. Phys.*, **21**, 1295 (1953).
12) D. Eisenberg and W. Kauzmann, "The Structure and Properties of Water," Oxford University Press, London (1960).
13) F. Humbel, F. Jona, and P. Scherrer, *Helv. Phys. Acta*, **26**, 17 (1953).
14) F. J. Ewing, *J. Chem. Phys.*, **3**, 203 (1935).
15) J. B. Forsyth, I. G. Hedley, and C. E. Johnson, *Proc. Phys. Soc., London, Solid State Phys.*, **1**, 179 (1968).
16) J. H. Watson, R. R. Cardell, Jr., and W. Heller, *J. Phys. Chem.*, **66**, 1757 (1962).
17) A. Szytula, M. Balanda, and Z. Dimitrijevic, *Phys. Stat. Sol.* (a), **3**, 1033 (1970).
18) F. J. Ewing, *J. Chem. Phys.*, **3**, 420 (1935).
19) A. F. Wells, "Structural Inorganic Chemistry," Oxford University Press, London (1962), Third Ed. p. 71.
20) T. Ishikawa and K. Inouye, This Bulletin, **46**, 2665 (1973).
21) T. Ishikawa and K. Inouye, *ibid.*, **48**, 1580 (1975).
22) A. Byström and A. M. Byström, *Acta Crystallogr.*, **3**, 146 (1950).
23) J. Gallagher, *Nature*, **226**, 1225 (1970).

A Theory of Ion Association as a Complement of the Debye-Hückel Theory*

Haruhiko YOKOYAMA and Hideo YAMATERA

Department of Chemistry, Faculty of Science, Nagoya University, Chikusa-ku, Nagoya 464

(Received December 23, 1974)

The classical Debye-Hückel theory of strong electrolyte solutions was re-examined in order to explain ion association. Regarding a symmetrical electrolyte in very dilute solutions, a more precise expression was derived for excess chemical potential due to electrostatic ion-ion interactions. This expression has, in addition to the Debye-Hückel term, a supplementary term resulting from a more proper account of the energy of the interactions of ions existing near each other. If the concept of ion association is taken as a complement of the Debye-Hückel theory, the contribution to the chemical potential of the electrolyte from ion association should correspond to the supplementary term. The following equation was thus obtained for the ion-association constant:

$$K=(8\pi Na^3/1000)\sum_{n=1}^{\infty} b^{2n+2}/[(2n+2)!\ (2n-1)]$$

This equation is in agreement with that derived by Ebeling on the basis of the cluster theory and has an asymptotic representation (at $b\to\infty$) in common with Bjerrum's. For practical b values, the present equation has the merit that it gives moderate K values, decreasing monotonously with an increase in the a value, and eliminates the disadvantages of Fuoss's result, giving a minimum K value at $b=3$, and of Bjerrum's, giving $K=0$ at $b\leqq 2$.

Debye and Hückel[1] have been successful in explaining the behavior of ions in dilute solutions of strong 1 : 1 electrolytes. For polyvalent ions, however, their theory was not satisfying, and the theoretical prediction evidently deviates from the experimental results even for dilute solutions.

Gronwall, LaMer, and Sandved[2] made an attempt to improve the Debye-Hückel theory by solving the Poisson-Boltzmann equation more accurately. However, the accurate solutions obtained by them and by other authors[3] were found to lack self-consistency.[4,5]

On the other hand, Bjerrum[6] introduced the concept of so-called ion association to explain the deviation of the experimental results from the Debye-Hückel theory. Thereafter, many other theories of ion association have been proposed by Denison and Ramsey,[7] Gilkerson,[8] Fuoss,[9] Ebeling,[10] and other authors.[11] These theories of ion association, with the probable exception of Ebeling's theory, have been based on specific models of the ion-pair.

Although evidence can be given for the formation of ion-pairs in solution, the geometrical configurations of the ion-pairs can hardly be specified. There may be solvent-separated ion-pairs in addition to contact ion-pairs.[12] If, as in Bjerrum's theory, all pairs of oppositely charged ions within a certain critical distance of each other are regarded as ion-pairs, some arbitrariness will be involved in the choice of the critical distance. Moreover, there seems to be a chance that fast-moving unassociated ions momentarily exist within the critical distance of each other. Thus, no geometrical models of the ion-pairs can be free from arbitrariness.

In our opinion, a theory of ion-association dealing with ion-pairs must be complementary to the theory describing the behavior of free ions (usually, the Debye-Hückel theory). We therefore re-examined the Debye-Hückel theory to see what correction could be made to improve the theory. Then, relating the correction to ion association, we obtained a theoretical expression for the ion-association constant of symmetrical electrolytes. The expression includes no arbitrary parameters except for the one representing the closest distance of approach of ions, and incidentally, it is in agreement with the expression derived by Ebeling on the basis of the cluster theory.

We shall describe the derivation of the expression for ion-association constants and compare the results with those deduced by other authors.[6,7,9,10]

Symbols

a	closest distance of approach of ions
b	Bjerrum's parameter [Eq. (14)]
c	concentration of electrolyte
e	elementary charge
k	Boltzmann's constant
n_i	number of i-type ions in V cm^3 of solution
q	$=z^2s/2$
r	distance from central ion
s	$=e^2/\varepsilon kT$
y	activity coefficient
z_i	charge number of i-type ion
z_j	charge number of central j-ion
z	absolute value of charge number of ions of symmetrical electrolytes
A	constant to be determined from condition of electrical neutrality [Eqs. (11) and (13)]
G^{el}	Gibbs free energy of electrostatic interactions between ions
K	ion-association constant
N	Avogadro's number
R	gas constant
T	absolute temperature
V	volume of solution
α	degree of association
γ	Euler's constant ($\gamma=0.5772\cdots$)
ε	dielectric constant of solvent
κ	reciprocal thickness of ionic atmosphere [Eq. (4)]
λ	charging parameter
μ	chemical potential per mole of electrolyte
μ^{el}	contribution of ion-ion interactions to μ
μ_i^{el}	contribution of ion-ion interactions to chemical potential of one i-type ion

* Presented in part at the 27th Annual Meeting of the Chemical Society of Japan, Nagoya, October, 1972, and at the 15th International Conference on Coordination Chemistry, Moscow, USSR, June, 1973. A preliminary report has been published: H. Yokoyama and H. Yamatera, *Chem. Lett.*, **1973**, 337.

ρ charge density
ψ electrostatic potential due to all the ions
ψ^{cloud} electrostatic potential due to all the ions except central j-ion
A_{DH}, ρ_{DH}, ψ_{DH}, and $\psi_{\text{DH}}^{\text{cloud}}$ approximate expressions for A, ρ, ψ, and ψ^{cloud} respectively, under Debye-Hückel conditions

Boltzmann Distribution and Poisson Equation. In the following discussions, the solvent is considered to be a continueous medium of a dielectric constant, ε, and the ions to be rigid spheres. The ion-ion interactions are assumed to be purely electrostatic.

If a particular ion is selected as the center of a coordinate system, the Boltzmann distribution law gives the charge density, ρ, as a function of the radial coordinate, r:

$$\rho(r) = \sum_i \frac{n_i z_i e}{V} \exp\left(-\frac{z_i e\psi(r)}{kT}\right) \tag{1}$$

where n_i is the number of i-type ions in V cm^3 of the solution, $z_i e$ the charge of the i-type ions, and $\psi(r)$ the electrostatic potential. We shall use in the following the subscripts 1 and 2 to denote, respectively, the cation and the anion of a single electrolyte. For a symmetrical electrolyte:

$$n_1 = n_2 \quad \text{and} \quad z_1 = -z_2 = z(z>0)$$

With n_1 and z, Eq. (1) can be rewritten as follows:

$$\rho(r) = \frac{n_1 ze}{V}\left[\exp\left(-\frac{ze\psi(r)}{kT}\right) - \exp\left(\frac{ze\psi(r)}{kT}\right)\right] \tag{2}$$

By expanding the exponential functions in Eq. (2) and introducing the parameter κ (the reciprocal thickness of the ionic atmosphere), one obtains:

$$\rho(r) = -\frac{\varepsilon\kappa^2}{4\pi}\sum_{n=0}^{\infty}\frac{1}{(2n+1)!}\left(\frac{ze}{kT}\right)^{2n}[\psi(r)]^{2n+1} \tag{3}$$

The parameter κ is defined by the expression:

$$\kappa^2 = \frac{8\pi n_1 z^2 s}{V} \tag{4}$$

or by the general expression:

$$\kappa^2 = \frac{4\pi\sum_i n_i z_i^2 e^2}{V\varepsilon kT} = \frac{4\pi s\sum_i n_i z_i^2}{V} \tag{5}$$

where s is a parameter with the dimension of length** and is defined by:

$$s = \frac{e^2}{\varepsilon kT}$$

The potential, $\psi(r)$, and the charge density, $\rho(r)$, are related to each other by the Poisson equation:

$$\frac{1}{r^2}\cdot\frac{\mathrm{d}}{\mathrm{d}r}\left(r^2\frac{\mathrm{d}\psi(r)}{\mathrm{d}r}\right) = -\frac{4\pi\rho(r)}{\varepsilon}$$

Debye-Hückel Approximation. For a very dilute solution, Debye and Hückel[1] simplified Eq. (3), ignoring the terms with $n \geqq 1$ under the condition of $|ze\psi(r)/kT| \ll 1$:

$$\rho(r) \simeq \rho_{\text{DH}}(r) = -\frac{\varepsilon\kappa^2}{4\pi}\psi_{\text{DH}}(r) \tag{6}$$

** In an aqueous solution at 25.0 °C with $\varepsilon = 78.30_3$, s has a value of 7.157 Å.

where the subscript DH indicates that the Debye-Hückel condition is assumed to be satisfied. Then they solved the Poisson equation and derived the expression:

$$\psi_{\text{DH}}(r) = A_{\text{DH}}\frac{\exp(-\kappa r)}{r} \tag{7}$$

The constant, A_{DH}, can be determined by means of the condition of electrical neutrality:

$$\int_a^{\infty} 4\pi r^2\rho(r)\mathrm{d}r = -z_j e \tag{8}$$

where $z_j e$ is the charge of the central j-ion and a is the closest distance of approach of ions. Equation (8) was solved with Eqs. (6) and (7) to give:

$$A_{\text{DH}} = \frac{z_j e\exp(\kappa a)}{\varepsilon(1+\kappa a)} \tag{9}$$

The potential, $\psi(r)$, is in general represented by the sum of the potential due to the j-ion, $z_j e/\varepsilon r$, and the potential due to all the other ions, $\psi^{\text{cloud}}(r)$. With the Debye-Hückel approximation,

$$\psi^{\text{cloud}}(r) \simeq \psi_{\text{DH}}^{\text{cloud}}(r)\left(=\psi_{\text{DH}}(r) - \frac{z_j e}{\varepsilon r}\right)$$
$$= \frac{z_j e}{\varepsilon r}\left[\frac{\exp(\kappa a - \kappa r)}{1+\kappa a} - 1\right]$$

Since the j-ion is present inside a cavity with a radius of a surrounded by an ionic cloud, the potential, $\psi^{\text{cloud}}(r)$, at the j-ion is given by the potential, $\psi^{\text{cloud}}(r)$, at $r=a$:

$$\psi^{\text{cloud}}(a) \simeq \psi_{\text{DH}}^{\text{cloud}}(a) = -\frac{z_j e\kappa}{\varepsilon(1+\kappa a)} \tag{10}$$

Contribution of the Ions Existing in the Vicinity of the j-ion to the Potential, $\psi^{\text{cloud}}(a)$. The contribution of the ions existing in the vicinity of the j-ion to the potentials, $\psi(r)$, $\psi^{\text{cloud}}(r)$, and $\psi^{\text{cloud}}(a)$, was ignored in the Debye-Hückel approximation. More exact expressions for these potentials including the ignored contribution can be derived by using a closer approximation to the original equation [Eq. (3)] for the charge distribution. In Eq. (3), the Debye-Hückel-type expression [a modification of Eq. (7)]:

$$\psi(r) = A\frac{\exp(-\kappa r)}{r} \tag{11}$$

can be used as an approximation to $\psi(r)$. A is a constant to be determined from the conditions of electrical neutrality. Since, for our purposes in this paper, we are primarily interested in the potential, $\psi^{\text{cloud}}(a)$, we shall describe below only the derivation of the potential, $\psi^{\text{cloud}}(a)$, of a closer approximation.

The time-averaged number of i-type ions in a unit volume at a certain distance, r, from the j-ion is given by the Boltzmann distribution law. Thus, their contribution to the potential at the j-ion can be expressed by:

$$\frac{1}{\varepsilon r}\cdot\frac{n_i z_i e}{V}\exp\left(-\frac{z_i e\psi(r)}{kT}\right)$$

The superposition of the contributions of the ions (except the j-ion) of all types in the whole space gives the potential at any one place within the distance

$r \leqq a$ due to the ionic cloud, $\psi^{\text{cloud}}(a)$:

$$\psi^{\text{colud}}(a) = \int_a^\infty \frac{1}{\varepsilon r} \sum_i \left[\frac{n_i z_i e}{V} \exp\left(-\frac{z_i e \psi(r)}{kT} \right) \right] 4\pi r^2 \mathrm{d}r$$

or

$$\psi^{\text{colud}}(a) = \frac{4\pi}{\varepsilon} \int_a^\infty r\rho(r)\mathrm{d}r$$

Using Eq. (11) for $\psi(r)$, one obtains:

$$\begin{aligned}\psi^{\text{cloud}}(a) &= -\kappa^2 \sum_{n=0}^{\infty} \frac{1}{(2n+1)!} \left(\frac{ze}{kT} \right)^{2n} A^{2n+1} \\ &\quad \times \int_a^\infty \frac{\exp[-(2n+1)\kappa r]}{r^{2n}} \mathrm{d}r \\ &= -\kappa A \exp(-\kappa a) \\ &\quad - (\kappa a)^2 \sum_{n=1}^{\infty} \frac{\exp[-(2n+1)\kappa a]}{(2n+1)!(2n-1)a^{2n+1}} \left(\frac{ze}{kT} \right)^{2n} A^{2n+1} \\ &\quad + (\kappa a)^3 (\cdots\cdots) + \cdots\cdots \end{aligned} \tag{12}$$

(For details of the calculation of the integral, see the footnote.***) The constant A in Eq. (12) is determined by the condition of electrical neutrality [Eq. (8)] as follows. The whole charge in all the volume outside the sphere of radius a is given by:

$$\begin{aligned}&\int_a^\infty 4\pi r^2 \rho(r)\mathrm{d}r \\ &= -\varepsilon\kappa^2 \sum_{n=0}^{\infty} \frac{1}{(2n+1)!} \left(\frac{ze}{kT} \right)^{2n} A^{2n+1} \int_a^\infty \frac{\exp[-(2n+1)\kappa r]}{r^{2n-1}} \mathrm{d}r \\ &= -\varepsilon(1+\kappa a) A \exp(-\kappa a) \\ &\quad - \varepsilon(\kappa a)^2 \left\{ -\frac{\ln(3\kappa a)+\gamma}{6a^2} \left(\frac{ze}{kT} \right)^2 A^3 \right. \\ &\quad \left. + \sum_{n=2}^{\infty} \frac{\exp[-(2n+1)\kappa a]}{(2n+1)!\,(2n-2)a^{2n}} \left(\frac{ze}{kT} \right)^{2n} A^{2n+1} \right\} \\ &\quad + (\kappa a)^3 (\cdots\cdots) + \cdots\cdots \end{aligned}$$

where γ is Euler's constant ($\gamma = 0.5772\cdots$.) Since this charge must be equal to $-z_j e$, the constant A becomes:

$$\begin{aligned}A = \frac{z_j e \exp(\kappa a)}{\varepsilon(1+\kappa a)} &\left\{ 1 - (\kappa a)^2 \left[-\frac{\ln(3\kappa a)+\gamma}{6} b^2 \left(\frac{z_j}{z} \right)^2 \right. \right. \\ &\left. \left. + \sum_{n=2}^{\infty} \frac{b^{2n} (z_j/z)^{2n}}{(2n+2)!\,(2n-1)} \right] \right\} \end{aligned} \tag{13}$$

where the $(\kappa a)^3$ and higher-order terms are disregarded. b is Bjerrum's parameter and is defined by:

$$b = \frac{|z_1 z_2| s}{a} = \frac{|z_1 z_2| e^2}{\varepsilon k T a} \tag{14}$$

or, for a symmetrical electrolyte,

$$b = \frac{z^2 s}{a} \tag{15}$$

By substituting Eq. (13) into Eq. (12) and by disregarding the $(\kappa a)^3$ and higher-order terms, one obtains:

$$\psi^{\text{Cloud}}(a) = -\frac{z_j e \kappa}{\varepsilon(1+\kappa a)} - (\kappa a)^2 \frac{z_j e}{\varepsilon a} \sum_{n=1}^{\infty} \frac{b^{2n} (z_j/z)^{2n}}{(2n+1)!\,(2n-1)} \tag{16}$$†

The second term on the right-hand side has been added as the first correction term to the Debye-Hückel expression [Eq. (10)].

The Gibbs Free Energy of the Electrostatic Interactions between Ions, G^{el}. According to the Debye charging process,[1] G^{el} can be evaluated as the electric work of charging up all the ions simultaneously from zero to their actual values at the same relative rate:[4,5]

$$G^{\text{el}} = \int_0^1 \sum_j z_j e \psi^{\text{cloud}}(a, \lambda z, \lambda\kappa) \mathrm{d}\lambda \tag{17}$$

where the summation is made over all the ions in V cm^3 of the solution, λ denotes the fraction of their final charges which the ions have at any stage of the integration, and $\psi^{\text{cloud}}(a, \lambda z, \lambda\kappa)$ is given by:

$$\begin{aligned}\psi^{\text{cloud}}(a, \lambda z, \lambda\kappa) &= -\frac{\lambda z_j e \lambda\kappa}{\varepsilon(1+\lambda\kappa a)} \\ &\quad - (\lambda\kappa a)^2 \frac{\lambda z_j e}{\varepsilon a} \sum_{n=1}^{\infty} \frac{(\lambda^2 b)^{2n}}{(2n+1)!\,(2n-1)} \end{aligned}$$

This expression is obtained by substituting $\lambda z_j e$ and $\lambda z e$ for $z_j e$ and ze respectively in Eq. (16). Then the right-hand side of Eq. (17) can be calculated as follows:

$$\begin{aligned}G^{\text{el}} &= -\frac{\sum_j z_j^2 e^2 \kappa}{\varepsilon} \int_0^1 \frac{\lambda^2}{1+\lambda\kappa a} \mathrm{d}\lambda \\ &\quad - \frac{\sum_j z_j^2 e^2}{\varepsilon a} (\kappa a)^2 \sum_{n=1}^{\infty} \frac{b^{2n}}{(2n+1)!\,(2n-1)} \int_0^1 \lambda^{4n+3} \mathrm{d}\lambda \\ &= -\frac{\sum_i n_i z_i^2 e^2}{3\varepsilon} \kappa\tau(\kappa a) \\ &\quad - \frac{\sum_i n_i z_i^2 e^2}{2\varepsilon a} (\kappa a)^2 \sum_{n=1}^{\infty} \frac{b^{2n}}{(2n+2)!\,(2n-1)} \end{aligned} \tag{18}$$

where

$$\tau(x) = \frac{3}{x^3} \left[\ln(1+x) - x + \frac{1}{2} x^2 \right]$$

The relation, $\sum_j z_j^2 e^2 = \sum_i n_i z_i^2 e^2$ (where i denotes the type of ion), is used in the last step of the calculation.

Contribution of Ion-Ion Interactions to the Chemical Potential of an Ion of Type i, μ_i^{el}. We have two ways for the derivation of μ_i^{el} as follows:

A) Derivation of μ_i^{el} from G^{el} (According to the Debye Charging Process). μ_i^{el} can be defined by the equation:

$$\mu_i^{\text{el}} = \frac{\partial G^{\text{el}}}{\partial n_i} \tag{19}$$

***

$$-\int_a^\infty \frac{\exp[-(2n+1)\kappa r]}{r} \mathrm{d}r = \ln[(2n+1)\kappa a] + \gamma - (2n+1)\kappa a + \frac{[(2n+1)\kappa a]^2}{2\cdot 2!} - \cdots\cdots + \frac{[-(2n+1)\kappa a]^p}{p\cdot p!} + \cdots\cdots$$

$$\int_a^\infty \frac{\exp[-(2n+1)\kappa r]}{r^m} \mathrm{d}r = \frac{\exp[-(2n+1)\kappa a]}{(m-1)a^{m-1}} \times \left\{ 1 + \frac{-(2n+1)\kappa a}{(m-2)} + \frac{[-(2n+1)\kappa a]^{m-2}}{(m-2)!} \right\} + \frac{[-(2n+1)\kappa a]^{m-1}}{(m-1)!\,a^{m-1}} \int_a^\infty \frac{\exp[-(2n+1)\kappa r]}{r} \mathrm{d}r$$

(when $m \geqq 2$)

† The $(\kappa a)^2$ term in Eq. (13) contributes only to the $(\kappa a)^3$ and higher-order terms, which are ignored in Eq. (16); therefore, the use of A_{DH} [Eq. (9)] instead of A [Eq. (13)] leads to the same result.

Using Eq. (18) and Eq. (5), Eq. (19) becomes:

$$\mu_i^{el} = -\frac{z_i^2e^2\kappa}{2\varepsilon(1+\kappa a)} - kT(\kappa a)^2\sum_{n=1}^{\infty}\frac{b^{2n+1}}{(2n+2)!\,(2n-1)} + \frac{kT(\partial V/\partial n_i)}{24\pi a^3}(\kappa a)^3\sigma(\kappa a) + \frac{kT(\partial V/\partial n_i)}{8\pi a^3}(\kappa a)^4\sum_{n=1}^{\infty}\frac{b^{2n}}{(2n+2)!\,(2n-1)} \quad (20)$$

where

$$\sigma(x) = \frac{3}{x^3}\left[-2\ln(1+x) + (1+x) - \frac{1}{1+x}\right] = 1 - 3\cdot\frac{2}{4}x + 3\cdot\frac{3}{5}x^2 - 3\cdot\frac{4}{6}x^3 + 3\cdot\frac{5}{7}x^4 - \cdots$$

The Debye-Hückel approximation corresponds to the first and third terms on the right-hand side of Eq. (20).[4,5] For a very dilute solution, the second term is more important than the third term.

B) Direct Derivation of μ_i^{el} (According to the Güntelberg Charging Process). μ_i^{el} is the electrostatic work done when a single ion of the i type is added to an assembly consisting of the rest of the ions and the solvent. If we disregard the work due to the volume change $(\partial V/\partial n_i)$, which is negligibly small compared with the other electric work in dilute solutions, μ_i^{el} can be evaluated as the electric work of increasing the charge of the particular ion from zero to z_ie in the solution.[4,5] Thus, according to Güntelberg, one has:

$$\mu_i^{el} = \int_0^1 z_ie\psi^{cloud}(a, \lambda z_i)\mathrm{d}\lambda \quad (21)$$

where $\psi^{cloud}(a, \lambda z_i)$ is given by Eq. (16), with the substitution of λz_i for z_j:

$$\psi^{cloud}(a, \lambda z_i) = -\frac{\lambda z_ie\kappa}{\varepsilon(1+\kappa a)} - (\kappa a)^2\frac{\lambda z_ie}{\varepsilon a}\sum_{n=1}^{\infty}\frac{\lambda^{2n}b^{2n}}{(2n+1)!\,(2n-1)}$$

By integration, Eq. (21) becomes:

$$\mu_i^{el} = -\frac{z_i^2e^2\kappa}{2\varepsilon(1+\kappa a)} - kT(\kappa a)^2\sum_{n=1}^{\infty}\frac{b^{2n+1}}{(2n+2)!\,(2n-1)} \quad (22)$$

This equation can also be derived from the Debye charging process, if $(\partial V/\partial n_i)$ is so small or if the solution is so dilute that the $(\kappa a)^3$ and $(\kappa a)^4$ terms can be ignored [see Eq. (20)].

A more involved expression for μ_i^{el} was derived by Gronwall *et al.*[2] from a more accurate solution of the Poisson-Boltzmann equation. However, these authors' expression has disadvantages in that it is too complicated to be applied to actual systems and involves the inconsistency that the two charging processes give different expressions for μ_i^{el}.[4,5] This inconcistency can be avoided only for very dilute solutions, where the correction terms derived by these authors can in practice be expressed by the first two terms of the progression in Eq. (22). Kaneko[3] made another correction to the Debye-Hückel theory. Although his expression for μ_i^{el} involves the same kind of problem as mentioned above, his expression is consistent with Eq. (22) for very dilute solutions. By advancing the approximation, we might obtain a more accurate result for solutions of moderate concentration, but the difficulties encountered by Gronwall *et al.* and Kaneko will remain. Therefore, no further efforts will be made to derive an expression for the μ_i^{el} of a closer approximation than Eq. (22). Although Eq. (22) in itself is valid only for solutions of sufficiently low concentrations, an attempt will be made to extend the application of Eq. (22) up to higher concentrations by connecting it with the concept of ion association.

Concept of Ion Association and the Derivation of the Ion-Association Constant. It is a common practice to attribute deviations from the Debye-Hückel theory to ion association. The ion-association equilibrium for a symmetrical electrolyte is expressed by:

	M	+	A	$\rightleftharpoons$	MA
concentration	$c(1-\alpha)$		$c(1-\alpha)$		$c\alpha$

(23)

where c denotes the concentration of the electrolyte and α the degree of association. When the ion-association equilibrium is assumed, the cation, M, and the anion, A, are usually considered to be free ions in the sense that they behave as predicted by the Debye-Hückel theory. The activity coefficients, y_M and y_A, of the ions, M and A, respectively are given by:

$$\ln y_M = \ln y_A = -\frac{z^2e^2\kappa}{2\varepsilon kT(1+\kappa a)} \quad (24)$$

Now, the chemical potential μ of the electrolyte is:

$$\mu = \mu_M^0 + \mu_A^0 + 2RT\ln c + RT\ln(y_My_A) + 2RT\ln(1-\alpha) \quad (25)$$

where μ_M^0 and μ_A^0 represent the chemical potentials of the two ionic species, M and A, respectively in the standard state. The contribution of ion-ion interactions to the chemical potential of the electrolyte, μ^{el}, is equal to the last two terms of Eq. (25). Using Eq. (24) and considering $\alpha \ll 1$ in very dilute solutions, one obtains:

$$\mu^{el} = RT\ln(y_My_A) + 2RT\ln(1-\alpha) \simeq -\frac{Nz^2e^2\kappa}{\varepsilon(1+\kappa a)} - 2RT\alpha \quad (26)$$

where N is the Avogadro number.

Since μ_i^{el} given by Eq. (22) is the contribution of ion-ion interactions to the chemical potential of an ion of the i type, μ_i^{el} multiplied by the total number of ions, $2N$, gives μ^{el}:

$$\mu^{el} = 2N\mu_i^{el} = -\frac{Nz^2e^2\kappa}{\varepsilon(1+\kappa a)} - 2RT(\kappa a)^2\sum_{n=1}^{\infty}\frac{b^{2n+1}}{(2n+2)!\,(2n-1)} \quad (27)$$

A comparison of Eqs. (26) and (27) leads to:

$$\alpha = (\kappa a)^2\sum_{n=1}^{\infty}\frac{b^{2n+1}}{(2n+2)!\,(2n-1)} \quad (28)$$

The equilibrium constant, K, of the ion-association reaction [Eq. (23)] is given by:

$$K = \frac{\alpha y_{MA}}{c(1-\alpha)^2y_My_A} \quad (29)$$

where y_{MA} is the activity coefficient of the ion-pair MA. In very dilute solutions, Eq. (29) can be written as:

TABLE 1. VALUES OF THE SUM $\sum_{n=1}^{\infty} \frac{b^{2n+2}}{(2n+2)!\,(2n-1)}$ (abbreviated to Σ) AND ITS LIMITING EXPRESSION $\frac{\exp(b)}{2b}$

b	$\log\Sigma$	$\log\frac{\exp(b)}{2b}$	b	$\log\Sigma$	$\log\frac{\exp(b)}{2b}$	b	$\log\Sigma$	$\log\frac{\exp(b)}{2b}$	b	$\log\Sigma$	$\log\frac{\exp(b)}{2b}$
0.1	−5.3802	0.7424	3.6	0.9118	0.7061	12.5	4.2388	4.0307	50.0	19.7518	19.7147
0.2	−4.1759	0.4848	3.7	0.9634	0.7377	13.0	4.4263	4.2309	55.0	21.8783	21.8448
0.3	−3.4713	0.3521	3.8	1.0139	0.7695	13.5	4.6158	4.4316	60.0	24.0090	23.9785
0.4	−2.9712	0.2706	3.9	1.0633	0.8017	14.0	4.8069	4.6330	65.0	26.1433	26.1152
0.5	−2.5831	0.2171	4.0	1.1117	0.8341	14.5	4.9997	4.8349	70.0	28.2804	28.2545
0.6	−2.2659	0.1814	4.1	1.1592	0.8668	15.0	5.1939	5.0373	75.0	30.4201	30.3960
0.7	−1.9974	0.1579	4.2	1.2058	0.8998	15.5	5.3893	5.2402	80.0	32.5620	32.5394
0.8	−1.7648	0.1433	4.3	1.2516	0.9330	16.0	5.5859	5.4436	85.0	34.7058	34.6846
0.9	−1.5593	0.1356	4.4	1.2965	0.9664	16.5	5.7836	5.6473	90.0	36.8512	36.8312
1.0	−1·3754	0.1333	4.5	1.3408	1.0001	17.0	5.9822	5.8515	95.0	38.9981	38.9792
1.1	−1.2088	0.1353	4.6	1.3843	1.0340	17.5	6.1817	6.0561	100.0	41.1463	41.1284
1.2	−1.0565	0.1409	4.7	1.4272	1.0681	18.0	6.3819	6.2610	110.0	45.4462	45.4300
1.3	−0.9162	0.1496	4.8	1.4694	1.1023	18.5	6.5828	6.4662	120.0	49.7500	49.7351
1.4	−0.7861	0.1609	4.9	1.5111	1.1368	19.0	6.7844	6.6718	130.0	54.0570	54.0433
1.5	−0.6649	0.1743	5.0	1.5522	1.1715	19.5	6.9865	6.8777	140.0	58.3667	58.3541
1.6	−0.5512	0.1897	5.2	1.6329	1.2413	20.0	7.1892	7.0838	150.0	62.6789	62.6670
1.7	−0.4443	0.2068	5.4	1.7117	1.3118	21.0	7.5960	7.4969	160.0	66.9930	66.9820
1.8	−0.3432	0.2254	5.6	1.7889	1.3828	22.0	8.0046	7.9110	170.0	71.3090	71.2986
1.9	−0.2475	0.2454	5.8	1.8646	1.4545	23.0	8.4147	8.3260	180.0	75.6265	75.6167
2.0	−0.1564	0.2665	6.0	1.9391	1.5266	24.0	8.8261	8.7418	190.0	79.9455	79.9362
2.1	−0.0696	0.2888	6.2	2.0124	1.5992	25.0	9.2386	9.1584	200.0	84.2657	84.2568
2.2	0.0134	0.3120	6.4	2.0848	1.6723	26.0	9.6523	9.5756	250.0	105.8817	105.8746
2.3	0.0929	0.3361	6.6	2.1563	1.7458	27.0	10.0669	9.9936	300.0	127.5161	127.5102
2.4	0.1693	0.3611	6.8	2.2271	1.8197	28.0	10.4824	10.4121	350.0	149.1630	149.1580
2.5	0.2427	0.3868	7.0	2.2973	1.8939	29.0	10.8987	10.8311	400.0	170.8191	170.8147
2.6	0.3134	0.4132	7.5	2.4709	2.0811	30.0	11.3157	11.2507	450.0	192.4822	192.4783
2.7	0.3818	0.4402	8.0	2.6428	2.2702	32.0	12.1517	12.0912	500.0	214.1508	214.1472
2.8	0.4478	0.4678	8.5	2.8142	2.4611	34.0	12.9900	12.9335	600.0	257.5004	257.4975
2.9	0.5117	0.4960	9.0	2.9860	2.6534	36.0	13.8303	13.7773	700.0	300.8626	300.8600
3.0	0.5737	0.5247	9.5	3.1590	2.8470	38.0	14.6723	14.6224	800.0	344.2338	344.2315
3.1	0.6339	0.5539	10.0	3.3336	3.0419	40.0	15.5159	15.4687	900.0	387.6120	387·6098
3.2	0.6924	0.5836	10.5	3.5102	3.2379	42.0	16.3608	16.3161	1000.0	430.9955	430.9934
3.3	0.7494	0.6136	11.0	3.6890	3.4348	44.0	17.2070	17.1645			
3.4	0.8049	0.6441	11.5	3.8700	3.6327	46.0	18.0543	18.0138			
3.5	0.8590	0.6749	12.0	4.0533	3.8313	48.0	18.9026	18.8639			

$$K \simeq \frac{\alpha}{c} \tag{30}$$

By noticing that $c=1000n_1/NV$, $\kappa^2=8\pi n_1 z^2 s/V$ [Eq. (4)], and $b=z^2 s/a$ [Eq. (15)], Eqs. (30) and (28) give:

$$K = \frac{8\pi N a^3}{1000}\cdot\frac{b^{2n+2}}{(2n+2)!\,(2n-1)} \quad \text{when } b\to\infty \tag{31}$$

The sum of the progression terms is shown in Table 1 for a variety of b values and is compared with the corresponding value of $\exp(b)/2b$. Obviously, it approaches $\exp(b)/2b$ with an increase in the b value, so that the ion-association constant becomes:

$$K \simeq \frac{4\pi N a^3}{1000}\frac{\exp(b)}{b} \quad \text{when } b\to\infty \tag{32}$$

This is in agreement with the limiting case ($b\to\infty$) of the Bjerrum theory.[6,13]

Comparison of This Theory with Other Theories of Ion Association. In this work the Debye-Hückel treatment was extended and correction terms were derived on the assumption that the solution is very dilute. By using these results and by assuming the ion-association equilibrium, we obtained an expression for the ion-association constant [Eq. (31)] which includes no arbitrary parameters except for a. (The other parameter, b, is a function of a.) Although the same expression for K was previously derived by Ebeling[10] from the cluster theory, the much simpler method of derivation given above will make the thermodynamical understanding of the ion association easier and clearer.

We shall now compare our results with those of the Bjerrum theory,[6] in which the ion-association constant is given by:

$$K = \frac{4\pi N}{1000}(z^2 s)^3 Q(b) \tag{33}$$

$$Q(b) = \int_2^b \frac{\exp(x)}{x^4}\mathrm{d}x$$

In the derivation of this equation, Bjerrum assumed a so-called "critical distance of ion association,"

Table 2. Thermodynamic parameters for ion-pair formation

Parameter	Yokoyama-Yamatera, Ebeling, and Bjerrum ($b\to\infty$)	Fuoss	Denison-Ramsey
K	$\frac{4\pi Na^3}{1000}\cdot\frac{\exp(b)}{b}$	$\frac{4\pi Na^3}{3000}\exp(b)$	$\exp(b)$
$\Delta G°$	$-RT\left(\ln\frac{4\pi Na^3}{1000b}+b\right)$	$-RT\left(\ln\frac{4\pi Na^3}{3000}+b\right)$	$-bRT$
$\Delta S°$	$R\ln\frac{4\pi Na^3}{1000b}-bRT\frac{\partial\ln\varepsilon}{\partial T}$	$R\ln\frac{4\pi Na^3}{3000}-bRT\frac{\partial\ln\varepsilon}{\partial T}$	$-bRT\frac{\partial\ln\varepsilon}{\partial T}$
$\Delta H°$	$-bRT^2\left(\frac{\partial\ln\varepsilon}{\partial T}+\frac{1}{T}\right)$	$-bRT^2\left(\frac{\partial\ln\varepsilon}{\partial T}+\frac{1}{T}\right)$	$-bRT^2\left(\frac{\partial\ln\varepsilon}{\partial T}+\frac{1}{T}\right)$

$q(=z^2s/2)$, and regarded a pair of oppositely charged ions within the cririca distance of each other as an ion-pair, and an ion with no other ions within the critical distance, as a free ion.†† In the present theory, an ion-pair is treated as a chemical species of unknown geometrical configuration, and the ion-association constant is derived from a thermodynamical consideration of the ion-ion interaction. A comparison between $\rho(r)$, the time-averaged charge distribution around an ion due to the Boltzmann distribution law [Eq. (1)], and $\rho_{DH}(r)$, the charge distribution assumed by the Debye-Hückel theory, shows that the latter underestimates the charge distribution in the vicinity of an ion. The excess (negative) free energy arising from the interaction of the ion with the additional opposite charge in excess of $\rho_{DH}(r)$ is regarded as resulting from the ion-pair formation, assuming that a free ion is such an ion as is described by the Debye-Hückel theory [Eq. (24)].

For very large values of b ($b\to\infty$), both expressions, (31) and (33), can be approximated by Eq. (32). This probably results from the fact that an approximate classification of ions into free ions and contact ion-pairs can be made at large b values. With a decrease in the value of b, the discrepancy between the ion-association constants predicted by Eqs. (31) and (33) gradually increases. The greatest discrepancy is found at $b\leqq 2$ (*i.e.*, $a\geqq q$), where the Bjerrum theory gives $K=0$, while the present theory predicts a definite value for K. This situation is illustrated by Fig. 1, where log K for 2 : 2 electrolytes in aqueous solutions at 25.0 °C is plotted against a in accordance with Eqs. (31) and (33). According to our opinion that the ion association is a working hypothesis for interpreting the deviation of the behavior of actual electrolyte solutions from that predicted by the Debye-Hückel theory, the ion-association constants should have finite values even at $b\leqq 2$, corresponding to non-zero values of the second term on the right-hand side of Eq. (22).

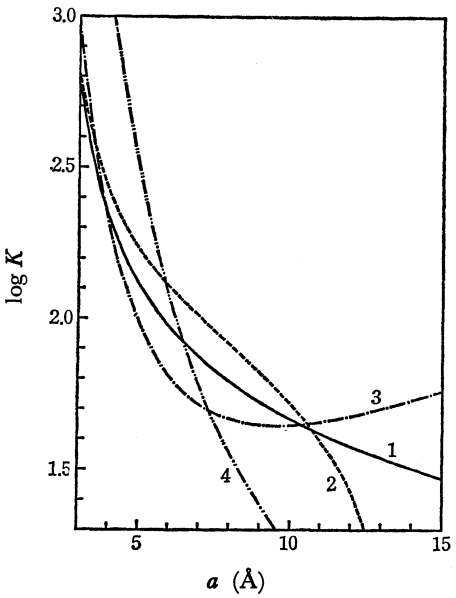

Fig. 1. Theoretical log K values for 2 : 2 electrolytes in aqueous solutions at 25.0 °C.
1: Present theory and Ebeling's theory (——)
2: Bjerrum's theory (— —)
3: Fuoss's theory (— · —)
4: Denison-Ramsey's theory (— · · —)

The Fuoss 1958 theory[9] is different from the Bjerrum theory in that a pair of ions in physical contact is meant by ion-pair. Although it gives a clearer idea of ion-pairs, it seems to be less adequate for complementing the Debye-Hückel theory. Fuoss's expression for the ion-association constant (Table 2) gives a minimum value of K at a certain value of a and then increasingly large values with an increase in a, as is shown in Fig. 1. For usual values of a, however, it gives K values not very much different from those predicted by the present theory. This seems to be a reason why the Fuoss theory gives a good explanation of the experimental results.

Denison and Ramsey[7] proposed the expression for the ion-association constant:

$$K=\exp(b)$$

†† Guggenheim[5,14] and other authors[15] introduced another parameter, d, as a variable critical distance or the distance defining the association, and made a generalization of Bjerrum's expression [Eq. (33)] using:

$$Q(b)=\int_{d/s}^{b}\frac{\exp(x)}{x^4}dx$$

Thus, they introduced flexibility in the critical distance of the Bjerrum theory. In addition, the parameter d can be considered to be the closest distance of approach of free ions and can be used in place of a in the Debye-Hückel expression (24).

in preference to the Fuoss theory. Their theory is based on the assumption of the Born thermodynamic cycle for the dissociation of an ion-pair, and is similar to the Fuoss theory[9] in that the contact ion-pair is assumed. However, the ion-association constants predicted by Denison-Ramsey's expression decrease with an increase in a, similarly to those predicted by the present theory.

The Gibbs free-energy change, $\Delta G°$, the enthalpy change, $\Delta H°$, and the entropy change, $\Delta S°$, for ion-pair formation were derived from the theoretical expressions for the ion-association constant; they are shown in Table 2, where Eq. (31) for the present and Ebeling's theories[10] and Eq. (33) for the Bjerrum theory[6] are approximated by the limiting equation (32). The thermodynamic parameters derived from Eq. (32) are not very different from those from Fuoss's and Denison-Ramsey's expressions; indeed, the formulas for $\Delta H°$ are identical with each other. (It should be noted that this remark is concerned with the limiting case of a large value of b.)†††

In a subsequent paper,[16] the ion-association constants predicted by the theories will be compared with the experimental results obtained from measurements of the electric conductivity and the osmotic coefficient.

The authors wish to thank the Ministry of Education for the financial support granted for this research. Thanks are also due to Nagoya University Computation Center for the use of a FACOM 230–60 computer.

††† At a large value of b, contact ion-pairs predominate over other kinds of ion-pairs in contributing to the chemical potential arising from ion-ion interactions. This seems to be the reason why all the theories give similar results in the limiting case.

References

1) P. Debye and E. Hückel, *Physik. Z.*, **24**, 185 (1923).
2) T. H. Gronwall, V. K. LaMer, and K. Sandved, *Physik. Z.*, **29**, 358 (1928).
3) S. Kaneko, *Denki Kagaku*, **2**, 348 (1934); *Nippon Kagaku Kaishi*, **56**, 411 (1935).
4) R. H. Fowler and E. A. Guggenheim, "Statistical Thermodynamics," Cambridge University Press (1939), p. 377.
5) E. A. Guggenheim and R. H. Stokes, "Equilibrium Properties of Aqueous Solutions of Single Strong Electrolytes," Pergamon Press (1969).
6) N. Bjerrum, *Kgl. Danske Videnskab. Selskab.*, **7**, No. 9 (1926).
7) J. T. Denison and J. B. Ramsey, *J. Amer. Chem. Soc.*, **77**, 2615 (1955).
8) W. R. Gilkerson, *J. Chem. Phys.*, **25**, 1199 (1956); *J. Phys. Chem.*, **74**, 746 (1970).
9) R. M. Fuoss, *J. Amer. Chem. Soc.*, **80**, 5059 (1958).
10) W. Ebeling, *Z. Physik. Chem.* (Leipzig), **238**, 400 (1968); H. Falkenhagen and W. Ebeling, "Ionic Interactions," Vol. 1, ed. by S. Petrucci, Academic Press (1971), p. 1.
11) L. D. Pettit and S. Bruckenstein, *J. Amer. Chem. Soc.*, **88**, 4783 (1966); H. Reiss, *J. Chem. Phys.*, **25**, 400, 408 (1956).
12) M. Eigen, *Discuss. Faraday Soc.*, **24**, 25 (1957); T. R. Griffiths and C. R. Symons, *Mol. Phys.*, **3**, 90 (1960); G. Atkinson and S. K. Kor, *J. Phys. Chem.*, **69**, 128 (1965), **71**, 673 (1967); H. Yokoyama and H. Yamatera, This Bulletin, **44**, 1725 (1971).
13) R. M. Fuoss and C. A. Kraus, *J. Amer. Chem. Soc.*, **55**, 1019 (1933).
14) E. A. Guggenheim, *Discuss. Faraday Soc.*, **24**, 53 (1957).
15) P. G. M. Brown and J. E. Prue, *Proc. Roy. Soc. Ser. A*, **232**, 320 (1955); J. E. Prue, "Ionic Equilibria," Pergamon Press (1966); M. R. Christoffersen and J. E. Prue, *Trans. Faraday Soc.*, **66**, 2878 (1970); R. A. Matheson, *J. Phys. Chem.*, **72**, 3330 (1968).
16) To be published in This Bulletin.

Theoretical Calculations of the Raman Intensities by the Vibronic Method

Hiroyuki SHINODA

Department of Applied Chemistry, Faculty of Science and Engineering, Waseda University, Nishi-Ohkubo, Shinjuku-ku, Tokyo 160

(Received September 30, 1974)

The values of the transition moment of Raman scattering have been calculated according to the formula derived from the vibronic expansion approach. The calculations have been performed for the symmetry coordinates of several small molecules and for the normal vibrations of methane. The electronic wave functions were calculated by the CNDO/2-CI method. The calculated results are large in comparison with the experimental ones. The calculated Raman intensities for the symmetric stretching vibrations were almost all contributed by the term *A* in the vibronic expansion theory. From the calculated results for the normal vibrations of methane, it was found that the vibronic method used in this work leads to more appropriate values than those obtained from the polarizability theory which was used in the previous paper.

The development of the research technique using the laser Raman instrument has aided the discussion of the problem of the Raman intensity. Therefore there is now enhanced interest in the theoretical calculation of the Raman intensity. The theory of the Raman intensity has been discussed on the basis of the Kramers-Heisenberg dispersion formula.[1] Placzek[2] approximated the term of the transition moment of Raman scattering in this formula by the term of the polarizability derivative of the ground state in the nuclear coordinate, provided that the incident light is far away from the resonance region and the ground state of the molecule is not degenerate. There have since been several reports[3] in which the Raman intensities of H_2 and H_2^+ have been calculated according to Placzek's polarizability theory. Recently the calculations of the polarizability derivatives for small polyatomic molecules have been performed by several investigators, the electronic wave functions being evaluated by the LCAO-ASMO-SCF method.[4] By the use of the wave functions obtained from the finite perturbation method within the CNDO version, Hush and Williams[5] calculated the polarizabilities for some diatomic molecules and estimated their polarizability derivatives. They concluded that these polarizability derivatives are suitable for interpreting the factors determining the Raman transition probabilities within a valence orbital scheme. Yamada[6] calculated the polarizability derivatives with the symmetric stretching vibrations of four hydrocarbons, CH_4, C_2H_2, C_2H_4, and C_2H_6, the polarizabilities being calculated according to the expression derived from the second-order perturbation theory. She concluded that the CNDO calculations might useful in understanding the Raman intensities, although the calculated results were small in comparison with the experimental ones. Moreover the present author and Miyazaki[7] calculated the polarizability derivatives for several small molecules by the use of the formula derived from the time-dependent perturbation theory. The calculations described above were performed on the basis of Placzek's polarizability theory. On the other hand, there have been several reports[8–12] in which the theory of the Raman intensity has been discussed. In this work, then, the values of the Raman intensity have been calculated according to the formula derived from the vibronic expansion approach.[8–10] The electronic wave functions were evaluated by the CNDO/2-CI method. For the symmetric stretching vibrations of small molecules, the transition moments of Raman scattering were calculated in the approximation of the symmetry coordinate. Moreover, the intensities and the depolarization ratios of the Raman scattering for the normal vibrations of methane were calculated. The calculated results were discussed in comparison with the experimental ones and with the results obtained from the polarizability method, based on Placzek's theory, which was used in the previous work.[7]

Methods of Calculations

Raman Intensity. The vibronic expansion approach for the Raman intensity used in these calculations has been discussed in detail in Ref. 13. The total intensity of a Raman line after averaging all the molecular orientations is given as follows:

$$I_{mn} = \frac{2^3\pi}{3^2c^4} I_0\omega^4 \sum_{\rho,\sigma} |(\alpha_{\rho\sigma})_{mn}|^2, \tag{1}$$

where c is the velocity of light; I_0 is the intensity of the incident light; ω is the frequency of the scattered light; m is the initial state; n is the final state and $(\alpha_{\rho\sigma})_{mn}$ is the $\rho\sigma$-th component of the polarizability tensor for the $m\rightarrow n$ transition; the sum goes over $\rho=x,y,z$, and $\sigma=x,y,z$, which independently refer to the molecule fixed coordinate system. As has been described in Ref. 13, the general vibronic representation of $(\alpha_{\rho\sigma})_{mn}$ has been given as following equation, involving the terms A, B, and C:

$$(\alpha_{\rho\sigma})_{mn} = A + B + C, \tag{2}$$

$$A = \sum_{r\neq g}\sum_{i}\left[\frac{1}{E_{ri}-E_{gm}-E_0}+\frac{1}{E_{ri}-E_{gn}+E_0}\right] \times \langle g^0|R_\rho|r^0\rangle\langle r^0|R_\sigma|g^0\rangle\langle\psi_m^g|\psi_i^r\rangle\langle\psi_i^r|\psi_n^g\rangle, \tag{3}$$

$$B = \sum_{a}\sum_{r\neq g}\sum_{i}\sum_{s\neq r}\left[\left\{\frac{\langle g^0|R_\rho|r^0\rangle\langle r^0|h_a|s^0\rangle\langle s^0|R_\sigma|g^0\rangle}{(E_{ri}-E_{gm}-E_0)(\varepsilon_r^0-\varepsilon_s^0)} + \frac{\langle g^0|R_\sigma|r^0\rangle\langle r^0|h_a|s^0\rangle\langle s^0|R_\rho|g^0\rangle}{(E_{ri}-E_{gn}+E_0)(\varepsilon_r^0-\varepsilon_s^0)}\right\} \times\langle\psi_m^g|\psi_i^r\rangle\langle\psi_i^r|Q_a|\psi_n^g\rangle + \left\{\frac{\langle g^0|R_\rho|s^0\rangle\langle s^0|h_a|r^0\rangle\langle r^0|R_\sigma|g^0\rangle}{(E_{ri}-E_{gm}-E_0)(\varepsilon_r^0-\varepsilon_s^0)}\right.$$

$$+\frac{\langle g^0|R_\rho|s^0\rangle\langle s^0|h_a|r^0\rangle\langle r^0|R_\tau|g^0\rangle}{(E_{ri}-E_{gn}+E_0)(\varepsilon_r^0-\varepsilon_s^0)}\Big\}$$
$$\times\langle\psi_m^g|Q_a|\psi_i^r\rangle\langle\psi_i^r|\psi_n^g\rangle\Big], \quad (4)$$

and

$$C=\sum_a\sum_{r\neq g}\sum_i\sum_{s\neq g}\Big[\Big\{\frac{\langle g^0|h_a|s^0\rangle\langle s^0|R_\tau|r^0\rangle\langle r^0|R_\rho|g^0\rangle}{(E_{ri}-E_{gm}-E_0)(\varepsilon_g^0-\varepsilon_s^0)}+\frac{\langle g^0|h_a|s^0\rangle\langle s^0|R_\tau|r^0\rangle\langle r^0|R_\rho|g^0\rangle}{(E_{ri}-E_{gn}+E_0)(\varepsilon_g^0-\varepsilon_s^0)}\Big\}\times\langle\psi_m^g|Q_a|\psi_i^r\rangle\langle\psi_i^r|\psi_n^g\rangle$$
$$+\Big\{\frac{\langle g^0|R_\tau|r^0\rangle\langle r^0|R_\rho|s^0\rangle\langle s^0|h_a|g^0\rangle}{(E_{ri}-E_{gm}-E_0)(\varepsilon_g^0-\varepsilon_s^0)}+\frac{\langle g^0|R_\tau|r^0\rangle\langle r^0|R_\sigma|s^0\rangle\langle s^0|h_a|g^0\rangle}{(E_{ri}-E_{gn}+E_0)(\varepsilon_g^0-\varepsilon_s^0)}\Big\}\times\langle\psi_m^g|\psi_i^r\rangle\langle\psi_i^r|Q_a|\psi_n^g\rangle\Big], \quad (5)$$

where E_{gm} and E_{gn} are the energies of the initial vibronic state, $|g\rangle|\psi_m^g\rangle$, and the final vibronic state, $|g\rangle|\psi_n^g\rangle$, respectively; here $|g\rangle$ is the wave function of the electronic ground state, and $|\psi_m^g\rangle$ and $|\psi_n^g\rangle$ are the wave functions of the m-th and n-th vibrational states respectively in the electronic ground state; E_{ri} is the energy of the intermediate vibronic state, $|r\rangle|\psi_i^r\rangle$; here $|r\rangle$ is the wave function of the electronic excited state and $|\psi_i^r\rangle$ is the wave function of the i-th vibrational state in the $|r\rangle$ electronic state; E_0 is the energy of the incident light; ε_g^0 is the energy of the $|g^0\rangle$ electronic ground state; ε_r^0 and ε_s^0 are the energies of the $|r^0\rangle$ and $|s^0\rangle$ electronic states respectively; here the superscript 0 denotes the equilibrium nuclear position in the ground state; R_ρ and R_σ are the operators of the ρ- and σ-components respectively of the electronic dipole moment; Q_a is the normal coordinate of the a vibrational mode, and $h_a=(\partial H/\partial Q_a)$, the first-order vibronic coupling operator introduced initially by Herzberg and Teller.[14] Equations (3)—(5) can not be used directly in the calculation of $(\alpha_{\rho\sigma})_{mn}$ because we have meager knowledge of the vibrational wave function of a molecule in the electronic excited state. Therefore, we have to rearrange the equations in order to express $(\alpha_{\rho\sigma})_{mn}$ in a form without the vibrational wave functions. The expression of the term A is rearranged by Verlan's technique,[10] an expansion of the energy denominators around a fixed energy in a power series. When only the first-order terms in the expansion are retained, and when E_{gn} and E_{gm} are put approximately equal to ε_g^0, the term A is given by:

$$A=-\sum_a\sum_{r\neq g}\Big[\frac{\langle g^0|R_\sigma|r^0\rangle\langle r^0|h_a|r^0\rangle\langle r^0|R_\rho|g_0\rangle}{(\varepsilon_r^0-\varepsilon_g^0-E_0)^2}+\frac{\langle g^0|R_\sigma|r^0\rangle\langle r^0|h_a|r^0\rangle\langle r^0|R_\rho|g^0\rangle}{(\varepsilon_r^0-\varepsilon_g^0+E_0)^2}\Big]\langle\psi_m^g|Q_a|\psi_n^g\rangle. \quad (6)$$

The terms B and C are simplified as follows by the use of the approximation that the energy, E_{ri}, is regarded as constant over i and put equl to ε_r^0:

$$B=-\sum_a\sum_r\sum_{s\neq r}\Big[\frac{\langle g^0|R_\sigma|r^0\rangle\langle r^0|h_a|s^0\rangle\langle s^0|R_\tau|g^0\rangle}{(\varepsilon_r^0-\varepsilon_g^0-E_0)(\varepsilon_s^0-\varepsilon_g^0-E_0)}+\frac{\langle g^0|R_\rho|s^0\rangle\langle s^0|h_a|r^0\rangle\langle r^0|R_\sigma|g^0\rangle}{(\varepsilon_r^0-\varepsilon_g^0+E_0)(\varepsilon_s^0-\varepsilon_g^0+E_0)}\Big]\langle\psi_m^g|Q_a|\psi_n^g\rangle \quad (7)$$

and

$$C=-\sum_a\sum_{r\neq g}\sum_{s\neq g}\Big[\frac{\langle g^0|h_a|s^0\rangle\langle s^0|R_\sigma|r^0\rangle\langle r^0|R_\rho|g^0\rangle}{(\varepsilon_r^0-\varepsilon_g^0-E_0)(\varepsilon_s^0-\varepsilon_g^0)}+\frac{\langle g^0|h_a|s^0\rangle\langle s^0|R_\rho|r^0\rangle\langle r^0|R_\sigma|g^0\rangle}{(\varepsilon_r^0-\varepsilon_g^0+E_0)(\varepsilon_s^0-\varepsilon_g^0)}+\frac{\langle g^0|R_\tau|r^0\rangle\langle r^0|R_\rho|s^0\rangle\langle s^0|h_a|g^0\rangle}{(\varepsilon_r^0-\varepsilon_g^0-E_0)(\varepsilon_s^0-\varepsilon_g^0)}+\frac{\langle g^0|R_\rho|r^0\rangle\langle r^0|R_\sigma|s^0\rangle\langle s^0|h_a|g^0\rangle}{(\varepsilon_r^0-\varepsilon_g^0+E_0)(\varepsilon_s^0-\varepsilon_g^0)}\Big]\langle\psi_m^g|Q_a|\psi_n^g\rangle. \quad (8)$$

By using the expressions in Eqs. (6)—(8), the equation for $(\alpha_{\rho\sigma})_{mn}$ can be written as:

$$(\alpha_{\rho\sigma})_{mn}=\sum_a(\alpha_{\rho\sigma}^a)'\langle\psi_m^g|Q_a|\psi_n^g\rangle, \quad (9)$$

where:

$$(\alpha_{\rho\sigma}^a)'=\sum_{r\neq g}\sum_{s\neq g}\Big[\frac{\langle g^0|R_\sigma|r^0\rangle\langle r^0|h_a|s^0\rangle\langle s^0|R_\rho|g^0\rangle}{(\varepsilon_r^0-\varepsilon_g^0+E_0)(\varepsilon_s^0-\varepsilon_g^0-E_0)}+\frac{\langle g^0|R_\sigma|r^0\rangle\langle r^0|h_a|s^0\rangle\langle s^0|R_\rho|g^0\rangle}{(\varepsilon_r^0-\varepsilon_g^0+E_0)(\varepsilon_s^0-\varepsilon_g^0+E_0)}+\frac{\langle g^0|h_a|s^0\rangle\langle s^0|R_\tau|r^0\rangle\langle r^0|R_\rho|g^0\rangle}{(\varepsilon_r^0-\varepsilon_g^0-E_0)(\varepsilon_s^0-\varepsilon_g^0)}+\frac{\langle g^0|h_a|s^0\rangle\langle s^0|R_\rho|r^0\rangle\langle r^0|R_\sigma|g^0\rangle}{(\varepsilon_r^0-\varepsilon_g^0+E_0)(\varepsilon_s^0-\varepsilon_g^0)}+\frac{\langle g^0|R_\sigma|r^0\rangle\langle r^0|R_\rho|s^0\rangle\langle s^0|h_a|g^0\rangle}{(\varepsilon_r^0-\varepsilon_g^0-E_0)(\varepsilon_s^0-\varepsilon_g^0)}+\frac{\langle g^0|R_\rho|r^0\rangle\langle r^0|R_\sigma|s^0\rangle\langle s^0|h_a|g^0\rangle}{(\varepsilon_r^0-\varepsilon_g^0+E_0)(\varepsilon_s^0-\varepsilon_g^0)}\Big]$$
$$-2\sum_{r\neq g}\frac{1}{(\varepsilon_r^0-\varepsilon_g^0-E_0)(\varepsilon_r^0-\varepsilon_g^0-E_0)}\times[\langle g^0|R_\tau|r^0\rangle\langle r^0|h_a|g^0\rangle\langle g^0|R_\rho|g^0\rangle+\langle g^0|R_\tau|g^0\rangle\langle g^0|h_a|r^0\rangle\langle r^0|R_\rho|g^0\rangle]. \quad (10)$$

In the above expression, all the terms have been multiplied by (-1). $(\alpha_{\rho\sigma}^a)'$ corresponds to the polarizability derivative $(\partial\alpha_{\rho\sigma}/\partial Q_a)_0$ in Placzek's theory and will hereafter be called the $\rho\sigma$-component of the Raman tensor for a normal vibration, a.

Electronic Wave Functions. One-electron wave functions, φ_n's, were obtained by the CNDO/2 method, an approximate self-consistent molecular orbital theory, proposed by Pople *et al.*[4] The wave function of the ground state, $|g^0\rangle$, was given by an antisymmetrized product with a closed-shell structure, Φ_0. The wave functions of the excited states, $|r^0\rangle$ and $|s^0\rangle$, in Eq. (10) were described by a linear combination of singly-excited configurations, $\Phi_{(i-k)}$'s.[15] By the use of the coefficients, $C_{(i-k)}^r$'s, of the configurations, the integrals in Eq. (10) could be rewritten as follows:

$$\langle g^0|H'|g^0\rangle=\langle\Phi_0|H'|\Phi_0\rangle, \quad (11)$$

$$\langle g^0|H'|r^0\rangle=\sum_i^{\text{occ}}\sum_k^{\text{unocc}}C_{(i-k)}^r\langle\Phi_0|H'|\Phi_{(i-k)}\rangle, \quad (12)$$

and

$$\langle r^0|H'|s^0\rangle = \sum_{i,j}^{occ}\sum_{k,l}^{unocc} C^r_{(i-k)}C^s_{(j-l)}\langle\Phi_{(i-k)}|H'|\Phi_{(j-l)}\rangle, \quad (13)$$

where H' denotes R_ρ, R_σ, or h_a. Since H' is defined as the sum of one-electron operators, $H'=\sum f$; the integrals on the right-hand sides of Eqs. (11)—(13) can thus be described by the integral terms with the one-electron wave functions:

$$\langle\Phi_0|H'|\Phi_0\rangle = 2\sum_{n}^{occ}\langle\varphi_n|f|\varphi_n\rangle, \quad (14)$$

$$\langle\Phi_0|H'|\Phi_{(i-k)}\rangle = \sqrt{2}\langle\varphi_i|f|\varphi_k\rangle, \quad (15)$$

and

$$\langle\Phi_{(i-k)}|H'|\Phi_{(j-l)}\rangle = \delta_{ij}\delta_{kl}\,2\sum_{n}^{occ}\langle\varphi_n|f|\varphi_n\rangle + \delta_{ij}\langle\varphi_k|f|\varphi_l\rangle - \delta_{kl}\langle\varphi_i|f|\varphi_j\rangle, \quad (16)$$

where the sums in the above equations go over the occupied orbitals in the ground state. When H' is R_ρ or R_σ, the integrals, $\langle\varphi_i|f|\varphi_k\rangle$'s, are calculated by the method described in a previous report.[16] When H' is h_a, the integrals are expressed as follows:[17]

$$\langle\varphi_i|f|\varphi_k\rangle = \sum_{\beta}\sum_{\mu}\sum_{\nu} e^2Z_\beta d_{i\mu}d_{k\nu}\left(\frac{\partial \boldsymbol{r}_\beta}{\partial Q_a}\right)\cdot\left\langle\chi_\mu\left|\frac{\boldsymbol{r}_{i\beta}}{r^3_{i\beta}}\right|\chi_\nu\right\rangle, \quad (17)$$

where e is the charge of the electron; Z_β is the core charge of the β atom; $\boldsymbol{r}_{i\beta}$ is the distance vector of the electron, i, from the β atom; $r_{i\beta}$ is the norm of the vector; $\boldsymbol{r}_\beta$ is the position vector of the β atom, and $d_{k\nu}$ is the coefficient of the atomic orbital, χ_ν, in the molecular orbital, φ_k. $(\partial\boldsymbol{r}_\beta/\partial Q_a)$ in Eq. (17) indicates the elements of the L_x matrix obtained by the usual **GF** method. In this work, the integrals on the right-hand side of Eq. (17) were calculated with the approximation that the integrals were neglected unless the atomic orbitals, χ_μ and χ_ν, belong to the same atom. This is consistent with the CNDO version used to obtain electronic wave functions. When χ_μ and χ_ν belong to an A atom which differs from the β atom, the integral is approximated by the following expression:

$$\left\langle\chi_\mu\left|\frac{\boldsymbol{r}_{i\beta}}{r^3_{i\beta}}\right|\chi_\nu\right\rangle = \delta_{\mu\nu}\frac{\boldsymbol{r}_{A\beta}}{r^3_{A\beta}}, \quad (18)$$

where $r_{A\beta}$ is the norm of the distance vector, $\boldsymbol{r}_{A\beta}$. When χ_μ and χ_ν belong to the β atom, the integration is performed rigorously.

Polarizability Method. According to Method I, described in a previous paper,[16] the polarizabilities were calculated for the molecule distorted in the manner dictated by the normal coordinate. The values of the Raman tensor were obtained by fitting the calculated polarizabilities to a cubic function with respect to the normal coordinate and by taking the first derivative at the equilibrium position.

Results and Discussions

In the calculations according to the vibronic method, the wavelength of the incident light was fixed at 5145 Å, which is the wavelength of an Ar^+ laser line, but in the calculation of the polarizabilities in the polarizability method, the energy of the incident light was taken to be zero.

Symmetric Stretching Vibrations: The symmetric stretching coordinates discussed in this work were the C–H and C–C vibrations of acetylene, ethylene, and ethane, the C–H vibration of methane, and the N–H vibration of ammonia. Since the Raman tensor with respect to symmetry coordinate, S_a's, were calculated with reference to the symmetric stretching modes, $(\partial\boldsymbol{r}_\beta/\partial Q_a)$ in Eq. (17) had to be replaced by $(\partial\boldsymbol{r}_\beta/\partial S_a)$, which was approximated as will be described below. For the C–H and N–H stretching modes, $(\partial\boldsymbol{r}_\beta/\partial S_a)$ was zero unless β denoted the hydrogen atom, while for C–C stretching modes $(\partial\boldsymbol{r}_\beta/\partial S_a)$ was zero unless β denoted the carbon atom. The vector $(\partial\boldsymbol{r}_\beta/\partial S_a)$ had a direction along the bond referring to the symmetry coordinate involving the displacement of the β atom.

The calculated results of $\bar{\alpha}_a'$ and $(\gamma_a')^2$ are listed in Table 1, where $\bar{\alpha}_a'=[(\partial\alpha_{xx}/\partial S_a)+(\partial\alpha_{yy}/\partial S_a)+(\partial\alpha_{zz}/\partial S_a)]/3$ and $(\gamma_a')^2=[\{(\partial\alpha_{xx}/\partial S_a)-(\partial\alpha_{yy}/\partial S_a)\}^2+\{(\partial\alpha_{yy}/\partial S_a)-(\partial\alpha_{zz}/\partial S_a)\}^2+\{(\partial\alpha_{zz}/\partial S_a)-(\partial\alpha_{xx}/\partial S_a)\}^2+6\{(\partial\alpha_{xy}/\partial S_a)^2+(\partial\alpha_{yz}/\partial S_a)^2+(\partial\alpha_{zx}/\partial S_a)^2\}]/2$. In the table, the calculated results in the polarizability method and the experimental results are also given. It is found that the values of $\bar{\alpha}'$ calculated by the vibronic method are 2—6 times larger than the experimental ones. The values in the parentheses in Table 1 are those obtained by the calculation using only the term A in Eq. (6). It is indicated that the Raman tensor for the symmetric stretching vibration is almost entirely explained by the term A. This fact supports the conclusion suggested by Verlan.[10] Practically,

Table 1. Trace terms, $\bar{\alpha}'$, and anisotropy terms, $(\gamma')^2$, of Raman tensor with respect to symmetry coordinates for symmetric stretching modes

Molecule		$\bar{\alpha}'$ [Å²]			$(\gamma')^2$ [Å⁴]	
		vib.[a]	pol.[a]	obsd.[b]	vib.[a]	pol.[a]
CH_4	S_{CH}	4.271(4.302)	0.876	2.08	0.0	0.0
C_2H_2	S_{CH}	4.707(4.716)	0.638	1.44	80.57	2.827
	S_{CC}	6.652(6.911)	1.655	2.94	159.8	14.23
C_2H_4	S_{CH}	13.36 (13.53)	1.243	2.08	431.1	3.242
	S_{CC}	10.47 (10.03)	1.130	1.89	314.7	18.76
C_2H_6	S_{CH}	13.87 (14.03)	1.373	2.65	0.006	0.656
	S_{CC}	7.628(7.965)	−0.362	0.92	0.883	0.809
NH_3	S_{NH}	5.198(5.375)	0.991		17.29	1.616

a) The abbreviations vib. and pol. mean vibronic and polarizability methods, respectively. b) From Ref. 18.

TABLE 2. L_x MATRIX ELEMENTS OF METHANE USED IN THE CALCULATION

		Equilibrium position of atom[a] [Å]	L_x matrix elements $\times N_0^{-1/2}$ [$g^{-1/2}$][b]			
			$Q_1(A_1)$	$Q_2(E)$	$Q_3(T_2)$	$Q_4(T_2)$
			(2919.4 cm^{-1})	(1548.1 cm^{-1})	(3015.9 cm^{-1})	(1319.2 cm^{-1})
C^1	x	0.0	0.0	0.0	0.03534	−0.01583
	y	0.0	0.0	0.0	0.02909	−0.07063
	z	0.0	0.0	0.0	−0.07493	0.08931
H^2	x	0.63104	0.28753	0.24678	0.22629	0.34453
	y	−0.63104	−0.28753	−0.15649	−0.21285	−0.07378
	z	0.63104	0.28753	−0.40327	0.20329	−0.16416
H^3	x	0.63104	0.28753	0.24678	−0.43682	−0.25022
	y	0.63104	0.28753	0.15649	−0.43812	0.01492
	z	−0.63104	−0.28753	0.40327	0.42857	−0.10529
H^4	x	−0.63104	−0.28753	−0.24678	−0.25135	0.01243
	y	0.63104	0.28753	0.15649	0.26479	0.40589
	z	0.63104	0.28753	−0.40327	0.24310	−0.36794
H^5	x	−0.63104	−0.28753	−0.24678	0.04082	0.08189
	y	−0.63104	−0.28753	−0.15649	0.03952	0.34703
	z	−0.63104	−0.28753	0.40327	0.01783	−0.42680

a) In molecule fixed coordinate. b) N_0 is the Avogadro number.

the calculated values of the terms B and C were very small.

The anisotropy term $(\gamma_a')^2$ is an effective factor for the theoretical calculation of a Raman intensity and is closely related to the depolarization ratio, ρ_n; $\rho_n = 6(\gamma_a')^2/[45(\bar{\alpha}_a')^2+7(\gamma_a')^2]$. In comparing the values of ρ_n calculated from the Raman tensor with respect to the symmetry coordinates, it is found that the values of ρ_n obtained from the vibronic method are smaller than those obtained from the polarizability method, with the exception of the C–H stretching in ethylene. In order to discuss the magnitude of $(\gamma_a')^2$ relative to the values of $\bar{\alpha}_a'$ in the calculated results, these values were compared with the experimental results. From the measurement by Schrötter and Bernstein,[18] the depolarization ratios of the Raman spectrum of acetylene are 0.27 and 0.06 for the C–H and C–C stretching vibrations respectively. The corresponding values are 0.310 and 0.308 in the vibronic method, and 0.445 and 0.383 in the polarizability method. It may be said that the theoretical calculations lead to an overestimation of the anisotropy terms in comparison with the magnitudes of $\bar{\alpha}'$.

Normal Vibrations of Methane: The normal modes were obtained by the usual **GF** method, using the **F** matrix reported by Shimanouchi *et al.*[19] The L_x matrix elements used in the calculations are given in Table 2. The calculated results of the Raman intensities, I/I_0, and the depolarization ratios, ρ_n, are listed in Table 3. In the table, the results calculated by the polarizability method and the experimental results are also listed. At a glance it may be seen that the results of the vibronic method show an entirely different tendency with respect to the relative intensities in comparison with the results calculated from the polarizability method. In the results of the vibronic method, the Raman intensity of the ν_1 vibration is strong, while those of the other vibrations are

TABLE 3. RAMAN INTENSITIES AND DEPOLARIZATION RATIOS OF STOKES LINES OF METHANE

	$I/I_0\times 10^{30}$ [cm^2]			ρ_n	
	vib.[a]	pol.[a]	obsd.[b]	vib.[a]	pol.[a]
ν_1	101.4	4.260	vs	0	0
ν_2	0.000	12.68	w	0.015	0.857
ν_3	0.021	3.881	w	0.857	0.857
ν_4	0.124	0.116		0.857	0.857

a) See footnote a in Table 1. b) From Refs. 20—22.

nearly equal to zero. In the results of the polarizability method, however, the Raman intensity of the ν_2 vibration is larger than that of the ν_1 vibration. In the experiments[20-22] a ν_1 vibration with a very strong intensity and ν_2 and ν_3 vibrations with weak intensities are observed. Moreover, for the depolarization ratio of the ν_2 vibration the two methods give different values. The values of the elements of the Raman tensors calculated in the vibronic method are listed in Table 4. The values for the ν_2 vibration are very small; they may be regarded as zero in comparison with those for the other vibrations. For the ν_3 and ν_4 vibrations, the values of the diagonal elements are zero. However the values from the terms A and B are not zero, and the absolute value of one element, for example $(\alpha_{xx})'$, from the term A is equal to that of the corresponding element from the term B, and their signs are opposite. The values of the $\bar{\alpha}'$ calculated by the use of only the term A or the term B are zero. Then, the depolarization ratio calculated by the use of one term, A, B, or C, is the same value, 0.857, as that calculated with the total values of the elements. This is not the case for the ν_2 vibration. The Raman tensors calculated in the polarizability method are shown in Table 5. The values of the three diagonal elements of the Raman tensor for the

TABLE 4. RAMAN TENSORS OF METHANE CALCULATED BY THE VIBRONIC METHOD $(\alpha^{a}_{\rho\sigma})' \times 10^4$ [cm^2 g$^{-1/2}$]

		Term A[a]	Term B[a]	Term C[a]	Total[b]
$\nu_1(A_1)$	$(\alpha_{xx})'$	−3.326	−0.0051	0.0289	−3.302
	$(\alpha_{yy})'$	−3.326	−0.0051	0.0289	−3.302
	$(\alpha_{zz})'$	−3.326	−0.0051	0.0289	−3.302
	$(\alpha_{xy})'=(\alpha_{yx})'$	0.0	0.0	0.0	0.0
	$(\alpha_{xz})'=(\alpha_{zx})'$	0.0	0.0	0.0	0.0
	$(\alpha_{yz})'=(\alpha_{zy})'$	0.0	0.0	0.0	0.0
$\nu_2(E)$	$(\alpha_{xx})'$	0.1198×10^{-6}	0.0057×10^{-6}	-0.0011×10^{-6}	0.1244×10^{-6}
	$(\alpha_{yy})'$	0.1252×10^{-6}	0.0003×10^{-6}	-0.0011×10^{-6}	0.1244×10^{-6}
	$(\alpha_{zz})'$	0.1310×10^{-6}	-0.0055×10^{-6}	-0.0011×10^{-6}	0.1244×10^{-6}
	$(\alpha_{xy})'=(\alpha_{yx})'$	-0.0042×10^{-6}	0.0015×10^{-6}	-0.0161×10^{-6}	-0.0188×10^{-6}
	$(\alpha_{xz})'=(\alpha_{zx})'$	-0.0006×10^{-6}	-0.0006×10^{-6}	-0.0074×10^{-6}	-0.0086×10^{-6}
	$(\alpha_{yz})'=(\alpha_{zy})'$	0.0033×10^{-6}	-0.0016×10^{-6}	0.0105×10^{-6}	0.0122×10^{-6}
$\nu_3(T_2)$	$(\alpha_{xx})'$	−0.0311	0.0311	0.0	0.0000
	$(\alpha_{yy})'$	−0.0022	0.0022	0.0	0.0000
	$(\alpha_{zz})'$	0.0333	−0.0333	0.0	0.0000
	$(\alpha_{xy})'=(\alpha_{yx})'$	−0.0496	0.0333	0.0678	0.0515
	$(\alpha_{xz})'=(\alpha_{zx})'$	0.0123	−0.0059	−0.0263	−0.0199
	$(\alpha_{yz})'=(\alpha_{zy})'$	0.0069	0.0008	−0.0320	−0.0243
$\nu_4(T_2)$	$(\alpha_{xx})'$	0.0289	−0.0289	0.0	0.0000
	$(\alpha_{yy})'$	0.0007	−0.0007	0.0	0.0000
	$(\alpha_{zz})'$	−0.0296	0.0296	0.0	0.0000
	$(\alpha_{xy})'=(\alpha_{yx})'$	0.0669	−0.0474	−0.0808	−0.0613
	$(\alpha_{xz})'=(\alpha_{zx})'$	−0.0324	0.0170	0.0639	0.0485
	$(\alpha_{yz})'=(\alpha_{zy})'$	0.0156	−0.0191	0.0143	0.0108

a) See text. b) Sum of the terms A, B, and C.

TABLE 5. RAMAN TENSORS OF METHANE CALCULATED BY THE POLARIZABILITY METHOD $(\alpha^{a}_{\rho\sigma})' \times 10^4$ [cm^2 g$^{-1/2}$]

	$\nu_1(A_1)$	$\nu_2(E)$	$\nu_3(T_2)$	$\nu_4(T_2)$
$(\alpha_{xx})'$	0.6768	0.6233	0.0	0.0
$(\alpha_{yy})'$	0.6768	0.3927	0.0	0.0
$(\alpha_{zz})'$	0.6768	−1.0161	0.0	0.0
$(\alpha_{xy})'=(\alpha_{yx})'$	0.0	0.0	−0.6940	−0.0595
$(a_{xz})'=(\alpha_{zx})'$	0.0	0.0	0.2689	0.0470
$(\alpha_{yz})'=(\alpha_{zy})'$	0.0	0.0	0.3289	0.0106

ν_2 vibration are different from one another. This contradicts the conclusion obtained from the group-theoretical consideration, as indicated in the review by Loudon.[23]

In comparison with the experimental results, the results of methane calculated by the vibronic method will now be discussed in detail. Schrötter and Bernstein[18] determined the Raman intensity by the use of the rotational Raman line, $J=1\rightarrow3$, of hydrogen as the standard. From their experimental results, the Raman intensity of the ν_1 vibration is 23.6×10^{-30} cm^2, this value being, in magnitude, about one-fourth of the calculated result. Furthermore, the Raman line from the ν_2 and ν_3 vibrations are also observed to have weak intensities. However, Dickinson *et al.*[21] reported, from the experimental results, that the relative intensity of the ν_3 vibration is 5 in comparison with the value of 20 for the intensity of the ν_1 vibration. On the other hand, this calculation showed that the Raman intensity of ν_4 is stronger than those of the ν_2 and ν_3 vibrations, although their intensities are so small as to be unobserved. The experimental results for the ν_2 and ν_3 vibrations may be explained by a theoretical calculation involving factors which are not considered in this work.

Conclusions

For the symmetric stretching vibrations of several small molecules and the normal vibrations of methane, the theoretical calculations of Raman tensors were performed in the vibronic method. From the results, the following conclusions can be drawn:

(a) Verlan's conclusion that the intensity for symmetric stretching vibration is almost entirely contributed by the term A is confirmed.

(b) The calculated intensities for the symmetric stretching vibrations are large in comparison with the experimental values.

From a comparison of the results for the normal coordinates of methane in the vibronic method with those in the polarizability method:

(c) The vibronic method is more suitable for theoretical calculations of the Raman intensity than is the polarizability method.

I would like to thank Professor Tomoo Miyazaki for his helpful advice and for his critical reading of the manuscript.

References

1) H. A. Kramers and W. Heisenberg, *Z. Phys.*, **31**, 681 (1925).

2) G. Placzek, "Handbuch der Radiologie," ed. by E. Marx, Akademische Verlagsgesellschaft, Leipzig, (1934), Vol. 6, Pt. 2.

3) J. O. Hirschfelder, *J. Chem. Phys.*, **3**, 555 (1935); W. Kolos and L. Eolniewicz, *ibid.*, **46**, 1426 (1967); R. P. Bell and D. A. Long, *Proc. Roy. Soc. Ser. A*, **203**, 364 (1950); E. Ishiguro, T. Arai, M. Mizushima, and M. Kotani, *Proc. Phys. Soc.* (London), **A65**, 178 (1952).

4) J. A. Pople, D. P. Santry, and G. A. Segal, *J. Chem. Phys.*, **43**, S129 (1965); J. A. Pople and G. A. Segal, *ibid.*, **43**, S136 (1965); J. A. Pople and G. A. Segal, *ibid.*, **44**, 3239 (1966).

5) N. S. Hush and M. L. Williams, *Theoret. Chim. Acta* (Berl.), **26**, 141 (1972).

6) H. Yamada, *Kwansei Gakuin Univ. Ann. Studies*, **21**, 95 (1972).

7) H. Shinoda and T. Miyazaki, *Chem. Lett.*, **1973**, 563.

8) A. C. Albrecht, *J. Chem. Phys.*, **34**, 1476 (1961).

9) F. A. Savin, *Opt. Spectry.*, **19**, 308,412 (1965); **20**, 549 (1966).

10) E. M. Verlan, *ibid.*, **20**, 341,447 (1966).

11) J. Tang and A. C. Albrecht, *J. Chem. Phys.*, **49**, 1144 (1968).

12) W. L. Peticolas, L. Nafie, P. Stein, and B. Fanconi, *ibid.*, **52**, 1576 (1970).

13) J. Tang and A. C. Albrecht, "Raman Spectroscopy," ed. by H. A. Szymanski, Vol. 2, Plenum Press, New York-London (1970), p. 33—68.

14) G. Herzberg and E. Teller, *Z. Phys. Chem.* (Leipzig), **B21**, 410 (1933); see also Ref. 17.

15) The notation $\Phi_{(i-k)}$ means the configuration χ_i^k as Murrell and McEwen's notation in *J. Chem. Phys.*, **25**, 1143 (1956).

16) T. Miyazaki and H. Shinoda, This Bulletin, **46**, 1216 (1973).

17) J. N. Murrell and J. A. Pople, *Proc. Phys. Soc.*, **A69**, 245 (1956).

18) H. W. Schrötter and H. J. Bernstein, *J. Mol. Spectrosc.*, **12**, 1 (1964).

19) T. Shimanouchi, I. Nakagawa, J. Hiraishi, and M. Ishii, *ibid.*, **19**, 78 (1966).

20) G. E. MacWood and H. C. Urey, *J. Chem. Phys.*, **4**, 402 (1936).

21) R. G. Dickinson, R. T. Dillon, and F. Rosetti, *Phys. Rev.*, **34**, 582 (1928).

22) M. A. Thomas and H. L. Welsh, *Can. J. Phys.*, **38**, 1291 (1960).

23) R. Loudon, *Advan. Phys.*, **13**, 423 (1964).

Solubility of Transition Metal Complexes in Aqueous Salt Solutions. I. Tris(1,10-phenanthroline)iron(II) Perchlorate

Katsuhiko MIYOSHI, Toshiaki TAURA, Chiyori SHIMADA, and Hayami YONEDA
Department of Chemistry, Faculty of Science, Hiroshima University, Higashi-senda-machi, Hiroshima 730
(Received January 16, 1975)

Solubility of tris(1,10-phenanthroline)iron(II) perchlorate was determined at 25 °C by spectrophotometry in aqueous solutions of sodium halides, sulfate, acetate, and trichloroacetate up to ionic strength of 0.5. It was found that the solubility is higher in the presence of water-structure breaking anions but is lower in the presence of water-structure making anions than is expected from the change in activity coefficients with ionic strength. This was interpreted in terms of compatibility and incompatibility of the influence of the complex cation on the water structure with that of added anions, and the hydrophobic nature of the complex cation was noted.

According to Gurney[1] or Frank,[2] ions in aqueous solution are classified into three groups on the basis of their interaction with water.[1-4] The first group consists of so-called electrostrictive water-structure makers, which attract surrounding water molecules so tightly through ion-dipole interaction that their co-spheres[1] cause a local increase in the viscosity. Typical examples are provided by Li^+, F^-, SO_4^{2-}, and other highly charged ions. The second group consists of water-structure breakers, which render the motion of water molecules more vivid around them than that of bulk ones (so-called negative hydration[5]). K^+, Rb^+, I^-, and other ions with low charge-to-radius ratio belong to this group and lead to a decrease in the viscosity of the solution. The last one consists of hydrophobic water-structure makers and is quite unique in that, when they are dissolved in water, though hardly soluble in general, water-water interaction is strengthened, *i.e.*, "iceberg" is formed in the vicinity of their hydrophobic parts (hydration of the second kind[6] or hydrophobic hydration) and sometimes so-called hydrophobic bonding[7] may take place. This behavior is characteristic of aqueous solutions and has attracted the attention of biochemists in recent years. Tetraalkylammonium homologues[8] and some organic ions including surfactants belong to this group.

As for coordination compounds, however, the above classification has not been well established,[3] though they can be permitted to have a variety of physical and chemical properties by substituting metal ions or coordinated ligands. In a series of our study on the solubility of transition metal complexes, we intend to focus our attention on the nature of their interaction with water and also with coexisting ions and to try to classify them into some groups.

Recently Steigman and Dobrow,[9] and Desnoyers *et al.*[4,10] succeeded in interpreting most excess thermodynamic functions of aqueous electrolyte solutions on the following assumptions: ions belonging to the first group are antagonistic with those belonging to the second and third groups with respect to their influence on the water structure, while those belonging to the second and third groups are cooperative with each other. On the basis of the above assumptions, it follows that electrolytes composed of cooperative ion pairs tend to have lower activity coefficients in water and the reverse holds for antagonistic pairs.[2,11] This phenomenon is often called a mutual or structural salting-in and -out, respectively and has been recently discussed quantitatively by Friedman *et al.*[12]

In our recent study on the Pfeiffer effect,[13] it was proposed that $[Zn(phen)_3]^{2+}$ (phen=1,10-phenanthroline) is classified into the third group in spite of its relatively high charge. However, the complex is so labile that it is not easy to examine its hydrophobic nature by usual techniques such as electrolytic conductance or viscosity measurements.[14] Since $[Zn(phen)_3]^{2+}$ and $[Fe(phen)_3]^{2+}$ are closely matched in many respects, particularly with regard to their interaction with water in which we are interested and the latter is extremely stable, the solubility of $[Fe(phen)_3](ClO_4)_2$ was measured in place of $[Zn(phen)_3](ClO_4)_2$ in various aqueous salt solutions as a function of the total ionic strength of these solutions. These data are expected to provide a valuable information on the hydrophobic nature of $[Fe(phen)_3]^{2+}$ as well as $[Zn(phen)_3]^{2+}$ if the concept of compatibility and incompatibility of the water structure influenced by ions,[9,10] is suitably applied.

Experimental

Preparation. Tris(1,10-phenanthroline)iron(II) perchlorate monohydrate was prepared by dissolving Mohr's salt, $FeSO_4(NH_4)_2SO_4 \cdot 6H_2O$ and 1,10-phenanthroline monohydrate in a mole ratio of 1 : 3 in hot water containing *ca.* 10% of methanol, followed by adding sodium perchlorate monohydrate. The resulting crystal was washed with water and recrystallized from water. Its purity was checked by elemental analysis.

Reagents. Added salts were sodium halides, sulfate, acetate, and trichloroacetate, all of which were of reagent grade and used without further purification.

Procedure. Solution equilibration was attained in a small glass bottle (100 ml) dipped in a water bath kept at 25±0.1 °C with a mercury-in-glass thermoregulator. The salt solution to which solid $[Fe(phen)_3](ClO_4)_2$ had been added, was continuously stirred in the water bath by a magnetic stirrer for 5 to 6 hours. Then an aliquot of the solution was pippetted out through a glass filter and was diluted appropriately in a volumetric flask with water. After 1 or 2 hours, an aliquot of the same solution was again pippetted out and diluted as before. $[Fe(phen)_3]^{2+}$ in the two diluted solutions was determined with a Shimadzu UV-200 spectrophotometer by use of its charge-transfer band with the maximum absorption at 510 nm. When the solution equilibration proved incomplete within experimental error, a similar procedure was done again after 1 to 2 hours. The time taken to reach solution equilibrium was usually from 5 to 6 hours. The molar absorption coefficient of $[Fe(phen)_3]^{2+}$

at 510 nm was 11100 and was not affected at all by added salts.

Results and Discussion

If K is defined as a thermodynamic solubility product[15] for $[Fe(phen)_3](ClO_4)_2$, K in water is expressed as

$$K = [[Fe(phen)_3]^{2+}][ClO_4^-]^2 f_{\pm(0)}{}^3 = 4S_{(0)}{}^3 f_{\pm(0)}{}^3 \quad (1)$$

where S and $f_\pm$ denote the solubility in mol/l and the mean activity coefficient of the complex salt, respectively, and the subscript (0) refers to water. In salt solutions, on the other hand, K is given by

$$K = 4S^3 f_\pm{}^3 \quad (2)$$

In the above two equations, ion association is ignored on the ground that $S_{(0)}$ is so small (8.99×10^{-4} mol/l) that there is little contribution from ion association to the solubility when the amount of added salts is small and if any, it does not differ greatly as long as halide ions are concerned[16] (the Bjerrum's critical distance[17] amounts to 7.1 Å for halides). From the identity of Eq. (1) with Eq. (2), it follows that

$$S/S_{(0)} = f_{\pm(0)}/f_\pm \quad (3)$$

If the Debye-Hückel approximation[18] for activity coefficients is employed, Eq. (3) is rearranged to

$$\log S/S_{(0)} = 1.018[I^{1/2}/(1+0.329aI^{1/2}) - I_{(0)}^{1/2}/(1+0.329aI_{(0)}^{1/2})] \quad (4)$$

at 25 °C, where I denotes the total ionic strength of the salt solution in which $[Fe(phen)_3](ClO_4)_2$ is dissolved and a the distance of closest approach in Å. Equation (4) suggests that $S/S_{(0)}$ should be greater than unity, increase with I, and should not be dependent on the kind of added salts.

Figure 1 shows the ratios $S/S_{(0)}$ as a function of square root of I and clearly indicates that they are in fact greater than unity but differ considerably from salt to salt added when they are compared at the same ionic strength. Since the cation (sodium ion) is common to all salt solutions and the concentration of ClO_4^- is much lower than that of added salts, the differences in $S/S_{(0)}$ are attributed to these added anions and the co-sphere of $[Fe(phen)_3]^{2+}$ overlaps predominantly with those of added anions rather than that of ClO_4^-. As a result, it can be concluded to a good approximation that the increase in $S/S_{(0)}$ with I depends on whether the complex cation is co-operative or antagonistic with added anions with regard to their influence on the water structure. In Fig. 1 are also drawn the two curves estimated by Eq. (4) with a=8 and 9 Å, which are chosen because the radius of $[Fe(phen)_3]^{2+}$ in water has been determined to be 6.5 and 5.3 Å by viscosity[19] and conductance[16] measurements, respectively and that of ClO_4^- to be 2.92 Å.[20]

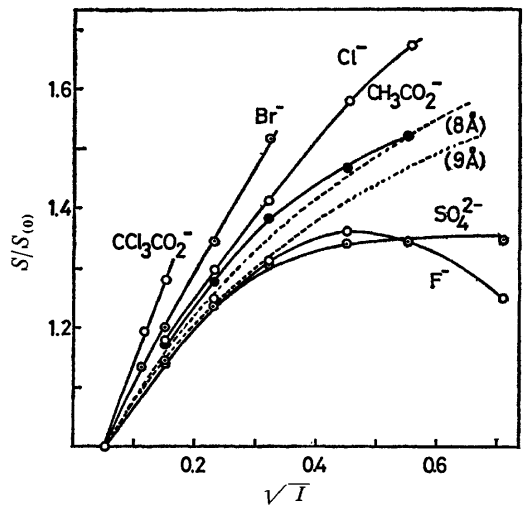

Fig. 1. Dependence of the solubility ratio $S/S_{(0)}$ on square root of ionic strength I. Dotted lines represent the theoretical values estimated by Eq. (4).

A close inspection of Fig. 1 indicates that the deviations of $S/S_{(0)}$ from theoretically estimated values are observed even at low salt concentrations at which the Debye-Hückel approximation is taken valid[18] and that the order of increasing ratio $S/S_{(0)}$ is $CCl_3COO^- > Br^- > Cl^- > CH_3COO^- > F^- \sim SO_4^{2-}$, which is in good agreement with the order of increasing water-structure breaking power of anions[9] (NaI could not be examined because of the precipitation of $[Fe(phen)_3]I_2$). Therefore, it is certain that $[Fe(phen)_3]^{2+}$ is cooperative with structure breakers, *i.e.*, it belongs to the third group. It is probably due to the ion association between $[Fe(phen)_3]^{2+}$ and SO_4^{2-} that the curve for sulfate tends to level off at high salt concentration, since the Bjerrum's critical distance amounts to 14.3 Å in this case (the association constant of $[Ru(phen)_3]SO_4$ in water has been reported to be 47 by Yokoyama and Yamatera[21]). Otherwise, the ratio should begin to decrease like that for fluoride at high salt concentrations.

The authors would like to express their deep gratitude to Prof. Y. Yamamoto, Hiroshima University, for helpful discussions.

References

1) R. W. Gurney, "Ionic Processes in Solution," McGraw-Hill Book Co., New York, N. Y. (1953).
2) H. S. Frank, *Z. Phys. Chem.* (Leipzig), **228**, 365 (1965).
3) E. R. Nightingale, "Chemical Physics of Ionic Solutions," ed. by B. E. Conway and R. G. Barradas, John Wiley & Sons, Inc., New York, N. Y. (1966), p. 87.
4) J. E. Desnoyers and C. Jolicoeur, "Modern Aspects of Electrochemistry", Vol. 5, ed. by J. O'M. Bockris and B. E. Conway, Plenum publishing Corp., New York, N. Y. (1969), p. 1.
5) O. Ya. Samoilov, *Discuss. Faraday Soc.*, **24**, 141 (1957).
6) H. G. Hertz and M. D. Zeidler, *Ber. Bunsenges. Phys. Chem.*, **68**, 821 (1964); H. G. Hertz, *ibid.*, **68**, 907 (1964).
7) G. Némethy, *Angew. Chem. Int. Ed. Engl.*, **6**, 195 (1967) and references cited therein.
8) W. -Y. Wen, "Water and Aqueous Solutions," ed. by R. A. Horne, John Wiley & Sons, Inc., New York, N. Y. (1972), p. 613; *J. Solution Chem.*, **2**, 253 (1973); T. S. Sarma and J. C. Ahluwalia, *Chem. Soc. Rev.*, **2**, 203 (1973).
9) J. Steigman and J. Dobrow, *J. Phys. Chem.*, **72**, 3424 (1968).
10) J. E. Desnoyers, M. Arel, G. Perron, and C. Jolicoeur, *ibid.*, **73**, 3346 (1969).
11) R. M. Diamond, *J. Amer. Chem. Soc.*, **80**, 4809 (1958).

12) P. S. Ramanathan and H. L. Friedman, *J. Chem. Phys.*, **54**, 1086 (1971); P. S. Ramanathan, C. V. Krishnan, and H. L. Friedman, *J. Solution Chem.*, **3**, 237 (1972).
13) H. Yoneda, K. Miyoshi, and S. Suzuki, *Chem. Lett.*, **1974**, 349; K. Miyoshi, K. Sakata, and H. Yoneda, *ibid.*, **1974**, 1087; K. Miyoshi, K. Sakata, and H. Yoneda, submitted to *J. Amer. Chem. Soc.*
14) R. L. Kay, "Trace Inorganics in Water," Advances in Chemistry Series, No. 73, ed. by R. A. Baker, Amer. Chem. Soc., Washington, D. C. (1968), p. 1 and references cited therein.
15) A thermodynamic solubility product denotes a hypothetical solubility product at infinite dilution where the activity coefficients of ions are regarded unity.
16) Y. Yamamoto, E. Sumimura, K. Miyoshi, and T. Tominaga, *Anal. Chim. Acta*, **64**, 225 (1973).
17) R. A. Robinson and R. H. Stokes, "Electrolyte Solutions," Butterworth and Co., Ltd., London (1959), p. 392.
18) Ref. 17, p. 223.
19) T. Kurucsev, A. M. Sargeson, and B. O. West, *J. Phys. Chem.*, **61**, 1567 (1957).
20) E. R. Nightingale, *ibid.*, **63**, 1381 (1959).
21) H. Yokoyama and H. Yamatera, *Chem. Lett.*, **1973**, 337.

The Solvent Extraction-Polarographic Determination of Cadmium(II) as the Tris(2,2′-bipyridine)iron(II) Tetraiodocadmate(II) Complex*

Kiyoshi Hasebe, Tsukasa Ohtsuki, and Tomihito Kambara

Department of Chemistry, Faculty of Science, Hokkaido University, Kita-ku, Sapporo 060

(Received March 18, 1974)

A new method for the solvent extraction-polarographic determination of cadmium has been proposed. The quaternary complex formed by the tris(2,2′-bipyridine)iron(II) cation and the tetraiodocadmate(II) anion can be readily extracted into benzyl alcohol. The extracted complex shows a well-defined reduction wave in the ternary electrolyte-solvent mixture, composed of benzyl alcohol, an aqueous electrolyte solution, and methyl cellosolve. The available range of the present method covers from 5.7×10^{-6} to 91.4×10^{-6} M of cadmium(II) in the aqueous phase. The optimum pH range for extraction is 3—9, and the extracted species is stable in the ternary solvent mixture for 5 hr. Zinc (II), bromide, and chloride ions do not interfere, but copper (II), mercury(II), and iron(III) do interfere.

Among the several methods devised for the determination of cadmium, especially the spectrophotometric method using dithizone[1] and the polarographic method,[2] are the most useful. 2,2′-Bipyridine (bpy) and related compounds are well known as remarkably useful colorimetric reagents for analytical use.[3] As to the determination of cadmium, for example, a spectrophotometric determination employing the ion-pair formation of the tetraiodocadmate(II) anion with the tris(2,2′-bipyridine)iron(II) cation has been reported.[4] However, this method makes it necessary to pay careful attention to the absorbance of the reagent blank solution. Fujinaga *et al.*[5] and the present authors[6,7] have already reported a polarography in a ternary solvent mixture consisting of chloroform, water, and methyl cellosolve (MCS). Recently, Kitagawa and Ichimura[8] have reported an interesting extraction-polarography of an extracted complex of tris(acetylacetonato)iron(III) and similar complexes in the methyl iso-butyl ketone. These methods are very useful since the concentration and separation can be achieved simultaneously. In the present paper, the solvent extraction-polarographic method is applied to the quaternary complex of tris(2,2′-bipyridine)iron(II) tetraiodocadmate(II) $[Fe(bpy)_3][CdI_4]$.

Experimental

Reagents. *2,2′-Bipyridine solution*: An aqueous 2×10^{-2} M solution was prepared.

Standard Iron(II) Solution: Mohr's salt was dissolved in water containing a small amount of sulfuric acid to give a 2×10^{-2} M solution. This was then standardized by EDTA titration.

Standard Cadmium(II) Solution: Guaranteed cadmium nitrate (Wako Chemicals) was dissolved in water containing sufficient nitric acid to give a 2×10^{-3} M solution. This was then standardized by EDTA titration with Eriochrome Black T as the indicator. This stock solution was used after accurate dilution.

Buffer Solutions: The pH was adjusted with the following solutions: hydrochloric acid (pH 1—3), acetic acid-sodium acetate (pH 3—6), and potassium dihydrogen phosphate-sodium borate (pH 9—10).

All the reagents used were of an analytical reagent grade.

Apparatus. A Yanagimoto polarograph, model PA-102, was used for recording the DC and AC polarograms. The DME had these characteristics: $m=1.88$ mg s^{-1} in pure water and $t=4.96$ s in the electrolysis solution at open circuit at $h=39$ cm. The experiments were carried out by using a cell with a mercury pool or a modified H-type cell with an SCE in a water bath thermostated at (20+0.1) °C. Before each polarographic measurement, all the solutions were deaerated by bubbling through for 15 min nitrogen gas which has been presaturated with the same solution as that used in the measurements.

A Hitachi-Horiba glass electrode pH meter, model F-5, was used. An Iwaki shaker, model KM, was used for the shaking.

Results and Discussion

Established Procedure. Twenty millilitres of a 2×10^{-2} M 2,2′-bipyridine solution was pipetted into a 100-ml separatory funnel. Five millilitres of a 3 M iron(II) solution, 3 ml of a 3 M sodium acetate solution, 1 ml of a 3 M potassium iodide solution and the sample solution containing the cadmium ion were pipetted into the funnel in that sequence. After adjusting the volume to 35 ml with water, the solution was let stand for about 2 min. It was then shaken with 10 ml of benzyl alcohol for 3 min. After the separation of the two phases, a 6-ml portion of the extract was pipetted into a 20-ml volumetric flask, and then 6 ml of aqueous 1 M potassium iodide was added as a supporting electrolyte. The flask was filled up to the mark with MCS. After deaeration with nitrogen gas, a polarogram was recorded.

Choice of Extracting Solvent. Five of the extracting solvents examined—namely, nitrobenzene, methyl *iso*-butyl ketone, 1, 2-dichloroethane, cyclohexanone, and chloroform, all of which have a relatively large dielectric constant,—extracted only a small amount of cadmium (II) in the form of the quaternary complex of $[Fe(bpy)_3CdI_4]$, and some of the above-mentioned solvents also caused a film at the interface between the two phases. Therefore, the above solvents were not suitable. When benzyl alcohol was used, however, tetraiodocadmate (II) was extracted quantitatively as the quaternary complex with the tris(2, 2′-bipyridine)iron(II) complex. Benzyl alcohol was, therefore, used in the present work.

Extractability. In order to confirm that tetraiodocadmate(II) anions were quantitatively extracted into benzyl alcohol as a quaternary complex, hydrogen

* Presented at the 19th Annual Meeting of the Polarographic Society of Japan, Sapporo, October, 1973.

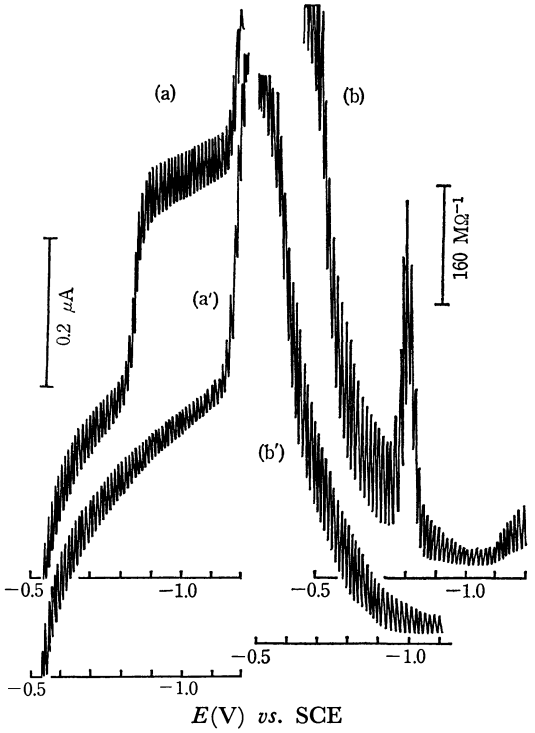

Fig. 1. The polarograms of the quaternary complex composed of tetraiodocadmate(II) anion with tris(2,2'-bipyridine)iron(II) cation into the ternary solvent mixture.
Concentration of iodide ion in aq. phase: $[I^-]_w = 8.58 \times 10^{-2}$ M, Concentration of bpy in aq phase: $[bpy]_w = 1.14 \times 10^{-2}$ M, Concentration of iron(II) in aq. phase: $[Fe(II)]_w = 2.86 \times 10^{-3}$ M, pH 7.5, Volume of aq. phase $V_w = 35$ ml, Volume of org. phase $V_0 = 10$ ml, (a) and (b): 6.86×10^{-5} M of Cadmium(II) in aq. phase, (a') and (b'): Without cadmium(II), (a) and (a'): DC polarogram, (b) and (b'): AC Polarogram.

sulfide was bubbled into the aqueous phase after the extraction. No yellow precipitate was formed. Upon carrying out a second extraction, cadmium could not be found in the aqueous phase; *i.e.*, the cadmium has been removed completely from the aqueous phase by a single extraction.

Polarograms of the Extracted Quaternary Complex in the Ternary Solvent Mixture. The polarograms obtained by the use of the established procedure are shown in Fig. 1. The half-wave potential of the complex was about −0.80 V *vs.* SCE. As may be seen from Fig. 1, no DC polarographic wave and no AC peak appeared in the absence of cadmium.

Effect of pH. The effect of the pH on the extraction of the quaternary complex was studied with several buffer solutions and sodium acetate. An approximately constant DC wave height and AC peak height were obtained between pH 3.72 and 9.39. Thus, the pH of the aqueous solution was adjusted to about 7 by adding sodium acetate solution, according to the Kotsuji method.[4]

Effect of Shaking Time and Standing Time. A constant DC wave height, or the corresponding AC peak height, was obtained by shaking for more than

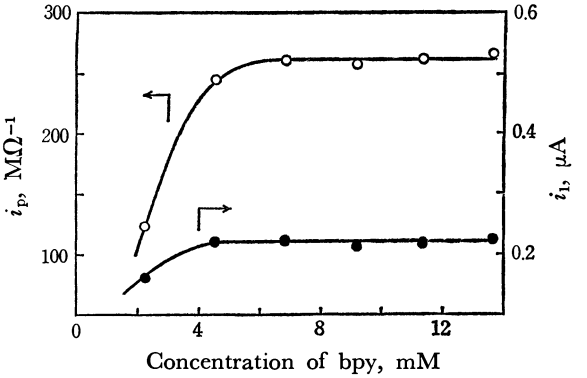

Fig. 2. Effect of 2,2'-bipyridine concentration on the extraction of the quaternary complex, $[Fe(bpy)_3CdI_4]$. ○: AC peak height, ●: DC wave height, $[Cd(II)]_w = 5.72 \times 10^{-5}$ M. Other conditions are the same as in Fig. 1.

1 min; we chose the shaking time of 3 min. The extracted species was very stable, its polarographic DC wave height in the ternary solvent mixture showed no change for 5 hours, and the corresponding AC peak height also remained unchanged.

Effect of the 2,2'-Bipyridine Concentration. With the concentrations of cadmium(II), iodide ion, and iron(II) kept constant, various amounts of 2,2'-bipyridine were added, after which the extraction was carried out according to the above procedure. The DC wave height, or the corresponding AC peak height of the ternary mixture, was found to be constant and at its maximum when the mole ratio of bipyridine to cadmium(II) was in the range from 100 to 250, as is shown in Fig. 2.

Effect of the Iodide and Iron(II) Concentrations. The DC wave height and the corresponding AC peak height in the ternary solvent mixture consisting of the extract, aqueous electrolyte, and MCS were found to be constant when the concentrations of iodide and iron(II) ions in the aqueous phase were higher than 4×10^{-2} M and 3×10^{-3} M respectively. Figure 3 shows the effect of the iron(II) concentration on the DC polarographic wave height, and the corresponding AC peak height. When the concentration of iron(II) was lower than

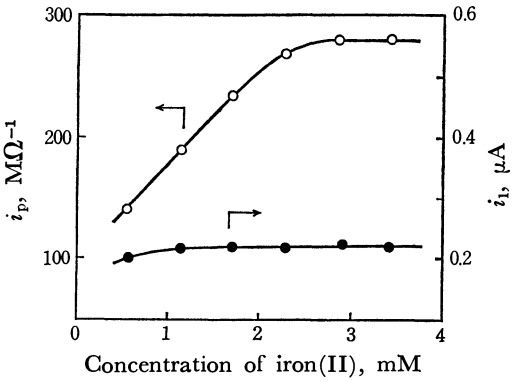

Fig. 3. Effect of iron(II) concentration on the extraction of the quaternary complex.
○: AC peak height, ●: DC wave height, $[Cd(II)]_w = 5.72 \times 10^{-5}$ M. Other conditions are the same as in Fig. 1.

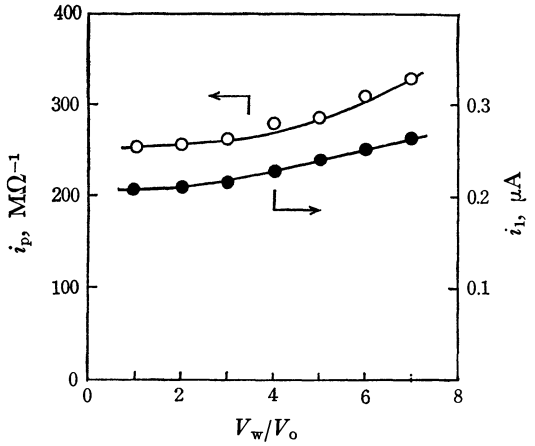

Fig. 4. Effect of aqueous-to-organic volume ratio (V_w/V_o) on DC wave height, or the corresponding AC peak height.
$V_o = 10$ ml, $V_w = 10$—70 ml, $[Cd(II)]_w = 5.72 \times 10^{-5}$ M.
Other conditions are the same as in Fig. 1.

3×10^{-3} M in the aqueous phase, a decrease of the AC peak height was observed. It can be seen that the excess of bpy reacts with cadmium(II) and produces a non-reducible complex, which is more stable than the tetraiodocadmate(II) complex.[9] Therefore, it is desirable that the excess of bpy be changed into the tris(2,2′-bipyridine)iron(II) chelate,[9,10] by the addition of an excess amount of iron(II).

Effect of the Aqueous-to-Organic Volume Ratio on the Polarogram. While keeping other conditions constant, the effect of the aqueous-to-organic volume ratio on the polarogram was studied by the polarographic method. The results are shown in Fig. 4, from which it is found that an increase in the volume ratio produced an increase in the DC wave height and also in the corresponding AC peak height. This is caused by the decrease in the volume of the organic phase by the mutual dissolution. Consequently, the aqueous-to-organic volume ratio should be adjusted to an approximately constant value.

Choice of Supporting Electrolyte. Several supporting electrolytes were investigated; the results are summarized in Table 1. As the supporting electrolyte, potassium iodide was the most suitable for the polarographic measurement.

Miscible Organic Solvent. As possible miscible solvents, methanol, ethanol, dioxane, and MCS were selected and investigated. Methanol and ethanol were found not to be suited for being miscible solvents, however, because these solvents were easily evaporated by bubbling nitrogen gas and did not mix well. The other two solvents were found to be very miscible. However, a better-defined polarogram was obtained by using MCS rather than dioxane.

Effect of Diverse Ions. The interference of diverse ions was examined; the results are given in Table 2. According to the familiar *t*-tests, not even a 100 : 1 mole ratio of zinc and bromide ions, or a 50 : 1 mole ratio of the chloride ions to cadmium(II) ions interfered with the solvent extraction-polarographic measurement. Copper(II), iron(II), and mercury(II) ions interfered seriously, however.

Calibration Curve. According to the established procedure described above, the calibration curve was drawn; the results are given in Fig. 5. It was found that the difference between the two averages of the two days was not found to be significant at the 95% level by the familiar *t*-test, using the data obtained

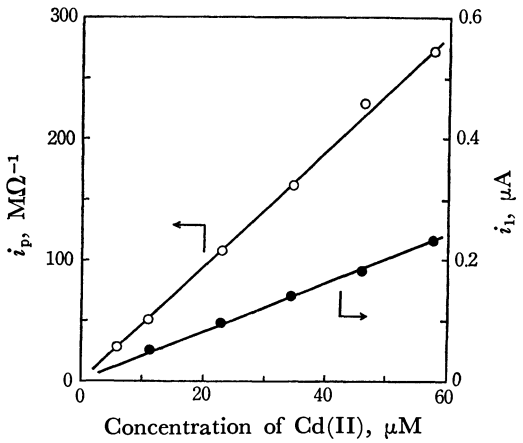

Fig. 5. Calibration curve of cadmium(II) in aqueous phase.
Data obtained under the same conditions as in Fig. 1.

Table 1. List of aqueous supporting electrolyte solutions utililized in preparation of the water-benzyl alcohol-MCS ternary mixture

Supporting electrolyte		Remark	
Name	Final Concn., M	DC Wave	AC Peak
H_2SO_4	0.3	Good Adsorption wave appears	Adsorption wave appears
$HClO_4$	0.3—0.9	Bad Adsorption wave appears	Bad
HCl	0.3—1.2	Bad	Good
HNO_3	0.3	Maximum wave appears	Good
LiCl	0.3	Not well-defined	Good
NaCl	0.3	Not well-defined	Good
KCl	0.3	Not well-defined	Good
KI	0.09—0.9	Very good When the concn. is decreased, adsorption wave appears.	Very good

TABLE 2. EFFECT OF INTERFERENCE OF DIVERSE IONS ON THE EXTRACTION OF 5.72×10^{-5} M Cd(II)

Ion	Molar concn. ratio to cadmium(II)	DC wave height and AC peak observed					
		DC (μA)			AC ($M\Omega^{-1}$)		
None		0.226	0.222	0.224	268	276	266
Cu^{2+}	10	a)			264	270	274
(as $CuSO_4$)	50	a)			194	192	196
	100	a)			160	162	160
Zn^{2+}	10	0.224	0.222	0.226	262	256	262
(as $ZnSO_4$)	50	0.218	0.216	0.214	258	264	260
	100	0.222	0.220	0.222	280	276	280
Fe^{3+}	10	0.230	0.226	0.222	264	272	264
(as iron alum)	50	b)					
	100	b)					
Hg^{2+}	10	c)			164	158	164
(as $HgSO_4$)	50	c)			136	136	136
	100	c)			56	52	54
Br^-	10	0.234	0.234	0.228	266	252	260
(as KBr)	50	0.216	0.210	0.210	264	266	268
	100	0.210	0.212	0.208	266	268	264
Cl^-	10	0.218	0.218	0.218	252	252	252
(as KCl)	50	0.206	0.200	0.208	264	266	258
	100	0.206	0.210	0.206	248	248	254

a) Well-defined DC polarogram is not obtainable. b) An inhomogeneous solution is formed. c) Mercury(II) ion behaves similarly to cadmium(II), therefore, the tris(2,2′-bipyridine)iron(II) complex cation concentration decreases.

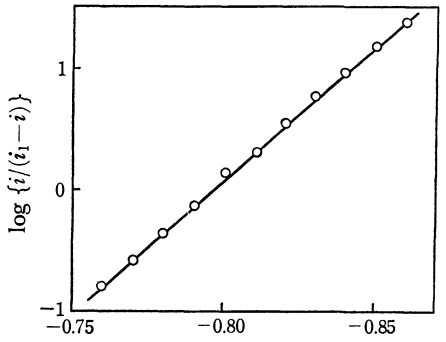

Fig. 6. Relationship between E and $\log\{i/(i_1-i)\}$. $[Cd(II)]_w=6.67\times10^{-5}$ M, $[I^-]_w=0.1$ M, $[bpy]_w=1.33\times10^{-2}$ M, $[Fe(II)]_w=3.33\times10^{-3}$ M, pH 7.5; Slope=45 mV, iR-drop: not corrected.

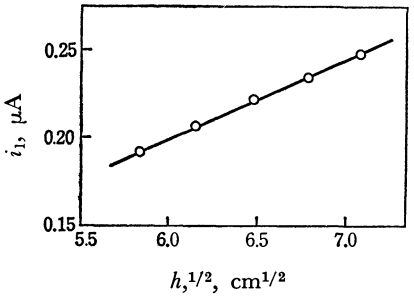

Fig. 7. Variation of i_l with the height of mercury column, h.
$[Fe(II)]_w=2.86\times10^{-3}$ M. Other conditions are the same as in Fig. 3.

with the 4.75×10^{-5} M cadmium(II) ion in the aqueous phase.

Characteristics of Limiting Current. The tetraiodocadmate(II) ion undergoes a two-electron reduction to the cadmium amalgam in a single step. An analysis of the log plot indicated the quasi-reversible nature of the process, the value of the slope being 45 mV at 20 °C, as is shown in Fig. 6. The reduction was diffusion-controlled as is evident from the linear plot of i_l against $h^{1/2}$, shown in Fig. 7. The relative temperature coefficient of the limiting current was 1.83% K^{-1} at 20 °C.

The authors wish to thank the Ministry of Education for the financial support granted for this research.

References

1) The Japan Society for Analytical Chemistry, ed., "Bunseki Kagaku Binran," Maruzen Publishers, Tokyo (1971), p. 142.
2) B. Breyer and H. H. Bauer, "Alternating Current Polarography and Tensammetry," Interscience Publishers, New York, N.Y. (1963), p. 147.
3) A. A. Schilt, "Analytical Applications of 1, 10-Phenanthroline and Related Compounds," Pergamon Press, London (1969).
4) K. Kotsuji, This Bulletin, **38**, 988 (1965).
5) T. Fujinaga, H. Brodowsky, T. Nagai, and K. Yamashita, *Rev. Polarog.* (Japan), **11**, 217 (1963).
6) T. Kambara and K. Hasebe, *Bunseki Kagaku*, **14**, 491 (1965).
7) T. Kambara, T. Ishii, and K. Hasebe, *Nippon Kagaku Kaishi*, **1972**, 920.
8) T. Kitagawa and A. Ichimura, *Bunseki Kagaku*, **22**, 1042 (1973).
9) H. Freiser and Q. Fernando, "Ionic Equilibria in Analytical Chemistry," John Wiley & Sons Inc., New York, N. Y. (1963), p. 310; translated in Japanese by T. Fujinaga and E. Sekido, Kagakudojin, Kyoto (1967), p. 256, 257.
10) L. G. Sillen and A. E. Martell, ed., "Stability Constants of Metal-Ion Complexes," The Chemical Society, London (1964), pp. 616, 617.

The Rapid Determination of Heavy Metals in Sediment by Means of X-ray Fluorescence Analysis* Modification of the X-ray Intensity Using Scattered Radiation

Hideki TANAKA** and Genzo HASHIZUME***

Environmental Science Institute of Hyogo Prefecture, Hyogo-ku, Kobe 652

(Received June 25, 1974)

The present method was developed as a way of modifying intensity using the mass-absorption coefficient of the matrix, which is itself obtained from the measurement of the intensity at an arbitrary scattered wavelength. This modification, derived from the simplified equation by the utilization of the known matrix composition, has been empirically demonstrated, and it has been applied to various river-sediment samples. Repeated analyses on copper and zinc in representative sediments were carried out, and the average ($\bar{x}$) and the coefficient of the variation (*c.v.*) obtained by the present method and by the atomic-absorption method were compared. In the former method, $\bar{x}$=1,550 μg/g, *c.v.*=4.25% on copper, $\bar{x}$=4,400 μg/g, and *c.v.*=7.11% on zinc; in the latter method, $\bar{x}$=1,500 μg/g, *c.v.*=9.87% on copper, $\bar{x}$=4,330 μg/g, and *c.v.*=13.03% on zinc.

The X-ray fluorescence method, the atomic-absorption method, and the colorimetric method have all been used to determine the elements in a samples with a homogeneous composition of samples. Of these analytical methods, the X-ray fluorescence method has these advantages compared with the others;

(1) many elements can be analyzed rapidly, (2) the samples need not be destroyed, and (3) the X-ray spectro-chemical analysis of heavy metals does not generally depend on any of the chemical properties of the elements in which they are present.

There is, however, a problem related to the analysis of sediments by the X-ray fluorescence method-the matrix effect. Therefore, many investigators have reported modifications.

There have been modifications derived from the theoretical equation on the basis of the absorption and excitation effects of X-ray emission,[1-3] and experimental modifications derived by assuming a definite relation between the X-ray intensities and constituent elements of a sample.[4-6]

Taylor and Andermann[7-8] adopted a technique which involves the utilization of a modification using the value of the ratio of the $K\alpha$- or $L\alpha$-ray intensity to the scattered radiation at an empirically selected wavelength. With this method, the variation in the X-ray intensity with the matrix effect could be modified at lower concentrations (less than 500 μg/g content of copper).[9] However, at higher concentrations, differences in the mass-absorption coefficients at the constituent elements of the substructure for both wavelengths appeared in the intensity ratio, an example is shown in Fig. 1.

The present modification was developed by using the modification factor of the variation in the fluorescence intensity, which was determined from the measurement of the scattered radiation at an arbitrary wavelength.

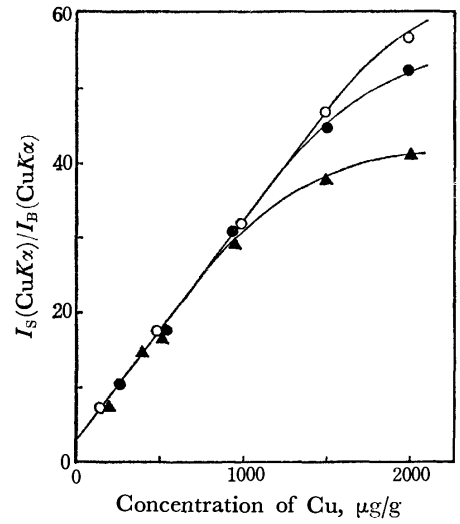

Fig. 1. Calibration curves of Cu on $I_S(CuK\alpha)/I_B(CuK\alpha)$ ratio.
○: H_3BO_3, ●: Cellulose powder, ▲: Silicic acid.

This paper will deal with the modification and with the analytical results on metals in the river- and sea-sediments.

Experimental

Sample Treatment and Analytical Conditions of the X-ray Measurements. The sediment was sufficiently separated from water and then displaced on the evaporating dish. After dehydration for three hr at 110 °C in a drying oven, the sample was moderately crushed by a pestle, sieved to obtain a fine fraction, and finally crushed by means of a mixer-mill until the particle size became smaller than 100 μ. The specimen was molded at a pressure of 15 t/cm² and then analyzed by using a X-ray spectrometer.

A Rigaku Denki Geigerflex X-ray spectrometer equipped with a D9C-type constant-potential X-ray generator and a KG-X-type goniometer was used for the X-ray emission measurements.

The analytical conditions of the X-ray spectra are shown in Table 1.

* Investigation Concerning the X-ray Fluorescence Analysis of Microgram Metals, Part III.

Part II: Hideki Tanaka, Yuzo Moriguchi, Tadashi Yamamoto, and Genzo Hashizume, *Bunseki Kagaku*, **21**, 1456 (1972).

** Present address: Environmental Science Institute of Hyogo Pref., Arata-cho, Hyogo-ku, Kobe-shi.

*** Industrial Research Institute of Hyogo Pref., Yukihira-cho, Suma-ku, Kobe-shi.

Table 1. Analytical conditions of X-ray

X-Ray tube	Tungsten target
Generator suplied	47.5 kV-40 mA
Analyzing crystal	LiF
Detector	Scintillation countor
Path	About 10^{-2} Torr
Counting time	10 s (Fix time)
Measuring method	To detect by using the pulse height analyzer and the differential method

Results and Discussion

The Intensity of the Scattered Radiation and the Mass-absorption Coefficient. The background of the X-ray fluorescence analysis is composed of the coherent scattering of photons of the given wavelength by the sample, the Compton scattering of the photons of the given wavelength by the sample, the scatter of radiation by the analyzing crystal, and fluorescence by the crystal. The intensity of the scattered radiation is approximately equal to that of the background, therefore, it can be expressed by the following equation.[10]

$$I_B = K_1[\{J_{(\lambda k)}\Sigma(C_iF_i^2/A_i)\}/\{\mu_{m(\ k)}(\sec\theta_1+\sec\theta_2)\} + \{J_{(\lambda k)}\Sigma C_i(Z_i-f_i^2)r\}/\{\mu_{m(\lambda c)}(\sec\theta_1+\sec\theta_2)\}] \quad (1)$$

where J is the photon flux which is the intensity distribution of the exciting source; λ_k is the $K\alpha$ wavelength for the i element; μ is the mass-absorption coefficient; m is the matrix; θ_1 and θ_2 are the angles of incidence and excitation (from the normal state to the sample surface); λ_c is the Compton scattering of the photons of the given wavelength; K is a factor which is decided by the k element and the geometrical conditions of the instrument; C is the concentration; A is the atomic number; F is the atomic scattering power, f is the incoherent scattering power, and r is a recoil factor. Equation(1) is expressed as the background intensity underneath a peak.

Now, if the k element to be analyzed is rarely present in the sample, this intensity can be regarded as that of the radiation scattered at the same arbitrary wavelength. Therefore, λ_k was experimentally selected to be 0.906 Å of the scattered radiation at an arbitrary wavelength which was not influenced by the coexisting elements and which was obtained with a relatively high intensity.

Equation (1) can be simplified by noting that, since $\lambda_k-\lambda_c=0.03$ Å$\doteqdot 0$, $\mu_{(\lambda c)}=\mu_{(\lambda k)}$.
Thus,

$$I_B = K_2\cdot K_s/\mu_{m(0.906\text{Å})} \quad (2)$$

where:

$$K_s = \Sigma\{C_i(K_s)_i\} \text{ and } (K_s)_i=\{F_i^2+(Z_i-f_i^2)r\}/A_i$$

$$K_2 = K_1\cdot J_{(\lambda k)}/(\sec\theta_1+\sec\theta_2) = \text{const.}$$

The values of $(K_s)_i$ for each element can be calculated from the values of F and f^2, which are available in the standard text by Lonsdal.[11]

Equation (3) can be obtained by the conversion of the logarithms with regard to two variables, I_B and μ_m (0.906 Å), on both sides of Eq. (2):

$$\log I_B + \log \mu_{m(0.906\text{Å})} = K_3 \quad (3)$$

The mass-absorption coefficient of the X-ray is expressed as a function of the wavelength, containing the photoelectric absorption coefficient (τ) and the scattering coefficient (δ). The photoelectric absorption coefficient increases in proportion to the third power of the wavelength in the region from a remote absorption edge. On the other hand, however, the scattering coefficient is constant and independent of the wavelength in the first approximation.[12] Therefore, the mass-absorption coefficient of the X-ray is generally expressed as $\mu=\delta+\tau$. Then, $\tau=CZ^m\lambda^3$; thus, $\mu=\delta+n\lambda^3$.

The mass-absorption coefficient of the scattered radiation at the arbitrary wavelength is

$$\mu_{m(0.906\text{Å})} = \delta + n(0.906)^3, \quad (4)$$

while that of the $K\alpha$-line to be analyzed is expressed as

$$\mu_{m(\lambda s)} = \delta + n\cdot\lambda_s^3, \quad (5)$$

where λ_s is the wavelength of the $K\alpha$-line to be analyzed.

The relation between $\mu_{m(\lambda s)}$ and $\mu_{m(0.906\text{Å})}$ can be expressed as follows from Eqs. (4) and (5):

$$\log \mu_{m(0.906\text{Å})} = \log \mu_{m(\lambda s)} + K_4 \quad (6)$$

When Eq. (6) is substituted in Eq. (3), Eq. (7) is obtained:

$$\log I_B + \log \mu_{m(\lambda s)} = K_5 \quad (7)$$

Thus, Eq. (7) shows that the mass-absorption coefficient for the given wavelength, λ_s, can be determined by the measurement of I_B.

The relation between the background intensity at 0.906 Å and the mass-absorption coefficient for the $K\alpha$-line to be analyzed on various model matrices was examined. Copper oxide, zinc carbonate, chromium oxide, arsenic trioxide, cadmium oxide, and stannous chloride were used as the standards. The concentrations of copper, zinc, chromium, arsenic, cadmium, and tin were adjusted to 1000 μg/g for each portion of boric acid, anhydrous aluminium sulfate, potassium sulfate, sodium sulfate, and sodium carbonate respectively used as the model materices.

The calculated results of the mass-absorption coefficients with the Cu$K\alpha$-, Zn$K\alpha$-, Cr$K\alpha$-, Cd$K\alpha$-, As$K\alpha$, and Sn$K\alpha$-emission spectra for the matrices are shown in Table 2.

The relation between the background intensity at 0.906 Å and the mass-absorption coefficient for Cu$K\alpha$-

Table 2. Values of mass absorption coefficient of K-emission spectra for various matrices

K-Emission spectrum	Matrix				
	H_3BO_3	Na_2CO_3	Na_2SO_4	$Al_2(SO_4)_3$	K_2SO_4
Cu$K\alpha$	10.56	17.15	28.53	31.43	63.30
Zn$K\alpha$	8.60	13.97	23.27	25.64	51.76
Cr$K\alpha$	32.21	53.09	87.54	96.12	155.64
As$K\alpha$	4.24	6.58	10.74	11.81	23.76
Cd$K\alpha$	0.74	1.02	1.55	1.69	3.27
Sn$K\alpha$	0.60	0.84	1.25	1.34	2.56

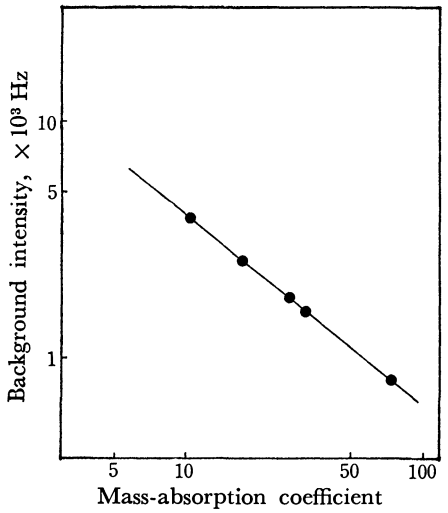

Fig. 2. Relationship between mass-absorption coefficient for Cu$K\alpha$-line and background intensity at 0.906 Å.

line is shown in Fig. 2 as representative of the standard elements.

A satisfactory reciprocity was obtained between I_B and $\mu_m(\mathrm{Cu}K\alpha)$.

Fluorescence X-Ray Intensity and Mass-absorption Coefficient. Kalman and Heller[13] have shown that the intensity of the fluorescence X-ray can be represented by:

$$I_S = K_6 C_s / \{\mu_{m(\bar{\lambda})} \sec\theta_1 + \mu_{(\lambda s)} \sec\theta_2\} \quad (8)$$

where I_S is the intensity of the fluorescence peak of the s element, $\bar{\lambda}$ is the effective exciting wavelength, and K_6 is a factor which is decided by the s element and the geometrical conditions of the instrument. The constancy of $\bar{\lambda}$ in the case of a measurable $K\alpha$-line excited by operating an X-ray tube continuously with a constant power input has been verified.[11]

Equation (8) can be simplified as follows:

$$I_S = K_6 C_s / N \cdot \mu_{m(\lambda s)} \quad (9)$$

where:

$$N = \mu_{m(\bar{\lambda})} / \mu_{m(\lambda s)} + \sec\theta_2 / \sec\theta_1 \quad (10)$$

Compton has proved that N can be considered a constant if, for all the matrices, $\mu_{(\lambda)} \propto \lambda^n$ (where n is independent of the matrix) over the range from $\bar{\lambda}$ to λ_s.[10]

As is shown Eq. (9), the intensity of the fluorescence is a function of the concentration and the mass-absorption coefficient. The relation between I_S and C_s can be represented as the calibration curve on an identical matrix; however, the relation between the $\mu_{m(\lambda s)}$ obtained from Eq. (8) and I_S should be examined further.

The result obtained by taking a intensity ratio on any matrix (m_i) and the standard model matrix (m_1) of the element to be analyzed at a constant concentration is shown in Eq. (11):

$$I_{S_1}/I_{S_i} = K_7 \mu_{m_1(\lambda s)} / \mu_{m_i(\lambda s)} \quad (11)$$

Equation (12) is obtained by the conversion of the logarithms on both sides Eq. (11), when the value of $\mu_{m_1(\lambda s)}$ is a unit:

$$\log I_{S_1}/I_{S_i} + \log \mu_{m_i(\lambda s)} = K_8 + \log \mu_{m_1(\lambda s)} \quad (12)$$

The main components in river- and sea-sediments are light elements, such as silicon and aluminium; the heavy metals to be analyzed in these samples usually comprize less than 0.2—0.3% of the total (by weight). Therefore,

$$C_s \ll C_1 + C_2 + C_3 + \cdots\cdots + C_n \text{ and } \mu_s \lesssim \mu_i$$
$$i = 1, 2, 3, \cdots\cdots, n$$

Then,

$$\mu_m = \mu_1 C_1 + \mu_2 C_2 + \mu_3 C_3 + \cdots\cdots + \mu_n C_n + \mu_s C_s$$
$$\fallingdotseq \mu_1 C_1 + \mu_2 C_2 + \mu_3 C_3 + \cdots\cdots + \mu_n C_n$$

If it should happen that the metal content in the standard model sample varies, the value of the mass-absorption coefficient for the measurable metal can be regarded as approximately constant in the range of lower concentrations.

The relation between I_{S1}/I_{Si} and $\mu_{m(\lambda s)}$ was examined on various matrices. Boric acid, sodium sulfate, anhydrous alminium sulfate, potassium sulfate, and sodium carbonate were used as the model matrices. The standard model matrix selected was anhydrous alminium sulfate, which had a mass-absorption coefficient close to that of the usual sediments. The samples containing 1000 μg/g copper in each matrix were used; the results are shown in Fig. 3.

The technique for the quantitative determination of elements in unknown samples is as follows: first, I_{S1}/I_{Si} is calculated from the value of $\mu_{mi(\lambda s)}$ (Fig. 3), which can be obtained by measuring the background intensity at 0.906 Å (Fig. 2); the peak intensity (I_{Si}) of an element in the sample is determined subsequently. Then, I_{Si} multiplied by I_{S1}/I_{Si} is transformed into I_{S1} for the matrix based on $\mu_{m_1(\lambda s)}$, and the concentration of the element with the transformed I_{S1} is determined from the calibration curve between C_s and I_{S1} on the standard model matrix.

Calibration Curves for Copper on Various Matrices. The calibration curves for copper in the concentration range

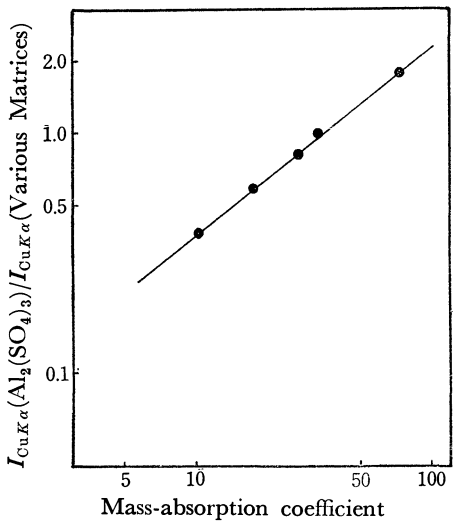

Fig. 3. Relationship between mass-absorption coefficient and intensity ratio of Cu$K\alpha$-line.

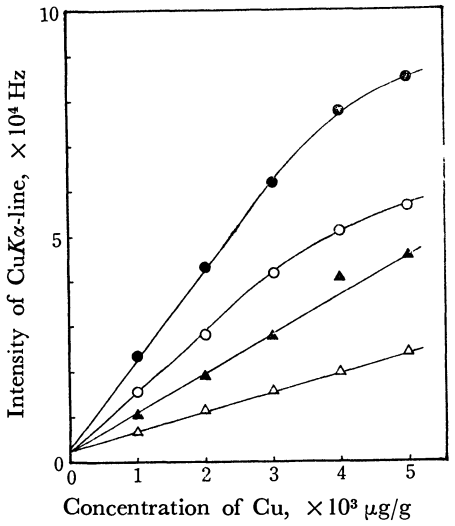

Fig. 4. Calibration curves for Cu on various matrices.
○: H_3BO_3, ●: Na_2CO_3, △: $Al_2(SO_4)_3$, ▲: K_2SO_4

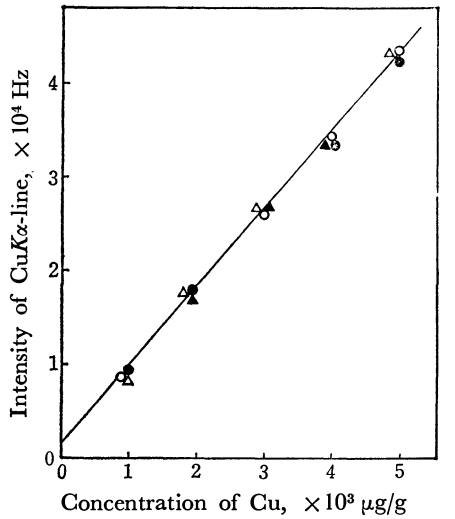

Fig. 5. Calibration curve for Cu converted into $Al_2(SO_4)_3$ matrix.
○: H_3BO_3, ●: Na_2CO_3, △: $Al_2(SO_4)_3$ ▲: K_2SO_4

of 500—5000 μg/g prepared in the various matrices described above are shown in Fig. 4. Each calibration curve for copper shows that the intensities become weak and become very different with an increase in the mass-absorption coefficient of the matrix for the $K\alpha$-emission spectrum. Therefore, each calibration curve agreed very closely with that of the standard model matrix ($Al_2(SO_4)_3$ matrix) when this modification technique was used. The results are shown in Fig. 5.

Theoretically, this relation can be applied to any element except for an element in the vicinity of the absorption edges with the constituent element of the matrix. On the other hand, it is unnecessary to consider the excitation effect of measurable X-rays by the coexisting elements on the measurement of heavy metals in the sediments, because the elements forming the matrices of the sediments are mainly silicate and organic compounds.

The modification technique for the fluorescence intensities of other metals may be examined similarly.

Precision of Analytical Values. The results of the measurement of the copper and zinc contents by the present method and by the atomic-adsorption method on 10 specimens drawn as 1-lot sediment specimens are shown in Table 3.

The pretreatment of a sediment for the atomic-absorption method was carried out as follows: the metals to be analyzed, consisting of 10 g of portions the dried sediment, were extracted with 50 ml of 2 M-HNO_3 for 2 hr and then filtered. The extracted solution was heated and concentrated in a Kjeldahl flask, and the organic compounds in the sample were decomposed with 10 ml of 98% sulfuric acid and 10—20 ml

Table 3. Measurement of Cu and Zn content by X-ray fluorescence method and atomic absorption method on 10 specimens drawn 1 lot sediment

No.	X-Ray fluorescence method		Atomic absorption method	
	Cu (μg/g)	Zn (μg/g)	Cu (μg/g)	Zn (μg/g)
1	1530	4260	1520	4360
2	1540	4430	1510	4380
3	1520	4400	1490	4760
4	1590	4510	1550	4450
5	1570	4320	1420	4160
6	1540	4450	1500	4220
7	1550	4530	1510	4080
8	1580	4390	1450	4410
9	1570	4210	1510	4320
10	1540	4460	1560	4190
$\bar{x}$	1550	4400	1500	4330
c.v.%	4.52	7.11	9.87	13.03

Table 4. Comparison of several metals content by X-ray fluorescence method and atomic absorption method

Sample No.	Cu		Zn		Cr		Sn	
	X[a] (μg/g)	A[b] (μg/g)	X[a] (μg/g)	A[b] (μg/g)	X[a] (μg/g)	A[b] (μg/g)	X[a] (μg/g)	A[b] (μg/g)
1	530	450	1250	1120	38	42	56	32
2	1940	1760	3620	3300	225	257	432	410
3	850	820	970	940	62	53	196	177
4	3750	3420	4820	4810	530	475	1260	1190
5	420	430	560	485	28	25	186	180
6	125	120	320	305	15	13.5	73	52

a) X-Ray fluorescence method. b) Atomic absorption method.

of 60% nitric acid. Then, the sample was analyzed by using the standard addition method.

The averages ($\bar{x}$) of the series of values obtained by the two analytical methods were approximately similar, but the coefficient of variation (*c.v.*) by the atomic-absorption method was larger than that by the X-ray fluorescence method.

Analysis of Several Metals in Sediments. The analytical values of copper, zinc, chromium, and tin in sediments obtained by the X-ray fluorescence method and the atomic-absorption method were compared. The results are listed in Table 4.

The standard addition technique was used for the atomic-absorption analysis. The values obtained by the two analytical methods agreed approximately.

The time required from pretreatment to the measurement of the sediments is shortened to about 30 min per sample, while 3 hr is needed for the atomic-absorption method. The present method is thus suitable for the rapid analysis of a number of samples, and good results are obtained for the concentration of each element in the range of 50—5000 μg/g.

References

1) H. J. Beattie and R. M. Brissey, *Anal. Chem.*, **26**, 980 (1954).
2) G. Andermann and J. W. Kemp, *ibid.*, **30**, 1306 (1958).
3) T. J. Cullen, *ibid.*, **34**, 812 (1962).
4) S. Suzuki, S. Matsumoto, and J. Itoh, *Bunseki Kagaku*, **19**, 1523 (1970).
5) M. Sugimoto, *ibid.*, **11**, 1168 (1962).
6) S. Matsumoto, *ibid.*, **21**, 342 (1972).
7) K. P. Champion, J. C. Taylor, and R. N. Whittem, *Anal. Chem.*, **38**, 109 (1966).
8) D. L. Taylor and G. Andermann, *ibid.*, **43**, 712 (1971).
9) H. Tanaka, Y. Moriguchi, and G. Hashizume, *Bunseki Kagaku*, **21**, 1457 (1972).
10) A. H. Compton and S. K. Allison, "X-Ray in Theory and Experiment," 2nd Ed., Van Nostrand, Princeton, N.J., (1935).
11) N. F. M. Henry and K. Lonsdale ed., "International Tables for X-Ray Crystallography," Vol. III, Chap. 3 (1962), (the Kynock Press Birmingham).
12) F. K. Richmyer, *Phys. Rev.*, **30**, 755 (1927).
13) Z. H. Kalman and L. Heller, *Anal. Chem.*, **34**, 946 (1962).

The Solubility of Elemental Mercury Vapor in Water

Isao SANEMASA

Department of Chemistry, Faculty of Science, Kumamoto University, Kurokami-machi, Kumamoto 860

(Received September 17, 1974)

The solubility of mercury vapor in water has been measured by means of atomic absorption spectrophotometry over the temperature range of 5—60 °C under atmospheric pressure. The aqueous solubility obeys Henry's law at each temperature. The solubilities and the Henry coefficients are reported. From the solubility data, the heat of the solution of mercury vapor in water is found to be −5.3 kcal/mol. The relationship between the Henry coefficient, k, and the solution temperature, T, is expressed by $\log k = -1078 \times 1/T + 6.250$. From this equation, the solubilities at 70—100 °C are estimated. The solubility of the mercury vapor in sea water has also been measured over the temperature range of 5—30 °C. A salting-out effect on the solubility is observed. The practical application of the aqueous solubility of the mercury vapor is discussed from the analytical point of view.

Bonhoeffer and Reichart[1] showed that the absorption spectrum of an aqueous solution of mercury was essentially the same as that of mercury vapor. At about the same time, Stock *et al.*[2] reported the solubilities of the metallic mercury in water. Since then, the solubilities of mercury have been studied by many workers. There is, however, a considerable disagreement among the literature values. This may be ascribed to the different experimental techniques used. The conventional techniques for the measurement of the mercury solubilities are as follows: colorimetric analysis, Pariaud and Archinard;[3] radioactive-tracer technique, Moser and Voigt;[4] neutron-activation method, Choi and Tuck;[5] atomic absorption spectrophotometry, Glew and Hames.[6] The most recent work is that by Onat,[7] who studied the dissolved mercury by means of ultraviolet spectrophotometry. The principle of measuring the dissolved mercury employed by Moser and Voigt and by Onat is different from that of other workers; it is based on the disproportionation reaction of the mercurous dimer into mercuric ions and free mercury. However, the procedures to attain the solubility equiliblium are essentially similar to those employed by other workers: they brought water into contact with metallic mercury. In the present work, mercury is treated as a vapor, and the solubility is determined based on Henry's law. The present study is different in this respect from those of the other workers.

Mercury, because of its high vapor pressure at room temperature, is introduced into the atmosphere through the impingement of the vapor and the fallout of particulate matters derived from the industrial process. During the past few years, considerable attention has been directed toward the potential hazards of mercury and its compounds in our environment. There have also been several articles[8-11] dealing specifically with the presence of mercury in air.

The generally accepted procedure for the determination of trace amounts of mercury is the cold-vapor atomic absorption technique, because it exhibits a high sensitivity. It is essentially based on a reduction-aeration method found by Kimura and Miller;[12] mercury present in solution as Hg(II) is reduced with Sn(II), and the resulting mercury vapor is separated by aeration. The most commonly utilized method at present was originally described by Hatch and Ott,[13] who combined the closed system reduction-aeration principle with atomic absorption spectrophotometry. The aqueous solubility of mercury vapor is, therefore, a common topic in analytical laboratories.

There are various forms of mercury found in nature, such as metal, inorganic, and organic compounds. Although most of the mercury reported in fish tissue is in the methyl form,[14] very little metylmercury has been discovered in sediments or river waters. Spangler *et al.*[15] demonstrated that demethylation processes by microbes in sediments probably reduce some or all of the methyl form to metallic mercury. It is also of interest, from this aspect, to study the aqueous solubility of elemental mercury.

Experimental

Reagents. All the chemicals were of an analytical reagent grade unless otherwise specified. The solutions used were: stannous chloride, 10% solution in 1 M HCl; sulphuric acid, 50% solution; potassium permanganate, 6% solution. The standard mercury stock solution of 0.5 mg/ml was prepared by dissolving the required amount of mercury (II) chloride in water. This solution was used to prepare a working standard containing 0.5 mg/l by dilution before each use. The metallic mercury was purified by distilation under reduced pressure after the air oxidation of the contaminated metal through successive aeration in water and by passing it through a column filled with a diluted HNO_3 solution.

Apparatus. The atomic absorption measurements were made with a Hitachi Model 508 atomic absorption spectrophotometer equipped with a mercury hollow-cathode lamp. A 10-cm-long gas cell with a 9.1-cm^2 cross-section and quartz windows was used. The instrumental settings were as follows: hollow-cathode lamp current, 6 mA; wavelength, 253.7 nm; band width, 0.32 nm. The solubility apparatus used was a simple closed system, as is shown in Fig. 1. It was composed of four glass flasks, a circulating pump (P) the metallic part of which was covered with plastic, and polyethylene tubes to connect them. Flask A is a 300 ml three-necked flask; the center neck is stoppered, while the other two are connected to a condenser and a gas inlet-type adapter with a stopcock. Flask B is a 1-l three-necked flask; the center neck is stoppered, while the other two are connected to a gas inlet-type adapter and an adapter, each with a stopcock. Flasks C and D, used as traps for the water vapor, are gas-washing-type, long-necked bottles with capacities of 500 ml and 2 l respectively. Flask A and Flasks B, C, and D were immersed in separate thermostats controlled within ±0.05 °C. The inlet of the circulating pump was connected

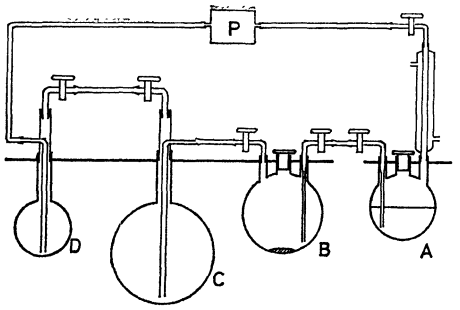

Fig. 1. Mercury vapor solubility apparatus.

to Flask A through the condenser, which was maintained at the same temperature as Flask B by circulating the water of the thermostat. The outlet of the pump was connected to Flask B, before which Flasks C and D were placed. The temperature of the room was always maintained higher than that of Flask B. The pressure in the closed system was always kept under atmospheric pressure.

Procedure. About a 20-g portion of metallic mercury is dropped into Flask B. A water sample (100 to 200 ml) is then poured into Flask A. After the mercury and the solution reach the desired temperatures, mercury vapor is introduced, bubbled into Flask A, and circulated by means of the pump. The circulation rate is adjusted to 100 to 200 ml/min. by using a Variac. After solubility equiliblium is attained, a suitable aliquot (1 to 20 ml) of the solution is withdrawn from Flask A and immediately added to a reduction-aeration bottle in the atomic absorption spectrophotometer. Measurements were made at least three times.

Measurement. The analytical procedure for determining the dissolved mercury by the flameless atomic absorption method is essentially similar to that reported by Omang.[16] Introduce a 100 ml portion of distilled water, 2 ml of 9 M sulphuric acid, and 2 ml of 10% tin(II) chloride solution into a 300-ml reduction-aeration bottle. Connect the bottle to an aeration apparatus equipped with a circulating pump and exhaust any mercury arising from contaminated reagents. When the recorder pen has returned to the base line, add the sample solution to the bottle and turn on the circulating pump at a constant flow rate of 1.5 l/min. Record the absorption peak of the mercury vapor. Carry the mercury working standard (0.05 to 0.5 μg) in the same manner as in the sample. In this case, care must be taken to adjust the total volume and the salt concentration in the bottle to make them constant. Determine the mercury concentration in the sample solution by means of a calibration curve.

Results and Discussion

The Time Required for the Attainment of the Solubility Equilibrium. The attainment of an equilibrium is important for solubility determinations and is checked in the following manner. A part of the solubility apparatus is disconnected and combined directly to the gas cell of the atomic absorption spectrophotometer. Drop metallic mercury into Flask B in the same manner as has been described in the Experimental section in the absence of water in Flask A, and then turn on the circulating pump and the recorder. The absorbance reading then begins to rise, reaches a maximum within 5 to 30 min. in accordance with the surface area of the mercury, and thereafter remains constant. Add an aqueous solution of about 100 ml to Flask A and monitor the absorbance reading. This monitoring shows that the reading, after a temporary sinking, returns slowly to the former constant line within 10 to 30 min. From the practical point of view, the liquid phase will reach equilibrium with the circulating mercury vapor within an hour.

The Effect of Oxygen on the Solubility. It has been said that mercury is readily oxidized in humid air.[2] In order to clarify this, experiments were made under conditions of both sufficiently aerating and bubbling nitrogen gas through the water. As a result, no appreciable differences in the solubility of mercury vapor were observed under the present experimental conditions.

The State of Mercury Gas Dissolved in Aqueous Solutions. In order to obtain information about the state of the mercury gas dissolved in pure and sea water, atomic absorption measurements were made with and without the addition of a reductant, Sn(II)-H_2SO_4 solution, to sample solutions in a reduction-aeration bottle. In the absence of the reductant, the readings of the absorption peaks were lowered by 1 to 2%. This is probably because of the relatively high salt concentrations in the liquid phase upon the addition of the reductant-that is, the salting-out effect. Indeed, the absorption peak increased gradually with an increase in the additional reductant. The same situation was also found in the case of the standard mercury solution. From the facts mentioned above and from the fact that the solubility obeys Henry's law, it may be concluded that the mercury gasses dissolved in pure and sea waters are in the elemental form.

Solubility of the Mercury Vapor in Water. In Figs. 2 and 3, the solubilities of mercury vapor in water in the temperature range from 5 to 60 °C are plotted against its vapor pressure; they are in equilibrium with the metallic mercury at the desired temperatures. The solubility at 5 °C may be less reliable. Figures 2 and 3 show that the aqueous solubility of mercury vapor obeys Henry's law at each solution temperature except at 5 °C. When the temperatures

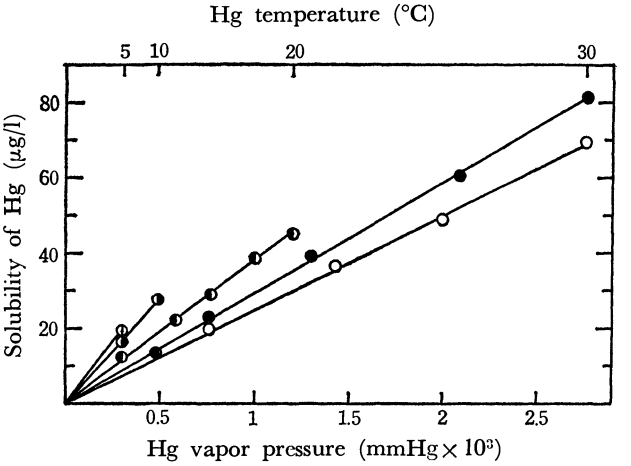

Fig. 2. The dependence of mercury solubility on mercury vapor pressure in pure water at 5 °C(◑), 10 °C(◑), 20 °C(◐), 30 °C(●) and in sea water at 30 °C(○).

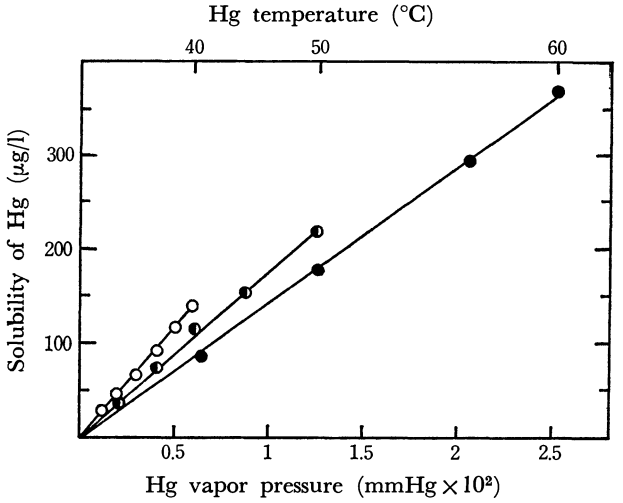

Fig. 3. The dependence of mercury solubility on mercury vapor pressure in pure water at 40 °C(○), 50 °C(◐), and 60 °C(●).

Table 1. Hg solubility and Henry coefficients

Temp. (°C)	Solubility (μg/l)[a)]	Henry coefficient
Pure water		
5	19.2	233
10	27.4	262
20	45.0	391
30	81.3	500
40	137	650
50	218	852
60	368	1010
70	5.6×10^{2}	13×10^{2}
80	8.5	15
90	12	19
100	18	23
Sea water		
5	17.2	
10	23.6	
15	31.6	
20	40.6	
25	54.9	
30	69.7	

a) Solubility is expressed in μg/l for convenience which is transformed into mole fraction by multiplying 8.98×10^{-11}.

of mercury are higher than those of solutions, the solubility values become lower than those expected from Henry's law because of the condensation of the vapor. The solubility data are summarized in Table 1, together with the Henry coefficients. The Henry coefficients are determined by dividing the partial pressures of mercury vapor (atm) by the mole fractions of the mercury dissolved.

The Temperature Dependence of the Solubility. The Henry coefficients are plotted in Fig. 4 according to the van't Hoff equation:

$$d\ln k/dT = \Delta H/RT^2 \quad (1)$$

where k is the Henry coefficient. The heat of solution, ΔH, is calculated from the slopes of the log k *vs.* $1/T$ plots to be −5.3 kcal/mol. The relationship between the Henry coefficient and the solution temperature is expressed in the following empirical equation:

$$\log k = -1078\times 1/T + 6.250 \quad (2)$$

The solubility data and the Henry coefficients at 70—100 °C listed in Table 1 are calculated from Eq. (2) and the mercury-vapor pressures at the corresponding solution temperatures on the assumption that Henry's law holds up to those pressures.

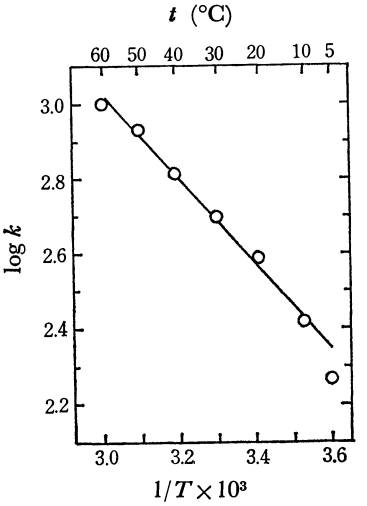

Fig. 4. log k *vs.* $1/T$ plot. The temperature dependence of solubility of mercury vapor in water.

Comparison of the Present Results with the Literature. This paper has presented the solubility results of mercury vapor in water. The aqueous solubility of mer-

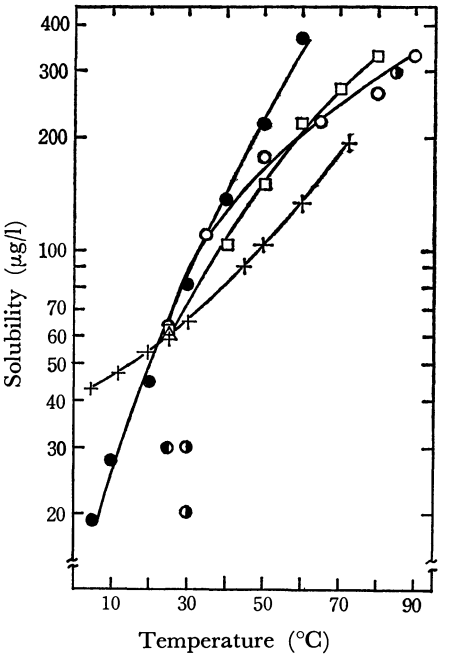

Fig. 5. Comparison of the solubilities reported in the literature: ●, this work; □, Onat; ○, Choi and Tuck; +, Glew and Hames; △, Moser and Voigt; ◐, Pariaud and Archinard; ◑, Stock *et al.*

TABLE 2. SOLUBILITY OF MERCURY AT 25 °C

Solubility (μg/l)	Literature
63.9	This work[a]
63.1	Choi and Tuck
58.8	Glew and Hames
61	Onat
60	Moser and Voigt
30	Pariaud and Archinard
20—30	Stock *et al.*[b]

a) Calculated from Eq. (2). b) Value at 30 °C.

cury in the metallic and gaseous states shoud be identical, provided that the dissolved metal mercury is in the elemental form. The results reported in the literature are illustrated in Fig. 5, together with those of the present work. The solubility data at 25 °C, summarized in Table 2, are in good agreement except for the earlier measurements by Stock *et al.* and Pariaud and Archinard. Above 50 °C, however, the present results are higher than those reported by other workers. Below 20 °C, the present results are considerably lower than those by Glew and Hames. However, their results are definitely too high, in view of the temperature dependences of the other two studies. The discrepancies in the present results at moderately higher temperatures may be caused by the different procedures used to attain the solubility equilibrium.

The Solubility in Sea Water. The solubility of mercury vapor in sea water was measured in the interest of practicality. The total mercury contained in the sample was analyzed prior to the solubility measurements. The blank concentration was found to be less than 0.1 μg/l. For this low content, the solubility data obtained were uncorrected. As is shown in Fig. 2, it is also confirmed that the solubility of mercury vapor in sea water at 30 °C obeys Henry's law. The solubility data at 5—30 °C are given in Table 1. It can be said, from Fig. 2 and Table 1, that the salting-out effect is observed on the aqueous solubility of mercury vapor, just as is observed in atomic absorption measurements. "Salting-out" is the decrease in the solubility of a non-electrolyte in ionic solutions.[17]

The Practical Application of the Aqueous Solubility of Mercury Vapor. According to the literature, the concentrations of mercury vapor in several laboratory atmospheres were determined to be 2—8,[8] 0.012,[9] or 1—30 μg/m³.[11] Based on the emission standard for mercury (1 μg/m³) promulgated by the U. S. Environmental Protection Agency,[10] the estimation of the aqueous solubility of the mercury vapor has been attempted. As a result, it has been found to be 0.0034 μg/l at 20 °C. In general, the concentration range of mercury in natural waters is from 0.5 to 364 ng/l.[18] Because of its low abundance, care must be taken in the discussion of the results when analytical experiments are made in the laboratory of the several μg/m³ level.

The author is indebted to Professor Hideo Nagai and Mr. Toshio Deguchi of Kumamoto University for their encouragement and discussions. Thanks are also due to the members of the Marine Biological Station of Kumamoto University for sampling the sea water.

References

1) K. F. Bonhoeffer and H. Reichart, *Z. Phys.*, **67**, 780 (1931).
2) A. Stock, F. Cucuel, F. Gerstner, H. Köhle, and H. Lux, *Z. Anorg. Allgem. Chem.*, **217**, 241 (1934).
3) J. C. Pariaud and P. Archinard, *Bull. Soc. Chim. Fr.*, **1952**, 454.
4) H. C. Moser and A. F. Voigt, *J. Amer. Chem. Soc.*, **79**, 1837 (1957).
5) S. S. Choi and D. G. Tuck, *J. Chem. Soc.*, **1962**, 4080
6) D. N. Glew and D. A. Hames, *Can. J. Chem.*, **49**, 3114 (1971).
7) E. Onat, *J. Inorg. Nucl. Chem.*, **36**, 2029 (1974).
8) C. W. Christian and J. W. Robinson, *Anal. Chim. Acta*, **56**, 470 (1971).
9) D. H. Anderson, J. H. Evans, J. J. Murphy, and W. W. White, *Anal. Chem.*, **43**, 1511 (1971).
10) F. P. Scaringelli, J. C. Puzak, B. I. Bennet, and R. L. Denny, *ibid.*, **46**, 278 (1974).
11) J. W. Robinson, P. J. Slevin, G. D. Hindman, and D. K. Wolcott, *Anal. Chim. Acta*, **61**, 431 (1972).
12) Y. Kimura and V. L. Miller, *ibid.*, **27**, 325 (1962).
13) W. R. Hatch and W. L. Ott, *Anal. Chem.*, **40**, 2085 (1968).
14) C. A. Bache, W. H. Gutenmann, and D. J. Lisk, *Science*, **172**, 951 (1971).
15) W. J. Spangler, J. L. Spigarelli, J. M. Rose, and H. M. Miller, *ibid.*, **180**, 192 (1973).
16) S. H. Omang, *Anal. Chim. Acta*, **53**, 415 (1971).
17) P. Ruetschi and R. F. Amilie, *J. Phys. Chem.*, **70**, 718 (1966).
18) J. Ôlafsson, *Anal. Chim. Acta*, **68**, 207 (1974).

The Chemical Behavior of Low Valence Sulfur Compounds. IX.[1] Photometric Determination of Thiosulfate, Trithionate and Tetrathionate in Mixture

Tadaaki MIZOGUCHI* and Taijiro OKABE

Department of Applied Chemistry, Faculty of Engineering, Tohoku University, Sendai 980

(Received September 26, 1974)

The cyanolysis and photometric determination of thiosulfate, trithionate and tetrathionate have been investigated under the various conditions. The cyanolysis of thiosulfate catalyzed by cupric ions proceeded quantitatively in the presence of acetate buffer solution of pH 4.5, while the degree of cyanolysis of trithionate and that of tetrathionate were 0.3 and 0.6%, respectively. The degree of cyanolysis of trithionate was not so depressed as to a negligible extent by the methods previously proposed, but was depressed to 0.7% or less by the addition of such organic solvents as acetone, methanol, *etc.* The determination of thiosulfate, trithionate and tetrathionate in the concomitant presence of them could be made with a high accuracy.

A simple analytical method for 0—10 μmol of thiosulfate and polythionates has been a subject in the study on the chemical behavior of low valence sulfur compounds in biological systems. The classical iodometric method for the determination of these compounds,[2] which was used in our previous studies, has been found inapplicable to the analysis of systems in which reducing organic compounds are contained.

A colorimetric method depending on the photometric determination of thiocyanate formed in the reaction with cyanide seems superior in the possibility of fractional determination of these compounds, to many other methods proposed previously.[3,4] This method was proposed by Nietzel *et al.*[5] to determine tetrathionate, and was then extended to the colorimetric determination of thiosulfate by Sörbo.[6] Urban has described the cyanolysis of thiosulfate[7] and polythionates,[8,9] obtaining only the mean value *n* in the formula $S_nO_6^{2-}$.[10] Koh *et al.* have fully investigated the cyanolysis and photometric determination of trithionate,[11] tetrathionate,[12] pentathionate[13] and hexathionate,[14] and also have reported a highly sensitive analytical method for thiosulfate[15] and polythionates[16] by means of solvent extraction. The application, however, has been restricted to the determination of two-component mixtures excluding trithionate.[17] Kelly *et al.*[18] have proposed a fractional determination method for thiosulfate, trithionate and tetrathionate, but the measured values fluctuate within 10 to 20%, requiring a more accurate analytical method to investigate the reaction mechanism of low valence sulfur compounds.

The reactions of thiosulfate and polythionates with cyanide are given by Eqs. (1)—(4). As the velocity of the reactions largely depends on the conditions applied,

$$S_2O_3^{2-} + CN^- \overset{Cu^{2+}}{=} SCN^- + SO_3^{2-} \quad (1)$$

$$S_3O_6^{2-} + CN^- + 2OH^- = SCN^- + SO_3^{2-} + SO_4^{2-} + H_2O \quad (2)$$

$$S_4O_6^{2-} + CN^- + 2OH^- = SCN^- + S_2O_3^{2-} + SO_4^{2-} + H_2O \quad (3)$$

$$S_4O_6^{2-} + 2CN^- + 2OH^- \overset{Cu^{2+}}{=} 2SCN^- + SO_3^{2-} + SO_4^{2-} + H_2O \quad (4)$$

it may be expected that special reactions proceed exclusively under the suitable conditions. However, it has not been shown systematically to what degree the side reactions can be depressed.

From a result of investigation of the respective reaction under the various conditions, it has become clear that three sorts of procedures shown in Table 1 can be employed with satisfactory accuracy, and that the determination of thiosulfate, trithionate and tetrathionate in mixtures can be made by those procedures. The present paper is concerned with the result of this investigation.

Experimental

Materials. All chemicals, except polythionates, were analytical reagent grade, and were used without further purification. Potassium trithionate and potassium tetra-

TABLE 1. PROCEDURES AND THE EQUIVALENTS OF THIOCYANATE EXPECTED

Procedure	Outline of the procedure	Reactions	Equivalents of SCN^- expected
A	Cupric ion-catalyzed cyanolysis of thiosulfate at pH 4.5	(1)	$S_A^{a)} = (S_2O_3^{2-})^{a)}$
B	Cyanolysis of tetrathionate in the presence of acetone followed by cupric ion-catalyzed cyanolysis of thiosulfate	(1), (4)	$S_B = (S_2O_3^{2-}) + 2(S_4O_6^{2-})$
C	Cyanolysis of trithioate and tetrathioate in boiling water bath followed by cupric ion-catalyzed cyanolysis of thiosulfate	(1), (2), (4)	$S_C = (S_2O_3^{2-}) + (S_3O_6^{2-}) + 2(S_4O_6^{2-})$

a) Denotes the amount in mole unit.

* Present address: Chemical Research Institute of Non-Aqueous Solutions, Tohoku University, Sendai 980

Table 2. Analysis of polythionate samples (wt%)

	$K_2S_3O_6$		$K_2S_4O_6$	
	K[a]	S[b]	K	S
Theoretical values	28.92	35.57	25.86	42.40
Measured values	28.97	35.74	25.85	42.93

a) Determined by gravimetry as potassium sulfate after ignition at 700 °C. b) Determined by gravimetry as barium sulfate after oxidation with potassium chlorate.

thionate were prepared by Stamm's method[19] and Martin's method[20], respectively, and were found to be free from thiosulfate as well as other polythionates by paper chromatography.[21] The results of analyses of the polythionates are shown in Table 2, indicating that these polythionate samples are pure enough for the purpose of this study.

Standard Trithionate Solution (0.01 M): Dissolve 0.5407 g of potassium trithionate in distilled water, and dilute to 200 ml. Prepare working solutions by suitable dilution.

Standard Tetrathionate Solution (0.01 M): Dissolve 0.6049 g of potassium tetrathionate in distilled water, and dilute to 200 ml. Prepare working solutions by suitable dilution.

Standard Thiocyanate Solution (0.05 M): Dissolve potassium thiocyanate in distilled water, and standardize by Volhard's method. Prepare working solutions by suitable dilution.

Standard Thiosulfate Solution (0.01 M): Dissolve sodium thiosulfate pentahydrate in distilled water, and standardize by iodometry. Prepare working solutions by suitable dilution.

Potassium Cyanide Solution (0.5 M): Dissolve 17.2 g of potassium cyanide in distilled water and dilute to 500 ml.

Cupric Chloride Solution (0.2 M): Dissolve 17.6 g of cupric chloride dihydrate in distilled water, dilute to 500 ml, and add a drop of concentrated hydrochloric acid to prevent the hydrolysis of cupric ions.

Buffer Solutions: Buffer solutions of desired pH values are obtained by mixing the following two solutions in a suitable ratio.

2 M acetate buffer solution: 2 M acetic acid with 2 M ammonium acetate,

0.2 M phosphate buffer solution: 0.2 M sodium dihydrogen phosphate with 5 M sodium hydroxide.

Ferric Nitrate-Perchloric Acid Solution:[13] Dissolve 303 g of ferric nitrate, $Fe(NO_3)_3 \cdot 9H_2O$, in a small volume of distilled water containing 217 ml of concentrated perchloric acid (60 wt%), and then dilute to 500 ml with distilled water.

Recommended Procedures. Procedure A. Cupric Ion-Catalyzed Cyanolysis of Thiosulfate at pH 4.5: Transfer an aliquot of the sample solution to a 50-ml volumetric flask. To this, add 10 ml of acetate buffer of pH 4.5, 1 ml of 0.5 M potassium cyanide solution, and 1.5 ml of 0.2 M cupric chloride solution, in this order, with mixing. Finally, add 5 ml of ferric nitrate-perchloric acid solution with continuous mixing, and make up to 50 ml with distilled water. Measure the absorbance of the solution against reagent blank at 460 nm in a glass cell of 10 mm thick. The content must be kept at 20 °C or lower to prevent the cyanolysis of higher polythionates. The thiocyanate equivalent can be obtained from the calibration curve prepared by using standard thiosulfate or thiocyanate solutions.

Procedure B. Cyanolysis of Tetrathionate in the Presence of Acetone Followed by Cupric Ion-Catalyzed Cyanolysis of Thiosulfate: Transfer an aliquot of the sample solution to a 50-ml volumetric flask, and add water to give a total volume of about 15 ml. Neutralize with 1 M ammonia water to thymolphtalein, add 10 ml of acetone, and cool to 20 °C. Add 2 ml of 0.5 M potassium cyanide solution and maintain at 20 °C for 20 min. Add 1.5 ml of 0.2 M cupric chloride solution, and apply the same ensuing manipulation as that in Procedure A.

Procedure C. Cyanolysis of Trithionate and Tetrathionate in Boiling Water Bath Followed by Cupric Ion-Catalyzed Cyanolysis of Thiosulfate: Transfer an aliquot of the sample solution to a 50-ml volumetric flask. Add a few drops of 0.1% thymolphtalein as well as 2 ml of 0.5 M potassium cyanide solution, and also 1 M ammonia water until a blue color comes out. Keep the flask in a boiling water for 30 min, and then cool to room temperature. Add 1.5 ml of 0.2 M cupric chloride solution and apply the same ensuing manipulation as that in Procedure A.

Unless otherwise stated, the concentrations mentioned in this report are values presented when the solutions are made up to 50 ml. The term of "cyanolysis" denotes "cyanolysis in the absence of cupric ions", and is distinct from "cupric ion-catalyzed cyanolysis". The degree of cyanolysis in each procedure is expressed as the ratio of equivalents of thiocyanate obtained to those expected to be obtained which are shown in Table 1. The concentrations of the stock solution of trithionate and of tetrathionate were determined on the assumption that the purities of both samples were 100%, since the impurities are not correctly determined by any of the methods previously reported. A Hitachi spectrophotometer model 101 was used to measure the absorbance.

Results and Discussion

Procedure A. Cupric Ion-Catalyzed Cyanolysis of Thiosulfate at pH 4.5. In Procedure A, the reaction shown by Eq. (1) is expected to proceed exclusively.

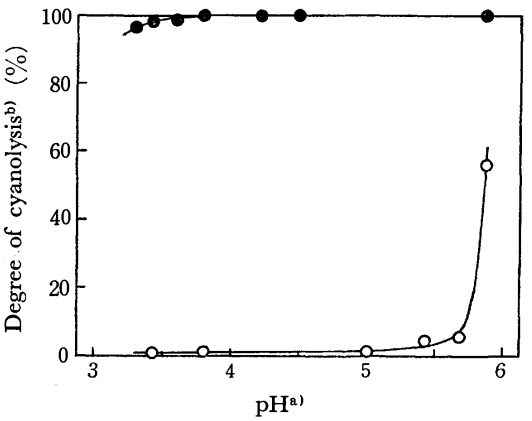

Fig. 1. Effect of pH on the cyanolysis of thiosulfate and tetrathionate.
Concn of KCN: 10 mM, concn. of $CuCl_2$: 6 mM, $S_2O_3^{2-}$(●) and $S_4O_6^{2-}$(○) taken: 5.00 μmol/50 ml.
a) pH values are those shown after $CuCl_2$ addition, which differed from those of the buffer solutions used by less than 0.2.
b) The degree of cyanolysis at each pH value was calculated by [(the absorbance obtained when such solutions as sample, buffer, KCN, $CuCl_2$ and $Fe(NO_3)_3$-$HClO_4$ were mixed in this order)/(the absorbance obtained when such solutions as sample, KCN, $CuCl_2$, $Fe(NO_3)_3$-$HClO_4$ and buffer were mixed in this order)] × 100. In the cyanolysis of tetrathionate, the reaction mixtures were maintained at the room temperature for 5 min before an addition of $CuCl_2$ solution.

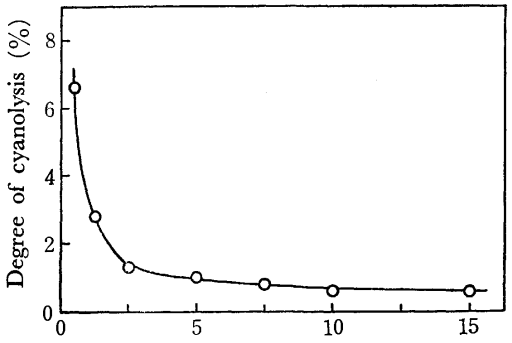

Fig. 2. Effect of the amount of acetate buffer solution of pH 4.5 on the cyanolysis of tetrathionate.
Concn. of KCN: 10 mM, concn. of $CuCl_2$: 6 mM, $S_4O_6^{2-}$ taken: 5.00 μmol/50 ml.

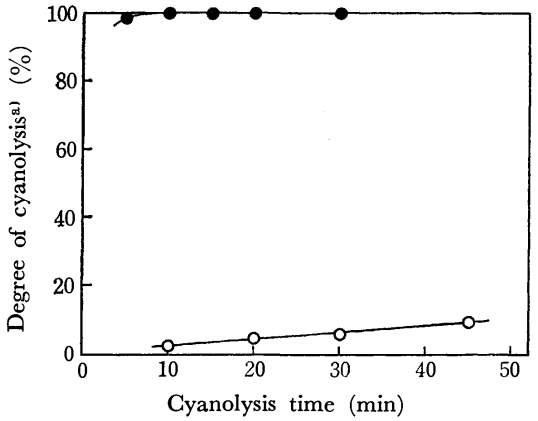

Fig. 3. Cyanolysis of trithionate and tetrathionate by Kelly's method.
○: trithionate, ●: tetrathionate.
Temp.: 5 °C, concn. of KCN: 20 mM, cyanolysis pH: 9.7, $S_3O_6^{2-}$ taken: 10.13 μmol/50 ml, $S_4O_6^{2-}$ taken: 5.00 μmol/50 ml.
a) Determined by using a calibration curve prepared from a standard thiocyanate solution. See Table 1 for the theoretical equivalents of thiocyanate.

It has been cleared by Urban[7] that the reaction shown by Eq. (1), catalyzed by cupric ions, proceeds selectively if the pH is carefully controlled, but the procedure is complicated. Figure 1 shows the results of the cyanolysis of thiosulfate and tetrathionate in the presence of acetate buffer solutions of various pH values. It is clear that the reaction shown by Eq. (1) takes place quantitatively above the pH value of 4, while the cyanolysis of tetrathionate hardly proceeds below the pH value of 5. These results are almost consistent with those by Urban.[7] Koh *et al.*[17] have reported that thiosulfate is not converted quantitatively to thiocyanate below the pH value of 5. This discrepancy may be attributed to their determination of pH values after an addition of cyanide solution. Figure 2 shows the effect of the amount of buffer solution added on the degree of cyanolysis of tetrathionate. It is clear that the addition of more than 5 ml has little effect. The amount added in the recommended procedure has been decided to be 10 ml per 50 ml so as to depress the fluctuation of pH in the analysis of practical samples.

The cyanolysis degree of 10 μmol of trithionate and that of 5 μmol of tetrathionate were 0.3 and 0.6%, respectively, showing that the cyanolysis of thiosulfate shown by Eq. (1) proceeds exclusively in the presence of acetate buffer of pH 4.5.

Procedure B. Cyanolysis of Tetrathionate in the Presence of Acetone Followed by Cupric Ion-Catalyzed Cyanolysis of Thiosulfate. In Procedure B, the reactions shown by Eqs. (1) and (4) are expected to proceed, while the cyanolysis of trithionate shown by Eq. (2) must be depressed. Kelly *et al.*[18] have described that the cyanolysis of trithionate can be depressed under the conditions of reaction temperature 5 °C and pH 9.65, but the actual degree of cyanolysis of trithionate is not shown.

The procedure proposed by Kelly *et al.* (Treatment I) was applied to analyses of trithionate and tetrathionate. The results in Fig. 3 show that tetrathionate undergoes a quantitative conversion according to Eq. (3), while the degree of cyanolysis of trithionate cannot be ignored. One of the reasons why recoveries of tetrathionate in the analysis of mixtures tend to be high, and those of thiosulfate correspondingly low by their method, may be that the cyanolysis of trithionate is not depressed quantitatively.

Several sorts of organic solvents were added to lower the dielectric constant of the solution, so as to prevent the cyanolysis of trithionate. Organic solvents were added after the regulation of pH. As is evident from the results shown in Table 3, the degree of cyanolysis of trithionate is depressed greatly by the addition of organic solvents, which, however, cannot be related simply to the dielectric constant of the solution. The cyanolysis in the presence of methanol and acetone was

Table 3. Effect of organic solvents on the cyanolysis of trithionate and tetrathionate in the absence of cupric ions

Organic solvent added (vol.%)	Degree of cyanolysis[a] (%)	
	$S_3O_6^{2-}$	$S_4O_6^{2-}$
None	24.4	100.0
Methanol (20)	2.9	100.4
Ethanol (20)	3.4	100.2
Isopropanol (20)	3.8	99.6
Ethylene glycol (20)	4.9	98.2
Dioxane (10)	6.2	117.5
(20)	3.4	133.8
(30)	2.3	144.0
Acetone (20)	4.2	100.4

Temp.: 25 °C, time: 30 min, concn. of KCN: 20 mM, $S_3O_6^{2-}$ taken: 9.90 μmol/50 ml, $S_4O_6^{2-}$ taken: 5.02 μmol/50 ml. Ferric nitrate-nitric acid solution[6], which is obtained by dissolving 50 g of ferric nitrate in water containing 100 ml of concentrated nitric acid followed by diluting to 500 ml with water, was used. a) Determined by using a calibration curve prepared from a standard thiocyanate solution. See Table 1 for the theoretical equivalent of thiocyanate.

Table 4. Cyanolysis of trithionate and tetrathionate in the presence of methanol

Concn. of KCN (mM)	Concn. of MeOH (vol.%)	Temp. (°C)	Time (min)	Absorbance[a]	
				$S_3O_6^{2-}$	$S_4O_6^{2-}$
10	20	10	30	0.0005	0.402
10	20	30	15	0.013	0.409
10	20	30	60	0.037	0.410
10	30	10	30	0.000	0.377
10	30	20	30	0.0045	0.423
10	30	30	30	0.012	0.425
10	40	30	30	0.007	0.434
15	30	20	15		0.416, 0.418
15	30	20	30	0.000	0.420
20	20	25	30	0.012	0.410
20	30	10	5		0.293
20	30	10	10		0.379
20	30	10	15		0.407
20	30	10	20		0.418
20	30	10	30	0.001	0.420
20	30	20	15	0.001, 0.000	0.423, 0.424
20	30	20	30	0.006	0.423
20	30	25	15	0.008, 0.008	
20	30	30	30	0.026	0.422
20	40	30	30	0.016	0.437

$S_3O_6^{2-}$ taken: 9.90 μmol/50 ml, $S_4O_6^{2-}$ taken: 5.04 μmol/50 ml. a) Ferric nitrate-nitric acid solution was used. Optimum conditions: methanol 30 vol.%, KCN 20 mM, temp. 20 °C, time 15 min.

Table 5. Cyanolysis of trithionate and tetrathionate in the presence of acetone

Concn. of KCN (mM)	Concn. of acetone (vol.%)	Time (min)	Absorbance	
			$S_3O_6^{2-}$	$S_4O_6^{2-}$
15	20	10	0.0035	0.421
15	20	15		0.447
15	20	20	0.005	0.456
15	20	25		0.460
15	20	30	0.0085	0.460
15	20	40	0.010	
20	20	5		0.400
20	20	10	0.004	0.4525
20	20	15		0.4615
20	20	20	0.007	0.4615
20	20	30	0 0125	
20	20	40	0.014	
20	30	10	0.003	0.419
20	30	15		0.453
20	30	20	0.005	0.467
20	30	25		0.472
20	30	30	0.0075	0.471
20	30	35		0.472
20	30	40	0.009	

$S_3O_6^{2-}$ taken: 9.90 μmol/50 ml, $S_4O_6^{2-}$ taken: 5.04 μmol/50 ml. Optimum conditions: acetone 20 vol.%, KCN 20 mM, temp. 20 °C, time 20 min.

investigated in detail, results of which being shown in Tables 4 and 5, respectively. Under each table are described the optimum conditions, where at as near as 20 °C, in a short time, the cyanolysis of tetrathionate is saturated, and that of trithionate shows its minimum.

In the case when methanol was added, ferric nitrate–nitric acid solution[6] was used instead of ferric nitrate–perchloric acid solution, so as potassium perchlorate not to precipitate. As is evident from Table 6, the conditions shown under Table 5 seem to be superior to those shown under Table 4, in respect that the ab-

Table 6. Effect of foreign substances on the cupric ion-catalyzed cyanolysis of thiosulfate in the presence of methanol and acetone

		Organic solvent added (vol.%)	
Fe reagent		Methanol (30) $Fe(NO_3)_3$-HNO_3[6]	Acetone (20) $Fe(NO_3)_3$-$HClO_4$[13]
Na_2SO_4	50 mg/50 ml	93.3%[a]	100.0%
	100	88.5	100.4
	200	80.4	100.9
Na_2HPO_4	4	98.9	99.8
	20	97.5	99.8
	40	80.3	97.2
	100	40.7	95.6
	200	7.6	88.9
NaCl	50	98.6	100.6
	100	97.9	102.8
	250	95.5	111.9
	500	96.5	134.2
Na_2SO_3	1	94.4	99.2
	2	91.7	96.1
	5	87.5	92.4
	10	85.4	91.9

$S_2O_3^{2-}$ taken: 5.00 μmol/50 ml, concn. of KCN: 20 mM, concn. of $CuCl_2$: 6 mM. a) The figures show the recoveries of thiosulfate in per cent.

Table 7. Cyanolysis of thiosulfate, trithionate and tetrathionate under the optimum conditions

Organic solvent		MeOH	Acetone
Amount added (vol.%)		30	20
Concn. of KCN (mM)		20	20
Temp. (°C)		20	20
Time (min)		15	20
Degree of cyanolysis (%)	$S_2O_3^{2-}$	0.6	0.8
	$S_3O_6^{2-}$	0.1	0.7
	$S_4O_6^{2-}$	100.4	100.4

Amount of sample taken (μmol/50 ml): $S_2O_3^{2-}$ 10.00, $S_3O_6^{2-}$ 9.90, $S_4O_6^{2-}$ 5.04.

sorbance is not affected so much by co-existing ions. Accordingly, the authors have concluded that acetone is superior to methanol as a solvent to be added for depressing the cyanolysis of trithionate. Nietzel *et al.*[5] have reported that the sensitivity of analysis is increased by the addition of acetone in the cyanolysis of tetrathionate. However, it may be a new finding that the degree of cyanolysis of trithionate is depressed by the addition of organic solvents.

The degrees of cyanolysis of thiosulfate, trithionate and tetrathionate under the recommended conditions are given in Table 7. It is clear that the degree of cyanolysis of trithionate is extremely low, compared with the value of 4.7% under the conditions proposed by Kelly *et al.* (see Ref. 18, Treatment I). On the other hand, the degree of cyanolysis of tetrathionate was almost 100%. However, it may be well considered that 1% of thiosulfate formed as shown by Eq. (3) is converted to thiocyanate, since the purity of tetrathionate sample is not necessarily pure, and the cyanolysis of thiosulfate proceeds by 0.8% under these above-mentioned conditions. The reason why the discrepancy between expected value and obtained value in Treatment I is much larger than the discrepancies obtained in Treatments II and III proposed by Kelly *et al.*, may be also related to the phenomena of partial cyanolysis of thiosulfate as described above. On the other hand, the error due to the partial cyanolysis of thiosulfate may be eliminated, if all of the thiosulfate are converted to thiocyanate in the presence of cupric ions.

Now Procedure B′ will be discussed below. This procedure denotes the cyanolysis procedure for only tetrathionate in the absence of cupric ions and is identical, in principle, with Treatment I proposed by Kelly *et al.* As a relation of $S_B=S_A+2S_{B'}$ exists between the thiocyanate equivalents(S) of three sorts of procedures, one of the three procedures can be omitted for the determination of thiosulfate, trithionate and tetrathionate. It seems that Procedure B′ is most apt to produce error among the three procedures, so the authors have not adopted this procedure as one of the recommended procedures. Procedure B′, however, is useful for judging if higher polythionates are present or not in the sample solutions.

In Table 8, the thiosulfate concentration obtained in the presence of acetone is compared with that obtained in the absence of acetone, showing that the cyanolysis of thiosulfate proceeds quantitatively in

Table 8. Effect of acetone on the cupric ion-catalyzed cyanolysis of thiosulfate[a]

Addition (vol.%)	$S_2O_3^{2-}$ obtained (mM)
None	1.042
Acetone (20) (=Procedure B)	1.036

Concn. of KCN: 20 mM, concn. of $CuCl_2$: 6 mM, $S_2O_3^{2-}$ concn. determined by iodometry: 1.035 mM.
a) The calibration curves were prepared by using a standard thiocyanate solution. The figures are the means of three measurements.

Procedure B. The purity of potassium tetrathionate sample used in the present study was found to be 99.0% by means of Procedure B.

Procedure C. Cyanolysis of Trithionate and Tetrathionate in Boiling Water Bath Followed by Cupric Ion-Catalyzed Cyanolysis of Thiosulfate. In Procedure C, not only thiosulfate and tetrathionate but also trithionate must be converted to thiocyanate. Urban[8] has reported the conditions under which the cyanolysis of trithionate proceeds quantitatively. These conditions, however, are not practical due to the extremely long reaction time. Kelly *et al.*[18] have proposed a procedure for the determination of trithionate by means of its cyanolysis at 100 °C and pH 9.6, followed by cupric ion-catalyzed cyanolysis of thiosulfate formed by the side reaction shown by Eq. (5).

$$S_3O_6^{2-} + H_2O = S_2O_3^{2-} + SO_4^{2-} + 2H^+ \quad (5)$$

The principle of Procedure C in the present study is wholly identical with that proposed by Kelly *et al.* The addition of a large amount of phosphate, however, decreased the absorbance, as in the case of Procedure B, so the present authors decided to adopt the recommended procedure as shown above. There seems to be sufficient probability that thiosulfate and tetrathionate undergo the quantitative cyanolysis under the conditions of Procedure C.

The cyanolysis of trithionate without cupric ions was investigated at various temperatures, the results of which are shown in Fig. 4. It is obvious that the maximum

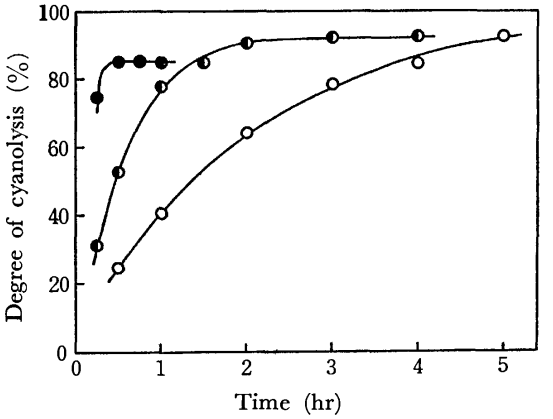

Fig. 4. Cyanolysis of trithionate at various temperatures.
Temp. (°C): ○ 50, ◐ 70, ● 90—95.
Concn. of KCN: 20 mM, $S_3O_6^{2-}$ taken: 4.95 μmol/50 ml.

recovery of trithionate decreases gradually with the increase of the cyanolysis temperature. On the other hand, the recoveries of trithionate under the following two sorts of cyanolysis conditions for 3 hr at 50 °C and 30 min at 95 °C, were the same and amounted to 97.6%, in the case when cupric ions were added after the cyanolysis. A difference of 2.4% between the expected value and the found value may be attributed to the impurities of the sample. Accordingly, it seems that trithionate undergoes the side reaction as shown by Eq. (5) during the cyanolysis at high temperature, and that Procedure C can be performed with a satisfactory accuracy for trithionate as well as thiosulfate and tetrathionate, as having been shown by Kelly *et al.* The purity of potassium tetrathionate sample used in the present study was found to be 99.3% by means of Procedure C.

Precision and Range of Determination. The precisions of Procedures A, B and C were evaluated by determining the concentrations of thiosulfate, tetrathionate and trithionate solutions, respectively, the results of which are shown in Table 9. An absorbance of 1.0 was obtained, when Procedures A, B and C were carried out, taking 12, 11 and 12 μ equivalents of thiocyanate in a 50-ml volumetric flask, respectively.

TABLE 9. REPLICATE DETERMINATION OF THE CONCENTRATIONS OF THIOSULFATE, TETRATHIONATE AND TRITHIONATE SOLUTIONS

Sample solution / Procedure applied		$S_2O_3^{2-}$ A	$S_4O_6^{2-}$ B	$S_3O_6^{2-}$ C
Analysis	1	0.495 mM	0.495 mM	0.489 mM
	2	0.496	0.495	0.488
	3	0.496	0.496	0.487
	4	0.495	0.495	0.487
	5	0.495	0.495	0.488
	6	0.495	0.494	0.488
Average		0.4953	0.4950	0.4878
CV (%)		0.23	0.28	0.34

TABLE 10. APPLICATION TO THE ANALYSIS OF MIXTURES OF THIOSULFATE, TRITHIONATE AND TETRATHIONATE (unit: mM)

		$S_2O_3^{2-}$	$S_3O_6^{2-}$	$S_4O_6^{2-}$	Procedures
Expt. 1	Expected	0	0	0.494	
	Found	0.002	0.004	0.486	A, B, C
2	Expected	0.364	0	0.368	
	Found	0.371	0.008	0.358	A, B, C
3	Expected	0.414	0.393	0.401	
	Found	0.418	0.382	0.395	A, B, C
		0.418	0.358	0.407	A, B', C
		0.394	0.382	0.407	B', B, C

The sample solutions were prepared by mixing the individual stock solutions. Procedure B' is identical with Procedure B; the only difference is that cupric chloride is not added in Procedure B'. In the case when Procedure B' is adopted, the amount of thiosulfate, trithionate and tetrathionate are given as follows: $(S_2O_3^{2-}) = S_B - 2S_{B'}$, $(S_3O_6^{2-}) = S_C - S_A - 2S_{B'}$, $(S_4O_6^{2-}) = S_{B'}$.

Absorbance and concentration showed a good linear relation between them within this concentration range.

Application to the Analyses of Mixtures. From the results described above, it is concluded that Procedures A, B and C can be performed without any noticeable side reactions. The following equivalents of thiocyanate(S) are formed by the three procedures (see Table 1):

$$S_A = (S_2O_3^{2-})$$
$$S_B = (S_2O_3^{2-}) + 2(S_4O_6^{2-})$$
$$S_C = (S_2O_3^{2-}) + (S_3O_6^{2-}) + 2(S_4O_6^{2-}).$$

Then, the amount of the species are given as follows:

$$(S_2O_3^{2-}) = S_A$$
$$(S_3O_6^{2-}) = S_C - S_B$$
$$(S_4O_6^{2-}) = \frac{1}{2}(S_B - S_A).$$

Table 10 shows the results of analyses of the mixtures consisting of thiosulfate, trithionate and tetrathionate. The values determined by Procedures A, B and C agree well with the expected values with a maximum discrepancy of 3%. This discrepancy seems to arise mainly by assuming that the polythionate samples are pure. On the other hand, it is noted that in the case when Procedure B' is adopted, recoveries of tetrathionate tend to be high, while those of thiosulfate or trithionate tend to be correspondingly low. This phenomena may be explained by the fact that the cyanolysis of thiosulfate and trithionate cannot be depressed completely in Procedure B'.

In the analytical method described here, polythionates above tetrathionate were not considered. Investigation on the photometric determination method for thiosulfate, trithionate, tetrathionate and pentathionate are currently under way. If polythionates above tetrathionate react with cyanide quantitatively in Procedure B as shown in Eq. (6), the value of $1/2(S_B - S_A)$

$$S_nO_6^{2-} + (n-2)CN^- + 2OH^- = (n-2)SCN^- + SO_3^{2-} + SO_4^{2-} + H_2O \quad (6)$$

would be as follows: $((S_4O_6^{2-}) + 3/2(S_5O_6^{2-}) + 2(S_6O_6^{2-}) + \cdots\cdots)$. Paper chromatography[21] may be useful for judging the presence of such higher polythionates.

In the reaction of low valence sulfur compounds, a few sorts of polythionates often appear together with the familiar compounds such as thiosulfate, sulfite and sulfate. However, the analysis of sulfite and sulfate is not a serious problem. Accordingly, the present analytical method, by which the determination of thiosulfate, trithionate and tetrathionate in the concomitant presence of them can be made with a great simplicity and a high accuracy, may be used widely in various fields.

References

1) Part VIII of this series: M. Takizawa, A. Okuwaki, and T. Okabe, This Bulletin, **46**, 3785 (1973).

2) A. Kurtenacker and E. Goldbach, *Z. Anorg. Allg. Chem.*, **166**, 177 (1927); *ibid.*, **134**, 265 (1924).

3) R. R. Jay, *Anal. Chem.*, **25**, 288 (1953).

4) L. Szekeres, *Talanta*, **21**, 1 (1974).
5) O. A. Nietzel and M. A. DeSesa, *Anal. Chem.*, **27**, 1839 (1955).
6) B. Sörbo, *Biochim. Biophys. Acta*, **23**, 412 (1957).
7) P. J. Urban, *Z. Anal. Chem.*, **179**, 415 (1961).
8) P. J. Urban, *ibid.*, **179**, 422 (1961).
9) P. J. Urban, *ibid.*, **180**, 110 (1961).
10) P. J. Urban, *ibid.*, **180**, 116 (1961).
11) T. Koh, A. Wagai, and Y. Miura, *Anal. Chim. Acta*, **71**, 367 (1974).
12) T. Koh and I. Iwasaki, This Bulletin, **39**, 352 (1966).
13) T. Koh, *ibid.*, **38**, 1510 (1965).
14) T. Koh and I. Iwasaki, *ibid.*, **38**, 2135 (1965).
15) T. Koh, *Bunseki Kagaku*, **22**, 322 (1973).
16) T. Koh and N. Saito, *Anal. Chim. Acta*, **61**, 449 (1972).
17) T. Koh and I. Iwasaki, This Bulletin, **39**, 703 (1966).
18) D. P. Kelly, L. A. Chambers, and P. A. Trudinger, *Anal. Chem.*, **41**, 898 (1969).
19) H. Stamm, M. Goehring, and U. Feldmann, *Z. Anorg. Allg. Chem.*, **250**, 226 (1942).
20) F. Martin and L. Metz, *ibid.*, **127**, 83 (1923).
21) P. A. Trudinger, *J. Bacteriol.*, **93**, 550 (1967).

Phase Equilibria in the $Fe-Fe_2O_3-Eu_2O_3$ System at 1200 °C

Tadashi SUGIHARA, Noboru KIMIZUKA,* and Takashi KATSURA

Department of Chemistry, Tokyo Institute of Technology, Ookayama, Meguro-ku, Tokyo 152

**National Institute for Researches in Inorganic Materials, Sakuramura, Niiharigun, Ibaragi 300-31*

(Received October 9, 1974)

The standard Gibbs energies of the reaction of $EuFeO_3$ and $Fu_3Fe_5O_{12}$ were determined to be -63300 ± 200 cal and -297800 ± 600 cal respectively at 1200 °C by means of following reactions: $Fe+1/2\ Eu_2O_3+3/4\ O_2=EuFeO_3$ and $5\ Fe+3/2\ Eu_2O_3+15/4\ O_2=Eu_3Fe_5O_{12}$, based on the phase equilibria in the $Fe-Fe_2O_3-Eu_2O_3$ system.

Many works on the double oxides involving rare earth sesquioxide and iron oxide have been investigated from the standpoint of crystal chemistry and the magnetic properties of perovskite and garnet structures.[1] Recently, Bedford and Catalano[2] have confirmed the existence of EuO, Eu_3O_4, and Eu_2O_3 at 1500 °C; they were first found by Bärnighausen.[3] McCarthy and Fischer[4] have also studied the Eu–Fe–O system at 1200 °C in a flowing argon atmosphere; they have also confirmed these compounds in addition to $EuFeO_3$ and $Eu_3Fe_5O_{12}$. However, very few studies have been done on the Gibbs energy of the reaction of lanthanoid-iron -perovskite or -garnet.

Recently, Kimizuka and Katsura[5] have determined the standard Gibbs energy of the reaction of $LaFeO_3$ from metallic iron, La_2O_3, and oxygen on the basis of the phase equilibria in the $Fe-Fe_2O_3-La_2O_3$ system at 1204 °C. They[6] have also established the phase equilibria in the $Fe-Fe_2O_3-Y_2O_3$ system at 1200 °C and determined the Gibbs energy of the reactions of $YFeO_3$, $Y_3Fe_5O_{12}$, and YFe_2O_4.

In the present study, we have determined the standard Gibbs energy of the reaction of $EuFeO_3$ and $Eu_3Fe_5O_{12}$ at 1200 °C on the basis of the phase equilibria in the $Fe-Fe_2O_3-Eu_2O_3$ system.

Experimental

Materials. High-purity-grade (99.9%) Eu_2O_3 and guaranteed-reagent-grade Fe_2O_3 were employed as the starting substances. Eu_2O_3 was heated at 1200 °C in air for 2 days to obtain B-type Eu_2O_3.[7] Fe_2O_3 was heated at 900 °C in air for 1 day. The subsequent procedures to obtain the sintered mixtures were the same as those described in a previous paper.[5]

Apparatus and Procedures. The quenching and thermogravimetric methods were adopted in the present study; the details of the procedures have been described by Kimizuka and Katsura.[5,6] The weight of the sample in oxygen was chosen as the reference for thermogravimetry. The equilibrium composition was determined by means of two side reactions. The quenching method employed in the present study is the same as that described in a previous paper,[6] the phases in quenched samples were identified by the powder X-ray diffraction method, with Mn-filtered Fe-$K\alpha$ radiation. The Fe^{2+}/Fe^{3+} ratio in the quenched nonstoichiometric $EuFeO_3$ was determined by the wet chemical method.[8]

Results and Discussion

Phase Equilibria. The equilibrium data at 1200 °C are summarized in Table 1 and are illustrated in Fig. 1. The following phases were stable under the present ex-

TABLE 1. DATA FOR EQUILIBRIA IN THE $Fe-Fe_2O_3-Eu_2O_3$ SYSTEM AT 1200°C

$\log P_{O_2}$ (±0.02)	Fe	Fe_2O_3 (mole %)	Eu_2O_3	Phases
0.00	0.00	38.00	62.00	E+Pv
	0.00	50.00	50.00	Pv
	0.00	57.00	43.00	Pv+G
	0.00	62.50	37.50	G
	0.00	78.56	21.44	H+G
	0.00	80.00	20.00	H+G
	0.00	90.00	10.00	H+G
3.88	0.00	57.00	43.00	Pv+G
	0.00	62.50	37.50	G
	10.14	70.92	18.94	M+G
	9.36	70.20	20.44	M+G
	15.05	75.70	9.25	M+G
9.14	3.75	53.39	42.91	M+Pv
	6.01	57.61	36.38	M+Pv
	12.50	67.40	20.10	M+Pv
	13.10	68.21	18.69	M+Pv
	16.92	73.93	9.15	M+Pv
9.27	6.42	51.96	41.62	W+Pv
	11.01	53.55	35.44	W+Pv
	23.39	57.68	18.93	W+Pv
	24.26	58.16	17.58	W+Pv
	30.96	60.60	8.44	W+Pv
9.80	25.44	57.10	17.46	W+Pv
10.26	26.68	55.99	17.33	W+Pv
10.82	28.06	54.74	17.20	W+Pv
11.26	29.31	53.62	17.07	W+Pv
11.92	8.45	50.37	41.18	W+Pv
	14.47	50.74	34.79	W+Pv
	29.29	52.42	18.31	W+Pv
	30.65	52.41	16.91	W+Pv
	38.49	53.44	8.07	W+Pv
12.09	23.59	38.48	37.93	Fe+Pv
	40.10	29.92	29.98	Fe+Pv
	72.25	14.05	13.70	Fe+Pv
	75.15	12.36	22.49	Fe+Pv
	88.75	5.69	5.56	Fe+Pv
12.51	0.69	37.53	61.78	E+Pv
	1.58	48.84	49.58	Pv
13.02	76.69	0.19	23.12	Fe+E
	87.61	0.34	12.05	Fe+E
	88.71	0.16	11.13	Fe+E
	94.56	0.17	5.27	Fe+E
15.80	66.66	0.01	33.33	Fe+E
	54.97	0.07	44.96	Fe+E
	72.22	0.31	27.47	Fe+E

Abbreviations have the following meaning: E=Eu_2O_3, Pv=$EuFeO_3$, G=$Eu_3Fe_5O_{12}$, H=Fe_2O_3, M=Fe_3O_4, W=FeO, Fe=metallic iron.

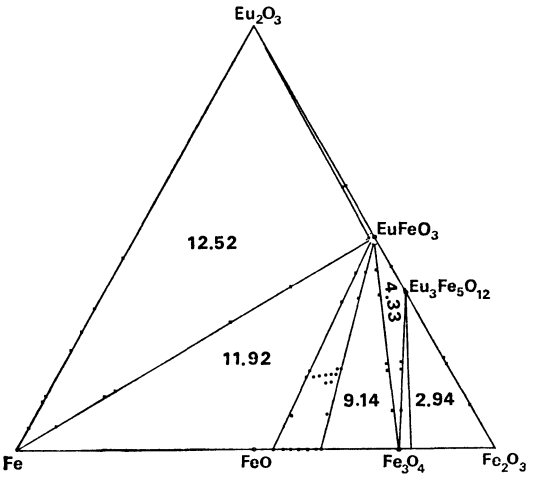

Fig. 1. Phase equilibria in the Fe-Fe_2O_3-Eu_2O_3 system at 1200 °C.
Numbers in the Figure mean values of $-\log P_{O_2}$ at which three crystalline phases are in equilibrium state. Small dots show the experimental results given in Table 1.

perimental conditions: Europium sesquioxide (Eu_2O_3), hematite (Fe_2O_3), magnetite (Fe_3O_4), wüstite (FeO), metallic iron (γ-Fe), europium-iron-perovskite ($EuFeO_3$), and europium-iron-garnet ($Eu_3Fe_5O_{12}$). The equilibria among the three condensed phases are as follows: (1) $EuFeO_3$, Eu_2O_3, and metallic iron, (2) $EuFeO_3$, wüstite, and metallic iron, (3) $EuFeO_3$, magnetite, and wüstite, (4) $EuFeO_3$ $Eu_3Fe_5O_{12}$, and magnetite, and (5) $Eu_3Fe_5O_{12}$, magnetite, and hematite. The following phases were characterized with respect to the stoichiometry: (a) Pure Eu_2O_3 was stable down to an oxygen partial pressure of $10^{-15.80}$ atm. However, it showed a small degree of non-stoichiometry at $10^{-15.80}$ atm. McCarthy and White[9] have reported the approximate phase relation of the Eu–Eu_2O_3 system at elevated temperatures up to 2200 °C; they showed the non-stoichiometry for Eu_2O_3 at 1200 °C and about 10^{-15} atm P_{O_2}, but they did not ascertain the extent of this non-stoichiometry. In the present study, by means of the thermogravimetric method, we determined the composition of the non-stoichiometric Eu_2O_3 phase to be $Eu_2O_{2.98\pm0.02}$ at $10^{-15.80}$ atm P_{O_2}: The lattice constants of both stoichiometric and non-stoichiometric Eu_2O_3 are given in Table 2. It is supposed that the non-stoichiometric Eu_2O_3 has a larger unit cell volume than the stoichiometric Eu_2O_3; this may be caused by the substitution of Eu^{2+} for Eu^{3+}. (b) The deviation from the stoichiometric composition of $Eu_3Fe_5O_{12}$ was not observed, and the lattice constants of the respective $Eu_3Fe_5O_{12}$ compounds equilibrated with Fe_2O_3, $EuFeO_3$ and with Fe_3O_4 were identical with each other. The values of stoichiometric $Eu_3Fe_5O_{12}$ are identical with those obtained by Espinosa.[10] (c) $EuFeO_3$ showed a significant deviation from the stoichiometry at relatively low oxygen partial pressures. The degree of non-stoichiometry was determined by both thermogravimetry and wet chemical analysis. These results were consistent with each other. The maximum deviation was

Table 2. Lattice constants of Eu_2O_3 and $EuFeO_3$

a) Eu_2O_3 (monoclinic B-type)

Lattice constants	Stoichiometric Eu_2O_3	Non-stoichiometric Eu_2O_3	Hoekstra[12]
a (Å)	14.102±0.005	14.113±0.004	14.12
b (Å)	3.601±0.001	3.603±0.001	3.600
c (Å)	8.806±0.004	8.808±0.003	8.801
β(deg)	100.02 ±0.3	100.05 ±0.2	99.98
V (Å^3)	440.3 ±0.3	441.0 ±0.2	

b) $EuFeO_3$ (Space group: D_{2h}^{16}-Pbnm, orthorhombic perovskite structure)

Lattice constants	$EuFeO_3$ coexisting with		Non-stoichiometric $EuFeO_3$	Stoichiometric $EuFeO_3$	Geller and Wood[13]
	Eu_2O_3	$Eu_3Fe_5O_{12}$			
a (Å)	5.373	5.371	5.373	5.373	5.371
b (Å)	5.607	5.605	5.607	5.604	5.611
c (Å)	7.683	7.684	7.685	7.684	7.686
V (Å^3)	231.4	231.3	231.5	231.3	231.6

Deviations in *a*, *b*, and *c* are ±0.001 by the least squares method, and those of *V* ±0.1.

determined to be $EuFeO_{2.976}$ at an oxygen partial pressure of $10^{-12.52}$ atm; at this point the non-stoichiometric $EuFeO_3$ was in equilibrium with both metallic iron and stoichiometric Eu_2O_3. $EuFeO_3$ shows a small but equivocal solubility of the three components. Since we could not determine the exact boundary of the $EuFeO_3$ field, the $EuFeO_3$ field was approximately bounded by the dotted line shown in Fig. 1. The lattice constants of $EuFeO_3$ in equilibrium with Eu_2O_3 and $Eu_3Fe_5O_{12}$, and of non-stoichiometric $EuFeO_3$ with the composition of $EuFeO_{2.976}$, were compared with those of stoichiometric $EuFeO_3$ given in Table 2.

(2) Calculation of the Standard Gibbs Energy of the Reaction of $EuFeO_3$ and $Eu_3Fe_5O_{12}$. On the basis of the phase equilibria, we may determine the following two standard Gibbs energies of the reaction of $EuFeO_3$ and $Eu_3Fe_5O_{12}$ from metallic iron, Eu_2O_3, and oxygen:

$$Fe + 1/2\,Eu_2O_3 + 3/4\,O_2 = EuFeO_3 \quad (1)$$

$$5\,Fe + 3/2\,Eu_2O_3 + 15/4\,O_2 = Eu_3Fe_5O_{12} \quad (2)$$

Since the $EuFeO_3$ component in equilibrium with metallic iron and Eu_2O_3 has the composition of $EuFeO_{2.976}$, it is convenient to choose the reference activity of the $EuFeO_3$ component as unity at this composition. As has been described before, the Eu_2O_3 component had a small compositional variation at lower oxygen partial pressures. However, the composition of Eu_2O_3 was nearly stoichiometric at an oxygen partial pressure of $10^{-12.52}$ atm, at which Reaction (1) was in the equilibrium state. Thus, with reference to Eq. (1), we may determine the standard Gibbs energy of the reaction of $EuFeO_3$ as follows

$$\Delta G^0(1) = 3/4\,RT \ln P_{O_2} = -63300\pm200\ \text{cal}\cdot\text{mol}^{-1},$$

where R and T indicate the gas constant and the absolute temperature respectively. The experimental error was estimated on the basis of the fluctuations of both temperature and the oxygen partial pressure.

Because the stoichiometric $Eu_3Fe_5O_{12}$ was in equilibrium with both stoichiometric $EuFeO_3$ and Fe_3O_4 at an oxygen partial pressure of $10^{-4.33}$ atm, the standard Gibbs energy change, referred to the following equation (3), may be calculated to be -4900 ± 200 cal:

$$3\,EuFeO_3 + 2/3\,Fe_3O_4 + 1/6\,O_2 = Eu_3Fe_5O_{12} \quad (3)$$

According to Darken and Gurry,[11] the activity of metallic iron in stoichiometric magnetite in equilibrium with wüstite is $10^{-1.545}$ at 1200 °C, while the oxygen partial pressure related to the wüstite-magnetite equilibrium in $10^{-9.14}$ atm. Thus, the standard Gibbs energy of the formation of Fe_3O_4, $\Delta G^0(4)$, referred to the following equation (4) may be calculated to be -154500 ± 300 cal at 1200 °C:

$$3\,Fe + 2\,O_2 = Fe_3O_4 \quad (4)$$

By adding $\Delta G^0(3)$, $2/3\Delta G^0(4)$, and $3\Delta G^0(1)$, we obtain the standard Gibbs energy of the reaction of $Eu_3Fe_5O_{12}$, $\Delta G^0(2)$, referred to Equation (2), as -297800 ± 600 cal.

It is interesting to compare the present Gibbs energy data with those of $LaFeO_3$, $YFeO_3$, and $Y_3Fe_5O_{12}$ which have been determined by Kimizuka and Katsura.[5,6] Comparing these data, we may observe that the standard Gibbs energy of the reaction of lanthanoid-iron perovskite from metallic iron, lanthanoid sesquioxide, and oxygen increases with decrease in the ionic radii of lanthanoid ions. The relationship between the ionic radii and the Gibbs energy will be discussed in more detail in the near future.

The authors wish to express their thanks to Dr. Kenzo Kitayama and Mr. Toshimori Sekine, Tokyo Institute of Technology.

References

1) G. Brauer, in "Progress in the Science and Technology of the Rare Earths," (L. Eyring, Ed.), Vol. 1, pp. 152—166, Pergamon Press, New York (1964): R. S. Roth, *ibid.*, pp. 167—210: E. F. Westrum, *ibid.*, pp. 310—350: N. A. Toropov, V. P. Barzakovskii, V. V. Lapin, and N. N. Kurtseva, in "Handbook of Phase Diagrams of Silicate Systems," Vol. 1, pp. 603—610, translated from Russian, Israel Program for Scientific Translations, Israel (1972): R. S. Roth, *J. Res. Natl. Bur. Stand*, **58**, No. 2, 75 (1957): R. S. Roth and S. J. Schneider, *J. Res. Nat. Bur. Stand.*, **64A**, No. 4, 309 (1960): S. J. Schneider, R. S. Roth, and J. L. Waring, *ibid.*, **65A**, No. 4, 345 (1961).

2) R. G. Bedford and E. Catanalo, *J. Solid State Chem.*, **3**, 112 (1971).

3) H. Bärnighausen, *J. Prakt. Chem.*, **34**, 1 (1965).

4) G. J. McCarthy and R. D. Fischer, *J. Solid State Chem.*, **4**, 340 (1972).

5) N. Kimizuka and T. Katsura, This Bulletin, **47**, 1801 (1974).

6) N. Kimizuka and Katsura, *J. Solid State Chem.*, **13**, 176 (1975). Standard Free Energy of Formation of $YFeO_3$, $Y_3Fe_5O_{12}$, and a New Compound YFe_2O_4 in the Fe-Fe_2O_3-Y_2O_3 system at 1200 °C.

7) R. S. Roth and S. J. Schneider, *J. Res. Nat. Bur. Stand.*, **64A**, 309 (1960).

8) I. Iwasaki, T. Katsura, M. Yoshida, and T. Tarutani, *Bunseki Kagaku*, **6**, 211 (1957).

9) G. J. McCarthy and W. B. White, *J. Less Common Metals.*, **22**, 409 (1970).

10) G. P. Espinosa, *J. Chem. Phys.*, **37**, 2344 (1962).

11) L. S. Darken and R. W. Gurry, *J. Am. Chem. Soc.*, **67**, 1398 (1945).

12) H. R. Hoekstra, *Inorg. Chem.*, **5**, 754 (1966).

13) S. Geller and E. A. Wood, *Acta Crystallogr.*, **9**, 563 (1956).

Thermochemical Properties of Lanthanoid-Iron-Perovskite at High Temperatures

Takashi KATSURA, Kenzo KITAYAMA, Tadashi SUGIHARA, and Noboru KIMIZUKA*

Department of Chemistry, Tokyo Institute of Technology, Ookayama, Meguro-ku, Tokyo 152

**National Institute for Researches in Inorganic Materials, Kurakake, Sakuramura, Niihari-gun, Ibaragi 300-31*

(Received October 9, 1974)

The standard Gibbs energy of formation of $\bar{C}FeO_3$($\bar{C}$=La, Nd, Sm, Eu, Gd, Tb, and Dy) from metallic iron, $\bar{C}_2O_3$, and oxygen has been determined at temperatures from 1473 to 1673 K. Based on the free-energy data, the heat of reaction and the entropy change resulting from the reaction have been calculated. The values of the heat of reaction of $LaFeO_3$, $NdFeO_3$, $SmFeO_3$, $EuFeO_3$, and $GdFeO_3$ (the first group) were identical, -107 kcal/mol, at the present temperature interval. However, the values of the heat of reaction of $TbFeO_3$ and $DyFeO_3$ (the second group) decreased with an increase in the temperature. The entropy change of each reaction in the first group was constant, independent of the temperature, and each value decreased in the sequence from $LaFeO_3$ to $GdFeO_3$. The entropy change of the second group decreased with an increase in the temperature. The change of the standard Gibbs energy was intimately related to the ionic radii of $\bar{C}$-ions, and the relationship between the Gibbs energy and the tolerance factor has been clarified.

Recently, Kimizuka and Katsura[1,2] and Sugihara *et al.*[3] have determined the standard Gibbs energy of the formation of $LaFeO_3$, $YFeO_3$, $Y_3Fe_5O_{12}$, $EuFeO_3$, and $Eu_3Fe_5O_{12}$ at 1200 °C on the basis of the phase equilibria in the Fe–Fe_2O_3–La_2O_3, Fe–Fe_2O_3–Y_2O_3, and Fe–Fe_2O_3–Eu_2O_3 systems. Sugihara *et al.*[3] suggested that the standard Gibbs energy of formation of lanthanoid-iron-perovskite from metallic iron, lanthanoid sesquioxides and oxygen would decrease in negative value with a decrease in the ionic radii of lanthanoid ions with 12 coordination number. Kimizuka and Katsura[2] and Kimizuka *et al.*[4,5] have found two series of new compounds, $\bar{A}Fe_2O_4$ ($\bar{A}$=Y, Ho, Er, Tm, Yb, and Lu) and $\bar{B}_2Fe_3O_7$ ($\bar{B}$=Yb and Lu), and determined the standard Gibbs energy of formation of YFe_2O_4. Tannieres *et al.*[6] and Evrard *et al.*[7] have also found the $\bar{A}Fe_2O_4$ and $Lu_2Fe_3O_7$ compounds, but they did not show any equilibrium relation in the Fe–Fe_2O_3–$\bar{A}_2O_3$ systems which could be used for calculating the standard Gibbs energy. It would be expected from the present knowledge about lanthanoid-iron-complex oxides that the $\bar{C}FeO_3$($\bar{C}$= La, Nd, Sm, EU, Gd, Tb, and Dy) would decompose straightforwardly to form metallic iron and $\bar{C}_2O_3$ at any definite oxygen partial pressure. On the other hand, the situation with $\bar{A}FeO_3$ is somewhat complicated because of the presence of the $\bar{A}Fe_2O_4$ and $\bar{B}_2Fe_3O_7$ compounds, and we can determine the standard Gibbs energy of formation of $\bar{A}FeO_3$ only after determining the standard Gibbs energy of formation of $\bar{A}Fe_2O_4$ and $\bar{B}_2Fe_3O_7$.

In the present study, we determine the standard Gibbs energy of formation of $\bar{C}FeO_3$ from metallic iron, $\bar{C}_2O_3$, and oxygen by the method of controlling the oxygen partial pressure by using a mixed gas of CO_2 and H_2. Temperatures were changed from 1473 to 1673 K. Based on the standard Gibbs energy data, we calculate the heat of reaction and entropy change resulting from the reaction, Fe+1/2 $\bar{C}_2O_3$+ 3/4 O_2=$\bar{C}FeO_3$. The relationship between the tolerance factor of the $\bar{C}FeO_3$ compounds and the standard Gibbs energy will also be presented.

Experimental

The experimental methods and apparatus adopted in this study are the same as those described by Kimizuka and Katsura.[1] Every equilibrium value of p_{O_2} was measured by means of a solid electrolyte cell composed of $(ZrO_2)_{0.85}(CaO)_{0.15}$. The values of P_{O_2} calculated from the thermochemical data[8] were in good agreement with those measured, and the differences were within ± 0.02 at most in terms of log P_{O_2} over the temperature and P_{O_2} ranges studied. The temperature was kept constant within ± 1 °C and was calibrated against the gold point.

A guaranteed reagent-grade Fe_2O_3 and a 99.9% pure-grade of each lanthanoid sesquioxide were used as the starting substances. The mixture of $Fe_2O_3/\bar{C}_2O_3=1$ was thoroughly mixed under ethyl alcohol and calcined at 1200 °C for from 20 to 30 hr in air. The subsequent procedures were the same as those described by Kimizuka and Katsura.[1] The weight change accompanying the reaction was followed by the thermogravimetric method within an error of ± 0.5 mg per about 3 g of every sample. The equilibrated sample was quenched rapidly, and the phases present were identified by an X-ray powder method.

Results and Discussion

The $\bar{C}FeO_3$ compounds decomposed straightforwardly to form metallic iron and $\bar{C}_2O_3$ at any definite oxygen partial pressure, and the reverse reaction occurred at the same P_{O_2} value.

We may write the general reaction scheme as follows:

$$Fe(s) + 1/2\bar{C}_2O_3(s) + 3/4O_2(g) = \bar{C}FeO_3(s) \quad (1)$$

In Equation (1), Fe(s) is in the form of γ-iron at temperatures from 910 to 1390 °C, while it is in the form of δ-iron from 1390 to 1534 °C.[9] Thus, in the present study, metallic iron is almost in the form of γ-iron except for $LaFeO_3$ at 1673 K. A recent study by Roth and Schneider[10] showed that La_2O_3 and Nd_2O_3 belong to the A-type with the hexagonal crystal system, Sm_2O_3, Eu_2O_3, and Gd_2O_3 to the B-type with the monoclinic crystal system, and Tb_2O_3 and Dy_2O_3, to the C-type with the cubic crystal system at the temperatures covered by the present study. The $\bar{C}FeO_3$ compounds are all perovskite-like compounds and all

belong to the orthorhombic crystal system. McCarthy and White[11] have studied the lower oxides of the Sm, Eu, Yb, Bedford anf Catalano[12] have also studied the Eu–Eu_2O_3, Sm–Sm_2O_3, and Yb–Yb_2O_3 systems at 1500 °C. As verified by them, $\bar{C}_2O_3$ is so stable at very low oxygen partial pressures that we cannot reduce them to lower oxidation states by the present techniques.

The most interesting fact in Equation (1) is that all the Fe^{3+} ions with the coordination numbers of 6 in the perovskite structure are reduced to metallic iron without passing through the state of Fe^{2+} ions.

Non-stoichiometry in $\bar{C}FeO_3$. It has been pointed out by Sugihara *et al.*[3] that $EuFeO_3$ has a non-stoichiometric composition, represented by $EuFeO_{3-x}$. This is also found in $\bar{C}FeO_3$, when the $\bar{C}$'s are Gd, Tb, and Dy. The deviated compositions of these compounds were determined to be approximately $\bar{C}FeO_{2.98}$ when the compounds were in equilibrium with metallic iron and Gd_2O_3, Tb_2O_3, or Dy_2O_3. We ascertained in addition no significant solubility of other components in the $\bar{C}_2O_3$ phases. The lattice constants of these non-stoichiometric compounds, synthesized at various temperatures and oxygen partial pressures, were obtained by the least-squares method. The results were almost identical with those for stoichiometric compounds. The lattice constants of stoichiometric $\bar{C}FeO_3$ were identical with those reported by Geller and Wood[13] and by Eibschütz.[14]

The Standard Gibbs Energy of Formation of $\bar{C}FeO_3$ from Metallic Iron, $\bar{C}_2O_3$, and Oxygen. In the present study, we define the activity of each $\bar{C}FeO_3$ component as being unity at the composition where each $\bar{C}FeO_3$ component is in equilibrium with both metallic iron and $\bar{C}_2O_3$ at the respective definite oxygen partial pressure. Thus, the standard Gibbs energy of formation $\bar{C}FeO_3$ from metallic iron, $\bar{C}_2O_3$, and oxygen can readily be calculated by measuring the equilibrium oxygen partial pressure in each assembly. Here, the $\bar{C}_2O_3$ phases are all in the stoichiometric composition, as has been mentioned before. The results are given in Table 1. The errors due to the fluctuations of both temperature and oxygen partial pressure may be estimated to be ±200 cal at most.

Figure 1 shows the relationship between $\Delta G^0/T$ and $1/T$, where T is the absolute temperature. As may be seen in Fig. 1, the slope for each $\bar{C}FeO_3$ except for $TbFeO_3$ and $DyFeO_3$ is straight and identical with all others. This means that the heat of reaction of each compounds except for $TbFeO_3$ and $DyFeO_3$ is constant, with an identical value of −107 kcal per mol. In the cases of $TbFeO_3$ and $DyFeO_3$, the heats of reaction change with temperature. The calculated heats of reaction at various temperatures are given in Table 1.

The Entropy Change. The entropy change, ΔS^0, is determined either by $(\Delta H^0-\Delta G^0)/T$ or $d\Delta G^0/dT$. The results are given in Table 1. As may be seen in Table 1, the entropy value of each compounds except for $TbFeO_3$ and $DyFeO_3$ is independent of the temperature and is constant with a good accuracy when we adopt the values of $(\Delta H^0-\Delta G^0)/T$.

Table 1. Values of standard Gibbs energy, heat of reaction, and entropy change

	Temp. (K)	$-\log P_{O_2}$ (atm.)	$-\Delta G^0$ (kcal/mol)	$-\Delta H^0\left(\frac{d\Delta G^0/T}{d(1/T)}\right)$ (kcal/mol)	$-\Delta S^0$ (eu) $-(\Delta H^0-\Delta G^0)/T$	$-\Delta S^0$ (eu) $(d\Delta G^0/dT)$
$LaFeO_3$	1473	13.63	68.9		26.14	
	1523	12.91	67.5		26.21	26.2±0.1
	1570	12.27	66.1		26.30	
	1673	11.04	63.4		26.31	28
$NdFeO_3$	1473	12.99	65.7		28.33	
	1523	12.27	64.1		28.41	28.3±0.1
	1570	11.67	62.9		28.36	
	1620	11.08	61.6		28.27	28
$SmFeO_3$	1473	12.68	64.1		29.40	
	1523	11.99	62.7	107±2	29.37	29.4±0.05
	1570	11.38	61.3		29.35	29
$EuFeO_3$	1473	12.52	63.3		29.95	
	1497	12.21	62.7		29.84	29.9±0.08
	1523	11.86	62.0		29.82	
	1570	11.24	60.6		29.83	29
$GdFeO_3$	1473	12.49	63.1		30.05	
	1497	12.15	62.4		30.05	30.0±0.05
	1523	11.80	61.7		30.02	
	1570	11.18	60.2		30.04	30
$TbFeO_3$	1473	12.22	61.8	76	10	8
	1497	11.96	61.5	94	22	18
	1523	11.62	60.7	117	37	38
	1548	11.21	59.6	138	51	(63±5)
$DyFeO_3$	1473	12.11	61.2	78	11	10
	1497	11.83	60.8	96	24	24
	1523	11.46	59.9	123	41	48
	1548	11.04	58.7	147	57	(65±5)

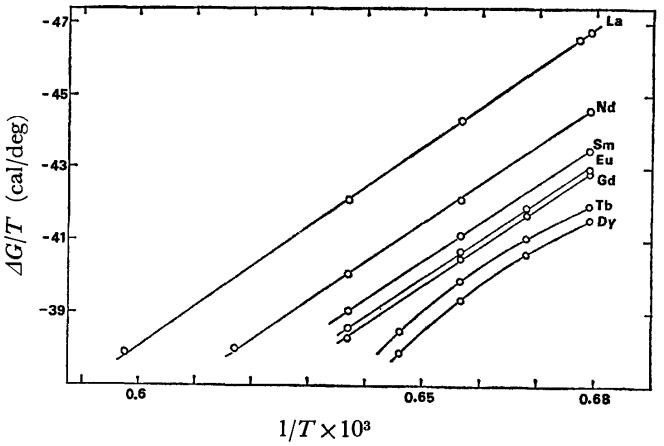

Fig. 1. The relationship between $\Delta G^0/T$ and $1/T$. The value at 1204 °C was cited from the paper by Kimizuka and Katsura.[1]

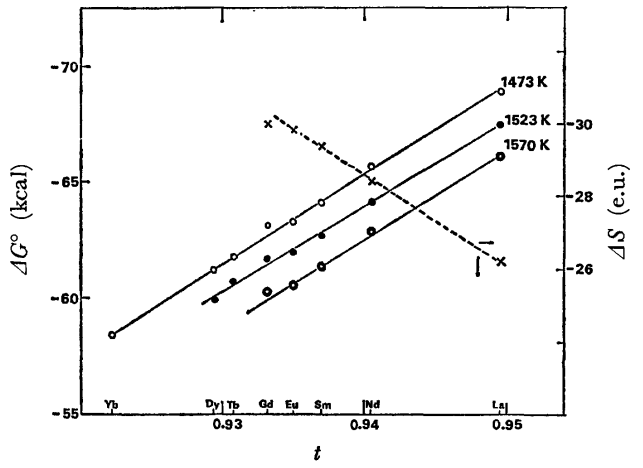

Fig. 2. The relationship between ΔG^0 and the tolerance factor t.

The values from $d\Delta G^0/dT$ seem to have some larger errors than those from $(\Delta H^0-\Delta G^0)/T$. On the other hand, the entropy change of $TbFeO_3$ and $DyFeO_3$ increases in negative value with an increases in the temperature.

It should be emphasized here that there are two groups of compounds in $\bar{C}FeO_3$ in respect to thermochemistry; the first includes $LaFeO_3$, $NdFeO_3$, $SmFeO_3$, $EuFeO_3$, and $GdFeO_3$, and the second, $TbFeO_3$ and $DyFeO_3$. This trend should be investigated furthermore with reference to the $\bar{A}FeO_3$ compounds.

The Relationship between the Tolerance Factor and the Standard Gibbs Energy of Formation of $\bar{C}FeO_3$. Figure 2 shows the relationship between the tolerance factor defined by Goldschmidt,[15] $[r_a+r_o=t\sqrt{2}(r_b+r_o)]$, and the standard Gibbs energy of formation of $\bar{C}FeO_3$ from metallic iron, $\bar{C}_2O_3$, and oxygen. In the tolerance-factor equation, r_a, r_b, and r_o mean the ionic radii of $\bar{C}$, Fe, and O ions in the perovskite structure respectively, and t is the tolerance factor. Here, we adopt the values reported by Espinosa[16] for ions of $\bar{C}$ with the coordination number of 12 in the perovskite structure. The ionic radii of Fe^{3+} and O^{2-} are 0.645 Å and 1.40 Å respectively; these values are given by Shannon and Prewitt.[17] The ΔG^0 value of $YbFeO_3$[18] is also given in Fig. 2. As may be seen in Fig. 2, the ΔG^0 value is proportional to the tolerance factor except for the case of $GdFeO_3$. The deviation in $GdFeO_3$ from the general trend is significant though within the range of experimental error; we cannot explain the reason for this deviation.

The entropy change resulting from the reaction is also plotted in Fig. 2. As is illustrated in Fig. 2, the entropy change decreases with a decrease in the tolerance factor.

References

1) N. Kimizuka and T. Katsura, This Bulletin, **47**, 1801 (1974).
2) N. Kimizuka and T. Katsura, *J. Solid State Chem.*, **13**, 176 (1975).
3) T. Sugihara, N. Kimizuka, and T. Katsura, This Bulletin, **48**, 1806 (1975).
4) N. Kimizuka, A. Takenaka, Y. Sasada, and T. Katsura, *Solid State Commun.*, **15**, 1321 (1974).
5) N. Kimizuka, A. Takenaka, Y. Sasada, and T. Katsura, *ibid.*, **15**, 1199 (1974).
6) N. Tannieres, O. Evrard, and J. Aubry, *C. R. Akad. Sc. Paris*, **278**, 241 (1974).
7) O. Evrard, B. Malaman, F. Jeannot, N. Tannieres, and J. Aubry, *ibid.*, **278**, 413 (1974).
8) "JANAF" Thermochemical Tables, U. S. Department of Commerce/Nat. Bur. Stand. (1965—1966).
9) M. Hansen, "Contribution of Binary Alloys," McGraw-Hill Book Co., New York (1958).
10) R. S. Roth and S. J. Schneider, *J. Res. Nat. Bur. Stand., A. Phys. Chemi.*, **64A**, 309 (1960).
11) G. J. McCarthy and W. B. White, *J. Less Common Metals*, **22**, 409 (1970).
12) R. G. Bedford and E. Catalano, *J. Solid State Chem.*, **3**, 112 (1971).
13) S. Geller and E. A. Wood, *Acta Crystallogr.*, **9**, 563 (1956).
14) M. Eibschutz, *ibid.*, **19**, 337 (1965).
15) V. M. Goldschmidt, T. Barth, G. Lunde, and W. Zachariasen, Pt. VII Skrifter Norske Videnskaps-Akad. Oslo, I. Mat. Naturv. K. I. No. 2 (1926).
16) G. P. Espinosa, *J. Chem. Phys.*, **37**, 2344 (1962).
17) R. D. Shannon and C. T. Prewitt, *Acta Crystallogr.*, B **25**, 925 (1969); *ibid.*, B **26**, 1046 (1970).
18) N. Kimizuka and T. Katsura, *J. Solid State Chem.*, **13**, in press.

The Fluorometric Determination of Gallium in Aluminum Metal with 8-Quinolinethiol[1]

Kunihiro WATANABE and Kyōzō KAWAGAKI

Faculty of Science and Technology, Science University of Tokyo, Yamazaki, Noda-shi, Chiba 278

(Received December 18, 1974)

A method for the fluorometric determination of gallium in aluminum metal is presented which involves extraction with the methyl isobutyl ketone (MIBK) of the gallium 8-quinolinethiolate complex. The extracted complex has a greenish-yellow fluorescence, with an emission maximum at 505 nm. The maximum fluorescence intensity is obtained at a pH of the initial aqueous phase of around 3.3; the fluorescence remains stable for at least 2 hr. When 50 ml of a sample aqueous solution containing gallium and 0.2 ml of a 0.2% 8-quinolinethiol solution is subjected to extraction with 10 ml of MIBK, the quantity of gallium which can be present for determination in the sample solution amounts to 1 to 30 μg. For the removal of the interfering effects of zinc, cadmium, copper, and nickel on the fluorometric determination, gallium was extracted with isopropyl ether from a 7 M HCl solution. The relative error of this method was 5% for 0.019% gallium in aluminum metal.

The fluorometric determination of gallium with such reagents as oxine and rhodamine B has been proposed, and the application to gallium in aluminum metal has also been tested.[2,3]

A benzene-extraction method for the fluorometric determination of gallium with 8-quinolinethiol was investigated by Korenman *et al.*[4] and chloroform extraction, by Davis.[5] However, in these studies no metal of any practical use was tested. Details on the analytical conditions are not available, and there exists disagreement between these studies as to the optimum conditions. 8-quinolinethiol does not react with aluminum and magnesium, but forms a stable complex with gallium. In view of these facts, the present authors examined the conditions in the determination of gallium in aluminum metal. MIBK was used as the extraction solvent.

Experimental

Reagents. Standard solution of gallium: A stock solution of gallium was prepared by dissolving 0.1819 g of 99.999% gallium metal (Mitsubishi Kinzoku Kogyo) in 6 M hydrochloric acid. The standard solution was prepared by diluting the stock solution. 0.2% 8-quinolinethiol solution: 0.1 g of 8-quinolinethiol hydrochloride (Dojin Yakka) was dissolved in 50 ml of 6 M hydrochloric acid.

10% L-ascorbic acid solution: 10 g of L-ascorbic acid was dissolved in water, and the mixture was diluted to 100 ml. This solution was freshly prepared for every experiment. 0.1% *O*-phenanthroline solution: 0.25 g of *O*-phenanthroline was dissolved in 10 ml of ethyl alcohol, and the mixture was diluted to 250 ml with water.

0.2 μg/ml uranine solution: 0.10 g of uranine was dissolved in water and diluted to 100 ml. The solution was then further diluted with water to make a solution containing 0.20 μg uranine per ml. The resultant solution was used as a reference standard to adjust the sensitivity of the fluorescence spectrophotometer.

Other reagents: The MIBK used as an extraction solvent and all the other chemicals were of an analytical grade. Under some conditions, ammonia was washed with an 8-quinolinethiol solution and MIBK.

Apparatus. The fluorometric measurements were carried out using a Hitachi fluorescence spectrophotometer, Model 203, with a mercury lamp. A 120 W Xenon lamp was used as the exciting source for the measurements of the fluorescence and excitation spectra. A 1 cm × 1 cm quartz cell was used. A Toa Denpa Model HM-5 A glass electrode pH meter was used for the pH measurements. An Iwaki KM shaker was used.

Procedure. A sample solution containing less than about 10 μg of gallium was transferred into a beaker. Then, 0.2 ml of the 0.2% 8-quinolinethiol solution and 5 ml of the 10% ascorbic acid solution were added to the solution. After the solution has been diluted to 50 ml with water, the pH of the solution was adjusted to 3.3 with dilute hydrochloric acid or ammonia. The resultant aqueous solution was then transferred into a separatory funnel. The gallium complex was extracted for 5 min with 10 ml of MIBK. After the separation of the aqueous phase, the fluorescence intensity of the organic phase was measured using a uranine solution as a reference standard. The amount of gallium was evaluated from the calibration curve. The excitation and fluorescence wavelengths used were 365 and 505 nm (exciting source: a mercury lamp) respectively.

Results and Discussion

Excitation and Fluorescence Spectra. 8-Quinolinethiol reacts with gallium to form a complex of a yellowish-green fluorescence. The complex showed an excitation maximum at 395 nm and a fluorescence maximum at

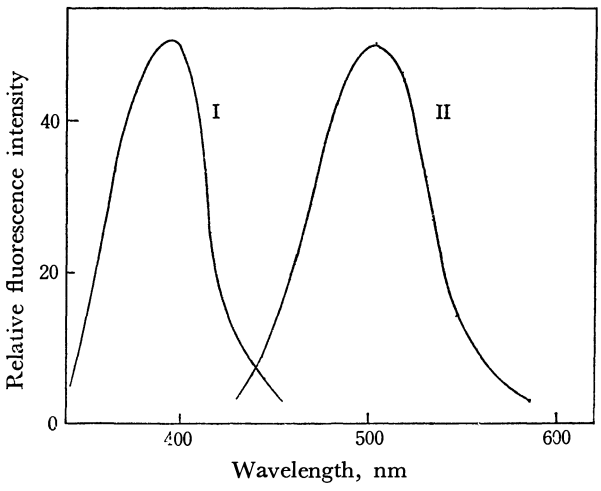

Fig. 1. Excitation and fluorescence spectra.
Excitation spectrum(I): Excited with xenon lamp and analyzed at wavelength for maximum fluorescence intensity.
Emission spectrum(II): Excited at 395 nm.

505 nm (exciting source: Xenon lamp). The apparent spectra are shown in Fig. 1.

Effect of the Amount of 8-quinolinethiol. The effect of the concentration of 8-quinolinethiol was investigated by adding various amounts of the reagent to a solution containing 5.8 μg of gallium. As is shown in Fig. 2, the maximum fluorescence intensity was obtained by the use of 0.1—0.2 ml of the 0.2% 8-quinolinethiol solution; above 0.2 ml of 8-quinolinethiol the fluorescence intensity decreased gradually in direct proportion to the amount of the reagent added. The fluorescence intensity of the reagent blank was found to be constant.

Effect of pH. The effect of the pH of the aqueous phase on the extraction was also studied. The results are shown in Fig. 3. The fluorescence intensity showed a maximum at pH 3.2—3.4. When the pH was higher than 3.5, the intensity decreased and became negligibly low at pH 11. Therefore, all the extractions were carried out at pH 3.3. According to Korenman, the optimum pH in a benzene extraction was 5, but Davis found that it was 3. The present result is in agreement with that of Davis.

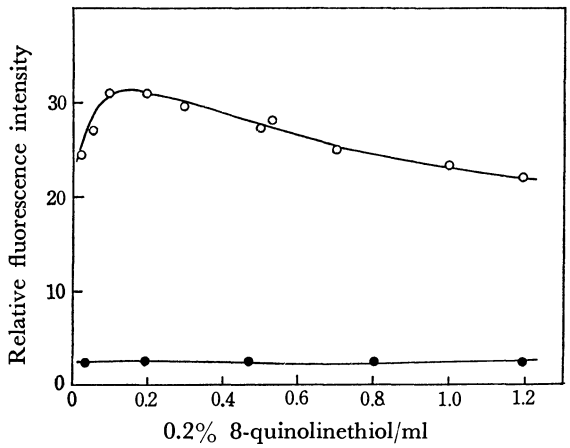

Fig. 2. Effect of amount of reagent.
—○— Ga: 5.8 μg pH: 3.5
—●— Reagent blank

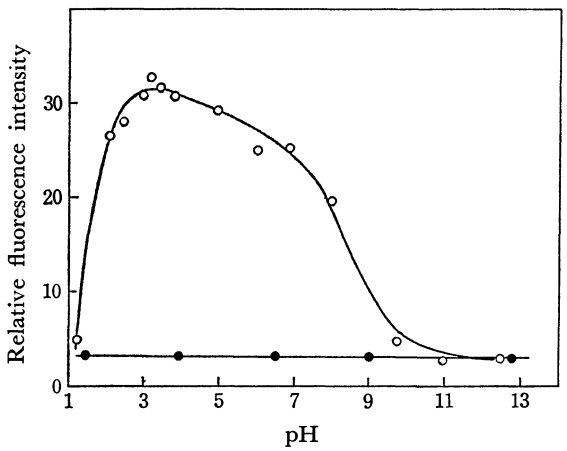

Fig. 3. Effect of pH on fluorescence intensity.
—○— Ga: 5.8 μg 0.2% 8-quinolinethiol: 0.2 ml
—●— Reagent blank

The pH was adjusted by adding hydrochloric acid or ammonia. The buffer solution used was a L-ascorbic acid solution. As the old ascorbic acid solution reduced the fluorescence intensity of the gallium complex, the solution was freshly prepared for each experiment.

Effect of the Shaking Time. The effect of the shaking time was tested in the range from 0.5 to 10 min. It was found that a 3-min shaking was sufficient. 5 min was chosen for shaking in the present experiments, though. The fluorescence intensity of an extracted complex was stable for at least 2 hr at room temperature.

Effect of the Volume of Aqueous Solution. When MIBK was used for the extraction of the chelate in water, a small amount of MIBK dissolved in the aqueous layer. For the investigation of the effect of the aqueous solution, the volume of the organic phase of MIBK was kept at 10 ml, while that of the aqueous phase was varied from 40 ml to 140 ml. As is shown in Fig. 4, the fluorescence intensity gradually increased in proportion to the volume of the aqueous phase, although no great effect of the volume of the aqueous solution on the intensity was observed.

Effect of Foreign Ions. The effect of 25 kinds of ions coexistent with 5.8 μg gallium was studied. The results are summarized in Table 1. The following ions did not interfere: aluminum, magnesium, calcium, chromium, scandium, lanthanum, titanium, zirconium, manganese, barium, and strontium ions. Zinc ions gave a positive error. A small amount of cobalt, nickel, copper, bismuth, iron, and silver ions reduced the fluorescence intensity. One milligram of vanadium ions (VO_3^-) reduced by ascorbic acid did not interfere. To remove some interfering ions in the above ions contained in aluminum metals, an isopropyl ether extraction method[6] was used.

The gallium chloride complex is extracted from the 7 M hydrochloric acid solution with isopropyl ether; then the organic phase is washed with 7 M hydrochloric acid, so that some interfering ions are completely removed from the gallium in the organic layer. In this separating method, zinc (up to 5 mg), cadmium (1.7 mg), copper (5 mg), nickel (1 mg), and cobalt (1 mg) do not interfere. Iron (III) is reduced to iron (II), masked with *O*-phenanthroline. However, the

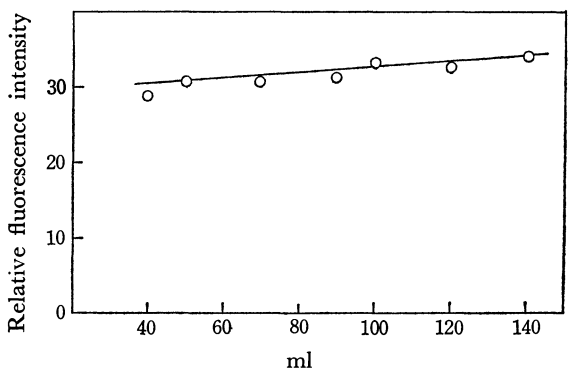

Fig. 4. Effect of volume of aqueous solution.
Ga: 5.8 μg 0.2% 8-quinolinethiol: 0.2 ml
pH: 3.5

TABLE 1. EFFECT OF FOREIGN IONS

Ions	(mg)	Added as	Ga found (μg)
Al^{3+}	10.0	$Al(NO_3)_3 \cdot 9H_2O$	5.8
	250.0	$Al(NO_3)_3 \cdot 9H_2O$	5.8
Ca^{2+}	2.0	$Ca(NO_3)_2$	5.8
Mg^{2+}	200.0	$MgSO_4$	5.8
Cr^{3+}	1.0	$Cr(NO_3)_3 \cdot 9H_2O$	5.8
Mn^{2+}	1.0	$MnSO_4$	5.8
La^{3+}	1.5	La_2O_3+HCl	5.8
Sc^{3+}	1.0	Sc_2O_3+HCl	5.8
Pb^{2+}	0.1	$Pb(NO_3)_2 \cdot H_2O$	5.8
Bi^{3+}	0.1	$Bi(NO_3)_3 \cdot 5H_2O$	3.3
Ba^{2+}	1.0	$BaCl_2 \cdot 2H_2O$	5.8
Sr^{2+}	1.0	$Sr(NO_3)_2$	5.7
ZrO^{2+}	1.0	$ZrOCl_2 \cdot 8H_2O$	5.4
Tl^{+}	0.1	$TlNO_3$	5.2
Ag^{+}	0.1	$AgNO_3$	0.2
Cu^{2+}	0.008	$CuSO_4 \cdot 5H_2O$	5.5
	0.02	$CuSO_4 \cdot 5H_2O$	4.8
Fe^{3+}	0.02	$NH_4Fe(SO_4)_2 \cdot 12H_2O$	5.4
	0.1	$NH_4Fe(SO_4)_2 \cdot 12H_2O$ + 5% ascorbic acid 5 ml	5.6
Ni^{2+}	0.02	$NiSO_4 \cdot 6H_2O$	3.2
Zn^{2+}	0.006	Zn+HCl	8.5
Ti^{4+}	0.1	$Ti(SO_4)_2$	5.8
VO_3^{-}	1.0	NH_4VO_3	1.3
	1.0	NH_4VO_3 + 5% ascorbic acid 5 ml	5.8
Hg^{2+}	0.1	$HgCl_2$	4.4
Co^{2+}	0.02	$Co(NO_3)_2 \cdot 6H_2O$	3.4
Sn^{2+}	0.04	$SnCl_2 \cdot 2H_2O$	5.8
In^{3+}	0.015	In + HCl	5.7
Sb^{3+}	0.1	$SbCl_3$	5.9

Ga taken: 5.8 g; 0.2% 8-quinolinethiol: 0.2 ml; pH: 3.3

iron *O*-phenanthroline complex increases the blank value slightly; therefore, a large amount of iron ions interferes.

Calibration Curves. The calibration curves for the determination of gallium were prepared under optimum conditions. The results are shown in Fig. 5. The I calibration curve was obtained by setting up the fluorometer at 50 using the standard uranine solution. The II curve was set at 25.

A linear relationship between the fluorescence intensity and the concentration of gallium was obtained over the concentration range of 0−10 μg of gallium per 10 ml of MIBK. The possible range for the accurate determination of gallium was 1—30 μg.

Synthetic Samples. The determination of gallium in some synthetic samples was done. For a synthetic sample containing copper, cobalt, nickel, and iron, which interfere significantly when present in even small amounts, both the gallium and the iron (III) were extracted with isopropyl ether from a 7 M hydrochloric acid solution. Then the iron (III) was reduced by an ascorbic acid solution, masked with *O*-phenanthroline. Table 2—4 shows the results of the determination of gallium. The samples containing zinc were

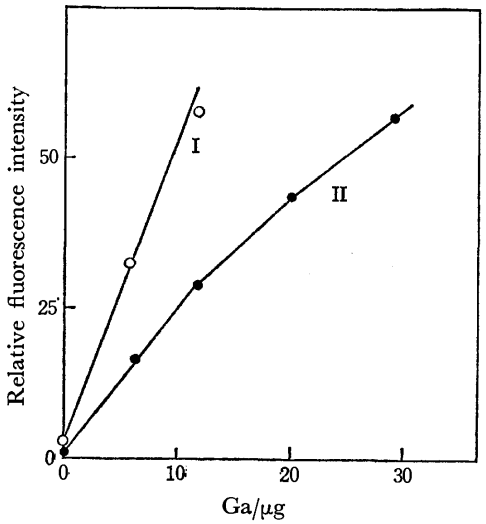

Fig. 5. Calibration curves for gallium.
Fluorometer reading was set at 50 div. (curve I) or 25 div. (curve II) with the uranine reference solution (0.2 μg uranine/ml)

TABLE 2. ANALYTICAL RESULTS FOR SYNTHETIC SAMPLES

Sample No.	Ga taken (μg)	Foreign ions (mg)	Ga found (μg)
1	3.2	Al^{3+} 50, Mg^{2+} 10, Mn^{2+} 1, Fe^{3+} 0.5, VO_3^{-} 0.1	3.3, 3.4, 3.4
2	6.3	(Al^{3+} 60, Zn^{2+} 5)	6.5, 6.2, 6.4
3	0.0	(Zn^{2+} 2.5, Cd^{2+} 1.7)	0.0, 0.0, 0.1
4	3.2 6.3	Cu^{2+} 5, Ni^{2+} 1, Co^{2+} 1, Mn^{2+} 1, Fe^{3+} 0.1	3.5, 3.2, 3.3 6.4, 6.5, 6.5
5	3.2 6.3	Al^{3+} 30, Mg^{2+} 10, Zn^{2+} 2.5 Cu^{2+} 2, Cr^{3+} 1, SiO_3^{2-} 1	3.0, 3.2, 3.4 6.5, 6.5, 6.3

treated in the same way as above (Tables 2-2, 3, 5). For a sample containing aluminum, magnesium, iron, and vanadium, the ether extraction was omitted and the gallium 8-quinolinethiolate was directly extracted with MIBK. The results are shown in Table 2-1.

In all of the cases studied in these synthetic samples, the gallium could be determined with an average error of 3 percent.

Determination of Gallium in Aluminum Metal. From the experimental results described above, a recommendable procedure is as follows: Dissolve 0.1—0.3 g of a sample in 50 ml of hot 7 M hydrochloric acid. Transfer the resultant solution to a 100-ml volumetric flask. Bring up to the mark with a 7 M hydrochloric acid solution. Pipet a 10 ml aliquot into a 100-ml beaker, and add 20 ml of 7 M hydrochloric acid. Transfer the solution to a separatory funnel and shake for 5 min with 20 ml of isopropyl ether. After this extraction has been repeated twice using 10 ml of isopropyl ether, discard the aqueous phase. Wash the resultant ether solution two times, with 20-ml and 10-ml portions of 7 M hydrochloric acid. Then add 20 ml of water to the ether phase. Evaporate only the ether phase on a sand bath, and then cool the water phase. Add 5 ml of 5% ascorbic acid solution and 2 ml of a 0.1% *O*-phenanthroline solution to the

Table 3. Analytical results for standard sample NBS 85 B

Amount of sample taken 2.651 mg/ml	Present method		2-Methyl-8-quinolinol method[3,7]	
	Ga found (μg)	Ga %	Ga found (μg)	Ga %
10 ml	5.3	0.020	5.1	0.019
	5.1	0.019	5.3	0.020
	5.3	0.020	5.2	0.020
20 ml	11.2	0.021		
	10.9	0.021		

Relative error: 5% for 0.019% gallium (standard sample NBS 85 B).

aqueous solution remaining in the beaker. After the dilution of the solution to 50 ml, add 0.2 ml of 0.2% 8-quinolinethiol and adjust the pH of the solution to 3.3. Transfer the solution to a separatory funnel, and then extract the gallium 8-quinolinethiolate complex by shaking for 5 min with 10 ml of MIBK. Then filter out the organic phase through a cotton plug. Transfer the extract to a quartz cell. The fluorescence intensity at 505 nm is measured at an excitation wavelength of 365 nm with reference to a 0.2 μg/ml uranine solution.

The accuracies of the amount of gallium in a sample as determined by the present method and by the conventional 2-methyl-8-quinolinol method[3,7] are shown in Table 3. The present method is shown to be accurate enough for the determination of gallium in the aluminum metal.

The authors would like to thank Mr. Hideto Kasagi for his assistance to experiments in the initial stage.

References

1) Determination of metals with thiooxine. II, Part I of this series: K. Watanabe and K. Kawagaki, *Bunseki Kagaku*, **22**, 581 (1973).
2) Y. Nishikawa, *Nippon Kagaku Zasshi*, **79**, 631 (1958).
3) K. Mukai, *Bunseki Kagaku*, **9**, 631 (1960).
4) I. M. Korenman, F. R. Sheyanova, and N. I. Starodubova, *Tr. Po Khim. i Khim. Teknol.*, **1963**, 243.
5) R. Davis, Univ. Microfilms (Ann Arbor. Mich.) Order No. 667874.
6) E. B. Sandell, "Colorimetric Determination of Traces of Metals," 3rd Ed., Interscience Publishers, New York (1959), p. 471.
7) M. Ishibashi, T. Shigematsu, and Y, Nishikawa, *Nippon Kagaku Zasshi*, **78**, 1139 (1957).

The Mechanism of Thermal Reactions in Apatites–Silica–Water Vapor Systems[1)]

Hideki MONMA and Takafumi KANAZAWA

Department of Industrial Chemistry, Faculty of Technology, Tokyo Metropolitan University, Fukazawa, Setagaya-ku, Tokyo 158

(Received December 18, 1974)

The reactions of fluor-, hydroxy-, and chlorapatites with silica in the presence of water vapor have been studied under various conditions—*i.e.*, various amounts of added silica, various temperatures (up to 1300 °C), and various heating times and water-vapor pressures (0.6—760 mmHg). As the pressure increased, the decomposition rate of hydroxyapatite with silica decreased considerably. Fluorapatite and chlorapatite were found to be decomposed with silica after being partially defluorinated or dechlorinated. In the case of fluorapatite, no effect of silica addition was recognized under a low water-vapor pressure (0.6 mmHg). This effect was observed under a high water-vapor pressure (760 mmHg), accompanied by rapid increases in the fluorine volatility and the destruction rate of the apatite in their time-dependence plots. In the reaction using chlorapatite, a similar effect was found under both low and high pressures. The results for the defluorination and dechlorination could mostly be interpreted by assuming the following changes: (1) halogen-oxyapatite formation, (2) the substitution of hydroxyl ions for halogen ions, and (3) the decomposition of apatite with silica.

Fluorine volatilization during the heat-treatment of rock phosphate in the presence of water vapor is accelerated by adding silica. In fact, thermal treatments above 1300 °C can be carried out by applying this reaction process to produce a defluorinated phosphate. Some thermodynamic considerations and a preliminary experiment on the fluorapatite (FAp)–silica–water vapor system were described in previous papers by the present authors.[2,3)] On the basis of these studies, it was estimated that silica can react with partially or completely hydroxylated FAp, but not stoichiometric FAp. A similar estimation may also hold for chlorapatite (CAp).

The purpose of the present investigation is to obtain some information concerning the mechanisms of the destruction, defluorination, and dechlorination of apatites in the presence of both silica and water vapor.

Experimental

Materials. The FAp was prepared by heating a stoichiometric mixture of $Ca_3(PO_4)_2$ (thermally synthesized material) and CaF_2 (special-grade reagent) at 1150 °C for 2.5 hr in a N_2 gas flow. Another substance, CaF_2, was placed upstream near the mixture to minimize volatilization of fluorine from the reactant. This synthetic FAp contained 3.76% F. The hydroxyapatite (HAp) was synthesized by heating a mixture of $Ca_2P_2O_7$ and CaO (added as $CaCO_3$) in the molar ratio of 1 : 2.7 at 1200 °C for 3 hr in water vapor (p_{H_2O}=150—230 mmHg), and was then purified by washing it with an aqueous solution of NH_4Cl to remove the excess CaO. The CAp was prepared by heating a mixture of $Ca_2P_2O_7$, $CaCO_3$ and $CaCl_2$ in the molar ratio of 1 : 1 : 2.5 at 1200 °C for 3 hr, followed by air quenching and by washing with a NH_4Cl aqueous solution to remove the calcium salts other than apatite. The chlorine content in this synthetic CAp was 6.72%. Apatite–silica mixtures with molar ratios in silica/apatite of from 1/1 to 18/1 were prepared by manual mixing in an agate-mortar. As the SiO_2 sample, silica sand (α-quartz) for optical glass making was adopted after it had been purified with hydrochloric acid. All the samples thus prepared were ground to 200 mesh and then used.

Heat-treatment and Analyses. The reaction runs were carried out by heating the samples at various temperatures (up to 1300 °C) and times (up to 9 hr) in a Na–H_2O mixed gas flow of 150 ml/min (p_{H_2O}=0.6—760 mmHg). The partial water-vapor pressure in the flow of the N_2 gas used here was determined to be 0.6 mmHg from a comparison of the data shown in Fig. 2 with the thermal stability curve of HAp reported by Riboud.[4)]

The decomposition rate of FAp or HAp was determined from a calibration curve of the apatite content *vs.* the relative X-ray diffraction intensity. This intensity means $I_{AP}/(I_{AP}+I_{\alpha-T}+I_{\beta-T})$, where the I's are the diffraction intensities obtained by using CuKα radiation at 31.8 °, 30.6 °, and 31.0 ° in 2 θ for apatite, α-, and β- tricalcium phosphates respectively.[5,6)] The procedure described above was, however, inapplicable to the measurement of the CAp decomposition because of a considerable change in the diffraction pattern of CAp itself upon heating.[7)] In this case, we investigated qualitatively whether or not the decomposition occurred.

The fluorine and chlorine contents were determined by thorium-nitrate and potassium-thiocyanate titrarions respectively. DTA was conducted in air from room temperature to 1350 °C at a rate of 10 °C/min. The sample weight was 400—600 mg, and the reference material used was α-Al_2O_3.

Results and Discussion

Thermodynamic Considerations. FAp and CAp are considered to be thermally stable up to their melting temperatures, whereas the thermal stability of HAp is strongly dependent on the pressure of the coexisting water vapor.[4,5)] The reactivities of apatites with silica were determined by the calculation of the standard free-energy changes (ΔG°_r) in these reactions, assuming $Ca_3(PO_4)_2$, Ca_2SiO_4, $CaSiO_3$, CaO, H_2O, HF, HCl, SiF_4, and $SiCl_4$ as reaction products. On the basis of these calculations, the following results were obtained: the ΔG°_r values for a reaction of HAp–SiO_2 system became negative above 600—700 °C, and even above 760 mmHg of coexisting water vapor it was considered possible for the decomposition of HAp to occur. On the other hand, the ΔG°_r values for the reactions of FAp–SiO_2 and CAp–SiO_2 systems were always positive in the range of 25—1300 °C. However, silica possibly reacts with FAp or CAp during heat-treatment in the presence of water vapor. The reason for this is that the standard free energies of formation of these apatites become close to the value of HAp with an increase in the substitution

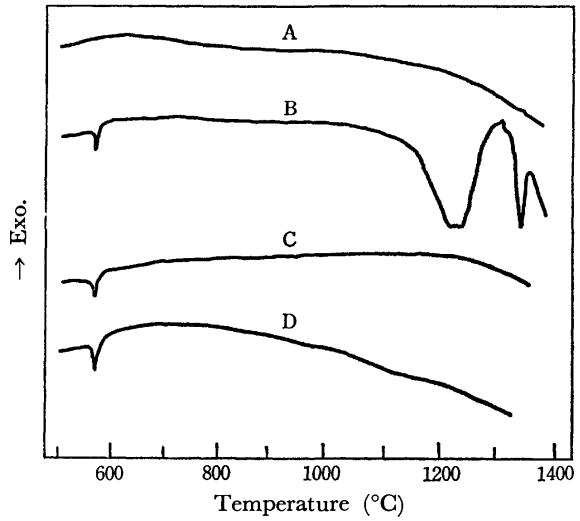

Fig. 1. DTA curves of HAp and apatites-silica mixtures.
Mixing molar ratio: apatite/silica = 1/3.
A: HAp, B: HAp-SiO_2, C: FAp-SiO_2, D: CAp-SiO_2.

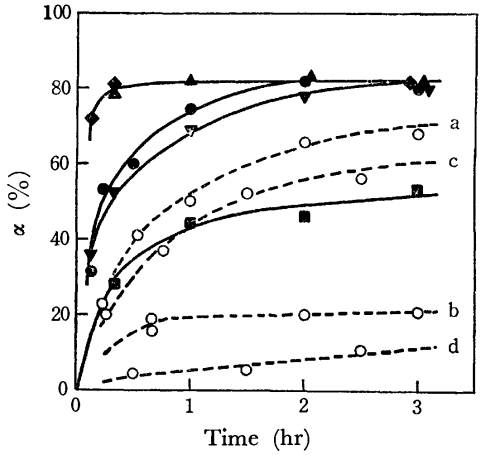

Fig. 3. Effects of heating condition and amount of added silica on decomposition (α) of HAp.
Sample: HAp-SiO_2 mixtures with various molar ratios; ▲: (1 : 13), ◆: (1 : 8), ●: (1 : 3), ○: (1 : 3), ▼: (1 : 2), ■: (1 : 1).
——: 1200 °C in N_2, ----a: 1100 °C in N_2, ----b: 1000 °C in N_2, ----c: 1200 °C in H_2O (760 mmHg), ----d: 1100 °C in H_2O (417 mmHg)

degree of OH^- for F^- or Cl^-.[8]

DTA. Each apatite and apatite–silica mixture was examined by DTA (Fig. 1). The broad endothermic peak at 1000—1300 °C was due to a decomposition reaction of HAp with silica, and the peak above 1300 °C suggested a thermal change due to the formation of different phosphates, such as $4CaO \cdot P_2O_5$, $Ca_7P_2Si_2O_{16}$, and $Ca_5P_2SiO_{12}$. HAp to which silica was added was completely decomposed to produce α-tricalcium phosphate after the heating test. On the other hand, the apatitic structures of all the samples except for the HAp–SiO_2 mixtures were maintained even after the heating.

Effect of the Addition of Silica to HAp. HAp and a HAp–SiO_2 mixture were heated at various temperatures for 3 hr in a flow of N_2 gas, and the decomposition rate (α) of HAp was measured (Fig. 2). The only product detected by X-ray powder diffraction was tricalcium phosphate. The decomposition apparently started from 1200—1250 °C for HAp and from 850—900 °C for the HAp–SiO_2 mixture. The former and the latter were due to the self-decomposition of HAp and the reaction of HAp with silica respectively.

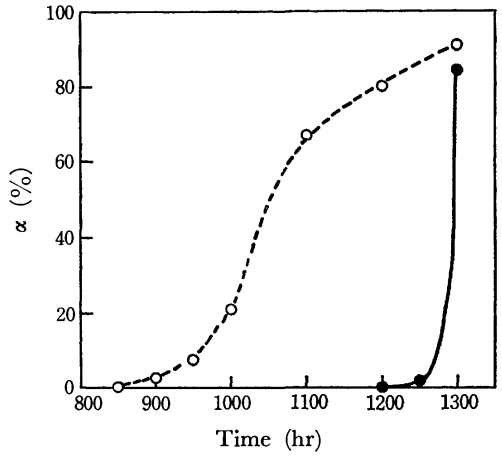

Fig. 2. Effect of added silica on decomposition (α) of HAp.
Heat-treatment: for 3 hr in N_2.
—●—: HAp, --○--: HAp-SiO_2 mixture (1 : 3).

Figure 3 shows the effects of the amount of added silica and the heating condition on α. The values of α were largely influenced by the heating temperature and the water-vapor pressure (p_{H_2O}) in the atmosphere.

In order to find further quantitative relations between α and p_{H_2O}, α was plotted against p_{H_2O} and its logarithm (Fig. 4). From these plots, nearly linear relations were obtained as follows:

$$\alpha = K p_{H_2O} + C \quad \text{(at 1200 °C)}$$
$$\alpha = K \log p_{H_2O} + C \quad \text{(at 1000—1100 °C)}$$

where α is a value after an apparent steady state had been reached, both K and C are constants depending on the heating temperature.

Effect of the Addition of Silica to FAp. The FAp and FAp–SiO_2 mixtures were heated at 1000—1300 °C for 3 hr under various water-vapor pressures. Their heating weight losses were 0.1—0.7%. Table 1 represents the volatilities of fluorine upon the reactions. The difference in the volatilities between the samples with and without silica was negligible at 1000—1200 °C, while it was clear at 1300 °C under a high water-vapor pressure. On the other hand, the decomposition rates of FAp were less than 1% at 1100—1300 °C in a N_2 gas flow, regardless of the presence or absence of silica. Under a pressure of 760 mmHg of water vapor, however, the rate at 1300 °C was 45% for a 1 : 18 mixture of FAp and SiO_2, compared with the value of less than 1% for FAp without silica.

Figure 5 indicates the changes in the fluorine volatility and the decomposition rate with the heating time at 1300 °C under a pressure of 760 mmHg. No

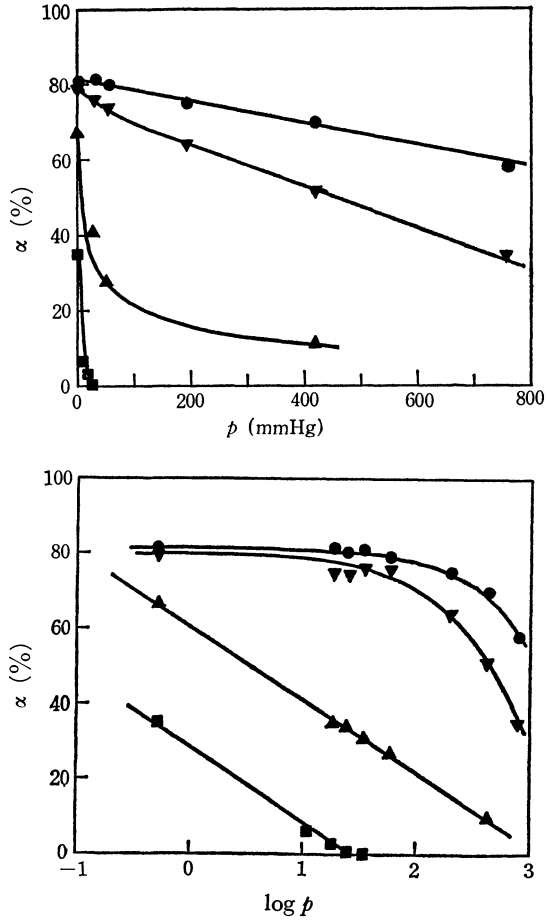

Fig. 4. Relation between docomposition (α) of HAp and water-vapor pressure (p_{H_2O}).
Sample: HAp-SiO_2 mixture (1 : 3).
●: 1200 °C-3 hr, ▼: 1170 °C-3 hr, ▲: 1100 °C-3 hr, ■: 1000 °C-9 hr.

Table 1. Effects of temperature, water-vapor pressure and amount of added silica on fluorine volatility

Sample[a]	Temperature (°C)	Fluorine volatility (%)[b] 0.6 mmHg[c]	18 mmHg	93 mmHg	234 mmHg	760 mmHg
FAp	1100	5.1	10.1	17.1	25.3	42.6
	1200	5.6	12.0	19.4	27.9	53.5
	1300	8.0	—	—	—	54.3
FAp-SiO_2 (1 : 3)	1100	5 0	9.4	17 6	23.9	38.7
	1200	7.2	11.3	20.8	28.0	56.3
	1300	7.2	—	—	—	67.6
FAp-SiO_2 (1 : 18)	1100	3.4	11.8	15.2	25.8	38.2
	1200	3.9	11.8	20.8	27.5	55.1
	1300	8.2	—	—	—	78.9

a) Value in parentheses shows mixing molar ratio of SiO_2 to FAp. b) Value after heating for 3 hr. c) Pressure of water vapor in the N_2 gas flow used here.

effect of silica addition on the volatility was observed up to 2 hr. The effect, however, was clearly observed after 2 hr; this time agreed approximately with the beginning of a rapid increase in the decomposition. The fluorine volatilization within 0—2 hr is based on

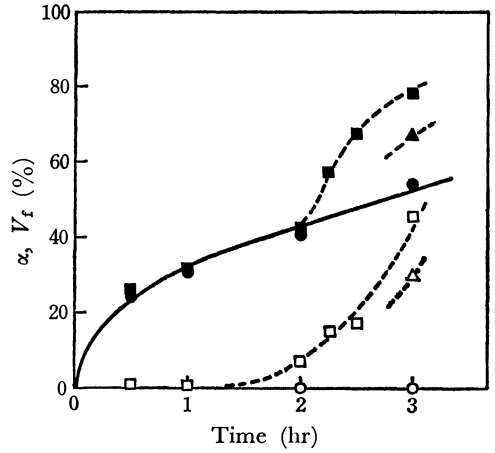

Fig. 5. Effects of added silica on decomposition (α) of FAp and fluorine volatility (V_f).
Heat-treatment: at 1300 °C in H_2O (760 mmHg).
●(FAp), ▲(FAp-SiO_2 (1 : 3)), ■(FAp-SiO_2 (1 : 18)) indicate volatility—time plots.
○(FAp), △(FAp-SiO_2 (1 : 3)), □(FAp-SiO_2 (1 : 18)) indicate decomposition rate—time plots.

the substitution of OH^- for F^-. Hence, the substitution degree required to decompose the apatite with silica was estimated to be about 40% under those heating conditions. In other words, no effect of silica addition is due to a low degree of substitution, which can rise upon further heating. For example, the defluorination is observed even at 1200 °C in a similar test using rock phosphate.[9]

Effect of the Addition of Silica to CAp. The effect of added silica on the chlorine volatility in the N_2 gas flow was also tested (Fig. 6). The chlorine volatilization was generally greater than the fluorine volatilization. The dechlorination due to silica addition was observed at all times; an especially rapid increase in the volatility appeared in the heating at 1300 °C. The starting point of this rapid increase was found to be about a 2-hr heating time and a 30% volatility; this agreed with the point at which tricalcium phosphate was first detected. On the other hand, the values of the volatility under a water-vapor pressure of 760 mmHg were unexpectedly decreased by adding silica at all times (Fig. 7). However, when the decom-

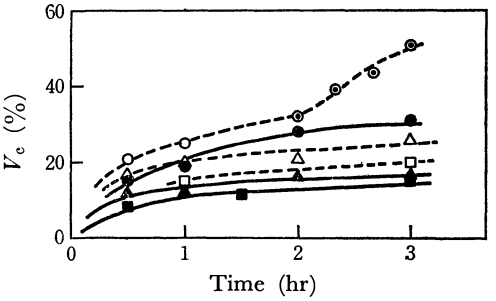

Fig. 6. Effect of added silica on chlorine volatility (V_c) in nitrogen gas.
—: CAp; ● 1300 °C, ▲ 1200 °C, ■ 1100 °C.
----: CAp-SiO_2 mixture (1 : 18); ○⊙ 1300 °C, △ 1200 °C, □ 1100 °C.
⊙: tricalcium phosphate was detected.

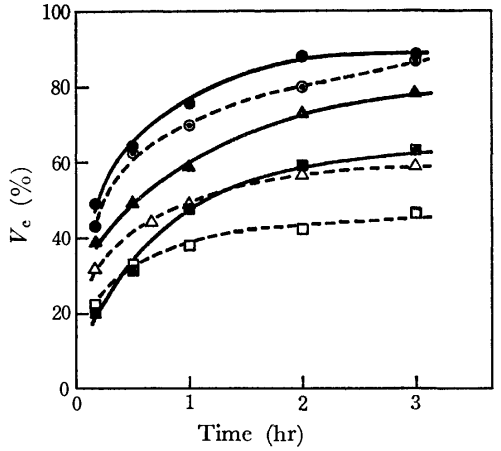

Fig. 7. Effect of added silica on chlorine volatility (V_c) in water vapor (760 mmHg).
——: CAp, ----: CAp-SiO_2 mixture (1 : 18). Symbols refer to Fig. 6.

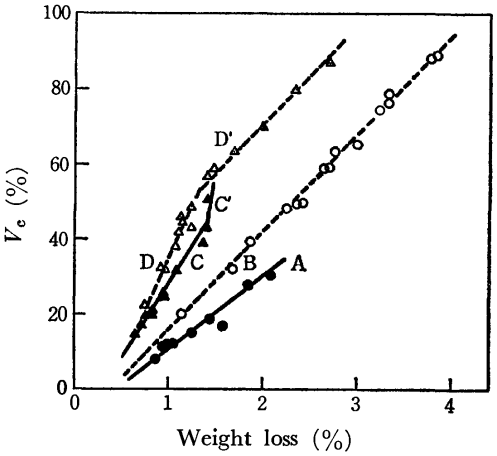

Fig. 8. Relationship between chlorine volatility (V_c) and weight loss after heating at various temperatures and times.
——: in N_2, ----: in H_2O (760 mmHg).
●○: CAp, ▲△: CAp-SiO_2 mixture (1 : 18).

position of a partially dechlorinated CAp began, its decreasing rate seemed to be reduced.

Figure 8 shows the relation between the chlorine volatilities and the heating losses. The fact that the extrapolated values are 0.3—0.4% in the loss may be ascribed to the evaporation of the water adsorbed on the samples. The changes in the slope from the (C) line to the (C') line, and from the (D) to the (D') line, in Fig. 8 were considered to be accompanied by the destruction of the apatite. The slopes of the (A), (B), (C), and (D) lines suggested the existence of some dechlorination processes, with a retention of the apatitic structure. Table 2 shows a comparison of the slopes calculated from the assumed reactions given in the footnote with the slopes determined from Fig. 8. The slopes of (A) and (C) agreed with that of chlor-oxyapatite formation.[10] The slopes of (B) and (D) agreed approximately with that of chlor-hydroxyapatite formation.

Table 2. Slopes for chlorine volatility-heating loss plots with linear relation

Method of calculation		Slope (Volatility (%)/Loss (%)) CAp	CAp-SiO_2 (1 : 18)
From reactions assumed			
Chlor-oxyapatite formation[a]		19.0	38.6
Chlor-hydroxyapatite formation[b]		28.2	57.4
From straight lines in Fig. 8	(A)	19.5	—
	(B)	26.0	—
	(C)	—	38.0
	(D)	—	57.5

a) $Ca_{10}(PO_4)_6Cl_2 \rightarrow Ca_{10}(PO_4)_6Cl_{2(1-x)}(OH)_{2x} \rightarrow Ca_{10}(PO_4)_6Cl_{2(1-x)}O_x\square_x$, where □ shows vacancy. b) $Ca_{10}(PO_4)_6Cl_2 \rightarrow Ca_{10}(PO_4)_6Cl_{2(1-x)}(OH)_{2x}$.

Summarizing the above results, the following interpretation may be given concerning the dechlorination processes: (1) Under low water-vapor pressures, chlor-oxyapatite is produced by the dehydration of the chlor-hydroxyapatite formed intermediately. (2) The substitution of OH^- for Cl^- proceeds under high water-vapor pressures. (3) In the presence of silica, a partially dechlorinated CAp is decomposed with silica.

References

1) This paper was read at the 31st Autumn Annual Meeting of the Chemical Society of Japan, Sendai, October, 1974.
2) T. Kanazawa, H. Monma, and T. Umegaki, *Sekko to Sekkai*, No. **112**, 31 (1971).
3) T. Kanazawa, H. Monma, and S. Ishii, *Kogyo Kagaku Zasshi*, **74**, 157 (1971).
4) P. V. Riboud, *Bull. Soc. Chim. Fr.*, **1968**, 1701.
5) H. Monma and T. Kanazawa, *Nippon Kagaku Kaishi*, **1972**, 339.
6) G. Otalora and H. H. Hess, *Amer. J. Sci.*, **267**, 822 (1969).
7) T. Kanazawa and H. Monma, *Kogyo Kagaku Zasshi*, **73**, 687 (1970).
8) E. J. Duff, *J. Chem. Soc., A*, **1971**, 1895.
9) G. M. Il'in, *Tr. Nauchn. Inst. po Udobr. i Insektofung.*, No. **208**, 133 (1965); *Chem. Abstr.*, **63**, 9503 (1965).
10) J. S. Prener, W. W. Piper, and R. M. Chrenko, *J. Phys. Chem. Solid*, **30**, 1465 (1965).

Studies on the Hexagonal Hydrate of Molybdenum Trioxide. The Physical Properties of the Hydrate and Its Changes on Heat Treatments in Air, in Hydrogen, and in a Hydrogen–thiophene Mixture

Noriyuki SOTANI

College of Liberal Arts, Kobe University, Tsurukabuto, Nada, Kobe 657

(Received December 20, 1974)

The hexagonal hydrate(I) of molybdenum trioxide, which has been newly found and reported, was studied by X-ray diffraction analysis, IR and NMR spectroscopies, and by other methods. Also studied was the change in (I) on heat treatments in air, in hydrogen, and in a hydrogen–thiophene mixture. The crystal was found to belong to a hexagonal system. The air-dried sample has about 0.46 mol of water. This water is included as a water molecule, not as hydroxyl. By the dehydration of (I), anhydrous molybdenum trioxide (I′), which has the same crystal structure as (I), is obtained. Another new form of (I′) is the hexagonal trioxide, which is hygroscopic and which easily absorbs water when standing in air. This (I′) is metastable and is irreversibly transformed to rhombic molybdenum trioxide(II) at 420—430 °C. In hydrogen and in a hydrogen–thiophene mixture, reduction and sulfurization occur in addition to transformation, which can be shown schematically as: (I)→(I′)→(II)$\begin{cases}\nearrow MoO_2\\ \searrow MoS_2\end{cases}$. Transformation in hydrogen and in the hydrogen–thiophene mixture proceeds faster than in air. Reduction occurs more quickly in the hydrogen–thiophene mixture than in hydrogen.

Molybdenum trioxide is usually prepared by the calcination of hydrate, the so-called molybdic acid or ammonium salt. Many works have been reported on the hydrates of molybdenum trioxide[1–4] and hydrates.[5–10] Among the hydrates of molybdenum trioxide, though only a rhombic MoO_3 is well known.[4] In addition to the rhombic MoO_3, there are several oxides the composition of which are very close to MoO_3, such as Mo_4O_{11},[11] Mo_8O_{23},[12] and Mo_9O_{26}.[12] All of these oxides show specific deep colours. As for the hydrate, the yellow dihydrate has been studied by many workers[5–10] and its precise structure was recently determined by Krebs.[13] Besides, yellow monohydrate and white monohydrate were found, but their precise natures have not yet been reported.

In a previous paper,[14] the present author reexamined in detail the nature of these hydrates of molybdenum trioxide. In these studies, a new form of hydrate, with a hexagonal structure, was found. By heat treatment, this new hydrate was transformed to anhydrous trioxide, which has the same structure as the initial hydrate. This anhydrous trioxide has never been reported, either. This hydrate and this oxide have smaller densities than other oxides and show interesting properties.

In the present paper, the author will report on his research into the precise physical properties of the hexagonal hydrate by X-ray diffraction analysis, IR and NMR spectroscopies, and by other methods. Also reported on will be research into their changes on heat treatments in air, in hydrogen, and in a hydrogen–thiophene mixture, this research was undertaken with a view to revealing the natures of the hydrate when used as a catalyst.

Experimental

Preparation of the Hexagonal Hydrate. The new hydrate of molybdenum trioxide was prepared by precipitation from a saturated ammonium paramolybdate solution by the addition of conc. HNO_3, to give an acidity of 2—3 M at about 70 °C. (HCl can be also used instead of HNO_3.) The sample (denoted as 'Sample A') was dried in air at room temperature.

To obtain an ammonia-free sample (denoted as 'Sample B'), the precipitate was prepared from a saturated sodium molybdate solution under the same conditions as the sample A. It probably contains a small amount of sodium ions, unlike Sample A, which contains ammonium ions.

X-Ray Diffraction, IR, and NMR Studies. The precise methods of the X-ray diffraction analysis, and IR and NMR spectroscopies were described previously.[14] Electron microscopic observation was carried out with a scanning-electron microscope (JAPAN ELECTRONICS LAB.-JSM U3 Type).

Measurements on Heat Treatments. Diffrential thermal analysis (DTA) and thermogravimetric analysis (TGA) were performed in air. The rate of weight decrease was measured by means of a quartz spring balance[15] with helices 15 mm in diameter and with 135 turns, with a capacity of 2 g and with a sensitivity of 0.1 mg/div. After heat treatment at each temperature, the sample was subjected to X-ray diffraction analysis, IR spectroscopy, and chemical analysis.

The behavior of the sample upon heat treatment in atmospheric hydrogen and in the hydrogen–thiophene mixture was studied in the same way. The purified hydrogen flowed at a rate accurately controlled to 0.1 mol/hr by means of a needle valve and an auxiliary regulator. The thiophene was fed into a stream of hydrogen by means of a calibrated hypodermic pump, at the feed rate of 1.4×10^{-2} mol/hr.[16]

Analysis of Ammonia and Sulfur. The ammonia was analyzed by the Kjeldahl method[17] and the sulfur, gravimetrically by the $BaSO_4$ method.[18]

Results

Air-dried Sample A. The X-ray pattern of the sample A, as shown in Fig. 1 (this pattern is not seen on the ASTM cards), belongs to a hexagonal system with a lattice constant of $a=6.09$Å and $c=9.14$Å. The indecies and the calculated spacings of lattice planes are listed in Table 1. Observation by the scanning-electron microscope also shows that the crystal belongs to the hexagonal system, as is shown in the photo.

The amount of ammonia in the air-dried sample A was about 1.6%, according to chemical analysis, this value corresponds to 0.15 mol of NH_3 per mol of MoO_3. According to thermogravimetric analysis, the sample has 0.54 mol of water per MoO_3, therefore, the

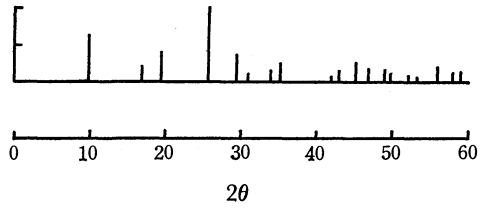

Fig. 1. The X-ray diffraction pattern of the sample A.

TABLE 1. THE X-RAY DIFFRACTION DATA OF THE SAMPLE

Index	*d* Spacings		Intensity
	Calcd	Obsd	
001	9.14	9.12	0.49
100	5.27	5.31	0.14
002, 101	4.57	4.57	0.30
102	3.45	3.46	1.00
110, 003	3.05	3.02	0.48
111	2.89	2.89	0.06
200, 103	2.64	2.64	0.09
201, 112	2.53	2.54	0.34
113	2.15	2.16	0.05
104	2.10	2.10	0.13
203, 210	1.99	1.99	0.20
211	1.95	1.95	0.14
		1.86	0.14
114, 212, 122	1.83	1.83	0.08
300	1.76	1.76	0.04
301	1.73	1.73	0.05
213	1.67	1.67	trace
302	1.64	1.64	0.21
		1.59	0.13
		1.57	0.07

composition can be represented as $(NH_3)_{0.15}\cdot MoO_3\cdot 0.54\,H_2O$ or $(NH_4)_{0.15}\cdot MoO_{3.08}\cdot 0.46\,H_2O$. However, the amounts of ammonia and water are indefinite and vary slightly with the conditions of preparation.

As can be seen from Fig. 2, which shows the IR spectrum of the A sample, the intensities of the bands at 3478 and 1610 cm^{-1} decrease when heated at a temperature below 300 °C, the bands can be attributed to the OH stretching and deformation vibrations of hydrated water respectively. The band at 1610 cm^{-1} shows that the water is present as water molecules, not as hydroxyl. The bands at 3170 and 1409 cm^{-1} agree exactly with the frequencies of the stretching and deformation vibrations of the ammonium ion.[19,20]

In the range below 1000 cm^{-1} of Mo-O-bond stretching and bending vibrations and of the librational motion of H_2O, the sample has a relatively sharp band at 976 cm^{-1}, a broad band at 916 cm^{-1}, a shoulder at 869 cm^{-1}, and a broad absorption in the range from 750 cm^{-1} to 450 cm^{-1}.

The NMR absorption was measured at room temperature and at that of liquid nitrogen. The peak-to-

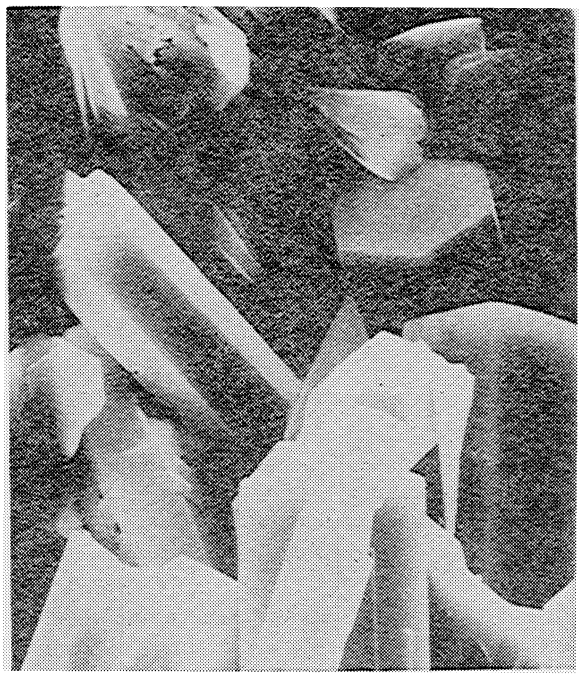

Photo. The sample A observed by the scanning electron microscope (×6000).

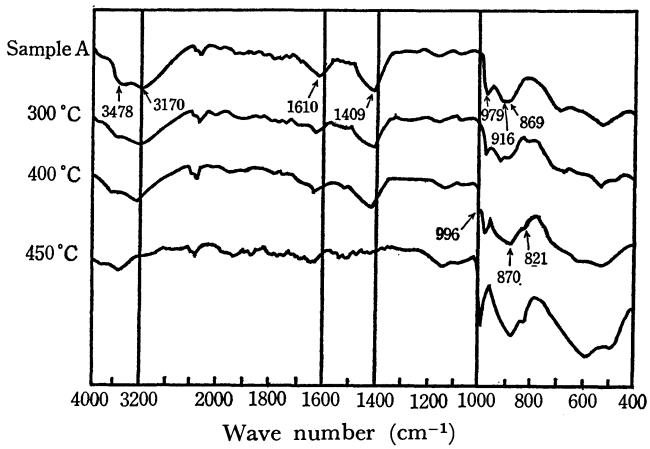

Fig. 2. IR spectra of the sample A.

peak values of the A sample at the temperature of liquid nitrogen, as shown in Fig. 3, are 1.4 G (I) and 11.7 G (II) respectively. (The values are the mean of at least five measurements.) As has been reported in a previous paper,[14] the peak-to-peak value of the II band may be attributed to absorption by the water molecule. The I band is attributed to the ammonium ion, which is mobile at the temperature of liquid nitrogen (probably in flip-flop motion).

The number of protons contained as water molecules was determined by free induction decay after a 90° pulse at 10 MHz; it agreed well with the value obtained by chemical and thermal analyses.

The density of the sample A was determined pycnometrically with cyclohexane at 25 °C. The density of the sample A is 3.73 g/cm^3, and that of the anhydrous hexagonal trioxide is 3.58 g/cm^3. These values are smaller than the 4.175 g/cm^3 of rhombic MoO_3[21] and the 6.47 g/cm^3 of MoO_2,[4] and are closer to the 3.117 g/cm^3 of the yellow dihydrate.[13]

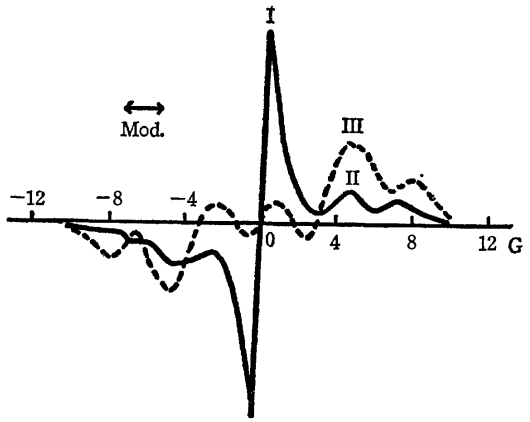

Fig. 3. NMR spectra of the samples A and B at liquid nitrogen temperature.
——: sample A, ----: sample B.

Air-dried Sample B. The B sample from sodium salt gives an X-ray diffraction pattern identical with that of the sample A except for a small difference in intensity.

The IR spectrum of the B sample is identical with that of the A sample except for the disappearance of the bands due to the ammonium ion.

The peak-to-peak value (III) of the NMR derivative curve of the B sample at the temperature of liquid nitrogen, which is also shown in Fig. 3, is nearly equal to that of the II band of the A sample and is due to the water molecule. In the case of the B sample, no band due to the ammonium ion was observed.

The X-ray and IR spectra show that the B sample is exactly the same compound as the A sample. The B sample probably contains a small amount of the sodium ion, unlike the A sample, which contains the ammonium ion, but the fact that the crystal structures are identical seems to show that these ions are contained as impurities in the crystal.

Behavior on Heat Treatment in Air. The DTA-TGA measurement of the A sample was done up to 500 °C. As can be seen from the typical DTA-TGA curve shown in Fig. 4, the weight of the sample decreases continuously up to 300 °C, without any definite

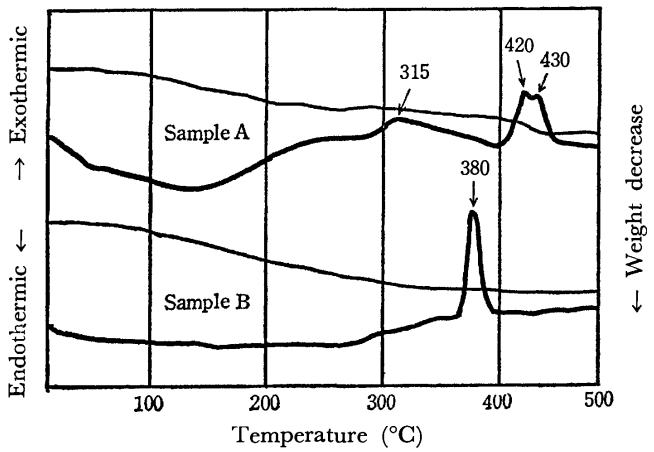

Fig. 4. DTA-TGA curves of the samples A and B.
—: DTA, —: TGA

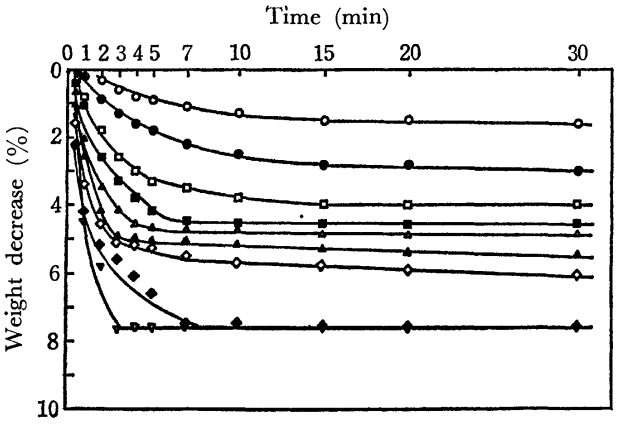

Fig. 5. Isothermal curves of weight decrease of the sample A by heat treatment in air.
○: 100 °C, ●: 150 °C, □: 200 °C, ■: 250 °C, △: 300 °C, ▲: 350 °C, ◇: 400 °C, ◆: 450 °C, ▽: 500 °C.

decomposition temperature, which corresponds to 0.46 mol of H_2O per mol of MoO_3. At 315 ° and 420—430 °C, an exothermal transformation, accompanied by a small weight loss, is observed. The transformation temperature, however, was not reproducible, because, for samples from different lots, one to three exothermal peaks appeared in the range from about 300 to 430 °C.

Figure 5 shows the rate of the weight loss measured in air at various temperatures by means of a quartz spring balance. At every temperature below 300 °C, the rate of weight loss rapidly decreases for several minutes, while the weight is kept nearly constant by further heating. The weight loss is about 5% at 300 °C. By heating at a temperature above 300 °C, after an initial rapid weight loss of about 5%, the weight exponentially approaches a certain minimum value, which is quickly attained by 450 and 500 °C heating. Thus, these curves seem to show weight decreases by two different processes—one below 300 °C and the other above 300 °C. These two processes correspond exactly to the endothermal change at the temperature below 300 °C and the exothermal transformation above 300 °C, observed on the DTA-TGA curve, respectively.

The quantities of ammonia included in the A sample heated for 30 min at various temperatures, as determined

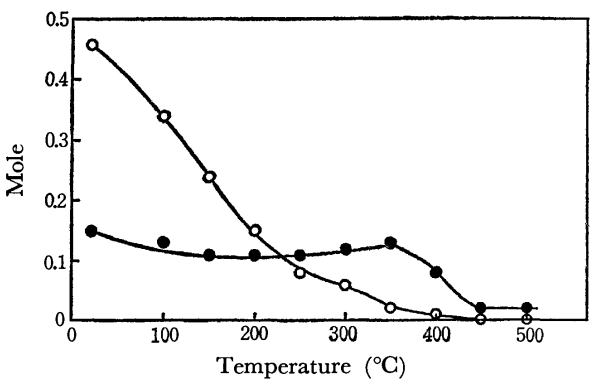

Fig. 6. Amounts of ammonia and water in the sample A after 30 min heating.
●: ammonia, ○: water.

Table 2. The results of X-ray diffraction analysis of the sample A after heat treatments, in air, in hydrogen and in a hydrogen-thiophene mixture

Time (min)		5	10	20	30	40	60	100	180	360
Air	350 °C	I	I	I	I	I	I	I	I	I+II
	400 °C	I	I	I	I+II		I+II		II	
Hydrogen	350 °C	I	I			I	I*+II+III	II+III		
	400 °C		I*+II+III			II+III				
Hydrogen + thiophene	350 °C	I+II	I+II	II+III		III				
	375 °C	I+II	II+III	III						
	400 °C	II+III	III							

I(I'); hexagonal oxide, II; rhombic MoO_3, III; MoO_2, *; trace

by chemical analysis, are plotted against the heating temperature in Fig. 6. The amount of ammonia content decreases slightly at below 150 °C, probably because of the desorption of the absorbed ammonia, is kept nearly constant up to 350 °C, and begins to decrease above 350 °C. The amount of residual water in the heated sample, as calculated from the total weight loss and the weight loss due to the deammoniation, is also shown in Fig. 6, on the assumption that the ammonia was contained as ammonium ions.

According to the above results, the weight loss below 300 °C is mainly to the liberation of the hydrated water, and the small weight decrease accompanied by the exothermal transformation at 420—430 °C in the DTA-TGA measurement is due to deammoniation. However, as the deammoniation must be endothermic, the transformation at 420—430 °C is essentially a solid-phase transformation. The small deammoniation is, therefore, considered to be an evolution of an ammonia impurity induced by the crystal rearrangement.

In the case of the B sample also, it evolves water as does the A sample below 300 °C and undergoes an exothermal transformation at about 380 °C, as is shown in Fig. 4, but no detectable weight loss is observed.

The results of the X-ray diffraction analysis of the A sample treated in air are summarized in Table 2. No change is observable in the diffraction pattern on heating at 350 °C for 360 min, even though most of the hydrated water is liberated in several minutes at that temperature, showing the conversion of the hydrated sample A (I) to anhydrous hexagonal oxide (I'). After 360 mins' heating at the same temperature, a weak pattern of rhombic MoO_3(II) is detectable. At 400 °C, II appears in 30 min; the X-ray pattern gradually increases in intensity as the duration of heating increases.

In the previous paper,[14] the present author reported that the transformation of I' to II was observed at 420—430 °C. However, a small exothermal peak appears at 315 °C on the DTA curve. The X-ray studies show that a small amount of II is observed when I' is heated in air at 350 °C for 360 min. It may, therefore, be assumed that the small peak at 315 °C can be the transformation of I' to II.

I' below the transformation temperature is highly hygroscopic, as is clearly shown by the fact that it absorbs easily about half of the water in heating. On the other hand, the sample heated above the transformation temperature absorbs water only slightly.

The IR spectra of the sample after heat treatment are shown in Fig. 2. The IR absorption bands at 3478 and 1610 cm^{-1} due to H_2O sharply decrease in intensity below 300 °C. The bands at 3170 and 1409 cm^{-1} due to the ammonium ion are retained up to near 350 °C, the intensities begin to decrease temperatures above 400 °C, as is to be expected from the results of thermal analysis, while the bands below 1000 cm^{-1} do not show any appreciable change at 300 °C. Above 400 °C, new bands at 996, 876, and 821 cm^{-1} due to II appear, and at 450 °C the spectrum changes completely to that of II.

Heat Treatment in Hydrogen (Reduction). The A sample was treated in hydrogen under an atmospheric pressure at 350 °C and 400 °C, and the structural changes were observed by X-ray diffraction (see Table 2). At 350 °C, no change is observable for 40 min, but at 60 min the intensity of the original hexagonal pattern is markedly reduced and patterns due to II and MoO_2(III) appear. At 100 min, most of the sample is reduced to III. A similar change is observable at 400 °C, though the rate is steep.

According to the X-ray results, II always coexists with the III phase. This suggests that no abrupt reduction of I' to III occurs; rather, the reduction passes through II—that is, I'→II→III.

Heat Treatment in the Hydrogen-thiophene Mixture. The changes in the A sample in the hydrogen–thiophene mixture were studied at 350, 375, and 400 °C. In this case, the hydrodesulfurization of thiophene also takes place, and the sample acts as a catalyst for the reaction. The results of the X-ray diffraction analysis of the A sample are listed in Table 2.

As in hydrogen, the transformation to II and the reduction to III also occur. II appears before III is detected. This fact suggests, as in the case of hydrogen, that the reaction proceeds in this sequence: I'→II→III. In the hydrogen–thiophene mixture, however, the transformation and reduction proceed far more quickly than in hydrogen. II, for example, appears in 5 min at 350 °C, and III, in 20 min. The change is even faster at higher temperatures.

The sulfur contents of the A sample when treated in the hydrogen–thiophene mixture were analyzed by the $BaSO_4$ method. Though MoS_2 was not detected by X-ray diffraction analysis, the sulfur contents increased with the time of treatment, as is shown in Fig. 7. The sulfurization did not exceed 5%, however, the rate of sulfurization was slower than those of transformation and reduction. As III was not easily sulfurized

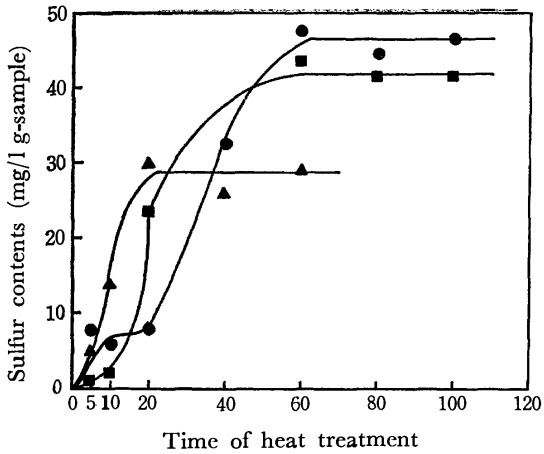

Fig. 7. Sulfur contents in the sample A after heat treatment for 30 min in a hydrogen-thiophene mixture.
●: 350 °C, ■: 375 °C, ▲: 400 °C.

under the same conditions,[16] II was assumed to selectively sulfurized in this experiment.

Discussion

As has been described above, I′, with the same hexagonal crystal structure as I, is obtained by dehydration. Neither I nor I′ have ever been reported previously; they may, then, be regarded as a new form.

The results of IR and NMR spectroscopies show that the water included in I is contained as water molecules, not as hydroxyl. The fact that I′ has the same crystal structure as I means that I′ has a structure with vacancies, in which the water molecule can be occluded.

The postulation of this structure is supported by the following facts: (i) I has no definite decomposition temperature upon dehydration. (ii) I′ is highly hygroscopic, in contrast with the nonhygroscopic nature of II. (iii) The density, when the substance A treated in air, changes from 3.75 g/cm^3 of I to 3.58 g/cm^3 of I′, without any change in the crystal structure.

I′ is surely transformed to II at 420—430 °C. II is not, on the other hand, transformed to I′ on cooling, and, so is regarded as a stable phase at low temperatures. I′ is, therefore, a metastable phase, and the transformation at 420—430 °C is from a metastable to a stable phase. The variation in the transformation temperature is probably due to the above fact. As has previously been described, the transformation is always accompanied by the decomposition of a small amount of ammonium ions. At the same time, the endothermal deammoniation overlaps the exothermal change. The exothermal change in the DTA curve is, therefore, somewhat compensated for by the endothermal deammoniation. This is another reason for the irreproducibility of the DTA curve. In the case of the B sample, which is free from ammonium ions, the transformation shows a simple single exothermal peak, with no endothermal change. Such impurities as the ammonium ion or the Na^+ ion, which may be contained in the vacancies of the oxide, are assumed to stabilize the hexagonal phase; therefore, the transformation temperature may have something to do with the amount of such impurities.

In addition to dehydration, the reduction and sulfurization of I′ occur in hydrogen and in the hydrogen-thiophene mixture. It is clear from Fig. 5 that the dehydration proceeds more quickly than the reduction and the sulfurization. Thus, it may be concluded that the reduction and the sulfurization occur after dehydration.

On the other hand, the X-ray results suggest, as has been described previously, that the reduction occurs consecutively as I′→II→III.

Sulfurization also occurs along with reduction in the hydrogen-thiophene mixture. As has been described previously, it is assumed that II is preferentially sulfurized. Consequently, in the hydrogen-thiophene mixture I changes as is shown in Fig. 8. The X-ray diffraction analysis confirms that the I′→II transformation in hydrogen proceeds faster than in air, and that, in the hydrogen-thiophene mixture, the transformation proceeds much faster still. An interesting fact is that the existence of hydrogen or thiophene accelerates the I′→II transformation. The precise mechanism is not known, but it seems to be certain that these gases have some catalytic function in the transformation.

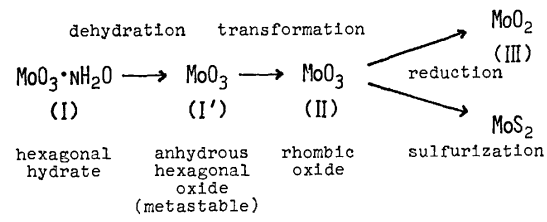

Fig. 8. Changes of the state of the hydrate by heat treatment, in air, in hydrogen and in a hydrogen-thiophene mixture.

The author is grateful to Professor Masatomo Hasegawa for his encouragement and helpful advice. He is also indebted to Professor Yushiro Saito for his NMR measurements and inspiring suggestions, and to Dr. Itaru Moto-oka for his DTA-TGA measurements and useful discussions. Also, the author is grateful to Mr. Yoshihiro Nishimitsu for his kind suggestions with respect to the format of this manuscript.

References

1) H. Braekken, *Z. Krist.*, **78**, 484 (1931).
2) N. Wooster, *ibid.*, **80**, 504 (1931).
3) G. Anderson and A. Magneli, *Acta Chem. Scand.*, **4**, 793 (1950).
4) L. Kihlborg, *Arkiv Kemi.*, **21**, 357, 417 (1963).
5) G. Carpéni, *Bull. Soc. Chim. Fr.*, **1947**, 484.
6) L. Lindquvist, *Acta Chem. Scand.*, **4**, 650 (1950), **10**, 1362 (1956).
7) K. Funaki and T. Segawa, *Denki Kagaku*, **18**, 305 (1950).
8) S. Maricic and J. Smith, *Acta Chem. Scand.*, **10**, 1362 (1956).
9) S. Asbrink, B. Brandt, and P. Kiegaarb, *ibid.*, **23**, 2196 (1969).
10) B. Krebs, *Chem. Commun.*, **1970**, 50.
11) A. Magneli, *Acta Chem. Scand.*, **2**, 861 (1948).

12) A. Magneli, *ibid.*, **2**, 501 (1948).
13) B. Krebs, *Acta Crystallogr.*, **B28**, 2222 (1972).
14) N. Sotani, Y. Saito, M. Oita, and M. Hasegawa, *Nippon Kagaku Kaishi*, 673 (1974).
15) P. L. Kirk and F. L. Schaffer, *Rev. Sci. Instrum.*, **19**, 785 (1948).
16) N. Sotani and M. Hasegawa, This Bulletin, **46**, 25 (1973).
17) "Jikken Kagaku Koza," ed. by M. Kotake, Vol. 23, p. 34, Maruzen, Tokyo (1957).
18) Anal. Chem. Soc. Japan, "Bunseki Kagaku Binran," p. 495, Maruzen, Tokyo (1961).
19) L. J. Bellamy, "The Infrared Spectra of Complex Molecules," p. 346, Mathuen and Co., London (1966).
20) Herzberg, "Molecular Spectra and Molecular Structure," p. 167, D. Van Norstrand Co., New Jersy (1968).
21) Hagg and A. Magneli, *Arkiv Kemi., Mineral Geol.*, **19A**, 12 (1935).

Preparation and Reaction of Some Di-*tert*-butylnitroxidopalladium(II) Complexes, $PdX(Bu^t_2NO)L$ ($L=PPh_3$, $AsPh_3$, $P(OPh)_3$; $X=Cl$, Br, I)

Masaaki OKUNAKA, Gen-etsu MATSUBAYASHI, and Toshio TANAKA

Department of Applied Chemistry, Faculty of Engineering, Osaka University, Yamada-kami, Suita, Osaka 565

(Received January 23, 1975)

$PdX(Bu^t_2NO)L$ ($L=PPh_3$, $AsPh_3$, $P(OPh)_3$; $X=Cl$, Br, I) was isolated by the reactions of $[PdCl(Bu^t_2NO)]_2$ with L and by the halogen exchange reactions of the chloro complexes with $LiBr\cdot H_2O$ or NaI. PMR and IR spectra revealed that $PdX(Bu^t_2NO)(PPh_3)$ and $PdX(Bu^t_2NO)(AsPh_3)$ exist as only one geometrical isomer with the halogen atom *trans* to the oxygen atom of the nitroxide ligand, while two isomers of $PdX(Bu^t_2NO)[P(OPh)_3]$ coexist in solution. The reaction of $PdX(Bu^t_2NO)(PPh_3)$ ($X=Cl$, I) with triphenylphosphine was found to give $Pd(PPh_3)_4$ together with $Pd X_2(PPh_3)_2$ and $Bu_2NO\cdot$. A similar reaction proceeded between $PdCl(Bu^t_2NO)$-$[P(OPh)_3]$ and triphenylphosphite to yield $Pd[P(OPh)_3]_3$, while a not well-defined complex $[PdCl(AsPh_3)_2]_n$ was obtained in the reaction of $PdCl(Bu^t_2NO)(AsPh_3)$ with triphenylarsine.

The interactions between stable nitroxide radicals and metal halides have been studied by several workers.[1-8]

Some time ago, Beck and Schmidtner[2] reported that di-*tert*-butyl nitroxide reacts with palladium chloride to give a diamagnetic chloro-bridged complex $[PdCl(Bu^t_2NO)]_2$ (I), in which $Bu^t_2NO^-$ coordinates to the palladium through both the nitrogen and oxygen atoms to form a three-membered ring. The chloro-bridge is expected to undergo a cleavage reaction by nucleophiles. In addition, the unique three-membered

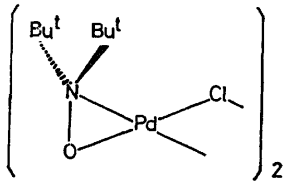

I

ring moiety is supposed to be reactive.

In these respects, it is of interest to investigate the reaction of I with some nucleophiles. This paper reports the preparation of $PdX(Bu^t_2NO)L$ ($L=PPh_3$, $AsPh_3$, $P(OPh)_3$; $X=Cl$, Br, I), and the reactions of $PdX(Bu^t_2NO)L$ with L to give low-valent palladium complexes.

Experimental

Di-*tert*-butyl nitroxide radical was prepared as described by Hoffmann *et al.*[9] $[PdCl(Bu^t_2NO)]_2$ was prepared according to the literature.[2] All the manipulations in the reaction of $PdX(Bu^t_2NO)L$ with L ($L=PPh_3$, $AsPh_3$, $P(OPh)_3$; $X=Cl$, I) were carried out under dry nitrogen.

Preparation of $PdX(Bu^t_2NO)L$ ($L=PPh_3$, $AsPh_3$, $P(OPh)_3$; $X=Cl$, Br, I). To a benzene solution of $[PdCl(Bu^t_2NO)]_2$ (0.57 g, 1.0 mmol) was added dropwise a benzene solution of triphenylphosphine (0.53 g, 2.0 mmol) with stirring for 30 min at room temperature. The solvent was evaporated to dryness under reduced pressure. The product obtained was dissolved in diethyl ether to give a suspension. It was filtered, and the filtrate was evaporated to dryness again under reduced pressure. The resulting solid was recrystallized from a benzene solution by adding petroleum ether to afford orange crystals of $PdCl(Bu^t_2NO)(PPh_3)$ (0.74 g, yield 68%).

$PdCl(Bu^t_2NO)(PPh_3)$ and a large excess amount of $LiBr\cdot H_2O$ were mixed in ethanol. After stirring for 30 min, the solution was evaporated to dryness and the product was recrystallized from ligroin to give dark red needles of $PdBr(Bu^t_2NO)(PPh_3)$. $PdI(Bu^t_2NO)(PPh_3)$ was synthesized by

TABLE 1. MELTING POINTS, ANALYTICAL DATA AND MOLECULAR WEIGHTS OF THE COMPLEXES

Complex	Mp (°C)	C% Found (Calcd)	H% Found (Calcd)	N% Found (Calcd)	M. W. Found (Calcd)
$PdCl(Bu^t_2NO)(PPh_3)$	152—153 (dec)	56.96 (56.71)	6.07 (6.30)	2.55 (2.69)	548 (503)
$PdBr(Bu^t_2NO)(PPh_3)$	175—183 (dec)	52.54 (52.68)	5.85 (5.61)	2.55 (2.36)	581 (593)
$PdI(Bu^t_2NO)(PPh_3)$	165—173 (dec)	49.18 (48.81)	5.47 (5.21)	2·34 (2.19)	646 (640)
$PdCl(Bu^t_2NO)(AsPh_3)$	155—156 (dec)	52.28 (52.71)	5.74 (5.63)	2.25 (2.37)	579 (592)
$PdBr(Bu^t_2NO)(AsPh_3)$	150—156 (dec)	48.98 (49.04)	5.25 (5.23)	2.40 (2.20)	608 (636)
$PdI(Bu^t_2NO)(AsPh_3)$	136—141 (dec)	45.48 (45.67)	4.93 (4.87)	2.24 (2.05)	645 (684)
$PdCl(Bu^t_2NO)[P(OPh)_3]$	104—105	52.15 (52.36)	5.68 (5.58)	2.36 (2.35)	579 (596)
$PdBr(Bu^t_2NO)[P(OPh)_3]$	123—126	48.79 (48.73)	5.37 (5.20)	2.29 (2.19)	638 (641)
$PdI(Bu^t_2NO)[P(OPh)_3]$	110—112	45.50 (45.40)	4.99 (4.85)	2.07 (2.03)	681 (689)

the reaction of the chloro complex with excess NaI in a similar manner. Six other complexes were similarly prepared. The melting points and analytical data are summarized in Table 1.

Reaction of $PdCl(Bu^t_2NO)(PPh_3)$ with Triphenylphosphine. To a benzene solution of $PdCl(Bu^t_2NO)(PPh_3)$ (0.55 g, 1.0 mmol) was added dropwise a benzene solution of triphenylphosphine (1.57 g, 6.0 mmol) with stirring at room temperature. The solution changed from orange to yellow *via* red, and finally a light yellow precipitate was obtained. Stirring was continued for 6 hr to force the reaction to completion. Then the solution was evaporated under reduced pressure, and the resulting solid was washed with diethyl ether to remove unreacted triphenylphosphine and liberated di-*tert*-butyl nitroxide. The product was recrystallized from ethanol to give pale yellow crystals of $Pd(PPh_3)_4$ (0.13 g, 0.11 mmol), mp 103—105 °C (decomp.) [lit,[10] 100—105 °C (decomp.)]. Found: C, 72.97; H, 5.56%. Calcd for $Pd(PPh_3)_4$: C, 74.83; H, 5.24%. From the component insoluble in ethanol $PdCl_2(PPh_3)_2$ (0.33 g, 0.47 mmol) was obtained, mp above 220 °C. Found: C, 61.36; H, 4.38%. Calcd for $PdCl_2(PPh_3)_2$: C, 61.60; H, 4.32%. ν(Pd–Cl) 360 cm^{-1}.

An equimolar amounts of $PdCl(Bu^t_2NO)(PPh_3)$ and triphenylphosphine were mixed in benzene and stirred for 42 hr at room temperature. The solution was concentrated under reduced pressure to give a yellow precipitate, which was washed with diethyl ether and collected by filtration. The IR spectrum of this product showed ν(Pd–Cl) band at 303 and 360 cm^{-1} arising from $PdCl(Bu^t_2NO)(PPh_3)$ and $PdCl_2(PPh_3)_2$, respectively.

Reaction of $PdI(Bu^t_2NO)(PPh_3)$ with Triphenylphosphine. A benzene solution containing $PdI(Bu^t_2NO)(PPh_3)$ (0.30 g, 0.47 mmol) and triphenylphosphine (0.74 g, 2.82 mmol) was allowed to react overnight at room temperature to form pale yellow crystals of $Pd(PPh_3)_4$ (0.18 g, 0.16 mmol) and red brown crystals of $PdI_2(PPh_3)_2$ (0.20 g, 0.23 mmol). They were identified by IR spectra and decomposition points.

Reaction of $PdCl(Bu^t_2NO)[P(OPh)_3]$ with Triphenylphosphite. To a benzene solution of $PdCl(Bu^t_2NO)[P(OPh)_3]$ (0.45 g, 0.76 mmol) was added dropwise a benzene solution of triphenylphosphite (1.40 g, 4.53 mmol) with stirring at room temperature. Immediately, the yellow color of the solution faded away. The solution was concentrated under reduced pressure to give an oily product, which was dissolved in petroleum ether. The resulting white precipitate was collected by filtration and recrystallized from ethanol to give colorless crystals of $Pd[P(OPh)_3]_3$ (0.14 g, 0.14 mmol), mp 128—130 °C (decomp.) under dry nitrogen [lit,[11] 118—129 °C (decomp.) under argon]. Found: C, 62.02; H, 4.35%. Calcd for $Pd[P(OPh)_3]_3$: C, 62.52; H, 4.38%. $PdCl_2[P(OPh)_3]_2$ (0.12 g, 0.14 mmol) was obtained from the petroleum ether solution, mp 177—179 °C (lit,[12] 175—180 °C).

Reaction of $PdCl(Bu^t_2NO)(AsPh_3)$ with Triphenylarsine. $PdCl(Bu^t_2NO)(AsPh_3)$ (0.95 g, 1.60 mmol) and tripenylarsine (2.95 g, 9.63 mmol) were mixed in benzene and stirred for 7 days at room temperature to form a yellow precipitate, which was filtered, washed with diethyl ether and dried *in vacuo* (0.92 g), mp 154—156 °C (decomp.). Found: C, 57.14; H, 4.65%. Calcd for $[PdCl(AsPh_3)_2]_n$: C, 57.32; H, 4.02%. ν(Pd–Cl), 318 cm^{-1}.

Physical Measurements. IR spectra were recorded in Nujol mulls or in chloroform on a Hitachi EPI-L (700—200 cm^{-1}) spectrophotometer. PMR spectra were recorded on a JOEL JNM-PS-100 spectrometer, using tetramethylsilane as the internal reference. ESR spectra were recorded on a JOEL JES-ME-3X spectrometer. Molecular weights were determined in chloroform using a Mechrolab vapor pressure osmometer.

Results and Discussion

Preparation and Configuration of $PdX(Bu^t_2NO)L$ ($L=PPh_3$, $AsPh_3$, $P(OPh)_3$; $X=Cl$, Br, I). The reaction of $[PdCl(Bu^t_2NO)]_2$ with L ($L=PPh_3$, $AsPh_3$, $P(OPh)_3$) gave $PdCl(Bu^t_2NO)L$ (Eq. 1), which underwent halogen exchange reactions to yield the corresponding bromo and iodo complexes (Eq. 2). Molecular

$$[PdCl(Bu^t_2NO)]_2 + 2L \longrightarrow 2PdCl(Bu^t_2NO)L \quad (1)$$
($L=PPh_3$, $AsPh_3$, $P(OPh)_3$)

$$PdCl(Bu^t_2NO)L + \text{excess } LiBr\cdot H_2O \text{ or } NaI \longrightarrow PdX(Bu^t_2NO)L \quad (X=Br, I) \quad (2)$$

weight determination indicates that these complexes are essentially monomeric in chloroform (Table 1), which is consistent with the fact that the IR spectra of $PdCl(Bu^t_2NO)L$ show an intense band at 303—316 cm^{-1} assigned to the terminal Pd–Cl stretch as shown in Table 2. These facts reveal that the cleavage reaction took place at the bridging moiety.

In these complexes obtained two geometrical isomers, *A* and *B*, are possible. PMR spectra of $PdX(Bu^t_2NO)(PPh_3)$ and $PdX(Bu^t_2NO)(AsPh_3)$ show only one *tert*-butyl signal (Table 2). In view of a large steric repulsion between *tert*-butyl and phenyl groups in *B*, but the insignificant one in *A*, this signal would be assigned to the isomer *A*. On the other hand, $PdX(Bu^t_2NO)[P(OPh)_3]$ exhibits another weak *tert*-butyl signal, which is probably arising from the isomer *B*. This is

Table 2. PMR and IR data of the complexes

Complex	δ (Bu^t) in $CDCl_3$ at 23 °C	ν(Pd-Cl), cm^{-1}	
		in Nujol mull	in $CHCl_3$
$PdCl(Bu^t_2NO)(PPh_3)$	1.74	303	305
$PdBr(Bu^t_2NO)(PPh_3)$	1.67	—	—
$PdI(Bu^t_2NO)(PPh_3)$	1.78	—	—
$PdCl(Bu^t_2NO)(AsPh_3)$	1.75	304	305
$PdBr(Bu^t_2NO)(AsPh_3)$	1.80	—	—
$PdI(Bu^t_2NO)(AsPh_3)$	1.75	—	—
$PdCl(Bu^t_2NO)[P(OPh)_3]$	1.35, 1.31(w)	316	305, 312(w)
$PdBr(Bu^t_2NO)[P(OPh)_3]$	1.38, 1.34(w)	—	—
$PdI(Bu^t_2NO)[P(OPh)_3]$	1.35, 1.32(w)	—	—

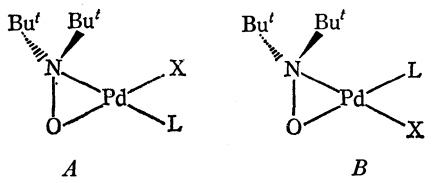

A *B*

supported from the smaller steric hindrance of triphenylphosphite than triphenylphosphine[13] (and probably triphenylarsine, too). In accordance with the PMR observations, IR spectra of $PdCl(Bu^t_2NO)(PPh_3)$ and $PdCl(Bu^t_2NO)(AsPh_3)$ in chloroform show only one ν(Pd–Cl) band, while two ν(Pd–Cl) bands appear in $PdCl(Bu^t_2NO)[P(OPh)_3]$ (Table 2).

ESR Spectra. The ESR spectrum of $PdCl(Bu^t_2NO)(PPh_3)$ in dichloromethane at room temperature shows a weak triplet with a spacing of 16.5 gauss (Fig. 1), which indicates a little dissociation of the complex in solution to produce di-*tert*-butyl nitroxide radical. The intensity of this signal is enourmously enhanced by the addition of triphenylphosphine as depicted in Fig. 1. These observations confirm that a redox reaction of the complex took place in the presence of triphenylphosphine. That is to say, $Bu^t_2NO^-$ which had coordinated as an anion was oxidized to $Bu^t_2NO\cdot$ radical, and, as an inevitable consequence, some reduced palladium species must be formed in solution. Thus, we

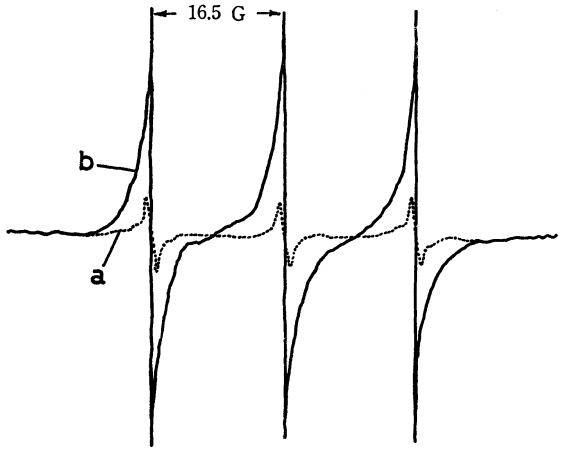

Fig. 1. ESR spectra of (a) $PdCl(Bu^t_2NO)(PPh_3)$ and (b) $PdCl(Bu^t_2NO)(PPh_3)+2PPh_3$, both in CH_2Cl_2 at 25 °C.
The concn. of the complex: 1.3×10^{-2} M; the signal is considered to be caused by $Bu^t_2NO\cdot$ produced by decomposition.

investigated the reaction of $PdX(Bu^t_2NO)L$ with L in order to clarify the reduced palladium complex.

Reaction of $PdX(Bu^t_2NO)L$ with L. $PdX(Bu^t_2NO)(PPh_3)$ (X=Cl, I) reacted readily with triphenylphosphine to give $Pd(PPh_3)_4$ and $PdX_2(PPh_3)_2$. Since $Bu^t_2NO^-$ works clearly as a one electron reducing agent, a monovalent palladium complex must be formed as an intermediate in the course of the reaction (Path 3 in Scheme 1). Recently, Otsuka *et al*[14] reported the preparation of monovalent palladium complexes $[PdX(Bu^tNC)_2]_2$, for which they proposed a dimeric halide-bridged structure (II). Thus, an

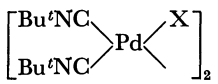

(X=Cl, Br, I)

II

equilibrium 4 between monomer and dimer will be most probable in solution. Further, the dimeric complex may disproportionate to $Pd(PPh_3)_4$ and $PdCl_2(PPh_3)_2$ by assist of another triphenylphosphine molecule (Path 5). However, the assumed intermediate involving monovalent palladium could not be isolated even in the equimolar reaction of $PdCl(Bu^t_2NO)(PPh_3)$ with triphenylphosphine (see Experimental).

Similarly, $Pd[P(OPh)_3]_3$ and $PdCl_2[P(OPh)_3]_2$ were obtained by the reaction of $PdCl(Bu^t_2NO)[P(OPh)_3]$ with excess triphenylphosphite. This reaction is thought to proceed through a similar way to Scheme 1.

In contrast to the results obtained for triphenylphosphine and triphenylphosphite complexes, no zerovalent complex could be isolated in the reaction of $PdCl(Bu^t_2NO)(AsPh_3)$ with excess triphenylarsine. Instead, a yellow complex whose IR spectrum shows a ν(Pd–Cl) band at 318 cm^{-1} was obtained. This complex is suggested to be $[PdCl(AsPh_3)_2]_n$ from analytical data. This complex is stable in air so far as it is in solid state. It is almost insoluble in common organic solvents, and at elevated temperatures decomposes in suspension in benzene even under dry nitrogen. The detailed structure of this complex has to await further studies in the solid state.

References

1) W. Beck, K. Schmidtner and H. J. Keller, *Chem. Ber.*, **100**, 503 (1967).
2) W. Beck and K. Schmidtner, *Chem. Ber.*, **100**, 3363 (1967).
3) R. A. Zelonka and M. C. Baird, *J. Amer. Chem. Soc.*, **93**, 6066 (1971).

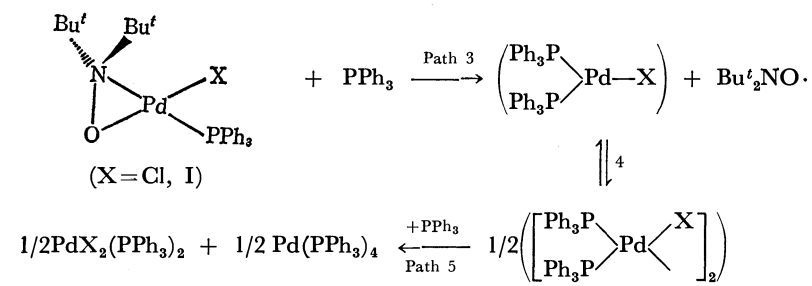

Scheme 1

4) D. Wilbur and R. Kreilick, *J. Chem. Phys.*, **52**, 1643 (1970).
5) T. B. Eames and B. R. Hoffman, *J. Amer. Chem. Soc.*, **93**, 3141 (1971).
6) Y. Y. Lim and R. S. Drago, *Inorg. Chem.*, **11**, 1334 (1972).
7) N. M. Karayannis, C. M. Paleos, C. M. Mikulski, L. L. Pytlewski, H. Blum and M. M. Labes, *Inorg. Chim. Acta.*, **7**, 74 (1973).
8) A. H. Cohen and B. M. Hoffmann, *Inorg. Chem.*, **13**, 1484 (1974).
9) A. Hoffman, A. M. Feldman and E. Gelblum, *J. Amer. Chem. Soc.*, **86**, 646 (1964).
10) L. Malatesta and M. Angoletta, *J. Chem. Soc.*, **1186** (1957).
11) W. Kuran and A. Musco, *J. Organometal. Chem.*, **40**, C47 (1972).
12) N. Ahmad, E. W. Ainscough, T. A. James and S. D. Robinson, *J. Chem. Soc. Dalton*, 1148 (1973).
13) C. A. Tolman, *J. Amer. Chem. Soc.*, **92**, 2956 (1970).
14) S. Otsuka, Y. Tatsuno and K. Ataka, *ibid.*, **93**, 6705 (1971).

Studies of the Preparation and Physical Properties of Multivalent Metal Condensed Phosphates. Part XI.[1] The Preparation of Various Aluminum Phosphates and Their Thermal Transformation

Mitsutomo TSUHAKO, Kazuko HASEGAWA, Tsuneo MATSUO, Itaru MOTOOKA,* and Masamitsu KOBAYASHI*

Kobe Women's College of Pharmacy, Motoyama-kitamachi, Higashinada-ku, Kobe 658

** Department of Chemistry, Kobe University, Nada-ku, Kobe 657*

(Received February 3, 1975)

In the reaction of Al_2O_3 or $Al(OH)_3$ with phosphoric acid, the conditions of the formation of the I and II types of aluminum dihydrogen tripolyphosphate, $AlH_2P_3O_{10}$, and the A and B types of aluminum tetrametaphosphate, $Al_4(P_4O_{12})_3$, were established. The I and II types of $AlH_2P_3O_{10}$ were chiefly obtained at 300 °C; the formation of the I type predominated when the water content of the primary product was 15—30%, while the II type was more readily formed at a water content of 10—15%. Also, the I and II types were easily formed at vapor pressures of 1—5 atm. $Al_4(P_4O_{12})_3$ was produced when the water content was less than 10% or more than 30%. On the other hand, the A and B types of $Al_4(P_4O_{12})_3$ were easily formed at 500 °C; the A type was chiefly formed when the water content was below 10% or above 25%, while the B type was produced at the water content of 10—25%. The water content of the primary product is presumably due to the dehydration caused by the condensation of the P–OH. Thus water, effective for the formation of aluminum phosphates, is the structural water (P–OH). Further, the B type was liable to be formed on rapid dehydration, while the A type was more readily produced on slow dehydration. Accordingly, the formation of aluminum phosphate has been confirmed to be greatly dependent on the water content of the primary product and on the vapor pressure in the secondary heat treatment.

Although many kinds of aluminum phosphates have been discovered as minerals[2-4] and synthesized by many investigators,[5-9] their structures, methods of preparation, and physical properties are not yet well known. The existence of the A, B, C, D and E types of aluminum tetrametaphosphate, $Al_4(P_4O_{12})_3$,[10,11] and the I and II types of aluminum dihydrogen tripolyphosphate, $AlH_2P_3O_{10}$,[12-14] has already been reported by d'Yvoire, but he isolated each phosphate from its mixture by dissolution with an alkaline solution or by decantation. Therefore, their formation conditions have not yet been established. Especially, the difference between the conditions of the formation of the I and II types or those of the A and B types is not clear. According to the authors' experience, it is very difficult to establish a preparation method of aluminum phosphates, because various phosphates are formed depending on the kind of aluminum and phosphorus starting material employed, their mixing ratio, and the heating temperature.[16-19] Therefore, in this study the relationship between the water content or the dehydration velocity and the yields of aluminum phosphates was studied; the formation of phosphates in various heating atmospheres was also examined in order to investigate the influence of the vapor pressure.

Experimental

Preparation of Aluminum Phosphate. Al_2O_3 or $Al(OH)_3$ and phosphoric acid were mixed in a gold or porcelain crucible in the molar ratios Al_2O_3/P_2O_5 (R) of 1/2, 1/3, 1/4, and 1/5; the mixture was then dehydrated by heating over a weak flame with vigorous agitation to obtain a white, highly viscous product in each case. (This is designated as the primary heat treatment, giving the primary products.) A small amount (0.5—0.6 g) of the product was accurately weighed, and the content of water liberated upon heating at 300 or 500 °C was determined by the Karl-Fischer method; meanwhile, another portion was heated for 5 or 20 hr in a thermostated electric furnace, in a vacuum (0.01 mmHg), in a nitrogen stream (50 ml N_2/min, vapor pressure (vp) 0—1 mmHg), in dry air (50 ml/min, vp 0—1 mmHg), in wet air (15—20 mg H_2O/hr, vp 20—25 mmHg), in water vapor (500 g H_2O/hr, vp 760 mmHg), and in a sealed tube[20] (vp 1.5—5 atm). (This is designated as the secondary heat treatment, giving the secondary products.) The experimental method may be shown schematically as follows:

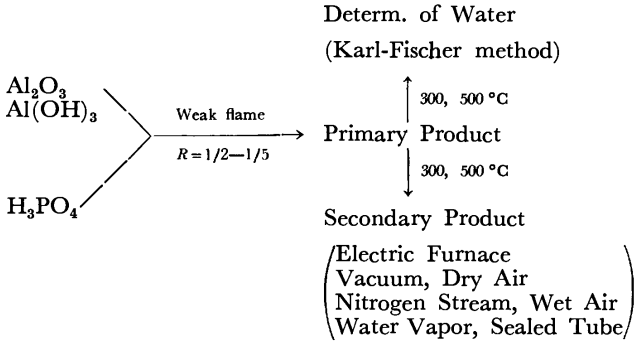

The temperature of the primary heat treatment is dependent on the aluminum materials used, their amounts, and the molar ratio R, it generally being 250—270 °C in the α-Al_2O_3—H_3PO_4 system, 140—160 °C in the γ-Al_2O_3 system, and 130—150 °C in the $Al(OH)_3$ system.

Measurement of the Dehydration Velocity. About 0.5 g of the primary product was weighed and elevated from room temperature to 500 °C at heating rates of 20, 6—7, and 0.8—1.0 °C/min, while the water content was continuously measured by the Karl-Fischer method.

Reaction of $Al(OH)_3$ or Al_2O_3 with P_2O_5. $Al(OH)_3$ or Al_2O_3 and P_2O_5 was rapidly mixed to give a molar ratio of $R=1/3$ in a dry box; the mixture was then heated in an electric furnace at 300 or 500 °C for 20 hr to form aluminum phosphates.

The aluminum phosphates thus obtained were relatively hard, but those obtained at 300 °C absorbed moisture when left in air; the phosphates were taken off the crucible as thin

plates. Especially, the I type of $AlH_2P_3O_{10}$ readily absorbed moisture to form dihydrate $AlH_2P_3O_{10}\cdot 2H_2O$ and separated from the crucible easily.

Apparatus and Methods. The X-ray analysis was carried out with a Rigaku Denki Geigerflex X-ray diffractometer, using Ni filtered Cu$K\alpha$ radiation. A Kyoto Denshi Karl-Fischer Titrator was used for the determination of water. A Rigaku Denki Diffrential Thermogravimetric Analyzer, 8002 HD, was used for the DTA and TG. The X-ray analysis, differential thermal analysis, and thermogravimetry (DTA, TG) of aluminum phosphate were carried out by the methods described in the previous papers.[18,19] The amounts of $AlH_2P_3O_{10}\cdot 2H_2O$, the II type of $AlH_2P_3O_{10}$, and the A and B types of $Al_4(P_4O_{12})_3$ formed in the secondary heat treatment were determined from the integrated intensities of their characteristic X-ray diffraction peaks; *i.e.*, $AlH_2P_3O_{10}\cdot 2H_2O$ was determined by the peak at $2\theta=11.2°$; the II type, by that at 26.4°; the A type, by that at 20.4°; and the B type, by that at 16.2°.

Results and Discussion

Relationship Between the Yield of Aluminum Dihydrogen Tripolyphosphate and the Water Content. It is very difficult to produce the I and II types of $AlH_2P_3O_{10}$ purely, because any attempts give a mixture of $AlH_2P_3O_{10}$ and $Al_4(P_4O_{12})_3$. Therefore, for the purpose of establishing the formation conditions of the I and II types, we studied the relationship between the yields of the I and II types and the water content of the primary product. The results are shown in Fig. 1. As can be seen, the II type was obtained in a good yield when the water content of the primary product was 10—15%, while the I type was obtained at the water content of 15—30%. Also, the water content of the primary product is 8—30% in the α-Al_2O_3–H_3PO_4 system, 15—28% in the γ-Al_2O_3 system, and 15—35% in the $Al(OH)_3$ system. Therefore, the I type is most readily formed, irrespective of the aluminum materials employed, but the II type is easily produced in the α-Al_2O_3–H_3PO_4 system. The water in the primary product is considered to be composed of the structural water (P–OH), the loose water, and coordinated water, though it is found from the results of DTA and TG (Fig. 2) that the amount of the loose and coordinated water is much less than that of the

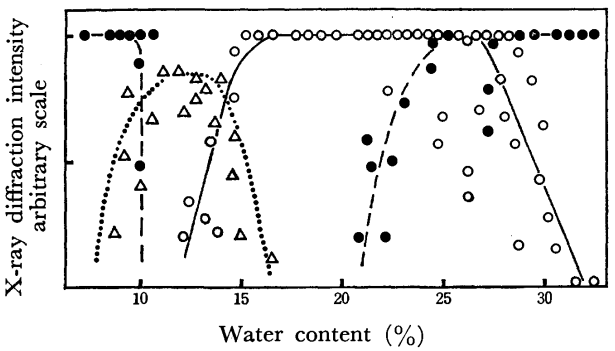

Fig. 1. Relationship between water content and the yields of various aluminum phosphates at 300 °C.
—○—: $AlH_2P_3O_{10}\cdot 2H_2O$,
···△···: II type of $AlH_2P_3O_{10}$,
—●—: Mixture of A and B types of $Al_4(P_4O_{12})_3$.

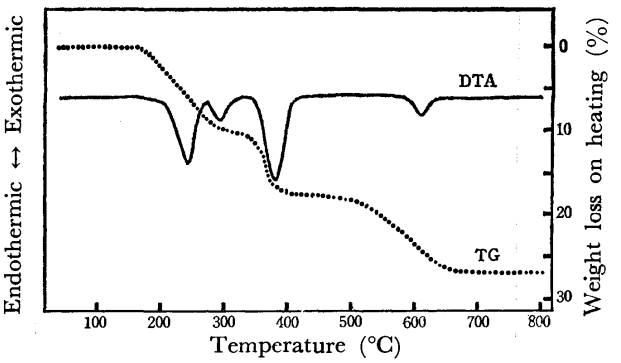

Fig. 2. DTA and TG of the primary product in the system of α-Al_2O_3–H_3PO_4.
Sample; 22 mg, Heating rate; 10 °C/min, $Al_2O_3/P_2O_5(R)=1/3$

structural water. This may be because the primary heat treatment was carried out at high temperatures (over 130—150 °C). In Fig. 2, the endothermic peaks with weight loss at 250—300, 360—390, and 620—630 °C are due to the dehydration caused by the condensation of the P–OH. Therefore, the formation of aluminum phosphates is confirmed to be greatly dependent on the amount of the structural water. On the other hand, $Al_4(P_4O_{12})_3$ was chiefly formed when the water content of the primary product was below 10% or above 30%, but the formation region of the A and B types was not clear at 300 °C. This may be because $Al_4(P_4O_{12})_3$ was generally formed under such special conditions as a large molar ratio and a low or high water content. $AlH_2P_3O_{10}\cdot 2H_2O$ can not be directly obtained by the secondary heat treatment at 300 °C, but when the I type of $AlH_2P_3O_{10}$ was allowed to stand in air, it readily absorbed moisture and was completely transformed into dihydrate $AlH_2P_3O_{10}\cdot 2H_2O$. Thus, the amount of the I type formed corresponds to the amount of $AlH_2P_3O_{10}\cdot 2H_2O$; accordingly, the amount of the latter is expressed as that of the former in Fig. 1. From the mixture of the composition of $R=1/2$, $AlPO_4$ (Berlinite) was found to be formed in addition to $AlH_2P_3O_{10}$ and $Al_4(P_4O_{12})_3$, though the amount of $AlPO_4$ is omitted in Fig. 1.

Relationship Between the Yield of Aluminum Tetrametaphosphate and the Water Content. Figure 3 shows the relationship between the yields of the A and B

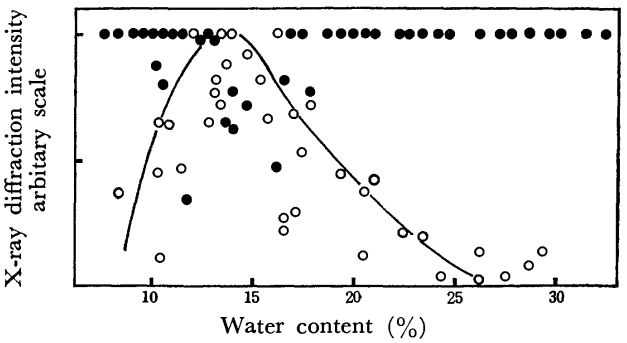

Fig. 3. Relationship between water content and the yields of A and B types of $Al_4(P_4O_{12})_3$ at 500 °C.
●: A type of $Al_4(P_4O_{12})_3$, —○—: B type

Table 1. Formation of aluminum phosphates in various heating atmospheres at 300 °C

	$\frac{1}{R}$	Water content (%)	Electric furnace 5 hr	Electric furnace 20 hr	Sealed tube	Water vapor	Wet air	Nitrogen stream	Dry air	Vacuum
$Al(OH)_3$	3	18.3	I(vs)	I(vs)	I(vs)	I(s), A(w)	A(m), B(m)	I(w), A(w), B(s)	A(m), B(s)	B(vs)
		20.5	I(vs)	I(vs)	I(vs)	I(s), A(w)	A(s), B(m)	I(w), A(m), B(s)	A(w), B(vs)	B(vs)
		22.7	I(vs)	I(vs)	I(vs)	I(vs)	A(s), B(m)	I(w), A(w), B(s)	A(w), B(vs)	B(vs)
		25.0	I(vs)	I(vs)	I(vs)	I(s), A(m)	A(s), B(s)	I(w), A(w), B(vs)	B(vs)	B(vs)
	4	17.6	I(vs)	I(vs)	I(vs)	I(m), A(vs)	A(vs), B(w)	A(m), B(s)	A(w), B(s)	B(vs)
		22.5	I(vs)	I(vs)	I(vs)	I(m), A(vs)	I(w), A(s), B(w)	A(s), B(m)	A(s), B(m)	B(vs)
		23.3	I(vs)	I(vs)	I(vs)	I(m), A(vs)	I(w), A(s), B(m)	A(m), B(m)	A(m), B(s)	B(vs)
	5	22.6	I(vs)	I(vs)	I(vs)	I(w), A(vs)	A(vs), B(w)	A(w), B(vs)	A(m), B(s)	B(vs)
		26.1	I(vs), A(w)	I(vs)	I(vs)	I(w), A(vs)	A(s), B(w)	A(m), B(s)	A(s), B(s)	B(vs)
α-Al_2O_3	3	10.9	II(s), A(w)	II(s), A(w)	II(s)	II(s)	A(s), B(w)	II(w), A(m), B(m)	A(s), B(s)	B(vs)
		12.6	II(s)	II(s)	II(s)	II(s)	A(vs), B(w)	II(w), A(s), B(w)	A(m), B(s)	B(vs)
		13.8	I(w), II(s)	I(w), II(s)	I(m), II(s)	I(m), II(s)	A(vs), B(w)	II(w), A(s), B(w)	A(s), B(m)	B(vs)
		18.3	I(vs)	I(vs)	I(vs)	I(vs)	A(s), B(w)	I(w), A(m), B(m)	A(m), B(s)	B(vs)
	4	11.2	II(s)	II(s)	II(s)	II(s)	A(s), B(m)	II(m), A(w)	A(w), B(s)	B(vs)
		13.6	II(s)	II(s)	II(s)	II(m), A(w)	A(vs)	II(m), A(m), B(m)	A(m), B(s)	B(vs)
		19.3	I(vs)	I(vs)	I(vs)	I(vs)	A(s), B(s)	A(m), B(s)	A(w), B(s)	B(vs)
	5	11.4	II(s)	II(s)	II(s)	II(m), A(w)	A(vs), B(w)	A(vs)	A(vs)	A(w), B(vs)
		13.8	I(m), II(s)	I(m), II(s)	I(m), II(s)	II(m), A(m)	A(vs)	A(vs)	A(vs)	A(w), B(vs)

X-ray diffraction intensity, vs; very strong, s; strong, m; medium, w; weak, vw; very weak
Products, I; $AlH_2P_3O_{10}\cdot 2H_2O$, II; II type of $AlH_2P_3O_{10}$, A; A type of $Al_4(P_4O_{12})_3$, B; B type

Table 2. Formation of aluminum phosphates in various heating atmospheres at 500 °C

	$\frac{1}{R}$	Water content (%)	Electric furnace 5 hr	Electric furnace 20 hr	Sealed tube	Water vapor	Wet air	Nitrogen stream	Dry air	Vacuum
$Al(OH)_3$	3	15.4	A(w), B(vs)	A(w), B(vs)	A(vs)	A(vs), Ber(w), Cri(m)	A(vs), B(w)	A(s), B(vs)	A(vs), B(m)	B(vs)
		19.8	A(m), B(m)	A(m), B(m)	A(vs)	A(vs), Ber(w), Cri(m)	A(vs), B(m)	A(m), B(vs)	A(vs), B(m)	B(vs)
		23.6	A(s), B(vw)	A(s), B(vw)	A(vs)	A(vs), Ber(w), Cri(m)	A(vs), B(m)	A(s), B(s)	A(vs), B(m)	B(vs)
		28.7	A(vs)	A(vs)	A(vs)	A(vs), Ber(w), Cri(m)	A(vs), B(m)	A(s), B(m)	A(vs), B(m)	B(vs)
	4	18.3	A(m), B(m)	A(m), B(m)	A(vs)	A(vs), Cri(m)	A(vs), B(w)	A(vs), B(w)	A(vs), B(w)	B(vs)
		20.1	A(s), B(w)	A(s), B(w)	A(vs)	A(vs), Cri(s)	A(vs)	A(vs), B(w)	A(vs), B(w)	B(vs)
		24.8	A(vs)	A(vs)	A(vs)	A(vs)	A(vs)	A(vs)	A(vs), B(w)	B(vs)
	5	23.7	A(vs)	A(vs)	A(vs)	A(vs), Cri(m)	A(vs)	A(vs), B(w)	A(vs), B(w)	B(vs)
		25.1	A(vs)	A(vs)	A(vs)	A(vs), Cri(w)	A(vs)	A(vs)	A(vs)	A(w), B(vs)
α-Al_2O_3	3	8.3	A(vs)	A(vs)	A(vs)	A(s), Ber(vw), Cri(m)	A(vs), B(w)	A(vs), B(w)	A(vs), B(w)	B(vs)
		10.8	A(vs)	A(vs), B(w)	A(vs)	A(s), Ber(w), Cri(m)	A(vs), B(w)	A(vs), B(w)	A(s), B(m)	B(vs)
		15.6	A(w), B(vs)	A(w), B(vs)	A(vs)	A(vs), Cri(m)	A(s), B(m)	A(s), B(m)	A(s), B(m)	B(vs)
		18.9	A(m), B(s)	A(m), B(s)	A(vs)	A(s), Ber(w), Cri(m)	A(s), B(m)	A(vs), B(w)	A(vs), B(w)	B(vs)
	4	11.3	A(s), B(w)	A(s), B(w)	A(vs)	A(s), Cri(m)	A(vs)	A(vs), B(w)	A(vs), B(w)	B(vs)
		14.6	A(m), B(s)	A(m), B(s)	A(vs)	A(vs), Cri(w)	A(vs), B(m)	A(vs), B(m)	A(s), B(w)	B(vs)
		17.1	A(m), B(vs)	A(m), B(vs)	A(vs)	A(vs), Cri(w)	A(vs), B(w)	A(vs), B(w)	A(vs), B(w)	B(vs)
	5	9.4	A(vs)	A(vs)	A(vs)	A(vs), Cri(w)	A(vs)	A(vs)	A(vs)	A(m), B(s)
		12.1	A(vs)	A(vs)	A(vs)	A(vs), Cri(w)	A(vs)	A(vs)	A(vs)	A(m), B(s)

X-ray diffraction intensity, vs; very strong, s; strong, m; medium, w; weak, vw; very weak
Products, A; A type of $Al_4(P_4O_{12})_3$, B; B type, Ber.; Berlinite, Cri.; Cristobalite type

types of $Al_4(P_4O_{12})_3$ and the water content liberated upon heating the primary product at 500 °C. The A type can be readily formed when the water content of the primary product is below 10% or above 25%, while the B type is obtained at a water content of 10—25%. The results show that the region of formation of the B type is more limited than that of the A type, it consequently being very difficult to prepare the pure B type. The authors repeated the experiment by this procedure 500—600 times, but only in 2—3% of the experiments could the pure B type be obtained, the product in most cases being a mixture of the A and B types. The A type was more likely to be obtained when the molar ratio, R, was low ($R=1/4$—$1/5$), that is, at larger amounts of phosphoric acid. The I and II types of $AlH_2P_3O_{10}$ were not formed at all at 500 °C, possibly because of the thermal transformation of the I and II types into $Al_4(P_4O_{12})_3$ at this temperature. The thermal transformation of the I and II types will be considered in detail latter.

Relationship Between the Formation of Aluminum Tetrametaphosphate and the Dehydration Velocity. As has been described above, the formation of $Al_4(P_4O_{12})_3$ was greatly affected by the water content of the primary product. The rate of dehydration of the primary product was examined in order to investigate the influence of dehydration in the preparation of the A and B types of $Al_4(P_4O_{12})_3$, using several samples with equal water contents. Figure 4 shows the relationship between the heating temperature and the weight loss (the degree of dehydration) at the heating rate of 6—7 °C/min. The ultimate weight loss of each sample was about 24—25%. Naturally, the amount of product may differ with the water content of the primary product, but in the primary product containing same water content it is also seen that the higher the dehydration velocity, the more readily the B type is formed, whereas the slower the dehydration velocity, the more A type is produced. Almost the same results were obtained at heating rates of 0.8—1.0 and 20 °C/min. About 70 to 75% of the

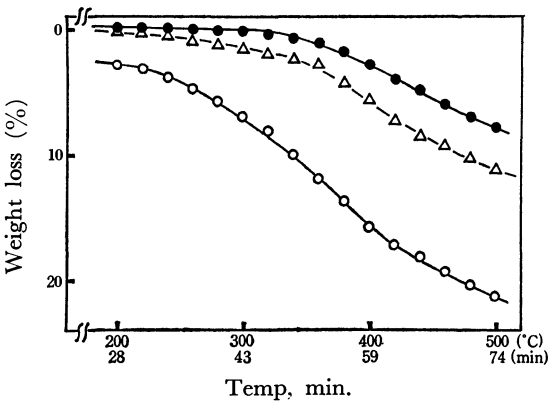

Fig. 4. Relationship between the formation of $Al_4(P_4O_{12})_3$ and dehydration velocity.
—●—: A type of $Al_4(P_4O_{12})_3$,
--△--: Mixture of A and B types
—○—: B type
Heating rate; 6—7 °C/min
Final weight loss; 24—25%

$Al_4(P_4O_{12})_3$ prepared in this experiment gave the A or B types or a mixture of the A and B types, according to dehydration velocity.

Preparation of Aluminum Phosphate in Various Heating Atmospheres. The relationship between the heating atmosphere and the products obtained at 300 °C is shown in Table 1. On heating in an electric furnace, the I type of $AlH_2P_3O_{10}$ was the product chiefly formed when the water content was 15—30%, while the II type was obtained at a water content of 10—15%. This is in good agreement with the above-mentioned results. A comparison of the products obtained in dry air, a nitrogen stream, wet air, water vapor, and in a sealed tube shows that both the I and II types are readily formed by heating the primary product in atmospheres containing much water, while neither of them is produced at all in dry air. In particular, it was proved that the type of product obtained in a sealed tube is dependent entirely on the water content of the primary product. Thus, it is clear that a high vapor pressure is required for the formation of the I and II types. On the contrary, on heating in a vacuum, no $AlH_2P_3O_{10}$ was obtained at all, and only the B type was formed. This shows that the B type is readily formed by rapid dehydration, as has been described above. The product becomes hygroscopic as the molar ratio R decreases ($R=1/4$—$1/5$), that is, with an increase in the amount of phosphoric acid. The relationship between the heating atmosphere and the products formed at 500 °C is given in Table 2. In both the α-Al_2O_3–H_3PO_4 and $Al(OH)_3$–H_3PO_4 systems at $R=1/3$, although some difference in products was observed according to the water content of the primary product, a mixture of the A and B types of $Al_4(P_4O_{12})_3$ was the product chiefly formed, regardless of the heating atmosphere; this shows that the kind of atmosphere had very little influence here. On the contrary, only the A type was obtained in a sealed tube, irrespective of the aluminum materials used, the molar ratio, and the water content. This may be because of the difficulty of the evaporation of water, *i. e.*, by the very low dehydration velocity. The formation of a mixture of the A type and $AlPO_4$ (berlinite and cristobalite type) in an atmosphere of water vapor can be interpreted in terms of the evaporation of the white P_2O_5 fumes caused by the flow of water vapor. The complete absence of the formation of the B type may also be due to the low dehydration velocity in water vapor, such as in a sealed tube. On the other hand, only the B type was obtained in a vacuum, *i. e.*, under conditions of rapid dehydration. The formation of the A type became dominant with a decrease in the molar ratio ($R\leqq 1/5$), regardless of the heating atmosphere, except in a vacuum, where the B type was still the product chiefly formed. The conditions for the formation of the A and B types could not be determined at 300 °C, but were clearly distinguished at 500 °C. No I or II type was formed at all at 500 °C. At $R=1/2$, a mixture of $Al_4(P_4O_{12})_3$ and $AlPO_4$ (berlinite and cristobalite type) was formed in any heating atmosphere. $AlPO_4$ (berlinite) was formed more readily in the $Al(OH)_3$–H_3PO_4 system than in the α-Al_2O_3–H_3PO_4 system. This may be

explained in terms of the higher reactivity of $Al(OH)_3$ than that of α-Al_2O_3 with phosphoric acid.

Reaction of α-Al_2O_3 or $Al(OH)_3$ with P_2O_5. Reactions in the systems of α-Al_2O_3–P_2O_5 and $Al(OH)_3$–P_2O_5 were carried out in order to investigate the preparation of aluminum phosphate in a much lower water content. At 500 °C, almost only the A type was formed in the α-Al_2O_3–P_2O_5 system, but the A type was contaminated by the B type in the $Al(OH)_3$–P_2O_5 system. This may be because of the water contained in $Al(OH)_3$. Thus, these experimental results show that the A type is liable to be produced in the absence of water.

Thermal Transformation of Aluminum Dihydrogen Tripolyphosphate. Although the present authors have already reported data on the thermal transformation of $Al_4(P_4O_{12})_3$,[21] little is yet known about that of $AlH_2P_3O_{10}$. The results of the DTA and TG of $AlH_2P_3O_{10}\cdot 2H_2O$ and the II type are shown in Fig. 5. For $AlH_2P_3O_{10}\cdot 2H_2O$, an endothermic reaction with a weight loss of $2H_2O$ was observed at about 150—160 °C; further, another endothermic reaction with a weight loss of the structural water occurred at about 520—530 °C, and the B type was formed. For the II type, an endothermic reaction occurred at 560—570 °C, and losing its structural water, the II type was transformed into a mixture of the A and B types of $Al_4(P_4O_{12})_3$. The determination of the water by the Karl-Fischer method proved that the weight loss seen in the TG curve was caused only by the loss of water. Figures 6 and 7 show the results obtained on heating the I and II types in air at 400—1200 °C for 5 hr. The I type was transformed into the D type of $Al_4(P_4O_{12})_3$ when heated at 450—500 °C; into the B type, at 500—800 °C, and into the A type, above 900 °C. The thermal transformation from the D type to the B type or from the B type to the A type could not be confirmed by the DTA method. On the other hand, the thermal transformation of the II type was quite different from that of the I type, a mixture of the A and B types being directly obtained

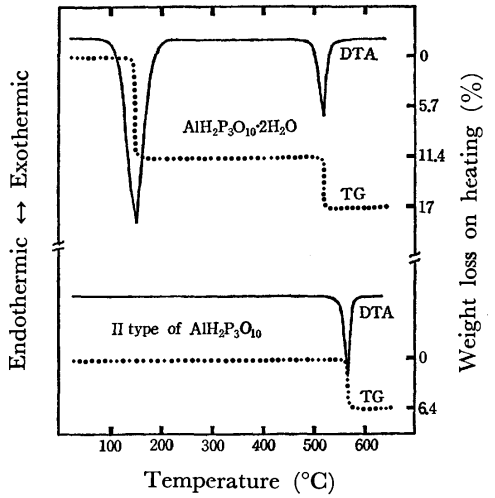

Fig. 5. DTA and TG of aluminum dihydrogen tripolyphosphate.
Sample; 30 mg, Heating rate; 10 °C/min.

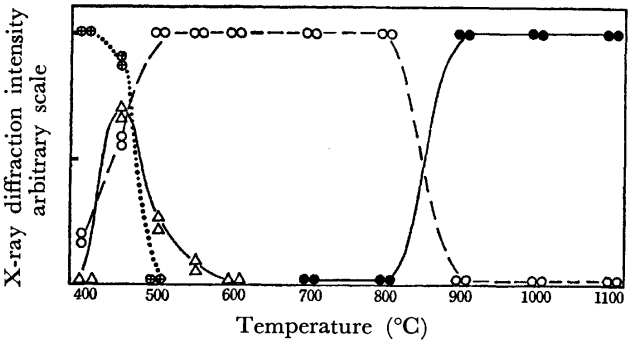

Fig. 6. Thermal transformation of I type of $AlH_2P_3O_{10}$.
···⊕···: I type of $AlH_2P_3O_{10}$. —△—: D type,
—○—: B type, —●—: A type

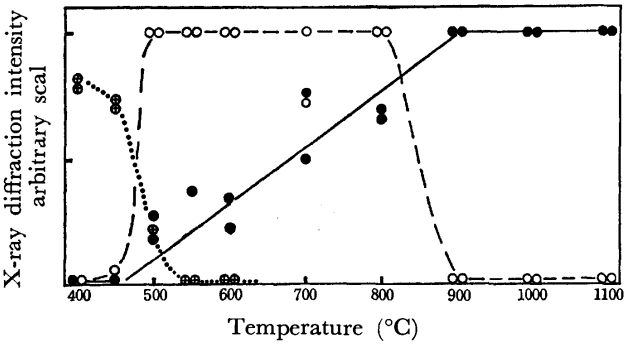

Fig. 7. Thermal transformation of II type of $AlH_2P_3O_{10}$.
···⊕···: II type of $AlH_2P_3O_{10}$, --○--: B type,
—●—: A type.

with no intermediate D type. The B type was readily obtained at 500 to 800 °C, but it was always contaminated by the A type; while only the A type was formed above 900 °C. Further, both the I and II types were vitrified by heating at 1200 °C for 5 hr. From these results, it may be concluded that the thermal transformation of the I and II types and of $AlH_2P_3O_{10}\cdot 2H_2O$ heated in air occurs as follows:

$$AlH_2P_3O_{10}\cdot 2H_2O \underset{}{\overset{150-160\,^\circ C}{\rightleftharpoons}} AlH_2P_3O_{10}\ \text{I type}$$

$$\xrightarrow{450-500\,^\circ C} Al_4(P_4O_{12})_3\ \text{D type} \xrightarrow{500\,^\circ C} \text{B type} \xrightarrow{900\,^\circ C}$$

$$\text{A type} \xrightarrow{1200\,^\circ C} \text{Metaphosphate glass}$$

$$AlH_2P_3O_{10}\ \text{II type} \xrightarrow{560-570\,^\circ C} \text{A + B type} \xrightarrow{900\,^\circ C}$$

$$\text{A type} \xrightarrow{1200\,^\circ C} \text{Metaphosphate glass}$$

Conclusions

The experimental results can be summarized as follows:

1) The formation of aluminum phosphates is greatly dependent on the water content of the primary product and on the vapor pressure in the secondary heat treatment.

2) The water effective in the formation of phosphates is that resulting from the dehydration caused by the condensation of the P-OH.

3) The I and II types of $AlH_2P_3O_{10}$ are produced

by heating the primary product at 300 °C; the I type can be most readily obtained when the water content of the primary product is 15—30%.

4) The II type is readily formed when the water content is 10—15%. Both the I and II types are formed under the conditions of a high vapor pressure.

5) $Al_4(P_4O_{12})_3$ is chiefly formed at a heating temperature above 500 °C. The A type is easily obtained when the water content is below 10% or above 25%.

6) The B type is formed at a water content of 10—25%.

7) $AlH_2P_3O_{10}\cdot 2H_2O$ undergoes the following thermal transformation in air: $AlH_2P_3O_{10}\cdot 2H_2O \rightleftarrows$ I type $\rightarrow$D type$\rightarrow$B type$\rightarrow$A type$\rightarrow$Metaphosphate glass.

References and Footnotes

1) Part X, M. Tsuhako, I. Motooka, and M. Kobayashi, *Chem. Lett.*, **1974**, 435.

2) J. W. Mellor, "A Comprehensive Treatise on Inorganic and Theoretical Chemistry," Longmans, 1935, **14**, p. 403.

3) Duncan McConnel, *Am. Mineral.*, **25**, 719 (1940).

4) Robert L. Manly, *ibid.*, **35**, 108 (1950).

5) Ferdinand d'Yvoire, *Bull. Soc. Chim. Fr.*, **1961**, 2277, 2283.

6) Philip E. Stone, Edward P. Egan, and James R. Lehr, *J. Amer. Ceram. Soc.*, **39**, 89 (1956).

7) A. A. Chistyakova, V. A. Sivkina, V. I. Sadkov, A. P. Khashkovskaya, and L. G. Povyskeva, *Neorg. Meter.*, **5**, 1573 (1969).

8) E. Z. Arlidge, V. C. Farmer, B. D. Mitchell, and W. A. Mitchell, *J. Appl. Chem.*, **13**, 17 (1963).

9) T. Kobayashi, *Yogyo Kyokaishi*, **71**, 115 (1963).

10) Ferdinand d'Yvoire, *Compt. rend.*, **251**, 2958 (1960).

11) Ferdinand d'Yvoire, *Bull. Soc. Chim. Fr.*, **1962**, 1224.

12) Ferdinand d'Yvoire, *Compt. rend.*, **251**, 2182 (1960).

13) Ferdinand d.Yvoire, *Bull. Soc. Chim Fr.*, **1962**, 1237, 1243.

14) This phosphate was submitted to two-dimensional paper chromatography according to Kroupa's method,[15] the spot corresponding to the constituent being detected by spraying ammonium molybdate solution with subsequent color development by ultraviolet irradiation. The results, together with those of DTA, TG, IRS, and chemical analysis, prove that these aluminum phosphates are aluminum dihydrogen tripolyphosphate $AlH_2P_3O_{10}$.

15) E. Karl-Kroupa, *Anal. Chem.*, **28**, 1091 (1956).

16) M. Tsuhako, I. Motooka, and M. Kobayashi, *Nippon Kagaku Zasshi*, **92**, 318 (1971).

17) M. Tsuhako, I. Motooka, and M. Kobayashi, *ibid.*, **92**, 1131 (1971).

18) M. Tsuhako, K. Hasegawa, T. Matsuo, I. Motooka, and M. Kobayashi, *Chem. Lett.*, **1973**, 367, 573.

19) M. Tsuhako, I. Motooka, and M. Kobayashi, This Bulletin, **46**, 2343 (1973).

20) About 0.1 to 0.2 g of the primary product was placed in a 20 ml test tube of special made which was then degassed and sealed.

21) M. Tsuhako, I. Motooka, and M. Kobayashi, *Nippon Kagaku Kaishi*, **1974**, 1028.

Cobalt(III) Complexes Containing Large Chelate Rings. I. Syntheses and Properties of Bis(ethylenediamine)-1,ω-diaminoalkanecobalt(III) Complexes[1)]

Hiroshi OGINO and Junnosuke FUJITA*

Department of Chemistry, Faculty of Science, Tohoku University, Aoba, Sendai, 980

(Received February 24, 1975)

New cobalt (III) complexes, $[Co(en)_2(H_2N(CH_2)_nNH_2)]X_3$ (n=4, 10, 12 and 14), $[Co_2(en)_4(H_2N(CH_2)_n-NH_2)_2]X_6$ (n=4, 5, 6, 8, 10 and 12), $[Co(en)_2(H_2N(CH_2)_4NH_3)_2]X_5$ and $[CoCl(en)_2(H_2N(CH_2)_{12}NH_3)]X_3$ were isolated from the products of reactions between $[CoCl_2(en)_2]Cl$ and 1,ω-diaminoalkane in dimethylsulfoxide, with the aid of SP-Sephadex column chromatography. For n=5, 6 and 8, no monomeric $[Co(en)_2(H_2N(CH_2)_nNH_2)]^{3+}$ was observed. This result is compatible with instability of the medium size rings in organic compounds. The elution behaviors on Sephadex column and the visible and ultraviolet absorption spectra of the new complexes were also described.

Although several reports on the isolation of metal complexes containing large chelate rings have been presented, no conclusive evidence for the ring formation has ever been obtained.[2)] Attempts to prepare metal complexes with 1,ω-diaminoalkanes, $H_2N(CH_2)_nNH_2$ (n>3) have also been made extensively.[3-10)] However, only Pfeiffer[11)] succeeded in isolating copper(II) complexes of bis(1,4-diaminobutane) and of bis- and tris-(1,6-diaminohexane), although his brief report did not give any evidence for the formation of seven- or nine-membered chelate rings. As shown later, these diamines tend to coordinate to a metal ion as a unidentate ligand or to two metal ions as a bridging ligand.

This paper will present the syntheses and properties of cobalt(III) complexes containing various 1,ω-diaminoalkanes. The diamines, $H_2N(CH_2)_nNH_2$, used in this work are as follows; n=2(en), 3(tn), 4(tmd), 5(pmd), 6(hxn), 8(ocn), 10(den), 12(don) and 14(tden). Some part of this work have been reported briefly in two communications.[12,13)] Very recently, Pryde *et al.*[14)] obtained platinum(II) and iridium(I) complexes containing $Bu^t_2P(CH_2)_nPBu^t_2$ (n=9 or 10).

Experimental

Materials. Guaranteed reagent grade dimethyl sulfoxide (DMSO) and 1,ω-diaminoalkanes (N-N) were obtained from Tokyo Kasei Co. and used without further purification. Column chromatography was carried out by use of SP-Sephadex C-25 (Pharmacia, Sweden).

Preparation of Cobalt(III) Complexes. All bis(ethylenediamine)-1,ω-diaminoalkanecobalt(III) complexes were obtained from the products of reactions of *cis*- or *trans*-$[CoCl_2(en)_2]Cl$ with N-N in DMSO. The *cis*-isomer of $[CoCl_2(en)_2]Cl$ seems to be a better starting material than the *trans*-isomer, because the *cis*-isomer is more soluble in DMSO.

The analytical data for the complexes prepared in this work are summarized in Table 1.

1) *$[Co(en)_2(tmd)]Br_3$ and $[Co_2(en)_4(tmd)_2]Br_6\cdot 6H_2O$*: To 550 ml of DMSO containing 4.3 g of *cis*- or *trans*-$[CoCl_2(en)_2]Cl$ (0.015 mol) was added 1.4 g of tmd (0.016 mol). The solution was kept at 50 °C for 20 hr and then cooled to room temperature. The reddish orange solution resulted was neutralized with concd HCl and diluted to 3 l with water. This was poured on a Sephadex ion exchange column (ϕ 5×40 cm). After washing the column with water, 1 l of an 0.1 M KBr solution was passed through the column. At this stage, the column showed four bands; pink (very small amount), red (small amount), yellow and yellowish orange bands from bottom to top of the column. After the first and second bands had been eluted with an 0.2 M KBr solution, the third yellow band was eluted with an 0.4 M KBr solution. The eluate was concentrated with a rotary evaporator to a small volume. A mixture of yellowish orange crystals of $[Co(en)_2(tmd)]Br_3$ and solid KBr was collected on a glass filter and washed with a small amount of water to remove KBr. The crude product thus obtained was recrystallized from water by the addition of solid NaBr. Pure crystals were filtered off and washed with ethanol and then with ether. Yield: 5.4 g (70%).

The last yellowish orange band was eluted with a warm 1 M KBr solution. Yellowish orange crystals of $[Co_2(en)_4(tmd)_2]Br_6\cdot 6H_2O$ were obtained from the eluate by a procedure similar to the above. Yield: 0.3 g.

2) *$[Co(en)_2(tmdH)_2]Br_5\cdot 4H_2O$*: To 100 ml of DMSO containing 2.9 g of *cis*-$[CoCl_2(en)_2]Cl$ (0.01 mol) was added 1.9 g of tmd (0.02 mol). The solution was stirred for 3 hr at room temperature. The reddish orange solution resulted was treated by a method similar to 1). When 2 l of an 0.2 M NaBr solution and then 4 l of an 0.25 M NaBr solution were passed through the column, five bands were observed on the column; red, yellow, reddish orange, yellow and orange bands from bottom to top of the column. They were eluted with 0.3—1 M NaBr solutions successively. The second yellow band gave $[Co(en)_2(tmd)]Br_3$ (0.15 g) and the fourth yellow band, $[Co(en)_2(tmdH)_2]Br_5\cdot 4H_2O$ (1.5 g). When the fourth band was eluted from the column, the fifth band was found to be separated into several bands, from one of which $[Co_2(en)_4(tmd)_2]Br_6\cdot 6H_2O$ (0.6 g) was obtained. Species in eluates obtained from other bands were not characterized.

3) *$[Co_2(en)_4(pmd)_2]Br_6\cdot 2H_2O$, $[Co_2(en)_4(hxn)_2]Br_6\cdot 4H_2O$, $[Co_2(en)_4(ocn)_2]Br_6\cdot 4H_2O$, $[Co(en)_2(den)]Br_3\cdot 2H_2O$ and $[Co_2(en)_4(den)_2]Br_6\cdot 3H_2O$*: To 550 ml of DMSO containing 4.3 g of *cis*-$[CoCl_2(en)_2]Cl$ (0.015 mol) was added 0.015 mol of N-N (1.5 g for pmd, 1.7 g for hxn, 2.2 g for ocn and 2.6 g for den). The solution was kept at 65 °C for 30 hr and then treated in a similar way to 1). By developing the adsorbed band with an 0.3 M KBr solution, the column gave the following eight bands regardless of the kind of N-N used; pale pink (very small amount, characterized as Co^{2+} species), reddish violet, yellow (this band is refered to as A band), reddish orange, yellowish orange, reddish orange, yellowish orange (B band) and orange from bottom to top of the column. The last orange band seems to be a mixture of highly charged species, because the band was separated into several bands with progression of the elution.

After the pale pink and reddish violet bands had been

* Present address: Department of Chemistry, Faculty of Science, Nagoya University, Nagoya, 464.

TABLE 1. SUMMARY OF ANALYTICAL DATA FOR THE COMPLEXES PREPARED IN THIS WORK

Complex	Formula	C, %		H, %		N, %	
		Calcd	Found	Calcd	Found	Calcd	Found
$[Co(en)_2(tn)]Br_3$	$[CoC_7H_{26}N_6]Br_3$	17.06	16.81	5.32	5.46	17.05	16.80
$[Co(en)(tn)_2]Br_3\cdot 4H_2O$	$[CoC_8H_{28}N_6]Br_3\cdot 4H_2O$	16.59	16.66	6.27	6.97	14.51	14.71
$[Co(en)_2(tmd)]Br_3$	$[CoC_8H_{28}N_6]Br_3$	18.95	18.71	5.57	5.76	16.58	16.58
$[Co(en)_2(den)]Br_3\cdot 2H_2O$	$[CoC_{14}H_{40}N_6]Br_3\cdot 2H_2O$	26.81	26.72	7.07	6.88	13.40	13.73
$[Co(en)_2(don)]Br_3\cdot H_2O$	$[CoC_{16}H_{44}N_6]Br_3\cdot H_2O$	30.16	29.91	7.28	7.31	13.19	13.04
$[Co(en)_2(tden)]Br_3\cdot 2.5H_2O$	$[CoC_{18}H_{48}N_6]Br_3\cdot 2.5H_2O$	31.23	31.35	7.72	7.61	12.14	12.37
$[CoCl(en)_2(donH)]Br_3\cdot 2.5H_2O$	$[CoClC_{16}H_{45}N_6]Br_3\cdot 2.5H_2O$	27.43	26.91	7.19	6.78	11.99	12.16
$[Co(en)_2(tmdH)_2]Br_5\cdot 4H_2O$	$[CoC_{12}H_{42}N_8]Br_5\cdot 4H_2O$	17.39	17.43	6.08	6.06	13.52	13.50
$[Co_2(en)_4(tmd)_2]Br_6\cdot 6H_2O$	$[Co_2C_{16}H_{56}N_{12}]Br_6\cdot 6H_2O$	17.12	17.01	6.11	6.16	14.98	15.09
$[Co_2(en)_4(pmd)_2]Br_6\cdot 2H_2O$	$[Co_2C_{18}H_{60}N_{12}]Br_6\cdot 2H_2O$	20.05	19.92	5.98	5.96	15.59	15.68
$[Co_2(en)_4(hxn)_2]Br_6\cdot 4H_2O$	$[Co_2C_{20}H_{64}N_{12}]Br_6\cdot 4H_2O$	21.03	20.95	6.35	6.35	14.72	14.30
$[Co_2(en)_4(ocn)_2]Br_6\cdot 4H_2O$	$[Co_2C_{24}H_{72}N_{12}]Br_6\cdot 4H_2O$	24.06	23.68	6.73	6.35	14.03	14.03
$[Co_2(en)_4(den)_2]Br_6\cdot 3H_2O$	$[Co_2C_{28}H_{80}N_{12}]Br_6\cdot 3H_2O$	27.20	26.92	7.01	6.74	13.59	13.83
$[Co_2(en)_4(don)_2]Cl_6\cdot 6.5H_2O$	$[Co_2C_{32}H_{88}N_{12}]Cl_6\cdot 6.5H_2O$	35.30	35.52	9.35	9.25	15.44	15.09

eluted with an 0.3 M KBr solution, the A band was eluted with an 0.4 M KBr solution and its yellow eluate was concentrated. A small amount of yellow crystals of $[Co(en)_3]Br_3\cdot 3H_2O$ was obtained and no formation of $[Co(en)_2(N\text{–}N)]^{3+}$ was observed for all the diamines except the den. In the case of den, the eluate gave yellowish orange crystals of $[Co(en)_2(den)]Br_3\cdot 2H_2O$. They were recrystallized similarly from water by the addition of solid KBr. Yield: 0.24 g (2.5 %).

After the A band had been eluted from the column, the concentration of eluent was increased to 0.6 M and then 1 M or more with progression of the elution. However, the use of such KBr solutions caused sometimes crystallization of $[Co_2(en)_4(N\text{–}N)_2]Br_6\cdot nH_2O$ in the column, so that a warm KBr solution (40—70 °C) was used. In the case of the den system, it was still difficult to avoid the crystallization. Therefore, the layer of B band was transfered to a beaker and a colored species was extracted with a hot 0.6 M KBr solution repeatedly. Yellowish orange crystals which were obtained from each eluate or extract by concentration were $[Co_2(en)_4(pmd)_2]Br_6\cdot 2H_2O$, $[Co_2(en)_4(hxn)_2]Br_6\cdot 4H_2O$, $[Co_2(en)_4(ocn)_2]Br_6\cdot 4H_2O$ and $[Co_2(en)_4(den)_2]Br_6\cdot 3H_2O$. The yields of $[Co_2(en)_4(N\text{–}N)_2]^{6+}$ ranged from 30% (pmd) to 12% (den) depending on the length of the methylenic chain of the N–N.

4) *$[CoCl(en)_2(donH)]Br_3\cdot 2.5H_2O$, $[Co(en)_2(don)]Br_3\cdot H_2O$ and $[Co_2(en)_4(don)_2]Cl_6\cdot 6.5H_2O$*: These complexes were obtained from 4.3 g of *cis-* or *trans-*$[CoCl_2(en)_2]Cl$ (0.015 mol) and 3.0 g of don (0.015 mol) by a method similar to 3). By developing the reaction product on a Sephadex column with an 0.2 M NaBr solution, eight bands were observed; pink (small amount), red (A band), yellow (B band), yellowish orange, reddish orange, yellowish orange, yellowish orange (C band) and orange from bottom to top of the column. The last band seems also to be a mixture of several highly charged species. After the first pink band had been eluted with an 0.2 M NaBr solution, the red A band was eluted with an 0.3 M NaBr solution. By evaporating the eluate, reddish violet crystals of $[CoCl(en)_2(donH)]Br_3\cdot 2.5\,H_2O$ were obtained and recrystallized from water by the addition of NaBr. The eluate of the A band contained a small amount of $[Co(en)_3]^{3+}$, but it was separated easily from the desired complex by the recrystallization.

The B band was eluted with an 0.4 M NaBr solution and the eluate was concentrated. Yellowish orange crystals of $[Co(en)_2(don)]Br_3\cdot H_2O$ were obtained and recrystallized from water by the addition of solid NaBr. Yield: 0.87 g (9%).

Then the column was washed with water. The layer of C band was transfered to a beaker and a colored species was extracted with a hot 1 M NaCl solution repeatedly. Upon cooling the extract to room temperature, fine crystals of $[Co_2(en)_4(don)_2]Cl_6\cdot 6.5H_2O$ were precipitated, filtered off and recrystallized from water.

5) *$[Co(en)_2(tden)]Br_3\cdot 2.5H_2O$*: This complex was prepared similarly by warming a DMSO (500 ml) solution containing 2.9 g of *cis-*$[CoCl_2(en_2)]Cl$ (0.01 mol) and 2.3 g of tden (0.01 mol) at 60 °C for 20 hr. The Sephadex column gave six bands on developing the product with an 0.2 M KBr; pale pink (small amount), yellow (small amount of $[Co(en)_3]^{3+}$), reddish violet, yellowish orange, reddish orange and brownish orange from bottom to top of the column. After the first three bands had been eluted with an 0.3 M KBr solution, the fourth yellowish orange band was eluted with a warm 0.6 M KBr solution. A gummy oil was separated from the solution by concentrating the eluate. The oil was dissolved into a small amount of warm water and the solution was cooled gradually to room temperature. Yellowish orange crystals of $[Co(en)_2(tden)]Br_3\cdot 2.5H_2O$ were precipitated, filtered off and recrystallized from water. Yield: 0.38 g (6%).

6) *$[Co(en)_2(tn)]Br_3$*: This complex was prepared by the procedure reported by Bailar and Work.[10] The product contained a considerable amount of $[Co(en)_3]Cl_3\cdot 3H_2O$. Pure crystals of $[Co(en)_2(tn)]Br_3$ were obtained by recrystallizing the product several times from water by the addition of a KBr solution.

Alternatively, a method similar to 1) was employed; to 100 ml of DMSO containing 2.9 g of *cis-*$[CoCl_2(en)_2]Cl$ (0.01 mol) was added 0.74 g of tn (0.01 mol). The solution was allowed to stand overnight at room temperature, neutralized with conc. HCl and subjected to Sephadex column chromatography. The fastest moving band seemed to be Co^{2+} species. The second band was pink and was followed by a yellow band. The yellow band was eluted with an 0.2 M KBr solution. Some bands remained on the column after elution of the yellow band. Evaporation of the yellow eluate gave crystals of $[Co(en)_2(tn)]Br_3$ which also contained $[Co(en)_3]Br_3\cdot 3H_2O$. They were recrystallized similarly from water by the addition of a KBr solution to give pure $[Co(en)_2(tn)]Br_3$. Yield: 1.2 g.

7) *$[Co(en)(tn)_2]Br_3\cdot 4H_2O$*: To 40 ml of an aqueous solution containing 12 g of $CoCl_2\cdot 6H_2O$ (0.05 mol) were added 11 g of tn (0.15 mol), 3 g of en (0.05 mol), 8.3 ml of 6 M HCl (0.05 mol) and 1 g of active carbon. Air was passed through the solution for 12 hr at room temperature. After removal of active carbon by filtration, solid KBr was added to the filtrate. A mixture of $[Co(en)_2(tn)]Br_3$ and $[Co(en)(tn)_2]Br_3\cdot 4H_2O$ was obtained. The latter was more soluble than the former and the desired complex was obtained by the fractional crystallization.

When solid $[CoCl_2(tn)_2]Cl$ was added in small portions to a DMSO solution containing equimolar amount of en, the desired complex was also formed together with $[Co(en)_3]^{3+}$ and $[Co(en)_2(tn)]^{3+}$

Apparatus. Visible and ultraviolet absorption spectra of aqueous solutions of the complexes were recorded on a Hitachi EPS-3 recording spectrophotometer.

Results and Discussion

Chromatographic Properties and Characterization of the Complexes. Both yellowish orange complexes of the monomeric $[Co(en)_2(N\text{–}N)]X_3$ and the dimeric $[Co_2(en)_4(N\text{–}N)_2]X_6$ obtained here have the same chemical composition, but their complex cations have different charges. The difference in the charge of the complex ion may be reflected on the chromatographic properties.

Sephadex resin charged with two kinds of complex ion was placed carefully on the top of a Sephadex column (ϕ 1.6×20 cm) by 1 mm thickness. The adsorbed complex ions were eluted with an 0.25 M KBr solution adjusted to pH 3 with HBr at a rate of about 1.6 ml/min. The relative R_f values to that of $[Co(en)_3]^{3+}$ are summarized in Table 2 where those of the authentic samples of the known charge are given for comparison. Table 2 shows that the R_f value increases by four to ten times as the charge of the complex ion decreases by one and that the complexes, $[Co(en)_2(N\text{–}N)]^{3+}$ give values expected for a monomeric tripositive ion, although a slight deviation from unity is observed for the complexes containing larger diamine chelate.

Table 2. The relative R_f values of various complexes
(Eluent: 0.25 M KBr solution adjusted to pH 3 with HBr.)

Complex ion	Relative R_f value
$[CoCl(NH_3)_5]^{2+}$	7.6[a]
$[Co(en)_3]^{3+}$	1[b]
$[Co(NH_3)_6]^{3+}$	0.65
$[CoCl(en)_2(donH)]^{3+}$	~1
$[Co(en)_2(tn)]^{3+}$	1.0
$[Co(en)_2(tmd)]^{3+}$	1.0
$[Co(en)_2(den)]^{3+}$	0.87
$[Co(en)_2(don)]^{3+}$	0.54
$[Co(en)_2(tden)]^{3+}$	0.43
$[Co(en)_2(tmdH)_2]^{5+}$	0.16
$[Co_2(en)_4(tmd)_2]^{6+}$	0.01_8
$[Co_2(en)_4(hxn)_2]^{6+}$	<0.02
$[Co_2(en)_4(don)_2]^{6+}$	<0.01
$[Cr\{(OH)_2Cr(en)_2\}_3]^{6+}$	~0.008

a) This value was determined by the elution of resins charged with $[CoCl(NH_3)_5]^{2+}$ and $[Co(en)_3]^{3+}$. (Eluent: 0.1 M KBr solution adjusted to pH 3 with HBr.) b) The R_f value of this complex ion is taken as unity.

Under the same elution condition, other yellowish orange complexes assignable to $[Co_2(en)_4(N\text{–}N)_2]^{6+}$ show such slow flow rates that their R_f values are determined with difficulty. However, these ions flow with an 0.5 M KBr solution at rates similar to that of $[Cr\{(OH)_2Cr(en)_2\}_3]^{6+}$, indicating that they are dimeric with hexapositive charge.

The R_f value of the yellowish orange complex whose elemental analysis gives correct value for $[Co(en)_2(tmdH)_2]Br_5\cdot 4H_2O$ is 0.16 and the complex ion can be concluded to be pentapositive. This complex will be the first example of cobalt(III) complex containing two unidentate diamines.

For the $[Co(en)_2(N\text{–}N)]^{3+}$, two nitrogen atoms of the N–N can occupy *cis* or *trans* positions as shown in Fig. 1A, if the methylenic chain of the N–N is long enough. However, all the N–N used in this work will occupy only *cis* positions. Molecular models reveal that the non-bonding interaction between the en and the N–N chelates make *trans* spanning difficult even in the case of tden with 14 methylenes. This will be supported by the fact that $[Co(en)_2(tmd)]^{3+}$ and $[Co(en)_2(don)]^{3+}$ were resolved into optical isomers by SP-Sephadex column chromatography using an 0.15 M potassium tartratoantimonate(III) solution as an eluent.[12,15]

Many isomers are possible for the dimeric complexes, $[Co_2(en)_4(N\text{–}N)_2]^{6+}$. As shown later, the formation of $[Co_2(en)_6]^{6+}$ was never observed, indicating that en will be unfavorable as a bridging ligand. Molecular models suggest that the structures in Fig. 1B are most probable. The catenane structures of which one example is shown in Fig. 1C are also possible, if the methylenic chain of

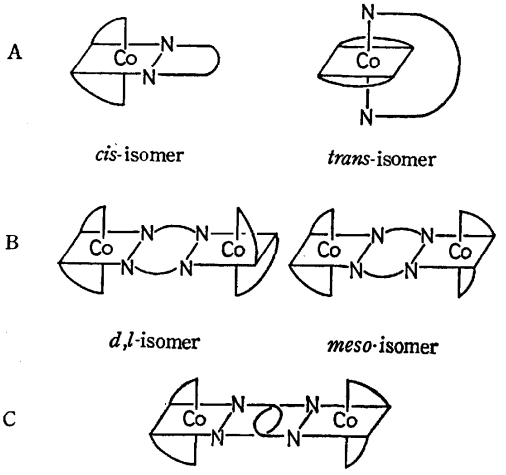

Fig. 1. Possible structures for the monomer ($[Co(en)_2(N\text{–}N)]^{3+}$) and the dimer ($[Co_2(en)_4(N\text{–}N)_2]^{6+}$). ⌒ and N⌒N denote en and N–N, respectively.
A: Possible structure of the monomer.
B: Most probable structures of the dimer.
C: One example of the catenane structures for the dimer.

the N–N becomes long enough.

The red complex assigned to $[CoCl(en)_2(donH)]Br_3 \cdot 2.5H_2O$[16] gives the R_f value almost the same as that of $[Co(en)_3]^{3+}$. This complex shows the first and the second absorption band at 18900 cm^{-1} with a shoulder at 21300 cm^{-1}, and at 27400 cm^{-1}, respectively. This spectral pattern is characteristic of a $[CoClN_5]$ type.[17,18] The complex is converted into aqua complex $[Co(H_2O)(en)_2(donH)]^{4+}$ when treated with silver nitrate in an acidic aqueous solution. The aqua complex exhibits a symmetrical first absorption band at 20400 cm^{-1}. Alexander and Spillert[19] prepared $[CoCl(en)_2(enH)]Cl_3 \cdot H_2O$ and assigned it to *cis* configuration. The present chloro complex may have the same *cis* structure.

Mechanism of the Reaction of $[CoCl_2(en)_2]Cl$ with N–N in DMSO. In order to elucidate the mechanism of the reaction of $[CoCl_2(en)_2]Cl$ with N–N, the preparations have been carried out under various conditions. The change of concentration of the reactants affects the distribution of products considerably. The yield of $[Co(en)_2(tmd)]^{3+}$ amounts to 70%, when 0.015 mol of tmd is allowed to react with an equivalent amount of $[CoCl_2(en)_2]Cl$ in 550 ml of DMSO. However, when the solvent DMSO is reduced to 50 ml, the yield of this monomer decreases to a few percent and that of the $[Co_2(en)_4(tmd)_2]^{6+}$ increases. In this case, formation of $[Co(en)_2(tmdH)_2]^{5+}$ and other very highly charged species than the hexapositive dimer is observed, some of the latter species remaining on the Sephadex column even after washed with a 1 M KBr solution. The mole ratio of $[CoCl_2(en)_2]Cl$ to N–N also affects the distribution of the products. As stated in the experimental section, the reaction of 0.01 mol of $[CoCl_2(en)_2]Cl$ with 0.02 mol of tmd in 100 ml of DMSO gives a small amount of $[Co(en)_2(tmd)]^{3+}$ and a large amount of $[Co(en)_2(tmdH)_2]^{5+}$ and $[Co_2(en)_4(tmd)_2]^{6+}$.

From these experimental results, the following mechanism can be deduced for the reaction of $[CoCl_2(en)_2]Cl$ with N–N:

cis- or *trans*-$[CoCl_2(en)_2]^+ + N\text{-}N \xrightarrow{\text{fast}}$

cis- or *trans*- 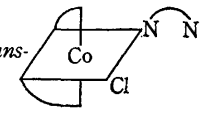 Intermediate(Int) (1)

Int— Intramolecular reaction → 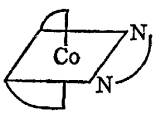 (2)

Int— Intermolecular reaction → dimer and higher polymers (3)

The reaction of $[CoCl_2(en)_2]Cl$ with N–N gives an intermediate species (Int) rapidly. The formation of the Int will be supported by the isolation of $[CoCl(en)_2(donH)]Br_3 \cdot 2.5H_2O$. An intramolecular ring closure of the Int leads to the formation of the monomer, while an intermolecular reaction of the Int results in the formation of the dimer and higher polymers. The former reaction is of the first-order and the half-time of the reaction should be independent of the concentration of the Int. On the other hand, the intermolecular reaction is bimolecular, so that the half-time of this reaction should decrease with increase of the concentration of the Int. Therefore, the reaction in a dilute solution favors the formation of the monomer in agreement with the experimental results.

The formation of $[Co(en)_2(tmdH)_2]^{5+}$ in a concentrated solution can be interpreted by a mechanistic consideration similar to that mentioned above; the bimolecular reaction of the Int with tmd would yield $[Co(en)_2(tmd)_2]^{3+}$ containing two unidentate tmd. The half-time of this reaction in a concentrated solution will be shorter than that in a dilute solution and hence the yield of $[Co(en)_2(tmdH)_2]Br_5 \cdot 4H_2O$ would increase with increase of the concentration of reactants.

A partial reduction of cobalt(III) to cobalt(II) were found for almost all the reactions in DMSO. The formation of a small amount of $[Co(en)_3]^{3+}$ may be related to this reduction reaction.

Relation between the Yield of $[Co(en)_2(N\text{–}N)]^{3+}$ and the Size of the Chelate Ring formed by N–N. The yields of monomeric complexes, $[Co(en)_2(N\text{–}N)]^{3+}$ are markedly dependent on the methylenic chain length of the N–N. In Fig. 2 is plotted the yield of $[Co(en)_2(N\text{–}N)]^{3+}$ obtained from $[CoCl_2(en)_2]Cl$ (0.015 mol), N–N (0.015 mol) and 550 ml of DMSO, against the number of ring members of the N–N in the complex ion. The reaction of $[CoCl_2(en)_2]Cl$ with en gives $[Co(en)_3]^{3+}$ almost quantitatively and no dimeric complex is detected even under the reaction in a highly concentrated solution. The yield of the monomer decreases sharply at pmd, which should form an eight membered chelate ring. The formation of the monomer is virtually zero for pmd, hxn and ocn. However, the monomer is again formed when the number of methylene groups becomes more than nine. The yield increases with increase of the number of methylene groups and seems to show a maximum at don, forming a fifteen membered chelate ring. This tendency is strikingly similar to that observed in the syntheses of organic ring

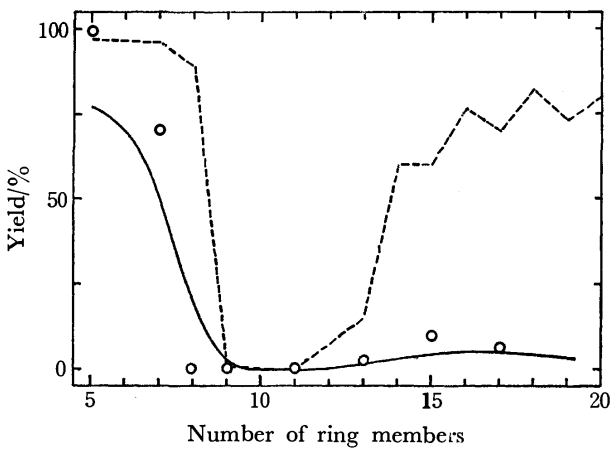

Fig. 2. Relation between the yield of compounds and the number of ring members. Open circles indicate the yields of $[Co(en)_2(N\text{–}N)]^{3+}$. Solid line and dashed line indicate the yield of ring ketones[22] obtained by Ruzicka and Ziegler, respectively.

Table 3. Absorption spectral data for the complexes prepared in this work and the related complexes
Wave numbers are in 10^3 cm^{-1} and the intensities given by log ε in parentheses.

Complex	I Band	II Band	Charge Transfer Band
$[Co(en)_3](ClO_4)_3$	21.3 (1.94)	29.6 (1.89)	47.5 (4.36)
$[Co(en)_2(tn)](ClO_4)_3$	21.0 (1.98)	29.2 (1.97)	45.9 (4.37)
$[Co(en)(tn)_2](ClO_4)_3$	20.7 (1.91)	28.8 (1.91)	44.4 (4.34)
$[Co(tn)_3](ClO_4)_3$	20.3 (1.88)	28.5 (1.87)	43.5 (4.36)
$[Co(en)_2(tmd)]Cl_3 \cdot H_2O$	20.9 (1.95)	29.1 (1.94)	45.9 (4.35)
$[Co(tmd)_3]Br_3$ [a]	19.9 (1.89)	27.9 (1.85)	43.1 (4.35)
$[Co(en_2)(den)]Br_3 \cdot 2H_2O$	20.8 (2.00)	28.9 (1.98)	45.5 (4.43)
$[Co(en)_2(don)]Br_3 \cdot H_2O$	20.8 (2.01)	29.0 (2.00)	
$[Co(en)_2(tden)]Br_3 \cdot 2.5H_2O$	20.8 (2.01)	29.0 (2.00)	45.5 (4.33)
$[Co(en)_2(tmdH)_2]Br_5 \cdot 4H_2O$	20.7_5 (2.00)	28.8 (1.97)	45.5sh(4.45)
$[Co_2(en)_4(tmd)_2]Br_6 \cdot 6H_2O$ [b]	20.8 (2.29)	28.9 (2.36)	46sh (4.72)
$[Co_2(en)_4(pmd)_2]Br_6 \cdot 2H_2O$ [b]	20.8 (2.26)	28.9 (2.26)	$45._5$ (4.72)
$[Co_2(en)_4(hxn)_2]Br_6 \cdot 4H_2O$ [b]	20.8 (2.28)	28.9 (2.28)	45.2 (4.41)
$[Co_2(en)_4(ocn)_2]Br_6 \cdot 4H_2O$ [b]	20.7_5 (2.31)	29.0 (2.29)	45.0 (4.74)
$[Co_2(en)_4(den)_2]Br_6 \cdot 3H_2O$ [b]	20.8 (2.29)	29.0 (2.27)	45.0 (4.71)
$[Co_2(en)_4(don)_2]Cl_6 \cdot 6.5H_2O$ [b]	20.8 (2.34)	29.0 (2.31)	45.0 (4.75)
$[CoCl(en)_2(donH)]Br_3 \cdot 2.5H_2O$	18.9 (1.89), 21sh(1.74)	27.4 (1.98)	44 (4.38)

a) From ref. 13. b) The intensities are given per one complex ion, *i.e.*, per two cobalt(III) ions.

ketones from bifunctional aliphatic molecules.

Ruzicka[20] succeeded in preparing large ring ketones by pyrolysis of metal salts of dicarboxylates. Ziegler *et al.*[21,22] improved Ruzicka's method and obtained the same compounds from dinitriles by employing the high dilution method. The relations between the yields of ring ketones prepared by both methods and the ring size are also given in Fig. 2. In organic chemistry, medium size ring compounds which correspond to eight to eleven membered ring systems are known to be less stable owing to such strains as bond angle deformations, bond opposition forces and trans-annular interactions.[23,24] Larger ring compounds than eleven members will be released from such strains sterically and becomes more stable than the medium size compounds. Existence of a minimum in the yields of the ring ketones in Fig. 2 has been interpreted in terms of such strains and entropy factor in the ring closure process.[23-26] Similar situation must exsist in the present complexes containing N–N. Molecular models reveal that the complexes containing pmd, hxn or ocn are seriously strained. With more increase of the ring members, the complex is formed but its yield decreases again over fifteen ring members. This second decrease can be understood by a concept similar to that widely accepted for the ring closure process of bifunctional organic compounds; the longer the chain the smaller probability of encounter between the cobalt(III) center and the terminal nitrogen atom of diamine in the Int. Parallelism between the chelate ring complexes and the ring ketones provides an additional support for the formulation of the present monomeric complexes containing a large chelate ring.

Spectral Properties of the Complexes. Numerical data for visible and ultraviolet absorption spectra of the complexes are summarized in Table 3.

The successive substitution of en in $[Co(en)_3]^{3+}$ with tn or tmd causes shifts in the first and second absorption bands to longer wave length. In Fig. 3 are plotted the

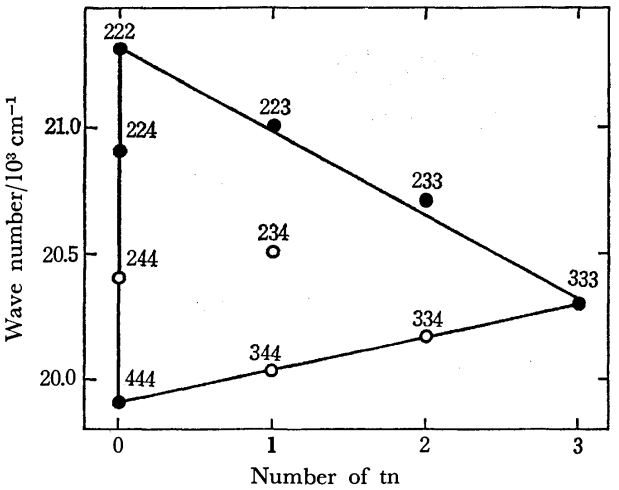

Fig. 3. Positions of the first absorption bands of $[Co(en)_a(tn)_b(tmd)_{3-a-b}]^{3+}$.
In the figure, 2, 3 and 4 indicate en, tn and tmd in the complex, respectively. For example, 234 denotes $[Co(en)(tn)(tmd)]^{3+}$. Open circles are the estimated values.

positions of the first absorption band maxima of $[Co(en)_a(tn)_b(tmd)_{3-a-b}]^{3+}$ against the number of tn in the complexes. The magnitude of the shifts is additive. Hence, the positions of the first absorption maxima of unknown complexes consisting of en, tn or tmd can be estimated from Fig. 3.

Figure 4 compares the maximum positions of the first absorption bands of various tris(diamine)cobalt(III) complexes. The absorption bands of $[Co(en)_2(N–N)]^{3+}$ shift to longer wave-length as the methylenic chain of the N–N becomes longer. However, the magnitude of the shifts becomes smaller with increase of the number of methylenic chain. A similar trend is observed for $[Co(en)(N–N)_2]^{3+}$ and $[Co(N–N)_3]^{3+}$.

Table 3 shows that the $[Co_2(en)_4(N–N)_2]^{6+}$ give the

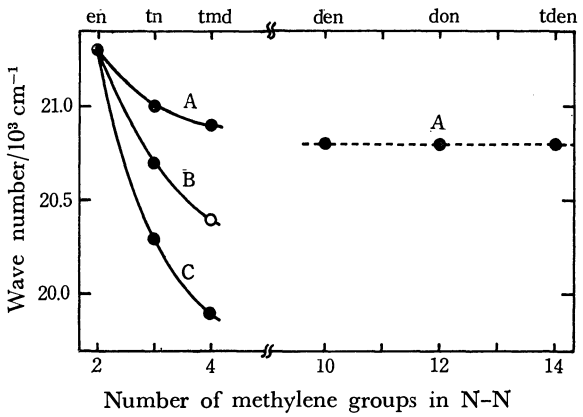

Fig. 4. Relation between the maximum potitions of the first absorption bands and the methylenic chain length of the N-N in $[Co(en)_2(N\text{-}N)]^{3+}$ (A), $[Co(en)(N\text{-}N)_2]^{3+}$ (B) and $[Co(N\text{-}N)_3]^{3+}$ (C). Absorption maximum of $[Co(en)(tmd)_2]^{3+}$ is taken from Fig. 3 (open circle).

absorption bands at almost the same positions as those of $[Co(en)_2(N\text{-}N)]^{3+}$. Their molar extinction coefficients are approximately 2 times larger than those of the monomeric complexes, the intensities of the dimeric complexes per one cobalt(III) ion being almost the same as those of the monomeric complexes.

The authors wish to thank Prof. Nobuyuki Tanaka and Prof. Kazuo Saito, Tohoku University, for their encouragement and support.

References

1) H. Ogino and J. Fujita, Presented at the 23rd Symposium on Coordination Chemistry, Fukuoka, Oct., 1973.
2) J. C. Bailar, Jr. ed., "The Chemistry of the Coordination Compounds," Reinhold Publishing Coorporation, New York (1956).
3) P. Pfeiffer and M. Haimann, *Ber.*, **36**, 1063 (1903).
4) L. Tschugaeff, *ibid.*, **39**, 3190 (1906).
5) A. Werner, *ibid.*, **40**, 15 (1907).
6) L. Tschugaeff, *J. prakt. Chem.*, **75**, 153 (1907).
7) A. Werner, *Ann. Chem.*, **386**, 1 (1911).
8) H. D. K. Drew and H. J. Tress, *J. Chem. Soc.*, **1933**, 1335.
9) P. Pfeiffer and E. Lübbe, *J. Prakt. Chem.*, **136**, 321 (1933).
10) J. C. Bailar, Jr. and J. B. Work, *J. Amer. Chem. Soc.*, **68**, 232 (1946).
11) P. Pfeiffer, *Naturwissenschaften*, **35**, 190 (1948).
12) H. Ogino and J. Fujita, *Chem. Lett.*, **1973**, 517.
13) J. Fujita and H. Ogino, *ibid.*, **1974**, 57.
14) A. J. Pryde, B. L. Shaw, and B. Weeks, *Chem. Commun.*, **1973**, 947.
15) The details will be published elsewhere.
16) In the previous communication,[12] this complex was formulated tentatively as $[Co(H_2O)(en)_2(donH)]Br_4$ from the result of elemental analyses.
17) M. Linhard and M. Weigel, *Z. anorg. Chem.*, **266**, 49 (1951).
18) M. D. Alexander and D. H. Busch, *Inorg. Chem.*, **5**, 602 (1966).
19) M. D. Alexander and C. A. Spillert, *ibid.*, **9**, 2344 (1970).
20) L. Ruzicka, M. Stoll, and H. Schinz, *Helv. Chim. Acta*, **9**, 249 (1926).
21) K. Ziegler, H. Eberle, and H. Ohlinger, *Ann. Chem.*, **504**, 94 (1933).
22) K. Ziegler and R. Aurnhammer, *ibid.*, **513**, 43 (1934).
23) S. Sicher, *Progr. Stereochem.*, **3**, 202 (1962).
24) E. L. Eliel, N. L. Allinger, S. J. Angyal, and G. A. Morrison, "Conformational Analysis," John Wiley & Sons, Inc., New York, N. Y. (1965).
25) L. Ruzicka, *Chem. Ind.* (London), **54**, 2 (1935).
26) G. Illuminati, L. Mandolini, and B. Masci, *J. Amer. Chem. Soc.*, **96**, 1422 (1974).

The ^{13}C Magnetic Resonance Study on the Effects of Divalent Paramagnetic Metal Acetylacetonates on Pyridine, Quinoline, and Isoquinoline. Specific Interactions with $Mn(AA)_2$

Kikuko HAYAMIZU, Makoto MURATA,* and Osamu YAMAMOTO

National Chemical Laboratory for Industry, 1-1-5 Honmachi, Shibuya-ku, Tokyo 151

(Received October 24, 1974)

^{13}C nuclear magnetic resonance studies of pyridine solutions containing paramagnetic Ni(II), Co(II), Cu(II), or Mn(II) acetylacetonate are made by observing the induced chemical shift, the line width, and the spin-lattice relaxation time due to the paramagnetism of these metals. The origin of the paramagnetic effects on the ^{13}C spectra induced by Ni, Co, or Cu acetylacetonate is mainly the contact interaction, while the ^{13}C spectra of the pyridine–$Mn(AA)_2$ system can not be interpreted by the same interaction. The ^{13}C spectra of quinoline and isoquinoline containing $Mn(AA)_2$ are also studied; the results indicate that the predominant mechanism is the dipole-dipole interaction.

Up to now, the influences of paramagnetic metals on the ^{13}C nuclear magnetic resonance (NMR) spectra have been studied mainly from two different viewpoints. The ^{13}C spectra of *N*-heterocyclic compounds with addition of Ni(II) acetylacetonate, $Ni(AA)_2$, were investigated in order to observe the ^{13}C contact shift, where the molecule under study interacts with the paramagnetic $Ni(AA)_2$ at the position of the nitrogen atom.[1-4] In magnetic resonances of nuclei other than ^{13}C, especially in the ^1H NMR, the contact shifts induced by paramagnetic metals have been studied for many molecules and metals, and the nature of the interaction between them have been elucidated.[5] From the studies of the induced ^{13}C shift, much information has been obtained about the electronic structure of the carbon skelton of the molecules.[1-4]

Another study is the observation of the quenching of the nuclear Overhauser effect (NOE), which is characteristic of the ^{13}C resonance.[6-11] In this case, the molecule under study does not have any special interacting site with the paramagnetic metals in solution. The roles of the paramagnetic metals are to accelerate the slow ^{13}C relaxation and to reduce the NOE enhancement. An attempt has been made to use various paramagnetic metals as "paramagnetic relaxation agents" for this purpose, but clearly the utility of the paramagnetic metals is limited since many molecules are known to associate with metals.

Morishima and his co-workers[1-4] have studied the ^{13}C contact shifts induced by $Ni(AA)_2$ and indicated that the induced ^{13}C contact shifts show an alternation in sign and an attenuation in magnitude, depending on the distance from the nitrogen atom of the interacting site. They interpreted this phenomenon in terms of the electron spin densities on the carbon s atomic orbitals. The line broadening of the ^{13}C spectra of *N*-heterocyclic compounds due to $Ni(AA)_2$ is in the order of the β, α, and γ-carbons to the nitrogen atom attached by $Ni(AA)_2$; this order is the same as that of the absolute magnitude of the ^{13}C contact shift induced by $Ni(AA)_2$.

On the other hand, Kotowycz and Hayamizu first observed that when the paramagnetic Mn^{2+} ion was added to the aqueous adenosine monophosphate (AMP) solution, the ^{13}C line broadening was observed from the nearest position of the metal-binding site.[12] This trend has been shown to be the same for pyrimidine nucleoside and nucleotide in the presence of the Mn^{2+} ion,[13] while a different trend was observed upon the addition of the Cu^{2+} ion in similar aqueous solutions.[14] Clearly these results suggest that different paramagnetic metals affect the ^{13}C spectra in different manners.

Although many studies have been made to observe the ^{13}C contact shifts induced by $Ni(AA)_2$ for various *N*-heterocyclic compounds or to quench the NOE enhancement using various paramagnetic metals, only a few observations have been reported for the effects due to various paramagnetic metals on the ^{13}C parameters of *N*-heterocyclic compounds. In this paper we wish to report on the influences of four kinds of divalent paramagnetic metals, *i.e.*, Ni, Co, Cu, and Mn on the ^{13}C spectra of pyridine by observing the ^{13}C chemical shift, the line width, and the spin-lattice relaxation time, T_1. The behavior of these parameters upon the addition of $Ni(AA)_2$, $Co(AA)_2$, and $Cu(AA)_2$ is approximately similar, but $Mn(AA)_2$ gives quite different effects on the induced ^{13}C shifts and the line broadening. To confirm whether or not this is a general trend, the ^{13}C spectra of quinoline and isoquinoline were also studied upon the addition of $Mn(AA)_2$.

Experimental

The ^1H-decoupled ^{13}C spectra were obtained by an NV-14 spectrometer, NEVA Ltd., Tokyo, operating at 15.1 MHz with a Fourier transform mode. The deuterium signal from the solvent, $CDCl_3$, was used for the heteronuclear lock. The FID signals were accumulated in 8192 data points of a Varian 620 l computer, and the spectral width was 800 Hz. To obtain reliable values, 16 to 1000 accumulations were made, depending on the line width, the tip angle being about 30°. The sample temperature was maintained at about 28°C by blowing in compressed air. As the chemical shift reference, internal benzene was used for pyridine and quinoline, while external benzene was used for isoquinoline in order to prevent overlapping of the signals. The chemical shift accuracy was within ± 0.2 Hz. T_1 was measured by the usual 180°—90° pulse method. The rms errors of the semi-logarithmic plot of $(M_0 - M(\tau))/M_0$ *vs.* τ were within 5%.

All the substances were obtained from commercial sources. The materials were used without further purification except for pyridine, which was distilled. The concentrations

* Present address: Nippon Electric Varian Ltd., 5-8-1 Yotsuya, Fuchu-shi, Tokyo 183.

of the $CDCl_3$ solutions were 62, 41, and 41 mole % for pyridine, quinoline, and isoquinoline, respectively. The stock solution of various metal acetylacetonates, $M(AA)_2$, in $CDCl_3$ or in pyridine was added successively by means of a microsyringe to obtain 5 to 7 different concentration of $M(AA)_2$.

Results and Discussion

Effects of Paramagnetic Metals on the ^{13}C Chemical Shift, the Line Width, and the Spin-Lattice Relaxation Time. The chemical shift induced by paramagnetic species in solution, $\Delta\delta_M$, consists of two terms, *i.e.*, the pseudocontact and contact terms.[15]

$$\Delta\delta_M = -\left[f(g)\frac{\beta^2}{kT}\frac{3\cos^2\theta-1}{r^3}+A\frac{\gamma_e}{\gamma_N}\frac{g\beta}{3kT}\right]S(S+1) \quad (1)$$

where $f(g)$ is the function of g component of the electron spin and other notations have the usual meanings. It has been reported that the pseudocontact term may be negligible for the ^{13}C shift induced by $Ni(AA)_2$ and that the contact term plays the main role.[1-4]

In a solution containing the paramagnetic species, the nuclear spin-lattice relaxation time, T_{1M}, and the nuclear spin-spin relaxation time, T_{2M}, due to the metal are written by [15]

$$\frac{1}{T_{1M}} = \frac{Nn_h}{N_p}S(S+1)\left[\frac{2}{15}\frac{g^2\beta^2\gamma_I^2}{r^6}\left(3\tau_c+\frac{7\tau_c}{1+\omega_s^2\tau_c^2}\right)+\frac{2}{3}\frac{A^2}{\hbar^2}\left(1+\frac{\tau_e}{1+\omega_s^2\tau_e^2}\right)\right] \quad (2)$$

$$\frac{1}{T_{2M}} = \frac{Nn_h}{N_p}S(S+1)\left[\frac{1}{15}\frac{g^2\beta^2\gamma_I^2}{r^6}\left(7\tau_c+\frac{13\tau_c}{1+\omega_s^2\tau_c^2}\right)+\frac{1}{3}\frac{A^2}{\hbar^2}\left(\tau_e+\frac{\tau_e}{1+\omega_s^2\tau_e^2}\right)\right] \quad (3)$$

where

$$\frac{1}{\tau_c} = \frac{1}{\tau_r} + \frac{1}{\tau_s}$$

and

$$\frac{1}{\tau_e} = \frac{1}{\tau_h} + \frac{1}{\tau_s}$$

τ_s is the electron spin relaxation time, τ_r is the characteristic time for the tumbling motion of the paramagnetic complex, and τ_h is the chemical exchange time for the ligand molecule between the coordination sphere and the bulk medium. n_h is the number of the ligand molecule in the solvation sphere, N_p is the molar concentration of the ligand molecule, and N is the molar concentration of paramagnetic metals.

The line broadening, $\Delta\nu_M$, induced by the paramagnetic metals is obtained from the difference between the full line width, $\Delta\nu_{obs}$, with the metal and $\Delta\nu_0$ without the metal:

$$\Delta\nu_M = \Delta\nu_{obs} - \Delta\nu_0$$

In a rough approximation, T_{2M} may be obtained from $\Delta\nu_M$ by the following relation:

$$1/T_{2M} = \pi\Delta\nu_M \quad (4)$$

Equations (2) and (3) show that T_{1M} and T_{2M} are functions of the contact correlation time, τ_e, and the dipolar correlation time, τ_c, and at the same time, they depend upon the magnitude of the isotropic coupling constant, A, and the distance between the metal and the nuclei.

Table 1. The effects of various metal acetylacetonates on the ^{13}C resonance of pyridine[a]

	S		α	β	γ
$Cu(AA_2)$	1/2	$1/T_{1M}(s^{-1})$	0.32	0.13	0.11
		$\Delta\nu_M$(Hz)	0.61	8.0	0.85
		$\Delta\delta_M$(Hz)	0.8	−1.8	0.3_5
$Ni(AA)_2$	1	$1/T_{1M}(s^{-1})$	0.20	0.17	0.04
		$\Delta\nu_M$(Hz)	0.30	1.75	0.08
		$\Delta\delta_M$(Hz)	1.4	−3.9	0.7
$Co(AA)_2$	2/3	$1/T_{1M}(s^{-1})$	0.018	0.012	0.008
		$\Delta\nu_M$(Hz)	0.032	0.032	0.013
		$\Delta\delta_M$(Hz)	1.6	−1.8	0.5
$Mn(AA)_2$	5/2	$1/T_{1M}(s^{-1})$	0.06	0.02	0.006
		$\Delta\nu_M$(Hz)	0.25	0.18	0.03
		$\Delta\delta_M$(Hz)	−1.1	−1.1	-0.3_5

a) These values are obtained from the linear plots of the parameters *vs.* the metal concentration at 5×10^{-3} M and normalized by $S(S+1)$.

In this paper, $\Delta\delta_M$, T_{1M}, and $\Delta\nu_M$ of the ^{13}C NMR spectra are measured in order to observe the influences of the four paramagnetic metals and to discuss the different effects according to Eqs. (1) to (4).

Interactions between Pyridine and Ni(AA)$_2$, Co(AA)$_2$, Cu(AA)$_2$, and Mn(AA)$_2$. To observe the paramagnetic effects due to $M(AA)_2$ (M=Ni, Co, Cu, and Mn) on the ^{13}C spectra, a pyridine solution was used with $M(AA)_2$ added successively. In Table 1 the values observed for $\Delta\delta_M$, $\Delta\nu_M$, and T_{1M} of each carbon of pyridine due to the four kinds of $M(AA)_2$ are summarized. These values are obtained from the plots of these parameters *vs.* the concentrations of $M(AA)_2$ at the point of 5×10^{-3} M, the mole ratio of pyridine to $M(AA)_2$ being approximately 1500 : 1. All the parameters, P_M, are calculated by means of

$$P_M = (P_{Mobs}-P_0)\frac{1}{S(S+1)}$$

where P_{Mobs} and P_O are the values with and without paramagnetic metals, and S is the electron-spin quantum number for each metal. In order to discuss the nature of the metal–pyridine interaction, all the parameters due to the presence of the metal must be normalized by $S(S+1)$, as is indicated by Eqs. (1) to (3).

Figure 1 shows the effects of various amounts of $M(AA)_2$ on the induced ^{13}C shifts of pyridine in $CDCl_3$, where the $\Delta\delta_M$'s are not normalized by $S(S+1)$. When the metals are Ni and Co, the $\Delta\delta_M$ values show a similar trend, *i.e.*, an increased concentration of the metals brings a larger shift. The singals of α and γ-carbons move to the higher field and that of β-carbons moves to the lower field, and the absolute magnitudes of $\Delta\delta_M$ are ordered as: $|\Delta\delta_M(\beta)|>|\Delta\delta_M(\alpha)|>|\Delta\delta_M(\gamma)|$. This trend was interpreted for the $Ni(AA)_2$–pyridine system in terms of the electron-spin densities on the carbon orbitals by Morishima and his co-workers.[1]

When $Cu(AA)_2$ was added to the pyridine solution (Figure 1(C)), each carbon signal behaves in a different manner from those of the $Ni(AA)_2$ and $Co(AA)_2$ systems, and the magnitudes of $\Delta\delta_M$ are rather small and not

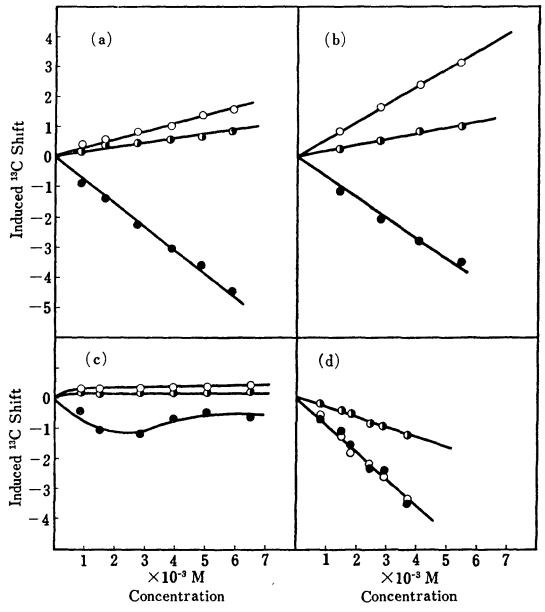

Fig. 1. The linear plots of the induced ^{13}C shifts for α(○), β(●), and γ(◑)-carbons of pyridine *vs.* the concentration of (a) $Ni(AA)_2$, (b) $Co(AA)_2$, (c) $Cu(AA)_2$, and (d) $Mn(AA)_2$.

linear to the concentration of $Cu(AA)_2$. However, the direction of the induced ^{13}C shifts for each carbon upon the addition of $Cu(AA)_2$ shows a trend similar to that in the addition of $Ni(AA)_2$ or $Co(AA)_2$.

The line broadening due to $Ni(AA)_2$, $Co(AA)_2$, and $Cu(AA)_2$ for each carbon resonance of pyridine arises in the same order as the magnitude of $\Delta\delta_M$, *i.e.*, $\Delta\nu_M(\beta) > \Delta\nu_M(\alpha) > \Delta\nu_M(\gamma)$. However, when $Cu(AA)_2$ was added, the line width of the β-carbon of pyridine was broadened to a large extent. It is known that $Cu(AA)_2$ takes a dimer structure in a pyridine solution; the non-linearity of $\Delta\delta_M$ *vs.* the concentration of $Cu(AA)_2$ and the particularly large line broadening of the β-carbon resonance line may be related to this fact.

Surprisingly, upon the addition of $Mn(AA)_2$ the carbon signals behave in a very different way, as is shown in Fig. 1(d); all the carbon signals move to a lower field, and the magnitudes of $\Delta\delta_M$ are ordered as: $|\Delta\delta_M(\alpha)| > |\Delta\delta_M(\beta)| > |\Delta\delta_M(\gamma)|$. The line broadening, $\Delta\nu_M$, due to $Mn(AA)_2$ occurs in the same way as the magnitude of $\Delta\delta_M$. This remarkable differences in the $\Delta\delta_M$ and $\Delta\nu_M$ may imply different mechanisms of the interactions between the metal and pyridine in the case of $Mn(AA)_2$.

To make clearer the pyridine–metal interaction mechanism, the T_{1M} values were measured; the results are shown in Table 1. The magnitude of $1/T_{1M}$ decreases in the order of the α, β, and γ-carbons of pyridine for all the $M(AA)_2$ systems, which suggests that $1/T_{1M}$ is mainly governed by the distance between the metal and each carbon of pyridine. Equation (2) shows that both the dipolar and scalar terms contribute to $1/T_{1M}$, but in this case the dipolar contribution is considered to be predominant, since this term is a function of $1/r^6$.

It is clear from Eq. (2) that, if $\omega_s\tau_e \gg 1$, the scalar term can be neglected. At the field of 15 MHz of the carbon resonance, the electron-spin resonance frequency, $\omega_s \approx 2.4\times10^{10}\ s^{-1}$,[16] and τ_s is known to be 3×10^{-9} and $4\sim7\times10^{-10}$ s for Mn^{2+} and Cu^{2+} respectively;[17] therefore, $\omega_s\tau_e \gg 1$ is valid for these two $M(AA)_2$ systems, and the scalar contribution to $1/T_{1M}$ can be neglected.

The τ_s of Co^{2+} is known to be rather short,[17] so that τ_e and τ_c are considered to be short also. The small values of $1/T_{1M}$ and $\Delta\nu_M$ upon the addition of $Co(AA)_2$ (see Table 1) may be due to the short correlation times. Here, the main mechanism for the spin-lattic relaxation is thought to be also a dipolar interaction.

For the system containing $Ni(AA)_2$, it is not obvious that the contribution of the scalar term to $1/T_{1M}$ of each carbon is negligible, although the $1/T_{1M}$ of the α-carbon is larger than that of the β-carbons. The ratio of the $1/T_{1M}$ of the α to the β-carbons in the $Ni(AA)_2$ system is a little smaller (1.2 : 1) than the other $M(AA)_2$ systems (about 3 : 1). However, the discussion of the $\Delta\delta_M$ values has indicated $|A_{\alpha\text{-carbon}}| < |A_{\beta\text{-carbon}}|$, and a remarkable line broadening is observed at the β-carbon resonance, but not at the α-carbon resonance. Therefore, as far as $1/T_{1M}(\alpha)$ is concerned, the contribution of the contact term may also be small and negligible in this system.

As has been discussed above, the values of the $1/T_{1M}$ of the α-carbons of pyridine containing these $M(AA)_2$ may be determined by the dipolar term. Actually assuming the distance between the metal and nitrogen atom of pyridine to be 3 Å, and using the observed values of $1/T_{1M}$ and Eq. (2), the τ_c values are calculated to be 4, 2.5, 0.76, and 0.23×10^{-11} s for the Cu-, Ni-, Mn-, and $Co(AA)_2$-pyridine complexes respectively. From these values, $\omega_s\tau_c \ll 1$ is shown to hold; therefore,

$$\frac{1}{T_{1M}} = \frac{Nn_h}{N_p} S(S+1)\frac{4}{5}\frac{g^2\beta^2\gamma_I^2}{r^6}\tau_c \qquad (5)$$

The stability constants of metal-pyridine systems have been obtained by various methods.[18] Although the stability constants for the $M(AA)_2$–pyridine systems in $CDCl_3$ solution are not known, the order of the stability of the complexes of $M(AA)_2$ may be estimated to be Cu>Ni>Mn>Co from similar systems. This order agrees with that of the $1/T_{1M}$ values of the α-carbons in Table 1, and at the same time with the τ_c value of each $M(AA)_2$–pyridine complex. Since the τ_c is a measure of the duration time for the dipolar coupling between the ligand and the paramagnetic metal, it is reasonable that the stability constants of the complexes are proportional to τ_c. Therefore, T_1 measurement is shown to give useful information about the stability constants of paramagnetic metal–ligand complexes.

Unlike the mechanism of the spin-lattice relaxation due to the paramagnetic metals, both the scalar and the dipolar relaxation mechanisms are effective in the spin-spin relaxation, as is shown in Eq. (3), even if the two assumptions $\omega_s\tau_c \ll 1$ and $\omega_s\tau_e \gg 1$ (in the case of Cu and Mn), or $\omega_s\tau_e \ll 1$ (in the case of Co), are used. From equation (4), $\Delta\nu_M$ may be used as a measure of $1/T_{2M}$. In the system containing $Cu(AA)_2$ and $Ni(AA)_2$, the values of $1/T_{2M}$ as well as $\Delta\delta_M$ of the β-carbons are the largest, indicating that the scalar coupling is one of the most important mechanisms of

the spin-spin relaxation. However, in the $Mn(AA)_2$–pyridine system, the $\Delta\nu_M$ values of the β-carbons are not the largest and takes place in the order of α, β, and γ-carbons, the same as the absolute magnitude of $\Delta\delta_M$. The different trends in both the $\Delta\delta_M$ and $\Delta\nu_M$ values of pyridine containing $Mn(AA)_2$ from the other $M(AA)_2$ suggest that the interaction between pyridine and $Mn(AA)_2$ seems to be quite different from the other metal systems.

Since pyridine is soluble in water, the ^{13}C spectra were observed for aqueous pyridine solutions containing the divalent metal ions. To D_2O solution of pyridine, Ni^{2+}, Co^{2+}, Cu^{2+}, or Mn^{2+} was added. The $\Delta\delta_M$ and $\Delta\nu_M$ due to these ions showed trends similar to those in the systems of pyridine–$CDCl_3$ solutions containing the corresponding $M(AA)_2$. In the D_2O system also, Mn^{2+} brings all the ^{13}C signals to a lower field, and the absolute magnitudes of $\Delta\delta_M$ are in the order of $|\Delta\delta_M(\alpha)| > |\Delta\delta_M(\beta)| > |\Delta\delta_M(\gamma)|$ and $\Delta\nu_M$ arises in the same way, *i.e.*, $|\Delta\nu_M(\alpha)| > |\Delta\nu_M(\beta)| > |\Delta\nu_M(\gamma)|$, while the paramagnetic effects due to the other ions are the largest in the β-carbon resonance line in both the induced shift and the line broadening.

Since the same trends are observed in $CDCl_3$ and the aqueous solutions containing Mn, the origin of the characteristic effects on the ^{13}C resonance due to Mn may come from the nature of the Mn–nitrogen bond. Thus, we extended our work to the systems of quinoline and isoquinoline interacting with $Mn(AA)_2$ in $CDCl_3$, in order to observe the paramagnetic effects on the ^{13}C resonance lines of nine carbons of these compounds.

The Interactions of Quinoline and Isoquinoline with Mn(AA)$_2$. When $Mn(AA)_2$ is added to quinoline or isoquinoline in $CDCl_3$ solutions, the $\Delta\delta_M$, $\Delta\nu_M$, and $1/T_{1M}$ of each carbon resonance increase linearly as the concentration of the metal increases, just as in the pyridine–$CDCl_3$ solution. Table 2 shows the effects of $Mn(AA)_2$ on the ^{13}C resonance parameters of pyridine, quinoline, and isoquinoline. These values were obtained from the slopes of the linear plots of the observed parameters *vs.* the concentration of $Mn(AA)_2$, and were calculated as the values relative to the corresponding parameters of a particular carbon of the γ-position to the nitrogen atom, *i.e.*, C-4 of pyridine and quinoline and C-10 of isoquinoline, which are set at unity. In the systems of quinoline and isoquinoline, the effect of $Mn(AA)_2$ on T_{1M} decreases in magnitude according to α, β, γ, $\cdots$ carbons, which is the same trend as that observed in the system of pyridine containing $Mn(AA)_2$ discussed above. All the $\Delta\delta_M$ values of quinoline and isoquinoline as well as those of pyridine due to $Mn(AA)_2$ shift to a lower field, and their magnitudes decrease in the order of the α, β, γ, $\cdots$ carbons. The $\Delta\nu_M$ value also shows the same trend, quite unlike the systems containing other $M(AA)_2$.

The facts described above suggest that the magnitudes of the paramagnetic effects on the ^{13}C resonance induced by $Mn(AA)_2$ mainly depend upon the distance between Mn and the carbon atoms. Equation (5) indicates that $1/T_{1M}$ is proportional to $1/r^6$; if the scalar interaction were neglected, $\Delta\delta_M$ and $1/T_{2M}$ would also become only a function of the geometric factor, as shown in Eqs. (1) and (3). Actually, the values of $1/T_{1M}$ and $\Delta\nu_M$ are plotted against $1/r^6$, together with the plot of $\Delta\delta_M$ against $(1-3\cos^2\theta)/r^3$, in Fig. 2. The molecular structures of quinoline and isoquinoline were assumed from those of pyridine and benzene. The metal–nitrogen distances in the crystal structures of the pyridine complexes have been reported to range from 2.0 to 2.3 Å,[19] but in solutions it is considered to become larger. Furthermore, the distance in a solution is assumed to be the averaged distance when the ligand molecule exchanges in the coordination sphere and in the bulk medium. The best fit of $1/T_{1M}$ as a function of $1/r^6$ was obtained for the metal–N distances at 3.3, 3.4, and 2.8 Å in pyridine, quinoline, and isoquinoline respectively. However, when the experimental errors are considered, it may be adequate to estimate 3 Å as

Table 2. The effects of $Mn(AA)_2$ on the ^{13}C spectra of pyridine, quinoline, and isoquinoline[a]

Pyridine	α(2,6)-positions	β(3,5)-positions	γ(4)-position
$1/T_{1M}$	10.0	2.3	1.0
$\Delta\delta_M$[b]	3.7	3.7	1.0
$\Delta\nu_M$	7.9	5.9	1.0

Quinoline	α-positions		β-positions			γ-positions			δ-position
	2	9	8	3	10	4	5	7	6
$1/T_{1M}$	9.4	7.7	5.5	2.0	1.9	1.0	0.9	1.2	1.2
$\Delta\delta_M$[b]	1.9	1.8	1.4	1.3	1.1	1.0	1.1	0.6	0.0
$\Delta\nu_M$	11.3	12.7	6.7	3.3	2.7	1.0	0.0	0.6	0.0

Isoquinoline	α-positions		β-positions		γ-positions		δ-positions		ε-position
	1	3	4	9	10	8	7	5	6
$1/T_{1M}$	11.8	13.1	2.0	2.4	1.0	0.5	0.5	0.4	0.4
$\Delta\delta_M$[b]	2.9	2.2	2.0	2.0	1.0	1.0	0.5	0.0	0.8
$\Delta\nu_M$	18.1	11.9	6.4	5.9	1.0	0.9	0.0	0.0	0.0

a) These values are obtained from the slopes of the linear plots of the parameters *vs.* $Mn(AA)_2$ concentration and normalized to those of C_4-carbon of pyridine and quinoline, and C_{10}-carbon of isoquinoline, which are set to unity. b) All the induced ^{13}C chemical shifts move to the lower field.

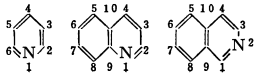

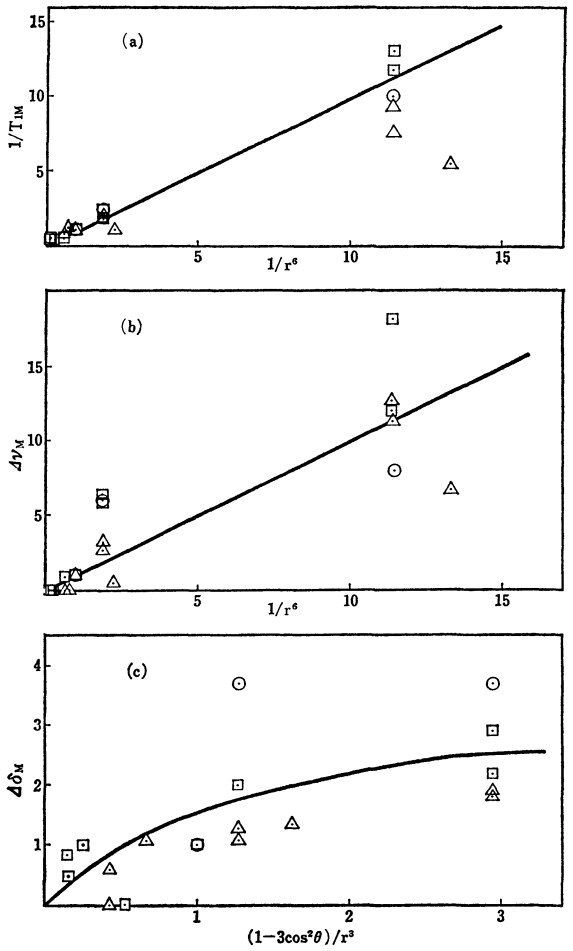

Fig. 2. The plots of (a) $1/T_{1M}$ and (b) $\Delta\nu_M$ against $1/r^6$, and (c) $\Delta\delta_M$ against $(1-3\cos^2\theta)/r^3$, where r is the distance between Mn and each carbon of pyridine (⊙), quinoline (△), and isoquinoline (⊡). All the values including the geometric factors are referred to C_4 of pyridine and quinoline, and C_{10} of isoquinoline.

the approximate averaged metal–N distance for these compounds; this value is used in Fig. 2. Since the parameter values relative to a particular γ-carbon resonance are used, the geometric parameters are also normalized to the same carbon. In other words, both the ^{13}C resonance parameters and the geometric values of the γ-carbon are set at unity.

As is shown in Fig. 2, although the linearity is not very good, there are apparent correlations between $1/T_{1M}$ and $1/T_{2M}$ and $1/r^6$, and between $\Delta\delta_M$ and $(1-3\cos^2\theta)/r^3$. This indicates that the ^{13}C resonance parameters induced by $Mn(AA)_2$ are mainly governed by the geometric factors. The scalar interaction is very small, and its extent may be the order of the deviation from the observed correlation between the induced parameters and the geometric factors. This conclusion seems a little surprising when we consider the results of the many studies of the interactions between $Ni(AA)_2$ and various *N*-heterocyclic compounds,[1-4] which clearly show that the induced ^{13}C shift can be interpreted in terms of the scalar interaction, with the complete neglect of the dipolar term.

The lanthanide shift reagents are also paramagnetic and induce large pseudocontact shifts without any significant line broadening in most cases. The unpaired electrons of the lanthanide metals, which induce the paramagnetic shift, occupy the inner shell. This may be one of the most important reasons why the contact term is negligible.[5]

On the other hand, Mn is a d-transition metal such as Cu, Co, and Ni; therefore we can expect that the paramagnetic effects on the NMR parameters would be induced in a similar way by these metals. However, the present study indicates that the contact interaction is very small in the manganese complexes in the ^{13}C resonance, quite unlike the cases of Cu, Co, and Ni complexes, where the contact interaction is predominant. The negligible contact interaction in the ^{13}C resonance of Mn complexes implies that the unpaired electron spin density does not exist on the carbon atoms of the ligand molecules. From the discussion of $1/T_{1M}$ and $1/T_{2M}$, the Mn metal approaches the nitrogen atom of the ligand molecule and forms the Mn–N bond, which persists for the duration of the dipolar correlation time. In that period the unpaired electron from Mn does not transfer into the ligand molecule through the Mn–N bond. It is not certain why the Mn-complexes are different from other paramagnetic metal complexes, but the difference is evident in the ^{13}C NMR spectra shown in the present study.

This fact is very valuable for the studies of metal binding in biological systems. When a manganous ion is added to an aqueous solution in biological systems, the effects of the paramagnetism on the ^{13}C NMR will appear in the chemical shift, the line width as well as the spin-lattice relaxation time, and their magnitudes will depend upon the distance between the carbon atom and the Mn metal. In other words, Mn is a very useful paramagnetic metal for studying the binding site, and in a favorable case, the averaged distance between the metal and the molecule under study may be estimated.

References

1) I. Morishima, T. Yonezawa, and K. Goto, *J. Amer. Chem. Soc.*, **92**, 6651 (1970).
2) I. Morishima, K. Okada, T. Yonezawa, and K. Goto, *ibid.*, **93**, 3922 (1971).
3) I. Morishima, K. Okada, and T. Yonezawa, *ibid.*, **94**, 1425 (1972).
4) I. Morishima, K. Yoshikawa, K. Okada, T. Yonezawa, and K. Goto, *ibid.*, **95**, 165 (1973).
5) G. N. La Mar, W. De W. Horrocks, Jr., and R. H. Holm, "NMR of Paramagnetic Molecules," Academic Press, New York (1973).
6) G. N. La Mar, *J. Amer. Chem. Soc.*, **93**, 1040 (1971).
7) G. N. La Mar, *Chem. Phys. Lett.*, **10**, 230 (1971).
8) R. Freeman, K. G. R. Pachler, and G. N. La Mar, *J. Chem. Phys.*, **55**, 4586 (1971).
9) S. Barcza and N. Engstrom, *ibid.*, **94**, 1762 (1972).
10) G. C. Levy and J. D. Cargloli, *J. Mag. Res.*, **10**, 231 (1973).
11) G. C. Levy and R. A. Komoroski, *J. Amer. Chem. Soc.*, **96**, 678 (1974).
12) G. Kotowycz and K. Hayamizu, *Biochemistry*, **12**, 517

(1973).
13) G. Kotowycz and O. Suzuki, *ibid.*, **12**, 3434 (1973).
14) G. Kotowycz, *Can. J. Chem.*, **52**, 924 (1974).
15) C. S. Johnson, Jr., "Advances in Magnetic Resonance," Vol. 1, ed. by J. S. Waugh, Academic Press, New York (1965).
16) A. Carrington and A. D. McLachlan, "Introduction of Magnetic Resonance", Harper & Row, New York (1967).
17) N. Bloembergen and L. O. Morgan, *J. Chem. Phys.*, **34**, 842 (1961).
18) "Stability Constants," Supplement No. 1. The Chemical Society, London (1971).
19) "Crystal Data, Determinative Table," 3rd Edition, ed. by J. D. H. Donnay and H. M. Ondik, National Bureau of Standard, Washington, D.C. (1973).

Thermal Bleaching of the Colored Form in the Photochromism of 2-Hydroxy-2′,4,4′-trimethoxytriphenylmethanol in Acetonitrile

Sanyo HAMAI and Hiroshi KOKUBUN

Department of Chemistry, Faculty of Science, Tohoku University, Aoba, Aramaki, Sendai 980

(Received November 1, 1974)

The photochromism of 2-hydroxy-2′,4,4′-trimethoxytriphenylmethanol (HTMM) in acetonitrile differs from that of other 2-hydroxytriphenylmethanol derivatives in some aspects. The colored form, 2′,4,4′-trimethoxy-*o*-fuchsone (TMF), of HTMM partly converts to 2-hydroxy-2′,4,4′-trimethoxytriphenylmethyl cation (Cat) at an early stage of the bleaching reaction. At a later stage a slow bleaching of TMF to HTMM becomes the main decay process. Bleaching of the produced Cat is so slow that Cat remains even after complete disappearance of TMF. The formation of Cat was concluded to be a reaction between adsorbed TMF and water on the cell surface. The rate determining step is not a diffusion process since the activation energy found is much larger than that of viscosity. Cat decays by the reaction with water, not with hydroxide ion.

2-Hydroxytriphenylmethanol derivatives show photochromism[1] as well as thermochromism.[2] The reaction scheme is as follows:

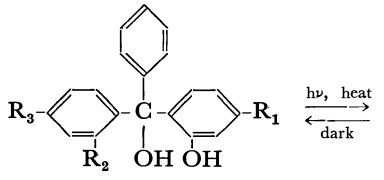

I

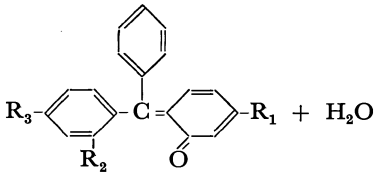

II

Ia $R_1=R_2=R_3=H$, 2-hydroxytriphenylmethanol (HM)
Ib $R_1=OCH_3$, $R_2=R_3=H$, 2-hydroxy-4-methoxytriphenylmethanol (HMM)
Ic $R_1=R_2=R_3=OCH_3$, 2-hydroxy-2′,4,4′-trimethoxytriphenylmethanol (HTMM)
IIa $R_1=R_2=R_3=H$, *o*-fuchson (F)
IIb $R_1=OCH_3$, $R_2=R_3=H$, 4-methoxy-*o*-fuchson (MF)
IIc $R_1=R_2=R_3=OCH_3$, 2′,4,4′-trimethoxyfuchson (TMF)

The colored form of HM, F, decays according to pseudo-first order kinetics.[1] However, MF, the colored form of HMM, shows an unusual bleaching pattern in saturated hydrocarbons such as *n*-hexane, but in polar solvents the bleaching reaction becomes the pseudo-first order.[3] Both substituents and solvent polarity have a critical effect on the bleaching mechanism. TMF which has three electron donating methoxy groups shows no unusual bleaching pattern in *n*-hexane as in the case of MF. However, in acetonitrile it was found to decay in a different pattern. We have investigated the thermal bleaching of TMF in acetonitrile in detail, the reuslts being given in the following.

Experimental

HTMM was synthesized from 2-hydroxy-2′,4,4′-trimethoxybenzophenone by the Grignard reaction with phenylmagnesium bromide and recrystallized several times from ether-*n*-hexane and ethanol-water mixtures. 2-Hydroxy-2′,4,4′-trimethoxybenzophenone was synthesized from 3-methoxyphenol and 2,4-dimethoxybenzoic acid in the presence of boron trifuoride-ethyl ether complex.[4] HTMM; mp 129—131 °C. Found: C, 72.34; H, 6.29%. Calcd for $C_{22}H_{22}O_5$: C, 72.10; H, 6.06%.

Acetonitrile was distilled over phosphorous pentoxide. A 6 W germicidal mercury lamp was used as a light source for 253.7 nm illumination. Absorption spectra were measured with a Hitachi EPS-3T spectrophotometer. A Haake FJ regulater was employed for temperature control.

The initial concentrations of HTMM were chosen to be *ca.* 2×10^{-4} M in all the experiments. The illuminated sample solutions were shaken before the measurements in order to make the concentration of TMF in the cell uniform.

Results and Discussion

The absorption spectral change with time for the solution of HTMM in acetonitrile after illumination for 20 s is shown in Fig. 1. Beside the absorption of TMF there is an absorption band due to other species at 438 nm. This band increases rapidly at the expense of the TMF band with isosbestic points at 420 and 456 nm at an early stage of bleaching. After the absorbance at 438 nm attains maximum, the absorption band due to TMF decreases slowly. The 438 nm band reamins even after TMF has disappeared completely. This absorption spectrum is iden-

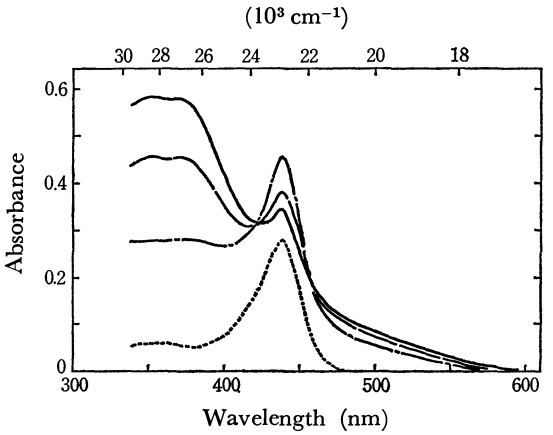

Fig. 1. Spectral change of the colored form of HTMM in acetonitrile.
——; immediately after illumination, — —; 4 min after, —·—; 14 min after, ----; 14 min after.

tical with that of 2-hydroxy-2′,4,4′-trimethoxytriphenylmethyl cation (Cat) prepared by adding sulfuric acid or an oxidizing agent to the HTMM acetonitrile solution. Only TMF is produced photochemically, since the absorption band of Cat does not appear by illumination of HTMM at 77 K.

Since the absorption spectra of TMF and Cat are superposed immediately after illumination, we should know the shapes of individual absorption spectra in order to analyze the growth and the decay of individual species. The absorption spectrum of Cat is known. The absorption spectrum of TMF was obtained by addition of triethylamine to the illuminated solution. Triethylamine forms a colorless complex with Cat selectively. Similar complexing phenomena are reported between crystal violet and primary amines and other triphenylmethyl cation derivatives and amines.[5] The resulting absorption spectrum of THF is given in Fig. 2.

Simultaneous measurement of absorbances at two different wavelengths discriminates the contribution of individual species to the measured absorbances. The wavelengths at 350 nm and 438 nm were chosen which correspond respectively to the absorption maxima of TMF and Cat. The absorbances of TMF and

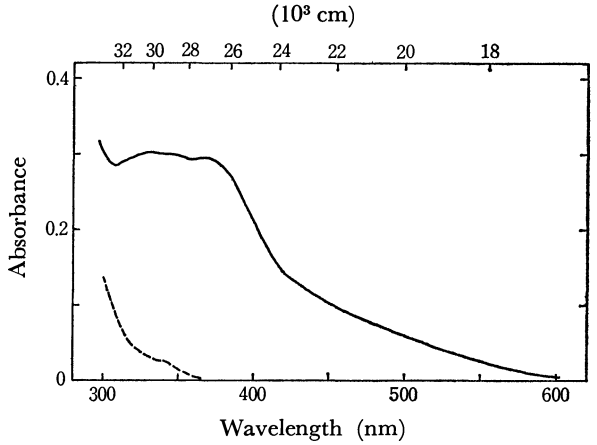

Fig. 2. ——; absorption spectrum of TMF in acetonitrile containing 7.2×10^{-2} M triethylamine, ----; *ca.* 24 hr illumination.

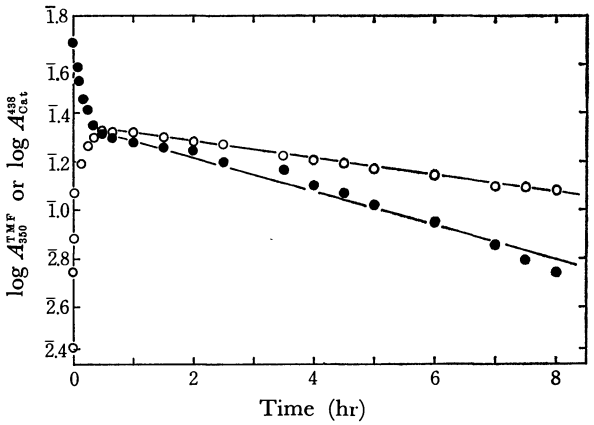

Fig. 3. Semilogarithmic plots of absorbances with time at 23 °C.
●: TMF, ○: Cat.

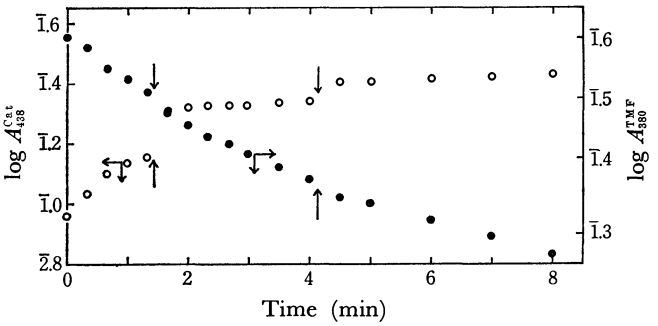

Fig. 4. Absorbance changes of TMF and Cat at the initial period of the reaction at 23 °C.
Arrows indicate the points at which a sample cell was shaken.
●; TMF, ○; Cat.

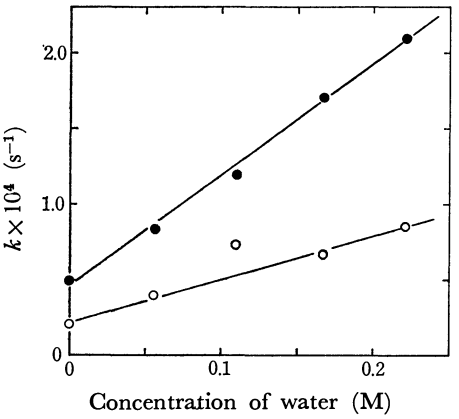

Fig. 5. Effect of water on the decay rates of TMF and Cat.
●: TMF, ○: Cat.

Cat as functions of time are plotted in the logarithmic scale in Fig. 3. The rapid growth of Cat corresponds to the initial decrease of TMF. Mechanical shaking of a sample cell at the stage where Cat is growing causes an increase in the absorbance of Cat and a slight decrease in the absorbance of TMF (Fig. 4). A similar phenomenon was also observed at 35 °C.

In the later stage both TMF and Cat show the first order decay (Fig. 3). In acetonitrile containing water less than 0.3 M, the type of concentration change of TMF and Cat is similar to that in neat acetonitrile. The first order decay rate constants for TMF and Cat at the later stage are proportional to the concentration of water added (Fig. 5).

With increasing water concentration, the concentration of Cat immediately after illumination becomes so high that the growth of Cat can not be followed. Moreover, the concentrations of TMF and Cat change in a complicated way.

In the solution containing a small amount of water, Cat seems to react with water yielding a starting material HTMM. This differs from other triphenylmethane cation dyes which react with anion to give their leuco forms.[6,7] The formation of Cat occurs only in the initial stage of the TMF decay. This suggests that the reaction is a kind of an inhibited reaction.

The molar absorption coefficient of TMF is not known. It seems to be of the order of 10000 at 350 nm, since that of an analogous compound F is 7830 at the absorption maximum at 77 K in methanol–ethanol (1 : 1). The molar absorption coefficient of Cat was found from the chemically prepared Cat solution to be 62200, being more than six times larger than that of TMF. Since the amounts of the decrease and increase in the absorbances, respectively, of TMF and Cat do not differ significantly from each other at the initial stage, it is probable that a part of TMF converts to Cat and another portion to HTMM.

An effect of mechanical stirring indicates that TMF reacts with water on a cell surface to give Cat. When TMF and Cat occupy the same adsorption sites, the adsorbed amount are given by $[\mathrm{Cat}]_{ads}=\alpha_1[\mathrm{Cat}]/(1+\beta_1[\mathrm{Cat}]+\beta_2[\mathrm{TMF}])$ for Cat and $[\mathrm{TMF}]_{ads}=\alpha_2[\mathrm{TMF}]/(1+\beta_1[\mathrm{Cat}]+\beta_2[\mathrm{TMF}])$ for TMF, respectively, where α's and β's are constants. If Cat is adsorbed much more strongly than TMF, the adsorbed amount of TMF can be given by $[\mathrm{TMF}]_{ads}=C[\mathrm{TMF}]/[\mathrm{Cat}]$, where C is a constant. Hence, the reaction rate is given for TMF by Eq. 1 and for Cat by Eq. 2.

$$-\frac{\mathrm{d[TMF]}}{\mathrm{d}t}=k_1\frac{[\mathrm{TMF}][\mathrm{H_2O}]}{\mathrm{Cat}}+k_1'[\mathrm{TMF}][\mathrm{H_2O}] \quad (1)$$

$$\frac{\mathrm{d[Cat]}}{\mathrm{d}t}=k_2\frac{[\mathrm{TMF}][\mathrm{H_2O}]}{[\mathrm{Cat}]}-k_2'[\mathrm{Cat}][\mathrm{H_2O}] \quad (2)$$

At the initial stage of reaction, the second terms of the right hand of Eqs. 1 and 2 can be neglected as compared with the first terms. The concentration of water is expected to be practically unchanged. Thus we obtain

$$\ln([\mathrm{TMF}]/[\mathrm{TMF}]_0)=-k_{\mathrm{TMF}}\int \mathrm{d}t/[\mathrm{Cat}] \quad (3)$$

$$[\mathrm{Cat}]^2-[\mathrm{Cat}]_0^2=k_{\mathrm{Cat}}\int[\mathrm{TMF}]\mathrm{d}t \quad (4)$$

Plots according to Eqs. 3 and 4 are linear (Figs. 6 and 7, respectively), indicating that the proposed mechanism is highly probable. The activation energies for k_{TMF} and k_{Cat} were found to be 17.8 and 25.6 kcal/mol, respectively, considerably larger than that of viscosity for acetonitrile, 0.8 kcal/mol. The rate determining step is, therefore, not diffusion process unlike the bleaching reaction of MF in *n*-hexane. A mechanical stirring may cause a forced convection which accelerates the reaction between TMF and water on a cell surface. Thus, the absorbance of TMF decreases in smaller amount than the corresponding increase in the absorbance of Cat, being consistent with the larger molar absorption coefficient of Cat.

Equations similar in form to Eqs. 3 and 4 can be derived from another mechanism in which dissociated proton from water reacts with TMF to give Cat in acetonitrile instead of on the cell surface. However, this is not the case, since the presence of sulfuric acid affects neither the growth rate now the initial yield of Cat when the acid concentration is lower than 2×10^{-5} M. A feature differing from the neat acetonitrile solution is that the growth of Cat is not monotonic but stepwise. The reason for the stepwise growth is not clear at all. In the solution containing acid

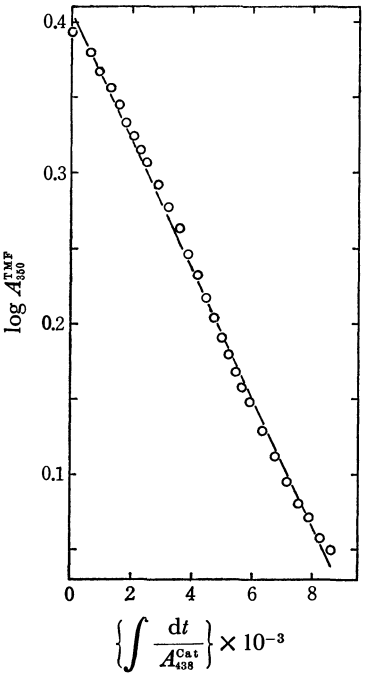

Fig. 6. Reaction analysis of TMF at the initial period at 23 °C.

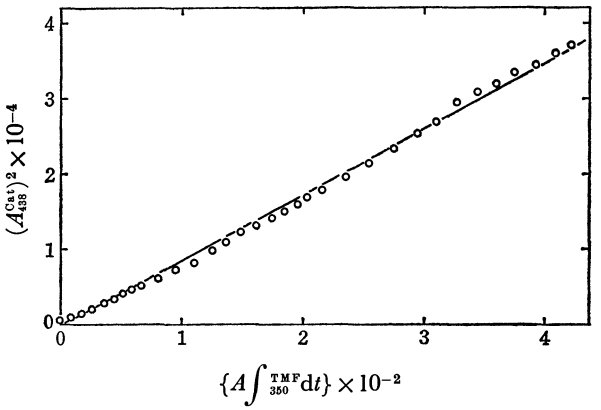

Fig. 7. Reaction analysis of Cat at the formation period at 23 °C.

of higher concentration, a considerable amount of Cat is produced immediately by the addition of acid.

The decay rate of TMF at the later stage is faster in solutions containing aqueous sulfuric acid as compared with solutions containing the same amount of water. The effect of added acid is not the simple protonation of TMF to give Cat, since Cat also decays. The following may be a possible reaction:

$$\mathrm{TMF}+(\mathrm{H_3O^+})_{solv}\rightarrow \mathrm{HTMM}+(\mathrm{H^+})_{solv}.$$

The decay rate of Cat, however, is slower in acidic solutions. The slower decay of Cat may be due to the slow production of Cat from the reaction between acid and HTMM. An enhanced stability of Cat in acidic solution may also be responsible.

In solutions containing triethylamine, the absorption due to Cat does not appear, although the bleaching pattern of TMF is the same as in neat acetonitrile. Cat once produced, therefore, is complexed with

triethylamine quickly. The resulting complex cation would be adsorbed on the cell surface as in the case of Cat. Consequently, the bleaching pattern of TMF is the same as in solution without triethylamine. The decay rate of TMF at the later stage is proportional to the triethylamine concentration. The reaction $TMF+(Et)_3N\cdot H_2O \rightarrow HTMM+(Et)_3N$ is plausible.

References

1) S. Hamai and H. Kokubun, *Z. Phys. Chem.* (Frankfurt), **88**, 211 (1974).
2) M. Gomberg and D. Nishida, *J. Amer. Chem. Soc.*, **45**, 190 (1923).
3) S. Hamai and H. Kokubun, This Bulletin, **47**, 2085 (1974).
4) K. Kurosawa, Y. Sasaki, and M. Ikeda, *ibid.*, **46**, 1498 (1973); and K. Kurosawa, private communication.
5) E. Kwiatkowski, *Roczniki Chem.*, **40**, 361 (1966).
6) S. Hochberg and V. K. LaMer, *J. Amer. Chem. Soc.*, **63**, 3110 (1941).
7) R. J. Goldacre and J. N. Phillips, *J. Chem. Soc.*, **1949**, 1724.

Photoelectron Spectra of Substituted Naphthalenes

Chikatoshi UTSUNOMIYA, Tsunetoshi KOBAYASHI, and Saburo NAGAKURA
The Institute for Solid State Physics, The University of Tokyo, Roppongi, Minato, Tokyo 106
(Received December 27, 1974)

The photoelectron spectra (PES) of 1- and 2-substituted naphthalenes (naphthols, aminonaphthalenes, *N,N*-dimethylaminonaphthalenes, acetylnaphthalenes, and cyanonaphthalenes) were measured in the region from 6 to 20 eV. The observed PES were assigned with the aid of the CNDO/2 calculations and the substituent effect. The lower energy bands of the compounds with the electron-donating group were found to be due to the ionization from the orbitals caused by the interaction of the highest three occupied π orbitals of the naphthalene ring with the nonbonding orbital of the substituent group. The second bands of the 1-substituted naphthalenes are commonly assigned to π orbitals almost completely localized on the naphthalene ring. The dimethylamino group of 1-dimethylaminonaphthalene was found to be twisted to a great extent from the ring plane.

Photoelectron spectroscopy is effective in getting information concerning electronic structures, especially concerning occupied orbitals, of molecules. In the preceding papers,[1-4] we have studied the PES of substituted benzenes. In this paper we extend the study to substituted naphthalenes. The PES of substituted naphthalenes have scarcely been studied and a few papers have hitherto been published. For example, Bock and his co-workers[5] studied the PES of 1- and 2-methoxy- and 1- and 2-methylthionaphthalenes. Maier[6] reported quite recently on the PES of aminonaphthalenes.

Experimental and Calculations

Naphthols, aminonaphthalenes, dimethylaminonaphthalenes, acetylnaphthalenes, and cyanonaphthalenes used in the present study were purified in usual ways and their purities were checked with the aid of NMR spectra. The PES of these compounds were measured as described previously,[3] the He I 584 Å resonance line being used as the excitation source and Xe gas as the internal standard for the energy-scale calibration. The CNDO/2[7] calculations of these compounds were carried out by a FACOM 230-60 computer at the Institute of Physical and Chemical Research. The geometrical structures of these compounds were assumed on the basis of the data for naphthalene and the corresponding benzene derivatives given in Refs. 8 and 9.

Results and Discussion

Naphthols. The PES of 1-naphthol and 2-naphthol are shown in Fig. 1. The vertical ionization potentials, I_v, of these compounds derived from the observed PES are summarized in Table 1.

As is seen in Fig. 1, naphthols show three lower-energy bands in the region from 7 eV to 10.1 eV. This is the region for the highest three occupied π orbital I_v's of naphthalene.[10] Therefore, these bands are reasonably due to the naphthalene π orbitals mixed with the hydroxyl n orbital, the energy of which is -10.96 eV for methanol.[11]

As is seen in Fig. 1 and Table 1, the I_v's of the first and third bands of 1-naphthol are smaller than the corresponding ones of naphthalene, but the second band I_v's agree with each other for both compounds. This fact demonstrates that the highest occupied π orbital of naphthalene (a_u) and the third one (b_{3g}) interact with the n orbital of the hydroxyl group, while

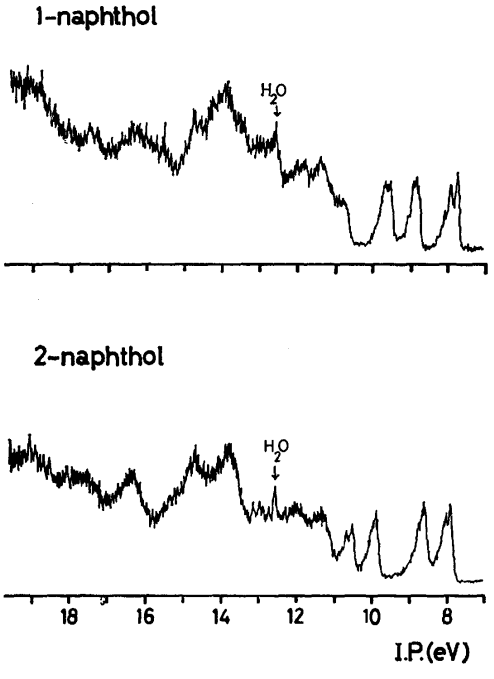

Fig. 1. Photoelectron spectra of naphthols.

the second one does not because the b_{1g} π orbital of naphthalene has nodes at the α-positions. On the other hand, the first three highest occupied orbital I_v's of 2-naphthol are smaller than the corresponding ones of naphthalene. This is because all the highest three occupied π orbitals of naphthalene have no node at the β-positions and can interact with the n orbital of the hydroxyl group. The CNDO/2 calculations (Fig. 2(b)) also support this conclusion. The orbital energy diagram given by the CNDO/2 method (Fig. 2(b)) qualitatively agrees with the observed one obtained on the assumption of Koopmans' theorem,[12] $\varepsilon = -I_v$, (Fig. 2(a)).

Aminonaphthalenes and Dimethylaminonaphthalenes. The PES of 1-aminonaphthalene, 2-aminonaphthalene, 1-dimethylaminonaphthalene, and 2-dimethylaminonaphthalene are shown in Figs. 3 and 4, the I_v's of these compounds being summarized in Table 1. These compounds show four lower-energy bands in the region from 7 eV to 10.5 eV except for 1-dimethylaminonaphthalene; the latter apparently shows only three bands in this region, but the second band consists

Table 1. Vertical ionization potentials ($I_v(J)$ in eV) of substituted naphthalenes

	$I_v(J)$			
J	1	2	3	4
Naphthalene[a)]	8.15	8.88	10.00	10.86
1-Naphthol	7.78	8.89	9.57	
2-Naphthol	7.90	8.63	9.91	10.54
Methanol[b)]	10.96	12.62	15.21	15.64
1-Aminonaphthalene	7.46	8.66	9.26	10.49
2-Aminonaphthalene	7.56	8.32	9.65	10.14
Methylamine[c)]	9.7	13.2	14.5	15.6
1-Dimethylamino-naphthalene	7.59	8.59	8.59	9.88
2-Dimethylamino-naphthalene	7.12	8.13	9.16	9.81
Trimethylamine[c)]	8.5	12.4	12.9	14.0
1-Acetylnaphthalene	8.23	8.99	9.18	10.12
2-Acetylnaphthalene	8.31	9.00	9.21	10.19
Acetone[d)]	9.72	12.6	13.4	13.9
Acetophenone[e)]	9.37	9.55	9.77	11.91
1-Cyanonaphthalene	8.61	9.35	10.31	
2-Cyanonaphthalene	8.64	9.33	10.51	11.18
Acetonitrile[f)]	12.21	13.14		

a) Ref. 10a. b) Ref. 11. c) Ref. 13. d) C. R. Brundle, M. B. Robin, N. A. Kuebler, and H. Basch, *J. Amer. Chem. Soc.*, **94**, 1451 (1972). e) Ref. 4. f) Ref. 15.

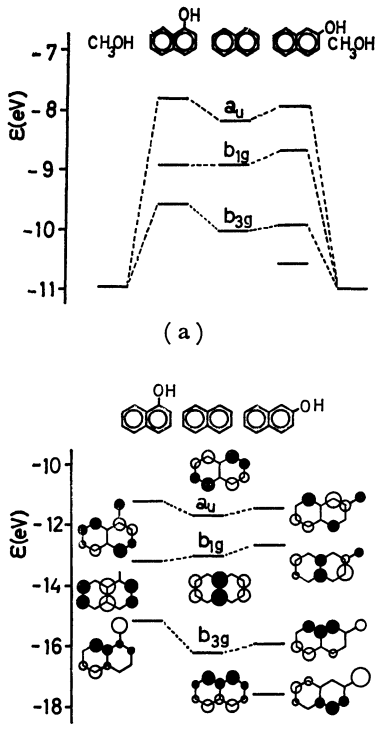

Fig. 2. Orbital energy diagrams for the higher occupied orbitals of naphthols; (a) experimental, (b) calculated.

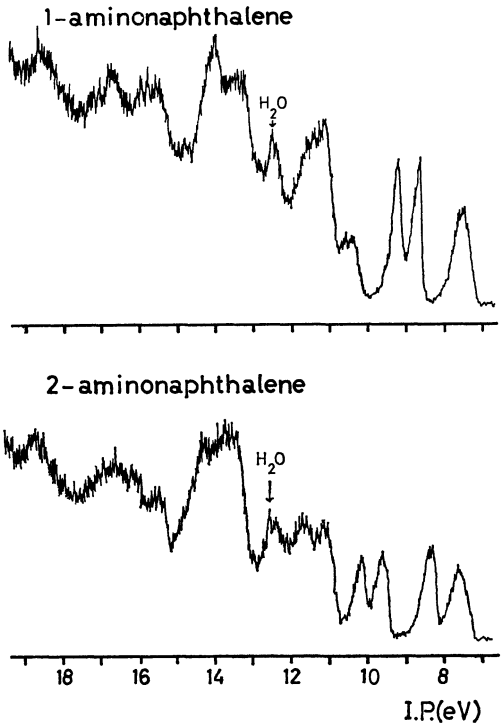

Fig. 3. Photoelectron spectra of aminonaphthalenes.

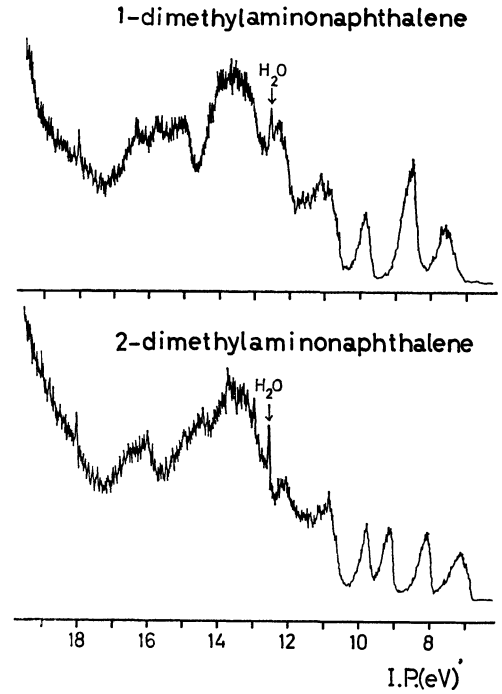

Fig. 4. Photoelectron spectra of dimethylamino-naphthalenes.

of two overlapping bands, judging from its integrated intensity. After all, all of these compounds show four bands in this region. This region includes the first three π bands of naphthalene, the methylamine n band,[13] and the trimethylamine n band.[13] Therefore, these bands are regarded as due to the four π orbitals constructed by the interaction between the highest three occupied π orbitals of naphthalene and the n orbital of the amino or dimethylamino group.

The observed orbital energy diagram estimated according to Koopmans' theorem and the calculated

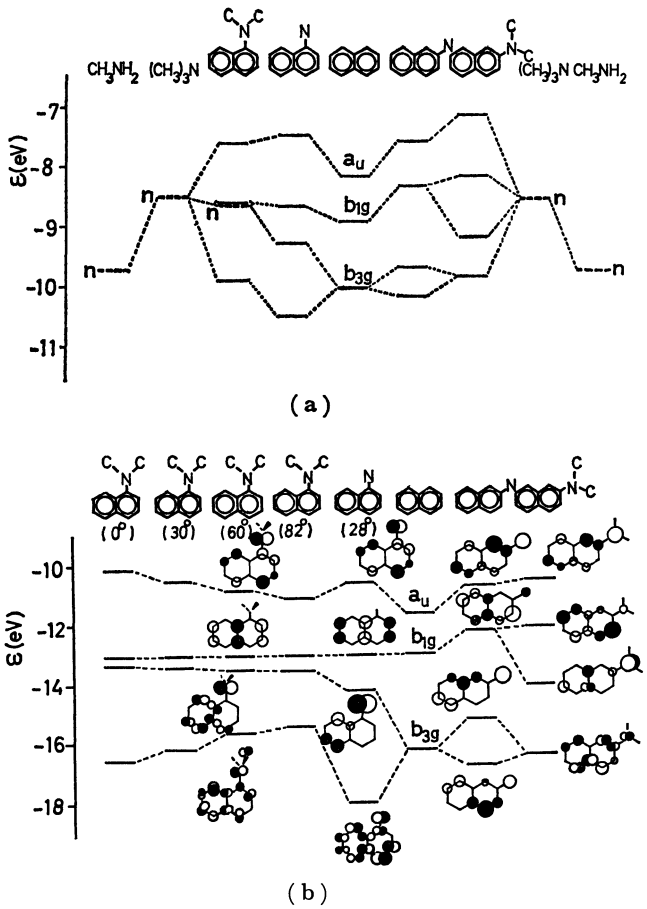

Fig. 5. Orbital energy diagrams for the higher occupied orbitals of aminonaphthalenes and dimethylaminonaphthalenes; (a) experimental, (b) calculated.

orbital energy diagram are shown in Figs. 5(a) and 5(b), respectively. In the calculations, the twist angle of the amino group from the naphthalene ring plane was assumed to be 28° for 1-aminonaphthalene on the basis of the molecular polarizability data.[14] The angle was assumed to be 0° for 2-aminonaphthalene and 2-dimethylaminonaphthalene. As for 1-dimethylaminonaphthalene, the calculations were carried out for the following twist angles of the dimethylamino group: 0°, 30°, 60°, and 82°. The last value, 82°, was estimated from van der Waals' radii.

As is seen in Fig. 5(a), the highest and second highest occupied orbitals of 1-aminonaphthalene and 2-aminonaphthalene are higher in energy than the corresponding first and second ones of naphthalene, respectively, but their fourth orbitals are lower in energy than the third highest π orbital of naphthalene. This indicates that the n orbital of the amino group is located between the second and third highest occupied π orbitals of the naphthalene ring. This is supported by the fact that the methylamine n I_v is 9.7 eV.[13] From the location of the methylamine n orbital, the third bands of 1-aminonaphthalene and 2-aminonaphthalene are due to the ionization from the orbitals which mainly consist of the nitrogen n orbital. This is supported by the fact that the band of 2-aminonaphthalene is more sensitive to *N,N*-dimethylation than the other lower-energy bands and also by the CNDO/2 calculations.

Judging from the fact that the energy of the second highest occupied orbital of 1-aminonaphthalene is scarcely changed by *N,N*-dimethylation, it is concluded that the second highest occupied π orbitals of 1-aminonaphthalene and 1-dimethylaminonaphthalene are almost completely localized on the naphthalene ring. This is supported by the sharpness of these bands and by the CNDO/2 calculations.

The first I_v of 1-aminonaphthalene can be expected to be reduced by *N,N*-dimethylation because of the electronic effect of methyl groups so long as the twist angle of the amino group from the naphthalene plane is not changed by *N,N*-dimethylation. In reality, however, the first I_v of 1-aminonaphthalene is increased by *N,N*-dimethylation. This indicates that the amino group of 1-aminonaphthalene is twisted further by the *N,N*-dimethylation because of the increment in steric hindrance. As is seen in Figs. 5(a) and 5(b), the overall pattern of the observed orbital energy diagram for the higher occupied orbitals of 1-aminonaphthalene, 1-dimethylaminonaphthalene, and naphthalene is qualitatively well reproduced by the result calculated for the 1-dimethylaminonaphthalene model with a twist angle at least of 60°. The total energy calculated by the CNDO/2 method also indicates that the 60° model is more stable than the others. These results suggest that the dimethylamino group of 1-dimethylaminonaphthalene is twisted by about 60°. This is consistent with Maier's result obtained with HMO level model calculations.[6]

According to the CNDO/2 calculations, the third highest occupied orbital of 1-dimethylaminonaphthalene consists mainly of the n orbital of the dimethylamino group. The band due to the ionization from this orbital is expected to appear around 8.5 eV, in view of the fact that the n orbital energy of trimethylamine is 8.5 eV.[13] Therefore, the band corresponds to one of the overlapping bands around 8.59 eV of 1-dimethylaminonaphthalene.

The observed I_v's of 2-aminonaphthalene and 1-dimethylaminonaphthalene agree with those reported by Maier.[6] As for 1-aminonaphthalene, however, our results are rather different from the values reported by him. We repeated the measurements carefully and confirmed our results.

Cyanonaphthalenes. The PES of 1-cyanonaphthalene and 2-cyanonaphthalene are shown in Fig. 6, the I_v's of these compounds being summarized in Table 1. We can see that cyanonaphthalenes show three lower-energy bands in the region from 8 eV to 10.6 eV. The highest three occupied π orbital bands of naphthalene fall in this region, and the first band of acetonitrile appears at 12.21 eV.[15] Therefore, the three lower-energy bands may be ascribed to the highest three occupied π orbitals of naphthalene mixed with the cyano group π orbital. According to Koopmans' theorem, the correlation diagram for these orbitals may be drawn as is shown in Fig. 7(a).

As is seen in Fig. 7(a), the third highest occupied orbital of 2-cyanonaphthalene is lower in energy than the corresponding one of 1-cyanonaphthalene. Since the third highest occupied π orbital of naphthalene has

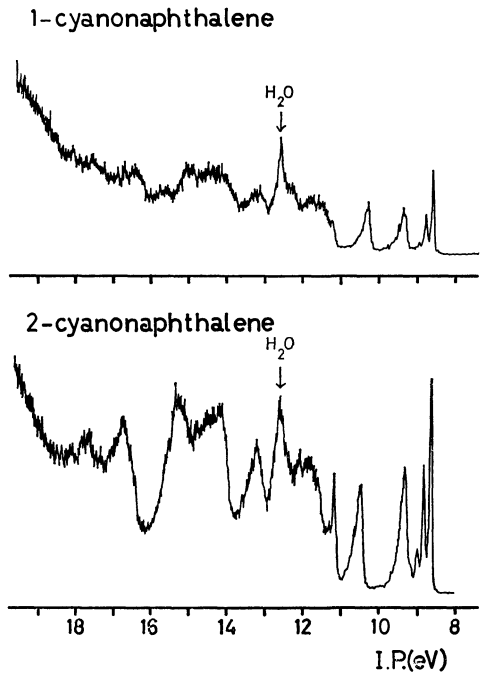

Fig. 6. Photoelectron spectra of cyanonaphthalenes.

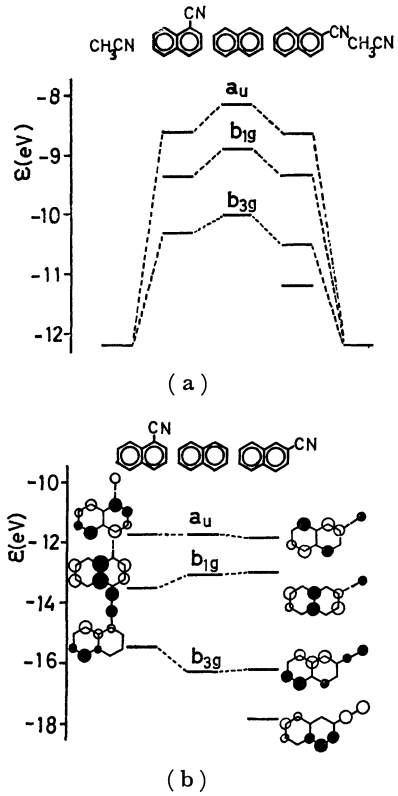

Fig. 7. Orbital energy diagrams for the higher occupied orbitals of cyanonaphthalenes; (a) experimental, (b) calculated.

a larger AO coefficient on carbon atom 1 than on carbon atom 2, this finding can be explained by considering the interaction of the orbital with the occupied π orbital of the cyano group located below. The same tendency was observed for the highest occupied π orbitals of these cyanonaphthalenes. However, the difference between the first I_v's of these compounds is considerably smaller than that between their third I_v's. This may be explained by considering the following two factors. 1) The third highest occupied π orbital of the naphthalene ring interacts more strongly with the occupied π orbital of the cyano group than the highest occupied one does. 2) The energy lowering due to the interaction with the vacant π orbital of the cyano group is more effective in the highest occupied π orbitals of the cyanonaphthalenes than in the third highest occupied ones.

In contrast with the first and third bands, the second band I_v of 2-cyanonaphthalene is smaller, though only slightly, than that of 1-cyanonaphthalene. This is because the second highest occupied π orbital of 1-cyanonaphthalene is almost completely localized on the naphthalene ring, while that of 2-cyanonaphthalene is composed of the naphthalene second highest occupied π orbital mixed with the occupied π orbital of the cyano group, as suggested by the CNDO/2 calculations (Fig. 7(b)).

As is seen in Fig. 7(a), the highest three occupied orbitals of these cyanonaphthalenes are much lower in energy than the corresponding ones of naphthalene. This indicates that the electron-withdrawing effect of the cyano group is very effective.

The fourth sharp band of 2-cyanonaphthalene at 11.18 eV may be ascribed to the fourth highest occupied π orbital constructed by the interaction of the naphthalene ring fourth highest occupied π orbital with the cyano group π orbital.

Acetylnaphthalenes. The PES of 1-acetylnaphthalene and 2-acetylnaphthalene are shown in Fig. 8, and the I_v's of these compounds are summarized in Table 1. Both compounds show three lower-energy bands in the region from 8 eV to 10.2 eV. Their

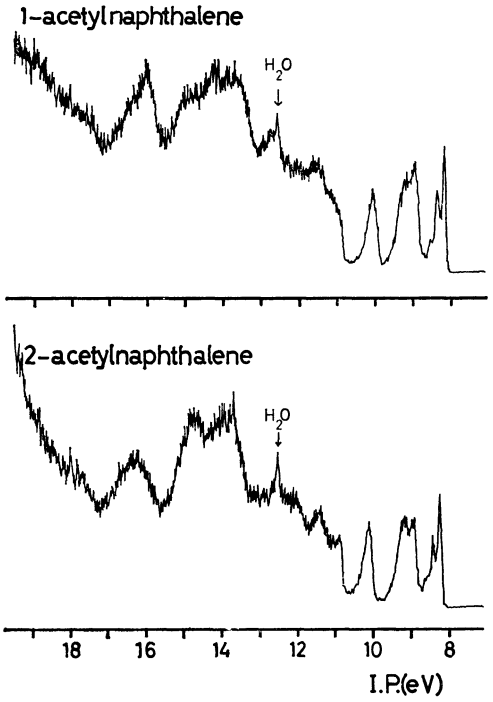

Fig. 8. Photoelectron spectra of acetylnaphthalenes.

second bands seem to consist of two overlapping bands, judging from the integrated intensities. Thus, there are four bands in the region from 8 eV to 10.2 eV for the acetylnaphthalenes. This region is for the first three π bands of naphthalene and the acetyl n orbital band (for example, acetophenone: 9.37 eV[4]). Therefore, the four observed bands may be ascribed to three orbitals caused by the interaction of the highest three occupied π orbitals of the naphthalene ring with the occupied π orbital of the acetyl group and to the acetyl n orbital.

According to the CNDO/2 calculations (Fig. 9(b)), in which the twist angle of the acetyl group was estimated to be 42° for 1-acetylnaphthalene from the polarizability data[16] and was assumed to be 0° for 2-acetylnaphthalene, the occupied orbitals of these compounds are located in the following order, from the top: π, n, π, π, $\cdots$.

First, let us consider the overlapping bands around 9.2 eV of each compound. One of them is assigned to the ionization from the n orbital of the acetyl group in view of the fact that the n orbital I_v of acetophenone is 9.37 eV.[4] According to the CNDO/2 calculations, the second highest occupied π orbital of 1-acetylnaphthalene is the orbital localized mainly on the naphthalene ring; its energy scarcely changes compared with that of naphthalene (−13.04 eV for naphthalene; −13.17 eV for 1-acetylnaphthalene). Therefore, the lower-energy band of the overlapping bands of 1-acetylnaphthalene is assigned to the ionization from this orbital. The second band at 9.00 eV of 2-acetylnaphthalene may also safely be assigned to the second highest occupied π orbital.

The remaining first and fourth bands of acetylnaphthalenes are assigned to the ionization from the orbitals constructed by the interaction mainly between the first and third highest occupied π orbitals of naphthalene and the π orbital of the acetyl group, respectively.

The observed correlation diagram for the orbital energies obtained on the assumption of Koopmans' theorem is shown in Fig. 9(a). The calculated relative ordering of the n and π orbitals of acetylnaphthalenes (Fig. 9(b)) is different from the experimental one (Fig. 9(a)). This discrepancy is often found in the CNDO/2 calculation of closely located n and π orbitals.

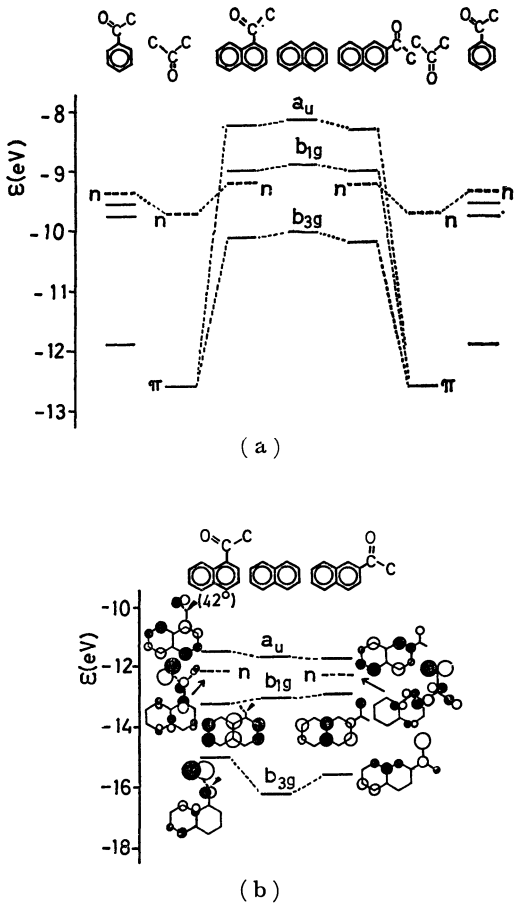

Fig. 9. Orbital energy diagrams for the higher occupied orbitals of acetylnaphthalenes; (a) experimental, (b) calculated.

References

1) T. Kobayashi and S. Nagakura, *Chem. Lett.*, **1972**, 903.
2) T. Kobayashi and S. Nagakura, *ibid.*, **1972**, 1013.
3) T. Kobayashi, K. Yokota, and S. Nagakura, *J. Electron Spectrosc.*, **2**, 449 (1973).
4) T. Kobayashi and S. Nagakura, This Bulletin, **47**, 2563 (1974).
5) H. Bock, G. Wagner, and J. Kroner, *Chem. Ber.*, **105**, 3850 (1972).
6) J. P. Maier, *Helv. Chim. Acta*, **57**, 994 (1974).
7) J. A. Pople and G. A. Segal, *J. Chem. Phys.*, **44**, 3289 (1966).
8) "Interatomic Distances," Sp. Pub. No. 11, ed. by L. E. Sutton, The Chem. Soc., London (1958).
9) "Interatomic Distances," Sp. Pub. No. 18, ed. by L. E. Sutton, The Chem. Soc., London (1965).
10) a) F. Brogli, E. Heilbronner, and T. Kobayashi, *Helv. Chim. Acta*, **55**, 274 (1972). b) J. H. D. Eland and C. J. Danby, *Z. Naturforsch.*, **23a**, 355 (1968).
11) M. B. Robin and N. A. Kuebler, *J. Electron Spectrosc.*, **1**, 13 (1972).
12) T. Koopmans, *Physica*, **1**, 104 (1934).
13) A. B. Cornford, D. C. Frost, F. G. Herring, and C. A. McDowell, *Can. J. Chem.*, **49**, 1135 (1971).
14) R. J. W. Le Fèvre and A. Sundaram, *J. Chem. Soc.*, **1962**, 4756.
15) D. W. Turner, C. Baker, A. D. Baker, and C. R. Brundle, "Molecular Photoelectron Spectroscopy," John Wiley & Sons, London (1970), p. 346.
16) P. H. Gore, J. A. Hoskins, C. K. Thadani, R. J. W. Le Fèvre, L. Radom, and G. L. D. Ritchie, *J. Chem. Soc. (B)*, **1969**, 426.

Dry Grinding on a Pigment Mixture. I. The Effect of α-Copper Phthalocyanine as a Lubricant on the Mechanochemical Transformation of Calcium Carbonate

Norimichi KAWASHIMA and Kenjiro MEGURO

Department of Chemistry, Faculty of Science, Science University of Tokyo, 1-3 Kagurazaka, Shinjuku-ku, Tokyo 162

(Received January 24, 1975)

α-Copper phthalocyanine and calcium carbonate were mixed and ground with a grinder, and then the surface properties of the mixtures were investigated in comparison with the grinding time by means of X-ray diffraction analysis, electron-micrograph observation, and the specific surface area as obtained by the B.E.T. method. In the grinding process, the crystal decays of both α-copper phthalocyanine and calcium carbonate were observed. Particularly, the calcite-aragonite transformation occurred in the case of calcium carbonate. However, the addition of some α-copper phthalocyanine to calcium carbonate interfered with the transformation of calcium carbonate. As a conclusion, it was evident that the surface of calcium carbonate was covered with α-copper phthalocyanine and that the grinding of calcium carbonate was interfered with by the lubricating action of α-copper phthalocyanine.

In some cases, not only are changes in the particle shape and size found in mechanical treatments such as crushing, grinding, and rolling, but also the physical and chemical properties of the particles become different from the original intrinsic properties.[1-5]

Many reports have been published on the mechanochemical changes in inorganic single material[6-8] and in inorganic–inorganic material mixed systems.[9-11] In the field of the paint industry, mixed-type pigments are used to obtain various color pigments. However, few studies have dealt with the grinding of mixtures of an organic pigment and an inorganic one.

In a previous work, we ourselves examined the mechanochemical change in the surface properties of α-copper phthalocyanine–titania, γ-quinacridone–titania mixed systems[12] and α-copper phthalocyanine–alumina mixed systems.[13] In this paper, the grinding process of a mixture of an organic pigment and an inorganic one was investigated by means of X-ray diffraction analysis, the observation of electron micrographs, and also surface-area measurements.

Experimental

The α-copper phthalocyanine (abbrev. α-CuPc) used here was supplied by Dainippon Ink Chemical, Ltd. The calcium carbonate was supplied by the Kokusan Kagaku Co., Ltd. The specific surface areas of α-CuPc and calcium carbonate, as measured by the B.E.T. method, were about 50 m^2/g and 2 m^2/g respectively. These pigments were ground with an Ishikawa-type grinder in a closed chamber at room temperature at the following mixed ratios of weight: α-CuPc *vs.* $CaCO_3$: (1 : 1), (1 : 9) and (1 : 19); these mixtures were abbreviated as follows;

Sample A: a (1 : 1) mixture of α-CuPc and $CaCO_3$
Sample B: a (1 : 9) mixture of α-Cupc and $CaCO_3$
Sample C: a (1 : 19) mixture of α-CuPc and $CaCO_3$

The grinding was done after; 2, 4, 6, 8, and 10 hr.

The X-ray diffractions were measured by using a nickel-filtered copper radiation at 35 kV and 10 mA as the X-ray diffraction source, with a scanning speed of 1/2° per min., a time constant of 2 s, a divergence slit of 1°, and a receiving slit of 0.2 mm. The X-ray diffraction diagrams were recorded by means of an X-ray diffractometer (Geigerflex).

The electron micrographs were taken by means of a Hitachi HU-200-type electron microscope.

The specific surface areas were measured by the B.E.T. method from the nitrogen-gas adsorption at the temperature of liquid nitrogen. The specimens were pretreated under a pressure of 10^{-5} Torr at room temperature for about one hour.

Results and Discussion

The Results for Calcium Carbonate and α-CuPc Alone. Calcium carbonate is well known to have two crystal forms, such as a stable type (calcite) and a metastable type (aragonite) as morphisms at an ordinary temperature and pressure.[14] The X-ray diffraction traces in the grinding process of calcium carbonate are given in Fig. 1. The intensities of all the reflections in the X-ray diffraction diagrams decrease and become weaker during the grinding process. The prominent peak of calcite corresponding to the (104) crystal face decreases more than those of the others. The aragonite peaks are detected for the first time in the specimen ground for 6 hr. After 10 hr grinding, aragonite become the main component of the mixture.

The X-ray diffraction traces of α-CuPc at various stages of the mechanical treatment are given in Fig. 2.

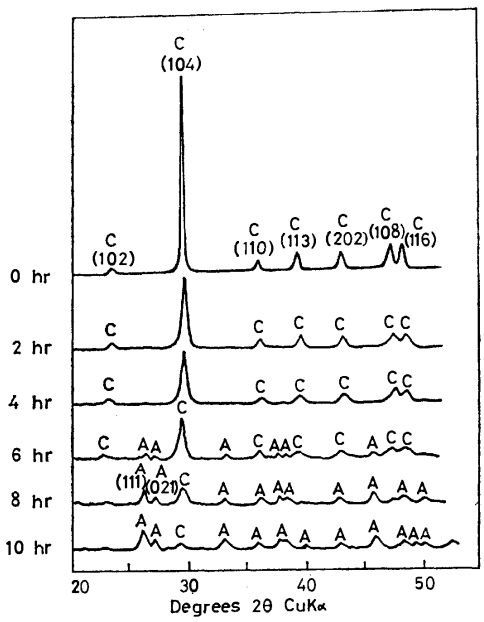

Fig. 1. X-ray diffraction patterns of $CaCO_3$ at different grinding times.

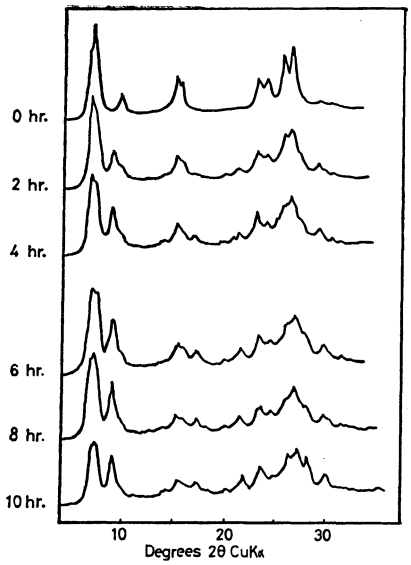

Fig. 2. X-ray diffraction patterns of α-CuPc at different grinding times.

The reflections characteristic of α-CuPc at the (200) and (002) crystal faces near 5°—8° in 2θ and four succesive medium reflections are observed to become broad with the grinding; they become hard to resolve in the specimen ground for 10 hr, much unlike the original situation. The reflection characteristic of β-CuPc corresponding to the $(20\bar{1})$ crystal face is observed in the specimen ground for 2 hr. In general, β-CuPc is known to be transformed to α-CuPc when comminution media are used.[15] However, α-CuPc may be considered to be transformed partially to the β-CuPc by absorbing the grinding energy.

The electron micrographs of the nongrinding specimens and the specimens ground for 10 hr of both calcium carbonate and α-CuPc alone are shown in Fig. 3. The micrograph of the calcium carbonate ground for 10 hr shows it to be finely divided particles. On the other hand, the particles of α-CuPc, compared with the case of calcium carbonate alone, aggregate considerably in the specimen ground for 10 hr. These facts are also confirmed by the specific-surface-area measurements.

The specific surface areas of both calcium carbonate and α-CuPc alone are plotted against the time of grinding in Fig. 4. It can be seen from this figure that the specific surface area of calcium carbonate gradually increases with the treatment, while that of α-CuPc decreases. Two factors may be considered to be the causes of the change in the specific surface area which take place in the process of grinding. One is associated with changes in the crystallite or particle size, the shapes of the particles, an dthe growth of cracks—that is, with primary structural changes. The other factor is related to the formation of secondary particles, which grow as a result of the aggregation or agglomeration of primary particles.[16] In the case of calcium carbonate alone, as has been described above, the particles are divided finely and no formation of secondary particles is observable. On the other hand, the specific surface area of α-CuPc may be considered to decrease with the grinding because of the aggregation.

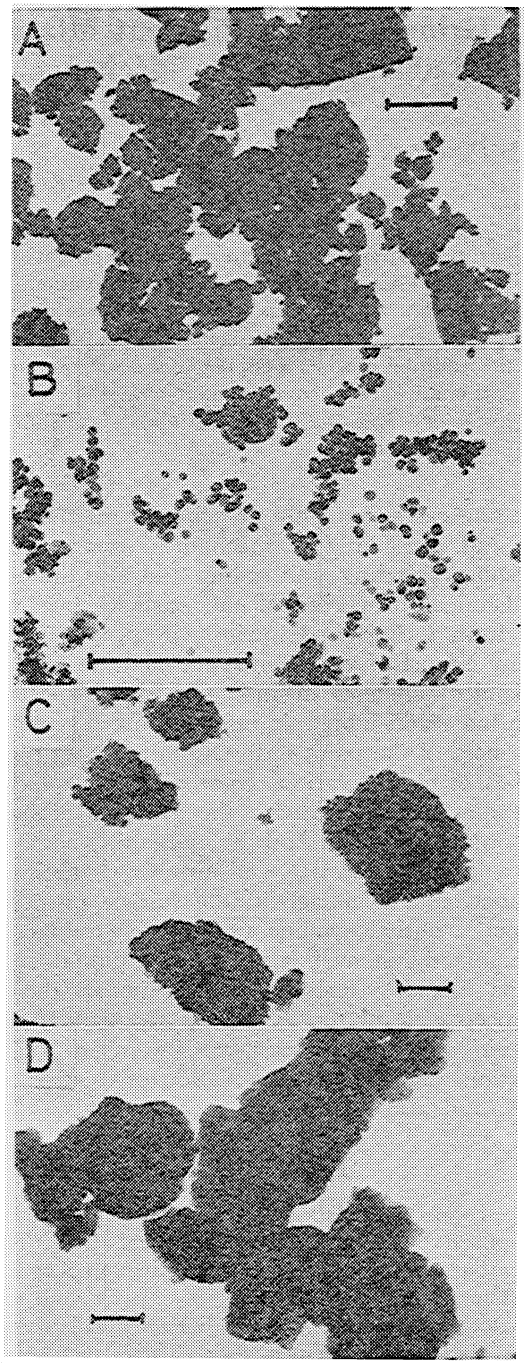

Fig. 3. Electron micrographs of $CaCO_3$ and α-CuPc. The linear dimension on the micrograph represents 1 μ.
A: original $CaCO_3$, B: $CaCO_3$ ground for 10 hr, C: original α-CuPc, D: α-CuPc ground for 10 hr.

The Results for Mixtures of Calcium Carbonate and α-CuPc. As with α-CuPc and calcium carbonate alone, the change in the surface properties of mixtures of several weight ratios of α-CuPc and calcium carbonate during the grinding process are estimated by a method similar to that used above.

The X-ray diffraction patterns of the mixtures (Samples A, B, and C) in the grinding process are given in Fig. 5. The reflections characteristic of α-CuPc in Sample A corresponding to the (200) and (002) crystal

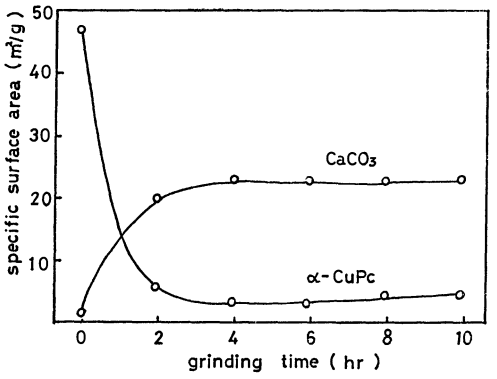

Fig. 4. The change of specific surface areas of α-CuPc and $CaCO_3$ with the time of grinding.

faces become broad, and the medium reflections at higher range become hard to resolve as the grinding proceeds. On the other hand, the (104) reflection of calcium carbonate in the mixtures does not decrease during the treatment more than in the case of calcium carbonate alone.

The calcite-aragonite transition is not observed in the specimen ground for 10 hr in Samples A and B; it is detected only in Sample C. The fact that the calcite-aragonite transition does not occur when the calcium carbonate is mixed with α-CuPc suggests that the calcium carbonate may be considered to be covered with α-CuPc; that is, the grinding of calcium carbonate may be interfered with by the lubricating action of α-CuPc. The strength of the lubricating action is also observed to increase with the amount of α-CuPc in the mixture system.

The electron micrographs of the specimens ground for 10 hr are shown in Fig. 6. In the case of Sample A, the particles of the mixture aggregate with each other, and the growth of secondary particles take place in the specimen ground for 10 hr, as in the case of α-CuPc alone. As is to be expected from Fig. 5-a, the calcium carbonate is also observed to be covered with α-CuPc and the grinding of calcium carbonate may be interfered with by the lubricating action of α-CuPc. In the case of Sample B, however, the ground particles of α-CuPc adhere around calcium carbonate particles. As is to be expected from the X-ray diffraction traces, the calcium carbonate in Sample C is ground considerably more than that of the other mixture systems. The electron micrograph of this specimen ground for 10 hr is similar to that of calcium carbonate alone in Fig. 3.

The calcium carbonate in the mixture is hardly ground more than calcium carbonate alone by the lubricating action of α-CuPc, judging from the results of the X-ray diffraction analysis and the observation of the electron micrographs. Consequently, though the specific surface area of calcium carbonate alone increases with grinding, the lubricating action of α-CuPc is expected to prevent an increase in the specific surface area of a mixture. Therefore, it is possible to determine the extent that the lubricating action of α-CuPc prevents the grinding of calcium carbonate by comparing the experimental curve with the theoretical one obtained by evaluating the specific surface areas of both α-CuPc and calcium carbonate alone, as based on the assumption of additivity.

The specific surface areas of mixtures are plotted against the time of grinding in Figs. 7, 8, and 9. It is interesting that the specific surface areas of Sample C gradually increase with the treatment, as with that of calcium carbonate alone, and those of Sample B decrease in the early stage of grinding and afterward gradually increase, while those of Sample A decrease, as with that of α-CuPc alone.

The experimental curves are observed to become lower than the theoretical one. This fact can be explained as follows. As has been described above, if the lubricating action of α-CuPc prevents the grinding of calcium carbonate, the specific surface area of calcium carbonate will not increase as the grinding continuos; that is, as the particle surfaces of calcium carbonate are covered with α-CuPc particles, aggregation is considered to occur. These facts agree with the results of the X-ray diffraction analysis and the elcctron-micrograph study.

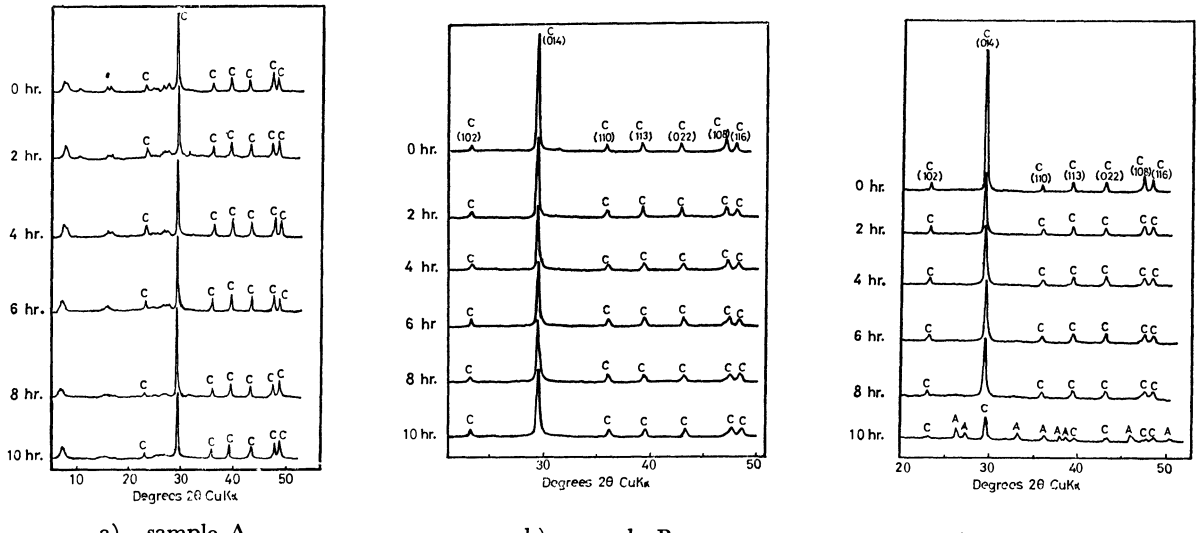

a) sample A b) sample B c) sample C

Fig. 5. X-Ray diffraction patterns of mixtures at different grinding times.

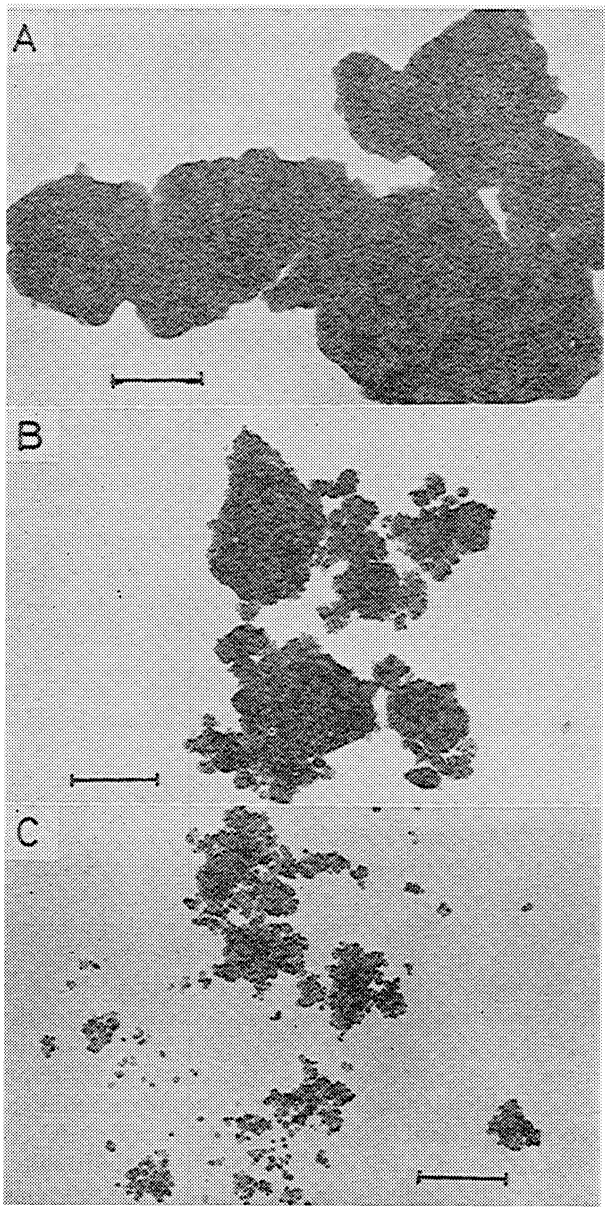

Fig. 6. Electron micrographs of ground mixtures.
The linear dimension on the micrograph represents 1 μ.
A: sample A ground for 10 hr, B: sample B ground for 10 hr, C: sample C ground for 10 hr.

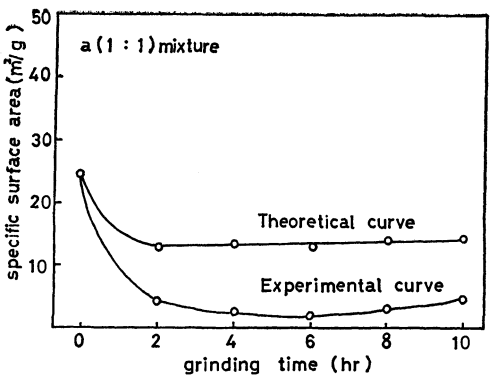

Fig. 7. The change of specific surface areas of sample A with the time of grinding.

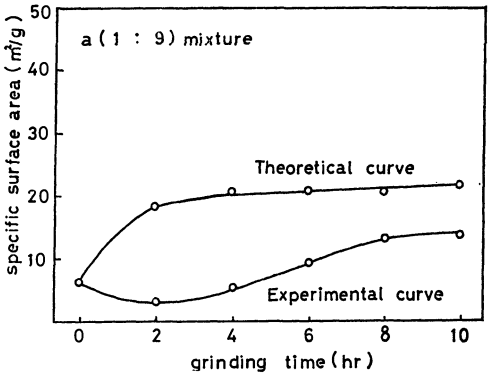

Fig. 8. The change of specific surface areas of sample B with the time of grinding.

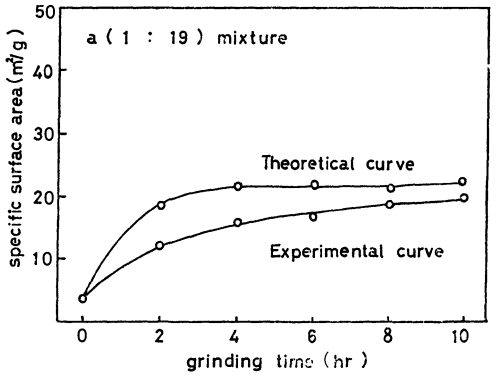

Fig. 9. The change of specific surface areas of sample C with the time of grinding.

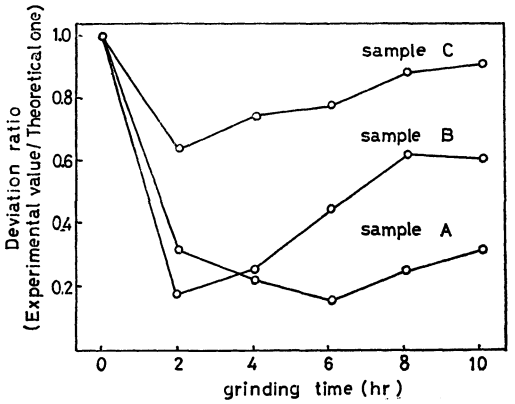

Fig. 10. The change in deviation ratio (Experimental value/Theoretical one) of pigment mixtures with the time of grinding.

The change in the deviation ratios (experimental value/theoretical one) for the mixtures with the time of grinding are shown in Fig. 10. The point at which the deviation ratio equals 1.0 coincides with the value at which the experimental value equals the theoretical one. That is, the lubricating action of α-CuPc is observed in the region in which the deviation ratio becomes lower than 1.0. The lubricating action of α-CuPc is observed in every mixture system, the order of the strength is as follows; Sample A > Sample B > Sample C.

The main conclusions obtained from these results are

as follows: when α-CuPc is mixed with calcium carbonate, the surface of the calcium carbonate is covered with that of α-CuPc, and the grinding of calcium carbonate is interfered with by the lubricating action of α-CuPc.

References

1) S. R. Rao, *Ind. J. Phys.*, **6**, 24 (1937).
2) S. S. Bhatnager, *Kollid-Z.*, **78**, 9 (1937).
3) H. Prasad and S. S. Dharmatti, *Ind. J. Phys.*, **11**, 393 (1938).
4) J. W. Axelson and E. L. Piret, *Ind. Eng. Chem.*, **42**, 665 (1950).
5) P. D. Dempster and P. D. Ritchie, *Nature*, **169**, 538 (1952).
6) H. Takahashi, This Bulletin, **32**, 374 (1958).
7) H. Takahashi, *ibid.*, 32, 381 (1958).
8) T. Kubo, S. Kato, M. Mitarai, and K. Uchida, *Kogyo Kagaku Zasshi*, **66**, 403 (1963).
9) R. Rasch, *Ber. Dtsch. Keram. Ges.*, **40**, 635 (1967).
10) G. Hashizume and A. Amita, *Kogyo Kagaku Zasshi*, **71**, 1379 (1968).
11) Y. Arai, T. Yasue, H. Takiguchi, and T. Kubo, *Nippon Kagaku Kaishi*, **1974**, 1611.
12) K. Meguro and I. Koga, *Farbe Lack*, **79**, 503 (1973).
13) N. Kawashima and K. Meguro, *Shikizai Kyokaishi*, **46**, 670 (1973).
14) J. H. Burns and M. A. Bredig, *J. Chem. Phys.*, **25**, 1281 (1956).
15) Y. Bansho, S. Suzuki, I. Saito, and T. Sekiguchi, *Kogyo Kagaku Zasshi*, **67**, 168 (1964).
16) H. Takahashi and K. Tsutsumi, This Bulletin, **40**, 7 (1967).

The Reaction of *N*-Substituted Carbonimidic Dihalides with Grignard Reagents. The Generation of Alkyl or Aryl Halides from Grignard Reagents

Sakuya TANAKA, Masaya OKANO*, and Shigeo TANIMOTO
Institute for Chemical Research, Kyoto University, Uji, Kyoto 611
(Received July 1, 1974)

The reaction of *N*-alkyl- or *N*-aryl-carbonimidic dihalides with Grignard reagents afforded α-elimination products, isocyanides, rather than substitution ones. Two kinds of alkyl or aryl halides were produced concomitantly in this reaction: one kind consisted of halides generated from the Grignard reagents used, and the other, of halides the halogens of which had been derived from the dihalides. The ease of formation of these halides was found to decrease in the order: iodide> bromide> chloride, regardless of which substrate served as the source of a halogen atom. A probable reaction mechanism is proposed.

The Grignard reactions of various carbonate derivatives (*e.g.*, phosgene,[1] chloroformates, and carbonates), as well as acyl chlorides and esters, which involve the replacement of one or two chlorine or alkoxy groups by alkyl or aryl groups of Grignard reagents have been well-established.[2] A very similar replacement has been reported for iminocarbonates,[3a] imidoyl chlorides,[3b] and imidates;[3a] and we have also observed that a chloroformimidate behaved similarly.[4] In contrast to these results, we found that *N*-alkyl- or *N*-aryl-carbonimidic dihalides reacted with Grignard reagents to afford α-elimination products, isocyanides, and that two kinds of alkyl or aryl halides were formed concomitantly. One of the latter products consisted of halides generated from the Grignard reagents used. A closely related observation has been reported for (dichloroiodo)-benzene by Melnikov.[6] This compound reacted with phenylmagnesium bromide to afford diphenyliodonium chloride (a substitution product), iodobenzene, chlorobenzene, bromobenzene (products corresponding to the present elimination), and biphenyl. The formations of all these products, except for that of bromobenzene, may be explained by either an ionic or radical mechanism; the pathway to afford bromobenzene has not yet been explored. The present paper will describe our results regarding the Grignard reaction of carbonimidic dihalides, which involves a novel generation of alkyl or aryl halides from the Grignard reagents.

Results and Discussion

When *N*-alkyl- or *N*-aryl-carbonimidic dihalides were treated in ether with Grignard reagents with a different halogen atom, the reaction occurred exothermally to afford isocyanides (**1**), two kinds of alkyl or aryl halides (**2** and **3**), magnesium halides, and a tarry product. Since the reaction of **1** with Grignard reagents is known, we adopted an inverse addition procedure (*i.e.*, the addition of a Grignard reagent to the dihalide) for the present reaction. Some typical data are shown in Table 1. Though the recorded yields of **1**, **2**, and **3** were not always those obtained under the optimum conditions for each reaction, their yields appeared to depend on the structures of both substrates.

$$\underset{}{R\text{-}N{=}CX_2} + R'MgX' \rightarrow \underset{\mathbf{1}}{R\text{-}N{\equiv}C} + \underset{\mathbf{2}}{R'X'} + \underset{\mathbf{3}}{R'X}$$

No liberation of isocyanides from *N*-substituted carbonimidic dihalides was observed, at least under the reaction conditions without Grignard reagents; therefore, it is obvious that the elimination reaction is promoted by the use of Grignard reagents. The halides **2** are produced only by the present reaction, since the absence of the remaining halides in the Grignard reagents was confirmed in each case before their use.

The preference for elimination over substitution in the present reaction appears to arise from the structual characteristics of *N*-substituted carbonimidic dihalides. It is well-known that the Grignard reactions of carboxylic acid derivatives, such as acid chlorides and esters, proceed by means of an addition-elimination mechanism, in which the initial coordination of the carbonyl O with the Mg atom of the Grignard reagent is involved. Thus, in the present reaction, the failure of the substitution of X in the dihalides may be attributed to a considerable decrease in the electron density on the imino N, which is caused by the presence of two electron-withdrawing groups (X) on the carbonimidoyl C. Further, it may be considered that the formation of stabilized products, isocyanides, may favor the elimination process.

It is worthwhile to present some information regarding the formation of **2** from Grignard reagents, because only one such transformation has been known.[6] The reactions of *N*-alkyl- or *N*-aryl-carbonimidic dichlorides with aryl magnesium bromides or iodides gave only **2**, while reactions with alkylmagnesium bromides or iodides yielded both **2** and **3**, the former being predominant. When *N*-phenylcarbonimidic dibromide was used as the substrate,[7] both halides were generally formed; **2** predominated over **3** when the halogen atom in the Grignard reagents was iodine, and the reverse was true when the halogen was chlorine. Further, the yields of **1** were roughly equal to the combined yields of **2** and **3** in general, except for some cases in which alkyl- or aryl-magnesium iodides were used.[8] To explain all these results, we tentatively proposed a mechanism involving the formation of a coordinated complex, **4**, followed by its synchronous decomposition to give **1** and either **2** or **3**.

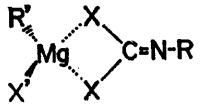

4

The effect of R in carbonimidic dichlorides on the

Table 1. Results of the reaction of carbonimidic dihalides with organometallic reagents
(Solvent; Ether, 50 ml)

R-N=CX$_2$ 0.05 mol	R'MgX' 0.05 mol	Temp. °C	Time hr	Reaction products, Yield (%)[a]			
				R-NC **1**	R'X' **2**	R'X **3**	Unreacted dihalide
c-$C_6H_{11}N$=CCl_2	C_6H_5MgBr	35	0.5	40	46	0	16
c-$C_6H_{11}N$=CCl_2	*p*-$CH_3C_6H_4MgBr$	35	0.5	37	40	0	17
c-$C_6H_{11}N$=CCl_2	C_6H_5MgI	35	0.5	24	66	0	trace
c-$C_6H_{11}N$=CCl_2	C_2H_5MgBr	25	3	31	—[b]	—[b]	6
c-$C_6H_{11}N$=CCl_2	*n*-$C_6H_{13}MgBr$	25	3	66	46	7	trace
c-$C_6H_{11}N$=CCl_2	*n*-$C_6H_{13}MgI$	25	0.5	22	34	1	43
n-C_4H_9N=CCl_2	C_6H_5MgBr	35	0.5	6	18	0	34
C_6H_5N=CCl_2	C_6H_5MgBr	35	0.5	trace	12	0	37
C_6H_5N=CBr_2[c]	C_6H_5MgI[c]	0	0.5	59	27	9	—[b]
C_6H_5N=CBr_2[c]	C_6H_5MgCl[c,d]	15	0.5	34	3	51	—[b]
C_6H_5N=CBr_2[c]	*n*-$C_6H_{13}MgCl$[c]	0	0.5	79	7	50	—[b]
C_6H_5N=CBr_2[c]	*n*-$C_6H_{13}MgI$[c]	0	0.5	32	37	26	—[b]
c-$C_6H_{11}N$=CCl_2	C_6H_5ZnBr	35	0.5	24	30	0	10
c-$C_6H_{11}N$=CCl_2	C_6H_5HgBr[e]	80	6	0	0	0	100
c-$C_6H_{11}N$=CCl_2	C_6H_5Li	0	0.5	40	0	35	30

a) Based on carbonimidic dihalide charged (determined by glc). b) Not determined. c) Both substrates, 0.02 mol each; solvent, 30 ml. d) THF was used as solvent. e) Benzene (10 ml) was used as solvent.

yields of the reaction products shows that their reactivity toward a fixed Grignard reagent decreases in this order: cyclohexyl>*n*-butyl>phenyl. We also observed a similar substituent effect on the reaction of the dichlorides with SCN^- in ethanol,[9] suggesting an S_N1 character for the fission of the C–Cl bond. Thus, it may be anticipated that the decomposition of **4** will be started by the loosening of the C–$X_{(1)}$ bond and that this will result in bond formation between $X_{(1)}$ and Mg atoms. If the induced nucleophilic attack of the R' group on $X_{(2)}$ or X' and the subsequent electron-transfer from the C–$X_{(2)}$ bond to the C atom (when the attack of R' occurred on X', an additional electron-transfer from Mg–X' to Mg–$X_{(2)}$ should be involved) take place before the complete fission of the C–$X_{(1)}$ bond, the transition state affording **1** and **3**, and that affording **1** and **2**, can be pictured as **5** and **6** respectively. Here the assumption that a geometrically and electronically approximate equivalence can be attained in the transition states appears not unreasonable. The reason will be given below. If this is true, the relative ease of the halide formation can be expected to decrease in this order: iodide>bromide>chloride, whichever participates X or X', because the susceptibilities of X and X' toward R' are considered to correlate with their electronegativities. The selectivity data in the halide formation from the reactions with *N*-phenylcarbonimidic dibromide were in qualitative agreement with this expectation. In the reaction with *N*-cyclohexylcarbonimidic dichloride, aromatic Grignard reagents showed a higher selectivity for the halide formation (*i.e.*, only **2** is formed), than that from aliphatic Grignard reagents. This may be because aryl carbanions are generally less reactive than alkyl ones.

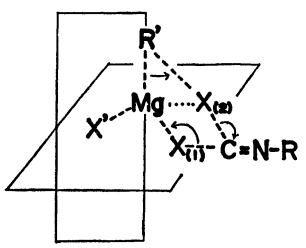

5

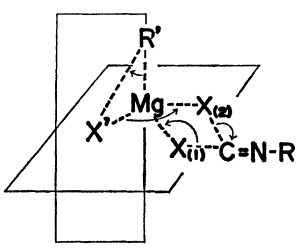

6

An extension of this reaction to other organometallic reagents was also attempted. When phenylzinc bromide was treated with *N*-cyclohexylcarbonimidic dichloride, a similar reaction occurred, though the yields of the products were unsatisfactory as expected. The reaction with much less reactive phenylmercuric bromide, however, did not afford any products; rather, most of the starting materials were recovered. Phenyllithium reacted with the dichloride to give the corresponding isocyanide and chlorobenzene.

Experimental

Materials. All the carbonimidic dihalides were prepared by the method of Kühle *et al.*[10] R=*cyclo*-C_6H_{11} in RN=CCl_2, bp 88—91 °C/23 mmHg (lit,[10] 79—82 °C/13 mmHg); R=*n*-C_4H_9, bp 40—42 °C/11 mmHg (lit,[10] 45—45.5 °C/14 mmHg); R=C_6H_5, bp 79—80 °C/8 mmHg (lit,[10] 83—85 °C/11 mmHg); R=C_6H_5 in RN=CBr_2, bp 104 °C/10 mmHg (lit,[10] 76.5—77.5 °C/0.15 mmHg). In the preparation of Grignard reagents, the complete conversion of the halides was confirmed by glc analyses. Phenylzinc bromide was prepared *in situ* by the exchange reaction[11] of phenylmagnesium bromide with zink chloride in ether. Phenylmercuric bromide was prepared from tetraphenyltin and mercuric bromide as has been described by Seyferth *et al.*[12] (mp 274—280 °C, lit,[12] 280 °C).

Reaction of Carbonimidic Dihalides with Grignard Reagents. Several examples are given below.

a) Reaction of Cyclohexylcarbonimidic Dichloride with Phenylmagnesium Bromide. An ethereal solution of the Grignard

reagent, prepared from 7.9 g (0.05 mol) of bromobenzene and 1.2 g (0.05 mol) of magnesium turnings in 50 ml of ether in the usual way[13] except that the solution was refluxed for an additional 30 min after the addition of all the bromobenzene, was gradually added to 9.0 g (0.05 mol) of cyclohexylcarbonimidic dichloride, the temperature being kept below 10 °C. After the mixture had then been allowed to stand at room temperature, the reaction started spontaneously and a white precipitate began to come out; then the mixture was refluxed for 30 min. The brown reaction mixture, with a characteristic odor of isocyanide, was poured into ice-water; the ethereal layer was separated, and then it was combined with a chloroform extract of the aqueous phase. The organic layer was dried, and the solvents were removed. The subsequent distillation of the residue gave 7.9 g of the distillate (bp 40—78 °C/23 mmHg), which was revealed to contain bromobenzene (46% yield), cyclohexyl isocyanide (40%), and the recovered dichloride (16%), leaving 2.1 g of a tarry product. No chlorobenzene was formed in this reaction.

b) Reaction of Cyclohexylcarbonimidic Dichloride with n-Hexylmagnesium Bromide. The Grignard reagent prepared from 8.3 g (0.05 mol) of *n*-hexyl bromide and 1.2 g (0.05 mol) of Mg in 50 ml ether was added to 9.0 g (0.05 mol) of the dichloride, after which the mixture was treated as has been described above. Distillation afforded 7.9 g of the distillate (bp 57—82 °C/55 mmHg) and left a tarry residue (2.7 g). The yields of the products were as follows: *n*-hexyl chloride, 7%; *n*-hexyl bromide, 46%; cyclohexyl isocyanide, 66%; and a trace amount of recovered dichloride.

c) Reaction of Phenylcarbonimidic Dibromide with Phenylmagnesium Iodide. A solution of the Grignard reagent obtained from 4.1 g (0.02 mol) of iodobenzene and 0.5 g (0.02 mol) of Mg in 20 ml of ether was slowly added to 5.3 g (0.02 mol) of the dibromide in 10 ml of ether at 0 °C. During the addition, the reaction occurred spontaneously and the temperature of the reaction mixture rose to *ca.* 30 °C, even under external cooling with an ice-salt mixture. After the reaction had subsided, the brown reaction mixture was refluxed for 15 min and then worked-up as has been described above. Distillation gave 2.6 g of the distillate (bp 40—74 °C/23.5 mmHg), leaving a tarry residue (1.5 g). The yields of the products were as follows: bromobenzene, 9%; iodobenzene, 27%; and phenyl isocyanide, 59%. Neither benzophenone anil nor benzanilide (the expected substitution products) could be detected in the tarry residue.

Reaction of Cyclohexylcarbonimidic Dichloride with Phenyllithium. An ethereal solution of phenyllithium, prepared from 7.9 g (0.05 mol) of bromobenzene and 0.8 g (0.12 mol) of lithium, was treated with 9.0 g (0.05 mol) of the dichloride at 0 °C. Glc analysis showed that the reaction products were chlorobenzene (35% yield) and cyclohexyl isocyanide (40%).

Authentic Samples for Glc. All the isocyanides were prepared from the corresponding formamides by the method of Ugi *et al.*[14]

Glc Analysis. The analysis was carried out on a Shimadzu GC-5A apparatus, using Apiezon L (25%)-Shimalite (3 m) and PEG 6000 (25%)-Chromosorb W (3 m) columns (carrier gas, N_2).

References

1) V. Grignard, *C. R. Acad. Sci., Paris*, **136**, 816 (1903).
2) For example, J. March, "Advanced Organic Chemistry," McGraw-Hill, New York (1968), p. 362.
3) a) J. Pornet and M. L. Miginiac, *C. R. Acad. Sci. Paris, Ser. C*, **273**, 1763 (1971); *Tetrahedron Lett.*, **1971**, 967. b) M. Busch and M. Fleishmann, *Ber.*, **43**, 2553 (1910); M. Busch and F. Falco, *ibid.*, **43**, 2557 (1910).
4) In the reaction of ethyl *N*-phenylchloroformimidate (prepared by the method of Kühle[5]) with phenylmagnesium bromide (in ether at 35 °C for 0.5 hr), ethyl *N*-phenylbenzimidate was obtained as the main product (over a 50% yield). Lesser amounts of benzanilide and *N*-(diphenylmethylene)aniline were also formed, neither phenyl isocyanide nor bromobenzene were found in the products (unpublished data).
5) E. Kühle, *Angew. Chem. Int. Ed. Engl.*, **8**, 20 (1969).
6) N. N. Melnikov, *J. Gen. Chem.* (*USSR*), **5**, 28 (1935); *Chem. Abstr.*, **29**, 4745 (1935).
7) The aromatic dibromides are generally isolable, while the less stable aliphatic ones are not. Therefore, the reaction with the aliphatic dibromides could not be undertaken.
8) In view of the comparatively high reactivity of these Grignard reagents, their consumption as a result of the reaction with alkyl or aryl halides may be considered.
9) The consumption of SCN^- at 20 °C was found to be as follows. For R=cyclohexyl, 58% after 5 min, and for R=phenyl, 44% after 45 min (unpublished data).
10) E. Kühle, B. Anders, and G. Zumach, *Angew. Chem.*, **79**, 663 (1967).
11) For general procedure, see "Jikken Kagaku Koza," ed. by M. Kotake and others, Vol. 20, Part II, Maruzen, Tokyo (1956), p. 93.
12) D. Seyferth and J. M. Burlich, *J. Organometal. Chem.*, **4**, 127 (1965).
13) C. F. H. Allen and S. Converse, "Organic Syntheses," Coll. Vol. 1, p. 226 (1941).
14) I. Ugi, O. Feezer, U. Eholzev, H. Knupfer, and K. Offermann, *Angew. Chem. Int. Ed. Engl.*, **4**, 472 (1965).

The Birch Reduction of Heterocyclic Carboxylic Acids. I. The Birch Reduction of 3-Furoic Acid

Takamasa KINOSHITA, Kouichi MIYANO, and Toshio MIWA
Faculty of Science, Osaka City University, Sumiyoshiku, Osaka 558

(Received July 26, 1974; in revised form, March 4, 1975)

The reduction of 3-furoic acid with sodium and 2-propanol in liquid ammonia gave 2,3-dihydro-3-furoic acid, which was isolated as a methyl ester (**1**) in 85% yield. The acid-catalyzed addition of methanol, ethanol, or 2-propanol to the ester **1** yielded 5-alkoxytetrahydro-3-furoate ester, **2**, **3**, or **4**, respectively, in a quantitative yield. When methanol or ethanol was used as a proton source in the reduction, work-up of the reaction mixture gave 5-alkoxytetrahydro-3-furoic acid, which was isolated as the methyl ester, **2** or **3**, in 87 or 92% yield, respectively. A mechanism for the Birch reduction of aromatic carboxylic acids is proposed.

The Birch reduction of the aromatic molecules has been extensively studied and widely applied to synthetic reactions.[1] Nevertheless, only few papers concerned with the Birch reduction of furan derivatives. Furan and its alkyl derivatives resist the Birch reduction.[2] Recently, Bedenbaugh *et al.* reduced simple furans with lithium in methylamine.[3] 2-Furoic acid has been reduced under the condition of the Birch reduction,[4] as expected from a facile reduction of benzoic acid.[5] The Birch reduction of 3-furoic acid into 2,3-dihydro-3-furoic acid and its application to a one-step synthesis of 5-alkoxytetrahydro-3-furoic acids will be described in this paper. The Birch reduction of 3-furoic acid provides a useful entry into the total synthesis of the branched-chain sugars.[6]

Results and Discussions

The Birch Reduction of 3-Furoic Acid. The reduction of 3-furoic acid with sodium and 2-propanol in liquid ammonia gave an acid, which, after esterification with diazomethane, was isolated as a methyl ester in 85% yield. The molecular formula, $C_6H_8O_3$, was determined by the elemental analysis and mass spectrometry ($M^+=128$). The IR spectrum of the ester showed the presence of a saturated ester function (1735 cm^{-1}) and an enol ether (3120 and 1620 cm^{-1}),[7] suggesting the product to be methyl 2,3-dihydro-3-furoate (**1**). The NMR spectrum of this compound shows a pattern characteristic of 3-substituted 2,3-dihydrofurans[8] as indicated in the experimental part.

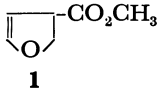

1

Syntheses of Methyl 5-Alkoxytetrahydro-3-furoates. Treatment of the ester **1** in methanol with acid catalyst gave methyl tetrahydro-5-methoxy-3-furoate (**2**) in a quantitative yield. The fact that the acid-catalyzed addition of alcohols to the α,β-unsaturated ether is a well-established reaction[9] may suffice to assign the structure **2** to the ether. Disappearance of the C=C stretching band due to enol ether function of **1** in its IR spectrum supports the structure.

Although the methyl peaks of **2** show sharp singlets in the NMR spectrum, the signal for H-5 is rather complex, inferring that the product is a mixture of stereoisomers. Actually, the gas chromatography of **2** gave two peaks in a ratio of 2 : 1. The major fraction was assumed to have a *trans* configuration from a stereochemical consideration of the addition of methanol. This was further confirmed by the downfield shift of the proton H-3 (δ 3.16) deshielded by the 5-methoxy group compared to that of the *cis* isomer (δ 3.04).[10]

Treatment of the ester **1** with ethanol or 2-propanol in the presence of acid gave an ethyl ether **3** or an isopropyl ether **4** corresponding to **2**, respectively, in a quantitative yield. They also were mixtures of stereoisomers, showing a signal for H-5 similar to that of the methyl ether **2**; however, no attempts were made to separate the isomers.

The reduction of 3-furoic acid with sodium and methanol or ethanol in liquid ammonia produced the methyl ether **2** or the ethyl ether **3** in 87 or 92% yield, respectively, after the methylation with diazomethane. Apparently, these ethers, **2** and **3**, were formed by the addition of alcohols to 2,3-dihydro-3-furoic acid in the course of work-up of the reaction mixture.[11]

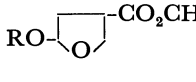

2: R=CH_3
3: R=C_2H_5
4: R=$CH(CH_3)_2$

Reaction Mechanism for the Birch Reduction of Aromatic Carboxylic Acids. The Birch reduction is initiated with the addition of an electron to the substrate molecule to form a radical anion, followed by the rapid protonation at the position with the highest electron density. The addition of another electron produces an anion, which is kinetically protonated to give an unconjugated cyclohexadiene.[12] According to the molecular orbital theory,[13] the extra electron in the first step of the Birch reduction will be introduced to the lowest unoccupied molecular orbital of symmetric or anti-symmetric character depending upon whether the substituent is electron-withdrawing or electron-releasing. Protonation at the highest electron density will occur at the 1- or 4-position in the former case and at the *o*- or *m*-position in the latter. The Birch reduction of benzoic acid gave 1,4-dihydrobenzoic acid,[14] indicating the carboxylate group is sufficiently electron-withdrawing in the Birch reduction. The highest spin density at the para position of the radical dianion derived from benzoate anion was also verified by the ESR study.[15] Apart from the MO argument, the products of the Birch reduction of the aromatic carboxylic acids may be rationalized as follows. All the aromatic carbonyl compounds, including benzoate anion, are assumed to add the electron not to the

aromatic nucleus but to the carbonyl group.[16] In the case of benzoate anion, the negative charge of the carboxylate anion will repel the charge of the resulting radical dianion **5a** as far as possible, favoring the contributing structure **5b** with the highest electron density at the carbon-4. As a corollary, benzamides may be well reduced on their aromatic nucleus only when the amide proton can be removed by a base to form amide anion. Thus, more acid benzamide substituted by methoxy groups at the meta positions can be reduced in good yield.[14]

The same argument may be valid for the Birch reduction of furoic acids. The addition of an electron to 2-furoate anion will produce a radical dianion with the highest electron density at the carbon-5 in its most favorite contributing structure **6**, followed by protonation at the position. The kinetic protonation of the dianion formed by the addition of another electron should occur at the carbon-2, forming the unconjugated acid, 2,5-dihydro-2-furoic acid. On the other hand, the radical dianion formed by the addition of an electron to 3-furoate anion will have the highest electron density at the carbon-2 in the most important contributing structure **7**; thus, the product of the Birch reduction of 3-furoic acid is 2,3-dihydro-3-furoic acid.

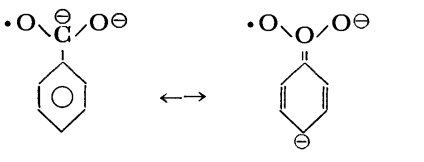

5a **5b**

6 **7**

Experimental

General. IR spectra were taken neat on a JASCO Model IR-E IR spectrometer and were calibrated against the 1600 cm^{-1} band of polystyrene. NMR spectra were recorded in deuteriochloroform solution at 100 MHz with a JEOL Co PS-100 spectrometer using tetramethylsilane as an internal reference. Mass spectra were recorded with a Hitachi RMU-6 mass spectrometer.

The Birch Reduction of 3-Furoic Acid. All the Birch reductions were carried out as follows: To a mixture of 3-furoic acid and *ca.* 8 molar equivalents of alcohol in liquid ammonia (*ca.* 10 ml per mole of acid) was added 3 equivalent atoms of sodium little by little with constant stirring under reflux. The mixture was stirred for an additional hour and excess of ammonium chloride was added. After evaporation of liquid ammonia at room temperature, the residue was dissolved in water. The aqueous solution was washed with several portions of ether to remove alcohol, acidified and immediately extracted continuously with ether for 24—48 h. The ether extract was esterified with excess of diazomethane and, after evaporation of the solvent, the residue distilled under reduced pressure.

With 2-Propanol: Methyl 2,3-dihydro-3-furoate (**1**), bp 83—84 °C/30 mmHg, was obtained in 85% yield. MS: (80 eV) *m/e* (rel intensity) 128 (20), 69 (100), 41 (26), 39 (16). NMR: δ 3.72 (s, 3, ester CH_3), 3.75 (m, 1, H-3), 4.44 (q, 1, $J_{2,3}=11$, $J_{2,2'}=-9.5$ Hz, H-2), 4.69 (q, 1, $J_{2',3}=7$ Hz, H-2'), 5.03 (t, 1, $J_{3,4}=3$, $J_{4,5}=3$ Hz, H-4), 6.42 ppm (t, 1, $J_{3,5}=2$ Hz, H-5).

Found: C, 56.08; H, 6.41%. Calcd for $C_6H_8O_3$: C, 56.24; H, 6.29%.

With Methanol: Methyl tetrahydro-5-methoxy-3-furoate (**2**), bp 90—92 °C/10 mmHg, n_D^{25} 1.4325, was isolated in 87% yield. IR: 1735 cm^{-1}. MS: (80 eV) *m/e* (rel intensity) M^+ absent[17], 159 (1.3), 145 (1.8), 129 (55), 115 (12), 103 (29), 99 (28), 87 (14), 71 (18), 69 (100), 59 (25), 58 (35), 55 (14), 45 (15), 41 (41), 39 (12). NMR: δ 2.00—2.45 (m, 2, H-4), 3.00—3.25 (m, 1, H-3), 3.27 (s, 3, ether CH_3), 3.65 (s, 3, ester CH_3), 4.05 (d, 2, H-2), 5.0 ppm (m, 1, H-5).

Found: C, 52.31; H, 7.44%. Calcd for $C_7H_{12}O_4$: C, 52.49; H, 7.55%.

Preparative gas chromatography of **2** was performed on a Varian Aerograph Model 90-P instrument equipped with a 4 mm × 2 m column of 20% Carbowax 20M at 150 °C with a flow rate of 40 ml/min. Two peaks of retention times of 9.1 and 10.8 min appeared in a ratio of 2 : 1. The faster-moving fraction showed the following NMR spectrum: δ 2.0—2.45 (m, 2, H-4), 3.16 (quintet, 1, H-3), 3.27 (s, 3, ether CH_2), 3.65 (s, 3, ester CH_3), 4.05 (d, 2, H-2), 5.02 ppm (q, 1, H-5). The slower-moving fraction showed the following NMR spectrum: δ 2.20—2.35 (m, 2, H-2), 3.04 (quintet, 1, H-3), 3.27 (s, 3, ether CH_3), 3.65 (ester CH_3), 4.05 (d, 2, H-2), 5.00 ppm (t, 1, H-5).

With Ethanol: Methyl 5-ethoxytetrahydro-3-furoate (**3**), bp 106—110 °C/15 mmHg, was obtained in 92% yield.[18] IR: 1735 cm^{-1}. MS: (80 eV) *m/e* (rel intensity) M^+ absent, 173 (0.7), 159 (2.7), 143 (12), 129 (47), 115 (10), 100 (24), 99 (13), 87 (15), 85 (17), 72 (19), 69 (100), 59 (17), 57 (12), 55 (15), 45 (11), 41 (28), 32 (22). NMR: δ 1.16 (t, 3, C–CH_3), 1.95—2.45 (m, 2, H-4), 2.90—3.40 (m, 1, H-3), 3.49 (q, 2, OCH_2), 3.64 (s, 3, OCH_3), 4.08 (d, 2, H-2), 5.18 ppm (m, 1, H-5).

Found: C, 55.05; H, 8.10%. Calcd for $C_8H_{14}O_4$: C, 55.16; H, 8.10%.

Acid-catalyzed Addition of Alcohols to Ester **1**. A solution of the ester **1** in appropriate amount of alcohol containing Dowex 50 (W-X8, H^+) ion-exchange resin (200—400 mesh) was stirred at room temperature overnight. After filtration of the resin followed by evaporation of the solvent, the residue was distilled under reduced pressure. The yields were quantitative. The esters, **2** and **3**, obtained by the Birch reduction were identified with the compounds produced by the acid-catalyzed addition of methanol and ethanol, respectively, by NMR spectrometry. The addition of 2-propanol gave methyl tetrahydro-5-isopropyloxy-3-furoate (**4**), bp 120—121 °C/30 mmHg. IR: 1735 cm^{-1}. MS: (80 eV) *m/e* (rel intensity) M^+ absent, 189[19] (0.6), 187 (0.4), 173 (3.1), 145 (13), 129 (89), 128 (11), 115 (16), 100 (40), 87 (37), 85 (10), 69 (100), 59 (13), 55 (11), 45 (10), 43 (22), 41 (26), 39 (13). NMR: δ 1.16 (d, 3, C–CH_3), 1.18 (d, 3, C–CH_3), 1.95—2.45 (m, 2, H-4), 2.90—3.45 (m, 1, H-3), 3.65 (s, 3, OCH_3), 3.84 (m, 1, O–CH), 4.00—4.15 (m, 2, H-2), 5.3 ppm (m, 1, H-5).

Found: C, 57.03; H, 8.46%. Calcd for $C_9H_{16}O_4$: C, 57.43; H, 8.57%.

The authors are greatly indebted to Dr. Yoshio Hirose and Mr. Kazuo Yoshihara of the Institute of Food Chemistry, Osaka, for the recording and analyses of the mass spectra and to Mr. Jun'ichi Gōda for the elemental analyses.

References

1) H. O. House, "Modern Synthetic Reactions," Ben-

jamin, Inc., Menlo Park, Cal. (1972), p. 145. R. G. Harvey, *Synthesis*, 161 (1970). E. M. Kaiser, *ibid.*, 391 (1972).

2) A. J. Birch, *J. Chem. Soc.*, **1945** 809.

3) A. O. Bedenbaugh, J. H. Bedenbaugh, J. D. Adkins, and W. A. Bergin, *J. Org. Chem.*, **35**, 543 (1970).

4) L. Rosenblum, Ph. D. Thesis, Ohio State Univ., 1952 [*Chem. Abstr.*, **52**, 11807d (1958)]. Unfortunately, this work was erroneously cited in A. P. Dunlop and F. N. Peters, "The Furan," Reinhold Publ. Co., New York, N. Y. (1953), p. 52. Rosenblum obtained 2,5-dihydro-2-furoic acid by the reduction of 2-furoic acid with 3 atom equivalents of sodium and ethanol in liquid ammonia. He also obtained 2-hydroxypentanoic, 2-oxopentanoic, and tetrahydro-2-furoic acids along with dimeric products on the reduction with 5 atom equivalents of sodium in liquid ammonia followed by addition of ammonium chloride. Unaware of the above results, we reached substantially the same results as Rosenblum. The product distribution of the reduction with 5 atom equivalents of sodium and ethanol in liquid ammonia was as follows (glc analysis): Pentanoic (1.0), 2-oxopentanoic (1.8), 2-hydroxypentanoic (6.1), 2,5-dihydro-2-furoic (1.9), tetrahydro-2-furoic acid (10.0). (Abstracts, the 24th Annual Meeting of the Chemical Society of Japan, 1463 (1971), Osaka).

5) A. P. Krapcho and A. A. Bothner-By, *J. Amer. Chem. Soc.*, **81**, 3658 (1959).

6) T. Kinoshita and T. Miwa, *Carbohyd. Res.*, **28**, 175 (1973).

7) G. D. Meakins, *J. Chem. Soc.*, **1953** 4171.

8) C. Botteghi, G. Consiglio, G. Cecarelli, and A. Stefani, *J. Org. Chem.*, **37**, 1835 (1972).

9) E. Schmitz and I. Eichhorn, "The Chemistry of the Ether Linkage," ed. by S. Patai, Interscience Publishers, New York, N. Y. (1967), p. 322.

10) J. R. Dyer, W. E. McGoningal, and K. C. Rice, *J. Amer. Chem. Soc.*, **87**, 654 (1965). C. Barbier, D. Gargnaire, and P. Vottero, *Bull. Soc. Chim. Fr.*, **1968** 2330.

11) In the case of 2-propanol, simple ether extraction of the reaction mixture removed the alcohol rather completely, while, in these cases, apparently more alcohol remained in the mixture and caused the addition during continuous extraction of the acidified reaction mixture with ether.

12) A detailed mechanism of the Birch reduction is discussed by C. Eaborn, R. A. Jackson, and R. Pearce, *J. Chem. Soc., Perkin I*, **1974**, 2055.

13) J. A. Bedford, J. R. Bolton, A. Carrington, and R. H. Prince, *Trans. Faraday Soc.*, **59**, 53 (1963).

14) M. E. Kuehne and B. F. Lambert, *J. Amer. Chem. Soc.*, **81**, 4278 (1959).

15) A. R. Buick, T. J. Kemp, G. T. Neal, and T. J. Stone, *J. Chem. Soc., A*, **1970**, 2227. P. Neta and R. W. Fessenden, *J. Phys. Chem.* **77**, 620 (1973).

16) Camps *et al.* proposed a formula suggesting the electron addition to the carbonyl group in the explanation for the reduction of a conjugated acid in the course of the Birch reduction; however, they assumed the first addtion of an electron to occur at the aromatic nucleus. F. Camps, J. Coll, and J. Pascual, *J. Org. Chem.*, **32**, 2563 (1967).

17) α-Alkoxytetrahydrofurans show very weak or no parent peak. *Cf.* D. R. Morton, E. Lee-Ruff, R. M. Southam, and N. J. Turro, *J. Amer. Chem. Soc.*, **92**, 4349 (1970). J. Srogl, M. Janda, J. Hajkova, and V. Kubelka, *Coll. Czch. Chem. Commun.*, **35**, 3462 (1970).

18) Five equivalent atoms of sodium was used.

19) M+1 peak is noticeable with compounds having many ether oxygens. The absence of the peak in the spectra of esters, **2** and **3**, might be due to low sample pressure. *Cf.* D. C. De Jongh and K. Biemann, *J. Amer. Chem. Soc.*, **86**, 67 (1964).

Studies of Polyphenyls and Polyphenylenes. I. The Syntheses and Infrared and Electronic Spectra of Several Sexiphenyls

Eiichi IBUKI, Shigeru OZASA, and Kazue MURAI

Department of Organic Chemistry, Kyoto College of Pharmacy, Yamashina, Higashiyama-ku, Kyoto 607

(Received July 26, 1974)

Seven linear sexiphenyls were synthesized by the Ullmann reaction of iodobiphenyl and diiodobiphenyl. Infrared studies indicated that the fine structure in the 780—810 cm^{-1} region suggests the presence of consecutive *m*-phenylene units, and that the positions of the strong or medium bands in the 820—840 cm^{-1} region indicate approximately the number of continuous *p*-phenylene units. The electronic spectra commonly displayed a prominent E-band in the narrow region of 192—207 nm. The intense K-band above 260 nm was considered to be an indication of the presence of one or more *p*-phenylene units.

It has been known that a twist of the pivot bond in a conjugated system of polyphenyls influences the interaction of π-electrons across the pivot bond and also the conjugation of the system, and consequently affects the spectral features.[1-3] In order to investigate the relationship between the number and arrangement of the benzene rings and the physical properties of polyphenyls and polyphenylenes, a series of symmetrical linear sexiphenyls, with closely related structures, have been prepared and their infrared and electronic spectra have been measured.

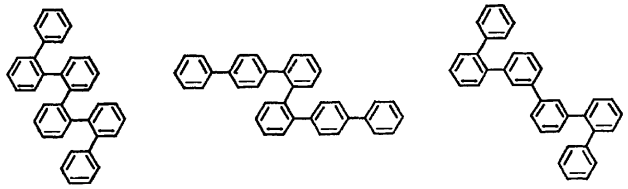

X XIII XVI

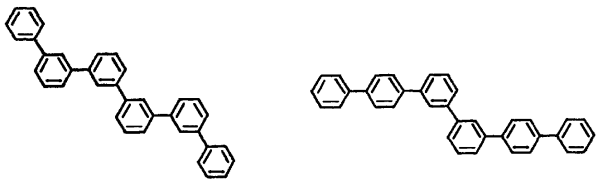

XVIII XX

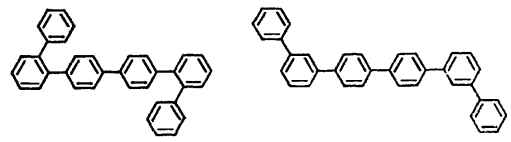

XXI XXII

The convenient route generally used for the preparation of polyphenyls is based on the reaction of arylcyclohexenone or arylcyclohexanone with an appropriate Grignard reagent or a corresponding lithium compound, followed by dehydration and dehydrogenation.[4,5] The resultant polyphenyl, however, is liable to be contaminated with a partially hydrogenated product.[6]

To avoid this disadvantage, the Ullmann coupling of aryl halides has been used in the present work. There are two forms of coupling in the syntheses of a series of symmetrical sexiphenyls: a) the coupling of iodoterphenyl, and b) the coupling of iodobiphenyl and diiodobiphenyl. In this work, the b method has been adopted in spite of the troublesome separation of polyphenyl from the reaction products, because the b method has the advantage of synthesizing both iodo compounds with ease from commercially available materials. Thus, iodobiphenyls (2- [I], 3- [II], and 4-iodobiphenyl[III]) and diiodobiphenyls (2,2'- [IV], 3,3'- [V], and 4,4'-diiodobiphenyl[VI]) were prepared from commercial aminonitrobenzene, chloronitrobenzene, aminobiphenyls, and benzidine. Then a mixture of mono- and diiodo compounds in the molar ratio of 2 to 1 was subjected to the Ullmann reaction at 260—270 °C with copper powder. The sexiphenyls and by-products thus obtained are shown in Table 1.

Table 1. Ullmann syntheses oe sexiphenyls

Iodides	Sexiphenyls (Yield, %)	By-products
I+IV	X (5.4)	VII VIII IX XI
II+IV	—	VII VIII XI XIV XVII
III+IV	XIII (1.6)	VII VIII XII XIV XV
I+V	XVI (5.5)	VII IX
II+V	XVIII (8.6)	VII XVII
III+V	XX (9.7)	VII XV XIX
I+VI	XXI (9.0)	VII IX XV
II+VI	XXII (14.0)	VII XVII XIX

Four sexiphenyls, X, XIII, XVI, and XXI, were found by the mixed-melting-point method and the IR spectra to be identical with authentic samples synthesized by the Ullmann coupling of the corresponding iodoterphenyls. An alternative synthesis of six sexiphenyls (X, XIII, XVIII, XX, XXI, XXII) has been reported earlier by other workers. Whereas the melting points of XIII and XX[7] do not coincide with those of the previous authors, those of the four remaining sexiphenyls fall within 1—2 °C of those of the other authors (X, XVIII,[8] XXI,[9] XXII[10,11]).

In all of the Ullmann coupling experiments, biphenyl and one or two kinds of quaterphenyls were isolated as by-products. Beside these substances, biphenylene and 1-phenyltriphenylene were separated from the product of I+IV, and biphenylene and 2-phenyltriphenylene, from III+IV.[12]

The yields of all the pure sexiphenyls except XIII were 5—14%. In the coupling reactions using IV

Table 2. Positions and tentative assignments of the characteristic bands of the infrared spectra (675—910 cm^{-1}) of sexiphenyls[a]

	X		
698	s	γ_{C-C}	
734	s	γ_{C-H}	(M, *o*)
743	s		
753	s		
776	s	γ_{C-H}	(*o*)
	XIII		
698	s	γ_{C-C}	
726	w		
744	sh, m	γ_{C-H}	(M, *o*)
754	s		
778	m	γ_{C-H}	(*o*)
834	sh, m	γ_{C-H}	(*p*)
842	s		
	XVI		
702	s	γ_{C-C}	
709	sh, s		
744	s	γ_{C-H}	(M, *o*)
759	s		
776	m	γ_{C-H}	(*o*)
796	m	γ_{C-H}	(*m*)
901	w	γ_{C-H}	(*m*)
907	w		
	XVIII		
690	sh, m	γ_{C-C}	
699	s		
754	s	γ_{C-H}	(M)
776	m	γ_{C-H}	(*m*)
786	m		
803	w		
817	vw		
873	m	γ_{C-H}	(*m*)
883	m		
897	w		
907	vw		
	XX		
687	s	γ_{C-C}	
698	sh, s		
707	m		
723	w		
759	s	γ_{C-H}	(M)
781	m	γ_{C-H}	(*m*)
800	vw		
839	s	γ_{C-H}	(*p*)
880	w	γ_{C-H}	(M, *m*)
912	w		
	XXI		
703	s	γ_{C-C}	
709	s		
747	s	γ_{C-H}	(M, *o*)
761	s		
773	vw	γ_{C-H}	(*o*)
786	m		
821	sh, m	γ_{C-H}	(*p*)
832	s		
	XXII		
699	s	γ_{C-C}	
724	vw		
755	s	γ_{C-H}	(M)
761	s		
793	s	γ_{C-H}	(*m*)
826	m	γ_{C-H}	(*p*)
833	m		
837	m		
888	m	γ_{C-H}	(*m*)

a) v: very, s: strong, m: medium, w: weak, sh: shoulder. γ_{C-C} and γ_{C-H} refer to vibrations which are primarily out-of-plane C-C, and out-of-plane C-H bending motions. M, *o*, *m*, *p* in parentheses refer to mono-, *ortho*-, *meta*-, and *para*-substituted rings.

as one of the iodo compounds (I+IV, and III+IV), the sexiphenyls were obtained only in low yields; furthermore, in the case of II+IV, no corresponding sexiphenyl was isolated, but biphenylene, 1- and 2-phenyltriphenylene were obtained. Hence, the Ullmann coupling of appropriate iodoterphenyl is preferable for these three sexiphenyls with an *o*-quaterphenyl unit in the middle of their structure.

For the separation of polyphenyl from a mixture of several products, liquid column chromatography, using alumina as the adsorbent and a cyclohexane or cyclohexane–benzene mixture as the eluent, was found to be a satisfactory technique.[13]

The IR spectra of the sexiphenyls were measured by the KBr-disk method. All the sexiphenyls commonly show the following absorptions: a group of prominent bands due to C–H out-of-plane deformation vibrations in the 675—910 cm^{-1} region; intense bands due to C–C out-of-plane deformation vibrations in the fairly narrow region of 685—710 cm^{-1};[14] medium bands due to C–C in-plane deformation vibrations near 1000 cm^{-1}, and weak bands due to C–H in-plane deformation vibrations in the 975—1350 cm^{-1} region. In addition, groups of medium bands due to C–C stretching vibrations and a weak band due to aromatic C–H stretching vibrations in the 1350—1600 cm^{-1} and 3000—3100 cm^{-1} regions respectively were observed.

The most characteristic bands of sexiphenyls in the 675—910 cm^{-1} region are shown in Table 2; the table indicates that these bands are consistent with the kinds of phenylene rings in each sexiphenyl.

Let us now discuss the assignment of the strong bands in the 734—761 cm^{-1} region of X, XIII, XVI, and XXI, in all of which one or more *o*-phenylene rings are present. Stewart and Hellman[16] have pointed out that the bands at 733—757 cm^{-1} of *o*-quaterphenyl must be due to C–H out-of-plane deformation vibrations of terminal rings; Sandroni and Geiss[17] have proposed a similar assignment for the intense bands in the 753±10 cm^{-1} region of polyphenyls. However, the strong bands near 745—755 cm^{-1} were also observed in the spectra of some polyphenylenes, which contain no terminal rings. Thus, tetraphenylene, *o*-hexaphenylene, *o*-octaphenylene,[20] and *o,p,o,p,o,p*-hexaphenylene[21] showed strong

bands at 745—755 cm^{-1}. Consequently, in the case of polyphenyls containing *o*-phenylene rings, the intense bands in the 734—761 cm^{-1} region should be assigned not only to the C–H out-of-plane bending bands of terminal rings, but also to those of *o*-phenylene rings.

Then the prominent bands observed commonly in the spectra of X, XIII, XVI, and XXI at 776—786 cm^{-1} should be assigned to the C–H out-of-plane bending vibrations of *o*-phenylene rings, as has been suggested by Stewart and Hellman[16] and Sandroni and Geiss,[17] because the medium or weak bands at 766—773 cm^{-1} were found commonly in the spectra of four polyphenylenes.

The four bands at 776, 786, 803, and 817 cm^{-1} in the spectra of XVIII were assigned to the C–H out-of-plane bending vibrations of *m*-phenylene rings. Stewart and Hellman[16] have pointed out that the characteristic C–H bands of some *m*-polyphenyls in the 780—810 cm^{-1} region are observed as a multiplet with an increase in the complexity, in accordance with the progression of *m*-phenylene rings, and have concluded that the fine structure can be attributed to the interaction bands between a ring and its nearest neighbors. The spectrum of XVIII supports strongly their opinion.

In the spectra of XIII, XX, XXI, and XXII, strong C–H out-of-plane bending vibration bands of two adjacent hydrogen atoms of *p*-phenylene rings were clearly observed at 842; at 839; at 832, and at 826, 833, and 837 cm^{-1} respectively. While XIII and XX have two *p*-linkages separated, respectively, by *o*- and *m*-phenylene groups, XXI and XXII have two consecutive *p*-linkages. A red shift of the characteristic bands was observed in the spectra of the latter two compounds. A similar red shift has been reported by Doss[19] and others[17] in the spectra of compounds with consecutive *p*-phenylene units.

These results show that the fine structure in the 780—810 cm^{-1} region suggests the presence of consecutive *m*-phenylene units, and that the positions of strong or medium bands in the 820—840 cm^{-1} region serve as an indication of the number of continuous *p*-phenylene units.

The electronic spectra of the seven sexiphenyls were measured in a cyclohexane solution. The absorption curves are shown in Figs. 1—4. The absorption maxima above 220 nm coincide within 1—2 nm for XIII, XVIII, XX, and XXI, and within 3—4 nm for X and XXII, with those of other workers.[8–10,22]

Gillam[1] has reported that the first intense band of the first four *p*-polyphenyls is shifted progressively toward a longer wavelength and increases in intensity with an increase in the number of rings. In the *m*-series, terphenyl and compounds containing 9—16 benzene rings absorb at substantially the same wavelength and with an intensity which is approximately proportional to the number of ring units.[1] In the case of *o*-polyphenyls, however, Dale[2] and others[20] have observed a blue shift and a weakening of the conjugate band as compared with those of the corresponding *m*-polyphenyls; these are results of reduced π-π interaction across the pivot bond.

In the present study, all seven sexiphenyls displayed two groups of intense bands: one in the fairly narrow region of 192—207 nm (ε=72800—98700) and another

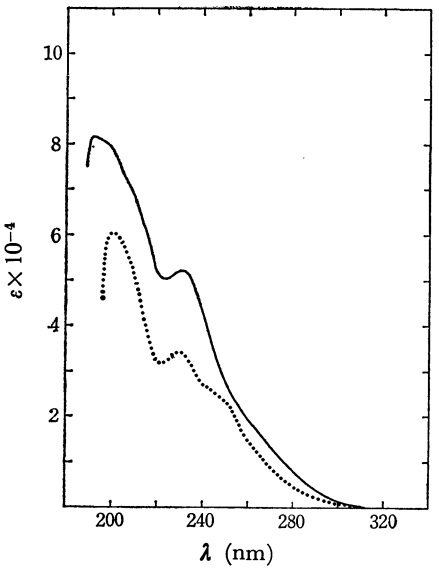

Fig. 1. Electronic spectra of quaterphenyl and sexiphenyl in cyclohexane.
·····: *o*-Quaterphenyl (IX),
——: *o*-Sexiphenyl (X).

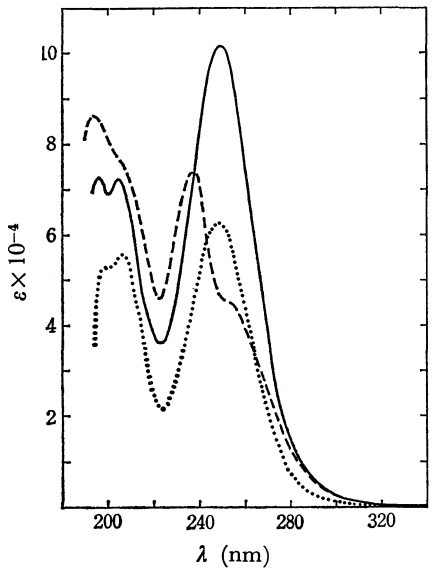

Fig. 2. Electronic spectra of quaterphenyl and sexiphenyls in cyclohexane.
·····: *m*-Quaterphenyl (XVII),
——: *m*-Sexiphenyl (XVIII),
----: 3,3′-Di(2-biphenylyl)biphenyl (XVI).

in the broad region of 230—300 nm with a high intensity. While the band position for the former was found to be rather independent of the structure, that for the latter was substantially affected by the nature and number of linkages formed between benzene rings. The first one, corresponding to the band at 203 nm (ε=49600) of biphenyl, is considered to be the E-band (the notation is according to Braude[23]), which is presumably due to the transitions between localized π-orbitals within each benzene ring.[2,3] The other one, corresponding to the band at 248 nm (ε=18500) of biphenyl, is regarded as the K-band (Burawoy's notation[23]), which should originate from

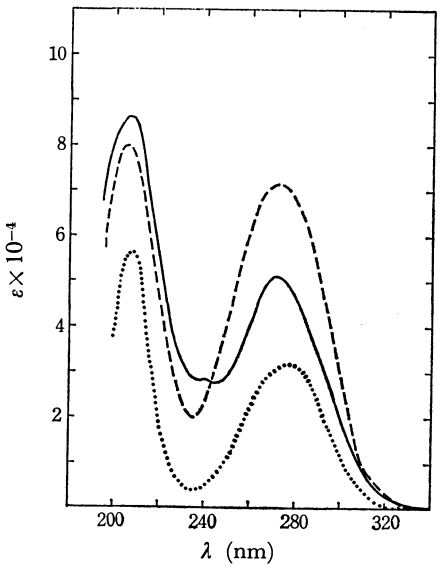

Fig. 3. Electronic spectra of terphenyl and sexiphenyls in cyclohexane.
·····: *p*-Terphenyl,
——: 2,2′-Di(4-biphenylyl)biphenyl (XIII),
----: 3,3′-Di(4-biphenylyl)biphenyl (XX).

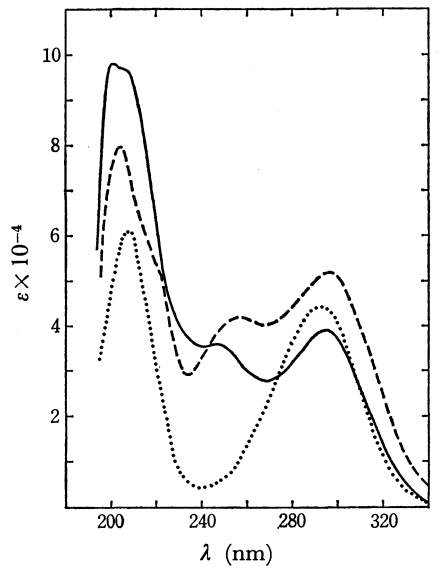

Fig. 4. Electronic spectra of quaterphenyl and sexiphenyls in cyclohexane.
·····: *p*-Quaterphenyl (XV),
——: 4,4′-Di(2-biphenylyl)biphenyl (XXI),
----: 4,4′-Di(3-biphenylyl)biphenyl (XXII).

transitions between whole-molecular π-orbitals made up of ring orbitals with no longitudinal node.[2,3]

Thus, the spectrum of X has the K-band with λ_{max} at 231 nm and an ε_{max} value of 52200, slightly stronger in its intensity than, but very similar in its location to, *o*-quaterphenyl (230; 34100) (Fig. 1). The spectra of XVIII and XVII (*m*-quaterphenyl) revealed intense bands at substantially the same wavelength, 248± 1 nm, with intensities about five times and three times respectively those of the biphenyl band. Therefore, the intensity of the K-band in the *m*-series may be correlated with the maximum number of biphenyl units in each compound (Fig. 2). In the case of XVI, in which *o*- and *m*-linkages are present, the spectrum revealed a strong K-band at 237 nm (ε=74100) which may correspond to the band near 230 nm of *o*-polyphenyls, but the characteristic band of *m*-polyphenyls near 250 nm was observed only as a shoulder.

Then in the spectra of XIII, XX, XXI, and XXII, all of which have *p*-linkage, a remarkable red shift of the K-band as compared with that in biphenyl was distinctly observed, as is shown in Figs. 3 and 4. Thus, XIII and XX have two *p*-terphenyl units in each structure and show a distinct band at about 270 nm, while XXI and XXII each have one *p*-quaterphenyl unit and both reveal a strong band near 300 nm. It may be considered that the arrangement of the *p*-phenylene units in the four sexiphenyls, even in the presence of *o*- or *m*-phenylene units, has a tendency to maintain a coplanarity of the rings; a distinct bathochromic shift of K-band results because of the elongation of the conjugated system.

On the basis of these results, the intense K-band above 260 nm in the spectra of sexiphenyl may be considered to be an indication of the presence of one or more *p*-phenylene units.

Experimental

All the melting points and boiling points are uncorrected. The IR spectra were recorded with a Leitz IIIG spectrophotometer. The electronic spectra were measured on a Shimadzu QV-50 spectrometer and a Hitachi EPS-2 spectrophotometer, using spectral-grade cyclohexane as the solvent. In the measurement in the short-wavelength region, 2-mm silica cells were used. The molecular weights were determined with a Mechrolab 301A vapor-pressure osmometer unless otherwise noted.

2-Iodobiphenyl (I). Commercial 2-aminobiphenyl (20 g, 0.12 mol) dissolved in sulfuric acid was diazotized with sodium nitrite. The suspension of the diazonium salt thus formed was treated with a potassium iodide solution. The product was purified by distillation *in vacuo* to give a pale yellow liquid; bp 130—134 °C/4 mmHg (lit,[24] bp 158 °C/6 mmHg); yield, 26.3 g (79.8%). (Found: C, 51.51; H, 3.26%.)

3-Iodobiphenyl (II). 3-Nitroaniline (69 g, 0.50 mol) in sulfuric acid (33 ml) and water (500 ml) were treated with sodium nitrite (36 g) in water (76 ml) at 0—5 °C with stirring. To the cold suspension of diazonium salt thus formed, benzene (1000 ml) and sodium acetate (160 g) in water (330 ml) were added in portions, after which the mixture was stirred at an ambient temperature for 7 hr and then at 30—35 °C for 40 hr. The benzene layer was separated, washed with water, and then dried. After the removal of the benzene, the residue was distilled *in vacuo* to afford a pale yellow oil; bp 166—170 °C/8 mmHg. Recrystallization from methanol gave 3-nitrobiphenyl as pale yellow needles; mp 59—60 °C (lit,[25] mp 61 °C); yield, 50.0 g (50.3%).

3-Nitrobiphenyl (20 g, 0.10 mol) was dissolved in hot benzene (800 ml) and treated with activated iron by a method similar to that of Hazlet and Dornfeld.[26] After filtration, hydrogen chloride was passed into the filtrate. The precipitate was separated off, washed with benzene, and dried. Then the salt was treated in the usual manner with 20% aqueous alkali. The benzene extract was washed with water and dried. The evaporation of the solvent, followed by

distillation *in vacuo*, yielded 3-aminobiphenyl as a colorless oil; mp 30 °C; bp 175—177 °C/13 mmHg (lit,[27] mp 31—31.5 °C; bp 177—178 °C/18 mmHg); yield, 12.3 g (72.4%).

3-Iodobiphenyl was prepared by the method described for the preparation of I to give a pale yellow oil; mp 25—26 °C; bp 175—178 °C/15 mmHg (lit,[27] bp 149—152 °C/1 mmHg); yield, 78.6%. (Found: C, 51.58; H, 3.48%.)

4-Iodobiphenyl (III). 4-Iodobiphenyl was prepared from 4-aminobiphenyl in the manner described above. Colorless plates from ethanol; mp 112.5—113.5 °C (lit,[28] mp 112 °C); yield, 70.8%. (Found: C, 51.51; H, 3.41%.)

2,2′-Diiodobiphenyl (IV). 2-Chloronitrobenzene (40 g, 0.25 mol) was heated with copper powder (80 g, 1.26 g-atom) at 215—225 °C and then at 225 °C for 1 hr. The subsequent extraction of the cooled mass with hot benzene, followed by evaporation, and the recrystallization of the residue from ethanol gave 2,2′-dinitrobiphenyl as pale yellow prisms; mp 122.5—124.5 °C (lit,[29] mp 123.5—124.5 °C); yield, 18.8 g (60.7%).

2,2′-Dinitrobiphenyl was reduced with activated iron in hot benzene in a manner previously described. Recrystallization from petroleum benzine afforded colorless prisms; mp 79—80 °C; yield, 73.0%.

The 2,2′-diaminobiphenyl (10 g, 0.054 mol) thus obtained was subjected to tetrazotization, followed by treatment with potassium iodide. The product was purified by distillation *in vacuo*; the subsequent recrystallization of the distillate (bp 130—170 °C/4 mmHg) from methanol gave 2,2′-diiodobiphenyl as pale yellow needles; mp 107.5—108.5 °C; yield, 8.8 g (40.0%). (Found: C, 35.63; H, 2.28%.)

3,3′-Diiodobiphenyl (V). 3-Iodonitrobenzene was prepared from 3-aminonitrobenzene by a method similar to that of Daines and Eberly;[30] mp 35.5—36.5 °C; yield, 55.4%. 3,3′-Diiodobiphenyl was obtained by the Ullmann reaction of 3-iodonitrobenzene, followed by reduction with tin and hydrochloric acid, and the Gries reaction of the product. Colorless needles from petroleum benzine; mp 71—72 °C (lit,[31] mp 72 °C); yield, 23.2% (based on 3-iodonitrobenzene). (Found: C, 35.59; H, 2.09%.)

4,4′-Diiodobiphenyl (VI). Commercial benzidine (18.4 g, 0.10 mol) was tetrazotized and then treated with potassium iodide in the manner described above to give VI as colorless leaves from benzene; mp 202—203 °C (lit,[32] mp 202 °C); yield, 35.0 g (86.3%). (Found: C, 35.78; H, 2.19%.)

Preparation of o-Sexiphenyl (X). A mixture of I (5.6 g, 20.0 mmol) and IV (4.0 g, 9.9 mmol) in a test tube (ϕ 2.5×20 cm) was heated in an oil bath at 265—270 °C, and then copper powder (28 g, 440 mg-atom) was stirred in in portions over a 1.5-hr period, after which the mixture was heated at 270 °C for an additional 1.5 hr. After cooling, the mixture was extracted with hot benzene, and the solvent was distilled off. The resulting solid (4.98 g) was subjected to chromatography on alumina, with cyclohexane and then with a cyclohexane-benzene (5 : 1 v/v) mixture (C–B (5 : 1)) as the eluents. The cyclohexane eluted three fractions, which, upon the evaporation of the solvent and recrystallization from ethanol, afforded VII, VIII, and IX. The mixture eluted two fractions, which, upon treatment as above, yielded X and XI. The properties of these compounds are as follows.

i) Biphenyl (VII): colorless leaves; mp 70—71 °C; yield, 11 mg.

ii) Biphenylene (VIII): pale yellow needles; mp 110—111 °C (lit,[33] mp 111—112 °C); yield, 322 mg.

Found: C, 94.45; H, 5.56%. Calcd for $C_{12}H_8$: C, 94.70; H, 5.30%. Picrate: 121—122 °C. (Found: C, 56.67; H, 3.11; N, 10.83%.) Styphnate: 160—162 °C. (Found: C, 54.43; H, 3.01; N, 10.60%.)

iii) *o*-Quaterphenyl (IX): colorless cubes; mp 118—119 °C (lit,[15] mp 118 °C); yield, 1880 mg.

Found: C, 93.87; H, 6.18%; mol wt (Rast), 324. Calcd for $C_{24}H_{18}$: C, 94.08; H, 5.92%; mol wt, 306.

iv) *o*-Sexiphenyl (X): colorless cubes from ethanol; mp 217—217.5 °C (lit,[8] mp 216—217 °C); yield, 249 mg (5.4%). UV: λ_{max} (ε) 192(82100), 231 nm (52200).

Found: C, 94.14; H, 5.98%; mol wt, 451. Calcd for $C_{36}H_{26}$: C, 94.28; H, 5.72%; mol wt, 458.

v) 1-Phenyltriphenylene (XI): colorless needles from ethanol; mp 160—161 °C (lit,[34] mp 162 °C); yield, 245 mg.

Found: C, 94.46; H, 5.47%; mol wt, 298. Calcd for $C_{24}H_{16}$: C, 94.70; H, 5.30%; mol wt, 304.

Reaction of II and IV. A mixture of II (8.4 g, 30.0 mmol) and IV (6.0 g, 14.8 mmol) was treated with copper powder (27.0 g, 430 mg-atom) at 270—280 °C for 1 hr. The hot benzene extract of the mixture was then chromatographed on an alumina column in a manner previously described. The three fractions which were eluted with a C–B (5 : 1) mixture gave VII (876 mg), VIII (545 mg), and XVII; the one fraction which was eluted with C–B (5 : 2) afforded XI (158 mg), and a last fraction which was eluted with benzene yielded XIV.

i) *m*-Quaterphenyl (XVII): colorless needles from ethanol; mp 86—87 °C (lit,[6] mp 85.5—86 °C); yield, 1250 mg.

Found: C, 93.80; H, 6.06%; mol wt (Rast), 314. Calcd for $C_{24}H_{18}$: C, 94.08; H, 5.92%; mol wt, 306.

ii) 2-Phenyltriphenylene (XIV): colorless needles from the C–B (5 : 2) mixture; mp 183—183.5 °C (lit,[34] mp 185 °C); yield, 200 mg.

Found: C, 94.74; H, 5.53%; mol wt, 306. Calcd for $C_{24}H_{16}$: C, 94.70; H, 5.30%; mol wt, 304.

Preparation of 2,2′-Di(4-biphenylyl)biphenyl (XIII). A mixture of III (9.8 g, 35 mmol) and IV (7.0 g, 17.5 mmol) was treated with copper powder (32 g, 500 mg-atom) at 265—270 °C for 1 hr and then at 270—280 °C for 1.5 hr. The hot benzene extract of the mixture was treated with the C–B (5 : 2) mixture to separate it into soluble and insoluble parts. Filtration and several crystallizations of the latter from benzene provided XV. The former, after the removal of the solvent, was dissolved in cyclohexane and subjected to chromatography on alumina. The cyclohexane eluted two fractions, which, upon recrystallization from ethanol, afforded VII (406 mg) and VIII (1357 mg). A mixture of C–B (5 : 1) eluted three fractions, which, after recrystallization, provided XII, XIII, and XIV (640 mg).

i) 2,4′-Diphenylbiphenyl (XII): colorless prisms from cyclohexane; mp 116—118 °C (lit,[35] mp 119—119.5 °C); yield, 50 mg.

Found: C, 94.45; H, 5.76%; mol wt, 307. Calcd for $C_{24}H_{18}$: C, 94.08; H, 5.92%; mol wt, 306.

ii) 2,2′-Di(4-biphenylyl)biphenyl (XIII): colorless rhombs from benzene; mp 192—194 °C (lit,[8] mp 189—190 °C); yield, 125 mg (1.6%). UV: λ_{max} (ε) 207 (86700), 240 (sh) (28100), 272 nm (51200).

Found: C, 94.43; H, 5.60%; mol wt, 451. Calcd for $C_{36}H_{26}$: C, 94.28; H, 5.72%; mol wt, 458.

iii) *p*-Quaterphenyl (XV): colorless plates from benzene; mp 318—319 °C (lit,[36] mp 317.7—318.7 °C); yield, 2200 mg.

Found: C, 94.38; H, 6.02%. Calcd for $C_{24}H_{18}$: C, 94.08; H, 5.92%.

Preparation of 3,3′-Di(2-biphenylyl)biphenyl (XVI). A mixture of I (3.5 g, 12.5 mmol) and V (2.5 g, 6.2 mmol) was heated with copper powder (13 g, 204 mg-atom) at 260—265 °C for 2 hr and at 270 °C for 1 hr. The hot benzene extract of the mixture was separated into three fractions by chromatography on alumina. A C–B (5 : 3) mixture eluted

two fractions, which provided VII (17 mg) and IX (1950 mg). Benzene eluted the third fraction, which, upon recrystallization from methanol, gave XVI. The elution with benzene afforded a colorless oil which was unidentified (1210 mg).

3,3′-Di(2-biphenylyl)biphenyl (XVI): colorless needles; mp 151.5—152 °C; yield, 155 mg (5.5%). UV: λ_{max} (ε) 194 (86500), 237 (74100), 252 nm(sh)(45400).

Found: C, 94.43; H, 5.90%; mol wt, 458. Calcd for $C_{36}H_{26}$: C, 94.28; H, 5.72%; mol wt, 458.

Preparation of m-*Sexiphenyl (XVIII).* A mixture of II (2.8 g, 10 mmol) and V (2.0 g, 5 mmol) was treated with copper powder (10 g, 160 mg-atom) under conditions similar to those used in the preparation of XVI. The hot benzene extract of the reaction mixture was chromatographed on an alumina column in the manner previously described. The two fractions which were eluted with a C–B (5 : 2) mixture gave VII (159 mg) and XVII (440 mg) respectively, while the next fraction, which was eluted with C–B (5 : 3), afforded XVIII.

m-Sexiphenyl (XVIII): colorless needles from cyclohexane; mp 145—146 °C (lit,[8] mp 146—147 °C); yield, 195 mg (8.6%). UV: λ_{max} (ε) 196 (72800), 205 (72300), 249 nm (101700).

Found: C, 94.05; H, 5.78%; mol wt (Rast), 465. Calcd for $C_{36}H_{26}$: C, 94.28; H, 5.72%; mol wt, 458.

Preparation of 3,3′-Di(4-biphenylyl)biphenyl (XX). A mixture of III (3.7 g, 13 mmol) and V (2.7 g, 6.6 mmol) was treated with copper powder (9.5 g, 150 mg-atom) at 260 °C for 1 hr and then at 280 °C for an additional hour. The hot benzene extract of the reaction mixture was digested with 120 ml of the C–B (5 : 2) mixture to give soluble and insoluble parts. Upon filtration, the filtrate was chromatographed on alumina, with the same solvent as the eluent, to give VII (8 mg) and XIX. The insoluble part was dissolved in benzene and then subjected to chromatography on alumina with benzene. Several crystallizations of the eluate afforded XX and XV (57 mg).

i) 3,4′-Diphenylbiphenyl (XIX): colorless needles from ethanol; mp 164—165 °C (lit,[4] mp 166—167 °C); yield, 201 mg.

Found: C, 94.04; H, 6.12%; mol wt (Rast), 309. Calcd for $C_{24}H_{18}$: C, 94.08; H, 5.92%; mol wt, 306.

ii) 3,3′-Di(4-biphenylyl)biphenyl (XX): colorless small plates from benzene; mp 257—258 °C (lit,[8] mp 247.5 °C); yield, 295 mg (9.7%). UV: λ_{max} (ε) 206 (79800), 273 nm (71200).

Found: C, 94.34; H, 5.83%; mol wt (Rast), 461. Calcd for $C_{36}H_{26}$: C, 94.28; H, 5.72%; mol wt, 458.

Preparation of 4,4′-Di(2-biphenylyl)biphenyl (XXI). A mixture of I (4.2 g, 15 mmol) and VI (3.0 g, 7.4 mmol) was heated with copper powder (15 g, 236 mg-atom), as has been described in the preparation of XVIII. The benzene extract was chromatographed on alumina in a manner previously used. A C–B (5 : 2) mixture eluted three fractions, which, upon treatment as above, gave VII (47 mg), IX (1063 mg), and XXI. Benzene eluted one fraction, which, upon recrystallization from benzene, provided XV (164 mg).

4,4′-Di(2-biphenylyl)biphenyl (XXI): colorless plates from benzene; mp 233—236 °C (lit,[10] mp 237.9—238.1 °C); yield, 304 mg (9.0%). UV: λ_{max} (ε) 202 (98700), 205 (sh) (97000), 250 (35700), 297 nm (38900).

Found: C, 94.08; H, 5.70%; mol wt (Rast), 470. Calcd for $C_{36}H_{26}$: C, 94.28; H, 5.72%; mol wt, 458.

Preparation of 4,4′-Di(3-biphenylyl)biphenyl (XXII). A mixture of II (6.3 g, 22.5 mmol) and VI (4.5 g, 11 mmol) was treated with copper powder (22.5 g, 350 mg-atom) as has been described in the preparation of XX. The benzene extract of the mixture was digested with 150 ml of the C–B (5 : 2) mixture to separate it into soluble [A] and insoluble [B] parts. After filtration, the filtrate was chromatographed on alumina, with the same solvent as the eluent, to give VII (510 mg) and XVII (1470 mg); further elution with benzene gave XIX (410 mg) and XXII. The insoluble part [B] and the xylene extract of the reaction mixture also gave additional XXII after chromatography on alumina with benzene, followed by several recrystallizations.

4,4′-Di(3-biphenylyl)biphenyl (XXII): slender, colorless plates from benzene; mp 287—288 °C (lit,[9] mp 280—281 °C; lit,[10] mp 287—288 °C); yield, 710 mg (14.0%). UV: λ_{max} (ε) 204 (80000), 256 (41700), 296 nm (51900).

Found: C, 94.13; H, 5.84%; mol wt, 465. Calcd for $C_{36}H_{26}$: C, 94.28; H, 5.72%; mol wt, 458.

The authors are indebted to the members of the Center of Elemental Analysis, Faculty of Pharmacy, Kyoto University, for the elemental analyses. Thanks are also due to Nippon Shinyaku Co., Ltd., for the measurements of IR spectra.

References

1) A. E. Gillam and D. H. Hey, *J. Chem. Soc.*, **1939**, 1170.
2) J. Dale, *Acta Chem. Scand.*, **11**, 650 (1957).
3) H. Suzuki, This Bulletin, **32**, 1340 (1959).
4) G. F. Woods and I. W. Tucker, *J. Amer. Chem. Soc.*, **70**, 3340 (1948).
5) W. Ried and D. Freitag, *Angew. Chem. Int. Ed. Engl.*, **7**, 835 (1968).
6) G. F. Woods and F. T. Reed, *J. Amer. Chem. Soc.*, **71**, 1348 (1949).
7) Cade has reported lower melting points 189—190 °C for XIII and 247.5 °C for XX (Ref. 8).
8) J. A. Cade and A. Pilbeam, *J. Chem. Soc.*, **1964**, 114.
9) G. F. Woods, D. D. Centola, H. E. Ruskie, and C. D. Miller, *J. Amer. Chem. Soc.*, **82**, 5227 (1960).
10) C. Beaudet, J. Horlait, A. Marcq, and G. Belpaire, *EUR* 31. f (1962).
11) Woods has noted lower melting point 280—281 °C (Ref. 9).
12) These by-products VII, IX, XI, XV, XVII, and XIX were identified by means of the mixed melting point measurements with each of authentic samples.
13) Some close correlations between the structure of polyphenyls and the order of their elution were observed in the chromatographic separation of the products. The result will be reported later.
14) The assignment agrees with those of Dale, Stewart, and others (Ref. 15—17). It seems inadequate to assign them as C–H out-of-plane bending bands of terminal rings as noted by Doss and Solomon (Ref. 18, 19).
15) J. Dale, *Acta Chem. Scand.*, **11**, 640 (1957).
16) J. E. Stewart and M. Hellmann, *J. Res. Natl. Bur. Stand.*, **60**, 125 (1958).
17) S. Sandroni and F. Geiss, *Z. Anal. Chem.*, **220**, 321 (1966).
18) L. J. Bellamy, "The Infrared Spectra of Complex Molecules," John Wiley & Sons, Inc., New York, N. Y. (1954), p. 64.
19) R. C. Doss and P. W. Solomon, *J. Org. Chem.*, **29**, 1567 (1964).
20) G. Wittig and G. Lehmann, *Chem. Ber.*, **90**, 875 (1957).
21) E. Ibuki, S. Ozasa, Y. Fujioka, M. Maeda, and Y. Hayashi, presented at The 91st Annual Meeting of the Pharm. Soc. of Japan, Fukuoka, April 8, 1971.

22) R. L. Alexander, *J. Org. Chem.*, **21**, 1464 (1956).
23) R. M. Silverstein and G. C. Bassler, "Spectrometric Identification of Organic Compounds," 2nd Ed., John Wiley & Sons, Inc., New York·London·Sydney (1967), p. 152.
24) H. Gilman, J. E. Kirby, and C. R. Kinney, *J. Amer. Chem. Soc.*, **51**, 2252 (1929).
25) J. Elks, J. W. Haworth, and D. H. Hey, *J. Chem. Soc.*, **1940**, 1284.
26) S. E. Hazlet and C. A. Dornfeld, *J. Amer. Chem. Soc.*, **66**, 1781 (1944).
27) E. Campaigne and Wm. B. Reid, *ibid.*, **68**, 1663 (1946).
28) W. Schlenk, *Ann. Chem.*, **368**, 295 (1909).
29) R. C. Fuson and E. A. Cleveland, "Organic Syntheses," Coll. Vol. III, p. 339 (1955).
30) F. B. Dains and F. Eberly, *ibid.*, Coll. Vol. II, p. 355 (1943).
31) L. Mascarelli and M. Piroma, *Gazz. Chim. Ital.*, **68**, 117 (1938).
32) C. Willgerodt and G. Hilgenberg, *Ber.*, **42**, 3826 (1909).
33) W. S. Rapson, R. G. Shuttleworth, and J. N. van Niekerk, *J. Chem. Soc.*, **1943**, 326.
34) P. G. Copeland, R. E. Dean, and D. McNen, *ibid.*, **1960**, 4522.
35) G. F. Woods and F. Scotti, *J. Org. Chem.*, **26**, 312 (1961).
36) J. J. E. Schmidt and J. A. Krimmel, *ibid.*, **25**, 252 (1960).

The Reaction of Cycloalkanones with Copper(II) Halides. II.[1] The Reaction of Cyclohexanones with Copper(II) Bromide

Kyoko Nishizawa* and J. Yasuo Satoh

Department of Chemistry, St. Paul's (Rikkyo) University, Nishi-Ikebukuro, Toshima-ku, Tokyo 171

(Received August 9, 1974)

The reaction of cyclohexanones with copper(II) bromide gave polybrominated cyclohexanediones in all cases except for the case of 3,5-dimethylcyclohexanone. Moreover, in this reaction, a pyrocatechol and a phenol derivative were obtained from 4-methyl- and 3,5-dimethylcyclohexanone respectively. The mechanism of this reaction was discussed.

Previously, the present authors reported that cyclohexanones reacted with copper(II) chloride in 50% dioxane to give polychlorinated cyclohexanediones in fairly good yields.[1,2] In this reaction, mono-, di-, and trichlorinated cyclohexanediones were obtained in good yields by controlling the quantity of copper(II) chloride and the reaction times. However, chlorocyclohexanone, which seems to be an intermediate from cyclohexanone to the cyclohexanediones, could not be isolated. This seems to be because α- and α,α'-chloro ketones are not as easy to crystallize as bromo ketone. Consequently, in the present work, in order to confirm the reaction mechanism by isolating bromo intermediates, the reaction of cyclohexanones with copper(II) bromide instead of copper(II) chloride was carried out.

Experimental

All the melting points are uncorrected. Thin-layer chromatography was carried out on silica gel (Wakogel B-5), and detected by means of iodine or an *o*-phenylenediamine–ethanol solution. Column chromatography was carried out on silica gel (Wakogel C-100). The IR spectra were measured with a Hitachi 215 grating infrared spectrophotometer by the KBr disk method, and the UV spectra, with a JASCO ORD/UV-5 spectrometer and a Hitachi 323 recording spectrophotometer in an EtOH solution. The NMR spectra were recorded in $CDCl_3$, unless otherwise noted, with TMS as the internal standard, with a Hitachi R-20A nuclear magnetic resonance spectrometer. The chemical shifts are presented in terms of the δ value. The mass spectra were obtained with a Hitachi RMU-7M mass spectrometer at 70 eV.

Reaction of Cyclohexanones with Copper(II) Bromide. The typical procedure was in accordance with that used in the case of copper(II) chloride described previously[1] under reflux for 0.5—2.5 hr. The reaction mixture was extracted with ether, and the extracts, after being washed and dried over Na_2SO_4, were evaporated under reduced pressure. The residue was purified by column chromatography to give the pure product.

Results and Discussion

The results are summarized in Tables 1 and 2. The NMR and IR spectra of the product from cyclohexanone showed the absorptions due to α-hydroxy-α,β-unsaturated ketone similar to those of the reaction product from cyclohexanone with copper(II) chloride; the product was identified as 3,6,6-tribromo-2-hydroxycyclohex-2-en-1-one (**3**).

In the reaction of 2- and 3-methylcyclohexanone, a product was obtained which, from its spectroscopic data, was identified as 6,6-dibromo-2-hydroxy-3-methylcyclohex-2-en-1-one (**4**), corresponding to the chloro compound.

In the case of 4-methylcyclohexanone, two products were isolated by column chromatography. The first product was determined to be 3,6-dibromo-2-hydroxy-5-methycyclohex-2-en-1-one (6), since it showed the absorptions due to an α-hydroxy-α,β-unsaturated ketone in the NMR and IR spectra and also a peak at 4.43 ppm (doublet, $J=3$ Hz) attributable to –CH(Br)– in the NMR spectrum. The second product had a peak at 2.61 ppm (singlet) attributable to aromatic methyl protons and a peak at 5.76 ppm (broad) attributable to the phenolic hydroxyl group; the ratio of their protons was 3 : 2 in the NMR spectrum. However, no peak due to aromatic protons was observed in the NMR spectrum. Accordingly, the product was identified as a hexasubstituted benzene derivative (**10**). In order to confirm that **10** can be formed through **6**, the reaction with 4-methylcyclohexanone was carried out for a longer time (2.5 hr). As a result, **6** was not obtained, but the yield of Compound **10** doubled (18%).

In the case of 3,4-dimethylcyclohexanone, it was deduced from the spectroscopic data that the product was 6,6-dibromo-2-hydroxy-3,4-dimethylcyclohex-2-en-1-one (**18**).

From the reaction of 3,5-dimethylcyclohexanone, three products were isolated by column chromatography. In the NMR spectrum of the first product, peaks were observed at 2.60 ppm (singlet) attributable to aromatic methyl protons and at 5.82 ppm (singlet) attributable to a phenolic hydroxyl group, the ratio of their protons being 6 : 1. Just as in the case of **10**, the absorption due to aromatic protons was not observed. Thus, this product was identified as a hexasubstituted benzene derivative (**17**). This identification was further confirmed by comparing the product with the sample produced from 3,5-dimethylphenol in a previously described manner.[3] The second product showed the absorptions due to an α,β-unsaturated ketone (1683 and 1607 cm^{-1}) in the IR spectrum. There was a peak at 1.43 ppm (doublet, $J=6$ Hz) due to methyl protons and one at 2.20 ppm (singlet) due to allylic methyl protons, but there were no peaks attributable to –CH(Br)– or hydroxyl groups in the NMR

* Present address: Meiji College of Pharmacy, 1-22-1 Yato-machi, Tanashi, Tokyo 188.

Table 1. Reaction of cycrohexanones with copper(II) bromide

Starting material	Mole ratio per ketone	Time (hr)	Products		Yield (%)
Cycylohexanone	30	1.5	3,6,6-tribromo-2-hydroxycyclohex-2-en-1-one	(**3**)	60
2-Methylcyclohexanone	20	1.5	6,6-dibromo-2-hydroxy-3-methylcyclohex-2-en-1-one	(**4**)	14
3-Methylcyclohexanone	20	1.5	6,6-dibromo-2-hydroxy-3-methylcyclohex-2-en-1-one	(**4**)	15
4-Methylcyclohexanone	30	0.5	3,6-dibromo-2-hydroxy-5-methylcyclohex-2-en-1-one	(**6**)	28
4-Methylcyclohexanone	30	1.5	3,6-dibromo-2-hydroxy-5-methylcyclohex-2-en-1-one	(**6**)	19
			3,4,6-tribromo-5-methylpyrocatechol	(**10**)	9
4-Methylcyclohexanone	30	2.5	3,4,6-tribromo-5-methylpyrocatechol	(**10**)	18
3,4-Dimethylcyclohexanone	20	1.5	6,6-dibromo-2-hydroxy-3,4-dimethylcyclohex-2-en-1-one	(**18**)	14
3,5-Dimethylcyclohexanone	20	1.0	2,6-dibromo-3,5-dimethylcyclohexan-1-one	(**11**)	9
3,5-Dimethylcyclohexanone	20	1.5	2,6-dibromo-3,5-dimethylcyclohexan-1-one	(**11**)	9
			2,6,6-tribromo-3,5-dimethylcyclohex-2-en-1-one	(**14**)	12
			2,4,6-tribromo-3,5-dimethylphenol	(**17**)	16

Table 2. Physical properties and elemental analyses of products

Product	Mp (°C)	IR (cm^{-1})	UV (nm)	NMR (ppm)	C (%) Found (Calcd) [Mol. formula]	H (%) Found (Calcd)
3	120—122	3413 1674 1622	301 (ε=8600)	2.97(s, 4H) 6.26(s, 1H)	(decomp.)	
4	135—138	3401 1669 1641	296 (ε=9100)	1.95(s, 3H) 2.08—3.52(m, 4H) 6.35(s, 1H)	29.59 (29.61) [$C_7H_8O_2Br_2$]	2.88 (2.84)
6	136—137	3400 1669 1638	295 (ε=9000)	1.15(d, J=6 Hz, 3H), 2.09—2.64(m, 1H) 2.71(d, J=4.5 Hz, 1H) 2.75(d, J=8.2 Hz, 1H) 4.43(d, J=3 Hz, 1H), 6.29(s, 1H)	Found 281.8904 [$C_7H_8O_2Br_2$]	Calcd[a] 281.8892
10	125—130 (subl.)	3528 3417 1631 1581		2.61(s, 3H) 5.76(b, 2H)	Found 357.7873 [$C_7H_5O_2Br_3$]	Calcd[a] 357.7841
18	150—151 (subl.)	3402 1670 1639	296 (ε=7100)	1.17(d, J=6 Hz, 3H), 1.89(s, 3H) 1.53—2.85(m, 1H), 2.69(d, J=8.4 Hz, 1H) 2.74(d, J=3.2 Hz, 1H), 6.32(b, 1H)	32.44 (32.25) [$C_8H_{10}O_2Br_2$]	3.34 (3.38)
11	175—179 (subl.)	1725		1.25(d, J=6 Hz, 6H) 1.31—2.43(m, 4H) 4.34 (d, J=11.2Hz, 2H)	Found 281.9246 [$C_8H_{12}OBr_2$]	Calcd[a] 281.9256
14	117—120	1683 1607	269 (ε=9800)	1.43(d, J=6 Hz, 3H), 2.20(s, 3H) 2.28—2.66(m, 1H) 2.46(d, J=2.5 Hz, 2H)	26.85 (26.62) [$C_8H_9OBr_3$]	2.55 (2.51)
17	160—163 (166)[3]	3420 1545		2.60(s, 6H) 5.82(s, 1H)	26.40 (26.75) [$C_8H_7OBr_3$]	2.06 (1.97)

a) Analyzed by high resolution mass spectrometry.

spectrum. From these data, the product was identified as 2,6,6-tribromo-3,5-dimethylcyclohex-2-en-1-one (**14**). The third product showed an absorption due to a saturated ketone (1725 cm^{-1}) in the IR spectrum, and no absorption due to unsaturated ketone in the UV spectrum. There was a peak at 1.25 ppm (doublet, J=6 Hz) attributable to methyl protons and one at 4.34 ppm (doublet, J=11.2 Hz) attributable to -CH(Br)-, the ratio of their protons being 3 : 1. Hence, the product was identified as a dibrominated cyclohexanone derivative (**11**).

In conclusion, the results of the present investigation of the reactions of cyclohexanones with copper(II) bromide can be summarized as follows: cyclohexanedione derivatives were obtained in all cases except in the case of 3,5-dimethylcyclohexanone; polysubstituted aromatic compounds were obtained in the cases of 4-methyl- and 3,5-dimethylcyclohexanone.

Now, the pathway for the formation of the polybrominated cyclohexanediones will be considered. The question of whether or not the liberated molecular bromine (Eq. 1) participates in the reaction of organic compounds with copper(II) bromide has been discussed in earlier reports:[4]

$$CuBr_2 \longrightarrow 1/2Br_2 + CuBr \quad (1)$$

Hence, the reaction of cyclohexanone with comparable amounts of bromine (15-fold molar) was carried out under the same conditions. 2,2,6,6-Tetrabromocyclohexanone [mp 118—120 °C (lit,[5] 122—123 °C)] was obtained in a quantitative yield, but neither **1**, **2**, nor **3** was obtained. Thus, it can be concluded that the reaction leading to cyclohexanedione derivatives is a specific reaction with copper(II) bromide. Considering this finding, together with previous results in the cases of reactions with copper(II) chloride,[1] a plausible mechanism for the formation of polyhalogenated cyclohexanediones is that shown in Scheme 1. **1** may be formed by the hydrolysis and dehydration of *gem*-dihalogen of Compound (**c**), followed by enolization.

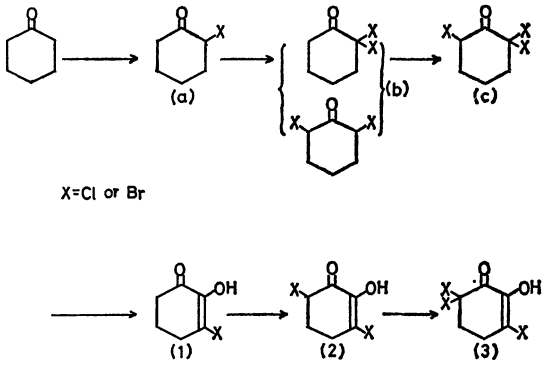

Scheme 1.

Next, the pathway to the pyrocatechol derivative will be considered. When the reaction with 4-methylcyclohexanone was stopped after only 30 min, the major product was **6**. In addition, the NMR spectrum indicated that Compound **7** [1.45 ppm (doublet, J= 6 Hz, $-CH_3$) and 2.05—2.88 ppm (multiplet, -CH- and $-CH_2-$)] exists in the filtrate as the minor product. From all the results in the case of 4-methylcyclohexanone, the following pathway was thus demonstrated (see Scheme 2). In the first stage of the reaction, **5** was produced through the pathway shown in Scheme 1, not affected by the methyl group because the methyl group in **5** was located in the γ-position with respect to the carbonyl group. The resulting **5** was further brominated to give **6** and then **7**. **7** was then led to **8** by dehydrobromination between the *gem*-bromine and the hydrogen on the adjacent tertiary carbon because of the larger steric hindrance due to the methyl group in **7** as compared with that in Compound **3**. **8** was subjected to enolization to give a more stable aromatic compound, **9** followed by bromination to the tetrasubstituted pyrocatechol derivative (**10**).

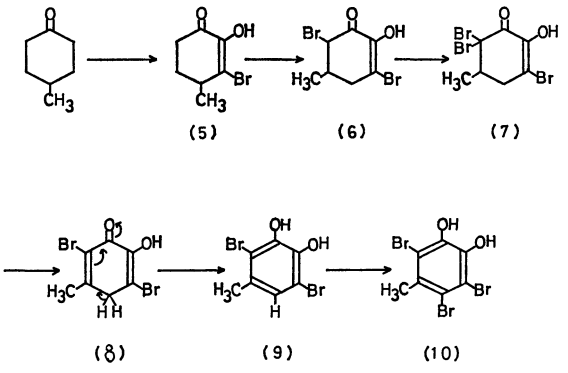

Scheme 2.

Lastly, the pathway to the phenol derivative will be considered. When the reaction with 3,5-dimethylcyclohexanone was stopped for 1 hr and the reaction mixture then treated in the usual way, the only resulting product was **11**. Hence, we propose the following pathway for the formation of **17** (see Scheme 3). The dehydrobromination and bromination of **12**, which is derived from **11**, gives **14**. The resulting **14** was subjected to dehydrobromination, followed by enolization to give a more stable aromatic compound, **16**. **16** was then brominated to give **17**. The last step is supported by a report[6] of halogenation at the *p*-position in the reaction of a phenol derivative with copper(II) halide.

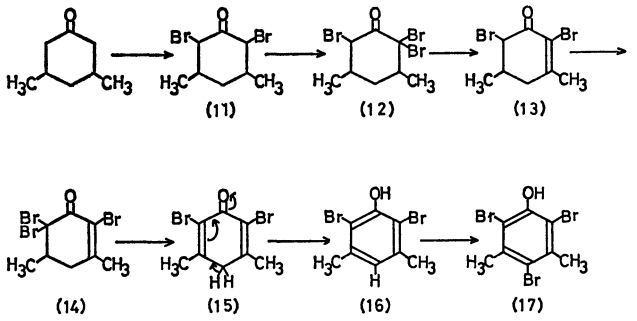

Scheme 3.

We wish to express our appreciation to Professor A. Hagitani of Rikkyo University for his kind guidance and helpful suggestions in this work. Thanks are also due to Dr. S. Hishida, Naka Works, Hitachi Ltd., for his measurement of the high-resolution mass spectra.

References

1) Part I: K. Nishizawa and J. Y. Satoh, This Bulletin, **48**, 1276 (1975).
2) J. Y. Satoh and K. Nishizawa, *Chem. Commun.*, **1973**, 83.
3) L. C. Raiford and J. H. Scott, *J. Org. Chem.*, **2**, 213 (1937).
4) C. E. Castro, E. J. Gaughan, and D. C. Owsley, *ibid.*, **30**, 587 (1965); T. Koyano, This Bulletin, **44**, 1158 (1971).
5) J. Petrissans and J. Deschamps, *Tetrahedron*, **26**, 2575 (1970); F. Boudroux and F. Taboury, *C. R. Acad. Sci., Paris*, **154**, 1509 (1912).
6) W. C. Baird, Jr. and J. H. Surridge, *J. Org. Chem.*, **35**, 3436 (1970).

NMR Studies of the Conformations of 3-Aryl-1,2,3-oxathiazolidine 2-Oxides

Fukiko YAMADA, Tomihiro NISHIYAMA, and Hiroshi SAMUKAWA

Department of Applied Chemistry, Faculty of Engineering, Kansai University, Senriyama, Suita, Osaka 564

(Received October 30, 1974)

Proton magnetic resonance spectroscopy has been used to investigate the conformations of a series of 3-aryl-1,2,3-oxathiazolidine 2-oxides. Their conformations were assigned on the basis of the vicinal coupling constants between four methylene protons at the C-4 and C-5 positions. The oxathiazolidine 2-oxides prefer twist-envelope forms, and their conformations vary with both the situation and the nature of the ring substituent. Postulated collision complexes based on the data of the observed solvent-shifts can also be explained in terms of the differences in the conformations.

Recently, considerable attention has been directed to the elucidation of the conformations of heterocyclic compounds by NMR spectroscopy. However, only a few studies have been reported on the stereochemistry of the 1,2,3-oxathiazolidine 2-oxides. For example, Deyrup and Moyer reported that the sulfoxide bond was known to have an acetylenic-like anisotropy and that, therefore, the NMR spectra of the two isomeric 4- or 5-substituted 3-*t*-butyl-1,2,3-oxathiazolidine 2-oxides permitted the assignment of *cis* and *trans* geometry.[1] On the other hand, we ourselves have reported that twelve new 3-aryl-5-methyl- and 3-aryl-5-chloromethyl-1,2,3-oxathiazolidine 2-oxides have been prepared in good yields, and the configurations of their stereoisomers have been discussed on the basis of the NMR spectral data.[2] In continuation of our previous reports concerning the formation of 3-aryl-1,2,3-oxathiazolidine 2-oxides and their NMR and mass spectra,[3,4] this paper will report the results of NMR analyses of a series of 3-aryl-1,2,3-oxathiazolidine 2-oxides (**1**).

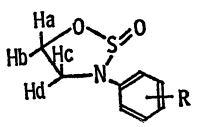

1

I, R=H
IIa, R=*o*-CH_3
IIb, R=*m*-CH_3
IIc, R=*p*-CH_3
IIIa, R=*o*-OCH_3
IIIb, R=*m*-OCH_3
IIIc, R=*p*-OCH_3
IV, R=*p*-Br
Va, R=*o*-Cl
Vb, R=*m*-Cl
Vc, R=*p*-Cl
VI, R=2,4,6-tri-Cl

Experimental

Measurements. All the boiling and melting points are uncorrected. All the NMR spectra were determined at 100- and 60-MHz with Japan Electron Optics Model JNM-PS-100 and JNM-3H-60 spectrometers respectively. The chemical shifts were reported in ppm downfield from the internal TMS (δ). The coupling constants were determined from the spectra with a 270 Hz sweep width and a sweep time of 0.5—1.0 Hz/s. The IR spectra were recorded on a Shimadzu Model 27-G grating spectrophotometer on a KBr disk for the solid materials or a NaCl plate for the liquid materials. The glc analysis was carried out on a Shimadzu gas chromatograph, Model GC-5AP$_3$T, using a 2.15-m column packed with silicone SE-30 (10 wt%). The percentage composition of the product was estimated by means of the relative peak areas (uncorrected).

Compounds. A series of **1** was prepared by the reaction of the corresponding *N*-sulfinylanilines with ethylene oxide in the presence of lithium chloride as a catalyst, and was purified by distillation or recrystallization, as has been described in our previous papers.[2,3] The above reaction conditions and the properties of the compounds thereby obtained are listed in Table 1.

Results and Discussion

Sulfoxide Bond. The IR spectra of all the **1** compounds showed a characteristic band of the S=O group at 1155—1172 cm^{-1} (Table 1). In trimethylene sulfites, the S=O group prefers to be axial,[5] and the same conformational preference is found in six-membered ring sulfoxides.[6,7] The assignment of the axial and equatorial S=O groups has been made on the basis of the positions of the S=O stretching bands in trimethylene sulfites: 1190 cm^{-1} for an axial oxygen and 1230 cm^{-1} for an equatorial oxygen. In the case of ethylene sulfite, the position of the S=O stretching band 1193 cm^{-1} (neat) to 1214 cm^{-1} (cyclohexane) indicates a predominance of pseudoaxial conformers.[8] If this consideration can be extended to the **1** compounds, and assuming an equilibrium between pseudoaxial and pseudoequatorial conformers, the position of the S=O stretching bands of **1**, 1172 (neat) to 1182 cm^{-1} (carbon tetrachloride) would indicate a predominance of pseudoaxial conformers. An inspection of the molecular model also reveals that the **1** compounds exist in pseudoaxial conformers.

Methylene Protons. The NMR spectra of the methylene protons of the IIa, IIIc, IV, and VI compounds are shown in Fig. 1. All the **1** compounds displayed similar sets of methylene-proton multiplets of the representative ABCD pattern. That is, the two well-separated multiplets of an unequal height and width correspond to the two protons at the 5 position, while the other ones further upfield correspond to the protons at the 4 position.[2] Besides, according to S=O bond anisotropy, which exerts a stronger deshielding effect at the *cis*-position than at the *trans*-position,[1,2] the NMR signals of the H_a and H_c protons can be assigned multiplets in a lower field than those of H_b and H_d respectively.

The appearance of the NMR spectra of **1** gave well-defined patterns for the methylene-proton signals. We have, therefore, segregated the spectra into four types—A, B, C, and D, as can be seen in Fig. 1. The signals of Compounds I, IIb, IIc, IV, Vb, and Vc may all be

Table 1. Data for the 3-aryl-1,2,3-oxathiazolidine 2-oxides

Compd. No.[a]	Reaction conditions		Yield %	Mp °C or Bp(mmHg)	IR (S=O) cm^{-1}	Elementary analysis (%), (Calcd value)				
	Temp., °C	Time, hr				C	H	N	S	halogen
I	50	8	90	45.0—46.8	1172	—	—	—	—	
IIa	45	13	74	79(0.1)	1162	71.20[b] (71.49)	8.66 (8.67)	9.12 (9.26)	—	
IIb	50	4	60	38.2—38.8	1161	54.60 (54.80)	5.61 (5.62)	7.15 (7.10)	16.22 (16.25)	
IIc	30	7	47	74.8—75.6	1169	—	—	—	—	
IIIa	40	6	80	120—125(0.1)	1157	64.07[b] (64.65)	7.91 (7.84)	8.10 (8.38)	—	
IIIb	30	13	10	34.0—36.0	1163	50.77 (50.69)	5.36 (5.20)	6.60 (6.57)	14.81 (15.03)	
IIIc	15	16	65	52.8—53.2	1163	50.83	5.25	6.62	14.72	
IV	50	7	60	87.5—88.2	1155	36.93 (36.66)	3.14 (3.08)	5.41 (5.34)	12.19 (12.23)	30.96 (30.48)
Va	20	14	47	58.0—59.9	1162	55.84[b] (55.99)	5.88 (5.87)	8.15 (8.16)		20.59 (20.67)
Vb	50	5	86	84.7—85.0	1161	44.07 (44·14)	3.65 (3.70)	6.44 (6.43)	14.82 (14.73)	16.29 (16.29)
Vc	50	5	79	68.5—71.5	1158	—	—	—	—	—
VI	45	4	50	115.3—115.8	1165	33.48 (33.53)	2.07 (2.11)	4.90 (4.89)	11.11 (11.19)	37.50 (37.12)

a) IIa, IIb, IIIa, IIIb, IIIc, IV, Va, Vb, and VI are newly-prepared compounds. b) These compounds are unstable even at room temp. and easily decompose by exposure to air. Therefore, the values of the elementary analyses were obtained for the corresponding *N*-(*β*-hydroxyethyl)aniline.[2]

Table 2. NMR spectral data of the compounds, 1.[a]

Compd. No.	Chemical Shifts, δ ppm							
	H_a	H_b	H_c	H_d	CH_3 or OCH_3	Aromatic ring proton[c]	H_a-H_b	H_c-H_d
I	4.89	4.55	3.77	3.52	—	6.82—7.35 (m)	0.34	0.25
IIa	4.82	4.41	4.00	3.49	2.36	7.05—7.26 (m)	0.41	0.51
IIb	4.85	4.51	3.72	3.49	2.27	2,4,6 : 6.62—6.82 5 : 7.10, J=7.5	0.34	0.23
IIc	4.86	4.50	3.74	3.49	2.29	2,6 : 6.84, J=8.3 3,5 : 7.05, J=8.3	0.36	0.25
IIIa	4.82	4.44	3.84	3.57	3.92	6.99 (s) 6.80—7.20 (m)	0.38	0.27
IIIb	4.86	4.52	3.73	3.50	3.73	2,4,6 : 6.42—6.60 (m) 5 : 7.12 (q)	0.34	0.23
IIIc	4.76	4.39	3.72	3.46	3.63	2,6 : 6.87 or 6.66 3,5 : 6.66 or 6.87	0.37	0.26
IV[b]	4.99	4.64	3.80	3.57	—	2,6 : 6.87, J=8.5 3,5 : 7.37, J=8.5	0.35	0.23
Va	4.84	4.44	3.95	3.65	—	7.04—7.46 (m)	0.40	0.30
Vb[b]	4.96	4.62	3.79	3.57	—	2,4,6 : 6.82—7.04 (m) 5 : 7.19	0.34	0.22
Vc	4.87	4.52	3.72	3.46	—	2,6 : 6.78, J=8.5 3,5 : 7.15, J=9.0	0.35	0.26
VI[b]	5.06	4.70	3.99	3.51	—	7.43 (s)	0.36	0.48

a) The data refer to 0.5 mmol/ml solutions in CCl_4 unless otherwise indicated. Chemical shifts are believed to be significant to ±0.02 ppm and coupling constants to ±0.2 Hz. b) Data for $CDCl_3$ (30%)—CCl_4 solution. c) Coupling constant, Hz.

considered to belong to Type A. Similarly, those of Compounds IIa, IIIa, and Va appear to belong to Type B, and those of IIIb and IIIc, to Type C. Only the signal of VI belongs to a different Type, D.

The NMR spectra of **1** are of an almost pure first-order type, and all the coupling constants can be obtained by inspection. Small second-order effects can be observed on the basis of a comparison of the peak pattern at 100 MHz with that of 60 MHz. Theoretically, one of these methylene protons is individually split to octet lines because of coupling with the three other protons. Computor simulations of the observed signals were carried out using the five-spin system (No. 396) of the Japan Electron Opt. Co., Ltd., program.

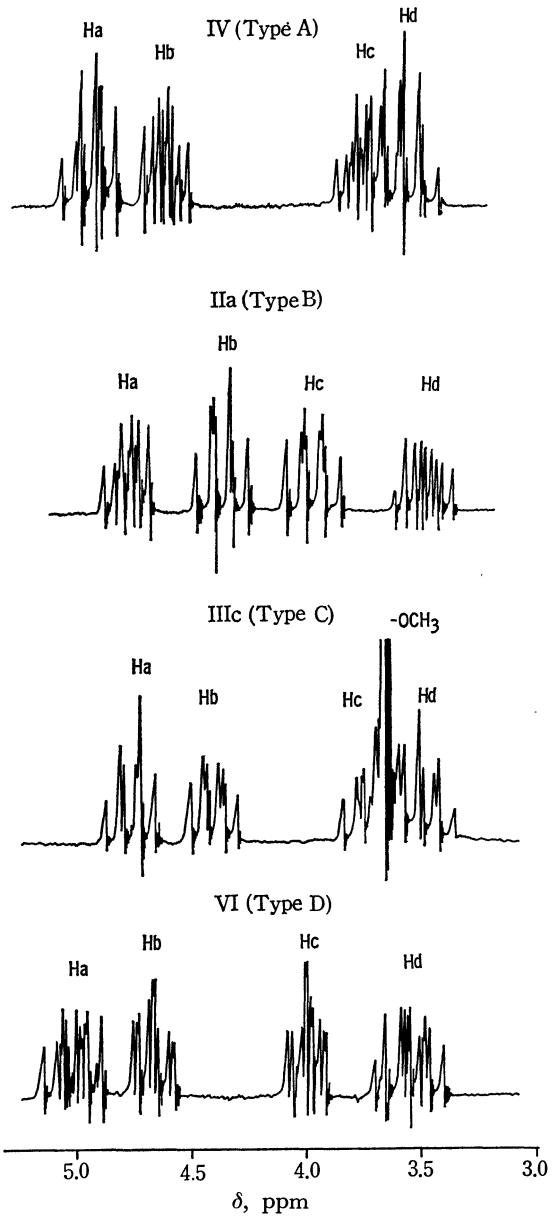

Fig. 1. 100 MHz NMR spectra of the methylene protons of **1** in CCl_4.

The agreement between the observed and calculated spectra was excellent. The NMR spectral data are listed in Table 2, while their coupling constants are summarized in Table 3.

As can be seen in Table 2, the differences between the chemical shift values for the geminal protons (H_a-H_b and H_c-H_d, δ ppm) may be due to the conformation of the oxathiazolidine ring. In the case of the compounds of Types A and C, the values of H_a-H_b and H_c-H_d are 0.34—0.37 and 0.22—0.26 ppm respectively. On the other hand, in the compounds of Types B and D, the above values are 0.36—0.41 and 0.27—0.51 ppm respectively. From the above results, it may be thought that the conformations of **1** vary with both the situation and the nature of the ring substituent, and that it is possible to distinguish them by the appearances of their methylene-proton signals.

Geminal Coupling. Two geminal coupling have been determined in this study (in Table 3); they were found to be in agreement with the values obtained for the other 3-aryl-5-methyl-1,2,3-oxathiazolidine 2-oxides (J_{cd}=8.3—8.8 Hz).[2]

Vicinal Coupling and Stereochemistry. In view of the results of the present investigation, the relevant distortions from the idealized stereochemistry of the **1** system, in which H_a is completely eclipsed by H_c and in which H_b is also eclipsed by H_d, involve torsional changes about the C-4 and C-5 bonds. These changes are most likely to be of two kinds, represented by the projections of **2** and **3** in Fig. 2.

A comparison of the pairs of entries in Table 3, where the electronegativities of the substituents are the same or similar, but where the substituents differ in position, leads to some suggestions. Thus, the much greater J_{ad} constants for Compounds IIb, IIc, IIIb, IIIc, Vb, and Vc than those of IIa, IIIa, and Va suggest that the distortions of the compounds with an *m*- or *p*-substituent are in the direction of the **2** projection, while those with *o*-substituents cause a distortion toward the **3** projection.

Williamson[9] and Laszlo and Schleyer[10] reported that the magnitudes of coupling constants between protons on adjacent saturated carbon atoms vary significantly with

TABLE 3. THE DATA OF THE COUPLING CONSTANTS[a] FOR THE METHYLENE PROTONS OF **1**

Compd. No.	Coupling Constants, Hz						J_{ad}/J_{bc} (r value)	θ (degree)	
	Geminal		Vicinal					A=8	A=7
	J_{ab}	J_{cd}	J_{ac}	J_{ad}	J_{bc}	J_{bd}			
I	8.5	8.5	6.6	8.9	4.1	7.0	2.2	15	12
IIa	7.8	9.0	7.2	4.5	7.9	6.8	1.8[b]	−11	−9
IIb	8.5	8.6	6.6	8.2	4.3	6.9	1.9	12	10
IIc	8.6	8.4	6.5	8.4	4.7	6.6	1.8	11	9
IIIa	8.4	8.9	7.1	5.4	7.1	7.0	1.3[b]	−5	−4
IIIb	8.6	8.6	6.5	8.5	4.1	7.0	2.1	14	11
IIIc	8.4	8.3	6.8	6.8	5.5	6.7	1.2	4	4
IV	8.4	8.6	6.5	8.6	4.1	6.9	2.1	14	11
Va	7.9	8.9	7.1	4.5	8.0	6.9	1.8[b]	−11	−9
Vb	8.4	8.4	6.6	8.8	4.0	6.9	2.2	15	12
Vc	8.4	8.4	6.6	8.2	4.3	6.8	1.9	12	10
VI	8.4	8.2	6.0	10.3	2.2	6.8	4.7	≥30	27

a) Coupling constants are believed to be significant to 0.2 Hz. b) Values for J_{bc}/J_{ad}.

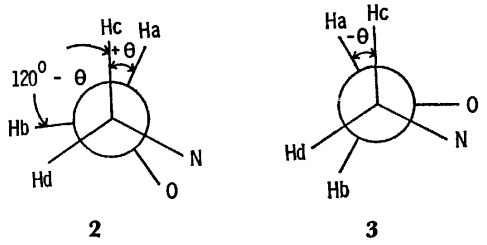

2 3

Fig. 2. Diagrams of **2** and **3** forms of the parts of methylene protons of **1**.
Dihedral angle (ϕ) = 120°±torsion angle (θ).

changes in the electronegativity (ER) of the adjacent substituent and that the internal chemical shifts for the same protons also depend on the ER of the substituent. From this literature, values of approximately 1—2 ppm/ER unit for the chemical shift and 1—1.5 Hz/ER for the coupling constant are given. Such values, which can be obtained from Tables 2 and 3, are quite small in comparison with the values mentioned above. Besides, the plots of J vicinal *vs.* ER of **1** showed a considerable scatter. There seems to be no unequivocal correlation between the ER and the coupling constant. These facts indicate that the chemical shifts and the coupling constants in the series of **1** do not depend on the ER of the ring substituent. Furthermore, the nature of our system assures the constancy of other variables, for example, the C–C bond length and the H–C–C angle. It is, therefore, probable that the vicinal coupling constants of **1** depend only on each dihedral angle.

Assuming, as is mentioned above, that the most important factor determining the magnitude of the vicinal coupling constant is the dihedral angle, one may conclude that the J_{trans}(J_{ad} or J_{bc}) in **1** is more sensitive to distortions from perfect eclipsing than J_{cis} (J_{ac} or J_{bd}) because of the shape of the Karplus function. In this series of 12 compounds, J_{ad} varies from 4.5 to 10.3 Hz, and J_{ac} varies from 6.0 to 7.2 Hz (Table 3).

When the envelope conformation and various other conformational extremes are considered, there is found to be a wide range of variability in the stereochemical relationships between methylene protons of **1**. For the molecule existing in the ideal envelope conformation, the coupling constants, J_{ad} and J_{bc}, correspond to the dihedral angles of approximately 120 and 120° respectively. In this case, the ratio (r) of J_{ad} to J_{bc} in the five-membered ring of **1** is close to 1.0. On the other hand, Lambert[11] reported that the ratio (R) of the average $^3J_{trans}$ to the average $^3J_{cis}$ in the six-membered ring compounds is nearly independent of the ER of the substituents and become a direct measure of the conformational effects, and that the ratio was close to 2.0 for the molecules in the perfect-chair conformation. In our system, a further inspection of molecular model reveals that a decrease in θ will decrease J_{ad} (Projection **2** in Fig. 2) or J_{bc} (Projection **3**), whereas it will increase J_{bc} (Projection **2**) or J_{ad} (Projection **3**). Thus, the coupling constant caused by each torsion angle, θ, is given by the following Karplus eq.:[12]

$$r = (J_{ad}/J_{bc}) \text{ or } (J_{bc}/J_{ad}) = \frac{A - B\cos(120+\theta) + C\cos 2(120+\theta)}{A - B\cos(120-\theta) + C\cos 2(120-\theta)} \quad (1)$$

For the above eq. (1), a reasonable set of empirical parameters, $A=+7$, $B=+1$, and $C=+5$,[12] was employed. Then we attempted to use the $A=+8$ parameter in eq. (1) in order to get good results. The changes in θ caused by the distortions and the corresponding changes in J and r are listed in Tables 4 and 5 ($+30° \geq \theta \geq -30°$).

The tortion angles corresponding to the calculated r values (in Table 5) with the best agreement with the observed r values (Table 3) were found out to be as is shown in Table 3. Figure 3 shows the plots of the observed vicinal coupling constants *vs.* the dihedral angles with the calculated Karplus curves for both of the parameters, $A=+7$ and $A=+8$. In the case of the $A=+8$ parameter, the data clearly fall on the Karplus curve.

Table 4. J values calculated by the Karplus Eq. in Eq. (1)

θ°	J, Hz		θ°	J, Hz	
	A=8	A=7		A=8	A=7
0	6.00	5.00			
1	6.17	5.17	−1	5.84	4.84
4	6.69	5.69	−4	5.36	4.36
5	6.86	5.86	−5	5.21	4.21
10	7.77	6.77	−10	4.51	3.51
11	7.96	6.96	−11	4.39	3.39
12	8.15	7.15	−12	4.26	3.26
13	8.33	7.33	−13	4.15	3.15
14	8.52	7.52	−14	4.04	3.04
15	8.71	7.71	−15	3.93	2.93
20	9.63	8.63	−20	3.48	2.48
25	10.53	9.53	−25	3.16	2.16
30	11.37	10.37	−30	3.00	2.00

Table 5. Correlation between θ and r obtained from Eq. (1)

θ°	r	
	A=8	A=7
0	1.00	1.00
1	1.06	1.07
4	1.25	1.31
5	1.32	1.39
10	1.72	1.93
11	1.81	2.05
12	1.91	2.19
13	2.01	2.33
14	2.11	2.47
15	2.22	2.63
20	2.77	3.48
25	3.33	4.41
30	3.79	5.19

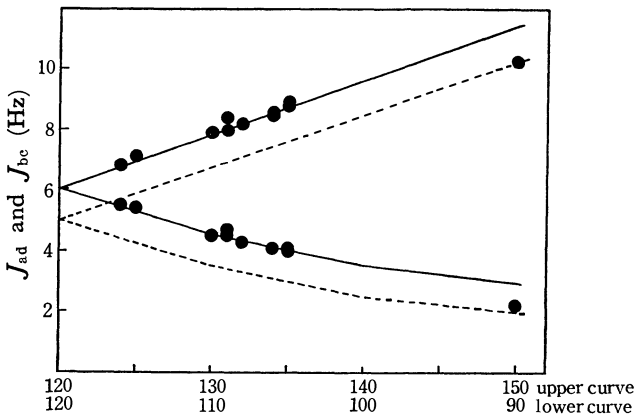

Fig. 3. Plots of the vicinal coupling constants, J_{ad} and J_{bc}, *vs.* the dihedral angles.
Calculated Karplus curves {—— in $A=8$ ---- in $A=7$

From these results, the conformations of **1** may be divided roughly into the following four groups:

Group 1. $\theta=10$—$15°$, $r=1.8$—2.2. The compounds of Type A, —that is, I, IIb, IIc, IV, Vb, and Vc, and IIIb—show this type of conformation.

Group 2. $\theta=-5$——$11°$, $r=1.3$—1.8. The compounds of Type B, IIa, IIIa, and Va, all with an *o*-substituent, show this type of conformation.

Group 3. $\theta=-5$—$+4°$, $r=1.2$—1.3. In IIIa and IIIc (Types B and C respectively), the two methylene groups are nearly eclipsed.

Group 4. $\theta\geq30°$, $r=4.7$. Compound VI, Type D, shows this conformation.

In Group 1, r is approximately 2.0 ± 0.2 (within 10—15%). In Group 3, both the r values are close to 1.0. The r of Group 4 shows an extremely large value; this indicates the presence of severe distortion in VI. Thus, deviations from $r=1$ indicate distortions from the envelope conformation.

It is interesting to compare these conformations with their chemical stabilities. Group 1 and Group 4 compounds are stable at room temperature. On the contrary, Group 2 and Group 3 compounds are unstable even at room temperature and are easily decomposed by water to the corresponding *N*-(β-hydroxyethyl)-anilines, as can be seen in Table 1.

Solvent-shift Studies. The NMR spectral data of **1** in a deuterobenzene solution exhibit benzene-induced shifts, as can be seen in Table 6. The proposed geometry of a benzene–solute collision complex of **1** is shown in Fig. 4. The results furnish considerable information on the stereochemical structure of the collision complex. (1a) In the case of Compounds I, IIb, IIc, and IIIb the solvent-shifts, $\Delta\delta_H$ ppm, for the different protons are in this order: $H_d>H_b>H_c>H_a$.

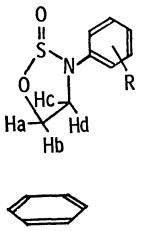

Fig. 4. Proposed geometry of benzene-solute collision complex of the oxathiazolidines.

This fact confirms the finding that the torsion angles in these compounds (Group 1) are found in the 10—15° range. In each compound, the $\Delta\delta_{Ha}$ value is smaller than the other three values; they are approximately 1.5 times H_a. This means that the co-ordinated benzene molecule exists rather closer to the C-4 atom than to the C-5 atom. (1b) On the other hand, Compounds IV, Vb, and Vc, all with a halogen substituent in Group 1, show this order of $\Delta\delta_H$ values; $H_d>H_c>H_b>H_a$. The values of the different four protons are somewhat greater than those of the corresponding protons in (1a) (*e.g.* $\Delta\delta_{Ha}$ in 1b$>\Delta\delta_{Ha}$ in 1a). These facts suggest that the co-ordinated benzene molecule in these compounds (1b) comes closer to the oxathiazolidine ring than with that of the compounds of (1a). (2) In the compounds with an *o*-substituent, IIa, IIIa, and Va, the $\Delta\delta_{Hc}$ values are somewhat smaller than the other three values. This indicates that the sign of the torsion angle of this group is negative compared with that of the compounds in Group 1.

TABLE 6. BENZENE-INDUCED SOLVENT SHIFTS $\Delta=[\delta(CCl_4)-\delta(C_6D_6)]$ FOR THE DIFFERENT PROTONS IN **1**

Compd. No.	Resonance					$(\Delta\delta_{Hc}-\Delta\delta_{Ha})/(\Delta\delta_{max}-\Delta\delta_{min})$
	H_a	H_b	H_c	H_d	CH_3 or OCH_3	
I	0.515	0.780	0.745	0.820	—	0.75
IIa	0.552	0.759	0.481	0.741	0.170	−0.26
IIb	0.475	0.725	0.675	0.760	0.240	0.70
IIc	0.445	0.680	0.605	0.715	0.215	0.59
IIIa	0.510	0.655	0.487	0.701	0.560	−0.11
IIIb	0.461	0.727	0.697	0.772	0.355	0.76
IIIc	0.485	0.770	0.580	0.725	0.390	0.39
IV[a)]	0.720	0.955	1.025	1.105	—	0.79
Va	0.620	0.705	0.520	0.805	—	−0.35
Vb[a)]	0.710	0.940	1.070	1.140	—	0.84
Vc	0.575	0.805	0.900	0.985	—	0.79
VI[a)]	0.590	0.820	0.745	0.730	—	—

a) $\Delta=\delta(CDCl_3(30\%)\text{-}CCl_4)-\delta(C_6D_6)$.

In IIa, the $\Delta\delta_H$ values show the order of $H_b > H_d > H_a > H_c$, and while in IIIa and Va the values show the order of $H_d > H_b > H_a > H_c$. (3) Compounds IIIa and IIIc, with a methoxy substituent, are considered to belong to this section. The $\Delta\delta_{Hb}$ value of IIIa is the smallest of all those of **1**; the value of $\Delta\delta_{Ha} - \Delta\delta_{Hc}$ is also the smallest of those of the compounds with an *o*-substituent,—that is, IIa, IIIa, and Va. In IIIc the $\Delta\delta_{Hd}$ value is relatively small and the value of $\Delta\delta_{Hc} - \Delta\delta_{Ha}$ is the smallest of the compounds in Group 1 and VI. In IIIa, the $\Delta\delta_H$ values show the order of $H_a > H_c$ and $H_d > H_b$, while in IIIc the order is $H_c > H_a$ and $H_b > H_d$. These facts indicate that the torsion angles of IIIa and IIIc are small and have either a positive or a negative sign. This result is quite consistent with the near-ideal envelope conformation of Group 3. (4) Compound VI, with tri-chloro substituents, shows the following effects. (a) The value of $\Delta\delta_{max} - \Delta\delta_{min}$, that is, $\Delta\delta_{Hb} - \Delta\delta_{Ha}$, is 0.230 ppm, the smallest of all those of **1**. (b) $\Delta\delta_{Hc}$ and $\Delta\delta_{Hd}$ are almost the same. From the above facts, we suggest that the co-ordinated benzene molecule exists at almost the same distance from both the H_c atom and the H_d atom.

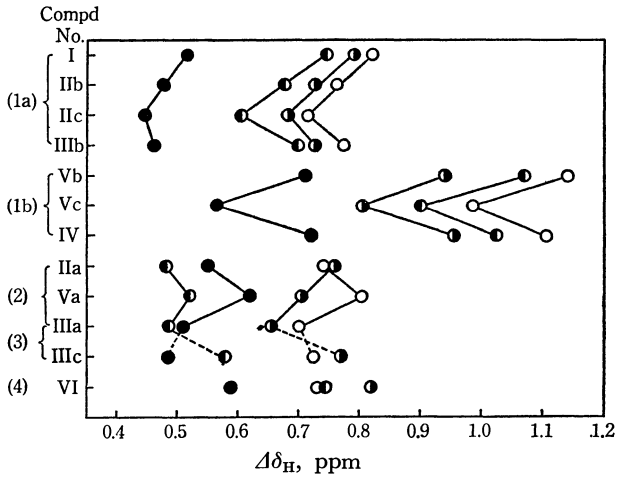

Fig. 5. Solvent-shift changes ($\Delta\delta_H$ obsd) of the methylene protons of **1**.
—●— H_a, —◑— H_b, —◐— H_c, —○— H_d

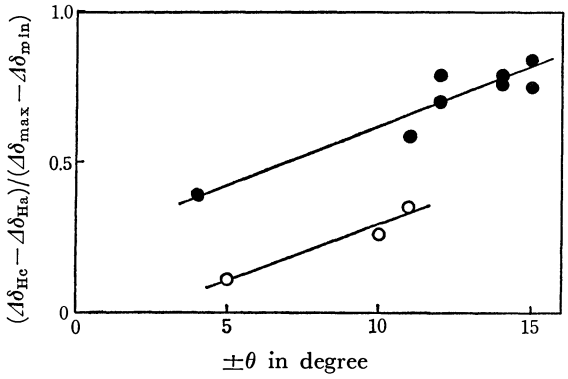

Fig. 6. Relationships between the values of $(\Delta\delta_{Hc} - \Delta\delta_{Ha})/(\Delta\delta_{max} - \Delta\delta_{min})$ and torsion angles θ.
●: I, IIb, IIc, IIIb, IIIc, IV, Vb, and Vc.
○: IIa, IIIa, and Va.

All the above phenomena are easily recognizable in Fig. 5. All the values of $(\Delta\delta_{Hc} - \Delta\delta_{Ha})/(\Delta\delta_{max} - \Delta\delta_{min})$ in **1**, except for VI, gave the proportional relationship with the θ angle, as can be seen in Fig. 6.

We are greatly indebted to Dr. Tadao Kamikawa of Osaka City University for recording the 100 MHz NMR spectra.

References

1) J. A. Deyrup and C. L. Moyer, *J. Org. Chem.*, **34**, 175 (1965).
2) T. Nishiyama and F. Yamada, This Bulletin, **44**, 3037 (1971).
3) F. Yamada, T. Nishiyama, M. Kinugasa, and M. Nakatani, *ibid.*, **43**, 3611 (1970).
4) F. Yamada, T. Nishiyama, Y. Fujimoto, and M. Kinugasa, *ibid.*, **44**, 1152 (1971).
5) C. G. Overberger, T. Kurtz, and S. Yaroslavsky, *J. Org. Chem.*, **30**, 4363 (1965).
6) K. W. Buck, A. B. Foster, W. D. Pardoe, M. H. Qadir, and J. M. Webber, *Chem. Commun.*, **1966**, 758.
7) C. R. Johnson and D. McCants, Jr., *J. Amer. Chem. Soc.*, **86**, 2935 (1964); J. C. Martin and J. J. Uebel, *ibid.*, **86**, 2936 (1964).
8) P. Haake, J. P. McNeal, and E. J. Goldsmith, *ibid.*, **90**, 715 (1968).
9) K. L. Williamson, *ibid.*, **85**, 516 (1963).
10) P. Laszlo and P. R. Schleyer, *ibid.*, **85**, 2709 (1963).
11) J. B. Lambert, *ibid.*, **89**, 1836 (1967).
12) A. A. Bothner-By, "Advances in Magnetic Resonance," Vol. 1, Academic Press, New York and London (1965), p. 195.

The High Resolution Mass Spectra of Shionane and Friedelane Derivatives

Hiroshi HIROTA, Yoshihiko MORIYAMA, Takahiko TSUYUKI, Yoshiaki TANAHASHI, Takeyoshi TAKAHASHI, Yoshiaki KATOH,* and Hiroshi SATOH*

Department of Chemistry, Faculty of Science, The University of Tokyo, Hongo, Bunkyo-ku, Tokyo 113

**Application Laboratory, Naka Works, Hitachi Ltd., Ichige, Katsuta-shi, Ibaragi 312*

(Received November 8, 1974)

High resolution mass spectra of shionane and friedelane derivatives were measured and characteristic fragmentation patterns were described.

In the course of structure study of shionone (**1**),[1] a triterpene ketone, $C_{30}H_{50}O$, isolated from roots of *Aster tataricus* L., low resolution mass spectra of shionone (**1**) and several derivatives were measured.[2] We now wish to describe studies on the characteristic fragmentation patterns of a shionane-type skeleton (**2a**) as well as those of a friedelane-type skeleton (**3a**) by high resolution mass spectrometry. These two frameworks bear a common partial structure in respect to A/B/C/D rings.

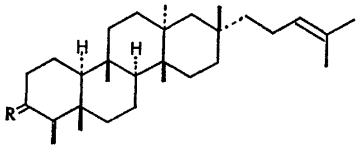

1 R=O
9 R=β-OH, α-H

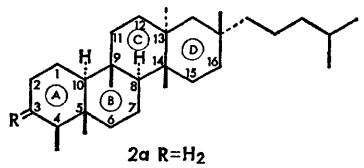

2a R=H_2
2b R=O

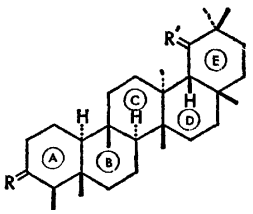

3a R=H_2; R'=H_2
3b R=O; R'=H_2
14 R=β-OH, α-H; R'=H_2
15 R=H_2; R'=O

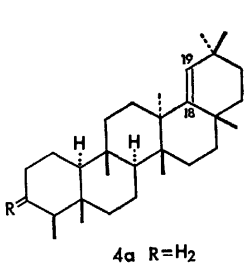

4a R=H_2
4b R=O

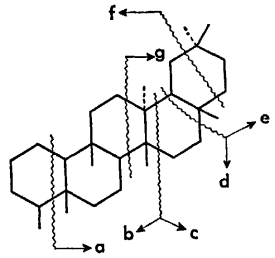

A

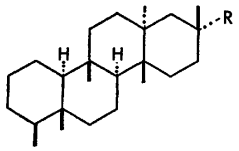

5 R=-$CH_2CH_2CO_2Me$
6 R=-CH_2CO_2Me
7 R=-CO_2Me
8 R=-$CH_2CH_2CH{=}C(Me)Me$
11 R=-$CH_2CH_2CH_2C(Me){=}CH_2$
12 R=-$CH_2CH_2CH_2COMe$

Courtney *et al.* examined the mass spectra of several friedelin derivatives and described fission patterns as shown in **A**. The cleavages **c**, **e**, and **f** were described to be characteristic for friedelin derivatives with a hydroxyl, an acetoxyl or a carbonyl group in ring E, **a** and **d** for compounds with a carbonyl group at C_3, and **b** and **g** for a friedelane skeleton.[3]

Later, Budzikiewicz *et al.* reported cleavages **b** and **g** as well as the subsequent fragmentations for friedel-18-ene (**4a**) and friedel-18-en-3-one (**4b**)[4].

In the high resolution mass spectra of methyl tri-, tetra-, and pentanorshionanoates (**5**, **6**, and **7**), obtained by degradation reactions of the side chain of shion-24-ene (**8**), prominent peaks are classified into two groups: one group consists of peaks which vary with the side chain length, and the other is composed of peaks which are independent of the side chain (Table 1).

The peaks due to $(M-15)^+$, $(M-31)^+$, $(M-71)^+$, $(M-139)^+$, $(M-179)^+$, $(M-194)^+$, $(M-207)^+$, and $(M-239)^+$ showed characteristic shifts by 14 mass units for **5** and **6**, and for **6** and **7**. It is obvious that these peaks are due to the species including the side chain. These compounds exhibit the molecular ions and the $(M-15)^+$ ions with high intensities, as well as the $(M-31)^+$ ions due to a fission between the acyl group and the oxygen atom with weak intensities.

Species $(M-71)^+$, $(M-139)^+$, $(M-179)^+$, and $(M-207)^+$ due to fissions **a**, **h**, **i**, and **g**, respectively, are derived from the two-bond fission between a quarternary and a tertiary carbon atoms and between a tertiary or a quarternary and a secondary carbon atoms, followed by loss of an additional hydrogen from the charged species.

The species due to $(M-194)^+$ is originated by rupture of bonds C_8–C_{14} and C_{11}–C_{12}. Although the latter is a bond between two secondary carbon atoms, the fission **j** occurred with relative ease (relative intensities: 20, 10, and 36% for **5**, **6**, and **7**, respectively).

The (M–239) peaks, observed in the spectra of **5** and

6, are considered to be due to species **p** which could be derived by the fission **g** followed by loss of a methoxyl group and two hydrogen atoms. These fissions are shown as in **B**.

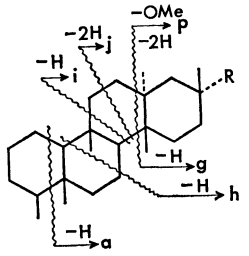

B

On the other hand, the peaks at *m/e* 329, *m/e* 259, *m/e* 233, *m/e* 217, *m/e* 205, *m/e* 193, *m/e* 191, *m/e* 179, *m/e* 177, *m/e* 149, *m/e* 137, *m/e* 135, *m/e* 123, *m/e* 109, *m/e* 95, *m/e* 81, *m/e* 69, and *m/e* 55 are independent of the side chain length.

The fragment **k** at *m/e* 329 ($C_{24}H_{41}$) is derived from the scission of the side chain of **5**, **6**, and **7**.

It has been reported that fission **b** due to two-bond fission between C_{13} and C_{18} and between C_{14} and C_{15} in friedelin (**3b**)[3,4] and friedel-18-ene (**4a**)[4] followed by loss of one hydrogen atom gives species at *m/e* 273 and 259, respectively. Although intense peaks due to fission **b** were observed in the spectra of friedelane derivatives (**3a**, **14**, and **15**), these peaks due to fission **b** in the spectra of **6** and **7** were rather weak. Friedelane derivatives and a few shionane derivatives were accompanied by species **b'**, derived from the two-bond fission **b** without loss of one hydrogen atom.

Peaks at *m/e* 233 ($C_{17}H_{29}$) were observed in the spectra of **5**, **6**, and **7**. The fragmentation process has remained obscure, because four alternative scissions such **1**$_1$, **1**$_2$, **1**$_3$, or **1**$_4$ including three-bond fission in ring C and D could be considered (**C**$_1$—**C**$_4$). The fragment **q** at *m/e* 217 ($C_{16}H_{25}$) observed for **2a**, **5**, **6**, and **8** is seemed to be due to scission **l** accompanied by loss of one hydrogen atom and a methyl group (**C**$_1$—**C**$_4$).

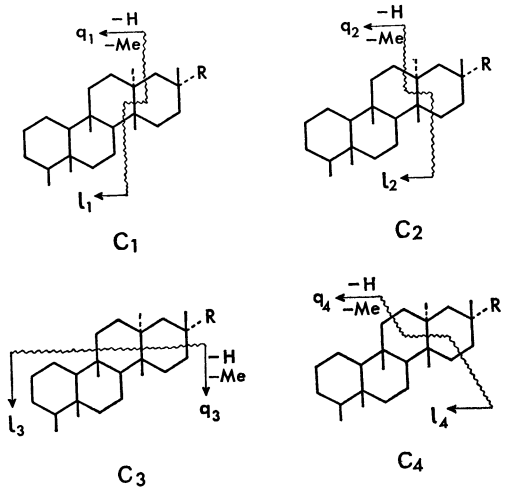

In a friedelane series, the corresponding scission **q** gives the peak at *m/e* 217 for **3a**, **4a**, and **15**, and a peak at *m/e* 233 for **14**.

By the two-bond fission of C_{12}—C_{13} and C_8—C_{14}, a charged species **m** (*m/e* 206) containing rings A and B was formed, which was followed by loss of a hydrogen atom to give species **m'** (*m/e* 205) for **5** and **6**. The counterpart to give a species **g** was discussed above.

The two-bond fission of C_{11}—C_{12} and C_8—C_{14} could produce either a charged species containing rings A and B or ring D. The latter charged species gives a species **j**, mentioned above. The former charged species, on removal of a hydrogen atom, affords a species **n** (*m/e* 191) for **5**, **6**, and **7**, whereas by abstraction of an additional hydrogen atom from the leaving moiety gives species **n'** (*m/e* 193).

The species at *m/e* 177 due to fragmentation **o** is formed by cleavage of two bonds (C_8–C_{14} and C_9–C_{11}) followed by loss of an additional hydrogen atom from the charged species. This fission is visualized by the rupture involving the quarternary C_9 and C_{14} centers. In the case of **5**, the species **o** ($C_{13}H_{21}$, *m/e* 177.1642, obs. 177.1637) was accompanied by $C_{12}H_{17}O$ (*m/e* 177.1279, obs. 177.1280) with weak intensity, which was likely due to a species **p** derived from the two-bond fission of C_{12}–C_{13} and C_8–C_{14} accompanied by loss of two hydrogen atoms and a methoxyl group (*cf.* **B**). This was supported by the appearance of the corresponding peak at *m/e* 163.1106 ($C_{11}H_{15}O$) in the mass spectrum of **6**. The fragment ion **o** constitutes the counterpart of ion **i**.

The above mentioned fission of the two bonds (C_8–C_{14} and C_9–C_{11}) and a subsequent hydrogen abstraction gave species **o'**, which were observed with nearly the same intensities as those due to the species **o**.

Peaks **r** were observed at *m/e* 149 for **2a**, **5**, **6**, **7**, and **8** with considerably high intensities. It is considered that this peak is produced from the three-bond fission of C_6–C_7, C_8–C_9, and C_{11}–C_{12} followed by loss of one methyl group and one hydrogen atom. In friedelane derivatives, the corresponding rupture **r** gives peaks at *m/e* 149 for **15**, at *m/e* 163 for **3b**, and at *m/e* 165 for **9** and **14**.

Fragmentation patterns independent of the side chain length can be depicted as in **D**.

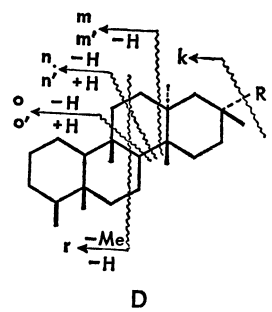

D

Although we can find other common peaks at *m/e* 263 ($C_{17}H_{27}O_2$ for **5** and **6**) and *m/e* 249 ($C_{16}H_{25}O_2$ for **5**, **6**, and **7**) for these compounds, it is likely that each fragment may be produced by a different mode of scission in each compound. These fragmentation patterns are therefore left undetermined.

Compositions of the species in low mass range less

Table 1. High resolution mass spectral data

	M^+	$(M-15)^+$	a	h	i	i′	j
Shionone (**1**)	426.3836 (92)	411.3604 (16)	341.3170 (100)	273.2546 (21)			218.2022 (27)
Shonane (**2a**)	414.4246 (48)	399.3971 (57)	343[b]	275.2746 (71)			220.2151 (36)
Shionanone (**2b**)	428.4019 (15)	413.3756 (6)	343.3353 (32)	275.2739 (16)			220.2181 (29)
Methyl trinor-shionanoate (**5**)	416.3679 (93)	401.3437 (28)	345.2762 (18)	277.2154 (56)	237.1842 (10)		222.1620 (30)
Methyl tetranor-shionanoate (**6**)	402.3483 (66)	387.3266 (33)	331.2643 (9)	263.2011 (47)	223.1682 (5)		208.1437 (19)
Methyl pentanor-shionanoate (**7**)	388.3331 (100)	373.3082 (100)	317.2494 (67)	249.1828 (80)			194.1292 (27)
Shion-24-ene (**8**)	412.4065 (63)	397.3861 (22)	341.3197 (6)	273.2578 (24)			218.2035 (15)
Shion-24-en-3β-ol (**9**)	428.4027 (54)	413.3794 (14)	341[b]	273.2589 (19)			218.2038 (14)
Friedelane (**3a**)	412.4065 (33)	397.3813 (16)	341[b]	273.2564 (4)	233.2266[d] (49)		218.2014 (42)
Friedelin (**3b**)	426.3870 (90)	411.3638 (63)	341.3209 (26)	273[b]			218.2022 (26)
Friedel-18-ene (**4a**)	410.3919 (53)	395.3692 (100)		271.2389 (16)			[g]
Friedelan-3β-ol (**14**)	428.4014 (84)	413.3758 (44)		273.2585 (7)			218.2003 (9)
Friedelan-19-one (**15**)	426.3822 (41)		[c]	287.2353 (2)		248.2145 (8)	233.1903 (5)

	g	k	d	b	b′	l	m
Shionone (**1**)	205.1958 (43)	343.3022 (42)			274.2296 (19)	247.2039 (30)	220.1807 (28)
Shionane (**2a**)	207.2105 (19)	329.3213 (36)		259[b]	260[b]	233.2278 (79)	
Shionanone (**2b**)	207.2109 (16)	343.3010 (22)				247.2058 (16)	220.1820 (21)
Methyl trinor-shionanoate (**5**)	209.1555 (24)	329.3194 (13)				233.2264 (73)	206.2045 (11)
Methyl tetranor-shionanoate (**6**)	195.1366 (26)	329.3192 (26)		259.2449 (5)	260.2504 (22)	233.2257 (78)	
Methyl pentanor-shionanoate (**7**)	181[b]	329.3188 (40)		259.2409 (20)		233.2262 (47)	
Shion-24-ene (**8**)	205.1944 (23)	329.3220 (31)		259.2427 (16)		233.2267 (58)	206.2016 (13)
Shion-24-en-3β-ol (**9**)	205.1954 (19)	345[b]			276.2439 (9)	249.2214 (9)	
Friedelane (**3a**)	205.1947[e] (45)		288.2817 (5)	259.2404 (70)	260.2489 (26)	233.2266[d] (49)	206.2012 (27)
Friedelin (**3b**)	205.1965 (42)		302[b]	273[b]	274.2344 (68)	247.2048 (32)	220.1846 (16)
Friedel-18-ene (**4a**)	203.1789 (47)		288.2804 (11)		260.2480 (16)	233.2267 (21)	206.2027 (11)
Friedelan-3β-ol (**14**)	205.1955 (19)		304[b]	275.2374 (41)	276.2438 (25)	249.2224 (20)	
Friedelan-19-one (**15**)	[f]		288.2847 (8)	259.2417 (69)	260.2467 (19)		

than *m/e* 137 were examined by high resolution mass spectrometry. Since these species would be formed through multi-step fissions, their fragmentation patterns are not discussed here.

The high resolution mass spectra of shionone (**1**), shionane (**2a**), shionanone (**2b**), shion-24-ene (**8**), and shion-24-en-3β-ol (**9**) and the low resolution mass spectra of shion-3-ene (**10**), shion-25-ene (**11**), norshionan-25-one (**12**), and shionan-3β,29-olide (**13**) are well interpreted by the fragmentation patterns above mentioned (Tables 1 and 2).

The $C_{14}H_{23}^+$ (*m/e* 191) peaks in the mass spectra of shionone (**1**), shionanone (**2b**), and friedelin (**3b**) are considered to be derived from the fragment **m′** and subsequent loss of a carbon monoxide molecule.

Introduction of a carbonyl group at C_{19} causes con-

OF SHIONANE AND FRIEDELANE DERIVATIVES[a)]

	m′	n	n′	o	o′	p	q
Shionone (**1**)	219.1739 (10)	205.1596 (27)	207.1753 (30)	191.1441 (13)	193.1578 (12)		231.1738 (12)
Shionane (**2a**)	205.1961 (17)	191.1764 (17)	193[b)]	177.1663 (28)	179.1792 (29)		217.1931 (19)
Shionanone (**2b**)	219.1733 (6)	205.1602 (11)	207.1746 (11)	191.1429 (6)	193.1599 (8)		
Methyl trinor-shionanoate (**5**)	205.1944 (13)	191.1803 (8)	193.1952 (11)	177.1637 (29)	179.1796 (13)	177.1280 (5)	217.1954 (19)
Methyl tetranor-shionanoate (**6**)	205.1928 (9)	191.1785 (19)	193.1930 (10)	177.1619 (43)	179.1776 (28)	163.1106 (5)	217.1947 (9)
Methyl pentanor-shionanoate (**7**)		191.1779 (27)	193[b)]	177.1631 (33)	179[b)]		
Shion-24-ene (**8**)	205.1944 (23)	191.1801 (32)	193.1957 (14)	177.1634 (32)	179.1796 (32)		217.1960 (14)
Shion-24-en-3β-ol (**9**)				193.1577 (9)			
Friedelane (**3a**)	205.1947[e)] (45)	191.1754 (33)	193.1906 (3)	177.1630 (41)	179.1784 (50)		217.1951 (51)
Friedelin (**3b**)		205.1607 (42)	207.1738 (16)		193.1601 (32)		
Friedel-18-ene (**4a**)	205.1946 (16)	191.1794 (21)		177.1643[h)] (68)	179.1770 (16)		217.1973 (47)
Friedelan-3β-ol (**14**)		207.1716 (7)		193.1586 (15)	195.1742 (10)		233.1902 (35)
Friedelan-19-one (**15**)	205.1970 (11)	191.1806 (22)		177.1637 (19)			217.1945 (55)

	r	f	c	e	m′−CO	i−CO	Base peak
Shionone (**1**)					191.1804 (21)		341.3170
Shionane (**2a**)	149.1310 (67)						123.1153
Shionanone (**2b**)					191.1787 (7)		109.1013
Methyl trinor-shionanoate (**5**)	149.1326 (62)						109.1012
Methyl tetranor-shionanoate (**6**)	149.1317 (71)						121.1020
Methyl pentanor-shionanoate (**7**)	149.1301 (27)						373.3082 388.3331
Shion-24-ene (**8**)	149.1335 (56)						109.1017 123.1169
Shion-24-en-3β-ol (**9**)	165.1271 (19)						109.1014
Friedelane (**3a**)	149.1312 (100)						109.1013 149.1312
Friedelin (**3b**)	163.1111 (62)				191.1825 (42)		109.1011
Friedel-18-ene (**4a**)	149.1329 (26)						111.1170 395.3692
Friedelan-3β-ol (**14**)	165.1273 (100)						165.1273
Friedelan-19-one (**15**)	149.1318 (27)	357.3148 (8)	165.1289 (5)	139.1119 (100)		219.2092 (16)	139.1119

a) Peaks higher than *m/e* 100 are registered. Numbers in parentheses refer to relative intensities. b) *m/e* Value, observed in a low resolution mass spectrum, but not detected in a high resolution mass spectrum, because error of the *m/e* value exceeded ±5 milli mass units. c) A peak at *m/e* 355 was not observed, but *m/e* 357.3148 ($C_{25}H_{41}O$), due to fission **a** followed by addition of H, was observed. d) Maybe due to fissions **i** and **l**. e) Maybe due to fissions **g** and **m′**. f) A peak at *m/e* 219 was not observed, but *m/e* 221.1900 ($C_{15}H_{25}O$), due to fission **g** followed by addition of H, was observed. g) A peak at *m/e* 216 was not observed, but *m/e* 217.1973 ($C_{16}H_{25}$), due to fission **j** followed by loss of H (not 2H), was observed. h) Or due to a species "**jj**", described in the reference 4.

Table 2. Low resolution mass spectral data of shionane derivatives

	M+	(M-15)+	a	h	j	g	k	b′	l	m	m′	n	n′	o
Shion-3-ene (**10**)	412	397	343	275	220	207	327		231	204	203	189	191	175
Shion-25-ene (**11**)	412	397	341	273	218	205	329	260	233	206	205	191	193	177
Norshionan-25-one (**12**)	414	399	343	275	220	207	329	260	233	206	205	191	193	177
Shionan-3β,29-olide (**13**)	442	427	373	275	220	207	357		261	234	233	219	221	205

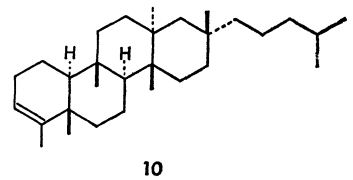

10

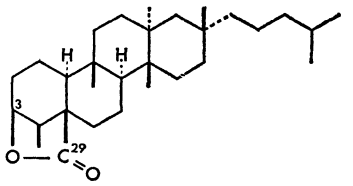

13

siderable changes in the fragmentation pattern of the friedelane skeleton. Among the fissions **b**, **c**, **d**, **e**, and **f** which are characteristic of a friedelane skeleton[3], two prominent peaks due to fissions **e** and **b** were observed in the mass spectrum of friedelan-19-one (**15**). The cleavage **f** seems to be not so important in the fragmentation of **15** (Figure **E**). A peak at *m/e* 219 was also observed. This ion could be explicable by the fragmentation (**i**—CO).

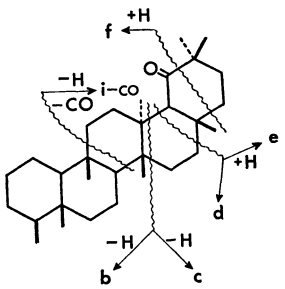

E

In conclusion, the cleavages **a**, **g**, **h**, **j**, **k**, **l**, **m** (**m**′), **n** (**n**′), **o** (**o**′), **q**, and **r** were shown to be characteristic of a shionane-type skeleton (**B**, **C**, and **D**).

The high resolution mass spectra of friedelin (**3b**), friedelane (**3a**), friedel-18-ene (**4a**), friedelan-3β-ol (**14**), and friedelan-19-one (**15**) confirmed the characteristic scissions **b**′ (or **b**) and **g** described earlier.[3,4] The fissions **h**, **j**, **l**,† **m** (**m**′), **n**, **o** (**o**′), **q**,† and **r** were also considered to be characteristic of a friedelane-type skeleton (**F** and **F**′).

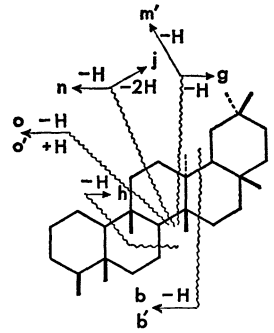

F

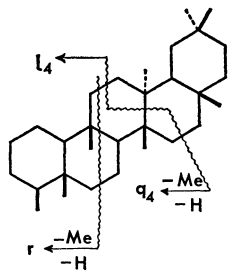

F′

Peaks due to the species **a** appeared for all shionane derivatives. The cleavages **b** and/or **b**′ were observed constantly for friedelane derivatives, while peaks due to these scissions were absent in the spectra of some shionane derivatives (Tables 1 and 2). These observations are considered to be due to structure differences between the two skeletons of shionane and friedelane.

Experimental

The high and low resolution mass spectra were determined with a Hitachi RMU-7M double-focusing and a Hitachi RMU-6-Tokugata mass spectrometers, respectively, operating at 70 eV. The samples were introduced by direct inlet system at 100 to 180 °C. Shionane and friedelane derivatives were available from earlier studies.[1,2,5]

References

1) (a) Y. Moriyama, Y. Tanahashi, T. Takahashi, and G. Ourisson, *Bull. Soc. Chim. France*, **1968**, 2890; (b) T. Tsuyuki, T. Hoshino, M. Ito, and T. Takahashi, *ibid.*, **1968**, 2895. And references cited therein.

2) Y. Tanahashi, Y. Moriyama, T. Takahashi, F. Patil, J.-F. Biellmann, and G. Ourisson, *ibid.*, **1966**, 1670.

3) (a) J. L. Courtney and J. S. Shannon, *Tetrahedron Lett*, **1963**, 13. (b) J. S. Shannon, C. G. Macdonald, and J. L. Courtney, *ibid.*, **1963**, 173.

4) H. Budzikiewicz, J. M. Wilson, and C. Djerassi, *J. Amer. Chem. Soc.*, **85**, 3688 (1963); They also described a formation of ion "**q**" and its related ions (analogues of species "**g**" in their text) from friedelin, friedelane, friedel-18-en-3-one and friedel-18-ene. However, the mass numbers of these ions are not compatible with their formulae.

5) T. Fukuda, T. Tsuyuki, Y. Tanahashi, and T. Takahashi, This Bulletin, **40**, 370 (1967).

† In Fig. **F**′, cleavages **l** and **q** are shown by $\mathbf{l}_4$ and $\mathbf{q}_4$, respectively. Other scissions $\mathbf{l}_1$, $\mathbf{l}_2$, and $\mathbf{l}_3$, and $\mathbf{q}_1$, $\mathbf{q}_2$, and $\mathbf{q}_3$ analogous to those shown in $\mathbf{C}_1$, $\mathbf{C}_2$, and $\mathbf{C}_3$, are also applicable for these cleavages **l** and **q**, respectively.

The Reaction of Aroyl Alkyl Carbonates with Isocyanates

Yuzuru UCHIDA and Seizi KOZUKA*

Department of Applied Chemistry, Osaka Institute of Technology, Asahi-ku, Osaka 535

**Department of Applied Chemistry, Faculty of Engineering, Osaka City University, Sumiyoshi-ku, Osaka 558*

(Received November 25, 1974)

Aroyl alkyl carbonates were treated with isocyanates with or without addition of sodium methoxide and alkyl *N*-aroylcarbanilates were obtained as the major products. Based on ^{18}O tracer study and catalytic effect of alkoxide ion, a base catalyzed ionic reaction process was confirmed for the mechanism of the carbanilate formation.

Thermal decomposition of acyl alkyl carbonates giving esters has been known to proceed through two different mechanisms.[1] The one is a cyclic unimolecular process and the second one is an ionic mechanism involving alkoxide ion as a chain carrying agent. The structure of the starting material and the nature of the solvent are considered to have important roles in making a choice between the two mechanisms. These results suggest that if the reaction carried out with a second reactant, such as isocyanate which reacts facilely with alkoxide ion, the formation of the product through alkoxide ion as an intermediate would be interrupted.

Acyl alkyl carbonates, on the other hand, are also known as acylating reagents.[2] Thus, alkoxy-acylation of isocyanates giving *N*-acylcarbanilates can be expected by the reaction with acyl alkyl carbonates. We have now tried the reaction and wish to report our results focusing our attention mainly to the synthesis of *N*-aroylcarbanilate and the formation mechanism.

Results and Discussion

Cyclohexyl benzoyl carbonate (**1**) was heated with phenyl isocyanate (**2**) in *o*-dichlorobenzene as a solvent at 150—160 °C. As expected, the product obtained was cyclohexyl *N*-benzoylcarbanilate (**3**), along with the products apparently formed by thermal decomposition of the carbonate[3] such as esters, acid anhydrides and symmetrical carbonates.

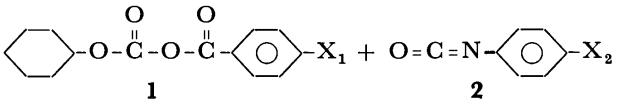

1 **2**

X_1: NO_2, CN, Br, H, OCH_3

X_2: NO_2, H, CH_3

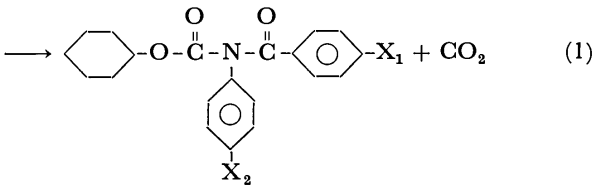

3 (1)

At the biginning of this study, the reaction was carried out without base. In the meantime, however, addition of a small amount of methoxide ion in the solution was found to complete the reaction much faster and with better result. Accordingly, the reaction was carried out with a small amount (*ca.* 15 mol%) of sodium methoxide. The results are given in Table 1.

The structure of the product was determined by the following observations. Namely, aroyl hydrazides (**4**)

Table 1. Reaction of aroyl alkyl carbonate and isocyanate

Reactant					Producct	
1	X_1	**2**	X_2	$NaOCH_3$	**3**	Yield %[a]
1a	CN	**2a**	H	none[b]	**3a**	36
1b	NO_2	**2a**	H	added[c]	**3b**	68
1c	Br	**2a**	H	added	**3c**	59
1d	H	**2a**	H	added	**3d**	54
1e	CH_3O	**2a**	H	added	**3e**	52
1d	H	**2b**	NO_2	added	**3f**	46
1d	H	**2c**	CH_3	added	**3g**	56

a) Yields of **3** were calculated based on **1**. b), c) See Experimental.

and cyclohexyl carbanilates (**5**) were obtained on treating **3** with hydrazine hydrochloride and ammonia in ether.

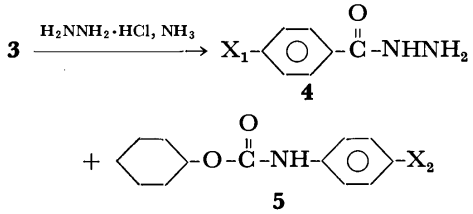

4 **5** (2)

Spectroscopic evidences and elemental analysis also confirmed this structure. The carbanilate **3b** was also prepared by the reaction of *p*-nitrobenzanilide, sodium hydride and cyclohexyl chloroformate.

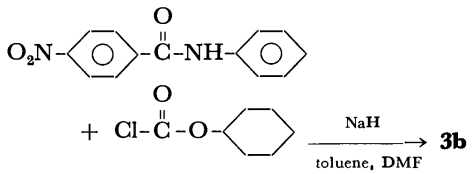

(3)

The reaction of phenyl isocyanate with a carboxylic acid or anhydride, which appears to be an analogous reaction to the present reaction, was studied by Ötvös *et al.*[4] An unstable mixed anhydride **6** was suggested as an intermediate which led to an amide or imide **7** on decarboxylation.

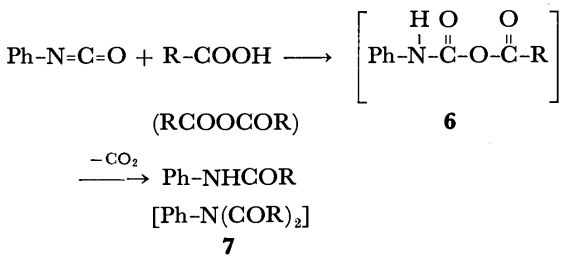

(RCOOCOR) **6**

$-CO_2$

Ph-NHCOR

$[Ph\text{-}N(COR)_2]$

7 (4)

By analogy with this mechanism, there are two possible processes that can be shown for the present reaction as shown below.

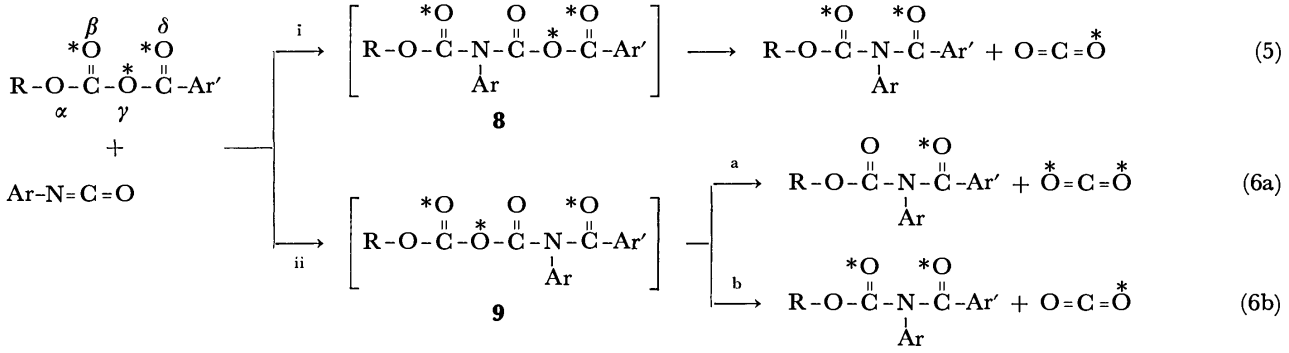

Nucleophilic attack of the aroyloxy group on the isocyanate results in formation of **8**. Attack of the γ-oxygen atom on the isocyanate with acyl-oxygen bond fission forms **9** as an intermediate. Decarboxylation of those intermediates lead to the product **3**.

The other possible process to give **3** is a base catalyzed reaction involving alkoxide ion as a catalyst. These processes can be distinguished by using ^{18}O labeled **1** at β, γ and δ oxygens as shown as asterisk in the equations, although the processes (6a) and (9) give the same results.

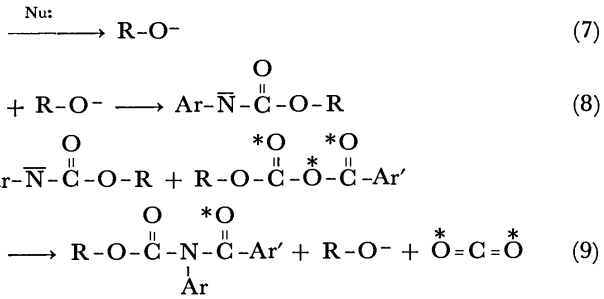

^{18}O Labeled **1a'** was prepared as follows:[5] The reaction of *p*-cyanobenzoic acid-^{18}O (0.826 excess atom%) with cyclohexyl chloroformate gave the carbonate **1a** which was then allowed to scramble ^{18}O by heating at 70 °C in CCl_4 for 12 hr. The ^{18}O distribution in **1a'** after heating was analyzed obtaining nearly complete ^{18}O scramblings among β, γ and δ oxygens. The reaction of the labeled **1a'** with phenyl isocyanate (**2a**) was carried out in *o*-dichlorobenzene without addition of sodium methoxide. After heating for 16 hr at 160 °C, **3a** was obtained in 36% yield. ^{18}O Content and distribution in **3a** were measured after the cleavage reaction shown in Eq. (2). The result is given in Scheme 1.

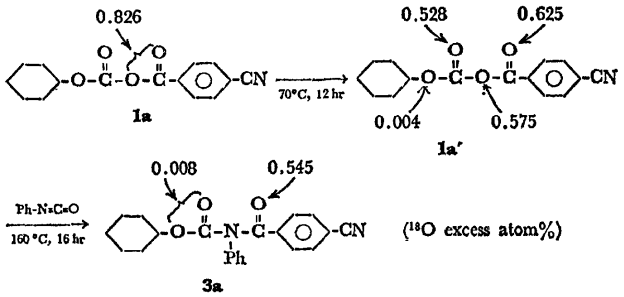

Scheme 1.

The ^{18}O in **3a** was found only at the benzoyl oxygen and the incorporation (0.545 excess atom%) concurred well to that of mean value of β, γ and δ oxygens of the starting **1a** (0.551 excess atom%). The result indicates that the starting **1a** scrambled ^{18}O completely among the three oxygens before reacting with the isocyanate. This was quite reasonable since the reaction with the isocyanate required a higher temperature (160 °C) than the oxygen scrambling reaction of the carbonate (70 °C).[5]

These results clearly ruled out the processes shown in Eqs. (5) and (6b) because only a negligible amount of ^{18}O was found in the carbanilate moiety in **3a**. The very small amount of ^{18}O seems to have originated from the ^{18}O in the alkoxide oxygen (α) of the starting material.

The base catalyzed reaction process shown in Eqs. (7)—(9) is the most probable mechanism between the two remaining possibilities because the reaction was catalyzed markedly by the addition of alkoxide ion.[6]

Experimental

Preparation of Aroyl Alkyl Carbonates. ^{18}O Labeled **1a** and **1d** were prepared in a similar manner reported in the previous paper. **1a**: mp 54.5—55.0 °C (lit,[5] mp 54.5—55.0 °C). **1d**: mp 21.0—22.0 °C (lit,[5] mp 21.0—21.5 °C). Carbonate **1b** was prepared as follows: An ether (50 ml) solution of triethylamine (15.0 g) was added dropwise into an ether (500 ml) suspension of *p*-nitrobenzoic acid (24.7 g) and cyclohexyl chloroformate (25.5 g) cooled in an ice bath. After stirring the mixture for additional 4 hr, water (200 ml) was added. The ether layer separated, was washed with dil. HCl, dil. aqueous $NaHCO_3$ and water then dried over Na_2SO_4. The solvent was evaporated under reduced pressure to give **1b** in 57% yield. mp 49.0—50.0 °C (from ether). Found: C, 57.31; H, 5.11; N, 4.77%. Calcd for $C_{14}H_{15}O_6N$: C, 57.33; H, 5.16; N, 4.78%. Carbonates **1c** and **1e** were obtained similarly in 79 and 87% yields, respectively. **1c**: mp 19.5—20.5 °C. Found: C, 51.41; H, 4.50%. Calcd for $C_{14}H_{15}O_4Br$: C, 51.39; H, 4.62%. **1e**: mp 59.5—60.5 °C. Found: C, 65.03; H, 6.34%. Calcd for $C_{15}H_{18}O_5$: C, 64.73; H, 6.52%.

Reaction of Aroyl Alkyl Carbonates with Isocyanates. A typical run was as follows: A mixture of **1b** (5.96 g), phenyl isocyanate (3.10 g) and sodium methoxide (0.15 g) in *o*-dichlorobenzene (25 ml) was heated at 160 °C for 1.5 hr. After evaporation of the solvent under reduced pressure, the residual

oily material was dissolved in ether (50 ml) and washed with water, dil. HCl, dil. aqueous $NaHCO_3$ and water then dried over Na_2SO_4. The crude product was purified through a colum chromatography on silica gel with benzene as an eluent then recrystallized from methanol obtaining **3b** (4.60 g). mp 103—104 °C. IR: 1735 and 1690 cm^{-1} ($\nu_{C=O}$). Found: C, 65.34; H, 5.48; N, 7.53%. Calcd for $C_{20}H_{20}O_3N_2$: C, 65.21; H, 5.47; N, 7.61%. Physical propaties and analytical results of other carbonates are as follows: **3a**: mp 105.0—105.5 °C. Found: C, 72.69; H, 5.66; N, 7.98%. Calcd for $C_{21}H_{20}O_3N_2$: C, 72.39; H, 5.79; N, 8.04%. **3c**: mp 90—91 °C. Found: C, 60.05; H, 4.93; N, 3.41%. Calcd for $C_{20}H_{20}O_3NBr$: C, 59.71; H, 5.01; N, 3.48%. **3d**: mp 77—78 °C. Found: C, 74.54; H, 6.59; N, 4.31%. Calcd for $C_{20}H_{21}O_3N$: C, 74.28; H, 6.55; N, 4.33%. **3e**: bp 228—233 °C/3 mmHg. **3f**: mp 97—98 °C. Found: C, 65.23; H, 5.42; N, 7.54%. Calcd for $C_{20}H_{20}O_5N_2$: C, 65.21; H, 5.47; N, 7.61%. **3g**: mp 81.5—82.5 °C. Found: C, 75.84; H, 6.96; N, 4.14%. Calcd for $C_{21}H_{23}O_3N$: C, 74.75; H, 6.87; N, 4.15%.

^{18}O Tracer Experiment. A solution of ^{18}O labeled **1a** (6.0 g) in CCl_4 (50 ml) was heated at 70 °C for 12 hr. The solvent was removed under reduced pressure and the residue was used for the reaction with **2a**. The same procedure described in the previous paper[5] was used for the determination of ^{18}O distribution in **1a** and **1a'**.

*Reaction of **3** with Hydrazine.* Anhydrous ammonia was bubbled into a mixture of **3a** (0.80 g) and hydrazine hydrochloride (0.80 g) in dry ether (50 ml) for 20 min with stirring at room temperature. The mixture was stirred for additional 7 hr. Cyclohexyl carbanilate (**5**) (0.50 g) was obtained from the ether solution by filtration. mp 83.5—84.5 °C (from $CHCl_3$-pet. ether) (lit,[7] mp 81—82 °C). The residue of the filtration gave *p*-cyanobenzhydrazide (0.20 g) on recrystallization. mp 197—198 °C (from methanol-CCl_4) (lit,[8] mp 198—199 °C).

^{18}O-Analysis was done by the same way as reported previously.[5]

*Preparation of Cyclohexyl N-(p-Nitrobenzoyl)carbanilate (**3b**).* A mixture of *p*-nitrobenzanilide (6.7 g) and NaH (1.5 g as 50% paste) in dry toluene (100 ml) was refluxed for 1 hr with stirring. Into the mixture, cyclohexyl chloroformate (4.5 g) in DMF (20 ml) was added with stirring at 70 °C. After stirring for additional 30 min, the mixture was then washed with dil. HCl, dil. aqueous $NaHCO_3$ and water then dried over Na_2SO_4. Removal of the solvent gave crude **3b** (7.2 g) which was recrystallized from methanol. mp 103—104 °C.

References

1) T. B. Windholz, *J. Org. Chem.*, **25**, 1703 (1960); E. J. Longosz and D. S. Tarbell, *ibid,*. **26**, 2161 (1961); C. J. Michejda, D. S. Tarbell and W. H. Saunders Jr., *J. Amer. Chem. Soc.*, **84**, 4113 (1962); C. J. Michejda and D. S. Tarbell, *J. Org. Chem.*, **29**, 1168 (1964); T. Kashiwagi, S. Kozuka, and S. Oae, *Tetrahedron*, **26**, 3619 (1970); C. J. Michejda and D. V. Riesen, *J. Org. Chem.*, **37**, 3021 (1972).

2) D. S. Tarbell and J. A. Price, *J. Org. Chem.*, **22**, 245 (1957); N. A. Leister and D. S. Tarbell, *ibid.*, **23**, 1152 (1958); D. S. Tarbell and J. R. Price, *ibid.*, **21**, 144 (1956); B. R. Baker, J. P. Joseph, R. E. Schab, and H. Williams, *ibid.*, **19**, 1786 (1954); J. R. Vaughan Jr. and R. L. Osato, *J. Amer. Chem. Soc.*, **73**, 5553 (1951).

3) D. S. Tarbell and E. L. Longosz, *J. Org. Chem.*, **24**, 774 (1959); T. B. Windholz, *ibid.*, **25**, 1703 (1960); R. C. L. Chow and D. S. Tarbell, *ibid.*, **32**, 2188 (1967).

4) L. Ötvös, J. Marton, and J. M. Agoston, *Tetrahedron Lett.*, **1960**, No. 2, 15.

5) S. Oae, K. Fujinori and Y. Uchida, *Tetrahedron*, **26**, 3169 (1970); S. Oae, Y. Uchida, K. Fujimori, and S. Kozuka, This Bulletin, **46**, 1741 (1973).

6) The reaction without sodium methoxide required about 15 hr to complete. With sodium methoxide (*ca.* 15 mol%), on the other hand, the reaction was completed within 1.5 hr. These were observed by following the change of IR spectra of the reaction mixtures.

7) C. W. Whitehead and J. J. Traverso, *J. Amer. Chem. Soc.*, **77**, 5872 (1955).

8) G. M. Filho and J. G. da Cosa, *Anais escola super. quim. Univ. Recife*, **1**, No. 1, 41 (1959); *Chem. Abstr.*, **55**, 3601 (1961).

The Mannich Reaction of Alicyclic α-Diketones. A Novel Synthesis of 2-Hydroxy-3-methyl-2-cyclohexen-1-one[1]

Masao ŌHASHI*, Tadashi TAKAHASHI, Seiichi INOUE, and Kikumasa SATO**

Department of Applied Chemistry, Faculty of Engineering, Yokohama National University, Minami-ku, Yokohama 233

**Chemical Laboratory, Seimi Chemical Co., Ltd., Chigasaki, Chigasaki-shi, Kanagawa 253*

(Received December 13, 1974)

A new synthesis of 2-hydroxy-3-methyl-2-cyclohexen-1-one (**1**) is described. The Mannich reaction of cyclohexane-1,2-dione (**2**) or 2-morpholino-2-cyclohexen-1-one (**3**) with morpholine and formalin gave a Mannich base (**4**), which was then hydrogenolized to afford **1**. However, the Mannich reaction of **1** merely gave a bis-Mannich base (**22**), which was then similarly hydrogenolized to afford 3,6-dimethyl-2-hydroxy-2-cyclohexen-1-one (**7**) along with 3,6-dimethyl-2-hydroxy-6-morpholinomethyl-2-cyclohexen-1-one (**26**); 2-hydroxy-3,6,6-trimethyl-2-cyclohexen-1-one could not be obtained under these conditions. The Mannich reaction of other alicyclic α-diketones and the hydrogenolysis of their Mannich bases are also described.

2-Hydroxy-3-methyl-2-cyclohexen-1-one (**1**) has been known as a flavor constituent in coffee aroma.[2] Previous papers have described several routes to synthesize **1** from 2-ethoxycarbonyl-2-methylcyclohexanone.[3]

In this paper, we will investigate the orientation and reactivities of several alicyclic α-diketones in the Mannich reaction for the synthesis of **1**.

The Mannich reaction of cyclohexane-1,2-dione (**2**),[4] which exists almost entirely in the enolic form[5] with 1 equivalent of both morpholine and formalin in dioxane, afforded 2-hydroxy-3-morpholinomethyl-2-cyclohexen-1-one (**4**) in a good yield.

Furthermore, 2-hydroxy-3,6-bismorpholinomethyl-2-cyclohexen-1-one (**5**) was easily obtained by the treatment of **2** with two equivalents of both morpholine and formalin. On the other hand, the Mannich reaction of cyclopentane-1,2-dione with excess morpholine and formalin in dioxane have been shown to give 2-hydroxy-3-morpholinomethyl-2-cyclopenten-1-one (**6**) as the sole product. This is supposed to be attributable to the significant difference in the solubility of the mono-Mannich bases, **4** and **6**.

The Mannich base **4** was hydrogenolized with zinc powder in glacial acetic acid to give **1** in a 51% yield. Similarly, the Mannich base **5** afforded 3,6-dimethyl-2-hydroxy-2-cyclohexen-1-one (**7**) by a similar hydrogenolysis.

Then we examined the Mannich reaction of 2-morpholino-2-cyclohexen-1-one (**3**). Enaminoketone (**3**) could be obtained by refluxing **1** with morpholine in benzene.

The Mannich reaction of **3** with morpholine and formalin in various solvents, for example, dioxane, ethanol, and isopropyl ether, resulted in recovery of only the starting material. However, **4** was successfully attained in a good yield by the refluxing of **3** with morpholine hydrochloride and with paraformaldehyde in dioxane–ethanol, while no bis-Mannich base (**5**) could be isolated even when **3** was treated with two molar equiv. of both morpholine hydrochloride and paraformaldehyde.

Although no 2-morpholino-3-morpholinomethyl-2-cyclohexen-1-one could be obtained, the above results suggest that the substrate underwent morpholinomethylation in the form of enaminoketone. On the other hand, the Mannich reaction of 2-morpholino-2-cyclopenten-1-one with morpholine and formalin did not afford the corresponding mono-Mannich adduct, but it did readily give the bis-Mannich base.[6]

Enaminoketone may be represented by three principally contributing resonance structures.[7] The Mannich reactions of enaminoketones have revealed an interesting relationship between the product and the ring size, but the detail are uncertain. Cycloalkanones have been shown to give the corresponding Mannich bases by treatment with paraformaldehyde and with secondary amine hydrochloride.[8]

Since **3** is enolizable, it can not easily be determined whether the morpholinomethylation occurs at the enol site or at the enamine site. Therefore, we studied the Mannich reactions of nonenolizable ketons such as 6-ethoxycarbonyl-6-methyl-2-cyclohexen-1-one (**9**).[3]

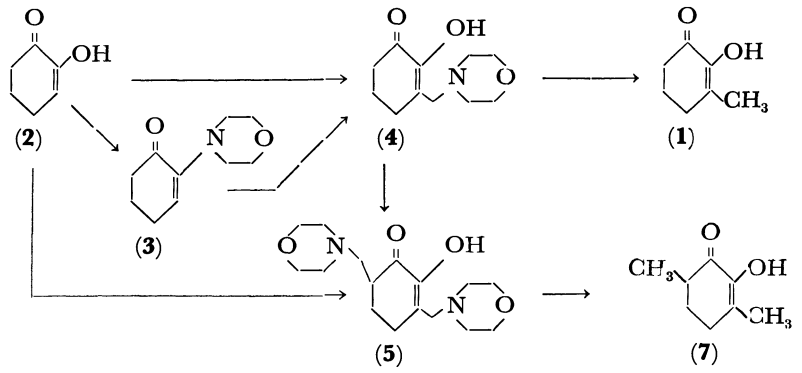

** To whom all correspondence should be addressed.

6-Ethoxycarbonyl-2-hydroxy-6-methyl-2-cyclohexen-1-one (**8**) easily reacted with morpholine and formalin in dioxane at room temperature to give a Mannich base (**10**); this base was then hydrogenolized to afford 6-ethoxycarbonyl-2-hydroxy-3,6-dimethyl-2-cyclohexen-1-one (**11**).

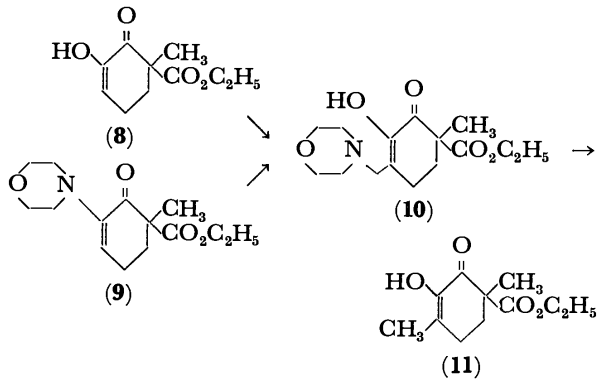

(**8**) (**9**) (**10**) (**11**)

Under the same conditions, **9** did not react even when warmed at 55 °C. However, **9** reacted with morpholine hydrochloride and with formalin in dioxane-water at room temperature to form **10**. In this case, however, it is not clear whether the substrate undergoes morpholinomethylation in the form of **9** or **8**, which is formed after the hydrolysis of **9** under the present reaction conditions.[3] At least these results imply that α-diketone is more subject to morpholinomethylation than is enaminoketone.

On the basis of these results, it may be supposed that the Mannich reactions of enolizable enaminoketons proceed *via* electrophilic substitution by morpholinomethylation through the hydrogen-bonded complex between enol and amino nitrogen.[9]

Then we examined the Mannich reactions of 2-hydroxy-3-methyl-2-cycloalken-1-ones. Tonari and his co-workers[10] reported the Mannich reaction of 2-hydroxy-3-methyl-2-cyclopenten-1-one (**12**) to give a mono-Mannich adduct (**14**) in a 30% yield and obtained 2-hydroxy-3,5-dimethyl-2-cyclopenten-1-one by subsequent hydrogenolysis. However, their characterization of the mono-Mannich base was inadequate. Therefore, we reexamined the Mannich reaction of **12** with various secondary amines.

The Mannich reaction of **12** under the conditions previously reported[10] afforded 2-hydroxy-5-methyl-3,5-bismorpholinomethyl-2-cyclopenten-1-one (**13a**) in a 34% yield. The melting point of this crude crystals was compatible with the reported[10] mp of 115—6°C. The structure of **13a** was confirmed by analytical and spectral data, and no mono-adduct (**14**) could be obtained. This reaction was examined with various ratios of reagents; these ratios are shown in Table 1. Moreover, we examined the Mannich reaction of 3-ethyl-2-hydroxy-2-cyclopenten-1-one (**15**) under the various conditions listed in Table 1.

When diketone (**15**) was treated with equimolar amounts of formalin and morpholine in dioxane at room temperature, 5-ethyl-3,5-bis-morpholinomethyl-2-cyclopenten-1-one (**16**) was obtained as the sole product; the best yield was attained with two molar equivalents of both formalin and morpholine,

Table 1. The Mannich reaction of **12** and **15** under various conditions

Formalin (equiv.)	Amine	(equiv.)	Mannich base	Yield[a] (%)
1.0	Morpholine hydrochloride	1.0	**13a**	34.8[b]
1.0	Morpholine	1.0	**13a**	38.4
2.0	Morpholine	2.0	**13a**	70.3
1.0	Pyrrolidine	1.0	**13b**	34.5
2.0	Pyrrolidine	2.0	**13b**	53.6
2.0	Piperidine	2.0	**13c**	90.0
1.0	Morpholine	1.0	**16a**	30.9
2.0	Morpholine	2.0	**16a**	85.3
2.0	Pyrrolidine	2.0	**16b**	40.8
2.0	Piperidine	2.0	**16c**	80.6

a) Yields are based on diketone. b) Procedure by Tonari and coworkers.[10]

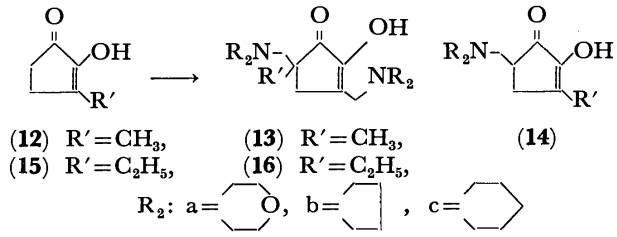

(**12**) R′=CH_3, (**13**) R′=CH_3, (**14**)
(**15**) R′=C_2H_5, (**16**) R′=C_2H_5,
R_2: a=O, b=, c=

The chemical properties and analytical characterization of **13** and **16** are summarized in Table **2**.

Then we studied the Mannich reactions of 2-cyclopentnones derived from **12**. The Mannich reaction of 2-pyrrolidino-5-methyl-2-cyclopenten-1-one (**17**)[11] with both formalin and pyrrolidine at −10 °C provided the bis-Mannich base (**13b**). However, efforts to introduce an aminomethyl group into such 2-cyclopenteneones with an electron-withdrawing group as 2-acetoxy-3-methyl-2-cyclopenten-1-one (**18**)[12] or 1-methyl-3-oxo-1-cyclopenten-2-yl *p*-toluene sulfonate (**19**) failed.

The hydrogenolysis of the Mannich bases **13a—c** with zinc powder in glacial acetic acid at 80 °C for 5 hr was accompanied by deaminomethylation to afford 3,5-dimethyl-2-hydroxy-2-cyclopenten-1-one (**20**); no trimethyl derivative (**21**) could be obtained under these conditions.

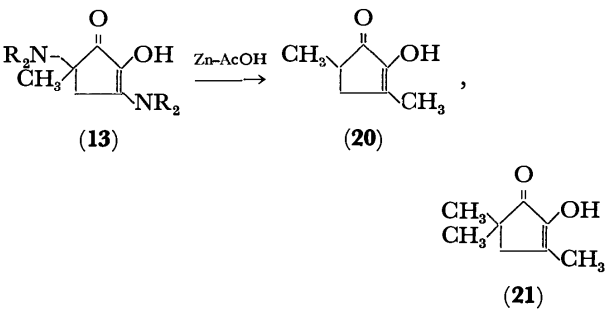

(**13**) (**20**) (**21**)

Then we examined the Mannich reaction of **1**. When **1** was treated with equimolar amounts of both morpholine and formalin, 2-hydroxy-6-methyl-3,6-bis-morpholinomethyl-2-cyclohexen-1-one (**22**) was obtained along with the recovered **1**.

The analytical data of **22** agreed with the $C_{17}H_{28}N_2O_4$

Table 2. Identification of bis-mannich bases

Compd.	mp. (°C)	IR (KBr) (cm^{-1}) O-H	IR (KBr) (cm^{-1}) C=O	IR (KBr) (cm^{-1}) C=C	UV_{max} (EtOH) nm (ε)	NMR ($CDCl_3$) δ_{ppm}[b]	Anal. Found (Calcd) C%	H%	N%
13a	123—123.5[a]	3400 (2600—2300)[c]	1690	1650	262 (7100)	1.06(s, 3H), 2.12—2.92 (m, 12H), 3.55—3.90 (m, 10H), 7.71(s, 1H)	62.07 (61.91)	8.56 (8.44)	8.39 (8.63)
13b	110.5—111.5[d]	3380 (2650—2300)[c]	1690	1660	260 (6990)	1.11(s, 3H), 1.50—2.05 (m, 8H), 2.09—2.99(m, 12H), 3.55(m, 2H), 7.60 (s, 1H)	69.25 (69.03)	9.42 (9.41)	9.77 (10.06)
13c	135[a]	3400 (2650—2400)[c]	1700	1665	262 (10800)	1.05(s, 3H), 1.15—1.93 (m, 12H), 2.09—2.95(m, 12H), 3.38(m, 2H), 8.87 (s, 1H)	70.61 (70.55)	9.85 (9.87)	8.95 (9.14)
16a	157—158[a]	3450 (2650—2450)[c]	1700	1660	265 (7880)	0.76(t, 3H, 6.8Hz), 1.30 —1.97(m, 2H), 2.18—2.95 (m, 12H), 3.40—3.94(m, 10H), 7.85(bs, 1H)	63.21 (62.94)	8.66 (8.70)	8.63 (8.63)
16b	113—114[d]	3450 (2650—2350)[c]	1700	1665	265 (5980)	0.74(t, 3H, 6.8Hz), 1.34 —2.06(m, 10H), 2.16—3.06 (m, 12H), 3.53(m, 2H), 8.46 (s, 1H)	69.59 (69.83)	9.64 (9.65)	9.33 (9.58)
16c	133—114[a]	3400 (2650—2400)[c]	1700	1660	264 (6690)	0.75(t, 3H, 6.8Hz), 1.30 —1.92(m, 14H), 2.05—2.85 (m, 12H), 3.35(m, 2H), 8.43(s, 1H)	71.21 (71.21)	10.16 (10.06)	8.63 (8.74)

a) Recrystallization from ethanol. b) TMS was used as an internal standard. c) Hydrogen-bonded O-H. d) Recrystallization from petroleum ether-ethanol.

formula, and the structure was assigned on the basis of its IR, NMR, and UV spectra. This reaction was run with the various ratios of reagents listed in Table 3; the best yield was obtained with 2 molar equivalents of both morpholine and formaline.

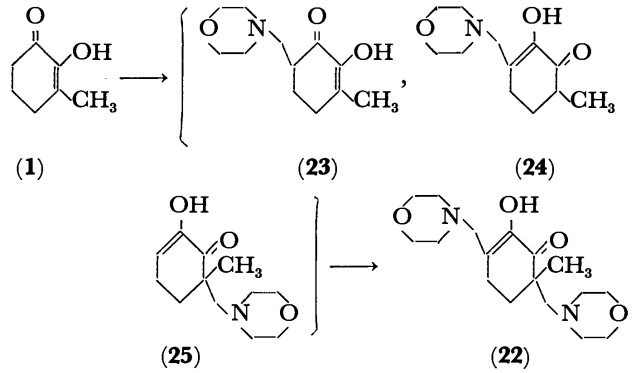

(1) (23) (24)

(25) (22)

Table 3. The Mannich reaction of **1** under various conditions in dioxane

Morpholine (equiv.)	Formalin (equiv.)	Reaction Temp. (°C)	Reaction Time (hr)	Yield (**22**)[a] (%)
1.0	1.0	27—28 and 55—56	2.5 5.0	40[b]
1.6	1.6	34—35 and 55—56	22.0 3.0	67[b]
2.0	2.0	25—27	60.0	79.2

a) Isolated yield based on diketone. b) Diketone 1 was recovered.

In no case, could any mono Mannich adducts (**23**, **24**, or **25**) be isolated. These results imply that the second morpholinomethylation is faster than the first.

The hydrogenolysis of **22** with zinc powder in acetic acid at 73—76 °C for 6 hr also afforded a demorpholinomethylation product (**7**) (60%) and 2-hydroxy-3,6-dimethyl-6-morpholinomethyl-2-cyclohexen-1-one (**26**) (6.8%). Under these conditions, no trimethyl diketone (**27**) could be isolated.

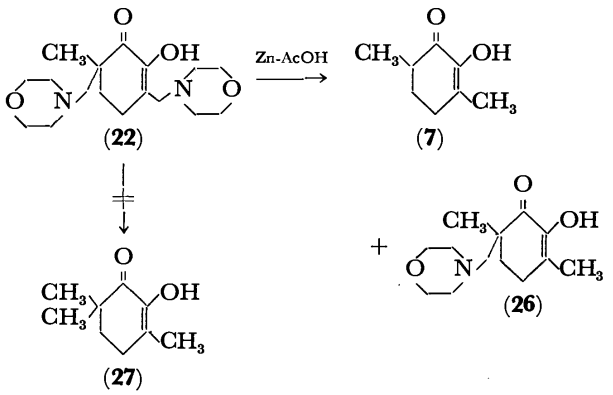

(22) (7) (26) (27)

On the basis of these facts, it was supposed that the Mannich bases with a tertiary aminomethyl group could easily undergo deaminomethylation[13] in the hydrogenolyses described above.

The NMR spectra of 6-substituted-2-cyclohexenones (**7**, **11**, and **26**) indicate that the allylic methyl protons appear as a doublet (J=0.6 Hz) at 1.83—1.89 ppm. Further work is under way to elucidate the reason for the splitting of these allylic methyl protons.

Experimental

All the melting points are uncorrected. The IR spectra were recorded with a Hitachi Model 215 spectrophotometer, and the UV spectra, with a Hitachi Model EPS-3T spectrophotometer. The NMR spectra were obtained on a JEOL Model C-60H spectrometer, with tetramethylsilane as the internal reference. The mass spectra were determined on a Hitachi RMU-6E spectrometer.

*2-Morpholino-2-cyclohexen-1-one (**3**).* A mixture of 4.6 g (41 mmol) of cyclohexane-1,2-dione, 4.5 g (51 mmol) of morpholine, and 100 ml of benzene was refluxed, while the water was removed, for 5 hr. After the removal of the benzene and the surplus morpholine, the residue was solidified. Recrystallization from isopropyl ether-ethanol gave 6.7 g (90.4%) of **3** as colorless crystals; mp 52.5—53 °C (lit,[14] mp 53—54 °C); IR(KBr) 3050 (=C-H), 1667 (C=O), 1605 cm^{-1} (C=C); NMR (CCl_4) δ *ca.* 1.95 (m, 2H), *ca.* 2.30 (m, 4H), *ca.* 2.70 (m, 4H), *ca.* 3.60 (m, 4H), 5.69 (t, 1H, J=3.9 Hz); UVmax (95% EtOH) 294 nm (ε=2450). Found: C, 66.24; H, 8.24; N, 7.58%. Calcd for $C_{10}H_{15}NO_2$; C, 66.27; H, 8.38; N, 7.73%.

*2-Hydroxy-3-morpholinomethyl-2-cyclohexen-1-one (**4**). A):* To a mixture of 2.80 g (25 mmol) of cyclohexane-1,2-dione in 3 ml of dioxane and 2.18 g (25 mmol) of morpholine, formalin (2.0 g, (25 mmol)) was added drop by drop, at room temperature and the mixture was then stirred for 3 hr. After the removal of the dioxane *in vacuo*, the residue was solidified. Recrystallization from isopropyl ether-ethanol gave 4.6 g (87.1%) of colorless crystals of **4**; mp 72—73 °C; IR(KBr) 3400 (O-H), 1665 (C=O), 1643 cm^{-1} (C=C); NMR (CCl_4) δ *ca.* 1.96 (m, 2H), *ca.* 2.38 (m, 8H), 3.08 (s, 2H), *ca.* 3.55 (m, 4H), *ca.* 5.73 (s, 1H); UVmax (95% EtOH) 274 nm (ε=8670). Found: C, 62.52; H, 8.06; N, 6.55%. Calcd for $C_{11}H_{17}NO_3$: C, 62.54; H, 8.11; N, 6.63%.

B): A mixture of 18.1 g (10 mmol) of **3**, 1.48 g (12 mmol) of morpholine hydrochloride, 0.36 g (4 mmol) of paraformaldehyde in 10 ml of dioxane, and 5 ml of ethanol was stirred for 6 hr under reflux. After cooling, the precipitated morpholine hydrochloride was separated, and the resulting mixture was diluted with ether, washed with water, and dried. After the evaporation of the solvent, trituration with isopropyl ether gave 1.75 g (83%) of **4**.

*2-Hydroxy-3,6-bismorpholinomethyl-2-cyclohexen-1-one (**5**).* To a mixture of 2.80 g (25 mmol) of **2** in 3 ml of dioxane and 5.22 g (60 mmol) of morpholine, formalin (4.8 g, (60 mmol)) in 1 ml of dioxane was added, drop by drop, at room temperature and the mixture was then stirred for 4.5 hr. After the removal of the dioxane *in vacuo*, the residual solid was recrystallized from isopropyl ether-ethanol to afford 6.28 g (85.2%) of **5**: mp 126.5—7.5 °C; IR (KBr) 3320 (O-H), 1672 (C=O), 1641 cm^{-1} (C=C); NMR (CCl_4) δ *ca.* 2.0 (m, 3H), 2.20—2.55 (m, 12H), 2.76 (s, 1H), 3.10 (s, 2H), *ca.* 3.45 (m, 8H); UVmax (95% EtOH) 277 nm (ε=6680). Found: C, 61.83; H, 8.53; N, 9.19%. Calcd for $C_{16}H_{26}N_2O_4$: C, 61.91; H, 8.44; N, 9.03%.

*2-Hydroxy-3-methyl-2-cyclohexen-1-one (**1**).* A mixture of 2.32 g (11 mmol) of **4**, 18.5 ml of glacial acetic acid, and 4.8 g (73 mg-atom) of zinc powder was stirred at 78—80 °C for 5 hr. After the zinc had then been filtered off and the acetic acid had been removed under reduced pressure, a small amount of water was added. The solution was subsequently extracted with chloroform. After drying, the chloroform was removed and the residue was chromatographed on a silica gel column. Elution with benzene-ethyl acetate (10 : 1) yielded 0.71 g (51.4%) of **1**; mp 60.5—61.5 °C (lit, [5] mp 63 °C). The spectral data were identical with those of an authentic sample.[3]

*2-Hydroxy-3,6-dimethyl-2-cyclohexen-1-one (**7**).* A mixture of 3.83 g (13 mmol) of **5**, 30 ml of acetic acid, and 8.45 g (0.13 g-atom) of zinc powder was stirred at 75—76 °C for 5 hr. After the zinc had then been filtered off and the acetic acid had been removed under reduced pressure, a small amount of water was added and the solution was extracted with chloroform. After drying, the solvent was evaporated and the residue was chromatographed on a silica gel column using benzene-ethyl acetate (10 : 1) to give 0.36 g (20%) of **7**; mp 61.5—62.5 °C; IR (KBr) 3420 (O-H), 1675 (C=O), 1650 cm^{-1} (C=C): NMR (CCl_4) δ 1.13 (d, 3H, J=7.0 Hz), 1.83 (d, 3H, J=0.6 Hz), 1.6—2.7 (m, 5H), 5.90 (s, 1H); UVmax (95% EtOH) 273 nm (ε=11900); mass *m/e* (%) 140 (41), 111 (80), 70 (83), 41 (100). Found: C, 68.08; H, 8.91%. Calcd for $C_8H_{12}O_2$: C, 68.55; H, 8.63%.

*6-Ethoxycarbonyl-2-hydroxy-3,6-dimethyl-2-cyclohexen-1-one (**11**). A):* To a mixture of 1.0 g (5 mmol) of **8** in 5 ml of dioxane and 0.40 g (5 mmol) of morpholine, formalin (0.4 g, (5 mmol)) in 1 ml of dioxane was added, at 14—15 °C and the mixture was then stirred for 3 hr. After removal of the dioxane *in vacuo*, we obtained a crude Mannich base (**10**) which was used without further purification for the next step. A mixture of the crude **10**, 18 ml of acetic acid, and 1.64 g (25 mg-atom) of zinc powder was stirred at 72—74 °C for 7 hr. After the zinc had then been filtered off and the acetic acid had been removed under reduced pressure, a small amount of water was added. After extraction with chloroform and drying with magnesium sulfate, the solvent was evaporated and the residue was chromatographed on a silica gel column. Subsequent elution with benzene-ethyl acetate (10 : 1) yielded 0.28 g (26%) of **11**; mp 46—48 °C; IR(KBr) 3440 (O-H), 1715, 1670 (C=O), 1640 cm^{-1} (C=C); NMR ($CDCl_3$) δ 1.22 (t, 3H, J=7.0 Hz), 1.40 (s, 3H), 1.89 (d, 3H, J=0.6 Hz), *ca.* 2.36 (m, 3H), 4.13 (q, 2H, J=7.0 Hz), 5.99 (s, 1H). Found: C, 61.87; H, 7.30%. Calcd for $C_{11}H_{16}O_4$: C, 62.25; H, 7.60%.

B): A mixture of 1.34 g (5 mmol) of **9**, 5 ml of dioxane, 0.62 g (5 mmol) of morpholine hydrochloride, and 0.40 g (5 mmol) of formalin was stirred at 50—55 °C for 4 hr. After having been worked up, the resulting mixture gave 1.20 g of crude **10**. To this Mannich base, 18 ml of acetic acid and 1.64 g (25 mg-atom) of zinc powder was added, the mixture was then stirred for 7 hr at 75 °C. A subsequent work-up in a manner similar to that described above afforded 266 mg (25%) of **11**.

*The Mannich Reaction of **12** with Secondary Amines: 2-Hydroxy-5-methyl-3,5-bismorpholinomethyl-2-cyclopenten-1-one (**13a**).* To 5.6 g (0.05 mol) of **12** in 50 ml of dioxane and 8.7 g (0.1 mol) of morpholine, a 8.1 g portion (0.1 mol) of formalin was added, drop by drop, at 0 °C. The mixture was then stirred at room temperature for several hours and allowed to stand overnight. After the subsequent removal of the dioxane under reduced pressure, the residue was solidified. Recrystallization from ethanol afforded 10.9 g (70.3%) of **13a**: mp 123—123.5 °C. The results with individual compounds under various conditions are shown in Table 1. The analytical data for **13a—c** are presented in Table 2.

*The Mannich Reaction of **15** with Secondary Amines: 5-Ethyl-2-hydroxy-3,5-bismorpholinomethyl-2-cyclopenten-1-one (**16**).* To 2.6 g (21 mmol) of **15** in 20 ml of dioxane and 3.7 g (42 mmol) of morpholine, formalin (3.4 g, (42 mmol)) was added at O °C. The mixture was then stirred at room temperature for several hours and kept overnight. The precipitated solid was recrystallized from ethanol to give 5.8 g (85.3%) of **16a**; mp 157—158 °C. The other results under various conditions are

shown in Table 1, while individual analytical data for **16a—c** are presented in Table 2.

*The Mannich Reaction of **17**: 2-Hydroxy-5-methyl-3,5-bispyrrolidinomethyl-2-cyclopenten-1-one (**13b**).* To 10.0 g (60 mmol) of **17** in 30 ml of dioxane and 8.6 g (0.12 mol) of pyrrolidine, a 9.8 g portion (0.12 mol) of formalin was slowly added, drop by drop at −10 °C, after while the mixture was stirred for 6 hr. The mixture was then stirred for 30 min at room temperature. After the subsequent removal of the solvent *in vacuo*, the resulting solid was recrystallized from petroleum ether-ethanol (10 : 1) to give 7.8 g (45.9%) of **13b**; mp 110.5—111.5 °C.

*1-Methyl-3-oxo-1-cyclopenten-2-yl p-Toluene Sulfonate (**19**).* To a stirred solution of 13.7 g (0.072 mol) of *p*-toluensulfonyl chloride in 4.7 g of pyridine, 6.7 g (0.06 mol) of **12** in 2.4 g of pyridine was added, drop by drop, with ice-water-bath cooling. The mixture was then stirred for 5 hr at 14—15 °C and the resulting mixture was poured into 60 ml of ice water. The precipitated crystals were filtered and recrystallized from petroleum ether-ethanol to afford 8.0 g (50.3%) of **19**; IR (KBr) 1710 (C=O), 1640 (C=C), 1585 cm^{-1} (aromatic (C=C); UVmax (99% EtOH) 229.5 nm (ε=24500); NMR ($CDCl_3$) δ 2.06 (s, 3H), 2.19—2.81 (m, 4H), 7.40 (m, 4H). Found: C, 58.97; H, 5.43%. Calcd for $C_{13}H_{14}O_4S$: C, 58.63; H, 5.30%.

*3,5-Dimethyl-2-hydroxy-2-cyclopenten-1-one (**20**). A)*: A mixture of 31.0 g (0.1 mol) of **13a**, 250 ml of glacial acetic acid, and 65.4 g (1 g-atom) of zinc powder was stirred at 80 °C for 5 hr. After the zinc had then been filtered off and the acetic acid removed *in vacuo*, 30 ml of water was added. The solution was then extracted with chloroform. After drying, the chloroform was evaporated and the residue was recrystallized from water to afford 5.1 g (40.5%) of **20**; mp 91—92.5 °C (lit,[6] mp 91—92 °C); IR (KBr) 3250 (O–H), 1690 (C=O), 1640 cm^{-1} (C=C); NMR ($CDCl_3$) δ 1.14 (d, 3H, J=7.5 Hz), 1.97 (t, 3H, J=0.6 Hz), 2.50 (m, 3H), 6.79 (s, 1H): UV max (99% EtOH) 261 nm (ε=12100). mass *m/e* (%) 126 (100), 111 (42), 83 (38), 79 (44), 56 (51). Found: C, 66.61; H, 8.10%. Calcd for $C_7H_{10}O_2$: C, 66.65; H, 7.99%.

B): Similarly, from 3.5 g (12.6 mmol) of **13b**, 35 ml of acetic acid, and 8.2 g (0.126 g-atom) of zinc powder, 0.50 g (31.4%) of **20** was obtained.

C): Similarly, from 3.10 g (10 mmol) of **13c**, 40 ml of acetic acid, and 6.5 g (0.1 g-atom) of zinc powder, 0.70 g (55.6 %) of **20** was obtained.

*2-Hydroxy-6-methyl-3,6-bismorpholinomethyl-2-cylohexen-1-one (**22**).* To a mixture of 0.60 g (4.75 mmol) of **1** in 3 ml of dioxane and 0.825 g (9.5 mmol) of morpholine, formalin (0.78 g, (9.5 mmol)) in 1 ml of dioxane was added slowly drop by drop at room temperature, and the mixture was stirred for 60 hr. After the removal of the dioxane *in vacuo*, the residue was diluted with a small amount of isopropyl ether to give white crystals. Recrystallization from isopropyl ether-ethanol afforded 1.22 g (79.8%) of **22**; mp 112—113 °C; IR (KBr) 3300 (O–H), 1674 (C=O), 1648 (C=C); NMR ($CDCl_3$) δ 1.05 (s, 3H), 1.6—2.3 (m, 4H), *ca.* 2.45 (m, 10H), 2.77 (s, 1H), *ca.* 3.69 (m, 8H); UVmax (99% EtOH) 274.5 nm (ε=8800). Found: C, 62.96; H, 8.68; N, 9.00%. Calcd for $C_{17}H_{28}N_2O_4$: C, 62.94; H, 8.70; N, 8.63%.

*Hydrogenolysis of **22** in Glacial Acetic Acid with Zinc Powder.* A mixture of 1.20 g (3.7 mmol) of **22**, 9 ml of glacial acetic acid, and 2.0 g (30.6 mg-arom) of zinc powder was stirred at 73—76 °C for 6 hr. After the zinc had then been filtered off and the acetic acid removed *in vacuo*, a small amount of water was added. The solution was then extracted with chloroform. After drying, the solvent was evaporated and the residue was chromatographed on 12 g of silica gel, using a 10 : 1 mixture of benzene-ethyl acetate as the eluent. An early fraction afforded 0.31 g (59.8%) of **7**: mp 61.5—62.5 °C. This compound was identical with the **7** derived from **4** as has been described above.

A later fraction gave 60 mg (6.8%) of **26**; mp 70—72 °C; IR (KBr) 3420 (O–H), 1670 (C=O), 1640 cm^{-1} (C=C); NMR (CCl_4) δ 1.00 (s, 3H), 1.83 (d, 3H, J=0.6 Hz), 1.90—3.0 (m, 10 H), *ca.* 3.49 (m, 4H), *ca.* 5.70 (broad s, 1H); UV_{max} (95% EtOH) 275 nm (ε=11800). Found: C, 65.58; H, 9.13; N, 5.88%. Calcd for $C_{13}H_{21}NO_3$: C, 65.25; H, 8.84; N, 5.85%.

References

1) Partly presented at the 29th Annual Meeting of the Chemical Society of Japan, Hiroshima, October, 1973.

2) M. A. Gianturco, A. S. Giammarino, and R. G. Pitcher, *Tetrahedron*, **19**, 2051 (1963); M. A. Gianturco, A. S. Giammarino, and P. Friedel, *Nature*, **210**, 1358 (1966).

3) K. Sato, S. Inoue, and M. Ōhashi, This Bulletin, **47**, 2519 (1974).

4) C. C. Hach, C. V. Bank, and H. Diehl, "Organic Syntheses," *Coll. Vol.* IV, p. 229 (1963).

5) C. W. N. Cumper, G. B. Leton, and A. I, Vogel, *J. Chem. Soc.*, **1965**, 2067.

6) K. Sato, S. Inoue, T. Kitagawa, and T. Takahashi, *J. Org. Chem.*, **38**, 551 (1973).

7) E. J. Cone, R. H. Garner, and A. W. Hayes, *ibid.*, **37**, 4436 (1972).

8) H. J. Roth and M. Mühlenbruch, *Arch. Pharm.*, **303**, 156 (1970); J. Brugidou and H. Christol, *C. R. Acad. Sci. Paris.*, **262**, 1595 (1965).

9) B. B. Thompson, *J. Pharm. Sci.*, **57**, 715 (1968); M. Tramontini, *Synthesis*, **1973**, 703 and, refernces cited therein.

10) K. Tonari, I. Ichimoto, H. Ueda, and C. Tatsumi, *Nippon Nogei Kagaku Kaishi*, **44**, 55 (1970).

11) R. T. Dahill, Jr. *J. Org. Chem.*, **31**, 2694 (1966).

12) L. E. Erickson, F. E. Collins, and R. T. Dahill, *ibid.*, **30**, 1050 (1965).

13) V. M. Behkov, Y. N. Belokon, M. M. Dolgaya, and N. S. Martinkova, *Tetrahedron*, **26**, 1199 (1970); V. M. Behkov, Y. N. Belokon, M. M. Dolgaya, and N. S. Martinkova, *Izt. Akad. Nauk. SSSR, Ser Khim*, **1967**, 471, 1721, 2234.

14) M. A. Tobias, J. G. Strong, and R. P. Napier, *J. Org. Chem.*, **35**, 1709 (1970).

A Study of the Kinetic Resolution of DL-Propylene Oxide with Optically Active Co(I)(salen) Type Complexes

Haruhiko Aoi, Michihiro Ishimori, and Teiji Tsuruta

Department of Synthetic Chemistry, Faculty of Engineering, University of Tokyo, Bunkyo-ku, Tokyo 113

(Received December 18, 1974)

An optically active Co(I)(salen) type complex, lithium *N,N'*-bis-(salicylaldehyde)-1(*R*),2(*R*)-1,2-*trans*-cyclohexanediiminatocobaltate (I), was prepared by reducing the Co(II) complex, *N,N'*-bis-(salicylaldehyde)-1(*R*),2(*R*)-1,2-*trans*-cyclohexanediiminatocobalt(II), with butyllithium. The structure of the Co(I) complex was determined by means of its absorption and circular dichroism (CD) spectra. D-Propylene oxide was found to react preferentially (*e.g.*, $\ll D/D+L \gg = 68\%$ in a dioxane solution) in a kinetic resolution of DL-propylene oxide using the above Co(I) complex as a catalyst. On the contrary, L-propylene oxide reacted selectively when Lewis acids were added to the system of the lithium Co(I) complex. The Lewis acids were demonstrated to interact with the Co(I) complex and to play a significant role in the asymmetric selectivity of the Co(I) species.

The square-planar tetradentate Schiff-base complexes of cobalt, such as cobaloxime[1] and Co(salen),[2] have been studied in relation to the coenzyme B_{12}. Few studies, however, have been done to explore the possibilities of an optically active Co(salen) type complex as a catalyst for any of the asymmetric reactions.

We reported in one of our previous papers[3] the kinetic resolution of DL-propylene oxide using an optically active Co(I) complex prepared by reducing an optically active Co(II)(salen) type complex, *N,N'*-bis(salicylaldehyde)-1(*R*),2(*R*)-1,2-*trans*-cyclohexanediiminatocobalt(II), Co(II)(sal)$_2$(*R*-CHXDA), with $LiAlH_4$; L-propylene oxide* was reacted in 95% selectivity.

In the course of further studies, it was found that D-propylene oxide, instead of the L-isomer, reacted preferentially when the Co(I) complex, prepared by reducing Co(II)(sal)$_2$(*R*-CHXDA) with butyllithium (BuLi), was used as a catalyst. This paper will describe the features of the kinetic resolution of DL-propylene oxide by use of the Co(I) complex prepared with BuLi. The effects of several metal alkyls and solvents on the asymmetric selectivity of the Co(I) complex will also be discussed in comparison with the case of the Co(II)(sal)$_2$(*R*-CHXDA)/$LiAlH_4$ system.

Experimental

Measurements. The absorption spectra were measured using a Shimadzu automatic recording spectrophotometer, Model MPS-50L. The CD spectra were taken on a Jasco Model J-20 spectrometer. The optical rotations were observed using a Perkin-Elmer Polarimeter Model 241. The glc analyses were carried out with a Hitachi Model K-53 Gas Chromatograph equipped with a column containing PEG.

Preparation of Cobalt Complexes. The reagents used were purified by the usual methods, as described elsewhere.[4] BuLi was prepared from *n*-butyl chloride and lithium metal; a cyclohexane solution of BuLi at the concentration of 1.42 mol/l was used. The Co(II)(sal)$_2$(*R*-CHXDA) was prepared by the method described in the previous paper.[3]

The Co(I) complex, Li$^+$[Co(I)(sal)$_2$(*R*-CHXDA)]$^-$, was prepared as follows: 0.05 mmol of Co(II)(sal)$_2$(*R*-CHXDA) was suspended in 50 ml of THF; then an equimolar amount of BuLi in cyclohexane added, and the solution was stirred for 1 hr at room temperature under a dry nitrogen atmosphere. A blue-green solution of the Co(I) complex was thus obtained. The evolved gases were analyzed by glc and calculated based on the amount of BuLi used. The Li$^+$[Co(I)(sal)$_2$(*R*-CHXDA)]$^-$/Lewis acid system was prepared by addition of an equimolar amount of a Lewis acid to the above solution of Li$^+$[Co(I)(sal)$_2$(*R*-CHXDA)]$^-$.

Reaction of the Co(I) Complex with DL-Propylene Oxide. 0.36 mmol of the Co(II) complex was suspended in a benzene (10 ml)/dioxane (5 ml) solvent (Tables 1 and 2) or an appropriate solvent (Tables 1 and 3); to which a cyclohexane solution of BuLi was added at the Co(II)/BuLi ratio of 1.0 or 2.0, after which the mixture was stirred for 2 hr at room temperature under a dry nitrogen atmosphere. In the case of the Co(I)/Lewis acid system (Table 2), a Lewis acid was added to the above solution at the ratio BuLi/Lewis acid=1.0 or 2.0, after which the mixture was stirred for 1 hr. Then 70 mmol of DL-propylene oxide was added to the above Co(I) solution. The mixture was sealed in an ampule under dry nitrogen and allowed to stand at 25 °C. After an appropriate reaction time, the non-reacted epoxide and acetone formed were analyzed by gas chromatography. The optical rotation of the recovered propylene oxide was measured.

The reaction of DL-propylene oxide with the Co(I) species prepared from the Co(II)/$LiAlH_4$ system was carried out similarly.

Results and Discussion

Preparation of Li$^+$[Co(I)(sal)$_2$(R-CHXDA)]$^-$. It has been reported that Co(II)(sal)$_2$(*R*-CHXDA) is a low-spin square-planar cobalt(II) complex with a λ conformation of the central chelate ring.[3] The absorption and CD spectra of the Co(I) species prepared by reducing Co(II)(sal)$_2$(*R*-CHXDA) with an equimolar amount of BuLi are shown in Figs. 1 and 2. The absorption spectrum in Fig. 1 is very similar to those of the reported Co(I) species[3] prepared by reducing Co(II)(sal)$_2$(*R*-CHXDA) with $LiAlH_4$ and with Na sand. The spectrum is also similar to that of Na$^+$[Co(I)(salen)]$^-$ observed by Calderazzo and Floriani.[5] Furthermore, by comparing the CD spectrum of the Co(I) species obtained from the Co(II) complex/BuLi system with that[3] of the Co(II) complex/$LiAlH_4$ system, these two Co(I) complexes are considered to have almost the same structure as to the co-planar ligand.

When the reaction of Co(II)(sal)$_2$(*R*-CHXDA) with

* L-propylene oxide: (*S*)-L-(−)-propylene oxide, D-propylene oxide: (*R*)-D-(+)-propylene oxide.

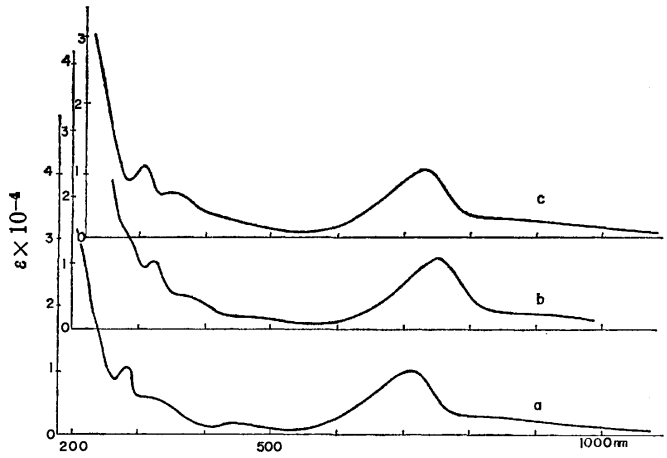

Fig. 1. The absorption spectra of the Co(I) species in THF.
(a) Co(II)(sal)$_2$(*R*-CHXDA)/BuLi
(b) Co(II)(sal)$_2$(*R*-CHXDA)/LiAlH$_4$
(c) Co(II)(sal)$_2$(*R*-CHXDA)/Na

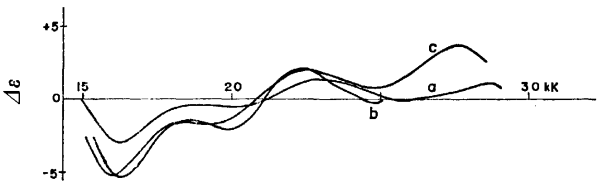

Fig. 2. The CD spectra of the Co(I) species in THF.
(a) Co(II)(sal)$_2$(*R*-CHXDA)/BuLi
(b) Co(II)(sal)$_2$(*R*-CHXDA)/LiAlH$_4$
(c) Co(II)(sal)$_2$(*R*-CHXDA)/Na

BuLi was carried out in a benzene or toluene solvent, butane and 1- and 2-butene were evolved, while butane was evolved quantitatively in a dioxane solution. It is thus concluded that the Co(I) species, Li$^+$[Co(I)(sal)$_2$(*R*-CHXDA)]$^-$ was prepared with simultaneous formation of the butyl radical by the reaction between Co(II)(sal)$_2$(*R*-CHXDA) and BuLi.

Resolution of DL-*Propylene Oxide with Li$^+$[Co(I)(sal)$_2$(R-CHXDA)]$^-$.* According to a previous study,[3] L-propylene oxide was reacted selectively in a kinetic resolution of DL-propylene oxide using an optically active Co(I) complex prepared by the reaction of Co(II)(sal)$_2$(*R*-CHXDA) with LiAlH$_4$. The reacted propylene oxide was isomerized to acetone quantitatively in the system at the ratio Co(II)/LiAlH$_4$=3.0, where the asymmetric selectivity** was very high, $\ll$L/D+L$\gg$ = 95%. On the other hand, at the ratios Co(II)/LiAlH$_4$ =1.5 and 1.0 the apparent percentage of acetone formed** and the asymmetric selectivity had lower values. This phenomenon was ascribed to side reactions involving the LiAlH$_4$ which remained in the system because of the incomplete reaction between LiAlH$_4$ and the Co(II) complex.

On the other hand, the reaction of BuLi with the Co(II) complex proceeds almost completely, resulting in the formation of a simple system of the Co(I) complex, which may be anticipated from the spectral similarity to behave as a catalyst similar to the Co(II)(sal)$_2$(*R*-CHXDA)/LiAlH$_4$ system.

** See the equations in Table 1.

Table 1. Asymmetric reaction of Co(II)(sal)$_2$(*R*-CHXDA)/BuLi system with propylene oxide (PO) in various solvents*

Solvent[a]	Time (day)	Conv.[b] (%)	$[\alpha]_{589}^{20}$[c] (°)	$\ll$D/D+L$\gg$[d] (%)	N[e]	Acetone formed[f] (%)
Diox	15	9.9	−0.59	68	20	100
Diox	18	11.3	−0.62	66	23	100
Bz/Diox	15	12.9	−0.33	58	25	95
Bz/Diox	16	14.0	−0.37	58	28	92
Bz/THF	18	14.0	−0.11	52	28	97
Tol	15	15.2	−0.32	56	31	94
o-Xyl	15	16.1	−0.06	51	33	100
m-Xyl	15	16.0	−0.06	51	32	90
Mes	16	16.3	−0.23	54	33	99
Bz/Tol	15	16.2	0	50	33	92
Bz/Tol[g]	15	13.4	+0.08	(52)[h]	27	99
Bz	15	16.5	+0.25	(54)[h]	33	94
Bz/CHAN	18	11.7	+0.09	(52)[h]	24	100

* Co(II)/BuLi=1(mol/mol), PO/Co(II)=200(mol/mol), temp.: 25 °C.
a) Bz: benzene, Diox: dioxane, THF: tetrahydrofuran, Tol: toluene, *o*-Xyl: *o*-xylene, *m*-Xyl: *m*-xylene, Mes: mesitylene, CHAN: cyclohexane; Bz/Diox=2(v/v), Bz/THF=2(w/w), Bz/Tol=2(w/w), Bz/CHAN=2(w/w). b) PO consumed(mol)/PO used(mol)×100. c) [α] for unreacted PO recovered. d) L-PO percent in the total conversion of D- and L-PO. $\ll$D/D+L$\gg = 1/2\left\{1+\left(\frac{D-L}{D+L}\right)\right\}\times 100$, where $\left(\frac{D-L}{D+L}\right)$ is the optical purity of the reacted monomer. The optical purity of the reacted monomer is evaluated by the eq. $\left(\frac{D-L}{D+L}\right) = \frac{[\alpha]}{[\alpha_0]}\times\frac{100-(\text{conv.})}{(\text{conv.})}$, where $[\alpha]/[\alpha_0]$ is the optical purity of the unreacted monomer. $[\alpha_0]_{589}^{21}=+15°$ for D-PO[6], (*cf.* Ref. 7). e) Recycling number for Li$^+$-[Co(I)(sal)$_2$(*R*-CHXDA)]$^-$. N=PO consumed/Li$^+$[Co(I)(sal)$_2$(*R*-CHXDA)]$^-$. Calcd on the assumption [Li$^+$[Co(I)(sal)$_2$(*R*-CHXDA)]$^-$]=[BuLi] used. f) Acetone formed(mol)/PO consumed(mol)×100. g) Bz/Tol=2.5(w/w). h) The values for $\ll$L/D+L$\gg$.

In a typical experiment carried out in a benzene/dioxane mixed solvent, the reacted propylene oxide was found to be isomerized to acetone quantitatively even at the Co(II)/BuLi ratio of 1.0, the Co(I) species being recycled as shown by the recycling number of the catalyst, given in Table 1. Contrary to the anticipation from the spectral similarity between the Co(II) complex/LiAlH$_4$ system and the Co(II) complex/BuLi system, D-propylene oxide was preferentially reacted in the reaction with the latter catalyst. Resolution reactions with the Co(II)/BuLi system were carried out in various solvents, as summarized in Table 1. A group of solvents, such as dioxane, tetrahydrofuran, toluene, and cyclohexane, was found to favor the reaction with D-propylene oxide over the L-isomer, whereas benzene exhibited the opposite effect. For comparison, the solvent effect on the reaction with the

Table 2. Asymmetric reaction of Co(II)(sal)$_2$(*R*-CHXDA)/LiAlH$_4$ system with propylene oxide in various solvents

Co(II)/LiAlH$_4$ (mol/mol)	PO/Co(II) (mol/mol)	Solvent[a]	Temp. (°C)	Time (day)	Conv.[b] (%)	$[\alpha]_{589}^{20}$[c] (°)	⟨L/D+L⟩[d] (%)
1.0	200	Diox	23	29	13.0	+1.39	81
1.0	100	Diox	28	14	30.2	+2.40	69
1.0	100	THF	22	13	13.2	+0.33	57
1.0	260	Tol	23	14	4.1	+0.30	73
2.0	100	Bz	22	15	11.9	+1.04	76

a), b), c), d) Description as in Table 1.

Table 3. Asymmetric reaction of Co(II)(sal)$_2$(*R*-CHXDA)/BuLi/Lewis acid system with propylene oxide#

Lewis acid[a]	Co(II)/BuLi/Lewis acid (mol/mol/mol)	Time (day)	Conv.[b] (%)	$[\alpha]_{589}^{20}$[c] (°)	≪L/D+L≫[d] (%)	N[e]	Acetone formed[f] (%)
B(i-Bu)$_3$	2/2/1	15	18.4	+0.07	51	37	96
	2/1/1	16	16.2	+0.16	53	65	94
	1/1/1	16	24.0	+0.75	58	24	94
Al(i-Bu)$_3$	2/2/1	15	23.0	+0.02	50	46	95
	2/1/1	16	31.5	+0.93	57	126	94
Zn(n-Bu)$_2$	2/2/1	15	8.7	+0.05	52	18	100
	2/1/1	16	6.5	+0.40	69	26	83
InEt$_3$	2/2/1	16	12.2	−0.29	(57)[g]	25	95
	2/1/1	15	15.2	+0.02	51	61	78
Co(II)/B(i-Bu)$_3$=1[h]		15	0	0	—	0	0

PO/Co(II)=200(mol/mol), temp.: 25 °C, Bz/Diox=2(v/v). a) B(i-Bu)$_3$: triisobutylborane, Al(i-Bu)$_3$: triisobutylaluminum, Zn(n-Bu)$_2$: dibutylzinc, InEt$_3$: triethylindium. b), c), d), e), f) Description as in Table 1. g) The value for ⟨D/D+L⟩. h) Co(II)(sal)$_2$(*R*-CHXDA)/B(i-Bu)$_3$=1(mol/mol) was used as a catalyst.

Co(II)/LiAlH$_4$ system was next examined. The Co(II)/LiAlH$_4$ system was found to attack L-propylene oxide selectively, regardless of the nature of the solvents used, as shown in Table 2. The selectivity is much higher than that of the Co(II)/BuLi system.

The remarkable difference in asymmetric selectivity between the Co(II)/BuLi and Co(II)/LiAlH$_4$ systems is of particular interest. It might be suspected that the AlH$_3$ moiety in the Co(II)/LiAlH$_4$ system interacts, as a Lewis acid, with the Co(I) species and plays a significant role in the asymmetric selectivity. Thus, the effect of a Lewis acid on the selectivity of the Co(I) species obtained from the Co(II) complex and BuLi was studied in the dioxane/benzene solvent. The results are summarized in Table 3. As expected, L-propylene oxide was preferentially consumed in a series of reactions involving triisobutylborane, triisobutylaluminum, dibutylzinc, and triethylindium as a Lewis acid, respectively. The results strongly suggest that the Lewis acids interact with the Co(I) species to form a "complex," for instance, Li$^+$[Co(I)]$^-$·Lewis acid. The selection for L-propylene oxide was observed even at the ratio Co(II)/BuLi/Lewis acid=2/2/1, where comparable amounts of Li$^+$[Co(I)]$^-$ and Li$^+$-[Co(I)]$^-$·Lewis acid are considered to co-exist, the apparent selectivity ≪L/D+L≫ being lowered by the presence of the Li$^+$[Co(I)]$^-$, which prefers D-propylene oxide. The low selectivity for L-propylene oxide at the ratio Co(II)/BuLi/InEt$_3$=2/1/1 and the selection of D-propylene oxide at the 2/2/1 ratio can be explained by the weak interaction between the Co(I) complex and InEt$_3$ because of the weak Lewis acidity of InEt$_3$.[8]

It has been reported that a Lewis acid such as trialkylaluminum reacts with acetone.[9] In the series of reactions in Table 3, however, the reacted propylene oxide was converted to acetone almost quantitatively, and no further reaction was observed. The Lewis acids may be stabilized by complexation with the Co(I) species, as has been described.

It is considered that the Co(I) species of the Co(II)/LiAlH$_4$ system is present as a complex, Li$^+$[Co(I)(sal)$_2$-(*R*-CHXDA)]$^-$·AlH$_3$, in accordance with the asymmetric selectivity being similar to that of the Co(II)/BuLi/Lewis acid system.

Mechanism for the Kinetic Resolution of DL-*Propylene Oxide.* A probable mechanism for the resolution of DL-propylene oxide and the isomerization of propylene oxide to acetone was previously discussed.[3] As shown in Scheme 1, the Co(I) species attacks the β-carbon of propylene oxide by an S_N2 mechanism, thus forming Co–C bonding; this is followed by isomerization of the propylene oxide moiety to acetone, the Co(I) species regenerated being recycled as a nucleophilic reagent.

The kinetic resolution is considered to take place at

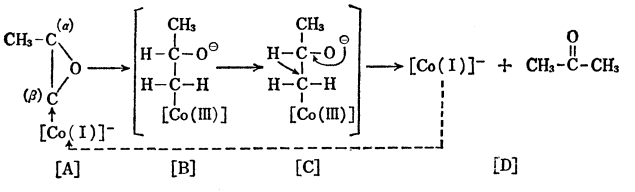

Scheme 1.

Table 4. The CD spectra of $Li^+[Co(I)(sal)_2(R\text{-CHXDA})]^-$, $Li^+[Co(I)(sal)_2(R\text{-CHXDA})]^-\cdot Al(i\text{-Bu})_3$ and $Li^+[Co(I)(sal)_2(R\text{-CHXDA})]^-\cdot AlH_3$ in THF

	$\tilde{\nu}\times10^{-3}$ cm^{-1} and $\Delta\varepsilon$ in parentheses			
$Li^+[Co(I)(sal)_2(R\text{-CHXDA})]^-$	28.3	23.0	19.8	16.1
	(+2.15)	(+1.21)	(−0.95)	(−3.03)
$Li^+[Co(I)(sal)_2(R\text{-CHXDA})]^-\cdot Al(i\text{-Bu})_3$	28.2	22.7	19.4	16.1
	(+1.84)	(+1.21)	(−0.97)	(−2.93)
$Li^+[Co(I)(sal)_2(R\text{-CHXDA})]^-\cdot AlH_3$	—	22.4	19.9	16.3
		(+2.08)	(−2.06)	(−5.39)

the stage [A] in Scheme 1. The Co(I) species reacts with either D- or L-propylene oxides preferentially, leaving unreacted propylene oxides containing a higher ratio of the other enantiomer. The CD spectra were measured in order to clarify the difference in asymmetric selectivity between the Co(II)/BuLi system and the Co(II)/BuLi/Lewis acid system. The CD spectra of the Co(II)/$LiAlH_4$ system and the Co(II)/BuLi/Lewis acid systems exhibit shapes similar to, but with slight band shifts† compared to, that of the Co(II)/BuLi system, as is shown in Table 4; this indicates that these Co(I) complexes have almost the same structure as to the inplane ligand, with a λ conformation of the central chelate ring similar to that of $Co(II)(sal)_2$-(*R*-CHXDA). In the light of the structure of trialkyltin-cobaloxime(I), Ph_3Sn–$Co(Dmg)_2$·Base, with a bond nature of Sn^+–$Co(I)^-$ reported by Schrauzer and Kralel,[10] it may be considered that the lithium cation is situated above the square plane of the Co(I) complex. Some information has been previously presented as to the site of Lewis acids in Co(salen) complexes. In Co(II)(salen)·$CHCl_3$,[11] Co(II)(salen)·InX_3,[12] Co(II)(salen)·SnX_4[13](X: halogen), and CH_3·Co(III)(salen)·H_2O-metal salt complexes,[14] it has been reported that $CHCl_3$ is combined with a phenolic oxygen by hydrogen bonding and that the metal atoms of Lewis acids form bonding with two phenolic oxygens.

On the basis of the above discussions, a possible structure for $Li^+[Co(I)(sal)_2(R\text{-CHXDA})]^-$·Lewis acid including $Li^+[Co(I)(sal)_2(R\text{-CHXDA})]^-\cdot AlH_3$ is depict-

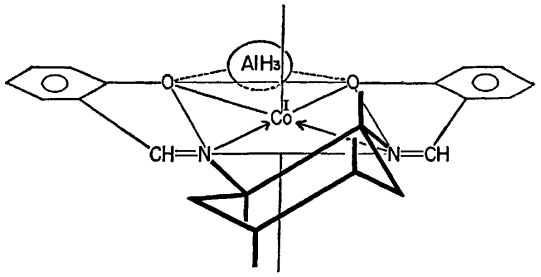

Fig. 3. A possible structure for $Li^+[Co(I)(sal)_2(R\text{-CHXDA})]^-\cdot AlH_3$.
The structure without AlH_3 moiety corresponds to that for $Li^+[Co(I)(sal)_2(R\text{-CHXDA})]^-$.

† The shifts are considered to reflect the interaction between the Co(I) species and Lewis acid.

†† The selectivities of the Co(II)/BuLi/Lewis acid systems can be interpreted in terms of those of mixed species, $Li^+[Co(I)(sal)_2(R\text{-CHXDA})]^-$·Lewis acid and $Li^+[Co(I)(sal)_2(R\text{-CHXDA})]^-$.

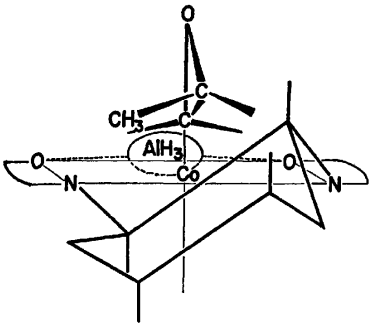

Fig. 4. Probable stereochemistry in the selection of a propylene oxide molecule by $Li^+[Co(I)(sal)_2(R\text{-CHXDA})]^-\cdot AlH_3$.

ed in Fig. 3. It should be easier for an incoming propylene oxide molecule to assume an orientation onto the active site as shown in Fig. 4; the bulky methyl group of propylene oxide and the Schiff-base ligand are far apart, because the left part of the diamine chelate is fixed below the square N_2O_2-plane due to the λ conformation. The chiral steric circumstance around the active site is established by the λ conformation of the central chelate ring, in co-operation with the Lewis acid moiety combined with pehnolic oxygens, which restricts the modes of orientation of the propylene oxide molecule. As shown in Fig. 4, L-propylene oxide would much more easily come to the Co(I) species, resulting in the high selectivity of the Co(II)/$LiAlH_4$ system to the L-isomer. Any orientation of D-propylene oxide could not be so easy as that of L-propylene oxide in Fig. 4 because of the steric hindrance caused by the right part of the diamine chelate fixed above the N_2O_2-plane and by the phenyl-azomethine parts and the AlH_3 placed on the same N_2O_2-plane, which were shown by the molecular-model consideration. In the absence of the Lewis acid moiety, the much smaller steric requirement around the active center would allow an incoming monomer to assume the orientation in a less specific way. According to our observation, D-propylene oxide exhibited a preference to the L-isomer in the reaction with $Li^+[Co(I)(sal)_2(R\text{-CHXDA})]^-$, though strong steric interaction between the Co(I) complex and the monomer may not be expected.†† The selection of L-propylene oxide by the Co(II)/BuLi system in benzene seems to be rather strange. Of interest, however, are the results of the X-ray analysis of the Co(II)(BAE)·benzene complex reported by Brückner *et al.*,[15] where benzene is fixed to the two phenolic oxygen atoms by the van der Waals distances. If such a specific fixation of benzene around phenolic

oxygens is also present in the Co(II)/BuLi system, a chiral structure similar to that of the $Li^+[Co(I)(sal)_2$-(*R*-CHXDA)]$^-$·Lewis acid system might be established around the active site.

References

1) a) G. N. Schrauzer, *Accounts Chem. Res.*, **1**, 97 (1968), b) G. N. Schrauzer, *J. Amer. Chem. Soc.*, **92**, 7078 (1970), c) K. Nguyen van Duong and A. Gaudemer, *J. Organometal. Chem.*, **22**, 473 (1970).

2) a) G. Costa, G. Mestroni, and G. Pellizer, *ibid.*, **11**, 333 (1968), b) C. Floriani, M. Puppis, and F. Calderazzo, *ibid.*, **12**, 209 (1968).

3) H. Aoi, M. Ishimori, S. Yoshikawa, and T. Tsuruta, *ibid.*, **85**, 241 (1975).

4) J. A. Riddick and W. B. Bunger, "Technique of Organic Chemistry," Vol. II, ed. by A. Weissberger, Wiley-Interscience, New York (1970).

5) F. Calderazzo and C. Floriani, *Chem. Commun.*, **1967** 139.

6) C. C. Price and M. Osgan, *J. Amer. Chem. Soc.*, **78**, 4787 (1956).

7) B. Franzus and J. H. Surridge, *J. Org. Chem.*, **31**, 4286 (1966).

8) O. Nakasugi, M. Ishimori, and T. Tsuruta, This Bulletin, **47**, 871 (1974).

9) a) K. Ziegler, K. Schneider, and J. Schneider, *Ann. Chem.*, **623**, 9 (1959), b) T. Eicher, "The Chemistry of Carbonyl Group," ed. by S. Patai, Interscience, New York (1966), p. 621.

10) G. N. Schrauzer and G. Kralel, *Chem. Ber.*, **102**, 2392 (1969).

11) M. Calligaris, G. Nardin, and L. Randaccio, *Coord. Chem. Rev.*, **7**, 385 (1972).

12) M. D. Hobday, and T. D. Smith, *J. Chem. Soc., Dalton*, **1972**, 2287.

13) M. D. Hobday and T. D. Smith, *J. Chem. Soc., A*, **1971**, 1453.

14) G. R. Tauszik, G. Pellizer, and G. Costa, *Inorg. Nucl. Chem. Lett.*, **9**, 717 (1973).

15) S. Brückner, M. Calligaris, G. Nardin, and L. Randaccio, *Inorg. Chim. Acta*, **2**, 386 (1968).

Component Amino Acids of the Antibiotic Longicatenamycin. Isolation of 5-Chloro-D-tryptophan[1]

Tetsuo SHIBA, Yasuo MUKUNOKI, and Hitoshi AKIYAMA

Department of Chemistry, Faculty of Science, Osaka University, Toyonaka, Osaka 560

(Received January 6, 1975)

An amino acid composition of the peptide antibiotic longicatenamycin was investigated. Four new amino acids, *i.e.*, *threo*-β-hydroxy-L-glutamic acid, L-2-amino-5-methylhexanoic acid, L-2-amino-6-methylheptanoic acid, and L-2-amino-7-methyloctanoic acid, which were reported by Shoji *et al.*, were reconfirmed by comparison with the synthetic specimens. Racemic forms of the latter three amino acids were synthesized through acetaminomalonate method. Furthermore, 5-chloro-D-tryptophan was newly isolated from the hydrolyzate of the antibiotic. This structure was assigned by NMR, MS and ORD. A steric configuration of this amino acid was certified by degradation to D-aspartic acid through ozonization. 5-Chloro-DL-tryptophan was synthesized from 3-cyanopropionaldehyde and *p*-chlorophenylhydrazine by Fischer's indole synthesis.

Longicatenamycin is an antibiotic isolated from the strain S-520 of *Streptomyces diastaticus* by Shoji and his collaborators in 1970 and tentatively named S-520.[2] This antibiotic is active against Gram-positive bacteria including *Diplococcus pneumoniae*. The hydrochloride of the antibiotic has extremely poor solubilities in water and almost all organic solvents except lower alcohol or dimethyl sulfoxide. Longicatenamycin showed the positive Ehrlich reaction and the characteristic UV absorptions at 299 nm, 290, 283 and 227.[2] According to the preliminary investigation by Shoji *et al.*, longicatenamycin is a peptide containing several unusual amino acids. They also suggested that the antibiotic is a complex mixture composed of several closely related peptides which have three exchangeable positions for amino acid residues in their molecules.[3] This feature seems to be rather common in many peptide antibiotics.[4-7] Among the component amino acids they reported, two kinds of new amino acids are involved. The one is *threo*-β-hydroxy-L-glutamic acid (**1**)[8] and the other is a group of three homologous amino acids with long carbon chains, *i.e.*, L-2-amino-5-methylhexanoic acid (**2**), L-2-amino-6-methylheptanoic acid (**3**) and L-2-amino-7-methyloctanoic acid (**4**).[9] They assigned the structures of those four amino acids mainly by NMR studies.[8,9]

Since Dakin had pointed out a possibility of an existence of β-hydroxyglutamic acid in the hydrolyzate of casein in 1918,[10] much efforts have been made in vain for isolation of this amino acid. However, at the present time, an occurrence of the amino acid was denied after all negative results by many workers.[11,12] If Shoji's presumption is right,[8] this will be a first presentation for an occurrence of β-hydroxyglutamic acid in nature. In the present study, a sample of the acid **1** obtained from the hydrolyzate of longicatenamycin was compared with the authentic *threo* and *erythro*-β-hydroxy-DL-glutamic acids which had been early synthesized by Kaneko *et al.*[13] The natural L-amino acid **1** was completely identical with synthetic *threo* isomer in NMR, amino acid analysis and thin-layer chromatography.

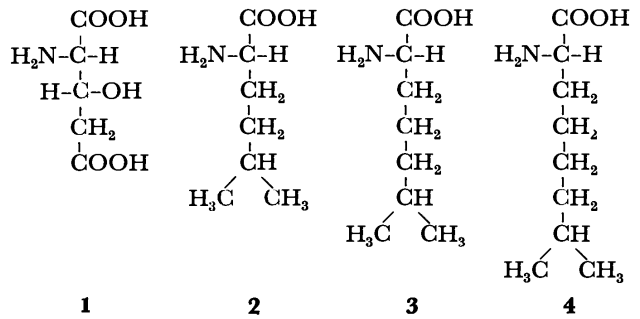

1 **2** **3** **4**

Fig. 1.

Three other new amino acids **2**, **3** and **4** exceed, in their carbon chain lengths, leucine which is known as the longest naturally occurring amino acid of $(CH_3)_2CH(CH_2)_nCH(NH_2)COOH$ type. We synthesized these amino acids by means of acetaminomalonate method. Thus, diethyl acetaminomalonate was coupled with isoamyl bromide, isohexyl bromide and isoheptyl bromide respectively and each coupling product was hydrolyzed to yield the corresponding DL-α-amino acids. Three natural L-amino acids **2**, **3** and **4**, were identified with the synthetic 2-amino-5-methylhexanoic acid, 2-amino-6-methylheptanoic acid and 2-amino-7-methyloctanoic acid respectively in NMR, amino acid analysis and thin-layer chromatography.

The amino acid composition of the acid hydrolyzate of longicatenamycin was reinvestigated in our study by amino acid analysis. Our result as shown in Table 1 coincides with that of Shoji *et al.*[2] within the experimental errors.

The molar ratio of amino acid composition indicates that there are three groups each comprising the homologous amino acids and corresponding to one mole respectively, *i.e.*, i) Val, Ile ii) **2**, **3**, **4** iii) Orn, Lys. The low value of **1** may be ascribed to the possible degradation *via* retroaldol condensation during the acid hydrolysis. The loss due to such decomposition was confirmed in the reference experiment with the authentic β-hydroxyglutamic acid.

At the stage of this investigation, the characteristic UV absorption and positive Ehrlich reaction of longicatenamycin cannot be explained by the component amino acids isolated so far. In addition, a difference between an apparent molecular weight (566) calculated based on a cyclic pentapeptide consisting of each one mole of Gly, **1**, Val (Ile), **2** (**3**, **4**) and Orn (Lys)[14] and the measured values of molecular weight of 2,4-dinitrophenyl (969) and acetyl (*ca.* 900) derivatives of longicatenamycin from extinction coefficients of the absorption spectra at 350 and 289 nm respectively, sug-

Table 1. The molar ratio of component amino acids of longicatenamycin[a)]

Gly[b)]	1	Val	Ile	2	3	4	Orn	Lys	Amm
1.00	0.45	0.77	0.17	0.20	0.36	0.38	0.76	0.28	0.68

a) The ratio of 5-chloro-D-trypophan is not included. b) Gly: glycine; Val: D-valine; Ile: D-isoleucine; Orn: D-ornithine; Lys: D-lysine; Amm: ammonia; **1**: *threo*-β-hydroxy-L-glutamic acid; **2**: L-2-amino-5-methylhexanoic acid; **3**: L-2-amino-6-methylheptanoic acid; **4**: L-α-2-amino-7-methyloctanoic acid.

gests strongly a presence of a tryptophan-like substance which might escape from the amino acid analysis because of a possible decomposition in the acid hydrolysis.

An experiment to trace such a predicted amino acid was done first by an alkaline hydrolysis of the antibiotic.[15] Thus, longicatenamycin was hydrolyzed with 10% barium hydroxide. From isobutyl alcohol extract of the hydrolyzate, a neutral amino acid with a molecular formula of $C_{11}H_{11}O_2N_2Cl$ was isolated in a crystalline state. This amino acid was positive to both ninhydrin and Ehrlich reactions, and showed UV absorptions at λ_{max}^{EtOH} 298 nm (ε 3800), 289 (5300), 282 (5200) and 226 (36700). From its NMR spectrum in C_5D_5N–D_2O as shown in Fig. 2 and mass spectrum, a structure of this new amino acid was assumed to be 5-chlorotryptophan. A position of chlorine atom on the indole nucleus was determined by the fact that a signal (Ha) in the lowest magnetic field can be assigned as H-4 in comparison with the spectrum of tryptophan itself and it shows only long range coupling of J=2 Hz with Hb.

A steric configuration of α-carbon atom cannot be clarified on this sample which was completely racemized during the alkaline hydrolysis. Therefore, the hydrolysis of longicatenamycin was carried out newly with 6 M hydrochloric acid in a sealed, evacuated tube. An optically active 5-chlorotryptophan thus obtained showed a positive ORD curve: $[\phi]_{320}$+3410° (peak), $[\alpha]_D^{25}$ +40° (methanol). Since L-tryptophan gave the negative ORD curve in methanolic solution, we assigned D-form for this amino acid. On the contrary, a configuration of α-carbon atom of *N*-carbethoxyacetyl-4-chlorotryptophan which was isolated as a hypocotyl swelling factor from immature seeds of *Pisum sativum* was assumed to be D-form by Marumo and Hattori only from the negative ORD curve.[16] Both conclusions seem to be controversy though there are differences in substitution groups. Since any contribution of acyl or chlorine substituent on tryptophan molecule to the sign of Cotton effect is not known well, a suspection of the configuration of tryptophan derivative from the sign of ORD curve must be very prudent.

Therefore, we now oxidized (+)-5-chlorotryptophan with ozone to lead to an optically active aspartic acid[17] which was purified as 2,4-dinitrophenyl (DNP) derivative. This DNP aspartic acid showed the negative value of the specific rotation: $[\alpha]_D^{20}$ −45° ($NaHCO_3$), indicating D-form of the amino acid unambiguously. Conclusively it is determined that (+)-5-chlorotryptophan in longicatenamycin has D-configuration at α-carbon atom.

For confirmation of the supposed structure of 5-chlorotryptophan, it was synthesized through the following novel method where the tryptophan synthesis by Komachiya *et al.*[18] was applied (Scheme 1). 3-Cyanopropionaldehyde (**5**)[19] was changed to 5-(2-cyanoethyl)-hydantoin (**6**) by Bücherer's method. A nitrile group in compound **6** was reduced to aldehyde using poisoned nickel catalyst according to the procedure by Komachiya *et al.*[18] The hydantoin aldehyde (**7**)

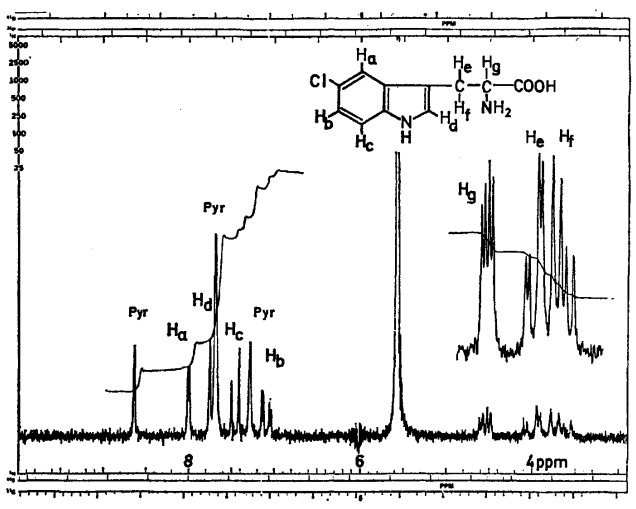

Fig. 2. NMR spectrum of 5-chlorotryptophan from longicatenamycin in C_5D_5N–D_2O (1 : 1) at 100 MHz.

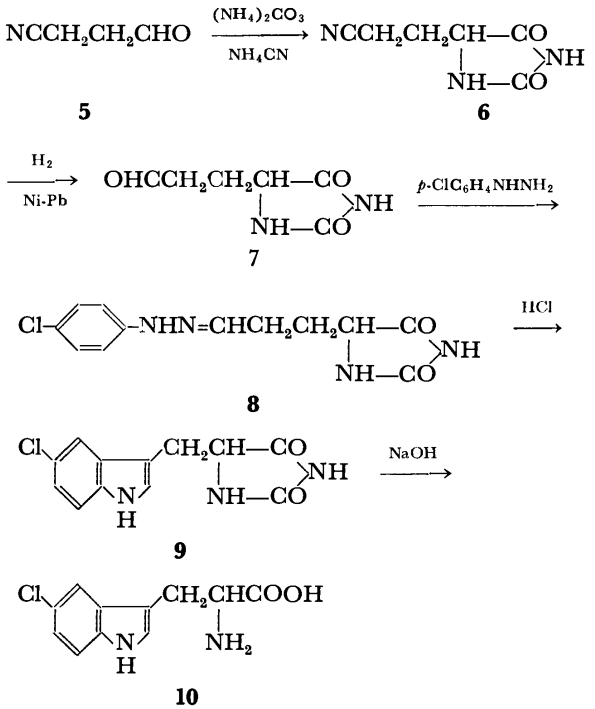

Scheme 1.

thus obtained was converted to *p*-chlorophenylhydrazone (**8**) which was then cyclized to indole hydantoin (**9**) through Fischer's indole synthesis using dilute hydrochloric acid. Alkaline hydrolysis of the product **9** gave 5-chloro-DL-tryptophan. The synthetic amino acid was completely identical with the natural compound in IR, NMR, amino acid analysis and mass spectrum. This is the first occurrence of 5-chlorotryptophan in nature.

This amino acid had been already synthesized by Rydon and his collaborators but through tedious long path.[20,21] One of the advantage in our synthetic method is that a single product of 5-chloroindole compound is obtained in principle even if the indole ring is formed at either *ortho* position of the compound **8** in Fischer's indole synthesis. Moreover, the overall yield from 3-cyanopropionaldehyde dimethyl acetal in this synthesis was as good as about 40%.

Now, the experimental formula of longicatenamycin becomes $C_{36.6}H_{54.3}O_{9.0}N_{8.0}Cl_{1.0}$ (MW 786) on the basis of the molar ratio of the component amino acids mentioned before added with one mole of 5-chlorotryptophan.[22] Apparent molecular weights of mono-DNP (953) and diacetyl (871) derivatives calculated from this formula are consistent with the observed values mentioned before. This indicated that there is no more amino acid unidentified in the molecule of longicatenamycin.

Other than these amino acids, Shoji *et al.* reported one spot of a-II in the acidic area of two-dimensional paper chromatogram of the hydrolyzate of longicatenamycin, although they could neither isolate nor detect it in amino acid analysis.[3] In our experiment where the antibiotic was hydrolyzed with hydrochloric acid in the evacuated tube, no such spot appeared on paper-chromatogram. Therefore, this spot would be due to some degradation of 5-chlorotryptophan during the acid hydrolysis in the presence of air.

From all of the above results, it can be now concluded that longicatenamycin is composed of each one mole of glycine, *threo*-β-hydroxy-L-glutamic acid, 5-chloro-D-tryptophan, D-valine (D-isoleucine), L-2-amino-5-methylhexanoic acid (L-2-amino-6-methylheptanoic acid, L-2-amino-7-methyloctanoic acid) and D-ornithine (D-lysine).[14]

Experimental

All melting points are uncorrected. The following apparatuses were employed: Jasco Model IR-S Infrared Spectrophotometer, Hitachi 124 Spectrophotometer, Jasco Model ORD/UV-5-Optical Rotatory Dispersion Recorder, Varian T-60 Spectrometer, Varian XL-100 Spectrometer and Hitachi Amino Acid Analyzer KLA-3. For NMR measurement, tetramethylsilane was used as an internal reference substance. Paper electrophoresis was carried out in a pyridine-acetic acid-water (30 : 4 : 966) buffer solution using Toyo filter paper No. 51. For thin-layer chromatography on silica gel G, the solvent systems of *n*-butanol–acetic acid–water (4 : 1 : 2) and methyl ethyl ketone–pyridine–water–acetic acid (35 : 5 : 5 : 1) were employed mainly.

DL-2-Amino-5-methylhexanoic Acid (2). To a solution of diethyl acetaminomalonate (13.0 g, 0.06 mol) and sodium metal (1.38 g, 0.06 mol) in absolute ethanol (100 ml), there was added isoamyl bromide (8.72 g, 0.06 mol) and the mixture was heated under reflux for 36 hr. To an oily residue obtained after evaporation of the solvent, water (100 ml) was added and the product was extracted with ether (500 ml). Extract was washed with water and dried with magnesium sulfate. Oily substance obtained after evaporation of ether was crystallized on addition of *n*-hexane. The product was recrystallized from ether to give needles, yield, 5.5 g. These were hydrolyzed by refluxing with 47% hydrobromic acid (100 ml) for 18 hr. The amino acid obtained was purified by Dowex 50×8 (H^+ form) column. From the eluate with M ammonium hydroxide, crystals of DL-2-amino-5-methylhexanoic acid were obtained and recrystallized from hot water, yield, 2.2 g (25%); mp 273—275 °C (decomp.). R_f value on thin-layer chromatogram: 0.38 (methyl ethyl ketone–pyridine–water–acetic acid, 35 : 5 : 5 : 1).

Found: C, 57.86; H, 10.41; N, 9.67%. Calcd for $C_7H_{15}O_2N$: C, 57.90; H, 10.41; N, 9.65%.

DL-2-Amino-6-methylheptanoic Acid (3). Isohexyl bromide was prepared by bromination of isohexyl alcohol with mixed acid of 47% hydrobromic acid and concentrated hydrochloric acid.[23] Isohexyl alcohol was obtained by reduction of 4-methylpentanoic acid with lithium aluminum hydride.[24] The latter compound was synthesized from isoamylbromide by Grignard reaction with carbon dioxide.[25] A coupling reaction of isohexyl bromide (5.0 g, 30 mmol) with diethyl acetaminomalonate (6.5 g, 30 mmol) was carried out in a similar manner to that for **2**. Elution of the amino acid from Dowex-50 column was done using a mixed solvent of 1 M ammonium hydroxide and methanol (1 : 1), yield, 1.6 g (33%); mp 286—290 °C (decomp.). R_f value on thin-layer chromatogram: 0.50 (methyl ethyl ketone–pyridine–water–acetic acid, 35 : 5 : 5 : 1).

Found: C, 60.24; H, 10.70; N, 8.77%. Calcd for $C_8H_{17}O_2N$: C, 60.34; H, 10.76; N, 8.80%.

DL-2-Amino-7-methyloctanoic Acid (4). Isoheptyl bromide was prepared from isohexylbromide through Grignard reaction, lithium aluminum hydride reduction and bromination successively. Coupling of isoheptyl bromide (4.60 g, 26 mmol) and diethyl acetaminomalonate (5.56 g, 26 mmol) was carried out in a similar way to that mentioned above, yield, 1.57 g (35%); mp 271—273 °C (decomp.). R_f value on thin-layer chromatogram: 0.54 (methyl ethyl ketone–pyridine–water–acetic acid, 35 : 5 : 5 : 1).

Found: C, 62.16; H, 10.99; N, 8.07%. Calcd for $C_9H_{19}O_2N$: C, 62.39; H, 11.05; N, 8.09%.

Isolation of 5-Chloro-DL-tryptophan (Alkaline Hydrolysis). Longicatenamycin (1.0 g) was refluxed with 10% aqueous barium hydroxide (50 ml) for 48 hr. The reaction mixture was diluted with water (50 ml) and then neutralized with 2 M sulfuric acid. Precipitate of barium sulfate was filtered, and the filtrate was extracted with isobutyl alcohol (100 ml) three times. After evaporation of the solvent, the brown powder was obtained. This was purified by repeated crystallization with aqueous methanol and ether to obtain colorless crystals, yield, 50 mg; mp 250—255 °C (decomp.). UV: λ_{max}^{MeOH} 298 nm (ε 3800), 289 (5300), 282 (5200), 226 (36700). NMR (100 MHz, C_5D_5N–D_2O (1 : 1): H-4: δ 8.03 (1H, d, J=2.0 Hz), H-6: 7.11 (1H, dd, J=2.0, 9.0), H-7: 7.49 (1H, d, J=9.0), H-2: 7.78 (1H, s), H-β: 3.66 (1H, dd, J=4.0, 16.0), H-β′: 4.00 (1H, dd, J=10.0, 16.0), H-α: 4.55 (1H, dd, J=4.0, 10.0), MS: *m/e*, 238, 193, 164, 127.

Found: C, 55.04; H, 4.89; N, 11.74; Cl, 14.68%. Calcd for $C_{11}H_{11}O_2N_2Cl$: C, 55.35; H, 4.65; N, 11.74; Cl, 14.86%.

Isolation of 5-Chloro-D-tryptophan (Acid Hydrolysis). A suspension of longicatenamycin (250 mg) in 6 M hydrochloric acid (10 ml) was heated at 110 °C for 1 hr in a sealed, evacu-

ated tube. After dilution with water (20 ml), the hydrolyzate was neutralized with 2 M sodium hydroxide and extracted with isobutyl alcohol (300 ml). The residue obtained after evaporation of the solvent from the extract was dissolved in a mixture of methanol–acetic acid–water (1 : 1 : 1) and subjected to Dowex 50×2 column (1.5×30 cm) bufferized with 0.2 M pyridine–acetic acid buffer of pH 3.1. Elution was carried out gradiently with 0.2 M pyridine buffer of pH 3.1 (200 ml) and 2 M pyridine buffer of pH 5.0 (200 ml) successively. From fractions No. 32—40 of each 8 g, colorless crystals were obtained, yield, 10 mg; mp 238—245 °C (decomp.); ORD, $[\phi]_{320}+3410°$ (peak) (*c* 0.58, methanol), $[\alpha]_D^{25}$ +40° (*c* 0.58, methanol). This compound was identified with DL-isomer obtained by the alkaline hydrolysis in UV spectrum, thin-layer chromatography and amino acid analysis.

Ozonization of 5-Chloro-D-tryptophan. Optically active 5-chlorotryptophan (5 mg) obtained above was dissolved in 0.5 M hydrochloric acid (2 ml) and ozone was passed through the solution on ice-cooling for 2 hr. After addition of 30% aqueous hydroperoxide (0.3 ml), the reaction mixture was heated on boiling water bath for 10 min. Crystals obtained after evaporation were dissolved in a small amount of water and subjected to Dowex 50×2 column (0.5×10 cm) bufferized with 0.2 M pyridine–acetic acid of pH 3.1. Elution was carried out with the same buffer solution and fractions of each 4 g were collected fractionally. From fractions No. 11 and 12, colorless crystals of aspartic acid were obtained. This amino acid was 2,4-dinitrophenylated using sodium hydrogencarbonate in the usual manner. Crystals of DNP-aspartic acid were obtained from ether extract after acidification. These were purified by silica gel column (0.5×15 cm) using a mixed solvent of *n*-hexane–ether (9 : 1). $[\alpha]_D^{18}$ −8.0° (c 0.03, methanol), $[\alpha]_D^{30}$ −45° (*c* 0.11, 1% $NaHCO_3$).

5-[2-(4-Chlorophenylhydrazonoformyl)-ethyl]-hydantion (8). i) 5-(2-Cyanoethyl)-hydantoin (**6**) was prepared from 3-cyanopropionaldehyde (**5**)[26] through Bücherer's reaction.[18] According to the method by Komachiya *et al.*,[18] nitrile group in the hydantoin **6** was reduced to aldehyde using Raney nickel catalyst poisoned with lead acetate in acetic acid to yield 5-(2-formylethyl)-hydantoin (**7**). The reaction mixture starting from 15.3 g (0.10 mol) of **6** was filtered to remove the catalyst, and a solution of *p*-chlorophenylhydrazine (14.3 g, 0.10 M) in 100 ml of 1 M hydrochloric acid was added with stirring. Crystals deposited were collected by filtration and recrystallized from ethanol–water, to give the hydrazone **8**, yield, 15.4 g (55%); mp 147—149 °C (decomp.).

Found: C, 51.25; H, 4.70; N, 19.80; Cl, 12.56%. Calcd for $C_{12}H_{13}O_2N_4Cl$: C, 51.34; H, 4.67; N, 19.96; Cl, 12.63%.

ii) The same hydrazone **8** was obtained from semicarbazone of **7** (9.98 g, 47 mmol) and *p*-chlorophenylhydrazine 6.70 g (47 mM) in a similar way, yield, 12.3 g (94%), mp 147—148 °C (decomp.).

5-(5-Chloroindolyl-3-methyl)-hydantoin (9). The hydrazone **8** (1.40 g, 5.0 mmol) was dissolved in hot water (80 ml) containing 3 M hydrochloric acid (3.72 ml) on heating at 100 °C. After keeping at this temperature for 80 min, the reaction mixture was evaporated *in vacuo*. The residue was crystallized in addition of a small amount of water. The crystals were filtered off, washed with water and dried to give the crude product, yield, 1.15 g (85%). A pure sample was obtained by purification on silica gel column chromatography using chloroform–methanol (95 : 5) as an elution solvent, mp 127—132 °C (decomp.).

Found: C, 53.10; H, 4.18; N, 15.74%. Calcd for $C_{12}H_{10}O_2N_3Cl\cdot 1/2H_2O$: C, 52.85; H, 4.07; N, 15.41%.

5-Chloro-DL-tryptophan (10). The chloroindole derivative **9** (540 mg, 2.0 mM) was dissolved in M sodium hydroxide and heated at 150—155 °C for 1 hr in a sealed tube in which air was displaced with nitrogen. After neutralization to pH 5.9 with 3 M hydrochloric acid, the reaction mixture was extracted with isobutyl alcohol (80 ml). Extract was washed with water and evaporated *in vacuo*. A small amount of undissolved material in ethanol was removed, and the filtrate was again evaporated. The residue thus obtained was crystallized from methanol–ether, yield, 260 mg (55%). A pure sample was obtained by Dowex 50×2 column chromatography using a gradient buffer of 0.2 M pyridine–acetic acid of pH 3.1 and 2.0 M buffer of pH 5.0, mp 254—256 °C (decomp.).[27] R_f values on thin-layer chromatogram: 0.71 (*n*-butanol–acetic acid–water, 4 : 1 : 2); 0.10 (chloroform–methanol–water, 45 : 12 : 1).

Found: C, 55.14; H, 4.83; N, 11.79; Cl, 14.40%. Calcd for $C_{11}H_{11}O_2N_2Cl$: C, 55.35; H, 4.65; N, 11.74; Cl, 14.86%.

The authors are deeply indebted to Dr. Hideo Otsuka and Dr. Junichi Shoji of Shionogi Co., Ltd. for their kind supply of longicatenamycin and encouragement throughout this work.

References

1) This study was presented at the 30th Annual Meeting of the Chemical Society of Japan, Osaka, April, 1974; A part was reported in a preliminary form: T. Shiba, Y. Mukunoki, and H. Akiyama, *Tetrahedron Lett.*, **1974**, 3085.
2) J. Shoji, S. Kozuki, M. Mayama, and N. Shimaoka, *J. Antibiotics*, **23**, 429 (1970).
3) J. Shoji and R. Sakazaki, *ibid.*, **23**, 432 (1970).
4) H. Brockmann, *Fortsch. Chem. Org. Naturstoffe*, **18**, 1 (1960).
5) H. Otsuka and J. Shoji, *Tetrahedron*, **23**, 1535 (1967).
6) M. Bodanszky and M. A. Ondetti, *Antimicr. Agents Chemoth.*, **1964**, 360.
7) K. Hayashi, Y. Suketa, K. Tsukamoto, and T. Suzuki *Experientia*, **22**, 354 (1966).
8) J. Shoji and R. Sakazaki, *J. Antibiotics*, **23**, 418 (1970).
9) J. Shoji and R. Sakazaki, *ibid.*, **23**, 519 (1970).
10) H. D. Dakin, *Biochem. J.*, **12**, 290 (1918); *ibid.*, **13**, 398 (1919).
11) C. E. Dent and D. I. Fowler, *ibid.*, **56**, 54 (1954).
12) T. Kaneko, T. Shiba, S. Tsuchida, and M. Shimamoto, *Nippon Kagaku Zasshi*, **80**, 69 (1959).
13) T. Kaneko, R. Yoshida, and H. Katsura, *ibid.*, **80**, 316 (1959).
14) The exchangeable amino acids in each group are shown in parentheses.
15) The results on the isolation of 5-chloro-D-tryptophan was reported in a preliminary form: T. Shiba, Y. Mukunoki, and H. Akiyama, *Tetrahedron Lett.*, **1974**, 3085.
16) S. Marumo and H. Hattori, *Planta*, **90**, 208 (1970).
17) Y. Maeno and S. Seno, *Nippon Kagaku Zasshi*, **87**, 1240 (1966).
18) Y. Komachiya, K. Suzuki, T. Yamada, H. Miyayashiki, and S. Sakurai, *ibid.*, **86**, 856 (1965).
19) The name of this compound was mistyped in the preliminary report.[15]
20) H. N. Rydon and C. A. Long, *Nature*, **164**, 575 (1949).
21) H. N. Rydon and J. C. Tweddle, *J. Chem. Soc.*, **1955**, 3499.
22) Longicatenamycin is a cyclohexapeptide with a free

ω-amino group of ornithine or lysine. The formula is based on this information. The study on total structure of longicatenamycin will be reported soon in the following paper.

23) O. Kamm, "Organic Synthesis," Coll. Vol. I, p. 9 (1956).

24) R. F. Nystrom and W. G. Brown, *J. Amer. Chem. Soc.*, **69**, 2548 (1947).

25) H. Gilman and R. H. Kirby, "Organic Synthesis," Coll. Vol. I, p. 361 (1956).

26) This aldehyde was prepared from its dimethyl acetal which was supplied from Ajinomoto Co., Inc.

27) This melting point agreed with that of DL-isomer from the natural source. Rydon *et al.* reported mp 278—279 °C (decomp.) for the same compound.

Absolute Configurations and Chiroptical Properties of Optically Active Derivatives of Tricyclo[4.3.0.0^{3,8}]nonane ("Twist-brendane")

Masao NAKAZAKI, Koichiro NAEMURA, and Sigeyuki HARITA

Department of Chemistry, Faculty of Engineering Science, Osaka University, Toyonaka, Osaka 560

(Received January 13, 1975)

(+)-Tricyclo[4.3.0.0^{3,8}]nonane ("twist-brendane") was synthesized *via* (+)-tricyclo[4.3.0.0^{3,8}]nonan-9-one from (+)-*endo*-2-carboxybicyclo[2.2.2]oct-5-ene. Optically active derivatives of twist-brendane with two functional groups such as (−)-2,9-twist-brendanedione and (−)-9-methylenetwist-brendan-2-one were synthesized from (−)-*endo*-2-carboxybicyclo[2.2.2]oct-5-ene. Absolute configurations of the compounds were established and their chiroptical properties were discussed.

Tricyclo[4.4.0.0^{3,8}]decane ("twistane")[1] belongs to point group D_2 and is one of the representatives of tricyclodecanes whose carbon frameworks are inherently chiral. We were the first to obtain twistane in optically active form, and assigned to configuration (**1a**) to (+)-twistane on the basis of the chiroptical property of the intermediate, (+)-2-twistanone.[2] In recent years, Tichý reinvestigated this problem and assigned the opposite configuration (**1b**) to the same dextrorotatory enantiomer.[3]

1a **1b**

In the preceeding paper, we reported the preparation of (−)-twist-brendane[4] from (−)-*endo*-2-carboxybicyclo[2.2.1]hept-5-ene (**3**) with known absolute configuration[5], and assignment of the absolute configuration (**2**) to (−)-twist-brendane.

2 **3**

In this paper, we wish to report an alternative synthesis of optically active twist-brendane from bicyclo[2.2.2]octane derivative (**4**) which eventually correlates the configuration of (−)-twist-brendane with that of twistane. Since twist-brandane derivatives have rigid structures with well-defined molecular geometry and may afford a suitable model to study intramolecular interactions between the functional groups held in these fixed relative orientations, the syntheses and chiroptical properties of various twist-brendane derivatives will be also described in this paper.

Our first task was the preparation of optically active 9-twist-brendanone (**5**)[6] from *endo*-2-carboxybicyclo-[2.2.2]oct-5-ene (**4**) $[\alpha]_D^{26}$ +31.8°[7] which was obtained through the optical resolution of racemic acid with the aid of (+)-2-(1-aminoethyl)naphthalene. Reduction of the (+)-carboxylic acid with lithium aluminum hydride followed by oxidation with Collins' reagent gave (+)-unsaturated aldehyde (**7**) which was smoothly converted into the (+)-oxetane (**8**) upon intramolecular Paterno-Büchi photoreaction.[8] Reductive cleavage of (+)-oxetane (**8**) with lithium aluminum hydride in *N*-methylmorpholine[9] afforded (+)-tricyclic alcohol (**9a**), which was oxidized with Jones' reagent to give (+)-ketone. Among two possible courses of the reductive ring fission of the (+)-oxetane (**8**), apparently the one leading to 2-hydroxytwist-brendane (**9b**) was not followed, because the (+)-ketone obtained showed a carbonyl absorption at 1765 cm^{-1} in its IR spectrum and was found to be different from 2-twist-brendanone (**10**) whose structure had been established by unambigous synthesis. These facts indicated that our (+)-ketone was the desired (+)-9-twist-brendanone (**5**). Wolff-Kishner reduction of this (+)-9-twist-brendanone gave a dextrorotatory hydrocarbon (11) $[\alpha]_D^{21}$ +177°, which was purified by chromatography and sublimation. Comparison of its NMR, IR, mass spectrum and vpc retention time with those of (−)-twist-brendane (**2**) confirmed that they are enantiomeric. This result gave us a clear information about the configurational relationship between (+)-twist-brendane (**11**) and our starting material (+)-*endo*-2-carboxybicyclo[2.2.2]oct-5-ene (**4**)[10] as shown below.

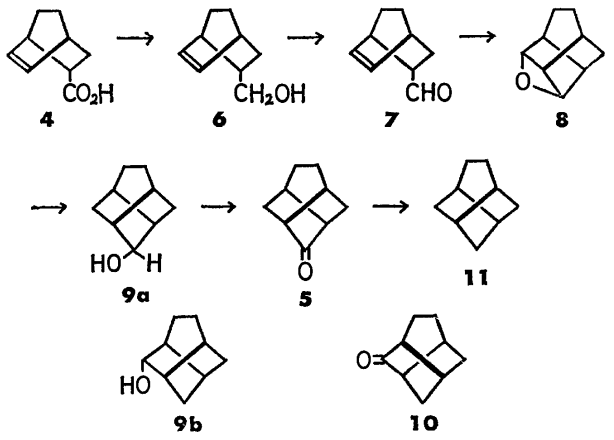

4 **6** **7** **8** **9a** **5** **11** **9b** **10**

Since (+)-twistane was derived from this bicyclo-[2.2.2]octane derivative (**4**), our previous assignment of the absolute configuration to (+)-twistane by chiroptical method has to be reversed confirming Tichý's new result.

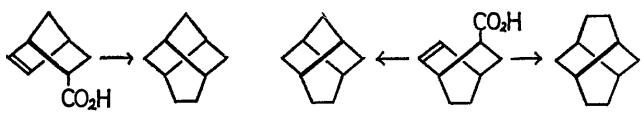

3 **2** **11** **4** **1b**

Next our attention was turned to prepare optically active twist-brendane derivatives with two functional groups and investigate their intramolecular interaction in their rigid molecular frameworks. (−)-Aldehyde (**14**) prepared *via* (−)-alcohol (**13**) from (−)-*endo*-2-carboxybicyclo[2.2.2]oct-5-ene (**12**) $[\alpha]_D^{24}$ −27.8° was treated with methylmagnesium iodide to give (−)-alcohol (**15**), which was oxidized with Collins' reagent to yield (−)-ketone (**16**). The ring closure leading to twist-brendane framework was again achieved by the Paterno-Büchi reaction. Irradiation of a solution of (−)-ketone (**16**) in benzene with mercury lamp gave a liquid product which was purified by distillation to give (−)-oxetane (**17**). Reductive cleavage of (−)-oxetane (**17**) with lithium aluminum hydride in *N*-methylmorpholine yielded alcohol (**18**), which, without purification, was treated with Collins' reagent to give (−)-ketone (**19**). The structural evidence was obtained on the basis of its following spectral data. The NMR spectrum exhibited sharp doublet signals centered at δ 1.11 (J=7 Hz) for the methyl group and the IR spectrum showed a carbonyl absorption at 1753 cm^{-1}.

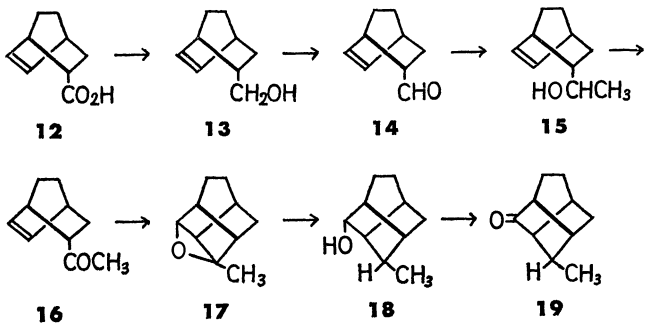

For the preparation of olefinic ketone (**20**), (−)-oxetane (**17**) was treated with perchloric acid in methanol and the product was chromatographed on alumina to give two products. To the minor product (22% yield) eluted with pentane was assigned the structure (**21**) on the basis of its IR spectrum which showed characteristic absorptions at 2839 cm^{-1} due to methoxy group and 3020 and 805 cm^{-1} due to trisubstituted olefin. Elution with ether–pentane afforded the major product (28% yield) whose IR spectrum (3450 cm^{-1} for hydroxyl group and 3050, 1675, 890 and 870 cm^{-1} for terminal methylene group) indicated the structure (**22**) for this olefinic alcohol. Upon Collins' oxidation, (−)-alcohol (**22**) gave (−)-ketone (**20**) whose structure was confirmed by the NMR spectrum data; δ 4.80 and 4.65 (olefinic protons) and 2.95 and 2.70 (two bridge head protons at C_1 and C_3). The olefinic alcohol (**22**) in hand, we diverted our effort to preparation of the twist-brendane with two oxo groups at C_2 and C_4 positions. After protection of hydroxyl group by acetylation, the resulted acetate (**23**) was ozonolyzed in chloroform (at −78 °C) to provide the ketoacetate (**24**) which was purified by chromatography followed by vaccum distillation. Failure in removing the acetyl group by hydrolysis with methanolic potassium hydroxide forced us to take a detour. Reduction of the ketoacetate (**24**) with lithium aluminum hydride followed by Collins' oxidation afforded a solid and the product was purified by sublimation to give diketone (**25**) which showed two carbonyl absorptions at 1785 and 1740 cm^{-1}. The specific rotation of the diketone (**25**) observed in chloroform solution was $[\alpha]_D$ −225° at 17 °C. When the substance was dissolved in methanol and the specific rotation of the solution was observed, there was a gradual change in the rotation from initial value $[\alpha]_D^{17}$ −153° to an equilibrium value $[\alpha]_D^{17}$ +32.0° during 4 hr.

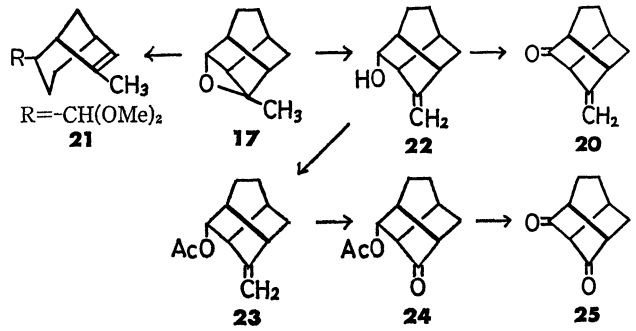

Since inspection of a molecular model of the olefinic ketone (**26**) reveals an interesting feature about the interaction of the double bond and carbonyl group in this unique twist-brendane framework, our final effort was directed to the preparation of this twist-brend-4-en-2-one (**26**). The key intermediate selected for the ketone (**26**) was a new oxetane (**27a**) which was obtained from 2-formylmethylbicyclo[2.2.1]hept-5-ene (**33**) by the Paterno-Büchi reaction. The Diels-Alder reaction of cyclopentadiene with allyl alcohol gave an *endo* and *exo* mixture of 2-hydroxymethylbicyclo[2.2.1]hept-5-ene (**28**) which was converted into the nitrile (**30**) *via* the tosylate (**29**). Upon hydrolysis with alkaline, the nitrile (**30**) afforded carboxylic acid (**31**) which was reduced with lithium aluminum hydride to yield alcohol (**32**). Oxidation of the alcohol (**32**) with Collins' reagent gave a mixture of *endo* and *exo*-2-formylmethylbicyclo[2.2.1]hept-5-ene (**33**). Irradiation was carried out on *endo* and *exo*-mixture of aldehydes (**33**) in benzene. Oxetane (**27a**) was smoothly produced and purified by sublimation to give a solid. Although there are two alternative ways of ring closure leading to (**27a**) and (**27b**), we assigned the structure (**27a**) to the oxetane since this compound could be transformed into 2-twist-brendanone (**10**) *via* 2-twist-brendanol (**34**) by reductive cleavage followed by Collins' oxidation.

28: R=OH, **31**: R=CO_2H **27a**
29: R=OTs, **32**: R=CH_2OH
30: R=CN, **33**: R=CHO

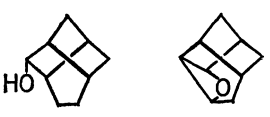

34 **27b**

Oxetane (**27a**) was treated with perchloric acid in methanol to give an alcoholic product. The product was oxidized with Collins' reagent to yield ketone which was chromatographed on silica gel. A fraction eluted with ether–pentane was distilled to give a ketone, to which the structure (**36**) was assigned to the basis of the following facts. The NMR spectrum exhibited signals at δ 3.75—3.55 due to a proton at C_4 and did not exhibit any signal at the region for olefinic proton. The IR spectrum showed a carbonyl absorption at 1750 cm^{-1} and absorptions for methoxy group at 2830 and 1105 cm^{-1}. The elementary analysis and mass spectrum (*m/e* 166 M^+) were in agreement with the calculated value for $C_{10}H_{14}O_2$. An expected alcohol (**37**) could not be obtained from the oxetane (**27a**) by the method.

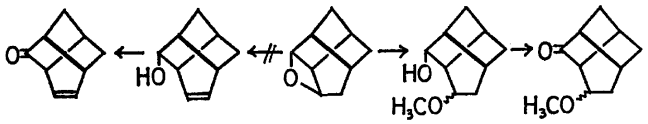

26 **37** **27** **35** **36**

Chiroptical Properties

(−)-*endo*-2-Methylbicyclo[2.2.1]heptan-7-one (**38**) is a bicyclic ketone being compared with (+)-9-twist-brendanone (**5**) and shows a positive Cotton effect at about 295 nm in its CD.[11] But (+)-9-twist-brendanone (**5**) exhibited a negative Cotton effect at 285 nm (Fig. 1). An ethano bridge of the tricyclic ketone twisted a center six-membered ring, hached in the formula (**39**) and a projection formula (**40**), where the C=O lies in the "point" of the twist,[12] is drawn for (+)-9-twist-brendanone (**5**). Then the octant rule is applied to both "outer" five-membered rings in this projection formula (**40**). It is obvious that negative contributions coming from the two "outer" rings determine the sign of the Cotton effect.

The chirality of carbon framework of (−)-9-methyltwist-brendan-2-one (**19**) is the opposite sense in contrast to that of (+)-9-twist-brendanone (**5**). However,

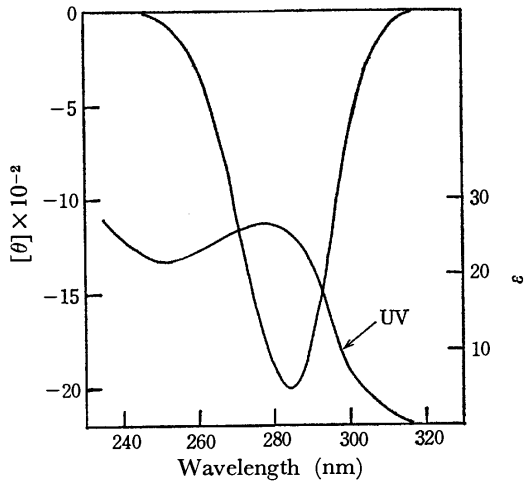

Fig. 1. CD and UV spectra of (+)-9-twist-brendanone (**5**).

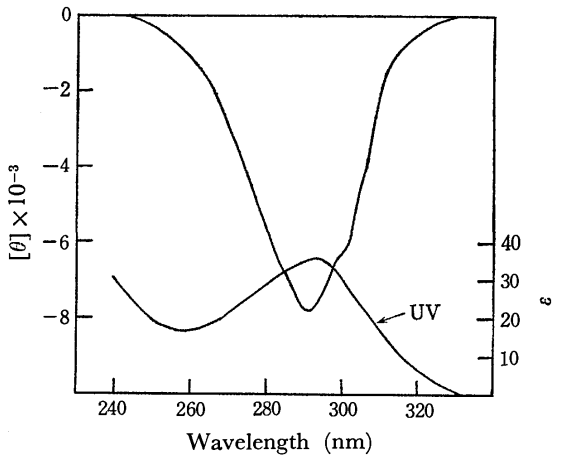

Fig. 2. CD and UV spectra of (−)-9-methyltwist-brendan-2-one (**19**).

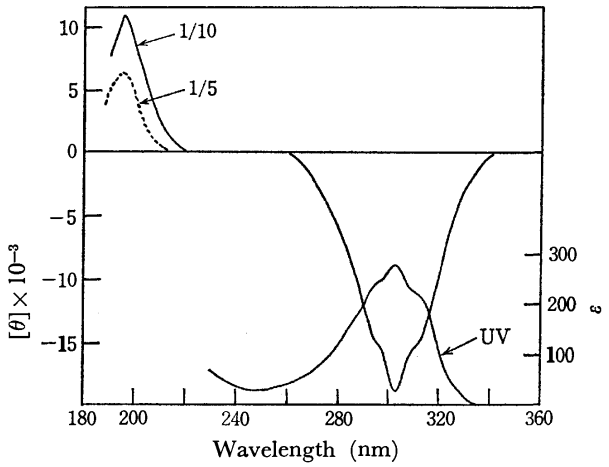

Fig. 3. CD (----) spectrum of (−)-9-methylenetwist-brendan-2-ol (**22**) and CD (——) and UV (——) spectra of (−)-9-methylenetwist-brendan-2-one (**20**).

(−)-9-methyltwist-brendan-2-one (**19**) exhibited also a negative Cotton effect at 292 nm (Fig. 2). The fact is explained by the same rule as mentioned above. Negative contributions coming from the two "outer" rings of the projection formula (**41**) determine the sign of the Cotton effect. (−)-9-Methylenetwist-brendan-2-ol (**22**) exhibited a strong positive Cotton effect at 195 nm (Fig. 3). (−)-9-Methylenetwist-brendan-2-one (**20**) exhibited a positive Cotton effect at 195 nm and a negative one at 302.5 nm and the intensities of both maximum were increased in contrast to those of the alcohol (**22**) and the saturated ketone (**19**). The negative Cotton effect at around 300 nm is also predictable from the same rule. These facts showed us that the sign of the Cotton effect at around 300 nm exhibited by twist-brendanones was essentially predictable from application of the octant rule to "outer" rings in the projection formula. In other word, the sign of the Cotton effect exhibited twist-brendanones is unequivocally related to a chirality of a middle ring of the projection formula and the concept is adopted for twistanones.[12] For the ketones exhibited a negative Cotton effect, the middle ring adopts P-helicity.

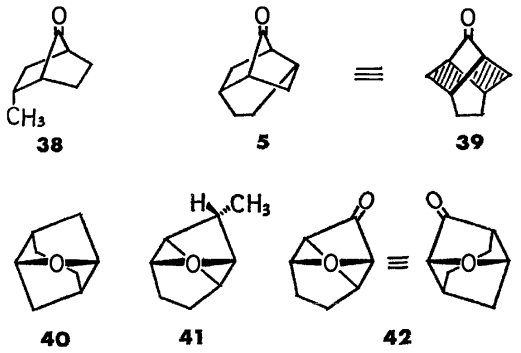

There are P-helicity six-membered ring and M-helicity seven-membered ring in (+)-2,9-twist-brendandione (**25**) as shown in the projection formula (**42**) and the diketone exhibited complicating maxima in its CD (Fig. 4). We have never offered a pertinent explanation for the fact.

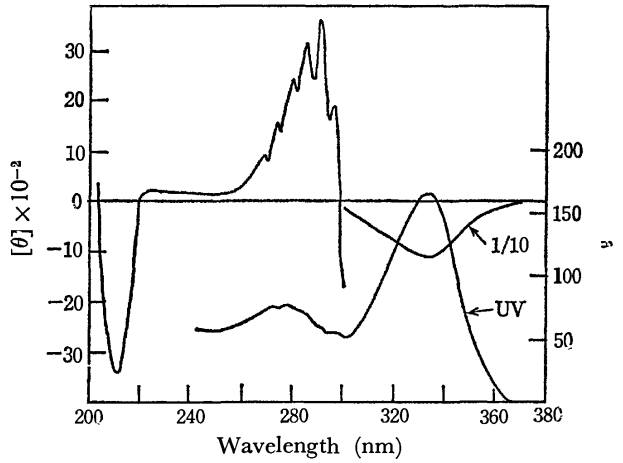

Fig. 4. CD and UV spectra of (+)-2,9-twist-brendandione (**25**).

Experimental

All the melting points and the boiling points are not corrected. The IR spectra were measured with Hitachi EPI-S2 spectrophotometer. The NMR spectra were obtained on LNM-C-60HL and JNM-MH-100 spectrometers. The UV spectra were measured with Beckman DB spectrometer. The optical rotations were measured with JASCO DIP-SL automatic polarimeter. The CD spectra were obtained on JASCO J-20 spectropolarimeter with CD attachment.

(+)-endo-*2-Carboxybicyclo[2.2.2]oct-5-ene (4).* A salt of *endo*-2-carboxybicyclo[2.2.2]oct-5-ene with (+)-2-(1-aminoethyl)naphthalene was recrystallized from ethanol and then a dextrorotatory salt was treated with hydrochloric acid to give (+)-carboxylic acid (**4**) mp 42—43 °C, $[\alpha]_D^{26}$ +31.8° (*c* 0.54, methanol).

Found: C, 71.21; H, 8.02%. Calcd for $C_9H_{12}O_2$: C, 71.02; H, 7.95%.

(+)-endo-*2-Hydroxymethylbicyclo[2.2.2]oct-5-ene (6).* Reduction of 10.9 g of (+)-carboxylic acid (**4**) with lithium aluminum hydride in ether gave 8.49 g of alcohol (**6**) bp 95 °C at 5 Torr, $[\alpha]_D^{25}$ +4.5° (c 1.1, methanol).

IR (neat film): 3350(s), 3050(w), 2950(s), 2880(m), 1055(m), 1035(m), 1015(m), and 710(s) cm^{-1}.

Found: C, 78.03; H, 10.35%. Calcd for $C_9H_{14}O$: C, 78.21; H, 10.21%.

(+)-endo-*2-Formylbicyclo[2.2.2]oct-5-ene (7).* To a solution of 59 ml of dry pyridine in 1.34 l of dry methylenechloride was added 36.4 g of chromium trioxide and the mixture was stirred at room temperature for 15 min. Then a solution of 8.4 g of (+)-alcohol (**6**) in 10 ml of dry methylenechloride was added to the mixture and it was stirred at room temperature for further 15 min. An organic layer was separated and a residue was rinsed with the same solvent. Combined organic solutions were washed with dilute hydrochloric acid, satd. aqueous sodium bicarbonate, water and dried over magnesium sulfate. After evaporation of the solvent a residue was distilled to give 6.53 g of (+)-aldehyde (**7**) bp 58 °C at 2 Torr, $[\alpha]_D^{26}$ +5.1° (*c* 1.2, methanol).

IR(neat film): 3050(w), 2950(s), 2880(m), 2820(w), 2750(w), 1720(s), 930(w) and 715(s) cm^{-1}.

Since the aldehyde was very sensitive to air, a correct elementary analysis datum was not obtained.

Photoreaction of (+)-Aldehyde (7). A solution of 6.08 g of (+)-aldehyde (**7**) in 500 ml of benzene was irradiated for 20 hr with mercury lamp (SHL-100 UV, Toshiba) under nitrogen atmosphere. After evaporation of the solvent, a residue was chromatographed on neutral alumina (Woelm Activity III) and a solid eluted with pentane was sublimed to give 2.85 g of (+)-oxetane (**8**) mp 167—170 °C (in sealed tube), $[\alpha]_D^{23}$ +148° (*c* 0.78, methanol).

IR(KBr): 2950(s), 2880(m), 1025(m), 935(m), 915(m), 895(m), 870(m), 840(m), 830(m) and 808(w) cm^{-1}.

NMR($CDCl_3$): δ 0.9—1.9(m, 7H), 2.1—2.5(m, 2H), 3.1—3.2(m, 1H), 4.3—4.5(m, 1H) and 4.6—4.8(m, 1H).

Found: C, 79.24; H, 8.86%. Calcd for $C_9H_{12}O$: C, 79.37; H, 8.88%.

(+)-Tricyclo[4.3.0.0^{3,8}]nonan-9-ol (9a). To a solution of 2.78 g of (+)-oxetane (**8**) in 170 ml of *N*-methylmorpholine was added 5.7 g of lithium aluminum hydride and the mixture was heated at reflux for 60 hr. After cooling, a few ml of methanol was added to the reaction mixture and then it was acidified with dilute hydrochloric acid. The mixture was extracted with ether. The extract was washed with satd. aqueous sodium bicarbonate, water and dried over magnesium sulfate. After evaporation of the solvent, a residue was chromatographed on neutral alumina (Woelm, activity III) and a solid eluted with ether-pentane was sublimed to give 1.22 g of (+)-tricyclic alcohol (**10**) mp 162—165 °C (in sealed tube), $[\alpha]_D^{23}$ +164° (*c* 0.66, methanol).

IR(KBr): 3350(s), 2930(s), 2880(m), 1090(s), 1075(m), 1030(m), 1010(m) and 875(w) cm^{-1}.

NMR($CDCl_3$): δ 1.2—2.2(m, 12H), 2.34(s, 1H) and 4.12(m, 1H).

Found: C, 78.09; H, 10.43%. Calcd for $C_9H_{14}O$: C, 78.21; H, 10.21%.

(+)-Tricyclo[4.3.0.0^{3,8}]nonan-9-one (5). A solution of 1.38 g of (+)-alcohol (**9a**) in 20 ml of acetone was treated with excess of 8 N Jones' reagent for 2 hr with ice cooling. The reaction mixture was poured into water and it was extracted with ether. The extract was washed with satd. aqueous sodium bicarbonate, water and dried over sodium sulfate. After evaporation of the solvent, a residue was chromatographed on neutral alumina (Woelm, Activity III) and a solid eluted with pentane was sublimed to give 711 mg of ketone (**5**) mp 159—161 °C (in sealed tube) (lit,[9] racemic: mp 141—143 °C), $[\alpha]_D^{19}$ +176° (*c* 0.57, methanol).

IR(KBr): 2900(s), 2830(m), 1765(s), 1470(m), 1190(m), 1140(m), 1115(m), 1070(w), 880(m), 840(m), 790(w) and 735(w) cm^{-1}.

NMR(CCl_4): δ 1.4—2.1 (m, 12H).

UV: $\lambda_{max}^{isooctane}$ (ε) 379 (27) nm.

CD (c 4.03×10^{-2}, isooctane): $[\theta]_{245}$ 0, $[\theta]_{285}$ −2020, $[\theta]_{320}$ 0.

Found: C, 78.64; H, 8.82%. Calcd for $C_9H_{12}O$: C, 79.37; H, 8.88%.

(+)-Tricyclo[4.3.0.0^{3,8}]nonane (**11**). A solution of 400 mg of 9-twist-brendanone (**5**), 219 mg of potassium hydroxide and 0.38 ml of 80% hydrazine hydrate in 3.5 ml of triethylene glycol was heated at reflux for 2 hr. Then water was allowed to boil out of the solution and the resulting solution was heated at 210 °C for further 5 hr. The reaction mixture was diluted with water and it was extracted with pentane. The extract was washed with water and dried over magnesium sulfate. After evaporation of the solvent, a residue was sublimed to give 134 mg of twist-brendane (**11**) mp 154—157 °C (in sealed tube), $[\alpha]_D^{21}$ +177° (c 0.46, ethanol). The NMR, IR, mass spectra and vpc retention time (10% SE-30 2m at 110 °C) were identical with those of (−)-enantiomer.[4]

(−)-endo-*2-Formylbicyclo[2.2.2]oct-5-ene* (**14**). Reduction of 34.0 g of (−)-*endo*-2-carboxybicyclo[2.2.2]oct-5-ene (**12**) $[\alpha]_D^{20}$ −27.8° with lithium aluminum hydride gave 27.7 g of (−)-*endo*-2-hydroxymethylbicyclo[2.2.2]oct-5-ene (**13**) $[\alpha]_D^{18}$ −4.0° (c 0.12, methanol). Upon oxidation with chromium trioxide, pyridine in dry methylene chloride, 13.8 g of (−)-alcohol (**13**) yielded 9.9 g of (−)-*endo*-2-formylbicyclo[2.2.2]oct-5-ene (**14**) bp 90—4 °C at 18 Torr, $[\alpha]_D^{18}$ −4.5° (c 1.86, methanol).

(−)-2-(1-Hydroxyethyl)bicyclo[2.2.2]oct-5-ene (**15**). A solution of 41.1 g of methyl iodide in 150 ml of dry ether was slowly added to a mixture of 6.4 g of magnesium with 100 ml of dry ether at room temperature and then the mixture was gently refluxed for 1 hr. After cooling to room temperature, a solution of 19.8 g of (−)-aldehyde (**14**) in 150 ml of dry ether was added to the Grignard reagent and the reaction mixture was boiled for 4 hr. It was cooled with ice and satd. aqueous ammonium chloride solution was added to the chilled mixture. A separated solid was filtered off and washed with ether. Combined ether solutions were washed with water and dried over magnesium sulfate. After evaporation of the solvent, a residue was distilled to give 20.2 g of (−)-alcohol (**15**) bp 108—110 °C at 20 Torr, $[\alpha]_D^{20}$ −0.23° (c 1.20, methanol).

IR(neat film): 3350(s), 3030(w), 2930(s), 2880(m), 1135(m), 1085(s), 1030(m), 925(m), 880(m) and 710(s) cm^{-1}.

Found: C, 78.62; H, 10.59%. Calcd for $C_{10}H_{16}O$: C, 78.89; H, 10.59%.

(−)-2-Acetylbicyclo[2.2.2]*oct-5-ene* (**16**). A solution of 9.60 g of (−)-alcohol (**15**) in 10 ml of dry methylene chloride was added to a mixture which was prepared from 42.0 g of chromium trioxide, 67.0 g of dry pryidine and 1000 ml of dry methylene chloride by the usual manner. The mixture was stirred for 15 min at room temperature. After working up as usual, a product was distilled to give 8.14 g of (−)-ketone (**16**) bp 102 °C at 20 Torr, $[\alpha]_D^{18}$ −8.1° (c 2.90, methanol).

IR (neat film): 3050(w), 2950(s), 2880(m), 1710(s), 1355(m), 1170(m) and 710(m) cm^{-1}.

Found: C, 79.97; H, 9.42%. Calcd for $C_{10}H_{14}O$: C, 79.95; H, 9.39%.

Photoreaction of (−)-2-acetylbicyclo[2.2.2]oct-5-ene (**16**). A solution of 7.00 g of (−)-ketone (**16**) in 600 ml of benzene was irradiated with mercury lamp (SHL-100UV, Toshiba) for 35 hr. After evaporation of the solvent, a residue was distilled to give 6.03 g of (−)-oxetane (**17**) bp 83—85 °C at 20 Torr $[\alpha]_D^{17}$ −177° (c 1.32, methanol).

IR (neat film): 2950(s), 2880(m), 1390(m), 1155(m), 1105(m), 1025(m), 955(m), 905(m), 890(m), 860(m) and 835(m) cm^{-1}.

Found: C, 79.50; H, 9.53%. Calcd for $C_{10}H_{14}O$: C, 79.95; H, 9.35%.

(−)-9-Methyltricyclo[4.3.0.0^{3,8}]nonan-2-one (**19**). To a solution of 2.78 g of (−)-oxetane (**17**) in 280 ml of *N*-methylmorpholine was added 6.9 g of lithium aluminum hydride at room temperature and the mixture was heated at reflux for 65 hr at which time it was cooled and added carefully with methanol, water and hydrochloric acid. The mixture was extracted with ether. The extract was washed with satd. aqueous sodium bicarbonate, water and dried over magnesium sulfate. After evaporation of the solvent, a residue was distilled to yield 1.62 g of the recovered oxetane (**17**) and a residual liquid was used to the following reaction. A solution of the residue in 5 ml of dry methylene chloride was added to a mixture of 1.58 g of chromium trioxide, 2.5 g of dry pryidine and 50 ml of dry methylene chloride and then the reaction mixture was stirred at room emperature for 15 min. After working up as usual, a crude product was chromatographed on neutral alumina (Woelm, activity III) and an elute with pentane was distilled to give 240 mg of (−)-ketone (**19**) bp 95—100 °C at 20 Torr, $[\alpha]_D^{15}$ −139° (c 0.38, methanol).

IR (neat film): 2950(s), 2870(m), 1753(s), 1455(m), 1380(w), 1300(w), 1180(w) and 1075(w) cm^{-1}.

NMR (CCl_4): δ 1.02(d, J=7 Hz, 3H), 1.4—2.2(m, 9H) and 2.3—2.5 (m, 2H).

UV: $\lambda_{max}^{isooctane}$ (ε) 292.5 (37) nm.

CD (c 5.00×10^{-2}, isooctane): $[\theta]_{240}$ 0, $[\theta]_{292}$ −7792, $[\theta]_{299}$ −6433, $[\theta]_{330}$ 0.

Found: C, 79.86; H, 9.45%. Calcd for $C_{10}H_{14}O$: C, 79.95; H, 9.39%.

(−)-9-Methylenetricyclo[4.3.0.0^{3,8}]nonan-2-ol (**22**). To a solution of 2.99 g of (−)-oxetane (**17**) in 200 ml of methanol was added 100 μl of 70% perchloric acid and then the mixture was kept at 18—20 °C for 20 hr. After dilution with 200 ml of water and saturation with sodium chloride, it was extracted with ether and the extract was washed with water. After drying over magnesium sulfate and evaporation of the solvent, a residue was chromatographed on neutral alumina (Woelm, activity III). First elution with pentane gave a bicyclic compound which was further purified by distillation to give 0.86 g of **21** bp 127—130 °C at 20 Torr, $[\alpha]_D^{18}$ +26.7° (c 1.22, methanol). Followed fraction eluted with pentane gave 1.10 g of the recovered oxetane (**17**). Fractions eluted with ether-pentane (2 : 8 volume) gave an alcoholic product which was distilled to yield 845 mg of **22** bp 135 °C at 20 Torr, $[\alpha]_D^{15}$ −319° (c 1.16, methanol).

17: IR(neat film): 3030(w), 2930(s), 2850(m), 1135(s), 1100(s), 1065(s), 970(m), 900(m) and 800(m) cm^{-1}.

Found: C, 73.18; H, 10.08%. Calcd for $C_{12}H_{20}O$: C, 73.43; H, 10.27%.

22: IR(neat film): 3450(s), 3050(w), 2950(s), 2880(m), 1675(m), 1100(s), 1080(s), 1060(s), 1045(m) 985(m), 890(s), 870(s) and 815(m) cm^{-1}.

Found: C, 79.68; H, 9.42%. Calcd for $C_{10}H_{14}O$: C, 79.95; H, 9.39%.

CD (c 2.60×10^{-2}, isooctane): $[\theta]_{195}$ $+3.09\times10^4$, $[\theta]_{218}$ 0.

(−)-9-Methylenetricyclo[4.3.0.0^{3,8}]nonan-2-one (**20**). A solution of 595 mg of (−)-unsaturated alcohol (**22**) in 5 ml of dry methylene chloride was added to a mixture which was prepared from 4.8 g of dry pyridine, 3.0 g of chromium trioxide and 900 ml of dry methylene chloride. The reaction mixture was stirred at room temperature for 20 min. An organic layer was separated and a residue was rinsed with the same solvent. Combined organic solutions were

washed with dilute hydrochloric acid, satd. aqueous sodium bicarbonate, water and dried over magnesium sulfate. After evaporation of the solvent, a residue was distilled to give 522 mg of (−)-ketone (**20**) bp 130 °C at 20 Torr, $[\alpha]_D^{17}$ −450° (*c* 0.92, methanol).

IR (neat film): 3050(w), 2950(s), 2870(m), 1750(s), 1675(m), 1075(m), 890(m), 860(m) and 810(m) cm^{-1}.

NMR (CCl_4): δ 1.4—2.0(m, 6H), 2.2—2.6(m, 2H), 2.74—2.95(m, 2H), 4.65(s, 1H) and 4.80(s, 1H).

UV: $\lambda_{max}^{isooctane}$ (ε) 296 sh (245), 303 (278) and 312 sh (213) nm.

CD (*c* 3.71×10^{-3}, isooctane): $[\theta]_{195}$ 1.099×10^5, $[\theta]_{220}$ 0. $[\theta]_{260}$ 0, $[\theta]_{294sh}$ -1.469×10^4, $[\theta]_{302.5}$ -1.900×10^4, $[\theta]_{311sh}$ -1.509×10^4 and $[\theta]_{338}$ 0.

Found: C, 81.52; H, 8.14%. Calcd for $C_{10}H_{12}O$: C, 81.04; H, 8.16%.

*(−)-2-Acetoxy-9-methylenetricyclo[4.3.0.0^{3,8}]nonane (**23**).* To a solution of 3.51 g of (−)-alcohol (**22**) in 15 ml of pyridine was added 5 ml of acetic anhydride at 0—5 °C and then the reaction mixture was stirred for 1 hr at this temperature and for 24 hr at room temperature. After dilution with water, it was extracted with ether. The extract was washed with dilute hydrochloric acid, satd. aqueous sodium bicarbonate, water and dried over magnesium sulfate. After evaporation of the solvent, a residue was distilled to give 4.24 g of acetate (**23**) bp 118—120 °C at 20 Torr, $[\alpha]_D^{17}$ −122° (*c* 1.53, methanol).

IR (neat film): 3050(w), 2950(m), 2870(m), 1730(s), 1685(w), 1365(m), 1250(s), 1230(s), 1053(m), 1040(m) and 880(m) cm^{-1}.

NMR (CCl_4): δ 1.4—1.5 (m, 2H), 1.6—1.8 (m, 4H), 1.88 (s, 3H), 1.9—2.2 (m, 2H), 2.3—2.7 (m, 2H), 4.50 (s, 1H), 4.56 (s, 1H) and 4.60 (s, 1H).

Found: C, 74.81; H, 8.49%. Calcd for $C_{12}H_{16}O_2$: C, 74.97; H, 8.39%.

*(−)-2-Acetoxytricyclo[3.4.0.0^{3,8}]nonan-9-one (**24**).* A solution of 4.00 g of (−)-acetate (**23**) in 140 ml of chloroform was cooled to −78 °C and treated with ozone until blue color persisted. Then the solution was allowed to warm to room temperature and nitrogen was bubled through the solution. The solution was added to a mixture of 5.4 g of zinc dust, 9 ml of acetic acid, 220 ml of chloroform and 900 ml of water and the mixture was stirred for 12 hr at room temperature. An organic layer was separated, washed with aqueous sodium carbonate and then with water, and dried over magnesium sulfate. After evaporation of the solvent, a residue was chromatographed on neutral alumina (Woelm, activity III) and fractions eluted with ether–pentane (2 : 8 volume) were distilled to give 1.33 g of ketone (**24**) bp 138—140 °C at 5 Torr, $[\alpha]_D^{15}$ −137° (*c* 0.54, methanol).

IR (neat film): 2950(s), 2870(m), 1775(s), 1735(s), 1370(m), 1250(s), 1230(s), 1205(m), 1190(m), 1050(m), and 1040(s) cm^{-1}.

Found: C, 67.87; H, 7.33%. Calcd for $C_{11}H_{14}O_3$: C, 68.02; H, 7.27%.

*(−)-Tricyclo[4.3.0.0^{3,8}]nonane-2,9-dione (**25**).* A solution of 1.10 g of (−)-acetate (**24**) in 40 ml of dry ether was added to a suspension of 0.32 g of lithium aluminum hydride in 30 ml of dry ether at room temperature and the mixture was heated at reflux for 2 hr. After cooling, saturated aqueous ammonium chloride solution was added to the chilled mixture and a separated solid was filtered off. A filtrate was dried over magnesium sulfate. After evaporation of the solvent a residual diol, without purification, was used to the next reaction. A solution of 0.50 g of the diol in 10 ml of dry methylene chloride was added to a mixture which was prepared from 3.90 g of chromium trioxide, 6.24 g of dry pyridine and 100 ml of dry methylene chloride. After stirring for 15 min at room temperature, an organic layer was separated and a residue was rinsed with the same solvent. Combined organic solutions were worked up by the usual manner and removal of the solvent gave a brown solid, which was sublimed to give 340 mg of diketone (**25**) mp 146—150 °C (in sealed tube), $[\alpha]_D^{17}$ −225° (*c* 0.40, chloroform).

IR(KBr): 2950(m), 2870(m), 1785(s), 1740(s), 1450(w), 1185 (w), 1175(w), 1085(w), 1070(w) and 850(w) cm^{-1}.

UV: $\lambda_{max}^{isooctane}$ (ε) 268 sh (72), 273 (76), 278.5 (77), 282 sh (71), 297 (55) and 334 (167) nm.

CD (*c* 4.01×10^{-2}, isooctane): $[\theta]_{203}$ 0, $[\theta]_{211}$ −3440, $[\theta]_{219}$ 0, $[\theta]_{269}$ +989, $[\theta]_{274}$ +1547, $[\theta]_{279}$ +2446, $[\theta]_{284.5}$ +3194, $[\theta]_{290}$ +3644, $[\theta]_{295.5}$ +1897, $[\theta]_{298}$ 0, $[\theta]_{334}$ −11180 and $[\theta]_{370}$ 0.

Found: C, 72.00; H, 7.16%. Calcd for $C_9H_{10}O_2$: C, 71.98; H, 6.71%.

A Mixture of endo *and* exo*-2-Cyanomethylbicyclo[2.2.1]hept-5-ene (**30**).* A solution of 26.9 g of a mixture of *endo* and *exo*-2-hydroxymethylbicyclo[2.2.1]hept-5-ene (**28**) which was prepared by the Diels-Alder reaction of allyl alcohol with cyclopentadiene in 95 ml of pyridine was added with 50.0 g of *p*-toluenesulfonyl chloride. The reaction mixture was stirred for 5 hr at 0—5 °C and then kept for further 24 hr at room temperature. It was poured into ice-water and acidified with hydrochloric acid. The mixture was extracted with ether. The extract was washed with saturated aqueous sodium bicarbonate, water and dried over magnesium sulfate. Removal of the solvent gave 56.4 g of tosylate (**29**), which, without purification, was used to the next reaction. A mixture of 56.4 g of tosylate (**29**), 32.5 g of sodium cyanide and 300 ml of dimethylformamide was heated for 12 hr at 120—140 °C. After cooling to room temperature, a solid was filtered off and a filtrate was concentrated under reduced pressure. A residue was added into ice-water and it was extracted with ether. The extract was washed with dilute hydrochloric acid, saturated aqueous sodium bicarbonate and water, and dried over magnesium sulfate. After evaporation of the solvent, a residue was distilled to give 20.5 g of a mixture of *endo* and *exo*-nitrile (**30**) bp 108—110 °C at 17 Torr.

IR (neat film): 3030(w), 2950(s), 2850(m), 2260(w), 1420(w), 1345(w), 1330(w) and 720(s) cm^{-1}.

Found: C, 81.27; H, 8.34; N, 10.31%. Calcd for $C_9H_{11}N$: C, 81.16; H, 8.33; N, 10.52%.

A Mixture of endo *and* exo*-2-(2-Hydroxyethyl)bicyclo[2.2.1]-hept-5-ene (**32**).* A mixture of 20.2 g of nitrile (**30**), 26.0 g of potassium hydroxide and 200 ml of ethylene glycol was heated for 7 hr at 140—160 °C. After cooling to room temperature, 300 ml of water was added to the reaction mixture and it was washed with ether to remove neutral compounds. Then the aqueous solution was acidified with hydrochloric acid and it was extracted with ether. The extract was washed with water and dried over magnesium sulfate. After evaporation of the solvent, a residue was distilled to give 20.1 g of carboxylic acid (**31**) bp 103—110 °C at 3 Torr. A solution of 19.8 g of carboxylic acid (**31**) in 150 ml of dry ether was slowly added to a suspension of 5.5 g of lithium aluminum hydride in 150 ml of dry ether and the reaction mixture was gently refluxed for 4 hr. After cooling with ice, saturated aqueous ammonium chloride solution was added to the chilled reaction mixture. A separated solid was filtered off and a filtrate was washed with water and dried over magnesium sulfate. After evaporation of the solvent, a residue was distilled to yield 17.1 g of a mixture of *endo* and *exo*-2-(2-hydroxyethyl)bicyclo[2.2.1]hept-5-ene (**32**) bp 77—79 °C at 4 Torr.

Found: C, 78.08; H, 10.23%. Calcd for $C_9H_{14}O$: C, 78.21; H, 10.21%.

A Mixture of endo *and* exo-*2-Formylmethylbicyclo[2.2.1]hept-5-ene (**33**).* To a mixture of 24.0 g of chromium trioxide, 38.0 g of dry pyridine and 580 ml of dry methylene chloride was added a solution of 5.52 g of alcohol (**32**) in 10 ml of dry methylene chloride. The reaction mixture was stirred for 15 min at room temperature. An organic layer was separated and a residue was rinsed with the same solvent. Combined organic solutions were worked up the usual manner. After evaporation of the solvent, a residue was distilled to yield 3.67 g of aldehyde (**33**) bp 89—91 °C at 20 Torr.

IR (neat film): 3050(w), 2950(s), 2860(m), 2730(w), 1720(s), 903(w), 830(w) and 725(m) cm^{-1}.

Found: C, 79.24; H, 8.98%. Calcd for $C_9H_{12}O$: C, 79.37; H, 8.88%.

*Photoreaction of Aldehyde (**33**).* A solution of 3.47 g of aldehyde (**33**) in 300 ml of benzene was irradiated for 15 hr with mercury lamp (SHL-100 UV, Toshiba) under nitrogen atmosphere. After evaporation of the solvent, a residue was chromatographed on neutral alumina (Woelm, acitivity III). An elution with pentane gave a solid which was sublimed to give 1.13 g of oxetane (**27a**) mp 161—163 °C (in sealed tube).

IR (KBr): 2950(s), 2880(m), 1330(s), 1050(s), 985(s), 955(m), 885(m), 840(m) and 800(m) cm^{-1}.

NMR ($CDCl_3$): δ 1.1—2.6 (m, 9H), 3.32—3.50 (m, 1H) and 4.50—4.80 (m, 2H).

Found: C, 78.92; H, 8.91%. Calcd for $C_9H_{12}O$: C, 79.37; H, 8.88%.

*Tricyclo[4.3.0.0^{3,8}]nonan-2-ol (**34**).* A solution of 848 mg of oxetane (**27a**) in 60 ml of *N*-methylmorpholine was added with 2.0 g of lithium aluminum hydride and the reaction mixture was heated at reflux for 68 hr. After cooling with ice, methanol was carefully added to the chilled reaction mixture and then it was acidified with dilute hydrochloric acid. The mixture was extracted with ether. The extract was washed with saturated aqueous sodium bicarbonate, water and dried over magnesium sulfate. After evaporation of the solvent, a residue was sublimed to yield 655 mg of alcohol (**34**) mp 188—191 °C (in sealed tube).

IR (KBr): 3400(s), 2950(s), 1305(w), 1280(w), 1160(w), 1130(w), 1095(m), 1065(m), 1025(m) and 810(w) cm^{-1}.

NMR ($CDCl_3$): δ 1.1—2.4 (m, 12H) and 3.9—4.1 (m, 1H).

Found: C, 77.72 H, 10.35%. Calcd for $C_9H_{14}O$: C, 78.21; H, 10.21%.

*Tricyclo[4.3.0.0^{3,8}]nonan-2-one (**10**).* A solution of 522 mg of alcohol (**34**) in 3 ml of dry methylene chloride was added to a mixture of 3.8 g of dry pyridine, 2.4 g of chromium trioxide and 58 ml of dry methylene chloride and then the reaction mixture was stirred for 15 min at room temperature. After working up as the usual manner, the solvent was evaporated and a residue was chromatographed on neutral alumina (Woelm, activity III). A fraction eluted with pentane gave a solid, which was sublimed to yield 329 mg of tricyclo-[4.3.0.0^{3,8}]nonan-2-one (**10**) mp 173—174 °C (in sealed tube). The IR, NMR and mass spectra were in complete agreement with those of authentic sample.[4]

*4-Methoxytricyclo[4.3.0.0^{3,8}]nonan-2-one (**36**).* A solution of 340 mg of oxetane (**27a**) in 20 ml of methanol was added with 20 μl of 70% perchloric acid and the reaction mixture was kept for 24 hr at room temperature. After dilution with water, it was extracted with ether. The extract was washed with water and dried over magnesium sulfate. After evaporation of the solvent, a residue was chromatographed on silica gel and fractions eluted with pentane-ether (8 : 2 volume) gave 290 mg of an oily product, which was used for the next reaction. To a solution of 290 mg of the product in 5 ml of acetone was added excess of 8 N Jones' reagent with ice cooling. After stirring for 15 min at room temperature, it was diluted with water and extracted with pentane. The extract was washed with saturated aqueous sodium bicarbonate and water, and dried over magnesium sulfate. After evaporation of the solvent, a residue was chromatographed on silica gel and fractions eluted with pentane gave an oily product which was distilled to yield 218 mg of 4-methoxytricyclo[4.3.0.0^{3,8}]-nonan-2-one (**36**) bp 125 °C (bath temperature) at 18 Torr.

IR (neat film): 2950(s), 2880(m), 2820(m), 1750(s), 1365(m), 1240(m), 1210(m), 1170(m), 1105(s), 1085(m), 1075(m), 1065(m), 1025(m) and 930(m) cm^{-1}.

NMR (CCl_4): δ 1.6—1.8 (m, 4H), 1.9—2.2 (m, 2H), 2.3—2.6 (m, 4H), 3.24 (s, 3H) and 3.5—3.7 (m, 1H).

Found: C, 71.90; H, 8.36%. Calcd for $C_{10}H_{14}O_2$: C, 72.26; H, 8.49%.

The authors are grateful to Dr. H. Ogura for measurement of the CD spectra.

References

1) H. W. Whitlock, Jr., *J. Amer. Chem. Soc.*, **84**, 3412 (1962). J. Gauthier and P. Deslongchamps, *Can. J. Chem.*, **45**, 297 (1967). A Belanger, J. Poupart, and P. Deslongchamps, *Tetrahedron Lett.*, **1968** 2127. A. Belanger, Y. Lambert, and P. Deslongchamps, *Can. J. Chem.*, **47**, 795 (1969).

2) K. Adachi, K. Naemura, and M. Nakazaki, *Tetrahedron Lett.*, **1968**, 5467.

3) M. Tichý, *ibid.*, **1972**, 2001. M. Tichý and J. Sicher, *Collect. Czech. Chem. Commum.*, **37**, 3106 (1972).

4) K. Naemura and M. Nakazaki, This Bulletin, **46**, 888 (1973).

5) J. A. Berson, J. S. Walia, A. Remanick, S. Suzuki, P. Reynolds-Warnhoff, and D. Willner, *J. Amer. Chem. Soc.*, **83**, 3986 (1961).

6) Presented at the 28th Annual Meeting of the Chemical Society of Japan, Tokyo, April, 1973, Preprint, Vol. III, p. 1343.

7) Tichý reported that *endo*-2-carboxybicyclo[2.2.2]oct-5-ene of specific rotation +48.2° was 95% optically pure.

8) R. Srinivasan, *J. Amer. Chem. Soc.*, **82**, 775 (1960). N. C. Yang, M. Nussin, and D. R. Coulson, *Tetrahedron Lett.*, **1965**, 1925.

9) R. R. Sauers and J. A. Whittle, *J. Org. Chem.*, **34**, 3579 (1969). R. R. Sauers, W. Schinski, M. M. Mason, E. O'Hara, and Byrne, *ibid.*, **38**, 642 (1973).

10) K. Mislow and J. G. Berger, *J. Amer. Chem. Soc.*, **84**, 1956 (1962). J. A. Berson and D. Willner, *ibid.*, **84**, 675 (1962). J. A. Berson, R. T. Luibrand, N. G. Kundu, and D. G. Morris, *ibid.*, **93**, 3074 (1971).

11) D. A. Lightner and D. E. Jackman, *ibid.*, **96**, 1939 (1974).

12) G. Snatzke and F. Werner-Zamojska, *Tetrahedron Lett.*, **1972**, 4275.

Coenzyme Models. II. Effect of Micellar Environments on the Acid-Catalyzed Hydration of 1,4-Dihydropyridine Derivatives[1]

Seiji SHINKAI, Reiko ANDO, and Toyoki KUNITAKE

Department of Organic Synthesis, Faculty of Engineering, Kyushu University, Fukuoka 812

(Received February 8, 1975)

An effect of micelles on the acid-catalyzed modification reaction of two dihydropyridines is reported in connection with the NADH function bound to alcohol dehydrogenase, and the hydration equilibrium of dihydronicotinamides was found to be quite susceptible to the ionic environment. The absorption maximum at 357 nm of 1-benzyl-1,4-dihydronicotinamide(NBzNH) was not affected by the presence of cationic micelles, while that of 1-lauryl-1,4-dihydronicotinamide(NLaNH) shifted by 5—6 nm to shorter wavelengths, probably due to the neighboring cationic charge. The hydration rates for dihydronicotinamides were prompted by NaLS micelle and retarded by CTAB micelle. The rate augmentation in the NaLS micelle, compared with the non-micellar system, was 1.7-fold for NBzNH and 33-fold for NLaNH. On the other hand, CTAB micelle pronouncedly depressed the hydration rate of NLaNH, which is 414-fold slower than in NaLS. The micelle of 1-lauryl-3-carbamoylpyridinium(NLaN), which forms the charge transfer complex with NLaNH, was found to inhibit the acid-catalyzed hydration more efficiently(1400-fold slower). Thus, it is suggested that the ammonium ion adjacent to the dihydronicotinamide group in alcohol dehydrogenase-NADH complex performs some biological functions.

NADH and its model compounds, 1,4-dihydronicotinamide derivatives, undergo rapid structural alternations in acidic solutions, and their UV spectra result in a shift of the characteristic absorption band in the 340—360 nm region downward to around 290 nm with tight isosbestic points.[2] Metzler and co-workers have studied the acid transformation of NADH and NPrNH[3] in the presence of a series of acids, and established that the observed spectral shift of NPrNH is completely reversible until the much slower secondary decay takes place.[4] They claimed acid-catalyzed hydration for the initial acid modification reaction (Eq. 1 or 2).

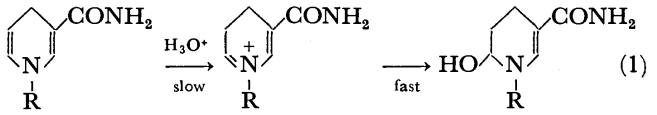

(1)

or

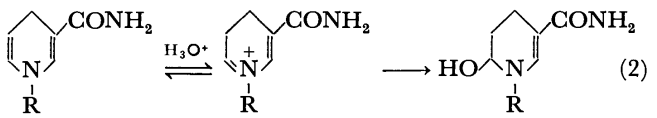

(2)

The 290 nm-absorbing compound was referred to as the "primary acid modification compound," and was later identified as 6-hydroxy-1,4,5,6-tetrahydronicotinamide by X-ray crystallography.[5] This compound is also unstable in acid, and the absorption at 290 nm disappears through the much slower, so-called "secondary acid reaction."

This reaction may be biologically important in connection with the fact that NADH bound to glyceraldehyde-3-phosphate dehydrogenase is characterized by a change in the UV spectrum similar to that which accompanies the primary acid reaction.[6,7] Reaction schemes (1) and (2) involve the formation of a cationic intermediate that is established to be a rate-determining step in aqueous media.[5] One would anticipate that the anionic environment would result in the acceleration of the apparent hydration rate as seen in acetal hydrolyses.[8,9] On the other hand, the cationic environment would retard the hydration rate. If this expectation is correct, it is conceivable that the lysine residue of the alcohol dehydrogenase which is postulated to exist very close to the bound NADH[10] performs some biological function by affecting the NADH reactivity.

In this paper we describe the effect of ionic micelles on the apparent hydration rate of acid-modifications of a few 1,4-dihydropyridines. Sodium laurylsulfate (NaLS), cetyltrimethylammonium bromide (CTAB) and 1-lauryl-3-carbamoylpyridinium bromide (NLaN) were used as surfactants. In order to study the micellar effect we chose 1-lauryl-1,4-dihydronicotinamide (NLaNH) in addition to 1-benzyl-1,4-dihydronicotinamide (NBzNH).

Surfactants: $CH_3(CH_2)_{11}SO_4Na$ (NaLS)

$CH_3(CH_2)_{15}N(CH_3)_3Br$ (CTAB)

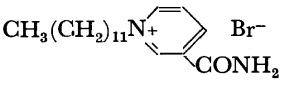

(NLaN)

Dihydropyridines:

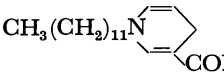

(NLaNH)

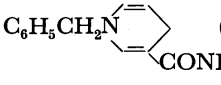

(NBzNH)

Experimental

Materials. Surfactants were products of Wako Pure Chemical Ind., NaLS(biochemical use) was used without further purification, and CTAB was recrystallized from ethanol before use.

NBzNH was prepared according to the method of Kim and Chaykin,[5] and recrystallized from ethanol-water, yellow needles, mp 110—112 °C (lit,[5] mp 110—112 °C). NLaN was obtained from lauryl bromide and nicotinamide[11], and reduced to NLaNH with sodium dithionite by the procedure used to prepare NPrNH.[12] The yellow precipitates were collected and recrystallized twice from petroleum ether-ether, mp 45—48 °C. An NMR spectrum taken in $CDCl_3$ was identical to that of NPrNH except for the resonance of the 1-alkyl group: $CH_3(CH_2)_{10}$–, 0.8—1.6 ppm, 23.1H; N–CH_2- and C_4–H_2, 3.0—3.2 ppm, 4.2H; C_5–H, 4.5—4.8 ppm, 1.0H; C_6–H and NH_2, 5.4—5.8 ppm, 2.8H; C_2–H, 7.0 ppm, 1.0H. This dihydropyridine was unstable to heat and slowly decomposed to the orange-colored oil even at room tempera-

ture. The crystals were preserved in a refrigerator, and stock solutions for kinetic measurements were prepared on the day of use.

Kinetics. The kinetic and spectroscopic measurements were carried out at 30±0.1 °C at a calculated ionic strength (with KCl) using a Hitachi 124 spectrophotometer. Reaction rates of hydration (NBzNH and NLaNH) were estimated by following the increase of absorbance at 292 nm or the decrease of absorbance at 357 nm, and both methods provided the identical result. The pseudo first-order rate constants were determined from the time-course of reaction thus obtained.

Results

Electronic Spectra. In order to assess the environmental effect of micelles on the absorption maxima of dihydronicotinamides, spectra of NLaNH and NBzNH were taken in various solvents (Table 1). The absorption maximum of NLaNH could not be determined in water because of the sparing solubility. If the hypothetical λ_{max} value of NLaNH in water is assumed to be the same as that of NPrNH in water, λ_{max} of NLaNH in cationic micelles is estimated to shift to the shorter wavelength by 5—6 nm by transferring from the aqueous to micellar phase. A similar hypsochromic shift was observed in ethanol.

Table 1. Electronic spectra of dihydropyridines in various media.[a]

Medium	λ_{max} (nm)		
	NLaNH	NPrNH	NBzNH
Diethyl ether			340[c]
Methanol		354[b]	
Ethanol	355		354[c]
52wt% Methanol-water		362[b]	
Water		362[b]	357[c]
CTAB micelle	356		357
NLaN micelle	357		357

a) 30 °C. b) S. Shinkai and T. C. Bruice, *Biochemistry*, **12**, 1750 (1973). c) From Ref. 10.

The λ_{max} value of NBzNH in water was not affected by the addition of cationic surfactants. Presumably, the equilibrium constant for the association of NBzNH with surfactants is rather small, resulting in the smaller micellar effect.

Hydration of 1-Benzyl-1,4-dihydronicotinamide (NBzNH). The absorption spectrum of the acid modification product of NBzNH are essentially the same as that of reference 4 with tight isosbestic points. In Fig. 1, pseudo first-order rate constants (k_{obsd}) for the hydration of NBzNH in the phosphate buffer were plotted against the concentration of surfactants, CTAB and NaLS. The concentration-rate profile is multiphasic. The rate constants are independent of the surfactant concentration below cmc, while they rapidly rise or descent with increasing concentration of surfactants above cmc. From Fig. 1 the cmc is estimated to be 4×10^{-4} M for CTAB and 3×10^{-3} M for NaLS under the reaction condition employed (lit,[13] cmc at 25 °C for CTAB, 9.2×10^{-4} M; for NaLS, 8.1×10^{-3} M).

The existence of the NaLS micelle raises the reaction

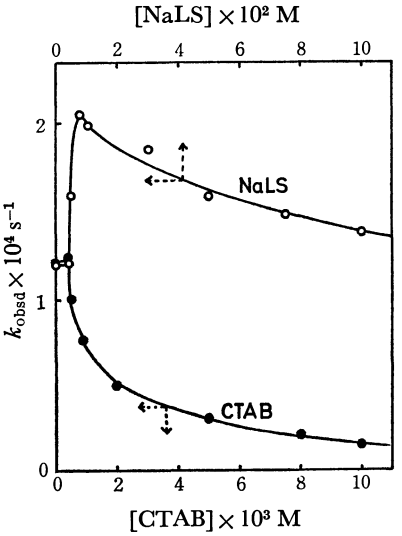

Fig. 1. Pseudo first-order rate constants for the acid-catalyzed hydration of NBzNH in aqueous solution. 30 °C, pH 6.30 with 0.01 M phosphate.

rate, and a rate augmentation of 1.7-fold is observed at the optimal surfactant concentration. Since the rate enhancement is slight, it is presumed that most of NBzNH is dissolved in the bulk phase and that the small amount of NBzNH bound to the micelle contributes to the rise of the total reaction rate.

On the contrary, CTAB depressed the hydration rate above the cmc, and the rate constant is 8.4-fold smaller at [CTAB]$=10^{-2}$ M, compared with that obtained without surfactant.

Hydration of 1-Lauryl-1,4-dihydronicotinamide (NLaNH). NBzNH is moderately soluble in aqueous solution (solubility: *ca.* 10^{-2} M), while NLaNH is sparingly soluble in water. In fact, precipitation of NLaNH (1.67×10^{-4} M) was recognized with less than 3.0×10^{-3} M of NaLS. Therefore, it would be reasonable to infer that the acid-catalyzed hydration reaction of this dihydronicotinamide entirely proceeds in the micelle. The surfactant concentration-rate profile for NLaNH is shown in Fig. 2. In the CTAB micelle the decay of NLaNH was extremely inhibited, so that

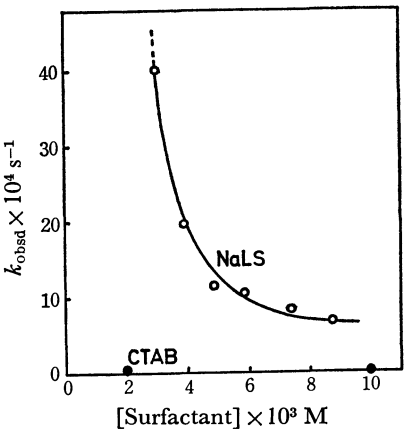

Fig. 2. Pseudo first-order rate constants for the acid-catalyzed hydration of NLaNH in aqueous solution. 30 °C, pH 6.30 with 0.01 M phosphate, [NLaNH]$=1.67\times10^{-4}$ M.

the first-order rate constant was calculated by means of the Guggenheim's equation: $k_{obsd}=9.7\times10^{-6}$ s^{-1} ($t_1/_2=$ *ca.* 20 hr) at [CTAB]$=1.0\times10^{-2}$ M. This reaction rate is about 12-fold slower than that of NBzNH in the non-micellar system. Since the NADH- or 1,4-dihydronicotinamide-mediated reduction reaction is generally much faster,[2] it may be said that dihydronicotinamides in the CTAB cationic micelle are almost completely stabilized in weakly acidic solutions.

In the accompanying paper we showed that NLaNH forms the charge transfer complex with NLaN in micellar systems (association constant, $K=22$—45 M^{-1}).[14] The hydration reaction in NLaN micelle is of much interest from the biological standpoint because the glyceraldehyde-3-phosphate dehydrogenase-NAD complex involves the charge transfer interaction between the 3-carbamoylpyridinium group of NAD and the enzyme residue, probably an indole nucleus.[15] The pseudo first-order rate constant for the hydration reaction of NLaNH was estimated to be 2.8×10^{-6} s^{-1} at [NLaN]$=1.56\times10^{-2}$ M, which is 3.5 times slower than in CTAB micelle. It seems, therefore, that the charge transfer interaction inhibits the acid-catalyzed hydration reaction more efficiently.

In NaLS micelle the hydration rates were conspicuously accelerated (Fig. 2). Shiny crystals of NLaNH were recognized in the presence of NaLS below 3.0×10^{-3} M. The rate rapidly increases as the surfactant concentration approaches the cmc, and, at [NaLS]$=3.0\times10^{-3}$ M, a remarkable rate augmentation of 414-fold (relative to that in the CTAB micelle) was observed. This enhanced rate is 33-fold greater than the hydration rate of NBzNH in non-micellar solution. The protonated intermediate (or the transition state) of the hydration reaction should be significantly stabilized by the anionic environment consisting of the NaLS micelle.

Discussion

Absorption Maxima of Dihydronicotinamides. The absorption maximum of dihydropyridines is known to shift depending on the environment. This phenomenon is of particular interest in connection with the observation that the complex of alcohol dehydrogenase and NADH has an absorption maximum at 325 nm in contrast to that of NADH at 340 nm.[16] This observation has been repeated and extended to NADH analogs and NAD-addition products.[17,18] Although the shift to shorter wavelengths is also brought forth by non-polar environments, Kosower rather claimed that a positively-charged nitrogen(probably ammonium ion of a lysine residue) which is located 3 Å apart from the nitrogen of the dihydropyridine ring produces the shift by destabilization of the polar excited state of the dihydropyridine.[10]

In the present study λ_{max} of NLaNH shifted by 6 nm to shorter wavelengths in the CTAB micelle compared with NPrNH in water (Table 1). NLaN efficiently forms the charge transfer complex with NLaNH in micellar systems,[14] and the complex probably possesses the face-to-face orientation. Despite the expectation that the remarkable hypsochromic shift may occur, the observed shift was only 5 nm in the micelle of NLaN. Therefore, the ring nitrogen of NLaNH may not be located very close to the cationic charge of surfactant molecules enough to perturb the spectrum.

Hydration Rates of Dihydronicotinamides. Although the hypsochromic shift of dihydronicotinamides caused by the adjacent cationic charge of the surfactant is only 5—6 nm, it is interesting to assess the acid-catalyzed hydration rates in reference to the shifts.

The experimentally observed first-order rate constants for the hydration of a dihydronicotinamide can be satisfactorily described by a general acid catalysis equation (3), in which k_0 is the reaction rate with water and k_H and k_{HA} are the catalytic constants of hydronium ion and buffer acid, respectively.[4]

$$k_{obsd} = k_0 + k_H[H_3O^+] + k_{HA}[HA]$$

Since the k_0 term is negligible in comparison with other terms,[4] one can consider that hydronium ion and buffer acid catalyze the hydration reaction. Under the condition employed, the hydration reaction is mainly catalyzed by $H_2PO_4^-$ ion,[4] that is, k_{HA} [HA]$>$ k_H [H_3O^+]. The CTAB micelle would localize $H_2PO_4^-$ ion around the Stern layer, while H_3O^+ ion would be expelled out of the micellar surface. Thus, one may expect that the hydration rates would be accelerated by concentrated $H_2PO_4^-$ ion. On the contrary, the presence of CTAB micelle depressed the reaction rates, so that the retardation should be caused by the cationic micelle itself. It is concluded, therefore, that a cationic micelle destabilizes a positively-charged intermediate (or the transition state to form the intermediate; Eqs. 1 and 2). A similar discussion would be possible to account for the acceleration effect by an anionic micelle. Thus, the effect of the cationic and anionic micelles on the hydration reaction is consistent with the previous proposition by Kim and Chaykin[5] that the protonation of dihydronicotinamides is involved in the rate-determining step.

The micellar effect on the hydration rate was most pronounced in the case of NLaNH. Though the decay of NLaNH is extremely depressed in CTAB micelle, it would not mean the dihydronicotinamide portion of NLaNH to be in the apolar core of the micelle. The hydration reaction is accelerated by the presence of NaLS micelle, and the acceleration phenomenon could not be expected for the functional group sinking in the micelle core. The dihydronicotinamide group probably exists in the Stern layer or at the vicinity. Our recent observation that NLaNH efficiently forms the charge transfer complex with the 3-carbamoylpyridinium group of NLaN in CTAB-micelle[14] would support this inference.

The relative rate augmentation and depression, compared with NBzNH in non-micellar system, are listed in Table 2. The surfactant concentration, where the rate difference is the greatest, was employed to demonstrate the susceptibility of the hydration reaction to the ionic environment. The conspicuous micellar effect is seen in the case of NLaNH. The NaLS micelle accelerates the hydration rate of NLaNH by 33-fold. This augementation corresponds to 414-fold of that in CTAB micelle, and, in fact, 1400-fold of that in NLaN micelle.

The cationic charge of CTAB and NLaN micelles is not located close to the nitrogen of the nicotinadmie

Table 2. Relative hydration rate[a)]

Dihydronicotinamide	Non-micelle	Micelle		
		LaLS	CTAB	NLaN
NBzNH	1.0	1.7	1/ 8.4	
NLaNH		33	1/12.6	1/44

a) 30 °C, pH 6.30 with 0.01 M phosphate. Surfactant concentrations which provide the greatest difference are as follows: for NBzNH, $[NaLS]=8.00\times10^{-3}$ M, $[CTAB]=1.00\times10^{-2}$ M; for NLaNH, $[NaLS]=3.00\times10^{-3}$ M, $[CTAB]=1.00\times10^{-2}$ M, $[NLaN]=1.56\times10^{-2}$ M.

group enough to cause the significant spectral shift. However, it exerts the remarkable inhibitory effect on the hydration. In the complex between NADH and alcohol dehydrogenase, a positively-charged nitrogen in the form of an ammonium ion is located at the distance of 3 Å from the nitrogen of the dihydropyridine ring, which does generate the spectral shift.[10] It is conceivable from the present results that the hydration reaction of the bound NADH to alcohol dehydrogenase would be greatly affected by the presence of such a closely neighboring ammonium ion. At present, however, it is uncertain if any biological function is associated with the presence of such a positive charge. The present work suggests that the positive charge protects the bound NADH from the hydration decay, and that it would enable the dihydronicotinamide group to act as a reducing function over a wide pH range.

Concluding Remark. As described above, the acid-catalyzed hydration of 1,4-dihydronicotinamide is quite susceptible to the influence of the ionic environment. This finding in a model system may be of importance bearing to an attempt to understand the function of the bound NADH to alcohol dehydrogenase. Micelles would be a typical model system such that the dihydronicotinamide group is located close to the ionic group. A similar system is possible in polyelectrolytes containing the dihydronicotinamide function (Eq. 4).[19]

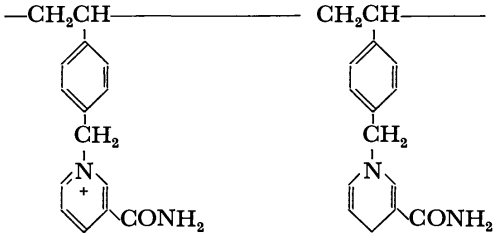

(4)

References

1) Contribution No. 343 from this department.
2) T. C. Bruice and S. J. Benkovic, "Bioorganic Mechanisms," Vol II, New York, N.Y., W. A. Benjamin, (1966) Chapter 9.
3) Abbreviations employed are: nicotinamide adenine dinucleotide and its reduced form, NAD and NADH; 1-R-1,4-dihydronicotinamide, R=Pr(NPrNH), R=benzyl(NBzNH), R=lauryl(NLaNH); 1-lauryl-3-carbamoylpyridinium bromide, NLaN.
4) C. C. Johnston, J. L. Gardner, C. H. Suelter, and D. E. Metzler, *Biochemistry*, **2**, 689 (1963).
5) C. S. Y. Kim and S. Chaykin, *ibid.*, **7**, 2339 (1968).
6) G. M. Rafter, S. Chaykin, and E. G. Krebs, *J. Biol. Chem.*, **208**, 799 (1953).
7) J. O. Meinhart, S. Chaykin, and E. G. Krebs, *ibid.*, **220**, 821 (1956).
8) R. B. Dunlop, G. A. Ghanim, and E. H. Cordes, *J. Phys. Chem.*, **73**, 1898 (1969).
9) B. M. Dunn and T. C. Bruice, *J. Amer. Chem. Soc.*, **92**, 6589 (1970).
10) E. M. Kosower, *Biochim. Biophys. Acta*, **56**, 474 (1962).
11) J. Baumrucker, M. Calzadilla, M. Centeno, G. Lehrmann, M. Uradaneta, P. Lindquist, D. Dunham, M. Price, B. Sears, and E. H. Cordes, *J. Amer. Chem. Soc.*, **94**, 8164 (1972).
12) Y. Paiss and G. Stein, *J. Chem. Soc.*, **1958**, 2905.
13) E. J. Fendler and J. H. Fendler, "Advances in Physical Organic Chemistry," Vol. 8, ed. by V. Gold, Academic Press, New York, N.Y. (1970), p. 271.
14) S. Shinkai, K. Tamaki, and T. Kunitake, This Bulletin, **48**, 1918 (1975).
15) G. Cilento and D. L. Sanito, *Arch. Biochem. Biophys.*, **110**, 133 (1965).
16) H. Theorell and R. K. Bonnicksen, *Acta Chim. Scand.*, **5**, 1105 (1951).
17) J. van Eys, F. E. Stolzenbach, L. Sherwood, and N. O. Kaplan, *Biochim. Biophys. Acta*, **27**, 163 (1958).
18) S. Shifrin, *Biochemistry*, **3**, 829 (1964).
19) T. Kunitake, S. Shinkai, and K. Tamaki, to be submitted.

Coenzyme Models. III. Enhanced Charge Transfer Interaction between the Oxidized and Reduced Forms of Nicotinamide in Micellar and Polymeric Systems. NAD Coenzyme Model[1]

Seiji SHINKAI, Kiyoshi TAMAKI, and Toyoki KUNITAKE

Department of Organic Synthesis, Faculty of Engineering, Kyushu University, Fukuoka 812

(Received February 8, 1975)

The micelle of 1-lauryl-3-carbamoylpyridinium bromide(NLaN) and poly-1-(*p*-vinylbenzyl)-3-carbamoylpyridinium chloride (PVCC) were shown to form charge transfer complexes with dihydronicotinamides and several aromatic compounds in aqueous media. A broad charge transfer absorption at longer wavelengths was easily detected, and the association constant of 1 : 1 complexes which was estimated from the CT band was enhanced by 6.2—220 times in the NLaN micelle and by 14—66 times in the polymeric system, compared with non-micellar, monomeric system. The enhancement of the interaction between NLaN and its reduced from (NLaNH) was similar in the CTAB micelle and in a nonionic micelle. The increased electron-acceptabilities of the pyridinium group in micellar and polymeric systems were discussed in reference to NAD coenzyme.

The oxidized and reduced forms of flavin mononucleotide produce a charge transfer complex which is a precursor of the semiquinone-type free radical.[2] The charge transfer interaction is similarly expected to exist in NAD coenzyme, and, in fact, a new broad absorption which appears to be due to a 1 : 1 charge transfer complex between NAD and NADH was observed at the longer wavelength.[3] In the nonenzymatic system the charge transfer interaction could be recognized only at abnormally high concentrations (0.14—1.5 M),[3] in the intramolecular charge transfer systems,[4,5] and in the frozen system at −78 °C.[6] Though it is quite important to prove the existence of the charge transfer interaction in connection with the hydrogen transfer reaction involving NAD coenzyme, the conditions employed in the previous model systems seem to be far from the original milieu where the enzymic reaction proceeds. Thus, it occurs to us that the charge transfer interaction may be more easily detected in microheterogeneous systems such as micelles and water-soluble polyelectrolytes. This paper describes charge transfer interactions of poly-1-(*p*-vinylbenzyl)-3-carbamoylpyridinium chloride(PVCC) and 1-lauryl-3-carbamoylpyridinium bromide (NLaN) with dihydronicotinamides (NBzNH, NLaNH) and several aromatic compounds, and the results obtained were compared with the corresponding monomeric compound.

Acceptor: $CH_3(CH_2)_{11}N^+$ (pyridinium, $CONH_2$) Br^- NLaN

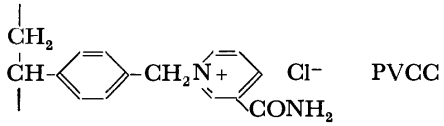

Donor: $CH_3(CH_2)_{11}N$ (dihydropyridine, $CONH_2$) NLaNH

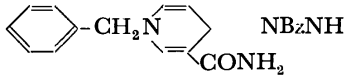

Experimental

Materials. *p*-Chloromethylstyrene was prepared according to the method of Miyake and Tanimoto,[7] bp 58—61 °C/0.13 mmHg (lit,[7] 58—62 °C/0.4 mmHg).

1-(*p*-Vinylbenzyl)-3-carbamoylpyridinium chloride (VCC) was prepared by quaternization of nicotinamide by *p*-chloromethylstyrene in methanol. Recrystallization of the resulting precipitates from methanol gave colorless needles; yield 86—92%, mp 235—238 °C. Found: C, 64.16; H, 6.21; N, 10.16%. Calcd for $C_{15}H_{15}N_2OCl \cdot 0.33\ H_2O$: C, 64.16; H, 6.35; N, 9.88%.

Polymerizations of VCC were conducted using potassium persulfate as initiator at 65 °C in water solvent. After 24 hr viscous polymer solutions were poured into acetone, and the recovered polymers were purified by dialysis to give white powders, yield 90%.

The syntheses of NLaN and NLaNH were described in the accompanying paper.[8] Other materials used in this paper were products of Wako Pure Chemical Ind.

Electronic Spectra. Absorption spectra were taken on a Hitachi 124 spectrophotometer at a slow scan speed to permit accurate determination of extinction coefficients. Spectra were recorded at 30 °C in aqueous solutions adjusted to pH 9.30 with 0.02 M borate buffer.

Association Constants. Association constants (K) in polymeric systems were determined by varying the concentration of PVCC while maintaining the concentration of donor compounds(D) constant. Data thus obtained were plotted according to Eq. 1 which holds for formation of a 1 : 1 complex,[9]

$$\frac{\Delta OD}{[PVCC]} = K \cdot \varepsilon [D] - K \Delta OD \qquad (1)$$

where [PVCC] represents the concentration of the VCC unit in the polymer, ε is the apparent molar absorption coefficient of the complex, and ΔOD represents the difference of optical density between the observed value and the sum of the individual absorptions. From the least-squares procedure of ΔOD *vs.* $\Delta OD/[PVCC]$ plots, slopes and intercepts were evaluated, and K and ε values are determined according to Eq. 1.

In micellar systems it was experimentally difficult to attain the conditions mentioned above, so that Eq. 1 was modified to Eq. 2 and ΔOD values were measured at two different NLaN concentrations.

$$\Delta OD = \frac{\varepsilon K}{\left(K + \frac{1}{[NLaN]}\right)} \cdot [D] = A \cdot [D] \qquad (2)$$

From the slope of [D] *vs.* ΔOD plots at different NLaN concentrations were determined two A values, the simultaneous equation of which gave K and ε values.

Results and Discussion

Charge Transfer Absorption Spectra. The absorption spectrum of NLaNH obtained in a micellar solution of cetyltrimethylammonium bromide (CTAB: 2.50×10^{-2} M) was essentially the same as that in absolute ethanol. On the other hand, the addition of NLaNH to a NLaN-micellar solution provided a colored solution (yellow-light orange). A new, diffused absorption appeared at 430—550 nm (Fig. 1) as previously reported for NAD[3] and for 1-benzyl-3-carbamoylpyridinium[9] in non-micellar systems at higher concentrations. In the NLaN-micelle, addition of 10^{-3}—10^{-4} M of NLaNH was found to be sufficient to detect the charge transfer absorption. According to Ludowieg and Levy,[3] the charge transfer absorption between 1-propyl-3-carbamoylpyridinium chloride (NPrN) and its reduced form (NPrNH) is very susceptible to the dilution effect. Although mixing of a 10^{-2} M colorless solution of NPrN with a 10^{-2} M light-yellow solution of NPrNH gave a solution with little increase in color intensity, an instantaneous orange color was observed at higher concentrations (0.7—1.5 M).[3] Therefore, the enhanced charge transfer interaction observed in the present micellar system may be associated with increased concentrations of the nicotinamide groups of NLaN and NLaNH in the thin Stern layer. The intensity of the charge transfer absorption was proportional to the concentration of NLaNH, when the concentration of NLaN was maintained constant under the condition of [NLaN] $\gg$ [NLaNH]. Thus, Eq. 2 is applicable to the present system, *i.e.*, the 1 : 1 complex is formed between NLaN and NLaNH even in a micellar system.

The interaction between NLaN and NLaNH was enhanced to a similar extent in a nonionic micelle of polyoxyethylene (10) oleyl alcohol as well as in CTAB micelle, and the spectra observed were almost the same as that observed in NLaN micelle (Fig. 1). Evidently, the ionic environment, characteristic of ionic micelles, is not obligatory to enhanced interaction. The concentration effect must play a decisive role for the enhancement of the charge transfer interaction in micellar systems.

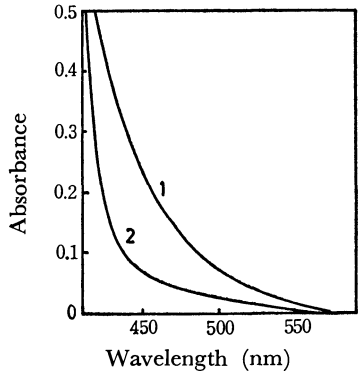

Fig. 1. Absorption spectra of NLaNH in micellar systems.
[NLaNH] $=4.0\times10^{-3}$ M, 30 °C, pH 9.30 with 0.02 M borate, 8 vol % ethanol.
1: [NLaN] $=1.56\times10^{-2}$ M, 2: [CTAB] $=2.50\times10^{-2}$ M.

Enhanced charge transfer interactions with NLaN and with PVCC were also observed for naphthalene, acenaphthene, adenosine and indole derivatives. Complexes with indole derivatives showed strong charge transfer absorptions at 320—450 nm and a difference spectrum indicated absorption maxima at 303—324 nm (ε=2600—900, Fig. 2).[10] These spectra are of particular interest because of their similarity to the spectrum of the NAD-glyceraldehyde-3-phosphate dehydrogenase complex (λ_{max} 360 nm).[11] This enzyme is the only one which is known to form a charge transfer complex between NAD and the enzyme residue, probably an indole nucleus. Velick[12] suggested that the NAD coenzyme is bound at the top or bottom of a tryptophan stack in the enzyme. A similar spectrum is observed in a model compound, 1-(β-indolylethyl)-3-carbamoylpyridinium chloride, which possesses the intra-

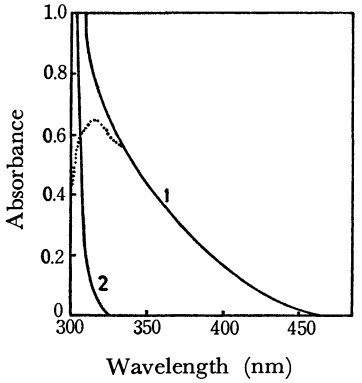

Fig. 2. Absorption spectra of (3-indolyl)acetic acid in micellar systems. The dotted curve indicates a difference spectrum (λ_{max} 317 nm).
[(3-Indolyl)acetic acid] $=1.0\times10^{-3}$ M. Other conditions are the same as a note of Fig. 1.

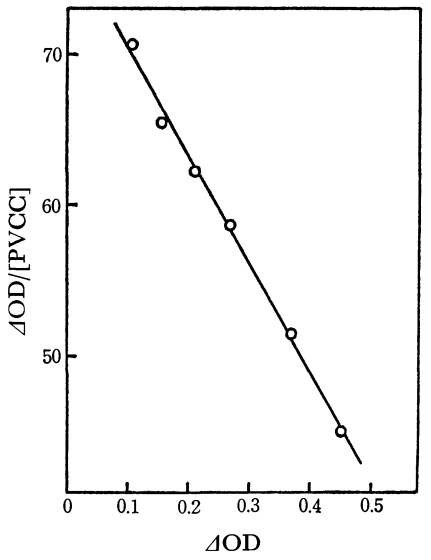

Fig. 3. Spectrophotometric determination of the association constant for the complex of indole with PVCC in water.
30 °C, pH 9.30 with 0.02 M borate, [indole] $=3.0\times10^{-3}$ M. See text (Experimental, Eq. 1) for details of the method.

molecular interaction between 3-carbamoylpyridinium and indole moieties (λ_{max} 325 nm, $\varepsilon=1000$).[4,5]

Association Constants. Association constants were determined according to the method of Cilento *et al.*[9,13,14] as described in the experimental section. The wavelengths employed are the same as in their system. The plots of ΔOD *vs.* ΔOD/[PVCC] in the polymeric systems gave good linear relationships and the correlation coefficients were better than 99% (Fig. 3). Association constants (K) and molar absorption coefficient (ε) determined using the least squares method are recorded in Table 1. It is seen that ε values are one half to two thirds of those of monomeric 3-carbamoylpyridinium.[9,13,14] On the other hand, the association constant was enhanced by 14—66 times. These results indicate that PVCC provides a better environment in forming the charge transfer complex compared to the monomeric compound and that a 1 : 1 complex is formed between a donor molecule and a VCC unit in the polymer. In the polymeric system two VCC units could interact with a donor molecule from both sides. However, this is not the case. And the better acceptor property observed may suggest that adjacent VCC units function to increase the electron-acceptability of the complex-forming VCC unit. As expected, the association constant of (3-indolyl)acetic acid was the greatest.

The plots of [D] *vs.* ΔOD for micellar systems gave linear relationships (Fig. 4), and association constants and molar absorption coefficients were computed from Eq. 2. The result is summarized in Table 2. Association constants for indole derivatives were enhanced by only 6—10 times in NLaN micelle, compared with non-micellar system. The enhancement was greater in the polymeric system than in the micellar system. On the other hand, association constants for naphthalene and acenaphthene were enhanced by 129—220 times in NLaN micelle. This large augmentation would be associated with solubilization by micellar systems, that is, water-insoluble aromatics like naphthalene and acenaphthene should be fixed in and/or near the Stern layer of NLaN micelle, resulting in strong charge transfer interactions. These aromatic compounds are insoluble in the aqueous solution of PVCC.

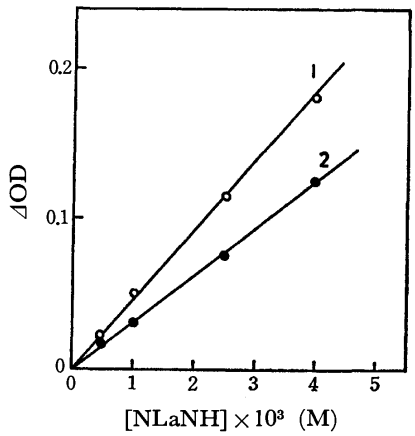

Fig. 4. Spectophotometric determination of the association constant for the complex of NLaNH with NLaN.
30 °C, pH 9.30 with 0.02 M borate, 8 vol % ethanol. 1: [NLaN] = 1.56×10^{-2} M, 2: [NLaN] = 1.00×10^{-2} M. See test (Experimental, Eq. 2) for details of the method.

Table 1. Association constants of PVCC[a]

Donor	λ[b] (nm)	NBzN[c] ε	NBzN[c] K (M^{-1})	PVCC ε	PVCC K (M^{-1})
NBzNH	440	307	3.76	180	51
Adenosine	325	145	2.29	100	140
Indole	380	890	2.21	360	72
(3-Indolyl)acetic acid	380	1060	4.09	440	271

a) 30 °C, pH 9.30 with 0.02 M borate buffer. b) Wavelength employed to evaluate ΔOD values of Eq. 1. c) Determined by Cilento *et al.*[9,13,14]

Association constants of aromatic compounds with NLaN decreased in CTAB and nonionic micelles. On the other hand, those of NLaNH with NLaN increased, or were unaffected in these micelles (Table 2). Presumably, the formation of a charge transfer complex between NLaNH and NLaN is favored because both of them possess the surfactant structure.

NAD Coenzyme Model. The foregoing observations establish that micellar and polymeric systems provide favorable environmentals in forming the 1 : 1 charge transfer complex between NLaN and donors including NLaNH, indole derivatives, and other aromatic compounds. These findings imply that these systems would act as a proper NAD coenzyme model, since it has been known that the interaction between pyridine

Table 2. Association constants of NLaN in micellar systems[a]

Donor	λ (nm)	NBzN[c] ε	NBzN[c] K (M^{-1})	Micellar system ε	Micellar system K (M^{-1}) NLaN	CTAB	Non-ion
NLaNH	440	307	3.76[b]	180	22	46	23
Naphthalene	326	850	0.17	490	38	9.2	4.6
Acenaphthene	330	1550	0.32	1040	41	19	1.9
Indole	380	890	2.21	600	14	5.6	4.9
(3-Indolyl)acetic acid	380	1060	4.09	690	41	14	11
DL-Tryptophan	380	650	2.52	420	22	13	—

a) 30 °C, pH 9.30 with 0.02 M borate, 8 vol% ethanol. b) Association constant between 1-benzyl-3-carbamoylpyridinium and 1-benzyl-1,4-dihydronicotinamide.[14] c) Determined by Cilento *et al.*[9,13,14]

and adenine rings produced by the folded conformation plays an important role to adjust the oxidation-reduction reactivity in the enzymic system.[15,16] It would be interesting to assess the effect of such an interaction on the oxidation-reduction reaction in a model system.

References

1) Contribution No. 345 from this department.
2) Q. H. Gibson, V. Massey, and N. M. Atherton, *Biochem. J.*, **85**, 369 (1962).
3) J. Ludowieg and A. Levy, *Biochemistry*, **3**, 373 (1964).
4) S. Shifrin, *Biochim. Biophys. Acta*, **81**, 205 (1964).
5) Idem, *Biochemistry*, **3**, 829 (1964).
6) M. J. Spiegel and G. R. Drysdale, *J. Biol. Chem.*, **235**, 2498 (1960).
7) T. Miyake and S. Tanimoto, *Yuki Gosei Kagaku Kyokai Shi*, **31**, 1050 (1973).
8) S. Shinkai, R. Ando, and T. Kunitake, This Bulletin, **48**, 1914 (1975).
9) G. Cilento and S. Schreier, *Arch. Biochem. Biophys.*, 107, 102 (1964).
10) A. Difference spectrum was obtained by subtracting the absorption of indole in CTAB micelle from that in NLaN micelle.
11) E. M. Kosower, *J. Amer. Chem. Soc.*, **78**, 3497 (1956).
12) S. F. Velick, *J. Biol. Chem.*, **233**, 1455 (1958).
13) G. Cilento and D. L. Sanioto, *Arch. Biochem. Biophys.*, **110**, 133 (1965).
14) G. Cilento and P. Tedeschi, *J. Biol. Chem.*, **236**, 907 (1961).
15) G. Weber, *Nature*, **180**, 1409 (1957).
16) S. Shifrin and N. O. Kaplan, *ibid.*, **183**, 1529 (1959).

Reaction of Group IV Organometallic Compounds. XXXII[1] Modified Synthesis of Imidazolidines with *N,N'*-Bis(trimethylsilyl)-1,2-diamines

Hiroharu Suzuki, Masayasu Ohashi, Kenji Itoh,* Isamu Matsuda, and Yoshio Ishii

Department of Synthetic Chemistry, Faculty of Engineering, Nagoya University, Nagoya 464

(Received February 28, 1975)

N,N'-Bis(trimethylsilyl)-1,2-diamines gave imidazolidine derivatives accompanied with the elimination of hexamethyldisiloxane in excellent yields by condensation reactions with carbonyl compounds under mild conditions. These reactions are regarded as the typical addition-elimination reaction of group IV organometallics.

Imidazolidine derivatives have been synthesized by a dehydration condensation reaction between diamine and carbonyl compounds. This preparative reaction, however, is reversible, and removal of generated water is required to complete the reaction. This operation takes generally long time and is inadequate to prepare water-sensitive homologues.

In this paper we describe a modified preparation of imidazolidine skeleton by means of *N,N'*-bis(trimethylsilyl)ethylene- and -*o*-phenylenediamines. Elimination of unreactive hexamethyldisiloxane should favor an irreversible generation of imidazolidine under mild reaction conditions. In addition, the present manipulation is easy to carry out simple separation of hexamethyldisiloxane *in vacuo*. These condensation reactions constitute an extension of addition-elimination reactions of main group organometallics from the standpoint of organometallic chemistry.

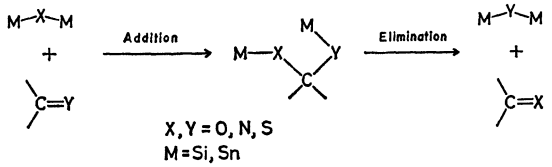

(1)

The most important driving force in either β-addition-β-elimination of heptamethyldimetallazane (M=Me_3Si,[2,3] Me_3Ge,[4] and Me_3Sn[2,5] X=NMe), or β-addition-ω-elimination (M=$^nBu_3Sn$; Y=$O(CH_2)_nO$,[6] $NR(CH_2)_2O$,[7] $NR(CH_2)_2NR$[7]) was the organometallic affinity differences between product (with stable M–Y bonds) and starting materials (with labile M–X bonds).[8]

This work is devoted to examine the possibility of utilization of the strong silicon-oxygen bond formation (a hard-hard interaction) in the imidazolidine cyclizations, because we previously elucidated that an inverse soft-soft interaction of tin-sulfur bond formation had substantial synthetic potential in iminocarbonylation or cyclization to thione-carbonate and spiro-orthoesters.

Results and Discussion

Reactions of electronically and sterically different various *N,N'*-bis(trimethylsilyl)-1,2,-diamines with aldehyde or ketones gave corresponding imidazolidine derivatives in excellent yields.

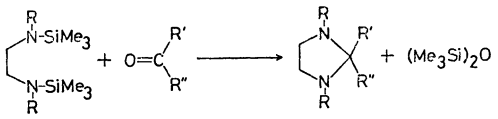

(2)

Hexamethyldisiloxane generated as a sole by-product could be removed completely by evaporation *in vacuo* at room temperature. When dimethylformamide was used as a reactant with *N,N'*-bis(trimethylsilyl)ethylenediamine and -*o*-phenylenediamine, subsequent elimination of dimethylamine induced the generation of 2-imidazoline and 2-benzimidazole, respectively. Preparative results are summarized in Table 1. Analytical and spectroscopic results are shown in Table 2.

Reaction of N,N'-*Bis(trimethylsilyl)ethylenediamine (**1**).* *N,N'*-Bis(trimethylsilyl)ethylenediamine (**1**) reacted with diethyl ketone and cyclohexanone to give the expected imidazolidines (**4b**) and (**4a**), which were readily purified by distillation. Analytical and spectral informations are in consistent with the depicted structures.

Dimethylformamide reacted with **1** at 120 °C to give imidazoline (**4c**) by way of further elimination of dimethylamine. Although 2-substituted imidazolines have been prepared by dehydration condensation under highly drastic conditions (200—220 °C), parent skeleton of 2-imidazoline has not been obtained. This method is extremely useful to prepare simplest 2-imidazoline (**4c**). The mechanism of this reaction was discussed later. Benzaldehyde did not give expected imidazolidine by ω-elimination of hexamethyldisiloxane but afforded *N,N'*-dibenzylideneethylenediamine (**4d**), which was definitely identified by analysis, IR ($\nu_{C=N}$ 1640 cm^{-1}), and NMR [τ_{CH} 1.80 (2H, s), τ_{CH_2} 6.16 (4H, s)].

Reaction of N,N'-*Bis(trimethylsilyl)*-N,N'-*dimethylethylenediamine (**2**).* Introduction of methyl groups on each nitrogen atom of **2** increased both electron density and steric hindrance around the nitrogen atom. The reaction of **2** with diethyl ketone, cyclohexanone, and even benzaldehyde, however, gave quantitatively the corresponding imidazolidines, **5b**, **5a**, and **5c**, which were unambiguously identified by analytical and spectral informations. Dimethylformamide did not react with **2** even at 120 °C for 6 hr indicative of the participation of steric effect to some extent.

Reaction of N,N'-*Bis(trimethylsilyl)*-o-*phenylenediamine (**3**).* Benzimidazoline derivatives (**6b** and **6a**) were obtained successfully by the reaction of **3** with benzaldehyde or cyclohexanone in excellent yields,

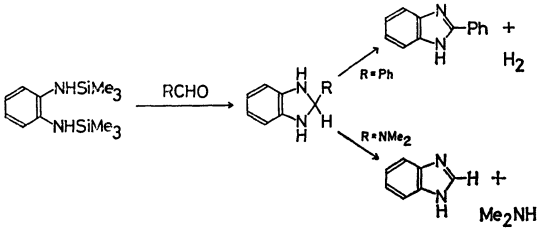

(3)

Table 1. Cyclization reaction of bis(trimethylsilyl)diamines with carbonyl compounds

Bis(TMS)-diamine	Carbonyl compound	Method[a]	Reaction conditions	Product	Bp (°C/mmHg) [mp] (°)	Yield[b] (%)
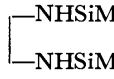 (1)		A	20 °C/2 min	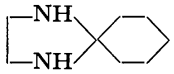 (4a)	41/0.2	59 (98)
(1)	$Et_2C=O$	B	120 °C/1 hr	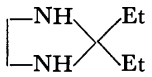 (4b)	31/2	59 (98)
(1)	Me_2NCHO	B	120 °C/1 hr	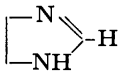 (4c)	50/1	87
(1)	PhCHO	A	20 °C/2 min	$(PhCH{=}N{-}CH_2)_2$ (4d)	152/0.8	98
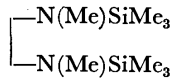 (2)		A	20 °C/2 min	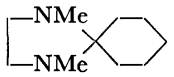 (5a)	72/50	56 (100)
(2)	$Et_2C=O$	B	180 °C/24 hr	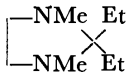 (5b)	40/7	33 (100)
(2)	Me_2NCHO	B	120 °C/6 hr	No reaction		
(2)	PhCHO	A	20 °C/2 min	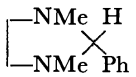 (5c)	63/1	93 (100)
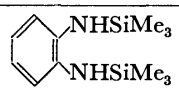 (3)		A	20 °C/2 min	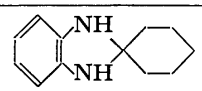 (6a)	[131—133]	66 (100)
(3)	$Et_2C=O$	B	180 °C/24 hr	No reaction		
(3)	Me_2NCHO	B	120 °C/12 hr	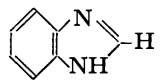 (6d)	[173—175]	97
(3)	PhCHO	B	50 °C/3 hr	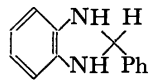 (6b)	[63—65]	91 (100)
(3)	PhCHO	B	120 °C/12 hr	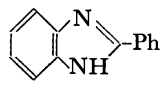 (6c)	[298—300]	29

a) See experimental section. b) Yield is isolated yield and that in parentheses is determined by NMR.

whereas diethyl ketone did not react with **3** even at 180 °C.

When **3** was reacted with benzaldehyde and with dimethylformamide at elevated temperature (120 °C), 2-phenylbenzimidazole (29%) and benzimidazole (97%) were generated respectively by way of the successive β-elimination of hydrogen and dimethylamine. In fact, 2-phenylbenzimidazoline (**6b**), prepared from **3** and benzaldehyde at room temperature, caused smooth elimination reaction of hydrogen to aromatize to benzimidazole at 120 °C.

Mechanism. Above-mentioned preparative reactions are reasonably explained by a β-addition-ω-elimination reaction controlled by the affinity difference between labile Si–N and stable Si–O bonds. The primary step is the nucleophilic attack of either nitrogen atom in *N,N'*-bis(trimethylsilyl)-1,2-diamines to the carbonyl carbon atom, followed by the rapid migration of trimethylsilyl group to oxy anion to give intermediate insertion product [A]. Formation of extremely stable hexamethyldisiloxane is the driving force of the ω-elimination reaction to give imidazolidine [B] as cyclization product. The reaction between **1** and benzaldehyde belongs to an exceptional case and facile β-elimination of trimethylsilanol is induced to give [C] which captures the second benzaldehyde at

Table 2. Analytical and spectroscopic results of products

	Analysis (Found)			^{1}H NMR (τ)	IR (cm^{-1})
4a	C	68.91	(68.54)	7.18 (4H, s)[a]	3250 (ν_{NH})[a]
	H	11.71	(11.50)	8.55 (10H, m)	
	N	19.38	(19.98)	8.82 (2H, s)	
4b	C	65.30	(65.59)	7.20 (4H, s)[a]	3260 (ν_{NH})[a]
	H	12.41	(12.58)	8.40—9.34 (12H, overlapping of NH, CH_2, and CH_3)	
	N	22.29	(21.85)		
4c	C	52.05	(51.41)	3.01 (1H, m)[b]	3420 (ν_{NH})[c]
	H	9.05	(8.62)	5.89 (1H, m)	
	N	38.89	(39.96)	6.49 (4H, m)	
4d	C	81.54	(81.34)	1.80 (2H, s)[a]	1640 ($\nu_{C=N}$)[a]
	H	7.06	(6.83)	2.55 (10H, m)	
	N	11.40	(11.85)	6.16 (4H, s)	
5a	C	72.04	(71.36)	7.35 (4H, s)[a]	2770 (ν_{N-CH_3})[a]
	H	11.98	(11.91)	7.89 (6H, s)	
	N	16.05	(16.64)	8.60 (10H, m)	
5b	C	69.47	(69.16)	7.27 (4H, s)[a]	2770 (ν_{N-CH_3})[a]
	H	13.10	(12.90)	7.75 (6H, s)	
	N	17.43	(17.92)	8.79 (4H, q, J=7Hz)	
				9.33 (6H, t, J=7Hz)	
5c	C	75.27	(74.96)	2.75 (5H, m)[a]	2760 (ν_{N-CH_3})[a]
	H	9.30	(9.15)	6.89 (1H, s)	
	N	15.43	(15.89)	7.20 (4H, AA'BB')	
				7.97 (6H, s)	
6a	C	76.94	(76.53)	3.55 (4H, m)[a]	3320, 3230 (ν_{NH})[d]
	H	8.57	(8.57)	6.54 (2H, s)	
	N	14.48	(14.88)	8.38 (10H, m)	
6b	C	79.31	(79.56)	1.60 (1H, s)[a]	3470, 3370 (ν_{NH})[d]
	H	5.89	(6.16)	2.42 (5H, m)	
	N	14.00	(14.27)	3.27 (4H, m)	
				6.00 (2H, s)	
6c	C	80.25	(80.39)	sparingly soluble	mass m/e 194 (M^+)
	H	5.08	(5.19)		
	N	14.31	(14.42)		
6d	C	70.60	(71.19)	1.85 (1H, s)[e]	mass m/e 118 (M^+)
	H	5.28	(5.12)	2.63 (4H, m)	
	N	23.92	(23.72)		

a) in CCl_4, b) in $CDCl_3$, c) in $CHCl_3$, d) in KBr, e) in $(CD_3)_2CO$

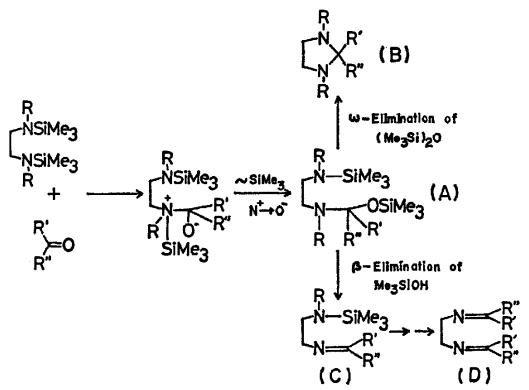

the another end to generate *N,N'*-dibenzylideneethylenediamine [D].

Experimental

IR spectra were recorded with a Japan Spectroscopic Co., Ltd. IR-S instrument. ^{1}H NMR spectra were measured with a Japan Electron Optics Lab. Co., Ltd. C-60 HL instrument. *N,N'*-Bis(trimethylsilyl)diamines were prepared according to Birkofer, Kühlthau, and Ritter.[9] Carbonyl compounds were freshly distilled before use.

Synthesis of Imidazolidines. To the *N,N'*-bis(trimethylsilyl)diamine (3.5—13.5 mmol) were added dropwise equimolar amounts of carbonyl compounds under an atmosphere of nitrogen at 0 °C.

In *Method* **A** the reaction mixture was warmed to room temperature. In *Method* **B** the mixture was heated in a sealed tube. In both methods formed hexamethyldisiloxane was removed from the reaction mixture to leave imidazolidine under reduced pressure (*ca.* 30 mmHg). For the purpose of elemental analysis, imidazolidines were distilled under reduced pressure. The elemental analyses, ^{1}H NMR spectra, IR spectra and other properties provided an adequate support for the structure assigned.

Reaction of N,N'-*Bis(trimethylsilyl)ethylenediamine with Benzaldehyde. Synthesis of* N,N'-*Dibenzylideneethylenediamine (**4d**).* To *N,N'*-bis(trimethylsilyl)ethylenediamine (2.75 g, 13.5 mmol) was added benzaldehyde (1.36 g, 12.8 mmol) dropwise under nitrogen at −78 °C. When the reaction mixture was warmed gradually to room temperature, exothermic reaction occurred to give transparent liquid separated into two layers. The reaction mixture was then distilled under reduced pressure (152 °C/0.8 mmHg) to yield colorless needles (1.48 g, 98% yield based on benzaldehyde used). Mp 52.0—54.0 °C. Found: C, 81.54; H, 7.06; N, 11.40%. Calcd for $C_{16}H_{16}N_2$: C, 81.34; H, 6.83; N, 11.85%. IR (in KBr) 1640 cm^{-1} ($\nu_{C=N}$). ^{1}H NMR (in CCl_4) τ 6.16 (4H, s), 2.25 (10H), and 1.80 (2H, s).

*Conversion of 2-Phenylbenzimidazoline (**6b**) to 2-Phenylbenzimidazole (**6c**).* By the heating of the benzene solution of 2-phenylbenzimidazoline (1.00 g, 5.11 mmol) in sealed tube at 120 °C for 12 hr, colorless precipitates sparingly soluble in benzene separated out. Upon recrystallization from acetone 2-phenylbenzimidazole precipitated as colorless prisms (0.291 g) in a 29% yield. The mp and spectroscopic data of the product were in good agreement with those of authentic sample.

References

1) Part XXXI, H. Suzuki, I. Matsuda, K. Itoh, and Y. Ishii, This Bulletin, **47**, 2737 (1974).
2) K. Itoh, I. K. Lee, I. Matsuda, S. Sakai, and Y. Ishii, *Tetrahedron Lett.*, **1967**, 2667.
3) K. Itoh, N. Kato, S. Sakai, and Y. Ishii, *J. Chem. Soc., C*, **1969**, 2005.
4) K. Itoh, I. Matsuda, T. Katsuura, S. Kato, and Y. Ishii, *J. Organometal. Chem.*, **34**, 75 (1972).
5) K. Itoh, Y. Fukumoto, and Y. Ishii, *Tetrahedron Lett.*, **1968**, 3199.
6) S. Sakai, Y. Kiyohara, K. Itoh, and Y. Ishii, *J. Org. Chem.*, **35**, 2347 (1970).
7) S. Sakai, Y. Asai, Y. Kiyohara, K. Itoh, and Y. Ishii, *Organometal. Chem. Syn.*, **1**, 45 (1970/1971).
8) K. Itoh, "Synthesis *via* Organometallic Compounds," (in Japanese) Maruzen (1974), p. 79.
9) L. Birkofer, H. Kühlthau, and A. Ritter, *Chem. Ber.*, **93**, 2802 (1960).

Selenocyanatodethallation in Organothallium(III) Compounds

Sakae UEMURA,* Akio TOSHIMITSU, Masaya OKANO, and Katsuhiko ICHIKAWA**

Institute for Chemical Research, Kyoto University, Uji, Kyoto 611

***Department of Hydrocarbon Chemistry, Faculty of Engineering, Kyoto University, Yoshida, Kyoto 606*

(Received March 3, 1975)

Substitution of thallium moiety in organothallium(III) compounds by selenocyanate is reported. Arylthallium (III) compounds react with KSeCN and $CuSO_4 \cdot 5H_2O$ or with $Cu(SeCN)_2$ in dioxane to give aryl selenocyanates in good yields. Alkoxythallates of styrene react smoothly with KSeCN in methanol to afford 1-alkoxy-1-phenyl-2-selenocyanatoethanes almost quantitatively. The oxyselenocyanation of terminal olefins is conducted by the *in situ* oxythallation of olefins, followed by the reaction with KSeCN.

Substitution of thallium moiety in organothallium-(III) compounds, such as aryl-,[1] vinyl-,[2] and alkylthallium(III) compounds,[3,4] by halogen (I, Br, and Cl) or pseudohalogen (CN and SCN) by use of copper and/or potassium salts has been reported. As another example of such substitution reactions we now wish to report the result of selenocyanatodethallation in aryl- and alkyl-thallium(III) compounds. This reaction would be a convenient method for the preparation of aryl and alkyl selenocyanates.

Results and Discussion

Reaction of Arylthallium(III) Compounds with Copper and/or Potassium Selenocyanates. When a mixture of arylthallium(III) compound (**1**), potassium selenocyanate and copper(II) sulfate hydrate was stirred in such solvents as dioxane, acetonitrile, methanol, and pyridine under reflux for 0.5 hr, aryl selenocyanate (**2**) was obtained in a good yield together with a small amount of aryl cyanide (**3**) (Scheme 1). Dioxane was revealed to be a solvent of choice for the preparation of **2**.

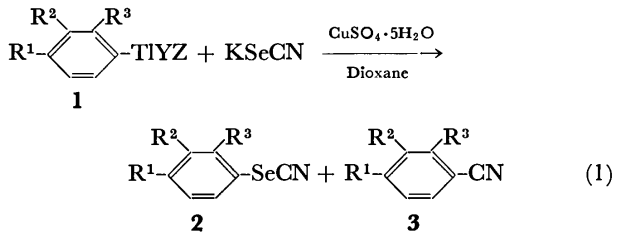

(1)

As in the case of the previously reported halogeno- and pseudohalogeno-dethallation,[1] the replacement of thallium moiety by SeCN occurred at the position where thallium was attached previously to aromatic ring. In contrast to thiocyanatodethallation which was accompanied by protodethallation forming aromatic hydrocarbon,[1d] almost no protodethallation occurred in this case. Sandmeyer reaction for preparing **2** has been known to be accompanied by the formation of diaryl selenide,[5] while none of such product was detected in the reaction products in this case. Typical results are summarized in Table 1.

The reaction proceeded even in the absence of copper-(II) sulfate, but the yield of **2** was low. Since the preparation of copper(II) thiocyanate from copper-(II) sulfate and potassium thiocyanate has been known,[6] it seems to be reasonable to assume that **2** was mainly formed by the interaction of **1** with copper(II) selenocyanate which may be formed in a reaction mixture. In order to ascertain this possibility, we prepared copper-(II) selenocyanate separately and examined the reaction of some arylthallium(III) compounds with this salt in dioxane. As a result, **2** was obtained in a good yield irrespective of the presence or absence of KSeCN, the formation of **3** being minimized (Table 1). Thus it is highly probable that the reaction affording **2** essentially involves the attack of $Cu(SeCN)_2$, formed *in situ*, on **1**. The reaction is ionic in nature since no effect was observed by the introduction of oxygen into the reaction mixture and no acrylonitrile polymer or phenylated acrylonitrile was obtained from the reaction in the presence of acrylonitrile.[1b] Reaction scheme seems to be a concerted nucleophilic substitution after coordination of copper to a ligand on thallium as proposed in the cases of halogeno- and pseudohalogeno-dethallation (Scheme 2).[1b-d]

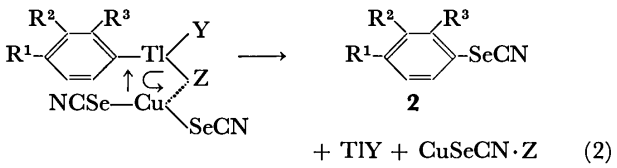

(2)

As to the formation of a side-product **3**, we confirmed in separate experiments that **3** was not derived from **2** under the present reaction conditions; *i.e.*, no deselenation from **2** occurred by heating **2** in the presence of KSeCN, $CuSO_4 \cdot 5H_2O$ or $Cu(SeCN)_2$ in dioxane. Although the exact pathway for **3** is not yet clear, one possibility is that commercial KSeCN may contain KCN, since the former is prepared by heating Se and KCN, which reacts with copper salt to form CuCN or $Cu(CN)_2$ in the reaction mixture. Cyanodethallation of arylthallium(III) compounds by these salts has been reported.[1d]

Reaction of the Alkoxythallate of Styrene with KSeCN. When a mixture of the alkoxythallate of styrene and KSeCN was stirred in methanol under reflux for 15—30 min, 1-alkoxy-1-phenyl-2-selenocyanatoethane (**5**) was obtained almost quantitatively (100% yield when R = CH_3, C_2H_5, and n-C_3H_7; 80—83% yield when R = i-C_3H_7, n-C_4H_9, and i-C_4H_9) (Scheme 3). The reaction did not occur at 25 °C for 2 hr. An elongation of the reaction time at refluxing temperature decreased the yield of **5**, because of the secondary reaction of **5** giving unidentified resinous products. When the reaction was applied to the alkoxythallate of α-methylstyrene and the acetoxythallate of norbornene, the compounds corresponding to **5** were scarcely obtained

* To whom correspondence should be addressed.

Table 1. Preparation of aryl selenocyanate

1 (5 mmol)					Cu^{2+} salt (mmol)	KSeCN (mmol)	Solvent (25 ml)	React. temp. (°C)	React. time (hr)	Products and yields(%)[a]	
R^1	R^2	R^3	Y	Z						**2**	**3**
					$CuSO_4 \cdot 5H_2O$						
H	H	H	OAc	ClO_4	0	20	Dioxane	101	4	24	0
H	H	H	OAc	ClO_4	10	40	Dioxane	101	0.5	78	6
H	H	H	OAc	ClO_4	10	40	Dioxane	101	2	76	6
H	H	H	OAc	ClO_4	10	20	Dioxane	101	2	59	8
H	H	H	OAc	ClO_4	10	40	MeCN	86	0.5	57	5
H	H	H	OAc	ClO_4	10	40	MeOH	65	0.5	22	2
H	H	H	OAc	ClO_4	10	40	Pyridine	115	0.5	28	2
H	H	H	$OCOCF_3$	$OCOCF_3$	10	40	Dioxane	101	0.5	38	1
Me	H	H	OAc	ClO_4	10	40	Dioxane	101	0.5	68	3
Me	Me	H	OAc	ClO_4	10	40	Dioxane	101	0.5	70	5
Me	Me	H	$OCOCF_3$	$OCOCF_3$	10	40	Dioxane	101	0.5	79	1
Me	H	Me	OAc	ClO_4	10	40	Dioxane	101	0.5	79	13
Me	H	Me	$OCOCF_3$	$OCOCF_3$	10	40	Dioxane	101	0.5	89	2
MeO	H	H	OAc	ClO_4	10	40	Dioxane	101	0.5	95	1
Cl H	H	H[b] Cl	$OCOCF_3$	$OCOCF_3$	10	40	Dioxane	101	0.5	60[b]	1
					$Cu(SeCN)_2$						
H	H	H	OAc	ClO_4	10	0	Dioxane	101	0.5	94	trace
H	H	H	OAc	ClO_4	10	20	Dioxane	101	0.5	89	1
H	H	H	NO_3	OH	10	0	Dioxane	101	0.5	50	1
Me	H	H	OAc	ClO_4	10	0	Dioxane	101	0.5	77	trace
Me	H	H	NO_3	OH	10	0	Dioxane	101	0.5	53	trace
Me	Me	H	$OCOCF_3$	$OCOCF_3$	10	0	Dioxane	101	0.5	78	1
Me	H	Me	$OCOCF_3$	$OCOCF_3$	10	0	Dioxane	101	0.5	83	4

a) Based on **1**. Determined by glc. b) A mixture of *o*- and *p*-isomers (*o*-/*p*-=30/70).

Table 2. Oxyselenocyanation of olefins[a]

Olefin (5 mmol)	Solvent (25 ml)	React. time (hr) at 15—20 °C[b]	React. time (hr) at reflux[c]	Products, Yield (%)[d]	
Styrene	MeOH	2	0.5	$PhCH(OMe)CH_2SeCN$	80
Styrene	MeOH	1	0.5	$PhCH(OMe)CH_2SeCN$	68
1-Octene	MeOH	2	0.25	$n\text{-}C_6H_{13}CH(OMe)CH_2SeCN$	80
1-Octene	MeOH	1	0.25	$n\text{-}C_6H_{13}CH(OMe)CH_2SeCN$	70
1-Hexene	MeOH	2	0.5	$n\text{-}C_4H_9CH(OMe)CH_2SeCN$	76
o-Allylphenol	MeOH	2	0.25	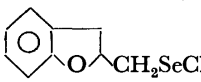	50
$EtOCH{=}CH_2$	EtOH	2	0.25	$(EtO)_2CHCH_2SeCN$	83
				$\begin{matrix}EtO\\AcO\end{matrix}\!\!>\!CHCH_2SeCN$	10
$AcOCH{=}CH_2$	EtOH	2	0.25	$(EtO)_2CHCH_2SeCN$	53
				$\begin{matrix}EtO\\AcO\end{matrix}\!\!>\!CHCH_2SeCN$	24
$CH_2{=}CH{-}CH{=}CH_2$	MeOH	2	0.25	$CH_2{=}CH{-}\underset{\displaystyle OMe}{\underset{\vert}{CH}}{-}CH_2SeCN$	61

a) $Tl(OAc)_3$ 8 mmol, KSeCN 20 mmol. b) Time for oxythallation. c) Time for Tl-SeCN replacement. d) Based on olefin charged.

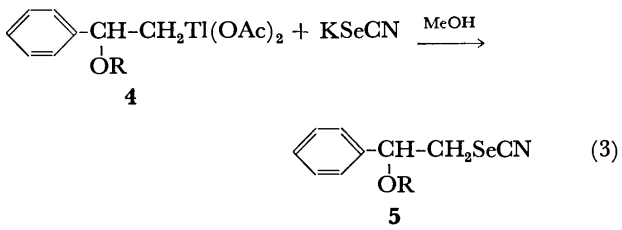

under room or refluxing temperature for 0.5 hr, and the oxidation products of olefins and/or the deoxythallation products were obtained. For example, benzyl methyl ketone and α-methylstyrene were obtained in 50% and 32% yields respectively in the former case, while norbornene was mainly formed in the latter.

The in situ Oxyselenocyanation of Olefins. The result of the reaction of the alkoxythallate of styrene with KSeCN described above and the report[3] of the *in situ* oxythiocyanation of olefins by $Tl(OAc)_3$ and KSCN prompt us to examine the *in situ* oxyselenocyanation of olefins. After a mixture of olefin and thallium(III) acetate was stirred in alcohol at 15—20 °C for 1—2 hr (oxythallation), an alcoholic solution of KSeCN was added and the mixture was then heated under reflux for 15—30 min to afford oxyselenocyanated compound, **6** (Scheme 4). Typical results are summarized in

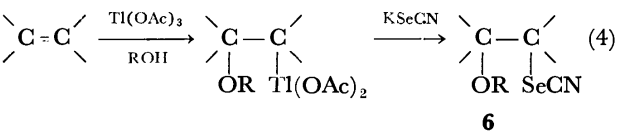

Table 2. Terminal olefins reacted smoothly to give **6**, while internal olefins such as cyclohexene and 2-octene gave only the oxidation products. This may be due to the difference of the stability between the intermediate alkoxythallates of olefins. From isoprene, two oxyselenocyanated compounds which seem to be 1,2- and 3,4-addition products were obtained, but the yield was very low (<10% yield) compared to the case of butadiene. Application of the reaction to isopropenyl acetate and α-methylstyrene resulted in only a slight formation of **6**, while methyl vinyl ketone and β-methylstyrene did not react at all under the conditions described above. The reaction with allyl chloride as a substrate afforded only allyl selenocyanate (bp 80 °C/20 mmHg; lit,[7] bp 75 °C/12 mmHg) quantitatively, irrespective of the presence or absence of thallium(III) acetate. The reaction of alkyl halide with KSeCN affording alkyl selenocyanate is well-known.[8]

Experimental

The IR spectra were taken with a Hitachi EPI-S2 spectrometer in paraffin mull and KBr disc. The NMR spectra were recorded with a Varian A-60 spectrometer in CCl_4, using TMS as an internal standard. Glc analyses were carried out on a Shimadzu 5APTF apparatus, using DEGS (25%)-Shimalite(1m) column (N_2 as carrier gas).

Materials. Arylthallium (III) acetate perchlorate monohydrate[9] and ditrifluoroacetates,[10] and the alkoxythallates of styrene and α-methylstyrene[4] were prepared by the reported methods. Arylthallium(III) nitrate hydroxide was prepared by heating aromatics with $Tl(NO_3)_3 \cdot 3H_2O$ in CCl_4.[11] Commercial butadiene, $CuSO_4 \cdot 5H_2O$, and KSeCN were used without purification. Other organic materials were purified before use by distillation.

Cu(SeCN)$_2$: An aqueous (20 ml) solution of KSeCN (10.8 g, 70 mmol) was added to an aqueous (50 ml) solution of $CuSO_4 \cdot 5H_2O$ (12.5 g, 50 mmol) at room temperature to afford the black precipitates immediately. After the mixture was stirred vigorously for 0.5 hr, the black precipitates were filtered off and washed with water and methanol to afford pure $Cu(SeCN)_2$. Yield, 9 g (94% yield based on KSeCN). It turns to pale brown at 200—210 °C and decomposes at about 260—280 °C. Found: C, 8.69; N, 9.77%. Calcd for $C_2CuN_2Se_2$: C, 8.79; N, 10.25%. IR 2150 cm^{-1}.

Reaction of Arylthallium(III) Compounds with KSeCN in the Presence of $CuSO_4 \cdot 5H_2O$. The following preparation of **2** ($R^1=CH_3$, $R^2=R^3=H$), *p*-tolyl selenocyanate, shows a typical procedure. To a brown heterogeneous solution of KSeCN (5.76 g, 40 mmol) and $CuSO_4 \cdot 5H_2O$ (2.50 g, 10 mmol) in dioxane (15 ml) was added a dioxane (10 ml) solution of **1**($R^1=CH_3$, $R^2=R^3=H$, X=OAc, $Y=ClO_4 \cdot H_2O$) (2.36 g, 5 mmol) at 15—20 °C. The mixture was then refluxed for 30 min under stirring to give a black heterogeneous solution. The solution was cooled down and filtered from the dark-grey precipitates. The filtrate was added by water (150 ml) and extracted with benzene. The extract was washed with aqueous $NaHCO_3$ and dried over Na_2SO_4. Glc analysis with dibenzyl as an internal standard showed the presence of 3.4 mmol of **2** ($R^1=CH_3$, $R^2=R^3=H$) (68% yield) and 0.2 mmol of *p*-tolunitrile (4% yield). Distillation gave pure *p*-tolyl selenocyanate; bp 86 °C/2 mmHg, mp 52—53 °C (lit,[12] mp 55—56 °C). IR 2140 (ν_{SeCN}) and 804(1,4-substituted phenyl) cm^{-1}. NMR δ 2.38 (s. 3H), 7.17 (d. 2H, J=8.5 Hz), and 7.50 (d. 2H, J=8.5 Hz).

Characterization of other aryl selenocyanates is as follows. **2**($R^1=R^2=R^3=H$); bp 111 °C/8 mmHg (lit,[13] 134 °C/10 mmHg). **2**(R^1=MeO, $R^2=R^3=H$); bp 115 °C/3 mmHg, mp 61—63 °C (lit,[14] mp 65 °C). IR 2140 (ν_{SeCN}) and 823 (4-substituted phenyl cm^{-1}. NMR δ 3.77 (s. 3H), 6.85 (d. 2H, J=9 Hz), and 7.53 (d. 2H, J=9 Hz). **2** (R^1 or R^3=Cl, $R^2=H$), chlorophenyl selenocyanate (*o*-/*p*-=3/7); bp 92 °C/2 mmHg (lit,[15] *o*-isomer; bp 152–153 °C/20 mmHg, *p*-isomer; mp 55 °C). **2** ($R^1=R^2$=Me, $R^3=H$); bp 105 °C/4 mmHg. IR 2150 (ν_{SeCN}) and 802 (phenyl)cm^{-1}. NMR δ 2.24 (s. 6H) and 7.0—7.35 (m. 3H). Found: C, 51.92; H, 4.49; N, 6.67%. Calcd for C_9H_9NSe: C, 51.47; H, 4.32; N, 6.67%. **2** ($R^1=R^3$=Me, $R^2=H$); bp 96—100 °C/3.5 mmHg (lit,[16] bp 138—139 °C/5 mmHg).

Reaction of the Alkoxythallates of Styrene with KSeCN. A methanol solution (25 ml) of KSeCN (2.88 g, 20 mmol) was added to **4**($R^1=CH_3$) (2.28 g, 5 mmol) and the mixture was heated under reflux for 30 min during which period the yellow solids formed at first turned to white precipitates. The solution was cooled down and filtered from white precipitates (1.51 g, TlSeCN). The filtrate was treated as described above. Glc analysis with benzophenone as an internal standard showed the presence of 5 mmol of **5** ($R^1=CH_3$), 1-methoxy-1-phenyl-2-selenocyanatoethane (100% yield). Distillation gave pure compound; bp 150—151 °C/6.5 mmHg. IR 2150(ν_{SeCN}), 1103(ν_{C-O}), 761(phenyl), and 698(phenyl)cm^{-1}. NMR δ 3.25 (s. 3H, methoxy), 3.27 (d. 1H, J=5.5 Hz, methylene), 3.29 (d. 1H, J=7.5 Hz, methylene), 4.42 (q. 1H, J=5.5 and 7.5 Hz, methine), and 7.30 (s. 5H, phenyl). Found: C, 50.04; H, 4.76; N, 5.52%. Clacd for $C_{10}H_{11}NOSe$: C, 50.02; H, 4.62; N, 5.83%.

Characterization of the products obtained by a similar treatment with other oxythallates is as follows. **5**(R^1=Et): bp 133 °C/5 mmHg. IR 2150 (ν_{SeCN}), 1095 (ν_{C-O}), 760

(phenyl), and 700 (phenyl) cm^{-1}. NMR δ 1.17 (t. 3H, J= 7 Hz), 3.31—3.45 (m. 4H), 4.53 (q. 1H, J=5.5 and 7.5 Hz), 7.28 (s. 5H). Found: C, 52.20; H, 5.26; N, 5.38%. Calcd for $C_{11}H_{13}NOSe$; C, 52.00; H, 5.16; N, 5.51%. **5**(R^1=*n*-Pr): bp 120 °C/3 mmHg. IR 2150 (ν_{SeCN}), 1097 (ν_{C-O}), 762 (phenyl) and 700 (phenyl) cm^{-1}. NMR δ 0.92 (t. 3H, J= 7 Hz), 1.57 (sex. 2H, J=7 Hz), 3.2—3.4 (m. 4H), 4.52 (q. 1H, J=5.5 and 8 Hz), and 7.30 (s. 5H). Found: C, 53.46; H, 5.86; N, 5.05%. Calcd for $C_{12}H_{15}NOSe$: C, 53.75; H, 5.64; N, 5.22%. **5** (R^1=*i*-Pr): bp 115 °C/2.5 mmHg. IR 2150 (ν_{SeCN}), 1120 (ν_{C-O}), 1088 (ν_{C-O}), 762 (phenyl) and 700(phenyl) cm^{-1}. NMR δ 1.07 (d. 3H, J=6 Hz), 1.20(d. 3H, J=6 Hz), 3.25(d. 1H, J=5.5 Hz), 3.27 (d. 1H, J=8 Hz), 3.55 (sep. 1H, J=6 Hz), 4.66 (q. 1H, J=5.5 and 8 Hz), and 7.30 (s. 5H). Found: C, 53.72; H, 5.75; N, 5.18%. **5** (R^1=*n*-Bu): bp 121 °C/3 mmHg. IR 2150 (ν_{SeCN}), 1100 (ν_{C-O}), 762 (phenyl), and 701(phenyl) cm^{-1}. NMR δ 0.8—1.7 (m. 7H), 3.25—3.40 (m. 4H), 4.52 (q. 1H, J=5.5 and 8 Hz), and 7.30 (s. 5H). Found: C, 55.54; H, 6.25; N, 5.16%. Calcd for $C_{13}H_{17}NOSe$: C, 55.33; H, 6.07; N, 4.96%. **5**(R^1=*i*-Bu): bp 128 °C/3 mmHg. IR 2150(ν_{SeCN}), 1100(ν_{C-O}), 762(phenyl), and 700(phenyl) cm^{-1}. NMR δ 0.90 (d. 6H, J=6.5 Hz), 1.4—2.2 (m. 1H), 3.10 (d. 1H, J=5.5 Hz), 3.11 (d. 1H, J=6.5 Hz), 3.29 (d. 1H, J=5.5 Hz), 3.32 (d. 1H, J=8 Hz), 4.50 (q. 1H, J=5.5 and 8 Hz), and 7.29 (s. 5H). Found: C, 55.33; H, 6.21; N, 4.97%.

The in situ *Oxyselenocyanation of Olefins.* The following preparation of α-selenocyanatomethylcoumaran shows a typical procedure. To a suspension of $Tl(OAc)_3$ (3.05 g, 8 mmol) in methanol (10 ml) was added *o*-allylphenol (0.67 g, 5 mmol) at 15—20 °C to give a pale yellow homogeneous solution. After the solution was kept at 15—20 °C for 2 hr under stirring, a methanolic solution (15 ml) of KSeCN (2.88 g, 20 mmol) was added to give the voluminous yellow precipitates. The mixture was then rapidly heated to refluxing temperature and kept for 15 min to give the white precipitates of TlSeCN (2.2 g, 7 mmol). The reaction mixture was cooled down and treated as described above. Glc analysis with benzyl phenyl ketone as an internal standard showed the presence of 2.5 mmol of α-selenocyanatomethylcoumaran (50% yield). Distillation gave pure compound; bp 132 °C/ 2 mmHg. IR 2150 (ν_{SeCN}), 1480 (δ_{CH_2}), 1229 (ν_{C-O}), and 751(phenyl) cm^{-1}. NMR δ 2.7—3.6 (m. 2H, CH_2Se–), 3.24 (d. 2H, J=5.5 Hz, $ArCH_2$), 4.75—5.2 (m. 1H, methine), and 6.6—7.2 (m. 4H, aryl). Found: C, 50.51; H, 3.92; N, 5.79%. Calcd for $C_{10}H_9NOSe$: C, 50.45; H, 3.81; N, 5.88%.

Characterization of other oxyselenocyanatoalkanes in Table 2 is as follows. 1-Selenocyanato-2-methoxyoctane: bp 131 °C/ 6 mmHg. IR 2150 (ν_{SeCN}) and 1093 (ν_{C-O}) cm^{-1}. NMR δ 0.7—1.7 (m. 13H), 3.15—3.35 [m. 3H, –CH(OR)–CH_2Se–], and 3.35 (s. 3H, methoxy). Found: C, 48.63; H, 8.16; N, 5.60%. Calcd for $C_{10}H_{19}NOSe$: C, 48.40; H, 7.72; N, 5.64%. 1-Selenocyanato-2-methoxyhexane: bp 90 °C/4 mmHg. IR 2150 (ν_{SeCN}) and 1090 (ν_{C-O}) cm^{-1}. NMR δ 0.8—1.7 (m. 9H), 3.1—3.5 [m. 3H, –CH(OR)–CH_2Se–], and 3.36 (s. 3H, methoxy). Found: C, 43.69; H, 7.19; N, 6.38%. Calcd for $C_8H_{15}NOSe$: C, 43.65; H, 6.87; N, 6.36%. 1,1-Diethoxy-2-selenocyanatoethane: bp 81 °C/2.5 mmHg. IR 2150 (ν_{SeCN}), 1120 (ν_{C-O}), and 1060 (ν_{C-O}) cm^{-1}. NMR δ 1.21 (t. 6H, J=7 Hz, methyl), 3.21 (d. 2H, J= 5.5 Hz, $-CH_2Se$-), 3.58 (q. 2H, J=7 Hz, $-OCH_2$–), 3.62 (q. 2H, J=7 Hz, $-OCH_2$–), and 4.70 (t. 1H, J=5.5 Hz, methine). Found: C, 37.95; H, 6.13; N, 5.64%. Calcd for $C_7H_{13}NOSe$: C, 37.86; H, 5.90; N, 6.31%. 1-Acetoxy-1-ethoxy-2-selenocyanatoethane: This compound was characterized from a mixture with 1,1-diethoxy-2-selenocyanatoethane. The analysis of each component in the mixture was carried out by glc using PEG 6000(25%)-Chromosorb W(1 m) column. IR 1747($\nu_{C=O}$) cm^{-1}. NMR δ 2.10 (s. 3H, acetoxy) and 5.96 (t. 1H, methine). (CH_3– and CH_2Se– protons were not resolved.) 3-Methoxy-4-selenocyanato-1-butene: bp 83 °C/4 mmHg. IR 2150 (ν_{SeCN}), 1640 ($\nu_{C=C}$), 1100 (ν_{C-O}), 990 (vinyl), and 938 (vinyl)cm^{-1}. NMR δ 3.19 (d. 1H, J=7 Hz, methylene), 3.20 (d. 1H, J=6 Hz, methylene), 3.30 (s. 3H, methoxy), 3.87 (q. 1H, J=6.5 Hz, methine), and 5.1—6.0 (m. 3H, vinyl). Found: C, 37.77; H, 4.89; N, 7.20%. Calcd for C_6H_9NOSe: C, 37.92; H, 4.77; N, 7.37%.

References

1) a) K. Ichikawa, Y. Ikeda, and S. Uemura, *Chem. Commun.*, **1971**, 169. b) S. Uemura, Y. Ikeda, and K. Ichikawa, *Tetrahedron*, **28**, 3025 (1972). c) S. Uemura, Y. Ikeda, and K. Ichikawa, *ibid.*, **28**, 5499 (1972). d) S. Uemura, S. Uchida, M. Okano, and K. Ichikawa, This Bulletin, **46**, 3254 (1973).

2) S. Uemura, H. Tara, M. Okano, and K. Ichikawa, *ibid.*, **47**, 2663 (1974).

3) H. Mitani, T. Ando, and Y. Yukawa, *Chem. Lett.*, **1972**, 455.

4) S. Uemura, K. Zushi, A. Tabata, A. Toshimitsu, and M. Okano, This Bulletin, **47**, 920 (1974).

5) O. Behaghel and H. Seibert, *Ber.*, **65**, 812 (1932).

6) C. L. Jenkins and J. K. Kochi, *J. Org. Chem.*, **36**, 3095 (1971).

7) H. Brintzinger, K. Pfannstiel, and H. Vogel, *Z. Anorg. Allg. Chem.*, **256**, 85 (1948).

8) "Methoden der Organischen Chemie," (Houben-Weyl), Vol. 9, ed. by E. Müller, Georg Thieme Verlag, Stuttgart (1955), pp. 939—942.

9) K. Ichikawa, S. Uemura, T. Nakano, and E. Uegaki, This Bulletin, **44**, 545 (1971).

10) A. McKillop, J. D. Hunt, M. J. Zelesko, J. S. Fowler, E. C. Taylor, G. McGillivray, and F. Kienzle, *J. Amer. Chem. Soc.*, **93**, 4841 (1971).

11) S. Uemura, A. Toshimitsu, and M. Okano, unpublished data.

12) F. Challenger, A. T. Peters, and J. Halévy, *J. Chem. Soc.*, **1926**, 1648.

13) F. Challenger and A. T. Peters, *ibid.*, **1928**, 1364.

14) O. Behaghel and M. Rollman, *J. Prakt. Chem.*, **123**, 336 (1929).

15) O. Behaghel and H. Seibert, *Ber.*, **66**, 708 (1933).

16) L. Chierici and R. Passerini, *Boll. Sci. Fac. Chim. Ind. Bologna*, **12**, 131 (1954); *Chem. Abstr.* **49**, 6868h (1955).

Behaviour of Some Selenium Bases in Disulphuric Acid. Conductometric and Cryoscopic Studies of Selenides, Selenoxides and Selenones in Disulphuric Acid

Ashok BALI and K. C. MALHOTRA

Department of Chemistry, Himachal Pradesh University, Simla 171001, India

(Received August 23, 1974)

Dimethylselenoxide is fully ionized in disulphuric acid whereas diphenyl selenoxide and its nitro derivatives behave as weak bases. In the case of selenones, alkyl selenones are completely ionized in disulphuric acid, diphenyl selenone and its nitro derivatives behave as weak electrolytes. From the extent of protonation it is observed that selenones are stronger bases than the corresponding sulphones. Amongst the selenides, diphenyl selenide is sulphonated whereas its nitro derivatives behave as weak bases in it.

In a continuation of our investigations,[1-5] we report here a study on the behaviour of selenides and compounds containing selenium–oxygen bonds in disulphuric acid. These data may be helpful in determining their relative basic strengths and also in determining their basicity with respect to sulphones. Szmant and Lapinski[6] and Szmant and Brost,[7] from their cryoscopic and spectroscopic studies on diphenyl sulphoxide in sulphuric acid concluded that it formed diphenyl sulphedium ion. This conclusion has been refuted by various workers.[8-9] Most alkyl sulphones behave as non electrolytes in sulphuric acid[9] and are protonated in disulphuric acid,[10] consequently their relative strengths have been differentiated in fluorosulphuric acid.[11] In the present study, the behaviors of selenides, selenoxides and selenones have been investigated and comparative studies with the analogous sulphur compounds have been made.

Results and Discussion

Disulphuric acid is a molecularly dissociated and slightly self ionized solvent. Its mode of dissociation and ionization may be represented[12] as in Eq. (1).

$$2H_2S_2O_7 \longrightarrow H_2SO_4 + H_2S_3O_{10} \rightleftharpoons H_3SO_4^+ + HS_3O_{10}^- \quad (1)$$

Because of its high acidic nature, most of the solutes behave as bases in it. The behaviour of a base in disulphuric acid may be represented by the general Eq. (2).

$$\text{Solute} + sH_2S_2O_7 \longrightarrow aX^+ + aHS_3O_{10}^- + bY + cH_2SO_4 \quad (2)$$

where Y represents uncharged species. Sulphuric acid formed in the reaction does not contribute significantly to the value of γ, the number of $HS_3O_{10}^-$ ions, or to ν, the number of particles or ions produced per mole of solute as it is one of the products of self dissociation of the acid. Methods of determining the values of γ, ν and c have been discussed in detail in the experimental section.[10,11,13-15] In the case of the compounds which are not fully protonated in disulphuric acid, dissociation constants have been determined by a method, already used by various workers.[16,17]

Interpolated values of the specific conductance and the depression in freezing points of various solutes at different concentrations are given in Tables 1 and 2 respectively. The dissociation constants for solutes which are not fully ionised have been determined and are reported in Table 4. In order to compare the relative basic strength of selenium compounds with those of sulphur compounds, dissociation constants previously reported for sulphur compounds are also included in Table 4.

Like dimethyl sulphoxide, dimethyl selenoxide is stable in disulphuric acid and forms a highly conducting stable solution. From the values of γ, ν, and c, it is evident that it is completely protonated as:

$$(CH_3)_2SeO + 2H_2S_2O_7 \longrightarrow (CH_3)_2SeOH^+ + HS_3O_{10}^- + H_2SO_4 \quad (3)$$

The solutions are colourless which suggests that there is no disproportionation to form elemental selenium which would have produced a green or yellow solution.[18] But in the case of diphenyl selenoxide, conductances of the solutions are quite low and increase

TABLE 1. SPECIFIC CONDUCTANCES OF SOLUTIONS OF VARIOUS SOLUTES IN DISULPHURIC ACID AT 25 °C

Specific Conductance $\times 10^3$ (ohm^{-1} cm^{-1})

Solute	Molality $\times 10^2$								
	2	4	6	8	12	14	16	18	20
Dimethyl selenoxide	4.186	4.703	5.342	5.983	6.932	7.689	8.324	9.164	9.866
Diphenyl selenoxide	3.824	3.958	4.088	4.390	4.713	5.127	5.396	5.682	5.27
4′-Nitrodiphenyl selenoxide	3.952	4.386	4.624	4.936	5.292	5.634	6.012	6.824	7.397
4,4′-Dinitrodiphenyl selenoxide	3.908	4.214	4.438	4.729	5.032	5.724	5.938	6.318	6.874
Dimethyl selenone	4.187	4.704	5.343	5.984	6.938	7.701	8.324	9.165	9.867
Diethyl selenone	4.186	4.703	5.344	5.983	6.937	7.698	8.326	9.164	9.866
4-Nitrodiphenyl selenone	3.964	4.392	4.701	5.014	5.438	5.826	6.134	7.012	7.523
4,4′-Dinitrodiphenyl selenone	3.987	4.362	4.582	4.864	4.986	5.598	5.762	6.468	6.682

Table 2. Freezing points of solutions of various solutes in disulphuric acid (°C)

Solute	Molality $\times 10^2$									
	2	4	6	8	10	12	14	16	18	20
Dimethyl selenoxide	34.82	34.76	34.64	34.58	34.46	34.32	34.26	34.18	34.06	33.92
Diphenyl selenoxide	35.06	35.02	34.98	34.86	34.80	34.76	34.68	34.58	34.49	34.36
4′-Nitrodiphenyl selenoxide	35.01	34.92	34.84	34.76	34.70	34.62	34.54	34.46	34.32	34.18
4,4′-Dinitrodiphenyl selenoxide	35.04	34.98	34.86	34.79	34.70	34.62	34.58	34.48	34.38	34.24
Dimethyl selenone	34.82	34.75	34.64	34.58	34.45	34.31	34.24	34.16	34.02	33.89
Diethyl selenone	34.81	34.76	34.62	34.56	34.44	34.30	34.26	34.12	34.04	33.88
Diphenyl selenone	35.06	35.03	34.96	33.84	34.76	34.66	34.58	34.46	34.32	33.92
4-Nitrodiphenyl selenone	35.02	34.96	34.84	34.80	34.72	34.64	34.52	34.42	34.36	34.24
4,4′-Dinitrodiphenyl selenone	34.98	34.88	34.78	34.70	34.64	34.56	34.48	34.39	34.29	34.18

with time. Simultaneously the solutions develop a dirty brown color but when the solutions are poured onto crushed ice, nothing separates out. This suggests that diphenyl selenoxide is sulphonated and the sulphonated product behaves as a weak base. A slight increase in the conductance of the solution is due to the formation of sulphuric acid which is known to behave as a weak base in disulphuric acid (*loc. cit.*). There has been no indication of the existence of dipositive selenidium ions as was proposed by Szmant and Lapanski for sulphoxide (*loc. cit.*) since that would have produced highly conducting solutions.

Table 3. Summary of the values of γ, ν and c for various selenium compounds in $H_2S_2O_7$

Compound	γ	ν	c		
			Conductivity	Cryoscopy	Titration
Dimethyl selenoxide	1	2	1	1.1	1
Diphenyl selenoxide	—	1	1	—	1
Dimethyl selenone	1	2	1	1.1	1.1
Diethyl selenone	1	2	1	1.1	1.1
Diphenyl selenone	1	2.1	1	1.1	1.1
p-Nitrophenyl selenide	1	2	—	—	—
Selenyl chloride	—	1	—	—	—
Selenyl fluoride	—	1	—	—	—

Table 4. Dissociation constants of various compounds containing sulphur–oxygen and selenium–oxygen bond in disulphuric acid

Compound	$K_b \times 10^2$
4-Nitrodiphenyl sulphoxide	86.42
4-Nitrodiphenyl selenoxide	92.38
4,4′-Dinitrodiphenyl sulphoxide	49.56
4,4′-Dinitrodiphenyl selenoxide	63.74
4-Nitrodiphenyl sulphone	78.46
4-Nitrodiphenyl selenone	82.58
4,4′-Dinitrodiphenyl sulphone	60.92
4,4′-Dinitrodiphenyl selenone	72.54

The introduction of an electron withdrawing group in one of the rings deactivates both of the rings towards sulphonation as 4-nitrodiphenyl selenoxide gives a stable pink solution in disulphuric acid. The conductance and the freezing point of the solution do not change with time. From the cryoscopic and conductance studies, it is evident that it behaves as a weak base. The dissociation constant is reported in Table 4. The introduction of a nitro group in the other ring further reduces the basicity of the Se–O group as is evident from the behavior of 4,4′-dinitrodiphenyl selenoxide, which in disulphuric acid forms an orange colored solution that becomes darker with time. However, there is no significant change with time in the values of γ, ν and c indicating that the solutions are fairly stable. From the experimental data it is evident that 4,4′-dinitrodiphenyl selenoxide behaves as a weak base. When solutions of both the mono- and di-nitro compounds are poured onto crushed ice, both the compounds are recovered quantitatively suggesting that in these compounds there is no sulphonation of the ring. From the cryoscopic and conductance data only, we do not feel qualified to specify the site of the protonation in these compounds. However, it may be reasonable to believe that the π electrons in the Se=O group are more labile and therefore the Se=O group will be protonated in preference to the ring NO_2 group. From the extent of the protonation of selenoxides, it is evident that selenoxides are more basic than sulphoxide *i.e.* the extent of the $d\pi$-$p\pi$ overlap between sulphur and oxygen is more than that between selenium and oxygen and consequently sulphoxide are less basic.

Alkyl sulphones are known to behave as weak electrolytes in sulphuric acid[9] but behave as strong bases in both fluorosulphuric[11] and disulphuric acids.[10] Dimethyl and diethyl selenones are monoprotonated and completely ionized in disulphuric acid. Becasue of the higher acid strength of the medium, the basicity of all these alkyl selenones is leveled to that of $HS_3O_{10}^-$ and it does not seem to be possible to differentiate their relative basicity. It is also observed that as compared to diphenyl selenoxide, diphenyl selenone is more stable towards sulphonation by the solvent as the conductance and the freezing point of the solutions do not change with time. It may be that unlike selenone, the deactivating inductive effect of the selenoxide group is counter balanced by the conjugation of the shared pairs of electrons on the selenium atom with the aromatic ring. Conjugation of the Se=O with the aromatic ring may be negligible and therefore diphenyl selenoxide undergoes sulphonation whereas the selenones are comparatively stable.

From the conductance and cryoscopic studies, it is evident that diphenyl selenone bahaves as a strong base

and the introduction of a deactivating group in one or both of the rings decreases the basicity of the Se=O group to a large extent as 4-nitro- and 4,4′-dinitrodiphenyl selenones behave as weak bases in disulphuric acid. Their dissociation constants have been determined and are included in Table 4. Our observations are at varience with those of Szmant and Lapinski (*loc. cit.*) who observed that the introduction of a nitro group in the *para* position of the ring increases the basicity of the SO group in sulphones and are in agreement with our earlier observations in fluorosulphuric acid. These observations are supported by the results of a theoretical molecular orbital treatment of sulphones by Koch and Moffitt[19] who have shown that there is only a slight conjugation between the double bond of S=O and the aromatic ring in diphenyl sulphone. This conclusion is supported by IR and UV spectroscopic measurements. By analogy similar arguments can be put forward for selenones.

In order to compare the basicity of compounds containing the selenium–oxygen bond and to determine the effects of substitution on their basicity, investigations have been extented to the behavior of SeO_2Cl_2, SeO_2F_2 and diethyl selenate in disulphuric acid. It is interesting to observe that the value of ν for these electrolytes is one, but there is a decrease in the conductance of the solution. This suggests that these compounds behave as non-electrolytes in disulphuric acid. This behaviour of non-electrolytes is similar to the one observed in the solvo-system sulphuric acid.[20] This decrease in the conductance of the solution may be attributed to a decrease in the mobilities of $H_3SO_4^+$ or $HS_3O_{10}^-$ ions caused by the non-electrolyte or to a reduction in the concentration of the autoprotolysis ion. A decrease in the mobilities of the characteristic solvent ions could be attributed to strong hydrogen bonding interactions between these solutes and the solvent molecules which would hinder the orientation of the latter and decrease their effectiveness in the proton-transfer conduction process. Diethyl selenate behaves as a weak base. The increase in the conductance is so insignificant that it is not possible to determine its dissociation constant.

It has been of interest to investigate the behaviour of selenides in disulphuric acid. Sulphides undergo sulphonation and oxidation in both sulphuric and disulphuric acids but in fluorosulphuric acid they are strong bases. The solutions of diphenyl selenides in disulphuric acid are not very stable as the solutions are green and the conductance of the solution changes with time. Even *p*-nitrophenyl selenide does not form stable solutions when dissolved in disulphuric acid. However, initial conductance and freezing point data indicate that it may be singly protonated. For each addition of the solute the changes in the conductance and freezing point have been observed with time and then extrapolated to zero time to get the initial conductance and freezing point. The introduction of a nitro group to each of the rings decreases the basicity of the selenide group to the extent that 4,4′-dinitrodiphenyl selenide behaves as a weak electrolyte. The solutions become intensely coloured. The intensity of the colour increases very much after 24 hr although there is no significant change in the conductance of the solution. The properties may be due to the presence of a quinonoid structure for the protonated species.

It may thus be concluded that compounds containing selenium–oxygen bonds are more basic than the corresponding compounds containing sulphur–oxygen bonds. Thus suggesting that the extent of $d\pi$-$p\pi$ overlap is greater in the sulphur–oxygen compounds than in the selenium–oxygen compounds.

Experimental

The design of the conductivity cell and the cryoscopic set up has been described earlier. Conductance measurements were made in an oil thermostat regulated at 25.00 ± 0.02 °C using a precision measuring bridge WBR No. 108 with logarithmic indicator amplifier type TAV, IKC No. 034 (Wissenchaftlich Technische Werkstatten) Wielheim Oby/ Germany. The composition of disulphuric acid was determined from its conductance in conductometric studies and from its freezing point in the cryoscopic studies. Addition of powdered solids was made with a weight burette having a wide bore tap while liquids were added with a weight dropper which was fitted with quickfit joints to avoid contact with moisture.

The conductometric factors γ ($HS_3O_{10}^-$) were obtained by comparison of the conductance at various concentrations of the solute with that of nitromethane in disulphuric acid. The temperature at which all conductance measurements were made (25 °C) was below the freezing point of all the solutions studied but since disulphuric acid super cools readily no problems were encountered with spontaneous crystallization of the solutions during the measurements.

In the case of the cryoscopic measurements, the observed freezing points were corrected for the super cooling by adding the correction ($\delta=0.014S\theta$) where S is the amount of super cooling and θ is the depression of the freezing point. The value of ν (the number of particles or ions produced per mole of the solute) has been calculated by equation:

$$\nu = \frac{\theta(1-0.178mS)}{5.9m}$$

where m is the molality, S is the number of the solvent molecules used and θ is the depression of the freezing point obtained by subtracting the observed freezing points from 35.82° which is the freezing point of a hypothetical solvent containing zero concentration of ionic self dissociation products. The factor c, the amount of sulphuric acid produced per mole of the solute has been found out by titrating these solutions against sulphur trioxide. Freezing point rises because of the reaction $H_2SO_4+SO_3\rightarrow H_2S_2O_7$, passes through a maximum and then decreases. The maximum in the freezing point represents the number of moles of sulphuric acid produced in a particular reaction. This technique has already been used by Wyatt and Dacre.

Dimethyl selenoxide was purified by fractional distillation under reduced pressure. Diphenyl selenoxide was prepared by the oxidation of diphenyl selenide with an equimolar amount of a 30% solution of hydrogen peroxide in glacial acetic acid. 4-Nitro- and 4, 4′-dinitro-diphenyl selenoxide were prepared by the oxidation of the corresponding selenides which in turn were prepared by refluxing ethanol solution of 1-chloro-4 nitrobenzene with freshly prepared concentrated solution of sodium selenide. The compounds were recrystallized from acetic acid. Diethyl selenone (Aldrich) was

purified by several recrystallization from absolute alcohol. 4-Nitro- and 4,4′-dinitro-diphenyl selenones were prepared by the oxidation of the corresponding selenoxides with an excess of 30% H_2O_2 in acetic acid. Alkyl selenates were purified by distillation under reduced pressure.

References

1) R. C. Paul, V. P. Kapila, and K. C. Malhotra, *J. Chem. Soc., A*, **1970**, 2267.
2) R. C. Paul, J. K. Puri, V. P. Kapila, and K. C. Malhotra, *J. Inorg. Nucl. Chem.*, **34**, 2141 (1972).
3) K. C. Malhotra and R. D. Sharma, *Ind. J. Chem.*, **10**, 430 (1972).
4) R. C. Paul, V. P. Kapila, J. K. Puri, and K. C. Malhotra, *ibid.*, **9**, 992 (1971).
5) K. C. Malhotra and S. M. Sehgal, *ibid.*, **12**, 1190 (1974).
6) H. H. Szmant and R. L. Lapinski, *J. Amer. Chem. Soc.*, **74**, 4395 (1952).
7) H. H. Szmant and G. A. Brost, *ibid.*, **74**, 5175 (1952).
8) R. J. Gillespie and R. C. Passerni, *J. Chem. Soc.*, **1956**, 3850.
9) S. K. Hall and E. A. Robinson, *Can. J. Chem.*, **42**, 1113 (1964).
10) R. C. Paul, J. K. Puri, and K. C. Malhotra, *J. Inorg. Nucl. Chem.*, **33**, 991 (1971).
11) K. C. Malhotra, S. K. Sharma, and K. K. Paul, *Ind. J. Chem.*, **9**, 250 (1971).
12) R. J. Gillespie and K. C. Malhotra, *J. Chem. Soc., A*, **1967**, 1994.
13) R. J. Gillespie and K. C. Malhotra, *ibid.*, **1968**, 1933.
14) R. C. Paul, D. Singh, and K. C. Malhotra, *ibid.*, **1969**, 1396.
15) R. J. Gillespie and K. C. Malhotra, *Inorg. Chem.*, **8**, 1751 (1969).
16) R. C. Paul, V. P. Kapila, J. K. Puri, and K. C. Malhotra, *Ind. J. Chem.*, **9**, 469 (1971).
17) R. C. Paul, V. P. Kapila, J. K. Puri, and K. C. Malhotra, *J. Chem. Soc., A*, **1971**, 2132.
18) J. Barr, R. J. Gillespie, R. Kapoor, and K. C. Malhotra, *Can. J. Chem.*, **46**, 149 (1969).
19) H. P. Koch and W. E. Moffitt, *Trans. Faraday Soc.*, **47**, 7 (1951).
20) R. J. Gillespie and C. Solomons, *J. Chem. Soc.*, **1957**, 1796.

Mössbauer and Magnetic Study of Mononuclear and Oxo-bridged Binuclear Iron(III) Complexes of 1,10-Phenanthroline and 2,2′-Bipyridine

V. K. GARG*, P. G. DAVID**, Takao MATSUZAWA***, and Teruya SHINJO***

*Department of Physics, University of Brasilia, Brasilia, Brazil

**Department of Chemistry, University of Brasilia, Brasilia, Brasil

***Institute for Chemical Research, Kyoto University, Kyoto 611

(Received October 28, 1974)

The oxo-bridged binuclear iron(III) complexes $[L_2(NCS)Fe–O–Fe(NCS)L_2]^{2+}$ (L=1,10-phenanthroline or 2,2′-bipyridine) were prepared recently in spite of the earlier report that they could not be prepared. The unperturbed and perturbed Mössbauer spectral and magnetic susceptibility data on these compounds are reported here and compared with those for the well characterized oxo-bridged compounds $[L_2XFe–O–FeXL_2]^{2+}$ (X= Cl^-, Br^-, $SO_4^{2-}/2$ or NO_3^-). The effect of Fe–X bond (X=Cl^-, Br^-, $SO_4^{2-}/2$, NO_3^-, or NCS^-) on the Mössbauer parameters was investigated, and the results are discussed in terms of the bonding properties of these anionic ligands. The data indicate that the electronegativity of the X ligands has no significant effect on the Mössbauer parameters. Another system, the mononuclear iron(III) complexes $[FeL_2(NCS)_2](NCS)$, investigated in this work showed no Mössbauer resonance at or above 223 K and below this temperature the unperturbed spectra exhibited a broad asymmetric singlet. Magnetic susceptibilities and magnetically perturbed Mössbauer spectra indicated that iron(III) ion in these mononuclear complexes was paramagnetic with $S=5/2$.

The Mössbauer parameters of isomer shift (*I.S.*) and quadrupole splitting (*Q.S.*) have been utilized in elucidating the structure and bonding in a large series of organometallic and coordination compounds.[1–6] Mössbauer studies have indicated that *I.S.* values are an approximate additive property of the type and number of ligands, and Erickson[7] has suggested a relative covalency scale. The *Q.S.* values provide complementary information on the nature of σ- and π-bonding in low-spin and high-spin compounds.

Binuclear complex of iron(III) with 1,10-phenanthroline (phen) or 2,2′-bipyridine (bipy), $[Fe_2L_4OCl_2]Cl_2$ (L=phen or bipy) has been of considerable interest since its first isolation by Gains *et al.*[8] It is now established that these complexes contain a linear Fe–O–Fe bridge[9–12]. Mössbauer studies on binuclear complexes $[Fe_2(phen)_4OX_2]X_2\cdot YH_2O$ (X=Cl^-, Br^- or $SO_4^{2-}/2$; $Y=2$—7) have been reported[4,10,12] while only one bipy complex, $Fe_2(bipy)_4O(SO_4)_2\cdot 9H_2O$ has received attention[4,10].

The exchange of Cl^- ligands in $[Fe_2L_4OCl_2]^{2+}$ by SO_4^{2-}, ClO_4^-, and Br^- to form $[Fe_2L_4X_2]^{2+}$ (where X=$SO_4^{2-}/2$, ClO_4^-, or Br^-) has been described.[9,13a,14] But it was reported by Driver and Walker[14] that an attempt to prepare $[Fe_2(phen)_4O(NCS)_2]^{2+}$ by analogous procedure resulted in the reduction product $Fe(II)(phen)_2(NCS)_2$. David[13] recently investigated in detail the reaction between $[Fe_2L_4OCl_2]^{2+}$ and NCS^- and reported that the observations of Driver and Walker were incorrect. David[13] prepared the binuclear complexes $[Fe_2L_4O(NCS)_2](NCS)_2$. We report here the Mössbauer spectral and magnetic susceptibility data on these compounds. The present data are in firm support of the conclusions reached earlier by David[13] based on electronic and infrared spectral data, and conductivity studies. Further, the Mössbauer spectral and magnetic susceptibility data for these compounds are in fair agreement with those reported for similar oxo-bridged binuclear compounds.

The effect of the anionic ligand X^- on the Mössbauer spectra of the binuclear complexes $[Fe_2L_4OX_2]X_2$ (where X=Cl^-, Br^-, $SO_4^{2-}/2$, NO_3^-, or NCS^-) are also presented here. Preparations of these anhydrous compounds have been reported recently. Even though Mössbauer investigation on a few of these complexes has been carried out,[4,10,12] there has been no systematic study to decide on the effect of the bonding properties of these anionic ligands on the Mössbauer parameters.

Yet another purpose of this article is to present data on Mössbauer spectra and magnetic susceptibility on the mononuclear iron(III) complexes $[FeL_2(NCS)_2]NCS$. The preparations of these compounds were reported recently by David and were characterized to be iron(III) compounds based on electronic and infrared spectral data and conductivity studies. Our Mössbauer and magnetic susceptibility data confirmed the conclusions of David while proving to be incorrect the earlier report of Driver and Walker that reduction of iron(III) to iron(II) occured during the attempted preparation of $[FeL_2(NCS)_2]^+$.

Experimental

Preparations. The following binuclear and mononuclear complexes were prepared by literature procedures: $Fe_2(phen)_4OCl_4$,[8] $Fe_2(phen)_4OBr_4$,[14] $Fe_2(phen)_4O(SO_4)_2$,[14] $Fe_2(phen)_4O(NO_3)_4$,[9] $Fe_2(phen)_4O(NCS)_4$,[13] $Fe_2(bipy)_4OCl_4$,[13] $Fe_2(bipy)_4OBr_4$,[13] $Fe_2(bipy)_4O(SO_4)_2$,[14] $Fe_2(bipy)_4O(NCS)_4$,[13] $Fe(phen)_2(NCS)_3$,[13] and $Fe(bipy)_2(NCS)_3$.[13] All these complexes were dried at room temperature in a vacuum desiccator for 3—5 days to effect complete removal of water of hydration.

The compound $Fe_2(bipy)_4O(NO_3)_4$ was prepared by a modification of the method used for the corresponding phen complex. In this procedure 2.34 g (0.015 mol) of 2,2′-bipyridine was added to a solution containing 3.03 g of $Fe(NO_3)_3\cdot 9H_2O$ (0.0075 mol) in 20 ml of water. The resulting dark brown solution was nearly saturated with sodium nitrate. The solution was filtered and the filtrate cooled in a refrigerator for 2—3 days, during which time dark brown crystals of $Fe_2(bipy)_4O(NO_3)_4$ separated out. The crystals were collected by filtration, washed with small quantities of ice-cold water

followed by *n*-hexane, and dried at room temperature in a vacuum desiccator.

Found: C, 47.40; H, 3.22; N, 16.60; Fe, 10.88%. Calcd for $Fe_2O(C_{40}N_8H_{32})(NO_3)_4$: C, 47.27; H, 3.17; N, 16.53; Fe, 10.98%.

Methods. The Mössbauer spectra were recorded in the standard transmission geometry with a constant acceleration Doppler velocity transducer, ^{57}Co in copper, and Ar–CH_4 filled proportional counter, and a 400 channel analyser. The data were least square fitted. To avoid possible corrections of solid angle, fairly small distance of detector-to-absorber, and large distance of source-to-absorber of the order of four times the window for detection were used. The velocity scale of the spectrometer was calibrated using an enriched iron foil. For calibration of temperature a copper-constantan thermocouple was used. For low temperature spectra in external magnetic field a Westinghouse superconducting solenoid with a stainless steel cryostat was used.

Magnetic susceptibility measurements were made with a torsion balance type magnetometer, Shimadzu MB-2, equipped with cryostatic arrangements for low temperature measurements.

Infrared spectra were recorded using a Perkin-Elmer 237 grating spectrophotometer. The samples were in the form of Nujol mulls. The potassium bromide disk method was considered but rejected owing to the possibility of exchange of the anionic ligands with Br^- which may lead to ambiguous results.

Results and Discussion

Binuclear Complexes. The binuclear oxygen-bridged complexes I—X (Table 1) are octahedral, the oxygen sharing the two octahedra. The presence of an oxygen bridge has been supported by infrared spectra.[10,15] It is known that in the solid phase $Fe_2L_4OX_4$ (X=Cl^-, NO_3^-, or $SO_4^{2-}/2$) exhibits an effective paramagnetic moment of the order of 1.5 B.M. per iron indicating the ground state multiplicities of iron(III) ions to be either $S=5/2$ corresponding to the d^5 high-spin configuration in the octahedral symmetry or $S=3/2$ corresponding to an electronic configuration $t_{2g}^4 e_g^1$ in octahedral symmetry.[9,10] Simple magnetic data do not clearly indicate the spin state $S=3/2$ or

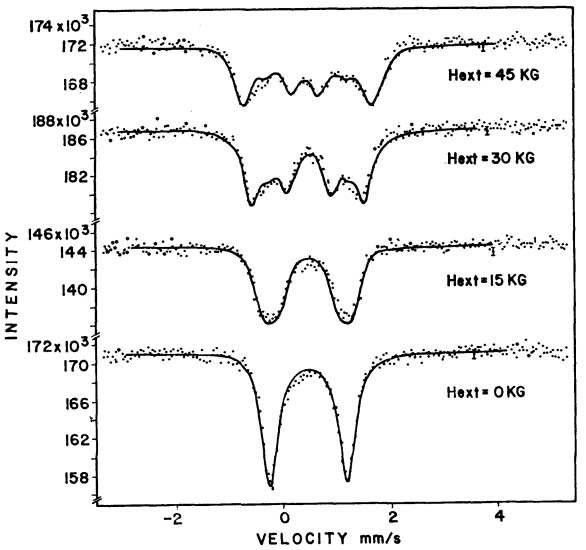

Fig. 1. Mössbauer spectra of $Fe_2(bipy)_4O(NCS)_4$ in externally applied magnetic fields at 4.2 K. The solid lines are the theoretical best fit curve for $\eta=1.0$ and $H_{ext}=H_{int}$.

Table 1. Mössbauer parameters

	Compound	Temperature (K)	*I.S.*/Fe (mm/s)	*Q.S.* (mm/s)	Γ (mm/s)
I	$Fe_2(phen)_4O(NCS)_4$	77	0.50±0.03	1.43±0.04	0.65
		4.2	0.81±0.14	1.52±0.14	
II	$Fe_2(phen)_4OCl_4$	300	0.36±0.02	1.65±0.02	0.24
		77	0.46±0.02	1.70±0.02	0.27
III	$Fe_2(phen)_4OBr_4$	300	0.43±0.02	1.62±0.02	
		77	0.50±0.02	1.62±0.02	
IV	$Fe_2(phen)_4O(SO_4)_2$	300	0.40±0.02	1.52±0.02	
		77	0.52±0.02	1.60±0.02	
V	$Fe_2(phen)_4O(NO_3)_4$	300	0.36±0.02	1.45±0.24	
		77	0.47±0.02	1.48±0.24	
VI	$Fe_2(bipy)_4O(NCS)_4$	77	0.50±0.02	1.23±0.02	0.36
		4.2	0.60±0.02	1.67±0.02	0.44
VII	$Fe_2(bipy)_4OCl_4$	300	0.37±0.02	1.48±0.02	
		77	0.47±0.02	1.52±0.02	
VIII	$Fe_2(bipy)_4OBr_4$	300	0.36±0.02	1.60±0.02	
		77	0.51±0.02	1.60±0.02	
IX	$Fe_2(bipy)_4O(SO_4)_2$	300	0.41±0.02	1.31±0.02	
		77	0.49±0.02	1.45±0.02	
X	$Fe_2(bipy)_4O(NO_3)_4$	300	0.37±0.02	1.48±0.02	
		77	0.48±0.02	1.50±0.02	
XI	$Fe(phen)_2(NCS)_3$	77	0.55±0.03		0.62
		4.2	0.55±0.02		0.80
		1.3	0.52±0.20		0.60
XII	$Fe(bipy)_2(NCS)_3$	77	0.34±0.02		0.72
		4.2	0.55±0.01		0.80
		1.3	0.46±0.01		0.60

$S=5/2$. But recent NMR contact shift,[13] Mössbauer,[10,16,17] and ESR[18] data have been interpreted to support that both iron(III) ions in the binuclear complexes are high-spin ($S=5/2$). The two $S=5/2$ ground state ions couple, through the intramolecular π-bonding interaction of the two oxygen p-orbitals and the metal d_{xz} and d_{yz} orbitals, to form a singlet ground state ($S=0$) for the complex as a whole. Our Mössbauer results in external magnetic field give further support to this singlet ground state (see below).

The effect of an external magnetic field on the Mössbauer spectra of the binuclear complex VI is shown in Fig. 1. All other binuclear complexes investigated in the present study shows similar effects in an external magnetic field. Similar study on $[Fe_2(salen)_2O]$, a compound similar to those investigated in our work, was carried out by Okamura *et al.*[19] They assigned a positive electric field gradient to their compound conforming to the observation that the quadrupole split lines underwent further splitting in the external field, one at the low velocity into a triplet and the other at the higher velocity into a doublet. In our oxo-bridged compounds the low velocity and the high velocity peaks split further into doublets in the external magnetic fields (Fig. 1) giving rise to a nearly symmetrical spectrum. Hence, the assignment of the sign to the electric field is not feasible. The nearly symmetrical spectrum may arise from the large asymmetry parameter.[20] The least square fit curves assuming $\eta=1.0$ and $H_{ext}=H_{int}$ closely approximate the experimental points, thus conforming to the asymmetry parameter close to 1.0.

The observed field in all our binuclear complexes is equal to the externally applied one within the experimental error of ±5.0 KG. Even if the moment for each iron(III) ion is 1 B.M., the internal field would be observable when the external field is close to 45 KG at 4.2 K. Hence, this is a clear evidence for the singlet ground state in these binuclear complexes, in agreement with the previous studies.[9,10,12]

In the solid phase the binuclear complexes have the structure $[L_2XFe\text{–}O\text{–}FeXL_2]^{2+}$ ($X=Cl^-$, NO_3^-, SO_4^{2-}/2, or NCS^-). The evidence for the coordination of these X ligands to iron(III) is obtained from the infrared spectral data. Khedekar *et al.*[9] observed the Fe–Cl stretching vibrations at 253 cm^{-1} in the infrared spectrum of $Fe_2(phen)_4OCl_4$, while our results in Table 2 prove the existence of coordination between iron(III) and the anionic ligands NO_3^-, SO_4^{2-}, and NCS^-. Our results are in fair agreement with the literature results for compounds containing coordinated NO_3^-, SO_4^{2-}, or NCS^- to metal.[21–24] There is no experimental evidence for the coordination of Br^- to iron(III) in the binuclear compound $Fe_2L_4OBr_4$. But considering the coordination of weak ligands like NO_3^- to iron(III) we tend to believe that Br^- is also coordinated.

Table 2. Infrared vibrartional frequencies of the anionic ligands

Compound	Anionic Ligand	$\bar{\nu}$, cm^{-1}
$Fe_2(phen)_4O(SO_4)_2$	SO_4^{2-}	1173(s), 1035(s), 975(s)[a]
$Fe_2(bipy)_4O(SO_4)_2$	SO_4^{2-}	1160(s), 1039(s), 930(s)[a]
$Fe_2(phen)_4O(NO_3)_4$	NO_3^-	1280(s, b), 1030(v, s)[a]
$Fe_2(bipy)_4O(NO_3)_4$	NO_3^-	1500(s),[a,b] 1282(s, b), 1010(v, s)[a]
$Fe_2(phen)_4O(NCS)_4$	NCS^-	2080(s, sh),[a] 2040(s)
$Fe_2(bipy)_4O(NCS)_4$	NCS^-	2080(s, sh),[a] 2040(s)

s=strong, v=very, b=broad, sh=shoulder
a) These peaks clearly indicate the presence of coordination of these anionic ligands to iron(III). b) This peak was partially obscured by the Nujol peaks.

The Mössbauer parameters for the binuclear complexes in which the anionic ligands are Cl^-, Br^-, NO_3^-, SO_4^{2-}, or NCS^- are depicted in Table 1. Within the experimental uncertainty the *I.S.* values do not show any appreciable change with the variation of the anionic ligands. By virtue of the strong antiferromagnetic coupling through the π-bonding interaction of the metal d-orbitals and the p-orbitals of O^{2-} the change in bonding properties, if any, of the X ligands may not have any significant effect on the Mössbauer parameters. The bonding is influenced by the combined effects of the electronegativity and the resonance of the X ligands concerned. While the electronegativity may fall in the order $Cl^->Br^->SO_4^{2-}>NO_3^->NCS^-$, the last named three ligands can withdraw electrons away from the coordination site by virtue of the resonance effects. The failure of these ligands to influence the *I.S.* values to any appreciable extent suggests that the electron density at the metal due to the (L→M) σ-donation is essentially identical.

The replacement of phen by bipy does not change the *I.S.* values and the π-back bonding of iron to both O^{2-} and bipy ligands (Table 1). Comparing the phen complex to the corresponding bipy complex, the *Q.S.* value is always greater for the phen complex although the same value of *I.S.* is obtained. This points out that the phen ligand is a better π-acceptor and/or a poorer σ-donor while the total σ-donor+π-acceptor ability is similar for both. In view of the lack of detailed information of the sign of *Q.S.* and the contribution from the lattice charge one cannot specifically refer to the d-orbitals which participate in the π-back

Table 3. Magnetic susceptibilities and magnetic moments

	Compound	Temperature (K)	$\chi\cdot10^6$/Fe (cgs)[a]	μ_{eff}/Fe (B.M.)[b]
I	$Fe_2(phen)_4O(NCS)_4$	294	5413	1.79[c]
VI	$Fe_2(bipy)_4O(NCS)_4$	299	3583	1.49[c]
VII	$Fe_2(bipy)_4OCl_4$	295	4123	1.57
XI	$Fe(III)(phen)_2(NCS)_3$	9	432198	5.50
		80	48886	5.62
		293	13163	5.65
XII	$Fe(III)(bipy)_2(NCS)_3$	8	611870	6.28
		80	60817	6.23
		300	16266	6.28

a) The molar susceptibility after correction for diamagnetism. The diamagnetic corrections ($\times10^6$ cgs/mol): Fe^{3+}, 13; bipy, 105; phen, 128; Cl^-, 23; NCS^-, 35; O^{2-}, 6 (Ref. 10). b) all ±0.05 B.M. c) These are in fair agreement with the literature results for similar binuclear compounds (Refs. 8—10).

bonding.

The effect of temperature on the Mössbauer parameters (Table 1) is insignificant. The compounds $Fe_2L_4O(NCS)_4$ are remarkable for the absence of any detectable Mössbauer resonance at room temperature and slight absorption around 223 K, the absorption increasing as the temperature is decreased. It is considered that the absence of any resonance at temperatures above 223 K is a consequence of low Debye temperature for iron in these compounds.

Mononuclear Iron(III) Complexes. The magnetic susceptibility data indicate that iron(III) ion in $[FeL_2(NCS)_2]NCS$ is in the high-spin state with $S=5/2$ at room temperature and temperatures to about 8 K (Table 3). The Mössbauer parameters for these complexes are given in Table 1. Without any external magnetic field at temperatures below 223 K the spectrum has a broad asymmetric line, and no resonance at room temperature or down to around 223 K. This lack of absorption at temperatures above 223 K may be the result of low Debye temperature. The comparable results for the corresponding binuclear complexes $Fe_2L_4O(NCS)_4$ show the significant influence of NCS^- ligands on the Mössbauer spectra of these complexes. Very broad peaks for the compounds $[FeL_2(NCS)_2]NCS$ (compounds XI and XII) could possibly be due to spin-spin relaxation.

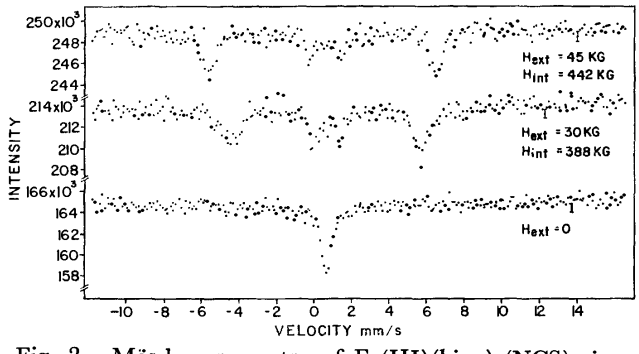

Fig. 2. Mössbauer spectra of $Fe(III)(bipy)_2(NCS)_3$ in externally applied magnetic fields at 4.2 K.

The Mössbauer spectra of $[Fe(bipy)_2(NCS)_2]NCS$ with the external magnetic fields are shown in Fig. 2. The compound $[Fe(phen)_2(NCS)_2]NCS$ shows identical effects. The results indicate that iron(III) ions in these complexes are in the high-spin state ($S=5/2$), in agreement with the magnetic susceptibility results. When the external field of 45 kG is applied the observed effective field is of the order of 442 kG. Because the sign of the internal field is negative, the induced field should be $442+45=487$ kG. Assuming purely paramagnetic case, the hyperfine field for $T\rightarrow 0$ and $H_{ext}\rightarrow\infty$ can be calculated for a d^5 system using a Brillouin function, the calculated value being -550 kG.[25] This is the limiting value arising from the exchange polarization of 1s and 2s electron cores with the d-shell electrons. Since the iron(III) complexes have 3s as well as 4s electrons which are expected to produce a positive electric field, the actual internal field will be the difference between these negative and positive contributions. This may at least partially account for the low experimental value. Saturation core polarization fields of the order of 500 kG are common in iron(III) compounds.[26,27] Hence, this further supports the $S=5/2$ spin state for iron(III) in our mononuclear complexes.

The authors are grateful to BNDE and CNPq (contract No. VKG–TC 17–174) of Brasil for partial support to this work and to Professor S. P. Puri for helpful suggestions.

References

1) R. L. Collins, R. Petit, and W. A. Baker, *J. Inorg. Nucl. Chem.*, **28**, 1001 (1966).
2) G. M. Bancroft, M. J. Mays, and B. E. Prater, *Discuss. Faraday Soc.*, **47**, 136 (1969); *J. Chem. Soc., A*, **1970**, 956.
3) R. H. Herber, R. B. King, and G. K. Wertheim, *Inorg. Chem.*, **3**, 101 (1964).
4) a) V. K. Garg, N. Malathi, and S. P. Puri, *Chem. Phys. Lett.*, **11**, 393 (1971); *b*) V. K. Garg, Ph. D. Thesis, University of Roorkee, India, 1971.
5) R. A. Prados and M. L. Good, *J. Inorg. Nucl. Chem.*, **33**, 3733 (1971).
6) K. J. Lurta, A. V. Ablov, V. I. Goldanskii, N. V. Gerbeleu, and R. A. Stukan, *Dokl. Akad. Nauk. USSR*, **196**, 1383 (1971); *b*) *Dokl. Phys. Chem.*, **196**, 190 (1971).
7) N. E. Erickson, in "The Mössbauer Effect and its Applications in Chemistry," American Chemical Society Publication, No. 68, 1971, pp. 86—125.
8) A. Gains, Jr., L. P. Hammett, and G. H. Walden, Jr., *J. Amer. Chem. Soc.*, **58**, 1668 (1936).
9) A. V. Khedekar, J. Lewis, F. E. Mabbs, and H. Weigold, *J. Chem. Soc., A*, **1968**, 1561.
10) W. M. Reiff, W. A. Baker, and N. E. Erickson, *J. Amer. Chem. Soc.*, **90**, 4794 (1968).
11) M. Wicholas and D. Jayne, *Inorg. Nucl. Chem. Lett.*, **7**, 443 (1971); b) M. Wicholas, *J. Amer. Chem. Soc.*, **92**, 4141 (1970).
12) W. M. Reiff, *J. Chem. Phys.*, **54**, 4718 (1971).
13) a) P. G. David, Ph. D. Thesis, Indiana University, Indiana, U. S. A., 1971, pp. 15—17; b) *J. Inorg. Nucl. Chem.*, **35**, 1463 (1973).
14) R. Driver and W. R. Walker, *Aust. J. Chem.*, **20**, 1375 (1967).
15) A. Earnshaw and J. Lewis, *J. Chem. Soc.*, **1961**, 396.
16) C. Bargeron and H. G. Drikamer, *J. Chem. Phys.*, **54**, 2285 (1971).
17) R. R. Berrett, B. W. Fitzsimmons, and A. A. Owusu, *J. Chem. Soc., A*, **1968**, 1585.
18) M. Y. Okamura and B. M. Hofman, *J. Chem. Phys.*, **51**, 3128 (1969).
19) M. Y. Okamura, I. M. Koltz, C. E. Johnson, M. R. C. Winter, and R. J. P. Williams, *Biochem.*, **8**, 1951 (1969).
20) A. J. Nozik and M. Kaplan, *Phys. Rev.*, **159**, 273 (1967).
21) K. Nakamoto, "Infrared Spactra of Inorganic and Coordination Compounds," 2nd Ed., John Wiley, New York (1970), pp. 173—175.
22) B. M. Gatehouse, S. E. Livingstone, and R. S. Nyholm, *J. Inorg. Nucl. Chem.*, **8**, 75 (1968).
23) C. C. Addison and B. M. Gatehouse, *J. Chem. Soc.*, **1960**, 613.
24) M. M. Chamberlain and J. C. Bailar, Jr., *J. Amer. Chem. Soc.*, **80**, 6412 (1959).
25) N. N. Greenwood and T. C. Gibb, "Mössbauer Spectroscopy," Chapman and Hall, London (1971), p. 103.
26) T. X. Carroll and M. Kaplan, *Phys. Lett.* **41A**, 145 (1972).
27) M. Takano, T. Shinjo, M. Kiyama, and T. Takada, *J. Phys. Soc. Japan*, **35**, 53 (1973).

NOTES

BULLETIN OF THE CHEMICAL SOCIETY OF JAPAN, VOL. 48(6), 1937—1938 (1975)

Changes in the Catalytic Activity of Cold-worked Platinum during the Oxidation of Carbon Monoxide

Shozo KISHIMOTO

Department of Chemistry, Faculty of Science, Kobe University, Rokkodai, Nada, Kobe 657

(Received June 29, 1974)

Synopsis. The rate of the oxidation of carbon monoxide was measured on cold-worked platinum to study the influence of annealing on the catalytic behavior. It was found that the presence of lattice defects (dislocations) in the crystal plays a role in initiating the reaction and serves to create new active sites during an acceleration period of the reaction.

Many experiments have been shown that the presence of lattice defects in a metal for various reactions plays an important role in governing the catalytic activity.[1-16] The reactions used in these experiments, in most cases, were hydrogenations and dehydrogenations. There are very few reports about the nature of active sites of metals for oxidation reactions effected by molecular oxygen. Very important contributions to this problem have been carried out by Gwathmey and his colleagues.[17,19] They found that the morphological changes of crystal faces of copper occur during the catalytic oxidation of hydrogen and suggested that these changes are initiated at the special sites of emergence of imperfections in the crystal. The purpose of the present study is to investigate the effects of lattice defects in platinum produced by cold-working on the rate of the catalytic activity change during the oxidation of carbon monoxide. This reaction was chosen as a typical reaction because of the simplicity of the reacting system. The reason for selecting platinum is that this metal is one of the most commonly used catalyst for oxidation reactions and is resistant to bulk oxidation at effective temperatures.

In order to introduce lattice defects, well annealed Pt wire (99.97% purity) with a diamer 0.5 mm was rolled to a thickness of 0.1 mm at room temperature. After being washed with acetone and distilled water, these specimens were annealed again at different temperatures between 300 and 800 °C in hydrogen and under vacuum for 1 hr. The catalytic activity was determined in a static system by measuring the decrease in the total pressure. A stoichiometric mixture of CO and O_2 was used for all experiments at a total pressure of 100 Torr. The product, CO_2, was continuously condensed by a liquid nitrogen trap connected to the reaction vessel. The apparent surface area of specimens used as the catalyst was about 15 cm^2. The gases, obtained from Takachiho Co., Ltd., were carefully purified by passing through adsorbent traps and fractionating *in vacuo*.

Some typical results at a reaction temperature of 295 °C are given in Fig. 1. Curve (A) shows the course of reaction as a function of time on the fresh specimen

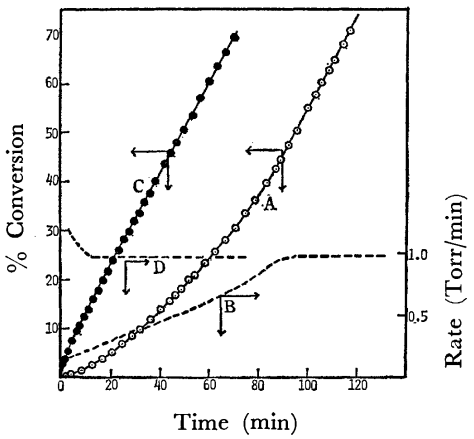

Fig. 1. Oxidation of CO on Pt annealed at 350 °C (reaction temperature 295 °C).
(A) and (B), first run: (C) and (D), second run.

annealed at 350 °C (first run). The change in the rate during the reaction is shown as curve (B) obtained from each point in curve (A). It is found that the rate increases at first with the progress of the reaction and attains to a steady limiting value. That is, two periods in the course of reaction can be defined: an acceleration period, and a steady state period, during which the rate of reaction is constant. These two periods are always observed under the conditions of present experiments when the freshly annealed specimens are used as the catalysts. The steady state rate is independent of the annealing temperatures (300—800 °C), however, the length of the acceleration period is strongly dependent on both the annealing temperatures and the reaction temperatures. Curves (C) and (D) are the results of the second run which is obtained with a new dose of the reacting gases after the first run. After an initial decrease, the rate becomes equal to the stationary value and no acceleration period is observed. Such a constant activity is found to remain unchanged even after several reaction runs. These results may suggest that the acceleration period is the process of the production of new active sites by the reaction itself. It is probable that the initial decrease in the rate (curve D) is due to CO poisoning on special active sites which are revealed by the evacuation after the first run. Figure 2(A) indicates the effect of annealing temperature on the catalytic activities in the range of the acceleration process at a reaction temperature of 295 °C. (The activities are expressed as a per cent conversion to CO_2 at a fixed reaction time, 50 min.) The change in the activity is considerable in the range 500—600 °C. According to

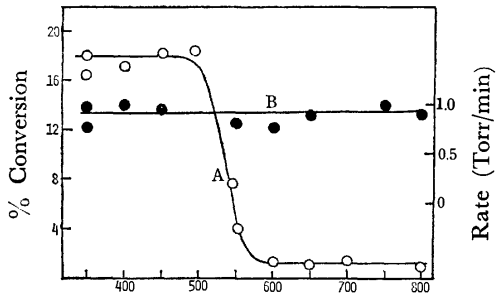

Fig. 2. Dependence of the catalytic activity in the acceleration period (A) and the steady period (B) on the annealing temperatures.
(A) Per cent conversion at a fixed reaction time, 50 min.
(B) Steady state rate, (Torr/min)

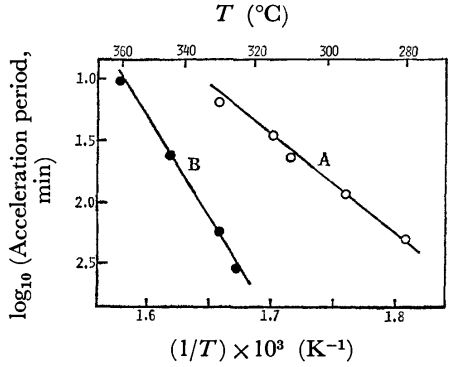

Fig. 3. Dependence of the length of the acceleration period on the reaction temperatures.
(A) Catalysts annealed at 350 °C.
(B) Catalysts annealed at 600 °C.

our previous results, this range approximately corresponds to the recovery temperature range involving the disappearance of dislocations produced by cold-working.[8] Figure 2(B) indicates that the catalytic activities in the stationary state is independent of the annealing temperatures. The dependence of the length of the acceleration period on the reaction temperature is given in Fig. 3. The length of the acceleration period increases with decreasing the reaction temperature, and the Arrhenius plots give the slopes equivalent to the activation energies of 35 and 79 kcal over the range 280—360 °C for the catalysts annealed at 350 and 600 °C, respectively. These results indicate that the activation of the surface by the reaction is very difficult when the catalyst is well annealed. Further, it can be concluded that under the conditions of the present experiments, the surface terminations of dislocations play an important role in initiating the oxidation reaction and serve greatly to create new active sites during the acceleration period. For the nature of these active sites, we have no complete explanation but it seems likely that these sites can be related to a kind of surface defects created by the cyclic oxidation-reduction process of the surface involved in the catalytic reaction. On the other hand, it may be considered that the possible reasons for affecting the catalytic activity on annealing are the decrease in surface area and active lattice planes at the surface, however, these factors do not seem to explain the sudden decrease in the activity in a limiting annealing range (500—600 °C) as discussed in previous papers.[6,7,15,16] Furthermore, it is clear that the annealing at temperatures above 600 °C has direct effects on a length of crystallite boundaries, crystal edges, and angular points at the surface. However, the results also indicate that these factors have no influence on the activity.

A few experiments were also carried out on cold-worked gold at a reaction temperature of 390 °C. It was found that no acceleration period is observed and the activity is not influenced by annealing in the range 400—800 °C. According to the previous paper, the recovery temperature range of cold-worked Au is in the range of 100—200 °C.[15] Accordingly, in this case, dislocations produced by cold-working cannot be responsible for the catalytic activity, since the catalysts are already annealed out at 400 °C before the measurements are made.

The author wishes to express his gratitude to Professor I. Uhara for reading the manuscript and for helpful discussions.

References

1) J. Eckell, *Z. Elektrochem.*, **39**, 433 (1933).
2) G. Rienäcker, *ibid.*, **46**, 369 (1940).
3) L. E. Cratty and A. V. Granato, *J. Chem. Phys.*, **26**, 96 (1957).
4) H. F. Farnsworth and R. F. Woodcock, *Advan. Catal.*, **9**, 123 (1957).
5) H. M. C. Sosnovsky, *J. Phys. Chem. Solid*, **10**, 304 (1959).
6) I. Uhara, S. Yanagimoto, K. Tani, G. Adachi, and S. Teratani, *J. Phys. Chem.*, **66**, 2691 (1962).
7) I. Uhara, S. Kishimoto, T. Hikino, Y. Kageyama, H. Hamada, and Y. Numata, *ibid.*, **67**, 996 (1963).
8) S. Kishimoto, *ibid.*, **67**, 1161 (1963).
9) I. Uhara, S. Kishimoto, Y. Yoshida, and T. Hikino, *ibid.*, **69**, 880 (1965).
10) M. A. Bhakta and H. A. Taylor, *J. Chem. Phys.*, **44**, 1264 (1966).
11) K. B. Keating, A. G. Rozner, and J. L. Youngblood, *J. Catal.*, **4**, 608 (1969).
12) Y. Inoue and I. Yasumori, *J. Phys. Chem.*, **75**, 880 (1971).
13) E. Miyazaki, T. Fukushima, K. Kawasaki, and K. Nakada, This Bulletin, **44**, 291 (1971).
14) Y. Takasu and T. Yamashina, *ibid.*, **45**, 2997 (1972).
15) S. Kishimoto and M. Nishioka, *J. Phys. Chem.*, **76**, 1907 (1972).
16) S. Kishimoto, *ibid.*, **77**, 1719 (1973).
17) H. Leidheiser, Jr., and A. T. Gwathmey, *J. Amer. Chem. Soc.*, **70**, 1200 (1948).
18) A. T. Gwathmey and R. E. Cunningham, *Advan. Catal.*, **10**, 57 (1958).
19) R. Y. Meelheim, R. E. Cunningham, K. R. Lawless, S. Azim, R. H. Kean, and A. T. Gwathmey, Proc. Int. Congr. Catal. 2nd, Paris, **1**, 2005 (1961).

BULLETIN OF THE CHEMICAL SOCIETY OF JAPAN, VOL. 48(6), 1939—1940 (1975)

Studies on the Catalytic Properties of Synthetic Zeolite A. V.[1] Site Selectivity of Silver Ion in (Ag^{ex}, Ca^{ex})-A

Masahiro NITTA, Kiyoshi OGAWA, and Kazuo AOMURA

Faculty of Engineering, Hokkaido University, Sapporo 060

(Received September 25, 1974)

Synopsis. The X-ray diffraction pattern and the propane-adsorption capacity of (Ag^{ex}, Ca^{ex})-A zeolites were determined as a function of the degree of ion exchange. From the change in diffraction intensity and the molecular sieving effect, it was deduced that Ag^+ ion prefers site I to site II.

It is well-known that synthetic zeolites A replaced by various cations are very useful as catalyst and adsorbent. The physicochemical property of zeolite A has been investigated in detail by many workers, but many points concerning the cation positions and the exchange scheme remain unclarified. We reported that Ag^+ ions were introduced into Na-A in an order of exchanging cations differing from that known for K^+ ions,[2] though both cations have a similar ionic radius larger than Na^+ ion. In this paper the site selectivity of Ag^+ ion in the (Ag^{ex}, Ca^{ex})-A* system is discussed.

The unit cell composition of $Ca^{ex}_{1.00}$-A is denoted by Ca_6 ($12AlO_2$ $12SiO_2$) nH_2O (M_{12} instead of Ca_6 for the monovalent cation form). From X-ray crystallography[3] and sorption study[4,5] of (Ca^{ex}, Na)-A, it was shown that all the $6Ca^{2+}$ ions occupy positions near the centers of the six-oxygen rings (site I) corresponding to the (111) plane. Other positions occupied by monovalent cations are sites near the centers of the eight-oxygen rings (site II) corresponding to the (100) plane, and site near a four-oxygen ring (site III) corresponding to the (110) plane.[6] In the hydrated Na-A, there are $4Na^+$ ions in site II and $8Na^+$ ions in site I. No X-ray structural data for (Ag^{ex}, Ca^{ex})-A seem to have been published. A recent study[7] suggests that Ag^+ ions occupy similar positions to those of Na^+ and K^+ ions.

The scattering power of silver for X-ray is much greater than that of calcium. Thus, when $Ca^{ex}_{1.00}$-A is replaced by Ag^+ ions, the intensity change in the X-ray diffraction of the above planes of (Ag^{ex}, Ca^{ex})-A should indicate the sites replaced by Ag^+ ions. As is shown in Fig. 1, the peak intensity of the (111) plane of hydrated samples decreased sharply with an increase in the degree of exchange, and reduced to zero at *ca.* 60%, while the intensity of the (100) plane did not decrease until 40% and then decreased gradually. This suggests that Ag^+ ions first occupy site I ($\leqq 8/12=66\%$), and then site II ($\geqq 5/12=41\%$). That is, Ag^+ ion prefers site I to site II. This is supported by the results of molecular sieving properties of (Ag^{ex}, Ca^{ex})-A and (K^{ex}, Ca^{ex})-A as given in the following.

Figure 2 shows the adsorption isobars of propane on (Ag^{ex}, Ca^{ex})-A and (K^{ex}, Ca^{ex})-A as a function of the degree of exchange. Since site II of $Ca^{ex}_{1.00}$-A is vacant, propane is rapidly diffused into the zeolite cavity and is adsorbed. In the case of K^+-exchange, propane was excluded by a $K^{ex}_{0.41}$, $Ca^{ex}_{0.69}$-A ($=5/12$). As is well known,[4] this is due to the siting of the initial K^+ ions into site II, which diminishes the apparent pore size. Takaishi *et al.*[5] have also confirmed from molecular sieving effects of (Ca^{ex}, K)-A with various adsorbates that K^+ ion prefers site II to site I. On the other hand, the replacement by Ag^+ ions permitted propane-sorption up to 70% ($\approx 8/12$) exchange, and then suddenly interfered with the sorption to *ca.* one fifth. This clearly indicates that the filling-up of site II by Ag^+ ions is completed after site I is completely filled

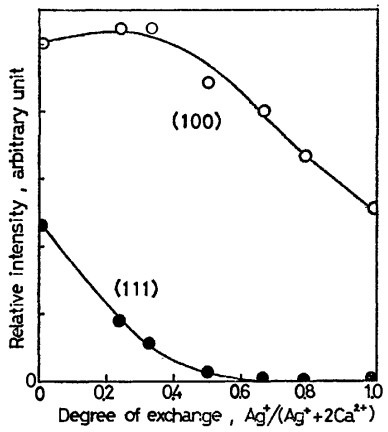

Fig. 1. Relationship between X-ray powder diffraction intensity and the degree of ion exchange.

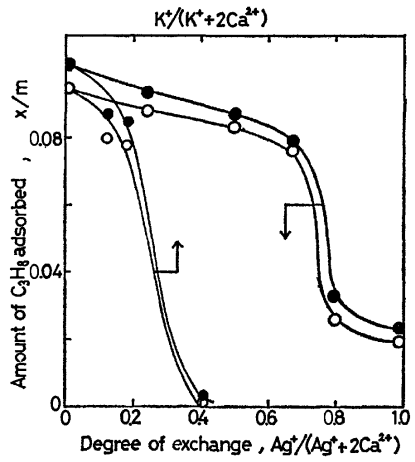

Fig. 2. Effects of silver and potassium exchanges for calcium on the sieving property.
○: 100 Torr, ●: 250 Torr, x/m: amount adsorbed in grams per gram of adsorbent.

* The nomenclature of cation-exchanged zeolite A obeyed Barrer's rule.[1] Superscript ex of M^{ex} indicates that M^{n+} ion was indroduced by ion-exchange.

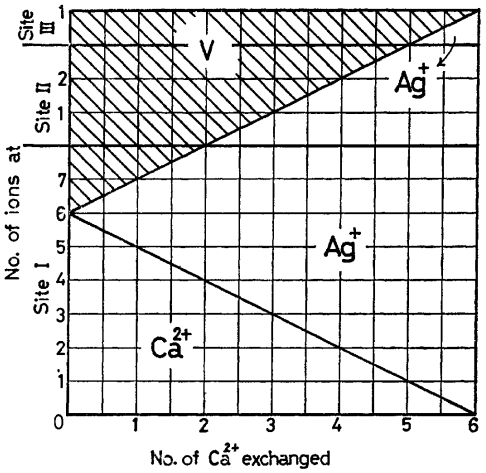

Fig. 3. Distribution of cations in (Ag^{ex}, Ca^{ex})-A.
V: Vacancies.

with $8Ag^+$ ions. That is to say, Ag^+ ion prefers site I to site II, in contrast with K^+ ion. This can be well interpreted by X-ray observation, and is consistent with the result of the (Ag^{ex}, Na)-A system.[2] The incomplete hindrance of $Ag^{ex}_{0.70-1.00}Ca^{ex}_{0.30-0}$-A for propane-sorption is due to the small ionic radius of Ag^+ (1.26 Å) compared to K^+ (1.33 Å).

From these results, the following diagram can be given to the dehydrated (Ag^{ex}, Ca^{ex})-A (Fig. 3). Such a diagram may be used as a guide line to future structural studies, and the true locations of Ag^+ ions should be determined only by X-ray structural analysis.

This work was supported by a Grant in Aid for Research from the Hokkaido Government.

Experimental

$Ca^{ex}_{1.00}$-A was prepared first from the original sodium-form zeolite A (Na-A) (Linde Molecular Sieve 4A powder). (Ag^{ex}, Ca^{ex})-A and (K^{ex}, Ca^{ex})-A were then prepared. The ion-exchange was carried out at 85±1 °C for 10 hr as already described.[1] Precaution was taken to shield the sample from light during ion-exchange and operations. The crystallinity of the samples was confirmed from the specific surface area to be unchanged by ion-exchange.

The X-ray powder diffraction pattern of the hydrated sample was obtained on a scintillation counter spectrometer using filtered Cu K_α radiation. The samples were exposed to air at room temperature while their spectra were measured.

The propane-adsorption was measured volumetrically at 0 °C on the sample activated at 250 °C in a vacuum at 10^{-3} Torr. Commercial propane (purity>99.5%) was subjected to two freeze-pump-thaw cycles before use.

References

1) Part IV of this series: S. Matsumoto, M. Nitta, K. Ogawa, and K. Aomura, This Bulletin, **48**, 1169 (1975).
2) M. Nitta, S. Matsumoto, and K. Aomura, *J. Catal.*, **35**, 317 (1974).
3) K. Seff and D. P. Shoemaker, *Acta Crystallogr.*, **22**, 162 (1967).
4) D. W. Breck, W. G. Eversole, R. M. Milton, T. B. Reed, and T. L. Thomas, *J. Amer. Chem. Soc.*, **78**, 5963 (1956); T. B. Reed and D. W. Breck, *ibid.*, **78**, 5972 (1956).
5) T. Takaishi, Y. Yatsurugi, A. Yusa, and T. Kuratomi, *J. Chem. Soc., Faraday I*, **71**, 97 (1975).
6) R. Y. Yanagida, A. A. Amaro, and K. Seff, *J. Phys. Chem.*, **77**, 805 (1973).
7) J. J. P. M. de Kanter, I. E. Maxwell, and P. J. Trotter, *Chem. Commun.*, **1972**, 733.

BULLETIN OF THE CHEMICAL SOCIETY OF JAPAN, VOL. 48(6), 1941—1942 (1975)

Fluorescence Polarization of Intramolecular EDA Complexes in (9,10-Dicyanoanthracene)-$(CH_2)_n$-(Naphthalene)

Tsutomu MIMURA, Michiya ITOH,* and Toshihiko OKAMOTO

Faculty of Pharmaceutical Sciences, The University of Tokyo, Bunkyo-ku, Tokyo 113

(Received September 26, 1974)

Synopsis. Fluorescence of the intramolecular EDA complex was observed below ~140 K in the nonpolar solution of (9,10-dicyanoanthracene)-$(CH_2)_n$-(naphthalene), $n=2$. The fluorescence and excitation polarizations of these EDA ($n=2$ and 3) complexes at 77 K were determined.

During the course of investigations of EDA complexes at low temperatures in the nonpolar solution of EDA system exhibiting exciplex fluorescence at room temperature, Itoh *et al.* reported on the intramolecular exciplex (above ~200 K) and fluorescence of the EDA complex (below ~160 K) in (9, 10-dicyanoanthracene)-$(CH_2)_n$-(naphthalene) (abbreviated as $\beta\alpha$(III) and $\beta\beta$(III), $n=3$), fluorescent states of which were found to be quite different from each other.[1,2] Recently, Itoh and Mimura reported on experimental evidence of an identical fluorescent state of the intermolecular exciplex and EDA complex between 9,10-dicyanoanthracene (DCA) and various naphthalenes;[3] CT absorption bands in these EDA systems lie in the region of the ^1L_a band of the electron acceptor with the aid of photoselection studies in 3-methylpentane (MP) solutions at 77 K.[4,5]

We have observed fluorescence of the intramolecular EDA complex in the MP solution of $\beta\alpha$(II) below ~140 K, but no exciplex formation at temperatures from room temperature to ~140 K. The fluorescence and excitation polarizations of intramolecular EDA complexes of $\beta\alpha$(II), $\beta\alpha$(III) and $\beta\beta$(III) were determined in MP solutions at 77 K.[6] The sample $\beta\alpha$(II) was synthesized and purified by preparative thin layer chromatography and recrystallized before use.

Synthesis of 1-(9,10-Dicyano-2-anthryl)-2-(1-naphthyl)-ethane. *N-(2-Anthrylmethylene)aniline (anile):* 2-Anthraldehyde (1 mol) and aniline (1 mol) were refluxed in benzene for several hours; yellow crystals separated out from a cooled solution. Recrystallized from benzene; mp 246 °C; yield 84%; IR(KBr) 1590, 1615, 1419, 900 and 750 $cm.^{-1}$

1-(2-Anthryl)-2-(1-naphthyl)ethylene: 1-Methylnaphthalene (180 mg) and potassium *tert*-butoxide (300 mg) were dissolved in DMF, and then the anile (350 mg) was added. The mixture was stirred for 3 hr at 95 °C, and poured into water and extracted with benzene. The solvent was evaporated and extracted with warm hexane. Yellow green product was purified through silica gel chromatography (benzene–hexane); mp 235 °C; yield 12%;

Found: C, 94.36; H, 5.45%. Calcd for $C_{26}H_{18}$: C, 94.55; H, 5.45%. IR(KBr) 745, 772, 795, 895 and 957 cm^{-1}.

1-(2-Anthryl)-2-(1-naphthyl)ethane: The ethylene derivative (92 mg) was hydrogenated over 5% Pd/C for 6 hr in THF and ethanol (1 : 1). Colorless crystals were obtained. Recrystallized from benzene–hexane; mp 157 °C; yield 95%.

Found: C, 94.21; H, 6.16%. Calcd for $C_{26}H_{20}$: C, 93.98; H, 6.02%. IR (KBr) 745, 778 and 900 cm^{-1}.

The substituted ethane was brominated and cyanogenated as described previously.[1]

1-(9,10-Dibromo-2-anthryl)-2-(1-naphthyl)ethane: Recrystallized from benzene; mp 155 °C.

Found: C, 63.94; H, 3.63%. Calcd for $C_{26}H_{18}Br_2$: C, 63.67; H, 3.67%. IR(KBr) 1255, 925, 745 and 768 cm^{-1}.

1-(9,10-Dicyano-2-anthryl)-2-(1-naphthyl)ethane: Recrystallized from benzene; mp 230 °C.

Found: C, 87.92; H, 4.73; N, 7.30%. Calcd for $C_{28}H_{18}N_2$: C, 87.96; H, 4.71; N, 7.33%. IR(KBr) 2220, 772 and 760 $cm.^{-1}$

Results and Discussion

An MP solution of $\beta\alpha$(II) at room temperature shows fluorescence due to the DCA moiety alone in $\beta\alpha$(II) (quantum yield; 0.92)[7] and no fluorescence in the 500-nm region. Exciplex fluorescence in MP or 2-methyltetrahydrofuran (MTHF) solutions of $\beta\alpha$(III) and $\beta\beta$(III) was observed.[1] The electronic absorption spectrum was the sum of the each component moiety. Although a remarkable fluorescence quenching of DCA moiety and a weak structureless fluorescence in the 450—550 nm region were observed in an MTHF solution of $\beta\alpha$(II) at room temperature, no distinct exciplex fluorescence was observed in either the polar or nonpolar solutions.

The fluorescence intensity due to the DCA moiety of an MP solution of $\beta\alpha$(II) decreased markedly at 77 K, a new broad fluorescence spectrum (λ_{max} 540 nm) being observed as shown in Fig. 1. The fluorescence excitation spectrum (monitored at 560 nm) and the absorption spectrum of an MP solution of $\beta\alpha$(II) differ from those of the DCA moiety at room temperature, and are very similar to the fluorescence excitation spectra and also the absorption spectra of MP solutions of $\beta\alpha$(III) and $\beta\beta$(III).[1] Fluorescence maximum and lifetime (540 nm, 100 ns) of an MP solution of $\beta\alpha$(II) at 77 K show similar values to those of $\beta\alpha$(III) (540 nm, 125 ns) and $\beta\beta$(III) (540 nm, 150 ns). The intramolecular EDA complex might be formed in an MP solution of $\beta\alpha$(II) below ~140 K, while no exciplex was detected at room temperature.

In intermediate temperatures, ~140—240 K, an MP solution of $\beta\alpha$(II) shows also a long wavelength fluorescence spectrum (500—600 nm), its excitation spectrum differing somewhat from that of the DCA

* To whom correspondence should be addressed

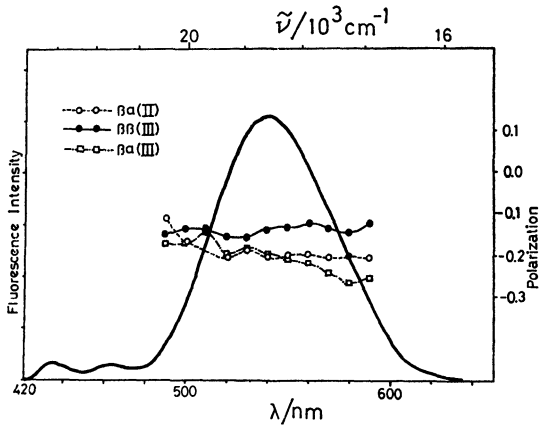

Fig. 1. The fluorescence spectrum of $\beta\alpha$(II) and the fluorescence polarizations of $\beta\alpha$(II), $\beta\alpha$(III) and $\beta\beta$(III) in MP at 77 K (excited at 360 nm; concentration: $\sim 10^{-6}$ M) The fluorescence intensity is in an arbitrary unit.

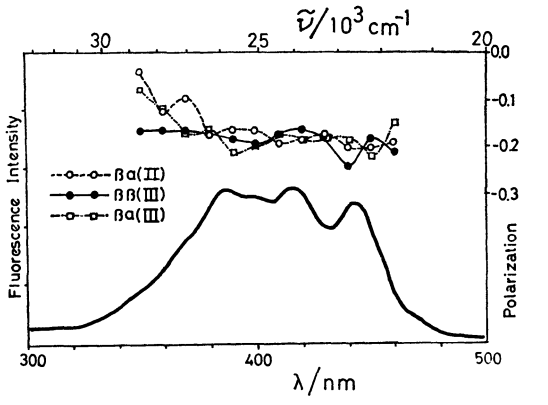

Fig. 2. The excitation spectrum of $\beta\alpha$(II) and the excitation polarizations of $\beta\alpha$(II), $\beta\alpha$(III) and $\beta\beta$(III) in MP at 77 K (monitored at 550 nm; concentration: $\sim 10^{-6}$ M) The fluorescence intensity is in an arbitrary unit. The excitation spectrum is not corrected for the intensity.

moiety (room temperature) and the EDA complex (77 K). An absorption spectrum corresponding to the excitation spectrum was also detected at almost the same intermediate temperature. These fluorescence and absorption spectra at ~140—240 K suggest an intramolecular electronic interaction in the ground state, geometrical and electronic structures of which seem to differ from those of the EDA complex at 77 K.

The fluorescence and excitation polarizations of MP solutions of $\beta\alpha$(III), $\beta\beta$(III) and $\beta\alpha$(II) were determined at 77 K by the photoselection method. Figure 1 shows negative polarization of these three compounds with excitation at 360 nm. Excitation polarization monitored at 550 nm exhibits negative values almost flat in the 440—360 nm range, as shown in Fig. 2. It is therefore unlikely that CT absorption bands in these intramolecular EDA complexes lie in this region. CT absorption bands in the EDA complexes between DCA and various naphthalenes lie in the wavelength region.[4,5] Since the electronic absorption band in the range 350—440 nm was ascribed to a local excitation (mostly ^1L_a transition) in the EDA complex, the negative fluorescence polarization by the excitation at 360 nm suggests that the long wavelength fluorescence (λ_{max} 540 nm) in these compounds is the CT fluorescence between DCA and naphthalene moieties,[8] if it is mixed with local excitations.

The average distance between the electron donor and acceptor seems to be larger in the intramolecular interaction than in the intermolecular interaction of DCA and naphthalene by a steric factor of the trimethylene chain in $\beta\alpha$(III) and $\beta\beta$(III). This is consistent with the results of the dipole moments in the fluorescent state of the exciplex, which are larger in $\beta\alpha$(III) and $\beta\beta$(III) (8.7—9.5 D)[1] than in the intermolecular systems of DCA and naphthalenes (5.9—8.6 D).[5] Thus, the CT state in the EDA complex may be higher in the former, and the CT band seems to shift to the shorter wavelength region than the first excited state of DCA by mixing with local excitations.

References

1) M. Itoh, T. Mimura, H. Usui, and T. Okamoto, *J. Amer. Chem. Soc.*, **95**, 4388 (1973).
2) M. Itoh, T. Mimura, and T. Okamoto, This Bulletin, **47**, 1078 (1974).
3) M. Itoh and T. Mimura, *Chem. Phys. Lett.*, **24**, 551 (1974).
4) M. Itoh, *ibid.*, **26** 505 (1974).
5) M. Itoh, *J. Amer. Chem Soc.*, **96**, 7390 (1974).
6) Determination of fluorescence and absorption spectra, and fluorescence (excitation) polarizations was made according to the method described previously. (See Ref.1)
7) The fluorescence quantum yield was measured as in the previous paper.
8) M. Chowdhury and L. Goodman, *J. Amer. Chem. Soc.*, **86**, 2777 (1964).

BULLETIN OF THE CHEMICAL SOCIETY OF JAPAN, VOL. 48(6), 1943—1944 (1975)

On the Phase Transition of Cyclic Tris(ethylene terephthalate)

Yukishige KITANO,* Michio KASHIWAGI,** and Yasuyuki EBATA
Basic Research Laboratories, Toray Industries, Inc., Tebiro, Kamakura 248
(Received October 31, 1974)

Synopsis. The crystal data of the Type B modification of the cyclic tris(ethylene terephthalate) showed it to be hexagonal, with the unit-cell dimensions of $a=15.42\pm0.03$ and $c=20.78\pm0.05$ Å (space group, $P6_1$ or $P6_5$). The effects of some organic reagents on the stability of Type B were studied qualitatively, and some information about the phase changes was obtained by the X-ray-diffraction and thermal-analysis techniques.

Because of their industrial importance and structural interest, the oligomers of poly(ethylene terephthalate), especially the cyclic trimer, have been investigated by many workers. The existence of two different forms, Type A and Type B,*** of the cyclic trimer was first found by Binns *et al.*,[1] and the discrepancies among the data previously reported[2-5] have been adjusted. Further observations were made by Ito and Okajima.[6] However, the Type B structure has not yet been unequivocally described. In this study we prepared stable Type B single crystals at room temperature and obtained crystal data on this material and some information concerning the effects of several organic reagents on the stability of the material.

The samples of the Type A cyclic trimer were extracted from a piece of poly(ethylene terephthalate) film with chloroform and were recrystallized repeatedly from a DMF solution. The samples of Type B were prepared by heating the Type A powder above 200 °C and by subsequently cooling it to room temperature. The X-ray diffraction data taken on the Type A samples were generally in agreement with those of Farrow *et al.*[7] and of Ito and Okajima.[6] The data for the Type B samples were similar to those of Binns *et al.*[1] and of Ito and Okajima,[6] but the X-ray pattern contained a number of reflections other than those previously reported. Single crystals of the Type B cyclic trimer were also prepared by the sublimation of the Type A powder. They are white platelet crystals of a size between 3 and 5 mm. The single-crystal X-ray pattern was identical to that of the Type B sample prepared by heating Type A and was completely indexed on the basis of the computer-refined hexagonal lattice parameters of $a=15.42\pm0.03$ and $c=20.78\pm0.05$ Å. The results are shown in Table 1. On the basis of six cyclic tris(ethylene terephthalate) per unit cell, the theoretical density is calculated to be 1.342 g·cm^{-3}; this should be compared with the observed density of 1.351 g·cm^{-3} obtained by floatation in a $ZnCl_2$ solution. Systematic absences are observed on the Weissenberg photographs for the $(00l)$ reflections with $l=6n$, where n is any integer. These data, combined with the Laue symmetry, 6/m, indicated the space group to be $P6_1$ or $P6_5$. Moreover, it is quite remarkable that the $(00l)$ reflections with $l=6n$ show a diffuse scattering elongated in the direction perpendicular to [001]. Such diffuse scattering is undoubtedly due to some disordering in the packing of molecules in the crystal.

Next, the stability of Type B at room temperature was investigated. The endothermic transition peaks from Type A to B in the differential thermal analysis of

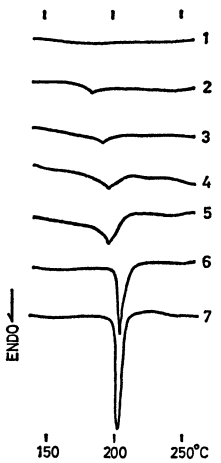

Fig. 1. DTA diagrams of the Type B samples exposed in the vapor of ethanol.
1: 0 hr, 2: 1 hr, 3: 2 hr, 4: 4 hr, 5: 6 hr, 6: 24 hr, 7: 72 hr.

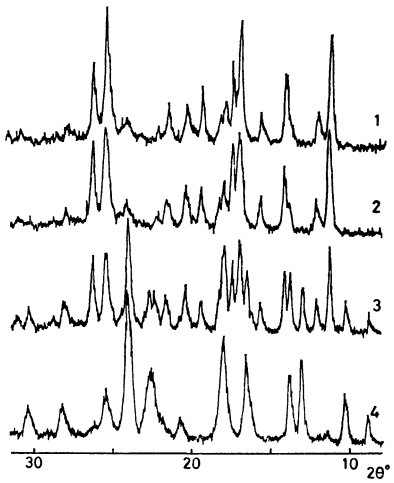

Fig. 2. X-Ray diffraction diagrams of the Type B samples exposed in the vapor of ethanol.
1: 0 hr, 2: 1 hr, 3: 4 hr, 4: 24 hr.

* Present address: Pioneering Research and Development Laboratories, Toray Industries, Inc., Sonoyama, Otsu 520.

** Present address: Engineering Research Laboratories, Toray Industries, Inc., Sonoyama, Otsu 520.

*** Type A and Type B, which have been designated by Binns *et al.*,[1] are stable at low and high temperatures respectively. The transition point of Type A to Type B is about 200 °C.

Table 1. X-Ray powder diffraction data for type B cyclic tris(ethylene terephthalate)[a)]

h	k	l	d_{obsd}	d_{calcd}	I_{obsd}	h	k	l	d_{obsd}	d_{calcd}	I_{obsd}
0	1	1	11.200	11.231	9	1	2	5	3.206	3.208	3
0	1	2	8.194	8.188	3	2	1	5			
1	1	0	7.687	7.708	56	0	4	2	3.179	3.178	7
1	1	1	7.225	7.227	20	1	1	6	3.156	3.158	9
0	2	1	6.354	6.355	12	2	2	4	3.081	3.095	8
1	1	2	6.172	6.190	56	0	2	6		3.074	
0	1	3		6.147		2	3	0		3.063	
0	2	2	5.615	5.616	13	0	4	3	3.006	3.007	4
1	1	3	5.149	5.151	60	0	1	7	2.897	2.897	3
1	2	0	5.032	5.046	70	1	4	1	2.885	2.885	3
1	2	1	4.901	4.904	21	4	1	1			
2	1	1				1	2	6	2.856	2.855	8
0	2	3	4.795	4.806	12	2	1	6			
1	2	2	4.540	4.539	17	2	2	5	2.825	2.826	3
2	1	2				0	4	4	2.805	2.808	3
0	3	1	4.353	4.352	8	1	4	2		2.805	
1	1	4	4.312	4.307	23	4	1	2			
0	2	4	4.114	4.099	7	1	2	7	2.557	2.558	4
0	3	2	4.080	4.091	16	0	1	8	2.550	2.549	3
1	2	3		4.078		1	5	1	2.383	2.382	3
0	1	5	3.969	3.967	7	5	1	1			
0	3	3	3.745	3.744	3	4	2	3	2.373	2.371	3
1	3	0	3.703	3.703	4	4	3	1	2.182	2.183	3
1	1	5	3.658	3.657	18	0	2	9		2.182	
1	3	1		3.645		2	5	1	2.127	2.127	3
1	2	4	3.612	3.619	9	5	2	1			
2	1	4				0	6	3	2.118	2.118	9
2	2	2		3.613		5	2	2	2.093	2.094	3
0	2	5	3.527	3.527	13	4	3	3		2.092	
3	1	2	3.488	3.488	25	4	1	7	2.080	2.079	3
0	0	6	3.463	3.463	100	5	2	3	2.041	2.043	3
0	3	4	3.373	3.379	30	2	4	6		2.039	3
2	2	3		3.368		4	2	6			
0	1	6	3.353	3.352	60	1	6	0	2.036	2.036	4
0	4	0	3.339	3.338	5	1	6	1	2.026	2.026	3
0	4	1	3.298	3.295	5	0	6	5	1.962	1.962	3
1	3	3	3.265	3.265	3	0	1	12	1.717	1.717	3
3	1	3									

a) $d=_{obsd}$, From diffractometer pattern calibrated by silicon powder; d_{calcd}, based on hexagonal lattice parameters, $a=15.42$ and $c=20.78$ Å; I_{obsd}, peak intensities from diffractometer pattern (Cu$K\alpha$ radiation).

the samples were found to vary when Type B was exposed to the vapor of such reagents as methanol, ethanol, acetone, DMF, benzene, and chloroform. Figure 1 shows the DTA diagrams of a sample treated with ethanol. After the sample had been treated for one hour, a small peak appeared at 187 °C. This peak grew larger and sharper, and, moreover, it shifted to high temperatures with time. After 24 hr of treatment, the peak reached 204 °C. In the course of this treatment, structural changes occurred, as assessed by X-ray diffraction. As is shown in Fig. 2, initial Type B structure gradually changed with time; finally it was almost entirely transformed into the Type A structure. Similar phenomena were observed when the samples were treated with other organic reagents.

X-Ray diffraction diagrams taken after the samples had been kept in air with a relative humidity of 30 to 50% for different lengths of time are given in Fig. 3. The peaks gradually broadened, showing that the samples became amorphous with time; one month later the Type B structure completely changed into Type A. On the other hand, when the Type B samples were kept in a desiccator over silica gel, no such phenomena were observed. This means that the Type B cyclic trimer is stable at room temperature in dry air.

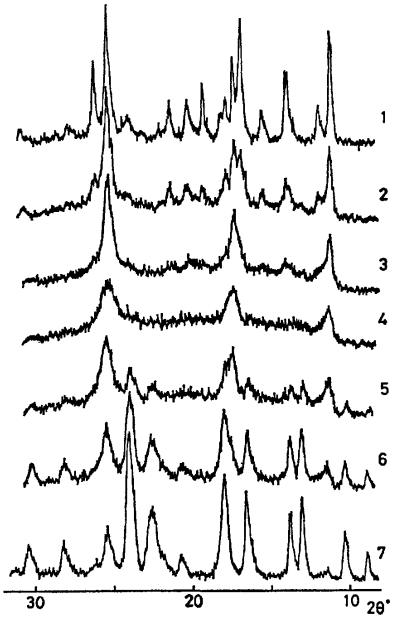

Fig. 3. X-Ray diffraction diagrams of the Type B samples kept in the air of 30 to 50% relative humidity.
1: 0 hr, 2: 1 day, 3: 2 days, 4: 7 days, 5: 10 days, 6: 15 days, 7: 30 days.

References

1) G. L. Binns, J. F. Frost, F. S. Smith, and E. C. Yeadon, *Polymer*, **7**, 583 (1966).
2) I. Goodman and B. F. Nesbitt, *ibid.*, **1**, 384 (1960).
3) D. Grime and I. M. Ward, *Trans. Faraday Soc.*, **54**, 959 (1958).
4) B. Seidel, *Z. Elektrochem.*, **62**, 214 (1958).
5) H. Zahn and B. Seidel, *Makromol. Chem.*, **29**, 70 (1959).
6) E. Ito and S. Okajima, *Polymer Lett.*, **7**, 483 (1969), *Polymer*, **12**, 650 (1971).
7) G. Farrow, J. McIntosh, and I. M. Ward, *Makromol. Chem.*, **38**, 147 (1960).

BULLETIN OF THE CHEMICAL SOCIETY OF JAPAN, VOL. 48(6), 1945—1946 (1975)

A Fluorometric Determination of Zinc in Portland Cement with 8-Quinolinethiol

Kunihiro WATANABE and Kyōzō KAWAGAKI

Faculty of Science and Technology, Science University of Tokyo, Yamazaki, Noda-shi, Chiba 278

(Received September 20, 1974)

Synopsis. A method for the fluorometric determination of zinc in cement with 8-quinolinethiol is presented. *o*-Phenanthroline and sodium thiosulfate have been found to be useful as masking reagents of interfering ions.

Atomic absorption[1] and polarographic[2] methods, among others, have been proposed in the literature for the determination of the zinc contained in a cement. In the fluorometric determination method of zinc[3] with 8-quinolinethiol previously reported by the present authors in connection with the removal of interfering ions, it was found that 8-quinolinethiol forms a stable complex with zinc and that most of the main constituent elements of a cement except iron do not interfere. In view of these findings, a fluorometric method has been developed for the determination of zinc in cement.

Good agreements were obtained between the results of the present method and those of conventional atomic absorption method.[1] The relative error of this method was from 1 to 5%.

Experimental

Reagents and Apparatus. A stock solution of zinc was prepared by dissolving 1.5286 g of zinc metal (Wako Junyaku Co.) in dilute hydrochloric acid. A 0.2% 8-quinolinethiol solution was prepared by dissolving 0.1 g of 8-quinolinethiol hydrochloride (Dojin Yakka Co.) in 50 ml of 6 M hydrochloric acid. The other reagents used were of an analytical reagent grade. The 8-quinolinethiol solution and chloroform were used for washing some of the reagents.

A Hitachi fluorescence spectrophotometer, Model 203, with a mercury lamp, was used for the fluorometric measurements. A Toa Denpa, Model HM5A, glass electrode pH meter was used for the pH measurements. An Iwaki KM shaker was also used.

Standard Procedure. Put 10 ml of a sample solution containing less than 30 μg of zinc into a beaker. Add 5 ml of a 10% ascorbic acid solution as well as 0.2 ml of a 0.2% 8-quinolinethiol solution (6 M HCl solution).

Dilute to about 50 ml with water, and adjust the pH of the solution to 4.0. Then transfer the solution to a separatory funnel and extract the zinc chelate with 10 ml of chloroform by shaking the funnel for 2 min. Measure the fluorescence intensity of the extract with reference to a 0.2 μg/ml uranine solution.

Results and Discussion

Effect of Diverse Ions. The effects of the main components of a cement on the fluorometric dermination of zinc have been intensively studied. The results are shown in Table 1. Calcium, aluminum, magnesium, sodium, potassium, and silicate ions do not interfere. However a large amount of aluminum forms hydroxides in an aqueous solution of pH 4; therefore, this element must be masked by ascorbic acid. Titanium and chromium do not interfere. Manganese does not interfere when zinc chelate is extracted at pH 4. Iron interferes strongly. Among the minor elements[4] in a cement, nickel, cobalt, copper, lead, and cadmium interfere.

Table 1. Effect of diverse ions

Ions	(mg)	Added	Zn found (μg)
Ca^{2+}	340	$Ca(NO_3)_2 \cdot 4H_2O$	7.6
Mg^{2+}	25	$Mg(NO_3)_2 \cdot 6H_2O$	7.6
Al^{3+}	36	$Al(NO_3)_3 \cdot 9H_2O$	7.6
Na^{+}	1000	NaCl	7.6
K^{+}	1000	KCl	7.6
Mn^{2+}	0.25	$MnSO_4 \cdot 6H_2O$	7.6
Fe^{2+}	0.1	$Fe+HNO_3+0.1\%$ *o*-phen 3 ml + ascorbic acid	7.5
Cd^{2+}	0.007	$Cd+HNO_3+Na_2S_2O_3 \cdot 5H_2O$ 1 g	7.9
Pb^{2+}	0.1	$Pb(NO_3)_2+Na_2S_2O_3 \cdot 5H_2O$ 1 g	7.6
Ti^{4+}	0.46	$TiO_2+H_2SO_4$	7.6
Hg^{2+}	0.1	$Hg(NO_3)_2$	5.2
SO_4^{2-}	2000	$(NH_4)_2SO_4$	7.6
VO_3^{-}	2	NH_4VO_3	7.4
PO_4^{3-}	1	$(NH_4)_2HPO_4$	7.6
SiO_3^{2-}	20	Na_2SiO_3	7.6

Zn taken: 7.6 μg; pH: 4.0; *o*-phen: *o*-phenanthroline

Masking and Removal of Interfering Ions. The uses of potassium cyanide and *o*-phenanthroline as masking reagents of iron ions were examined. The amount of potassium cyanide has little effect on the fluorescence intensity of zinc chelate. However, because of the use of the masking reagent in an alkaline solution, some ions from hydroxides, thus interfering with the fluorescence intensity. Potassium cyanide was less effective in masking than *o*-phenanthroline. In view of these results, *o*-phenanthroline was chosen as the masking reagent.

The effect of the concentration of *o*-phenanthroline is shown in Fig. 1. The extractability of chelate decreases upon the addition of more than 5 ml of a 0.1% *o*-phenanthroline solution. However, less than 5 ml of *o*-phenanthroline has very little effect on the fluorescence intensity.

The amount of iron ions to be masked by *o*-phenanthroline was also examined. As is shown in Fig. 2, a 5-ml portion of 0.1% *o*-phenanthroline is required to mask 0.3 mg of iron ions.

The procedure used to remove some interfering ions is as follows: Add *o*-phenanthroline and 8-quinolinethiol to the sample solution to form the zinc chelate. Then extract the zinc chelate with chloroform. Repeat the extraction. Combine the organic extracts. To

separate the zinc from the organic phase, shake with a 0.1 M hydrochloric acid solution. In this back-extraction, copper (up to 0.1 mg) and cobalt (up to 0.1 mg) ions remain in the organic phase, but the zinc, lead, cadmium, and nickel are transferred into the aqueous phase. Lead and cadmium react with sodium thiosulfate to form thiosulfate complex ions; therefore, lead (up to 1 mg) and cadmium (up to 10 μg) are masked with sodium thiosulfate. In the case of the coexistence of *o*-phenanthroline, nickel does not interfere up to 50 μg.

Synthetic Sample. For the synthetic sample of cement shown in Table 2, the separation of the chloroform layer from the aqueous layer after the extraction of the zinc chelate was difficult. For quick separation into two layers, a 10-ml portion ethyl alcohol was added to the sample solution.

Determination of Zinc in Cement Samples. In view of the experimental results described above, the recommended procedure for the determination of zinc in cement samples is: Take about 0.25 g of a cement sample, and 0.5 g of ammonium chloride, and add 5 ml of hydrochloric acid to the mixture. Then heat on a steam bath for 30 min, and add 20 ml of hot water to the solution for the complete dissolution of the soluble components of the cement sample. Filter the solution, and wash the precipitate with hot water. Cool the filtrate, and dilute the solution to 250 ml in a volumetric flask.

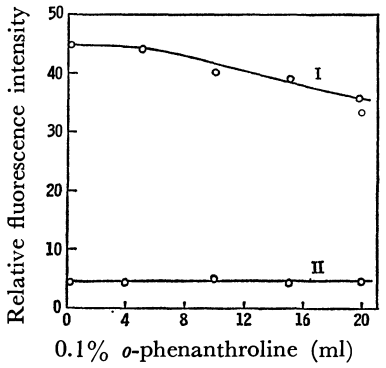

Fig. 1. Effect of amount of *o*-phenanthroline.
0.2% 8-quinolinethiol: 0.2 ml; pH: 4.0;
I: Zn 7.6 μg; II: Zn 0 μg; Wavelength: 365 nm/520 nm

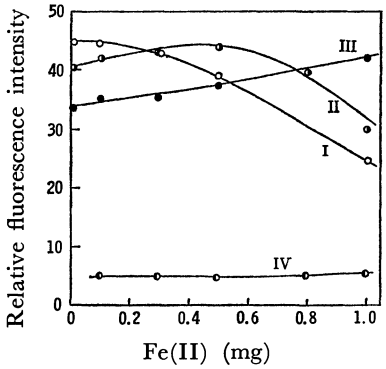

Fig. 2. Masking of Fe(II) with *o*-phenanthroline.
0.1% *o*-phenanthroline (I: 5 ml; II: 10 ml; III: 20 ml; IV: 20 ml)
Zn: 7.6 μg (I, II, III); Zn: 0 μg (IV); Wavelength: 365 nm/520 nm

Table 2. Analytical results of synthetic samples

Sample No.	Zn taken (μg)	Diverse ions (mg)	Zn found (μg)
I	7.6	Al^{3+} 6, Mg^{2+} 3, Ca^{2+} 120, Fe^{3+} 1, Cr^{3+} 0.1, Mn^{2+} 0.1, Ti^{4+} 0.08, Ni^{2+} 0.04, Cu^{2+} 0.04, Pb^{2+} 0.04, SiO_3^{2-} 1, PO_4^{3-} 0.1	7.5, 7.6, 7.5
	3.8		3.8, 4.0, 3.9
II	7.6	Ca^{2+} 240, Mg^{2+} 6, Mn^{2+} 0.1, Al^{3+} 12, SiO_3^{2-} 1, PO_4^{3-} 0.1, Cr^{3+} 0.1	7.6, 7.6, 7.5

Table 3. Analytical results of portland cements

Portland cement	Sample taken (g)	Zn found (%)	
		Proposed method	Atomic absorption method
I	0.2706	0.06_4	0.06_1
II	0.2171	0.04_0	0.04_4
III	0.2143	0.05_8	0.05_8

Pipet a 10- or 20-ml aliquot into a 100-ml beaker, add 5 ml of a 10% ascorbic acid solution, and 5 ml of a 0.1% *o*-phenanthroline solution to each 10 ml of the sample solution and 10 ml of ethyl alcohol. Then dilute the solution to 50 ml, add 0.3 ml of a 0.2% 8-quinolinethiol solution, and adjust the pH to 4. Extract the zinc chelate with 10 ml of chloroform by shaking for 2 min. Put the aqueous phase into a beaker, add 0.2 ml of 0.2% 8-quinolinethiol, adjust the pH to 4, and repeat this extraction twice. Combine the organic extracts. To back-extract zinc chelate from the organic phase, shake with 40 ml of 0.1 M hydrochloric acid for 2 min. Separate the aqueous phase, neutralize with a sodium hydroxide solution, and add 1 g of sodium thiosulfate to the solution. After the complete dissolution of the sodium thiosulfate, add 0.2 ml of 0.2% 8-quinolinethiol, adjust the pH to 4, and extract the zinc chelate with 10 ml of chloroform. Measure the fluorescence intensity with respect to a uranine solution. The zinc content (0— 30 μg) can then be calculated from the calibration curve.

The zinc in synthetic and Portland cement samples was determined by the proposed method. The results are shown in Tables 2 and 3. The present method is rapid and accurate enough for the determination of zinc in cement. The relative error of this method was from 1 to 5% for from 0.01 to 0.1% of zinc.

References

1) H. Ishii, H. Einaga, and M. Numata, *Onoda Kenkyu Hokoku*, **19**, 61 (1967).
2) H. Ishii, H. Einaga, and E. Aoki, *Bunseki Kagaku*, **14**, 149 (1965).
3) K. Watanabe, and K. Kawagaki, *ibid.*, **22**, 581 (1973).
4) H. Ishii, *ibid.*, **17**, 533 (1968).

BULLETIN OF THE CHEMICAL SOCIETY OF JAPAN, VOL. 48(6), 1947—1948 (1975)

Synthesis of *trans*-Dibromo-bis{(2-pyridyl)methylamine} and -bis{*S*-1-(2-pyridyl)ethylamine} cobalt(III) Complexes

Toshishige M. SUZUKI,* Yoshiko WATANABE, Junnosuke FUJITA,** and Kazuo SAITO
Department of Chemistry, Faculty of Science, Tohoku University, Aoba, Sendai 980

(Received January 8, 1975)

Synopsis. Light green crystals of *trans*-dibromo-bis{(2-pyridyl)-methylamine} and -bis{*S*-1-(2-pyridyl)-ethylamine}cobalt(III) bromide have been prepared. The latter complex shows a circular dichroism (CD) spectrum enantiomeric with that of the corresponding *S*-propylenediamine complex in the first absorption band region.

Several cobalt (III) complexes with (2-pyridyl)-methylamine (pma)[1,2,3] (I) and optically active 1-(2-pyridyl)ethylamine (pea)[4] (II) have been prepared. However, these complexes are limited to tris- and *cis*-bis-diamine types, and no *trans*-bis type complex has been reported. Michelsen[3] claimed that the *trans* type

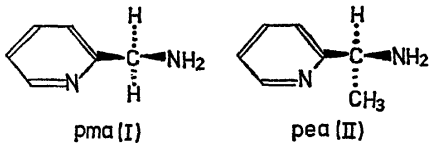

complexes were not formed in the preparation of bis type complexes. In the course of our preparative work on cobalt (III) complexes with the same ligands, we have obtained *trans*-dibromo-bis(pma) and -bis(pea) cobalt (III) complexes for the first time. This paper reports the preparation of these complexes as well as circular dichroism spectrum of the pea complex.

Experimental

Ligands: (2-Pyridyl)methylamine (pma) was purchased from Aldrich Chemical Co., and used without further purification. 1-(2-Pyridyl)ethylamine (pea) was prepared according to the method described in the literature[5] and resolved with (−)$_D$-tartaric acid by a method similar to that given by Michelsen.[4] (−)$_D$-Isomer of pea is known to have *S*-configuration.[6,7] *trans*-Dibromo-bis{*S*-1-(2-pyridyl)ethylamine}-cobalt(III) hydrogen dibromide, *trans*-[$CoBr_2$(*S*-pea)$_2$]-Br·HBr: A mixture of $NH_4[Co(SO_3)_2(NH_3)_4]$[8] (3.0 g, 0.01 mol) and *S*-pea (2.44 g, 0.02 mol) in 20 ml of water was heated at 60 °C for 2 hr with stirring. The brownish yellow solution was evaporated to dryness under reduced pressure at 60 °C and the residue dissolved in 20 ml of 48% hydrobromic acid. The solution was warmed at 60 °C for 2 hr to give light green crystals, which were filtered off, washed with a small amount of ethanol and then with ether. Found: C, 26.95; H, 3.39; N, 8.98%. Calcd for $C_{14}H_{20}N_4CoBr_4$: C, 26.50; H, 3.78; N, 9.13%. *trans*-Dibromo-bis{(2-pyridyl)-methylamine}cobalt(III) bromide monohydrate, *trans*-[$CoBr_2$(pma)$_2$]Br·H_2O: This complex was prepared by a similar method by use of pma instead of *S*-pea. Found: C, 27.39; H, 3.18; N, 10.54%. Calcd for $C_{12}H_{18}N_4OCoBr_3$: C, 27.07; H, 3.40; N, 10.51%.

Absorption and CD spectra were recorded with a Shimadzu Double 40-R spectrophotometer and a Jasco J-20 spectropolarimeter, respectively, at room temperature.

Results and Discussion

The two dibromo complexes have light green color, characteristic of *trans*-dibromo-diamine complexes. Figure 1 shows that their absorption spectra are very similar to that of the corresponding *S*-propylenediamine (*S*-pn) complex. The present *trans*-dibromo complexes with two unsymmetrical bidentate ligands have further geometrical isomers, *cis* and *trans* with respect to the configuration of the pyridyl groups (py). However, the *cis* isomer involves a big steric hindrance between the hydrogen atoms of the two pyridyl groups and the present complex can be assigned to *trans*(Br-Br)*trans*(py-py) configuration. This assignment may be supported by the *trans*(py-py) configuration of $[Cu(S\text{-pea})_2]Cl_2\cdot 2H_2O$.[7]

Isolation of the corresponding dichloro complexes was not successful because of their high solubility.

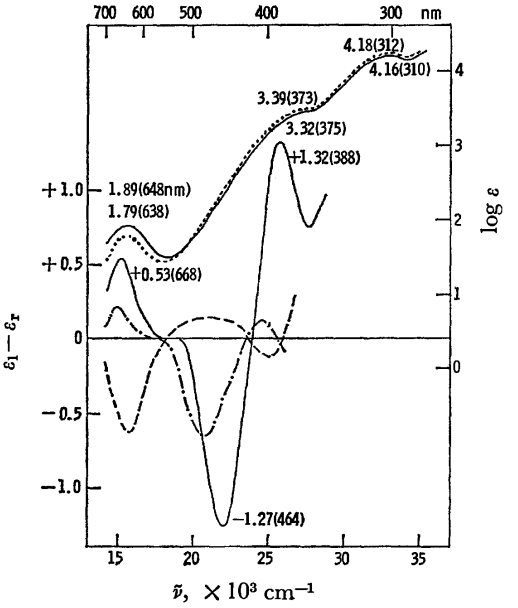

Fig. 1. Absorption spectra of (·····) *trans*-[$CoBr_2$(pma)$_2$]$^+$ and (——) *trans*-[$CoBr_2$(*S*-pea)$_2$]$^+$ in methanol. CD spectra of (——) *trans*-[$CoBr_2$(*S*-pea)$_2$]$^+$ (----) *trans*-[$CoBr_2$(*S*-pn)$_2$]$^+$ [9] and (—·—) *trans*-[$CoCl_2$(*N*-Me(*R*)-en)$_2$]$^+$ [11] in methanol.

* Present Adress: Government Industrial Research Institute, Tohoku, Nigatake, Haranomachi, Sendai 983.

** Present Adress: Department of Chemistry, Faculty of Science, Nagoya University, Chikusa, Nagoya 464.

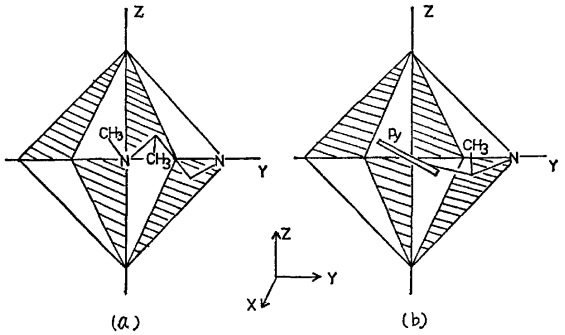

Fig. 2. The hexadecadal regional rule proposed by Mason.[13]

The CD spectrum of *trans*-$[CoBr_2(S\text{-pea})_2]^+$ gives a positive and a negative CD band in the region of the Ia($A_{1g}\rightarrow E_g$) and Ib ($A_{1g}\rightarrow A_{2g}$) absorption component (D_{4h} approximation), respectively (Fig. 1). This spectrum is virtually enantiomeric with that of *trans*-$[CoX_2(S\text{-pn})_2]^+$ (X = Cl^-, Br^-),[9] but very similar to those of *trans*(Cl,Cl) *trans*(*N*-CH_3, *N*-CH_3)-$[CoCl_2(N\text{-}CH_3(R)\text{-}S\text{-pn})_2]^{+}$[10] (*N*-$CH_3$(*R*)-*S*-pn = *N*-methyl(*R*)-*S*-propylenediamine) and -$[CoCl_2(N\text{-}CH_3(R)\text{-en})_2]^{+}$[11] (*N*-$CH_3$(*R*)-en = *N*-methyl(*R*)-ethylenediamine). X-Ray diffraction method[12] showed that three complexes have a similar conformational structure to one another.

Mason[13] proposed a hexadecadal regional rule (Fig. 2(a)) to account for the CD sign of a *trans*-dihalogeno-diamine complex. The *N*-methyl group in an unhatched region gives contribution to a negative CD for the $A_{1g}\rightarrow A_{2g}(D_{4h})$ component, while the *S*-pn has no such *N*-methyl group and its chain alkyl group lies in a hatched region where contribution to the sign is reversed. The CD sign of the $A_{1g}\rightarrow E_g(D_{4h})$ component is usually opposite to that of the $A_{1g}\rightarrow A_{2g}(D_{4h})$ owing to the partial sum-rule.[12] Detailed structure of the present dibromo complex is unknown. However, the *S*-pea chelates in $[Cu(S\text{-pea})_2]Cl_2\cdot H_2O$[7] have slightly puckered structures and the chelates and the pyridyl rings are not co-planar. On the analogy of this X-ray analysis, the *S*-pea chelate ring in the bromo complex is depicted in Fig. 2(b). Such a twisted structure can be expected whenever the methyl group tends to take an equatorial orientation to the chelate ring. Hence most atoms in the pyridyl group seem to occupy the unhatched region and will give a CD with negative sign for the $A_{1g}\rightarrow A_{2g}(D_{4h})$ component. The *N*-methyl-*S*-pn(en) complex has asymmetric nitrogen atom but the *S*-pea complex does not. The similarity in the CD spectra between the *S*-pea and the *N*-methyl(*R*)-*S*-pn(en) complexes will thus be understood by the hexadecadal rule.

The *trans*-$[CoBr_2(S\text{-pea})_2]^+$ react readily with *S*-pea in DMSO at room temperature to give $[Co(S\text{-pea})_3]^{3+}$ consisting of all possible four diastereomers. Of these, *fac*-*Δ*, *fac*-*Λ* and *mer*-*Λ* were separated and isolated by SP-Sephadex column chromatography, but *mer*-*Δ* isomer was too little to be isolated. Michelsen[4] obtained also the first three isomers from $[CoCl_2\,py_4]Cl\cdot 6H_2O$ and *S*-pea in pyridine using a similar column chromatography. The origin of such a stereoselective complex formation remains unknown.

References

1) G. J. Sutton, *Aust. J. Chem.*, **13**, 74, 222, 473 (1960).
2) K. Michelsen, *Acta Chem. Scand.*, **24**, 2003 (1970).
3) K. Michelsen, *ibid.*, **26**, 769 (1972).
4) K. Michelsen, *ibid.*, *A*, **28**, 428 (1974).
5) F. B. Laforge, *J. Amer. Chem. Soc.*, **50**, 2477 (1928).
6) H. E. Smith, L. J. Schaad, R. B. Banks, C. J. Wiant, and C. F. Jordan, *ibid.*, **95**, 811 (1973); O. Cervinka, O. Belovsky, and P. Rejmanova, *Z. Chem.*, **10**, 69 (1970); *Chem. Abstr.*, **72**, 110653j (1970).
7) K. Matsumoto and H. Kuroya, Private communication.
8) A. Werner and H. Gruger, *Z. Anorg. Chem.*, **16**, 398 (1898).
9) H. Ito, J. Fujita, and K. Saito, This Bulletin, **42**, 1286 (1969).
10) M. Saburi, Y. Tsujito, and S. Yoshikawa, *Inorg. Nucl. Chem. Lett.*, **5**, 203 (1969); *Inorg. Chem.*, **9**, 1476 (1970).
11) D. A. Buckingham, L. G. Marzilli, and A. M. Sargeson, *Inorg. Chem.*, **7**, 915 (1968); M. Kojima and T. Ishii, *Inorg. Nucl. Chem. Lett.*, **10**, 1095 (1974).
12) Y. Saito and H. Iwasaki, This Bulletin, **35**, 1131 (1962); W. T. Robinson, D. A. Buckingham, G. Chandler, L. G. Marzilli, and A. M. Sargeson, *Chem. Commun.*, **1970**, 539.
13) S. F. Mason, *J. Chem. Soc.*, *A*, **1971**, 667.

BULLETIN OF THE CHEMICAL SOCIETY OF JAPAN, VOL. 48(6), 1949—1950 (1975)

The Regioselective Addition of Alcohols to Isoprene with Rhodium Trichloride Hydrates

Hiroshi KAWAZURA,* Toshihisa TAKAGAKI, and Yoshio ISHII

Department of Synthetic Chemistry, Faculty of Engineering, Nagoya University, Furo-cho, Chikusa-ku, Nagoya 464

(Received October 7, 1974)

Synopsis. Rhodium trichloride hydrates gave predominantly the 1,2-addition product, 2-alkoxy-2-methylbut-3-ene, in the addition reaction of alcohols to isoprene. The regioselective path was established by assuming the formation of the π-(2-methylbut-3-en-2-yl)rhodium complex.

The almost exclusive formation of 2-alkoxybut-3-ene in the addition reaction of alcohols to 1,3-butadiene with rhodium trichloride hydrates[1] prompted us to examine the same reaction with isoprene, with special attention, paid to its regioselectivity, which was not noticed in the pioneering work.[2]

Table 1 summarizes the results of the addition reactions of various alcohols to isoprene carried out at 50 °C for 96 hr under nitrogen in the presence of a catalytic amount of $RhCl_3 \cdot 3H_2O$. The addition products were fractionated by preparative glc, and all the structures, as described in the table, were unambiguously determined by IR and PMR. The predominant formation of 2-alkoxy-2-methylbut-3-ene, a 1,2-addition product, accounting for more than 70% of the total products, proved the regioselectivity of the reaction.

The ionic nature of the reaction is evident, since the total yields of the addition products hold a parallel correlation with the intensities of the OH stretching vibrations of the alcohols, as in the case of butadiene.[1]

The regioselective path of the reaction may be understood if one assumes the formation of π-allylic rhodium complexes originating from an alcoholic proton attack on isoprene, as is delineated in the following scheme. The overwhelming formation of the **A** complex can be understood in view of the higher electron density of the C^1 carbon in comparison with the C^4 carbon in isoprene. Consequently, the predominant formation of the 1,2-addition product may be well explained as an attack

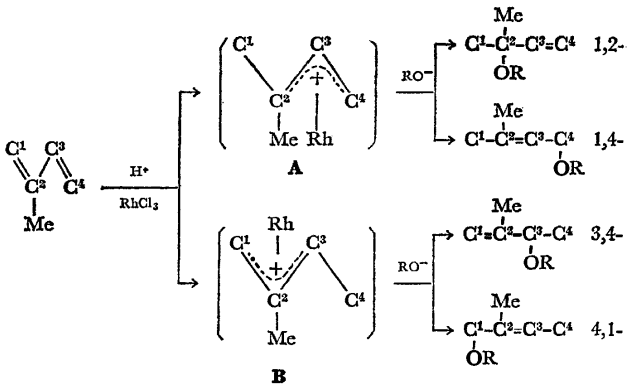

of alkoxy nucleophile on the electron-deficiently stabilized C^2 tertiary carbon in the **A** complex. The nil to minor formations of 3-alkoxy-2-methylbut-1-ene, the 3,4-addition product and the total absences of 1-alkoxy-2-methylbut-2-ene, the 4,1-addition product may be reflections of the electronically unfavored formation of the **B** complex.

Eventually the regioselectivity to the 1,2-addition may be ascribed to the predominant formation of the π-(2-methylbut-3-en-2-yl)rhodium complex, to whose tertiary carbenium carbon occurs the highly directive addition of the alkoxy nucleophile.

Experimental

Reaction of n-*BuOH to Isoprene.* A mixture of *n*-BuOH (25.0 ml) containing $RhCl_3 \cdot 3H_2O$ (62.0 mg, 0.24 mmol) and isoprene (15.0 ml, 150 mmol) was heated at 50 °C for 96 hr with stirring under nitrogen. The reaction mixture was then filtered, and the filtrate was subjected to preparative glpc (PEG 6000, 3 m, 60 °C, H_2 50 ml/min) to give three

Table 1. Addition reaction of alcohols to isoprene

Alcohol (25 ml)	$RhCl_3 \cdot 3H_2O$ mmol	Addition products: 1,2- 2-Alkoxy-2-methylbut-3-ene mmol	% [a]	1,4- 4-Alkoxy-2-methylbut-2-ene mmol	% [a]	3,4- 3-Alkoxy-2-methylbut-1-ene mmol	% [a]	Total mmol	% [a]	Intensity of ν_{OH} [b] (l mol^{-1} cm^{-1}) 10^4
Me-	0.22	22.6	15.1	4.6	3.1	0	0	27.2	18.1	0.53
Et-	0.20	24.9	16.6	7.7	5.1	trace	—	32.6	21.7	0.62
Pr^n-	0.32	23.0	15.3	2.1	1.4	4.5	3.0	29.6	19.7	—
Bu^n-	0.24	33.0	22.0	5.7	3.8	8.1	5.4	46.8	31.2	0.72
Bu^t-	0.21	11.4	7.6	0.9	0.6	2.0	1.3	14.3	9.5	—
Bu^s-	0.21	2.3	1.5	0.9	0.6	0	0	3.2	2.1	0.58
Bu^i-	0.22	0		0		0		0		0.42

a) On the basis of fed isoprene 150 mmol. b) Cited from Ref. 3.

* Present address: Faculty of Pharmaceutical Sciences, Josai University, Keyaki-dai, Sakado, Saitama 350-02.

addition products. Isolated were 2-*n*-butoxy-2-methylbut-3-ene (1,2-addition product) (4.77 g (33.0 mmol); bp 12—13 °C/2 mmHg; IR (liquid, cm^{-1}) 1650 ($\nu_{C=C}$), 1093 (ν_{C-O}), 1000 and 920 (δ_{CH} in $-CH=CH_2$); PMR (CCl_4 with TMS, τ) 4.21 (1H, dd, $J=18$ and $J=10$ Hz, proton at C^3), 5.01 (1H, dd, $J=18$ and $J=2$ Hz, *trans* proton at C^4), 5.04 (1H, dd, $J=10$ and $J=2$ Hz, *cis* proton at C^4), 6.75 (2H, t, $J=6.0$ Hz, $-CH_2O-$), 8.58 (4H, m, $-(CH_2)_2-$), 8.75 (6H, s, protons of two methyls at C^2), and 9.08 (3H, t, $J=6.2$ Hz, methyl protons in butoxy)), 3-*n*-butoxy-2-methylbut-1-ene (3,4-addition product) (1.07 g (8.1 mmol); bp 12—13 °C/2 mmHg; IR (liquid, cm^{-1}) 1650 ($\nu_{C=C}$), 1090 ($\nu_{C=C}$), and 920 (δ_{CH} in $>C=CH_2$); PMR (CCl_4 with TMS, τ) 5.16 (2H, m, protons at C^1), 6.21 (1H, q, $J=6.0$ Hz, proton at C^3), 6.75 (2H, t, $J=6.0$ Hz, $-CH_2O-$), 8.35 (3H, s, methyl protons at C^2), 8.58 (4H, m, $-(CH_2)_2-$), 8.77 (3H, d, $J=6.0$ Hz, protons at C^4-methyl), and 9.08 (3H, t, $J=6.2$ Hz, methyl protons in butoxy)), and 4-*n*-butoxy-2-methylbut-2-ene (1,4-addition product) (0.81 g (5.7 mmol); bp 23—25°C/2 mmHg; IR (liquid, cm^{-1}) 1650 ($\nu_{C=C}$), 1095 (ν_{C-O}), and 1000 (δ_{CH} in $>C=CH-$); PMR (CCl_4 with TMS, τ) 4.78 (1H, t, $J=6.0$ Hz, proton at C^3), 6.21 (2H, d, $J=6.2$ Hz, protons at C^4), 6.73 (2H, t, $J=6.0$ Hz, $-CH_2O-$), 8.30 (3H, s, C^1-methyl protons), 8.38 (3H, s, methyl protons at C^2), 8.56 (4H, m, $-(CH_2)_2-$), and 9.10 (3H, t, $J=6.3$ Hz, methyl protons in butoxy).

Reaction of the Other Alcohols to Isoprene. According to the procedure described above, the addition reaction and the products analysis were carried out for the other alcohols to give the glpc fractions, which were determined, as is shown in the table, by their IR and PMR, in which were found a characteristic pattern attributable to the 1,2-, 3,4-, or 1,4-addition product.

References

1) H. Kawazura and T. Ohmori, This Bulletin, **45**, 2213 (1972).
2) K. C. Dewhirst, *J. Org. Chem.*, **32**, 1297 (1967).
3) G. M. Barrow, *J. Phys. Chem.*, **59**, 1129 (1955).

BULLETIN OF THE CHEMICAL SOCIETY OF JAPAN, VOL. 48(6), 1951—1952 (1975)

The Photolysis of Dimethyl Diazomalonate in Alcohols. The Detection of Triplet Carbene

Wataru ANDO, Tsuneo HAGIWARA, and Toshihiko MIGITA
Department of Chemistry, Gunma University, Kiryu, Gunma 376

(Received November 7, 1974)

Synopsis. The photolysis of dimethyl diazomalonate n alcohols gave the O–H insertion product of biscarbomethoxycarbene and dimethyl malonate as the major products. The dimethyl malonate might be formed by the hydrogen abstraction of a triplet carbene.

There have been a few reports which show the occurrence of a triplet carbene in the direct photolysis of diazo compounds, whereas its benzophenone-sensitized photolysis is generally accepted to produce a triplet carbene.[1,2]

This paper will report some examples in which substantial amounts of hydrogen abstraction from alcoholic solvents and of non-stereospecific addition to olefin result from the biscarbomethoxycarbene produced through the photolysis of dimethyl diazomalonate in alcoholic media.

The direct irradiation of a methanol solution of dimethyl diazomalonate (0.16 g in 2.5 ml) was carried out with a high-pressure mercury lamp until the disappearance of the diazo compound. A gas chromatographic analysis of the reaction mixture gave dimethyl methoxymalonate and dimethyl malonate in 78 and 10% yields respectively; the structures of the products were established by NMR, IR, and elemental analyses. Appropriate control experiments showed that the products are stable under the present reaction conditions.

The photolysis in ethanol gave four products; dimethyl ethoxymalonate (I-b), ethyl methyl ethoxymalonate (II-b), ethyl methyl methoxymalonate (III-b), and dimethyl malonate (IV). From the photolysis of the diazomalonate in 2-propanol, the Wolff rearrangement product (III) was obtained together with the O–H insertion (I) and ester exchange (II) products, as minor products, while dimethyl malonate became the major product.

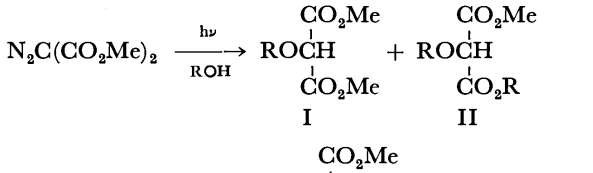

		I	II	III	IV
a	R=Me	78%	—	—	10%
b	R=Et	33	2%	13%	34
c	R=*iso*-Pr	21	4	12	41
d	R=*tert*-Bu	40	5	12	0

It is noteworthy that the photolysis of diazomalonate produced substantial amounts of dimethyl malonate, which increased with an increase of the H-donor abilities of the alcohols. Furthermore, a change of the concentration of the diazomalonate from 1 mmol to 0.2 mmol in 5 ml 2-propanol resulted in an increase in the yield of dimethyl malonate from 41 to 77%, with the formation of pinacol (27%) and the O–H insertion product (10%).

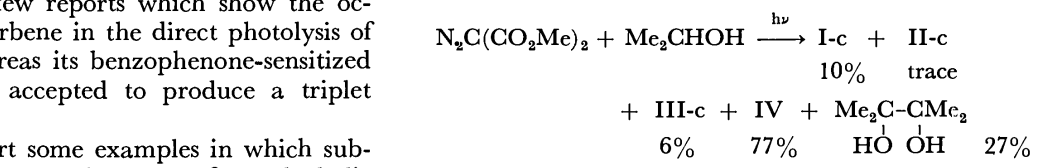

Although I and III are quite familiar products of the reaction of the singlet carbene derived from the diazo compound in alcohols,[3,4] the formation of malonate and pinacol can be though to be rather characteristic for the triplet carbene, which can abstract the α-hydrogen atom from alcohol. Indeed, the benzophenone-sensitized photodecomposition of dimethyl diazomalonate in ethanol and 2-propanol gave dimethyl malonate in 74—80% yields.

It is also worth noting that the photolysis of diazomalonate in mixtures of *cis*-4-methyl-2-pentene and alcohols gave cyclopropane derivatives in a non-stereospecific manner, but rather similar to the case of the photosensitized reaction,[5] especially in the presence of methanol, although the total yields of the adducts were quite low.

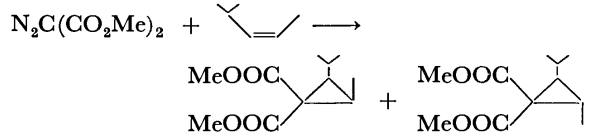

hν	92%	8%
hν + Ph_2C=O	14%	86%
hν + MeOH[a]	18%	82%
hν + EtOH[a]	66%	34%
hν + *iso*-PrOH[a]	75%	25%

a) The mole ratio of *cis*-4-methyl-2-pentene and alcohol is 1 : 10.

These findings strongly support the idea that the triplet species are involved in the direct photolysis of diazomalonate in alcohols. Singlet carbene reacts with alcohols to give either O–H insertion or Wolff-rearrangement products, while the residual carbene, which contains the triplet, abundantly reacts with olefin to give non-stereospecific adducts.

At present, the occurrence of the triplet carbene in the direct photolysis of diazomalonate in alcohols is thought to be brought about through some intersystem crossing processes. The small amounts of triplet carbene thus formed abstract a hydrogen atom from

Table 1. Reaction of dimethyl diazomalonate with *cis*-4-methyl-2-pentene in methanol

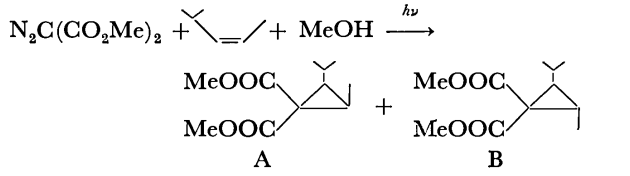

Mole ratio MeOH/	Product ratio, % A	B
1	63%	37%
2	42	58
4	38	62
10	18	82

alcohol, and the α-hydroxalkyl radical may induce the decomposition of diazomalonate by chain processes, giving substantial amounts of dimethyl malonate, since the thermal decomposition of diazomalonate in the presence of benzoyl peroxide in alcohol has been known to give dimethyl malonate in a good yield.[6]

Experimental

General. Solutions of dimethyl diazomalonate were placed in clean 10×100 mm Pyrex tubes. The tubes were corked (non-degassed), placed in a water-cooled bath, and then irradiated by means of a Rikosha 400-W high-pressure mercury lamp, with a maximum output at 3650—3660 Å. Photolyses were carried out until the diazo band in the infrared region disappeared. The solutions were analyzed on an Ohkura gas chromatograph with a calibrated 2 m×4 mm stainless steel column of 15% silicon SF-96 on Celite 545. The products were characterized by NMR (see the table shown below), IR and elemental analyses.

Reaction of Dimethyl Diazomalonate with Methanol. A solution of 187 mg of dimethyl diazomalonate in 1 ml of methanol was cooled with running water and irradiated through Pyrex with a high-pressure mercury lamp for 5 hr. After the distillation of the solvent, the residue was fractionated by gas chromatography. The major product was then collected. I-a: Found: C, 44.15; H, 6.02%. Calcd for $C_6H_{10}O_5$: C, 44.44; H, 6.22%.

Reaction of Dimethyl Diazomalonate with Ethanol. A solution of 155 mg of dimethyl diazomalonate in 1 ml of ethanol was similarly irradiated for 3 hr. Subsequent gas chromatography gave 34% of dimethyl malonate and 33% of a major product identified as dimethyl ethoxymalonate(I-b). The minor products were collected in 2% (II-b) and 13% (III-b) yields. I-b: Found: C, 47.58; H, 6.93%. Calcd for $C_7H_{12}O_5$: C, 47.72; H, 6.87%. II-b: Found: C, 50.29; H, 7.18%. Calcd for $C_8H_{14}O_5$: C, 50.52; H, 7.42%. III-b: Found: C, 47.86; H, 6.75%. Calcd for $C_7H_{12}O_5$: C, 47.72; H, 6.87%.

Reaction of Dimethyl Diazomalonate with 2-Propanol. Irradiation of a solution of 160 mg of dimethyl diazomalonate in 1 ml of 2-propanol gave I-c and IV as major products, and II-c and III-c as minor products. When a solution of 160 mg of dimethyl diazomalonate in 5 ml of 2-propanol was irradiated, the five products were isolated by gas chromatography at 160 °C. The two major products were pinacol (47% yield) and dimethyl malonate (64% yield). The minor products were found to to be I-c (8%), II-c (trace), and III-c (5%). I-c: Found: C, 50.43; H, 7.32%. Calcd for $C_8H_{14}O_5$: C, 50.52; H, 7.42%. II-c: Found: C, 54.93; H, 8.12%. Calcd for $C_{10}H_{18}O_5$: C, 55.03; H, 8.21%. III-c: Found: C, 50.16; H, 7.39%. Calcd for $C_8H_{14}O_5$: C, 50.52; H, 7.42%.

Reaction of Dimethyl Diazomalonate with tert*-Butyl Alcohol.* A solution of 152 mg of dimethyl diazomalonate in 1 ml of *tert*-butyl alcohol was irradiated for 5 hr through Pyrex tubes. The products were analyzed by gas chromatography at 170 °C. The major product was identified as I-d by spectral analysis. The minor products were collected in 5% (II-d) and 12% (III-d) yields. I-d: Found: C, 52.45; H, 7.95%. Calcd for $C_9H_{16}O_5$: C, 52.93; H, 7.90%. II-d: Found: C, 58.37; H, 8.95%. Calcd for $C_{12}H_{22}O_5$: C, 58.51; H, 9.00%. III-d: Found: C, 52.78; H, 8.12%. Calcd for $C_9H_{16}O_5$: C, 52.93; H, 7.90%.

Sensitized Decomposition of Diazomalonate in Alcohols. A solution of 170 mg of dimethyl diazomalonate and 0.95 g of benzophenone in 2.5 ml of alcohol was placed in a Pyrex tube under a nitrogen atmosphere and irradiated with the high-pressure mercury lamp for 5 hr. Gas-chromatographic analysis gave only dimethyl malonate as a major product.

Decomposition of Dimethyl Diazomalonate in cis*-4-Methyl-2-pentene and Alcohols.* All the samples, in Pyrex tubes, were irradiated under nitrogen with the same light source for the same long time. The products were analyzed by gas chromatography. The results of a typical run, in which dimethyl diazomalonate and *cis*-4-methyl-2-pentene were dissolved in methanol, are shown in Table 1.

NMR Data of the Products

Compd	NMR spectrum in CCl_4 (ppm)
I-a	3.48(s, 3H), 3.08(s, 6H), 4.30(s, 1H).
I-b	1.28(t, 3H), 3.62(q, 2H), 3.76(s, 6H), 4.33(s, 1H).
II-b	1.28(t, 3H), 1.32(t, 3H), 3.63(q, 2H), 3.76(s, 3H), 4.22(q, 2H), 4.32(s, 1H).
III-b	1.30(t, 3H), 3.45(s, 3H), 3.74(s, 3H), 4.23(q, 2H), 4.26(s, 1H).
I-c	1.20(d, 6H), 3.4—3.8(m, 1H), 3.75(s, 6H), 4.38(s, 1H).
II-c	1.18(d, 6H), 1.26(d, 6H), 3.4—3.8(m, 1H), 3.73(s, 3H), 4.11(s, 1H), 4.8—5.3(m, 1H).
III-c	1.27(d, 6H), 3.44(s, 3H), 3.75(s, 3H), 4.20(s, 1H), 4.7—5.4(m, 1H).
I-d	1.20(s, 9H), 3.73(s, 6H), 4.45(s, 1H).
II-d	1.22(s, 9H), 1.45(s, 9H), 3.72(s, 3H), 4.31(s, 1H).
III-d	1.48(s, 9H), 3.45(s, 3H), 3.75(s, 3H), 4.14(s, 1H).

References

1) W. Kirmse, "Carbene Chemistry," 2nd ed., Academic Press, New York, N.Y. (1971).

2) M. Jones, Jr., and R. A. Moss, "Carbenes," Vol. 1, Wiley-Interscience, New York, N.Y. (1973).

3) A. P. Padwa and R. Layton, *Tetrahedron Lett.*, **1965**, 2167.

4) O. P. Strausz, T. DoMinh, and H. E. Gunning, *J. Amer. Chem. Soc.*, **90**, 1660 (1968).

5) M. Jones, Jr., W. Ando, M. E. Hendrick, A. Kulczycki, Jr., P. M. Howley, K. M. Hummel, and D. S. Malamet, *ibid.*, **94**, 7469 (1972); and references cited therein.

6) L. Horner and H. Schwarz, *Ann.*, **747**, 1 (1971).

BULLETIN OF THE CHEMICAL SOCIETY OF JAPAN, VOL. 48(6), 1953—1954 (1975)

Sucrose Chemistry. 6. Synthesis of Amino Derivatives of Sucrose

Tetsuo SUAMI, Toshihide IKEDA, Shigeru NISHIYAMA, and Ryoichi ADACHI

Department of Applied Chemistry, Faculty of Engineering, Keio University, Hiyoshi, Yokohama 223

(Received December 6, 1974)

Synopsis. 6'-Amino-6'-deoxy- and 1',6'-diamino-1',6'-dideoxysucrose have been prepared by azidolysis of the corresponding tosylates, followed by catalytic hydrogenation.

In connection with the preceding papers on sucrose chemistry,[1a-e] we have attempted to prepare amino derivatives of sucrose. Two triamino-trideoxysucroses[2,3] and 6-amino-6-deoxysucrose[4] have been described in the literature. In the present paper, we wish to report the synthesis of 6'-amino-6'-deoxy- (**3**) and 1',6'-diamino-1,'-6'dideoxysucrose (**9**).

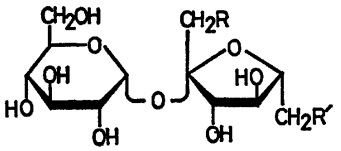

	R	R'
3:	OH	NH_2
9:	NH_2	NH_2

2,3,4,6,1',3',4'-Hepta-*O*-acetylsucrose[5-7] was treated with tosyl chloride in pyridine to give 2,3,4,6,1',3',4'-hepta-*O*-acetyl-6'-*O*-tosylsucrose (**1**). Nucleophilic replacement of **1** with an azide ion gave 6'-azido-6'-deoxysucrose heptaacetate (**2**). Catalytic hydrogenation of **2**, followed by de-*O*-acetylation afforded **3**.

2,3,4,6,3',4'-Hexa-*O*-acetyl-1',6'-di-*O*-tosylsucrose (**7**) was prepared by tosylation of 2,3,4,6,3',4'-hexa-*O*-acetylsucrose (**6**).[8] 1',6'-Diazido-1',6'-dideoxysucrose hexaacetate (**8**) was obtained by azidolysis of **7**. Compound **8** was de-*O*-acetylated and subsequently hydrogenated to afford **9**. Compounds **3** and **9** showed faint astringent taste.

PMR spectra of the acetyl derivatives of **3** and **9** were determined and the methyl group signals at highest field (δ 2.00 and 2.02) were assigned definitively to those of the acetamido methyl groups on C-6' and C-1' by the specific deuteration technique.[11-13]

Experimental

General. Melting points were determined in capillary tubes, and are uncorrected. Solutions were evaporated under diminished pressure below 40 °C. Optical rotations were measured on a Japan Spectroscopic DIP-SL polarimeter. PMR spectra were determined at 60 MHz on a Varian A-60D spectrometer in chloroform-*d* or deuterium oxide with tetramethylsilane or sodium 4,4-dimethyl-4-silapentane-1-sulfonate as an internal standard. The peak position is given in δ-value. Tlc was performed on a silica gel (Wakogel B-10) plate, and silica gel (Wakogel C-200) was used for column chromatography.

*2,3,4,6,1',3',4'-Hepta-*O*-acetyl-6'-*O*-tosylsucrose (**1**).* To a solution of 2,3,4,6,1',3',4'-hepta-*O*-acetylsucrose[5-7] (790 mg, 1.2 mmol) in dry pyridine (20 ml), tosyl chloride (1.22 g, 6.4 mmol) was added and the mixture was agitated for 72 hr. The mixture was poured into ice cold water and extracted with chloroform repeatedly. The combined extracts were evaporated and the residue was crystallized from aqueous methanol to give **1** (780 mg, 80%), mp 120—122 °C. $[\alpha]_D^{24}$ +62.0° (*c* 1.0, chloroform). PMR data ($CDCl_3$): δ 1.99 (s, 3H, OAc), 2.02 (s, 3H, OAc), 2.06 (s, 12H, 4 OAc), 2.12 (s, 3H, OAc) and 2.45 (s, 3H, aryl-CH_3).

Found: C, 50.37; H, 5.27; S, 3.67%. Calcd for $C_{33}H_{42}O_{20}S$: C, 50.13; H, 5.35; S, 4.06%.

*2,3,4,6,1',3',4'-Hepta-*O*-acetyl-6'-azido-6'-deoxysucrose (**2**).* A mixture of **1** (696 mg, 0.9 mmol) and sodium azide (350 mg, 5.4 mmol) in *N*,*N*-dimethylformamide (14 ml) was heated at 130—133 °C for 24 hr under agitation. The mixture was filtered and the filtrate was evaporated. The residue was acetylated with acetic anhydride in pyridine in the usual manner to a product (515 mg). The product was subjected to chromatography on a silica gel column and the fractions which showed a single spot at R_f 0.58 in butanone–toluene(2 : 5, v/v) were collected. The solution was evaporated to give **2** (411 mg, 71%) as a glassy solid. $[\alpha]_D^{21}$ +52.4° (*c* 8.6, chloroform). PMR data ($CDCl_3$): δ 2.03 (s, 3H, OAc), 2.06 (s, 3H, OAc), 211 (s, 12H, 4 OAc), 2.18 (s, 3H, OAc) and 5.64 (d, 1H, $J_{1,2}$ 3.4 Hz, H-1).

Found: C, 47.43; H, 5.49; N, 6.35%. Calcd for $C_{26}H_{35}N_3O_{17}$: C, 47.20; H, 5.33; N, 6.35%.

*6'-Amino-6'-deoxysucrose (**3**).* Compound **2** (401 mg) was hydrogenated in ethanol (60 ml) in the presence of platinum catalyst (85 mg) at 3.4 kg/cm² of hydrogen atmosphere at 40 °C for 20 hr. After the catalyst was removed, the solution was concentrated. The residue was de-*O*-acetylated in 0.1 M sodium methoxide in methanol (13 ml) for 2 hr and the solution was neutralized with Amberlite IR-120 (H^+). The solution was evaporated and the residue was crystallized from ethanol–methanol–water (3 : 3 : 4, v/v) in a refrigerator for two weeks to give **3** (110 mg, 53%), mp 132—135 °C (dec). $[\alpha]_D^{24}$ +57.5° (*c* 1.8, water). PMR data (D_2O): δ 5.46 (d, 1H, $J_{1,2}$ 2.9 Hz, H-1).

Found: C, 42.47; H, 6.54; N, 3.93%. Calcd for $C_{12}H_{23}NO_{10}$: C, 42.22; H, 6.79; N, 4.10%.

*2,3,4,6,1',3',4'-Hepta-*O*-acetyl-6'-acetamido-6'-deoxysucrose (**4**).* Compound **3** (92 mg) was acetylated in the usual manner to give **4** (138 mg, 76%) as an amorphous solid. $[\alpha]_D^{25}$ +56.0° (*c* 0.54, chloroform). PMR data ($CDCl_3$): δ 2.00 (s, 6H, OAc and NAc), 2.04 (s, 3H, OAc), 2.09 (s, 6H, 2 OAc), 2.10 (s, 6H, 2 OAc), 2.17 (s, 3H, OAc) and 5.60 (d, 1H, $J_{1,2}$ 3.5 Hz, H-1).

Found: C, 49.33; H, 5.90; N, 2.27%. Calcd for $C_{28}H_{39}NO_{18}$: C, 49.63; H, 5.80; N, 2.07%.

*2,3,4,6,1',3',4'-Hepta-*O*-trideuterioacetyl-6'-acetamido-6'-deoxysucrose (**5**).* Compound **4** (96 mg) was dissolved in methanol (20 ml) previously saturated with ammonia. After settled overnight, the solution was evaporated and the residue was acylated with acetic anhydride-d_6 in pyridine. The product was purified on a silica gel column in acetone–chloroform (1 : 4, v/v) to give **5** (92 mg, 93%). $[\alpha]_D^{14}$ +55.1° (*c* 1.4, chloroform). PMR data ($CDCl_3$): δ 2.00 (s, 3H, NAc) and 5.62 (d, 1H, $J_{1,2}$ 3.5 Hz, H-1).

*2,3,4,6,3',4'-Hexa-*O*-acetylsucrose (**6**).* This compound

was prepared from 2,3,4,6,3′,4′-hexa-*O*-acetyl-1′,6′-di-*O*-tritylsucrose[8,9] by detritylation with hydrogen bromide in glacial acetic acid[10] in a yield of 75%. Mp 131—132 °C. $[\alpha]_D^{18}$ +40.4° (*c* 2.24, chloroform). Found: C, 48.88; H, 5.94%. Lit,[9] mp 132 °C, $[\alpha]_D$+40.1° (*c* 2.07, chloroform). PMR data ($CDCl_3$): δ 2.00 (s, 3H, OAc), 2.04 (s, 3H, OAc), 2.07 (s, 3H, OAc), 2.08 (s, 6H, 2 OAc), 2.19 (s, 3H, OAc), 2.56 (s, 2H, 2 OH) and 5.66 (d, 1H, $J_{1,2}$ 3.5 Hz, H-1).

*2,3,4,6,3′,4′-Hexa-*O*-acetyl-1′,6′-di-*O*-tosylsucrose (**7**).* Compound **6** (830 mg, 1.4 mmol) was treated with tosyl chloride (1.33 g, 7.0 mmol) in pyridine (10 ml) for 44 hr. The reaction mixture was poured into ice cold water (100 ml) to give the crude product (1.22 g, 97%), mp 62—67 °C. $[\alpha]_D^{21}$ +57° (*c* 1.0, chloroform). PMR data ($CDCl_3$): δ 2.02 (s, 3H, OAc), 2.03 (s, 6H, 2 OAc), 2.08 (s, 6H, 2 OAc), 2.13 (s, 3H, OAc) and 2.50 (s, 6H, 2 CH_3).

Found: C, 50.64; H, 5.07; S, 6.80%. Calcd for $C_{38}H_{46}O_{21}S_2$: C, 50.55; H, 5.14; S, 7.10%.

*2,3,4,6,3′,4′-Hexa-*O*-acetyl-1′,6′-diazido-1′,6′-dideoxysucrose (**8**).* A mixture of **7** (1.22 g, 1.4 mmol) and sodium azide (0.7 g, 10.8 mmol) in DMF (30 ml) was heated and subsequently treated as described in the preparation of **2** to give **8** (0.51 g, 59%) as a glassy solid. $[\alpha]_D^{24}$ +53.7° (*c* 1.42, chloroform). PMR data ($CDCl_3$): δ 2.01 (s, 3H, OAc), 2.02 (s, 3H, OAc), 2.08 (s, 9H, 3 OAc), 2.15 (s, 3H, OAc) and 5.60 (d, 1H, $J_{1,2}$ 3.5 Hz, H-1).

Found: C, 44.61; H, 5.03; N, 12.62%. Calcd for $C_{24}H_{32}N_6O_{15}$: C, 44.72; H, 5.01; N, 13.04%.

*1′,6′-Diamino-1′,6′-dideoxysucrose (**9**).* Compound **8** (356 mg) was dissolved in 0.1 M sodium methoxide in methanol (10 ml). After settled for 2 hr, the solution was neutralized with Amberlite IR-120 (H^+), and the solution was hydrogenated as described in the preparation of **3**. The crude product was dissolved in aqueous methanol and precipitated by adding acetone to give **9** (113 mg, 60%), mp 119—124 °C (dec). $[\alpha]_D^{20}$ +77.3° (*c* 0.97, water).

*2,3,4,6,3′,4′-Hexa-*O*-acetyl-1′,6′-diacetamido-1′,6′-dideoxysucrose (**10**).* Compound **9** (157 mg) was acetylated in the usual manner and the crude product was purified by column chromatography to give an amorphous solid (119 mg, 38%). $[\alpha]_D^{21}$ +51.8° (*c* 0.74, chloroform). PMR data ($CDCl_3$): δ 2.00 (s, 3H, NAc), 2.02 (s, 6H, OAc and NAc), 2.04 (s, 3H, OAc), 2.08 (s, 6H, 2 OAc), 2.12 (s, 3H, OAc), 2.17 (s, 3H, OAc) and 5.64 (d, 1H, $J_{1,2}$ 3.5 Hz, H-1).

Found: C, 49.78; H, 6.01; N, 3.92%. Calcd for $C_{28}H_{40}N_2O_{17}$: C, 49.70; H, 5.96; N, 4.14%.

*2,3,4,6,3′,4′-Hexa-*O*-trideuterioacetyl-1′,6′-diacetamido-1′,6′-dideoxysucrose (**11**).* Compound **10** (70 mg) was de-*O*-acetylated and subsequently acylated as described in the preparation of **5** to give **11** (70 mg, 97%). $[\alpha]_D^{20}$ +51.2° (*c* 3.7, chloroform). PMR data ($CDCl_3$): δ 1.99 (s, 3H, NAc), 2.01 (s, 3H, NAc) and 5.62 (d, 1H, $J_{1,2}$ 3.5 Hz, H-1).

References

1) a) T. Suami, T. Otake, S. Ogawa, T. Shoji, and N. Kato, This Bulletin, **43**, 1219 (1970); b) T. Suami, N. Kato, M. Kawamura, and T. Nishimura, *Carbohyd. Res.*, **19**, 407 (1971); c) T. Suami, T. Otake, N. Kato, T. Nishimura, and T. Ikeda, *ibid.*, **21**, 451 (1972); d) T. Suami, T. Otake, T. Nishimura, and T. Ikeda, *ibid.*, **26**, 234 (1973); e) *Idem.*, This Bulletin, **46**, 1014 (1973).

2) S. Umezawa, T. Tsuchiya, S. Nakada, and K. Tatsuta, *ibid.*, **40**, 395 (1967).

3) R. Khan, K. S. Mufti, and M. R. Jenner, *Carbohyd. Res.*, **30**, 183 (1973).

4) I. Jezo, *Chem. Zvesti*, **25**, 364 (1971).

5) T. Otake, This Bulletin, **43**, 3199 (1970).

6) J. G. Buchanan, D. A. Cummerson, and D. M. Turner, *Carbohyd. Res.*, **21**, 283 (1972).

7) J. M. Ballard, L. Hough, and A. C. Richardson, *ibid.*, **24**, 152 (1972).

8) T. Otake, This Bulletin, **45**, 2895 (1972).

9) J. G. Buchanan and D. A. Cummerson, *Carbohyd. Res.*, **21**, 293 (1972).

10) H. Bredereck, H. Zinner, L. Wagner, G. Faber, W. Greider, and W. Huber, *Chem. Ber.*, **91**, 2824 (1958).

11) D. Horton, J. B. Hughes, J. S. Jewell, K. D. Philips, and W. N. Turner, *J. Org. Chem.*, **32**, 1073 (1967).

12) D. Horton, W. E. Mast, and K. D. Philips, *ibid.*, **32**, 1471 (1967).

13) T. Suami, S. Ogawa, Y. Naito, and H. Sano, *ibid.*, **33**, 2831 (1968).

BULLETIN OF THE CHEMICAL SOCIETY OF JAPAN, VOL. 48(6), 1955—1956 (1975)

The Formation of 1,1′-Oligomeric Ferrocenes from Chloromercuriferrocene and Bis(chloromercuri)ferrocene

Taeko IZUMI and Akira KASAHARA

Department of Applied Chemistry, Faculty of Engineering, Yamagata University, Yonezawa, Yamagata 992

(Received December 18, 1974)

Synopsis. A series of 1,1′-oligomeric ferrocenes, including biferrocene, 1,1′-biferrocenylene, 1,1′-terferrocene, 1,1′-quaterferrocene, 1,1′-quinqueferrocene, and 1,1′-sexiferrocene, was formed by the reaction between chloromercuriferrocene and 1,1′-bis(chloromercuri)ferrocene in the presence of palladium(II) salt.

The increasing interest in systems containing directly bonding ferrocene nuclei has been focused on the study of the synthesis of oligomeric ferrocene.[1] Nesmeyanov *et al.*[2] reported a mixed Ullmann reaction with bromoferrocene and 1,1′-dibromoferrocene to give a series of 1,1′-oligomeric ferrocenes. Watanabe *et al.*[3] also described the formation of the 1,1′-oligomeric ferrocenes from the reaction of a mixture of mono- and dilithioferrocenes with cobalt chloride. More recently, Roling and Rausch[4] reported a mixed Ullmann reaction between haloferrocene and 1,1′-diiodoferrocene.

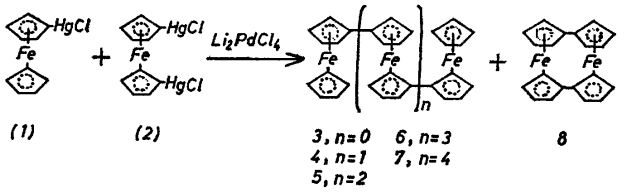

Fig. 1.

In this report, we wish to describe the synthesis of ferrocene oligomers from the reaction between a palladium(II) salt and a mixture of chloromercuriferrocene (**1**) and 1,1′-bis(chloromercuri)ferrocene (**2**).

In the presence of lithium chloropalladite, the reaction between **1** and **2** was accomplished in a polar solvent, such as ethanol or acetonitrile, under an atmosphere of nitrogen. The reaction products were separated by a combination of crystallization and chromatography on alumina and were found to be biferrocene (**3**), 1,1′-terferrocene (**4**), 1,1′-quaterferrocene (**5**), 1,1′-quinqueferrocene (**6**), 1,1′-sexiferrocene (**7**), and 1,1′-biferrocenylene (**8**). As may be seen in Table 1, different product ratios were obtained depending on the ratio of **1** to **2**. Roling and Rausch[4] reported that **8** could not be detected in a mixed Ullmann reaction; however, the **8** prepared in this study agreed in its properties with the 1,1′-biferrocenylene obtained by Hedberg and Rosenberg.[5]

Table 1. Reaction of chloromercuriferrocene (**1**) and 1,1′-bis(chloromercuri)ferrocene (**2**) with palladium(II) salt

Run	Ratio of **1** to **2**	Solvent	Percentage yields[a] of products						
			3	**4**	**5**	**6**	**7**	**8**	total
1	2 : 1[b]	EtOH	44	9	2			3	58
2	2 : 1[b]	CH_3CN	48	10	2	1		4	65
3	1 : 1[c]	EtOH	31	16	4	1	1	4	57
4	1 : 1[c]	CH_3CN	30	18	6	2	1	3	59
5	1 : 2[d]	EtOH	16	24	6	3	1	6	56
6	1 : 2[d]	CH_3CN	20	18	5	3	1	4	51

a) Yields are based on the limiting reagent in each reaction. b) Six mmol of **1** and 3 mmol of **2** were used. c) Four mmol of **1** and 4 mmol of **2** were used. d) Two point four mmol of **1** and 4.8 mmol of **2** were used.

Heck[6] previously reported that the reaction of olefins with arylmercuric chloride and palladium(II) salt produces the arylated olefinic compounds, accompanied by biaryl; he suggested that the mechanism of the formation of biaryl as a by-product involves a coupling reaction of arylpalladium chloride or a reaction of arylpalladium chloride and arylmercuric chloride. The formation of ferrocene oligomers may, therefore, be accounted for as follows:

$$FcHgCl + Li_2PdCl_4 \rightarrow [FcPdCl] + HgCl_2 + 2LiCl$$

$$Fcl(HgCl)_2 + 2Li_2PdCl_4 \rightarrow [Fcl(PdCl)_2] + 2HgCl_2 + 4LiCl$$

$$2[FcPdCl] \rightarrow Fc\text{-}Fc + PdCl_2 + Pd$$

or

$$[FcPdCl] + FcHgCl \rightarrow Fc\text{-}Fc + HgCl_2 + Pd$$

$$2[FcPdCl] + Fcl(HgCl)_2 \rightarrow Fc\text{-}Fc\text{-}Fc + 2HgCl_2 + 2Pd$$

$$2[FcPdCl] + [Fcl(PdCl)_2] \rightarrow Fc\text{-}Fc\text{-}Fc + 2PdCl_2 + 2Pd$$

$$[FcPdCl] + [Fcl(PdCl)_2] \rightarrow [Fc\text{-}FcPdCl] + PdCl_2 + Pd$$

$$2[Fc\text{-}FcPdCl] \rightarrow Fc\text{-}Fc\text{-}Fc\text{-}Fc + PdCl_2 + 2Pd$$

$$2[Fc\text{-}FcPdCl] + [Fcl(PdCl)_2] \rightarrow Fc\text{-}Fc\text{-}Fc\text{-}Fc\text{-}Fc + 2PdCl_2 + 2Pd$$

$$[Fc\text{-}FcPdCl] + [Fcl(PdCl)_2] \rightarrow [Fc\text{-}Fc\text{-}FcPdCl] + PdCl_2 + Pd$$

$$2[Fc\text{-}Fc\text{-}FcPdCl] \rightarrow Fc\text{-}Fc\text{-}Fc\text{-}Fc\text{-}Fc\text{-}Fc + PdCl_2 + Pd$$

$$2[Fcl(PdCl)_2] \rightarrow Fcl\text{-}Fcl + 2PdCl_2 + 2Pd$$

$$[Fcl(PdCl)_2] + Fcl(HgCl)_2 \rightarrow Fcl\text{-}Fcl + 2HgCl_2 + 2Pd$$

Fc=ferrocenyl, $FeC_{10}H_9$; Fcl=1,1′-ferrocenylene, $Fe(C_5H_4)_2$.

Experimental

Materials. All the melting points are uncorrected. The chloromercuriferrocene[7] (**1**) and 1,1′-bis(chloromercuri)-ferrocene[7] (**2**) were prepared by the standard literature method. The IR spectra were measured using a Hitachi 215 spectrometer. The NMR spectra were measured using a Hitachi R-22 (90 MHz) spectrometer. The chemical shifts were expressed in downfield from TMS as an internal standard. The mass spectra were recorded on a Hitachi RMU-6E mass spectrometer at 70 eV.

General Procedure for the Preparation of Oligomeric Ferrocenes. The lithium chloropalladite solutions were prepared by stirring 1.01 g (24 mmol) of anhydrous lithium chloride and 2.12 g (12 mmol) of anhydrous palladium chloride overnight at room temperature in 100 ml of ethanol. On the other hand, in the case of acetonitrile, a 12-mmol portion instead of a 24-mmol portion of lithium chloride was used.

To this lithium chloropalladite solution, a mixture of **1** and **2** was added, after which the mixture was stirred at room temperature for 48 hr under nitrogen. After the separation of the precipitated palladium, the solvent was evaporated under reduced pressure to yield Substance A. The precipitated palladium was further extracted with boiling toluene until the toluene extracts were colorless; the toluene was then evaporated to yield Substance B. Finally, the precipitated palladium was extracted with boiling bromobenzene, the extracts were allowed to cool, and the resulting precipitate was collected to give Substance C.

Substance A was dissolved in 30 ml of benzene, and 30 ml of hexane was added. The precipitate, thus formed was collected to yield a yellow product, which was crystallized from benzene and identified as 1,1′-quinqueferrocene (**6**); mp 258—260 °C (lit, 240—245 °C,[3] 262—264 °C[4]). IR (KBr) 1105, 1100, 1020, 998, 805 cm^{-1}. The NMR spectrum of **6** is not available, for **6** is insoluble in the solvent necessary for the observation of the NMR spectrum.

Found: C, 64.88; H, 4.47%; mol wt, 922 (mass spectrometry). Calcd for $C_{50}H_{42}Fe_5$: C, 65.13; H, 4.59%; mol wt, 922.

The filtrate was chromatographed on neutral alumina. The first elution with hexane-benzene (4 : 1) afforded orange-yellow crystals; they were identified as biferrocene (**3**) (mp 236—238 °C) by a mixed-melting-point determination with an authentic sample (mp 238—239 °C[8]). IR (KBr) 1105, 1100, 1028, 1000, 818 cm^{-1}. NMR ($CDCl_3$) δ 3.95 (s, 10H, unsubstituted cyclopentadienyl ring protons), 4.17 (m, 4H, β protons on the substituted ring), 4.31 ppm (m, 4H, α protons on the substituted ring). Found: mol wt, 370 (mass spectrometry). Calcd for $C_{20}H_{18}Fe_2$: mol wt, 370.

The second band was eluted with hexane-benzene (1 : 1) to yield a yellow material, which was then cryatallized from a mixture of hexane-benzene. This material was 1,1′-terferrocene (**4**); mp 223—224 °C (dec.) (lit,[3] 226.5—227.2 °C (dec.)). IR (KBr) 1105, 1100, 1020, 1000, 815 cm^{-1}. NMR ($CDCl_3$) δ 3.94 (s, 10H, unsubstituted cyclopentadienyl ring protons), 4.06—4.28 ppm (m, 16H, α and β protons on the substituted ring).

Found: C, 64.92; H, 4.61%; mol wt 554 (mass spectrometry). Calcd for $C_{30}H_{26}Fe_3$: C, 65.03; H, 4.73%; mol wt, 554.

The third band was eluted with benzene to give a orange-yellow compound, which was then crystallized from benzene to yield 1,1′-quaterferrocene (**5**); mp 275—280 °C (dec.) (lit,[3] mp 280 °C). IR (KBr) 1105, 1100, 1025, 1000, 810 cm^{-1}. The NMR spectrum of **5** is not available, for **5** is insoluble in the solvent necessary for the observation of the NMR spectrum.

Found: C, 64.89; H, 4.60%; mol wt, 738 (mass spectrometry). Calcd for $C_{40}H_{34}Fe_4$: C, 65.09; H, 4.64%; mol wt 738.

The last band was eluted with benzene-chloroform (1 : 1) to give reddish-orange crystals, which were then crystallized from benzene to yield 1,1′-biferrocenylene (**8**) (mp 370 °C (dec) (lit,[5] mp 380 °C (dec))). IR (KBr) 1110, 1105, 1027, 1005, 824 cm^{-1}. NMR (C_6D_6) δ 3.79 (t, 8H), 5.25 ppm (t, 8H).

Found: C, 65.48; H, 4.31%; mol wt 368 (mass spectrometry). Calcd for $C_{20}H_{16}Fe_2$: C, 65.54; H, 4.39%; mol wt, 368.

Substance B was purified in a similar manner to yield **3**, **4**, **5**, **6**, and **8**.

Substance C was extracted with boiling benzene until the extracts were colorless. The benzene was then allowed to cool to yield a yellow-brown material, 1,1′-sexiferrocene (**7**) (mp 265—268 °C (dec.), (lit, mp 252—256 °C,[3] mp 270—272 °C[4])). IR (KBr) 1105, 1100, 1020, 995, 802 cm^{-1}. The NMR spectrum of **7** is not available, for **7** is insoluble in the solvent necessary for the observation of the NMR spectrum.

Found: C, 65.01, H, 4.46%; mol wt, 1106 (mass spectrometry). Calcd for $C_{60}H_{50}Fe_6$: C, 65.15; H, 4.56%; mol wt, 1106.

The results are summarized in Table 1.

The Preparation of Biferrocene (3) and 1,1′-Biferrocenylene (8). To a solution of 10 mmol of lithium chloropalladite in acetonitrile, a 5-mmol portion of **1** was added, after which the mixture was stirred at room temperature for 24 hr under nitrogen. The product was isolated by filtration to remove a precipitated palladium and by distillation under reduced pressure to remove the solvent. The residue was dissolved in hexane-benzene (1 : 1); subsequent chromatography on alumina afforded yellow crystals (mp 236—238 °C, 66% yield), which were identical as biferrocene (**3**) by a comparison of the IR and NMR spectra and by a mixed-melting-point determination with an authentic sample.[8]

1,1′-Biferrocenylene (**8**) (mp 370 °C, 48% yield) was also obtained from the reaction of 10 mmol of lithium chloropalladite and 2.5 mmol of **2** in a manner similar to that used for **3**.

References

1) a) D. E. Bublitz and K. L. Rinehart, Jr., "Organic Reaction," Vol. 17, p. 1 (1969); b) M. D. Rausch, P. V. Roling, and A. Siegel, *Chem. Commun.*, **1970**, 502; c) S. I. Goldberg and J. G. Breland, *J. Org. Chem.*, **36**, 1499 (1971).

2) A. N. Nesmeyanov, V. N. Drozd, V. A. Sazonova, V. I. Romanoko, A. K. Prokof'ev, and L. A. Nokonova, *Izv. Akad. Nauk SSR, Otd. Khim. Nauk*, **1963**, 667.

3) N. Watanabe, I. Motoyama, and K. Hata, This Bulletin, **39**, 790 (1966).

4) P. V. Roling and M. D. Rausch, *J. Org. Chem.*, **37**, 729 (1972).

5) F. L. Hedberg and H. Rosenberg, *J. Amer. Chem. Soc.*, **91**, 1258 (1969).

6) R. F. Heck, *ibid.*, **90**, 5518 (1968), and following papers.

7) R. E. Fish and M. Rosenblum, *J. Org. Chem.*, **26**, 1034 (1965).

8) M. D. Rausch, *ibid.*, **26**, 2802 (1961).

BULLETIN OF THE CHEMICAL SOCIETY OF JAPAN, VOL. 48(6), 1957—1958 (1975)

The C–O Bond Cleavage of Allyl Ethers by Rhodium Compounds

Masami WAYAKU, Kiyotomi KANEDA, Toshinobu IMANAKA, and Shiichiro TERANISHI
Department of Chemical Engineering, Faculty of Engineeing Science, Osaka University, Toyonaka, Osaka 560
(Received January 6, 1975)

Synopsis. Allyl ethers were cleaved by rhodium compounds under mild conditions to give aldehydes and hydrocarbons. This reaction can be extended to allyl esters.

The cleavage of allyl or benzyl ethers has hitherto been known—*e.g.*, i) by hydrogenolysis over Raney-nickel,[1] ii) by treatment with strong bases or rhodium compounds to generate an enol ether followed by acid hydrolysis or oxidation,[2] and iii) by oxidation with SeO_2 in acetic acid.[3] The reaction products were usually alcohols and aldehydes. Also, the reactions of allyl ethers with transition metals are known to give a metal hydride or π-allyl complex.[4]

In this paper, we wish to report that the C–O bonds of cinnamy and benzyl ethers have been easily cleaved to the corresponding aldehydes and hydrocarbons in

TABLE 1. THE CLEAVAGE OF CINNAMYL AND BENZYL ETHERS

	Catalyst	Solvent	Reaction time, hr	Reaction temp, °C	Products and yields, %[a]
Cinnamyl ethers					
Dicinnamyl ether 1.2 mmol	$RhCl_3$-PPh_3-EtOH	Dioxane	2	100	(II), 97 (III), 96
p-Methylcinnamyl hydrocinnamyl ether 1.2 mmol	$RhCl_3$-PPh_3-EtOH	Dioxane	2	100	*p*,*β*-Dimethylstyrene, 48 *β*-Phenylpropionaldehyde, 41 *p*-Methylcinnamaldehyde, 27 *n*-Propylbenzene, 21 Allylbenzene, 14
Cinnamyl *n*-propyl ether 3.0 mmol	$RhCl_3$-PPh_3-EtOH	Dioxane	2	100	(II), 40 (III), 37 Cinnamyl alcohol, 3.3 Propionaldehyde, Propane Propylene
Cinnamyl isopropyl ether 3.0 mmol	$RhCl_3$-PPh_3-EtOH	Dioxane	2	100	(II), 33 (III), 17 Acetone, Propane, Propylene
Cinnamyl allyl ether 5.0 mmol	$RhCl_3$-PPh_3-EtOH	Tetrahydrofuran	2	60	(II), 44 (III), 34 Acrolein, Propylene
	$RhCl(PPh_3)_3$	Tetrahydrofuran	2	60	(II), 12 (III), 9.5
	$RhCl(CO)(PPh_3)_2$	Tetrahydrofuran	2	60	(II), 19 (III), 18
Benzyl ethers					
Dibenzyl ether[c] 1.2 mmol	$RhCl_3$-PPh_3-EtOH	Dioxane	8	100	Toluene, 3.0 Benzaldehyde, 2.4
p-Anisyl benzyl ether 1.2 mmol	$RhCl_3$-PPh_3-EtOH	Dioxane	8	100	*p*-Methylanisole, 17 Benzaldehyde, 16 *p*-Anisaldehyde, 4.5 Toluene, 3.6
p-Nitrobenzyl benzyl ether 1.2 mmol	$RhCl_3$-PPh_3-EtOH	Dioxane	8	100	*p*-Nitrobenzaldehyde, 16 Toluene, 15 Benzaldehyde, 0.6 *p*-Nitrotoluene, 0.5
Benzyl allyl ether 5.0 mmol	$RhCl_3$-PPh_3-EtOH	Tetrahydrofuran	16	60	Toluene, 24 Benzaldehyde, 17 Propylene, Acrolein
Cyclic ethers[b]					
2,5-Dihydrofuran 5.0 mmol	$RhCl_3$-PPh_3-MeOH	Tetrahydrofuran	16	60	Crotonaldehyde, 21
	$RhCl(PPh_3)_3$	Tetrahydrofuran	16	60	Crotonaldehyde, 15
Cinnamyl esters					
Cinnamyl *n*-butyrate 5.0 mmol	$RhCl(CO)(PPh_3)_2$	——	6	150	(II), 34 (III), 22 Styrene, 2.5 Cinnamyl *n*-propyl ether, trace
Cinnamyl isobutyrate 5.0 mmol	$RhCl(CO)(PPh_3)_2$	——	6	150	(II), 37 (III), 15 Styrene, 1.1 Cinnamyl isopropyl ether, trace
Cinnamyl acetate 5.0 mmol	$RhCl(CO)(PPh_3)_2$	——	6	150	(II), 23 (III), 16 Cinnamyl methyl ether, trace
Benzyl ester					
Benzyl acetate[c] 5.0 mmol	$RhCl(CO)(PPh_3)_2$	——	24	150	Benzyl methyl ether, 4.0 Toluene, 1.2 Benzaldehyde, 0.9

a) Yields are based on the reactants. b) Cyclic ethers such as tetrahydrofuran, tetrahydropyran, and 3,4-dihydro-α-pyran were not cleaved under these conditions. c) Unreacted ether and ester were recovered.

the presence of rhodium compounds under mild conditions.

The reaction of cinnamyl alcohol with $RhCl_3$ and PPh_3 in dioxane gave dicinnamyl ether (I), β-methylstyrene (II), and cinnamaldehyde (III). In an early stage of the reaction, the ether formation was remarkable. Therefore, the reaction of ether (I) with $RhCl_3$ and PPh_3 was carried out. As expected, C–O bond cleavage products (II) and (III) were obtained in high yields.[5]

$$PhCH{=}CHCH_2OH \longrightarrow \underset{(I)}{(PhCH{=}CHCH_2)_2O}$$
$$\longrightarrow \underset{(II)}{PhCH{=}CHCH_3} + \underset{(III)}{PhCH{=}CHCHO}$$

$RhCl(PPh_3)_3$ and $RhCl(CO)(PPh_3)_2$ were also active as catalysts, but $PdCl_2$, $RuCl_3$, and $IrCl_3$ were not good catalysts.

The generality of this cleavage reaction was demonstrated for cinnamyl alkyl, cinnamyl allyl, dibenzyl, and benzyl allyl ethers. In the case of *p*-substituted benzyl ethers, the bonds between the carbon of a benzyl group containing a more electron-donating substituent and oxygen were selectively cleaved. However, non-allylic ethers, such as hydrocinnamyl isopropyl and dihydrocinnamyl ether, did not react. The cleavage of cyclic allyl ether to unsaturated aldehyde was also observed.

In addition, this reaction could also be applied to allyl esters. Cinnamyl *n*-butyrate afforded (II), (III), propionaldehyde, propylene, and cinnamyl propyl ether. The reaction was accompanied by a decarbonylation of the ester to ether. These results are summarized in Table 1.

This C–O bond cleavage reaction is characteristic of allyl and benzyl ethers. Presumably the allyl rhodium complex might play an important role as an intermediate species.

Experimental

Materials. The dibenzyl ether, 2,5-dihydrofuran, and benzyl acetate were purchased from Nakarai Kagaku. The other ethers and esters were prepared by the methods of the literature.[6]

Cleavage of Cinnamyl or Benzyl Ethers. To a solution of $RhCl_3 \cdot 3H_2O$ (0.25 mmol) and PPh_3 (0.25 mmol) in ethanol (2.5 mmol) and dioxane or tetrahydrofuran (5 ml), we added cinnamyl or benzyl ether (1.2—5.0 mmol). After 2 hr (or 8 hr) of refluxing under a nitrogen stream, the solvent was removed and the residue was treated by gas chromatography (25% Apiezon grease L on Neopak) to isolate the products. The structures of the products were determined by means of the IR and NMR spectra. From cinnamyl allyl ether, β-methylstyrene (II) (2.30 mmol), cinnamaldehyde (III) (1.72 mmol), acrolein, and propylene were obtained.

Decarbonylation of Cinnamyl or Benzyl Esters. A mixture of the ester (5 mmol) and $RhCl(CO)(PPh_3)_2$ was heated at 150 °C for 6 hr. The resulting solution was treated as has been mentioned above. $RhCl(CO)(PPh_3)_2$ was recovered quantitatively.

References

1) a) H. Gilman, "Organic Chemistry," Vol. 1, John Wiley & Sons, New York (1958), p. 822.
b) S. Mitsui, S. Imaizumi, and Y. Esashi, This Bulletin, **43**, 2143 (1970).
2) a) J. Cunningham, R. Gigg, and C. D. Warren, *Tetrahedron Lett.*, **1964**, 1191. b) E. J. Corey and J. W. Suggs, *J. Org. Chem.*, **38**, 3224 (1973).
3) a) R. Gigg and C. D. Warren, *J. Chem. Soc., C*, **1968**, 1903. b) K. Kariyone and H. Yazawa, *Tetrahedron Lett.*, **1970**, 2885.
4) a) A. Bright, J. F. Malone, J. K. Nicholson, J. Powell, and B. L. Shaw, *Chem. Commun.*, **1971**, 712. b) H. C. Clark and H. Kurosawa, *Inorg. Chem.*, **12**, 1566 (1973).
5) Addition of 3-fold excess of PPh_3 to $RhCl_3$ concentration depressed this reaction.
6) a) J. M. Senheimer and J. Link, *Ann.*, **479**, 211 (1930). b) R. C. Cookson and S. R. Wakkus, *J. Chem. Soc., B*, **1966**, 1245. c) E. Cherbuliez, F. Neumeier, and H. Lozeron, *Helv. Chim. Acta*, **14**, 186 (1931). d) H. B. Gans and A. B. Holton, *Chem. Abstr.*, **29**, 6902 (1935). e) J. V. Braun, *Ber.*, **43**, 1352 (1910). f) Sh. Mamedov and D. N. Khydyrov, *Chem. Abstr.*, **57**, 11073 (1962). g) I. Lin and A. R. Day, *J. Amer. Chem. Soc.*, **74**, 5133 (1952). h) V. K. Hess and W. Wustrow, *Ann.*, **437**, 273 (1924). i) S. G. Powell and R. Adams, *J. Amer. Chem. Soc.*, **42**, 646 (1920).

BULLETIN OF THE CHEMICAL SOCIETY OF JAPAN, VOL. 48(6), 1959—1960 (1975)

The Optical Rotatory Dispersion and Circular Dichroism of Levoglucosenone

Akio OHNISHI, Eriko TAKAGI, and Kunio KATŌ

Central Research Institute, The Japan Tobacco & Salt Public Corporation, 6-2 Umegaoka, Midori-ku, Yokohama 227

(Received December 27, 1974)

Synopsis. The ORD and CD of levoglucosenone were measured in order to elucidate its abnormally large $[\alpha]_D$ value of $-524°$.[1] The complicated pattern observed was considered to contain three Cotton effects—at 357, 231 and 207 nm; the first one at 357 nm seems to be responsible for the large $[\alpha]_D$ value.

In our previous paper,[1] anhydro sugar homologues, such as levoglucosan (1,6-anhydro-β-D-glucopyranose) (II), 1,6-anhydro-3-deoxy-β-D-glucopyranosen (III),[1,2] and levoglucosenone (1,6-anhydro-3,4-dideoxy-β-D-glucopyranosen-2-one) (IV),[1,3] were determined to be the primary pyrolysis products of cellulose using Curie-point pyrolysis-gas liquid chromatography. Compound IV was first identified by Halpern *et al.*[3] in 1973; its abnormally large $[\alpha]_D$ value has been reported to be $-460°$ ($CHCl_3$, *c* 1.0)[3] and $-524°$ (C_2H_5OH, *c* 1.0),[1] while those of D-glucose (I), II and III are of the usual magnitude, as Table 1 shows. To elucidate this abnormality, the optical rotatory dispersions (ORDs) and circular dichroisms (CDs) of IV and its related compounds were measured in the wavelength region of 600—190 nm using a JASCO model J-20 spectropolarimeter. The results are shown in Figs. 1 and 2.

Compounds I and III showed a simple positive dispersion of the ORD curves, whereas Compound II showed a simple negative dispersion, as may be seen in Fig. 1. On the contrary, IV showed a complicated ORD curve with peaks at 328 ($[\phi]=+6500°$), 246 ($+15000°$), and 195 ($+31500°$) nm and troughs at 390 ($-6000°$), 293 ($+4500°$), and 217 ($-66500°$) nm, as may be seen in Fig. 2. From the CD curves of IV, the first negative Cotton effect, involving the 390 nm

TABLE 1. THE OPTICAL ROTATION AT 589 nm

Compound	Formula	$[\alpha]_D$	Solvent	Reference
I	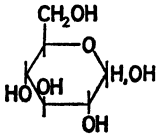	+52.7°	H_2O	4)
II	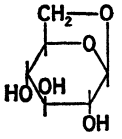	−66.5°	H_2O	5)
III	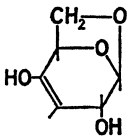	+86°	C_2H_5OH	2)
IV	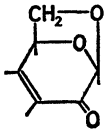	−460° −524°	$CHCl_3$ C_2H_5OH	3) 1)

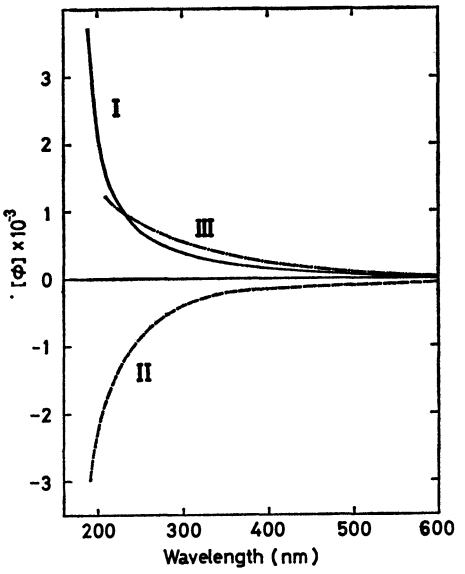

Fig. 1. The ORD curves of D-glucose (I), levoglucosan (II) and 1,6-anhydro-3-deoxy-β-D-glucopyranosen (III) measured in H_2O (I, II) or in C_2H_5OH (III) at 20 °C.
The ordinate is expressed in terms of molar rotation, $[\phi]$.

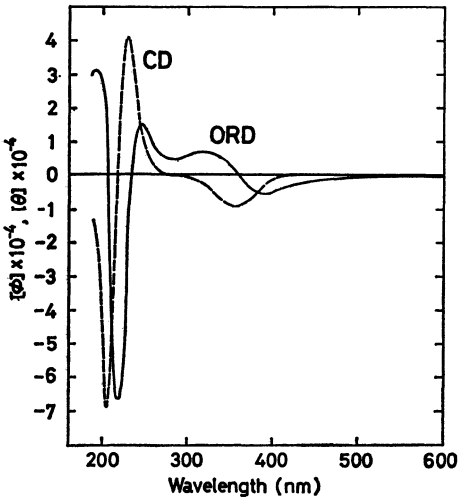

Fig. 2. The ORD and CD curves of levoglucosenone measured in C_2H_5OH at 20 °C.
The ordinate is expressed in terms of molar rotation, $[\phi]$, or molar ellipticity, $[\theta]$.

trough and the 328 nm peak of the ORD curve, was observed at 357 nm. The second positive Cotton effect, involving the 246 nm peak and the 217 nm trough of the ORD curve, was observed at 231 nm. The third negative Cotton effect, involving the 217 nm trough and the 195 nm peak of the ORD curve, was observed at 207 nm. The negative Cotton effect at 357 nm seems to correspond to the absorption band at 355 nm (ε 85, n–π^*)[1] of the carbonyl group while the other two Cotton effects may correspond to the absorption band at 217 nm (ε 6000, π–π^*).[1]

The abnormally large $[\alpha]_D$ value of IV seems to be due to the negative Cotton effect at 357 nm.

References

1) A. Ohnishi, K. Katō, and E. Takagi, *Polym. J.*, **7**, 431 (1975).
2) A. Ohnishi, E. Takagi, and K. Katō, *Chem. Lett.*, **1974**, 1361.
3) Y. Halpern, R. Riffer, and A. Broido, *J. Org. Chem.*, **38**, 204 (1973).
4) H. S. Isbell and W. W. Pigman, *J. Res. Nat. Bur. Stand.*, **18**, 141 (1937).
5) R. M. Hann and C. S. Hudson, *J. Amer. Chem. Soc.*, **64**, 2435 (1942).

Temperature-Dependent Infrared Study on L- and DL-α-Alanine

Norio KANEKO, Hiroaki TAKAHASHI, and Keniti HIGASI

Department of Chemistry, School of Science and Engineering, Waseda University, Tokyo 160

(Received November 21, 1974)

Infrared spectra from 4000 to 30 cm^{-1} of L- and DL-α-alanine and their *N*-deuterated analogues were measured at temperatures ranging from 295 to 100 K. Highly temperature-dependent bands were observed at 972 cm^{-1} (at 100 K) for L-α-alanine and 975 cm^{-1} for DL-α-alanine. The temperature dependence of the half-widths of these bands indicates that above 200 K the vibrational modes are considerably modulated by some motions, possibly arising from breaking of hydrogen bonds. These bands are thus assigned to the first overtone of the NH_3^+ torsional mode.

Temperature studies of vibrational spectra of amino acids would provide valuable information on the nature of hydrogen bonding as well as molecular motions in these biologically important substances. Although numerous studies have been published on amino acids, temperature studies of the infrared and Raman spectra are very scarce.[1-5]

It is the purpose of this paper to report on the changes due to the temperature variation observed in the infrared spectra of L- and DL-α-alanine and their *N*-deuterated analogues.

Experimental

L-Alanine and DL-α-alanine were recrystallized several times from aqueous solution. *N*-Deuterated analogues were prepared by successive exchanges with D_2O.

Infrared spectra were recorded on a Hitachi EPI-G3 spectrophotometer for the 4000 to 400 cm^{-1} range and a Hitachi FIS-3 spectrophotometer for the 400 to 30 cm^{-1} range. The spectra were obtained from Nujol mulls between KRS-5 or polyethylene plates (depending on the frequency range). A Dewar-type low temperature cell with a copper-constantan thermocouple was used. The frequencies are estimated to be accurate within ± 2 cm^{-1}.

Results

L-α-Alanine. Infrared spectra from 1800 to 30 cm^{-1} of L-α-alanine at both room and liquid nitrogen temperatures are given in Fig. 1. A band appears at 972 cm^{-1} which does not seem to have been reported

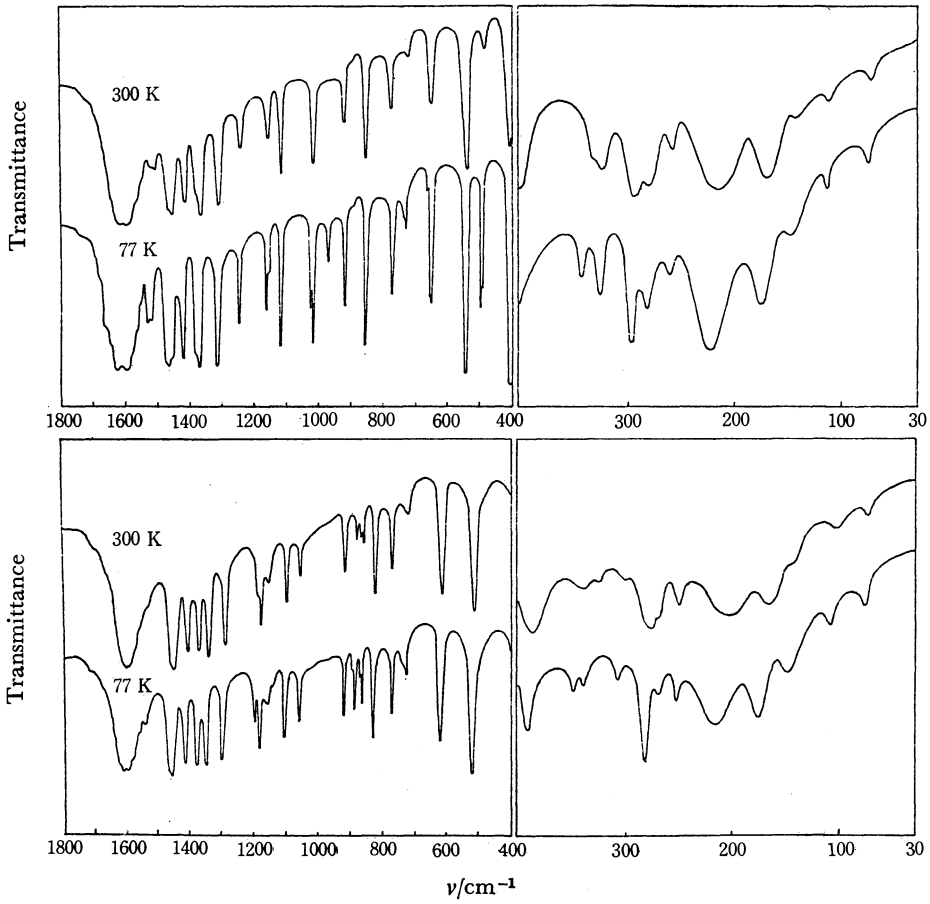

Fig. 1. Infrared spectra of L-α-alanine (upper) and its *N*-deuterated powder (bottom) suspended in Nujol, observed at room temperature and liquid nitrogen temperature.

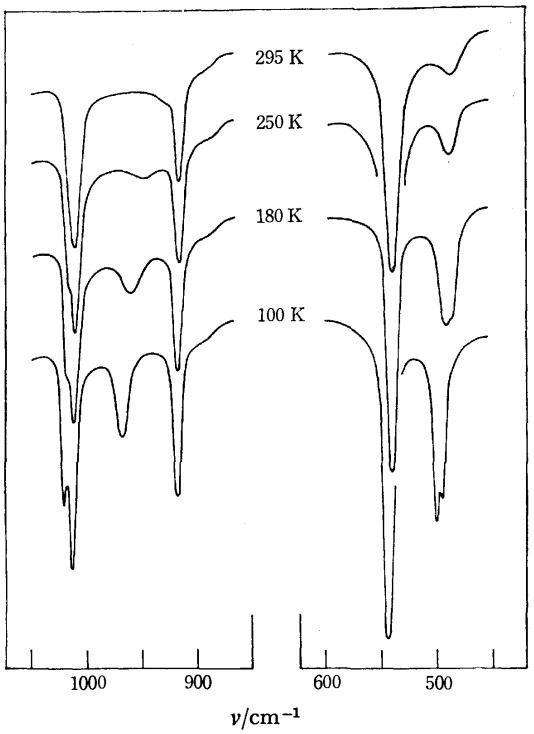

Fig. 2. Temperature dependence of the bands at 972 and 487 cm^{-1} for L-α-alanine.

before—this is the most interesting feature of the liquid nitrogen temperature spectrum. This band disappears by deuteration of the NH_3^+ group as shown in Fig. 1.

The temperature variation of the band is shown in Fig. 2 together with that of the band at 487 cm^{-1}. At room temperature the band is recognizable as a very weak and rather broad shoulder on the 920 cm^{-1}. With a fall in temperature the shoulder becomes sharper, the intensity increasing and shifting towards higher frequency. A similar behavior is observed for the band at 487 cm^{-1}, except that it exhibits splitting as well. This band has been assigned to the NH_3^+ torsional vibration.[2]

DL-α-*alanine.* The liquid nitrogen temperature spectrum from 1800 to 30 cm^{-1} of DL-α-alanine is shown in Fig. 3 along with the room temperature spectrum. The very weak and broad band at 975 cm^{-1} and the band at 497 cm^{-1} show a similar temperature effect to that of the bands at 972 cm^{-1} (at 100 K) and 487 cm^{-1} of L-α-alanine. See Fig. 4 for its detailed feature. The 497 cm^{-1} band has been assigned to the NH_3^+ torsional vibration.[6] The 975 cm^{-1} band, not previously reported, is absent from the spectrum of the *N*-deuterated analogue as shown in Fig. 3.

Infrared spectra of α- and γ-glycine, L- and DL-valine and DL-leucine were also measured at various low temperatures. Although NH_3^+ torsional frequencies were

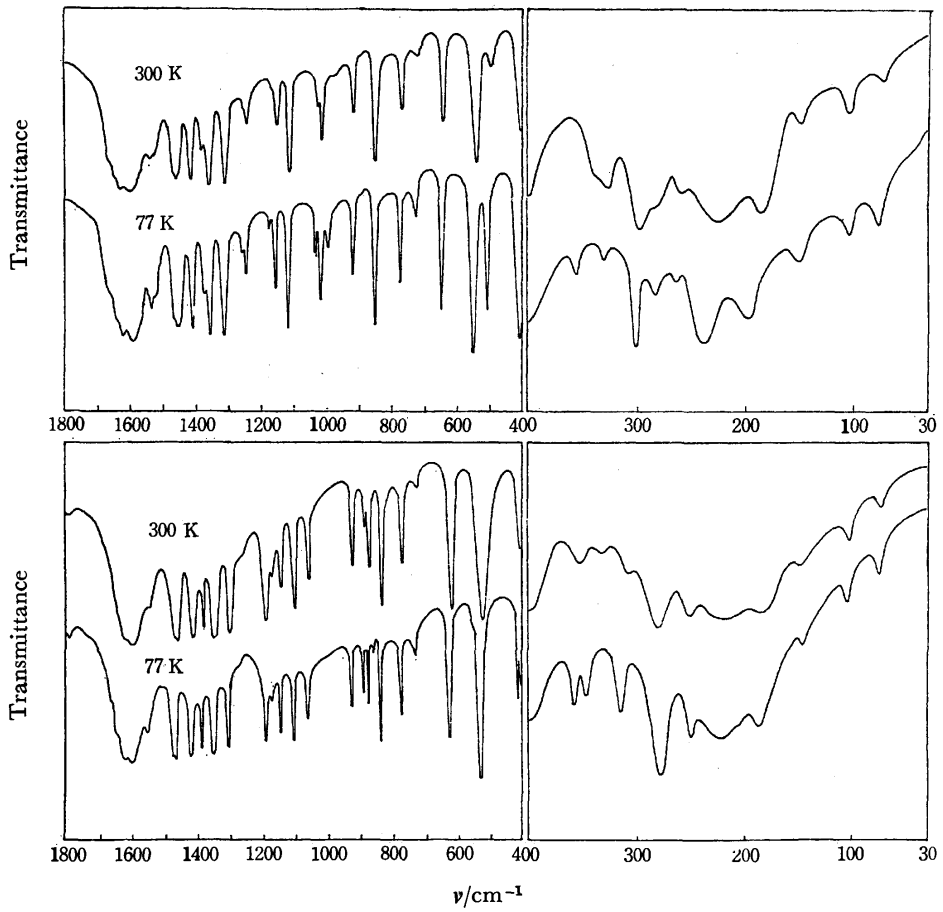

Fig. 3. Infrared spectra of DL-α-alanine (upper) and its *N*-deuterated powder (bottom) suspended in Nujol, observed at room temperature and liquid nitrogen temperature.

observed respectively at 525, 560, 575, 565, and 580 cm^{-1} for α-, γ-glycine, L-, DL-valine, and DL-leucine, no temperature-dependent band was detected between 1200 and 900 cm^{-1}.

Discussion

Since the bands at 972 cm^{-1} (at 100 K) for L-α-alanine and at 975 cm^{-1} for DL-α-alanine are both far (over 40 cm^{-1}) from adjacent bands, it is unlikely that they arise from crystal-field splitting.

We find that the temperature effect of the bands at 972 and 975 cm^{-1} is very similar to that of the NH_3^+ torsional vibrations at 487 and 497 cm^{-1} and that the frequencies are about twice as high as the corresponding torsional frequencies. We may infer that the temperature dependence of overtone vibrations is analogous to that of the fundamental vibrations, and, hence, the newly observed bands at 972 cm^{-1} for L-α-alanine and at 975 cm^{-1} for DL-α-alanine should be assigned to the first overtone of the NH_3^+ torsional vibration.

The above assignment can be substantiated by the spectra of *N*-deuterated analogues. Disappearance of the bands at 972 and 975 cm^{-1} by deuteration of the NH_3^+ group indicates that they originate from the motion of the NH_3^+ group. However, the location of the first overtone of the ND_3^+ torsional vibration is not clear. We see from Figs. 1 and 3 that the ND_3^+ torsional fundamental is observed at 346 cm^{-1} for L-α-alanine and at 354 cm^{-1} for DL-α-alanine at room temperature. The first overtone is thus expected to appear around 700 cm^{-1} at liquid nitrogen temperature. However, no new band is detected around this frequency. It is possible that the overtone bands are hidden under the Nujol band at 720 cm^{-1} or the intensities are too low to be observed.

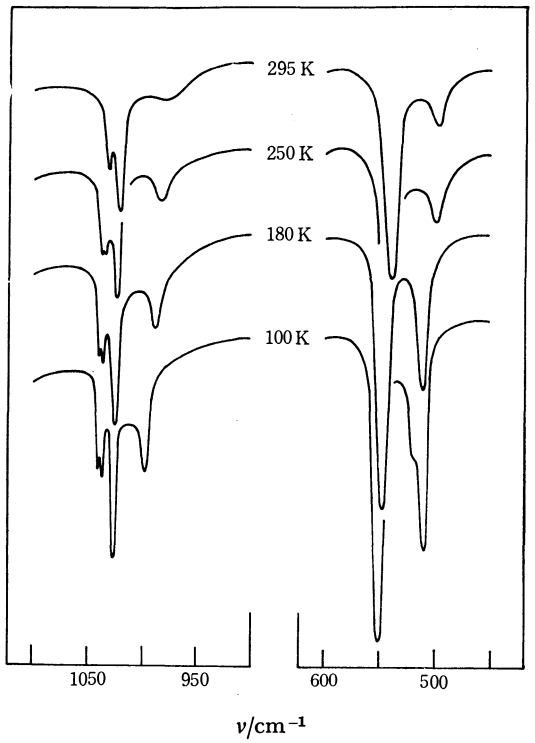

Fig. 4. Temperature dependence of the bands at 975 and 497 cm^{-1} for DL-α-alanine.

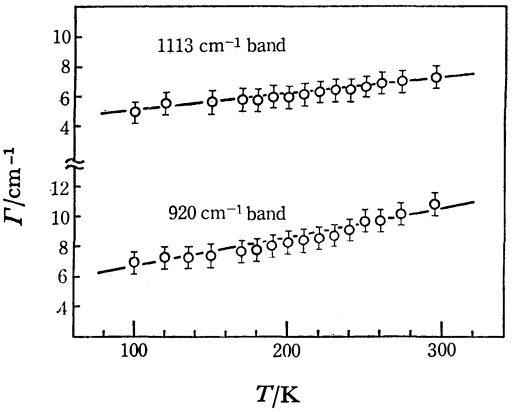

Fig. 5. The half-width of the band at 1113 cm^{-1} (CH_3 rock[4]) and that of the band at 920 cm^{-1} (CCN sym. stretch[4]) for L-α-alanine *versus* absolute temperature. The spectral slit-width is 3 cm^{-1}.

The appearance of the first overtone of the NH_3^+ torsional vibrations in the infrared spectra can be explained if we assume that the NH_3^+ torsions in L-α-alanine and DL-α-alanine are very anharmonic, as one would expect from any vibration associated with hydrogen bonds.

The theory given by Maradudin and Fein[7] predicts that the phonon width due to anharmonicity increases linearly with increasing temperature when the temperature is sufficiently high and is proportional to the square of the cubic force constant. The half-width of the band at 1113 cm^{-1} (CH_3 rock[4]) and that of the

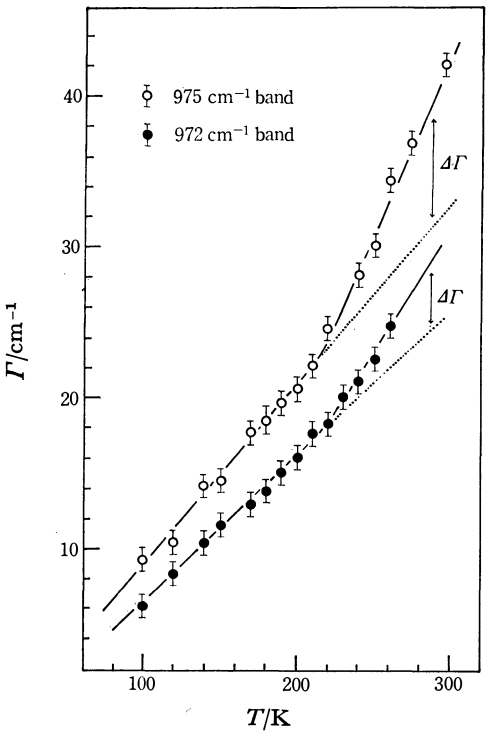

Fig. 6. The half-width of the band at 972 cm^{-1} for L-α-alanine and that of the band at 975 cm^{-1} for DL-α-alanine *versus* absolute temperature. The spectral slit-width is 3 cm^{-1}.

band at 920 cm^{-1} (CCN sym. stretch[4]) of L-α-alanine are plotted against temperature as shown in Fig. 5. They show a gradual temperature dependence, varying linearly with temperature, which indicates that the anharmonicity is small. In Fig. 6, the half-width of the 972 cm^{-1} band for L-α-alanine as well as that of the 975 cm^{-1} band for DL-α-alanine are plotted as a function of temperature. In the temperature range from 100 to 200 K, the half-widths of both bands also increase linearly with increasing temperature. However, the slopes are much steeper in this case, indicating considerable anharmonicity. An interesting feature in this figure is that the deviation from the linearity starts at about 200 K.

Wang and Storms[2,3] reported that a similar deviation was observed above 220 K for the half-width of the NH_3^+ torsional Raman band at 484 cm^{-1} for L-α-alanine. They explained the deviation as due to the modification of the NH_3^+ torsional mode by breaking of a –NH···O– hydrogen bond above 220 K.

If the extra broadening of the 972 and 975 cm^{-1} bands is also caused by relaxation induced by the rupture of a –NH···O– hydrogen bond, it is reasonable to assume that the extra broadening $\Delta\Gamma$ can be expressed as

$$\Delta\Gamma = \Delta\Gamma_0 \exp(-\Delta E/RT)$$

where ΔE is the activation energy of the hydrogen breaking process. In fact, a straight line was obtained when the observed values of $\ln(\Delta\Gamma)$ were plotted against $1/T$. From the slope of this straight line, ΔE was calculated to be 3.6 ± 0.6 kcal/mol for L-α-alanine and 3.7 ± 0.7 kcal/mol for DL-α-alanine.

These values are quite reasonable for the energy of a –NH···O– hydrogen bonding, being in good agreement with the hydrogen bonding energy of 3.5 ± 0.6 kcal/mol calculated by Wang and Storms from the half-width of the torsional Raman band at 484 cm^{-1} for L-α-alanine This may be regarded as additional evidence that the newly observed infrared bands at 972 cm^{-1} for L-α-alanine and at 975 cm^{-1} for DL-α-alanine are due to the first overtone of the NH_3^+ torsional mode.

The half-widths of the NH_3^+ torsional infrared bands at 487 cm^{-1} for L-α-alanine and at 497 cm^{-1} for DL-α-alanine were also measured at various temperatures. However, the splitting of these bands at low temperatures (Figs. 2 and 4) made it almost impossible to evaluate half-width accurately and ΔE was not calculated for these bands.

References

1) W. R. Feairheller and J. T. Miller, *Appl. Spectrosc.*, **25**, 175 (1971).
2) C. H. Wang and R. D. Storms, *J. Chem. Phys.*, **55**, 3291 (1971).
3) C. H. Wang and R. D. Storms, *ibid.*, **55**, 5110 (1971).
4) R. Adamowicz and E. Fishman, *Spectrochim. Acta*, **28A**, 889 (1972).
5) Y. Grenie and C. Garrigou-Lagrange, *J. Mol. Spectrosc.*, **41**, 240 (1972).
6) J. F. Jacovitz, T. A. Durkin, and J. L. Walter, *Spectrochim. Acta*, **23A**, 67 (1967).
7) A. A. Maradudin and A. E. Fein, *Phys. Rev.*, **128**, 2589 (1962).

The Photovoltaic Effect in Naphthacene-Gold Layers

Michio MATSUMURA, Hiromichi UOHASHI,* Masaki FURUSAWA,**
Naoto YAMAMOTO, and Hiroshi TSUBOMURA
Department of Chemistry, Faculty of Engineering Science, Osaka University, Toyonaka, Osaka 560
(Received November 25, 1974)

The photovoltaic effect in gold–naphthacene thin layers has been studied. By excitation in the region of the visible absorption band of naphthacene (2.4—3.0 eV), it was found that the photovoltage consists of two components; one with a short response time, caused by the electron transfer across the boundary between gold and naphthacene, and the other with a long response time, attributable to a diffusion process in the naphthacene film. The lifetime of carriers produced by the former process was estimated to be 0.08 s at least, decaying by the recombination of trapped holes in naphthacene with electrons in gold. Photovoltage was also observed in a region of wavelengths greater than the visible absorption band of naphthacene.

Photovoltaic effects of organic compounds have been investigated by many authors.[1] It is known that the photovoltage for a semiconductor is produced by the transport of charge carriers across contact barriers.[2] Other processes such as the Dember effect[3] are also known. However, in the case of organic compounds such as anthracene and naphthacene, analysis of the phenomena is more difficult because of complicated features and poor reproducibility.

In order to clarify the mechanism of photovoltage by illumination in the region of the absorption band of naphthacene, we have made a detailed study of the photovoltaic effect across the gold-naphthacene interface. The photovoltage for a similar system was reported by Reucroft *et al.*[4] Ghosh and Feng investigated the photovoltage for a gold-naphthacene–aluminum system, attributing the photovoltage to the difference in the work function of the two electrode materials.[5]

Experimental

The specimens are made in the form of successive thin layers of gold(Au^1), naphthacene, inositol[$C_6H_6(OH)_6$], and gold (Au^2), obtained by evaporation onto a quartz substrate at less than 10^{-5} Torr (Fig. 1). The gold layers at the two ends, serving as electrodes, are semi-transparent. The deposition rate of naphthacene was about 2 nm/s. The thickness of the naphthacene layer was determined, by measurements of the optical density, to be in the range 0.05—1.0 μ. The area covered by both electrodes was about 0.2 cm^2. The photovoltage was measured by two methods, (a) with exciting light chopped at 30 Hz and a lock-in amplifier(NF circuit design block, LI-573), and (b) with a steady light and vibrating reed electrometer (Takeda Riken, TR-84M). Throughout this paper, the photovoltage is defined as the voltage at the Au^1 electrode taking that at the other electrode (Au^2) as zero. An Ushio 500 W xenon lamp and an Ushio 500 W halogen lamp were used as light sources. A Japan Jarrel-Ash, 0.25 m Ebert-type monochromator was used. The light intensity was measured with a thermopile (Eppley, Bismus-silver type). Most measurements were made under ordinary atmosphere.

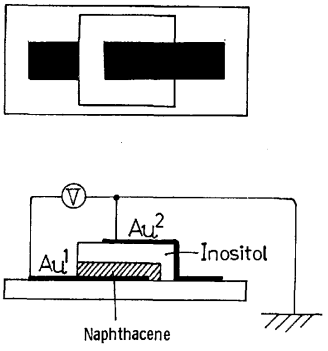

Fig. 1. A diagrammatic picture of a specimen used for photovoltaic measutements.

Results

The photovoltage of the Au^1–naphthacene–inositol–Au^2 system measured with the aid of a vibrating reed electrometer by exciting the visible absorption band of naphthacene is shown in Fig. 2. When the light was turned on, the photovoltage showed a quick negative response, followed by a slow rise toward the positive direction. When the light was turned off, it became more positive for an instant and then degraded slowly. It is obvious from this behavior that there are two components in the photovoltage (shown by broken lines): One has a negative polarity and a fast response and the other a positive polarity and a slow response. This photovoltaic behavior did not change with the direction of illumination, *i.e.*, illumination from either side of the Au electrodes. The response time and the intensity of

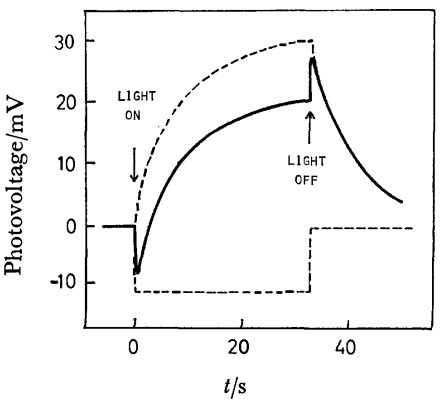

Fig. 2. The photovoltage measured as a function of time with steady illumination (λ=500 nm) by use of a vibrating reed electrometer.

* Present address: Engineering Plastics Ltd., Higashiosaka, Osaka.
** Present address: Sony Corp., Osaki, Tokyo.

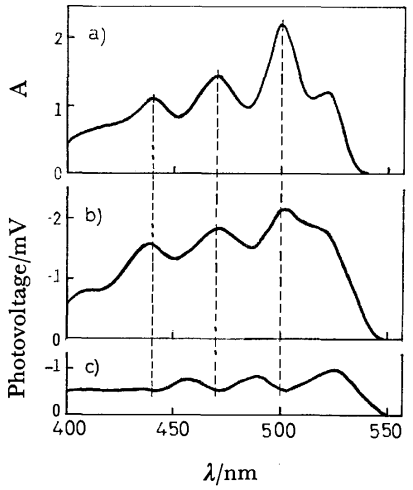

Fig. 3. (a) The absorption spectrum of a naphthacene film. (b) The photovoltage action spectrum, illuminated from the side of Au[1]. (c) The photovoltage action spectrum, illuminated from the side of Au[2]. The thickness of naphthacene layer is about 0.6 μ throughout. The photovoltage was measured by using a lock-in amplifier. The curves (b) and (c) are corrected so as to give photovoltages at the illumination intensity of 5.4×10^{13} photons/cm^2·s throughout the spectral region.

the slow component differed to some degree with specimen.

The visible absorption spectrum of a naphthacene layer deposited on a quartz glass plate is shown in Fig. 3a. The spectrum nearly coincides with the absorption spectrum of the single crystal of naphthacene assigned to a ^{1}La transition.[6]

The action spectra for the photovoltages measured with a lock-in amplifier are shown in Figs. 3b and c. It should be noted that only the component of photovoltage alternating at 30 Hz is given by this method and the resulting action spectra correspond to the fast-response component of the photovoltage shown in Fig. 2. Curve b, the action spectrum for illumination from the Au[1] side, closely resembles the absorption spectrum of curve a, while curve c, the action spectrum for illumination from the Au[2] side, is entirely different.

One of the action spectra for the photovoltage measured with the vibrating reed electrometer is shown in Fig. 4, with illumination from the Au[1] side and the wavelength scanned from short to long wavelengths at the speed of 25 nm/min. Contrary to the case shown in Fig. 3b, the action spectrum has a shape quite different from the absorption spectrum. The position of the minima indicated by arrows correspond well with the absorption peaks. Since there are two components in the photovoltage, the action spectrum should contain spectra for the positive and negative components. The fast-response, negative component should have a structure similar to the absorption spectrum, and therefore the action spectrum can be regarded as the difference between the slow-response, positive component, shown by the broken line, and the fast-response, negative component (hatched part).

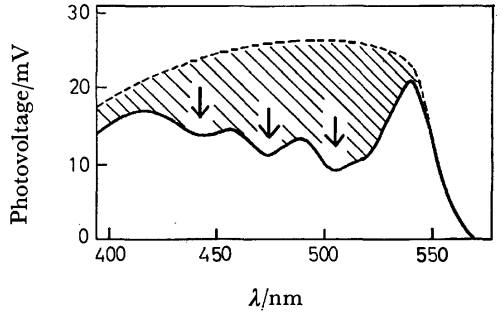

Fig. 4. The photovoltage action spectrum observed by using a vibrating reed electrometer under steady illumination.

The dependence of photovoltage on the exciting light intensity for each of the components is shown in Fig. 5. The photovoltage of the slow-response component (Fig. 5a) was measured with light at 535 nm and a vibrating reed electrometer. In the region where the light is weak, the photovoltage is proportional to light intensity,

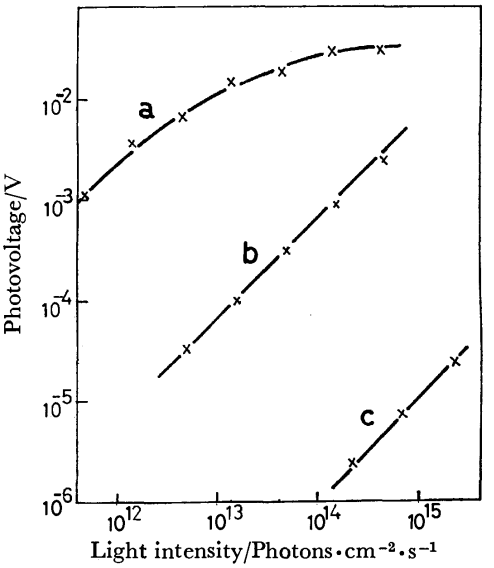

Fig. 5. The dependence of the photovoltages on light intensity. (a) Slow-response component, measured with a vibrating reed electrometer, λ 535 nm. (b) Fast-response component, measured with a lock-in amplifier, λ 500 nm. (c) Photovoltage in the long wavelength region, measured with a lock-in amplifier, λ 820 nm.

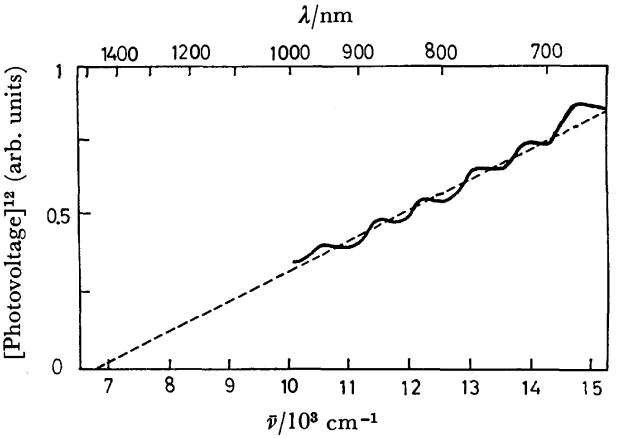

Fig. 6. Photovoltage action spectrum measured with the aid of a lock-in amplifier in the region of wavelength longer than the absorption band of naphthacene.

but shows saturation in the strong light region. The light intensity at which saturation began differed a little with specimen. It also shifted to the weaker intensity side day by day. The fast-response component of the photovoltage, measured with light at 500 nm and the lock-in amplifier, was proportional to the light intensity (Fig. 5b).

Weak photovoltages were also observed even with light at wavelengths longer than the absorption band of naphthacene. The action spectrum measured by using the lock-in amplifier is shown in Fig. 6. The dependence on light intensity is shown in Fig. 5c. The polarity was the same as that of the fast-response component observed for the excitation in the region of the absorption band.

Discussion

Mechanism for the Photovoltaic Effect. *a. The Fast-response Component*: The fast-response component makes the Au^1 electrode negative, and can be selectively measured by means of the chopped light method. When the light comes from the Au^1 side, the action spectrum agrees with the absorption spectrum of the naphthacene layer (Fig. 3b). When the light comes from the other side, the maxima of the action spectrum do not agree with the absorption peaks, but agree in wavelength with those of the absorption bottoms. In the case where the layer of naphthacene was thinner than 0.2 μ, the action spectra did not change with the direction of the illumination and agreed with the absorption spectra. These results suggest that the fast-response component of the photovoltaic effect takes place near the interface between gold (Au^1) and naphthacene, because the light coming from the side of Au^2 is absorbed more strongly at the absorption peaks in the naphthacene layer before reaching the naphthacene-Au^1 boundary than at the bottoms. The charge transfer process caused by the exciton at the interface may be suitable for explaining the results. The negative polarity shows electron trasfer from the naphthacene exciton to Au^1. A similar mechanism was proposed by Killesreiter and Baessler for an aluminum electrode-anthracene crystal system.[7,8] They attributed the photocurrent to a charge carrier generated by the exciton-metal interaction, and concluded that the electron transfer from the exciton takes place mainly within 20 Å from the boundary.

The depths of light absorption (the distance at which the light intensity becomes 1/e) of the naphthacene layer can be approximately estimated from the absorbances to be 0.12 μ at λ 500 nm (at the absorption maximum) and about 0.3 μ at the minima. When illuminated from the side of Au^2 into the naphthacene layer 0.6 μ or more in thickness, the exciting light hardly reaches the interface. The fact that we obtained photovoltage to a considerable magnitude under these conditions (Fig. 3c) shows that some species with long diffusion length (>0.1 μ) participate in the electron transfer process at the boundary. The diffusion length of the singlet exciton in naphthacene single crystal is determined to be 120 Å[9] by fluorescence studies, and that of triplet exciton to be 0.4 μ[10] by photocurrent studies. For a thin film made by evaporation, the values should be smaller. It might be concluded that the participation of triplet excitons formed from singlet excitons is predominant in the charge carrier generation for the case of excitation from the Au^2 side. When illuminated from the Au^1 side, both singlet and triplet excitons can participate in the electron transfer process.

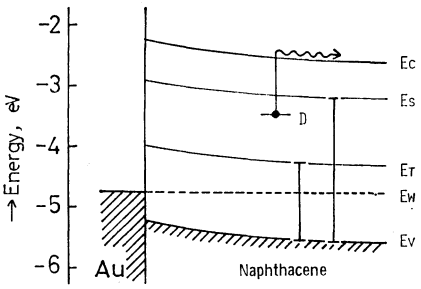

Fig. 7. A band model for the gold-naphthacene interface. E_C, E_V, and E_W designate the energies of the conduction band, the valence band and the work function of gold, respectively. E_S and E_T are the energies of the singlet and triplet excitons of naphthacene. *D* indicates a hypothetical donor level.

The work function of gold (E_w) is about 4.8 eV,[11] the ionization potential of naphthacene (I_p) is about 5.25 eV[12] and the band gap of naphthacene (E_g) is 3.0 eV.[13] If one takes the position of the valence band of naphthacene (E_v) to be 5.25 eV, then, that of the conduction band (E_c) is 2.25 eV. The energies of the singlet exciton (E_s) and the triplet exciton (E_T) from the valence band are 2.4 eV[13] and 1.25 eV,[14] respectively (Fig. 7). The electron transfer from naphthacene to gold requires an energy higher than $E_v - E_w$, *viz.*, 0.45 eV. For the case of the electron transfer from gold to naphthacene, the energy of $E_w - E_c$, *viz.*, 2.55 eV or more, is required. The energies of both singlet and triplet excitons are therefore large enough to cause an electron transfer from naphthacene to gold, but not to cause an electron transfer from gold to naphthacene. This conclusion is compatible with the polarity of photovoltage observed.

b. The Slow-response Component: The photovoltage curve in Fig. 4 can be interpreted to be the superposition of a slow-response, positive component and a fast-response, negative one. When the light is not very strong, the two components of the photovoltage are nearly proportional to the light intensity, as shown in Figs. 5a and b. One can therefore conclude that the action spectrum when illuminated from the Au^1 side should have the same fine structure as that of the absorption spectrum. But the slow-response component is strong in the region of the tails of absorption band of naphthacene (Fig. 4), which implies that the slow component of the photovoltaic effect takes place, not at the interface but inside the naphthacene layer.

Jortner proposed an exciton-exciton interaction mechanism for free carrier generation in the bulk.[15] This mechanism, however, does not explain the dependence on light intensity we obtained. The exciton-impurity (electron donor or electron acceptor) interaction or exciton-trapped carrier interaction, leading to carrier

formation as indicated in Fig. 7, seems to be a plausible mechanism for the slow response component.

As is usual in the band theory for semiconductors, we assume that the naphthacene energy bands are bent near the boundary due to the difference of work functions between gold and naphthacene. Since the work function of naphthacene is reported to be 4.51 eV,[16] we can assume that the bands for naphthacene are bent downwards toward the interior as shown in Fig. 7 by an amount of (4.87—4.51) eV. When free carriers are produced in the naphthacene, the electrons move to the interior of the naphthacene layer and the holes move to the gold electrode according to the energy gradient. It is therefore expected that the polarity of the photovoltaic effect becomes positive at the electrode, regardless of the species of the mobile carrier. Thus we can conclude that the slow-response component arises from the charge carrier generation in the interior of naphthacene layer.

Some of the carriers might be captured by shallow traps. The trapped carriers can be thermally excited and recombine slowly with the counter charge carriers. The decay of the slow-response component can be interpreted by such a thermal recombination process.

c. Photovoltaic Effect in the Region of Long Wavelength: A very weak photovoltage was observed in the region of wavelength longer than the absorption band of naphthacene with a lock-in amplifier. The polarity and the light intensity dependence are the same as those of the fast-response component caused by light in the region of the absorption band. The action spectrum is shown in Fig. 6, where the square root of the photovoltage is plotted against wave number. The photovoltage could be observed even with light at 1000 nm. The small humps in the spectrum are due to the interference of light in the sample. No peak can be observed which corresponds to S–T absorption band of naphthacene. It is seen that the plot lies roughly on a straight line (dotted line). From the intersection of the straight line with abscissa, the threshold energy for the photovoltage is found to be about 6800 cm^{-1} (0.84 eV). Williams and Dresner reported the threshold value of photoemission of holes from gold to anthracene crystal to be 1.17 eV[17] from the photocurrent measurement. Based on their result, 0.77 eV is estimated as the threshold of photoemission of holes from gold to naphthacene, since naphthacene has an ionization potential 0.40 eV smaller than anthracene. This nearly coincides with the value derived experimentally by us. Our result also shows that the photoemission occurs for an organics-metal system without external electric field.

A slow-response, positive component of the photovoltage was observed with the light at wavelengths greater than the absorption edge of naphthacene, in addition to the fast-response, negative one. The former component might be caused by the direct excitation of the trapped carriers.

Since the photovoltage measured with the aid of a lock-in amplifier gives only the alternating part of the voltage caused by chopped light, there should be no effect by an additional steady illumination, if the photovoltage is proportional to light intensity. Contrary to expectation, the photovoltage remarkably increased by steady illumination in the region of the absorption band of naphthacene in addition to the chopped light at wavelengths greater than that of absorption band. It was also observed that this enhancement grew slowly on application of the steady light, as in the case of the slow-response component. It is plausible that the long wavelength light stimulates the detrapping of the trapped carriers produced by the steady light in naphthacene layer.

Carrier Formation and Recombination at the Boundary. The excitons at the boundary between gold and naphthacene inject holes into the naphthacene layer.

The rate of transfer is formulated as

$$dN/dt = I\Phi\eta - kN, \quad (1)$$

where N is the density of holes in the naphthacene layer [holes·m^{-2}], I the light intensity [phtons·m^{-2}·s^{-1}], Φ the quantum yield of the excitons which can reach the boundary per photon, η the efficiency that the exciton causes electron transfer, and k is the rate constant for the recombination of holes with the electrons in the gold electrode [s^{-1}].

In the stationary state, N is given by Eq. 2 taking $dN/dt=0$

$$N = I\Phi\eta/k, \quad (2)$$

For the sake of simplicity we assume that the holes lie on a plane parallel to the boundary with a distance d. Then the photovoltage (V_{ph}) can be given by

$$V_{ph} = Ned/\varepsilon\varepsilon_0, \quad (3)$$

where e is the elementary electronic charge, ε the dielectric constant of naphthacene, and ε_0 the vacuum permittivity. From Eqs. 2 and 3, we find that V_{ph} is proportional to the light intensity, in agreement with the experimental result (Fig. 5b). The experimental value of V_{ph} was obtained to be 20 mV, at $I=10^{18}$ photons·m^{-2}·s^{-1}, at $\lambda=500$ nm, measured with the aid of a vibrating reed electrometer and using the specimen whose slow-response component was weak. η and ε can be taken to be 0.2[7] and 3.8,[18] respectively, according to Baessler *et al.* d can be reasonably assumed to be 5 Å, and Φ 0.5 at most. We can then get k to be 12 s^{-1} or less. This corresponds to a lower limit of the lifetime of the holes produced at the boundary of 0.08 s. The lifetime thus obtained is much longer than the value of 1.2—2.0 μs[19] reported by Bogus. Bogus derived the lifetime of the hole produced at the boundary between an anthracene crystal and silver from measurement of the photocurrent, where free carriers only participate. It should be noted that the photovoltage is caused not only by free carriers but also by trapped carriers. Thus it is concluded that the holes produced in our experiment are trapped within a few microseconds, and the trapped holes then recombine with electrons in the metal within some hundreds of milliseconds. Although no detailes on the state of trapped holes are known, they might either be localized on naphthacene cation or impurity cation stabilized near the boundary. Our studies on the photovoltaic effect have thus revealed the existence of trapped holes with a long lifetime at the boundary between an organic substance and a metal.

References

1) F. Gutmann and L. E. Lyons, "Organic Semiconductors," John Wiley & Sons, New York (1967), p. 790.
2) T. S. Moss, G. J. Burrell, and B. Ellis, "Semiconductor Opt-Electronics," Butterworth & Co., London (1973), p. 153.
3) T. S. Moss, L. Pincherle, and A. M. Woodward, *Proc. Phys. Soc.* (London) B, **66**, 743 (1953).
4) P. J. Reucroft, P. L. Kronick, and E. E. Hillman, *Mol. Cryst. Liq. Cryst.*, **6**, 247 (1969).
5) A. K. Ghosh and T. Feng, *J. Appl. Phys.*, **44**, 2781 (1973).
6) A. Bree and L. E. Lyons, *J. Chem. Soc.*, **1960**, 5206.
7) H. Killesreiter and H. Baessler, *Chem. Phys. Lett.* **11**, 411 (1971).
8) H. Killesreiter and H. Baessler, *Phys. Status Solidi B*, **51**, 657 (1972).
9) G. Vaubel and H. Baessler, *Mol. Cryst. Liq. Cryst.*, **12**, 47 (1970).
10) G. Vaubel and H. Kallmann, *Phys. Status Solidi*, **35**, 789 (1969).
11) P. A. Anderson, *Phys. Rev.*, **115**, 553 (1959).
12) M. Pope, J. Burgos, and J. Giachino, *J. Chem. Phys.*, **43**, 3367 (1965).
13) N. Geacintov, M. Pope, and H. Kallmann, *ibid.*, **45**, 2639 (1966).
14) Y. Tomkiewicz, R. P. Groff, and P. Avakian, *ibid.*, **54**, 4504 (1971).
15) J. Jortner, *Phys. Rev. Lett.*, **20**, 244 (1968).
16) M. Kotani and H. Akamatu, *Discuss. Faraday Soc.*, **51**, 94 (1971).
17) R. Williams and J. Dresner, *J. Chem. Phys.*, **46**, 2133 (1967).
18) H. Baessler, G. Herrmann, N. Riehl, and G. Baubel, *J. Phys. Chem. Solids*, **30**, 1579 (1969).
19) C. Bogus, *Z. Phys.*, **207**, 281 (1967).

Hydrogen Bonding Interactions of Carboxylic Acids with *N,N*-Dimethylacetamide and Pyrazine as Studied by Means of NMR Dilution Shifts

Hideaki FUJIWARA, Nobuyuki YOSHIDA, and Tsuneo IKENOUE

Chemical Research Institute of Non-Aqueous Solutions, Tohoku University, Katahira 2-1-1, Sendai 980

(Received December 9, 1974)

The NMR dilution shifts of OH proton in several carboxylic acids have been studied for mixtures with *N,N*-dimethylacetamide (DMA) or pyrazine. The acids treated were acetic, propionic isobutyric, and trifluoroacetic acids. The dilution shifts curve of OH proton in each acid–DMA system showed a characteristic *v*-type curve with the minimum value at 0.65—0.75 mol fraction of the acid. The curve for the isobutyric acid–pyrazine system was linear below 0.45 mol fraction of the acid, taking the minimum at 0.75 mol fraction. These curves were explained by assuming the formation of both 1: 1 and 2 (acids): 1(base) complexes in the chemical equilibrium. The formation constants of the complexes and the shifts of OH proton in the 2: 1 complex were estimated for each system. Liability of the complex formation and the structure possible for the 2: 1 complex were discussed.

The amide-acid interaction has been of interest to many NMR investigators.[1-6] Gillespie and Birchall[1] studied the proton NMR spectra of several amides in FSO_3H at low temperatures and concluded that amides were protonated at the oxygen atom. It was found that the addition of trifluoroacetic acid (TFA)[3] or dichloroacetic acid[4] to an amide leads to the unrestricted internal rotation around the C–N bond, which was interpreted as resulting from the occurrence of *N*-protonation in the amide. The examination of the absorption spectra of amides in sulfuric acid by Goldfarb *et al.*[7] indicates the presence of two equilibria in the mixture, one corresponding to the protonation of the amide and the other to the hydrogen bonding of the protonated amide with the solvent. Edward and Wang,[8] however, explained the spectral data only in terms of a protonation equilibrium of the amide considering the difference in the hydration number between a protonated amide and a protonated Hammett indicator which was used to establish the H_0 scale. Thus the simultaneous interaction of the amide with two acidic protons has not been corroborated yet.

The interaction of *N,N*-dimethylacetamide (DMA) with some carboxylic acids has been studied also by measuring the density, viscosity, electric conductivity, melting point, and infrared and Raman spectra.[3,9-11] For the acetic acid–DMA system, the formation of 1: 1 and 2 (acids): 1(DMSO) complexes has been suggested, the former from the fact that the glass formation occurred in the range 0.4—0.6 mol fraction of the acid,[10] and the latter from the fact that the viscosity and electric conductivity became maximum in the range 0.6—0.7 mol fraction.[11] The presence of the 1: 1 and 2: 1 complexes in the acetic acid–DMA system was also suggested by Khazova and Chesnokov[11] as a result of the measurements of their infrared and Raman spectra, though the importance of the Fermi resonance to interpret the spectra had been pointed out by Haurie and Novak.[9]

In a previous paper,[12] the NMR dilution shifts for the binary systems of some carboxylic acids and dimethyl sulfoxide (DMSO) were examined and the shift curves were explained assuming the formation of both 1: 1 and 2 (acids): 1 (DMSO) complexes in the chemical equilibrium. A similar examination for the systems of some carboxylic acids in DMA has been carried out. To ascertain the participation of 2: 1 complex in such acid-base interaction, pyrazine was also chosen as a base which possesses two equivalent basic sites in a molecule. Acetic, propionic, isobutyric, and trifluoroacetic acids were used as the acid.

Experimental

All the procedures for the purification of carboxylic acids and the preparation of solutions are the same as reported previously.[12] Commercial DMA was dried by returning the forerun through barium oxide into a still pot after the addition of toluene by 30 volume %. After drying had been accomplished, toluene was removed by distillation under reduced pressure. When methanol was mixed with the purified DMA, the NMR fine structure of OH proton was clearly observed, in particular below 0.5 mol fraction of the alcohol,[13] showing the marked efficiency of DMA to retard the exchange rate of the OH proton.

Pyrazine was handled in a liquid state with use of a constant temperature box at about 65°C. Commercial pyrazine was purified in a similar way to that for DMA.

NMR spectra were obtained with a Hitachi R-20B high resolution NMR spectrometer (60 MHz, at 34.5 °C). The chemical shift was measured with a frequency counter, the error being within $\pm$0.1 Hz. NMR measurements at high temperatures were carried out with a Hitachi R-20VTP prove. The sample temperatures were determined with a ethylene glycol "chemical shift thermometer". The NMR spectra for the isobutyric acid–pyrazine system at ordinary temperature were measured with a Varian V-4300B NMR spectrometer (60 MHz). The shift was determined by the side band technique with accuracy of $\pm$0.15 Hz. The probe temperature was 33 °C.

Results

The shifts of OH proton (δ_{OH}) in the carboxylic acid–DMA systems plotted against acid mol fraction (X) are shown in Figs. 1 and 2. The dilution shift curves for isobutyric and propionic acids exhibit the *v*-type pattern (Fig. 1), the curve for TFA being linear below 0.45 mol fraction of the acid (Fig. 2). These curves are similar to those obtained for the carboxylic acid–DMSO systems.[12] The curve for acetic acid (Fig. 1) exceptionally shows no minimum in the intermediate con-

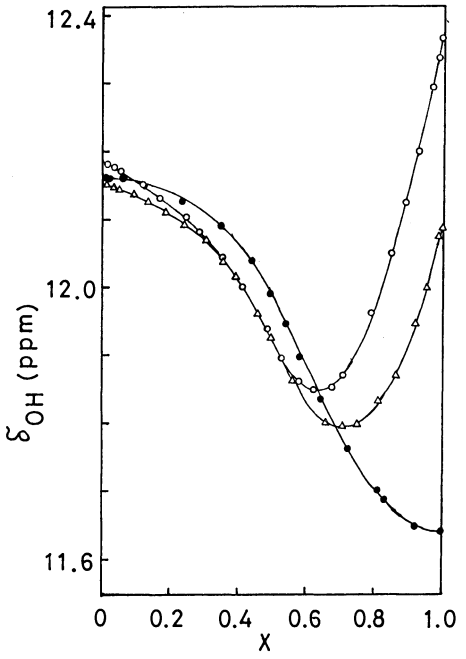

Fig. 1. Dilution shift curves observed for the acid–DMA systems.
○: Isobutyric acid. △: Propionic acid. ●: Acetic acid.

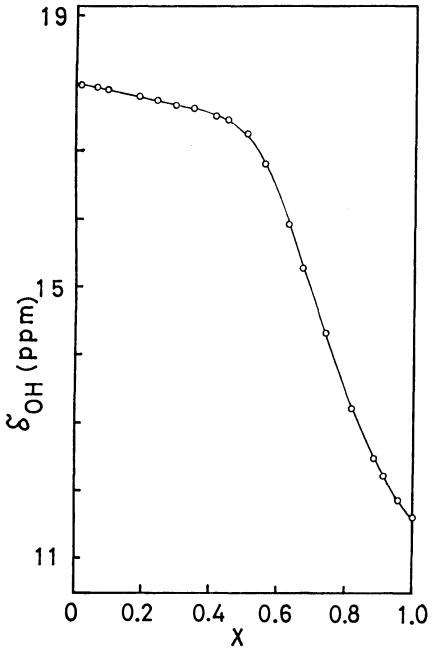

Fig. 2. A dilution shift curve observed for the TFA –DMA system.

centration. This is understandable from the following facts: (1) the difference between the minimum shift and the shift for the neat solution decreases in the order of isobutyric, propionic, and acetic acids for the acid-DMSO systems, (2) the difference is smaller in the acid-DMA systems than that in the acid-DMSO systems for isobutyric and propionic acids.

The dilution shift curve for the isobutyric acid-pyrazine system at ordinary temperature (curve a,

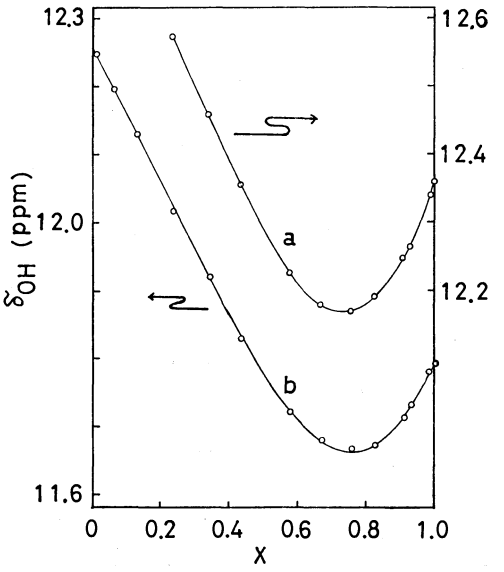

Fig. 3. Dilution shift curves observed for the isobutyric acid-pyrazine system.
a: At 33 °C. b: At 80.5 °C.

Fig. 3) also goes through the minimum at 0.75 mol fraction of the acid. The measurements for this system at two high temperatures of 80.5 °C (curve b) and 127 °C (not shown but similar to curve b in Fig. 3) revealed that the concentration corresponding to the minimum shift does not vary with temperature and the curves are practically linear below 0.45 mol fraction of the acid.

The dilution shift curve of the TFA-pyrazine system at 60 °C was similar to the curves for the TFA-DMA (Fig. 2) and TFA-DMSO[12] systems.

Two proton signals due to the two *N*-methyl groups of DMA in the TFA-DMA system coalesced into a singlet above 0.55 mol fraction of the acid.[3] The acid concentration where the coalescence occurred was temperature dependent; it decreased from 0.55 mol fraction at 34.5 °C to 0.35 mol fraction at 40.0 °C. No such coalescence was observed for the systems containing isobutyric, propionic, or acetic acid instead of TFA at 34.5 °C.

The shift of CH proton in the acid and base changed monotonously with the acid concentration. The variation of the shift was less than 1/5 of that for the OH proton.

Discussion

An acid-base interaction in solution generally produces either the ionic species such as the conjugate acid or base of the initial species, or the hydrogen bonded complex. The former is important in the case of a strong acid against a strong base, and the latter in the case of a weak acid against a weak base. Measurements of the infrared spectra on the systems of acetic acid-DMA,[14] formic acid-DMA,[15] and formic acid-DMSO[15] revealed no ionic species. Examination of the absorption spectra of pyrazine in the mixture of isobutyric acid and *n*-hexane did not show any evidence of the presence of ionic species,[16] though the dissolu-

tion of pyrazine in aqueous sulfuric acid clearly produces the ionic species such as pyrazinium ions.[17-19]

It can thus be assured that only the hydrogen bond formation is important in interpreting the NMR data for the OH protons of acetic, propionic, and isobutyric acids in DMSO, DMA, and pyrazine. Since the presence of ionic species has been reported for the systems containing TFA with DMSO,[3] DMA,[14] or pyrazine,[20] the contribution of ionic species may be unavoidable in interpreting the data for these systems.

The characteristic ν-type shift curves (Figs. 1 and 3) are interpreted by assuming that the carboxylic acid dimer produces the 2: 1 and 1: 1 complexes with a base[12] as follows:

$$A_2 + B \rightleftarrows A_2 \cdot B \qquad K_1$$

$$A_2 \cdot B + B \rightleftarrows 2(A \cdot B) \qquad K_2$$

where A_2 and B denote the carboxylic acid cyclic dimer and the base, respectively, and $A_2 \cdot B$ and $A \cdot B$ the 2: 1 and 1: 1 complexes, respectively. The procedure for analysis of the ν-type shift curve is summarized below, the detailes having been given previously.[12] Under the above conditions, the shift of OH proton can be calculated in terms of the following six parameters:

δ_D=the shift of OH proton in the cyclic dimer of the acid. The value was evaluated by extrapolating the straight part of the dilution shift curve in cyclohexane to infinite dilution of the acid,

$\delta_{C\beta}$=the shift of OH proton in the 1: 1 complex. The value was substituted by the value of δ_{OH} (the shift observed) at infinite dilution of the acid in DMA or pyrazine,

$\delta_{C\alpha}$=the shift of OH proton in the 2: 1 complex,

K_1=the formation constant of the 2: 1 complex,

K_2=the formation constant of the 1: 1 complex, and

X=initial mol fraction of the acid in monomer unit.

Of these, $\delta_{C\alpha}$, K_1, and K_2 remain to be determined. δ_D, $\delta_{C\beta}$, and X were obtained experimentally. These three parameters can be determined by calculation so as to give the best fit between the calculated and observed dilution shift curves. This process of the least squares was achieved by the trial and error method, only one set of parameters being obtained for each system within an acceracy of the measurement of shifts and concentrations. Parameters obtained experimentally or by calculation for each system are summarized in Table 1, together with those for the acid-DMSO systems.[12] The shift data above 0.6 mol fraction of the acid were omitted in the calculation, since the deviation between the calculated and observed shifts never diminished in that region.

Table 1. Parameters obtained experimentally or by calculation[a] for carboxylic acid–DMSO, DMA, and pyrazine systenms (34.5 °C)

Base	Acid	δ_D	$\delta_{c\beta}$	K_1	K_2	$\delta_{c\alpha}$
DMSO	Acetic	13.36	11.88	100	9	11.13
	Propionic	12.49	11.89	60	9	11.00
	Isobutyric	12.64	11.92	40	9	10.87
	TFA	12.03	16.44	c	c	c
DMA	Acetic	12.36	12.162	220	10	11.70
	Propionic	12.49	12.155	60	8	11.52
	Isobutyric	12.64	12.185	90	5	11.59
	TFA	12.03	18.00	c	c	c
Pyrazine[b]	Isobutyric	12.19	12.257	20	1.7	11.353

a) δ_D and $\delta_{c\beta}$ are obtained experimentally and K_1, K_2, and $\delta_{c\beta}$ by calculation. The accuracy of calculation is $\pm 20\%$ for K_1 and K_2 and ± 0.05 ppm for $\delta_{c\alpha}$. b) The isobutyric acid–pyrazine system is investigated at 80.5 °C. c: Not fully analyzed.

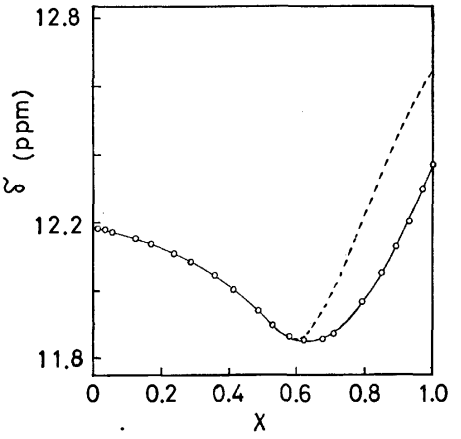

Fig. 4. A comparison of the observed and the calculated dilution shift curves for the isobutyric acid-DMA system.
——: Observed. ----: Calculated. ○: Experimental points.

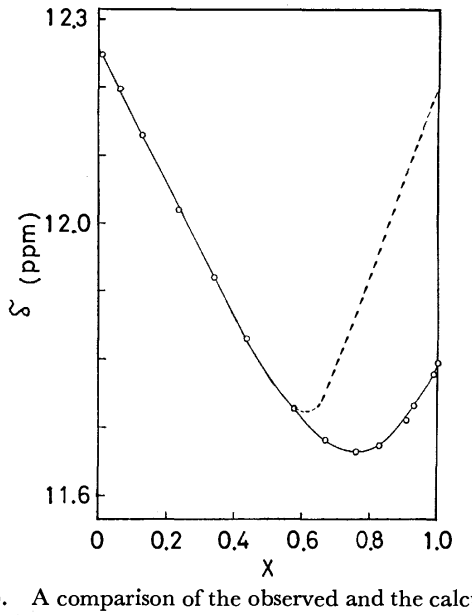

Fig. 5. A comparison of the observed and the calculated dilution shift curves for the isobutyric acid-pyrazine system (at 80.5 °C).
——: Observed. ----: Calculated. ○: Experimental points.

The deviation of δ_{calcd} (shift value calculated) from δ_{OH} (shift value observed) above 0.6 mol fraction of the acid is shown in Figs. 4 and 5. It is larger in the isobutyric acid-pyrazine system than in the isobutyric acid-DMA system. The larger deviation for the pyrazine system is presumably due to the fact that the measurement temperature was higher. Since a rise in

temperature usually causes a larger contribution of the monomer and/or chain oligomer of carboxylic acid,[21] higher temperature may be responsible for the larger deviation of δ_{calcd} from δ_{OH}.

The K_1 values are always more than five times larger than the K_2 values (Table 1). The large K_1 value implies the low concentration of the cyclic dimer in solution and a remarkable tendency of the acid molecule to form complexes with the base. The Raman spectral data[9] also show a negligibly small amount of the cyclic dimer for the solutions of about 0.5 mol fraction of acetic acid in DMSO or DMA.

Although pyrazine is known to be more basic than DMSO and DMA,[22] K_1 in pyrazine is smaller than that in either DMSO or DMA. This is partly ascribed to the higher measurement temperature of pyrazine system than that of DMSO and DMA systems. The polarity of each species in a solution may also explain the small K_1 in pyrazine. Pyrazine is a non-polar solvent, while DMSO and DMA are dipolar solvents. While the cyclic dimer of carboxylic acid will be less polar, the complexes of the acid with these basic solvents may be well supposed to be polar. The polar species is stabilized in a polar medium to a larger extent than the less polar species such as the cyclic dimer, leading to the large K_1 value in a polar medium.

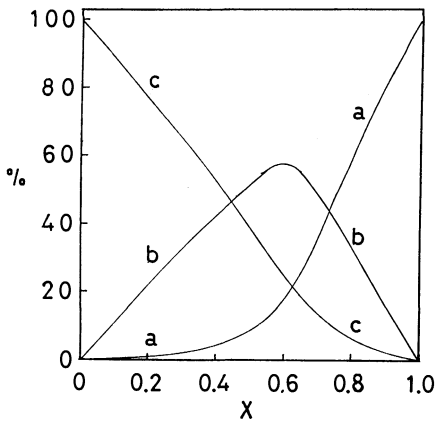

Fig. 6. A distribution curve of the acid molecule to each species in the isobutyric acid-pyrazine system.
a: Cyclic dimer. b: 2: 1 Complex. c: 1: 1 Complex.

For the isobutyric acid-pyrazine system, the dilution shift curve is linear below 0.45 mol fraction of the acid, an apparent difference from the curves for the acid-DMA systems. As seen from Fig. 6, the 1: 1 and 2: 1 complexes predominate below 0.45 mol fraction of the acid, and the shift depends almost on the K_2 value which is decisive to the ratio of 1: 1 complex to 2: 1 complex. Thus, the linearity in the dilution shift curve of the isobutyric acid-pyrazine system may be due to the smallness of the K_2 value.

It is noteworthy that $\delta_{C\alpha}$ lies in a higher field side than $\delta_{C\beta}$ and δ_D (Table 1). This is closely related to an appearance of the minimum in the shift curve at a higher acid concentration. The structure possible for the 2: 1 complex of the acid with DMA and pyrazine are readily given as I and II, respectively, in which two basic sites of the base interact simultaneously with the acids.

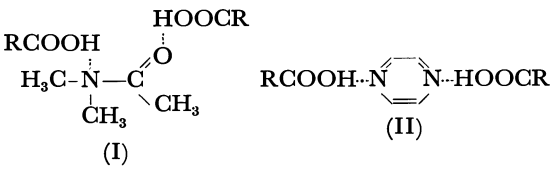

The authors are grateful to Professor Y. Ikegami and Mr. M. Kumano for their helpful discussions. They are also indebted to Mr. K. Fujieda for discussing the accuracy of NMR measurements.

References

1) R. J. Gillespie and T. Birchall, *Can. J. Chem.*, **41**, 148 (1963).
2) G. A. Olah, D. L. Brydon, and R. D. Porter, *J. Org. Chem.*, **35**, 317 (1970).
3) C. F. Nawrot and A. Veis, *J. Amer. Chem. Soc.*, **92**, 3903 (1970).
4) P. A. Temussi and R. Bellofiore, *Ric. Sci.*, **39**, 419 (1969).
5) A. R. Katritzky and R. A. Y. Jones, *Chem. Ind.*, (London), **1961**, 722.
6) R. B. Homer and C. D. Johnson in "The Chemistry of Amides," ed. by J. Zabicky, John Wiley & Sons, London (1970), Chapter 3.
7) A. R. Goldfarb, A. Mele, and N. Gutstein, *J. Amer. Chem. Soc.*, **77**, 6194 (1955).
8) J. T. Edward and I. C. Wang, *Can. J. Chem.*, **40**, 966 (1962).
9) M. Haurie and A. Novak, *J. Chim. Phys.*, **64**, 679 (1967).
10) V. F. Chesnokov and I. M. Bokhovkin, *Zh. Obshch. Khim.*, **39**, 1189 (1969).
11) I. V. Khazova and V. F. Chesnokov, *ibid.*, **40**, 7 (1970).
12) H. Fujiwara, *J. Phys. Chem.*, **78**, 1662 (1974).
13) The fine structure of OH proton had never been observed clearly in the methanol-DMA system; C.R. Kanekar, C. L. Khetrapal, K. V. Ramiah, and C. A. Indirachary, *Proc. Indian Acad. Sci., Sect. A*, **66**, 189 (1966).
14) P. Combelas, F. Cruege, J. Lascombe, C. Quivoron, and M. Rey-Lafon, *J. Chim. Phys.*, **66**, 668 (1969).
15) C. W. Chao, A. Veis, and F. Jacobs, *J. Amer. Chem. Soc.*, **89**, 2219 (1967).
16) H. Fujiwara and T. Ikenoue, *Sci. Rept. RITU., A*, **25**, 145 (1975).
17) A. S. Chia and R. F. Trimble, Jr., *J. Phys. Chem.*, **65**, 863 (1961).
18) R. H. Linnell and A. Kaczmarczyk, *ibid.*, **65**, 1196 (1961).
19) M. Iwaizumi and H. Azumi, *Nippon Kagaku Zasshi*, **84**, 694 (1963).
20) H. Kamei, *J. Phys. Chem.*, **69**, 2791 (1965).
21) M. Haurie and A. Novak, *C. R. Acad. Sci., Paris, Ser. B*, **264**, 694 (1967).
22) pK_{BH^+} values of DMSO, DMA, and pyrazine are -2.8,[23] -0.19,[7] and 0.65,[17] respectively, in aqueous sulfuric acid.
23) P. Haake and R.D. Cook, *Tetrahedron Lett.*, **1968**, 428.

Photolysis of Cyclopropane at 1470 and 1634 Å

Kazuhiko SHIBUYA, Kin-ichi OBI, and Ikuzo TANAKA

Department of Chemistry, Tokyo Institute of Technology, Ohokayama, Meguro-ku, Tokyo 152

(Received December 18, 1974)

The vacuum-ultraviolet photolysis of cyclopropane in the gas phase has been investigated at room temperature at excitation wavelengths 1470 and 1634 Å. Primary processes are discussed in terms of variations of product yield as a function of conversion and in the presence of additives such as NO, C_2D_4, and H_2. The relative yields of decomposition are determined at both wavelengths. The main primary process is cyclo-$C_3H_6+h\nu\rightarrow C_2H_4+CH_2$, the yield being 67% at 1470 Å (69% at 1634 Å). The observed product yield responsible for methylene is much less than that for ethylene. However, the yields become equal in the photolysis of cyclopropane with excess hydrogen. The other primary processes are as follows in order of decreasing importance; cyclo-$C_3H_6+h\nu\rightarrow C_2H_3+CH_3$, 19% (18%), cyclo-$C_3H_6+h\nu\rightarrow C_3H_4+2H$, 9% (7%), cyclo-$C_3H_6+h\nu\rightarrow C_2H_2+CH_3+H$, 3% (4%), cyclo-$C_3H_6+h\nu\rightarrow C_2H_2+CH_4$, 1% (1%).

Numerous studies have been carried out on the vacuum ultraviolet photolysis of simple hydrocarbons.[1,2] However, less attention has been paid to the photolysis of cycloalkanes than to typical alkanes and alkenes.

Photolysis of the simplest cycloalkane, cyclopropane, was first carried out at 1470 Å by Currie, Okabe, and McNesby.[3] Using an isotopic technique, they postulated the following primary processes in order of decreasing importance:

$$\text{cyclo-}C_3H_6 + h\nu \begin{cases} \longrightarrow CH_2 + C_2H_4 \\ \longrightarrow H_2 + C_3H_4 \\ \longrightarrow H + C_3H_5 \end{cases}$$

Scala and Ausloos[4] proposed the following reaction as the major primary process in the photolysis at 1470 and 1236 Å:

$$\text{cyclo-}C_3H_6 + h\nu \longrightarrow CH_2CH_2CH_2^*$$

The highly excited trimethylene intermediate, formed by the primary act of the photoexcited cyclopropane molecule, undergoes two kinds of decomposition,

$$CH_2CH_2CH_2^* \begin{cases} \longrightarrow C_2H_4 + CH_2 \\ \longrightarrow C_3H_4 + 2H \end{cases}$$

or isomerization to excited propylene which is always followed by fragmentation.

Dhingra and Koob[5] suggested, on the basis of two kinds of experimental evidence, that there is no need to postulate the trimethylene formation in the primary process, at least as a source of methylene and ethylene. First, no collisional conversion of singlet to triplet trimethylene is observed, and secondly, *cis*- and *trans*-1,2-dimethylcyclopropane yield only *cis*- and *trans*-2-butene, respectively. Since no direct method was available to detect the proposed trimethylene intermediate chemically, they concluded that if it exists it must be very short lived.

In the present work, the photolysis of cyclopropane at 1470 and 1634 Å has been studied with and without additives. Nitric oxide was used to suppress the radical reactions, and hydrogen was employed to scavenge methylene formed in the primary act. Major attention is focused upon quantitative features of the primary processes; the relative yields of the primary processes have been determined.

Experimental

Most of the experimental procedures used in the present study have been described previously.[6] The xenon lamp was equipped with a sidearm containing zeolite as a gettering agent and activated by a microwave generator. The bromine lamp was provided with a quartz window and a cold finger. The vapor pressure of bromine was maintained constant by cooling the cold finger with dry-ice.

Cyclopropane, hydrogen, methane, and nitric oxide were obtained from Takachiho Chem. Ind. Co., and ethylene-d_4 from Merck, Sharp, & Dohme, Ltd. Cyclopropane was purified by gas chromatography of a 9 m long squalane column at room temperature and subsequently distilled at dry-ice temperature. The resulting cyclopropane contained about 0.002% propylene. Nitric oxide was distilled at -160 °C and degassed at -196 °C. The other materials were used without further purification.

After irradiation, the products and the remaining reactants were collected in a sample tube with a Teopler pump and analyzed by gas chromatography; products of C_1 and C_2 were analyzed with a 2 m long silica gel column with 5% squalane or 3 m long activated charcoal column, and those of C_3 and C_4 were analyzed with a 9 m long squalane column. All products were identified by authentic gas samples. Mass spectrometric analyses of hydrogen and methane were carried out in the experiments of isotopic mixture of cyclopropane and ethylene-d_4.

Results and Discussion

Primary Processes. The products observed in the photolysis at both wavelengths were identical but somewhat different in proportions. The measured products were methane, acetylene, ethylene, ethane, propylene, propane, methylacetylene, allene, *n*-butane, butene isomers, and methylcyclopropane. Of these products, ethane, propylene, propane, and *n*-butane completely disappeared with the addition of 10% nitric oxide.

Ethylene, the most abundant product in the photolysis of cyclopropane at 1470 and 1634 Å, was hardly suppressed by added nitric oxide, so that the major primary process would be

$$\text{cyclo-}C_3H_6 + h\nu \longrightarrow C_2H_4 + CH_2, \quad \Delta H = 92 \text{ kcal/mol.} \qquad (1)$$

If ethylene formed has sufficient energy to decompose into acetylene and hydrogen competing with the collisional deactivation, the ratio of acetylene to ethylene

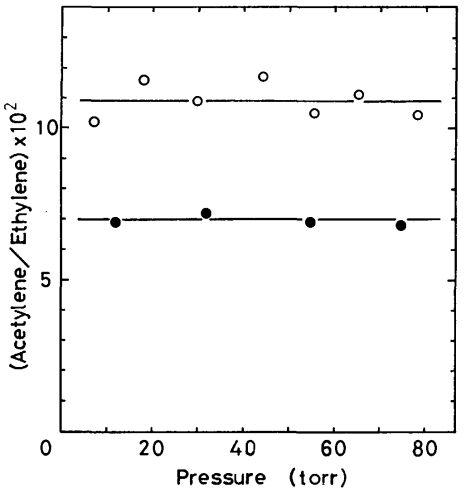

Fig. 1. Ratio of acetylene to ethylene as a function of total pressure in the photolysis of cyclopropane at 1470 Å:
○, *without NO;* ●, *with 10% NO.*

would decrease with the pressure of cyclopropane. Formation of such an energized ethylene has been confirmed in the photolysis of ethane, propane, *n*-butane, and cyclobutane at 1470 Å,[7,8] where the maximum available energy for ethylene is in the range of 160—175 kcal/mol. In order to examine whether energized ethylene is produced in our system, cyclopropane was photolysed in the pressure region of 7—77 Torr. The results are shown in Fig. 1. Since the ratio is evidently independent of pressure, it might be concluded that ethylene produced in the photolysis of cyclopropane at 1470 Å hardly decomposes. Considering the lower available energy of 102 kcal/mol for the 1470 Å photolysis of cyclopropane than that for other paraffins, the result seems reasonable. This would also be the case for the 1634 Å photolysis, in which the maximum energy carried by ethylene formed in the process (1) is 82 kcal/mol.

Yields of the products at both wavelengths are expressed relative to the yield of allene (allene=10) and plotted as a function of the allene/cyclopropane ratio in Figs. 2a—3b. Under the conditions of our experiments, the allene/cyclopropane ratio can be used as a scale proportional to conversion for the following reasons. 1) Within experimental error, the yield of allene was almost proportional to the irradiation time and equal both with and without nitric oxide in the photolysis of cyclopropane. Allene is therefore considered to be produced molecularly by the primary step and its yield never varies with occurrence of the secondary reactions. 2) The relative yield of ethylene, the most abundant product at the both wavelengths, changes during the period of the photolysis without nitric oxide (Figs. 2a and 3a). However, if the secondary reactions with regard to ethylene are taken into account, the amount of ethylene produced by the primary step remains constant relative to that of allene throughout the irradiation period.

The existence of vinyl radicals in this system is confirmed by the following experimental results. 1) Propylene, disappearing entirely with the addition of 10% nitric oxide, is formed *via* radical reactions,[9] namely the recombination reaction of C_3H_5 and H, or C_2H_3 and CH_3. If the association of C_3H_5 with H yields propylene, the formation rate of propylene should be depressed with increasing conversion since the concentration of hydrogen atom is lowered with the increasing amount of ethylene formed. The results show, however, that the rate of propylene formation is constant as a function of conversion. Thus, the following reaction is plausible for the formation of propylene:

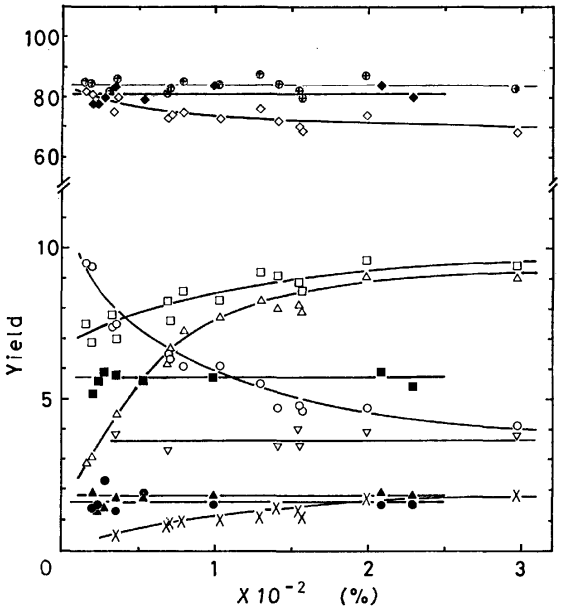

Fig. 2a. Relative yield of product as a function of ratio of allene to cyclopropane in the photolysis of cyclopropane at 1470 Å:
○, CH_4; □, C_2H_2; ◇, C_2H_4; ▽, C_3H_6; △, C_3H_8+methylacetylene; ×, n-C_4H_{10}; ⊕, ϕ_1 calculated by Eq. (I). The closed points represent the results obtained from the experiments with 10% NO.

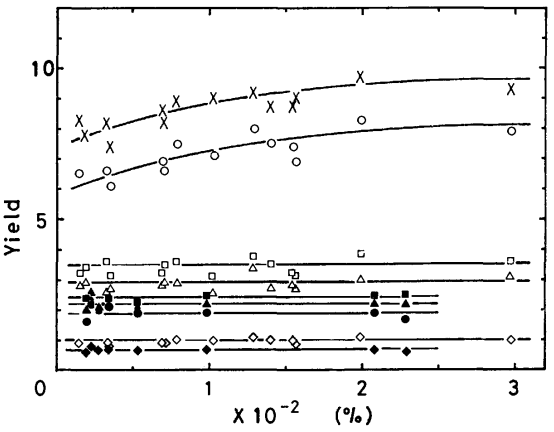

Fig. 2b. Relative yield of product as a function of ratio of allene to cyclopropane in the photolysis of cyclopropane at 1470 Å:
×, C_2H_6; ○, 1-C_4H_8; □, *cis*-2-C_4H_8+cyclo-$C_3H_5CH_3$; △, *trans*-2-C_4H_8; ◇, *iso*-C_4H_8. The closed points represent the results obtained from the experiments with 10% NO.

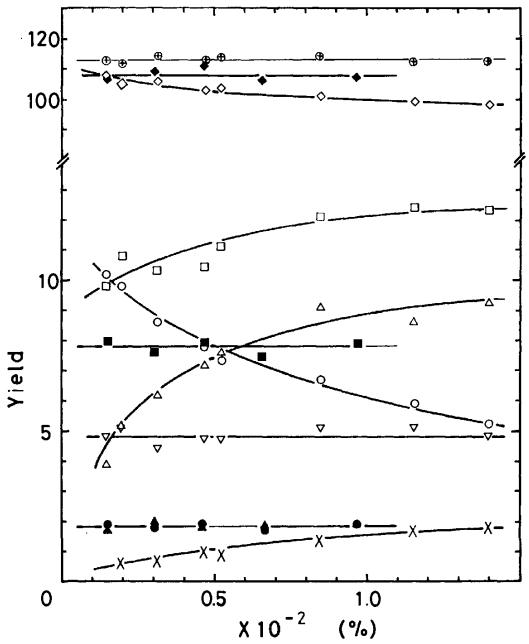

Fig. 3a. Relative yield of product as a function of ratio of allene to cyclopropane in the photolysis of cyclopropane at 1634 Å:
○, CH_4; □, C_2H_2; ◇, C_2H_4; ▽, C_3H_6; △, C_3H_8+methylacetylene; ×, n-C_4H_{10}; ⊕, ϕ_1 calculated by Eq. (I).

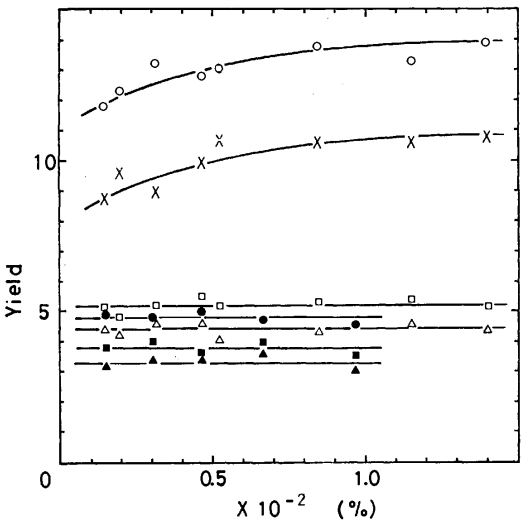

Fig. 3b. Relative yield of product as a function of ratio of allene to cyclopropane in the photolysis of cyclopropane at 1634 Å:
×, C_2H_6; ○, 1-C_4H_8+*iso*-C_4H_8; □, *cis*-2-C_4H_8+cyclo-$C_3H_5CH_3$; △, *trans*-2-C_4H_8. The closed points represent the results obtained from the experiments with 10% NO.

$$C_2H_3 + CH_3 \longrightarrow C_3H_6. \quad (2)$$

2) Since some part of acetylene formation is depressed by addition of nitric oxide, it is formed *via* radical reactions. The following processes might be possible for the acetylene formation:

$$2C_2H_3 \longrightarrow C_2H_2 + C_2H_4, \quad (3)$$
$$\longrightarrow CH_2{=}CH{-}CH{=}CH_2 \quad (4)$$

Although the reported values[10,11] of k_3/k_4 lie between 0.02 and 3, only a trace amount of 1,3-butadiene was observed in our experiments. Therefore, Reaction (3) would contribute little to the formation of acetylene. Another possible reaction sequence forming acetylene through radical reactions is as follows:

$$C_2H_4 + H \longrightarrow C_2H_5, \quad (5)$$
$$C_2H_5 + C_2H_3 \longrightarrow 1\text{-}C_4H_8, \quad (6)$$
$$\longrightarrow 2C_2H_4, \quad (7)$$
$$\longrightarrow C_2H_2 + C_2H_6, \quad (8)$$

where ethylene is the reaction product formed by primary process (1).

In order to examine whether the reaction sequence (5) to (8) occurs, the photolysis of cyclopropane at 1470 Å was carried out with the same irradiation time with and without 10% nitric oxide. The results are given in Table 1. The relative yields are normalized to the yield of allene because it is independent of the addition of nitric oxide. In the presence of nitric oxide the yields of the other products were reduced but not suppressed completely. The portions of the remaining C_4 products, which are not scavenged by 10% nitric oxide, seem to be formed by the insertion reaction of methylene into cyclopropane. The behavior of chemically activated methylcyclopropane has been studied by several researchers[12,13] who suggested the following reaction sequence for the formation of C_4H_8 isomers;

Table 1. Relative yields with the same irradiation time in the photolysis of cyclopropane at 1470 Å[a]

Products	without NO	with 10% NO
C_2H_2	7.7	5.8
$CH_2{=}C{=}CH_2$	10.0	9.9
1-C_4H_8	6.6	1.7
iso-C_4H_8	0.9	0.9
trans-2-C_4H_8	2.6	2.0
cis-2-C_4H_8+cyclo-$C_3H_5CH_3$	3.3	2.6

a) The total pressure was kept at 21 Torr in all the experiments with and without 10% NO. The yield of allene in the photolysis of cyclopropane without NO is taken to be ten. The two kinds of experiments were alternately repeated with the same irradiation time, the values listed being the averages over the five runs.

$$CH_2 + \text{cyclo-}C_3H_6 \longrightarrow CH_3 + C_3H_5, \quad (9)$$
$$\longrightarrow \text{cyclo-}C_3H_5CH_3{*}, \quad (10)$$
$$\text{cyclo-}C_3H_5CH_3{*} \xrightarrow{+M} \text{cyclo-}C_3H_5CH_3, \quad (11a)$$
$$\longrightarrow \text{butene isomers}, \quad (11b)$$
$$CH_3 + C_3H_5 \xrightarrow{+M} \text{cyclo-}C_3H_5CH_3, \quad (12a)$$
$$\longrightarrow \text{butene isomers}. \quad (12b)$$

If these reactions occur even in the photolysis of cyclopropane, then the C_4H_8 isomers would be formed not only by Reaction (11a, 11b) but also by Reaction (12a, 12b). In the presence of 10% nitric oxide the latter reaction would be suppressed, while the former is opera-

tive both with and without nitric oxide. As seen from the yields of *iso*-C_4H_8, *trans*-2-C_4H_8, and *cis*-2-C_4H_8 plus cyclo-$C_3H_5CH_3$ in Table 1, the amount of each C_4H_8 isomer formed by Reaction (12a, 12b) was equal to 0.3 times of that formed by Reaction (11a, 11b), respectively. Applying this value to the case of 1-C_4H_8, the fraction of 2.2 ($=1.7\times1.3$) should be expected to be formed by Reactions (11a, 11b) and (12a, 12b) in the experiment without nitric oxide, and the remainder of 1-C_4H_8 (the fraction of 4.4) should be ascribed to Reaction (6). Moreover, since the yield of acetylene in the presence of nitric oxide is attributed to the molecular detachment, the fraction of 1.9 results from Reaction (8). We can finally obtain the value 2.3 for k_6/k_8 which is almost equal to the value 2.1 reported by Ibuki and Takezaki.[11] We thus conclude that the reaction sequence (6) to (8) surely occurs, and vinyl radical plays an important role as an intermediate. Occurrence of these reactions might be suggested by the fact that the increments of acetylene, ethane, and 1-butene *vs.* conversion show a similar trend and correspond to the increase of ethyl radical formation (Figs. 2a—3b). The following primary process would be the proper mode forming vinyl radicals,

$$\text{cyclo-}C_3H_6 + h\nu \longrightarrow C_2H_3 + CH_3. \quad (13)$$

Figures 2a and 3a show that the yield of methane decreases with increasing conversion without nitric oxide. This would reflect the variation of ethylene concentration. Since ethylene formed in the main primary process (1) scavenges hydrogen atom, Reaction (5), the stationary state concentration of hydrogen atom would decrease as a greater amount of ethylene is produced, which turns out that the association of methyl radical with hydrogen atom,

$$CH_3 + H \xrightarrow{+M} CH_4, \quad (14)$$

is suppressed, while the formation of propane and *n*-butane,[3]

$$CH_3 + C_2H_5 \longrightarrow C_3H_8, \quad (15)$$

$$2C_2H_5 \longrightarrow n\text{-}C_4H_{10}, \quad (16)$$

is promoted. Although the yield of methane is in opposite variation to that of propane, their sum remained constant, which implies that the decrement of methane is virtually compensated by the increment of propane. Reaction (8) was presented as a mechanism of ethane formation. The recombination of methyl radicals should be added as another step:

$$2CH_3 \xrightarrow{+M} C_2H_6. \quad (17)$$

Methane would also be formed in a primary process, because it was found even with nitric oxide. The molecular production of methane should be accompanied by formation of acetylene:

$$\text{cyclo-}C_3H_6 + h\nu \longrightarrow C_2H_2 + CH_4. \quad (18)$$

However, there was several times as much acetylene as methane in the photolysis with the radical scavenger and it is concluded that the following step is another mode of acetylene formation.

$$\text{cyclo-}C_3H_6 + h\nu \longrightarrow C_2H_2 + CH_3 + H. \quad (19)$$

The alternative explanation of acetylene formation from energized ethylene for an excess of acetylene over methane has been rejected since there exists no energized ethylene in our system.

Currie *et al.*[3] proposed that allene and methylacetylene are formed by the molecular elimination of hydrogen,

$$\text{cyclo-}C_3H_6 + h\nu \longrightarrow C_3H_4 + H_2, \quad (20)$$

from the isotopic composition of hydrogen molecule formed in the photolysis of the mixture of cyclopropane-d_0 and -d_6. On the other hand, Scala and Ausloos[4] demonstrated that they are formed substantially by the following reaction sequence,

$$\text{cyclo-}C_3H_6 + h\nu \longrightarrow C_3H_5^* + H, \quad (21)$$

$$C_3H_5^* \longrightarrow C_3H_4 + H, \quad (22)$$

on the basis of the isotopic composition of hydrogen molecule formed from the mixture of cyclopropane-d_6 and H_2S. They concluded that the majority of the allyl and/or cyclopropyl radicals formed in the primary process (21) dissociate further to form C_3H_4. We carried out the photolysis of the mixture of cyclopropane-d_0 and ethylene-d_4 ([cyclo-C_3H_6]/[C_2D_4]$\simeq$30). If the molecular elimination of hydrogen is the dominant process for the C_3H_4 formation, the ratio H_2/C_3H_4 should be close to unity. It was obtained as 0.18 and 0.15 by mass spectrometry and gas chromatography for the 1470 and 1634 Å photolysis, respectively. Thus, it may be concluded that the majority of C_3H_4 are produced by the atomic elimination of hydrogen:

$$\text{cyclo-}C_3H_6 + h\nu \longrightarrow CH_2{=}C{=}CH_2 + 2H, \quad (23)$$

$$\text{cyclo-}C_3H_6 + h\nu \longrightarrow CH_3{-}C{\equiv}CH + 2H. \quad (24)$$

Relative Yields of the Primary Processes. We can determine the relative weights of the primary processes according to the foregoing discussion. To facilitate comparison, weight of the primary process (23) is taken as ten at both wavelengths ($\phi_{23}=10$) and the yields of the other primary processes (ϕ_1, ϕ_{13}, ϕ_{18}, ϕ_{19}, and ϕ_{24}) are expressed relative to ϕ_{23}.

We have noted that the most abundant product, ethylene, scavenges hydrogen atoms and the resultant ethyl radicals undergo the association or disproportionation reactions with themselves or the other radicals. The stationary state assumption leads to the relation,

$$\phi_1 = (C_2H_4) + (C_3H_8) + 2(n\text{-}C_4H_{10}) + \left(\frac{k_6}{k_8} - \frac{k_7}{k_8} + 1\right)(C_2H_2)_r, \quad (I)$$

where $(C_2H_2)_r$ represents the yield of acetylene formed by Reaction (8); *viz.*, that reduced by adding nitric oxide. The value of $(C_2H_2)_r$ was attributed to the difference between the acetylene yields with and without nitric oxide in Fig. 2a at 1470 Å and Fig. 3a at 1634 Å. By means of Eq. (I) and the values[11] of $k_6/k_7=0.89$ and $k_8/k_7=0.43$, the values of ϕ_1 *vs.* conversion at 1470 and 1634 Å are illustrated in Figs. 2a and 3a, respectively. We obtain 83 at 1470 Å and 113 at 1634 Å as the constant values of ϕ_1. The relative weight of the primary process (13) is estimated from the amount of vinyl radical. Since vinyl radicals react with methyl or ethyl radicals, Reaction (2) or Reactions (6)—

(8), the yield of vinyl radical is nearly equal to the sum of propylene and $(C_2H_2)_r \times (k_6+k_7+k_8)/k_8$ at high conversion. Thus, the relative weights of the primary process (13), ϕ_{13}, are 24 and 30 at 1470 and 1634 Å, respectively. Primary process (18) is the only molecular mechanism forming methane and therefore methane formed in the presence of nitric oxide should be attributed to Reaction (18); *viz.*, its relative weights (ϕ_{18}) are equal to 1.6 and 1.8 at 1470 and 1634 Å, respectively. Although Reaction (18) yields molecularly the same amounts of acetylene and methane, the former is obtained in much larger quantities (Figs. 2a and 3a). The difference should be attributed to another step forming acetylene molecularly, or Reaction (19). Thus, we obtain $\phi_{19}=4.0$ at 1470 Å and 6.0 at 1634 Å. Since methylacetylene is formed only by Reaction (24), the yield should be equal to the relative weight of this process, $\phi_{24}=1.7$ and 1.8 at 1470 and 1634 Å, respectively. The total value of ϕ's is normalized to 100, the resulting values (ϕ) being summarized in Table 2.

TABLE 2. RELATIVE YIELDS OF PRIMARY PROCESSES IN THE PHOTOLYSIS OF CYCLOPROPANE AT 1470 AND 1634 Å[a)]

Primary process		Relative yield	
		1470 Å	1634 Å
$C_2H_4+CH_2$	(ϕ_1)	67	69
$C_2H_3+CH_3$	(ϕ_{13})	19	18
$CH_2=C=CH_2+2H$	(ϕ_{23})	8	6
$C_2H_2+H+CH_3$	(ϕ_{19})	3	4
$C_2H_2+CH_4$	(ϕ_{18})	1	1
$CH_3-C\equiv CH+2H$	(ϕ_{24})	1	1

a) The relative yields are noramlized to $\phi_1+\phi_{13}+\phi_{18}+\phi_{19}+\phi_{23}+\phi_{24}=100$.

Although the same amounts of ethylene and methylene are formed in Reaction (1), the observed yield of the products resulting from methylene is much less than that from ethylene.[4)]

A polymer is a major product in the mercury photosensitized reaction of cyclopropane. Strausz *et al.*[14)] stressed that hexyl and allyl radicals are most likely to be precursors of polymer formation. We supposed that C_3H_5 radicals obtained according to Reaction (9) do act as a precursor of polymerization and hence the yield of methylene estimated from the products becomes much smaller than expected. We therefore added a large amount of hydrogen as methylene scavenger to the pure cyclopropane system. Methylene obtained by primary process (1) is converted into methyl radical or methane by the following reaction sequence[15)]:

$$^1CH_2 + H_2 \longrightarrow CH_4^* \begin{cases} \longrightarrow CH_3 + H, & (25) \\ \xrightarrow{+M} CH_4, & (26) \end{cases}$$

$$^1CH_2 \xrightarrow{+M} {}^3CH_2, \quad (27)$$

$$^3CH_2 + H_2 \longrightarrow CH_3 + H. \quad (28)$$

In the presence of excess hydrogen, the reaction of methylene with hydrogen has an advantage over that with cyclopropane. When the $[H_2]/[\text{cyclo-}C_3H_6]$ ratio exceeded four, methylcyclopropane and butene isomers except 1-butene almost disappeared while the yields of methane, ethane, and propane increased to a great extent. This means that Reactions (9) and (10) become unimportant while Reactions (25) to (28) become the ruling steps as regards methylene. In the photolytic system without hydrogen where polymerization occurs, methyl radicals would make a large contribution to polymer formation process. Consequently, the total yield of products resulting from methylene becomes apparently small. The yields of products responsible for ethylene and methylene, $Y(C_2H_4)$ and $Y(CH_2)$, are given by

$$Y(C_2H_4) = \phi_1, \quad (II)$$

and

$$Y(CH_2) = (CH_4) + 2\{(C_2H_6) - (C_2H_6)_r\} + C_3H_6 + (C_3H_8) - (\phi_{13}+\phi_{18}+\phi_{19}), \quad (III)$$

respectively, when cyclopropane is photolysed with no additives. On the other hand, with excess hydrogen, we have

$$Y(C_2H_4) = (C_2H_4) + (C_3H_8) + 2(n\text{-}C_4H_{10}) + 0.36(1\text{-}C_4H_8), \quad (IV)$$

and

$$Y(CH_2) = (CH_4) + 2\{(C_2H_6) - 0.48(1\text{-}C_4H_8)\} + (C_3H_6) + (C_3H_8) - (\phi_{13}+\phi_{18}+\phi_{19}). \quad (V)$$

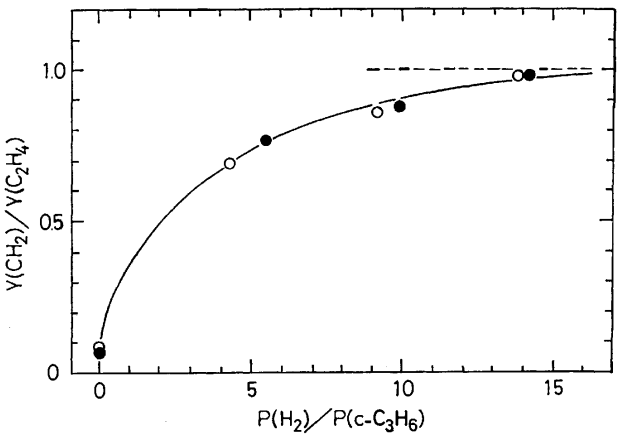

Fig. 4. $Y(CH_2)/Y(C_2H_4)$ as a function of $P(H_2)/P$ (cyclo-C_3H_6) in the photolysis of cyclopropane with an excess of hydrogen:
●, 1470 Å photolysis; ○, 1634 Å photolysis. The pressure of cyclopropane, P(cyclo-C_3H_6), was kept at 21 Torr.

The ratios of $Y(CH_2)$ to $Y(C_2H_4)$ are plotted *vs.* the ratio of $P(H_2)$ to P(cyclo-C_3H_6) in Fig. 4, where $P(H_2)$ and P(cyclo-C_3H_6) are the pressure of hydrogen and cyclopropane, respectively. We see that the ratio of $Y(CH_2)$ to $Y(C_2H_4)$ is asymptotic to unity at high pressure of hydrogen. This implies that the yield of products resulting from methylene becomes almost equal to that from ethylene in the presence of excess hydrogen. Thus, it can be shown that Reaction (1) is the main primary process and that the same amounts of methylene and ethylene are surely produced.

The Crystal and Molecular Structure of the *p*-Bromobenzoate of Sterigmatocystin

Keiichi FUKUYAMA, Tomitake TSUKIHARA, Yukiteru KATSUBE, Nobuo TANAKA,*
Takashi HAMASAKI,** and Yuichi HATSUDA**
Faculty of Engineering, Tottori University, Koyama, Tottori 680
(Received December 23, 1974)

The crystals of the *p*-bromobenzoate of sterigmatocystin, $C_{25}H_{15}O_7Br$, are monoclinic, with the space group of $P2_1$, and with two molecules per unit cell with the dimensions of $a=13.062(7)$, $b=9.029(4)$, $c=8.942(4)$ Å, and $\beta=102.25(5)°$. The structure was refined by a least-squares method to $R=0.055$ for 1292 non-zero reflections. The absolute configuration of the molecule was determined by using the anomalous dispersion effect of the bromine atom. The absolute configuration of the bisdihydrofuran ring agrees with that in aflatoxin B_1.

Sterigmatocystin is one of the carcinogenic metabolites of the mold *Aspergillus versicolor* (Vuillemin) Tiraboschi. A preliminary report on the X-ray structural analysis of the *p*-bromobenzoate of sterigmatocystin has already been published.[1] In the series of studies of the structures of the metabolites of this mold,[1-3] the refinement of the structure and the determination of the absolute configuration of the *p*-bromobenzoate of sterigmatocystin have been undertaken.

Refinement of the Structure

The title compound, $C_{25}H_{15}O_7Br$, was prepared by the method described in the previous paper.[1] The unit-cell constants were remeasured on a Toshiba four-circle diffractometer with Ni-filtered Cu$K\alpha$ radiation ($\lambda=1.5418$ Å). The crystal data are: monoclinic, space group $P2_1$, $a=13.062$ (7), $b=9.029$ (4), $c=8.942$ (4) Å, $\beta=102.25$ (5)°, $V=1030.6$ Å^3, $Z=2$, $M=507.3$, $D_m=1.640$ g·cm^{-3}, $D_x=1.635$ g·cm^{-3}, $\mu=34.4$ cm^{-1}. The structure found in the previous paper[1] was refined by the block-diagonal least-squares procedure using the three-dimensional intensity data obtained by the Weissenberg method. Out of 1580 measured reflections,*** 1292 non-zero reflections were used for the refinement. After several cycles of refinement with individual anisotropic temperature factors, the discrepancy factor (R value) was reduced to 0.065. The difference electron density map at this stage revealed peaks corresponding to fifteen hydrogen atoms. Three cycles of refinement, including hydrogen atoms, brought the R value down to 0.057.

Determination of the Absolute Configuration

In the final stage of the analysis, the absolute configuration of the molecule was determined by using the anomalous scattering of Cu$K\alpha$ radiation by the bromine atom.[4] The structure factors were calculated for the two enantiomorphs with a scattering factor for bromine of the $f_{Br}=f^{\circ}_{Br}+\Delta f_{Br}'+i\Delta f_{Br}''$ form, where $\Delta f_{Br}'=-0.9$ and $\Delta f_{Br}''=1.5$. Sixteen Friedel pairs of reflections strongly affected by the anomalous dispersion effect were selected for accurate intensity measurements. The intensities were obtained by the $\omega-2\theta$ scan technique using Ni-filtered Cu$K\alpha$ radiation on the four-circle diffractometer with a specimen with dimensions of *ca.* $0.07\times0.04\times0.30$ mm^3. The absolute configuration was established by a comparison of the observed and calculated intensities shown in Table 1. Three further cycles of refinement including the anomalous dispersion effect reduced the R value to 0.055 for 1292 non-zero reflections. The unit weight was applied for all the non-zero reflections. The final atomic parameters are shown in Table 2. The absolute configuration is correctly represented by the atomic parameters of Table 2 if a right-handed coordinate system is adopted.

TABLE 1. FRIEDEL PAIRS OF REFLECTIONS USED IN DETERMINING THE ABSOLUTE CONFIGURATION
The right-handed coordinate system is adopted.

k	h	l	$F_c(hkl)$	$F_c(\bar{h}\bar{k}\bar{l})$	$I_o(hkl)$ $I_o(\bar{h}\bar{k}\bar{l})$
5	3	0	108	92	$>$
3	5	0	107	119	$<$
0	2	1	175	185	$\simeq$
5	3	1	118	131	$<$
2	1	2	163	180	$<$
4	2	2	142	127	$>$
0	3	4	153	143	$>$
0	1	4	86	71	$>$
1	1	3	69	80	$<$
3	1	$\bar{4}$	109	98	$>$
1	3	$\bar{2}$	159	170	$\simeq$
2	4	$\bar{2}$	161	174	$<$
3	4	$\bar{2}$	95	107	$\simeq$
5	2	$\bar{2}$	125	115	$>$
2	1	$\bar{1}$	175	150	$>$
4	3	$\bar{1}$	63	73	$<$

The atomic scattering factors were taken from the International Tables for X-ray Crystallography.[5] A list of the observed and calculated structure factors is kept by the office of the Chemical Society of Japan, (Document No. 7511). The computations were performed on a TOSBAC 3400 computer at the Tottori University Computing Center and on a NEAC 2200—N700 computer at the Computation Center of Osaka University.

* Present address: Institute for Protein Research, Osaka University, Suita 565.

** Faculty of Agriculture, Tottori University, Koyama, Tottori 680.

*** The reflections in the blind regions of the Weissenberg method were measured on the diffractometer.

TABLE 2(a). FINAL ATOMIC PARAMETERS AND e.s.d.'s ($\times 10^4$) FOR NON-HYDROGEN ATOMS
The anisotropic temperature factors are of the form: $\exp(-\beta_{11}h^2-\beta_{22}k^2-\beta_{33}l^2-\beta_{12}hk-\beta_{13}hl-\beta_{23}kl)$.

	x	y	z	β_{11}	β_{22}	β_{33}	β_{12}	β_{13}	β_{23}
Br	−616(1)	2484(3)	11595(2)	114(1)	265(3)	254(2)	−2(4)	178(3)	−5(6)
C(1)	1994(10)	−4562(14)	2848(12)	124(11)	104(24)	137(16)	−73(25)	83(22)	−5(30)
C(2)	1916(8)	−3363(13)	3790(11)	79(8)	112(21)	127(15)	18(21)	20(18)	26(28)
C(3)	2515(7)	−2058(12)	3841(10)	72(7)	93(23)	114(13)	−32(19)	35(15)	−21(25)
C(4)	2463(8)	−804(14)	4811(11)	66(7)	140(22)	141(16)	3(21)	43(17)	18(31)
C(5)	3119(7)	498(12)	4628(10)	62(7)	80(21)	114(13)	8(17)	23(15)	−9(24)
C(6)	3144(8)	1872(14)	5399(11)	87(8)	154(25)	119(15)	13(21)	62(18)	−60(28)
C(7)	3752(9)	3024(13)	5201(12)	111(10)	113(27)	155(17)	−79(24)	63(21)	−20(29)
C(8)	4402(9)	2872(17)	4144(12)	90(8)	206(31)	152(17)	−50(28)	23(19)	−42(36)
C(9)	4426(8)	1568(14)	3372(11)	82(8)	141(22)	112(14)	−44(22)	33(17)	−25(28)
C(10)	3789(8)	403(13)	3604(11)	64(7)	131(24)	122(15)	21(20)	14(16)	0(28)
C(11)	3218(7)	−2024(12)	2855(10)	59(6)	86(23)	118(13)	−5(17)	22(14)	−27(24)
C(12)	3320(9)	−3167(12)	1915(11)	97(9)	58(20)	119(15)	38(19)	36(18)	−19(24)
C(13)	2738(10)	−4409(13)	1936(12)	135(12)	37(22)	140(17)	67(23)	24(22)	22(27)
C(14)	3738(11)	−4999(16)	259(13)	138(13)	152(25)	158(19)	48(31)	91(25)	−15(36)
C(15)	3196(9)	−3528(15)	−1808(13)	86(9)	175(25)	173(18)	−33(25)	99(21)	−26(35)
C(16)	3581(7)	−2594(17)	−750(10)	74(7)	141(21)	153(15)	−10(27)	98(16)	−47(36)
C(17)	3992(9)	−3409(15)	720(12)	82(8)	164(24)	154(18)	4(24)	70(20)	−89(32)
C(18)	580(12)	−4680(19)	4699(15)	154(15)	259(36)	206(24)	−128(38)	151(31)	24(48)
C(19)	2689(8)	1515(13)	7796(11)	77(8)	87(20)	141(16)	10(21)	9(17)	−40(27)
C(20)	1867(8)	1768(13)	8657(10)	73(7)	114(21)	108(14)	22(18)	28(16)	−20(25)
C(21)	953(8)	2543(19)	8102(11)	102(9)	146(22)	164(17)	41(33)	46(19)	−29(41)
C(22)	234(9)	2840(17)	8987(13)	94(9)	168(30)	204(20)	90(27)	100(21)	86(40)
C(23)	385(8)	2183(16)	10391(11)	93(9)	161(28)	141(16)	−10(25)	81(19)	−35(33)
C(24)	1256(9)	1382(16)	10985(13)	91(9)	168(26)	171(19)	14(26)	67(21)	−7(36)
C(25)	2008(8)	1169(16)	10113(12)	78(8)	184(26)	133(16)	49(24)	14(18)	49(32)
O(1)	1221(6)	−3385(10)	4732(8)	100(6)	175(16)	136(11)	−100(16)	94(13)	−54(21)
O(2)	1933(6)	−794(10)	5829(9)	105(7)	172(11)	214(14)	−89(18)	169(16)	−110(25)
O(3)	2426(5)	2085(8)	6348(7)	77(5)	133(16)	121(9)	42(13)	53(11)	1(18)
O(4)	3849(5)	−840(9)	2760(7)	72(5)	117(13)	123(10)	−9(14)	54(11)	−65(19)
O(5)	2903(8)	−5521(10)	962(9)	172(9)	102(16)	171(13)	−23(19)	102(18)	−85(22)
O(6)	3345(8)	−5014(12)	−1352(9)	171(10)	210(19)	170(14)	−60(24)	129(19)	−206(26)
O(7)	3506(5)	950(10)	8261(8)	70(5)	203(17)	158(12)	11(16)	43(13)	49(24)

TABLE 2(b). FINAL POSITIONAL PARAMETERS ($\times 10^3$) AND ISOTROPIC TEMPERATURE FACTORS FOR HYDROGEN ATOMS

Attached to		x	y	z	B
H(1)	C(24)	136(9)	103(15)	1218(13)	5.6(33)Å^2
H(2)	C(25)	264(11)	48(18)	1046(16)	9.9(47)
H(3)	C(21)	78(7)	296(13)	685(11)	4.1(28)
H(4)	C(22)	−44(9)	351(15)	863(13)	6.3(36)
H(5)	C(7)	375(10)	399(18)	567(15)	8.6(43)
H(6)	C(8)	483(9)	375(15)	400(12)	5.3(32)
H(7)	C(9)	490(8)	131(13)	249(11)	3.4(26)
H(8)	C(17)	473(8)	−322(13)	119(12)	5.1(33)
H(9)	C(16)	359(7)	−138(12)	−95(10)	1.7(22)
H(10)	C(15)	281(10)	−327(17)	−302(15)	9.0(45)
H(11)	C(14)	436(11)	−570(19)	47(16)	9.8(46)
H(12)	C(1)	151(10)	−550(18)	269(15)	8.5(43)
H(13)	C(18)	19(8)	−441(13)	560(11)	3.6(28)
H(14)	C(18)	20(8)	−488(15)	371(12)	4.9(30)
H(15)	C(18)	94(8)	−559(14)	521(12)	4.7(30)

Description of the Structure and Discussion

The present X-ray analysis has established the absolute configuration of the *p*-bromobenzoate of sterigmatocystin. Figure 1 shows a view of the packing of the molecules in the crystal and the numbering of atoms, while Fig. 2 shows the stereoscopic view of the molecule. Both figures are illustrated with the correct absolute configuration. As has been shown by Holker *et al.*,[7]

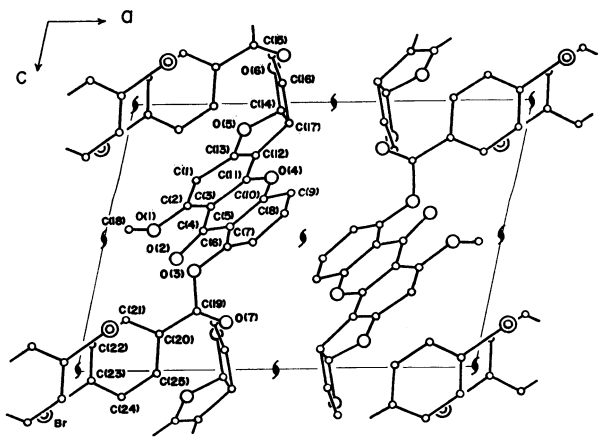

Fig. 1. The crystal structure viewed along the *b* axis and the numbering of atoms. Hydrogen atoms are omitted in the figure.

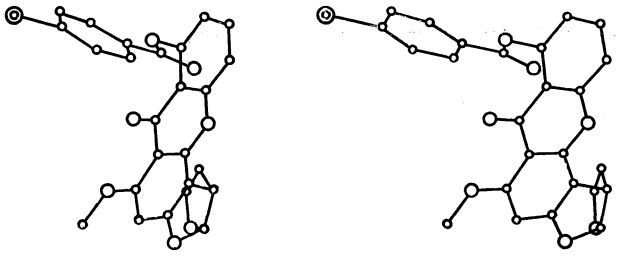

Fig. 2. Stereoscopic view of the molecule.

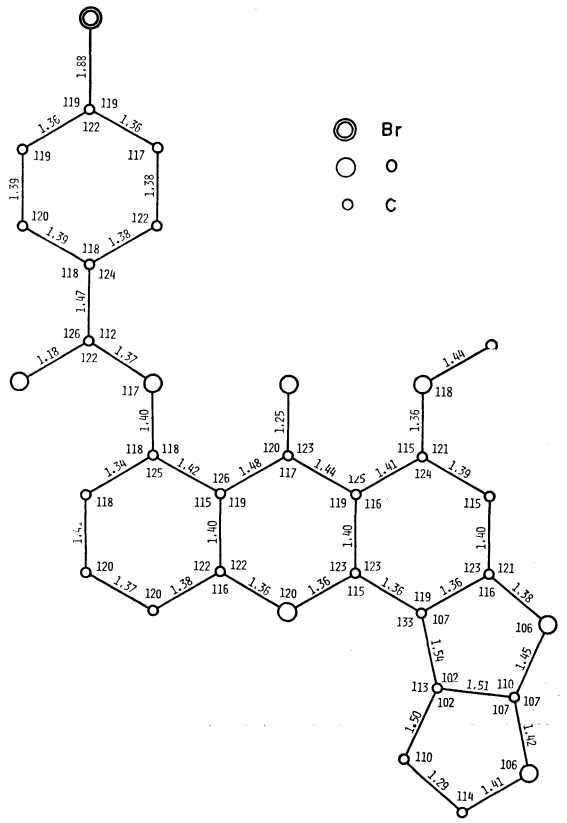

Fig. 3. The bond lengths (Å) and angles (°). The e.s.d.'s of the bond lengths and angles are about 0.02 Å and 1.2 °, respectively.

the absolute configuration of the bisdihydrofuran ring in this compound agrees with that found in aflatoxin B_1.[6] The bond lengths and angles for non-hydrogen atoms are illustrated in Fig. 3. The e.s.d.'s of the bond lengths and the angles for non-hydrogen atoms are about 0.02 Å and 1.2 ° respectively. The bond angles of C(3)–C(4)–C(5), C(9)–C(10)–O(4), and O(4)–C(11)–C(12) are 117 °, 116 °, and 115 ° respectively; these values are smaller than the trigonal sp^2 hybrid angle. On the other hand, the bond angles of C(2)–C(3)–C(4) and C(4)–C(5)–C(6) are larger than 120 °. This structural situation has also been found in the xanthone skeleton in sterigmatin.[3] The dimensions of the bisdihydrofuran ring are close to those in the compounds, such as aflatoxin B_1[6] and sterigmatin,[3] within the limit of experimental error.

The least-squares planes through the xanthone skeleton with O(1) and O(3) atoms, through the terminal five-membered ring, through the benzene ring, and through the C(19), C(20), O(3), and O(7) atoms are represented by the equations;

$$0.580X - 0.370Y + 0.726Z = 4.592 \quad \text{(I)}$$

$$0.973X - 0.055Y - 0.225Z = 4.956 \quad \text{(II)}$$

$$0.405X + 0.831Y + 0.383Z = 4.533 \quad \text{(III)}$$

and

$$0.345X + 0.880Y + 0.325Z = 4.135 \quad \text{(IV)}$$

respectively, where $X=ax+cz\cos\beta$, $Y=by$, and $Z=$

Table 3. Deviations of atoms from each least-squares plane and dihedral angles

(a) Deviations

(I) From xanthone-skeltone with O(1) and O(3) atoms					
C(1)	0.07 Å	C(2)	0.03 Å	C(3)	−0.01 Å
C(4)	−0.06	C(5)	−0.03	C(6)	0.01
C(7)	0.03	C(8)	0.04	C(9)	0.00
C(10)	−0.03	C(11)	−0.02	C(12)	0.02
C(13)	0.03	O(1)	0.06	O(2)	−0.19
O(3)	0.12	O(4)	−0.05	C(14)[a]	−0.04
C(17)[a]	0.05	O(5)[a]	0.04		
(II) From terminal five-membered ring					
C(14)	−0.05 Å	C(15)	−0.03 Å	C(16)	0.01 Å
C(17)	0.01	O(6)	0.06		
(III) From benzene ring					
C(20)	−0.01 Å	C(21)	0.04 Å	C(22)	−0.04 Å
C(23)	0.02	C(24)	0.00	C(25)	−0.01
Br[a]	0.01	C(19)[a]	−0.03		
(IV) From the plane through C(19), C(20), O(3), and O(7) atoms					
C(19)	0.01 Å	C(20)	0.00 Å	O(3)	0.00Å
O(7)	−0.01				

(b) Dihedral angles

	I	II	III
II	65.1°		
III	78.2°	74.8°	
IV	83.7°	77.6°	5.5°

a) Not included in the least-squares calculation.

Table 4. Intermolecular contacts less than 3.6 Å

Br	C(15)[a]	3.54 Å	C(21)	C(18)[a]	3.49 Å
C(21)	O(1)[a]	3.48	C(22)	C(2)[a]	3.50
Br	O(2)[b]	3.52	C(19)	O(6)[c]	3.29
C(20)	O(5)[c]	3.30	C(20)	O(6)[c]	3.49
C(24)	O(5)[c]	3.53	C(25)	O(5)[c]	3.24
O(3)	O(6)[c]	3.39	C(25)	C(10)[d]	3.54
C(25)	O(4)[d]	3.50	O(1)	C(15)[d]	3.59
O(2)	C(15)[d]	3.43	O(7)	C(16)[d]	3.32
C(7)	C(1)[e]	3.52	C(8)	C(13)[e]	3.58
C(8)	O(5)[e]	3.42	C(7)	O(4)[f]	3.43
C(8)	C(10)[f]	3.58	C(8)	O(4)[f]	3.40
C(17)	O(7)[g]	3.25	C(18)	O(2)[h]	3.37
O(1)	C(21)[h]	3.48			

The superscripts refer to the following positions relative to the reference molecule at x,y,z; a) $-x,1/2+y,1-z$. b) $-x,1/2+y,2-z$. c) $x,1+y,1+z$. d) $x,y,1+z$. e) $x,1+y,z$. f) $1-x,1/2+y,1-z$. g) $1-x,-1/2+y,1-z$. h) $-x,-1/2+y,1-z$.

$cz \sin\beta$. Table 3 shows the deviations of the atoms from these planes and the dihedral angles between these planes. The dihedral angle between the I and II planes is 65.1 °; this value is close to the corresponding angle found in aflatoxin B_1.[6] The deviations of the atoms from the plane of the xanthone skeleton in this compound are large in comparison with those in sterigmatin;[3] the xanthone skeleton bends slightly about the O(2)–O(4) axis. The intermolecular distances for non-hydrogen atoms of less than 3.6 Å are listed in Table 4, which indicates that there is no abnormally short contact.

The authors wish to thank Professor Tamaichi Ashida of Nagoya University for his permission to use the block-diagonal least-squares program.

References

1) N. Tanaka, Y. Katsube, Y. Hatsuda, T. Hamasaki, and M. Ishida, This Bulletin, **43**, 3635 (1970).
2) Y. Katsube, T. Tsukihara, N. Tanaka, K. Ando, T. Hamasaki, and Y. Hatsuda, *ibid.*, **45**, 2091 (1972).
3) K. Fukuyama, T. Tsukihara, Y. Katsube, T. Hamasaki, Y. Hatsuda, N. Tanaka, T. Ashida, and M. Kakudo, *ibid.*, **48**, 1639 (1975).
4) J. M. Bijvoet, A.F. Peerdeman, and A.J. van Bommel, *Nature*, **168**, 271, (1951).
5) "International Tables for X-ray Crystallography," Vol. III, Kynoch Press, Birmingham (1962), p. 202.
6) T. C. van Soest and A. F. Peerdeman, *Acta Crystallogr.*, **B26**, 1940 (1970).
7) J. S. E. Holker and L. J. Mulheirn, *Chem. Commun.*, **1968**, 1576.

Molecular Structure of 2-Fluoropropane as Determined By Gas Electron Diffraction

Hironobu KAKUBARI,* Takao IIJIMA, and Masao KIMURA**
Department of Chemistry, Faculty of Sciences, Hokkaido University, Sapporo 060
(Received December 23, 1974)

The skeletal parameters, C–C, C–F, and C···F distances, of 2-fluoropropane have been determined by means of gas electron diffraction. The r_g-values obtained are: C–C 1.514±0.004 Å, C–F 1.405±0.005 Å and C···F 2.366 ±0.006 Å.*** By a joint analysis of the diffraction data and the spectroscopic moments of inertia, determination of the remaining structural parameters has also been attempted, and the ϕ_z value of the CCC angle being found to be 114.6±1.5 °.

It is well-known that systematic elongations of both C–C and C–Cl distances are observed in the series of chloroalkanes, *viz.*, from methyl to ethyl to isopropyl to *t*-butyl chlorides.[1-3] In the corresponding series of fluorides,[4] however, the structure of isopropyl fluoride, or 2-fluoropropane, was not determined until recently. The microwave spectrum of this molecule was observed by Griffiths, Owen, and Sheridan, and the rotational constants were obtained.[5] However, they did not determine the structural parameters since their spectrum was only for the normal species. Saito and co-workers measured the microwave spectra of the normal and six isotopic species and found a reasonable set of the r_0-structure.[6]

The molecule is unfavorable for determining the structure from spectroscopic data, because the central carbon is close to the center of gravity and there is no stable isotope for fluorine. The C–C and C–F distances are especially difficult to determine accurately. Such being the case, it is desirable to obtain information on the skeletal structure by means of gas electron diffraction to complement the spectroscopic r_0-structure.

In the present diffraction study, the C–C and C–F bonded distances and the C···F non-bonded distance were determined. Furthermore, by a joint analysis of the diffraction and spectroscopic data, determination of the complete structure of this molecule was attempted.

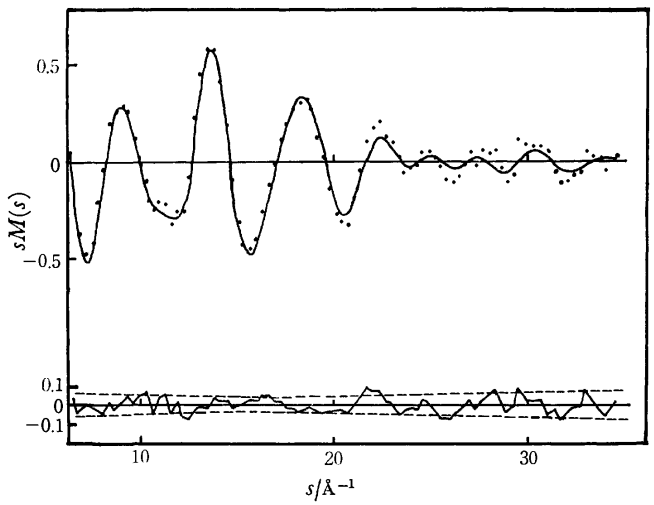

Fig. 1. Molecular intensity curve of 2-fluoropropane. Experimental values (dots) are compared with the best-fit theoretical (solid curve). The residuals are shown below, where the broken curves represent the estimated uncertainty in the intensity measurement.

Experimental

The sample was synthesized by Dr. Shuji Saito, Sagami Chemical Research Center, the purity being checked by him to be about 99.5% by gas-chromatography. The diffraction photographs were taken at room temperature by a unit with an r^3-sector[7] under the following conditions: camera length, 109.3 mm; accelerating voltage, 40 kV; beam current, 0.2 μA; exposure time, 2—4 min; sample pressure, 50—20 Torr. The scale factor was calibrated by the diffraction pattern of carbon disulfide. The total range of s covered was from 7 to 36 Å^{-1}. Five plates were selected for the least square analysis. The observed reduced molecular intensity is shown in Fig. 1, together with the calculated intensity for the best-fit model.[8]

Analysis of the Diffraction Data

The skeletal parameters, C–C, C–F, and C···F distances, were determined by a least square adjustment for molecular intensity. Routine procedure[9,10] was followed for scattering factors, anharmonicity constants and other details of the analytical processes. The final results obtained from the analysis of five plates are given in Table 1. Other structural parameters were fixed

Table 1. Results of the least square analysis of the diffraction data for 2-fluoropropane[a]

Adjusted parameters		Fixed parameters[b]	
r_g(C–F)	1.405(5)	r_a(C···C)	2.535
r_g(C–C)	1.514(4)	r_a(C–H_{Methyl})	1.091
r_g(C···F)	2.366(6)	r_a(C–H_{sec})	1.096
index of resolution	0.97—1.05	ϕ_α(CCH_{sec})	109.2
		ϕ_α(HCH_{Methyl})	107.7

a) Distances in Å and angles in degrees. The numbers in parentheses indicate the limits of error attached to the last significant digit. For the definitions of r_g, r_a and ϕ_α see Ref. 11. b) Those non-bonded distances not shown in the Table were computed by use of the parameters listed here. The local C_{3v} symmetry of the methyl groups is assumed. The C–H bonds which lie on the CCC plane are in the *trans* position to the C–C bond.

* Present address: Oki Electric Industry, Co. Ltd., Higashikanagawa, Hachioji, Tokyo.
** To whom correspondence should be addressed.
*** 1 Å=100 pm is used throughout this paper.

to appropriately assumed values, also listed in Table 1. Most of the assumed values were taken from the r_s-structure of propane.[12] These values were eventually replaced by those obtained by a joint analysis of the diffraction results and the spectroscopic moments of inertia, given in Table 4, and the least square calculation was repeated for the molecular intensity of a plate or two. The most probable values of the adjusted parameters did not vary significantly.

The mean amplitudes of vibration were also fixed to the calculated values. The force constants were adjusted by the method of Cyvin and Cyvin[13] so as to reproduce the fundamental frequencies observed by Griffiths, Owen and Sheridan[5] and Crowder and Koger.[14] The method is an iterative process based on the relation, $\boldsymbol{F}=\tilde{\boldsymbol{L}}_0^{-1}\boldsymbol{\Lambda}\boldsymbol{L}_0^{-1}$, where $\boldsymbol{L}_0$ is the transformation matrix obtained from a trial set of the force constants, $\boldsymbol{\Lambda}$ is the eigenvalue matrix of the observed values and $\boldsymbol{F}$ is the improved force-constant matrix. The calculation is iteratively repeated until the calculated eigenvalues converge exactly to the observed values. The force constants thus obtained are still approximate, since the set can only be one of the many possible sets which could reproduce the observed vibrational frequencies. However, it is considered to be sufficient for evaluating mean amplitudes as long as the initial trial set is properly chosen.

Table 2. Calculated values of the mean amplitudes of vibration at 298 K (in Å units)

C–F	0.0540	H···H	0.13—0.26[a]
C–C	0.0562	C···H	0.11—0.16
C···F	0.0814	F···H	0.11—0.16
C–H	0.0784		

a) The range indicates the distribution of the calculated values among the non-equivalent non-bonded distances.

The set of force constants of 2-chloropropane determined by Cyvin and Cyvin[13] was used as the initial trial, where the diagonal constant for the C–F stretching of CH_3F,[15] 3.135 mdyn/Å, was used. The mean amplitudes at 298 K thus calculated are listed in Table 2.

Joint Analysis of the Diffraction Results and the Spectroscopic Rotational Constants

Determination of the structural parameters which were not obtained by analysis of the diffraction data was carried out by means of a joint analysis of the diffraction intensity and the rotational constants on the basis of the zero-point average structure. The vibrational corrections for both r_g-distances and rotational constants were carried out by the ordinary method.[16] All the normal modes including the torsional motion of the methyl tops were treated as small-amplitude motions, since the barrier to internal rotation as high as 3.0—3.5 kcal/mol[5] makes it unnecessary to rely on the large-amplitude theory for the vibrational correction.[17,18] The moments of inertia and the calculated values of the vibrational correction are listed in Table 3. The values of r_g—r_α^0 are 0.0029 Å, 0.0024 Å, and 0.0007 Å for C–F, C–C, and C···F distances, respectively.

Table 3. Moments of inertia of 2-fluoropropane[a] (in amu Å² units)

	$I^{(0)}$	ΔI	$I^{(z)}$
a	58.131	0.065	58.196(7)[b]
b	62.373	0.091	62.464(9)
c	105.533	0.064	105.597(7)

a) $I^{(0)}$; Observed effective values for the ground vibrational state (Refs. 5 and 6). Conversion factor 505376 MHz amu Å² was used. ΔI; Calculated values of the vibrational correction. $I^{(z)}$; Moments of inertia for the zero-point average structure.
b) Estimated uncertainties to be attached to the last significant digit.

Table 4. Structure parameters of 2-fluoropropane compatible with both the diffraction data and the spectroscopic moments of inertia[a]

C–F	r_g	1.405±0.005
C–C	r_g	1.514±0.004
C···F	r_g	2.366±0.006
∠CCC	ϕ_z	114.6±1.5
$C–H_{Methyl}$ $C–H_{sec}$	r_g	1.13±0.03[b]
$\angle HCH_{Methyl}$	ϕ_z	110±3
$\angle CCH_{sec}$	ϕ_z	109.0 (assumed)

a) Distances in Å and angles in degrees. b) The values of $r_g-r_\alpha^0$ for $C–H_{Methyl}$ and $C–H_{sec}$ are 0.020 Å and 0.016 Å, respectively.

For a complete description of the structure of this molecule, eight independent parameters given in Table 4 are necessary. Three distances from electron diffraction and three moments of inertia from microwave spectroscopy are therefore insufficient. Although the rotational constants of ^{13}C-species and singly deuterated species are available,[6] none of them effectively provide independent additional information. The following two assumptions were then made: (1) The $C–H_{Methyl}$ and $C–H_{sec}$ are equivalent in their r_g-values. (2) The CCH_{sec} angle is within the range of 109±2 °. The implication of the first assumption is essentially the same as the equivalence of C-H distances in r_e-values. As for the second assumption, it was found that the moments of inertia $I^{(z)}$ are very insensitive to the CCH_{sec} angle. A variation of CCH_{sec} as much as 2 ° produces changes in $I^{(z)}$ of only about 0.01 amu Å².

Since there remain six parameters for the six independent observables, they can be determined uniquely for each combination of the six observed values which are allowed to vary within their stated uncertainties. Therefore, for the three distances from electron diffraction, the uncertainties can not be reduced by the joint analysis as in other more favorable cases.[17,19] The other three parameters can only be determined with large uncertainties, since they are strongly correlated with the three distances from diffraction. Numerical results are summarized in Table 4. The uncertainties for ∠CCC, C–H, and ∠HCH represent the maxima and minima of the ranges of these parameters in which the values compatible with the moments of inertia are

found, as the C–F, C–C, and C···F distances are varied within the stated limits of error. The uncertainties associated with the limits of error of $I^{(z)}$ are much smaller. The CCC angle is determined with a reasonable range of uncertainty. The C–H distance and the HCH angle shown in Table 4 are larger than the commonly accepted range of methyl structure. Nevertheless, both C–H and HCH would decrease if the C···F distance decreases. This seems to suggest that the anharmonicity of the non-bonded C···F distances, which was assumed negligible in the present study, is substantially nonzero.

Discussion

The C–C and C–F distances of 2-fluoropropane are compared with those of other fluoroalkanes in Table 5. Although the comparison is somewhat obscured by lack of the r_g-distances for some of the compounds concerned, the trends that both C–C and C–F distances increase from methyl to ethyl, isopropyl, and *t*-butyl are observed in the same way as in the chlorides. The C–C distances of fluorides are smaller than those of *n*-alkanes, *e.g.*, propane.[10] The shortening seems to be similar in nature to that often encountered in fluorine substitution.[23]

TABLE 5. COMPARISON OF THE STRUCTURAL PARAMETERS OF FLUORO-ALKANES (IN Å UNITS)

		C–C	C–F	Ref.
CH_3F	r_0		1.3852(1)	20
CH_3CH_2F	r_0	1.505(3)	1.398(5)	4
$(CH_3)_2CHF$	r_0	1.515(1)	1.407(2)	6
	r_g	1.514(4)	1.405(5)	a)
$(CH_3)_3CF$	r_0	1.516(5)	1.43(2)	21
	r_g	1.522(8)	1.427(8)	22[b]
$(CH_3)_2CH_2$	r_g	1.532(3)		10

a) The present study. b) Estimated from the reported r_a-values, 1.520 and 1.425, respectively.

The r_0-structure reported by Saito and co-workers[6] is consistent with the r_g-structure determined in the present study. However, since the difference between r_0 and r_g values is often as large as 0.01 Å, the closeness of r_0 and r_g seen in Table 5 can be fortuitous.

The authors wish to thank Dr. Shuji Saito, Sagami Chemical Research Center, for the sample and for his helpful discussions. Numerical computation was performed on a FACOM 230-60 of the Hokkaido University Computing Center and also on a FACOM 270-20 in the laboratory of Professor Kimio Ohno, to whom the authors' thanks are due.

References

1) D. R. Lide, Jr. and M. Jen, *J. Chem. Phys.*, **38**, 1504 (1963).
2) F. L. Tobiason and R. H. Schwendeman, *ibid.*, **40**, 1014 (1964).
3) R. L. Hilderbrandt and J. D. Wieser, *ibid.*, **56**, 1143 (1972).
4) L. Nygaard, *Spectrochim. Acta*, **22**, 1261 (1966).
5) J. H. Griffiths, N. L. Owen, and J. Sheridan, *J. Chem. Soc. Faraday II*, **69**, 1359 (1973).
6) K. Yoshida, F. Makino, and S. Saito, private communication. A preliminary report was read at the Spring 26 th National Meeting of the Chemical Society of Japan (Tokyo, 1972).
7) Y. Murata, K. Kuchitsu, and M. Kimura, *Jap. J. Appl. Phys.* **9**, 591 (1970).
8) Numerical experimental data of the leveled total intensity and the background, together with the correlation matrix, have been deposited with the Chemical Society of Japan. (Document No. 7514).
9) S. Konaka and M. Kimura, This Bulletin, **43**, 1693 (1970).
10) T. Iijima, *ibid.*, **45**, 1291 (1972).
11) K. Kuchitsu and S. J. Cyvin, "Molecular Structures and Vibrations," ed. by S. J. Cyvin, Chapter 12, Elsevier, Amsterdam (1972).
12) D. R. Lide, Jr., *J. Chem. Phys.*, **33**, 1514 (1960).
13) B. N. Cyvin and S. J. Cyvin, *Acta Chem. Scand.*, **26**, 3943 (1972).
14) G. A. Crowder and T. Koger, *J. Mol. Struct.*, **23**, 311 (1974). The observed values of frequencies are consistent with those given in Ref. 5, although the assignments slightly differ.
15) S. Mizushima and T. Shimanouchi, "Infrared Absorption and Raman Effect," (in Japanese), Kyoritsu, Tokyo (1958).
16) K. Kuchitsu, "MTP International Review of Science. Physical Chemistry Series One," vol. 2, ed. by G. Allen, Chapter 6, Medical and Technical Publishing Co. Ltd., Oxford (1972).
17) T. Iijima and S. Tsuchiya, *J. Mol. Spectrosc.*, **44**, 88 (1972).
18) We also applied the large-amplitude treatment to the analysis of this molecule and found that either method leads to the same result if the distances are represented in terms of the r_g-structure.
19) T. Iijima, This Bulletin, **45**, 3526 (1972).
20) F. A. Andersen, B. Bak, and S. Brodersen, *J. Chem. Phys.*, **24**, 989 (1956).
21) D. R. Lide, Jr. and D. E. Mann, *ibid.*, **29**, 914 (1958).
22) B. Haase, J. Haase, and W. Zeil, *Z. Naturforsch.*, **22a**, 1646 (1967).
23) A. Yokozeki and S.H. Bauer, "The Geometric and Dynamic Structures of Fluorocarbons and Related Compounds," in "Topics in Current Chemistry," Springer Verlag, Berlin (1974).

Theoretical Determination of the Principal Axes of ^{13}C Chemical Shielding Tensors and their Relationship to the Anisotropies in Some Organic Compounds

Isao ANDO, Atsuo NISHIOKA, and Masahiro KONDO

Department of Polymer Chemistry, Tokyo Institute of Technology, Ookayama, Meguro-ku, Tokyo 152

(Received January 27, 1975)

The principal axes and values for the ^{13}C chemical shielding tensors of carbonyl compounds (formaldehyde, acetaldehyde, acetone, and formic acid), methanol, and *n*-paraffins (propane and *n*-butane) have been determined theoretically by the LCGI-MO theory using the MINDO/2 method. Further, their anisotropies have been estimated. These results have then been discussed by comparing them with the observation of Pines *et al.* and in part compared with the anisotropies in the literature calculated by using other theoretical methods.

The chemical shielding constant of a molecule in NMR is a symmetric second-rank tensor quantity with nine components. In gases and liquids one can observe only the isotropic value of the chemical shielding tensor, that is, the average of the three diagonal components resulting from the rapid molecular reorientation. On the other hand, in solid states the molecular motion is greatly reduced. Thus, in principle, it is possible to determine the six independent components of the tensor; in practice, however, it is normally difficult. To know the full tensor would be extremely valuable for, especially, the theoretical study of the chemical shielding constant. In the last several years significant progress has been achieved in experimental techniques and also in the calculation of the ^{13}C chemical shift.[1] The present authors[2] recently concerned themselves with a theoretical study of the anisotropy of the ^{13}C chemical shielding constant in several organic compounds in order to interpret the experimental data measured by Pines *et al.*[3] Although it is very important to know the exact directions of the principal axes of the ^{13}C shielding tensor for each carbon atom in any molecule, we have not enough information about them at present.

Recently Waugh *et al.*[4] and others[5] have determined experimentally the relative orientation of the principal axes of the ^{13}C shielding tensors using single crystals of several organic compounds, and have shown that such information is more easily obtained from NMR than from X-ray diffraction. In this work we will be concerned with the theoretical determination of the principal axes of the ^{13}C shielding tensors and their relations to the shielding tensor in several compounds, such as formaldehyde, acetaldehyde, acetone, formic acid, methanol, propane, and *n*-butane(*n*-paraffins are known to be planar in the solid state).

There are two theoretical approaches to the determination of the principal axes and values. In one, the six independent shielding elements of the tensor are calculated, the principal values are obtained by diagonalizing the complete tensor, and then, from these, the corresponding axes are determined. In the other, the dependence of the diagonal elements of the tensor on the rotation of the coordinate system chosen is calculated, and then, from this, the principal axes and the principal values are determined. In this work the latter method was used because of its simplicity and its applicability to our case.

Theoretical

The shielding tensor, $\boldsymbol{\sigma}'$, is expressed as follows:

$$\sigma' = \begin{pmatrix} \sigma'_{xx} & \sigma'_{yx} & \sigma'_{zx} \\ \sigma'_{xy} & \sigma'_{yy} & \sigma'_{zy} \\ \sigma'_{xz} & \sigma'_{yz} & \sigma'_{zz} \end{pmatrix} \quad (1)$$

The value of each element in the shielding tensor depends upon the coordinate system chosen in any specific molecule. Therefore, in order to determine the principal axes and values, the dependence of the values of the diagonal terms upon the rotation of the coordinate system chosen must be known.

Now, a coordinate system, $\mathbf{X}$ (x,y,z) for the inherent principal axes is defined for $\boldsymbol{\sigma}$ (diagonalized shielding tensor). The transformation of an arbitrary coordinate system, $\mathbf{X}'$ (x',y',z'), into the coordinate system, $\mathbf{X}$-(x,y,z), by rotation is as follows:

$$\mathbf{X} = \mathbf{T}\cdot\mathbf{X}' \quad (2)$$

where $\mathbf{T}$ is the transformation matrix. All the molecules concerned are planar. Thus, one of the three principal axes is along the direction perpendicular to the molecular plane due to their symmetry; this axis is defined as the z axis. The rotation of the right-handed coordinate system is about the z axis. Thus, $\mathbf{T}$ is defined as:

$$\mathbf{T} = \begin{pmatrix} \cos\theta & -\sin\theta & 0 \\ \sin\theta & \cos\theta & 0 \\ 0 & 0 & 1 \end{pmatrix} \quad (3)$$

The coordinate system rotates counterclockwise about the z axis. As $\mathbf{T}$ is an unitary matrix, the inverse matrix, $\mathbf{T}^{-1}$, is identical to the transposed matrix, $\tilde{\mathbf{T}}$. From the character of a tensor, we can write the following relation by choosing an appropriate value of θ:

$$\begin{aligned} \sigma &= \mathbf{T}^{-1}\cdot\sigma'\cdot\mathbf{T} \\ &= \tilde{\mathbf{T}}\cdot\sigma'\cdot\mathbf{T} \end{aligned} \quad (4)$$

Then, as $\tilde{\mathbf{T}}\cdot\mathbf{T}=\mathbf{E}$ ($\mathbf{E}$: unit matrix),

$$\sigma' = \mathbf{T}\cdot\sigma\cdot\tilde{\mathbf{T}} \quad (5)$$

As has been described above, one of the three principal axes is the z axis perpendicular to the molecular plane. In obtaining the remaining principal axes, we first calculate the angle (relative to the principal axes) at which the value of σ'_{xx} and σ'_{yy} are equal to each other:

$$\sigma'_{xx} = \sigma'_{yy} \quad (6\text{-}1)$$

then

$$\sigma_{xx} + (\sigma_{yy}-\sigma_{xx})\sin^2\theta = \sigma_{yy} - (\sigma_{yy}-\sigma_{xx})\sin^2\theta \quad (6\text{-}2)$$

$$(\sigma_{yy}-\sigma_{xx})(2\sin^2\theta-1) = 0 \quad (6\text{-}3)$$

From this equation, the value of θ is found to be 45 degrees when $\sigma_{yy}\neq\sigma_{xx}$. This result may be true only in this case. Therefore, the position where $\sigma'_{xx}=\sigma'_{yy}$ is found to deviate by 45 degrees from the principal axis. This shows that, in the principal axis systems, the values of σ'_{xx} and σ'_{yy} take the maximum or minimum value. Thus, we can find the principal axes and values by calculating the dependence of the values of σ'_{xx}, σ'_{yy} and σ'_{zz} upon the rotation of the coordinate system chosen.

The paramagnetic term governing predominatly the ^{13}C chemical shielding constant is estimated using the LCGI-MO theory of Pople[6] according to a previous paper[2] as follows (*e.g.*, σ'^{p}_{xx}):

$$\sigma'^{p}_{xx} = -(2e^2\hbar^2/m^2c^2)\langle r^{-3}\rangle_{2p}\sum_{i}^{occ}\sum_{k(\neq i)}^{unocc}\Delta E_{k-i}^{-1} \times (C_{iy_A}C_{kz_A}-C_{iz_A}C_{ky_A})\sum_{B}(C_{iy_B}C_{kz_B}-C_{iz_B}C_{ky_B}) \quad (7)$$

where C_{ix_A} is the coefficient of the $2p_x$ atomic orbital on the A atom of the i-th molecular orbital in the LCAO MO theory, where $\sum_{i}^{occ}$ and $\sum_{k(\neq i)}^{unocc}$ are the summations over occupied and unoccupied orbitals, respectively, where $\sum_{B}$ runs over all the atoms in the molecule, and where ΔE_{k-i} is the singlet-singlet excitation energy between the i-th occupied and the k-th unoccupied orbitals. $\langle r^{-3}\rangle_{2p}$ represents the atomic 2p orbital dimension given by:[7]

$$\langle r^{-3}\rangle_{2p} = 34.33a_0^{-3}(1-0.323q_A')/24 \quad (8)$$

where a_0 is the Bohr radius and where $-q_A'e$ is the net charge. The MINDO/2 method[8] was used as the molecular orbital method.

The bond lengths and bond angles used were as follows:[9] Bond length (the notation of Xn is used for an atom, X, with an elemental symbol being bonded to n neighbours. For example, the carbon atoms in propane and formaldehyde will be described as C4 and C3, respectively):

$l_{C4-H}=1.09$, $l_{C3-H}=1.08$, $l_{C4-C4}=1.54$,
$l_{C4-C3}=1.52$, $l_{C3-O1}=1.22$, $l_{C4-O2}=1.43$,
$l_{C3-O2}=1.36$, $l_{O2-H}=0.96$ (Å)

Bond angle:

$$\angle C\text{-}C\text{-}C=\angle C\text{-}C\text{-}H=\angle H\text{-}C\text{-}H=\angle H\text{-}O\text{-}C=\angle O\text{-}C\text{-}H=109°28'$$

$$\angle C\text{-}C\text{=}O=\angle H\text{-}C\text{=}O=\angle O\text{-}C\text{=}O=120°$$

All the calculations were carried out by means of the HITAC-8800 computer of the Computer Center of the University of Tokyo.

Results and Discussion

The calculated dependences of the σ'^{p}_{xx}, σ'^{p}_{yy}, and σ'^{p}_{zz} of the molecules concerned here upon the rotation of the coordinate system chosen are shown in Fig. 1, where the coordinate system of each carbon rotates

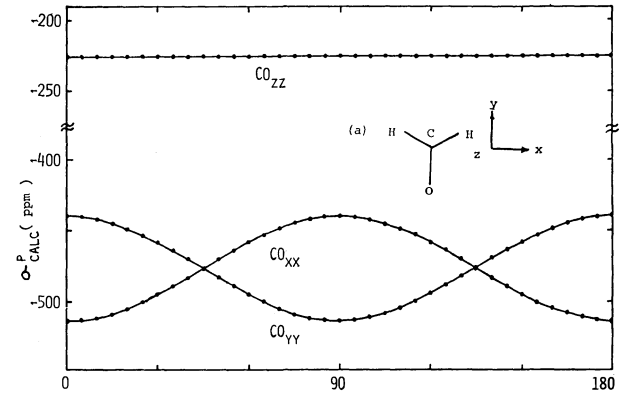

Angle of rotation about z axis (Degrees)

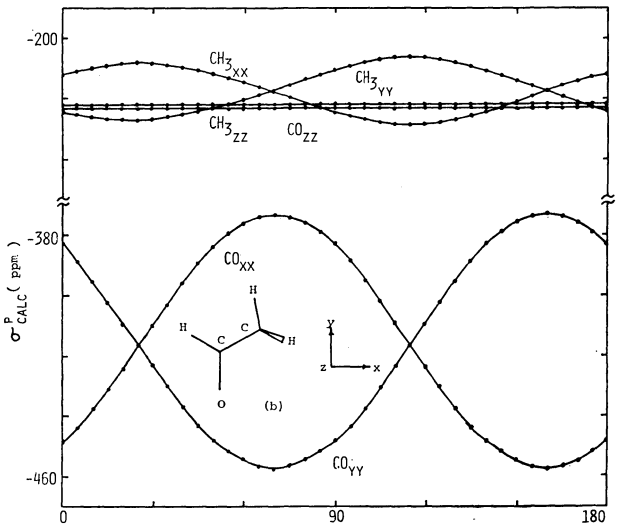

Angle of rotation about z axis (Degrees)

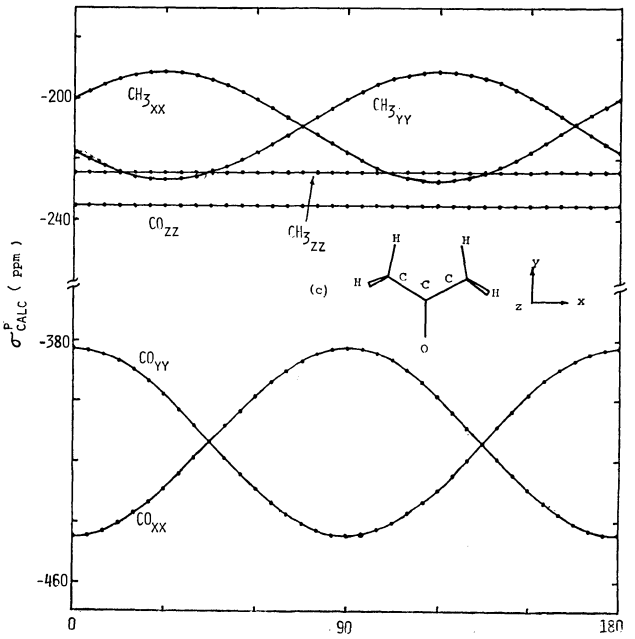

Angle of rotation about z axis (Degrees)

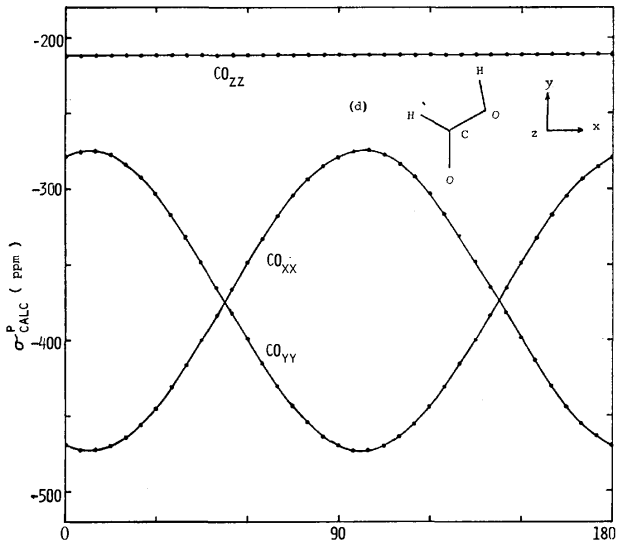

Angle of rotation about z axis (Degrees)

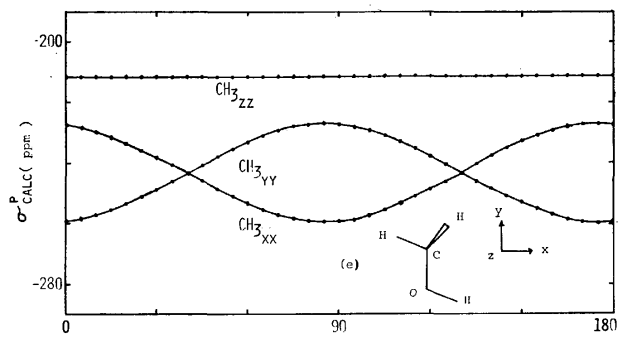

Angle of rotation about z axis (Degrees)

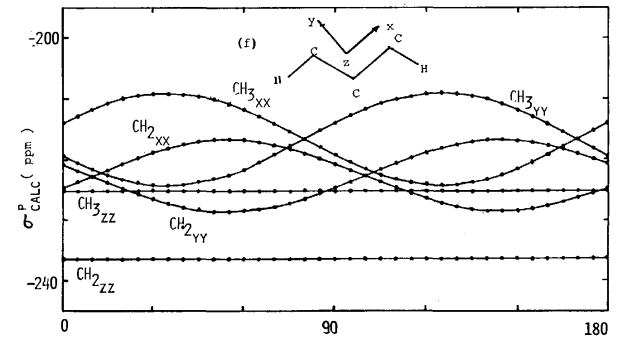

Angle of rotation about z axis (Degrees)

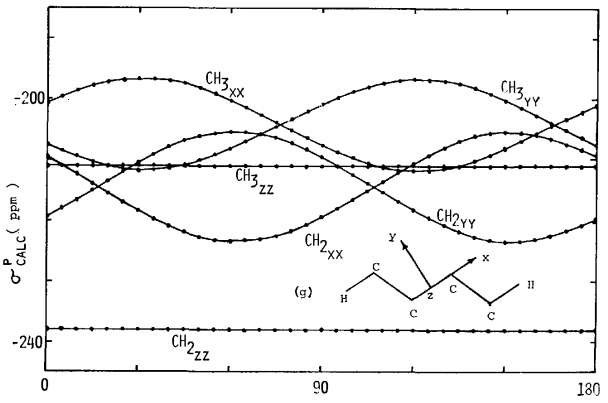

Angle of rotation about z axis (Degrees)

Fig. 1. Dependence of the calculated ^{13}C shielding tensor components σ^P_{calc} upon the rotation of the coordinate system for (a) formaldehyde, (b) acetaldehyde, (c) acetone, (d) formic acid, (e) methanol, (f) propane, (g) *n*-butane. For example, CH_{3xx} denotes the xx component of the shielding tensor for the methyl carbon.

counterclockwise from the position shown in the figure; the interval of the plots of the calculated value is 5 degrees, and the conformations of *n*-paraffins are taken as of the *trans* zig-zag form.

Let us first discuss the position of the principal axes by dividing the compounds concerned into two groups, carbonyl compounds and methanol, and *n*-paraffins. In the former group, if the carbonyl carbon is involved, we can expect that one of the principal axes in formaldehyde and acetone is along the C=O bond axis, as is predicted by the molecular symmetry, but the axes for acetaldehyde and formic acid are not always along the C=O bond axis (*cf.* Fig. 1). As for acetaldehyde and formic acid, the corresponding axes deviate by 20 degrees clockwise and by 8 degrees counterclockwise from the C=O bond axis, as is shown in the figure. Therefore, the axis of the former is oriented approximately along the direction bisecting the O–C–C angle, and the deviation of the latter from the C=O bond axis is very slight, contrary to expectations. These results show that the influence of the OH group neighbouring the carbonyl carbon on the position of the principal axes concerned is smaller than that of the CH_3 group. As for the methyl groups of acetaldehyde, acetone, and methanol, it is found that the principal axis corresponding to the C_{3v} axis of the CH_3 group is oriented at the positions of 25 degrees counterclockwise, 30 degrees counterclockwise, and 6 degrees clockwise respectively from the fixed coordinate system defined in the figure; therefore, these corresponding principal axes are found to deviate by 5 degrees clockwise, and about 0 degree and 6 degrees clockwise respectively from the C_{3v} axis of the CH_3 group. In these compounds, one of the principal axes is found to be oriented approximately along the C_{3v} axis, although this axis, speaking strictly, deviates slightly from the C_{3v} axis.

Next, let us discuss the *n*-paraffins. As for the methyl carbons of propane and *n*-butane, it is found that their principal axes corresponding to the above-mentioned axis deviate by 35 and 30 degrees counterclockwise respectively from the fixed coordinate system; therefore, these principal axes are found to deviate by 16 and 10.5 degrees respectively from the C_{3v} axis of the CH_3 group. The deviation of the former is slightly larger than that of the latter. This may be due to the difference between the CH_3 and CH_2 groups in its next nearest-neighbour group. However, it may still be said that these axes are oriented approximately along the C_{3v} axis. As for the CH_3 groups of these molecules, one of the principal axes is found to deviate by 54.7 and 62 degrees counterclockwise respectively from the fixed coordinate system; therefore, in propane this axis bisects the angle formed by the directions of the CH_3–CH_2 and CH_2–CH_3 bonds, and in *n*-butane it deviates slightly by 7.3 degrees

counterclockwise from the corresponding axis, probably because of the symmetry.

Next, let us discuss the principal values and the anisotropies of the shielding constants of the compounds concerned. Here, for convenience, we will define the principal values in terms of σ_{11}, σ_{22}, and σ_{33} (the magnitude of shielding is $\sigma_{11} \lesssim \sigma_{22} \lesssim \sigma_{33}$) instead of σ^{p}_{xx}, σ^{p}_{yy}, and

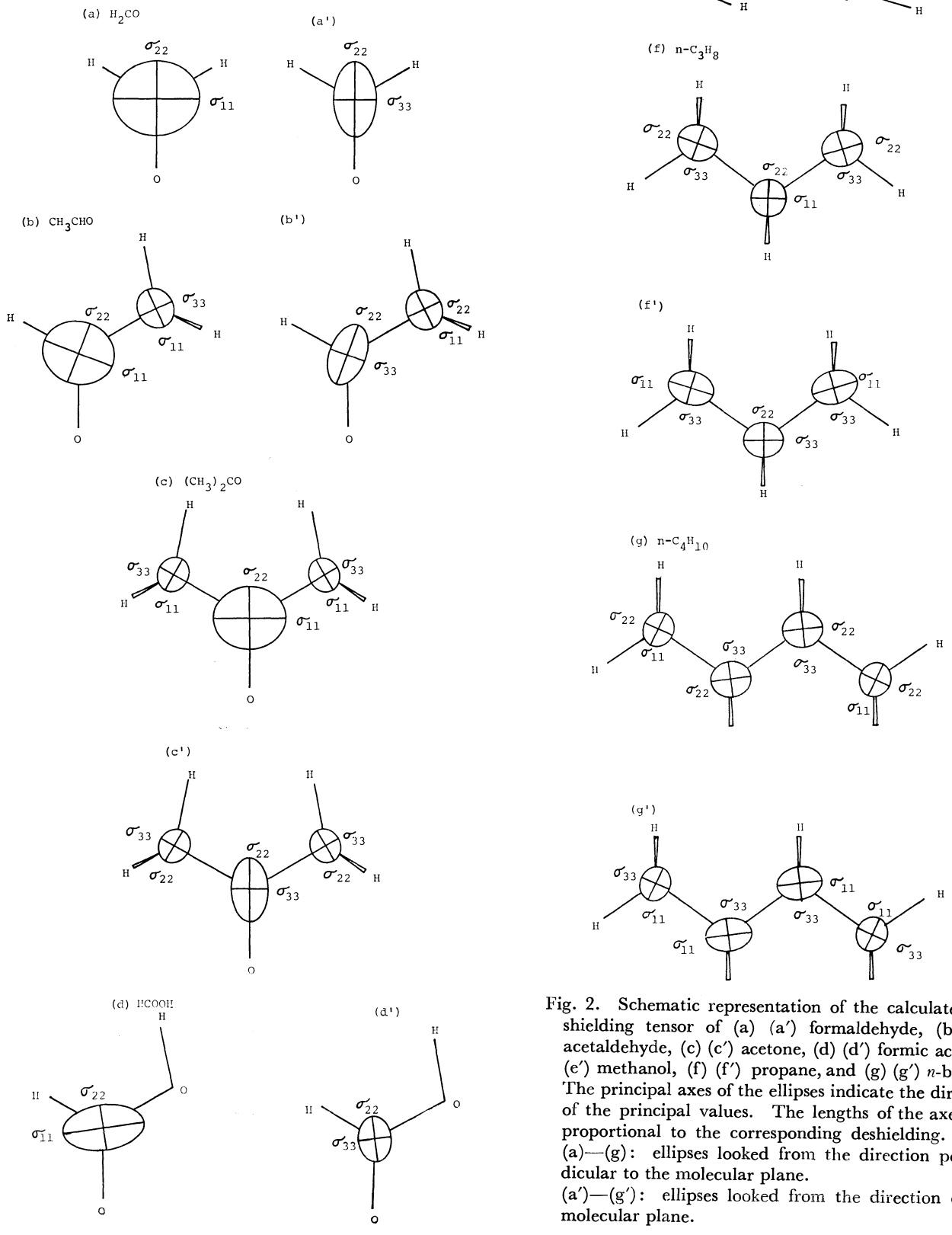

Fig. 2. Schematic representation of the calculated ^{13}C shielding tensor of (a) (a′) formaldehyde, (b) (b′) acetaldehyde, (c) (c′) acetone, (d) (d′) formic acid, (e) (e′) methanol, (f) (f′) propane, and (g) (g′) *n*-butane. The principal axes of the ellipses indicate the direction of the principal values. The lengths of the axes are proportional to the corresponding deshielding.
(a)—(g): ellipses looked from the direction perpendicular to the molecular plane.
(a′)—(g′): ellipses looked from the direction of the molecular plane.

TABLE 1. THE CALCULATED PRINCIPAL VALUES AND ANISOTROPIES OF ^{13}C SHIELDING TENSORS IN SOME ORGANIC COMPOUNDS
(For the comparison, the experimental data in the literature are indicated.)

Compounds	calculated (ppm)				experimental[b] (ppm)			
	σ_{11}	σ_{22}	σ_{33}	$\Delta\sigma$[a]	σ_{11}	σ_{22}	σ_{33}	$\Delta\sigma$
$H_2C{=}O$	−514	−439	−226	250.5	——	——	——	——
CH_3CHO CH_3	−227	−223	−208	17	74±6	86±6	126±7	46±7
CH_3CHO CO	−458	−374	−222	194	−147±7	−105±6	42±6	168±7
$(CH_3)_2CO$ CH_3	−227	−225	−191	35	81±6	81±6	131±6	50±6
$(CH_3)_2CO$ CO	−445	−383	−235	179	−150±6	−136±6	50±7	193±7
$HCOOH$	−474	−275	−212	162.5	——	——	——	——
CH_3OH	−260	−227	−212	31.5	55±6	55±6	118±6	63±6
$CH_3CH_2CH_3$ CH_3	−224	−220	−209	13	——	——	——	——
$CH_3CH_2CH_3$ CH_2	−237	−229	−217	16	——	——	——	——
$CH_3CH_2CH_2CH_3$ CH_3	−212	−211	−197	14.5	——	——	——	——
$CH_3CH_2CH_2CH_3$ CH_2	−238	−224	−206	25	——	——	——	——

a) $\Delta\sigma=\sigma_{33}-(\sigma_{11}+\sigma_{22})/2$ b) Shifts are in ppm relative to benzene liquid.

σ^{p}_{zz}, because the physical meaning for the xx, yy, and zz suffixes sometimes becomes obscure in this case. The calculated results of the principal values and the anisotropies for the compounds concerned are tabulated in Table 1, together with the experimental data in the literature. For further clarification, the principal axes and values are shown by a schematic representation in Fig. 2. In the carbonyl carbons it is found that the principal value of the shielding tensor perpendicular to the molecular plane is the largest one, that the order of the magnitude of their anisotropies ($\Delta\sigma=\sigma_{33}-(\sigma_{11}+\sigma_{22})/2$) is $\overset{H}{H}\!>\!C{=}O > \overset{CH_3}{H}\!>\!C{=}O > \overset{CH_3}{CH_3}\!>\!C{=}O > \overset{H}{HO}\!>\!C{=}O$, and that the magnitude of $\Delta\sigma$ is sensitive to the substituents. As for the methyl carbons in all the compounds concerned the axis of the most shielding component is found to be oriented approximately along the C_{3v} axis except for CH_3OH (*cf.* Fig. 2).

Next, we will discuss the individual compounds separately. As for the anisotropy of formaldehyde, Appleman *et al.*[1] and Tokuhiro *et al.*[10] have reported values of 250.8 and 294.9 ppm respectively, calculated using the *ab initio* method. Our results agree well with the former. For acetaldehyde, the value of the carbonyl carbon in this work increases slightly compared with the previous case[2b] ($\Delta\sigma=192.8$ ppm); one of the principal axes is assumed to lie on the C=O bond and is very much smaller than the value of 280 ppm calculated by Appleman *et al.*[1] On the other hand, for the methyl carbon our value is larger than their value of 2.9 ppm. The experimental values of Pines *et al.*[3] are found to agree with our results. As for acetone, the value of the methyl carbon in this work increases compared to the previous case;[2a] one of the principal axes is assumed to lie on the C=O bond.[11] The value in this work is found to be consistent with the experimental value.[3] As for formic acid, the value in this work is smaller than that of 198.4 ppm calculated by Appleman *et al.*[1] In general, their calculated results are larger than our results for carbonyl carbons. As for methanol, the calculated value is somewhat smaller than the experimental data. One of the reasons for this discrepancy may be that it partly arises from the neglect of the hydrogen bonding among the molecules. Further, it should be noted that the most shielded component is not along the C_{3v} axis, but along the direction perpendicular to the fixed molecular plane, contrary to the results for the other methyl groups. As for *n*-paraffins, the value of $\Delta\sigma$ for the methylene carbon in propane is found to be larger than that in *n*-butane. This may be because in the former the neighbouring groups are the methyl groups, while in the latter they are the methyl and methylene groups. The value of $\Delta\sigma$ is found to be very sensitive to the environment of the specified carbon. As for the methyl carbons, it is found that there is a slight difference between the values of $\Delta\sigma$ in the two paraffins; this must also be due to the above-mentioned reason. The observation of these molecules has not yet been done; after it has, we hope to measure $\Delta\sigma$ to get important information for the study of the molecular motion in a solid.

References

1) B.R. Appleman and B.P. Dailey, *Advan. Mag. Reson.*, **7**, 231 (1974).
2) a) I. Ando, A. Nishioka, and M. Kondo, *Chem. Phys. Lett.*, **25**, 212 (1974); b) I. Ando and A. Nishioka, This Bulletin, **48**, 841 (1975).
3) A. Pines, M.G. Gibby, and J.S. Waugh, *Chem. Phys. Lett.*, **15**, 373 (1972).
4) a) P. Van Hecke, J.C. Weaver, B.L. Neff, and J.S. Waugh, *J. Chem. Phys.*, **60**, 1668 (1974); b) S. Pausak, J. Tegenfeldt, and J.S. Waugh, *ibid.*, **61**, 1338 (1974); c) J.L. Ackerman, J. Tegenfeldt, and J.S. Waugh, *J. Amer. Chem. Soc.*, **96**, 6843 (1974).
5) J. Kempf, H.W. Spiess, U. Haeberlen, and H. Zim-

mermann, *Chem. Phys.*, **4**, 269 (1974).
6) J. A. Pople, *J. Chem. Phys.*, **37**, 53 (1962).
7) J. A. Pople, *Mol. Phys.*, **7**, 301 (1964).
8) M. J. S. Dewar and E. Haselbach, *J. Amer. Chem. Soc.*, **92**, 590 (1970).
9) J. A. Pople and D. L. Beveridge, "Approximate Molecular Orbital Theory," McGraw-Hill, New York (1970), p. 111.
10) T. Tokuhiro, B. P. Appleman, G. Fraenkel, C. W. Kern, and P. K. Pearson, *J. Chem. Phys.*, **57**, 20 (1972).
11) In this calculation l_{C-H} is taken as 1.09 Å. Therefore the shielding components of the carbonyl carbon differ slightly.

Inhibition Effects of Some Polymers on Electroreduction of Anions at the Mercury/Solution Interface

Tetsuya OHSAKA, Yasuo IIDA, and Tadashi YOSHIDA

Applied Electrochemistry Laboratory, Graduate School of Science and Engineering, Waseda University, Nishi-Okubo, Shinjuku-ku, Tokyo 160

(Received May 8, 1974)

The present work was conducted to investigate the electroreduction of anions (typically $S_2O_8^{2-}$ and BrO_3^-) under the influence of the adsorption of polymers (polyethyleneglycol, alkylphenoxy polyethoxy ethanols and polyvinylpyrrolidone) on the electrode surface. The limiting current of $S_2O_8^{2-}$ reduction was depressed by the polymers in the region from nearly the zero-charge potential to the more negative potential. The half-wave potential of BrO_3^- reduction shifted towards more negative potential by adding the polymers. In the potential range where the cathodic current was mainly controlled by mass transfer of the anions, the time (t_m) needed to complete the formation of a monolayer was obtainable conveniently from the instantaneous current *vs.* time ($I-t$) curve as reported previously for the inhibited reduction of Cd^{2+} or Cu^{2+}.[2,3,8] In the potential range where the current was mainly controlled by charge transfer, an exact determination of t_m, by which the maximum surface concentration of polymer was given, was possible only when the instantaneous current density (i) was plotted against $t^{1/2}$. In such a potential range, i was expressed as follows.

$$i = i_0 - (i_0 - i_1)(t/t_m)^{1/2} \quad \text{for } t \leqslant t_m$$

or

$$i = i_1 \quad \text{for } t > t_m$$

Moreover,

$$\bar{I}_{ads}/\bar{I}_0 = 1 - \frac{10}{13}\frac{i_0 - i_1}{i_0}(t_d/t_m)^{1/2} \quad \text{for } t_d \leqslant t_m$$

$$\bar{I}_{ads}/\bar{I}_0 = 1 - \frac{10}{13}\frac{i_0 - i_1}{i_0} - \frac{3}{13}\frac{i_0 - i_1}{i_0}\{1 - (t_d/t_m)^{-5/3}\} \quad \text{for } t_d > t_m$$

where i_0 and i_1 are the instantaneous current densities at $\theta=0$ and 1, $\bar{I}_{ads}$ and $\bar{I}_0$ the polarographic currents with and without polymers, t_d the drop time, t_m the time required to attain the saturated adsorption. The relationship between the shift of half-wave potential and $(t_d/t_m)^{1/2}$ (for $t_d \leqslant t_m$) or $(t_d/t_m)^{-5/3}$ (for $t_d > t_m$), was introduced and the results were verified for the inhibition effects of polymer on the electroreduction of BrO_3^- as well as for that on VO^{2+} reduction.

The adsorption of polymers at the mercury/solution interface has been investigated by differential capacity measurements,[1] and it was found that the adsorption is mainly controlled by diffusion process at the initial stage. The inhibition due to an adsorbed polymer on the electroreduction of Cd^{2+} or Cu^{2+} scarcely took place until the attainment of a certain high coverage when the sharp increase of inhibition occured. Such inhibition effects might be characterized by the diffusion process of depolarizer.[2,3]

The present paper is mainly concerned with the inhibition effects of polymer on the electroreduction of some anions, which will be compared with those on Cd^{2+} reduction. The process of electroreduction of anion is characterized by the interference owing to the influence of electric field in the double layer on the reacting entities, and the interference arises markedly in a dilute supporting electrolyte solution.[4] In consideration of polyvalent anions including $S_2O_8^{2-}$, $Fe(CN)_6^{3-}$, and $PtCl_4^{2-}$ or monovalent anions such as BrO_3^-, NO_3^-, and IO_3^- under the double layer effects,[5] the electroreduction of $S_2O_8^{2-}$ [4,6] and BrO_3^- [7] will be investigated typically.

Experimental

A DME (dropping mercury electrode) was used as the test electrode. All the potentials were referred to a saturated calomel electrode (SCE). A Yanagimoto P-8 Type Polarograph with three electrodes system was used for the measurements of current-potential curves. The instantaneous current *vs.* time curves were determined from the iR drop observed with a recorder or an oscilloscope in parallel with 2 kΩ resistance which was connected in series with the DME and the polarization circuit. Water-soluble polymers PVP (BASF), PEG (Sanyo Chemical Industry), and Triton X (Rohm and Haas) were used without further purification. The depolarizers were reagent-grade $CdSO_4$, $K_2S_2O_8$, $KBrO_3$, and $VOSO_4$. Observation was carried out in the atmosphere of purified nitrogen at 25 °C.

Results and Discussion

Inhibition Effects of Polymer on the Electroreduction of $S_2O_8^{2-}$. For the Case Where the Current Is Mainly Controlled by Mass Transfer: Figure 1 shows the polarograms of $S_2O_8^{2-}$ reduction inhibited by the adsorption of PVP. It was confirmed by the differential capacity measurements[1] that the adsorption of PVP occurs within the potential range in Fig. 1. The polarographic currents were inhibited in the range from the vicinity of zero-charge potential to *ca.* −1.5 V. Similarly, PEG or Triton X inhibited the reduction of $S_2O_8^{2-}$. The decrease of inhibition effects in the range from *ca.* −1.2 to −1.8 V may be ascribed to sufficient polarization. It is interesting that the inhibition effects of polymers on $S_2O_8^{2-}$ reduction are similar to the "supporting electrolyte effect"[5] which results from the double layer effects on anion reduction in the absence of adsorbates.

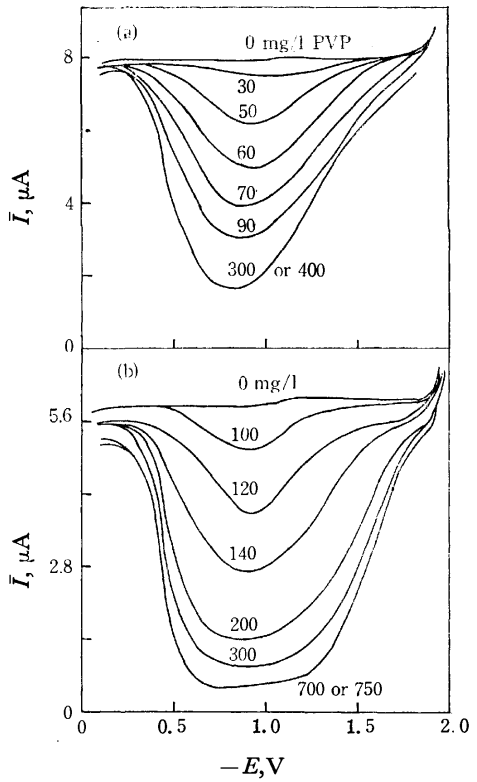

Fig. 1. Polarograms of $K_2S_2O_8$ inhibited by PVP.
(a) 0.5 M sodium sulfate+1.5 mM $K_2S_2O_8$+various contents of PVP $\bar{M}=10000$.
(b) 0.5 M sodium sulfate+1.0 mM $K_2S_2O_8$+various contents of PVP $\bar{M}=750000$.

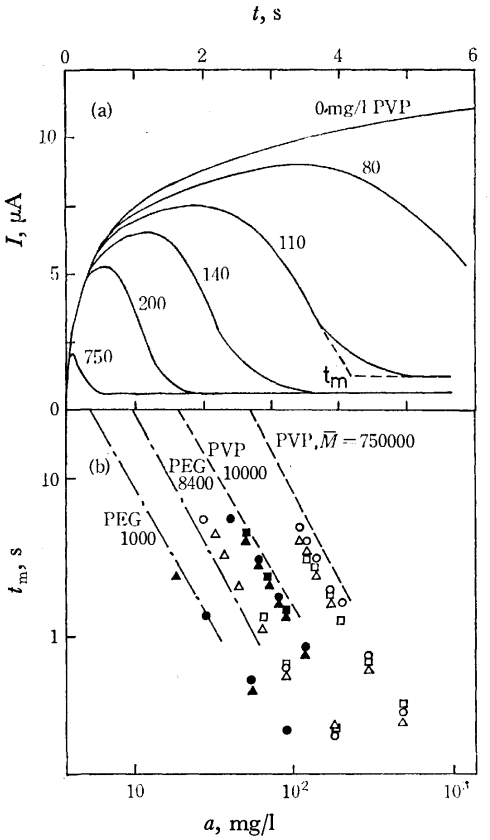

Fig. 2. Instantaneous current measurements for $K_2S_2O_8$ reduction.
(a) $I-t$ curves: 0.5 M sodium sulfate+1.0 mM $K_2S_2O_8$+various contents of PVP $\bar{M}=750000$, $E=-0.8$ V.
(b) log t_m *vs.* log a plots: 0.5 M sodium sulfate+1.0 mM $K_2S_2O_8$+various adsorbates, PVP $\bar{M}=750000$ observed at potentials (○: −0.4 V, △: −0.8 V, □: −1.2 V), PVP $\bar{M}=10000$ (●: −0.5 V, ▲: −1.0 V, ■: −1.5 V), PEG $\bar{M}=8400$ (○: −0.5 V, △: −0.9 V, □: −1.5 V), PEG $\bar{M}=1000$ (●: −0.5 V, ▲: −1.0 V), dashed lines for PVP observed at −0.5 V and one-dotted lines for PEG observed at −0.6 V are derived from differential capacity measurements in 0.5 M sulfuric acid.

In the case of diffusion-controlled adsorption in a dilute PVP solution, PVP of low $\bar{M}$ was more effective on the inhibition than that of high $\bar{M}$ as shown by the results for 50 mg/l of $\bar{M}=10000$ and 100 mg/l of $\bar{M}=750000$ in Fig. 1. Such results may be due to the diffusion coefficient which decreases with $\bar{M}$. On the contrary, PVP of high $\bar{M}$ took more the effect on the inhibitive action as compared with that of low $\bar{M}$ when the adsorption attained the saturation in concentrated PVP solution. The tendency similar to the cases of PVP was also revealed by PEG in the inhibition effects. However, the inhibition of Triton X became more effective with the decreases of $\bar{M}$ in each case of diffusion-controlled or saturated adsorption, which might be due to the increase of adsorbability of Triton X with the decrease of $\bar{M}$ in contrast with the cases of PVP and PEG.

We have investigated the determination of the maximum surface concentration (Γ_m) of polymer at the interface, and it was derived from the time t_m, at which the formation of a monolayer of polymer was achieved. The time t_m required to attain the saturated adsorption of polymer was obtained previously by the differential capacity measurements,[1] while it was also determined from the time dependence of instantaneous limiting current.[2,3] Such time dependence was observed at the potential where the polarogram was most depressed. Figure 2(a) shows the instantaneous limiting current *vs.* time ($I-t$) curves for $S_2O_8^{2-}$ at $E=-0.8$ V in the solution containing PVP of $\bar{M}=750000$. These curves are similar to those in Refs. 2, 3, and 8 where the limiting current is inhibited by diffusion-controlled film formation of polymer. The time t_m can be obtained conveniently by extrapolating the sharply decreasing region in $I-t$ curve to the minimum one. The plots of log t_m *vs.* log a (a: bulk concentration of adsorbates) obtained from $I-t$ curves are shown in Fig. 2(b) in comparison with those derived from the differential capacity measurements. In Fig. 2(b), the broken and one-dotted lines are derived from the capacity method,[1-3] and their slopes of *ca.* −2 are in approximate agreement with those plotted with t_m values obtained from $I-t$ curves, which supports the Koryta equation[9] as described in the previous papers.[1-3] Therefore, in the case as shown in Fig. 2, t_m can be conveniently determined by the instantaneous limiting current, which makes the estimation of Γ_m (maximum surface concentration of adsorbates) easy.

For the Case Where the Current Is Mainly Controlled by Charge Transfer: Figure 3(a) shows the polarograms of $S_2O_8^{2-}$ in 0.005 M sodium sulfate, where the limiting

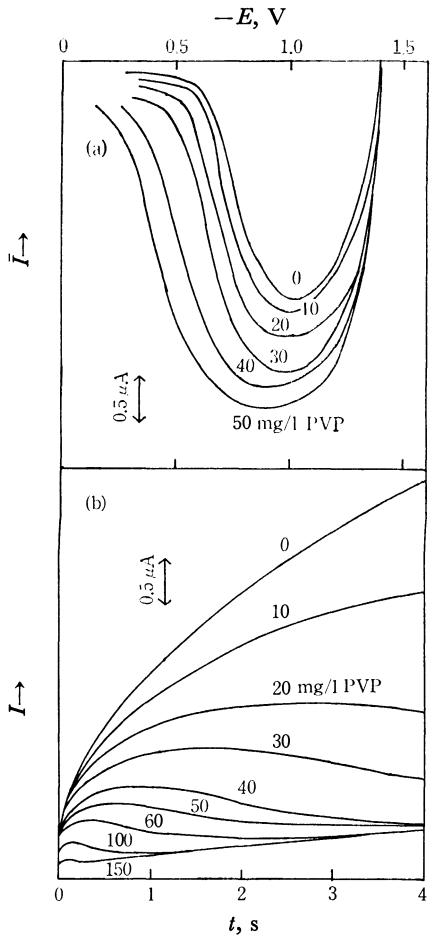

Fig. 3. Polarograms of 1.5 mM $K_2S_2O_8$ in 0.005 M sodium sulfate inhibited by PVP $\bar{M}=10000$ and their instantaneous current *vs.* time curves observed at −1.0 V.
(a) Polarograms, (b) $I-t$ curves.

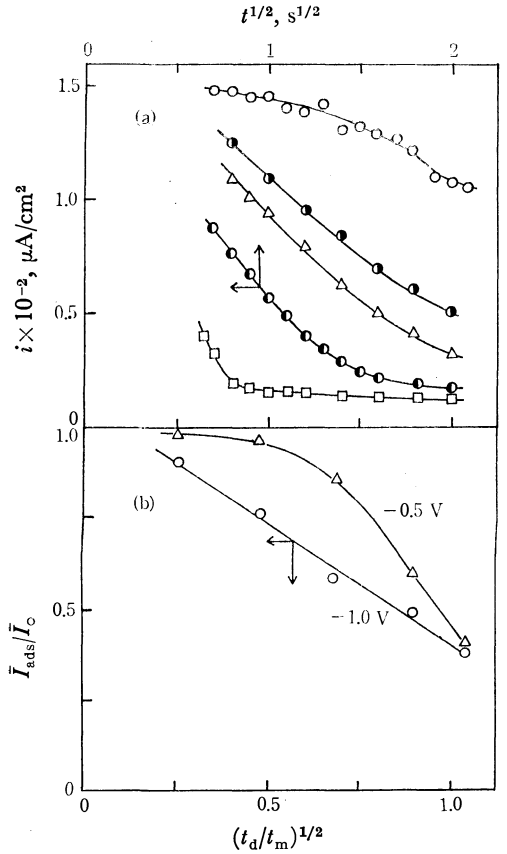

Fig. 4. Behaviors of instantaneous current density for $K_2S_2O_8$ reduction in the presence of polymer in a dilute supporting electrolyte.
1.5 mM $K_2S_2O_8$+0.005 M sodium sulfate+various contents of PVP $\bar{M}=10000$,
(a) $i-t^{1/2}$ plots at −1.0 V, contents (○: 0 mg/l PVP, ◑: 20 mg/l, △: 30 mg/l, ◐: 50 mg/l, □: 150 mg/l),
(b) $\bar{I}_{ads}/\bar{I}_0$ *vs.* $(t_d/t_m)^{1/2}$ plots at −0.5 and −1.0 V.

current without adsorbates is depressed by the double layer effects in the range from *ca.* −0.6 V to −1.4 V. In the above range, the current is mainly controlled by charge transfer rather than mass transfer.[4,5] The inhibition effects of polymer in a dilute supporting electrolyte are larger than those in a concentrated electrolyte, as shown by the results for 50 mg/l PVP in Fig. 3(a) and Fig. 1(a). The $I-t$ curves in Fig. 3(b) were observed at $E=-1.0$ V where the maximum inhibition by polymer was shown. In the $I-t$ curve without adsorbates, I becomes the function of $t^{2/3}$ instead of $t^{1/6}$ which means limiting current. Further, the $I-t$ curves with adsorbates always show the ambiguous transition range from diffusion-controlled to saturated adsorption, which makes the graphical determination of t_m difficult.

For the purpose of determining the time t_m, $I-t$ curves in Fig. 3(b) were rewritten as i *vs.* $t^{1/2}$ plots in Fig. 4(a) in view of diffusion-controlled film formation. In the absence of adsorbates, the instantaneous current density somewhat decreases with time owing to the influence of diffusion process of depolarizer, though the value is expected to be constant independently of time. In the presence of adsorbates, the instantaneous current density decreases linearly with $t^{1/2}$ in the range of diffusion-controlled adsorption of polymer, whereas i becomes nearly constant after the attainment of saturated adsorption. Then, the inhibition effects of polymer on the instantaneous current density in the potential range where the current is mainly controlled by charge transfer of depolarizer can be given by Eqs. (1) and (2) shown later. This tendency is similar to that of C (differential capacity) *vs.* $t^{1/2}$ curves, and the time t_m can be easily determined by the graphical extrapolation in the same manner as described previously for $C-t^{1/2}$ curves.[1]

Relationship between Polarographic Current and Instantaneous Current Density. When the current is mainly controlled by charge transfer, the inhibition is assumed to be ascribed mainly to the blocking effect of adsorbates by considering the behavior of Fig. 4(a). The instantaneous current density before the attainment of saturated adsorption can be regarded as the sum of the instantaneous current densities on the covered (i_1) and the "clean" areas (i_0) as follows.

$$i = i_0(1-\theta) + i_1\theta = i_0 - (i_0-i_1)(t/t_m)^{1/2} * \quad \text{for } t \leqslant t_m \qquad (1)$$

* $\theta = \dfrac{\Gamma}{\Gamma_m} = \dfrac{0.736D^{1/2}at^{1/2}}{0.736D^{1/2}at_m^{1/2}} = (t/t_m)^{1/2}$, where D and a are the diffusion coefficient and bulk concentration of adsorbates.

When the saturated adsorption is achieved,

$$i = i_1 \qquad \text{for } t > t_m \qquad (2)$$

where i_0 and i_1 are the instantaneous current densities at θ (coverage)=0 and 1. These equations are supported by three conditions for $i-t^{1/2}$ curves: (i) instantaneous current density at $t=0$ (i_0) becomes constant regardless of polymer concentration, (ii) instantaneous current density in the presence of adsorbates decreases linearly with $t^{1/2}$, and (iii) instantaneous current density in the case of saturated adsorption becomes constant value i_1.

The relation between polarographic current and instantaneous current density can be derived from Eq. (1) or (2).

For $t_d \leq t_m$

$$I = A\{i_0-(i_0-i_1)(t/t_m)^{1/2}\}$$

Then,

$$\bar{I}_{ads}/\bar{I}_0 = \frac{\frac{1}{t_d}\int_0^{t_d} 0.85(mt)^{2/3}\{i_0-(i_0-i_1)(t/t_m)^{1/2}\}dt}{\frac{1}{t_d}\int_0^{t_d} 0.85(mt)^{2/3}i_0 dt}$$

$$= 1 - \frac{10}{13}\frac{i_0-i_1}{i_0}(t_d/t_m)^{1/2} \qquad (3)$$

where $\bar{I}_{ads}$ and $\bar{I}_0$ are the polarographic currents with and without adsorbates, and A, t_d, and m are the surface area ($=0.85\ m^{2/3}\ t^{2/3}$), the drop time, and the mercury flow rate, respectively.

For the purpose of investigating Eq. (3), the relation of $\bar{I}_{ads}/\bar{I}_0$ *vs.* $(t_d/t_m)^{1/2}$ was plotted in Fig. 4(b). $\bar{I}_{ads}/\bar{I}_0$ *vs.* $(t_d/t_m)^{1/2}$ curve becomes linear at -1.0V where the current is mainly controlled by charge transfer, whereas at -0.5 V it deviates from the linearity because of the mass transfer becoming predominant at -0.5 V.[4,5] Then, Eq. (3) holds for the system where the current being mainly controlled by charge transfer, is inhibited by polymer.

For $t_d > t_m$,

$$\bar{I}_{ads}/\bar{I}_0 = \frac{\frac{1}{t_d}\int_0^{t_m} A\{i_0-(i_0-i_1)(t/t_m)^{1/2}\}dt + \frac{1}{t_d}\int_{t_m}^{t_d} Ai_1 dt}{\frac{1}{t_d}\int_0^{t_d} Ai_0 dt}$$

$$= 1 - \frac{10}{13}\frac{i_0-i_1}{i_0} - \frac{3}{13}\frac{i_0-i_1}{i_0}\{1-(t_d/t_m)^{-5/3}\} \qquad (4)$$

Eq. (4) is expected to hold as well as Eq. (3) within the potential range where the current is mainly controlled by charge transfer.

Inhibition Effects of Polymer on the Electroreduction of BrO_3^-. Figure 5 shows the polarograms of BrO_3^- reduction in 0.05 M sulfuric acid where the half-wave potential shifts from -0.4 V to more negative side by adding PEG, and this tendency differs from that of polarograms for $S_2O_8^{2-}$ reduction in 0.5 M sodium sulfate. The shift of half-wave potential is relatively large in a dilute polymer solution where the adsorption is controlled by the diffusion of polymer, while the shift tends to be saturated in the polymer solution so concentrated as to attain rapidly the saturated adsorption. PVP and PEG of small $\bar{M}$ have greater influence on polarograms as compared with those of large $\bar{M}$ in the range of diffusion-controlled adsorption, however, the reverse is the case in the range of saturated adsorption.

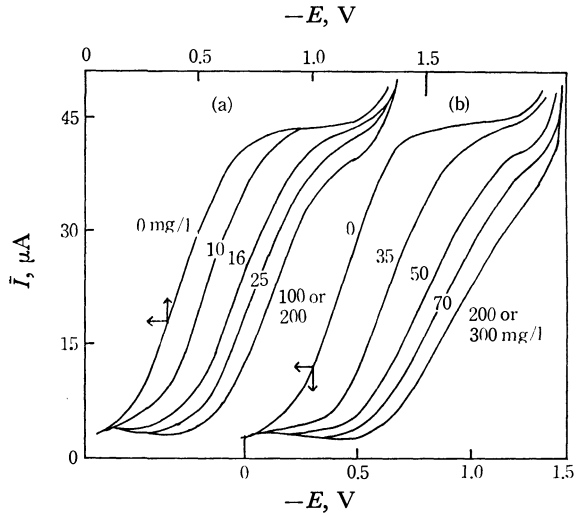

Fig. 5. Polarograms of $KBrO_3$ inhibited by PEG.
0.05 M sulfuric acid+1.0 mM $KBrO_3$+various contents of PEG,
(a) PEG $\bar{M}$=1000, (b) PEG $\bar{M}$=8400.

In the case of Triton X, the smaller the mean molecular weight ($\bar{M}$), the larger the influence on polarograms in each case of diffusion-controlled and saturated adsorption.

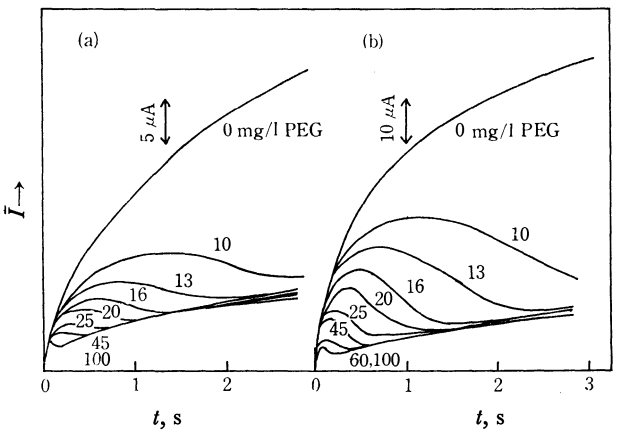

Fig. 6. Instantaneous current *vs.* time curves for $KBrO_3$ reduction inhibited by PEG.
0.05 M sulfuric acid+1.0 mM $KBrO_3$+various contents of PEG $\bar{M}$=1000,
(a) $E=-0.3$ V, (b) $E=-0.5$ V.

For the BrO_3^- reduction inhibited by PEG in 0.05 M sulfuric acid, $I-t$ curves were observed at two potentials along the waves in Fig. 5; -0.3 V is a typical potential at the foot of polarograms (Fig. 6(a)), and -0.5 V is that in the neighborhood of limiting current (Fig. 6(b)). The time t_m can be easily determined from $I-t$ curves at -0.5 V shown in Fig. 6(b) in the same way as described in Fig. 2(a). However, from the $I-t$ curves at -0.3 V in Fig. 6(a) the determination of t_m is difficult because of the indistinct transition range from the diffusion-controlled to the saturated adsorption.

The inhibition effects of polymers on BrO_3^- reduction are examined in detail at the foot of polarographic wave where the current is predominantly controlled by charge transfer (Fig. 7). Figures 7(a) and (b) are the results

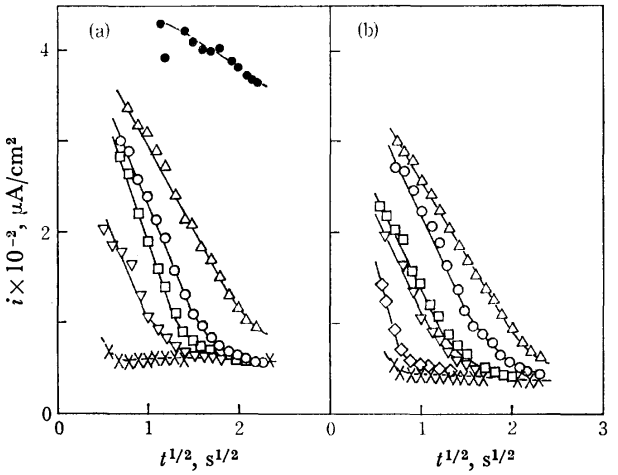

Fig. 7. Instantaneous current density *vs.* square root of time curves for $KBrO_3$ reduction inhibited by polymers. 0.05 M sulfuric acid+1.0 mM $KBrO_3$+polymers, $E=-0.3$ V,
(a) contents of PEG $\bar{M}=8400$ (●: 0 mg/l, △: 25 mg/l, ○: 35 mg/l, □: 40 mg/l, ▽: 50 mg/l, ×: 200 or 300 mg/l),
(b) contents of Triton X-405 $\bar{M}=2000$ (△: 15 mg/l, ○: 20 mg/l, □: 25 mg/l, ▽: 30 mg/l, ◇: 50 mg/l, ×: 70 or 100 mg/l).

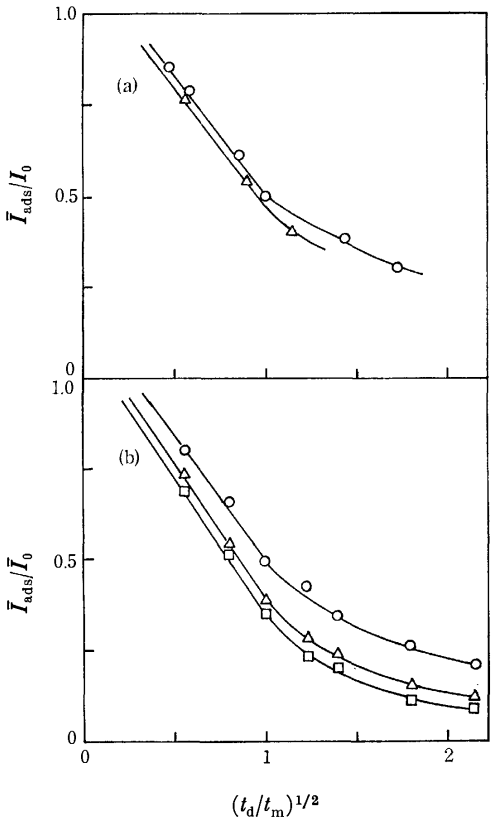

Fig. 8. $(\bar{I}_{ads}/I_0)$ *vs.* $(t_d/t_m)^{1/2}$ plots for $KBrO_3$ reduction in the presence of polymer.
(a) 0.05 M sulfuric acid+1.0 mM $KBrO_3$+PVP (○: $\bar{M}=10000$, △: $\bar{M}=750000$), $E=-0.3$ V,
(b) 0.05 M sulfuric acid+1.0 mM $KBrO_3$+Triton X-205 $\bar{M}=1100$, (○: observed at -0.2 V, △: -0.3 V, □: -0.4 V).

with PEG of $\bar{M}=8400$ and Triton X-405 of $\bar{M}=2000$. In the solution containing adsorbates, i decreases linearly with $t^{1/2}$ in the range of the diffusion-controlled adsorption prior to the saturated adsorption where nearly constant i of *ca.* 60 μA/cm² is obtained, while roughly constant i of *ca.* 400 μA/cm² is observed for the solution without polymer. These phenomena can be explained well by Eqs. (1) and (2).

On the relationships introduced in the foregoing paragraph, $\bar{I}_{ads}/\bar{I}_0$ *vs.* $(t_d/t_m)^{1/2}$ plots are shown in Fig. 8. For $t_d \leqslant t_m$, these plots result in a linear relation having the intercept of *ca.* 1, while for $t_d > t_m$, they approach to the asymptotic value of i_1/i_0, as expected from Eq. (3) or (4), respectively. The slopes of Eq. (3) and the asymptotic values of Eq. (4) for $t \to \infty$ obtained from $\bar{I}_{ads}/\bar{I}_0$ *vs.* $(t_d/t_m)^{1/2}$ plots are shown in Table 1, in comparison with those calculated from the instantaneous current densities at -0.3 V. The intercepts of Eq. (3) obtained by $\bar{I}_{ads}/\bar{I}_0$ *vs.* $(t_d/t_m)^{1/2}$ plots are also listed in Table 1. The slopes and the asymptotic values obtained from the figures like Fig. 8 agree approximately with those calculated with the instantaneous current densities except for the slopes with PVP. The intercept values at $t=0$ obtained from $\bar{I}_{ads}/\bar{I}_0$ *vs.* $(t_d/t_m)^{1/2}$ plots are somewhat larger than the theoretical values of unity expected from Eq. (3). Then, it follows that the current density (i_0) on free surface in the solution containing adsorbates is somewhat higher than that (i_0') in the solution without adsorbates, though Eq. (3) holds on the assumption of $i_0=i_0'$ (*cf.* the derivation of Eq. (3)). Such results might be attributed to the interaction between adsorbates and depolarizer on the surface or to the characteristics of capillary.[10]

Table 1. Slopes, asymptotic values, and intercepts of $\bar{I}_{ads}/\bar{I}_0$ *vs.* $(t_d/t_m)^{1/2}$ plots

Adsorbates		$-E$,V	Slopes[a] for $t_d \leqslant t_m$		Asymp. value for $t \to \infty$		Intercept at $t=0$
			obsd[b]	calcd[c]	obsd[b]	calcd[c]	
PEG	$\bar{M}=$ 1000	0.3	0.74	0.60	0.22	0.22	1.02
	$\bar{M}=$ 8400	0.3	0.74	0.67	0.18	0.13	1.08
PVP	$\bar{M}=$ 10000	0.3	0.73	0.41	0.27	0.27	1.20
	$\bar{M}=$ 750000	0.3	0.74	0.46	0.25	0.33	1.20
Triton	X-205	0.3	0.79	0.71	0.10	0.08	1.18
	X-405	0.3	0.77	0.69	0.18	0.10	1.09

a) Absolute values. b) The values observed directly from $\bar{I}_{ads}/\bar{I}_0$ *vs.* $(t_d/t_m)^{1/2}$ plots. c) The values calculated from instantaneous current densities (slope=$\frac{10}{13}\frac{i_0-i_1}{i_0}$, asymptotic value=$i_1/i_0$).

Table 2 shows the values of αn and $E''_{1/2}$ (half-wave potential at the saturated adsorption) for the inhibition effects of polymer on BrO_3^- reduction. The values of αn were obtained from the potential dependence of log $(\bar{I}_d-\bar{I}_{ads})/\bar{I}_{ads}$, where α, n, and $\bar{I}_d$ were the transfer coefficient, the number of electrons involved in the reduction, and the polarographic limiting current. From the results of $E_{1/2}''$ and αn in Table 2, Triton X is found to be most effective on the inhibition of BrO_3^- reduction. The shift of half-wave potential in the presence of

TABLE 2. HALF-WAVE POTENTIAL AT MAXIMUM SHIFT $E''_{1/2}$ AND αn FOR BrO_3^- ELECTROREDUCTION UNDER SATURATED ADSORPTION OF POLYMERS

Adsorbates		a mg/l	$-E''_{1/2}$, V	αn[a)]
PEG $\bar{M}=$	1000	45	0.82	0.18
$\bar{M}=$	8400	200	0.97	0.15
PVP $\bar{M}=$	10000	300	0.67	0.19
$\bar{M}=$	750000	600	0.68	0.19
Triton	X-205	250	1.20	0.14
	X-405	300	0.88	0.16

In the solution without adsorbates, half-wave potential and αn for BrO_3^- reduction are -0.40 V and 0.23.
a) The values of αn are calculated from the relation of $\log\{(\bar{I}_d-\bar{I}_{ads})/\bar{I}_{ads}\}$ *vs.* E.

polymer will be derived from the change of the apparent rate constant (k_{app}) with polymer and its potential dependence. The instantaneous current in the absence of polymer is given by,

$$I_0 = nFAk_0a^* \tag{5}$$

where k_0 and a^* are the rate constant at $\theta=0$ and the concentration at electrode surface.

For the case with polymer,

$$I_{ads} = nFAk_{app}a^* \tag{6}$$

The apparent rate constant can be assumed as the sum of rate constants on covered (k_1) and uncovered surface (k_0) as follows,[11]

$$k_{app} = k_0(1-\theta) + k_1\theta = k_0 - (k_0-k_1)(t/t_m)^{1/2} \quad \text{for } t \leqslant t_m \tag{7}$$

$$k_{app} = k_1 \quad \text{for } t > t_m \tag{8}$$

Then,

$$(I_{ads})_A = nFAa^*\{k_0-(k_0-k_1)(t/t_m)^{1/2}\} \quad \text{for } t \leqslant t_m \tag{9}$$

or $$I_{(ads)_B} = nFAk_1a^* \quad \text{for } t > t_m \tag{10}$$

The potential dependence of k_0 or k_1 is expressed as follows,

$$k_0 = k_0^s \exp\left\{-\frac{\alpha nF}{RT}(E-E_0)\right\} \tag{11}$$

$$k_1 = k_1^s \exp\left\{-\frac{\alpha nF}{RT}(E-E_0)\right\} \tag{12}$$

where k_0^s and k_1^s are the standard rate constants for $\theta=0$ and 1, and E_0 the standard potential of the system in question. The concentration at the electrode surface can be expressed by the instantaneous current, that is,

$$a^* = \frac{\delta}{D}(I_d-I_0) \tag{13}$$

where D and δ are the diffusion coefficient and the thickness of diffusion layer.

(a) Potential *vs.* polarographic current relation in the absence of adsorbates; Substituting Eqs. (11) and (13) into the expression for the polarographic current $\bar{I}_0$ which is given by integrating Eq. (5) and dividing its results by the drop life, we can obtain the potential *vs.* polarographic current relation.

$$E = E_0 + \frac{RT}{\alpha nF}\ln(0.85m^{2/3}nF\bar{\delta}D^{-1}) + \frac{RT}{\alpha nF}\ln\frac{\bar{I}_d-\bar{I}_0}{\bar{I}_0} + \frac{RT}{\alpha nF}\ln\frac{3}{5}k_0^s t_d^{2/3} \tag{14}$$

(b) Potential *vs.* polarographic current relation in the presence of adsorbates; When $t_d \leqslant t_m$, the $E-\bar{I}$ relation is given by substituting Eqs. (11), (12), and (13) into the polarographic current of $\bar{I}_{ads}$ obtained from Eq. (9),

$$E = E_0 + \frac{RT}{\alpha nF}\ln(0.85m^{2/3}nF\bar{\delta}D^{-1}) + \frac{RT}{\alpha nF}\ln\frac{\bar{I}_d-\bar{I}_{ads}}{\bar{I}_{ads}} + \frac{RT}{\alpha nF}\ln\left\{\frac{3}{5}k_0^s t_d^{2/3} - \frac{6}{13}(k_0^s-k_1^s)t_m^{-1/2}t_d^{7/6}\right\} \quad \text{for } t_d \leqslant t_m \tag{15}$$

When $t_d > t_m$, the polarographic current of $\bar{I}_{ads}$ is the sum of $(\bar{I}_{ads})_A = \frac{1}{t_d}\int_0^{t_m}(I_{ads})_A\,dt$ and $(\bar{I}_{ads})_B = \frac{1}{t_d}\int_{t_m}^{t_d}(I_{ads})_B\,dt$. Substituting Eqs. (11), (12), and (13) into $\bar{I}_{ads}$ above mentioned, we obtain

$$E = E_0 + \frac{RT}{\alpha nF}\ln(0.85m^{2/3}nF\bar{\delta}D^{-1}) + \frac{RT}{\alpha nF}\ln\frac{\bar{I}_d-\bar{I}_{ads}}{\bar{I}_{ads}} + \frac{RT}{\alpha nF}\ln\left\{\frac{9}{65}(k_0^s-k_1^s)t_m^{5/3}t_d^{-1} + \frac{3}{5}k_1^s t_d^{2/3}\right\} \quad \text{for } t_d > t_m \tag{16}**$$

The half-wave potentials $E_{1/2}$ without polymer and $E'_{1/2}$ with polymer can be derived from Eqs. (14), (15), and (16) by putting $\bar{I}_0 = 1/2\bar{I}_d$ and $\bar{I}_{ads} = 1/2\bar{I}_d$, respectively. Thus, the shift of half-wave potential ($\Delta E_{1/2} = E'_{1/2} - E_{1/2}$) is shown as follows,

$$\Delta E_{1/2} = \frac{RT}{\alpha nF}\ln\left\{1-\frac{10}{13}\left(1-\frac{k_1^s}{k_0^s}\right)\left(\frac{t_d}{t_m}\right)^{1/2}\right\} \quad \text{for } t_d \leqslant t_m \tag{17}$$

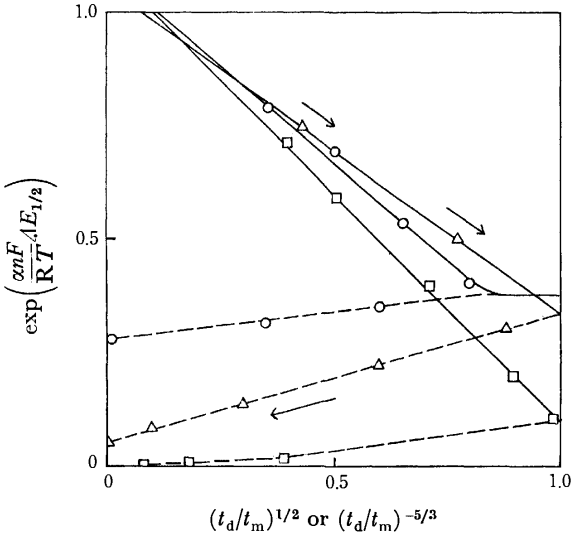

Fig. 9. Shifts of half-wave potential for $KBrO_3$ reduction in the presence of polymers.
0.05 M sulfuric acid+$KBrO_3$+polymers (○: 1.5 mM $KBrO_3$ with various content of PVP $\bar{M}=10000$, △: 1.0 mM $KBrO_3$ with PEG $\bar{M}=8400$, □: 1.0 mM $KBrO_3$ with TritonX-205 $\bar{M}=1100$),
solid lines: $\exp\left(\frac{\alpha nF}{RT}\Delta E_{1/2}\right)$ *vs.* $(t_d/t_m)^{1/2}$ plots, dashed lines: $\exp\left(\frac{\alpha nF}{RT}\Delta E_{1/2}\right)$ *vs.* $(t_d/t_m)^{-5/3}$ plots.

** $t_d\bar{I}_{ads} = \int_0^{t_m}(I_{ads})_A dt + \int_{t_m}^{t_d}(I_{ads})_B dt$

or

$$\Delta E_{1/2} = \frac{RT}{\alpha nF} \ln\left[\frac{k_1^s}{k_0^s} + \left\{1 - \frac{k_1^s}{k_0^s} - \frac{10}{13}\left(1 - \frac{k_1^s}{k_0^s}\right)\right\}\left(\frac{t_d}{t_m}\right)^{-5/3}\right] \quad \text{for } t_d > t_m \qquad (18)$$

On the basis of these relationships, the plots of $\exp\left(\frac{\alpha nF}{RT}\Delta E_{1/2}\right)$ *vs.* $(t_d/t_m)^{1/2}$ or $(t_d/t_m)^{-5/3}$ are shown in Fig. 9, where the arrows indicate the increase of adsorbates contents.

Since $\exp\left(\frac{\alpha nF}{RT}\Delta E_{1/2}\right)$ decreases linearly with $(t_d/t_m)^{1/2}$ for $t_d \leqslant t_m$ and increases with $(t_d/t_m)^{-5/3}$ for $t_d > t_m$, the shift of $E_{1/2}$ is explained by Eq. (17) or (18).

Examination of Eq. (17) or (18) for the Inhibition Effects of Polymers on Cation Reduction. The characteristics for the inhibition effects of polymer on the electroreduction are assumed to be independent of the ionic charge of depolarizer except for the double layer effects within the potential range where the current is predominantly controlled by charge transfer. In the irreversible reduction of VO^{2+}, the polarogram in the acetate

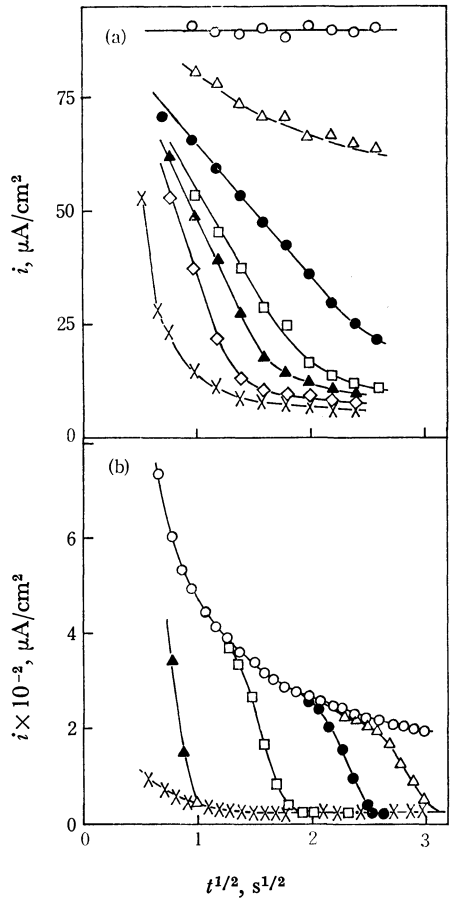

Fig. 10. Instantaneous current density *vs.* square root of time curves for cation reduction inhibited by polymer.
(a) (0.5 M CH_3COOH+0.5 M CH_3COONa)+1.0 mM $VOSO_4$+PVP $\bar{M}$=750000, $E=-1.1$ V, contents of PVP (○: 0 mg/l, △: 80 mg/l, ●: 110 mg/l, □: 140 mg/l, ▲: 170 mg/l, ◇: 250 mg/l, ×: 500 mg/l),
(b) 1 N sulfuric acid+1.0 mM $CdSO_4$+PVP $\bar{M}$=750000, $E=-0.9$ V, contents of PVP (○: 0 mg/l, △: 80 mg/l, ●: 100 mg/l, □: 150 mg/l, ▲: 400 mg/l, ×: 800 mg/l).

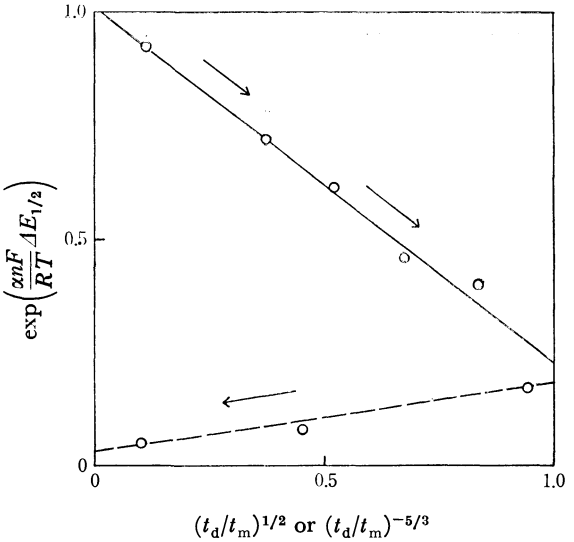

Fig. 11. Shift of half-wave potential for $VOSO_4$ reduction in the presence of polymers.
(0.5 M CH_3COOH+0.5 M CH_3COONa)+1.0 mM $VOSO_4$+various contents of PVP $\bar{M}$=750000, Solid line: $\exp\left(\frac{\alpha nF}{RT}\Delta E_{1/2}\right)$ *vs.* $(t_d/t_m)^{1/2}$ plot, dashed line: $\exp\left(\frac{\alpha nF}{RT}\Delta E_{1/2}\right)$ *vs.* $(t_d/t_m)^{-5/3}$ plots.

buffer of pH 4.7 was inhibited by the polymer in the same way as that for BrO_3^-, that is, the half-wave potential became more negative with the addition of the polymers. In this case, the exact determination of t_m was possible by the $i-t^{1/2}$ plot shown in Fig. 10(a) in the potential range where the charge transfer was predominant. The results in Fig. 10(a) show that Eqs.(1) and (2) hold well for the inhibited reduction of VO^{2+} where the current is mainly controlled by charge transfer. Then, it follows that Eq. (17) or (18) based on Eq. (1) or (2) is applicable to the above case. In Fig. 11, the plot of $\exp\left(\frac{\alpha nF}{RT}\Delta E_{1/2}\right)$ *vs.* $(t_d/t_m)^{1/2}$ or $(t_d/t_m)^{-5/3}$ becomes linear as expected from Eq. (17) or (18), respectively. The arrows in the figure indicate the increase of adsorbate contents. Meantime, typical results in contrast with $i-t^{1/2}$ plots in Fig. 10(a) are shown in Fig. 10(b), which reveals the inhibition effects of polymer on the instantaneous limiting current density of Cd^{2+} reduction. In the absence of adsorbates, the results reveal the process mainly controlled by linear diffusion of depolarizer, since the instantaneous current density decreases with the function of $1/t^{1/2}$ which is expected from the Ilković equation.[12] In the presence of adsorbates, the depression of instantaneous current density is not expressed as a linear relation of i *vs.* $t^{1/2}$ which implies the blocking effect of polymer, but shows the sharp change after a certain adsorption time. Such results may be due to the inhibition which is dependent not only on the blocking effect of adsorbates but also on the variation of diffusion path of depolarizer having fast reaction rate.[3]

Summary. So far as the present research is concerned, the inhibition effects of polymer on reduction current may be classified into two typical cases regard-

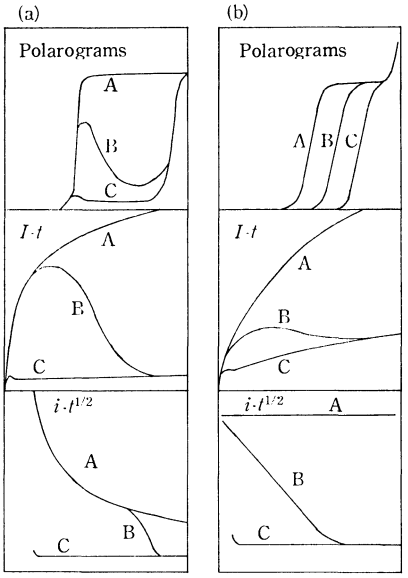

Fig. 12. Models for inhibition effects of polymer on electroreduction current.
A: with no polymer, B: with polymer in the case of diffusion-controlled adsorption, C: with polymer in the case of saturated adsorption,
(a) inhibition effects on reaction in the potential ranges of limiting current,
(b) inhibition effects on reaction in the potential ranges where the current is mainly controlled by charge transfer.

less of the ionic charge of depolarizer. Fig. 12(a) shows the typical inhibition effects of polymer when the current is predominantly controlled by mass transfer of ions. In such a case, the time t_m needed to complete a monolayer of polymer can be obtained directly from $I-t$ curve, which results in a convenient determination of Γ_m of polymer. In these cases, $i-t^{1/2}$ plots differ markedly from those in Fig. 12(b) for the process mainly controlled by charge transfer. Meanwhile, Fig. 12(b) shows the other type of inhibition effects of polymer when the current is mainly controlled by charge transfer. In such cases, the time t_m can be obtained exactly from $i-t^{1/2}$ relation instead of $I-t$ curve.

Moreover, Eqs. (17) and (18) for the shift of half-wave potential in the presence of adsorbates were verified with regard to the system of Fig. 12(b), *i.e.*, the inhibition effects of polymer on the electroreduction of BrO_3^- or VO^{2+}.

References

1) T. Yoshida, T. Ohsaka, and S. Tanaka, This Bulletin, **45**, 362 (1972); T. Yoshida, T. Ohsaka, and S. Nomoto, *ibid.*, **45**, 1585 (1972).
2) T. Yoshida, T. Ohsaka, and M. Suzuki, *ibid.*, **45**, 3245 (1972).
3) T. Ohsaka, H. Yamamoto, and T. Yoshida, *ibid.*, **46**, 1320 (1973).
4) A. N. Frumkin and G. M. Florianovich, *Zh. Fiz. Khim.*, **29**, 1827 (1955).
5) T. N. Anderson and H. Eyring, "Physical Chemistry an Advanced Treatise," Vol. IXA, ed. by H. Eyring, D. Henderson, and W. Jost, Academic Press, New York, (1960), p. 310; R. Parsons, "Advances in Electrochemistry and Electrochemical Engineering," Vol. 1, ed. by P. Delahay and C. W. Tobias, Interscience Publishers, New York, (1961), p. 41.
6) A. N. Frumkin, *Z. Electrochem.*, **59**, 807 (1955); I. Müller, *Electrochim. Acta.*, **14**, 293 (1969).
7) J. J. Lingane and I. M. Kolthoff, *J. Amer. Chem. Soc.*, **61** 825 (1939); V. I. Zykov, *Dokl. Akad. Nauk SSSR*, **136**, 1158 (1961); A. M. Shams El Din, T. M. H. Saber, and H. A. El Shayeb, *J. Electroanal. Chem.*, **36**, 411 (1972).
8) T. Yoshida and T. Ohsaka, *Bull. Sci. Eng. Res. Lab. Waseda Univ.*, **58**, 34 (1972).
9) J. Koryta, *Collect. Czech. Chem. Commun.*, **18**, 206 (1953).
10) J. Kůta and I. Smoler, "Progress in Polarography," Vol. 1, ed. by P. Zuman and I. M. Kolthoff, Interscience Publishers, New York, (1962), p. 49.
11) J. Kůta, J. Weber, and J. Koutecký, *Collect. Czech. Chem. Commun.*, **25**, 2376 (1960); J. Kůta and I. Smoler, *Z. Electrochem.*, **64**, 285 (1960).
12) L. Meites, "Polarographic Techniques," Second Ed., Interscience Publishers, New York, (1965), p. 113.

Studies on Bond Character in Phosphorus Ylides by Combustion Heat and X-Ray Photoelectron Spectroscopy

Manabu SENŌ, Shinji TSUCHIYA, Hideo KISE, and Teruzo ASAHARA

Institute of Industrial Science, The University of Tokyo, 7-22, Roppongi, Minato-ku, Tokyo 106

(Received October 24, 1974)

In order to clarify the electron structure of carbonyl-stabilized phosphorus ylides, measurements of X-ray photoelectron spectroscopy (XPS) and combustion heat were performed. NMR and IR spectra were also measured as complementary methods. The results suggest that carbomethoxymethylenetriphenylphosphorane has a major contribution of polar bond ($\overset{+}{P}$–$\bar{C}$) structure, whereas benzoylmethylenetriphenylphosphoranes have a larger contribution of covalent bond (P=C). A dπ—pπ interaction in the P–C bond was interpreted for XPS and NMR. The data for heat of combustion suggest that a large contribution of the polar bond structure brings about stabilization of the ylide molecule. These results show that XPS and combustion heat measurements are useful means for the analysis of ylide bonding.

It has been considered that the phosphorus atom in phosphorus ylides has an oxidation number between P(IV) and P(V) and forms a multiple bond with an adjacent atom possessing lone-pair electrons *via* a dπ-pπ bonding. The nature of the P–C bonding in phosphorus ylides has been discussed mainly on the basis of their chemical properties. Recently, IR, NMR, dipole moment, and X-ray diffraction techniques have also been used for the elucidation of the bond character, but an uncertainty still seems to remain especially on the variation of the character with the substituents on the carbon atom.

It has been reported that X-ray photoelectron spectroscopy (XPS) is especially useful in the investigation of the bonding or the formal oxidation state of atoms in a variety of compounds.[1] This induced us to use XPS as a tool for probing the bond character of the phosphorus ylides, expecting the direct elucidation of the electronic environment of the phosphorus atom.

In the present work, we have analyzed the bonding mainly by means of XPS, and the ambiguities in electronic structure have been clarified through the examination of the binding energies. The measurement of combustion heat is also considered to give useful pieces of information on the bond energy in thermodynamic sense, and the results on the phosphorus ylides will be described as well as the data of IR, and NMR spectroscopy.

Results and Discussion

The compounds used for the present investigation are the carbonyl-stabilized phosphorus ylides, which have been already studied by IR,[2] NMR,[3] dipole moment,[4] and X-ray diffraction.[5] Measurement of p*K*a value and chemical reactivities[6] have also been carried out in order to clarify the effect of substituent on the carbonyl carbon. By these investigations, three resonance structures shown below have been presented:

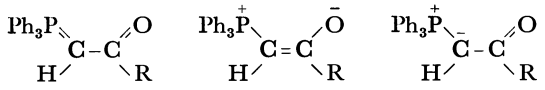

Ia **Ib** **Ic**

The contribution of each structure is considered to vary with the substituents R through their inductive, mesomeric and steric effects. In the present investigation, we tried to clarify the degree of contribution of each resonance structure in differently substituted ylides.

IR Studies. The C=O stretching bands in phosphorus compounds are summarized in Table 1. The bands of the phosphonium salts appear at higher frequencies by 135—189 cm^{-1} than those of the ylides. This suggests that the contribution of the structure **Ib** is large in the ylides, whereas the phosphonium salts have not the contribution of this type of resonance structure.

TABLE 1. STRETCHING BANDS OF C=O GROUPS IN THE YLIDES AND THEIR SALTS

Compounds	C=O band (cm^{-1})
1 Ph_3P=CHCO–C$_6$H$_4$–NO_2	1540—1500
2 Ph_3P=CHCO–C$_6$H$_5$	1527
3 Ph_3P=CHCO–C$_6$H$_4$–OMe	1503
4 Ph_3P=CHCO–OMe	1620
5 [$Ph_3\overset{+}{P}$–CH_2CO–C$_6$H$_4$–NO_2]Br^-	1689
6 [$Ph_3\overset{+}{P}$–CH_2CO–C$_6$H$_5$]Br^-	1662
7 [$Ph_3\overset{+}{P}$–CH_2CO–C$_6$H$_4$–OMe]Cl^-	1652
8 [$Ph_3\overset{+}{P}$–CH_2CO–OMe]Br^-	1725

In the salts (**5**), (**6**), and (**7**) an electron donating substituent on phenyl ring yields a low frequency shift by the conjugation of the carbonyl group with the phenyl ring.

In the ylides (**1**), (**2**), and (**3**), we also find the same aspect of the effect of substituents on phenyl ring with that mentioned above in the salts (**5**), (**6**), and (**7**).

Thus, we should consider not only the resonance structure **Ib**, but also **IIa** and **IIb**:

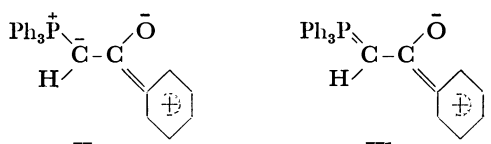

IIa **IIb**

The ylide (**4**) exhibits a C=O band at higher frequency by as much as about 100 cm^{-1} than those of other ylides. Furthermore, the difference of the C=O frequency between the salt (**8**) and the ylide (**4**) is the smallest (105 cm^{-1}) among the pairs of the salt and the ylide listed in Table 1. These results indicate that the contribution of the resonance structure **Ia** and/or **Ic** is significant in the ylide (**4**).

NMR Studies. The chemical shift and coupling constant of methylene and methine protons are summarized in Table 2.

Table 2. NMR data of the ylides and their salts

Compounds	^1H (methylene or methine) Shift (ppm)	^1H (methylene or methine) J_{P-C-H} (Hz)	^{31}P (ppm)	^{13}C[a] Shift (ppm)	^{13}C[a] J_{P-C} (Hz)
1	4.46	21.6	−16.8	52.5	108
2	4.40	24.3	−16.3	49.7	108
3	4.34	24.3	−16.7	48.4	107
4	2.82	—	−17.4	28.9	131
5	6.60	13.5	−20.5	—	—
6	6.40	13.5	−20.6	—	—
7	6.36	13.5	−20.4	—	—
8	5.25	15.8	−20.5	32.6	57

a) Methylene or methine carbons.

Comparison of the salts with ylides shows that the methylene signals of the salts appear in lower magnetic field than methine signals of the ylides. This may be attributed to higher electron densities on methine carbon atoms in the ylides than those on methylene carbon atoms in the salts, although, as generally observed, the partially olefinic character of the methine proton in the ylides would compensate the high field shift. Moreover, the difference in coupling constants between the ylides and the salts shows the existence of $d\pi$-$p\pi$ interaction in P–C bond of the ylides.

The methylene protons in the salts (**5**), (**6**), and (**7**) give signals at lower field by 1.11—1.35 ppm than that of the salt (**8**). The same tendency is observed between the ylides (**1**), (**2**), (**3**), and (**4**), and this may be attributed to the electron releasing character of the phenyl ring. The ylide (**4**) is distinct from others also in that the shift of the signal in going from the salt (**8**) to the ylide (**4**) is large (2.43 ppm) compared to the shift in other pairs of the salts and the ylides (2.00—2.14 ppm). It was supposed from the IR measurement that the ylides (**1**), (**2**), and (**3**) have a larger contribution of the resonance structure **Ib**, whereas the ylide (**4**) is considered to have the major resonance structure **Ia** or **Ic**. The present results of NMR suggest a high degree of negative charge on the methine carbon and this seem to support the structure **Ic** rather than **Ia** for the ylide (**4**).

The signals of ^{31}P NMR of the salts appear at lower magnetic field than those of the ylides as shown in Table 2; this may be attributed to less positive charge on phosphorus atoms in the ylides. The substituent effect is not found for the phosphonium salts. In the case of the ylides, the substituents on carbonyl carbon have a clear effect on phosphorus atom through $d\pi$-$p\pi$ bonding. The ^{31}P NMR peak of the ylide (**4**) appears at the lowest magnetic field among the ylides, probably because of the more positive charge on the phosphorus atom of the ylide. These results are consistent with those of IR and ^1H NMR, indicating the large contribution of resonance structure **Ic** in the ylide (**4**). The shift of the ylides (**1**), (**2**), and (**3**) suggests that the nature of P–C bonding in these ylides is of more double bond character. Hence, it is likely that the ylides (**1**), (**2**), and (**3**) have a larger contribution of resonance structure **IIb**.

The ^{13}C chemical shift and ^{13}C–^{31}P nuclear spin coupling constant are especially useful in the investigation of the bondings of phosphorus ylides. The shifts in Table 2 were assigned on the basis of previous studies.[3k,31] Gray showed that the ylides such as $Ph_3P(CR)CO_2R'$ should not be considered to have primarily **Ib** type electron structure, on the basis of comparison with value, $\delta_{13C}=70.92$ ppm and $J_{C-P}=99.2$ Hz, for C-1 of enol form **III**.

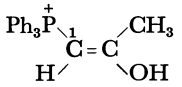

III

The results in Table 2 suggest a considerable carbanion character of P–C carbons especially for ylide (**4**), whereas the ylides (**1**), (**2**), and (**3**) seem to have considerable olefinic character by comparison with data for **III**. Especially, the values of the ^{13}C–^{31}P coupling constant are close to that of **III**. That is, since the ^{13}C–^{31}P coupling constant reflects the s character of the ylide bond,[31] the ylide bond in (**1**), (**2**), and (**3**) is considered to have the character of sp^2.

The substituent effect on ^{13}C NMR is consistent with IR and other NMR data shown above, and the order of ^{13}C NMR chemical shift is parallel with p*K*a values.[6]

Combustion Heat Studies. Two main factors have been suggested to account for bond strengthening in covalent bonds. The first reflects a certain amount of polar character of the bond. This ionic-covalent resonance causes lowering of energy of the molecule and a strengthening of the bonds. Another factor of bond strengthening has been attributed to some additional π-bonding. Pi-bonding involving d-orbital is often found in phosphorus compounds. It is of interest to see whether this type of bonding makes an important contribution to the overall energy content of the molecule. For phosphorus compounds there are much thermochemical data available and the effects of $d\pi$-$p\pi$ bonding are much more apparent.[7] Thus, the measurement of combustion heat may be useful for the studies of bonding of phosphorus ylides. The data of combustion heat of the ylides $Ph_3P{=}CHCOR$ and related compounds are summarized in Table 3. Now we consider the thermochemical cycle shown below:

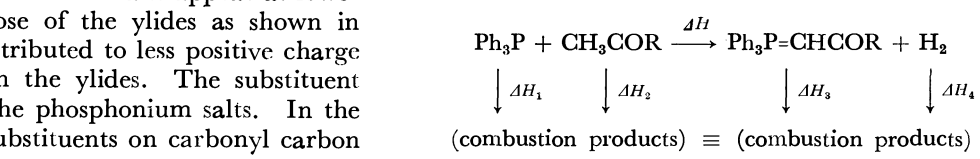

Thus, the enthalpy change ΔH of the P–C bond formation is derived from the combustion heats, ΔH_1, ΔH_2, ΔH_3, and ΔH_4

$$\Delta H = (\Delta H_1 + \Delta H_2) - (\Delta H_3 + \Delta H_4) \quad (1)$$

where $\Delta H_4 = -68$ kcal·mol^{-1}. The results calculated by the above equation are given in Table 3.

Table 3. Combustion heats (ΔH_{comb}) and enthalpy changes of the P–C bond formation (ΔH) of ylides

R	ΔH_2 of CH_3COR (kcal·mol^{-1})	ΔH_3 of Ph_3P=CHCOR (kcal·mol^{-1})	ΔH (kcal·mol^{-1})
p-$NO_2C_6H_4$	−940.0	−3398.1	−0.9
Ph	−989.6	−3420.9	−27.7
p-$MeOC_6H_4$	−1116.1	−3535.4	−39.7
OMe	−378.3	−2701.7	−135.6

Ph_3P; $\Delta H_1 = -2527.0$ kcal·mol^{-1}

The value for the ylide with substituent R=OMe shows that this substituent brings about a large decrease in ΔH, compared to the other substituents R=p-NO_2-C_6H_4, Ph, and p-$MeOC_6H_4$. Since the decrease in ΔH indicates the stabilization of the P–C bond, the bond of the ylide (**4**) is thought to be most stable among four ylides.

According to NMR data, the ylide (**4**) is considered to have the smaller contribution of the covalent bond through dπ–pπ interaction, and the results obtained from the combustion heat measurement seem to show that a large contribution of **Ic** brings about stabilization of the ylide molecule. We also found a substituent effect in the combustion heat of the ylides (**1**), (**2**), and (**3**), and the change in these values is consistent with that of NMR data. Furthermore, Jolly *et al.* have shown that XPS shifts do correlate well with thermochemical data.[8] It is expected that a relation is established between XPS shifts and combustion heat data for phosphorus ylides.

XPS Studies. A survey of the literature reveals the utility of X-ray photoelectron spectroscopy (XPS) on the investigation of the electronic environment of anomalous covalent atom and this induced us to use XPS as a tool for probing the ylide bonds. Most recently, Mixan *et al.* reported the XPS measurement on sulfur-nitrogen ylides and related compounds attempting to probe the nature of the S–N polar bonds.[1f]

Table 4. P-2p electron binding energies in phosphorus ylides and their salts, the rate constants of Wittig reaction and basicities, pK_a[a]

Compounds	Binding energies (eV)	log k of Wittig reaction (k; l·mol^{-1}·s^{-1})	pK_a
Ph_3P=O	131.5		
Ph_3P=S	131.6		
1	130.8	−5.19	4.2
2	131.2	−3.92	6.0
3	131.3	−3.39	6.7
4	131.7	−1.84	8.8
5	131.8		
6	132.0		
7	132.0		
8	132.5		

a) Reaction with benzaldehyde.[6]

The electron binding energies in phosphorus atom measured in the present work are summarized in Table 4.

The phosphorus 2p binding energies were recorded with reference to the C ls line at 284 eV. Distinct differences are found between the spectra of the ylides and those of their salts; the binding energies of the salts are higher than those of the corresponding ylides. It is also found that P-2p electron binding energies in the ylides decrease in the order (**4**)>(**3**)>(**2**)>(**1**), reflecting the substituent effect. It is likely that the large binding energy of the ylide (**4**) is due to a large contribution of resonance structure **Ic** rather than **Ia** and **Ib**, as revealed already by the measurements of IR, NMR, and combustion heat. Aryl substituents seem to bring about an increase in the electron density on phosphorus atom, compared to the methoxy group in the ylide (**4**). By considering the results of IR and NMR, the increase of electron density is thought to be the result of a large contribution of the structure **IIb** rather than that of **Ib**.

The binding energy of the ylide (**4**) is almost the same with those of Ph_3P=O and Ph_3P=S, and this implies that the polarity of P–C bond in (**4**) is comparable to those of P–O and P–S bonds in the phosphine oxide and sulfide. For the salts (**5**), (**6**), and (**7**), the substituent effect on the binding energies is not found; a distinct difference in chemical shift of the salt (**8**) has not been explained yet.

Siegbahn *et al.* demonstrated[9] that the chemical shift in the total screening constant can be written as

$$\Delta\sigma_A = \frac{-\Delta E_A}{3mc^2} + \frac{\pi e}{3mc\mu_0 g_A}\Delta\sum_\alpha C_{A,\alpha\alpha} I_{\alpha\alpha} \quad (2)$$

where ΔE_A: XPS shift, $C_{A,\alpha\alpha}$: spin-rotation constant for nucleus A along the αth molecular inertial axis, $I_{\alpha\alpha}$: corresponding principal moment of inertia of the molecule, μ_0: nuclear magneton, g_A: g-factor for nucleus A. From this relation, they concluded that the first term in equation (2) is the part of the shift in the diamagnetic constant and is proportional to the XPS shift. This term is only of the size of a few ppm. The second term is the part of the shift in the paramagnetic constant and is one or two orders of magnitude larger than the first term. Thus, no linear correlation between XPS and NMR shift can be expected even for the same kind of compounds.

In the present work, the shifts in the compounds having different kind of bondings vary largely as seen among Ph_3P=O, Ph_3P=S, and phosphorus ylides, and the correlation between XPS and NMR shift is not observed. However, in the series of phosphorus ylides and their salts, a correlation between XPS and ^{31}P NMR is found. The results seem to indicate that both the phosphorus ylides and salts used for the present investigation have almost the same contribution of paramagnetic term, and the diamagnetic term contributes mainly to the change in the shift of these spectra. For quaternary phosphonium compounds, Swartz *et al.* also reported that a linear relationship was established between the P-2p binding energies and the ^{31}P NMR

chemical shifts.[1c]

It has been elucidated that the overall rate of the Wittig reaction depends on the rate of electrophilic reaction of ketones or aldehydes onto the α-carbon of ylide compounds.[10] This step would be affected by the electronic character as well as the steric one. With respect to a series of ylides used here, a linear relationship between the basicity of the ylides and the reaction rate with benzaldehyde has been established.[6] This indicates that the rate determining step mentioned above is affected only by the electronic effect. Thus, more positive charge on phosphorus atom would favor the reaction. Since the binding energy of XPS is proportional to the positive charge, a relationship between the binding energy and the reactivity is expected, and this is actually the case as shown in Table 4.

Conclusion

1) In the present investigation it was concluded that the electronic structure of carbomethoxymethylenetriphenylphosphorane (**4**) has a major contribution of resonance structure **Ic**. Measurements of ^{31}P NMR and XPS support localization of positive charge on phosphorus atom, and combustion heat data also convince us of the large contribution of resonance structure **Ic**.

2) With respect to ylides (**1**), (**2**), and (**3**), the large lower shift of C=O stretching bands show that the carbonyl groups in the ylides are polar ($>\overset{\delta+}{C}-\overset{\delta-}{O}$), and it was clarified by ^{13}C NMR that the hybrid orbital of the methine carbon is close to sp^2 hybrid. These results indicate that these ylides have a large contribution of resonance structure **Ib**, **IIa**, and **IIb**. However, ^{31}P NMR and XPS measurements show that these ylides have less positive charge on phosphorus atom than ylide (**4**). Thus, the resonance structure **IIb** is considered to have a primary contribution.

3) In the ylides (**1**), (**2**), and (**3**), the substituent effect is found on both the methine proton and the phosphorus atom, whereas in the salts (**5**), (**6**), and (**7**), the substituent effect is observed only on methylene protons. This observation indicates that P–C bonds in the ylides are semipolar with $d\pi$-$p\pi$ interaction. P–C–H Coupling constant in Table 2 also support the above discussion. Thus, these results experimentally clarify $d\pi$-$p\pi$ interaction in phosphorus ylides.

4) The result of the analysis by XPS is consistent with those by IR and NMR, and gives additional informations on polar bondings. A correlation between P-2p binding energies of XPS and ^{31}P NMR shifts was observed in phosphorus ylides and phosphonium salts, and a relation was also established between the binding energies and combustion heat of ylides. These suggest that XPS may be a useful tool for the elucidation of the electronic structure of some organic compounds.

Experimental

The compounds used in this study were prepared, purified and characterized according published methods.[4,6,11] All the ylides were prepared by dehydrohalogenation of corresponding phosphonium salts. The results of elemental analyses are as follows.

	Calcd			Found		
	C	H	N	C	H	N
(**1**)	73.30	4.95	3.28	73.11	4.75	3.35
(**2**)	82.08	5.58	—	82.09	5.61	—
(**3**)	79.10	5.64	—	79.03	5.68	—
(**4**)	75.41	5.74	—	75.65	5.74	—

IR Spectroscopy. All the infrared spectra were obtained as mulls with Nujol on a JASCO IRA-2 infrared spectrometer. All the spectra have sharp absorption bands of C=O stretching except that of ylide (**1**) which has a broad peak due to the overlap with the absorption peak of the nitro group.

NMR Spectroscopy. ^1H NMR spectra were recorded on a Hitachi R-22 spectrometer (90 MHz) using deuteriochloroform as a solvent and TMS as an internal standard.

The measurement of ^{31}P NMR were made using a Hitachi R-20A NMR spectrometer at 24.3 MHz using 85% phosphoric acid as an external reference. The spectra were taken in chloroform; the concentration 1.0—0.5 M was needed for detection of the signals.

^{13}C NMR spectra were obtained using a Hitachi R-26 NMR spectrometer in Fourier transform mode, and was operated at 10 MHz. ^{13}C–H Couplings were eliminated using broad band ^1H-noise-modulated decoupling. The ylides and salts were run in saturated deuteriochloroform solutions in 10 mm sample tubes, and TMS was used as an internal standard.

X-Ray Photoelectron Spectroscopy. The measurements were performed with a JASCO ESCA-1 or a McPherson ESCA-36 electron spectrometer with Mg$K\alpha$ radiation. The spectra were obtained on powdered samples mounted on an aluminum plate. In order to compensate for the charging of the insulating samples during the phtoelectron ejection process, all the spectra were referenced to the photoelectron line of C ls; E_b=284 eV. An attempt was also made to reference the spectra to the Au $4f_{7/2}$; E_b=83 eV by vacuum deposition of gold onto the samples, and the results from the two methods were consistent with each other. The binding energies were read at the midway point of the full peak at half height.

Combustion Heat. Combustion heat data were obtained using a Shimadzu automatic bomb calorimeter CA-3. Powdered samples were wrapped in Gampi paper, and liquid samples were placed in gelatin capsule. The given data were averaged values of ten measurements.

References

1) (a) M. Plavin, D. N. Hendrickson, J. M. Hollander, and W. L. Jolly, *J. Phys. Chem.*, **74**, 1116 (1970). (b) W. E. Morgan, W. T. Stec, R. G. Albridge, and J. R. V. Wazer, *Inorg. Chem.*, **10**, 926 (1971). (c) W. E. Swartz and D. M. Hercules, *Anal. Chem.*, **43**, 1066 (1971). (d) W. E. Swartz, J. K. Ruff, and D. M. Hercules, *J. Amer. Chem. Soc.*, **94**, 5227 (1972). (e) W. T. Stec, W. E. Moddeman, R. G. Albridge, and T. R. V. Wazer, *J. Phys. Chem.*, **75**, 3975 (1971). (f) C. E. Mixan and J. B. Lambert, *J. Org. Chem.*, **38**, 1350 (1973).

2) (a) A. J. Speziale and K. W. Ratts, *J. Amer. Chem. Soc.*, **85**, 2790 (1963). (b) A. J. Speziale and K. W. Ratts, *J. Org. Chem.*, **28**, 465 (1963).

3) (a) K. W. Ratts and A. N. Yao, *J. Org. Chem.*, **31**, 1185 (1967). (b) J. E. Lancaster, *Spectrochim. Acta*, **23A** 1449 (1967). (c) F. J. Randall and A. W. Johnson, *Tetrahedron Lett.*, 2841 (1968). (d) H. J. Bestmann and J. P. Snyder, *J. Amer. Chem. Soc.*, **89**, 3936 (1967). (e) D. M. Crouse, A. T. Wehman, and E. E. Schweizer, *Chem. Commun.*, **1968**, 866. (f) A. W.

Johnson, "Ylide Chemistry," Academic Press, Inc., New York (1966), p. 76. (g) M. Halman and I. Blatzner, *J. Phys. Chem.*, **70**, 580 (1966). (h) M. M. Crutchfield, J. R. V. Wazer *et. al.*, "Topics in Phosphorus Chemistry," vol. 5, John Wiley & Sons, New York (1967), p. 227. (i) H. Schmidbaur and W. Fronic, *Chem. Ber.*, **101**, 604 (1968). (j) S. O. Grim *et. al.*, *J. Chem. Eng. Data*, **15**, 497 (1970). (k) G. A. Gray, *J. Amer. Chem. Soc.*, **95**, 5092 (1973). (l) G. A. Gray, *ibid.*, **95**, 7736 (1973).

4) F. Ramirez and S. Dershowitz, *J. Org. Chem.*, **22**, 41 (1957).

5) (a) A. J. Speziale and K. W. Ratts, *J. Amer. Chem. Soc.*, **87**, 5603 (1965). (b) J. C. J. Bart, *J. Chem. Soc. B*, **1969**, 350. (c) J. C. J. Bart, *Angew. Chem.*, **80**, 697 (1968).

6) S. Flizar, R. F. Hudson, and G. Salvadori, *Helv. Chim. Acta*, **172**, 1580 (1963).

7) (a) H. H. Jaffe, *J. Inorg. Nucl. Chem.*, **4**, 372 (1957). (b) C. L. Chernick and H. A. Skinner, *J. Chem. Soc.*, **1956**, 1401. (c) H. O. Prichard and H. A. Skinner, *Chem. Rev.*, **55**, 745 (1955). (d) C. T. Mortimer, "Reaction Heats and Bond Strengths," Pergamon Press Ltd., London (1962). (e) R. T. Sanderson, "Chemical Bonds and Bond Energy," Academic Press, New York and London (1971).

8) W. L. Jolly, "Electron Spectroscopy," ed. by D.A. Shirley North-Holland Publ. Co., Amsterdam (1972). (b) W. L. Jolly and D. N. Hendrickson, *J. Amer. Chem. Soc.*, **92**, 1863 (1970). (c) W. L. Jolly, *ibid.*, **92**, 3260 (1970).

9) U. Gelius, G. Johansson, H. Siegbahn C. J. Allan, D. A. Allison, J. Allison, and K. Siegbahn, *J. Electron Spectrosc. Relat. Phenomena*, **1**, 285 (1972/1973).

10) A. J. Speziale and D. E. Bissing, *J. Amer. Chem. Soc.*, **85**, 3875 (1963).

11) (a) O. Isler, H. Guttman, M. Motaron, R. Ruegg, G. Ryser, and P. Zeller, *Helv. Chim. Acta*, **40**, 1242 (1957). (b) C. Screttas and A.F. Isbell, *J. Org. Chem.*, **27**, 2573 (1962).

The Free Energy of Transfer from a Binary to a Ternary Solution by the Isopiestic Measurements

Hatsuho UEDAIRA

Research Institute for Polymers and Textiles, Sawatari 4, Kanagawa-ku, Yokohama 221

(Received January 11, 1975)

A new method of calculating the free energy of transfer of a solute from a binary to a ternary solution on the mole fraction scale from isopiestic measurements is reported. It was proved that only the new method is consistent.

A knoledge of thermodynamic properties of aqueous ternary solutions is necessary for clear understanding of the interactions in many aqueous ternary systems containing two electrolytes, an electrolyte and a nonelectrolyte, and two nonelectrolytes. The knowledge is also fundamental to a comprehension of the mechanism of the denaturation of proteins and the interactions in complex biological systems.

It is shown that the chemical potential of each component in ternary solution can be calculated at various concentrations by the isopiestic vapor pressure method. The free energy of transfer of a solute from a binary to a ternary solution is obtained at various concentrations from the chemical potentials in these solutions.

In actual biological systems, the concentrations of some solutes are very low, while, for instance, the average local concentrations of amino acids and peptides within the protein molecule are very high.[1] Further, the free energy of transfer is found to alter even its sign at some concentration range.[2] Consequently, not only the interactions at the standard state but also the concentration dependence of the interactions are very important.

Unfortunately, contradiction is found in the calculation of the transfer free energy on the mole fraction scale in recent papers.[3,4]

Here we report a new consistent expression for the free energy of transfer from isopiestic measurements.

The Free Energy of Transfer on Molality Scale

Since the concentration of the solute is measured on molality scale in the isopiestic method, we start with the free energy of transfer on the molality scale. The chemical potentials of solute 1 in a binary and in a ternary (solute 2 and water) solution on the molality scale, $\mu_{10}(m)$ and $\mu_1(m)$, are expressed as follows,

$$\mu_{10}(m) = \mu_{10}^0(m) + \nu_1 RT \ln m_{10}\gamma_{10} \quad (1)$$

$$\mu_1(m) = \mu_1^0(m) + \nu_1 RT \ln m_1\gamma_1 \quad (2)$$

where $\mu_{10}{}^0(m)$ and $\mu_1{}^0(m)$ are the standard states in a binary and in a ternary solution, respectively. m_{10} and γ_{10} are the molality and the activity coefficient of solute 1 in a binary solution, and m_1 and γ_1 are the corresponding quantities in a ternary solution. γ_1 is the number of moles of ions formed from 1 mole of solute 1.

The immediate result of isopiestic vapor pressure measurements is the chemical potential of the volatile solvent (water) in the ternary solution. The chemical potentials of the solutes are calculated by Gibbs-Duhem equation,

$$n_w d\mu_w = -n_1 d\mu_1 - n_2 d\mu_2 \quad (3)$$

where

$$d\mu_i = \nu_i RT d\ln m_i\gamma_i \quad (i = 1 \text{ or } 2) \quad (4)$$

Equation (4) implies the assumption that $d\mu_j{}^0 = 0$. In other words, the activity coefficient of solute 1 is unity in the standard state in water and not in the standard state in a water-solute 2 solvent,[5]

$$\mu_{10}^0(m) = \mu_1^0(m) \quad (4a)$$

Consequently, the free energy of transfer of solute 1 from a given molality in water to the same molality in water-solute 2 solution is given by,

$$\Delta G_t(m) = \mu_1 - \mu_{10} = \nu_1 RT \ln (\gamma_1/\gamma_{10}) \quad (5)$$

The $\Delta G_t(m)$ in Eq. (5) has the same value as that of $\Delta G_t(m)$ which is defined by the change in excess free energy,

$$\Delta G_t(m) = \mu_1^{ex} - \mu_{10}^{ex}$$

where μ_1^{ex} and μ_{10}^{ex} are the excess free energy (or non-ideal free energy) defined by Friedman.[6]

The values of $\Delta G_t(m)$ of glycylglycine (solute 1) from water to urea-water solutions at various concentrations of glycylglycine (m_1) and urea (m_2) are shown in Table 1.

TABLE 1. FREE ENERGY OF TRANSFER ON MOLALITY SCALE (in J/mol) OF GLYCYLGLYCINE FROM WATER TO UREA SOLUTIONS

m_1	m_2					
	1.0	2.0	3.0	4.0	5.0	6.0
0	−232	−430	−587	−705	−793	−865
0.5	−147	−280	−391	−478	−546	−606
1.0	−102	−202	−289	−358	−411	−455
1.5	−82.8	−167	−238	−288	−317	−327

The Free Energy of Transfer on Mole Fraction Scale

The Examination of Previous Experessions.[4] When solute 2 is treated as a component of the mixed solvent, the appropriate concentration scale for solute 1 is the mole fraction. According to the definition in the previous paper,[4]

$$\Delta G_t(N) = \nu_1 RT \ln (f_1/f_{10}) \quad (6)$$

where $\Delta G_t(N)$ is the free energy of transfer of solute 1 from water to water-species 2 solution at constant mole fraction. f_{10} and f_1 are the activity coefficients of solute 1 in mole fraction scale in a binary and in a ternary solution, respectively. The activity coefficient of the

solute in molality scale is converted into the rational activity coefficient as usual by

$$f_{10} = \gamma_{10}(1+0.001 W_{A0}\nu_1 m_{10}) \tag{7}$$

where W_{A0} is the molecular weight of pure solvent. Let m_1' denote the molality of solute 1 in the ternary solution when the mole fraction of solute 1 in the ternary solution is the same as in a binary solution, then we have,

$$m_1' = (1+0.001 W_{A0}\nu_2 m_2)m_{10} \tag{8}$$

In the ternary solution, f_1 is related to γ_1' by

$$f_1 = \gamma_1'(1+0.001 W_A \nu_1 m_1') \tag{9}$$

where γ_1' is the activity coefficient of solute 1 at m_1' and W_A is the molecular weight of mixed solvent (water-species 2) defined by[3,4]

$$W_A = \frac{55.51 W_{A0} + W_2 m_2}{55.51 + m_2} \tag{10}$$

where W_2 and m_2 are the molecular weight and molality of species 2 in the mixed solvent, respectively.

To examine whether these definitions are consistent or not, we subtract $\Delta G_t(m)$ from $\Delta G_t(N)$. Then, at any concentration, using Eqs. (5) to (10), we obtain

$$\frac{\Delta G_t(N)-\Delta G_t(m)}{\nu_1 RT} = \ln\left\{\frac{1+0.001 W_A \nu_1 m_1'}{1+0.001 W_{A0}\nu_1 m_{10}}\right\} + \ln(\gamma_1'/\gamma_1) \tag{11}$$

At infinite dilution, $\gamma'_1=\gamma_1$, then,

$$\frac{\Delta G_t(N)-\Delta G_t(m)}{\gamma_1 RT} = 0 \tag{12}$$

On the other hand, since the chemical potential of solute 1 in a binary solution on mole fraction scale is,

$$\mu_{10}(N) = \mu_{10}^0(N) + \nu_1 RT \ln N_{10} f_{10} \tag{13}$$

Combining Eqs. (1) and (13), in a binary solution we have,

$$\ln f_{10} = \ln \gamma_{10} + \ln(m_{10}/N_{10}) + \frac{\mu_{10}^0(m)-\mu_{10}^0(N)}{\nu_1 RT} \tag{14}$$

Similarly in a ternary solution,

$$\ln f_1 = \ln \gamma_1' + \ln(m_1'/N_1) + \frac{\mu_1^0(m)-\mu_1^0(N)}{\nu_1 RT} \tag{15}$$

Substituting Eqs. (14) and (15) into Eq. (6) and combining Eqs. (5) and (6), we obtain

$$\frac{\Delta G_t(N)-\Delta G_t(m)}{\nu_1 RT} = \frac{\mu_1^0(m)-\mu_{10}^0(m)}{\nu_1 RT} - \frac{\mu_1^0(N)-\mu_{10}^0(N)}{\nu_1 RT} + \ln(m_1' N_{10}/N_1 m_{10}) + \ln(\gamma_1'/\gamma_1) \tag{16}$$

where $N_1=N_{10}$. Substituting Eqs. (4a) and (8) into (16), we have

$$\frac{\Delta G_t(N)-\Delta G_t(m)}{\nu_1 RT} = -\frac{\mu_1^0(N)-\mu_{10}^0(N)}{\nu_1 RT} + \ln(1+0.001 W_{A0}\nu_2 m_2) + \ln(\gamma_1'/\gamma_1) \tag{16a}$$

Combining Eqs. (11) and (16a), we obtain,

$$\frac{\mu_1^0(N)-\mu_{10}^0(N)}{\nu_1 RT} = \ln(1+0.001 W_{A0}\nu_2 m_2) - \ln\left\{\frac{1+0.001 W_A \nu_1 m_1'}{1+0.001 W_{A0}\nu_1 m_{10}}\right\}$$

which becomes at infinite dilution of solute 1,

$$\frac{\mu_1^0(N)-\mu_{10}^0(N)}{\nu_1 RT} = \ln(1+0.001 W_{A0}\nu_2 m_2) \tag{17}$$

Equation (17) shows that the difference between standard states on mole fraction scale in a binary and in a ternary solution depends on the concentration of solute 2. The free energy of transfer, defined by Eqs. (6), (7), (9), and (10) does not mean the difference in chemical potentials in the two states, but it means,

$$\Delta G_t(N) = \mu_1(N) - \mu_{10}(N) - \nu_1 RT \ln(1+0.001 W_{A0}\nu_2 m_2) \tag{17a}$$

Furthermore, using Eq. (17), we can examine Eq. (9). The usual relation between $\mu_{10}^0(m)$ and $\mu_{10}^0(N)$ is obtained from Eq. (14),

$$\frac{\mu_{10}^0(m)-\mu_{10}^0(N)}{\nu_1 RT} = -\ln\left(\frac{1000}{W_{A0}}\right) \tag{14a}$$

Then, using Eqs. (4a), (14a), and (17),

$$\frac{\mu_1^0(m)-\mu_1^0(N)}{\nu_1 RT} = \frac{\mu_1^0(m)-\mu_{10}^0(m)}{\nu_1 RT} - \frac{\mu_1^0(N)-\mu_{10}^0(N)}{\nu_1 RT} - \frac{\mu_{10}^0(N)-\mu_{10}^0(m)}{\nu_1 RT} = -\ln\left(\frac{1000}{W_{A0}}+\nu_2 m_2\right) \tag{18}$$

Equation (18) is substituted in Eq. (15), we obtain

$$f_1 = \gamma_1'\left(1+\frac{\nu_1 m_1'}{\frac{1000}{W_{A0}}+\nu_2 m_2}\right) = \gamma_1'\left(1+0.001\frac{1000}{\frac{1000}{W_{A0}}+\nu_2 m_2}\nu_1 m_1'\right) \tag{19}$$

Equation (19) differs from Eq. (9). For consistency, 1000 in the numerator in the second term in parenthesis of Eq. (19) should be $(1000+W_2 m_2)$. That is, the definition of f_1 by Eqs. (9) and (10) is not right.

The Consistent Expression for ΔG_t(N). Here $\Delta G_t(N)$ is defined by Eq. (6), and Eqs. (7) and (8) hold too. The difference between this and previous section is only in the definition of f_1. f_1 is defined by

$$f_1 = \gamma_1'\{1+0.001 W_{A0}(\nu_1 m_1' + \nu_2 m_2)\} \tag{20}$$

Now, at any concentration, from Eqs. (5), (6), (7), (8), and (20), we obtain

$$\frac{\Delta G_t(N)-\Delta G_t(m)}{\nu_1 RT} = \ln\left\{\frac{1+0.001 W_{A0}(\nu_1 m_1'+\nu_2 m_2)}{1+0.001 W_{A0}\nu_1 m_{10}}\right\} + \ln(\gamma_1'/\gamma_1) \tag{21}$$

At infinite dilution of solute 1, $\gamma'_1=\gamma_1$, so, Eq. (21) gives

$$\frac{\Delta G_t(N)-\Delta G_t(m)}{\nu_1 RT} = \ln(1+0.001 W_{A0}\nu_2 m_2) \tag{22}$$

which differs from Eq. (12) in previous section.

On the other hand, Eq. (16a) also holds here, consequently, combining Eqs. (16a) and (21), we obtain

$$\frac{\mu_1^0(N)-\mu_{10}^0(N)}{\nu_1 RT} = \ln(1+0.001 W_{A0}\nu_2 m_2) - \ln\left\{\frac{1+0.001 W_{A0}(\nu_1 m_1'+\nu_2 m_2)}{1+0.001 W_{A0}\nu_1 m_{10}}\right\}$$

which becomes at infinite dilution of solute 1,

TABLE 2. FREE ENERGY OF TRANSFER ON MOLE FRACTION SCALE (in J/mol) OF GLYCYLGLYCINE FROM WATER TO UREA SOLUTIONS

m_{10}	N_1	m_2					
		1.0	2.0	3.0	4.0	5.0	6.0
0	0	−189	−342	−456	−533	−579	−611
0.5	0.008927	−108	−201	−272	−319	−348	−369
1.0	0.017696	−64.0	−126	−174	−204	−216	−218
1.5	0.026311	−44.8	−90.4	−122	−129	−110	−82.4

$$\frac{\mu_1^0(N)-\mu_{10}^0(N)}{\nu_1 RT}=0 \tag{23}$$

That is, the standard states in a binary and in a ternary solution are the same on mole fraction scale too, and $\Delta G_t(N)$ means the difference in chemical potentials of the solute in a ternary and binary solution, as in the case of $\Delta G_t(m)$. The difference between the standard states in the ternary solution on molality and on mole fraction scale is obtained by combining Eqs. (4a), (14a), and (23),

$$\frac{\mu_1^0(m)-\mu_1^0(N)}{\nu_1 RT}=-\ln(1000/W_{A0}) \tag{24}$$

By substituting Eq. (24) into Eq. (15), we obtain the same equation for f_1 as Eq. (20). Consequently, the definition of $\Delta G_t(N)$ by Eq. (6) and f_1 by Eq. (20), results in the consistent relation.

The value of $\Delta G_t(N)$ at infinite dilution which is expressed by Eq. (22) has the same value as the quantity defined by Bower and Robinson as a measure of the medium effect.[7]

The values of $\Delta G_t(N)$ of glycylglycine from water to urea-water mixture are tabulated in Table 2. $\Delta G_t(N)$ has less negative values than $\Delta G_t(m)$.

The author wishes to acknowledge Prof. W. Y. Wen and Dr. H. Uedaira for their helpful discussions.

References

1) I. M. Klotz, *Brook Heaven Symposia in Biol.*, **13**, 25 (1960).
2) H. Uedaira and H. Uedaira, The 12th Annual Meeting of the Biophys. Soc. of Japan (1973).
3) W. Y. Wen and C. M. L. Chen, *J. Phys. Chem.*, **73**, 2895 (1969).
4) H. Uedaira, This Bulletin, **45**, 3068 (1972).
5) H. S. Harned and R. A. Robinson, "Multicomponent Electrolyte Solutions," Pergamon Press Inc., London (1968), p. 94.
6) H. L. Friedman, "Ionic Solution Theory," Interscience Publishers, New York (1962), p. 194.
7) V. E. Bower and R. A. Robinson, *J. Phys. Chem.*, **67**, 1524 (1963).

Microwave Spectrum of 2-Pyridinecarbaldehyde

Yoshiyuki KAWASHIMA, Masao SUZUKI, and Kunio KOZIMA*

Laboratory of Molecular Spectroscopy, Tokyo Institute of Technology, O-okayama, Meguro-ku, Tokyo 152

(Received January 29, 1975)

The microwave spectrum of 2-pyridinecarbaldehyde has been observed in the region 8—22 GHz. The rotational constants of the ground state are $A=5362.52\pm2.19$ MHz, $B=1620.07\pm0.03$ MHz, and $C=1244.42\pm0.03$ MHz and the inertia defect is -0.075 amu·Å^2. This value demonstrates that the molecule is planar in its equilibrium position. The total dipole moment is 3.56 ± 0.07 D, the components of which are $\mu_a=3.48\pm0.05$ D and $\mu_b=0.76\pm0.08$ D. From these facts it is concluded that the conformation of the molecule is of the O–N *s-trans* form. The rotational constants of the five vibrationally-excited states have also been determined.

Several studies of the microwave spectra have been done to determine the structural isomerism of conjugated aldehyde compounds. While two isomers, *i.e.*, the *s-trans* and the *s-cis* isomer, have been observed for furfural,[1,2] only the *s-trans* isomer has been found for 2-thiophenecarbaldehyde,[1] acrolein,[3] and crotonaldehyde.[4,5] By means of the microwave spectrum it is also known that only one isomer exists in the vapor of methacrolein and the structure of this isomer is quite similar to that of crotonaldehyde, except for the methyl group.[6]

By measuring the NMR spectrum of 2-pyridinecarbaldehyde in solution it has been suggested that the molecules are of the O–N *s-trans* form to the extent of 70—80 per cent.[7] However, in the study of the far infrared spectrum only one torsional frequency has been observed.[8] In order to know whether or not the two isomers exsist for this compound and to ascertain the stable conformation, this investigation was carried out.

Experimental

The sample of 2-pyridinecarbaldehyde, obtained from a commercial source, was purified by distillation at 53 °C/7 Torr before use. The microwave spectrum was measured over the frequency range from 8- to 22-GHz with a conventional 100-kHz square-wave Stark modulation spectrometer. The measurements were made by using a 6-m absorption cell cooled by ice.

Results and Discussion

Microwave Spectrum and its Assignments. By assuming that the stable conformation is of the O–N *s-trans* form and the form is planar in its equilibrium configuration and by using the normal values of the structural parameters, the rotational constants were roughly calculated. The low-J R-branch transitions of the a-type for the vibrationally-ground state could be found near the frequencies calculated from the preliminary rotational constants by using the rigid rotor approximation. The splittings caused by the nuclear quadrupole of the nitrogen atom were not observed. The $J=4\leftarrow3$ transitions were ascertained by their characteristic features in the Stark effect. By using the least-squares method the rotational constants were determined so as to get the best fit between the observed and the calculated frequencies. The transition frequencies thus assigned are listed in Table 1, together with the differences between the observed and the calculated frequencies. A search was made for b-type transitions at the expected frequencies, but none could be detected unambiguously. As can be seen from Table 1, the agreement is such that the effect of centrifugal distortion can be said to be negligible in the range studied. The rotational constants determined are shown in

Table 1. Assigned transition frequencies of 2-pyridinecarbaldehyde in the vibrationally-ground state (in MHz)

Transition	ν_{obsd}[a]	$\Delta\nu$[b]	Transition	ν_{obsd}[a]	$\Delta\nu$[b]
$3_{13}\leftarrow2_{12}$	8013.92	0.14	$5_{14}\leftarrow4_{13}$	15130.92	0.01
$3_{03}\leftarrow2_{02}$	8487.09	0.22	$6_{16}\leftarrow5_{15}$	15876.29	−0.04
$3_{22}\leftarrow2_{21}$	8593.60	0.11	$6_{06}\leftarrow5_{05}$	16367.69	−0.09
$3_{21}\leftarrow2_{20}$	8699.90	−0.22	$6_{25}\leftarrow5_{24}$	17066.21	−0.24
$3_{12}\leftarrow2_{11}$	9139.48	−0.04	$6_{52}\leftarrow5_{51}$	17254.42	0.07
$4_{14}\leftarrow3_{13}$	10656.16	−0.20	$6_{51}\leftarrow5_{50}$	17254.42	0.06
$4_{04}\leftarrow3_{03}$	11197.18	0.10	$6_{34}\leftarrow5_{33}$	17303.64	0.31
$4_{23}\leftarrow3_{22}$	11437.38	0.32	$6_{33}\leftarrow5_{32}$	17369.06	−0.24
$4_{32}\leftarrow3_{31}$	11508.70	0.38	$6_{24}\leftarrow5_{23}$	17883.92	−0.14
$4_{31}\leftarrow3_{30}$	11515.50	−0.03	$6_{15}\leftarrow5_{14}$	18064.18	−0.07
$4_{22}\leftarrow3_{21}$	11697.93	0.01	$7_{17}\leftarrow6_{16}$	18452.54	0.02
$4_{13}\leftarrow3_{12}$	12151.68	−0.07	$7_{07}\leftarrow6_{06}$	18856.56	0.14
$5_{15}\leftarrow4_{14}$	13277.70	−0.02	$7_{26}\leftarrow6_{25}$	19844.40	0.16
$5_{05}\leftarrow4_{04}$	13822.00	0.03	$7_{35}\leftarrow6_{34}$	20206.18	0.18
$5_{24}\leftarrow4_{23}$	14262.81	0.03	$7_{34}\leftarrow6_{33}$	20351.12	−0.06
$5_{42}\leftarrow4_{41}$	14382.45	0.25	$7_{16}\leftarrow6_{15}$	20936.70	−0.12
$5_{41}\leftarrow4_{40}$	14382.45	−0.11	$7_{25}\leftarrow6_{24}$	21033.96	−0.02
$5_{33}\leftarrow4_{32}$	14403.00	0.13	$8_{18}\leftarrow7_{17}$	21008.22	0.07
$5_{32}\leftarrow4_{31}$	14427.60	−0.34	$8_{08}\leftarrow7_{07}$	21314.90	−0.25
$5_{23}\leftarrow4_{22}$	14763.04	0.10			

a) Maximum experimental uncertainty in frequency measurements is ±0.1 MHz. b) $\Delta\nu=\nu_{obsd}-\nu_{calcd}$.

Table 2. Rotational constants and inertia defect of 2-pyridinecarbaldehyde in the vibrationally-ground state

Rotational constants	Moments of inertia[a]
$A=5362.52\pm2.19$ MHz	$I_a=94.243$ amu·Å^2
$B=1620.07\pm0.03$	$I_b=311.947$
$C=1244.42\pm0.03$	$I_c=406.113$
asymmetric parameter $\kappa=-0.81756$	
inertia defect $\Delta=I_c-I_a-I_b=-0.075\pm0.038$ amu·Å	

a) Conversion factor: 5.05377×10^5 MHz·amu·Å^2

* To whom correspondence should be addressed. Present address: Department of Chemistry, Chuo University, Kasuga 1-chome, Bunkyo-ku, Tokyo 112.

Table 2. The small negative value of the inertia defect demonstrates that the molecule is planar in its equilibrium configuration.

By assuming the molecular parameters of the r_s structure of pyridine[9] for the ring and the parameters of furfural[1] for the aldehyde group, the distance, C_2–C, between the C_2 atom and the carbon atom of the CHO group and the angle of $\angle$N–C_2–C were determined so as to get a good fit between the observed and the calculated rotational constants, where the ring carbons are numbered from the nitrogen starting with C_2. The results obtained for the *s-trans* isomer are shown in Table 3, where the hydrogen atom attached to C_n is designated as H_n. The rotational constants thus calculated from these parameters were A=5362.5 MHz, B=1620.1 MHz, and C=1244.2 MHz, in good agreement with the observed values. By using these parameters the molecular configurations calculated for the *s-trans* and the *s-cis* isomer are schematically shown in Fig. 1. When the *s-cis* form is assumed for this compound, it seems hard to adjust the parameters to fit the calculated rotational constants with those observed, unless the parameters of the CHO group, for instance, are varied beyond the reasonable values. Therefore, it is probable that the molecule is of the O–N *s-trans* isomer. Some evidence for this is given by the data of the dipole moments.

TABLE 3. MOLECULAR PARAMETERS OF 2-PYRIDINECARBALDEHYDE

Assumed structural parameters[a]	
Distances	Angles
N–C_2: 1.340 Å	$\angle C_6$–N–C_2: 116°50′
C_2–C_3: 1.395	$\angle$N–C_2–C_3: 123°53′
C_3–C_4: 1.394	$\angle C_2$–C_3–C_4: 118°32′
C_2–H_2: 1.081	$\angle C_3$–C_4–C_5: 118°20′
C_4–H_4: 1.077	$\angle$N–C_6–H_6: 115°53′
C_6–H_6: 1.084	$\angle C_4$–C_3–H_3: 121°18′
C=O: 1.250*	$\angle C_2$–C=O: 121°36′*
C–H: 1.088*	$\angle C_2$–C–H: 116°55′*
Fitted structural parameters	
C_2–C: 1.477	$\angle$N–C_2–C: 112°0′

a) Parameters are quoted from Ref. 9 and, for those with asterisk, from (1).

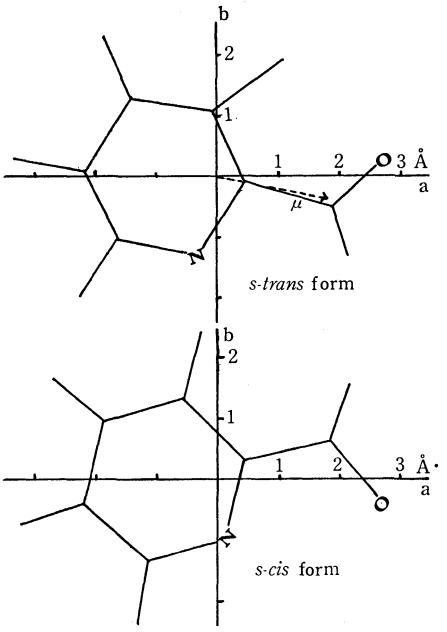

Fig. 1. Two isomers of 2-pyridinecarbaldehyde.

Dipole Moment. In order to determine the electric dipole moment, the Stark displacements of the six transitions, shown in Table 4 were measured. These lines fit the quadratic Stark displacements nicely. The absorption cell was calibrated using the J=1←0 transition of OCS, taking the dipole moment of OCS as 0.7152 D.[10] The observed and calculated Stark coefficients are given in Table 4, together with the value of the total dipole moment, μ, and those of its components along the a and b principal axes, μ_a and μ_b.

TABLE 4. (a) STARK EFFECT AND OBSERVED VALUES OF DIPOLE MOMEMNTS OF 2-PYRIDINECARBALDEHYDE

Transition		$\Delta\nu/E^2$[MHz/(kV/cm)^2] observed	calculated
4_{04}←3_{03}	M=1	−6.03±0.87	−6.12
	M=2	7.72±0.41	7.71
4_{14}←3_{13}	M=0	−7.15±0.67	−6.99
	M=1	4.08±0.41	4.01
4_{13}←3_{12}	M=1	−6.64±0.32	−6.59
	M=2	−22.41±0.67	−22.47

μ_a=3.48±0.05; μ_b=0.76±0.08 D

μ=3.56±0.07 D; $\tan^{-1}(\mu_b/\mu_a)$=12.3°

(b) Calculated values of dipole moments.

	μ_a	μ_b	$\tan^{-1}(\mu_a/\mu_b)$
s-trans form	3.83 D	0.78 D	11.5°
s-cis form	4.47	2.84	32.4°

It is reasonable to consider that the dipole moment of this compound is approximately given by the vector sum of the moment of benzaldehyde and that of pyridine.

Our recent study of the microwave spectrum of benzaldehyde has elucidated that the value of the component of the dipole moment parallel to the C=O bond is 2.95 D, pointing the negative end toward the oxygen atom, and that perpendicular to the C=O bond is 1.28 D, pointing the negative end toward the hydrogen atom of the aldehyde group.[11] By using the microwave spectrum the value of the dipole moment of pyridine is found to be 2.15 D.[12] There is no doubt that the C_2 axis of the pyridine molecule coincides with the orientation of the moment vector, the negative end of which points to the nitrogen atom. By considering that the molecular parameters of the *s-cis* form are not so different from those of the *s-trans* form, it can be calculated from the parameters that for the *s-trans* or the *s-cis* form the C_2 axis of the pyridine ring makes an angle of 66.7 ° or 43.5 ° with the a principal axis, and the C=O bond makes an angle of 43.3 ° or 48.5 ° with the same axis, respectively.

By adding the vectors mentioned above, the a and b components of the moment were calculated for the *s-trans* and the *s-cis* isomer. The results obtained are

shown in Table 4(b). From the table it can be concluded that the compound in the vapor exists mainly as the O–N *s-trans* isomer, in agreement with the preliminary result described above. Of the four possible directions of the dipole moment, the direction supported by the calculation is shown by an arrow in Fig. 1.

From the dielectric constant measurements, the value of the dipole moment has been reported as 3.35D in the benzene solution at 25 °C,[13,14] and the values of the moments for the *s-trans* and the *s-cis* form have been estimated as 3.51 D and 5.05 D, respectively.[13] These values estimated in the benzene solution seem almost to agree with the values of 3.91 D and 5.30 D estimated in the vapor, respectively, as can be calculated from the values shown in Table 4(b).

In the case where two isomers of a compound exist in equilibrium, it is well known that the abundance ratio of the molecules of the more polar isomer to those of the less polar isomer generally increases when the state changes from vapor to a benzene solution. Therefore, as the barrier to internal rotation of the CHO group of this molecule is considered to be comparable to that of benzaldehyde,[15] from the fact that the value of the moment obtained in the vapor is larger than that obtained in the benzene solution it can be said that no considerable amount of the molecules of the *s-cis* isomer exists even in the benzene solution.

Vibrationally-excited states. As the spectrum is very rich, an attempt should be made to find the lines due to the *s-cis* form. Therefore, the measurements were carefully made near the frequencies estimated by using the rotational constants of the *s-cis* form, which were tentatively calculated from the molecular parameters listed in Table 3. However, we could not observe

Table 5. Assigned transition frequencies of 2-pyridinecarbaldehyde in the vibrationally-excited states (in MHz)

Transition	v_1		v_2		v_3	
	ν_{obsd} [a]	$\Delta\nu$ [b]	ν_{obsd} [a]	$\Delta\nu$ [b]	ν_{obsd} [a]	$\Delta\nu$ [b]
$3_{03}\leftarrow2_{02}$	8494.30	−0.10	8477.45	0.23	8500.20	−0.32
$3_{22}\leftarrow2_{21}$	8600.60	−0.26	—		—	
$3_{21}\leftarrow2_{20}$	8707.30	−0.02	—		8709.40	−0.11
$3_{12}\leftarrow2_{11}$	9144.88	−0.07	9121.87	0.39	9150.31	−0.13
$4_{14}\leftarrow3_{13}$	10668.68	−0.20	10654.67	0.49	10673.93	−0.05
$4_{04}\leftarrow3_{03}$	11207.56	0.24	11184.93	0.28	11217.15	−0.31
$4_{23}\leftarrow3_{22}$	11446.93	0.02	11424.35	0.47	11452.65	−0.19
$4_{32}\leftarrow3_{31}$	11518.10	0.04	11495.10	0.16	—	
$4_{22}\leftarrow3_{21}$	11707.57	0.21	11684.30	0.35	—	
$4_{13}\leftarrow3_{12}$	12158.93	−0.10	12127.96	0.23	12166.95	−0.10
$5_{15}\leftarrow4_{14}$	13293.66	0.21	13275.52	0.34	13300.28	−0.19
$5_{05}\leftarrow4_{04}$	13835.02	−0.10	13807.73	0.31	13849.88	−0.24
$5_{24}\leftarrow4_{23}$	14275.20	0.06	14246.42	0.03	14283.01	−0.18
$5_{42}\leftarrow4_{41}$	14394.40	0.01	14365.70	0.17	—	
$5_{33}\leftarrow4_{32}$	14415.00	−0.01	14386.20	0.18	—	
$5_{32}\leftarrow4_{31}$	14439.60	−0.48	14411.60	0.27	—	
$5_{23}\leftarrow4_{22}$	14774.27	−0.16	14745.00	0.44	14774.30	0.12
$5_{14}\leftarrow4_{13}$	15140.06	−0.02	15100.79	−0.13	15151.68	0.30
$6_{16}\leftarrow5_{15}$	15895.14	−0.18	15873.67	0.07	15904.61	0.10
$6_{06}\leftarrow5_{05}$	16383.72	−0.40	16352.02	−0.24	16404.06	0.18
$6_{25}\leftarrow5_{24}$	17081.49	0.13	17045.95	−0.96	17092.30	0.38
$6_{52}\leftarrow5_{51}$	17268.92	−0.06	17233.77	−0.59	—	
$6_{51}\leftarrow5_{50}$	17268.92	−0.07	17233.77	−0.60	—	
$6_{42}\leftarrow5_{41}$	17294.14	0.05	17259.00	−0.47	—	
$6_{43}\leftarrow5_{42}$	—		—		17298.70	−0.40
$6_{34}\leftarrow5_{33}$	17318.12	0.29	17282.73	−0.14	—	
$6_{33}\leftarrow5_{32}$	17383.74	−0.08	17348.74	−0.72	17388.33	0.31
$6_{24}\leftarrow5_{23}$	17896.96	−0.40	17860.30	0.14	17897.00	0.44
$6_{15}\leftarrow5_{14}$	—		—		18091.30	0.25
$7_{17}\leftarrow6_{16}$	18474.74	−0.09	18449.68	−0.15	18486.48	0.15
$7_{07}\leftarrow6_{06}$	18876.54	0.29	18841.00	−0.39	18899.50	−0.13
$7_{26}\leftarrow6_{25}$	19861.74	0.00	19821.30	−0.32	—	
$7_{35}\leftarrow6_{34}$	20222.70	−0.14	—		20230.30	0.56
$7_{34}\leftarrow6_{33}$	20368.10	0.04	20327.74	−0.47	20371.00	0.32
$7_{16}\leftarrow6_{15}$	20949.90	−0.02	20895.00	0.25	20971.80	0.34
$7_{25}\leftarrow6_{24}$	21049.12	0.29	21003.32	0.18	21049.12	0.15
$8_{18}\leftarrow7_{17}$	21034.00	0.16	21006.00	0.23	—	
$8_{08}\leftarrow7_{07}$	21338.04	−0.68	21301.76	−0.18	—	

a) Maximum experimental uncertainty in frequency measurements is ±0.1 MHz. b) $\Delta\nu=\nu_{obsd}-\nu_{calcd}$.

Table 5. (Continued)

Transition	v_4		v_5	
	ν_{obsd}[a]	$\Delta\nu$[c]	ν_{obsd}[b]	$\Delta\nu$[c]
$3_{03}\leftarrow2_{02}$	8496.30	0.01	—	
$3_{12}\leftarrow2_{11}$	9150.31	0.17	9157.0	0.08
$4_{14}\leftarrow3_{13}$	10667.60	0.02	10682.8	0.18
$4_{04}\leftarrow3_{03}$	11209.65	0.16	11221.2	−0.25
$4_{23}\leftarrow3_{22}$	11449.70	−0.06	11461.8	−0.01
$4_{31}\leftarrow3_{30}$	11528.50	0.17	—	
$4_{22}\leftarrow3_{21}$	11710.88	−0.07	11723.0	−0.09
$4_{13}\leftarrow3_{12}$	—		12175.3	0.43
$5_{15}\leftarrow4_{14}$	13291.95	0.27	13310.6	0.10
$5_{05}\leftarrow4_{04}$	13837.16	−0.07	—	
$5_{24}\leftarrow4_{23}$	14278.58	−0.04	14293.7	0.05
$5_{42}\leftarrow4_{41}$	14398.30	−0.12	—	
$5_{41}\leftarrow4_{40}$	14398.30	0.24	—	
$5_{33}\leftarrow4_{32}$	14419.30	0.41	—	
$5_{32}\leftarrow4_{31}$	14443.80	−0.16	14458.8	−0.37
$5_{23}\leftarrow4_{22}$	14779.46	0.03	14794.5	0.03
$5_{14}\leftarrow4_{13}$	15148.57	0.08	15159.3	−0.36
$6_{16}\leftarrow5_{15}$	15892.86	−0.15	15915.5	−0.12
$6_{06}\leftarrow5_{05}$	16385.40	−0.35	16404.1	−0.17
$6_{25}\leftarrow5_{24}$	17085.53	0.13	17103.5	0.08
$6_{52}\leftarrow5_{51}$	17273.51	−0.01	—	
$6_{51}\leftarrow5_{50}$	17273.51	−0.02	—	
$6_{42}\leftarrow5_{41}$	17298.70	0.01	—	
$6_{34}\leftarrow5_{33}$	17323.00	0.41	17341.0	0.39
$6_{33}\leftarrow5_{32}$	17388.33	−0.25	17406.5	−0.45
$6_{24}\leftarrow5_{23}$	17904.30	0.18	17921.9	0.16
$6_{15}\leftarrow5_{14}$	18085.40	0.15	18098.4	−0.12
$7_{17}\leftarrow6_{16}$	18471.92	0.04	18498.3	−0.03
$7_{07}\leftarrow6_{06}$	18876.54	−0.41	18899.5	0.19
$7_{26}\leftarrow6_{25}$	19866.10	−0.16	19887.5	0.25
$7_{34}\leftarrow6_{33}$	20373.92	0.16	20395.5	0.12
$7_{16}\leftarrow6_{15}$	20961.00	−0.18	20976.0	−0.42
$7_{25}\leftarrow6_{24}$	21057.80	0.05	21077.5	0.07
$8_{18}\leftarrow7_{17}$	21029.80	−0.34	21060.2	−0.32
$8_{08}\leftarrow7_{07}$	21338.04	−0.10	—	

a) Maxmium experimental uncertainty in frequency measurements is ±0.1 MHz. b) The uncertainty is ±0.2 MHz. c) $\Delta\nu=\nu_{obsd}-\nu_{calcd}$.

any lines which might be assigned to the *s-cis* form, while we could find the five sets of the spectra due to the vibrationally-excited states near the spectrum of the ground state. The excited states will be designated hereafter by the symbol of v_i, the suffix, i, being numbered from one upward in the order of decreasing intensity. By using the least-squares procedure, the five sets of the rotational constants were determined so as to get the best fit between the observed and the calculated frequencies. Of the observed frequencies for each set, several values, which do not seem to be precise, were omitted in this calculations. The assigned transition frequencies for the excited states are listed in Table 5, together with the differences between the observed and the calculated frequencies. The rotational constants thus obtained are shown in Table 6.

From the values of the inertia defects shown in Table 6, it is concluded that the v_1, v_2, and v_5 states are the excited ones for the out-of-plane deformation vibrations.

Table 6. ROTATIONAL CONSTANTS AND INERTIA DEFECTS OF 2-PYRIDINECARBALDEHYDE IN VIBRATIONALLY-EXCITED STATES

	Rotational constants (MHz)			Inertia defect (amu·Å²)
	A	B	C	
v_1	5342.21 ±2.71	1620.65 ±0.04	1246.31 ±0.04	−0.937 ±0.048
v_2	5256.60 ±4.22	1615.70 ±0.07	1245.49 ±0.05	−3.167 ±0.077
v_3	5432.22 ±4.66	1621.67 ±0.06	1246.67 ±0.04	0.709 ±0.076
v_4	5374.64 ±2.94	1622.03 ±0.03	1245.65 ±0.03	0.112 ±0.051
v_5	5342.23 ±2.92	1622.79 ±0.04	1247.91 ±0.04	−1.047 ±0.051

It should be noted that the values of the inertia defects for the v_1 and v_2 states are almost the same as those of the $v=1$ and $v=2$ states of benzaldehyde obtained by Kakar *et al.*,[15] respectively.

Table 7. LOW-FREQUENCY VIBRATIONS OF 2-PYRIDINECARBALDEHYDE

	Microwave spectrum	Far-infrared spectrum	Raman spectrum
v_1	127±20 cm⁻¹	111[a] cm⁻¹	117 cm⁻¹
v_2	187±15	—	—
v_3	219±19	225 (broad)	230
v_4	239±13		
v_5	312±35	—	—

a) This value is quoted from Ref. 8.

By measureing the relative intensities of the satellite lines with respect to the ground state transitions, the vibrational energy separations were estimated from the Boltzmann factor. The results are shown in Table 7, together with the corresponding wave numbers obtained from the far-infrared and the laser Raman spectrum of the liquid state for comparison. The broad infrared band near 225 cm⁻¹ may be a doublet.

References

1) F. Mönnig, H. Dreizler, and H. D. Rudolph, *Z. Naturforsch.*, A, **20**, 1323 (1965).
2) F. Mönnig, H. Dreizler, and H. D. Rudolph, *ibid.*, A, **21**, 1633 (1966).
3) E. A. Cherniak and C. C. Costain, *J. Chem. Phys.*, **45**, 104 (1966).
4) M. Suzuki and K. Kozima, This Bulletin, **42**, 2183 (1969).
5) S. L. Hsu and W. H. Flygare, *Chem. Phys. Lett.*, **4**, 317 (1969).
6) M. Suzuki and K. Kozima, *J. Mol. Spectrosc.*, **38**, 314 (1971).
7) G. J. Karabattos and F. M. Vane, *J. Amer. Chem. Soc.*, **85**, 3886 (1963).
8) F. A. Miller, W. G. Fateley, and R. E. Witkowski, *Spectrochim. Acta*, **23A**, 891 (1967).
9) B. Bak, L. Hansen-Nygaard, and J. Rastrup-Andersen, *J. Mol. Spectrosc.*, **2**, 361 (1958).
10) J. S. Muenter, *J. Chem. Phys.*, **48**, 4544 (1968).

11) Y. Kawashima and K. Kozima, This Bulletin, **47**, 2879 (1974).
12) B. B. DeMore, W. S. Wilcox, and J. H. Goldstein, *J. Chem. Phys.*, **22**, 876 (1954).
13) J. Barassin and H. Lumbroso, *Bull. Soc. Chim. Fr.*, **1959**, 1947.
14) R. J. W. Le Fèvre and P. J. Stiles, *J. Chem. Soc., B*, **1966**, 420.
15) R. K. Kakar, E. A. Rinehart, C. R. Quade, and T. Kojima, *J. Chem. Phys.*, **52**, 3803 (1970).

Ligand-Ligand Interaction in Tris(2,2'-bipyridyl) and Tris (1,10-phenanthroline) Complexes of Nickel(II)

Takeshi OHNO and Shunji KATO

Institute of Chemistry, College of General Education, Osaka University, Toyonaka, Osaka 560

(Received February 1, 1975)

UV spectra of $[Ni(2,2'\text{-bipyridyl})_3]Cl_2$ and $[Ni(2,2'\text{-bipyridyl})(H_2O)_4]Cl_2$ in the mixed solvent of methanol and water (4: 1) were measured at 4.2 K. No difference between the spectra indicates a small splitting (<90 cm^{-1}) between the exciton states extending through the three 2,2'-bipyridyls. Since the UV spectrum of $[Ni(1,10\text{-phenanthroline})_3]Cl_2$ has a band with the progression as that of $[Ni(1,10\text{-phenanthroline})(H_2O)_4]SO_4$, a molecular exciton interaction between the three 1,10-phenanthrolines is not strong.

When some aromatic molecules coordinate to a metal ion through hetero atom(s) of the group(s) such as >C=O >O$^-$, and >N, they suffer from such ligand-ligand interactions as a molecular exciton interaction and a Coulomb exchange interaction between the neighbouring ligands.[1-3] We have investigated the ligand-ligand interactions by comparing the excited states of the bis- or the tris-bidentate complexes with those of the corresponding mono-bidentate complexes in the cases of β-diketones, 2,2'-bipyridyl,* 1,10-phenanthroline,** and *N*-alkylsalicylideneimine[4] at 77 K, and have obtained some remarks as follows; (a) the higher intensity of 0–0' band (absorption) and 0'-0 band (fluorescence) compared to those of the mono-bidentate complex suggests a delocalization of the excited singlet state through the two or three chelating ligands, (b) the increase in the yield of the triplet state formation is attributed to the overlap between the ligands nearly perpendicular with each other, (c) there was no distinct splitting of the absorption band, indicating a weak ligand-ligand interaction, (d) the depolarized fluorescence of $[Zn(bipy)_3]^{2+}$ at 77 K suggests that the energy splitting due to ligand-ligand interaction is so small (<70 cm^{-1}) that the upper state fluoresces as the lower does.

In contrast to the small splitting of the molecular exciton states, Mason *et al.* had concluded on the assumption of the strong coupling scheme that the molecular exciton splittings were nearly equal to differences (1200—2000 cm^{-1}) between the peaks of the positive and the negative bands of the circular dichroism observed at room temperature in the cases of trisacetylacetonato,[5] tris-phen[6] and tris-bipy[6] complexes. Recently, however, it was demonstrated[7] that either a medium or a weak coupling scheme was a suitable one, because the absorption and the circular dichroism spectra with a fine structure were observed in the case of $[Ni(bipy)_3]^{2+}$ below 0 °C: a small splitting value (<70 cm^{-1}) was inferred on the basis of the vibronic coupling theory proposed by Perrin and Gouterman.

In order to obtain the splitting in $[Ni(bipy)_3]^{2+}$, we tried to measure the well resolved absorption spectrum in a mixed solvent at 4.2 K, where the compound is free from a (crystal) exciton.

* 2,2'-Bipyridyl will be hereafter abbreviated to "bipy."

** 1,10-Phenanthroline will be hereafter abbreviated to "phen."

Experimental

Materials $[Ni(bipy)_3]Cl_2$, $[Ni(phen)_3]Cl_2$, and $[Ni(bipy)(H_2O)_4]SO_4$ were prepared from appropriate nickel (II) salts and the ligands and purified by recrystallization. G.R. methanol of Wako Chemical Co., and twice distilled water were used for the mixed solvent.

Procedure All the sample solutions except for $[Ni(phen)(H_2O)_4]^{2+}$ solution were prepared by dissolving a com plex in the mixed solvent of the methanol and the water (4:1 by volume). The sample solution of $[Ni(phen)(H_2O)_4]^{2+}$ is obtained by dissolving $NiSO_4 \cdot H_2O$ of $\sim 2 \times 10^{-4}$ M and the phenanthroline of 2×10^{-5} M in the solvent. It is assumed on the basis of the large formation constant (log $K_1 = 8.60$[8]) that the free phen was reduced to 0.1% at most. The absorption spectra at 4.2 K were measured by using a thin cell (0.1×10 mm) plunged in the liq. He in a Dewar vessel, which was kindly offered by prof. N. Mataga. Although the sample solutions had a great number of fine cracks at 4.2 K, the cracks did not interfere with the measurement of the absorption spectrum owing to the following reasons. One is that the fine cracks running perpendicular to the window of the cell do not seriously scatter the light beam. The other is that a head-on-type photomultiplier with a wide aperture (A=12 cm^2) can catch the most of the scattered light. Though a polyvinylalcohol film (PVA) and a rod of polymethylmethacrylate (PMM) containing a complex, had no crack at 4.2 K, the doped complex has a broader spectrum, which is probably attributed to many kinds of doping cite in PVA or a thermal decomposition of the complex during the thermal polymerization.

Results

Absorption spectra of $[Ni(bipy)_3]^{2+}$ and $[Ni(bipy)(H_2O)_4]^{2+}$ in the region of the UV are shown in Figs. 1 and 2, respectively. The absorption bands at 4.2 K (solid line in Figs. 1 and 2) have well resolved structure which are almost common to the two ions. Figure 3 shows the absorption spectra of $[Ni(phen)_3]^{2+}$, $[Ni(phen)(H_2O)_4]^{2+}$ and the free phen in the region of the UV at 77 K. The three compounds have similar and weakly resolved spectra at 77 K.

Discussion

$[Ni(bipy)_3]Cl_2$. Since $[Ni(bipy)(H_2O)_4]^{2+}$ has a similar absorption spectrum to that of $[Zn(bipy)(H_2O)_4]^{2+}$ in the region of the UV, the well resolved spectrum is mainly attributed to the coordinating bipy with *cis*-conformation (not to d-d transition). The

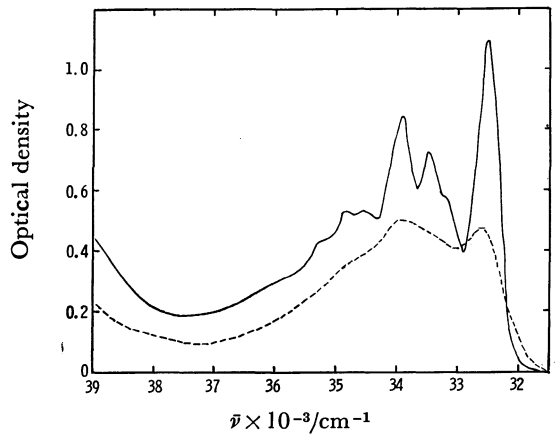

Fig. 1. Absorption spectra of 6×10^{-4} M solution of $[Ni(bipy)_3]^{2+}$
—— at 4.2 K, ---- at room temperature.

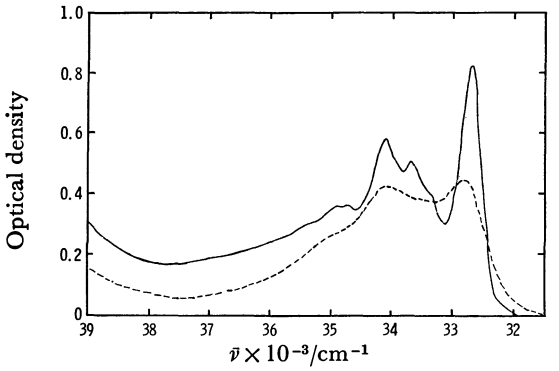

Fig. 2. Absorption spectra of $[Ni(bipy)(H_2O)_4]^{2+}$
—— [complex]: 1.28×10^{-3} M and at 4.2 K,
---- [complex]: 2.0×10^{-3} M and at room temperature.

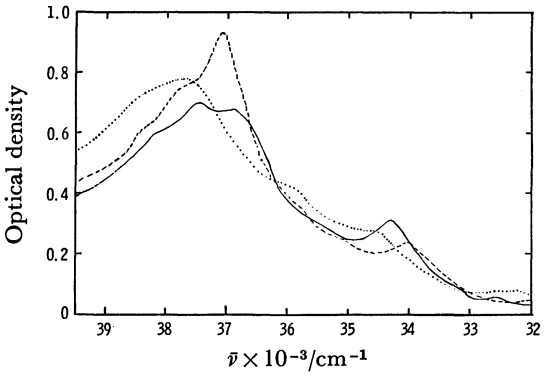

Fig. 3. Absorption spectra of phen and the phen complexes at 77 K
—— $[Ni(phen)_3]^{2+}$: 6.6×10^{-5} M,
---- $[Ni(phen)(H_2O)_4]^{2+}$ ($NiSO_4$: 2×10^{-4} M and phen: 2×10^{-5} M),
..... phen: 2×10^{-5} M.

coordinating bipy in the nickel complex is assumed to have practically one kind of transition ($A_1 \rightarrow B_1$) with the moment which is a several tens times as large as the other one ($A_1 \rightarrow A_1$),[9] as in the case of $[Zn(bipy)(H_2O)_4]^{2+}$ whose strong fluorescence at 77 K has a good mirror image relation to the absorption spectrum. Therefore, several sub-bands of $[Ni(bipy)(H_2O)_4]^{2+}$ are assigned to vibronic ones of the transition, $A_1 \rightarrow B_1$.

It is easily seen that the tris-bipy complex of nickel (II) keeps the vibronic band system of the mono-bipy complex and has neither new band nor splitting of the vibronic bands, which should be observed if there are any strong or intermediate coupling between the three ligands. The common width (460 cm^{-1}) of the 0–0′ bands to the two complexes, offers a contradictory proof to the inter-ligand interaction.

It is assumed that in the weak interaction scheme, a splitting of the vibronic band is produced by the interaction between the same vibronic states, the one of the splitted bands of the lower frequency is assigned to the transition to the E state and the other of the higher frequency to the A_2 state of $[Ni(bipy)_3]^{2+}$ with D_3 symmetry. And the spacing between the two 0–0′ bands may be equal to the splitting between the E and the A_2 states. When the splitting is much smaller than a spacing between the adjacent progression bands, the bands do not split but become broader. On assuming a Gaussian band shape and a moment ratio, 1 : 2, of $A_1 \rightarrow E$ to $A_1 \rightarrow A_2$, it is obtained that a greater bandwidth (473 cm^{-1}) than that (460 cm^{-1}) of the mono-bipy complex may be observed for $[Ni(bipy)_3]^{2+}$ when the splitting is 90 cm^{-1}. Therefore, the common band width (460 cm^{-1}) to the complexes implies a splitting less than 90 cm^{-1} between the two states. This possible largest value is supported by the fact that the splitting of $[Zn(bipy)_3]^{2+}$ is less than 70 cm^{-1}, which had been obtained by a measurement of the fluorescence polarization. Assuming that the total coupling energy is four times as great as the splitting of the 0–0′ band, of which the intensity is one-fourth of the total intensity, the possible maximum value of the coupling energy (360 cm^{-1}) is consistent with 210 cm^{-1} which Hawkins *et al.*[7] have obtained by the spectrum simulation of the circular dichroism on the basis of Perrin-Goutermans' vibronic coupling theory.

On the other hand, Mason has obtained a larger coupling energy (1050 cm^{-1}) by fitting the observed intensity of the circular dichroism with the calculated one on the Hückel M.O.[10] However, the reconstituted circular dichroism was so complex as to contain some extra shoulders (as Fig. 2 in the reference 10 shows). Because a surplus of shoulders or bands is originated from a larger coupling, the phantom shoulders of the reconstituted spectrum may be explained by an overestimation of the coupling energy.

$[Ni(phen)_3]^{2+}$. As in the case of the bipy complexes, all the absorption bands of the tris-phen and the mono-phen complexes in the region of $30—40 \times 10^3$

Table 1. The fine structure of the highest band

$[Ni(phen)(H_2O_4)]^{2+}$		$[Ni(phen)_3]^{2+}$	
ν cm^{-1}	$\Delta\nu$ cm^{-1}	ν cm^{-1}	$\Delta\nu$ cm^{-1}
37040		37760	
(37740)[a]	700	37450	690
(38460)	720	(38170)	720

a) Parenthesis shows shoulder.

cm^{-1} are assigned to the transition localized in the ligand(s). The mono-phen complex holds a weakly resolved structure for the transition of the largest wave number (^1B_a in the free phen). The structure may be caused by a metal effect, because the ^1B_a band of the free phen has no structure (but a great band width). Since the structure has a common spacing between the adjacent sub-bands (700 cm^{-1}) as Table 1 shows, the sub-bands are assigned to the vibronic bands. In the tris-phen complex, the less clear progression with the spacing of 700 cm^{-1} was observed and the feature of the band was similar to that of the free phen. It is probable that the less clear structure is caused by a sharing of the metal effect with the three ligands. A similar situation has been observed in the case of $[Zn(phen)_2(H_2O)_2]^{2+}$.[3]

Hawkins *et al.* has offered another explanation to the less stronger 0–0′ band of $[Ni(phen)_3]^{2+}$ than the 0–0′ band of $[Ni(phen)(H_2O)_4]^{2+}$; this explanation was that a molecular exciton interaction in $[Ni(phen)_3]^{2+}$ produced a broading of the 0–0′ band.[7] However, it must be noticed that $[Ni(phen)_3]^{2+}$ has a common spacing between the sub-bands as $[Ni(phen)(H_2O)_4]^{2+}$ has.

References

1) T. Ohno and S. Kato, This Bulletin, **47**, 1901 (1974).
2) J. Mason and S.F. Mason, *Tetrahedron*, **23**, 1919 (1967).
3) T. Ohno and S. Kato, This Bulletin, **47**, 2953 (1974).
4) T. Ohno and S. Kato, unpublished.
5) E. Larsen, S. F. Mason, and G. H. Searle, *Acta Chem. Scand.*, **20**, 191 (1966).
6) S. F. Mason, *J. Chem. Soc.*, **1969**, 1428.
7) R. G. Bray, J. Ferguson, and C. J. Hawkins, *Aust. J. Chem.*, **22**, 209 (1969).
8) D. W. Margerum, R. L. Bystroff, and C. V. Banks, *J. Amer. Chem. Soc.*, **78**, 4211 (1956).
9) Y. Gondo, *J. Chem. Phys.*, **41**, 3928 (1969), I. Hanazaki and S. Nagakura, *Inorg. Chem.*, **8**, 648 (1969).
10) S. F. Mason, B. J. Peart, and R. E. Waddell, *J. Chem. Soc. Dalton*, **1973**, 944.

Core-electron Spectra of Mono-substituted Benzenes Obtained by the Gas-phase X-Ray Photoelectron Spectroscopy

Toshiaki OHTA, Takashi FUJIKAWA, and Haruo KURODA

Department of Chemistry, Faculty of Science, The University of Tokyo, Hongo, Tokyo 113

(Received February 7, 1975)

The gas-phase X-ray photoelectron spectra were observed on benzene and its eight mono-substituted derivatives; C_6H_5X, X=H, CH_3, NH_2, OH, F, Cl, Br, NO_2 and CN. Binding energies of core levels were determined from the observed spectra by using the spectrum simulation technique, and they were compared with the chemical shift predicted from the CNDO/2 charge densities on the basis of the electrostatic potential model. It is shown that the C1s binding energies of benzene derivatives can be generally correlated with atomic charges, q_j, by the following equation;

$$E_i(\text{C 1s}) = 290.2 + 22.67q_i + \sum_{j\neq i}(q_j/R_{ij}) \quad \text{eV.}$$

By using this relation and the observed C1s binding energies, the atomic charge analysis is carried out. Satellite bands were observed in the C1s spectra as well as in some other core-electron spectra of benzene derivatives. Theoretical calculations are carried out on the energies and probabilities of shake-up transitions. It is concluded that the observed satellites are mainly due to the shake-up processes associated with the excitations of π electrons.

The effects of substituent groups on the charge distributions in benzene derivatives are of great interest from chemical point of view, and have been studied by means of various theoretical methods. However, hitherto, there has been no experimental method which directly gives the atomic charges of a molecule. The core electron binding energies of atoms in a molecule can be determined by means of X-ray photoelectron spectroscopy. It has been well established that the core electron binding energy varies more or less depending on the chemical bonds in the ground state of molecule, and this effect, called "chemical shift," is directly reflecting the charge distribution in the molecule. Thus X-ray photoelectron spectroscopy provides a way to investigate the atomic charges of a molecule.

On several benzene derivatives, Clark *et al.*[1] observed the X-ray photoelectron spectra of their frozen solid states, and discussed the correlation between CNDO/2 charge densities and observed binding energies. In particular, detailed investigations were carried out on fluorobenzenes.[2] In a previous paper,[3] we studied the charge distributions of *p*-benzoquinone, hydroquinone and their halogen-substituted derivatives from the X-ray photoelectron spectra of the solid states of these compounds.

However, the X-ray photoelectron spectrum of a solid sample is unavoidally affected by the so-called solid state effects, so that there always remain some ambiguities in the analyses of chemical-shift data obtained from the solid-state X-ray photoelectron spectroscopy. It is desirable to use the gas-phase X-ray photoelectron spectra in order to study molecular properties. The atomic charges of fluorobenzenes were investigated by Thomas[4] by this technique.

In the present paper, we report the gas-phase X-ray photoelectron spectra of monosubstituted benzenes and the results of the analyses of the observed spectra by means of the electrostatic potential model. We will also report the natures of the satellite bands accompanying the core electron peaks.

Experimental

The gas-phase X-ray photoelectron spectra were measured with a McPherson ESCA 36 electron spectrometer, by employing Mg$K\alpha$ radiation (1253.6 eV), on benzene and its monosubstituted derivatives: C_6H_5X (X=H, OH, NH_2, CH_3, CN, NO_2, F, Cl and Br). Each sample, purified by distillation in advance, was repeatedly out-gassed by the freezing and pumping technique, and then its vapor was introduced into gas-handling system of the spectrometer through a needle valve. In most of the present experiments, the pressure of sample vapor read at the position just after the needle valve, was maintained at about 0.2 Torr. Since this position is considerably separated with fine tubing from the gas-ionization cell of the spectrometer, the actual vapor pressure within the ionization cell must be very much lower, possibly one order less, than the above value.

The binding energies of core electron peaks, referred to the vacuum level, were calibrated by using the N1s peak of nitrogen gas, mixed in the sample vapor, as the reference; the binding energy of the N1s level of nitrogen molecule was taken as 409.9 eV. The energy calibration was repeated at least twice for each sample by independent experiments, and confirmed to be reproducible within 0.2 eV.

Results and Discussion

Binding Energies of Core Electron Levels. In the case of monosubstituted benzenes, there are four inequivalent positions of carbon atom in their benzene rings; we will label these positions as C_1, C_2, C_3, and C_4 as illustrated in Fig. 1. Thus we should expect that C1s levels of a monosubstituted benzene will split into four because of the chemical shifts. In the cases of toluene

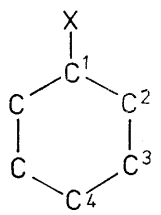

Fig. 1.

TABLE 1. TOTAL CHARGE DENSITIES OF MONOSUBSTITUTED BENZENES OBTAINED FROM CNDO/2 CALCULATION

	Benzene ring							Susbtituents				
	C_1	C_2	C_3	C_4	H_1	H_2	H_3	C	N	O	X[a)]	H
C_6H_6	0.006	0.006	0.006	0.006	−0.006	−0.006	−0.006					−0.006
$C_6H_5CH_3$	0.043	−0.010	0.012	−0.003	−0.008	−0.008	−0.008	−0.021				0.005
$C_6H_5NH_2$	0.137	−0.046	0.026	−0.022	−0.002	−0.008	−0.008		−0.228			0.091
C_6H_5OH	0.196	−0.061	0.032	−0.021	0.001	0.009	−0.008			−0.252		0.143
C_6H_5F	0.236	−0.055	0.028	−0.015	0.018	−0.000	−0.001				−0.199	
C_6H_5Cl	0.085	0.015	0.005	0.013	0.012	0.003	0.001				−0.169	
C_6H_5CN	0.058	0.010	0.006	0.009	0.003	0.000	−0.001	0.084	−0.166			
$C_6H_5NO_2$	0.051	0.011	0.007	0.023	0.036	0.010	0.003		0.471	−0.338		

a) X means halogen atoms

and benzonitrile, there will be another Cls level associated with the carbon atom of substituent group. However, the splittings of Cls levels are not large enough to give well resolved peaks in the observed Cls spectra. In effect, the Cls spectra of monosubstituted benzenes were observed only as a broad and asymmetrical peak with or without a shoulder. Therefore, we used the spectrum simulation technique to determine the binding energy of each Cls level. In applying this technique, we must first determine the peak shape of a single component. The Cls peak of benzene can be used for this purpose since there should be no splitting of Cls level in the case of benzene. In effect, the observed Cls spectrum of benzene gave a sharp symmetrical peak, its width (FWHM) being 1.05 eV under the present experimental condition. We tried to fit the observed peak with a modified Lorentz function described as follows;

$$f(E-E_0) = I\cdot\left[\frac{1-s}{1+\left(\frac{E-E_0}{w/2}\right)^2}+\frac{s}{1+\left(\frac{E-E_0}{w/2}\right)^4}\right] \quad (1)$$

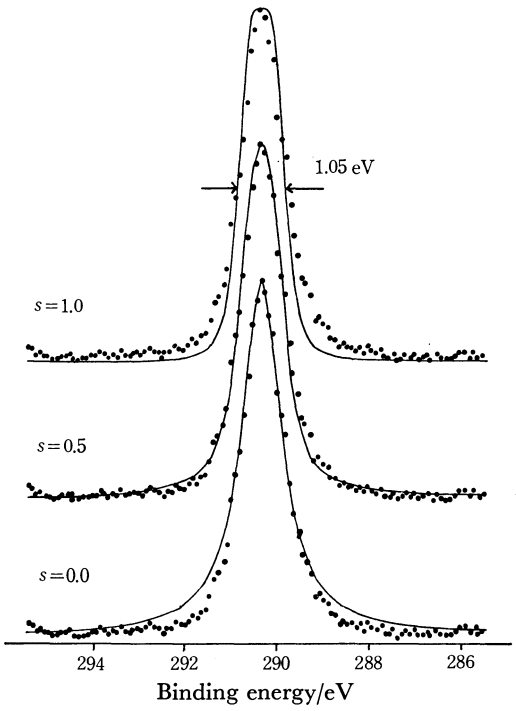

Fig. 2. X-Ray photoelectron spectrum of Cls electrons of benzene. The calculated curve (see text) are shown by solid lines.

where I, E_0 and w are the height, position and width of the peak, respectively, and s is a parameter determining the peak shape. In Fig. 2, the peak shapes calculated for $s=0.0$, 0.5, and 1.0 are compared with the observed Cls peak of benzene. The best agreement was obtained when $s=0.5$. Thus we decided to set $w=1.05$ eV and $s=0.5$ in the following process. Next, we examined the expected order of different Cls levels of each monosubstituted benzene. This information is desirable to have, though not indispensable, in order to carry out the spectrum simulation procedures. For this purpose, we estimated the relative chemical shift, ΔE_i, from the CNDO/2 charge densities by the following equation given by the electrostatic potential model;[5)]

$$\Delta E_i = k_c q_i + \sum_{j\neq i}(1/R_{ij})\cdot q_j \quad (2)$$

where q_i and q_j are the charge densities of the i-th and j-th atoms, respectively, R_{ij} is the interatomic distance (in atomic units), and k_c is a constant which we tentatively assumed as 22.1 eV/unit charge. The charge densities obtained by CNDO/2 calculations are given in Table 1. In the case of bromobenzene, we did not carry out the CNDO/2 calculation, but assumed that the order of the C ls levels is the same as in fluorobenzene.

Taking the intensity ratio of the peaks corresponding to C_1, C_2, C_3, and C_4 as 1 : 2 : 2 : 1, we adjusted the peak positions until the best agreement was obtained between the calculated and observed C ls spectra. The final

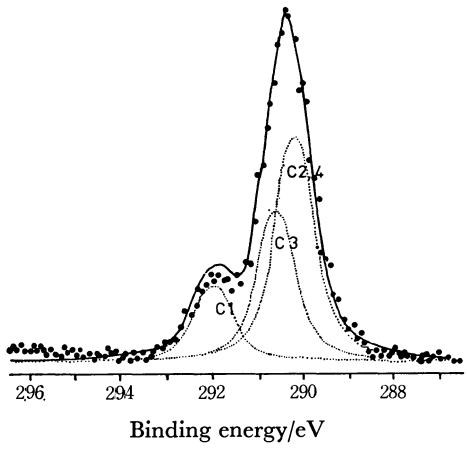

Fig. 3. Decomposition of the Cls spectrum of phenol into the constituent bands. The results of decomposition are shown with broken lines.

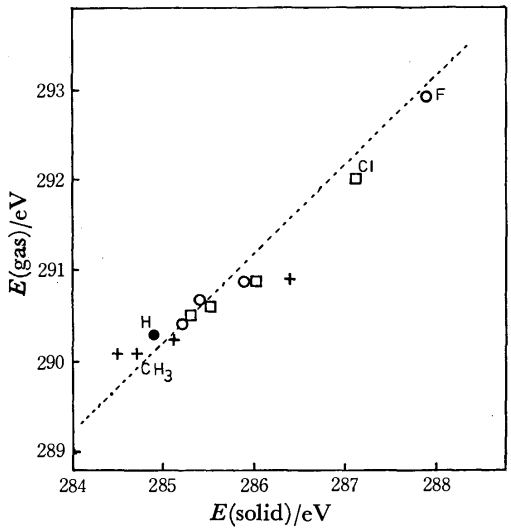

Fig. 4. Comparison of the C 1s binding energies obtained by the gas phase experiments with those reported from the studies of frozen solids.[1]

result of such a procedure is illustrated in Fig. 3, which is the one obtained of phenol. By the above technique, we were able to determine the binding energy of each C 1s level with an accuracy of ± 0.1 eV. The values thus obtained are given in Table 2 together with the binding energies of other core electron levels.

Clark *et al.*[1] reported the C 1s binding energies of benzene, toluene, chlorobenzene and fluorobenzene, obtained from the similar analyses of the shapes of the C 1s spectra of the frozen solid states. In Fig. 4, their values are compared with our gas-phase values. We can conclude that there is a nearly constant energy difference, 5.2 eV, between the solid and gas-phase values. It should be noted first that the solid-state values are the ones referred to the Fermi levels of the samples whereas our gas-phase values are referred to the vacuum level, and second that the binding energy obtained of a solid sample is necessarily affected by the fact that the core-hole ion state is stabilized by polarizing its surroudings. In other words, the binding energies determined from the X-ray photoelectron spectra of solid samples are dependent on the work function and polarization energy of the solid state, both of which should, in principle, vary from sample to sample. Therefore, it is rather surprising to find that the difference between the solid and gas-phase values is almost the same for a variety of monosubstituted benzenes.

Effects of Substituent Group on C 1s Levels. The binding energies of the C 1s levels of monosubstituted benzenes are compared in Fig. 5. We note that, in all cases, the C 1s level of the carbon atom at the substituted position is considerably shifted to higher binding energy as the result of substitution, while those of other carbon atoms of benzene ring show much smaller shifts except in the cases of nitrobenzene and benzonitrile.

As we compare the four molecules, C_6H_5X with X= H, Br, Cl, and F, the shifts of the C 1s level of the atom at the substituted position is the larger as the electronegativity of the substituent atom is the higher. The four substituents, CH_3, NH_2, OH, and F, are mutually

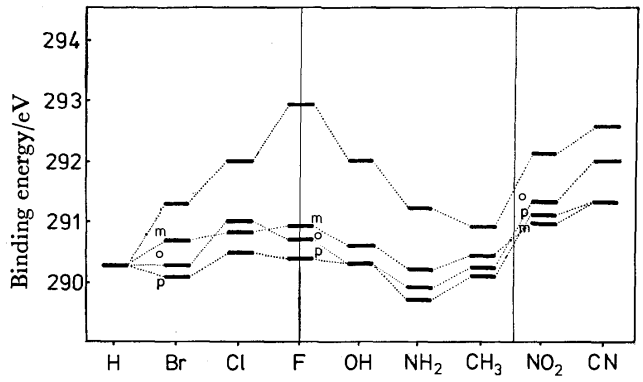

Fig. 5. C 1s Binding energies of benzene derivatives.

isoelectronic, and the electronegativity increases in the order, C<N<O<F. Here again, the core electron level of the carbon atom at the substituted position increases with the increase of electronegativity of the substituent.

In the cases of the six substituents mentioned above, the core electron binding energies of the carbon atoms at *ortho*-, *meta*-, and *para*-positions are in the order, *para*< *ortho*<*meta*, except for chlorobenzene.[6]

The CN and NO_2 groups are known to be electron attractive substituents, whose π-electron systems can interact strongly with those of benzene ring. These can be clearly distinguished from other substituents by looking their effects on the C 1s levels; In benzonitrile and nitrobenzene, all C 1s levels are considerably shifted to higher binding energy as compared with the C 1s level of benzene.

Charge Distribution and Chemical Shift. According to the electrostatic potential model, the binding energy E_i of a core electron level of the i-th atom in a molecule is given by the following equation,

$$E_i = E_0^{\mathrm{A}} + k_{\mathrm{A}} q_i + \sum_{j \neq i} (q_j / R_{ij}) \qquad (3)$$

where E_0^{A} and k_{A} are constants dependent on the kind of atom. Strictly speaking, the value of E_0^{A} must be slightly different for different molecules since it is affected by the molecular reorganization energy, but we could reasonably assume that it remains the same among benzene derivatives.[7]

We can rewrite Eq. (3) in the following form;

$$E_i - \sum_{j \neq i} (q_j / R_{ij}) = E_0^{\mathrm{A}} + k_{\mathrm{A}} q_i \qquad (4)$$

This means that one should obtain a straight line when $E_i - \sum_{j \neq i} (q_j / R_{ij})$ is plotted against q_i. Using the CNDO/2 charge densities and observed C 1s binding energies E_i(obsd), we calculated $E_i(\mathrm{obsd}) - \sum_{j \neq i} (q_j / R_{ij})$ and plotted it against q_i. The result is shown in Fig. 6. We see that the plots are, in effect, well on a straight line except a few points concerned with benzonitrile and chlorobenzene. The inclination of the above straight line gives the value of k_{C} as 22.67 eV/unit charge, which is in good agreement with the value, 22.0 eV/unit charge, calculated from Slater orbitals for the carbon atom by Siegbahn, *et al.*[5] The intercept of the line at $q_i=0$ gives the E_0^{A} value. This found to be 290.2 eV. Thus we obtain the following equation;

TABLE 2. BINDING ENERGIES OF CORE LEVELS (unit: eV)

	C_1	C_2	C_3	C_4	C	N	O	X
C_6H_6	290.3	290.3	290.3	290.3				
$C_6H_5CH_3$	290.9	290.2	290.4	290.1	290.1			
$C_6H_5NH_2$	291.2	289.9	290.2	289.7		405.3		
C_6H_5OH	292.0	290.2	290.6	290.2			538.9	
C_6H_5F	292.9	290.7	290.9	290.4				693.3[1]
C_6H_5Cl	292.0	291.0	290.5	290.8				207.5, 206.3[2]
C_6H_5Br	291.3	290.3	290.7	290.1				196.3, 189.3[3]
C_6H_5CN	292.5	292.0	291.3	291.3	291.0	405.0		
$C_6H_5NO_2$	292.1	291.3	291.0	291.1	291.0	411.5	538.3	

1) F 1s, 2) Cl $2p_{1/2,3/2}$ 3) Br $3p_{1/2,3/2}$

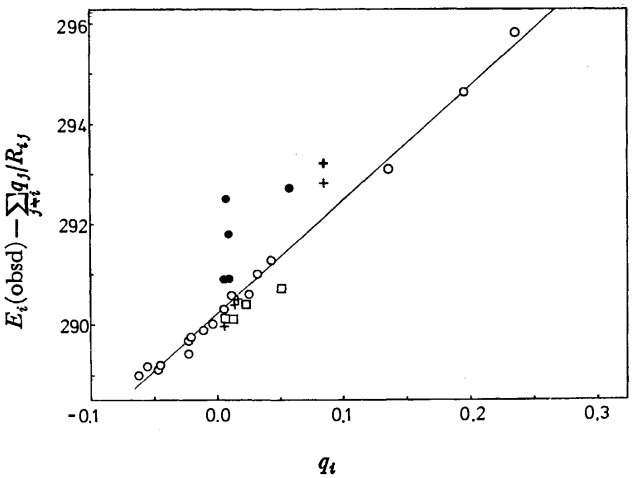

Fig. 6. Correlation of between $E_i(\text{obsd})-\sum_{j\neq i}q_j/R_{ij}$ and q_i. The data points shown by filled circles, open squares and crosses are those of benzonitrile, nitrobenzene and chlorobenzene, respectively. The data points related with other compounds are shown by open circles.

$$E_i(\text{Cls}) = 290.2 + 22.67q_i + \sum_{j\neq i}(q_j/R_{ij}) \qquad (5)$$

We propose the above equation as the one generally applicable for the analyses of Cls binding energies of benzene derivatives.

By Eq. (5) we calculated the binding energies of Cls levels of monosubstituted benzenes from the CNDO/2 charge densities listed in Table 1, and calculated the Cls spectrum of each compound. The results are compared in Fig. 7. The calculated spectra almost completely agree with the observed ones in the cases of toluene, aniline, phenol and fluorobenzene. In comparison with the above cases, the agreement is less satisfactory in the cases of chlorobenzene, nitrobenzene and benzonitrile. We think that this is reflecting the poor reliabilities of the charge densities estimated for these compounds by CNDO/2 calculations.

Atomic Charge Analysis. According to Eq. (3), the relative chemical shift, $\Delta E_i=E_i-E_0^{\text{A}}$, of each core level can be expressed by a linear combination of charge densities. Thus we have a series of linear equation of the following form;

$$\Delta E_i = \sum_j a_{ij}q_j \qquad (6)$$

In a matrix presentation, they can be summarized as follows

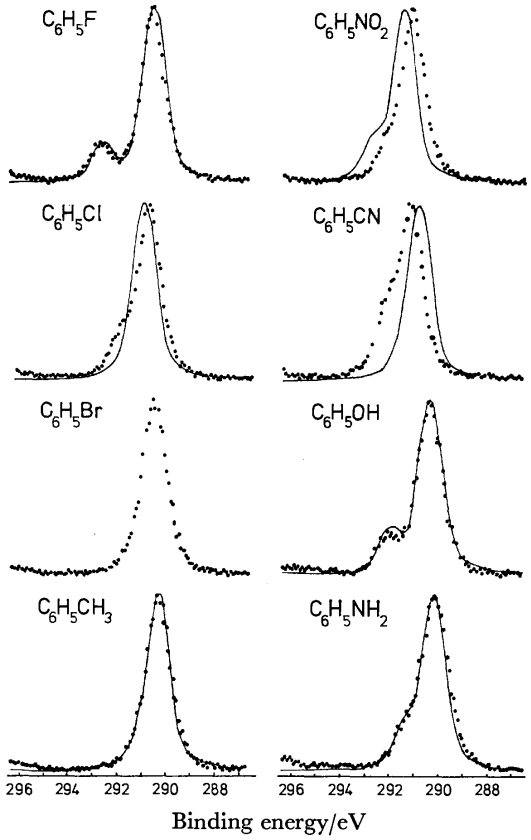

Fig. 7. Cls Spectra of benzene derivatives. The observed data are shown by points. The spectra calculated from the CNDO/2 charge densities are shown by lines.

$$\boldsymbol{\delta} = \mathbf{Aq} \qquad (7)$$

where $\boldsymbol{\delta}$ and $\mathbf{q}$ are vectors whose components are the ordered sets $\{\Delta E_i\}$ and $\{q_j\}$, respectively, and $\mathbf{A}$ is the matrix whose elements are a_{ij}. By comparing Eq. (6) with Eq. (3), one can easily see that an off-diagonal element a_{ij} of $\mathbf{A}$ matrix is equal to $1/R_{ij}$ which can be known from the molecular geometry, and a diagonal element a_{ii} is equal to k_{A}. Thus, if we know the $\boldsymbol{\delta}$ vector, we can, in principle, calculate the $\mathbf{q}$ vector. In other words, the charge densities can be estimated from the observed chemical shifts of core electron levels. This method has been used by several authors[3,4,8] and named "atomic charge analysis" (ACHARGE analysis).

In the preceeding section, we have determined the E_0^{A} and k_{A} values for Cls level, but not for other core levels. Furthermore, the components of $\boldsymbol{\delta}$ vector,

Table 3. Charge densities determined by ACHARGE analysis

	C_1	C_2	C_3	C_4	C	N	O	X
$C_6H_5CH_3$	0.125	−0.042	0.006	0.010	−0.037			
$C_6H_5NH_2$	0.161	−0.044	0.037	−0.042		−0.256		
C_6H_5OH	0.204	−0.034	0.028	−0.040			−0.306	
C_6H_4F	0.265	−0.035	0.032	−0.024				−0.270
C_6H_5Cl	0.161	−0.016	0.061	−0.051				−0.230
C_6H_5Br	0.105	−0.027	0.034	−0.031				−0.086
C_6H_5CN	0.087	0.004	0.008	0.066	0.181	−0.364		

associated with hydrogen atoms are not experimentally available. Thus we have to reduce the dimension of δ vector by introducing a few assumptions. First, we used the condition of electrical neutrality of molecule, which is expressed as;

$$\sum_j q_j = 0 \tag{8}$$

Second, we assumed that the charge densities of hydrogen atoms are the same as the values obtained by the CNDO/2 calculations, and excluded from the unknown quantities which should be obtained by solving the equation. This assumption may not be legitimate, but seems allowable, since hydrogen atoms of benzene ring are likely to have small charges as indicated by the CNDO/2 calculations (see Table 1), so that the above assumption should not significantly affect the results of ACHARGE analysis. When we use the two assumptions described above, the dimension of $\mathbf{q}$ vector can be reduced to four for aniline, phenol, chlorobenzene, bromobenzene and fluorobenzene, and five for toluene, benzonitrile, and nitrobenzene. Thus we were able to carry out ACHARGE analysis using only the binding energies of C 1s levels in all cases except nitrobenzene. In the case of nitrobenzene, the analysis is possible if we use the N 1s or O 1s binding energy, but we did not carry out the analysis since reliable values of E_0^A and k_A are not available at present for nitrogen and oxygen atoms of benzene derivatives.

The charge densities thus obtained from the analyses of the C 1s spectra of benzene derivatives are listed in Table 3. In most compounds studied here, we found a good agreement between the charge densities derived from the ACHARGE analyses and those by the CNDO/2 calculations. It should be noted that ACHARGE analysis can be carried out without the aid of molecular orbital calculation once the values of E_0^A and k_A have been established. In this sence, we could regard its results as "experimental charge densities."

In Table 4, the results of the ACHARGE analysis of fluorobenzene reported by different authors are compared with those of the present study. They are in satisfactory agreement although the actual procedures of analysis differ a little between different authors.

Table 4. Atomic charges of fluorobenzene

Atom	CNDO/2	ACHARGE analysis		
		Thomas[4]	Clark *et al.*[2]	present work
C_1	0.236	0.23	0.209	0.265
C_2	−0.055	−0.04	−0.028	−0.035
C_3	0.028	0.01	0.005	0.032
C_4	−0.015	0.00	0.003	−0.024
F	−0.199	−0.19	−0.203	−0.270

We note in Table 3 that the net charge on the substituent group (CN) of benzonitrile is negative in agreement with the chemical intuition that CN group is an electron attractive substituent. The situation seems to be not so simple in the case of aniline where the substituent is an electron donative one. As shown in Table 3, the nitrogen atom of the NH_2 group has a considerably large negative charge, so that the net charge on the NH_2 group becomes negative even if we took into account the positive charges on the hydrogen atoms. The same conclusion is derived also from the CNDO/2 charge densities. However, if we examine the π-electron population predicted from the CNDO/2 molecular orbitals, we see that the amount of π electron transferred from NH_2 group to benzene ring amounts to 0.278 *e*. Thus we can conclude that the nitrogen atom of the NH_2 group is donating its π electron to the benzene ring, but attracting σ electron primarily from the carbon atom which is directly bonded to the nitrogen atom, so that the net charge of NH_2 group becomes negative. The situation seems to be more or less similar in the cases of other electron donative substituents.

Satellite Bands of Core Electron Peaks. Core electron peaks of X-ray photoelectron spectra are often accompanied by satellites associated with the two-electron process where an ejection (shake-off) or excitation (shake-up) of an outer-shell electron occurs simultaneously with the photoionization of a core level.[9,10] Figure 8 shows the satellite of the C 1s peak of benzene.

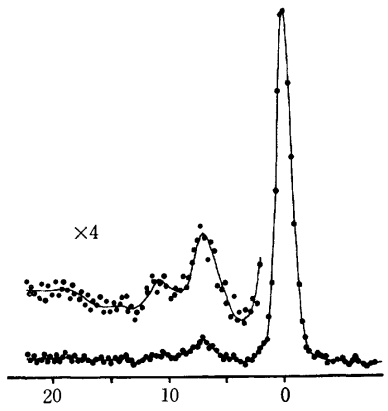

Fig. 8. C 1s Spectrum of benzene. The high-energy region of the spectrum is also shown by expanding the intensity scale to show the satellites. The energy difference from the main peak is given in the abscissa.

We can see two bands in the high binding-energy side of the C 1s peak, their maxima being at 7.0 and 11.0 eV, respectively, from the main peak. The intensity relative to the main peak is 10.5 and 2.5 percent for the 7.0 and 11.0 eV bands, respectively. We examined the pressure dependences of these bands, and confirmed that their energies and intensities relative to the C 1s peak are practically unaffected by the change of the vapor pressure of benzene. This fact indicates that the above bands are not due to the inelastic scattering of photoelectron, but due to the shake-up or shake-off process. Beside the above two bands, we observed several very weak bands at much higher binding energies. For these bands, however, we were not able to confirm whether they are really due to two-electron process or not.

Satellites by two-electron processes were also observed in the C 1s spectra of the monosubstituted benzenes. Their shapes and intensities were found to vary more or less depending on the substituent group. In the case of nitrobenzene, satellite appeared in the O 1s region as well as in the C 1s region, but not in the N 1s region. The O 1s satellite was composed of three bands located at 3.0, 10.0, and 13.0 eV, respectively, from the main peak. A considerably sharp satellite band was observed in the N 1s region of the spectrum of benzonitrile at 5.0 eV from the main peak. No satellite definitely attributable to two-electron process was found in the regions other than C 1s in the cases of other monosubstituted benzenes studied here.

According to the theory based on the sudden approximation, the probability of a shake-up process which yields the final state Ψ_k where a secondary excitation (or ejection) of a valence electron has occurred simultaneously with the photoionization of a core level, can be given as follows;[11]

$$P_k = |\langle\Phi_0|\Psi_k\rangle|^2 \tag{9}$$

where Φ_0 is the wave function in which the valence-electron orbitals are the same as in the ground state of the molecule without a core hole.

We calculated the molecular orbitals of valence electrons by means of the CNDO/2 method. In order to calculate the molecular orbitals of the core-hole ion, we assumed the localized-core-hole model[12] and used the equivalent-core approximation.[13] The wave functions Φ_0 and Ψ_k were then expressed in the form of a Slater determinant constructed from the above orbitals, and the shake-up probability was calculated by use of Eq. (9). A part of the results thus obtained of benzene are shown in Table 5 in order to illustrate the general trend of the predicted shake-up probabilities. It should be noted that the shake-up probability is predicted to be quite small for σ—σ^* transitions. This was also the case for other σ—σ^* transitions which we have omitted in Table 5. On the other hand, a π—π^* transition ($2b_1 \rightarrow 3b_1$) is predicted to have a considerably large shake-up probability. We carried out similar calculations on monosubstituted benzenes, and found that, like in benzene, the shake-up probability is generally quite small (less than 0.5 percent) in the case of σ—σ^* transition, and the transitions of significant shake-up probability can be found only among π—π^* transitions. Seemingly, the above results are reasonable since we can generally expect that, in a π-conjugated system, π electrons would play the most important role in the relaxation process accompanying the ejection of a core electron because of the labile nature of π electrons.

TABLE 5. SHAKE-UP PROBABILITIES(%) OF C 1s FOR BENZENE OBTAINED BY CNDO/2 CALCULATION

Occupied orbital	Vacant orbital							
	$3b_1(\pi)$	$2a_2(\pi)$	$8a_1$	$9a_1$	$6b_2$	$10a_1$	$11a_1$	$4b_1(\pi)$
$1b_1(\pi)$	0.51	—	—	—	—	—	—	0.06
$3b_2$	—	—	—	—	0.25	—	—	—
$5a_1$	—	—	0.08	0.16	—	0.32	0.0	—
$6a_1$	—	—	0.50	0.17	—	0.08	0.0	—
$4b_2$	—	—	—	—	0.06	—	—	—
$2b_1(\pi)$	5.26	—	—	—	—	—	—	0.09
$5b_2$	—	—	—	—	0.39	—	—	—
$7a_1$	—	—	0.0	0.09	—	0.03	0.08	—
$1a_2(\pi)$	—	0.04	—	—	—	—	—	—

The energy separation of a satellite band from the main core electron peak must be equal to the excitation energy of the core-hole ion. This will be given as follows;

$$\Delta E_k = \langle\Psi_k|H|\Psi_k\rangle - \langle\Psi_0|H|\Psi_0\rangle \tag{10}$$

where Ψ_k and Ψ_0 are the wave function of the excited state and that of the ground state of the core-hole ion, respectively. Unfortunately, however, the CNDO/2 method generally provides only poor predictions as regards the energies of π—π^* transitions which are most important to understand the satellites of benzene derivatives. As we have already pointed out, there is a good reason to suppose that, in π-conjugated molecules, the contributions of π electrons are of primary importance in the relaxation process accompanying the ionization of a core level. Therefore, it would be allowable, at least as a first approximation, to attribute the relaxation entirely to π electrons by freezing the states of σ electrons the same as in the initial state without a core hole, and estimate the energies of π—π^* transitions of the core hole ion by means of a semi-empirical SCF-MO-CI method within the framework of π electron approximation. Here again, we took the localized-core-hole model. This means that, for a monosubstituted benzene, we have to consider four different core-hole states corresponding to four inequivatent locations of C 1s hole in benzene ring. We carried out the calculation on each of these core hole state. The semiempirical parameters related to the core-hole atoms C($1s \cdot tr \cdot tr \cdot tr \cdot \pi$), N($1s \cdot tr^2 \cdot tr \cdot tr \cdot \pi$)| and O($1s \cdot tr^2 \cdot tr^2 \cdot tr \cdot \pi$) were assumed to be the same as those of $N^+(1s^2 \cdot tr \cdot tr \cdot tr \cdot \pi)$, $O^+(1s^2 \cdot tr^2 \cdot tr \cdot tr \cdot \pi)$ and $F^+(1s^2 \cdot 2s^2 \cdot 2p^2 \cdot 2p^2)$, respectively, according to the equivalent-core approximation. We used the Katagiri-Sandrofy's formula[14] for resonance integral and the Nishimoto-Mataga's formula[15] for two-center repulsion integral, and took into account not only the nearest-neighbor resonance integrals, but also the non-nearest-neighbor ones.[16] In the calculations of configuration interactions, we took into account all singly-excited con-

TABLE 6. SHAKE-UP ENERGIES(eV) AND PROBABILITIES(%) OF PHENOL OBTAINED BY π-ELECTRON APPROXIMATION

Transition	Localized core-hole model				Weighted average	Exp.
	C_1	C_2	C_3	C_4		
4→5	4.99(0)	4.69(0.48)	4.51(0.39)	5.53(3.34)	6.81(4.68)	6.8(8.5)
4→6	6.62(0.53)	5.70(0.32)	5.37(0.66)	6.27(0)		
3→5	5.82(4.62)	7.43(2.83)	6.52(1.58)	5.05(0)		
3→6	6.80(0)	7.74(0.00)	7.11(0.11)	6.76(0.47)		
4→7	8.02(0)	7.04(0.01)	7.22(0.03)	7.84(0.05)		
2→5	7.90(0.03)	8.46(0.80)	8.62(1.48)	9.40(0.95)		
3→7	8.64(0.15)	9.41(0.12)	8.91(0.01)	8.19(0)		
2→6	8.54(0)	8.86(0.16)	9.37(0.00)	9.32(0)		
2→7	10.76(0.06)	11.22(0.01)	11.30(0.00)	11.56(0.12)	12.39(2.39)	9.5(2.3)
1→5	13.21(2.56)	12.60(2.00)	12.34(2.57)	12.43(2.26)		
1→6	13.06(0)	12.78(0.00)	12.57(0.00)	12.24(0)		
1→7	15.59(0.01)	15.06(0.01)	14.77(0.01)	14.65(0.10)		

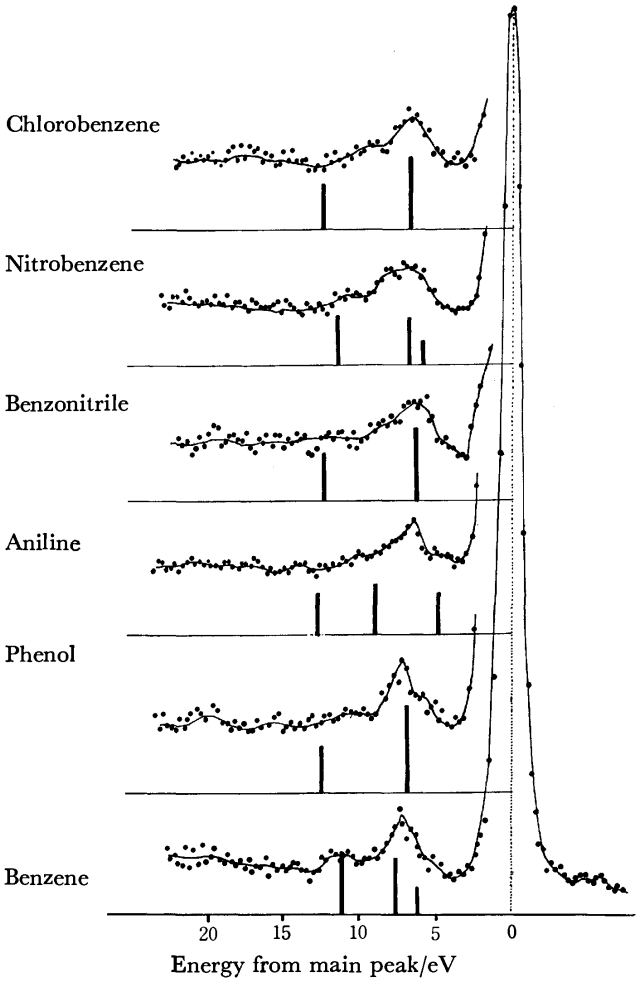

Fig. 9. Satellites accompanying the C 1s peaks of X-ray photoelectron spectra of benzene derivatives. Calculated results are shown as vertical bars, whose positions and heights indicate the predicted energies and intensities, respectively.

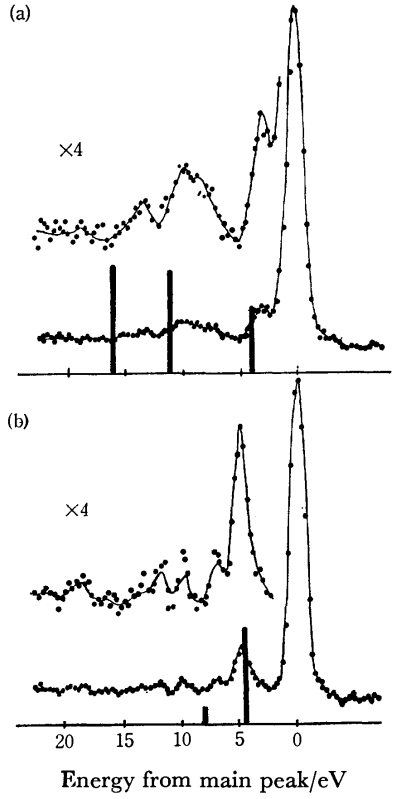

Fig. 10. Satellites accompanying the core electron peaks of the X-ray photoelectron spectra.
(a) O 1s spectrum of nitrobenzene (b) N 1s spectrum of benzonitrile. Satellite region is shown by expanding the intensity scale.
Calculated results are shown as vertical bars.

figurations. By means of the above method, we estimated the energies of π—π^* transitions of the core-hole state. The shake-up probability was then calculated by Eq. (9) by using the CI wave functions obtained by the above calculations.

The results obtained of phenol are listed in Table 6.

It should be noted that the location of C 1s hole does significantly affect not only the transition energies but also the shake-up probabilities. The observed satellite is to correspond to the superposition of the satellites associated with each C 1s peak. Unfortunately, however, the resolution of the observed spectrum is not high enough to discuss the fine structures of satellite. Thus, we tentatively took the weighted average of predicted satellites for the purpose to compare with the observed spectra. We see that the predicted satellites are in reasonable agreement with the observation (see Table 6).

Similar calculations were carried out on other monosubstituted benzenes, the results of which are compared in Fig. 9 with the observed satellites. The agreement between the prediction and observation is generally satisfactory. We also performed the calculations on the shake-up satellites of N ls peak of benzonitrile and O ls peak of nitrobenzene. The results are shown in Fig. 10. Here again, we see that the general features of the observed satellites are satisfactorily explained by the calculations.

From the results described above, we can conclude that the prominent satellites accompanying the core electron peaks of the X-ray photoelectron spectra of monosubstituted benzenes are mainly due to the shake-up of π electrons.

References

1) D. T. Clark, D. Kilcast, and W. K. R. Musgrave, *J. Chem. Soc. D*, **1971**, 516.
2) D. T. Clark, D. Kilcast, D. B. Adams, and W. K. R. Musgrave, *J. Electron Spectrosc.*, **1**, 227 (1972/73).
3) T. Ohta, M. Yamada, and H. Kuroda, This Bulletin, **47**, 1158 (1974).
4) T. D. Thomas, *J. Chem. Phys.*, **52**, 1373 (1970).
5) K. Siegbahn, C. Nordling, G. Johansson, J. Hedman, P. F. Hedén, K. Hamrin, U. Gelius, T. Bergmark, L. O. Werme, R. Manne, and Y. Baer. "ESCA Applied to Free Molecules," North-Holland, Amsterdam (1969).
6) There is an uncertainty in the order of binding energies for chlorobenzene because CNDO/2 calculations are less reliable for the molecules containing second-row elements.
7) This is supported by the theoretical investigation by D. W. Davis and D. A. Shirley who found the reorganization energies are almost constant for several benzene derivatives. (D. W. Davis and D. A. Shirley, *J. Electron Spectrosc.*, **3**, 137 (1974).)
8) D. T. Clark, D.B. Adams, and D. Kilcast, *Chem. Phys. Lett.*, **13**, 439 (1972).
9) M. O. Krause, T. A. Carlson, and R. D. Dismukes, *Phys. Rev.*, **170**, 37 (1968).
10) U. Gelius, C. J. Allan, D. A. Allison, H. Siegbahn, and K. Siegbahn, *Chem. Phys. Lett.*, **11**, 224 (1971).
11) R. Manne and T. Åberg, *ibid.*, **7**, 282 (1970).
12) W. L. Jolly and D. N. Hendrickson, *J. Amer. Chem. Soc.*, **92**, 1863 (1970).
13) L. C. Snyder, *J. Chem. Phys.*, **55**, 95 (1971).
14) S. Katagiri and C. Sandorfy, *Theoret. Chim. Acta, (Berl.)* **8**, 203 (1967).
15) K. Nishimoto and N. Mataga, *Z. Phys. Chem.*, (Frankfurt) **13**, 140 (1957).
16) T. Ohta, H. Kuroda, and T.L. Kunii, *Theoret. Chim. Acta*, **19**, 167 (1970).

Electron Pair Concept and an Extension of the Penney-Dirac Bond Order

Takashi OKADA and Takayuki FUENO

Department of Chemistry, Faculty of Engineering Science, Osaka University, Toyonaka, Osaka 560

(Received March 24, 1975)

The density functions representing electron pairs are extracted from two-electron density matrices by operating irreducible tensor operators in a two-electron spin space. Properties of these functions are examined, and the generalized Penney-Dirac bond orders are defined between atomic orbitals. Significance of the bond orders in chemical valence problems is discussed.

The concept of electron pair first introduced by Lewis[1] has long been accepted as the concisest and most fundamental notion of chemical valence. Ever since Heitler and London[2] and Sugiura[3] unveiled the nature of chemical binding of the hydrogen molecule, quantum theory has gained a great deal of success in the description of bondings in molecules as well as electron pairs. Thus, in valence bond theory, the electron pair concept is cast into the premise that an electron pair bond is associated with perfect singlet pairing of spins of electrons in the valence orbitals of the atoms concerned. The picture of electron pair bond was further extended by the introduction of the resonance concept.[4] On the other hand, molecular orbital theory in its simplest form explains the electron pair concept from the viewpoint that for each chemical bond there exists a bonding orbital which is occupied by two electrons in a singlet spin coupling. The methods of equivalent orbitals[5] and localized orbitals[6] are considered to be a reformulation of Lewis' concept in the molecular orbital formalism.

The recent development of computers has made more exact and complicated wavefunctions available, and more sophisticated types of wavefunctions which preserve the electron pair concept have been examined by several authors.[7] However, all these attempts to interpret the electron pair concept are still liable to depend upon the forms of the wavefunctions adopted. It is desirable to reformulate Lewis' concept in terms of fundamental quantities that may be applicable to general types of wavefunctions.

For this purpose, the reduced density matrices, which were introduced by Hushimi[8] and developed by Löwdin[9] and McWeeny,[10] would be the most adequate tool. The first- and second-order reduced density matrices (hereafter referred to as 1- and 2-matrices, respectively) are defined, in the Löwdin normalization,[9] for an N-electron wavefunction $\Psi(x_1, x_2\, x_3, \cdots x_N)$ by the expressions

$$\rho^{(1)}(x_1; x_1') = N\int \Psi(x_1, x_2, \cdots x_N) \times \Psi^*(x_1', x_2, \cdots x_N)\mathrm{d}x_2 \cdots \mathrm{d}x_N \quad (1)$$

$$\rho^{(2)}(x_1, x_2; x_1', x_2') = \binom{N}{2}\int \Psi(x_1, x_2, x_3, \cdots x_N) \times \Psi^*(x_1', x_2', x_3, \cdots, x_N)\mathrm{d}x_3 \cdots \mathrm{d}x_N \quad (2)$$

The diagonal elements of 1-matrix, $\rho^{(1)}(x_1; x_1)$, are interpreted as the electron density at point x_1. A number of useful valence concepts such as various types of populations,[11-14] valence atomic orbitals[10,15] and force concept,[16] have emerged from 1-matrix. By contrast, 2-matrix has hitherto been scarcely employed in electronic structure interpretations despite its fundamental importance.[17]

In this article, we consider Lewis' electron pairs as singlet coupled pairs of electrons possible in an N-electron system and intend to extract these pairs from the total $N(N-1)/2$ pairs represented by 2-matrix. First, we will obtain the distribution of these pairs in an N-electron singlet state by applying to 2-matrix the operator, $-(4/3)\boldsymbol{S}(1)\cdot\boldsymbol{S}(2)$, which was used to define the Penney-Dirac bond order.[18] Then, we will define generalized bond orders from this distribution, which will prove to give spinless 1-matrix on integration. The characteristics of the pair distribution and the bond order will be examined. Finally, we will extend the formulation to nonsinglet states by introducing spin density as well as triplet coupled electron pairs.

I. Definitions of the Spin Coupling Matrix Q^0 and the Bond Order P^0_{ab} in a Singlet State

In the Dirac vector model,[19,20] the problem of permutation degeneracy is replaced by vector couplings between spin angular momenta. The Hamiltonian is equivalent to

$$H = \text{const.} - \frac{1}{2}\sum_{a>b}(1+4\boldsymbol{s}_a\cdot\boldsymbol{s}_b)J_{ab} \quad (3)$$

the summation being over all pairs. Here, J_{ab} is the exchange integral between orbitals a and b, and $\boldsymbol{s}_a$ is the spin vector of an electron in orbital a.

If the spins in orbitals a and b are antiparallel, as in the hydrogen molecule, $\boldsymbol{s}_a\cdot\boldsymbol{s}_b=-3/4$. However, if the spins are mutually random, $\boldsymbol{s}_a\cdot\boldsymbol{s}_b=0$. Penney defined the fractional bond order P_{ab} by a linear interpolation between the two limits. Thus,

$$P_{ab} = -(4/3)\overline{\boldsymbol{s}_a\cdot\boldsymbol{s}_b} \quad (4)$$

$$= (1+2\partial E/\partial J_{ab})/3 \quad (5)$$

Equation (5) shows that, once the energy has been obtained as a function of exchange integrals, the Penney-Dirac bond orders are easy to compute.[21] This definition of P_{ab} may be extended to general types of wavefunctions.[17]

Alternatively, we may think of a bonding electron pair as a pair of electrons with singlet coupled spins and generalize the original idea of Penney by operating $-(4/3)\boldsymbol{S}(1)\cdot\boldsymbol{S}(2)$ to 2-matrix for an N-electron singlet system. We define a matrix Q^0 with space variables

alone such that[22-24]

$$Q^0(r_1, r_2; r_1', r_2') = \int_{s_1=s_1', s_2=s_2'} -(4/3)\boldsymbol{S}(s_1)\cdot\boldsymbol{S}(s_2) \times \rho^{(2)}(x_1, x_2; x_1', x_2')ds_1ds_2 \quad (6)$$

where r_i and s_i are the space and spin variables, respectively. The spinless matrix Q^0 may be termed the spin coupling matrix.

For an eigenstate of $\boldsymbol{S}^2$ and $\boldsymbol{S}_z$ (with $M_s=0$), 2-matrix can always be decomposed into four components:[24]

$$\begin{aligned}\rho^{(2)}(x_1, x_2; x_1', x_2') &= P_2^{\tau_1\tau_1}\tau_1(s_1, s_2)\tau_1^*(s_1', s_2') \\ &+ P_2^{\tau_2\tau_2}\tau_2(s_1, s_2)\tau_2^*(s_1', s_2') + P_2^{\tau_3\tau_3}\tau_3(s_1, s_2)\tau_3^*(s_1', s_2') \\ &+ P_2^{\sigma\sigma}\sigma(s_1, s_2)\sigma^*(s_1', s_2') \end{aligned} \quad (7)$$

where $P_2^{\tau_1\tau_1}$, *etc.*, are the space functions that depend on r_1, r_2, r_1', r_2'. The four possible spin functions are abbreviated as τ_1, τ_2, τ_3 and σ:

$$\begin{aligned}\tau_1 &= \alpha(1)\alpha(2) \\ \tau_2 &= \beta(1)\beta(2) \\ \tau_3 &= [\alpha(1)\beta(2)+\beta(1)\alpha(2)]/\sqrt{2} \\ \sigma &= [\alpha(1)\beta(2)-\beta(1)\alpha(2)]/\sqrt{2}\end{aligned} \quad (8)$$

For a singlet state, three functions $P_2^{\tau_1\tau_1}$, $P_2^{\tau_2\tau_2}$ and $P_2^{\tau_3\tau_3}$ are identical,[24] so that they can be written as $P_2^{\tau\tau}$. Considering $\overline{\boldsymbol{S}(1)\cdot\boldsymbol{S}(2)}=-3/4$ and $1/4$ for singlet and triplet pairs, respectively, the Q^0 matrix is represented by

$$Q^0(r_1, r_2; r_1', r_2') = P_2^{\sigma\sigma} - P_2^{\tau\tau} \quad (9)$$

When we operate $-4\boldsymbol{S}_z(1)\cdot\boldsymbol{S}_z(2)$ on 2-matrix and integrate over spin variables, we obtain a quantity equal to

$$P_2^{zz} = P_2^{\sigma\sigma} + P_2^{\tau_3\tau_3} - P_2^{\tau_1\tau_1} - P_2^{\tau_2\tau_2} \quad (10)$$

For a singlet state, this quantity coincides with that of the Q^0 matrix (Eq. (9)). $\boldsymbol{S}_z(1)\cdot\boldsymbol{S}_z(2)$ givens an expectation value $1/4$ for parallel spins and $-1/4$ for antiparallel spins. Thus, we may interpret the Q^0 matrix of a singlet state as indicating the difference in the probabilities of two electrons at r_1 and r_2 being with antiparallel and parallel spins. Note that the terms *antiparallel* and *parallel* are used strictly as an attribute of $\boldsymbol{S}_z(1)\cdot\boldsymbol{S}_z(2)$, whereas the *singlet* and *triplet* pairs are defined on the basis of $\boldsymbol{S}(1)\cdot\boldsymbol{S}(2)$.

On the other hand, the following trace conditions hold[24]:

$$\mathrm{Tr}P_2^{\sigma\sigma} = N(N+2)/8 - S(S+1)/2 \quad (11)$$

$$\frac{1}{3}\mathrm{Tr}(P_2^{\tau_1\tau_1}+P_2^{\tau_2\tau_2}+P_2^{\tau_3\tau_3}) = N(N-2)/8+S(S+1)/6 \quad (12)$$

Therefore, the trace for our Q^0 matrix is given by:

$$\mathrm{Tr}Q^0(r_1, r_2; r_1', r_2') = N/2 - 2S(S+1)/3 \quad (13)$$

We regard the $N/2$ pairs represented by the Q^0 matrix in a singlet state ($S=0$) as electron pairs in the chemical sense.

It seems natural to base bond orders on the Q^0 matrix. To this end, we use a normalized atomic orbital basis set (a, b, c,$\cdots$) and introduce spatial "Heitler-London-like" geminals among these atomic orbitals:

$$\begin{aligned}S_{aa}(r_1, r_2) &= a(r_1)a(r_2) \\ S_{ab}(r_1, r_2) &= [a(r_1)b(r_2)+b(r_1)a(r_2)]/\sqrt{2} \\ T_{ab}(r_1, r_2) &= [a(r_1)b(r_2)-b(r_1)a(r_2)]/\sqrt{2}\end{aligned} \quad (14)$$

S_{ab} and T_{ab} are not necessarily normalized; the overlaps between atomic orbitals are generally nonzero. Using Eq. (14), we define the bond orders P_{aa}^0 and P_{ab}^0 as

$$\begin{aligned}P_{aa}^0 &= \int S_{aa}^*(r_1, r_2)Q^0(r_1, r_2; r_1', r_2')S_{aa}(r_1', r_2')dr_1dr_2dr_1'dr_2' \\ &= \int a^*(r_1)a^*(r_2)Q^0(r_1, r_2; r_1', r_2')a(r_1')a(r_2')dr_1dr_2dr_1'dr_2' \\ P_{ab}^0 &= \int S_{ab}^*(r_1, r_2)Q^0(r_1, r_2; r_1', r_2')S_{ab}(r_1', r_2')dr_1dr_2dr_1'dr_2' \\ &+ \int T_{ab}^*(r_1, r_2)Q^0(r_1, r_2; r_1', r_2')T_{ab}(r_1', r_2')dr_1dr_2dr_1'dr_2' \\ &= 2\int a^*(r_1)b^*(r_2)Q^0(r_1, r_2; r_1', r_2')a(r_1')b(r_2')dr_1dr_2dr_1'dr_2'\end{aligned} \quad (15)$$

By definition of Eq. (15), we may assign the bond order P_{aa}^0 and P_{ab}^0 to ionic and covalent terms, respectively. It should be noted that the bond orders proposed in this paper are not directly related to bond strength but are some topological indices concerning the electron spin coupling.

II. Characteristics of the Bond Order

Our bond orders and Q^0 matrix have been derived from 2-matrix, and so it is useful to investigate their relations with 1-matrix. By integrating the Q^0 matrix of a singlet state with respect to the second electron, we obtain the following relation:

$$P_1(r_1; r_1') = 2\int Q^0(r_1, r_2; r_1', r_2)dr_2 \quad (16)$$

where $P_1(r_1; r_1')$ is the ordinary spinless 1-matrix defined by

$$P_1(r_1; r_1') = \int_{s_1=s_1'} \rho^{(1)}(x_1; x_1')ds_1 \quad (17)$$

The proof of Eq. (16) will be given in the Appendix.

Equation (16) means that the spatial distribution of N electrons in $N/2$ paris as represented by the Q^0 matrix is identical to the charge density distribution, which has been accepted as a fundamental quantity in usual theories of molecular electronic structure.

The physical meaning of Eq. (16) becomes apparent when this relation is considered on the atomic orbital basis. The spinless 1-matrix is expanded by atomic orbital basis set (a, b,$\cdots$) in the following way:

$$P_1(r_1; r_1') = \sum_{a,b}\gamma_{ab}^0 a(r_1)b^*(r_1') \quad (18)$$

If we assume an orthogonalized atomic orbital basis set (OAO set), the integration over the one-electron Hilbert space can be divided into subspaces of the atomic orbitals involved. Then, from Eqs. (15), (16) and (18), we obtain

$$\begin{aligned}\gamma_{aa}^0 &= \int a^*(r_1)P_1(r_1; r_1')a(r_1')dr_1dr_1' \\ &= 2\sum_b\int a^*(r_1)b^*(r_2)Q^0(r_1, r_2; r_1', r_2')a(r_1')b(r_2')dr_1dr_2dr_1'dr_2' \\ &= 2P_{aa}^0 + \sum_{b\neq a}P_{ab}^0\end{aligned} \quad (19)$$

Once we have calculated bond orders on OAO basis, the electron population of each AO is easily computed according to Eq. (19). The contribution is two electrons from the ionic term and one electron from the covalent terms, in agreement with usual chemical concepts.

A similiar relation obtains for γ^0_{ab}, if we define $P^0_{\substack{ac\\bc}}$ as follows:

$$P^0_{\substack{ac\\bc}} = \int S^*_{ac}(r_1, r_2)Q^0(r_1, r_2; r_1', r_2')S_{bc}(r_1', r_2')dr_1dr_2dr_1'dr_2' + \int T^*_{ac}(r_1, r_2)Q^0(r_1, r_2; r_1', r_2')T_{bc}(r_1', r_2')dr_1dr_2dr_1'dr_2' \quad (20)$$

The resulting γ^0_{ab} is

$$\gamma^0_{ab} = \sqrt{2}(P^0_{\substack{aa\\ba}} + P^0_{\substack{ab\\bb}}) + \sum_{c\neq a,b} P^0_{\substack{ac\\bc}} \quad (21)$$

The meaning of Eq. (21) is to be discussed in a later section.

For single-determinant wavefunctions, 2-matrix can be expressed in terms of the products of 1-matrix.

$$\rho^{(2)}(x_1, x_2; x_1', x_2') = \frac{1}{2}\left\{\rho^{(1)}(x_1; x_1')\rho^{(1)}(x_2; x_2') - \rho^{(1)}(x_2; x_1')\rho^{(1)}(x_1; x_2')\right\} \quad (22)$$

By a straight manipulation using Eq. (18) we obtain the following expression for Q^0 matrix:

$$Q^0(r_1, r_2; r_1', r_2') = \frac{1}{4}\sum_{a,b,c,d}\gamma^0_{ad}\gamma^0_{bc}a(r_1)b(r_2)c^*(r_1')d^*(r_2') \quad (23)$$

The corresponding expressions for bond orders are

$$P^0_{aa} = {n^0_{aa}}^2/4,\ P^0_{ab} = {n^0_{ab}}^2/2 \quad (24)$$

where n^0_{aa} and n^0_{ab} are the diagonal and the off-diagonal elements of $\boldsymbol{n}^0$ matrix,

$$\boldsymbol{n}^0 = \boldsymbol{s}\boldsymbol{\gamma}^0\boldsymbol{s} \quad (25)$$

which was first defined by Davidson[13] and further discussed by Roby[14] in electronic population analysis. Here $\boldsymbol{s}$ is the ordinary overlap matrix between atomic orbitals and γ^0 is the matrix whose elements are γ^0_{ab} given in Eq. (18). On an OAO basis set, $\boldsymbol{n}^0$ simply reduces to γ^0.

We immediately see that Wiberg's bond indices[25]

$$W_{aa} = {\gamma^0_{aa}}^2,\ W_{ab} = {\gamma^0_{ab}}^2 \quad (26)$$

are simply related to our bond orders. Further, the bond index partitioning of atomic charge proposed by Trindle[26] may be regarded as a special case of Eq. (19), and the localization procedure by bond index maximization[27] has a clear physical meaning that each localized orbital contributes most to covalent electron pairing between the atomic orbitals concerned.

More generally, molecular wavefunctions are expressed as a linear combination of determinants made up of orthonormal spin orbitals. It will be convenient, therefore, to evaluate the Q^0 matrix elements and bond orders explicitly for these wavefunctions.

We consider a many-determinant wavefunction,

$$\Psi = \sum_\kappa a_\kappa\Phi_\kappa \quad (27)$$

The density matrix for the case of the present concern is a simple weighted sum of the transition density matrices connecting all different pairs of determinants which arise from the expansion.

$$Q^0(\kappa\lambda|r_1, r_2; r_1', r_2') = \binom{N}{2}\int_{s_1=s_1', s_2=s_2'}\Phi_\kappa(x_1, x_2, \cdots x_N) \times\left(-\frac{4}{3}\boldsymbol{S}(s_1)\cdot\boldsymbol{S}(s_2)\right)\Phi_\lambda^*(x_1', x_2', \cdots x_N)ds_1ds_2dx_3\cdots dx_N \quad (28)$$

$$Q^0(r_1, r_2; r_1', r_2') = \sum_{\kappa,\lambda}a_\kappa a_\lambda^*Q^0(\kappa\lambda|r_1, r_2; r_1', r_2') \quad (29)$$

We denote by $P^0_{aa}(\kappa\lambda)$ and $P^0_{ab}(\kappa\lambda)$ the bond orders pertaining to $Q^0(\kappa\lambda|r_1, r_2; r_1', r_2')$. Thus

$$P^0_{aa} = \sum_{\kappa,\lambda}a_\kappa a_\lambda^*P^0_{aa}(\kappa\lambda) \text{ and } P^0_{ab} = \sum_{\kappa,\lambda}a_\kappa a_\lambda^*P^0_{ab}(\kappa\lambda) \quad (30)$$

The transition densities and bond orders for determinants representing spin orbital configurations,

$$\kappa = (\phi_1\theta_1, \phi_2\theta_2, \cdots, \phi_i\theta_i, \cdots) \text{ and}$$
$$\kappa' = (\phi_1'\theta_1', \phi_2'\theta_2', \cdots, \phi_i'\theta_i', \cdots)$$

follow at once from Slater's rules:

(i) $\kappa = \kappa' = (\phi_1\theta_1, \phi_2\theta_2, \cdots, \phi_i\theta_i, \cdots)$

$$Q^0(\kappa\kappa|r_1, r_2; r_1', r_2') = \frac{1}{2}\sum_{i,j}\{\varepsilon_1\phi_i(r_1)\phi_j(r_2)\phi_i^*(r_1')\phi_j^*(r_2') - \varepsilon_2\phi_j(r_1)\phi_i(r_2)\phi_i^*(r_1')\phi_j^*(r_2')\}$$

$$P^0_{aa}(\kappa\kappa) = \frac{1}{2}\sum_{i,j}(\varepsilon_1-\varepsilon_2)c_{ia}{}^2c_{ja}{}^2$$

$$P^0_{ab}(\kappa\kappa) = \frac{1}{2}\sum_{i,j}\{\varepsilon_1(c_{ia}{}^2c_{jb}{}^2+c_{ja}{}^2c_{ib}{}^2)-2\varepsilon_2c_{ia}c_{ib}c_{ja}c_{jb}\}$$

(ii) $\kappa = (\phi_1\theta_1, \phi_2\theta_2, \cdots, \phi_i\theta_i, \cdots, \phi_j\theta_j \cdots)$
$\kappa' = (\phi_1\theta_1, \phi_2\theta_2, \cdots, \phi_i'\theta_i, \cdots, \phi_j\theta_j, \cdots)$

$$Q^0(\kappa\kappa'|r_1, r_2; r_1', r_2') = \frac{1}{2}\sum_{j\neq i}\{\varepsilon_1\phi_i(r_1)\phi_j(r_2)\phi_i'^*(r_1')\phi_j^*(r_2') + \varepsilon_1\phi_j(r_1)\phi_i(r_2)\phi_j^*(r_1')\phi_i'^*(r_2') - \varepsilon_2\phi_j(r_1)\phi_i(r_2)\phi_i'^*(r_1')\phi_j^*(r_2') - \varepsilon_2\phi_i(r_1)\phi_j(r_2)\phi_j^*(r_1')\phi_i'^*(r_2')\}$$

$$P^0_{aa}(\kappa\kappa') = \sum_{j\neq i}(\varepsilon_1-\varepsilon_2)c_{ja}{}^2c_{ia}c_{i'a}$$

$$P^0_{ab}(\kappa\kappa') = \sum_{j\neq i}\{\varepsilon_1(c_{jb}{}^2c_{ia}c_{i'a}+c_{ja}{}^2c_{ib}c_{i'b}) - \varepsilon_2c_{ja}c_{jb}(c_{ia}c_{i'b}+c_{ib}c_{i'a})\}$$

(iii) $\kappa = (\phi_1\theta_1, \phi_2\theta_2, \cdots, \phi_i\theta_i, \cdots, \phi_j\theta_j, \cdots)$
$\kappa' = (\phi_1\theta_1, \phi_2\theta_2, \cdots, \phi_i'\theta_i, \cdots, \phi_j'\theta_j, \cdots)$

$$Q^0(\kappa\kappa'|r_1, r_2; r_1', r_2') = \frac{1}{2}\{\varepsilon_1\phi_i(r_1)\phi_j(r_2)\phi_i'^*(r_1')\phi_j'^*(r_2') + \varepsilon_1\phi_j(r_1)\phi_i(r_2)\phi_j'^*(r_1')\phi_i'^*(r_2') - \varepsilon_2\phi_i(r_1)\phi_j(r_2)\phi_j'^*(r_1')\phi_i'^*(r_2') - \varepsilon_2\phi_j(r_1)\phi_i(r_2)\phi_i'^*(r_1')\phi_j'^*(r_2')\}$$

$$P^0_{aa}(\kappa\kappa') = (\varepsilon_1-\varepsilon_2)c_{ia}c_{ja}c_{i'a}c_{j'a}$$

$$P^0_{ab}(\kappa\kappa') = \varepsilon_1(c_{ia}c_{jb}c_{i'a}c_{j'b}+c_{ib}c_{ja}c_{i'b}c_{j'a}) - \varepsilon_2(c_{ia}c_{jb}c_{i'b}c_{j'a}+c_{ib}c_{ja}c_{i'a}c_{j'b})$$

In all the above equations, ε_1 and ε_2 are defined as follows:

If ϕ_i and ϕ_j have the same spin,

$$\varepsilon_1 = \varepsilon_2 = -1/3;$$

If ϕ_i and ϕ_j have different spins,

$$\varepsilon_1 = 1/3 \text{ and } \varepsilon_2 = -2/3.$$

c_{ia}, *etc.*, are the overlap between orbital ϕ_i and atomic orbital a

$$c_{ia} = \langle\phi_i|a\rangle = \sum_b d_{ib}s_{ab} \tag{31}$$

d_{ib} being the usual LCAO coefficients.

For a special case in which $\kappa=\kappa'=(\phi_1\alpha,\ \phi_1\beta,\cdots\phi_i\alpha,\ \phi_i\beta\cdots)$, the bond orders $P^0_{aa}(\kappa\kappa)$ and $P^0_{ab}(\kappa\kappa)$ reduce to

$$P^0_{aa}(\kappa\kappa) = (\sum_i c_{ia}{}^2)^2 \tag{32}$$

$$P^0_{ab}(\kappa\kappa) = 2(\sum_i c_{ia}c_{ib})^2 \tag{33}.$$

Noting that

$$\gamma^0_{\mu\nu} = 2\sum_i d_{i\mu}d_{i\nu}, \tag{34}$$

Eqs. (32) and (33) can readily be verified to be identical with Eq. (24) for a single determinant case.

Incidentally, it will be appropriate to define an atom-atom bond order, P^0_{AB}, as a simple sum of the bond orders between the atomic orbitals on atoms A and B

$$P^0_{AB} = \sum_a^{\text{on A}} \sum_b^{\text{on B}} P^0_{ab} \tag{35}.$$

If atomic orbitals on a given atom are assumed to be orthogonal, as is usually the case, the atom-atom bond order remains invariant under a unitary transformation of AO basis within each atom. This invariance is easily derived from the fact that the one-electron Hilbert space for each atom is constant under the transformation.

III. Bond Order and Molecular Binding

As has already been stated, the bond order defined in the present paper has no bearing with energy derivatives but is a topological index of spin coupling. Thus, the bond order of dissociated hydrogen molecule is 1 but there exists no energy stabilization. None the less, it is expected that one may gain some insight into molecular binding, using the present bond order concept.

In molecular orbital theory the binding energy is ascribed to resonance integrals, β_{ab}. Slater[28] and McWeeny[29] pointed out that this integral is also responsible for molecular binding in valence bond theory. Generally, the expression of total electronic energy contains a term $\sum_{a,b}\gamma^0_{ab}\beta_{ab}$, and γ^0_{ab} is considered to be some measure of binding. Fortunately, the electronic structure of stable molecules can well be represented by a single-determinant wavefunction. In this case the bond order, P^0_{ab}, simply reduces to $\gamma^0_{ab}{}^2/2$. Therefore, P^0_{ab} might also be a measure of binding, which varies more sharply than γ^0_{ab}.

In this connection, use of an effective one-electron Hamiltonian

$$h(1) = T(1) + V_a(1) + V_b(1) \tag{36}$$

is suggestive. The expectation values of this hamiltonian between "Heitler-London-like" geminals are

$$\langle S_{ab}|h(1)|S_{ab}\rangle = (E_a+E_b+2s_{ab}\beta_{ab})/2 \tag{37}$$

and

$$\langle T_{ab}|h(1)|T_{ab}\rangle = (E_a+E_b-2s_{ab}\beta_{ab})/2 \tag{38}$$

which show that the energy stabilization, $s_{ab}\beta_{ab}$, results if electrons in a and b couple into a singlet pair, whereas there appears a repulsive interaction of $-s_{ab}\beta_{ab}$ in triplet coupling. It can be concluded that the bond order, P^0_{ab}, which assures a net stabilization roughly proportional to s^2_{ab}, is a certain measure of the latent capability with which an electron pair can enter into covalent binding when the overlap between the relevant atomic orbitals becomes sufficiently large.

On the OAO basis set, we must turn to Eq. (21). $P^0_{\substack{aa\\ba}}$, $P^0_{\substack{ab\\bb}}$ and $P^0_{\substack{ac\\bc}}$ are interpreted as an intensity of resonance between the corresponding structures of electron pairing. Because γ^0_{ab} is a sum of many such terms, examination of its significance in chemical binding is somewhat boring to make. However, in single-determinant wavefunctions each term in Eq. (21) takes a simple form:

$$P^0_{\substack{aa\\ba}} = \gamma^0_{aa}\gamma^0_{ab}/2\sqrt{2},\quad P^0_{\substack{ab\\bb}} = \gamma^0_{bb}\gamma^0_{ab}/2\sqrt{2},$$
$$P^0_{\substack{ac\\bc}} = \gamma^0_{ac}\gamma^0_{bc}/2 \tag{39}$$

Substituting these expressions into Eq. (21), we obtain

$$\gamma^0_{ab} = (\gamma^0_{aa}+\gamma^0_{bb})\gamma^0_{ab}/2 + \sum_{c\neq a,b}\gamma^0_{ac}\gamma^0_{bc}/2 \tag{40}.$$

When the sum of populations on a and b equals 2, as is generally expected in electron pair bonds, γ^0_{ab} can in effect be imparted to $P^0_{\substack{aa\\ba}}$ and $P^0_{\substack{ab\\bb}}$ only. This result verifies the picture that the resonance between covalent and ionic structures is responsible for chemical binding depicted on the OAO basis.

IV. Extension to a Doublet State

It is desired to extend the analysis of electron pairs in previous sections to nonsinglet states. As can be seen from Eq. (13), the trace of the Q^0 matrix for these states is no longer equal to the number of singlet pairs. Obviously, we must add a certain quantity to make up the difference.

In this section we consider doublet states with N electrons which would be interpreted as $(N-1)/2$ pairs plus one odd electron. Integration of the Q^0 matrix over the second electron yields

$$P_1(r_1;r_1') - D_s(r_1;r_1') = 2\int Q^0(r_1,r_2;r_1',r_2)\mathrm{d}r_2 \tag{41}$$

where $D_s(r_1;r_1')$ is a normalized spin density matrix[30,31] defined by

$$D_s(r_1;r_1') = \frac{1}{M_s}\int_{s_1=s_1'} \mathbf{S}_z(s_1)\rho^{(1)}(x_1;x_1')\mathrm{d}s_1 \tag{42}$$

The relationship (41) will be proved in the Appendix.

Equation (41) can be interpreted as an indication that the electron distribution may be decomposed to $(N-1)/2$ pairs and an odd electron. The former distribution is represented by the same Q^0 matrix as in singlet states while the latter comes from the spin density matrix.

For an electron distribution represented by Eq. (41) the electron population on each atomic orbital is expressed by bond orders and spin density as follows:

$$\gamma^0_{aa} = 2P^0_{aa} + \sum_{b\neq a}P^0_{ab} + \gamma^s_{aa} \tag{43}$$

where γ^s_{aa} is an expansion coefficient of the spin density matrix

$$D_S(r_1; r_1') = \frac{1}{2S}\sum_{a,b}\gamma^s_{ab}a(r_1)b^*(r_1'). \quad (44)$$

As an example, we consider a linear H_3 system and show the distributions of one electron pair and one odd electron obtained from the HMO solution. Two configurations were considered: (a) an H_2 molecule plus an H radical; and (b) the linear symmetrical H_3 radical. The various bond quantities are as shown in Fig. 1.

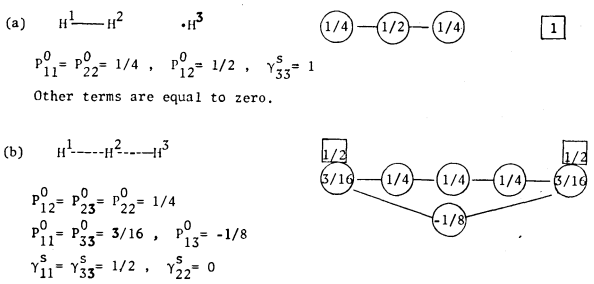

Fig. 1. Distribution of bond quantities in the linear H_n molecule. The quantities pertaining to electron pairs and odd electrons are shown in circles and squares, respectively.

V. States with Higher Spin Multiplicities

We may interpret the electronic structure of an N-electron system having a resultant spin $S \geq 1$ in the following two fashions. One is a system comprising $(N/2-S)$ electron pairs and $2S$ odd electrons while the other is $N/2$ pairs in which $(N/2-S)$ pairs are singlet type and the remaining S pairs are triplet type. Here we proceed along the latter line.

We now must seek for a density function which represents the distribution of triplet type pairs. The triplet type pairs of the present concern should be anisotropic ones which give the total spin angular momentum S, and are the origin of spin-spin dipolar interactions.[23,31,32] Further, it is preferred that this density function does not depend on the axis of spin quantization.

To meet these requirements, it seems appropriate to introduce the normalized spin-spin coupling function, $D_{ss}(r_1,r_2; r_1',r_2')$, defined by McWeeny.[31] This function is obtained by operating an irreducible tensor operator of rank 2, $3\boldsymbol{S}_z\cdot\boldsymbol{S}_z-\boldsymbol{S}\cdot\boldsymbol{S}$, to 2-matrix:

$$D_{ss}(r_1, r_2; r_1', r_2') = \frac{2}{S(2S-1)}\int_{s_1=s_1',s_2=s_2'}(3\boldsymbol{S}_z(s_1)\cdot\boldsymbol{S}_z(s_2) - \boldsymbol{S}(s_1)\cdot\boldsymbol{S}(s_2))\rho^{(2)}_{st}(x_1, x_2; x_1', x_2')ds_1ds_2 \quad (45)$$

where the subscript st on 2-matrix denotes that a standard state with $\langle \boldsymbol{S}_z\rangle = S$ is assumed. It has been shown that the function is invariant against different $\langle \boldsymbol{S}_z\rangle$values. The four spin functions in Eq. (8) are eigenfunctions of this operator.

$$3\boldsymbol{S}_z(s_1)\cdot\boldsymbol{S}_z(s_2)-\boldsymbol{S}(s_1)\cdot\boldsymbol{S}(s_2) \quad \begin{cases} \tau_1(s_1, s_2) = \frac{1}{2}\tau_1(s_1, s_2) \\ \tau_2(s_1, s_2) = \frac{1}{2}\tau_2(s_1, s_2) \\ \tau_3(s_1, s_2) = -\tau_3(s_1, s_2) \\ \sigma(s_1, s_2) = 0\ \sigma(s_1, s_2) \end{cases} \quad (46).$$

Obviously, neither of the electron pairs in singlet and random couplings contributes to D_{ss}.

We obtain $D_S(r_1; r_1')$ by integrating $D_{ss}(r_1,r_2; r_1',r_2')$ over the second electron.

$$D_S(r_1; r_1') = \int D_{ss}(r_1, r_2; r_1', r_2)dr_2 \quad (47)$$

On the other hand, the Q^0 matrix, upon integration, gives the following relation,

$$P_1(r_1; r_1') - \frac{4}{3}S(S+1)D_S(r_1; r_1') = 2\int Q^0(r_1, r_2; r_1', r_2)dr_2 \quad (48).$$

Equations (47) and (48) will be proved in the Appendix.

We are now at the position to define a matrix, Q^2, representing the distribution of triplet type pairs. It is most advantageous to define it by

$$Q^2(r_1, r_2; r_1', r_2') = \frac{2}{3}S(S+1)D_{ss}(r_1, r_2; r_1', r_2') \quad (49)$$

which leads to a simple relation

$$P_1(r_1; r_1') = 2\int\{Q^0(r_1, r_2; r_1', r_2) + Q^2(r_1, r_2; r_1', r_2)\}dr_2 \quad (50).$$

We define the corresponding bond order, P^2_{ab}, from Q^2 matrix as in Eq. (15).

$$P^2_{ab} = 2\int a^*(r_1)b^*(r_2)Q^2(r_1, r_2; r_1', r_2')a(r_1')b(r_2')dr_1dr_2dr_1'dr_2' \quad (51).$$

On the OAO basis, the electron population on each atomic orbital is expressed by P^0_{aa}, P^0_{ab} and P^2_{ab}:

$$\gamma^0_{aa} = 2P^0_{aa} + \sum_{b\neq a}(P^0_{ab}+P^2_{ab}) \quad (52).$$

Alternatively, in chemical interpretations, it is preferred that negative values are assigned to triplet coupled electron pairs. When we regard $N/2$ pairs as comprising $(N/2-S)$ singlet pairs and S triplet pairs, it is appropriate to use the following density function

$$Q^T = Q^0(r_1, r_2; r_1', r_2') + [(S-2)/(S+1)]Q^2(r_1, r_2; r_1', r_2') \quad (53)$$

and the bond order

$$P^T_{ab} = P^0_{ab} + [(S-2)/(S+1)]P^2_{ab} \quad (54).$$

On the OAO basis set, the sum of these bond orders is equal to $(N/2-2S)$, which is the difference in number between the singlet and triplet pairs.

In single-determinant wavefunctions with a definite spin angular momentum S, Q^0 and Q^2 matrices take the following forms:

$$Q^0(r_1, r_2; r_1', r_2') = \frac{1}{12}\sum_{a.b.c.d}(3\gamma^0_{ad}\gamma^0_{bc}-\gamma^s_{ad}\gamma^s_{bc}-2\gamma^s_{ac}\gamma^s_{bd}) \times a(r_1)b(r_2)c^*(r_1')d^*(r_2') \quad (55)$$

$$Q^2(r_1, r_2; r_1', r_2') = \frac{S+1}{3(2S-1)}\sum_{a.b.c.d}(\gamma^s_{ac}\gamma^s_{bd}-\gamma^s_{ad}\gamma^s_{bc}) \times a(r_1)b(r_2)c^*(r_1')d^*(r_2') \quad (56).$$

If we define $\boldsymbol{n}^s$ matrix by $\boldsymbol{n}^s = \boldsymbol{s}\gamma^s\boldsymbol{s}$ as in Eq. (25), the bond orders resulting from Eqs. (55) and (56) are

$$P^0_{aa} = (n^{0\,2}_{aa} - n^{s\,2}_{aa})/4 \quad (57)$$

$$P^0_{ab} = (3n^{0\,2}_{ab} - n^{s\,2}_{ab} - 2n^s_{aa}n^s_{bb})/6 \quad (58)$$

$$P^2_{ab} = [2(S+1)/3(2S-1)](n^s_{aa}n^s_{bb} - n^{s\,2}_{ab}) \quad (59).$$

These generalized bond orders can be applied to singlet

and doublet states as well.

We conclude the context by considering the H_4 system in a triplet state as an example. Three possible configurations are examined: (a) an H_2 molecule plus two H atoms; (b) an H_3 linear symmetrical doublet radical plus one H atom; and (c) an H_4 square planar configuration. The bond orders defined by Eq. (54) were calculated in the simple HMO approximation. The results are collected in Fig. 2.

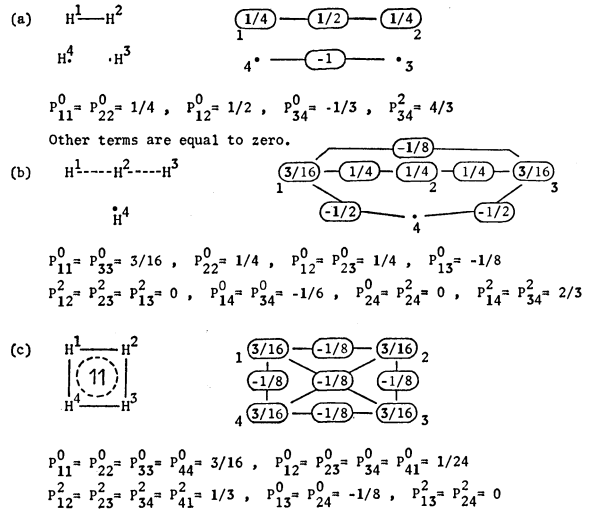

Fig. 2. Distribution of bond quantities in the triplet H_4 molecule. The bond orders defined by Eq. (54) are depicted.

VI. Concluding Remarks

We have shown in this introductory study that the electron pair concept as used in chemistry can be characterized adequately by the spin coupling matrices Q^0 and Q^2. These matrices in turn permit definitions of the generalized Penney-Dirac bond orders, from which the covalent and ionic characters of chemical binding can immediately be understood.

On the other hand, the contact nuclear spin-spin coupling constants are known to be a measure of the covalent bonding character.[33-35] Also, it has been shown implicitly that the bond order P^0_{ab} can be related to nuclear spin-spin coupling constants, provided a mean excitation energy approximation is adopted.[23,36-38] The situation endorses the usefulness of the bond order here defined.

The allowed and forbidden characters of chemical reactions are also a problem of current interest. Continuity of the bond order along reaction path has successfully been used for this purpose in connection with the space and spin symmetry conservations.[39,25] It was particularly with such uses for reactivity problems in mind that we decided to undertake the present analytical study. The concept of electron pair shift as was put forth by Robinson and Ingold[40] will be treated in a succeeding paper.

The authors would like to thank Dr. K. Yamaguchi for his helpful discussions.

TABLE 1. $\Phi^0_{ij}(r_1,r_2;\, r_1',r_2')$ AND $\Phi^2_{ij}(r_1,r_2,;\, r_1',r_2')$ IN TERMS OF "HEITLER-LONDON-LIKE" BASIS (STANDARD STATES)

	Q^0	$[3(2S-1)/4(S+1)]Q^2$
(a) $\phi_i \neq \phi_j$; $\phi_{i'} \neq \phi_{j'}$		
(i) Same island, $p_{ij}=-1$	$S_{ij}S'^*_{ij}$	0
(ii) Same island, $p_{ij}=+1$	$-\frac{1}{2}(S_{ij}S'^*_{ij}+T_{ij}T'^*_{ij})$	0
(iii) Different islands	$\frac{1}{4}(S_{ij}S'^*_{ij}-T_{ij}T'^*_{ij})$	0
(iv) i in island, j in O-chain	$\frac{1}{4}(S_{ij}S'^*_{ij}-T_{ij}T'^*_{ij})$	0
(v) Same O-chain, $p_{ij}=-1$	$S_{ij}S'^*_{ij}$	0
(vi) Same O-chain, $p_{ij}=+1$	$-\frac{1}{2}(S_{ij}S'^*_{ij}+T_{ij}T'^*_{ij})$	0
(vii) Different O-chains, $p_{ij}=+1$	$-\frac{1}{3}T_{ij}T'^*_{ij}$	$\frac{1}{2}T_{ij}T'^*_{ij}$
(viii) Different O-chains, $p_{ij}=-1$	$\frac{1}{2}S_{ij}S'^*_{ij}-\frac{1}{6}T_{ij}T'^*_{ij}$	$-\frac{1}{2}T_{ij}T'^*_{ij}$
(ix) Different E-chains, $p_{ij}=+1$	$-\frac{1}{2}S_{ij}S'^*_{ij}-\frac{1}{6}T_{ij}T'^*_{ij}$	$-\frac{1}{2}T_{ij}T'^*_{ij}$
(x) Different E-chains, $p_{ij}=-1$	$\frac{1}{2}S_{ij}S'^*_{ij}+\frac{1}{6}T_{ij}T'^*_{ij}$	$\frac{1}{2}T_{ij}T'^*_{ij}$
(b) $\phi_i \neq \phi_j$; $\phi_{i'}=\phi_{j'}$ or $\phi_i=\phi_j$; $\phi_{i'} \neq \phi_{j'}$		
(xi) Same island	$\frac{1}{\sqrt{2}}S_{ij}S'^*_{ij}$	0
(xii) Same O-chain	$\frac{1}{\sqrt{2}}S_{ij}S'^*_{ij}$	0
(c) $\phi_i=\phi_j$; $\phi_{i'}=\phi_{j'}$		
(xiii) Same island	$S_{ij}S'^*_{ij}$	0

Appendix

Our purpose is to prove Eqs. (47) and (48).

$$D_S(r_1; r_1') = \int D_{SS}(r_1, r_2; r_1', r_2)\mathrm{d}r_2 \tag{47}$$

$$P_1(r_1; r_1') - \frac{4}{3}S(S+1)D_S(r_1; r_1') = 2\int Q^0(r_1, r_2; r_1', r_2)\mathrm{d}r_2 \tag{48}$$

Both Eqs. (16) and (41) are special cases of Eq. (48).

To derive these relations it is convenient to use the results obtained by Cooper and McWeeny,[41,42] who expressed a wavefunction of configuration interaction type in the form

$$\Psi = \sum_\kappa a_\kappa \Psi_\kappa \tag{60}$$

where the Ψ_κ are general spin-coupled functions of valence bond type arising from arbitrary orbital configurations. They derived the general expressions of various transition density functions for any pair of standard states κ and λ. From Eq. (4.2) in reference (41) we can easily write Q^0 and Q^2 matrices in the following form:

$$Q(\kappa\lambda|r_1, r_2; r_1', r_2') = M_{\kappa\lambda}\Delta_{\kappa\lambda}\sum_{i,j}^{(\text{pairs})}\xi_{ij}\Phi_{ij}(r_1, r_2; r_1', r_2') \tag{61}$$

where Φ_{ij} is expressed in terms of the "Heitler-London-like" geminals as used in Eq. (14). The Φ_{ij}'s relevant to Q^0 and Q^2 matrices are listed in Table 1. For other symbols, original papers by Cooper and McWeeny are to be referred.

On the other hand, the P_1 and D_S matrices are written in the forms

$$P_1(\kappa\lambda|r_1; r_1') = M_{\kappa\lambda}\Delta_{\kappa\lambda}\sum_{i=1}^{N}\xi_i\phi_i(r_1)\phi_i^*(r_1') \tag{62}$$

$$D_S(\kappa\lambda|r_1; r_1') = (1/S)M_{\kappa\lambda}\Delta_{\kappa\lambda}\sum_{i=1}^{N}\xi_i x_i\phi_{i1}(r_1)\phi_i^*(r_1') \tag{63}$$

where
$$x_i = \frac{1}{2}p_i \quad \text{if } i \text{ is in an } O\text{-chain}$$
$$= 0 \quad \text{otherwise.}$$

It should be noted that no contribution occurs in this category if there are two or more orbital differences, or if any E-chain occurs.

The relations (47) and (48) are replaced by similar relations among the transition densities for each pair of standard states κ and λ. The two-body terms expressed by "Heitler-London-like" geminals give the following one-body terms by integrating over the second electron.

$$\int S_{ij}(r_1, r_2)S_{ij}'^*(r_1', r_2)\mathrm{d}r_2 =$$
$$\varepsilon\{\phi_i(r_1)\phi_i^*(r_1')\delta_{\phi_j\phi_{j'}} + \phi_j(r_1)\phi_{j'}^*(r_1')\delta_{\phi_i\phi_{i'}}\} \tag{64}$$

where

$\varepsilon = 1/2$ for $\phi_i \neq \phi_j$; $\phi_{i'} \neq \phi_{j'}$ or $\phi_i = \phi_j$; $\phi_{i'} = \phi_{j'}$

$\varepsilon = 1/\sqrt{2}$ for $\phi_i \neq \phi_j$; $\phi_{i'} = \phi_{j'}$ or $\phi_i = \phi_j$; $\phi_{i'} \neq \phi_{j'}$

$$\int T_{ij}(r_1, r_2)T_{ij}'^*(r_1', r_2)\mathrm{d}r_2 =$$
$$\frac{1}{2}\{\phi_i(r_1)\phi_i^*(r_1')\delta_{\phi_j\phi_{j'}} + \phi_j(r_1)\phi_{j'}^*(r_1')\delta_{\phi_i\phi_{i'}}\} \tag{65}.$$

It is verified from the above equations that Q^0 and Q^2 densities between standard states with more than two orbital differences do not contribute to the P_1 and D_S densities.

The proof is given for a case with no orbital difference. The contributions to $\phi_i(r_1)\phi_i^*(r_1')$ from Q^0 densities are obtained from Table 1 as follows.

[i in island]

(i), (xiii) $\rightarrow \frac{1}{2}\phi_i\phi_i^*$
(ii) $\rightarrow -\frac{1}{2}\phi_i\phi_i^*$
(iii), (iv) $\rightarrow 0$
$\Big\}$ — $\frac{1}{2}\phi_i\phi_i^*$

The number of pairs with $p_{ij} = -1$ is always more than that with $p_{ij} = +1$ by one, so that the sum of the above terms is $\phi_i\phi_i^*/2$.

[i in O-chain]

		$p_i=1$	$p_i=-1$
(iv)	$\rightarrow 0$		
(v)	$\rightarrow \frac{1}{2}\phi_i\phi_i^*$	0	$\phi_i\phi_i^*$
(vi)	$\rightarrow -\frac{1}{2}\phi_i\phi_i^*$		
(vii)	$\rightarrow -\frac{1}{6}\phi_i\phi_i^*$	$-\frac{1}{6}\phi_i\phi_i^*$	$\frac{1}{6}\phi_i\phi_i^*$
(viii)	$\rightarrow \frac{1}{6}\phi_i\phi_i^*$		

The results of summation are obtained by counting the number of pairs with $p_{ij} = +1$ and $p_{ij} = -1$. Further, the number of O-chains is equal to $2S$, where $S(S+1)$ is the eigenvalue of the S^2 operator. We get the expression of one-body terms in the following forms:

$$p_i = +1 \qquad \frac{1-2S}{6}\phi_i\phi_i^*$$
$$p_i = -1 \qquad \frac{2S+5}{6}\phi_i\phi_i^*$$

[i in E-chain]

(ix) $\rightarrow -\frac{1}{3}\phi_i\phi_i^*$
(x) $\rightarrow \frac{1}{3}\phi_i\phi_i^*$
$\Big\}$ — 0

The one-body terms from (ix) and (x) always cancel each other, so we can disregard the transition densities if any E-chain occurs.

On the other hand, the left-hand side of Eq. (48) is expressed by

$$M_{\kappa\lambda}\Delta_{\kappa\lambda}\sum_{i=1}^{N}\{1 - \frac{4}{3}(S+1)\times\frac{1}{2}p_i\}\phi_i(r_1)\phi_i^*(r_1') \tag{66}$$

where the second term in blackets is counted only if i is in O-chains. The expression (66) completely agrees with twice the sum of the various terms derived above.

We may obtain the contributions to $\phi_i(r_1)\phi_i^*(r_1')$ from Q^2 densities similarly.

[i in O-chain]

		$p_i=1$	$p_i=-1$
(vii)	$\rightarrow \frac{1}{4}\phi_i\phi_i^*$	$\frac{1}{4}\phi_i\phi_i^*$	$-\frac{1}{4}\phi_i\phi_i^*$
(viii)	$\rightarrow -\frac{1}{4}\phi_i\phi_i^*$		

[i in E-chain]

(ix) $\rightarrow -\frac{1}{4}\phi_i\phi_i^*$
(x) $\rightarrow \frac{1}{4}\phi_i\phi_i^*$
$\Big\}$ — 0

Then $[(2S-1)p_i/4]\phi_i(r_1)\phi_i^*(r_1')$ is the result of summation among all O-chains. Then, from Eq. (49) we obtain

$$\int D_{SS}(\kappa\lambda|r_1, r_2; r_1', r_2)dr_2 = M_{\kappa\lambda}\Delta_{\kappa\lambda}\sum_i^{\text{in } O\text{-chain}}(1/2S)p_i\phi_i(r_1)\phi_i^*(r_1')$$
$$= D_S(\kappa\lambda|r_1; r_1')$$

The proof for the case with one orbital difference can be obtained in a similar way and hence omitted.

References

1) G. N. Lewis, "Valence and the Structure of Atoms and Molecules," (1923), New York, Chemical Catalog Co.
2) W. Heitler and F. London, *Z. Phys.*, **44**, 455 (1927).
3) Y. Sugiura, *ibid.*, **45**, 484 (1927).
4) L. Pauling, "The Nature of the Chemical Bond," Cornell Univ. Press, New York (1940).
5) J. Lennard-Jones, *Proc. Roy. Soc., Ser. A*, **198**, 1, 14 (1949).
6) C. Edmiston and K. Ruedenberg, *Rev. Mod. Phys.*, **35**, 457 (1963).
7) For examples; J. M. Parks and R. G. Parr, *J. Chem. Phys.*, **28**, 335 (1958): W. A. Goddard, III, *Phys. Rev.*, **157**, 81 (1967): W. A. Goddard, III, T. H. Dunning, Jr., W. J. Hunt, and P. J. Hay, *Accounts Chem. Res.*, **6**, 368 (1973): K. J. Miller and K. Ruedenberg, *J. Chem. Phys.*, **48**, 3444 (1968).
8) K. Husimi, *Proc. Phys. Math. Soc. Japan*, **22**, 264 (1940).
9) P.-O. Löwdin, *Phys. Rev.*, **97**, 1474 (1955).
10) R. McWeeny, *Rev. Mod. Phys.*, **32**, 335 (1960).
11) C. A. Coulson, *Proc. Roy. Soc., Ser. A*, **169**, 413 (1939); A. Streitwieser, Jr., "Molecular Orbital Theory for Organic Chemists," John Wiley & Sons, Inc., New York (1961).
12) R. McWeeny, *J. Chem. Phys.*, **19**, 1614 (1951); R. S. Mulliken, *ibid.*, **23**, 1833 (1955).
13) E. R. Davidson, *ibid.*, **46**, 3320 (1967).
14) K. R. Roby, *Mol. Phys.*, **27**, 81 (1974); *Theoret. Chim. Acta*, **33**, 105 (1974) and references therein.
15) K. Ruedenberg, *Rev. Mod. Phys.*, **34**, 326 (1962).
16) B. M. Deb, *ibid.*, **45**, 22 (1973).
17) C. A. Coulson and R. G. A. R. MacLagan, *Adv. Chem. Phys.*, **21**, 303 (1971); R. G. A. R. MacLagan, *Mol. Phys.*, **22**, 821 (1971).
18) W. G. Penney, *Proc. Roy. Soc., Ser. A*, **158**, 306 (1937).
19) P. A. M. Dirac, *ibid., Ser. A*, **123**, 714 (1929).
20) J. Van Vleck and A. Sherman, *Rev. Mod. Phys.*, **7**, 167 (1935).
21) D. Clarkson, C. A. Coulson, and T. H. Goodwin, *Tetrahedron*, **19**, 2153 (1963).
22) The Q^0 matrix is the same as the D_{st} matrix defined by McWeeny and Mizuno[23] and the R_2^0 matrix defined by Kutzelnigg,[24] if proper multiplicative constants are included. The superscript 0 is attached because $\boldsymbol{S}(1)\cdot\boldsymbol{S}(2)$ is an irreducible tensor operator of rank 0.
23) R. McWeeny and Y. Mizuno, *Proc. Roy. Soc., Ser. A*, **259**, 554 (1961).
24) W. Kutzelnigg, *Z. Naturforsch.*, **18a**, 1058 (1963); **20a**, 168 (1965).
25) K. B. Wiberg, *Tetrahedron*, **24**, 1083 (1968).
26) C. Trindle, *J. Amer. Chem. Soc.*, **91**, 219 (1969).
27) C. Trindle, *ibid.*, **92**, 3251 (1970).
28) J. C. Slater, *J. Chem. Phys.*, **19**, 220 (1951).
29) R. McWeeny, *Proc. Roy. Soc., Ser. A*, **223**, 63, 306 (1953).
30) H. M. McConnell, *J. Chem. Phys.*, **28**, 1188 (1958).
31) R. McWeeny, *ibid.*, **42**, 1717 (1965).
32) A. D. McLachlan, *Mol. Phys.*, **5**, 51 (1962).
33) J. B. Stothers, "Carbon-13 NMR Spectroscopy," Academic Press, New York (1971).
34) M. H. Chisholm, H. C. Clark, L. E. Manzer, and J. B. Stothers, *J. Amer. Chem. Soc.*, **94**, 5087 (1972).
35) T. Ibusuki and Y. Saito, *Chem. Lett.*, **1973**, 1255.
36) H. M. McConnell, *J. Chem. Phys.*, **24**, 460 (1956).
37) L. Salem, "The Molecular Orbital Theory of Conjugated Systems," W. A. Benjamin, Inc., New York (1966).
38) M. Barfield and M. Karplus, *J. Amer. Chem. Soc.*, **91**, 1 (1969), and references therein.
39) K. Yamaguchi, *Chem. Phys. Lett.*, **28**, 93 (1974).
40) C. K. Ingold, "Structure and Mechanism in Organic Chemistry," Bell, London (1953).
41) I. L. Cooper and R. McWeeny, *J. Chem. Phys.*, **45**, 226 (1966).
42) I. L. Cooper, *ibid.*, **50**, 2166 (1969).

Stereoisomers of the Bis(L-hydrogenaspartato)-trimethylenediaminecobalt(III) Complex

Yoshihiro KOJIMA

Department of Chemistry, Faculty of Science, Kanazawa University, Kanazawa 920

(Received October 14, 1974)

The bis(L-hydrogenaspartato)trimethylenediaminecobalt(III) complex has been prepared by the reaction of the *trans*-$[CoCl_2(tn)_2]^+$ complex with L-aspartic acid, and its eight stereoisomers have been separated by an ion-exchange chromatographic method. The six isomers are *trans*(*O*)-*Λ* and -*Δ*, *cis*(*O*)*cis*(*N*)-*Λ* and -*Δ* and *trans*(*N*)-*Λ* and -*Δ* isomers, in which either aspartate ion forms the five-membered chelate ring through an N atom of the amino group and an O atom of the α-carboxylate group. The remaining isomers are *Λ*- and *Δ*-*trans*(*O*) ones containing a five-membered chelate ring and a six-membered ring of L-aspartate ions. On the other hand, stereoselective formations have been found in the *Λ*, *Δ*, and *Λ* isomers for the *trans*(*O*), *cis*(*O*)*cis*(*N*), and *trans*(*N*) isomers respectively. It has become apparent that these stereoselectivities agree with those found for the corresponding *l*-pn and en complexes, while the orders of the formation amounts for the three geometrical isomers disagree.

In order to study stereochemistry and stereoselectivity, we previously examined the mixed L-aspartato complexes with *l*-propylenediamine[1] and ethylenediamine;[2] all of the stereoisomers isolated were characterized by their electronic absorption, circular dichroism (CD), and proton magnetic resonance (PMR) spectra. It was also found that the order of the formation amounts of the isomers agrees well between the *l*-propylenediamine and the ethylenediamine complexes.

In the present work, the stereoisomers of a mixed bis(L-hydrogenaspartato)trimethylenediamine complex ion were chosen in order to examine the influence of the six-membered chelate ring of the γ-diamine on the stereochemistry and stereoselectivity. Through this work, all the diastereoisomers corresponding to the six isomers which had been obtained in the previous work[2] were isolated. In addition, a novel pair of diastereoisomers containing an usual five-membered ring of a chelating L-aspartate ion and a six-membered ring formed by NH_2 and β-COO^- of another aspartate ion have been isolated.

Experimental

Preparation. 1) *Carbonatobis(trimethylenediamine)cobalt(III) Chloride*, $[Co(CO_3)(tn)_2]Cl \cdot 1.5H_2O$: Boyle and Harris[3] synthesized this complex by allowing silver carbonate to react on an aqueous solution of the *trans*-dichlorotrimethylenediamine complex. We prepared this complex easily by allowing trimethylenediamine(tn) to react on a solution of potassium tricarbonatocobaltate(III).[4] Trimethylenediamine (8.8 g, 0.12 mol) was added to a cold solution of tricarbonatocobaltate(III) ($CoCl_2 \cdot 6H_2O$, 10 g (0.042 mol) scale), and the mixture was stirred continuously at about 50 °C for 1.5 hr; the solution turned red-violet. After that, the resulting solution was concentrated on a water-bath until its surface was covered with crystals. The concentrated solution was then kept in a refrigerator overnight. The yield of the crude crystals was 13 g. This was subsequently dissolved in the least possible amount of water. After ethanol had been added to the solution until fine crystals began to deposit, the solution was kept in a refrigerator. The desired complex thus obtained was washed successively with ethanol and ether, and then dried in air.

2) trans-*dichlorobis(trimethylenediamine)cobalt(III) Chloride*, trans-$[CoCl_2(tn)_2]Cl$: Bailar and Work[5] synthesized this complex by allowing trimethylenediamine to react on anhydrous cobalt(II) chloride in ethanol with bubbling air. We prepared the complex easily by allowing concd HCl to react on the $[Co(CO_3)(tn)_2]^+$ complex. The complex obtained in 1) (5 g, 0.016 mol) was dissolved in a small amount of water, and then concd HCl (100 ml) was stirred in, little by little. Then the mixture was evaporated to a small volume (~30 ml) on a water-bath at about 60 °C and allowed to stand for a day to give bright green crystals. They were collected, washed successively with cold concd HCl and ethanol, and finally dried in air. The yield was 3.5 g. The crude crystals were dissolved in the minimum amount of hot concd HCl and then an ethanol–ether mixture (1: 1) was added to the solution. By keeping the whole in a refrigerator, pure crystals of the desired complex were deposited.

3) *Bis(L-hydrogenaspartato)trimethylenediaminecobalt(III) Perchlorate*, $[Co(L\text{-}Hasp)_2(tn)]ClO_4$: The preparative reaction for this complex and the procedure for the chromatographic separation of the stereoisomers were essentially the same as those in the previous work:[1] The complex obtained in 2) (3.1 g, 0.01 mol) and L-aspartic acid (2.7 g, 0.02 mol) were allowed to react at 50 °C for 1 hr in the presence of active charcoal (1 g) and under alkaline conditions (pH~10). For the chromatographic separation, a cation-exchange column containing 100—200 mesh Dowex 50W-X8 resin in the H-form (5.5×35 cm) was used. By eluting a red-violet band at the top of the column with a 0.05 M $NaClO_4$ aqueous solution, five bands colored red or red-violet were completely separated. After the first band had been collected in a fraction, the remaining bands were again eluted with a 0.1 M $NaClO_4$ solution. The fractions collected from the bands were numbered according to the order of elution (No. 1—5). The red-brown band remaining at the top of the column was of the bis(trimethylenediamine) complex. The chromatographic separation was repeated in order to store the same fractions.

The first eluted band actually consisted of two overlapping bands differing in their sign of the main CD peak; the first band showed (+), and the second band, (−). As to the remaining bands, no such phenomenon was observed.

The isolation of the isomeric compounds from the fractions was carried out as follows. Fraction No. 1 was concentrated at 35 °C until red-violet crystals began to deposit, and then it was allowed to stand in a refrigerator for a day. The less soluble isomer thus obtained was recrystallized from water until the $\Delta\varepsilon$ of the main CD peak with the (+) sign reached a constant value. For the sake of convenience, this isomer was labeled E-1. The filtrate obtained after isolating the E-1 isomer was stored in order to isolate the other isomers.

The No. 2 fraction was evaporated to a small volume at 35

°C along with the simultaneous removal of the perchlorate used for the elution, and then a large amount of an ethanol–ether mixture (1:3) was added to the solution in order to precipitate the red material. After the solution had stood in a refrigerator for a day, the precipitated material was collected by means of a centrifuge and then dissolved in a small amount of water. After ethanol had been added to the solution, the whole was kept in a refrigerator for several days. The red isomer (E-2) thus obtained was recrystallized from water by adding ethanol.

The No. 3 fraction was first evaporated to near dryness at 35 °C, and simultaneously the perchlorate was removed. The residue was dissolved in the minimum amount of water, and to the solution a large amount of an ethanol–ether mixture (1:5) was added. After the solution had been allowed to stand for some time, the desired isomer was separated as an oil. After the solvent had been eliminated, a large amount of ethanol was added to the oil to precipitate the isomer. The precipitates were then collected by means of the centrifuge and washed with ethanol. They were again dissolved in the minimum amount of water, and then ethanol was added until the solution began to cloud over. The turbid solution was clarified by warming and then the solution was kept in a refrigerator for several days. The red isomer (E-3) thus obtained was recrystallized from water by adding ethanol.

The No. 4 fraction was concentrated to a small volume at 35 °C and then kept in a refrigerator for a day to give red crystals. This isomer (E-4) was recrystallized from water.

The No. 5 fraction was treated in the same way as the No. 3. The desired red isomer (E-5) was recrystallized from water by adding ethanol.

The filtrate preserved after the E-1 had been isolated was rechromatographed using a small column (Dowex 50W-X8, 100—200 mesh, 2×40 cm, H-form) and 0.05 M $NaClO_4$. Three bands were separated and collected in fractions. Judging from the sign of the main CD peak, it was recognized that the first band was formed by overlapping two bands: the band showing (+) was first eluted, and then the band showing (−) was eluted, overlapping the (+) band. The second band uniformly showed the (+) sign, and the third band, the (−) sign. The first fraction was treated in the same fashion as No. 3. The crude material thus obtained was dissolved in the minimum amount of water, and ethanol (a 3-fold volume) was then added to the solution. By keeping the solution in a refrigerator, red-violet crystals exhibiting the (−) sign of the main CD peak were deposited. The recrystallization was repeated until the $\Delta\varepsilon$ of the CD peak became constant. This isomer was labeled E-1′. The other isomer, with the (+) sign, was isolated from the filtrate of E-1′. Judging from the spectral data and the chromatographic behavior, this isomer was exactly the same as E-1. The second fraction, containing a very small amount of isomeric species, was concentrated to a small volume at 35 °C and then kept in a refrigerator. The red-violet isomer thus obtained was labeled S-1. Its CD spectrum exhibited the (+) sign at the main peak. The third fraction was treated in the same fashion as No. 3. The crude material thus obtained was dissolved in the minimum amount of water. After alcohol had been added, the solution was kept in a refrigerator for several days. The red-violet isomer thus obtained was recrystallized from water by adding ethanol and was labeled S-2.

Formation Ratios of the Isomers. The relative concentrations of the isomers in the fractions were spectrophotometrically estimated by the method described in previous papers,[1,2] and the formation ratios among the isomers were calculated from the results.

Measurements. The electronic absorption spectra were measured with a Hitachi Recording spectrophotometer, Model 323. The circular dichroism spectra were recorded on JASCO Model ORD/UV-5 spectrophotometer with a CD attachment. The proton magnetic resonance (PMR) spectra were recorded on JEOL Model JNM-PS-100 spectrometer (100 MHz) at 23 °C. The values of the chemical shifts were measured in relation to sodium 2,2-dimethyl-2-silapentane-5-sulfonate (DSS) as the internal reference. All the spectra were run in deuterium oxide. The E-1, E-1′, and E-4 isomers for the PMR samples were converted into chloride using an anion-exchange resin (Dowex 1-X8, 100—200 mesh) because of the poor solubility of the perchlorates.

Results and Discussion

From the results of elemental analysis (Table 1), it is obvious that all the compounds isolated are stereoisomers of the bis(L-hydrogenaspartato)trimethylenediaminecobalt(III) complex. However, elemental analysis was not performed for S-1 and S-2 because of their poor yields.

TABLE 1. ELEMENTAL ANALYSES OF THE COMPLEXES PREPARED

Label	Complex	C%	H%	N%
E-1	(+)-[Co(L-Hasp)$_2$-(tn)]ClO_4	26.70 (26.62	4.72 4.47	11.32 11.29)
E-1′	(−)-[Co(L-Hasp)$_2$-(tn)]ClO_4	26.52 (26.62	4.88 4.47	11.31 11.29)
E-2	(+)-[Co(L-Hasp)$_2$-(tn)]ClO_4	27.01 (26.62	4.92 4.47	11.28 11.29)
E-3	(−)-[Co(L-Hasp)$_2$-(tn)]ClO_4	26.47 (26.62	4.68 4.47	11.30 11.29)
E-4	(+)-[Co(L-Hasp)$_2$-(tn)]$ClO_4\cdot 0.5H_2O$	26.06 (26.13	4.69 4.58	10.99 11.03)
E-5	(−)-[Co(L-Hasp)$_2$-(tn)]$ClO_4\cdot 2.5H_2O$	24.29 (24.38	5.02 5.02	10.02 10.34)

( ): Calcd

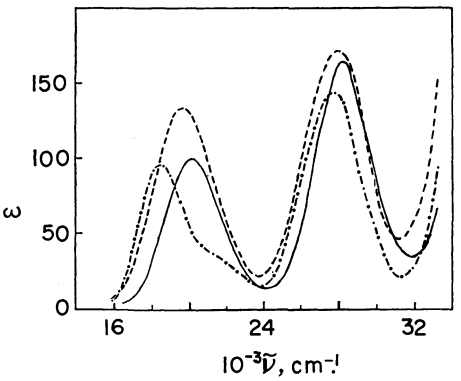

Fig. 1. The electronic absorption spectra of *trans*(*O*)-*cis*(*N*)-*Λ*-[Co(L-Hasp)$_2$(tn)]$^+$ (-·-·-), *cis*(*O*)*cis*(*N*)-*Λ*-[Co(L-Hasp)$_2$(tn)]$^+$ (——), and *cis*(*O*)*trans*(*N*)-*Λ*-[Co(L-Hasp)$_2$(tn)]$^+$ (——).

Characterization of Isomers. Some representative absorption spectra are shown in Fig. 1, while the numerical data are summarized in Table 2. The spectra of E-1, E-1′, S-1, and S-2 are essentially the same and showed a characteristic splitting in their first absorption bands. This fact indicates that these four isomers have *trans*(*O*)*cis*(*N*) geometry, because it is well known that the first band of a *trans*(*O*)-Co^{III}-

TABLE 2. ELECTRONIC ABSORPTION SPECTRA AND CD SPECTRA OF THE COMPLEXES

Label	Complex ion	Band I		Band II		CD	
		$10^{-3}\tilde{\nu}_{max}$ cm^{-1}	ε_I [a]	$10^{-3}\tilde{\nu}_{max}$ cm^{-1}	ε_{II} [a]	$10^{-3}\tilde{\nu}_{max}$ cm^{-1}	$\Delta\varepsilon$ [a]
E-1	*trans*(*O*)*cis*(*N*)-*Λ*-(+)-[Co(L-Hasp)$_2$(tn)]$^+$	18.6	95	27.8	144	18.9	+3.38
		ca. 21.7 sh				22.7	−0.44
E-1′	*trans*(*O*)*cis*(*N*)-*Λ*-(−)-[Co(L-Hasp)$_2$(tn)]$^+$	18.5	94	27.5	146	18.7	−2.15
		ca. 21.7 sh					
E-4	*cis*(*O*)*cis*(*N*)-*Λ*-(+)-[Co(L-Hasp)$_2$(tn)]$^+$	19.6	133	27.9	172	19.5	+1.52
E-3	*cis*(*O*)*cis*(*N*)-*Λ*-(−)-[Co(L-Hasp)$_2$(tn)]$^+$	19.8	114	28.0	148	19.8	−1.64
E-2	*cis*(*O*)*trans*(*N*)-*Λ*-(+)-[Co(L-Hasp)$_2$(tn)]$^+$	20.1	99	28.2	165	19.6	+2.37
						22.2	−0.48
E-5	*cis*(*O*)*trans*(*N*)-*Λ*-(−)-[Co(L-Hasp)$_2$(tn)$^+$	20.0	112	28.2	181	20.5	−2.24
S-1	*trans*(*O*)*cis*(*N*)-*Λ*-(+)-[Co(L-Hasp)$_2$(tn)]$^+$ [b]	18.6	(95)	27.6	(148)	19.0	(+3.17)
		ca. 21.7 sh				22.7	(−0.41)
S-2	*trans*(*O*)*cis*(*N*)-*Λ*-(−)-[Co(L-Hasp)$_2$(tn)]$^+$ [b]	18.7	(94)	27.7	(146)	18.8	(−2.02)
		ca. 21.7 sh					

a) mol^{-1} cm^{-1}. b) The ε and $\Delta\varepsilon$ values of S-1 and S-2 were estimated using the ε values of E-1 and E-1′, respectively, because the lack of the elemental analyses.

$(O)_2(N)_4$ type of complex shows a remarkable splitting.[1,2,6] On the other hand, the spectra of E-2, E-3, E-4, and E-5 reveal symmetrical patterns in their first bands. In addition, the values of $\varepsilon_{II}/\varepsilon_I$ for E-2, E-5, E-3, and E-4 have been calculated as 1.67, 1.62, 1.30, and 1.29 respectively. It has been found experimentally that the value of $\varepsilon_{II}/\varepsilon_I$ for the *cis*(*O*)*trans*(*N*) isomer is larger than that for the *cis*(*O*)*cis*(*N*) isomer.[2,6] These facts suggest that E-2 and E-5 have the *cis*(*O*)*trans*(*N*) geometry, while E-3 and E-4 have the *cis*(*O*)*cis*(*N*) structure. These absorption spectral assignments agree with those made by means of the PMR spectra, which will be discussed later.

The CD spectra are shown in Figs. 2—4, while the numerical data are summarized in Table 2. The spectrum of E-1 (*trans*(*O*)) shows a dominant (+) peak on the lower-energy-side in the first absorption band

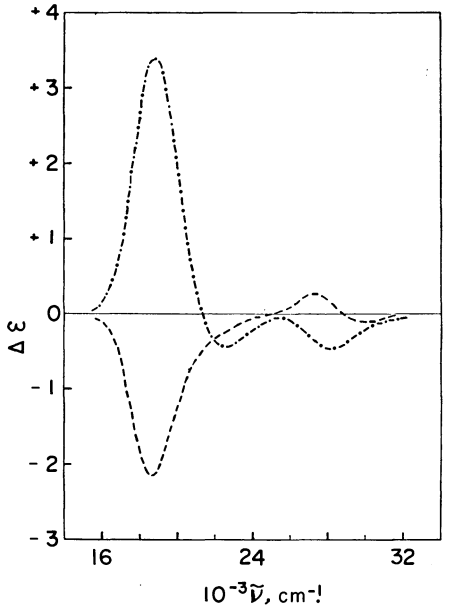

Fig. 2. The CD spectra for *trans*(*O*)*cis*(*N*)-*Λ*-(+)-[Co(L-Hasp)$_2$(tn)]ClO$_4$ (E-1) (·····) and *trans*(*O*)*cis*(*N*)-*Λ*-(−)-[Co(L-Hasp)$_2$(tn)]ClO$_4$ (E-1′) (——).

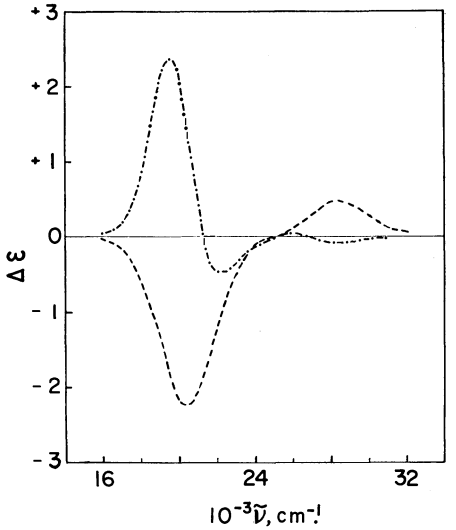

Fig. 3. The CD spectra for *cis*(*O*)*trans*(*N*)-*Λ*-(+)-[Co(L-Hasp)$_2$(tn)]ClO$_4$ (E-2) (·····) and *cis*(*O*)*trans*(*N*)-*Λ*-(−)-[Co(L-Hasp)$_2$(tn)]ClO$_4$ (E-5) (——).

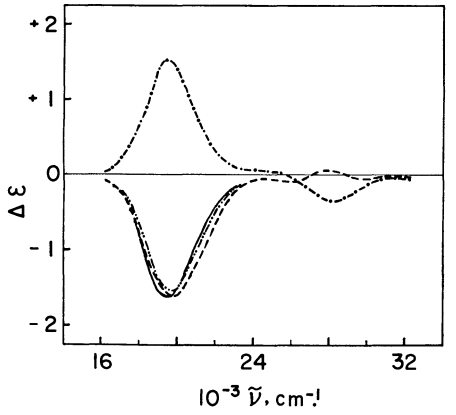

Fig. 4. The CD spectra for *cis*(*O*)*cis*(*N*)-*Λ*-(+)-[Co(L-Hasp)$_2$(tn)]ClO$_4$ (E-4) (·····) and *cis*(*O*)*cis*(*N*)-*Λ*-(−)-[Co(L-Hasp)$_2$(tn)]ClO$_4$ (E-3) (——), and the configurational effect curves of *cis*(*O*)*cis*(*N*)-*Λ*-(−)-[Co(L-Hasp)$_2$(tn)]$^+$ (·····) and *cis*(*O*)*cis*(*N*)-*Λ*-(−)-[Co(L-ala)$_2$(tn)]$^+$ (——).

region, while only one (−) peak is observed in the spectrum of E-1′ (*trans*(*O*)). E-2 and E-5 have a dominant (+) peak and only one (−) peak respectively in their CD spectra. E-3 shows a spectrum with a (−) peak, and E-4 shows a spectrum with a form nearly symmetrical to that of E-3.

The CD spectrum of the $(-)_{589}$-$[Co(tn)_3]^{3+}$ complex shows a minor (+) peak (E component) at a longer wave length and a major (−) peak (A_2 component) at a shorter wave length in the first band region.[7] The absolute configuration of this complex is determined to be *Λ*,[8,9] which is the same as that of the $(+)_{589}$-$[Co(en)_3]^{3+}$ complex.[10] As to the bis(diamine)-type complexes, the absolute configuration of the $(-)_{589}$-$[Co(acac)(tn)_2]^{2+}$ complex has been determined;[11] its CD spectrum shows only one (−) peak, and the *Λ* configuration is assigned to the complex. The corresponding ethylenediamine complex, $(-)_{589}$-$[Co(acac)(en)_2]^{2+}$, shows a similar spectrum.[12] This similarity suggests that, in the bis(diamine)-type complexes, the difference in tn and en has little influence upon the CD spectra. Accordingly, the absolute configuration of each isomer of the present complex, a bis(aminoacidato)diamine-type complex, was confidently determined by relating the sign of the dominant CD peak in the first absorption band region to that for the $[Co(L\text{-}Hasp)_2(en)]^+$ complex.[2] That is, the E-1, E-2, and E-4 isomers have the *Λ* configuration, and the E-1′, E-3, and E-5 isomers have the *Δ* configuration.

Applying Douglas' relationship,[13] the vicinal curves due to two L-aspartate chelates are calculated for the $[Co(L\text{-}Hasp)_2(tn)]^+$ and $[Co(L\text{-}Hasp)_2(en)]^+$ complexes. The results are shown in Fig. 5. The curves of the complexes resemble each other. This lends support

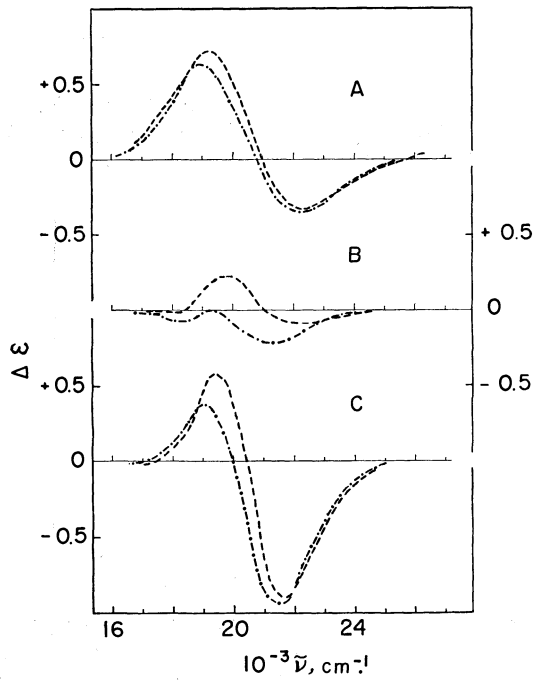

Fig. 5. The vicinal curves of $[Co(L\text{-}Hasp)_2(tn)]^+$ (-·-·-) and $[Co(L\text{-}Hasp)_2(en)]^+$ (——) complexes, A; *trans*(*O*)-*cis*(*N*), B; *cis*(*O*)*cis*(*N*), and C; *cis*(*O*)*trans*(*N*) isomers.

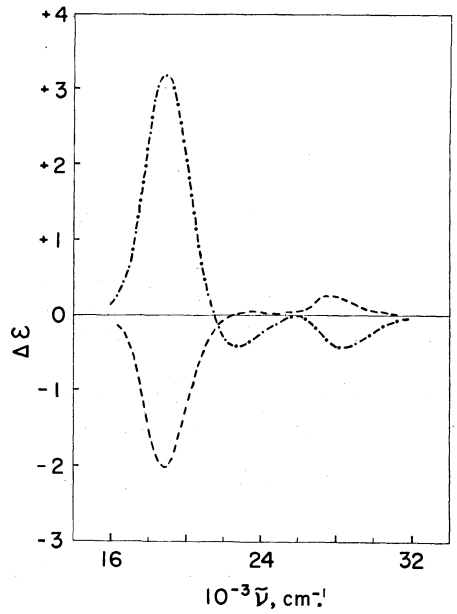

Fig. 6. The CD spectra for *trans*(*O*)*cis*(*N*)-*Λ*-(+)-$[Co(L\text{-}Hasp)_2(tn)]^+$ (S-1) (-·-·-) and *trans*(*O*)*cis*(*N*)-*Δ*-(−) $[Co(L\text{-}Hasp)_2(tn)]^+$ (S-2) (——).

to the previous assignment.

Figure 6 shows the CD curves of S-1 and S-2 drawn by assuming their ε values to be the same as those of E-1 and E-1′ respectively. The curve of S-1 is similar to that of E-1, while the curve of S-2 differs a little from that of E-1′. The absolute configurations of these isomers can also be determined tentatively from the sign of the main CD peak, similarly to the E isomers; S-1 has the *Λ* configuration, and S-2 has the *Δ* configuration. Accordingly, it may be concluded that the E-1 and S-1 isomers are of *trans*(*O*)*cis*(*N*)-*Λ*, while E-1′ and S-2 are *trans*(*O*)*cis*(*N*)-*Δ*.

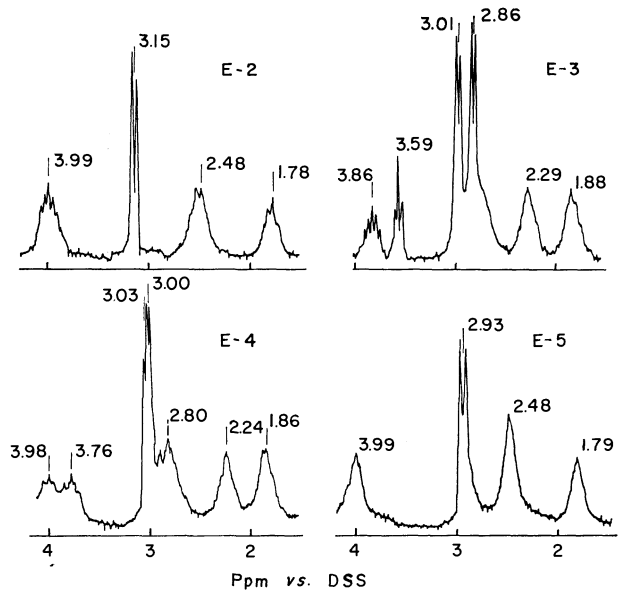

Fig. 7. The PMR spectra for *cis*(*O*)*trans*(*N*)-*Λ*-(+)-$[Co(L\text{-}Hasp)_2(tn)]^+$ (E-2), *cis*(*O*)*cis*(*N*)-*Δ*-(−)-$[Co(L\text{-}Hasp)_2(tn)]^+$ (E-3), *cis*(*O*)*cis*(*N*)-*Λ*-(+)-$[Co(L\text{-}Hasp)_2(tn)]^+$ (E-4), and *cis*(*O*)*trans*(*N*)-*Δ*-(−)-$[Co(L\text{-}Hasp)_2(tn)]^+$ (E-5).

The PMR spectra of the E-2, E-3, E-4, and E-5 isomers are shown in Fig. 7, with the signals of the NH_2 group and HDO eliminated. The resonance signals could be assigned on the basis of the signals of the $[Co(L\text{-Hasp})_2(en)]^+$ [2] and $[Co(CO_3)(tn)_2]^+$ complexes. The signal of the CH_2 protons (AB of ABX) of the β-carbon of the chelated aspartate ion was detected as a doublet, and its chemical shift is given as the center of the doublet. The signals due to the CH_2 and CH groups of the two aspartate ions are observed at 3.15 and 3.99 for E-2, and at 2.93 and 3.99 ppm for E-5. On the other hand, E-3 shows the CH_2 signals at 2.86 and 3.01 ppm and the CH signals at 3.59 and 3.86 ppm. Similarly, E-4 shows the CH_2 signals at 3.00 and 3.03 ppm and the CH signals at 3.76 and 3.98 ppm. Moreover, the signals of three CH_2 groups of the chelated diamine were observed as two peaks in the intensity ratio of 1 : 2 for E-2 and E-5, while the corresponding signals were observed as three peaks of equal intensities for the E-3 and E-4 isomers (a peak at the lowest-magnetic-field for E-3 overlaps with a CH_2 peak of the L-aspartate ion). These results indicate that the E-2 and E-5 isomers have a chemical environment of C_2 symmetry, while E-3 and E-4 have one of C_1 symmetry. Accordingly, it may be concluded that E-2 and E-5 are a pair of diastereoisomers of *cis(O)trans(N)*, while E-3 and E-4 are one of *cis(O)cis(N)*.

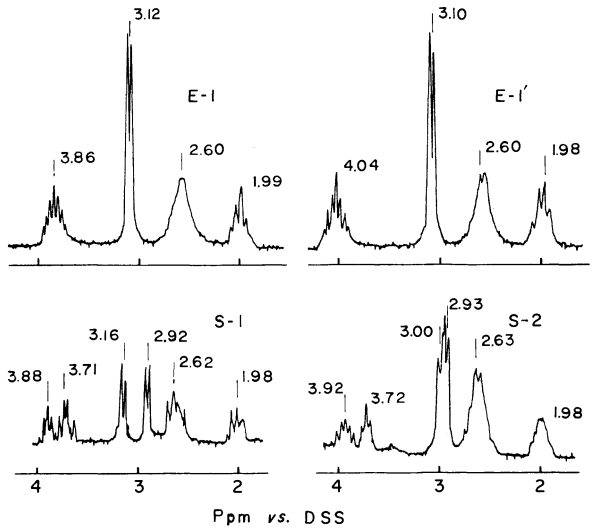

Fig. 8. The PMR spectra for *trans(O)cis(N)*-Λ-(+)-$[Co(L\text{-Hasp})_2(tn)]^+$ (E-1), *trans(O)cis(N)*-Λ-(−)-$[Co(L\text{-Hasp})_2(tn)]^+$ (E-1'), *trans(O)cis(N)*-Λ-(+)-$[Co(L\text{-Hasp})_2(tn)]^+$ (S-1), and *trans(O)cis(N)*-Λ-(−)-$[Co(L\text{-Hasp})_2(tn)]^+$ (S-2).

Figure 8 shows the PMR spectra for the E-1, E-1', S-1, and S-2 isomers, whose structure has been determined as *trans(O)cis(N)*. The CH and CH_2 protons of the chelated L-aspartate ions resonate at 3.86 and 3.12 ppm for E-1 and at 4.04 and 3.10 ppm for E-1'. These values are almost equal to those for a pair of diastereoisomers of the corresponding *l*-propylenediamine complex[1] and of the ethylenediamine complex[2] (Table 3). From these correspondences it may be assumed that the E-1 and E-1' isomers are a pair of diastereoisomers with *trans*(O_α)*cis(N)* geometry in respect

Table 3. Assignment of PMR signals[a] of *trans(O)-cis(N)*-$[Co(L\text{-Hasp})_2(diamine)]^+$ complexes

(A)

Diamine		Λ isomer asp CH_2	Λ isomer asp CH	Λ isomer tn CH_2	Ref.
tn	(E-1)	3.12	3.86	2.60, 1.99	
	(S-1)	3.16, 2.92	3.88, 3.71	2.62, 1.98	
		(2 : 2	: 1 : 1	: 2 : 1)[b]	
en		3.09	3.81		2
l-pn		3.11	3.85		1

(B)

Diamine		Λ isomer asp CH_2	Λ isomer asp CH	Λ isomer tn CH_2	Ref.
tn	(E-1')	3.10	4.04	2.60, 1.98	
	(S-2)	3.00, 2.93	3.92, 3.72	2.63, 1.98	
		(2 : 2	: 1 : 1	: 2 : 1)[b]	
en		3.00	4.02		2
l-pn		3.06	3.98		1

a) Values in ppm from DSS. b) Ratio of the integrated intensities of peaks.

to the donor O_α and N atoms of the glycinate backbone. As an alternative configuration of C_2 symmetry, the *trans*(O_β)*cis(N)* geometry due to the β-carboxylate ions of the chelated aspartate ions is possible. As may be seen in Fig. 3, the configurational effect curve of the E-3 (or *cis(O)cis(N)*-Λ) isomer is in close agreement with the curve of the *cis(O)cis(N)*-Λ-$[Co(L\text{-ala})_2(tn)]^+$ complex.[14] An agreement of the same kind is also observed for the other isomers labeled E. From these comparisons, it can be concluded that in every isomer labeled E two L-aspartate ions chelate to the central cobalt(III) ion, thus forming the five-membered rings.

Now let us characterize the S-1 and S-2 isomers. As compared with E-1 and E-1', the yields of these isomers were extremely poor. The ratios of the integrated intensities of all the signals for these isomers (Table 3) support the idea that both are complexes of the bis(L-aspartato)-type. Moreover, from the facts that the absorption spectra of the isomers show remarkable splittings of the first absorption band and that the $\Delta\varepsilon$ in the CD spectra estimated for S-1 and S-2 are almost equal to those for E-1 and E-1' respectively, it may be concluded that the S-1 and S-2 isomers are the stereoisomers of the *trans(O)cis(N)*-$[Co(L\text{-Hasp})_2(tn)]^+$ complex. The PMR spectra of these *trans(O)cis*(N) isomers differ from those of the other *trans(O)cis(N)* isomers (E-1 and E-1'); the CH protons of the two aspartate ions for S-1 resonate at 3.71 and 3.88 ppm, while those for S-2 resonate at 3.72 and 3.92 ppm. The splittings of the signals due to the CH_2 protons are also observed for the isomers labeled S. The chemical shifts of the CH signals and that of the CH_2 signals at the lower magnetic field for S-1 are in close agreement with the corresponding chemical shifts for E-1. The same relation helds for S-2 and E-1'. These

agreements in chemical shifts suggest that S-1 (or S-2) also has a chelate ring such as the E-1 (or E-1′) isomer. Since the actual spectra differ between S-1 and E-1 (or S-2 and E-1′), the alternative coordination mode of the L-aspartate ion must be taken into consideration. The pK values of the S-1 and E-1 isomers, which have been calculated from the concentration of the solution and its pH value, were roughly 11.0 and 7.0 respectively. These facts suggest that the S-1 isomer differs in its dangling carboxylate group from the E-1 isomer. Thus, the S-1 and S-2 isomers can now be characterized as a pair of diastereoisomers containing a five-membered ring and a six-membered ring, the latter due to the β-carboxylate of the L-aspartate ion. As far as we know, this is the first time that a complex with a six-membered chelate ring of the aspartate ion has been isolated.

Table 4. Formation ratios of $[Co(L\text{-}Hasp)_2(tn)]^+$ isomers

trans(O)cis(N)		*cis(O)cis(N)*		*cis(O)trans(N)*	
Λ	Δ	Λ	Δ	Λ	Δ
13	2.2	5.1	20	12	1
$\Lambda:\Delta=5.9:1$		$\Lambda:\Delta=1:3.9$		$\Lambda:\Delta=12:1$	

Stereoselectivity. The formation ratios among three geometrical isomers are summarized in Table 4. The stereoselective formations are found in the Λ, Δ, and Λ isomers for the *trans(O)cis(N)*, *cis(O)cis(N)*, and *cis(O)trans(N)* isomers respectively. This tendency agrees with those for the corresponding *l*-propylenediamine[1] and ethylenediamine complexes.[2] The amount formed in the present reaction decreased in this order: *cis(O)-cis(N)-*Δ > *trans(O)cis(N)-*$\Lambda \cong$ *cis(O)trans(N)-*Λ > *cis(O)-cis(N)-*Λ > *trans(O)cis(N)-*Δ > *cis(O)trans(N)-*Δ; this order differs from those of the *l*-pn and the en complexes.[2] The formation ratio of the *trans(O)cis(N)*: *cis(O)cis(N)*: *cis(O)trans(N)* isomer is about 29: 47: 24. On the other hand, the ratio of these three geometrical isomers in the *l*-pn complex is 61: 34: 5, and that in the en complex is 55: 34: 11. These facts show that the *trans(O)* isomer in the present complex is harder to form than the *cis(O)* isomers, compared with the *trans(O)* isomer in the *l*-pn and the en complexes. The orders in the *l*-pn and the en complexes have been explained on the basis of the consideration of the formation of hydrogen bonding between the β-carboxylate group and the amino group.[1,2] However, the order in the present complex can not be understood from the hydrogen bonding alone.

The author wishes to thank Professor M. Shibata for his kind instruction and continuous encouragement during this work.

References

1) Y. Kojima and M. Shibata, *Inorg. Chem.*, **10**, 2382 (1971).
2) Y. Kojima and M. Shibata, *ibid.*, **12**, 1009 (1973).
3) J. E. Boyle and G. M. Harris, *J. Amer. Chem. Soc.*, **80**, 782 (1958).
4) M. Shibata, *Nippon Kagaku Zasshi*, **67**, 771 (1966).
5) J. C. Bailar, Jr. and J. B. Work, *J. Amer. Chem. Soc.*, **68**, 232 (1946).
6) N. Matsuoka, J. Hidaka, and Y. Shimura, This Bulletin, **45**, 2491 (1972).
7) P. G. Beddoe and S. F. Mason, *Inorg. Nucl. Chem. Lett.*, **4**, 433 (1968).
8) The symbols Δ and Λ are based upon the convention proposed by the IUPAC in *Inorg. Chem.*, **9**, 1 (1970).
9) T. Nomura, F. Marumo, and Y. Saito, This Bulletin, **42**, 1016 (1969).
10) K. Nakatsu, M. Shiro, Y. Saito, and H. Kuroya, *ibid.*, **30**, 158 (1957).
11) H. Kawaguchi, K. Matsumoto, H. Kuroya, and S. Kawaguchi, *Chem. Lett.*, **1972**, 125.
12) A. J. McCaffery, S. F. Mason, and B. J. Norman, *J. Chem. Soc.*, **1965**, 5094.
13) C. T. Liu and B. E. Douglas, *Inorg. Chem.*, **3**, 1356 (1964); B. E. Douglas and S. Yamada, *ibid.*, **4**, 1561 (1965).
14) Unpublished.

The Steric Requirements of *N,N'*-Bis(salicylidene)-2-aminobenzylamines on Metal Chelate Formation

Hajime KANATOMI, Yoichi DEMURA, and Ichiro MURASE

Laboratory of Chemistry, College of General Education, Kyushu University, Ropponmatsu, Chuo-ku, Fukuoka 810

(Received December 27, 1974)

Copper(II), Ni(II), Co(II), Zn(II), and Be(II) chelates of *N,N'*-bis(salicylidene)-2-aminobenzylamine and its methyl and dimethyl salicylidene derivatives have been prepared and characterized. According to the molecular models, the ligands are favorable to tetrahedral arrangement on complex formation. The spectral and magnetic properties revealed that all the Co(II) and some of the Cu(II) chelates were pseudo-tetrahedral, while the Ni(II) and other Cu(II) chelates were square-planar, with a considerable angle strain. This ligand property is somewhat inconsistent with the conclusion derived from *N,N'*-bis(salicylidene)polymethylenediamine chelates, in which the trimethylene analogue could not take a pseudotetrahedral arrangement around a metal ion. The difference in stereochemistry between the two ligands with the same number of bridging carbon atoms will be discussed on the basis of the flexibility and the steric requirement of the central chelate ring.

Several reports have revealed that metal chelates of *N,N'*-bis(salicylidene)polymethylenediamine change in their stereochemistry with an expansion of the central chelate ring size.[1-7] *N,N'*-Bis(salicylidene)ethylenediamine imposes a square-planar structure for transition-metal chelates due to the steric requirement of the ligand in which the central chelate ring was five-membered. On the other hand, *N,N'*-bis(salicylidene)trimethylenediamine forms a high-spin Co(II) chelate with a structure of a very flattened tetrahedron,[5] and in the square-planar Cu(II) and Ni(II) chelates a significant decrease of the apparent ligand field strength is observed relative to the corresponding ethylenic chelates.[1] The fact that the Co(II) chelate could not take a pseudotetrahedral geometry was explained by the insufficient flexibility of the six-membered central chelate ring consisting of a trimethylene chain.

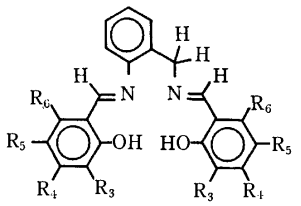

LH_2

LaH_2: $R_3=R_4=R_5=R_6=H$
LbH_2: $R_5=CH_3, R_3=R_4=R_6=H$
LcH_2: $R_3=R_5=CH_3$, $R_4=R_6=H$
LdH_2: $R_4=R_6=CH_3$, $R_3=R_5=H$

In this report, *N,N'*-bis(salicylidene)-2-aminobenzylamine (abbreviated LaH_2 hereafter) and its 5-methyl, 3,5-dimethyl, and 4,6-dimethylsalicylidene derivatives (LbH_2, LcH_2, and LdH_2 respectively) are chosen as quadridentate ligands in order to study the stereochemistry of the metal chelates with regard to the effect of the central chelate ring flexibility. When these ligands combine with metal ions to form three condensed chelate rings, the central ring is six-membered, as is the trimethylene analogue. The flexibility of the ring is, however, suppressed much more than that of the trimethylene analogue because the two carbon atoms of the benzene ring are constituents of the central chelate ring. Molecular models suggest that a square-planar configuration around a metal ion is difficult without a deformation of bond angles; otherwise, the two phenolic oxygen may overlap on the same plane. A favorable arrangement is one which is distorted from square-planar bending at the flexible methylenic linkage of the central chelate ring. In the derivatives, the methyl groups will exert an electronic influence on the ligand-field strength through the donor atoms; this may affect the chelating tendencies or the metal chelate configuration.

Experimental

The infrared spectra were determined in potassium bromide disks by means of a Hitachi EPI-S2 spectrophotometer, while the electronic spectra were measured with a Hitachi EPS-3T spectrophotometer. The PMR spectra were recorded at 60 MHz in $CDCl_3$ with a Hitachi Model R-24 NMR spectrometer, and the chemical shifts are quoted as ppm values relative to tetramethylsilane. The magnetic moments were measured at room temperature by means of a recording magnetometer specially designed by Hirakawa.[14]

Preparation of the Schiff Bases (LaH_2, LbH_2, LcH_2, and LdH_2). A mixture of 0.02 mol of salicylaldehyde (for LaH_2) and 0.01 mol of 2-aminobenzylamine in 30 ml of methanol was refluxed for 20 min. The yellow crystals which resulted from cooling the reaction mixture in an ice bath were recrystallized from methanol. For LbH_2, LcH_2, and LdH_2, 5-methylsalicylaldehyde, 3,5-dimethylsalicylaldehyde, and 4,6-dimethylsalicylaldehyde were reacted respectively in place of salicylaldehyde. The melting points were: LaH_2, 82—83.5 °C; LbH_2, 118—120 °C; LcH_2, 105—106.5 °C; LdH_2, 123—125.5 °C.

Preparation of the 1: 1 Chelates. A warm methanol solution of the Schiff base was mixed with an equimolar amount of a metal acetate[Cu(II), Ni(II), Co(II), and Zn(II)] or beryllium nitrate in a minimum amount of warm methanol, after which the mixture was refluxed for 20 min. The crystals of the desired chelates were deposited on refluxing or after cooling the reaction mixture. They were collected by filtration, recrystallized from an ethanol-chloroform mixture if necessary, and dried at 90 °C for 8 hr *in vacuo*. The yield was 70—80% for every chelate. The Cu(II) chelate of Lb prepared in this procedure consisted of brown crystals carrying 1/2 mol of water.

Preparation of the Green Cu(II) Chelate(LbCu). To each mol of *o*-aminobenzylamine and Cu(II)-acetate in a minimum amount of hot methanol, we added a slight excess of double

molar 5-methylsalicylaldehyde in methanol, after which the mixture was heated on a water bath for 30 min. After the solution had stood overnight at room temperature, the dark green crystals which resulted were filtered off, washed with a small amount of methanol, and dried at 90 °C *in vacuo*.

Preparation of the 1: 2 Ni(II) Chelates. Although the reaction of LaH_2 or LdH_2 with the Ni(II) ion under the conditions described above inevitably afforded the 1: 2 chelates, they were best prepared by reacting the ligands with a double amount of the metal ion. The reaction was carried out with Ni(II)-acetylacetonate in benzene for LaH_2 and with Ni(II)-acetate in dimethylformamide for LdH_2. The chelates were crystallized out by heating the reaction mixture; they were filtered after cooling, washed with methanol, and dried at 90°C *in vacuo*.

The results of the elemental analyses of the free ligands and the metal chelates are summarized in Table 1.

TABLE 1. ELEMENTAL ANALYSES OF THE SCHIFF BASES AND THEIR METAL CHELATES

Compound	Formula	Found (Calcd) C%	H%	N%
LaH_2	$C_{21}H_{18}N_2O_2$	76.40 (76.34	5.45 5.49	8.49 8.48)
LaCo	$C_{21}H_{16}N_2O_2Co$	65.05 (65.12	4.35 4.16	7.27 7.23)
LaZn	$C_{21}H_{16}N_2O_2Zn$	63.25 (64.06	4.24 4.10	6.83 7.12)
LaBe	$C_{21}H_{16}N_2O_2Be$	74.30 (74.76	4.88 4.78	8.18 8.30)
$(LaH)_2Ni$	$C_{42}H_{34}N_4O_4Ni$	70.37 (70.31	4.82 4.78	7.64 7.80)
LbH_2	$C_{23}H_{20}N_2O_2$	77.24 (77.07	6.20 6.19	7.81 7.81)
LbCu	$C_{23}H_{18}N_2O_2Cu$	65.60 (65.78	4.77 4.80	6.71 6.67)
LbCu $1/2H_2O$	$C_{23}H_{19}N_2O_{2.5}Cu$	64.65 (64.40	4.81 4.93	6.59 6.53)
LbNi	$C_{23}H_{18}N_2O_2Ni$	66.21 (66.54	4.83 4.86	6.67 6.75)
LbCo	$C_{23}H_{18}N_2O_2Co$	65.92 (66.51	4.88 4.85	6.58 6.75)
LcH_2	$C_{25}H_{26}N_2O_2$	77.42 (77.69	6.73 6.78	7.29 7.25)
LcCu	$C_{25}H_{24}N_2O_2Cu$	66.89 (67.02	5.53 5.40	6.24 6.25)
LcNi	$C_{25}H_{24}N_2O_2Ni$	67.88 (67.75	5.49 5.46	6.37 6.32)
LcZn	$C_{25}H_{24}N_2O_2Zn$	66.68 (66.75	5.39 5.38	6.25 6.23)
LdH_2	$C_{25}H_{26}N_2O_2$	77.52 (77.69	6.78 6.78	7.17 7.25)
LdCu	$C_{25}H_{24}N_2O_2Cu$	66.88 (67.02	5.36 5.40	6.22 6.25)
LdCo	$C_{25}H_{24}N_2O_2Co$	67.45 (67.72	5.49 5.46	6.29 6.32)
LdZn	$C_{25}H_{24}N_2O_2Zn$	66.77 (66.75	5.38 5.38	6.12 6.23)
$(LdH)_2Ni$	$C_{50}H_{30}N_4O_4Ni$	72.09 (72.38	6.06 6.08	6.84 6.75)

Results and Discussion

The infrared spectra of the free ligands reveal a difference between the two azomethine bondings. Each ligand shows two absorption bands in the 1600 cm^{-1} region, as is illustrated in Table 2. The higher one can be assigned to the double bond of the CH=N-(CH_2) stretching vibration, and the lower one, to the CH=N-(phenyl) stretching vibration, by analogy with the azomethine frequencies of salicylidenebenzylamine (1634 cm^{-1})[8] and salicylideneaniline (1625 cm^{-1})[9] respectively. In the case of LdH_2, only one band appeared, at 1625 cm^{-1}; this is because the bond order of the CH=N-(CH_2) was lowered by the electronic effect of the substituted methyl groups and the absorption overlapped with the CH=N-(phenyl) band.

TABLE 2. C=N STRETCHING FREQUENCIES OF *N,N'*-BIS-(SALICYLIDENE)-2-AMINOBENZYLAMINES AND THEIR 1: 1 METAL CHELATES (cm^{-1})

Ligand	Metal H_2	Cu(II)	Ni(II)	Co(II)	Zn(II)	Be(II)
La	1636	*	*	1608	1625	1632
	1625				1613	1618
Lb	1641	1627[a]	1628	1624	——	——
	1630					
Lc	1633	1627	1627	*	1624	——
	1629				1611	——
Ld	1625	1607	*	1604	1610	——

*: no chelate was isolated. —: no reaction was examined. a): anhydrous green chelate.

TABLE 3. PMR DATA RECORDED AT 60 MHz IN $CDCl_3$ (ppm VALUES RELATIVE TO INTERNAL TMS)

Compound	CH=N–(CH_2)	CH=N–(phenyl)	OH
LaH_2	8.63	8.49	13.10
LbH_2	8.50	8.36	12.82
LcH_2	8.48	8.33	13.05
LdH_2	8.86	8.72	13.41

The PMR spectra exhibit two peaks arising from different azomethine protons. The chemical shifts of the two pairs are about 0.15 ppm different, as may be seen in Table 3; the one at the higher magnetic field belongs to the CH=N–(CH_2) proton, while the lower one is due to the CH=N–(phenyl) proton. This assignment is supported by analogy with the azomethine PMR of salicylidenebenzylamine (8.23 ppm)[8] and of salicylideneaniline (8.50 ppm).[9] The methyl groups *ortho* and *para* to the azomethine groups increase, and the *meta* methyls decrease, the deshielding effect of the phenyl ring current. The OH proton resonance appears as a broad band; the band broadening is attributed to the proton exchange which is taking place at a high rate between the two OH bondings. The chemical shifts shown in Table 3 indicate the mean value due to the two OH protons. Judging from these values, the *para* and/or *ortho* methyl derivatives (LbH_2 and LcH_2) have more shielded OH protons than the nonsubstituted one (LaH_2), while that of the *meta* derivative (LdH_2) is less shielded.

Metal chelates isolated as pure crystals with the 1: 1 metal-ligand composition are listed in Table 2, which

shows the CH=N stretching frequencies. It may be seen that the two CH=N absorptions shift to lower frequencies on complex formation and that many of them are overlapped into one band. As is to be expected from the molecular model and from the fact that Cu(II) and Ni(II) chelates could not be isolated with La, the ligand is not likely to have a square-planar arrangement. Furthermore, the tetrahedrally distorted arrangement seems most likely for La because the ligand affords chelates with Zn(II) and Be(II) ions, which are believed to prefer to form tetrahedral complexes. It was shown that, in the case of *N,N'*-bis(salicylidene)-polymethylenediamine, the tetramethylene bridge was the smallest chain which would allow the four donor atoms to occupy truly tetrahedral sites around a metal ion. Since beryllium would not tolerate even a slight departure from tetrahedral stereochemistry, the trimethylene derivative did not form a 1:1 complex with the Be(II) ion, but instead gave a 1:2 complex in which the ligand functioned as a bidentate chelate.[3] This explanation is, however, inconsistent with the present finding, where La could form a 1:1 Be(II) chelate despite having a less flexible three-carbon bridge.

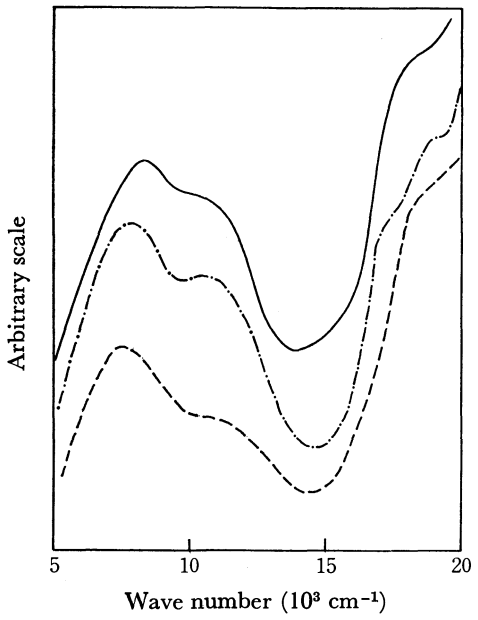

Fig. 1. Electronic reflectance spectra of La-Co(II), ----; Lb-Co(II), ——; Ld-Co(II), ——.

With La, Lb, and Ld, 1:1 Co(II) chelates were isolated as orange-red crystals. The spectral patterns of these chelates, shown in Fig. 1, are quite similar to that obtained for bis(*N*-phenylsalicylaldiminato)cobalt-(II), which exhibited absorption bands at 7600, 10700, 16700 (shoulder), and 19300 cm^{-1} in the near-infrared and visible region[10] and which has been shown by crystallographycal evidence to have a pseudotetrahedral geometry.[11] The magnetic moment of the Co(II) chelate with La was $\mu_{eff}=4.2$ B.M. ($\chi=18.69\times10^{-6}$ $egsu^{-1}$) at room temperature; this is in agreement with those expected for tetrahedral Co(II) complexes.[12] On the bases of these similarities in spectral and magnetic properties with complexes of a known structure, it may be concluded that these Co(II) chelates adopt the pseudotetrahedral geometry around the metal ion. In *N,N'*-bis(salicylidene)polymethylenediaminatocobalt-(II), those with four to six bridging methylene groups were found to be pseudotetrahedral; however, the trimethylene derivative showed an anomalous electronic spectrum and was assumed to be a highly flattened tetrahedron on the basis of the magnetic high-spin character (4.56 B.M.).[5]

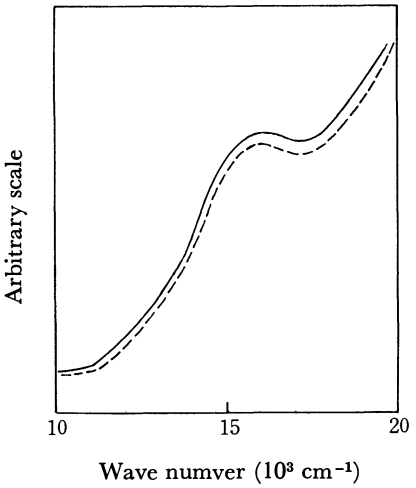

Fig. 2. Electronic reflectance spectra of Lb-Ni(II), ----; Lc-Ni(II), ——.

Nickel(II) chelates with a 1:1 metal-ligand composition were isolated with Lb and Lc. It is seen the presence of *para* and/or *ortho* methyl groups, which increase the electron density of the phenolic oxygens, is necessary for the chelate formation. These chelates were diamagnetic and exhibited *d-d* bands at 15900 cm^{-1} for the Lb-chelate and at 16000 cm^{-1} for the Lc-chelate in their reflectance spectra; the patterns are shown in Fig. 2. It thus appears that these chelates have a basically planar configuration, though it is not necessarily strictly planar. In *N,N'*-bis(salicylidene)polymethylenediaminatonickel(II), the planar structures were retained even when the bridging methylene groups increased to 3, 4, or 5, while a significant decrease in the apparent ligand-field strength was observed with an increase in the number of methylene groups.[1,7] The bands for the present Ni(II) chelates were in lower energy region than those of the tetra- and pentamethylene complexes; this may be attributed to the distortion of the bond angles produced when the ligand molecules are forced to adopt the square-planar configuration on the metal-chelate formation.

The PMR spectra of Ni(II) and Zn(II) chelates with Lc are shown in Fig. 3. It is interesting that the separate PMR peaks of the CH=N–(CH_2) and the CH=N–(phenyl) protons in the free ligand become a single peak in the Ni(II) chelate and shift to a higher magnetic field (7.34 ppm). Therefore, the two azomethine linkages are equivalent in the metal chelate rings; this agrees with the fact that the azomethine stretching vibration appears as a single band. On the contrary, the two PMR peaks in the corresponding Zn(II) chelate are merely shifted to the respective

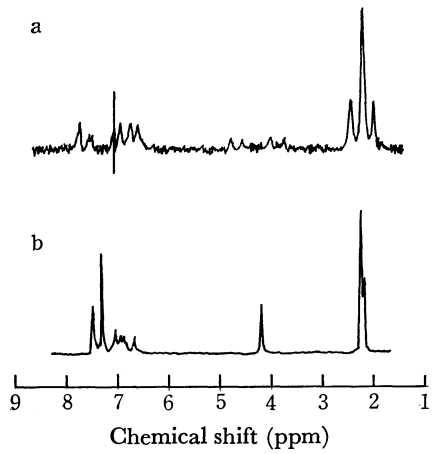

Fig. 3. PMR spectra of Lc-Zn(II) (a) and Lc-Ni(II) (b).

higher magnetic fields (7.87 and 7.77 ppm), indicating that each azomethine retains a different character in this case. Furthermore, the bridging methylene protons, which appear as a single peak at 4.76 ppm in the free ligand, shift to 4.28 ppm in the Ni(II) chelate, while it splits into an AB pattern centered at 4.30 ppm (J_{AB}=8 Hz) in the Zn(II) chelate. The different features; in the methylene PMR can be explained in terms of the central chelate ring flexibility when it is retained at the methylenic linkage in the Ni(II) chelate and fixed in the Zn(II) chelate. The characteristics of the ring flexibility probably arise from the difference in the configuration that is, the Ni(II) chelate is square-planar, while the Zn(II) chelate is tetrahedral.

La and Ld do not form 1:1 Ni(II)-chelates, but instead form 1:2 complexes in which these ligands function as a bidentate chelate. The presence of the uncoordinated salicylaldimino moiety in each ligand molecule is evidenced by the presence of a free OH group which exhibits a broad and weak infrared absorption around 2700 cm^{-1}. To distinguish the coordination site of the molecule, the CH=N stretching vibration were compared with the corresponding free ligand; however, they appeared as one rather broad band at 1618 cm^{-1} in $(LaH)_2Ni$ and at 1608 cm^{-1} in $(LdH)_2Ni$. Therefore, it was not clear that either CH=N–(CH_2) or CH=N–(phenyl) nitrogen coordinated to the metal ion. The reflectance spectral patterns are typical for a square-planar Ni(II) complex exhibiting one *d-d* band at 16000 cm^{-1} in the La-complex and at 16400 cm^{-1} in the Ld-complex.

Copper(II) chelates were isolated with Lb, Lc, and Ld. La could not be a chelate ligand; they must be due to an insufficient electron density of the donor atoms in the same sense as are the Ni(II) chelates. It should be noted that the chelate with Ld was brown and that with Lc was green, while Lb gave chelates of both color types, of which the brown one contained 1/2 mol of water. The difference in color was apparent in their reflectance spectral patterns, as may be seen in Fig. 4. The green chelates show a distinct absorption maximum at 16200 cm^{-1} in Lb-Cu(II) and 16400 cm^{-1} in Lc-Cu(II), with a shoulder both around 13500 cm^{-1}, while the brown chelates exhibit absorption only as a shoulder or broad band around 15000 cm^{-1}. According

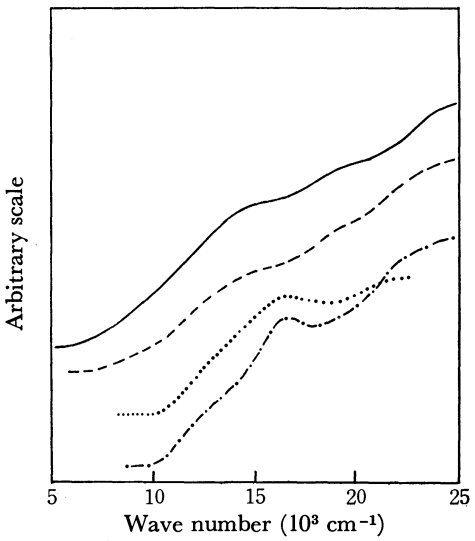

Fig. 4. Electronic reflectance spectra of Lb-Cu(II) (green), ·····; Lb-Cu(II) (brown), ——; Lc-Cu(II), -·-·-; Ld-Cu(II), ——.

to the criteria established by several investigators with regard to the Cu(II) chelates of bissalicylaldimines,[13] these types of absorptions are a result of tetrahedral distortion. The difference in the spectral patterns between the green and the brown chelates depends on the degree of distortion from a square-planar configuration; the green chelates are essentially square-planar, while the brown chelates are pseudotetrahedral.

In the present Cu(II) chelates, the degree of distortion may be attributed to the degree of the ligand-field strength, because the only structural difference in these ligands is in the presence of the methyl groups at the salicylidene moieties, which exert no steric effect on the chelate configuration. A relatively high electron density at the oxgen atoms, which is achieved by the electronic effect of *ortho* and *para* methyl groups, seems to be necessary to enforce the planar configuration on the chelate, as in the case of Lc. The ligand-field strength of Lb is likely to be intermediate in taking a planar or pseudotetrahedral arrangement, because it can from chelates of either type, depending upon the reaction conditions. However, this argument is partly hypothetical, since the role of the 1/2 mol of water has not been made clear.

Conclusion

In *N,N'*-carbon-bridging bissalicylaldimine derivatives, the three carbon-chain compounds are not necessarily unfavorable for tetrahedral arrangement around a particular metal ion. The stereochemistry of the metal chelates is governed not only by the steric requirement of the metal ion, but also by the steric preference of the bridging carbon linkages in addition to the chain flexibility. This has been evidenced by the present investigation, where *N,N'*-bis(salicylidene)-2-aminobenzylamines formed tetrahedral 1:1 chelates with Be(II) and Co(II) ions which were impossible with the trimethylene analogue. Since a Ni(II) ion enforced a square-planar coordination on the ligands, a

decrease in the ligand-field strength was observed and the derivatives with insufficient donor powder could not form a 1 : 1 chelate. In the Cu(II) chelates, the degree of tetrahedral distortion depended upon the donor power in each ligand. It may tentatively be considered that Lb is in a boundary condition in taking a planar or pseudotetrahedral arrangement around a Cu(II) ion.

References

1) R. H. Holm, *J. Amer. Chem. Soc.*, **82**, 5632 (1960).
2) H. Weigold and B. O. West, *J. Chem. Soc.*, A, **1967**, 1310.
3) G. E. Batley and D. P. Graddon, *Australian J. Chem.*, **21**, 267 (1968).
4) S. J. Gruber, C. M. Harries, and E. Sinn, *J. Inorg. Nucl. Chem.*, **30**, 1805 (1968).
5) M. Hariharan and F. L. Urbach, *Inorg. Chem.*, **8**, 556 (1969).
6) M. Hariharan and P. L. Urbach, *ibid.*, **10**, 2667 (1971).
7) W. C. Hoyt and G. W. Everett, Jr., *ibid.*, **8**, 2013 (1969).
8) G. C. Percy, *J. Inorg. Nucl. Chem.*, **34**, 3357 (1972).
9) G. C. Percy, *ibid.*, **34**, 3369 (1972).
10) L. Sacconi, M. Ciampolini, F. Maggio, and F. P. Carasino, *J. Amer. Chem. Soc.*, **89**, 3246 (1962).
11) E. Frasson and C. Panattoni, *Z. Krist.*, **116**, 154 (1961).
12) B. N. Figgis and R. S. Nyholm, *J. Chem. Soc.*, **1959**, 338.
13) M. Kato, K. Imai, Y. Muto, T. Tokii, and H. B. J. Jonassen, *J. Inorg. Nucl. Chem.*, **35**, 109 (1973), and the references herein.
14) K. Hirakawa, Ka. Hirakawa, and S. Yoneyama, *Jap. J. Appl. Phys.*, **2**, 816 (1963).

Iminophosphorane Complexes of Palladium(II)

Mitsuyo FUKUI, Kenji ITOH, and Yoshio ISHII

Department of Synthetic Chemistry, Faculty of Engineering, Nagoya University, Furo-cho, Chikusa-ku, Nagoya 464

(Received January 28, 1975)

Iminophosphorane complexes of palladium $[(C_6H_5)_3P{=}N{-}C_6H_4{-}X{-}p]PdCl_2(CH_3CN)$ (X=NO_2, **1A**; $COOC_2H_5$, **2A**; Cl, **3A**; H, **4A**; CH_3, **5A**) have been prepared by ligand-substitution reaction between $(C_6H_5CN)_2PdCl_2$ and the parent iminophosphoranes, followed by recrystallization from acetonitrile–ethyl acetate. Other iminophosphoranes (X=OCH_3, and $(C_6H_5)_2(CH_3)P{=}N{-}Si(CH_3)_3$), however, gave only dimeric complexes with the $[(\text{Iminophosphorane})PdCl_2]_2$ composition. Complexes **1A—5A** and $\{[(C_6H_5)_3P{=}N{-}C_6H_4{-}X{-}p]PdCl_2\}_2$ (X=NO_2, **1B**; $COOC_2H_5$, **2B**; Cl, **3B**; H, **4B**; CH_3, **5B**) are also discussed. The ligand-exchange reaction of **2B** and **5B** with α,α'-bipyridine, $(C_6H_5)_3P$, and $(CH_3O)_3P$ took place, liberating the parent iminophosphorane.

Iminophosphoranes represented as two resonance hybrides, $R_3\overset{+}{P}{-}\overset{-}{N}R' \leftrightarrow R_3P{=}NR'$, are isoelectronic with phosphorus ylides. Numerous transition metal complexes of phosphorus,[1–10] nitrogen,[11–13] and sulfur[14–16] ylides have recently been prepared. Information on iminophosphorane complexes has, however, been limited to those of V(0),[19] Co(II),[17,18] Cu(II),[17] Mo(0),[20] and W(0),[20] there is no known palladium complex. In this paper, the quantitative preparation of palladium(II) complexes with aryliminotriphenylphosphoranes and *N*-trimethylsilyliminodiphenylmethylphosphorane will be described, and the IR spectra of these complexes will be discussed.

Experimental

All the preparations of the iminophosphorane complexes were carried out under an atmosphere of nitrogen or argon. The IR spectra were recorded on a JASCO Model DS-403G spectrometer calibrated with polystyrene. The proton NMR spectra were recorded on a JEOL C60-HL instrument, with TMS as the internal reference. The analyses were carried out by the Microanalytical Center of Kyoto University, Japan.

Starting Materials. The dichlorobis(benzonitrile)palladium(II) was prepared according to the method of Kharasch *et al.*[21] The *p*-substituted phenyliminotriphenylphosphoranes were obtained by the interaction of dibromotriphenylphosphine with *p*-substituted anilines in the presence of triethylamine.[22] The *N*-trimethylsilyliminodiphenylmethylphosphorane was prepared by a method reported previously.[23]

Preparation of $[(C_6H_5)_3P{=}N{-}C_6H_4{-}X\text{-p}]PdCl_2(CH_3CN)$ *(X=NO_2, 1A; $COOC_2H_5$, 2A; Cl, 3A; H, 4A; CH_3, 5A).* The preparation of the phenyliminotriphenylphosphorane complex (**4A**) will be described as a representative example. A benzene suspension (10 ml) of dichlorobis(benzonitrile)palladium(II) (0.1046 g, 2.730 mmol) and phenyliminotriphenylphosphorane (0.0964 g, 2.730 mmol) was stirred overnight under an inert atmosphere. Dark brown precipitates (**4B**) were thus obtained quantitatively (0.1437 g). When **4B** was recrystallized from the mixed solvent of acetonitrile–ethyl acetate (1:2) at 0 °C for few days, a black violet microcrystalline complex (**4A**) was obtained. The time required for the recrystallization increased upon substitution of an electron-releasing group on the phenyl ring; it was overnight for *p*-NO_2(**1A**) and *p*-$COOC_2H_5$(**2A**), a few days for *p*-Cl(**3A**) and *p*-H(**4A**), and three months for *p*-CH_3(**5A**). The analytical data and melting points of the complexes are shown in Table 1. The dark brown precipitates, which must be dinuclear complexes **1B-4B**, could not be isolated in an analytical pure form except for **5B**. Consequently, a definitive determination was achieved by means of the monomeric complexes, **1A-5A**, which were obtained by a cleavage of dichlorobridging in the crude **1B-5B** by means of a large volume of acetonitrile.

Preparation of $\{[(C_6H_5)_3P{=}N{-}C_6H_4{-}OCH_3\text{-p}]PdCl_2\}_2$ *(6B).* A benzene suspension (10 ml) of dichlorobis(benzonitrile)palladium(II) (0.2763 g, 7.204 mmol) and anisyliminotriphenylphosphorane (0.2763 g, 7.204 mmol) was stirred under an inert atmosphere overnight. Dark brown precipitates (**6B**) were thus obtained quantitatively (0.4010 g); they were recrystallized from an acetonitrile–ethyl acetate (1:2) mixed solvent. The resulting crystals were dichlorodi-μ-chlorobis(*p*-anisyliminotriphenylphosphorane)dichloropalladium(II) with one molecule of acetonitrile as the solvent of crystallization; mp 143—145 °C. Found: C, 52.83; H, 4.04; N, 3.37%. Calcd for $C_{52}H_{37}Cl_4N_3O_2P_2Pd_2$: C, 53.73; H, 4.08; N, 3.61%. PMR ($CDCl_3$): τ 8.70 (s, CH_3), τ 6.30 (s, OCH_3), τ 2.16—2.76 (m, C_6H_5 and C_6H_4). IR (KBr disk): 1238 cm^{-1} [ν(P=N)], (free 1334 cm^{-1}; $\Delta\nu$ 96 cm^{-1}); 302, 310, 332, and 348 cm^{-1} [ν(Pd-Cl)].

Preparation of $\{[(C_6H_5)_2(CH_3)P{=}N{-}Si(CH_3)_3]PdCl_2\}_2$ *(7B).* To a benzene (8 ml) solution of dichlorobis(benzonitrile)palladium(II) (0.2421 g, 6.325 mmol), *N*-trimethylsilylimino-

TABLE 1. ANALYTICAL DATA AND MELTING POINTS OF ARYLIMINOPHOSPHORANE COMPLEXEXES OF PALLADIUM $[(C_6H_5)_3P{=}N{-}C_6H_4{-}X{-}p]PdCl_2(CH_3CN)$

Complex	X	Mp(°C)	Analyses (%) C Found(Calcd)	H Found(Calcd)	N Found(Calcd)
1A[a]	NO_2	209—211	50.38(50.63)	3.80(3.60)	6.66(6.81)
2A	$COOC_2H_5$	165—166	53.57(54.10)	4.39(4.23)	4.17(4.35)
3A	Cl	182—185	51.66(51.51)	3.84(3.66)	4.54(4.62)
4A	H	170—171	54.25(54.61)	4.03(4.05)	4.78(4.90)
5A	CH_3	170—172	54.74(55.36)	4.26(4.31)	4.99(4.78)
5B[b]	CH_3	229—230.5	54.94(55.12)	4.05(4.07)	2.97(2.57)

a) $[(C_6H_5)_3P{=}N{-}C_6H_4{-}X{-}p]PdCl_2(CH_3CN)$. b) $\{[(C_6H_5)_3P{=}N{-}C_6H_4{-}X{-}p]PdCl_2\}_2$

diphenylmethylphosphorane (0.1410 g, 6.285 mmol) was added under argon. The mixture was then stirred overnight. Orange precipitates were recrystallized from the dichloromethane–*n*-hexane (1: 1) mixed solvent or benzene (0.2301 g, 92%); mp 168—170 °C. Found: C, 41.39; H, 4.68; N, 2.83 %. Calcd for $C_{32}H_{44}Cl_4N_2P_2Si_2Pd_2$: C, 41.35; H, 4.77; N, 3.01%.

Reaction of α,α′-Bipyridine and Triphenylphosphine with Dichlorodi-μ-chlorobis(p-ethoxycarbonyliminotriphenylphosphorane)dipalladium-(II) (2B). A benzene (11 ml) solution of 2B (0.1610 g, 1.335 mmol) and α,α′-bipyridine (0.0417 g, 2.671 mmol) was stirred for one day. Dichloro(α,α′-bipyridine)palladium(II) was precipitated (0.0825 g, 96%) and the parent iminophosphorane was quantitatively liberated in a benzene solution. They were identified by comparison with authentic samples. A similar procedure was used in the reaction of 7B with four equimolar amounts of triphenylphosphine; the reaction gave quantitatively dichlorobis(triphenylphosphine)palladium(II) and the parent iminophosphorane. In the case of two equimolar amounts of triphenylphosphine, the reaction proceeded with one half mole of dichlorobis(triphenylphosphine)palladium(II); one half mol of **7B** was recovered.

Reaction of Trimethylphosphite with Dichlorodi-μ-chlorobis-(p-tolyliminotriphenylphosphorane)dipalladium(II) (5B). To a benzene (7 ml) solution of 5B (0.1627 g, 1.497 mmol), trimethylphosphite (0.0276 g, 5.990 mmol) was added under nitrogen. After the mixture had been stirred at room temperature for 3 hr, the solvent was evacuated. The white residue was recrystallized from chloroform–ether. Dichlorobis(trimethylphosphite)palladium(II) was thus obtained (0.1053 g, 81%).

Results and Discussion

The reaction between dichlorobis(benzonitrile)palladium(II) and aryliminotriphenylphosphorane in benzene took place at room temperature overnight under an inert atmosphere to give dark brown precipitates with the composition of $\{[(C_6H_5)_3P{=}N{-}C_6H_4{-}X\text{-}p]PdCl_2\}_2$ (X=NO_2, **1B**; $COOC_2H_5$, **2B**; Cl, **3B**; H, **4B**; CH_3, **5B**) in a quantitative yield. When these precipitates, **1B—5B**, were recrystallized from an acetonitrile–ethyl acetate (1: 2) mixed solvent, the palladium-chloride bridge of **1B—5B** was cleaved with acetonitrile to give $[(C_6H_5)_3P{=}N{-}C_6H_4{-}X\text{-}p]PdCl_2(CH_3CN)$ (X=NO_2, **1A**; $COOC_2H_5$, **2A**; Cl, **3A**; H, **4A**; CH_3, **5A**). The IR absorptions of the ν(P=N) stretching frequencies of free and complexed aryliminotriphenylphosphoranes, those of the ν(Pd–Cl) region, and those of the ν(C≡N) region are summarized in Table 2.

The difference in stretching frequencies, $\Delta\nu$(P=N), between free and complexed aryliminotriphenylphosphoranes shows that the electron-releasing substituent strengthens the bonding of the Pd–N bond except in the case of the *p*-methyl substituent, as is shown in Fig. 1.

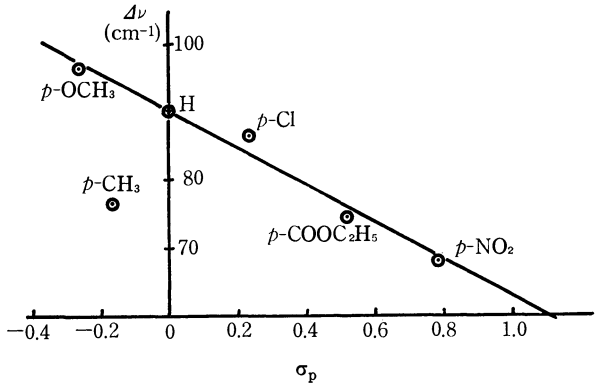

Fig. 1. A correlation between $\Delta\nu$(P=N) and Hammett constants (σ_p) in aryliminotriphenylphosphorane complexes.

There are four ν(Pd–Cl) absorptions in the initially formed dimeric complexes (B); they became a simple band after recrystallization from acetonitrile–ethyl acetate. This fact supports the view that readily coordinating acetonitrile cleaved the dichlorobridging to afford the monomeric complex (A). The PMR spectrum of **5A** also indicates the presence of coordinated acetonitrile at τ 8.00 as a sharp singlet.

Monomeric aryliminotriphenylphosphorane complexes containing acetonitrile as a coordinated ligand can be represented by two resonance structures, the zwitter-ionic form (**C**) and the coordinated form (**D**):

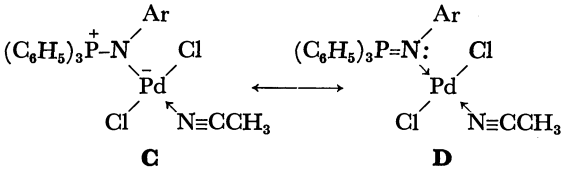

The *trans* configuration of acetonitrile and aryliminotriphenylphosphorane is favorable, since the ν(C≡N) band of the complex was at the higher frequencies [2311—2329 cm^{-1}; each value is closer in order to the complexed ν(P=N) and ν(Pd–Cl) bands] than is that of free acetonitrile (2255 cm^{-1}), as is shown in Table 2. Aryliminotriphenylphosphorane, which has an electron-attracting substituent, displays a weak

Table 2. Infrared spectra of parent iminophosphoranes, $(C_6H_5)_3P{=}N{-}C_6H{-}X\text{-}p$; bridging dimers, $\{[(C_6H_5)_3P{=}C{-}N{-}C_6H_4{-}X\text{-}p]PdCl_2\}_2$ (**B**); and mononuclear complexes, $[(C_6H_5)_3P{=}N{-}C_6H_4{-}X\text{-}p]PdCl_2(CH_3CN)$ (**A**)

Complex	X	ν (P=N) cm^{-1}		Δν(P=N) cm^{-1}	ν (Pd–Cl) cm^{-1}					ν (C≡N) cm^{-1}
		free	complexed **A** and **B**		**B**				**A**	**A**
1	NO_2	1364	1296	68	308	319	329	349	334	2311
2	$COOC_2H_5$	1356	1282	74	303	322	330	341	330	2313
3	Cl	1339	1253	86	295	310	333	361	330	2313
4	H	1338	1248	90	303	312	323	345	322	2315
5	CH_3	1325	1249	76	302	314	327	349	319	2329

trans effect on acetonitrile, which coordinates at the lone pair of the nitrogen atom. Alternatively, the monomeric complex (**A**) exhibits one distinct ν(Pd-Cl) frequency in the region of 319—334 cm^{-1}. This also suggests a *trans*-configuration structure with a higher symmetry.

When a strongly electron-releasing *p*-methoxy substituent was introduced, acetonitrile could not cleave the dichlorobridging and gave only the dimeric complexes (**B**), in contrast to the above complexes (**1**—**5**).

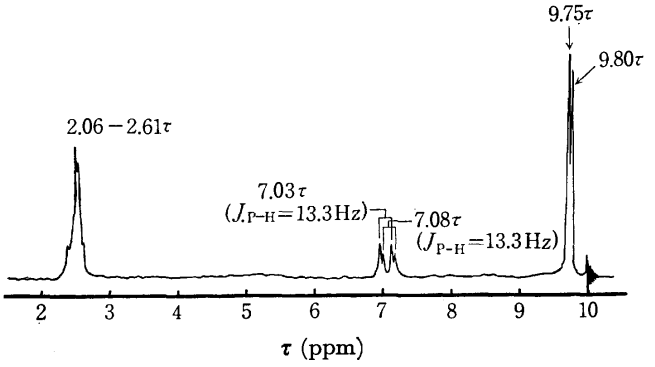

Fig. 2. Proton magnetic resonance spectrum of $\{[(C_6H_5)_2(CH_3)P{=}N{-}Si(CH_3)_3]PdCl_2\}_2$, **7B** in $CDCl_3$. Proton ratio at τ 7.03: 7.07=2: 1, and τ 9.75: 9.08 =2: 1.

When *N*-trimethylsilyliminodiphenylmethylphosphorane was used instead of *N*-aryliminotriphenylphosphoranes as a ligand, a stable dimeric complex (**7B**) was obtained. The PMR spectrum, shown in Fig. 2, suggests the presence of two isomers. Four ν(Pd-Cl) bands were observed at 306, 328, 350, and 361 cm^{-1}, indicative of a dimeric structure. The ν(P=N) in benzene was observed at 1070 cm^{-1}, 227 cm^{-1} lower than the free ligand (at 1307 cm^{-1} in benzene). Such a large absorption difference compared with the aryliminotriphenylphosphorane complexes may be ascribed to the exclusive contribution of the zwitter-ionic structure to **7B**. From the PMR spectrum, we concluded that **7B** is present as a mixture of *cis* and *trans* (1 : 2) isomers.

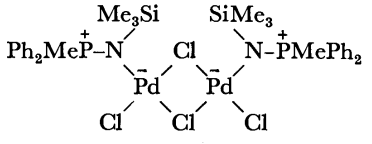

7B-*cis*

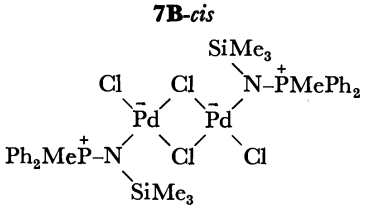

7B-*trans*

Ph=C_6H_5, Me=CH_3

Such a zwitter-ionic structure had previously been established by an X-ray analysis of the nickl-phosphorus ylide complex.[24] It is interesting that the Si–N bond in **7B** is quite stable to hydrolysis. Such a stabilization can be explained in terms of the enhanced (2p-3d)π interaction, which is induced by the transmission of the negative charge on the anionic palladium to vacant 3d orbitals on the silicon atom through rehybridized 2p orbitals on the central nitrogen atom.

Finally, the ligand substitution of aryliminotriphenylphosphorane complexes was attempted with **2B**. The coordinated *p*-ethoxycarbonylphenyliminotriphenylphosphorane was selectively liberated by α,α′-bipyridine or triphenylphosphine to give the dichloro(α,α′-bipyridine)palladium(II) or the dichlorobis(triphenylphosphine)palladium(II) complex. A similar result was obtained by the reaction of **5B** with trimethylphosphite. These results suggest that aryliminotriphenylphosphoranes are weaker ligands than α,α′-bipyridine, triphenylphosphine, and trimethylphosphite.

References

1) F. R. Kreissl, C. G. Kreiter, and E. O. Fischer, *Angew. Chem. Intern. Ed. Engl.*, **11**, 643 (1972).
2) H. H. Karsch, H. F. Klein, and H. Schmidbaur, *Chem. Ber.*, **107**, 93 (1974).
3) H. Schmidbaur and K. H. Räthlein, *ibid.*, **107**, 102 (1974).
4) W. Hieber, *ibid.*, **95**, 3070 (1962).
5) A. Greco, *J. Organometal. Chem.*, **43**, 351 (1972).
6) K. A. O. Starzewski, H. T. Dieck, K. D. Franz, and F. Hohmann, *ibid.*, **42**, C35 (1972).
7) D. K. Mitchell, W. D. Korte, and W.C. Kaska, *Chem. Commun.*, **1970**, 1384.
8) S. Z. Goldberg, D. K. Duesler, and K. N. Raymond, *ibid.*, **1971**, 826.
9) W. C. Kaska, D. K. Mitchell, and R. F. Reichelderfer, *J. Organometal. Chem.*, **47**, 391 (1973).
10) W. Malish, *ibid.*, **61**, C15 (1973).
11) N. A. Baily, R. D. Gillard, M. Keeton, R. Mason, and D. R. Russell, *Chem. Commun.*, **1966**, 396.
12) M. Keeton, R. Mason, and D. R. Russell, *J. Organometal. Chem.*, **33**, 259 (1971).
13) F. R. Kreissl and E. O. Fischer, *Chem. Ber.*, **107**, 183 (1974).
14) D. Bravo, G. Fronza, C. Ticozzi, and G. Gaudiano, *J. Organometal. Chem.*, **74**, 143 (1974).
15) G. Matsubayashi, M. Toriuchi, and T. Tanaka, *Chem. Lett.*, **1973**, 985.
16) H. Koezuka, G. Matsubayashi, and T. Tanaka, *Inorg. Chem.*, **13**, 443 (1974).
17) P. Appel and R. Schaaff, *Z. Naturforsch.*, **16b**, 405(1961).
18) K. B. Yatsimirskii, Z. A. Sheka, and E. I. Sinyavskaya, *Zh. Neorg. Khim.*, **15**, 1552 (1970).
19) W. Hieber, E. Winter, and E. Schubert, *Chem. Ber.*, **95**, 3070 (1962).
20) H. Bock and H. T. Dieck, *Z. Naturforsch.*, **21b**, 739 (1966); H. Bock and H. T. Dieck, *Z. Anorg. Chem.*, **345**, 9 (1966).
21) M. S. Kharasch, R. C. Seyler, and F. R. Mayo, *J. Amer. Chem. Soc.*, **60**, 882 (1938).
22) L. Horner and H. Oediger, *Ann. Chem.*, **627**, 142 (1959).
23) K. Itoh, M. Okamura, and Y. Ishii, *J. Organometal. Chem.*, **68**, 327 (1974).
24) C. Krüger, *Angew. Chem. Intern. Ed. Engl.*, **11**, 387 (1972).

Effect of Various Additives on Color Center Formation and Brightness Depreciation of Calcium Halophosphate Phosphors

Kazuo NARITA and Nobuyuki TSUDA

Toshiba Research and Development Center, 1 Komukai-Toshibacho, Saiwaiku, Kawasaki 210

(Received February 14, 1975)

Color center formation and brightness depreciation by 185 nm radiation were studied in calcium halophosphates containing various additives. Partial bleaching experiments show that the depreciation of plaque brightness is due to the absorption of 254 nm radiation by color centers, the reabsorption of luminescence by color centers being unimportant. In unactivated Ca halophosphates, the stronger the 185 nm absorption of additives, the weaker the color center formation. In Sb- and Mn-activated Ca halophosphates, however, no clear relation is found between the 185 nm absorption of additives and the brightness depreciation. The effect of cesium on improving lamp performance is described.

A great deal of information has been accumulated on the color centers of calcium halophosphate.[1-17] In fluorescent lamps, color centers are formed in halophosphate phosphors by exposure to 185 nm Hg radiation. It has been established that the decrease of lumen output in the first several minutes of lamp operation is closely related to the formation of color centers.[6,8] These centers are assumed to absorb a part of 254 nm exciting radiation and/or emitted luminescence energy in the visible region. It would be of great practical meaning to suppress, if not to prevent, the formation of color centers in halophosphate phosphors.

Aia and Poss[18] found that the initial light output of a fluorescent lamp is increased when a few percent of Cd is incorporated in halophosphate phosphors. Apple[6] explained the effect of Cd as follows. By introducing Cd, a strong absorption band appears in the wavelength region shorter than 200 nm in Ca halophosphate, which, in its pure state, is transparent down to 150 nm. In this manner, Cd provides a new process by which a considerable part of the deleterious 185 nm radiation is absorbed and dissipated without creating color centers. The major part of color centers is created in the first several minutes of lamp operation. It is, therefore, understandable why the "initial" lamp efficiency, which is usually measured after several tens of minutes of stabilization, appears to be increased.

If one follows Apple's explanation, other elements which would equal or surpass Cd in improving lamp efficiency might be found by examining whether the elements in question fulfill the following two conditions.

(I) In order to suppress the formation of color centers, such elements that give rise to strong absorption in the 185 nm region in the halophosphate matrix would be effective.

(II) The elements mentioned above should have little or no absorption at 254 nm and in the visible region, so that they absorb neither 254 nm exciting radiation nor the emitted fluorescence.

In this work, diffuse reflection spectra of Ca halophosphates with various metal additives were measured between 180 and 650 nm. Then it was checked whether any additive exists which satisfies the above conditions, and whether the element selected in this manner really brings about the expected decrease of depreciation.

Experimental

Materials. Samples prepared were: (1) Sb- and Mn-activated halophosphate $Ca_{9.5}Sb_{0.1}Mn_{0.2}(PO_4)_6(F_{0.9}Cl_{0.1})_2$, which has a composition close to that of commercial 4200 K phosphor (hereafter referred to as "Standard"), (2) unactivated halophosphate $Ca_{9.8}(PO_4)_6(F_{0.9}Cl_{0.1})_2$ ("Matrix"), (3) unactivated halophosphates with additives $Ca_{9.7}M_{0.1}(PO_4)_6(F_{0.9}Cl_{0.1})_2$ where M represents metal additives ("Series A" samples), and (4) $Ca_{9.4}M_{0.1}Sb_{0.1}Mn_{0.2}(PO_4)_6(F_{0.9}Cl_{0.1})_2$ ("Series B" samples). The raw materials ($CaHPO_4$, $CaCO_3$, CaF_2, $CaCl_2$, Sb_2O_3, $MnCO_3$ and a suitable compound of the desired metal M) were dry-mixed, ignited at 1150 °C for 30 min in air, ground thoroughly and ignited again under the same conditions.

Formation and Bleaching of Color Centers. Color centers were formed by 185 nm radiation from a 10 W, low pressure mercury lamp with a quartz envelope. Phosphor plaques were placed about 1 cm below the lamp. All the irradiation experiments were carried out in a vacuum. In order to bleach the color centers, samples were irradiated with a germicidal lamp or a 500 W Xenon arc lamp coupled with appropriate filters.

Measurements. Reflection spectra were measured with a Jarrel-Ash vacuum monochromator of Seya-Namioka type (model 78—660) in vacuum ultraviolet, and with a Perkin-Elmer monochromator (model E1) in the UV and visible regions.

Brightness of phosphor plaques was obtained by integrating the emission spectra. For this purpose, a ZV-1 spectroradiometer[19] equipped with a Perkin-Elmer printing integrator was used. The 254 nm exciting radiation was made as weak as possible to prevent the bleaching of color centers during the course of brightness measurements. It was confirmed that the emission spectra of investigated samples change little with the 185 nm irradiation.

Results and Discussion

Correlation between Plaque Brightness and 254 nm Absorption by Additives. Wachtel investigated thoroughly the relation between the concentration of various impurities and plaque brightness of a 3000 K Ca halophosphate phosphor.[20] In order to examine the above-mentioned condition II more quantitatively, an attempt was made to correlate the plaque brightness of Series B phosphors with the 254 nm absorption due to additives.

In the calculations described below, the following

assumptions are made:

(1) Additives absorb the exciting 254 nm light and dissipate it nonradiatively.

(2) They do not sensitize nor quench the luminescence of the activators.

(3) They do not absorb the visible emission.

The plaque brightness of Series B samples, I, is given by

$$I = cE_e(1-R_B(\lambda_e))\frac{k_{ac}(\lambda_e)}{k_{ac}(\lambda_e)+k_m(\lambda_e)+k_{ad}(\lambda_e)}, \quad (1)$$

where c is a constant, E_e the energy of 254 nm exciting radiation and $R_B(\lambda_e)$ the diffuse reflectance at 254 nm, while $k_{ac}(\lambda_e)$, $k_m(\lambda_e)$ and $k_{ad}(\lambda_e)$ are the 254nm absorption coefficients of activators, pure halophosphate matrix, and metal additives, respectively.

The plaque brightness of Standard, I_0, is given by

$$I_0 = cE_e(1-R_0(\lambda_e))\frac{k_{ac}(\lambda_e)}{k_{ac}(\lambda_e)+k_m(\lambda_e)}, \quad (2)$$

where $R_0(\lambda_e)$ is the diffuse reflectance of Standard at 254 nm.

The absorption coefficients are correlated with diffuse reflectance by the Kubelka-Munk formula[21]

$$\frac{k}{s} = \frac{(1-R)^2}{2R}, \quad (3)$$

where s is scattering coefficient. The ratio k/s is called remission function. It is assumed that s is constant for all the samples. The ratio $(1-R_B(\lambda_e))/(1-R_0(\lambda_e))$ is close to unity in the presence of strong absorption of activators. Thus, the relative plaque brightness of Series B phosphors compared to Standard, I/I_0, is given by

$$\frac{I}{I_0} \fallingdotseq \frac{k_{ac}(\lambda_e)+k_m(\lambda_e)}{k_{ac}(\lambda_e)+k_m(\lambda_e)+k_{ad}(\lambda_e)} = \frac{(1-R_0(\lambda_e))^2/2R_0(\lambda_e)}{\{(1-R_0(\lambda_e))^2/2R_0(\lambda_e)+(1-R_A(\lambda_e))^2/2R_A(\lambda_e) - (1-R_m(\lambda_e))^2/2R_m(\lambda_e)\}} \quad (4)$$

where $R_A(\lambda_e)$ and $R_m(\lambda_e)$ are diffuse reflectance of Series A samples and Matrix at 254 nm, respectively.

Figure 1 shows diffuse reflection spectra of Matrix,

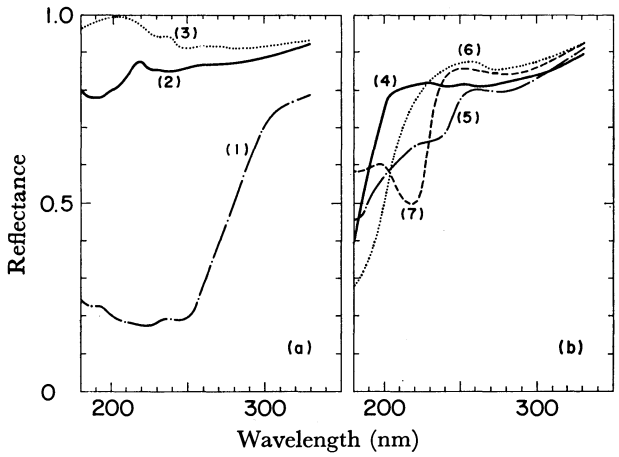

Fig. 1. Diffuse reflection spectra of Standard, Matrix and selected Series A samples (Additives are specified below).
(1) Standard. (2) Matrix. (3) Cs. (4) Cd. (5) Zr. (6) Ge. (7) Tb.

Standard and selected Series A samples. The $R_A(\lambda_e)$ values of all of Series A samples and the I/I_0 values of the corresponding Series B phosphors are given in Table 1. The same data are plotted also in Fig. 2. Using the observed values of $R_0(\lambda_e)=0.228$ and $R_m(\lambda_e)=0.865$, the dependence of I/I_0 on $R_A(\lambda_e)$ was calculated by Eq. (4) (solid line curve, Fig. 2).

TABLE 1. SUMMARY OF REFLECTANCE AND BRIGHTNESS DEPRECIATION DATA

Additive	$R_A(\lambda_e)$	I/I_0	$R_A(\lambda_1)$	$k_c(\lambda_e)/s$	I_1/I	$(I/I_0)\times(I_1/I)$
Standard	0.865	1.000	0.782	0.936	0.800	0.800
Li	0.700	0.907	0.702	1.02	0.821	0.745
Na	0.690	0.894	0.762	0.66	0.839	0.750
K	0.782	0.959	0.904	0.84	0.829	0.795
Rb	0.782	0.971	0.866	0.92	0.819	0.795
Cs	0.911	1.005	0.976	0.90	0.844	0.848
Cu	0.191	0.291	0.251	0.60	0.789	0.229
Ag	0.749	0.920	0.637	0.79	0.820	0.755
Au	0.798	0.787	0.848	0.74	0.755	0.594
Mg	0.860	0.952	0.875	0.86	0.780	0.743
Sr	0.811	0.993	0.804	0.85	0.800	0.795
Ba	0.821	0.971	0.735	0.96	0.806	0.782
Zn	0.780	0.866	0.476	0.96	0.816	0.706
Cd	0.815	0.999	0.500	0.66	0.834	0.833
Hg	0.824	1.018	0.799	0.82	0.809	0.824
Sc	0.766	0.948	0.789	0.86	0.765	0.725
Y	0.801	0.975	0.793	0.82	0.796	0.776
B	0.760	0.985	0.748	0.86	0.811	0.799
Al	0.831	1.001	0.829	0.86	0.795	0.796
Ga	0.719	0.758	0.482	0.76	0.776	0.588
In	0.481	0.831	0.204	0.68	0.744	0.618
Tl	0.829	0.986	0.666	0.86	0.797	0.786
Ti	0.252	0.259	0.139	0.44	0.799	0.207
Zr	0.789	0.971	0.469	0.60	0.820	0.797
Hf	0.618	0.894	0.466	0.60	0.860	0.768
Si	0.880	0.989	0.845	0.69	0.796	0.787
Ge	0.870	0.968	0.198	0.53	0.786	0.761
Sn	0.536	0.616	0.451	0.66	0.815	0.502
Pb	0.450	0.716	0.345	0.48	0.858	0.614
V	0.149	0.180	0.140	0.18	0.835	0.150
Nb	0.160	0.417	0.178	0.70	0.792	0.330
Ta	0.441	0.707	0.345	0.60	0.811	0.574
As	0.820	0.852	0.440	0.56	0.809	0.690
Bi	0.125	0.572	0.170	0.73	0.881	0.504
Cr	0.408	0.593	0.214	0.40	0.773	0.459
Mo	0.299	0.255	0.307	0.26	0.660	0.168
W	0.380	0.431	0.262	0.86	0.838	0.361
Fe	0.208	0.435	0.192	0.16	0.898	0.391
Co	0.802	0.158	0.190	0.18	0.850	0.134
Ni	0.631	0.347	0.242	0.22	0.857	0.297
La	0.830	0.966	0.793	0.86	0.784	0.757
Ce	0.502	0.814	0.618	0.61	0.815	0.663
Pr	0.850	0.799	0.411	0.42	0.797	0.637
Nd	0.842	0.599	0.366	0.47	0.801	0.480
Sm	0.780	0.885	0.364	0.43	0.779	0.689
Eu	0.441	0.785	0.445	0.48	0.775	0.609
Gd	0.838	0.945	0.950	0.70	0.798	0.754
Tb	0.859	0.969	0.601	0.56	0.790	0.765
Dy	0.850	0.909	0.623	0.67	0.776	0.703
Ho	0.820	0.765	0.581	0.65	0.795	0.608
Er	0.800	0.787	0.756	0.65	0.805	0.633
Tm	0.838	0.872	0.744	0.60	0.811	0.707
Yb	0.763	0.874	0.620	0.63	0.801	0.700
Lu	0.838	0.963	0.742	0.72	0.796	0.766

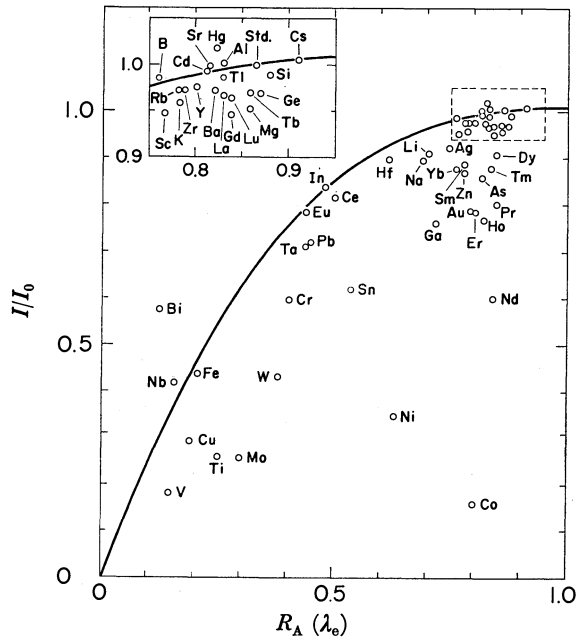

Fig. 2. Relation between 254 nm reflectance of Series A samples ($R_A(\lambda_e)$) and relative plaque brightness of corresponding Series B samples (I/I_0). Names of additives are indicated in the figure.

We see that the experimental I/I_0 values of such Series B samples as those containing K, Rb, Cs, Mg, Sr, Ba, Cd, Hg, Sc, Y, B, Al, Tl, Zr, Si, Ge, La, Gd, Tb, Lu, In, Eu, Fe and Nb are close to the calculated values. Of these, the first twenty additives might be of practical value, since their I/I_0 values are high. For the additives not mentioned above, I/I_0 is much lower than expected from Eq. (4), indicating that assumptions (2) and (3) are more or less invalid.

Change of Plaque Brightness due to Color Center Bleaching. As the absorption due to the color centers of Ca halophosphate extends from UV to visible region, both the 254 nm exciting radiation and the emission in the visible region may be absorbed by the color centers. In order to determine which of these two absorption processes is dominant in brightness depreciation, the effect of partial bleaching on plaque brightness was investigated.

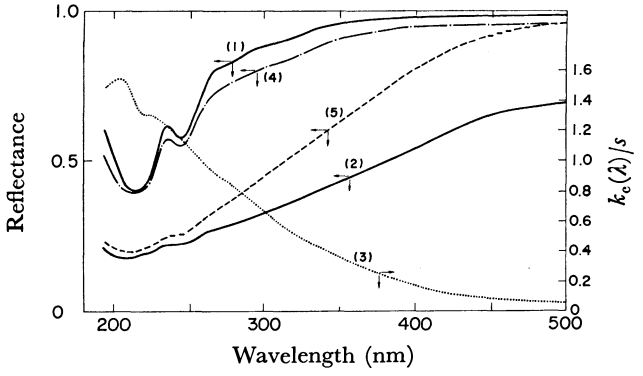

Fig. 3. Change of diffuse reflection spectrum of $Ca_{9.7}Sb_{0.03}(PO_4)_6(F_{0.9}Cl_{0.1})_2$ by 185 nm irradiation and by subsequent bleaching. (1) Before irradiation. (2) After 185 nm irradiation (6 hr in vacuum). (3) Spectrum of $k_c(\lambda)/s$ calculated from (1) and (2). (4) After bleaching by 254 nm light (1 hr). (5) After bleaching by blue light through UV 39+V-V 40 filters (10 hr).

Figure 3 shows the change of diffuse reflection spectra of a $Ca_{9.7}Sb_{0.03}(PO_4)_6(F_{0.9}Cl_{0.1})_2$ phosphor during the course of bleaching of color centers. The sample containing only a small amount of Sb was chosen because of ease of reflectance measurements. This sample has a weak absorption due to Sb in the UV region (curve (1)). The reflection spectrum after 185 nm irradiation (6 hr in a vacuum) is shown by curve (2). The remission function of the induced color centers, $k_c(\lambda)/s$, was calculated by

$$\frac{k_c(\lambda)}{s} = \frac{(1-R_i(\lambda))^2}{2R_i(\lambda)} - \frac{(1-R(\lambda))^2}{2R(\lambda)}, \qquad (5)$$

where $R(\lambda)$ and $R_i(\lambda)$ are diffuse reflectance before and after irradiation, respectively. The result is shown by curve (3). The color centers were then bleached, either by 254 nm light from a germicidal lamp or by blue light from a xenon lamp coupled with Toshiba UV-39 (sharp cut-off at 390 nm) and V-V 40 (band pass with peak at 400 nm) filters. The results are shown by curves (4) and (5), respectively. Note that 254 nm irradiation bleaches the color centers almost completely, while the blue light bleaches the color centers in the visible, with little change in the 254 nm region.

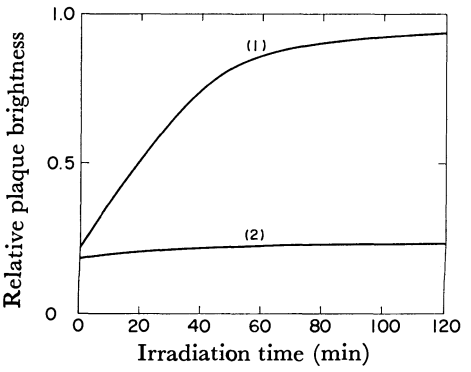

Fig. 4. Change of plaque brightness during bleaching. The sample was first irradiated by 185 nm light and then (1) by 254 nm light, (2) by blue light through UV 39+V-V 40 filters.

Figure 4 shows the change of plaque brightness of the same phosphor by bleaching. It is seen that the brightness, which has decreased to about 20% of the initial value due to 6 hr 185 nm irradiation, is almost completely restored by exposition to 254 nm light. On the other hand, little restoration of brightness is observed by blue light irradiation. It is thus concluded that the brightness depreciation is caused by the absorption of 254 nm light by color centers, the self-absorption of the emission in the visible region being unimportant. This might be due to the fact that the absorption of the color centers is very weak for the visible luminescence as compared with the absorption for the 254 nm radiation (Fig. 3, curve (3)). The same results as those shown in Figs. 3 and 4 were obtained for Standard phosphor.[22]

The nonradiative energy transfer from Sb to color

centers, proposed recently by Parodi,[17] does not seem to play a significant role in this case, since, in his concept, bleaching of color centers in the visible region should result in the recovery of brightness.

Relation between 185 nm Absorption and Color Center Formation. The next step is to investigate whether condition I can be used as a criterion to find other additives which are effective in suppressing the formation of color centers.

As a measure of the concentration of color centers, the remission function of the color centers at 254 nm, $k_c(\lambda_e)/s$, is used, since this value determines the extent of brightness depreciation.

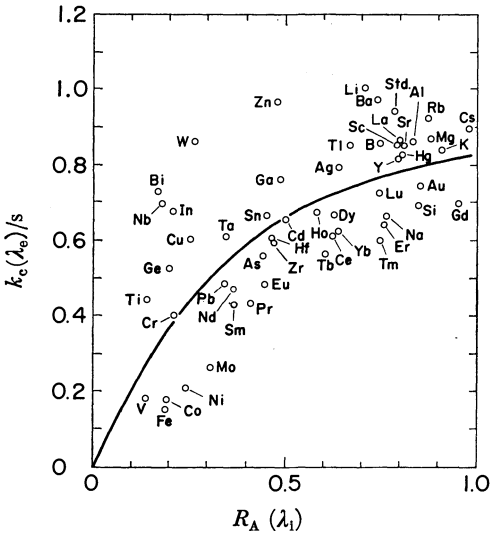

Fig. 5. Relation between 185 nm reflectance ($R_A(\lambda_i)$) and the extent of 254 nm absorption due to induced color centers ($k_c(\lambda_e)/s$) in Series A samples. Irradiation by 185 nm light was carried out for 6 hr in vacuum.

Figure 5 shows the relation between the reflectance at 185 nm ($R_A(\lambda_i)$) and the $k_c(\lambda_e)/s$ values induced by 6 hr of 185 nm irradiation in Series A samples. As expected, the stronger the 185 nm absorption due to additives, the weaker the color center formation. Of the twenty additives selected in accordance with condition II, Cd, Zr, Ge and Tb give rise to strong absorptions at 185 nm. Out of these additives, Cd, Zr and Tb suppress the formation of color centers to the extent expected for their $R_A(\lambda_i)$ values. Germanium also has such an effect, but less than expected for its strong absorption at 185 nm.

Relation between Color Center Formation and Brightness Depreciation. In order to calculate the relative brightness depreciation by color center formation, the view deduced from partial bleaching experiments is adopted. That is, a part of 254 nm light is absorbed and dissipated by color centers, the reabsorption of the emitted light being negligible. In a similar way to Eq. (4), the relative brightness in the presence of color centers, I_i/I, is given by

$$\frac{I_i}{I}=\frac{1-R_{Bi}(\lambda_e)}{1-R_B(\lambda_e)}\cdot\frac{k_{ac}(\lambda_e)+k_m(\lambda_e)+k_{ad}(\lambda_e)}{k_{ac}(\lambda_e)+k_m(\lambda_e)+k_{ad}(\lambda_e)+k_c(\lambda_e)}, \quad (6)$$

where I and I_i are the plaque brightness of Series B samples before and after 185 nm irradiation, respectively, and $R_{Bi}(\lambda_e)$ is 254 nm reflectance of Series B phosphors after irradiation.

In the first approximation, the term $k_{ad}(\lambda_e)$ is neglected, which in most cases is much smaller than the absorption coefficient of activators. Moreover, it is assumed that $k_c(\lambda_e)/s$ is related to $R_A(\lambda_i)$ by the solid line curve of Fig. 5. The values of I_i/I can then be calculated numerically as a function of $R_A(\lambda_i)$.

Figure 6 shows the result of this calculation (solid line curve) as well as experimental brightness depreciation data under 6 hr of 185 nm irradiation. The individual $R_A(\lambda_i)$ and I_i/I values are given in Table 1.

The calculation predicts that the brightness depreciation of Series B phosphors under this irradiation condition will be 15—25%. Another prediction is that the brightness would decrease, for example, by *ca.* 6% as compared to Standard, if one could find such an additive with $R_A(\lambda_i)=0.20$ with no absorption at 254 nm.

The experimental I_i/I_0 values are, as a whole, in rough agreement with the calculated one (Fig. 6). The dependence of I_i/I_0 on $R_A(\lambda_i)$ is, however, not so explicit as predicted by calculation. Some particular cases are discussed below.

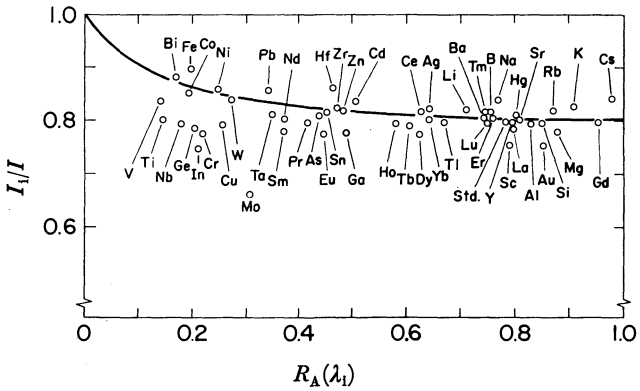

Fig. 6. Relation between 185 nm reflectance of Series A samples ($R_A(\lambda_i)$) and relative brightness after depreciation (I_i/I). Irradiation by 185 nm light was carried out for 6 hr in vacuum. Solid line curve was calculated by Eq. (6).

Considering the results mentioned in the previous section, particular attention was paid to Series B phosphors containing Cd, Zr, Ge and Tb. Cd- and Zr-containing phosphors show better performance than Standard under 185 nm radiation (Table 1 and Fig. 6). It was found, however, that Zr-containing phosphor has some disadvantages. Its initial brightness is inferior to that of Cd-containing phosphors. It tends to sinter slightly during lamp baking, thus giving an inhomogeneous phosphor layer.

Additives Ge and Tb were found, for unknown reasons, to be ineffective in improving performance. It seems that the absorption spectra of color centers in the presence of the activators differ considerably from those in the absence of activators. In short, application of conditions I and II did not lead to the finding of another additive having an advantage over Cd.

It was found unexpectedly that the addition of Cs improves not only the initial brightness, but also the maintenance. The increase of initial brightness can be understood in terms of the decreased absorption at 254 nm (Fig. 1, curve (3)). However, the reason for the brightness depreciation of the Cs-containing phosphor being even smaller than the Cd-containing phosphor (Table 1 and Fig. 6) is inexplicable, since Cs does not suppress color center formation at all (Fig. 5). Microscopic observation revealed that the Cs-containing phosphor is much more transparent or "porosity-free" than Standard. The optimum amount of Cs to be added depends strongly on the ignition conditions. In routine production, the best result was obtained when 0.03—0.1 g atom Cs was added to 1 mol phosphor. By chemical analysis, only a very small portion of the added Cs (<100 ppm) was found in the ignited phosphor. Moreover, the particle size of the Cs-containing phosphor was slightly greater than Standard. It is thus postulated that the added Cs compound (usually Cs_2CO_3) acts as a flux in the ignition process.

The promising outcome on the Cs-containing phosphor powder prompted a large scale lamp test using this phosphor. These lamps have 1—1.5% more initial lumen output than the reference lamps coated with Standard phosphor, and the decrease of the output after 1000 hr of operation is about 1% less than that of the reference. This result compares favorably with the Cd-containing phosphor, which gives 2% more initial lumens than the reference lamps, but no advantage in performance for long-term operation.

The authors wish to express their gratitude to Dr. Y. Uehara, presently at St. Marianna University, for suggesting this work. Thanks are also due to Dr. M. Tamatani for valuable discussions, A. Taya for sample preparation and M. Inoue and his group for lamp data.

References

1) H. Ikegami and M. Kobayashi, *Toshiba Review*, **13**, 51 (1958).
2) L. Suchow, *J. Electrochem. Soc.*, **108**, 847 (1961).
3) P. D. Johnson, *J. Appl. Phys.*, **32**, 127 (1961).
4) B. Segall, G. W. Ludwig, H. H. Woodbury, and P. D. Johnson, *Phys. Rev.*, **128**, 76 (1962).
5) J. H. Singleton and L. Suchow, *J. Electrochem. Soc.*, **110**, 36 (1963).
6) E. F. Apple, *ibid.*, **110**, 374 (1963).
7) R. K. Swank, *Phys. Rev.*, **135A**, 266 (1964).
8) L. E. Vrenken, T. H. De Vette, and R. W. Van der Wolf, *Illum. Eng.*, **59**, 59 (1964).
9) W. W. Piper, L. C. Kravitz, and R. K. Swank, *Phys. Rev.*, **138A**, 1802 (1965).
10) S. Kamiya and H. Shibata, *Denki Kagaku*, **33**, 895 (1965), **35**, 154 (1967) and **35**, 718 (1967).
11) E. F. Apple and J. O. Aicher, "Proc. Int. Conf. Luminescence," 2013, Akademiai Kiado, Budapest (1966).
12) G. Dejardin, R. Falgon, and J. Janin, *Compt. Rend.* **264B**, 481 (1967).
13) G. T. Bauer, *J. Electrochem. Soc.*, **115**, 1176 (1968).
14) D. I. M. Knotterus, H. W. Den Hartog, and W. Van der Lugt, *Phys. Stat. Solidi*, **13A**, 505 (1972).
15) R. W. Warren, *Phys. Rev.*, **6B**, 4679 (1972).
16) R. W. Warren, J. Van Broekhoven, and F. M. Ryan, *Electrochem. Soc. Meeting Abstract*, 97 (1974).
17) J. A. Parodi, *J. Luminescence*, **9**, 315 (1974).
18) M. A. Aia and S. M. Poss, U. S. 2965786 (1960).
19) Y. Uehara, T. Kushida, K. Hanada, and S. Kaneko, *Toshiba Rev.*, **17**, 857 (1962).
20) A. Wachtel, *J. Electrochem. Soc.*, **105**, 256 (1958).
21) P. Kubelka, *J. Opt. Soc. Amer.*, **38**, 448 (1948).
22) K. Narita and N. Tsuda, 28th Annual Meeting of Chemical Society of Japan, 1V33 (1973).

ESR Studies of the Structures and Spin-exchange Interactions of the Dimers of Nitro-substituted Salicylaldehyde Schiff-base Complexes of Copper(II) in Frozen Solutions*

Makoto CHIKIRA and Taro ISOBE

Chemical Research Institute of Non-Aqueous Solutions, Tohoku University, Katahira, Sendai 980

(Received March 3, 1975)

The computer simulations of the ESR spectra for the triplet-state dimers of the title complexes in frozen solutions revealed that the dimeric structures change markedly upon nitro-substitutions at the positions of 3 or 5 in the phenyl-rings of the Schiff bases. It was also found that some of these nitro-substituted copper(II) complexes form 1 : 1 molecular complexes with bis(*N*-salicylideneisopropylaminato)copper(II) in toluene. The dependence of the ESR spectral intensities for the $\Delta M=2$ transitions upon the temperature in the range of 1.57—4.2 K indicated that the intra-dimer spin-exchange interactions are weakly anti-ferromagnetic (0.7—2.2 cm^{-1}).

Recently, many mononuclear copper(II) complexes have been found to be dimerized in solutions.[1-10] In our previous paper, it has been revealed that the angle (ξ) between the $g_{//}$ axis and the copper-copper axis for the dimers of various quadridentate salicylaldehyde Schiff-base complexes of copper(II) in frozen toluene solutions is considerably smaller than that for the bidentate ones.[6] However, we have now obtained a new experimental result that the dimeric structures of the Schiff-base complexes of copper(II) in frozen solutions change markedly upon the introduction of nitro-groups into the phenyl-rings of the Schiff bases at the 3 or 5 position. Moreover, it has been found that the nitro-substituted bidentate Schiff-base complexes of copper(II) form 1 : 1 molecular complexes in toluene with bis(*N*-salicylideneisopropylaminato)copper(II), which has no ability to be dimerized in toluene.

The purpose of this paper is to estimate the dimeric structures and intra-dimer spin-exchange interaction energies for these dimers and to investigate the nature of these dimerizations in solutions.

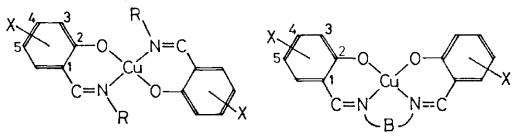

Cu(nX-RSal) Cu(nX-SalB)

Fig. 1. Schematic illustrations of salicylaldehyde Schiff-base complexes of copper(II). Following abbreviations were made.
Me=CH_3, Et=C_2H_5, *n*-Pr=C_3H_5, *iso*-Pr=$(CH_3)_2CH$, *t*-Bu=$C(CH_3)_3$, MeO=CH_3O, en=C_2H_4, pn=(CH_3)-$CHCH_2$, ibn=$(CH_3)_2CCH_2$, tren=$(CH_2)_3$.

Experimental

Materials. The copper(II) complexes generally represented as Cu($n$$NO_2$-RSal) and Cu($n$$NO_2$-SalB) (see Fig. 1) were prepared according to the method of Sacconi and Ciampolini.[11] Commercial toluene and nitroalkanes were purified by the usual methods.[12]

Measurements. The ESR spectra were measured at 77 K and in the range of 1.57—4.2 K. An improved insertion-type liquid helium Dewar in conjunction with a room-temperature cavity of a HITACHI 771 X-band ESR spectrometer was used for the measurements in the low-temperature range. The temperature below 4.2 K was obtained by pumping on liquid helium by means of a vacuum pump (150 l/min) and a manostat.

The sample solutions were transferred into thin quartz tubes (o. d. 2.0 mm). In order to secure thermal contact between the sample and liquid helium, the upper parts of the tubes were made open so that the tubes could be filled with the liquid helium. The relation between the microwave power and the intensity was examined at the lowest temperature of the measurement in every case in order to remove the effect of saturation in the measurement of the ESR spectral intensity.

Results and Discussion

Figure 2 shows the observed ESR spectra of Cu(5NO_2-EtSal) in toluene at 77 K. In general, the introduction of nitro-groups into the phenyl-rings of the Schiff base resulted in a decrease in the solubility of the copper(II) complexes in toluene. On the other hand, the ratio of dimers to monomers considerably increased with the nitro-substitutions. We have previously reported that, in the case of bidentate Schiff-base complexes of copper-(II) in toluene, the dimer formations are seriously inhibited by methyl or methoxy groups at the 3 positions in the phenyl-rings of the Schiff bases.[6] However, 3-nitro-groups did not hinder the dimerization at all. Moreover, the ratio of the triplet-state spectral intensity to the doublet-state one for Cu(3NO_2-EtSal) in toluene was larger than that for Cu(EtSal) at the same concentration. A similar correlation between the solubility and the ratio of dimers to monomers in solutions has been reported by Yokoi for bis(*t*-butylacetoacetato)-copper(II) in hydrocarbon solvents.[3]

The magnetic parameters for triplet-state dimers were defined in the manner previously described;[5,6] they are listed in Table 1, together with the data previously obtained for unsubstituted complexes.[5] In contrast to the parameters for the doublet-state monomers, those for the triplet-state dimers changed markedly with the nitro-substitutions. The triplet-state dimers of Cu-(3NO_2-EtSal) and Cu(5NO_2-EtSal) have the magnetic parameters characteristic of coaxial g and fine-structure tensors, that is, $g_2 \approx g_{M//}$ and $|A_{M//}/2| \approx A_1 \approx A_h$. In order to estimate the distance between the two copper ions and the ξ angle for theses dimers, the simulation

* Part of this report was preliminarily published in *Chem. Lett.*, **1974**, 865.

of the triplet ESR spectra was performed as has previously been described[5,10] on the basis of the spin-Hamiltonian expressed as:

$$\mathcal{H} = \beta g_{\perp}(S_xH_x+S_yH_y) + \beta g_{//}S_zH_z + A_{\perp}(S_xI_x+S_yI_y) + A_{//}S_zI_z+H_{dd}-JS_1\cdot S_2 \quad (1)$$

where H_{dd} is the point-spin-dipole interaction tensor; the other symbols have their usual meanings. The resonance magnetic fields were calculated by means of the perturbation calculations to the second order for both H_{dd} and hyperfine terms. The angular dependence of the transition probability was calculated by the use of the spin functions obtained from the first-order perturbation calculations only for H_{dd}.

As Fig. 2 shows, the observed spectra for Cu(5NO_2-EtSal) in toluene can be well simulated with the following spin-Hamiltonian parameters: $g_{//}=2.225$, $g_{\perp}=2.05$, $|A_{//}|=0.0095$ cm^{-1}, $|A_{\perp}|=0.0010$ cm^{-1}, r(copper–copper distance)=4.02 Å, and $\xi=15°$. The estimated values of r and ξ are very close to those for the dimers of Cu(EtSal) in methylcyclohexane[9] and for various quadridentate Schiff-base complexes of copper(II) in toluene.[6]

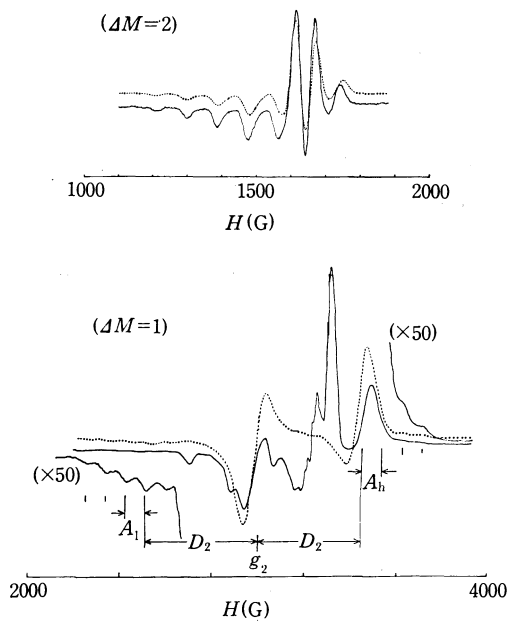

Fig. 2. ESR spectra of Cu(5NO_2-EtSal) in toluene at 77 K.
Broken lines: calculated spectra with the parameters, $g_{//}=2.225$, $g_{\perp}=2.050$, $|A_{//}|=0.0095$ cm^{-1}, $|A_{\perp}|=0.0010$ cm^{-1}, $r=4.02$ Å, $\xi=15°$, ΔH (Gaussian)=30 G ($\Delta M=1$) and 15 G ($\Delta M=2$). Microwave frequency; $\nu=9.2576$ GHz.

The triplet ESR spectra of Cu($n$$NO_2$-RSal) in toluene markedly changed in their line-shape upon the addition of a large excess of Cu(*iso*-PrSal). Figures 3 and 4 show the ESR spectra of Cu(5NO_2-EtSal) and Cu(5NO_2-*iso*-PrSal) respectively with a large excess of Cu(*iso*-PrSal) in toluene. The A_1 values (70 G) for these spectra are considerably smaller than those (87 G) for the dimers of Cu(5NO_2-EtSal) in toluene. The peaks near 3500 G are markedly broadened. It should be noted that neither Cu(*iso*-PrSal) nor Cu(5NO_2-*iso*-PrSal) in toluene exhibited triplet-sate ESR signals. Therefore, these triplet signals may be due to 1:1 molecular complexes of Cu(5NO_2-RSal) with Cu(*iso*-PrSal), although it remains uncertain whether these 1:1 complexes are the dimers of mixed-ligand complexes or the associated complexes of Cu($n$$NO_2$-RSal) and Cu(RSal).

Since the magnetic parameters for the monomers of Cu(5NO_2-*iso*-PrSal) are almost equal to those of Cu(*iso*-PrSal), Eq. (1) may still be a good approximated spin-Hamiltonian for the analysis of the triplet ESR

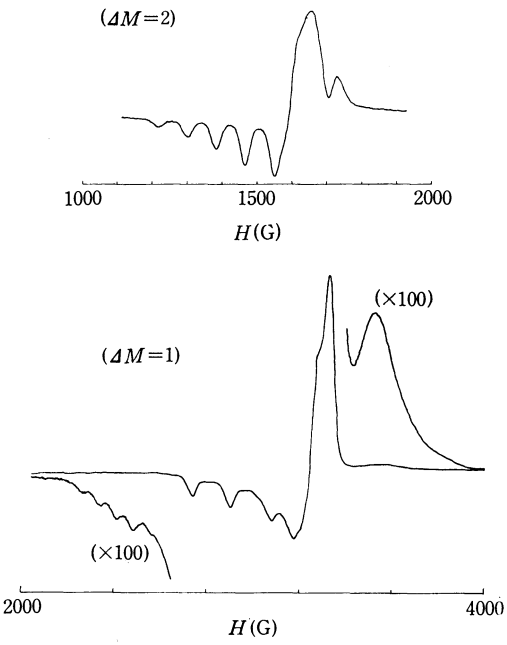

Fig. 3. ESR spectra of Cu(5NO_2-EtSal) with a large excess of Cu(*iso*-PrSal) in toluene at 77 K. $\nu=9.258$ GHz.

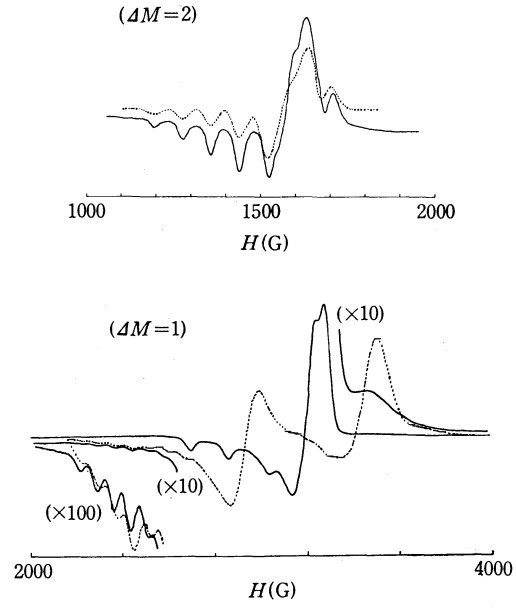

Fig. 4. ESR spectra of Cu(5NO_2-*iso*-PrSal) with a large excess of Cu(*iso*-PrSal) in toluene at 77 K. Broken lines: calculated spectra with the parameters, $g_{//}=2.230$, $g_{\perp}=2.040$, $|A_{//}|=0.0085$ cm^{-1}, $|A_{\perp}|=0.0015$ cm^{-1}, $r=3.75$ Å, $\xi=35°$, ΔH(Gaussian)=30 G ($\Delta M=1$) and 20 G ($\Delta M=2$).

spectra of the 1:1 molecular complexes. The best fit between observed and calculated spectra could be obtained with the following parameters: $g_{//}=2.23$, $g_{\perp}=2.04$, $|A_{//}|=0.0087$ cm^{-1}, $|A_{\perp}|=0.0015$ cm^{-1}, $r=3.75$ Å, and $\xi=35°$. These parameters are close to those of the dimers of Cu(*iso*-PrSal) in methylcyclohexane.[9]

In contrast with Cu(*iso*-PrSal), Cu(*t*-BuSal) did not form such 1:1 complexes with Cu(nNO$_2$-RSal) in toluene; the excess of Cu(*t*-BuSal) in the toluene solutions of Cu(5NO$_2$-RSal) did not alter the observed parameters of the triplet ESR spectra due to the dimers of Cu(5NO$_2$-RSal). In this case, only the broadenings of the spectra were observed. It has been reported by Yokoi that two species with different degrees of tetrahedral deformation exist for Cu(*iso*-PrSal) in toluene, while only one species with a high degree of that deformation exists for Cu(*t*-BuSal) in toluene.[14] It is of interest that the $g_{//}$ and $|A_{//}|$ values for the 1:1 complexes of Cu(5NO$_2$-RSal) with Cu(*iso*-PrSal) are closer to those for the species of Cu(*iso*-PrSal) with a lower degree of tetrahedral deformation. The difference between Cu(*t*-BuSal) and Cu(*iso*-PrSal) in the ability to form 1:1 complexes with Cu(nNO$_2$-RSal) is probably due to the differences in the tetrahedral deformation of the ligand coordination. A similar tendency in the dimer formation has been observed for Cu(RSal) in methylcyclohexane.[9]

The copper(II) complexes generally represented as Cu(nNO$_2$-SalB) are scarcely soluble in toluene, while Cu(3NO$_2$-Salpn) and Cu(3NO$_2$-Salibn) are considerably soluble in various nitroalkanes and exhibit intense ESR signals due to triplet dimers. The nitroalkane solutions of many other Cu(nX-SalB) complexes (X= H, Me, Br, and MeO) which were soluble in toluene did not exhibit the triplet ESR signals. The effect of the bridges between the iminoic nitrogens on the dimer formations of the 3-nitro-substituted Schiff-base complexes in nitroalkanes was quite analogous to that of the unsubstituted complexes in toluene:[6] Cu(3NO$_2$-Salen) is insoluble in nitroalkanes, and the amount of the dimers of Cu(3NO$_2$-Salpn) in nitroalkanes is larger than that of Cu(3NO$_2$-Salibn), while Cu(3NO$_2$-Saltren) is scarcely dimerized in nitroalkanes.

The ESR spectra of Cu(3NO$_2$-Salibn) in nitroethane at 77 K are shown in Fig. 5. In contrast with the dimers of Cu(nNO$_2$-RSal) in toluene, those for Cu-(3NO$_2$-SalB) in nitroalkanes have the parameters characteristic of the non-coaxial spin-Hamiltonian

TABLE 1. MAGNETIC PARAMETERS FOR COPPER(II) DIMERS (X-BAND)

Ligand	g_2	D_2 (G)	A_1 (G)	A_h (G)	$g_{M//}$	$A_{M//}$ (G)
5NO$_2$-EtSal	2.221	469	87	87	2.221	186
3NO$_2$-EtSal	2.222	466	86	86	2.226	184
(EtSal)[a]	2.171	564	80	67	2.227	180
5NO-*n*-PrSal			83		2.227	180
3NO$_2$-Salpn	2.156	548	89	80		
3NO$_2$-Salibn	2.153	544	84	77	2.212	196
(Salpn)[a]	2.190	428	100	100	2.197	207

a) Ref. 6.

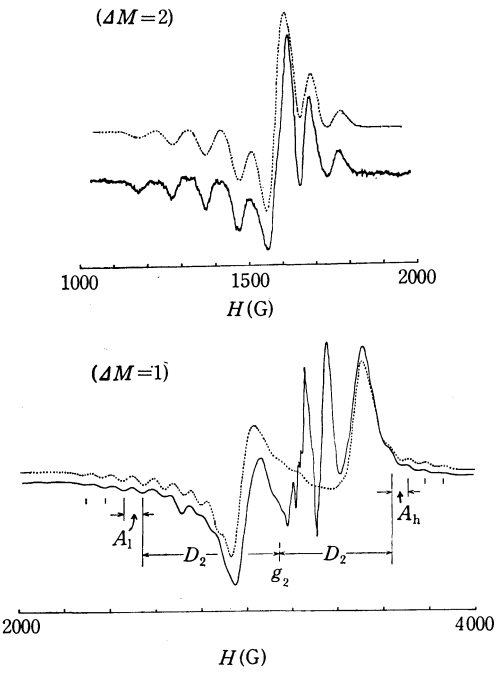

Fig. 5. ESR spectra of Cu(5NO$_2$-Salibn) in nitroethane at 77 K. Broken lines: calculated spectra with the parameters, $g_{//}=2.20$, $g_{\perp}=2.045$, $|A_{//}|=0.0100$ cm^{-1}, $|A_{\perp}|=0.0010$ cm^{-1}, $r=3.80$ Å, $\xi=35°$, ΔH (Gaussian) $=25$ G ($\Delta M=1$) and 22 G ($\Delta M=2$). $\nu=9.297$ GHz.

tensors- that is, $g_{M//}>g_2$ and $|A_{M//}/2|>A_1>A_h$. In addition, the D_2 values of Cu(3NO$_2$-SalB) is considerably larger than that of Cu(SalB) in toluene.[6] As Fig. 5 shows, the observed spectra could be simulated with those parameters: $g_{//}=2.20$, $g_{\perp}=2.045$, $|A_{//}|=0.0100$ cm^{-1}, $|A_{\perp}|=0.0010$ cm^{-1}, $r=3.80$ Å, and $\xi=35°$. These r and ξ values are closer to those of Cu(RSal) in toluene than to those of Cu(SalB) in toluene.[6] However, it is still uncertain whether the phenolic oxygen atoms in the Schiff base coordinate to the adjacent copper ions in the dimer at their apical positions, because we simulated the observed spectra with axially symmetric g and A tensors.

Intra-dimer Spin-exchange Interactions. When an ESR spectrum due to triplet-state dimers is not saturated, the spectral intensity (I) is proportional to the paramagnetic susceptibility of the dimer system; it can be expressed as:

$$I = c/T(3+\exp(-J/kT)) \qquad (2)$$

where c is an appropriate proportionality constant. Since the $\Delta M=2$ spectra for the present dimers are quite different in position from the allowed spectra due to both dimers and monomers, the I in Eq. (2) can be estimated from the intensity of the $\Delta M=2$ spectra alone.

Figure 6 shows the $\Delta M=2$ spectra of Cu(3NO$_2$-Salibn) in frozen nitroethane at 1.6 and 4.2 K. Since the line-shapes or linewidths of these spectra did not vary over this temperature range, the relative intensity of the triplet ESR spectra is equal to the relative peak height of a certain line (H) in the first derivative $\Delta M=2$ spectra. On the other hand, the shape of the $\Delta M=2$ spectra for Cu(5NO$_2$-EtSal) in toluene changed

with the temperature even at the minimum level of microwave power (0.48 mW) at which the $\Delta M=2$ spectra can be obtained with a satisfactory signal-to-noise ratio on our spectrometer. The examination of the relation between the spectral intensity and the microwave power revealed that the $\Delta M=2$ spectra at 4.2 K were saturated to some extent even at this microwave power. A similar change in the line-shape at 4.2 K could be observed at a stronger microwave power. These phenomena suggest that the modulations of the intradimer spin-exchange or spin-dipole interaction by thermal vibrations in this temperature range are not sufficient to make the spin-lattice relaxation time short enough to remove the saturation of the ESR signals. Because of the low solubility of Cu(5NO_2-EtSal) in toluene, the concentration of the sample cannot be made so high as that of Cu(3NO_2-Salibn) in nitroethane. Therefore, the modulation of the interdimer or dimer-monomer spin-dipole interaction in the toluene solutions of only Cu(5NO_2-EtSal) may be too weak to recover the spin-lattice relaxation.

This problem, however, could be solved by the addition of a large excess of Cu(*t*-BuSal) to the toluene solutions of Cu(5NO_2-EtSal). When an excess of Cu(*t*-BuSal), which does not combine with Cu(5NO_2-EtSal), coexists in the solution, the shape of the $\Delta M=2$ spectra no longer depends on the temperature and the intensity increases linearly with the square root of the microwave power over the range of 0.48—4.8 mW (see Fig. 7). This phenomenon indicates that the thermal contact between the spin system of Cu(5NO_2-EtSal) and that of Cu(*t*-BuSal) could recover the spin-lattice relaxations. Consequently, the J value for the dimers of Cu(5NO_2-EtSal) in toluene could be estimated in the way described above by the addition of excess Cu(*t*-BuSal) to the solutions.

In the case of the 1 : 1 complexes of Cu(5NO_2-RSal) with Cu(*iso*-PrSal) in toluene, the line shapes of the $\Delta M=2$ spectra depend on the temperature in a more complicated manner. Figure 8 shows the $\Delta M=2$ spectra for the 1 : 1 complexes of Cu(5NO_2-EtSal) with Cu(*iso*-PrSal) in toluene at 4.2 and 1.57 K. The linewidth at 1.57 K is quite broad compared to that at 4.2 K. In this case, the broadening of the spectrum is not due to the saturation effect, because the intensity

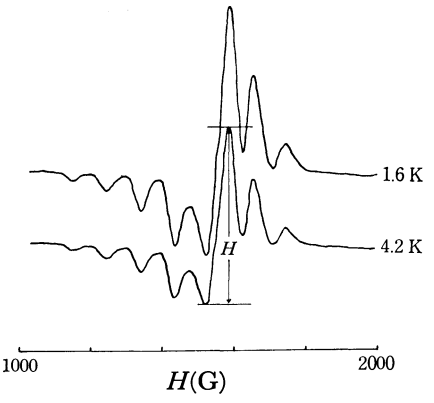

Fig. 6. $\Delta M=2$ spectra of Cu(5NO_2-Salibn) in nitroethane at 4.2 and 1.6 K.

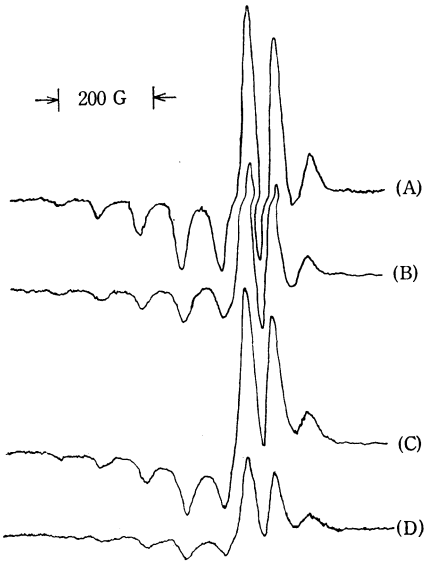

Fig. 7. $\Delta M=2$ spectra of Cu(5NO_2-EtSal) in toluene. (A): 1.57 K, (B): 4.2 K without Cu(*t*-BuSal). (C): 1.57 K, (D): 4.2 K with a large excess of Cu(*t*-BuSal).

of the $\Delta M=2$ spectra at 1.57 K increased linearly with the microwave power over the range of 0.48—4.8 mW. A similar change in the line-shape was observed for the 1 : 1 complexes of Cu(5NO_2-*iso*-PrSal) with Cu(*iso*-PrSal). These changes in the line-shape may be attributed to a considerable decrease in the T_2 (spin-spin relaxation time) and/or in the degree of the structural homogeniety of the 1 : 1 complexes, including their surroundings. Since the line-shape varied in a complicated manner, we did not attempt to estimate the J values for these complexes.

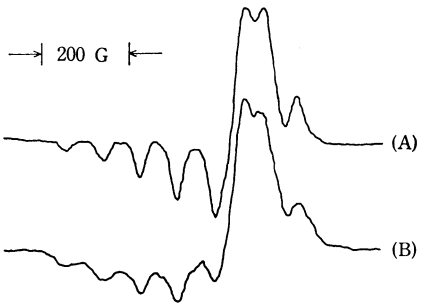

Fig. 8. $\Delta M=2$ spectra of Cu(5NO_2-EtSal) with a large excess of Cu(*iso*-PrSal) in toluene. (A): 4.2 K, (B): 1.57 K.

Figure 9 shows the calculated and experimentally determined relative intensity changes of the triplet ESR spectra for the dimers of Cu(5NO_2-EtSal) in toluene and of Cu(3NO_2-Salibn) in nitroethane, in units of the intensity at 4.2 K. The J values estimated from this figure are listed in Table 2, together with the r and ξ values determined by computer simulations. In this table, the corresponding parameters for the dimers of Cu(MeSal) and Cu(3Me-Salpn) in toluene are also listed. The J values for the dimers of Cu(5NO_2-EtSal) and Cu(3NO_2-Salibn) were antifer-

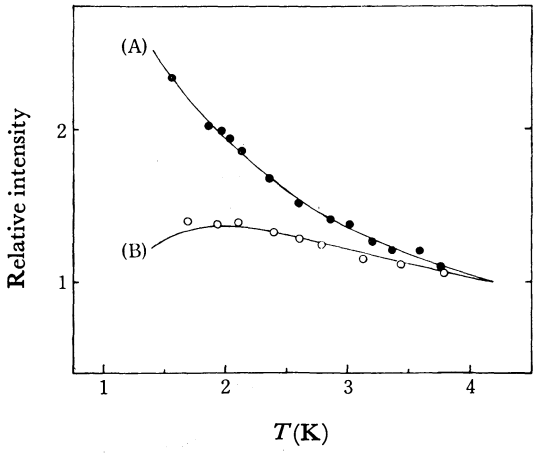

Fig. 9. Temperature dependence of relative intensities for $\Delta M=2$ spectra.
●: Cu(5NO_2-EtSal) with a large excess of Cu(*t*-BuSal) toluene, ○: Cu(3NO_2-Salibn) in nitroethane.
Full lines: calculated curves from Eq. (2). (A) $J=-0.7$ cm^{-1}, (B) $J=-2.2$ cm^{-1}.

TABLE 2. THE J, r, AND ξ VALUES FOR COPPER(II) DIMERS

	Medium	J(cm^{-1})	r(Å)	ξ(°)
Cu(5NO_2-EtSal)	Toluene	-0.7 ± 0.2	4.02	15
(Cu(MeSal))[a]	Toluene	-2.3 ± 0.2	3.75	35
Cu(3NO_2-Salibn)	Nitroethane	-2.2 ± 0.2	3.80	35
(Cu(3Me-Salpn)[a]	Toluene	-1.5 ± 0.3	4.05	15

a) Refs. 7 and 10.

romagnetic, as in the case of the other Schiff-base complexes of copper(II) in frozen solutions.[7,9,10]

We have previously reported that many Cu(*n*X-RSal) and Cu(*n*X-SalB) complexes (X=H, Me, MeO, Br; R=Me, Et, *n*-Pr; B=pn, ibn) in toluene are similar in dimeric structure to Cu(MeSal) and Cu(Salpn) in toluene respectively.[6] Corresponding to the changes in the r and ξ values with the nitro-substitutions, marked changes in the J values were observed. Since the nitro-groups in phenyl-rings have a strong electron-attracting power, the π-electron distribution over the copper(II) chelates will be severely modified with these groups. In particular, the affinity of the phenolic oxygen for the adjacent copper(II) ions at their apical positions may be reduced because of a decrease in the π-electron density on the oxygen atoms. Therefore, the contribution of such apical coordinations of the phenolic oxygen atoms to the spin-exchange interactions may decrease upon the nitro-substitutions. However, this is merely one possible explanation for the changes in the dimeric structure and in the J values with the nitro-substitutions. The fact that the dimer formation was markedly promoted by the nitro-groups suggests that the change in the dispersion or polarization forces between the ligands may play an important role in determining the dimeric structure and spin-exchange interactions.

Since the dimeric structures have still not been revealed in detail, it is impossible to discuss the mechanisms of the intradimer spin-exchange interactions further. However, the results obtained above support the previous conclusion that dimeric structures for copper(II) chelates in frozen solutions are determined by the subtle balance of many kinds of interactions between monomeric halves in the dimers and between the dimers and solvents.[3,6,9,10]

The authors wish to express their thanks to Dr. Hiroshi Yokoi for his valuable discussions and suggestions during this work.

References

1) T. D. Smith and J. R. Pilbrow, *Coordin. Chem. Rev.*, **13**, 173 (1974), and the references therein.
2) W. E. Hatfield, *Inorg. Chem.*, **11**, 216 (1972), and the references therein.
3) H. Yokoi and T. Isobe, This Bulletin, **44**, 1446 (1971); *ibid.*, **46**, 447 (1973); *ibid.*, **47**, 497 (1974).
4) H. Yokoi and T. Isobe, *Chem. Lett.*, **1972**, 95.
5) M. Chikira and T. Isobe, This Bulletin, **45**, 3006 (1972).
6) M. Chikira, H. Yokoi, and T. Isobe, *ibid.*, **47**, 2208 (1974).
7) M. Chikira and T. Isobe, *Chem. Phys. Lett.*, **30**, 498 (1975).
8) H. Yokoi and M. Chikira, *J. Amer. Chem. Soc.*, in press.
9) H. Yokoi and M. Chikira, *J. Chem. Soc.*, in press.
10) M. Chikira and T. Isobe, to be published.
11) L. Sacconi and M. Ciampolini, *J. Chem. Soc.*, **1964**, 276.
12) J. A. Riddick and W. B. Bunger, "Organic Solvents," John Wiley & Sons, New York, 1970.
13) Z. Matsumura, M. Chikira, S. Kubota, and T. Isobe, *Rev. Sci. Instrum.*, **45**, 596 (1974).
14) H. Yokoi, This Bulletin, **47**, 3037 (1974).

Ketyl Radicals Formed in Grignard Reaction. III.[1] Steric Effects on the Formation of Radicals

Masao ŌKUBO

Department of Chemistry, Faculty of Science and Engineering, Saga University, Honshō-chō, Saga 840

(Received February 20, 1974)

In the reaction of benzophenone with phenylmagnesium bromide, the concentration and life-time of the ketyl radical were influenced greatly by the substitution of *ortho*-hydrogen atoms of both the two reactants by methyl group. From the results of visible absorption and ESR measurements and also of product-analysis, the ketyl radical was considered to be a common intermediate towards normal and abnormal reaction products. The existence of an equilibrium between monomeric and dimeric states of the ketyl radical was also proposed.

The peculiarity of the ketyl radical observed in the Grignard reaction of *o*-methylbenzophenone was discussed in comparison with that of potassium-ketyl of the same ketone,[1] but the reason for the ketyl radical having a long "life time" remained ambiguous. The effects of the *o*-methyl group of benzophenone as well as those of the phenyl-Grignard reagent on the formation of ketyl radicals have been studied more precisely.

Results and Discussion

The formation of ketyl radicals was followed by observation of the characteristic coloration of the reaction solution by means of visible absorption spectroscopy and ESR spectroscopy. Results obtained by use of these techniques will be discussed separately.

"Life Time" of Ketyl Radicals. When *o*-methyl-substituted benzophenones were treated with arylmagnesium bromide (ArMgBr) in tetrahydrofuran (THF) under N_2-atmosphere or in vacuum and at room temperature, the colorless solution turned to purple or wine-red. The coloration, which is due to the formation of ketyl radicals,[1] lasted in most cases for as long as several months. Benzopinacol, as a minor product, has often been isolated from the reaction mixture of benzophenone and Grignard reagents, being considered to be the product formed by dimerization of the ketyl radical (Scheme 1).[2]

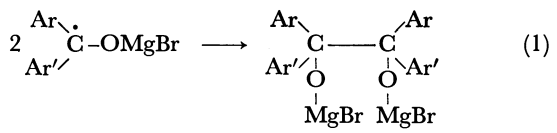

(1)

The time during which the characteristic coloration was observed is tentatively denoted in this paper as the "life time" of a ketyl radical. The "life time" at 50 °C was greatly influenced by the number of *o*-methyl groups. The "life times" of radicals and the yields of carbinols and pinacols are given in Table 1. The increasing number of *o*-methyl groups on the ketone prolongs the "life time" exceedingly (experiments 1, 2 and 3). That of *o*-methyl groups on ArMgBr also prolongs it, but the effect is smaller (experiments 1, 4 and 5). The fair yield of benzopinacol in experiment 5 can be attributed to the steric hindrance effect of *o*-methyl groups of mesityl-MgBr. However, the absence of the pinacol, despite the appearance of the characteristic color, in experiment 4 must be noted. This fact shows that the ketyl radical formed does not necessarily dimerize to the pinacol. When the velocity of the formation of *o*-methyltriphenylcarbinol in experiment 4 was compared with that of the same product in experiment 2, the unsubstituted benzophenone was

Table 1. "Life times" of radicals and yields of carbinols and pinacols

0.9 M ketone and 1.35 M ArMgBr, at 50 °C.

No.	ArMgBr	Ketone	"Life Time" (min)	Yield (%) Carbinol	Yield (%) Pinacol
1		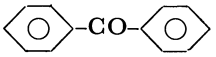	0	100	0
2		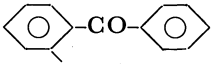	210	69	10
3		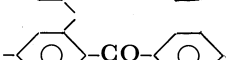	>1100	8	trace
4		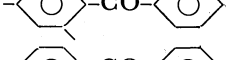	5	100	0
5		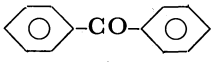	10	1.8	45

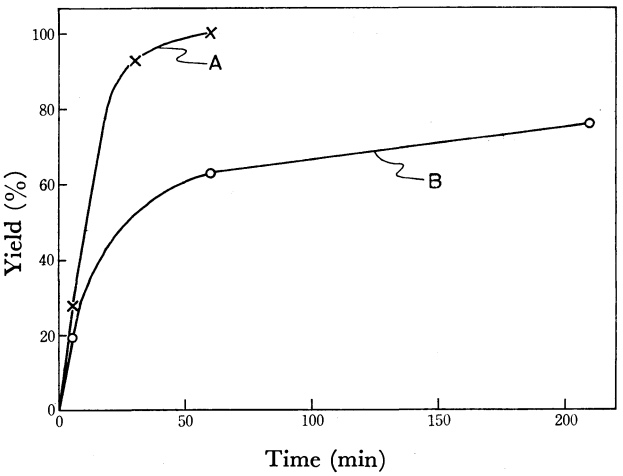

Fig. 1. Yields of *o*-methyltriphenylcarbinol at 50 °C.

A: 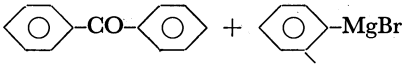

(experiment 4 in Table 1)

B: 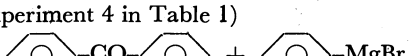

(experiment 2 in Table 1)

0.9×10^{-2} mol ketone and 1.35×10^{-2} mol ArMgBr.

found to yield the carbinol rapidly and quantitatively (Fig. 1). The short "life time" of the ketyl radical in experiment 4 can thus be attributed to the rapidity of the normal addition reaction.

These facts make it possible to assume that the ketyl radical is a common intermediate in Grignard reaction. If the ketyl radical is pictured tentatively as shown in

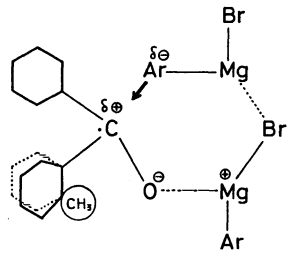

Fig. 2. Attempted depiction of ketyl-type radical intermediate.
At present, it cannot be decided on which of the two (or more) Ar groups delocalizes the other free electron.

Fig. 2, the normal addition product and the dimerization product can be explained in terms of steric hindrance, effects of which can be classified as (i) the effect caused by the Grignard moiety, and (ii) that caused by the ketone moiety. When (i) is large and (ii) small, the Grignard-aryl group cannot come close to the carbonyl-carbon atom and the radical would tend towards the sterically less-hindered dimerization process,[2] this being the case in experiment 5. The dimerization process is retarded by effect (ii), which is shown in experiment 3. In this case (i) is small and (ii) very large, and the Grignard reagent attacks the unsubstituted phenyl group of the ketone as reported by Fuson *et al.*[3] (Scheme 2). This nuclear phenylation has been explained recently on the basis of an electron-transfer mechanism.[4]

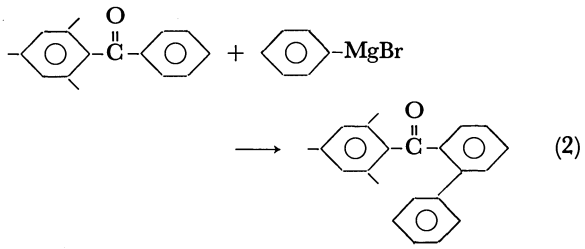

(2)

The rapidity of the formation of the carbinol in experiment 4 is explained in terms of the energy level of the reaction intermediate, ketyl radical. The delocalization of the free electron spin is favored owing to the small twisting angle of the two phenyl groups of benzophenone out of plane of its carbonyl group, thus lowering the energy level. The same effect can be expected also in experiment 5, but the enhanced effect of steric hindrance of the Grignard-mesityl group makes it impossible to produce the carbinol.

A considerable amount of mesitylene was found in experiment 5. When a larger scale reaction was carried out using 28% excess molar mesityl-MgBr and the reaction mixture was decomposed by D_2O-D_2SO_4, the content of monodeuteriomesitylene in the recovered sample of mesitylene was about 30% on the basis of NMR absorption. Thus the mesityl radical, produced as a result of the electron-transfer from the Grignard reagent to the ketone (Scheme 3), would abstract hydrogen from the THF molecule (Scheme 4).

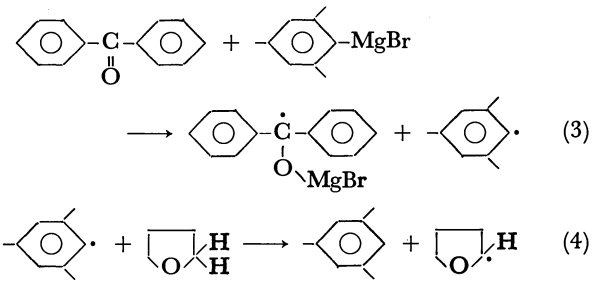

(3)

(4)

Table 2. Visible absorption bands of radical species
Ketone: 3.3×10^{-4}M, ArMgBr: 5.0×10^{-4}M
s: strong, m: medium, w: weak.

No.	Ketone	-MgBr λ_{max}(nm)	temp. (°C)	ε	-MgBr λ_{max} (nm)	temp. (°C)	Mg(Hg) λ_{max} (nm)
I	-CO-	553 s 610m	25	>8500	553 s, 610m	25	60—610 s (broad)
II	-CO-	434, 540 s, 580m	25	>8000	383, 530m, 570w	50	434, 540 s, 580w
III	-CO-	380, 534 s, 565m	25	>4000	380, 555w	50	438, 534 s, 565w
IV	-CO-	564 s, 620m	25	~2000	564 s, 620w	50	620 s
V	-CO-	450, 560m, 615w	50	~150	not observed	50	438, 570 s, 610w
VI	-CO-	430, 580w, 610w	50	~30	not observed	50	———

Thus, all the results are explained by considering the formation of a ketyl radical to be an essential process in the Grignard reaction.

Visible Absorption Spectra. Evacuated optical cells were used for the measurements of visible absorption spectra of ketyl radicals. Main absorption bands appear at 530—580 nm. They are accompanied by weaker bands at longer wavelength side (570—620 nm) in all cases. Absorption spectra of Mg-ketyls of respective ketones were also measured (Table 2).

The values of absorbance give a rough estimate obtained when the absorbance of main band becomes almost maximum after a certain time of reaction of each ketone with phenyl-MgBr. High absorbances observed in the cases of ketones bearing at least one unsubstituted phenyl group can be attributed to the spin delocalization given by:

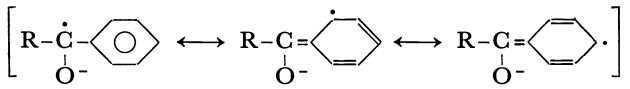

Though the nearly planar structure of unsubstituted benzophenone favors spin delocalization, the ketyl of this least-hindered ketone favors, at the same time, normal addition and/or dimerization (Table 1, experiments 1, 4 and 5). For this reason, any high absorbance cannot be realized in the Grignard reaction of benzophenone itself.

The temperatures listed in Table 2 are those necessary to realize a velocity of color development suitable for ordinary measurements under the conditions of the described molar concentrations. In reactions with phenyl-MgBr, ketones I—IV easily reveal colors at room temperature but V and VI need higher temperatures. In reactions with *o*-tolyl-MgBr, only ketone I reveals color at room temperature, II—IV need higher temperatures, and V and VI do not reveal color after warming for several hours. Thus the initial electron-transfer process is affected by two kinds of steric hindrance; one due to ketones, and the other to Grignard reagents.

The absorption bands at 380—450 nm appear when at least one of the two aryl groups of ketone twists almost perpendicularly out of plane of the carbonyl group, but these bands were not assigned in this work. The following discussion is concerned mainly with *o*-methyl- and *o,o'*-dimethylbenzophenone. The variation of the relative absorbance $\varepsilon_{564}/\varepsilon_{620}$ in the time-course of the reaction of *o,o'*-dimethylbenzophenone with phenyl-MgBr is interesting. For convenience, the relative height at λ_{max}'s of the respective band was taken as the value of $\varepsilon_{564}/\varepsilon_{620}$. The relative absorbance is small in the initial stage, and becomes larger as the reaction proceeds under each molar concentration (Fig. 3). It becomes smaller when the solution is diluted. The convergence of the relative absorbance to the value of 1.65—1.70 after 24 hr suggests the existence of an equilibrium. As the 620 nm band of the Grignard ketyl can be assigned to its monomeric state on the basis of the fact that the Mg-ketyl has a simple band at the same wavelength, the 564 nm band could be assigned to its dimeric state. This assignment is supported by the following results. When

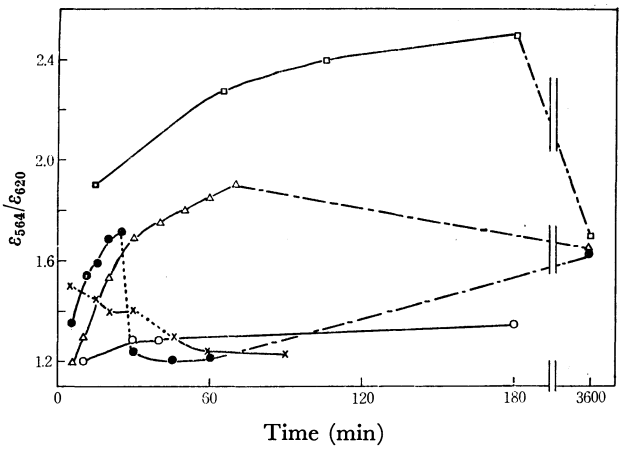

Fig. 3. Variation of relative absorbance $\varepsilon_{564}/\varepsilon_{620}$ with respect to time.

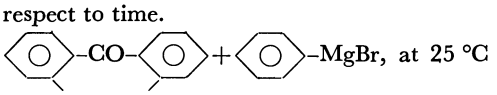

at 25 °C

·····: Diluted before the subsequent measurement.
-·-·-: Left to stand for 24 hr.
Molar concentration: [Grignard]/[Ketone], $\times 10^4$ M.
i) ○, 5.0/3.3=1.5 ii) ×, 30.0/3.3=9.0
iii) ●, 30.0/0.66=45.0 iv) △, 5.0/0.66=7.6
v) □, 1.0/0.66=1.5

the concentration of ketone is low (experiments iii, iv and v), the relative absorbance is larger as the molar ratio of ketone is higher (experiments iv and v). The higher relative absorbances in the initial stage of experiment iii than that of iv can be explained as follows: a much higher amount of the monomeric ketyl initially formed by the action of the much higher amount of Grignard reagent in experiment iii affords a higher amount of the dimeric aggregate than in experiment iv.[6] This is reasonable since the velocity of the initial developement of absorbance decreases in the order: ii>iii>i~iv>v (not represented in Fig. 3).

In the reaction of *o*-methylbenzophenone with *o*-tolyl-MgBr, a similar phenomenon was observed (Table 3). The absorption band of Mg-ketyl of this ketone broadened from 560 to 610 nm probably owing

Table 3. Variation of relative absorbance $\varepsilon_{553}/\varepsilon_{610}$ with respect to time

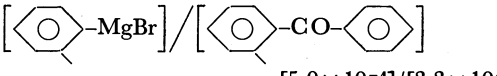

$=[5.0\times10^{-4}]/[3.3\times10^{-4}]$
$=1.5$

Reaction time (min)	Extent of dilution	temp. (°C)	$\varepsilon_{553}/\varepsilon_{610}$
5	×1	25	1.63
10	×1	25	2.12
20	×1	25	2.41
25	×1	25	2.45
45	×1	25	3.11
60	×5	25	2.09
⋮	⋮	⋮	⋮
3600	×5	25	1.25
3605	×5	5	1.32
3610	×5	25	1.25

to the unsymmetrical molecular structure. The twisting vibration of *o*-tolyl group out of plane of the benzoyl group is considered to be easier in Mg-ketyl than in Grignard-ketyl.[1] The mixing of the electronic transition corresponding to the benzoyl group with that corresponding to the *o*-tolyl group could be expected. In contrast to the Mg-ketyl, the Grignard-ketyl has bands at 553 and 610 nm, resembling the Grignard-ketyl of *o,o'*-dimethylbenzophenone. Taking into account the previous observation of the very high spin density on the unsubstituted phenyl group of the Grignard-ketyl of *o*-methylbenzophenone,[1] one could ascribe the absorption bands of this ketyl mainly to the electronic transition corresponding to the unsubstituted benzoyl group. A discussion on the relative absorbance is thus significant in this case. It becomes larger as the reaction proceeds, smaller when the solution is diluted, and again larger when the temperature is lowered.

The existence of another equilibrium between the original ketone and the monomeric ketyl is suggested from the effect of temperature and that of the steric hindrance caused by the Grignard reagent (Table 2). The existence of this equilibrium is also suggested from the relative velocity of the initial developement of absorbance found in the experiments (Fig. 3). A higher velocity was realized by the higher molar ratio of the Grignard reagent and also by the higher concentrations of the two reactants. The two equilibrium processes can be represented as follows (Scheme 5).

$$2G + 2B \overset{K_1}{\rightleftarrows} 2G^{\ddagger} + 2B^{\dashv} \overset{K_2}{\rightleftarrows} [B^{\dashv} \cdots G^{\ddagger} \cdots B^{\dashv}] + G^{\ddagger} \qquad (5)$$

G: Grignard reagents
B: Benzophenones

The ketyl radical in Fig. 2 depicts the monomeric state "$2G^{\ddagger}+2B^{\dashv}$," a part of which is the precursor of carbinol. The dimeric species $[B^{\dashv}\cdots G^{\ddagger}\cdots B^{\dashv}]$ is considered to be the precursor of pinacol. The Grignard reagent represented tentatively as monomeric in this scheme may exist as more aggregated state.[6,7]

Radical Concentration. The radical concentration, determined by ESR technique, was also affected by the structure of ketone and that of the Grignard reagent. A single sample tube was used throughout the measurement, and conditions of the ESR spectrometer were kept constant as far as possible. The results for the respective combinations of reactants differ considerably (Fig. 4), and thus it is feasible to discuss the relative effect of substituent.

The maximum concentration of the ketyl radicals formed in reactions with phenyl-MgBr decreases in the order:

2-*t*-Butyl- (C) > 2,6-Dimethyl- (D) > 2,2'-Dimethyl- (A) >
2-Methyl- (B) > 2,6,2'-Trimethylbenzophenone (F)

A different order, A>B>C>D>F, is found for the velocity of electron-transfer in the initial stage of the reaction. The two orders can be explained in terms

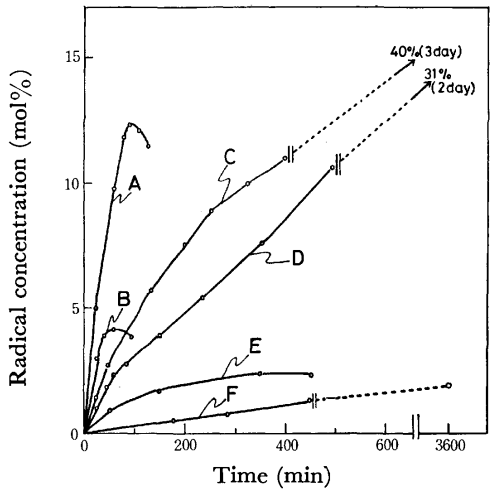

Fig. 4. Variation of radical concentration based on original ketones at 20 °C.
ArMgBr: 7.0×10^{-4}, Ketone: 3.3×10^{-4}.

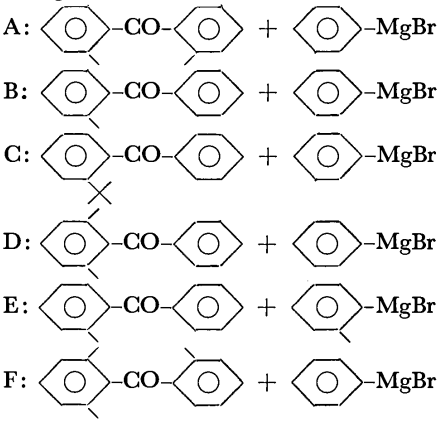

of steric hindrance. In cases A and B, the initial electron-transfer is relatively rapid owing to the small steric hindrance which in turn favors the subsequent normal addition and dimerization, and thus the concentration of the ketyl radicals begin to come down in short times. In cases C and D, the large steric hindrance retards the initial electron-transfer as well as the subsequent processes,[4] and thus the remarkably high radical concentrations are realized after long times of reaction. The high radical concentrations in these cases are ascribed to the small equilibrium constant K_2 of Scheme 5. The low concentration in case F would be due mainly to the largest (of cases A—F) steric hindrance against the initial electron-transfer. If case E is compared with B, the effect of *o*-methyl group of Grignard reagent can be discussed. The velocity of the initial electron-transfer from *o*-tolyl-MgBr, being lower than that from phenyl-MgBr, becomes comparable to that of subsequent processes, thus depressing the radical concentration.

ESR measurement provides further evidence for the existence of the monomer-dimer equilibrium. The effect of temperature in the case of mesityl phenyl ketone and phenyl-MgBr is as follows: the radical concentration decreased to 89—91% at −30 °C and to 69—73% at −50 °C based on a concentration observed at +20 °C, and the variation was reproducible.

Another evidence obtained from the effect of dilution is as follows: when a volume of the solvent twice as much as that of the reaction solution was added just after the radical concentration reached the maximum (reaction A, Fig. 4), the resulting concentration was 21% higher than that expected from the extent of dilution.

Conclusion. The characteristics of the Grignard reaction are considered by a large number of investigators to be ionic, and the contribution of radical processes has been recognized only in a few cases.[2] Ashby and his co-workers[8] proposed that heavy metal impurities in magnesium initiate the formation of benzopinacol in the reaction of benzophenone with methyl-MgBr. However, they later observed the formation of the ketyl radical in the reaction of *o*-methylbenzophenone with the same Grignard reagent.[9] The reason for the long "life time" of the Grignard–ketyl of *o*-methylbenzophenone[1] can now be given: (a) the steric hindrance of the ketyl radical against the normal addition and dimerization, or (b) the enhanced delocalization of the free spin on the phenyl group.[1] The latter may cause a trend towards a slow nuclear phenylation similar to that observed in the reaction of mesityl phenyl ketone, though the detection of such a minor product was difficult.[4]

The effect of steric hindrance on the formation of the ketyl radical due to the initial electron-transfer is evidently consistent with the same effect on the decay of the radicals due to the subsequent processes.

Experimental

Materials and Reaction. *ortho*-Methyl-substituted benzophenones were prepared according to the method previously reported.[10] Grignard reagents in THF were prepared as usual and transferred to storage bottles under N_2-atmosphere. A definite aliquot of Grignard solution was pipetted out under N_2-stream, and transferred to a reaction flask. Benzophenone and its derivatives dissolved in THF were added at once. The reaction mixture was stirred at 50 °C for a certain time as long as the characteristic color was observed, and hydrolyzed with aqueous ammonium chloride. The products were analyzed by means of glc and tlc.

Visible Absorption Measurements. The apparatus for measurements was constructed from an optical cell and a reaction vessel equipped with a container for ketone connected with a breakable seal. An aliquot of ArMgBr solution was transferred under N_2-stream to the reaction vessel, frozen with liquid N_2, evacuated by means of a vacuum line, and diluted to an appropriate volume by vacuum distillation of THF. The apparatus was sealed off. Immediately after the breakable seal was broken, the optical measurement was begun. A Hitachi EPS-3T model spectrophotometer was used.

ESR Measurements. The apparatus for measurements was constructed as described previously.[11] Preparation of samples was similar to that for the optical measurements. Radical concentration was determined by the over-modulation technique. JEOL ME-3X model and PE-1X model spectrometers were used.

The author is grateful to Professor Kazuhiro Maruyama, Kyoto University, for his stimulating discussions. He thanks Professor Yasuo Deguchi and Mr. Hideo Fujita, Kyoto University, for use of the ESR spectrometer in their laboratory.

References

1) Part I; M. Ōkubo, This Bulletin, **48**, 1057 (1975). Part II; M. Ōkubo, *ibid.*, **48**, 1327 (1975).
2) C. Blomberg and H. S. Mosher, *J. Organometal. Chem.*, **13**, 519 (1968) and literatures cited therein.
3) R. C. Fuson, M. D. Armstrong, and S. B. Speck, *J. Org. Chem.*, **7**, 297 (1942).
4) M. Ōkubo, This Bulletin, **48**, 1327 (1975).
5) K. Maruyama, R. Tanikaga, and R. Goto, *ibid.*, **36**, 1141 (1963).
6) K. Maruyama, *ibid.*, **37**, 897 (1964).
7) F. W. Walker and E. C. Ashby, *J. Amer. Chem. Soc.*, **91**, 3845 (1969).
8) E. C. Ashby, F. W. Walker, and H. M. Neumann, *Chem. Commun.*, **1970**, 330.
9) E. C. Ashby, J. Laemle, and H. M. Neumann, *J. Amer. Chem. Soc.*, **94**, 5421 (1972).
10) P. S. Hofmann, D. J. Reiding, and W. Th. Nauta, *Rec. Trav. Chim. Rays-Bas*, **79**, 790 (1960).
11) K. Maruyama, This Bulletin, **37**, 1013 (1964).

Photochemistry of *peri*-Substituted Naphthalenes. I. Photochemistry of Dimethyl 1,8-Naphthalenediacrylate

Koichi HONDA, Akira YABE, and Hideaki TANAKA

National Chemical Laboratory for Industry, 7th Division, 85 Shinshuku, Hiratsuka, Kanagawa 254

(Received October 29, 1974)

The photochemical reactions of dimethyl 1,8-naphthalene diacrylate (I) in solution are found to be *cis,trans* isomerization and concomitant intramolecular cycloaddition through a triplet state (E_T is *ca.* 40 kcal/mol). Cyclization reaction gives naphtho[1′,8′]bicyclo[3.1.1]hept-2-ene-6-*exo*,7-*endo*-dimethyl dicarboxylate (VI), its 6-*endo*, 7-*endo* substituted isomer (VII) and *cis-anti*-naphtho[1′,8′]bicyclo[3.2.0]hept-2-ene-6,7-dimethyl carboxylate (II) in a ratio of *ca.* 85: 10: 5. Predominant formation of crossed adducts is discussed, taking into consideration the ground-state conformations of (I). Biradical mechanism is proposed for the cyclization to explain the stereochemistry of the crossed products.

It is well-known that cinnamic acid derivatives photodimerize to yield stereospecific cyclobutane compounds in solid state, but isomerize to their geometrical isomers by irradiation in solution or in liquid state. The photochemical behavior differing according to state is attributable to the fixed distance and orientation between two olefin molecules in crystalline state. Schmidt[1] concluded in his topochemical studies that the photodimerization in crystalline state can take place only when the intermolecular distance between two olefin molecules is less than *ca.* 4 Å. Since the distance between 1 and 8 positions of naphthalene molecules is 2.57 Å, 1,8-naphthalene diacrylic acid derivatives are expected to undergo intramolecular photodimerization even in solution. As a part of photochemical studies of *peri*-substituted naphthalenes, we studied the photochemistry of *trans, trans*-dimethyl 1,8-naphthalenediacrylate (I) in solution.

Experimental

Spectral data of compounds I, II, III and VI are given in Table 1.

Preparation of I. Compound I was prepared by the Wittig condensation of naphthalaldehyde hydrate[2] with carbomethoxymethylene-triphenyl-phosphorane.[3] A solution of 5.0 g (25 mmol) of dialdehyde in 100 ml of benzene was heated at reflux temperature for 30 min. This hot benzene solution was then added dropwise to 200 ml of a refluxing benzene solution of 25 g (75 mmol) of the Wittig reagent over a period of 15 min. The solution was heated at reflux temperature for 5 hr with stirring in N_2 atmosphere and then filtered, the solvent being removed under reduced pressure. The residue was extracted with 300 ml of ether and the solvent of extract was evaporated off. The yellow residue enriched in I was chromatographed on a column of silica gel with ether to give, after recrystallization from ether, 2.8 g of pure product (I), mp 117—118 °C.

Preparation of II and III. Compound II was prepared from the photoproduct of maleic anhydride with acenaphthylene[4] by usual hydrolysis and esterification, mp 150—151 °C. Compound III was synthesized by base-catalysed epimerization of II. A solution of 0.5 g of II and 0.3 g of sodium methoxide in 5 ml dry methanol in a sealed tube was heated at 70 °C for 8 hr. Recrystallization of the product from methanol gave an equilibrated mixture of II and III in a 5: 95 ratio. Pure III was separated from the mixture by tlc (silica gel, elution

TABLE 1. SPECTRAL DATA OF I, II, III, AND VI

Compd.	Mp (°C)	NMR ($CDCl_3$) δ ppm	IR (KBr) cm^{-1}	UV in cyclohexane nm (log ε)	Mass (M^+)
I	117—118	3.80 (s, 6 methyl H) 7.25 (pair of d, J=15.4 Hz, 4 *trans* vinyl H) 7.2—8.0 (m, 6 aromatic H)	2960, 1710, 1630, 1435, 1370, 1312, 1275, 1197, 1172, 1035, 980, 872, 820, 780	209(4.49), 240(4.30) 265(sh), 332(4.26)	296
II	150—151	3.27 (m, 2 *endo* H) 4.51 (m, 2 benzyl H) 3.77 (s, 6 *exo* methyl H) 7.2—7.7 (m, 6 aromatic H)	2960, 1740, 1440, 1365, 1350, 1265, 1226, 1187, 1160, 829, 796	229(4.91), 278(3.82) 289(3.89), 300(3.71) 306(3.56), 316(2.97) 320(2.99)	296
III	125—128	3.40 (m, 1 *endo* H) 4.30 (m, 2 benzyl H, 1 *exo* H) 3.77 (s, 3 *exo* methyl H) 3.51 (s, 3 *endo* methyl H) 7.2—7.7 (m, 6 aromatic H)	2960, 1730, 1315, 1234, 1185, 1195, 1150, 1020, 784	229(5.15), 279(3.83) 290(3.90), 300(3.72) 306(3.58), 317(2.97) 320(2.83)	296
VI	98—99	2.92 (s, 1 *endo* H) 4.11 (s, 2 benzyl H, 1 *exo* H) 3.79 (s, 3 *exo* methyl H) 3.14 (s, 3 *endo* methyl H) 7.2—7.7 (m, 6 aromatic H)	2970, 1725, 1435, 1358, 1288, 1435, 1212, 1179, 1170, 1018, 829, 798, 789	213(4.53), 229(4.59) 236(4.59), 277(3.89) 288(3.98), 299(3.80) 317(2.88), 321(2.64)	296

with chloroform), mp 125—128 °C.

Photocyclization of I in a Preparative Scale. An immersion-well type photoreactor with a 100 W high pressure Hg arc lamp was used for the irradiation of I in a preparative scale. Ethanol solution of naphthalene was circulated as a filter solution to prevent light absorption by the cyclized products. The reaction temperature was maintained at 25 °C.

A solution of 400 mg of I in 1.1 *l* of cyclohexane (0.0013 M) was irradiated with the reactor with bubbling N_2 gas. The reaction was monitored by following the disappearance of the absorption peak at 332 nm in the UV spectrum of I, and the starting material was entirely consumed after 5 hr. The solvent was completely evaporated under reduced pressure, and the residual crystal was dissolved in ether and treated with activated charcoal. The recrystallization of the ether solution yielded 320 mg of VI, mp 98—99 °C.

Photocyclization of I in an Analytical Scale. A solution of I (0.0013 M) in a quartz cubic (1 cm in length, 4 ml in volume) was irradiated at room temperature with use of a 500 W high pressure Hg arc lamp. Toshiba UV D25 and UV 35 filters were used for direct irradiation. Toshiba filters VY 42, VY 43, VY 48 and VY 49 were used for benzil, benzanthraquinone, erythrosine and rose bengal sensitization, respectively. The reaction was also monitored by the change of UV spectrum except for some sensitized experiments, the irradiation time required to reach the complete disappearance of I being used as a measure of the reaction rate. After the reaction was complete, the solvent was removed under reduced pressure and 0.5 ml of benzene was added. The concentrated benzene solution was used for product analysis. Quantitative analysis was performed by glc (Carbowax 20 M on Chromosorb W, 80—100 mesh, 2 m, 240 °C). In almost all experiments, only intramolecular cyclization products were obtained, but in the case of benzil sensitization and piperylene addition, some by-products from the sensitizer or the quencher were formed. In the dye sensitized experiments, the sensitizers themselves were slightly photo-bleached.

Results and Discussion

Photocyclization Reaction. We found that the direct and sensitized photochemical reaction of I in solution underwent *cis, trans* isomerization with concomitant cyclization and ultimately led exclusively to the formation of cyclized products. Glc analysis of the final products showed the formation of three intramolecular cyclized products, and no intermolecular adducts were formed. Six structures II—VII were considered for the cyclized products. The main product was identified to be VI by comparing its spectral data with those of II and III which were obtained from the photoadduct of maleic anhydride and acenaphthylene.[4] One of the two minor products was identified to be II by comparing its glc retention time with that of an authentic sample of II. The other minor product, the first eluent in glc, was presumed to be V or VII, since the crossed adducts (intramolecular head-to-tail adducts, V—VII) were expected to be eluted more rapidly than the straight adducts (intramolecular head-to-head adducts, II—IV). Photoproducts mixture obtained from the methanol solution, in which this minor product was involved in *ca.* 20% yield, gave almost the same NMR spectrum as that of pure VI, but the peak ratio of *exo-* and *endo*-carbomethoxy protons at δ 3.79 and 3.14 respectively (Table 1) was about 1 : 1.4. The NMR spectrum suggested the inclusion of the crossed adduct having *endo*-carbomethoxy group except VI. Hence, the minor product unidentified was determined to be VII, which has two *endo*-carbomethoxy groups.

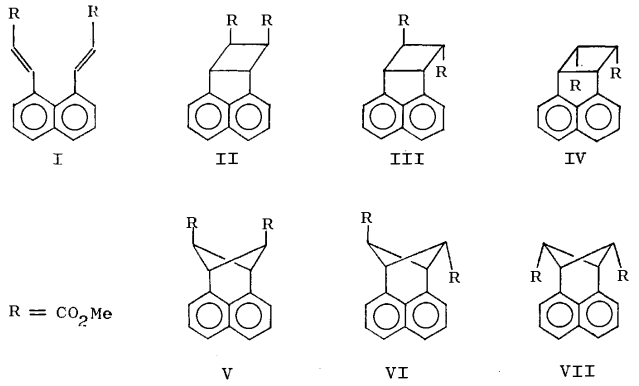

Table 2. Results of product analysis[a]

Solvent	Condition	Yields of products (%) VII	VI	II
Cyclohexane	Degassed	9	86	5
	N_2 Saturated	11	81	8
	Aerated	10	75	15
	O_2 Saturated	8	77	16
	Benzil Sensitized	10	85	5
	Benzanthraquinone Sensitized	10	86	4
	Piperylene Added	9	84	7
Methanol	N_2 Saturated	21	76	3
	Erythrosine Sensitized	19	79	2
	Rose Bengal Sensitized	17	80	3
	Rose Bengal Added	21	75	4
n-Propyl Bromide	Aerated	16	79	4
	N_2 Saturated	14	84	2

a) Sensitized or quenching experiments were performed in degassed or N_2 saturated solutions.

The results of the photochemical reaction in an analytical scale are summarized in Table 2. The product ratio in direct irradiation was almost the same as that of sensitized reaction. It is seen that benzil (the triplet energy, E_T=54 kcal/mol),[5] benz[*a*]anthraquinone (E_T=47 kcal/mol)[6] and erythrosine (E_T 42 kcal/mol)[7] are efficient sensitizers, while rose bengal (E_T=39 kcal/mol)[7] is a very inefficient one, acting rather as an effective quencher, whereas piperylene (E_T=47—49 kcal/mol)[8] shows no quenching action. The triplet energy of I was thus estimated to be *ca.* 40 kcal/mol, though the phosphorescence of I was not observed in the measurement in EPA solution at 77 K. In the presence of oxygen, II slightly increased and VI decreased complementarily, the reaction rate being suppressed at the same time. Decrease in the rate may be caused by triplet quenching since the fluorescence of I was scarcely quenched by oxygen. Dependence of product ratio on solvents was slightly seen. A larger amount of VII seemed to be produced in the more polar solvents. In addition, in *n*-propyl bromide

solution, the reaction rate was greatly accelerated probably by an external heavy atom effect.

The results suggest that the cyclization reaction proceeds predominantly through the triplet state of I, although from the oxygen addition experiments, II is considered to be formed from the singlet state to some extent.

Our results for the cyclization of I, in addition to those of Meinwald and Young[9] for 1,8-divinylnaphthalene (R=H in I) and 1,8-distyrylnaphthalene (R=Ph in I) seem to suggest that the intramolecular photocyclization of naphthalene-1,8-diolefins generally leads to crossed adducts. Interestingly, the photochemical tendency of naphthalene-1,8-diolefins to give predominantly crossed adducts differs from the well-known property of 1,6-dienes but is similar to that of 1,5-dienes,[10] although the present diolefins are 1,6-dienes.

We did not detect V in the photochemical reaction of I, but Meinwald and Young[9] found the product corresponding to V to be one of the main products in the photocyclization of distyrylnaphthalene. Since the reactive conformation should be common to the two diolefins, the difference in stereoselectivity might be due to different excited states or different intermediates, although they have not discussed what kind of excited state contributes to the reaction of distyrylnaphthalene.

Quantum Yields of Geometrical Isomerization, Cyclization and Fluorescence. Since attempts to isolate the geometrical isomers of I (*cis, trans* isomer, I′; *cis, cis* isomer, I″) were unsuccessful, an accurate quantum yield for the isomerization could not be determined. However, as a measure of photoreactivity under various conditions, we estimated the quantum yields for isomerization and cyclization from the disappearance rate of I followed by the UV spectral changes. The absorption spectrum changed with irradiation time on exciting with 365 nm light as follows. At first, the peak at 332 nm rapidly decreased and the shoulder peak at 265 nm disappeared, the cycloadducts even at this stage being detected by glc. Decrease of the 332 nm peak then became slow with concomitant appearance of adduct peaks (Table 1), and finally I was completely converted into adducts by prolonged irradiation. The change of spectrum with irradiation time is shown in Fig. 1. The spectral behavior of I would be explained by considering that the rapid decrease in the first stage is due to the superposition of rapid isomerization and considerably slow cyclization of I, and the slow decrease in the second stage is due only to cyclization of the *pseudo*-photostationary mixture of I and I′ (and I″)

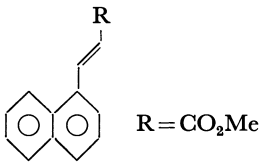

VIII

formed at first. In fact, *trans*-methyl-1-naphthaleneacrylate (VIII), where only geometrical isomerization is possible, showed a spectral change similar to that of I in the first stage. Namely, on exciting with 350 nm light, the peak of VIII at 318 nm decreased rapidly with irradiation time and reached a photostationary state, as shown in Fig. 2.

The plot of the optical density of I at λ_{max} (332 nm) against irradiation time (Fig. 3) showed two approximately linear parts corresponding to the two stages of

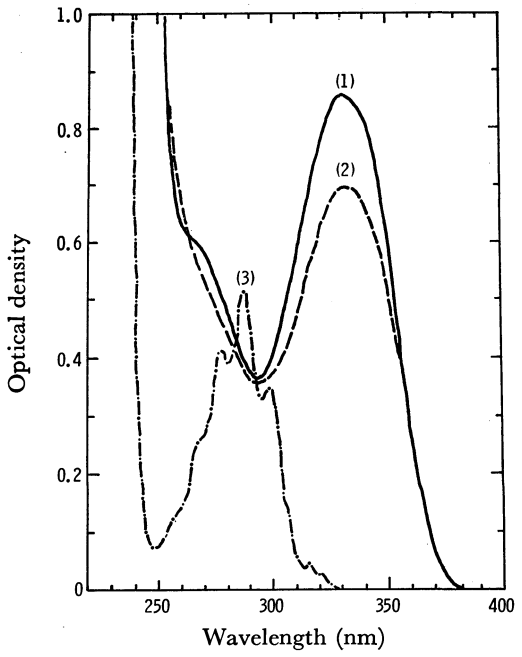

Fig. 1. UV absorption spectral change of (I) in cyclohexane solution with irradiation time on exciting 365 nm light.
(1); initial spectrum, (2); intermediate spectrum (*pseudo*-photostationary state between I and I′ (and I″), (3); final spectrum (intramolecular cycloadducts).

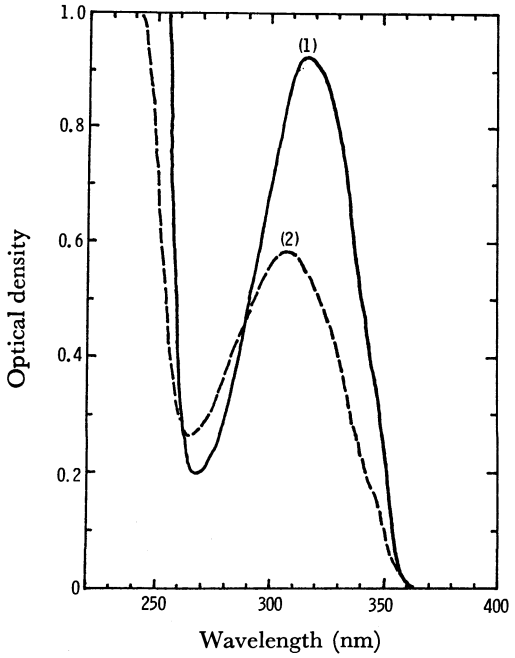

Fig. 2. UV absorption spectra change of VIII in cyclohexane solution with irradiation time on exciting 350 nm light.
(1); initial spectrum, (2); final spectrum (photostationary state between *trans*- and *cis*-isomer of VIII).

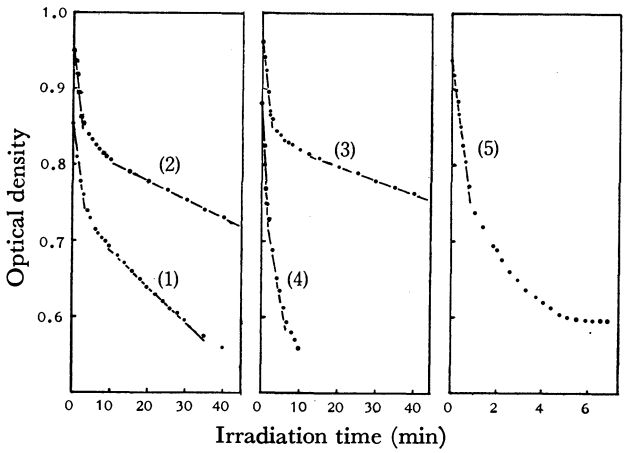

Fig. 3. The change of optical density of I and VIII at λ_{max} with irradiation time.
(1), (2), (3), and (4) denote respectively the conditions: degassed, N_2 saturated, O_2 saturated cyclohexane solution and N_2 saturated *n*-propyl bromide solution, in the change of (I) at 322 nm on exciting 365 nm light.
(5) denotes the change of VIII in N_2 saturated cyclohexane solution at 318 nm on exciting 350 nm light, when the intensity of the exciting light is normalized to that of 365 nm light.

the spectral change in small conversions. From the slope of the plot, we determined the quantum yields for isomerization and cyclization* without any corrections, since the absorptivity of I at 365 nm (exciting light) was almost constant in small conversions and the cyclized products did not absorb the exciting light. The results are given in Table 3 together with those of VIII. Both quantum yields for isomerization and cyclization decrease slightly with the addition of oxygen and increase remarkably on using *n*-propyl bromide as a heavy atom solvent. The quantum yield of fluorescence of I under various conditions is also summarized in Table 3. Anthracene was used as a fluorescence standard (the quantum yield is 0.30),[11] since the fluorescence peak of I is at about 410 nm. The yield of fluorescence in the heavy atom solvent is reduced to about one-half the yield in cyclohexane, although it is not affected by oxygen. The results on the quantum

Table 3. Quantum yields of reactions and fluorescence[a)]

		φ_i	φ_c	φ_f
I/Cyclohexane	Degassed	4.6×10^{-2}	0.57×10^{-2}	—
	N_2 saturated	4.5×10^{-2}	0.28×10^{-2}	3.5×10^{-2}
	O_2 saturated	4.3×10^{-2}	0.20×10^{-2}	3.5×10^{-2}
VIII/Cyclohexane	N_2 saturated	28×10^{-2}	—	—
I/*n*-PrBr	N_2 saturated	5.9×10^{-2}	2.5×10^{-2}	1.9×10^{-2}

a) φ_i, φ_c and φ_f denote the quantum yields of isomerization, cyclization and fluorescence, respectively. Potassium ferrioxalate is used as a chemical actinometer.

* Since the contribution of I″ is negligible, at least in small conversions, isomerization is that from I to I′, and cyclization is that of a *pseudo*-photostationary mixture of I and I′ (and I″).

yield measurement also suggest that the photochemical reaction of I proceeds mainly through the triplet state of I.

Photochemical reaction of a fairly concentrated solution of I (*ca.* 0.1 M $CDCl_3$ solution) was studied by following NMR spectral change with irradiation time (irradiated with 365 nm light). Rapid isomerization of I to I′ was confirmed by an appearance of NMR peaks based on *cis*-olefinic group (δ 6.16, doublet, J= 12.6 Hz, *cis*-vinyl H, another doublet peak is hidden in the peaks of aromatic protons; 3.59, methoxy H). Simultaneous appearance of peaks based on *trans*-vinyl protons (δ 6.24, 8.62, pair of doublet, J=15.4 Hz) differing from those of I (δ 6.29, 8.37, J=15.4 Hz) and lack of the peaks of intramolecular cyclization products on irradiating for a long time suggest that photochemical reaction of concentrated solution of I would be geometrical isomerization and intermolecular dimerization. Detailed analysis of dimerized products was not performed.

Since the predominant formation of VI is almost independent of irradiation time, namely independent of whether the *pseudo*-photostationary state between I and I′ (and I″) is attained or not, the main product from I′ is expected to be the same VI as that from I. The photocyclization of I and I′ greatly resembles that of 1,5-dienes. Scheffer and Wostradowski[12] reported that acetone sensitized photochemical reaction of *trans, trans*- and *trans,cis*-isomers of dimethyl octa-2,6-diene-1,8-dioate, $(-CH_2-CH{=}CH-CO_2Me)_2$, leads to *cis, trans* isomerization with concomitant formation of the cyclized products corresponding to VI and VII in the same 65: 35 ratio.

Reaction Mechanism. The predominant formation of crossed adducts in photochemical reaction of naphthalene-1,8-diolefins irrespective of their substituents (H, Ph or CO_2Me) suggests that ground-state conformations contribute strongly to the course of cyclization. Examination of molecular models suggests that two ground-state conformers, I-A and I-S, are stable sterically, where two olefinic groups rotate to a considerable extent from naphthalene plane due to their steric inhibition.

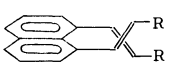

I-A

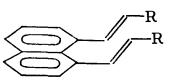

I-S

R=CO_2Me

From *anti* conformer I-A, only crossed adducts formation would be possible, and both crossed and straight adducts could be produced from *syn* conformer I-S. However, I-S is less favorable than I-A due to larger nonbonding interactions between two olefinic groups. Hence, the contribution of I-S to the crossed adducts formation is considered to be less important.

From the observations that (1) stereochemistry of crossed products VI and VII cannot be explained by the concerted mechanism, (2) isomerization and cyclization take place concomitantly through the triplet state and (3) both geometrical isomers I and I′ yield the same main product VI, we propose the reaction mechanism for the formation of crossed adducts as

follows, assuming intermediate 1,4-biradicals from *anti* conformers, I-A and I'-A.

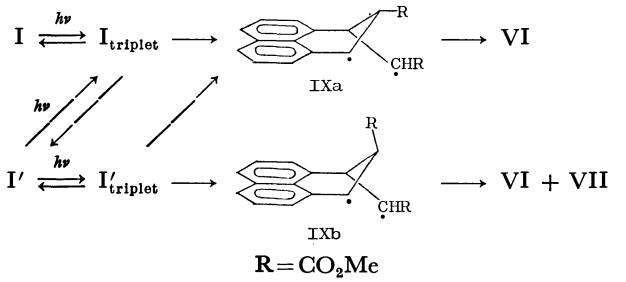

The back reactions of the biradicals to the ground state or the triplet state of I or I' are omitted to avoid complexity of the scheme.

Sole biradical IXa could be formed from I-A, but formation of two biradicals IXa and IXb would be possible from I'-A. Since the spin of the biradicals is expected still to be parallel, spin inversion is necessary for ring closure. The biradicals would be long-lived enough to change into the most stable conformation. For ring closure of biradical IXa, rapid rotation of the terminal carbomethoxy methine site into the satble conformation, where the interaction with an *equatrial* carbomethoxy group is minimized, would lead to preferential formation of main product VI. If the lifetime of the biradical is comparable to the rotational rate of terminal site, V and VI would be produced from the biradical. Cyclization of distyrylnaphthalene would be the case, if the reaction proceeds through the biradical corresponding to IXa. Biradical IXb would yield VI and minor product VII for ring closure.

Formation of VII from less-favored conformer I-S would be possible, if ring inversion of biradical IXc is considered as follows.

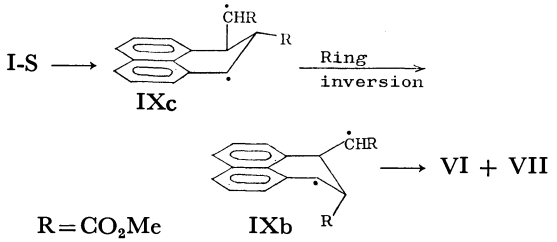

However, considering the reduced importance of I-S and the formation of most products from *pseudo*-photostationary mixture of I and I' (and I''), most of minor product VII would be formed from I' through the biradical IXb. Although details are not available since neither I' nor I'' is isolated, the observed solvent effect (increase of VII in polar solvents) could be interpreted, if the portion of I' in the *pseudo*-stationary mixture increases in polar solvents.

Formation of straight adduct II would be related to less-favored conformer I-S. In fact, this is supported by the predominant formation of straight adducts in the photochemical reaction of the compound fixed to *syn* conformer, 1,7-(1',8'-naphthalene)-1,6-heptadienes (RR=$(-CH_2-)_3$ in I and I''). However, a biradical mechanism would be unreasonable for the formation of II, since straight adducts other than II are not detected. Two possible biradicals, IXd and IXe, from the conformer I-S are expected to give at least two straight adducts for ring closure with nearly equivalent probability.[14]

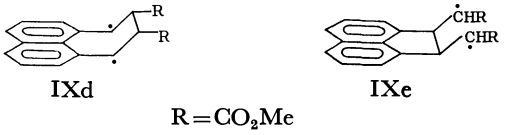

R=CO_2Me

If the observed oxygen effect (increase of II in the presence of oxygen) is considered, a concerted mechanism from singlet state would be more reasonable than a biradical one for the formation of another minor product II, although the formation of a small amount of II by triplet sensitization cannot be explained in a satisfactory manner.

Increase in cyclization efficiency by *n*-propyl bromide is much greater than that in isomerization efficiency (Table 3), even if experimental errors are considered. This suggests that the intermediate biradicals formed from the triplet state of I must be again affected by the heavy atom solvent, since the enhancement of triplet yield by heavy atom effect should increase the quantum yields of cyclization and isomerization at the same ratio. The additional heavy atom effect should cause an acceleration of spin-inversion rate of biradicals, resulting in an increase in the rate of their ring-closure to cyclized products.

Irradiation in Rigid Matrix and in Solid State. Prolonged irradiation of I in EPA rigid glassy solution at 77 K did not bring about any UV spectral changes. The unreactivity would be attributed to the reduced triplet-yield of I, since the fluorescence yield increases remarkably under these conditions (φ_f=*ca.* 0.5).

When I is irradiated in a crystalline state, the IR absorption peaks based on the olefinic groups of I disappear completely but the amount of cyclization products is negligible. Although further detailed analysis of the products was not performed, polymeric substances could be produced.

The authors are grateful to Prof. Makoto Takahasi, the University of Tokyo, for his valuable discussions, and to Mr. Kazuo Sato for his assistance in experiments.

References

1) G. M. J. Schmidt, *J. Chem. Soc.*, **1964**, 2014.
2) F. W. Lichtenthaler and A. El-Scherbiney, *Chem. Ber.*, **101**, 1799 (1968).
3) O. Isler, H. Gutmann, M. Montavon, R. Rüegg, G. Ryser, and P. Zeller, *Helv. Chim. Acta*, **40**, 1242 (1957).
4) W. Hartmann and H. G. Heine, *Angew. Chem. Int. Ed. Engl.*, **10**, 272 (1971), J. E. Shields, D. Gavrilovic, J. Kopecky, W. Hartmann, and H. G. Heine, *J. Org. Chem.*, **39**, 515 (1974).
5) N. J. Turro, "Molecular Photochemistry," Benjamin, New York (1967), p. 132.
6) The triplet energy was estimated from the phosphorescence spectrum.
7) K. Gollnick, "Advances in Photochemistry," **6**, p. 14, John Wiley & Sons, Inc. (1968).
8) A. A. Lamola and G. S. Hammond, *J. Chem. Phys.*, **43**, 2129 (1965).
9) J. Meinwald and J. W. Young, *J. Amer. Chem. Soc.*, **93**,

725 (1971).
10) J. J. Bloomfield and D. C. Owsley, *Tetrahedron Lett.*, **21**, 1795 (1973) and references cited therein.
11) J. B. Birks, "Photophysics of Aromatic Molecules," Wiley Interscience, (1970), p. 251.
12) J. R. Scheffer and R. A. Wostradowski, *Chem. Commun.*, **1971**, 144 and *J. Org. Chem.*, **37**, 4317 (1972).
13) S. F. Nelsen and J. P. Gillespie, *J. Amer. Chem. Soc.*, **95**, 2940 (1973).
14) R. M. Pagni and C. R. Watson, Jr., *ibid.*, **96**, 2291 (1974); R. M. Pagni, C. R. Watson, Jr., J. E. Bloor, and J. R. Dodd, *ibid.*, **96**, 4064 (1974).

Photoreduction and Photoaddition of *N*-Acetyldiphenylmethyleneamine in Alkylbenzenes

Shuichiro Asao, Naoki Toshima, and Hidefumi Hirai

Department of Industrial Chemistry, Faculty of Engineering, The University of Tokyo, Hongo, Bunkyo-ku, Tokyo 113

(Received December 19, 1974)

Irradiation of *N*-acetyldiphenylmethyleneamine (II) in toluene solution gave *N*-(1,1,2-triphenylethyl)acetamide and *N*-(1,1-diphenylmethyl)acetamide in 11% and 4.4% yields, respectively. The former is an addition product of toluene to the C=N bond of imine II, and the latter a hydrogenation product of II. The same kind of addition and hydrogenation products as those in toluene were obtained on irradiation of imine II in ethylbenzene, cumene, *o*-, *m*-, and *p*-xylene, mesitylene, *p*-methoxytoluene, and *p*-cyanotoluene, respectively. Two kinds of competitive reaction processes are proposed from the results of the substituent effects for the phenyl ring of toluene, the effect of the additives such as sensitizers and quenchers, and the dependence of the photoreaction yields on the concentration of the additive. The photoreaction proceeds not only by the "chemical sensitization" mechanism derived from the ketyl radical of benzophenone, a hydrolyzed product of II, but also by the mechanism through the excited state of II itself.

The photochemical behavior of acyclic imines is not very clear,[1-12] although it is well-known that heteroaromatic compounds containing nitrogen actively undergo photochemical reactions.[13] The photoreduction of benzophenone imine derivatives in particular has been investigated in detail.[1,3,4] On irradiation of diphenylmethyleneamine (I) in 2-propanol, benzhydrylamine and *N*-benzhydrylidenebenzhydrylamine were produced instead of a dihydro dimer of I corresponding to benzpinacol given by the photoreduction of benzophenone.[3] *N*-Alkyldiphenylmethyleneamine was also reduced photochemically on its C=N bond, the reaction mechanism being proposed by Fischer and Padwa as a "chemical sensitization" process.[1,4,14-18] "Chemical sensitization" means that the ketyl radical, derived photochemically from the carbonyl compound present in the starting materials as an impurity, transfers a hydrogen atom to the imine without any energy transfer. On the other hand, high photochemical reactivity of α,β-unsaturated ketones suggests that the imino ketone, the N-analogue of an enone, would undergo the photochemical reaction expected to be brought about *via* the excited state of itself.

In a previous paper,[19] the photoreduction of *N*-acetyldiphenylmethyleneamine (II) (*N*-acetyldiphenylketimine) in 2-propanol was reported to give *N*-diphenylmethylacetamide (IV). We now wish to report that the addition product and the hydrogenation product on the C=N bond were obtained on irradiation of imine II in several alkylbenzenes, indicating that the excited state of imine II has the character of hydrogen abstraction though it was generally proposed that the C=N group should scarcely abstract a hydrogen.[20]

Results

Photoreaction of N-*Acetyldiphenylketimine (II) with Toluene.* The toluene solution of *N*-acetyldiphenylketimine (II) in a quartz tube was irradiated under nitrogen atmosphere with a 500 W high pressure mercury lamp for 100 hr. After irradiation toluene was distilled off and three products were separated by column chromatography on silica gel: *N*-diphenylmethylacetamide (IV), *N*-(1,1,2-triphenylethyl)acetamide (Va), and dibenzyl (VIa) in 4.4%, 11%, and 3.4% yields, respectively.

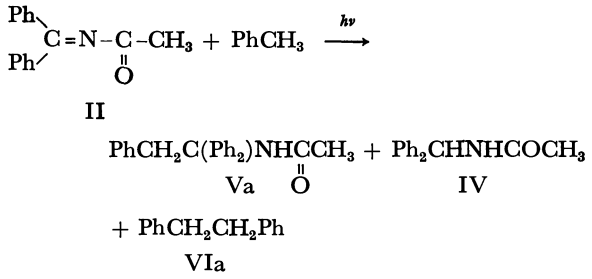

The remainder was the starting material. Compound IV was the same as that given on irradiation of II in 2-propanol: *i.e.*, it was identified by spectral data which included infrared absorption (3245, 1646, 1544 cm^{-1}) for the amide group, and the NMR spectrum at δ 7.07—7.46 (10H, m) for aromatic protons, δ 6.00—6.51 (m) for an amide proton, δ 1.97 (3H, s) for acetyl protons, and δ 1.77 (m) for a methine proton. Structure IV was further confirmed by comparing the spectral data with those of the authentic sample. Compound VIa was the coupling product of benzyl radicals brought about on hydrogen abstraction. Amide Va was the adduct of toluene to II. This kind of adduct was obtained on the photoreaction of II in cyclohexene[8] but not in 2-propanol. Structure Va was inferred from its composition ($C_{22}H_{21}NO$) and spectral data which included the infrared absorption bands for an amide group (3326, 1657, 1546 cm^{-1}), and confirmed by the NMR spectrum showing acetyl protons (3H, δ 1.94, s), aromatic protons (15H, δ 6.40—7.42), an amide proton (δ 6.17, m), and methylene protons (2H, δ 3.92) originating from toluene.

Photoreaction of N-*Acetylketimine II with Alkylbenzenes and Relative Reactivities of Alkylbenzenes.* On irradiation of II in substituted toluenes, the reactions proceeded *via* hydrogen atom abstraction from alkylbenzenes, the adducts, hydrogenation products and dimeric hydrocarbons being obtained. Irradiation of II in *p*-methyltoluene (*p*-xylene) gave Vb (37%) and IV (14%). Structure Vb was determined as *N*-[1,1-diphenyl-2-(*p*-tolyl)ethyl]acetamide by its NMR spectrum data. It showed signals for methyl protons (δ 2.22) derived from *p*-xylene, and fourteen aromatic protons, four

TABLE 1. PHOTOREACTION OF *N*-ACETYLKETIMINE II WITH ALKYLBENZENES(III)[a]

Subscript	Alkylbenzene (III)	Product yield (%)[b]		Relative reactivity toward $^3Ph_2CO$[c]
		Hydrogenation product (IV)	Adduct (V)	
a	Toluene	4.4	11	1.0
b	*p*-Xylene	14	37	4.3
c	Mesitylene	18	38	5.6
d	Ethylbenzene	11	25	3.3
e	Cumene	16	40	2.3

a) Irradiation was carried out in a quartz tube with an Eikōsha 500 W high pressure mercury lamp for 100 hr. Concentration of II was 0.14 mol/l and volume of III was 30 ml. b) Yields refer to the conversion in this paper, *i.e.*, the remainder is the starting imine. c) See Ref. 21.

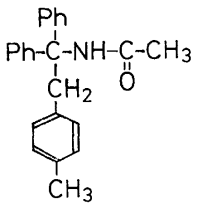

Vb

of which showed the typical A_2B_2 signal pattern of *p*-disubstituted benzene. Only one methyl group of *p*-xylene was concerned with the addition reaction. In ethylbenzene *N*-(1,1,2-triphenyl-*n*-propyl)acetamide (Vc, yield 25%), *d,l*- and *meso*-2,3-diphenylbutane, and IV (yield 11%) were obtained. The reaction occurred *via* hydrogen atom abstraction in a benzylic position, not in a methyl group. These results and the yields of the reaction in other alkylbenzenes are summarized in Table I. Product yields were determined by glpc (Apiezon greese L on Chromosorb W(HP)). As the adduct of ethylbenzene was not detectable by glpc, the yield of Vd was given by the remainder after subtracting the yield of IV in glpc from that of the mixtures of Vd and IV obtained by column chromatography on silica gel. The same method was applied to the yield of the adduct of cumene.

TABLE 2. DEPENDENCE OF THE PHOTOREACTION YIELD OF *N*-ACETYLKETIMINE II WITH TOLUENE IN THE PRESENCE OF SEVERAL ADDITIVES[a]

Additive	E_T[b] (kJ/mol)	Yield (%)	
		Adduct	Hydrogenation product
None		2.5	0.94
Xanthone	310	10	28
Triphenylamine	295	1.2	1.1
Benzophenone	290	12	12
Triphenylene	280	1.1	1.2
Diacetyl	235	6.6	1.4
Benzil[c]	220	5.2	1.7
Fluorenone	220	0.40	0.27
1-Methylnaphthalene	250	0.36	0.20

a) Irradiation was carried out in toluene (10 ml) solution with 0.23 mol/l of II and 4.3×10^{-2} mol/l of additives in a pyrex tube for 30 hr unless otherwise stated. b) See Ref. 22. c) Irradiation with light of wave lengths greater than 390 nm for 60 hr.

Effect of Additives on the Photoreaction of N-*Acetylketimine II with Toluene upon Additives.* The photoreaction of II with toluene was carried out in the presence of several additives (Table 2). The toluene (10 ml) solution of II (0.23 mol/l) with benzophenone (0.043 mol/l) in a pyrex tube under nitrogen was irradiated with a 500 W high pressure mercury lamp at 25 °C. After 30 hr irradiation IV (yield 12%) and Va (yield 12%) were obtained.

When 1-methylnaphthalene was used in this photoreaction instead of toluene, no photoreaction of II was observed. This can be explained by quenching of the photoreaction of II with 1-methylnaphthalene. On the basis of this result, quenching studies were carried out with naphthalene. The results indicate a Stern-Volmer relationship for product appearance (Fig. 1). The slope for Va is 2.46×10^2 l/mol and that for IV is 1.00×10^2 l/mol.

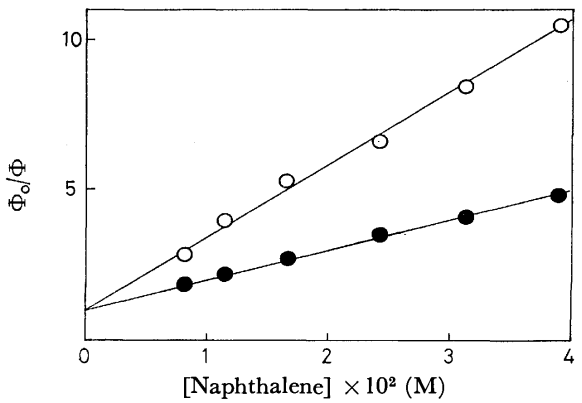

Fig. 1. Quenching of the photoreaction of *N*-acetylketimine II with toluene by naphthalene: Adduct (○), Hydrogenation product (●); [*N*-Acetylketimine] 0.23 mol/l, [Toluene] 10 ml; Irradiation was carried out with above 300 nm for 30 hr at 25 °C.

Dependence of the Photoreaction of N-*Acetylketimine II with Toluene upon the Concentration of Benzil.* The reaction yield increased in the presence of benzil (Table 2). The influence of benzil in the photoreaction was investigated on irradiation of II (0.23 mol/l) in toluene (10 ml) at wavelengths greater than 390 nm with various concentration of benzil. Benzil exhibits its absorption at 370 nm (ε_{max} 78) due to an n-π^* transition, the shoulder of the absorption appearing in the region of wavelengths greater than 390 nm. On the other hand,

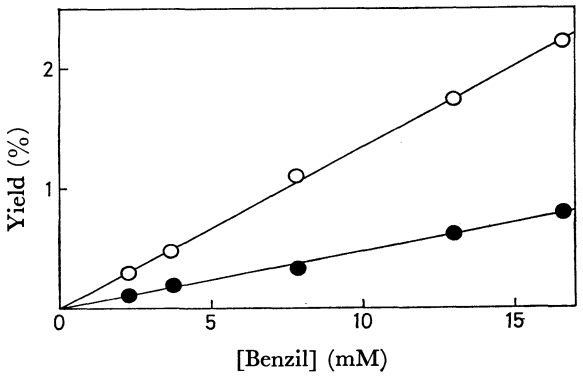

Fig. 2. Dependence of the yields of the photoreaction of *N*-acetylketimine II with toluene on the concentration of benzil: Adduct (○), Hydrogenation product (●); [*N*-Acetylketimine] 0.23 mol/l, [Toluene] 10 ml; Irradiation was carried out above 390 nm for 60 hr at 25 °C.

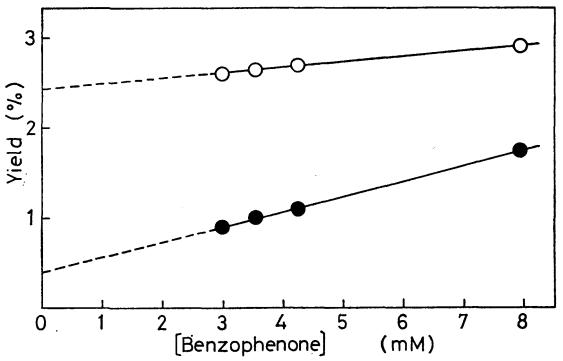

Fig. 3. Dependence of the yields of the photoreaction of *N*-acetylketimine II with toluene on the concentration of benzophenone: Adduct (○), Hydrogenation product (●); [*N*-Acetylketimine] 0.23 mol/l, [Toluene] 10 ml; Irradiation was carried out above 300 nm for 30 hr at 25 °C.

II shows no absorption in the region above 390 nm (Fig. 4, Experimental). No products were obtained at a light above 390 nm without sensitizers, the same results being obtained even with benzophenone under these conditions.[23] Figure 2 shows the results of the sensitization experiments with II using benzil, the reaction yields increasing linearly with added benzil. The same kind of dependence was observed on the reaction of II with diacetyl. Thus benzil and diacetyl were found to be effective to the reaction as additives.

Dependence of the Photoreaction of N-*Acetylketimine II with Toluene on the Concentration of Benzophenone.* The starting sample II contains a small amount of benzophenone, hydrolysis product of II which is easily hydrolyzed. Benzophenone was added as a chemical sensitizer and was recovered without any change after irradiation. Figure 3 shows the relations of the photoreaction yields *vs.* the total amount of benzophenone which should be the sum of an added amount and a hydrolyzed amount determined by glpc. The full lines indicate the experimental data and the dotted lines the extrapolation of the results. Both products increase in yields linearly with the concentration of benzophenone.

Photoreaction of N-*Acetylketimine II with Substituted Toluenes.* The results of the photoreaction of II with various substituted toluenes are summarized in Table 3. The total yields of the adducts and the hydrogenation products are shown in relative values using the value in toluene as a standard. For the sake of comparison, the relative reactivity of substituted toluenes toward benzophenone triplet is cited.[21] It is apparent that the reactivity of II differs a great deal from that of benzophenone, in the case of *p*-methoxytoluene. On the reaction of II with three isomers of methyltoluenes (xylenes), the yields decreased in the order $p\text{-}CH_3 > m\text{-}CH_3 > o\text{-}CH_3$.

Discussion

Effect of Additives. The mechanism of the photoreaction of II with alkylbenzenes appears to be complicated, since the energy of the excited triplet state of sensitizers is not concerned directly with the sensitization of the reaction of II (Table 2). As an example, benzophenone (E_T=290 kJ/mol) was effective in the reaction as a sensitizer, but not triphenylene (E_T=280 kJ/mol) with nearly the same triplet energy as that of benzophenone. Padwa and co-workers[1] suggested that benzophenone works as a so-called "chemical sensitizer" in the photoreduction of *N*-benzoyldiphenylketimine (VIII) in 2-propanol. Benzophenone was regarded as not transferring its triplet energy to VIII because of the fact that phosphorescence of benzophenone was not appreciably quenched by VIII. If the photoreduction and photoaddition reaction of II with toluene occurs by "chemical sensitization," the species with a hydrogen abstracting character can play the role of a chemical

Table 3. Photoreaction of *N*-acetylketimine II with substituted toluene (III)[a]

Substituted toluene (III)	Yields (%)			Relative reactivity	
	Hydrogenation product (IV)	Adduct (V)	Total (IV+V)	Imine II	$^3Ph_2CO$[b]
Toluene	1.2	4.2	5.4	1.00[c]	1.00[c]
p-Xylene	10	14	24	4.4	4.3
m-Xylene	3.4	8.8	12.2	2.3	2.9
o-Xylene	4.1	6.8	10.9	2.0	—
p-Methoxytoluene	2.0	3.7	5.7	1.1	10.6
p-Cyanotoluene	2.9	2.5	5.4	1.0	—

a) Photoreactions were carried out in a solution of substituted toluene (5 ml), benzene (5 ml), and II (0.23 mol/l) in a pyrex tube with light above 300 nm for 30 hr. b) See Ref. 21. c) Standard.

sensitizer to increase the product yields, regardless of the excitation energy. In fact, triphenylamine with triplet energy higher than that of benzophenone did not sensitize the reaction, but xanthone with a hydrogen atom abstracting character was effective. On irradiation of II above 390 nm, no reaction occurred with or without benzophenone.[23,24] Irradiation of II above 390 nm in toluene in the presence of benzil or diacetyl gave IV and Va. Benzil (E_T=220 kJ/mol) and diacetyl (E_T=235 kJ/mol) with a hydrogen abstracting character exhibit maxima at 370 nm (ε_{max} 78) with tailing and at 422 nm (ε_{max} 22), respectively,[24,25] indicating n-π^* absorption. Benzil or diacetyl is considered to abstract a hydrogen atom of the triplet state after excitation with light above 390 nm and to transfer it to II. In contrast, fluorenone, whose lowest triplet state is (π, π^*) with E_T=220 kJ/mol, retarded the reaction above 300 nm. Fluorenone is not able to abstract a hydrogen atom from toluene on irradiation,[26] and probably acts as a quencher on irradiation of II in toluene.

Chemical Sensitization of the Reaction of II by Benzil. Benzil is effective as a sensitizer (Table 2) and the photochemical reaction yields of both the adduct and the hydrogenation product increased linearly with benzil added at the wavelengths above 390 nm (Fig. 2). The reaction scheme is proposed as follows (Scheme 1).

$$\mathrm{Ph{-}\underset{\underset{O}{\|}}{C}{-}\underset{\underset{O}{\|}}{C}{-}Ph} \xrightarrow{h\nu} \mathrm{Bz^*(S_1)} \longrightarrow \mathrm{Bz^*(T_1)}$$

(Bz)

$$\mathrm{Bz^*(T_1)} \xrightarrow{k_d} \mathrm{Bz}$$

$$\mathrm{Bz^*(T_1) + PhCH_3} \xrightarrow{k_r} \mathrm{Ph{-}\underset{\underset{HO}{|}}{\dot{C}}{-}\underset{\underset{O}{\|}}{C}{-}Ph + Ph\dot{C}H_2}$$

(RH) (BzH) (R)

$$\mathrm{BzH + Ph_2C{=}NAc} \xrightarrow{k_H} \mathrm{Ph_2\dot{C}{-}NHAc + Bz}$$

(D) (DH)

$$\mathrm{DH + Ph\dot{C}H_2} \xrightarrow{k_{cc}} \mathrm{PhCH_2C(Ph_2)NHAc}$$

(R) (Ad)

$$\mathrm{2DH} \xrightarrow{k_D} \mathrm{Ph_2CHNHAc + D}$$

(DH_2)

$$\mathrm{2Ph\dot{C}H_2} \xrightarrow{k_c} \mathrm{PhCH_2CH_2Ph}$$

Scheme 1.

Only benzil (Bz) can absorb light above 390 nm to cause excitation, since imine II (D) and benzophenone cannot absorb light in that region. The excited triplet state of benzil [Bz* (T_1)] abstracts a hydrogen atom from toluene (RH) and α-amino radical (DH) is formed by hydrogen atom transfer from BzH to II. An adduct (Ad) is obtained by cross-coupling between DH and R. A hydrogenation product (DH_2) is produced by disproportionation.

The usual steady-state treatment of Scheme 1 gives the following two equations for the adduct (Ad) and the hydrogenation product (DH_2).

$$\frac{d[DH_2]}{dt} = k_D[DH]^2 = \frac{k_r[Bz^*(T_1)][RH]}{1+k_{cc}(k_Dk_c)^{-1/2}}$$

$$\frac{d[Ad]}{dt} = k_{cc}[DH][R] = \frac{k_r[Bz^*(T_1)][RH]}{1+(k_Dk_c)^{1/2}(k_{cc})^{-1}}$$

These equations show that yields of the adduct and the hydrogenation product should be proportional to the concentration of benzil, since [Bz*(T_1)] is proportional to [Bz]. The results in Fig. 2 indicate that Scheme 1 is valid. Consequently, the reaction *via* "chemical sensitization" is promoted linearly with the quantity of chemical sensitizer.

Quenching of the Photoreaction of N-*Acetylketimine II in Toluene.* Padwa and co-workers reported on the photoreduction of *N*-(diphenylmethylene)methylamine (IX) in 2-propanol[1] and suggested that the photoreduction of IX occurs *via* "chemical sensitization" due to the fact that a quantum yield of the photoreduction of IX was very low ($\Phi<10^{-3}$) and that only such the sensitizers with a hydrogen abstracting power as benzophenone (Φ=0.66) are effective.

If the photoreaction of II with toluene proceeds only *via* "chemical sensitization," the reaction does not involve the excited state of II as an intermediate and II serves as a hydrogen atom capture. The reaction path on the basis of "chemical sensitization" mechanism in the presence of a quencher can be considered to be that outlined in Scheme 2.

$$\mathrm{Ph_2CO} \xrightarrow{h\nu} \mathrm{Ph_2CO^*(S_1)} \longrightarrow \mathrm{Ph_2CO^*(T_1)}$$

$$\mathrm{Ph_2CO^*(T_1)} \xrightarrow{k_d} \mathrm{Ph_2CO}$$

$$\mathrm{Ph_2CO^*(T_1) + PhCH_3} \xrightarrow{k_r} \mathrm{Ph_2\dot{C}OH + Ph\dot{C}H_2}$$

$$\mathrm{Ph_2\dot{C}OH + Ph_2C{=}NAc} \xrightarrow{k_H} \mathrm{Ph_2\dot{C}NHAc + Ph_2CO}$$

$$\mathrm{Ph_2\dot{C}NHAc + Ph\dot{C}H_2} \xrightarrow{k_{cc}} \mathrm{PhCH_2C(Ph_2)NHAc}$$

$$\mathrm{2Ph_2\dot{C}NHAc} \xrightarrow{k_D} \mathrm{Ph_2CHNHAc + Ph_2C{=}NAc}$$

$$\mathrm{2Ph\dot{C}H_2} \xrightarrow{k_c} \mathrm{PhCH_2CH_2Ph}$$

$$\mathrm{Ph_2CO^*(T_1) + Q} \xrightarrow{k_q} \mathrm{Ph_2CO + Q^*}$$

Scheme 2.

The usual steady-state treatment of Scheme 2 gives the Stern–Volmer equation:

$$\frac{\Phi_A^\circ}{\Phi_A} = \frac{\Phi_R^\circ}{\Phi_R} = 1 + \frac{k_q[Q]}{k_r[RH]+k_d}$$

where Φ is the quantum yield of the reaction in the presence of a quencher, Φ^0 is that without a quencher, and subscripts A and R denote the adduct and the reduction product, respectively.

This equation being exactly the same as that for benzophenone, the Stern-Volmer plot should coincide with that of benzophenone. In the plot for Φ_A°/Φ_A *vs.* [Q], the slope for the adduct was 2.46×10^2 l/mol. But the slope of the Stern-Volmer plots on the photoreaction of benzophenone in toluene was reported to be *ca.* 10^3 l/mol[27–32] differing from that for the reaction of II. This difference cannot be explained by the difference of viscosity of the solution between benzo-

phenone and II. In fact, the viscosity of the solution of II in the experiment is 0.573 cp and does not influence the assumption of diffusion control. On the other hand, the slope of the plot for the adduct differs from that of the hydrogenation product. These results suggest that the photoreaction of II with toluene is not explicable by "chemical sensitization" of benzophenon , and that the excited state of II should influence the reaction.

Mechanistic Consideration on the Sensitization Effect of Benzophenone. The photoreaction yields increase linearly with the amount of a chemical sensitizer, and additives such as benzil and benzophenone act as chemical sensitizers.

The photoreaction of II with toluene in the presence of various amounts of benzophenone equal to the sum of an impurity in II and the added compound was investigated to see if the excited state of II could abstract a hydrogen atom from toluene. The linear dependence of the reaction yields on the total concentration of benzophenone (Fig. 3) agrees with the result of the reaction in the presence of benzil (Fig. 2). From the linearity, the plot of the experimental data can be extrapolated to the zero concentration of benzophenone. If the excited state of II cannot abstract a hydrogen atom, the reaction yields should converge on 0% at the point of no benzophenone. Actually, however, Fig. 3 indicates clearly the formation of the adduct and the hydrogenation product in about 2.5% and 0.4% yields, respectively, without benzophenone. These figures indicate exactly the yields of the reactions through the excited state of II.

Consequently, the present photoreaction is explained by the competition reactions between *via* "chemical sensitization" and *via* the excited state of II (Scheme 3).

$$Ph_2C{=}NAc \xrightarrow{h\nu} Ph_2C{=}NAc^*(S_1) \longrightarrow Ph_2C{=}NAc^*(T_1)$$
$$Ph_2C{=}NAc^*(T_1) + PhCH_3 \longrightarrow Ph_2\dot{C}{-}NHAc + Ph\dot{C}H_2$$
$$Ph_2\dot{C}{-}NHAc + Ph\dot{C}H_2 \longrightarrow PhCH_2C(Ph_2)NHAc$$
$$2Ph_2\dot{C}{-}NHAc \longrightarrow Ph_2CHNHAc + Ph_2C{=}NAc$$
$$2Ph\dot{C}H_2 \longrightarrow PhCH_2CH_2Ph$$
$$Ph_2CO \xrightarrow{h\nu} Ph_2CO^*(S_1) \longrightarrow Ph_2CO^*(T_1)$$
$$Ph_2CO^*(T_1) + PhCH_3 \longrightarrow Ph_2\dot{C}OH + Ph\dot{C}H_2$$
$$Ph_2\dot{C}OH + Ph_2C{=}NAc \longrightarrow Ph_2\dot{C}{-}NHAc + Ph_2CO$$

Scheme 3.

Comparison of the Photoreactivity between N-*Acetylketimine II and Benzophenone.* The ability of hydrogen abstraction by the excited state of II is further emphasized by comparison of the photoreactivity of II with that of benzophenone. Walling and Gibian reported on the photoreduction of benzophenone in substituted toluenes.[21] The rate-determining step of the photoreduction was the process of a hydrogen abstraction,[27-32] the rate constant of formation of benzpinacol by radical reaction of benzophenone ketyl radicals being $3.6\times10^9\ M^{-1}\ s^{-1}$.[32] In the case of the reaction of II (0.15 mol/l) with large excess of alkylbenzenes in the presence of 0.25 molar equivalent of benzophenone, benzpinacol was not obtained, at least below 50% conversion, and added benzophenone was recovered without any change. If the reaction proceeds *via* "chemical sensitization" by benzophenone in II as an impurity, the rate for hydrogen atom transfer from a ketyl radical to II should be greater than that of disproportionation of the ketyl radicals. That is, if the situation were contrary, benzpinacol should have been formed on irradiation. In order to explain the photoreaction of II with toluene by "chemical sensitization," the rate-determining step should be the process of hydrogen atom abstraction by benzophenone. The photoreactivity of II with substituted toluenes should then coincide with that of benzophenone. However, the relative reactivity of II with *p*-methoxytoluene differs greatly from that of benzophenone. Furthermore, on irradiation of II with *p*-halotoluenes the adduct and the hydrogenation product increased in yields in the order *p*-F<*p*-Cl<*p*-Br.[33] The order is reverse to that in the photoreduction of benzophenone in *p*-halotoluenes. These findings support existence of the reactive excited state of II.

Hammond and co-workers reported on the photoreaction of benzophenone with alkylbenzenes which gives rise to the formation of benzpinacol, a reduction product, and a cross coupling product of benzophenone ketyl radical with benzyl radical.[34] Their results are shown in Table 4 with the present data of II.

Table 4. Comparison of the photoreactivity of *N*-acetylketimine II and benzophenone

Ketone or imine	Alkylbenzene	Yield (%)[a]		
		Benzpinacol	Hydrogenation product	Adduct
Ph_2CO[b]	$PhCH_3$	51	—	43
Ph_2CO[b]	$PhCH(CH_3)_2$	24	—	48—60
II	$PhCH_3$	—	29	71
II	$PhCH(CH_3)_2$	—	29	71

a) Yield based on the consumed benzophenone or II.
b) See Ref. 34.

The proportion of a cross coupling product in the photoproducts of *N*-acetylketimine II with alkylbenzenes is higher than that of benzophenone. This can be interpreted by the difference between the reaction mechanism of II and that of benzophenone. Although there is no band indicating an intermolecular interaction in the electronic spectra of II with toluene, the differences mentioned above suggest that II interacts with alkylbenzenes weakly in some way.

Experimental

Materials. Alkylbenzene such as toluene, ethylbenzene, *p*-xylene, cumene, and mesitylene (Yoneyama Chemical Industry), and *o*-, *m*-xylene, and, *p*-methylanisole (Tokyo Chemical Industry) were dried over sodium by refluxing and then distilled. Benzophenone (Yoneyama Chemical Industry), xanthone, fluorenone, and benzil (Tokyo Chemical Industry) were recrystallized from ethanol. Triphenylene and triphenylamine (Tokyo Chemical Industry) were used without further purification. Eluting solvents for column chromatography such as cyclohexane, benzene, methylene chloride, chloroform, and ethanol were used in the state they were received.

Instrumentations. Irradiation was performed with a 500

W Halos high pressure mercury lamp (Eikōsha Ltd.). Most comparative runs were carried out on a merry-go-round type reactor (Rikōkagaku Ltd.) with a turntable device holding the rotating pyrex tubes. This turntable also rotated around the lamp in a water cooled quartz immersion well. The turntable and tubes were held in a constant temperature water bath maintained at 25 °C. Glpc analysis was performed with a Ohkura Rikagaku gaschromatograph with a flame ionization detector, equipped with a 2 m × 3 mm ϕ stainless steel column packed with 10% Apiezon Grease L on 60—80 mesh Diasolid A or on 60—80 mesh Chromosorb W(HP). Infrared spectra were obtained using a JASCO IR-E spectrometer. Ultraviolet measurements were carried out on a Shimadzu MPS-50L spectrophotometer. The NMR spectra were recorded on a JEOL PS-100 or a Hitachi Perkin-Elmer R-20B spectrometer. A Hitachi RMS-4 mass spectrometer was used for mass spectrometry. Melting points were determined with a Yanagimoto micro melting point apparatus. Vapor pressure osmometer analyses were carried out on a Mechrolab Inc. Model 301A osmometer.

Preparation of N-*Acetyldiphenylmethyleneamine(II) (*N-*Acetyldiphenylketimine).*[6,35,36] An ethereal solution of the Grignard reagent from bromobenzene was treated with a stoichiometric amount of benzonitrile. Completion of the decomposition of the Grignard-nitrile complex by addition of methanol gave a pale yellow slurry. The slurry was filtered, and the filtrate was distilled a few times. The fraction of bp 125 °C (1.0 mmHg) was diphenylketimine [lit,[36] bp 127 °C (3.5 mmHg)]. *N*-acetyldiphenylketimine (II) was prepared by refluxing diphenylketimine in twice the number of moles of acetic anhydride for six hr. bp 168—170 °C (1.0 mmHg)] [lit,[35] bp 168—171 °C (1 mmHg)]. UV spectrum of II is shown in Fig. 4.

Preparative Irradiation Procedure. The solution of *N*-acetylketimine II (0.14 mol/l) in toluene (30 ml) in a quartz tube was degassed in three succesive freeze-thaw cycles and irradiated under nitrogen with a 500 W high pressure mercury lamp for 100 hr. The photoreaction mixtures were worked up by evaporation of the solvent at a reduced pressure and separated by column chromatography on silica gel. The reaction mixtures were eluted in succession with 500 ml of cyclohexane, benzene, methylene chloride, chloroform, and ethanol. The coupling products of benzyl radicals were eluted with cyclohexane, and *N*-acetylketimine II and benzophenone, almost the entire amount of which is a hydrolysis product in the silica gel column, were eluted with benzene. The fractions eluted by chloroform contained both the adduct and the reduction product separately. Both products were purified by repeated recrystallization from the mixed solvent of cyclohexane and ethanol, or that of *n*-hexane and ethanol. The structure of the adducts and the coupling products were determined from their spectral data and elemental analyses. The analytical and spectral data are show in Tables 5 and 6. The hydrogenation product [*N*-(1,1-diphenylmethyl)acetamide, IV] was identi-

Table 5. Adducts of *N*-acetylketimine II with alkylbenzenes

Alkylbenzene	mp (°C)	Formula	MW	Elemental Analysis					
				Found			Calcd		
				C	H	N	C	H	N
Toluene	167.3—168.0	$C_{22}H_{21}NO$	315	83.74	6.73	4.47	83.77	6.71	4.44
p-Xylene	198.6—199.0	$C_{23}H_{23}NO$	329	83.96	7.09	4.21	83.85	7.04	4.25
m-Xylene	187.5—188.0	$C_{23}H_{23}NO$	329	84.07	7.14	4.47	83.85	7.04	4.25
o-Xylene	186.6—187.3	$C_{23}H_{23}NO$	329	83.69	7.02	4.55	83.85	7.04	4.25
Mesitylene	192.3—193.0	$C_{24}H_{25}NO$	343	83.62	7.46	3.96	83.92	7.34	4.08
Ethylbenzene	189.5—190.2	$C_{23}H_{23}NO$	329[a]	83.46	6.85	4.36	83.85	7.04	4.25
Cumene	171.2—171.7	$C_{24}H_{25}NO$	343	83.73	7.32	3.88	83.92	7.34	4.08
p-Methylanisole	181.5—181.8	$C_{23}H_{23}NO_2$	345	79.97	6.72	4.40	79.97	6.72	4.06
p-Cyanotoluene	253.3—254.0	$C_{23}H_{23}N_2O$	340	81.41	5.93	8.08	81.15	5.92	8.23

a) Analyzed by a vapour pressure osmometer in ethyl acetate at 37 °C.

Table 6. Spectral data of the adducts of alkylbenzenes to *N*-acetylketimine II

Alkylbenzene	IR (cm^{-1})		NMR δ in $CDCl_3$				
	ν_{NH}	ν_{CO}	Phenyl protones	NH	CH_2	Acetyl	Other protons
Toluene	3326	1657	7.48—6.60(15H)	6.16	3.91	1.94	
p-Xylene	3358	1656	7.34—6.66(10H) 6.39, 6.81, 6.56, 6.43 (4H, J=7.5 Hz)	6.13	3.83	1.89	*p*-CH_3 2.22
m-Xylene	3300	1656	7.54—6.62(14H)	6.30	3.89	1.91	*m*-CH_3 1.31
o-Xylene	3320	1660	7.39—6.75(14H)	6.30	3.89	1.91	*o*-CH_3 1.32
Mesitylene	3305	1662	7.47—6.87(10H) 6.80(1H), 6.25(2H)	6.30	3.80	1.87	CH_3 2.11(6H)
Ethylbenzene	3300	1657	7.70—7.54(15H)	6.19	—	1.81	CH 4.72, CH_3 1.25 J_{CH-CH_3}=7.2 Hz
Cumene	3340	1655	7.52—6.70(15H)	6.52	—	2.00	CH_3 1.38(6H)
p-Methylanisole	3380	1659	7.39—6.75(14H)	6.30	3.98	1.91	CH_3 1.32
p-Cyanotoluene	3360	1656	7.55—6.83(10H) 7.25, 7.17, 6.89, 6.81(4H, J=8 Hz)	6.23	4.05	1.98	

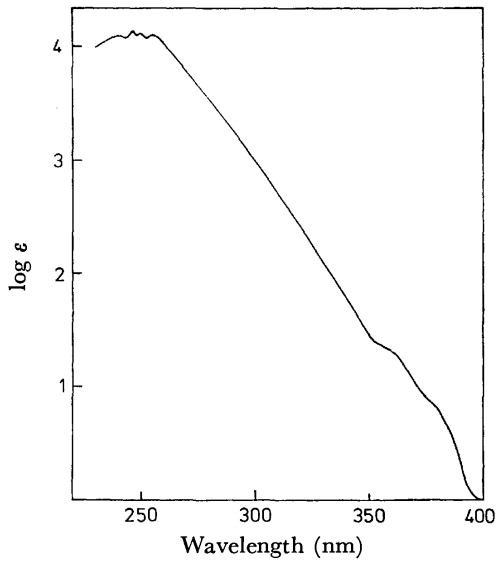

Fig. 4. UV spectrum of *N*-acetyldiphenylmethyleneamine (II) in *n*-hexane.

fied by comparing its spectral data with those of an authentic sample prepared otherwise, and by its inability to depress the melting point.

Irradiation for Mechanistic Study. A degassed solution of *N*-acetylketimine II (0.23 mol/l), substituted toluene (5 ml), and benzene (5 ml) in a pyrex tube under nitrogen was irradiated with a 500 W high pressure mercury lamp at 25±1 °C for 30 hr using a merry-go-round type reactor. The reaction mixtures were worked up by evaporation of the solvent at reduced pressure, and analysed by glpc. Column was a 2 m×3 mm ϕ in 10% Apiezon Grease L on 60—80 mesh Diasolid A or on 60—80 mesh Chromosorb W (HP). The results are summarized in Tables 1 and 3 in the case of alkylbenzenes and *p*-substituted toluenes, respectively. Yields are given in percentage of the starting imine II. No other products of the imine II except those in Table 3 could be obtained, and the remaining imine was recovered after the reaction.

Mechanistic Study in the Presence of Additives. A degassed solution of II (0.23 mol/l) in toluene (10 ml) in the presence of additives in a pyrex tube under nitrogen was irradiated with a 500 W high pressure mercury lamp at 25±1 °C for 30 hr with a merry-go-round type reactor described above. After irradiation, toluene was distilled off in a reduced pressure, and yields of both products, the adduct (Va) and the hydrogenation product (IV), were determined by glpc equipped with a 2 m× 3 mm ϕ column packed with 10% Apiezon Grease L on 60—80 mesh Chromosorb W (HP) at 222 °C at a nitrogen flow rate of 55 ml/min. The results are summarized in Table 2. Yields are shown in percentage with respect to the starting imine II. The remainder of imine was recovered in each case.

References

1) A. Padwa, W. Bergmark, and D. Pashayan, *J. Amer. Chem. Soc.*, **91**, 2653 (1969); A. Padwa and T. Smolanoff, *ibid.*, **93**, 548 (1971); A. Padwa and M. Dharan, *Tetrahedron Lett.*, **1972**, 1053; P. Beak and C. R. Payet, *J. Org. Chem.*, **35**, 3281 (1970).

2) T. Okada, K. Saeki, M. Kawanisi, and H. Nozaki, *Tetrahedron*, **26**, 3661 (1970); B. Fraser-Reid, A. McLean, and E. W. Usherwood, *Can. J. Chem.*, **47**, 4511 (1969).

3) N. Toshima, H. Hirai, and S. Makishima, *Kogyo Kagaku Zasshi*, **72**, 184 (1969); E. S. Huyser, R. H. S. Wang, and W. T. Short, *J. Org. Chem.*, **33**, 4323 (1968).

4) M. Fischer, *Tetrahedron Lett.*, **1966**, 5273; *Chem. Ber.*, **100**, 3599 (1967).

5) Y. Ogata and K. Takagi, *Tetrahedron*, **27**, 2785 (1971).

6) H. Ohta and K. Tokumaru, *Chem. Ind.*, **1971**, 1301.

7) N. Toshima and H. Hirai, *Tetrahedron Lett.*, **1970**, 433; R.L. Furey and R.O. Kan, *Tetrahedron*, **24**, 3085 (1968).

8) N. Toshima, S. Asao, K. Takada, and H. Hirai, *Tetrahedron Lett.*, **1970**, 5123.

9) T. H. Koch and D. A. Brown, *J. Org. Chem.*, **36**, 1934 (1971); T. H. Koch and R. M. Rodehorst, *Tetrahedron Lett.*, **1972**, 4039; T. H. Koch, M. A. Geigel, and C. C. Tsai, *J. Org. Chem.*, **38**, 1090 (1973); T. H. Koch, R. J. Sluski, and R. H. Moseley, *J. Amer. Chem. Soc.*, **95**, 3957 (1973).

10) A. Padwa and F. Albrecht, *ibid.*, **94**, 1000 (1972); H. Hiraoka, *Chem. Comm.*, **1970**, 1306.

11) R. W. Binkley, *J. Org. Chem.*, **35**, 2796 (1970); T. Tezuka, A. Yanagi, and T. Mukai, *Tetrahedron Lett.*, **1970**, 637.

12) R. W. Binkley, *J. Org. Chem.*, **34**, 3218 (1969); J. Gorse, III. and R. W. Binkley, *ibid.*, **37**, 575 (1972).

13) P. Beak and W. R. Messer, "Organic Photochemistry," O. L. Chapman Ed., Marcel Dekker, New York (1969), Vol. 2, p. 117; P. Claus, *et al.*, *Pure Appl. Chem.*, **33**, 339 (1973).

14) B. M. Monroe and S. A. Weiner, *J. Amer. Chem. Soc.*, **91** 450 (1969).

15) P. S. Engel and B. M. Monroe, "Advances in Photochemistry," W. A. Noyes, Jr., G. S. Hammond, and J. N. Pitts, Jr., Ed., Wiley-Interscience, New York (1971), Vol. 8, p. 245.

16) J. G. Pacifici and G. Irick, Jr., *Tetrahedron Lett.*, **1969**, 2207.

17) H. E. Zimmermen and V. J. Hull, *J. Amer. Chem. Soc.*, **92**, 6515 (1970).

18) M. B. Rubin and J. M. Ben-Bassat, *Mol. Photochem.*, **3**, 155 (1971).

19) T. Okada, M. Kawanisi, H. Nozaki, N. Toshima, and H. Hirai, *Tetrahedron Lett.*, **1969**, 927.

20) H. Ohta and K. Tokumaru, *ibid.*, **1974**, 2965; H. Hart and R. W. Peiffer, *Chem. Commun.*, **1974**, 126; H. Hart and R. W. Peiffer, *J. Amer. Chem. Soc.*, **96**, 4849 (1974).

21) C. Walling and M. J. Gibian, *ibid.*, **87**, 3361 (1965).

22) W. G. Herkstroeter, A. A. Lamola, and G. S. Hammond, *ibid.*, **86**, 4537 (1964).

23) The n-π^* absorption band of benzophenone has maximum at 375 nm. See V. L. Ermolaev and A. N. Terenin, *Soviet Phys.*, **3**, 423 (1960).

24) N. J. Leonard and E. R. Blout, *J. Amer. Chem. Soc.*, **72**, 484 (1950).

25) C. J. Timmons, "UV Atlas of Organic Compounds," Butterworths, Verlag Chemie, London and Weinheim (1966), No. B5/1.

26) W. E. Bachaman, *J. Amer. Chem. Soc.*, **55**, 391 (1933).

27) G. Porter and F. Wilkinson, *Trans. Faraday Soc.*, **57**, 1686 (1961).

28) A. Beckett and G. Porter, *ibid.*, **59**, 2038 (1963).

29) A. Beckett and G. Porter, *ibid.*, **59**, 2051 (1963).

30) J. N. Pitts, Jr., H. W. Johnson, and T. Kuwana, *J. Phys. Chem.*, **66**, 2456 (1962).

31) J. A. Bell and H. Linschitz, *J. Amer. Chem. Soc.*, **85**, 528 (1963).

32) S. A. Weiner, *ibid.*, **94**, 581 (1972).

33) Unpublished results.

34) G. S. Hammond, W. P. Baker, and W. M. Moore, *J. Amer. Chem. Soc.*, **83**, 2795 (1961).

35) J. E. Banfield, G. M. Brown, F. H. Davey, W. Davies, and T. H. Ramsay, *Australian J. Sci. Res.*, **A1**, 330 (1948).

36) P. L. Pickard and T. L. Tolbert, *J. Org. Chem.*, **26**, 4886 (1961).

Carboxymethylation of Organic Halides by Palladium Complexes under Mild Conditions[1)]

Masanobu HIDAI, Tomoji HIKITA, Yoshimasa WADA, Yuzo FUJIKURA, and Yasuzo UCHIDA
Department of Industrial Chemistry, The University of Tokyo, Hongo, Bunkyo-ku, Tokyo 113
(Received January 8, 1975)

Palladium complexes, $Pd(CO)(PPh_3)_3$, $Pd_3(CO)_3(PPh_3)_4$, $Pd_3(CO)_3(PPh_3)_3$, and $PdCl_2(PPh_3)_2$ were found to be excellent catalysts for the carboxymethylation of various organic halides under very mild conditions. The carboxymethylation reaction is considered to proceed *via* acyl complexes as the intermediates.

In previous papers we reported syntheses of palladium(0) carbonyl complexes, $Pd(CO)(PPh_3)_3$ (**1**), $Pd_3(CO)_3(PPh_3)_4$ (**2**), and $Pd_3(CO)_3(PPh_3)_3$ (**3**),[2)] and the oxidative addition of various organic halides to **1** affording acyl complexes of palladium.[3)] In the present paper is described carboxymethylation of various organic halides under ambient conditions catalyzed by **1**, **2**, **3**, and also $PdCl_2(PPh_3)_2$ (**4**).

A number of papers on the carbonylation of organic halides by transition metal complexes have been reported, but the reactions required high temperature and pressure. Recently there appeared several reports on the carbonylation of organic halides under ambient conditions, in which $Ni(CO)_4$,[4-7)] $NaCo(CO)_4$,[8)] or a nickel-thiourea complex[9)] was used as the catalyst in combination with base. However, the yields of carbonylated products were below one mole or at best a few mole per mole of the transition metal complex used, and reaction temperatures of *ca.* 100° were sometimes required. In contrast, the palladium complexes **1**—**4** show remarkable catalytic activities in the carboxymethylation of various organic halides under very mild conditions.

Results and Discussion

When carbon monoxide is bubbled through a mixture of iodobenzene, methanol, diethylamine, and the palladium(0) complex (**1**, **2**, or **3**) at room temperature, methyl benzoate is produced with the formation of diethylammonium iodide. The yield of the ester was determined by means of gas chromatography and observed to increase linearly with the reaction time. Table 1 shows the yields exceeding far 100% based on palladium atom, along with other results which will be described hereinafter. As shown in Table 1, catalytic activities of **2** and **3** are comparable and higher than that of **1**.

Since **1** and **2** are formed by the treatment of **4** with methanol, diethylamine, and carbon monoxide,[10)] **4** can be conveniently used as the catalyst for the carboxymethylation instead of **1**, **2**, or **3**. Complex **4** is a stable compound and easy to handle compared with **1**, **2**, and **3** which are appreciably air-sensitive. Therefore carboxymethylation of various organic halides was carried out by employing **4** as the catalyst, and the

TABLE 1. CATALYTIC CARBOXYMETHYLATION OF ORGANIC HALIDES BY PALLADIUM COMPLEXES

$$RX \xrightarrow[CO,\ MeOH,\ Et_2NH]{Pd\ Complex} RCOOMe + Et_2NH\cdot HX$$

Complex	Halide	Temp. °C	CO Press. atm	Time hr	Yield of methyl ester	mol/Pd
1[a)]	Iodobenzene	18	1	5	Benzoate	6.0
2[a)]	Iodobenzene	18	1	5	Benzoate	10.0
3[a)]	Iodobenzene	18	1	5	Benzoate	10.0
4[a)]	Iodobenzene	18	1	5	Benzoate	9.5
5[a)]	Iodobenzene	18	1	5	Benzoate	9.0
6[a)]	Iodobenzene	18	1	5	Benzoate	13.5
1+PPh_3[a,d)]	Iodobenzene	18	1	5	Benzoate	2.7
4+PPh_3[a,d)]	Iodobenzene	18	1	5	Benzoate	5.0
4[b)]	*p*-Iodotoluene	24	1	5	*p*-Toluate	18.3
4[b)]	Bromobenzene	50	1	6	Benzoate	8.8
4[b)]	Bromobenzene	100	45	10	Benzoate	57.0
4[b)]	*p*-Dibromobenzene	80	10	1	*p*-Bromobenzoate Terephthalate	17.8 12.0
4[b)]	*β*-Bromostyrene	24	1	11	Cinnamate	21.3
4[b)]	1-Bromo-2-ethoxyethylene	50	1	2.5	*β*-Ethoxyacrylate	1.4
1[c)]	Benzyl Bromide	19	1	3	Phenylacetate	13.5
1[c)]	Methyl Iodide	20	1	3	Acetate	trace

a) Molar ratio of the complex: iodobenzene: diethylamine: methanol is 0.01: 1: 1: 5. In case of **2** or **3**, the molecular weight is reduced to a mononuclear basis. b) Molar ratio of the complex: halide: diethylamine is 0.01 to 0.02 : 1: 1. c) Calcium oxide is used as the base in place of diethylamine. Molar ratio of **1**: halide: CaO: methanol is 0.01: 0.8: 0.2: 10. d) One molar equivalent of PPh_3 is added.

results are listed also in Table 1. The reaction procedure is essentially the same as in the case of **1**, **2**, or **3**. The methyl esters are formed after an induction period of about 30 min, and the yields increase linearly with the reaction time even after 22 hr. As shown in Table 1, iodobenzene, *p*-iodotoluene, bromobenzene, *p*-dibromobenzene, *β*-bromostyrene, and 1-bromo-2-ethoxyethylene are converted catalytically by **4** to corresponding esters in high yields under mild conditions. Organic halides such as vinyl chloride, vinyl bromide, 1,2-dichloroethylene, 1,2-dibromoethylene, and chlorobenzene did not afford corresponding esters under the same conditions.

Amines other than diethylamine, *e.g.* dicyclohexylamine, can be used as the base. Organic halides that readily form ammonium salts with amines cannot be used as the substrate. But the use of calcium oxide as the base in place of amines enables carboxymethylation of benzyl bromide as well as iodobenzene at room temperature and under 1 atm carbon monoxide. As indicated in the lowest lines of Table 1, benzyl bromide was converted catalytically to methyl phenylacetate by **1**, while methyl iodide gave only a trace amount of methyl acetate.

In order to elucidate the reaction mechanism, two kinds of benzoyl complexes of palladium were also employed as the catalyst for the carboxymethylation of iodobenzene. One is $PdI(COPh)(PPh_3)_2$ (**5**), which is obtained by the reaction of **1** with iodobenzene in toluene under carbon monoxide at room temperature, and has an IR absorption at 1634 cm^{-1} assignable to $\nu_{O=O}$.[3] The other one is [$PdI(COPh)(PPh_3)$·toluene] (**6**), which is obtained by the reaction of **2** or **3** with iodobenzene in toluene (in the reaction of **2**, **6** is obtained together with **5**), and has an absorption at 1660 cm^{-1} also assignable to $\nu_{C=O}$. Both of **5** and **6** give molar equivalent of methyl benzoate by the treatment with methanol and diethylamine under nitrogen at room temperature. Moreover, they show similar catalytic activities in the carboxymethylation of iodobenzene as shown in Table 1. These results suggest that the benzoyl complexes **5** and **6** are the reaction intermediates of the carboxymethylation, and the following scheme is proposed.[11]

$$Pd(CO)(PPh_3)_n \xrightarrow{RX} PdX(COR)(PPh_3)_n \quad (n=1 \text{ or } 2)$$

MeOH, CO, base

RCOOMe, base·HX

In the absence of base, the palladium complexes show no catalytic activities. That is, when carbon monoxide is bubbled through a mixture of **1**, iodobenzene, and methanol for several hours, no ester formation is observed. And when diethylamine is added to the mixture after carbon monoxide is expelled by nitrogen bubbling, stoichiometric amount of benzoate is obtained. This indicates the reductive elimination of benzoyl iodide hardly occurs in the absence of base. Therefore the base is considered to rather enhance the direct attack of methoxide anion on the Pd-COPh moiety than neutralize the acidity being formed during the reaction. The acidity constant of methanol is 10^{-16}, while the equilibrium constant of $MeOH+R_2NH \leftrightarrows MeO^- + R_2NH_2^+$ is about 10^{-6}.[12]

As shown in Table 1, the yield of methyl benzoate from iodobenzene depends on the palladium complexes used and increases in the order **1**<**4**<**2**—**3**. When one molar equivalent of triphenylphosphine is added to the reaction mixture catalyzed by **4**, the yield observed is similar to that with **1**. This is compatible with the fact that **1** is prepared by treatment of **4** with diethylamine and methanol in the presence of one molar equivalent of triphenylphosphine under carbon monoxide. The addition of triphenylphosphine to **1** lowers the yield of ester formation since the ligand added shifts the equilibrium $\mathbf{1} \leftrightarrows Pd(CO)(PPh_3)_2 + PPh_3$ to the left-hand side and prevents the oxidative addition of iodobenzene.[3]

Experimental

Syntheses of complexes **1**, **2**, **3**, and **5** were already described in previous papers.[2,3,10] The complex **1** was also prepared by treatment of **4** with diethylamine and methanol in the presence of one molar equivalent of triphenylphosphine under carbon monoxide (yield, 60%). These complexes are air-sensitive and their handling must be conducted in oxygen-free, dry atmosphere. Complex **4** was prepared according to the published method.[14] Methanol, toluene, and diethylamine were purified according to the usual methods and distilled under nitrogen atmosphere. Organic halides were commercially obtained and were degassed and saturated with carbon monoxide before use. 1-Bromo-2-ethoxyethylene was prepared according to the published method.[15] Esters used as the standard material in gas chromatography analyses were commercially obtained.

Carboxymethylation Reaction under 1 atm Carbon Monoxide. When carbon monoxide was bubbled at room temperature (18°C) through a stirred mixture of **1** (0.100 g, 0.109 mmol), iodo benzene (2.22 g, 10.9 mmol), methanol (1.76 g, 55.0 mmol), and diethylamine (0.80 g, 11.0 mmol), the mixture became a yellow, homogeneous solution and then white powder of ammonium salt precipitated gradually with the formation of benzoate. After 5 hr the amount of benzoate determined by gas chromatography was 0.65 mmole (6.0 times molar equivalent of **1**). The above procedure was applied to all other similar reactions.

Another reaction system containing **4** (0.100 g, 0.285 mmole), iodobenzene (5.50 g, 27.0 mmole), dicyclohexylamine (3 ml), and methanol (5 ml) afforded methyl benzoate of 15.7 times molar equivalent of **4** for 6.5 hr, and 48.6 times for 22 hr at room temperature. Still other system containing **1** (0.100 g, 0.109 mmol), benzyl bromide (1.44 g, 8.42 mmol), calcium oxide (0.100 g, 1.78 mmol), and methanol (3.95 g, 123 mmol) gave methyl phenylacetate of 1.47 mmol (13.5 times molar equivalent of **1**) for 3 hr at 19 °.

Carboxymethylation under Elevated Pressures. In a 50 ml stainless-steel autoclave were placed **4** (0.200 g, 0.285 mmol), *p*-dibromobenzene (6.37 g, 27.0 mmol), methanol (20 ml), and diethylamine (3 ml). The reaction mixture was magnetically stirred at 80 °C under carbon monoxide pressure of 10 kg/cm^2, and 1 hr after the pressure dropped to zero. The mixture was extracted by 100 ml of toluene, in which methyl *p*-bromobenzoate (5.13 mmol), dimethyl terephthalate (3.46 mmol), and unreacted *p*-dibromobenzene (18.4 mmol) were analyzed.

Preparation of [PdI (COPh) (PPh_3)·toluene] (6). When carbon monoxide was bubbled through a toluene solution (10 ml) of **2** (0.173 g, 0.126 mmol) and iodobenzene (3 ml), the original red color of the solution turned into yellow in 15 min. After the solution was allowed to stand overnight, yellow crystals of **6** precipitated (0.148 g (55% based on Pd), $\nu_{C=O}$ at 1660 cm^{-1}). Cryoscopic molecular weight measurement could not be conducted because of the insufficient solubility of the complex. Found: C, 54.99; H, 4.00; P, 4.88%. Calcd for $C_{32}H_{28}OPIPd$: C, 55.50; H, 4.04; P, 4.48%. By adding *n*-hexane to the filtrate of the above solution, yellow crystals of **5** precipitated (0.050 g (16% based on Pd), $\nu_{C=O}$ at 1634 cm^{-1}). When the reaction was carried out in methanol in place of toluene, was obtained yellow powder which was a mixture of **5** and **6**.

Stoichiometric Ester Formation from 5 or 6. When the benzoyl complex **5** (0.119 g) was treated with methanol (2.5 ml) and diethylamine (1.5 ml) under nitrogen at room temperature, the original yellow color turned into brown, and 99.9% molar equivalent of methyl benzoate resulted. As for **6**, the procedure was almost the same.

References

1) A part of this work was presented at the 30th Annual Meeting of the Chemical Society of Japan, Osaka, April, 1974. Recently similar reactions have been found by Heck *et al.* (*J. Org. Chem.*, **39**, 3318 (1974)).

2) K. Kudo, M. Hidai, and Y. Uchida, *J. Organometal. Chem.*, **33**, 393 (1971).

3) K. Kudo, M. Sato, M. Hidai, and Y. Uchida, This Bulletin, **46**, 2820 (1973).

4) E. J. Corey and L. S. Hegedus, *J. Amer. Chem. Soc.*, **91**, 1233 (1969).

5) L. Cassar and M. Foá, *Inorg. Nucl. Chem. Lett.*, **6**, 291 (1970).

6) M. Nakayama and T. Mizorogi, This Bulletin, **44**, 508 (1971).

7) L. Cassar and M. Foá, *J. Organometal. Chem.*, **51**, 381 (1973).

8) R. F. Heck and D. S. Breslow, *J. Amer. Chem. Soc.*, **85**, 2779 (1963).

9) G. P. Chiusoli, M. Dubini, M. Ferraris, F. Guerrieri, S. Merzoni, and G. Mondelli, *J. Chem. Soc., C*, **1968**, 2889.

10) M. Hidai, K. Kokura, and Y. Uchida, *J. Organometal. Chem.*, **52**, 431 (1973).

11) A carbomethoxy complex, $PdCl(COOMe)(PPh_3)_2$, which was obtained by the reaction of **4** with methanol and carbon monoxide in the presence of a tertiary amine,[10] did not give methyl benzoate by treatment with iodobenzene even at 50 °C. This might exclude the possibility that the reaction proceeds *via* a carbomethoxy complex as an intermediate.

12) J. B. Hendrickson, D. J. Cram, and G. S. Hammond, "Organic Chemistry," McGraw-Hill, New York, 3rd Ed., (1970), p. 304.

13) The complex **4** affords a mixture of **1** and **2** by the treatment with carbon monoxide, methanol, and diethylamine, while in the presence of one molar equivalent of triphenylphosphine **4** is converted to **1** exclusively.

14) F. R. Hartley, *Organometal. Chem. Rev.*, **6**, 119 (1970).

15) G. Stork and M. Tomasz, *J. Amer. Chem. Soc.*, **86**, 471 (1964).

The Sesquiterpenes of Ginseng

Kazuo YOSHIHARA and Yoshio HIROSE

The Institute of Food Chemistry, 475 Shimamotocho, Mishimagun, Osaka 618

(Received January 21, 1975)

The sesquiterpenes of ginseng have been studied. From the volatile oil, fifteen compounds were characterized. Three of those compounds, α-panasinsene, β-panasinsene and β-neoclovene, were new compounds and were characterized in this paper. Panasinsenes are considered as intermedial compounds in isomerization of caryophyllene to neoclovene.

The root and rootlet of ginseng (*Panax ginseng* C.A. Meyer) have long been used as Chinese medicine. A large number of reports on saponines and triterpenes have been published,[1] but no study of the volatile oil of ginseng has yet been made. Here we have investigated the volatile oil in detail and have isolated several interesting hydrocarbons.

The ginseng used in this investigation consisted of commercial dried rootlets gathered in Korea and in Japan, and fresh roots and rootlets gathered in Japan. There is little difference between the gas chromatograms of the volatile oils of dried Korean rootlets and dried Japanese rootlets. There is also little difference between the fresh root and fresh roots. The characterized compounds are listed in Table 1. As Japanese

TABLE 1. THE LIST OF COMPOUNDS FROM GINSENG

Compound	Ratio in the voltatile oil	
	Fresh ginseng	Dried ginseng
β-Gurjunene	2%	3%
β-Panasinsene	8	20
α-Panasinsene	5	4
Caryophyllene	8	6
β-Farnesene	3	4
α-Neoclovene	7	15
α-Humulene, β-Humulene	5	6
γ-Selinene	—	4
β-Neoclovene	3	5
β-Selinene	—	3
α-Selinene	—	5
Selina-4(14), 7(11)-diene	—	2
Caryophyllene alcohol	—	2
Bicyclogermacrene	36	—

fresh roots obtained from another source showed a similar composition, we regarded the difference in the volatile oils is due to the different treatment of the roots and the rootlets. It is remarkable that bicyclogermacrene is a main component in the volatile oil of fresh ginseng root. This compound has been found only in *Citrus Junos* Sieb. ex Miquel,[2] yet it is expected to be of wide distribution as a precursor of bicyclogerelemene, aromadendrene, ledol, maaliene, *etc.*

The acidity of fresh root homogenate is pH 4.8—4.6, on standing for one week, the homogenate showed a change in its volatile constituents, whereby the amount of bicyclogermacrene decreased markedly and three selinene type compounds, α-selinene, β-selinene, and selina-4(14),7(11)-diene, appeared.

We will describe below the four hydrocarbons, α-neoclovene, β-neoclovene, α-panasinsene, and β-panasinsene, which were isolated for the first time from a natural source.

α-Neoclovene (I) was identified by comparing its spectral data with those of authentic neoclovene, which had been known as the product of the concd H_2SO_4-catalyzed isomerization of caryophyllene.[3]

β-Neoclovene (II) was isolated as a minor component in the oil of dried rootlets. From the spectral data, it was supposed that there were three tertiary methyl groups and an exocyclic methylene group in II, and that two of the tertiary methyl groups occupied geminal positions. II gave two dihydroderivatives on catalytic hydrogenation. Those two dihydroderivatives were identical with two dihydro-neoclovenes obtained by the hydrogenation of α-neoclovene. Therefore, II must be an isomer of α-neoclovene in respect to the position of the double bond, and represented by the structure II in Fig. 1. In order to distinguish those two isomers, we named I, which had previously been called by the name of neoclovene, and II α-neoclovene and β-neoclovene, respectively.

The spectral data of α-panasinsene (III) exhibits the existence of three tertiary methyl groups, an olefinic methyl group, and a trisubstituted double bond in III. The fact that the hydrogenation of III resulted in two dihydroderivatives and the molecular ion peak of III at *m/e* 204 showed III is tricyclic hydrocarbon.

β-Panasinsene (IV) is also a sesquiterpene hydrocarbon (molecular weight, 204). The NMR spectrum shows the existence of three tertiary methyl groups and an exocyclic methylene group. The IR spectrum shows that two tertiary methyl groups are geminal. The catalytic hydrogenation of IV gave two dihydroderivatives, which were identified with two dihydroderivatives of III. Therefore, III and IV are isomers of the same carbon skeleton, differing only in the position of the double bond. On isomerization with concd H_2SO_4 in ether, IV was transformed to three hydrocarbons, α-neoclovene, β-neoclovene, and α-panasinsene. On the basis of the results mentioned above and the spectral data, we supposed that α-panasinsene and β-panasinsene had to be assigned the structure III and IV, respectively. The framework of III and IV appeared in Parker's report[4] in connection with his explanation of the pathway leading from caryophyllene to neoclovene in the presence of H_2SO_4. Furthermore, the ozonolysis of IV gave a ketone (V).[5] Therefore, we have elucidated the structure III and IV

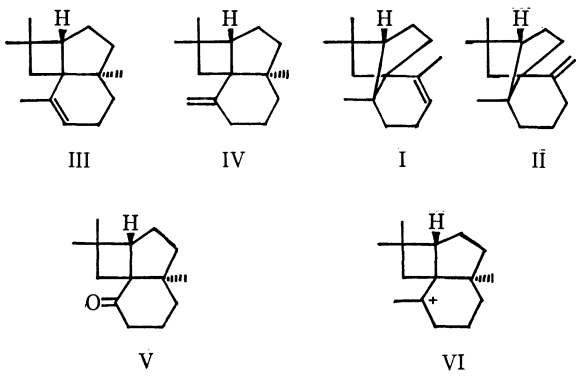

Fig. 1.

as mentioned above.

The discovery of intermediate tricyclic hydrocarbon, β-panasinsene, strongly supports Parker's explanation that caryophyllene rearranges through the panasinsene type cation (VI) to neoclovene with acid.

Most araliacean plants in Japan show a rather simple and common feature on their volatile constitutions, which contain β-farnesene, caryophyllene, and humulene as the main components. However, we found a few remarkable instance in Araliaceae. Two example are *Panax japonicum* C.A. meyer and *Acanthopanax sciadophylloides* Franch et Sav., which contain germacrene-D as the sole component,[6] and the third one is *Panax ginseng*. In the latter, caryophyllene is transformed to neoclovenes through panasinsenes, and a novel hydrocarbon, bicyclogermacrene, is accumulated.

Experimental

Analytical Instruments. As an analytical gas chromatograph, Hitachi-Perkin F6-D-type apparatus fitted with a HB-2000 capillary column (45 m by 0.25 mm) was used. N_2 gas was flowed through as the carrier gas. For the measurement of the physical data, a Hitachi EPI-G2-type infrared absorption spectrometer with NaCl cell, a JEOL-JNM-C-60-type nuclear magnetic resonance spectrometer, a Hitachi RMU-6-type mass spectrometer (operated at an accelerating voltage of 2 kV, an ionization voltage of 80 eV, and an ion source temperature of 250 °C), and a Perkin-Elmer's 141-type polarimeter were used.

Extraction and Isolation. Commercial dried rootlets of ginseng (5 kg) were extracted with ethanol, and the extract was concentrated and steam-distilled. About a 5 g portion of a volatile oil was thus obtained. The volatile oil dissolved in ethyl ether was washed with an aqueous $NaHCO_3$ solution, and a 4.3 g portion of the neutral fraction was obtained from the ethyl ether layer. The neutral oil obtained thus was subjected to column chromatography on Merck's Al_2O_3 column (activity II-III), and then separated into 3.5 g of the hydrocarbon fraction (eluted with n-hexane) and 0.5 g of the oxygenated compound fraction (eluted with ethyl ether). The former was further subjected to column chromatography on Al_2O_3 impregnated with 15 wt% $AgNO_3$ and was eluted with *n*-hexane and ethyl ether. Each eluted fraction was separated into pure compounds by means of a Varian MODEL 90-P-type gaschromatograph fitted with an aluminum column (20 ft by 3/8 in) packed with Carbowax 20 M on Diasolid L. The gas chromatograph was operated at a bath temperature of 180—200 °C, He gas was used as the carrier gas.

Fresh root (4 kg) was mashed, filtered, and then washed with acetone. The acetone in the filtrate was then evaporated, and the residue was extracted with *n*-hexane. When this extract was concentrated and distilled under diminished pressure, 500 mg of oil were obtained. The same procedure was carried out for the fresh rootlets. The oil from the fresh rootlets was used for comparison. Another 500 g portion of fresh ginseng was homogenized, and the pH of this homogenate was measured using B.T.B. and B.C.G. After standing for one week at room temperature covered with benzene, the homogenate was treated by the procedure described above. The oil of the homogenate was then examined by mean of analytical gas chromatography.

Physical Properties and Chemical Reactions. α-Neoclovene (1), $[\alpha]_D^{25}$ −56° (in MeOH), NMR: τ 8.99(s, 6H), 8.81 (s, 3H), 8.41 (m, 3H), and 4.91 (m, 1H), IR: 1650, 1140, 980, 840, 815, 790, and 775 cm^{-1}, MS: *m/e* 204 (M^+, $C_{15}H_{24}$), 189 (base peak), 175, 161, 147 and 105.

β-Neoclovene (II), $[\alpha]_D^{25}$ −30° (in MeOH), NMR: τ 9.16 (s, 3H), 8.98 (s, 3H), 8.81 (s, 3H), 5.37 (t, J=2 Hz 1H), and 5.62 (t, J=2 Hz 1H), IR: 3050, 1625, 1365, 1355 and 890 cm^{-1}, MS: *m/e* 204 (M^+, $C_{15}H_{24}$), 189, 176, 161 (base peak), 147, 148, 133, 119, and 91, (Found; C, 88.14; H, 11.82%. $C_{15}H_{24}$ requires C, 88.16; H, 11.84%).

α-Panasinsene (III), NMR: τ 9.12 (s, 3H), 9.05 (s, 3H), 8.77 (s, 3H), 8.05 (allyl coupled m, 3H) and 4.60 (m, 1H), IR: 1640, 1370, 1360, 1200, 1110, 1070, 1000, 940 and 800 cm^{-1}, MS: *m/e* 204 (M^+, $C_{15}H_{24}$), 189, 161, 122 (base peak) and 107, (Found; C, 88.13; H, 11.83%. $C_{15}H_{24}$ requires C, 88.16; H, 11.84%).

β-Panasinsene (IV), $[\alpha]_D^{25}$ −3° (in MeOH), NMR: τ 9.26 (s, 3H), 9.14 (s, 3H), 8.92 (s, 3H), 5.22 (d, J=2 Hz 1H) and 5.16 (d, J=2 Hz 1H), IR: 3080, 1620, 1365, 1360, 1260, 1080, 930, and 885 cm^{-1}, MS: *m/e* 204 (M^+, $C_{15}H_{24}$), 189, 175, 161 (base peak), 146, 133, 122, 109 and 107.

The Hydrogenation of I and II. I and II were hydrogenated in methanol over platinum oxide. Both gave the same products in analytical gas chromatography, and by preparative gas chromatography two isomeric compounds, neoclovane-A and neoclovane-B, were isolated.

Neoclovane-A, NMR: τ 9.07 (d, J=6 Hz 3H), 8.97 (s, 3H), and 8.80 (s, 6H), IR: 1370, 1360, 1305, 1165, 1135, 970, and 945 cm^{-1}, MS: *m/e* 206 (M^+, $C_{15}H_{26}$), 191, 178, 163, 150, 135, 123, 109, 81 (base peak), 82, 69 and 55, (Found; C, 87.28; H, 12.70%. $C_{15}H_{26}$ requires C, 87.30; H, 12.70%).

Neoclovane-B, NMR: τ 9.25 (d, J=6 Hz 3H), 8.98 (s, 3H), 8.93 (s, 3H) and 8.80 (s, 3H), IR: 1380, 1365, 1315, 1295, 1155, 1140 and 965 cm^{-1}, MS: *m/e* 206 (M^+, $C_{15}H_{26}$), 191, 178, 163, 150, 135, 123, 109, 81 (base peak), 82, 69 and 55, (Found; C, 87.27; H, 12.70%. $C_{15}H_{24}$ requires C, 87.30; H, 12.70%).

The Hydrogenation of III and IV. III and IV were hydrogenated in methanol using platinum oxide as the catalyst. The products were subjected to preparative gas chromatography, and two dihydroderivatives, panasinsane-A and panasinsane-B, were isolated from both hydrogenation products.

Panasinsane-A, NMR: τ 9.15 (s, 3H), 9.11 (s, 3H), 9.05 (d, J=6 Hz 3H) and 8.85 (s, 3H), IR: 1370, 1365, 1265, 1110 and 1050 cm^{-1}, MS: *m/e* 206 (M^+, $C_{15}H_{26}$), 191, 178, 163, 150, 135 (base peak), 123, 122, 109, 93 and 81, (Found; C, 78.27; H, 12.69%. $C_{15}H_{26}$ requires C, 87.30; H, 12.70%).

Panasinsane-B, NMR: τ 9.12 (s, 3H), 9.08 (s, 3H), 8.86 (s, 3H) and 8.84 (d, J=3 Hz 3H), IR: 1375, 1360, 1160, 1140, 1010 and 985 cm^{-1}, MS: *m/e* 206 (M^+, $C_{15}H_{26}$), 191, 177, 163, 150, 135 (base peak), 124, 109, 93 and 81, (Found; C, 87.28; H, 12.69%. $C_{15}H_{26}$ requires C, 87.30; H, 12.70%).

Isomerization of IV. IV (150 mg) was dissolved in 20 ml

of ethyl ether, and then 2 ml of concd H_2SO_4 were added. After 10 min, the resultant solution was poured into a saturated $NaHCO_3$ solution and extracted with ethyl ether. After drying with Na_2SO_4, the solvent was removed; about 130 mg of oil were thus obtained. The oil was examined by means of gas chromatography. Three new peaks in ratio of 3: 1: trace; they were identified with α-neoclovene, β-neoclovene, and α-panasinsene respectively.

The Ozonolysis of IV. The *n*-hexane solution of IV was subjected to ozonization, and the reaction mixture was shaked with water. After drying with Na_2SO_4, the solvent was removed. The product was purified by mean of gas chromatography.

Tricyclic ketone (V), NMR: τ 9.13 (s, 6H) and 9.02 (s, 3H), IR: 1695, 1470, 1430, 1385, 1375, 1325 and 1920, MS: *m/e* 206 (M^+, $C_{13}H_{22}O$), 191, 178, 173, 163, 151 (base peak), 135 and 107.

The authors wish to express their hearty thanks to Mr. Minoru Shiga of the Shiono Koryo Kaisha, Ltd., for providing the caryophyllene and to Mr. Katsumasa Okamura of Nagano Nogyo Shikensho for provinding the fresh ginseng.

References

1) M. Nagai, T. Ando, N. Tanaka, O. Tanaka, and S. Shibata, *Chem. Pharm. Bull.*, **20**, 1212 (1972), and references cited therein.

2) K. Nishimura, N. Shinoda, and Y. Hirose, *Tetrahedron Lett.*, **1969**, 3097.

3) W. Parker, R. A. Raphael, and J. S. Roberts, *J. Chem. Soc., C*, **1969**, 2634.

4) W. Parker, R. A. Raphael, and J. S. Roberts, *Tetrahedron Lett.*, **1965**, 2313.

5) T. F. W. Mckillop, J. Martin, W. Parker, J. S. Roberts, and J. R. Stevenson, *J. Chem. Soc.*, **1971**, 3375.

6) K. Yoshihara and Y. Hirose, *Phytochemistry*, **12**, 468 (1973).

Synthesis of (2*R*, 3*S*, 4*S*)-4-Amino-3-hydroxy-2-methyl-5-(3-pyridyl)-pentanoic Acid Present in Antibiotic Pyridomycin

Mitsuhiro KINOSHITA and Satoshi MARIYAMA

Department of Applied Chemistry, Faculty of Engineering, Keio University, Hiyoshi, Kohoku-ku, Yokohama 223

(Received April 12, 1975)

Natural (2*R*,3*S*,4*S*)-4-amino-3-hydroxy-2-methyl-5-(3-pyridyl)pentanoic acid (**1**) present in antibiotic pyridomycin was synthesized. The 5,6-anhydro-1,2-*O*-isopropylidene-3-*C*-methyl-α-D-allofuranose (**4**) was prepared from (the known) 3-deoxy-1,2;5,6-di-*O*-isopropylidene-3-*C*-methyl-α-D-allofuranose (**2**). Regiospecific introduction of 3-pyridyl group to the C-6 of **4** was effected by 3-pyridyllithium. The product (**5**) was converted to the 5-azido derivative (**7**) by the S_N2 substitution reaction of the 5-mesylate (**6**) of **5**. Hydrolysis of **7** followed by two-stage oxidation with periodate-bromine in aqueous acetic acid afforded (2*R*,3*S*,4*S*)-4-azido-3-formyloxy-2-methyl-5-(3-pyridyl)pentanoic acid (**9**), which was transformed to the dihydrochloride of **1**.

A novel amino acid, 4-amino-3-hydroxy-2-methyl-5-(3-pyridyl)pentanoic acid (**1**) present in antimycobacterial antibiotic pyridomycin[1,2] was isolated as a degradation product of pyridomycin by Ogawara, *et al.*[3] Its absolute configuration was established as "2*R*,3*S*,4*S*" (structure **1**) based on the complete structure of the parent antibiotic determined by X-ray crystallographic analysis.[4] This paper presents a synthesis of **1** with the natural configuration from an appropriate sugar derivative through regiospecific and stereospecific routes as shown in the Chart.

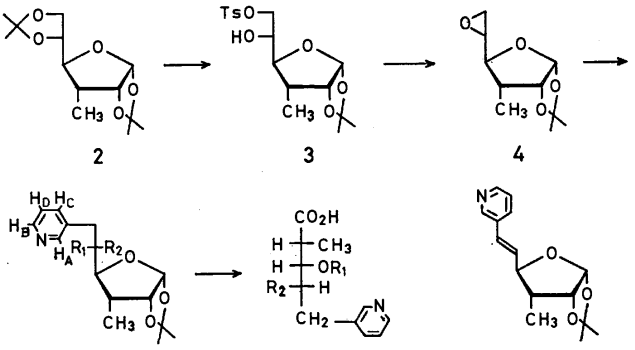

Chart.

Removal of 5,6-*O*-isopropylidene group of (the known) 3-deoxy-1,2; 5,6-di-*O*-isopropylidene-3-*C*-methyl-α-D-allofuranose[5] (**2**) with a warm 91% aqueous acetic acid followed by selective *O*-tosylation in the usual way afforded the 6-tosylate (**3**) in a 65% yield. Treatment of **3** with sodium methoxide in chloroform gave 5,6-anhydro-3-deoxy-1,2-*O*-isopropylidene-3-*C*-methyl-α-D-allofuranose (**4**) in a 76% yield. The epoxide ring of **4** was regiospecifically opened with 3-pyridyllithium[6] in ether at −10 °C to afford 3,6-dideoxy-1,2-*O*-isopropylidene-3-*C*-methyl-6-*C*-(3-pyridyl)-α-D-allofuranose (**5**) in an 88% yield, whose structure was confirmed by PMR spectroscopy. Mesylation of **5** with mesyl chloride in pyridine gave crystalline 5-mesylate (**6**) in a 75% yield. Substitution reaction of **6** with sodium azide in dimethylsulfoxide at 85 °C afforded two kinds of products, which were separated from each other by silica gel column chromatography in homogeneous states. Structural elucidations of the reaction products isolated on the basis of elemental and spectroscopic analyses revealed that the reaction produced one substitution reaction product and one elimination reaction product in 70 and 23% yield, respectively, none of the rearrangement reaction product being formed. Since this substitution reaction seemed to be very characteristic of the S_N2 reaction which should theoretically have only one alternation (*E*2 reaction),[7] the major product above-obtained was considered the expected S_N2 substitution reaction product, 5-azido-3,5,6-trideoxy-1,2-*O*-isopropylidene-3-*C*-methyl-6-*C*-(3-pyridyl)-β-L-talofuranose (**7**), the C-5 configuration of which was opposite to that of **6**. The structure of the minor product assigned to the elimination reaction product was determined as 3,5,6-trideoxy-1,2-*O*-isopropylidene-3-*C*-methyl-6-*C*-(3-pyridyl)-α-D-*ribohex-trans*-5-enofuranose (**8**) by PMR analysis. When the mesylate (**6**) was kept without the nucleophile (azide ion) in dimethyl sulfoxide at ~85 °C, the formation of **8** was never observed. This fact indicated that the compound (**8**) should be formed in the *E*2 reaction of **6** under S_N2 condition. Moreover, the fact that in the case of **6**, such an *E*2 reaction practically occured to some extent, may demonstrate that the 3-pyridylmethyl hydrogens at C-6 of **6** are so active that they are removed by the weakly basic azide ion.

Hydrolysis of **7** in a boiling 20% aqueous acetic acid, followed by successive oxidations of the resultant free sugar with sodium periodate and with bromine in the same aqueous acetic acid at room temperature afforded (2*R*,3*S*,4*S*)-4-azido-3-formyloxy-2-methyl-5-(3-pyridyl)pentanoic acid (**9**) as needles in a 59% yield. It should be noted that the two-stage oxidation of the free sugar must be carried out in the acidic condition at pH≤2, in order to prevent the complicated side reactions including the β-elimination of the formyloxy group which may probably be catalysed by the free pyridyl residue present in its own molecule at heigher pH values than 2.

De-*O*-formylation of **9** with dilute hydrogen chloride in aqueous dioxane at room temperature gave the corresponding azido hydroxy acid (**10**) as a crystalline hydrochloride in an 81% yield. The hydrochloride of **10** was hydrogenolyzed on palladium black in methanol to afford the title compound (**1**) as a monohydrochloride in a 97% yield, from which the dihydrochloride of **1**

was obtained as a colorless hygroscopic powder with a negative rotation ($[\alpha]_D$ −2° in 5 M hydrochloric acid). The synthetic dihydrochloride of **1** proved to be identical with the natural amino acid dihydrochloride derived from pyridomycin according to Ogawara, *et al.*[3] in all respects.

Experimental

Melting points were determined on a Mitamura Riken micro hot-stage and are uncorrected. IR spectra were taken on a Hitachi 225 spectrophotometer, PMR spectra were recorded on a Varian A-60D spectrometer using TMS as an internal standard. Specific rotations were determined with a Zeiss Photoelectric Precision Polarimeter. Tlc was performed on WAKO-GEL B-5 and silica gel column chromatography on WAKO-GEL C-200 which was activated at 110 °C for 1 hr. Paper chromatography was conducted on Toyoroshi No. 525 with butanol–acetic acid–water (3: 1: 1). Paper electrophoresis was carried out with a Savant 1V-5000A in formic acid–acetic acid–water (1: 3: 36). pK_a values were measured with a Metrohm Herisau Potentiograph E436. In general, all concentration were carried out under reduced pressure below 40 °C.

3-Deoxy-1,2-O-isopropylidene-3-C-methyl-6-O-tosyl-α-D-allofuranose (3). Treatment of **2** (7.00 g) prepared according to Rosenthal, *et al.*[5] with a 91% aqueous acetic acid (38.8 ml) at 60 °C for 30 min followed by evaporation afforded a syrup, which was chromatographed through silica gel (140 g) with benzene–ethyl acetate (1: 1) to give a practically pure sample of the de-5,6-*O*-isopyridenation product (5.36 g, 90.5% yield). The product (4.15 g, 18.9 mmol) was tosylated with tosyl chloride (3.99 g, 20.9 mmol) in pyridine by the usual way to afford **3** (5.06 g, 72%) as a colorless syrup: $[\alpha]_D^{28}$ +23° (*c* 1.15, chloroform); $\nu_{max}^{CCl_4}$ 3550 (OH) and 1175 cm^{-1} (sulfonate); $\delta(CDCl_3)$, 1.15 (d, 3-CH_3, J_{3,CH_3}=6.8 Hz), 1.32 and 1.48 [each s, $(CH_3)_2C$], 3.33—4.08 (m, OH and H-3), 4.13 (s, Ar–CH_3), 3.62—4.33 (m, H-4, H-5, and H-6), 4.57 (dd, H-2, $J_{2,3}$=4.9 Hz), 5.77 (d, H-1, $J_{1,2}$=3.9 Hz), and 7.33—7.97 (m, Ar).

Found: C, 55.09; H, 6.53; S, 8.30%. Calcd for $C_{17}H_{24}O_7S$: C, 54.83; H, 6.50; S, 8.60%.

5,6-Anhydro-3-deoxy-1,2-O-isopropylidene-3-C-methyl-α-D-allofuranose (4). A 2.12M solution of sodium methoxide in methanol (6.5 ml) was added dropwise with stirring to a solution of **3** (5.06 g, 13.6 mmol) in dry chloroform (20 ml) under ice-cooling. After the cooled mixture was vigorously stirred, it was allowed to stand at room temperature for 2 hr. The resultant solution was poured into cold water (20 ml) and the mixture was extracted with chloroform. The chloroform layer was washed with satd. aq. NaCl, dried, and evaporated. The syrupy residue (2.69 g) was chromatographed through silica gel (150 g) with benzene–ethyl acetate (5: 1) to afford **4** (2.06 g, 76%) as a colorless syrup: $[\alpha]_D^{25}$ +12° (*c* 0.85, chloroform); $\nu_{max}^{CCl_4}$ 1250 and 870 cm^{-1} (epoxide); $\delta(CDCl_3)$, 1.18 (d, 3-CH_3, J_{3,CH_3}=6.8 Hz), 1.35 and 1.52 [each s, $(CH_3)_2C$], 1.75—2.42 (m, H-3), 2.58—3.17 (m, H-5 and H-6), 3.58 (dd, H-4, $J_{3,4}$= 10.0 Hz and $J_{4,5}$=5.9 Hz), 4.63 (dd, H-2, $J_{2,3}$=4.9 Hz), and 5.88 (d, H-1, $J_{1,2}$=3.9 Hz).

Found: C, 59.84; H, 7.88%. Calcd for $C_{10}H_{16}O_4$: C, 59.98; H, 8.05%.

3,6-Dideoxy-1,2-O-isopropylidene-3-C-methyl-6-C-(3-pyridyl)-α-D-allofuranose (5). The reaction was carried out under nitrogen. An ethereal solution (16.6 ml) of butyllithium (8.61 mmol) was cooled to −35 °C in a dry ice-methanol bath and there was added dropwise with stirring, a solution of 3-bromopyridine (1.82 g, 11.5 mmol) in ether (8 ml) during a period of 30 min. After 15 min, to the bright yellow colored suspension was added dropwise with stirring, a solution of **4** (573 mg, 2.87 mmol) in ether (7 ml), the mixture being maintained at −10 °C for 1.5 hr. The resultant brown mixture was then poured into cold water and extracted with ether twelve times. The ether extracts were washed with satd. aq. NaCl, dried and evaporated to afford a brown syrup (1.24 g). The syrup was chromatographed through silica gel (80 g) with benzene–acetone (1: 1) to give pale yellow crystals of **5** (700 mg, 88%). Recrystallization from ethyl acetate–petroleum ether afforded an analytical sample as a colorless needle: mp 114.0—115.0 °C; $[\alpha]_D^{14}$ +39° (*c* 0.74, chloroform); ν_{max}^{KBr} 3460 (OH), 1585, 1430, 795 and 710 cm^{-1} (pyridine); $\delta(CDCl_3)$, 1.23 (d, 3-CH_3, J_{3,CH_3}=6.8 Hz), 1.38 and 1.55 [each s, $(CH_3)_2C$], 1.83—2.50 (m, H-3), 2.75—3.01 (m, H-6 and OH), 3.75—4.17 (m, H-4 and H-5), 4.65 (dd, H-2, $J_{2,3}$=4.9 Hz), 5.87 (d, H-1, $J_{1,2}$= 3.9 Hz), 7.30 (m, H_D, $J_{A,D}$=1.0 Hz, $J_{B,D}$=5.0 Hz and $J_{D,C}$= 8.3 Hz), 7.73 (m, H_C, $J_{A,C}$=2.6 Hz and $J_{B,C}$=2.0 Hz), 8.40 (m, H_B, $J_{A,B}$=0.5 Hz), and 8.55 (m, H_A).

Found: C, 64.73; H, 7.59; N, 4.91%. Calcd for $C_{15}H_{21}O_4N$: C, 64.49; H, 7.58; N, 5.01%.

3,5,6-Trideoxy-1,2-O-isopropylidene-5-O-mesyl-3-C-methyl-6-C-(3-pyridyl)-α-D-allofuranose (6). Mesylation of **5** (1.20 mmol) with mesyl chloride (1.44 mmol) in dry pyridine (3.4 ml) at room temperature followed by work up in the usual manner afforded a crystalline solid of **6**(540 mg), which was recrystallized from ethyl acetate–petroleum ether to give a pure sample of **6** (333 mg, 75%): mp 111.5—112.0 °C; $[\alpha]_D^{18}$ +31° (*c* 0.89, chloroform); ν_{max}^{KBr} 1360 and 1175 cm^{-1} (sulfonate); $\delta(CDCl_3)$, 1.23 (d, 3-CH_3, J_{3,CH_3}=6.8 Hz), 1.37 and 1.51 [each s, $(CH_3)_2C$], 4.47 (s, $-SO_3CH_3$), 1.83—2.33 (m, H-3), 3.17 (d, H-6, $J_{5,6}$=6.0 Hz), 3.98 (dd, H-4, $J_{3,4}$=10.0 Hz and $J_{4,5}$=4.5 Hz), 4.65 (dd, H-2, $J_{2,3}$=4.8 Hz), 5.01 (dt, H-5), 5.88 (d, H-1, $J_{1,2}$=3.8 Hz), 7.3—7.9 and 8.5—8.9 (each m, 3-pyridyl).

Found: C, 53.67; H, 6.47; N, 3.77; S, 9.02%. Calcd for $C_{16}H_{23}O_6NS$: C, 53.77; H, 6.49; N, 3.92; S, 8.96%.

5-Azido-3,5,6-trideoxy-1,2-O-isopropylidene-3-C-methyl-6-C-(3-pyridyl)-β-L-talofuranose (7) and 3,5,6-Trideoxy-1,2-O-isopropylidene-3-C-methyl-6-C-(3-pyridyl)-α-D-ribohex-trans-5-enofuranose (8). A solution of **6** (331 mg, 0.925 mmol) in dimethylsulfoxide (1.7 ml) was heated with sodium azide (181 mg, 2.78 mmol) at 85 °C for 2 hr: tlc [benzene–acetone (3: 1)] revealed the absence of **6** (R_f 0.37) and the presences of the two products (R_f 0.60 and 0.52). The cooled solution was diluted with water (2 ml) and extracted with ethyl acetate seven times. The extracts were washed with satd. aq. NaCl, dried and evaporated to afford a yellow syrup (295 mg). Column chromatography [silica gel 45 g, benzene–acetone (10: 1)] of the syrup afforded the substitution product (**7**) [R_f 0.60, colorless syrup, 196 mg (70%)] and the elimination product (**8**) [R_f 0.52, colorless needle, 54 mg (23%)].

7: $[\alpha]_D^{15}$ +11° (*c* 1.40, chloroform); $\nu_{max}^{CCl_4}$ 2105 cm^{-1} (N_3); $\delta(CDCl_3)$, 1.02 (d, 3-CH_3, J_{3,CH_3}=6.8 Hz), 1.36 and 1.46 [each s, $(CH_3)_2C$], 2.0—2.6 (m, H-3), 3.0—3.5 (m, H-5 and H-6), 3.80 (dd, H-4, $J_{3,4}$=10.2 Hz and $J_{4,5}$=1.3 Hz), 4.66 (dd, H-2, $J_{2,3}$=4.0 Hz), 5.93 (d, H-1, $J_{1,2}$=3.6 Hz), 7.2—7.9 and 8.5—8.8 (each m, 3-pyridyl).

Found: C, 59.21; H, 6.67; N, 18.55%. Calcd for $C_{15}H_{20}O_3N_4$: C, 59.19; H, 6.62; N, 18.41%.

8: mp 80.0—81.5 °C (two recrystallizations from petroleum ether); $[\alpha]_D^{20}$ +13° (*c* 0.75, chloroform); $\nu_{max4}^{CCl_4}$ 965 cm^{-1} (disubstituted *trans*-olefine); δ ($CDCl_3$), 1.12 (d, 3-CH_3, J_{3,CH_3}=6.8 Hz), 1.38 and 1.59 [each s, $(CH_3)_2C$], 1.7—2.1 (m, H-3), 4.13 (dd, H-4, $J_{3,4}$=10.0 Hz and $J_{4,5}$=7.0 Hz), 4.78 (t, H-2, $J_{2,3}$= 3.9 Hz), 6.07 (d, H-1, $J_{1,2}$=3.9 Hz), 6.37 (dd, H-5, $J_{5,6}$=16.3 Hz), 6.91 (d, H-6), 7.3—8.1 and 8.6—9.1 (each m, 3-pyridyl).

Found: C, 68.80; H, 7.33; N, 5.31%. Calcd for $C_{15}H_{19}O_3N$: C, 68.94, H, 7.33; N, 5.36%.

(2R,3S,4S)-4-Azido-3-formyloxy-2-methyl-5-(3-pyridyl)-pentanoic Acid (9). A solution of **7** (506 mg, 0.172 mmol) in a 20% aqueous acetic acid (25 ml) was refluxed for 5 hr. After evaporation, the residual syrup (free sugar) was dissolved in a 33% aqueous acetic acid (15 ml) and then cooled at 5 °C, there was added dropwise under stirring a solution of $NaIO_4$ (716 mg) in water (7.2 ml). After 20 min, bromine (0.45 ml) was added to the reaction mixture (pH 2) and allowed to stand at room temperature overnight. The resultant solution was aerated to remove an excess of bromine and evaporated. The residual solid mass was extracted with ethanol (*ca.* 5 ml) and the extract was evaporated to give a yellow syrup (958 mg). Column chromatography [silica gel 50 g, chloroform–methanol–acetic acid (80:5:1)] of the syrup afforded a yellow solid, which was recrystallized twice from acetone to give a pure sample of **9** (275 mg, 59%) as colorless needles: mp 127.5—129.5 °C (decomp.); $[\alpha]_D^{26}$ −114° (*c* 0.57, methanol); ν_{max}^{KBr} 2100 (N_3) and 1725 cm^{-1} (OCHO and COOH); $\delta(CDCl_3)$, 1.34 (d, 2-CH_3, J_{2,CH_3}=7.1 Hz), 2.73 (dd, H-5, $J_{4,5}$=11.0 Hz, $J_{5,5'}$=14.5 Hz), 3.16 (dq, H-2, $J_{2,3}$=4.5 Hz), 3.54 (dd, H-5′, $J_{4,5'}$=3.6 Hz), 4.13 (dq, H-4, $J_{3,4}$=8.0 Hz), 5.53 (dd, H-3), 7.4—8.2 and 8.7—9.1 (each m, 3-pyridyl), 8.47 (s, OCHO), and 12.0—12.3 (broad s, COOH).

Found: C, 52.00; H, 5.06; N, 19.90%. Calcd for $C_{12}H_{14}O_4N_4$: C, 51.79; H, 5.07; N, 20.14%.

(2R,3S,4S)-4-Azido-3-hydroxy-2-methyl-5-(3-pyridyl)pentanoic Acid (10) Hydrochloride. Treatment of **9** (21.7 mg) with 2 ml of a 2% HCl (in 50% (v/v) aq. dioxane) at room temperature for 1 hr followed by evaporation afforded a crystalline solid, which was recrystallized twice from methanol–ether to give a pure sample of **10** hydrochloride (19.2 mg, 81%) as colorless needles: mp 127.0—132.0 °C (decomp.); $[\alpha]_D^{19}$ −40° (c 0.63, methanol); ν_{max}^{KBr} 3340 (OH), 2090 (N_3), and 1720 cm^{-1} (COOH).

Found: C, 45.97; H, 5.40; N, 19.75; Cl, 12.46%. Calcd for $C_{11}H_{14}O_3N_4 \cdot HCl$: C, 46.08; H, 5.27; N, 19.54; Cl, 12.37%.

(2R,3S,4S)-4-Amino-3-hydroxy-2-methyl-5-(3-pyridyl)pentanoic Acid (1). A solution of the hydrochloride of **10** (18.2 mg) in methanol (2 ml) was stirred with palladium black for 1 hr in a hydrogen atmosphere to afford a monohydrochloride of **1** (17.1 mg, 97%) as a hygroscopic monohydrate: mp 140—143 °C (decomp.); $[\alpha]_D^{24}$ −12° (*c* 0.35, methanol).

Found: C, 46.86; H, 6.91; N, 9.62; Cl, 13.08%. Calcd for $C_{11}H_{16}O_3N_2 \cdot HCl \cdot H_2O$: C, 47.40; H, 6.87; N, 10.05; Cl, 12.72 %. The dihydrochloride of **1** was obtained as a monohydrate in a quantitave yield by treatment of aqueous solution of the monohydrochloride with 0.1M hydrochloric acid: colorless hygroscopic powder, mp 175—180 °C (decomp.) [lit,[3] mp 177—180 °C (decomp.)]; $[\alpha]_D$ −2°, $[\alpha]_{546}$ −4°, $[\alpha]_{436}$ −8°, $[\alpha]_{405}$ −10° and $[\alpha]_{365}$ −11° (*c* 0.53, 5M HCl at 24 °C) [A natural specimen of the dihydrochloride monohydrate isolated from pyridomycin by authors gave the following rotations: $[\alpha]_D$ −2°, $[\alpha]_{546}$ −4°, $[\alpha]_{436}$ −8°, $[\alpha]_{405}$ −10° and $[\alpha]_{365}$ −11° (c 0.37, 5M HCl at 27 °C)]; pK_a, 3.20, 4.70, and 8.70 (titration equivalent 305) [lit,[3] pK_a, 3.25, 4.75, and 8.80 (300)].

Found: C, 41.74; H, 6.58; N, 9.06; Cl, 22.61%. Calcd for $C_{11}H_{16}O_3N_2 \cdot 2HCl \cdot H_2O$: C, 41.91; H, 6.40; N, 8.89; Cl, 22.50%. The IR (KBr) and PMR (D_2O) spectra of the synthetic specimen of **1** were identical with those[8] of authentic sample of natural amino acid. R_f-values on paper chromatography and mobilities of paper electrophoresis of the synthetic product and the natural one (above described) were all identical.

The authors wish to express their sincere thanks to Dr. Kenji Maeda, National Institute of Health of Japan, for his helpful advice and kind supply of pyridomycin and to Mr. Saburo Nakada, Keio University, for the elemental analyses. We also wish to thank gratefully Dr. Hamao Umezawa, Institute of Microbial Chemistry and Prof. Sumio Umezawa, Keio University, for their encouragements.

References

1) K. Maeda, H. Kosaka, Y. Okami, and H. Umezawa, *J. Antibiot.* (Tokyo), **6A**, 140 (1953).

2) Y. Okami, K. Maeda, and H. Umezawa, *ibid.*, **7A**, 55 (1954).

3) H. Ogawara, G. Koyama, H. Naganawa, K. Maeda, and H. Umezawa, *Chem. Pharm. Bull.*, **16**, 679 (1968).

4) G. Koyama, Y. Iitaka, K. Maeda, and H. Umezawa, *Tetrahedron Lett.*, **1967**, 3587.

5) A. Rosenthal and M. Sprinze, *Can. J. Chem.*, **47**, 3941 (1969).

6) H. Gilman and S. M. Spatz, *J. Amer. Chem. Soc.*, **62**, 446 (1940); A. Murray, W. W. Foreman, and W. Langham, *ibid.*, **70**, 1037 (1948).

7) J. B. Hendrickson, D. J. Cram, and G. S. Hammond, "Organic Chemistry," McGraw-Hill Book Company, 1970, p. 401.

8) The IR and PMR spectral charts of the authentic sample were generously supplied by Dr. Hiroshi Ogawara, the National Institute of Health of Japan, to whom the authors' thanks are due.

The Facile Synthesis of 5′-Nucleotides by the Selective Phosphorylation of a Primary Hydroxyl Group of Nucleosides with Phosphoryl Chloride*

Tsuneo Sowa and Shunji Ouchi

Research Section, Foodstuff Plants, Asahi Chemical Industry Co., Ltd., Nobeoka, Miyazaki 882

(Received June 6, 1974)

5′-Nucleotides were directly prepared by selective phosphorylation with phosphoryl chloride in the presence of water and pyridine in acetonitrile. The rate of phosphorylation with phosphoryl chloride was markedly improved by the addition of suitable amounts of water and pyridine; the maximal formation of 5′-nucleotides was obtained by mixing these three reactants phosphoryl chloride, water, and pyridine in a molar ratio of 2:1:2 at a low temperature, followed by adding nucleosides corresponding to a one-fourth or one-fifth of the phosphoryl chloride. By mixing phosphoryl chloride, water, and pyridine in acetonitrile under controlled conditions, a hygroscopic complex (Complex 1), an active phosphorylating agent in the present phosphorylation of nucleosides, was isolated. It was identified as an adduct composed of tetrachloropyrophosphate and pyridinium chloride by means of its infrared spectra and by its chromatographic behavior. One of the proposed structures of the adduct is trichloropyrophosphopyridinium chloride. Both the selectivity in the 5′-hydroxyl group of the nucleosides and the yield of 5′-nucleotides increase upon the addition of pyridinium chloride in the phosphorylation of the unprotected nucleosides with tetrachloropyrophosphate. In the phosphorylation with tetrachloropyrophosphate, the H^+ derived from pyridinium chloride in acetonitrile is considered to increase the selectivity for the 5′-hydroxyl group by decreasing the reactivity of the hydroxyl groups in the ribose moiety of the nucleosides with the adduct. Similar results were obtained in the phosphorylation with phosphoryl chloride in the presence of pyridinium chloride in acetonitrile. Thus, several procedures for the selective phosphorylation of unprotected nucleosides to 5′-nucleotides are available.

Several attempts at the direct and selective phosphorylation of the 5′-hydroxyl group of nucleosides in the unprotected form have been made. Along those lines, 5′-nucleotides have been prepared from the corresponding nucleosides by direct phosphorylation with phosphoryl chloride in pyridine.[1,2] However, all of these methods are far from practical either in the laboratory or for commercial application because of the low conversion of nucleosides into nucleotides and because of the low selectivity in the formation of 5′-nucleotides.

Recently, Yoshikawa *et al.*[3] reported the preparation of 5′-nucleotides in good yields from the corresponding nucleosides by direct phosphorylation with phosphoryl chloride in trialkylphosphates; they also reported that, by the addition of an adequate amount of water to the reaction mixture, the competitive phosphorylation of the 2′ (or 3′)-hydroxyl group was strongly inhibited.

In the present paper, the authors will describe the methods of preparing the 5′-nucleotides by direct phosphorylation, with a complete selectivity for the primary hydroxyl group of nucleosides in acetonitrile, and will discuss the possible reaction mechanisms.

The nucleosides used in this experiment are adenosine (An-R), guanosine (Gn-R), inosine (Hx-R), xanthosine (Xn-R), uridine (Un-R), cytidine (Cn-R), 1-β-D-arabinofuranosyl uracil (Ara–Un), 1-β-D-arabinofuranosyl cytosine (Ara-Cn), 9-β-D-arabinofuranosyl adenine (Ara-An), 2′-deoxycytidine (Cn-dR), 2′-deoxyuridine (Un-dR), 8-bromoadenosine (Br-AnR), 8-hydroxyadenosine (8-OH-AnR), 8-mercaptoadenosine (8-SH-AnR), 8-bromoguanosine (8-Br-GnR), N^6-*n*-butyladenosine (N^6-Bu-AnR), 8,2′-*S*-anhydro(9-β-D-arabinofuranosyl) 8-mercaptoadenine (*S*-Anhyd-An), 2,2′-*O*-anhydro(1-β-D-arabinofuranosyl) cytosine hydrochloride (Anhyd-Cn), 2,2′-*O*-anhydro(1-β-D-arabinofuranosyl) uracil (Anhyd-Un), and 5-amino-1-β-D-ribofuranosylimidazole-4-carboxamide (AICAR).

Results and Discussion

Phosphorylation of Unprotected Nucleosides. When inosine was subjected to the addition of phosphoryl chloride in the presence of water and pyridine in acetonitrile, inosine-5′-phosphate (5′-IMP) was exclusively obtained; the yield reached 92.4%. 5′-Nucleotides with the other base components listed in Table 1 could similarly be obtained with an almost complete selectivity in the 5′-hydroxyl group, but the nucleoside containing 8-bromoguanine was resistant to direct phosphorylation by phosphoryl chloride.

One of the advantages of the present phosphorylation method was distinctly demonstrated in the preparation of 5′-arabinonucleotides. Since the arabinonucleoside has no 2′,3′-*cis*-diol group, which could be easily protected with the isopropylidene or the benzylidene group, it has been difficult to prepare 5′-arabinonucleotides by a conventional phosphorylation method. For example, when Schreckel *et al.*[4] prepared 1-β-D-arabinofuranosyl cytosine 5′-monophosphate by the phosphorylation of 2′,3′-*O*-benzylidene cytidine with polyphosphoric acid, the yield amounted to only 10%. It was found that the present method was much superior to Schreckel's method for preparing 5′-arabinonucleotides because the phosphorylation of the arabinonucleosides could be accomplished directly without the introduction of any protecting groups to the secondary hydroxyl groups in the sugar moiety.

Similarly, 2′-deoxyuridine, 2′-deoxycytidine, 2,2′-*O*-

* Most of this study was presented at the 22nd Annual Meeting of the Chemical Society of Japan, Tokyo, April, 1969.

Table 1. Direct phosphorylation of nucleosides

	H_2O (mmol)	Reaction time, hr	Yield of 5′-nucleotide, mol %	Selectivity of 5′-nucleotide, %
Gn-R	25	6	89.5	93.0
An-R	25	4	91.3	92.9
Hx-R	28	4	92.4	93.3
Xn-R	24	6	90.0	99.4
Un-R	25	6	86.3	98.1
Cn-R	20	2	98.6	100.0
Ara-Un	25	6	84.8	90.0
Ara-Cn	20	2	97.5	99.1
Ara-An	25	4	90.4	93.4
2′-An-dR[a]	25	4	—	—
2′-Cn-dR	20	2	95.1	98.4
2′-Un-dR	25	4	85.1	90.6
8,2′-*S*-Anhyd-AnR	25	4	98.8	100.0
2,2′-*O*-Anhyd-AnR	25	5	81.3	94.3
8-Br-AnR	25	4	84.3	91.7
8-OH-AnR	26	4	91.1	93.7
8-SH-AnR	26	6	80.0	92.8
N^6-Bu-AnR	25	4	88.8	93.4
8-Br-GnR	25	6	25.1	—
AICAR[b]	27	1	76.9	—

Experimental conditions:
CH_3CN 10 ml, $POCl_3$ 44 mmol, C_5H_5N 48 mmol
H_2O listed in above Table, nucleoside 10 mmol at 2 °C.

a) Adenine was produced in almost quantitative yield.
b) AICNR-5′MP was produced as a by-product.

anhydro(1-β-D-arabinofuranosyl) uracil, and 8,2′-*S*-anhydro(1-β-D-arabinofuranosyl)-8-mercaptoadenine, all with no 2′,3′-*cis*-diol group, could be easily phosphorylated to prepare the corresponding 5′-nucleotides in good yields. All attempts at the phosphorylation of 2′-deoxyadenosine and 2′-deoxyguanosine failed because of the lability of their glycosidic linkage and their low solubilities.

The phosphorylation of 5-amino-1-β-D-arabinofuranosylimidazole-4-carboxamide (AICAR) under the present conditions gave 5-amino-1-β-D-arabinofuranosylimidazole-4-carboxamide 5′-phosphate (AICAR-5′-MP).[5] In addition to the expected 5′-phosphomonoester, its dehydrated derivative, 1-β-D-arabinofuranosyl-4-cyano-5-aminoimidazole 5′-phosphate (AICNR-5′-MP, λ_{max} at pH 2.0, 240—242 nm),[6] was detected on the paper electrophoresis of the phosphorylation mixture. AICAR-5′MP was readily isolable from AICNR-5′MP by precipitating the former as its free acid from an acidic aqueous solution at pH 2.5.

In the present phosphorylation, the amounts of the three reagents were held to a definite value. That is, phosphoryl chloride, water, and pyridine were mixed in the molar ratio of 2: 1: 2 at a low temperature, and then nucleosides corresponding to one-fourth or one-fifth of the phosphoryl chloride was added. No reaction was observed without water, and the amount of water was thought to be critical. As is shown in Fig. 1, the formation of inosine 5′-phosphate obviously depended on the amount of water in the reaction

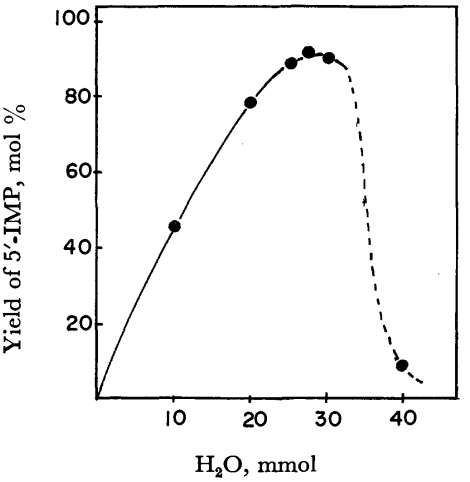

Fig. 1. Effect of water.
Experimental conditions: CH_3CN 10 ml, $POCl_3$ 44 mmol, C_5H_5N 48 mmol, H_2O: figured above, inosine 10 mmol at 2 °C.

media. When about 0.6 mol of water per mole of phosphoryl chloride was added, the yield of inosine 5′-phosphate rose to 90%. Either an increase or a decrease in the amount of water remarkably decreased the formation of inosine 5′-phosphate.

Yoshikawa *et al.*[3] reported that 5′-nucleotides were selectively obtained by treating the unprotected nucleosides with phosphoryl chloride in trialkylphosphates in the presence of a half amount of water per mole of phosphoryl chloride. In the present phosphorylation, however, there was no reaction without pyridine, the amount of pyridine was thus thought to be critical, too. When an amount of pyridine equimolar to phosphoryl chloride was added, the best result was obtained, as is shown in Fig. 2. The reaction temperature also influenced the phosphorylation yield and selectivity toward the 5′-hydroxyl group. In the present phosphorylation, the maximal formation of 5′-nucleotides was obtained in the reaction at a temperature between 0 and 2 °C (Fig. 3). A reaction at a higher temperature brought about an unfavorable formation of inosine 2′ (or 3′), 5′-diphosphate, and of hypoxanthine

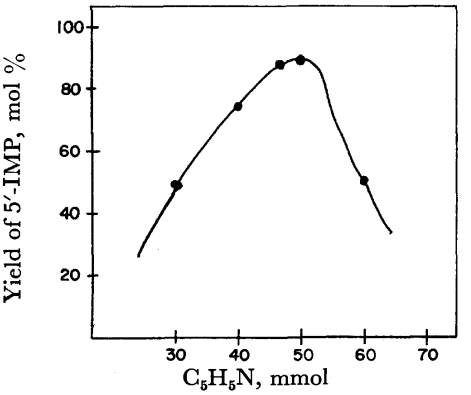

Fig. 2. Effect of pyridine on the direct phosphorylation of nucleosides.
Experimental conditions: CH_3CN 10 ml, $POCl_3$ 44 mmol, H_2O 28 mmol; C_5H_5N: figured above, inosine 10 mmol at 2 °C.

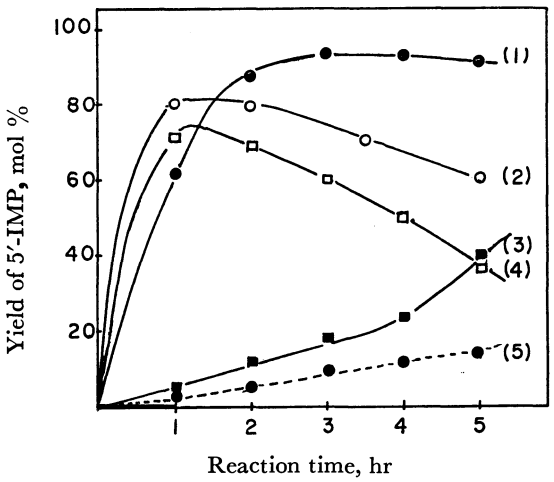

Fig. 3. Effect of reaction temperature.
Experimental conditions: CH_3CN 10 ml, $POCl_3$ 44 mmol, H_2O 28 mmol, C_5H_5N 48 mmol, inosine 10 mmol.
reaction temp.: (1) at 2 °C, (2) at 10 °C, (3) at 20 °C, (4) inosine 2′ (or 3′),5′-diphosphate produced at 20 °C, (5) hypoxanthine produced at 20 °C.

due to the cleavage of the glycosidic linkage.

Possible Mechanisms of the Selective Phosphorylation of the Unprotected Nucleoside. In the present phosphorylation described above, it was requisite to maintain the molar ratio of phosphoryl chloride, water, and pyridine at 2: 1: 2. On the basis of the evidence obtained so far, the real phosphorylating agent was assumed to be a species different from phosphoryl chloride. Phosphoryl chloride was partially hydrolyzed to dichlorophosphoric acid,[7] which was then further hydrolyzed provided an excess of water was present:

$$POCl_3 + H_2O + C_5H_5N \longrightarrow POCl_2(OH) + C_5H_5NHCl$$

In the present phosphorylation, the amount of water was strictly controlled, and only one-half of phosphoryl chloride was hydrolyzed to dichlorophosphoric acid. Moreover, in this hydrolysis only one mole of water and of pyridine was utilized; the stoichiometry of these reactants effected a phosphomonoester formation shown to have a molar ratio of phosphoryl chloride, water, and pyridine not of 1: 1: 1 but of 2: 1: 2. This seems to show that dichlorophosphoric acid might not be a phosphorylating agent. It is known that dichlorophosphoric acid is capable of reacting with phosphoryl chloride to give tetrachloropyrophosphate:[13]

$$HOPOCl_2 + POCl_3 + C_5H_5N \longrightarrow P_2O_3Cl_4 + C_5H_5NHCl$$

In this formation of tetrachloropyrophosphate from dichlorophosphoric acid, one mole of phosphoryl chloride and of pyridine were utilized, and the amounts of phosphoryl chloride, water, and pyridine were in the molar ratio of 2: 1: 2. Thus, the real species acting for the phosphorylation was considered to be tetrachloropyrophosphate, which dichlorophosphorylated the 5′-hydroxyl group in the reaction with the nucleoside. The pyrophosphate linkage in the tetrachloro-derivative of pyrophosphoric acid is extremely sensitive to hydrolysis with a base. The necessity to keep the amount of water limited and to keep the temperature low during the phosphorylation has been explained by the above discussion.

If tetrachloropyrophosphate is the species causing the selective phosphorylation at the 5′-hydroxyl group, dichlorophosphoric acid should be produced as an intermediate during the reaction. The transient formation of dichlorophosphoric acid is further indicated by the following evidence. The reaction of *t*-butanol with phosphoryl chloride is known to give dichlorophosphoric acid:[3,7]

$$POCl_3 + t\text{-}C_4H_9OH \longrightarrow POCl_2(OH) + t\text{-}C_4H_9Cl$$

If water provides a hydroxyl group to substitute for a chlorine atom in phosphoryl chloride, and if dichlorophosphoric acid is then actually formed, *t*-butanol might be utilized in place of water. Since *t*-butanol acts as an acceptor of the chlorine atom (as in the above equation), the molar ratio of phosphoryl chloride, *t*-butanol, and pyridine for the preparation of tetrachloropyrophosphate should be kept at 2: 1: 1. In the present study, in fact, under these conditions, 5′-nucleotides were similarly obtained by the direct phosphorylation of common nucleosides, in good agreement with the results obtained in the phosphorylation with phosphoryl chloride in the presence of water and pyridine, as is shown in Table 2. Though it was shown

Table 2. Direct phosphorylation by $POCl_3$ in the presence of alcohol and pyridine

Compd	Alcohol[a]	Reaction time, hr	Yield of 5′-*N*-tide, mol %	Selectivity of 5′-*N*-tide %
Hx–R	MeOH	4	94.4	96.4
Hx–R	EtOH	6	87.7	95.5
Hx–R	*t*-BuOH	6	93.8	95.1
Hx–R	*n*-BuOH	8	10.0	—
An–R	MeOH	4	85.6	93.9
Gn–R	MeOH	7	80.4	88.1
Cn–R	MeOH	6	98.2	100
Un–R	MeOH	7	76.6	89.6

Experimental conditions: CH_3CN 10 ml, $POCl_3$ 44 mmol, alcohol 24 mmol, C_5H_5N 24 mmol, nucleoside 10 mmol, at 2 °C.
a) MeOH: methanol, EtOH: ethanol, *t*-BuOH: *t*-butyl alcohol.

that *t*-butanol could be replaced by methanol or ethanol without affecting the reaction yield and selectivity** in the phosphorylation, its isomeric *n*-butanol gave poor results. *n*-Butanol was shown not to produce dichlorophosphoric acid, but to provide its phosphomonoester by reacting with phosphoryl chloride; it was not considered to be suitable for the preparation of tetrachloropyrophosphate in the presence of pyridine.

However, when the unprotected nucleosides were subjected to a reaction with tetrachloropyrophosphate in acetonitrile, it was found that the reaction went

** Selectivity of 5′-nucleotides is defined as the molar ratio (%) of 5′-nucleotides to all of the phosphorylated product.

Table 3. Direct phosphorylation with $P_2O_3Cl_4$

Compd.	Reaction time, hr	Yields of product, mol %		Selectivity of 5′-*N*-tide %
		5′-*N*-tide	by-pro[a)]	
An-R	0.5	81.4	16.6	83.3
Gn-R	0.5	61.7	33.5	64.8
Hx-R	0.5	80.5	19.5	80.5
Xn-R	2.0	94.1	t	100
Un-R	0.5	90.3	8.6	91.3
Cn-R	0.5	60.3	37.7	62.5

Experimental conditions:
nucleoside 10 mmol, $P_2O_3Cl_4$ 24 mmol, CH_3CN 10 ml
reaction temp. at 2 °C
a) nucleoside 2′ (or 3′), 5′-diphosphate

essentially to completion within half an hour, that the 5′-nucleotides, except for uridine 5′-phosphate and xanthosine 5′-phosphate, were obtained in yields between 60 and 80%, and that considerable amounts of the phosphorylated by-products, nucleoside 2′ (or 3′), 5′-diphosphate, were formed (Table 3). Similar results had been obtained by the direct phosphorylation of nucleosides with tetrachloropyrophosphate in trialkylphosphate.[3] Therefore, it can not be concluded that tetrachloropyrophosphate acts alone in the efficient selective phosphorylation of the 5′-hydroxyl group of nucleosides.

When phosphoryl chloride, water, and pyridine were mixed in acetonitrile at a low temperature and when the reaction mixture was then treated with dry ether, hygroscopic crystals (Complex 1) were obtained; they began to soften at 40 °C and were completely molten at 50—51 °C. The thin-layer chromatography of this hygroscopic product showed a different behavior from tetrachloropyrophosphate (Fig. 4). The infrared spectra of the product was not the same as that of tetrachloropyrophosphate. Moreover, a crystalline product (Complex 2) which has been prepared by reacting tetrachloropyrophosphate with pyridinium chloride in the molar ratio of 1:2 showed the same hygroscopic

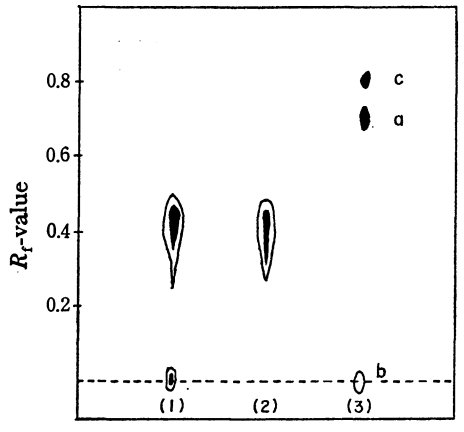

Fig. 4. Thin-layer chromatography
Solvent: ethylene glycohol dimethyl ether.
(1) Complex 1, (2) Complex 2, (3) authentic samples
a: $P_2O_3Cl_4$, b: $C_5H_5N \cdot HCl$, c: $POCl_3$.
●: detected with the Allen method.
○: detected with U.V. light.

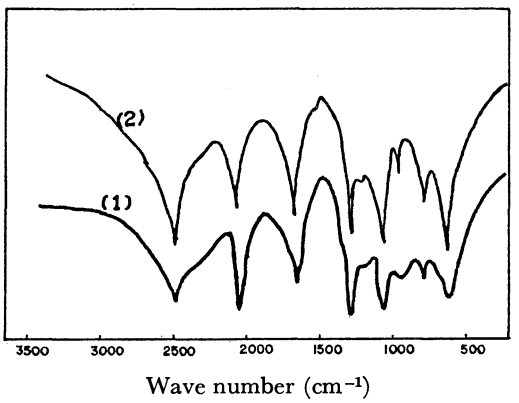

Fig. 5. Infrared spectra of Complex 1 and Complex 2.
(1) Complex 1, (2) Complex 2

properties, and its chromatographic behavior was quite similar to that of Complex 1. The identity of Complex 1 with Complex 2 was further confirmed by a comparison of their infrared spectra (Fig. 5). The infrared spectra of Complex 1 and Complex 2 both included a broad strong band due to P=O stretching at 1280 cm^{-1}, a broad band associated with the P–O–P group at 980 cm^{-1} and three fairly sharp bands at 2500, 2200, and 1680 cm^{-1} (–C=N$^+$–stretching). The fact that both Complex 1 and Complex 2 absorb ultraviolet light strongly suggests the presence of pyridine as a constituent of both these complexes.

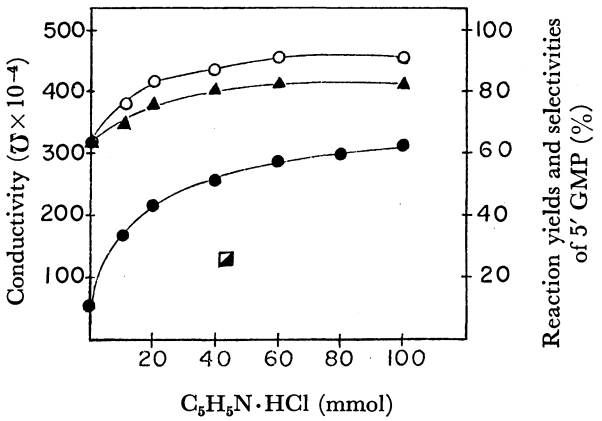

Fig. 6. Effect of pyridinium chloride.
Experimental conditions: $P_2O_3Cl_4$ 22 mmol, CH_3CN 10 ml, at 0 °C.
Phosphorylation of guanosine was performed by adding guanosine (10 mmol) into the above mixture.
○: selectivity of 5′-guanylic acid (5′ GMP), ●: reaction yield of 5′ GMP, ▲: conductivity, ◪: conductivity in the absence of $P_2O_3Cl_4$.

Figure 6 shows the conductivity of mixtures of tetrachloropyrophosphate with varying amounts of pyridinium chloride in acetonitrile. The conductivity increases with the addition of pyridinium chloride to four times the initial value when pyridinium chloride equivalent to twice the molar amount of tetrachloropyrophosphate is present. Similar results were obtained on the addition of water after the mixing of phosphoryl chloride and pyridine in acetonitrile, and the same conductivity was obtained when water was

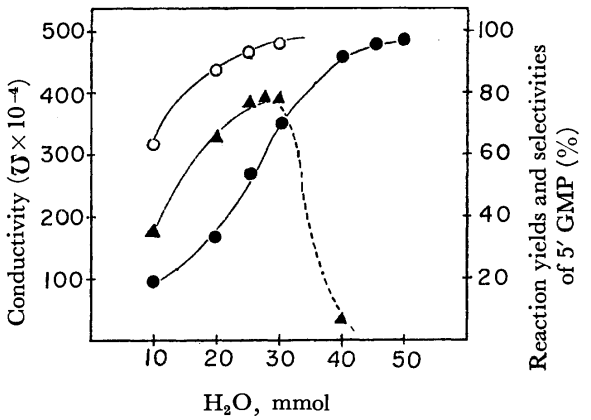

Fig. 7. Effect of water on conductivity, the reaction yield and selectivity of 5′ GMP.
Experimental conditions: $POCl_3$ 22 mmol, C_5H_5N 48 mmol, CH_3CN 10 ml, at 2 °C.
The phosphorylation was performed by adding guanosine (10 mmol) into the above solution.
●: conductivity, ○: selectivity of 5′ GMP, ▲: reaction yield of 5′ GMP.

added in half the molar amount of phosphorus oxychloride (Fig. 7). On the other hand, the conductivity of pyridinium chloride was only 105×10^{-4} ℧ at the same concentration in anhydrous acetonitrile, as is plotted in Fig. 6. The results obtained suggest that the active phosphorylating agent formed by the reaction of phosphoryl chloride with pyridine containing water is an adduct of tetrachloropyrophosphate with pyridinium chloride, which is readily dissociated into charged species in solution.

In order to test the potency of the adduct for selective phosphorylation, a common nucleoside was reacted with tetrachloropyrophosphate in the presence of varying amounts of pyridinium chloride. A typical example is shown in Fig. 6. Both the reaction yield and the selectivity of phosphorylation were obviously influenced by the amount of pyridinium chloride. The results presented in Table 4 showed a good agreement with those obtained in the mixture of phosphoryl chloride, water, and pyridine.

Although, at the present stage of the investigation, no definite determination of the structure of the adduct of tetrachloropyrophosphate with pyridinium chloride has been made, one proposed structure is trichloropyrophosphopyridinium chloride, which would be formed as in the following equations:

$$C_5H_5NHCl \rightleftharpoons C_5H_5N^+H + Cl^- \quad (1)$$

$$C_5H_5N^+H \rightleftharpoons C_5H_5N + H^+ \quad (2)$$

$$Cl_2P(O)-O-P(O)Cl_2 + C_5H_5N \longrightarrow \left[Cl_2P(O)-O-P(O)(Cl)-N^+C_5H_5\right] Cl^- \quad (3)$$

One possible hypothesis is that H^+ derived as indicated in the above equations increases the conductivity of the mixture in acetonitrile, and also increases the selectivity for the 5′-hydroxyl group by decreasing the reactivity of the hydroxyl groups in the ribose moiety of nucleosides with the adduct.

5′-Nucleotides could not be obtained by reacting nucleosides with phosphoryl chloride in the presence of water and strong bases, such as triethylamine, morpholine, or pyrolidine, in acetonitrile (Table 5). In the phosphoylation with tetrachloropyrophosphate,

Table 4. Direct phosphorylation with $P_2O_3Cl_4$ in the presence of $C_5H_5N\cdot HCl$

Compd	Reaction time, hr	Yield of 5′-*N*-tide, mol %	Selectivity of 5′-*N*-tide %
An–R	3.0	92.1	93.8
Gn–R	4.0	90.0	95.0
Hx–R	2.0	93.7	95.1
Xn–R	6.0	89.2	98.6
Un–R	2.0	87.2	90.8
Cn–R	1.5	98.2	98.2
Ara–Un	2.0	88.6	91.4
Ara–Cn	2.0	95.4	97.2

Experimental conditions: nucleoside 10 mmol, $P_2O_3Cl_4$ 22 mmol, $C_5H_5N\cdot HCl$ 44 mmol, CH_3CN 10 ml, at 2 °C.

Table 5. Effect of organic amine

Organic amine	pK_a value	Yields of the products, mol %			
		5′ IMP[1]	Hx′-R	Hx[2]	others[3]
γ-Picoline	5.18	91.3	2.7	1.0	5.0
2,6-Lutidine	5.03	90.4	3.6	0.8	5.2
Pyridine	6.02	92.8	1.5	0.8	4.9
Dimethylaniline	5.10	91.7	2.9	1.6	2.5
Pyrrole	11.3	31.7	40.2	28.1	—
Pyrrolidine		32.7	36.1	30.2	—
Morpholine	9.6	40.7	33.8	21.6	4.2
Triethylamine	10.9	28.8	69.7	1.6	—

Experimental Conditions:
CH_3CN 10 ml, $POCl_3$ 44 mmol, H_2O 28 mmol, organic amine 48 mmol, inosine 10 mmol, at 2 °C for 4 hr.
1) 5′-Inosinic acid. 2) Hypoxanthine. 3) Inosine 2′(3′), 5′-diphosphate.

Table 6. Direct phosphorylation by $P_2O_3Cl_4$ in the presence of organic amine hydrochloride

Org. amine hydrochloride	Reaction time, hr	Yields of product, mol %		Selectivity of 5′ IMP
		5′ IMP[a]	others[b]	
Pyridine	4	94.9	3.6	96.3
γ-Picoline	4	93.8	5.6	94.3
Morpholine	6	90.7	4.5	93.3
Pyrolidine	6	95.6	1.8	98.1
Triethylamine	6	89.6	3.6	93.1
Ethylamine	6	85.0	3.4	92.0

Experimental conditions:
inosine 10 mmol, $P_2O_3Cl_4$ 22 mmol, CH_3CN 10 ml, org. amine hydrochloride 44 mmol, at 2 °C.
a) 5′-Inosinic acid. b) Inosine 3′(or 2′),5′-diphosphate.

however, interesting evidence was obtained that the above organic amine hydrochloride could replace pyridinium chloride (Table 6). The reaction of morpholine with phosphoryl chloride is knwon to give morpholinophosphorodichloridate or dimorpholinophosphorochloridate.[8,9] This means that, in the reaction of the free base with phosphoryl chloride, no adducts were derived because the strong base is too reactive to permit the substitution of a chlorine atom by a hydroxyl group; thus, no formation of dichlorophosphoric acid as an intermediate occurs.

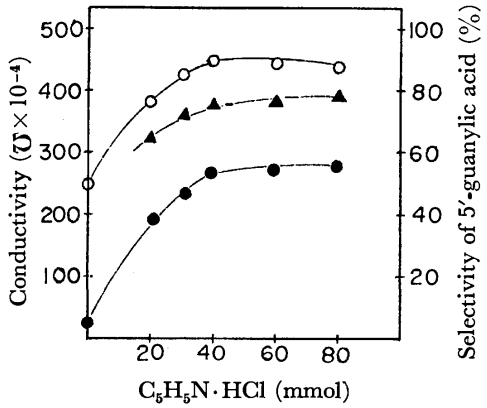

Fig. 8. Effect of pyridinium chloride on conductivity and selectivity of 5′-guanylic acid.
Experimental conditions: CH_3CN 10 ml, $POCl_3$ 44 mmol, at 2 °C.
The phosphorylation was performed by adding guanosine (10 mmol) into the above solution.
○: selectivity of 5′ GMP, ▲: reaction yield of 5′ GMP
●: conductivity.

The addition of pyridinium chloride to phosphoryl chloride in acetonitrile also increased the conductivity of the mixture (Fig. 8). This shows that a dissociable adduct, dichlorophosphopyridinium chloride, similar to trichloropyrophosphopyridinium chloride was probably present in this mixture, suggesting the selective formation of 5′-nucleotides by directly reacting nucleosides with phosphoryl chloride in the presence of pyridinium chloride. As expected, 5′-nucleotides were formed in yields between 85 and 98% from the corresponding nucleosides under the above conditions, as is shown in Table 7.

Table 7. Direct phosphorylation by $POCl_3$ in the presence of $C_5H_5N·HCl$

Compd.	Reaction time, hr	Yield of 5′-*N*-tide, mol %	Selectivity of 5′-*N*-tide, %
An–R	4	89.4	93.4
Gn–R	6	85.7	89.9
Hx–R	4	91.2	93.1
Xn–R	6	88.9	92.1
Cn–R	6	98.0	100
Un–R	6	95.4	98.3
Ara–Cn	6	96.3	100
Ara–Un	6	97.5	99.0

Experimental Conditions: nucleoside 10 mmol, $POCl_3$ 25 mmol, $C_5H_5N·HCl$ 48 mmol, CH_3CN 10 ml, at 2 °C.

The phosphorylation of nucleosides at the 5′-hydroxyl group was not much affected by the polarity of the solvents used in the present reactions. Among the solvents, acetonitrile was superior to the others in both the formation of 5′-nucleotides and the selectivity in

Table 8. Effect of the solvent

Solvent	Reaction time, hr	Yield of 5′-inosinic acid, mol %	Selectivity of 5′-inosinic acid, %
CH_3CN	4	93.5	95.2
CH_3NO_2	5	90.0	95.4
$(CH_3)_2C=O$[a]	4	74.3	83.3
THF[b]	6	71.3	98.0
Dioxane	8	78.9	84.3
CH_2Cl_2	4	89.7	94.6
DMF[c]	6	28.9	—
t-C_4H_9OH	6	1.7	—
$CHCl_3$	8	44.0	92.8

Experimental Conditions: organic solvent 10 ml, $POCl_3$ 44 mmol, H_2O 28 mmol, C_5H_5N 48 mmol, inosine 10 mmol, at 2 °C.
a) The reaction mixture was treated with acid to eliminate the protecting group. b) Tetrahydrofuran. c) Dimethylformamide.

Table 9. R_f-values and the electrophoretic mobilities of nucleosides and nucleotides

Compound	R_f values		Electrophoretic mobilities (cm)	
	Solv. A	Solv. B	pH 2.5	pH 8.8
An–R	0.17	0.51		4.5
An–R–5′MP	0.35	0.14	6.0	15.0
Gn–R	0.33	0.32		5.5
Gn–R–5′MP	0.46	0.19	7.0	16.0
Hx–R	0.44	0.33	−1.0	8.0
Hx–R–5′MP	0.67	0.10	13.0	17.5
Xn–R	0.35			14.0
Xn–R–5′MP	0.52			19.0
Cn–R	0.53	0.52		6.0
Cn–R–5′MP	0.74	0.11	−2.0	17.5
Un–R	0.54	0.51		6.0
Un–R–5′MP	0.69	0.14	8.0	17.0
Ara–Cn	0.65	0.33		−2.5
Ara–Cn–5′MP	0.72	0.13		15.5
Ara–Un	0.58	0.48		−1.0
Ara–Un–5′MP	0.78			15.0
Ara–An	0.19	0.45		−1.0
Ara–An–5′MP	0.38	0.13		13.0
8-Br–AnR	0.08	0.62		4.0
8-Br–AnR–5′MP	0.24	0.14		14.0
8-SH–AnR	0.14	0.68		5.9
8-SH–AnR–5′MP	0.30	0.21		16.5
8-OH–AnR	0.25	0.31		8.0
8-OH–AnR–5′MP	0.44	0.15		18.5
8,2′-*S*-Anhyd AnR	0.12	0.61		−1.0
8,2′-*S*-Anhyd–AnR–5′MP	0.23	0.18		10.0
2,2′-*O*-Anhyd–UnR	0.67	0.48		−2.0
2,2′-*O*-Anhyd–UnR–5′MP	0.81	0.09		17.0
AICAR	0.36	0.39	−10.0	
AICAR–5′MP	0.50	0.15	0	
AICNR–5′MP		0.20	6.5	

the 5′-hydroxyl group (Table 8). Nitromethane and methylene chloride, which dissolve nucleosides completely, are useful as reaction solvents in place of acetonitrile. However, no 5′-nucleotides were formed in dimethylformamide (DMF) or *n*-butanol, presumably because both the amide and alcohol were so reactive to phosphoryl chloride. In acetone, the isopropylidenation reaction took place in inosine at the same time to give 2′,3′-*O*-isopropylidene inosine 5′-phosphate in a 38% yield.

The methods described here simple, direct ways to effect phosphorylation with a complete selectivity to the primary hydroxyl group of nucleosides under mild conditions; they have been adapted to produce the 5′-nucleotides economically.

Experimental

The ultraviolet spectra were recorded on a Hitachi EPS-2T spectrophotometer, and the infrared spectra, on a Hitachi EPI-G2. The conductivity experiments were run on a Shimadzu conduction meter. The paper chromatography was carried out by the ascending technique on Toyo-Roshi No. 51 paper (40×40 cm), using the following solvent systems: Solvent A, isopropyl alcohol–saturated ammonium sulfate–1M-sodium acetate, 2: 79: 19, Solvent B, *n*-butanol–acetic acid–water 4: 1: 5. The paper electrophoresis of the product was performed on the same paper with a 0.05M-borate buffer (pH 8.8) and a 0.05M-citrate buffer (pH 2.5) at a potential gradient of 1.5 kV/cm, for 1 hr. The structure of 5′-nucleotides was confirmed by both a sodium periodate–benzidine test[10] and a 5′-nucleotidase of bull-seminal-plasma treatment.[11] Thin-layer chromatography was used for the identification of the reaction product obtained by mixing phosphoryl chloride, water and pyridine; it was carried out on Wakogel B-5F with Solvent C, ethyleneglycohol dimethyl ether, in a dry box. The location of the products on the layer was determined by the Allen method[12] and by ultraviolet absorption. The nucleotides were identified by a comparison of the R_f-values with those of the authentic samples, as summarized in Table 9.

Preparation of Tetrachloropyrophosphate. Tetrachloropyrophosphate was readily obtained by the method of Craft.[8] A mixture of phosphoric oxide (42.6 g, 0.15 mol) and phosphorus pentachloride (97.8 g, 0.47 mol) was heated at 105 °C for 8 hr, and then cooled and filtered. The solid was washed with carbon tetrachloride, and the combined filtrate and washings were distilled, giving tetrachloropyrophosphate (18.3 g, 31.3 %). Bp 101—103 °C/10 mmHg, d_4^{20}, 1.81.

Preparation of Complex 1. Into a mixture of freshly distilled phosphoryl chloride (20.2 g), water (1.18 g) pyridine (10.4 g), and acetonitrile (23 g) were vigorously stirred at a temperature of 2 °C. Dry ether (100 ml) was then added to the reaction mixture; the precipitate was separated by filtration, washed with ether, and then dried. The hygroscopic crystals (25.8 g) began to soften at 40 °C and was completely molten at 50—51 °C.

Preparation of Complex 2. The hygroscopic crystal (22.3 g) were prepared by mixing tetrachloropyrophosphate (15 g) and pyridinium chloride (13.8 g) in acetonitrile, followed by adding ethyl ether (300 ml) in essentially the same manner as has been described above. Mp 82—88 °C.

Phosphorylation of Nucleosides in the Unprotected Form.

Method A: To a mixture of freshly distilled phosphoryl chloride (44 mmol), water (28 mmol), pyridine (48 mmol), and acetonitrile (189 mmol), which was maintained at 2 °C with stirring, we added a nucleoside (10 mmol, dried at 120 °C for 4 hr), after which the mixture was maintained for 4 hr. The reaction mixture was poured into ice water and stirred further for 1 hr at 5 °C. The resulting solution was analyzed by the paper electrophoretic method described above. The results obtained are listed in Table 1.

Method B: A nucleoside (10 mmol) was dissolved in a mixture of tetrachloropyrophosphate (22 mmol) and acetonitrile (190 mmol), after which the resulting mixture was poured into ice water and analyzed by the paper-electrophoretic method. The results obtained are listed in Table 3.

Method C: A solution which contained a 5′-nucleotide was obtained by reacting the nucleoside (10 mmol) with a mixture of phosphoryl chloride (44 mmol), alcohol (24 mmol), and pyridine (24 mmol) in acetonitrile (190 mmol) in essentially the same manner as that described for Method A. The results obtained are listed in Table 2.

Method D: A solution which contained a 5′-nucleotide was obtained by reacting the nucleoside (10 mmol) with phosphoryl chloride (24 mmol) or tetrachloropyrophosphate (24 mmol) in the presence of pyridinium chloride (44 mmol) in acetonitrile (190 mmol) in the same way as in Method A. The results obtained are listed in Table 4 and Table 7.

References

1) J. M. Gulland and G. I. Hobday, *J. Chem. Soc.*, **1940**, 746.
2) G. R. Baker and G. E. Fall, *J. Chem. Soc.*, **1957**, 3798.
3) M. Yoshikawa, T. Kato, and T. Takenishi, This Bulletin, **42**, 3505 (1969).
4) A. M. Schrecker, J. A. R. Meed, and M. J. Urshel, *Biochem. Pharmacology*, **15**, 1443 (1966).
5) M. Kikkawa, *J. Patent Publication* 42–4348.
6) T. Meguro, *ibid.*, 41–1534.
7) M. Yoshikawa and T. Kato, This Bulletin, **40**, 2849 (1967).
8) H. A. C. Montogomery and J. H. Turnbell, *Proc. Chem. Soc.*, **1957** 178, *J. Chem. Soc.*, **1958** 1963.
9) M. Ikehara and E. Ohtsuka, *Chem. Pharm. Bull.*, **10**, 536 (1962), *ibid.*, **11**, 435 (1963).
10) M. Viscontini, D. Hoch, and P. Karrei, *Helv. Chim. Acta*, **38**, 642 (1955).
11) L. A. Leppel and R. J. Hilmae, *J. Biol. Chem.*, **188**, 655 (1951).
12) R. J. L. Allen, *Biol. J.*, **34**, 858 (1940).
13) R. W. Chambers, J. G. Moffatt, and H. G. Khorana, *J. Amer. Chem. Soc.*, **79**, 3747 (1957).

Effect of Base on Palladium-Black Catalyzed Carbonylation of Iodobenzene

Takeshi Ito, Kunio Mori, Tsutomu Mizoroki, and Atsumu Ozaki

Research Laboratory of Resources Utilization, Tokyo Institute of Technology, Ohokayama, Meguro-ku, Tokyo 152

(Received October 22, 1974)

It was found that palladium-black is a highly active catalyst for the carbonylation of iodobenzene with carbon monoxide and methanol in the presence of potassium acetate, triethylamine, or tributylamine to give methyl benzoate. The kinetic study of the carbonylation showed that the oxidative addition of iodobenzene to a palladium(0) complex is rate-determining, and that the bases affect considerably the rate-determining step.

It is known that relatively stable alkoxy-enyl complexes such as **1** are quantitatively carbonylated in the presence of sodium acetate in methanol[1] and that a complex containing Pd–C sigma-bond reacts extremely rapidly with carbon monoxide in the presence of sodium methoxide in methanol–benzene to give the corresponding ester almost quantitatively.[2] Maitlis, *et al.* demonstrated that an acyl–Pd bond is much less readily cleaved by acid than by base.[2] The styrene-palladium complex can be carbonylated with carbon monoxide and alcohol in the presence of tertiary amines to give cinnamate and phenylsuccinate *via* carbomethoxy palladium as an intermediate.[3,4] Hidai, *et al.* obtained $Pd(CO)(P\phi_3)_3$ and $Pd_3(CO)_3(P\phi_3)_3$ by the reaction of $PdCl_2(P\phi_3)_2$ with carbon monoxide in methanol-amine systems by use of primary or secondary amines, while a carbomethoxy complex, $(P\phi_3)_2PdCl(COOCH_3)$, was isolated by use of tertiary amines.[5]

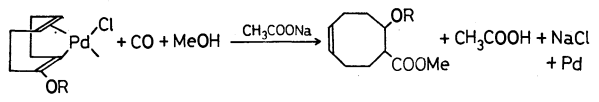

1

The present work was undertaken to examine whether these stoichiometric reactions in a basic medium is reflected in a palladium-catalyzed carbonylation. Palladium(0) complexes is readily oxidized by aryl iodide and bromide to give σ-arylpalladium(II) complexes.[6,7] This reaction was successfully utilized for the palladium-black catalyzed phenylation of olefin with iodobenzene in the presence of potassium acetate in methanol.[8] In a basic medium, palladium-black is also highly active for the carbonylation of iodobenzene. Thus, the effect of bases on the carbonylation was kinetically investigated.

Experimental

Procedure. All the carbonylations were carried out using a Ti–Mn alloy autoclave (100 ml) equipped with a magnetic stirrer. The experimental procedure is illustrated by the carbonylation of iodobenzene with carbon monoxide and methanol to give methyl benzoate. Iodobenzene (40 mmol), methanol (1—30 ml), palladium-black (0.01—1.0 mmol), and a base selected from potassium acetate, triethylamine, and tributylamine were placed in the autoclave. Benzene or toluene (30 ml) was used as the solvent, if necessary. The autoclave was heated up to a desired temperature (60—130 °C) within 20 min, and carbon monoxide (purity 98%) was then introduced up to 5—70 kg/cm². The pressure was kept constant during the reaction by supplying carbon monoxide from a high pressure vessel. After the reaction, the autoclave was rapidly cooled by water, and then carbon monoxide was purged out.

Analysis. Liquid products were quantitatively determined by gas chromatography. A DC-550 columun (3 m) with hydrogen carrier was used at 130 °C for the determination of methyl benzoate, iodobenzene, benzaldehyde, and propiophenone by use of bromobenzene as an internal standard. The amounts of benzal acetophenone and benzanilide were determined using the same columun at 190—230 °C with benzophenone or 1-bromonaphthalene as an internal standard. All the materials were obtained from commercial sources, and utilized without purification.

Results and Discussion

Formation of Methyl Benzoate. As shown in Table 1, the yield of methyl benzoate increased with increase in the amount of potassium acetate. Most of iodobenzene is consumed for the carbonylation when the amount (mmol) of potassium acetate exceeds that of iodobenzene used. Benzoic acid was always found as a product, although its amount was not determined. Accordingly the selectivity based on the amount of iodobenzene consumed is higher than that described in Table 1. The reaction mixtures were always colourless, and most of the catalyst was present in the form of palladium-black. Triethylamine and tributhylamine were also effective, while pyridine was much less

Table 1. Effect of base on yield of methyl benzoate
C_6H_5I 40 mmol, CH_3OH 30 ml, P_{CO} 45 kg/cm² (at r.t.), Temp. 98 °C, Time 90 min.

Pd-black mmol	Base mmol	Conv. %	$C_6H_5COOCH_3$ mmol	Select. %
1.0	AcOK —	14	0.90	16
1.0	AcOK 15	44	13	73
1.0	AcOK 25	64	19	74
1.0	AcOK 50	77	23	74
1.0	AcOK 60	81	24	75
0.1	AcOK 50	80	29	90
0.25	AcOK 50	79	28	88
0.50	AcOK 50	76	28	91
1.0	Py 50	14	5.6	100
1.0	NEt_3 50	51	17	83
1.0	NBu_3 50	28	10	85

(AcO=CH_3COO, Py=C_5H_5N, Et=C_2H_5, Bu=n-C_4H_9)

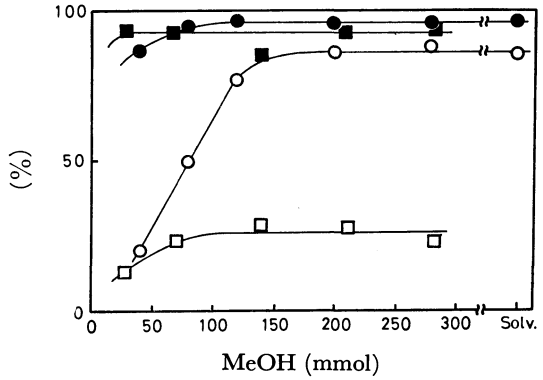

Fig. 1. Effect of amount of methanol.
C_6H_5I 40 mmol, C_6H_6 30 ml, NEt_3 50 mmol, Pd-black 0.5 mmol, P_{co} 20 kg/cm² (Const.), Time 90 min.
□ (Conv.), ■ (Select.) at 73 °C, ○ (Conv.), ● (Select.) at 98 °C.

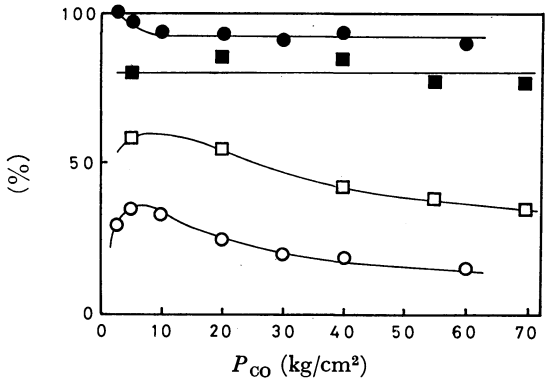

Fig. 2. Effect of the pressure of CO.
○ (Conv.) and ● (Select.) under the condition that C_6H_5I 40 mmol, C_6H_6 30 ml, MeOH 280 mmol, NEt_3 50 mmol, Pd-black 0.5 mmol, and Time 90 min.
□ (Conv.) and ■ (Select.) under the condition that C_6H_5I 40 mmol, MeOH 30 ml, AcOK 50 mmol, Pd-black 0.25 mmol and Time 90 min.

effective giving a reddish reaction mixture, from which a palladium(II) compound, $Pd(C_5H_5N)_2I_2$, was isolated. In any case, neither diphenyl nor anisole was detected in the products. The effect of the amount of palladium-black is also represented in Table 1. Palladium-black is so active that it was difficult to examine the effect of the amount of palladium-black in detail.

The effects of the amount of methanol and the pressure of carbon monoxide on the yield of methyl benzoate using triethylamine ($C_6H_5I/N(C_2H_5)_3=1/1.25$ in mol) and benzene as the solvent, are shown in Figs. 1 and 2 respectively. The yield of methyl benzoate is independent of the amount of methanol when the molar ratio of methanol to iodobenzene is more than 3 (Fig. 1). The carbonylation is slightly retarded under higher pressures of carbon monoxide (Fig. 2). The rate of carbonylation was determined under a constant pressure of carbon monoxide (20 kg/cm²) in the presence of enough amounts of methanol ($MeOH/C_6H_5I=7/1$ in mol) and triethylamine or tributhylamine (amine/$C_6H_5I=1.25/1$ in mol) as the base. The results are shown in Fig. 3, where C_t is the conversion of iodobenzene. The yield of methyl benzoate significantly

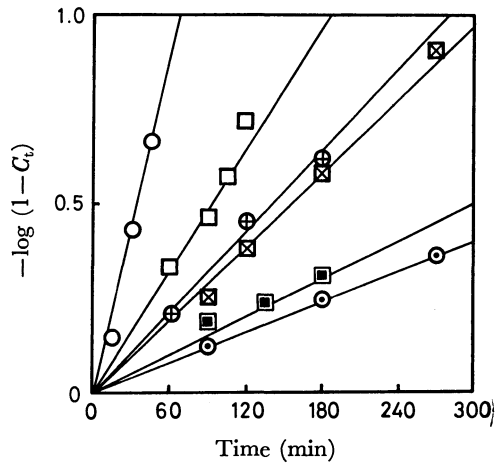

Fig. 3. Plot of $-\log(1-C_t)$ against time in the presence of NEt_3 or NBu_3.
C_6H_5I 40 mmol, C_6H_6 30 ml, Amine 50 mmol, MeOH 280 mmol, Pd-black 0.5 mmol, P_{co} 20 kg/cm².
NEt_3; ○ (98 °C), ⊕ (82 °C), and ⊙ (73 °C).
NBu_3; □ (137 °C), ⊠ (122 °C), and ▣ (110 °C).

depends not only on the base used, but also its amount as described in Table 1. It was confirmed, however, that in the presence of an enough amount of a base (base/$C_6H_5I\geq1$), the carbonylation rate was almost independent of its amount. Potassium acetate was not used for this kinetic study because of its low solubility in benzene. Admitting that the concentration of an active palladium species is constant during the reaction with an equilibrium apparently established among the enough amount of amine, carbon monoxide, and palladium-black, the rate is proportional to the amount of iodobenzene. The rate constants are obtained from the gradients of these linear plots, and the Arrehenius plot is shown in Fig. 4. Tributhylamine needs higher reaction temperature than triethylamine does, while the apparent activation energy in the former case (14 kcal/mol) is smaller than that in the latter case (25 kcal/mol).

In the arylation of olefin with iodobenzene catalyzed by palladium-black, it was considered that the palla-

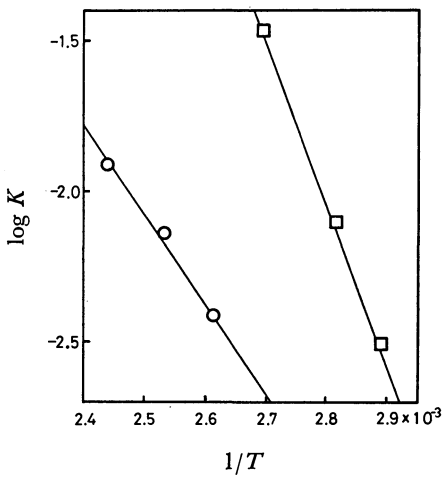

Fig. 4. The Arrhenius plot.
□ NEt_3 25 kcal/mol. ○ NBu_3 14 kcal/mol.

Table 2. Formation of benzoyl derivatives

C_6H_5I 40 mmol, NEt_3 50 mmol, Pd-black 0.5 mmol, $C_6H_5CH_3$ 30 ml.

Reactant	p_{CO} (Kg/cm²)	Temp. (°C)	Time (hr)	Conv. (%)	Prod. (mmol)		Select.[d] (%)
$C_6H_5NH_2$ 50 mmol	20[a]	98	1	36	$C_6H_5CONHC_6H_5$	14	100
$C_6H_5NH_2$ 50 mmol	20[a]	98	2	66	$C_6H_5CONHC_6H_5$	25	96
$C_6H_5NH_2$ 50 mmol	20[a]	98	3	71	$C_6H_5CONHC_6H_5$	27	94
H_2 60 kg/cm²[b]	60[b]	150	4.5	49	C_6H_5CHO	16	82
C_2H_4[c] 30 kg/cm²[b]	30[b]	160	3	77	$C_6H_5COC_2H_5$	12	39

a) The pressure was kept constant during the reaction. b) At the room temperature. c) NBu_3 was used as the base. d) Based on the amount of C_6H_5I consumed.

dium-black supplied an active palladium complex of low oxidation state during the reaction, and that the arylation proceeded *via* σ-arylpalladium intermediate.[8] Four processes were proposed as essential for the arylation of olefin. The kinetics of carbonylation of iodobenzene with carbon monoxide and methanol can also be understood by the following scheme similar to that of the arylation. The fact that the rate of car-

$$\underset{\mathbf{2}}{PdL_n} + C_6H_5I \longrightarrow \underset{\mathbf{3}}{C_6H_5PdIL_{n-2}} + 2L \quad (1)$$

$$C_6H_5PdIL_{n-2} + CO \longrightarrow \underset{\mathbf{4}}{C_6H_5COPdIL_{n-2}} \quad (2)$$

$$C_6H_5COPdIL_{n-2} + CH_3OH \longrightarrow C_6H_5COOCH_3 + \underset{\mathbf{5}}{HPdIL_{n-2}} \quad (3)$$

$$HPdIL_{n-2} + 2L + \text{base} \longrightarrow PdL_n + (\text{H-base})^+ I^- \quad (4)$$

(L=CO, base, or solvent)

bonylation is proportional to the amount of iodobenzene as shown in Fig. 3, indicates the oxidative addition of iodobenzene to the palladium complex 2, where n is probably 4 as seen in $Pd(CO)(P\phi_3)_3$ and $Pd(P\phi_3)_4$, to be rate-determining. The acylpalladium intermediate 4 must be formed rapidly, because of no increase in the yield of methyl benzoate with increasing the pressure of carbon monoxide as shown in Fig. 2. This is consistent with the fact that neither diphenyl nor anisole was detected in the product. Methyl benzoate must be also formed rapidly by the attack of methanol to the acylpalladium 4, because the yield of methyl benzoate is almost independent of the amount of methanol as shown in Fig. 1. This is consistent with the result of stoichiometric reaction that acylpalladium sigma-bond is readily cleaved in a basic medium.[1,2] No detection of palladium(II) compound in the products obtained on using potassium acetate, triethylamine, or tributylamine as the base, suggests that the equilibrium of the reaction (4) is much inclined to the right.

It is worthy of notice that the rate of carbonylation depends significantly on the base used. The difference in the rate and the apparent activation energy shown in Fig. 4 demonstrates that the amines work as ligand to control the concentration of palladium complex **2** and its reactivity for the oxidative addition of iodobenzene. This difference can be explained by assuming that less crowded triethylamine coordinates to the complex **2** more tightly than tributhylamine. That is, triethylamine will keep the concentration of complex **2** higher than tributhylamine during the course of carbonylation, resulting in increasing the rate of reaction (1). Triethylamine, however, needs higher activation energy, since the oxidative addition of iodobenzene to the complex **2** must be accompanied by dissociation of the ligand (amine, CO, and solvent) coordinate to the complex **2**. Pyridine is less effective. It probably stabilizes the intermediate **3**, **4**, or **5**, and retards the regeneration of the active complex **2**.

The other possible scheme, *via* carbomethoxy palladium intermediate, is worthy of metnion here, since carbomethoxy palladium was suggested as an intermediate in the carbonylation of olefin or acetylene.[3,4] Neither of carbomethoxy nor the other palladium(II) complexes, however, were detected in the carbonylation products of iodobenzene. Hidai, *et al.* reported that the stoichiometric reaction of carbomethoxy palladium, $(P\phi_3)_2PdCl(COOCH_3)$, with methyl iodide at 90 °C or with benzyl bromide at 140 °C gave quantitatively methyl acetate or methyl phenylacetate respectively,[5] while the reaction with iodobenzene gave no methyl benzoate even at higher temperature.[9] These facts positively eliminate the scheme *via* carbomethoxy palladium intermediate in the carbonylation of iodobenzene catalyzed by palladium-black.*

Formation of Benzoyl Derivatives. The carbonylation of iodobenzene with carbon monoxide and aniline or hydrogen was examined in benzene or toluene. As summarized in Table 2, the carbonylation in aniline–benzene gives benzanilide selectively. The rate is almost proportional to the amount of iodobenzene. The carbonylation with carbon monoxide and hydrogen also gives benzaldehyde selectively, although it needs an enforced reaction condition. In the absence of carbon monoxide, iodobenzene was hydrogenated quantitatively to benzene under the condition specified in

* Yoshida *et al.* independently reported on the carbonylation of C_6H_5I with CO and methanol catalyzed by $PdCl_2$–Py system (*Nippon Kagaku Kaishi*, **1974**, 1386), where Py seemed to be most effective as the base, and they postulated kinetically the scheme *via* carbomethoxy palladium(II) intermediate. The present carbonylation using palladium-black, however, was strongly retarded by the addition of Py as shown in Table 1, and the catalyst was mostly converted into $Pd(Py)_2I_2$ after the carbonylation. This fact also eliminates the carbomethoxy palladium(II) intermediate.

Table 2, while only a trace amount of benzene was detected in the carbonylation product. The carbonylation with carbon monoxide and ethylene gives a considerable amount of propiophenone and a polymer, contrary to our expectation that acrylophenone would be formed. The sources of hydrogen to give propiophenone remains unclarified. The carbonylation with styrene gives a small amount of benzal acetophenone as determined by retention time of gas chromatograph. The arylation of ethylene or styrene was observed only in the absence of carbon monoxide. The formation of these benzoyl derivatives can also be explained by an acylpalladium intermediate.

References

1) L. F. Hines and J. K. Stille, *J. Amer. Chem. Soc.*, **94**, 485 (1972).
2) T. Hosokawa and P. M. Maitlis, *ibid.*, **95**, 4924 (1973).
3) T. Yukawa and S. Tsutsumi, *J. Org. Chem.*, **34**, 738 (1969).
4) R. F. Heck, *J. Amer. Chem. Soc.*, **94**, 2712 (1972).
5) M. Hidai, M. Kokura, and Y. Uchida, *J. Organometal. Chem.*, **52**, 431 (1973).
6) P. Fitton and E.R. Vick, *ibid.*, **28**, 287 (1971).
7) K. J. Klabunde and J. Y. F. Low *ibid.*, **51**, C33 (1973).
8) K. Mori, T. Mizoroki, and A. Ozaki, This Bulletin, **46**, 1505 (1973).
9) M. Hidai, private communication.

Photosensitized Oxygenation of Unconjugated Cyclic Dienes[1]

Akio HORINAKA, Ruka NAKASHIMA, Masaharu YOSHIKAWA, and Teruo MATSUURA
Department of Synthetic Chemistry, Faculty of Engineering, Kyoto University, Sakyo-ku, Kyoto **606**
(Received December 21, 1974)

The present investigation was undertaken in order to see whether singlet oxygen-oxidation of unconjugated cyclic dienes having spatially close double bonds causes a particular transannular reaction as previously observed with 1,5-cyclooctadiene which gave 4-hydroxy-5-cyclooctenone. Most cyclic dienes tested underwent normal "ene" reaction to give allylic hydroperoxides. Thus, on dye-sensitized photooxygenation followed by reduction with sulfite, dicyclopentadiene, *cis,trans*-1,5-cyclodecadiene, *trans,trans,trans*-1,5,9-cyclododecatriene, 1,4-cyclooctadiene, 1,3-cyclooctadiene, and germacrone yielded a stereoisomeric mixture of tricyclo[5.2.1.$0^{2,6}$]decan-4,8-diene-3-ols, *cis,cis*-2,7-cyclodecadienol, a stereoisomeric mixture of two 2,5,9-cyclododecatrienols, 2,4-cyclooctadienol, *endo*-3,8-peroxide of cyclooctene, and germacra-3,7(11),10(14)-trien-9-ol-6-one(*E*), respectively. Under similar conditions, norbornadiene, and *cis,cis*-1,6-cyclodecadiene remained virtually unchanged.

It was reported[2] that the rose bengal-sensitized photooxygenation of 1,5-cyclooctadiene gives 6-hydroperoxy-1,4-cyclooctadiene, a normal "ene" reaction product by singlet oxygen,[3] and 4-hydroxy-5-cyclooctenone which resulted from an unusual transannular reaction of the hydroperoxide, possibly due to the proximity of the reacting groups. As an extension of this type of transannular reaction, the photosensitized oxygenation of various unconjugated cyclic dienes and a triene, some of which are known to often undergo transannular reactions,[4] was investigated.

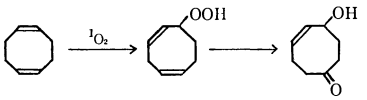

The photosensitized oxygenation of cyclic polyenes I—VIII was carried out in methanol or methylene chloride containing rose bengal or methylene blue as a sensitizer under irradiation with visible light. The reaction mixture was treated with aqueous sodium sulfite in order to reduce the initially formed peroxides. Contrary to our expectation, in most cases the main products were allylic alcohols resulting from a normal "ene" reaction, no particular transannular reaction product being obtained.

Photosensitized oxygenation of dicyclopentadiene (I) followed by reduction gave a 9: 1 mixture of *exo*- (IXa) and *endo*- (IXb) allylic alcohols in 72% yield, which was converted into a single α,β-unsaturated ketone X[5] by treating with active manganese dioxide. On reduction with lithium aluminum hydride X underwent a less-hindered side attack of hydride ion to give exclusively IXb. The structure of the *exo* isomer IXa was confirmed by its synthesis by the oxidation of I with selenium dioxide.[5] The results indicate that I undergoes "ene" reaction with predominant attack of singlet oxygen to the less hindered side of the molecule to give isomeric allylic hydroperoxides corresponding to IXa and IXb.

Under similar conditions, norbornadiene (II), and *cis,cis*-1,6-cyclodecadiene (III) remained virtually unchanged, although the former gave a complex mixture of products in a small yield on prolonged photooxygenation. However, *cis,trans*-1,5-cyclodecadiene (IV) suffered photosensitized oxygenation to give, after reduction, a single crystalline cyclodecadienol in 44% yield, for which one of two structures XIa and XIb is possible because of the absence of IR band around 970 cm^{-1} characteristic of a *trans* double bond.[6] Structure XIb was excluded by the fact that the MNR spectrum showed no signal of diallylic methylene protons (C=C–CH_2–C=C) usually appearing at δ 2.78.[7] Predominant formation of XIa from IV indicates that the *trans* double bond of IV is more susceptible to the attack of singlet oxygen than the *cis* double bond, probably due to the more strained nature of the *trans* double bond or to the more axial-like conformation of hydrogens allylic to the *trans* double bond.[8]

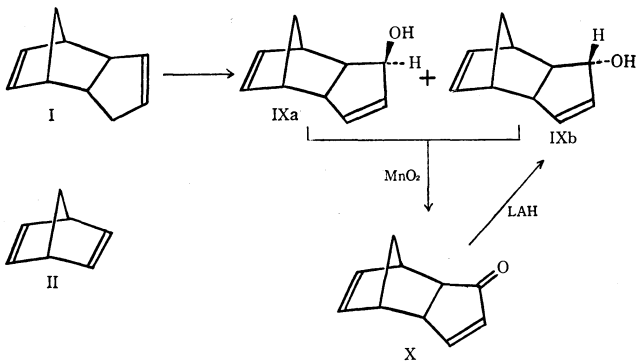

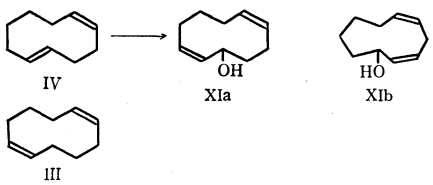

Litt and Nickon reported the photosensitized oxygenation of *trans,trans,trans*-1,5,9-cyclododecatriene (V).[9] They pointed out that no *cis-trans* isomerization occurred during photooxygenation but did not describe the reaction products. Photooxygenation of V under the usual conditions gave an about 1: 1.3 mixture of two 2,5,9-cyclododecatrienols in 41% yield and crystalline products in 3% yield. The structures of these two cyclododecatrienols were tentatively assigned as XIIa and XIIb on the basis of the following facts. The NMR spectrum of the mixture was in accord with these structures (see Experimental), and on catalytic hydrogenation the mixture gave cyclodecanol as the sole single product. The crystalline product appeared

to be a mixture of cyclododecatrienediols but was not further examined.

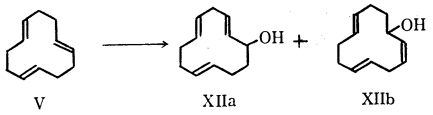

V XIIa XIIb

Similar sensitized photooxygenation of 1,4-cyclooctadiene (VI) gave a single product for which structure XIII was deduced from its spectral data (see Experimental).

The photosensitized oxygenation of a conjugated cyclic diene, 1,3-cyclooctadiene (VII) was also examined. Both sensitized[10] and unsensitized[11] photooxygenations of VII have been reported. By sensitized photooxygenation, VII is known to give an *endo*-peroxide XIV formed by the 1,4-addition of singlet oxygens to a conjugated diene system.[10] We observed also that methylene blue-sensitized photooxygenation of VII in methylene chloride gave XIV in 53% yield, and that rose bengal-sensitized photooxygenation in methanol gave a complex mixture of products, probably due to participation of the solvent methanol. Peroxide XIV was converted into *cis*-cyclooctane-1,4-diol (XV)[11] and *cis*-2-cyclooctene-1,4-diol (XVI) by controlled hydrogenation.

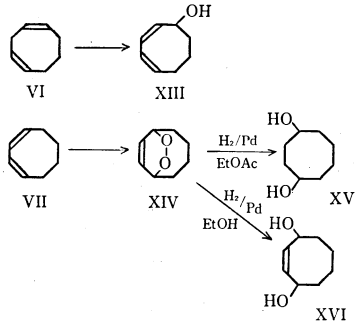

VI XIII VII XIV XV XVI

Germacra-3,9-diene derivatives have been considered to be important precursors of various types of bicyclic sesquiterpenes, which may be formed by transannular cyclisation *in vivo*.[12] Such types of biogenetic-type syntheses have drawn considerable attention.[13] In an attempt to obtain such a germacradiene precursor having an alcoholic oxygen function, the photosensitized oxygenation of germacrone (VIII) was carried out. Rose bengal-sensitized oxygenation of VIII in methanol yielded a complex mixture of products, from which a crystalline substance was obtained in a low yield. Its IR spectrum showed bands at 3400 (hydroxyl), 1660 (α,β-enone), and 895 cm^{-1} (end methylene). In the NMR spectrum new signals due to vinyl protons at δ 4.86 (singlet) and 5.05 (singlet) and a triplet signal due to a $-\underline{C}H-OH$ proton at δ 3.78 (J=6 Hz) appeared, instead of one of the two methyl signals, δ 1.45 and 1.62, and one of the two di-π-methylene signals at δ 3.16 in VIII. These data suggest two possible structures XVIIa and XVIIb for the product. However, assignment of the NMR spectrum of the photooxygenation product in comparison with those of germacrone (VIII)[14] and of germacrone epoxides XVIII and XIX[15] reveals that the correct structure must be XVIIa, since a doublet signal at δ 2.6 (J=6 Hz), which couples with the $-\underline{C}H-OH$ proton, is not assignable to structure XVIIb. It should be noted that in the photosensitized oxygenation of germacrene (1(10),4,7(11)-germacratriene(E,E)) singlet oxygen attacks predominantly the exocyclic double bond at 7 position but the triphenylphosphite–ozone adduct attacks the most strained double bond at 5 position.[16]

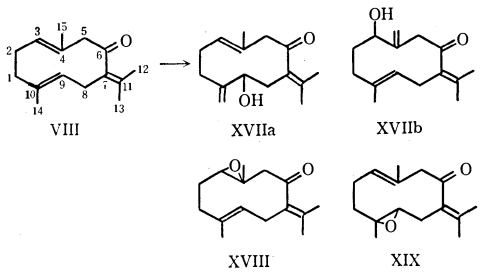

VIII XVIIa XVIIb

XVIII XIX

Experimental

Materials. Commercial olefins, dicyclopentadiene (I), norbornadiene (II), *trans, trans, trans*-1,5,9-cyclododecatriene (V), and 1,3-cyclooctadiene (VII) were used. The preparation of 1,4-cyclooctadiene (VI) was carried out according to the method of Moon and Gang.[7] *cis, cis*-1,6-Cyclodecadiene (III) and *cis,trans*-1,5-cyclodecadiene (IV) were supplied by Dr. P. Heinbach, Max-Planck-Institut für Kohlenforschung, Mülheim/Ruhr, and germacrone (VIII) by Dr. Y. Hirose, Institute of Food Chemistry, Osaka, and Dr. Y. Tomita, Shionogi Research Laboratories, Osaka.*

Photosensitized Oxygenation of Dicyclopentadiene (I). A solution of I (10 g) and rose bengal (200 mg) in methanol (230 ml) was irradiated with a tungsten–bromine lamp under bubbling oxygen until 0.45 mol equivalent of oxygen (810 ml) was consumed. The reaction mixture was diluted with methanol to 250 ml. In order to determine the peroxide content, an aliquot was analyzed by iodometry which showed that the mixture contained 91 mol % of peroxide based on the consumed oxygen. The reaction mixture was treated with sodium sulfite (7 g) in water (300 ml) under ice-cooling and vigorously stirring for 1 hr. The mixture was concentrated and the aqueous residue was extracted with light petroleum and then with ether. Evaporation of the extracts followed by vacuum distillation gave a mixture of tricyclo[5.2.1.$0^{2,6}$]deca-4,8-diene-3-ols (IXa and IXb) as an oil (3.17 g; 72% yield based on the consumed oxygen); bp 95 °C (bath temperature)/2 mmHg; Mass: m/e 148 (M^+); IR (neat): 3300 (OH), 2940, and 1035 cm^{-1}; NMR (CCl_4): δ 5.4—6.0 (m, 4H), 4.0 (br. s, 1H), 3.8 (br. s, 1H, OH), 3.4 (m, 1H), 3.02 (br. s, 1H), 2.8 (m, 1H), 2.6 (m, 1H), and 1.2—1.7 (m, 2H). Vpc analysis (Silicon DC 550; 180 °C; carrier gas, hydrogen; 1 kg/cm^2) of the oil revealed that it consisted of a 9: 1 mixture of IXa (retention time, 5.0 min) and IXb (4.2 min). The identity of IXa and IXb was confirmed by comparison of their vpc retention times with those of authentic samples, and also by their conversion into X (see below). The authentic samples of IXa and IXb were prepared by selenium dioxide oxidation of I[5] and lithium aluminum hydride reduction of X.[17] The IR spectrum of the oil was almost identical with that of IXa prepared as above.

Oxidation of IXa and IXb into Tricyclo[*5.2.1.*$0^{2,6}$]*decan-4,8-*

* The authors are grateful for the generous supply of these samples.

diene-3-one (X). A 9:1 mixture of IXa and IXb (865 mg) in light petroleum (100 ml) was stirred vigorously with active manganese dioxide (9 g) for 5 hr. After filtration the mixture was concentrated and the residue was purified by sublimation followed by recrystallization from *n*-hexane to give X (582 mg) as colorless prisms; mp 61—63 °C (lit, mp 65.3—65.6 °C[5]); 59—59.5 °C[17]); λ_{max}^{EtOH} 225 nm (ε 8600); NMR (CCl_4) δ 7.3 (dd, 1H, J=2.2 and 6 Hz) and 5.6—6.1 (m, 3H). (Found: C, 81.97; H, 7.14%. Calcd for $C_{10}H_{10}O$: C, 82.11; H, 6.90%).

Photosensitized Oxygenation of cis,trans-*1,5-Cyclodecadiene (IV).* A solution of IV (1.5 g) and rose bengal (200 mg) in methanol (230 ml) was photooxygenated. After being treated with sodium sulfite, the mixture was worked up in a similar manner to the case of I to give XIa (660 mg, 44%) as crystals; mp 96—96.5 °C (from light petroleum); Mass: *m/e* 152 (M^+); NMR (CCl_4): δ 5.3 (m, 4H), 4.32 (m, 1H), 2.34 (s, 1H, OH), 2.22 (m, 2H), 1.85 (m, 4H), and 1.62 (m, 4H).

Found: C, 78.61; H, 10.82%. Calcd for $C_{10}H_{16}O$: C, 78.89; H, 10.59%.

Photosensitized Oxygenation of trans,trans,trans-*1,5,9-Cyclododecatriene.* A solution of V (16.2 g) and rose bengal (300 mg) in methanol (310 ml) was photooxygenated for 25 hr, consuming 0.22 mole equivalent of oxygen (490 ml). After treatment with sodium sulfite, the mixture was worked up as above. Evaporation of the light petroleum extract followed by vacuum distillation gave an oil (1.49 g; 41% based on the consumed oxygen); bp 103 °C/2 mmHg; Mass: *m/e* 178 (M^+); IR (neat): 3300, 2900, 1650, 1440, and 970 cm^{-1}. Vpc analysis revealed that it consisted of 1:1.3 mixture of XIIa and XIIb. A solution of the oil (0.21 g) in ethyl acetate (10 ml) was hydrogenated in the presence of platinum black (25 mg). After filtration, the mixture was evaporated. Recrystallization of the residue from *n*-hexane gave cyclododecanol as crystals, mp 79—80 °C, which were identified by comparison of IR, glc and tlc with those of a commercial sample.

Ether extraction of the original aqueous layer followed by evaporation gave a solid, which on recrystallization from ethyl acetate yielded crystals (110 mg; 3% yield); mp 131—139 °C; IR (Nujol) 3150, 2850, 1660, 1440, 1025, 1010, and 970 cm^{-1}. (Found: C, 74.19; H, 9.44%. Calcd for $C_{12}H_{18}O_2$: C, 74.19; H, 9.34%). These crystals appear to be a mixture of cyclododecatrienediols but were not further examined.

*Photosensitized Oxygenation of 1,4-Cyccloctadiene (VI).*** A solution of VI (1.64 g) and rose bengal (100 mg) in methanol (130 ml) was photooxygenated for 13 hr, consuming 0.81 mol equivalent of oxygen (275 ml). After treatment with sodium sulfite, the mixture was worked up as above to give an oil (806 mg) which on vacuum distillation afforded 2,4-cyclooctadienol (XIII) as an oil (530 mg; 39% based on the consumed oxygen); bp 105 °C (bath temperature)/3 mmHg; Mass: *m/e* 124 (M^+); IR (neat) 3330, 3005, 2925, 2850, 1690, 1445, and 1040 cm^{-1}; NMR (CCl_4): δ 5.9—5.4 (m, 4H), 4.6—4.2 (m, 1H), 2.32 (s, 1H, OH), and 2.7—1.2 (m, 6H); λ_{max}^{EtOH} 210 nm (ε 5600).

Found: C, 77.13; H, 9.70%. Calcd for $C_8H_{12}O$: C, 77.37; H, 9.74%.

Photooxygenation of 1,3-Cyclooctadiene (VII). A solution of VII (5.40 g) and methylene blue (100 mg) in methylene chloride (240 ml) was photooxygenated for 23 hr, consuming 0.6 mol equivalent of oxygen (875 ml). The mixture was washed with water and dried over anhydrous sodium sulfate. Evaporation of the solvent followed by vacuum distillation gave *endo*-3,8-peroxide of cyclooctene (XIV) as crystals (2.58 g; 53% based on the consumed oxygen); bp 80—97 °C/2 mmHg; mp 60—65 °C (lit, mp 50.5—55.5 °C[10]); IR (Nujol,): 1000, 975, 920, and 760 cm^{-1}; NMR (CCl_4): δ 6.23—6.07 (q) 2H), 4.76 (m, 2H), and 2.3—1.3 (m, 8H).

Catalytic Hydrogenation of XIV. Palladium Black: A solution of XIV (100 mg) in ethyl acetate (10 ml) was hydrogenated in the presence of palladium black (30 mg). After removal of the catalyst, the mixture was evaporated to give an oil which was chromatographed on a neutral alumina column (30 g). Elution with 1:1 benzene-acetone yielded 1,4-cyclooctanediol (XV) (54 mg; 55%). Recrystallization from ethyl acetate gave crystals, mp 84—87 °C (lit, mp for *cis*-diol 85—86.5 °C[11]). (Found: C, 66.06; H, 11.42%. Calcd for $C_8H_{16}O_2$: C, 66.63; H, 11.18%).

Palladium Charcoal: A solution of crude XIV prepared by the methylene blue-sensitized photooxygenation of VII (2.7 g) in ethanol (20 ml) was hydrogenated in the presence of palladium charcoal (200 mg) and treated in the same manner as above to give *cis*-2-cyclooctene-1,4-diol (XVI) (105 mg; 38% based on the consumed oxygen in the photooxygenation). Recrystallization from ethyl acetate gave crystals; mp 143—151 °C; IR (Nujol) 3200, 1050, 1030, 960, and 750 cm^{-1}; Mass: *m/e* 142 (M^+).

Found: C, 67.57; H, 9.93%. Calcd for $C_8H_{14}O_2$: C, 68.00; H, 9.95%.

Photosensitized Oxygenation of Germacrone (VIII). A solution of VIII (6 g) and rose bengal (200 mg) in methanol (350 ml) was photooxygenated for 4 hr until VIII was completely consumed. The mixture was found by iodometry to contain 0.75 mol equivalent of peroxide on the basis of the consumed oxygen (1.1 l). The mixture was treated with sodium sulfite (4.8 g) in water (200 ml) under ice cooling, concentrated under reduced pressure and then extracted with light petroleum and ether successively. The organic layers were dried over anhydrous sodium sulfate and evaporated. The residue from the light petroleum extract was recrystallized from carbon terachloride to give germacra-3,7(11),10(14)-trien-9-ol-6-one(*E*) (XVIIa) as crystals (153 mg; 2.5%); mp 91.5—92.5 °C; IR (KBr): 3400, 1660, 1015, and 895 cm^{-1}; NMR (CCl_4): δ 1.60 (d, 3H, J=1 Hz), 1.78 (s, 3H), 1.81 (s, 3H), 2.2 (m, 4H), 2.3 (s, 1H, OH), 2.60 (d, 2H, J=6 Hz, $-CH(OH)-CH_2-$), 3.15 (s, 2H, $=C-CH_2-CO-$), 3.78 (t, 1H, J=6 Hz), 4.86 (s, 1H), 5.05 (s, 1H), and 5.35 (m, 1H).

Found: C, 76.79; H, 9.69%. Calcd for $C_{15}H_{22}O_2$: C, 76.88; H, 9.46%.

The mother liquor from XVIIa and the ether extract (1.91 g) were found to be complex mixtures, from which isolation of pure products was unsuccessful.

References

1) Photoinduced Reactions. LXXXVI. Part LXXXV: I. Saito, M. Takami, and T. Matsuura, This Bulletin, in press (1975).

2) T. Matsuura, A. Horinaka, H. Yoshida, and Y. Butsugan, *Tetrahedron*, **27**, 3095 (1971).

3) For reviews of singlet oxygen chemistry see: a) C. S. Foote, *Accounts Chem. Res.*, **1**, 104 (1968); b) K. Gollnick, *Advan. Photochem.*, **6**, 1 (1968); c) T. Matsuura, *Yuki Gosei Kagaku Kyokai Shi*, **26**, 217 (1968); d) D. R. Kearns, *Chem. Rev.*, **71**, 395 (1971); e) R. W. Denny and A. Nickon, *Org. Reactions*, **20**, 133 (1973).

4) A. C. Cope, M. M. Martin, and M. A. Mckervey, *Quart. Rev.*, **20**, 119 (1966).

5) R. B. Woodward and T. J. Katz, *Tetrahedron*, **5**, 70 (1959).

6) K. Nakanishi, "IR Absorption Spectroscopy-Practical", Nankodo Publ., Tokyo (1960), p. 30.

** The authors are indebted to Mr. Y. Usagawa for carrying out this experiment.

7) S. Moon and C. R. Gang, *J. Org. Chem.*, **34**, 465 (1969).
8) T. Matsuura, A. Horinaka, and R. Nakashima, *Chem. Lett.*, **1973**, 887.
9) F. A. Litt and A. Nickon, "Oxidation of Organic Compounds-III", Advan. Chem. Ser., No. 77, Amer. Chem. Soc. Publ., Washington D. C. (1971), p. 118.
10) Y. Kayama, M. Oda, and Y. Kitahara, The 24th Annual Meeting of Chem. Soc. Japan, Osaka (1971), Papers of Abstracts-III, p. 1360; *Chem. Lett.*, **1974**, 345.
11) A. C. Cope, A. H. Keough, P. E. Peterson, H. E. Simmons, Jr., and G. W. Wood, *J. Amer. Chem. Soc.*, **79**, 3900 (1957).
12) a) J. B. Hendrickson, *Tetrahedron*, **7**, 82 (1959); b) C. Kaneko and S. Nozoe, "Natural Product Chemistry-'67", (Y. Kitahara, N. Tamiya, K. Nakanishi, and S. Ito Ed.), Kagaku no Ryoiki Special Issue No. 80, Nankodo Publ., Tokyo (1967), p. 66.
13) For example see: a) E. D. Brown, M. D. Solomon, J. K. Sutherland, and A. Tore, *Chem. Commun.*, **1967**,111; b) T. C. Jain and J. E. McCloskey, *Tetrahedron Lett.*, 2917 (1969); c) S. C. Bhattacharyya, *Tetrahedron*, **22**, 2331 (1968); d) K. Yoshihara, Y. Ohta, T. Sakai, and Y. Hirose, *Tetrahedron Lett.*, **1969**, 2263; e) M. Iguchi, M. Niwa, and S. Yamamura, *Chem. Commun.*, **1971**, 974; **1972**, 689; *Tetrahedron Lett.*, **1973**, 1687.
14) C. Ganter and B. Keller-Wojtkiewicz, *Helv. Chim. Acta*, **54**, 183 (1971).
15) H. Hikino, C. Konno, T. Nagashima, T. Kohama, and T. Takemoto, *Tetrahedron Lett.*, **1971**, 337.
16) T. W. Sam and J. K. Sutherland, *J. Chem. Soc. Chem. Commun.*, **1972**, 424.
17) M. Rosenblum, *J. Amer. Chem. Soc.*, **79**, 3179 (1957).

Potentiometric Analysis and Fundamental Technique

Yoshihiro SHIGEMASA, Masayuki SHIMAO, Chikahiro SAKAZAWA, and Teruo MATSUURA*

Department of Industrial Chemistry, Faculty of Engineering, Tottori University, Tottori 680

**Department of Synthetic Chemistry, Faculty of Engineering, Kyoto University, Kyoto 606*

(Received January 13, 1975)

The formose reaction, the calcium hydroxide-catalyzed condensation of formaldehyde to monosaccharides, was potentiometrically analyzed. The oxidation-reduction potential varied in a characteristic way and gave information of considerable importance. Some appreciable transition points in the oxidation-reduction potential curve showed satisfactorily the occurrence of a phase change such as an induction period and saccharide-forming and saccharide-decomposing stages. With regard to the fundamental operating conditions, vigorous stirring and an increase in the dissolved oxygen elongated the induction period. Furthermore, the latter diminished the yield of saccharide under the lower limit of the critical range of the calcium hydroxide concentration.

The formose reaction, in which monosaccharides result from formaldehyde in the presence of an alkaline catalyst in an aqueous medium, was first reported by Butlerow.[1] Thereafter, much attention has been directed to studies of catalysts for saccharide-forming reactions. Of these, some alkali earth- and alkali-hydroxides and organic bases, such as pyridine and picoline, have been recognized as active catalysts.[2,3] Especially, $Ca(OH)_2$ is widely used for the investigation of the above reaction. From their experiments using a dilatometer, Belezin and Surykina[4] observed the existence of a time lag prior to the saccharide condensation; this period was shortened by adding glucose or fructose.

Pfeil and Schroth[5] prepared saccharides using TlOH as a catalyst, and recognized the formation of substances which accelerate the formose reaction during the induction time by pursuing the consumption of formaldehyde or products, followed by the Cannizzaro reaction. Subsequently, they supposed that the substances would form a calcium complex and contributed to the saccharide formation. Furthermore, they demonstrated that the extent of formose reaction is greatly affected by the kind of alkaline cations used.

Recently, in their series of studies of the formose reaction, Weiss *et al.*[6-9] followed the reaction in a continuously stirred tank reactor. They derived a kinetic expression for the formose condensation, and pointed out the instabilities observed in both the Cannizzaro reaction and the formose reaction were obviously attributable to changes in the $Ca(OH)_2$ concentration. Fujino *et al.*[10] have obtained evidence for the formation of soluble complexes consisting of alkali earth-saccharides or alkali earth-formaldehyde and recognized the presence of a relationship between their catalytic activity and their complex-forming ability.

In certain situations, the oxidation-reduction potential (ORP) has often been employed to estimate a state or a mechanism of reaction systems.[11,12] As has been mentioned above, with regard to the formose synthesis, much information concerning the activity of catalysts and the reaction mechanism has been accumulated. However, there have been few attempts to elucidate the nature of this reaction by employing ORP estimation. In an earlier paper[13] dealing with the potentiometric analysis of the formose reaction, it was shown that the changes in ORP show a good correlation with the characteristic reaction phases. The object of this paper is to present more details of the previous work and to describe some additional experiments concerning the fundamental techniques in the reaction.

Experimental

Procedure. Under N_2 an aqueous formaldehyde was treated with $Ca(OH)_2$ in an apparatus attached to a potentiometer.

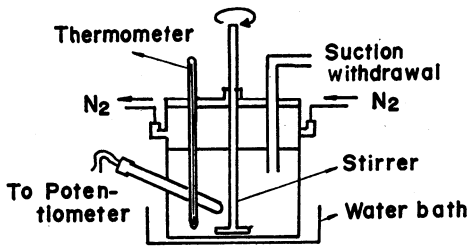

Fig. 1. Apparatus.

These are shown in Fig. 1. The bath temperature was kept in the range of 60±1 °C, and the rate of stirring remained at 320 rpm through the experiment. A representative method of the reaction was as follows. The reactor, which contained 90 ml of 37% formalin (commercial) and 790 ml of water, was pre-equilibrated at 60±1 °C in a thermostat; the reaction was then initiated, followed by the addition of 8.5 g of $Ca(OH)_2$. At convenient intervals, *ca.* a 10-ml aliquot was withdrawn into a 50 ml flask and immediately acidified with 1M HCl; these aliquots were analyzed for formaldehyde, the total saccharides, and organic acids as follows.

The formaldehyde was determined by the method of Bricker *et al.*,[14] only the optical density being measured at 579 nm.

The calculation of the formaldehyde concentration was done by means of a previously prepared calibration curve.

The total saccharides were determined using the phenol-sulfuric acid method,[15] the concentration being calculated as glucose from a calibration curve. The organic acids was determined by back titration with 1M KOH after the aliquot had been acidified. When A ml of 1M HCl was added to the solution and subsequently B ml of 0.1M KOH was consumed to neutralize the solution, the organic acid concentration, x M, was given by the following equation:

$$x = 2 \times 8.5 \times 1000/74 \times 880 + 0.01B - 0.1A$$

The dissolved oxygen was estimated by following a modification of the Winkler method,[16] while the stirring speed was measured using a stroboscope.

The UV spectra were measured using a Shimadzu Spectro-

photometer, MPS-50L. A sample solution withdrawn from the reaction mixture was cooled immediately in a dry ice–acetone bath to about 0 °C, at which the reaction would virtually not proceed at all. Next, the solution was centrifuged under a high speed to remove the turbidity of the medium. Even when the sample was simply cooled and not acidified, it was stable enough for the determination of the UV spectra so long as it was stored in a refrigerator.

Results and Discussion

As is shown in Fig. 2, a representative ORP curve for the formose reaction apparently has four characteristic steps. The first step: Almost no change in ORP is observed, and no production of saccharides can be detected with a little consumption of formaldehyde. This step may be an induction period, after which only a small amount of organic acids (mainly formic acid) is detected. The period of this step varies depending upon the reaction conditions. For example, it is shortened when a known promoter, such as glucose,[5] fructose,[17] xylose, or glycolaldehyde,[18] is added. The second step: After the induction period, the ORP curve begins to turn downward and reaches to a minimum point (the time up to this point is termed T_{min}). At this point, the yield of saccharides is only approximately 3% (as glucose based on formaldehyde), and the formaldehyde condensation to saccharides is initiated slowly, whereas as much as 20—30% of the formaldehyde is consumed. The rate of organic acid production is similar to that in the previous step. The third step: The ORP curve turns upwards from the minimum point and reaches a small maximum (the time up to this point is termed T_{max}), whereupon a little drop is observed, while the color of the solution simultaneously turns to pale yellow (the so-called yellowing point). As the ORP of the solution increases, the reaction proceeds rapidly with a rise in the temperature up to the maximum, 70—75 °C. At the termination of this step, the formaldehyde consumption is raised to 95% and the yield of the saccharides amounts to 50—70%. The fourth step: A steady state appears again in ORP, while the saccharides formed begin to decompose and the total amount of saccharides decreases successively as time passes. The temperature of the mixture slowly becomes lower, on the other hand, the color of the mixture changes from light yellow to light brown or brown.

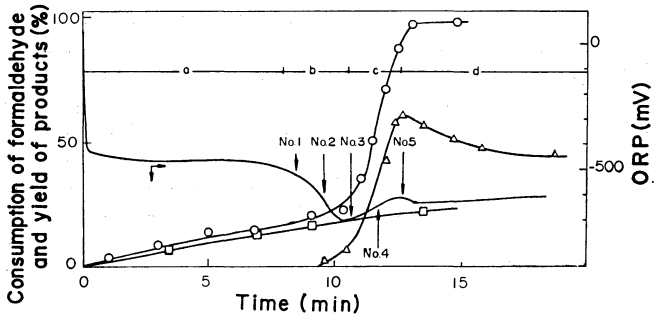

Fig. 2. Potentiometric and product analyses of the formose reaction.
[HCHO]=1.4 M; [Ca(OH)$_2$]=0.13 M; ○, Formaldehyde; △, Total sugars; □, Organic acids; T_{min}=a+b; T_{max}=a+b+c; ΔORP=maxORP−minORP.

In order to ascertain the optimum conditions for the saccharide formation, some basic experimental conditions, such as the influences of the stirring speed and the dissolved oxygen, were investigated. The stirring speed has a negligible influence on the saccharide yield within the rage of 200—1200 rpm. However, vigorous stirring causes the ΔORP (the ORP difference between T_{max} and T_{min}) to decrease (Fig. 3) and results in an increase in the period up to both T_{min} and T_{max} (Fig. 4). The results indicate that the stirring speed need not necessarily be high; hence, 320 rpm would seem an adequate speed for usual experiments.

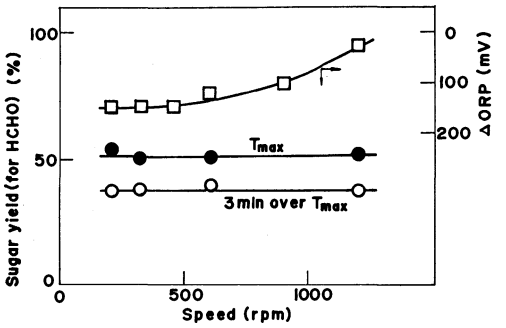

Fig. 3. Effect of agitation on sugar yield and ΔORP.
[HCHO]=2.0 M; [Ca(OH)$_2$]=0.2 M.

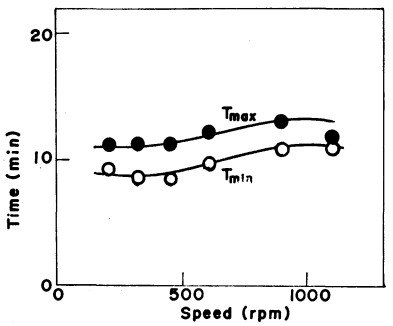

Fig. 4. Effect of agitation on T_{min} and T_{max}.
Reaction condition; Same as Fig. 3.

Concerning the influence of dissolved oxygen, a set of experiments were carried out in which the periods up to T_{min} and T_{max} were determined with an increase in the concentration of dissolved oxygen (Fig. 5). The oxygen concentrations were adjusted by introducing limited amounts of oxygen and nitrogen into the reactor. As may be seen in Fig. 5, slight elongation in the time up to both T_{min} and T_{max} is observed with an increase in the oxygen concentration. On the other hand, at a comparatively lower level of the Ca(OH)$_2$ concentration (0.17 M), the dissolved oxygen at a high concentration diminishes the sugar yield, while at a little higher concentration (0.20 M), the sugar yield remains unchanged within this range of oxygen concentration (Fig. 6). The results show that oxygen acts as a weak inhibitor of the formose reaction. Therefore, the progress of the reaction under a nitrogen atmosphere seems to be favorable for obtaining saccharides in a high yield.

The ORP measurements of the formose reaction were carried out under various conditions. Whenever the

Table 1. Changes of UV absorption in the formose reaction

Sample number[a]	Supernatant			Neutralized			Acidified		
	pH	λ_{max}(nm)	Abs.	pH	λ_{max}(nm)	Abs.	pH	λ_{max}(nm)	Abs.
No. 1	11.2	272	—	4.2	272	0.33	1.0	272	0.31
No. 2	11.2	272	—	6.0	272	0.24	1.2	272	0.20
No. 3	11.2	288	0.35	5.2	288	0.43	1.0	288	0.38
No. 4	11.1	290	1.90	6.1	290	1.99	1.0	290	1.73
No. 5	11.0	292	5.96	6.2	287	4.48	1.0	282	3.03

a) Shown in Fig. 2.

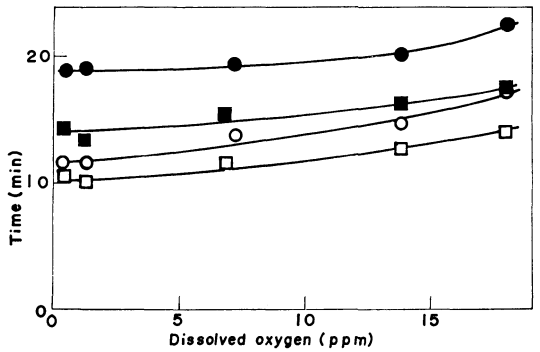

Fig. 5. Effect of oxygen on T_{min} and T_{max}.
T_{min} (-○-) and T_{max} (-●-); [HCHO]=2.0 M and [$Ca(OH)_2$]=0.17 M. T_{min} (-□-) and T_{max} (-■-); [HCHO]=2.0 M and [$Ca(OH)_2$]=0.2 M. HCHO; Prepared from paraformaldehyde.

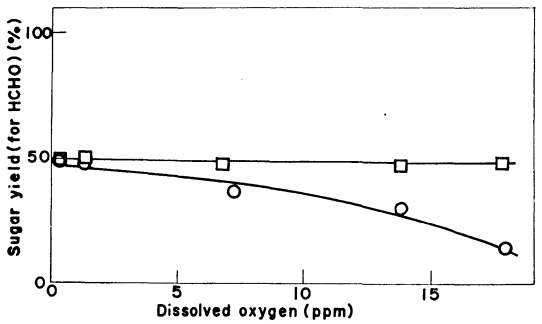

Fig. 6. Effect of oxygen on sugar yield.
Reaction conditions; Same as Fig. 5. [$Ca(OH)_2$]: ○, 0.17 M; □, 0.20 M.

conditions under which the formose reaction took place smoothly to give saccharides were employed, the minimum (2nd step) and maximum (3rd step) points necessarily appeared. On the contrary, under such conditions where the formose reaction would not take place, when, for example, the reaction was initiated under the lower limit of the critical of the $Ca(OH)_2$ concentration, the ORP did not show significant change but, rather, rose slowly. In these cases, the pH of the mixture was gradually lowered because of the organic acids resulting from the Cannizzaro reaction.

With regard to the saccharide formation, trioses may be produced at the early stage of the second step, followed by the additional formation of tetroses at the minimum ORP point, and then higher saccharides are accumulated up to the maximum ORP point, as may be seen from the paperchromatographic analysis of aliquots.[13]

The UV spectra data with samples withdrawn intermittently during the course of the reaction are shown in Table 1. Some absorption maximum at 290 nm is first observed at T_{min}, and the amount of optical absorption continues to increase until T_{max}. Immediately after the yellowing point (T_{max}), λ_{max} is shifted beyond the wavelength of 300 nm. The substance with the λ_{max} value of 290 nm may be considered to be an intermediate produced during the induction period and may play some role in the subsequent step of sugar formation. However, the substance has not yet been successfully isolated, and its nature remains to be elucidated. In view of the above facts, emphasis may be placed on the utility of ORP measurements in the formose reaction. Although there may not be completely satisfactory arguments for the observed ORP changes, it should be noted that some important features of the formose reaction, such as the initiation and the end of the reaction, can be characterized by means of the ORP curve; this is worthy of future investigation. For example, the visual method (yellowing point), which has been employed for obtaining the highest yield of saccharides, might better be placed by ORP measurements because of some disadvantages with the operation and accuracy of the former method.

In conclusion, the ORP-determination method might make some contributions to future studies of the formose reaction in searching for the optimum reaction conditions and for active catalysts; moreover, it might well be used in technological development.

References

1) A. Butlerow, *C. R. Acad. Sci. Paris*, **53**, 145 (1861); *Ann.*, **120**, 295 (1861).
2) K. Runge and R. Mayer, *Ann.*, **707**, 161 (1967).
3) T. Mizuno, T. Mori, N. Shiomi, and H. Nakatsuji, *J. Agr. Chem. Soc. Japan*, **44**, 324 (1970).
4) J. A. Balezin and E. K. Surykina, *Zh. Prikl. Khim.*, **39**, 1826 (1966).
5) E. Pfeil and G. Schroth, *Chem. Ber.*, **85**, 293 (1952).
6) A. H. Weiss, R. Lapierre, and J. Shapira, *J. Catal.*, **16**, 332 (1970).
7) A. H. Weiss and H. Tambawala, *ibid.*, **26**, 388 (1972).
8) A. H. Weiss and J. Shapira, *J. Hydrocarbon Process.*, **49**, 119 (1970).
9) A. H. Weiss and T. John, *J. Catal.*, **32**, 216 (1974).
10) K. Fujino, J. Kobayashi, and I. Higuchi, *Nippon Kagaku Kaishi*, **1972**, 2287; **1972**, 2292.
11) T. Nawano, *Water Purification and Liquid Wastes Treatment*, **13**, 25 (1972).
12) S. Huenig and H. Steinmetzer, *Tetrahedron*, **1972**, 4835.

13) T. Matsuura, Y. Shigemasa, and C. Sakazawa, *Chem. Lett.*, **1974**, 713.
14) C. E. Bricker and H. R. Johnson, *Ind. Eng. Chem.*, **17**, 400 (1945); M. Lambert and A. C. Neish, *Can. J. Research*, **28B**, 83 (1950).
15) M. Bubois, K. A. Gilles, J. K. Hamilton, P. A. Rebers, and F. Smith, *Anal. Chem.*, **28**, 350 (1956).
16) JIS, K-0102, p. 76 (1971).
17) H. Schmalfuss, *Biochem. Z.*, **185**, 70 (1927).
18) A. Kusin, *Chem. Ber.*, **68**, 619 (1935).

A Novel Preparation of Enamine Phosphonates from Ketene *O,N*-, *S,N*-, and *N,N*-Acetals with Diethyl Phosphite

Masahiro FUKUDA, Kazuhito KAN, Yoshiki OKAMOTO, and Hiroshi SAKURAI

The Institute of Scientific and Industrial Research, Osaka University, Yamada-kami, Suita-shi, Osaka **565**

(Received January 22, 1975)

1-Dimethylamino-1-methoxy-1-alkenes (ketene *O,N*-acetals), 1-dimethylamino-1-ethylthio-1-alkenes (ketene *S,N*-acetals) and 1,1-bis(dimethylamino)ethylene (ketene *N,N*-acetal) reacted with diethyl phosphite to give the corresponding (*E*)-diethyl 1-dimethylamino-1-alkenylphosphonates. Although ketene diethylacetal (ketene *O,O*-acetal) reacted with diethyl phosphite to give diethyl 1,1-diethoxy-1-ethylphosphonate, 1,1-bis(ethylthio)-1-alkenes (ketene *S,S*-acetals) did not react with diethyl phosphite.

Enamine phosphonates have been synthesized by Horner's olefination method of tetraethyl dimethylaminomethylenediphosphonate with aldehydes,[1] and also by addition of diethyl phosphite to ynamines.[2] In this paper we wish to report a new method of preparation of enamine phosphonates by the reaction of ketene *O,N*-, *S,N*-, and *N,N*-acetals with diethyl phosphite. The method has the following adventages over the methods described above. The reaction proceeds smoothly under mild conditions, and the procedure is quite simple.

Results and Discussion

Ketene *O,N*- (Ia—c), *S,N*- (IIa—c), and *N,N*-acetals (III) reacted exothermally with diethyl phosphite at room temperature to give the corresponding enamine phosphonates (Va—c) in 50—80% yields (Table 1), according to the following scheme.

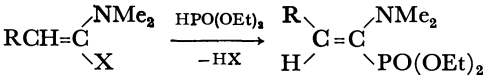

(1)

Ia R=H X=OMe
b R=Me X=OMe
c R=Et X=OMe
IIa R=H X=SEt
b R=Me X=SEt
c R=Et X=SEt
III R=H X=NMe_2

Va R=H
b R=Me
c R=Et

The structures of Va—c were identified by elemental analysis and NMR, mass, and IR spectral data. NMR spectra indicate that the enamine phosphonates obtained by this method are only *E*-isomer. The PCCH coupling constant of Vb and Vc was observed to be 13.5 Hz, which is the same as that reported by Schindler and Plöger.[2a]

TABLE 1. ENAMINE PHOSPHONATES FROM KETENE O,N-, S,N-, AND N,N- ACETALS WITH DIETHYL PHOSPHITE

Ketene Acetal	Product	Bp (°C)/ mmHg	Yield (%)
Ia(R=H, X=OMe)	Va(R=H)	92—94/1	75
Ib(R=Me, X=OMe)	Vb(R=Me)	114—115/5	58
Ic(R=Et, X=OMe)	Vc(R=Et)	116—123/6	47
IIa(R=H, X=SEt)	Va(R=H)		54
IIb(R=Me, X=SEt)	Vb(R=Me)		77
IIc(R=Et, X=SEt)	Vc(R=Et)		81
III(R=H, X=NMe_2)	Va(R=H)		55

The reaction was carried out without solvent at 60—80 °C for 0.5—1 hr.

Since the compounds (I, II, and III) are the analog of enamine or ketene acetal, it is expected that β-carbon of I, II, and III would exhibit a strong nucleophilic character due to the conjugation of the double bond with electron donor groups.[3] Thus, it seems reasonable to speculate that an intermediate(IV) was formed by addition of diethyl phosphite to the C=C double bond of I, II, or III, although our attempt to isolate IV was unsuccessful. Enamine phosphonate (V) would be produced immediately by the elimination of HX from IV.

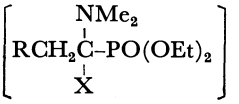

(IV)

It was found that the adduct (VI) derived from *N,N*-dialkylacetamide and dimethyl sulfate reacted with diethyl phosphite to give VII in 30—40% yields. In this case also, the intermediate (IV) would be formed and undergo elimination of methanol *in situ* to give VII.

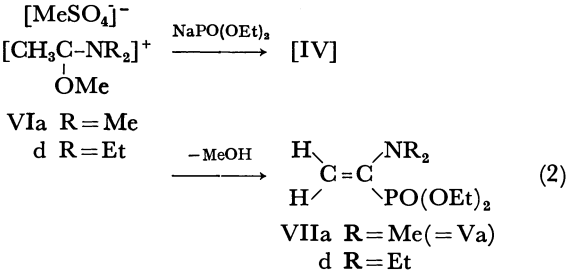

(2)

VIIa R=Me(=Va)
d R=Et

It is noteworthy that *N*-methylpyrrolidone diethylacetal (VIII) reacted with an excess diethyl phosphite to give the corresponding enamine phosphonate (IX).

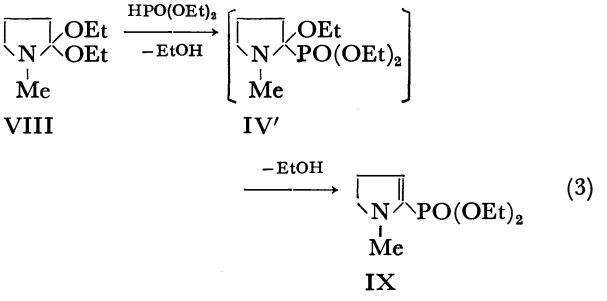

(3)

The reaction process can be explained by considering the intermediate (IV') which will rapidly loose ethanol *in*

situ and give IX in 60% yield. The product (IX) obtained did not react with another diethyl phosphite, and the excess diethyl phosphite was recovered by distillation *in vacuo*.

In the case of ketene *O,O*-acetal (X), an addition reaction occurred at room temperature. One mole of diethyl phosphite reacted with one mole of X to give diethyl 1,1-diethoxy-1-ethylphosphonate (XI). The structure of XI was confirmed by its NMR spectrum.

$$\underset{\text{X}}{CH_2{=}C(OEt)_2} \xrightarrow{HPO(OEt)_2} \underset{\text{XI}}{CH_3C(OEt)_2PO(OEt)_2} \quad (4)$$

This seems to be the first example of diethyl phosphite being added to the activated unsaturated system in the absence of a base or free radical initiator.[4] The compound (XI) remained unchanged by refluxing over metallic sodium for 3 hr.

The contribution of dialkylamino group to the β-elimination of HX from the intermediate (IV) might be of great importance.

$$[RCH_2\text{-}\overset{\overset{\delta+}{\curvearrowleft}NR_2}{\underset{\underset{\delta-}{\curvearrowleft}X}{C}}\text{-}PO(OEt)_2] \qquad \text{IV}$$

Vinyl ethers reacted with diethyl phosphite to give aldehydes, no addition products of vinyl ether and diethyl phosphite being obtained.[5]

Thus, ketene *N,N*-, *O,N*-, and *S,N*-acetals react with diethyl phosphite to form the intermediate (IV, IV') and loose HX from IV or IV'. Ketene *O,O*-acetal is led only to the formation of 1:1 adduct (XI). Ketene *S,S*-acetals did not react with diethyl phosphite even under base-catalyzed conditions.

The nucleophilicity of β-carbon of ketene *N,N*-, *O,N*-, *S,N*-, and *O,O*-acetals, vinyl ethers, and ketene *S,S*-acetals decreases in the order given in literature.[3] The order is essentially the same as that obtained for this experiment on the reactivities of these compounds toward diethyl phosphite.

These enamine phosphonates (V, VII, and IX) have good thermal stabilities, but readily react with moisture to decompose to acylphosphonates. The acylphosphonates are further hydrolyzed to acids and diethyl phosphite.[1]

Experimental

All the boiling points are uncorrected. The NMR spectra were obtained at 100 MHz on a JNM-TS-100 spectrometer, with TMS as an internal reference in deuteriochloroform. The mass spectra were obtained on a Hitachi RMU-6 or RMU-7 spectrometer with an indirect inlet. The gas chromatographic analysis were carried out using a Shimadzu GC-3AF on a 1 m×3 mmϕ column packed with 5% SE-30 on Cellite.

Preparation of N,N-*Dialkylacetamide–Dimethyl Sulfate-Adduct (VI).* *N,N*-Dimethylacetamide and dimethyl sulfate-adduct (VIa) was prepared from *N,N*-dimethylacetamide and dimethyl sulfate according to the method of Bredereck *et al.*[6] Unreacted starting material was removed by extraction with dry ether. *N,N*-Diethylacetamide–dimethyl sulfate-adduct (VId) was prepared from the corresponding amide and dimethyl sulfate, in a similar manner.

Preparation of Ketene O,N-*Acetals (I).* 1-Dimethylamino-1-methoxyethylene (Ia) was prepared from IVa and sodium methoxide in methanol by the method of Bredereck *et al.*,[7] except that the mixture of Ia and *N,N*-dimethylacetamide dimethyl acetal was refluxed over sodium instead of calcium in order to purify the product (Ia). Yield 81%, bp 104 °C. (lit,[7] bp 104—105 °C). 1-Dimethylamino-1-methoxy-1-propylene (Ib) was prepared from *N,N*-dimethylpropionamide-dimethyl sulfate-adduct and sodium methoxide. The product, bp 117—118 °C, was obtained in 34% yield. (lit,[7] bp 117—120 °C). In a similar manner, 1-dimethylamino-1-methoxy-1-butene (Ic) was obtained in 30% yield, bp 128—136 °C.

Preparation of Ketene S,N-*Acetals (II).* 1-Dimethylamino-1-ethylthioethylene (IIa) was prepared from *N,N*-dimethyl-*S*-ethylthioacetamidium iodide and sodium ethylmercaptide in dry ether by the method of Mukaiyama *et al.*[8] The product was obtained in 72% yield, bp 58—59 °C/20 mmHg. (lit,[8] bp 58—59 °C/21 mmHg). In a similar manner, compounds IIb and IIc were obtained, respectively. 1-Dimethylamino-1-ethylthio-1-propylene (IIb); yield 58%, bp 68—71 °C/24 mmHg. 1-Dimethylamino-1-ethylthio-1-butene (IIc); yield 85%, bp 70—71 °C/17 mmHg. The purity of these compounds was confirmed by gas chromatography.

Preparation of Ketene N,N-*Acetal (III).* This was prepared from tetramethylacetamidinium methyl sulfate and sodium hydride by the method of Bredereck *et al.*[7] Yield 11%, bp 115—118 °C. (lit,[7] bp 115 °C).

Preparation of N-*Methylpyrrolidone Diethylacetal (VIII).* This acetal was prepared from *N*-methylpyrrolidone–dimethyl sulfate-adduct and sodium ethoxide by the method described above.[7] Yield 46%, bp 67 °C/12 mmHg. (lit,[7] bp 57—58 °C/10 mmHg). This acetal did not loose one mole of ethanol, even under reflux over metallic sodium for several hours.

Preparation of Ketene S,S-*Acetals.* These were prepared by pyrolysis of ethyl orthothioester in the presence of potassium bisulfate by the method of Volger and Arens.[9] 1,1-Bis(ethylthio)ethylene was obtained in 43% yield, bp 75 °C/12 mmHg. (lit,[9] bp 80—81 °C/17 mmHg). 1,1-Bis(ethylthio)-1-propylene was obtained in 70% yield, bp 79 °C/12 mmHg. (lit,[9] bp 60—60.2 °C/4 mmHg).

Preparation of Ketene O,O-*Acetal (X).* This was obtained from α-bromoacetaldehyde diethyl acetal by treatment with potassium *t*-butoxide.[10] Yield 40%, bp 82—84 °C/200 mmHg. (lit,[10] bp 83—86 °C/200 mmHg).

Reaction of Ketene O,N-*Acetals (I) with Diethyl Phosphite.* To 30 g (217 mmol) of diethyl phosphite in a flask equipped with a reflux condenser was added 22 g (106 mmol) of Ia at room temperature. An exothermic reaction took place and the temperature was raised to 60—80 °C. The methanol produced as the by-product was refluxed. The mixture was kept at 60—80 °C for 0.5 hr. After removal of the alcohol by means of an aspirator, the residue was distilled and purified by redistillation *in vacuo*. This was confirmed to be (*E*)-diethyl 1-dimethylaminovinylphosphonate (Va). Yield 34 g (75.4%), bp 92—94 °C/1 mmHg. IR; 1250 cm^{-1} (P=O). Mass; *m/e* (relative intensity) 207 (M^+, 17.5) 178 (16.3) 150 (17.5) 71 (93.8) 70 (100). NMR; δ 1.32 (t, 6H, $-OCH_2\underline{CH_3}$) 2.72 (s, 6H, $-NMe_2$) 3.65 (d, 1H, $^{H=}{}_P$, J_{PCCH}=11.2 Hz) 4.03 (d-q, 4H, $-O\underline{CH_2}CH_3$) 4.75 (d, 1H, $^{H=}{}_P$, J_{PCCH}=15.8 Hz). Found: C, 46.42; H, 8.66; N, 6.67%. Calcd for $C_8H_{18}NPO_3$: C, 46.33; H, 8.76; N, 6.78%.

In a similar manner, Ib and Ic reacted with diethyl phos-

Restricted Rotation Involving the Tetrahedral Carbon. XV. Restricted Rotation about a C_{sp^3}–C_{sp^2} Bond in 9-Aryltriptycene Derivatives[1)]

Mikio NAKAMURA and Michinori ŌKI*

Department of Chemistry, Faculty of Science, The University of Tokyo, Tokyo 113

(Received January 25, 1975)

A series of 9-aryltriptycene derivatives have been prepared and their internal rotation about the C_{Ar}–C_9 bond has been examined by DNMR technique. The PMR behavior of these compounds is best interpreted by assuming a back and forth rotation rather than a full rotation. The barriers to rotation of compounds with one substituted benzo group have been found to be in the range 13—15 kcal/mol, whereas those with two substituted benzo bridges are lower than 9 kcal/mol. The low barrier of these compounds relative to 9-alkyltriptycenes is attributed to the rise in energy of the ground state. The stable conformation of the 9-aryltriptycenes is also discussed.

Barriers to rotation of alkyl groups are extraordinarily high when the alkyl group is bonded to the bridge head carbon of the triptycene skeleton. The barrier to rotation of the *t*-alkyl group in compound **1** is so high that the rotational isomers can be isolated as stable entities at room temperature.[2)] Even the methyl group in compound **2** has a high barrier to rotation showing clear AB_2 type signals below −70 °C.[3)]

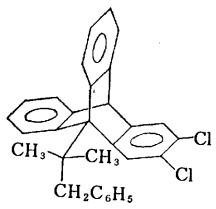

1

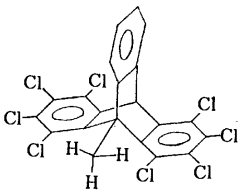

2

These findings have stimulated us to study whether the rotational barriers are also high when an aryl group is bonded to the bridge head carbon of the triptycene molecule. Several 9-*o*-tolyl- and 9-*o*-anisyl-triptycene derivatives (**3**—**10**) were synthesized. The methyl or the methoxy group in the aryl ring is introduced to identify the isomers, if possible, by the NMR technique, because the methyl should show signals at different chemical shift when it is located at different environments and the life time is long enogh to be detected.

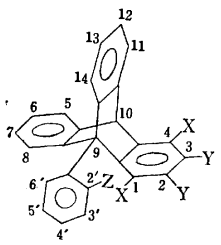

	X	Y	Z
3	H	H	CH_3
4	F	F	CH_3
5	Cl	Cl	CH_3
6	CH_3	H	CH_3
7	Cl	Cl	OCH_3
8	CH_3	H	OCH_3

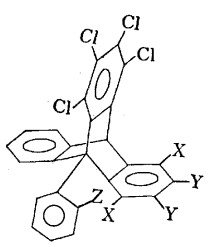

9	Cl	Cl	CH_3
10	CH_3	H	OCH_3

The purpose of this paper is to describe the results of the study on the barrier of these compounds and to discuss the possible rate process. Various factors which govern the barrier heights to rotation are also discussed.

Results and Discussion

Rate Process and Conformation. The PMR spectrum of compound **4** at room temperature shows two methyl signals with an interval of 1.5 Hz at 60 MHz. The same interval was also observed for these signals at 100 MHz which indicates that the signal is split by coupling. Irradiation at the aromatic region produced no collapse of the signals. The coupling between the methyl protons and fluorine nucleus takes place in this compound at room temperature. PMR spectra of **4** at low temperature show little change from the spectrum obtained at room temperature except for the aromatic region (Fig. 1), both the chemical shift and coupling constant remaining almost constant. On the other hand, two distinct signals are found at low tem-

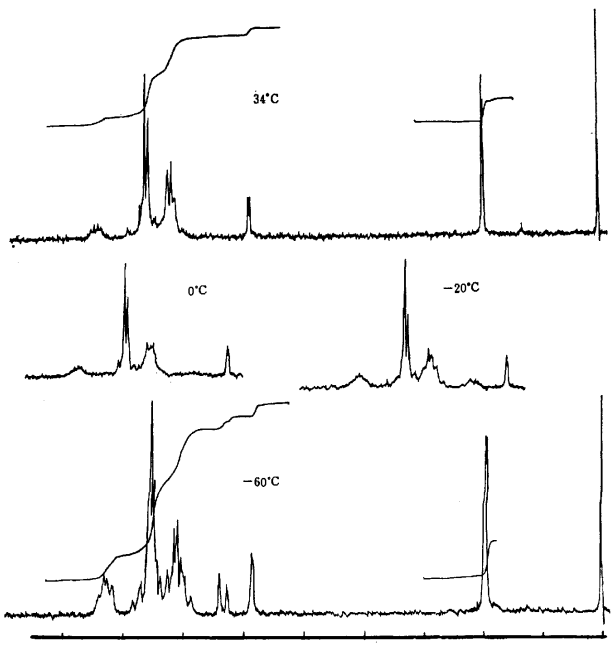

Fig. 1. Temperature dependent PMR spectra of compound **4**.

perature apart from the main aromatic signals, two peaks at δ 6.17 and a multiplet at δ *ca.* 8.1, each corresponding to 1 proton. Since there is a multiplet peak at δ *ca.* 8.1 at room temperature, the latter signal now corresponds to 2 protons. The former two peaks seem to be the A (or B) part of an AB quartet from the shape of the signals and coalescence behavior. The coupling constant is 7.5 Hz.

The peak at δ *ca.* 8.1 present in the spectrum at room temperature is assigned to the 6′-H for the following reasons. The PMR spectrum of **11** shows a broad singlet with the intensity of 2 protons at δ 7.77. This signal is most reasonably assigned to the protons at 2′ and 6′ positions. The assignment is confirmed by the strong intensification of the signal upon irradiation of the methyl signal. Jackman and Sternhell[4] stated that, in benzene derivatives, a methyl group causes a 0.17, 0.09 and 0.17 ppm upfield shift of the *ortho*, *meta* and *para* protons respectively, and a methoxy group causes a 0.1 ppm upfield shift of the *meta* protons. Taking these substituent effect into consideration, we can calculate the chemical shift of the 6′-H of compound **4** to be δ 8.1, which is in good agreement with the observed chemical shift.

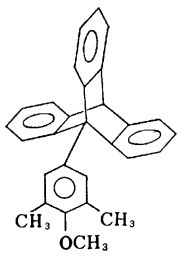

11

The PMR spectrum of compound **4** was examined at 136 °C, but no change was observed from that at room temperature. Thus the rate process which occurs in this molecule should conform to the fact that the methyl signals are not affected by temperature although the rotation in question is fast on the NMR time scale at room temperature and is slow at low temperatures.

We assume that the ground state is the conformation in which the aryl group does not eclipse the benzo group, although there are some examples that the ground state is the conformation in which one of the substituents in the alkyl group eclipses the phenyl ring.[5] We believe this assumption is reasonable because the benzo is a large group. Two mechanisms may be considered to account for the above findings.

The first mechanism comprises a partial rotation shown in Scheme 1. In this process, the transition state of rotation is conformation (**13**) in which 6′-H passes over the substituent X. The ground state shown by **12** and **12′** are mirror images of each other and the

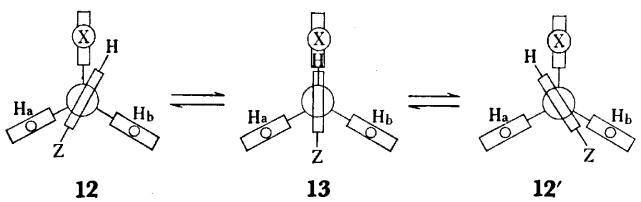

12 **13** **12′**

Scheme 1.

energy level should be the same. The locations of the Z group (methyl or methoxy) in **12** and **12′** are identical and the average of the chemical shifts of **12** and **12′** is the same as that of either **12** or **12′**. On the other hand, the *peri*-protons (H_a and H_b) experience different chemical shifts when the rotation is slow: in **12**, H_b must give a signal at a high magnetic field and H_a at a low field due to the anisotropy of the 9-aryl group while in **12′** the reverse is the case. When the rotation is fast, the chemical shifts of these protons are averaged out. In this mechanism, the barrier for the Z group to pass over the benzo group (H_a or H_b) must be very high, since otherwise it would be impossible to account for the small spectral change of the methyl group at various temperatures. This mechanism is called mechanism A in the later discussion.

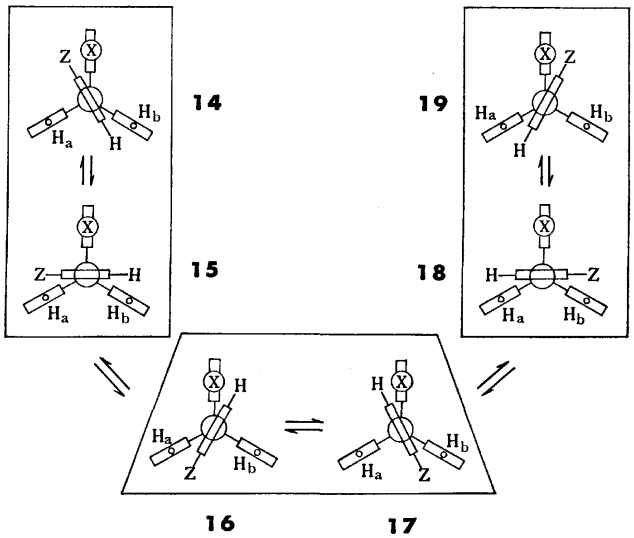

Scheme 2.

Another possible mechanism is shown in scheme 2. The barrier by which the 6′-H group passes over the unsubstituted benzo group is assumed to be so low that the corresponding motion is not detected by the present technique. Thus we assume that conformations **14** and **15** are not distinguishable even at low temperatures. A combination of **14** and **19** and that of **15** and **18** constitute pairs of *dl*-isomers. The averaged spectrum of **14** and **15** and that of **18** and **19** should then be identical. For an exchange of **14**—**15** and **18**—**19**, two possible ways may be considered, one which has a conformation in which Z eclipses the substituted benzo group as a transition state, and the other which occurs *via* **16** and **17**. Since the transition state of the former process, formed by eclipsing Z with the substituted benzo bridge, would be of too high an energy to pass over, it is reasonable to assume that the latter way is more plausible.

The substituent Z in a conformation of **14** and **15** will be in an identical magnetic environment with that in **18**—**19**, whereas the magnetic environment of Z in **16** and **17** is different. Thus in order to explain the small change in the methyl region of the PMR spectra, it is necessary to assume that conformations **16** and **17** are so unstable that their populations can be neglected or that the chemical shifts of the methyl protons in **16** and

17 coincide with those in **14**—**15** and **18**—**19**. These assumptions are referred to as mechanisms B and B′ respectively in the following discussions.

The possibility of these three cases can be discussed on experimental evidence. The first is the coupling of the methyl protons with the fluorine atom at a benzo bridge in compound **4**. If the coupling occurs through bonds, the number of the intervening bonds is seven including an sp^3-hybridized carbon. No such example has been found, though there are some examples of coupling through more than seven bonds in some conjugated systems.[6] On the other hand, the through space coupling of protons with a fluorine atom is well-known,[7] if they are close to each other in space. Thus the methyl-fluorine coupling is more easily explained by assuming mechanism B or B′.

The low temperature PMR spectra of compound **5** showed almost the same change as those of **4**. New signals appeared at δ 6.18 and 8.2 at low temperature, each corresponding to 1 proton, whereas the methyl signal at δ 1.77 showed little change. The free energy of activation for rotation was roughly estimated to be 14.5 kcal/mol, that of compound **4** being 13.2 kcal/mol. This small rise in the free energy of activation by going from the fluoro compound **4** to the chloro compound **5** again favors mechanism B or B′. If mechanism A were the case, the barrier would have been raised to a considerable extent by the substituent change. The PMR spectrum of **3** at low temperature shows one proton at a low field (δ 7.9) but no signal at a high field of the aromatic region. If mechanism A is assumed in which the barrier is the eclipsing of 6′-H with one of the benzo bridges, conformations **20** and **21** correspond to the ground state. H_a will give a signal at a low field, whereas H_b and H_c become non-equivalent, when the rotation is frozen. Thus there is no reason for a signal not to appear at a high field in mechanism A. On the other hand, mechanism B and B′ can explain the absence of a signal at a high field. Since mechanism B and B′ postulate that the barrier is the eclipsing of Z with one of the benzo groups and the exchange between **20** and **21** is fast, the signal of H_a at low temperature should appear at a low field, whereas those of H_b and H_c should appear at an average field. The averaged signal will be hidden by other aromatic signals.

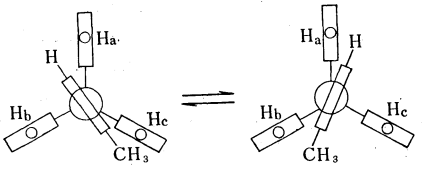

20 **21**

The PMR spectra of **11**, wflich has no methyl group at 2′ and 6′ positions, should be temperature dependent if mechanism A were the case, since the magnetic environment of H_b differs from that of H_c when the rotation is frozen. On the other hand, mechanism B and B′ predict that the signals of compound **11** will not be temperature dependent down to −90 °C because the transition state where the Ar-H eclipses the unsubstituted benzo group is of low energy. An experimental

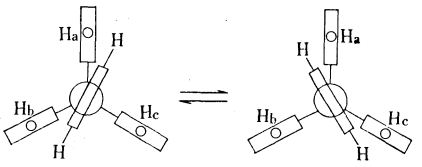

Compound **11** (Mechanism A).

fact that the spectra are independent on temperature down to −95 °C clearly supports mechanism B and B′.

All the experimental results favor mechanism B and B′, but a problem remains as to which of the two is more plausible. As regard this the fact that signals corresponding to one proton each appear at a low and a high field is of importance. Since the chemical shifts of *peri*-protons are mainly determined by the anisotropy effects of the aromatic ring, we must consider the stable conformation of the molecule.

In conformation **16**, the repulsive interaction between the substituent X and the Ar-H tends to widen the dihedral angle θ at the expense of the dihedral angle θ' in **16′**. The decrease in θ', however, necessarily increases the repulsive interaction between Z and the benzo bridge. Consequently, there will be a tendency that θ becomes small and θ' large. The result is that neither H_a nor H_b gives a signal at a high or a low field, even though the rotation is frozen. In the case where

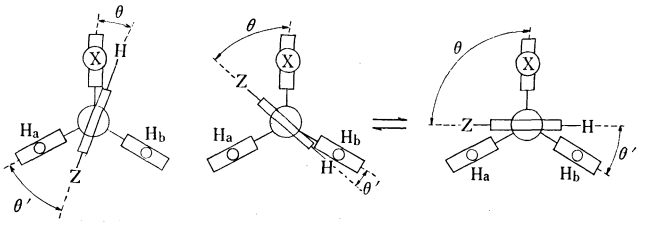

16′ **14′** **15′**

this barrier is small, the chemical shifts of H_a and H_b are averaged even at a low temperature. Thus the conformation **16** contradicts the experimental results. On the other hand, in conformation **14** the repulsive interaction between Z and X will tend to enlarge the dihedral angle θ and minimize the dihedral angle θ' in **14′**. In this conformation, H_a will give a signal at a high field and H_b at a low field. With the aid of conformation **15**, the large difference in the chemical shift between H_a and H_b cannot be explained, since these protons are located in almost the same magnetic environment with respect to aryl ring (see **15′**). Thus the appearance of signals at a low and a high field, each corresponding to one proton, is consistent with conformation **14** only. The above discusssion favors mechanism B over B′. Absence of conformations **16** and **17** seems strange, but the instability arises because of the repulsive force between X and Ar-H and that between Z and the benzo bridge.

Information on the dihedral angle θ is obtained from the large chemical shift difference between two *peri* protons, H_a and H_b (*ca.* 2.0 ppm for compounds **4**—**8**). Using the Johnson-Bovey diagram, we can calculate the difference to be *ca.* 1.8 ppm when the dihedral angle θ in **14′** is 60 °. Increasing the dihedral angle gives much smaller values.

Further evidence for the value of the dihedral angle is obtained from the rather large difference in chemical shifts (0.6 ppm) of two methyl groups at positions 1 and 4 in compounds **6** and **8**. Since it can be assumed that the methyl group at position 4 is not influenced by the 9-aryl group, signals at δ *ca.* 2.5* can be assigned to the 4-methyl group. This means that the anisotropy of the benzene ring causes a high field shift of the 1-methyl protons by *ca.* 0.5 ppm. Such a shift is possible only when θ is almost 60 °. When θ is below this, the chemical shift of 1-methyl protons becomes lower. When θ is almost 90 °, the chemical shift difference increases to the same extent as that of the methyl groups in compound **12**. In this compound the dihedral angle is predicted to be almost 90 ° from the dihedral angles of analogous biphenyls and the chemical shift difference amounts to as great as 0.9 ppm.

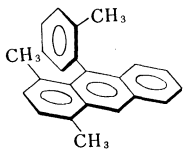

12

Conformation **14'** is also consistent with the through space coupling between 1-methyl and fluoro groups. Since the distance between these groups becomes large in other conformations, the coupling will be very small, if any.

The rationale for the stability of conformation **14** may be either or both of the following: a) there is attractive interaction between the methyl group and a halogen atom at a *peri* position, b) the repulsive interaction between the Ar-H and the substituent X and that between the methyl and the benzo bridge is large as was the case in conformations **16** and **17**. If the attractive interaction between the methyl and the halogen atom stabilizes conformation **14**, then the introduction of a repulsive group may cause the appearance of unstable conformations such as **16** and **17**. Thus compound **6** was prepared. However, the aromatic region of its PMR spectra is almost the same as that of other compounds at low temperatures: one proton at δ 6.20 and another at δ 8.1. Neither of the PMR spectra of **7** and **8** gave any sign of presence of conformations **16** and **17**. Thus the origin of instability of conformations **16** and **17** seems to be the steric effect.

Having found the unexpectedly low barrier to rotation in compounds **3**—**8**, we were interested in increasing the steric effect. Thus triptycene derivatives **9** and **10**, which have two benzo bridges with substituents, were prepared. Two points in the PMR spectra of these compounds at room temperature were found to differ from those with one substituted benzo group **4**—**8**. Namely, there is a proton which gives a signal at a considerably high field (δ 5.8), and the 6'-H does not give a signal at a low field. These characteristics are best interpreted by assuming conformations **22** and **23**, since H_c in these conformations should give signals at a high field. An alternative form **24** or **25** cannot explain the high field shift of H_c. The shift of 6'-H to the higher field should be attributed to the chloro group at *peri*-position. Since compound **9** has two benzo bridges with chloro groups, appearance of 6'-H of this compound at a high field supports this discussion. Although the chloro group has been known to shift the signals to lower field in alkyltriptycenes,[2] a different steric situation could cause the different effect. Absence of a signal due to 6'-H of compound **10** at a low field may be taken as an indication that the stable conformation of **10** is **22** which has 6'-H close to the chloro group.

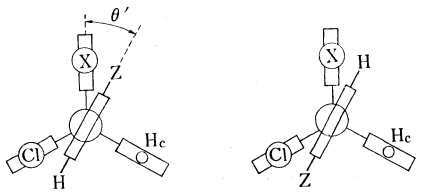

22 **23**

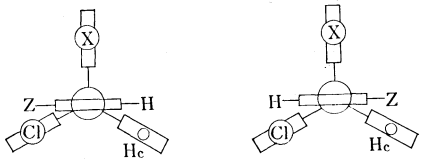

24 **25**

The chemical shifts of H_c in **9** and **10** are higher than those in **4**—**8** by *ca.* 0.3—0.4 ppm. If it is assumed that the main group which gives shielding to the H_c nucleus is the benzene ring, then H_c should be located just above the benzene ring of the 9-aryl group. This indicates that the dihedral angle θ' given in conformation **22** is close to 30 °. The small difference (0.07 ppm) in chemical shifts of 1- and 4-methyls of compound **10** also supports this conformation.

Barriers to Rotation. The temperature dependent behavior of the PMR spectra of 9-aryltriptycenes was a striking contrast to that of 9-alkyltriptycenes. The insensitiveness of the spectra at higher temperatures is possibly an indication of the frozen rotation of the aryl group and the temperature dependence of the spectra might be caused by freezing the motion of other parts of the molecule. In order to rule out this possibility, we undertook another experiment. The idea arose from the fact that the Diels-Alder reaction in making the triptycene skeleton is highly stereoselective and in the case of 9-*t*-alkyltriptycenes, it was possible to synthesize *dl* and *meso* forms separately.[2] If this technique is applied to the present case, the reaction of 9-*o*-tolylanthracene with tetrachlorobenzyne should give a different product from that obtained by the reaction between 1,2,3,4-tetrachloro-9-*o*-tolylanthracene and benzyne. An identical product, however, was obtained. Thus it is concluded that the rotation about C_{Ar}–C_9 bond in these compounds is fast at room temperature.

It was difficult to obtain the accurate values of rotational barriers, since the exchanging system contains 8

*) If compounds **6** and **8** only are taken into consideration, it is difficult to assign the signals since the other pair of signals appears also at δ 1.9. However, the data of compound **10** clearly suggest that the signal at δ 2.5 should be assigned to the methyl at position 4.

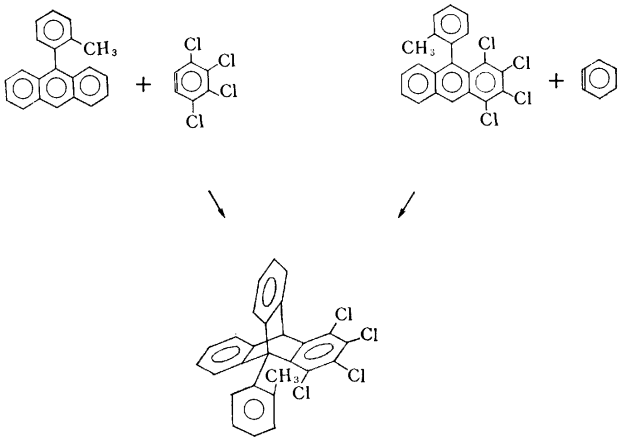

spins in these compounds. Fortunately, however, the signals of two protons at *peri*-positions, H_a and H_b, appear at a high and a low field. A rough estimation of the free energy of activation for internal rotation is possible by the usual method of coalescence temperature.[9] In Tables 1 and 2 chemical shift differences of H_a and H_b, coalescence temperatures and free energies of activation are listed.

TABLE 1. CHEMICAL SHIFT

	H_a	H_b	H_c	Z	X	6'-H
3	6.8—6.9	7.90	—	1.72	—	8.48
4	6.17	8.05	—	1.90	—	8.15
5	6.18	8.18	—	1.77	—	8.23
6	6.20	8.14	—	1.73	1.85 2.51	8.40
7	6.10	8.12	—	3.50	—	8.14
8	6.07	8.00	—	3.50	1.90 2.42	8.26
9	—	—	5.80	1.87	—	7.6—7.6
10	—	—	5.75	3.53	2.42 2.49	7.6

TABLE 2. ACTIVATION FREE ENERGY

	$\Delta\nu$ (Hz)	T_c (°C)	ΔG_c^* (kcal/mol)
3	60—66	—	—
4	113	5	13.2
5	120	34	14.6
6	116	10	13.4
7	121	40	14.8
8	116	0	12.9
9	—	—	—
10	—	−90>	9>

The free energy of activation is between 13 and 15 kcal/mol. However, we see that replacing a chloro group with a methyl group decreases the free energy of activation by more than 1 kcal/mol. Although the error involved in estimation of the energy may be large, it is evident that the coalescence temperatures of the methyl compounds **6** and **8** are lower than those of the chloro compounds **5** and **7**, whereas the chemical shift differences of H_a and H_b are almost the same. We have pointed out that the main factor governing the energy of the transition state for the rotation is the repulsive interaction between the aryl-substituent and the *peri*-proton. Thus the energy of the transition state should not vary too much from compound to compound. The reduction of the barrier height should be attributed to the raise of the ground state. In the ground state conformations **14** or **19**, the repulsive interaction between Z and X increases when X becomes larger, whereas this strain cannot be relieved by changing the dihedral angle, since the change results in increase of the interaction between Ar-H and H_a or H_b. Thus the ground state of the methyl compounds should be higher than that of the chloro compounds. This type of rise in ground state levels is also observed in compounds **9** and **10**. Since they have two *peri*-substituents, the ground state should be raised considerably. This is reflected in the low coalescence temperature of the PMR spectra. PMR spectra of **9** showed little change whereas that of **10** showed a little temperature dependence when the temperature is lowered to −90 °C. The methoxy signal broadened to show a half band width of 6 Hz at −90 °C. If we assume that the chemical shift difference of the methoxy group in conformations **22** and **23** is 10 Hz and the coalescence temperature is −100 °C, the barrier becomes 8.8 kcal/mol. We believe this is the maximum value for the barrier, since it is not likely that the chemical shift difference is less.

In conclusion, the 9-aryltriptycene studied here shows a lower barrier relative to 9-alkyltriptycenes. The highest barrier obtained corresponds to that of a 9-methyltriptycene derivative. Since the energy level of the transition state should be very high in 9-aryltriptycenes, this striking decrease in barrier height must be attributed to the rise of the ground state energy. Because of the required geometry of the 9-aryl group and the triptycene skeleton, the repulsive interaction between these groups seems to be severe in these compounds, raising the ground state.

Experimental

Syntheses. *9-o-Tolylanthracene*: To a vigorously stirred tetrahydrofuran solution of *o*-tolylmagnesium iodide, prepared from 21.8 g. (0.1 mol) of *o*-iodotoluene and 2.4 g (0.1 mol) of magnesium, was added 16.0 g (0.08 mol) of anthrone at 0 °C. The reaction mixture was stirred for 3 hr at room temperature and was then heated with stirring for 1 hr, cooled, and treated with concentrated hydrochloric acid. The organic layer was washed with aqueous sodium bicarbonate and dried over sodium sulfate. After evaporation of the solvent, the product was purified by chromatography on alumina. Elution with hexane gave a pure product, mp 126 °C (lit,[10] 125—126 °C), in 85% yield based on anthrone.

9-o-Anisylanthracene, mp 177—178 °C, was similarly prepared by treating *o*-anisylmagnesium iodide in tetrahydrofuran with anthrone. The yield was 82% based on anthrone. Found: C, 88.89; H, 5.50%. Calcd for $C_{21}H_{16}O$: C, 88.70; H, 5.67%. NMR ($CDCl_3$, δ) 3.52 (3H, s), 6.9—7.7 (12H, m), 8.38 (1H, s).

9-(4-methoxy-3,5-xylyl)anthracene, mp 178 °C, was similarly prepared by treating 4-methoxy-3,5-xylylmagnesium bromide in tetrahydrofuran with anthrone. The yield was 80% based on anthrone. Found: C, 88.54; H, 6.63%. Calcd for $C_{23}H_{20}O$: C, 88.42; H, 6.45%. NMR ($CDCl_3$, δ): 2.35 (6H, s), 3.82 (3H, s), 6.9—8.1 (10H, m), 8.43 (1H, s).

1,2,3,4-Tetrachloro-9-o-tolylanthracene. To a vigorously

stirred tetrahydrofuran solution of *o*-tolylmagnesium iodide, prepared from 21.8 g. (0.1 mol) of *o*-iodotoluene and 2.4 g (0.1 mol) of magnesium, was added a solution of 3 g (0.09 mol) of 1,2,3,4-tetrachloroanthrone[11] in 200 ml of benzene at room temperature over a period of 2 hr. The reaction mixture was heated for 1 hr and then cooled to 0 °C. About 10 ml (0.22 mol) of condensed chlorine was trapped at −70 °C and then introduced into the reaction vessel.** After stirring for 1 hr concentrated hydrochloric acid was added. Treatment of the product as above gave yellow crystals, mp 170—171 °C. The yield was 45% based on the anthrone. Found: C, 62.27; H, 2.91; Cl, 34.73%. Calcd for $C_{21}H_{12}Cl_4$: C, 62.10; H, 2.98; Cl, 34.92%. NMR ($CDCl_3$, δ): 1.86 (3H, s), 6.9—8.2 (8H, m), 9.0 (1H, s).

1,4-Dimethyl-9-o-tolylanthracene (**12**) was prepared by treating *o*-tolylmagnesium iodide with 1,4-dimethylanthrone[12] in tetrahydrofuran. This compound was obtained as a liquid after chromatography on alumina. The yield was 75%. Found: C, 93.40; H, 6.50%. Calcd for $C_{23}H_{20}$: C, 93.20; H, 6.80%. NMR ($CDCl_3$, δ): 1.89 (3H, s), 1.92 (3H, s), 2.80 (3H, s), 6.8—7.6 (9H, m), 7.8—8.1 (1H, m), 8.50 (1H, s).

1,4-Dimethyl-9-o-anisylanthracene, mp 135—136 °C, was prepared by treating *o*-anisylmagnesium iodide with 1,4-dimethylanthrone in tetrahydrofuran. The yield was 72%. Found: C, 88.72; H, 6.48%. Calcd for $C_{23}H_{20}O$: C, 88.42; H, 6.45%. NMR ($CDCl_3$, δ): 2.02 (3H, s), 2.79 (3H, s), 3.62 (3H, s), 6.9—7.7 (9H, m), 7.9—8.1 (1H, m), 8.58 (1H, s).

9-o-Tolyltriptycene (3). To a vigorously stirred refluxing solution of 1 g (0.0037 mol) of 9-*o*-tolylanthracene and 1 ml (0.009 mol) of butyl nitrite in 20 ml of methylene chloride was added 0.7 g (0.005 mol) of anthranilic acid in 5 ml of tetrahydrofuran over a period of 2 hr. The reaction mixture was refluxed for 2 hr, and evaporated *in vacuo* after cooling. The residue was taken up in ether, washed with aqueous sodium bicarbonate and dried over sodium sulfate. After evaporation, the product was purified by chromatography on alumina. Elution with hexane followed by recrystallization from benzene–hexane gave pure product, mp 249.5—250.5 °C, in 57% yield. Found: C, 94.29; H, 5.84%. Calcd for $C_{27}H_{20}$: C, 94.15; H, 5.85%. NMR ($CDCl_3$, δ): 1.72 (3H, s), 5.37 (1H, s), 6.7—7.6 (15H, m), 8.48 (1H, m).

1,2,3,4-Tetrafluoro-9-o-tolyltriptycene (**4**) was similarly prepared by treating 9-*o*-tolylanthracene and butyl nitrite in methylene chloride with tetrafluoroanthranilic acid[13] in purified acetone. The reaction mixture was purified by chromatography on alumina. Recrystallization from ethanol gave pure material, mp 163—164 °C. The yield was 48%. Found: C, 77.49; H, 4.22; F, 18.41%. Calcd for $C_{27}H_{16}F_4$: C, 77.28; H, 3.84; F, 18.88%. NMR ($CDCl_3$, δ): 1.90 (3H, d), 5.80 (1H, d), 6.8—7.7 (11H, m), 8.15 (1H, m).

1,2,3,4-Tetrachloro-9-o-tolyltriptycene (**5**), mp 288.5—289.0 °C, was prepared similarly by treating 9-*o*-tolylanthracene and butyl nitrite in methylene chloride with tetrachloroanthranilic acid[14] in purified acetone. The yield was 65%. Found: C, 67.13; H, 3 .08;Cl, 29.51%. Calcd for $C_{27}H_{16}Cl_4$; C, 67.25: H, 3.34; Cl, 29.41%. NMR ($CDCl_3$, δ): 1.77 (3H, s), 5.97 (1H, s), 6.7—7.7 (11H, m), 8.23 (1H, m).

1,4-Dimethyl-9-o-tolyltriptycene (**6**), mp 208—209 °C, was prepared by treating 1,4-dimethyl-9-*o*-tolylanthracene and butyl nitrite in methylene chloride with anthranilic acid in purified acetone. The yield was 72%. Found: C, 93.69; H, 6.26%. Calcd for $C_{29}H_{24}$: C, 93.51; H, 6.49%. NMR ($CDCl_3$, δ): 1.73 (3H, s), 1.85 (3H, s), 2.51 (3H, s), 5.57 (1H, s), 6.55, 6.64 (2H, AB quartet, J=8 Hz), 6.8—7.6 (11H, m), 8.40 (1H, m).

1,2,3,4-Tetrachloro-9-o-anisyltriptycene (**7**), mp 210—211 °C, was prepared similarly by treating 9-*o*-anisylanthracene with tetrachloroanthranilic acid in purified acetone. The yield was 57%. Found: C, 64.80; H, 3.31; Cl, 28.72%. Calcd for $C_{27}H_{16}Cl_4O$: C, 65.09; H, 3.24; Cl, 28.46%. NMR ($CDCl_3$, δ): 3.50 (3H, s), 5.95 (1H, s), 6.6—7.8 (11H, m), 8.14 (1H, m).

1,4-Dimethyl-9-o-anisyltriptycene (**8**): mp 216—217 °C, was similarly prepared by treating 1,4-dimethyl-9-*o*-anisylanthracene and butyl nitrite in dimethoxyethane with anthranilic acid in purified acetone. The yield was 23%. Found: C, 89.99; H, 6.20%. Calcd for $C_{29}H_{24}O$: C, 89.65; H, 6.23%. NMR ($CDCl_3$, δ): 1.90 (3H, s); 2.42 (3H, s), 3.50 (3H, s), 5.59 (1H, s), 6.53, 6.60 (2H, AB quartet, J=8 Hz), 6.8—7.7 (11H, m) 8.26 (1H, m).

1,2,3,4,5,6,7,8-Octachloro-9-o-tolyltriptycene (**9**), mp>300 °C, was prepared by treating 1,2,3,4-tetrachloro-9-*o*-tolylanthracene and butyl nitrite in methylene chloride with tetrachloroanthranilic acid in purified acetone. The yield was 35%. NMR ($CDCl_3$, δ): 1.87 (3H, s), 5.80 (1H, d, J=8 Hz), 6.71 (1H, s), 6.8—7.7 (7H, m).

1,4-Dimethyl-5,6,7,8-tetrachloro-9-o-anisyltriptycene (**10**), mp >300 °C, was prepared from 1,4-dimethyl-9-*o*-anisylanthracene, butyl nitrite, and tetrachlorothranilic acid. The yield was 44%. Found: C, 66.45; H, 3.90; Cl, 26.99%. Calcd for $C_{29}H_{20}Cl_4O$: C, 66.18; H, 3.83; Cl, 26.95%. NMR ($CDCl_3$, δ): 2.42 (3H, s), 2.49 (3H, s), 3.53 (3H, s), 5.75 (1H, d, J= 8 Hz), 6.27 (1H, s), 6.6—7.7 (9H, m).

9-(4-Methoxy-3,5-xylyl)triptycene (**11**), mp 255—256 °C, was similarly prepared from 9-(4-methoxy-3,5-xylyl)anthracene, butyl nitrite, and anthranilic acid. The yield was 82%. Found: C, 89.86; H, 6.02%. Calcd for $C_{29}H_{24}O$: C, 89.65; H, 6.23%. NMR ($CDCl_3$, δ): 2.42 (6H, s), 3.84 (3H, s), 5.37 (1H, s), 6.8—7.5 (12H, m), 7.75 (2H, broad s).

NMR Measurement. The PMR spectra at various temperatures were recorded as described previously.

**) This treatment is necessary because one of the chloro groups seems to undergo exchange. Without this treatment addition of water causes the formation of products with less chlorine content.

References

1) Preceding paper: F. Suzuki and M. Ōki, This Bulletin, **48**, 596 (1975).
2) G. Yamamoto and M. Ōki, *Chem. Commun.*, **1974**, 713.
3) a) M. Nakamura, M. Ōki, and H. Nakanishi, *J. Amer. Chem. Soc.*, **95**, 7169 (1973). b) M. Nakamura, M. Ōki, H. Nakanishi, and O. Yamamoto, This Bulletin, **47**, 2415 (1974).
4) L. M. Jackman and S. Sternhell, "Application of Nuclear Magnetic Resonance Spectroscopy in Organic Chemistry," Pergamon Press (1969), p. 202.
5) A. Mannschreck and L. Ernst, *Chem. Ber.*, **104**, 228 (1971).
6) M. Barfield and B. Chakrabart, *Chem. Rev.*, **1969**, 757.
7) P. C. Myhre, J. M. Edmands, and J. Kruger, *J. Amer. Chem. Soc.*, **88**, 2459 (1966).
8) C. E. Johnson and F. A. Bovey, *J. Chem. Phys.*, **29**, 1012 (1958).
9) H. Kessler, *Angew. Chem. Int. Ed. Engl*, **9**, 219 (1970).
10) F. A. Vingiello, M. O. L. Spangler, and J. E. Bondurant, *J. Org. Chem.*, **25**, 2091 (1960).
11) P. Kniel, *Helv. Chim. Acta*, **46**, 492 (1963).
12) F. Bell and D. H. Waring, *J. Chem. Soc.*, **1949**, 267.
13) S. Hayashi and N. Ishikawa, *Nippon Kagaku Zasshi*, **91**, 1000 (1970).
14) V. Villiger and L. Blangey, *Chem. Ber.*, **42**, 3549 (1909).

Reaction of Tetrachloroxylenes with Fuming Nitric Acid.[1] Side-chain Nitrooxylation and Quinol Nitrate Formation

Hitomi SUZUKI, Katsuro ISHIZAKI, Shigeru MARUYAMA, and Terukiyo HANAFUSA
Department of Chemistry, Faculty of Science, Hiroshima Uninersity, Higashi-sendamachi, Hiroshima 730
(Received February 18, 1975)

Direct action of fuming nitric acid upon tetrachloro-*o*- and -*m*-xylenes at room temperatur led to the formation of 3,5,6-trichloro-1,2-dimethyl-4-oxocyclohexa-2,5-dienyl nitrate and 2,5,6-trichloro-1,3-dimethyl-4-oxocyclohexa-2,5-dienyl nitrate, respectively, as the major products. In contrast, tetrachloro-*p*-xylene was simply converted into 2,3,5,6-tetrachloro-4-methylbenzyl nitrate. Plausible reaction sequences as well as criteria as a basis for predicting the propensity of polysubstituted alkylaromatics towards unusual nitration have been discussed.

Action of nitrating agent upon lightly substituted alkylbenzenes usually results in the replacement of one of the ring hydrogen atoms by nitro group. The increase in number of alkyl groups, however, tends to divert the reaction from the normal course into branch pathways leading to the production of unexpected products.[2] The most typical of these anomalous nitrations are the side-chain nitrooxylation (path a) and oxidation to unsaturated cyclic ketones (path b).

With substituted polymethylbenzenes these two processes are often in competition and as far as the substrate contains two methyl groups in *para* relationship, preference for the side-chain substitution dominates. We have previously suggested that the dichotomy of the reaction would presumably be determined by the structure of a benzenium ion intermediate;[3]

i) If the ion has the structure **1** in which the nitro group is attached to the nuclear carbon atom bearing a methyl group which is *para* to another methyl group, proton release would occur from the latter group to give a nitromethylene cyclohexadiene (**2**) which could be transformed into benzyl nitrate (**3**) (path a).

ii) If the ion has the structure **4** in which the nitro group is attached to the ring carbon atom bearing a methyl group which is *para* to a halogen atom, capture of the nitrate ion by the halogen-bearing carbon would occur to give an addition product (**5**), which will then be converted to the unsaturated carbonyl compound (**6**), usually isolated as *p*-quinol (**7**) (path b).

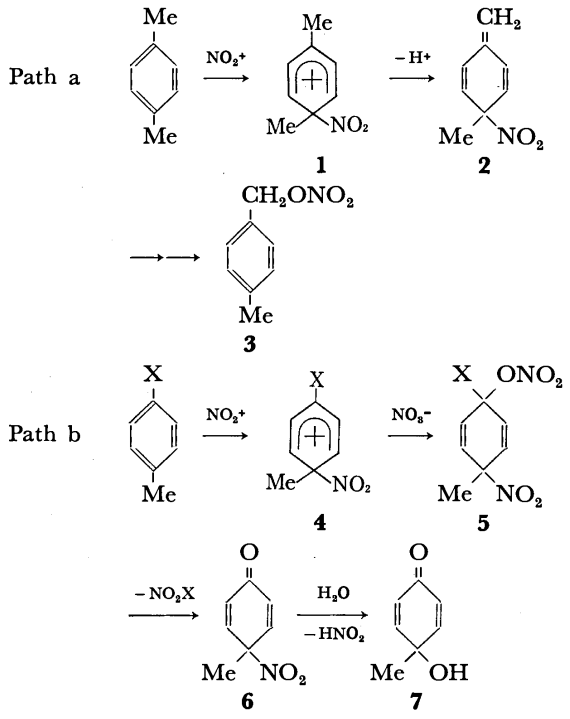

Scheme 1.

In order to test the reliability of the above criteria as a basis for predicting the propensity of polysubstituted alkylaromatics towards unusual nitration, as well as to obtain further insight into factors involved in the competition between side-chain substitution and nuclear oxidation, our studies were extended to the reaction of tetrachloroxylenes with fuming nitric acid.

A suspension of tetrachloro-*o*-xylene (**8**) in cold fuming nitric acid (d=1.50) was set aside with stirring overnight. **8** disappeared slowly to give a clear light brown solution which, on pouring into excess of water, gave a good yield of a pale yellow solid. Chromatography of the product on deactivated alumina resulted in the separation of some unchanged material and two new crystalline compounds melting at 166—167 °C and 145—146 °C, respectively. The high-melting compound had the formula $C_8H_7Cl_3O_2$ and showed mass peaks at m/e 240 (M^+), 225 (M^+—Me), and 205 (M^+—Cl). Proton NMR spectrum showed two methyl singlets at δ 1.68 and 2.32 and one hydroxyl peak at *ca.* 2.6 ppm (broad, exchangeable with D_2O). Its infrared spectrum contained carbonyl absorption at 1680 cm^{-1}, carbon-carbon double bond absorptions at 1637 and 1600 cm^{-1}, and hydroxyl absorption at 3400—3200 cm^{-1}, suggesting a cross-conjugated hydroxyketone. Its ultraviolet spectrum exhibited absorption maxima at 251—252 (log ε=4.08) and 291—292 nm (log ε=3.33) characteristic of a 2,5-cyclohexadienone system. Thus, the structure of dienone could be either 3,5,6-trichloro-1,2-dimethyl-4-oxocyclohexa-2,5-dienol (**12**) or 2,5,6-trichloro-1,3-dimethyl-4-oxocyclohexa-2,5-dienol (**19**). An unequivocal structure assignment to **12** was obtained by the zinc-acetic acid reduction of the ketone, which resulted in the isolation of a good yield of 2,5,6-trichloro-3,4-xylenol (**15**). The identity of the latter was confirmed by the independent synthesis starting with 3,4-xylenol according to the sequence shown in Scheme 2.[4]

The low-melting product had the formula $C_8H_6Cl_3NO_4$ and showed mass peaks at m/e 285 (M^+), 239 (M^+—NO_2), 223 (M^+—NO_3), and 221 (M^+—NO_2—CO). Its infrared spectrum showed prominent bands at 1683 (CO), 1646 (ONO_2), 1600 (C=C), 1292 (ONO_2), 1188,

1140, and 1042 cm^{-1}. The proton NMR spectrum displayed two methyl singlets at δ 1.71 and 2.27 ppm. The ultraviolet spectral pattern with maxima at 254—255 (log ε=4.05) and 286—290 nm (log ε=3.44) was typical of a 2,5-cyclohexadienone system. Given the presence of a cross-conjugated cyclohexadienone skeleton, two methyl groups, three chlorine atoms, and a nitrooxyl group, we could write twenty possible structures, nineteen of which, however, could readily be eliminated on the following chemical and spectral grounds:

1) Two methyl groups are magnetically non-equivalent.

2) Ring carbon atom bearing geminal chlorine atom and nitrooxyl group would be converted into carbonyl group.

3) Chlorine atoms are unable to undergo the intramolecular migration during the course of nitration.

4) Nitrooxyl group placed on a double bond would be subject to a facile nitrogen-oxygen single bond fission in protic acid medium.

5) When dissolved into nitric acid, **12** was converted into this nitrooxyl compound, which on prolonged contact with the nitrating agent was further converted into trichloro-*p*-toluquinone (**14**). These leave the structure 3,5,6-trichloro-1,2-dimethyl-4-oxocyclohexa-2,5-dienyl nitrate (**13**).

When the reaction mixture was quenched immediately after the dissolution of **8** in cold nitric acid, a yellow crystalline solid was obtained. Since this product showed infrared bands at 1690, 1610, and 1570 cm^{-1} and proton NMR peaks at δ 2.10 and 2.19 ppm, and since it gradually converted to **12** and other unidentified substances on standing, it was assigned the structure 2,5,6-trichloro-3,4-dimethyl-4-nitrocyclohexa-2,5-dienone (**11**).

A plausible mechanism to account for the formation of **12** and **13** is outlined in Scheme 2. In this mechanism an electrophilic attack on the methyl-bearing carbon by nitronium ion results in the formation of benzenium ion (**9**) which would take up nitrate anion to form addition product (**10**), from which nitryl chloride is eliminated to yield ketone **11**. The nitro group on the doubly activated allylic carbon atom undergoes a facile solvolytic replacement, yielding **13** as the major product. Minor amount of **12** would arise from the hydrolysis of **11** during aqueous work-up. The possibility of some secondary reactions occurring on the alumina column during elution is excluded since **12** and **13** are also obtained directly from the reaction product by fractional crystallization from ethanol.

A similar treatment of tetrachloro-*m*-xylene (**16**) with nitric acid resulted in the formation of a mixture of two carbonyl compounds **19** and **20** melting at 151—152 °C and 135—136 °C, respectively. Elemental analysis and molecular weight determination revealed that **19** is isomeric with **12** and **20** is isomeric with **13**. The high-melting ketone was uniquely established as 2,5,6-trichloro-1,3-dimethyl-4-oxocyclohexa-2,5-dienol (**19**), since the alternative structure **12** had been assigned to the isomeric product from **8**.

The low-melting ketone with a formula $C_8H_6Cl_3NO_4$ (*m/e*, 285 (M^+)) exhibited two methyl singlet peaks

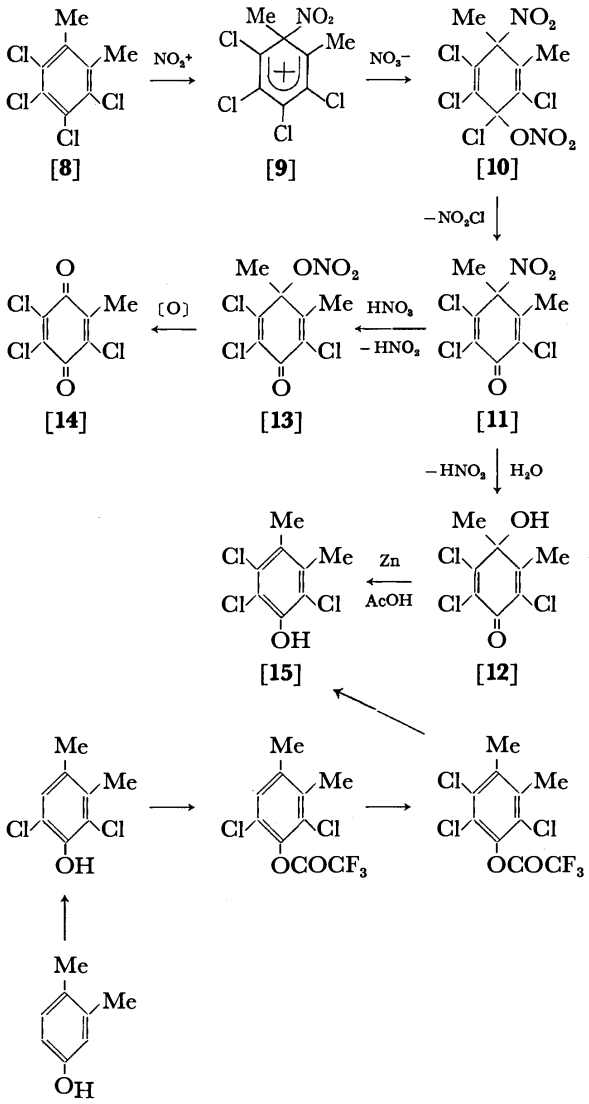

Scheme 2.

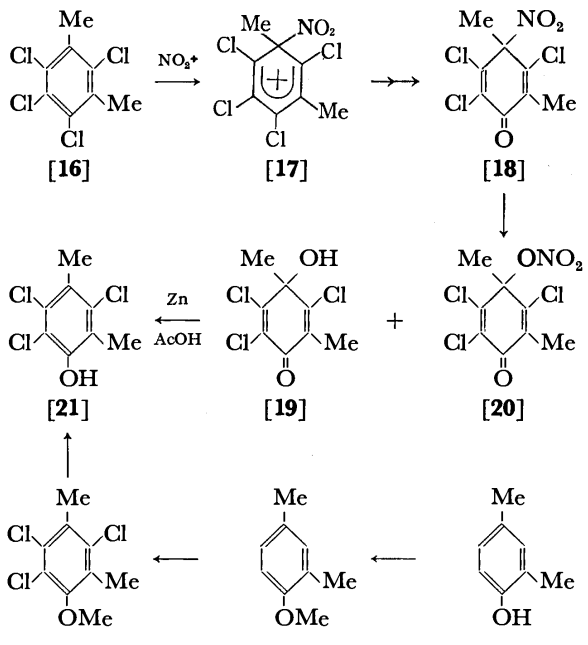

Scheme 3.

at δ 1.66 and 2.16 ppm. Its infrared spectrum showed absorptions at 1650, 1604, 1296, 1169, and 1051 cm^{-1}, and its ultraviolet spectrum with maxima at 255 (log ε=4.15) and 289—290 nm (log ε=3.46) indicated the presence of a 2,5-cyclohexadienone structure. Thus, the ketone is presumed to be a trichlorodimethyl-4-oxocyclohexa-2,5-dienyl nitrate and a similar consideration made for **13** allowed for **20** the structure 2,5,6-trichloro-1,3-dimethyl-4-oxocyclohexa-2,5-dienyl nitrate possible. Conclusive proof that the low-melting ketone has structure **20** was obtained through its transformation into 3,5,6-trichloro-2,4-xylenol (**21**) and comparing melting point, infrared spectrum and proton NMR spectrum of the latter with those of the authentic specimen prepared from 2,4-xylenol according to the sequence shown in Scheme 3.[4]

When the reaction mixture was worked up several minutes after mixing the reactants at room temperature, the predominant constituent of the product was an unstable nitroketone (**18**) which, however, could not be separated in pure form.

Tetrachloro-*p*-xylene (**22**) was treated with excess of nitric acid at room temperature to give a single clean product, which was isolated in 82% yield and identified as 4-methyl-2,3,5,6-tetrachlorobenzyl nitrate (**25**) by comparison with the authentic specimen. When the reaction mixture was allowed to stand for several weeks, initial product **25** was completely converted into 4-nitro-2,3,5,6-tetrachlorotoluene (**26**). Scheme 4 outlines the pathway from **22** to **26**. Attack on **22** by nitronium would result in the formation of a benzenium ion **23**, which would be converted to the expected nitrate **25** *via* diene **24**.

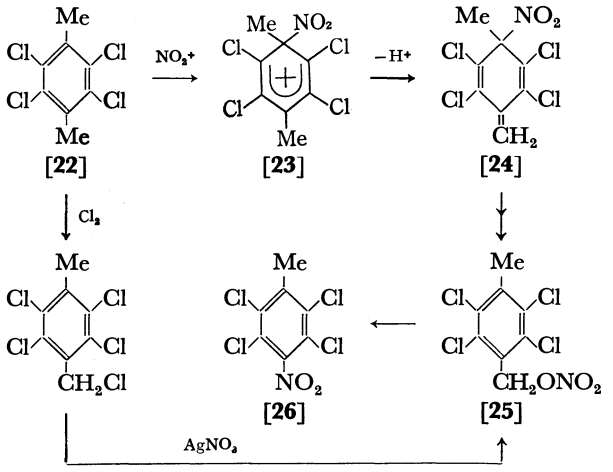

Scheme 4.

The presence of a pair of methyl group in *para* relationship is critical for the facile formation of benzyl nitrates. **22** with a pair of *para* methyl groups undergoes side-chain nitrooxylation to form benzyl nitarte **25**, whereas **8** and **16** both bearing no paired methyl groups in *para* positions undergo only nuclear oxidation to give unsaturated cyclic carbonyl compounds **12** and **13**, or **19** and **20**, respectively. No side-chain substitution was observed with the latter two substrates. Thus, the present results serve to reinforce the previous suggestion and augment the applicability of the above-mentioned guides *i* and *ii* as a basis for foreseeing the predisposition of substituted polyalkylaromatics towards the unusual nitration: electrophilic attack of the nitronium ion on three isomeric tetrachloroxylenes **8**, **16**, and **22** will lead to the formation of benzenium ions **9**, **17**, and **23**, respectively. Ion **23** satisfies the requirement *i* to follow the path a, giving the side-chain substitution product, while ions **9** and **17** comply with the requirement *ii* to follow the addition-elimination sequence (path b), resulting in the formation of unsaturated cyclic ketones. Our result, in addition to its mechanistic interest, provides a novel method for the synthesis of quinol nitrates. Further works to extend the method as an easy entry to quinols and related compounds are now in progress.

Experimental

All melting points were determined on a hot-stage apparatus and are uncorrected. Infrared spectra were obtained in Nujol mulls with a Jasco 402G spectrophotometer. Ultraviolet spectra were recorded in methanol on a Shimadzu QV-50 spectrophotometer. Proton NMR spectra were taken using a Varian T-60 instrument. All measurements were made on 5—10% deuteriochloroform solutions using TMS as an internal reference at probe temperature. Mass spectra were obtained on a Hitachi RMS-4 spectrometer.

Three tetrachloroxylene isomers were prepared by the chlorination of the corresponding hydrocarbons and purified through alumina chromatography.

Procedure for the Nitration of Tetrachloroxylenes. The procedures used for tetrachloro-*o*-xylene (**8**) and tetrachloro-*m*-xylene (**16**) were essentially the same and the only one experiment shall be reported here.

A suspension of **8** (10.0 g, 0.41 mol) in nitric acid (d=1.5, 130 g) was stirred at room temperature for 10 hr. The solid gradually dissolved giving a clear dark brown solution, which was then quenched by pouring into a large excess of ice water. The pale yellow solid precipitate (7.46 g) was collected by filtration, washed with dilute aqueous sodium hydrogen carbonate, and sucked as dry as possible. Aqueous washings were combined and extracted three times with ether and the extract was evaporated to give crude **12** (0.96 g) as pale yellow solid. A part of the product (1.0 g) was placed on the top of alumina column (deactivated by 10% acetic acid) and eluted with light petroleum to give **13** (0.33 g, 33%) as white needles, mp 145—146 °C with decomposition.

Found: C, 33.73; H, 2.05; N, 4.92; O, 22.14; Cl, 36.91%. Calcd for $C_8H_6Cl_3NO_4$: C, 33.54; H, 2.11; N, 4.89; O, 22.34; Cl, 37.12%.

Further elution with light petroleum containing benzene yielded **12** (0.39 g, 33%), which was recrystallized from ethanol to give white prisms, mp 166—167 °C.

Found: C, 40.07; H, 2.91%. Calcd for $C_8H_7Cl_3O_2$: C, 39.79; H, 2.92%.

Direct crystallization of the crude product mixture (3.25 g; air-dried for several weeks) from ethanol gave pure **13** (0.84 g). When a solution of **8** (0.63 g) in cold nitric acid (20 ml) was diluted with water immediately after complete dissolution, nitroketone **11** was obtained as pale yellow precipitate (0.34 g), mp 64—66 °C, which gradually decomposed to **12** and other unidentified substances. Its elemental analysis was not satisfactory.

Found: C, 33.07; H, 2.09; N, 4.90%. Calcd for $C_8H_6Cl_3NO_3$: C, 35.52; H, 2.24; N, 5.18%.

Similar treatment of **16** gave a mixture of several carbonyl compounds, the major components being **19** and **20**, although yields were lower under comparable conditions (20—30 and 15—24%, respectively).

19: mp 151—152 °C. ^{1}H NMR: δ 1.63 (s, 3H), 2.12 (s, 3H), and *ca.* 2.8 ppm (broad, 1H, exchangeable with D_2O); IR: 3400—3200, 1673, 1643, 1606, 1168, and 1070 cm^{-1}; UV: 249—251 (log ε=4.36) and 286—287 nm (log ε=3.75); Mass: *m/e* 240 (M^+), 225 (M^+-Me), and 205 (M^+-Cl).

Found: C, 39.62; H, 2.83%. Calcd for $C_8H_7Cl_3O_2$: C, 39.79; H, 2.92%.

20: mp 135—136 °C. Mass: *m/e* 285 (M^+), 239 (M^+-NO_2), and 223 (M^+-ONO_2).

Found: C, 33.84; H, 2.20; N, 4.59%. Calcd for $C_8H_6Cl_3NO_4$: C, 33.54; H, 2.11; N, 4.89%.

When the reaction mixture was diluted with water several minutes after mixing the reactants, there resulted a precipitate, mp 69—71 °C, which showed infrared bands at 1670, 1605, and 1570 cm^{-1} and proton NMR peaks at δ 2.15 and 2.19 ppm. These features are in line with the structure **18**, but attempt to obtain the ketone in pure form failed. On standing **18** gradually decomposed to **19** and other unidentified substances.

A suspension of tetrachloro-*p*-xylene (**22**; 0.51 g, 0.0021 mol) in nitric acid (13 g) was allowed to stand with stirring overnight. The dark mixture was poured into ice water and the precipitated solid was filtered off, washed with aqueous sodium hydrogen carbonate, and dried. The crude product (0.64 g; mp 69—72 °C) was recrystallized from ethanol to give **25** as white leaflets, mp 80—82 °C. Yield, 0.523 g (82%). IR: 1649, 1620, and 1276 cm^{-1}; ^{1}H NMR; δ 2.67 (s, 3H) and 5.85 ppm (s, 2H).

Found: C, 31.72; H, 1.63; N, 4.65%. Calcd for $C_8H_5Cl_4NO_3$: C, 31.51; H, 1.65; N, 4.59%.

When the reaction mixture was left to stand at room temperature for several weeks, the usual work-up followed by crystallization of the solid precipitate from ethanol gave 4-nitro-2,3,5,6-tetrachlorotoluene as the sole significant product. Mp 156—159 °C. The product was identical with an authentic specimen.[5]

Financial supports for this work from the Ministry of Education and the Saneyoshi Scientific Foundation are gratefully acknowledged.

References

1) The Reaction of Polysubstituted Aromatics. Part XLI; Part XL: H. Suzuki, K. Ishizaki, and T. Hanafusa, *Nippon Kagaku Kaishi*, **1975**, 566. A preliminary report has been published: H. Suzuki, K. Ishizaki, S. Maruyama, and T. Hanafusa, *Chem. Commun.*, **1975**, 51.

2) For reviews, see S. R. Hartshorn, *Chem. Soc. Rev.*, **3**, 167 (1974); H. Suzuki, *Bull. Inst. Chem. Res. Kyoto Univ.*, **50**, 407 (1972). A possible role of nitromethylene cyclohexadiene as an intermediate in the side-chain substitution has been discussed in some detailed manner: A. Fischer and N. Ramsay, *Can. J. Chem.*, **52**, 3691 (1974).

3) H. Suzuki, S. Maruyama, and T. Hanafusa, This Bulletin, **47**, 876 (1974), and other papers in this series.

4) Synthesis of the reference compounds has been published separately: H. Suzuki, K. Ishizaki, and T. Hanafusa, *Nippon Kagaku Kaishi*, **1975**, 566.

5) W. Qvist and N. Holmberg, *Acta Acad. Aboensis Math. Phys.*, **6**, 3 (1932); *Chem. Abstr.*, **27**, 5727 (1933).

Nitration of 9,10-Dialkylphenanthrenes. Side-chain Nitrooxylation in Competition with Side-chain Nitration[1]

Hitomi SUZUKI, Hajime YONEDA, and Terukiyo HANAFUSA

Department of Chemistry, Faculty of Science, Hiroshima University, Higashi-sendamachi, Hiroshima 730

(Received March 12, 1975)

9,10-Dimethylphenanthrene and 9-methyl-10-ethylphenanthrene gave 9-methyl-10-nitromethylphenanthrene and 9-ethyl-10-nitromethylphenanthrene, respectively, as major product, when treated with fuming nitric acid in dichloromethane at low temperatures. In contrast, 9,10-diethylphenanthrene yielded a comparable mixture of products arising from side-chain nitration and side-chain nitrooxylation, which on chromatography over deactivated alumina gave 9-ethyl-10-(α-nitroethyl)phenanthrene and 9-ethyl-10-(α-hydroxyethyl)phenanthrene as main isolable products. 9-Methylphenanthrene and 9-ethylphenanthrene were both simply nitrated at the ring position to give the corresponding 9-alkyl-10-nitrophenanthrenes in good yields. No side-chain attack was observed. Factors responsible for determining which one of the competitive pathways will be followed have been discussed.

Reaction of polymethylbenzenes with fuming nitric acid often leads to the formation of products resulting from side-chain nitrooxylation (path a). In contrast, polymethylnaphthalenes and polymethylanthracenes can be attacked at the side-chain to yield naphthylnitromethanes and anthrylnitromethanes, respectively (path b). Both substitution processes have been suggested to involve nitromethylene cyclohexadiene intermediate with *para*-quinoid structure (**1**),[2] and a marked change in the modes of reaction towards the nitrating agent, observed on going from the benzenes to naphthalenes and anthracenes, has been related to the change in the development of carbonium ion character on the methylene carbon atom of intermediate ion pair (**2**) (Scheme 1).[3] In order to learn more about the mechanism of side-chain substitution and also to gain further insight into factors which determine whether path a or path b is followed, we have investigated the reaction of several alkylphenanthrenes with fuming nitric acid.

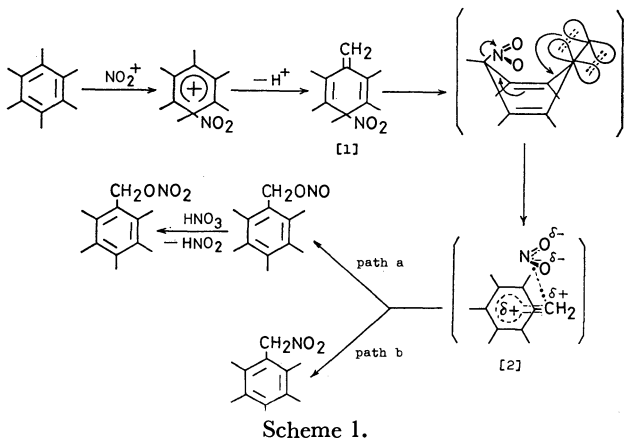

Scheme 1.

A dilute solution of 9,10-dimethylphenanthrene (**3a**) in purified dichloromethane was treated with an equivalent amount of nitric acid (d=1.5) at −10 °C and the dark brown mixture was allowed to stand in the refrigerator until the color had lightened. Quenching with water followed by chromatography of the crude product on deactivated alumina and recrystallization from chloroform–light petroleum resulted in the isolation of a new crystalline compound (**7a**), mp 175—176 °C, as principal product. **7a** had a molecular formula $C_{16}H_{13}NO_2$ and exhibited infrared bands due to nitro group at 1550 and 1361 cm^{-1}; proton NMR resonances at δ 2.81 (s, 3H), 6.09 (s, 2H), and 7.55—8.85 ppm (m, 8H). The mass spectrum showed the expected peaks at m/e 251 (M^+) and 205 (M^+-NO_2). These data are consistent with its formulation as 9-methyl-10-nitromethylphenanthrene (**7a**). This compound is unique in that it presents the first clear example of side-chain substitution which has occurred *via* nitromethylene cyclohexadiene with *ortho* quinoid structure (**5**). The overall reaction sequence is depicted in Scheme 2.

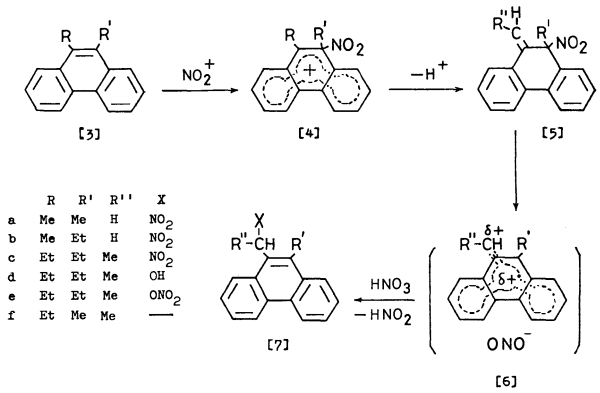

Scheme 2.

A similar reaction with 9-methyl-10-ethylphenanthrene (**3b**) yielded a yellow solid, the predominant component of which was readily separated by crystallization from ethanol and identified as 9-ethyl-10-nitromethylphenanthrene (**7b**) by its analysis and the usual spectroscopic measurements. Spectral inspection on a yellow syrupy residue from the mother liquor obtained in the recrystallization of the crude product indicated no appreciable formation of nitrate ester, which was not further sought for.

When 9,10-diethylphenanthrene (**3c**) was similarly allowed to react with nitric acid, a thick dark red liquid was obtained. It showed strong infrared bands at 1631—1635, 1278, and 860 cm^{-1}, indicating that the nitrate ester formation was a distinctly important process here. Proton NMR spectrum exhibited the characteristic

methyl and methylene splittings of two α-substituted ethyl groups, suggesting the presence of two major products arising from the attack in the α-position of ethyl groups. The signal integration revealed that these products were formed in almost equal amounts. When the product mixture was chromatographed over silica gel, slightly yellow needles melting at 107—110 °C was obtained from cyclohexane containing benzene eluates, and a low-melting glassy substance eluted from a mixture of benzene and methanol. The former compound with an elemental composition of $C_{18}H_{13}NO_2$ showed infrared bands for nitro group at 1548 cm^{-1}; proton NMR peaks due to ethyl group at 1.39 (t, 3H) and 3.23 (q, 2H), one methyl group at 2.16 (d, 3H), one methine proton at 6.33 (q, 1H), and aromatic protons at 7.36—8.89 ppm (m, 8H). On the basis of these evidences structure 9-ethyl-10-(α-nitroethyl)phenanthrene (**7c**) was assigned to the compound. The latter product with an approximate composition $C_{18}H_{18}O$ had the strong, broad infrared band due to hydroxyl group at 3540 cm^{-1}; proton NMR peaks at δ 1.38, 1.80, 3.26, 5.95, and *ca.* 7.5—9.2 ppm with the respective integrated peak area ratio of 3:3:2:1:8. These data support the assignment of structure 9-ethyl-10-(α-hydroxyethyl)phenanthrene (**7d**) to the product, characterization of which then allowed identification of a second major component in the original product mixture as 9-ethyl-10-(α-nitrooxymethyl)phenanthrene (**7e**). This would be the first case reported of the extensive nitrooxylation which occurs on an alkyl group of polycyclic aromatics and is contrasted with the reaction of 9,10-diethylanthracene (**8**) in which the only reaction that proceeds is the addition reaction.[3]

Under comparable conditions both 9-methylphenanthrene and 9-ethylphenanthrene were simply nitrated at the ring position and gave a good yield of 9-methyl-10-nitrophenanthrene and 9-ethyl-10-nitrophenanthrene, respectively. No side-chain attack was observed.

So far little work has been made of the nitration of alkyl derivatives of phenanthrene, but it is clear that 9- and 10-positions would maintain their reactivity.[4] Thus, nitronium ion attaches to the position carrying alkyl group to form arenium ion (**4**), which loses proton from the activated alkyl group on the adjacent carbon atom to give nitromethylene cyclohexadiene intermediate (**5**). **5** could collapse by heterolytic C-N bond fission to give a phenantrylmethylium-nitrite ion pair (**6**), the cationic component of which can dissipate its positive charge from the *exo*-cyclic carbon atom into two intact benzene nuclei. In a nitrite ion the the nitrogen atom has a much less electron density than oxygen atoms. A preferential bonding of 9-phenantrylmethylium ions (**6a** and **6b**) to the nitrogen atom of the ambident anion would then yield the observed nitro compound (**7a** and **7b**) (Scheme 2).

In contrast to **5a** and **5b**, diene **5c** affords a carbonium ion with branched structure (**6c**). This would mean the increase in the development of carbonium ion character in the cationic component of the ion pair **6c**. The greater the carbonium contribution, the greater would be the tendency for nitrite ion to form a covalent linkage at the atom having the higher electron density. Thus in recombining with the cationic center, oxygen atoms can effectively compete with the nitrogen atom, leading to the concurrent formation of nitro compound and nitrite ester. The latter compound is not stable in the presence of nitric acid and rapidly converted into the corresponding nitrate **7e**. The order of nitrate-forming tendencies as derived from the present work is **3c**≫**3b**>**3a**, which suggests that the mode of reaction is determined by the same factors that govern selectivity in the alkylation of the ambident anions.[5] The results are just what would have been predicted on the basis of the concept of "hard and soft acids and bases."[6]

One may ask why the nitrate formation is prominent in the nitration of **3c**, but is not in the nitration of 9,10-diethylanthracene (**8**). The answer would appear to be related to a lesser degree of steric hindrance involved when arenium ion (**4**) comes in to form a nitromethylene cyclohexadiene **5c** than when ion **9** comes in to form diene **10**. Consequently, with **8** the addition product formation wins out over the side-chain substitution (Scheme 3).[3]

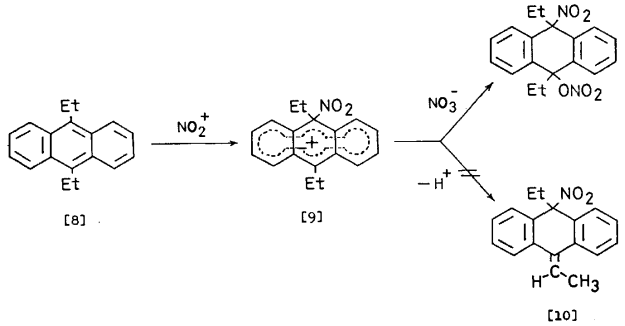

Scheme 3.

Spectral inspectrion of a product mixture from **3b** revealed that methyl group is much more reactive than ethyl group towards side-chain substitution. This result would be expected if one takes into account: 1) the greater contribution of intermediate ion **4b** relative to **4f** due to the partial relief of steric strain and the favorable inductive effect of ethyl group, 2) the relative ease of hyperconjugative proton release from the activated alkyl groups, and 3) the increase in steric interference with *peri*-hydrogen atom when the cyclohexadiene **5f** is formed.

An alternative possible route, which we have previously suggested for side-chain nitrooxylation of polymethylbenzenes[7] and could equally well explain the results, involves a nucleophilic attack of nitrate or nitrite anions at the *exo*-methylene group of **5** with simultaneous loss of the nitro group as nitrite anion (Scheme 4). The increase in nitrate-formation on going from **3a** to **3c** to polymethylbenzenes could con-

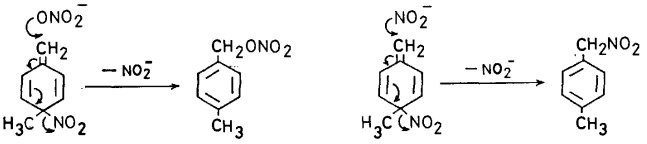

Scheme 4.

ceivably derive from difference in the proportion of S_N1' and S_N2' character in the transition state. Unfortunately, this pathway lacks good formal analogies in the literature as far as the authors are aware. In a recent paper,[8] some detailed discussion in favor of this mechanism has been made by Fischer and Ramsay in connection with their work on the adduct formation in the nitration of polymethylbenzenes. We do not feel, however, that sufficient data are yet available to be able to dismiss in a definite manner either of the two mechanisms proposed.

Experimental

All melting points are uncorrected. Infrared spectra were run in Nujol mulls on a Jasco DS-402G spectrophotometer. Proton NMR spectra were taken for deuteriochloroform solutions on a Varian T-60 spectrometer using TMS as internal standard. Mass spectra were obtained on a Hitachi RMS-4 spectrometer. Thin-layer chromatography on silica gel G was used for monitoring reactions and chromatographic separations. Indication was effected with iodine vapor or ultraviolet light.

9,10-Dialkylphenanthrenes were prepared by the reaction of 10-lithio derivatives of related 9-alkylphenanthrenes[9] with methyl and ethyl iodides, and purified by chromatography over alumina followed by recrystallization from benzene–light petroleum. Physical properties of some phenanthrene derivatives obtained in connection with the present work are summarized in Table 1. To our knowledge, compounds **7a** to **7e** are not previously described in the literature.

Dichloromethane used as solvent for the nitration was purified according to our procedure described in a previous paper of this series.[3] Yields are based on product isolation.

Procedure for the Nitration of 9,10-Dialkylphenanthrenes. 9,10-Dialkylphenanthrene (0.002 mol; 0.41 g for **3a**; 0.44 g for **3b**, and 0.47 g for **3c**) was dissolved in dichloromethane (5 ml) and vigorously stirred with external cooling at −10 °C. After slow addition of nitric acid ($d=1.5$; 0.002 mol, 0.86 ml) in the same solvent (5 ml) through a syringe over a period of 30 min, the mixture was kept in the dark at 0 °C for 2 hr and at room temperature for 30 min, and then quenched by the addition of water. The organic layer was separated, washed with dilute aqueous sodium hydrogen carbonate, and dried over anhydrous magnesium sulfate. The light yellow crystalline residue or syrupy liquid obtained after removal of the solvent was examined by infrared and proton NMR spectroscopy as well as thin-layer chromatography.

1) A crude product from **3a** was crystallized from a mixture of benzene and cyclohexane to give **7a** as faintly yellow needles, mp 175—176 °C. Yield, 0.43 g (86%).

Found: C, 76.57; H, 5.21; N, 5.53%. Calcd for $C_{16}H_{13}NO_2$: C, 76.48; H, 5.21; N, 5.57%.

2) A crude product from **3b** was crystallized from chloroform–pentane to give **7b** as white, fine needles, mp 172—174 °C. Yield, 0.34 g (64%). IR: 1548, 1328, 756, and 717 cm^{-1}; Mass: *m/e* 265 (M^+) and 219 (M^+-NO_2).

Found: C, 77.32; H, 5.84; N, 5.02%. Calcd for $C_{17}H_{15}NO_2$: C, 76.96; H, 5.70; N, 5.28%.

A syrupy residue obtained from the mother liquor showed infrared bands at 1632, 1276, and 853 cm^{-1}, indicating the presence of slight amounts of nitrate ester.

3) An oily product from **3c** failed to produce a solid on standing in refrigerator. It was then placed on a column of silica gel developed with cyclohexane. Elution with cyclohexane followed by a mixture of cyclohexane and benzene yielded unchanged hydrocarbon and **7c**. The latter recrystallized from benzene–chloroform appeared as slightly yellow needles, mp 107—110 °C. Mass: *m/e* 279 (M^+) and 233 (M^+-NO_2).

Found: C, 77.40; H, 6.07; N, 4.98%. Calcd for $C_{18}H_{17}NO_2$: C, 77.40; H, 6.14; N, 5.01%.

Further elution with benzene followed by 10%-methanol in benzene yielded a sticky glass, which we were unable to obtain in pure form but identified as **7d** by its NMR and IR spectra.

Found: C, 85.86; H, 7.15%. Calcd for $C_{18}H_{18}O$: C, 86.36; H, 7.25%.

Finally, elution of the column with methanol produced a trace of red-brown oil that was not further characterized.

Products from 9-methylphenanthrene and 9-ethylphenanthrene were recrystallized from a mixture of light petroleum and ether, and melted at 171—172 °C and 101—103 °C, respectively. Structural assignments were made on the basis of the analyses, NMR, and IR, spectra. Minor isomeric

Table 1. Physical properties of some 9,10-disubstituted phenanthrenes

Compound	R	R′	Mp (°C)	^1H NMR Spectra (δ)
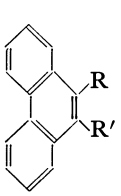	CH_3	CH_3	145—147[11]	2.73 (s, 6H), 7.35—7.78 (m, 4H), 7.97—8.29 (m, 2H), 8.56—8.89 (m, 2H)
	CH_3	C_2H_5	81—83[12]	1.27 (t, 3H), 2.70 (s, 3H), 3.30 (q, 2H), 7.53—9.05 (m, 8H)
	C_2H_5	C_2H_5	102—104[11]	1.38 (t, 6H), 3.27 (q, 4H), 7.48—8.92 (m, 8H)
	CH_3	CH_2NO_2	175—176	2.81 (s, 3H), 6.09 (s, 2H), 7.55—8.85 (m, 8H)
	C_2H_5	CH_2NO_2	172—174	1.38 (t, 3H), 3.19 (q, 2H), 6.12 (s, 2H), 7.50—8.94 (m, 8H)
	C_2H_5	$CH(CH_3)NO_2$	107—110	1.39 (t, 3H), 2.16 (d, 3H), 3.23 (q, 2H), 6.33 (q, 1H), 7.36—8.89 (m, 8H)
	C_2H_5	$CH(CH_3)OH$	—[a]	1.38 (t, 3H), 1.80 (d, 3H), 3.26 (q, 2H), 5.95 (q, 1H), 7.5—9.2 (m, 8H)

a) Glassy substance with no definite melting range.

products were not sought for.

9-Methyl-10-nitrophenanthrene:[10] IR: 1517 and 1228 cm^{-1}; ^1H NMR: δ 2.64 (s, 3H) and *ca.* 7.4—8.9 ppm (m, 8H).

Found: C, 75.83; H, 4.55; N, 5.96%. Calcd for $C_{15}H_{11}NO_2$: C, 75.94; H, 4.67; N, 5.90%.

9-Ethyl-10-nitrophenanthrene: IR: 1519 and 1368 cm^{-1}; ^1H NMR: δ 1.40 (t, 3H), 2.05 (q, 2H), and 7.51—8.87 ppm (m, 8H).

Found: C, 76.52; H, 5.20; N, 5.50%. Calcd for $C_{16}H_{15}NO_2$: C, 76.52; H, 5.21; N, 5.57%.

Financial support of our work by the Ministry of Education and the Saneyoshi Scientific Foundation is gratefully acknowledged.

References

1) The Reaction of Polysubstituted Aromatics. Part XLII; Part XLI: H. Suzuki, K. Ishizaki, S. Maruyama, and T. Hanafusa, This Bulletin, **48**, 2112 (1975).

2) Methylene cyclohexadienes have apparently not been observed directly in electrophilic substitutions of polymethylbenzenes and related substances, although the possibility of their formation in such reactions has been considered by numerous workers. For a recent review of methylene cyclohexadiene as possible intermediate in non-conventional electrophilic substitutions, see S. R. Hartshorn, *Chem. Soc. Rev.*, **3**, 167 (1974). See also discussion in Ref. 8.

3) H. Suzuki, H. Yoneda, and T. Hanafusa, This Bulletin, **47**, 3106 (1974).

4) G. M. Badger, "The Structures and Reactions of the Aromatic Compounds," Cambridge University Press, Cambridge (1954).

5) E. S. Gould, "Mechanism and Structure in Organic Chemistry," Holt, Reinhart and Winston, New York (1959), p. 297; N. Kornblum, R. A. Smiley, R. K. Blackwood, and D. C. Iffiand, *J. Amer. Chem. Soc.*, **77**, 6269 (1955).

6) R. G. Pearson and J. Songstad, *ibid.*, **89**, 1827 (1967).

7) K. Nakamura, This Bulletin, **44**, 133 (1971).

8) A. Fischer and N. Ramsay, *Can. J. Chem.*, **52**, 3691 (1974).

9) B. M. Mikhailov and N. E. Chernova, *Zh. Obshch. Khim.*, **21**, 1517 (1951); P. W. Rabideau and R. G. Harvey, *J. Org. Chem.*, **35**, 25 (1970).

10) H. Heaney, A. J. Jones, and I. T. Millar, *J. Chem. Soc.*, **1965**, 2587.

11) C. K. Bradsher and W. J. Jackson, Jr., *J. Amer. Chem. Soc.*, **76**, 4140 (1954).

12) C. K. Bradsher and S. T. Amore, *ibid.*, **65**, 2016 (1943).

The Structure of Yuzurimine-C

Shosuke YAMAMURA, Hajime IRIKAWA,* Yasuaki OKUMURA,* and Yoshimasa HIRATA**

Faculty of Pharmacy, Meijo University, Showa-ku, Nagoya 468
**Department of Chemistry, Shizuoka University, Oya, Shizuoka 422*
***Chemical Institute, Nagoya University, Chikusa-ku, Nagoya 464*

(Received April 1, 1975)

The structure of yuzurimine-C, one of the yuzurimine-type alkaloids, was unambiguously determined on the basis of chemical evidences coupled with its spectral data. Particularly, application of the ^{13}C NMR spectra plays an important role in the structural elucidation.

As described in the previous paper,[1] yuzurimine-C was isolated, as one of the minor components, from the plant *Daphniphyllum macropodum* Miquel (Japanese name "Yuzuriha"). In the present paper, we wish to describe the structure of yuzurimine-C on the basis of chemical evidences coupled with comparison of its ^{13}C NMR spectrum with those of yuzurimine and its derivatives.

Yuzurimine-C (**1**, mp 186—187 °C; $C_{23}H_{29}O_5N$) is one of the minor alkaloids, that has a secondary methyl group [δ 1.04 ppm (2H, d, J=6 Hz)] and a carbomethoxyl group [ν_{max} 1736 cm^{-1} and δ 3.58 ppm (2H, s)] analogous to those of yuzurimine (**2**).[2] The IR spectrum of **1** indicates the presence of two different carbonyl groups (ν_{max} 1736 and 1723 cm^{-1}), one of which can be due to an aldehyde group [ν_{max} 1723 cm^{-1} and δ 9.99 ppm (1H, s)], instead of a tertiary acetoxymethyl group in yuzurimine (**2**). Furthermore, two sharp doublets at δ 5.61 (1H, d, J=10 Hz) and 6.20 ppm (1H, d, J=10 Hz) in the NMR spectrum must be due to two olefinic protons 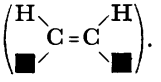 . From a biogenetic point of view, the above spectral data suggests that yuzurimine-C, which co-occurs with yuzurimine (**2**) in the plant, may have a tentative structure (**1**). In fact, this tentative structure (**1**) can be confirmed, as follows.

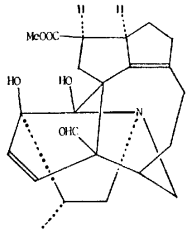

(**1**)

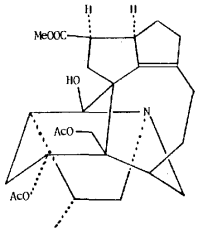

(**2**)

When heated with methyl iodide in acetone under reflux for 6 hr,* yuzurimine-C was converted into the corresponding methiodide (**3**, mp 209—210 °C; $C_{24}H_{32}O_5NI$) in almost quantitative yield. In the mass spectra of the methiodides corresponding to daphniphylline[3] and daphnilactone-B,[4] usually, they have the fragment peaks resulting from the loss of MeI from each molecular ion. In the case of **3**, however, the strong peak can be observed at m/e 413 resulting from the loss of HI, indicating that the original alkaloid (**1**) must have a HO-C-N< grouping. In fact, yuzurimine-C methiodide (**3**) was readily converted into a keto-amine (**4**, mp 199—200 °C; $C_{24}H_{31}O_5N$) only by contact with aqueous alkaline solution, as seen in the case of yuzurimine methiodide.[2] In the IR spectrum of **4**, extraordinary low C=O frequency (ν_{max} 1640 cm^{-1}) assigned to the newly formed keto-group must result from proximity of the nitrogen atom with a lone pair of electrons.

The presence of a vicinal glycol [HO-C-C(OH)-N<] can be confirmed on the basis of the following experiments. When treated with $NaIO_4$ in aqueous MeOH-THF (room temp., 16 hr), yuzurimine-C was converted into a keto-lactam [**5**, mp 179—181 °C; $C_{23}H_{27}O_5N$ (m/e 397 (M^+))], in good yield. In the IR spectrum of **5** [ν_{max} 1737, 1705 br. and 1660 cm^{-1}; no OH band], the absorption band at 1660 cm^{-1} is attributable to the newly formed lactam carbonyl. Furthermore, it is clear from the molecular model of **5** that the other newly formed keto-group can not conjugate well with the disubstituted double bond [ν_{max} 1705 br. cm^{-1} and λ_{max} 215 nm (ε, 6590)] which is readily reduced on catalytic hydrogenation leading to the formation of a dihydro-compound [**6**, mp 168—169 °C; $C_{23}H_{29}O_5N$ (m/e 399 (M^+))]. Further information of the disubstituted double bond can be obtained from the NMR spectrum of the keto-lactam (**5**), which has two doublets assigned to the grouping [δ 5.61 (1H, d, J=14 Hz) and 6.01 ppm (1H, d, J=14 Hz)]. Clearly, this disubstituted double bond in **5** (J=14 Hz) must be included in a medium ring, and not in the original six-membered ring (J=10 Hz in **1**, **3**, and **4**).[5]

As mentioned earlier, yuzurimine-C (**1**) seems to have an aldehyde group (-C-CHO) instead of the acetoxymethyl group in yuzurimine (**2**). This is also supported by the following chemical evidences: when treated with limited amounts of $LiAlH_4$ in THF (room temp., 5 hr), yuzurimine-C (**1**) was converted into the corresponding hydroxy-compound [**7**, mp 168—170 °C; $C_{23}H_{31}O_4N$ (m/e 385 (M^+) ν_{max} 3470, 3420, and 1715 cm^{-1}]. The NMR spectrum of **7** indicates two doublets at δ 3.75 and 4.06 ppm (each one proton, J=12 Hz) due to the newly formed hydroxymethyl group instead of the aldehyde group in yuzurimine-C (**1**). These doublets in **7** are further shifted to δ 4.48 ppm (2H, br. s) on acetylation with Ac_2O-pyridine (room temp., overnight) leading to the formation of the corresponding mono-acetate [**8**, mp 171—173 °C; $C_{25}H_{33}O_5N$ (m/e 427 (M^+)); ν_{max} 3440,

* The starting material was recovered under milder conditions (room temp., overnight).

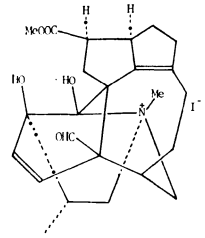

(3)

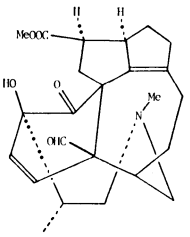

(4)

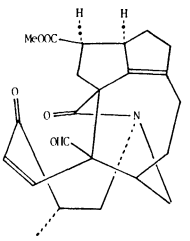

(5)

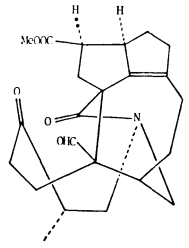

(6)

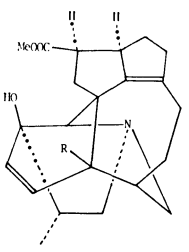

(7) R=CH_2OH
(8) R=CH_2OAc

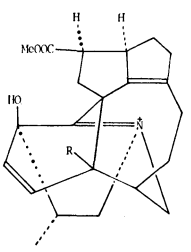

(9) R=CHO
or CH_2OH

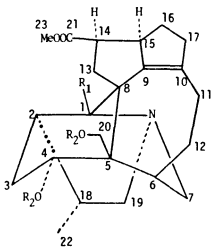

(10) R_1=OH R_2=H
(11) R_1=H R_2=Ac

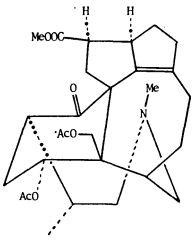

(12)

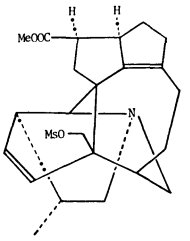

(13)

1745, and 1735 cm^{-1}]. In the course of reduction, an anti-Bredt's rule imine (**9**) as an unstable intermediate must be produced,[6] as found in the case of yuzurimine (**2**).[2] Finally, the structure (**1**) for yuzurimine-C is supported by comparison of its ^{13}C NMR spectrum with those of yuzurimine (**2**) and its derivatives (**10**—**13**).[2]

Generally, partially relaxed Fourier transform (PRFT) ^{13}C NMR technique[7] is known to be very useful in the structural study on complex natural products, because methyl, methylene, methine and quaternary carbon signals are easily differentiated.

Thus, proton noise decoupled (PND) and partially relaxed FT ^{13}C NMR spectra of yuzurimine-C were measured, as shown in Fig. 1, in which the PRFT spectrum was obtained by using the pulse sequence (180 °–τ–90 °–T).

In the PRFT spectrum at τ=0.6 s, methylene and disubstituted olefin peaks appear as positive signals, while methine and secondary methyl peaks are nulled. Quaternary carbon and tetrasubstituted olefin peaks remain negative. The results of ^{13}C NMR experiments of yuzurimine-C (**1**), yuzurimine (**2**), and several derivatives (**10**—**13**) are summarized in Table 1.

In the Table 1, the signals of the quaternary carbon C-1 connected to the hydroxyl group and the nitrogen atom are seen in the spectra of **1** (δ 91.6 ppm), **2** (δ 96.8 ppm), and **10** (δ 97.3 ppm), whereas the spectra of **11**, **12**, and **13** lack the signal attributed to the above quaternary carbon. Nine methylene and six methine signals are observed in the spectra of **4** and **10**, whereas seven methylene, four methine, and one carbonyl (δ 207.0 ppm) signals are found in the case of yuzurimine-C (**1**). Furthermore, four olefinic signals are seen in the

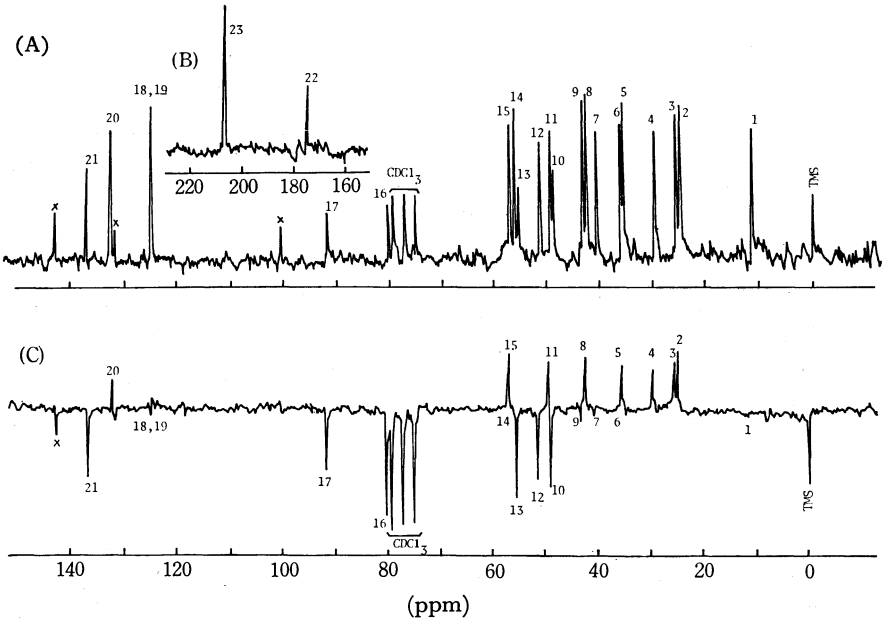

Fig. 1. (A, B) Proton noise decoupled (PND) natural abundance FT ^{13}C NMR spectra of yuzurimine-C (1) in $CDCl_3$ (100 mg/1.7 ml) at 15.04 MHz; (A): recycle time=1 s, number of scans=3600, sweep width=2500 Hz; (B): low field part, recycle time=1 s, number of scans=5400, sweep width=5000 Hz. (C): PRFT ^{13}C NMR spectrum of yuzurimine-C (1); interval time τ=0.6 s, recycle time T=10 s, number of scans=5000, sweep width=2500 Hz.

TABLE 1. ^{13}C CHEMICAL SHIFTS OF YUZURIMINE-C (**1**), YUZURIMINE (**2**), AND ITS DERIVATIVES (**10**—**13**)

Functional group	Compound						Assignment
	1	**2**	**10**	**11**	**12**	**13**	
-Me	11.4	14.7	14.9	15.5	14.2	18.4	C-22
	51.2	51.0	51.5	51.1	51.1	51.3	C-23
					a)47.6*	b)37.2*	a) N-Me b) $-SO_2-Me$
$-CH_2-$	24.8	25.2	25.6	25.4	24.9	25.1	C-3, 11, 12, 13,
	25.6	27.1	27.4	26.9	26.8	25.6	16, 17
	29.6	27.3	29.7	27.2	28.7	27.7	
	35.5	28.7	30.7	28.2	29.8	39.9	
	42.4	37.4	36.7	39.1	40.4	43.3	
		43.1	43.3	42.8	42.4		
	49.1	58.6	59.2	58.1	67.1	51.7	C-7, 19, 20
	56.8	64.4	64.8	64.8	67.1	63.7	
		67.0	66.7	67.1	68.4	71.6	
C=O	a)207.0				b)189.3		a) C-20 b) C-1
-CH-	36.0	34.3	32.3*	35.1*	39.0**	32.9	C-6
	40.6	34.3	34.4*	37.6*	39.7**	35.1**	C-18
		42.2*	42.5**	38.3*	41.9**	39.2**	C-2
	43.0	43.1*	43.6**	42.8	43.2**	42.9	C-15
	55.9	57.5	57.9	54.0	56.7	54.8	C-14
		72.9	71.7	73.4	71.5		C-4
				67.0		66.8	C-1
-C-	48.7	45.0	45.9	41.1	44.3*	39.9*	C-5
	55.2	52.1	51.7	46.4	60.0	42.9*	C-8
	91.6	96.8	97.3				C-1
	80.1						C-2
-COOMe	175.6	175.3	177.6	175.0	175.5	175.2	C-21
>C=C<	125.0	136.7	136.7	133.4	132.9	138.6	C-9, 10
	136.9	144.0	144.0	144.5	145.0	140.2	
	125.0					127.8	C-3, 4
	132.5					131.5	
AcO-		21.0		21.1	21.1		Me-COO-
		21.0		21.1	21.1		
		170.1		170.1	170.1		Me-COO-
		170.8		170.8	170.6		

1) Chemical shifts are given in ppm relative to TMS. 2) Assignment of chemical shifts for close-lying peaks marked with asterisk may be reversed. 3) The ketonic ^{13}C NMR signal in **12** is observed at extraordinary high field (δ 189.3 ppm), indicating the presence of a strong interaction between the keto-group and the nitrogen atom, as suggested by the IR spectrum (ν_{max} 1633 cm^{-1})[2].

spectra of **1** and **13**. These facts are in good agreement with the partial structures, as shown below. The

Yuzurimine-C (**1**)

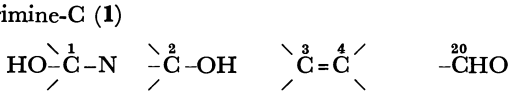

2 and **10**

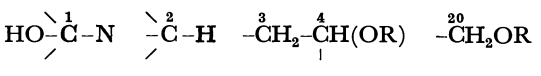

presence of the hydroxyl group on C-2 in yuzurimine-C (**1**) rationalized the upfield shift of C-19 and C-22 signals and the down field shift of C-18 signal. The PRFT spectrum of **1** which lacks the signal at δ 125.0 ppm clearly indicates that the signal of one disubstituted olefinic carbon overlaps with that of one of the two tetra-substituted olefinic carbon atoms. The other signals show the one to one correspondence to each carbon atom.

The present study indicates that partially relaxed Fourier transform ^{13}C NMR technique must be very useful in the structural study on the daphniphyllum alkaloids of undetermined complex structure.[8,9]

From a structural point of view,[8] yuzurimine-C (**1**) belongs to be yuzurimine group of alkaloids as suggested in the previous paper,[1] and is the most highly oxygenated product among them.

Experimental

All mps were uncorrected. The IR and UV spectra were recorded on a JASCO Model IR-S and on a Perkin-Elmer 202 spectrophotometer, respectively. The ^1H and ^{13}C NMR spectra were obtained on a Nihondenshi JNM-PS 100 (100 MHz) and on a Nihondenshi JNM-PFT 60 (15.04 MHz), respectively. Chemical shifts for all NMR spectra are given in ppm from TMS as an internal standard using $CDCl_3$ as

solvent, unless otherwise stated. Only prominent peaks are cited. (d, doublet; m, multiplet; q, quartet; s, singlet; t, triplet). The mass spectra were recorded on a Hitachi RMU-6C mass spectrometer with an ionization energy of 70 eV. Column chromatography was carried out on basic alumina (Nakarai Chemical Co. Ltd., *ca.* 200 mesh). Thin layer chromatography (tlc) was performed on Kieselgel 60 PF_{254} using *n*-hexane–ether–diethylamine (10: 10: 1), unless otherwise stated.

Physical Properties of Yuzurimine-C (1). Mp 186—187 °C (from *n*-hexane–acetone); $[\alpha]_D^{25} = +28°$ ($c=1.33$ in $CHCl_3$); ν_{max} (KBr) 3450 br. s, 1736, 1722, and 1660 cm^{-1}; λ(EtOH) 210 nm (ε, 8410), end absorption; δ 1.04 (3H, d, $J=6.0$ Hz), 3.58 (3H, s), 5.61 (1H, d, $J=10.0$ Hz), 6.20 (1H, d, $J=10.0$ Hz), and 9.99 ppm (1H, s); *m/e* 399 (M^+), 381, 353, 352, and 324 (Found: C, 69.01; H, 7.22; N, 3.57%. Calcd for $C_{23}H_{29}O_5N$: C, 69.15; H, 7.32; N, 3.51%).

Formation of Yuzurimine-C methiodide (3). A solution of yuzurimine-C (20 mg) and MeI (2 ml) in acetone (5 ml) was heated under reflux for 6 hr, and then concentrated under reduced press to leave pale yellow crystals in quantitative yield, which were recrystallized from acetone–Et_2O to give needles of the corresponding methiodide (**3**), mp (decomp.) 209—210 °C; ν_{max} (Nujol) 3280, 1745, and 1720 cm^{-1}; δ($CDCl_3$–CD_3OD) 1.17 (3H, d, $J=6.0$ Hz), 3.20 (3H, s), 3.65 (3H, s), 3.56—4.60 (4-5H, complex), 5.88 (1H, d, $J=10$ Hz), 6.45 (1H, d, $J=10$ Hz) and 9.99 ppm (1H, s); *m/e* 413 (M^+—HI), 398, 384, 370, 356, and 327 (Found: C, 53.15; H, 6.04; N, 2.09%. Calcd for $C_{24}H_{32}O_5NI$: C, 53.24; H, 5.96; N, 2.59%).

Formation of the Keto-amine (4). A solution of **3** (30 mg) in $CHCl_3$ (20 ml) was shaken well with water (15 ml) containing Na_2CO_3 (30 mg). The chloroform solution was washed with sat. NaCl aq. solution, and then dried over anhydrous Na_2SO_4. Removal of the solvent afforded white crystals of **4** in almost quantitative yield, mp 199—200 °C (from acetone–*n*-hexane); ν_{max} (Nujol) 3400, 1725, 1715 sh., and 1640 cm^{-1}; δ 0.92 (3H, d, $J=7.0$ Hz), 2.17 (3H, s), 3.63 (3H, s), 4.08 (2H, br.), 5.83 (1H, d, $J=10$ Hz), 6.34 (1H, d, $J=10$ Hz), and 10.1 ppm (1H, s); *m/e* 413 (M^+), 398, 384, 370, 356, and 327 (Found: C, 69.27; H, 7.52; N, 3.20%. Calcd for $C_{24}H_{31}O_5N$: C, 69.70; H, 7.51; N, 3.39%).

Oxidation of Yuzurimine-C (1) with $NaIO_4$. To a solution of yuzurimine-C (100 mg) in MeOH–THF (4: 1; 8 ml) was added a solution of $NaIO_4$ (150 mg) in 50% aq. MeOH (3 ml) with stirring. The resulting solution was further stirred at room temperature for 16 hr, and then concentrated under reduced press. The remaining reaction mixture was dissolved in water and extracted with $CHCl_3$. The extract was washed with sat. NaCl aq. solution and then dried over anhydrous Na_2SO_4. Removal of the solvent gave an amorphous solid (*ca.* 107 mg), which was chromatographed on alumina (0.5 g) and eluted with Et_2O to give colorless needles of the keto-lactam (**5**), mp 179—181 °C (from Et_2O); ν_{max} (Nujol) 1737, 1705 br., and 1660 cm^{-1} (no OH absorption band); λ_{max} (MeOH) 215 nm (ε, 6590); δ 1.01 (3H, d, $J=7.0$ Hz), 3.06—3.50 (3H, complex), 3.64 (3H, s), 3,85 (1H, q, $J=13$, 8 Hz), 4.40 (1H, q, $J=12$, 8 Hz), 5.61 (1H, d, $J=14$ Hz), 6.01 (1H, d, $J=14$ Hz), and 9.95 ppm (1H, s); *m/e* 397 (M^+), 383, 369, 355, 350, 337, 311, and 310 (Found: C, 69.83; H, 7.02; N, 3.56%. Calcd for $C_{23}H_{27}O_5N$: C, 69.50; H, 6.85; N, 3.52%).

Catalytic hydrogenation of the Keto-lactam (5). Catalytic hydrogenation of **5** (15 mg) in EtOAc (2 ml) was carried out over 10% Pd–C (5 mg) at room temp. overnight, and then the catalysts were filtered. The filtrates were evaporated under reduced press. to give an almost colorless oil, which was chromatographed on alumina. Elution with Et_2O afforded white crystals (13 mg) which were recrystallized from Et_2O–*n*-hexane to give colorless plates of **6**, mp 168—169 °C; ν_{max} (Nujol) 1735, 1710, 1695, and 1623 cm^{-1}; δ 1.02 (3H, d, $J=7.0$ Hz), 3.05—3.50 (3H, complex), 3.64 (3H, s), 3.66 (1H, q, $J=13$, 8 Hz), 4.56 (1H, q, $J=12.5$, 8 Hz), and 10.01 ppm (1H, s); *m/e* 399 (M^+), 371, 339, 313, 312, 311, and 301 (Found: C, 69.12; H, 7.32; N, 3.35%. Calcd for $C_{23}H_{29}O_5N$: C, 69.15; H, 7.32; N, 3.51%).

$LiAlH_4$ Reduction of Yuzurimine-C (1). To a solution of yuzurimine-C (69 mg) in THF (3 ml) was added $LiAlH_4$ (14 mg) with stirring, and then the heterogeneous solution was continuously stirred at room temperature for 5 hr. After excess $LiAlH_4$ was decomposed with EtOH, the reaction mixture was poured into sat. potassium sodium tartarate aq. solution and extracted with $CHCl_3$. The extract was washed with sat. NaCl aq. solution and then dried over anhydrous Na_2SO_4. Removal of the solvent gave a white solid (56 mg) which was recrystallized from Et_2O–acetone to afford white crystals of **7**, mp 168—170 °C; ν_{max}(Nujol) 3470, 3420, and 1715 cm^{-1}; δ 1.16 (3H, d, $J=7.0$ Hz), 3.62 (3H, s), 3.75 (1H, d, $J=12$ Hz), 4.06 (1H, d, $J=12$ Hz), 5.69 (1H, d, $J=10$ Hz) and 5.83 ppm (1H, d, $J=10$ Hz); *m/e* 385 (M^+ for $C_{23}H_{31}O_4N$), 368, 354, and 326.

Acetylation of 7. A solution of **7** (15 mg) in dry pyridine (1 ml) and acetic anhydride (1 ml) was allowed to stand at room temperature overnight, and then concentrated under reduced press. to give a pale brown oil, which was chromatographed on alumina and eluted with EtOAc to give colorless needles of **8** (12 mg), mp 171—173 °C (from *n*-hexane–acetone); ν_{max} (Nujol) 3440, 1745, and 1735 cm^{-1}; δ 1.12 (3H, d, $J=7.0$ Hz), 2.09 (3H, s), 3.66 (3H, s), 4.48 (2H, br. s) and 5.72 ppm (2H, br. s); *m/e* 427 (M^+), 387, 368, 345, and 300 (Found: *m/e* 427.2336. Calcd for $C_{25}H_{33}O_5N$: *m/e* 427.2359).

References

1) M. Toda, H. Irikawa, S. Yamamura, and Y. Hirata, *Nippon Kagaku Zasshi*, **91**, 103 (1970); M. Toda, Y. Hirata, and S. Yamamura, *Tetrahedron*, **28**, 1477 (1972).

2) H. Irikawa, S. Yamamura, and Y. Hirata, *Tetrahedron*, **28**, 3727 (1972).

3) H. Irikawa, N. Sakabe, S. Yamamura, and Y. Hirata, *ibid.*, **24**, 5691 (1968).

4) M. Toda, H. Niwa, H. Irikawa, Y. Hirata, and S. Yamamura, *ibid.*, **30**, 2683 (1974).

5) S. Sternhell, *Quart. Rev.*, **23**, 236 (1969) and references cited therein.

6) M. Toda, Y. Hirata, and S. Yamamura, *Chem Commun.*, **1970**, 1597.

7) G. C. Levy and G. L. Nelson, "Carbon-13 Nuclear Magnetic Resonance for Organic Chemists," Wiley-Interscience, New York, N. Y. (1972), p. 176.

8) S. Yamamura and Y. Hirata, "The Alkaloids," Vol. XV, ed. by R. H. F. Manske, Academic Press, New York (1975), in press. See also MTP International Review of Science," ed. by K. Wiesner, Butterworths, London (1975), in press.

9) S. Yamamura, J. A. Lamberton, M. Toda, and Y. Hirata, *Tetrahedron*, in press (1975).

Synthesis of 1-*N*-[(*S*)-4-Amino-2-hydroxybutyryl]lividomycin A[1]

Isamu WATANABE, Tsutomu TSUCHIYA, Sumio UMEZAWA, and Hamao UMEZAWA*

Department of Applied Chemistry, Faculty of Engineering, Keio University, Hiyoshi, Yokohama 223

**Institute of Microbial Chemistry, Kamiosaki, Shinagawa-ku, Tokyo 141*

(Received April 16, 1975)

The title compound (**7**), which is active against resistant bacteria producing phosphotransferase I, was synthesized from lividomycin A through a cyclic carbamate derivative (**3**). Selective hydrolysis of the carbamate ring followed by acylation of the free C-1-amino group with (*S*)-2-hydroxy-4-aminobutyric acid by the active ester method led to **7**.

As already described,[2] (*S*)-4-amino-2-hydroxybutyrylation of 1-NH_2 of ribostamycin gives butirosin B which is active against kanamycin-resistant strains such as *E. coli* K–12 ML 1629 and ML 1630 producing neomycin-kanamycin phosphotransferase I[3] (P-ase I). The 5″-hydroxy group of lividomycins,[4] and ribostamycin undergoes this enzyme reaction and these antibiotics do not inhibit growth of these resistant organisms. We designed, therefore, to attach the above-mentioned side chain to the 1-NH_2 of lividomycin A, hoping that this antibiotic could be converted to a derivative with the activity against resistant strains.

Lividomycin A was treated with benzyl chloroformate to give penta-*N*-benzyloxycarbonyl derivative (**1**), which was treated with benzaldehyde dimethyl acetal in the presence of acidic catalyst according to the method described by Bissett, Evans, and Parrish.[5] Chromatographic separation of the products gave the tri-*O*-benzylidene derivative (**2**) in a yield of 48%. It should be noted that cyclohexylidenation of tetra-*N*-benzyloxycarbonylribostamycin with cyclohexanone dimethyl ketal gave a 5″-*O*-(1-methoxycyclohexyl) derivative.[6]

Selective removal of the protecting group at 1-NH_2 was successful through the cyclic carbamate method.[2] Treatment of **2** with sodium hydride in DMF afforded the 1,6-cyclic carbamate (**3**) in a yield of 52%. The presence of the cyclic carbamate was confirmed by the absorption peak[7] at 1765 cm^{-1}. Another cyclic carbamate formation between 2-NH_2 and 3-OH groups in the L-idose moiety was not recognized, suggesting that the 2,6-diamino-2,6-dideoxyidose moiety may be in 1C-like conformation which hinders the carbamate formation.

In order to determine the positions of the benzylidene and cyclic carbamate groups, **3** was mesylated in pyridine and the tri-*O*-mesyl derivative (**4**) was subjected to acidic hydrolysis in methanol. On examination of the hydrolyzate by thin-layer chromatography, the formation of 3′-deoxyparomamine[8] and methyl mannoside was clearly discerned, but formation of methyl riboside and methyl 2,6-diamino-2,6-dideoxyidoside was not observed. Since *O*-mesyl group is generally resistant to acid hydrolysis,[9] the above result indicates that the benzylidene groups are attached to 4′,6′-*O*, 2″″,3″″-*O*, and 4″″,6″″-*O*, and the cyclic carbamate is formed between 1-NH_2 and 6-OH groups. Observation of no OMe group of hemiacetal in the NMR spectrum of **3** also supported the structure **3**.

Protection of the hydroxyl groups with benzylidene groups is not required for the formation of 1,6-cyclic carbamate[7]; treatment of **1** with sodium hydride in DMF gave the corresponding cyclic carbamate in a yield of 45%. However, benzylidenation increased the solubility in organic solvents and facilitated later 1-*N*-acylation.

Selective hydrolysis of the cylic carbamate by gradual addition of barium hydroxide in a manner as already described[2] gave the aminol (**5**), which was then condensed with (*S*)-2-hydroxy-4-phthalimidobutyric acid[10] (HPBA) by the active ester method, using *N*-hydroxysuccinimide and dicyclohexylcarbodiimide (DCC) in tetrahydrofurane. The condensation product (**6**) was then treated with hydrazine to remove the phthaloyl group and with palladium black and hydrogen to remove the benzyloxycarbonyl and benzylidene groups to give the titled compound (**7**).

A mild acid hydrolysis of **7** gave 1-*N*-((*S*)-4-amino-2-hydroxybutyryl)-3′-deoxyparomamine (**8**), and this fact confirmed the structure of **7**.

The synthetic 1-*N*-((*S*)-4-amino-2-hydroxybutyryl)-lividomycin A showed antibacterial activity[1] against organisms producing P-ase I.

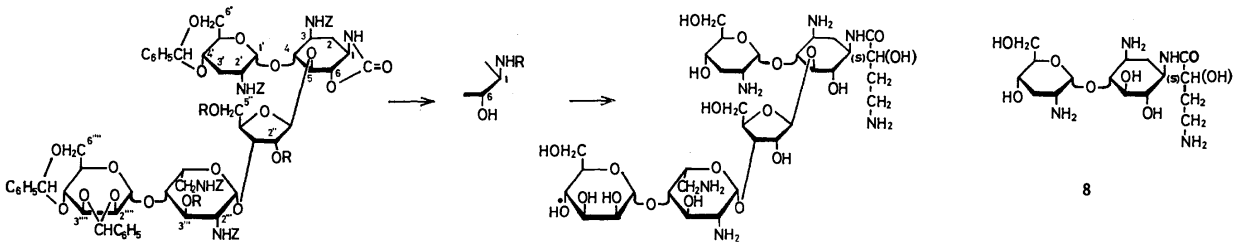

R

3 H

4 SO_2CH_3

R

5 H

6 $COCH(OH)CH_2CH_2N$=Phth

7

Z : $CO_2CH_2C_6H_5$

Phth : $(OC)_2C_6H_4$

8

Eoperimental

Thin layer chromatography (tlc) was carried out on silica gel (Silica Rider 5B, Daiichi Pure Chemicals Co., Ltd.)unless otherwise stated. Paper chromatography (ppc) was carried out on Toyo-Roshi paper No. 50, developed with 1-butanol-pyridine–water–acetic acid (6: 4: 3: 1) and detected by ninhydrin.

1,3,2′,2‴,6‴-Penta-N-*benzyloxycarbonyllividomycin A (1).* To a mixture of lividomycin A sulfate (21.4 g, approximately 20 mmol of lividomycin A base) and anhydrous sodium carbonate (16 g) in aqueous methanol (1: 4, 500 ml, ice-salt cooled), benzyl chloroformate (22.8 g) was added dropwise under stirring and stirring was continued for 3 hr at −5∼0 °C. The reaction mixture was evaporated to dryness and the residue was extracted with hot acetone (170 ml×3). The combined solution was evaporated to ∼100 ml. Addition of ether (300 ml) gave colorless precipitates, 30 g. On tlc with chloroform–methanol (6: 1), it gave a single spot at R_f 0.57. Purification by column chromatography on silica gel with chloroform–methanol (10: 1) as a solvent gave **1**, 26.07 g (91%); $[\alpha]_D^{22}$ +40 ° (*c* 1, MeOH). Found: C, 57.73; H, 6.14; N, 4.60 %. Calcd for $C_{69}H_{85}N_5O_{28}$: C, 57.86; H, 5.98; N, 4.89%.

4′,6′; 2‴,3‴; 4‴,6‴-Tri-O-*benzylidene-1,3,2′,2‴,6‴-penta*-N-*benzyloxycarbonyllividomycin A (2).* To a solution of **1** (5.5 g) in dry DMF (80 ml), anhydrous *p*-toluenesulfonic acid (140 mg) and benzaldehyde dimethyl acetal (8 g) were added and the solution was heated at 30 °C for 6 hr under reduced pressure (10—15 Torr). On tlc with chloroform–methanol (20: 1), the solution showed a major spot (R_f 0.68) and other several minor spots. Methanol (100 ml) was added and the solution was allowed to stand for 30 min. After addition of saturated sodium hydrogen carbonate solution (3 ml), the mixture was evaporated with the aid of toluene. The residue was extracted with chloroform (150 ml×2). The organic layer was washed with water, dried over sodium sulfate and the solvent was removed by evaporation. The residue (7 g) was chromatographed on a column of silica gel with chloroform–ethanol–triethylamine (25: 1: 0.05). The fractions containing **2** was evaporated to give a solid of **2**, 3.14 g (48%); $[\alpha]_D^{25}$ +32.5 °(*c* 1, $CHCl_3$). Found: C, 63.92; H, 5.92; N, 4.11%. Calcd for $C_{90}H_{97}N_5O_{28}$: C, 63.71; H, 5.76; N, 4.13%. Mono and di-*O*-benzylidene derivatives were also obtained (2.1 g).

4′,6′;2‴,3‴;4‴,6‴-Tri-O-*benzylidene-3,2′,2‴,6‴-tetra*-N-*benzyloxycarbonyllividomycin A 1,6-Carbamate (3).* To an ice-cold solution of **2** (550 mg) in dry DMF (5 ml) under nitrogen, 50% oily sodium hydride (70 mg) was added and the mixture was stirred for 3 hr under cooling. After addition of acetic acid (0.2 ml), the resulting viscous, pale-brown solution was poured into a mixture of chloroform (70 ml) and saturated sodium chloride solution (70 ml) under vigorous stirring. The organic layer was separated, washed with sodium chloride solution, dried over sodium sulfate and evaporated. The residue was chromatographed on a short column of silica gel with chloroform–methanol–triethylamine (20: 1: 0.1) to give a solid of **3**, 270 mg (52%); $[\alpha]_D^{25}$ +34° (*c* 1, $CHCl_3$); IR (KBr): 1765 cm^{-1} (*trans*-fused cyclic carbamate[7]). R_f 0.36 on tlc with chloroform–methanol (20: 1). Found: C, 62.49; H, 5.53; N, 4.21%. Calcd for $C_{83}H_{89}N_5O_{27}$: C, 62.75; H, 5.65; N, 4.41%.

4′,6′;2‴,3‴;4‴,6‴-Tri-O-*benzylidene-3,2′,2‴,6‴-tetra*-N-*benzyloxycarbonyl-2″,5″,3‴-tri*-O-*mesyllividomycin A 1,6-Carbamate (4).* To a solution of **3** (95 mg) in pyridine (2 ml), mesyl chloride (0.1 ml) was added and the solution was allowed to stand at room temperature overnight. Isolation of the product in a usual manner gave a solid of **4**, 105 mg (96%); $[\alpha]_D^{24}$ +28.5° (*c* 1, $CHCl_3$); IR (KBr): 1175 (ν_s SO_2), 1350 (ν_{as} SO_2) ,1770 cm^{-1}; NMR (in $CDCl_3$): δ 2.93 (3H s, SO_2CH_3), 3.06 (6H s, SO_2CH_3). Found: C, 56.39; H, 5.23; N, 3.99; S, 5.54%. Calcd for $C_{86}H_{95}N_5O_{33}S_3$: C, 56.67; H, 5.25; N, 3.84; S, 5.28%.

Acidic Methanolysis of 3 and 4. Procedure 1. A suspension of **3** or **4** in 1 M methanolic hydrogen chloride was heated at 80 °C and the reaction mixture was examined by ppc and ninhydrin coloration. After overnight heating, the reaction mixture of **3** gave a spot of 3′-deoxyparomamine[8] (the R_f-value was taken as 1) and a spot of R_f 3.5. The reaction mixture of **4** gave spots of R_f 4.75 and 3.31 (slight) and 1 (very slight). After 3 days heating, the chromatographic pattern of the reaction mixture of **3** did not changed but that of **4** changed to give a clear spot of 3′-deoxyparomamine. Other spots did not changed.

Procedure 2. A suspension of **3** or **4** in 0.5 M methanolic hydrogen chloride was heated at 80 °C for 2 days and the reaction mixture was examined by tlc (Kieselgel 60 F-254 from E. Merck in Germany) with benzene–methanol (1: 1) and detected by 5% anisaldehyde in ethanolic sulfuric acid. Each of the reaction mixtures gave a spot of methyl mannoside (R_f 0.28).

4′,6′;2‴,3‴; 4‴,6‴-Tri-O-*benzylidene-3,2′,2‴,6‴-tetra*-N-*benzyloxycarbonyllividomycin A (5).* To a solution of **3** (600 mg) in dioxane (35 ml), 0.025 M barium hydroxide solution (6 ml) was added and the mixture was stirred at 60 °C for 30 min to the completeness of neutralization. Additional aliquots (6 ml×2) of the barium hydroxide solution were added and treated similarly. Carbon dioxide was introduced and the mixture was filtrated. After evaporation of the filtrate, the residue was taken up in chloroform, washed with water, dried over sodium sulfate and freed of solvent. The crude product (620 mg) was chromatographed on a short column of silica gel with chloroform–methanol–triethylamine (10: 1: 0.03) to give a solid of **5**, 320 mg (54%); $[\alpha]_D^{20}$ +28° (*c* 1, $CHCl_3$). Found: C, 62.75; H, 6.00; N, 4.26%. Calcd for $C_{82}H_{91}N_5O_{26}$: C, 63.03; H, 5.87; N, 4.48%.

4′,6′; 2‴,3‴;4‴,6‴-Tri-O-*benzylidene-3,2′,2‴,6‴-tetra*-N-*benzyloxycarbonyl-1*-N-[*(S)-2-hydroxy-4-phthalimidobutyryl*]-*lividomycin A (6).* To an ice-cold solution of HPBA (42 mg) and *N*-hydroxysuccinimide (19 mg) in THF (1 ml), DCC (37 mg) was added and the mixture was stirred for 1 hr under cooling. To the resulting suspension, a solution of **5** (205 mg) and triethylamine (30 mg) in THF (2 ml) was added and the mixture was stirred for 2 hr under cooling. After filtration, the solution was evaporated and the residue was extracted with acetone. The solvent was removed and the residue (240 mg) was chromatographed on a short column of silica gel with chloroform–ethanol–triethylamine (20: 1: 0.05) to give a solid of **6**, 172 mg (73%); $[\alpha]_D^{22}$ +37° (*c* 1, $CHCl_3$); IR (KBr): 1713, 1655 (sh), 1525 cm^{-1}. Found: C, 62.73; H, 5.62; N, 4.60%. Calcd for $C_{94}H_{100}N_6O_{30}$: C, 62.94; H, 5.62; N, 4.68%.

1-N-[*(S)-4-Amino-2-hydroxybutyryl*]*lividomycin A (7).* To a suspension of **6** (185 mg) in aqueous ethanol (7: 1, 5 ml), hydrazine hydrate (200 mg) was added and the solution was heated at 60°C for 1.5 hr. After evaporation of the solvent, the residue was washed with water and extracted with chloroform. The solvent was removed and the residue was extracted with dioxane. To the solution (4 ml), water (1 ml) and acetic acid (0.3 ml) were added and the mixture was hydrogenated over palladium black at room temperature overnight. The mixture was filtered and evaporated. The residue was extracted with water and, after addition of a few drops of acetic acid, the aqueous solution was again treated with palladium black and hydrogen likewise. The hydrogenation was repeated once again. After filtration, the filtrate was evaporated and the residue was chromatographed on a column of CM-Sephadex C-25 (NH_4 form). Elution with a linear gradient of am-

monia (0—0.2 M) gave a single peak of chromatographically homogeneous **7**, 63 mg (69%); $[\alpha]_D^{22}$ +68° (*c* 1, H_2O); ppc, $R_{\text{flividonycin A}}$ 0.52; IR (KBr): 1660, 1575 cm^{-1}. Found: C, 44.81; H, 7.13; N, 9.30%. Calcd for $C_{33}H_{62}N_6O_{20}\cdot H_2O$: C, 45.00; H, 7.32; N, 9.54%.

1-N-((S)-4-Amino-2-hydroxybutyryl)-3'-deoxyparomamine (8). A suspension of **7** (100 mg) in 0.4 M methanolic hydrogen chloride (5 ml) in a sealed tube was shaken at 70 °C for 15 hr. Powdered sodium hydrogen carbonate was added and the neutral mixture was filtered and the filtrate was evaporated. The residue was chromatographed on a column of CM-Sephadex C-25 (NH_4 form). Elution with a linear gradient of ammonia (0—0.15 M) gave a single peak of chromatographically homogeneous **8**, 25 mg (47%); $[\alpha]_D^{19}$ +19° (*c* 0.7, H_2O); ppc, $R_{f\ 3'\text{-deoxyparomamine}}$ 0.45; IR (KBr): 1640, 1550 cm^{-1}. Found: C, 43.62; H, 7.41; N, 11.72%. Calcd for $C_{16}H_{32}N_4O_8\cdot H_2CO_3$: C, 43.40; H, 7.28; N, 11.90%.

References

1) Preliminary communication: I. Watanabe, T. Tsuchiya, S. Umezawa, and H. Umezawa, *J. Antibiot.* (Tokyo), **26**, 310 (1973).

2) D. Ikeda, T. Tsuchiya, S. Umezawa, and H. Umezawa, *ibid.*, **25**, 741 (1972).

3) H. Umezawa, H. Yamamoto, M. Yagisawa, S. Kondo, T. Takeuchi, and Y. A. Chabbert, *ibid.*, **26**, 407 (1973).

4) T. Oda, T. Mori, H. Ito, T. Kunieda, and K. Munakata, *ibid.*, **24**, 333 (1971).

5) F. H. Bissett, M. E. Evans, and F. W. Parrish, *Carbohyd. Res.*, **5**, 184 (1967).

6) D. Ikeda, T. Suzuki, T. Tsuchiya, S. Umezawa, and H. Umezawa, This Bulletin, **46**, 3210 (1973).

7) S. Umezawa, Y. Takagi, and T. Tsuchiya, *ibid.*, **44**, 1411 (1971).

8) T. Oda, T. Mori, and Y. Kyotani, *J. Antibiot.* (Tokyo), **24**, 503 (1971).

9) R. S. Tipson, Advances in Carbohydrate Chemistry, Vol. 8, 107 (1953); D. H. Ball and F. W. Parrish, *ibid.*, Vol. 23, 233 (1968).

10) E. Akita, Y. Horiuchi, and T. Ito, Japanese Patent, 49-20166, Feb. 22 (1974).

The Substituent Effect. V. NMR Chemical Shifts of Hydrogen-bonding Hydroxyl Proton of Phenols in DMSO

Mizue FUJIO, Masaaki MISHIMA, Yuho TSUNO,[1)]
Yasuhide YUKAWA* and Yoshio TAKAI*

Department of Chemistry, Faculty of Science, Kyushu University, Hakozaki, Fukuoka 812

**Institute of Scientific and Industrial Research, Osaka University, Yamada-kami, Suita, Osaka 565*

(Received December 10, 1974)

The chemical shifts of the hydrogen bonded OH proton of *m*- and *p*-substituted phenols, and 4-substituted 2-cresols, 3-cresols, and 2,6-xylenols were determined in DMSO. The effects of substituents on the hydroxyl chemical shift of these series were correlated linearly with each other (correlation coefficient$>$0.999), except for the bulky planar substituents in the 3-cresol series which may be subject to the steric loss of their coplanarity with the benzene ring. The substituent effects were treated successfully with the equation, $\Delta\delta=\rho(\sigma^0+r^-\Delta\bar{\sigma}_R^-)$. The phenol series gave $r^-=0.673$ and $\rho=1.530$. The same r^- value appeared to be applicable to all the other series with negligible changes in the ρ value. Deviations from the correlation of particular substituents, in particular those having acidic hydrogen, were attributed to the modification of the electronic nature of substituents arising from the strong substituent-DMSO interaction.

Concerning the substituent effects, we discussed in detail the application of the LArSR Eq. (1) and LSFE Eq. (2)[2)] to the correlational analysis of the hydroxyl proton chemical shifts of *m*- and *p*-substituted phenols in DMF.[3)]

$$\log(k/k_0) \text{ or } P-P_0=\rho\bar{\sigma}=\rho(\sigma^0+r^+\Delta\bar{\sigma}_R^++r^-\Delta\bar{\sigma}_R^-) \quad (1)$$

$$\log(k/k_0)_p=\rho\bar{\sigma}_p=\rho(\sigma_i+q_r^+\sigma_\pi^++q_r^-\sigma_\pi^-) \quad (2)$$

$$\log(k/k_0)_m=\rho\bar{\sigma}_m=\rho(1.17\sigma_i+0.50\sigma_\pi^\pm) \quad (2')$$

The substituent chemical shifts of the hydrogen bonded hydroxyl proton were described in terms of inductive and resonance parameters derived from the chemical reactivity. This might be due to the fact that the hydrogen-bonding of phenols resembles the dissociation of phenols in the electronic situation. The results indicated that the electronic nature of substituents in DMF solution was effectively modified, in reference to those in aqueous solutions, by the particular substituent-solvent interactions. We tentatively derived a set of inductive and resonance substituent constants for such DMF-modified substituent groups. The validity of such a treatment should be verified for systems other than the substituted phenols in DMF solution. Further, the consistency of solvent-modified parameters therefrom should be verified in various systems whose resonance requirements with substituents differ; the constancy of parameters independent of the systems of different combinations of inductive-resonance effects should be examined. Since the chemical shifts of ordinary protons of substituted benzene derivatives are usually determined in non-aqueous aprotic solvents, similar modification of the substituent effect may be involved in these chemical shift data. In order to shed further light on these problems, we have studied substituent effects on the hydrogen-bonded proton NMR chemical shifts of various series of phenols, naphthols,[4)] anilines,[4)] and acetanilides[5)] in several aprotic solvents.

The proton resonance spectra of NH groups generally have a broadened line due to quadrupole of nitrogen, which hinders the ultimate accuracy of the chemical shift measurement of substituted anilines and acetanilides in DMF. However, such a difficulty due to broadening was found to be much reduced in measurements in DMSO solution. A similar improvement was also observed in the determination of OH chemical shifts of some hindered phenol systems such as substituted cresols and xylenols. DMSO is now being extensively used as a solvent and the substituent chemical shift data in DMSO solution have recently become available from our studies which include not only proton NMR but ^{13}C and ^{19}F NMR chemical shift data.[4)] Determination of the set of substituent parameters from the phenol substituent chemical shifts in the particular solvent thus becomes necessary as a reference for this series of studies. The phenol-hydroxyl chemical shifts in DMSO have been studied by several investigators[6-8)] and treated with σ^- constants. Our treatment stands on a different basis and appears to be more consistent.

The present paper gives brief discussions on our LArSR analysis of substituent effects on the chemical shifts of phenols in DMSO solution. A similar treatment of substituent chemical shifts of series of hindered phenols is included for comparison. A forthcoming paper[9)] will give the LSFE analysis and a comparison with relevant treatments of the same material by means of Taft[10)] and Swain and Lupton[11)] equations.

Experimental

The chemical shifts were measured from the low field ^{13}C–H satellite of dimethyl sulfoxide as an internal standard with a Hitachi-Perkin Elmer R-20 Spectrometer operating at 60 MHz.

Dimethyl sulfoxide was fractionally distilled from calcium hydride under reduced pressure and stored over molecular sieves.

All the phenols, cresols and xylenols were thoroughly purified by repeated fractionation or recrystallization from appropriate solvents, and for some phenols purification was effected by further sublimation of purified samples. Melting points and other physical constants agreed well with established values. The preparation of most *m*- and *p*-substituted phenols was previously described.[3)]

m- *and* p-*Hydroxyphenyltrimethylammonium Iodides* were prepared from corresponding aminophenols by exhaustive meth-

ylation with methyl iodide in aqueous sodium carbonate solution; *m*-$(Me)_3N^+I^-$ derivative, mp 198.5 °C, recrystallized from ethanol, lit,[12] mp 179 °C, and *p*-$(Me)_3N^+I^-$ derivative, mp 210.5 °C, recrystallized from ethanol, lit,[12] mp 195 °C.

m-*and* p-*Hydroxyphenyldimethylsulfonium Iodides* were prepared from methylmercaptophenols by methylation on heating with methyl iodide in a sealed tube at 110 °C for 12 hr; *m*-isomer, mp 79—80 °C, from methanol-ether, lit,[13] mp 97—98 °C; *p*-isomer, mp 127—128 °C, from ethanol-ether, lit,[14] mp 123—124 °C.

m-Methylmercaptophenol afforded m-*hydroxyphenyl methyl sulfoxide* on oxidation. The phenol was allowed to react with methanesulfonyl chloride in acetic anhydride for 24 hr at 0—−5 °C, to give the methanesulfonate (mp 36—37 °C, lit,[15] mp 38—39 °C). Oxidation of the sulfonate on standing the mixture with fuming nitric acid ($d=1.52$) in acetic anhydride for 24 hr at below 0 °C, yielded *m*-methylsulfinylphenyl methanesulfonate (mp 89—90 °C, lit,[15] mp 89—90 °C), which was hydrolyzed with 10% aq. sodium hydroxide solution at 50 °C for 24 hr to give the final product; mp 55—55.5 °C; from benzene-chloroform, lit,[15] mp 61—62 °C.

Several 3-cresols, available from commercial sources, were purified by appropriate methods; 3-*cresol*, bp 101 °C/20 mmHg, lit,[16] mp 202 °C; 3,4-*dimethylphenol*, mp 62—63 °C, from benzene-petroleum ether, lit,[16] mp 62.5 °C; 4-*chloro*-3-*cresol*, mp 63—63.5 °C, from *n*-hexane, lit,[17] mp 66 °C; 4-*nitro*-3-*cresol*, mp 133—133.5 °C, from ethanol-benzene, lit,[18] mp 129 °C; 4-*methylthio*-3-*cresol*, mp 56.8—57.2 °C, from benzene-*n*-hexane, lit,[12] mp 55—56 °C.

4-*Amino*-3-*cresol* was prepared from 4-nitro-3-cresol by reduction with stannous chloride in alcoholic hydrochloric acid and purified by sublimation under 1 mmHg at 120 °C (mp 180—181 °C, lit,[16] mp 179 °C), which was converted by acetylation with acetic anhydride-water into 4-*acetamino*-3-*cresol* (mp 132—133 °C, from aq. ethanol, lit,[16] mp 130 °C) and by methylation with methyl iodide into 2-*methyl*-4-*hydroxyphenyltrimethylammonium iodide*, mp 216—217 °C, from ethanol, lit,[12] mp 194.8—195 °C.

4-Dimethylamino-3-cresol was also derived from 4-amino-3-cresol. The aminocresol was converted into the methyl ether with diazomethane and then into *N,N,N*-trimethyl-4-methoxy-2-methylanilinium iodide with methyl iodide. The anilinium iodide was converted by the method given by Cope *et al.*,[19] reductive fission with lithium aluminum hydride in boiling THF, into 4-dimethylamino-3-methylanisole (bp 163 °C/26 mmHg), which yielded 4-*dimethylamino*-3-*cresol* (mp 89—89.2 °C, from ligroin. Found: C, 71.37; H, 8.57; N, 9.17%. Calcd for $C_9H_{13}NO$: C, 71.49; H, 8.67; N, 9.26%.) by the ether-fission with boiling hydroiodic acid.

4-Methoxy-3-cresol and 3-methylhydroquinone were prepared from 4-amino-2-cresol. 4-Amino-2-cresol was allowed to react with diazomethane to give 4-amino-2-methylanisole, which was diazotized in dil. sulfuric acid at 0 °C and decomposed at elevated temperature. The phenolic product gave two distillates, bp 120 °C/18 mmHg and bp 160 °C/18 mmHg, on fractionation. 4-*Methoxy*-3-*cresol*, mp 43.5—45.2 °C (lit,[20] mp 46 °C), was obtained from the former fraction by recrystallization from petroleum ether, and 3-*methylhydroquinone*, mp 131.5—132 °C, lit,[21] mp 124—125 °C, from the latter, by recrystallization from benzene.

Oxidation of 4-methylthio-3-cresyl acetate with hydrogen peroxide in acetic acid according to the method given by Bordwell and Boutan[15] gave 4-methylsulfonyl-3-cresyl acetate, which was hydrolyzed with 10% aq. potassium hydroxide solution to give 4-*methylsulfonyl*-3-*cresol* in good yield (mp 105.5—106.5 °C, from chloroform. Found: C, 51.38; H, 5.21; S, 17.28%. Calcd for $C_8H_{10}SO_3$: C, 51.60; H, 5.41; S, 17.22%.). 4-Methylthio-3-cresol was converted into 4-*methylsulfinyl*-3-*cresol* (mp 120.8—121 °C, from benzene-chloroform; Found: C, 56.28; H, 5.82; S, 18.70%. Calcd for $C_8H_{10}SO_2$: C, 56.44; H, 5.92; S, 18.84%.) *via* 4-methylthio-3-cresyl methanesulfonate, by the same oxidation procedure for *m*-hydroxyphenyl methyl sulfoxide. 4-*Hydroxy*-2-*tolyldimethylsulfonium iodide* (mp 113.5—114 °C, from ethanol-ether, lit,[12] mp 110—111 °C) was obtained by the same method as that for hydroxyphenyldimethylsulfonium iodide. 4-*Thiocyano*-3-*cresol* was prepared by the procedure given by Bordwell and Boutan[22] and was purified by recrystallization from benzene-ligroin; mp 79 °C, lit,[23] mp 76 °C.

4-*Acetyl*-3-*cresol* (mp 134 °C, from benzene, lit,[24] mp 128 °C) was obtained by the Fries rearrangement of 3-cresyl acetate with $AlCl_3$, being allowed to stand at room temperature for 24 hr in nitrobenzene.

4-*Bromo*-3-*cresol* was given by the bromination of *m*-cresol according to the reported method.[25] The bromination product obtained by the dropwise addition of bromine to *m*-cresol in chloroform was carefully fractionated to remove the 6-bromo derivative. The fraction, bp 140—145 °C at 20 mmHg, gave 4-bromo-3-cresol and purification was further effected by repeated recrystallization from petroleum ether; mp 59 °C, lit,[26] mp 58.5—59.2 °C and[25] 60—61 °C. 4-Bromo-3-cresol was converted into 4-*cyano*-3-*cresol* (mp 140—140.2 °C, from benzene. Found: C, 72.06; H, 5.21; N, 10.32%. Calcd for C_8H_7NO: C, 72.16; H, 5.30; N, 10.52%.) by the method given by Friedman and Shechter.[27] The 4-cyano derivative was hydrolyzed and esterified with methanol to give 4-*carbomethoxy*-3-*cresol*; mp 115.5—116 °C recrystallized from benzene (lit,[28] mp 109 °C).

2-*Cresol* (bp 128—129 °C/110 mmHg, lit,[16] bp 130 °C/112 mmHg) and 2,4-*xylenol* were obtained by purification of commercial products.

By the usual diazonium method, 4-chloro-2-toluidine was converted into 4-*chloro*-2-*cresol* (mp 48.5—49 °C, from petroleum ether, lit,[17] mp 49 °C), and 4-nitro-2-toluidine into 4-*nitro*-2-*cresol* (mp 95—95.5 °C, from benzene-ligroin, lit,[29] mp 94.4—95 °C).

4-Nitro-2-cresol was reduced with stannous chloride in alcoholic hydrochloric acid into 4-*amino*-2-*cresol* (mp 178 °C subl. at 100 °C/3.5 mmHg, lit,[16] mp 175 °C) which was followed by acetylation with aq. acetic acid and acetic anhydride into 4-*acetylamino*-2-*cresol* (mp 185—185.5 °C from aq. ethanol, lit,[16] mp 179 °C), and also by exhaustive methylation with methyl iodide into 4-*hydroxy*-3-*methyl phenyltrimethylammonium iodide* (mp 226.8—227 °C, from ethanol. Found: C, 40.84; H, 5.60; N, 4.70; I, 42.99%. Calcd for $C_{10}H_{16}ONI$: C, 40.97; H, 5.50; N, 4.78; I, 43.29%.).

4-*Dimethylamino*-2-*cresol* was prepared from 4-amino-2-methylanisole by same procedure as that for 3-cresol derivative, mp 84—85 °C, recrystallized from benzene-ligroin. Found: C, 71.20; H, 8.67; N, 8.98%. Calcd for $C_9H_{13}NO$: C, 71.49; H, 8.67; N, 9.26%.

4-Bromo-2-methylacetanilide was saponified to give 4-bromo-2-methylaniline, which was converted by the diazonium method into 4-*bromo*-2-*cresol*; mp 65—65.5 °C, from ligroin, lit,[16] mp 64 °C. Similarly, 4-*cyano*-2-*cresol* (mp 97.5—97.8 °C, from benzene-ligroin, lit,[16] mp 93 °C) was prepared from 4-cyano-2-methylaniline, and was converted by saponification and esterification into 4-*carbomethoxy*-2-*cresol*; mp125.8—126 °C, from ligroin-benzene. Found: C, 64.87; H, 5.98%. Calcd for $C_9H_{10}O_3$: C, 65.05; H, 6.07%.

4-*Acetyl*-2-*cresol* (mp 112—112.2 °C, from benzene, lit,[30] mp 104 °C) was obtained by the same method as that for 3-cresol.

4-*Methoxy*-2-*cresol* was synthesized according to the reported meth od[31]; 4-methoxyphenol was converted into 2-cresol by

direct introduction of 2-methyl group with dimethylamine and formaldehyde followed by hydrogenolysis (120 atom H_2, 200 °C, 16 hr) in the presence of CuCrO in dioxane; mp 72 °C, from benzene–ligroin, lit,[31] mp 70.5 °C.

4-*Thiocyano*-2-*cresol* was obtained by the same method as that for the 3-cresol derivative; mp 70.5—71 °C, from benzene–ligroin, lit,[23] mp 71 °C.

The following 4-substituted 2,6-xylenols were employed for measurements after repeated recrystallization of commercial products from appropriate solvents; 2,6-*xylenol*, mp 45—45.2 °C, from *n*-hexane, lit,[32] mp 46—47 °C; 2,4,6-*trimethylphenol*, mp 73.8—74.2 °C, from *n*-hexane, lit,[31] mp 70—71 °C; 4-*methylthio*-2,6-*xylenol*, mp 63 °C, from *n*-hexane, lit,[33] mp 62.5—64 °C.

4-*Nitro*-2,6-*xylenol* was prepared by the following procedure. 2,6-xylenol was converted into its methyl ether with dimethyl sulfate and then nitrated with nitric acid in acetic anhydride. 4-Nitro-2,6-xylenol methyl ether obtained was demethylated with hydrobromic acid–acetic acid mixture to give the final compound; mp 172.5—173 °C, from benzene, lit,[32] mp 170—172 °C. 4-*Hydroxy*-2,6-*xylenol* was obtained from the above 4-nitro-2,6-xylenyl methyl ether successively by reduction with tin in hydrochloric acid–ethanol, diazotization of the resulting aniline to give the phenol, and demethylation; mp 153—154 °C, sublimation 120 °C at 4 mmHg, lit,[16] mp 149—151 °C.

4-*Bromo*-2,6-*xylenol* was prepared[34,35] from 2,6-xylenol by bromination in acetic acid at 15°C and purified by recrystallization from *n*-hexane, mp 79—79.5 °C, lit,[35] mp 79 °C. The above 4-bromo compound was converted into 4-*cyano*-2,6-*xylenol* (mp 125 °C, from aq. ethanol, lit,[32] mp 124—125 °C) by the usual procedure[27] with cuprous cyanide in boiling DMF. 4-*Carbomethoxy*-2,6-*xylenol* was given by saponification of the 4-cyano compound and esterification of the 4-carboxylic acid with methanol–conc. sulfuric acid; mp 131.5—132 °C, from benzene, lit,[16] mp 130 °C.

4-*Acetyl*-2,6-*xylenol* was obtained by the Fries rearrangement of 2,6-xylenyl acetate and recrystallized from ethanol–benzene; mp 156—157 °C, lit,[32] mp 151—152 °C. 4-*Benzoyl*-2,6-*xylenol* was prepared by the same procedure from 2,6-xylenyl benzoate; mp 145 °C, from aq. ethanol, lit,[36] mp 142—142.5 °C.

4-*Methoxy*-2,6-*xylenol* was synthesized according to the procedure described for 4-methoxy-2-cresol; mp 78.2—78.5 °C, from ligroin, lit,[31] mp 77 °C.

4-*Hydroxy*-3,5-*dimethylphenyldimethylsulfonium iodide* was prepared from 4-methylthio-2,6-xylenol with methyl iodide by heating under reflux for 30 min; mp 130 °C, from methanol–ether. Found: C, 38.69; H, 5.10; S, 10.52; I, 40.51%. Calcd for $C_{10}H_{15}OSI$: C, 38.72; H, 4.87; S, 10.34; I, 40.91%.

4-*Methylsulfonyl*-2,6-*xylenol* was prepared from 4-methylthio-2,6-xylenol by oxidation by the same procedure as that for *p*-substituted cresol and recrystallized from chloroform–benzene–ethanol, mp 158—159 °C, lit,[37] mp 149—150 °C.

4-*Hydroxy*-3,5-*dimethylphenyl methyl sulfoxide* was prepared by the same procedure as that for *m*-hydroxyphenyl methyl sulfoxide; 4-methylthio-2,6-xylenol was converted into the corresponding methanesulfonate (mp 77—78.5 °C, from chloroform–*n*-hexane) which was oxidized with fuming nitric acid–acetic anhydride to 4-methanesulfoxy-3,5-dimethylphenyl methyl sulfoxide (mp 122.5—123.5 °C, from benzene–chloroform) and then followed by saponification to give the final compound, mp 76—77 °C, from benzene–chloroform–petroleum ether. Found: C, 58.56; H, 6.49; S, 17.23%. Calcd for $C_9H_{12}O_2S$: C, 58.67; H, 6.56; S, 17.40%.

4-*Acetamino*-2,6-*xylenol* was prepared by reduction of 4-nitro-2,6-xylenol with stannous chloride in ethanolic hydrochloric acid, followed by direct acetylation of the aniline obtained with aqueous acetic acid–acetic anhydride mixture and recrystallized from benzene, mp 142.5—143 °C; Found: C, 66.84; H, 7.44; N, 7.56%. Calcd for $C_{10}H_{13}NO_2$: C, 67.02; H, 7.31; N, 7.82%.

Results

In the hydroxyl chemical shift measurement in DMSO solution, relatively sharp and stable signals were obtained for various phenols even under conditions of highest possible dilution (about 0.065 M). The dilution shift was generally insignificant in this solvent, at most *ca.* 2 Hz on 4-fold dilution, and was practically negligible in the case of hindered phenols. Most phenols gave hydroxyl signals of half-height width within 1.5 Hz. Although Traynham[6] did not find the OH signal of *p*-aminophenol, we succeeded in observing a sharp signal of the OH proton with regular intensity by using the sample purified by repeated sublimation immediately before use. Fischer *et al.*[38] reported that 4-formyl- and 4-nitro-2,6-xylenols exhibited very broad peaks, especially the latter a peak of half-height width of 1.4 ppm. According to the present results, 2,6-xylenols generally gave slightly broader signals for the hydroxyl proton than unhindered phenols, but the nitro derivative gave a signal of width within 5 Hz, benzoyl and cyano derivatives 7 Hz, and at the worst, acetyl derivative 12—17 Hz.

The non-equivalent OH protons of 2-methyl- and 2,6-dimethyl-hydroquinones gave two separated signals of the ordinary half-height width in this solvent. This suggests that no rapid proton exchange occurs between the two OH groups. The assignment was made on the basis of correlations between substituent chemical shifts for different structural classes of phenols.

The hydroxyl proton chemical shifts extrapolated to the infinite dilution are summarized in Table 1. Since

Table 1. Chemical shifts of hydroxyl protons of phenols, cresols and xylenols in DMSO

No.	Subst.	Phenol		2-Cresol	2,6-Xylenol	3-Cresol
		$\Delta\delta_p^{TMS}$	$\Delta\delta_m^{TMS}$	$\Delta\delta_{2\text{-Me}}^{TMS}$	$\Delta\delta_{2,6\text{-Me}_2}^{TMS}$	$\Delta\delta_{3\text{-Me}}^{TMS}$
1	NO_2	10.963	10.353	10.907	9.782	10.717
2	CN	10.540	10.140	10.455	9.353	10.418
3	SO_2CH_3	10.510	10.160		9.295	10.367
4	$SOCH_3$	10.010	9.895		8.757	9.855
5	SCN	10.140		10.056		10.070
6	$SMe_2^+I^-$	10.665	10.352		9.513	10.557
7	$NMe_3^+I^-$	10.085	10.168	9.990		10.012
8	COC_6H_5	10.373	9.793		9.185	
9	$COCH_3$	10.250	9.703	10.175	9.047	10.050
10	$COOCH_3$	10.257	9.765	10.172	9.058	10.065
11	H	9.253		9.128	8.072	9.142
12	Br	9.623	9.813	9.515	8.418	9.497
13	Cl	9.600	9.810	9.480		9.468
14	SCH_3	9.370	9.425		8.160	9.252
15	NHAc	9.078	9.262	8.930	7.887	9.127
16	CH_3	9.002	9.140	8.865	7.822	8.885
17	OCH_3	8.828	9.295	8.660	7.617	8.695
18	OH	8.535	9.077	8.382	7.357	8.432
19	NMe_2	8.535	8.928	8.365		8.815
20	NH_2	8.267	8.755	8.078		8.200

the values for *m*- and *p*-substituted phenols were already reported,[3] the Table 1 includes only new data and those necessary for comparison with substituent shifts of other derivatives. The results for *m*- and *p*-substituted phenols are in good agreement with those reported by Traynham[6] and Ouellette[7] within ±0.01 ppm. The data for *p*-acetyl and *p*-trifluoromethyl derivatives are identical with Traynham's values but not with those of Ouellette. Socrates[8] also reported a set of data under the same conditions, differing from ours by more than ±0.1 ppm for 13 derivatives and more than ±0.3 ppm for 6 in 45 derivatives where comparisons are possible. The discrepancies appear to be out of the usual limit of conceivable errors when compared to the fact that the data of Tribble and Traynham differed from ours only at most by 0.03 ppm.

The chemical shifts of 4-substituted 2,6-xylenols are generally in good agreement with those reported by Fischer *et al.*[38]

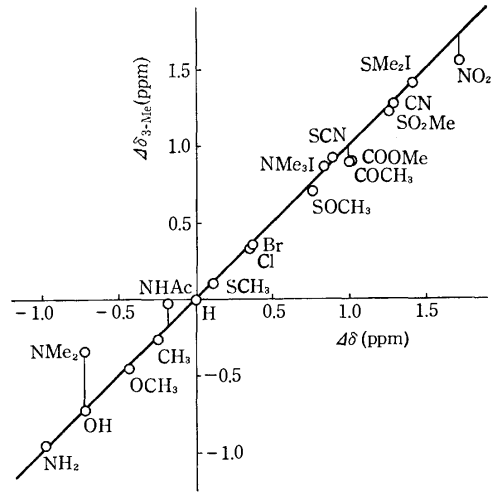

Fig. 1. The linear relation between the substituent chemical shifts of 3-cresols and phenols.

Discussion

In *m*- and *p*-substituted phenols, the electron attracting substituents gave a lower field shift and the releasing groups a higher field shift. This can be interpreted reasonably in terms of the stabilization or the dispersion of the acquired negative charge at the hydroxyl oxygen by the strong OH–DMSO hydrogen-bonding. The stronger hydrogen-bonding by the acid-strengthening substituents should bring about the greater shifts toward down field. Thus the substituent chemical shift may be in principle related to the Hammett-type substituent constants.

The substituent chemical shifts of 4-substituted 2-cresols correlate linearly to those of 4-substituted phenols with excellent precision (correlation coefficient 0.99995 and standard deviation ±0.009) by

$$\Delta\delta_{2\text{-Me}} = 1.047\Delta\delta - 0.008$$

Similarly 4-substituted 2,6-xylenols correlate with phenols by

$$\Delta\delta_{2,6\text{-Me}_2} = 0.999\Delta\delta - 0.009$$

with a correlation coefficient 0.9999 and a standard deviation ±0.013. Introduction of two methyl groups at both *ortho* positions to the phenol hydroxyl markedly shifts the correlation line to up field but does not affect the susceptibility of the hydroxyl chemical shift to changes in 4-substituent. 4-Substituted 3-cresols also give a good linear plot of the substituent chemical shifts against phenols, as shown in Fig. 1 with the slope= 1.000, except dimethylamino, acetamino, and nitro derivatives, deviations of which can of course be referred to the steric loss of coplanarity of substituents with the benzene ring.

Socrates[8] pointed out that the substituent chemical shifts of various phenols, including *ortho*-substituted derivatives, in DMSO solution were correlated linearly to the pK_a of corresponding phenols in water. Figure 2 shows a plot of the chemical shifts obtained in the present study against the corresponding pK_a values in water. Because of their leveling effect, strongly electron releasing substituents in the dissociation of

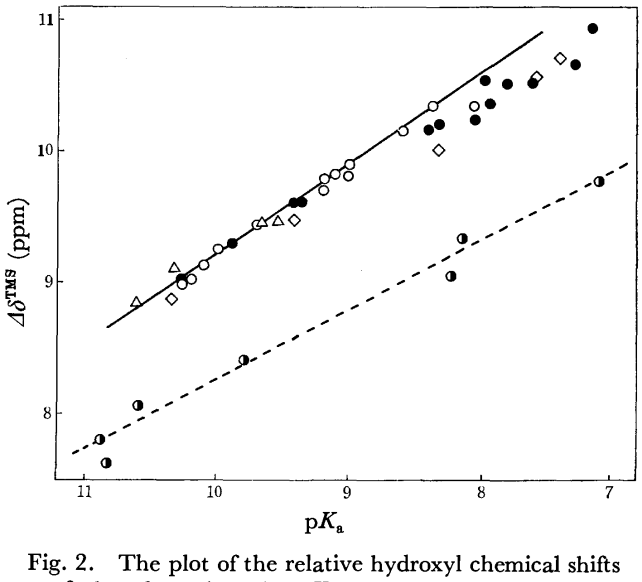

Fig. 2. The plot of the relative hydroxyl chemical shifts of phenols against the pK_a values: *m*-substituted ○, *p*-substituted ● phenols, 3-cresols ◇, 2-cresols△, and 2,6-xylenols ◑.

phenols could not be included in this comparison. *m*-Substituents appear to fall on a straight line and all +*R* class 4-substituted derivatives deviate substantially below the line. These systematic deviations should be significant in view of the excellent correlations of hydroxyl chemical shifts among different classes of phenols above. It is worthy to note that the 2,6-xylenols fall on a parallel line. Thus, Socrates' correlation does not seem to be an accurate description of the substituent effect on the hydroxyl chemical shift of various phenols in DMSO. The systematic deviations of *para* substituents evidently suggest that the resonance contribution (relative to the inductive contribution) of +*R* class *para* substituents is less important in the hydrogen-bonding hydroxyl chemical shifts with DMSO than in the dissociation of phenols in water.

The relative chemical shifts for 17 well-behaving *m*-substituents on phenol in DMSO give a linear Hammett correlation with the standard σ_m constants,[3]

$$\Delta\delta = 1.529\sigma_m - 0.004 \quad (3)$$

with standard deviation ± 0.022 and correlation coefficient 0.9987.[39] Fischer *et al.* applied a similar treatment to each of three sets of literature data[6,7] to give ρ values of 1.4—1.53.[38] In Eq. (3) of *meta* derivatives, deviations are obvious for amino, hydroxyl, and acetamino groups which were not included in the calculation. *m*-Acetyl, *m*-carboalkoxy, and *m*-methoxy groups exhibited slightly less electron-attracting effects than expected from the standard σ_m values and are fitted closer to the correlation line by employing the $\bar{\sigma}$ values, 0.291, 0.31, and 0.06, respectively, which were derived from pK_a of corresponding benzoic acids in aqueous organic solutions.[40] All the results suggest the importance of the solvent-substituent interaction. Amino, acetamino, and hydroxyl groups act as effective hydrogen-bond donors to DMSO. The negative charge acquired at hydroxyl oxygen or amino nitrogen due to hydrogen bonding with an acceptor solvent can make these groups more electron releasing. The loss of hydrogen-bond donation in non-aqueous aprotic solution can explain the deviations of *m*-methoxy, *m*-acetyl, and *m*-carboalkoxy groups. The substituent parameters of a given group should change due to the modification of its electronic nature by the solvent-substituent interaction.[3] Since the ordinary substituent parameters were derived from the data in aqueous solutions where donative hydrogen bonding to substituents is highly important, they may not correlate well with the data in aprotic solvents. We have denoted the overall effect as "the solvent-modification of substituent effects" or "the effect of solvent-modified substituents."[3] There should be a number of possible causes for the deviations, but we assume that the deviations observed in the above correlation can be referred primarily to the effect of the solvent-modification of substituents. Thus, all substituents would be modified more or less in the present system. However, most *meta* substituents except for the few groups mentioned above follow Eq. (3) and the range of fitting covers chemical shift changes over 1.2 ppm. Accordingly the ρ value obtained above appears to be sufficiently reliable.

We see from Socrates' correlation (Fig. 2) that the conjugatively electron attracting ($+R$) *para* substituents exhibit more enhanced resonance effects than those estimated from corresponding σ_p^0 values. Traynham applied σ_p^- values for correlating these substituents and gave slightly different ρ values for *para* and *meta* derivatives.[6] From the systematic deviations in Fig. 2 it is evident that neither σ_p^0 nor σ_p^- could represent appropriately the effects of $+R$ *para* substituents in this system with the same ρ value as *meta* substituents. In order to describe the effects of both *para* and *meta* substituents, an introduction of certain parameter weighting resonance contribution relative to the inductive or unexalted polar contribution appears to be necessary. The LArSR equation can be applied to this system as a useful approximation, giving a satisfactory correlation (for 30 *m*- and *p*-derivatives),

$$\Delta\delta = 1.530(\sigma^0 + 0.673\Delta\bar{\sigma}_R^-) - 0.004 \quad (4)$$

with standard derivation ± 0.024 and correlation coefficient 0.9990.[41] This confirms that the substituent effect on the hydrogen-bonded hydroxyl chemical shift can be treated in the same way as that on chemical reactivities in terms of the Hammett-type substituent parameters. The $-R$ *para* substituents appear to give a better fit to the σ_p than to σ_p^0 constants,[3,42] but the deviations due to the solvent-modification may also be expected for certain *para* substituents as observed in the *meta* correlation. When the $-R$ *para* groups are correlated with the standard σ_p^0 values, the *p*-amino, hydroxy, acetamino and some other groups deviate from the correlation to a comparative extent as the *meta* analogues do. The $+R$ groups generally satisfy Eq. (4), while carbonylamido and sulfonamido groups show significant derivations. Deviations of the trimethylammonium and dimethylsulfonium groups are remarkable. Nevertheless, it is evident from the satisfactory fit to Eq. (4) that modification of the electronic nature of substituents with DMSO is not significant at least as far as the ordinary $+R$ substituents are concerned.

Table 2. Apparent substituent constants in DMSO

No.	Subst.	$\bar{\sigma}_p$				
		Phenols $\bar{\sigma}_m$	Phenols $\bar{\sigma}_p$	2-Cresols $\bar{\sigma}_{2\text{-Me}}$	2,6-Xylenols $\bar{\sigma}_{2,6\text{-Me}_2}$	3-Cresol $\bar{\sigma}_{3\text{-Me}}$
1	NO_2	0.722	1.121	1.118	1.128	1.033
2	CN	0.583	0.844	0.836	0.848	0.838
3	SO_2CH_3	0.596	0.825		0.809	0.804
4	$SOCH_3$	0.422	0.498		0.475	0.469
5	SCN		0.583	0.587		0.609
6	$SMe_2^+I^-$	0.721	0.926		0.952	0.928
7	$NMe_3^+I^-$	0.601	0.547	0.546		0.571
8	COC_6H_5	0.356	0.735		0.737	
9	$COCH_3$	0.297	0.655	0.661	0.647	0.596
10	$COOCH_3$	0.337	0.658	0.659	0.655	0.606
11	H		0.002	0.007	0.008	0.002
12	Br	0.369	0.244	0.249	0.236	0.235
13	Cl	0.367	0.229	0.227		0.216
14	SCH_3	0.115	0.079		0.066	0.074
15	NHAc	0.008	−0.112	−0.116	−0.113	−0.007
16	CH_3	−0.071	−0.162	−0.157	−0.155	−0.166
17	OCH_3	0.030	−0.276	−0.285	−0.290	−0.290
18	OH	−0.113	−0.467	−0.459	−0.457	−0.462
19	NMe_2	−0.210	−0.467	−0.469		−0.211
20	NH_2	−0.323	−0.643	−0.648		−0.614

The ρ values obtained by means of Eqs. (3) and (4) being identical, the apparent $\bar{\sigma}$ values of this system (Table 2) are calculated by using the ρ value of 1.529. The excellent linear correlations of the 4-substituent chemical shifts among phenols, 2- and 3-cresols, and xylenols indicate that these sets of data may give an identical set of apparent $\bar{\sigma}$ values for 4-substituents and that the degree of resonance exaltation of $+R$ 4-substituents, $r^-=0.673$ in Eq. (4), remains practically constant. The ρ value for each structural class is obtained by $1.529\,\lambda$, where λ is the slope of the plot of $\Delta\delta$ for a respective system aganist those of the phenol system. The sets of apparent $\bar{\sigma}$ values for all 4-substituents derived from 2-cresols and 2,6-xylenols are

identical within experimental uncertainty with the values from the parent phenols (Table 2). The same $\bar{\sigma}$ values are also given from the 3-cresol system for most 4-substituents, excluding the bulky planar groups which require the coplanarity with the benzene ring for resonance.

The agreement of these values suggests that the deviations from the calculated set of apparent substituent constants with standard parameters are not due to the experimental error but are inherent to substituents. Apparent $\bar{\sigma}$ values for most substituents are slightly more electron releasing than σ_p^0 for $-R$ groups and the calculated $\bar{\sigma}$ values for $+R$ groups. This can be attributed to the decrease in the electron-attracting effect of substituents in aprotic DMSO due to the absence of hydrogen-bonding from water in which the standard substituent parameters were determined. Significant deviations are observed for the substituents carrying an active hydrogen such as NH_2, OH, $NHCOCH_3$, $CONH_2$ and SO_2NH_2, whose particularly enhanced electron-releasing effects may be explained as to be due to the effect of the negative charge gained through the hydrogen-bonding with DMSO, in addition to the regular enhancement. The decreased electron attraction of charged groups NMe_3^+ and SMe_2^+ should not be unreasonable if the difference in solvation between the charged and dipolar substituents in aprotic and protic solvents is considered. The effect of solvent modification of respective substituents may thus be estimated at least qualitatively by the difference of apparent $\bar{\sigma}$ from the calculated values. However, since the $\bar{\sigma}$ values for $+R$ groups should only measure the apparent effects in reference to a given intermediate r value of 0.673, they cannot be taken as a proper set of substituent parameters for the solvent-modified substituents with DMSO, unless they can be in some way referred to the standard σ^0 scale ($r=0$) or σ^- scale ($r=1.00$).

The effect of the 3-methyl group in the 3-cresol system remains constant regardless of changes in 4-substituents, and the additivity of substituent effects holds giving an apparent $\bar{\sigma}$ of -0.07 for the 3-methyl group, except for the case where the steric loss of resonance of 4-substituents exists. In the 2-cresol system, the effect of the *o*-methyl group is represented similarly in an additive manner giving an apparent -0.075 effect in σ unit for the methyl group, even though the ρ value 1.579 is slightly higher than that for the parent phenol system. Introduction of another *o*-methyl group also exhibits a constant additive effect throughout the series, but the apparent -0.77 effect in σ unit appears too large for it to be referred to the electronic effect of two methyl groups. The effect of the 2,6-dimethyl group would not arise from electronic modification of the system but predominantly from a certain non-electronic effect due to its proximity to the phenol hydroxyl functionality.

The phenomenon was ascribed to the steric loss of coplanarity of the DMSO-hydrogen bonding OH function with the benzene ring and consequently to the enhanced shielding due to an acquired negative charge at the oxygen atom.[6] Deviation from the coplanarity of the detection function should produce a marked decrease in the resonance interaction with $+R$ *para* substituents and this is reflected in the apparent $\bar{\sigma}$ values. However, the difference between the $\bar{\sigma}_p$ values for the hindered and unhindered phenol series is hardly detectable. Further information is obtained from results of the 4-substituted 3-cresol system. 4-Dimethylamino and 4-acetamino groups exhibit a significant loss of electron-releasing effect (Fig. 1), while the 4-hydroxyl group which is effectively stabilized through hydrogen bonding with DMSO shows none. This is in line with the fact that the *o*-cresols exhibit an up-field shift no more significant than expected from the additivity of substituent effects, and does not conflict with the above argument. On the other hand, the chemical shift difference 0.618 of the unhindered hydroxyl proton of 3,5-dimethylhydroquinone relative to 3,5-dimethylphenol provides an apparent $\bar{\sigma}$ value of -0.40 for the sterically hindered hydrogen-bonding 4-OH substituent in the 3,5-xylenol system, on the assumption $\rho=1.53$. The decrease of the $\bar{\sigma}$ value from -0.46 for unhindered systems (Table 2) is insignificant in contrast to the marked reduction observed in the case of the methoxy group from the ordinary value of -0.27 to -0.12 for the hindered one. Thus, the coplanarity of the hydrogen-bonding OH is not lost effectively, even in the presence of two *ortho* methyl groups. The proximity of the DMSO molecule will be determined by the steric effects in the neighborhood of the phenol site and the steric restriction of approach of DMSO to the site should be sufficient to cause a minor loss (*ca.* 10%) in the electron releasing effect of the hydroxyl group. The data appear to be insufficient to draw any decisive conclusion, but it is conceivable that the up-field shift of the hindered hydroxyl proton is caused largely by the change in the extent of transfer of hydrogen-bonding proton between the donor and acceptor molecules.

References

1) To whom inquiries should be addressed.

2) a) Y. Yukawa and Y. Tsuno, This Bulletin, **32**, 960, 965, 971 (1959); Y. Yukawa, Y. Tsuno, and M. Sawada, *ibid.*, **39**, 2274 (1966); Y. Yukawa, Y. Tsuno, and M. Sawada, *ibid.*, **45**, 1198 (1972). b) Y. Yukawa and Y. Tsuno, *Nippon, Kagaku Zasshi*, **86**, 873 (1965); Y. Yukawa and Y. Tsuno, *Memoir, ISIR Osaka Univ.*, **23**, 71 (1966).

3) Y. Tsuno, M. Fujio, Y. Takai, and Y. Yukawa, This Bulletin, **45**, 1519 (1972).

4) Y. Tsuno, M. Fujio, M. Mishima, and Y. Yukawa, unpublished.

5) M. Fujio, Y. Tsuno, Y. Yukawa, and Y. Takai, This Bulletin, in press.

6) J. G. Traynham and G. M. Knesel, *J. Org. Chem.*, **31**, 3350 (1966); M. T. Tribble and J. G. Traynham, *J. Amer. Chem. Soc.*, **91**, 379 (1969).

7) R. J. Ouellette, *Can. J. Chem.*, **43**, 707 (1965).

8) G. Socrates, *Trans. Faraday Soc.*, **66**, 1052 (1970).

9) Y. Tsuno, M. Fujio, and Y. Yukawa, This Bulletin, in press.

10) S. Ehrenson, R. T. C. Brownlee, and R. W. Taft, *Progr. in Phys. Org. Chem.*, **10**, 1 (1973)

11) C. G. Swain and E. C. Lupton, Jr., *J. Amer. Chem.*

Soc., **90**, 4328 (1968).
12) S. Oae and C. C. Price, *ibid.*, **80**, 3425 (1958).
13) T. Zincke and C. Evel, *Ber.*, **47**, 923 (1914).
14) T. Zincke and C. Evel, *ibid.*, **47**, 1100 (1914).
15) F. G. Bordwell and P. J. Boutan, *J. Amer. Chem. Soc.*, **79**, 717 (1957).
16) Dictionary of Organic Compounds (1953).
17) P. T. Sah and H. H. Anderson, *J. Amer. Chem. Soc.*, **63**, 3164 (1941).
18) A. Proskouriakoff and R. J. Titherington. *ibid.*, **52**, 3978 (1930).
19) A. C. Cope, E. Ciganek, L. J. Fleckenstein, and M. A. P. Meisinger, *ibid.*, **82**, 4651 (1960).
20) W. Baker and N. C. Brown, *J. Chem. Soc.*, **1948**, 2303.
21) R. H. C. Nevile and A. Winther, *Ber.*, **15**, 2976 (1882).
22) F. G. Bordwell and P. J. Boutan, *J. Amer. Chem. Soc.*, **78**, 854 (1956).
23) H. P. Kaufmann and E. Weber, *Archiv. Pharm.*, **267**, 192 (1929).
24) A. H. Blatt, Organic Reaction, Vol. 1, p. 354; K. W. Rosenmund and W. Schnurr, *Ann.*, **460**, 56 (1928).
25) E. J. O'Bara, R. B. Balskey, and I. Starer, *J. Org. Chem.*, **35**, 16 (1970).
26) R. C. Huston and A. H. Neeley, *J. Amer. Chem. Soc.*, **57**, 2176 (1935).
27) L. Friedman and H. Shechter, *J. Org. Chem.*, **26**, 2522 (1961).
28) D. Peltier, *Bul. soc. sci. Bretagne*, **31**, 7 (1956); *Chem., Abstr.*, **52**, 9016f (1958).
29) W. R. Vaughan and G. K. Finch, *J. Org. Chem.*, **21**, 1201 (1956).
30) J. Klingel, *Ber.*, **18**, 2687 (1885).
31) W. Peeve and A. Sadle, *J. Amer. Chem. Soc.*, **72**, 3252 (1948).
32) A. Fischer, G. J. Leary, R. D. Topsom, and J. Vaughan, *J. Chem. Soc., B*, **1966**, 782.
33) E. Geothals and P. Radzitzky, *Bull. Soc. Chim. Belges*, **73**, (5–6), 546 (1964); *Chem. Abstr.*, **61**, 10614a (1964).
34) T. C. Bruice, N. Kharasch, and R. J. Winzler, *J. Org. Chem.*, **18**, 83 (1953).
35) H.-J. Brielig and G. Lutzel, *Ann.*, **608**, 140 (1957).
36) K. v. Auweres and E. Jansen, *ibid.*, **483**, 44 (1930).
37) J. Yates and E. Haddock, *Brit.* 128217; *Chem. Abstr.*, **70**, 19804g (1969).
38) A. Fischer, M. C. A. Opie, J. Vaughan, and G. J. Wright, *J. Chem. Soc., B*, **1972**, 319.
39) The following 17 *meta* substituents were included in the calculation; *m*-substituents 1, 2, 8, 9, 10, 11, 12, 13, 14, 16, and 19 of Table 1, and CHO, CF_3, COOEt, F, *t*-Bu, and 3, 5-Me_2 groups.
40) These values were determined from reported data; M. Fujio and Y. Tsuno, unpublished: See also Y. Yukawa, Y. Tsuno, and M. Sawada, This Bulletin, **45**, 1198 (1972).
41) The following *para* substituents were included in addition to the 17 *meta* substituents in Eq. (3); *p*-substituents 1, 2, 5, 8, and 10 of Table 1, and CHO, CF_3, COOEt, $C_6H_5N{=}N$, $C_6H_5N{=}CH$, $C_6H_5CH{=}N$, C_6H_5, SCN, and 3,5-Cl_2 groups.
42) See, Refs. 6, 7, and also M. T. Tribble and J. G. Traynham, "Advances in Linear Free Energy Relationships," Chap. 4, ed. by N. B. Chapman and J. Shorter, Plenum, New York (1972), p. 143.

Studies of the Fragment-ion Distribution and Reaction with a Charge Spectrometer. VI. A New Interpretation of the Fragmentation Mechanism in CH_3X Based on the Molecular Orbital Method. (2)*

Shigeru IKUTA, Kenji YOSHIHARA, and Takanobu SHIOKAWA

Department of Chemistry, Faculty of Science, Tohoku University, Aoba, Aramaki, Sendai 980

(Received September 6, 1974)

We have proposed a new fragmentation mechanism and successfully applied it to various monosubstituted alkanes RX. The fragmentation mechanism can be described as follows: (1) The bond scission first occurs where the electrons exist densely in the particular occupied molecular orbital correlated to the particular ionization. (2) Process (1) competes with the electron redistribution. (3) In the higher-energy region, secondary scission also occurs. The breakdown curves of the $CH_3NH_2^+$, CH_3SH^+, and CH_3Br^+ produced by charge-exchange reactions have been obtained by the use of a perpendicular double-mass spectrometer. The experimental results can be satisfactorily explained by the proposed mechanism on the basis of the calculated eigenvectors of the various molecular orbitals.

The fragmentation mechanism of molecules by electron or photon impact has usually been interpreted by the quasiequilibrium theory (QET) first proposed by Rosenstock *et al.*[1] and later improved by other researchers.[2] Nevertheless, this theory does not have a wide applicability, especially in cases of very large and very small molecules.[3,4]

Hirota[5] and Lorquet[6] have suggested that the scission probability of the skeletal bonds is proportional to the electron densities of the highest occupied molecular orbital at the corresponding bond. However, this theory cannot completely explain the energy dependence of the mass spectra, as was pointed out in a previous paper.[7] Furthermore, in the cases of molecules with lone-pair electrons, the highest occupied MO is non-bonding, and the ionization caused by the loss of the non-bonding electron results in the formation of the stable molecular ion and does not result in the formation of the fragment ions. Therefore, in these molecules, Hirota's proposal is incomplete as an explanation of the production of the fragment ions.

In a previous paper[8] on the breakdown curves of various CH_3X substances (X=NH_2, OH, SH, Cl, Br, and I), we found that the C–X bond in methyl halides (Group A) easily dissociates, while that in methylamine, methanol, or methyl mercaptan (Group B) does not. This difference can be interpreted in terms of the main character of the various occupied MO's calculated by the Extended Hückel Molecular Orbital method,[9] on the assumption that fragmentation occurs at the bond at which an electron is ejected.

In this study we have improved our earlier proposal,[8] put forward a new theory based on the molecular orbital method for fragmentation mechanism, and succeeded in interpreting the fragmentation in several typical cases (CH_3NH_2, CH_3SH, and CH_3Br).

Experimental

The fragmentation of CH_3X^+ produced by charge-exchange reactions was studied using a perpendicular-type double-mass spectrometer. The details of the apparatus have already been described.[10] In this work, H_2S^+, $C_2H_2^+$, Xe^+, H^+, Kr^+, Ar^+, Xe^{++}, Ne^+, and He^+ ions were used as the primary incident ions; they were led into the reaction chamber, where the charge exchange between these ions and CH_3X occurred. The pressure in the reaction chamber was kept below 8×10^{-6} Torr in order to avoid consecutive ion-molecule reactions between the fragment ions and neutral molecules.

Calculation

The eigenvectors of the molecular orbitals of various CH_3X substances were calculated according to the Extended Hückel Molecular Orbital method.[9] The molecular orbitals to describe these molecules are represented by a linear combination of valence atomic orbitals. The Coulomb integrals of the atomic orbitals, H_{ii}, are shown in Table 1. The resonance integral between the i th and j th atomic orbitals, H_{ij}, was calculated by means of this equation: $H_{ij}=0.5\ K(H_{ii}+H_{jj})S_{ij}$, where S_{ij} was the overlap integral and where the value of K was taken to be 1.75, as in Hoffmann's paper.[9] For the calculation of the overlap integral, Slater μ-values for the valence-shell ns and np atomic orbitals were used as in Mulliken's paper,[11] and 4 was taken as the effective quantum number, n^* for bromine.[11] The calculation was performed at the Computer Center of Tohoku University.

TABLE 1. H_{ii} VALUES IN THIS CALCULATION

	H	C	N	O	F	S	Cl	Br	I
H_{ii}(ns)	13.60[b]	18.00[a]	24.00[c]	24.00[a]	31.00[a]	16.00[a]	18.00[a]	27.00[a]	24.00[c]
H_{ii}(np)		11.26[b]	14.49[b]	13.62[b]	17.42[b]	10.36[b]	12.97[b]	11.81[b]	10.45[b]

a) A. D. Baker and D. Betteridge, "Photoelectron Spectroscopy," Pergamon Press, London (1972). b) J. Mály and M. Hussonnois, *Theoret. Chim. Acta* (Berl.), **31**, 137 (1973). c) J. A. Bearden and A. F. Burr, *Rev. Mod. Phys.*, **39**, 125 (1967).

* Part 1 of this series of studies has been published in *Mass Spectroscopy, Japan*, **22**, 233 (1974).

Results and Discussion

Hirota[5] has proposed the molecular orbital theory to account for the mass spectra resulting from electron impact. According to his theory, the scission probability of the skeletal bonds is proportional to the electron densities of the highest occupied MO at the corresponding bond of the bombarded molecule. However, this theory cannot apply to the following fragmentation processes: (i) the fragmentation to produce the hydrogen-deficient ion from the molecular ion, and (ii) the fragmentation of the molecular ions involving lone-pair electrons. Also, his theory has difficulty in explaining the energy dependence of the fragmentation of the molecular ions as a function of an absorbed energy.[7]

Therefore, we considered the fragmentation mechanism to be as follows:

(1) The bond scission first occurs where the electrons exist densely in the particular occupied MO correlated to the particular ionization.

(2) Process (1) competes with the electron redistribution.

(3) In a higher-energy region, secondary scission also occurs.

Based on Process (1), the primary fragment ions from the molecular ions can be predicted by the main character of the particular MO which is correlated to the particular ionization. For example, if the occupied MO is non-bonding, the ionization caused by the loss of the non-bonding electron should result in the formation of the stable molecular ion. If the occupied MO is C-X bonding, the ionization caused by the loss of the electron in this orbital should result in the scission of the C-X bond. The absorbed-energy dependence of the fragmentation processes of the molecular ions can be explained by Processes (2) and (3) in addition to Process (1). Although we have obtained the breakdown curves of CH_3X (X=NH_2, OH, SH, Cl, Br, and I), this paper will deal with the typical fragmentation mechanism of methylamine (CH_3NH_2), methyl mercaptan (CH_3SH), and methyl bromide (CH_3Br).

Table 2. Calculated ionization potentials, eigenvectors, main character of MO and model employed for calculation on methylamine

	Ionization potential (eV)			
Calcd	16.17	15.55	14.19	13.44
Obsd[12]	15.6	14.5	13.2	9.7
	Eigenvectors			
C(2s)	0.0008	−0.0184	0.0000	0.0019
C(2pX)	0.0000	−0.0000	0.5662	−0.0000
C(2pY)	−0.3179	−0.2959	−0.0000	0.0073
C(2pZ)	0.2723	−0.3252	−0.0000	−0.4262
H_1	0.2973	−0.1579	−0.0000	−0.3936
H_2	−0.0089	0.2140	0.4062	0.1766
H_3	−0.0089	0.2140	0.4062	0.1766
N(2s)	−0.1419	0.0174	0.0000	−0.1105
N(2pX)	−0.0000	−0.0000	−0.3518	0.0000
N(2pY)	0.3942	0.5620	−0.0000	−0.1798
N(2pZ)	0.4978	−0.3593	−0.0000	0.7377
H_4	0.1236	0.0563	−0.1620	0.0570
H_5	0.1236	0.0563	0.1620	0.0570
	Main character			
	σ (C–N) σ (C–H)	π (CH_3) σ (C–N)	π (CH_2).	n (N) σ (C–H)

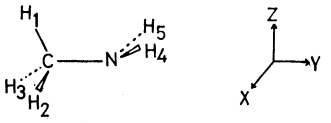

Methylamine (CH_3NH_2). The electronic configuration and the model employed for this calculation on methylamine are shown in Table 2. The highest occupied MO(HOMO) is non-bonding (n(N)) and C–H bonding (σ(C–H)), because there is a larger population of the eigenvectors in the N(2pZ), C(2pZ), and H_1 atomic orbitals. The second occupied MO (SOMO) is C–H bonding (π(CH_2)), the third occupied MO (TOMO) is C–H bonding (π(CH_3)) and C–N bonding (σ(C–N)), and the fourth occupied MO(FOMO) is C–N bonding (σ(C–N)), N–H bonding (π(NH_2)), and C–H bonding (σ(C–H)).

According to Mechanism (1) the mechanism may be considered to be as follows. The ionization caused by the loss of the N(2pZ) non-bonding electron in HOMO results in the formation of the stable molecular ion, P^+, while the ionization caused by the loss of the C–H bonding electron in HOMO results in the formation of the $(P–H)^+$ ion, followed by the scission of the C–H bond. The ionization caused by the loss of the electron in SOMO results in the formation of the $(P–nH)^+$ ion, while the ionization caused by the loss of the electron in TOMO or FOMO results in the formation of the $(P–nH)^+$, and CH_3^+ or NH_2^+ ions, where $(P–nH)^+$ ion indicates a hydrogen-deficient species ($(P–H)^+$, $(P–2H)^+$, or $(P–3H)^+$) from the molecular ions. One hydrogen-deficient ion $(P–H)^+$ is considered to have the formula of $CH_2NH_2^+$ instead of CH_3NH^+, because the highest occupied MO is C–H bonding (and n(N)), while the second occupied MO is also

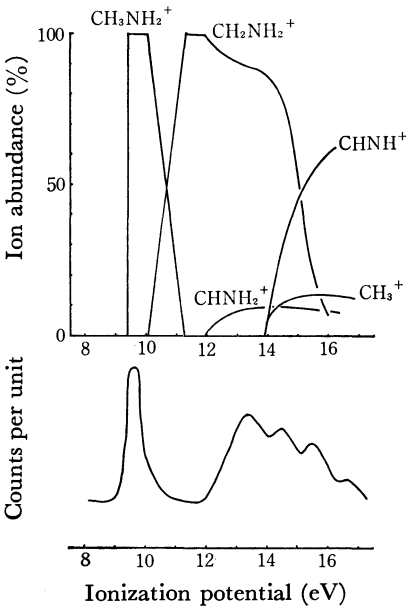

Fig. 1. Comparison of the observed breakdown curve with the photoelectron spectrum[13] for methylamine.

C–H bonding.

The photoelectron spectrum[13] and the breakdown curves of methylamine[14,15] are shown in Fig. 1. Although the bands (above the second one) of the photoelectron spectrum cannot be discriminated well because of the overlapping, there is an agreement between the appearance potentials of the fragment ions obtained by the charge-exchange and those of the bands in the photoelectron spectrum. That is, the appearance potential of $CHNH_2^+$ and that of $CHNH^+$ (or CH_3^+) correspond to the ionization potentials of the second and third bands respectively in the photoelectron spectrum. Although the appearance potential of CH_2-NH_2^+ does not seem to be equal to the ionization potential of the first band in the photoelectron spectrum, this discrepancy may be ascribed to the dissociation of the vibrationally excited ions. In the region of 10.5—12.0 eV, the cross section for photoelectron emission is small; this phenomenon is also observed in the charge-exchange reaction. The relative abundance of $CH_2NH_2^+$ obtained by the charge-exchange reactions is large in this region.

Table 3. Calculated ionization potentials, eigenvectors, main character of MO and model employed for calculation on methyl mercaptan

	Ionization potential (eV)		
Calcd	13.89	11.52	10.38
Obsd[13]	13.67	12.08	9.44
	Eigenvectors		
C(2s)	−0.0830	0.0469	−0.0000
C(2pX)	0.0000	0.0000	0.1514
C(2pY)	−0.5329	0.1276	0.0000
C(2pZ)	0.1600	0.1332	0.0000
H_1	0.1937	0.0153	0.0000
H_2	0.0319	−0.0188	0.0154
H_3	0.0319	−0.0188	−0.0154
S(3s)	−0.0909	−0.4544	0.0000
S(3pX)	0.0000	−0.0000	0.9881
S(3pY)	0.4293	−0.4206	−0.0000
S(3pZ)	−0.2494	−0.7056	0.0000
H_4	0.2805	0.1844	−0.0000
	Main character		
	σ (C–S) σ (S–H)	σ (S–H)	n (S)

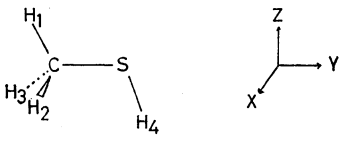

Methyl Mercaptan (CH_3SH). The electronic configuration and the model employed for this calculation of methyl mercaptan are shown in Table 3. The highest occupied MO is non-bonding (n(S)), and the ionization caused by the loss of the non-bonding electron results in the formation of only the stable molecular ion. The second occupied MO is S–H bonding (σ(S–H)), and the ionization caused by the loss of the S–H bonding electron results in the formation of the $(P–H)^+$ ion.[16] As the third occupied MO is C–S, C–H, and S–H bonding, the ionization caused by the loss of the electron in this orbital results in the formation of CH_3^+ or SH^+ and of hydrogen-deficient species from the molecular ions.

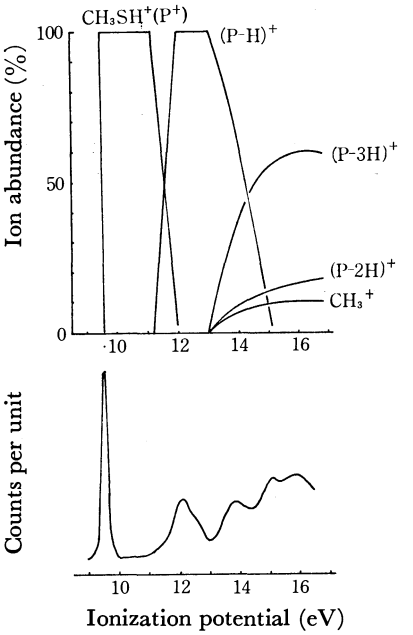

Fig. 2. Comparison of the observed breakdown curve with the photoelectron spectrum[13] for methyl mercaptan.

The photoelectron spectrum[13] and breakdown curves of methyl mercaptan[17] are shown in Fig. 2. The appearance potential of $(P–H)^+$ is equal to the appearance of the second band of the photoelectron spectrum and the appearance potentials of the $(P–3H)^+$ and CH_3^+

Table 4. Caluculated ionization potentials, elgenvectors, main character of MO and model employed for calculation on methyl bromide

	Ionization potential (eV)				
Calcd	14.98	14.98	13.77	11.79	11.79
Obsd[18]	15.85	15.14	13.52	10.85	10.53
	Eigenvectors				
C(2s)	−0.0000	−0.0000	−0.0203	0.0000	0.0000
C(2pX)	0.5825	−0.0000	0.0000	−0.1808	0.0000
C(2pY)	0.0000	0.0000	0.4079	−0.0000	−0.0000
C(2pZ)	0.0000	0.5825	−0.0000	0.0000	0.1808
H_1	0.0000	0.4848	0.0448	0.0000	0.0147
H_2	0.4198	−0.2424	0.0448	−0.0127	−0.0073
H_3	−0.4198	−0.2424	0.0448	0.0127	−0.0073
Br(4s)	−0.0000	−0.0000	−0.1946	−0.0000	−0.0000
Br(4pX)	0.1251	−0.0000	0.0000	0.9833	−0.0001
Br(4pY)	−0.0000	−0.0000	−0.7324	−0.0000	−0.0000
Br(4pZ)	0.0000	0.1251	−0.0000	−0.0001	−0.9833
	Main character				
	π(CH2)	π(CH3)	σ(C–Br)	n(Br)	n(Br)

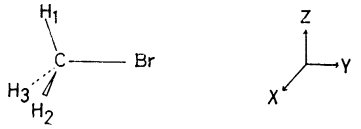

ions are equal to that of the third band. This means that the production of the fragment ions is correlated to the electronic configuration of the molecule. It is clearly shown in Fig. 2 that the stable molecular ion is obtained after the ionization caused by the loss of the electron in the highest occupied MO, the $(P-H)^+$ ion is obtained after that in the second occupied MO, and the $(P-3H)^+$ and CH_3^+ ions are obtained after that in the third occupied MO. These results are in good accordance with our theoretical consideration for the production of the fragment ions.

Methyl Bromide (CH_3Br). The electronic configuration and the model employed for this calculation of methyl bromide are shown in Table 4. As may clearly be seen from the table, the highest occupied MO (which is degenerate) is non-bonding (n(Br)), and the ionization caused by the loss of the non-bonding electron results in the formation of a stable molecular ion. The second occupied MO is C–Br bonding (σ(C–Br)), and the ionization caused by the loss of the C–Br bonding electron results in the formation of CH_3^+ or Br^+. The third occupied MO is C–H bonding, and the ionization of the C–H bonding electron results in the formation of the CH_2Br^+ ion.

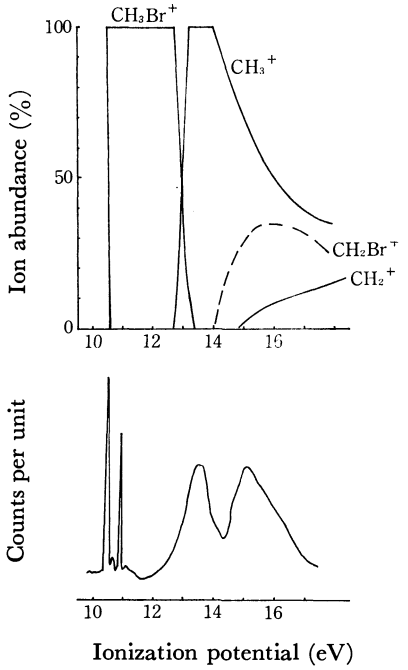

Fig. 3. Comparison of the observed breakdown curve with the photoelectron spectrum[18] for methyl bromide.

The photoelectron spectrum[19] and the breakdown curves of CH_3Br[20] are shown in Fig. 3. The appearance potential of CH_3^+ is equal to that of the second band of the photoelectron spectrum, while the appearance potential of CH_2Br^+ is equal to that of the third band. Accordingly, these results are also in good accordance with our theoretical consideration for the production of the fragment ions.

The energy dependence of the scission probability of the C–X bond in various CH_3X^+ substances (X=NH_2, OH, SH, Cl, Br, and I) obtained by the charge-exchange reactions is shown in Fig. 4. The sum of the abundance of the CH_3^+ and X^+ (produced by the ionization caused by the loss of the C–X bonding electron) was plotted as a function of the absorbed energy of CH_3X. The main characteristics of the highest, second, and third occupied MO's on various CH_3X are shown in Table 5. There are outstanding differences in the main characters in the second and third occupied MO's between Groups A and B. These differences are directly related to the fragmentation processes between the two groups (as is shown in Figs 1. (or 2) and 3, or 4). Moreover, it may be suggested that the order of the scission probability of the C–X bond shown in Fig. 4 corresponds to that of the bond population ($C_iC_jS_{ij}$, where C_i and C_j are the eigenvectors of the i th and j th atomic orbitals, and where S_{ij} is the overlap integral between them) in the second or third occupied MO.[21]

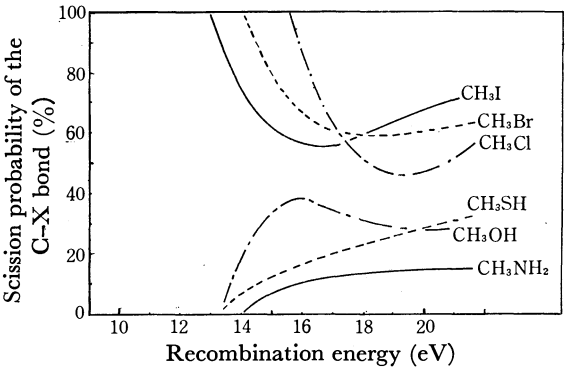

Fig. 4. The observed scission probabilities of the C–X bond in various CH_3X as a function of recombination energy.

Table 5. Main character in the highest, second, and third occupied molecular orbitals on various CH_3X

	Group A		
	Cl	Br	I
Highest	n(Cl)[a]	n(Br)[a]	n(I)[a]
Second	σ(C–Cl)	σ(C–Br)	σ(C–I)
Third	$\pi(CH_3)$[a]	$\pi(CH_3)$[a]	$\pi(CH_3)$[a]

	Group B		
	NH_2	OH	SH
Highest	n(N), $\pi(CH_3)$	n(O)	n(S)
Second	$\pi(CH_2)$	$\pi(CH_3)$	σ(S–H)
Third	σ(C–N),$\pi(CH_3)$	σ(C–O),σ(C–H)	σ(C–S),σ(S–H)

a) Orbital is degenerate

From these results it is obvious that the bond scission first occurs where the electrons exist densely in the particular occupied MO correlated to the particular ionization [Mechanism (1)]. The scission probability can be well predicted by means of the main characteristics and the bond populations of various occupied MO's (which fit the ionization energy) in the cases of simple compounds of CH_3X. Considerations of Mechanism (2), the redistribution of electrons, may become more significant for the more complicated systems, such as C_2H_5X, C_3H_7X, and C_4H_9X.[22] This subject will be discussed in succeeding papers.

References

1) H. M. Rosenstock, M. B. Wallenstein, A. L. Wahrhaftig, and H. Eyring, *Proc. Natl. Acad. Sci.*, U.S., **38**, 667 (1952).
2) M. L. Vestal, *J. Chem. Phys.*, **43**, 1356 (1965).
3) E. Lindholm, "Ion-Molecule Reactions," Vol. 2, ed. by Franklin, Plenum Press, New York (1972), p. 457.
4) H. M. Rosenstock, J. T. Larkins, and J. A. Walker, *Int. J. Mass Spectrom. Ion Phys.*, **4**, 309 (1973).
5) for example; K. Hirota, *Nippon Kagaku Zasshi*, **91**, 585 (1970).
6) J. C. Lorquet, *Mol. Phys.*, **9**, 101 (1965).
7) S. Ikuta, K. Yoshihara, and T. Shiokawa, This Bulletin, **46**, 3648 (1973).
8) S. Ikuta, K. Yoshihara, and T. Shiokawa, *Mass Spectroscopy, Japan*, **22**, 233 (1974).
9) R. Hoffmann, *J. Chem. Phys.*, **39**, 1397 (1963).
10) T. Shiokawa, K. Yoshihara, M. Yagi, T. Omori, H. Kaji, M. Hiraga, T. Nagatani, and Y. Takita, *Mass Spectroscopy, Japan*, **18**, 1230 (1970).
11) R. S. Mulliken, C. A. Rieke, D. Orloff, and H. Orloff, *J. Chem. Phys.*, **17**, 1248 (1949).
12) A. B. Cornford, D. C. Frost, F. G. Herring, and C. A. McDowell, *Can. J. Chem.*, **49**, 1135 (1971).
13) H. Ogata, H. Onizuka, Y. Nihei, and H. Kamada, This Bulletin, **46**, 3026 (1973).
14) H. Sjögren, *Arkiv Fysik*, **29**, 565 (1965).
15) T. Nagatani, K. Yoshihara, and T. Shiokawa, This Bulletin, **46**, 3036 (1973).
16) This $(P-H)^+$ ion is considered to have a formula of CH_3S^+ because ionization of the electron in SOMO which is S–H bonding will produce this ion by the scission of the S–H bond.
17) K. Yoshihara, M. Kobayashi, S. Ikuta, and T. Shiokawa, This Bulletin, in press.
18) J. L. Ragle, I. A. Stenhouse, D. C. Frost, and C. A. McDowell, *J. Chem. Phys.*, **53**, 178 (1970).
19) D. W. Turner, "Molecular Photoelectron Spectroscopy", John Wiley & Sons, New York, N. Y. (1969).
20) S. Ikuta, K. Yoshikawa, and T. Shiokawa, *Mass Spectroscopy, Japan*, to be published.
21) The values of the bond population of the C–X bond in the second or third occupied molecular orbitals are as follows.

CH_3–NH_2: 0.052, CH_3–OH: 0.057, CH_3–SH: 0.110,
CH_3–Cl: 0.125, CH_3–Br: 0.144, CH_3–I: 0.143

The order of the scission probability of the C–X bond shows reverse tendency for CH_3OH and CH_3SH concerning the calculated and observed ones (see Fig. 4). This may be influenced by the degree of elimination of H_2O and/or H_2S from the molecular ions.
22) S. Ikuta, K. Yoshihara, and T. Shiokawa, This Bulletin, to be published.

The Computation of the Thermodynamic Properties of Aqueous Electrolyte Solutions by Means of the Perturbation Theory of Fluids

Fumio HIRATA and Kiyoshi ARAKAWA
Research Institute of Applied Electricity, Hokkaido University, Sapporo 060
(Received November 13, 1974)

A useful method to investigate the thermodynamic properties of aqueous electrolyte solutions was presented on the basis of the perturbation theory of fluids, where a *primitive model* was used as a reference system. A perturbation potential of a square type was applied. An analytical solution of the mean spherical model (MSM) equation obtained by Waisman and Lebowitz was used as the thermodynamic functions of the reference system, and an ionic distribution function in electrolyte solutions was derived. The values of the energy parameters which represent the depth of the well were determined by a comparison of the observed values of the thermodynamic quantities with the calculated ones.

Some remarkable progress in the field of electrolyte solution theory has been made recently,[1–7] the most important example coming from the application of the methods developed in the theory of liquids.[8–10] In many of these studies a simple model ("primitive model"[5]) has been used, where each ion behaves as a charged hard sphere imbedded in a continuum with a macroscopic value of the dielectric constant.

An analytical solution of the drirect correlation function for the model was obtained from the mean spherical model (MSM)[9] equation by Waisman and Lebowitz.[5] It may be said to be the only analytical solution which has been obtained through the statistical thermodynamic treatment of electrolyte solutions since the proposition of the Debye-Hückel theory.

A way to improve the primitive model is to take into account the effect of ions upon the liquid structure of solvents. It is well-known that water molecules around ions are not always bound strictly about the ions in aqueous solutions.[11–13] At room temperature, water molecules around very small (Li^+) or polyvalent (Mg^{2+}, Ca^{2+}) ions are considered to be less mobile than those in bulk water due to ion-water interactions (*positive hydration*), while in the case of comparatively large ions, such as Cs^+ and I^-, water molecules around ions become more mobile than those in bulk water (*negative hydration*).[11–13] Such ion-water interaction produces very complicated effects upon ion-ion interactions. Gurney represented the additional interactions by a term of the overlapping of cospheres in which solvent molecules are in a different state from those in bulk water.[11] Rasaiah[6] and Ramanathan and Friedman[7] solved numerically the hypernetted chain (HNC) equation,[8] where the interaction potential of an ion pair cotains a contribution from the overlapping of the cospheres.

On the basis of a model similar to that mentioned above, an alternative method for the improvement of the "primitive model" will be presented in this paper using the perturbation method in the theory of liquids;[10,14] the primitive model is used as a reference system, and the contribution from the overlapping of cospheres is regarded as a perturbation.

Perturbation Method

The basic idea of the perturbation theory is to represent the potential energy of a system as a sum of two terms:

$$U = U^{(0)} + U^{(1)}, \tag{1}$$

where $U^{(0)}$ is the potential energy of the unperturbed system ("reference system"), and $U^{(1)}$, the perturbation energy. It is assumed that $U^{(0)}$ and $U^{(1)}$ are a sum of pair potentials. The equation for the Helmholtz free energy of a multicomponent system is expressed straightforwardly by the perturbation theory as follows:

$$\beta A/N = \beta A^{(0)}/N + (2\pi\beta/\rho)\sum_{i,j=1}^{\sigma}\rho_i\rho_j\int_0^\infty g_{ij}^{(0)}(r)u_{ij}^{(1)}(r)r^2\mathrm{d}r. \tag{2}$$

Here, the subscripts i and j are used to distinguish the species in the system; $A^{(0)}$ and $g_{ij}^{(0)}(r)$, the Helmholtz free energy and the radial distibution function of the reference system, respectively; $u_{ij}^{(1)}(r)$, the perturbation potential of a pair of molecules; ρ_i, the number density of i-th component; N, the total number of molecules; ρ, the total number density ($=\sum_i^\sigma \rho_i$) and $\beta=(kT)^{-1}$.

In the present case, the pair potential, $u_{ij}^{(0)}(r)$, of the reference system is givn by:

$$\begin{aligned} u_{ij}^{(0)}(r) &= \infty, & r \leq R_{ij}, \\ &= e_ie_j/\varepsilon r, & r > R_{ij}, \end{aligned} \tag{3}$$

where e_i is the charge of the i-th type of ions; R_{ij}, the distance of the closest approach between ions of the i and j types, $R_{ij}=(R_{ii}+R_{ij})/2$, and ε, the macroscopic dielectric constant of the solvent. The interaction attributed to the effect of the overlap of cospheres, which is regarded as a perturbation, must have a very complicated form. Here, we will represent the potential by a simple form,[6,15] that is, a square well or a square mound potential, as follows:

$$\begin{aligned} u_{ij}^{(1)}(r) &= 0, & r \leq R_{ij}, \\ &= d_{ij}, & R_{ij} < r < R_{ij} + b_{ij}, \\ &= 0, & R_{ij} + b_{ij} \leq r. \end{aligned} \tag{4}$$

Here, d_{ij} is the depth (the height) of the well (mound), and b_{ij}, the width of the well (mound). Since the $u_{ij}^{(1)}(r)$ used here is the potential of the mean force averaged over the coordinate of the solvent molecules, which means the free energy of pair interaction between ions, the thermodynamic quantities derived are "osmotic quantities." For instance, the derivative of the free energy by the volume of solution is not the pressure

but the osmotic pressure.[16] From Eq. (2), we obtained this equation for the energy per unit volume:[2,6]

$$E = E^{(0)} + \frac{1}{2}\sum_{i,j=1}^{\sigma}\rho_i\rho_j\int_0^{\infty}\frac{\partial[\beta u_{ij}^{(1)}(r)]}{\partial\beta}g_{ij}^{(0)}(r)4\pi r^2\mathrm{d}r, \quad (5)$$

where $E^{(0)}$ is the energy per unit volume of the reference system given by:

$$E^{(0)} = \frac{1}{2}\sum_{i,j=1}^{\sigma}\rho_i\rho_j\int_0^{\infty}\frac{\partial[\beta u_{ij}^{(0)}(r)]}{\partial\beta}g_{ij}^{(0)}(r)4\pi r^2\mathrm{d}r. \quad (6)$$

By substituting Eq. (3) into Eq. (6), we obtained the following expression:

$$E^{(0)} = \left(1+\frac{\partial \ln \varepsilon}{\partial \ln T}\right)E^{el}. \quad (7)$$

E^{el} is given by:

$$E^{el} = (1/2)\sum_{i,j=1}^{\sigma}\rho_i\rho_j\int_0^{\infty}\frac{e_ie_j}{\varepsilon r}g_{ij}^{(0)}(r)4\pi r^2\mathrm{d}r. \quad (8)$$

Description of the Reference System

Analytical Solution of MSM Equation. We use the analytical solution of the MSM equation for the primitive model, which was derived by Waisman and Lebowitz,[5] as the reference system in the perturbation method.[6] According to MSM,

$$\begin{aligned} g_{ij}^{(0)}(r) &= 0, & r \le R_{ij} \quad (9)\\ C_{ij}^{(0)}(r) &= -\beta e_ie_j/\varepsilon r, & r > R_{ij} \end{aligned}$$

where $C_{ij}^{(0)}(r)$ is the direct correlation function of the reference system. Using the conditions in Eq. (9), Waisman and Lebowitz solved the Ornstein-Zernike equation by a method which was identical with Wertheim's[17] way of solving the Percus-Yevick (PY) equation[8] for a single-component fluid of hard spheres. The final solution was obtained only for the case in which the hard-sphere diameter of all the species were the same. The direct correlation function, $C_{ij}^{(0)}(r)$, derived was:

$$\begin{aligned} C_{ij}^{(0)}(r) &= \tilde{C}(r;\xi;\beta) - (\beta/\varepsilon R)e_ie_j(2B-B^2r/R), & r \le R\\ &= -\beta e_ie_j/\varepsilon r, & r > R \quad (10) \end{aligned}$$

where $\tilde{C}(r;\xi,\beta)$ is the Wertheim solution, and R, the distance of the closest approach of the ion pair which is common to all the pairs. ξ and B are the parameters given by:

$$\xi = \pi R^3\rho/6, \quad (11)$$

$$B = x^{-2}[x^2+x-x(1+2x)^{1/2}], \quad (12)$$

where x is the product of the Debye-Hückel parameter, κ, and the hard-sphere diameter, R,

$$x^2 = \kappa^2R^2 = [(4\pi\beta/\varepsilon)\sum_i^{\sigma}\rho_ie_i^2]R^2. \quad (13)$$

Thermodynamic Functions. The free energy and energy per unit volume were given by:

$$\beta a(x,\beta;\xi) = \beta\tilde{a}(\xi,\beta) - (12\pi R^3)^{-1}[3x^2+6x+2 - 2(1+2x)^{3/2}], \quad (14)$$

$$E^{el}(x,\beta) = (1/2)\sum_{i,j}^{\sigma}\rho_i\rho_j\int\frac{e_ie_j}{\varepsilon r}g_{ij}^{(0)}(r)4\pi r^2\mathrm{d}r = -\frac{x^2+x-x(1+2x)^{1/2}}{4\pi\beta R^3}. \quad (15)$$

Here, $\tilde{a}(\xi,\beta)$ is the free energy per unit volume of a hard-sphere fluid, which is derived by integrating the Wertheim's formula for the equation of state over the density.[17]

Radial Distribution Function. We have derived the radial distribution function, $g_{ij}^{(0)}(r)$, by an inverse Laplace transform from the function given by Waisman and Lebowitz.[5] The mathematical details are described in the Appendix. The resulting equation consists of the following two terms:

$$g_{ij}(y) = \tilde{g}_{ij}(y) + g_{ij}^{el}(y), \quad (16)$$

where y is the separation between an ion pair reduced by the distance of the closest approach, R. The first term of Eq. (16) is the radial distribution function obtained as the solution of the PY equation for the hard-sphere fluid, which was calculated by Bearman and his coworkers in the range of $1 \le y \le 6$.[18,19] The second term is the part related to the charge distribution, which is given by (see Appendix):

$$\begin{aligned} g^{el}(y) &= g_1^{el}(y), & \text{for } 1 \le y \le 2,\\ &= g_1^{el}(y) + g_2^{el}(y), & \text{for } 2 \le y \le 3,\\ &= g_1^{el}(y) + g_2^{el}(y) + g_3^{el}(y), & \text{for } 3 \le y \le 4, \quad (17) \end{aligned}$$

where $g_1^{el}(y)$, $g_2^{el}(y)$, and $g_3^{el}(y)$ are:

$$\begin{aligned} g_1^{el}(y) &= (\pm 2q^2/12\xi y)\{\sin[q(y-1)] - \cos[q(y-1)]\}\exp[-q(y-1)], \quad (18a)\\ g_2^{el}(y) &= (\pm 1/12\xi y)[2(y-2)q^3\{\cos[q(y-2)] + \sin[q(y-2)]\} - 2q^2\sin[q(y-2)]] \times \exp[-q(y-2)], \quad (18b)\\ g_3^{el}(y) &= (\pm 1/12\xi y)[2q^4(y-3)^2\{\cos[q(y-3)] - \sin[q(y-3)]\} - 2q^3(y-3) \times \{3\cos[q(y-3)] + \sin[q(y-3)]\} + 6q^2\sin[q(y-3)]]\exp[-q(y-3)]. \quad (18c) \end{aligned}$$

Here, q is a parameter given by:

$$q = \{(1+2\kappa R)^{1/2}-1\}/2. \quad (19)$$

The form of $g_{ij}(y)$ calculated in the range of $1 \le y \le 4$ is shown in Figs. 1(a)—(c). Eq. (16) shows that the distribution law of ions in electrolyte solutions is influenced by two different factors: the distribution law characteristic of hard-sphere fluids, which originates from the short-range repulsion between molecules, and a distribution law similar to the Debye-Hückel type which is caused by the long-range Coulombic interaction. While the Debye-Hückel-like distribution is dominant at low concentrations, the total distribution approaches that of a hard-sphere fluid at high concentrations. The change in the shape of the distribution curves with the concentration (Fig. 1) appears to represent such a feature in the distribution of ions.

The curve of $g_{ij}(y)$ has an oscillation that becomes outstanding with an increase in the concentration. This property of $g_{ij}(y)$ in electrolyte solutions was first predicted by Kirkwood and Poirier;[20] it was later formulated by Stillinger and Lovett[21] as a "second moment condition." Recently, Card and his coworkers confirmed the property through a Monte Carlo calculation.[22]

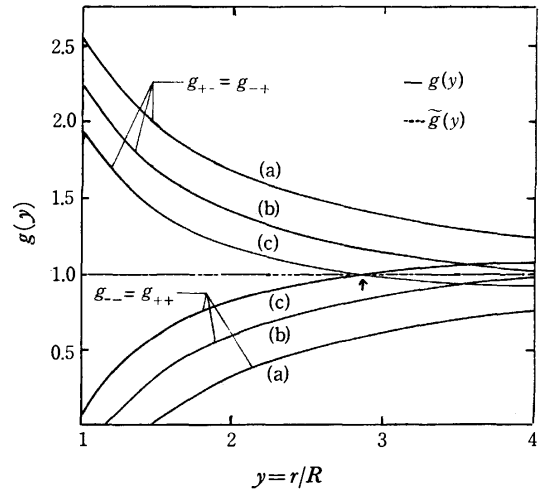

Fig. 1(a). The radial distribution functions computed from MSM equation for the primitive model at $\rho R^3=0.001$, 0.01, and 0.05 at 25 °C assuming that $R=4.0$ Å and $\tilde{g}(y)\simeq 1.0$ for $y>1$. (a) $\rho R^3=0.001$, (b) $\rho R^3=0.01$, (c) $\rho R^3=0.05$. In the curve (c), the inversion (oscillation) occurs at the point which is indicated by an arrow.

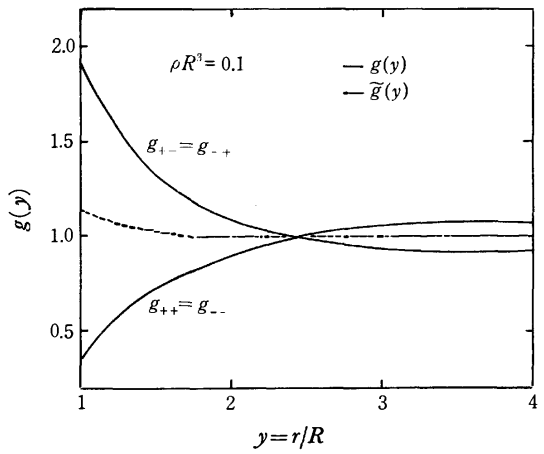

Fig. 1(b). The radical distribution function at $\rho R^3=0.1$. Values calculated by Throop and Bearman is used for $g(y)$ in this figure and the following.

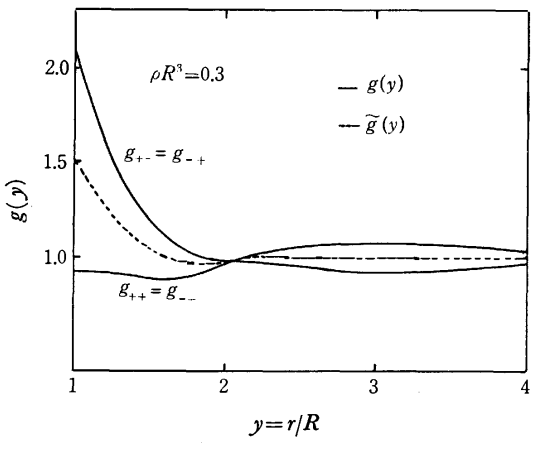

Fig. 1(c). The radial distribution functions at $\rho R^3=0.3$.

Computation of Thermodynamic Functions

Free Energy. After substituting Eq. (4) and changing the variable, r, to a reduced variable, y, we obtain from Eq. (2):

$$\beta(A-A^{(0)})/N = 3\xi J\beta d_{ij}, \tag{20}$$

$$J = \int_1^{1+a} g_{ij}(y)y^2 dy, \tag{21}$$

where a is b_{ij}/R. The contribution from like-like terms in Eq. (2) is ignored. Since the values of $\xi(=\pi R^3\rho/6)$ are smaller than 0.05 in this concentration range (smaller than 1.0 M in molarity),[23] we can safely suppose that $\tilde{g}_{ij}(y)=1$. Thus, Eq. (16) is written as:

$$g_{ij}(y) = 1 + g_{ij}^{el}(y). \tag{16'}$$

After substituting Eqs. (16'), (17), and (18) into Eq. (21), we get:

$$\begin{aligned} J &= (1/3)\{(1+a)^3-1\}+(1/12\xi)\{[(2q+2aq+1)\sin(aq) \\ &\quad +\cos(aq)]\exp(-aq)-1\}, \quad \text{for } R\geq b_{ij}, \\ &= (1/3)\{(1+a)^3-1\}+(1/12\xi)\{[(2q+2aq+1)\sin(aq) \\ &\quad +\cos(aq)]\exp(-aq)+[2(a^2-1)q^2+(3a+1)q-1] \\ &\quad \times\cos[q(a-1)]\exp[-q(a-1)]-[5(1+a)q-2q \\ &\quad +3]\sin[q(a-1)]\exp[-q(a-1)]-4q\}, \\ &\quad \text{for } R\leq b_{ij}\leq 2R. \end{aligned} \tag{24}$$

As the hard-sphere radii of ions, Pauling's crystal radii are used.[24] The width of the well, b_{ij}, is equal to the diameter of the water molecule, 2.76 A.[6] The parameter, d_{ij}, is dtermined by fitting the calculated values of A with the one observed at 0.5 M. In this paper, the experimental values of the thermodynamic quantities are transformed into the McMillan-Mayer system according to Friedman's procedure, and the comparison between the calculated and observed values is made in the McMillan-Mayer system.[25] The values of

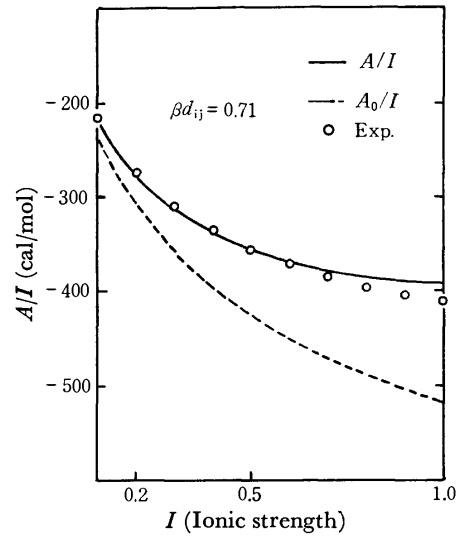

Fig. 2. Calculated and experimental Helmholtz free energy for aqueous solutions of NaCl at 25 °C. The broken line and the solid one are calculated values for the reference system and the system with a square well (or mound) potential as a perturbation, respectively and circles the experimental ones. It is assumed that $\beta d_{+-}=0.71$ and $\beta d_{++}=\beta d_{--}=0$.

TABLE 1. THE VALUES OF βd_{ij} WHICH GIVE THE BEST FIT BETWEEN OBSERVED AND CALCULATED VALUES OF FREE ENERGY

	Li^+	Na^+	K^+	Rb^+	Cs^+
F^-		0.72	0.65		
Cl^-	1.84	0.71	0.09	−0.16	−0.53
Br^-	1.74	0.72	0.07	−0.26	−0.61
I^-	2.02	0.73	0.08	−0.41	−0.76

d_{ij} are tabulated for some 1-1 electrolytes in Table 1. In Fig. 2, the agreement between the observed and calculated values of free energy in the concentration range up to 1.0 M is shown for NaCl as an example.

Energy. The second term of Eq. (5) becomes:

$$\frac{1}{2}\sum_{i,j=1}\rho_i\rho_j E_{ij}\int_R^{R+b_{ij}} g_{ij}^{(0)}(r)4\pi r^2 dr, \tag{25}$$

where E_{ij} is defined by:

$$E_{ij} = d_{ij} - T\frac{\partial d_{ij}}{\partial T}. \tag{26}$$

Eq. (5) is given by:

$$\frac{\beta(E-E^{(0)})}{\rho/2} = 6\xi J\beta E_{ij}. \tag{27}$$

The observed value with which the calculated value of E is compared is the relative apparent molal heat content.[6,7] The values of E_{ij} determined by a comparison of the observed values of E with the calculated ones are tabulated in Table 2, together with the values of $(-\partial d_{ij}/\partial T)$. The agreement between the observed and calculated values of E in the concentration range up to 1.0 M is very good, as is shown for NaCl in Fig. 3.

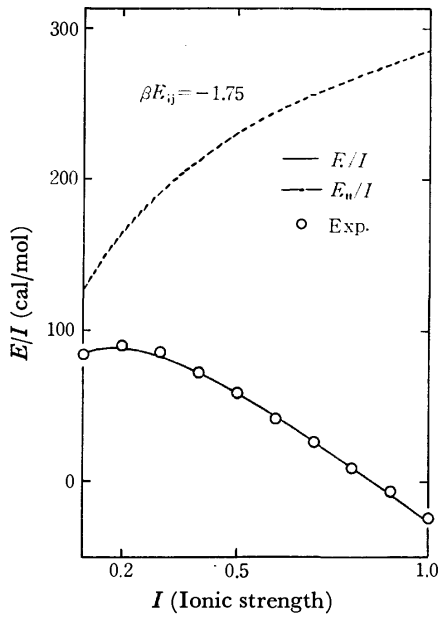

Fig. 3. Calculated and experimental excess energy for aqueous solution of NaCl at 25 °C. The broken line and the solid one are calculated values for the reference system and the system with a square well (or mound) potential as a perturbation, respectively. It is assumed that $\beta E_{+-} = -1.75$, $\beta E_{++} = \beta E_{--} = 0$.

TABLE 2. THE VALUES OF βE_{ij} (UPPER RIGHT HALF OF TABLE) AND $k^{-1}(-\partial d_{ij}/\partial T)$ (LOWER LEFT HALF)

	Li^+	Na^+	K^+	F^-	Cl^-	Br^-
Li^+					0.03	−0.03
Na^+					−1.75	−1.80
K^+				−0.66	−1.55	−1.80
F^-			−1.31			
Cl^-	−1.81	−2.46	−1.84			
Br^-	−1.77	−2.52	−1.81			

Discussion

Interpretation of the Parameter, d_{ij}. In the present computation, an energy parameter, d_{ij}, is used as an adjustable one. We will here discuss the physical meaning of the parameter. When two ions come close enough together so that their cospheres overlap each other, as is shown in Fig. (4), some of the water molecules in the cospheres are displaced. Thus, if the water molecules in the cospheres are in a state of lower free energy than those in bulk water, the overlap of the cospheres gives rise to an increase in the free energy of the water molecules which were in the cosphere before the overlap occurres, and the resulting contribution to the interaction between two ions is repulsive. When the water molecules in the cospheres are in a state of higher free energy than those in bulk water, the converse effect appears by the overlap of the cospheres, which is attractive. Thus, the plus and minus which appear in the sign of d_{ij} in Table 1 can be reasonably interpreted. This interpretation of the parameter, d_{ij}, coincides with that of Rasaiah.[6]

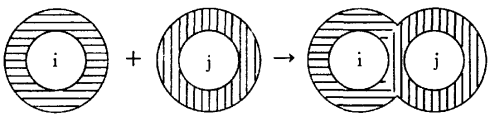

Fig. 4. Schematic representations of the process in which cospheres overlap.

Temperature Dependence of d_{ij}. As may be seen in Table 2, the signs of all the values of $(-\partial d_{ij}/\partial T)$ are minus. In the case of K^+, this sign is consistent with an intuitive picture, since the cospheres around the ions are considered to constitute a structure-breaking region, where water molecules are in a state of higher "entropy" than those in bulk water; the overlap of cospheres would thus lead to a net decrease in the "entropy." In the case of Li^+, it is difficult to interpret the sign of $(-\partial d_{ij}/\partial T)$, because the cospheres around the ions are expected to be in a state of lower "entropy." One possible explanation, which was given by Rasaiah,[6] is that $(-\partial d_{ij}/\partial T)$ is determined by the outer region far away from the nearest neighbor cosphere. This is plausible, since the structure-breaking region is considered to extend outside the cosphere in the case of very small ions, such as Li^+ and polyvalent ions (Mg^{2+}, Ca^{2+}, *etc.*).

Appendix

The Derivation of the Radial Distribution Function, $g_{ij}(y)$, from the Function Given by Waisman and Lebowitz. It is convinient

to start from Eq. (23) in Ref. (5a), which defines a function $\boldsymbol{L}(s)$.[5] That is:

$$\boldsymbol{L}(s) = \boldsymbol{G}(s)\boldsymbol{H}^T(-s). \tag{A,1}$$

Here, $\boldsymbol{G}(s)$ is a matrix whose (i,j)-element is a Laplace transform of the radial distribution function, $g_{ij}(y)$, of ions of the j type around an ion of i type:

$$G_{ij}(s) = 12(\eta_i\eta_j)^{1/2}\int_{R_{ij}}^{\infty} rg_{ij}(r)e^{-sr}dr, \tag{A,2}$$

where η_i is $\pi\rho_i/6$. $\boldsymbol{H}^T(-s)$ is a transpose of a matrix, $\boldsymbol{H}(-s)$, in which the sign of variables is changed to give this equation:

$$\boldsymbol{H}(s) = \boldsymbol{A} - s^2\boldsymbol{F}(s) - (\gamma^2/4)(s\boldsymbol{D}+2\boldsymbol{V}), \tag{A,3}$$

where γ and D_{ij}, the (i,j)-element of $\boldsymbol{D}$, are:

$$\gamma^2 = 8\pi\beta/\varepsilon \text{ and } D_{ij} = (\rho_i\rho_j)^{1/2}e_ie_j,$$

respectively. In Eq. (A, 3), $\boldsymbol{F}(s)$ is a matrix whose (i,j)-element is a Laplace transform of the direct correlation function.

$$F_{ij}(s) = -12(\eta_i\eta_j)^{1/2}\int_0^{R_{ij}} r\left(C_{ij}(r)+\frac{\beta e_ie_j}{\varepsilon r}\right)e^{-sr}dr. \tag{A,4}$$

The (i,j)-element of $\boldsymbol{L}(s)$ in Eq. (A,1) has been shown, on the basis of a consideration of the analyticity in the complex s-plane, to have this form:[5]

$$L_{ij}(s) - s^{-2}A'_{ij} = 2M_{ij}. \tag{A,5}$$

When the hard-sphere diameters of all species are equal, we get the following equalities:

$$A_{ij} = A_{ji} = A_{ii} = A_{jj} = A, \tag{A,6a}$$

$$A'_{ij} = A'_{ji} = A'_{ii} = A'_{jj} = A', \tag{A,6b}$$

$$V_{ij} = V_{ji} = -V_{ii} = -V_{jj} = -V, \tag{A,6c}$$

$$M_{ii} = M_{jj}, \quad M_{ij} = M_{ji} \tag{A,6d}$$

and $A' = 12\,\eta A$, where $\eta = \sum_i \eta_i$. By virtue of these equalities, the quadratic equations (28a)—(28e) in Ref. (5a) are reduced to a readily solvable form, and the solutions are:

$$A = 6\eta\frac{(2\xi+1)^2}{(1-\xi)^4}, \quad A' = 72\eta^2\frac{(2\xi+1)^2}{(1-\xi)^4},$$

$$M_{ij} = -\frac{6\eta}{R^2}\left\{\frac{6R\xi(1+\xi/2)^2}{(1-\xi)^4}+\frac{\beta e_ie_jB^2}{\varepsilon}\right\},$$

$$V_{ij} = -\frac{12\eta\beta e_ie_jB}{R(\gamma^2/2)\varepsilon},$$

$$M \equiv M_{ii} + M_{ij} = -\frac{72\eta R\xi(1+\xi/2)^2}{R^2(1-\xi)^4},$$

$$M' \equiv M_{ii} - M_{ij} = -\frac{12\eta\beta e^2B^2}{\varepsilon R^2}. \tag{A,7}$$

Now, multiplying the two sides of Eq. (A, 1) by an inverse of the matrix, $\boldsymbol{H}^T(-s)$, we get:

$$\boldsymbol{G}(s) = \boldsymbol{L}(s)\boldsymbol{H}^T(-s)^{-1} \tag{A,8}$$

Therefore, the (i,j)-element, $G_{ij}(s)$, of the matrix, $\boldsymbol{G}(s)$, is given by:

$$G_{ij}(s) = \{L_{ij}(s)H_{ii}(-s) - L_{ii}(s)H_{ji}(-s)\}D(s)^{-1}. \tag{A,9}$$

Here, $D(s)$ is a determinant of the matrix, $\boldsymbol{H}^T(-s)$; it is given by:

$$D(s) = \{A_{ii}-s^2F_{ii}(-s)-(\gamma^2/4)(-sD_{ii}+2V_{ii})\}^2 - \{A_{ij}-s^2F_{ji}(-s)-(\gamma^2/4)(-sD_{ji}+2V_{ji})\}^2. \tag{A,10}$$

Condisering the equalities in Eqs. (A, 7), the right-hand side of Eq. (A, 10) can be factores to give:

$$D(s) = \{-s^2[F_{ii}(-s)-F_{ji}(-s)]-2(\gamma^2/4)(-sD+2V)\} \times \{2A-s^2[F_{ii}(-s)+F_{ji}(-s)]\}. \tag{A,11}$$

By reference to Eqs. (A, 6) and (A, 7), the numerator of the right-hand side of Eq. (A, 9) is found to be given by:

$$\begin{aligned} &L_{ij}(s)H_{ii}(-s) - L_{ii}(s)H_{ji}(-s) \\ &= -(s^{-2}A'+2M_{ii})\{A-s^2F_{ji}(-s)-(\gamma^2/4)(sD-2V)\} \\ &\quad +(s^{-2}A'+2M_{ij})\{A-s^2F_{ii}(-s)-(\gamma^2/4)(-sD+2V)\} \\ &= (s^{-2}A'+M)\{-s^2[F_{ii}(-s)-F_{ji}(-s)] \\ &\quad -2(\gamma^2/4)(-sD+2V)\}-M'\{2A-s^2[F_{ii}(-s) \\ &\quad +F_{ji}(-s)]\}. \end{aligned} \tag{A,12}$$

Thus,

$$G_{ij}(s) = \frac{s^{-2}A'+M}{2A-s^2[F_{ii}(-s)+F_{ji}(-s)} - \frac{M'}{-s^2[F_{ii}(-s)-F_{ji}(-s)]-2(\gamma^2/4)(-sD+2V)}. \tag{A,13}$$

By the substitution of the expression for $F_{ij}(-s)$, which is obtained by combining Eq. (10) with Eq. (A, 4), Eq. (A,13) becomes:

$$G_{ij}(s) = \frac{1}{2}\frac{sL_1(s)}{L_1(s)+S_1(s)e^{Rs}} - \frac{1}{2}\frac{sL_2}{L_2+S_2(s)e^{Rs}}. \tag{A,14}$$

Here, $L_1(s)$, L_2, $S_1(s)$, and $S_2(s)$ are given by:

$$L_1(s) = 12\xi[(1+\xi/2)Rs+(2\xi+1)], \tag{A,15a}$$

$$S_1(s) = (1-\xi)^2(sR)^3 + 6\xi(1-\xi)(sR)^2 + 18\xi^2(sR) - 12\xi(1+2\xi), \tag{A,15b}$$

$$L_2 = -2p^2, \tag{A,15c}$$

$$S_2(s) = (s^2+2ps+2p^2)e^{sR} - 2p^2, \tag{A,15d}$$

where p is a parameter defined by:

$$p = \{(1+2\kappa R)^{1/2}-1\}/2R. \tag{A,16}$$

The expression for the radial distribution function is obtained by taking an inverse Laplace transform of Eq. (A, 14). Changing r and s to y and t respectively through the $r=Ry$ and $s=t/R$ relations, we get the final equation:

$$g_{ij}(y) = \tilde{g}_{ij}(y) + g^{01}_{ij}(y). \tag{A,17}$$

Here, $\tilde{g}_{ij}(y)$, $g_{ij}(y)$, and $g^{01}_{ji}(y)$ are given by:

$$g_{ij}(y) = \frac{1}{2\pi iy}\int_{\delta-i\infty}^{\delta+i\infty}\frac{1}{12\xi}G_{ij}(y)e^{ty}dt, \tag{A,18a}$$

$$g_{ij}(y) = \frac{1}{2\pi iy}\int_{\delta-i\infty}^{\delta+i\infty}\frac{tL_1(t)e^{yt}dt}{12\xi[L_1(t)+S_1(t)e^t]}, \tag{A,18b}$$

$$g^{01}_{ij}(y) = \frac{1}{2\pi iy}\int_{\delta-i\infty}^{\delta+i\infty}\frac{tL_2e^{yt}dt}{12\xi[L_2+S_2(t)e^t]}, \tag{A,18c}$$

where $L_1(t)$, $S_1(t)$, L_2, and $S_2(t)$ are:

$$L_1(t) = 12\xi[(1+\xi/2)t+(2\xi+1)], \tag{A,19a}$$

$$S_1(t) = (1-\xi)^2t^3 + 6\xi(1-\xi)t^2 + 18\xi^2t - 12\xi(1-2\xi), \tag{A,19b}$$

$$L_2(t) = -2q^2, \tag{A,19c}$$

$$S_2(t) = t^2 + 2qt + 2q^2, \tag{A,19d}$$

and

$$q = \{(1+2\kappa R)^{1/2}-1\}/2. \tag{A,20}$$

In Eq. (A, 17), the first term is Wertheim's solution of the PY equation for a hard-sphere fluid; the integral in Eq. (A, 18b) was evaluated by Bearman and his co-workers using the res-

idue theorem in the range of $1<y<6$.[18,19] The second term, which is characteristic of electrolyte solutions, can also be evaluated in a similar way. After the denominator of the integrand is expanded to the power series in $L_2/S_2(t)$, Eq. (A, 18c) is written by:

$$g_{ij}^{el}(y) = \frac{1}{12\xi y}\sum_{n=1}^{\infty}\frac{(-1)^{n+1}}{2\pi i}\int_{\delta-i\infty}^{\delta+i\infty}\exp[t(y-n)]\left[\frac{L_2}{S_2(t)}\right]^n t\,dt. \tag{A,21}$$

The path of integration is to be taken to the right of all the poles of $1/S_2(t)$. Thus, the integral for $y<n$ is zero and that for $y>n$ is evaluated by means of the residue theorem. The resulting equations in the range of $1\leq y\leq 4$ are:

$$\begin{aligned} g^{el}(y) &= g_1^{el}(y), \quad \text{for } 1\leq y\leq 2, \\ &= g_1^{el}(y) + g_2^{el}(y), \quad \text{for } 2\leq y\leq 3, \\ &= g_1^{el}(y) + g_2^{el}(y) + g_3^{el}(y), \quad \text{for } 3\leq y\leq 4, \end{aligned} \tag{A,22}$$

where $g_1^{el}(y)$, $g_2^{el}(y)$, and $g_3^{el}(y)$ are

$$\begin{aligned} g_1^{el}(y) &= (\pm 2q^2/12\xi y)\{\sin[q(y-1)] \\ &\quad - \cos[q(y-1)]\}\exp[-(y-1)], \end{aligned} \tag{A,23a}$$

$$\begin{aligned} g_2^{el}(y) &= (\pm 1/12\xi y)[2(y-2)q^3\{\cos[q(y-2)] \\ &\quad - \sin[q(y-2)]\} - 2q^2\sin[q(y-2)]] \\ &\quad \times \exp[-q(y-2)], \end{aligned} \tag{A,23b}$$

$$\begin{aligned} g_3^{el}(y) &= (\pm 1/12\xi y)[2q^4(y-3)^2\{\cos[q(y-3)] \\ &\quad + \sin[q(y-3)]\} - 2q^3(y-3) \\ &\quad \times \{3\cos[q(y-3)] + \sin[q(y-3)]\} \\ &\quad + 6q^2\sin[q(y-3)]]\exp[-q(y-3)]. \end{aligned} \tag{A,23c}$$

References

1) A. R. Allnat, *Mol. Phys.*, **8**, 533 (1964).
2) J. C. Rasaiah and H. L. Friedman, *J. Chem. Phys.*, **48**, 2742 (1968); *ibid.*, **50**, 3965 (1969).
3) G. Stell and J. L. Lebowitz, *ibid.*, **48**, 3706 (1968).
4) H. C. Andersen and D. Chandler, *ibid.*, **53**, 547 (1970); *ibid.*, **54**, 26 (1971).
5) E. Waisman and J. L. Lebowitz, a) *ibid.*, **56**, 3086 (1972); b) *ibid.*, **56**, 3093 (1972).
6) J. C. Rasaiah, *J. Chem. Phys.*, **52**, 704 (1970); *J. Solution Chem.*, **2**, 301 (1973).
7) P. S. Ramanathan and H. L. Friedman, *J. Chem. Phys.*, **54**, 1086 (1971).
8) "The Equilibrium Theory of Classical Fluids," ed. by H. L. Frisch and J. L. Lebowitz, W. A. Benjamin Company, Inc., (1964).
9) J. L. Lebowitz and J. Percus, *Phys. Rev.*, **144**, 251 (1966).
10) J. A. Barker and D. Henderson, *J. Chem. Phys.*, **47**, 2856, 4714 (1967).
11) R. W. Gurney, "Ionic Processes in Solution," Dover, New York (1953).
12) H. S. Frank and W. Y. Wen, *Discuss. Faraday Soc.*, **24**, 133 (1957).
13) O. Ya. Samoilov, *ibid.*, **24**, 141 (1957).
14) P. J. Leonard, D. Henderson, and J. A. Barker, *Trans. Faraday Soc.*, **66**, 2439 (1970).
15) J. C. Rasaiah and G. Stell, *Mol. Phys.*, **18**, 249 (1970).
16) M. G. McMillan, Jr. and J. E. Mayer, *J. Chem. Phys.*, **13**, 276 (1945).
17) M. Wertheim, *Phys. Rev. Lett.*, **8**, 321 (1963), *J. Math. Phys.*, **5**, 643 (1964).
18) G. J. Throop and R. J. Bearman, *J. Chem. Phys.*, **42**, 2408 (1965).
19) F. Mandel, R. J. Bearman, and M. Y. Bearman, *ibid.*, **52**, 3315 (1970).
20) J. G. Kirkwood and J. C. Poirier, *J. Phys. Chem.*, **58**, 591 (1954).
21) F. H. Stillinger, Jr. and R. Lovett, *J. Chem. Phys.*, **49**, 1991 (1968).
22) J. C. Rasaiah, D. H. Card, and J. P. Valleau, *ibid.*, **56**, 248 (1972).
23) In the concentration range up to 1.0 M, the values of ξ are smaller than 0.036 even in the case of CsI. As shown in Fig. 1 (b), where the value of $\xi(=\pi\rho R^3/6)$ is about 0.05, $\tilde{g}(y)$ is nearly equal to one.
24) L. Pauling, "The Nature of the Chemical Bond," 3rd Ed., Cornell University Press, Ithaca, New York (1960).
25) H. L. Friedman, *J. Chem. Phys.*, **32**, 1351 (1960).

Studies of the $\pi \rightarrow \pi^*$ Absorption Bands of 9,10-Phenanthrenequinone

Akira KUBOYAMA, Fumio KOBAYASHI, and Satomi MOROKUMA
National Chemical Laboratory for Industry, Shibuya-ku, Tokyo 151
(Received November 13, 1974)

The $\pi \rightarrow \pi^*$ S–S absorption spectra of 9,10-phenanthrenequinone and 3-bromophenanthrenequinone in solutions up to the vacuum UV region were obtained. On the other hand, MO calculations of the π-electronic systems of these quinones were carried out by means of the P–P–P method. The $\pi \rightarrow \pi^*$ absorption bands of these quinones were assigned on the basis of the calculated results. The blue-shift of the longest-wavelength $\pi \rightarrow \pi^*$ band of phenanthrenequinone due to the bromine-atom substitution at its 3-position was observed. Similar facts are found in aromatic carbonyl compounds, fluorenone and acetophenone.

Previously, we have theoretically and experimentally studied the $\pi \rightarrow \pi^*$ singlet-singlet absorption bands of *p*-quinones (*p*-benzoquinone, α-naphthoquinone, and anthraquinone) and *o*-benzoquinone.[1] The $\pi \rightarrow \pi^*$ absorption bands of 9,10-phenanthrenequinone(PHQ) have been studied by few workers. We have obtained the electronic spectra of PHQ and 3-bromo-PHQ in solutions up to the vacuum UV (VUV) region, and carried out MO calculations of their π-electronic systems by means of the P-P-P method. Their $\pi \rightarrow \pi^*$ singlet-singlet bands have been assigned on the basis of the calculated results.

Experimental

Measurements. The absorption spectra were measured in the same manner as in the previous work.[1] *n*-Heptane, 1,1,1,3,3,3-hexafluoro-2-propanol (HFIP), and ethanol were used as solvents. The measurement of the absorption spectrum of PHQ in the gas phase was also carefully carried out at *ca.* 200 °C with a 5-cm-path cell wrapped with a ribbon heater, using a Cary 14M recording spectrophotometer.

Materials. Commercially-available PHQ was purified by vacuum sublimation (mp 209.5—210.5 °C). The 3-bromo-PHQ was prepared according to Schmidt *et al.*'s method[2] and recrystallized five times from acetic acid (mp 272.5—273.5 °C). The *n*-heptane was the same as that used in the previous work, while the ethanol was of the spectrograde from the Dozin Yakugaku Co. The HFIP of the Eastman Co. was used without further purification.

Results. The $\pi \rightarrow \pi^*$ absorption spectra obtained are shown in Figs. 1—3. The wavelengths and molar absorption coefficients of the absorption maxima in these spectra are shown in Table 1. The solubility of these quinones in *n*-heptane was too poor for us to determine their concentration. Especially, the absorption spectrum of 3-bromo-PHQ in the *n*-heptane solution in the VUV region could not be accurately measured because of its very poor solubility. The longer-wavelength $\pi \rightarrow \pi^*$ bands of PHQ in the gas phase could not be accurately measured because of their weak intensities.

Calculations

Method. As for the electronic integral values in the P-P-P method, various kinds of integral values were tentatively used, based on the results obtained in the previous calculations. The set of electronic integral values which brought about the best agreement between the calculated and the experimental results will now be described. The values of the one-center core integrals, the two-center core integral of the C–O bonds, and electron repulsion integrals are the same as those used in the previous calculations.[1] The two-center core integral values of the C–C bonds were obtained with the Pariser-Parr method.[3] In this calculation, the bromine atom substituted for PHQ is considered to participate in the π-electronic system of PHQ with a 3p lone electron-pair. The one-center

Table 1. Wavelengths and molar absorption coefficients of the absorption maxima (the values in parentheses are the latter)

PHQ				3-Bromo-PHQ		Band name
Gas	*n*-Heptane	Alcohol	HFIP	*n*-Heptane	HFIP	
~372 (nm)	398	414.5 (1480)	442 (1370)	390	~435 (1260)	a
	~332			~340		b′
~298	314	321 (4290)	333.5 (6080)	317.5	331 (9030)	b
			~275 (13500)	279.5	284 (14200)	c′
249	263	264.5 (31500)	261 (31500)	261.5	262.5 (32000)	c
	256	256 (29400)	253.5 (31500)			
				~220		d′
200.5	209.5	210 (31400)	210 (37000)	~200	205 (27700)	d
	178		182 (31600)	~178	182 (27500)	e

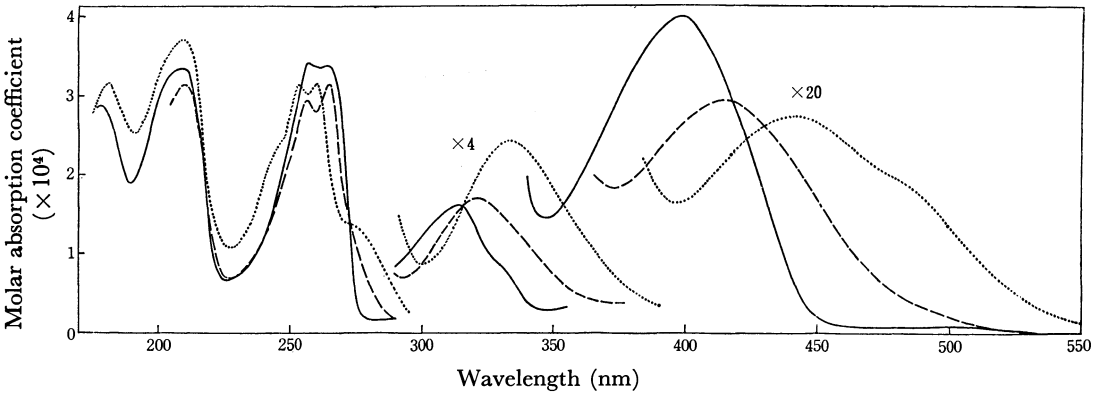

Fig. 1. Absorption spectra of phenanthrenequinone in solutions.
——: *n*-Heptane, — —: ethanol, ——: HFIP
In the *n*-heptane solution the scale of the ordinate is arbitrary.

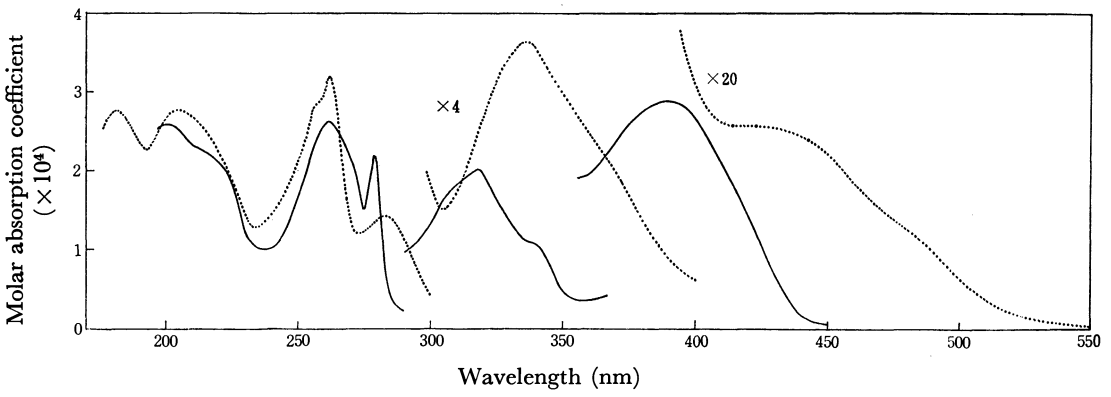

Fig. 2. Absorption spectra of 3-bromophenanthrenequinone in solutions.
——: *n*-Heptane, ——: HFIP.
In the *n*-heptane solution the scale of the ordinate is arbitrary.

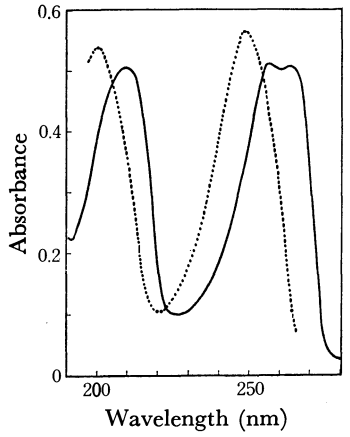

Fig. 3. Absorption spectra of phenanthrenequinone.
——: *n*-Heptane, ——: gas phase.
The scale of the ordinate is arbitrary.

core integral value of the bromine atom (−20.00 eV) and the two-center core integral value of the carbon-bromine bond (−1.00 eV) were determined so that the results calculated with them might be reasonable.

In the calculation, the forty lowest singly-excited configurations were included. The calculations were carried out with a FACOM 270-30 computer. The dimensions of PHQ assumed are shown in Fig. 4. The molecular structure of PHQ has not yet been elucidated.[4] PHQ is considered to take the planar structure of C_{2v} The dimensions shown in Fig. 4 were assumed considering the reported dimensions of its related compounds[5] (fluorene, triphenylene, anthraquinone, and acenaphthenequinone). The lengths of all the bonds in the benzene rings in PHQ were assumed to be 1.40 Å. The bond length of the carbon-bromine bond in 3-bromo-PHQ was assumed to be 1.91 Å.[6]

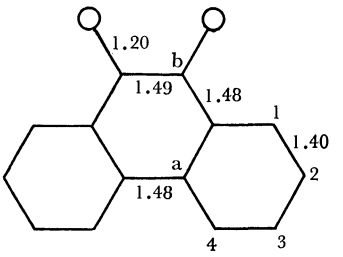

Fig. 4. Dimension of phenanthrenequinone (Å).
a: 120 °, b: 121.5 °.

Results. The calculated excitation energies (E), oscillator strengths (f), and symmetry species of the excited singlet states are shown in Table 2, along with the observed results in *n*-heptane solutions (for energies) and HFIP solutions (for f-values). The molecular plane and symmetry axis of PHQ are regarded as the yz-plane and the z-axis respectively.[7] The first column

Table 2. The calculated excitation energies, oscillator strengths, and symmetry species of the singlet excited states and the corresponding observed results

Calculated				Observed		
No.	Symmetry	E (eV)	f	Band name	E (eV)	f
		(1) PHQ				
1	$B_2(y)$	4.220	0.130	a	3.1	0.03
2	$A_1(z)$	4.302	0.001	b′	3.7	0.13
3	B_2	4.458	0.104	b	3.9	
4	B_2	5.138	0.504	c	4.8	0.78
5	A_1	5.155	0.461	c′		
9	B_2	5.925	0.625	d	5.9	1.0
10	A_1	6.046	0.641	d′		
18	B_2	6.638	0.297			
20	A_1	6.871	0.204			
21	A_1	6.932	0.274	e	7.0	~0.7
22	A_1	7.178	0.618			
23	B_2	7.207	0.596			
		(2) 3-Bromo-PHQ				
1		4.215	0.109	a	3.2	~0.02
2		4.272	0.014	b′	3.7	0.15
3		4.422	0.091	b	3.9	
4		5.057	0.548	c′	4.4	~0.2
5		5.162	0.486	c	4.7	~0.5
9		5.899	0.513	d′	5.6	0.9
10		5.972	0.423	d	6.2	
18		6.718	0.194			
19		6.763	0.353			
22		7.009	0.445	e	7.0	~0.8
23		7.218	0.304			
24		7.316	0.315			

of this table indicates the numbering of the magnitude of E. The letters, y and z, in parentheses denote the direction of polarization in the electronic transition. In this table, the data on the higher excited states with small f-values have been omitted.

Discussion

As may be seen in Fig. 1, PHQ in the n-heptane solution appears to have five distinct $\pi\rightarrow\pi^*$ bands–near 400, 315, 260, 210, and 180 nm. These five $\pi\rightarrow\pi^*$ bands are denoted as, respectively, the a-, b-, c-, d-, and e-bands. As for the very weak shoulder near 490 nm of the a-band in the HFIP solution, it may be assigned to the $n\rightarrow\pi^*$ band, since the $n\rightarrow\pi^*$ band is observed near 500 nm in the n-heptane solution.[8] The $n\rightarrow\pi^*$ band in the HFIP solution seems to be somewhat intensified, compared with that in the n-heptane solution, through a vibronic coupling of the two closely-situated excited states of the $n\rightarrow\pi^*$ band and the a-band. In the b- and c-bands, a shoulder is clearly found on the longer-wavelength side of the b-band in the n-heptane solution and of the c-band in the HFIP solution. These weak shoulders show that another $\pi\rightarrow\pi^*$ band may exist there. In the case of 3-bromo-PHQ, as may be seen in Fig. 2, a distinct shoulder is found on the longer-wavelength side of the b- and d-bands, and a new absorption peak is found on the longer-wavelength side of the c-band. These shoulders and peak on the longer-wavelength side of the b- and c-bands may correspond respectively to the above-mentioned shoulders of PHQ. As for the shoulder on the longer-wavelength side of the d-band, another $\pi\rightarrow\pi^*$ band may exist there. The corresponding band of PHQ may be hidden in its d-band. Therefore, eight $\pi\rightarrow\pi^*$ bands are noticeable in 3-bromo-PHQ, and PHQ may be supposed to have the corresponding eight $\pi\rightarrow\pi^*$ bands. These other $\pi\rightarrow\pi^*$ bands are denoted as b′-, c′-, and d′-bands respectively, as is shown in Table 1. The large energy changes of the $\pi\rightarrow\pi^*$ bands in HFIP solutions compared with those in n-heptane solution, as may be seen in Figs. 1 and 2, may be mainly due to a strong hydrogen-bond formation between the quinones and HFIP, because HFIP, containing six electronegative fluorine atoms in its molecule, is thought to be a strong proton-donor.

Since longer-wavelength $\pi\rightarrow\pi^*$ bands usually show a red-shift due to the substitution of such an electron-donating group as a bromine atom to a π-electronic system, it is noticeable that the a-band of PHQ shifts towards shorter wavelengths due to the bromine-atom substitution at its 3-position, as may be seen in Figs. 1 and 2. Similar facts are found in the longest-wavelength weak $\pi\rightarrow\pi^*$ band near 380 nm of fluorenone[9] and that near 280 nm of acetophenone,[10] using 3-bromo, 3-methyl, and 3-methoxyfluorenones[11] and p-methyl and p-chloroacetophenones respectively. In all these cases, the electron-donating groups are substituted at the para-position of benzene rings to carbonyl groups. Therefore, similar facts may be expected to be generally observed in other aromatic carbonyl compounds.

As for the assignments of the $\pi\rightarrow\pi^*$ bands of PHQ and 3-bromo-PHQ, the five bands, a-, b-, b′-, c-, and c′-bands, can be reasonably assigned on the basis of the calculated results, as may be seen in Table 2. The c′-band can be reasonably assigned on the basis of the relatively large decrease in its excitation energy with the bromine-atom substitution. As for the higher-energy bands, the d-, d′-, and e-bands, the assignments based on the calculated results are not clear.

As for the above-mentioned blue-shift of the a-band upon the bromine-atom substitution, the calculated energy changes of the a-band with the bromine-atom substitutions at the various positions are shown in Table 3. In addition, those with the alkyl-group

Table 3. The changes of the calculated excitation energies of the a-band of PHQ with the bromine-atom and the alkyl-group substitutions at its various positions

Position	ΔE (eV)[a]	
	Bromine atom	Alkyl group
1	−0.042	−0.006
2	−0.046	−0.035
3	−0.005	+0.011
4	−0.072	−0.033

a) ΔE denotes the remainders where the excitation energies of PHQ are subtracted from the corresponding ones of 3-bromo-PHQ.

substitutions are also shown in Table 3. The calculations of the alkyl-group substituted PHQ's were carried out taking the one-center core-integral value of the substituted carbon atoms as -9.00 eV, in consideration of the inductive effect of the alkyl group, but disregarding its resonance effect, as in the previous work.[1] As may be seen in Table 3, the calculated energy decrease of the a-band in 3-bromo-PHQ is far smaller than those in the other bromo-PHQ's. Therefore, the calculated results are not inconsistent with the observed results. On the basis of the calculated results shown in Table 3, a blue-shift of the a-band of 3-alkyl-PHQ compared with that of PHQ can also be expected.

As for the comparison of our theoretical assignment of the $\pi\rightarrow\pi^*$ bands of PHQ with the experimental facts[12-14] previously reported, our assignment of the a-, c-, and c'-bands is consistent with the dichroic absorption spectra of PHQ in the stretched PVA sheet, reported by Inoue *et al.*[12] but that of the b-band is inconsistent. The pattern of the calculated energies and f-values of the π, π^* excited states of PHQ are far more sensitive to the electronic integral values used than those in the quinones previously studied.[1] Therefore, further studies of the assignment of the $\pi\rightarrow\pi^*$ bands of PHQ are desirable.

As may be seen in Fig. 3, the shapes of the $\pi\rightarrow\pi^*$ bands of PHQ in the gas phase are similar to those in the *n*-heptane solution.[15] The broad shape of the $\pi\rightarrow\pi^*$ bands in the gas phase may be due to the measurement at a high temperature. It is noticeable that all the energies of the $\pi\rightarrow\pi^*$ bands in the gas phase are considerably larger than those in the *n*-heptane solution as may be seen in Table 1. The energy differences (in wave number) between the former and the latter are *ca.* 1760, *ca.* 1710, 1630, and 2140 cm^{-1} for the a-, b-, c-, and d-bands respectively. A similar fact is observed in anthraquinone.[16]

The authors are grateful to Mr. Toshihiro Kamada of this Laboratory and Mr. Yoshikuni Sato of the Tokyo Metropolitan Industrial Technology Center for their helpful cooperation in the experiments.

References

1) A. Kuboyama, S. Matsuzaki, M. Takagi, and H. Arano, This Bulletin, **47**, 1604 (1974); A. Kuboyama and K. Wada, *ibid.*, **38**, 1709 (1965).

2) J. Schmidt and M. Eitel, *J. Prakt. Chem.*, (2), **134**, 167 (1932).

3) R. G. Parr, "Quantum Theory of Molecular Electronic Structure," W. A. Benjamin, New York (1964), p. 503; R. Pariser and R. G. Parr, *J. Chem. Phys.*, **21**, 767 (1953).

4) M. Alleaume, R. Darrouy, and J. Housty, *Acta Crystallogr.*, **14**, 1202 (1961).

5) a) G. M. Brown and M. H. Bortner, *ibid.*, **7**, 139 (1954); b) A. Klug, *ibid.*, **3**, 165, 176 (1950); c) B. V. R. Murty, *Z. Krist.*, **113**, 445 (1960); K. Lonsdale, H. J. Millege, and K. El-Sayed, *Acta Crystallogr.*, **20**, 1 (1967); d) T. C. W. Mak and J. Trotter, *ibid.*, **16**, 811 (1963).

6) C. A. Coulson, "Valence," Clarendon Press, Oxford (1952), p. 180.

7) H. Eyring, J. Walter, and G. E. Kimball, "Quantum Chemistry," J. Wiley & Sons, New York (1944), p. 376.

8) A. Kuboyama and M. Anze, *Nippon Kagaku Kaishi*, **1972**, 229; A. Kuboyama, This Bulletin, **33**, 1027 (1960).

9) A. Kuboyama, *ibid.*, **37**, 1540 (1964).

10) J. Tanaka, S. Nagakura, and M. Kobayashi, *J. Chem. Phys.*, **24**, 311 (1956).

11) a) A. Kuboyama, unpublished work; b) E. D. Bergman, G. Berthier, Y. Hirshberg, E. Loewenthal, B. Pullman, and A. Pullman, *Bull. Soc. Chim. France*, **17**, 669 (1951); c) S. Cohen, *J. Amer. Chem. Soc.*, **79**, 1500 (1957).

12) H. Inoue and Y. Tanizaki, *Z. Phys. Chem. N. F.*, **73**, 48 (1970).

13) M. Titz and M. Nepras, *Collection Czechoslov. Chem. Commun.*, **37**, 2674 (1972).

14) In this work, the dichroism of the excitation spectrum of the phosphorescence band[8] of PHQ in *n*-heptane solution at 77 K was measured, but an unambiguous result could not be obtained (A. Kuboyama and S. Matsuzaki (Yabe), This Bulletin, **40**, 2475 (1967).

15) J. Aihara, K. Ohno, and H. Inokuchi, This Bulletin, **43**, 2435 (1970); L. B. Clark, G. G. Peschel, and I. Tinoco, Jr., *J. Phys. Chem.*, **69**, 3615 (1965); L. E. Jacobs and J. R. Platt, *J. Chem. Phys.*, **16**, 1137 (1948).

16) F. Kobayashi and A. Kuboyama, unpublished work.

Some Properties of the Salt between Inosine and L-Lysine

Yoshihisa SUZUKI, Kentaro HARA, and Tsuneo HIRAHARA
Central Research Laboratories, Ajinomoto Co., Inc., Suzuki-cho, Kawasaki 210
(Received December 2, 1974)

Among several basic amino acids, only the L-lysine free base was found to form a crystalline salt with inosine. A specific stereochemical arrangement of these two molecules, inosine and L-lysine, is considered to be involved in such a crystalline salt-formation on the basis of the fact that D-lysine did not form a crystalline salt with inosine. Part of the equilibria were determined at 10 °C for the inosine–L-lysine–water and inosine–L-lysine–60 w/w % aqueous ethanol systems. The salt was unstable against water, while it was stable against aqueous ethanol (containing more than about 40% ethanol). The solubility of the salt in water was summarized as follows: $\log S$ (w/w %) $= 0.0219\,t + 0.624$. The X-ray powder diffraction data of the salt are given.

In the course of a study of the interactions between nucleic acid components and amino acids, L-lysine and L-(or D-)tryptophan have both been found to form 1 : 1 crystalline compounds with inosine.[1,2] It has also been demonstrated that the optical resolutions of these two amino acids are performed through these crystalline compounds with inosine.[2,3] Such a crystalline compound of inosine with L-lysine is considered to be a salt, while with tryptophan it is considered to be a molecular complex, on the basis of the facts that lysine is basic and tryptophan is neutral. This paper will describe some properties of the crystalline salt of inosine with L-lysine.

Results and Discussion

Inosine possesses a pK_a value of 8.8, due to the hydroxyl group at the 6 position, and can form salts with various inorganic basic substances.[4,5] However, among several basic amino acids tested, only L-lysine formed a crystalline salt with inosine. An equimolecular solution of inosine and one of the basic amino acids (free bases) including L-arginine, L-histidine, L-ornithine, L-citrulline, and L-creatine was evaporated to dryness. The powder X-ray diffraction data revealed that the residue was an equimolecular mixture of crystals of inosine and individual amino acid. (The L-ornithine free base was dried in the amorphous solid.) The characteristic X-ray diffraction patterns, shown in Table 1, were obtained only when the L-lysine free base was employed.

Such a specific ability of the salt-formation of L-lysine with inosine cannot be interpreted merely in terms of the basicity of amino acid. L-Arginine shows no salt-formation despite the fact that basicity is higher than that of L-lysine.

The solubilities of amino acids (free bases) may explain to a certain extent such a salt-formation. The L-arginine free base or the L-histidine free base is not so soluble in water, and it is easily precipitated independently before the precipitation of the salt. On the other hand, L-lysine is very soluble and it is not easily

Table 1. The X-ray powder diffraction data of the salt between inosine and L-lysine

d (Å)	I/I_0 [a]
10.28	50
9.18	20
6.29	90
5.16	10
4.98	10
4.87	5
4.56	80
4.49	100
4.44	30
4.16	50
4.06	70
4.00	20
3.92	20
3.77	20
3.72	30
3.56	50
3.41	10
3.29	10
3.23	70

a) The scale of the intensity is so chosen as to make the most intense line have the value 100.

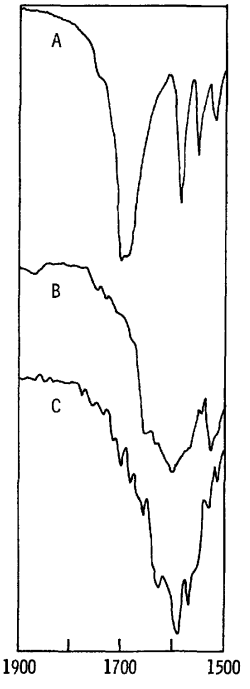

Fig. 1. Infrared spectra (KBr) of the crystals.
A: Inosine in the α-form.
B: The salt between inosine and L-lysine.
C: Sodium salt of inosine.

precipitated alone, and so there is a large possibility for the crystallization of the salt. However, the explanation in terms of the solubilities is not yet enough for the salt-formation, since L-ornithine was not associated with inosine in spite of its high solubility, like that of L-lysine.

It is also confusing that D-lysine cannot easily form a crystalline salt with inosine. This fact is advantageous for the resolution of racemic lysine.[3] When an equimolecular aqueous solution of inosine and D-lysine was evaporated to dryness, it gave an amorphous solid, or an almost amorphous solid plus a small quantity of inosine crystals in the α-form.[6] A specific stereochemical arrangement of these two molecules, inosine and L-lysine, may be involved in such a crystalline salt-formation, as is a molecular complex.

However, there is no doubt that an ionic bond is involved in this interaction. The infrared spectrum of the crystalline salt (Fig. 1) showed a strong absorbance at 1600 cm^{-1}, like that of sodium salt of inosine. This fact indicates an anionic dissociation of the hydroxyl group at the 6 position of the inosine molecule. The absence of the absorption band at 1680—1700 cm^{-1} also indicates an absence of any carbonyl group in the inosine molecule.

A part of the equilibria for the inosine–L-lysine–water and inosine–L-lysine–60%(w/w) aqueous ethanol systems were determined at 10 °C. In order to attain to the equilibrium, the mixture of the crystals and the solution was shaken for 16 hr, 40 hr, or 48 hr; the different shaking times revealed no significant difference in the composition data of the solution phase with the shaking period.

Table 2 shows the composition data of a part of the equilibrium for the inosine–L-lysine–water system at 10 °C. Figure 2 illustrates the solution phase of this system. The solubility of inosine increases linearly with an increase in the amount of L-lysine until its L-lysine salt is precipitated (Point A in Fig. 2), and then it

Table 2. Composition data of the equilibrium for the inosine–L-lysine–water system at 10 °C

Run No.	Solution (wt%)		Wet residue[b] (wt %)		Solid phase[a]
	Inosine	L-Lysine	Inosine	L-Lysine	
1	0.95	0.00	—	—	I2
2	4.55	2.48	—	—	I2
3	6.65	4.78	90.3	2.59	I2
4	9.34	6.55	87.2	1.57	I2
5	9.37	6.25	75.8	3.24	I2
6	15.1	10.6	84.8	2.91	I2
7	19.9	15.7	84.0	3.30	I2
8	20.8	15.5	88.7	4.60	I2
9	25.1	19.4	69.2	29.0	I2+I·L
10	24.5	19.7	61.4	36.7	I·L
11	22.7	19.2	56.6	40.0	I·L
12	22.3	19.4	51.8	33.9	I·L
13	15.2	28.6	57.8	33.9	I·L

a) I2: Inosine dihydrate, $C_{10}H_{12}N_4O_5 \cdot 2H_2O$. I·L: L-Lysine salt of inosine, $C_{10}H_{12}N_4O_5 \cdot C_6H_{14}N_2O_2$. b) Inosine+L-Lysine+Water=100 (%).

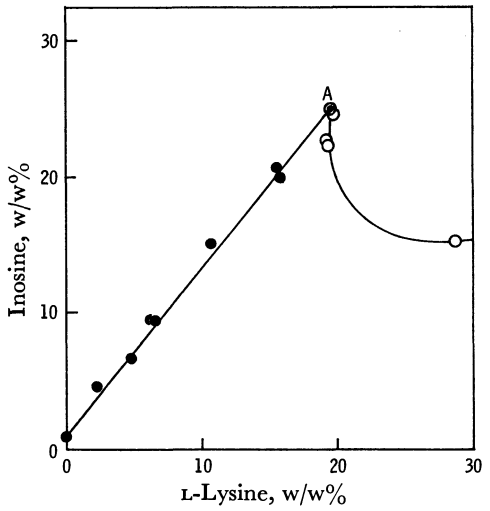

Fig. 2. An illustration of the solution phase of the equilibrium for the inosine–L-lysine–water system at 10 °C. (An extracted part from the phase diagram.) The symbolic marks of the residues are as follows:
●: Inosine dihydrate,
○: The salt between inosine and L-lysine.

decreases with a further increase in L-lysine. The slope of the initial linear increase is, however, not unity in relation to the molar ratio of inosine to L-lysine, but is, instead, about 0.7. The molar ratio at Point A is, consequently, also about 0.7. Accordingly, the L-lysine salt of inosine is unstable in the solution in which the molar ratio is unity; in other words, the salt is incongruent and unstable against water. When an excess amount of the salt is added to water at 10 °C, the suspended salt is changed into inosine dihydrate. For the stable crystallization of the salt, it is desirable that the solution possesses an excess amount of L-lysine; the molar ratio of L-lysine to inosine must be more than 1.4 (a reciprocal of 0.7).

On the other hand, the salt is stable against about 60%(w/w) aqueous ethanol, as is shown in Table 3 and Fig. 3. Table 3 shows the composition data of a part of the equilibrium for the inosine–L-lysine–60% aqueous ethanol system at 10 °C, while Fig. 3 illustrates

Table 3. Composition data of the equilibrium for the inosine–L-lysine–60% (w/w) ethanol system at 10 °C

Run No.	Solution (wt %)		Wet residue[b] (wt %)		Solid phase[a]
	Inosine	L-Lysine	Inosine	L-Lysine	
1	0.93	0.00	—	—	I(α)
2	1.47	0.48	99.3	0.7	I(α)
3	2.70	1.34	61.2	16.7	I(α)+I·L
4	2.39	2.12	64.8	34.4	I·L
5	2.55	4.00	62.7	36.2	I·L
6	2.58	5.92	66.9	33.2	I·L
7	2.52	8.05	62.0	32.1	I·L
8	2.47	13.8	64.1	35.7	I·L

a) I(α): Inosine in the α-form.[7] I·L: L-Lysine salt of inosine, $C_{10}H_{12}N_4O_5 \cdot C_6H_{14}N_2O_2$. b) Inosine+L-Lysine+Water=100 (%).

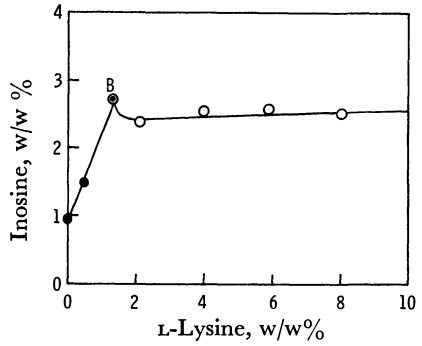

Fig. 3. An illustration of the solution phase of the equilibrium for the inosine–L-lysine–60 w/w% aqueous ethanol system at 10 °C. (An extracted part from the phase diagram.) The symbolic marks of the residues are as follows:
●: Inosine in the α-form,
○: The salt between inosine and L-lysine.

the solution phase of this system. The solubility of inosine in 60% ethanol increases linearly with an increase in the amount of L-lysine until its L-lysine salt is precipitated (Point B in Fig. 3). However, the molar ratio of inosine to L-lysine at Point B is about 1.1. Accordingly, the salt is stable against a 60% ethanol solution, whereas it is unstable against water.

A stabilizing effect in the presence of ethanol was observed when the concentration of ethanol was more than 40 w/w%. Therefore, the stable crystallization of the salt is performed from an equimolar solution of inosine and L-lysine by means of the addition of ethanol to make the concentration more than 40%.

Table 4. The solubility of inosine, and the L-lysine salt of inosine in water

Temp. (°C)	Solubility (w/w %)		
	Inosine in the α-form[7]	The salt, inosine·L-lysine	(Inosine-content in the solution of the salt)
10	0.95	7.03	(4.56)
30	3.1	18.4	(11.9)
50	8.2	52.5	(34.0)

The precise determination of the solubility of the salt in water was difficult because of the instability of the salt against water. However, a brief determination was performed by the addition of the salt, a little at a time, to water at a constant temperature until no more salt was dissolved; we thus made clear solution. The results are summarized in Table 4, which also shows the solubility of inosine in the α-form for comparison of the inosine-content in the solution. The logarithm of the solubility is linear to the temperature; it is expressed as follows:

$$\log S\,(\%) = 0.0219\,t + 0.624$$

where S represents the weight of the salt contained in 100 g of the solution and where t is the temperature (°C). The inosine-content in the solution of the salt thus obtained is about four times as much as that in the saturated solution of inosine in the α-form.[7] An aqueous solution of a high concentration of inosine for medical use can be prepared by dissolving the salt of inosine with L-lysine into water.

Experimental

Materials. The crystals of inosine, the L-arginine free base and the L-histidine free base used were of a commercial grade of the Ajinomoto Co., Inc. The aqueous concentrated solutions of the free bases of L-ornithine, L-lysine, and D-lysine were prepared from their respective hydrochlorides through the ion-exchange method. The free bases of L-citrulline and L-creatine were commercially obtained. The salt between inosine and L-lysine was prepared according to Suzuki *et al.*[1]

Examination of the Salt-formation. Inosine (0.005 M) and one of the basic amino acids (0.005 M) were dissolved in water, after which the mixture was evaporated to dryness *in vacuo*. The resulting solids were examined by the X-ray powder diffraction method. The IR spectra (KBr) were measured with a Nippon Bunkoh Model IR-S instrument.

Analysis. The inosine was determined with the absorbance at 250 nm in 0.1 M HCl, using the molar extinction coefficient of 11800. The lysine was determined according to the ninhydrin method by Yamagishi *et al.*[8]

Determination of the Inosine–L-Lysine–Water System. An excess amount of the crystals collected from inosine and the L-lysine salt of inosine were added to water or an aqueous solution of the L-lysine free base to make a slurry in tightly-capped glass bottles at 10±0.2 °C. The equilibria were achieved by tumbling the bottles for 16 hr (Runs No. 2, 3, 5, 7, 8, and 11) or 40 hr (Runs No. 4, 6, 9, 10, 12, and 13) at a constant temperature. A tumbling period of at least 16 hr was employed so as to avoid any more significant variation in the composition data of the solution phase. The prolonged period of 40 hr was employed for the convenience of the experimental schedule. Then, the mixtures were quickly filtered by means of a glass filter. The clear solutions and wet residues were submitted to analysis. The residues were examined by means of the X-ray diffraction method (Cu$K\alpha$) in order to identify the crystal form.

Determination of the Inosine–L-Lysine–60% Ethanol System. The same method was used except that the solvent was not water but 60 w/w% ethanol containing a definite amount of L-lysine. The tumbling period for the equilibrium was 48 hr.

Stability of the Salt in Relation to Aqueous Ethanol. An excess amount of the salt between inosine and L-lysine was added to an aqueous ethanol which had a definite concentration of ethanol. After the mixture had been shaken overnight at 10 °C, the suspended solid was examined by means of the X-ray method in order to confirm whether or not the form of the crystals was changed.

The Solubility of the Salt in Water. The salt between inosine and L-lysine was added to water, little by little, with vigorous shaking in order to dissolve it at a constant temperature (10, 30, or 50 °C). When a very small amount of a suspended solid remained undissolved in the solution, the mixture was filtered; the clear supernatant was then submitted to the analysis of inosine. The amount of the salt dissolved was calculated from the stoichiometry of 1 : 1.

The authors wish to thank Mr. Takashi Sato for his technical assistance in a part of the present study.

References

1) Y. Suzuki, T. Hirahara, and T. Nakamura, Japan

Patent 43 29011 (1968).
2) Y. Suzuki, T. Hirahara, T. Akashi, and T. Nakamura, U.S.P. 3532684 (1970); Brit. 1180635 (1970); Fr. 1601066 (1970); West Ger. Offen. 1645977 (1970).
3) Y. Suzuki, T. Hirahara, K. Hara, and N. Sato, Japan Patent 46 24006 (1971).
4) Y. Suzuki and Y. Nomura, This Bulletin, **47**, 2553 (1974).
5) Y. Suzuki and T. Toki, *ibid.*, **47**, 2556 (1974).
6) Y. Suzuki and N. Nagashima, *ibid.*, **43**, 1600 (1970).
7) Y. Suzuki, *ibid.*, **47**, 2549 (1974).
8) M. Yamagishi and T. Yoshida, *Yakugaku Zasshi*, **73**, 675 (1953).

The Calculation of the Primary Radiolysis Yield of Water Vapor Irradiated by 10-keV Electrons

Shin-ichi OHNO, Hisashi NAGAYAMA, Kiyoshi OKAZAKI,* and Shin SATO*

Japan Atomic Energy Research Institute, Tokai-mura, Ibaraki-ken 319-11

**Department of Applied Physics, Tokyo Institute of Technology, Ookayama, Meguro-ku, Tokyo 152*

(Received December 13, 1974)

The yields for the ionization and excitation from each molecular orbital of a water molecule irradiated by 10 keV electrons were calculated using the classical binary-encounter approximation. On further assuming fragmentation processes of the excited or ionized states consistent with the photochemical and mass spectrometrical results in the literature, we obtained, as the radiolysis yields of water vapor: G(electron)=2.96; $G(OH^-)=0.04$; $G(H_3O^+)=3.00$; G(H)=4.83—5.21, including G('hot' H-atoms)$\leq$0.87; $G(H_2)=0.28$—1.15; G(O)=0.83—1.21; G(OH)=6.70—7.08, and $G(-H_2O)=G$(ionized water)$+G$(excited water)$=2.91+4.96=7.87$.

The ideal study of radiation chemistry consists of (i) the experimental determination of the radiation-chemical products, and (ii) the interpretation of their formation by means of a detailed analysis, specifying the primary products in the physical stage[1] (chiefly molecules in the electronically excited or ionized state) and following their fate in temporal sequence until observable chemical changes appear. Thus, a knowledge of the nature and yields of the primary products is extremely important to radiation chemists.

The primary products are formed as a result of the interaction of molecules with electrons in an energy distribution given by the degradation spectrum.[2,3] Fast electrons in the degradation spectrum interact with molecules in an "optical" collision, for which the cross section is expressed by the Bethe-Born approximation. For slow electrons of the degradation spectrum ($T\lesssim100$ eV), however, this approximation loses its validity.[4]

We have chosen another possible approach to this problem of the calculation of the primary yields. Our method is a combination of the binary-encounter collision theory and a procedure for calculating the degradation spectrum. We previously applied it to the case of noble gases from He to Xe[5,6] and obtained results in reasonable agreement with the experimental ones.

The present paper is an extension of our work to a molecular system. The G-values of the ionization and excitation from each molecular orbital of the water molecule will be given. Then, we assume the mode with which the primary products decompose to give fragments on the basis of knowledge from photochemistry, mass spectrometry, and photoelectron spectroscopy. The yields of the fragments thus obtained may be compared with those estimated from the experimental work. The agreements are quite satisfactory, as will be shown later.

Method of Calculation

The "binary-encounter" collision theory, first presented by Thomas in 1927[7] and formulated and discussed in detail by Gryzinski,[8,9] Vriens,[10] and Burgess,[11] involves the following approximations:[10]

(i) the incident electron interacts with only one electron in the molecule.

(ii) the interaction between the molecular electrons and nucleus can be disregarded during the collision. In other wors, the collision takes place in a region small compared to the molecular dimensions. Thomas cosidered[7] the case of an electron with a kinetic energy of T moving through a cloud of free target electrons moving in random directions with kinetic energy of E_i. He gave this differential cross section per unit of energy interval for transferring an energy, E, to a target electron:

$$\sigma_{E,dir}=\frac{\pi e^4}{T+I_i+E_i}\left(\frac{1}{E^2}+\frac{4E_i}{3E^3}\right) \qquad (I)$$

for $T+I_i\geq E$. Here, I_i is the binding energy of the target electron in the i-th molecular orbital (M.O.). The target electron on receiving the energy, E, may jump to a higher M.O. with the excitation energy, E_n, if $E\geq E_n$. Ionization occurs if E is larger than I_i, the kinetic energy of the ejected electron being $E-I_i$. One may also apply the above formula to an excitation induced by the exchange between the incident electron and a molecular electron ($\sigma_{E,exc}$). In this case, E in Eq. I should be replaced by $T+I_i-E$.

The stopping power, the degradation spectrum, and the total number of the primary products were all calculated on the basis of Eq. I. The details of the formulation were the same as those presented previously,[6] except for a slight modification of the stopping power formula (Eq. IV in Ref. 6).

Stopping Power. In the present work we used the stopping power expressed as follows:

$$S(T)=N\sum_i S_i(T)$$

$$S_i(T)=n_i\left\{\int_{E_{si}}^{(T+I_i)/2}E(\sigma_{E,dir}+\sigma_{E,exc})dE+\frac{1}{2}\int_{E_{ti}}^{E_{si}}E\sigma_{E,exc}dE\right\} \qquad (II)$$

for $T\geq I_i$. Here, N is the number of molecules in a unit of volume, $S_i(T)$ is the stopping power due to the n_i-electrons in the i-th M.O., and E_{si} and E_{ti} are the excitation energies of the lowest singlet and triplet levels respectively for the electrons in the i-th M.O. When $T\leq I_i$, the upper limit of the first integral should be replaced by T. When $T<E_{si}$, the first term disappears and the E_{si} in the second integral should be replaced by T.

Double Collision. A molecule undergoing interac-

tion with an impacting electron may result in a simultaneous excitation and/or ionization of two electrons. Gryzinski formulated two such processes:[9] one in which two electrons in the molecule are excited and/or ionized by two successive collisions of the incident electron, and another in which the incident electron ejects the first electron, which in turn excites or ionizes the second electron in the same molecule. According to the treatment of Gryzinski,[9] and using Eq. I as the cross sections for transferring energy on collision, we derived the cross-section formulas[12] for double ionization (designated as $\sigma(H_2O^{++})$), double excitation $\sigma(H_2O^{ee})$, and simultaneous excitation and ionization $\sigma(H_2O^{e+})$ in order to estimate their yields with the help of the degradation spectrum obtained on the basis of single collisions alone.

Constants Used for Calculation

The ground-state electronic configuration of the H_2O molecule is:

$$(1a_1)^2(2a_1)^2(1b_2)^2(3a_1)^2(1b_1)^2, \quad {}^1A_1$$

For the present calculation, we must know the binding energies, I_i, of the electrons in each M.O., their average kinetic energies, E_i, and their lowest singlet and triplet excitation energies, E_{si} and E_{ti}. Table 1 summarizes the values used. The lowest excited states:

$$\cdots (1b_2)^2(3a_1)^2(1b_1)(4a_1), \quad {}^3B_1\ (5\text{ eV}), \quad {}^1B_1(7.5\text{ eV})$$

$$\cdots (1b_2)^2(3a_1)(1b_1)^2(4a_1), \quad {}^1A_1\ (9.6\text{ eV})$$

heve been identified by UV-absorption or electron-impact experiments.[14-16] The E_{si} values of the other M.O.'s given in Table 1 were estimated from the differences in the I_i-values. Selection rules for transitions were taken into account. All the E_{ti}-values, except for the lowest, were set equal to the respective E_{si} values; they are only provisional.

TABLE 1. THE BINDING ENERGY (I_i), THE KINETIC ENERGY (E_i), AND THE LOWEST SINGLET (E_{si}) AND TRIPLET (E_{ti}) LEVELS OF ELECTRONS IN THE WATER MOLECULE (IN eV)

M.O.	I_i	E_i	E_{si}	E_{ti}
$1b_1$	12.6	70.4	7.5	5.0
$3a_1$	14.7	42.0	9.6	9.6
$1b_2$	18.4	42.0	13.3	13.3
$2a_1$	32.2	70.4	27.1	27.1
$1a_1$	540	806	535	535

More difficult to ascertain are the average kinetic energies, E_i. Since the M.O. $1a_1$, $2a_1$, and $1b_1$ are composed mainly of the atomic orbitals of oxygen (1s, 2s+2pz, and 2px respectively), the E_i values of these M.O.'s may be calculated using Slater's rule.[17] The E_i values for $1b_2$ and $3a_1$ were set equal to the mean of the kinetic energies calculated for the corresponding atomic orbitals of oxygen and hydrogen.[18]

For the calculation of the double-collision cross-sections, we assumed, to simplify the computation, that double collisions occur only among the 6-electrons in the $1b_1$, $3a_1$, and $1b_2$ orbitals. The 6-electrons are situated uniformly on the surface of the sphere with a radius of 0.5 Å, so that the mean distance between two of these electrons is 0.8 Å. The first ionization energy, $\bar{I}(\mathrm{I})$, the first excitation energy, $\bar{E}_s(\mathrm{I})$, and the kinetic energy, $\bar{E}_i$, are taken to be the averages of the respective values of the $1b_1$, $3a_1$, and $1b_2$ electrons. The second ionization energy, $\bar{I}(\mathrm{II})$, and the second excitation energy, $\bar{E}_s(\mathrm{II})$, are tentatively taken to be $2\times\bar{I}(\mathrm{I})$ and $2\times\bar{E}_s(\mathrm{I})$ respectively.

Results

Figure 1 shows the $y(T)$ for a 10 keV electron in H_2O (1 atm, 0 °C). Once $y(T)$ is obtained, the calculation of the yields of the ionization and excitation is straightforward if we use the total cross-section, $Q_s(T)$, for each process.[6] Figures 2 and 3 show the $T\cdot y(T)\cdot Q_s(T)$ *vs.* $\ln T$ plots; according to Platzman[2] the area under the curve is proportional to the yield of the s process (Fig. 2 refers to ionizations, while Fig. 3 refers to excitations).

Tables 2—4 summarize the G-values of all the primary products obtained in the present calculation. All the integrations were carried out by means of a computer, HITAC 8700, with a mesh of $(0.5)^{1/40}$ for the energy.

Since the cross-sections for the dissociative-electron capture of the H_2O molecule have been previously reported,[19] we can estimate the order of magnitude of the yield of this process using the $y(T)$-curve obtained

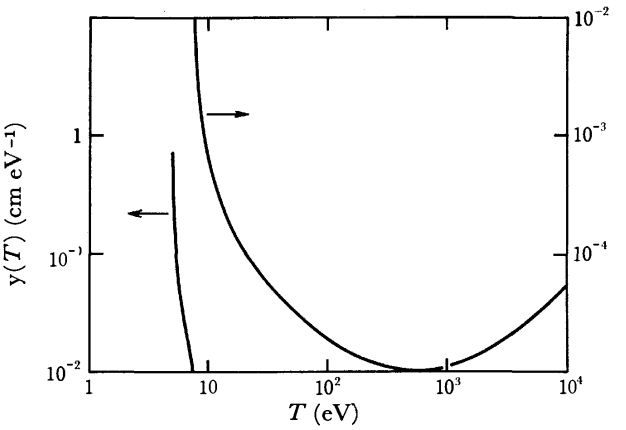

Fig. 1. The degradation spectrum for a 10 keV electron in water vapor (0 °C, 1 atm).

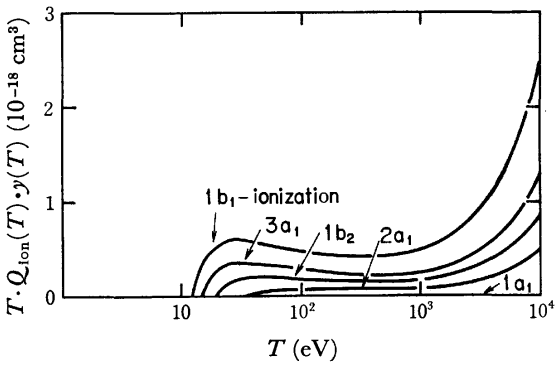

Fig. 2. Contribution of different portions of the electron degradation spectrum to ionizations from each M.O. in H_2O.

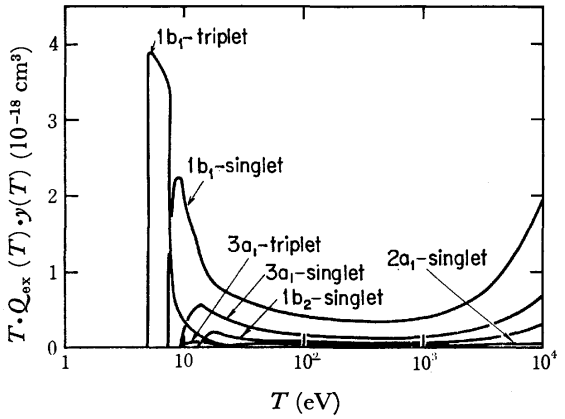

Fig. 3. Contribution of different portions of the electron degradation spectrum to excitations from each M.O. in H_2O.

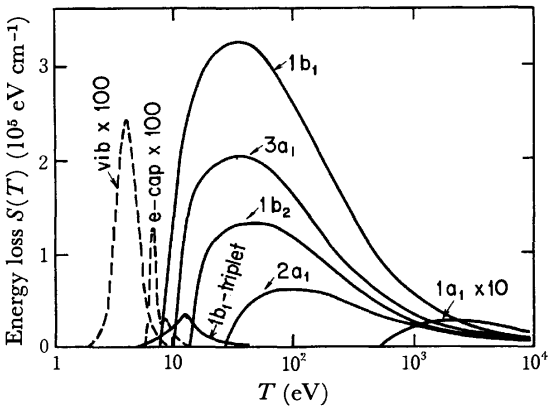

Fig. 4. The stopping power for electrons in water vapor. The contribution from electronic excitation and ionization of each M.O., dissociative electron capture (e-cap) and vibrational excitation (vib) of the H_2O molecule.

Table 2. The *G*-values of excitations in the H_2O molecule

M.O.	Singlet	Triplet	Mode of decomposition
$1b_1$	2.80	1.00	H+OH
$3a_1$	0.96	0.029	H+OH* (75%), H_2+O (25%)
$1b_2$	0.39	0.011	"hot H"+OH, or H_2+O*
$2a_1$	0.076	0.0016	Ion. frag.[a]
$1a_1$	0.000079	1.5×10^{-6}	Ion. frag.

a) Ionizing fragmentation.

Table 3. The *G*-values of ionizations in the H_2O molecule

M.O.	*G*	Mode of decomposition
$1b_1$	1.26	H_2O^++e
$3a_1$	0.68	H_2O^++e
$1b_2$	0.44	Ion. frag.
$2a_1$	0.21	Ion. frag.
$1a_1$	0.005	H^++OH^++2e *via* HO^{2+}

Table 4. The *G*-values for double collisions in the H_2O molecule

Primary product	Excitation energy (eV)	*G*	Mode of fragmentation
H_2O^{++}	45.6	0.09	H^++OH^++2e
H_2O^{ee}	30.6	0.12	H_2O^++e
H_2O^{+e}	35.6	0.31	Ion. frag.

in the present work. This gives $G\approx0.04$ for this reaction:

$$H_2O + e \longrightarrow H^- + OH \quad (1)$$

An alternative mode of dissociation:

$$H_2O + e \longrightarrow H_2 + O^- \quad (2)$$

has a much lower probability.[19]

Figure 4 shows the contribution from the electrons in each M.O. of the H_2O molecule to the stopping power for electrons in water vapor. Here are also shown, for convenience of comparison, the stopping power due to the dissociative-electron capture (Reaction 1) and the stopping power due to the vibrational excitations of water previously estimated by Mozumder.[20]

Yields of the Radiolytic Fragments

In order to obtain the radiolysis yields so as to compare them with the experimental results, we must know the fate or fragmentation process of the primary products listed in Tables 2 to 4.

The Ionized States. As to the ionized states, useful information is available from experimental photoelectron spectroscopy.[21] When an electron is removed from the $1b_1$ orbital, non-bonding in nature, the resulting ion is left practically unexcited. The loss of an electron from $3a_1$ will cause a bending vibration. If an electron is lost from a bonding $2a_1$ or $1b_2$ orbital, the O-H bond strength is weakened and its length is increased. In fact, the peaks of the band corresponding to the ionization from $1b_2$ in the P.E.S. spectrum are diffuse, suggesting a short lifetime prior to dissociation.[21]

The ejection of a $1a_1$-electron produces a doubly-charged ion by a well-known Auger process; the ion will then decompose.[22]

The Excited States. The UV absorption experiments threw light on the neutral excited states listed in Table 3. The continuous band ranging from 7 to 9 eV is due to the $\cdots\cdots(1b_1)^2$, $^1A_1\rightarrow\cdots\cdots(1b_1)(4a_1)$, $^1B_1$ transition, where the higher state is repulsive because of the anti-bonding nature of the $4a_1$ orbital.[23] The photochemical experiments have enabled us to conclude that the fragments are OH and H.[24] The excitation of an electron from $3a_1$, responsible for the bent shape of the molecule, to an anti-bonding $4a_1$ orbital will strain it towards its linear form and at the same time dissociate it. The photochemical experiments show that O, $OH(^2\Sigma^+)$, and $OH(^2\Pi)$ are formed simultaneously, their abundances being 25, 5, and 70% respectively.[24,25]

Nothing is known at present about the fate of the excited water molecules formed by promoting an electron from $1b_2$, $2a_1$, or $1a_1$ to $4a_1$ or a higher orbital. Since the excitation energy in these cases exceeds the lowest ionization energy of H_2O, both ionization and dissocia-

tion are possible. Therefore, we tentatively assume that the excitation of a $1b_2$-electron leads to dissociation to "hot H"+OH or H_2+O, while the excitation of a $2a_1$- or $1a_1$-electron leads to dissociative ionization. In the former case, the "hot H"-atoms might further react with water:

$$\text{"hot H"} + H_2O \longrightarrow H_2 + OH \quad (3)$$

as has been evidenced in the photochemical experiments.[24]

Double Collision. The doubly charged water and the excited water ion, designated as H_2O^{++} and H_2O^{+e} respectively in Table 4, would dissociate because of their large excitation energy. The doubly excited state, H_2O^{ee}, would lead to preionization.

The Ionizing Fragmentation. The yield of the primary products which will produce ionizing fragmentation amounts to $G\approx1$. Mass spectrometry provides information on the fragments. The mass spectrum of water obtained with an extremely high ion-extraction efficiency[26] shows that both H^+ and OH^+ are very abundant ions, about 25—30% of the parent ion, H_2O^+. The intensities of the other ions, O^+ and H_2^+, are low enough to be excluded from the present consideration. Thus, we may assume that the processes designated as Ion. frag. in Tables 2—4 are represented by:

$$H_2O \longrightarrow \begin{cases} H + OH^+ + e\ (50\%) & (4) \\ H^+ + OH + e\ (50\%) & (5) \end{cases}$$

It is possible that these fragments have a kinetic energy or an electronic excitation energy. Thus, the H-atoms formed in Reaction 4 can possibly react further according to Reaction 3.

Ion-molecule Reactions. The ionic fragments produced by the decomposition of the primary products of the water radiolysis may react with a water molecule to yield another ion. The following reactions are well known:[27]

$$H_2O^+ + H_2O \longrightarrow H_3O^+ + OH \quad (6)$$

$$OH^+ + H_2O \longrightarrow H_3O^+ + O \quad (7)$$

$$H^- + H_2O \longrightarrow H_2 + OH^- \quad (8)$$

The proton may react with several water molecules succesively to form a clustered state. We will represent this state as merely H_3O^+ for the sake of simplicity.

Final Results. We can now use the results shown in Tables 2 to 4 to estimate the G-values of the radiolytic fragments of water vapor in accordance with the above assumptions. The results are summarized in Table 5.

Table 5. The G-values of the fragments in the radiolysis of water vapor

Fragment	G
electron	2.96
OH^-	0.04
H_3O^+	3.00
H	4.83—5.21[a]
H_2[b]	0.28—1.15
O	0.83—1.21
OH	6.70—7.08

$G(-H_2O)=G$(ionized water)$+G$(excited water) $=2.91+4.96=7.87$

a) G("hot H")$\leq$0.87 is included. b) "molecular" H_2.

Discussion

The experimental W values which have been reported for water vapor lie around 30 eV.[27] Thus, G(ionization) $=3.3$. The values of G(electron) can be obtained experimentally from the difference in the radiolytic yields of water vapor with and without added electron scavengers; the values of 3.0 ± 0.4[28] and 2.7 ± 0.6[29] have been reported. The value for $G(-H_2O)$ was estimated by means of the total hydrogen yields from water vapor containing various organic additives. There is a reasonable agreement on $G(-H_2O)=8\pm1$.[27] Molecular hydrogen is also formed,[28,30] with a yield ($G\approx0.6$), not influenced by additives. More recently Boyd *et al.*[31] reported that the yields of hydrogen from the Febetron radiolysis of water vapor with HCl are $G(H_2)=7.9\pm0.2$ and $G(H_2)=4.6\pm0.2$ with 1 mol% SF_6. They combined their results, taking G("molecular" H_2)$=0.45$, with the relative primary ion yields of the radiolysis of water vapor as: G(e)$=3.3$, G(H)$=4.15$, G(OH)$=6.25$, and G(O)$=1.05$. It is of interest to compare all these results with the values compiled in Table 5. The agreement is satisfactory.

The important role of kinetically hot or electronically excited H-atoms has often been noticed.[32,33] According to the scheme discussed above, they are possibly formed either by the decomposition of the excited water molecule (itself formed by the promotion of a $1b_2$-electron) or by way of Reaction 4. Thus, the present results predict 0.9 as the maximum G-value of "hot" or excited H-atoms.

The yield of the doubly charged water, H_2O^{++}, amounting to $G=0.1$ should be noted in view of the radiolysis of frozen aqueous solutions. Molecular decomposition by Coulomb repulsion would bring about the atomic displacement in the solid phase,[34] the result of which may be the formation of trapped species.

The O-atoms, to which little attention has been paid, may be produced with a high yield ($G\approx1$) and may play an important role in the radiation chemistry of water.[35]

It is of some interest to know the mean energy, $\tilde{I}_1$, imparted to the molecule undergoing ionization. In an ionizing collision, the impacting electron loses the energy, E, which is the sum of the energy imparted to the molecule and the kinetic energy of the ejected electron. Using the results in Tables 2 to 4, one obtains:

$$\tilde{I}_i = \frac{\sum(I_i \times G_i)}{\sum G_i} = 19\,\text{eV}$$

which largely exceeds the lowest ionization energy, 12.6 eV. This is due to the electronic excitation of the ions formed or to excitation to repulsive ionic states, leading to the formation of fragments with a high kinetic energy.

We must further note that Santar and Bednar[4] calculated the yields of the excitation and ionization of valence electrons in the water molecule. They

treated separately the contributions to the yield from "fast" and "slow" electrons of the degradation spectrum. They used the available optical data for H_2O to calculate the yields due to "fast" electrons. They also utilized the optical data to ascertain the number and initial kinetic energy of the "slow" electrons, which are produced predominantly by "fast" collisions. They further used the experimental W value for water, considered the energy balance, and finally obtained results which are close to those found experimentally.

The present method is obviously more straightforward and simpler than that employed by Santer and Bednar. It requires neither the optical data nor the W value. Instead, it requires data on the binding energy, the excitation energy, and the kinetic energy of each electron in the molecule. In conclusion, we should mention that the "binary-encounter" approximation may be very useful, not only for getting a general idea about the primary process of radiolysis, but also for estimating non-empirically the radiation-chemical yields.

The authors wish to thank Dr. Kazuhiko Izui for his helpful discussions and Dr. Tsutomu Watanabe, University of Tokyo, for suggesting a procedure for the estimation of the E_i values.

References

1) E. J. Hart and R. L. Platzman, "Mechanisms in Radiobiology," ed. by A. Forssberg and M. Errera, Academic Press, New York (1961), Vol. 1, Chap. 2.
2) R. L. Platzman, "Radiation Research," ed. by G. Silini, North-Holland, Amsterdam (1967), p. 20.
3) L. V. Spencer and U. Fano, *Phys. Rev.*, **93**, 1172 (1954).
4) I. Santar and J. Bednar, *Collection Czechoslov. Chem. Commun.*, **32**, 953 (1967); **33**, 1 (1968).
5) S. Ohno, *Chem. Lett.*, **1973**, 817.
6) S. Sato, K. Okazaki, and S. Ohno, This Bulletin, **47**, 2174 (1974).
7) L. H. Thomas, *Proc. Camb. Phil. Soc.*, **23**, 829 (1927).
8) M. Gryzinski, *Phys. Rev.*, **115**, 374 (1959).
9) M. Gryzinski, *ibid.*, **A138**, 305, 322, 336 (1965).
10) L. Vriens, "Case Studies in Atomic Collision Physics I," ed. by E. W. McDaniel *et al.*, North-Holland, Amsterdam (1969), p. 335.
11) A. Burgess and I. C. Percival, "Advances in Atomic and Molecular Physics," Vol. 4, ed. by D. R. Bates and I. Estermann, Academic Press, New York (1968), p. 109.
12) K. Okazaki, S. Sato, and S. Ohno, This Bulletin, **48**, 1411 (1975).
13) K. Siegbahn *et al.*, "ESCA Applied to Free Molecules," North-Holland, Amsterdam (1971).
14) G. Herzberg, "Electronic Spectra of Polyatomic Molecules," Van Nostrand, Princeton, N. J., (1966).
15) C. R. Claydon, G. A. Segal, and H. S. Taylor, *J. Chem. Phys.*, **54**, 3799 (1971).
16) S. Trajmar, W. Williams, and A. Kuppermann, *ibid.*, **58**, 2512 (1973).
17) B. B. Robinson, *Phys. Rev.*, **A140**, 764 (1965).
18) This procedure for a rough estimation of E_i is due to the suggestion made by Dr. T. Watanabe, University of Tokyo.
19) R. N. Compton and L. G. Christophorou, *Phys. Rev.*, **154**, 110 (1967).
20) A. Mozumder, "Advances in Radiation Chemistry," Vol. 1, ed. by M. Burton and J. Magee, Wiley-Interscience, New York (1970), p. 1.
21) C. R. Brundle and D. W. Turner, *Proc. Roy. Soc.* (London), *Ser. A*, **307**, 27 (1968).
22) A. Ore, in Ref. 2, p. 54.
23) F. O. Ellison and H. Shull, *J. Chem. Phys.*, **23**, 2348 (1955).
24) M. Cottin, J. Masanet, and C. Vermeil, *J. Chim. Phys.*, **63**, 959 (1966).
25) J. R. McNesby, I. Tanaka, and H. Okabe, *J. Chem. Phys.*, **36**, 605 (1962).
26) J. Schutten, E. J. de Heer, H. R. Moustafa, A. J. H. Boerboom, and J. Kistemaker, *ibid.*, **44**, 3924 (1966).
27) R. S. Dixon, *Radiat. Res. Rev.*, **2**, 237 (1970).
28) J. H. Baxendale and G. P. Gilbert, *J. Amer. Chem. Soc.*, **86**, 516 (1964); *Sciences*, **147**, 1571 (1965).
29) G. R. A. Johnson and M. Simic, *J. Phys. Chem.*, **71**, 1118, 2775 (1967).
30) A. R. Anderson, R. Knight, and J. A. Winter, *Nature* (London), **201**, 1026 (1964).
31) A. W. Boyd, C. Willis, and O. A. Miller, *Can. J. Chem.*, **51**, 4048 (1973).
32) R. L. Platzman, *Radiat. Res.*, **17**, 419 (1962).
33) Y. Hatano, S. Shida, and S. Sato, This Bulletin, **41**, 1120 (1968).
34) J. Durup and R. L. Platzman, *Discuss. Faraday Soc.*, **31**, 156 (1951).
35) A. O. Allen, *Radiat. Res., Suppl.*, **4**, 54 (1964).

The Radiation-induced Decoloration of Azo Dye in Aqueous Solutions

Nobutake Suzuki, Takeshi Nagai, Hiroshi Hotta, and Masamitsu Washino

Japan Atomic Energy Research Institute, Takasaki Radiation Chemistry Research Establishment, Takasaki 370-12

(Received December 25, 1974)

The decoloration yield of an Acid Red 265 neutral aqueous solution, G(-Dye), equaled 1.00 ± 0.04, regardless of the dose rate and the initial dye concentration in the early stage. The G(-Dye) increased to 1.46 in the presence of nitrous oxide, but was independent of the presence of oxygen and acetone. In nitrogen-saturated solutions, the G(-Dye) increased markedly upon the addition of alcohols—for example, up to 1.83 upon the addition of 2 mM *n*-butyl alcohol. On the other hand, in oxygen-saturated solutions, the G(-Dye) decreased markedly upon the addition of even a small amount of alcohols. The effects of alcohols, namely, the G(-Dye) in both the solutions were in the order of their reactivity with OH radicals. The decoloration is attributable to the attack of the OH radicals formed by the radiolysis of water to the dye. The increase in the G(-Dye) for the nitrogen-saturated solutions containing alcohols is attributable to the attack of the alcohol radicals ($R\dot{C}HOH$) formed by the reactions of alcohols with OH radicals. In the oxygen-saturated solutions, the $R\dot{C}HOH$ radicals are converted to the peroxides, which do not react with the dye. The rate constant for the reaction of the OH radical with Acid Red 265, obtained by using various additives from the competition reaction method, is $9.3\pm1.4\times10^9$ $M^{-1}s^{-1}$. The effects of CNS^-, glucose, and phenol were also examined.

The decoloration of organic dyes in aqueous solutions induced by ionizing radiation has recently been reviewed by Grossweiner.[1] However, the radiation chemistry of azo dyes in aqueous solutions has not been extensively studied. A few authors[2,3] have, though, reported on its radiation-induced decoloration of azo dye in aqueous solutions. Korgaonkar *et al.*[2] discussed the possibility that the color changes of azo dye solution induced by ionizing radiation might serve as convenient radiation dosimeters. Mytelka *et al.*[3] have studied the radiation-induced decoloration of azo dye waste water.

In this paper, the effects of alcohols and other additives on the radiation-induced decoloration of Acid Red 265 in aqueous solutions will mainly be discussed, and the rate of its decoloration reaction will be estimated.

Experimental

Reagents. The Acid Red 265 (Kayaku Acid Brilliant Red BL; see Fig. 1), obtained from the Nippon Kayaku Co., Ltd., was further purified by recrystallization from a methyl alcohol-ethyl alcohol mixture. The recrystallized Acid Red 265 was then dried overnight in a vacuum desiccator containing silica gel. A test by thin-layer chromatography showed only a single component in the sample. The nitrous oxide (99.0%) was used without further purification. The other reagents used were of a reagent grade.

Fig. 1. Schematic of the sodium salt of Acid Red 265.

Irradiation Procedure and Analysis. The dye solution was prepared by dissolving recrystallized Acid Red 265 in triply distilled water. The solution was bubbled with nitrogen for 40 min or with oxygen for 15 min prior to irradiation. In some experiments, a nitrous oxide-saturated solution was prepared by bubbling for about 20 min. The solutions were placed in Pyrex glass tubes (30 ml) with a stopper and then irradiated with cobalt-60 gamma rays at room temperature. The dose rate (1.1×10^5 rad/hr) was determined by Fricke dosimetry ($G(Fe^{3+})=15.6$).

The degree of decoloration was determined by the measurement of the optical density at 542 nm with a Shimadzu spectrophotometer UV-200.

Results

Decoloration of Acid Red 265 in Aqueous Solutions. The degrees of decoloration for the nitrogen- and oxygen-saturated 0.1 mM Acid Red 265 aqueous solutions are shown as a function of the dose in Fig. 2. The degree of decoloration increased linearly with the dose below 4.8×10^4 rad, following the first-order kinetics. The degree of decoloration was independent of the presence of oxygen, at least below 6.4×10^4 rad. The pH of the solution changed from 6.4 to 4.7 at 4.8×10^4 rad. When the initial pH of the solution was changed by the addition of sulfuric acid, the degree of decoloration was independent of the initial pH between 4.3 and 6.4.

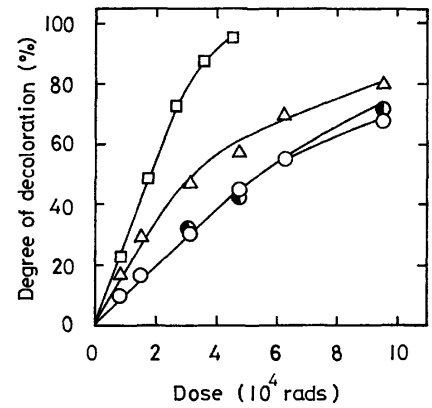

Fig. 2. Effects of additives on degree of decoloration. Dye concentration: 0.1 mM; ○: N_2 saturation, ◐: O_2 saturation, △: N_2O saturation, □: 2 mM *n*-butyl alcohol+N_2O.

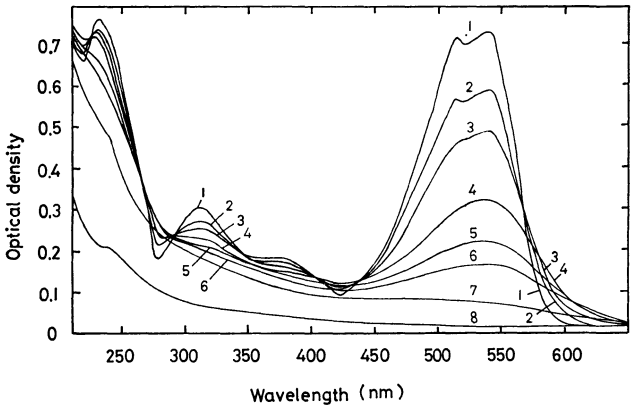

Fig. 3. Absorption spectra of unirradiated and irradiated oxygen-saturated Acid Red 265 aqueous solutions. Dye concentration: 0.1 mM; Curve 1 corresponds to the unirradiated sample. Curves 2—8 represented the spectra of solutions irradiated at the total doses of 1.6×10^4, 3.2×10^4, 6.4×10^4, 9.5×10^4, 1.3×10^5, 1.9×10^5, 2.8×10^5 rad, respectively.

The absorption spectra, shown in Fig. 3 as measured for the oxygen-saturated aqueous solution, indicate that the absorption band at 542 nm decreases with the dose, and that, below 6.4×10^4 rad (Curve 4), the isosbestic points appear at six different wavelengths, namely, 564, 439, 403, 290, 263, and 224 nm. Above 9.5×10^4 rad (Curve 5), the absorption band of the Acid Red 265 aqueous solution at 542 nm practically disappears and the isosbestic points disappear completely.

The results for the nitrous oxide-saturated similar solution are shown by open triangles in Fig. 2. The degree of decoloration for the nitrous oxide-saturated solution was higher than that for the nitrogen- and oxygen-saturated solutions. This suggests that nitrous oxide promotes the decoloration reaction.

When the decoloration yield, G(-Dye), was estimated as the number of dye molecules decolored per 100 eV of energy absorbed, from the concentration of the dye decolored, the G(-Dye) in the early stage equaled 1.00 ± 0.04, regardless of the dose rate in the range from 1×10^4 to 1.9×10^5 rad/hr and regardless of the initial dye concentration from 0.05 to 0.4 mM.

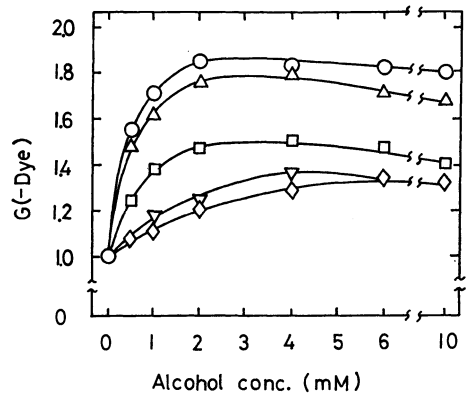

Fig. 4. Effect of alcohols on the G(-Dye) in the nitrogen-saturated solutions. Dose: 4.8×10^4 rad, Dye concentration: 0.1 mM, ◇: methyl alcohol, □: ethyl alcohol, △: *n*-propyl alcohol, ○: *n*-butyl alcohol, ▽: *tert*-butyl alcohol.

Effect of Alcohols. The degrees of decoloration for the nitrogen-saturated 0.1 mM Acid Red 265 aqueous solutions containing 4 mM alcohols increased linearly with the dose up to 4.8×10^4 rad in all cases. The values of the G(-Dye) for the nitrogen-saturated solutions containing *n*-alcohols and *tert*-butyl alcohol at 4.8×10^4 rad are shown as a function of the alcohol concentration in Fig. 4. Similar results for other isomers of butyl alcohol were also obtained. The G(-Dye) increased steeply with an increase in the concentration of alcohols up to 2 mM; then it decreased gradually except in the cases of methyl alcohol and *tert*-butyl alcohol.

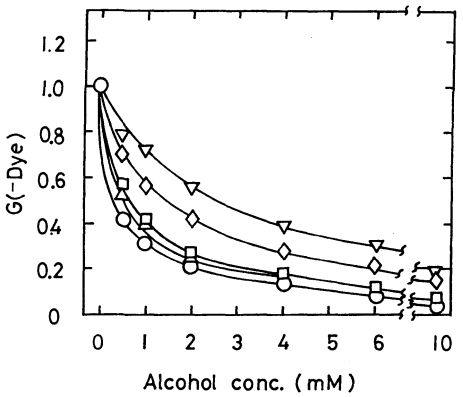

Fig. 5. Effect of alcohols on the G(-Dye) in the oxygen-saturated solutions. Dose: 4.8×10^4 rad, Dye concentration: 0.1 mM, ◇: methyl alcohol, □: ethyl alcohol, △: *n*-propyl alcohol, ○: *n*-butyl alcohol, ▽: *tert*-butyl alcohol.

On the other hand, the values of the G(-Dye) for the oxygen-saturated solutions containing *n*-alcohols and *tert*-butyl alcohol at 4.8×10^4 rad are shown as a function of the alcohol concentration in Fig. 5. Similar results for other isomers of butyl alcohol were also obtained. The G(-Dye) decreased with an increase in the concentration of alcohols.

Effect of Other Organic Additives. The values of the G(-Dye) for the nitrogen-saturated 0.1 mM Acid Red 265 aqueous solutions containing glucose and phenol are shown in Fig. 6 as a function of the organic additive concentration by open triangles and open squares respectively. The G(-Dye) increased up to 2 mM glucose, and thereafter decreased gradually with an increase in the concentration of glucose above 2 mM. The effect of phenol was in contrast to that of alcohols and glucose; that is, the G(-Dye) decreased upon the addition of phenol.

The results for the oxygen-saturated solutions containing glucose and phenol are shown in Fig. 7 as a function of the organic additive concentration by open triangles and open squares respectively. The G(-Dye) decreased steeply up to 2 mM glucose and phenol, and then decreased gradually above 2 mM. This tendency was almost the same as that for the solution containing alcohols.

The values of the G(-Dye) for the nitrogen- and oxygen-saturated solutions containing acetone are shown

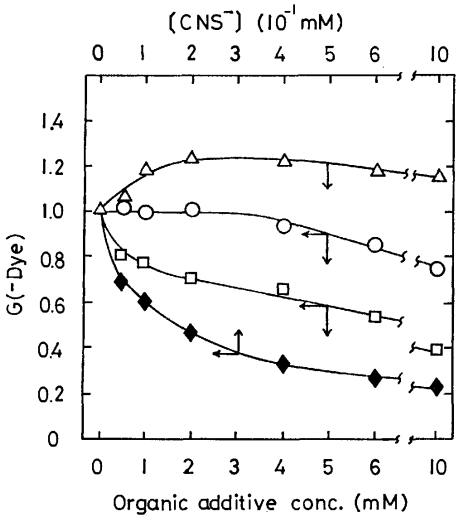

Fig. 6. Effect of organic additives and CNS^- on the G(–Dye) in the nitrogen-saturated solutions.
Dose: 4.8×10^4 rad, Dye concentration: 0.1 mM, △: glucose, □: phenol, ○: acetone, ◆: CNS^-.

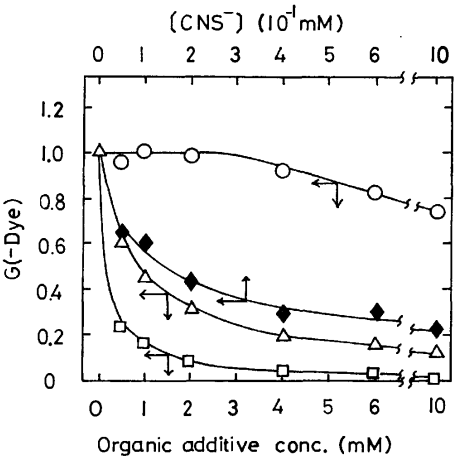

Fig. 7. Effect of organic additives and CNS^- on the G(-Dye) in the oxygen-saturated solutions.
Dose: 4.8×10^4 rad, Dye concentration: 0.1 mM, △: glucose, □: phenol, ○: acetone, ◆: CNS^-.

by open circles in Figs. 6 and 7 respectively. The G(-Dye) for neither solution was affected by the addition of acetone, at least not in the range from 0.5 to 2 mM. The effect of acetone for both the solutions is very different from those for the solutions containing alcohols and other organic additives.

Effect of CNS⁻. The G(-Dye) for the nitrogen- and oxygen-saturated 0.1 mM Acid Red 265 aqueous solutions containing CNS^- at 4.8×10^4 rad decreased markedly with an increase in the CNS^- concentration, as is shown in Figs. 6 and 7 respectively by solid lozenges. The two curves are almost the same. The effect of CNS^- for the nitrogen-saturated solution is, though, different from those for the solutions containing alcohols and other organic additives.

Effect of n-*Butyl Alcohol in N_2O-saturated System.* The degree of decoloration for the nitrous oxide-saturated 0.1 mM Acid Red 265 aqueous solution containing 2 mM *n*-butyl alcohol is shown by open squares in Fig. 2 as a function of the dose. The degree of decoloration increased linearly in the early stage. The G(-Dye) for the nitrous oxide-saturated aqueous solution containing 2 mM *n*-butyl alcohol was 2.56; this value was the highest of all the values for the nitrogen-saturated solutions.

Discussion

When a neutral aqueous solution is irradiated with cobalt-60 gamma rays, radicals and molecular products are formed from water:

$$H_2O \rightsquigarrow OH,\ H,\ e^-_{aq},\ H_2O_2,\ H_2, \qquad (1)$$

and in the presence of oxygen:

$$H + O_2 \longrightarrow HO_2 \qquad (2)$$

$$e^-_{aq} + O_2 \longrightarrow O_2^- \qquad (3)$$

As may be seen in Figs. 2, 6, and 7, the G(-Dye) was independent of the presence of oxygen; it was not even affected by the addition of 2 mM acetone. Acetone effectively scavenges hydrated electrons:[4,5]

$$e^-_{aq} + (CH_3)_2CO \longrightarrow (CH_3)_2CO^- \qquad (4)$$

and the rate of the reaction of acetone with the OH radical is slow.[6] This indicates that hydrated electrons do not contribute to the decoloration reaction. On the other hand, the G(-Dye) decreased markedly in the nitrogen- and oxygen-saturated solutions upon the addition of CNS^-, which is an efficient scavenger of OH radicals:[7]

$$OH + CNS^- \longrightarrow OH^- + CNS\cdot \qquad (5)$$

It is concluded from these findings that the decoloration of Acid Red 265 aqueous solutions is attributable to the attack of OH radicals formed from the radiolysis of water, and the species formed from water other than the OH radical contribute little to the decoloration reaction.

The G(-Dye) equals 1.00 ± 0.04 for the neutral aqueous solution. The primary yield of the OH radical, G(OH), formed from the radiolysis of water is 2.74 for neutral water.[8] This fact indicates that more than a half of the primary OH radicals are consumed by reactions other than the decoloration reaction.

On the basis of the results described above, the radiation-induced decoloration reaction of Acid Red 265 in aqueous solutions may be represented as follows:

$$A + OH \xrightarrow{k_6} AOH \text{ (decolored product)} \qquad (6)$$

$$A + OH \longrightarrow AOH' \text{ (colored product)} \qquad (7)$$

where A is Acid Red 265. The dye molecule has three kinds of sites for Reactions 6 and 7: (a) the azo group, (b) aromatic rings connecting directly to the azo group, (c) the benzene ring, not conjugated to the azo group. The attack of the OH radical on Site c would be independent of the decoloration reaction and would cause little change in the absorption spectra. This is represented as Reaction 7.

In Fig. 3, the absorption bands near 310 and 542 nm are attributable to the azo group and its auxochromic effect.[9,10] The absorption band near 230 nm is attri-

butable to substituted aromatic rings.[9,10] The optical density at 230 nm does not decrease with the dose so much as do those at 310 and 542 nm, and the isosbestic points at 224 and 263 nm appear below 6.4×10^4 rad (Curve 4). This suggests that the decoloration reaction is not necessarily accompanied by the destruction of substituted aromatic rings.

Azo group (Site a) is stabilized by hydrogen bonding with an adjacent OH group in a naphthalene ring.[11] Furthermore, the masking of the azo group can be expected because of the steric effect of the adjacent SO_3Na and CH_3 groups. Therefore, the direct attack on Site a would be minor. On the other hand, the attack of the OH radical on Site b clearly makes the dye decolor. This attack is, then, the main process for Reaction 6, as will be described later. Since the skeleton of the dye molecule is not necessarily destroyed by this reaction, the decrease in the optical density at 230 nm is small, as may be seen in Fig. 3.

When the attack of the OH radical on Site a occurs, this reaction may follow to scissor the C–N–N–C bridge. As aromatic rings after this scission may give a spectrum near 230 nm similar to that of the attack on Site b, the two attacks can not be distinguished by means of these spectra.

Nitrogen-saturated Solutions Containing Alcohols. Alcohols are also efficient scavengers of OH radicals.[12,13]

$$RCH_2OH + OH \xrightarrow{k_8} \dot{R}CHOH + H_2O \quad (8)$$

However, the addition of alcohols makes the G(-Dye) increase in the nitrogen-saturated solutions. This means that alcohol radicals ($R\dot{C}HOH$) contribute to the decoloration reaction in the nitrogen-saturated solutions, while some of alcohol radicals as well as OH radicals may be consumed by a reaction other than the decoloration reaction, like Reaction 7.

$$A + RCHOH \longrightarrow ARCHOH \text{ (decolored product)} \quad (9)$$

$$A + RCHOH \longrightarrow ARCHOH' \text{ (colored product)} \quad (10)$$

Ekstrom and Garnett have reported that, in the radiolysis of air-free binary mixture, that is, benzene–methyl alcohol[14] and polycyclic aromatic compounds–methyl alcohol,[15] $\cdot CH_2OH$ radicals add to benzene and the polycyclic aromatic compound. This supports the addition of alcohol radicals on aromatic rings (Reactions 9 and 10).

As may be seen in Fig. 4, the G(-Dye) increases steeply up to 2 mM alcohols and decreases gradually with an increase in the concentration of alcohols above 2 mM. The maximum values of the G(-Dye) and the concentration of alcohols for them are shown in Table 1. The increase in the G(-Dye) upon the addition of alcohols was in the order of *n*-butyl alcohol>*n*-propyl alcohol> *iso*-butyl alcohol, *sec*-butyl alcohol>ethyl alcohol>*tert*-butyl alcohol>methyl alcohol. The G(-Dye) increased up to 1.83 upon the addition of 2 mM *n*-butyl alcohol from 1.00 for the non-alcoholic aqueous solution. The order of the G(-Dye) in Table 1 almost corresponds to the order of the rate constants for the reaction of alcohols with OH radicals, as measured by the pulse-radiolysis technique; these rate constants are listed in Table 2.[6,7] The concentrations for the maximum G(-Dye) are high for methyl alcohol and *tert*-butyl alcohol, whose rate constants are low in comparison with others. The present findings indicate that the $R\dot{C}HOH$ radical destroys the dye chromophore more effectively than does the OH radical.

The small decrease in the G(-Dye) at 10 mM alcohol in Fig. 4 may be explained in terms of the following spur effect. Since alcohol molecules exist inside the spur of gamma rays at such a high concentration, they

Table 1. G(-DYE) FOR THE AQUEOUS SOLUTIONS CONTAINING VARIOUS ADDITIVES

Additives	Additive concn. (mM)	G(-Dye)
a) Nitrogen-saturated solutions.		
None	0	1.00
Methyl alcohol	6	1.34
Ethyl alcohol	2	1.47
n-Propyl alcohol	2	1.75
n-Butyl alcohol	2	1.83
iso-Butyl alcohol	2	1.64
sec-Butyl alcohol	2	1.64
tert-Butyl alcohol	4	1.37
Glucose	2	1.23
Phencl	2	0.71
Acetone	2	1.00
CNS^-	1	0.22
b) Oxygen-saturated solutions.		
None	0	1.00
Methyl alcohol	2	0.42
Ethyl alcohol	2	0.27
n-Propyl alcohol	2	0.25
n-Butyl alcohol	2	0.20
iso-Butyl alcohol	2	0.22
sec-Butyl alcohol	2	0.23
tert-Butyl alcohol	2	0.56
Glucose	2	0.31
Phenol	2	0.08
Acetone	2	0.98
CNS^-	1	0.22
c) Nitrous oxide-saturated solutions.		
None	0	1.46
n-Butyl alcohol	2	2.56

Table 2. RATE CONSTANTS FOR REACTIONS 6 AND 8

Additives	k_6[a] ($M^{-1}s^{-1}$)	k_8[b] ($M^{-1}s^{-1}$)
Methyl alcohol	8.1×10^9	4.8×10^8
Ethyl alcohol	8.1×10^9	1.1×10^9
n-Propyl alcohol	1.03×10^{10}	1.5×10^9
n-Butyl alcohol	9.9×10^9	2.2×10^9
iso-Butyl alcohol	1.03×10^{10}	2.0×10^9
sec-Butyl alcohol	1.05×10^{10}	1.9×10^9
tert-Butyl alcohol	7.9×10^9	2.5×10^8
Glucose	8.7×10^9	1.0×10^9
Phenol[c]	7.2×10^9	4.2×10^9
	1.81×10^{10}	1.06×10^{10}
CNS^-	1.02×10^{10}	6.6×10^9

a) Initial pH 6.4. b) Rate constants for reaction of OH radical with additives from references 6) and 7). c) See a text for the values of phenol.

react with a fraction of the OH radical larger than that predicted from the ratio of the concentration of alcohol to that of azo dye. The local concentration of the alcohol radicals produced is high in the spur or in the neighborhood of the spur, and the dye concentration is low. Therefore, some of the alcohol radicals are consumed through the following process,[16] that is, disproportionation or dimerization in advance of Reaction 9:

$$2RCHOH \longrightarrow RCHO + RCH_2OH \quad (11a)$$
$$\searrow (RCHOH)_2 \quad (11b)$$

According to Taub and Dorfman, the rate of the bimolecular reaction of two α-ethyl alcohol radicals in water is very fast and the absolute rate constant is $1.1\pm0.3\times10^9$ $M^{-1}s^{-1}$.[17]

Oxygen-saturated Solutions Containing Alcohols. In the oxygen-saturated solutions, the alcohol radicals ($R\dot{C}HOH$) react rapidly with oxygen, leading to the formation of peroxyradicals:

$$R\dot{C}HOH + O_2 \longrightarrow RC(O_2\cdot)HOH \quad (12)$$

As may be seen in Table 1, the G(-Dye) for the oxygen-saturated solutions decrease upon the addition of alcohols. This means that the peroxyradicals from Reaction 12 do not react with the dye. These peroxyradicals are easily converted to aldehydes (or ketones), glycols, and peroxide.[18,19]

The decrease in the G(-Dye) upon the addition of 2 mM alcohols for the oxygen-saturated solutions, as is shown in Table 1, was in the order of *n*-butyl alcohol> *iso*-butyl alcohol>*sec*-butyl alcohol>*n*-propyl alcohol> ethyl alcohol>methyl alcohol>*tert*-butyl alcohol. The order of the decrease in the G(-Dye) corresponds exactly to that of the rate constants for the reaction of alcohols with OH radicals in Table 2, because the role of alcohols in the above reaction scheme is simpler in the oxygen-saturated solutions than in the nitrogen-saturated solutions.

N_2O-saturated Solutions. As may be seen in Table 1, the $G(\text{-Dye})_{N_2O}$ for the nitrous oxide-saturated solution is 1.46; it increases to 2.56 upon the addition of 2 mM *n*-butyl alcohol. These values are remarkably larger than those for the nitrogen-saturated solutions. It is well known that nitrous oxide reacts rapidly with hydrated electrons, produced in an aqueous solution by ionizing radiations, thus leading to the formation of the OH radical:[20]

$$e^-_{aq} + N_2O \longrightarrow OH + OH^- + N_2 \quad (13)$$

Therefore, such a large G(-Dye) is attributable to an increase in the OH radical through Reaction 13 in addition to the primary radical.

Since the G(-Dye) for the nitrogen- and oxygen-saturated solutions equals 1.0 for $G(OH)=2.7$, the $G(\text{-Dye})_{N_2O}$ for the nitrous oxide-saturated solutions should be at least 2.0 for $G(OH)_{N_2O}=G(OH)+G(e^-_{aq})=5.6$, according to the scheme proposed above. The observed value of the $G(\text{-Dye})_{N_2O}$ indicates only a half of the expected increase, suggesting that OH radicals are consumed through another path, such as their recombination because of the high concentration.

Effects of Glucose and Phenol. The effect of glucose on the G(-Dye) is similar to that of alcohols in Table 1. The order of the decrease in the G(-Dye) for the oxygen-saturated solutions containing glucose in Table 1 corresponds exactly to that of the rate constant for the reactions of glucose with the OH radical shown in Table 2. However, in the nitrogen-saturated solution, glucose is less effective than methyl alcohol, even though the rate constant for glucose is larger than that for methyl alcohol (see Table 2). This may be due to the dependence of the rate constant of Reaction 9 on the structure of R- that is, a steric effect.

The effect of phenol on the G(-Dye) for the oxygen-saturated solution in Table 1 can be explained on the basis of the above reaction scheme; that is, phenol gives the smallest G(-Dye) in Table 1 and has the largest rate constants in Table 2. The G(-Dye) for the nitrogen-saturated solution also decreases upon the addition of phenol. This suggests that a $C_6H_5(OH)_2\cdot$ radical formed by the addition reaction of the OH radical to phenol hardly contributes to the decoloration reaction. According to Land and Ebert,[21] the $C_6H_5(OH)_2\cdot$ radical subsequently undergoes either the unimolecular elimination of water to form a more resonance-stabilized phenoxy radical($C_6H_5O\cdot$), or bimolecular radical-radical reactions.

Rate Constant for Reaction 6. The rate constant for Reaction 6 can be determined by using a competition reaction with additives. If G_r is the yield of the OH radicals consumed by Reactions 6 and 8, then:

$$\frac{1}{G(\text{-Dye})} = \frac{1}{G_r}\left(1+\frac{k_8[RCH_2OH]}{k_6[A]}\right) \quad (14)$$

where [A] and [RCH_2OH] are initial concentrations of Acid Red 265 and additives respectively. Since Reaction 9 is also attributable to the decoloration in the nitrogen-saturated solutions, the experiment of the competition reaction was carried out in the oxygen-saturated solution. The plots of $1/G$(-Dye) are linear against the additive concentration, in good agreement with Eq. 14. From Eq. 14, the slope of the curve gives the k_8/k_6 ratio and the intercept gives the G_r value by means of the least-squares method. The k_6 values listed in Table 2 were obtained from the observed k_8/k_6 ratio by using the corresponding k_8 values in Table 2. These k_6 values are in good agreement with each other. The average k_6 value is $9.3\pm1.4\times10^9$ $M^{-1}s^{-1}$. This value is near to the rate constants of the reactions of the OH radical with benzene (3.0×10^9 $M^{-1}s^{-1}$), toluene ($3.0\times10^9 M^{-1}s^{-1}$), and phenol ($4.2\times10^9$ and 1.06×10^{10} $M^{-1}s^{-1}$).[6] This fact supports the idea that the decoloration reaction is mainly attributable to the addition of the OH radical to aromatic rings adjacent to chromophore. The rate constants for the reactions of various dyes with the OH radical reported by some investigators are also of an order of about 10^9—10^{10} $M^{-1}s^{-1}$.[1,22]

Since the k_8 values for phenol in the reference are scattered, the k_6 value for phenol in Table 2 is calculated by using the two k_8 values, excluding the above average value.

References

1) L. I. Grossweiner, *Radiat. Res. Rev.*, **2**, 345 (1970).

2) K. S. Korgaonkar and M. S. Tarakanath, *Int. J. Appl. Radiat. Isotopes.*, **14**, 405 (1963).
3) A. I. Mytelka and R. Manganelli, *J. Water Pollution Control Federation*, **40**, 260 (1968).
4) E. J. Hart, S. Gordon, and J. K. Thomas, *J. Phys. Chem.*, **68**, 1271 (1964).
5) P. Riesz, *Radiat. Res.*, (*Suppl.*), **4**, 152 (1964).
6) M. Anbar and P. Neta, *Int. J. Appl. Radiat. Isotopes*, **18**, 493 (1967).
7) G. E. Adams, J. W. Boag, J. Currant, and B. D. Michael, "Pulse Radiolysis," Proceedings of the International Symposium held at Manchester, April, 1965, pp. 131—143, Academic Press, London, 1965.
8) B. H. J. Bielski and A. O. Allen, *Int. J. Radiat. Phys. Chem.*, **1**, 153 (1969).
9) A. E. Gillam and E. S. Stern, "An Introduction to Electronic Absorption Spectroscopy in Organic Chemistry," Edward Arnold LTD., London, 1960.
10) J. R. Dyer, "Applications of Absorption Spectroscopy of Organic Compounds," Prentice-Hall, Inc., New Jersey, 1965.
11) H. Zollinger, "Azo and Diazo Chemistry Aliphatic and Aromatic Compounds," Interscience Pub., Inc., New York, 1961.
12) A. Henglein, *J. Phys. Chem.*, **63**, 1852 (1959).
13) G. E. Adams and R. L. Willson, *Trans. Faraday Soc.*, **65**, 2981 (1969).
14) A. Ekstrom and J. L. Garnett, *J. Phys. Chem.*, **70**, 324 (1966).
15) A. Ekstrom and J. L. Garnett, *J. Chem. Soc., A*, **1968**, 2416.
16) M. Simic, P. Neta, and E. Hayon, *J. Phys. Chem.*, **73**, 3794 (1969).
17) I. A. Taub and L. M. Dorfman, *J. Amer. Chem. Soc.*, **84**, 4053 (1962).
18) A. J. Swallow, "Radiation Chemistry of Organic Compounds," Chapter IV, Pergamon Press, New York, 1960.
19) G. G. Jayson, G. Scholes, and J. Weiss, *J. Chem. Soc.*, **1957**, 1358.
20) F. S. Dainton and D. B. Peterson, *Proc. Roy. Soc.*, (London), **A267**, 443 (1962).
21) E. J. Land and M. Ebert, *Trans. Faraday Soc.*, **63**, 1181 (1967).
22) B. L. Gupta and E. J. Hart, *Radiat. Res.*, **48**, 8 (1971).

The Crystal and Molecular Structure of *cis*-2,2-Diphenyl-3,4-dichlorothietane 1,1-Dioxide

Shigekazu KUMAKURA

Department of Chemistry, Saitama University, 255 Shimo-okubo, Urawa 338

(Received January 31, 1975)

The title compound crystallizes in the space group $C2/c$ with $a=18.85(2)$, $b=6.15(1)$, $c=27.94(2)$ Å, $\beta=111.3(1)°$, and $Z=8$. The structure was determined from the photographic X-ray data and was refined by the block-diagonal least-squares method to $R=0.10$ for 1006 observed reflections. Centrosymmetrically related molecules in the crystal form a dimer by means of weak intermolecular C-H···O hydrogen bonds. The thietane skeleton of the compound is bent with the dihedral angle, $C_\alpha SC_\alpha/C_\alpha C_\beta C_\alpha$, of 148.7°. The average distance of the C–S bonds is 1.87 Å, while that of the C–C's in the thietane ring is 1.58 Å. The conformation of the C–Cl bonds with respect to the thietane ring is (3a4e). The transannular S···Cl distance is 3.42 Å. The CNDO/2 calculation reveals that the 3*d*–3*p* bonding overlap is present between these atoms. The bond angles involving the ring substituents deviate greatly from those observed for *cis*-2,2-diphenyl-3,4-dichlorothietane. These deformations may be explained in terms of dipole-dipole interactions.

cis-2,2-Diphenyl-3,4-dichlorothietane 1,1-dioxide (abbreviated hereafter as *cis*-SO_2-DCTE) was prepared by the oxidation of *cis*-2,2-diphenyl-3,4-dichlorothietane (*cis*-DCTE) by using 30% H_2O_2 as an oxidizing agent.[1]

The crystal-structure analysis of *cis*-SO_2-DCTE was undertaken, and the molecular geometry was compared with that of *cis*-DCTE[2] in order to establish the geometry of the thietane ring and to know the effect of changing the ring substituents, which may alter the structure of the thietane ring.

Experimental

Single crystals of this compound grown from an ethanol solution are thin colorless plates with well-developed {001} planes and with a perfect {100} cleavage. The cell constants, determined from Weissenberg and oscillation photographs, are listed in Table 1, together with other crystal data.

TABLE 1. CRYSTAL DATA

Monoclinic	
$a=$	18.85 (2) Å
$b=$	6.15 (1) Å
$c=$	27.94 (2) Å
$\beta=$	111.3 (1)°
$V=$	3018 Å^3
Formula	$C_{15}H_{12}Cl_2SO_2$, F.W.=327.13
$D_m=$	1.44 g/cm^3
$D_x=$	1.440 g/cm^3
$Z=$	8
$\mu=$	51.20 cm^{-1} (Cu$K\alpha$)
Possible space group:	*Cc* or *C2/c*
(Absent spectra:	*hkl* when $h+k$ is odd, and *h0l* when *l* is odd.)

It was difficult to select a suitable crystal for the intensity measurements, because the crystals were thin, brittle plates. Specimens with dimensions of $0.05\times0.07\times0.2$ mm, $0.05\times0.1\times0.08$ mm and $0.1\times0.1\times0.05$ mm were used for the collection of the intensity data around the *b*, *a*, and *c* axes respectively. Equi-inclination Weissenberg photographs were taken for *h0l*—*h4l*, *0kl*, and *hk0* using byCu$K\alpha$ radiation ($\lambda=$ 1.542 Å). The intensities of 1006 reflections were estimated visually and were corrected for the Lorentz, polarization, and spot-shape factors by the usual procedures. Absorption and extinction corrections were not applied.

Structure Analysis

The positions of the sulfur and chlorine atoms were determined from a Patterson synthesis, sharpened by a factor $\exp(B\sin^2\theta/\lambda^2)$ ($B=3.0$ Å^2), while the positions of the remaining non-hydrogen atoms were determined from the subsequent Fourier syntheses of the electron density. The space group, $C2/c$, is consistent with this structure. A block-diagonal least-squares refinement using anisotropic temperature factors reduced the R value ($R=\sum||F_o|-|F_c||/\sum|F_o|$) to 0.10. In the final cycles of the refinement, all the hydrogen atoms located by assuming a suitable geometry were included in the structure-factor calculations. The temperature factors of hydrogen atoms were assumed to be isotropic; the values of 3.0 Å^2 and 4.0 Å^2 were given for those atoms in the thietane skeleton and in the phenyl groups respectively. At every stage of the refinement, the scale factor, S, for F_0 was calculated for each layer-line data according to the following relation:

$$S\times\sum|F_o(hkl)|=\sum|F_c(hkl)|,$$

where the summation is taken over all the values of h and l for each k. A weighting scheme for the least-squares procedure, $w=1$ when $|F_o|\geq5.0$ and 0.3 otherwise, was employed.

The final difference map is flat within the range of ±0.2 eÅ^{-3}. The final atomic and thermal parameters are listed in Table 2. A list of the observed and calculated structure factors has been deposited with the Chemical Society of Japan.[3]

The atomic scattering factors were taken from the International Tables for X-ray Crystallography, Vol. III.

The calculations were carried out on a HITAC 5020E computer at the Computer Center of the University of Tokyo and on a TOSBAC 3400 of Saitama University.

Description and Discussion of the Structure

Figure 1 shows the molecular conformation, the bond distances, the bond angles, and the atomic numbering scheme. The molecule is dissymmetric, but both

TABLE 2. ATOMIC PARAMETERS

Positional parameters for the atoms in the asymmetric unit with their standard deviations ($\times 10^4$)

	x/a	*y/b*	*z/c*
S	−114(2)	−1223(9)	796(2)
Cl(1)	−1486(2)	1760(10)	369(2)
Cl(2)	−528(2)	2470(10)	1569(1)
O(1)	−593(6)	−2415(24)	1001(5)
O(2)	168(6)	−2375(23)	444(4)
C(2)	630(8)	505(29)	1276(5)
C(3)	18(9)	2392(33)	1163(5)
C(4)	−487(9)	1550(30)	612(7)
C(11)	1267(9)	930(33)	1072(6)
C(12)	1296(7)	2891(30)	808(6)
C(13)	1910(11)	3305(34)	646(7)
C(14)	2471(9)	1637(36)	747(6)
C(15)	2399(8)	−274(32)	994(6)
C(16)	1809(8)	−591(29)	1159(6)
C(21)	978(8)	−3(32)	1860(6)
C(22)	1498(10)	1360(40)	2174(6)
C(23)	1821(10)	914(44)	2702(7)
C(24)	1591(12)	−960(49)	2887(7)
C(25)	1088(14)	−2468(52)	2561(7)
C(26)	777(12)	−1876(39)	2045(6)

Thermal parameters ($\times 10^3$)

The temperature factor is of the form:

$T=\exp[-2\pi^2(U_{11}a^{*2}h^2+U_{22}b^{*2}k^2+U_{33}c^{*2}l^2+2U_{12}a^*b^*hk+2U_{13}a^*c^*hl+2U_{23}b^*c^*kl)]$

	U_{11}	U_{22}	U_{33}	U_{12}	U_{13}	U_{23}
S	48	77	76	2	60	12
Cl(1)	51	117	64	42	12	−9
Cl(2)	57	102	52	27	48	−50
O(1)	46	102	116	10	27	34
O(2)	79	86	71	11	62	191
C(2)	53	73	45	36	33	4
C(3)	84	91	52	−123	77	−189
C(4)	76	56	113	71	144	212
C(11)	82	87	53	−29	79	−133
C(12)	15	71	95	−50	28	−192
C(13)	112	64	116	−50	138	12
C(14)	59	111	86	−49	76	−174
C(15)	34	81	86	2	28	−272
C(16)	33	71	76	48	30	−68
C(21)	44	85	65	74	62	141
C(22)	70	163	50	−40	8	−289
C(23)	74	176	76	9	11	−147
C(24)	98	200	76	80	−4	17
C(25)	192	199	79	18	152	400
C(26)	138	106	74	63	92	76

enantiomers are present in the crystal because the requirement of the space group.

The thietane ring is bent with a dihedral angle, C(2)SC(4)/C(2)C(3)C(4), of 148.7°. The average length of the C–S bonds is 1.87 Å, while that of the ring C–C's is 1.58 Å. The mean value of the S–C–C bond angles and the C–C–C in the ring are 88.8° and 95.3° respectively. The C–S–C of 77.6(8)° is much smaller than that of dimethyl sulfone (103.0°).[4] The average distance of the S=O bonds is 1.45 Å, and the

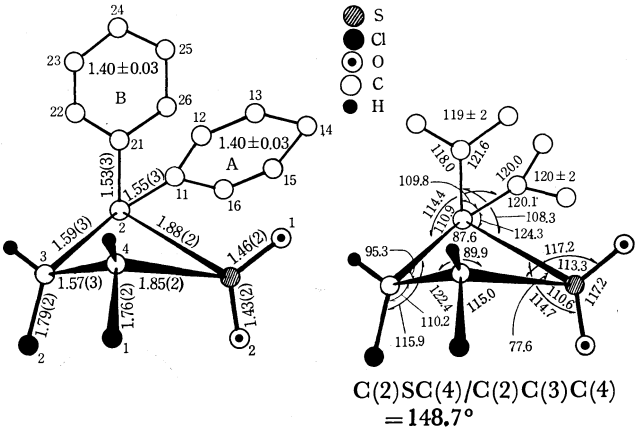

Fig. 1. Bond lengths (Å). E.s.d.'s are shown in parentheses. Bond angles (°). The e.s.d.'s of the bond angles involving Cl and S atoms are ±0.8 °∼1.3 ° and those of the others are ±1.4 °∼1.8 °.

O–S–O angle is 117.2°. These values agree with those observed for dimethyl sulfone (1.445(15) Å and 117.9(8)°). The C(3)–Cl(2) and C(4)–Cl(1) bond distances are 1.79(2) Å and 1.76(2) Å respectively. The directions of these bonds are axial and equatorial respectively, as is shown in Fig. 1, and differ from those, (3e4a), observed for *cis*-DCTE. This fact suggests an inversion of the thietane ring by the oxidation of *cis*-DCTE in the course of the preparation of *cis*-SO_2-DCTE. The non-bonded S·····Cl(2) distance in the *cis*-SO_2-DCTE molecule is 3.42 Å, significantly shorter than the usual van der Waals contact (3.65 Å). If the *cis*-SO_2-DCTE molecule could retain the conformation observed for *cis*-DCTE in its crystalline state, it would take the (3e4a) conformation, in which the transannular S····· Cl(2) distance would be 4.07 Å. Hence, the (3a4e) conformer seems not to be favored in view of the non-bonded repulsions between the Cl atom and the sulfonyl group. In order to explain the ring inversion, a molecular orbital calculation using the CNDO/2 method was carried out for the model molecules assumed for both the conformers.[5] It was found that the (3a4e) conformer may be more stable than the (3e4a) conformer. The electronic energy mainly participates in stabilizing the (3a4e) conformer. The ring inversion can be explained in terms of this contribution. It is noteworthy that the 3*d*-3*p* interaction between the S and Cl(2) atoms is bonding, while that in the (3e4a) conformer is approximately non-bonding.

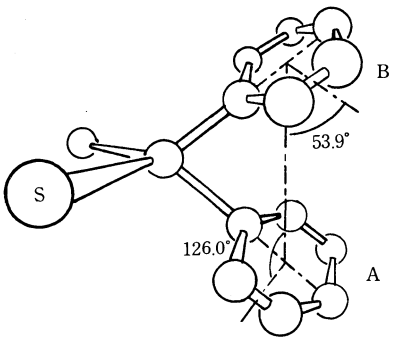

Fig. 2. Orientations of the phenyl groups.

The phenyl groups, A and B, are practically planar; their orientations are shown in Fig. 2. The non-bonded distances, O(1)·····C(26), S·····C(26), O(2)·····C(16), and S···C(16), are 3.21 Å, 3.41 Å, 3.13 Å, and 3.30 Å respectively. Non-bonded repulsions caused by these close contacts might play an important role in determining the phenyl orientations.

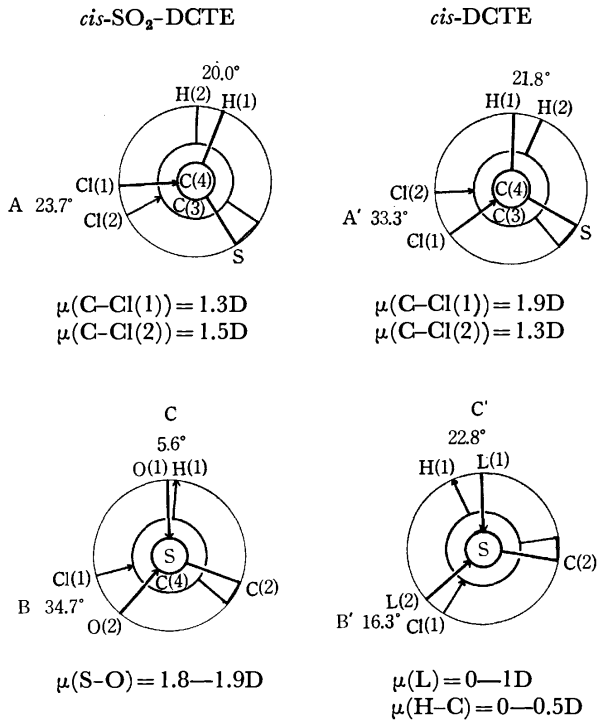

Fig. 3. Newman projections of the torsion angles involving the thietane-ring atoms in *cis*-SO_2-DCTE and in *cis*-DCTE. L(1) and L(2) represent the lone pairs in the axial and equatorial directions, respectively.

Figure 3 shows the torsion angles around the thietane rings observed for *cis*-SO_2-DCTE and *cis*-DCTE as Newman projections, where the arrows superposed on the projected bonds indicate the directions of the bond moments assigned to the respective bonds. The direction of the lone pairs of the sulfur atom in *cis*-DCTE is deduced by assuming a tetrahedral disposition around the sulfur atom. A comparison of the two molecules reveals that the bond angles in *cis*-SO_2-DCTE deviate greatly from the corresponding angles of *cis*-DCTE. The torsion angle, A, is smaller than A'; B is larger than B'; and C smaller than C'. These deformations can be explained qualitatively in terms of dipole-dipole interactions between the ring substituents by taking into account the values of the bond moments[6] given in Fig. 3.

The crystal structure viewed along the *b* axis is illustrated in Fig. 4. The relevant intermolecular contacts are listed in Table 3. These distances are all normal except for the C(4^{i})···O(2) of 3.26 Å, which is found in a pair of enantiomers. Using the calculated position of the hydrogen atom, H(1^{i}), attached to C(4^{i}), it is found that this atom is on a line connecting O(2) and C(4^{i}) and that the distance between O(2) and H(1^{i}) is 2.23 Å, much smaller than the usual van der Waals contact (2.6 Å). These facts suggest a weak C-H···O hyhrogen bond between O(2) and C(4^{i}). Similar hydrogen bonds have been found in the crystal of di-(*p*-chlorophenyl) sulfone.[7] The enantiomers in the crystal of *cis*-SO_2-DCTE form a dimer by this hydrogen bond, as is shown in Fig. 4.

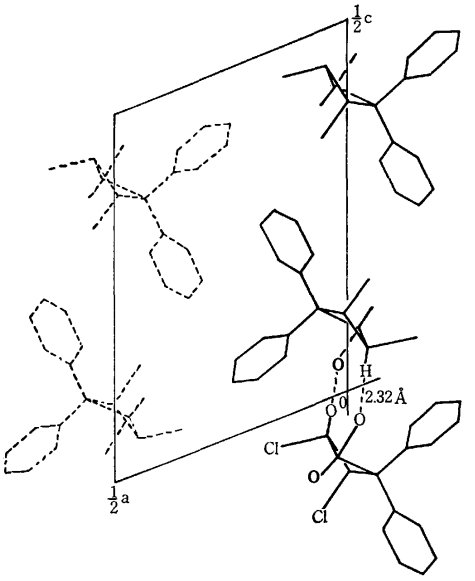

Fig. 4. Projection of the crystal structure viewed along the *b* axis.

TABLE 3. RELEVANT INTERMOLECULAR CONTACTS

S···O(2^{i})	4.08 Å
S···C(13^{i})	4.41
Cl(1)···O(2^{i})	3.95
Cl(2)···C(24^{ii})	3.60
O(2)···O(2^{i})	3.74
O(2)···C(4^{i})	3.26

i=$-x$, $-y$, $-z$ ii=$-x$, $1/2+y$, $1/2-z$

The author is grateful to Dr. Atsuyoshi Ohno and Dr. Yutaka Ohnishi of the Sagami Chemical Research Center for kindly supplying the crystals of *cis*-SO_2-DCTE and to Professor Takashi Shimozawa for his keen interest and valuable discussions. This research was supported in part by a Scientific Research Grant from the Ministry of Education, for which the author's thanks are also due.

References ane Notes

1) A. Ohno, Y. Ohnishi, and G. Tsuchihashi, *Tetrahedron Lett.*, **1969**, 161.

2) S. Kumakura and T. Kodama, This Bulletin, to be published.

3) The table of the F_o-F_c values is kept as a document at the office of the Bulletin of the Chemical Society of Japan. (Document No. 7515).

4) D. E. Sands, *Z. Krist.*, **119**, 245 (1963).

5) A CNDO/2 calculation has been carried out by using a published program (J. A. Pople and D. L. Beveridge, "*Approximate Molecular Orbital Theory*," McGraw-Hill, New York, 1970) on a HITAC 8700/8800 computer at the Computer

Center of the University of Tokyo. For great savings in computer time, the phenyl groups in *cis*-SO_2-DCTE were ignored. Calculations were made for the model molecules, that is, for *cis*-2,3-dichlorothietane 1,1-dioxide taking either the (2a3e) conformation or the (2e3a), the skeletal dimension of which is assumed to be equal to that of *cis*-SO_2-DCTE (3a4e) observed in its crystalline state. The (2e3a) conformer, corresponding to the *cis*-SO_2-DCTE (3a4e), is found to be more stable by 5.1 kcal/mol than the (2a3e).

6) The values of the bond moments for *cis*-DCTE were cited from Ref. 2. The values for *cis*-SO_2-DCTE were obtained from the results of an analysis carried out on the dipole moments of *cis*- and *trans*-SO_2-DCTE molecules by using the molecular dimensions observed for the *cis*-compound in its crystalline state.

7) D. J. Sutor, *J. Chem. Soc.*, **1963**, 1105.

ENDOR Studies in the Conformation of 3,3′- or 3,4′-Polymethylenebiphenyl Anion Radicals.

Kazuhiko ISHIZU, Fujito NEMOTO, Koji YAMAMOTO,* and Masao NAKAZAKI*

Department of Chemistry, Faculty of Science, Ehime University, Bunkyo-cho, Matsuyama 790

**Department of Chemistry, Faculty of Engineering Science, Osaka University, Toyonaka, Osaka 560*

(Received February 3, 1975)

The ENDOR spectra have been observed for the anion radicals of 3,3′- and 3,4′-polymethylenebiphenyl with various chain lengths. The hyperfine coupling constants of the ring protons of the 3,3′-derivatives are comparable with those of the reference derivative, *m,m′*-bitolyl, and the biphenyl ring is considered to take the planar conformation. When the chain length is shortened and the polymethylene chain increases its probability of being held on the biphenyl aromatic plane, strong through-space interactions are observed between the aromatic π and the polymethylene pseudo-π orbital. In 3,4′-polymethylenebiphenyl with shorter chain lengths, the coplanar phenyl rings are twisted out by the polymethylene span and the magnitudes of the spin densities at the *ortho*-position are reduced by the resonance inhibition between two phenyls. McLachaln's MO calculations predict that the twisting angles between the two phenyls are similar to the value reported for 2,2′-bitolyl anion radical. In contrast to the case of the 2,2′-bitolyl anion radical, however, a conformational change in biphenyl resulting from the delocalization of the unpaired electron is suppressed by a tight lock of the rotation of the phenyl groups in the polymethylene derivatives.

Polymethylenebiphenyls bridged by a suitable polymethylene chain at the 3,3′- or 3,4′-positions were synthesized, and the conformation of the diamagnetic neutral molecule was investigated by means of UV and NMR absorption spectroscopies.[1,2] The UV absorption parameters of the 3,3′-polymethylenebiphenyls indicated that the biphenyl rings are coplanar.

On the other hand, in the cases of the 3,4′-polymethylenebiphenyls, the polymethylene span prevents the biphenyl ring from having the coplanar conformation and inhibition of the resonance between the two phenyls was observed in the conjugation band of the UV absorption. In the previous studies of hindered biphenyl anion radicals, one of the present authors, K.I., proposed that the coplanar character of the biphenyl ring is enhanced by delocalizations of the unpaired electron.[3–5]

In the cases of the polymethylenebiphenyls, the rotation of each phenyl ring is tightly locked in certain conformations, thus, little conformational change could be expected due to the presence of the unpaired electron.

A comparative study of the steric hindrance with the anion radical of the 2,2′-alkylbiphenyl and that of the polymethylenebiphenyl is of considerable interest, since the rotation of the phenyl group can be partially allowed and since interchange between the *trans*- and *cis*-conformations may be possible in 2,2′-dialkylbiphenyls.

However, the ESR technique is not suitable for this study, because the hyperfine multiplets may be very complicated as a result of the lower molecular symmetry. Furthermore, the possibility of the long-range interaction of the polymethylene may give an additional complexity to the ESR hyperfine structures, as may be expected from the anomalous NMR shift of the polymethylene protons observed in the neutral molecules.[1]

In the present work, ENDOR studies were made for 3,3′-polymethylenebiphenyl (n=8 and 10) and 3,4′-polymethylenebiphenyl (n=9, 10, 11), bridged by different chain lengths (n).

The spin densities of the *ortho*- and *para*-positions were determined, and the degrees of the steric hindrance were estimated from McLachlan's MO calculations carried out for the twisted biphenyls. In addition, it was clearly demonstrated that the long-range interaction of the polymethylene group varies with both the chain lengths and the bridging positions.

Experimental

The synthesis and physicochemical properties of the materials used here were reported in the previous paper.[1] The radical anions were prepared by reduction with a potassium metal in DME (Dimethoxyethane), letting the reaction mixtures stand in a dry ice–acetone bath. The stability of the anion radicals depends strongly on the polymethylene chain lengths. In paticular, the radical anions of the 3,4′-polymethylene derivative with n=9 are stable only at temperatures lower than −70 °C. The ENDOR spectra were recorded by a JEOL-type ES-EDX-1 spectrometer under operating conditions similar to those described elsewhere.[6] The ESR intensities began to saturate at a microwave output of about 2 mw on the dial scale of the JES-ME-3 ESR spectrometer, and the ENDOR spectra were successfully recorded in the vicinity of −80 °C.

Results and Discussion

3,3′-Polymethylenebiphenyl. The ESR spectra of 3,3′-bridged polymethylene derivatives showed merely the broadened nine-line hyperfine structures; these structures were not further resolved into any lines, as may be seen in Fig. 1. The ENDOR spectra shown in Fig. 2, however, were resolved to show the details of complicated hyperfine couplings. The hyperfine coupling constants of the *ortho*- and *para*-protons, (a_2^H, a_6^H, and a_4^H) were easily identified with reference to the ENDOR spectrum of the *m,m′*-bitolyl anion radical. The hyperfine coupling constants assumed in the ESR measurement of the *m,m′*-bitolyl anion radicals were reconfirmed by the present work; the absolute values of the hyperfine coupling constant determined by ENDOR also gave an excellent agreement with the

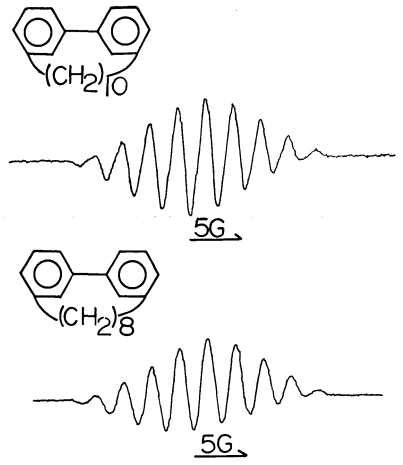

Fig. 1. ESR spectra of 3,3′-polymethylenebiphenyl anion radical recorded at −85 °C.

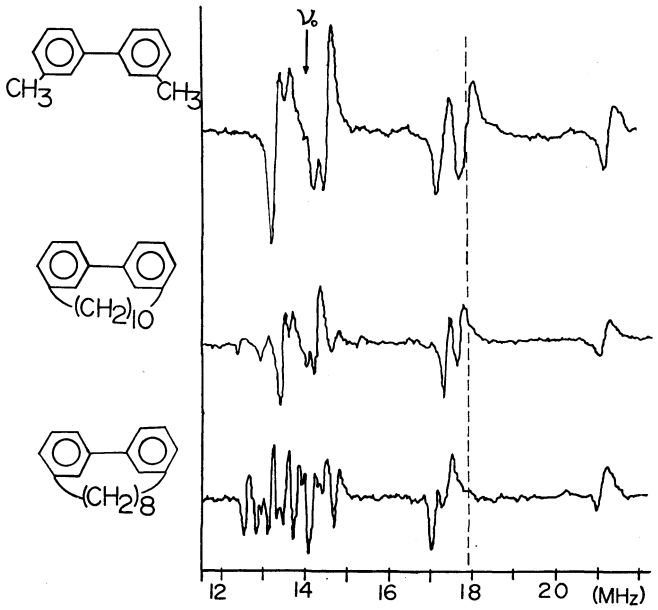

Fig. 2. Higher frequency halves of ENDOR spectra of 3,3′-bitolyl and 3,3′-polymethylenebiphenyl anion radicals. ν_0: free proton frequency.

results of the recent NMR measurements.[7]

As compared with the ENDOR hyperfine structures of the *meta*-ring protons of the reference derivative, the polymethylene derivatives exhibited rather complicated structures around the free proton frequency.

Beside the β-proton splitting (0.15 gauss) and the ring-proton splitting (0.29 gauss) at the *meta*-position, the derivative with $n=10$ gave two extra splittings (0.58, 1.02 gauss); they probably resulted from the long-range interaction attributable to the polymethylene chain.

Similar long-range interactions attributable to long alkyls have already been demonstrated by the previous ENDOR study of the Banfield-Kenyon radical.[8] More substantial evidence of the long-range interactions can be seen in the derivative with $n=8$. The multiple hyperfine structures composed of six different splittings cannot be explained without taking into account the contribution from the long-range interactions.

It is quite intersting that the polymethylene derivatives bridged by the shorter chain length ($n=8$) give strong long-range interactions. In the 3,3′-polymethylene derivatives, the polymethylene strain may force the polymethylene chain to take a coplanar structure with the biphenyl aromatic plane. Thus, the through-space interaction between the aromatic-π and the polymethylene pseudo-π orbital must be effectively enhanced in the derivatives bridged by shorter chain lengths.

The hyperfine coupling constants of the 3,3′-polymethylenebiphenyl anion radicals are summarized in Table 1. It may be seen that the magnitude of the *ortho*(a_2^H, a_6^H)- and *para*(a_4^H)-splittings for the 3,3′-polymethylene derivatives resembles that for the *m,m*′-bitolyl and biphenyl anion radicals. This means that the biphenyl ring probably takes the planar conformation in 3,3′-polymethylene derivatives.

3,4′-Polymethylenebiphenyl. The ESR spectra of the 3,4′-polymethylenebiphenyl anion radical are shown in Fig. 3.

Since the molecule has no symmetry, the ESR spectra are very complicated as a result of the overlap of the unresolved hyperfine components. The resolution of the ESR spectrum is reduced with an increase in the chain length; thus, the undecamethylene derivative exhibits no resolvable hyperfine structures. As one may expect from the ESR observation, the ENDOR spectrum of the derivative with $n=11$ exhibits the most complicated structures. As is shown in Fig. 4, more than eight hyperfine splittings were detected in the frequency region of the *meta*-ring and β-methylene protons, indicating the possibility of a long-range interaction due to the polymethylene group.

Contrary to the cases of the 3,3′-polymethylene derivatives, the number of the hyperfine lines is reduced with a decrease in the polymethylene chain length. A molecular model suggests that a part of the polymethylene chain located around the 4′-position separates

Table 1. Hyperfine coupling constant of 3,3′-polymethylenebiphenyl anion radicals (G)

Compound	Position								
	a_3^H, a_5^H, and a^R						a_2^H	a_6^H	a_4^H
3,3′-Bitolyl	(0.27	0.44) [a]					2.43	2.81	5.22
	(0.27	0.49) [b]					2.33	2.82	5.15
	(0.284	0.494) [c]					2.37	2.78	5.25
Decamethylene	0.15	0.29	0.58	1.02			2.53	2.77	5.13
Octamethylene	0.11	0.21	0.37	0.48	0.57	0.76	2.43	2.61	5.22

a) ENDOR b) ESR c) NMR

Table 2. Hyperfine coupling constant of 3,4′-polymethylenebiphenyl anion radicals (G)

Compound	(a_3^R $a_3^{R'}$ a_5^H $a_5^{H'}$)	a_6^H	$a_2^{H'}$	$a_6^{H'}$	a_6^H	$a_4^{R'}$	$a_4^{H'}$
Nonamethylene	(0.08, 0.26, 0.45, 0.75)	1.54	1.72	2.30	2.68	3.71	4.97
Decamethylene	(0.07, 0.17, 0.31, 0.42, 0.67)	1.19	1.87	2.10	2.43	3.56	5.11
Undecamethylene	(0.05, 0.18, 0.38, 0.55, 0.59, 0.72, 1.00, 1.05)	1.88	2.16	2.62	2.86	3.56	4.93

Hyperfine coupling constants at the *ortho*- and the *para*-positions are assigned with reference to predictions of the MO calculations.

from the aromatic plane and becomes perpendicular to the 4′-substituted phenyl ring as the twist of the phenyl group increases. In this situation, the probability of the orbital overlap between the polymethylene group and the aromatic ring may be considerably reduced.

The four lines appearing in the frequency range from 16 MHz to 18 MHz are assigned to the absorption due to the *ortho*-protons, while the two lines at 19 MHz and 21 MHz are attributed to the splittings of the β-methylene ($a_4^{R'}$) and the ring (a_4^H), respectively both at the *para*-positions.

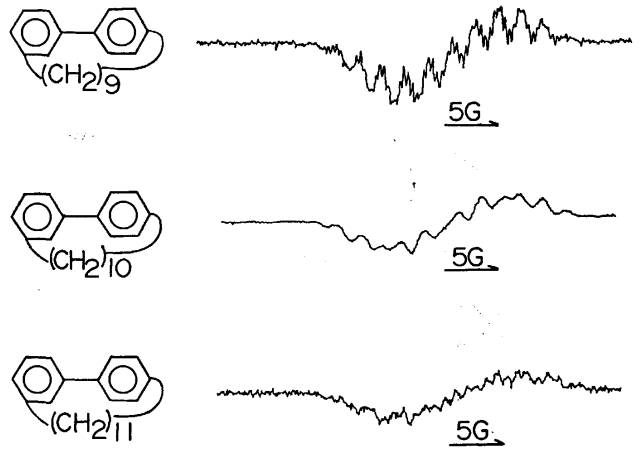

Fig. 3. ESR spectra of 3,4′-polymethylenebiphenyl anion radicals recorded at −85 °C.

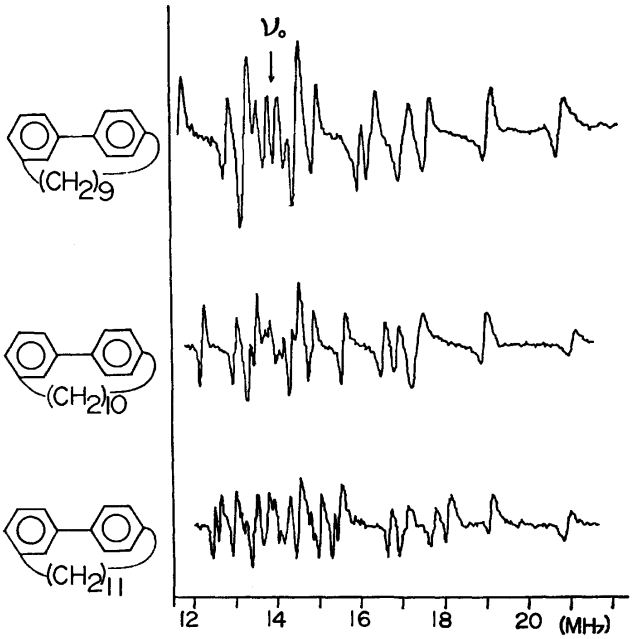

Fig. 4. Higher frequency halves of ENDOR spectra of 3,4′-polymethylenebiphenyl anion radicals.
ν_0: free proton frequency.

In the previous studies, an exceptionally hindered internal rotation of the alkyl chain was reported for the 4,4′-di-*n*-propylbiphenyl and 4,4′-polymethylenebiphenyl anion radicals, where a normal quintet splitting of the four methylene protons splits into two sets of triplet splittings.[9,10] A similar situation is probable for the present cases. Based on the observed methylene proton splitting ($a_4^{\beta'}$) and McLachlan's spin density ($\rho_4^{\pi'}$) at the 4′-position, the equilibrium dihedral angles, φ, of the β-methylene group were calculated tentatively, assuming McConnell-Heller's equation:[11]

$$a_{4'}^{\beta} = (B_0 + B_2 \cos^2 \varphi)\rho_{4'}^{\pi} \quad (1)$$

Taking the B_0/B_2 ratio to be +0.06 with B_2=50 gauss,[12] the dihedral angles were estimated to be 48°, 49°, and 53° for n=9, 10 and 11 respectively.

If the segment motion of the β-methylene group is tightly locked, one of the two β-methylene protons may give rise to the splitting ($a_4^{\beta'}$) in the range from 16 MHz to 17 MHz, as one would expect from a similar calculation using $\varphi' = 70°$. In the present case, however, it is difficult to identify this splitting because of the overlap of the absorption with those of the *ortho*-protons observed in the same frequency region.

The experimental spin densities of the ring carbon ρ_i^{π}, were calculated from the ring proton splitting (a_i^H) using Copla-Bolton's equation:[13]

$$a_i^H = Q_{CH}(0)\rho_i^{\pi} - K_{CH}^H[\rho_i^{\pi}]^2 \quad (2)$$

where $Q_{CH}^H(0) = -27$ and $K_{CH}^H = -12$ gauss. The Coulomb integrals of the ring carbons attached to the methylene were estimated to be $\alpha_i = \alpha - 0.2\beta$, and the resonance integral between the bridgehead carbons was taken to be $\beta_{11} = \beta\cos\theta$ as a function of the twisting angles (θ) of the phenyl groups. McLachlan's parameter, λ, is estimated to be 1.1 for any derivative. McLachlan's spin densities (ρ_2^{π}, $\rho_{2'}^{\pi}$, ρ_6^{π}, $\rho_{6'}^{\pi}$, and ρ_4^{π}) of the derivative with n=11 indeed show an excellent agreement with the experimental values when the biphenyl ring is assumed to take the planar conformation, that is, when θ=0. On the other hand, the MO calculation carried out on the twisted biphenyls taking θ=50° gives results which account for the observed spin densities of the derivatives with n=9 and 10, as may be seen in Table 3.

In the UV absorption maxima of the conjugation band observed for the neutral molecules, the derivatives bridged by shorter chains (n=9 and 10) display a blue shift as compared with the UV absorption parameters of the derivative with a longer chain (n=11); that is,

Table 3. Experimental and theoretical spin densities of polymethylenebiphenyls

Chain length	Spin densities						Twisting angle
n	4	4′	2	6	2′	6′	θ
Exp. 9	0.202	—	0.104	0.058	0.066	0.088	
10	0.208	—	0.093	0_045	0.071	0.080	
Calcd.	0.216	0.157	0.139	0.048	0.082	0.082	50°
Exp. 11	0.200	—	0.111	0.071	0.101	0.102	
Calcd.	0.197	0.183	0.141	0.082	0.117	0.117	0°

Table 4. Parameters of the steric hindrance for polymethylenebiphenyls

	ρ_p/ρ_o		ρ_p/ρ_o
Biphenyl	2.12	*o,o*′-Bitolyl	2.46[a]
m,m′-Bitolyl	2.09	3,4′-Nonamethylene	2.28[b]
3,3′-Decamethylene	2.04	3,4′-Decamethylene	2.52
3,3′-Octamethylene	2.19	3,4′-Undecamethylene	1.97

a) $Q^{H}_{CH_2}$ is estimated to be 28 G. b) $\rho^{\pi}_{4'}$ -values are estimated from the McLachlan's MO calculations. c) ρ_p/ρ_o values are calculated to be $\frac{(\rho^{\pi}_4+\rho^{\pi}_{4'})/2}{(\rho^{\pi}_2+\rho^{\pi}_{2'}+\rho^{\pi}_6+\rho^{\pi}_{6'})/4}$.

3,4′-nonamethylenebiphenyl (λ_{max}=250 nm, ε=14500), 3,4′-decamethylenebiphenyl (λ_{max}=248 nm, ε=16700) and 3,4′-undecamethylenebiphenyl (λ_{max}=252 nm, ε=18800). The regular blue-shift of the absorption maxima from the undecamethylene to the nonamethylene derivative is accompanied by a decrease in the extinction coefficient. This can be understood in terms of the resonance inhibition resulting from the steric hindrance.

No detailed investigation of the structure of the neutral molecules has been reported, so the twisting angles, θ, of the two phenyls are assumed to be between the two values for biphenyls (θ=30°, λ_{max}=247 nm, ε=18050) and 2-methylbiphenyls (θ=58°, λ_{max}=235 nm, ε=10500).[14]

The present calculations of the twisting angles in the anion radicals are more or less qualitative. Therfore, the ratios of the averaged spin densities at the *para*- and the *ortho*-positions, $\rho_p{}^{\pi}/\rho_o{}^{\pi}$, which have often been used as parameters to estimate the degree of the steric hindrance, are tentatively compared with those for the usual alkyl derivatives in Table 4.

It is very interesting that the values for the 3,4′-nona- and decamethylene derivatives are close to that for *o,o*′-bitolyl, while the value for the 3,4′-undecamethylene derivative is rather akin to those of biphenyl and the 3,3′-polymethylene derivatives. Since the twisting angles of the 2,2′-dialkylbiphenyl anion radicals are assumed to be around 45°, one may see that the MO prediction of the steric hindrance is also valid for the present derivatives. In addition, it may be speculated that the same magnitude of the steric hindrance can be assumed for both the neutral molecules and the anion radicals of the hindered polymethylenebiphenyls.

In contrast to this situation, it has been known that the biphenyl rings of the 2,2′-dialkylbiphenyl anion radicals are likely to increase in planar character because of a delocalization of the unpaired electron.

In 2,2′-dialkylbiphenyl, the rotations of the two phenyl groups are partially allowed, and the extra delocalization energy of the unpaired electron may compenasate for the repulsion energy between the two phenyls so as to increase the coplanarity of the biphenyl ring. On the other hand, the rotation of each phenyl group is tightly locked in the hindered polymethylene derivatives and the conformation of the biphenyl ring may be fixed in a certain twisting angle by the strong polymethylene strain.

References

1) K. Yamamoto, T. Hirokawa, and M. Nakazaki, *Tetrahedron Lett.*, **1969**, 4551.
2) K. Yamamoto, Y. Naito, Y. Tanaka, and M. Nakazaki, This Bulletin, **46**, 2900 (1973).
3) K. Ishizu, *ibid.*, **37**, 1093 (1964).
4) K. Ishizu, H. Hasegawa, H. Chikaki, H. Nishiguchi, and Y. Deguchi, *Kogyo Kagaku Zasshi*, **68**, 1522 (1965).
5) K. Ishizu, K. Mukai, H. Hasegawa, K. Kubo, H. Nishiguchi, and Y. Deguchi, This Bulletin, **42**, 2808 (1969).
6) T. Yamamoto, K. Sato, and T. Miyamae, *Japan. J. Appl. Phys.*, **11**, 1508 (1972).
7) J. W. M. de Boer, M. R. Arick, and E. de Boer, *J. Chem. Phys.*, **59**, 638 (1973).
8) K. Ishizu, T. Yamamoto, M. Kohno, A. Nakajima, and Y. Deguchi, *Tetrahedron Lett.*, **1974**, 1537.
9) F. Nemoto, K. Ishizu, and H. Hasegawa, *Chem. Lett.*, **1972**, 267.
10) K. Ishizu, F. Nemoto, H. Hasegawa, K. Yamamoto, and M. Nakazaki, This Bulletin, **46**, 140 (1973).
11) C. Heller and H. M. McConnell, *J. Chem. Phys.*, **32**, 1535 (1960).
12) K. Ishizu, F. Nemoto, K. Mukai, M. Kohno, and H. Hasegawa, This Bulletin, to be published.
13) J. P. Copla and J. R. Bolton, *Mol. Phys.*, **6**, 273 (1963).
14) H. Suzuki, This Bulletin, **32**, 1350 (1959).

The Cadmium-photosensitized Reaction of Water, Alcohols, and Ethers. The Quenching of the Resonance Radiation at 326.1 nm and the Photosensitized Luminescence

Shunzo YAMAMOTO,* Kazuyuki TANAKA, and Shin SATO

Department of Applied Physics, Tokyo Institute of Technology, Ookayama, Meguro-ku, Tokyo 152

(Received March 5, 1975)

A luminescence similar to the photosensitized luminescence of ammonia was observed in the cadmium-photosensitized reaction of water, alcohols, and ethers. The quantum yields of the luminescence with these compounds were much smaller than that with ammonia. The rate constants for the formation of the excited complexes between the excited cadmium atoms and the substrates generally increased with a decrease in the ionization potentials of the substrates. This shows that the complex has the characteristics of a charge-transfer type. On the other hand, the efficiencies of the quenching of the resonance radiation at 326.1 nm by ethers were smaller than those of alcohols. It is concluded that the quenching through the formation of the complex is a minor process in the quenching of the resonance radiation by water, alcohols, and ethers.

By analogy with the mercury-photosensitization, it can be expected that such electron-donor molecules as ammonia and water react with excited cadmium atoms to form excited complexes, and that such complexes fluoresce.

In previous papers,[1-3] such luminescence was found in the cadmium-photosensitized reactions of ammonia and some aliphatic amines. The quantum yields of the luminescence, the wavelength at the peak, and the rate constants for the formation of excited complexes were measured. From the relationship between these values and the structure of the amines, it was concluded that the complexes are of the charge-transfer type. Further, we discussed a mechanism for the formation and the deactivation of the complexes on the basis of the pressure dependences of the intensities of the resonance line at 326.1 nm and of the luminescence.

It now seems valuable to observe the similar luminescence in the cadmium-photosensitized reactions of water, alcohols, and ether, to measure the rates of the quenching of the resonance radiation and of the formation of the complex, and to determine the effects of the structure of the alcohols and ethers on the quantum yields of the luminescence and the position of the emission band, in order to gain a further understanding of the cadmium-photosensitized luminescence.

Experimental

The apparatus and procedure were the same as those previously described.[1] The reaction cell and the cadmium resonance lamp were kept at 220 ± 1 °C. The vapor pressure of cadmium at this temperature is 1.04×10^{-3} Torr. The lamp was operated by an alternating current (50 Hz). As was described previously,[4] since the lifetimes of $Cd(5^3P_{1,0})$ are very short, the observed intensity of the light from the cell is not affected by the periodic change in the light intensity of the lamp.

The cadmium metal used was high-purity cadmium (99.9999%) manufactured by the Osaka Asahi Metal Co. Distilled water and 99.9% D_2O were freed of dissolved gases by alternate freezing and thawing under a vacuum. Spectro-grade methanol and ethanol were used after having been degassed. The dimethylether and ethylene oxide (G.R. grade) were used after having been degassed at the temperature of liquid nitrogen. The diethylether and tetrahydrofuran were used after having been dried by Na-K and repeated trap-to-trap distillations. In order to minimize the pressure dependence of the absorption intensity at 326.1 nm, the substrates were diluted with argon and the total pressure in the cell was kept constant.

Results

In Fig. 1 the emission bands obtained with water, methanol, and ethanol are shown, together with the analogous band with ammonia. The bands for ethers studied had the same basic shape and so are not given here. We could not detect an emission band with ethylene oxide. The band shapes are very similar to that observed with ammonia (the band widths for water and alcohols are slightly narrower than that for ammonia), but the intensities are much smaller than that for ammonia. The wavelengths at the peaks are listed in Table 1.

The quantum yields of the luminescence with water, alcohols, and ethers were determined by a comparison of the integrated intensity of the emission band for the compound in question that for ammonia under

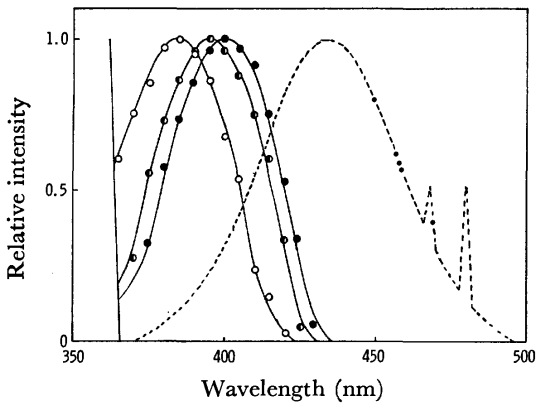

Fig. 1. Emission band contours for H_2O (open circles), methanol (half-filled circles), and ethanol (filled circles). The curve for NH_3, given by the broken line, is derived from Ref. (1).

* Present address: Department of Chemistry, Faculty of Science, Okayama University, Tsushima, Okayama 700.

Table 1. Wavelength at the peak of the emission band and quantum yield of the luminescence

Compounds	I_p (kcal/mol)	λmax (nm)	Quantum yield
H_2O	291.3	385	1.2×10^{-3}
D_2O		385	5.7×10^{-3}
Methanol	250.6	395	3.1×10^{-3}
Ethanol	242.6	400	1.5×10^{-3}
Dimethylether	230.6	390	4.8×10^{-3}
Diethylether	220.1	398	1.1×10^{-3}
Tetrahydrofuran	217.6	398	8.5×10^{-3}

Table 2. Half-quenching pressure for the quenching of 326.1 nm resonance radiation

Compound	Torr
H_2O	5.38
D_2O	31.5
Methanol	2.95
Ethanol	0.82
Dimethylether	92.6
Diethylether	11.2
Ethylene oxide	0.13
Tetrahydrofuran	26.8

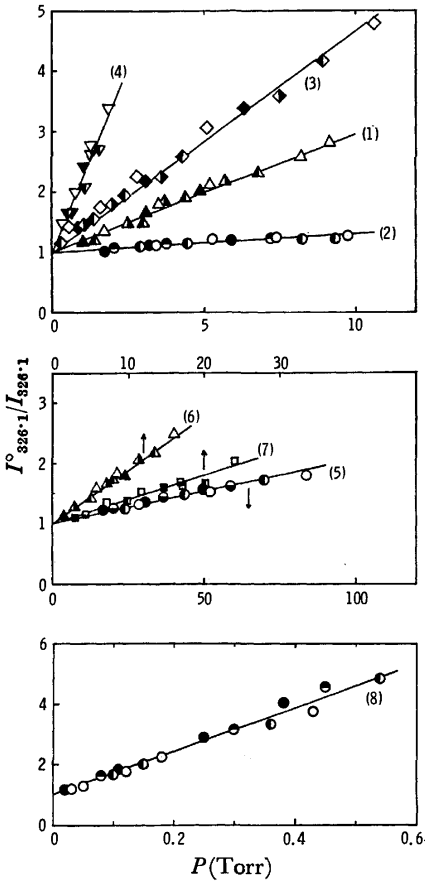

Fig. 2. Stern-Volmer plots for the quenching of the resonance radiation at 326.1 nm by water, alcohols, and ethers diluted with argon.
1) H_2O; Total pressure are 80(△), 67(▲), 56(▲), and 48(▲) in Torr.
2) D_2O; 80(○), 67(◐), 56(◓), and 48(●).
3) methanol; 80(◇), 67(◈), 56(◈), and 48(◆).
4) ethanol; 80(▽), 67(▼), 56(▼), and 48(▼).
5) dimethylether; 210(○), 177(◐), 148(◒), and 126(●).
6) diethylether; 80(△), 67(▲), 56(▲), and 48(▲).
7) tetrahydrofuran; 80(□), 67(◧), 56(⬓), and 48(■).
8) ethylene oxide; 80(○), 67(◐), 56(◓), and 48(●).

the same conditions. The results are also listed in Table 1.

In order to estimate the efficiency of the quenching of the 326.1 nm resonance line, the emission intensity at 326.1 nm was measured as a function of the pressure

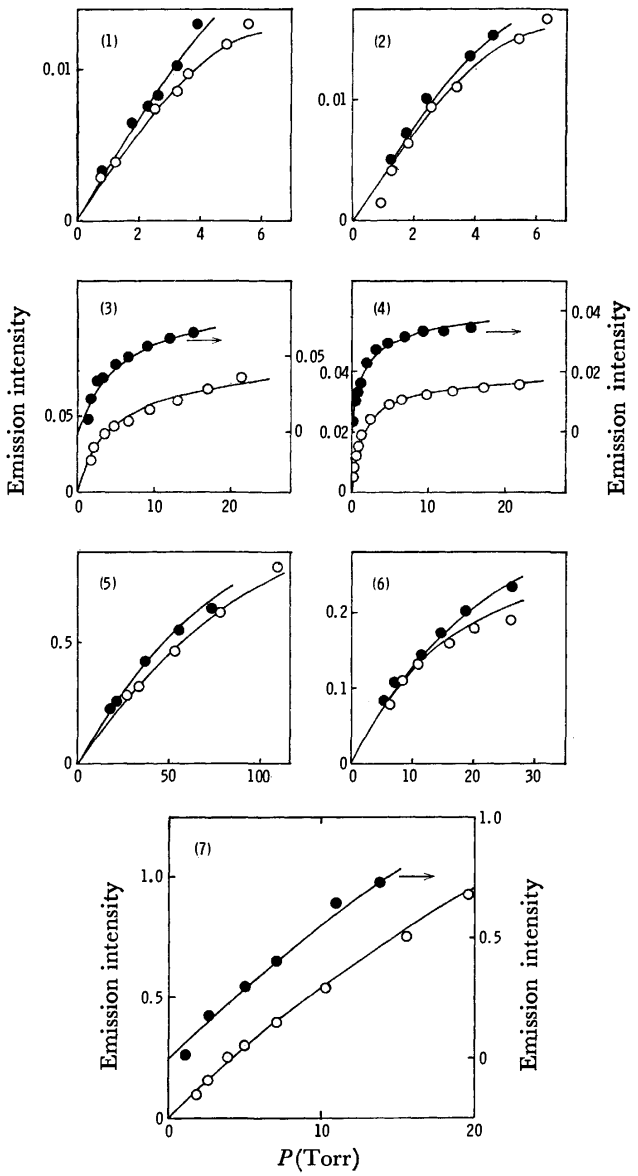

Fig. 3. The intensity at the peak of the emission band from the complex as a function of the partial pressure of substrates. The total pressures are 80(○) and 56(●) in Torr, except for dimethylether, and those for dimethylether are 210(○) and 148(●) in Torr. The plots for 48 Torr in the cases of methanol, ethanol, and tetrahydrofuran are displaced upwards for clearity.
1) H_2O; 2) D_2O; 3) methanol; 4) ethanol; 5) dimethylether; (6) diethylether; 7) tetrahydrofuran.

of the substrates. The Stern-Volmer plots are shown in Fig. 2, where I_0 and I are the intensities of the resonance lines in the absence and in the presence of the substrates respectively. As the intensity decreased with the increase in irradiation time, the I values shown in Fig. 2 were obtained by extrapolation to zero irradiation time. As is shown in Fig. 2, the plots for each substrate at various total pressures lie on one straight line; no total pressure dependence can be seen. The half-quenching pressure obtained from the slopes of the straight lines in Fig. 2 are listed in Table 2. The values for ethers are generally larger than those for alcohols.

The pressure dependence of the intensity at the peak of the emission band is shown in Fig. 3. The intensities were again obtained by extrapolation to zero irradiation time. As was shown in a previous paper,[3] the emission intensities for amines have maximum values, but those for water, alcohols, and ethers increase monotonously with an increase in the pressure.

Discussion

Let us first consider the effect of the structure of the substrates on the position of the emission band. In the mercury-photosensitized luminescence,[5,6] it was previously reported that the band given by the deuterated species is slightly shifted to longer wavelengths. In the present experiment, however, the bands obtained with H_2O and D_2O appeared at the same wavelength. As was described in the previous paper,[3] it would be expected that the decrease in the ionization potential of the substrate would cause the peak of the emission band to shift to a longer wavelength. In fact, as is shown in Table 1, the substitution of alkyl groups for hydrogen atoms in water, which increases the electron-donating ability of the oxygen atom, generally causes a red-shift of the emission band. An inspection of Table 1, however, shows that the peak for methanol is at a longer wavelength than that for dimethylether, while the peak for ethanol is at a longer wavelength than those for diethylether and tetrahydrofuran. It seems that the position of the emission band cannot be explained by the ionization potential alone. Freeman *et al.*[7] found a similar red-shift in Hg–alcohols system. However, they did not detect an emission band with ethers, so the effect of replacing both of the hydrogen atoms in water by alkyl groups remains an open question.

With respect to the quenching of the resonance line, the following reactions may be considered in a manner similar to that described in previous paper:[2,3]

$$Cd^*(^3P_1) \longrightarrow Cd(^1S_0) + h\nu \qquad k_0 \qquad (1)$$

$$Cd^* + M \rightleftarrows Cd^0(^3P_0) + M \qquad k_1, k_{-1} \qquad (2)\ (3)$$

$$Cd^* + A \longrightarrow \text{products} \qquad k_2 \qquad (4)$$

$$Cd^0 + A \longrightarrow \text{products} \qquad k_3 \qquad (5)$$

$$Cd^* + A \rightleftarrows CdA_v^* \qquad k_4, k_{-4} \qquad (6)\ (7)$$

where M stands for Ar or A and where A respesents the substrates. Since Reaction (2) and (3) are very fast in the presence of foreign gases, an equilibrium is established between $Cd(^3P_1)$ and $Cd(^3P_0)$. In the above mechanism, CdA_v^* is an unstabilized complex between the triplet cadmium atoms and the substrates. Reaction (7) was important in the case of ammonia,[2] but in the cases of water, alcohols, and ethers it does not seem to be important, since the Stern-Volmer plots lie on a straight line in the present experiment.[3] The overall rates of the quenching of the resonance line ($k_2+k_1k_3/k_{-1}+k_4$; $k_1/k_{-1}=1.68$ at 220 °C) were evaluated from the values of the half-quenching pressure in Table 2 by the method described in a previous paper;[2] they are listed in Table 3.

Table 3. Overall rate constants of the quenching of the resonance radiation and relative rate for the formation of the complex

Compounds	$k_2+1.68k_3+k_4$ (cm^3 $molecule^{-1}s^{-1}$)	$k_4/_4k^{NH_3}$
H_2O	3.9×10^{-12}	0.035
D_2O	6.7×10^{-13}	0.038
Methanol	7.2×10^{-12}	0.081
Ethanol	2.6×10^{-11}	0.091
Dimethylether	2.3×10^{-13}	0.044
Diethylether	1.9×10^{-12}	0.139
Ethylene oxide	1.6×10^{-10}	—
Tetrahydrofuran	7.8×10^{-13}	0.189

As was described previously,[3] the efficiency of the quenching by amines increases with an increase in the molecular complexity. However, as is shown in Table 3, the quenching by alcohols is generally more efficient than that by ethers.

From the pressure dependence of the intensity at the peak of the emission band, the relative values of k_4 can be estimated by a method described previously.[3] These values are also listed in Table 3. The values of k_4 increase in this order: $H_2O < D_2O <$ dimethylether $<$ methanol $<$ ethanol $<$ diethylether $<$ tetrahydrofuran. This order is in agreement with the order of the decrease in the ionization potential, except for the case of dimethylether. This tendency was also found in the cadmium-photosensitized reaction of amines; this indicates that the complex formed between the excited cadmium atoms and water, alcohols, and ethers is of the charge-transfer type.

The quantum yields of the luminescence for water, alcohols, and ethers given in Table 1 are much smaller than those for amines. As was mentioned in the previous paper,[3] the quenching of the resonance line by amines occurs mainly through the formation of the complex. However, it seems likely that the formation of the complex is not the predominant process in the quenching of the resonance line in the cases of water, alcohols, and ethers. In actuality, the k_4 values for water, alcohols, and ethers are about two or three orders of magnitude smaller than those for amines.

The ratio of the overall rates of the quenching of the resonance line for H_2O and D_2O is 5.9: 1. This value is considerably larger than the value of 1.91: 1 for the quenching of the Hg-253.7 nm resonance line by H_2O and D_2O. On the other hand, the ratio of the k_4 values for H_2O and D_2O is about unity. These findings also show that the quenching through the formation of the complex is not very important, as has been described

above. In the cadmium photosensitization, the available energy is only 87.7 kcal mol^{-1}. It is quite small compared with the O-H bond energy of H_2O (117 kcal mol^{-1}), even if the CdH formation is taken into account. The quenching of the excited cadmium atoms by water seems, then, to occur through the vibrational excitation of water. Therefore, the large isotope effect of H_2O and D_2O on the quenching rates may be due to the difference in the vibrational energies of O-H and O-D.

As was mentioned above, the quenching of the resonance line by alcohols is generally more efficient than that by ethers. Further, contrary to the expectation based on the ionization potential, the k_4 value for dimethylether is quite small. Thus, in the systems of Cd-alcohols and Cd-ethers, these values cannot be explained in terms of the electron-donating ability of the oxygen atom alone. In order to understand the effect of the higher substitution, we examined the effect of the replacement of the hydrogen atoms of ammonia by one, two, and three alkyl groups on the values of k_4 and $k_2+1.68k_3+k_4$. The results are shown in Table 4.

Table 4. The rate constants of the quenching of the resonance radiation and of the formation of the complex for primary-, secondary-, and tertiaryamines

Amines	$k_2+1.68k_3+k_4$ (cm^{3}molecule^{-1} s^{-1})	$k_4/k_4^{NH_3}$
Ammonia	2.4×10^{-12}	1.0
Methylamine	2.4×10^{-11}	10.7
Dimethylamine	2.9×10^{-11}	10.0
Trimethylamine	1.9×10^{-11}	5.1
Ethylamine	6.1×10^{-11}	15.8
Diethylamine	1.7×10^{-10}	43.1[a]
Triethylamine	1.1×10^{-10}	15.3[a]

a) These values were evaluated from the intensity at 450 nm (not at the peak) owing to the interference of the scattered light from the lamp, and therefore, they may be somewhat smaller than true values.

In both series of substitutions, methyl and ethyl, k_4 and $k_2+1.68k_3+k_4$ decrease on going from dialkyl amines to trialkyl amines. These tendencies are similar to those between methanol and dimethylether, and between ethanol and diethylether. As has been described in the previous paper,[3] in the series of primary amines a good relationship between k_4 and the ionization potential of amines was found. When secondary and tertiary amines are included, however, k_4 (and the efficiency of the quenching of the resonance line) cannot be explained in terms of the ionization potential (or the electron-donating ability of the nitrogen atom of amine) alone.

The relationship between k_4 and the ionization potential of substrates is shown in Fig. 4. The k_4 values for primary amines are quoted from Ref. (3). In general, k_4 increases with a decrease in the ionization potential. Especially for primary amines and alcohols, there is a good correlation between k_4 and the ionization potential. However, the k_4 values for secondary amines, tertiary amines, and ethers are somewhat smaller than the values predicted from the correlation mentioned above. In this manner, the reactivity of amines, alcohols, and ethers must be mainly governed by the electron-donating ability of the nitrogen and oxygen atoms, but partly by an other factor. This additional factor suppresses the formation of the excited complex in the cases of secondary amines, tertiary amines, and ethers. We tried to identify this factor, but we could not. Moreover, the origin of this factor remains an open question.

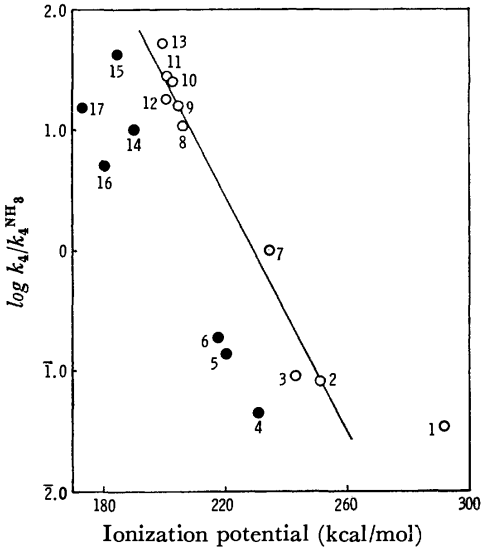

Fig. 4. Relationship between the relative rate constants for the formation of the excited complex and the ionization potential of substrates.
1) H_2O; 2) methanol; 3) ethanol; 4) dimethylether; 5) diethylether; 6) tetrahydrofuran; 7) ammonia; 8) methylamine; 9) ethylamine; 10) *n*-propylamine; 11) *n*-butylamine; 12) *sec*-butylamine; 13) *tert*-butylamine; 14) dimethylamine; 15) diethylamine; 16) trimethylamine; 17) triethylamine.
The plots for *s*- and *t*-amines and ether are shown as filled circles.

References

1) S. Tsunashima, T. Toyono, and S. Sato, This Bulletin, **46**, 2654 (1973).
2) S. Yamamoto, S. Tsunashima, and S. Sato, *ibid.*, **48**, 1172 (1975).
3) S. Yamamoto and S. Sato, *ibid.*, **48**, 1382 (1975).
4) S. Yamamoto, M. Takaoka, S. Tsunashima, and S. Sato, *ibid.*, **48**, 130 (1975).
5) R. H. Newman, C. G. Freeman, M. J. McEwan, R. F. C. Claridge, and L. F. Phillips, *Trans. Faraday Soc.*, **66**, 2827 (1970).
6) C. G. Freeman, M. J. McEwan, R. F. C. Claridge, and L. F. Phillips, *ibid.*, **66**, 2974 (1970).
7) C. G. Freeman, M. J. McEwan, R. F. C. Claridge, and L. F. Phillips, *ibid.*, **67**, 67 (1971).

A Polarographic Cell for the Continuous Monitoring of Column Effluents and Its Application to the Determination of Nitropyridine Derivatives

Tamotsu WASA and Soichiro MUSHA

Department of Applied Chemistry, College of Engineering, University of Osaka Prefecture, Sakai 591

(Received August 30, 1974)

The construction of a microdetector, based on the principle of polarography, for liquid chromatography and its application are described. The characteristics of the flow cells with a horizontal dropping mercury electrode (HDME), a vertical dropping mercury electrode (DME), and a mercury plated platinum electrode (Hg–Pt) are compared with each other. The flow cell has been applied to the analysis of a mixture of nitropyridine derivatives, such as 2-amino-3-nitropyridine (A3N), 2-amino-5-nitropyridine (A5N), 2-hydroxy-3-nitropyridine (O3N), 2-hydroxy-5-nitropyridine (O5N), and 2-nitroaminopyridine (NA), by means of a reversed-phase partition column or an ion-exchange column. In quantitative analysis, a standard deviation of better than 3% can be obtained.

Various physicochemical detectors, *e.g.*, refractometric,[1] colorimetric,[2] thermometric,[3] and ionization detector,[4] for the continuous analysis of column effluents are well established, and measurements have been made successfully in recent years. Some of these detectors are excellent in sensitivity and stability, but all add to the complexity and expense of the liquid chromatographic equipment.

On the other hand, the polarographic method was first used for the continuous monitoring of the column effluents by Drake;[5] the technique was later extensively developed with the powerful studies by Kemula.[6,7] Thereafter, various investigations of the apparatus[8–15] and its application[16–23] have been reported by several authors.

The present paper will describe a polarographic cell for the continuous measurement of a flowing solution, the characteristics of the flow cell, and its application to the determination of nitropyridine derivatives separated by either a reversed-phase partition column or an ion-exchange column.

Experimental

Apparatus. *Polarographic Flow Cell*: Three cells for a horizontal dropping mercury electrode (HDME),[24] a vertical dropping mercury electrode (DME), and a mercury plated platinum electrode (Hg–Pt) were designed and compared with each other. As is shown in Fig. 1, the cell for HDME was constructed of a Teflon plate (5) on which an effluent canal (2×2 mm) (1) and depressions for a mercury pool electrode (2), a detector electrode (3), and a thermostated water passageway (4) were caved. The Teflon plate was sandwiched between two plates of transparent acrylics (6). Polyethylene film (7) was used to prevent the swelling of acrylics with an organic solvent contained in the effluent. Though the cell for DME was constructed in the same way as for HDME, the cell was modified for DME. The capillary had the following characteristics in Britton-Robinson's buffer (pH 9.0) containing 0.2 M sodium sulfite at −0.9 V *vs.* SCE, at $h=35$ cm: $m=1.64$ mg/s for both electrodes, $t=1.51$ for HDME and 5.54 s/drop for DME. The cell for Hg–Pt was the same as for HDME. The Hg–Pt was a mercury plated platinum wire (0.3 mm in diameter×0.5 mm in length) which was plated electrolytically in a plating mixture containing 0.05 M mercuric chloride, 0.1 M EDTA, and 0.5 M sodium carbonate.

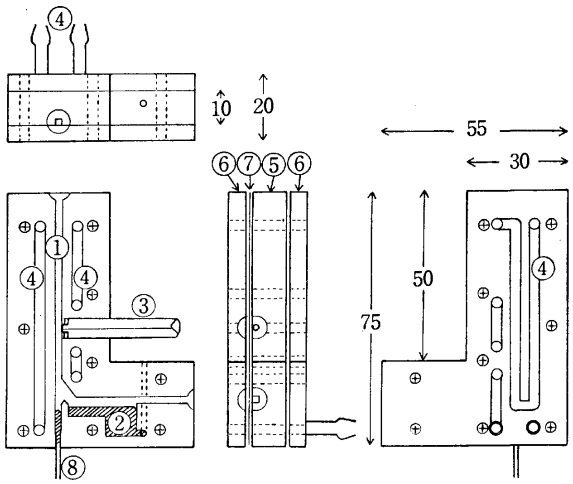

Fig. 1. Polarographic flow cell.
1) Effluent canal, 2) Hg pool anode, 3) HDME, 4) Thermostated water passageway, 5) Teflon, 6) Acrylics, 7) Polyethylene film, 8) Teflon tubing to Hg reservoir; ⊕: Setscrew; Scale in mm.

Voltage-applying and Current-measuring Equipment: The fundamental polarographic and chromato-polarographic measurements were carried out by using a Yanagimoto Automatic Recording Polarograph (PA-101) with a Toa Polyrecorder (EPR-2T). Simple equipment, as is shown in Fig. 2 (G and H), was also used for the practical chromato-polarography.

Chromatographic System: A schematic diagram of the apparatus used for liquid chromatography is shown in Fig. 2. The carrier liquid from an eluate reservoir (A) was conveyed into a saturator (C) by a Shibata micropump (SP-100; 0—120 ml/hr) (B). The saturator, made of glass (1 cm i.d. ×15 cm long) and filled with an organic solvent such as is used for the stationary phase in the column up to 10 cm from the bottom, ensures the proper equilibration of the moving phase with the stationary liquid. The carrier from the saturator passes through a sample injection device (D)[4] and is then delivered into the separation column (E) made of glass (0.5—0.9 cm i.d. × 5—30 cm long). The sample is introduced onto the top of the column by means of either a pipette or a calibrated syringe. Chromatographic peaks, leaving the column, pass through the flow cell (F) and are then presented on the recorder (H). The pulsing movement of the effluent due to the pump was damped by placing a nitrogen bubble (1—5 cm^3) on the top of the saturator and the column. The

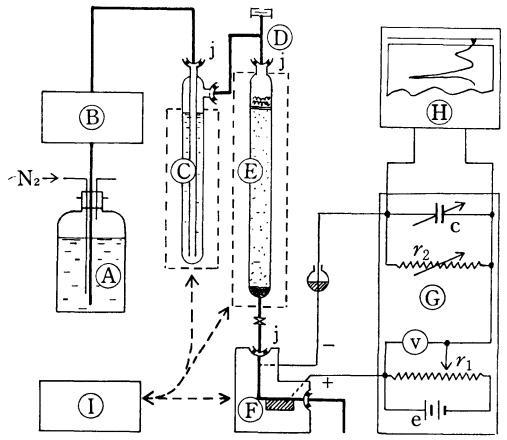

Fig. 2. Schematic diagram of chromato-polarograph.
A) Eluate reservoir, B) Elution pump, C) Saturator, D) Sample injection device, E) Separation column, F) Flow cell, G) Polarograph, H) Recorder, I) Thermostat; e: battery (3 V), r_1: resistor (100 Ω), v: voltmeter (0—3 V), r_2: standard resistor (0.1 Ω—100 kΩ), c: damping capacitor (0—200 μF), j: O-ring joint.

Teflon tubing (0.9 mm i. d. and 1.7 mm o. d.) and various fittings were obtained from the Shibata Chemical Apparatus Mfg. Co., Ltd., Tokyo.

Preparation of the Column: The column packing was prepared as follows: after spherical polystyrene grains had been sufficiently swollen with an organic solvent (TCE or DCB), the excess solvent was removed by filtration with a small glass filter. The swollen polystyrene grains, which had been effectively washed with 10% ethanol, were suspended in 10% ethanol, and then the air bubbles cohesively attached to the grains were removed under reduced pressure. The suspension of the filler was quietly poured into the glass column plugged with a small wad of cotton and filled with 10% ethanol, while the filler liquid was quietly drained at the same rate. The column was then pressed under nitrogen pressure (about 2 atm) until the height of the carrier liquid above the packing was about 1 cm. These processes were repeated until the desired bed height was obtained. After filling the column, the top was then plugged with a small wad of cotton. The ion-exchange column was 0.5 cm i. d. × 5.6 cm long, and it was packed with Dowex 1×8 (100—200 mesh, nitrate form).

Materials and Reagents. The spherical polystyrene grains (7.1% cross-linked with divinylbenzene) employed as the support of the stationary phase were prepared by suspension polymerization according to the method of Winslow and Matreyek.[25] The polymer grains were sieved to five fractions of 100—115, 115—150, 150—200, 200—250, and above 250 mesh. The ion-exchange resin was Dowex 1×8 (100—200 mech), and the resin, supplied in the chloride form, was converted into the nitrate form by treating it with 1 M sodium hydroxyde and 1 M nitric acid. After having been washed with distilled water, the resin was stored in 1 M potassium nitrate. As for the stationary phase of the partition column, 1,1,2,2-tetrachloroethane (TCE) and *o*-dichlorobenzene (DCB) from Wako Pure Chemical Ind., Ltd., were used without further purification. The 2-amino-3-nitropyridine (A3N), 2-amino-5-nitropyridine (A5N), 2-hydroxy-3-nitropyridine (O3N), and 2-hydroxy-5-nitropyridine (O5N) were kindly donated by Professor Eiji Imoto of the University of Osaka Prefecture; their mp's were 164, 165—166, 226—228, and 192.5—193.5 °C respectively. The stock solutions (about 10^{-2} M) were prepared by dissolving the specimen in 10% ethanol. All the other chemicals were of a reagent grade or an equivalent. Britton-Robinson's buffer (BR) and 1 M potassium nitrate were used as the carrier liquid of the reversed partition and the ion-exchange chromatography respectively.

Procedures. After pre-conditioning the separation column under a fixed flow rate for 30—60 min at a constant temperature, an aliquot of the sample solution was introduced onto the top of the column and the current through the polarographic-flow cell at the constant applied voltage was recorded. The deaeration of the carrier liquid was carried out by means of either the addition of sodium sulfite (0.2 M) for neutral and alkaline solutions or a stream of nitrogen gas for an acidic solution.

Results and Discussion

Characteristics of the Flow Cell. To obtain some information concerning the characteristics of the three different flow cells described above, 2×10^{-4} M A3N in a BR buffer (pH 9.1) containing 0.2 M sodium sulfite was passed through the cell at a given flow rate and the polarographic current was recorded at an applied voltage of −0.9 V *vs.* Hg pool, which was sufficient for the reduction of A3N. The results obtained are presented in Fig. 3, where the current is plotted

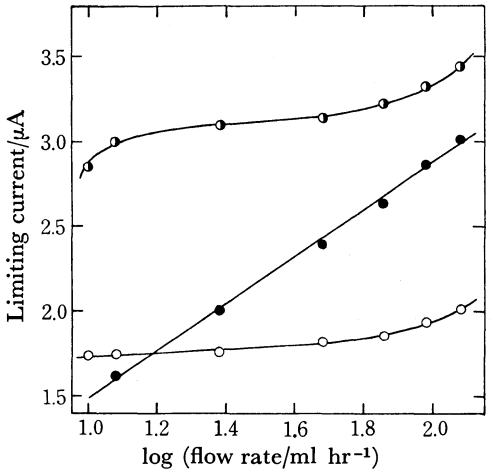

Fig. 3. Effect of flow rate on the polarographic current.
●: Hg–Pt, ◑: DME, ○: HDME.

against the logarithm of the flow rate. The effect of the flow rate on the current obtained with the HDME and DME is less pronounced than that on Hg–Pt. However, the slopes of the curves for both the dropping mercury electrodes exhibit a tendency to increase with the flow rate and to become similar to that for the stationary electrode[26] at a flow rate above 100 ml/hr. In the following experiments, the cell with HDME was used because the current oscillation, accompanied by the dropping of the mercury, can be easily reduced by the connection of a parallel capacitor (Fig. 2,c) and a good stability and reproducibility can be obtained.

The relationship between the limiting current in the flowing electrolyte and the height of the mercury reservoir is presented in Fig. 4; the change of the current with the mercury head was greater than that for the normal diffusion-controlled current, even in the

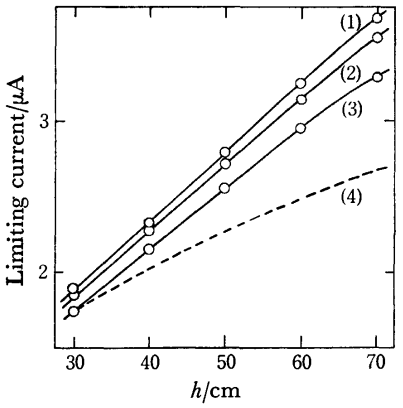

Fig. 4. Relationship between the limiting current (i) and the height (h) of Hg reservoir.
Flow rate of effluent: 1) 120, 2) 24, 3) 0 ml/hr, 4) diffusion current.

stationary solution. The steep increase in the current may be due to the stirring effect[27] of the rapidly dropping electrode in a narrow cavity. Takemori and Honda[15] found that the current through the particular cell designed as the detector of the liquid chromatography showed a constant value irrespective of the height of the mercury reservoir over a limited range. The discrepancy from the present observation seems to be caused by the difference in the flow rate in the electrode cavity and by the wall effect related to the electrode position.

Polarographic Behavior and Chromato-polarographic Separation of Nitropyridine Derivatives. Polarography: The course of the polarographic reduction was observed to be very similar in all the nitropyridines used (A3N, A5N, O3N, and O5N); they showed a diffusion-controlled and well-defined reduction wave (1st wave), followed by an ill-defined wave (2nd wave), at a potential, 0.8 V, more negative than that of first wave in an acidic buffered solution. The second wave became more ill-defined with an increase in the pH. The height of the first wave, except in the case of O5N, was observed to remain constant over the whole pH range studied and to be proportional to the concentration of the compounds in the range of $(0.5—20)\times10^{-4}$ M. On the other hand, at pH values heigher than 7 the splitting of the first wave for O5N into two waves was observed. The ratio of the two heights changed with the pH, the sum remaining constant.

As may be seen in Fig. 5, which presents the changes in the half-wave potentials of the nitropyridines with the pH, the polarographic separation of the mixtures in the normal manner seems to be difficult because the half-wave potentials are so close to each other.

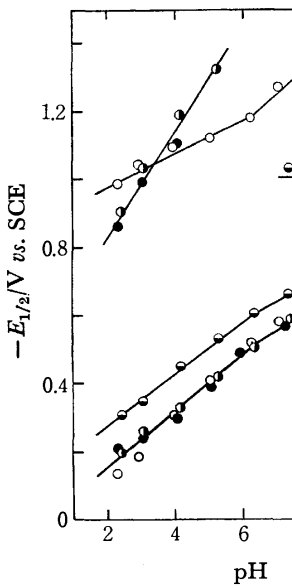

Fig. 5. pH-Dependence of the half-wave potentials of nitropyridines in BR buffer.
○: A3N, ●: A5N, ◑: O3N, ◒: O5N; Concn of nitropyridine: 2×10^{-4} M.

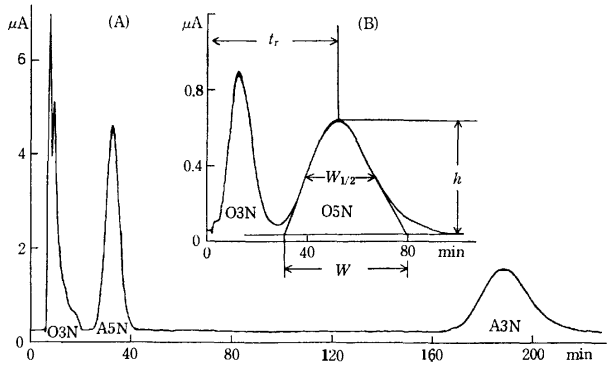

Fig. 6. Chromato-polarograms of nitropyridine mixtures at 30 °C.
A) Reversed-phase partition column (TCE), B) Ion-exchange column (Dowex 1×8, R-NO_3).

Chromato-polarography: Figure 6 (A) shows a typical chromato-polarogram obtained for a mixture of O3N, A5N, and A3N using a 0.9×10 cm column packed with spherical polystyrene grains (150—200 mesh) swollen by TCE, with a BR buffer (pH 9.1) containing 0.2 M sodium sulfite as a mobile phase, at a flow rate of 24 ml/hr. The current passing through the flow cell was recorded at an applied voltage of −0.8 V *vs.* Hg pool, which was sufficient for the reduction of all three compounds.

To examine the effect of the pH on the retention times of O3N, A5N, and A3N, such operating conditions as the sample size (1 μmol), the flow rate (24 ml/hr), and the column temperature (30 °C) were kept constant;

Table 1. The effect of pH on the retention times of niteopyridines
Column: 0.9×11.5 cm, polystyrene grains (150—200 mesh) swollen by TCE

pH	Retention time/min		
	O3N	A5N	A3N
1.82	8.3	8.3	23.5
3.02	8.3	14.1	79.0
5.02	6.0	19.5	110.0
7.02	7.1	21.3	117.2
9.16	7.0	22.7	111.7
11.0	5.0	22.7	110.0

only the pH of the mobile phase (BR buffer) was changed. The results obtained are listed in Table 1. From the table it can be seen that, whereas the retention times of A5N and A3N are practically unaffected by the pH in the pH range above 5, the retention time decreases steeply with the change in pH in the acidic range below 5 because of the protonation of pyridine derivatives, and that the retention time of O3N is smaller than that of the former in the whole pH range studied. In the following experiments, the BR buffer with a pH of 9 was mainly used as the mobile phase, since a good separation can be obtained and since the dissolving oxygen can be removed easily by adding sodium sulfite.

The effects of the size of the packing polystyrene particle, the column temperature, the flow rates of the mobile phase, and the concentration of methanol in the mobile phase on the height equivalent to a theoretical plate (HETP) and the resolving power (R) of the column were also investigated; the results obtained are summarized in Fig. 7.

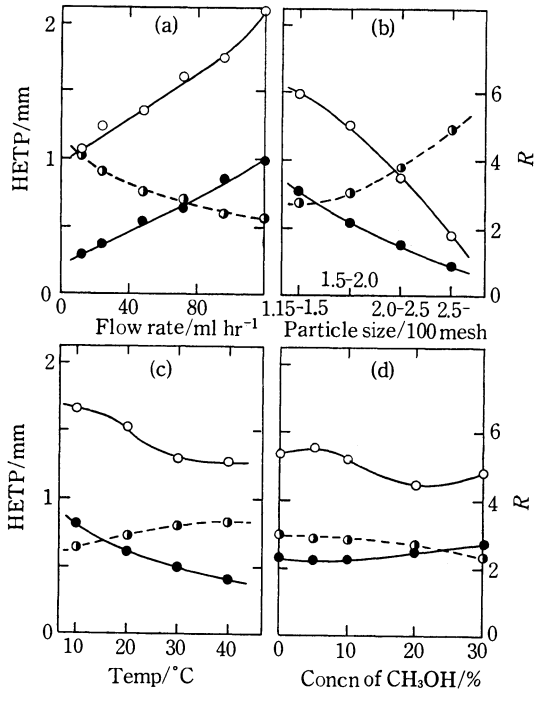

Fig. 7. Effect of flow rate (a), particle size (b), temperature (c), and methanol concentration (d) on the the HETP (——) and the resolving power (R,——) of the column.
Concn of nitropyridine: 1 μmol; ●: A3N, ○: A5N.

The efficiency of the column was calculated by means of Eq. (1) of the plate theory:[4,28]

$$n = 16(t_r/W)^2 \quad (1)$$

where n is the number of the theoretical plate in the column, t_r is the retention time (min), and W is the peak width in min at the base. HETP was calculated from:

$$\text{HETP} = \text{column length in mm}/n \quad (2)$$

The resolving power (R) for the separation of A5N and A3N was calculated from:

$$R = 2\Delta t_r/\sum W \quad (3)$$

where Δt_r is the difference in the retention times of the two peaks and $\sum W$ is the sum of the peak widths at the base.

From Figs. 7a, b, and c, it can be seen that both the efficiency and the resolving power of the column used under the controlled experimental conditions increase with a decrease in the flow rate and the particle sizes and with an increase in the column temperature. With an increase in the methanol concentration in the mobile phase, no significant changes in the efficiency or the resolving power could be observed (Fig. 7 d), but the operating time for the separation was shortened.

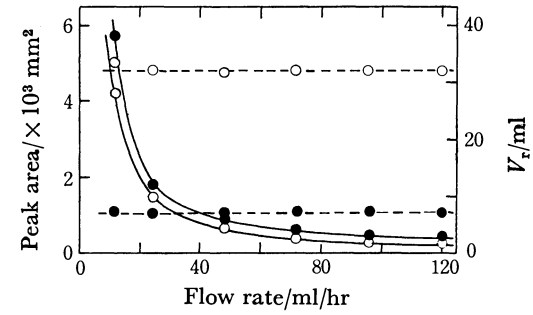

Fig. 8. Effect of flow rate on the peak area ($W_{1/2}\times h$, ——) and the retention volume (V_r,-----) at 30 °C.
Column: 0.9×5.7 cm, polystyrene grains (150—200 mesh) swollen by TCE; Elution: BR buffer (pH 9.2) contg. 0.2 M Na_2SO_3; Applied potential: −0.9 V *vs.* Hg pool; Sample: A5N (●, 1.29 μmol)+A3N (○, 1.26 μmol).

The changes in the peak areas corresponding to A5N and A3N with the flow rate are presented in Fig. 8, together with their retention volume, with the sample size and the experimental conditions being kept constant. With an increase in the flow rate, the peak areas for both A5N and A3N decreased hyperbolically, while their retention volumes showed fixed values independent of the flow rate. In determining components by means of chromato-polarography, therefore, the flow rate should be kept constant.

In order to obtain information concerning the reproducibility of the chromato-polarograms, the separation of a mixture of A5N (1.29 μmol) and A3N (1.26 μmol) was repeated five times under the same conditions; the results obtained are summarized in Table 2. The standard deviations of the peak heights and the peak areas (peak height×half-peak width) corresponding to each component were within 3.5 and 1.5% respectively; no appreciable change in the retention time was observed, even with ten runs of the separation.

The relationships between the chromato-polarographic responses obtained and the sample amounts added to the top of the column under the same operating conditions are presented in Table 3; linear relations were observed between the responses, the peak height, the peak areas (peak height×half-peak width and cutting-and-weighing method), and the amounts of A5N and A3N. In the analysis of the components in the sample by using the peak height, however, attention must be paid to keep the conditions strictly

TABLE 2. THE REPRODUCIBILITY OF CHROMATO-POLAROGRAMS FOR NITROPYRIDINES
Column: 0.9×5.3 cm, polystyrene grains (150—200 mesh) swollen by TCE, 30 °C; Elution; BR buffer (pH 9.15) contg. 0.2 M Na_2SO_3, 48 ml/hr; Applied potential: −0.9 V *vs.* Hg pool

Exp. No.	Peak height/mm		Peak area/mm²		Retention time/min	
	A5N	A3N	A5N	A3N	A5N	A3N
1	81.3	37.8	667	937	7.9	36.3
2	80.0	38.4	672	937	7.9	36.2
3	77.4	38.5	658	933	7.9	35.9
4	84.2	39.8	672	945	7.9	35.4
5	78.3	36.4	658	928	7.8	35.6
ave.	80.2_4	38.1_8	$665._4$	$936._0$	7.8_8	35.8_8

TABLE 3. THE RELATIONSHIP BETWEEN THE CHROMATO-POLAROGRAPHIC RESPONSES AND THE SAMPLE SIZE OF NITROPYRIDINES
Column: 0.9×7.5 cm, polystyrene grains (150—200 mesh) swollen by TCE, 30 °C; Elution: BR buffer (pH 9.15) contg. 0.2 M Na_2SO_3, 60 ml/hr; Applied potential: −0.9 V *vs.* Hg pool; Recorder sens.: 0.0266 μA/mm; Chart speed: 180 mm/hr

Sample added /μmol		Peak height /mm		Peak area[a] /mm²		Peak area[b] /mg		Retention time /min		*R*
A5N	A3N	A5N	A3N	A5N	A3N	A5N	A3N	A5N	A3N	
0.2	1.0	19.5	42.7	156	1132	7.2	47.8	8.53	41.4	2.0
0.4	0.8	41.8	33.4	334	878	14.8	38.0	8.70	40.8	2.1
0.6	0.6	61.2	25.3	490	665	21.8	29.0	8.67	40.3	2.2
0.8	0.4	78.8	17.0	643	450	27.8	20.4	8.64	40.2	2.3
1.0	0.2	99.5	8.2	796	221	34.9	10.0	8.64	40.3	2.5

a) Peak height (h)×half-peak width ($W_{1/2}$). b) Cutting-and-weighing method.

controlled, since the height is markedly affected by even a small change in the operating conditions. The retention times for A5N and A3N were not pronouncedly affected by changes in the sample size, but the resolving power was observed to decrease slightly with an increase in the amounts.

Though all of the 2-hydroxy isomer could be easily separated from the mixture of 2-hydroxy and 2-amino nitropyridines by means of the reversed-phase partition column described above, as is shown in Fig. 6 (A), the separation of the mixture of 2-hydroxy isomers was not successful since they are sparingly soluble to such organic solvents as TCE and DCB. Thereupon, an ion-exchange column (5×56 mm) packed with Dowex 1×8 of 100—200 mesh was also used to separate the mixture of 2-hydroxy isomers. After adding the sample to the top of the column, the elution was carried out with 1 M potassium nitrate containing 0.2 M sodium sulfite at the flow rate of 24 ml/hr at 30 °C; a typical chromato-polarogram thus obtained is shown in Fig. 6 (B).

Application to the Determination of 2-Amino Nitropyridines in Nitrating Mixtures. The nitration was carried out by adding 5 ml of a nitrating reagent containing 1 ml of fuming nitric acid (d 1.52) in 20 ml of concentrated sulfuric acid to 100 ml of a concentrated sulfuric acid solution containing 0.5 g of 2-aminopyridine under continuous stirring at a temperature lower than 5 °C. One ml of the reaction mixture was pipetted out at a given time interval and transferred into a 25-ml volumetric flask. After having been neutralized with 5 M sodium hydroxyde under cooling by ice-water, the mixture was diluted to the desired volume with distilled water.

In a run, after a further tenfold dilution of the neutralized sample with a BR buffer (pH 7.1), the solution was polarographed in the usual way at 25 °C.

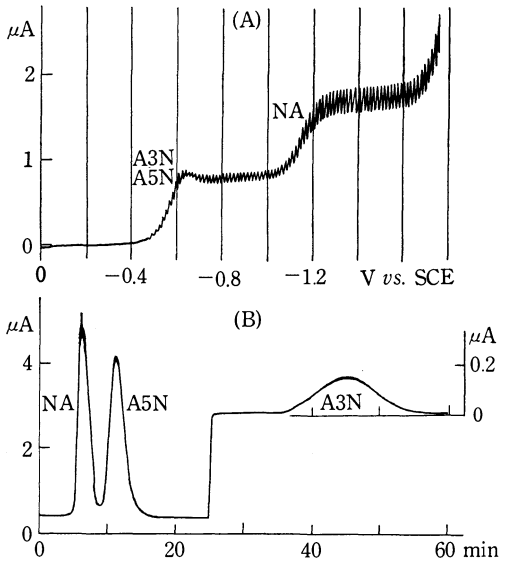

Fig. 9. Polarogram (A) and chromato-polarogram (B) of nitropyridines formed by nitration of 2-amino-pyridine.
Nitration: 5 °C, 30 min; Column: 0.5×10 cm, polystyrene grains swollen by DCB; Elution: 24 ml/hr; Applied potential: −1.5 V *vs.* Hg pool.

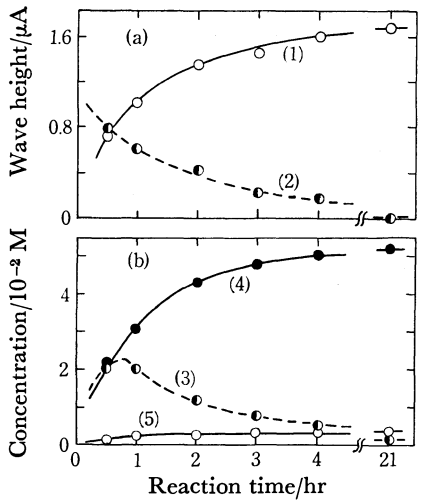

Fig. 10. Change of polarogram (a) and chromato-polarogram (b) during nitration.
1) 1st wave (A3N, A5N), 2) 2nd wave (NA), 3) 1st peak (NA), 4) 2nd peak (A5N), and 5) 3rd peak (A3N)

The polarogram thus obtained and the changes in the wave heights with the reaction times are shown in Figs. 9 (A) and 10 (a) respectively. From the latter figure, it can be seen that the second wave attains its maximum value rapidly after the addition of the nitrating reagent, while the first wave increases slowly at the expense of the second wave with the reaction time; the half-wave potential of the first wave coincides with that of A5N or A3N under the same conditions.

In another run, 0.5 ml of the neutralized sample was added to the top of the column described above and the column was eluted with BR buffer (pH 9) containing 0.2 M sodium sulfite at 30 °C. A typical chromato-polarogram is shown in Fig. 9 (B). The retention times of the second and the third peaks agreed with those for A5N and A3N respectively. The product corresponding to the second wave in Fig. 9 (A) and the first peak in Fig. 9 (B) may be concluded to be 2-nitroaminopyridine (NA).[29] Figure 10 (b) shows the changes in the concentration of the nitro compound formed in the reaction mixture with the reaction time, where the concentration of each substance was calculated by comparing the peak area obtained with that of a pure substance. From the findings described above, it may be deduced that 2-nitroaminopyridine forms rapidly at the first stage of the nitration and is then converted to A5N and A3N in the ratio of 14.5 to 1.

The authors wish to thank Professor Eiji Imoto for the gift of nitropyridine derivatives. They are also indebted to Mr. Hideo Oshima for his assistance in the experimental work.

References

1) R. D. Conlon, *Anal. Chem.*, **41**, 107A (1969).
2) J. J. Kirkland, *ibid.*, **40**, 391 (1968).
3) K. P. Hupe and E. Bayer, *J. Gas. Chromatog.*, **5**, 197 (1967).
4) T. E. Young and R. J. Maggs, *Anal. Chim. Acta*, **38**, 105 (1967).
5) B. Drake, *Acta Chem. Scand.*, **4**, 554 (1950); *Chem. Abstr.*, **44**, 8408g (1950).
6) W. Kemula, *Roczniki Chem.*, **26**, 281 (1952); *Chem. Abstr.*, **47**, 7344d (1953).
7) W. Kemula, "Proceeding of the International Symposium on Microchemistry 1958," Pergamon, London (1959), p. 248; "Progress in Polarography," Interscience, New York (1962), p. 397.
8) C. K. Mann, *Anal. Chem.*, **29**, 1385 (1957).
9) W. J. Blaedel and J. W. Todd, *ibid.*, **30**, 1821 (1958).
10) R. L. Robertus, R. J. Cappell, and G. W. Bond, *ibid.*, **30**, 1825 (1958).
11) W. J. Blaedel and J. H. Strohl, *ibid.*, **33**, 1631 (1961); **36**, 445 (1964).
12) E. B. Buchanan, Jr. and J. R. Bacon, *ibid.*, **39**, 615 (1967).
13) J. Janata and H. B. Mark, Jr., *ibid.*, **39**, 1896 (1967).
14) J. G. Koen, J. F. K. Huber, H. Poppe, and G. den Boef, *J. Chromatog. Sci.*, **8**, 192 (1970).
15) Y. Takemori and M. Honda, *Rev. Polarog.*, **16**, 96 (1970).
16) E. Sándi, *Z. Anal. Chem.*, **167**, 241 (1959).
17) W. Blaedel and J. W. Todd, *Anal. Chem.*, **33**, 205 (1961).
18) M. C. Corfield and A. Robson, *Biochem. J.*, **84**, 146 (1962).
19) M. Mohnke, R. Schmunk, and H. Schütze, *Z. Anal. Chem.*, **219**, 137 (1966).
20) W. Kemula, K. Butkiewicz, and D. Sybilska, "Modern Aspects of Polarography," Plenum, New York (1966), p. 36.
21) S. Tustanowski, *J. Chromatog.*, **31**, 266 (1967).
22) W. Kemula and D. Sybilska, *Anal. Chim. Acta*, **38**, 97 (1967).
23) P. Lanza, V. Concialini, and A. Benati, *J. Electroanal. Chem.*, **17**, 395 (1967).
24) I. Smoleń, *Collection Czech. Chem. Commun.*, **19**, 238 (1954).
25) F. H. Winslow and M. Matreyek, *Ind. Eng. Chem.*, **43**, 1108 (1951).
26) O. H. Müller, *J. Amer. Chem. Soc.*, **69**, 2992 (1947).
27) J. J. Lingane and B. A. Loveridge, *ibid.*, **72**, 438 (1950).
28) I. Rosenthal, A. R. Weiss, and V. R. Usdin, "Treatise on Analytical Chemistry," Part I, Vol. 3, ed. by I. M. Kolthoff and P. J. Elving, Interscience, New York (1961), p. 1411.
29) H. Meyer and E. R. von Beck, *Monatsh.*, **36**, 731 (1915).

The Reactions of Recoil Tritium Atoms with Water. II. Reactivity Integral- and Moderator-Isotope Effects in H_2O-D_2O Binary Mixtures

Enzo TACHIKAWA and Yasuyuki ARATONO

Division of Chemistry, Japan Atomic Energy Research Institute, Tokai-Mura, Ibaraki 319-11

(Received October 25, 1974)

The HT and DT yields from the nuclear transformation of $^6Li(n,\alpha)T$ in H_2O-D_2O binary mixtures were studied in the liquid phase. The $(HT/H_2O)/(DT/D_2O)$ ratio was nearly constant at 1.60 ± 0.08 over the whole range of mol fractions of D_2O in the presence of I_2 as a scavenger. Using the kinetic model with reasonable assumptions, the relative efficiencies for the kinetic moderation of H_2O, HDO, and D_2O were determined. The results indicate that the collision of recoil T atoms with HDO, with a large fractional energy loss, must occur as frequently as with H_2O.

As is the case with organic compounds,[1-3] the two most important energetic reactions of recoil T atoms with H_2O or D_2O are the hydrogen abstraction and the hydrogen substitution;

$$T + H_2O(D_2O) \longrightarrow HT + OH(DT+OD) \quad (1)$$

$$T + H_2O(D_2O) \longrightarrow HTO + H(DTO+D) \quad (2)$$

The yields of Reactions 1 and 2 are 11 and 68% with H_2O and 10.6 and 68% with D_2O respectively.[4,5] The apparent absence of the isotope effect must result from the fact that the preference of the abstraction of H over D atoms is counterbalanced by the "moderator" isotope effects[6] of H_2O and D_2O on recoil T atoms.

In a previous paper,[5] the "moderator" isotope effect was estimated to be 1.5 by comparing the acetone-*t* yield at zero mol fraction (m.f.) of acetone in the H_2O-acetone and D_2O-acetone binary systems. This, in turn, gives the "reactivity integral"[6] isotope effect of 1.5.

The present paper will deal with the recoil T reactions in the H_2O-D_2O mixture. This system has the advantage that the relative reactivity of recoil T atoms is directly proportional to the observed HT/DT at any given m.f. of D_2O; thus, no correction for the "moderator" isotope effect is required.

Experimental

The experimental procedure has been described in detail in the previous paper.[5] Five-ml portions of various mixtures of H_2O and D_2O containing 0.025 g of $LiNO_3$ were sealed in a 13-ml quartz ampoule with a breakable tip. The neutron irradiation was carried out in the JRR-4 in a flux of 3×10^{13} $n\cdot cm^{-2}\cdot s^{-1}$ for 1 min. The dose rate of γ-rays at the irradiation port was estimated to be 1×10^8 $r\cdot h^{-1}$. During the irradiation, samples were cooled by letting cooling water flow through and were maintained at 20—30 °C.

After the irradiation, the gaseous products collected by means of a Toepler pump were divided into two parts. One of them was injected into an alumina column, 6 m long, for the determination of the product yield. The other was subjected to the isotopic separation. A 5-m ferric oxide-γ-alumina column was used. The γ-alumina was 40—60 mesh, chemically coated with Fe_2O_3. The column was operated at the temperature of liquid N_2. The activity measurement was performed using a gas-flow proportional counter.

The activity of the condensates was measured by means of a liquid scintillation counter. One hundred μl of a solution was dissolved in 10 ml of the liquid scintillator, prepared by dissolving 112 g of naphthalene, 275 mg of POPOP, and 6 g of DPO in 1 l of dioxane.

The conversion factor required to correlate the activities measured by the two different methods was obtained in the following experiments. An aliquot of the tritiated water of a known specific activity was passed through a carbon-wool column heated at 1100 °C. The resulting hydrogen was directly introduced into the radio-gas chromatograph. Another aliquot of the water was radio-assayed by means of the liquid scintillation counter. The counting efficiency of the radio-gas chromatograph was 1/3.8 of that of the liquid scintillation counter. The activities of the gaseous products can, then, be compared with those of the liquid phase.

Results and Discussion

Relative Reactivities of O–H and O–D Bonds. In Fig. 1 the HT and DT yields in 0.07 M $LiNO_3$ solution containing 1.2×10^{-3} M I_2 are plotted as a function of the m.f. of D_2O. It seems that H_2O is more efficient than D_2O as a moderator for recoil T atoms, since the HT yield curve is slightly convex upward, while the DT yield curve is concave. However, at a given composition of H_2O and D_2O, a comparison of the relative reactivities of O–H and O–D bonds does not require any correction for the "moderator" isotope

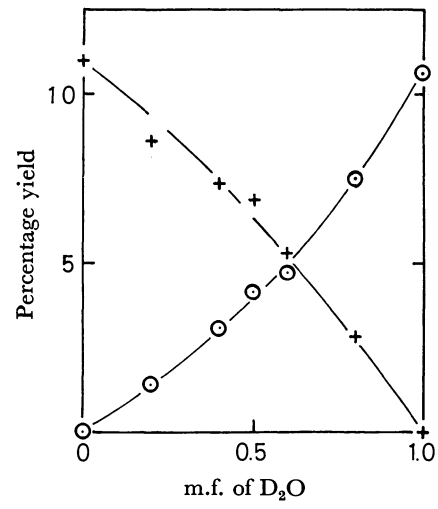

Fig. 1. Yields of HT and DT formed by reactions of recoil T atoms in H_2O-D_2O binary mixtures.
⊙: percentage yield of DT, + : percentage yield of HT.

Table 1. Relative reactivities of O–H and O–D bonds, and relative moderating abilities of H_2O, HDO, and D_2O in H_2O–D_2O binary mixtures

m.f. of D_2O	HT/H_2O (%/m. f.)	DT/D_2O (%/m. f.)	$\frac{HT/H_2O}{DT/D_2O}$	$\alpha_{HDO}/\alpha_{H_2O}$	$\alpha_{HDO}/\alpha_{D_2O}$
1.0	—	10.6	—	—	—
0.8	14.0	9.38	1.49	1.01	1.35
0.6	13.3	7.83	1.69	0.91	1.57
0.5	12.5	8.20	1.68	0.76	1.33
0.4	12.3	7.75	1.59	0.90	1.40
0.2	10.8	7.00	1.54	1.13	1.62
0.0	11.0	—	—	—	—
			av. 1.60 ± 0.08	α_{H_2O}: α_{HDO}: α_{D_2O} $=1.56\pm0.16:1.45\pm0.12:1$	

effect, since both bonds are exposed to the same tritium flux. Thus, the $(HT/H_2O)/(DT/D_2O)$ ratio is directly proportional to the reactivity of these bonds. The values summarized in Table 1 are almost constant at 1.60 ± 0.08 over the whole range of the m.f. of D_2O. This suggests that the hot reactions with the two bonds have very similar energy dependences and can be used for estimates of the magnitude of the "reactivity integral" isotope effect, I_{HT}/I_{DT}.

In the present case, the $(HT/H_2O)/(DT/D_2O)$ ratio is related to I_{HT}/I_{DT} by the following equation;[7]

$$\frac{(HT/H_2O)}{(DT/D_2O)} = \frac{S_{OH}}{S_{OD}} \cdot \frac{I_{HT}}{I_{DT}} \tag{3}$$

where S_{OH} and S_{OD} are the collision cross sections for the T atoms with O–H and O–D bonds, averaged over the proper range of energies.

With the value of 1.60 ± 0.08 for the $(HT/H_2O)/(DT/D_2O)$ ratio, Eq. 3 can be simplified as;

$$\frac{I_{HT}}{I_{DT}} = 1.60 \times \frac{S_{OD}}{S_{OH}} \tag{4}$$

Therefore, if the collision cross sections of these bonds are equal, the "reactivity integral" isotope effect is determined to be 1.60 ± 0.08.

However, in the mixtures of H_2O and D_2O isotopic mixing occurs;

$$H_2O + D_2O \rightleftharpoons 2HDO \tag{5}$$

Its equilibrium constant has been reported to be 3.78 ± 0.03 by Pyper *et al.*[8] and 3.94 ± 0.03 by Gold *et al.*[9] Thus, the actual reaction systems are composed of H_2O, HDO, and D_2O, and the value of 1.60 must be the overall "reactivity integral" isotope effect between the O–H and O–D bonds in these chemical forms. In the abstraction of hydrogen from D_2O, both the primary and the secondary isotope effects exist, while from HDO either the primary or the secondary isotope effect exists, depending upon which hydrogen atom is abstracted. If the secondary isotope effect on the abstraction of hydrogen is as important as in the substitution of hydrogen[1,2] the yield must be larger from H_2O than from HDO on a per-bond basis. The HT/DT ratios from various reaction systems, including the CH_4–CD_4, CH_2D_2, and CH_3F–CD_3F systems, always stay within the range of 1.28—1.35.[2] These results are consistent only with the view that the primary isotope effect makes a major contribution to the isotope effect observed. Thus, although no unequivocal data are available, it may be considered that, in the present reaction system, the secondary isotope effect is less important than the primary isotope effect.

Relative Moderating Abilities of H_2O, HDO, and D_2O. The Estrup-Wolfgang kinetic theory[2] incorporates no mechanistic assumptions and has successfully been applied to various reaction systems. However, it has very seldom been applied to the condensed phases,[12] since therein the reactions of recoil atoms are often influenced by the various effects characteristic of the liquid phase, such as the cage effect and the local heating of the matrix.

Data on the reactions of recoil T atoms in condensed phases are, in virtually all cases, completely consistent with the model based on reactions in the gaseous phases. It has been reported that the reactions with various hydrocarbons gave similar yields in the gas and liquid phases.[2] The only differences found could be attributed to the more rapid collisional deactivation of excited products in the liquid phases. This clearly indicates that the effects which usually play a significant role in the liquid phase make only a minor contribution to the reactions of recoil T atoms in the liquid phases. Thus, the application of the kinetic theory to the present reaction systems is reasonable.

According to the kinetic theory, the probability that a hot atom will react with the component, j, to form the product, i, is expressed by this equation;[13]

$$P_i = \left(\frac{N_i}{N_s}\right) = \left(\frac{f_j}{\alpha}\right) I_i - \left(\frac{f_j}{\alpha}\right)^2 K_i + \cdots \tag{6}$$

where I_i and K_i are the "reactivity integral"[14] and the "energy shadowing" terms respectively. The f_j is the collision probability of a hot atom with the component, j. In the present reaction mixtures,

$$\begin{aligned} f_{H_2O} &= (X_{H_2O} \cdot S_{H_2O})/(\textstyle\sum X_j S_j) \\ f_{HDO} &= (X_{HDO} \cdot S_{HDO})/(\textstyle\sum X_j S_j), \text{ and} \\ f_{D_2O} &= (X_{D_2O} \cdot S_{D_2O})/(\textstyle\sum X_j S_j) \end{aligned} \tag{7}$$

where $\sum X_j S_j = X_{H_2O} \cdot S_{H_2O} + X_{HDO} \cdot S_{HDO} + X_{D_2O} \cdot S_{D_2O}$ and where X_j is the m.f. of the component, j. The α is the weighted sum of the average energy loss upon collision with H_2O, HDO, and D_2O:

$$\alpha = \alpha_{H_2O} \cdot f_{H_2O} + \alpha_{HDO} \cdot f_{HDO} + \alpha_{D_2O} \cdot f_{D_2O} \tag{8}$$

The sum of the HT and DT yields is not large and is almost constant at 11% over the whole range of the

m.f. of D_2O. Thus, if the energy range of the recoil T atoms needed to produce HT or DT lies entirely above the range to produce HTO or DTO, one can reasonably ignore the "energy shadowing" term. On the other hand, as it is probable that the former lies below the latter, or that both energy ranges overlap each other, one must take into account the "energy shadowing" effects caused by the substitution reactions.

However, as for the reactions among the isotopic water molecules, it is considered unlikely that the shapes and the energy ranges of the excitation curves for the abstraction and substitution of hydrogen vary significantly with the reactant molecules. This consideration leads to the view that a fraction of recoil T atoms, eliminated by the substitution reaction prior to the abstraction reaction, is close to the constant, K, among the samples. This is consistent with the fact that the total water-t yield is almost constant over the whole range of the m.f. of D_2O. Thus, the $(1-K)\cdot N_s$ atoms of tritium are available for abstraction reaction. Consequently, as a reasonable approximation, one can derive the following equations on the assumption that $S_{H_2O}=S_{HDO}=S_{D_2O}$:

i) for the case of a single reactant of H_2O or D_2O;

$$\frac{N_{HT}}{(1-K)\cdot N_s}=\frac{f_{H_2O}}{\alpha_{H_2O}}I_{H_2O},\quad \frac{I_{H_2O}\cdot(1-K)}{\alpha_{H_2O}}=0.11 \tag{9}$$

$$\frac{N_{DT}}{(1-K)\cdot N_s}=\frac{f_{D_2O}}{\alpha_{D_2O}}I_{D_2O},\quad \frac{I_{D_2O}\cdot(1-K)}{\alpha_{D_2O}}=0.106 \tag{10}$$

ii) for the case of a binary mixture;

a. the HT yield from the reactions with H_2O;

$$\left(\frac{N_{HT}}{N_s}\right)_{H_2O}=(1-K)\cdot\frac{f_{H_2O}}{\alpha}\cdot I_{H_2O}$$

$$=\frac{(1-K)\cdot(X_{H_2O}/\alpha_{H_2O})\cdot I_{H_2O}}{X_{H_2O}+(\alpha_{HDO}/\alpha_{H_2O})\cdot X_{HDO}+(\alpha_{D_2O}/\alpha_{H_2O})\cdot X_{D_2O}} \tag{11}$$

b. the HT yield from the reactions with HDO;

$$\left(\frac{N_{HT}}{N_s}\right)_{HDO}=\frac{(1-K)\cdot(X_{HDO}/\alpha_{H_2O})\cdot I_{HDO}}{X_{H_2O}+(\alpha_{HDO}/\alpha_{H_2O})\cdot X_{HDO}+(\alpha_{D_2O}/\alpha_{H_2O})\cdot X_{D_2O}} \tag{12}$$

By equating I_{HDO} with $(I_{H_2O})/2$ and by substituting Eq. 9 into Eqs. 11 and 12, we obtain the following equation for the total HT yield from the H_2O–D_2O binary mixtures:

$$\left(\frac{N_{HT}}{N_s}\right)=\frac{0.11\cdot X_{H_2O}+0.055\cdot X_{HDO}}{X_{H_2O}+(\alpha_{HDO}/\alpha_{H_2O})\cdot X_{HDO}+(\alpha_{D_2O}/\alpha_{H_2O})\cdot X_{D_2O}} \tag{13}$$

The corresponding equation for the total DT yield from the mixture is;

$$\left(\frac{N_{DT}}{N_s}\right)=\frac{0.106\cdot X_{D_2O}+0.053\cdot X_{HDO}}{X_{D_2O}+(\alpha_{HDO}/\alpha_{D_2O})\cdot X_{HDO}+(\alpha_{H_2O}/\alpha_{D_2O})\cdot X_{H_2O}} \tag{14}$$

Thus, if we know the $(\alpha_{H_2O}/\alpha_{D_2O})$ value, the relative efficiency of H_2O, HDO, and D_2O as the kinetic moderators can be determined using Eqs. 13 and 14. In Table 1 are also included the values of $(\alpha_{HDO}/\alpha_{H_2O})$ and $(\alpha_{HDO}/\alpha_{D_2O})$. For the calculation, the $\alpha_{H_2O}/\alpha_{D_2O}$ value of 1.5 was used, this value has previously been determined from the ratios of the acetone-t yields at zero m.f. of acetone in the H_2O–acetone and D_2O–acetone systems.[5] As an average, the values of 1.56 ± 0.16 for $\alpha_{H_2O}/\alpha_{D_2O}$ and of 1.45 ± 0.12 for $\alpha_{HDO}/\alpha_{D_2O}$ are deduced. Although the qualitative and quantitative significance of the present relative moderating abilities is largely dependent on the model and the asumptions introduced, the uncertainties involved do not affect the semiquantitative conclusion: $\alpha_{H_2O}\approx\alpha_{HDO}>\alpha_{D_2O}$.

A non-reactive collision of a recoil T atom with a molecule is very "cushioning".[7] In such a collision, a large fraction of the excess kinetic energy of the atom is transferred to the various degrees of freedoms in the struck molecule. The complexity of the molecule and the case of the energy transfer through the bonds are considered to be the important parameters governing the efficiency of the energy transfer. The consequence of the former is well demonstrated by the experimental results[7,15]: the α values increase in this order, D_2, CH_4, C_2H_6, n-C_3H_8, n-C_4H_{10}, n-C_5H_{12}, and iso-C_5H_{12}, indicating their dependence on the number of atoms involved and the complexity of the molecule. On the other hand, the latter parameter is closely related to the vibrational frequency of the bonds, since the energy transfer occurs through the bond vibrations: as the frequency becomes higher, the transfer becomes faster. The present results are consistent with this consideration: the O–H bond has a vibrational frequency higher than that of the O–D bond,[16] and the collision of recoil T atoms with HDO, with a large fractional energy loss, must occur as frequently as with H_2O.

References

1) F. S. Rowland, in MTP Inter. Rev. of Science, Phys. Chem. Series One, Vol. 9, J. C. Polanyi, ed., p. 109, Butterworths, London (1972).
2) R. Wolfgang, *Progr. Reaction Kinetics*, **3**, 97 (1965).
3) D. S. Urch, in MTP Inter. Rev. of Science, Inorg. Chem. Series One, Vol. 8, A. G. Maddock, ed., p. 149, Butterworths, London (1972).
4) T. Kambara, R. M. White, and F. S. Rowland, *J. Inorg. Nucl. Chem.*, **21**, 210 (1961).
5) E. Tachikawa and Y. Aratono, presented at the 18th Discussion Meeting of the Radiochemistry, Sendai, Miyagi (Oct. 1974), *J. Inorg. Nucl. Chem.*, in press (1975).
6) E. K. C. Lee and F. S. Rowland, *J. Amer. Chem. Soc.*, **85**, 2907 (1963).
7) J. W. Root and F. S. Rowland, *J. Chem. Phys.*, **46**, 4299 (1967).
8) J. W. Pyper, R. S. Newbury, and G. W. Barten, Jr., *ibid.*, **6**, 2253 (1967).
9) V. Gold and C. Tomlinson, *Chem. Commun.*, **1970**, 472.
10) E. K. C. Lee, J. W. Root, and F. S. Rowland, *Chem. Eff. Nucl. Transform. Proc. Symp.*, 1964, **1**, 55 (1965).
11) J. W. Root and F. S. Rowland, *J. Amer. Chem. Soc.*, **85**, 1021 (1963).
12) N. A. Katanos and M. I. Stamouli, *Radiochimica Acta*, **7**, 126 (1967).
13) R. Wolfgang, *J. Chem. Phys.*, **39**, 2983 (1963).
14) D. S. Urch, M. J. Welch, and R. J. Arthy, *Trans. Faraday Soc.*, **66**, 1642 (1970).
15) D. S. Urch and M. J. Welch, *ibid.*, **64**, 154 (1968).
16) D. Eisenberg and W. Kauzmann, The Structure and Properties of Water, Oxford University Press (1969), p. 228.

The CD Spectra of (L-Aspartato) (L-2,4-diaminobutyrato) cobalt (III) Complexes

Masatoshi WATABE and Sadao YOSHIKAWA*

General Education Department, Kogakuin University, Hachioji, Tokyo 193

**The Department of Synthetic Chemistry, Faculty of Engineering, The University of Tokyo, Hongo, Bunkyo-ku, Tokyo 113*

(Received October 30, 1974)

Systematic correlations in CD spectra are found when the CD spectra of the isomers of the [Co(L-aspartato)-(L-2,4-diaminobutyrato)] complex, the $[Co(N)_3(O)_3]$ type, are compared with those of the isomers of the [Co-(L-2,4-diaminobutyrato)$_2$]$^+$, the $[Co(N)_4(O)_2]$ type, and those of the isomers of the [Co(L-aspartato)$_2$]$^-$, the $[Co(N)_2(O)_4]$ type.

The coordination of two optically active tridentate ions such as aspartate (=asp) or 2,4-diaminobutyrate (=2,4-dba), with cobalt(III) can result in three geometric isomers. One of these isomers has been easily characterized, without ambiguity, on the basis of the electronic absorption spectra. The assignment of the other two isomers has been attempted by using the CD spectra, but no distinct characterization has yet been established.[1-5] The CD spectra of these complexes are different from those of the complexes containing bidentate and tetradentate ligands. The two *cis*(*N*) isomers of the [Co(L-2,3-dpa)$_2$]$^+$(L-2,3-dpa= L-2,3-diaminopropionate ion)[2] were assigned by using X-ray analysis, while the isomers of the [Co(L-2,4-dba)$_2$]$^+$ were characterized by using the PMR spectra in comparison with those of the [Co(L-2,3-dpa)$_2$]$^+$. The CD spectra of the complexes containing asp, dba, and dpa did not show any distinct relation between the sign of the CD components and the absolute configuration of these isomers. Legg and Neal, by comparing these CD spectra with those of the [Co(EDDS)]$^-$-(EDDS=ethylenediaminedisuccinate) and the [Co(EDDAMS)]$^-$(EDDAMS=ethylenediamine-*N*,*N*-diacetic-*N'*-monosuccinate),[6] proposed that the assignment done by Douglas[4] for the configuration of the two *cis*(*N*) isomers of the [Co(L-asp)$_2$]$^-$ had better be reversed.

We ourselves have previously reported the preparation and the separation of the isomers of the [Co(L- or D-asp)(L-2,4-dba)] complex.[7] These isomers have been characterized by using the PMR spectra. They have the same membered chelate rings as the [Co(L-2,4-dba)$_2$]$^+$ and the [Co(L-asp)$_2$]$^-$. This paper will describe whether the CD spectra of the isomers of the [Co(L-asp)(L-2,4-dba)] join those of the [Co(L-asp)$_2$]$^-$ and those of the [Co(L-2,4-dba)$_2$]$^+$.

Experimental

The preparation and the separation of the isomers were reported in a previous paper.[7] Three geometrical isomers were obtained for the [Co(L-asp)(L-2,4-dba)], they were designated L1, L2, and L3 in the order of elution in the ion-exchange chromatography. The electronic absorption spectra and the CD spectra were measured with a JASCO J-20 spectrophotometer. The measurements were carried for an aqueous solution except for the L1 isomer, the solution of which contains *ca.* 50% H_2SO_4.

Results and Discussion

Figure 1 shows the possible geometric isomers of the [Co(L-asp)(L-2,4-dba)]. The facial isomer (L3) can easily be distinguished from meridional isomers by comparing the electronic spectra of the three isomers of the [Co(L-asp) (L-2,4-dba)].

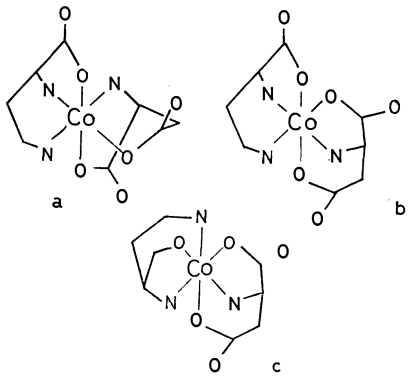

Fig. 1. The three possible geometrical isomers of the [Co(L-asp)(L-2,4-dba)] a: *trans*(*O*)*cis*(*N*), b: *cis*(*O*) *trans*(*N*), c: *cis*(*O*)*cis*(*N*). The isomers are named by considering 5-membered N and O atoms.

CD Spectra. The L-2,4-dba and the L-asp coordinated have 5-membered, 6-membered, and 7-membered chelate rings. When γ-amine nitrogen atoms of the L-2,4-dba for the [Co(L-2,4-dba)$_2$]$^+$ are replaced by oxygen atoms, one by one, the [Co(L-2,4-dba)$_2$]$^+$ may change to the [Co(L-asp)(L-2,4-dba)], and then to the [Co(L-asp)$_2$]$^-$. At this time, the relative positions of the 5-, 6-, and 7-membered chelate rings are not changed. The observed CD spectra may be classified into three groups (the A, B, and C rows in Fig. 2) by assuming that: (1) the difference between the N and O atoms coordinated may be disregarded, (2) the γ_{max} of the CD spectra varies with the change in the number of *X* and *Y* for the $[Co(N)_x(O)_y]$ system, and (3) the additivity of the vicinal effect holds for these nine isomers. Each of the three groups is composed of three isomers containing a different $[Co(N)_x(O)_y]$ type. In each series, one exact geometrical configuration is revealed by the electronic absorption spectra, *trans*(*O*)-*cis*(*N*) for [Co(L-2,4-dba)$_2$]$^+$, *cis*(*O*)*cis*(*N*) for [Co(L-asp)(L-2,4-dba)], and *cis*(*O*)*trans*(*N*) for [Co(L-asp)$_2$]$^-$ (see Fig. 2). The CD spectrum of the α isomer (the

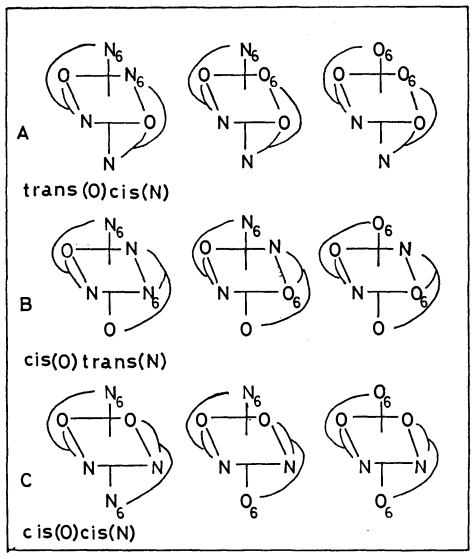

Fig. 2. Configurational analogies of the [Co(L-2,4-dba)$_2$]$^+$ (left), the [Co(L-asp)(L-2,4-dba)] (middle), and the [Co(L-asp)$_2$]$^-$ complexes (right).

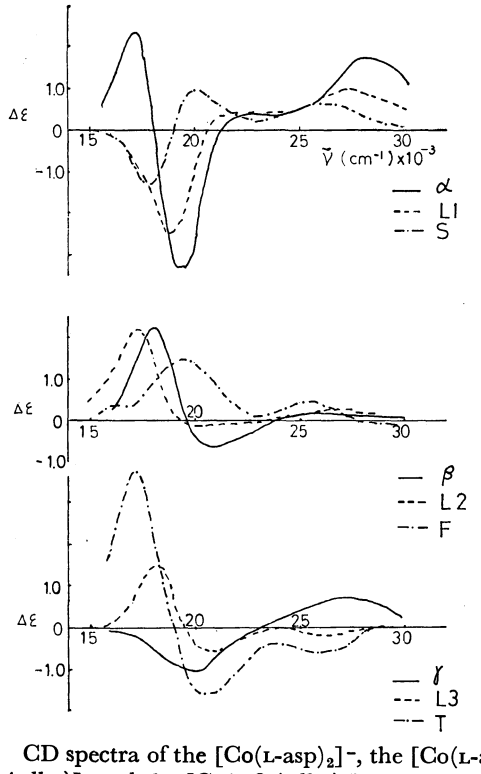

Fig. 3. CD spectra of the [Co(L-asp)$_2$]$^-$, the [Co(L-asp)-(L-2,4-dba)], and the [Co(L-2,4-dba)$_2$]$^+$.

three isomers obtained for the [Co(L-2,4-dba)$_2$]$^+$ are named α, β, and γ in the order of elution in ion-exchange chromatography), the configuration of which has the *trans(O)* geometry, resembles that of L1 of the [Co(L-asp)(L-2,4-dba)] rather than that of L2 (Fig. 3). The L1 isomer is assigned to the *trans(O)cis(N)* according to the above assumption (Fig. 2-A). Since the CD spectrum of L1 resembles that of the S isomer (the three isomers obtained are named F, S, and T in the order of elution in ion-exchange chromatography) of the [Co(L-asp)$_2$]$^-$, S must have the *trans(O)cis(N)* configuration. This last assignment, while not consistent with that of Douglas *et al.*,[4] agrees with that done by Legg and Neal.[6] When these three CD spectra are compared with each other in the order of [Co(L-2,4-dba)$_2$]$^+$→[Co(L-asp)(L-2,4-dba)]→[Co(L-asp)$_2$]$^-$, the value of the large negative peak at about 18×10^3 cm^{-1} is found to decrease gradually and the ν_{max} is found to shift to the longer wavelength side. The intensities of these CD spectra in the second absorption band region are also aligned in the order of α>L1>S. The β isomer for the [Co(L-2,4-dba)$_2$]$^+$ has the *cis(O)trans(N)* configuration.[3] The *cis(O)trans(N)* of [Co(L-asp)(L-2,4-dba)] lies in the same series as the *cis(O)trans(N)* isomer of the [Co(L-2,4-dba)$_2$]$^+$ (Fig. 2-B), and the CD spectrum of the L2 isomer considerably resembles that of the β isomer (Fig. 3). The configuration of the L2 isomer must be *cis(O)trans(N)*. The *cis(O)trans(N)* of the [Co(L-asp)$_2$]$^-$ lies also in the same series, and the CD spectrum of the F isomer resembles those of both the β isomer and the L2 isomer, especially by having the same $\Delta\varepsilon$ in the second absorption region, except for the large splitting in the first absorption band as a result of the *trans(N)* configuration. In the last series, the CD spectrum of the L3 isomer resembles that of the T isomer, but neither resembles that of the γ isomer. However, the CD intensities in the second absorption region of these complexes are aligned in the order of γ>L3>T. This indicates a gradual change in the vicinal effect.

We have also confirmed the alternative assignment of the two *cis*(N) isomers of the [Co(L-asp)$_2$]$^-$ and the [Co(L-asp)(ida)]$^-$, first identified by Legg and Neal.[6]

The authors wish to thank Drs. M. Saburi and S. Yano for helpful discussions.

References

1) J. I. Legg and D. W. Cooke, *J. Amer. Chem. Soc.*, **89**, 6854 (1967).
2) W. A. Freeman and C. F. Liu, *Inorg. Chem.*, **7**, 764 (1968).
3) W. A. Freeman and C. F. Liu, *ibid.*, **9**, 1191 (1970).
4) S. Yamada, J. Hidaka, and B. E. Douglas, *ibid.*, **10**, 2187 (1971).
5) J. Hidaka, S. Yamada, and B. E. Douglas, *J. Coord. Chem.*, **2**, 123 (1972).
6) J. I. Legg and J. A. Neal, *Inorg. Chem.*, **12**, 1805 (1973).
7) M. Watabe, K. Onuki, and S. Yoshikawa, This Bulletin, **48**, 687 (1975).

The Formation and Structure of Copper(II) Complexes with Cyclodextrins in an Alkaline Solution

Yoshihisa MATSUI, Toyoaki KURITA, Masao YAGI, Tetsuo OKAYAMA, Kazuo MOCHIDA, and Yoshio DATE

Department of Agricultural Chemistry, Shimane University, Nishikawazu, Matsue 690

(Received January 24, 1975)

Copper(II) forms a 2: 1 complex with cyclodextrin in an alkaline solution. The complexes with α- and β-cyclodextrins were isolated from solutions by the addition of ethanol. They are labile, and, upon heating, the Cu(II) is reduced to Cu(0). The role of the hydroxide ion was examined by means of potentiometric and conductometric titrations; it was found that the reaction of 1 mol of α-cyclodextrin with 2 mol of $Cu(OH)_2$ consumes 2 mol of the hydroxide ion, whereas 3 mol of the hydroxide ion are consumed for the reaction of β-cyclodextrin. Polarimetric measurements showed that the optical rotation of cyclodextrin changes from dextrorotatory to levorotatory upon the formation of the Cu(II)–cyclodextrin complex. It was suggested, with a molecular model, that the two pairs of C_2 and C_3' secondary hydroxyl groups of contiguous glucose units are cross-linked by the $Cu(OH^-)_2Cu$ ion bridge in the α-cyclodextrin complex and by $Cu(OH^-)(O^{2-})Cu$ ion bridge in the β-cyclodextrin complex. Furthermore, the circular ring of cyclodextrin may be distorted to the ellipsoidal form by the complex formation, causing a pronounced change in the optical rotation.

Cyclodextrins are cyclic oligomers composed of six or more α-D-glucopyranose units linked 1→4 as in amylose. The molecular shape of cyclodextrin is schematically depicted as a torus.[1] One side of the torus is hemmed round by the C_2 and C_3 secondary hydroxyl groups of the glucopyranoses. Even the smallest one of the cyclodextrins, α-cyclodextrin, has 12 hydroxyl groups arranged side by side around one edge of the torus. The analogy with the structure of porphyrin, which has four amino groups in the vicinity of one another in a molecule, suggests the possibility that cyclodextrins are good ligands for metallic cations. Although the hydroxyl group has a poor ability for coordinating to metallic cations, some diol compounds can form complexes with copper(II).[2] Therefore, copper(II) was selected for the study of the formation of cyclodextrin complexes with metallic cations. Some preliminary results have previously been reported.[3]

Experimental

Materials. The α-, β-, and γ-cyclodextrins were prepared by the method of Lane and Pirt.[4] They were separated and purified according to the directions of Cramer and Henglein.[5] The $CuSO_4 \cdot 5H_2O$ was purified by recrystallization from water. The EDTA, murexide (ammonium purpurate), methyl α-D-glucopyranoside, and potassium chloride, all of a reagent grade, were used without further purification.

Methods and Procedures. The solubilization of $Cu(OH)_2$ in an alkaline solution containing cyclodextrin: Two aqueous solutions, 0.2 to 2.0 M NaOH and 0.02 M $CuSO_4$, of an equal volume were mixed. The precipitate of $Cu(OH)_2$ was formed immediately. The supernatant was virtually colorless. Solid cyclodextrin was then added to the mixture. The mixture was stirred well and then allowed to stand at 25 °C for about 1 hr. The supernatant thus became blue. The concentration of the dissolved Cu(II) was titrimetrically determined by the use of EDTA and murexide, as a titrant and an indicator respectively, after the neutralization of the supernatant by aqueous HCl and the addition of a few drops of 30% NH_4OH.

Isolation of Cu(II)–Cyclodextrin Complexes: To 10 ml of 0.5 M NaOH containing 0.02 M cyclodextrin, we added 15 ml of 0.04 M $CuSO_4$. The Cu(II) thus precipitated was filtered off, and 25 ml of ethanol was added to the filtrate. A blue precipitate appeared; this was then filtered off, washed with aqueous ethanol, and air-dried at room temperature. The Cu(II) content in the isolated complex was titrimetrically determined with EDTA as has been described above. The Cu(I) content was spectrophotometrically determined by the use of ammonium molybdate(VI)[6] after the complex had been dissolved in water. The Cu(0) content was determined by subtracting the Cu(II) and Cu(I) contents from the total Cu content, which was titrimetrically determined with EDTA after the complex had been oxidized by heating in concentrated HNO_3. The cyclodextrin content was determined by the measurement of the optical rotation of an aqueous solution of the complex buffered at pH *ca.* 7, where the complex dissociates into Cu(II) and cyclodextrin. In this determination, the specific rotations of the α- and β-cyclodextrins were taken to be 150.5 and 162.5 ° respectively.[7]

The potentiometric titration was carried out by the use of a Toa Electronics pH meter, Model HM-5A, with an indicator electrode for a high alkaline solution, Model HG-4005, and a reference electrode, Model HC-205. To a 50-ml beaker, we added 25 ml of 0.02 M $CuSO_4$ in 2.5 M KCl containing 0.01 M cyclodextrin or 0.02 M methyl α-D-glucopyranoside. The solution was then stirred and degassed with N_2 for 30 min. An indicator electrode and a reference electrode were immersed in the solution, to which, then, 2.28 M KOH was added, drop by drop with a syringe, at room temperature.

The polarograms of the Cu(II)–cyclodextrin complexes were measured by means of a Yanagimoto polarograph, Model P-8. The saturated calomel electrode, used as a reference electrode, was connected with the cell solution by means of a KCl-agar bridge. The cell solution was degassed and thermostated at 25 °C. The dropping mercury electrode had the following characteristics in 1 M NaOH: $m=2.314$ mg/s, $t=3.53$ s.

The polarimetric measurements were carried out at room temperature with an automatic polarimeter of the Japan Spectroscopic Co., Model DIP-SL. A Hitachi spectrophotometer, Model 124, was used for the colorimetric determination of Cu(I).

Results and Discussion

Copper(II) hydroxide is practically insoluble in aqueous NaOH. However, upon the addition of cyclodextrins, the Cu(II) ion does dissolve to form a blue solution.[3] Figure 1 shows the plots of the concentrations of the dissolved Cu(II) *vs.* those of cyclodextrins added in alkaline solutions. Each plot was linear, with a slope of about 2.0. The solubilization of $Cu(OH)_2$ in an alkaline solution also took place on the addition of methyl α-D-glucopyranoside. However, the slope of the similar plot in this case was not 2.0, but 1.0.

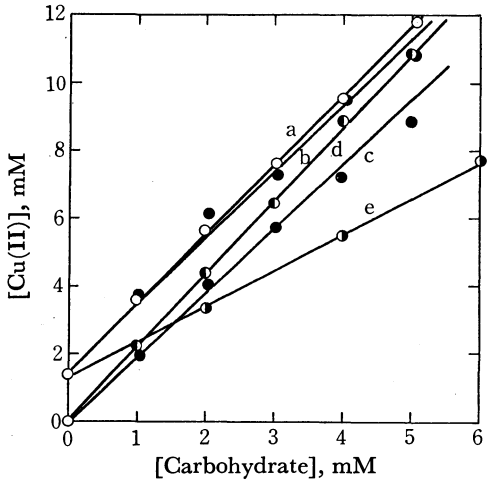

Fig. 1. Plots of the concentration of the dissolved Cu(II) *vs.* those of carbohydrates added.
a, α-cyclodextrin in 1.0 M NaOH; b, β-cyclodextrin in 1.0 M NaOH; c, β-cyclodextrin in 0.2 M NaOH; d, γ-cyclodextrin in 0.2 M NaOH; e, methyl α-D-glucopyranoside in 1.0 M NaOH.

The complexes of Cu(II) with α- and β-cyclodextrins were isolated as has been described in the Experimental section. The isolated complexes were not very stable. Thus, when the complexes were allowed to stand at room temperature for a week or were heated at 110 °C *in vacuo* for a few hours, the color of the complexes changed from blue to green. The contents of Cu(II), Cu(I), Cu(0), and cyclodextrin in the air-dried and heated samples were determined (Table 1). The results clearly show the formation of 2:1 complexes between Cu(II) and cyclodextrins. However, upon heating, the Cu(II) in the complexes is reduced in part to Cu(0). It is not yet obvious which of the substances–cyclodextrin and ethanol used as a precipitant–acts as a reductant.

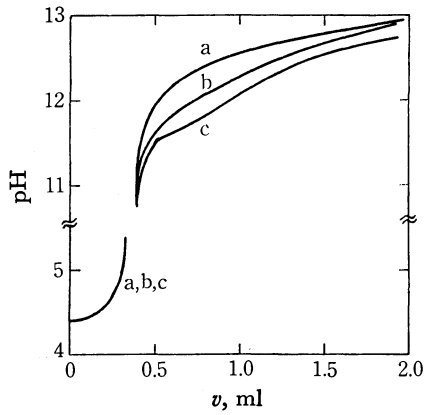

Fig. 2. Potentiometric titration of 0.02 M $CuSO_4$ in 2.5 M KCl with 2.28 M KOH in the absence (a) and in the presence of 0.01 M α- and β-cyclodextrins (b and c, respectively).

Potentiometric Titration. Cyclodextrins form complexes with Cu(II) only in an alkaline solution. In order to examine the role of the hydroxide ion, the potentiometric titration of $CuSO_4$ was carried out in the absence and in the presence of cyclodextrins, using aqueous KOH as a titrant. The ionic strength of the Cu(II) solution was kept at about 2.5 M with 2.5 M KCl. The reproducibility of the experiments was very good when an indicator electrode for high alkaline solutions was used (Fig. 2). In the absence of cyclodextrin, $Cu(OH)_2$ was precipitated by the addition of a drop of a KOH solution and did not dissolved even at a high alkaline pH. In the presence of α-cyclodextrin, on the other hand, the $Cu(OH)_2$ precipitated in the acidic pH region was re-dissolved at alkaline pH. A blue transparent solution was obtained at pH 12.4. Curves a and b in Fig. 2 are the potentiometric titration curves for $CuSO_4$ solutions in the absence and in the presence of α-cyclodextrin respectively. The pH value for the latter was always lower than that for the former at every volume of the titrant over the whole alkaline pH region. This fact suggests that the hydroxide ion is consumed in the formation of the Cu(II)–cyclodextrin complex. Curve c in Fig. 2 shows the potentiometric titration curve for a $CuSO_4$ solution containing β-cyclodextrin. The $Cu(OH)_2$ precipitated in the acidic pH region was re-dissolved at pH 12.2 to form a bluish transparent solution. The pH value at every volume of the titrant throughout the alkaline region was not only lower than that for a solution containing no

Table 1. The contents of coppers and cyclodextrins in the isolated complexes

		Content, mmol/l				mole ratio	
		Cu(0)	Cu(I)	Cu(II)	CD[a]	Cu(II)/CD	Cu[b]/CD
α-CD	air-dried	0.00	0.00	0.82	0.42	1.95	1.95
α-CD	heated to 110 °C	0.15	0.00	0.90	0.53	1.69	1.98
β-CD	air-dried	0.00	0.00	0.73	0.36	2.03	2.03
β-CD	heated to 110 °C	0.16	0.00	0.73	0.45	1.62	1.98

a) CD: Cyclodextrin. b) Cu=Cu(O)+Cu(I)+Cu(II).

cyclodextrin, but also lower than that for a solution containing α-cyclodextrin. On the other hand, the potentiometric titration curve for a $CuSO_4$ solution containing methyl α-D-glucopyranoside was virtually identical with that for a solution containing no carbohydrate. The $Cu(OH)_2$ precipitated in the acidic pH region did not completely dissolve until the pH value reached 13.1.

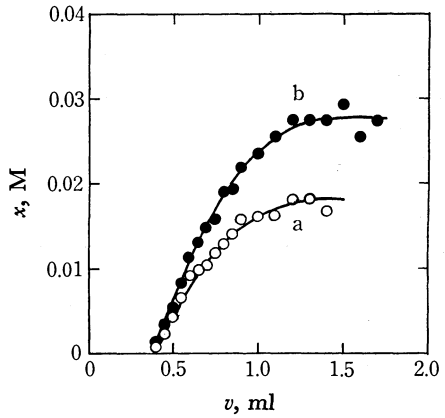

Fig. 3. Plots of the amount (x) of the hydroxide ion consumed for the formation of the complexes between 0.02 M $Cu(OH)_2$ and 0.01 M α- and β-cyclodextrins (a and b, respectively) *vs.* the volume (v) of 2.28 M KOH added.

Figure 3 shows the plots of the amount (x) of the hydroxide ion consumed for the complex formation *vs.* the volume (v) of the titrant. The x value was calculated from the difference of pH at each volume of the titrant on the assumption that the activity coefficient of the proton equals unity.[8] The x values for the reaction of 0.97 mmol of $Cu(OH)_2$ with cyclodextrin were 0.90 and 1.37 mmol for α- and β-cyclodextrins respectively. This fact suggests that, to form one mol of the Cu(II)–α-cyclodextrin and Cu(II)-β-cyclodextrin complexes, two and three mol respectively of the hydroxide ion are consumed. The reaction may be represented as follows:

$$2Cu(OH)_2 + AH_4 \rightleftarrows \underset{\mathbf{A}}{[Cu_2(AH_2^{2-})(OH^-)_2]} + 2H_2O$$

$$\mathbf{A} + OH^- \rightleftarrows \underset{\mathbf{B}}{[Cu_2(AH^{3-})(OH^-)_2]^-} + H_2O \qquad (1)$$

$$\mathbf{B} + OH^- \rightleftarrows \underset{\mathbf{C}}{[Cu_2(A^{4-})(OH^-)_2]^{2-}} + H_2O$$

$$\mathbf{C} + OH^- \rightleftarrows [Cu_2(A^{4-})(OH^-)(O^{2-})]^{3-} + H_2O$$

where AH_4 means cyclodextrin. Among these complexes, the $[Cu_2(A^{4-})(OH^-)_2]^{2-}$ complex may be the most stable one for α-cyclodextrin, whereas the $[Cu_2(A^{4-})(OH^-)(O^{2-})]^{3-}$ complex may be the most stable for β-cyclodextrin.

Conductometric Titration. The role of the hydroxide ion in the Cu(II)–cyclodextrin complex formation was also examined by means of conductometric titration. In Eq. (1), $Cu(OH)_2$ is practically insoluble and cyclodextrin is a neutral molecule, so that the contribution of these compounds to the specific conductance

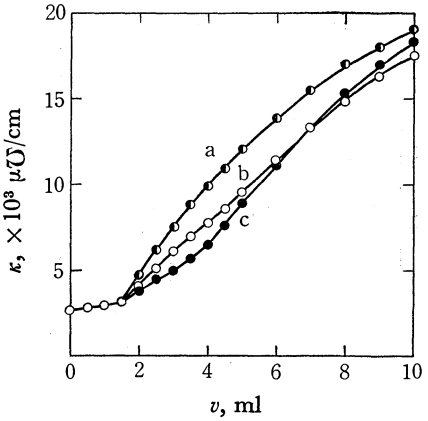

Fig. 4. Conductometric titration of 0.02 M $CuSO_4$ with 0.5 M NaOH in the absence (a) and in the presence of 0.01 M α- and β-cyclodextrins (b and c, respectively).

of a solution is negligible. Since there is no doubt that the ionic equivalent conductance of the hydroxide ion is much greater than that of the complex ion, the specific conductance of an alkaline solution would be appreciably decreased by the formation of a complex between $Cu(OH)_2$ and cyclodextrin.

When an aqueous solution of 0.5 M NaOH was added, drop by drop, to 25 ml of 0.02 M $CuSO_4$, the specific conductance (κ) of the solution changed, as is shown by Curve a of Fig. 4. No significant increase in κ was observed until *ca.* 2.0 ml of NaOH had been added. It was also observed that this process is accompanied by the precipitation of $Cu(OH)_2$ in the conductivity cell. Since the ionic equivalent conductance of Cu(II) and Na^+ (53.6 and 50.1 $cm^2℧$/equiv. respectively at 25 °C[9]) are approximately equal, a decrease in κ due to the consumption for the formation of insoluble $Cu(OH)_2$ may almost be compensated for by an increase in κ due to the addition of Na^+. The value of κ then increased with the continued addition of NaOH over 2.0 ml. A similar titration was carried out in the presence of 0.01 M α-cyclodextrin (Curve b of Fig. 4). After the addition of NaOH over 2.0 ml, the value of κ was somewhat less than that for the solution containing no cyclodextrin. This fact indicates that a part of the hydroxide ion is consumed for the formation of the Cu(II)–cyclodextrin complex. No clear inflection point was observed, although it could be said that an inflection point exists at v=*ca.* 4.0 ml. This may be due to the fact that the cyclodextrin is a weak acid and does not fully ionize even in the presence of Cu(II) until the pH of the solution becomes sufficiently high.

In order to estimate more accurately the amount of the hydroxide ion consumed, the difference ($\Delta\kappa$) in κ between the two solutions was plotted against the volume (v) of NaOH added. As is shown in Fig. 5, the value of $\Delta\kappa$ increased rapidly after the value of v exceeded 1.5 ml. Then, it reached its maximum. After that, $\Delta\kappa$ decreased almost linearly with an increase in v. The decrease in $\Delta\kappa$ may be due to an increase in the volume of the cell solution, to an increase in the ionic strength, and/or to the consumption of the hydroxide ion to form $Cu(OH)_4^{2-}$ in a strong alkaline solution

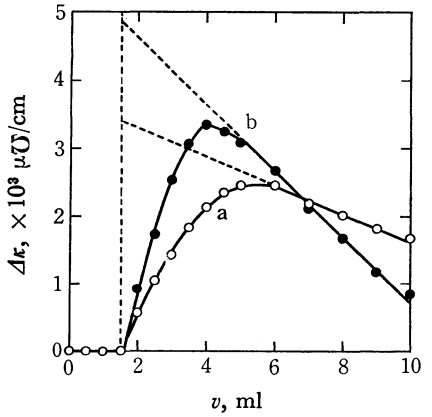

Fig. 5. Plots of $\Delta\kappa$ *vs.* the volume of 0.5 M NaOH added.
a, 0.01 M α-cyclodextrin; b, 0.01 M β-cyclodextrin.

containing no cyclodextrin. To exclude these effects on $\Delta\kappa$, the linear portion of the $\Delta\kappa$ *vs.* v plot was extrapolated to $v=1.5$ ml, where the solubilization of $Cu(OH)_2$ began to occur in the presence of cyclodextrin. The value of $\Delta\kappa$ thus obtained ($\Delta\kappa_0$) was 3.40×10^3 μ℧/cm. Similar results were obtained with regard to the formation of the complex between Cu(II) and β-cyclodextrin (Curve c's of Figs. 4 and 5). The $\Delta\kappa_0$ value was 4.85×10^3 μ℧/cm in this case.

If the ionic equivalent conductance of the complex ion (λ_a) is known, the amount (x) of the hydroxide ion consumed for the complex formation can be estimated by means of the following equation:

$$x = \Delta\kappa_0/(\lambda_b-\lambda_a) \qquad (2)$$

where λ_b is the ionic equivalent conductance of the hydroxide ion (198.3 cm^2℧/equiv. at 25 °C[9]). This was done by means of polarography. Figure 6 shows the

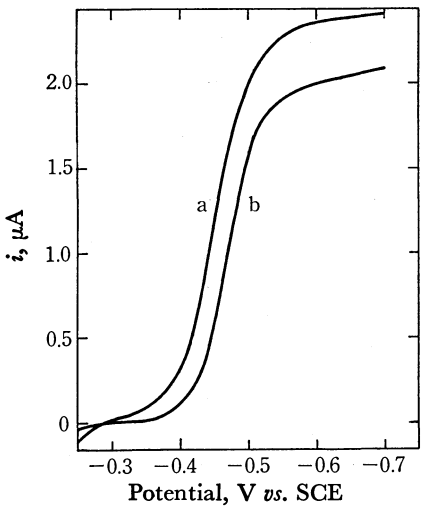

Fig. 6. Polarograms of the Cu(II) complexes with α- and β-cyclodextrins (a and b, respectively) in 1 M NaOH.
[Cu(II)], 0.466 mM; [Cyclodextrin], 20.0 mM

polarograms of the Cu(II)-cyclodextrin complexes in 1 M NaOH. The limiting current for each wave was proportional to the square root of the effective pressure on the mercury drop; this fact indicates that each wave is diffusion-controlled. The diffusion constants of the Cu(II)-α- and β-cyclodextrin complexes were evaluated to be 3.13×10^{-6} and 2.32×10^{-6} cm^2/s respectively on the basis of the Ilkovic equation.[10] The diffusion constant (D) is related to the ionic equivalent conductivity (λ) by the Nernst equation:[11]

$$D = \lambda RT/ZF^2 \qquad (3)$$

where R is the gas constant; T, the temperature; Z, the ionic valence, and F, the Coulomb constant. To calculate the value of λ_a, the value of Z was assumed to be 2 for the α-cyclodextrin complex and 3 for the β-cyclodextrin complex on the basis of Eq. (1). The λ_a values thus obtained were 23.4 and 26.0 cm^2℧/equiv. for the α- and β-cyclodextrin complexes respectively. Accordingly, the x values were determined to be 0.019 and 0.028 M for the α- and β-cyclodextrin complexes respectively; that is, about 2 mol of the hydroxide ion was consumed for the reaction of one mole of α-cyclodextrin with 2 mol of $Cu(OH)_2$, whereas 3 mol of the hydroxide ion were consumed for the same reaction of β-cyclodextrin. These results agree with those of the potentiometric titration.

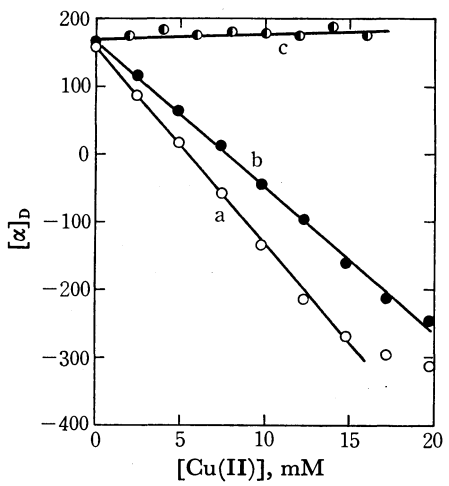

Fig. 7. Plots of the specific rotations of α- and β-cyclodextrins (a and b, respectively) and methyl α-D-glucopyranoside (c) *vs.* the concentration of Cu(II) in 1 M NaOH.

Optical Rotation of Cu(II)–Cyclodextrin Complexes. The specific rotation of cyclodextrin was drastically changed by the formation of the Cu(II) complex. Cyclodextrins themselves are dextrorotatory. The specific rotations of α- and β-cyclodextrins in 1 M NaOH are virtually the same as those in distilled water. However, upon the addition of Cu(II) in an alkaline solution of each cyclodextrin, the specific rotation ($[\alpha]_D$) of the cyclodextrin became levorotatory. Figure 7 shows the plots of $[\alpha]_D$ *vs.* the concentration of Cu(II) added to a solution of 10.3 mM cyclodextrin in 1 M NaOH. The $[\alpha]_D$ value for each cyclodextrin decreased linearly with an increase in the concentration of Cu(II). The slope of the plot for α-cyclodextrin is larger than that for β-cyclodextrin. On the other hand, the specific rotation of methyl α-D-glucopyranoside in an alkaline solution showed virtually no change upon the addition of Cu(II) to form the complex between Cu(II) and

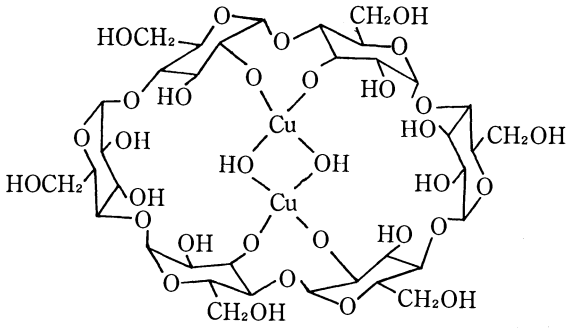

Fig. 8. The suggested structure of the Cu(II)–α-cyclodextrin complex.

methyl α-D-glucopyranoside. These results indicate that the conformation of cyclodextrin remarkably changes upon the formation of the Cu(II) complex and that the conformation change occurs in the whole cyclodextrin ring rather than in the glucopyranose-unit ring alone.

The structure of the complexes was studied with framework molecular models. It was presumed that two Cu(II) ions are bond by two hydroxide ions in the complex of $Cu_2(A^{4-})(OH^-)_2^{2-}$ for α-cyclodextrin.[3] The models showed that the secondary hydroxyl groups in α-cyclodextrin coordinate to the $Cu(OH^-)_2Cu$ residue, as is shown in Fig. 8; that is the C_2 and C_3' hydroxyl groups of contiguous glucopyranose units coordinate to the Cu(II) ions. It was impossible for the $Cu(OH^-)_2Cu$ residue to be bound to another combination of the hydroxyl groups, such as two pairs of the hydroxyl groups at C_2 and C_3, in the same glucopyranose unit. Furthermore, it was revealed that the distance between the two pairs of the C_2 and C_3' hydroxyl groups (*ca.* 10 Å) was considerably longer than that of the $Cu(OH^-)_2Cu$ ion bridge (*ca.* 6 Å). Accordingly, if the $Cu(OH^-)_2Cu$ residue was connected to the secondary hydroxyl groups of the cyclodextrin, the overall ring was significantly distorted from circular to ellipsoidal, as is depicted in Fig. 8. This fact may be related to the great change in the optical rotation of the cyclodextrin with the formation of the Cu(II) complex.

In the Cu(II)-β-cyclodextrin complex, the degree of the distortion of the overall ring may be somewhat smaller than that in the Cu(II)–α-cyclodextrin complex, for β-cyclodextrin is larger and more flexible than the α-cyclodextrin ring. This may be the reason why the

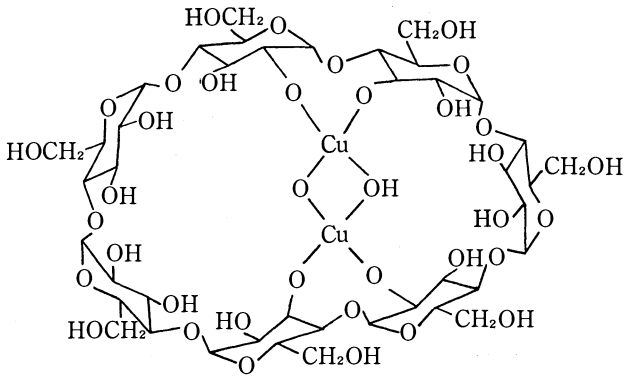

Fig. 9. The suggested structure of the Cu(II)–β-cyclodextrin complex.

slope of $[\alpha]_D$ *vs.* the concentration of Cu(II) for β-cyclodextrin is smaller than that for α-cyclodextrin (Fig. 7). The structure of the Cu(II)–β-cyclodextrin complex was presumed to be as is depicted in Fig. 9.

The spectrophotometrical and the detailed polarographical behavior of the Cu(II)–cyclodextrin complexes will be reported in subsequent articles.

The authors wish to thank Professor Kunio Okamoto, Kyoto University, for the use of a polarimeter.

References

1) For recent reviews, see D. W. Griffiths and M. L. Bender, *Advan. Catal.*, **23**, 209 (1973); T. Kuge and K. Takeo, *Denpun Kagaku*, **21**, 151 (1974).
2) R. E. Reeves and P. Bragg, *J. Amer. Chem. Soc.*, **84**, 2491 (1962).
3) Y. Matsui, T. Kurita, and Y. Date, This Bulletin, **45**, 3299 (1972).
4) A. G. Lane and S. J. Pirt, *J. Appl. Chem. Biotechnol.*, **21**, 330 (1971).
5) F. Cramer and F. M. Henglein, *Chem. Ber.*, **91**, 308 (1958).
6) N. Nelson, *J. Biol. Chem.*, **153**, 375 (1944).
7) D. French, *Advan. Carbohyd. Chem.*, **12**, 189 (1957).
8) The activity coefficient of HCl was reported to be 1.147 at the molality of 2.5 (Ref. 9, p. 491); this value indicates that the assumption is approximately valid.
9) R. A. Robinson and R. H. Stokes, "Electrolyte Solutions," Butterworth, London (1965), p. 463.
10) D. Ilkovic, *Collect. Czech. Chem. Commun.*, **6**, 498 (1934).
11) W. Nernst, *Z. Physik. Chem. (Leipzig)*, **2**, 613 (1888).

X-Ray Study of the Compound Obtained by the Reaction of N^{δ}-Salicylidene-L-ornithine and Palladium(II) acetate. The Crystal Structure of (N^{α}-Salicylidene-D-ornithinato) (N^{α}-Salicylidene-L-ornithinato)dipalladium(II)-Dimethyl Sulfoxide

Yoshitane KOJIMA, Masanori MATSUI,* and Keiji MATSUMOTO

Department of Chemistry, Faculty of Science, Osaka City University, Sumiyoshi-ku, Osaka 558
**Kanazawa Medical University, Uchinada-machi, Kahoku-gun, Ishikawa-ken 920-02*

(Received January 30, 1975)

X-Ray structure analysis has elucidated that the reaction of N^{δ}-salicylidene-L-ornithine and palladium(II) acetate in DMF results in the amine exchange and racemization of the ligand, yielding (N^{α}-salicylidene-D-ornithinato)(N^{α}-salicylidene-L-ornithinato)dipalladium(II). The yellow crystals are monoclinic, $a=15.15(2)$, $b=9.80(1)$, $c=15.67(2)$ Å, $\beta=111.3(1)°$, space group $P2_1/c$, and $Z=2$. The structure was solved by the Patterson and Fourier techniques and was refined by the least-squares method to $R=0.105$. The complex molecule has a center of symmetry by which D- and L-Schiff-base ligands are interrelated. Each Pd atom has a square-planar coordination by means of two O and N^{α} atoms of one ligand, and the N^{δ} atom of the other one, the two N atoms being in the *trans* position. The $H_2N^{\delta}-(CH_2)_3-\underset{|}{C}H-N^{\alpha}$ fragments of the two ligands bridge the two Pd atoms, giving a 14-membered ring.

The stereoselectivity of metal complex[1] is an important subject in the coordination chemistry. We planned to study the stereochemical behavior of the dissymmetric complexes of labile metal ions for some amino acids and attempted to prepare the optically active Ni(II), Cu(II), and Pd(II) complexes involving the quadridentate Schiff-base ligand N^{δ}-salicylidene-ornithine. However, none of the products obtained from the reactions of the acetates of these metal ions with the L-enantiomer of the ligand in DMF showed any optical activity. Since the Pd(II) complex was isolated as good crystals, an X-ray crystal structure analysis was undertaken in order to discover why the optical activity due to the dissymmetric ligand disappears during the reaction.

Experimental

Preparation. N^{δ}-Salicylidene-L-ornithine (sal-L-orn) was prepared following the procedure of Witkop *et al.*[2] The yellow crystals decompose at 201—202 °C; the temperature agrees well with the temperature reported by them. A suspension of equimolar amounts of sal-L-orn and palladium(II) acetate in DMF was stirred for several hours until they had been completely dissolved. Brownish yellow crystals were then precipitated by the addition of twice as many moles of dipyridyl as the sal-L-orn and subsequently recrystallized from hot DMSO. Since the compounds are efflorescent, the elemental analyses could not be carried out. The exact composition of the compound was determined by means of X-ray structure analysis, as will be described below.

X-Ray Measurement. Since the compound decomposes rapidly in air, the crystals were sealed in thin-walled Lindemann glass capillaries. Two well-formed specimens with the approximate dimensions of $0.12\times0.27\times0.23$ and $0.12\times0.25\times0.43$ mm were used for the intensity measurements, one mounted about the b axis and the other, about the c axis. The unit-cell dimensions were determined by a least-squares refinement of 45 independent measurements of the 2θ values from Weissenberg photographs calibrated by silicon powder ($a=5.4307$ Å). Crystal data: $Pd_2(C_{12}H_{14}N_2O_3)_2(C_2H_6SO)_4$, mol wt 993.7. Monoclinic, $a=15.15(2)$ Å, $b=9.80(1)$ Å, $c=15.67(2)$ Å, $\beta=111.3(1)°$, space group $P2_1/c$, $Z=2$ ($D_x=1.51$, $D_m=1.52$ g cm^{-3}), $F(000)=1008$, $V=2169$ Å^3, $\mu=90.7$ cm^{-1} (for Cu$K\alpha$).

Multiple film, equi-inclination Weissenberg photographs for the $h0l$-$h6l$ and $hk0$-$hk10$ layers were taken with Cu$K\alpha$ radiation ($\lambda=1.5418$ Å). The intensities were estimated visually by the use of a calibrated intensity scale. After corrections for the usual Lp-factor and the spot shape, the structure amplitudes were placed on a common arbitrary scale by internal correlation. A total of 3641 independent reflections were collected. However, 622 of these were too weak to be observed, and so they were assumed to be zero. No correction for absorption was made.

Structure Determination

In the beginning of the structure analysis we knew only that the crystal contains the palladium atoms, the salicylidene-ornithine ligand, and probably DMSO molecules. A trial calculation of the density indicated that there may be four Pd atoms in a unit cell. The initial coordinates for the Pd atom were determined from a three-dimensional Patterson map. Two sulfur and eight light atoms were located on a Fourier map phased by the heavy atom. The positions of all the remaining non-hydrogen atoms were found by successive Fourier syntheses. At this point it was revealed that the complex corresponded to dimeric(N^{α}-salicylidene-D-ornithinato) (N^{α}-salicylidene-L-ornithinato)-dipalladium(II)·4DMSO; the optically active N^{δ}-salicylidene-L-ornithine used initially seems to be isomerized to the N^{α} analogue and to be racemized during the reaction with palladium(II) acetate. Several cycles of block-diagonal least-squares refinement gave an R factor of 0.142, isotropic temperature factors being used for all the atoms. Five more cycles of the refinement with anisotropic temperature factors converged to $R=0.105$ for 3119 non-zero reflections. The weighting scheme employed was:

TABLE 1. FRACTIONAL POSITIONAL PARAMETERS ($\times 10^4$) AND ANISOTROPIC TEMPERATURE FACTORS ($\times 10^4$) WITH e. s. d. 's IN PARENTHESES

Temperature factors are of the form: $\exp[-(h^2B_{11}+k^2B_{22}+l^2B_{33}+hkB_{12}+hlB_{13}+klB_{23})]$.

Atom	x	y	z	B_{11}	B_{22}	B_{33}	B_{12}	B_{13}	B_{23}
Pd	460(1)	1856(1)	3996(1)	61(0)	72(1)	44(0)	−2(1)	45(1)	0(1)
C(1)	2343(10)	1120(12)	4060(9)	74(8)	99(13)	63(7)	15(17)	61(13)	14(16)
C(2)	3308(10)	1301(16)	4399(11)	69(9)	146(17)	76(9)	13(20)	52(15)	10(21)
C(3)	3900(12)	666(18)	3989(13)	78(10)	178(23)	105(12)	3(25)	73(19)	−12(28)
C(4)	3485(14)	−260(19)	3252(14)	123(15)	169(23)	122(15)	74(30)	129(25)	21(30)
C(5)	2524(11)	−493(15)	2913(12)	78(9)	125(17)	110(12)	22(21)	101(18)	6(24)
C(6)	1926(9)	185(11)	3310(9)	71(8)	88(12)	62(7)	10(15)	77(12)	12(15)
C(7)	952(9)	−150(12)	2871(8)	80(8)	89(12)	51(6)	25(16)	68(12)	25(14)
C(8)	−718(8)	52(12)	2603(8)	61(7)	100(13)	47(6)	−12(15)	31(11)	21(15)
C(9)	−1358(10)	1065(13)	2862(10)	74(8)	104(14)	63(8)	−1(18)	34(13)	2(17)
C(10)	−900(9)	−1417(11)	2863(8)	77(8)	87(11)	41(6)	−41(15)	38(11)	−19(13)
C(11)	−660(10)	−1602(11)	3883(8)	85(8)	70(11)	49(6)	−17(15)	53(12)	−12(13)
C(12)	992(10)	2994(12)	2906(8)	91(9)	97(13)	44(6)	−54(18)	59(12)	−18(15)
C(13)	7067(14)	4784(26)	5165(16)	99(14)	303(40)	137(18)	144(39)	76(26)	−73(44)
C(14)	7420(15)	2207(19)	4717(18)	111(15)	139(22)	171(21)	−66(29)	69(29)	5(34)
C(15)	3662(17)	1328(33)	7075(19)	99(16)	434(60)	149(22)	61(51)	2(30)	−149(63)
C(16)	4521(20)	−940(27)	8117(24)	161(25)	220(39)	234(34)	−46(49)	50(46)	84(60)
N(1)	292(7)	432(9)	3081(6)	73(6)	74(9)	44(5)	−8(12)	49(9)	17(11)
N(2)	492(6)	3332(8)	4928(6)	60(5)	63(9)	40(4)	−10(11)	42(8)	−6(10)
O(1)	1855(6)	1787(9)	4470(6)	61(5)	127(10)	57(5)	−16(12)	44(8)	−32(12)
O(2)	−942(6)	1960(8)	3479(6)	64(5)	84(8)	64(5)	7(11)	50(8)	−8(11)
O(3)	−2204(7)	980(11)	2491(8)	60(6)	162(14)	97(8)	0(14)	30(10)	−24(17)
O(4)	8746(7)	4012(9)	5272(7)	73(6)	109(10)	93(7)	−2(12)	82(11)	−15(14)
O(5)	5247(10)	1520(17)	8401(15)	78(9)	246(25)	228(19)	35(23)	20(20)	27(35)
S(1)	7716(3)	3882(4)	4626(3)	89(3)	141(5)	68(2)	−14(6)	52(4)	13(5)
S(2)	4308(4)	840(6)	8203(4)	85(3)	209(8)	130(4)	2(8)	56(6)	20(9)

$w = 0.2$ for $F_o < 7.2$

$w = 1.0$ for $7.2 \leqq F_o \leqq 43.0$

$w = (43.0/F_o)^2$ for $F_o > 43.0$

The scattering factors for the zerovalent Pd, S, N, C, and O atoms were taken from "International Tables for X-ray Crystallography." In the final cycle, the shifts in the atomic parameters were less than their standard deviations. A difference Fourier synthesis computed at this stage did not show the peaks corresponding to any of the hydrogen atoms. The final atomic parameters and their estimated standard deviations are listed in Table 1. A table of the observed and calculated structure factors is preserved by the Chemical Society of Japan (Document No. 7516).

Results and Discussion

A perspective view of the complex, which shows the coordination geometry and the numbering of the atoms, is given in Fig. 1. The complex assumes a dimeric structure. The two halves of this dimer are related by a crystallographic center of symmetry: thus, the molecule is of an inactive *meso* form, with two enantiomeric Schiff-base ligands. The H_2N^{δ}–$(CH_2)_3$–CH–N^{α} fragments of the two ligands bridge the two Pd atoms, giving the 14-membered ring, as is shown in Fig. 2. The two Pd atoms are separated by 5.31 Å. Each Pd atom has a square-planar coordination and is bonded to the phenolic oxygen, O(1); the carboxylate oxygen, O(2); and the imino nitrogen, N(1), of one salicylidene-

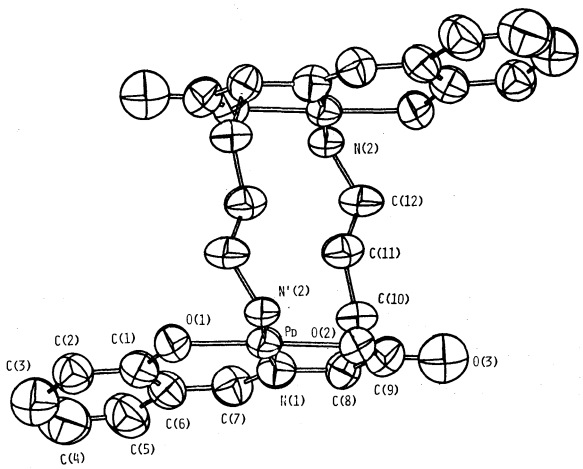

Fig. 1. Perspective view of (N^{α}-sal-D-orn) (N^{α}-sal-L-orn) dipalladium (II). The thermal ellipsoids are drawn at the 48% probability level.

ornithine ligand, and to the terminal amino nitrogen N(2) of the enantiomeric one. One of the hydrogen atoms attached to C(11) lies close to the Pd atom, as is shown in Fig. 2. (The coordinates of the H atoms were calculated by assuming the C–H distance to be 1.08 Å.) The Pd···H distance (2.93 Å) seems to be slightly shorter than the sum of the van der Waals radii (3.1 Å);[3] this suggests that there is a weak interaction between the Pd and H atoms, giving a distorted square-pyramidal coordination of the Pd atom. It is,

TABLE 2. DEVIATIONS OF THE ATOMS FROM LEAST-SQUARES PLANES (d/Å) AND DIHEDRAL ANGLES BETWEEN THEM

(A) Plane through N(1), N'(2), O(1), and O(2) (plane A)					
Pd	−0.01	N(1)	−0.03	N(2)	−0.03
O(1)	0.03	O(2)	0.03		
(B) Plane through Pd, C(8), C(9), N(1), and O(2) (plane B)					
Pd	−0.04	C(8)	−0.05	C(9)	0.01
N(1)	0.06	O(2)	0.03	O(3)	0.03
(C) Plane through Pd, C(1), C(6), C(7), N(1), and O(1) (plane C)					
Pd	0.06	C(1)	0.03	C(6)	0.04
C(7)	−0.02	N(1)	−0.03	O(1)	−0.08
(D) Plane through C(1), C(2), C(3), C(4), C(5), and C(6) (plane D)					
C(1)	0.01	C(2)	−0.02	C(3)	0.02
C(4)	−0.00	C(5)	−0.00	C(6)	−0.00

Dihedral angles between the planes (φ/°)

A and B	3.9	A and C	5.6	A and D	10.7
B and C	7.4	B and D	12.3	C and D	5.2

Equations of planes

(A) $0.289X + 0.698Y - 0.655Z + 3.005 = 0$
(B) $0.288X + 0.650Y - 0.703Z + 3.329 = 0$
(C) $0.197X + 0.728Y - 0.657Z + 2.878 = 0$
(D) $0.114X + 0.758Y - 0.642Z + 2.847 = 0$

where X, Y, and Z are coordinates in Å units relative to a, b, and c^* axes, respectively.

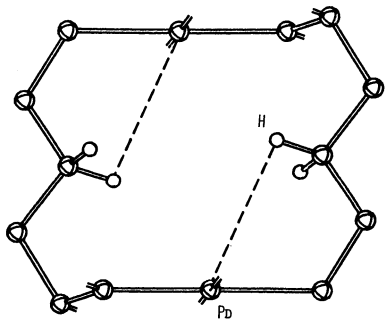

Fig. 2. Fourteen-membered ring formed from H_2N^{δ}-$(CH_2)_3$-CH-N^{α} fragments of the two ligands and two Pd atoms. Calculated positions of some H atoms are given in the Figure in order to show the short Pd···H contacts.

however, possible judging from the molecular models that the hydrogen atom merely sterically occupies the apical coordination position.

The least-squares planes of various parts of the complex and the dihedral angles between them are listed in Table 2. The Pd atom lies on the best least-squares plane (Plane A) defined by the four ligator atoms (Fig. 3). The salicylidene moiety is bent away from Plane A in the opposite direction of another salicylidene-glycinato Pd moiety, while the glycinato residue is bent in its direction.

The bond distances and angles are summarized in Table 3. The Pd–N(2) distance (2.04 Å) is in good agreement with the value found for that in bisethylenediamine palladium(II) (2.04 Å).[4] The Pd–O(2) and Pd–O(1) distances (1.98 and 1.97 Å) are approximately in agreement with the values found for those (2.02 and 1.99 Å) in bis(L-prolinato)palladium(II)[5] and bis(N-isopropyl-3-methylsalicylaldiminato)palladium(II)[6] respectively. The Pd–N(1) distance (1.95 Å) is shorter than those of 2.02 and 2.03 Å in bis(N-isopropyl-3-methylsalicylaldiminato)palladium(II).[6] The other bond distances and angles in the salicylidene-glycinato moiety are similar to those found in (N-salicylidene-glycinato)copper(II).[7]

The stereoview along the b axis and the numbering of the atoms of DMSO molecules are shown in Fig. 4. The crystal is composed of the dimeric Pd(II) complexes and the DMSO molecules. All the intermolecular atomic contacts are of the van der Waals type except for the N(2)–H···O(4) hydrogen bond (2.90 Å), which is shown by a dotted line in Fig. 4. The DMSO molecules are normal in their dimensions,[8] but the relatively large thermal motion suggests that there is some disorder in the molecular arrangement.

In the synthesis of the complex, we used only N^{δ}-salicylidene-L-ornithine as the ligand. Nevertheless, the product contained both the enantiomeric N^{α}-salicylidene-L- and -D-ornithinate anions. This means that, in the ligand, the amine-exchange reaction

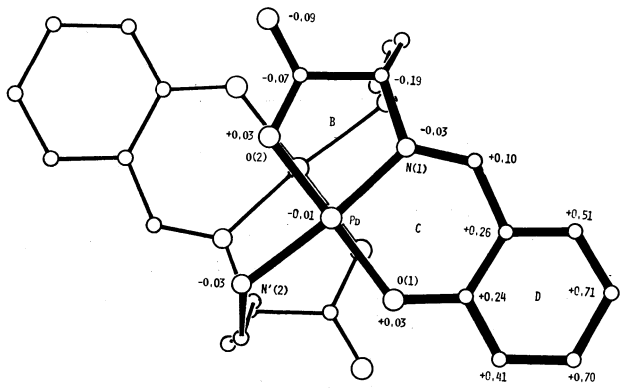

Fig. 3. Projection of (N^{α}-sal-D-orn) (N^{α}-sal-L-orn)-dipalladium(II) on the plane through N(1), N'(2), O(1), and O(2) and deviations (Å) of the atoms from the plane.

TABLE 3. BOND DISTANCES (d/Å) AND BOND ANGLES (φ/°)
E. s. d. 's are in parentheses

Pd–N(1)	1.95(1)	Pd–N(2)	2.04(1)	Pd–O(1)	1.97(1)
Pd–O(2)	1.98(1)	O(1)–C(1)	1.32(2)	C(1)–C(2)	1.38(2)
C(2)–C(3)	1.42(3)	C(3)–C(4)	1.42(3)	C(4)–C(5)	1.38(3)
C(5)–C(6)	1.44(2)	C(1)–C(6)	1.44(2)	C(6)–C(7)	1.42(2)
C(7)–N(1)	1.29(2)	N(1)–C(8)	1.49(2)	C(8)–C(9)	1.54(2)
C(9)–O(2)	1.29(2)	C(9)–O(3)	1.20(2)	C(8)–C(10)	1.55(2)
C(10)–C(11)	1.52(2)	C(11)–C(12)	1.53(2)	C(12)–N(2)	1.48(2)
O(1)–Pd–N(1)	95.0(4)	N(1)–Pd–O(2)	84.4(4)		
O(2)–Pd–N′(2)	90.0(3)	O(1)–Pd–N′(2)	90.6(3)		
Pd–O(1)–C(1)	123.3(9)	O(1)–C(1)–C(2)	117.1(13)		
O(1)–C(1)–C(6)	123.7(13)	C(2)–C(1)–C(6)	119.2(14)		
C(1)–C(2)–C(3)	121.7(16)	C(2)–C(3)–C(4)	118.7(18)		
C(3)–C(4)–C(5)	120.9(20)	C(4)–C(5)–C(6)	120.1(17)		
C(5)–C(6)–C(1)	119.3(13)	C(1)–C(6)–C(7)	127.7(13)		
C(5)–C(6)–C(7)	113.0(13)	C(6)–C(7)–N(1)	122.5(11)		
C(7)–N(1)–C(8)	120.7(11)	C(7)–N(1)–Pd	126.6(10)		
Pd–N(1)–C(8)	112.7(8)	N(1)–C(8)–C(9)	109.6(11)		
N(1)–C(8)–C(10)	110.5(10)	C(9)–C(8)–C(10)	109.9(11)		
C(8)–C(9)–O(2)	117.0(12)	C(8)–C(9)–O(3)	119.3(14)		
O(2)–C(9)–O(3)	123.7(14)	C(9)–O(2)–Pd	115.5(9)		
Pd–N′(2)–C′(12)	116.9(10)	C(8)–C(10)–C(11)	113.1(11)		
C(10)–C(11)–C(12)	111.3(11)	C(11)–C(12)–N(2)	109.8(11)		
S(1)–O(4)	1.53(1)	S(1)–C(13)	1.75(3)	S(1)–C(14)	1.72(3)
S(2)–O(5)	1.50(3)	S(2)–C(15)	1.75(3)	S(2)–C(16)	1.79(4)
O(4)–S(1)–C(13)	104.9(10)	O(4)–S(1)–C(14)	105.0(11)		
C(13)–S(1)–C(14)	103.5(13)	O(5)–S(2)–C(15)	103.3(15)		
O(5)–S(2)–C(16)	105.4(16)	C(15)–S(2)–C(16)	103.9(16)		

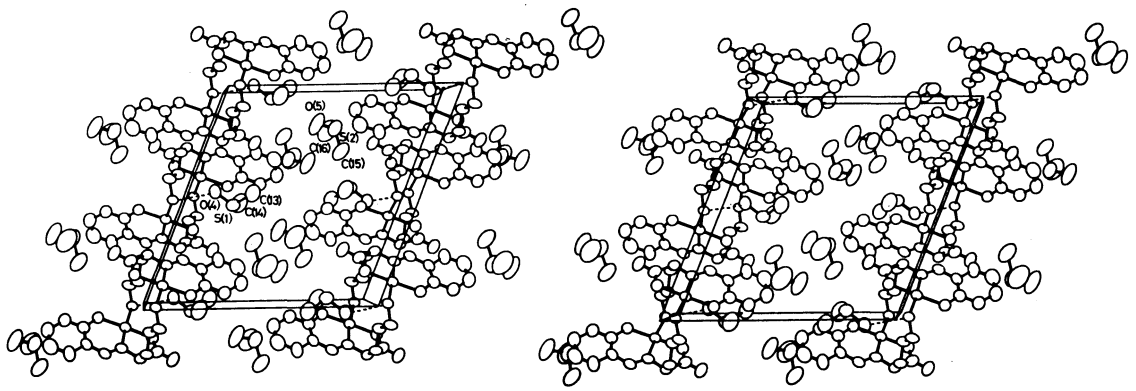

Fig. 4. Stereoscopic view of (N^{α}-sal-D-orn)(N^{α}-sal-L-orn)dipalladium(II)·4DMSO, looking down along the b axis. Dotted lines show the N(2)–H···O(4) hydrogen bonds.

proceeds thus:

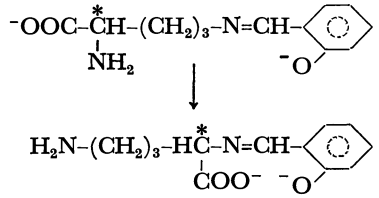

Furthermore, the recemization reaction apparently takes place during the reaction of N^{δ}-salicylidene-L-ornithine and palladium(II) acetate in DMF and the subsequent recrystallization from DMSO.

So far several studies have been made of the mechanisms of amine-exchange and racemization reactions in the metal chelates of some Schiff bases. Verter and his co-workers proposed the mechanism of amine-exchange reaction in bis[N-(phenyl derivatives)-salicylaldimine]copper(II) [9] whereas Weinstein *et al.* presented that of the racemization reaction in (N-pyridoxylidene-L-valinato)copper(II).[10] The former may be applicable to the present complex, though whether the reaction occurs by means of an intra- or an intermolecular mechanism is unknown. The latter is different in situation from the present case.

Most of the calculations were made by using a local version of the UNICS programs.[11] The authors wish to express their thanks to Dr. Ken Hirotsu and Dr.

Fusao Takusagawa, who adapted these programs to a FACOM 270-30 computer at Osaka City University. Figure 4 was drawn by using the TECS program written by Dr. Takusagawa.

References

1) For instance, R. Nakon, P. R. Rechani, and R. J. Angelici, *Inorg. Chem.*, **12**, 2431 (1973). J. H. Dunlop and R. D. Gillard, "Advances in Inorganic Chemistry and Radiochemistry" Vol. 9, edited by H. J. Emeleus and A. G. Sarpe, Academic Press, New York and London (1966), p. 185.

2) B. Witkop and T. W. Beiler, *J. Amer. Chem. Soc.*, **76**, 5589 (1954).

3) D. M. Roe, P. M. Bailey, K. Moseley, and P. M. Maitlis, *Chem. Comm.*, **1972**, 1273.

4) J. R. Wiesner and E. C. Lingafelter, *Inorg. Chem.*, **5**, 1770 (1966).

5) T. Ito, *Acta Crystallogr.*, **B27**, 1062 (1971).

6) P. C. Jain and E. C. Lingafelter, *ibid.*, **23**, 127 (1967).

7) T. Ueki, T. Ashida, Y. Sasada, and M. Kakudo, *ibid.*, **B25**, 328 (1969).

8) R. Thomas, C. B. Shoemaker, and K. Eriks, *ibid.*, **21**, 12 (1966). M. A. Viswamitra and K. K. Kannan, *Nature*, **209** 1016 (1966).

9) H. S. Verter and A. E. Frost, *J. Amer. Chem. Soc.*, **82**, 85 (1960).

10) G. N. Weinstein, M. J. O'Connor, and R. H. Holm, *Inorg. Chem.*, **9**, 2104 (1970).

11) T. Sakurai, Ed., The Universal Crystallographic Computation Program System (UNICS), The Crystallographic Society of Japan (1967).

Catalytic Activities of a Polyoxime-cobalt Complex for the Addition Reaction of an Alcohol to Acrylaldehyde and for the Polymerization of Styrene

Sung Jho KIM and Takeo TAKIZAWA

Faculty of Pharmaceutical Sciences, The University of Tokyo, Hongo, Bunkyo-ku, Tokyo 113

(Received March 14, 1974)

A new polymeric cobalt-chelate complex was prepared from cobalt acetate and a polyoxime consisting mainly of 1,2-bis(hydroxyimino)trimethylene units. The polymeric complex in the solid state at 77—300 K, both in air and under a vacuum, gives an ESR signal with a *g*-value of about 2 and can initiate the polymerization of styrene and catalyze the "Michael"-type addition reaction of an alcohol to acrylaldehyde, yielding exclusively *β*-alkoxypropionaldehyde, after being treated with phenylthiol and sodium borohydride. The catalytic activities depend greatly on the cobalt content and are much greater than those of its monomeric analogue in composition, bis(dimethylglyoximato)cobalt. The absorption spectrum of the polymeric complex treated with the reagents is similar to that of monomeric or polymeric analogues containing monovalent cobalt atoms.

The metal-chelate complexes of a new polyoxime have been investigated in terms of physical and chemical properties in comparison with those of the monomeric analogues corresponding in composition, the metal-chelate complexes of dimethylglyoxime. The polyoxime was derived from an alternating copolymer of ethylene and carbon monixide ($\left[-CH_2CH_2)_{1.2}\overline{C}-\right]_x$, $(C_{17}H_{24}O_5)_x$, $(308.4)_x$, molecular weight 4000): it is considered to consist mainly of 1 2-bis(hydroxyimino)trimethylene units ($\left[-(CH_2)_{1.6}\overline{(C}-\underset{HON}{\overset{\|}{C}})_{0.8}\overline{(C)}_{0.2}\right]_x$, $(C_{17}H_{24}N_8O_9)_x$, $(484.3)_x$). A reversible uptake of molecular oxygen by a polyoxime-cobalt complex(POX-Co) and catalytic activities of a polyoxime–copper complex have been reported.[1-3]

$$CO + C_2H_4 \longrightarrow -CH_2CH_2-\underset{O}{\overset{\|}{C}}- \longrightarrow$$

$$-CH_2-\underset{HON}{\overset{\|}{C}}-\underset{NOH}{\overset{\|}{C}}- \xrightarrow{Co(CH_3CO_2)_2\cdot 4H_2O} \text{POX-Co}$$

Here we will describe the catalytic activities of POX-Co in the polymerization of styrene and in the "Michael"-type addition reaction of an alcohol to acrylaldehyde, yielding exclusively *β*-alkoxypropionaldehyde. A di- or trivalent cobalt complex of dimethylglyoxime(cobaloxime (II) or (III)) can be converted into a monovalent cobaloxime(I) by treatment with reductants.[4] On the other hand, POX-Co does not show any change upon treatment with reductants alone. However, a combination of sodium borohydride and a polymeric complex prepared by the treatment of POX-Co with phenylthiol(POX-Co-S) or the resulting complex(POX-Co-R) shows catalytic activities.

Experimental

Materials. By adding 4.5, 2.5, 1.5, 1.2, or 0.8 g of bis(acetate) tetraaquocobalt ($Co(CH_3CO_2)_2 4H_2O$) into a solution of 3.0 g of the polyoxime in a mixture of dioxane and methanol (1:1 by volume, 5×10^{-3} g/ml) under nitrogen, a complex with a cobalt content of 19.12 (POX-Co-1), 14.84 (POX-Co-2), 10.38 (POX-Co-3), 7.83 (POX-Co-4), or 5.71% (w/w) (POX-Co-5) was prepared; these complexes correspond to the complexes with the composition ratios of Co*/OX= 1/4, 1/6, 1/8, 1/12, and 1/16 (where Co* and OX are the numbers of cobalt atoms and oxime groups in the complex). The catalysts employed were derived from POX-Co-1—5. As an example, the preparation of the catalyst derived from POX-Co-1 will be described. In a 50 ml flask we placed 1.0 g of POX-Co-1, 1.0 g of phenylthiol (excess) and 20 ml of methanol. The mixture was then stirred at room temperature for 24 hr under nitrogen. This yielded a red-purple powder, which was then separated by filtration, washed with methanol, and dried at 80 °C for 8 hr *in vacuo* (yield: 1.5 g, POX-Co-S-1). POX-Co-1 has a composition corresponding to a cobalt/phenylthio group of *ca.* 1/1. The IR spectrum of POX-Co-S-1 showed characteristic bands of the phenyl group (3040, 1485, 735, and 685 cm^{-1}, KBr disc). In a 50 ml flask we placed 1.6 g of POX-Co-S-1 with a cobalt content of 14.59%, 75 mg of $NaBH_4$ (a slight excess), and 20 ml of isopropyl alcohol. The mixture was stirred for 4 hr at 70 °C under nitrogen. After 0.5 hr it changed into a green solution (probably monovalent cobalts are present); the brown precipitate which was deposited was then washed with 1% of acetic acid and water and dried at 80 °C for 8 hr over P_2O_5 *in vacuo* (yield: 1.0 g POX-Co-R-1). The results of the elemental analysis and the IR spectrum of POX-Co-R-1 were almost the same as those of POX-Co-1. When the mixture was stirred in air, phenyldithiobenzene was formed catalytically, and the resulting red-purple powdery complex, with IR spectrum and elemental analysis almost the same as those of POX-Co-S-1, did not show any change upon treatment with $NaBH_4$. The other catalysts, with lower cobalt contents, POX-Co-S-2—5 and POX-Co-R-2—5, were derived from POX-Co-2—5 similarly. In the preparation of POX-Co-S-2—5, 280 (POX-Co-S-2), 210 (POX-Co-S-3), 140 (POX-Co-S-4) or 105 mg (POX-Co-S-5) of phenylthiol per 1.0 g of POX-Co-2—5 was employed; in that of POX-Co-R-2—5, a slight excess of $NaBH_4$ was used. These catalysts are insoluble powders. The elemental analyses of these compounds are summarized below. Found Copolymer: C, 65.80; H, 7.58%. Calcd for $\left[-(CH_2CH_2)_{1.2}\overline{C}-\right]_x$, $(C_{17}H_{24}O_5)_x$, $(308.4)_x$: C, 66.23; H, 7.79%. Found Polyoxime: C, 42.51; H, 4.98; N, 22.54%. Calcd for $\left[-(CH_2)_{1.6}\overline{(C}-\underset{HON}{\overset{\|}{C}})_{1.6}\overline{(C}-\underset{O}{\overset{\|}{C}})_{0.2}\right]_x$, $(C_{17}H_{24}N_8O_9)_x$, $(484.4)_x$: C, 42.15; H, 4.96; N, 23.14%. Found POX-Co-1: C, 34.35; H, 3.87; N, 18.15; Co, 19.12%. POX-Co-R-1: C, 33.86; H, 3.91; N, 18.36, Co, 19.38%. Calcd for Co*:OX=1:4, $(C_{17}H_{20}N_8O_9Co_2)_x$, $(598.3)_x$: C, 34.13; H,

3.37; N, 18.73; Co, 19.70%. Found POX-Co-S-1: C, 42.78; H, 4.16; N, 16.85; Co, 14.59; S, 7.76%. Calcd for Co*: OX: S*=1: 4: 1, $(C_{29}H_{30}N_8O_9S_2Co_2)_x$, $(816.5)_x$: C, 42.66; H, 3.70; N, 17.24; Co, 14.43, S, 7.85%. Found POX-Co-2: Co, 14.16%. POX-Co-R-2: Co, 14.12%. Calcd for Co*: OX= 1: 6: Co, 14.02%. Found POX-Co-S-2: Co, 11.20; S, 6.25%. Calcd for Co*: OX: S*=1: 6: 1: Co, 11.34; S, 6.18%. Found POX-Co-3: Co, 10.38%. POX-Co-R-3: Co, 10.27%. Calcd for Co*: OX=1: 8: Co, 10.89%. Found POX-Co-4: Co, 7.58%. POX-Co-R-4: Co, 7.42%. Calcd for Co*: OX= 1: 12: Co, 7.52%. Found POX-Co-S-4: Co, 6.51; S, 3.64%. Calcd for Co*: OX: S*=1: 12: 1: Co, 6.48; S, 3.53%. Found POX-Co-5: Co, 5.53%. POX-Co-R-5: Co, 5.42%.Calcd for Co*: OX=1: 16: Co, 5.45%. Found POX-Co-S-5: Co, 4.86; S, 2.73%. Calcd for Co*: OX: S*=1: 16: 1: Co, 4.83; S, 2.63% (S*: number of sulfur atoms.).

Procedures. *Polymerization*: In a three-necked flask equipped with a condenser, a gas-inlet tube, and a dropping funnel containing redistilled styrene, we placed the catalyst, the medium and the other reactants ($NaBH_4$, aq NaOH, *etc.*). The amounts of these reactants are given in Table 1. The mixture was stirred at 70 °C under nitrogen; after 0.5 hr it changed into a green solution (probably monovalent cobalts are present). The styrene was then added. After 3.0 hr the mixture was poured into methanol, and the resulting precipitate was collected by filtration. The precipitate was put in hot toluene, and the resulting solution was filtered to remove the catalyst. The filtrate was concentrated and then poured into methanol, after which the precipitated polystyrene (molecular weight, 5200—7400) was collected by filtration.

Addition Reaction: In a 25-ml glass tube we placed 0.1 g of POX-Co-R, 1/10 mol of purified acrylaldehyde, and 1/5 mol of an alcohol. The tube was then swept free of air with nitrogen, sealed, and stirred at 60—70 °C for 2 hr in a water bath. The product was characterized using IR, NMR, and gaschromatographic techniques.

Measurement. The absorption spectrum was measured at room temperature under nitrogen using a Cary-11 Recording Spectrophotometer. The ESR spectrum was taken with a Nihon Denshi Electron Spin Resonance Spectrometer, Model JEOL-P-10 X-band, using the 100 kHz field. The molecular weights of the ethylene/carbon monoxide copolymer and the polystyrene were determined using a Perkin-Elmer Molecular Weight Apparatus.

Results and Discussion

Table 1 shows that the polymeric complexes are much more effective than cobaloximes; this is obvious in the catalyst systems including a strong alkali. The addition of 1.0 ml of 15% aqueous potassium hydroxide or 300 mg of sodium isopropoxide instead of 15% aqueous sodium hydroxide had the same enhancing effect; however that of 1.0 ml of aqueous lithium hydroxide or calcium hydroxide did not. The absorption spectrum of the green solution obtained as a result of the reaction of POX-Co-S, POX-Co-R or phenylpyridinatocobaloxime(III) with sodium borohydride is similar to that of a cobaloxime(I) or vitamine B_{12s} (containing a Co(I)),[6] as is shown in Fig. 1. The formation of a cobaloxime(III) with a Co–C bond resulting from the reaction of a cobaloxime(I) with styrene has also previously been shown.[7] These facts suggest that a species containing a Co(I) plays an important role in the polymerization. It is well known that unstable monomeric binuclear Co(II) complexes including a cobaloxime(II) disproportionate into a Co(I) and a Co(III) complex in a strong alkaline solution.[8] POX-Co-R may consist partly of binuclear Co(II) units, which might contribute to make the polymeric catalyst more effective. However, a system containing a binuclear cobaloxime(II) (dimeric pyridinato- or aquocobaloxime(II)) could not polymerize styrene under the same conditions as those employed for the polymeric catalyst. POX-Co-R can be converted into POX-Co-S again by the addition of phenylthiol under nitrogen; this is supported by a comparison of their elemental analyses, IR spectra, and reactivities towards sodium borohydride.

Table 1. Polymerization of styrene

Catalyst system	Medium[b] ROH, R=	Product PS[c] (g)/Co (gram atom)
PhS-Co-Pyr[d]+I[e]	i-C_3H_7	4.0×10^3
PhS-Co-Ryr+I+II[f]	i-C_3H_7	3.4×10^3
POX-Co-S-1+I+II	CH_3	—
-S-1+I	i-C_3H_7	14.7×10^3
-S-1+I	t-C_4H_9	19.1×10^3
-S-1+I+II	i-C_3H_7	$26.0\times10_3$
-S-2+I+II	i-C_3H_7	7.0×10^3
-S-5+I+II	i-C_3H_7	0.2×10^3
POX-Co-R-1	i-C_3H_7	1.0×10^3
-R-1+I	i-C_3H_7	24.8×10^3
-R-1+II	i-C_3H_7	10.8×10^3
-R-2+II	i-C_3H_7	3.9×10^3
-R-3+II	i-C_3H_7	0.5×10^3
-R-4+II	i-C_3H_7	0.1×10^3

a) Carried out at 70 °C for 3 hr under nitrogen. b) 20 ml of each alcohol was used. c) Polystyrene. d) Phenylthiolatopyridinatocobaloxime.[5] e) 50 mg of $NaBH_4$. f) 1.0 ml of 15% (w/w) aq. NaOH. Catalysts used : 100 mg, Styrene used: 10.0 g.

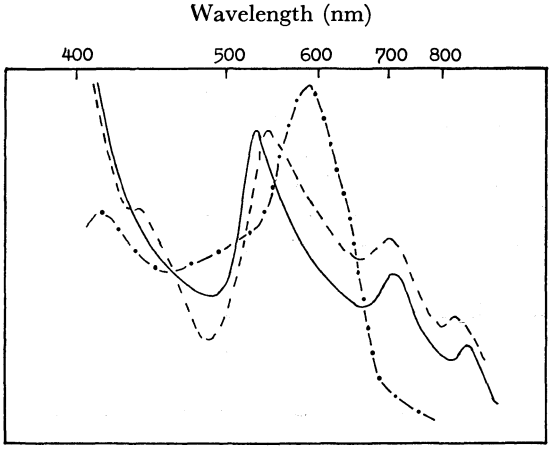

Fig. 1. Absorption spectra.
——: The green solution obtained by the reaction of POX-Co-S-1 with $NaBH_4$ (in 2-propanol).
----: Vitamine B_{12s} (in methanol)[6]
-●-: Tributylphosphinatocobaloxime(I) (in methanol)[6].

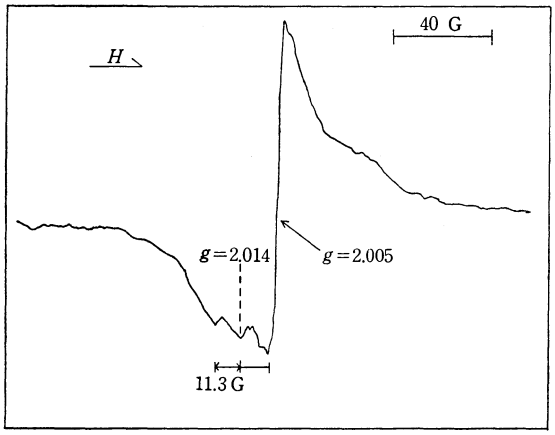

Fig. 2. ESR spectrum of the polyoxime–cobalt complex (POX–Co-R-1). Measured in the solid state (powder) at 77 K under vacuum.

Table 2. "Michael" type addition reaction of an alcohol to acrylaldehyde[a)]

Catalyst	Alcohol, ROH R=	Product, $ROCH_2CH_2CHO$ mol/gram atom of Co
POX–Co–1	CH_3	0.1×10
POX–Co–R–1	CH_3	13.1×10
–R–1	C_2H_5	2.2×10
–R–1	i-C_3H_7	0.1×10
–R–1	n- or t-C_4H_9	—
–R–2	CH_3	15.2×10
–R–3	CH_3	14.9×10
–R–4	CH_3	0.1×10
–R–5	CH_3	—

Catalyst used: 100 mg. ROH used: 1/5 mol. Acrylaldehyde used: 1/10 mol. a) Carried out at 60—70 °C for 2 hr under nitrogen.

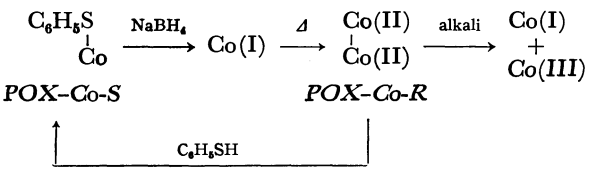

This interconversion was also confirmed by ESR spectroscopy. POX–Co-R exhibits an ESR signal at 77—300 K both in air and under a vacuum, as is shown in Fig. 2. The signal disappears as a result of the interconversion of POX–Co-R into –Co-S. The intensity of the signal increased with an increase in the cobalt content of the complex. The signal may be due to the low spin Co(II) of some units of POX–Co-R.

In the addition reaction, contrary to the results for the polymerization, the catalytic activity of POX–Co-R is not proportional to the cobalt content, and methanol is the most reactive among the alcohols used, as is shown in Table 2. When acrylonitrile, methyl acrylate or crotonaldehyde was employed instead of acrylaldehyde, it was recovered unchanged. On the other hand, bis(dimethylglyoximato)cobalt(II),[8)] which may be the monomeric analogue of POX–Co-R-1 in composition, and cyanopyridinato- and chloropyridinatocobaloxime-(III)[9)] catalyze like ordinary base-catalysts, such as sodium hydroxide and sodium acetate, the addition reaction of an alcohol not only to acrylaldehyde but also to acrylonitrile and methyl acrylate. The different behavior of the polymeric complexes in both catalyses must be partly ascribed to the varieties in the structure and properties of their units; however, there is, so far, no satisfactory explanation of the difference.

References

1) S. J. Kim and T. Takizawa, *Makromol. Chem.*, **175**, 125 (1974).
2) S. J. Kim and T. Takizawa, *Chem. Commun.*, **1974**, 356.
3) S. J. Kim and T. Takizawa, *Makromol. Chem.*, in press, "Activities of a New Polyoxime-Copper Complex in the Reversible Uptake of Molecular Oxygen and Carbon Monoxide, in the Polymerization of Acrylonitrile and in the Addition Reaction of Alcohols to Acrolein."
4) G. N. Schrauzer and R. J. Windgassen, *J. Amer. Chem. Soc.*, **88**, 3738 (1966).
5) G. N. Schrauzer and R. J. Windgassen, *ibid.*, **89**, 3607 (1967).
6) G. N. Schrauzer and J. Kohnle, *Chem. Ber.*, **98**, 3324 (1965).
7) G. N. Schrauzer and R. J. Windgassen, *J. Amer. Chem. Soc.*, **89**, 1999 (1967).
8) G. N. Schrauzer and R. J. Windgassen, *Chem. Ber.*, **99**, 602 (1966).
9) G. N. Schrauzer and J. Kohnle, *ibid.*, **97**, 3056 (1964).

Studies on Xanthenyl and Thioxanthenyl Derivatives. Reactions of Xanthenyl and Thioxanthenyl Halides with Substituted-Ethylenes

Sami Bassili AWAD,* Nadia Fouad ABDUL-MALIK, and Sadek Elsayed ABDOU

Department of Chemistry, Faculty of Science, University of Cairo, Giza, Egypt

(Received August 23, 1974)

Xanthenyl and thioxanthenyl chlorides (**1**) were added to 1,1-bis-(*p*-alkoxyphenyl)-2-substituted-ethylenes (**2**) to give 1,1-bis-(*p*-alkoxyphenyl)-2-substituted-2-[xanthen(or thioxanthen)-9-yl]ethylenes (**3**). The 2-nitro-derivatives (**3**) were converted in boiling methanolic potassium hydroxide into the allenes, 1,1-bis-(*p*-alkoxyphenyl)-2-[xanthen(or thioxanthen)-9-ylidene]ethylenes (**4**). The 2-methyl(or chloro)-derivatives (**3**) reacted with bromine in the presence of hydrogen bromide, to yield xanthylium or thioxanthylium tribromide (**5**) and the corresponding 2,2-disubstituted-ethylene (**6**). The tribromides (**5**) reacted with the ethylene (**2**, Z=H) to give, after spontaneous dehydrobromination, the corresponding 2-bromo-derivatives (**3**, Z=Br).

In a preceding publication,[1] it has been shown that xanthenyl and thioxanthenyl chlorides (**1a,b**) were added to 1,1-bis-(*p*-alkoxyphenyl)ethyleness (**2**, Z=H) and their 2-bromo(or chloro)-derivatives (**2**, Z=Br or Cl) to give the corresponding 1,1-bis-(*p*-alkoxyphenyl)-2-[xanthen (or thioxanthen)-9-yl]ethylenes (**3**, Z=H) and the orresponding 1,1-bis(*p*-alkoxyphenyl)-2-bromo(or chloro)-2-[xanthen(or thioxanthen)-9-yl]ethylenes (**3**, Z=Br or Cl), respectively. We now show that each of xanthenyl and thioxanthenyl chlorides (**1a, b**) was added to 1,1-bis-(*p*-alkoxyphenyl)-2-nitro(and methyl)ethylenes (**2a—f**) to give, after spontaneous dehydrochlorination, the corresponding 1,1-bis-(*p*-alkoxyphenyl)-2-nitro-(and methyl)-2-[xanthen(or thioxanthen)-9-yl]ethylenes (**3a—l**). The 1,1-bis-(*p*-alkoxyphenyl)-2-nitroethylenes (**2a—c**) are prepared by treating the corresponding 1,1-bis-(*p*-alkoxyphenyl)-2-bromoethylenes (**2**, Z=Br) with silver nitrite.

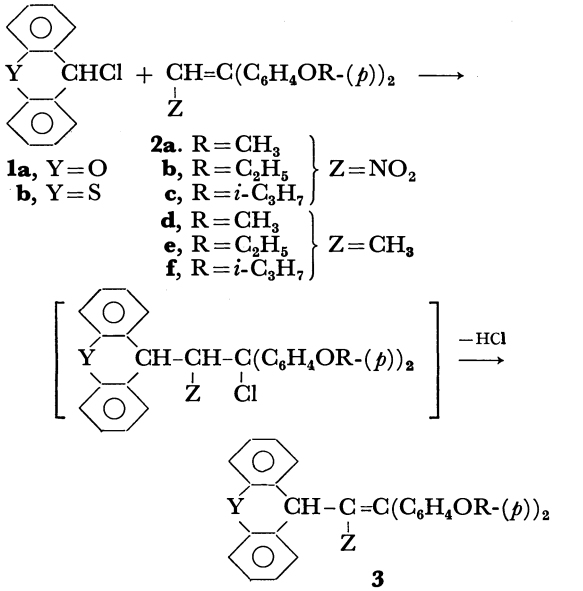

3a, R=CH_3; **b**, R=C_2H_5; **c**, R=*i*-C_3H_7 } Y=O, Z=NO_2

d, R=CH_3; **e**, R=C_2H_5; **f**, R=*i*-C_3H_7 } Y=S, Z=NO_2

3g, R=CH_3; **h**, R=C_2H_5; **i**, R=*i*-C_3H_7 } Y=O, Z=CH_3

j, R=CH_3; **k**, R=C_2H_5; **l**, R=*i*-C_3H_7 } Y=S, Z=CH_3

* The author to whom the correspondence is due to.

The structure of the 2-nitro-derivatives (**3a—f**) was confirmed by analytical and spectral data, and *via* treatment with methanolic potassium hydroxide to give the corresponding allenes namely, 1,1-bis-(*p*-alkoxyphenyl)-2-[xanthen(or thioxanthen)-9-ylidene]ethylenes (**4**) which were identical with the allenes previously obtained[1] by dehydrohalogenation of compounds **3** (Z=Br or Cl).

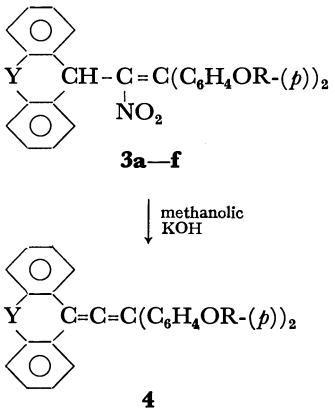

It has been shown[1] that xanthenyl(or thioxanthenyl)-ethylenes (**3**, Z=H or Br), in the presence of hydrogen bromide, cleaved with bromine to give mainly xanthylium or thioxanthylium tribromide (**5**) and 2-bromo-ethylenes **6** (Z=H or Br). The 2-methyl, and 2-chloro-xanthenyl(or thioxanthenyl)-derivatives (**3**, Z=CH_3 or Cl) cleaved similarly to give compounds **5** and **6**.

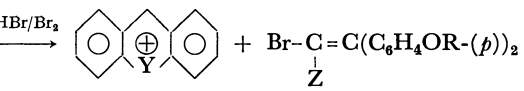

5: Y=O, S

6: Z=CH_3, Cl

On the other hand, the tribromides (**5**) reacted with 1,1-bis-(*p*-alkoxyphenyl)ethylenes (**2**, Z=H) to afford mainly in each case the corresponding 1,1-bis-(*p*-alkoxyphenyl)-2-bromo-2-[xanthen(or thioxanthen)-9-yl]ethylenes (**3**, Z=Br). This could be achieved through the reaction of the ethylenes **2** (Z=H) with the molecular bromine originated from the compounds **5** to give compounds **6** (Z=H) together with compounds **7**. The latter reacted readily, *in situ*, to give, after spontaneous dehydrobromination of the inter-

Table 1. 1,1-bis-(*p*-alkoxyphenyl)-2-nitro(and methyl)-2-[xanthen(and thioxanthen)-9-yl]ethylenes

Compd.	Mp (°C)	Mol formura	Microanalysis Found/Calcd C	H	N	S
3a	152	$C_{29}H_{23}NO_5$	74.40 74.84	4.60 4.95	3.50 2.01	
b	147	$C_{31}H_{27}NO_5$			3.30 2.83	
c	164	$C_{33}H_{31}NO_5$			2.90 2.69	
d	148	$C_{29}H_{23}NO_4S$	72.70 72.35	5.10 4.78	3.20 2.91	6.70 6.65
e	150	$C_{31}H_{27}NO_4S$			2.90 2.75	6.40 6.29
f	180	$C_{33}H_{31}NO_4S$			2.80 2.60	6.30 5.69
g	104	$C_{30}H_{26}O_3$	82.40 88.95	5.80 5.99		
h	106	$C_{32}H_{30}O_3$	83.40 83.12	6.50 6.71		
i	147	$C_{34}H_{34}O_3$	83.50 83.27	6.80 6.94		
j	110	$C_{30}H_{26}O_2S$	79.70 80.00	5.50 5.78		7.20 7.11
k	120	$C_{32}H_{30}O_2S$	80.40 80.29	6.20 6.28		6.50 6.69
l	115	$C_{34}H_{34}O_2S$	80.50 80.63	6.90 6.72		6.30 6.32

mediate **8**, the 2-bromo-derivatives **3** (Z=Br).

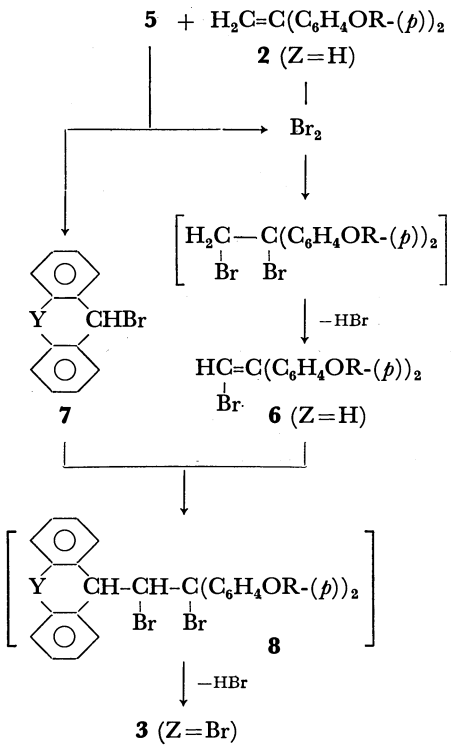

In support of the above scheme, the following may be mentioned:

(i) The tribromides **5** reacted readily with 1,2-di-*p*-methoxyphenylethylene to give mainly the relatively stable 1,2-di-*p*-methoxyphenyl-1,2-dibromoethane and the corresponding xanthenyl (or thioxanthenyl) bromide (**7**).

(ii) When treated with excess dimethylaniline, for one minute, the tribromides **5** afforded *p*-bromodimethylaniline together with 9-*p*-dimethylaminophenylxanthene(or thioxanthene).

(iii) It has been reported that compounds **5**[2,3] lost their halogen when treated with alkali or hydroxylic solvents, to give xanthene(or thioxanthene) and xanthone(or thioxanthone).

(iv) Xanthenyl(or thioxanthenyl) bromide (**7**) was added readily to 1,1-bis-(*p*-methoxyphenyl)-2-bromoethylene (**6**, Z=H) at room temperature or at −5 °C to give compound **3** (Z=Br).

Experimental

All melting points are uncorrected. The infrared spectra were recorded with a Pye-Unicam SP 1000 spectrophotometer.

*1,1-Bis-(*p*-alkoxyphenyl)-2-nitroethylenes (2a—c).* A mixture of each of 1,1-bis-(*p*-alkoxyphenyl)-2-bromoethylene (0.01 mol), silver nitrite (0.03 ml) and acetone (50%, 100 ml) was heated to boiling for 10 hr and then filtered while hot. The filtrate was cooled and the product was collected and purified by crystallization from 80% ethanol. Yields: 80, 75 and 60% respectively. **2a** Mp and mixed mp[4] 112 °C. Found: C, 67.12; H, 5.42; N, 4.72%. Calcd for $C_{16}H_{15}NO_4$: C, 67.36; H, 5.26; N, 4.91%. **2b** Mp 65 °C. Found: C, 69.35; H, 5.82; N, 4.87%. Calcd for $C_{18}H_{19}NO_4$: C, 69.00; H, 6.07; N, 4.50%. **2c** Mp 102 °C. Found: C, 69.95; H, 6.62; N, 3.91%. Calcd for $C_{20}H_{23}NO_4$: C, 70.38; H, 6.74; N, 4.10%.

*1,1-Bis-(*p*-isopropoxyphenyl)-2-methylethylene (2f).* 0.1 mol of *p,p'*-di-isopropoxybenzophenone was added to a solution of methylmagnesium iodide (0.2 mol) in dry ether (100 ml) and the mixture was left overnight. The reaction mixture was decomposed with a cold solution of ammonium chloride. The ethereal layer was separated, washed with water, dried (Na_2SO_4) and filtered. The solvent was recovered and the oily product was distilled *in vacuo* to give **2f**, Bp 120 °C /20 Torr. Found: C, 80.48; H, 8.12%. Calcd for $C_{21}H_{26}O_2$: C, 80.13; H, 8.39%.

*1,1-Bis-(*p*-alkoxyphenyl)-2-nitro(or methyl)-2-[xanthen(or thioxanthen)-9-yl]ethylenes (3a—1).* Ten mmol of each of compounds **2a—f** was added to a solution of ten mmol of each of xanthenyl and thioxanthenyl chlorides (**1a, b**) in ether (100 ml) (prepared by passing hydrogen chloride through a cold ethereal solution of 9-xanthenol[5] or 9-thioxanthenol[6] till saturation). The mixture was left overnight. Ether was distilled off and the product was crystallized from ethanol to give the corresponding derivatives **3a—1** (Table 1).

Yields: 50—60%. IR for each of compounds **3a—f**: 2990 (CH), 1525 and 1360—1290 (NO_2) cm^{-1}.

*1,1-Bis-(*p*-alkoxyphenyl)-2-[xanthen(or thioxanthen)-9-ylidene]-ethylene (4).* A solution of each of the 2-nitro-derivatives **3a—f** (1 g) in methanolic potassium hydroxide (2 g in 100 ml) was heated to boiling (water-bath) for 5 hr, cooled, diluted with water and extracted with ether. The solvent was washed with water, dried (Na_2SO_4) and recovered. The residue was crystallized from ethanol–ether to give almost colorless crystals identified (mp and mixed mp[1]) as compounds **4a—f**. Yield 90%.

*Reactions of Bromine with Compounds 3. (a) With 1,1-Bis-(*p*-alkoxyphenyl)-2-methyl-2-[xanthen(or thioxanthen)-9-yl]ethylenes (3g—1):* (i) Bromine (1.6 g, 0.01 mol) in chloroform (5 ml) was added to a solution of compound **3** g (2.17 g, 0.005 mol)

in the same solvent (20 ml) which was previously saturated with hydrogen bromide. Instantaneous deep orange precipitate of xanthylium tribromide (2.1 g), mp and mixed mp[2] 164 °C, was formed. The filtrate was evaporated *in vacuo* and the residue was crystallized from ethanol to give colorless crystals (1.5 g) identified (mp and mixed mp[7]) as 1,1-bis-(*p*-methoxyphenyl)-2-bromo-2-methylethylene.

(ii) The repetition of (i) using compound **3h** (2.25 g, 0.005 mol) gave thioxanthylium tribromide (2.2 g) as scarlet-red precipitate, mp and mixed mp[3] 185 °C, and 1,1-bis-(*p*-methoxyphenyl)-2-bromo-2-methylethylene (1.5 g).

(iii) The same reaction above using **3j** or **k** (0.005 mol) gave xanthylium tribromide (2.1 g) or thioxanthylium tribromide (2.2 g) together with, in each case, 1,1-bis-(*p*-ethoxyphenyl)-2-bromo-2-methylethylene (1.7 g), mp 71 °C. Found: C, 63.50; H, 5.46; Br, 22.20%. Calcd for $C_{19}H_{21}BrO_2$: C, 63.16; H, 5.81; Br, 22.16%.

*(b) With 1,1-Bis-(*p*-alkoxyphenyl)-2-chloro-2-[xanthen(or thioxanthen)-9-yl]ethylenes (6, Z=CH_3 or Cl).* When the above experiments (a; i, ii, iii) were repeated using the corresponding *p*-methoxy (or ethoxy)-2-chloro-derivatives (0.005 mol), similar results were obtained. Thus in each case the corresponding xanthylium tribromide (2.1 g) or thioxanthylium tribromide (2.2 g) together with 1,1-bis-(*p*-methoxyphenyl)-2-bromo-2-chloroethylene (1.6 g), mp and mixed mp[8] 103 °C or 1,1-bis(*p*-ethoxyphenyl)-2-bromo-2-chloroethylene, mp and mixed mp[8] 115 °C, were isolated respectively.

(c) When the above experiments, (a) and (b), were carried out using equimolecular quantities of bromine (0.005 mol), the same products were obtained together with unchanged derivatives equal to half the quantities of the corresponding starting materials.

*Reaction of Xanthylium(or thioxanthylium)-tribromide (5) with 1,1-Bis-(*p*-alkoxyphenyl)ethylenes (2, Z=H).* Compound **6** (0.005 mol) was added to a solution of each of the ethylenes **2**, (Z=H) (0.005 mol) in chloroform (50 ml) and the whole mixture was heated to boiling (water-bath) for 3 hr. The solvent was recovered and the residue was crystallized from ethanol to give colorless crystals identified (mp and mixed mp[9]) as 1,1-bis-(*p*-alkoxyphenyl)-2-bromo-2-[xanthen-9-yl]-ethylene (**3**, Z=Br) respectively. Yield 90%.

When the above experiments were repeated using compound **5** (Y=S) (0.005 mol), 1,1-bis-(*p*-alkoxyphenyl)-2-bromo-2-[thioxanthen-9-yl]ethylene with mp which showed no depression when mixed with authentic samples[1] was obtained. Yield 85%.

*Reactions of 5 with 1,2-Di-(*p*-methoxyphenyl)ethylene.* (a) A mixture of compound **5** (Y=O) (2.1 g) (0.005 mol), 1,2-di-(*p*-methoxyphenyl)ethylene (1.2 g) and chloroform (50 ml) was heated to boiling for 1 hr. The solvent was concentrated, diluted with petrol (60—80 °C) and cooled to give 1,2-dibromo-1,2-di-(*p*-alkoxyphenyl)ethane (1.9 g), mp and mixed mp[10] 178 °C. The filtrate was concentrated till near dryness and the residue was crystallized from dry petrol (40—60 °C) to give xanthenyl bromide (**7**) (1 g), mp and mixed mp[2] 87 °C.

(b) Repetition of experiment (a) using compound **5** (Y=S) (2.18 g, 0.005 mol) gave the 1,2-dibromo-1,2-di-(*p*-methoxyphenyl)ethane (1.9 g) and thioxanthenyl bromide (1.1 g).

Reactions of 5 (Y=O, S) with Dimethylaniline. A mixture of compound **5** (Y=O or S) (1 g) and dimethylaniline (10 ml) was heated to boiling for 1 min, cooled, made alkaline with aqueous sodium hydroxide and then steam-distilled. In each case, dimethylaniline passed over followed by *p*-bromodimethylaniline (0.3 g), mp and mixed mp[11] 55 °C. The non-steamable portion was cooled and filtered off. The product was crystallized from ethanol to give 9-*p*-dimethylaminophenylxanthene (0.6 g), mp and mixed mp[12] 157 °C, or 9-*p*-dimethylaminophenylthioxanthene (0.6 g), mp 175 °C. Found: N, 4.72; S, 9.94%. Calcd for $C_{21}H_{19}NS$: N, 4.41; S, 10.09%.

Addition of Xanthenyl Bromide (7) to Compound 6 (Z=H). Xanthenyl bromide (0.005 mol) in chloroform (20 ml) was added to a solution of compound **6** (Z=H, R=MeO) (0.005 mol) in chloroform (20 ml) cooled to −5 °C. The reaction mixture was kept at −5 °C for 1 hr and then chloroform was washed with cold sodium hydroxide solution (5%), water, dried, filtered and recovered. The residue was crystallised from ethanol to give colorless crystals identified (mp and mixed mp[1]) as 1,1-bis-(*p*-methoxyphenyl)-2-bromo-2-[xanthen-9-yl]ethylene. Yield 40%.

References

1) W. Tadros, A. B. Sakla, S. B. Awad, and N. F. Abdul-Malik, *Helv. Chim. Acta*, **56**, 1829 (1973).
2) M. Gomberg and L. H. Cone, *Ann.*, **376**, 193 (1910).
3) E. K. Fields, *J. Org. Chem.*, **30**, 937 (1965).
4) T. R. Govindachari, B. R. Pia, and U. Ramadas Rao, *Proc. Indian Acad Sci*, **48A**, 111 (1958); *Chem. Abstr.*, **53**, 1228f (1959).
5) F. G. Kny-Jones and A. M. Ward, *J. Chem. Soc.*, **1930**, 535.
6) T. P. Hilditch and S. Smiles, *ibid.*, **99**, 145 (1911).
7) P. Pfeiffer and R. Wizinger, *Ann.*, **461**, 132 (1928).
8) W. Tadros, A. B. Sakla, A. A. A. Helmy, and M. K. Khalil, *J. Chem. Soc.*, **1965**, 3994.
9) W. Tadros, A. B. Sakla, M. Gindy, and N. Fouad, *J. Chem. Soc., C*, **1970**, 1923.
10) P. Hoering and K. P. Gralert, *Ber.*, **42**, 1204 (1909).
11) A. Weber, *Ber.*, **8**, 715 (1875).
12) R. Fosses, *C. R. Acad. Sci. Paris*, **158**, 1435.

NOTES

BULLETIN OF THE CHEMICAL SOCIETY OF JAPAN, VOL. 48 (7), 2203—2204 (1975)

Enthalpies of Combustion of Organic Compounds. II. L- and D-Glutamic Acid

Minoru SAKIYAMA and Syûzô SEKI

Department of Chemistry, Faculty of Science, Osaka University, Toyonaka, Osaka 560

(Received November 1, 1974)

Synopsis. Enthalpies of combustion of L- and D-glutamic acid in the crystalline state have been measured by oxygen bomb calorimetry. Standard enthalpies of formation at 298.15 K have been determined.

Among optically active aliphatic amino acids, the enthalpy of combustion has been determined for both isomers in few compounds. The only exception is leucine in the crystalline state and the values obtained by Huffman *et al.*[1] of both isomers coincide with each other. In this paper the enthalpies of combustion of L- and D-glutamic acid in the crystalline state are reported. The idealized combustion reaction to which the energies and enthalpies of combustion refer is the following one at 25 °C:

$$C_5H_9O_4N(c) + 5.25O_2(g) = 5CO_2(g) + 4.5H_2O(l) + 0.5N_2(g).$$

Materials. L-Glutamic acid (Takara Kōsan Co. Ltd.) and D-glutamic acid (Ajinomoto Co. Ltd.) were purified by recrystallization from aqueous solution. Crystals were dried, pelletted and stored on silica gel for at least 72 h before combustion. X-Ray diffraction using Cu-Kα radiation shows that the crystals belong to the β-phase[2] (the most stable modification).

Apparatus, Procedures and Calculations. An isoperibol, rotating, precision bomb-calorimeter[3] was used without rotation. In order to facilitate complete combustion of the samples, *ca.* 0.2 g of liquid paraffin (Wakō Pure Chemical Co. Ltd.) was used as an auxiliary oil. No weight loss was observed when the liquid paraffin was placed in an open dish in air for several hours. The standard energy of combustion of the oil was determined by six combustion experiments. The results of the individual combustion experiments in term of $\Delta E_c^\circ/M$ at 298.15 K are −45909.9, −45924.5, −45905.4, −45913.0, and −45909.4 J g^{-1}. Mean and standard deviations of the mean are −45909.3±4.1 J g^{-1}. Calorimetric procedures and methods of calculation are similar to those described previously.[3] The energy equivalent of the standard calorimetric system[3] was found from six calibration experiments by using benzoic acid (Standard Reference Material 39i, National Bureau of Standards, U.S.A) to be 15164.4±0.8 J K^{-1}, where the uncertainty is the standard deviation of the mean.

Auxiliary Quantities. The molecular weights were computed on the basis of the 1961 table of atomic masses. The composition formula and the values (for 25 °C) of density, ρ, specific heat capacity, c_p, and $(\partial E/\partial p)_T$ for the combustible substances are given in Table 1. Two crucibles were used. One (#1, wt. 11.141 g) is made of Pt-10% Rh alloy with density and specific heat capacity of 20.50 g cm^{-3} and 0.1464 J K^{-1} g^{-1}, respectively, at 25 °C. The other (#2, wt. 11.137 g) is made of platinum with density and specific heat capacity of 21.40 g cm^{-3} and 0.1362 J K^{-1} g^{-1}, respectively, at 25 °C.

Table 1. Auxiliary quantities used in the calculation of standard energy of combustion

	ρ / g cm^{-3}	c_p / J K^{-1} g^{-1}	$(\partial E/\partial p)_T$ / J kPa^{-1}g^{-1}
L- and D-Glutamic acid $C_5H_9O_4N$	1.538	1.19	(−0.60)[a]
Auxiliary oil $CH_{1.855}$	0.882	2.22	−2.60
Fuse $CH_{1.860}O_{0.930}$	1.5	1.70	−2.94

a) Estimated value.

Results

Six combustion experiments were carried out with L- and D-glutamic acid. Data from combustions selected as typical are given in Table 2. Notations follow those given by Hubbard *et al.*[5] except for the following: Δm (H_2O cal.), excess water in the calorimeter can; ΔE (std. state), sum of items 81—85, 87—89, 93, and 94 in ref. 5. Results of the individual combustion experiment in terms of $\Delta E_c^\circ/M$ at 298.15 K are summarized as follows: −15298.6, −15293.1, −15293.8, −15307.3, −15299.3, −15307.1, mean and standard deviation of the mean −15300.3±2.5 J g^{-1} for L-glutamic acid and −15304.3, −15304.0, −15309.2, −15301.5, −15309.7,

Table 2. Typical combustion experiments

	L-Glutamic acid	D-Glutamic acid
m^1(compd.)/g	1.16927	1.17672
m^1(auxil. oil)/g	0.20518	0.19690
m^1(fuse)/g	0.00265	0.00234
m^1(H_2O tot.)/g	1.081	1.090
m^1(Pt)/g	11.141	11.157
Δm^1(H_2O cal.)/g	−0.074	0.104
P^1(gas)/MPa	3.040	3.040
T_i/°C	23.15799	23.17928
T_f/°C	24.98876	24.99227
ΔT_{corr}/°C	0.02458	0.02448
$n^f(HNO_3)$/mol	0.000793	0.000815
ΔE_{ign}/J	5.60	5.78
$\Delta E_{dil_n}(HNO_3)$/J	−0.11	−0.12
$\Delta E_{decomp}(HNO_3)$/J	46.69	48.00
ΔE(std. state)/J	17.71	17.70
ε^1(cont.)/J K^{-1}	18.17	18.08
ε^f(cont.)/J K^{-1}	20.39	20.28
ΔE°_c/J g^{-1}	−15299.3	−15301.5

Table 3. Thermodynamic quantities of L- and D- glutamic acid

	ΔE_c° / kJ mol^{-1}	ΔH_c° / kJ mol^{-1}	ΔH_f° / kJ mol^{-1}
L-Glutamic acid	-2251.09 ± 0.93	-2250.47 ± 0.93	-1003.32 ± 1.16
D-Glutamic acid	-2251.94 ± 0.68	-2251.32 ± 0.68	-1002.47 ± 0.97

-15305.1, mean and standard deviation of the mean -15305.6 ± 1.3 J g^{-1} for D-glutamic acid. Thermochemical quantities have been calculated from these results and are given in Table 3. In the calculation of the standard enthalpies of formation, CODATA key values[6] were employed for the standard enthalpy of formation of $H_2O(l)$ and $CO_2(g)$. Uncertainties in Table 3 are uncertainty interval recommended by Rossini,[7] *i. e.*, twice the final overall standard deviation of the mean.

Discussion

The difference in the standard enthalpies of combustion of L- and D-glutamic acids as observed in the present work is 0.85 kJ mol^{-1}, which is 0.038% of the ΔH_c° values and well within the sum of each uncertainty interval. It may be stated that no difference is found between the enthalpy of combustion values of L- and D-glutamic acid within the limit of precision of the present work.

The enthalpy of combustion of L-glutamic acid has been reported by Fischer and Wrede,[8] Emery and Benedict,[9] Huffman *et al.*,[10] Oka,[11] and Tsuzuki and Hunt.[12] In compilations published recently,[13,14] Tsuzuki's value[12] ($\Delta H_c^\circ=-2244.09\pm0.75$ kJ mol^{-1}, where uncertainty is the uncertainty interval) is adopted as a selected value. The present result on L-glutamic acid is in agreement with that of Huffman *et al.*[10] ($\Delta H_c^\circ=-2248.52\pm1.17$ kJ mol^{-1}, where uncertainty is the uncertainty interval) within the assigned uncertainty intervals, while the present result is 6.3 kJ mol^{-1} more negative than the selected value mentioned above. Nothing has ever been reported on the enthalpy of combustion of D-glutamic acid.

The authors would like to express their hearty thanks to Dr. K. Toi, Ajinomoto Co. Ltd., and Dr. F. Sakiyama, the Institute for Protein Research, Osaka University, for their cooperation in obtaining the purified samples. The assistance of Mr. A. Kamaguchi and Miss. T. Sato is appreciated.

References

1) H. M. Huffman, S. W. Fox, and E. L. Ellis, *J. Amer. Chem. Soc.*, **59**, 2144 (1937).
2) S. Hirokawa, *Acta Crystallogr.*, **8**, 637 (1955); H. Takahashi, T. Takenishi, and N. Nagashima, This Bulletin, **35**, 923 (1962).
3) M. Sakiyama, T. Nakano, and S. Seki, *ibid.*, **48**, 1705 (1975).
4) F. D. Rossini (ed.), "Experimental Thermochemistry," Vol. 1, Interscience Publishers, New York, 1956.
5) W. N. Hubbard, D. W. Scott, and G. Waddington, Ref. 4, pp. 75—128.
6) *J. Chem. Thermodynamics*, **4**, 331 (1972).
7) F. D. Rossini, Ref. 4, pp. 297—320.
8) E. Fischer and F. Wrede, *Sitzber. Preuss. Akad. Wiss.*, Math.-Phys. Kl. **1904**, 687.
9) A. G. Emery and F. G. Benedict, *Amer. J. Physiol.*, **28**, 301 (1911).
10) H. M. Huffman, E. L. Ellis, and S. W. Fox, *J. Amer. Chem. Soc.*, **58**, 1728 (1936).
11) Y. Oka, *Nippon Seirigaku Zasshi*, **9**, 365 (1944).
12) T. Tsuzuki and H. Hunt, *J. Phys. Chem.*, **61**, 1668 (1957).
13) J. D. Cox and G. Pilcher, "*Thermochemistry of Organic and Organometallic Compounds*," Academic Press, London and New York, 1970. In this monograph, the data of Huffman *et al.*[10] on L-glutamic acid seems to be erroneously cited as that of D-glutamic acid.
14) E. S. Domalski, *J. Phys. Chem. Reference Data*, **1**, 221 (1972).

BULLETIN OF THE CHEMICAL SOCIETY OF JAPAN, VOL. 48 (7), 2205—2206 (1975)

Oxidation of a Conductive Polymer-TCNQ Salt with Atmospheric Oxygen

Kenji NAKATANI, Tadayoshi SAKATA, and Hiroshi TSUBOMURA

Department of Chemistry, Faculty of Engineering Science, Osaka University, Toyonaka, Osaka 560

(Received February 3, 1975)

Synopsis. The oxidation reaction of conductive poly-4-vinylpyridinium ($P4VP^+$) tetracyano-*p*-quinodimethanide-($TCNQ^-$) with oxygen has been studied. The main product of this reaction is found to be α,α-dicyano-*p*-toluoylcyanide. An interesting difference in reactivity was observed between the polymer salt and the ethanol solution of the monomer salt.

In a previous paper,[1] we reported the electronic spectra of the $P4VP^+TCNQ^-$ and the complex salt including neutral TCNQ ($P4VP^+TCNQ^-TCNQ_x$), which form highly conductive films.[2] The conduction mechanism was discussed. The $P4VP^+TCNQ^-$ film is green in a vacuum but by the introduction of oxygen, the color changes gradually to light brown and the conductivity descreases. Hatano *et al.* reported the oxidation of the γ-methylpyridinium TCNQ salt in acetonitrile solution by oxygen.[3] Sanada *et al.* reported that the deterioration of TCNQ salts of cationic polymer was caused by oxygen and moisture.[4] However, the mechanism of the oxidation and its product have not been clarified.

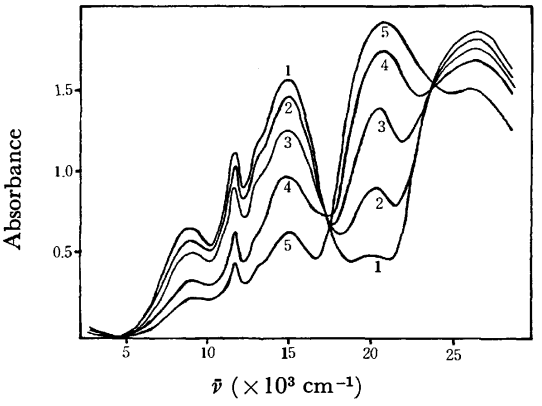

Fig. 1. Electronic absorption spectral change of the polymer film after the introduction of air at 288 K.
1: 2 min, 2: 1 hr 15 min, 3: 3 hr 50 min, 4: 20 hr, 5: 66 hr.

Coherent films of $P4VP^+TCNQ^-$ were deposited on quartz plates and kept in a vacuum. The change of absorption spectra after the introduction of oxygen was measured at various temperatures. As shown in Fig. 1, the intensities of the absorption bands attributable to TCNQ monomer at 845 nm, $TCNQ^-$ aggregate at 665 nm, and the charge transfer band between $TCNQ^-$ radicals at 1100 nm decreased with time after the introduction of oxygen, and a new absorption band appeared at 475 nm. Another absorption was found to appear in the infrared region above 1800 nm (Fig. 2), which disappeared with the lapse of time. Since this IR absorption is attributable to a charge resonance band between $TCNQ^-$ and neutral TCNQ, neutral TCNQ is concluded to be one of the products, formed by an electron transfer reaction such as:

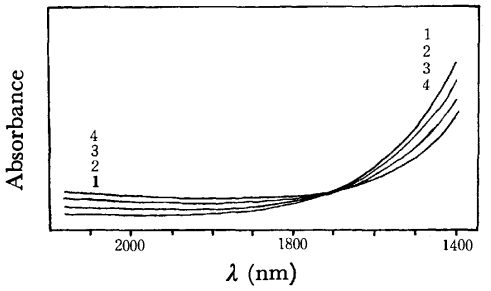

Fig. 2. Infrared absorption spectral change after the introduction of air at 300 K.
1: 0 min, 2: 15 min, 3: 40 min, 4: 90 min.

$$TCNQ^- + O_2 \longrightarrow TCNQ + O_2^-$$

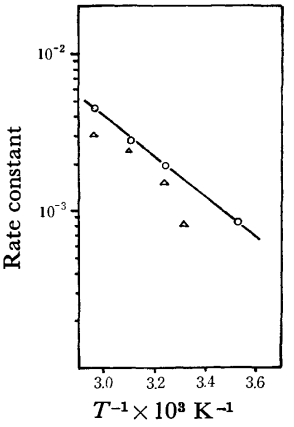

Fig. 3. Logarithmic rate constant plot *versus* inverse absolute temperature, calculated
○: from the change of TCNQ monomer band,
△: from the change of CT absorption band.

The logarithm of the absorbance of $TCNQ^-$ monomer band at 845 nm and that for the charge transfer band between $TCNQ^-$s at 1100 nm of the film under atmosphere of oxygen show a good linear relation with time, showing that the reaction is of the first order as regards the concentration of $TCNQ^-$. The activation energy obtained from the Arrhenius plot of the rate constants obtained from the absorption band is 5.7 kcal/mol. The reaction rate constant calculated from the decay of the monomer band was found to be larger than the one calculated from that of the charge transfer band.

The oxidized polymer film was extracted with ethanol and the extract was separated by thin-layer chromatography using acetone–benzene (1:1). The main orange-colored product was identified to be α,α-dicyano-*p*-toluoylcyanide, because the band shape and peak

positions (λ_{max}=476, 276 nm) of the electronic spectrum agreed with those of sodium α,α-dicyano-*p*-toluoylcyanide, synthesized according to the literature.[5] The IR spectra of the main reaction products also show all the strong bands of the synthesized sodium salt (for example, $\nu_{C=O}$=1645 cm^{-1}, $\nu_{C\equiv N}$=2200, 2160 cm^{-1}), together with some impurity bands.[6] The R_f value in the thin-layer chromatography of the orange-colored product agreed with that of the sodium α,α-dicyano-*p*-toluoylcyanide. The reaction might proceed as follows,

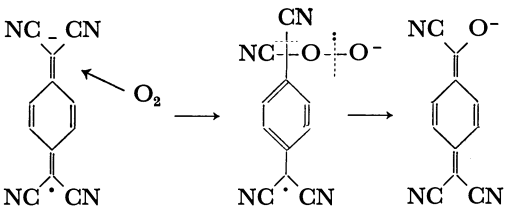

This deterioration reaction of the polymer TCNQ salt is sensitive to the environment of the anion. *N*-methylpyridinium TCNQ was not deteriorated by oxygen even when it was exposed to air for several weeks.

When the aerated ethanol solution of Li^+TCNQ^- was irradiated in the UV region, the color of the solution changed remarkably from green to orange. The resulting photochemical reaction product was found to be also α,α-dicyano-*p*-toluoylcyanide.

It is interesting that the polymer film reacts with oxygen in the dark, while the reaction of Li^+TCNQ^- in solution needs UV excitation.

References

1) K. Nakatani, T. Sakata, and H. Tsubomura, This Bulletin, **48**, (2) 657 (1975).

2) J. H. Lupinski, K. D. Kopple, and J. J. Hertz, *J. Polym. Sci.*, **C16**, 1561 (1967).

3) H. Nomori, M. Hatano, and A. Kanbara, *Kogyo Kagaku Zasshi*, **67**, 1608 (1964).

4) K. Sanada, A. Iwasawa, E. Tsuchida, and I. Shinohara, *Nippon Kagaku Kaishi*, **1974**, 961.

5) W. R. Hertler, H. D. Hartzler, D. S. Acker, and R. E. Benson, *J. Amer. Chem. Soc.*, **84**, 3387 (1962).

6) During extraction with ethanol and separation by thin-layer chromatography, a small part of the orange colored product changed into a colorless substance. Consequently, the material used for the IR measurement was considered to contain some impurities.

BULLETIN OF THE CHEMICAL SOCIETY OF JAPAN, VOL. 48 (7), 2207—2208 (1975)

Charge Transfer Interactions between Oxygen and the Anion Radicals of Tetracyanoquinodimethane and Tetracyanoethylene

Tadayoshi SAKATA, Toshihiro OKAI,* and Hiroshi TSUBOMURA

Department of Chemistry, Faculty of Engineering Science, Osaka University, Toyonaka, Osaka 560

(Received February 24, 1975)

Synopsis. The spectra of the anion radicals of tetracyanoquinodimethane and tetracyanoethylene formed on porous Vycor glass change by introducing O_2 at 77 K. The main features are broadening and slight energy shift of the bands and appearance of a new band. These changes are explained by assuming the charge transfer interactions between O_2 and the anion radicals.

Anion radicals are expected to act as strong electron donors, since their ionization potentials are very low. It is expected therefore that they interact or react easily with O_2, a weak electron acceptor. Tsubomura *et al.* studied extensively the charge transfer (CT) interactions between O_2 and a large number of organic molecules.[1-3] In this paper, the interactions between O_2 and anion radicals of tetracyanoquinomethane (TCNQ) and tetracyanoethylene (TCNE) formed on Vycor glass are reported.

TCNQ and TCNE were adsorbed on porous Vycor glass plates *in vacuo* and their anions were produced by introducing triethylamine. The electronic absorption spectra of the anions agreed well with those reported in the literature.[4,5] The sample was cooled down to 77K and oxygen was introduced into the sample cell, since these anion radicals react easily with O_2 at room temperature.

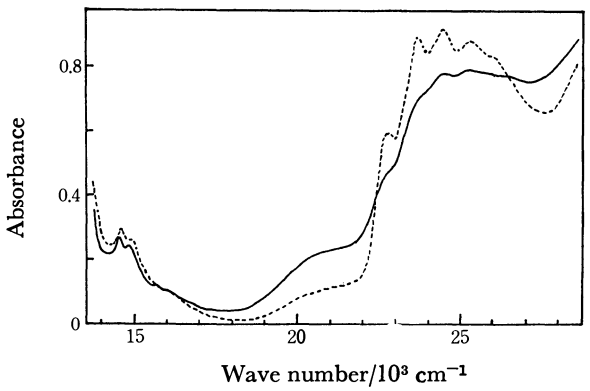

Fig. 1. Absorption spectra of $TCNQ^-$ at 77 K before (----) and after (——) the introduction of O_2.

Figure 1 shows the electronic absorption spectra of the anions before and after the introduction of O_2 at 77 K. The band systems at ~15000 cm^{-1} showing some vibrational structures are attributable to the first excited state of $TCNQ^-$.[6] The strong band systems centered at around 25000 cm^{-1} is attributable to the second excited state of the anion. The weak absorption at 20500 cm^{-1} might be due to an impurity because it cannot be observed in the spectrum of $TCNQ^-$.[7]

* Present address: Nippon Paint Co., Ltd., Osaka.

The spectra show that the second band system of the anion becomes broad and the first one shifts slightly to red (~50 cm^{-1}), its intensity decreasing by the introduction of O_2. It is also shown that the absorption from 18000 to 22000 cm^{-1} swells, suggesting the appearance of a new absorption band. When O_2 is removed, the spectrum is mostly restored, showing that these spectral changes due to O_2 are reversible. Swelling of the absorption around 18000—22000 cm^{-1} with the introduction of O_2 and its reversibility with removal of O_2 were also observed in the case where *N,N,N',N'*-tetramethyl-*p*-phenylenediamine was used as a reducing agent instead of triethylamine.

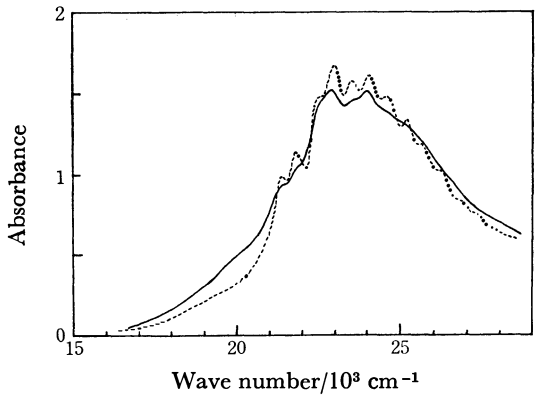

Fig. 2. Absorption spectra of $TCNQ^-$ at 77 K before (----) and after (——) the introduction of O_2.

Figure 2 shows similar results on $TCNE^-$. The vibrational structure characteristic of $TCNE^-$ almost disappears upon introduction of O_2, and the absorption around 20000 cm^{-1} swells, suggesting the appearance of a new band. The reversibility with O_2 removal was also observed.

These results can be explained by assuming weak charge transfer (CT) interactions between O_2 and the anion radicals (A^-). The vertical CT energy (E^v_{CT}) from A^- as an electron donor to O_2 can be expressed by[10]

$$E^v_{CT} = I^v_p(A^-) - E^v_A(O_2) + P(A\cdots O_2^-) - P(A^-\cdots O_2) \quad (1)$$

where I^v_P and E^v_A are the vertical ionization potential and the vertical electron affinity, respectively, and $\Delta P = P(A\cdots O_2^-) - P(A^-\cdots O_2)$ represents the change in the polarization energy during the optical transition. Taking $I^v_P(A^-)$ to be roughly equal to $E_A(A)$, $I^v_P(TCNQ^-)$ and $I^v_P(TCNE^-)$ are estimated to be 1.7 eV[11] and 2.0 eV,[12] respectively. The adiabatic electron affinity of O_2 was determined to be 0.43 eV.[13] The vertical one, $E^v_A(O_2)$, is probably a littly negative.[1] As a counter balance to the adoption of $E_A(A)$ values for $I^v_P(A^-)$ which must cause some underestimation, it seems most

appropriate here to take $E_A^V(O_2)$ to be roughly zero. Inspite of the difficulty in evaluating the polarization energies rigorously, it seems reasonable to assume 1.0 eV for the value of ΔP.[14] Under these evaluations, the transition energies E_{CT}^V for $TCNQ^-\cdots O_2$ and $TCNE^-\cdots O_2$ are obtained as 2.7 eV (22000 cm^{-1}) and 3.0 eV (24000 cm^{-1}), respectively, in fair agreement with the spectral position where swelling occurs.

The reversible change of the absorption spectra around 20000 cm^{-1} for both anions is thus reasonably attributable to the CT interactions between O_2 and the radical anions. The small red shift and intensity change for the first band of $TCNQ^-$ and the broadening of the band shape in both cases are then explained by the CT interaction between O_2 and the anion radicals.

References

1) H. Tsubomura and R. S. Mulliken, *J. Amer. Chem. Soc.*, **82**, 5966 (1960).

2) H. Ishida, H. Takahashi, H. Sato, and H. Tsubomura, *ibid.*, **92**, 275 (1970).

3) H. Ishida, and H. Tsubomura, *J. Photochem.*, **2**, 285 (1974).

4) L. R. Melby, R. J. Harder, W. R. Hertler, W. Mahler, R. E. Benson, and W. E. Mochel, *J. Amer. Chem. Soc.*, **84**, 3374 (1962).

5) M. Sofue and S. Nagakura, This Bulletin, **38**, 1048 (1965).

6) D. A. Lowitz, *J. Chem. Phys.*, **46**, 4698 (1967).

7) A very small amount of α,α-dicyano-*p*-toluoylcyanide might be formed, since this compound has a strong absorption at 480 nm.[8,9]

8) W. R. Hertler, H. D. Hartzler, D. S. Acker, and R. E. Benson, *J. Amer. Chem. Soc.*, **84**, 3387 (1962).

9) K. Nakatani, T. Sakata, and H. Tsubomura, This Bulletin, to be published.

10) T. Sakata, T. Okai, H. Sugimoto, and H. Tsubomura, This Bulletin, **46**, 2698 (1973).

11) G. Briegleb, *Angew. Chem.*, **76**, 326 (1964).

12) L. E. Lyons and L. D. Palmer, *Chem. Phys. Lett.*, **21**, 442 (1973).

13) J. L. Pack and A. V. Phelps, *J. Chem. Phys.*, **44**, 1870 (1966).

14) For the CT complex between O_2 and I^- in ethanol, E_{CT}^V is about 4.4 eV.[15] Using $I_P^V(I^-)=3.1$ eV and $E_A^V(O_2)=0.15$ eV, ΔP is obtained as 1.45 eV. Therefore $\Delta P=1.0$ eV in our case seems to be a reasonable value, taking the difference of the environments and the ionic radii into consideration.

15) H. Levanon and G. Navon, *J. Phys. Chem.*, **73**, 1861 (1969).

BULLETIN OF THE CHEMICAL SOCIETY OF JAPAN, VOL. 48 (7), 2209—2210 (1975)

The Syntheses and Properties of Mixed Cobalt(III) Complexes Containing 2-Mercaptoacetic Acid or 3-Mercaptopropionic Acid

Kiichi Hori

Department of Chemistry, Faculty of Science, Yamagata University, Yamagata 990

(Received December 6, 1974)

Synopsis. The following mixed cobalt(III) complexes were prepared and characterized: $[Co(SCH_2COO)en_2]X$ and $[Co(SCH_2CH_2COO)en_2]X$, where X is a chloride or iodide ion. Those complexes are common mononuclear complexes, in which the mercaptocarboxylic acids of the ligands function as bidentate ligands.

As a part of a series of the coordinating behavior of thiols in cobalt(III) complexes, mixed cobalt(III) complexes containing 2-aminoethanethiol[1] or 2-mercaptoethanol[2] have been reported. For those complexes, two type are found, one being mononuclear and the other binuclear; the coordinated thiolic sulfurs of the ligands are terminal and bridged respectively. This work was undertaken in order to prepare mixed cobalt(III) complexes containing 2-mercaptoacetic acid or 3-mercaptopropionic acid and to compare the results with the previous ones.

Experimental

Preparation. *$[Co(SCH_2COO)en_2]X$ (X is Cl or I)*: Twenty millilitters of an aqueous solution containing 0.9 g of 2-mercaptoacetic acid and 1.1 g of sodium hydroxide were stirred, drop by drop, into a solution of 2.8 g of *trans*-$[CoCl_2en_2]Cl$ in water (40 ml). The mixture was further stirred for 30 min and concentrated to half its volume *in vacuo*, and then we added 4 g of potassium iodide. On standing, a crude product of iodide was precipitated. Recrystallization was carried out from water.

Found: C, 18.64; H, 4.71; N, 14.35%. Calcd for $C_6H_{18}O_2N_4SICo$: C, 18.19; H, 4.59; N, 14.15%.

When the concentration of the starting solution was higher, $Na_3[Co_3(SCH_2COO)_6]$[3] was also obtained.

The solution of the corresponding chloride was obtained from the solution of iodide by passing it over chloride-form anion-exchange resin. The solution was concentrated *in vacuo* and then cooled. The chloride thus precipitated was recrystallized from a small volume of water by adding ethanol.

Found: C, 24.18; H, 5.88; N, 18.11%. Calcd for $C_6H_{18}O_2N_4SClCo$: C, 24.64; H, 5.97; N, 18.39%. Absorption maxima, nm(log ε): 518(2.14), 382(shoulder) (2.4), and 282 (4.03).

$[Co(SCH_2CH_2COO)en_2]X$ (X is Cl or I): These complexes were prepared by a method similar to that described above, except that 1.05 g of 3-mercaptopropionic acid were used instead of 2-mercaptoacetic acid.

Found (Iodide): C, 20.71; H, 5.31; N, 14.06%. Calcd for $C_7H_{20}O_2N_4SICo$: C, 20.49; H, 4.92; N, 13.66%. Found (Chloride): C, 26.25; H, 6.17; N, 17.33%. Calcd for $C_7H_{20}O_2N_4SClCo$: C, 26.37; H, 6.34; N, 17.58%. Absorption maxima, nm (log ε): 525(2.14), 385(shoulder) (2.4), and 291(4.10).

Apparatus. The same instruments as described previously were used.[2]

Results and Discussion

The absorption spectra of the complexes are shown in Fig. 1, together with those of the related complexes. The absorption spectra of the complexes are similar to that of $[Co(SCH_2CH_2NH_2)en_2]Cl_2$,[1] but they are not similar to that of $[Co_2(SCH_2CH_2NH_2)_2dien_2]Cl_4$,[1] which is a binuclear complex bridged by the thiolic sulfurs of ligands. The maximum values of the first absorption band for the present complexes and $[Co(SCH_2CH_2NH_2)en_2]Cl_2$ are regularly shifted to longer wavelengths in the order of the 2-aminoethanethiolato, 2-mercaptoacetate, and 3-mercaptopropionate complexes. The molar conductivities of the complexes show the values of 103—107 mho·cm^{-1}, indicating that they are 1:1-type electrolytes. From all of these facts, it was concluded that the complexes have configurations similar to that of $[Co(SCH_2CH_2NH_2)en_2]Cl_2$, in which a thiolic sulfur of the ligand is combined with a cobalt(III) ion.

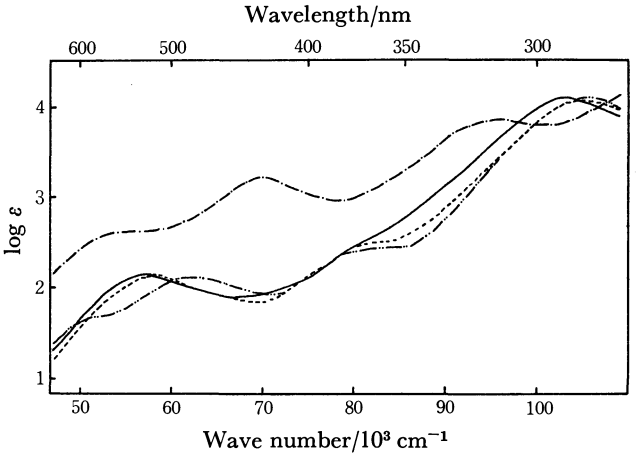

Fig. 1. Absorption spectra of the complexes.
-·-·-: $[Co(SCH_2CH_2NH_2)en_2]Cl_2$, ----: $[Co(SCH_2COO)en_2]Cl$, ——: $[Co(SCH_2CH_2COO)en_2]Cl$, -··-: $[Co_2(SCH_2CH_2NH_2)_2dien_2]Cl_4$.

The infrared spectral data of the complexes are summarized in Table 1, together with those of the related complexes. The assignments of the bands shown in the table were made tentatively by reference to the spectra of the related complexes. In all the complexes, the bands indicating the presence of the coordinated ethylenediamine and carboxylato groups are observed.[4,5] No ν(S–H) band are observed in the 2500—2600 cm^{-1} region. From the infrared spectra it was also considered that the complexes have the configurations shown above. In $[Co(SCH_2CH_2COO)en_2]Cl$, the wave number of the ν_a(COO) band is higher than those of usual carboxylato

Table 1. The main bands of infrared spectra of the complexes (cm^{-1})

$[Co(SCH_2CH_2NH_2)en_2]Cl_2$	$[Co(SCH_2CH_2NH_2)en_2]Cl_2$-D[9]	$[Co(SCH_2COO)en_2]Cl$	$[Co(SCH_2COO)en_2]Cl$-D[9]	$[Co(SCH_2CH_2COO)en_2]Cl$	$[Co(SCH_2CH_2COO)en_2]Cl$-D[9]	$[Co(SCH_2CH_2COO)en_2]I$	$[Co(SCH_2CH_2COO)en_2]I$-D[9]	Tentative assignments
3370 (s)		3365 (s)		3340 (s)				ν(N–H)
3190 (s)		3220 (s)		3250 (s)		3230 (s)		
3120 (s)		3120 (s)		3200 (s)		3135 (s)		
	2380 (s)		2375 (s)	3120 (s)		3095 (s)		
	2265 (s)		2280 (s)		2380 (s)		2410 (s)	ν(N–D)
		1618 (s)	1594 (s)		2280 (s)		2290 (s)	
1576 (s)		1562 (s)		1682 (m)	1580 (s)	1610 (s)	1578 (s)	ν_a(COO)
		1350 (s)	1340 (s)	1563 (s)		1552 (s)		δ(N–H)
	1162 (s)		1175 (s)	1394 (s)	1380 (s)	1377 (s)	1378 (s)	ν_s(COO)
515(sh)	467 (m)	504 (w)	470 (sh)		1150 (s)		1158 (s)	δ(N–D)
496 (m)	455 (w)	494 (m)		500 (m)	470 (m)	513 (w)	475 (m)	ν(Co–N)
		370 (m)	365 (m)	495 (m)		500 (m)	465 (sh)	
326 (m)	327 (w)	310 (w)	308 (w)	346 (m)	340 (m)	342 (m)	340 (m)	ν(Co–O)
				300 (w)	295 (sh)	298 (m)	298 (m)	ν(Co–S)

Abbreviation; s: strong, m: medium, w: weak, sh: shoulder.

complexes. It was assumed, comparing the spectra of the chloride and the related complexes and considering the deuterated effects, that the shift in the chloride is due to the intramolecular hydrogen bond. The ν(Co–N) and ν(Co–O) bands of the complexes were assigned by considerations similar to that of the cobalt(III) complexeswith (2-aminoethylthio) acetic acid.[6] The ν(Co–S) band for the present cobalt(III) complexes is expected, from the bands assignments of the related complexes,[7] to appear in the 280—370 cm^{-1} region. Therefore, among the bands appearing in those region for the complexes we selected the corresponding bands, considering the effects due to deuterations.

The complexes are changed by the reactions with alkyl halides to $[Co(R–SCH_2COO)en_2]X_2$ or $[Co(R–SCH_2CH_2COO)en_2]X_2$, in which the coordinated thiolic sulfurs are alkylated like $[Co(SCH_2CH_2NH_2)en_2]Cl_2$.[8]

References

1) K. Hori, *Nippon Kagaku Zasshi*, **90**, 561 (1969).
2) K. Hori, *ibid.*, **91**, 547 (1970).
3) K. Hori, *ibid.*, **92**, 322 (1971).
4) M. E. Baldwin, *J. Chem. Soc.*, **1960**, 4369; N. Sato and J. Fujita, *Spectrochim. Acta*, **22**, 577 (1966).
5) K. Nakamoto, "Infrared Spectra of Inorganic and Coordination Compounds," John Wiley & Sons, New York, (1970), p. 222.
6) K. Hori, unpublished work.
7) G. W. Watt, J. F. Knifton, and C. V. Senoff, *Inorg. Chem.*, **8**, 2252 (1969).
8) K. Hori, *Bull. Yamagata Univ. (Nat. Sci.)*, **8**, 403 (1974).
9) They represent the complexes in which the amino groups of the ligands in the corresponding complexes were deuterated.

BULLETIN OF THE CHEMICAL SOCIETY OF JAPAN, VOL. 48 (7), 2211—2212 (1975)

The Determination of Formation Constants by Measurements of Molar-volume Changes

Norio WATANABE and Susumu TAKAMOTO

Department of Chemistry, Faculty of Science, Gakushuin University, Mejiro, Toshima-ku, Tokyo 171

(Received February 7, 1975)

Synopsis. Density measurements were made with a solution containing equivalent amounts of diethylenetriamine and the copper(II) ion, and with solutions of different concentrations of potassium hydroxide. The measurements were also made with systems in which the above-mentioned solutions were mixed. The molar-volume changes due to the complex formation were calculated from the density.[1] The results were used for the calculation of the formation constant of the monohydroxo-diethylenetriamine-copper(II) ion.

When ions of opposite charges combine in aqueous solutions, the molar-volume change can be expected to increase as the electroconstriction is weakened.[2] This phenomenon has been established in various acid-base systems.[1,3,4] When a copper(II) ion is coordinated with dienthylenetriamine (abbreviated as dien) at a ratio of 1: 1, the copper(II) ion tends to assume a square-planar structure, with a water molecule at one of its four coordination sites.[5] With the increase in the pH of this solution, the coordinated water molecule easily dissociates a proton and the electric charge of the Cu-dien$(OH_2)^{2+}$ complex changes from +2 to +1. Therefore, the addition of hydroxide ions to a solution containing the 1: 1 complex of Cu(II) and dien is expected to bring about an increase in the molar-volume change of Cu(II). In this study, the molar-volume change of Cu(II) mentioned above was determined at various concentrations of hydroxide ions. The results indicated the presence of a correlation between the formation of the complex and the molar-volume change. Consequently, the formation constant of this hydroxo complex was determined on the basis of the molar-volume change, and a comparison was made with the results obtained by the potentiometric titration method.[5].

Experimental

The copper nitrate solution was standardized gravimetrically by using 8-quinolinol. The diethylenetriamine was distilled twice and diluted with decarbonated water. Its solution was standardized by potentiometric titration using nitric acid of a known concentration. The potassium hydroxide was standardized by the method used in the case of dien. The density measurement was made by means of a pycnometer (14 cm^3 in volume) in a constant-temperature bath maintained at 25.0±0.01 °C.

The initial compositions of the solutions before mixing were as follows:

Solution 1: 0.050 M Cu(II), 0.050 M dien, and the pH controlled at 4.7 by using nitric acid.

Solution 2: Potassium hydroxide in ten different concentrations ranging from 0 to 0.2 M.

Results and Discussion

Martell and his co-workers[4] indicate, on the basis of there potentiometric study, that, in solutions containing equivalent amounts of Cu(II) and dien, the three nitrogen atoms of dien are all coordinated with a copper(II) ion above pH 4 and that the possibility of the formation of a dimer and a dihydroxo complex is small. They also concluded that a normal complex, Cu-dien$(OH_2)^{2+}$, was completely formed in the pH range from 4 to 8. Therefore, the following equilibrium has been established above pH 8:

$$\text{Cu-dien}(OH_2)^{2+} = \text{Cu-dien}(OH)^{+} + H^{+} \qquad (1)$$

The molar-volume changes of Cu(II) due to the mixing of Solution 1 and Solution 2 are shown in Fig.1

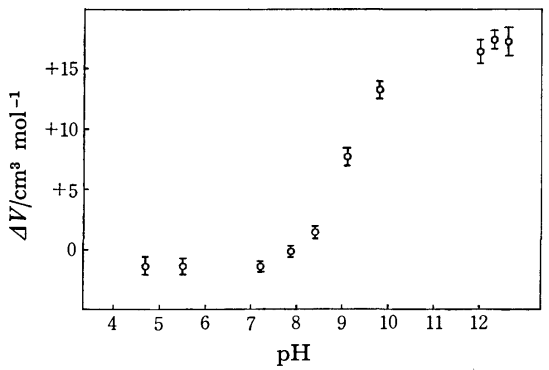

Fig. 1. Molar volume changes of Cu(II) due to the mixing of Solution 1 and Solution 2.

as a function of the pH of the mixed solution. In Solution 1 (pH 4.7 before mixing), Cu-dien$(OH_2)^{2+}$ complex ions are completely formed. In Fig. 1, the molar-volume change remains constant at −1.4 (cm^3 mol^{-1}) in the pH range from 4.7 to 7.2. This agrees with the finding obtained by the potentiometric titration, that the Cu-dien$(OH_2)^{2+}$ complex is completely formed in the solution of pH 4—8. The gradual increase in the molar-volume change in the pH range from 7.9 to 10 corresponds to the shift of the equilibrium (1) to the right, resulting in the increase in the Cu-dien$(OH)^{+}$ complex. At pH>12, the molar-volume change reaches a limiting value +17.1 (cm^3 mol^{-1}); this suggests that Cu-dien$(OH)^{+}$ complexes are completely formed in this pH range.

The molar-volume change of −1.4 (cm^3 mol^{-1}) at pH 4.7—7.2 is denoted by the symbol V(Cu-dien(OH_2)). Similarly, the molar-volume change of +17.1 (cm^3 mol^{-1}) at pH>12 is denoted by the symbol V(Cu-dien(OH)). By analogy with the equation commonly used in spectrophotometric studies,[5] the equilibrium concen-

trations of Cu-dien$(OH_2)^{2+}$ and Cu-dien$(OH)^+$, denoted by C_1 and C_2 respectively, can be expected to be given by Eq. (2) in terms of the molar-volume change, ΔV, at pH 8—11.

$$\frac{C_2}{C_1} = \frac{V(\text{Cu-dien}(OH_2)) - \Delta V}{\Delta V - V(\text{Cu-dien}(OH))} \quad (2)$$

Equation (2) can be used for the determination of the formation constant of Cu-dien$(OH)^+$, as can be expected from:

$$K_{\text{Cu-dien}(OH)} = \frac{C_2 \cdot [H^+]}{C_1} \quad (3)$$

The hydrogen-ion concentration $[H^+]$ was obtained by converting the reading of the pH meter using the hydrogen-ion activity coefficients by means of the Debye-Hückel equation. In order to eliminate the effects of other ions no foreign electrolytes such as KNO_3 was used in the present study. As a consequence, the ionic strength after mixing varies in the range from 0.15 to 0.2. By means of Eqs. (2) and (3), the formation constants of Cu-dien$(OH)^+$ were calculated to be:

$$pK_{\text{Cu-dien}(OH)} = 9.0 \text{ at pH } 9.1$$

$$pK_{\text{Cu-dien}(OH)} = 9.1 \text{ at pH } 9.8$$

The formation constants thus obtained from the molar-volume change data agree well with those of Martell and his co-workers ($pK=9.0$), determined by potentiometric titration.[4]

The authors wish to thank Dr. Reita Tamamushi and Dr. Takusei Hashitani for their helpful advice and encouragement.

References

1) T. Yasunaga and T. Sasaki, *Nippon Kagaku Zasshi*, **71**, 62 (1950).
2) T. G. Spiro, A. Revesz, and J. Lee, *J. Amer. Chem. Soc.*, **90**, 4000 (1968).
3) L. G. Hepler, *J. Phys. Chem.*, **69**, 965 (1965).
4) J. Rasper and W. Kauzman, *J. Amer. Chem. Soc.*, **84**, 1771 (1962).
5) R. C. Courtney, R. L. Gustafson, S. Chaberek, Jr., and A. E. Martell, *ibid.*, **81**, 519 (1959).
6) N. Watanabe, S. Ohe, and S. Takamoto, *Nippon Kagaku Kaishi*, **1975**, 298.

BULLETIN OF THE CHEMICAL SOCIETY OF JAPAN, VOL. 48 (7), 2213—2214 (1975)

The Intramolecular Hydrogen Bonding in *o*-Hydroxybenzyl Alcohol

Nobuo MORI and Kenzo MORIOKA

Department of Chemistry, Science University of Tokyo, Kagurazaka, Shinjuku-ku, Tokyo 162

(Received November 25, 1974)

Synopsis. IR and PMR spectral investigations showed that *o*-hydroxybenzyl alcohol in a dilute solution in CCl_4 existed predominantly in two internally bonded forms, **A** and **B**, and probably also in **C**.

The infrared ν_{OH} data of *o*-hydroxybenzyl alcohol (**1**) in a dilute solution in CCl_4 have previously been reported,[1] but not discussed in detail in relation to the hydrogen bonding, probably because of its complicated system involving two hydroxyl groups and three hydrogen-accepting sites. This problem will be elucidated in this note.

In our infrared reinvestigation, **1** in a dilute CCl_4 solution obviously showed, in the ν_{OH} region, three bonded OH bands at 3620, 3605, and 3429 cm^{-1}; the first two overlapped one another, and there was no significant band due to a free aliphatic OH absorption. From a comparison with the data of the corresponding methyl ethers (**2** and **3**) listed in Table 1, the 3429 cm^{-1} band can undoubtedly be assigned to the aromatic OH group bonded to the aliphatic OH-oxygen atom, and the 3605 cm^{-1} band probably masks a free aromatic OH band which should appear near 3610 cm^{-1}. The ε value of this masked band can be calculated to be *ca.* 24 by using the ε values of the other aromatic OH bands ($=20.2\times 90.0/75.7$).

The 3620 and the 3605 cm^{-1} bands must then be allocated to the aliphatic OH species bonded to two hydrogen-accepting sites, the aromatic OH-oxygen atom and the π-electrons; the weaker 3620 cm^{-1} band can correspond to the π-bonded OH absorption of α-unsubstituted benzyl acohols, which always appears near 3617 cm^{-1}, independently of the ring-substituent,[2] while the stronger 3605 cm^{-1} band can be assigned to the O-bonded OH group. **4** shows only a single O-bonded OH band at 3608 cm^{-1}.

The above assignments are consistent with the OH-PMR data. The OH chemical shifts from TMS for *m*- or *p*-substituted benzyl alcohols at an infinite dilution in CCl_4 decrease with an increase in the sigma value of the substituent and with a decrease in the integrated-intensity ratio of the infrared π-bonded OH band,[3] as Fig. 1 shows; this indicates that the π-bonded OH-protons are subject to a diamagnetic anisotropy effect of the benzene ring and that this effect is dominant over a possible deshielding effect of the OH···π-bond. On the contrary, the OH-proton of **3** and **4** resonates at a lower field, and this down-field shift increases with an increase in the relative intensity of the infrared 3605 cm^{-1} band. The PMR and IR data are consistent with one another if the 3605 cm^{-1} band is due to the O-bonded OH group and if a deshielding effect of the hydrogen bond is

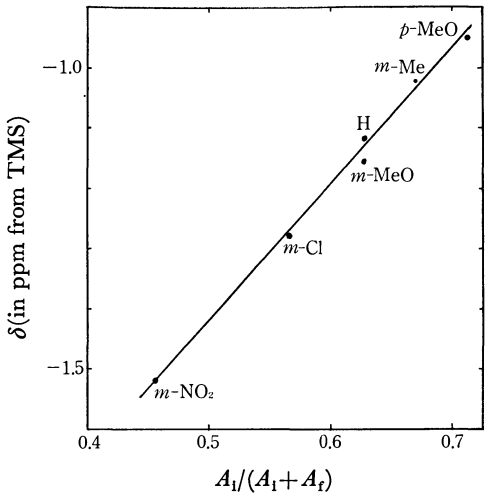

Fig. 1. Correlation between the OH-chemical shift (δ) and the relative population of the π-bonded OH species ($A_i/(A_i+A_f)$).

Table 1. Apparent data of *o*-hydroxybenzyl alcohol and related compounds

	Compound	ν_{OH} in cm^{-1} (ε) of			
		Free OH	π-bonded OH	O-bonded OH	
1		—	3620(45.3)*	3605(90.4)	3429(75.7)
2		3612(20.2)	—	—	3395(90.0)
3	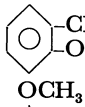	3639(20.6)*	3619(37.7)*	3605(46.7)	—
4	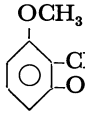	—	—	3608(76.5)	—

* Shoulder.

Table 2. Dilution shift for the OH-proton

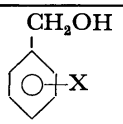	X							
	p-CH_3O	*m*-CH_3	H	*m*-CH_3O	*m*-Cl	*m*-NO_2	*o*-CH_3O	2,6-di-CH_3O
δ (in ppm from TMS)	−0.95	−1.02	−1.12	−1.16	−1.28	−1.52	−1.57	−1.82

operative on the OH-proton; in this case, the proton is further subject to an anisotropy effect of the ring-current, which will be rather paramagnetic, because it must be located nearby on the plane of the benzene ring.

On the basis of the above findings and considerations, and, further, if the ν_{OH} of a free OH group is not decreased by the bonding of the O atom with another OH group,[5] the monomeric *o*-hydroxybenzyl alcohol in CCl_4 may exist predominantly in two internally bonded forms: **A**, in which the aromatic OH group is bonded to the oxygen atom of the π-bonded aliphatic OH group, and **B**, in which the aliphatic OH group is bonded to the free aromatic OH-oxygen atom, and probably also in **C**, in which the aromatic and the aliphatic OH group are free and π-bonded respectively, but not in **D**, in which the aromatic OH group is bonded to the free aliphatic OH-oxygen atom:

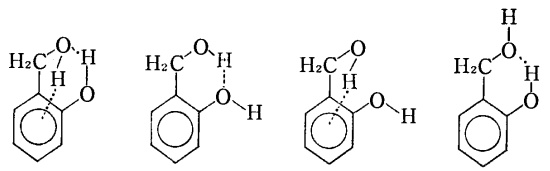

A **B** **C** **D**

In **A**, the aromatic OH group will lie substantially on the plane of the benzene ring, as was suggested in the case of 2,6-dialkylphenols,[8] and the C–O axis of the hydroxymethyl group will be staggered by θ around the ring plane and located at an O–H distance (r) which is not much longer than the O-H bond distance of 0.96 Å, in such a manner that one of the sp^3-orbitals occupied by the n-electrons of the oxygen atom is directed toward the aromatic O–H bond so as to overlap with the antibonding orbital of the latter, as is shown in the figure:

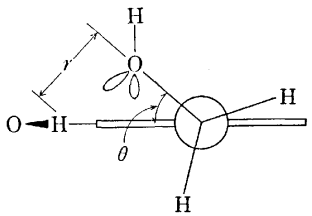

Such torsion of the C–O axis from the normal position[9] in relation to the ring plane must be caused by the hydrogen bonding with the aromatic OH group. A Büchi's Dreiding-model examination shows that, when θ is, *e.g.*, 30°, r is equal to *ca.* 1.5 Å; in this case, the two OH groups will be able to be O- and π-bonded respectively, because (1) this O···H distance corresponds empirically to a spectral shift of *ca.* 100 cm^{-1} of the bonded OH in aliphatic diols,[6] and to the much larger shift which can be expected for the bonded aromatic OH group in the figure, and (2) π-bonding is suggested in the quasi-equatorial form, with θ being somewhat larger than 30°, of 1-tetralols.[10]

Experimental

All the alcohols are known and those except commercially available products were prepared by the usual methods; their purity was checked by their physical constants, PMR spectra and/or chromatograms.

The IR spectra were recorded at *ca.* 25 °C on a JASCO-DS-403G spectrometer (concentration: 0.003 mol/l or less in CCl_4: cell-thickness: 5.0 cm).

The PMR spectra were recorded on a JEOL-LNM-4H-100 spectrometer operating at 100 MHz; dilution experiments were carried out at concentrations down to 0.01 mol/l in CCl_4. The results are summarized in Tables 1 and 2.

References

1) R. E. Richards and H. W. Thompson, *J. Chem. Soc.*, **1947**, 1260; M. M. Davies, *Trans. Faraday Soc.*, **36**, 1114 (1940); A. E. Martin, *Nature*, **166**, 474 (1950).

2) M. Ōki and H. Iwamura, This Bulletin, **32**, 955 (1959); and the value of A_l/A_f described in this paper was converted into the ratio of $A_l/(A_l+A_f)$ in Fig. 1, where A_l and A_f denote the integrated intensities of the π-bonded and the free OH bands, respectively.

3) Such a notable substituent-dependence of δ is not observed in α,α-dimethylbenzyl alcohols.[4]

4) M. Oki and H. Iwamura, *ibid.*, **36**, 1 (1963).

5) This assumption is consistent with the available data of intramolecular OH···OH bondings, as was evidenced particularly in 1,4-diols with spectral shifts of *ca.* 150—190 cm^{-1}.[6,7]

6) L. P. Kuhn, *J. Amer. Chem. Soc.*, **74**, 2492 (1952).

7) L. P. Kuhn, P. von R. Schleyer, W. F. Baitinger, and L. E. Eberson, *ibid.*, **86**, 650 (1964).

8) K. U. Ingold, *Can. J. Chem.*, **38**, 1092 (1960); Z. Yoshida, N. Ishibe, and K. Shobatake, *Kogyo Kagaku Zasshi*, **68**, 808 (1965).

9) J. C. Evans, *Spectrochim. Acta*, **17**, 129 (1961).

10) H. Iwamura and K. Hanaya, This Bulletin, **43**, 3901 (1970); N. Mori, M. Yoshifuji, Y. Asabe, and Y. Tsuzuki, *ibid.*, **44**, 1137 (1971).

BULLETIN OF THE CHEMICAL SOCIETY OF JAPAN, VOL. 48 (7), 2215—2216 (1975)

A Convenient Synthesis of Substituted Pyrocatechols

Kyoko NISHIZAWA and J. Yasuo SATOH*

Meiji College of Pharmacy, Yato-machi, Tanashi, Tokyo 188

* *Department of Chemistry, St. Paul's (Rikkyo) University, Nishi-Ikebukuro, Toshima-ku, Tokyo 171*

(Received January 28, 1975)

Synopsis. It was found that substituted pyrocatechol derivatives were formed by the reaction of polychlorinated cyclohexane-1,2-diones with lithium carbonate in DMF.

Substituted pyrocatechol derivatives have been reported to be formed from methyl substituted phenols and benzenes[1] in several steps. However, no report has appeared on their synthesis from cyclohexanone and methylcyclohexanones. In previous papers[2] we reported that polychlorinated cyclohexane-1,2-diones (**1a**—**1e**) were obtained in good yields from the reaction of cyclohexanones with a large excess of copper(II) chloride. The resulting products have a *gem*-dichloro functional group in the α-position with respect to the carbonyl group. It seems that this functional group would make them capable of leading to the following substituted pyrocatechol derivatives (**2a**—**2e**) by dehydrochlorination. We have studied the reaction of these polychlorinated compounds (**1a**—**1e**) with lithium carbonate in DMF.

The product obtained from **1a** showed no absorption of an α,β-unsaturated ketone, but showed the out-of-plane bending vibration of aromatic hydrogens in the IR spectrum (Table 1). In the NMR spectrum, there was no peak due to an aliphatic proton, but a peak at 5.71 ppm (broad, 2H) due to phenolic hydroxyl groups and a peak at 6.84 ppm (singlet, 2H) due to aromatic protons.

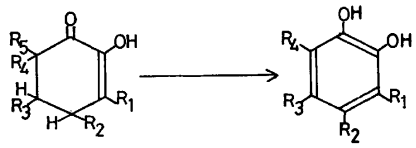

(1) (2)

1a: $R_1=R_4=R_5=Cl$, $R_2=R_3=H$ — **2a**: $R_1=R_4=Cl$, $R_2=R_3=H$

1b: $R_1=CH_3$, $R_2=R_3=H$, $R_4=R_5=Cl$ — **2b**: $R_1=CH_3$, $R_2=R_3=H$, $R_4=Cl$

1c: $R_1=R_4=R_5=Cl$, $R_2=CH_3$, $R_3=H$ — **2c**: $R_1=R_4=Cl$, $R_2=CH_3$, $R_3=H$

1d: $R_1=R_2=CH_3$, $R_3=H$, $R_4=R_5=Cl$ — **2d**: $R_1=R_2=CH_3$, $R_3=H$, $R_4=Cl$

1e: $R_1=R_3=CH_3$, $R_2=H$, $R_4=R_5=Cl$ — **2e**: $R_1=R_3=CH_3$, $R_2=H$, $R_4=Cl$

Fig. 1.

The results indicate that the product obtained is an *o,o'*-disubstituted pyrocatechol derivative, identified to be compound **2a**. In the same manner, the corresponding pyrocatechol derivatives **2b**, **2c**, **2d**, and **2e** were obtained from compounds **1b**, **1c**, **1d**, and **1e**, respectively. Physical properties of the products are given in Table 1.

The present work demonstrates that substituted pyrocatechol derivatives, which heretofore were prepar-

TABLE 1. PHYSICAL PROPERTIES AND ELEMENTAL ANALYSES OF PRODUCTS

Starting materials	Products	Mp (°C)	IR(KBr) (cm^{-1})	NMR($CDCl_3$) δ (ppm)	C (%) Found (Calcd) [Mol. formula]	H (%) Found (Calcd)	Yields (%)
1a	**2a**	109—111	3478 3397 1605 1589	5.71(b, 2H) 6.84(s, 2H)	40.36 (40.26) [$C_6H_4O_2Cl_2$]	2.17 (2.25)	60
1b	**2b**	66—67	3471 3370 1626 1590	2.21(s, 3H) 5.45(b, 2H) 6.60(d, J=8 Hz, 1H) 6.78(d, J=8 Hz, 1H)	52.98 (53.02) [$C_7H_7O_2Cl$]	4.33 (4.45)	50
1c	**2c**	62—63	3527 3248 1626 1604	2.22(s, 3H) 5.47(b, 2H) 6.67(s, 1H)	43.48 (43.56) [$C_7H_6O_2Cl_2$]	3.20 (3.13)	45
1d	**2d**	92.5—93.0	3497 3285 1629 1583	2.13(s, 3H) 2.16(s, 3H) 5.35(b, 1H) 5.55(b, 1H) 6.65(s, 1H)	55.51 (55.67) [$C_8H_9O_2Cl$]	5.57 (5.26)	67
1e	**2e**	86.5—87.5	3460 3250 1625 1602	2.17(s, 3H) 2.22(s, 3H) 5.32(b, 2H) 6.49(s, 1H)	55.61 (55.67) [$C_8H_9O_2Cl$]	5.33 (5.26)	70

ed with difficulty, can be synthesized readily from cyclohexanones *via* chlorination with copper(II) chloride followed by the above reaction.

Experimental

All melting points are uncorrected. Thin-layer chromatography was carried out on silica gel (Wakogel B-5), and detected with iodine. Column chromatography was carried out on silica gel (Wakogel C-100). The IR spectra were measured with a Hitachi 215 grating infrared spectrophotometer by the KBr disk method. The NMR spectra were recorded on $CDCl_3$ with TMS as an internal standard with a Hitachi R-20A nuclear magnetic resonance spectrometer. The chemical shifts are presented in terms of the δ value.

The general procedure was to reflux the polychlorocyclohexane-1,2-dione[2] (1 g) with 1.5 molar equiv. of Li_2CO_3 in DMF (20 ml) for 30 min in a nitrogen atmosphere. Ethereal extract of the reaction mixture was washed with 5% HCl. The product was chromatographed and crude material obtained from benzene–ether (9: 1) eluates was recrystallized from toluene.

The authors wish to thank Professor A. Hagitani, Rikkyo University, for his guidance and helpful suggestions.

References

1) L. Horner and E. Geyer, *Chem. Ber.*, **98**, 2016 (1965); W. Baker, H. F. Bondy, J. Gumb, and D. Miles, *J. Chem. Soc.*, **1953**, 1615; H. J. Teuber and G. Staiger, *Chem. Ber.*, **88**, 802 (1955); L. Horner and W. Spietschka, *Ann. Chem.*, **579**, 159 (1952); L. Horner and K. Sturm, *ibid.*, **597**, 1 (1955); R. Willstätter and H. E. Müller, *Chem. Ber.*, **44**, 2182 (1911).

2) J. Y. Satoh and K. Nishizawa, *Chem. Commun.*, **1973**, 83; K. Nishizawa and J. Y. Satoh, This Bulletin, **48**, 1276 (1975).

BULLETIN OF THE CHEMICAL SOCIETY OF JAPAN, VOL. 48 (7), 2217—2218 (1975)

A Facile Synthesis of 6-Chloro-D-tryptophan

Tamon MORIYA, Katsuaki HAGIO, and Naoto YONEDA

Research Laboratory of Applied Biochemistry, Tanabe Seiyaku Co., Ltd., 16-89, Kashima-3-chome, Yodogawa-ku, Osaka 532

(Received March 24, 1975)

Synopsis. A nonnutritive sweetener, 6-chloro-D-tryptophan (**4**), was synthesized from D-tryptophan (**1**) by nitration, hydrogenation and diazotization, followed by a reaction with cuprous chloride. The optical rotation of **4** agreed with that of an authentic sample which had been prepared by the resolution of racemic **4** methanesulfonate.

6-Chloro-D-tryptophan (**4**) is known as a nonnutritive sweetener with a good sucroselike taste.[1] The use of racemic **4** as a sweetening agent is undesirable because the L-isomer has a somewhat bitter taste. In respect of the synthetic method, it has been reported only that racemic **4** had been prepared from 6-chloroindole *via* its gramine derivative.[2] Now we wish to report that the D-isomer of **4** was successfully synthesized through three steps starting from D-tryptophan (**1**), which can readily be obtained on an industrial scale.

The nitration of **1** was carried out by a slight modification of Fazi's method.[3] A suspension of **1** in acetic acid was treated with fuming nitric acid, without any isolation of the nitrate of **1**, to give the nitrate of 6-nitro-D-tryptophan (**2**) (yellow needles, 59.7%), which was then converted to the free amino acid (**2**) [yellow needles, $[\alpha]_D^{25}$ +12.5° (c=0.2, 20% EtOH), 78.9%] by the addition of sodium carbonate.

The hydrogenation of **2** over palladium-carbon in aqueous hydrochloric acid furnished the amino derivative (**3**)[4] [colorless needles, $[\alpha]_D^{25}$ −13.1° (c=1, 1M HCl), 91.2%].

At the final step of the synthesis, the Sandmeyer reaction for **3** was examined. It was reported that the reactions of nitrous acid with tryptophan and its derivatives led to the deamination of the N^{α}-amino group[5] and to the formation of N^{1}-nitrosamine derivatives.[6] In this study, the 6-amino group of **3** was selectively diazotized in acetic acid, though the reaction using hydrochloric acid gave complicated products. The resulting diazotized compound was treated with cuprous chloride to give 6-chloro-D-tryptophan (**4**) [colorless prisms, $[\alpha]_D^{25}$ −11.3° (c=1, 1M HCl), 50.8%]. Both the spectral data and the optical rotation of **4** were in agreement with those of an authentic sample which had been obtained by the resolution of racemic **4** methanesulfonate by means of a preferential crystallization procedure in our laboratory.[7]

The new method promises to be both economical and convenient for the preparation of 6-chloro-D-tryptophan and would also serve for the synthesis of a variety of 6-substituted derivatives of optically active tryptophans.

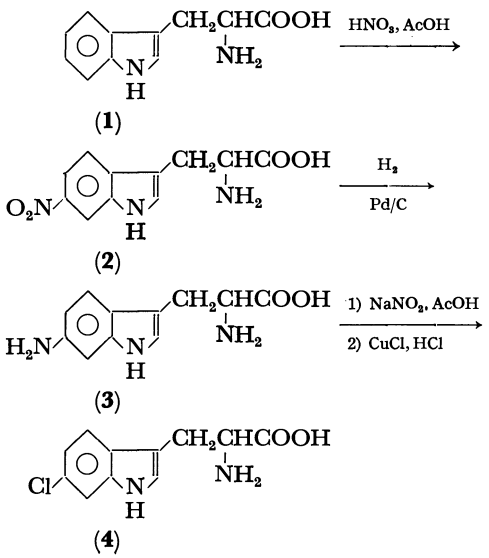

Experimental

All the melting points are uncorrected. The IR spectra were obtained on a Shimadzu IR-27G spectrophotometer. The NMR spectra were recorded on a Hitachi R-20A instrument, using TMS as the internal standard. The observed rotations were measured with a Perkin-Elmer Model 141 polarimeter.

6-Nitro-D-tryptophan (2). To a suspension of D-tryptophan (40.8 g, 0.2 mol) and urea (0.5 g) in glacial acetic acid (500 ml) was added a solution of fuming nitric acid (d 1.50, 7.5 ml) in glacial acetic acid (30 ml). The resulting yellow clean solution was stirred at 0 °C until it changed to a suspension. Then, to the suspension was slowly added, drop by drop at 15 °C, additional fuming nitric acid (d 1.50, 17.5 ml) in glacial acetic acid (70 ml). After stirring for 18 hr at 20—25 °C, the resulting yellow precipitate was collected by filtration to yield **2**·HNO_3·1/2H_2O (28.33 g, 44.1%). The filtrate was then diluted with 300 ml of water ,and the solution was concentrated to 300 ml *in vacuo*. On standing in a refrigerator overnight a further crop of **2**·HNO_3·1/2H_2O (10.01 g, 15.6%) was deposited from the remainder. The recrystallization of the crude **2**·HNO_3·1/2H_2O from diluted nitric acid gave hygroscopic yellow needles; mp 192—194 °C (decomp). IR (KBr); 1750, 1500, and 1330 cm^{-1}.

Found: C, 41.01; H, 4.40; N, 17.19%. Calcd for $C_{11}H_{11}N_3O_4$·HNO_3·1/2H_2O: C, 41.13; H, 4.08; N, 17.44%.

The crude **2**·HNO_3·1/2H_2O (25.0 g) in hot water (200 ml) was converted to the free amino acid (**2**·H_2O, 16.4 g, 78.9%) by the addition of sodium carbonate (4.2 g). Yellow needles (from ethanol), mp 250—252 °C (decomp). $[\alpha]_D^{25}$ +12.5 ° (c=0.2, 20% EtOH). IR (KBr); 3200, 1620, 1495, and 1330 cm^{-1}. NMR (D_2O–NaOH); δ 1.5—3.2 (2H, m), 3.3—3.6 (1H, m), 7.10 (1H, d, J=8.7 Hz), 7.23 (1H, s), 7.28 (1H, dd, J=2.2, 8.7 Hz) and 7.54 ppm (1H, d, J= 2.2 Hz).

Found: C, 49.50; H, 4.50; N, 16.18%. Calcd for $C_{11}H_{11}N_3O_4$·H_2O: C, 49.44; H, 4.90; N, 15.72%.

Hydrochloride: Yellow needles (from dil. HCl); mp 243 °C (decomp). IR (KBr); 3520, 3280, 3000, 1730, 1490, and 1340 cm^{-1}.

6-Amino-D-tryptophan (3). A mixture of **2**·H_2O (12.46

g, 0.047 mol) in 2.2% hydrochloric acid (320 ml) and methanol (200 ml) containing 10% palladium-carbon (1.0 g) was shaken at 25 °C under an atmospheric pressure of hydrogen until the absorption of hydrogen ceased. After 3.41 (3.2 molar equivalents) of hydrogen had been absorbed (3.5 hr), the catalyst was removed and the filtrate was concentrated to dryness *in vacuo*. The residue was dissolved in water (30 ml), and the pH of the solution was adjusted to 6.0 with a saturated aqueous sodium bicarbonate to separate **3**·H_2O as colorless needles (10.06 g, 91.2%); mp 252 °C (decomp). (from ethanol). $[\alpha]_D^{25}$ −13.1 ° (c=1, 1 M HCl), IR (KBr); 3580, 3290, 3150, 1590, 1400, 1345, and 802 cm^{-1}. NMR (DMSO-d_6); δ 2.7—3.3 (2H, m), 3.3—3.7 (1H, m), 6.34 (1H, dd, J=8.3, 1.5 Hz), 6.50 (1H, d, J=1.5 Hz), 6.86 (1H, s), 7.19 (1H, d, J=8.3 Hz) and 10.3 ppm (1H, broad).

Found: C, 55.82; H, 6.33; N, 17.59%. Calcd for $C_{11}H_{13}N_3O_2 \cdot H_2O$: C, 55.68; H, 6.37; N, 17.71%.

6-Chloro-D-tryptophan (4). To a solution of **3**·H_2O (4.75 g, 0.02 mol) in acetic acid (80%, 120 ml) was added an aqueous solution (20 ml) of sodium nitrite (1.38 g, 0.02 mol) drop by drop at 0 °C with stirring. The resulting solution was stirred for 20 min longer and then added to a solution of cuprous chloride [prepared from cupric sulfate pentahydrate (7.46 g, 0.03 mol)] in 15% hydrochloric acid (110 ml) at 0 °C over a 10-min period. After stirring at room temperature for 15 hr and then at 80 °C for an hour, the reaction mixture was concentrated to dryness *in vacuo*. The residue, in 400 ml of water, was treated with hydrogen sulfide, and then the cupric sulfide was removed by filtration. The filtrate was concentrated to separate colorless prisms of crude **4**·HCl. A solution of **4**·HCl in water (30 ml) was treated with active charcoal and neutralized (pH 6.0) with 10% sodium hydroxide. The precipitate was collected and recrystallized from aqueous alcohol to afford **4** as colorless prisms (2.42 g, 50.8%); mp 264—265 °C (decomp). $[\alpha]_D^{25}$ −11.3 ° (c=1, 1 M HCl). IR (KBr); 3400, 3080, 1665, 1585, 810, and 530 cm^{-1}. NMR (D_2O–NaOH); δ 2.8—3.4 (2H, m), 3.5—3.7 (1H, m), 7.06 (1H, dd, J=8.3, 2.0 Hz), 7.40 (1H, d, J=2.0 Hz) and 7.61 ppm (1H, d, J=8.3 Hz).

Found: C, 55.49; H, 4.54; N, 11.90; Cl, 14.74%. Calcd for $C_{11}H_{11}N_2O_2Cl$: C, 55.35; H, 4.65; N, 11.74; Cl, 14.86%.

The authors wish to thank Director Dr. Ichiro Chibata and Dr. Muneji Miyoshi for their encouragement in this study.

References

1) a) E. C. Kornfeld, J. M. Sheneman, and T. Suarez, Ger. 1917844 (Nov. 6. 1969): *Chem. Abstr.*, **72**, 30438c (1970); b) *idem.*, Japan 48—16624 (Apr. 23, 1973).

2) H. N. Rydon and J. C. Tweddle, *J. Chem. Soc.*, **1955**, 3499.

3) a) R. De Fazi, G. Berti, and A. Da Settimo, *Gazz. Chim. Ital.*, **89**, 2238 (1959). The L-isomer of **2**·HNO_3 [mp 160 °C (decomp)], **2**·HCl [mp 245 °C (decomp)] and **2** [mp 265 °C (decomp)] have been synthesized, but the optical rotations have not been described. b) T. Nagasaka and S. Ohki, *Yakugaku Zasshi*, **92**, 777 (1972).

4) L. Goodman, R. R. Spencer, G. Casini, O. P. Crews, and E. J. Reist, *J. Med. Chem.*, **8**, 251 (1965). The L-isomer of **3**·1/8H_2O [mp 210—212 °C, $[\alpha]_D^{24}$ +10.0 ° (c=1, 1 M HCl)] has been synthesized by hydrogenation of 6-nitro-L-tryptophan in water using platinic oxide as catalyst.

5) N. Y. Demiyanov and N. I. Putokhin, *Compt. Rend. Acad. Sci. USSR*, **2**, 390 (1935): *Chem. Abstr.*, **29**, 6889 (1935).

6) R. Bonnett and R. Holleyhead, *J. Chem. Soc. Perkin I*, **1974**, 962.

7) S. Yamada, M. Yamamoto, C. Hongo, and I. Chibata, *J. Agr. Food. Chem.*, in press.

BULLETIN OF THE CHEMICAL SOCIETY OF JAPAN, VOL. 48 (7), 2219—2220 (1975)

A Convenient Synthesis of α-Bromophenylacetic Acid from Benzaldehyde Using Methyl (Methylthio) methyl Sulfoxide

Katsuyuki OGURA, Shigeko FURUKAWA, and Gen-ichi TSUCHIHASHI

Sagami Chemical Research Center, Nishi-Ohnuma, Sagamihara, Kanagawa 229

(Received March 31, 1975)

Synopsis. 1-Methylsulfinyl-1-(methylthio)-2-phenylethylene (**2a**) and 1-methylsulfinyl-1-(methylthio)-2-(*p*-chlorophenyl)ethylene (**2b**) reacted with bromine in various solvents to give α-bromophenylacetic acid derivatives. It should be noted that α-bromophenylacetic acid and α-bromo(*p*-chlorophenyl)acetic acid were mainly obtained by the reaction of bromine with **2a** and **2b**, respectively, in acetic acid.

As previously reported,[1] methyl (methylthio) methyl sulfoxide (**1**)[2,3] can condense with aromatic aldehydes in the presence of trimethylbenzylammonium hydroxide (Triton B) to afford the corresponding 1-methylsulfinyl-1-(methylthio)-2-arylethylenes (**2**), which are easily converted into ethyl arylacetates (**3**) on treatment with hydrogen chloride in ethanol, providing a new method for the synthesis of ethyl arylacetates (Scheme 1). Further, the reaction of the condensation product (**2**) with bromine has been examined, and we now wish to describe on a novel synthetic route from benzaldehyde to α-bromophenylacetic acid.

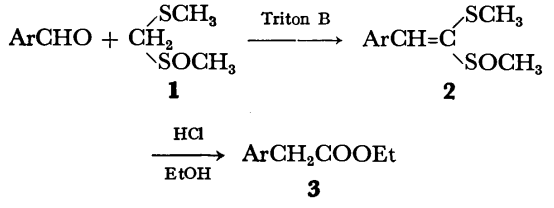

(a, Ar=C_6H_5; b, Ar=*p*-ClC_6H_4)

Scheme 1.

The reaction of 1-methylsulfinyl-1-(methylthio)-2-phenylethylene (**2a**) with bromine was carried out in carbon tetrachloride, methanol, and acetic acid. When **2a** was treated with bromine in carbon tetrachloride, methanethiol ester (**4a**) of α-bromophenylacetic acid was isolated in 25% yield. The structure of **4a** was assigned by its IR and NMR spectra and elemental analysis (see Experimental Section).

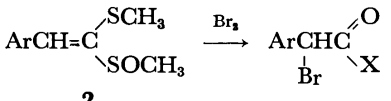

a	Ar=C_6H_5	X=SCH_3
b	=C_6H_5	=OCH_3
c	=C_6H_5	=OH
d	=*p*-ClC_6H_4	=OH
e	=*p*-ClC_6H_4	=OCH_3

Scheme 2.

In methanol, bromine reacted with **2a** to give methyl α-bromophenylacetate (**4b**) in 64% yield. It should be noted that a better result was obtained when acetic acid was used as a solvent. Thus, the reaction with bromine in acetic acid afforded α-bromophenylacetic acid in 73% yield.

By a similar reaction in acetic acid, α-bromo(*p*-chlorophenyl)acetic acid (**4d**) was also obtained in 60% yield, starting from 1-methylsulfinyl-1-(methylthio)-2-(*p*-chlorophenyl)ethylene (**2b**).[4,5] Since **2a** and **2b** were easily derived from the corresponding aldehydes by the reaction with methyl (methylthio) methyl sulfoxide (**1**),[1] the present reactions completed a simple two-step synthesis of α-bromophenylacetic acid and α-bromo(*p*-chlorophenyl)acetic acid from benzaldehyde (over-all yield: 66%) and *p*-chlorobenzaldehyde (over-all yield: 44%), respectively.

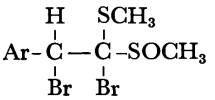

5

The transformation of **2** into **4** may be accounted for by a mechanism which involves an intermediacy of **5**, which is finally converted into **4** by the subsequent hydrolysis.

Experimental

*Reaction of 1-Methylsulfinyl-1-(methylthio)-2-phenylethylene (**2a**) with Bromine.* *a) In Carbon Tetrachloride*: Bromine (0.21 ml, 4.0 mmol) was added to a solution containing **2a** (798 mg, 3.8 mmol) in carbon tetrachloride (10 ml) under cooling with ice, and the resulting solution was stirred at room temperature for 2 hr. After the addition of water (5 ml) and extraction with methylene chloride, the organic layer was dried over anhydrous sodium sulfate and evaporated under reduced pressure. The residue was chromatographed (silica-gel column, eluted with *n*-hexane and benzene) to give 263 mg (0.95 mmol, 25%) of a pale yellow oil, which was identified as methanethiol ester (**4a**) of α-bromophenylacetic acid by its physical properties and elemental analysis. IR (neat): 1685 cm^{-1} ($\nu_{C=O}$); NMR ($CDCl_3$): δ 2.33 (s, 3H, $COSCH_3$), 5.36 (s, 1H, –CHBr–), 7.34 (m, 5H, C_6H_5); Found: C, 44.16; H, 3.50; S, 13.00%. Calcd for C_9H_9BrOS: C, 44.09; H, 3.70; S, 13.08%.

b) In Methanol: A solution containing **2a** (526 mg, 2.5 mmol) in methanol (5 ml) was stirred at room temperature for 41.5 hr after the addition of bromine (0.33 ml, 5.7 mmol) under cooling with ice. The solution was evaporated under reduced pressure, and the residue was chromatographed [silica-gel column, eluted with benzene–*n*-hexane (1 : 4)] to afford 363 mg (1.58 mmol, 64%) of a pale yellow oil, which was identified as methyl α-bromophenylacetate (**4b**) by the comparison of its IR and NMR spectra with those of an authentic specimen prepared by esterification (conc. sulfuric acid–methanol) of α-bromophenylacetic acid.

c) In Acetic Acid: Bromine (0.13 ml, 2.6 mmol) was added,

together with acetic acid (1 ml), to a solution containing **2a** (533 mg, 2.5 mmol) in acetic acid (1 ml). The resulting solution was stirred at room temperature for 17.5 hr and, after the evaporation under reduced pressure, the residue was chromatographed (silica-gel column, eluted with methylene chloride) to give 394 mg (1.83 mmol, 73%) of pale yellow crystals, which were once recrystallized from cyclohexane to afford colorless crystals, mp 51.5—52 °C; IR (KBr): 3100—2300 and 1700 cm^{-1}; NMR (CCl_4): δ 5.24 (s, 1H), 7.33 (m, 5H), 11.35 (s, 1H); Found: C, 44.82; H, 3.28%. Calcd for $C_8H_7BrO_2$: C, 44.68; H, 3.28%.

The structure of this product was assigned as α-bromophenyacetic acid (**4c**) by its physical properties and elemental analysis. Furthermore, its NMR and IR spectra were completely accordant with those of an authentic sample (mp 71.5—72 °C; lit,[6] mp 68—69 °C) obtained by the reaction of mandelic acid with hydrobromic acid and sulfuric acid.[6] The melting point of the crystals obtained by the reaction of **2a** with bromine was raised to 81—82 °C, after several recrystallizations from cyclohexane. This melting point is in accord with those reported in the other literatures (ranging from 78.5 to 84 °C).[7]

*Reaction of 1-Methylsulfinyl-1-(methylthio)-2-(*p*-chlorophenyl)-ethylene (2b) with Bromine.* *a) In Methanol*: Bromine (0.09 ml, 1.8 mmol) was added to a solution containing **2b** (408 mg, 1.7 mmol) in methanol (5 ml) and the resulting solution was stirred at room temperature for 22 hr. After the evaporation under reduced pressure, the residue was chromatographed [silica-gel column, eluted with benzene–*n*-hexane (1:4)] to give 189 mg (0.72 mmol, 43%) of methyl α-bromo(*p*-chlorophenyl)acetate (**4e**) and 198 mg (1.06 mmol, 52%) of methyl (*p*-chlorophenyl)acetate. The structures of these products were assigned by the comparison of their IR and NMR spectra with those of the corresponding authentic samples.

b) In Acetic Acid: Bromine (0.11 ml, 2.1 mmol) was added, together with acetic acid (1 ml), to a solution containing **2b** (502 mg, 2.0 mmol) in acetic acid (1 ml) and the resulting solution was stirred at room temperature for 19 hr. After the evaporation under reduced pressure, the residue was chromatographed [silica-gel column, eluted with benzene–*n*-hexane (1:4)] to give 342 mg of colorless crystals, which were shown by the NMR analysis to consist of (*p*-chlorophenyl)acetic acid (35 mg, 0.21 mmol, 10%) and α-bromo-(*p*-chlorophenyl)acetic acid (307 mg, 1.23 mmol, 60%). The latter was isolated by recrystallization from cyclohexane as colorless crystals, mp 83—86 °C (lit,[8] mp 95—96 °C), which were identified with α-bromo(*p*-chlorophenyl)acetic acid (**4d**) by the comparison of their NMR ($CDCl_3$) and IR ($CHCl_3$) spectra with those of an authentic specimen.[8]

References

1) K. Ogura and G. Tsuchihashi, *Tetrahedron Lett.*, **1972**, 1383.

2) K. Ogura and G. Tsuchihashi, This Bulletin, **45**, 2203 (1972).

3) We have also reported new synthetic methods for making aldehydes, α-hydroxyaldehydes, α-amino acids and cyclobutanone derivatives: K. Ogura and G. Tsuchihashi, *Tetrahedron Lett.*, **1971**, 3151; **1972**, 2681; K. Ogura, S. Furukawa, and G. Tsuchihashi, *Chem. Lett.*, **1974**, 659; K. Ogura and G. Tsuchihashi, *J. Amer. Chem. Soc.*, **96**, 1960 (1974); K. Ogura, M. Yamashita, M. Suzuki, and G. Tsuchihashi, *Tetrahedron Lett.*, **1974**, 3653.

4) The reaction of 2-(3′,4′-dimethoxyphenyl)-1-methylsulfinyl-1-(methylthio) ethylene resulted in the formation of α-bromo(3,4-dimethoxyphenyl)acetic acid (21%) and (3,4-dimethoxyphenyl)acetic acid (18%). The structures of these compounds were assigned by their NMR spectra.

5) When bromine was reacted with **2b** in methanol, methyl α-bromo(*p*-chlorophenyl)acetate and methyl (*p*-chloropheny)acetate were formed in 43% and 52% yields, respectively (see Experimental Section).

6) J. M. Bruce and F. K. Sutcliffe, *J. Chem. Soc.*, **1957**, 4789.

7) K. C. Kemp and D. Metsger, *J. Org. Chem.*, **33**, 4165 (1968); Distillers Co. Ltd., Belg. Pat. 622439 (1963), *Cf. Chem. Abstr.*, **59**, 11352c (1963); The literatures cited in Ref. 6.

8) J. Krapcho, U.S. Pat. 3166544 (1965), *Cf. Chem. Abstr.*, **62**, 13157e (1965).

BULLETIN OF THE CHEMICAL SOCIETY OF JAPAN, VOL. 48 (7), 2221—2222 (1975)

Rearrangement of Tetramethyl-*trans*-decalin Derivatives[1)]

Tochiro TATEE, Takahiko TSUYUKI, and Takeyoshi TAKAHASHI

Department of Chemistry, Faculty of Science, The University of Tokyo, Bunkyo-ku, Tokyo 113

(Received April 1, 1975)

Synopsis. The dihydroxydecalin (**6**) was treated with iodine at 140 °C to give the octalins (**13** and **14**). Treatment of the β-epoxide (**8**) with boron trifluoride etherate gave the octalins [**17** and **18** (or **19**)] and the oxide (**20**).

Backbone rearrangements in the steroid and terpenoid fields are well documented.[2a,b)] Intracyclic tension in the rigid polycyclic ring provokes of backbone rearrangements to give the products less constrained. Electronic effects resulting from the presence of functional groups and kinetic effects due to the nature of reagents can modify the development of rearrangement.[3a,b)]

It has been shown that a treatment of the decalols (**1** and **2**) with iodine at 140 °C gave a mixture of olefins (**3**, **4**, and **5**), respectively.[4)] It would be expected that a dihydroxydecalin (**6**) having a hydroxyl group at C-6 might effect a rearrangement to give a ketone (**7**). Similarly, a rearrangement of an epoxide (**8**) to form an enol benzoate (**9**) might be expected.

Recent communication on the epoxides of bisnorlabdane derivatives and on related epoxides[5)] prompted us to report our result.[1)] We wish to describe the rearrangements of **6** and **8**.

The hydroxyketone (**10**)[6)] was treated with methylmagnesium iodide to give a mixture of diols (**6** and **11**). Pure **6** was obtained by crystallization from light petroleum. The configuration of the tertiary hydroxyl group in **6** was confirmed by conversion of **6** into **1**[4)] *via* a ketol (**12**). Treatment of **6** with iodine at 140 °C gave the unsaturated alcohols (**13** and **14**).

A benzoate (**15**) derived from **13** was epoxidized with *m*-chloroperbenzoic acid to give **8** and **16**. The β-epoxide (**8**) was treated with boron trifluoride etherate in benzene to yield three products. The PMR and IR spectra of the most polar product showed the presence of a benzoyloxyl and a hydroxyl group and the absence of olefinic proton. Therefore the structure (**17**) was given for the most polar compound.

The presence of a benzoyloxyl and a hydroxyl group along with an olefinic proton in the second polar product was shown by its PMR and IR spectra, which led to the structure (**18** or **19**) for this substance. The PMR spectrum of the least polar product indicated the presence of one proton (δ 3.90, d, J=4 Hz) on a carbon atom attached to ethereal oxygen on a five membered ring[7)] and of a benzoyloxyl group. No signal due to olefinic proton was observed. The absence of hydroxyl absorption in the IR spectrum and the mass spectrum showing a molecular ion peak at *m/e* 328 along with the observations mentioned above suggested the structure (**20**) for the least polar product.

As a result, the dehydration of **6** with iodine and the treatment of **8** with boron trifluoride etherate gave the rearranged products in which the 1,3-diaxial interaction was released. A further rearrangement of a methyl group resulting in new formation of 1,3-diaxial interaction, did not take place. The hydroxyl group (at C-6 of **6**) and the benzoyloxyl group (at C-2 of **8**) did not develop further rearrangement to give **7** and **9**, respectively, under the conditions described above.

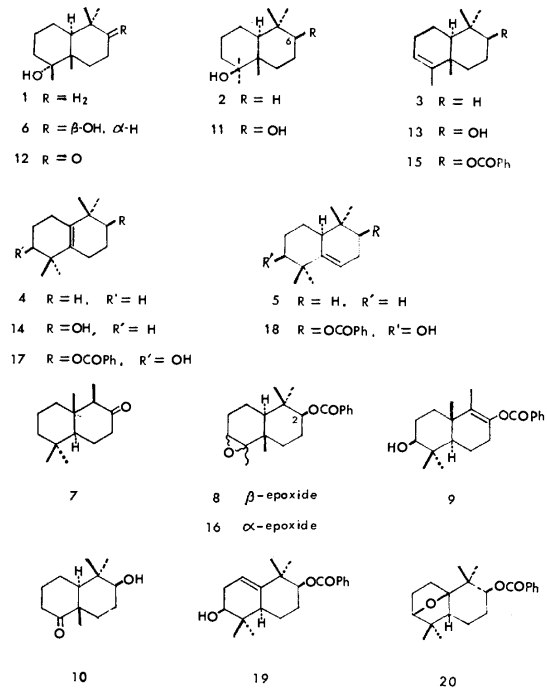

Experimental

Instruments utilized for measurements of spectral data and the other experimental indications were the same as those described in Ref. 4.

1α,6β-Dihydroxy-1β,5,5,9β-tetramethyl-trans-*decalin (6).* To the Grignard reagent prepared from methyl iodide (5 g) and magnesium (637 mg) in dry ether (25 ml) at 0 °C was added a solution of the ketol (**10**;[6)] 1.31 g) in dry ether (20 ml). The reaction mixture was stirred at 0 °C for 2 hr. After usual treatment, the residue (1.43 g) was chromatographed on a column of silica gel (150 g). Elution with a mixture of light petroleum and ether (2: 1) gave a mixture of epimeric diols (**6** and **11**; 1.07 g; yield: 76% from **10**), which was crystallized from light petroleum to afford the pure **6**, mp 151.5—152.5 °C, IR (Nujol) 3570, 3400, 3350 cm^{-1}; PMR ($CDCl_3$) δ 0.83, 0.97, 1.02, and 1.11 (each 3H, s; t-CH_3), 3.26 (1H, m; -CH-OH); mass *m/e* 226 (M^+; 1%) and *m/e* 43 (100%); Found: C, 74.04; H, 11.51%. Calcd for $C_{14}H_{26}O_2$: C, 74.28; 11.58%. The mother liquid of crystallization containing the epimeric diol (**11**) was not examined further.

The Decalol (1). The diol (**6**; 40 mg) in acetone (5 ml) was oxidized with Jones' reagent (0.1 ml) at 0 °C. After usual work-up, a ketol (**12**; 41 mg) was obtained as an oil, IR (liquid) 3480 and 1700 cm^{-1}; mass *m/e* 224 [M^+ ($C_{14}H_{24}O_2$); 26%] and *m/e* 43 (100%). To the ketol (**12**) were added

diethyleneglycol (2 ml), 80% hydrazine hydrate (0.3 ml) and potassium hydroxide (20 mg), and the resulting mixture was refluxed for 3 hr and the temperature of the reaction mixture was raised to 200 °C. Water was added and the mixture was extracted with ether. After usual work-up, the residue was chromatographed on a column of silica gel (5 g). Elution with a mixture of light petroleum and ether (10: 1) gave the known decalol (**1**;[4] 8 mg).

Dehydration of the Diol (6) with Iodine. The diol (**6**; 167 mg) was heated at 165 °C. To the resulting melted material cooled to 140 °C was added iodine (6.7 mg) and the mixture was kept for 20 sec. The cooled reaction mixture was extracted with ether. After usual work-up, the residue was chromatographed on a column of silica gel (12 g) impregnated with 20% silver nitrate. Elution with a mixture of light petroleum and ether (10: 1) gave 2-hydroxy-1,1,5,5-tetramethyl-1,2,3,4,5,6,7,8-octahydronaphthalene (**14**; 31 mg; y: 21%), as an oil, IR (liquid) 3380 cm^{-1}; PMR ($CDCl_3$) δ 0.97 (9H, s; $3\times t$-CH_3), 1.02 (3H, s; t-CH_3), and 3.47 (1H, q, J= 4 and 8 Hz; -C<u>H</u>-OH); mass *m/e* 208 [M^+($C_{14}H_{24}O$); 16%] and *m/e* 175 (100%). Elution with a mixture of light petroleum and ether (5: 1) gave 3β-hydroxy-4,4,8,8aβ-tetramethyl-*trans*-1,2,3,4,4a,5,6,8a-octahydronaphthalene (**13**; 70 mg; y: 45%), mp 99—99.5 °C (from light petroleum), IR (Nujol) 3280 and 1655 cm^{-1}; PMR ($CDCl_3$) δ 0.82 (3H, s; t-CH_3), 1.00 (6H, s; $2\times t$-CH_3), 1.58 (3H, d, J=2 Hz; C=C-CH_3), 3.25 (1H, q, J=5 and 11 Hz; -C<u>H</u>-OH), and 5.16 (1H, m; CH=C); mass *m/e* 208 [M^+; 14%] and *m/e* 175 (100%); Found: C, 80.97; H, 11.65%. Calcd for $C_{14}H_{24}O$: C, 80.71; H, 11.61%.

Benzoylation of the Unsaturated Alcohol (13). The unsaturated alcohol (**13**; 50 mg) in pyridine (0.5 ml) was heated at 95 °C with benzoic anhydride (143 mg) for 24 hr. After usual treatment, the unsaturated benzoate (**15**; 55 mg; y: 74%) was obtained; mp 146—147.5 °C, IR (Nujol) 1710 cm^{-1}; PMR ($CDCl_3$) δ 0.98 (3H, s; t-CH_3), 1.08 (6H, s; $2\times$ t-CH_3), 1.60 (3H, d, J=2 Hz; C=C-CH_3), 4.6—4.9 (1H, m; -C<u>H</u>-OBz), and 5.1—5.3 (1H, m; CH=C); mass *m/e* 312 [M^+; 4%] and *m/e* 105 (100%); Found: C, 80.67; H, 9.18%. Calcd for $C_{21}H_{28}O_2$: C, 80.73; H, 9.03%.

Epoxidation of the Unsaturated Benzoate (15). The unsaturated benzoate (**15**; 51 mg) in benzene (5 ml) was treated with *m*-chloroperbenzoic acid (33 mg) at room temperature for 24 hr. After usual work-up, the residue (107 mg) was chromatographed on a column of silica gel (10 g). Elution with benzene–ether (20: 1) afforded a mixture of the α- and β-epoxides (**16** and **8**). The mixture was subjected to further separation on a column of silica gel (8 g). Elution with a mixture of light petroleum-benzene-ether (25: 25: 2) gave 2β-benzoyloxy-5β,6β-epoxy-1,1,5α,10β-tetramethyl-*trans*-decalin (**8**; 13 mg; y: 24%), mp 190—190.5 °C (from light petroleum), IR (Nujol) 1710 cm^{-1}; PMR ($CDCl_3$) δ 0.95, 1.01, 1.15, and 1.23 (each 3H, s; CH_3), 2.96 (1H, triplet-like singlet; C<u>H</u>-C, with O bridge), and 4.6—4.9 (1H, m; -C<u>H</u>-OBz); mass *m/e* 328 [M^+; 0.5%] and *m/e* 105 (100%); Found: C, 76.93; H, 8.34%. Calcd for $C_{21}H_{28}O_3$: C, 76.79; H, 8.59%. Further elution with the same solvent mixture gave 2β-benzoyloxy-5α,6α-epoxy-1,1,5β,10β-tetramethyl-*trans*-decalin (**16**; 19 mg; y: 36%), mp 151—152 °C (from light petroleum), IR (Nujol) 1710 cm^{-1}; PMR ($CDCl_3$) δ 0.94, 1.04, 1.15, and 1.24 (each 3H, s; CH_3), 2.90 (1H, t, J=2.5 Hz, C<u>H</u>-C with O bridge), and 4.6—4.9 (1H, m; -CH-OBz), mass *m/e* 328 [M^+ ($C_{21}H_{28}O_3$); 0.1%] and *m/e* 105 (100%).

Treatment of the β-Epoxide (8) with Boron Trifluoride Etherate. The β-epoxide (**8**; 14 mg) in dry benzene (0.2 ml) was treated with freshly distilled boron trifluoride etherate at room temperature for 17 min. Aqueous sodium hydrogen carbonate solution (0.3 ml) was added and the ethereal extract was passed through a column of silica gel (2 g). Light petroleum–ether (1: 1) eluents, after evaporation of the solvents, were subjected to separation by preparative thin-layer chromatography [solv. benzene–ether (3: 1)]. The material corresponding to the most polar spot (R_f 0.45—0.55) gave 6β-benzoyloxy-2β-hydroxy-1,1,5,5-tetramethyl-1,2,3,4,5,6,7,8-octahydronaphthalene (**17**; 4 mg), as an oil, IR (liquid) 3500 and 1715 cm^{-1}; PMR ($CDCl_3$) δ 0.99, 1.03, 1.06, and 1.14 (each 3H, s; t-CH_3), 3.44 (1H, q, J=4 and 10 Hz; -C<u>H</u>-OH; axial-H), and 4.88 (1H, q, J=4 and 9 Hz; -C<u>H</u>-OBz; axial-H); mass *m/e* 328 [M^+ ($C_{21}H_{28}O_3$); 0.4%] and *m/e* 105 (100%). The product corresponding to the second polar spot (R_f 0.55—0.62) gave 6β-benzoyloxy-2β-hydroxy-1,1,5,5-tetramethyl-1,2,3,4,4a,5,6,7-octahydronaphthalene (**18**) or 2β-benzoyloxy-6β-hydroxy-1,1,5,5-tetramethyl-1,2,3,4,4a,5,6,7-octahydronaphthalene (**19**), as an oil, (3.5 mg), IR (liquid) 3520 and 1695 cm^{-1}; PMR ($CDCl_3$) δ 1.00 (6H, s; $2\times t$-CH_3), 1.09 (3H, s; t-CH_3), 1.16 (3H, s; t-CH_3), 3.48 (1H, br. s, $W_{1/2}$ *ca.* 5.5 Hz; -C<u>H</u>-OH; equatorial-H), 4.88 (1H, q, J=5.5 and 8 Hz; -C<u>H</u>-OBz; axial-H), and 5.42 (1H, triplet like singlet; CH=C); mass *m/e* 328 [M^+ ($C_{21}H_{28}O_3$); 0.2%] and *m/e* 105 (100%). The product corresponding to the least polar spot (R_f 0.71—0.86) gave 2β-benzoyloxy-6β,9β-epoxy-1,1,5,5-tetramethyl-*trans*-decalin (**20**; 4.5 mg), as an oil, IR (liquid) 1710 cm^{-1}; PMR ($CDCl_3$) δ 1.00 (3H, s; t-CH_3), 1.05 (6H, s; $2\times t$-CH_3); 1.08 (3H, s; t-CH_3), 3.90 (1H, d, J=4 Hz; -CH-O-C-), and 4.86 (1H, t, J=2.5 Hz; -C<u>H</u>-OBz; equatorial-H); mass *m/e* 328 [M^+ ($C_{21}H_{28}O_3$); 9%] and *m/e* 105 (100%).

References

1) A part of this paper was presented at the 31st Annual Meeting of the Chemical Society of Japan, Sendai, October 4, 1974 (Proceedings, Vol. I, p. 37).

2) a) *e.g.*: D. N. Kirk and M. P. Hartshorn, "Steroid Reaction Mechanism," Elsevier Publishing Company, Amsterdam (1968), p. 291 and p. 354. b) *e.g.*: P. de Mayo, "Molecular Rearrangements," Vol. 2, John Wiley & Sons, Inc., New York (1964), p. 821.

3) a) J. Bascoul and A. Crastes de Paulet, *Bull. Soc. Chim. Fr.*, **1969**, 189. b) M. M. Janot, C. Monneret, Q. Khuong-Huu, and R. Goutarel, *C. R. Acad. Sc. Paris*, **265C**, 1468 (1967).

4) T. Tatee, T. Tsuyuki, R. Aoyagi, and T. Takahashi, This Bulletin, **47**, 3158 (1974).

5) M. S. Hadley and T. G. Halsall, *J. Chem. Soc., Perkin I*, **1974**, 1334.

6) F. Sondheimer and D. Elad, *J. Amer. Chem. Soc.*, **80**, 1967 (1958).

7) J. H. Block and G. H. Constantine, Jr., *Photochemistry*, **11**, 3279 (1972). And the references cited therein.

BULLETIN OF THE CHEMICAL SOCIETY OF JAPAN, VOL. 48 (7), 2223—2224 (1975)

Effect of Alkylation on the Iodine 6s Rydberg States of Iodoalkanes

Shunji KATSUMATA, Hidechika WAKABAYASHI, and Katsumi KIMURA

Physical Chemistry Laboratory, Institute of Applied Electricity, Hokkaido University, Sapporo 060

(Received February 10, 1975)

Synopsis. In a series of alkyl iodides far UV absorption and photoelectron spectra indicate that, unlike higher Rydberg members, the lowest Rydberg states are rather sensitive to the alkyl groups, linearity holding between the term values and the first ionization potentials.

Previously, Kimura *et al.* studied the effects of alkyl groups on the ionization potentials (IP) of alkyl compounds by He(I) photoelectron (PE) spectroscopy[1-3] and used the PE data for the assignment of a far UV absorption spectrum of ethyl fluoride.[4] In the present work we have studied the far UV absorption spectra of a series of alkyl iodides $C_mH_{2m+1}I$(m=1—4), emphasis being laid on the effects of the alkyl groups on the lowest Rydberg states.

A far UV spectrum of methyl iodide has been interpreted in terms of several Rydberg series by Herzberg,[5] Price,[6] and many other workers.[7-10] Using a pressure broadening technique, Robin and Kuebler[8] confirmed that the absorption bands of methyl iodide in the 180—205 nm region can be attributed to the first members of the 5p→ns Rydberg series converging to the $^2E_{3/2}$ and $^2E_{1/2}$ ionic states. Boschi and Salahub[9,10] studied far UV spectra of many alkyl iodides in detail and indicated that the 5p→ns Rydberg series except the first members can be explained in terms of nearly constant quantum defects (about 4.2). In the course of our recent study of alkyl iodides, we found that only the lowest Rydberg states are sensitive to the alkyl groups.

Absorption measurements were carried out in vapor phase (0.06—0.25 Torr) in the region 165—210 nm by a 50 cm vacuum UV spectrophotometer previously used.[4] The experimental technique employed is essentially the same as that used before.[11,12] Except for the synthesized *s*- and *t*-butyl iodides, the commercial compounds were used. All the samples were purified by distillation.

Typical examples of the far UV spectra are shown in Fig. 1, indicating the Herzberg B, C, and D bands

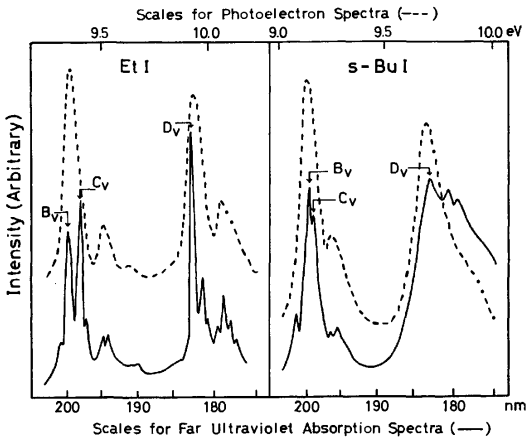

Fig. 1. Far UV absorption spectra of ethyl and *s*-butyl iodide in the 175—205 nm region, compared with the first two PE ionization bands.

due to the (5p→6s) transitions. Bands B and C correspond to the $^2E_{3/2}$ ionic state and band D to the $^2E_{1/2}$. The far UV spectra obtained for the compounds except *s*-butyl iodide which has not been studied so far are essentially the same as those reported by Boschi and Salahub.[9,10] The lowest Rydberg transition energies are summarized in Table 1, which were obtained from the mean positions of the vertical-transition peaks (B_V and C_V as shown in Fig. 1). The separation between the D_V peaks and the B_V—C_V average positions give rise to the spin-orbit splittings (Δ) summarized in Table 1 together with the corresponding PE data.

The term values (T) are the differences between the transition energies (E) and the first IP's (I_1) previously determined.[1,3] The term value is equivalent to the Rydberg-state IP. The Rydberg formula is expressed by $I_1-E=R/(n-\delta)^2$, where n is the principal quantum number and δ is the quantum defect. The lowest Rydberg bands largely deviate from the above formula with $\delta\approx4.2$.[9,10] We obtained the δ values (Table 1)

Table 1. The 5p→6s ($^2E_{3/2}$) Rydberg states of alkyl iodides

Compound	E (cm^{-1})	I_1[a] (eV)	T (cm^{-1})	δ	Δ (eV) Far UV	Δ (eV) PE[a]
MeI	49950	9.50[b]	26700	3.97	0.61_3	0.62
EtI	50050	9.35	25400	3.92	0.57_6	0.58
n-PrI	50050	9.26	24600	3.88	0.57_0	0.56
i-PrI	49900	9.18	24100	3.86	0.55_7	0.57
n-BuI	50100	9.23	24300	3.87	0.57_6	0.58
i-BuI	49950	9.18	24100	3.86	0.60_1	0.56
s-BuI	50150	9.13	23500	3.84	0.56_4	0.55
t-BuI	49250	9.09	24100	3.86	0.55_1	0.55

a) Refs. 1 and 3. b) J. L. Ragle, I. A. Stenhouse, D. C. Frost, and C. A. McDowell, *J. Chem. Phys.*, **53**, 178 (1970).

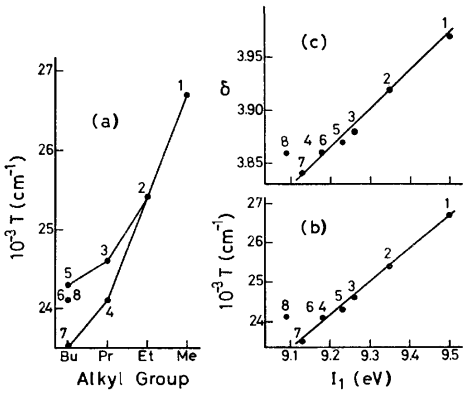

Fig. 2. (a) Variation of the lowest-Rydberg-state term values with increasing size of the alkyl group in a series of alkyl iodides. (b) Relationship between the term values and the first IP's. (c) Relationship between the quantum defects and the first IP's.
(1) MeI, (2) EtI, (3) *n*-PrI, (4) *i*-PrI, (5) *n*-BuI, (6) *i*-BuI, (7) *s*-BuI, and (8) *t*-BuI.
The solid lines are drawn to show the modes of variation.

from the Rydberg formula using the experimental T values. The following remarks may be added on the lowest Rydberg states of the alkyl iodides.

(1) The T's for the 5p→6s ($^2E_{3/2}$) Rydberg states are plotted against the number of carbon atoms in the alkyl group in Fig. 2(a), indicating a downward trend with increasing alkylation. Such a trend for other series of alkyl compounds has been indicated by Robin and Kuebler.[13,14]

(2) In Fig. 2(b), the T's are plotted against the first IP's, indicating a good linear relationship, although only *t*-butyl iodide deviates slightly from linearity. This linearity is important, being pointed out for the first time, and is based on the fact that the lowest Rydberg transition energies (Table 1) are almost constant throughout the series of compounds. For the higher members of the 5p→*n*s Rydberg series, however, no such linearity holds.

(3) The δ's are plotted against the first IP's in Fig. 2(c), indicating again approximate linearity. The δ values of 3.84—3.97 are considerably smaller as compared with that (about 4.2) used for the higher members.[9,10]

(4) The far UV absorption spectra are compared with the previously obtained PE spectra[1,3] (broken curves in Fig. 1). Both the optical and PE spectra are surprisingly similar in shape. Such similarity has already been pointed out for other simple compounds by Basch *et al.*[15] and Narayan.[16] As can be seen from Table 1, the spin-orbit splittings in the 5p→6s Rydberg states are very close to those in the first ionized states.

(6) The variation of the first IP's in the alkyl iodides was previously interpreted in terms of the mixing of the iodine 5p orbitals with the *p*-type alkyl-group orbitals.[1,3] In a large number of aliphatic compounds, Robin[13] pointed out the importance of the n=3 orbitals of the alkyl groups in the lowest Rydberg orbitals. In the present study, unlike the higher Rydberg states, the lowest Rydberg states and the first ionized states show striking similarities with respect to the alkyl-group substitution. This strongly suggests that, as the alkyl group changes from the methyl group to the higher one, the variation in the mixing of the iodine 6s orbital with the alkyl-group n=3 orbital in the lowest Rydberg states is approximately equal to the variation in the mixing of the iodine 5p orbitals with the alkyl-group *p*-type orbitals in the ground states. The longest-wavelength absorption bands of the alkyl iodides appearing in the 250—270 nm region were assigned earlier to the $n\rightarrow\delta^*$ transitions by Kimura and Nagakura.[17]

References

1) K. Kimura, S. Katsumata, Y. Achiba, H. Matsumoto, and S. Nagakura, This Bulletin, **46**, 373 (1973).
2) S. Katsumata, T. Iwai, and K. Kimura, *ibid.*, **46**, 3391 (1973).
3) A. Toba, S. Katsumata, and K. Kimura, This Bulletin, to be published.
4) T. Yamazaki, S. Katsumata, and K. Kimura, *J. Electron Spectrosc.*, **2**, 335 (1973).
5) G. Herzberg, "Molecular Spectra and Molecular Structure, III. Electronic Spectra and Electronic Structure of Polyatomic Molecules," Van Nostrand, New York (1966), p. 532.
6) W. C. Price, *J. Chem. Phys.*, **4**, 539, 546 (1936).
7) Papers cited in Ref. 5.
8) M. B. Robin and N. A. Kuebler, *J. Mol. Spectrosc.*, **33**, 274 (1970).
9) R. A. Boschi and D. R. Salahub, *Mol. Phys.*, **24**, 289 (1972).
10) R. A. Boschi and D. R. Salahub, *ibid.*, **24**, 735 (1972).
11) H. Tsubomura, K. Kaya, K. Kimura, J. Tanaka, and S. Nagakura, This Bulletin, **37**, 417 (1964).
12) K. Kimura and S. Nagakura, *Mol. Phys.*, **9**, 117 (1965); *Theoret. Chim. Acta*, **3**, 164 (1965); *J. Chem. Phys.*, **47**, 2916 (1967).
13) M. B. Robin, *Int. J. Quantum Chem. Symp.*, **6**, 257 (1972).
14) M. B. Robin and N. A. Kuebler, *J. Electron Spectrosc.*, **1**, 13 (1972).
15) H. Basch, M. B. Robin, N. A. Kuebler, C. Baker, and D. W. Turner, *J. Chem. Phys.*, **51**, 52 (1969).
16) B. Narayan, *Mol. Phys.*, **23**, 281 (1972).
17) K. Kimura and S. Nagakura, *Spectrochim. Acta*, **17**, 166 (1961).

BULLETIN OF THE CHEMICAL SOCIETY OF JAPAN, VOL. 48 (7), 2225 (1975)

Dielectric Relaxation and Molecular Structure. XVI. Dielectric Behavior of Tertiary Alcohols

Taro KOSHII, Hiroaki TAKAHASHI, and Keniti HIGASI

Department of Chemistry, Waseda University, Shinjuku, Tokyo 160

(Received April 2, 1975)

Synopsis. The relaxation time and the activation energy of the principal dispersion of tertiary alcohols do not increase but *decrease* with increase in the number of the carbon atoms in the molecule. This observation seems to be in accord with a hypothesis that the principal dispersion is associated with the size of the hydrogen-bonded cluster of alcohols.

It is well known for *n*-alkyl bromides[1] and alkyl acetates,[2,3] that the relaxation time and the activation energy regularly increase with increase in the number of carbon atoms in the molecular chain. The same trend has been found also in normal primary alcohols.[4] The purpose of this note is to report that an exception to this general tendency is found in the case of tertiary alcohols.

Recently, the dielectric behavior of 2-methyl-2-butanol and 3-methyl-3-pentanol have been studied by the method described before.[5] The relaxation times, τ, of these tertiary alcohols and 2-methyl-2-propanol[6] are plotted, in Fig. 1, against the carbon number of the alcohol. It will be seen that the τ curve in the full line decreases with increase in the number of carbon atoms; it exhibits a striking contrast to the broken curve for normal primary alcohols.[4] Moreover, the curves for the reduced relaxation time, τ/η,[7] against the number of carbon atoms also show a downward slope for tertiary alcohols. The activation enthalpies, ΔH^*, of these tertiary alcohols[8] are plotted in Fig. 2 together with those of normal primary alcohols.[4] The ΔH^* *vs.* carbon number curve shows a decrease for the tertiary alcohols, while that for normal alcohols increases. For tertiary alcohols treated here, the larger the molecule becomes, the smaller are the τ and ΔH^* values. This indicates that the principal dispersion of these alcohols is not determined by the molecular size; that is, their relaxation is not a property of a monomer. Since the steric hindrance around the OH group increases with increase in the carbon number, the size of clusters by hydrogen bonds would become smaller possibly in the order of 2-methyl-2-propanol>2-methyl-2-butanol>3-methyl-3-pentanol. The above statement seems to be in accordance with the hypothesis that the principal dispersion is associated with the size of the hydrogen-bonded cluster of alcohols.[8]

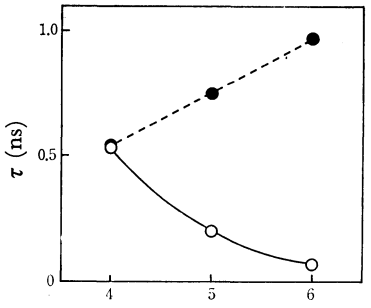

Fig. 1. Relaxation time, τ, *vs.* the number of carbon atoms of the alcohol at 25 °C.
○: tertiary alcohols, ●: normal alcohols.[4]

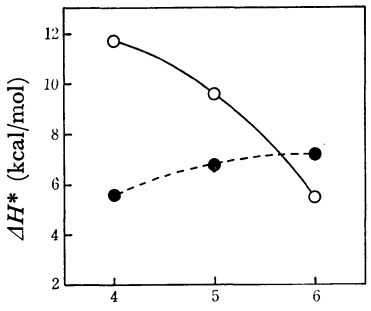

Fig. 2. Activation enthalpy, ΔH^*, *vs.* the number of carbon atoms of the alcohol.
○: tertiary alcohols, ●: normal alcohols.[4]

References

1) C. P. Smyth, "Dielectric Behavior and Structure," McGraw-Hill Book Co., Inc., New York (1955), pp. 114—116.
2) G. P. Srivastava, P. C. Mathur, and Mrs. Krishna, *J. Chem. Phys.*, **60**, 1894 (1974).
3) Y. Koga, H. Takahashi, and K. Higasi, This Bulletin, **47**, 84 (1974).
4) S. K. Garg and C. P. Smyth, *J. Phys. Chem.*, **69**, 1294 (1965).
5) T. Koshii, E. Arie, M. Nakamura, H. Takahashi, and K. Higasi, This Bulletin, **47**, 618 (1974).
6) H. Sato, T. Koshii, H. Takahashi, and K. Higasi, *Chem. Lett.*, **1974**, 579.
7) E. W. Washburn, "Internatioanl Critical Tables of Numerical Data, Physics, Chemistry and Technology," NRC, McGraw-Hill Book Co., Inc., New York (1926).
8) H. Sato, T. Koshii, H. Takahashi, and K. Higasi, *Chem. Lett.*, **1975**, 491.

BULLETIN OF THE CHEMICAL SOCIETY OF JAPAN, VOL. 48 (7), 2226 (1975)

Studies on Ferrocene and Its Derivatives. I. Reactions of Formylferrocene with α-Amino Acids

A. M. OSMAN, M. A. EL-MAGHRABY, and Kh. M. HASSAN
Faculty of Science, University of Assiut, Egypt

(Received May 2, 1973)

Synopsis. The condensation reactions of formylferrocene (I) with various α-amino acids and their esters were studied. The products are new Schiff bases (II) which may be of medicinal value.

From a medicinal point of view, ferrocene is considered to be potent for treatment of iron deficiency anaemia.[1,2] However, it needs to be prepared in the form of a suitable derivative.

The present investigation is an attempt to prepare some new derivatives of ferrocene, likely to be used as haematinics, by interaction of formylferrocene (I) with α-amino acids or their esters. The reaction proceeded smoothly in ethanol and in the presence of sodium carbonate to give quantitative yields of the Schiff bases (II). The time of reaction and purity of the products were controlled by thin layer chromatography (tlc):

$$\underset{\text{(I)}}{\text{Fc-CHO}} + \text{H}_2\text{N-CH(COOR')-R} \xrightarrow[\text{Na}_2\text{CO}_3]{\text{EtOH}} \underset{\text{(II)}}{\text{Fc-CH=N-CH(COOR')-R}}$$

(Fc=ferrocenyl; R=alkyl and others; R'=H or ethyl)

The prepared Schiff bases are brown crystals, sparingly soluble in hot water, easily soluble in ethanol and alkali solution, and insoluble in most organic solvents. They are easily hydrolyzed by dilute acids to their original components. Compounds (II) are likely to inherit the properties of the reactant entities and possess some new medicinal properties.

The results of the above reactions are given in Table 1.

Experimental

General Method of Preparation of Schiff Bases (II). An equimolecular mixture of formylferrocene (I) and an α-amino acid or its ester was refluxed for about two hours in absolute ethanol in the presence of 2 mol of anhydrous sodium carbonate. The reaction mixture was filtered while hot, whereby the Schiff base precipitated after concentration as a brown solid. In certain cases, addition of a few drops of absolute ether is necessary to precipitate the reaction product. The time of reaction and purity of the products were controlled by thin-layer chromatography. Purification of the Schiff bases was effected by dissolution in a minimum volume of absolute ethanol, and precipitation with absolute ether. The results are presented in Table 1: melting points were uncorrected, and the solvent used for tlc estimation of R_f value was a 20: 1 benzene–ethanol mixture.

Hydrolysis of Schiff Bases (II). A sample of the Schiff base (II; R=H, R'=Et) was covered with 2 M HCl, then heated for about half an hour. The reaction mixture was filtered while hot, whereby formylferrocene (I) was isolated as dark brown crystals (mp 223—224 °C). It was identified by means of the mixed melting point test with an authentic sample, and by the identical R_f value (0.26, benzene). The filtrate from the reaction mixture was concentrated and cooled to precipitate the amino acid hydrochloride, which on neutralisation deposited the free amino acid (identified by mp and R_f value).

References

1) British Pat. 819108, 26.8.59. (Imperial Chemical Industries, Ltd.)
2) British Pat. 869504, 31.5.61; 870949, 21.6.61. (Imperial Chemical Industries, Ltd.).

TABLE 1. Fc–CH=N–R″

Amino acid part (=N-R″)	Yield	Mp (°C)	R_f	Molecular formula	Obsd (%)			Calcd (%)		
					C	H	N	C	H	N
Glycine	92	270	0.65	$C_{13}H_{13}O_2NFe$	57.23	4.69	5.11	57.38	4.8	5.16
DL-Alanine	90	200—201	0.57	$C_{14}H_{15}O_2NFe$	58.85	5.19	4.90	58.93	5.26	4.91
β-Alanine	88	213—214	0.55	$C_{14}H_{15}O_2NFe$	58.84	5.15	4.90	58.94	5.26	4.91
DL-Valine	93	215	0.73	$C_{16}H_{19}O_2NFe$	61.17	5.93	4.45	61.32	6.07	4.47
DL-Leucine	90	204—205	0.64	$C_{17}H_{21}O_2NFe$	62.28	6.35	4.28	62.39	6.42	4.28
DL-Isoleucine	87	250	0.80	$C_{17}H_{21}O_2NFe$	62.25	6.40	4.29	62.39	6.42	4.28
L-Glutamic acid	95	265—267	0.63	$C_{16}H_{17}O_4NFe$	55.88	4.87	3.99	55.97	4.95	4.08
DL-Aspartic acid	95	232—233	0.59	$C_{15}H_{15}O_4NFe$	54.60	4.46	4.22	54.71	4.55	4.26
L-Tyrosine	90	230	0.72	$C_{20}H_{19}O_4NFe$	60.95	4.47	3.48	61.06	4.83	3.56
DL-Tyrosine	88	190—191	0.64	$C_{22}H_{20}O_2NFe$	52.71	3.92	5.67	52.80	4.00	5.60
L-Methionine	87	229—230	0.71	$C_{16}H_{19}O_2NSFe$	55.54	5.39	3.98	55.65	5.50	4.06
L-Cystine	88	260—261	0.61	$C_{28}H_{28}N_2O_4S_2Fe_2$	53.02	4.31	4.35	53.16	4.43	4.43
L-Arginine	87	238—239	0.51	$C_{28}H_{30}N_3O_2Fe$	59.23	5.19	9.81	59.36	5.30	9.89
Glycine ethyl ester	90	140	0.61	$C_{16}H_{17}O_2NFe$	59.89	5.51	4.63	60.02	5.69	4.70
DL-Alanine ethyl ester	89	173	0.63	$C_{16}H_{19}O_2NFe$	61.15	5.93	4.38	61.32	6.07	4.47
DL-Valine ethyl ester	91	230	0.65	$C_{18}H_{23}O_2NFe$	63.21	6.66	3.99	63.34	6.74	4.10
L-Leucine ethyl ester	90	291—292	0.62	$C_{19}H_{25}O_2NFe$	64.08	6.91	3.82	64.22	7.04	3.94

Fc=Ferrocenyl

BULLETIN OF THE CHEMICAL SOCIETY OF JAPAN, VOL. 48 (7), 2227—2228 (1975)

Synthesis of Succin-as-eins. II.[1] Dyes Derived from β-(2-Fluoroyl) propionic, β-(3-Phenanthroyl)propionic Acids and Carbazole-3,6-bis(γ-ketobutyric Acid)

R. GOPAL* and P. C. GUPTA
Department of Chemistry, University of Allahabad, India

(Received May 10, 1974)

Synopsis. A number of succin-as-eins have been prepared by condensing β-(2-fluoroyl)propionic, β-(3-phenanthroyl) propionic acids and carbazole-3,6-bis(γ-ketobutyric acid) with phenol, resorcinol, catechol, quinol, phloroglucinol, pyrogallol, and orcinol.

The γ-keto acids have been found to cyclize to their γ-hydroxylactones,[2] which yield acetyl derivatives[3,4] retaining their cyclic structures. The β-(2-fluoroyl) propionic acid[5] (I: R=$C_{13}H_9$) and β-(3-phenanthroyl) propionic acid[6] (I: R=$C_{14}H_9$) gave a new series of cyclic compounds, succin-as-eins (IIIa—g)[1] on condensation with phenols such as phenol, resorcinol, catechol, quinol, phloroglucinol, pyrogallol, and orcinol. Similarly, carbazole-3,6-bis(γ-ketobutyric acid) (VI)[7] gave a new series of cyclic bis-compounds (VIIa—g) on condensation with respective phenols. The condensation process proceeds through the equilibrium process of lactol (II) of acid (I) as described earlier.[1,8]

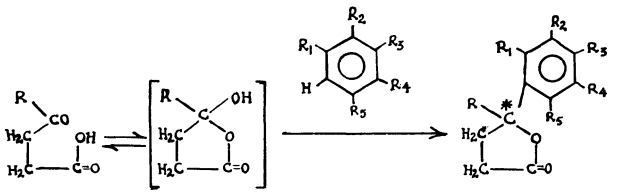

I II IIIa—g

(IIIa) $R_1=R_2=R_4=R_5=H$; $R_3=OH$
(IIIb) $R_2=R_4=R_5=H$; $R_1=R_3=OH$
(IIIc) $R_3=R_4=R_5=H$; $R_1=R_2=OH$
(IIId) $R_2=R_3=R_5=H$; $R_1=R_4=OH$
(IIIe) $R_2=R_4=H$; $R_1=R_3=R_5=OH$
(IIIf) $R_4=R_5=H$; $R_1=R_2=R_3=OH$
(IIIg) $R_2=R_4=H$; $R_5=CH_3$; $R_1=R_3=OH$
(IV) $R_2=R_4=R_5=H$; $R_1=R_3=OCOCH_3$
(V) $R_5=H$; $R_2=R_4=Br$; $R_1=R_3=OH$

Scheme 1.

The IR (KBr) spectra of IIIa—g, VIIa—g, VIII, and IX show strong bands between 1760—1750 cm^{-1} (γ-lactone). The respective diacetyl (IV: 1760, 1200, and 1125 cm^{-1}) and dibromo (V: 1760 cm^{-1}) derivatives of fluorenyl resorcinol succin-as-ein (IIIb: R=$C_{13}H_9$) and phenanthryl resorcinol succin-as-ein (IIIb: R=$C_{14}H_9$) are also indicative of γ-lactone and resorcinol molecule in it. The pentacetyl (VIII: four acetoxy and one *N*-acetyl) and tetrabromo (IX) derivatives of carbazole-3,6-bis-resorcinol succin-as-ein (VIIb) are indicative of two resorcinol molecules in it. The absorption maxima (λ_{max}) of IIIa—g given in Table 1

Table 1. Preparation and properties of 2-fluorenyl succin-as-eins (III: R=$C_{13}H_9$) and 3-phenanthryl succin-as-eins (III: R=$C_{14}H_9$)

Dyes	Condensation Temp. (°C)	Condensation Time (hr)	Mp (°C)	Appearance	λ_{max}^{EtOH} (nm); ε Neutral	λ_{max}^{EtOH} (nm); ε at (pH)	Found % C	Found % H	Calcd % C	Calcd % H
(IIIa; R=$C_{13}H_9$)[a]	150	3	320	Dark brown	—	400 (10.8); 6840	80.38	4.99	80.70	5.26
(IIIb; R=$C_{13}H_9$)	160	3/4	235	Dull red	450; 2828 & 480; 2577	500 (9.3); 716	76.98	5.17	77.09	5.02
(IIIc; R=$C_{13}H_9$)	160	1/4	270	Dark brown	—	b)	76.83	5.31	77.09	5.02
(IIId; R=$C_{13}H_9$)	170	1/3	225	Dark brown	—	b)	77.27	5.39	77.09	5.02
(IIIe; R=$C_{13}H_9$)	190	1/12	210	Dark yellow	—	430 (9.0); 5984	73.53	4.67	73.79	4.81
(IIIf; R=$C_{13}H_9$)	160	1/6	220	Yellow	—	b)	73.41	4.58	73.79	4.81
(IIIg; R=$C_{13}H_9$)	160	1/12	250	Deep red	—	b)	77.13	5.17	77.42	5.40
(IIIa; R=$C_{14}H_9$)	110	6	182	Pink	—	430 (9.7); 7080	80.98	5.31	81.35	5.08
(IIIb; R=$C_{14}H_9$)[a]	150	1	178	Red	450; 1184	500 (10.0); 2664	78.07	5.09	77.84	4.86
(IIIc; R=$C_{14}H_9$)	130	3	205	Brown	—	b)	77.52	4.49	77.84	4.86
(IIId; R=$C_{14}H_9$)	160	1/2	195	Olive green	—	b)	77.55	4.51	77.84	4.86
(IIIe; R=$C_{14}H_9$)	160	1/6	220	Light brown	—	420 (8.9); 3860	74.27	4.31	74.61	4.66
(IIIf; R=$C_{14}H_9$)	130	5/4	188	Dark brown	—	b)	74.91	4.33	74.61	4.66
(IIIg; R=$C_{14}H_9$)	140	3	180	Orange	—	b)	77.89	4.88	78.12	5.20

a) Excess phenol after condensation was removed by steam distillation. b) The alkaline solution decomposed during the measurement of λ_{max} values.

* Present address: Defence Laboratory, Jodhpur, India.

Table 2. Preparation and properties of carbazole-3,6-bis-succin-as-eins (VII)

Dyes	Condensation Temp. (°C)	Condensation Time (hr)	Mp (°C)	Appearance	λ_{max}^{EtOH} (nm); ε Neutral	λ_{max}^{EtOH} (nm); ε at (pH)	Found % C	Found % H	Found % N	Calcd % C	Calcd % H	Calcd % N
VIIa[a]	150	13½	>300	Dark brown	—	390 (10.8); 10380	73.68	4.73	2.58	73.98	4.81	2.69
VIIb	160	1/12	>300	Violet red	455; 2204	500 (8.9); 5069	69.29	4.82	2.43	69.69	4.52	2.54
VIIc	160	1/4	>300	Dark brown	—	470 (7.8); 2430	69.32	4.18	2.16	69.69	4.52	2.54
VIId	170	1/6	>300	Dark brown	—	b)	65.54	4.10	2.18	69.69	4.52	2.54
VIIe	190	1/15	>300	Scarlet red	—	430 and 450 (9.2); 4197	65.56	4.01	2.16	65.86	4.28	2.40
VIIf	150	1/2	>300	Dark brown	—	b)	66.18	4.56	2.65	65.86	4.28	2.40
VIIg	180	1/4	>300	Dark red	—	510 (9.2); 2663	70.14	4.66	2.11	70.46	5.00	2.41

a) Excess phenol after condensation was removed by steam distillation. b) The alkaline solution decomposed during the measurement of λ_{max} values.

(VIIa) $R_1=R_2=R_4=R_5=H$; $R_3=OH$, (VIIb) $R_2=R_4=R_5=H$; $R_1=R_3=OH$, (VIIc) $R_3=R_4=R_5=H$; $R_1=R_2=OH$, (VIId) $R_2=R_3=R_5=H$; $R_1=R_4=OH$, (VIIe) $R_2=R_4=H$; $R_1=R_3=R_5=OH$, (VIIf) $R_4=R_5=H$; $R_1=R_2=R_3=OH$, (VIIg) $R_2=R_4=H$; $R_5=CH_3$; $R_1=R_3=OH$, (VIII) $R_2=R_4=R_5=H$; $R_1=R_3=OCOCH_3$; $NH=NCOCH_3$, (IX) $R_5=H$; $R_2=R_4=Br$; $R_1=R_3=OH$.

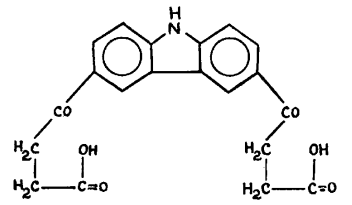

VI

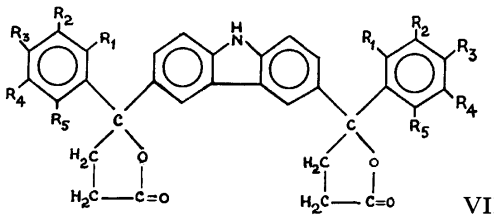

VIIa—g

Scheme 2

and V are comparable with their analogous succineins and phthaleins, but those of VII except that of VIIa given in Table 2 and IX have been found higher than their analogous phthaleins and succineins.

Experimental

All melting points are uncorrected. The λ_{max} (UV and visible) have been recorded on Model DU-2 Beckmann Spectrophotometer and IR determined using a Perkin-Elmer Infracord Spectrometer.

The preparation and purification of the compounds (III) were done in identical manner as described earlier[1,2,8] taking respective acids (I) and phenols (yield, 40—45%). In the preparation of VII, the phenols were taken in twice molar amounts for the acid (VI), and concd H_2SO_4 was used as condensing agent (yield, 45—50%).

Acetylation of IIIb. Each dye (IIIb: $R=C_{13}H_9$ and $R=C_{14}H_9$) (0.5 g), acetic anhydride (10 ml), and fused sodium acetate (2 g) were refluxed at 135—140 °C for 3.5 hr to give a curcumin yellow compound, (IV: $R=C_{13}H_9$) (0.5 g), mp 180 °C; λ_{max}^{EtOH} (ε): 365 nm (8840) and a light yellow compound (IV: $R=C_{14}H_9$) (0.51 g), mp 142 °C; λ_{max}^{EtOH} (ε): 350 nm (6810) which were recrystallized from 80% ethanol.

Found: C, 73.01; H, 4.68; CH_3CO, 19.12%. Calcd for $C_{27}H_{22}O_6$: C, 73.30; H, 4.97; CH_3CO, 19.45%.

Found: C, 73.76; H, 4.72; CH_3CO, 18.66%. Calcd for $C_{28}H_{22}O_6$: C, 74.00; H, 4.84; CH_3CO, 18.94%.

Bromination of IIIb. Each dye (IIIb; $R=C_{13}H_9$ and $R=C_{14}H_9$) (0.5 g) was dissolved in glacial acetic acid (10 ml) and to this a solution of bromine in glacial acetic acid (8 ml) was slowly added in cold to give deep red crystals (V: $R=C_{13}H_9$) (0.51 g), mp 300 °C; λ_{max}^{EtOH} (at pH 7.2) (ε): 520 nm (2476), and red crystals (V: $R=C_{14}H_9$) (0.51 g), mp 196 °C; λ_{max}^{EtOH} (at pH 9.1) (ε): 525 nm (2006) which were recrystallized from 90% ethanol.

Found: Br, 32.22%. Calcd for $C_{23}H_{16}O_4Br_2$: Br, 32.62%.
Found: Br, 29.88%. Calcd for $C_{24}H_{16}O_4Br_2$: Br, 30.27%.

Acetylation of Dye (VIIb). The dye (VIIb) (0.5 g) was treated similarly to the case of IIIb to give a red crystalline pentacetyl compound (VIII) (0.6 g), mp>300 °C (from acetone–ether); λ_{max}^{EtOH} (ε): 320 and 330 nm (6072).

Found: C, 66.51; H, 4.32; CH_3CO, 28.0%. Calcd for $C_{42}H_{35}O_{13}N$: C, 66.22; H, 4.59; CH_3CO, 28.25%.

Bromination of Dye (VIIb). To the dye (VIIb) (0.5 g) in glacial acetic acid (10 ml) was added saturated solution of bromine in acetic acid (15 ml). The contents were left at room temperature for 3 days to give a brown product. The acetone solution of brown product on refluxing with sodium acetate gave a deep red tetrabromo compound (IX) (0.54 g), mp>300 °C (from 80% ethanol); λ_{max}^{EtOH} (at pH 8.1) (ε): 510 and 520 nm (2167); (at pH 10.5): 580 and 600 nm (8670).

Found: Br, 36.50%. Calcd for $C_{32}H_{21}O_8NBr_4$: Br, 36.88%.

One of the authors (R.G.) thanks the C.S.I.R., New Delhi for a grant and fellowship and Director, Defence Laboratory, Jodhpur for granting permission to publish the work.

References

1) Part I: R. Gopal, P. C. Gupta, and S. P. Garg, This Bulletin, **47**, 1789 (1974).
2) P. R. Jones, *Chem. Rev.*, **63**, 465 (1963).
3) S. Gabriel, *Ber.*, **14**, 919 (1881).
4) P. R. Jones and S. L. Congdon, *J. Amer. Chem. Soc.*, **81**, 4291 (1959).
5) C. F. Koelsch, *ibid.*, **55**, 3886 (1933).
6) R. D. Haworth and C. R. Mavin, *J. Chem. Soc.*, **1933**, 1013; W. E. Bachmann and J. T. Bradbury, *J. Org. Chem.*, **2**, 175 (1937—1938).
7) D. R. Mitchell and S. G. P. Plant, *J. Chem. Soc.*, **1936**, 1295.
8) R. Gopal, P. C. Gupta, and S. P. Garg, *J. Indian Chem. Soc.*, **50**, 410 (1973).

BULLETIN OF THE CHEMICAL SOCIETY OF JAPAN, VOL. 48 (7), 2229—2230 (1975)

Calculation of the Ionization Yield in He by Incident Ar^+ and H^+ Ions with the Initial Energies of 1 and 0.1 MeV

Shin-ichi OHNO

Japan Atomic Energy Research Institute, Tokai-mura, Ibaraki 319-11

(Received November 18, 1974)

Synopsis. The classical binary-encounter theory was used to calculate the $G(He^+)$ due to the direct action of incident particles and that due to the secondary electrons. The results show that both values depend greatly on the quality of the radiation used.

The passage of heavy ions in matter causes the formation of various excited and ionized atoms through two processes: (i) the direct action of the incident ion and (ii) the indirect action resulting from the electrons ejected in (i). This note will present the results of calculation of the number of He^+ ions produced in (i) and (ii) respectively when a 1- or 0.1-MeV Ar^+ or the proton has been completely absorbed in He at 0 °C and 1 atm.

Method of Calculation

Non-empirical calculation was made on the basis of the classical binary-encounter approximation.[1] The advantage of this method is that it gives, in a simple way, an estimate of the cross sections as reasonable as the Born approximation over a wide range of energies of the incident particles.[2]

The incident particle with a mass of M, a charge of Ze, and a velocity of V_1 is assumed to collide with the atomic electron with a mass of m, a charge of e and a velocity of v_1. Let V_2 and v_2 be their respective velocities after the collision. When the energy transferred, $E=(1/2)m(v_2^2-v_1^2)$, exceeds the ionization energy, I, of the atomic electron, the ionization of the atom occurs, the kinetic energy of the ejected electron being $E-I$.

The differential cross section, σ_E, for transferring the energy, E, is expressed as:[2]

(i) If $2V_1 \geq v_2 + v_1$, $E \leq 2m_1V_1(V_1 - v_1)$,

$$\sigma_E = \frac{2\pi Z^2e^4}{mV_1^2}\left(\frac{1}{E^2}+\frac{2mv_1^2}{3E^3}\right) \quad (1)$$

(ii) If $v_2 - v_1 \leq 2V_1 \leq v_2 + v_1$, $2mV_1(V_1 - v_1) \leq E \leq 2mV_1(V_1 + v_1)$,

$$\sigma_E = \frac{\pi Z^2e^4}{3V_1^2v_1E^3}\left\{4V_1^3-\frac{1}{2}(v_2-v_1)^3\right\} \quad (2)$$

(iii) If $E/V_1 \geq m(v_2 + v_1)$,

$$\sigma_E = 0 \quad (3)$$

The energy spectrum, $y_p(T)$, of the incident particle as defined by Spencer and Fano,[3] can be expressed as the inverse of its stopping power. The stopping power may be obtained by integrating $E\sigma_E$ over E from E_{min} to E_{max}. E_{min} was set equal to 21.2 eV, the lowest singlet excitation energy of He. E_{max} is given by $2mV_1(V_1+v_1)$. Once $y_p(T)$ is obtained, the number of the He^+ ions produced directly by the incident particle of initial energy, T_0, may be calculated:

$$N_p(He^+) = N\int_I^{T_0} Q_{ion}(T)\cdot y_p(T)dT \quad (4)$$

Here, $Q_{ion}(T)$ is the probability that the He^+ ion will be formed in a collision with the particle with the energy of T and is obtained by integrating σ_E over a pertinent range of E. N is the number of He atoms per unit of volume, and I, the first ionization energy of He (24.6 eV). The G-value is given by $100\cdot N_p(He^+)/T_0$.

The ionization yield due to secondary electrons was calculated as follows. The energy spectrum of the electrons was obtained by Eqs. 1, 2, and 3, with the aid of the $y_p(T)$-curve mentioned above. Then, we could use the previous results[4] to calculate the ionization yields in He due to these ejected electrons.

It should be mentioned that, in the present calculation of the stopping power of the incident particle, we neglected the contributions from such modes of energy loss as the excitations and charge exchange of the projectile (Ar^+) and nuclear collisions. These omissions may slightly decrease the $G(He^+)$ due to incident particles, but the main features of the present results would not be changed.

The applicability of the present method is demonstrated by the facts that (i) the total yield of the ionization and excitation in He by incident 100-keV electrons calculated by the present method is in agreement with the experimental results,[4,5] and that (ii) the observed spectrum of the kinetic energy of the ejected electron on impacting 100-keV protons on He[6] can be well represented by Eq. 1, as is shown in Fig. 1.

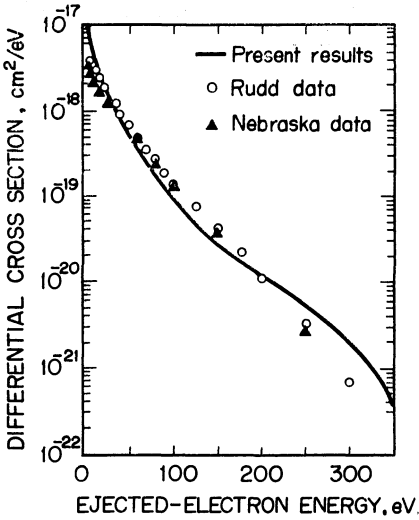

Fig. 1. Differential cross section for ejection of electrons by 100-keV protons in He.

Results

In Fig. 2, the values of $T\cdot Q_{ion}(T)\cdot y(T)$ are plotted againsnt $\ln(T)$ according to Platzman's method.[7] The

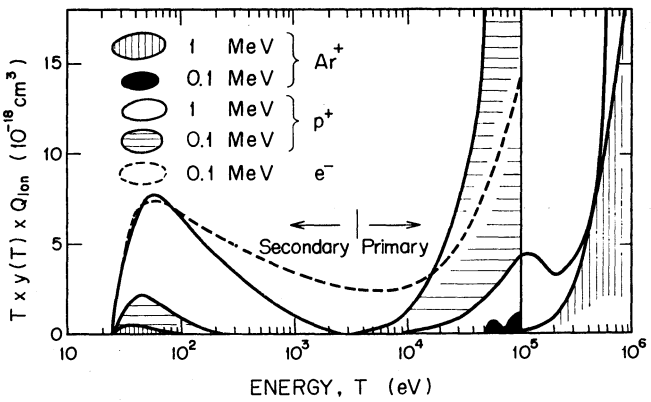

Fig. 2. Contribution of different portions of the slowing-down spectra of the incident particles ("Primary") and the ejected electrons ("Secondary") to the total ionization of He. Coordinate values for 1-MeV incident particles should be multiplied by 10.

area under the curve is proportional to the yield, thus demonstrating the contribution to the yield from a given energy range of the ion or the electrons. In the cases of 1- and 0.1-MeV Ar^+, the yield due to secondary electrons is small compared to that due to the interaction of the incident ion. In the case of the 1-MeV proton, the two processes give approximately the same yield. The energy spectrum of the secondary electrons in this case is similar to that in the case of the incident 100-keV electron.

The *G*-values of the two processes for each incident particle are compiled in Table 1.

Table 1. *G*-values of He^+ for different radiations

Incident particle	Energy (MeV)	Direct[a]	Indirect[b]	Total
Ar^+	1	0.59	0.02	0.61
Ar^+	0.1	0.016	0	0.016
p^+	1	1.75	1.04	2.79
p^+	0.1	1.35	0.15	1.50
e^-	0.1			2.42[c]

a) Ionization due to the direct action of incident particles.
b) Ionization due to the electrons ejected in a).
c) From Ref. 4.

Conclusion

The observed *G*-values of the radiolysis products generally depend on the type and energy of the radiation used. Many radiation chemists seem to ascribe this effect to the different spatial distributions and not to the different primary yields of the products initially formed in the radiation action. The present calculation has been concerned only with the primary yield and not with the spatial distribution. The results clearly show that the primary yield itself depends on the quality of the radiation used. Thus, the yields in addition to the spatial distributions must be taken into consideration for a better understanding of the "LET-effect" in radiation chemistry.

The author is indebted to Dr. Kazuhiko Izui, Japan Atomic Energy Research Institute, and Prof. Shin Sato, Tokyo Institute of Technology, for their helpful discussions.

References

1) L. H. Thomas, *Proc. Camb. Phil. Soc.*, **23**, 829 (1927).
2) L. Vriens, "Case Studies in Atomic Collision Physics I," ed. by E. W. McDaniel, North-Holland, Amsterdam (1969), p. 335.
3) L. V. Spencer and U. Fano, *Phys. Rev.*, **93**, 1172 (1954).
4) S. Ohno, *Chem. Lett.*, **1973**, 817.
5) S. Sato, K. Okazaki, and S. Ohno, This Bulletin, **47**, 2174 (1974).
6) M. E. Rudd, C. A. Sautter, and C. L. Bailey, *Phys. Rev.*, **151**, 20 (1966).
7) R. L. Platzman, *Int. J. Appl. Radiat. Isotopes*, **10**, 116 (1961).

Normal Vibrations of Benzenesulfonate and Benzene-d_5-sulfonate Ions

Toyozo Uno, Akio Kuwae, Yutaka Saito, and Katsunosuke Machida
Faculty of Pharmaceutical Sciences, Kyoto University, Sakyo-ku, Kyoto 606
(Received January 23, 1975)

Infrared and Raman spectra of sodium benzenesulfonate and its fully *C*-deuterated derivative have been recorded in the solid state and in the aqueous solution. The normal coordinate analysis has been made for $C_6H_5SO_3^-$ and $C_6D_5SO_3^-$ ions based on the C_{2v} symmetry. A valence force field was assumed and the force constants were refined by the least squares method. It was found that the diagonal force constants for the CH out-of-plane bending vibrations at the *ortho* and the *para* positions are greater than the corresponding constant for the *meta* position. This result reflects well the effect of the electron attractive substituent in monosubstituted benzene derivatives. The force constants obtained were transferred to *p*-toluenesulfonate ion successfully.

The infrared spectra of benzenesulfonic acid salts have been studied by a few investigators with limited interest in the asymmetric and the symmetric stretching frequencies of the SO_3^- group.[1-3] Exceptionally, Margoshes *et al.*[4,5] quoted a band at 750 cm^{-1} as a datum to illustrate a correlation between the out-of-plane CH deformation frequencies and the electronegativity and the mass of the substituent in a series of monosubstituted benzenes. No reports seem to have been published yet on the overall vibrational assignments for benzenesulfonate ion. In the present work, we have investigated the infrared and Raman spectra of sodium benzene- and benzene-d_5-sulfonates, assigning the fundamental frequencies in detail and carrying out the normal coordinate analysis for both the in-plane and the out-of-plane vibrations. Special attention has been drawn on the infrared band at 750 cm^{-1} due to the CH out-of-plane deformation vibration in which all the hydrogen atoms move in phase. This band appears normally in the region between 770 and 720 cm^{-1} for monosubstituted benzenes. As well known for the cases of nitrobenzene and benzoic acid derivatives, the in-phase CH out-of-plane deformation frequency is raised when the substituent becomes strongly electron attractive. Although the $-SO_3^-$ group is supposed to be an electron attractive substituent, benzenesulfonate ion shows this band in the middle of the normal range, 750 cm^{-1}. In this respect it is of interest to clarify the role of the mass and the electronegativity of the substituent in determining the CH out-of-plane deformation frequencies.

Experimental

Commercially available sodium benzenesulfonate and sodium *p*-toluenesulfonate were recrystallized from methanol. Sodium benzene-d_5-sulfonate was kindly supplied by Dr. Y. Tanaka of Okayama University. The infrared spectra were recorded on a Koken DS-301 spectrophotometer equipped with NaCl prisms (4000—650 cm^{-1}), on a Perkin Elmer Model 521 grating spectrophotometer (800—250 cm^{-1}) and on a Hitachi FIS-3 grating spectrophotometer (400—33 cm^{-1}). The measurements were made for the mulls with Nujol or hexachlorobutadiene over the whole range, and for the aqueous (H_2O and D_2O) solutions between 1700 and 650 cm^{-1}. The Raman spectra of the crystalline powder samples sealed in capillary tubes were measured on a JEOL S-1 laser Raman spectrophotometer. The slit width was 12 cm^{-1}. The Raman polarization measurement was made for the saturated aqueous solution. The 514.5 nm line of a Coherent 52 G Ar^+ laser was used as the excitation source. The infrared and the Raman specra of sodium benzene- and benzene-d_5-sulfonates are shown in Figs. 1 and 2. The observed fundamental frequencies are listed in Table 1 together with the assignments and the calculated frequencies.

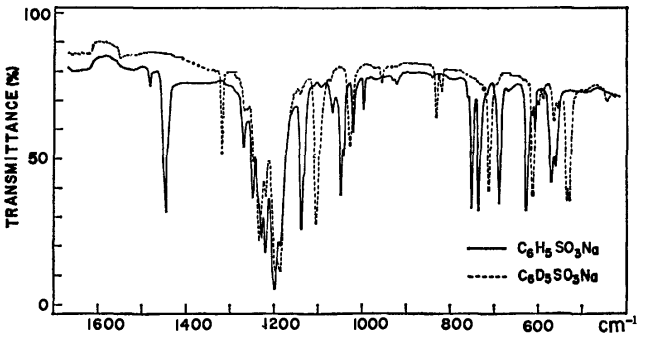

Fig. 1. Infrared spectra of sodium benzenesulfonate and sodium benzene-d_5-sulfonate.

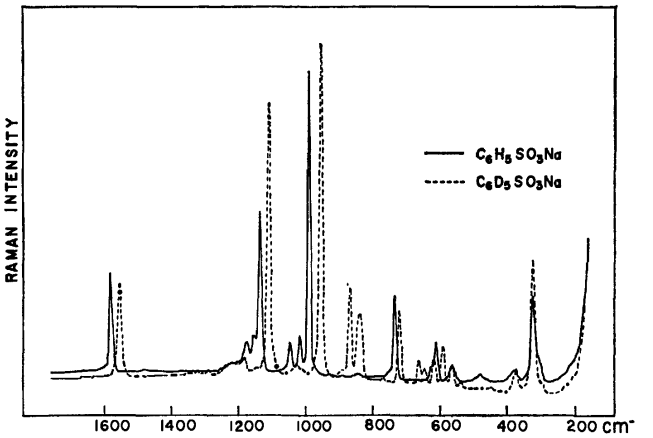

Fig. 2. Raman spectra of sodium benzenesulfonate and sodium benzene-d_5-sulfonate.

Assignments

For sodium benzene-d_5-sulfonate, one of the b_2 CD in-plane deformation frequencies expected around 850 cm^{-1} could not be found in either the infrared or the Raman spectrum. All the other fundamentals due to the ring in-plane vibrations of benzene- and benzene-d_5-sulfonate ions were easily assigned by referring to the available data for toluene,[6] chlorobenzene[7,8] and their ring deuterated compounds.[6,8,9]

Table 1. Observed and calculated fundamental frequencies (cm^{-1})

Species	Sodium benzenesulfonate				Sodium benzene-d_5-sulfonate			
	Obsd		Calcd	Assignment	Obsd		Calcd	Assignment
	IR	Raman			IR	Raman		
a_1		1584[a]	1588	νCC+βCH	1552 w	1555[a]	1549	νCC+δring
	1487 w	1489 vw	1492	βCH+νCC			1353	νCC+βCD
		1177 w	1190	βCH+νCC	1107 s	1110 s p	1117	νCS+ν_sSO$_3$+νCC
	1137 s	1136 s p	1137	νCS+νCC+ν_sSO$_3$	1030 m	1022 w p	1031	ν_sSO$_3$+νCC+δring
	1049 s	1048 w p	1048	ν_sSO$_3$+νCC	957 w	953 s p	950	δring+νCC
	1020 m	1022 w p	1024	νCC+δring		866 m p	854	βCD
	995 w	991 s p	998	δring+νCC	834 m[a]	837 m p	825	βCD+νCC
	735 s	735 m p	736	νCS+δring	711 s	718 m p	709	νCS+δring
	560 s	567 w	568	δ_sSO$_3$+δring	566 w	562 w	563	δ_sSO$_3$+δring
	330 m	322 m p	329	δ_sSO$_3$+δring+νCS	323 m	322 m p	322	δ_sSO$_3$+δring+νCS
b_2		1584 m dp	1588	νCC	1552 w	1555 m dp	1546	νCC
	1447 s	1448 vw	1450	βCH+νCC	1320 m		1316	νCC+βCD
	1310 vw		1323	βCH			1283	νCC
			1286	νCC	1193 vs[a]		1193	ν_aSO$_3$
	1194 vs[a]		1193	ν_aSO$_3$		1048 vw	1033	βCD
	1157 sh	1158 w	1161	βCH			835	βCD
	1069 w		1076	νCC+βCH	822 w		813	βCD
	628 s	624 sh	621	δring	611 s[a]	616 w	611	δ_aSO$_3$
	614 w	610 w dp	611	δ_aSO$_3$	589 w	590 w dp	599	δring
	383 w	376 w dp	383	ρSO$_3$+δCS	378 w[a]	372 w dp	378	ρSO$_3$
	218 m		219	δCS	207 m		207	δCS
b_1	1194 vs		1194	ν_aSO$_3$	1193 vs		1194	ν_aSO$_3$
	985 vw		984	γCH	834 m		837	γCD+tor
	921 w		919	γCH+tor	761 vw		765	γCD+tor
	750 s		748	tor+γCH+γCS	611 s	616 w	613	δ_aSO$_3$+tor
	688 s		687	tor+γCH	599 sh		604	δ_aSO$_3$+tor+γCD
	609 m		609	δ_aSO$_3$	531 s	536 vw	530	γCD+tor
	478 w	478 w	469	tor+ρSO$_3$+γCS	433 m		442	ρSO$_3$+tor+γCS
	383 w		385	tor+ρSO$_3$	378 w	372 w dp	361	tor+γCS+ρSO$_3$
	133 m		139	γCS	125 w		132	γCS
a_2	965 vw		962	γCH		772 vw	772	γCD+tor
	840[b]		853	γCH	655 vw		663	γCD
	407 sh		417	tor+γCH	371 sh		367	tor+γCD

a) Overlapped frequencies. b) Frequency estimated from combination band.

Table 2. Analysis of summation bands

Obsd	Calcd	Obsd	Calcd
1963	1970=985(b_1)+985(b_1)	1763	1761=840(a_2)+921(b_1)
1955	1950=965(a_2)+985(b_1)	1745	1735=750(b_1)+985(b_1)
1900	1906=921(b_1)+985(b_1)	1716	1715=750(b_1)+965(b_2)
1889	1886=921(b_1)+965(a_2)	1682	1680=840(a_2)+840(a_2)
1805	1805=840(a_2)+965(a_2)	1670	1671=750(b_1)+921(b_1)
1775[a]	1771=1157(b_2)+614(b_2)		

a) Combination band of in-plane fundamentals.

The infrared bands observed at 1194 and 1049 cm^{-1} for the crystal of sodium benzenesulfonate are assigned to the asymmetric and the symmetric SO_3^- stretching vibrations, respectively.[1] The former band is broad and splits complicatedly, but in the aqueous solution this splitting disappears and only a single broad absorption is observed in the same frequency region. The symmetric stretching band is sharp and shifts to 1033 cm^{-1} on going to the aqueous solution. Sodium benzene-d_5-sulfonate shows the corresponding infrared bands at 1193 and 1030 cm^{-1}. In analogy with the case of benzenesulfonyl chloride[10] the C-S stretching vibration is thought to couple with a ring vibration, contributing to the infrared bands at 1137 and 735 cm^{-1} of sodium benzenesulfonate and those at 1107 and 711 cm^{-1} of sodium benzene-d_5-sulfonate.

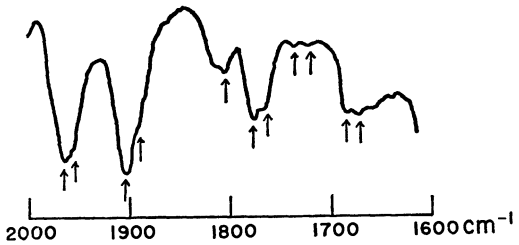

Fig. 3. Infrared summation bands in the region between 1600 and 2000 cm^{-1}. The arrows show the observed absorptions.

Except for the strong infrared band at 750 cm^{-1}, the assignments of the CH out-of-plane deformation frequencies were accomplished with the aid of an analysis of the summation bands in the region between 2000 and 1600 cm^{-1}.[11] (see Fig. 3) The agreements between the sums of the fundamentals and the observed summation frequencies are good as shown in Table 2. Among these summation bands, the band near 1800 cm^{-1} due to the combination of the two a_2 vibrations is the least sensitive to the change of the substituent, since the a_2 vibrations do not involve the motion of the substituent when it is approximated to be a point mass. One of the a_2 fundamentals of benzenesulfonate ion is observed at 965 cm^{-1} in the infrared spectrum probably because the molecular symmetry is lowered in the crystal. The remaining a_2 fundamental is easily estimated from the summation frequency 1805 cm^{-1}. The assignments of the b_1 out-of-plane ring deformation frequencies were made by analogy with toluene[6] and chlorobenzene[7,9,12], and by referring to the result of the normal coordinate calculation with the starting set of force constants.

After the ring vibrational frequencies were identified, the infrared and the Raman bands left unassigned below 700 cm^{-1} were attributed to the symmetric and the asymmetric deformation vibrations and the rocking vibrations of the SO_3^- group by referring to the corresponding frequencies of methanesulfonate ion.[13] The presently assigned SO_3^- group frequencies are reasonable in comparison with those for *p*-aminobenzenesulfonate ion.[14]

Normal Coordinate Analysis

The structure determination by the X-ray analssis has not yet been made for sodium benzenesulfonate. Accordingly, the structure of benzenesulfonate ion was estimated in this work from analogy with the results of the X-ray analysis for magnesium and zinc salts.[15] The benzene ring was assumed to be a regular hexagon being coplanar with one of the S–O bonds. The six angles around the sulfur atom were taken to be tetrahedral. We adopted the molecular symmetry C_{2v} for benzenesulfonate ion by eliminating the interaction terms between the ring and the substituent from the force field.[16] The torsional motion around the C–S bond was excluded from the calculation. Figure 4 shows the structure parameters and the internal coordinate system.

The force field was assumed to be of the valence type and the initial values of force constants for the ring

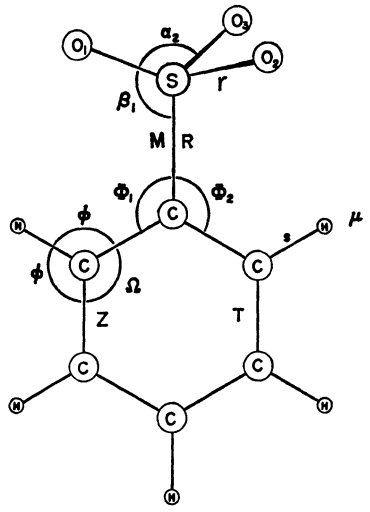

Fig. 4. The structure and the internal coordinates used in the calculation. Bond lengths(in Å): CH, 1.084; CC, 1.397; CS, 1.82; SO, 1.39.

part were taken from toluene.[6] For the sulfonate part, the initial constants were set equal to the F matrix elements obtained from the Urey-Bradley force constants for methanesulfonate ion.[13] In the region above 500 cm^{-1}, the transferred force constants reproduced fairly well the fundamental frequencies already assigned, and the remaining frequencies could be selected so as to reproduce the calculated values as closely as possible under the restriction from the Raman polarization and the isotope effects. Preliminary calculations showed, however, that the agreement between the observed and the calculated frequencies below 500 cm^{-1} could not be improved within the framework of the transferred force field, so that we introduced the interaction constants $F_{\Phi-\rho SO_3}$ and $F_{M-\rho SO_3'}$ with initial values zero. These constants are defined by the terms in the potential function

$$V = \cdots\cdots + F_{\Phi-\rho SO_3} S_\Phi S_{\rho SO_3} + F_{M-\rho SO_3'} S_M S_{\rho SO_3'} + \cdots\cdots,$$

where the coordinates S_Φ, $S_{\rho SO_3}$, S_M and $S_{\rho SO_3'}$ are given by

$$S_\Phi = (\Phi_2 - \Phi_1)/\sqrt{2}$$

$$S_{\rho SO_3} = (2\beta_1 - \beta_2 - \beta_3)/\sqrt{6}$$

$$S_M = M$$

and

$$S_{\rho SO_3'} = (\beta_2 - \beta_3)/\sqrt{2},$$

respectively.

We attributed zero weights to the CH stretching frequencies and accordingly fixed the CH stretching constant K_s to the transferred value. The simultaneous least squares refinement of all the other force constants was found to result in divergence. Accordingly, the iteration was performed alternately for the force constants related to the substituent and for those related to the benzene ring, until the sum of the squared residuals became stationary. In this process, any force constants showing large dispersions were fixed automatically, and for this reason most of the off-diagonal substituent constants were left highly indeterminate. Fortunately,

Table 3. Valence force constants of benzenesulfonate ion

	Type	Unit[a]	Value	Type	Unit	Value
(in-plane)	K_s[b]	1	5.0664	K_T	1	6.4266
	K_R	1	5.3908	H_ϕ	3	0.5161
	H_Φ	3	0.8943	H_Ω	3	0.9920
	F_{T^o}	1	0.7305	F_{T^m}	1	−0.3911
	F_{T^p}	1	0.3959	$F_{T\phi}$	2	0.1076
	$F_{T\Phi}$	2	0.0763	$F_{T\Omega}$	2	0.1187
	F_{TR}	1	0.4831	$F_{R\Phi}$	2	1.1137
	F_{ϕ^o}	3	0.0048	F_{ϕ^m}	3	−0.0074
	F_{ϕ^p}	3	0.0031			
(out-of-plane)	H_{μ^o}	3	0.4620[c]	H_{μ^m}	3	0.4166
	H_{μ^p}	3	0.4925	H_M	3	0.4524
	H_z	3	0.3440	f_{μ^o}	3	−0.0592
	f_{μ^m}	3	−0.0186	f_{μ^p}	3	−0.0093
	f_{z^o}	3	−0.0166	$f_{\mu z^o}$	3	−0.1708
	$f_{\mu z^m}$	3	−0.0061			
(SO_3 part)	K_r	1	8.1777	H_α	3	2.2993
	H_β	3	1.1144	F_{rR}	1	0.1559
	F_{rr}	1	0.3503	$F_{r\alpha}$	2	0.2799
	$F_{R\beta}$	2	0.2134	$F_{r\beta}$	2	0.2000
	$F_{\alpha\alpha}$	3	0.2004	$F_{\alpha\beta}$	3	0.0309
	$F_{\beta\beta}$	3	−0.6562	$F_{\Phi-\rho SO_3}$	3	−0.4487
	$F_{M-\rho SO_3'}$	3	0.3263			

a) 1. in mdyn/Å, 2. in mdyn/rad, 3. in mdyn Å/rad². b) The subscripts denote the coordinates involved. c) Standard errors for H_{μ^o}, H_{μ^m} and H_{μ^p} are 0.0243, 0.0292 and 0.0281 (mdyn Å/rad²), respectively.

the ring frequencies were hardly affected by these constants, and the force constants for the ring part were believed to converge to the best values. The diagonal constants for the CH out-of-plane deformation coordinates at the *meta* and the *para* positions of the substituent, H_{μ^m} and H_{μ^p}, respectively, were constrained to the same value in the calculation for toluene by Lau and Snyder[6], but they were treated as the independent parameters in the present work. The final set of force constants are listed in Table 3.

Discussion

The mixing between the CH out-of-plane deformation and the ring torsional vibrations of benzenesulfonate ion is appreciable in the a_2 and the b_1 species. The infrared bands at 750 and 688 cm^{-1} characteristic of monosubstituted benzenes are contributed almost equally from the CH out-of-plane deformation and the torsional vibrations. The C-S out-of-plane deformation vibration also contributes to the 750 cm^{-1} band, explaining the fact that this frequency is sensitive to the mass of the substituent.[5] For the deuterated compound, the b_1 SO_3^- asymmetric deformation vibration couples with the torsional vibrations in the fundamentals at 611 and 599 cm^{-1}. The infrared band of the undeuterated compound at 478 cm^{-1} corresponds to the X-sensitive band at 508 cm^{-1} of nitrobenzene[17] and also to the 460 cm^{-1} band of benzenesulfonyl chloride.[10] According to the present calculation, this band is due to a coupled mode of the SO_3^- out-of-plane rocking, the C-S out-of-plane deformation and the ring torsional vibrations.

In the presently obtained force field of benzenesulfonate ion, the CH out-of-plane deformation constants for the *ortho* and the *para* hydrogen atoms are appreciably greater than that for the *meta* hydrogen atoms. The electronic theory due to Margoshes *et al.* states that the increase of the local π-electron density on the ring carbon facilitates the rehybridization from sp_2 to sp_3 orbitals on the out-of-plane deformation of the CH bond.[4] The present result is consistent with the prediction of this theory for the *meta*-orienting substituent. A similar conclusion was already obtained by Kakiuchi *et al.* in their simplified treatment of the CH out-of-plane deformation vibrations of some monosubstituted benzenes.[18,19] Usually, the characteristic infrared band due to the in-phase CH out-of-plane deformation vibration of monosubstituted benzene derivatives shifts to the high-frequency side when the substituent becomes more electron-attractive. Margoshes *et al.* also pointed out that, in the case of mono-atomic substituent X, a negative correlation exists between the frequency of this band and the reduced mass of the bond C–X.[5] For benzenesulfonate ion, the electron drawing character of the substituent tends to raise this frequency, while the large mass of the sulfur atom tends to lower it, and these effects cancell each other. In order to estimate the mass effect we tried a calculation in which the mass of sulfur is replaced by that of carbon and the bond length C-S by that of C–C in toluene, leaving the force constants unchanged. This calculation gave rise to an increase of the in-phase CH out-of-plane deformation frequency by about 10 cm^{-1}, to which the diminutions in the mass and the bond length were found to con-

Table 4. Observed and calculated frequencies of *p*-toluenesulfonate ion (CH_3 and SO_3 vibrations are omitted) (cm^{-1})

	ν_{obsd}	ν_{calcd}	
		Initial	Final[a]
b_1 species	952	957	949
	813	818	897
	694	766	713
	622	609	609
	482	540	501
	406	412	409
	232	250	246
a_2 species	973	962	979
	846	852	848
	373	412	362

a) In the final calculation, $H_{\mu^o}=0.4881$, $H_{\mu^m}=0.4085$ and $H_z=0.2947$ mdyne Å/rad^2.

tribute equally.

In order to check the transferability of the force constants among related compounds, the normal coordinate calculation for *p*-toluenesulfonate ion was performed in the same way as that for benzenesulfonate ion. The force constants for the methyl group were transferred from toluene[6] and the others from the final set for benzenesulfonate ion. By using these constants, the observed frequencies of sodium *p*-toluenesulfonate were reproduced well except for two infrared frequencies 694 and 482 cm^{-1} to which the torsional vibrations contribute mainly. With the purpose to attain a better fit between the observed and the calculated frequencies, the force constants related to the CH out-of-plane deformation and the torsional vibrations were refined by the least squares method. After several cycles of refinements, the torsional constant H_z converged to an intermediate value between those of toluene and benzenesulfonate ion, and fairly good fit was obtained without large changes of the CH out-of-plane deformation constants. The results are shown in Table 4. The large differences in the torsional constants among differently substituted benzene derivatives indicate that the easiness of the torsional motion is highly sensitive to the ring-electron density, which in turn is related closely to the number and the kind of the substituents. For the other force constants, we may conclude that the transferability between benzenesulfonate and *p*-toluenesulfonate ions is fairly good.

The authors wish to express their thanks to Prof. T. Takenaka and Prof. S. Hayashi of Kyoto University for the use of Perkin-Elmer Model 521 and Hitachi FIS-3 grating infrared spectrophotometers. Thanks are also due to Dr. Y. Tanaka of Okayama University for supplying the sample of sodium benzene-d_5-sulfonate. Throughout this work, FACOM 230—60 and 230—75 computers of Kyoto University Computer Center were used.

References

1) B. J. Lindberg, *Acta Chem. Scand.*, **21**, 841 (1967).
2) B. J. Lindberg, *ibid.*, **21**, 2215 (1967).
3) S. Detoni and D. Hadzi, *Spectrochim. Acta*, **11**, 601 (1957).
4) R. D. Kross, V. A. Fassel, and M. Margoshes, *J. Amer. Chem. Soc.*, **78**, 1332 (1956).
5) M. Margoshes and V. A. Fassel, *Spectrochim. Acta*, **7**, 14 (1955).
6) C. La Lau and R. G. Snyder, *ibid.*, **27A**, 2073 (1971).
7) D. H. Whiffen, *J. Chem. Soc.*, **1956**, 1350.
8) J. R. Sherrer, *Spectrochim. Acta*, **20**, 345 (1964).
9) T. R. Nanney, R. T. Bailey, and E. R. Lippincott, *Spectrochim. Acta*, **21**, 1495 (1965).
10) T. Uno, K. Machida, and K. Hanai, *ibid.*, **24A**, 1705 (1968).
11) D. H. Whiffen, *ibid.*, **7**, 253 (1955).
12) J. R. Sherrer, *ibid.*, **23A**, 1489 (1967).
13) K. Fujimori, This Bulletin, **32**, 621 (1959).
14) L. Ganguly, C. I. Jose, and A. B. Biswas, *Spectrochim. Acta*, **24A**, 215 (1968).
15) J. M. Broomhead and A. D. I. Nicol, *Acta Crystallogr.*, **1**, 88 (1948).
16) B. L. Crawford, Jr. and E. B. Wilson, Jr., *J. Chem Phys.*, **9**, 323 (1941).
17) C. V. Stephenson, W. C. Coburn, Jr., and W. S. Wilcox, *Spectrochim. Acta*, **17**, 933 (1961).
18) Y. Kakiuchi, *Nippon Kagaku Zasshi*, **80**, 250 (1959).
19) Y. Kakiuchi, H. Saito, and T. Yokoyama, *J. Mol. Spectrosc.*, **32**, 247 (1969).

Lifetimes of Electrons in Irradiated Liquid Alkanes

Kenji FUEKI

Department of Synthetic Chemistry, Nagoya University Chikusa-ku, Nagoya 464

(Received March 26, 1975)

A calculation has been made of lifetimes of electrons in irradiated liquid alkanes on the basis of the lifetime distribution function for the geminate electrons derived from the exponential distribution function for electron ranges. The results show that the intrinsic electron lifetimes correlate with the electron mobilities and most of the geminate electrons recombine within 1 ns in the alkanes at room temperature. A consideration is given to the effect of pulse duration time on the apparent electron lifetime and the observable yield of electrons in *n*-hexane.

In recent years there has been much interest in the behavior and properties of electrons in nonpolar liquids in some branches of chemistry and physics. In radiation chemistry considerable efforts have been paid to this research field both theoretically and experimentally. As such an effort, a number of studies have been made of ranges of electrons in irradiated liquid hydrocarbons, in which various spatial distribution functions for the thermalized electrons have been used and tested by comparison with experiment. At present it appears that a Gaussian-power function[1] and an exponential function[2–4] are the best among the prescribed forms of electron distribution functions for liquid alkanes. As an alternative approach to an understanding of the behavior of electrons in irradiated liquid hydrocarbons, we may discuss the lifetime distribution of the thermalized electrons. Most of previous studies on this subject have dealt with only very limited hydrocarbons such as cyclohexane and *n*-hexane.[5–8] Also, values of the diffusion constant of the electron used in earlier studies are inappropriate in the light of recent electron mobility data. The diffusion constant of the electron is a crucial factor in determining electron lifetimes. More recent studies have used the appropriate values of the diffusion constant of the electron.[9,10] Schuler and his coworkers[11] have developed a phenomenological model for the description of electron lifetimes in irradiated liquid hydrocarbons which is based on their scavenging function.

In this work, we attempt to calculate the lifetime distribution of electrons in irradiated liquid alkanes on the basis of the exponential distribution function for electron ranges and recent experimental data on electron mobilities. Here we deal with seven alkanes (*n*-pentane, cyclopentane, neopentane, *n*-hexane, cyclohexane, 2,2-dimethylbutane and 2,2,4-trimethylpentane) for which the electron mobilities vary over three orders of magnitude.

Model and Lifetime Distribution Function

First, we assume a model in which an instantaneous pulse of radiation is given to dielectric liquids and ranges of electrons produced are expressed by the exponential distribution function as given by Eq. (1).

$$\begin{aligned} \phi(r) &= 0, && r \leq r_0 \\ \phi(r) &= (1/4\pi br^2)\exp[(r_0-r)/b], && r \geq r_0 \end{aligned} \tag{1}$$

where b is the range parameter and r_0 is the reaction radius. Using the time-distance relationship, $t=r^3/3Dr_c$, derived from the Nernst-Einstein relation[5] and $4\pi r^2\phi(r)\mathrm{d}r=f(t)\mathrm{d}t$, we get Eq. (2) for the lifetime distribution function or the existence function for geminate ion-electron pairs.

$$F(t) = \int_t^\infty f(t)\mathrm{d}t = \exp\{(3Dr_c)^{1/3}[t_0^{1/3}-(t+t_0)^{1/3}]/b\}, \quad 0 \leq t \leq t_f$$

$$t_0 = r_0^3/3Dr_c,\ r_c = e^2/\varepsilon kT \tag{2}$$

where D is the sum of the diffusion constants of the ion and electron, e is the electronic charge, ε is the dielectric constant of a liquid, k is Boltzmann's constant and T is the absolute temperature. Equation (2) represents the fraction of electrons present at time t after an instantaneous pulse of radiation. t_f is a characteristic time difined as $F(t_f)=G_{fI}/G_t$, where G_{fI} and G_t are the free ion yield and the total ion yield, respectively. t_f means the time at which the geminate recombination of ion-electron pairs practically completes.

We may define another characteristic time $t_{1/e}$ for the geminate recombination. $t_{1/e}$ is the time at which the value of $F(t)$ falls to 1/e of its value at $t=0$. Since t_0 is very small, $t_{1/e}$ is given, to a very good approximation, by Eq. (3).

$$t_{1/e} = b^3/3Dr_c \tag{3}$$

$t_{1/e}$ is exactly given by Eq. (3) for $r_0=0$.

Since the Nernst-Einstein relation neglects the effect of outward diffusive motion of electrons on the geminate recombination times, the use of this relation tends to underestimate the geminate recombination times. In the calculations of electron lifetimes, therefore, we have also attempted to correct for this effect in a similar manner to that used in Ref. 12. Such a corrected time t' is given by Eq. (4)

$$t' = t[1+(4/3r_c)(3Dr_c)^{1/3}t^{1/3}]^{3/2} \tag{4}$$

We now consider a square pulse of duration τ. In this case the existence function is expressed by Eq. (5), assuming $r_0=0$.

$$F(t) = (1/\tau)\int_0^\tau \exp[a(t^*-t)^{1/3}]\mathrm{d}t^* \tag{5}$$

where $a=(3Dr_c)^{1/3}/b$ and time is measured from the onset of the pulse. Performing the integration in Eq. (5) leads to Eq. (6).

$$\begin{aligned} F(t) &= (3/\tau a)\{(2/a^2) - [t^{2/3} + (2/a)t^{1/3} + (2/a^2)] \\ &\quad \times \exp(-at^{1/3})\}, \quad t \leq \tau \\ F(t) &= (3/\tau a)\{[(t-\tau)^{2/3} + (2/a)(t-\tau)^{1/3} + (2/a^2)] \\ &\quad \times \exp[-a(t-\tau)^{1/3}] - [t^{2/3} + (2/a)t^{1/3} + (2/a)^2] \\ &\quad \times \exp(-at^{1/3})\}, \quad t \geq \tau \end{aligned} \tag{6}$$

It can be shown that $F(t)$ in Eq. (6) for $\tau=0$ reduces $F(t)$ in Eq. (2) with $r_0=0$.

Values of physical parameters used in the calculations are listed in Table I. Since the diffusion constant of the electron is usually much greater than that of the ion, the diffusion, constant D may be approximated by the diffusion constant of the electron, D_e, which is related to the electron mobility μ_e by $D_e=kT\mu_e/e$. The electron mobility in n-hexane at -80 °C was calculated from a mobility equation $\mu_e=\mu_0\exp(-E/RT)$ where $\mu_0=120$ cm^{2}V^{-1} s^{-1} and $E=4.3$ kcal mole^{-1}.[16,22] The results of the calculations are given in Tables 2 and 3, and Figs. 1—3. The results in Table 2 and Fig. 1 were obtained using $r_0=5$ Å, and those in Table 3 and Figs. 2 and 3 were calculated with $r_0=0$.

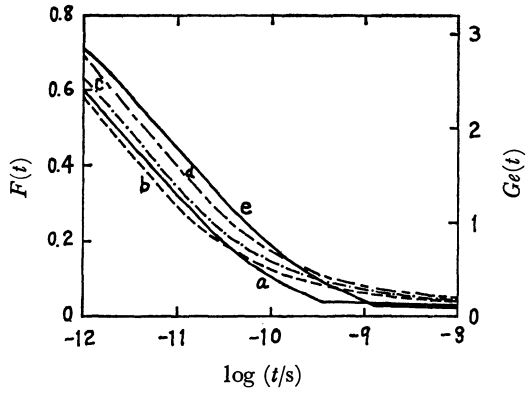

Fig. 1. Decay of electron population in cyclohexane and n-hexane at 23 °C. Time is measured from the input of an instantaneous pulse of radiation. a: cyclohexane, exponential function; b: cyclohexane, Schuler's function ($\alpha=12$ M^{-1}, $k=4.3\times10^{12}$ M^{-1} s^{-1}); c: cyclohexane, Schuler's function ($\alpha=12$ M^{-1}, $k=2.7\times10^{12}$ M^{-1} s^{-1}); d:cyclohexane, Schuler's function ($\alpha=12$ M^{-1}, $k=1.8\times10^{12}$ M^{-1} s^{-1}); e: n-hexane, exponential function.

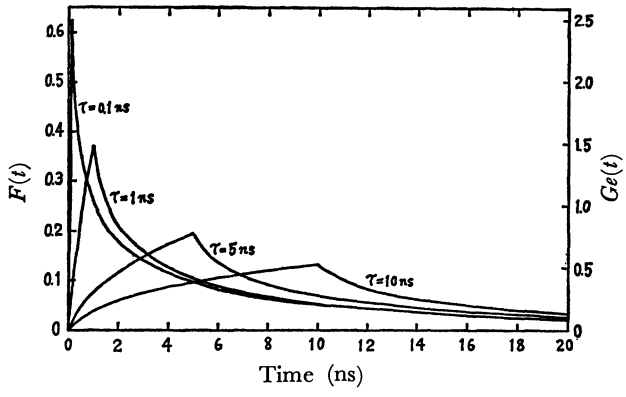

Fig. 2. Growth and decay of electron population in pulse-irradiated n-hexane at -80 °C. Time is measured from the onset of the pulse.

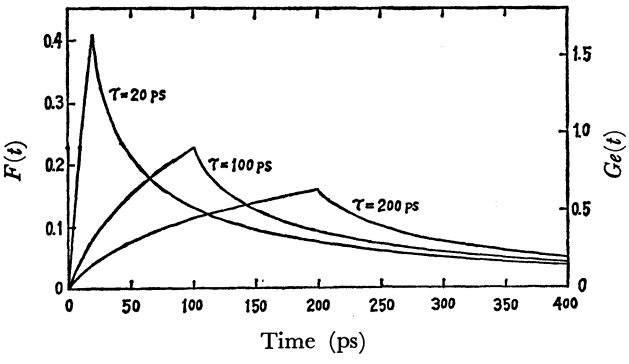

Fig. 3. Growth and decay of electron population in pulse-irradiated n-hexane at 23 °C. Time is measured from the onset of the pulse.

Results and Discussion

Lifetimes of Electrons in Liquid Alkanes. In Table 2 are presented the calculated characteristic times for the geminate recombination of ion–electron pairs in seven alkanes at 23 °C. In the calculations two approximations were used for the time-distance relation: one is the forced diffusion approximation (FD), in which the Nernst-Einstein relation is used; the other is the forced diffusion approximation with a random diffusion correction (FRD), in which Eq. (4) is used for the corrected time t'. It is seen in Table 2 that the FRD approximation yields the characteristic recombination times greater than does the FD approximation. The differences between values obtained with these two approximations are greater for t_f and t_f' than for $t_{1/e}$ and $t_{1/e}'$. This is understandable noting that $t_{1/e}$ or $t_{1/e}'$ represents the geminate recombination time for the electrons not very far away from their parent ions and on which the strong Coulomb field acts, while t_f or t_f' represents the recombination time for the electrons distant from their parent ions and being subjected to the thermal force almost as strong as the Coulomb force. It can be seen from Tables 1 and 2 that the greater is the electron mobility, the greater is the ratio of $t_{1/e}'$ to $t_{1/e}$, for instance, this ratio is the greatest for neopentane and the smallest for n-hexane, while the ratio of t_f' to t_f is about the same (~3) for all the hydrocarbons studied. The magnitude of t_f or t_f' decreases with increasing electron mobility. Similarly, the value of $t_{1/e}$ or $t_{1/e}'$ decreases with increasing electron mobility with one exception of neopentane for which $t_{1/e}$ or $t_{1/e}'$ is somewhat greater than expected from the electron mobility in neopentane. Such an exception is due to the fact that the electron range b in neopentane is much greater than those in the other hydrocarbons as shown in Table 1 and that $t_{1/e}$ is proportional to b^3 (see Eq. (3)). The use of $G_{fi}=0.86$ and $G_t=3.7$ for neopentane yields $b=250$ Å[2] which is close to the b value given in Table 1.

Figure 1 shows the calculated time dependence of electron population in cyclohexane and in n-hexane after an instantaneous pulse of radiation. In Fig. 1 $G_e(t)$ represents the yield of electrons present at time t, calculated setting $G_e(t)=G_t$. Curve a was calculated using the exponential distribution function and the FRD approximation for electrons in cyclohexane. Curves b, c and d for cyclohexane were calculated using S huler's distribution function for electron life times[11] with the reactivity parameter, $\alpha=12$ M^{-1},[23] and the absolute rate constant, $k=4.3\times10^{12}$,[24] 2.7×10^{12},[25] and 1.8×10^{12} M^{-1} sec^{-1},[18] respectively, for the reaction of electrons with carbon tetrachloride. It is seen in

TABLE 1. PHYSICAL PARAMETERS USED IN THE CALCULATIONS AT 23 °C

Liquid	r_c[a] (Å)	b[b] (Å)	μ_e ($cm^2/V \cdot s$)	G_{fi}[a]	G_t
n-pentane	306	65.3	0.16[d]	0.145	4.0[b]
Cyclopentane	288	62.2	1.1[d]	0.155	4.0[b]
Neopentane	318	232[c]	70[e,f]	1.2[c]	5.5[c]
n-Hexane	299	58.1	0.08[e,g]	0.131	4.0[b,h]
Cyclohexane	279	57.5	0.24[g]	0.148	4.0[b,i]
2,2-Dimethylbutane	293	92.8	12[f]	0.304	4.3[b]
2,2,4-Trimethyl-pentane	291	96.1	7[d]	0.332	4.8[j]

a) Ref. 13. b) Ref. 14. c) Ref. 3. d) Ref. 15. e) Ref. 16. f) Ref. 17. g) Ref. 18. h) Ref. 19. i) Ref. 20. j) Ref. 21.

TABLE 2. CHARACTERISTIC TIMES FOR GEMINATE ION-ELECTRON RECOMBINATION IN LIQUID ALKANES AT 23 °C

Liquid	FD		FRD	
	$t_{1/e}$ (ps)	t_f (ps)	$t'_{1/e}$ (ps)	t_f' (ps)
n-Pentane	7.4	290	11	800
Cyclopentane	0.99	37	1.4	100
Neopentane	0.73	2.7	2.0	11
n-Hexane	11	460	15	1200
Cyclohexane	3.7	140	5.3	390
2,2-Dimethylbutane	0.30	5.9	0.50	18
2,2,4-Trimethylpentane	0.57	12	0.98	38

TABLE 3. CALCULATED HALF-LIFE TIMES AND YIELDS OF ELECTRONS IN PULSE-IRRADIATED *n*-HEXANE

t (°C)	τ	$t_{1/2}$	G (e^-)
−80	ns	ns	
	10	13.5	0.52
	5	7.8	0.77
	1	2.4	1.5
	0.1	0.64	2.5
	0	0.13	4.0
23	ps	ps	
	200	290	0.63
	100	170	0.90
	20	53	1.6
	0	3.5	4.0

Fig. 1 that curves b and c are very close to curve a and that curve d gives somewhat higher values of $F(t)$ or $G_e(t)$ than does curve a, but curve d is also comparable to curve a on the time scale. It should be noted, however, that curve a underestimates considerably electron lifetimes in the long-time limit for the geminate ion-electron recombination. Schuler's lifetime distribution function predicts the time dependence of $t^{-1/2}$ in the long-time limit,[11] while Eq. (2) does not predict the $t^{-1/2}$ dependence. This discrepancy arises from the fact that the use of the Nernst-Einstein relation is not appropriate for the description of motion of electrons distant from their parent ions since Brownian motion of electrons is as important as the electron drift in the Coulomb field for such electrons. Curve e shows $F(t)$ or $G_e(t)$ calculated using the exponential distribution function and the FRD approximation for electrons in *n*-hexane. The shape of the curve is similar to that for cyclohexane, but the geminate recombination time in *n*-hexane is longer than that in cyclohexane. It is noted that in the calculations, an extremely low dose rate is assumed, resulting in an indefinitely long lifetime of the free electrons.

Lifetimes of Electrons in Pulse-Irradiated n-*Hexane.* Figures 2 and 3 show the growth and decay of electron population in *n*-hexane at −80 °C and 23 °C, respectively, calculated using Eq. (6) for a square pulse of duration τ. The duration time τ is taken as 0.1, 1, 5 and 10 ns at −80 °C and 20, 100 and 200 ps at 23 °C. It can be seen from Figs. 2 and 3 that the electron population increases with time, reaches a maximum at $t=\tau$ and then decreases with increasing time. It is also seen that the shorter is the duration time of the pulse, the higher is the maximum of electron population and the greater is the apparent decay rate of electrons. Table 3 summarizes the half-life time, $t_{1/2}$, for the decay of electrons and the yield of electrons, $G(e^-)$, at the maximum of electron population. The half-life time for $\tau=0$ is the shortest at each temperature and indicates the intrinsic lifetime of the geminate electrons at that temperature. The lifetimes of electrons at −80 °C are much longer than those at 23 °C. This difference arises from the fact that the electron mobility at −80 °C is much lower than that at 23 °C as shown by the temperature dependence of the mobility equation.

Comments on Pulse Radiolysis Observations of Electrons in Liquid Hydrocarbons. Optical absorption spectra of trapped electrons were observed by the pulse radiolysis technique in liquid hydrocarbons: *n*-hexane, cyclohexane, methylcyclohexane and isopentane at 20 °C;[26] *n*-hexane and 3-methylhexane at −80 °C;[27] methylcyclohexane at −113 °C;[28] squalane at −165∼−70 °C;[29] propane at −185 and −165°C.[30] The decay of electrons observed at room temperature obeys the second-order kinetic law and these electrons are regarded as the free electrons.[26] Studies of the decay of electrons at low temperatures suggest that the initial decay of electrons observed is due to the geminate recombination with their parent ions.[27-30] However, there are only very limited experimental data available for a quantitative comparison between theoretical calculations and the observed characteristics of decay of electrons. Such a comparison has recently been made successfully for electrons in pulse-irradiated liquid propane.[31] It is hoped that a more detailed experimental study will be undertaken on the decay of the geminate electrons in *n*-hexane to test the applicability of the present model.

References

1) J.-P. Dodelet, K. Shinsaka, U. Kortsch, and G. R. Freeman, *J. Chem. Phys.*, **59**, 2376 (1973).
2) G. C. Abell and K. Funabashi, *ibid.*, **58**, 1079 (1973).
3) J.-P. Dodelet and G. R. Freeman, *ibid.*, **60**, 4657 (1974).
4) A. Mozumder, *ibid.*, **60**, 4305 (1974).

5) F. Williams, *J. Amer. Chem. Soc.*, **86**, 3954 (1964).
6) G. R. Freeman, *Adv. Chem. Ser.*, **82**, 339 (1968).
7) A. Hummel, *J. Chem Phys.*, **49**, 4840 (1968).
8) A. Mozmuder, *ibid.*, **48**, 1659 (1968).
9) A. Mozumder, *ibid.*, **55**, 3026 (1971).
10) J.-P. Dodelet and G. R. Freeman, *Can. J. Chem.*, **50**, 2729 (1972).
11) R. H. Schuler and P. P. Infelta, *J. Phys. Chem.*, **76**, 3812 (1972).
12) F. Williams, *J. Chem. Phys.*, **48**, 4077 (1968).
13) W. F. Schmidt and A. O. Allen, *J. Phys. Chem.*, **72**, 3730 (1968).
14) M. Tanaka and K. Fueki, *ibid.*, **77**, 2524 (1973).
15) W. F. Schmidt and A. O. Allen, *J. Chem. Phys.*, **52**, 4788 (1970).
16) R. M. Minday, L. D. Schmidt, and H. T. Davis, *J. Phys. Chem.*, **76**, 442 (1972).
17) G. Bakale and W. F. Schmidt, *Chem. Phys. Lett.*, **22**, 164 (1973).
18) A. O. Allen and R. A. Holroyd, *J. Phys. Chem.*, **78**, 796 (1974).
19) J. M. Warman and S. J. Rzad, *J. Chem. Phys.*, **52**, 485 (1970).
20) J. M. Warman, K.-D. Asmus, and R. H. Schuler, *J. Phys. Chem.*, **73**, 931 (1969).
21) S. J. Rzad and K. M. Bansal, *ibid.*, **76**, 2374 (1972).
22) R. M. Minday, L. D. Schmidt, and H. T. Davis, *J. Chem. Phys.*, **54**, 3112 (1971).
23) G. W. Klein and R. H. Schuler, *J. Phys. Chem.*, **77**, 978 (1973).
24) J. H. Baxendale, J. P. Keene, and E. J. Rasburn, *J. Chem. Soc. Faraday I*, **70**, 718 (1974).
25) A. O. Allen, T. E. Gangwer, and R. A. Holroyd, *J. Phys. Chem.*, **79**, 25 (1975).
26) J. H. Baxendale, C. Bell, and P. Wardman, *J. Chem. Soc. Faraday I*, **69**, 776 (1973).
27) J. T. Richards and J. K. Thomas, *Chem. Phys. Lett.*, **10**, 317 (1971).
28) J. H. Baxendale, C. Bell, and P. Wardman, *ibid.*, 12, 347 (1971).
29) I. A. Taub and H. A. Gillis, *J. Amer. Chem. Soc.*, **91**, 6507 (1969).
30) H. A. Gillis, N. V. Klassen, G. G. Teather, and K. H. Lokan, *Chem. Phys. Lett.*, **10**, 481 (1971).
31) K. Fueki, to be published.

Ranges and Lifetimes of Electrons in Irradiated Liquid Hydrocarbons. Application of the Modified Exponential Distribution Function

Masatoshi BABA and Kenji FUEKI

Department of Synthetic Chemistry, Nagoya University, Chikusa-ku, Nagoya 464

(Received April 2, 1975)

A modified exponential function is developed for the description of the spatial distribution of electrons in irradiated liquid hydrocarbons. This distribution function is applied to calculations of ranges and lifetimes of electrons in a number of hydrocarbons. The temperature dependence of electron ranges is also investigated for some of the hydrocarbons. A calculation is made of electron scavenging in cyclohexane using this distribution function and the forced diffusion approximations.

Recently, there has been considerable interest in the behavior, properties and reactions of electrons in nonpolar liquids. Many studies have been made of spatial distributions[1-12] and lifetimes[13-18] of electrons in irradiated liquid hydrocarbons. It has been shown that the simple exponential distribution function can well account for some experimental results on electrons in liquid hydrocarbons.[6,10] However, the electron population probability derived from the simple exponential distribution function increases monotonously with decreasing ion-electron separation distance and becomes very large near or at zero distance. Such a behavior at very small distances seems unrealistic on general grounds.

In this work, we develop a modified exponential function for the spatial distribution of electrons, which removes the unrealistic behavior of the simple exponential distribution function at small distances and still retains the characteristics of the exponential distribution function at large distances, and apply it to calculations of ranges and lifetimes of electrons in a number of liquid hydrocarbons including alkanes, alkenes, dienes, alkynes and aromatics. We also investigate the temperature dependence of electron ranges in some of the hydrocarbons. Further, using this distribution function and the forced diffusion approximations, we attempt to calculate the dependence on the scavenger concentration of the yield of electrons scavenged in a cyclohexane solution, and compare these results with that obtained from Schuler's scavenging function.

Outline of Calculation

The Modified Exponential Distribution Function. The spatial distribution function for the thermalized electrons used in the present calculations is given by Eq. (1).

$$\phi(r) = (1/2)(\pi b_{ME} r)^{-3/2}\exp(-r/b_{ME}) \quad (1)$$

where r is the separation distance of an ion-electron pair, b_{ME} is the electron range parameter and determined from Eq. (6). $\phi(r)$ is a normalized function: $\int_0^\infty \phi(r)4\pi r^2 dr=1$, and unlike the simple exponential distribution function, the function $\Phi(r)=4\pi r^2\phi(r)$ behaves in such a way that it changes smoothly with r, taking a maximum value at a finite value of r and becoming zero at $r=0$.

We define the average electron range by Eq. (2).

$$\bar{r}_{ME} = \int_0^\infty r\phi(r)4\pi r^2 dr = (3/2)b_{ME} \quad (2)$$

The Geminate Ion-Electron Recombination Time. Using the Nernst-Einstein relation, we can derive Eq. (3a) which gives the time-distance relationship for the geminate ion-electron pair.[13]

$$t = r^3/3Dr_c \quad (3a)$$

Here D is the sum of the diffusion constants of the ion and electron, and r_c is the Onsager distance, $r_c=e^2/\varepsilon kT$, where e is the electronic charge, ε is the dielectric constant of a liquid, k is Boltzmann's constant and T is the absolute temperature. If we make a correction for the effect of outward diffusive motion of electrons on the geminate recombination times in a similar manner as that used in Ref. 14, we obtain Eq. (3b) as the corrected time-distance relationship.

$$t' = (r^3/3Dr_c)[1+(4r/3r_c)]^{3/2} \quad (3b)$$

It is seen in Eq. (3b) that the greater is the ion-electron separation distance r, the greater is the correction term $[1+(4r/3r_c)]^{3/2}$. We define by Eq. (4a) or (4b) the average recombination time for the geminate ion-electron pairs, namely, the average lifetime of the geminate electrons.

$$\tau_g = \bar{r}_{ME}^3/3Dr_c, \quad (4a)$$

$$\tau_g' = (\bar{r}_{ME}^3/3Dr_c)[1+(4\bar{r}_{ME}/3r_c)]^{3/2} \quad (4b)$$

Since the diffusion constant of the electron is usually much greater than that of the ion, the diffusion constant D may be approximated by the diffusion constant of the electron, D_e, which is related to the electron mobility μ_e by $D_e=kT\mu_e/e$.

The Free Ion Yield. The free ion yield G_{fi} is expressed by Eq. (5).

$$G_{fi} = G_t\int_0^\infty \phi(r)\exp(-r_c/r)4\pi r^2 dr \quad (5)$$

Substituting $\phi(r)$ given in Eq. (1) into Eq. (5) and integrating it, we get a simple equation in closed form (Eq. (6)).

$$G_{fi} = G_t[1+2(r_c/b_{ME})^{1/2}]\exp[-2(r_c/b_{ME})^{1/2}] \quad (6)$$

where G_t represents the total ion yield. In the present calculations G_t is assumed to be 4.3 for all the hydrocarbons. Equation (6) is used for determining b_{ME}.

The Yield of Electrons Scavenged by a Scavenger. The yield of electrons scavenged by a scavenger, $G(e_{sc}^-)$, is calculated using Eq. (7a) or (7b).

$$G(e_{sc}^-) = G_t\int_0^\infty \phi(r)[1-\exp(-kSt)]4\pi r^2 dr, \quad (7a)$$

$$G(e_{sc}^-) = G_t\int_0^\infty \phi(r)[1-\exp(-kSt')]4\pi r^2 dr \qquad (7b)$$

where k is the rate constant for reaction of electrons with the scavenger and S is the concentration of the scavenger. The time t or t' is given as a function of r by Eq. (3a) or (3b).

Results and Discussion

The results of the calculations are given in Tables 1—4 and Figs. 1 and 2.

Electron Ranges. In Tables 1, 2 and 3 are listed the ranges of electrons, b_{ME} and $\bar{r}_{ME}$, calculated from Eqs. (6) and (2) using experimental values of G_{fl} for alkanes; alkenes, dienes, and alkynes; and aromatics, respectively. For comparison the electron ranges, $\bar{r}_E$, obtained from the simple exponential distribution function, $\phi(r)=(4\pi b_E r^2)^{-1}\exp(-r/b_E)$, are also given for alkanes in Table 1. It should be noted that $\bar{r}_E$ is equal to b_E for the simple exponential distribution function. The value of $\bar{r}_{ME}$ or b_{ME} correlates with that of G_{fl}: the greater is the free ion yield, the greater is $\bar{r}_{ME}$ or b_{ME}. Such a correlation has been found with other spatial distribution functions for electron ranges.[12] It is seen in Table 1 that generally $\bar{r}_{ME}$ is somewhat greater than $\bar{r}_E$ for the same compound, although $\bar{r}_{ME}$ is equal to $\bar{r}_E$ for neopentane. Figure 1 illustrates a comparison between the modified and simple exponential distribution functions for electrons in cyclohexane at room temperature. In the calculations of these distribution curves, b_{ME}= 41.4 Å and b_E=57.5 Å were used, which were ob-

Table 1. Ranges and lifetimes of electrons in alkanes

Liquid	T (K)	G_{fl}	b_{ME} (Å)	$\bar{r}_{ME}$ (Å)	μ_e (cm²/V s)	τ_g (ps)	τ_g' (ps)	$\bar{r}_E$[k] (Å)
Methane	140	1.13[a]	448	672	430[f]	2.5	8.0	
Ethane	200	0.158[a]	72.2	108	0.97[f]	5.3	8.0	
Propane	238	0.166[a]	62.4	93.7	0.55[f]	6.1	9.1	
Cyclopropane	260	0.078[a]	39.7	59.5	0.011[f]	81	110	
n-Butane	296	0.19[b]	53.6	80.4				
	293	0.225[a]	56.4	84.5	0.27[f]	9.2	14	
Isobutane	294	0.31[c]	70.4	105.6				
n-Pentane	296	0.145[b]	45.0	67.4	0.14[g]	9.3	14	62.3
	293	0.12[d]	41.9	62.8				
Isopentane	296	0.17[b]	48.6	72.9				67.6
Neopentane	296	0.86[b]	142	212	70[h,i]	0.56	1.5	212
	294	1.09[e]	177	265	70[h,i]	1.1	3.4	
Cyclopentane	296	0.155[b]	43.6	65.4	1.1[j]	1.2	1.8	60.8
n-Hexane	296	0.131[b]	42.0	63.0	0.082[g]	14	20	57.9
	293	0.11[d]	39.3	59.0				
2-Methylpentane	296	0.148[b]	44.9	67.4				
3-Methylpentane	296	0.146[b]	43.8	65.7				60.6
2,3-Dimethylbutane	296	0.192[b]	48.6	72.8				68.0
2,2-Dimethylbutane	296	0.304[b]	62.8	94.2	12[h]	0.31	0.53	89.9
	293	0.40[d]	77.0	116				
Cyclohexane	296	0.148[b]	41.4	62.1	0.24[g]	4.7	6.9	57.5
					0.35[j]	3.2	4.7	
	293	0.11[d]	36.3	54.5	0.45[e]	1.7	2.4	
n-Heptane	296	0.131[b]	41.0	61.5				
2,4-Dimethylpentane	296	0.178[b]	48.2	72.2				
2,2,3-Trimethylbutane	296	0.290[b]	61.1	91.7				
n-Octane	296	0.124[b]	39.7	59.6				54.6
2,3,4-Trimethylpentane	296	0.174[b]	45.4	68.1				
2,2,4-Trimethylpentane	296	0.332[b]	65.6	98.4	7[j]	0.61	1.1	94.6
2,2,3,3-Tetramethylbutane	379	0.80[e]	101	151				
n-Nonane	296	0.117[b]	38.8	58.2				
2,2,4,4-Tetramethylpentane	295	0.83[e]	124	186	24[e]	1.2	3.1	
2,2,3,3-Tetramethylpentane	295	0.42[e]	71.9	108	5.2[e]	1.2	2.3	
n-Decane	296	0.117[b]	38.4	57.5				
2,2,5,5-Tetramethylhexane	293	0.67[e]	105	158	12[e]	1.5	3.4	
2,2,6,6-Tetramethylheptane	293	0.47[e]	81.3	122				
2,2,7,7-Tetramethyloctane	316	0.34[e]	56.7	85.0				
n-Tetradecane	296	0.120[b]	37.6	56.3				
Squalane	296	0.119[b]	36.7	55.1				

a) Ref. 4. b) Ref. 8. c) Ref. 5. d) Ref. 19. e) Ref. 2. f) Ref. 4. g) Ref. 20. h) Ref. 21. i) Ref. 22, Data at 300 K. j) Ref. 23. k) Ref. 22, values at 300 K.

Table 2. Ranges and lifetimes of electrons in alkenes, dienes, and alkynes

Liquid	T (K)	G_{fi}	b_{ME} (Å)	$\bar{r}_{ME}$ (Å)	μ_e (cm²/V s)	τ_g (ps)	τ_g' (ps)
Ethylene	170	0.010[a]	31.6	47.4	0.003[d]	150	180
Propylene	234	0.042[a]	32.9	49.3	0.008[d]	68	87
Butene-1	293	0.093[b]	36.8	55.3	0.064[e]	11	15
trans-Butene-2	293	0.080[b]	35.4	53.1	0.029[e]	22	30
cis-Butene-2	293	0.23[b]	52.5	78.7	2.2[e]	1.0	1.6
Isobutene	293	0.25[b]	52.7	79.0	1.44[e]	1.6	2.6
2-Methylbutene-2	292	0.26[b]	58.3	87.5	3.6[f]	0.83	1.4
2,3-Dimethylbutene-2	293	0.44[b]	76.9	115	5.8[e]	3.6	6.8
Hexene-1	293	0.10[b]	34.3	51.4			
	296	0.062[c]	28.6	42.8			
trans-Hexene-2	293	0.092[b]	34.7	52.0			
3,3-Dimethylbutene-1	296	0.17[c]	47.3	71.0			
trans-Hexene-3	293	0.10[b]	36.0	54.1			
cis-Hexene-3	293	0.13[b]	38.3	57.5			
Cyclohexene	293	0.20[b]	43.9	65.8	1.00[e]	1.5	2.3
	296	0.150[c]	37.9	56.9			
Propadiene	282	0.050[b]	28.8	43.2			
Butadiene-1,3	269	0.038[b]	26.3	39.5			
Pentadiene-1,4	293	0.067[b]	29.5	44.3			
Hexadiene-1,5	292	0.066[b]	28.5	42.7			
Heptadiene-1,6	292	0.067[b]	28.3	42.4			
Octadiene-1,7	292	0.065[b]	27.5	41.2			
Acetylene	198	0.020[b]	24.2	36.3			
Propyne	260	0.17[b]	32.8	49.1			
Butyne-2	293	0.32[b]	64.9	97.4			
Hexyne-1	253	0.10[b]	28.7	43.0			
Hexyne-2	293	0.19[b]	47.7	71.5			
Hexyne-3	293	0.212[b]	50.7	76.0			

a) Ref. 4. b) Ref. 3. c) Ref. 8. d) Ref. 4. e) Ref. 24. f) Ref. 25, data at 300 K.

Table 3. Ranges and lifetimes of electrons in aromatics

Liquid	T (°K)	G_{fi}	b_{ME} (Å)	$\bar{r}_{ME}$ (Å)	μ_e (cm²/V s)	τ_g (ps)	τ_g' (ps)
Benzene	292	0.081[a]	28.7	43.0	0.114[c]	3.7	5.0
	296	0.053[b]	28.4	42.6	0.6[d]	0.70	0.96
Toluene	292	0.093[a]	29.1	43.7	0.063[c]	7.3	10
t-Butylbenzene	296	0.09[b]	28.4	42.6			
1,2-Dimethylbenzene	292	0.094[a]	27.2	40.8	0.018[c]	22	31
1,3-Dimethylbenzene	292	0.082[a]	27.8	41.7	0.057[c]	7.0	9.6
1,4-Dimethylbenzene	292	0.073[a]	27.8	41.7	0.062[c]	6.1	8.2
1,2,3-Trimethylbenzene	292	0.12[a]	29.3	44.0	0.022[c]	24	34
1,2,4-Trimethylbenzene	292	0.083[a]	27.9	41.9	0.035[c]	12	16
1,3,5-Trimethylbenzene	293	0.087[a]	29.5	44.3	0.16[c]	2.9	4.0
1,2,3,4-Tetramethylbenzene	292	0.11[a]	29.3	43.9			
1,2,4,5-Tetramethylbenzene	353	0.15[a]	31.8	47.7			
Pentamethylbenzene	333	0.22[a]	38.3	57.5			
Hexamethylbenzene	448	0.6[a]	57.4	86.1			
Naphthalene	357	0.094[a]	22.4	33.7			
Anthracene	500	~0.1[a]	~16	~24			

a) Ref. 5. b) Ref. 8. c) Ref. 5. d) Ref. 25, data at 300 K.

TABLE 4. TEMPERATURE DEPENDENCE OF ELECTRON RANGES IN HYDROCARBONS

Liquid	T (K)	G_{fi}	b_{ME} (Å)	d (g/cm³)	$b_{ME}d$ (10^{-8} g/cm²)		Liquid	T (K)	G_{fi}	b_{ME} (Å)	d (g/cm³)	$b_{ME}d$ (10^{-8} g/cm²)	
n-Hexane[a]	296	0.131	42.1	0.656	28			383	0.22	42.3	0.577	24	
	297	0.138	43.0	0.656	28		Cyclohexene[b]	185	0.066	38.3	0.917	35	
	314	0.162	44.4	0.640	28			218	0.10	39.2	0.885	35	
	319	0.168	44.6	0.636	28			256	0.14	40.4	0.848	34	Av. 36
	328	0.183	45.6	0.627	29			293	0.20	43.9	0.813	36	
	333	0.195	46.5	0.621	29	Av. 29		331	0.27	47.9	0.776	37	
	348	0.217	47.7	0.609	29			358	0.33	51.7	0.750	39	
	352	0.226	48.4	0.604	29		Butadiene[b]	183	0.018	27.5	0.752	21	
	357	0.239	49.2	0.600	30			216	0.024	26.4	0.712	19	Av. 19
	363	0.248	49.8	0.594	30			240	0.030	26.2	0.684	18	
	371	0.256	50.0	0.586	29			269	0.038	26.3	0.650	17	
Cyclohexane[a]	296	0.149	41.5	0.776	32		Propyne[b]	183	0.090	27.5	0.760	21	
	305	0.169	43.1	0.767	33			210	0.12	29.9	0.725	22	Av. 22
	307	0.166	42.4	0.766	32			233	0.14	31.1	0.694	22	
	315	0.184	43.8	0.758	33			260	0.17	32.8	0.657	22	
	322	0.195	44.3	0.751	33		Benzene[c]	281	0.072	28.2	0.891	25	
	333	0.213	45.3	0.741	34	Av. 33		292	0.081	28.7	0.880	25	
	339	0.233	46.9	0.735	34			304	0.087	28.7	0.867	25	
	348	0.245	47.2	0.726	34			313	0.098	29.5	0.858	25	
	354	0.253	47.6	0.721	34			324	0.105	29.6	0.846	25	Av. 26
	357	0.263	48.2	0.718	35			333	0.12	30.7	0.837	26	
	368	0.279	48.8	0.707	34			345	0.13	31.0	0.823	26	
Hexene-1[b]	152	0.018	30.1	0.812	24			353	0.15	32.5	0.815	27	
	192	0.033	30.5	0.772	24			374	0.19	35.1	0.793	28	
	224	0.049	31.3	0.740	23		Toluene[c]	212	0.044	28.0	0.941	26	
	255	0.067	32.1	0.708	23			253	0.066	28.0	0.904	25	
	293	0.10	34.3	0.673	23	Av. 23.5		292	0.093	29.1	0.868	25	Av. 25
	323	0.13	36.2	0.640	23			322	0.12	30.3	0.840	25	
	354	0.18	39.9	0.607	24			354	0.15	31.3	0.811	25	

a) Ref. 7. b) Ref. 3. c) Ref. 5.

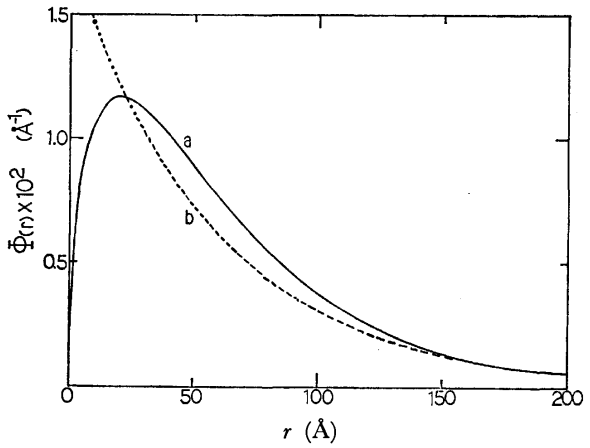

Fig. 1. Comparison between the spatial distribution functions for electrons in cyclohexane. a: modified exponential function, b: simple exponential function. See the text for the parameters used in the calculations.

tained using G_{fi}=0.148 and G_t=4.3. Table 4 shows the calculated temperature dependence of electron ranges b_{ME} for some of the hydrocarbons. It can be seen from Table 4 that b_{ME} increases with increasing temperature for these hydrocarbons except for butadiene where b_{ME} is nearly constant over the temperature range studied. Values of the parameter $b_{ME}d$ are also given in Table 4, where d is the liquid density. The value of $b_{ME}d$ is nearly constant for each of the hydrocarbons, although it decreases with increasing temperature for butadiene and tends to increase with increasing temperature for cyclohexene at higher temperatures. Thus, it appears that the electron range in liquid hydrocarbons is, approximately, inversely proportional to the medium density.

Geminate Recombination Times. The geminate ion-electron recombination times or the lifetimes of geminate electrons, τ_g and τ_g', are given for alkanes, alkenes and aromatics in Tables 1, 2 and 3, respectively. It can be seen from these tables that the values of τ_g or τ_g' are in the time range of 1—10 ps for most of the hydrocarbons and in the time range of 10—100 ps for some of the hydrocarbons. It is also seen that the geminate recombination time correlates with the electron mobility: the greater is the electron mobility, the shorter is the geminate recombination time. The geminate recombination times for electrons in liquid methane and neopentane are longer than expected from the electron mobilities in these liquids. This is due to the fact that the electron ranges are very large in methane and neopentane. It is interesting to note that the electrons in methane and neopentane are quasi-free electrons. The corrected

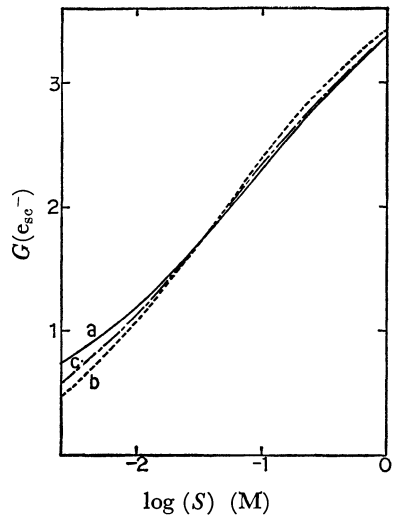

Fig. 2. Concentration dependence of the yield of electrons scavenged in a cyclohexane solution. a: calculated from Schuler's scavenging function, b: calculated from Eq. (7a), c: calculated from Eq. (7b). See the text for the parameters used in the calculations.

geminate recombination time, τ_g', is greater than the geminate recombination time, τ_g, derived directly from the Nernst-Einstein relation. The ratio of τ_g' to τ_g is different for individual compounds and depends on the value of $\bar{r}_{ME}/r_c$ as seen from Eqs. (4a) and (4b). For instance, the values of τ_g'/τ_g are large for methane and neopentane for which the values of $\bar{r}_{ME}/r_c$ are large.

Electron Scavenging in Cyclohexane. Figure 2 shows the yields of electrons scavenged, $G(e_{sc}^-)$, by a scavenger (carbontetrachloride) in cyclohexane, which were calculated as a function of the scavenger concentration. In Fig. 2, curve a was calculated using Schuler's scavenging function with $G_{fi}=0.12$, $G_t=4.2$ and $\alpha=12\ M^{-1}$.[26] It is well known that Schuler's scavenging function can satisfactorily reproduce the observed dependence on the scavenger concentration of the yield of electrons scavenged in irradiated liquid hydrocarbons. Curves b and c were calculated using Eqs. (7a) and (7b), respectively. The value of the parameter, k/D, involved in Eq. (7a) or (7b) was chosen so that the calculated curve fits reasonably curve a. The value of k/D thus chosen is 8.5×10^{14} $M^{-1}\,cm^{-2}$ in Eq. (7a) and $5.9\times10^{14}\,M^{-1}\,cm^{-2}$ in Eq. (7b). It is seen in Fig. 2 that curve a is closer to curve c than curve b and that curve c is very close to curve a at the scavenger concentrations higher than 10^{-2} M. However, curve c deviates from curve a at the scavenger concentrations lower than 10^{-2} M, and the deviation tends to increase with decreasing scavenger concentration. The value of k can be obtained from k/D making use of μ_e. Taking $\mu_e=0.24\ cm^2\,V^{-1}\,s^{-1}$,[20] k is calculated to be 5.2×10^{12} $M^{-1}\,s^{-1}$ from $k/D=8.5\times10^{14}\,M^{-1}\,cm^{-2}$ and $3.6\times10^{12}\,M^{-1}\,s^{-1}$ from $k/D=5.9\times10^{14}\,M^{-1}\,cm^{-2}$. The expermental values of k have been reported to be 4.3×10^{12},[27] 2.7×10^{12},[28] and $1.8\times10^{12}\,M^{-1}\,s^{-1}$ [20] for the reaction of electrons with carbon tetrachloride in cyclohexane. The values of k derived in the present work are reasonably compared with the experimental values, in particular, the value of $3.6\times10^{12}\,M^{-1}\,sec^{-1}$ is in good agreement with the experimental values. Thus, it appears that the present treatment can well account for the concentration dependence of electron scavenging in cyclohexane except for the low concentration region. Since the electrons scavengeable at low scavenger concentrations are mostly far away from their parent ions, Brownian motion of these electrons is as much effective as their drift motion in the Coulomb field and the use of the Nernst-Einstein relation is not appropriate for the description of the behavior of such electrons. The Smoluchowski equation must be properly solved for electrons in such a situation.[29]

References

1) J.-P. Dodelet and G. R. Freeman, *Can. J. Chem.*, **49**, 2643 (1971).
2) J.-P. Dodelet and G. R. Freeman, *ibid.*, **50**, 2667 (1972).
3) J.-P. Dodelet, K. Shinsaka, U. Kortsch, and G. R. Freeman, *J. Chem. Phys.*, **59**, 2376 (1973).
4) M. G. Robinson and G. R. Freeman, *Can. J. Chem.*, **52**, 440 (1974).
5) K. Shinsaka and G. R. Freeman, *ibid.*, **52**, 3495 (1974).
6) J.-P. Dodelet and G. R. Freeman, *J. Chem. Phys.*, **60**, 4657 (1974).
7) W. F. Schmidt and A. O. Allen, *J. Phys. Chem.*, **72**, 3730 (1968).
8) W. F. Schmidt and A. O. Allen, *J. Chem. Phys.*, **52**, 2345 (1970).
9) R. A. Holroyd, B. K. Dietrich, and H. A. Schwarz, *J. Phys. Chem.*, **76**, 3794 (1972).
10) G. C. Abell and K. Funabashi, *J. Chem. Phys.*, **58**, 1079 (1973).
11) M. Tanaka and K. Fueki, *J. Phys. Chem.*, **77**, 2524 (1973).
12) A. Mozumder, *J. Chem. Phys.*, **60**, 4305 (1974).
13) F. Williams, *J. Amer. Chem. Soc.*, **86**, 3954 (1964).
14) F. Williams, *J. Chem. Phys.*, **48**, 4077 (1968).
15) J.-P. Dodelet and G. R. Freeman, *Can. J. Chem.*, **50**, 2729 (1972).
16) A. Hummel, *J. Chem. Phys.*, **49**, 4840 (1968).
17) A. Mozumder, *ibid.*, **55**, 3026 (1971).
18) R. H. Schuler and P. P. Infelta, *J. Phys. Chem.*, **76**, 3812 (1972), and references therein.
19) P. H. Tewari and G. R. Freeman, *J. Chem. Phys.*, **49**, 4394 (1968).
20) A. O. Allen and R. A. Holroyd, *J. Phys. Chem.*, **78**, 796 (1974).
21) G. Bakale and W. F. Schmidt, *Chem. Phys. Lett.*, **22**, 164 (1973).
22) R. M. Minday, L. D. Schmidt, and H. T. Davis, *J. Phys. Chem.*, **76**, 442 (1972).
23) W. F. Schmidt and A. O. Allen, *J. Chem. Phys.*, **52**, 4788 (1970).
24) J.-P. Dodelet, K. Shinsaka, and G. R. Freeman, *J. Chem. Phys.*, **59**, 1293 (1973).
25) R. M. Minday, L. D. Schmidt, and H. T. Davis, *ibid.*, **54**, 3112 (1971).
26) G. W. Klein and R. H. Schuler, *J. Phys. Chem.*, **77**, 978 (1973).
27) J. H. Baxendale, J. P. Keene, and E. J. Rasburn, *J. Chem. Soc., Faraday I*, **70**, 718 (1974).
28) A. O. Allen, T. E. Gangwer, and R. A. Holroyd, *J. Phys. Chem.*, **79**, 25 (1975).
29) A. Hummel, *J. Chem. Phys.*, **48**, 3268 (1968).

The Electronic Structure of the Electron-donor-acceptor System in the Excited State. The Exciplex and the Fluorescent State of EDA Complex

Tsutomu MIMURA, Michiya ITOH,* Toshiaki OHTA,** and Toshihiko OKAMOTO

Faculty of Pharmaceutical Sciences, The University of Tokyo, Bunkyo-ku, Tokyo 113

***Department of Chemistry, Faculty of Science, The University of Tokyo, Bunkyo-ku, Tokyo 113*

(Received April 17, 1975)

The semiempirical SCF-MO-CI calculation was applied to the electron donor-acceptor (EDA) interaction in 9,10-dicyanoanthracene and naphthalene system which exhibits the exciplex fluorescence and also the fluorescence due to the EDA complex stable in the ground state. On the basis of energy contour maps of the ground and excited states and of electronic transitions in the EDA system, the relaxation process from the F.C. excited state of the EDA complex to an identical fluorescent state with the exciplex was discussed on the intermolecular interaction, and also on the intramolecular interaction in (9,10-dicyanoanthracene)-$(CH_2)_3$-(naphthalene) systems.

There are numerous investigations relating to the electronic and geometrical structures of excimers. Excimers are believed to have a sandwich structures and to be stabilized by the exciton as well as charge resonance interaction. For exciplex it has been thought that the CT interaction is more important than the exciton interaction from many points of view.[1] Most molecular orbital calculation of the EDA complex as well as the exciplex were based on the configuration interaction between the ground and locally excited states of each component molecule including the charge transfer interaction, which is so called the method of "composite molecules".[2] On the other hand, some of investigators attempted to calculate the electronic structure of the EDA complex as a single conjugate system of π-electrons.[3,4]

Ohta, Kuroda and Kunii reported a method to calculate the electronic structure of the EDA complex, where the complex was treated as a single conjugated system of π-electrons.[6] The electronic state was calculated by the semiempirical SCF-MO-CI method within π-electron approximation by including all β terms. They accounted well for electronic transitions of the EDA complex of tetracyanoethylene with polycyclic aromatic hydrocarbons by this method.[5,6]

We have reported both exciplex and EDA complex fluorescence in the same EDA systems of 9,10-dicyanoanthracene (DCA) and naphthalenes.[7-9] The previous paper suggested that the geometrical arrangement between the excited electron acceptor and the ground state donor in the primary process of the exciplex formation was different from that of the Frank-Condon (F.C.) excited state of the corresponding EDA complex formed in the ground state.[7] In the intermolecular system, however, the fluorescence behavior of EDA complex and exciplex led to the conclusion that the fluorescent state of the exciplex may be identical with that of the corresponding EDA complex.[8] On the other hand, the geometrical conversion from their F.C. excited state of the EDA complex to the fluorescent state is sterically forbidden in the intramolecular system of 1-(9,10-dicyano-β-anthryl)-3-(α or β-naphthyl)propane.[9]

* To whom all correspondence should be addressed.

In this paper, the electronic interactions between 9,10-dicyanoanthracene and naphthalene both in the ground and excited states were calculated by assuming the complex as a single π-conjugate system. On the basis of energy contour maps of the ground and excited states and of electronic transitions in this EDA system, the electronic and geometrical structures of the fluorescent state of the exciplex and the EDA complex were discussed.

Method of calculation

The Pariser-Parr-Pople type semiempirical LCAO-SCF-MO's including configuration interaction of the EDA complex are calculated by assuming the complex as a single π-conjugate system. The molecular orbitals of the complex are calculated within the zero-differential-overlap approximation but with the including all two center resonance integrals.[5,6] In this method two center resonance integrals were evaluated by Katagiri-Sandorfy's formula,[10]

$$H_{\mu\nu} = \frac{1}{4}(C_\mu + C_\nu + \gamma_{\mu\mu} + \gamma_{\nu\nu} - 2\gamma_{\mu\nu})S_{\mu\nu} \qquad (1)$$

where C_μ is one center penetration integral and $S_{\mu\nu}$ is the overlap integral of atomic orbitals. If two atomic orbitals are associated to same molecule in these systems, $S_{\mu\nu}$ is evaluated from single Slater atomic orbitals, and if two atomic orbitals are associated to different molecule, we used SCF-atomic orbitals.[11] Two center repulsion integrals, $\gamma_{\mu\nu}$, were evaluated by Nishimoto-Mataga's formula,[12] and one center repulsion integrals, $\gamma_{\mu\mu}$, were estimated according to the Pariser-Parr's method.[13] Core energy, $H_{\mu\mu}$, is assumed to be minus of the ionization potential, which is given by Hinze and Jaffe.[14] Intermolecular core-core repulsion integrals, $\gamma_{\mu\nu}{}^c$, were estimated by following Dewar-Klopman's formula modified by Ohta *et al.*[5,15,16]

$$\gamma_{\mu\nu}{}^c = \gamma_{\mu\nu} + \left(\frac{1}{R_{\mu\nu}} - \gamma_{\mu\mu}\right)\exp\left[\alpha(R_{\mu\nu} - D_\mu - D_\nu)\right] \qquad (2)$$

Table 1 shows parameters used here which were also adopted in the calculations of the EDA complexes between tetracyanoethylene (TCNE) and various polycyclic aromatic hydrocarbons and also various excimers of aromatic hydrocarbons.[5,6]

TABLE 1. USED PARAMETERS IN THIS CALCULATION

	$H_{\mu\mu}$ (eV)	$\gamma_{\mu\mu}$ (eV)	C (eV)	D (a.u.)	ζ
C+	−11.16	11.13	14.5	2.0	1.625
N+	−16.18	11.52	20.0	1.0	1.950

$\alpha = -1.75$

The iteration of SCF-MO calculation was repeated, until the deviation in the total electronic energy by iteration becomes less than 10^{-4}%. For the prediction of electronic transitions, the CI calculation was carried out taking into consideration of the forty lowest singly excited configurations. The character of MO and the nature of the electronic transition in the bimolecular system are derived with same procedures as those references.[5,6]

The ground state total energy of each geometrical conformation was calculated by subtracting the total energy of component molecules (DCA and naphthalene) from summation of the electronic and core-core repulsion energies. The total energy in the first excited singlet state was evaluated from the total energy in the ground state and the first electronic transition energy.[5,6]

The energy contour maps of the ground and the first singlet excited state were depicted by moving a center of naphthalene on DCA molecule, where the intermolecular distance was assumed to be 3.4Å and molecular planes were parallel each other.[17] The calculation to depict one contour map was performed with 20 conformations taking into account of symmetry. The angle between the long axes of DCA and naphthalene, θ, were adopted to be 30°, 60°, and 90°, as shown in Fig. 1. Actual computation was carried out by the use of HITAC 8700/8800 operating system of the University of Tokyo.

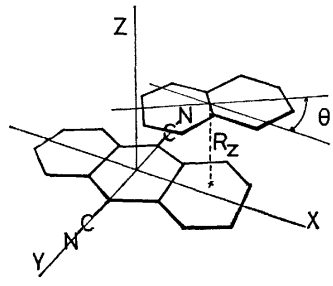

Fig. 1. The conformation and the geometrical parameters used for these calculations, where θ is the angle between the long axes and R_z is distance between the molecular planes (parallel) of these component molecules.

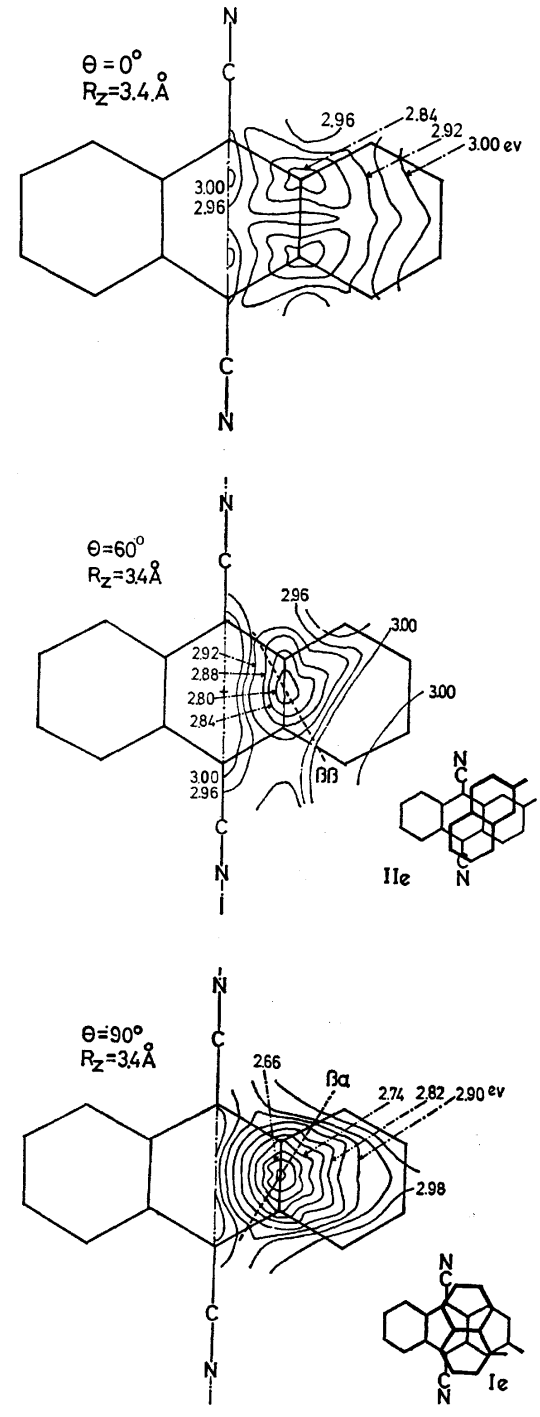

Figs. 2—4. The energy contour maps in the excited states for each angle of θ.

Results

The energy contour maps of the first excited singlet state obtained in the DCA and naphthalene system are shown in Figs. 2—4 for θ=0°, 60°, and 90°, respectively. Although there are minimum points in the excited state for θ=0° and 60°, the most stable structure in the excited state is in the conformation of θ=90° as shown in Figs. 4. The ground state energy contour maps also shown in Fig. 5—7 for each angle of θ. Here, the most stable geometries in the excited state are represented by Ie and IIe and those geometries in the ground state are Ig and IIg as shown in Figs. 3—6. Unfortunately, there is no minus point of the total energy in the ground state which might mean a stabilization in the complex formation in the ground state. However, this is not important in this stage because we don't take into account explicitly a solute-solvent interaction and fix an intermolecular distance at 3.4 Å. It seems that the relative total energy is more important in the EDA complex formation. Inspection of these energy contour maps reveals that the most stable

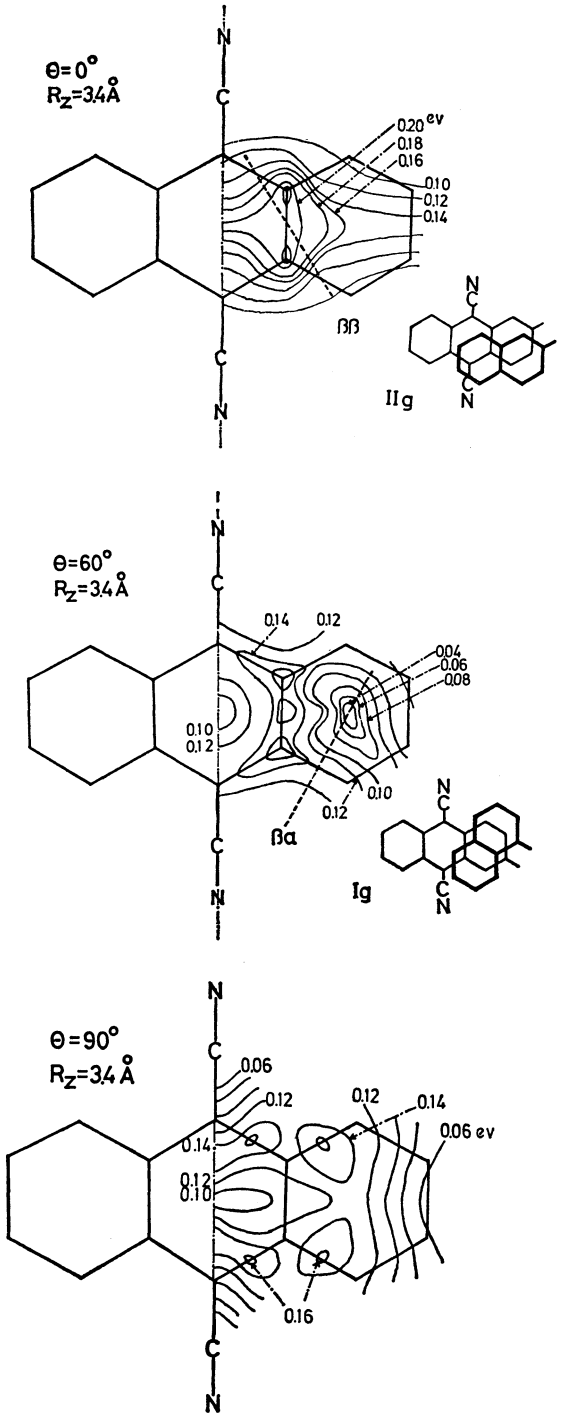

Figs. 5—7. The energy contour maps in the ground states for each angle of θ.

structure in the ground state is in the conformation of $\theta=60°$, as shown in Fig. 6.

The nature of excitation was estimated by following equation which are identical with those described in the previous paper by Ohta, Kuroda and Kunii,[6]

$$\left.\begin{aligned} \mathrm{LE(D^*A)} &= \sum_{ij} b_{ij}{}^2{}_{,m} D_i D_j, \\ \mathrm{LE(DA^*)} &= \sum_{ij} b_{ij}{}^2{}_{,m} A_i A_j, \\ \mathrm{CT(D^+A^-)} &= \sum_{ij} b_{ij}{}^2{}_{,m} D_i A_j, \\ \mathrm{CT(D^-A^+)} &= \sum_{ij} b_{ij}{}^2{}_{,m} A_i D_j, \end{aligned}\right\} \quad (3)$$

Table 2. The electronic excitation energies, oscillater strengths and characters of transition of the lowest three excitations

Structure	Excitation energy (eV)	Oscillater strength	Character of Transition[a] CT(D+A−)	LE(DA*)
Ig	2.96 (418 nm)	0.42	24%	74%
	3.16 (392)	0.15	66	28
	3.46 (358)	0.02	49	42
Ie	2.50 (495)	0.17	48	52
	3.41 (363)	0.02	43	45
	3.43 (361)	0.23	42	55
IIg	2.78 (446)	0.27	43	56
	3.22 (384)	0.17	46	53
	3.38 (366)	0.10	52	46
IIe	2.62 (472)	0.15	45	53
	3.10 (400)	0.22	46	52
	3.57 (347)	0.02	31	34

a) Residual characters are LE(D*A) and CT(D⁻A⁺) in mere trace amount.

where D_i, D_j, A_i, and A_j are expressed in Eq. (4), and $C_{i\mu}$ is coefficient of the atomic orbital, and $b_{ij,m}$ are coefficient of each excitation (i-th MO→j-th MO, Φ_{ij}) in CI calculation of the m-th excited state (Eq. (5)).

$$D_i = \sum_{\mu=1}^{n_d} C_{i\mu}{}^2, \quad A_i = \sum_{\mu=n_d+1}^{n_d+n_a} C_{i\mu}{}^2 \quad (4)$$

$$\Psi_m = \sum_{ij} b_{ij,m} \Phi_{ij} \quad (5)$$

In Eq. (4), n_a and n_d are given numbers to atoms in acceptor and donor molecules, respectively. The electronic transition and the character of transition are listed in Table 2 for several structures including Ig and Ie as mentioned above. The character of transition and oscillater strength are remarkably varied with the conformation of the EDA complex. These electronic transition characters summarized in Table 2 represent that the first electronic transition (absorption) from the ground state conformation (Ig or IIg) and also transition (fluorescence) from the excited singlet state (Ie or IIe) are the CT transition (D→A) equally mixed with the local excitation (^1L_a) of DCA.

Discussion

The great difference between the inter- and intramolecular systems is their degrees of freedom. In the intermolecular system each component molecule can take any conformation with no restriction. Therefore, the molecular conformation in the intermolecular EDA system may be dependent only on the electronic interaction in the ground state and also in the excited state of this system. Since the exciplex is the electronic interaction between the ground and the excited state molecules, the fluorescent conformation of the exciplex may be the energy minimum conformation in the energy contour map of the excited state. The energy minimum conformation for $\theta=90°$ seems to be most stable in the excited state than those for $\theta=0°$ and 60°, as shown in Figs. 2—4. Then, the exciplex and the

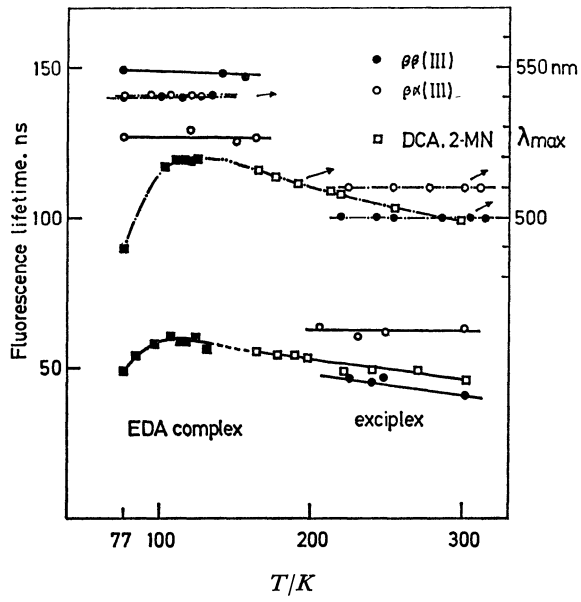

Fig. 8. The temperature dependence of the EDA complex and exciplex fluorescence maxima and fluorescence lifetimes of $\beta\alpha$-, $\beta\beta$(III) and DCA, 2-methylnaphthalene (2-MN) systems in 3-methylpentane. The broken lines and solid lines refer to the right and left ordinates, respectively. (extracted from the previous papers, Refs., 7) and 8)).

fluorescent state of the EDA complex, as will be mentioned later, seem to be in the geometrical conformation of Ie.

DCA and various naphthalenes form the corresponding EDA complex in the ground state as reported in the previous papers.[7-9] The fluorescence maxima and lifetimes of the exciplex (above~150 K) and EDA complex (below~120 K) were reported to continuously vary in the intermolecular system of DCA-naphthalenes, while these maxima and lifetimes were also reported to change discontinuously in the intramolecular system of 1-(9,10-dicyano-β-anthryl)-3-(α or β-naphthyl)propane (abreviated to $\beta\alpha$- and $\beta\beta$(III)) in the temperature region of 180—200 K.[7,8] The fluorescence behavior is illustrated in Fig. 8 extracted from previous papers for subsequent discussion. In the energy point of view, the conformation of these EDA complexes might be Ig for $\theta=60°$ as mentioned in the last section. Mataga and Murata,[18] and also Kobayashi *et al.*[19] reported that in fluid media the geometrical conformation of the F.C. excited state of the EDA complex of tetracyanobenzene (TCNB) and aromatic hydrocarbons reorient to a great extent to a fluorescent conformation. On the other hand, Itoh and Mimura demonstrated an experimental evidence of an identical fluorescent state of the exciplex and the EDA complex in the DCA and alkylnaphthalene system.[8] The geometrical conversion from the F.C. excited state of the complex (Ig) to the fluorescent equilibrium state (Ie) may be smoothly achieved in fluid media at low temperature. In the rigid matrix at 77 K, however, the fluorescence of the EDA complex seems to be from an non-relaxed or incompletely relaxed state near F.C. excited state of the EDA complex as mentioned in the previous paper.

As mentioned last section, the electronic transitions of the local excitation (^1L_a) and the CT transition are comparably mixed each other, and the electronic transition character of the first transition is dependent very much on the geometry. These results calculated here are consistent with the experimental results of the photoelection study that the fluorescence of the EDA complex of these systems has considerable CT character reported in the previous papers.[20-22] Furthermore, the electronic transition in Ig are in agreement with the absorption spectra of the EDA complexes of the DCA-naphthalene systems at 77 K.

In the intramolecular systems of $\beta\alpha$- and $\beta\beta$(III), the geometrical conformation between DCA and naphthalene moieties are restricted by trimethylene chain. The allowed traces of a center of naphthalene over the DCA molecule with an approximate spacing of 3.4 Å are shown by dotted lines in energy contour maps for $\beta\alpha$- and $\beta\beta$(III), respectively. A molecular model suggests that $\beta\alpha$(III) does not take the conformation of $\theta=0°$, while $\beta\beta$(III) does not take $\theta=90°$. Therefore, the geometry of the exciplex of the former may be Ie and that of the latter is IIe. On the other hand, the ground state geometry of $\beta\alpha$(III) seems to be Ig and that of $\beta\beta$(III) seems to be IIg by considering a steric hindrance of the trimethylene conformation.

In the intermolecular interaction, the geometrical conversion from the F.C. excited state of the EDA complex (Ig) to the fluorescent state (Ie) is not restricted in the fluid media, as mentioned above. In the intramolecular interaction, however, this kind of the geometrical conversion retaining the space of the electron donor and acceptor, *e.g.* Ig→Ie in $\beta\alpha$(III) and IIg→IIe in $\beta\beta$(III) seem to be forbidden by the trimethylene chain. As the result, the fluorescent state of the EDA complex in $\beta\alpha$- and $\beta\beta$(III) may be approximately the F.C. excited state of the complex formed in the ground state which are completely different from that of the corresponding exciplex. The electronic transitions calculated based on the geometrical conformations of Ig and IIg are consistent with the electronic absorption spectra and fluorescence polarizations of the corresponding EDA complexes reported previously.[22]

References

1) N. Mataga and T. Kubota, "Molecular Interactions and Electronic Spectra," Marcel Dekker, New York, N.Y., (1970) and references cited therein.
2) H. C. Longuet-Higgins and J. N. Murrell, *Proc. Phys. Soc.* (London), **A68**, 601 (1955).
3) T. Shida and S. Iwata, *J. Chem. Phys.*, **56**, 2858 (1972).
4) M. Itoh, This Bulletin, **46**, 821 (1973).
5) T. Ohta, Thesis, The University of Tokyo (1971).
6) T. Ohta, H. Kuroda, and T. L. Kunii, *Theor. Chim. Acta* (Berl.), **19**, 167 (1970).
7) M. Itoh, T. Mimura, H. Usui, and T. Okamoto, *J. Amer. Chem. Soc.*, **95**, 4388 (1973).
8) M. Itoh, and T. Mimura, *Chem. Phys. Lett.*, **24**, 551 (1974).

9) M. Itoh, T. Mimura, and T. Okamoto, This Bulletin, **47**, 1078 (1974).
10) S. Katagiri and C. Sandorfy, *Theor. Chim. Acta.* (Berl.), **4**, 203 (1966).
11) E. Clementi, C. C. J. Roothaan, and M. Yoshimine, *Phys. Rev.*, **127**, 1618 (1962).
12) K. Nishimoto and N. Mataga, *Z. Physik. Chem.* (Frankfurt), **13**, 140 (1957).
13) R. Pariser and R. G. Parr, *J. Chem. Phys.*, **21**, 466 (1953).
14) J. Hinze and H. H. Jaffe, *J. Amer. Chem. Soc.*, **84**, 540 (1962).
15) M. J. S. Dewar and G. Klopman, *ibid.*, **89**, 3089 (1967).
16) D_μ and D_ν are zero for intramolecular core-core repulsion, then the equation (2) become to be identical with Dewar-Klopman's formula.
17) On this kind of approximation, this value is applicable to various donor-acceptor systems, taking structures of parallel molecular planes and spacing of 3.4 Å.
18) N. Mataga and Y. Murata, *J. Amer. Chem. Soc.*, **91**, 3114 (1969).
19) T. Kobayashi, K. Yoshihara, and S. Nagakura, This Bulletin, **44**, 2603 (1971).
20) M. Itoh, *Chem. Phys. Lett.*, **26**, 505 (1974).
21) M. Itoh, *J. Amer. Chem. Soc.*, **96**, 7390 (1974).
22) T. Mimura, M. Itoh, and T. Okamoto, This Bulletin, **48**, 1941 (1975).

A Study of the Exchange Reaction between Water and Surface Hydroxyl Groups on Magnesium Oxide by Means of Infrared Diffuse Reflectance Spectroscopy

Nobutsune TAKEZAWA and Haruo KOBAYASHI

Department of Chemical Process Engineering, Hokkaido University, Sapporo 060

(Received October 9, 1974)

Infrared diffuse reflectance spectroscopy was applied to the study of the exchange reaction between water and surface hydroxyl groups on magnesium oxide. The results led to the conclusion that (i) no reaction occurs *via* the combination of hydroxyl groups, and (ii) the hydroxyl groups react with adsorbed water reversibly. Two types of hydroxyl groups present on the surface are involved in the rate determining step.

A study of adsorption by means of diffuse reflectance spectroscopy provides valuable information on the state of the adsorbed species.[1-3] In an earlier stage of investigation, experiments were carried out in the visible and ultraviolet regions. Little work had been done in the infrared region until Kortuem and Delfs published their work in this spectral region.[4] Since then, it has been applied to the study of adsorption or inorganic analysis,[5-11] but no kinetic study has been carried out on catalytic reactions.

Some infrared spectral studies of the adsorption were conducted on alkaline earth metal oxides.[8,9,12-16] We have applied the infrared diffuse reflectance method to the exchange reaction between water and surface hydroxyl groups on magnesium oxide.

Experimental

Experiments were carried out in a manner similar to that in the previous work.[7-9] About 50 mg of magnesium oxide* in powder form** (J. T. Baker Co., Ltd.) was packed in a cell to a thickness of about 2 mm. The cell was attached to a Nippon Bunko model DR-3 diffuse reflectance apparatus (Japan Spectroscopic Co., Ltd.), the spectra being recorded with a Nippon Bunko Model IR-G infrared spectrophotometer.

Prior to the experiments, the sample was heated at 310 °C for 5 hr in a stream of purified nitrogen. Deuterium oxide vapor saturated at room temperature or at 0 °C was allowed to flow over the sample with a nitrogen stream to react with surface hydroxyl groups at 240—310 °C. The reaction between water and surface deuteroxyl groups was also carried out in a similar manner.

The reflectivity of the sample was practically independent of its amount for a sample weighing more than 35 mg.*** No. emission band was observed.

Results and Discussion

Water Adsorption. Part of the original sample was in the form of magnesium hydroxide, as confirmed by the presence of a strong absorption band at 3700 cm^{-1}.[8,9] When the sample was heated at 310 °C for 5 hr, the band disappeared and two new absorption bands were observed at 3730 and 3610 cm^{-1}. These bands were previously assigned to the OH stretching vibrations of different types of surface hydroxyl groups.[8,9,17] According to Anderson *et al.*,[17] the model for chemisorbed water consists of hydroxyl group adsorbed on a surface magnesium ion, the remaining hydrogen forming another hydroxyl group with an adjacent surface O^{2-} ion. The former (referred to as OH_h) gives rise to the absorption band at 3730 cm^{-1} and the latter that at 3610 cm^{-1} (referred to as OH_l). After the sample is once heated as described above, the intensities of these bands change no more by further heating at 240—310 °C. It was confirmed that no water was desorbed under these conditions. The positions and the intensities of these bands remained unchanged in the presence of water vapor (H_2O).

Adsorption of water was carried out with a conventional adsorption apparatus. It was found that the adsorption of water is initially rapid followed by slow adsorption. The adsorbed amount slightly increases with time in the latter stage of the adsorption. Finally, 0.09 ml STP/g MgO of water was held on the sample at 23 mmHg 290 °C after 2 hr. Over 90% of adsorbed water was rapidly desorbed upon degassing. The amount of the reversibly adsorbed water is roughly proportional to 0.25 th power of the partial pressure of water. The retention volume of water was determined as a function of the temperature of the gas chromatographic column in which magnesium oxide was packed. The heat of adsorption of water was estimated to be 6.9 kcal/mol from the temperature dependence of the retention volume.

Thus, it is concluded that water is reversibly adsorbed on magnesium oxide. The amount of spectroscopically active hydroxyl groups on magnesium oxide was kept constant irrespective of the presence or absence of water vapor.†

The Reaction between Water and Surface Hydroxyl Groups. In contrast to the above results, the intensities of the absorption bands due to the hydroxyl groups decreased appreciably when deuterium oxide vapor was brought into contact with magnesium oxide. New bands due to surface deuteroxyl groups appeared at 2760 (OD_h) and 2670 (OD_l) cm^{-1}. The positions of OH_h and OH_l remained unchanged in the course of the reaction. When water vapor (H_2O) was allowed to flow

* The average particle size of the sample was about 12 μ.

** The surface area of magnesium oxide was 16 m^2/g.

*** The reflectivity of the sample should be independent of its amount for a quantitative analysis of the diffuse reflectance spectra.

† The total amount of hydroxyl groups was estimated from that of water released by heating at 750 °C for 1 hr. It was found that the water amounted to 0.92 ml STP/g MgO.

over the sample which had been partially deuterated, the bands due to the deuteroxyl groups decreased, whereas those due to hydroxyls increased according to the reaction between H_2O and OD. The reaction proceeded at a faster rate as compared to the reaction of D_2O with OH. When the partial pressure of water vapor was lowered to one fifth of that in the former run, the rate was reduced by 34%. The rate is, therefore, proportional to 0.25 power in the partial pressure of water, indicating that the reaction proceeds in proportion to the amount of reversibly adsorbed water.

Evaluation of the Rate of the Reaction. For estimating the rate of the reaction, the relation between the reflectivity and the adsorbed amount should be obtained. According to Frei *et al.*,[18] total reflectivity R at given wave number $\tilde{\nu}$ of binary system can be written with reference to the Kubelka-Munk equation[19] as

$$(1-R)^2/2R = k_1/s_1 + k_2/s_2, \quad (1)$$

where k_1 and k_2 are the absorption coefficients and s_1 and s_2 the scattering coefficients. The reflectivity R can be determined with reference to the standard material of $R=1$. Mamiya[7] recently pointed out that alkali halide particles can be used as a standard meterial and that its reflectivity decreases by only 4% with an increase in its size from 1—5 μ to 40—80 μ. Potassium bromide with an average particle size of 15 μ was therefore employed. It is assumed that the term k_1/s_1 in the right hand side of Eq. (1) is the reflectance function of the sample itself whereas k_2/s_2 is that due to hydroxyl or deuteroxyl groups. Since the value of k_1/s_1 can be estimated from the background spectrum by means of the Kubelka-Munk equation $(1-R_1)^2/2R_1=k_1/s_1$ (R_1: the reflectivity of the sample), the k_2/s_2 value is readily estimated from Eq. (1). The integrated intensity n_iI_i of surface species i can thus be given by the following equation, assuming that s_2 is independent of wave number for the absorption band in question:

$$n_iI_i = \int k_2/s_2 d\nu = \int\left[\frac{(1-R)^2}{2R} - \frac{(1-R_1)^2}{2R_1}\right]d\tilde{\nu} \quad (2)$$

where n_i is the amount of the species i and I_i its intensity per unit amount.

Figure 1 illustrates the plot of the n_iI_i-values for OH_h and OD_h against the time of the reaction D_2O+OH at 290 °C. We see that the intensity of OH_h monotonically decreases with time whereas that of OD_h increases. Similar results were obtained for OH_l and OD_l, whereas these trends were reversed for the reaction between OD and H_2O.

The difference $I_i\Delta n_i$ between the n_iI_i-values at $t=0$ and $t=t$ is proportional to the change in the amount of the species i in the course of the reaction. Figure 2 shows the relation between these difference for OH_h and OD_h. The linear relationship indicates that OH_h was replaced by OD_h in the course of the reaction. On the assumption that one OH_h was replaced by one OD_h, the slope α of the plot gives the ratio I_{OD_h}/I_{OH_h}. The total intensity $n_{OH_h}I_{OH_h}+n_{OD_h}(I_{OD_h}/\alpha)$ which is proportional to the sum of the

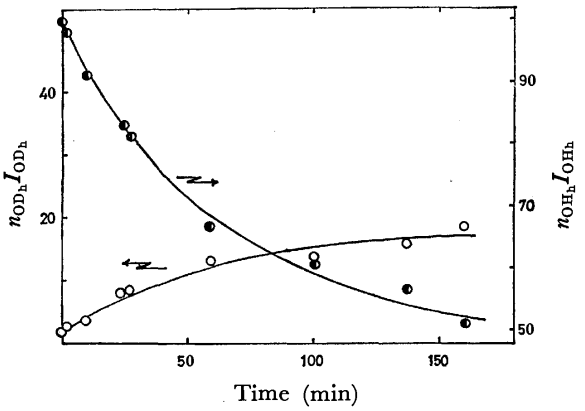

Fig. 1. The change in the intensities of surface OH_h and OD_h in the course of the reaction D_2O+OH at 290 °C.
◐: OH_h ○: OD_h

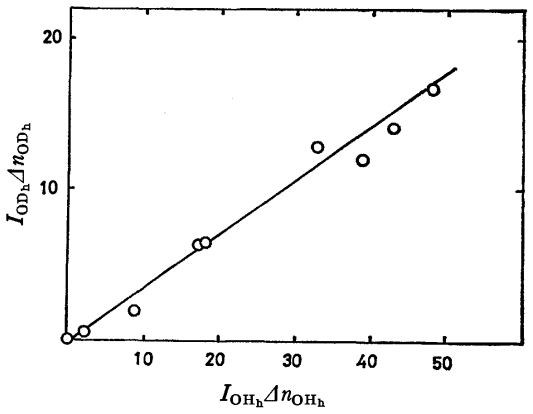

Fig. 2. The plots of the change in OH_h, $I_{OH_h}\Delta n_{OH_h}$ *versus* that in OD_h, $I_{OD_h}\Delta OD_h$.

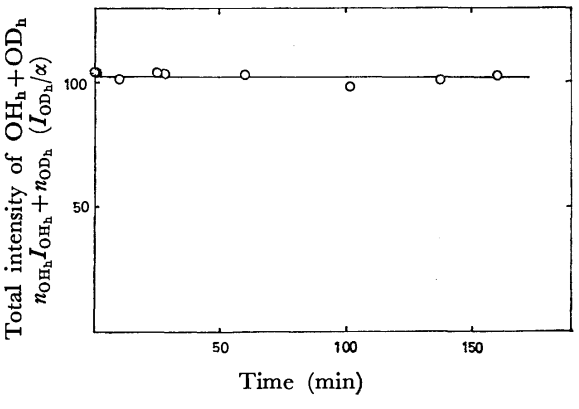

Fig. 3. Total intensity of OH_h+OD_h *versus* time of the reaction D_2O+OH at 290 °C.

amount of OH_h and OD_h was therefore determined from Eq. (2) and the value of α. Figure 3 shows the plot of the total intensity against the time of the reaction. This indicates that the sum of the amount of OH_h and OD_h remained practically constant during the course of the reaction. It is also valid for OH_l and OD_l although the intensities of these species could not be determined as accurately as those of OH_h and OD_h. The results were, therefore, consistent with those described above, indicating that the amount

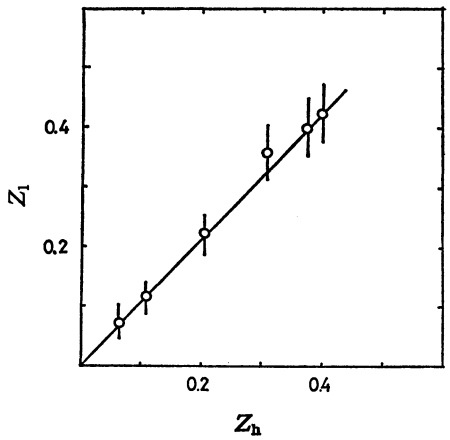

Fig. 4. Relation between the atomic fraction Z_l of OD_l and Z_h of OD_h in the course of the reaction D_2O+OH at 290 °C.

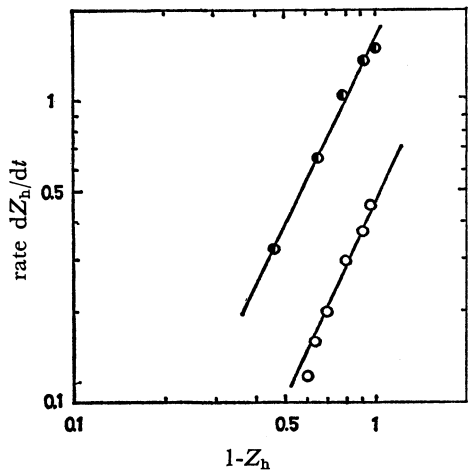

Fig. 5. Rate dZ_h/dt of the increase in the atomic fraction of OD_h *versus* atomic fraction $(1-Z_h)$ of OH_h. The reaction D_2O+OH was carried out at 290 °C(○) and at 310 °C(◐).

of hydroxyl groups can be determined by the Kubelka-Munk equation (1). The ratio of $n_{OD_h}(I_{OD_h}/\alpha)$ to the total intensity gives the atomic fraction of OD_h. Similarly, the atomic fraction of OD_l can be determined.

Mechanism of the Reaction. The amount of surface hydroxyl groups did not change unless deuterium oxide was present in ambient gas. No reaction occurred *via* the combination of a pair of hydroxyl groups. The exchange reaction proceeded at a rate proportional to the amount of reversibly absorbed deuterium oxide.

Figure 4 illustrates the relation between the atomic fractions Z_h of OD_h and Z_l of OD_l in the course of the reaction between D_2O and OH. The results indicate that the atomic fraction of OD_l is practically the same as that of OD_h in the course of the reaction. The rate of the reaction of D_2O with OH_h is illustrated as a function of the atomic fraction $(1-Z_h)$ of OH_h (Fig. 5). It is evident that the rate is proportional to $(1-Z_h)^2$. On the other hand, the rate of the reaction between H_2O and OD is proportional to Z_h^2 and is not proportional to $(1-Z_h)$ or Z_h as is often the case in exchange reactions. We conclude that two hydroxyl groups participate in the reaction. Since the atomic fraction of OH_h is the same as that of OH_l, both species might be simultaneously involved in the reaction. Under the present experimental conditions, reversibly adsorbed deuterium oxide reacts with both species in the rate determining step.

References

1) G. Kortuem and W. Braun, *Z. Phys. Chem. N. F.*, **18**, 242 (1958). Other papers published by G. Kortuem and his collaborators.
2) K. Klier, *Catal. Rev.*, **1**, 207 (1967).
3) M. Mamiya, *Bunseki Kiki* (Analytical Instrument), **4**, No. 2, 21 (1966).
4) G. Kortuem and H. Delfs, *Spectrohim. Acta*, **20**, 405 (1964).
5) G. Kortuem and H. Quabeck, *Ber. Bunsenges. Phys. Chem.*, **73**, 1020 (1969).
6) G. Kortuem and H. Quabeck, *ibid.*, **74**, 364 (1970).
7) M. Mamiya, *Hyomen* (Surface), **7**, 45 (1969).
8) N. Takezawa, K. Miyahara, and I. Toyoshima, *J. Res. Inst. Catal., Hokkaito Univ.*, **19**, 56 (1971).
9) N. Takezawa, This Bulletin, **44**, 3177 (1971).
10) N. Takezawa, *Chem. Commun.*, **1971**, 1451.
11) E. Ishii, M. Mamiya, and T. Murakami, *Nippon Kagaku Kaishi*, **1972**, 353.
12) M. J. D. Low, N. Takezawa, and A. J. Goodsel, *J. Colloid Interfac. Sci.*, **37**, 422 (1971).
13) M. J. D. Low, A. J. Goodsel, and N. Takezawa, *Environ. Sci. Technol.*, **5**, 1191 (1971).
14) A. J. Goodsel, M. J. D. Low, and N. Takezawa, *ibid.*, **6**, 268 (1972).
15) N. Takezawa and H. Kobayashi, *J. Catal.*, **25**, 179 (1971).
16) N. Takezawa and H. Kobayashi, *ibid.*, **28**, 335 (1972).
17) P. J. Anderson, R. F. Horlock, and J. F. Oliver, *Trans. Faraday Soc.* **61**, 2754 (1964).
18) P. W. Frei, D. E. Ryan, and V. T. Lieu, *Can. J. Chem.*, **44**, 1965 (1966).
19) P. Kubelka and F. Munk, *Z. Tech. Phys.*, **12**, 593 (1931). P. Kubelka, *Opt. Soc. Amer.*, **38**, 449, 1067 (1948).

Formulation of Stokes' Radii in DMF, DMSO and Propylene Carbonate with Solvent Structure Cavity Size as Parameter

Niro MATSUURA, Kisaburo UMEMOTO, and Yasuyuki TAKEDA

Department of Pure and Applied Sciences, College of General Education, The University of Tokyo, Komaba, Meguro-ku, Tokyo 153

(Received October 15, 1974)

Conductance of univalent ions in DMSO (dimethyl sulfoxide), DMF (dimethylformamide) and PC (propylene carbonate) was determined by use of tetrabutylammonium-tetrabutylborate as standard electrolyte of equal cationic and anionic conductance. Empirical formulation of Stokes' radius was attempted on the assumption of a structure-cavity affecting the ionic transport in a medium of aprotic and polar solvent as well as water. By application of classical fluid dynamics Stokes' radius r_s is given in terms of $-(2/3)\ r_c+(1/\sigma_s)\ (r_c-r_o)^2$, where r_c is crystal ionic radius, r_o and σ_s are parameters characteristic of the cavity and molecular sizes, respectively, with respect the solvent.

According to hydrodynamic theory the force acting on the hard shere with a radius a moving with a steady velocity of v_∞ in an incompressible fluid with a viscosity coefficient η is given by Eq. (1).

$$F = 4\pi\eta \cdot a \cdot v_\infty + 2\pi\eta \cdot a \cdot v_\infty \quad (1)$$

Equation (1) implies two terms of the friction drag acting tangentially on the sphere and the normal drag. The deviation from Stokes' law is obvious in ionic transport, if the crystal ionic radius is employed for a hard sphere chosen as a model. If the ion were to take as shape greatly deformed from the sphere under the influence of solvent structure according to the size fittness between the structure cavity and ions, the normal drag of the second term in (1) would be greatly reduced. A modification of Stokes' theory is required even in the frame of hydrodynamic theory by consideration of the sticky and slipping boundary.[1] The slippy boundary between the moving sphere and the medium leads to a Stokes' force of $4\pi\eta \cdot a \cdot v_\infty$ with the second term in (1) dropped. The solvation of ions explains qualitatively the deviation from Stokes' law, but a concept of negative solvation,[2] or some other hypotheses is inevitable. For a quantitative aspect of ionic transport, a number of more elaborate and sophisticated theories of solvation have been proposed, such as the Zwanzing theory of dielectric drag,[3] Uedaira's micro-viscosity of a solvent molecule just around the ions,[4] and a chemical-bond theory of solvent structure with a microscopic dipole moment.[5]

In recent works,[6~8] the transfer free energy of ions in aprotic solvents, involving PC, EC, DMF, and DMSO, were determined. These and similar data of enthalpy reported by Krishnan and Friedman[9] enable us to estimate the entropy of transfer of ions from water to the aprotic solvents. A large negative value of solvation entropy suggests that a certain liquid structure of solvent plays an important role in decreasing solvation entropy by producing an ordered arrangement even in these aprotic solvents. Accordingly, a comparative study of the Walden product was attempted in this work in various aprotic solvents other than water.

Unusual behavior of ionic conductance has been observed in some ionic species whose solvated radius (apparent Stokes' radius) is smaller than the crystal ionic radius. Kiso has compiled a large number of ionic conductance data with a variety of charges and sizes, concluding that a maximum ionic conductance can be seen for an ionic diameter of about 2.8 Å in aqueous medium which corresponds to the cavity size of water structure.[10] On this basis, Kiso proposed a slipped transport with a minimum friction involving a tangential shear alone, if the ionic size fits the size of a cavity present in the fluid medium. This model is helpful for understanding the apparent Stokes' radius which shows occasionally a radius smaller than the actual crystal ionic radius.

Experimental

Conductance of Cell. A conductance cell of 500 ml capacity was constructed according to the Erlenmeyer flask design of Kraus *et al.*[11] An electrode chamber is attached to the flask in such a way that the chamber liquid is thoroughly mixed with the solution in the main body of the cell. The electrodes were two platinum of 12 mm diameter, their distance being 10 mm. The cell constant of 0.4070 cm^{-1} was determined by eight KCl aqueous solutions in the concentration range from 3×10^{-3} to 8.5×10^{-3} M as referred to the value of 146.98×10^{-6} mho for KCl solution at 1×10^{-3} M at 25 °C.[12]

Procedure. Precaution was taken for precise conductance measurement particularly against pollution by impurities of water vapor, CO_2 and O_2. For preventing temperature and composition changes of liquid in the conductance cell, the temperature was controlled by a double chambered thermostat at 25±0.01 °C. The cell temperature change was readily detected by the shift of resistance readings exceeding 0.01%. The starting pure solvent was subjected to constant stirring with a teflon coated rotor of a magnetic stirrer for one hour, additional half-hour stirring being sufficient for each addition of electrolyte salt of about 100 mg. Direct transfer of the solvent from the 500 ml measuring flask kept in the thermostat to the conductance cell was made within 15 s. Stepwise increase of the electrolyte concentration was made by quick operation of transfer from weighing bottle to the conductance cell. Calibration for drainage on the wall of the flask, amounting to 0.5 ml or less, does not affect the acuracy of electrolyte concentration more than 0.1%. Repeated determination of cell constant was made for a series of runs with a given solvent system. Resistance was measured on a Model Yokogawa-Hewlette-Packard Universal Bridge.

Materials. The method of purification of solvent and electrolyte was as described.[6] The standard electrolyte of *n*-tetrabutylammonium *n*-tetrabutylborate, $(n\text{-Bu})_4N\cdot B(n\text{-Bu})_4$,[13] was synthesized from borontrifluoride etherate and *n*-butylmagnesium bromide as starting materials, purification

by recrystallization being repeated thrice for the crude preparation with a melting point of 110.6 °C to a final product with a melting point of 111.5 °C. All other chemicals were obtained from the Wako-Pure Chemicals Ltd.

Results and Discussion

The conductance of individual univalent ions at infinite dilution was studied in order to see how the ionic size regulates the ionic transport in non-aqueous solvent. The conductance at infinite dilution Λ° was determined by extrapolation of the observed Λ values from Λ-$\sqrt{c}$ plots for ten concentration points from 0.5×10^{-4} to 5×10^{-3} M. For dividing λ_∞ into each component of $\lambda_\infty^\pm$ an assumption was made of an equal conductance value for $(n\text{-Bu})_4\,N^+$ and $(n\text{-Bu})_4\,B^-$. The results on $\lambda_\infty^\pm$ are listed in Table 1 together with the calculated "apparent" Stokes' radius, r_s, according to the relation: $r_s=e\cdot E/6\pi\eta\lambda_\infty$. An empirical formulation of apparent Stokes' radius was attempted as a function of crystal ionic radius, r_c,[14] by introducting a solvent-dependent parameter, r_0. Starting with the assumption that hydrodynamic theory is valid even for ionic transport, we divided the force, for the sake of the formulation of r_s, into the tangential drag and the normal drag, corresponding to the first and the second terms, respectively, in Eq. (1). Hydrodynamic theory predicts that an air bubble of radius a passing through a liquid medium with velocity v_∞ has a drag force of $4\pi\eta a v_\infty$. If the moving ions make use of a vacant space of the solvent-structure cavity, the deviation of Stokes' law in ionic transport could be concentrated in the second ferm of the normal drag in Eq. (1) under the influence of the discrepancy between the ion-size and the cavity space. On this account, a correction was made by introducing a cavity-size parameter, r_0, for the second term of Eq. (1) in the form of Eq. (6) in consideration of the solvent-structure effect.

$$6\pi\eta\lambda_\infty r_s = 4\pi\eta\lambda_\infty r_c + f(r_c-r_0)$$

For finding the form of the function, $f(r_c-r_0)$, the value of $(r_s-(2/3)r_c)$ was plotted against r_c from the data shown in Table 1.

The results are shown in Figs. 1 and 2, in which $f(r_c-r_0)$ is approximated to a hyperbolic function in the form of $k(r_c-r_0)^2$.

It can be seen from the curves that a very small constant value, r_s°, is needed in some arbitary way for minimizing the deviation from $k(r_c-r_0)^2$ in Eq. (6).

Table 1. IONIC CONDUCTANCE OF INDIVIDUAL UNIVALENT IONS, λ_∞, AT 25 °C

Identical values have been reported in the reference marked with a number just behind the asterisk.

Solvent	DMSO		DMF		PC	
Viscosity η (Poise)	0.096		0.00796		0.0253	
	λ_∞	r_s	λ_∞	r_s	λ_∞[d]	r_s
Li^+	13.15	3.18	25.0	4.11	9.61	3.37
Na^+	13.8[a]	3.03	29.9[b]	3.44	10.45	3.10
K^+	14.4[a]	2.91	30.8[b]	3.34	11.79	2.75
Rb^+	16.1_3	2.59	32.4[b]	3.18	14.0_5	2.31
Cs^+	17.0_2	2.46	34.6	2.98	14.7_4	2.20
Me_4N^+	18.6_8	2.25	38.9[c]	2.65	14.8_5	2.18
Et_4N^+	16.8_2	2.49	35.6	2.89	13.8_2	2.34
Pr_4N^+	13.4	3.12	29.2[c]	3.53	11.0_0	2.95
Bu_4N^+	11.2_9	3.74	26.9	3.83	9.32_5	3.47
NH_4^+			38.7[b]	2.66	14.45	2.24
Cl^-	24.4_0	1.71	55.1[b]	1.87	15.9_4	2.03
Br^-	24.2[a]	1.73	53.6[b]	1.92	18.7_5	1.73
I^-	23.8[a]	1.76	53.3[b]	1.97	19.0_9	1.70
ClO_4^-	24.6_4[a]	1.70	52.9[b]	1.96	18.2_8	1.77
NO_3^-	27.0[a]	1.55	38.7[b]	2.66	22.1_2	1.47

Data referred to a) P.G. Shears, G. R. Lester, and L. R. Dawson, *J. Phys. Chem.*, **60**, 1433 (1956). b) R. C. Paul, I. R. Suigla, and S. P. Narmal, *J. Phys. Chem.*, **741** (1961). c) J. E. Prue and P. T. Sherrington, *Trans. Faraday Soc.*, **57**, 1795 (1961). d) Similar data were reported recently by M. L. Jansen and H. L. Yeager, *J. Phys. Chem.*, **77**, 3089 (1973).

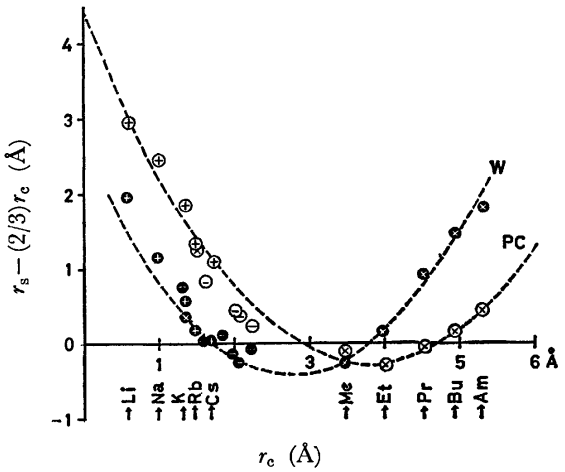

Fig. 1. Hyperbolic curves in the $\{r_s-(2/3)r_c\}$ plots against r_c for univalent ions with crystal ionic radius of r_c and with the apparent Stokes' radius r_s in water(W) and in propylene carbonate(PC), represented by; $r_s-(2/3)r_c=0.53(r_c-2.8)^2-0.6$ for water and $r_s-(2/3)r_c=0.31(r_c-3.8)^2-0.3$ for PC.

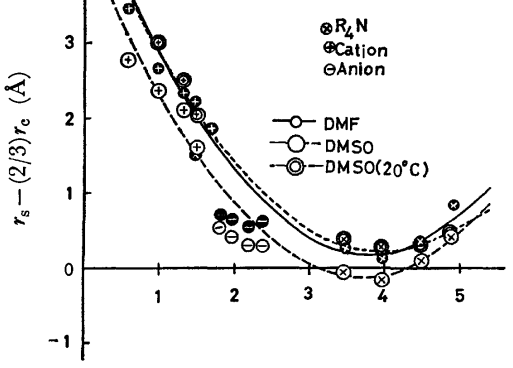

Fig. 2. Similar curves as Fig. 1 in DMF(dimethylformamide) and DMSO(dimethyl sulfoxide) represented by; $r_s-(2/3)r_c=0.32(r_c-3.75)^2+0.2$ for DMF and $r_s-(2/3)r_c=0.33(r_c-3.7)^2-0.2$ for DMSO.

Table 2. Parameters employed for the formulation of Stokes' radii by Eq. (6) from the plots shown in Figs. 1 and 2

Solvent	k Å^{-1}	r_0 Å	r_s^0 Å	σ_s Å	$1/\sigma_s$ Å^{-1}	Donor Number
PC	0.31	3.80	−0.3	3.23	0.31	15.1
DMF	0.32	3.75	+0.2	3.13	0.32	26.6
DMSO	0.33	3.70	−0.2	3.05	0.33	29.8
Water[a)]	0.53	2.80	−0.6	1.93	0.52	18.0

a) From the data of ionic conductance in aqueous system well established and available to be referred in the Hand-book (Landolt Bernstein Tabellen, II. Band, 7. Teil, 259, pp. 266 (1960)).

The correction r_s° is too small to affect greatly the accuracy in the predicted k and r_0 values which are required for the formulation. The parameters k and r_0 could be determined by application of least squares rule to the average values, $\sqrt{r_s-(2/3)\ r_c-r_s^\circ/r_c}$.

The results are given in Table 2.

It should be noted that the parameter k is a constant varying inversely with the size of a solvent molecule, σ_s, defined by $\sqrt[3]{(3/4\pi)V_s^\circ}$, where V_s° is the molar volume of solvent at 25 °C. In order to see if this observation on k values is right, works on conductance are extended to many other non-aqueous solvents whose data are available in literature. In a similar way to our treatment stated before, calculated Stokes' radii of univalent cations were formulated by a second order linear equation in a more general form of $a\cdot r_c^2+b\cdot r_c+c=r_s$, where a, b, and c are constants and a is identical with the constant k.

The results are given in Table 3 for a dozen solvents. In is interesting to see that a linear relationship between the molarvolume radius σ_s and the coefficient a or parameter k exsists in satisfactory agreement. Furthermore, the coefficient b has a value approximately equal to −2 and another constant coefficient c is proportional to the molecular radius of solvent, σ_s. The constant c

Table 3. Coefficients of a second order linear function of r_c (crystal ionic radius) employed for formulation of apparent Stokes' radius, r_s at 25 °C

Solvent	Molar Volume Radius Å		Coefficients in $r_s=ar_c^2+br_c+c$		Stokes' Radius Å	Reference
	σ_s	a (Å^{-1})	b (Å)	c (Å)	$(n\text{-Bu})_4N^+$	
1 Water	1.93	0.53	−2.30	3.56	4.77	a, b
2 Formamide	2.51	0.40	−1.97	4.06	3.80	c
3 Methanol	2.52	0.40	−2.13	5.08	3.85	d
4 Acetonitrile	2.75	0.36	−2.07	4.39	3.88	e, f, g, h, i
5 Ethanol	2.85	0.35	−2.13	5.55	3.84	j, p
6 NMF[1]	2.85	0.70	−3.81	6.17	4.83	k
7 DMSO[2]	3.05	0.33	−1.78	4.32	3.73	l, m
8 Acetone	3.08	0.29	−1.55	4.60	4.02	n, o
9 Propanol	3.10	0.32	−2.02	5.85	3.92	p
10 NMA[3]	3.12	0.34	−1.93	4.50	3.39	q (35 °C)
11 Pyridine	3.18	0.31	−1.79	4.80	3.87	s
12 DMF[4]	3.13	0.32	−1.84	4.70	3.69	r
13 PC[5]	3.23	0.31	−1.84	4.67	3.55	t, u
14 Butanol	3.31	0.28	−1.80	6.02	4.04	v
15 NMP[6]	3.34	0.25	−1.70	5.00	2.6	w
16 Nitrobenzene	3.46	0.31	−1.79	4.80	3.80	x, y, z
			Average: −2.03			

1 *N*-Methyl formamide, 2 Dimethyl sulfoxide, 3 *N*-Methylacetamide, 4 Dimethylformamide, 5 Propylene carbonate, 6 *N*-Methylpropionamide.

a) R. L. Kay and D. F. Evans, *J. Phys. Chem.*, **70**, 2325 (1966). b) R. A. Robinson and R. H. Stokes, "Electrolyte Solution," Butterworths, London (1955), pp. 25. c) J. M. Notley and M. Spiro, *J. Phys. Chem.*, **70**, 1502 (1966). d) J. A. Davis, R. L. Kay, and A. R. Gordon, *J. Chem. Phys.*, **19**, 749 (1951). e) R. L. Kay, D. F. Evans, and C. Zawoyski, *J. Phys. Chem.*, **69**, 3878 (1965). f) J. F. Coetzee and G. P. Cunningham, *J. Amer. Chem. Soc.*, **87**, 2529 (1965). g) A. C. Harknass and H. M. Daggett Jr., *Can. J. Chem.*, **43**, 1215 (1965). h) G. L. Kay, B. J. Hales, and G. P. Cunningham, *J. Phys. Chem.*, **71**, 3925 (1967). i) C. H. Springer, J. F. Coetzee, and R. L. Kay, *ibid.*, **73**, 471 (1969). j) J. R. Graham and A. R. Gordon, *J. Amer. Chem. Soc.*, **79**, 2350 (1957). k) R. D. Sigh, P. P. Rastogi, and R. Gopal, *Can. J. Chem.*, **46**, 3525 (1968). l) N. P. Yao and D. N. Bennion, *J. Phys. Chem.*, **175**, 1727 (1971). m) D. E. Arrington and E. Griswold, *ibid.*, **74**, 123 (1970). n) M. J. MacDowell and C. A. Kraus, *J. Amer. Chem. Soc.*, **73**, 3239 (1951). o) M. B. Reynold and C. A. Kraus, *ibid.*, **70**, 1709 (1948). p) D. F. Evans and P. Gardam, *J. Phys. Chem.*, **72**, 3281 (1968). q) R. Gopal and O. N. Bhatnagar, *ibid.*, **69**, 2382 (1965). r) J. E. Prue and P. J. Sherrington, *Trans. Faraday. Soc.*, **57**, 1795 (1961). s) D. S. Burgess and C. A. Kraus, *J. Amer. Chem. Soc.*, **70**, 706 (1948). t) L. M. Mukherjee and D. P. Boden, *J. Phys. Chem.*, **73**, 3969 (1969); **74**, 1942 (1970). u) M. L. Jansen and H. L. Yeager, *ibid.*, **77**, 3089 (1973). v) D. F. Evans and P. Gardam, *ibid.*, **73**, 158 (1969). w) R. D. Sigh and R. Gopal, This Bulletin, **45**, 2088 (1972). x) C. R. Witschonke and C. A. Kraus, *J. Amer. Chem. Soc.*, **69**, 247 (1947). y) E. G. Taylor and C. A. Kraus, *ibid.*, **69**, 1731 (1947). z) E. Hirsch and R. M. Fuoss, *ibid.*, **82**, 1018 (1960).

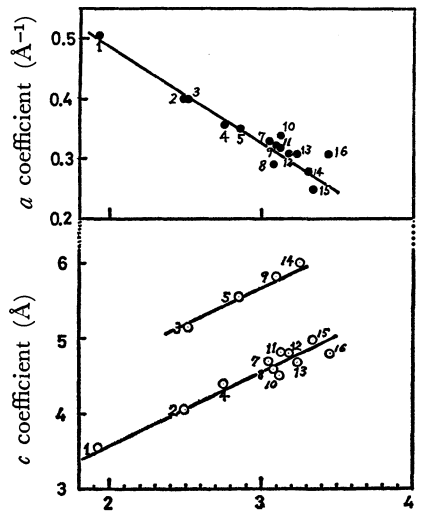

Fig. 3. A linear correlation between molar-volume radius σ_s of solvents and constant coefficients, a and c in the second order linear equation of r_c for representation of apparent Stoke's radius r_s. Solvent numbers refered to Table 3.

is a distance measured from the center of point charge, that is r_s at $r_c=0$, to a solvent molecule in a kinetically restricted movement, designated by $\sqrt{\mu \cdot e/\varepsilon kT}$, where μ and ε are the dipole moment and dielectric constant respectively, of solvent at T K. A linear dependence of c on σ_s can be understood from the fact that the solvation sphere of a point charge ion has a distance proportional to the molar-volume radius of solvent, σ_s. Figure 3 shows the plots of a (or k) and c against σ_s. A close correlation can be seen between the apparent Stokes' radii or Walden products and the molecular size of the solvent. One exceptional case was observed in a system of *N*-methylformamide whose unusually high association by hydrogenbond could be responsible.

Stokes' radii of Bu_4N^+ion (Table 3) have essentially the same value of 3.8, indicating that the Walden product rule holds in a large number of non-aqueous solvents, as far as this particular ion is concerned. The only exception is seen in *N*-methylformamide and its homologue, probably due to their strong hydrogen bonded association. In our formulation of r_s, the curves plotted against r_c differ very slightly among the solvents with an appreciable change of dielectric constant. For example, pyridine ($\varepsilon=12.3$, $\sigma_s=3.18$ Å), DMF ($\varepsilon=36.1$, $\sigma_s=3.13$ Å) and PC ($\varepsilon=64$, $\sigma_s=3.23$ Å), yield three very close curves (Fig. 4). On the other hand, there is a large difference in the shape of curves and the location of the minimum point discriminating one solvent from another between acetonitrile, formamide and water (Fig. 5). It seems likely that the donor number of the solvent is also no influential factor in the ionic transport, although it is a good measure of the medium effect of non-aqueous solvent.[7] From the second order linear equation a minimum Stokes' radius appears at r_c (minimum) $=-b/2a$, which can be regarded,

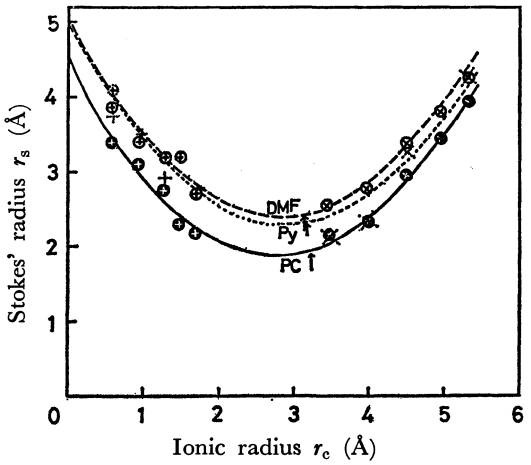

Fig. 4. Stokes' radius representation by crystal ionic radius in $a \cdot r_c^2+b \cdot r_c+c$ with constant coefficients a,b and c (in the Table 3), broken line with open circle for DMF, dotted line with cross for Pyridine and full line with black circle for PC.

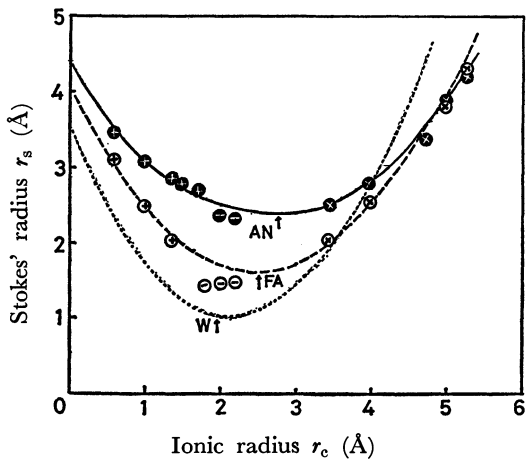

Fig. 5. Similar curves as Fig. 4. Full line for acetonitrile(AN), broken line for formamide and dotted line for water (Stokes' radius omitted).

to first approximation, as $1/a$ or k since the value of $-b$ is close upon 2 (Table 3). This is the reason why a minimum Stokes' radius appears when the ion radius fits well with the molar-volume radius of the solvent. These facts lead to the conclusion that there should be a contribution of a structure cavity or a free-volume space in the solvent medium to the ionic transport depending on the size of moving ions relative to the size of solvent molecules.

References

1) R. B. Bird, W. E. Stewart, and E. N. Lightfoot, "Transport Phenomena," John Wiley, N. Y. (1960); pp. 50–60.
2) O. Y. Samoilov, "Ionic Solvation-Structure of Electrolyte Solution," Translation by Uedaira, Chizin Shokan, Tokyo (1960).
3) R. Zwanig, *J. Chem. Phys.*, **52**, 3625 (1970); *J. Phys. Chem.*, **75**, 239 (1971).
4) H. Uedaira, *Zhur. Fiz. Khim.*, **42**, 3024 (1968); *ibid.*, **45**, 2550 (1971).
5) C. Howat and B. C. Webster, *J. Phys. Chem.*, **76**, 3714 (1972); K Fueki, D. F. Feng, L. Kevan, and R. E.

Christoffersen, *ibid.*, **75**, 2297 (1971).
6) N. Matsuura, K. Umemoto, and Z. Takeuchi, This Bulletin, **47**, 813 (1974).
7) N. Matsuura and K. Umemoto, *ibid.*, **47**, 1324 (1974).
8) N. Matsuura, K. Umemoto, M. Waki, Z. Takeuchi, and M. Omoto, *ibid.*, **47**, 806 (1974).
9) C. V. Krishnan and H. L. Friedman, *J. Phys. Chem.*, **73**, 3934 (1969).
10) Y. Kiso, "Zone Electrophoresis," Nankodo, Tokyo (1973), p. 28.
11) H. M. Daggett Jr., E. J. Bair, and C. A. Kraus, *J. Amer. Chem. Soc.*, **73**, 799 (1951).
12) J. E. Lind. Jr., J. J. Zwolenik, and R. M. Fuoss, *ibid.*, **81**, 1557 (1959).
13) R. Fuchs, J. L. Bear, and R. F. Rodewald, *ibid.*, **91**, 5797 (1969).
14) V. C. Zrumahliz, *Zhur. Fiz. Khim.*, **45**, 2559 (1971); L. Pauling, "The Nature of the Chemical Bond," 3rd Ed., Cornell University Press, Ithaca (1960).

Solvent Effects on the Absolute Intensities of Infrared Absorption Bands and the Dipole-Dipole Interaction

Masao KAKIMOTO and Tsunetake FUJIYAMA*

Department of Chemistry, Faculty of Science, The University of Tokyo, Hongo, Bunkyo-ku, Tokyo 113

**Department of Chemistry, Faculty of Science, Tokyo Metropolitan University, Fukazawa, Setagaya-ku, Tokyo 158*

(Received December 2, 1974)

The absolute intensities of the infrared absorption bands, ν_3 of methyl iodide, ν_2 of methyl cyanide, and ν_8 of methyl cyanide, were measured in various solvents at various concentrations. Even after the effect of the internal field is eliminated, very large solvent effects remain in the absorption intensities due to the intermolecular interactions. An equation based on the model of the dipole-dipole interaction is proposed to interpret the experimental results. Comparison with the experimental data confirms the validity of the model.

Much attention has been given to the change of infrared intensities in going from the gas to the liquid phase or from the gas phase to solutions. Many equations have been proposed to predict the ratio of the intensities of the gas and the liquid phases, among which that of Polo and Wilson[1] is the most familiar. Mallard and Straley[2] and Person[3] proposed an equation for the intensity ratio of the gas phase and solutions, which is identical to that of Polo and Wilson to the limit of pure liquid. These two equations deal with the integrated intensities and neglect the anomalous dispersion of the refractive index in the region of the adsorption band. The validity of the assumption of a single refractive index was studied theoretically by Schatz.[4] Although Schatz claims that the equation of Polo and Wilson is valid even for strong absorption bands if one chooses an appropriate value for the single refractive index, its usefulness is restricted to rather weak absorption bands.[5] The same problem has been treated by many other authors.[6-9] In the case of very strong absorption bands, one must take into account the frequency dependence of the refractive index rigorously, as shown theoretically and experimentally by Bakhshiev and coworkers[10] and by Crawford and coworkers.[11] These authors have presented an equation giving the relation between the apparent and the true absorption indices at each frequency. It is accepted that, when one compares the observed intensities at various phases, one must make a correction for the effect of the so-called internal field according to the scheme of Polo-Wilson or Mallard-Straley-Person for a weak absorption band and of Bakhshiev-Crawford for a strong absorption band. After being undergoing correction following the aforementioned schemes, the intensities of liquids or solutions agree well with the gas-phase intensities, if no specific solute-solute or solute-solvent interaction in liquids or solutions exists.[6,10-12]

It should be noted that the above treatment deals only with the change of the internal field surrounding an absorbing molecule and does not consider the effects of intermolecular interactions. Some authors such as Buckingham,[13] Mirone,[14] and Bakhshiev and coworkers[15] have discussed the effects of intermolecular interactions on infrared intensities. They used the reaction field of Onsager.[16] Experimental works concerning these theories are very scarce.[17-20]

In the present paper, the authors report the absolute intensities of a few absorption bands of methyl iodide and methyl cyanide in various solvents at various concentrations, and show that the effects of solvents are very large in some cases, even after the elimination of the effect of the internal field. The vibrational bands and solvents are as follows, ν_3 (the C-I stretching vibration) of methyl iodide, solvents: methyl cyanide and carbon disulfide, ν_2 (the C≡N stretching vibration) of methyl cyanide, solvents: carbon tetrachloride and 1,1,1-trichloroethane, and ν_8 (the CCN bending vibration) of methyl cyanide, solvents: carbon tetrachloride and nitromethane. In these systems no serious specific solute-solute or solute-solvent interaction is expected other than the dipole-dipole interaction. An equation is proposed to connect the absolute intensity of a pure liquid or a solution to that of the gas phase, based on the model of the dipole-dipole interaction.

Experimental

Commercial chemicals were used. Methyl iodide was distilled just before the observation to remove the pale yellowish color. Other samples were used without further purification although the infrared spectrum of methyl cyanide showed a samll amount (about 0.5 wt%) of water in it: the presence of water in methyl cyanide seems to cause no serious error.

Binary solutions were prepared just before the observation to attain appropriate concentrations by measuring the weight of each component. Mole percentage and molar concentrations were calculated by use of the density data.[21] Additivity of the volumes of both components was assumed.

The infrared spectra of the ν_2 band of methyl cyanide were measured in carbon tetrachloride- and 1,1,1-trichloroethane-solutions at various concentrations with a Perkin-Elmer 112G single-beam infrared spectrometer. A Perkin-Elmer 12C single-beam infrared spectrometer mounted with a CsBr prism was used to measure the ν_8 band of methyl cyanide in carbon tetrachloride- and nitromethane- solutions. The same spectrometer mounted with a KBr prism was used to measure the ν_3 band of methyl iodide in methyl cyanide- and carbon disulfide-solutions. The frequencies were calibrated following the standard method with the use of atmospheric water-vapour or carbon dioxide lines for the 112G spectrometer, and atmospheric water-vapour and methanol vapor lines for the 12C spectrometer.[22] The spectrometers were operated under a resolution of about 1 cm^{-1} except for the case of the ν_8 band of methyl cyanide, where the resolution was about 2 cm^{-1}. The effect of the finite slit width on the observed spectra was found to be very small. It was confirmed that the observed spectra were free of stray-light. All the measurements were carried out at room temperature

(25 °C). Each spectrum was measured at least twice.

A variable-length cell with KRS-5 window was used in the measurements. The thickness of the sample-cell was determined at each observation by the method of interference fringes.[23]

The observed spectra were reduced to the absorption-index curves, $k(\nu)$'s[24] where ν is the wavenumber in cm^{-1}, and the absolute intensities, Γ's, were calculated by means of the definition:[25]

$$\Gamma = \frac{4\pi}{c_m}\int_{band} k(\nu)\ d(\nu)$$

where c_m is the molar concentration (mol/cm^3). The integration of $k(\nu)$ over the absorption band was estimated by fitting a Lorentzian curve to the observed $k(\nu)$ curve by the method of least-squares. Care should be taken so that all the observed absorption bands contain hot bands in their lower-frequency sides. The hot bands cause the asymmetry of the main bands and it was found to be difficult to remove them by the usual method of least-squares. Thus, only the high-frequency sides of the bands were used in numerical calculations. The standard deviations were estimated from the deviations of the calculated Lorentzian curves from the observed absorption curves and from the maximum errors in the thicknesses of the sample-cell.

Since all the observed absorption bands are weak, Mallard-Straley-Person's scheme[2,3] was applied to the correction for the effect of the internal field, according to the equation

$$\Gamma_c = n_s\left[\frac{(n/n_s)^2+2}{n^2+2}\right]^2\Gamma$$

where n_s and n are the refractive indices of the solution and the solute, respectively, and Γ_c is the corrected intensity which is to be compared with the intensity of the gas phase. The refractive index was measured by the use of an Abbe's refractometer for each solution at the room temperature. The absolute intensity, Γ_c, is related to the transition dipole moment, m_1, of the vibrational transition by the equation[26]

$$\Gamma_c = \frac{8\pi^3}{3hc}N_a(m_1)^2$$

where h is Planck's constant, c the velocity of light, and N_a Avogadro's number. The observed intensity, Γ_c, is shown at each concentration in Figs. 1—4. The values of Γ's, Γ_c's, and $|m|$'s are given in Tables 1—3.

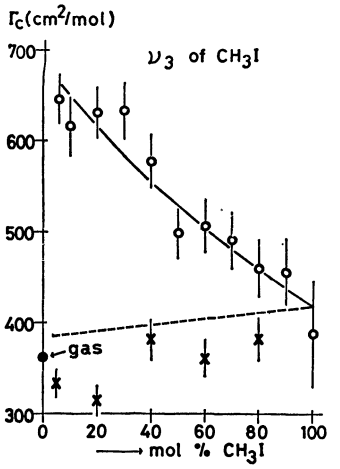

Fig. 1. Concentration-dependence of the absolute intensity of the ν_3 band of methyl iodide. The open circles and crosses indicate the observed intensities in methyl cyanide-solutions and in carbon disulfide-solutions, respectively. The vertical lines indicate standaed deviations. The solid line shows the concentration-dependence for methyl cyanide-solutions, calculated from the parameters of Table 4. The broken line shows the concentration-dependence for carbon disulfide-solutions, predicted from the same parameters of Table 4.

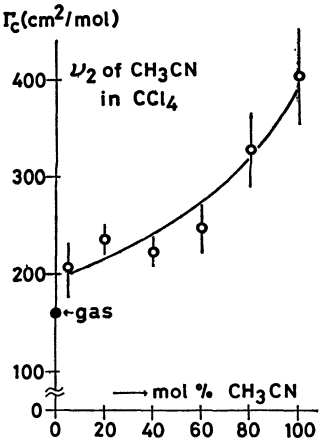

Fig. 2. Concentration-dependence of the absolute intensity of the ν_2 band of methyl cyanide in carbon tetrachloride-solutions. The open circles indicate observed intensities and the vertical lines standard deviations. The solid line shows the concentration-dependence calculated from the parameters of Table 4. The closed circle corresponds to the gas-phase intensity of Jesson and Thompson.[33]

Results and Discussion

We see from the figures that the absolute intensities greatly change in solutions even after correction for the internal fields. This indicates that the transition moment, m_1, changes in solutions as a result of intermolecular interactions. Thus we can obtain information on intermolecular interactions in liquids or solutions from the experimental data. In the following, we deal with the theoretical consideration on the change of infrared intensity in solutions.

The electric dipole moment, m, of a molecule under the influence of electric field, $\mathfrak{F}$, is given by

$$m = \mu + \alpha\langle\mathfrak{F}\rangle_{av} \qquad (1)$$

where μ and α are the electric dipole moment and the electric dipole polarizability, respectively, of an isolated molecule, and molecule, and $\langle\ \rangle_{av}$ means the average over all possible configurations of the surrounding molecules. All the quantities appearing in Eq. (1) can be expanded in powers of the normal coordinates of the vibrations. In the expansion of m, we take only the term that is linear on the normal coordinate, q, of the vibration:

$$m_1 = \mu_1 + \alpha_1\langle\mathfrak{F}_0\rangle_{av} + \alpha_0\langle\mathfrak{F}_1\rangle_{av} \qquad (2)$$

where the suffixes "0" and "1" mean respectively the zeroth and the first terms of the expansion, namely:

$$A_0 = \langle 0|A|0\rangle \qquad (3)$$

and

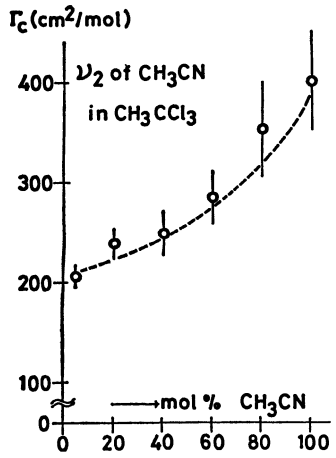

Fig. 3. Concentration-dependence of the absolute intensity of the ν_2 band of methyl cyanide in 1,1,1-trichloroethane-solutions. The open circles indicate observed intensities and the vertical lines standard deviations. The broken line shows the concentration dependence predicted from the parameters of Table 4.

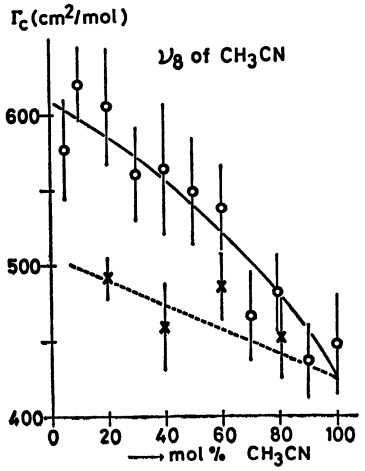

Fig. 4. Concentration-dependence of the absolute intensity of the ν_8 band of methyl cyanide. The open circles and crosses indicate the observed intensities in carbon tetrachloride-solutions and in nitromethane-solutions, respectively. The vertical lines indicate standard deviations. The solid line shows the concentration-dependence for carbon tetrachloride-solutions, calculated from the parameters of Table 4. The broken line shows the concentration-dependence for nitromethane-solutions, predicted from the same parameters of Table 4.

$$A_1 = \left(\frac{\partial A}{\partial q}\right)\langle 0|q|1\rangle \qquad (4)$$

The calculation of $\langle\mathfrak{F}_0\rangle_{av}$ and $\langle\mathfrak{F}_1\rangle_{av}$ has been made by Buckingham[13] and Bakhshiev and co-workers[15] using the reaction field of Onsager:[16] their results are expressed in terms of the dielectric constants of the surrounding macroscopic media. On the other hand, the present authors have recently calculated $\langle\mathfrak{F}_0\rangle_{av}$ based on a model of dipole-dipole interaction to explain the equilibrium of *trans*- and *gauche*-1,2-dibromoethanes in the liquid and in solutions,[27] and

Table 1. Concentration-dependence of the absolute intensity of the ν_3 band of methyl iodide
(Values in parentheses are standard deviations)
ν_3 of methyl iodide

mol%	Γ (cm²/mol)	Γ_c (cm²/mol)	$\lvert m_1(\text{obsd})\rvert$ (Debye)	$\langle\mathfrak{F}_p\rangle_{av}\times10^{-6}$ (Debye/cm³)
	—methyl cyanide-solution—			
100	531(79)	388(58)	0.0393	0.0151
90	621(49)	456(36)	0.0427	0.0232
80	622(42)	460(31)	0.0428	0.0333
70	660(41)	491(31)	0·0443	0.0410
60	678(39)	507(29)	0.0450	0.0501
50	662(36)	498(27)	0.0446	0.0600
40	762(39)	578(29)	0.0480	0.0699
30	831(40)	633(31)	0.0502	0.0827
20	823(36)	631(28)	0.0502	0.0912
10	799(42)	616(32)	0.0496	0.1044
6	836(35)	646(27)	0.0508	0.1087
	—carbon disulfide-solutions—			
80	525(32)	382(23)	0.0390	0.0121
60	498(27)	361(20)	0.0379	0.0091
40	527(30)	381(22)	0.0390	0.0061
20	436(23)	314(16)	0.0354	0.0031
5	463(21)	333(15)	0.0364	0.0008

Table 2. Concentration-dependence of the absolute intensisity of the ν_2 band of methyl cyanide
(Values in parentheses are standard deviations)
ν_2 of methyl cyanide

mol%	Γ (cm²/mol)	Γ_c (cm²/mol)	$\lvert m_1(\text{obsd})\rvert$ (Debye)	$\langle\mathfrak{F}_p\rangle_{av}\times10^{-6}$ (Debye/cm³)
	—carbon tetrachloride-solutions—			
100	480(59)	401(49)	0.0400	0.3980
80	393(44)	326(37)	0.0360	0.2717
60	298(29)	246(24)	0.0313	0.1776
40	272(19)	223(15)	0.0299	0.1051
20	288(18)	235(15)	0.0306	0.0463
5	254(29)	207(24)	0.0288	0.0111
	1,1,1-trichloroethane-solutions—			
80	426(57)	353(47)	0.0375	0.2724
60	345(32)	285(26)	0.0337	0.1837
40	303(27)	249(22)	0.0315	0.1188
20	292(19)	239(15)	0.0309	0.0661
5	251(14)	206(11)	0.0287	0.0334

have shown that the latter calculation explains well the part of the averaged electric field that changes in solutions, although the absolute value does not agree with that calculated from the reaction field. We calculate $\langle\mathfrak{F}_0\rangle_{av}$ and $\langle\mathfrak{F}_1\rangle_{av}$ following the same model of dipole-dipole interaction as before.

The basic idea of the model is that the solute and the solvent molecules are dispersed uniformly and homogeneously in a vacuum instead of in a continuous dielectric medium. Each molecule has its physical quantities (say, dipole moment, polarizability, *etc.*) identical with those in the gas phase, but since the density is so high (or the average intermolecular separation between the nearest neighbour is so short) in the

Table 3. Concentration-dependence of the absolute intensity of the ν_8 band of methyl cyanide
(Values in parentheses are standard deviations)
ν_8 of methyl cyanide

mol%	Γ (cm²/mol)	Γ_c (cm²/mol)	$\lvert m_1(\text{obsd})\rvert$ (Dybye)	$\langle\mathfrak{F}_p\rangle_{av}\times10^{-6}$ (Debye/cm³)
	—carbon tetrachloride-solutions—			
100	536(40)	447(33)	0.0422	0.3980
90	524(28)	436(24)	0.0417	0.3355
80	581(31)	481(25)	0.0438	0.2726
70	565(36)	466(29)	0.0431	0.2263
60	652(34)	537(28)	0.0463	0.1782
50	667(42)	548(35)	0.0468	0.1450
40	686(52)	563(43)	0.0474	0.1020
30	684(38)	560(31)	0.0473	0.0735
20	740(46)	605(38)	0.0491	0.0488
10	759(29)	620(24)	0.0497	0.0222
5	706(41)	577(33)	0.0480	0.0120
	—nitromethane-solutions—			
80	543(33)	452(28)	0.0425	0.3621
60	584(27)	485(22)	0.0440	0.3246
40	553(34)	459(28)	0.0428	0.2838
20	593(16)	491(13)	0.0443	0.2501

liquid phase or in solutions, the magnitudes of these quantities are modified as a consequence of intermolecular interactions, a typical example being Eq. (2). Following the same procedure as before, we obtain:[27]

$$\langle\mathfrak{F}_0\rangle_{av}=\frac{4\pi^2}{27}N_a^2\mu_0\left[\left(\frac{\mu_0^2}{kT}+\alpha_0\right)\frac{\rho}{W_m}c_m+\left(\frac{\mu_{0s}^2}{kT}+\alpha_{0s}\right)\right]+\frac{2\pi^4}{25\times243}N_a^4\mu_0\times\left[\frac{\mu_0^6}{(kT)^3}\left(\frac{\rho}{W_m}\right)^3c_m+\frac{\mu_0^2\mu_{0s}^4}{(kT)^3}\frac{8^3}{A^3}c_{ms}\right] \quad (5)$$

$$\langle\mathfrak{F}_1\rangle_{av}=\frac{4\pi^2}{27}N_a^2\mu_1\left[a_0\frac{\rho}{W_m}c_m+a_{0s}\frac{8}{A}c_{ms}\right] \quad (6)$$

where

$$A=\left\{\left(\frac{W_m}{\rho}\right)^{1/3}+\left(\frac{W_{ms}}{\rho_s}\right)^{1/3}\right\}^3 \quad (7)$$

and m_1, μ_1, α_0, and α_1 are those already described in Eq. (2), μ_0 is the permanent dipole moment of the solute molecule, W_m, ρ, and c_m are respectively the molecular weight, density, and molar concentration (mol/cm³) of the solute (the same symbols suffixed by "s" refer to those of the solvent), and N_a is the Avogadro number.

Calculation showed that $\langle\mathfrak{F}_1\rangle_{av}$ is very small as compared with $\langle\mathfrak{F}_0\rangle_{av}$ and that the terms containing α_0 and α_{0s} in the parentheses of the first term of Eq. (5) have much smaller contributions than the rest. We have therefore neglected these terms and analysed the experimental data by the following equation:[29]

$$m_1=\mu_1+\alpha_1\langle\mathfrak{F}_p\rangle_{av} \quad (8)$$

where

$$\langle\mathfrak{F}_p\rangle_{av}=\frac{4\pi^2}{27}N_a^2\mu_0\left[\frac{\mu_0^2}{kT}\frac{\rho}{W_m}c_m+\frac{\mu_{0s}^2}{kT}\frac{8}{A}c_{ms}\right]+\frac{2\pi^4}{25\times243}N_a^4\frac{\mu_0^3}{(kT)^3}\left[\mu_0^4\left(\frac{\rho}{W_m}\right)^3c_m+\mu_{0s}^4\frac{8^3}{A^3}c_{ms}\right] \quad (9)$$

Equation (8) relates the intensity data and the parameters, μ_1 and α_1. We can thus determine the magnitudes of μ_1 and α_1, using the intensity data at different concentrations and the calculated $\langle\mathfrak{F}_p\rangle_{av}$. In the calculation of $\langle\mathfrak{F}_p\rangle_{av}$, permanent dipole moments were taken to be 3.92 D for methyl cyanide,[30] 1.65 D for methyl iodide,[30] 1.79 D for 1,1,1-trichloroethane,[31] and 3.10 D for nitromethane.[30] For the ν_3 transition of methyl iodide, we obtained $\lvert\mu_1\rvert$ of 0.0391 D and $\lvert\alpha_1\rvert$ of 0.1134 Å³ from the experimental data of methyl cyanide-solutions by the method of least squares. Similarly, we obtained $\lvert\mu_1\rvert$ and $\lvert\alpha_1\rvert$ for the ν_2 and the ν_8 transitions of methyl cyanide, both from the data of carbon tetrachloride-solutions. The obtained values of $\lvert\mu_1\rvert$ and $\lvert\alpha_1\rvert$ are given in Table 4. The calculated concentration-dependence of the absolute intensities, corresponding to the determined $\lvert\mu_1\rvert$ and $\lvert\alpha_1\rvert$, is shown by solid lines in Figs. 1, 2, and 4.

In order to confirm the validity of the present theory and the obtained parameter-values, the concentration-dependencies of the absolute intensity for the other solvents were calculated using the values of $\lvert\mu_1\rvert$ and $\lvert\alpha_1\rvert$ of Table 4. The calculated curves are compared with the observed intensities in Figs. 1, 3, and 4 (broken lines).

We see that the agreement between the observed and the predicted concentration-dependence of the absolute intensities is fairly good for all the absorption bands. This indicates that the present model of dipole-dipole interaction can well represent the mechanism that causes a variation of the infrared absorption intensities in solutions. Incidentally, the gas-phase intensity data[32-34] are included in Figs. 1 and 2. It is seen that the calculated intensities approach the gas-phase intensities in the limit of the infinite dilution by nonpolar solvents, which indicates that the present estimation of $\lvert\mu_1\rvert$ is very reasonable. It should be noted that, although the signs of μ_1 and α_1 can not be determined from the intensity measurements, the signs of the products, $\mu_1\alpha_1$'s, can be determined from the solvent effect data. The conclusion is that $\mu_1\alpha_1>0$ for the ν_3 transition of methyl iodide, since as $\langle\mathfrak{F}_p\rangle_{av}$ becomes large so does $\lvert m_1\rvert$. Similarly we obtain the result $\mu_1\alpha_1>0$ for the ν_2 transition of methyl cyanide and $\mu_1\alpha_1>0$ for the ν_8 transition of methyl

Table 4. Values of $\lvert\mu_1\rvert$ and $\lvert\alpha_1\rvert$
(The values were determined by the method of least-squares from the data of methyl cyanide-solutions for ν_3 of methyl iodie, and from the data of carbon tetrachloride-solutions for ν_2 and ν_8 of methyl cyanide. Values in parentheses are standard deviations)

Transition	$\lvert\mu_1\rvert$ (D)	$\lvert\alpha_1\rvert$ (Å³)	$\mu_1\alpha_1$
ν_3 CH_3I	0.0391(0.0008)	0.1134(0.0114)	+
ν_2 CH_3CN	0.0280(0.0008)	0.0285(0.0039)	+
ν_8 CH_3CN	0.0493(0.0005)	0.0204(0.0022)	−

cyanide. Dickson *et al.*[32] concluded that $\mu_1<0$ for the ν_3 transition of methyl iodide. Thus we can say that $\alpha_1<0$ for this particular transition.

We must remember that the calculation of $\langle\mathfrak{F}_0\rangle_{av}$, based on the same model as in the present paper, resulted in very different values from those calculated on the basis of the reaction field in the case of 1,2-dibromoethane in liquid and in solutions,[27] although the former can well explain that part of the field which changes in concentration- or temperature-variation. The same situation is expected for the present cases. If we have data for the dielectric constant as each concentration, and calculate $\langle\mathfrak{F}_p\rangle_{av}$ by use of the reaction field formalism, somewhat different values for $|\alpha_1'|$s from the present results may be obtained. Thus the present values of $|\alpha_1|$'s can not be too much relied upon. In fact, we obtain $|\alpha_1|$ of 0.11 Å^3 for the ν_2 transition of methyl cyanide, if we use the gas-phase absolute intensity of Raman scattering measured by Schrotter and Bernstein.[39] neglecting the anisotropy of α_1. It seems, however, that the present approach has something to do with the real mechanism of molecular interaction that causes the intensity change, from the fact that the two-parameter equation, Eq. (8), can reproduce the intensity change very well.

The authors wish to express their gratitude to all the members of the Shimanouchi Laboratory for their valuable discussions. The authors are particularly grateful to Professor Takehiko Shimanouchi, the University of Tokyo, for giving them the opportunity to publish this work.

References

1) S. R. Polo and M. K. Wilson, *J. Chem. Phys.*, **23**, 2376 (1955).
2) W. C. Mallard and J. W. Straley, *ibid.*, **27**, 877 (1957).
3) W. B. Person, *ibid.*, **28**, 319 (1958).
4) P. N. Schatz, *Spectrochim. Acta*, **21**, 617 (1965).
5) Concerning this point, see references 10) and 11).
6) H. Ratajczak and W. J. Orville-Thomas, *Trans. Faraday Soc.*, **61**, 2603 (1965).
7) A. A. Clifford, *J. Mol. Structure*, **4**, 98 (1969).
8) B. Lefranc, J. Jacob, and J. Vincent-Geisse, *Spectrochim. Acta*, **22**, 1057 (1966); J. Vincent-Geisse, *J. Phys.* (Paris), **24**, 259 (1963); See also N. G. Bakhshiev, O. P. Girin, and V. S. Libov, *Opt. Spectrosc.*, **22**, 377 (1967).
9) K. H. Illinger, *J. Mol. Spectrosc.*, **15**, 440 (1965).
10) N. G. Bakhshiev, O. P. Girin, and V. S. Libov, *Opt. Spectrosc.*, **14**, 255, 336, 395 (1963); V. S. Libov, N. G. Bakhshiev, and O. P. Girin, *ibid.*, **16**, 549 (1964); V. S. Libov, O. P. Girin, and N. G. Bakhshiev, *ibid.*, **20**, 350 (1966); B. A. Mikhailov, V. M. Zolotzev, and N. G. Bakhshiev, *ibid.*, **34**, 627 (1973).
11) A. A. Clifford and B. Crawford, Jr., *J. Phys. Chem.*, **70**, 1536 (1966); T. Fujiyama and B. Crawford, *ibid.*, **72** 2174 (1968), **73**, 4040 (1969); B. Crawford, Jr., A. C. Gilby, A. A. Clifford, and T. Fujiyama, *Pure Appl. Chem.*, **18**, 373 (1969).
12) It is impossible to cite here all the publications which deal with this problem. The readers are referred to the following papers; J. C. Decius, *J. Chem. Phys.*, **35**, 1919 (1961); T. E. Thomas, W. J. Orville-Thomas, J. Chamberlain, and H. A. Gebbie, *Trans. Faraday Soc.*, **66**, 2710 (1970); L. P. Lindsay and P. N. Schatz, *Spectrochim. Acta*, **20**, 1421 (1964); J. Jacob and J. P. Benaich, *J. Chim. Phys.* (Paris), **64**, 1282 (1967).
13) A. D. Buckingham, *Proc. Roy. Soc., Ser. A*, **248**, 169 (1958), **255**, 32 (1960); *Trans. Faraday Soc.*, **56**, 753 (1960).
14) P. Mirone, *Spectrochim. Acta*, **22**, 1897 (1966); Mirone's treatment is erroneous in that he does not distinguish the dielectric constant and the square of the refractive index. In fact, his equation can not explain the present results. If corrections are made properly to Mirone's treatment, the result becomes essentially the same as that of Buckingham.[13]
15) O. P. Girin and N. G. Bakhshiev, *Opt. Spectrosc.*, **24**, 488 (1968); O. P. Girin, N. G. Bakhshiev, and O. I. Maksimova, *ibid.*, **25**, 22 (1968).
16) L. Onsager, *J. Amer. Chem. Soc.*, **58**, 1486 (1936).
17) G. L. Caldow, D. Cunliffe-Jones, and H. W. Thompson, *Proc. Roy. Soc.* (London), **A254**, 17 (1960).
18) A. R. H. Cole and A. J. Michell, *Spectrochim. Acta*, **20**, 747 (1964).
19) G. Levi and M. Chalaye, *C. R. Acad. Sci. Paris, B* **265**, 1093 (1962).
20) O. P. Girin, S. Kh. Akopyan, and N. G. Bakhshiev, *Opt. Spectrosc.*, **25**, 111 (1968); V. S. Smirmov, Yu. E. Zabiyakin, O. P. Girin, and N. G. Bakhshiev, *ibid.*, **27**, 138 (1969); O. P. Girin and N. G. Bakhshiev, *Soviet Phys. Uspekhi*, **6**, 106 (1963).
21) "International Critical Tables," National Research Council, McGraw-Hill, New York (1928).
22) A. R. Downie, M. C. Magoon, T. Purcell, and B. Crawford, Jr., *J. Opt. Soc. Amer.*, **43**, 941 (1953).
23) D. C. Smith and E. C. Miller, *J. Opt. Soc. Amer.*, **34**, 130 (1944).
24) M. Kakimoto and T. Fujiyama, This Bulletin, **45**, 3021 (1972), Eq. (1).
25) B. Crawford, Jr., *J. Chem. Phys.*, **29**, 1042 (1958), Eq. (2).
26) See, for example, J. Overend, "Quantitative Intensity Studies and Dipole Moment Derivatives," in "Infrared Spectroscopy and Molecular Structure," edited by M. Davies, Elsevier (1963).
27) M. Kakimoto and T. Fujiyama, This Bulletin, in press.
28) The second term of Eq. (5) arises from the third-order term in the expansion of the distribution function (see footnote 13) of the reference[27]). When the dipole moment is very large, as is the case for methyl cyanide, this term gives a significant contribution that can not be neglected.
29) The direction of $\langle\mathfrak{F}_0\rangle_{av}$ or $\langle\mathfrak{F}_p\rangle_{av}$ in the present model is always the same as that of the permanent dipole moment. Therefore the rigorous expression for α_1 should be $(\alpha_{\rho\sigma})_{01}$ according to the notation of Placzek,[40] where ρ and σ indicate the directions of μ_1 and μ_0, respectively, in the molecular frame.
30) C. H. Townes and A. L. Schawlow, "Microwave Spectroscopy," McGraw-Hill (1955).
31) A. A. Maryott, M. E. Hobbs, and P. M. Gross, *J. Amer. Chem. Soc.*, **63**, 659 (1941).
32) A. D. Dickson, I. M. Mills, and B. Crawford, Jr., *J. Chem. Phys.*, **27**, 445 (1957).
33) J. P. Jesson and H. W. Thompson, *Spectrochim. Acta*, **13**, 217 (1958), referred to in B. H. Thomas and W. J. Orville-Thomas, *J. Mol. Structure*, **7**, 123 (1971), in the unit of 10^3 darks. We converted the latter into the unit of cm^2/mol by the relation:

$$\Gamma(\text{cm}^2/\text{mol}) = \text{A(darks)} \times 10^3/\nu_0$$

where ν_0 is the wavenumber (cm^{-1}) at the band center.
34) Kondo's preliminary result[35] is 103 darks or 272 cm^2/mol for the gas-phase intensity of the ν_8 band of methyl

cyanide, which conflicts with the present result. Among other authors, Gordon[36] reports 113 darks and Hendricks[37] reports 130 darks. It seems that some unexplained cause exists which makes the intensity of this particular absorption band in carbon tetrachloride-solution very different from that of the gas phase.

35) S. Kondo, private communication.

36) A. V. Gordon, Dissertation (Oxford University, 1954).

37) Hendricks, Ph. D. Thesis (Brown University, 1956), cited in the report of Names and Orville-Thomas.[38]

38) L. Names and W. J. Orville-Thomas, *Trans. Faraday Soc.*, **61**, 2612 (1965).

39) H. W. Schrötter and H. J. Bernstein, *J. Mol. Spectrosc.*, **12**, 1 (1964). It should be noted that the value of α_1 appearing in the equation of the Raman-intensities should not be precisely the same as that in the present discussion, bacause the dispersion formula of α_1[40] includes the frequency of the incident light. In the present discussion, α_1 corresponds to a static field, while the Raman scattering is usually excited by a visible light.

40) G. Placzek, "The Rayleigh and Raman Scattering," U. S. At. Energy Comm. UCRL-TRANS-526(L), 1962 [translated from "Marx Handbuch der Radiologie," Akademischer Verlagsgeselschaft, Leipzig(1934), 2nd ed., Vol. 6, Pt. II, pp. 205—374].

The Raman Spectra of Surfactants and The Concentration Dependence of Their Molecular Conformations in Aqueous Solutions[1)]

Hirofumi Okabayashi, Masataka Okuyama, and Teizo Kitagawa*

Department of Engineering Chemistry, Nagoya Institute of Technology, Gokiso, Nagoya 466

**Institute of Protein Research, Osaka University, Yamada-kami, Suita, Osaka 565*

(Received January 21, 1975)

The laser Raman scattering by potassium *n*-alkyl carboxylates and sodium *n*-alkyl sulfates was measured in the solid state and aqueous solutions, and the concentration dependence of molecular conformations of these molecules was studied. For aqueous solutions of potassium *n*-hexanoate and potassium *n*-pentanoate, the Raman intensities of the accordion vibrations of the all-*trans* form relative to the skeletal deformation vibrations of the *gauche* isomers were found to increase with an increase in the concentration. This intensity change is remarkable at the critical micelle concentration. A concentration dependence of the intensity of the Raman lines was also observed in the frequency region of 1600—600 cm^{-1}. These observations revealed that the percentage of the all-*trans* form of the surfactant molecules increases with an increase in the concentration above the critical micelle concentration.

The infrared absorption spectra of straight-chain fatty acids and their salts have been extensively studied by many investigators,[2–15)] and the vibrational assignment of the infrared absorption bands has been almost completely established. However, very few Raman studies of these compounds have been reported.

In our preceding paper[16)] on the Raman spectra of a homologous series of sodium *n*-alkyl sulfates and of potassium *n*-alkyl carboxylates, the sulfate ions were found to take the *trans* form about the CH_2–O bond in an aqueous solution. Moreover, it was concluded that the conformational randomness of the *n*-alkyl hydrocarbon skeleton of these surfactant molecules increases with the number of carbon atoms.

In the present study, the concentration dependence of the relative Raman intensities was investigated for aqueous solutions of potassium *n*-alkyl carboxylates and sodium *n*-alkyl sulfates, and the conformation change in the surfactant molecules accompanying the formation of micelles was discussed.

Experimental

The samples of potassium *n*-butanoate (Pn-B), potassium *n*-pentanoate (Pn-P), potassium *n*-hexanoate (Pn-H), and potassium *n*-octanoate (Pn-O) were prepared from the corresponding aliphatic acids and potassium hydroxide, and were purified by recrystallization. The samples of sodium *n*-butyl sulfate (SBS), and sodium *n*-hexyl sulfate (SHS) were prepared from sulfuric acid, *n*-alkyl alcohol, and sodium hydroxide. The purity was checked by elementary analysis. Found for SBS: C, 26.94; H, 5.20%. Calcd for $C_4H_9O_4SNa$: C, 27.27; H, 5.15%. Found for SHS: C, 35.27; H, 6.70%. Calcd for $C_6H_{13}O_4SNa$: C, 35.11; H, 6.39%.

The measurements of the Raman spectra of these surfactants were carried out at room temperature with the use of a JEOL model-02AS Raman spectrometer and the 488.0 nm line of an Ar^+ gas laser. The temperature dependence of the intensities of the Raman lines was measured by the use of a JRS-S1 Raman spectrometer. The Raman spectra of the surfactants in the solid state were obtained by focusing the laser beam into a cavity of the small disk of samples. For the measurements of aqueous solutions, the potassium *n*-alkyl carboxylates were dissolved in a 0.1 M KOH solution to avoid hydrolysis, but the sodium *n*-alkyl sulfates were simply dissolved in water.

Results and Discussion

The Raman spectra of Pn-B, Pn-P, and Pn-H in aqueous solutions are shown in Fig. 1, while the frequencies observed in the solid state and in aqueous solutions are listed in Table 1. The vibrational assignment of these Raman lines was carried out on the basis of the infrared-absorption spectra of fatty acids and their salts.[13–15)]

A weak peak commonly observed at 1550 cm^{-1} in aqueous solutions corresponds to the infrared-absorption band of an aqueous solution at 1550 cm^{-1} and is assigned to the COO^- anti-symmetric stretching vibration. The two Raman lines of the solid surfactants at 1550 and 1580—1600 cm^{-1} may possibly

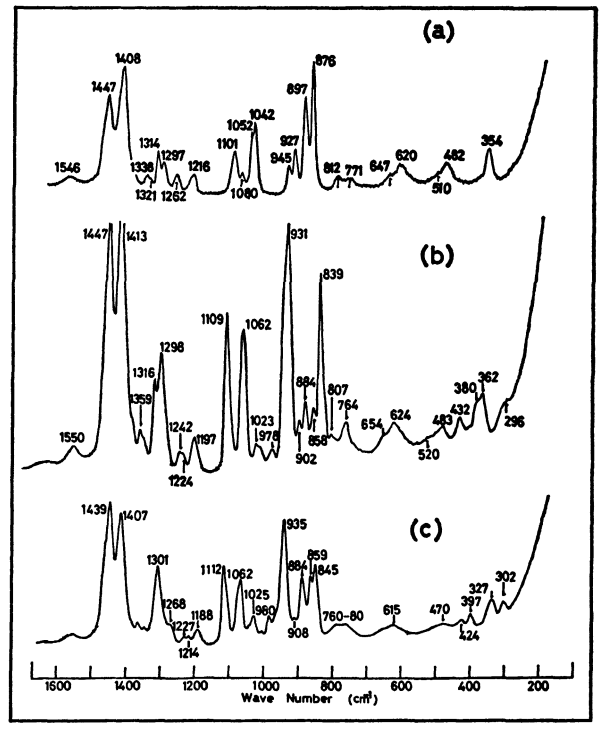

Fig. 1. Raman spectra of (a) Pn-B (500 mg/cc), (b) Pn-P (400 mg/cc) and (c) Pn-H (450 mg/cc) in aqueous solutions.

TABLE 1. RAMAN FREQUENCIES (cm^{-1}) AND RELATIVE INTENSITIES[a] OF Pn-B, Pn-P, Pn-H, AND Pn-O IN THE SOLID STATE AND AQUEOUS SOLUTIONS

Pn-B		Pn-P		Pn-H		Pn-O	
Solid	Soln	Solid	Soln	Solid	Soln	Solid	Soln
1581 m		1598 w		1582 m		1582 w	
	1546 wb	1550 vwb	1550 wb	1545 vwb	1550 vwb	1545 vw	1551 wb
						1473 sh	
1454 s	1447 s	1464 m	1465 sh	1457 m	1455 sh	1460 vs	1465 vs
		1448 w	1447 s			1445 sh	
1434 sh	1435 sh	1434 vs		1432 s	1439 vs	1435 s	
1420 vs	1408 vs	1406 w	1413 s	1413 s	1407 s	1417 sh	1415 s
1381 vwb	1379 sh	1379 vw	1380 sh	1381 vw	1380 sh	1384 vw	1371 vwb
		1356 vw	1359 w	1363 vwb	1363 vwb	1374 vw	
1345 wb	1338 w	1340 vw	1351 w	1341 vwb	1342 vwb	1345 vwb	1348 vwb
	1321 sh	1319 w			1320 sh		
1310 vwb	1314 m		1316 w				
1288 m	1297 w	1293 s	1298 m	1300 m	1301 m	1288 s	1300 s
				1290 w			
		1275 sh	1275 sh	1262 w	1268 vwb		
1257 w	1262 w					1256 vw	1257 vw
		1236 w	1242 vw			1233 vwb	1240 sh
1224 vwb	1216 w		1224 sh	1222 vwb	1227 vwb		
					1214 vw		
		1204 w	1201 w	1196 vwb		1207 vw	1201 vwb
					1188 wb	1185 vw	1175 w
1108 m	1101 m	1107 s	1109 s	1114 m	1112 m	1120 m	1117 m
						1112 vw	
			1090 sh				
1078 vw	1080 vw			1078 vw	1070 sh		1077 m
		1063 s	1062 m	1060 m	1062 m	1065 m	1064 m
	1052 sh		1058 sh			1050 w	
1040 s	1042 m				1039 sh	1034 w	1036 m
		1024 m	1023 vw	1027 w	1025 w		
			1017 vw				
				1010 vw	1005 vwb	1001 vw	1005 sh
			978 vw	982 sh	980 vw		
				965 vwb	965 sh	963 vwb	960 sh
939 w	945 w		936 sh				
922 vwb	927 m	927 vs	931 s	925 vs	935 s	920 m	926 s
			902 vw		908 vw		
891 vs	897 s	892 m	884 vw	886 w	884 m	896 m	897 m
	876 vs						875 m
858 w			858 vw	861 vw	859 w		
		838 vw	839 m	849 w	845 m	839 vw	844 m
	812 wb	809 vw	807 vwb				
779 vwb	771 vwb			786 vwb	781 vwb	772 vwb	775 wb
			764 w	767 vwb	758 vwb		
		730 vwb	740 sh			731 vw	
698 vwb		692 w		692 wb		695 vwb	
	647 sh		654 sh		650 sh		650 vw
	620 wb		624 wb				622 wb
				610 sh	615 wb		
585 vwb		584 w		587 wb		581 vwb	
		525 w	520 sh				530 sh
503 sh	510 sh						
				495 vw	499 sh		
478 m	482 wb		483 vwb				
				472 vw	470 wb		477 wb
			432 w			442 vw	
				420 w	424 vwb	424 vw	430 sh
					397 w		397 w
			380 sh				
356 m	354 m	355 s	362 m				350 sh
		318 w		325 s	327 m		
							314 vw
			296 sh	296 vw	302 w	293 vwb	
255 vwb		255 vw				248 s	254 sh

a) vs: very strong, s: strong, m: medium, w: weak, wb: weak and broad, vw: very weak, vwb: very weak and broad, sh: shoulder.

be the split components of the COO^- anti-symmetric stretching vibration. A strong Raman line at 1450—1465 cm^{-1} is commonly observed in the solid state and an aqueous solution, and is due to the CH_2 scissoring vibrations. A common Raman line of the surfactant solutions around 1400—1420 cm^{-1} also appears in the solid state; this line corresponds to the infrared-absorption band of the aqueous solutions at 1400 cm^{-1}, and is ascribed to the COO^- symmetric stretching vibration. A Raman line observed at 1380 cm^{-1} in the solid samples and aqueous solutions is due mainly to the terminal-methyl symmetric deformation.

The weak broad Raman line of the solid surfactants at 690—700 cm^{-1} corresponds to the infrared-absorption band at 690—700 cm^{-1}; it is assigned to the COO^- scissoring vibration. This vibrational mode is observed at 650 cm^{-1} in the aqueous solutions, with a considerable shift in the frequencies. A broad Raman line of the aqueous solutions is observed at 615—620 cm^{-1}; in the solid state this Raman line appears at 580—590 cm^{-1}, with a frequency shift, and is attributed to the COO^- wagging vibration. A broad Raman peak is commonly observed at 500—530 cm^{-1} in the solid surfactants and aqueous solutions; it is assigned to the COO^- rocking vibration. These Raman lines do not depend very much upon the chain length. However, there are several Raman lines which are characteristic of each molecule; they are related to the molecular conformations.

In the lower frequency region of the Raman spectrum of each solid sample a strong Raman line is observed, and its frequency is inversely proportional to the number of carbon atoms when it is greater than five. This relationship has been found for the accordion-like skeletal deformation frequencies of *n*-paraffins.[17,18] Accordingly, this line must be ascribed to an accordion vibration of the surfactant molecule. Moreover, in the aqueous solution of each sample there is a medium Raman line which closely corresponds to the accordion vibration observed in the solid state; its frequency is also proportional to the reciprocal number of the carbon atoms. This Raman line should be assigned to the accordion-like vibration due to the extended molecular form in the aqueous solution. This observation is also compatible with the fact that the extended molecular form is abundant in the liquid state for low homologous *n*-paraffins.[17,18]

Potassium n-*Butanoate.* The Raman lines of Pn-B at 812, 876, 1052, and 1321 cm^{-1} are not observed in the solid state; accordingly, these lines are ascribed to the rotational isomer about the CH_2–CH_2 bond. Two Raman lines are observed at 1080 and 1290—1300 cm^{-1} in the solid state and in an aqueous solution. They are not identified in the infrared-absorption spectra of Pn-B.[15] The two Raman lines of the solid Pn-B at 478 and 356 cm^{-1} are also observed at 482 and 354 cm^{-1} in an aqueous solution. These lines correspond closely to the infrared-absorption bands of *n*-butyric acid at 487 and 364 cm^{-1}, which have been assigned to the CCO deformation vibration and the CCC deformation vibration[14] respectively.

Potassium n-*Pentanoate.* The weak Raman lines of the Pn-P solution at 764, 858, 936, 978, 1017, and 1224 cm^{-1} are not found in the spectrum of the solid surfactant; accordingly, they are attributed to the *gauche* isomers about the CH_2-CH_2 bonds. Four Raman lines at 839, 884, 1023, and 1275 cm^{-1} are found for both the solid Pn-P and an aqueous solution, but they are not observed in the infrared-absorption spectra.[15] The accordion vibration of Pn-P is identified at 355 cm^{-1} in the solid state and at 362 cm^{-1} in an aqueous solution. Three Raman peaks of the aqueous solution at 380, 432, and 483 cm^{-1} are not found in the spectrum of the solid state; they are thus ascribed to the skeletal deformation vibrations of the *gauche* isomers.

Potassium n-*Hexanoate.* Three Raman lines of the aqueous solution at 908, 1039, and 1214 cm^{-1} disappear in the solid state and are, therefore, attributed to the *gauche* isomers. The Raman lines of Pn-H are observed at 780—785, 860, 1025—1030, 1070—1080, and 1260—1270 cm^{-1} in both the solid state and an aqueous solution, but none of these lines is observed in the infrared-absorption spectra of Pn-H.[15] The accordion vibration of Pn-H is observed at 325 cm^{-1} in the solid state and at 327 cm^{-1} in an aqueous solution. Since only the Raman peak of the aqueous solution at 397 cm^{-1} disappears in the solid state, it must be assigned to the skeletal deformation vibrations of the *gauche* isomers.

Potassium n-*Octanoate.* The three Raman lines of the aqueous solution at 850, 875, and 1077 cm^{-1} disappear in the solid Pn-O; accordingly, they can serve as indicators of the *gauche* isomers. Three Raman lines of Pn-O are also observed at 960, 1000, and 1120 cm^{-1} in the solid state and in aqueous solution, but these lines do not appear in the infrared-absorption spectra.[16] The accordion vibration of Pn-O gives rise to the Raman lines at 248 cm^{-1} in the solid state and at 250 cm^{-1} in an aqueous solution. The two Raman lines at 430 and 450 cm^{-1} are due to the coupled vibrational modes of the skeletal deformation vibrations and the CCO deformation vibration of the *trans* isomer. The three Raman lines of the aqueous solution at 314, 350, and 397 cm^{-1} are not observed in the solid state; accordingly, they are attributed to the skeletal deformation vibrations of the *gauche* isomers.

Temperature Dependence of Raman Spectra of Aqueous Solutions. Figures 2(a) and (b) show the Raman spectra of Pn-H and Pn-P, respectively, in the aqueous solutions at two different temperatures. The Raman intensity of the accordion vibration of the all-*trans* form seems to decrease as the temperature is raised. In the case of Pn-H, the Raman intensities of the peak at 327 cm^{-1} relative to the peaks at 397, 424, and 470 cm^{-1} are lower at 96 °C, while for Pn-P the intensities of the peak at 362 cm^{-1} relative to other peaks are lower at 96 °C than at 20 °C.

Concentration Dependence of the Relative Raman Intensities of Potassium Aliphatic Carboxylates. Figures 3(a) and (b) show the change in the intensities of Raman lines with the concentration of Pn-H and Pn-P in the skeletal deformation vibration region. The intensities of the Raman lines were found to be con-

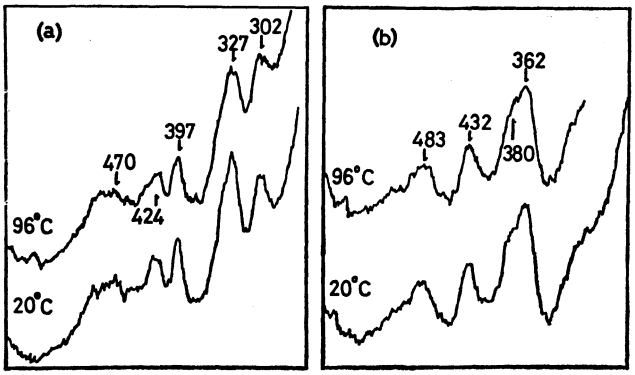

Fig. 2. Temperature dependence of the Raman spectra of (a) Pn-H (450 mg/cc) and (b) Pn-P (400 mg/cc) in aqueous solutions.

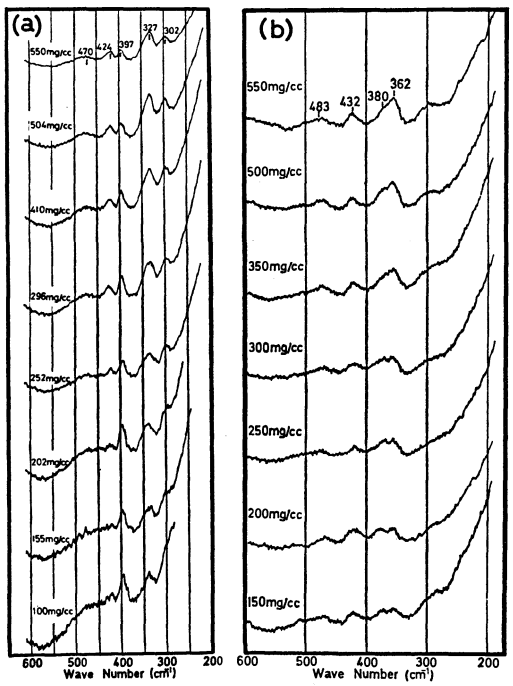

Fig. 3. Raman spectra of (a) Pn-H and (b) Pn-P in aqueous solutions at various concentrations.

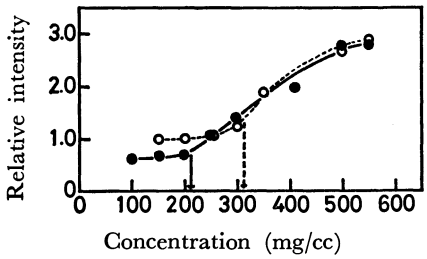

Fig. 4. Concentration dependence of the peak height ratio (I_{327}/I_{397}) of the Pn-H solution (solid line) and that (I_{362}/I_{432}) of the Pn-P solution (broken line). Weak background due to the water spectrum was substracted from the surfactant spectrum using the Raman scattering of distilled water as the base line. Solid and broken arrows indicate the critical micelle concentrations of Pn-H and Pn-P, respectively.

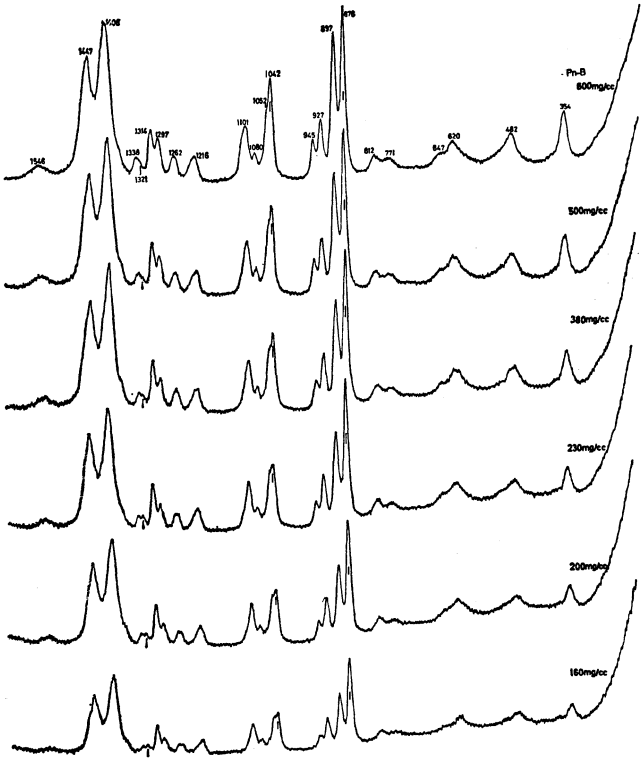

Fig. 5. Raman spectra of Pn-B in aqueous solution at various concentrations.

siderably influenced by the concentration. The relative Raman intensity of the accordion vibration of Pn-H at 327 cm^{-1} increases with an increase in the concentration, while the relative intensity of the peak at 397 cm^{-1} due to the *gauche* isomer decreases. The peak-height ratio of the two Raman lines, I_{327}/I_{397}, is plotted against the concentration in Fig. 4. It is almost constant below ca. 200 mg/cc, but gradually increases with the concentration above this point. Since this intensity change occurs around the critical micelle concentration (CMC), (210 mg/cc),[18] the spectral change is considered to be caused by the formation of micelles.

In the case of Pn-P, the intensity of the accordion vibration at 362 cm^{-1} increases with an increase in the concentration. In Fig. 4, the peak heights of the accordion vibration relative to the skeletal deformation vibration of the *gauche* isomer, I_{362}/I_{432}, are plotted against the concentration. The ratio is unchanged below the CMC (310 mg/cc),[19] but it increases gradually above this concentration. Thus, for Pn-P as well as for Pn-H, the all-*trans* form of the skeletal backbone seems to be more stable in the micelles than in the mono-molecular dispersion state.

For the aqueous solution of Pn-B, the concentration dependence of the relative intensities of the Raman lines was observed in the frequency region of 600—1600 cm^{-1} rather than in the region of 200—600 cm^{-1}. As is shown in Fig. 5, the relative intensities of the Raman lines at 897, 1042, and 1297 cm^{-1} increase with an increase in the concentration, but that of the peak at 1321 cm^{-1} decreases. Since the former three lines exist in the Raman spectrum of the solid

Pn-B, they are ascribed to the all-*trans* form, whereas the latter Raman line disappears in the solid state and is assigned to the *gauche* isomers. In Fig. 6(a), the peak heights of the Raman lines at 897 and 1042 cm^{-1} relative to the peak at 1101 cm^{-1} are plotted against the concentration of Pn-B. In the concentration region below the CMC (440 mg/cc),[18] both I_{897}/I_{1101} and I_{1042}/I_{1101} are constant and then increase above the CMC. On the contrary, the ratio of I_{1321}/I_{1338} decreases slightly above the CMC.

The concentration dependence of the Raman lines of Pn-P and Pn-H was found in the frequency region of 600—1600 cm^{-1} as well as in the low-frequency region. As is shown in Fig. 6(b), the peak heights of the Raman lines of Pn-P at 931, 1109, 1298, and 1447 cm^{-1} relative to the peak at 1062 cm^{-1} increase with an increase in the concentration above the CMC (310 mg/cc).[19] These lines correspond to the Raman lines of the solid Pn-P at 927, 1107, 1293, and 1448 cm^{-1}; therefore, they are attributed to the all-*trans* form. The intensity of the peak at 1224 cm^{-1} relative to that of 1242 cm^{-1} also decreases with an increase in the concentration above the CMC.

A similar variation was also observed for some of the Raman lines of Pn-H. As is shown in Fig. 6(c), the relative peak height of I_{935}/I_{1062} increases with an increase in the concentration above the CMC (210 mg/cc),[18] but that of I_{1214}/I_{1227} decreases. Since the Raman line of the aqueous solution at 935 cm^{-1} corresponds to the very strong line of the solid Pn-H at 925 cm^{-1}, this line must be due to the all-*trans* form.

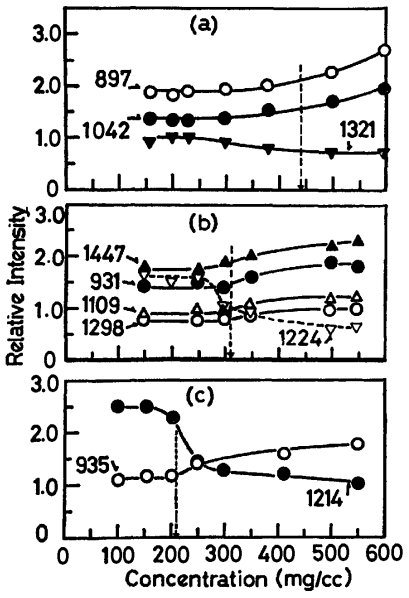

Fig. 6. Concentration dependence of the relative Raman peak heights in aqueous solutions; (a) Pn-B, the peak heights of the 897 and 1042 cm^{-1} lines relative to the 1101 cm^{-1} line; the peak height of the 1321 cm^{-1} line relative to the 1338 cm^{-1} line; (b) Pn-P, the peak heights of the 931, 1109, 1298, and 1447 cm^{-1} lines relative to the 1064 cm^{-1} line; the peak height of the 1224 cm^{-1} line relative to the 1242 cm^{-1} line; (c) Pn-H, the peak heights of the 935 cm^{-1} line relative to the 1062 cm^{-1} line; the peak height of the 1214 cm^{-1} line relative to the 1227 cm^{-1} line.
The baseline was simply drawn from the basin at *ca.* 1500 cm^{-1} to that at *ca.* 700 cm^{-1} in each spectrum.

For the aqueous solution of Pn-O, the relative peak height of I_{844}/I_{897} is almost constant below *ca.* 70 mg/cc, but this ratio decreases with the concentration over this point. On the contrary, the relative intensity of I_{1064}/I_{897} increases in the concentration region above *ca.* 70 mg/cc. Since the Raman line of the Pn-O solution is observed in the solid state, it must be attributed to the all-*trans* form. The concentration of 70 mg/cc is not exactly the CMC, but it is very close to the reported value of the CMC (70—110 mg/cc).[18]

For the surfactant molecules with longer chains, the CMC becomes lower; accordingly, the observation of the precise Raman intensity around the CMC is more difficult. However, it is evident that the formation of micelles causes the intensity change of the Raman spectra and that this spectral change is associated with the conformational changes in the *n*-alkyl hydrocarbon chains.

Concentration Dependence of the Raman Intensities of Sodium n-*Butyl Sulfate and Sodium* n-*Hexyl Sulfate.* In our previous study,[16] the Raman lines of SBS in an aqueous solution at 792 and 947 cm^{-1} were assigned to the CH_2 rocking vibration and the C–C stretching vibration of the *gauche* isomers respectively. The relative peak heights of these Raman lines were also found in the present study to decrease with an increase in the concentration. Similar behavior was observed for the Raman line of the *gauche* isomers at 824 cm^{-1}.

For the aqueous solution of SHS, the two Raman lines of the *gauche* isomers at 806 and 987 cm^{-1} show the concentration dependence of the Raman intensities. The relative peak heights of I_{806}/I_{896} and I_{987}/I_{896} decrease with an increase in the concentration, whereas the ratio of I_{1125}/I_{896} increases. These intensity changes also occur around the CMC (140 mg/cc).[19] The concentration dependence of the relative Raman intensities of sodium *n*-alkyl sulfates are also probably due to the conformation changes in the *n*-alkyl chains.

The authors wish to express their gratitude to Professor Tatsuo Miyazawa of the University of Tokyo for his interest and continuing encouragement during this work, and to Mr. Shuichi Muraishi of the Japan Electron Optics Laboratory for his measurements of the temperature dependence of the Raman spectra.

References

1) Presented at the Symposium on Molecular Structure, Nagoya, Japan, Oct., 1973, and Tokyo, Japan, Oct., 1974.
2) C. Duval, J. Lecomte, and F. Douvillé, *Ann. Phys.*, **17**, 5 (1942).
3) A. R. H. Cole and R. N. Jones, *J. Opt. Soc. Amer.*, **42**, 348 (1952).
4) D. Hadzi and N. Sheppard, *Proc. Roy. Soc.*, **A216**, 247 (1953).
5) L. H. Jones and E. McLaren, *J. Chem. Phys.*, **22**, 1796 (1954).

6) L. Robert and J. Favre, *Mikro. Chim. Acta*, **1955**, 517.
7) K. J. Wilmshurst, *J. Chem. Phys.*, **23**, 2463 (1955).
8) E. Childers and G. W. Struthers, *Anal. Chem.*, **27**, 737 (1955).
9) K. Ito and H. J. Bernstein, *Can. J. Chem.*, **34**, 170 (1956).
10) D. Chapman, *J. Chem. Soc.*, **1958**, 784.
11) B. Ellis and H. Pyszora, *Nature*, **181**, 181 (1958).
12) H. Susi, *J. Amer. Chem. Soc.*, **81**, 1535 (1959).
13) T. Shimanouchi and M. Kawano, This Bulletin, **32**, 894 (1959).
14) M. Kawano, *Nippon Kagaku Zasshi*, **81**, 1652 (1960); *ibid.*, **82**, 161 (1961); *ibid.*, **82**, 428 (1961).
15) R. Goto and T. Takenaka, *ibid.*, **84**, 392 (1963).
16) H. Okabayashi, M. Okuyama, T. Kitagawa, and T. Miyazawa, This Bulletin, **47**, 1075 (1974).
17) S. Mizushima and T. Shimanouchi, *J. Amer. Chem. Soc.*, **71**, 1320 (1949).
18) R. F. Schaufele, *J. Chem. Phys.*, **49**, 4168 (1968).
19) S. H. Herzfeld, *J. Phys. Chem.*, **56**, 953 (1952); K. Shinoda, T. Nakagawa, B. Tamamushi, and T. Isemura, "Colloidal Surfactants," Academic Press, New York and London (1963), p. 77; "Kagaku Binran," ed. by the Chemical Society of Japan, Maruzen, Tokyo (1966).
20) These CMC's were obtained by measurements of the refractive indices of the surfactant solutions in the present study.

Semiempirical Relations in Molecular Liquids. I. Molecular Structure, Melting Temperature, and Effective Hard Core Diameter of Molecules[1)]

Yoshitsugu OONO

Department of Applied Science, Faculty of Engineering, Kyushu University, Higashi-ku, Fukuoka 812

(Received January 29, 1975)

A simple method for the estimation of the effective hard core diameter of a molecule (at melting point), which is the only parameter in the application of the scaled particle theory to molecular liquids, is proposed. For a nearly spherical molecule, the effective hard core diameter a in Å can be given by

$$a = 1.072\, P^{2/5} T_m^{-1/10},$$

where P is the parachor of the molecule in cgs unit and T_m is the melting temperature in K. The factor 1.072 is equal to that predicted by the scaled particle theory.

The statistical mechanics of simple liquids has recently been developed and equilibrium properties can be calculated fairly accurately.[2)] On the other hand, statistical mechanical theories for molecular liquids remain undeveloped. Insight into the relationship between molecular structure and physical properties of molecular liquid is desirable.

The significant structure theory[3)] can predict physical properties of molecular liquids semiempirically, but its theoretical basis seems to be obscure. Another semiempirical theory so far developed is the scaled particle theory (SPT),[4)] which has a sound physical basis for a nearly spherical molecule. The SPT was originally developed[5)] to treat systems of hard spheres. However, it has been shown[6)] that, if the effective hard core diameters of the molecules are properly chosen, molecular liquids can be described by the SPT fairly well. So far, surface tension,[6,7)] isothermal compressibility,[7,8)] thermal expansivity,[8)] Henry's constant,[6)] heat capacity,[8)] and heat of vaporization[9)] have been calculated or correlated with each other by the SPT. The only parameter used in the SPT is the effective hard core diameter a of the molecule. If we know a and the density of the liquid, then we can calculate surface tension, isothermal compressibility, *etc.* The value of a can be estimated from density with the aid of information on the molecular structure.[4)] However, measurement of density at temperatures other than room temperature is not very easy.

In this paper we propose a method for estimating the effective hard core diameter of molecules at melting point from the knowledge of the molecular structure and the approximate value of the melting temperature which can be easily measured. This paper gives a simple method for estimation of da/dT, where T is temperature.

Theory

Outline of the Scaled Particle Theory. The semiphenomenological version of the SPT[4,6)] can be summarized as follows. The chance p_0 that the spherical cell of radius r is devoid of molecular centers satisfies the relation

$$d \ln p_0(r)/dr = -4\pi r^2 \rho G(r), \tag{1}$$

where ρ is the number density. $G(r)$ is so defined that $\rho G(r)$ measures the concentration of molecular centers just outside the spherical cell. According to fluctuation theory, we have

$$p_0(r) \propto \exp[-W(r)/kT], \tag{2}$$

where W is the reversible work required to produce a spherical hole of radius r. By thermodynamic consideration we have

$$dW = pdV + \sigma dA, \tag{3}$$

where p is the pressure, σ the surface tension which has the form $\sigma=\sigma_0(1-2\delta/r)$, V the volume of the hole, and A the surface area of the hole. Using Eqs. (1), (2) and (3), we obtain

$$G(r) = \frac{p}{\rho kT} + \frac{\sigma}{\rho kT}\frac{dA}{dV}. \tag{4}$$

On the other hand, we know $G(r)$ exactly for $r \leq a/2$:[4)]

$$G(r) = 1/(1-4\pi\rho r^3/3) \tag{5}$$

Equating G, dG/dr, and $G'' \equiv d^2G/dr^2$ calculated from both Eqs. (4) and (5) at $r=a/2$, we get p, σ_0, and δ as functions of $y=\pi\rho a^3/6$.

Some Remarks on the Application of the SPT to Molecular Liquids. Since it is known that G'' is not continuous at $r=a/2$, it is desirable not to use G'' in order to obtain p, σ_0 and δ. If G'' is not used, then not all the three quantities, p, σ_0, and δ, can be obtained. However, we can obtain σ_0 and δ as functions of y and p. For σ_0 we have

$$2\pi\sigma_0 a^2/3kT = 2y(1-y) + 3y^2/(1-y^2) - 2py. \tag{6}$$

Equation (1) is exact even if the particle has no hard core. The hard core assumption is used in Eq. (5), but the equation also holds in the case of the particle exerting attractive forces besides hard core repulsion. This implies that we can choose the so-called augmented van der Waals equation of state[10)] for the pressure p in Eq. (6), *i.e.*, attractive forces affect σ_0 and δ only through p.

If the molecule has a sufficiently hard core, then Eq. (5) is a good approximation, so that the SPT can be used for the case of molecular liquids with nearly spherical repulsion core. We can therefore use the observed pressure in Eq. (6). Then the last term on the right-hand side of Eq. (6) is negligible at higher densities. Consequently, surface tension scarcely depends on the details of van der Waals attractive forces at higher densities.

Basic Relation. With observed data on σ_0, ρ, and T, the quantity y can be determined from Eq. (6) with py discarded, *i.e.*,

$$\sigma_0 T^{-1} \rho^{-2/3} = 4.28 \times 10^{-17} y^{1/3}(2+y)/(1-y)^2, \tag{7}$$

Table 1. Table of the function $s(y)$ defined by Eq. (9)

y	$s(y)$
0.30	0.985
0.40	1.037
0.50	1.065
0.52	1.068
0.54	1.070
0.56	1.071
0.58	1.072
0.60	1.071
0.62	1.070

where σ_0 is in dyn/cm, T in K, and ρ in cm^{-3}. The effective hard core diameter obtained from Eq. (7) is a slightly decreasing function of temperature. Dependence of a on temperature has been estimated by Mayer.[11] However, since the data on gas viscosity are needed, his method is not useful.

Surface tension can be calculated semiempirically from the parachor P and the density by

$$P = \pi N_A \sigma_0^{1/4} a^3/6y, \quad (8)$$

where N_A is the Avogadro number. Eliminating σ_0 from Eqs. (7) and (8), we obtain

$$s(y) \equiv aP^{-2/5}T^{1/10} = 1.65y^{1/3}[(1-y)^2/y^{1/3}(2+y)]^{1/10}, \quad (9)$$

where P is in cgs unit and a in Å.

As can be seen from Table 1, $s(y)$ depends on y slightly. The function $s(y)$ is nearly constant when y is about 0.55. It can be shown that for many organic compounds the values of y at the melting point fall in the range 0.5—0.6. Thus we expect that the equation

$$aP^{-2/5}T^{1/10} = C, \quad (10)$$

where C is a constant, holds fairly accurately at melting point.

Validity of the Relation (10)

Validity of the relation (10) is demonstrated in Figs. 1—4. The effective hard core diameter a is calculated from surface tension data by means of Eq. (7) and extrapolated linearly to the melting point. Data are taken from Refs. 12—14, in which the values of calculated parachor are also cited. The linear relation between a and T is assumed to a first approximation. The lines in Figs. 1—4 denote Eq. (10) with $C=1.072$, the value being consistent with that in Table 1. It can be concluded from Figs. 1—4 that Eq. (10) holds fairly accurately when molecules are nearly spherical.

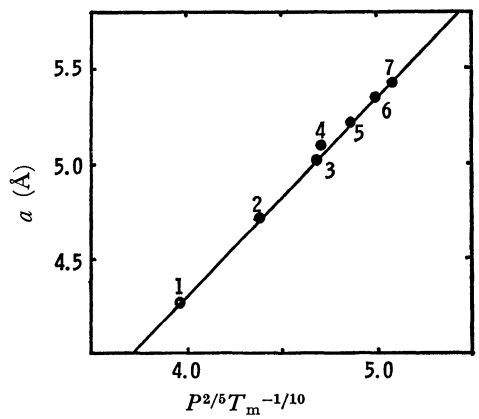

Fig. 1. Relation between a and $P^{2/5}T_m^{-1/10}$ for acetonitrile and haloalkanes.
1: acetonitrile, 2: dichloromethane, 3: 1,2-dichloroethane, 4: chloroform, 5: 1,2-dibromoethane, 6: carbon tetrachloride, 7: bromotrichloromethane.

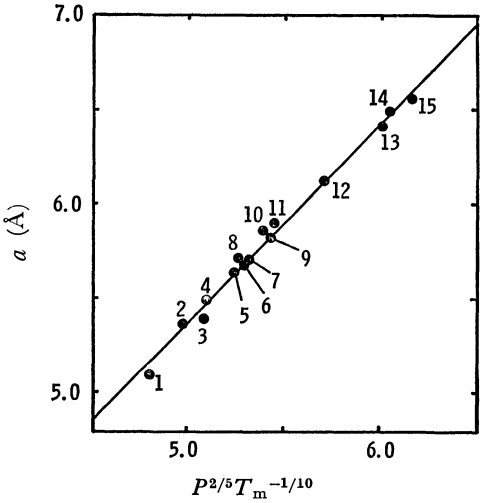

Fig. 2. Relation between a and $P^{2/5}T_m^{-1/10}$ for benzene, cyclohexane, and monosubstituted benzenes.
1: benzene, 2: fluorobenzene, 3: cyclohexane, 4: aniline, 5: chlorobenzene, 6: thiophenol, 7: bromobenzene, 8: nitrobenzene, 9: trifluoromethylbenzene, 10: toluene, 11: stylene, 12: ethylbenzene, 13: *n*-propylbenzene, 14: isopropylbenzene, 15: *t*-butylbenzene.

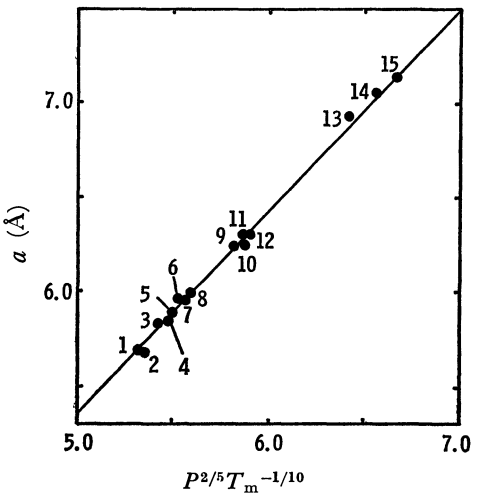

Fig. 3. Relation between a and $P^{2/5}T_m^{-1/10}$ for di- and tri- substituted benzenes.
1: *o*-chlorobenzaldehyde, 2: *p*-dichlorobenzene, 3: *p*-xylene, 4: *o*-dichlorobenzene, 5: *m*-dichlorobenzene, 6: *o*-xylene, 7: *p*-chloroacetophenone, 8: *m*-xylene, 9: 1,2,3-trimethylbenzene, 10: 1,3,5-trimethylbenzene, 11: 1,2,4-trimethylbenzene, 12: *o*-ethylnitrobenzene, 13: *p*-*t*-butylmethylbenzene, 14: *p*-diisopropylbenzene, 15: *o*-diisopropylbenzene.

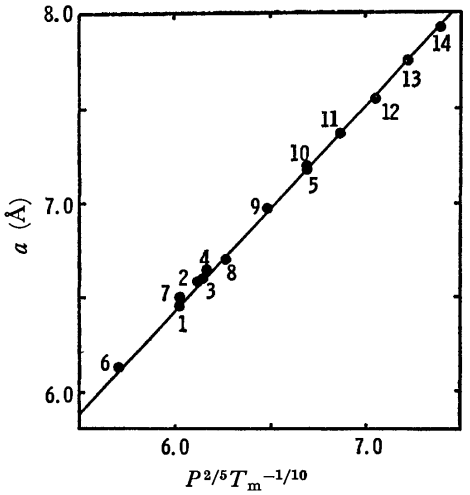

Fig. 4. Relation between a and $P^{2/5}T_m^{-1/10}$ for n-alkylbenzenes, naphthalenes, *etc.*
1: 1-methylnaphthalene, 2: *trans*-decalin, 3: 5-methyl-1,2,3,4-tetrahydronaphthalene, 4: *cis*-decalin, 5: 2-butylnaphthalene, 6: ethylbenzene, 7: n-propylbenzene, 8: n-butylbenzene, 9: n-pentylbenzene, 10: n-hexylbenzene, 11: n-heptylbenzene, 12: n-octylbenzene, 13: n-nonylbenzene, 14: n-decylbenzene.

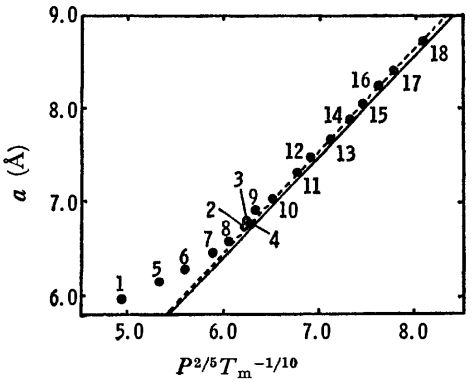

Fig. 5. Relation between a and $P^{2/5}T_m^{-1/10}$ for ethyl ether and alkanes.
1: ethyl ether, 2: 2-methylheptane, 3: 2,2,4-trimethylheptane, 4: 2-methyl-3-ethylpentane, 5: n-pentane, 6: n-hexane, 7: n-heptane, 8: n-octane, 9: n-nonane, 10: n-decane, 11: n-undecane, 12: n-dodecane, 13: n-tridecane, 14: n-tetradecane, 15: n-pentadecane, 16: n-hexadecane, 17: n-heptadecane, 18: n-nonadecane.

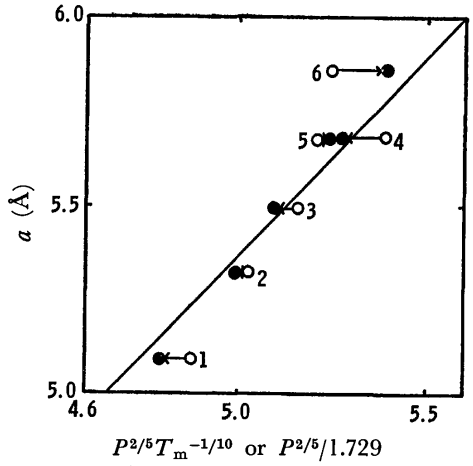

Fig. 6. Effect of $T_m^{-1/10}$ on the linear relation (10).
●: $P^{2/5}T_m^{-1/10}$, ○: $P^{2/5}/1.729$
1: benzene, 2: carbon tetrachloride, 3: aniline, 4: nitrobenzene, 5: chlorobenzene, 6: toluene.

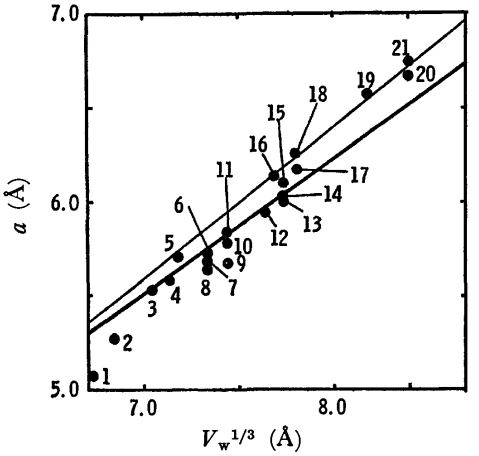

Fig. 7. Linear relation between a and $V_w^{-1/3}$.
——: $a=0.80\,V_w^{-1/3}$, ——: $a=0.79\,V_w^{-1/3}$
1: benzene, 2: fluorobenzene, 3: chlorobenzene, 4: bromobenzene, 5: toluene, 6: m-dichlorobenzene, 7: o-dichlorobenzene, 8: p-dichlorobenzene, 9: p-xylene, 10: o-xylene, 11: m-xylene, 12: 1,2-dichloro-4-methylbenzene, 13: 1,2,3-trimethylbenzene, 14: 1,3,5-trimethylbenzene, 16: isopropylbenzene, 17: 1-methylnaphthalene, 18: t-butylbenzene, 19: p-t-butylmethylbenzene, 20: p-diisopropylbenzene, 21: o-diisopropylbenzene.

Figure 5 shows that the relation (10) holds also for the case of non-spherical molecules. Normal alkanes asymptotically satisfy Eq. (10) with $C=1.080$, but this value cannot be explained in terms of the SPT (Table 1).

Discussion

For many organic liquids the factor $T^{-1/10}$ at melting point is *ca.* 0.6. Hence the main factor in Eq. (10) is $P^{2/5}$. Although $a \propto P^{2/5}$ holds approximately, the factor $T^{-1/10}$ markedly improves the approximate relation as shown in Fig. 6. Thus the factor $T^{-1/10}$ is indispensable for making C in Eq. (10) constant.

In the application of the SPT to molecular liquids the parameter a is considered to be the effective hard core diameter of the molecule. Thus if the physical picture of the SPT is correct, then a should be correlated with the actual dimension of a molecule. In the case of simple liquids, a and the distance where the repulsive potential is zero is almost the same.[5] In the case of molecular liquids, it is difficult to define or determine the dimension of complex molecules. For the sake of convenience, we choose, as a measure of actual dimension of a molecule, the cubic root of the van der Waals volume V_w estimated and tabulated by Bondi.[15] A roughly linear relation between a at melting point and $V^{1/3}$ is shown in Fig. 7. The physical picture of the

SPT is correct at least in the case of liquids consisting of nearly spherical molecules.

The value of a at room temperature can be calculated from the density at room temperature which can be measured very easily. The value of a at melting point can be estimated if the melting point is known. A rough measurement of the melting point is also very easy and da/dT can thus be estimated. We can therefore estimate a at desired temperature from density at room temperature, molecular structure and melting point. The da/dT estimated by the method mentioned above is rather large.[16] Hence the quantity should not be considered to represent the softness of the intermolecular repulsive force quantitatively but should be treated as a mere parameter for better applications of the SPT to molecular liquids.

The author wishes to express his thanks to Professor T. Oyama for critical reading of the manuscript.

References

1) This work was partly reported in *Technology Reports of the Kyushu University*, **47**, 363 (1974) (in Japanese).
2) L. Verlet, "Statistical Mechanics, New Concepts, New Problems, New Applications," ed. by S.A. Rice, K. F. Freed, and J. C. Light, Univ. of Chicago Press, Chicago (1972), p. 379.
3) M. S. Jhon and H. Eyring, "Physical Chemistry, an Advanced Treatise," VIIIA, ed. by D. Henderson, Academic Press, New York and London (1971), p. 335.
4) H. Reiss, "Advances in Chemical Physics," Vol. 9, ed. by I. Prigogine and S. A. Rice, Wiley, New York (1965), p. 1.
5) H. Reiss, H. L. Frisch, E. Helfand, and J. L. Lebowitz, *J. Chem. Phys.*, **31**, 369 (1959).
6) H. Reiss, H. L. Frisch, E. Helfand, and J. L. Lebowitz, *ibid.*, **32**, 119 (1960).
7) S. W. Mayer, *J. Phys. Chem.*, **67**, 2160 (1963).
8) S. J. Yosim, *J. Chem. Phys.*, **40**, 3069 (1964).
9) S. J. Yosim and B. B. Owens, *ibid.*, **39**, 2222 (1963).
10) H. C. Longuet-Higgins and B. Widom, *Mol. Phys.*, **8**, 549 (1964).
11) S. W. Mayer, *J. Chem. Phys.*, **38**, 1803 (1963).
12) R. R. Dreisbach, "Physical Properties of Chemical Compounds," American Chemical Society, Washington D.C. (1955).
13) R. R. Dreisbach, "Physical Properties of Chemical Compounds II," American Chemical Society, Washington D.C. (1959).
14) R. R. Dreisbach, "Physical Properties of Chemical Compounds III," American Chemical Society, Washington D.C. (1961).
15) A. A. Bondi, *J. Phys. Chem.*, **68**, 441 (1964).
16) R. A. Pierotti, *ibid.*, **71**, 2366 (1967).

The Syntheses and Spectroscopic Investigation of Copper(II), Nickel(II), and Cobalt(II) Complexes of 8-Quinolinecarboxamide

Masahide NOJI, Yoshinori KIDANI, and Hisashi KOIKE*

Faculty of Pharmaceutical Sciences, Nagoya City University, Tanabe-dori, Mizuho-ku, Nagoya 467

(Received August 20, 1974)

The syntheses of the bivalent metal complexes of 8-quinolinecarboxamide (abbreviated as 8-QCA) were attempted; the complexes obtained have the compositions of $M(8\text{-QCA})_2X_2$ (M=Cu(II), Ni(II), and Co(II) ions; X=Cl^-, Br^-, I^-, and NO_3^-) and $Cu(8\text{-QCA})Cl_2$. The diffuse reflectance, the infrared and far-infrared spectra, and the magnetic moments of these metal complexes were measured. The coordination sites of 8-QCA have been suggested for the amide oxygen and the quinoline nitrogen from the diffuse reflectance spectra and the infrared spectra. The values of 3.13—3.21 B.M. and 4.81—5.03 B.M. were observed for $Ni(8\text{-QCA})_2X_2$ and $Co(8\text{-QCA})_2X_2$ respectively. From these magnetic moments, an octahedral structure has been proposed for the nickel and the cobalt complexes, whose far-infrared spectra (600—200 cm^{-1}) also supported this structure, with a *trans*-planar coordination of the 8-QCA molecules around the metal ions. Since the $Cu(8\text{-QCA})_2X_2$ complexes are of the mononuclear form, judging from the magnetic moments of 1.87—1.93 B.M., and since the far-infrared spectra suggested a structure belonging to the C_{2h} point group, a distorted octahedral configuration is conceivable.

Some quinoline derivatives, such as 8-hydroxyquinoline and 8-mercaptoquinoline, which are able to form a chelate ring with metal ions are well known to show a strengthened antibacterial action upon the addition of some kinds of metal ions. The present authors have long been interested in the metal chelates of the quinoline derivatives because of their biological significance, in this investigation the syntheses of the bivalent metal complexes of 8-quinolinecarboxamide (abbreviated as 8-QCA in this paper) were attempted.

It has previously been reported that, when a carboxamide group participates in metal-complex formation, it can coordinate on metal ions with or without the proton released from the carboxamide group. The former is called a cationic complex, and the latter, a neutral complex; both of them have been found in the metal complexes of 2-pyridinecarboxamide.[1] However, 8-QCA does not form neutral complexes in an aqueous solution because of the formation of metal hydroxides; only the cationic complexes were obtained. The complexes have the compositions of $Cu(8\text{-QCA})Cl_2$ and $M(8\text{-QCA})_2X_2$ (M=Cu(II), Ni(II), and Co(II) ions; X=Cl^-, Br^-, I^-, and NO_3^-). The coordination sites and the structures of the cationic chelates of 2-pyridinecarboxamide and its related derivatives with the bivalent metal ions have been studied by Sekizaki and Yamasaki;[2-7] it has also been concluded that the chelate-ring formation took place through the amide oxygen and the pyridine nitrogen, as confirmed by X-ray analyses.[8-10]

The magnetic moments, the diffuse reflectance spectra, and the infrared and far-infrared spectra of the bivalent metal complexes of 8-QCA were measured as part of the analyses. The data will be compared with those of the metal complexes of 2-pyridinecarboxamide, and the coordination sites and the structures of the metal complexes of 8-QCA will be discussed.

* Present address: School of Medical Technology and Nursing, Fujita Gakuen University, Kutsukake, Toyoake City, Aichi Prefecture 470-11.

Experimental

Materials. The metal halides and metal nitrates were analytical-grade products of Wako Pure Chemical Industries, Ltd.

Synthesis of 8-Quinolinecarboxamide. To an excess of thionyl chloride (25 g) we added 5 g of 8-quinolinecarboxylic acid, which has been synthesized according to the method reported by Campbell *et al.*;[11] the resultant solution was refluxed for 4 hr at 80 °C on a water bath. When the excess of thionyl chloride was distilled away under reduced pressure, crude 8-quinolinecarbonyl chloride was obtained as a reddish brown residue, which was subsequently dissolved in 50 ml of methanol. The methanol solution was added gradually to a large excess of an ice-cold methanol solution of ammonia, from which crude 8-quinolinecarboxamide was then deposited as yellow crystals. It was recrystallized twice from water. Yield, 60%.

Found: C, 69.69; H, 4.78; N, 16.30%. Calcd for $C_{10}H_8N_2O$: C, 69.76; H, 4.68; N, 16.26%.

Preparations of Metal Complexes. *1) Dichloro(8-quinolinecarboxamide)copper(II), Bis(8-quinolinecarboxamide)copper(II) Bromide, Bis(8-quinolinecarboxamide)copper(II) Nitrate, and Bis(8-quinolinecarboxamide)cobalt(II) Bromide*: To 15 ml of an ethanol solution containing 1 mmol of the corresponding metal salt, we added 344 mg (2 mmol) of the ligand dissolved in 20 ml of ethanol; the mixture was then kept standing at room temperature. The objective complexes were obtained as a crystalline powder. They were collected by filtration and washed with hot ethanol.

2) Bis(8-quinolinecarboxamide)nickel(II)Chloride, Bis(8-quinolinecarboxamide)nickel(II) Bromide, and Bis(8-quinolinecarboxamide)cobalt(II) Iodide: These complexes were obtained by treating ethanol solutions containing 1 mmol of the corresponding metal salt with 2 mmol of the ligand in 20 ml of ethanol. The resultant solution was evaporated to 2/3 volume on a water bath. After it had been kept standing overnight at room temperature, a crystalline powder was deposited.

3) Bis(8-quinolinecarboxamide)nickel(II) Iodide, Bis(8-quinolinecarboxamide)nickel(II) Nitrate, and Bis(8-quinolinecarboxamide) cobalt(II) Iodide: After mixing 1 mmol of the corresponding metal salt in 20 ml of an ethanol solution containing 2 mmol of the ligand, the solution was warmed on a water bath; a crystalline powder was then deposited out.

The results of elemental analyses of the obtained metal

Table 1. Results of elemental analyses of bivalent metal complexes of 8-quinolinecarboxamide

Complexes	Found (%)				Calcd (%)				Yield (%)
	C	H	N	M	C	H	N	M	
$Cu(C_{10}H_8N_2O)Cl_2$	39.03	2.54	9.13	20.3	39.17	2.63	9.14	20.7	25
$Cu(C_{10}H_8N_2O)_2Br_2$	42.15	2.69	9.91	10.9	42.31	2.74	9.87	11.2	78
$Cu(C_{10}H_8N_2O)_2(NO_3)_2$	45.45	3.08	15.46	11.5	45.16	3.03	15.80	11.9	67
$Ni(C_{10}H_8N_2O)_2Cl_2\cdot 1/2H_2O$	48.70	3.68	11.22	12.3	48.94	3.70	11.42	12.2	32
$Ni(C_{10}H_8N_2O)_2Br_2$	42.61	2.87	9.95	10.0	42.67	2.87	9.96	10.4	50
$Ni(C_{10}H_8N_2O)_2I_2$	36.63	2.41	8.58	8.9	36.57	2.46	8.53	8.9	36
$Ni(C_{10}H_8N_2O)_2(NO_3)_2$	45.49	2.86	16.08	11.5	45.57	3.06	15.94	11.1	42
$Co(C_{10}H_8N_2O)_2Br_2\cdot 1/2H_2O$	41.67	2.94	9.60	10.4	41.98	2.99	9.79	10.3	70
$Co(C_{10}H_8N_2O)_2I_2$	36.64	2.33	8.52	9.3	36.56	2.45	8.53	9.0	43
$Co(C_{10}H_8N_2O)_2(NO_3)_2$	45.38	3.02	16.00	11.3	45.65	3.07	15.97	11.2	56

complexes are shown in Table 1.

Magnetic and Spectroscopic Measurements. The magnetic moments were measured with a Shimadzu MB-2-type magnetic balance. The diffuse reflectance spectra were measured with a Hitachi EPS-3T spectrophotometer equipped with an integrating-sphere accessory by means of the method described in a previous paper.[12] A JASCO IRA-2 spectrophotometer and a JASCO DS-701 spectrophotometer were used to record the infrared spectra in the region of 400—4000 cm^{-1} and in the region of 200—600 cm^{-1} respectively by the Nujol and HCB mull methods.

Results and Discussion

Magnetic Moments. The magnetic moments observed for the bivalent metal complexes of 8-QCA are shown in Table 2.

The copper complexes give normal magnetic moments in the region of 1.87—1.93 B.M., indicating no spin interaction among the adjacent copper ions. All the nickel complexes, $Ni(8\text{-}QCA)_2X_2$, give magnetic moments of 3.13—3.21 B.M., which fall within the region of 2.9—3.4 B.M. reported for octahedral complexes.[13] The magnetic moments observed for $Co(8\text{-}QCA)_2X_2$ are 4.81—5.03 B.M., corresponding to the reported values of 4.7—5.2 B.M. for octahedral cobalt complexes.[14]

Diffuse Reflectance Spectra. As is shown in Fig. 1, the absorption maxima (λ_{max}) in the diffuse reflectance spectra of $Cu(8\text{-}QCA)_2Br_2$ and $Cu(8\text{-}QCA)_2(NO_3)_2$ are observed at 700 and 675 nm.

Table 2. Magnetic moments of $M(8\text{-}QCA)_2X_2$ and $Cu(8\text{-}QCA)Cl_2$ (18—21 °C)

Complexes	Moments observed	Moments calcd for spin-only formula
$Cu(8\text{-}QCA)Cl_2$	1.90 B. M.	1.73 B. M.
$Cu(8\text{-}QCA)_2Br_2$	1.93	1.73
$Cu(8\text{-}QCA)_2(NO_3)_2$	1.87	1.73
$Ni(8\text{-}QCA)_2Cl_2$	3.13	2.82
$Ni(8\text{-}QCA)_2Br_2$	3.21	2.82
$Ni(8\text{-}QCA)_2I_2$	3.19	2.82
$Ni(8\text{-}QCA)_2(NO_3)_2$	3.19	2.82
$Co(8\text{-}QCA)_2Br_2$	4.98	3.88
$Co(8\text{-}QCA)_2I_2$	5.03	3.88
$Co(8\text{-}QCA)_2(NO_3)_2$	4.81	3.88

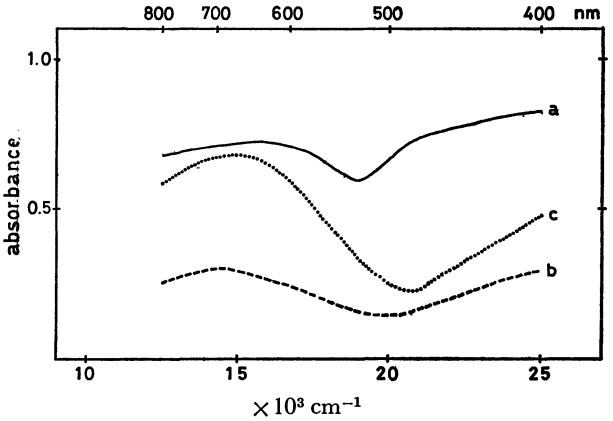

Fig. 1. Diffuse reflectance spectra of metal complexes.
a: $Cu(8\text{-}QCA)Cl_2$ b: $Cu(8\text{-}QCA)_2Br_2$,
c: $Cu(8\text{-}QCA)_2(NO_3)_2$

The λ_{max} values of these copper complexes are rather close to those of the metal chelates of 2-acetylpyridine[15] and 2-pyridinecarboxamide,[2] the N,O-coordination of the ligand having been determined. Therefore, the coordination sites of 8-QCA with a copper ion are considered to be the amide oxygen and the quinoline nitrogen.

The 1 : 1 complex, $Cu(8\text{-}QCA)Cl_2$, gives its absorption maximum at 650 nm, much like those of the 2 : 1 copper complexes; however, a new and characteristic shoulder is observed around 450—480 nm, as is shown in Fig. 1. The appearance of the shoulder may be due to the structural differences between the 1 : 1 complex and the 2 : 1 complexes. However, the λ_{max} value of the neutral copper chelate of 2-pyridinecarboxamide, $Cu(pia)_2$, the N,N-coordination of the ligand of which has been determined, was found at 530 nm in a chloroform solution.[1] The large difference in the λ_{max} values between $Cu(pia)_2$ and $Cu(8\text{-}QCA)Cl_2$ may indicate that the binding sites of 8-QCA are the amide oxygen and the quinoline nitrogen in the latter complex.

The nickel complexes, $Ni(8\text{-}QCA)_2X_2$, have the similar λ_{max} value of 680 nm, as is shown in Fig. 2.

Table 3. Main absorption peaks in infrared spectra

Complexes	ν_{NH_2}	$\nu_{asym(OCN)}$	δ_{NH_2}	$\nu_{sym(OCN)}$
8-QCA	3300, 3150	1665, 1648	1610	1370
$Cu(8\text{-}QCA)Cl_2$	3350, 3290, 3200	1643	1615	1380
$Cu(8\text{-}QCA)_2Br_2$	3200	1637	1615	1382
$Cu(8\text{-}QCA)_2(NO_3)_2$	3350, 3180	1656	1623	—
$Ni(8\text{-}QCA)_2Cl_2$	3300, 3130	1645	1615	1380
$Ni(8\text{-}QCA)_2Br_2$	3350, 3170	1643	1617	1380
$Ni(8\text{-}QCA)_2I_2$	3360, 3170	1642	1605	1380
$Ni(8\text{-}QCA)_2(NO_3)_2$	3350, 3180	1652	1620	—
$Co(8\text{-}QCA)_2Br_2$	3320, 3140	1637	1615	1380
$Co(8\text{-}QCA)_2I_2$	3350, 3300, 3170	1640	1603	1380
$Co(8\text{-}QCA)_2(NO_3)_2$	3350, 3180	1650	1620	—

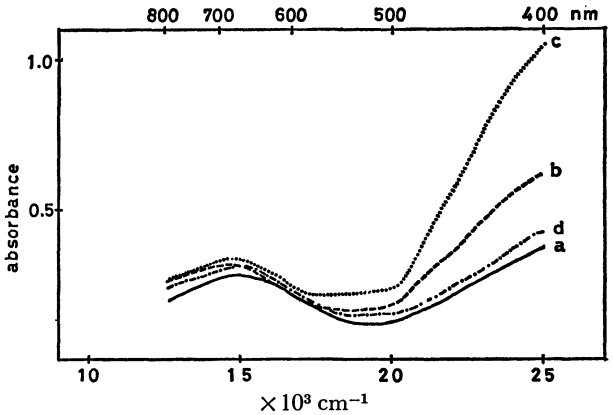

Fig. 2. Diffuse reflectance spectra of metal complexes.
a: $Ni(8\text{-}QCA)_2Cl_2$ b: $Ni(8\text{-}QCA)_2Br_2$
c: $Ni(8\text{-}QCA)_2I_2$ d: $Ni(8\text{-}QCA)_2(NO_3)_2$

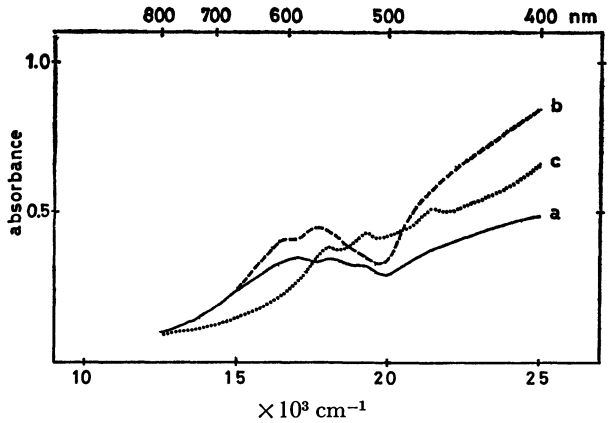

Fig. 3. Diffuse reflectance spectra of metal complexes.
a: $Co(8\text{-}QCA)_2Br_2$ b: $Co(8\text{-}QCA)_2I_2$
c: $Co(8\text{-}QCA)_2(NO_3)_2$

Since the octahedral nickel complexes of the ligand with the N,N-coordination like ethylenediamine and bipyridyl are known to show their d-d bands in the region of 560—570 nm,[16,17] the large difference in the λ_{max} values between $Ni(8\text{-}QCA)_2X_2$ and both the $Ni(en)_2^{2+}$ and $Ni(bip)_2^{2+}$ systems may exclude the possibility of the N,N-coordination, that is, coordination through the amide nitrogen and the quinoline nitrogen. The other possibility is the coordination through the amide oxygen and the quinoline nitrogen,

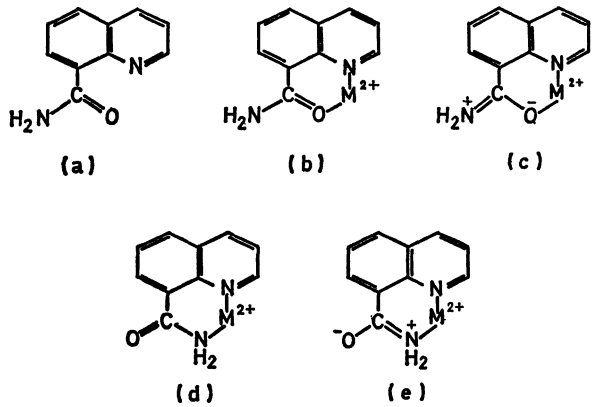

Fig. 4. Resonance forms for the ligand and the metal complexes.

this possibility is supported by the resemblance of the diffuse reflectance spectra between $Ni(8\text{-}QCA)_2X_2$ and both $Ni(piaH)Cl_2$ and $Ni(2AP)_2X_2$ (piaH= 2-pyridinecarboxamide; 2AP=2-acetylpyridine).[2,15]

The $Co(8\text{-}QCA)_2X_2$ complexes give rather complicated diffuse reflectance spectra, shown in Fig. 3, with two or three absorption bands in the wavelength region of 550—600 nm which are characteristic of octahedral cobalt complexes. However, no tendency to the longer-wavelength shift has been reported for cobalt complexes with the variation in the N,N-, N,O-, and O,O-coordinations, and the bonding sites of 8-QCA can not be deduced from the diffuse reflectance spectra.

Infrared Spectra. The infrared data of the $M(8\text{-}QCA)_2X_2$ complexes are summarized in Table 3, together with those of the ligand and the 1 : 1 copper complex. The ligand gives two peaks, at 3300 and 3150 cm^{-1}, due to the stretching vibrations of the amino group. The asymmetric OCN stretching frequency of the amide group[2] is observed as two peaks at 1665 and 1648 cm^{-1}, with its symmetric stretching peak at 1370 cm^{-1}.

The deformation mode of the amino group is observed at 1610 cm^{-1} as a shoulder.

Upon complex formation, the asymmetric N–H stretching frequencies either shift toward frequencies higher by 50—60 cm^{-1} or remain at nearly the same frequency as that of the ligand. The asymmetric and symmetric OCN stretching vibrations shift toward lower and higher frequencies respectively. These

Table 4. Assignments in far-infrared spectra (in cm^{-1})

Complexes	Chelate ring def.	ν_{M-N}	ν_{M-O}	ν_{M-X}	Amide torsion	Unassigned
$Cu(8\text{-}QCA)Cl_2$	480	—	244	290	360	
$Cu(8\text{-}QCA)_2Br_2$	486	271	240	—	349	
$Cu(8\text{-}QCA)_2(NO_3)_2$	483	275	236	—	356	210
$Ni(8\text{-}QCA)_2Cl_2$	488	254	227	—	340	
$Ni(8\text{-}QCA)_2Br_2$	480	257	225	—	320	208
$Ni(8\text{-}QCA)_2I_2$	476	255	220	—	323	
$Ni(8\text{-}QCA)_2(NO_3)_2$	478	258	220	—	330	242
$Co(8\text{-}QCA)_2Br_2$	478	239	217	—	322	
$Co(8\text{-}QCA)_2I_2$	475	242	216	—	323	
$Co(8\text{-}QCA)_2(NO_3)_2$	475	233	223	—	317	

results show that the ligand may take the resonance form (a), while for the $M(8\text{-}QCA)_2X_2$ complexes various forms, (b)—(e) in Fig. 4, are conceivable.

Since the asymmetric and symmetric OCN stretching vibrations arise mainly from the C=O and C-N stretching respectively, the N,N-coordination predicts that the contribution of the (d) resonance form would be larger that than of the (e) form because of the Coulombic repulsion in the latter form. In the (d) form the symmetric OCN stretchings are expected to shift toward the lower frequency side, while the asymmetric OCN stretchings remain at frequencies similar to that of the ligand. The observed frequency shifts of the amide group are opposite to the predicted shift for the N,N-coordination. However, when the $M(8\text{-}QCA)_2X_2$ complexes are in a resonance between the (b) and (c) forms, the *N,O*-coordination predicts the shifts of the asymmetric and symmetric OCN stretching to be to the lower- and higher-frequency side respectively. Therefore, the N,O-coordination seems reasonable for the $M(8\text{-}QCA)_2X_2$ complexes and $Cu(8\text{-}QCA)Cl_2$.

The same infrared spectral behavior of the amide group has been reported for $[M(H_2O)_2\ (piaH)_2]X_2$, where the N,O-coordination has been determined by *X*-ray analyses.[9-10]

Far-infrared Spectra. The ligand shows a peak at 233 cm^{-1} due to the amide torsion, a peak at 458 cm^{-1} assignable to the in-plane deformation of C=O, and other peaks due to quinoline-ring vibrations. Upon the complex formation, new peaks are observed in the region of 470—490 cm^{-1} and are assigned to the chelate-ring deformation. In the $M(8\text{-}QCA)_2X_2$ complexes, the peaks found around 320—360 cm^{-1} are assigned to the amide torsion.

$Cu(8\text{-}QCA)_2X_2$ and $Cu(8\text{-}QCA)Cl_2$: For $Cu(8\text{-}QCA)Cl_2$, a broad band due to the Cu-Cl stretching vibration is observed at 290 cm^{-1}, while the other peaks appear at 244 cm^{-1} below 300 cm^{-1}. The other 2 : 1 complexes give two common peaks in the regions of 271—275 cm^{-1} and 236—240 cm^{-1}, the peaks being assigned to the Cu-N (quinoline) and the Cu-O (amide) stretching respectively.

$Ni(8\text{-}QCA)_2X_2$: Since the $Ni(8\text{-}QCA)_2X_2$ complexes are supposed to be octahedral, the two nickel-ligand stretching vibrations can be expected to appear at relatively constant frequencies. In fact, the stretching vibrations assignable to the Ni-N (quinoline) and the Ni-O (amide) are found in the regions of 254—258 cm^{-1} and 220—227 cm^{-1} respectively.

$Co(8\text{-}QCA)_2X_2$: The peaks assignable to the Co-N (quinoline) and Co-O(amide) stretching vibrations are found in the regions of 239—242 cm^{-1} and 216—217 cm^{-1} for the bromide and iodide. For the nitrate, the peaks at 223 and 233 cm^{-1} are assigned to the Co–O (quinoline) and Co–O (amide) stretching vibrations.

Since the 2 : 1 complexes, $M(8\text{-}QCA)_2X_2$, do not give the peaks assignable to the metal-anion stretching vibrations above 200 cm^{-1}, the coordination of the anions on the metal ions can not be deduced. These assignments are summarized in Table 4.

In the assignments of the metal-ligand stretching vibrations in the $M(8\text{-}QCA)_2X_2$ complexes, the far-infrared data of the bivalent metal complexes of quinoline and oxine are used as references. Ohkaku and Nakamoto[18] reported that the octahedral bivalent metal chelates of oxine, $[M(oxine)_2(H_2O)_2]$, have their M-O and M-N stretching vibrations at the frequencies shown in Table 5. Frank and Rogers[19] studied the far-infrared spectra of the bivalent metal complexes of quinoline, $M(Q)_2Cl_2$(Q=quinoline), and assigned the M-N stretching vibrations as is shown in Table 5. In general, it is recognized that metal complexes with larger stability constants give the metal-ligand stretching vibrations at higher frequencies so long as the structures of the objective complexes are similar to one another. Though here no study has been made of the stability constants of 8-QCA with bivalent metal ions, it can be assumed that the stability constants of 8-QCA fall in between those of oxine and quinoline as far as the same metal ions are concerned. In other words, the

Table 5. Far infrared data reported for $M(oxine)_2(H_2O)_2$ and $M(Q)_2Cl_2$ (in cm^{-1})

Complexes	ν_{M-O}	ν_{M-N}
$Cu(oxine)_2(H_2O)_2$	310.5	289
$Ni(oxine)_2(H_2O)_2$	301.2	264
$Co(oxine)_2(H_2O)_2$	295	240
$Zn(oxine)_2(H_2O)_2$	264	207
$Cu(Q)_2Cl_2$		259
$Ni(Q)_2Cl_2$		223
$Co(Q)_2Cl_2$		226
$Zn(Q)_2Cl_2$		205

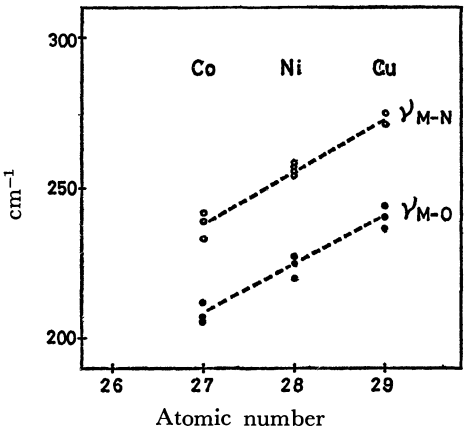

Fig. 5. A plot of M–N and M–O stretching frequencies *vs.* atomic number for $M(8\text{-QCA})_2X_2$.

copper 2 : 1 complexes should give the stretching vibration of the M–N (quinoline) in the frequency region of 259—289 cm^{-1}, and the nickel and the cobalt complexes, in the regions of 233—264 cm^{-1} and 226—240 cm^{-1} respectively. The M–O (amide) stretching frequencies are considered to be lower than the M–N (quinoline) stretching vibrations.

In order to ascertain the validity of the assignments, the stretching vibrations of the M–N (quinoline) and the M–O (amide) were plotted against the atomic number of the metal ions, as is shown in Fig. 5; linear relationships were found. The fact that the metal-ligand stretching vibrations number two throughout the metal complexes studied suggests a *trans*-planar coordination of the ligand molecules around the metal ions, since the octahedral structure with a *trans*-planar configuration of 8-QCA molecules on the metal ions belongs to the C_{2h} point group, which may be expected to produce two peaks due to the M–N (quinoline) and M–O (amide) stretching vibrations.

Conclusion

Through the analyses of the magnetic moments, the diffuse reflectance spectra, and the infrared and far-infrared spectra, the following conclusions have been deduced for the $M(8\text{-QCA})_2X_2$ complexes and $Cu(8\text{-QCA})Cl_2$:

1) The coordination sites seem to be the amide oxygen and the quinoline nitrogen.

2) For $Ni(8\text{-QCA})_2X_2$ and $Co(8\text{-QCA})_2X_2$, an octahedral structure with a *trans*-planar coordination of 8-QCA is suggested by the magnetic moments and the far-infrared spectra.

3) For $Cu(8\text{-QCA})_2X_2$, a distorted octahedral structure with a *trans*-planar coordination of 8-QCA is conceivable, judging from the magnetic moments and the far-infrared spectra. As for $Cu(8\text{-QCA})Cl_2$, no definite structure can be deduced from the present data.

The authors wish to thank Dr. N. Yamanaka of the Government Industrial Institute, Nagoya, for permitting them to use a Shimadzu MB-2 magnetic balance. Thanks are also due to Misses M. Ishiguro and S. Iwauchi of the Analytical Center of Nagoya City University for the elemental analyses.

References

1) M. Sekizaki and K. Yamasaki, *Nippon Kagaku Zasshi*, **87**, 1053 (1966).
2) M. Sekizaki, M. Tanase, and K. Yamasaki, This Bulletin, **42**, 399 (1969).
3) M. Sekizaki and K. Yamasaki, *Spectrochim. Acta*, **25A**, 475 (1969).
4) M. Sekizaki and K. Yamasaki, *Rev. Chim. Minerale*, **6**, 255 (1969).
5) M. Nonoyama and K. Yamasaki, *Inorg. Chim. Acta*, **3**, 585 (1969).
6) M. Sekizaki and K. Yamasaki, *ibid.*, **4**, 296 (1970).
7) M. Nonoyama and K. Yamasaki, *ibid.*, **7**, 373 (1973).
8) S. C. Chang, J. K. H. Ma, J. T. Wang, and N. C. Li, *J. Coord. Chem.*, **2**, 31 (1972).
9) A. Masuko, T. Nomura, and Y. Saito, This Bulletin, **40**, 511 (1967).
10) M. Sekizaki, F. Marumo, K. Yamasaki, and Y. Saito, *ibid.*, **44**, 1731 (1971).
11) K. N. Campbell, J. F. Kerwin, R. A. LaForge, and B. K. Campbell, *J. Amer. Chem. Soc.*, **68**, 1844 (1946).
12) M. Noji, Y. Kidani, and H. Koike, This Bulletin, **48**, 245 (1975).
13) F. A. Cotton and G. Wilkinson, The Japanese Translation of "Advanced Inorganic Chemistry," 2nd Ed., Baifukan Ltd., Tokyo (1973), p. 794.
14) F. A. Cotton and G. Wilkinson, *ibid.*, p. 784.
15) Y. Kidani, M. Noji, and H. Koike, This Bulletin, **48**, 239 (1975).
16) S. Utsuno and K. Sone, *ibid.*, **37**, 1038 (1964).
17) H. Ito, *Nippon Kagaku Zasshi*, **77**, 1385, 1397 (1956).
18) N. Ohkaku and K. Nakamoto, *Inorg. Chem.*, **10**, 798 (1971).
19) C. W. Frank and L. B. Rogers, *ibid.*, **5**, 615 (1966).

Synthesis and Thermochromic Properties of New Five-coordinate Copper Chelates

Noriko IWASAKI, Kozo SONE, and Heijiro OJIMA*

Department of Chemistry, Faculty of Science, Ochanomizu University, Otsuka, Bunkyo-ku, Tokyo 112

**Department of Chemistry, Aichi Kyoiku University, Kariya, Aichi 448*

(Received February 4, 1975)

Two new five-coordinate copper(II) chelates [Cu(PCdien)] and [Cu(PCenpn)] were prepared, and the thermochromism of the former in methanolic solution was studied. When this violet-blue solution (ν_{max}: 16500 cm^{-1}) was heated nearly to the boiling point of methanol, the color of the solution became gradually yellowish (ν_{max}: 21000 cm^{-1}). The absorption spectra of these cold and hot solutions were compared with those of similar four-coordinate Cu(II) complexes in various solvents, and the yellow color was ascribed to a tetra-coordinated species of [Cu(PCdien)], which is formed by the partial rupture of the pentacoordinated structure caused by the intramolecular steric strains. No thermochromic property of the PCenpn chelate was observed.

Recently we prepared two new five-coodinate copper(II) chelates shown below, and found that one of them shows a peculiar thermochromism in its methanolic solution. The results of these studies will be described in this paper.

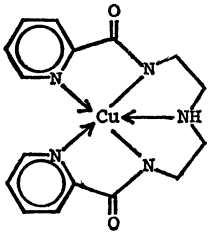

[Cu(PCdien)]=*N*-(picolinoyl)-*N'*-(picolinoylaminoethyl)-ethylenediaminato copper(II)

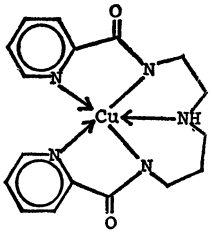

[Cu(PCenpn)]=*N*-(picolinoyl)-*N'*-(picolinoylaminoethyl)-propanediaminato copper(II)

Experimental

Synthesis of the Chelates. [Cu(PCdien)] can be prepared from diethylenetriamine and methyl picolinate; 13.7 g (0.1 mol) of the latter is added dropwise into 5.2 g (0.05 mol) of the former, and the mixture is heated at 140 °C for 1 hr and then at 160 °C for 2 hr. A concentrated aqueous solution containing 12.5 g (0.05 mol) of $CuSO_4 \cdot 5H_2O$ is added to it, and then one containing 4 g (0.1 mol) of NaOH. The deep green, tarry precipitate which separates out is washed with cold methanol, and the dark blue crude crystals which remain are recrystallized from hot methanol. The product obtained is the monohydrate of [Cu(PCdien)] (Found: Cu, 16.23; N, 17.59; H_2O, 4.20%. Calcd for $C_{16}H_{17}N_5O_2Cu \cdot H_2O$: Cu, 16.17; N, 17.82; H_2O, 4.58%.); the anhydrous chelate can be obtained by its dehydration in vacuum at 90 °C, (Found: Cu, 17.00%. Calcd for $C_{16}H_{17}N_5O_2$ Cu: Cu, 16.95%).

[Cu(PCenpn)] can be obtained in a similar way from 3-(aminoethylamino)-propanediamine and methyl picolinate. After heating the ligand mixture and mixing it with solutions of $CuSO_4 \cdot 5H_2O$ and NaOH, the mixture is evaporated under reduced pressure almost to dryness, and extracted with methanol. The extract is then evaporated to dryness again, and the residue is recrystallized from water (pH 9). The product has the composition of $[Cu(PCenpn)] \cdot 1.5H_2O$ (Found: Cu, 15.27; N, 16.93; H_2O, 6.70%. Calcd for $C_{17}H_{19}N_5O_2Cu \cdot 1.5H_2O$: Cu, 15.28; N, 16.84; H_2O, 6.50%.) and can be made anhydrous as in the case of [Cu(PCdien)] (Found: Cu, 16.53%. Calcd for $C_{17}H_{19}N_5O_2Cu$: Cu, 16.34%.).

Physical Measurements. The visible absorption spectra of the solutions were measured with a Shimadzu Multi-convertible Spectrophotometer Double-40, using 5 mm and 10 mm cells. Measurements with hot and cold solutions were carried out as promptly as possible after their preparation, without use of thermospacers; this is because the thermochromic changes are quite slow and no serious error was expected to result. All other measurements were carried out with conventional techniques.

Results and Discussion

Both of the chelates are violet-blue crystals, and dissolve in methanol forming violet-blue solutions with ν_{max} and ε_{max} values shown in Table 1. When these solutions are heated almost to boiling, the color of the solution of [Cu(PCenpn)] remains nearly unchanged, but that of [Cu(PCdien)] becomes gradually green, and then remarkably yellowish. This color change is fairly slow, and the solution must be refluxed

TABLE 1. CHARACTERISTIC DATA ON [Cu(PCdien)] AND [Cu(PCenpn)]

		[Cu(PCdien)]	[Cu(PCenpn)]
$\nu_{max}(\varepsilon_{max})$[a]		16500 cm^{-1}(140)	15400 cm^{-1}(250)
Molar conductivity[b] (mho cm^2 mol^{-1})		11.55	3.18
μ_{eff} (286 K) BM		1.79[c]; 1.81[d]	1.81[c]; 1.88[d]
IR spectra	ν_{N-H}	3440 cm^{-1}	3320 cm^{-1}
	amide I	1637	1620
		1620	
	py	1598	1598
		1581	1580
		1560	1557

a) Methanolic solutions. b) 10^{-3} M solutions in methanol: these data show that both of the chelates are only partially ionized in solution. c) Anhydrous chelate. d) Hydrated chelate.

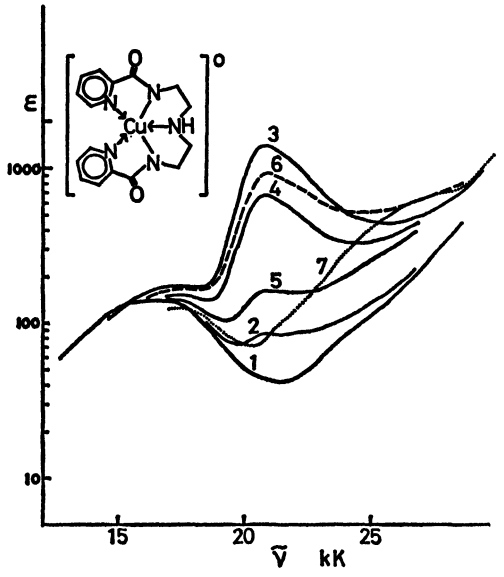

Fig. 1. Absorption spectra of [Cu(PCdien)] in methanol.

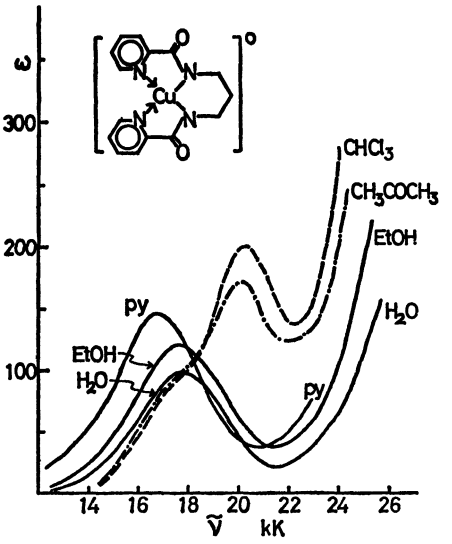

Fig. 2. Absorption spectra of I in various solvents.

for some minutes for its full development. The reverse change from yellow to violet-blue occurs on cooling, but this change is much slower, and the solution reverts to its original violet-blue state only after standing for several days in a freezer (*ca.* −15 °C).

The general outlook of the spectral changes observed in the course of this process is shown in Fig. 1. Curve 1 shows the spectrum of a fresh, cold solution (2.0×10^{-3} M) prepared by keeping the weighed sample together with methanol in a freezer overnight. When this solution is left standing at room temperature (26 °C) for some time (*ca.* 1/2 hr), a weak band at *ca.* 21000 cm^{-1} is observed (Curve 2).[1] This band becomes very much stronger by heating; Curve 3 is the spectrum of the same solution after refluxing at *ca.* 68 °C for 10 min, when the apparent color change appears to be nearly complete. Curve 4 is observed when the refluxed solution is cooled and kept in a freezer for a day; Curve 5, after four more days, and Curve 6 when the solution is then refluxed again.

The spectral changes can thus be repeated; however, as can be seen from these Curves, the amount of the observed spectral change tends to decrease in the course of repetition. This seems to be due to an irreversible decomposition of the chelate, which, also slowly, takes place in solution; in fact, when we let the solution stand for a long time (5 days) at room temperature, the solution becomes remarkably greenish and only poorly thermochromic. Curve 7 shows the absorption curve of such an "aged" solution.

Although the exact mechanism of this thermochromism is still unknown, a clue for its understanding can be found in the earlier work of Ojima.[2] Figure 2 shows his data on the absorption curves of the chelate I in various solvents.

It can be seen that the ν_{max} and ε_{max} values are largest in $CHCl_3$ (20200 cm^{-1} and 200, respectively), and the ν_{max} decreases in the order of $CHCl_3\rightarrow CH_3COCH_3\rightarrow H_2O\rightarrow EtOH\rightarrow py$, while the ε_{max} seems to pass through a minimum and then increases again. Table 2 summarizes these data, and similar data observed with the chelates II and III.[3]

In $CHCl_3$, which is a poorly coordinating solvent, we can expect the chelate I to assume a four-coodinate structure. This structure will be approximately planar, but the formation of a perfectly planar structure will be hindered by the strains in the chelate rings and by the repulsion between the hydrogen atoms on the pyridine rings. Going to a more strongly coordinating solvent, however, the chelate will become gradually tetragonal, and when the solvent becomes very basic (*e.g.* pyridine), the chelate may become eventually pentacoordinated. The spectral changes in Fig. 2 and Table 2 can probably be taken as the reflection of these structral changes.[4]

We now see that the absorption curves of [Cu(PCdien)] in cold and hot methanol are, respectively, very similar to those of I in pyridine and chloroform. Model studies show that the pentacoordinated structure of [Cu(PCdien)] is, although sterically possible (trigonal bipyramid seems to be more favorable than square pyramid), quite highly strained; therefore, though the chelate may retain its pentacoordinated structure in a very cold solution, a rupture of the chelate ring (probably at the Cu←NH bond) will take place on heating, leading to a tetracoordinated structure. The spectral analogy mentioned above can thus be understood, at least in a qualitative way. The tetracoordinated structure is, however, again expected from model studies to be considerably strained; indeed, the very high ε_{max} value of the high-temperature species observed in Fig. 1 (apparent value: 1400 at 20800 cm^{-1}) may be related to this high strain and poor

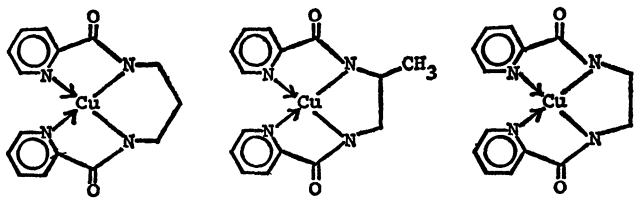

TABLE 2. ν_{max} AND ε_{max} VALUES OF THE CHELATES I—III IN VARIOUS SOLVENTS

Chelate	ν_{max} (10^3 cm^{-1}: ε_{max} in parentheses)				
	$CHCl_3$	CH_3COCH_3	H_2O	EtOH	py
I	20.2(198)	20.0(171)	17.7(97)	17.3(117)	16.3(145)
II	20.4(397)	—	18.5(225)	18.5(252)	17.4(252)
III	17.1(216)	—	18.7(212)	18.3(228)	17.5(256)

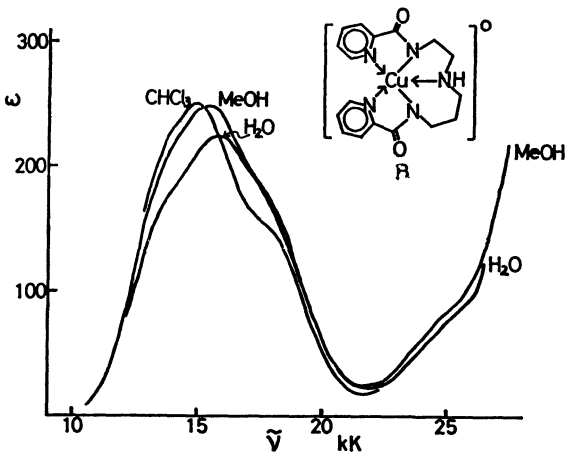

Fig. 3. Absorption spectra of [Cu(PCenpn)] in various solvents.

symmetry of the chelate. Moreover, the change between these two structures will need a large amount of conformational change, so that it (and the reverse reaction, too) will need a large activation energy, and a part of the chelate may be lost in the course of these changes by some kind of decomposition.

It is also of interest to note that the chelate [Cu(PCenpn)], which is not thermochromic in methanol (and H_2O and $CHCl_3$, in which it is also soluble), shows absorption curves which are all very similar (Fig. 3), and characteristic of the CuN_5-type pentacoordinated chelates already studied by Ojima and Nonoyama.[5] The slight structural change from [Cu(PCdien)] to [Cu(PCenpn)], *i.e.* the introduction of one 6-ring instead of a 5-ring, seems to greatly lessen the intramolecular strain, and avoid the rupture of the chelate ring upon heating.

Our thanks are due to Miss Junko Ida for her help in the experiments.

References

1) When the solution is kept longer at room temperature, however, this band does not gain in intensity so much, and the solution begins gradually to "age", *i.e.*, to show a curve similar to Curve 7 and to become poorly thermochromic.

2) H. Ojima, *Nippon Kagaku Zasshi*, **88**, 333 (1967).

3) A serious exception among these data is that of the chelate III in $CHCl_3$; here ν_{max} and ε_{max} are much lower than expected from other data. This, however, may be due to the effect of intermolecular association leading to an apparently higher coordimation number of copper(II), which will be favored in such a poorly coordinating solvent.

4) It may be pointed out that the spectral change from H_2O or EtOH to py resembles, to some extent, the change observed when $[Cu(NH_3)_4(OH_2)_2]^{2+}$ is transformed in aqueous solution into $[Cu(NH_3)_5(OH_2)]^{2+}$, which probably holds its water only very weakly; *cf.*, *e.g.*, B. J. Hathaway and A. A. G. Tomlinson, *Coord. Chem. Rev.*, **5**, 1 (1970).

5) H. Ojima and K. Nonoyama, *Z. Anorg. Allg. Chem.* **401**, 207 (1973).

Use of a Glass Electrode in the Potentiometric Study of Acid-Base Equilibria of Zinc and Cadmium Acetates in Acetic Acid

Kiyoshi SAWADA, Mitsuji NAKANO, Hidenari MORI, and Motoharu TANAKA

Laboratory of Analytical Chemistry, Faculty of Science, Nagoya University, Nagoya 464

(Received April 10, 1975)

Potentiometric study of acid-base equilibria of zinc and cadmium acetates in acetic acid was undertaken with a glass electrode filled with a LiCl-$HClO_4$ acetic acid solution. Potentiometric titration of 0.1 m $LiClO_4$ acetic acid solution with perchloric acid and lithium acetate reveals that the glass electrode gives rise to the Nernstian response. The equilibrium constant of the reaction, $HClO_4+LiOAc \overset{K_f}{\rightleftharpoons} LiClO_4+HOAc$ is found as $\log K_f=7.86$. The titration of zinc and cadmium acetate with perchloric acid and lithium acetate points to the following equilibria: $M(ClO_4)_2+LiOAc \overset{\beta_1}{\rightleftharpoons} M(OAc)(ClO_4)+LiClO_4$, $M(ClO_4)_2+2LiOAc \overset{\beta_2}{\rightleftharpoons} M(OAc)_2+2LiClO_4$, $M(ClO_4)_2+3LiOAc \overset{\beta_3}{\rightleftharpoons} LiM(OAc)_3+2LiClO_4$. Logarithmic overall formation constants of the acetato complexes, β_1, β_2 and β_3 were determined as 4.04, 7.00 and 9.2 respectively for zinc, and 3.43, 5.46 and 8.0 respectively for cadmium. In addition zinc forms tetraacetate complex with the overall formation constant of $\log \beta_4=12.4$.

Acetic acid has been used as a convenient solvent for the titration of weak bases.[1,2] The huge number of acid-base equilibria in the solvent have been investigated for the analytical purpose, and equilibrium constants of many systems have been obtained by potentiometry, colorimetry, conductometry and other methods.

Various hydrogen ion indicator electrodes have been utilized in potentiometric studies. The hydrogen electrode, being a fundamental electrode, has difficulty in handling and fails sometimes to give a satisfactory reproducibility.[3-6] Glass and chloranil electrodes have been used as indicator electrodes for the acid-base titration,[1] and dissociation constants of acids and bases have been estimated from the relative electromotive forces of the electrodes.[7-11]

In early works, because of a poor precision of instrument, a considerable error was inevitable in potentiometric measurements in acetic acid solution having high electrical resistance.[12] Mukherjee[5] and Bruckenstein and Kolthoff[8] have claimed the reproducibility to less than one millivolt. However the scatter of emf by the variation of electrolyte concentration and the deviation from reversible response point to the reproducibility of the electrodes to about five millivolts. According to studies on the reversibility of the electrode,[4,6,11,13-15] the reproducibility of a potentiometry in acetic acid does not seem to be as good as claimed.

Thus, as stated by Popov,[2] some of the problems can not be resolved without additional careful works on the electrode systems in acetic acid. The poor precision of some earlier works may be due to the absence of medium salt, which lowers the electrical resistance of the solution and keeps the activity coefficient constant, and the presence of impurities such as water.

In the present paper, the response of a glass–calomel electrode cell filled with acetic acid solution is investigated with care. The potentiometric study with this electrode system is undertaken on the acid-base equilibria of zinc and cadmium acetate, *i.e.*, the formation of acetato complexes, for which the formation of higher acetato complex has been pointed out as a result of solubility measurements.[16]

Experimental

Reagents. Acetic acid, perchloric acid and lithium acetate,[17] lithium perchlorate[18] and zinc acetate[19] were prepared by the methods described previously.

Cadmium Acetate: G. R. grade $Cd(OAc)_2\cdot 2H_2O$ was recrystallized twice from acetic acid containing acetic anhydride.

Measurements. *Glass Electrode*: The inner solution of a commercially available glass electrode was replaced by a 0.1 mol/kg LiCl-0.1 mol/kg $HClO_4$ acetic acid solution. An Ag-AgCl electrode was utilized as an inner reference electrode. After standing in 0.1 mol/kg $LiClO_4$ acetic acid solution for 2 days at 100 °C, the glass electode was stored in the same solution. The glass electrode prepared in this manner exhibits smaller drift of potential than the commercially available glass electrode containing aqueous inner solution.

Calomel Electrode: The method of preparation of the calomel electrode composed of 0.27 mol/kg LiCl acetic acid solution has been described elsewhere.[18] The reproducibility of the electrode was found to be less than 0.3 mV. The electrode was connected with the sample solution through a salt bridge. Both salt bridge and sample solution contain 0.1 mol/kg $LiClO_4$ as a medium salt.

Potentiometry. The chemical cell used is written as follows:

Ag|AgCl|0.1 mol/kg LiCl, 0.1 mol/kg $HClO_4$ AcOH soln.|glass electrode glass|sample soln. (0.1 mol/kg $LiClO_4$HOAc soln.)‖0.1 mol/kg salt $LiClO_4$ HOAc soln.‖0.27 mol/kg LiCl HOAc soln.|Hg_2Cl_2|Hg bridge calomel electrode

The potential was measured, in a water-jacketted vessel thermostated at 25.0±0.1 °C, with an Orion research digital pH/mV meter model 801.

The glass electrode shows a variation of about one millivolt of electrode potential in a few days, so the standard potential of the cell should be measured every day.

Results and Discussion

Response of Glass Electrode in Acetic Acid. The following two equilibria are relevant to lithium perchlorate in acetic acid:

$$HClO_4 + LiOAc \overset{K_f}{\rightleftharpoons} LiClO_4 + HOAc \quad (1)$$

and

$$Li^+ + ClO_4^- \overset{K_{LiClO_4}}{\rightleftharpoons} LiClO_4 \quad (2)$$

Perchloric acid and lithium acetate are weak electrolytes in this medium[1] and we have

$$H^+ + ClO_4^- \overset{K_{HClO_4}}{\rightleftharpoons} HClO_4 \quad (3)$$

$$Li^+ + OAc^- \overset{K_{LiOAc}}{\rightleftharpoons} LiOAc. \quad (4)$$

When perchloric acid is added to lithium perchlorate solution, we have the following relationship:

$$[H^+] + [HClO_4] - C_{HClO_4} = [OAc^-] + [LiOAc] \quad (5)$$

where C_{HClO_4} denotes the total concentration of the added perchloric acid. As the ionic dissociation in acetic acid is very weak,[1] Eq. (5) is approximated to Eq. (6).

$$[HClO_4] - C_{HClO_4} = [LiOAc] \quad (6)$$

Substitution of the formation constant of Eq. (1), K_f, into Eq. (6) leads to Eq. (7).

$$[HClO_4]^2 - C_{HClO_4}[HClO_4] - [LiClO_4]K_f^{-1} = 0. \quad (7)$$

Solving the quadratic equation, we obtain

$$[HClO_4] = \frac{1}{2}\{C_{HClO_4} + (C_{HClO_4}^2 + 4[LiClO_4]K_f^{-1})^{1/2}\}. \quad (8)$$

From the constant of the equilibrium (3), K_{HClO_4}, the free hydrogen ion concentration is given by:

$$[H^+] = [HClO_4]K_{HClO_4}^{-1}[ClO_4^-]^{-1}. \quad (9)$$

And from the condition of electroneutrality, we have

$$[H^+] + [Li^+] = [OAc^-] + [ClO_4^-]. \quad (10)$$

When the concentration of perchloric acid added, C_{HClO_4}, is much smaller than that of lithium perchlorate,

$$[OAc^-] \text{ and } [H^+] \ll [Li^+] \text{ and } [ClO_4^-]. \quad (11)$$

Consequently Eq. (10) is reduced to

$$[Li^+] = [ClO_4^-]. \quad (12)$$

Then the equilibrium constant of Eq. (2) is written as follows:

$$K_{LiClO_4} = [LiClO_4][Li^+]^{-1}[ClO_4^-]^{-1} = [LiClO_4][ClO_4^-]^{-2}. \quad (13)$$

The free lithium perchlorate concentration, $[LiClO_4]$, being approximated as the total concentration, C_{LiClO_4}, Eq. (13) is rewritten as follows:

$$[ClO_4^-]^2 = C_{LiClO_4}K_{LiClO_4}^{-1}. \quad (14)$$

Substitution of Eqs. (8) and (14) into Eq. (9) leads to

$$[H^+] = \frac{1}{2}\{C_{HClO_4} + (C_{HClO_4}^2 + 4C_{LiClO_4}K_f^{-1})^{1/2}\} \times K_{LiClO_4}^{1/2}/(C_{LiClO_4}^{1/2}K_{HClO_4}) \quad (15)$$

As the lithium perchlorate concentration may be regarded as constant,

$$[H^+] = \frac{1}{2}\{C_{HClO_4} + (C_{HClO_4}^2 + 4C_{LiClO_4}K_f^{-1})^{1/2}\}K \quad (16)$$

where $K = K_{LiClO_4}^{1/2}/(C_{LiClO_4}^{1/2}K_{HClO_4}) = \text{constant}$.

Thus, as the activity coefficient of hydrogen ion is kept constant, the electromotive force of the cell at 25.0 °C is given by:

$$E = E_0 + \frac{RT}{nF}\ln[H^+] = E_0' + 59.1 \log \frac{1}{2}\{C_{HClO_4} + (C_{HClO_4}^2 + 4C_{LiClO_4}K_f^{-1})^{1/2}\}. \quad (17)$$
$$(E_0' = E_0 + 59.1 \log K)$$

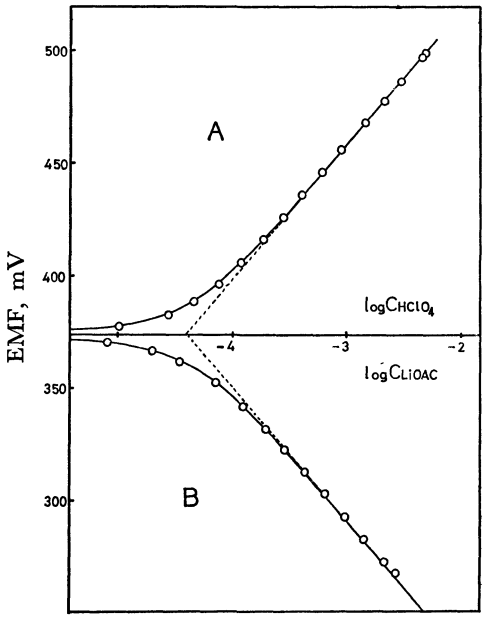

Fig. 1. Electromotive force of 0.1 mol/kg $LiClO_4$ acetic acid solution as a function of logarithmic concentration of perchloric acid (A) and lithium acetate (B). Solid lines are the normalized curve, $X = \log x$, $Y = 59.1 \log (x + \sqrt{x^2+4})$.

In Fig. 1 (A), electromotive force of 0.1 molal lithium perchlorate acetic acid solution is plotted as a function of logarithmic concentration of added perchloric acid. In order to compare the data with normalized curve, $X = \log x$, $Y = 59.1 \log (x + \sqrt{x^2+4})$, Eq. (17) is rewritten as follows:

$$E = E_0' + 59.1 \log \frac{1}{2} C_{LiClO_4}^{1/2} K_f^{-1/2} \times [C_{HClO_4} C_{LiClO_4}^{-1/2} K_f^{1/2} + \{(C_{HClO_4} C_{LiClO_4}^{-1/2} K_f^{1/2})^2 + 4\}^{1/2}] = E' + 59.1 \log [C_{HClO_4} C_{LiClO_4}^{-1/2} K_f^{1/2} + \{(C_{HClO_4} C_{LiClO_4}^{-1/2} K_f^{1/2})^2 + 4\}^{1/2}]. \quad (18)$$
$$\left(E' = E_0' + 59.1 \log \frac{1}{2} C_{LiClO_4}^{1/2} K_f^{-1/2}\right)$$

By the curve fitting, $\log C_{LiClO_4}^{-1/2} K_f^{1/2} = 4.44$ was obtained from the reading of abscissa in Fig. 1 (A). As $C_{LiClO_4} = 0.1$ mol/kg the formation constant of lithium perchlorate was found as $\log K_f = 7.88 \pm 0.05$; and by the extrapolation to $C_{HClO_4} = 1$ the apparent standard potential, E_0' was estimated as $E_0' = 636$ mV.

The titration of 0.1 mol/kg lithium perchlorate solution with lithium acetate is shown in Fig. 1 (B). In the same way as in the preceding case, the free acetate ion concentration is given as follows:

$$[OAc^-] = \frac{1}{2}\{C_{LiOAc} + (C_{LiOAc}^2 + 4C_{LiClO_4}K_f^{-1})^{1/2}\} \times K_{LiClO_4}^{1/2}/(C_{LiClO_4}^{1/2}K_{LiOAc}) \quad (19)$$

where C_{LiOAc} denotes the total concentration of added lithium acetate. By using Eq. (19) and autoprotolysis constant of acetic acid, $K_{HOAc}=[H^+][OAc^-]$, the electromotive force of lithium perchlorate solution ($C_{LiClO_4}=0.1$ mol/kg and $C_{LiOAc} \ll C_{LiClO_4}$) is written as

$$E = E_0 + \frac{RT}{nF}\ln\frac{K_{HOAc}}{[OAc^-]} = E_0 + 59.1 \log K' - 59.1 \log \frac{1}{2}\{C_{LiOAc} + (C_{LiOAc}^2 + 4C_{LiClO_4}K_f^{-1})^{1/2}\}. \quad (20)$$

($K'=K_{LiClO_4}^{1/2}/(C_{LiClO_4}^{1/2}K_{LiOAc})=$constant)

In the same manner as in the titration with perchloric acid, comparison of the experimental results with the normalized curve, Eq. (19), gives $\log C_{LiClO_4}^{-1/2}K_f^{1/2}=4.42$, *i.e.*, $K_f=7.84$ and $E_0+59.1 \log K'=113$ mV.

The experimental values are in excellent agreement with normalized curve (solid lines in Fig. 1), and the formation constant of lithium perchlorate, K_f, obtained by the titration with perchloric acid agrees well with the value obtained by the titration with lithium acetate. Thus the glass electrode described in the experimental section gives rise to a reversible electromotive force.

In addition, from the difference of the apparent standard potentials, $E_0'_{(HClO_4)}$ and $E_0'_{(LiOAc)}$, K_f is estimated as $\log K_f=7.86$.

As the concentrations of perchloric acid and lithium acetate are much smaller than that of lithium perchlorate, the fraction of the two aggregated species with lithium perchlorate, $HClO_4 \cdot LiClO_4$ and $LiOAc \cdot LiClO_4$, if any, would be constant.

$$HClO_4 + LiClO_4 \rightleftharpoons HClO_4 \cdot LiClO_4 \quad (21)$$

$$LiOAc + LiClO_4 \rightleftharpoons LiOAc \cdot LiClO_4 \quad (22)$$

In Fig. 1 (B) the deviation of data from the normalized curve at higher lithium acetate concentration should indicate the dimerization of lithium acetate, *i.e.*,

$$2LiOAc \rightleftharpoons (LiOAc)_2 \quad (23)$$

Formation of Zinc-Acetato Complex. Reaction of perchloric acid with zinc acetate in solution containing 0.1 mol/kg lithium perchlorate is written as follows:

$$pZn(OAc)_2 + qHClO_4 \rightleftharpoons Zn_p(OAc)_{2p-q}(ClO_4)_q + qHOAc \quad (24)$$

$$pZn(OAc)_2 + qLiClO_4 \rightleftharpoons Zn_p(OAc)_{2p-q}(ClO_4)_q + qLiOAc. \quad (25)$$

It has previously been confirmed that zinc acetate exists as a monomer in acetic acid [19]. When $q>2p$, the species formed should be written as $H_{q-2p}Zn_p(ClO_4)_q$ or $Li_{q-2p}Zn_p(ClO_4)_q$, which can be negligible as will hereinafter be mentioned.

The total concentration of perchlorate, C_{ClO_4}, is given by the following:

$$C_{ClO_4} = C_{LiClO_4} + C_{HClO_4} = [LiClO_4] + [HClO_4] + \sum q[Zn_p(OAc)_{2p-q}(ClO_4)_q], \quad (26)$$

$$\sum q[Zn_p(OAc)_{2p-q}(ClO_4)_q] = C_{LiClO_4} + C_{HClO_4} - [LiClO_4] - [HClO_4]. \quad (27)$$

The total lithium perchlorate concentration, C_{LiClO_4}, is given by Eq. (28).

$$C_{LiClO_4} = [LiClO_4] + [LiOAc]. \quad (28)$$

Substitution of Eq. (28) to Eq. (27) leads to

$$\sum q[Zn_p(OAc)_{2p-q}(ClO_4)_q] = C_{HClO_4} - [HClO_4] + [LiOAc] \quad (29)$$

Thus the formation function of perchlorate of zinc, $\bar{n}^*$, is written as follows:

$$\bar{n}^* = (\sum q[Zn_p(OAc)_{2p-q}(ClO_4)_q])C_{Zn}^{-1} = (C_{HClO_4} - [HClO_4] + [LiOAc])C_{Zn}^{-1} \quad (30)$$

As the free concentration of lithium perchlorate, $[LiClO_4]$, can be approximated by the total concentration, C_{LiClO_4}, Eq. (30) becomes

$$\bar{n}^* = (C_{HClO_4} - [HClO_4] + C_{LiClO_4}[HClO_4]^{-1}K_f^{-1})C_{Zn}^{-1} \quad (31)$$

In Fig. 2 the results of potentiometric titration of various concentration of zinc acetate solutions containing 0.1 mol/kg lithium perchlorate are plotted as a function of mole ratio $a \equiv C_{HClO_4}/C_{Zn}$. By using the following equation:

$$E = E_0' + 59.1 \log [HClO_4] \quad (E_0'=636 \text{ mV}), \quad (32)$$

free perchloric acid concentration, $[HClO_4]$, can be calculated from the electromotive force E.

The formation function, $\bar{n}^*$, calculated by Eq. (31) is plotted as a function of $\log [HClO_4]$ in Fig. 3 (open symbols). The plot lies on the same curve irrespective of the zinc acetate concentration. This implies that there is no difference in the degree of polymerization between zinc acetate and the species formed, *i.e.*, all species involved in this reaction are monomer (*i.e.*, $p=1$). Over a range of $\bar{n}^*$ not exceeding 2, the reaction of zinc acetate with perchloric acid is

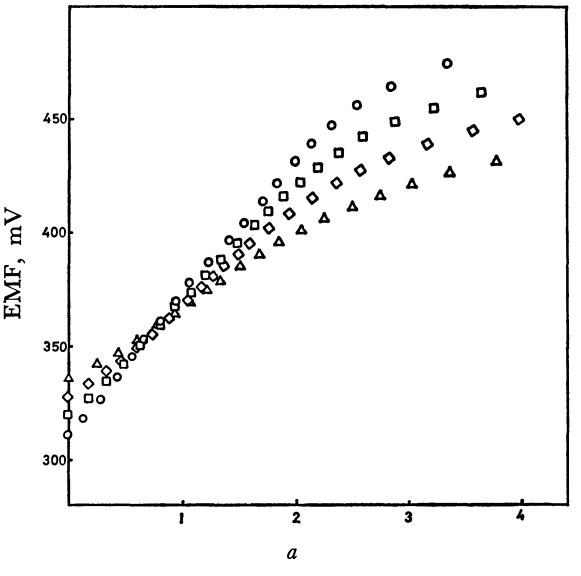

Fig. 2. Electromotive force of various concentrations of zinc acetate as a function of mol ratio $a \equiv C_{HClO_4}/C_{Zn}$. C_{Zn}: ○, 1.769; □, 0.885; ◇, 0.442; △, 0.221×10^{-3} mol/kg.

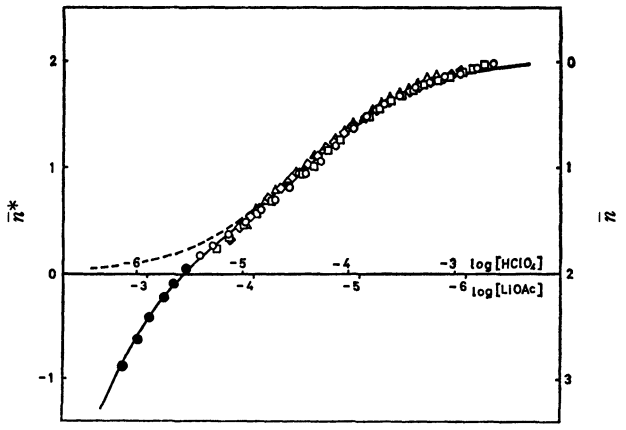

Fig. 3. Plot of formation function of zinc perchlorate, $\bar{n}^*$, and of zinc acetate complex, $\bar{n}$, ($\bar{n}=2-\bar{n}^*$), as a function of log [$HClO_4$] and log [LiOAc] ($=\log K_f^{-1}C_{LiClO_4}-\log$ [$HClO_4$]). Open symbols are the results of titration with perchloric acid. C_{Zn}: ○, 1.769; □, 0.885; ◇, 0.442; △, 0.221×10^{-3} mol/kg. Filled circle is the results with lithium acetate ($C_{Zn}=1.769\times10^{-3}$ mol/kg). Dotted line is the normalized curve, $X=\log x$, $Y=(ax+2x^2)/(1+ax+x^2)$. Solid line is the normalized curve, $X=\log x$, $Y=(ax+2x^2+3bx^3+4cx^4)/(1+ax+x^2+bx^3+cx_4)$.

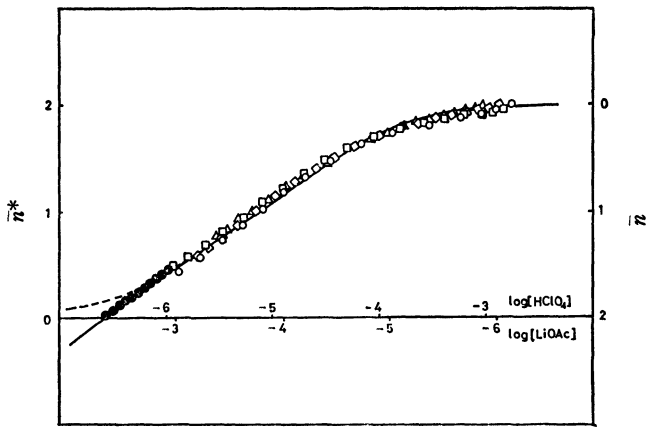

Fig. 4. Plot of formation function of cadmium perchlorate, $\bar{n}^*$, and of cadmium acetato complex, $\bar{n}(\bar{n}=2-\bar{n}^*)$, as a function of log [$HClO_4$] and log [LiOAc] ($=\log K_f^{-1}C_{LiClO_4}-\log$ [$HClO_4$]). Open symbols are the results of titration with perchloric acid. C_{Cd}: ○, 4.000; □, 2.000; ◇, 1.000; △, 0.500×10^{-3} mol/kg. Filled circle is the results with lithium acetate ($C_{Cd}=2.000\times10^{-3}$ mol/kg). Dotted line is the normalized curve, $X=\log x$, $Y=(ax+2x^2)/(1+ax+x^2)$. Solid line is the normalized curve, $X=\log x$, $Y=(ax+2x^2+3bx^3)/(1+ax+x^2+bx^3)$.

written as follows:

$$Zn(OAc)_2 + HClO_4 \overset{\beta_1}{\rightleftharpoons} Zn(OAc)(ClO_4) + HOAc \quad (33)$$

$$Zn(OAc)_2 + 2HClO_4 \overset{\beta_2}{\rightleftharpoons} Zn(ClO_4)_2 + 2HOAc. \quad (34)$$

By the use of equilibrium constants of Eqs. (33) and (34),

$$\beta_1^* = [Zn(OAc)(ClO_4)][Zn(OAc)_2]^{-1}[HClO_4]^{-1} \quad (35)$$

$$\beta_2^* = [Zn(ClO_4)_2][Zn(OAc)_2]^{-1}[HClO_4]^{-2}, \quad (36)$$

we obtain

$$\bar{n}^* = ([Zn(OAc)(ClO_4)] + 2[Zn(ClO_4)_2])C_{Zn}^{-1} = (\beta_1^*[HClO_4] + 2\beta_2^*[HClO_4]^2) \times (1+\beta_1^*[HClO_4] + \beta_2^*[HClO_4]^2)^{-1}. \quad (37)$$

Fitting the experimental results with the normalized curve, $X=\log x$, $Y=(ax+2x^2)/(1+ax+x^2)$, we obtained $\log\beta_1^*=4.92$ and $\log\beta_2^*=8.76$ (Fig. 3, dotted line).

Now, zinc acetate solution containing 0.1 mol/kg $LiClO_4$ was titrated with lithium acetate. The formation function calculated by Eq. (38) is plotted in Fig. 3 (filled circles).

$$\bar{n}^* = (-C_{LiOAc}+[HClO_4]-[LiOAc])C_{Zn}^{-1} \quad (38)$$

The plot deviates from the dotted line and goes down to under zero, the fact pointing to the formation of acetato complexes higher than diacetato species, *i.e.*, formation of $Li_{n-2}Zn(OAc)_n$ ($n>2$, $n=2-q$).

The reaction of zinc acetate with perchloric acid can be rewritten by the reaction of zinc perchlorate with lithium acetate as follows:

$$Zn(ClO_4)_2 + LiOAc \overset{\beta_1}{\rightleftharpoons} Zn(OAc)(ClO_4) + LiClO_4 \quad (39)$$

$$Zn(ClO_4)_2 + 2LiOAc \overset{\beta_2}{\rightleftharpoons} Zn(OAc)_2 + 2LiClO_4 \quad (40)$$

These equilibrium constants, β_1 and β_2, are related with β_1^* and β_2^* as follows:

$$\beta_1 = [Zn(OAc)(ClO_4)][LiClO_4][Zn(ClO_4)_2]^{-1}[LiOAc]^{-1} = K_f\beta_1^*\beta_2^* \quad (41)$$

$$\beta_2 = [Zn(OAc)_2][LiClO_4]^2[Zn(ClO_4)_2]^{-1}[LiOAc]^{-2} = K_f^2\beta_2^* \quad (42)$$

The free lithium acetate concentration, [LiOAc], and formation function of acetato complex, $\bar{n}$, are written as follows:

$$[LiOAc] = C_{LiClO_4}K_f^{-1}[HClO_4]^{-1} \quad (43)$$

$$\bar{n} = 2 - \bar{n}^*. \quad (44)$$

In Fig. 3 $\bar{n}$ going up to 3 at higher lithium acetate concentration, the formation of triacetato and tetraacetato complexes is anticipated.

$$Zn(ClO_4)_2 + 3LiOAc \overset{\beta_3}{\rightleftharpoons} LiZn(OAc)_3 + 2LiClO_4 \quad (45)$$

$$Zn(ClO_4)_2 + 4LiOAc \overset{\beta_4}{\rightleftharpoons} Li_2Zn(OAc)_4 + 2LiClO_4. \quad (46)$$

Thus the formation function of acetato complex is written as follows:

$$\bar{n} = ([Zn(OAc)(ClO_4)] + 2[Zn(OAc)_2] + 3[LiZn(OAc)_3] + 4[Li_2Zn(OAc)_4])C_{Zn}^{-1} = (\beta_1'[LiOAc] + 2\beta_2'[LiOAc]^2 + 3\beta_3'[LiOAc]^3 + 4\beta_4'[LiOAc]^4)(1+\beta_1'[LiOAc] + \beta_2'[LiOAc]^2 + \beta_3'[LiOAc]^3 + \beta_4'[LiOAc]^4)^{-1} \quad (47)$$

where conditional overall formation constants are defined as $\beta_1'=\beta_1[LiClO_4]^{-1}$, $\beta_2'=\beta_2[LiClO_4]^{-2}$, $\beta_3'=\beta_3[LiClO_4]^{-2}$ and $\beta_4'=\beta_4[LiClO_4]^{-2}$.

By comparison of the plot of $\bar{n}$ *vs.* log [LiOAc] with the normalized curve, $X=\log x$, $Y=(ax+2x^2+3bx^3+4cx^4)(1+ax+x^2+bx^3+cx^4)^{-1}$, β_3' and β_4' are determined from b ($=\beta_3'/\beta_2'^{3/2}$) and c ($=\beta_4'/\beta_2'^2$), where β_1' and β'_2 have been obtained previously. Thus from the

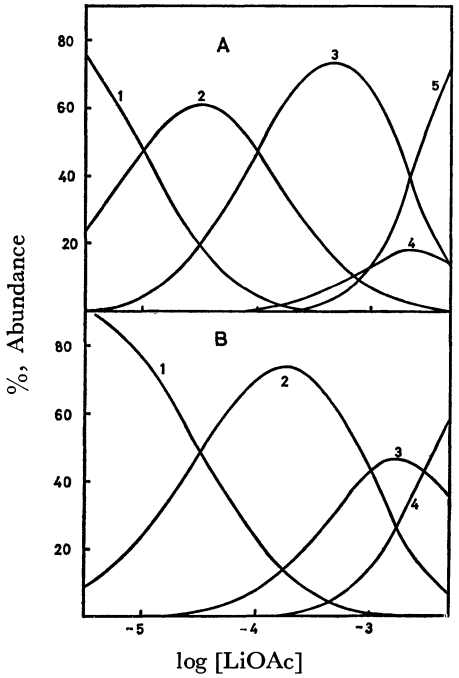

Fig. 5. Distribution diagram of acetato complexes of zinc (A) and cadmium (B) in 0.1 mol/kg $LiClO_4$ acetic acid solution.
1, $M(ClO_4)_2$; 2, $M(OAc)(ClO_4)$; 3, $M(OAc)_2$; 4, $LiM(OAc)_3$; 5, $Li_2M(OAc)_4$.

best fit curve (Fig. 3, solid line), the formation constants of acetato complexes are found as $\log \beta_1 = 4.04 \pm 0.1$, $\log \beta_2 = 7.00 \pm 0.1$, $\log \beta_3 = 9.2 \pm 0.3$ and $\log \beta_4 = 12.4 \pm 0.5$.

Formation of Cadmium-Acetato Complex. Potentiometric titration of cadmium acetate solution containing 0.1 mol/kg $LiClO_4$ with perchloric acid and lithium acetate has been carried out in the same manner as in the titration of zinc acetate. The results are shown in Fig. 4. In the case of cadmium complexes higher than triacetato complex are not observed over the studied range of lithium acetate concentration. The following equilibria are found to be relevant to the cadmium acetate:

$$Cd(ClO_4)_2 + LiOAc \overset{\beta_1}{\rightleftharpoons} Cd(OAc)(ClO_4) + LiClO_4 \quad (48)$$

$$Cd(ClO_4)_2 + 2LiOAc \overset{\beta_2}{\rightleftharpoons} Cd(OAc)_2 + 2LiClO_4 \quad (49)$$

$$Cd(ClO_4)_2 + 3LiOAc \overset{\beta_3}{\rightleftharpoons} LiCd(OAc)_3 + 2LiClO_2 \quad (50)$$

with overall formation constants of $\log \beta_1 = 3.43 \pm 0.1$, $\log \beta_2 = 5.46 \pm 0.1$ and $\log \beta_3 = 8.0 \pm 0.3$.

Fig. 5 depicts the distribution diagrams for acetato complexes of zinc (A) and cadmium (B) in 0.1 mol/kg $LiClO_4$ acetic acid solution calculated from the formation constants obtained in the present paper. Touller and Trémillon have investigated the formation of the acetato complexes of zinc, cadmium and other metals by the use of amalgam electrodes.[20] The formation constants of cadmium–acetato complexes reported by them are in fair accord with ours. The agreement of their constants for zinc with ours is poor presumably because they neglected the higher acetato complexes.

The financial support from the Ministry of Education is gratefully acknowledged.

References

1) G. Charlot and B. Trémillon, "Les Reactions Chimiques dans les Solvants et les Sels Fondus," Gauthier-Villars, Paris (1963).
2) A. I. Popov, in "The Chemistry of Nonaqueous Solvents" (J. J. Lagowski, ed.) Vol. III, p. 241. Academic press, New York (1970).
3) A. W. Hutchison and G. C. Chandlee. *J. Amer. Chem. Soc.*, **53**, 2881 (1931).
4) T. Yvernault, J. More, and M. Durand, *Bull. Soc. Chim. Fr.*, **16**, 542 (1949).
5) L. M. Mukherjee, *J. Amer. Chem. Soc.*, **79**, 4040 (1957).
6) A. T. Cheng, R. A. Howald, and D. L. Miller, *J. Phys. Chem.*, **67**, 1601 (1963).
7) P. Rochlin, D. B. Murphy, and S. Helf, *J. Amer. Chem. Soc.*, **76**, 1451 (1954).
8) S. Bruckenstein and I. M. Kolthoff, *ibid.*, **78**, 2974 (1956).
9) O. W. Kolling, *Anal. Chem.*, **40**, 956 (1968).
10) T. Medwick, G. Kaplan, and L. G. Weyer, *J. Pharm. Sci.*, **58**, 308 (1969).
11) O. W. Kolling and H. E. Gracey, *Inorg. Chem.*, **11**, 2556 (1972).
12) G. J. Hills in "Reference Electrodes," (D. J. G. Ives and G. J. Janz, ed.) p. 447. Academic press, New York (1961).
13) T. Higuchi, M. L. Danguilan, and A. D. Cooper, *J. Phys. Chem.*, **58**, 1167 (1954).
14) N. Petit, *C.E.A.-R*-3643(1963).
15) D. Wegmann, J. P. Escarfail, and W. Simon, *Helv. Chim. Acta*, **45**, 826 (1962).
16) A. W. Davidson and W. H. McAllister, *J. Amer. Chem. Soc.*, **52**, 519 (1930).
17) K. Sawada, H. Ohtaki, and M. Tanaka, *J. Inorg. Nucl. Chem.*, **34**, 625 (1972).
18) K. Sawada and M. Tanaka, *ibid.*, **36**, 1971 (1974).
19) K. Sawada and M. Tanaka, *ibid.*, **35**, 2455 (1973).
20) J.-C. Touller and B. Trémillon, *Anal. Chim. Acta*, **49**, 115 (1970).

The Cycloaddition Reaction of Isonitrile to Ketenimine Formed by the Reaction of Isonitrile with Carbene*

Naruyoshi OBATA, Haruo MIZUNO, Takeo KOITABASHI, and Takeo TAKIZAWA
Faculty of Pharmaceutical Sciences, University of Tokyo, Hongo, Bunkyo-ku, Tokyo 113
(Received March 10, 1975)

The reaction of several 2-, 4-, and/or 6-methyl-substituted phenylisonitrile with dihalocarbene and diphenylcarbene has been studied. The reaction of methyl-substituted phenylisonitrile with dihalocarbene gave indolenine or indoloquinoline derivatives *via* ketenimine intermediate which might be produced by α-addition of carbene to isonitrile. In contrast, the reaction of 2,6-dimethylphenylisonitrile with diphenylcarbene presumably formed by photolysis of diphenyldiazomethane gave *N*-(2,6-dimethylphenyl)diphenylketenimine, and further caused a cycloaddition reaction with isonitrile to yield indonimine derivatives. The structure of these products are discussed on the basis of the spectral data and chemical reactions. The mechanistic pathway of these reactions and the effect of methyl substituent in the cyclization stage are also discussed.

The reactivity of both carbene and isonitrile has been well recognized as divalent carbon.[1,2] It is expected that the reaction of electrophilic carbene with nucleophilic isonitrile gives the ketenimine derivatives in analogy with the superficial dimerization of carbene.[1,3] Halleux[4] discovered that the reaction of cyclohexylisonitrile with dichlorocarbene generated by $CHCl_3$-*t*-BuOK method[5] led to *N*-cyclohexyldichloroacetamidate. He showed that ketenimine was an intermediate in this reaction. The reactions of cyclohexyl- or *t*-butylisonitrile with diphenylcarbene to form ketenimine derivatives were also reported.[6]

The reactions of aromatic isonitrile with dihalocarbene or diphenylcarbene are of great interest not only with respect to the cycloaddition reaction of isonitrile to aromatic ring** of aryl-substituted ketenimine intermediate but also in connection with the mechanism of the oligomerization of phenylisonitrile to give indigodianil.[7] The reaction of phenylisonitrile with or without methyl substituent(s) at *ortho*-position with dihalocarbene and diphenylcarbene were investigated.

Results and Discussion

Reaction of Arylisonitrile with Dihalocarbene. The reaction of 2,6-dimethylphenylisonitrile with 2 mol equivalent of CHX_3-*t*-BuOK was carried out at 0 °C. After work-up in the usual way, indolenine derivative (Ia) (mp 135 °C, 40%) or (Ib) (mp 122 °C, 27%) was obtained. A similar result was also obtained in the reaction of 2,4,6-triphenylmethylisonitrile with dichlorocarbene giving (Ic) (mp 148 °C, 20%). No acetamidate derivatives reported by Halleux[4] was isolated in these reactions. Elemental analysis and molecular weight determination indicated that compounds Ia—Ic consisted of two molecules of isonitrile and one molecule of dihalocarbene. In the IR region, each of them showed characteristic four peaks at 1500—1700 cm^{-1} which were due to the C=C or C=N stretching. In the NMR spectrum, Ia and Ib showed multiplets at τ 3.05 (3H) and 3.5—4.7 (3H) and three sharp singlets at τ 7.85 (6H), 8.1 (3H) and 8.8 (3H). The signals at τ 3.05 and 3.5—4.7 showed that both aromatic protons and diene protons[9] were present in this compound. Three signals at high field might be attributed to the aromatic methyl protons, unsaturated methyl protons and saturated methyl protons. Consequently, it is most likely that an aromatic ring of two 2,6-dimethylphenylisonitrile was transformed into a cyclohexadiene ring. This was further evidenced by the NMR spectrum of compound Ic which showed three broad singlets at τ 3.15 (2H), 3.78 (1H) and 4.65 (1H) due to aromatic protons and uncoupled protons.

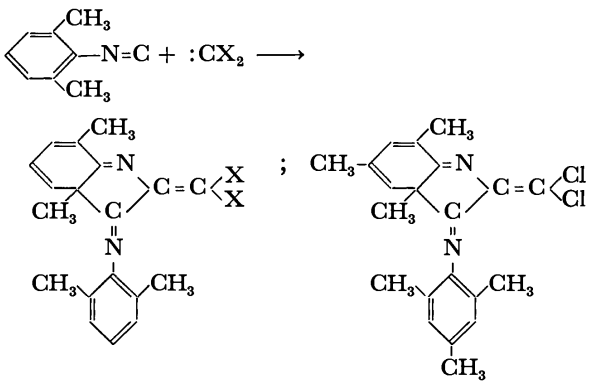

Ia: X=Cl
Ib: X=Br
Ic:

Scheme 1.

The structure of I was confirmed by the following reaction. Compound Ib was hydrolysed by dilute hydrochloric acid to give only polymer but silica gel-catalyzed hydrolysis gave amide (IIb) (mp 143 °C) in an appreciable yield. Elemental analysis and molecular weight determination indicated that compound IIb has a composition of one molecule each of Ib and H_2O. The characteristic peaks at 1640 ($\nu_{C=N}$), 1720 ($\nu_{C=O}$) and 3400 cm^{-1} (ν_{N-H}) in the IR spectrum of IIb suggested the presence of amide group. The NMR spectrum exhibited a complex multiplet at τ 3.0 (6H) and broad singlets at τ 1.43 (1H), 4.13

* A part of this work has been published. T. Takizawa, N. Obata, Y. Suzuki and T. Yanagida, *Tetrahedron Lett.*, **1969**, 3407, M. Muramatsu, N. Obata, and T. Takizawa, *Tetrahedron Lett.*, **1973**, 2133. It was also presented at the 20th Annual Meeting of the Chemical Society of Japan, Tokyo, April, 1967 and at the 23rd Annual Meeting of the Chemical Society of Japan, Tokyo, April, 1970.

** It was reported that the reaction of aromatic imine with *t*-butylisonitrile in the presence of boron trifluoride resulted in the formation of indole and azetidine derivatives.[8]

(1H), 7.7 (6H) and 7.88 (6H). The signals at τ 3.0 7.7 and 7.88 indicated the presence of two 2,6-dimethylphenyl group. The signal at τ 1.43 was assigned to the N-H proton of the amide group because of the disappearance of the signal by the addition of deuterium oxide. The signal at τ 4.13 was attributed to dibromomethin proton.[10] Thus the structure of the amide IIb is not enamine form (IIa) but imine form as shown in Scheme 2. Hydrolysis of Ib might take a route of the ring opening initiated by a protonation and resulting in regeneration of aromatic ring.

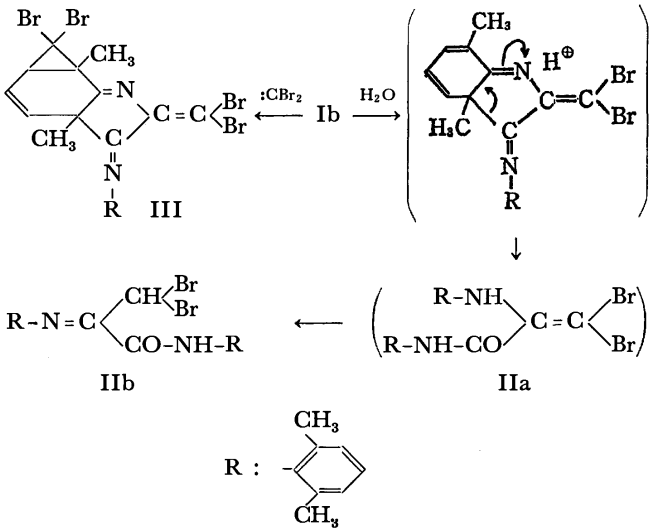

Scheme 2.

If the Seyferth method,[11] decomposition of phenyl(tribromomethyl)mercury, is employed for the generation of dibromocarbene, it might be expected to trap the intermediate giving compound I because of high reactivity of this carbene to multiple bond.[12]

Thus the reflux of the mixture of phenyl(tribromomethyl)mercury and 2 mol equivalent of 2,6-dimethylphenylisonitrile in benzene for 2 hr under nitrogen stream resulted in the formation of Ib (35%), IIb (22%), III (mp 193—195 °C following decomposition, 1.2%) and polymer.*** The identity of the structures Ib and IIb with that obtained above was established by mixing mp. Compound III was found to be the 1 : 1 adduct of Ib and dibromocarbene from elemental analysis and molecular weight determination. In fact the reaction of Ib with phenyl(tribromomethyl)-mercury in benzene gave III in an appreciable yield. In the IR region, III exhibited a characteristic absorption at 1020 cm^{-1} which was due to the cyclopropane skeleton.[13] On comparison of the NMR spectrum of III with that of Ib, it was found that III exhibited an extra multiplet at τ 4.40 (2H), but no multiplet at τ 3.7 (1H) observed in Ib. These spectral data indicated that III was produced by the addition of carbene to methyl substituted double bond[1,14] of cyclohexa-(1,3)-diene Ib. Thus the structure of III is formulated as shown in Scheme 2. Compound IIb might be formed in the hydrolysis of Ib at work-up stage by silica gel chromatography, since IIb could not be obtained on rapid treatment of reaction mixture with silica gel chromatography. The reaction of phenyl-(tribromomethyl)mercury with large excess isonitrile gave only Ib in good yield under the conditions without hydrolysis. On the other hand, the reaction of isonitrile with large excess phenyl(tribromomethyl)mercury gave III, carbene addition product to Ib, in good yield.

The reaction of 2,4-dimethylphenylisonitrile with dibromocarbene was carried out in the same way in order to investigate the effect of methyl substituent at *ortho* positions in this cycloaddition reaction. In contrast to the reaction mentioned above, a large quantity of polymer and a small amount of indoloquinoline derivative (IV) (mp 194—195 °C, 4%) were obtained. Compound IV was found to have the composition of HBr-elimination from 2 : 1 adduct of isonitrile and dibromocarbene on the basis of elemental analysis and the mass spectrum.

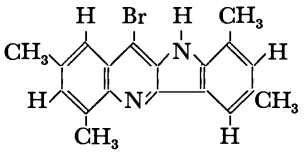

IV

In the IR region, IV exhibited characteristic absorption at 3240 cm^{-1} due to N-H stretching frequency. The UV absorption spectrum of IV showed characteristic maxima at 282 (log ε: 4.83), 350 (4.22), and 385 nm (3.67), which were similar to those of indolo (3′ : 2′—2 : 3)quinoline reported by Clemo and Felton.[15] This shows that compound IV has an indoloquinoline chromophore. The NMR spectrum exhibited five broad singlets at τ 2.05 (1H), 2.4 (1H), and 3.0 (1H) and four sharp singlets at τ 7.0 (3H), 7.45 (3H), 7.55 (3H) and 7.6 (3H). The singlet at τ 2.6 was assigned to N-H protone because of its broadness and the disappearance of the signal by addition of deuterium oxide. In fact, compound IV gave *N*-acetyl derivative (V) (mp 200—202 °C) in the reaction of IV with acetic anhydride. The other four broad signals at low field and four sharp singlets at high field were attributed to uncoupled aromatic protons and four methyl protons in a different atomosphere, respectively. Considering these spectral evidences, it was concluded that the structure of IV should be indoloquinoline derivative as shown in the figure.

The reaction of 4-methylphenylisonitrile, no substituent at *ortho* position, with dibromocarbene in the same condition as above resulted only in the formation of polymer. A similar result was obtained in the

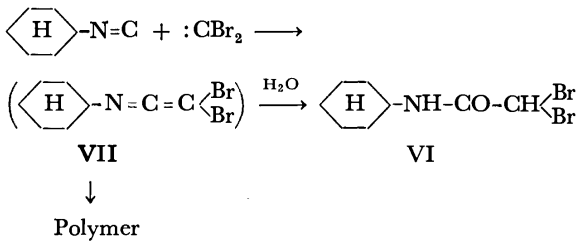

Scheme 3.

*** All polymers obtained in the reaction of arylisonitrile with dihalocarbene showed a similar absorption in the IR spectrum.

reaction of cyclohexylisonitrile with dibromocarbene, and a trace amount of *N*-cyclohexyldibromoacetamide (VI) (mp 142 °C) was isolated. Compound VI might be produced in the reaction of intermediate *N*-cyclohexyldibromoketenimine (VII) with H_2O which was present as an impurity.

When this reaction was carried out by the $CHCl_3$-*t*-BuOK method for generation of carbene, *N*-cyclohexyldibromoacetamidate was isolated as a result of the addition of *t*-BuOH or *t*-BuOK to VII[4]. The formation of polymer, main product in these cases, might also be taking a route of cationic polymerization initiated by the attack of isonitrile to ketenimine VII. This indicates that the reaction of aromatic isonitrile with dihalocarbene generated by either the CHX_3-*t*-BuOK method or the Seyferth method to give the cycloaddition products I and IV and/or polymer might proceed *via* *N*-aryldihaloketenimine intermediate VIII. In fact the reflux of *N*-(2,6-xylyl)dimethylketenimine (IX) prepared by a modification of the Stevens method[16] with 2,6-dimethylphenylisonitrile resulted in the formation of indolenine derivative (X) (mp 103 °C, 26%). The properties and spectra of compound X were essentially similar to those of I.

Thus it is clear that ketenimine VIII is the real intermediate in these cycloaddition reactions. The most reasonable mechanistic pathway of the reaction of arylisonitrile with dihalocarbene might be illustrated

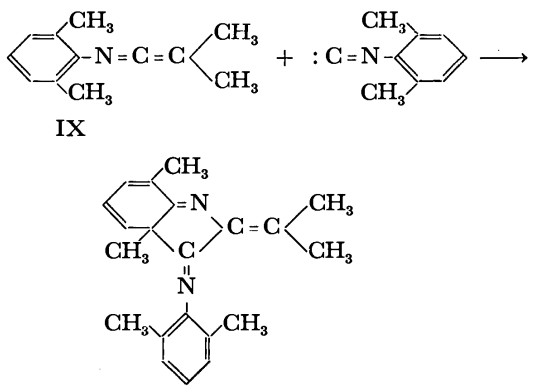

IX

Scheme 4.

by the following scheme (Scheme 5).

Indolenine Ia—Ic could be formed by 1,4-cycloaddition reaction of isonitrile to the ketenimine intermediate VIII formed by the α-addition of carbene or carbenoid† to isonitrile. The fact that the reaction of 2,6-dimethylphenylisonitrile with dihalocarbene generated by CHX_3-*t*-BuOK method gave no *N*-2,6-dimethylphenyldihaloacetamidate (XI) but indolenine derivatives I, might be due to the steric requirement of attacking species, *t*-butoxy anion and 2,6-dimethylphenylisonitrile to ketenimine VIII in the cyclization stage. It was considered that for the formation of IV primary cycloaddition products such as I caused

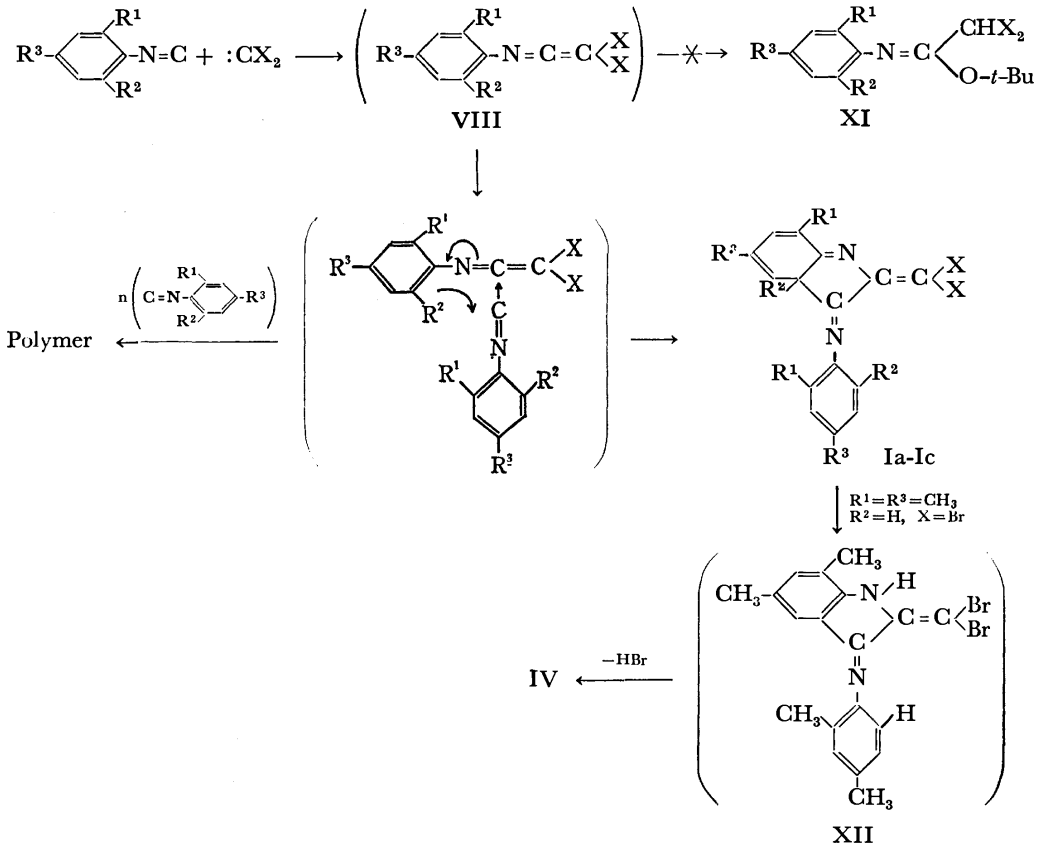

VIII XI Ia-Ic XII

Scheme 5.

† We believe that a ketenimine intermediate is formed by the reaction of isonitrile with carbene which is produced by the decomposition of Ph–Hg–CBr_3 and basic α-elimination from haloform, although other mechanisms cannot be excluded completely.

the prototropy to give indole derivative (XII), from which hydrogen bromide might be eliminated by phenyl(tribromomethyl)mercury or phenylmercuric bromide, decomposition product of carbene precursor.[17] The formation of polymer might also be taking a route of cationic polymerization initiated by the nucleophilic attack of isonitrile to ketenimine VIII, since the order of reactivity of the cationic polymerization of isonitrile,[18] *i.e.*, cyclohexyl-≳4-methylphenyl->2,4-dimethylphenyl->2,6-dimethylphenylisonitrile, was identical with that of the formation of polymer in these reactions. This reactivity of isonitrile must be controlled by the steric effect of methyl substituent at *ortho* positions.

Photolysis of Diphenyldiazomethane in the Presence of 2,6-*Dimethylphenylisonitrile.** For further investigation of the cycloaddition reaction of isonitrile with phenyl-substituted ketenimine at cumulated carbon, diphenyldiazomethane as a precursor of diphenylcarbene[1,2,7] was subjected to photolysis in the presence of 2,6-dimethylphenylisonitrile.

The *n*-hexane solution of diphenyldiazomethane and a molar equivalent of 2,6-dimethylphenylisonitrile was irradiated with a 500 W high pressure mercury lamp for 4 hr. IR absorption spectrum of the reaction mixture showed a new peak at 2020 cm^{-1} besides the peaks due to isonitrile and diazo compound. Subsequent removal of solvent at room temperature and rapid separation by means of alumina chromatography gave *N*-(2,6-xylyl)-diphenylketenimine (XIII) (mp 60—61 °C, 1%), *N*-(2,6-xylyl)-diphenylacetamide (XIV) (mp 210—211 °C, 24%) and a very small amount of 1-(2,6-dimethylphenylimino)-2-(2,6-dimethylanilino)-3-phenylindene (XV) (mp 197—198 °C). The structures of XIII and XIV were established by comparison with authentic samples prepared by a modification of the Stevens method.[16] The infrared and NMR spectra of XIII and XIV were consistent with the assigned structures. Ketenimine XIII was easily hydrolyzed by dilute hydrochloric acid or alumina to produce amide XIV in a quantitative yield. Consequently, the amide XIV corresponding to XIII was formed by hydration of ketenimine XIII on an alumina column.

The results indicate that ketenimine was formed in at least 25% yield in the photochemical reaction. We believe that the formation takes the route of photolysis of diphenyldiazomethane to produce diphenylcarbene and electrophilic attack of this carbene to isonitrile, although other mechanisms for the formation of ketenimine cannot be excluded completely.[6]

The reflex of benzene solution of equimolar mixture of ketenimine XIII and 2,6-dimethylphenylisonitrile resulted in the formation of XV in 73% yield. In the IR region, XV exhibited characteristic absorption bands at 3300, 1655 and 1620 cm^{-1} which might be attributed to N–H group, C=N or C=C double bond, respectively. The UV absorption spectrum of XV showed a characteristic peak at 272 nm (log ε: 4.61). The NMR spectra exhibited a multiplet at τ 3.0—4.0 (16H) and a singlet at τ 7.85 (12H). The structure of XV was further confirmed by the following reaction. Compound XV was hydrolyzed by

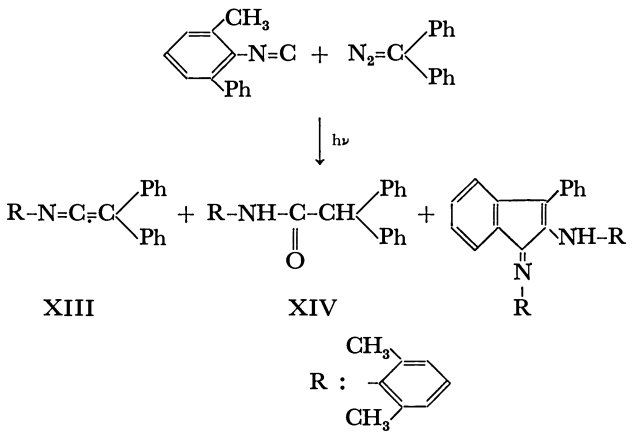

Scheme 6.

dilute hydrochloric acid in THF to give 2-(2,6-dimethylanilino)-3-phenylindone (XVI) (mp 133—134 °C) and 2,6-xylydine in good yield. The structure of XVI was established by elemental analysis, molecular weight determination and a comparison of spectral data, IR and UV, with those of known 2,3-diphenylindone.[19] Thus the structure of XV was established as shown in Scheme 6. Its formation indicated that the cycloaddition of isonitrile to ketenimine did not occur in the 2,6-dimethylphenyl ring but in phenyl ring of ketenimine preferentially in the fashion of 1,4-cycloaddition, as shown in the following scheme (Scheme 7).

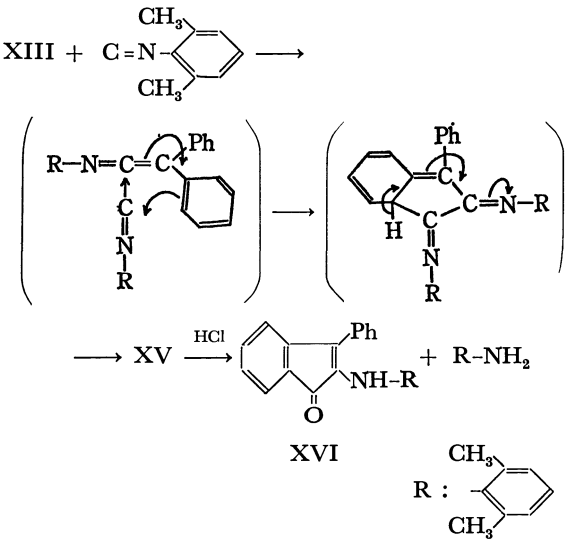

Scheme 7.

This reaction as well as that of 2,4-dimethylphenylisonitrile with dibromocarbene to give IV, *i.e.*, the cycloaddition of isonitrile to non-substituted phenyl ring, seems to show that the methyl substitution at *ortho* position did not favour the cycloaddition reaction of isonitrile to phenyl ring of ketenimine.

Also, all these cycloaddition reactions of isonitrile to ketenimine easily produced by the reaction of isonitrile with carbene seem to suggest the mechanism of the formation of indigodianil (XVII) in the oligomerization of phenylisonitrile. Grundmann[7] proposed the following mechanism for this oligomerization, the

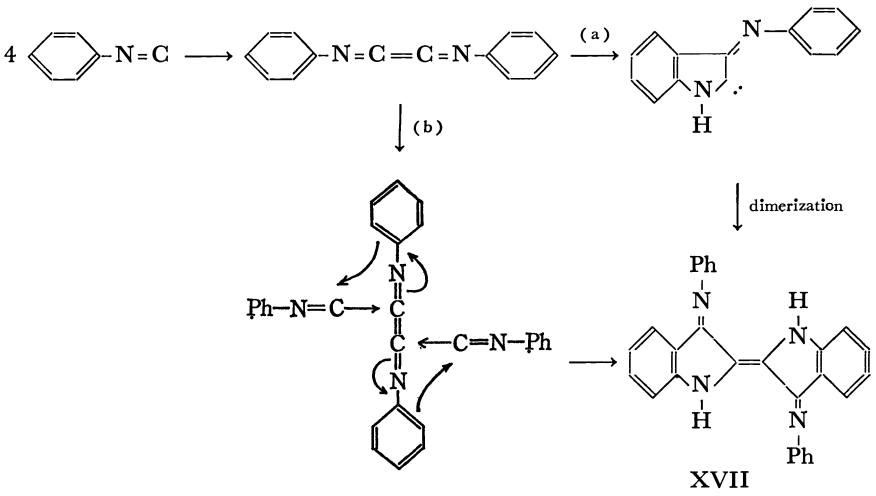

Scheme 8.

dimerization of isonitrile and intramolecular cyclization of the dimer to give carbene followed by its dimerization (path a). But the reactions we investigated so far suggest another possible mechanism, *i.e.*, dimerization and intermolecular double cycloaddition of isonitrile to cumulate double bond (path b).

In conclusion, the reaction of several methyl-substituted phenylisonitrile with dihalocarbene gave indolenine or indoloquinoline derivatives and/or polymer *via* ketenimine intermediate. This was evidenced by the reaction of *N*-(2,6-xylyl)dimethylketenimine with 2,6-dimethylphenylisonitrile to give indolenine such as I. This intermediate ketenimin was isolated only in the photolysis of diphenyldiazomethane in the presence of isonitrile, the formation of which might be taking a route of dimerization of divalent carbon, presumably diphenylcarbene and isonitrile. In the reaction of isonitrile with tri-aryl-substituted ketenimine, two possibilities to form indole and indene derivatives as the result of the cycloaddition of isonitrile to phenyl ring of ketenimine were indicated. Although the electronic effect of methyl group in these reactions does not seem to be an important factor, the steric effect of methyl substituent is supposed to play a more important role on both the direction of the cycloaddition of isonitrile to ketenimine and the reactivity of isonitrile, *i.e.*, the reactivity of cationic polymerization of isonitrile.

Experimental††

Starting Materials. Isonitrile was prepared by the I. Ugi procedure[20]. Phenyl(tribromomethyl)mercury was prepared by the Seyferth method[11].

Reaction of 2,6-Dimethylphenylisonitrile (A) with $CHCl_3$–t-BuOK, Indolenine Derivative (Ia). 2.4 g (0.02 mol) of chloroform was added, with cooling for 30 min, to a stirred suspension of 1.3 g (0.01 mol) of 2,6-dimethylphenylisonitrile and t-BuOK (0.02 mol) in 20 ml of peteroleum ether. The reaction mixture was poured into ice-water, extracted with petroleum ether, washed with water and dried, giving yellow solid. Recrystallization from ether gave 0.7 g (40%) of Ia, mp 135.5 °C. The structure of Ia was established by the following data.

Found: C, 65.80; H, 5.27; N, 8.01; Cl, 20.87%; mol. wt, 329. Calcd for $C_{19}H_{18}N_2Cl_2$; C, 66.08; H, 5.22; N, 8.11; Cl, 20.58%; mol. wt, 345. IR(KBr): 1680, 1630, 1595 cm^{-1} ($\nu_{C=C}$ or $\nu_{C=N}$). UV λ_{max}^{EtOH}: 305 (log ε: 3.99); 350 nm (4.14). NMR($CDCl_3$): τ 3.05 (m, 3H), 3.5—4.7 (m, 3H), 7.85 (s, 6H), 8.1 (s, 3H), 8.8 (s, 3H).

(B) with $CHBr_3$-t-BuOK, Indolenine Derivative (Ib). A similar reaction was carried out between 0.01 mol of 2,6-demethylphenylisonitrile and 0.02 mol of $CHBr_3$–*t*-BuOK in petroleum ether. After a similar work-up, 0.58 g (27%) yellow crystals of Ib, mp 122 °C was obtained, after recrystallization from ether–petroleum ether (1 : 1).

Found: C, 52.31; H, 4.28; N, 6.21; Br, 36.38%; mol. wt, 438. Calcd for $C_{19}H_{18}N_2Br_2$: C, 52.56; H, 4.71; N, 6.45; Br, 36.12%; mol. wt, 434. IR (KBr): 1680, 1630, 1590, 1505 cm^{-1} ($\nu_{C=C}$ or $\nu_{C=N}$). UV λ_{max}^{EtOH}: 230 (log ε: 4.30), 310 (3.86), 352 nm (4.04).

Reaction of 2,4,6-Trimethyphenylisonitrile with $CHCl_3$-t-BuOK, Indolenine derivative (Ic). A similar reaction was carried out between 1.45 g (0.01 mol) of 2,4,6-trimethylphenylisonitrile and 0.02 mol of $CHCl_3$–*t*-BuOK. The reaction mixture was poured into ice-water and extracted with ether. The extracts were washed with water and dried ($MgSO_4$). After removal of the solvent, the residue was chromatographed on a column of silica gel. Elution with hexane–benzene (3 : 2) gave yellow solid. Recrystallization of this material from ether gave 0.3 g (20%) of indolenine derivative (Ic), mp 148 °C.

Found: C, 67.41; H, 5.78; N, 7.85; Cl, 18.37%; Calcd for $C_{21}H_{22}N_2Cl_2$: C, 67.56; H, 5.94; N, 7.51; Cl, 18.72%. IR (KBr): 1680, 1615, 1600, 1520 cm^{-1} ($\nu_{C=C}$ or $\nu_{C=N}$). UV λ_{max}^{EtOH}: 230 (log ε: 4.48), 290 (4.05), 305 (3.02), 360 nm (4.12). NMR($CDCl_3$): τ 3.15 (broad s, 2H), 3.78 (broad s, 1H), 4.65 (broad s, 1H), 7.7 (s, 3H), 7.88 (s, 6H), 8.1 (s, 3H), 8.32 (s, 3H), 8.82 (s, 3H).

Hydrolysis of Ib. A solution of 100 mg (2.3 mmol) of Ib and 1 g of silica gel in 30 ml aqueous methanol was refluxed for 24 hr and allowed to stand for several days at room temperature. After silica gel chromatography, 16 mg

†† All melting points were uncorrected. IR spectra were determined using a Nihonbunko DS 402 G infrared spectrophotometer. UV spectra were recorded with a Carry 11 recording spectrophotometer. NMR spectra were obtained with a Varian A-60 spectrometer, using tetramethylsilane as an internal standard. The molecular weight was determined by use of a Hitachi 105 vapor pressure osmometer.

(15%) of amide IIb was obtained. The structure of IIb was established by the following data.

Found: C, 50.68; H, 4.65; N, 6.35; Br, 35.44%; mol. wt, 443. Calcd for $C_{19}H_{20}ON_2Br_2$: C, 50.44; H, 4.42; N, 6.19; Br, 35.39; mol. wt, 443. IR (KBr): 3400 (ν_{N-H}), 1720 ($\nu_{C=O}$), 1640 cm^{-1} ($\nu_{C=N}$). UV λ_{max}^{EtOH}: 255 nm ($\log \varepsilon$: 3.49). NMR($CDCl_3$): τ 1.43 (broad s, 1H), 3.0 (m, 6H), 4.13 (s, 1H), 7.7 (s, 6H), 7.88 (s, 6H).

Reaction of 2,6-Dimethylphenylisonitrile with Phenyl(tribromomethyl)mercury. A solution of 2.49 g (0.019 mol) of 2,6-dimethylphenylisonitrile and 5.03 g (9.5 mmol) of phenyl(tribromomethyl)mercury in 30 ml dry benzene was refluxed for 2 hr under nitrogen stream. The reaction mixture was cooled and filtered. The residue was washed with benzene and combined, and the combined benzene solution was evaporated. The residue was chromatographed on a column of silica gel. From the eluent with hexane, 1.15 g (35%) of Ib (from hexane) and 0.034 g (1.2%) of III were obtained mp 193—195 °C (from hexane). III gave the following analytical and spectral data. Found: C, 39.80; H, 2.86; N, 4.77; Br, 51.64%; mol. wt, 582. Calcd for $C_{20}H_{18}N_2Br_4$: C, 39.60; H, 2.97; N, 4.62; Br, 52.81%; mol. wt, 606. IR (KBr): 1680 ($\nu_{C=N}$), 1618 ($\nu_{C=C}$), 1020 cm^{-1} ($\nu_{cyclopropane}$). UV λ_{max}^{EtOH}: 230 ($\log \varepsilon$: 4.13), 290 nm (4.20). NMR($CDCl_3$): τ 3.05 (m, 3H) 4.4 (m, 2H), 7.85 (s, 3H), 8.05 (s, 3H), 8.4 (s, 1H), 8.75 (s, 3H).

From the eluent with benzene over 4 days, 0.92 g (22%) of IIb, mp 143 °C (from hexane) was obtained. However, IIb could not be obtained by rapid treatment with silica gel chromatography (one or two days).

When the reaction was carried out with the reverse mol ratio of 5 mmol of 2,6-dimethylphenylisonitrile to 10 mmol of phenyl(tribromomethyl)mercury, III was obtained in 10% yield. On the contrary, when 5 moles excess isonitrile to phenyl(tribromomethyl)mercury was used, the yield of Ib rose to 65% and IIb and III could not be obtained.

Reaction of Ib with Phenyl(tribromomethyl)mercury. A solution of 0.43 g (1 mmol) of Ib and 0.53 g (1 mmol) of phenyl(tribromomethyl)mercury in 30 ml dry benzene was refluxed for 2 hr under nitrogen stream. After the reaction mixture was filtered, the solvent was removed by evaporation and the residue was chromatographed on a column of silica gel. 51 mg (12%) of III and a trace amount of IIb were obtained.

Reaction of 2,4-Dimethylphenylisonitrile with Phenyl(tribromomethyl)mercury. A solution of 1.79 g (14 mmol) of 2,4-dimethylphenylisonitrile and 3.62 g (7 mmol) of phenyl(tribromomethyl)mercury in dry benzene 30 ml was refluxed for 2 hr under nitrogen stream. After work-up in the usual way and silica gel chromatography, 40 mg (2%) of IV, mp 194—195 °C (from hexane) and a large amount of polymer were obtained.

When a benzene solution of phenyl(tribromomethyl)-mercury was added to a refluxing solution of 2 equivalent isonitrile in benzene, the yield of IV rose to 4%. The structure of IV was established by the following data.

Found: C, 64.48; H, 4.98; N, 8.15; Br, 22.34%; mol. wt, (mass spectrum) 353. Calcd for $C_{19}H_{17}N_2Br$: C, 64.59; H, 4.82; N, 7.93; Br, 22.66%; mol. wt, 353. IR (KBr): 3240 cm^{-1} (ν_{N-H}). UV λ_{max}^{EtOH}: 282 ($\log \varepsilon$: 4.83), 350 (4.22), 385 nm (3.67). NMR (CCl_4): τ 2.05 (s, 1H), 2.4 (s, 1H), 2.6 (s, 1H), 3.0 (s, 1H), 7.0 (s, 3H), 7.45 (s, 3H), 7.55 (s, 3H), 7.6.

Reaction of Cyclohexylisonitrile with Phenyl(tribromomethyl)-mercury. A similar reaction was carried out between 0.9 g (8.2 mmol) of cyclohexylisonitrile and 2.19 g (4.1 mmol) of phenyl(tribromomethyl)mercury in benzene 20 ml. After silica gel chromatography, 18 mg (0.7%) of *N*-cyclohexyldibromoacetamide VI, mp 142 °C (from ether) and a large amount of polymer were obtained. Compound VI gave the following analytical and spectral data.

Found: C, 32.22; H, 4.46; N, 5.07%. Calcd for $C_8H_{13}NOBr_2$: C, 32.13; H, 4.38; N, 4.69%. IR (KBr): 3310 (ν_{N-H}), 1670 cm^{-1} ($\nu_{C=O}$).

N-acetyl Indoloquinoline V. A solution of 25 mg (0.071 mmol) of IV in 1.5 g of acetic anhydride was heated at 80 °C for 1 hr. The reaction mixture was poured into water, extracted with ether and dried ($MgSO_4$). The solvent was removed and recrystallization from ethanol gave 13 mg (47%) of *N*-acetyl indoroquinoline V, mp 200—202 °C.

Found: C, 64.04; H, 4.73; N, 7.98%. Calcd for $C_{21}H_{19}ON_2Br$: C, 63.80; H, 4.81; N, 7.09%.

Photolysis of Diphenyldiazomethane in the Presence of 2,6-dimethylphenylisonitrile. A equimolar mixture of diphenyldiazomethane 0.74 g and 2,6-dimethylphenylisonitrile 0.5 g in *n*-hexane 30 ml was irradiated with a 500 W high pressure mercury arc lamp at 15 °C in a quartz vessel. After photolysis for 4 hr, the solvent was evaporated at room temperature and the residue was subjected to alumina column chromatography. Elution with *n*-hexane gave *N*-(2,6-xylyl)diphenylketenimine (XIII), mp 61—62 °C, in 7 mg (0.7%) yield. The structure was established by the following data and by melting point determination with the authentic sample prepared by a modification of the Stevens method.[16] Compound XIII showed the characteristic infrared absorption at 2020 cm^{-1} ($\nu_{C=C=N}$).

Found: C, 89.15; H, 6.50; N, 4.97%. Calcd for $C_{22}H_{19}N$: C, 88.85; H, 6.44; N, 4.71%. Further elution with benzene gave a trace amount of purple crystalline 1-(2,6-dimethylphenylimino)-2-(2,6-dimethylanilino)-3-phenylindene (XV), mp 197—198 °C, formed by the reaction of XIII with 2,6-dimethylphenylisonitrile.

Finally *N*-(2,6-xylyl)-diphenylacetamide (XIV), mp 210—211 °C, was obtained in 0.25 g (24%) yield from the eluent with methylenedichloride. The structure of amide XIV corresponding to XIII was identified by comparison with the authentic sample prepared by the following method.

Preparation of Ketenimine: (A) N-(2,6-xylyl)dimethylketenimine(IX) was prepared by a modification of the Stevens method[16], bp 93—95 °C/0.5 mmHg. The characteristic infrared absorption was at 2020 cm^{-1} which was due to the heterocumulated double bond. (B) *N*-(2,6-xylyl)-diphenylketenimine (XIII) was also prepared by the same procedure[16]. Ketenimine XIII showed the mp 62° C (from *n*-hexane) and the characteristic infrared absorption band at 2020 cm^{-1} ($\nu_{C=C=N}$).

Reaction of 2,6-Dimethylphenylisonitrile with N-(2,6-Xylyl) dimethylketenimine (IX). Indolenine Derivative (X). A solution of 1.73 g (0.013 mol) of 2,6-dimethylphenylisonitrile and 2.29 g (0.013 mol) of *N*-(2,6-xylyl)dimethylketenimine in dry benzene 20 ml was refluxed for 6 hr. The solvent was removed and the residue was chromatograp ed on a colunm of alumina. Elution with hexane gave 0.34 g (26%) of X, mp 103 °C (from petroleum ether) and recovered isonitrile 1.18 g.

Found: C, 82.96; H, 7.95; N, 9.23%; mol. wt, 300. Calcd for $C_{21}H_{24}N_2$: C, 82.85; H, 7.95; N, 9.20%; mol. wt, 304. IR (KBr): 1665, 1635, 1625, 1595, 1535 cm^{-1}, UV λ_{max}^{EtOH}: 230 ($\log \varepsilon$: 4.24), 299 (3.95), 325 nm (3.90). NMR ($CDCl_3$): τ 3.05 (m, 3H), 3.7—4.6 (m, 3H), 7.65 (d, 6H), 7.85 (d, 6H), 8.05 (s, 3H), 8.9 (s, 3H).

Reaction of 2,6-Dimethylisonitrile with N-(2,6-Xylyl)diphenylketenimine (XIII). Indonimine Derivative (XV). A solution of 0.66 g (0.005 mol) of 2,6-dimethylphenylisonitrile and

1.50 g (0.005 mol) of *N*-(2,6-xylyl)diphenylketenimine in dry benzene 20 ml was refluxed for 3 hr. After the solvent was removed by evaporation, a precipitated purple solid was obtained. Recrystallization from hexane-methylenechloride resulted in 1.59 g (73%) of indone imine XV, mp 197—198 °C.

Found: C, 86.60; H, 6.69; N, 6.60%; mol. wt, 420. Calcd for $C_{31}H_{28}N_2$: C, 86.88; H, 6.59%; mol. wt, 429. IR (KBr): 3300 (ν_{NH}), 1655 ($\nu_{C=N}$), 1620 cm^{-1} ($\nu_{C=C}$). UV λ_{max}^{EtOH}: 272 nm (log ε: 4.61). NMR(CCl_4): τ 3.0—4.0 (m, 16H), 7.85 (s, 12H).

Hydrolysis of Indonimine XV. A solution of 0.3 g of XV in 0.3% HCl–THF (20 ml) was refluxed for 3 hr. The reaction mixture was extracted by methylenechloride. After removal of the solvent, the residue was subjected to alumina column chromatography. Elution with benzene gave 2-(2,6-dimethylanilino)-3-phenylindone XVI, mp 133—134 °C (*from petroleum ether*).

Found: C, 83.88; H, 6.07; N, 4.90%. Calcd for $C_{22}H_{19}NO$: C, 84.31; H, 6.17; N, 4.47%. IR (KBr): 3340 (ν_{N-H}), 1717 cm^{-1} ($\nu_{C=O}$). UV λ_{max}^{EtOH}: 269 (log ε: 4.36), 320 sh (3.44), 560 nm (2.80). NMR(CCl_4): τ 2.5—4.7 (m, 14H), 7.95 (s, 6H).

References

1) W. Kirmse, "Carbene Chemistry," Academic Press, New York (1964). J. Hine, "Divalent Carbon," The Ronald Press Company, New York (1964).

2) I. Ugi, "Newer Method of Preparative Organic Chemistry," Vol. IV, ed., by W. Foerest, Academic Press, New York and London (1968).

3) See for example, D. M. Lemal, E. P. Grosselind, and S. D. McGregor, *J. Amer. Chem. Soc.*, **88**, 582 (1966).

4) A. Halleux, *Angew. Chem.*, **76**, 899 (1964).

5) W. von E. Doering and K. Hoffmann, *J. Amer. Chem. Soc.*, **76**, 6162 (1954).

6) J. H. Boyer and W. Beverung, *Chem. Commun.*, **1969**, 1377. J. A. Green and L. A. Singer, *Tetrahedron Lett.*, **1969**, 5093. E. Ciganek, *J. Org. Chem.*, **35**, 862 (1970).

7) W. Madelung and M. Tencers, *Chem. Ber.*, **48**, 953 (1915). C. Grundmann, *ibid.*, **91**, 1380 (1958).

8) J. A. Deyrup, M. M. Vesting, W. W. Hagan, and H. Y. Yun, *Tetrahedron*, **25**, 1467 (1969).

9) L. M. Jackman and S. Sternhell, "Application of Nuclear Magnetic Resonace Spectroscopy in Organic Chemistry," 2nd Edition, Pergamon Press, Inc., New York, N. Y. (1969), pp. 188, 285.

10) H. A. Szymanski and R. E. Yelin, "NMR Band Handbook," IFI Plenum. New York-Washington (1968), p. 44.

11) D. Seyferth, J. M. Burlitch, *J. Organometal. Chem.*, **4**, 127 (1965).

12) D. Seyferth, J. M. Burlitch, R. J. Minasz, J. Yick-Pui Mui, H. D. Simmons, A. H. Treiber, and S. R. Dowd, *J. Amer. Chem. Soc.*, **87**, 4259 (1965).

13) L. J. Bellamy, "The Infrared Spectra of Complex Molecules," John Wiley and Sons, Inc., New York (1958), p. 29.

14) E. Chinoporos, *Chem. Rev.*, **63**, 235 (1963).

15) G. R. Clemo, D. G. I. Felton, *J. Chem. Soc.*, **1952**, 1658.

16) C. L. Stevens and J. C. French, *J. Amer. Chem. Soc.*, **76**, 4398 (1954). C. L. Stevens and G. H. Singhal, *J. Org. Chem.*, **29**, 34 (1964).

17) D. Seyferth, J. Y. P. Mui, L. J. Tood, and K. V. Darragh, *J. Organometal. Chem.*, **8**, 29 (1967).

18) T. Takizawa *et al.*, unpublished results.

19) E. D. Bergmann, *J. Org. Chem.*, **21**, 461 (1956).

20) I. Ugi and R. Meyr, *Chem. Ber.*, **93**, 239 (1960).

Synthetic Studies of Laurencin and Related Compounds. I. The Synthesis of *t*-3-Bromo-*r*-2,*c*-8-diethyl-3,4,7,8-tetrahydro-2*H*-oxocin

Tadashi MASAMUNE, Satoshi NUMATA, Hajime MATSUE, Akira MATSUYUKI, Takehiro SATO, and Hisashi MURASE

Department of Chemistry, Faculty of Science, Hokkaido University, Sapporo 060

(Received March 29, 1975)

The synthesis of the titled bromohydrooxocin (**2**), one of model compounds for synthetic approaches to laurencin (**1**), is described. *trans*- and *cis*-2,5-Diethyl-2,5-dihydrofurans (**25**), prepared by treatment of furan with bromine and then with ethyl magnesium bromide, was submitted, after oxidation with ozone, to the Robinson-Schöpf condensation with methylamine to give *trans*- and *cis*-2,4-diethylbicyclononanones (**19a** and **19b**), whose configurations were discussed on the NMR spectra. These compounds were converted into *trans*- and *cis*-diethylhydrooxocinones (**38a** and **38b**), respectively, according to a six-step process analogous to the Paquette procedure. It is to be noted that (i) thermally induced, intramolecular dienyl 1,5-hydrogen transfer (**36** to **37**), one of the key reactions in the process, took place without difficulty with *cis*-aminodiene (**36b**), while the rearrangement did not proceed smoothly with *trans*-aminodiene (**36a**), and (ii) *trans*-ketone (**38a**) was isomerized readily into *cis*-ketone (**38b**). Further hydride reduction of *cis*-ketone (**38b**) followed by bromination with carbon tetrabromide and triphenylphosphine yielded the aimed bromohydrooxocin (**2**) as a major product, which possessed the same relative configuration concerning the ring substituents as laurencin (**1**).

One decade ago, we reported the isolation and structure elucidation of laurencin (**1**), a bromine-containing, acetylenic seaweed component.[1] Many related compounds have since been identified as constituents of marine algae,[2] and these natural halogenocyclic ethers have been attractive as a synthetic target owing to their unusual skeleton. We describe herein the preparation of *t*-3-bromo-*r*-2,*c*-8-diethyl-3,4,7,8-tetrahydro-2*H*-oxocin (**2**), which possesses the same relative configuration concerning the ring substituents as laurencin (**1**). In view of the fact that the synthetic process involved no complexity due to the side chain with an enyne grouping and gave information of conformational change or isomerization caused by introduction of substituents into oxocanes,[3] this hydrooxocin (**2**) was a most useful model compound for the natural cyclic ethers.

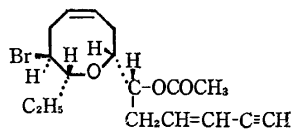

1

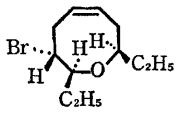

2

Although hydrooxocins are not readily accessible synthetically as compared with hydrooxoepine,[4,5] several methods for preparing the oxocins have been reported; namely, radical cyclization of olefinic alcohols,[6] dichlorocarbene homologation,[7] the Dieckmann condensation,[8] and so on.[9] In addition, Paquette and coworkers have recently published an elegant synthetic method,[10] which involves 9-methyl-9-aza-3-oxabicyclo-[3.3.1]nonan-7-one[11] (**3**) as an intermediate, prepared by the Robinson-Schöpf condensation, and leads to formation of 7,8-dihydro-2*H*-oxocin-3(4*H*)-one (**4**). While compound **4** possesses a most appropriate framework for the preparation of **2**, we first attempted to synthesize the compound in a manner analogous to the biogenesis, because "laurediols" (**5**), polyenyne glycols regarded as one of the precursors of the titled compounds, had been isolated from the seaweed.[12]

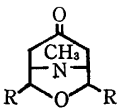

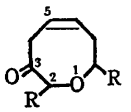

3 R=H
19a R=C_2H_5, *trans*
19b R=C_2H_5, *cis*

4 R=H
38a R=C_2H_5, *trans*
38b R=C_2H_5, *cis*

The preparation of undeca-5,8-dien-3-ol (**6**) a "laurediol" analog for **2**, was carried out as follows. The Grignard reagent from hex-1-yn-4-ol[13] (**7**) was coupled[14] with *trans*-pent-2-enyl bromide[15] (**8**) over cuprous bromide as catalyst to give *trans*-undec-8-en-5-yn-3-ol (**9**), oil, in 65% yield, which on hydrogenation over Lindler catalyst[16] afforded **6**, oil, in almost quantitative yield. Attempted cyclization reactions of **6** with lead tetraacetate or with hypobromous acid afforded complex tarry material, which resisted further purification. Compound **9** was then oxidized with

$C_2H_5CH^{t}{=}CHCH_2CH^{c}{=}CHCH_2CH(OH)R$

5 R=$CH(OH)CH_2CH{=}CH{-}C{\equiv}CH$
6 R=C_2H_5

$C_2H_5CH^{t}{=}CHCH_2C{\equiv}CCH_2CH(OH)C_2H_5$

9

$C_2H_5CH(O)CHCH_2C{\equiv}CCH_2CH(OH)C_2H_5$

10

$C_2H_5CH(O)CHCH_2CH^{c}{=}CHCH_2CH(OH)C_2H_5$

11

$C_2H_5{-}CH(OR,OH){-}CHCH_2CH^{c}{=}CHCH_2CH(OH)C_2H_5$

15 R=CH_3
16 R=C_4H_9
17 R=$CH_3C_6H_4SO_2$
18 RO=Cl

perbenzoic acid to the 8,9-epoxide (**10**), which was converted by hydrogenation under the same conditions as **9** into 8,9-epoxyundec-5-en-3-ol (**11**) in 95% yield from **9**. This was further hydrogenated over Adams platinum to give 8,9-epoxyundecan-3-ol (**12**). Treatment of **11** with potassium hydroxide in refluxing aqueous DMSO resulted in no expected cyclization and produced undeca-4,6-diene-3,9-diol (**13**). The same treatment of saturated epoxide (**12**), however, led to simple cleavage of the epoxy ring, giving undecane-3,4,9-triol (**14**), mp 91—93 °C. Likewise, unsaturated epoxide (**11**), when treated with sodium methoxide in refluxing methanol or with potassium *tert*-butoxide in refluxing *tert*-butyl alcohol, afforded the corresponding unsaturated alkoxyglycols (**15** and **16**). Furthermore treatment of **11** with acids, *p*-toluenesulfonic acid in benzene or hydrogen chloride in methanol, also effected only the cleavage of the epoxy ring to give unsaturated triol monotosylates (**17**) or diol chlorides (**18**). Thus, all attempts to cyclize **11** to hydrooxocins under various conditions failed.

The synthesis of compound **2** was then undertaken by a modification of the Paquette procedure,[10] which required the preparation of 2,4-diethyl-9-methyl-9-aza-3-oxabicyclo[3.3.1]nonan-7-ones (**19**) as key intermediates. Attempted preparation of 2,4-diethyl-3-oxaglutaraldehydes (**20**), necessary as the starting substance for **19**, by the Williamson synthesis of methyl acetal[17] of 2-hydroxybutyraldehyde (**21**) and that[17] of 2-chlorobutyraldehyde (**22**) with bases (NaH) followed by acid treatment gave only tarry material. On the other hand, the Robinson-Schöpf condensation of **21** with methylamine and acetonedicarboxylic acid afforded a basic mixture, which was expected to contain piperidone derivatives (**23**) convertible into bicyclononanones **19** by ring closure. However, attempted formation of cyclic ethers **19** by tosylation of the basic mixture followed by base treatment[18] or by acid treatement[19] again failed; only a small amount of non-basic, undecane-3,6,9-trione (**24**), mp 78—80 °C, was isolated by chromatography of the tarry product.

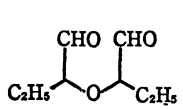

20

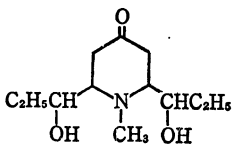

23

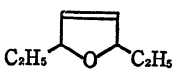

25

The synthesis of bicyclononanones **19** was finally achieved as described below. Treatment of furan (1 mol) with bromine (1 mol) at −40——45 °C in ether produced 2,5-dibromofurans,[20] which were treated with ethyl magnesium bromide (2 mol) at −40——10 °C.[21] The resulting 2,5-diethyl-2,5-dihydrofurans (**25**), bp 51—54 °C/35 mmHg, obtained in 20% yield, were ozonized at −78 °C in ethyl acetate to give oxaglutaraldehydes **20** in 70% yield. This dialdehyde mixture (**20**) reacted with methylamine and acetonedicarboxylic acid in an aqueous buffered solution of pH 5.0 at room temperature for 43 hr[11] to give basic products, from which a mixture of *trans*- and *cis*-2,4-diethylbicyclononanones (**19a** and **19b**), showing the same R_f value on tlc, was separated after chromatography. While the *trans*-isomer (**19a**), mp 89—90 °C, could be isolated in 9.8% yield from furan by fractional recrystallizations of the mixture, the *cis*-isomer (**19b**), mp 86—88 °C, was obtained in 1.8% yield in pure state as follows. The mixture of **19a** and **19b**, freed from pure **19a** obtained by the recrystallizations, was reduced with lithium aluminum hydride (LAH) to give a mixture of alcohols, from which two alcohols could be isolated by preparative tlc. The more polar alcohol (**26b**) was converted into the *cis*-ketone (**19b**) with chromic anhydride–pyridine complex in dichloromethane,[22] and the less polar alcohol (**26a**) into the *trans*-ketone (**19a**) by the same treatment (15 min). Interestingly, the latter alcohol (**26a**), when treated for a long time (overnight) under the oxidation conditions, produced *N*-formyl ketone (**27a**) in good yield. This compound (**27a**) showed two singlets (1H in total) due to a formyl proton in the NMR spectrum, which would result from slow rotation of the bond between the carbonyl carbon and nitrogen atoms.[23]

The *trans*- and *cis*-configurations of two ethyl groups in compounds **19a** and **19b** were deduced from the NMR spectra. These spectra, coupled with spin decoupling and/or contact shift [Eu(dpm)$_3$] studies, were interpreted by comparison with those of closely related compounds **28**,[24] **29**,[25] **30**[26] and **31**,[27] as well as by consideration of the influence of alkyl substituents on the chemical shifts of cyclohexane ring protons,[28] and the result is summarized in Table 1. As shown in Table 1, the signals due to equatorial and/or axial protons at C_1, C_2 and C_8 coincided with the corresponding protons at C_5, C_4 and C_6 in the spectrum of **19b**, indicating the existence of a plane of symmetry in the molecule. On the other hand, this equivalency was not observed in the spectrum of **19a**. Thus the two ethyl groups at C_2 and C_4 in question must be *cis*-oriented (β and β or α and α) in **19b**, and *trans*-oriented in **19a** (β and α or α and β). Since *cis*-2-acetoxy-4-ethyl-9-methyl-9-aza-3-oxabicyclo[3.3.1]nonan-7-one (**32**) exists in a double-chair conformation irrespective of the presence of the diaxial 2,4-substituents,[29] these and unsubstituted compounds (**19a**, **19b** and **3**) would undoubtedly adopt the double-chair conformation. The remaining problem was the conformation (and hence the configuration) of the two ethyl groups of **19b**. Judging from only the coupling constants, $J_{1,2}$ and $J_{4,5}$ (each 2 Hz) in **19b** and $J_{1,2}$ (0 Hz) and $J_{4,5}$ (2 Hz) in **19a**, it might not be unreasonable to assign equatorial conformations (α-configurations) to both the ethyl groups of the *cis*-isomer (**19b**). However, the constants in question depend delicately on the whole conformational change.[26] Furthermore, the ethyl methylene protons of **19b** (*cis*) appeared at remarkably low fields, as compared with those of **19a** (*trans*), the difference in δ-value being 0.20—0.35 ppm. In general, axial methyl protons at the α-carbon atom in oxacyclohexane systems absorb at lower fields than the corresponding equatorial protons[30] and are also deshielded when disposed 1,3-diaxially (*syn*-axially) to other methyl protons[31] and/or nitrogen lone pair electrons.[32] These facts strongly suggested that each of the relevant ethyl groups in **19b** would probably take an axial (and

TABLE 1. THE NMR SPECTRA OF 9-METHYL-9-AZA-3-OXABICYCLO[3.3.1]NONAN-7-ONES[a)]

Protons	Chemical shift (δ) Compounds			J	Coupling constants[b,c)] (Hz) Compounds		
	3	**19a**	**19b**		**3**	**19a**	**19b**
H_1	3.00 br d,	2.76 br d,	2.82 br d,	$J_{1,2e}$	0.0	0.0	2.0
H_5	3.00 br d,	2.76 br d,	2.82 br d,	$J_{5,4e}$	0.0	—	2.0
H_{2e}	3.62 d,	3.36 do d,	3.00 do t,	$J_{1,2a}$	1.0	—	—
H_{4e}	3.62 d,	— —	3.00 do t,	$J_{5,4a}$	1.0	2.0	—
H_{2a}	3.71 br d,	— —	— —	$J_{1,8e}$	0.0	0.0	0.0
H_{4a}	3.71 br d,	3.57 do do d,	— —	$J_{5,6e}$	0.0	0.0	0.0
H_{6e}	2.12 d,	1.96 d,	1.92 d,	$J_{1,8a}$	6.0	6.0	6.0
H_{8e}	2.12 d,	2.04 d,	1.92 d,	$J_{5,6a}$	6.0	4.0	6.0
H_{6a}	2.61 do d,	2.55 do d,	2.51 do d,	$J_{2,H}$	—	8.0	6.5
H_{8a}	2.61 do d,	2.30 do d,	2.51 do d,			6.0	6.5
			1.62 qui,	$J_{4,H}$	—	9.0	6.5
$CH_3\underline{CH_2}$	— —	1.40 m,	1.60 qui,			5.0	6.5
$\underline{CH_3}CH_2$	— —	0.89 t,	0.89 t,	$J_{6a,6e}$	15.5	15.5	15.5
$N\underline{CH_3}$	2.56 s,	2.48 s,	2.61 s,	$J_{8a,8e}$	15.5	15.5	15.5

a) The spectra were measured in CCl_4 at 100 MHz, and the abbreviations "H_{2e} and $J_{1,2e}$" refer to "equatorial proton at C_2 and coupling constant between H_1 and H_{2e}," respectively. b) The coupling constants were estimated by first-order approximations. c) The coupling constant, $J_{2a,2e}$ and $J_{4a,4e}$, in compound **3** were 11.5 and 11.5 Hz.

hence a β-configuration) rather than an equatorial conformation. The spectrum of the *trans*-isomer(**19a**) could be understood well on the same ground. This conformational assignment was consistent with that to the 7-deoxo derivatives (**33a** and **33b**) of **19a** and **19b**, which would also exist in a double-chair conformation; that is, the C_2- and C_4-proton signals were observed at δ 3.46 and 3.68 in the NMR spectrum of the *trans*-isomer (**33a**), while the corresponding signals coincided and appeared at higher field, δ 3.14, in that of *cis*-isomer (**33b**). The ethyl methylene protons in question of the *trans*-isomer (**33a**) were found by spin decoupling studies to be coupled to these C_2 and C_4 protons at higher field (near δ 1.35) than those of the *cis*-isomer **33b** (near δ 1.70).

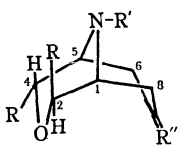

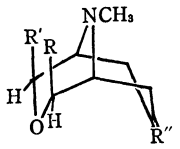

19a R=C_2H_5, R'=CH_3, R''=O
19b R=R'=C_2H_5, R''=O
26a R=C_2H_5, R'=CH_3, R''=β-H, α-OH
26b R=R'=C_2H_5, R''=β-H, α-OH
27a R=C_2H_5, R'=CHO, R''=O
32b R=CH_2OCOCH_3, R'=C_2H_5, R''=O
33a R=C_2H_5, R'=CH_3, R''=H_2
33b R=R'=C_2H_5, R''=H_2

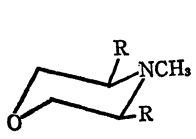

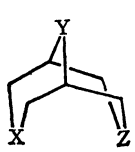

28 R=H
29 R=CH_3
30 X=O, Y=Z=CH_2
31 X=CH_2, Y=NCH_3, Z=O

Compound **19a** was reduced with lithium aluminum hydride in refluxing ether to give an epimeric alcohol mixture, consisting mainly of α-alcohol[11,26)] (**26a**). This alcohol mixture was dehydrated with sulfuric acid in acetic acid at 155 °C[33)] and produced a mixture of diastereoisomeric olefins (**34a**) in 95% yield from **19a**. This olefin mixture (**34a**) was converted quantitatively into the saturated *trans*-compound (**33a**) by hydrogenation over platinum in ethanol. Likewise, *cis*-ketone (**19b**) was convered into an epimeric alcohol mixture (main, **26b**) and then dehydrated under the comparable conditions to give an olefin (**34b**) in 90% yield, which on hydrogenation formed the *cis*-saturated compound (**33b**).

trans- and *cis*-Olefins (**34a** and **34b**) were converted into the corresponding methiodides, *trans*- (**35a**, a mixture of diastereoisomers), mp 179—182 °C, and *cis*-isomers (**35b**), mp 190—191 °C. These methiodides were submitted to the Hofmann degradation under the carefully controlled conditions to give *trans*- (**36a**, a mixture of diastereoisomers), oil, and *cis*-2,8-diethyl-3-dimethylamino-3,8-dihydro-2*H*-oxocins (**36b**), oil, in good yields, respectively.

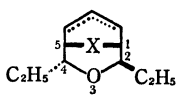

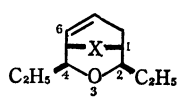

34a X=NCH_3
34b X=NCH_3
35a X=$\overset{+}{N}(CH_3)_2$ I^-
35b X=$\overset{+}{N}(CH_3)_2$ I^-

Heating of *cis*-aminodiene (**36b**), with 3-dimethylamino, and 2- and 8-ethyl groups all β-oriented, at 120—125 °C for 15 min resulted in facile intramolecular dienyl 1,5-hydrogen transfer, giving *cis*-dienamine (**37b**), oil, as a single product in almost quantitative yield. To the contrary, conversion of a mixture of *trans*-aminodienes (**36a**), one with the three groups β-, α- and β-oriented and the other with those β-, β- and

α-oriented, into the desired *trans*-dienamine (**37a**), oil, did not proceed smoothly as expected under the comparable conditions. The product was a multi-component mixture including **37a**, which was estimated to account for at most 60% of the total bases under the best conditions examined. The difference in reactivity between *trans*- and *cis*-aminodienes (**36a** and **36b**) indicated that this thermally induced, α-oriented-hydrogen shift from C_3 to C_7 in *trans*-isomer (**36a**), presumably concerted and suprafacial [1,5] sigmatropic rearrangement,[34] would be hindered by the presence of an α-oriented ethyl group either at C_2 or C_8.[35]

These *trans*- (without further purification) and *cis*-dienamines (**37a** and **37b**) were hydrolyzed in refluxing dil fluoroboric acid and produced *trans*- and *cis*-2,8-diethylhydrooxocinones (**38a** and **38b**), both oil, in 18 and 45% yields from bicyclononanones (**19a** and **19b**), respectively. In accordance with the assigned structures, both β,γ-unsaturated ketones (**38a** and **38b**) displayed absorption maxima near 310 nm (ε= 50—200) and near 1715 and 1650 cm^{-1} in the UV and IR spectra. Interestingly, the UV absorption intensity (ε 90—162) of the latter (**38b**) was about twice stronger than that (50—100) of the former (**38a**), indicative of larger overlap of π-electrons of the double bond and carbonyl group in *cis*-isomer (**38b**) as compared with that in *trans*-isomer (**38a**).

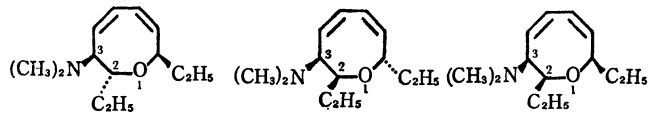

36a **36b**

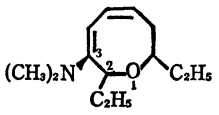

37a *trans*
37b *cis*

The NMR spectra of these isomers (**38a** and **38b**) indicated a noteworthy difference concerning the C_4-protons. The protons of the latter (**38b**) appeared at δ 2.78 and 3.82 as two doublets with the same vicinal coupling constants of 6 Hz ($J_{4,5}$), while those of the former (**38a**) at δ 2.93 and 3.52 as two double doublets with different vicinal coupling constants ($J_{4,5}$) of 3 and 2 Hz. If the Karplus equation[36] held for the constants in question, the observed values suggested that the dihedral angles between the C_4- and C_5-protons would become about 30° and 150° in the *cis*-isomer (**38b**), and the corresponding angles about 65° and 55° in the *trans*-isomer (**38a**). These angles implied that the olefinic proton at C_5 in *cis*-isomer (**38b**) would be located in the outer side of two planes formed by the two carbon at C_4 and C_5 and each of two hydrogen atoms at C_4 and that in *trans*-isomer (**38a**) in the inner side of the planes. On the other hand, the two ethyl groups would reasonably be oriented towards the outer side of the ring in each of the isomers so as to decrease the possible serious steric interaction. Examination of

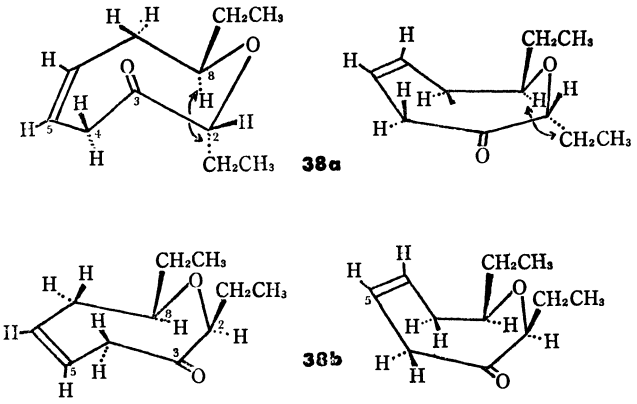

38a **38b**

Fig. 1.

the Dreiding model, considering these dispositions as well as the UV intensities, indicated that only two forms as shown in Fig. 1 were possible as plausible conformations for each of the *trans*- and *cis*-hydrooxocinones (**38a** and **38b**). These conformations suggested that the *trans*-ketone (**38a**) would be less stable than the *cis*-ketone (**38b**), because the α-ethyl group in either one of **38a** (Fig. 1) would be disposed 1,3-*syn*-axially to the α-oriented α-hydrogen to the oxygen atom. As expected, the *trans*-ketone (**38a**) was readily epimerized to the *cis*-isomer (**38b**) by treatment with base (5% KOH in ethanol, room temperature, 20 min) almost quantitatively. This isomerization was most valuable for further investigations, because the two side chains at C_2 and C_8 of laurencin (**1**) possesses the *cis*-configuration.

Reduction of *cis*-diethylhydrooxocin (**38b**) with sodium borohydride produced a mixture of alcohols, from which epimeric alcohols (**39** and **40**) were isolated after chromatography in 50 and 15% yields, respectively. These alcohols (**39** and **40**) displayed characteristic peaks due to one of the C_4-protons and the C_3-proton in the NMR spectra; the major alcohol (**39**) showed a double doublet (J=8 and 12 Hz) and a multiplet at δ 2.63 and 3.68, and the minor alcohol (**40**) a double doublet (J=3, 7 and 13 Hz) and a double triplet (J= 3, 3 and 9 Hz) at δ 2.81 and 3.75, respectively. The observed signal patterns in the latter (**40**), apart from the chemical shifts, were completely superimposable over those of the corresponding protons (C_4- and C_3-protons) in laurencin (**1**), indicating that the minor alcohol (**40**) possessed the same relative configuration as to the three substituents as **1**, while the major alcohol (**39**) took the different configuration only at the carbon atom bearing the hydroxy group.

The major alcohol (**39**) was then treated with carbon tetrabromide and triphenylphospine to give bromohydrooxocin (**2**), oil, as an only isolable product in moderate yield, which showed a pair of molecular ion peaks at *m/e* 248 and 246 in the mass spectrum. Since this bromination usually proceeds in S_N2 manner,[37] the C_3-configuration of **2** was expected to be inverted. In fact, compound **2** revealed a clear, double triplet with coupling constants of 3, 3 and 9 Hz at δ 4.05 due to the C_3-proton, though the C_4-proton in question near δ 3.15 was not discernible as a separate peak owing to overlap with the C_2- and C_8-protons. Thus, bromodiethylhydrooxocin (**2**) took the same relative

configuration concerning the three substituents at C_2, C_3 and C_8 as the aimed natural compound, laurencin (**1**).

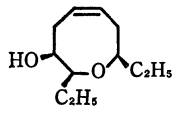

39

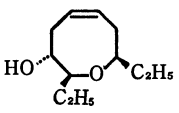

40

Experimental

All the mps and bps were uncorrected. The homogenity of each compound was always checked by tlc over silica gel (Wakogel B-5) and/or by glc (Hitachi K-53) over 10% SE-30. Column chromatographies were carried out over silicic acid (Merck, Kieselgel 60 or Mallinckrodt, silicic acid 100 Mesh). The UV and IR spectra were measured in ethanol and carbon tetrachloride, respectively, unless otherwise stated. The NMR spectra were obtained in carbon tetrachloride, unless otherwise stated, at 100 MHz, and the chemical shifts were given in δ-values, TMS being used as an internal standard. The abbreviations "s, d, t, q, qui, m, br, and do" in the NMR spectra denote "singlet, doublet, triplet, quartet, quintet, multiplet, broad, and double," respectively.

*(E)-Undec-8-en-1-yn-3-ol (**9**).* A stirred solution of hex-1-yn-4-ol[13] (**7**, 5.5 g) in anhydrous ether (50 ml) was mixed with ethyl magnesium bromide, prepared from ethyl bromide (13 g) and magnesium turnings (2.8 g) in ether (90 ml), and refluxed until evolution of ethane ceased. To the mixture cooled at 0 °C were added *trans*-pent-2-enyl bromide[15] (**8**) (9.4 g) and anhydrous cuprous chloride (0.6 g).[14] The whole mixture was refluxed for 2.5 hr, then stirred at room temperature for 14 hr and, after being cooled, treated with aqueous saturated ammonium chloride. After separation of the ether layer, the aqueous layer was extracted with ether repeatedly. All the ether solutions were combined, washed with 1 M hydrochloric acid, 5% aqueous sodium bicarbonate and water, dried over sodium sulfate, and evaporated to leave oil, which was distilled to give **9** (6.12 g), bp 111—114 °C/20 mmHg; IR, ν_{max} 3540, 2200, 1061, and 967 cm^{-1}; NMR (CCl_4 and D_2O), δ 0.93 and 0.98 (total 6H, each t J=7 Hz, $2CH_2CH_3$), 1.49 and 2.02 (each 2H, qui J=7 Hz, CH_2 at C_2 and C_{10}), 2.28 and 2.82 (each 2H, m, CH_2 at C_4 and C_7), 3.55 [1H, qui J=6.5 Hz, CH(OH)], 5.30 and 5.64 (each 1H, do t, J=14, 5, 5 and 14, 7, 7 Hz, CH=CH). Found: C, 79.35; H, 10.68%. Calcd for $C_{11}H_{18}O$: C, 79.46; H, 10.92%.

The acetate (**9a**) was prepared quantitatively by treatment of **9** (0.1 g) with acetic anhydride (1.0 ml) and pyridine (1.0 ml) at room temperature overnight; IR ($CHCl_3$), ν_{max} 1730, 1021, and 965 cm^{-1}; NMR, δ 1.97 (3H, s, $OCOCH_3$), and 4.72 [1H, qui, J=6.5 Hz, $CH(OCOCH_3)$].

*(5Z,8E)-Undeca-5,8-dien-3-ol (**6**).* Hydrogenation of **9** (1.0 g) was carried out over Lindlar catalyst[16] (1.5 g) at room temperature in ethanol and ceased after 1.5 hr, when 150 ml of hydrogen (1.0 mol) had been consumed. After removal of the catalyst and solvent, the residue was dissolved in dichloromethane, washed with saturated sodium chloride and water, dried and evaporated to dryness to give **6** (1.0 g); IR, ν_{max} 3570, 3470, 1015, and 968 cm^{-1}, NMR (CCl_4 and D_2O), δ 0.93 and 0.97 (total 6H, each t J=6.5 Hz, $2CH_2CH_3$), 1.41 (2H, qui J=6.5 Hz, CH_2 at C_2), 1.96 (2H, m, CH_2 at C_{10}), 2.16 (2H, t J=6.5 Hz, CH_2 at C_4), 2.73 (2H, br t J=4.5 Hz, CH_2 at C_7), 3.45 [1H, qui J=6.5 Hz, CH(OH)], and 5.38 [4H, m, 2(CH=CH)]. Found: C, 78.78; H, 11.80%. Calcd for $C_{11}H_{20}O$: C, 78.51; H, 11.98%.

*(Z)-8,9-Epoxyundec-5-en-3-ol (**11**).* To a solution of **9** (2.5 g) in chloroform (60 ml) was added perbenzoic acid (3.0 g) at 0 °C, and the solution was allowed to stand in a refrigerator for 20 hr. The reaction mixture was worked up as usual to yield 8,9-epoxyundec-5-yn-3-ol (**10**, 2.7 g); IR ($CHCl_3$), ν_{max} 3420, 974, 939, 908, and 878 cm^{-1}; NMR ($CDCl_3$ and D_2O), δ 0.94 and 0.99 (total 6H, each t J=7 Hz, $2CH_3CH_2$), 1.57 and 1.60 (total 4H, each qui J=6.5 Hz, $2CH_3CH_2$), 2.40 (4H, m, $2CH_2$ at C_4 and C_7), 2.84 (2H, m, 2CH at C_8 and C_9), 3.62 [1H, qui J=6.5 Hz, CH(OH)]. Found: C, 71.35; H, 11.16%. Calcd for $C_{11}H_{20}O_2$: C, 71.59; H, 10.94%.

Compound **10** (1.4 g) was hydrogenated over Lindlar catalyst (2.3 g) in the same manner as **9** and afforded **11** (1.35 g); IR, ν_{max} 3440, 974, and 888 cm^{-1}; NMR (CCl_4 and D_2O), δ 0.92 and 0.96 (total 6H, each t J=6 Hz, $2CH_3CH_2$), 1.42 (4H, m, $2CH_3CH_2$), 2.22 (4H, m, $2CH_2$ at C_4 and C_7), 2.62 (2H, m, 2CH at C_8 and C_9), 3.43 [1H, qui J=6 Hz, CH(OH)], and 5.48 (2H, m, CH=CH). Found: C, 70.68; H, 12.16%. Calcd for $C_{11}H_{22}O_2$: C, 70.92; H, 11.90%.

*8,9-Epoxyundecan-3-ol (**12**).* Compound **11** (320 mg) in ethanol (10 ml) was hydrogenated over Adams platinum (105 mg as $PtO_2 \cdot H_2O$) at room temperature. The reaction was ceased after 1.5 hr, when 44 ml of hydrogen (1.0 mol) had been absorbed. After being worked up as usual, the reaction mixture gave **12** (330 mg); IR ($CHCl_3$), ν_{max} 3590, 3430, 960, and 893 cm^{-1}. Found: C, 69.88; H, 12.68%. Calcd for $C_{11}H_{24}O_2$: C, 70.16; H, 12.85%.

*Undeca-4,6-diene-3,8-diol (**13**).* A solution of **11** (60 mg) in a mixture of dimethyl sulfoxide (DMSO, 20 ml), potassium hydroxide (1 g) and water (10 ml) was heated at 155—160 °C for 3 hr. After being cooled, the reaction mixture was poured onto ice and extracted with chloroform repeatedly. The chloroform extracts were washed with 2 M hydrochloric acid, 5% aqueous sodium bicarbonate and saturated aqueous sodium chloride, dried over magnesium sulfate and evaporated to give **13** (53 mg); IR, ν_{max} 3530, 3370, 1055, 990, and 951 cm^{-1}, which was treated with acetic anhydride (0.6 ml) and pyridine (0.6 ml) at room temperature for 4.5 hr to yield the diacetate (**13a**, 56 mg); UV, λ_{max} 231 nm (ε 15600); IR, ν_{max} 1736, 1224, and 1007 cm^{-1}; NMR, δ 0.90 and 0.92 (total 6H, each t J=6.5 Hz, $2CH_3CH_2$), 1.58 (4H, br m, $2CH_3CH_2$), 1.97 and 2.01 (total 6H, each s, $2CH_3COO$), 2.41 (2H, br t J=6.5 Hz, CH_2 at C_4), 4.77 and 5.28 [each 1H, qui and q J=6.5 Hz, $2CH(OCOCH_3)$], and 4.30 (4H, m, 2CH=CH). Found: C, 66.86; H, 9.11%. Calcd for $C_{15}H_{24}O_4$: C, 67.13; H, 9.02%.

*Undecane-3,4,9-triol (**14**).* Compound **12** (200 mg) was treated with the afore-mentioned alkaline DMSO solution (45 ml) in the same manner as **11**. The reaction mixture was worked up as usual to leave oily residue, which showed a practically single spot on tlc and crystallized on trituration with ether. The crystalline material was recrystallized from ether-hexane to give **14** (45 mg), mp 91—93 °C; IR (Nujol), ν_{max} 3280, 1072, and 969 cm^{-1}. Found: C, 64.80; H, 11.68%. Calcd for $C_{11}H_{24}O_3$: C, 64.71; H, 11.76%.

The triacetate (**14a**) showed the following spectra; IR ($CHCl_3$), ν_{max} 1723 cm^{-1}; NMR, δ 0.88 and 0.90 (total 6H, each t J=7 Hz, $2CH_3CH_2$), 1.45 (12H, br m, $6CH_2$), 2.03 (9H, s, $3CH_3COO$), and 4.85 [3H, br m, $3CH(OCOCH_3)$].

*Treatment of **11** with Sodium Methoxide.* Compound **11** (115 mg) was refluxed in a methanol solution containing sodium methoxide, prepared from sodium (345 mg) and methanol (15 ml), for 18 hr. The mixture was worked up as usual to give oil, which showed a single spot on tlc and

was identified as unsaturated methoxyglycols (**15**) on the spectral data; IR, ν_{max} 3420 and 1100 cm^{-1}; NMR (CCl_4 and D_2O), δ 0.93 (6H, t J=7 Hz, $2C\underline{H}_3CH_2$), 1.45 (4H, br m, $2CH_3C\underline{H}_2$), 2.18 (4H, br m, $2C\underline{H}_2CH{=}CH$), 3.33 (3H, s, $C\underline{H}_3O$), 3.52 (3H, br, 3C$\underline{H}$ at C_3, C_4 and C_9), and 5.48 (2H, m, C$\underline{H}$=C$\underline{H}$).

Treatment of ***11*** *with* p-*Toluenesulfonic Acid.* A solution of **11** (400 mg) in dry benzene (35 ml) containing *p*-toluenesulfonic acid (38 mg) was refluxed for 20 hr and, after being cooled, washed with a 5% sodium bicarbonate solution, dried and evaporated to leave oil (380 mg), which was found to consist of two components by tlc. The oil was separated into two fractions by chromatography over silicic acid (Mallinckrodt, 10 g) with a 3 : 1 mixture of benzene and ethyl acetate. The more polar fraction (197 mg) was identical with the unreacted starting epoxide **11**, and the less polar was identified as undecenetriol monotosylate(s) (**17**, 87 mg); IR, ν_{max} 3360, 1188, and 1176 cm^{-1}; NMR, δ 0.92 (6H, t J= 6.5 Hz, $2C\underline{H}_3CH_2$), 1.32 and 2.06 (4H and 2H, br, $3C\underline{H}_2$), 2.43 (3H, s, $C\underline{H}_3C_6H_4$), 3.50 [2H, m, 2C$\underline{H}$(OH)], 4.40 [1H, m, C$\underline{H}(OSO_2)$], 4.61 (2H, br s, 2O$\underline{H}$), 5.43 (2H, br, C$\underline{H}$=C$\underline{H}$), and 7.25 and 7.75 (each 2H, ABq J=8.5 Hz, $C_6\underline{H}_4$).

*The Robinson-Schöpf Condensation of 2-Hydroxybutyraldehyde (****21****) Followed by Acid Treatment.* The aldehyde (**21**) was prepared from the dimethyl acetal[17]; IR, ν_{max} 3600, 3490, 1079, 1062, and 970 cm^{-1}; NMR, δ 0.93 (3H, t J=7 Hz), 2.40 (1H, br s, disappeared on addition of D_2O), 3.32 and 3.37 (each 3H, s), and 4.03 (1H, d J=6 Hz), and was used for the next reaction without isolation. A solution of the acetal (13.5 g) in acetic acid (2.5 ml) and water (10 ml) was refluxed for 50 min and, after being cooled, poured into an aqueous solution (125 ml) containing anhydrous disodium phosphate (14.6 g) and citric acid (9.4 g). After addition of methylamine hydrochloride (6.1 g) and acetonedicarboxylic acid (14.6 g), the solution was adjusted to pH 5.0 by addition of aqueous sodium hydroxide, then diluted with water to 250 ml of the total volume, and stirred at room temperature for 48 hr. The solution was made acidic and shaken with dichloromethane to remove neutral and acidic substances. The acidic solution was made strongly basic and extracted with dichloromethane repeatedly. The dichloromethane solutions were combined and evaporated to leave dark brown oil, which was mixed with 20% sulfuric acid (20 ml). The mixture was refluxed for 2 hr, cooled, made basic, and again extracted with dichloromethane. The extracts were dried and evaporated to leave brown oil (3.9 g), which was chromatographed over silicic acid (Mallinckrodt, 100 g), using benzene–ethyl acetate (6 : 1). Several fractions gave crystalline material, which on recrystallization from hexane yielded undecane-3,6,9-trione (**24**) (0.34 g), mp 78—80 °C; IR ($CHCl_3$), ν_{max} 1714 cm^{-1}; NMR ($CDCl_3$), δ 1.05 (6H, t J= 7 Hz), 2.47 (4H, q J=7 Hz), and 2.70 (8H, s). Found: C, 66.62; H, 9.03%. Calcd for $C_{11}H_{18}O_3$: C, 66.67; H, 9.09%.

Compound **24** (55 mg) in dry methanol (10 ml) was reduced with sodium borohydride (100 mg) at 0 °C for 35 min and afforded oily alcohol (64 mg), which was treated with acetic anhydride (1.0 ml) and pyridine (1.5 ml) at room temperature overnight to give undecane-3,6,9-triol triacetate (88 mg), oil; IR, ν_{max} 1741, 1247, and 1018 cm^{-1}; NMR ($CDCl_3$), δ 0.88 (6H, t J=7 Hz), 2.02 (9H, s), and 4.81 (3H, m W_H=14 Hz). Found: C, 61.58; H, 9 02%. Calcd for $C_{17}H_{30}O_6$: C, 61.79; H, 9.15%. The triacetate (78 mg) was hydrolyzed with 5% potassium hydroxide in refluxing methanol (45 min) to give the triol (50 mg), which was reconverted into **24** (37 mg), mp 78—79 °C, by oxidation with Jones reagent (0.5 ml) in acetone (8 ml) at 0 °C for 1.75 hr.

trans- *and* cis-*2,5-Diethyl-2,5-dihydrofurans (****25****).* To a solution of freshly distilled furan (42 g) in ether (800 ml) cooled at −45 °C was dropwise added bromine (28 ml), and the solution was stirred at the temperature for 10 min. To the solution was added the Grignard reagent, prepared from ethyl bromide (210 g) and magnesium turnings (40.0 g) in ether (1000 ml), under stirring at such a rate that the temperature did not exceed −10 °C, and the whole mixture was kept at room temperature overnight. After careful addition of water under cooling to decompose excess of the Grignard reagent, the ether layer was separated, and the aqueous layer was extracted with ether. The ether solutions were combined, washed with water, dried and evaporated to leave oily residue, which was distilled to give **25** (25.0 g), bp 51—54 °C (35 mmHg); δ 0.88 (6H, t J=7 Hz), 1.50 (4H, m), 4.65 (2H, m), and 5.70 (2H, s). Found: C, 76.36; H, 11.02%. Calcd for $C_8H_{14}O$: C, 76.14; H, 11.18%.

trans- *and* cis-*2,4-Diethyl-9-methyl-9-aza-3-oxabicyclo[3.3.1]-nonan-7-ones (****19a*** *and* ***19b****).* Into a solution of **25** (11.0 g) in ethyl acetate (350 ml) cooled at −78 °C was bubbled ozone, until the solution became purplish. The solution was treated with potassium iodide and then with aqueous sodium thiosulfate at room temperature. The acetate solution was separated and the aqueous layer was extracted with ethyl acetate. The ethyl acetate solutions were combined, washed with water, dried and evaporated to leave crude 2,4-diethyl-3-oxaglutaraldehydes (**20**) (9.6 g), IR ($CHCl_3$), ν_{max} 1730 cm^{-1}, which were used for the next reaction without further purification.

To an aqueous solution (100 ml) containing anhydrous disodium phosphate (14.6 g) and citric acid (9.4 g) were added the crude aldehydes (**20**) (9.6 g), methylamine hydrochloride (6.1 g) and acetonedicarboxylic acid (14.6 g). The whole solution was adjusted to pH 5.0 by addition of conc sodium hydroxide solution, diluted with water to 250 ml of the total volume, and then stirred at room temperature for 43 hr. The reaction mixture, after being made acidic, was washed with ether, made basic and then extracted with chloroform repeatedly. The chloroform solutions afforded dark brown oil (8.4 g), which was separated by chromatography over alumina (Merck, 200 g), using benzene, benzene–ether (2 : 1, 1 : 1 and 1 : 2) and ether, successively. Fractions eluted with benzene and benzene–ether (2 : 1 and 1 : 1) gave oily (4.6 g) and crystalline bases (4.2 g), showing the same single spot on tlc. The latter was recrystallized twice from hexane to yield **19a** (2.5 g), mp 89—90 °C; Mass, *m/e* 211 (M^+) and 110 (base); IR (Nujol), ν_{max} 1705, 1164, 1059, 983, 908 and 843 cm^{-1}; NMR (Table 1). Found: C, 68.47; H, 10.29; N, 6.60%. Calcd for $C_{12}H_{21}O_2N$: C, 68.21; H, 10.02; N, 6.63%.

The remaining bases (1.7 g), obtained on the recrystallizations, were combined with the oily bases (4.6 g) and reduced with LAH (2.3 g) in ether (300 ml) at room temperature overnight and, after being worked up as usual, afforded a mixture of alcohols (6.3 g). These alcohols were separated into three fractions, more polar (0.5 g), middle (main **26b**, 1.8 g) and less polar fractions (main **26a**, 3.6 g), by preparative tlc (80 plates) over silica gel (Wakogel B-5), using ethanol as solvent; each plate was made of the gel (10 g) with area of 20×20 cm. The middle fractions (1.8 g) were oxidized with chromium trioxide (2.8 g), celite (4.5 g) and pyridine (4.5 ml) in dichloromethane (75 ml) at room temperature for 15 min. After removal of the celite by filtration, the dichloromethane solution was evaporated to leave oily residue, which was dissolved in chloroform and then extracted with dil hydrochloric acid. The acidic solution, after being

made basic, was extracted with chloroform repeatedly. The chloroform solution was washed with water, dried and evaporated to give crystalline substance, which on recrystallization from hexane yielded **19b** (1.0 g), mp 86—88 °C; Mass, *m/e* 211 (M^+) and 110 (base); IR (Nujol), ν_{max} 1714, 1167, 1026, 973, 917, and 853 cm^{-1}; NMR (Table 1). Found: C, 68.32; H, 10.20; N, 6.60%. Calcd for $C_{12}H_{21}O_2N$: C, 68.21; H, 10.02; N, 6.63%. The less polar fractions (3.6 g) were oxidized under the same conditions as mentioned above to give **19a** (1.9 g), mp 89--90 °C.

trans-*2,4-Diethyl-9-formyl-9-aza-3-oxabicyclo[3.3.1]nonan-7-one (27a).* A solution of the crude *trans*-alcohol (main **26a**, 0.97 g) in pyridine (30 ml) was treated with chromium trioxide (3.0 g) at room temperature overnight and poured into ice-water. After being worked up as usual, the reaction mixture gave crude amide (0.88 g), which was purified by chromatography over silicic acid to yield **27a** (0.63 g), oil; Mass, *m/e* 225 (M^+); IR ($CHCl_3$), ν_{max} 1722 and 1663 cm^{-1}; NMR ($CDCl_3$), δ 8.12 and 8.26 (each s, total 1H).

trans-*2,4-Diethyl-9-methyl-9-aza-3-oxabicyclo[3.3.1]nonanes (34a).* A solution of **19a** (5.55 g) in ether (50 ml) was refluxed with LAH (2.0 g) for 16 hr. After addition of water, the resulting precipitate was removed by filtration and washed with ether. The filtrate was separated into aqueous and ether layers, and the aqueous layer was extracted with ether. All the ether solutions were combined, washed with water, dried and evaporated to give an epimeric alcohol mixture (main **26a**, 5.55 g), oil; Mass, *m/e* 213 (M^+) and 112 (base); IR, ν_{max} 3410, 1123, 1074, 1024, and 947 cm^{-1}; NMR, δ 0.92 (6H, t J=7 Hz, $2CH_2C\underline{H}_3$), 2.41 (3H, s, $NC\underline{H}_3$), 3.57, 3.71 and 3.64 (total 3H, do d J=6 and 9 Hz, do do d J=2, 5 and 8 Hz, and br, 3H at C_2, C_4 and C_7, respectively), 4.87 and 5.00 (total 1H, each s, O$\underline{H}$).

To the alcohol mixture (4.75 g) cooled in glacial acetic acid (1.87 g) was added dropwise conc sulfuric acid (6.11 g). The mixture was heated at 150 °C for 2.5 hr, cooled and poured into ice-water. The aqueous solution was made basic and filtered to remove a small amount of tarry substance. The filtrate was extracted with chloroform, and the chloroform solution gave **34a** (4.13 g), oil; Mass, *m/e* 195 (M^+) and 94 (base); IR, ν_{max} 1125, 1067, and 980 cm^{-1}; NMR, δ 0.87 (3H, t J=6 Hz, $2CH_2C\underline{H}_3$), 2.23 (3H, s, $NC\underline{H}_3$), 3.40 (2H, complex m, 2H at C_2 and C_4), 5.40 and 5.80 (each 1H, m, C$\underline{H}$=C$\underline{H}$). Found: C, 73.98; H, 10.55; N, 7.30%. Calcd for $C_{12}H_{21}ON$: C, 73.79; H, 10.84; N, 7.17%.

cis-*2,4-Diethyl-9-methyl-9-aza-3-oxabicyclo[3.3.1]non-6-ene (34b).* A solution of **19b** (0.50 g) in ether (20 ml) was reduced with LAH (0.30 g) at room temperature for 17 hr. After being worked up as usual, the solution gave an epimeric alcohol mixture (main **26b**, 0.50 g), oil; Mass, *m/e* 213 (M^+) and 112 (base); IR, ν_{max} 3360, 1133, 1116, 1026, and 951 cm^{-1}; NMR, δ 0.91 (6H, t J=7 Hz, $2CH_2C\underline{H}_3$), 2.44 (3H, s, $NC\underline{H}_3$), 3.51 (2H, t J=7 Hz, 2H at C_2 and C_4), 3.30 and 3.75 (total 1H, each br, H at C_7), 4.92 and 5.04 (total 1H, each br s, O$\underline{H}$).

The alcohol mixture (0.50 g) was treated with conc sulfuric acid (0.60 g) and glacial acetic acid (0.20 g) at 160 °C for 2 hr. The mixture gave oily olefin (**34b**) (0.41 g); Mass, *m/e* 195 (M^+) and 94 (base); IR ($CHCl_3$), ν_{max} 1120, 1085, and 1050 cm^{-1}; NMR ($CDCl_3$), δ 0.94 (6H, t J=7 Hz, $2CH_2C\underline{H}_3$), 2.43 (3H, s, $NC\underline{H}_3$), 2.98 (1H, do d J=6 and 10 Hz, H at C_2 or C_4), 3.17 (1H, do t J=2, 7.5 and 7.5 Hz, H at C_4 or C_2), 5.64 and 5.72 (each 1H, ABq J=11 Hz, C$\underline{H}$=C$\underline{H}$). Found: C, 74.02; H, 10.83; N, 7.28%. Calcd for $C_{12}H_{21}ON$: C, 73.79; H, 10.84; N, 7.17%.

trans- *and* cis-*2,4-Diethyl-9-methyl-9-aza-3-oxabicyclo[3.3.1]nonanes (33a and 33b).* A mixture of olefins (**34a**) (0.41 g) was hydrogenated over platinum (0.20 g as $PtO_2 \cdot H_2O$) in ethanol at room temperature for 1 hr, when 48 ml of hydrogen (1 mol) had been consumed. After removal of the catalyst, the mixture was evaporated, diluted with water, and extracted with chloroform. The chloroform solution was washed with water, dried and evaporated to give **33a** (0.40 g), oil; Mass, *m/e* 197 (M^+) and 96 (base); IR, ν_{max} 1180, 1066, and 862 cm^{-1}; NMR, δ 0.85 and 0.88 (total 6H, each t J=7 Hz, $2CH_2C\underline{H}_3$), 2.46 (3H, s, $NC\underline{H}_3$), 3.46 (1H, do d J=6 and 9 Hz, H at C_4 or C_2), and 3.68 (1H, do do d J=2.5, 6 and 8 Hz, H at C_2 or C_4).

Compound **34b** (60 mg) was hydrogenated over platinum (50 mg) in ethanol (10 ml) at room temperature for 17 hr, when 7 ml of hydrogen (1 mol) had been absorbed. The mixture afforded **33b** (43 mg), oil; Mass; *m/e* 197 (M^+) and 96 (base); IR, ν_{max} 1066 and 1036 cm^{-1}; NMR, δ 0.92 (6H, t J=7.5 Hz, $2CH_2C\underline{H}_3$), 2.57 (3H, s, $NC\underline{H}_3$), and 3.14 (2H, do t J=4, 7 and 7 Hz, 2H at C_2 and C_4).

trans- *and* cis-*2,4-Diethyl-9,9-dimethyl-9-azonia-3-oxabicyclo-[3.3.1]nonene Iodides (35a and 35b).* A *trans*-olefin mixture (**34a**, 3.64 g) was treated with methyl iodide (10 ml) in refluxing ethanol (40 ml) for 2 hr. The mixture was evaporated to leave crude methiodides (6.14 g), which crystallized on trituration with ether and were recrystallized from acetone–isopropyl ether to give **35a** (5.58 g) mp 179—182 °C; Mass, *m/e* 195 ($M^+ - CH_3I$), 142 (CH_3I), and 94; IR (Nujol), ν_{max} 1110, 1076, 998, and 914 cm^{-1}; NMR ($CDCl_3$), too complex to be interpreted. Found: C, 46.10; H, 7.28; N, 4.10%. Calcd for $C_{13}H_{24}ONI$: C, 46.26; H, 7.12; N, 4.15%.

A solution of *cis*-olefin (**34b**, 0.35 g) in ethanol (20 ml) was refluxed with methyl iodide (5 ml) to give crude methiodide (0.60 g), which crystallized on trituration with ether and was recrystallized from acetone–isopropyl ether to yield **35b** (0.52 g), mp 190—191 °C; Mass, *m/e* 195 (M^+—CH_3I), 142 (CH_3I), and 94 (base); IR (Nujol), ν_{max} 1135, 1112, 1078, 1030, and 993 cm^{-1}; NMR ($CDCl_3$), δ 1.00 and 1.04 (total 6H, each t J=7 Hz, $2CH_2C\underline{H}_3$); 3.50 and 3.73 (each 3H, s, $2NC\underline{H}_3$), 3.90 (1H, br t J=6 Hz, H at C_2 or C_4), 4.52 (1H, br s, W_H=7 Hz, H at C_4 or C_2), 5.90 and 5.93 (each 1H, ABq J=10 Hz, C$\underline{H}$=C$\underline{H}$). Found: C, 46.15; H, 7.26; N, 4.20%. Calcd for $C_{13}H_{24}ONI$: C, 46.26; H, 7.12; N, 4.15%.

trans- *and* cis-*2,8-Diethyl-3-dimethylamino-3,8-dihydro-2H-oxocins (36a and 36b).* An aqueous solution of **35a** (765 mg) was eluted through a column of Amberlite IRA-400 (hydroxide form). The alkaline eluate was evaporated below 45 °C under reduced pressure (below 15 mmHg) to leave the quarternary methoxide (**36a**), which was decomposed by heating at 45—50 °C under nitrogen (15 mmHg) for 10 min. The resulting liquid was extracted with ether, dried and evaporated to give **36a** (403 mg), oil; Mass, *m/e* 209 (M^+); IR, ν_{max} 1130, 1100, 1082, 1036, 1008, and 686 cm^{-1}; NMR δ 0.89 and 0.95 (total 6H, each t J=7 Hz, $2CH_2C\underline{H}_3$), 1.51 (4H, m, $2C\underline{H}_2CH_3$), 2.16 (6H, s, $2NC\underline{H}_3$), 3.31 (2H, m, 2H at C_2 and C_3), 4.18 (1H, br m, H at C_8), 5.22 (1H, do d J=3 and 12 Hz, H at C_4), 5.68 (2H, m, 2H at C_5 and C_6), and 6.06 (1H, do d J=5 and 12 Hz, H at C_7).

Compound **35b** (310 mg) was treated in the same manner as **35a** and afforded **35b** (159 mg), oil; Mass, *m/e* 209 (M^+); IR ($CHCl_3$), ν_{max} 1117, 1108, 1060, 1041, and 1016 cm^{-1}; NMR ($CDCl_3$), δ 0.99 and 1.02 (total 6H, each t J=7 Hz, $2CH_2C\underline{H}_3$), 1.54 (4H, m, $2C\underline{H}_2CH_3$), 2.20 (6H, s, $2NC\underline{H}_3$), 3.34 (1H, br do d J=5 and 7.5 Hz, H at C_3), 3.57 (1H, br do d J=2, 5 and 10 Hz, H at C_2), 4.03 (1H, br t J=7 Hz, H at C_8), 5.36 (1H, do d J=2 and 12 Hz, H at C_7), 5.46 (1H, do d J=7.5 and 12 Hz, H at C_4), 5.66 (1H, br do d J=5 and 12 Hz, H at C_5), and 6.04 (1H, br do d J=5 and 12 Hz,

H at C_6).

*trans- and cis-2,8-Diethyl-3-dimethylamino-7,8-dihydro-2H-oxocins (**37a** and **37b**).* Compounds **36a** (1.40 g) were heated at 120—125 °C (bath temperature) for 15 min under nitrogen to give a 4 : 6 mixture (1.40 g) of unidentified product(s) (**38**) and **37a**. The ratio was estimated by comparison of the signals due to dimethylamino groups in the NMR spectrum of the whole reaction product with that in the spectrum of **38**, which remained unchanged as basic component(s) in the next transformation of **37a** to **38a**. Treatment of **36a** under other conditions [heating at 105 °C for 2 hr, heating at 145 °C for 2 min, or distillation *in vacuo* (15 mmHg) at 110 °C (each bath temperature)] did not increase the yield of **37a**. Compound **37a** showed the following spectra; IR, ν_{max} 1603 and 1063 cm^{-1}; NMR, δ 0.82 and 0.90 (total 6H, each t J=7 Hz, $2CH_2C\underline{H}_3$), 1.36 (4H, complex m, $2C\underline{H}_2CH_3$), 2.30 (2H, m, 2H at C_7), 2.56 (6H, s, $2NC\underline{H}_3$), 2.65 (1H, m, H at C_8), 4.36 (1H, t J=7 Hz, H at C_2), 4.98 (1H, d J=5 Hz, H at C_4), 5.38 (1H, do d J=5 and 12 Hz, H at C_5), and 5.82 (1H, do do d J=2, 4.5 and 12 Hz, H at C_6). The whole product was used in the next reaction without further purification.

Compound **36b** (750 mg) was heated at 70—80 °C (bath temperature) for 20 min under nitrogen to give a 1 : 1 mixture (750 mg) of **36a** and **37b**. However, **36b** (750 mg) when heated at 120—125 °C for 10 min, afforded **37b** (750 mg), as a sole product, as far as the product was examined by tlc and NMR. This dienamine (**37b**) was characterized by the following spectra and used for the next reaction without further purification: IR, ν_{max} 1603 and 1043 cm^{-1}; NMR ($CDCl_3$), δ 0.86 and 0.93 (total 6H, each t J=7 Hz, $2CH_2C\underline{H}_3$), 1.60 (4H, complex m, $2C\underline{H}_2CH_3$), 2.30 (2H, m, 2H at C7), 2.57 (6H, s, $2NC\underline{H}_3$), 2.86 (1H, br do do d J=6, 6 and 8 Hz, H at C_8), 3.60 (1H, do d J=6.5 and 9 Hz, H at C_2), 5.02 (1H, d J=4.5 Hz, H at C_4), 5.76 (1H, m, H at C_6), and 6.13 (1H, br do d J=4.5 and 12 Hz, H at C_5).

*trans-2,8-Diethyl-7,8-dihydro-2H-oxocin-3(4H)-one (**38a**).* An aqueous solution (14 ml) containing **37a** (1.40 g) and 7% fluoroboric acid (2.8 ml) was refluxed for 15 min, cooled, neutralized with aqueous sodium carbonate, and extracted with ether (100 ml) and then with dichloromethane (2×100 ml). The organic solutions were combined, dried and evaporated to leave oil (860 mg), which was dissolved in ether. The ether solution was shaken with 1 M hydrochloric acid to separate neutral (540 mg) and basic components (**38**, 320 mg). A part (470 mg) of the neutral substance, showing a single spot on tlc, was purified by chromatography over silicic acid (Merck, 20 g) with a 25 : 1 mixture of benzene and ethyl acetate to yield **38a** (307 mg) in pure state, oil; Mass, *m/e* 182 (M^+), 153, 96, and 81 (base); UV (isooctane), λ_{max} 295 nm (ε 96) (sh), 305 (108), 313 (76), and 325 (50) (sh); IR (film), ν_{max} 1717, 1660, 1120, 1089, 1081, 1048, and 1005 cm^{-1}; NMR ($CDCl_3$), δ 0.96 and 1.00 (6H, each t J=7 Hz, $2CH_2C\underline{H}_3$), 1.58 (2H, m, $C\underline{H}_2CH_3$ at C_8), 1.64 (2H, qui J=7 Hz, $C\underline{H}_2CH_3$ at C_2), 2.05 (2H, m, 2H at C_7), 2.93 and 3.52 (each 1H, do d J=16, 3 and 16 and 2 Hz, 2H at C_4), 3.70 (1H, m, H at C_8), 3.86 (1H, t J=7 Hz, H at C_2), and 5.63 (2H, m, 2H at C_5 and C_6). Found: C, 72.64; H, 9.95%. Calcd for $C_{11}H_{18}O_2$: C, 72.49; H, 9.96%.

*cis-2,8-Diethyl-7,8-dihydro-2H-oxocin-3(4H)-one (**38b**).* A solution of **37b** (700 mg) and 7% fluoroboric acid (1.5 ml) in water (7 ml) was refluxed for 15 min, cooled and then worked up as usual to leave oil (608 mg), showing a single spot. The oil was purified by chromatography in the same way as **37a**, giving **38b** (470 mg) in pure state, oil; Mass, *m/e* 182 (M^+), 153, 96, and 81 (base); UV (isooctane), λ_{max} 294 (ε 142) (sh), 303 (162), 313 (156), and 324 nm (90); IR (film), ν_{max} 1718, 1641, 1120, 1108, 1091, 1068, and 1013 cm^{-1}; NMR ($CDCl_3$), δ 0.99 (6H, t J=7 Hz, $2CH_2C\underline{H}_3$), 1.62 (4H, m, $2C\underline{H}_2CH_3$), 2.25 (2H, m, 2H, at C_7), 2.77 (1H, do d J=13 and 6 Hz, H at C_4), 3.36 (1H, m, H at C_8), 3.71 (1H, do d J=5 and 7 Hz, H at C_2), 3.82 (1H, do d J=13 and 6 Hz, H at C_4), 5.71 (2H, m, 2H at C_5 and C_6). Found: C, 72.23; H, 9.94%. Calcd for $C_{11}H_{18}O_2$: C, 72.49; H, 9.96%.

A solution of *trans*-ketone (**38a**, 10 mg) in methanol (4 ml) was stirred with base (5% KOH) at room temperature for 20 min, diluted with water (20 ml), and extracted with ether (2×30 ml). The ether solution, after being worked up as usual, gave oil (10 mg), which was identical with *cis*-ketone (**38b**) in all respects (tlc, IR, and NMR). Treatment of **38a** with acid (refluxing 7% HBF_4, 15 min, or *p*-TsOH in dichloromethane, room temperature, 20 hr) proved to give no **38b** by tlc.

*2,8-Diethyl-3,4,7,8-tetrahydro-2H-oxocin-3-ols (**39** and **40**).* Compound **38b** (60 mg) was reduced with sodium borohydride (40 mg) in methanol (10 ml) at 0 °C for 40 min. The reaction mixture was made acidic (pH 4—5) with 2 M hydrochloric acid, concentrated and extracted with ether (2×50 ml). The ether solution was washed with saturated brine, dried and evaporated to leave oil (65 mg), showing two spots on tlc. The oil was separated roughly into three fractions by column chromatography over silica gel (Merck, 2 g, benzene : methanol=9 : 1). Fractions (30 mg) eluted early showed a single spot and gave **39** (30 mg), oil; Mass, *m/e* 155 (M^+-C_2H_5), 137, and 108; IR (film), ν_{max} 3420, 1066, and 1010 cm^{-1}; NMR ($CDCl_3$), δ 0.94 and 0.97 (total 6H, each t J=7 Hz, $2C\underline{H}_3CH_2$), 1.56 (4H, m, $2CH_3C\underline{H}_2$), 2.30 (3H, m, 3H at C_4 and C_7), 2.63 (1H, do d J=8 and 12 Hz, H at C_4), 3.33 (2H, m, 2H at C_2 and C_8), 3.68 (1H, m, H at C_3), and 5.76 (2H, m, 2H at C_5 and C_6). Middle fractions (30 mg) consisted mainly of **39** (tlc). Fractions eluted later showed a single spot on tlc and gave **40** (5 mg), oil; Mass, *m/e* 155 (M^+—C_2H_5), 137, and 108, IR (film), ν_{max} 3400, 1066, and 1011 cm^{-1}; NMR ($CDCl_3$), δ 1.02 (6H, t J=7 Hz, $2C\underline{H}_3CH_2$), 1.58 (4H, m, $2CH_3C\underline{H}_2$), 1.62 (1H, s, O<u>H</u>), 2.30 (3H, m, 3H at C_4 and C_7), 2.82 (1H, do do d J=3, 7 and 13 Hz, H at C_4), 3.32 (2H, m, 2H at C_2 and C_8), 3.75 (1H, do t J=3, 3 and 9 Hz, H at C_3), and 5.88 (2H, m, 2H at C_5 and C_6).

*t-3-Bromo-r-2,c-8-diethyl-3,4,7,8-tetrahydro-2H-oxocin (**2**).* To a stirred solution of alcohol **39** (50 mg) and carbon tetrabromide (135.5 mg) in dichloromethane (4 ml, dried through molecular sieves) was added dropwise a solution of triphenylphosphine (71.3 mg) in dry dichloromethane (6 ml) at room temperature during 3 hr, and the whole mixture was stirred at the temperature overnight. After removal of the solvent under reduced pressure, the residue was extracted with pentane (total 30 ml) repeatedly. The pentane solution was evaporated carefully under atmospheric pressure to leave oily residue, which was passed through a column filled with silica gel (1 g), pentane being used as solvent. Early fractions gave a mixture (10 mg) of carbon tetrabromide and **2**, and the following fractions showed a single spot on tlc and afforded **2** (25 mg), oil; Mass, *m/e* 248 and 246 (M^+), 219 and 217 (M^+—C_2H_5), and 190 and 188 (M^+—$2C_2H_5$), and 109; IR (film), ν_{max} 1282, 1118, 1080, 1032, and 809 cm^{-1}; NMR ($CDCl_3$), δ 0.97 (6H, t J=7 Hz, $2C\underline{H}_3CH_2$), 1.28 (2H, br s, $CH_3C\underline{H}_2$), 1.57 (2H, m, $CH_3C\underline{H}_2$), 2.20 (3H, m, 3H at C_4 and C_7), 4.30 (3H, m, 3H at C_2, C_4 and C_8), 4.05 (1H, do t J=3, 3 and 9 Hz, H at C_3), and 5.90 (2H, m, 2H at C_5 and C_6).

References

1) T. Irie, M. Suzuki, and T. Masamune, *Tetrahedron*, **24**, 4193 (1968); *Tetrahedron Lett.*, **1965**, 1091.

2) A. Furusaki, E. Kurosawa, A. Fukuzawa, and T. Irie, *ibid.*, **1973**, 4579, and their previous papers; W. Fenical, K. B. Gifkins, and J. Clardy, *ibid.*, **1974**, 1507, and their previous papers.

3) F. A. L. Anet and P. J. Degen, *ibid.*, **1972**, 3613; L. A. Paguette and R. W. Begland, *J. Org. Chem.*, **32**, 2723 (1967).

4) a) J. Meinwald and H. Nozaki, *J. Amer. Chem. Soc.*, **80**, 3132 (1958). b) L. A. Paguette and R. W. Begland, *ibid.*, **90**, 5159 (1968).

5) R. Roulet, J. Wenger, M. Hardy, and P. Vogel, *Tetrahedron Lett.*, **1974**, 1479; L. Skattebøl, *J. Org. Chem.*, **35**, 3200 (1970); V. J. Traynelis, W. L. Hergenrother, H. T. Hanson, and J. A. Valicenti, *ibid.*, **29**, 123 (1964); J. Meinwald, D. W. Dicker, and N. Danieli, *J. Amer. Chem. Soc.*, **82**, 4087 (1960); E. E. Schweizer and W. E. Parham, *ibid.*, **82**, 4085 (1960).

6) M. Lj. Mihailović, Ž. Čeković, J. Stanković, N. Pavlovic, S. Konstantinovic, and S. Djokić-Mazinjanin, *Helv. Chim. Acta*, **56**, 3056 (1973); *cf.*, F. D. Gunstone and R. P. Inglis, *Chem. Commun.*, **1972**, 12.

7) F. Nerdel, J. Buddrus, W. Brodowski, and P. Weyerstahl *Tetrahedron Lett.*, **1966**, 5385.

8) N. J. Leonard, T. W. Milligan, and T. L. Brown, *J. Amer. Chem. Soc.*, **82**, 4075 (1960).

9) R. Clinging, F. M. Dean, and L. E. Houghton, *J. Chem. Soc. Perkin I*, **1974**, 66; H. S. Kasmai and H. W. Whitlock, Jr., *J. Org. Chem.*, **37**, 2161 (1972).

10) L. A. Paquette, R. W. Begland, and P. C. Storm, *J. Amer. Chem. Soc.*, **90**, 6148 (1968).

11) C. L. Zirkle, F. R. Gerns, A. W. Pavloff, and A. Burger, *J. Org. Chem.*, **26**, 395 (1961).

12) E. Kurosawa, A. Fukuzawa, and T. Irie, *Tetrahedron Lett.*, **1972**, 2121.

13) P. Lauger, M. Prost, and R. Charlier, *Helv. Chim. Acta*, **42**, 2379 (1959).

14) *cf.*, W. Oroshnik, G. Karmas, and A. D. Mebane, *J. Amer. Chem. Soc.*, **74**, 295 (1952); J. P. Danehy, D. B. Killian, and J. A. Nieuwland, *ibid.*, **58**, 611 (1936).

15) W. G. Young, L. Richard, and J. Azorlosa, *ibid.*, **61**, 3070 (1939).

16) H. Lindlar, *Helv. Chim. Acta*, **35**, 446 (1952).

17) C. L. Stevens, E. Farkas, and B. Gillis, *J. Amer. Chem. Soc.*, **76**, 2695 (1954).

18) *cf.*, A. C. Cope and T. -Y. Shen, *ibid.*, **78**, 5912 (1956).

19) *cf.*, L. N. Owen and A. G. Peto, *J. Chem. Soc.*, **1955**, 2383; M. Lj. Mihailović, S. Gojkorić, and Ž. Čeković, *J. Chem. Soc. Perkin I*, **1972**, 2460.

20) *cf.*, J. Fakstop, *J. Amer. Chem. Soc.*, **72**, 869 (1950).

21) *cf.*, L. Crombie, *J. Chem. Soc.*, **1950**, 1714.

22) *cf.*, R. Ratcliffe and R. Rodehorst, *J. Org. Chem.*, **35**, 4000 (1970).

23) H. Paulsen and K. Todt, *Angew. Chem.*, **78**, 943 (1966); *Chem. Ber.*, **100**, 3385, 3396 (1967); R. A. Johnson, *J. Org. Chem.*, **33**, 3627 (1968); T. Masamune, H. Hayashi, M. Takasugi, and S. Fukuoka, *ibid.*, **37**, 2343 (1972).

24) R. K. Harris and R. A. Spragg, *Chem. Commun.*, **1966**, 314.

25) H. Booth and J. H. Little, *J. Chem. Soc. Perkin II*, **1972**, 1846.

26) N. S. Zefirov and S. V. Ragozina, *Tetrahedron*, **30**, 2345 (1974); N. S. Zefirov, S. V. Rogozina, E. D. Kurkutova, V. Goncharov, and N. V. Belov, *Chem. Commun.*, **1974**, 260. *cf.*, P. Bucci, G. Lippi, and B. Macchia, *J. Org. Chem.*, **35**, 913 (1970); P. R. Stapp and J. C. Randall, *ibid.*, **35**, 2948 (1970).

27) C. -Y. Chen and R. J. W. LeFévre, *J. Chem. Soc. (B)*, **1966**, 539.

28) H. Booth, *Tetrahedron*, **22**, 615 (1966).

29) T. Masamune, H. Matsue, S. Numata, and A. Furukaki, *Tetrahedron Lett.*, **1974**, 3933.

30) T. A. Crabb and E. R. Jones, *Tetrahedron*, **26**, 1217 (1970); D. Tavernier and M. Anteunis, *ibid.*, **27**, 1677 (1971).

31) N. S. Bhacca and D. H. Williams, "Application of NMR spectroscopy in Organic Chemistry," Holden-Day, Inc., San Francisco, (1964), p. 21.

32) T. M. Moynehan, K. Schofield, R. A. Y. Jones, and A. R. Katritzky, *J. Chem. Soc.*, **1962**, 2637; M. Kotake, I. Kawasaki, T. Okamoto, S. Matsutani, S. Kusumoto, and T. Kaneko, This Bulletin, **35**, 1335 (1962); S. Ito, J. B. Stothers, and S. M. Kupchan, *Tetrahedron*, **20**, 913 (1964).

33) *cf.*, A. C. Cope, *J. Amer. Chem. Soc.*, **70**, 1433 (1948).

34) R. B. Woodward and R. Hoffman, "The Conservation of Orbital Symmetry," 1970 Verlag Chemie, GmbH, Weinheim/Bergstr., (1970), p. 114; G. B. Gill, *Quart. Rev.*, **22**, 338 (1968).

35) Stereochemical studies on this rearrangement, starting from isolation of each diastereoisomer of *trans*-aminodienes (**36a**) or their precursors (**35a** and **34a**), are now in progress.

36) M. Karplus, *J. Amer. Chem. Soc.*, **85**, 2870 (1963).

37) R. K. Boekman, Jr. and B. Genam, *Tetrahedron Lett.*, **1974**, 913; A. K. Bose and B. Lal, *ibid.*, **1973**, 3937; J. Hooz and S. S. Gilani, *Can. J. Chem.*, **46**, 86 (1968).

Synthesis of 6′-Amino-1-*N*-[(*S*)-4-Amino-2-Hydroxybutyryl]-6′-Deoxylividomycin A

Isamu WATANABE, Akio EJIMA, Tsutomu TSUCHIYA, Sumio UMEZAWA, and Hamao UMEZAWA*

Department of Applied Chemistry, Faculty of Engineering, Keio University, Hiyoshi, Yokohama 223

**Institute of Microbial Chemistry, Kamiosaki, Shinagawa-ku, Tokyo* 141

(Received April 16, 1975)

The titled compound (**11**) was prepared from lividomycin A. A partially protected cyclic 1,6-carbamate derivative (**6**), which has free hydroxyl groups at C-4′ and C-6′, was prepared, and the 6′-hydroxyl group was selectively tosylated. Replacement of the tosyl group by azido group, followed by partial hydrolysis of the carbamate ring gave the aminol (**9**). Acylation of the free C-1-amino group with (*S*)-4-amino-2-hydroxybutyric acid and hydrogenation of the azido group led to **11**. Preparation of 4′,6′-di-*O*-methyllividomycin A (**13**) was also described.

In the foregoing paper,[1] we reported the synthesis of 1-*N*-((*S*)-4-amino-2-hydroxybutyryl)lividomycin A (**1**). The compound had an improved antibiotic spectrum, being active against resistant organisms producing neomycin-kanamycin phosphotransferase I (P-ase I). We have further undertaken to prepare its 6′-amino-6′-deoxy derivative namely the titled compound which is synonymous with 1-*N*-((*S*)-4-amino-2-hydroxybutyryl)-3′-deoxy-4‴-*O*-mannosylneomycin B expecting to obtain a more effective compound, because introduction of an amino group at C-6′ of related aminoglycoside antibiotics generally enhances the antibacterial activity of the parent antibiotic.

Penta-*N*-benzyloxycarbonyllividomycin A (**2**) described in the foregoing paper[1] was treated with 1,1-dimethoxycyclohexane in the presence of acidic catalyst to give di-*O*-cyclohexylidene derivative (**3**) as the major product. It should be noted that the similar reaction of **2** with benzaldehyde dimethyl acetal gave a tri-*O*-benzylidene derivative[1] as the major product. Addition of methanol to the reaction mixture containing di-*O*-cyclohexylidene derivatives as major products caused hydrolysis of the minor products, and this treatment easily afforded the purified **3**. The positions of the cyclohexylidene groups in **3** were proved by periodate oxidation of **3** and by *O*-methylation of **6** that is later described. Periodate oxidation of **3** followed by acidic hydrolysis gave no trace of mannose, indicating the absence of a cyclohexylidene group at C-2 and C-3 of the mannose moiety. It is also noteworthy that **3** contains no 1-methoxycyclohexyl group, which is formed[2] at C-5 of the ribose moiety in the case of similar cyclohexylidenation of tetra-*N*-benzyloxycarbonylribostamycin; this result is compatible with the benzylidenation of penta-*N*-benzyloxycarbonyllividomycin A.[1]

Treatment of **3** with sodium hydride in DMF[1,3] gave the 1,6-cyclic carbamate (**4**) which was then benzoylated. The penta-*O*-benzoyl derivative (**5**) was more soluble in organic solvents than the corresponding tri-*O*-benzylidene derivative of lividomycin A described previously.[1] Controlled hydrolysis of **5** with aqueous acetic acid successfully removed only the cyclohexylidene group at C-4′,6′. Possibly this selectivity is due to participation of the *O*-benzoyl group at C-3‴′. We have experienced the similar phenomenon in the other examples which will be published elswhere. For structural confirmation, the mono-*O*-cyclohexylidene derivative (**6**) was methylated with diazomethane in the presence of BF_3-etherate to give the di-*O*-methyl derivative (**12**) and treated successively with barium hydroxide, acetic acid, and palladium and hydrogen to give the 4′,6′-di-*O*-methyllividomycin A (**13**), whose acidic methanolysis did not give 3′-deoxyparomamine in the hydrolyzate, indicating that the hydroxyl groups at C-4′ and C-6′ (not those at C-4‴′ and C-6‴′) were methylated.

Tosylation of **6** gave the 6′-*O*-tosyl derivative (**7**). The selective 6′-*O*-tosylation was supported by the fact that tritylation was difficult for **7**.

Compound **7** was treated with sodium azide in DMF to give the 6′-azido derivative (**8**). Treatment of **8** with dilute solution of barium hydroxide hydrolyzed the 1,6-cyclic carbamate as well as the benzoyl ester

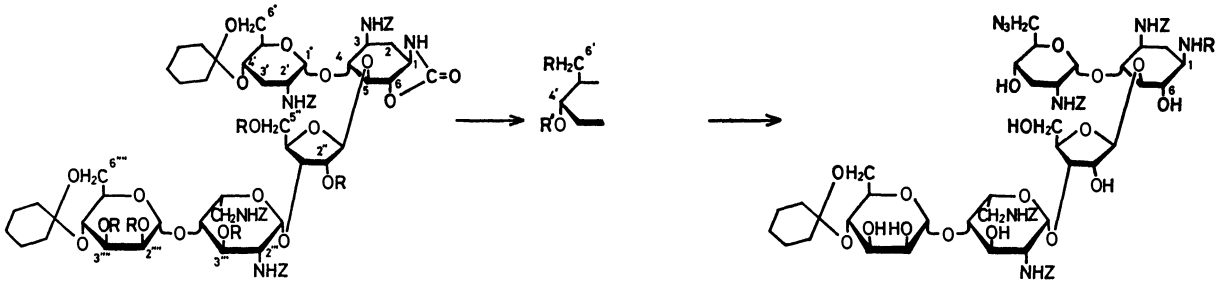

Z : $CO_2CH_2C_6H_5$

	R		R	R′
		6	OH	H
	R	7	$OSO_2C_6H_4$-*p*-CH_3	H
4	H	8	N_3	H
5	COC_6H_5	12	OCH_3	CH_3

	R
9	H (s)
10	$COCH(OH)CH_2CH_2NHZ$

groups to give **9** which has a free amino group at C-1. Condensation of **9** with (*S*)-4-benzyloxycarbonylamino-2-hydroxybutyric acid[4] by an active ester method using *N*-hydroxysuccinimide and dicyclohexylcarbodiimide (DCC) in THF gave the 1-*N*-acyl derivative (**10**). The cyclohexylidene group of **10** was removed by acidic treatment and the product was catalytically hydrogenated to remove the benzyloxycarbonyl groups and to reduce the azido to the amino group to afford the titled compound (**11**).

The derivative **11** showed antibacterial activity against resistant bacteria producing P-ase I as expected, but the activity did not exceed that of 1-*N*-((*S*)-4-amino-2-hydroxybutyryl)lividomycin A.[1] The 4',6'-di-*O*-methyllividomycin A (**13**) showed no antibacterial activity.

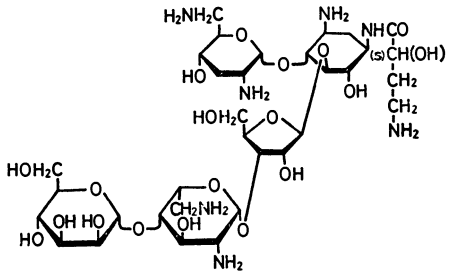

11

Experimental

General procedure was the same as described in the foregoing paper.[1]

*1,3,2',2''',6'''-Penta-*N*-benzyloxycarbonyl-4',6';4'''',6''''-di-O-cyclohexylidenelividomycin A (**3**).* To a solution of penta-*N*-benzyloxycarbonyllividomycin A (**2**) (7.87 g) in dry DMF (170 ml), *p*-toluenesulfonic acid (200 mg) and 1,1-dimethoxycyclohexane (18 ml) were added and the solution was heated at 30 °C for 3.5 hr under reduced pressure (~30 Torr). Methanol (80 ml) was added and the solution was allowed to stand for 30 min. Examination by tlc using chloroform–methanol (20 : 1) showed that by the methanol treatment, three spots initially observed collapsed to single major one (R_f 0.26). After addition of saturated sodium hydrogen carbonate solution, the solvent was removed by coevaporation with toluene. The residue was chromatographed on a column of silica gel with chloroform–methanol–triethylamine (30 : 1 : 0.1). The portion containing **3** was evaporated to give a solid of **3**, 3.73 g (43%); $[\alpha]_D^{27}$ +43° (*c* 1, $CHCl_3$).

Found: C, 60.92; H, 6.39; N, 4.22%. Calcd for $C_{81}H_{101}N_5O_{28}$: C, 61.08; H, 6.39; N, 4.40%.

*3,2',2''',6'''-Tetra-*N*-benzyloxycarbonyl-4',6';4'''',6''''-di-O-cyclohexylidenelividomycin A 1,6-Carbamate (**4**).* To an ice-cold solution of **3** (300 mg) in dry DMF (3 ml), 50% oily sodium hydride (40 mg) was added under a nitrogen atmosphere and the mixture was stirred for 3 hr in the cold. After neutralization with acetic acid, the resulting viscous solution was poured into a mixture of chloroform and saturated sodium chloride solution under stirring. The separated organic layer was washed with saturated sodium chloride solution and water, and dried over sodium sulfate. The solution was evaporated and the residue (270 mg) was chromatographed on a short column of silica gel with chloroform–methanol–triethylamine (25 : 1 : 0.1). The portion containing **4** was evaporated to give a solid of **4**, 195 mg (70%); $[\alpha]_D^{27}$ +41° (*c* 1, $CHCl_3$); IR (KBr): 1760 cm^{-1}.

Found: C, 59.58; H, 6.32; N, 4.45%. Calcd for $C_{74}H_{93}N_5O_{27}$: C, 59.87; H, 6.31; N, 4.72%.

*2'',5'',3''',2'''',3''''-Penta-*O*-benzoyl-3,2',2''',6'''-tetra-*N*-benzyloxycarbonyl-4',6';4'''',6''''-di-*O*-cyclohexylidenelividomycin A 1,6-Carbamate (**5**).* To a solution of **4** (210 mg) in dry pyridine (4.2 ml), benzoyl chloride (530 mg) was added and the solution was allowed to stand at −10 °C overnight. A few drops of water was added and the solution was allowed to stand for 1 hr. Powdered sodium hydrogen carbonate (300 mg) was added and the mixture was evaporated. The residue was extracted with chloroform and the solution was washed with water, potassium hydrogen sulfate solution, sodium hydrogen carbonate solution, and water and dried over sodium sulfate. After evaporation, the residue was dissolved in a mixture of ethyl acetate–benzene–triethylamine (2 : 5 : 0.02) and the solution was filtered through a short column of silica gel with aid of the above solvent system to remove impurities. Evaporation of the filtrate gave a solid, which was reprecipitated from benzene–*n*-hexane to give **5**, 220 mg (78%); $[\alpha]_D^{27}$ +13° (*c* 1, $CHCl_3$).

Found: C, 65.15; H, 5.70; N, 3.43%. Calcd for $C_{109}H_{113}N_5O_{32}$: C, 65.29; H, 5.68; N, 3.49%.

*2'',5'',3''',2'''',3''''-Penta-*O*-benzoyl-3,2',2''',6'''-tetra-*N*-benzyloxycarbonyl-4'''',6''''-*O*-cyclohexylidenelividomycin A 1,6-Carbamate (**6**).* To a solution of **5** (600 mg) in acetone (15 ml), acetic acid (6.25 ml) and water (3.75 ml) were added and the solution was allowed to stand at 37 °C for 8 hr. Sodium hydrogen carbonate (4 g) was added and the mixture was concentrated. The resulting sludge was shaken with chloroform. The separated organic layer was washed with saturated sodium hydrogen carbonate solution, and water, dried over sodium sulfate, and evaporated. On tlc with chloroform–methanol (30 : 1), the residue showed two main spots of R_f 0.71 (**5**) and R_f 0.29 (**6**) along with two faint spots. The residue was chromatographed on a column of silica gel (22 g) successively with chloroform–methanol–triethylamine (50 : 1 : 0.1, totally 120 ml) and chloroform–methanol–triethylamine (30 : 1 : 0.1). From the early fractions, **5** (240 mg, 40%) was recovered. From the later fractions, **6** was obtained; it was reprecipitated from chloroform–*n*-hexane, 290 mg (50%); $[\alpha]_D^{27}$ +11° (*c* 1, $CHCl_3$).

Found: C, 64.47; H, 5.53; N, 3.55%. Calcd for $C_{103}H_{105}N_5O_{32}$: C, 64.27; H, 5.50; N, 3.64%.

*2'',5'',3''',2'''',3''''-Penta-*O*-benzoyl-3,2',2''',6'''-tetra-*N*-benzyloxycarbonyl-4'''',6''''-O-cyclohexylidene-6'-O-tosyllividomycin A 1,6-Carbamate (**7**).* To a cold solution (−10 °C) of **6** (770 mg) in pyridine (16 ml), *p*-toluenesulfonyl chloride (390 mg) was added and the solution was allowed to stand at the temperature overnight and worked up in a similar manner as described for the preparation of **5** from **4**, 764 mg (92%); $[\alpha]_D^{31}$ +12.5° (*c* 2, $CHCl_3$); IR (KBr): 1175 cm^{-1} (Ts); NMR ($CDCl_3$): δ 2.39 (3H s, $SO_2C_6H_4C\underline{H}_3$).

Found: C, 63.23; H, 5.33; N, 3.14; S, 1.55%. Calcd for $C_{110}H_{111}N_5O_{34}S$: C, 63.55; H, 5.38; N, 3.37; S, 1.54%.

*6'-Azido-2'',5'',3''',2'''',3''''-Penta-*O*-benzoyl-3,2',2''',6'''-tetra-*N*-benzyloxycarbonyl-4'''',6''''-O-cyclohexylidene-6'-deoxylividomycin A 1,6-Carbamate (**8**).* To a solution of **7** (720 mg) in dry DMF (18 ml), sodium azide (230 mg) was added and the mixture was stirred at 60 °C for 6 hr. On tlc with chloroform–ethanol (30 : 1), **8** (R_f 0.40) appeared instead of **7** (R_f 0.47). Chloroform (200 ml) was added and the solution was washed with saturated sodium chloride solution (50 ml × 4), and water, and dried over sodium sulfate. After evaporation of the solvent, the residue was dissolved in a mixture of chloroform–ethanol–triethylamine (40 : 1 : 0.1)

and the solution was filtered through a short column (20 g) of silica gel with aid of the above solvent system to remove impurities. Evaporation of the filtrate gave **8**, 633 mg (94%); $[\alpha]_D^{28}$ +12.5° (*c* 2, $CHCl_3$); IR (KBr): 2100 (N_3), 1775 cm^{-1}.

Found: C, 63.26; H, 5.39; N, 5.61%. Calcd for $C_{103}H_{104}N_8O_{11}$: C, 63.44; H, 5.38; N, 5.75%.

*6′-Azido-3,2′,2‴,6‴′-tetra-*N*-benzyloxycarbonyl-4‴′,6‴′-O-cyclohexylidene-6′-deoxylividomycin A (**9**).* To a solution of **8** (520 mg) in dioxane (32 ml), 0.025 M barium hydroxide solution (16 ml) was added and the mixture was stirred at 60 °C for 30 min. Additional aliquot (16 ml) of the barium hydroxide solution was added and the mixture was stirred for 2 hr until the mixture became neutral. The treatment was repeated once again. Subsequent procedures were carried out as described for the preparation of **5** from **3** in the foregoing paper[1] except for the use of chloroform–methanol–triethylamine (6 : 1 : 0.01) for the chromatography, 340 mg (91%); $[\alpha]_D^{31}$ +48° (*c* 2, $CHCl_3$).

Found: C, 56.53; H, 6.08; N, 7.23%. Calcd for $C_{67}H_{86}N_8O_{25}\cdot 1/2H_2CO_3$: C, 56.52; H, 6.11; N, 7.81%.

*6′-Azido-3,2′,2‴,6‴′-tetra-*N*-benzyloxycarbonyl-1-*N*-[(S)-4-benzyloxycarbonylamino-2-hydroxybutyryl]-4‴′,6‴′-O-cyclohexylidene-6′-deoxylividomycin A (**10**).* To an ice-cold solution of (*S*)-4-benzyloxycarbonylamino-2-hydroxybutyric acid[4] (58.5 mg) and *N*-hydroxysuccinimide (26.6 mg) in THF (1 ml), DCC (47 mg) was added and the solution was allowed to stand for 1 hr under cooling. To the resulting suspension containing dicyclohexylurea, a solution of **9** (270 mg) and triethylamine (30 mg) in THF (2.5 ml) was added and the mixture was stirred at 0 °C for 1 hr and then at room temperature overnight. Filtration followed by evaporation gave a solid, which was chromatographed on a column of silica gel with chloroform–ethanol–triethylamine (10 : 1 : 0.2) to give **10**, 126 mg (40%); $[\alpha]_D^{20}$ +35° (*c* 1, $CHCl_3$); IR (KBr): 2090 cm^{-1} (N_3).

Found: C, 57.84; H, 6.25; N, 7.40%. Calcd for $C_{79}H_{98}N_9O_{29}$: C, 57.94; H, 6.03; N, 7.70%.

*6′-Amino-1-*N*-((S)-4-amino-2-hydroxybutyryl)-6′-deoxylividomycin A (**11**).* A solution of **10** (110 mg) in a mixture (10 ml) of acetone–acetic acid–water (3 : 5 : 2) was heated at 60 °C for 2 hr. Evaporation gave a residue, which was dissolved in aqueous dioxane (2 : 5, 4 ml). After addition of a few drops of acetic acid, the solution was hydrogenated over palladium black. Chromatography of the product on a column of CM-Sephadex C-25 (NH_4 form) with a linear gradient of aqueous ammonia (0∼0.3 M) gave a solid, which showed a single peak of **11**, 41 mg (64%); $[\alpha]_D^{20}$ +68° (*c* 1, H_2O); ppc, $R_{f\ \text{lividomycin A}}$ 0.6; IR (KBr): 1650, 1580 cm^{-1}.

Found: C, 42.46; H, 7.19; N, 10.19%. Calcd for $C_{33}H_{63}N_7O_{19}\cdot H_2CO_3\cdot 2H_2O$: C,42.54; H, 7.25; N, 10.21%.

*2‴,5‴,3‴′,2‴′,3‴′-Penta-O-benzoyl-3,2′,2‴,6‴′-tetra-*N*-benzyloxycarbonyl-4‴′,6‴′-O-cyclohexylidene-4′,6′-di-O-methyllividomycin A 1,6-Carbamate (**12**).* To a solution of **6** (140 mg) in dry dichloromethane (3 ml) in an ice-cold bath, boron trifluoride etherate (5 mg) was added, and diazomethane in dichloromethane was added until the solution became yellow. Triethylamine was added and the solution was evaporated to give a residue, which was dissolved in chloroform. The solution was washed with saturated sodium hydrogen carbonate solution, and water, dried over sodium sulfate, and evaporated. The residue was chromatographed on a column of silica gel with chloroform–ethanol–triethylamine (50 : 1 : 0.1); 65 mg (46%); $[\alpha]_D^{20}$ +21° (*c* 1, $CHCl_3$); NMR ($CDCl_3$): δ 3.22, 3.33 (each 3H s, OCH_3).

Found: C, 64.82; H, 5.63; N, 3.50%. Calcd for $C_{105}H_{109}N_5O_{12}$: C, 64.57; H, 5.63; N, 3.59%'

*4′-6′-Di-O-methyllividomycin A (**13**).* A sample of **12** was treated with barium hydroxide solution in a similar manner as described for the preparation of **9**. The product was treated with acetic acid and then with palladium black and hydrogen as described for the preparation of **11** to afford **13** (65%); $[\alpha]_D^{20}$ +83° (*c* 1, H_2O); PPC, $R_{f\ \text{lividomycin A}}$ 3.1; NMR (D_2O): δ 3.41 (6H s, OCH_3).

Found: C, 43.75; H, 7.10; N, 7.96%. Calcd for $C_{31}H_{59}N_5O_{18}\cdot H_2CO_3\cdot H_2O$: C, 44.19; H, 7.30; N, 8.05%.

*Acidic methanolysis of **13**.* A suspension of **13** in 0.4 M methanolic hydrogen chloride was heated at 80 °C for 10 hr. As a control experiment, lividomycin A was similarly treated. Paper chromatography of the both hydrolyzates gave the following results: Methanolysis of **13**: $R_{f\ \text{DST}}$* 1.4 (faint), 2.1 (3′-deoxy-4′,6′-di-*O*-methylparomamine), and 2.9 (methyl 2,6-diamino-2,6-dideoxyidoside?). Methanolysis of lividomycin A: $R_{f\ \text{DST}}$ 0.8 (3′-deoxyparomamine), 1.4 (faint), and 2.9.

References

1) I. Watanabe, T. Tsuchiya, S. Umezawa, and H. Umezawa, This Bulletin, **48**, 2124 (1975).

2) D. Ikeda, T. Suzuki, T. Tsuchiya, S. Umezawa, and H. Umezawa, *ibid.*, **46**, 3210 (1973).

3) D. Ikeda, T. Tsuchiya, S. Umezawa, and H. Umezawa, *ibid.*, **47**, 3136 (1974).

4) H. Kawaguchi, T. Naito, S. Nakagawa, and K. Fujisawa, *J. Anitibiot.* (Tokyo), **25**, 695 (1972).

* Relative R_f value, that of 2-deoxystreptamine being taken as 1.

The Rearrangement of 10-Bromo-10,11-dihydrodibenzo[*b,f*]thiepin-11-one and Related Compounds in an Alkaline Solution

Ikuo UEDA*

Research Laboratories, Fujisawa Pharmaceutical Co., Ltd., Kashima, Yodogawa-ku, Osaka 532

(Received December 2, 1974)

The reaction of 10-bromo-10,11-dihydrodibenzo[*b,f*]thiepin-11-one (**1**) with sodium methoxide in methanol has been shown to lead to thioxanthone (**4**) and 10-hydroxy-10,11-dihydrodibenzo[*b,f*]thiepin-11-one (**5**). If the reaction of **1** in an aqueous sodium hydroxide solution is carried out, six products, **4**, **5**, 9-hydroxy-thioxanthene-9-carboxylic acid (**6**), thioxanthene-9-carboxylic acid (**7**), thioxanthene (**8**), and 10,11-dihydrodibenzo[*b,f*]-thiepin-10-one (**9**), are formed. The structures of the products were established by elementary analysis, by an examination of the spectral data, by gas chromatography, and by an independent synthesis. The results were discussed in terms of the mechanism proposed.

The synthesis of 10-(4′-methylpiperazino)10,11-dihydrodibenzo[*b,f*]thiepin-11-one (**2**) for a biological evaluation has been described by Jílek *et al.*[1] The treatment of 10-bromo-10,11-dihydrodibenzo[*b,f*]thiepin-11-one (**1**) with 1-methylpiperazine has also been shown to lead to Compound **2** and to 10,11-dihydrodibenzo[*b,f*]thiepin-10,11-dione (**3**) and 10,11-dihydrodibenzo[*b,f*]thiepin-10-one (**9**).[1]

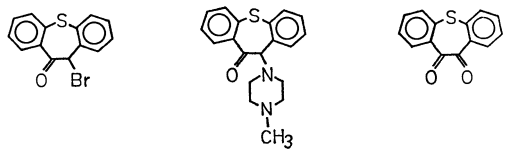

(**1**) (**2**) (**3**)

Chart 1.

As part of an investigation of the synthesis of the derivatives of dibenzo[*b,f*]thiepin with potential biological activity,[2] the present author has attempted to prepare 10-methoxy-10,11-dihydrodibenzo[*b,f*]thiepin-11-one(I) from **1** and sodium methoxide. However, instead of the expected compound I, a neutral product, thioxanthone (**4**), was obtained in a 23% yield.

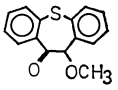

(I)

Chart 2.

The present paper will deal with detailed studies of the reaction of **1** and related compounds (**16**) and (**21**) with alkali.

Results and Discussion

In order to obtain information on the formation of **4**, the author first treated **1** with sodium methoxide in methanol under reflux. The reaction products separated by column chromatography on silica-gel from the reaction mixture were **4** and 10-hydroxy-10,11-dihydrodibenzo[*b,f*]thiepin-11-one (**5**) as is outlined in Scheme 1. Evidence for the **5** structure is based on

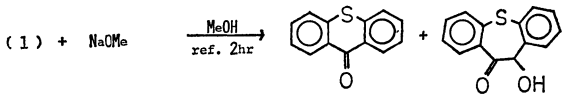

(**4**) (23%) (**5**) (<5%)

Scheme 1.

the NMR and IR spectra; NMR ($CDCl_3$, ppm) δ 4.9 and 6.21 (1H, d, J=5.5 Hz, 11-proton) and 7.0—9.0 (8H, m, aromatic protons), IR (nujol, cm^{-1}) 3400(OH) and 1650(CO). The yields shown are for isolated recrystallized products.

When Compound **1** was treated with a sodium hydroxide solution for 2 hr at 80 °C, six products were obtained, as is outlined in Scheme 2. The acidic product (**6**) separated from the aqueous phase in a 50% yield did not show a constant melting point. The IR spectrum of **6** in Nujol mull indicated absorption bands at 1675 cm^{-1} (CO) and 3450 cm^{-1} (OH), and the NMR spectrum exhibited a signal of aromatic protons at δ 7.2—7.8 in deuteriochloroform. The treatment of its potassium salt (**10**; R=OH) with methyl iodide in DMF at room temperature gave a yellow crystalline (mp 130—131 °C), which was identified as methyl 9-hydroxy thioxanthene-9-carboxylate(**11**) from the results of elementary analysis and its IR and NMR spectra. When **6** was treated with methanol containing a small amount of concentrated hydrochloric acid, methyl 9-methoxythioxanthene-9-carboxylate (**13**) was obtained in a 67% yield. From these experimental results, Compound **6** was identified as 9-hydroxythioxanthene-9-carboxylic acid. Thin-layer chromatography of the mother liquor of the recrystallization of **11** showed the presence of methyl thioxanthene-9-carboxylate (**12**)[3] upon comparison with a sample prepared by an independent route. Therefore, the tlc shows the formation of 9*H*-thioxanthene-9-carboxylic acid (**7**). It was proved therefore, that the acidic reaction products, **6**, contain a small amount of **7**.

Compounds **4** and **9** as neutral products were isolated from the reaction mixture and were found to be identical in IR and NMR spectra with authentic samples. The gas chromatography of the neutral reaction mixture showed the presence of **5** and thioxanthene (**8**) by comparison with the retention time of authentic samples.[4] The yield of **6** is for an isolated product; the

* Abstracted from a portion of a Ph. D. Dissertation submitted in March, 1974, to Osaka University.

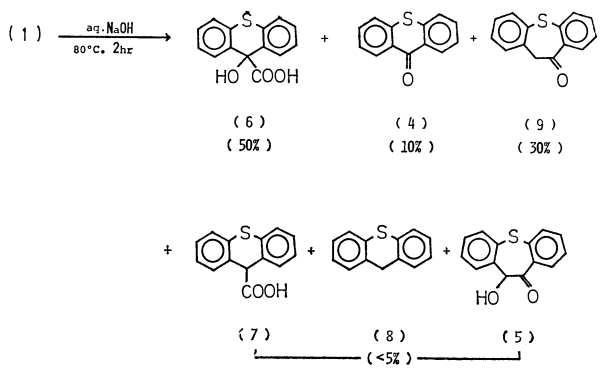

Scheme 2.

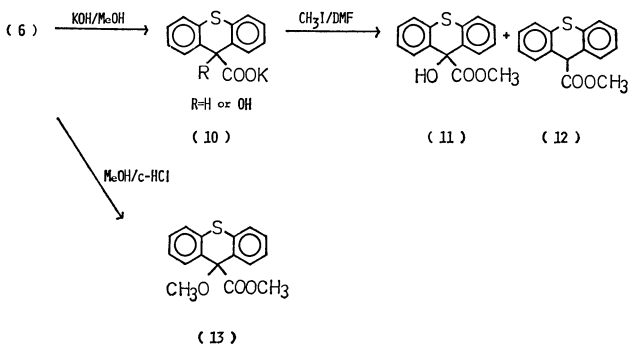

Scheme 3.

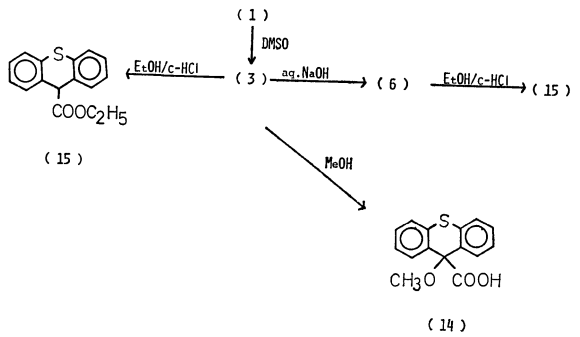

Scheme 4.

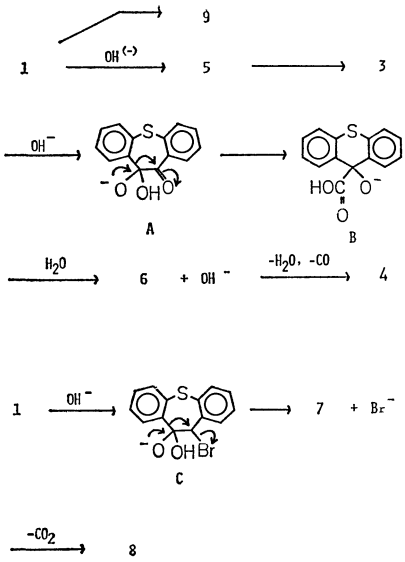

Scheme 5.

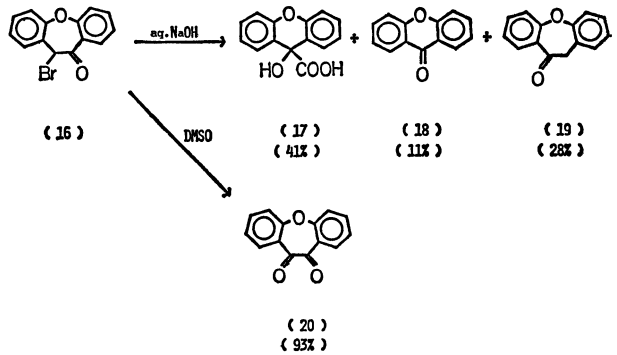

Scheme 6.

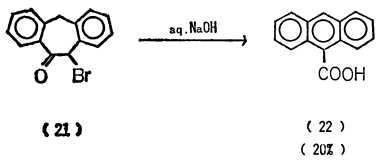

Scheme 7.

yields of **4**, **5**, **7**, **8** and **9** were determined by gas-chromatography of the crude reaction mixture, as is shown in Scheme 2.

The variation of the solvent in the reaction of **1** with alkali changed the products and the product ratios. For example, in water the acidic products were obtained in the highest yield. The formation of neutral products increased with an increase in the amount of methanol. Under anhydrous reaction conditions the acidic products were not isolated from the reaction mixture (see Experimental part).

The treatment of **1** in DMSO gave **3** in an 83.3% yield; it was converted to **6** in an aqueous sodium hydroxide solution.

Mechanisms. Compound **3** has been shown to lead to **6** in an aqueous sodium hydroxide solution and to 9-methoxythioxanthene-9-carboxylic acid (**14**) in methanol.[1] In acid hydrolysis, the formation of 9-Hydroxythioxanthene-9-carboxylate from both **3** and **6** has been reported.[5]

From the above-mentioned experimental results, the plausible mechanistic interpretations shown in Scheme 5 for the formation of **5**, **6**, **7**, and **9** from the reaction of **1** with a base can be advanced. The reaction of **1** with the hydroxy anion gives a secondary alcohol **5**, which is then dehydrogenated to afford diketone **3**.[6] The formation of **6** can be explained as resulting from the base-catalyzed benzilic acid rearrangement of the diketone **3**, as has been described in the literature.[1,9] Compound **9** may be formed by the reductive debromination of **1**. The formation of **7** from **1** and a base can also be explained as resulting from an intermediate, C, formed by the nucleophilic attack of the hydroxy anion on the carbonyl group of **1**. The two products, **4** and **8** appear to have been derived by the dehydration-decarbonylation of **6** and the decarboxylation of **7** respectively.

Table 1. Reaction of **1** with alkali

	Reaction condition[a]		Products		Product ratio[c]
	Base	Solvents (ml)	Acidic[b] (%)	Neutral (g)	
1	Na	MeOH(15)	—	0.5	—
2	NaOH	H_2O(7.5)/MeOH(7.5)	0.5(35.7)	0.4—0.5	1.0—1.2
3	NaOH	H_2O(15)	0.7(50.0)	0.3	2.3

a) 1.5 g of **1** and two equivalent of sodium or sodium hydroxide, are used for all of experiments. Alkali concentration; 2 to 3%, Reaction temperature; 80 °C, time; 2 hr. b) Percentage of acidic substances was calculated on the basis of **3**. c) Weight ratio of acidic and neutral substances.

Similarly, the treatment of 10-bromo-10,11-dihydrodibenz[*b,f*]oxepin-11-one (**16**)[7] in an aqueous sodium hydroxide solution gave 9-Hydroxyxanthene-9-carboxylic acid (**17**), xanthone (**18**), and 10,11-dihydrodibenz-[*b,f*]oxepin-11-one (**19**) in 41%, 11%, and 28% yields respectively. No xanthene-9-carboxylic acid or xanthene was isolated. The oxidation of **16** in DMSO gave **20** in a 93% yield (Scheme 6).

The treatment of 10-bromo-10,11-dihydro-5H-dibenzo[*a,d*]cyclohepten-11-one (**21**)[8] in an aqueous sodium hydroxide solution gave anthracene 9-carboxylic acid **21** in a 20% yield. No neutral products were obtained in this reaction.

Experimental

All the melting points are uncorrected. The IR spectra were taken with a Hitachi EPI-2 spectrometer. The NMR spectra were recorded by means of a Varian A-60 spectrometer in $CDCl_3$, using TMS as the internal standard.

Reaction of 10-Bromo-10, 11-dihydrodibenzo[b,f]*thiepin-11-one* ***1*** *with Alkali. The Reaction of* ***1*** *with Sodium Methoxide in Absolute Methanol*: A solution of 3.0 g of **1** in methanol containing sodium methoxide (prepared from 400 mg of sodium metal and 30 ml of methanol) was refluxed for 3 hr. After the removal of the methanol *in vacuo*, the residue was treated with a mixture of water and ethyl acetate. The ethyl acetate layer was washed with water, dried, and evaporated. A benzene solution of the oily residue (1.5 g) was adsorbed on 75 g of a silica gel (Mallinchrodt®, 100 mesh) and eluted with benzene. The subsequent evaporation of the eluent gave yellow crystals, which were recrystallized three times from cyclohexane to give 0.5 g (23%) of thioxanthone **4** as yellow needles; mp 210—212 °C; Found: C, 73.58; H, 3.65; S, 15.30%. Calcd for $C_{13}H_8OS$: C, 73.58; H, 3.80; S, 15.08%.

Rod-like crystals were obtained from the mother liquors of recrystallization and were crystallized from cyclohexane to give pale yellow, rod-like crystals; mp 121—124 °C. NMR($CDCl_3$, ppm) δ 4.90 and 6.21 (1 H, d, J=5.5 Hz, 11-proton), and 7.0—9.0(8H, m, aromatic protons). IR; ν_{max} (Nujol) 3400(OH), 1650(CO) and 1580 (aromatic)cm^{-1}. The structure of this compound was assumed to be 10-hydroxy-10,11-dihydrodibenzo[*b,f*]thiepin-11-one **5** on the basis of the IR and NMR spectra.

Reaction of ***1*** *with Aqueous Sodium Hydroxide.* A suspension of 3.0 g of **1** in an aqueous sodium hydroxide solution (sodium hydroxide, 0.8 g; water, 30 ml) was stirred for 2 hr at an inner temperature of 80 °C. After cooling, the oil was extracted with ethyl acetate, and the ethyl acetate layer was washed with water, dried, and evaporated. The residue thus obtained was recrystallized from cyclohexane to give 0.8 g (34.8%) of crystals **9**; mp 63—65 °C.

The aqueous layer was acidified with dil. hydrochloric acid and then allowed to stand to cool. The precipitate was filtered and air-dried at room temperature to give 1.3 g (50%) of crystals **6**.

Methyl 9-Hydroxy-thioxanthene-9-carboxylate ***11.*** A 0.4-g portion of **6** was dissolved in 10 ml of methanol containing 0.19 g of potassium hydroxide, and then the methanol was removed *in vacuo* below 30 °C. The colorless solid thus obtained was suspended in 15 ml of DMF. To the mixture we added 1 ml of methyl iodide, and the mixture was stirred for 48 hr at room temperature. To this solution we then added 1 ml of methyl iodide, after which stirring was continued for 48 hr. The reaction mixture was poured into 50 ml of water, made alkaline to pH 10 to 11 with a 10% sodium hydroxide solution, and extracted with ethyl acetate; the solution was then chromatographed on a silica-gel column using ethyl acetate as the eluent. The evaporation of the effluent offered pale yellow crystals, which were recrystallized from cyclohexane to give 0.3 g(67%) of pale yellow crystals **11**; mp 131—131.5 °C. Found: C, 66.15; H, 4.43; S, 11.80%. Calcd for $C_{15}H_{12}O_3S$: C, 66.17; H, 4.44; S, 11.76%.

Methyl 9-Methoxy-thioxanthene-9-carboxylate ***13.*** A 1.5-g portion of **6** was dissolved in a mixed solvent of 15 ml of methanol and 5 ml of conc. hydrochloric acid. The solution was then refluxed for 2 hr. After the removal of the methanol, the residue was extracted with ethyl acetate, and the ethyl acetate layer was dried over magnesium sulfate and evaporated. The solid thus obtained was recrystallized from cyclohexane to give **13**; mp 136.5—138 °C. Found: C, 67.17; H, 4.87; S, 11.06%. Calcd for $C_{16}H_{14}O_3S$: C, 67,12: H, 4.93; S, 11.18%. NMR($CDCl_3$, ppm) δ 2.98(3H, s, CH_3O-), 3.56(3H, s, $COOCH_3$), and 7.1—7.9(8H, m, aromatic protons). IR ν_{max} (Nujol) 1740(CO) and 1250(-O-)cm^{-1}.

10,11-Dihydrodibenzo[b,f]*thiepin-10,11-dione* ***3.*** *Oxidation of* ***9*** *by Selenium Oxide*: To a solution of 6.8 g of **9** in 15 ml of dioxane, we added a solution of 3.33 g of selenium oxide in a mixed solvent of 40 ml of dioxane and 2.5 ml of water. This solution was refluxed for 2 hr. The inorganic substance was then filtered off, and the filtrate was evaporated *in vacuo*. The residue thus obtained was recrystallized from cyclohexane to give 3.5 g (66.3%) of **3**; mp 135—136 °C (lit,[1] 135—136 °C).

Oxidation of ***1*** *by DMSO*: A solution of 1.5 g of **1** in 15 ml of DMSO was stirred for 1 hr on a boiling-water bath. After the subsequent removal of the DMSO *in vacuo*, the residue was recrystallized from cyclohexane to give 1.0 g(83.3%) of **3** as yellow needles; mp 135—136 °C.

10,11-Dihydrodibenz[b,f]*oxepin-10,11-dione* ***20.*** A solution of 2.5 g of **16** in 25 ml of DMSO was stirred for 2 hr on a boiling-water bath. After the subsequent removal of the DMSO *in vacuo*, the residue was recrystallized from benzene to give 1.8 g (93%) of **20**; mp 118—119 °C (lit,[9] 119 °C).

The Reaction of ***16*** *with Alkali.* A suspension of 5.0 g of **16** in an aqueous sodium hydroxide solution (sodium

hydroxide, 1.36 g; water, 50 ml) was stirred for 2 hr at 80 °C. After cooling, the oil was extracted with ethyl acetate. The aqueous layer was acidified with 10% hydrochloric acid, allowed to stand to cool, and then extracted with ethyl acetate. The ethyl acetate layer was washed with water, dried over magnesium sulfate, and evaporated. The residue thus obtained was recrystallized from a mixed solvent of benzene and hexane to give 1.75 g (14%) of **17**, IR; ν_{max} (Nujol) 2400(HO), 1740 and 1720(COO)cm^{-1}. NMR ($CDCl_3$, ppm) δ 7.2—7.8 and 8.2—8.3(8H, m, aromatic protons). The neutral reaction products were chromatographed on a silica-gel column using a mixture of benzene and cyclohexane (1 : 5) as the eluent. Compounds **18** and **19** were isolated in 11% and 28% yields respectively. These compounds were identical with samples of **18**[10] and **19**[11] obtained by an independent route as regards IR and NMR spectra.

*The Reaction of **21** with Alkali.* A solution of 2.1 g of **21**[8] in aqueous sodium hydroxide(sodium hydroxide, 0.5 g; water, 21 ml) was heated at 80 °C for 2 hr with stirring. The reaction mixture was then extracted with ethyl acetate, and the aqueous layer was acidified with dil. hydrochloric acid. The precipitate was filtered and recrystallized from a mixed solvent of acetone and *n*-hexane to give 0.3 g(20%) of crystals; mp 217 °C. NMR($CDCl_3$, ppm) δ 7.3—8.0 (aromatic protons). IR; ν_{max} (Nujol) 2700, 2500 (OH) and 1675(CO)cm^{-1}. The IR and NMR spectra of the compound were identical with those of anthracene 9-carboxylic acid, and the melting point of this compound was not depressed by admixture with the authentic sample.

The author wishes to thank H. Manabe for the spectra data, and T. Ikeda and his associates for the microanalyses.

References

1) J. O. Jílek, E. Svátek, J. Metysová, J. Pomykacek, and M. Protiva, *Collect. Czech. Chem. Commun.*, **32**, 3186 (1967).
2) I. Ueda, Y. Sato, S. Maeno, and S. Umio, *Chem. Pharm. Bull.* (Tokyo), in Press.
3) The ester **12** was obtained by esterification of 9*H*-thioxanthene-9-carboxylic acid.
4) The gas chromatograpy showed the presence of the diketone **3** at 30 min after the reaction bigan, but at the end of the reaction, **3** was not determined.
5) A. Lüttringhaus and G. Creutzburg, *Angew. Chem. Int. Ed. Engl.*, **7**, 128 (1968).
6) E. D. Bergmann and M. Rabinovitz, *J. Org. Chem.*, **25**, 827 (1960).
7) J. R. Geigy. A.-G. Neth. Appl., 6, 605, 741; *Chem. Abstr.*, **66**, 65, 507c (1967).
8) G. J. B. Corts and N. TH. Nauta, *Rec. Trav. Chim. Pays-Bas*, **85**, 389 (1966).
9) F. Mathys, V. Prelog, and R. B. Woodward, *Helv. Chim. Acta.*, **39**, 1095 (1956).
10) A. F. Holleman, "Organic Syntheses," Coll. Vol. I, p. 552 (1941).
11) S. Kimoto, K. Kimura, and S. Muramatsu, *Yakugaku Zasshi*, **74**, 426 (1954).

Synthesis of Chloro(organo-oxy)tin(IV) from Organo-hydroxylic Compound and Tin(II) Chloride

Mitsuo MASAKI, Kiyoshi FUKUI, Izuhiko UCHIDA, and Hiroshi YASUNO

Polymer Research Laboratory, Ube Industries, Ltd., Minami-kaigan, Goi, Ichihara, Chiba 290

(Received December 13, 1974)

The reaction of an organo-hydroxylic compound and tin(II) chloride with a chlorine compound containing positively polarizable chlorine was found to yield trichloro(organo-oxy)tin(IV) or its disproportionation products, dichlorobis(organo-oxy)tin(IV) and tin(IV) chloride. The reaction of tin(II) chloride and *N*-chlorosuccinimide (NCS) with methanol or ethanol afforded methoxy- or ethoxy-trichloro(succinimide)tin(IV) (**1**), while the reaction with *n*-butanol led to the formation of dibutoxydichlorotin(IV) (**2**) and tetrachlorobis(succinimide)tin(IV) (**3**). The reaction of tin(II) chloride and NCS with alcohols in the presence of cyclohexanone oxime gave dialkoxydichloro(cyclohexanone oxime)tin(IV) (**6**). Cyclohexanone oxime and hexahydro-2*H*-azepin-2-one (3,4,5,6-tetrahydro-2*H*-azepin-7-ol) could be used as the organo-hydroxylic reagent in the reaction, while 1-chloronitrosocyclohexane and *N*-chlorohexahydro-2*H*-azepin-2-one were also useful as the chlorine compound. Thus, dichlorobis(cyclohexanone oximato)tin(IV) (**9**), dichlorobis(hexahydro-2*H*-azepin-2-onato)tin(IV) (**13**), and an adduct of **9** with tetrachlorobis(hexahydro-2*H*-azepin-2-one)tin(IV) (1 : 1) were prepared. Two stable complexes, bis(benzophenone oximato)dichlorobis(hexahydro-2*H*-azepin-2-one)tin(IV) (**15**) and dichlorobis-(2-pyridinethiolato)tin(IV) (**11**), were synthesized by the reactions of **13** with benzophenone oxime and 2-pyridinethiol respectively. The complex **13** was also synthesized by the reaction of *N*-trimethylsilylhexahydro-2*H*-azepin-2-one with tin (IV) chloride.

Halogeno(organo-oxy)tin(IV), such as alkoxychlorotin(IV), can be prepared *via* substitution reactions from tin(IV) halides,[1] tetraalkoxytin(IV),[2] and other organotin(IV) compounds.[3] However, these reactions have some limitations on their use as general preparative methods, as has been shown in the literature. There have been two reports on the formation of halogeno (organo-oxy)tin(IV) from tin(II) halides. Nesmejanov and Kozechkow[4] have suggested the probable formation of dichlorodiethoxytin(IV) in the reaction of tin (II) chloride with diarylmercury in ethanol, based upon the isolation of the corresponding aromatic hydrocarbon and metallic mercury. Melinichenko *et al.*[5] reported briefly a reaction of mercury acetate with tin(II)chloride in acetic acid, the reaction gave diacetoxydichlorotin (IV) and mercury.

This paper will describe a new, convenient method for the synthesis of trichloro(organo-oxy)tin(IV) or dichlorobis(organo-oxy)tin(IV), which consists of the reaction of hydroxylic compounds with tin(II) chloride in the presence of a chlorine compound containing positively polarizable chlorine, such as *N*-chlorosuccinimide(NCS), *N*-chlorohexahydro-2*H*-azepin-2-one(NCC), and 1-chloro-1-nitrosocyclohexane(CNC). This reaction is illustrated in Scheme 1. In the first step of the reaction, trichloro(organo-oxy)tin(IV) is formed as a complex with a ligand(YH) derived from the chlorine compound (Y-Cl), which is isolated in a good yield in several cases. The second step is a disproportionation of the complex, giving dichlorobis-(organo-oxy)tin(IV) and a complex of tin(IV) chloride with the ligand (YH). The disproportionation occurs, depending on the nature of the organo-oxy group (RO-) and the ligand (YH), under the conditions used for the first-step reaction.

$$ROH + SnCl_2 + Y\text{-}Cl \xrightarrow{\text{1st step}} ROSnCl_3 \cdot YH$$

$$2\,ROSnCl_3 \cdot YH \xrightarrow{\text{2nd step}} (RO)_2SnCl_2 + (YH)_2SnCl_4$$

ROH: Methanol, Ethanol, *n*-Butanol, Cyclohexanone oxime, and Hexahydro-2*H*-azepin-2-one.

Y-Cl: *N*-Chlorosuccinimide, 1-Chloro-1-nitrosocyclohexane, and *N*-Chlorohexahydro-2*H*-azepin-2-one.

Scheme 1.

Results and Discussion

When methanol, tin(II) chloride, and NCS were allowed to react in a molar ratio of 1 : 1 : 1 in ethylene dichloride (EDC), trichloromethoxy(succinimide)tin (IV) (**1a**) was produced in an 86% yield. An analogous treatment of ethanol, in place of methanol, afforded trichloroethoxy(succinimide)tin(IV) (**1b**) in an 87% yield. However, the treatment of *n*-butanol, tin(II) chloride, and NCS under similar conditions gave di-*n*-butoxydichlorotin(IV) (**2c**) and tetrachlorobis(succinimide)tin(IV) (**3**) instead of *n*-butoxytrichloro(succinimide)tin(IV) (**1c**).

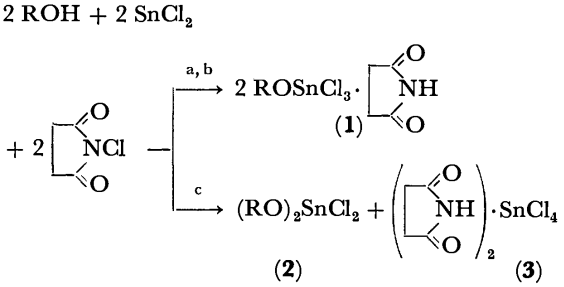

These facts indicate that **1c** readily undergoes disproportionation, while **1a** and **1b** are stable under similar conditions.

The complexes **1a** and **1b** were identified with specimensprepared by the reactions of trichloro(methanol)methoxytin(IV) (**4a**) and trichloro(ethanol)ethoxytin(IV) (**4b**) respectively with succinimide. Such a ligand-exchange reaction has also been reported by Paul *et al.*,[6] who, however, observed only the formation

of complexes of trichloromethoxytin(IV) with various ligands including amides, primary amines and nitrogen heterocycles. Analogously, ligand-exchange reactions occurred when **4a** was treated with an equimolar amount of hexahydro-2*H*-azepin-2-one, its *N*-methyl derivative, or cyclohexanone oxime.

However, when **4a** was treated with a 1.5 fold molar amount of cyclohexanone oxime (**5**), a disproportionation reaction occurred and dichloro(cyclohexanone oxime)dimethoxytin(IV) (**6a**) and tetrachlorobis(cyclohexanone oxime)tin(IV) (**7**) were formed in 94 and 97% yields respectively.

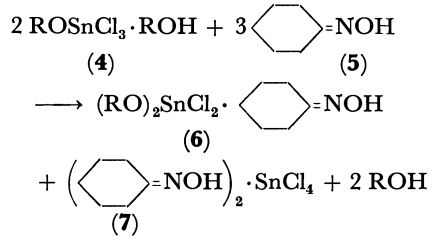

A similar treatment of **1b** or **4b** with **5** gave dichloro(cyclohexanone oxime)diethoxytin(IV) (**6b**) in a good yield. Di-*n*-butoxydichloro(cyclohexanone oxime)tin (IV) (**6c**) was obtained by the treatment of **2c** with an equimolar amount of **5**, providing a confirmation for the formation of **2c** in the reaction mentioned above. The complexes **6** were unexpectedly stable enough to be handled in atmosphere, while dialkoxydichlorotin (IV) or its complexes are, in general, very sensitive to moisture and readily decompose in atmosphere.

The complexes **6** could also be obtained by the reactions of **5**, tin(II) chloride and NCS in the alcohols. In these reactions, the development of blue color was transiently observed, indicating the formation of 1-chloro-1-nitrosocyclohexane (CNC) as one of the reaction intermediates. Since the reaction of **5** with NCS was experimentally confirmed to result in the formation of CNC and succinimide,[7] the use of CNC as a chlorine compound (Y-Cl)[8] in the reaction of Scheme 1 was examined.

As a variation of the hydroxylic compound in the reaction of Scheme 1, **5** was used. The reaction of **5**, tin(II) chloride, and CNC in a molar ratio of 1 : 1 : 1 afforded dichlorobis(cyclohexanone oximato)tin(IV) (**9**) and **7** in good yields. These results shows that trichloro(cyclohexanone oximato)(cyclohexanone oxime)tin(IV) (**10**), formed in the first step, readily undergoes a disproportionation, while trichloro(cyclohexanone oxime)methoxytin(IV) (**8**) is stable under similar conditions. The complex **9** is very sensitive to atmospheric moisture, and the formation of **9** was confirmed by several reactions. The treatment of **9** with alcohols afforded **6** in good yields, and the reaction of **9** with double the molar amount of 2-pyridinethiol gave dichlorobis(2-pyridinethiolato)tin(IV) (**11**) and **5** in 83 and 72% yields respectively.

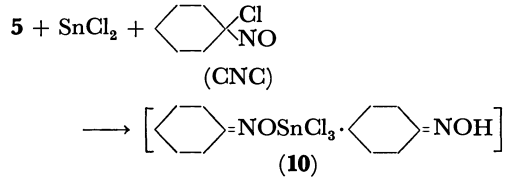

The complex **11** was very stable and was also obtained quantitatively from the reaction of bis(acetylacetonato)-dichlorotin(IV) with 2-pyridinethiol in a molar ratio of 1 : 2.

N-Chlorohexahydro-2*H*-azepin-2-one (NCC) was also useful as a chlorine compound for the reaction shown in Scheme 1. When hexahydro-2*H*-azepin-2-one (**12**), tin(II) chloride, and NCC were allowed to react in a molar ratio of 1 : 1 : 1 in benzene, dichlorobis(hexahydro-2*H*-azepin-2-onato)tin(IV) (**13**) and tetrachlorobis(hexahydro-2*H*-azepin-2-one)tin(IV) (**14**) were both formed in good yields. The complex **13** was isolated as an adduct with benzene (3 : 1), an alternative synthesis of which will be described below.

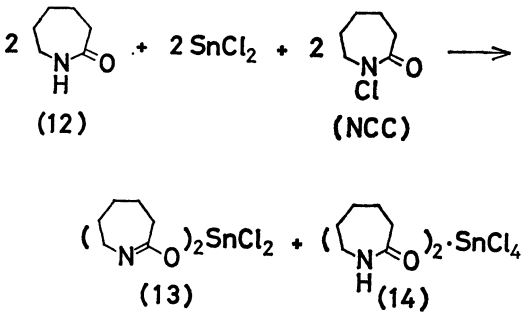

The formation of **13** was supported by two reactions. The first is the reaction with 2-pyridinethiol affording **11** and **12**, while the second reaction consists of a treatment with benzophenone oxime, yielding bis(benzophenone oximato)dichlorobis(hexahydro-2*H*-azepin-2-one)tin(IV) (**15**).[9]

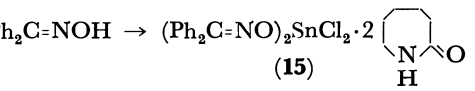

When **5**, tin(II) chloride, and NCC were allowed to react in a molar ratio of 1 : 1 : 1 in benzene, an adduct of **9** with **14** (1 : 1) (**16**) was formed in a good yield. The adduct **16**[10] was also isolated from the reaction of **13** with **7**.

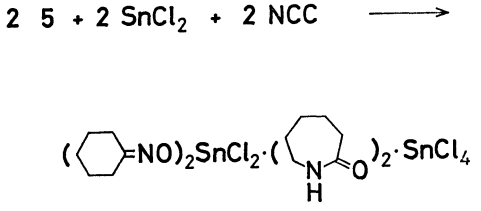

(16)

As an alternative synthesis of **13**, the reaction of *N*-trimethylsilylhexahydro-2*H*-azepin-2-one (**17**) with tin (IV) chloride was performed. When **17** was treated with tin(IV) chloride in a molar ratio of 2 : 1 in benzene, and when trimethylsilyl chloride and the solvent were then removed by evaporation, **13** was obtained as a residue in an elemental analytically pure state. The structural supports for **13** were obtained by a study of the IR, NMR, and mass spectra.

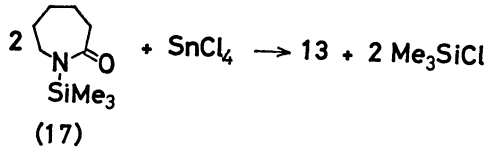

(17)

The IR spectrum of **13** exhibits three strong intensity bands at 1620, 1520, and 330 cm^{-1}. The last band[11] can be assigned to the Sn–Cl vibration in a six-coordinated octahedral tin(IV) complex,[6,12,13] the appearance of only one band in the 300—350 cm^{-1} region suggests a *trans* configuration for two Sn–Cl bonds.[13-15] The C=O stretching band of **12** at 1660 cm^{-1} shifts to a spectral region lower by 30 and 50 cm^{-1} on *O*-coordinated complex formation with boron trifluoride and tin(IV) chloride respectively, indicating that the band at 1620 cm^{-1} of **13** may be due to C=O stretching. Furthermore, the band at 1520 cm^{-1} can be assigned to C=N stretching on the basis of the facts that dichlorobis(3,4,5,6-tetrahydro-2*H*-azepin-7-yl sulfato)-tin(IV) shows only one band, at 1520 cm^{-1}, in the 1500—1700 cm^{-1} spectral region, a band which can be assigned to C=N stretching,[16] and that **17** exhibits no band in the 1500—1700 cm^{-1} spectral region except for a carbonyl band at 1630 cm^{-1}.[16,17]

The proton NMR spectrum of **13** shows three peaks, at 8.20 (12H in β, γ, and δ positions), 7.35 (4H in α) and 6.60 (4H, in ε), and no remarkable splitting of the peaks is observed. This indicates that the two azepine rings in **13** are identical or very similar, because the NMR peaks of α or ε protons may be expected to split when one azepine ring in **13** is bonded only on the nitrogen atom with the tin atom and the other is bonded only on the oxygen atom with the tin atom. This supposition follows from the NMR data of several *N*- or *O*-substituted **12** which are shown in Table 1.

Table 1. NMR-spectra of hexahydro-2*H*-azepin-2-one and its derivatives (τ, in $CHCl_3$)

Compounds	β,γ and δ(6H)	α(2H)	ε(2H)
Unsubstituted	8.25	7.55	6.80
O-Methyl-	8.30	7.60	6.58
N-Methyl-	8.30	7.47	6.60
N-Chloro-	8.20	7.40	6.10
N-Trimethylsilyl-	8.30	7.48	6.78

These spectral observations lead to a probable structure for **13**, which is shown in Fig. 1, although it is not yet clear whether the two oxygen-tin bonds are *cis* or *trans*.

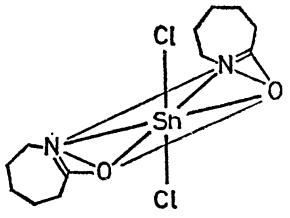

Fig. 1. A probable structure for **13**. An alternative structure, in which two oxygen-tin bonds are *trans*, is also possible.

The complex **13** could not be prepared by the conventional methods of synthesis mentioned in the above introductory part. The recrystallization of **13** from benzene-ethyl ether afforded the adduct with benzene (3 : 1).

Some comments can be made about the mechanism of the reaction shown in Scheme 1, although there has not, so far as we aware, been any report on the oxidation of bivalent tin into a tetravalent state with a halogen compound containing positively polarizable halogen under non-aqueous conditions.[18] Three modes of the pathway can be postulated for the first step reaction. The first involves an initial reaction of tin (II) chloride with the chlorine compound giving a trichlorotin(IV) derivative (A), followed by the replacement of the latter with the hydroxylic compound. The second involves the initial formation of a hypochlorite-type compound (B) from the hydroxylic compound and the chlorine compound and the subsequent reaction of B with tin(II) chloride. The third pathway consists of a concerted mechanism involving a cyclic transition state (C).

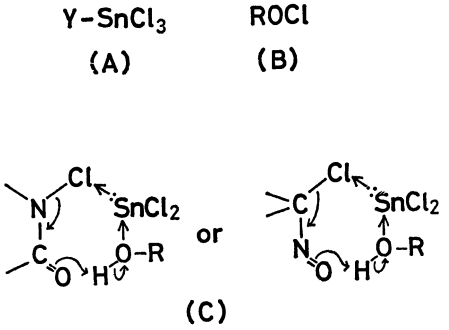

The first-step reaction or the overall reaction of Scheme 1 is independent of the order in which the hydroxylic compound or the chlorine compound is added to tin(II) chloride, although in several cases some reactions have been observed between the two reactants before the addition of the third reactant. For instance, a reaction was observed to occur when NCS was added to tin(II) chloride; the reaction gave a product which might be an *O*-coordination complex of tin(II) chloride with NCS or trichloro(succinimidato)-tin(IV). Although the product could not be confirmed because of its very hygroscopic character, the reaction is so slow as still to be incomplete after stirring for 12 hr at room temperature or for several hours at 80 °C. On the other hand, the reaction of NCS and tin(II) chloride with alcohols or **12** is essentially completed within several hours at room temperature or within 1 hr at 80 °C. Furthermore, the reaction between **5**, tin(II) chloride, and CNC proceeds smoothly in benzene at room temperature, while scarcely no reaction of CNC with tin(II) chloride occurred under the same conditions. It is clear, therefore, that the first pathway is not predominant. The second pathway seems also not to be favored, since NMR spectral investigations do not indicate an isomerization of CNC or NCC into the corresponding hypochlorite-type compound (B) in the presence of **5** or **12**, in spite of the successful reactions of **5**, tin(II) chloride, and CNC and of **12**, tin(II)

chloride, and NCC.

At present, in view of these observations, it seems that the first-step reaction of Scheme 1 can best be explained by the third pathway, although the first and second pathways may be competitive to some extent according to the combination of reactants.

Experimental

All the compounds containing tin or silicon atoms, except the $(acac)_2SnCl_2$, **6** and **11**, were handled in a dry nitrogen atmosphere. The reagents and organic solvents for the reactions were used as anhydrous states. All the melting points are uncorrected. The products were identified, unless otherwise mentioned, by comparisons of the melting points and IR spectra with those of authentic samples.

*Trichloromethoxy(succinimide)tin(IV) (**1a**).* *a) From Methanol, $SnCl_2$, and NCS*: To a solution of NCS (3.34 g, 25 mmol) in EDC (120 ml) was added $SnCl_2$ (4.74 g, 25 mmol) with stirring at room temperature. A slightly exothermic reaction occurred, and the temperature of the mixture rose by 3.5—5 °C. To the stirred mixture was added drop by drop a solution of methanol (0.9 g, 28 mmol) in EDC (30 ml) at room temperature, after which the mixture was refluxed for 1 hr. The resulting solid was collected by filtration, washed with EDC, and dried to give 7.62 g (86%) of **1a**; mp 192.5—197.5 °C(decomp). IR(KBr): 3140, 3050, 1785, 1700, 1640, 515, 445, 360, 340(sh), 320, 300 and 285 cm^{-1}.

Found: C, 16.95; H, 2.46; N, 3.79; C, 29.63%. Calcd for $C_5H_8Cl_3NO_3Sn$: C, 16.91; H, 2.27; N, 3.94; Cl, 29.95%.

*b) From **4a** and Succinimide*: A mixture of **4a**[1a] (7.20 g, 25 mmol) and succinimide (2.45 g, 25 mmol) in EDC (250 ml) was heated under atmospheric pressure until 100 ml of the solvent had been distilled off. The resultant solid was collected by filtration, washed with EDC, and dried to give 8.26 g (93%) of **1a**; mp 192.5—197.5 °C (decomp).

*Trichloroethoxy(succinimide)tin(IV) (**1b**).* *a) From Ethanol, $SnCl_2$ and NCS*: In a manner similar to Method *a)* used for **1a**, NCS (3.34 g, 25 mmol) was treated with $SnCl_2$ (4.74 g, 25 mmol) in EDC (120 ml) and subsequently with ethanol (1.2 g, 26 mmol) in EDC (30 ml), thus giving 8.0 g (87%) of **1b**; mp 188.5—189.5 °C (decomp). IR (KBr): Essentially identical in pattern with that described in *a)* for **1a**.

Found: C, 19.68; H, 2.87; N, 3.60; Cl, 28.63%. Calcd for $C_6H_{10}Cl_3NO_3Sn$: C, 19.52; H, 2.73; N, 3.79; Cl, 28.81%.

*b) From **4b** and Succinimide*: In a manner similar to Method *b)* used for **1a**, **4b**[1a] (7.90 g, 25 mmol) was treated with succinimide (4.90 g, 50 mmol) in benzene (250 ml) to give 8.42 g (91%) of **1b**.

*Trichloro(hexahydro-2H-azepin-2-one)methoxytin(IV) (**18**).* In a manner similar to Method *b)* used for **1a**, **4a** (14.41 g, 50 mmol) was treated with **12** (5.66 g, 50 mmol) in benzene (300 ml) to give 17.86 g (97%) of **18**; mp 196—199 °C (decomp). IR (KBr): 3350, 1610, 530, 510, 350, 320, 295 and 285 cm^{-1}.

Found: C, 22.95; H, 3.61; N, 3.51; Cl, 29.10%. Calcd for $C_7H_{14}Cl_3NO_2Sn$: C, 22.77; H, 3.61; N, 3.51; Cl, 28.80%.

*Trichloromethoxy(1-methylhexahydro-2H-azepin-2-one)tin(IV) (**19**).* In a manner similar to Method *b)* used for **1a**, **4a** (7.20 g, 25 mmol) was treated with 1-methylhexahydro-2*H*-azepin-2-one (3.18 g, 25 mmol) in benzene (170 ml) to give 8.76 g (91%) of **19**; mp 217.5—219 °C (decomp.) IR (KBr): 1600, 525, 450, 350, 325, 310 and 280 cm^{-1}.

Found: C, 25.04; H, 4.29; N, 3.63; Cl, 27.91%. Calcd for $C_8H_{16}Cl_3NO_2Sn$: C, 25.07; H, 4.21; N, 3.66; Cl, 27.75%.

*Trichloro(cyclohexanone oxime)methoxytin(IV) (**8**).* In a manner similar to Method *b)* used for **1a**, **4a** (14.41 g, 50 mmol) was treated with **5** (5.66 g, 50 mmol) in benzene (300 ml) to give 14.76 g (80%) of **8a**; mp 158.5—160 °C (decomp). IR (KBr): 3180, 3100, 1130, 1080, 1060, 510, 490, 345, 320 and 310 cm^{-1}.

Found: C, 22.70; H, 3.78; N, 4.05; Cl, 28.63%. Calcd for $C_7H_{14}Cl_3NO_2Sn$: C, 22.77; H, 3.82; N, 3.79; Cl, 28.80%.

*Dichloro(cyclohexanone oxime)dimethoxytin(IV) (**6a**).* *a) From **4a** and **5***: To a solution of **4a** (7.20 g, 25 mmol) in methanol (100 ml) was added **5** (4.24 g, 37.5 mmol): the mixture was then stirred for 2 hr at room temperature. The resulting precipitates were collected by filtration, washed with methanol and dried to give crude **6a** (4.28 g, 94%). Recrystallization from EDC-methanol gave an analytical sample as colorless crystals; mp 156 °C (decomp). IR (KBr): 2760—2260 (centered at 2500), 2200—1800 (centered at 2050), 1110, 1040, 1010, 590, 520, 475, 350, 310 and 275 cm^{-1}.

Found: C, 26.24; H, 4.74; N, 3.71; Cl, 19.47%. Calcd for $C_8H_{17}Cl_2NO_3Sn$: C, 26.30; H, 4.66; N, 3.84; Cl, 19.45%.

The methanolic filtrate and washings were concentrated to dryness, and the residue was treated with benzene to give colorless precipitates. Filtration afforded 5.92 g (97%) of **7**.[19]

*b) From Methanol, $SnCl_2$, NCS and **5***: To a suspension of NCS (3.34 g, 25 mmol) in methanol (100 ml) was added $SnCl_2$ (4.74 g, 25 mmol) at room temperature: the temperature of the mixture thereby rose by 11 °C. The resultant solution was stirred for 2 hr at room temperature. To the solution was added **5** (4.24 g, 37.5 mmol) at room temperature, after which stirring was continued for 2 hr. The resultant solid was collected by filtration, washed with methanol (50 ml), and dried to give 4.41 g (97%) of **6a**.

The combined filtrate and washings were then concentrated, and the residue was treated with EDC (150 ml) to give 5.19 g (85%) of **7** as colorless precipitates.

The EDC solution was concentrated, and the residue was extracted with boiling benzene (100 ml). After the insoluble residue had been removed by filtration, the hot benzene solution was allowed to stand at room temperature, thus affording 2.08 g (85%) of succinimide, as colorless crystals.

*Dichloro(cyclohexanone oxime)diethoxytin(IV) (**6b**).* *a) From **4b** and **5***: In a manner similar to Method *a)* used for **6a**, **4b** (7.90 g, 25 mmol) was treated with **5** (4.24 g, 37.5 mmol) in ethanol (200 ml), thus affording crude **6b** (4.51 g, 92%). Recrystallization from EDC-ethanol gave colorless crystals; mp 157—158 °C (decomp). IR (KBr): Essentially identical in pattern with that described in *a)* for **6a**.

Found: C, 30.47; H, 5.45; N, 3.47; Cl, 18.30%. Calcd for $C_{10}H_{20}Cl_2NO_3Sn$: C, 30.57; H, 5.39; N, 3.57; Cl, 18.05%.

The ethanolic filtrate and washing were concentrated and the residue was treated with EDC (100 ml), thus affording 5.75 g (94%) of **7** as colorless precipitates.

*b) From Ethanol, $SnCl_2$, NCS and **5***: In a manner similar to Method *b)* used for **6a**, NCS (3.34 g, 25 mmol) was treated with $SnCl_2$ (4.74 g, 25 mmol) in ethanol (200 ml) and subsequently with **5** (4.24 g, 37.5 mmol). 4.68 g (96%) of **6b** were thus obtained, together with 5.6 g (92%) of **7** and 1.99 (81%) of succinimide.

*Di-n-butoxydichloro(cyclohexanone oxime)tin(IV) (**6c**).* *a) From **2c** and **5***: The reaction of NCS (3.34 g, 25 mmol), $SnCl_2$ (4.74 g, 25 mmol), and *n*-butanol (1.9 g, 25.6 mmol) in EDC (120+30 ml) was performed in a manner identical with that described in *a)* for **1a**. The resulting reaction mixture was filtered to give 3.11 g (54%) of **3**. Recrystallization from EDC gave an analytical sample as colorless needles; mp 149.5—152.5 °C (decomp). Found C, 20.95;

H, 2.43; N, 5.90%. Calcd for $C_8H_{10}Cl_4N_2O_4Sn$: C, 20.95; H, 2.26; N, 6.11%.

Since it became clear that **3** was partially soluble in the EDC used as the solvent, but was scarcely soluble in benzene, the same reaction was repeated, but in benzene (90+30 ml), in order to make the separation of **3** from the reaction mixture easy. The resulting reaction mixture was filtered to give 4.76 g (83%) of **3**. To the filtrate was added **5** (2.83 g, 25 mmol) and the mixture was stirred for 2 hr at room temperature. The resultant solid was collected by filtration, washed by being suspended in EDC (50 ml×2), and dried to give 0.85 g of **7**. The combined filtrate and washings were concentrated, and the residue was treated with *n*-butanol to give 3.15 g (56%) of **6c** as colorless precipitates. Recrystallization from EDC-*n*-butanol gave an analytical sample; mp 152—156 °C (decomp). IR (KBr): Essentially identical in pattern with that described in *a)* for **6a**.

Found: C, 37.55; H, 6.24; N, 3.06; Cl, 16.00%. Calcd for $C_{14}H_{29}Cl_2NO_3Sn$: C, 37.45; H, 6.51; N, 3.21; Cl, 15.79%.

b) From n-*Butanol, $SnCl_2$, NCS and* **5**: In a manner similar to Method *b)* used for **6a**, NCS (3.34 g, 25 mmol) was treated with $SnCl_2$ (4.74 g, 25 mmol) in *n*-butanol and subsequently with **5** (4.24 g, 37.5 mmol). The resultant reaction mixture was filtered to give 8.71 g of a mixture of **6c** and **7** as a powdery solid. This mixture was then treated with EDC (100 ml) to give 2.49 g (41%) of **7** as an insoluble solid. The EDC solution separated from **7** was concentrated, and the residue was treated with *n*-butanol (100 ml) to afford 3.94 g (70%) of **6c** as colorless precipitates. The solution separated from **6c** was combined with the *n*-butanolic filtrate separated from the above mixture, and then concentrated. The residue was treated with boiling benzene (150 ml) to give 2.58 g (42%) of **7** as an insoluble solid. Thus, the total yield of **7** was 5.07 g (83%). The hot benzene solution separated from **7** was allowed to stand at room temperature to give 1.94 g (79%) of succinimide as colorless crystals. The benzene solution separated by filtration was concentrated, and the residue was treated with *n*-butanol (30 ml) to give a further 1.55 g portion (28%) of **6c**. Thus, the total yield of **6c** was 5.49 g (98%).

1-Chloro-1-nitrosocyclohexane (CNC). To a solution of **5** (11.31 g, 100 mmol) in benzene (100 ml) was added NCS (13.35 g, 100 mmol); the mixture was then stirred for 5 hr at room temperature, whereby a intensive blue color was developed. The resultant solid was collected by filtration, washed with benzene, and dried to give 9.18 g (93.6%) of succinimide. The combined filtrate and washing were washed with water (50 ml×2), dried over Na_2SO_4, and concentrated to give crude CNC (11.74 g, 80%). Distillation gave 7.42 g (50%) of CNC; bp 54—54.5 °C/15 mmHg (lit,[7a] 52 °C/12 mmHg).

*Dichlorobis(cyclohexanone oximato)tin(IV) (**9**).* To a stirred mixture of $SnCl_2$ (9.47 g, 50 mmol) and **5** (5.65 g, 50 mmol) in benzene (70 ml) was added drop by drop a solution of CNC (7.38 g, 50 mmol) in benzene (30 ml) below 12 °C with ice cooling. The mixture was stirred overnight at room temperature, and then the resulting solid was collected by filtration, washed with EDC (50 ml), and dried to give 11.96 g (98%) of **7**. The benzene filtrate was concentrated to dryness, giving crude **9** as a very hygroscopic, semicrystalline solid (10.58 g). IR (KBr): 2940, 2850, 1600, 1435, 990, 970 and 590 cm^{-1}.

Structural support for **9** was obtained by reactions with alcohols, and 2-pyridinethiol. The reaction with the latter reagent is described in the *b)* section for **11**.

Reaction with Alcohols: Crude **9** (3.0 g) was added to 50 ml of methanol, ethanol, or *n*-butanol, and the mixture was stirred for 1 hr at room temperature. The resulting precipitates were collected by filtration to give **6a** (1.79 g, 67%), **6b** (1.92 g, 67%) or **6c** (2.4 g, 74%). The products were confirmed by means of their melting points and IR spectra, which were identical with those of the respective authentic samples prepared above.

The alcoholic filtrate was concentrated, and the residue was extracted with boiling *n*-hexane (50 ml×3). The combined extracts were concentrated to dryness, giving **5** as a crystalline residue. The yields of **5** in reactions with methanol, ethanol and *n*-butanol were 0.70 g (85%), 0.64 g (79%) and 0.75 g (91%) respectively.

*Dichlorobis(hexahydro-2H-azepin-2-onato)tin(IV) (**13**). a) From **17** and $SnCl_4$*: To a stirred solution of **17**[17] (9.27 g, 50 mmol) in benzene (60 ml) was added drop by drop a solution of $SnCl_4$ (6.51 g, 25 mmol) in benzene at room temperature, after which the stirring was continued for 5 hr. The resultant solution was concentrated to dryness on an oil bath at 40 °C under reduced pressure in order to remove the benzene and trimethylsilyl chloride. **13** was obtained as a colorless crystalline residue (10.64 g, theoretical yield is 10.35 g); mp 85—86 °C. An analytical sample was obtained by drying the residue at 70 °C. IR (KBr): 1620, 1520, 1455, 530, 470, 330 and 275 cm^{-1}. MS (*m/e*): 414 (M^+), 379 (M−Cl), 302 (M−$C_6H_{10}NO$) and (M−Cl−$C_6H_{10}NO$).

Found: C, 34.95; H, 5.06; N, 6.63; Cl, 17.54%. Calcd for $C_{12}H_{20}Cl_2N_2O_2Sn$: C, 34.82; H, 4.87; N, 6.77; Cl, 17.13%.

*b) Adduct of **13** with Benzene (3 : 1)*: A solution of **13** (8.30 g of the crystalline residue obtained above) in benzene (50 ml) was stirred for 4 hr at room temperature and allowed to stand overnight. A trace of an insoluble substance was filtered off, and ethyl ether (60 ml) was added to the filtrate. After stirring for 7 hr, the resulting colorless solid was collected by filtration, washed with a small quantity of benzene, and dried at room temperature to give 1.15 g of the adduct; mp 100—101 °C. IR (KBr): 1620, 1550 and 680 cm^{-1}. MS: Identical peaks shown in *a)* for **13**.

Found: C, 38.22; H, 5.08; N, 6.10; Cl, 16.32%. Calcd for $(C_{12}H_{20}Cl_2N_2O_2Sn)_3C_6H_6$: C, 38.19; H, 5.00; N, 6.36; Cl, 16.14%.

*c) Preparation of a Solution of **13** (from **12**, $SnCl_2$, and NCC)*: To a suspension of $SnCl_2$ (4.74 g, 25 mmol) in benzene (60 ml) was added **12** (2.83 g, 25 mmol), after which the mixture was stirred for 30 min at room temperature. To the resultant solution was added drop by drop a solution of NCC[20] (3.69 g, 25 mmol; bp 55 °C/4×10^{-3} mmHg) in benzene (40 ml) below 10 °C, with ice cooling. After the addition, the mixture was stirred for 15 hr at room temperature, and then it was filtered to give **14**[21] as a colorless powdery solid (5.89 g, 96.7%) and a solution, which was confirmed to contain **13** (12.5 mmol in the theoretical yield) by treatment with 2-pyridinethiol or benzophenone oxime, and by the isolation of the adduct of **13** with benzene.

*d) Isolation of the Benzene Adduct from the Solution Prepared in c) for **13***: The solution was concentrated to give a caramel-like residue, which was then dissolved in benzene (10 ml) after which the solution was stirred for 20 hr at room temperature. The resultant solid was collected by filtration, washed with a small quantity of benzene, and dried at room temperature to give 2.61 g (47%) of the adduct, whose mp, IR and MS were identical with those of the specimen obtained in *b)* for **13**. Found: C, 38.23; H, 5.14; N, 6.01; Cl, 16.45%.

Dichlorobis(2-pyridinethiolato)tin(IV) (II). a) From Bis

*(acetylacetonato)dichlorotin(IV) (**20**) and 2-Pyridinethiol*: To a stirred solution of **20** (3.88 g, 10 mmol) in benzene (100 ml) was added 2-pyridinethiol (2.22 g, 20 mmol), after which the mixture was refluxed for 30 min. The resultant solid was collected by filtration, washed with EDC, and dried to give 3.86 g (94%) of **11** as a slightly pale yellow, powdery solid; mp 275—277 °C (decomp). IR (KBr): 1580, 1550, 1435, 1420, 410, 400, 310, 300 and 270 cm^{-1}. MS (*m/e*): 410 (M^+), 375 (M−Cl), 340 (M−Cl_2), 300 (M−PyS) and 265 (M−Cl−PyS).

Found: C, 29.38; H, 1.83; N, 6.87; Cl, 17.24; S, 15.81%. Calcd for $C_{10}H_8Cl_2N_2S_2Sn$: C, 29.30; H, 1.97; N, 6.83; Cl, 17.30; S, 15.64%.

*b) From **9** and 2-Pyridinethiol*: A solution of **9** was prepared by the reaction of 25 mmol portions of $SnCl_2$, **5**, and CNC in benzene (100 ml), followed by a separation from the resultant **7**. To the solution was added 2-pyridinethiol (2.78 g, 25 mmol) at room temperature, and the mixture was stirred for 2 hr. The resulting solid was collected by filtration, washed with EDC (50 ml), and dried to give 4.28 g (83%) of **11**; mp 275—277 °C (decomp.)

The combined filtrate and washings were concentrated, and the residue was extracted with boiling *n*-hexane (50 ml × 3). The combined extracts were then concentrated to dryness to give 2.05 g (72%) of **5** as crystals.

*c) From **13** and 2-Pyridinethiol*: To the solution of **13** in benzene, prepared by Method *c)* for **13** was added 2-pyridinethiol (2.78 g, 25 mmol), and the mixture was treated in a manner identical with that described in *b)* for **11**, thus giving 4.67 g (91%) of **11**.

*Bis(benzophenone oximato)dichlorobis(hexahydro-2H-azepin-2-one)tin(IV) (**15**).* To a solution of **13** (5.28 g, 12.75 mmol, prepared by Method *a)* for **13**) in benzene (100 ml) was added benzophenone oxime (5.03 g, 25.5 mmol), and the mixture was stirred overnight. The resultant solid was collected by filtration, washed with benzene (70 ml), and dried in a nitrogen atmosphere at room temperature to give 9.34 g (90.5%) of **15**; mp 178.5—180.5 °C. IR (KBr); 3280, 1630, 940, 700, 540, 450, 340(sh), 330, 320 and 295 cm^{-1}.

Found: C, 56.50; H, 5.05; N, 6.74; Cl, 8.75%. Calcd for $C_{38}H_{42}Cl_2N_4O_4Sn$: C, 56.41; H, 5.20; N, 6.93; Cl, 8.78%.

A similar treatment of the solution of **13** in benzene prepared by Method *c)* for **13** with benzophenone oxime (4.93 g, 25 mmol) afforded 8.39 g (83%) of **15**.

*An Adduct of **9** and **14** (1 : 1) (**16**).* *a) From **13** and **7***: To a solution of **13** (5.44 g, 13.15 mmol, prepared by Method *a)* for **13**) in benzene (100 ml) was added **7**[16] (6.40 g, 13.15 mmol), and the mixture was stirred for 15 hr at room temperature. The resultant solid was collected by filtration, washed with benzene (40 ml), and dried overnight at 70 °C under reduced pressure to give 11.19 g (94.5%) of **16** as a colorless, powdery solid; mp 103—108 °C (sintering begins at 98 °C). IR (KBr): 3330, 3280, 3190, 1630, 1010, 990, 525, 510, 350(sh), 320—310 and 290 cm^{-1}.

Found: C, 32.34; H, 4.72; N, 5.90; Cl, 23.83%. Calcd for $C_{24}H_{42}Cl_6N_4O_4Sn_2$: C, 31.97; H, 4.66; N, 6.22; Cl, 23.62%.

*b) From **5**, $SnCl_2$, and NCC*: A solution of NCC (7.38 g, 50 mmol) in benzene (30 ml) was added drop by drop to a stirred mixture of **5**, (5.66 g, 50 mmol) and $SnCl_2$ (9.48 g, 50 mmol) in benzene (90 ml) below 14 °C; the stirring was continued overnight at room temperature after the addition. The resulting solid was collected by filtration, washed with benzene, and dried at room temperature under reduced pressure for 7 hr to give 21.03 g (81%) of **16** containing benzene (1.82 mol per 1 mol of **16**) as a colorless powdery solid; mp 97—98 °C.

Found: C, 40.21; H, 5.07; N, 5.34; Cl, 20.68%. Calcd for $C_{24}H_{42}Cl_2N_4O_4Sn\cdot(C_6H_6)_{1.82}$: C, 40.22; H, 5.12; N, 5.37; Cl, 20.40%. The solid was further dried for 6.5 hr at 50 °C and then for 7.5 hr at 70 °C under reduced pressure to give benzene-free **16**. Found: C, 32.44; H, 4.75; N, 6.11; Cl, 23.94%.

The authors wish to express their gratitude to Professor Emeritus Masao Horio of Kyoto University and President Shotaro Sugiura of the Polymer Research Laboratory, Ube Industries, for their constant encouragement throughout this work. The authors also wish to express thanks to Professor Teruaki Mukaiyama of Tokyo Institute of Technology for his valuable suggestions.

References

1) a) D. C. Bradley, E. V. Caldwell, and W. Wardlaw, *J. Chem. Soc.*, **1957**, 3030, 4775. b) R. Piekos and A. Radecki, *Roczniki Chem.*, **39**, 765 (1965). c) R. Ueeda, Y. Kawasaki, T. Tanaka, and R. Okawara, *J. Organometal. Chem.*, **5**, 194 (1966). d) R. C. Mehrotra and V. D. Gupta, *J. Indian Chem. Soc.*, **40**, 911 (1963).

2) R. C. Mehrotra and V. D. Gupta, *ibid.*, **43**, 155 (1966).

3) a) W. H. Nelson and D. F. Martin, *J. Organometal. Chem.*, **4**, 67 (1965). b) Y. Kawasaki and R. Okawara, *J. Inorg. Nucl. Chem.*, **27**, 1168 (1965).

4) A. N. Nesmejanow and K. A. Kozeschkow, *Ber.*, **63**, 2496 (1930).

5) L. S. Melnichenko, N. N. Zemlyanski, K. A. Samurskaya, and K. A. Kozeschkow, *Dokl. Akad. Nauk SSSR*, **190**, 351 (1970): Eng. Ed. p. 48.

6) R. C. Paul, H. S. Makhni, P. Singh, and S. L. Chadha, *Z. Anorg. Allg. Chem.*, **377**, 108 (1970).

7) The reaction of **5** with *N*-bromosuccinimide is known to give 1-bromo-1-nitrosocyclohexane: a) D. C. Iffland and G. X. Criner, *J. Amer. Chem. Soc.*, **75**, 4047 (1953), but the reaction of **5** with NCS has not been reported, in spite that several methods for the preparation of CNC have been described: b) H. Diekmann and W. Luttke, *Angew. Chem. Int. Ed. Engl.*, **7**, 387 (1968) and references cited therein.

8) A positively polarizable character of chlorine in CNC has been observed in the reaction of CNC with triphenylphosphine; M. Ohno and J. Sakai, *Tetrahedron Lett.* **1965**, 4541.

9) An alternative structure, bis(benzophenone oxime)-dichlorobis(hexahydro-2*H*-azepin-2-onato)tin(IV), can be excluded on the basis of the fact that benzophenone oxime does not form a complex even with tin(IV) chloride, while **12** readily forms complexes with chlorotin(IV)'s, such as alkoxytrichlorotin(IV) and tin(IV) chloride.

10) The structural consideration of the adduct (**16**) is now in progress; the results will be published elsewhere, together with other experimental results.

11) A referee suggested the possibility that the band at 330 cm^{-1} may be due to the Sn–O vibration. Although positive evidence is lacking to date, we still favor the assignment of the band to the Sn–Cl vibration. This is based on the facts that, in the literature, [6,13,22] the strong-intensity bands in the 300—350 cm^{-1} region in the spectra of most hexa-coordinated tin(IV) complexes containing both Sn–O and Sn–Cl bonds have been assigned to the Sn–Cl vibration and the bands in the 400—600 cm^{-1} region have been assigned to the Sn–O vibration. The spectrum of **13** shows a medium-intensity band at 515 cm^{-1} which can be assigned to Sn–O vibration, because the complexes **1**, **18**, **19**, **8**, **6**, **15**,

and **16** exhibit absorption bands in the 500—550 cm^{-1} region in the respective spectra, while no band is observed in the 500—600 cm^{-1} region in the IR spectrum of **11**.

12) I. R. Beattie and M. Milne, *J. Inorg. Nucl. Chem.*, **28**, 1651 (1966).

13) R. C. Paul and S. L. Chadha, *Aust. J. Chem.*, **22**, 1381 (1969).

14) J. P. Clark and C. J. Wilkins, *J. Chem. Soc., A*, **1966**, 871.

15) I. R. Beattie, G. P. McQuilian, L. Rule, and M. Webster, *ibid.*, **1963**, 1514.

16) M. Masaki *et al.*, unpublished results.

17) K. Ruhlmann and B. Rupprich, *Ann. Chem.*, **686**, 226 (1965).

18) Although the oxidation of tin(II) halide with a molecular halogen is known to give tin(IV) halide, molecular chlorine can not be used as a chlorine compound in this method. Even if molecular chlorine caused the first step reaction competitively with the formation of tin(IV) chloride, the final product would be only a complex of tin(IV) chloride with an organo-hydroxylic compound, because the trichloro(organo-oxy)tin(IV) formed in the reaction would be immediately converted into the complex by the by-produced hydrogen chloride (Y=Cl, in Scheme 1).

19) M. Masaki, K. Fukui, M. Uchida, K. Yamamoto, and I. Uchida, This Bulletin, **46**, 3179 (1973).

20) G. Caprata, G. Lemetre, and A. Vercellone, *Ann. Chim.* (Rome), **49**, 1167 (1959).

21) Inventa AG., Swiss Pat. 326,165 (1958).

22) a) R. Chand and S. L. Chadha, *J. Inorg. Nucl. Chem.*, **31**, 2753 (1969). b) S. H. Hunter, V. M. Langford, G. A. Rodley, and C. J. Wilkins, *J. Chem. Soc., A*, **1968**, 305.

The Formation of Ethers from Nerol and *l*-Linalool in the Presence of Boron Trifluoride Etherate

Kimiko NAGAI

Department of Chemistry, Faculty of Science, Hiroshima University, Higashisenda-machi, Hiroshima 730

(Received January 6, 1975)

Upon treatment with boron trifluoride etherate at room temperature, *dl*-linaloyl neryl, *dl*-geranyl linaloyl, *dl*-neryl α-terpenyl, and dineryl ethers were obtained from nerol and linaloyl neryl, *l*-geranyl linaloyl, *dl*-neryl α-terpenyl, and *l*-linaloyl piperityl ethers, from *l*-linalool. Of these ethers, linaloyl piperityl ether was thought to be formed by the cyclization of linaloyl neryl and geranyl linaloyl ethers.

In connection with previous papers on the formation of ethers from geraniol,[1] *d*-borneol, *dl*-isoborneol,[2] and *l*-isopulegol,[3] the action of boron trifluoride etherate ($BF_3 \cdot Et_2O$) on nerol (I) and *l*-linalool (II) was examined in the present work; five ethers were obtained, and their structures were determined to be *dl*-linaloyl neryl (III), *l*-geranyl linaloyl (IV), *dl*-neryl α-terpenyl (V), dineryl (VI), and *l*-linaloyl piperityl (VII) ethers.

To date, several works have been reported on the reaction of I and II with an acidic catalyst, but they have dealt with the characterization of monomeric products; there are no descriptions of higher-boiling products.[4,5]

Results and Discussion

Nerol and *l*-linalool were treated with boron trifluoride etherate under the various conditions listed in Table 1. Each reacted mixture was fractionated into monomeric (bp 60—90 °C/4 mmHg) and dimeric (bp 90—120 °C/4 mmHg) fractions, and the monomeric fraction was further separated by elution chromatography into the two portions of hydrocarbons and the oxygen-containing compounds.

Characterization of Monomeric Products. The monomeric hydrocarbon portions thus separated from reacted mixtures of I and II commonly showed eight peaks in glc, although their relative intensities were different. The components, after being isolated through preparative glc, were identified as myrcene, α-terpinene, dipentene, β-ocimene X,[6] β-ocimene Y,[6] γ-terpinene, *p*-cymene, and terpinolene by mass and IR spectroscopy and by glc admixing authentic samples.

The monomeric oxygen-containing portions from reacted mixtures of I and II were examined by glc and IR, NMR, and mass spectroscopy; linalool, α-terpineol, and geraniol were identified in the case of I other than unreacted alcohol, and *d*-α-terpineol, nerol, and geraniol, in the case of II.

Characterization of Dimeric Products. The dimeric fractions from the reacted mixtures of I and II were eluted over a silica gel column with benzene to separate the individual components. Thus, III, IV, V, and VI were characterized in the case of I, and III, IV, V, and VII, in the case of II, as will be shown below.

dl-*Linaloyl Neryl Ether (III)*: A colorless, oily compound was isolated from dimeric fractions of both I and II as a less polar substance than geranyl linaloyl ether.[1] The molecular formula of this compound was determined to be $C_{20}H_{34}O$, which corresponds to that of terpene ether based on the molecular ion in the mass spectra; the IR spectrum showed characteristic ether bands at 1118, 1098, 1048, and 1039 cm^{-1}, and the NMR spectrum revealed proton signals of five vinylic methyl groups at δ 1.60 (6H), 1.67 (6H), and 1.72 (3H), whose chemical shifts are in good correspondence with those of the isopropyridene of II (δ 1.60, 1.67, each 3H, br. s)[8] and of isopropyridene (δ 1.60, 3H, br. s, δ 1.68, 3H, d, $J=1$ Hz) and the vinylic methyl signals (δ 1.72, 3H, d, $J=1$ Hz) of I.[8] The correspondence of the proton signals was also observed between vinylic methyls of geranyl linaloyl ether[1] and its mother alcohols. This evidence suggests that the compound is linaloyl neryl ether.

The ether was subjected to catalytic hydrogenation over an Adams catalyst in acetic acid to give an octahydro derivative, $C_{20}H_{40}O$, which was identified as tetrahydrolinaloyl tetrahydroneryl ether based on the coincidence of the IR and NMR spectra with those of an authentic ether synthesized from *dl*-tetrahydrolinalool and tetrahydronerol (tetrahydrogeraniol) according to Williamson's procedure.[7] Thus, it is certain that the compound was *dl*-linaloyl neryl ether (III).

l-*Geranyl Linaloyl Ether (IV)*: This ether, $C_{20}H_{34}O$, $[\alpha]_D^{18}$ −16.7°, was isolated as a secondary, eluted, colorless, oily compound from dimeric fractions of II. The IR, NMR, and mass spectra were superimposable on those of the geranyl linaloyl ether which had been obtained in the reaction of geraniol with boron trifluoride etherate and whose structure has been proposed.[1] The compound took up four molar equivalents of hydrogen in catalytic hydrogenation over platinum oxide in acetic acid to give an octahydro derivative which was identical with tetrahydrogeranyl tetrahydrolinaloyl ether in glc and spectroscopy. This ether, IV, was also detected as a trace in glc of the reacted mixture from I.

dl-*Neryl α-Terpenyl Ether (V)*: A third colorless, oily ether was isolated from dimeric fractions of I and II as a more polar substance than geranyl linaloyl ether.

The $C_{20}H_{34}O$ ether absorbed three molar equivalents of hydrogen in catalytic hydrogenation over platinum oxide in acetic acid to give a hexahydro derivative, $C_{20}H_{40}O$, which was identified as tetrahydroneryl dihydro-α-terpenyl ether by a comparison of the IR, NMR, and mass spectra with those of an authentic synthesized ether.

The IR and NMR spectra of the ether exhibited the presence of an ether linkage (1162, 1141, 1056, and 1040 cm^{-1}; δ 3.87, 2H, d, $J=7$ Hz) connecting an allylic methylene and a tertiary carbon, gem-dimethyls

TABLE 1. REACTION OF NEROL AND *l*-LINALOOL WITH BORON TRIFLUORIDE ETHERATE

No. of experiment	Nerol[a]			Linalool[a]			
	1	2	3	4	5	6	7
$BF_3 \cdot Et_2O$ (ml)	0.7	0.7	0.7	0.5	0.6	0.7	0.7
Reaction temp. (°C)	20	20	10	30	30	30	20
Reaction period (hr)	24	72	24	30	30	30	24
Conversion (%)[b]	68.0	96.0	31.0	75.0	83.0	87.0	65.0
C_{10}-Hydrocarbons acyclic (%)	0.3	2.0	0.8	0.5	0.9	1.6	1.0
C_{10}-Hydrocarbons cyclic (%)	0.7	5.0		1.5	2.5	4.0	5.0
Geraniol (%)	1.0	2.0	trace	2.0	2.5	1.5	3.0
Nerol (%)	—	—	—	1.0	0.8	0.5	1.0
α-Terpineol (%)	17.0	30.0	1.6	13.0	14.0	14.0	11.0
Linalool (%)	4.0	6.0	0.8	—	—	—	—
Linaloyl neryl ether (%)	6.0	7.0	2.4	3.0	2.2	2.7	3.0
Neryl α-terpenyl ether (%)	8.0	9.0	2.4	4.0	2.4	4.3	1.0
Dineryl ether (%)	6.0	7.0	3.0	—	—	—	—
Geranyl linaloyl ether (%)	trace	trace	trace	16.0	15.9	15.9	10.0
Linaloyl piperityl ether (%)	—	—	—	11.0	11.8	10.5	2.0
Residue (%)	25.0	28.0	20.0	23.0	30.0	32.0	28.0
Total cyclization (%)	25.7	44.0	4.0	29.5	30.7	32.8	19.0

a) Ten grams of the alcohol were used in each experiment. b) Composition of reacted mixtures was determined with the aid of gas chromatography.

on an oxygen-bearing carbon atom (1381 and 1369 cm^{-1}; δ 1.13, 6H, s), four vinylic methyls (1675 and 830 cm^{-1}; δ 1.60, 3H, br. s, δ 1.67, 6H, br. s. and δ 1.72, 3H, d, J=1 Hz), three vinylic protons (δ 5.30, 3H, m), and four allylic methylenes (δ 2.10, 8H, br. s). Moreover, the proton signals of the four vinylic methyls showed a good correspondence with those of a vinylic methyl and an isopropyridene group of nerol and of a vinylic methyl of α-terpineol. Thus, the ether could be characterized as *dl*-neryl α-terpenyl ether (V).

Dineryl Ether (VI): The $C_{20}H_{34}O$ ether, which was isolated as the most polar substance in the elution chromatography of the dimeric fractions from I, took up four molar equivalents of hydrogen in catalytic hydrogenation over platinum oxide in acetic acid to give an octahydroether, $C_{20}H_{42}O$, whose IR, NMR, and mass spectra were superimposable upon those of ditetrahydroneryl ether synthesized from tetrahydronerol.

The IR and NMR spectra of the ether showed the presence of an ether linkage connecting two allylic methylenes (1100, 1068 cm^{-1}; δ 4.03, 4H, d, J=7 Hz), each of which was coupled with a vinylic proton (1672 and 835 cm^{-1}; δ 5.30, 4H, m), and both of isopropyridene and vinylic methyl (δ 1.60, 6H, br. s and δ 1.67, 1.72, each 6H, d, J=1 Hz).[8] The methyl signals of the isopropyridene and vinylic methyl also corresponded to those of nerol. Thus, it is certain that this compound was dineryl ether (VI).

l-Linaloyl Piperityl Ether (VII): The most polar compound, $C_{20}H_{34}O$, $[\alpha]_D^{18}$ −38.3°, which was isolated from the dimeric fraction of II showed absorption bands attributable to an ether linkage at 1148, 1118, 1108, and 1085 cm^{-1} and an *m/e* 137 (14%) ion, $C_{10}H_{17}$, characteristic of the mass spectra of the terpene ethers mentioned above. The compound gave a dihydro derivative, $C_{20}H_{36}O$, in catalytic hydrogenation over platinum oxide in methanol and a saturated hexahydro derivative, $C_{20}H_{40}O$, in catalytic hydrogenation over the same catalyst in acetic acid. The evidence revealed the compound to be a mixed ether of acyclic and monocyclic terpene alcohols.

The NMR spectrum of the compound showed a typical ABX signal attributable to a terminal vinyl group (δ 5.95, q, J_{AX}=18 Hz, J_{BX}=10 Hz; δ 5.15, q, J_{AB}=2 Hz, J_{AX}=18 Hz; δ 4.95, q, J_{AB}=2 Hz, J_{AX}=10 Hz, each 1H), overlapped with signals of other olefinic protons. This signal disappeared in the spectrum of the dihydro derivative, which contained the proton signals attributable to two secondary methyls (δ 1.11 and 1.16, each 3H, d, J=6 Hz), three vinylic methyls (δ 1.60 and 1.68, 6H and 3H, each br. s), two vinylic protons (δ 5.08, 2H, m), two allylic methylenes (δ 2.00, 4H, br. s), an oxygen-bearing methine (δ 3.95, 1H, d, J=7 Hz), and a methyl attached to an oxygen-bearing tertiary carbon (δ 1.10, 3H, s); the signal of the last methyl showed an upper-field shift by 0.18 ppm compared with that of the corresponding methyl group in the original ether (δ 1.28, 3H, s), as well as those of the methyls attached to an oxygen-bearing tertiary carbon in both linalool (δ 1.28, 3H, s) and dihydrolinalool (δ 1.10, 3H, s). On the other hand, the hexahydro derivative of VII was heated with hydroiodic acid and also treated with acetic anhydride and boron trifluoride etherate to give menthyl iodide and menthyl acetate respectively. The evidence certainly indicates that the ether is linaloyl l-*p*-menthenyl ether.

As the position to which the linalooxy residue is attached, three carbons, $C_{(3)}$, $C_{(5)}$, and $C_{(6)}$, of the l-*p*-menthenyl moiety are possible.

As has been mentioned above, both oxygen-bearing

Table 2. Conversion of *dl*-linaloyl neryl ether and *dl*-geranyl linaloyl ether by boron trifluoride etherate

	Linaloyl neryl ether (%)	Geranyl linaloyl ether (%)
Unreacted ether	2.0	6.2
Monoterpene hydrocarbons	33.0	6.8
Linalool	—	8.2
α-Terpineol	20.1	4.7
Nerol	—	trace
Geraniol	—	2.3
Linaloyl piperityl ether	25.0	57.0
Polymer	13.5	10.1
Other compounds	6.4	4.7

methines of VII and its dihydro derivative commonly showed the doublet at δ 3.95 (J=7 Hz), while the methine group of the hexahydro derivative of VII showed the triplet at δ 3.40. Such an upward shift and change in the signal pattern depending upon the saturation of the 1-*p*-menthene residue picked up the $C_{(3)}$ from the above possible position as the ether-linked position. Thus, the structure of the ether is probably *l*-linaloyl piperityl ether.

The Dreiding model examination of VII, furthermore, showed the following facts: when the isopropyl group holds the pseudoequatorial conformation, the dihedral angle between $C_{(2)}$–H and $C_{(3)}$–H is approximately 80°, and that between $C_{(3)}$–H and $C_{(4)}$–H, 170°; when the isopropyl group holds the axial conformation, they are, respectively, 45° and 75°. On the other hand, the NMR spectra of VII and its dihydro derivative showed a doublet with 7 Hz as the proton signals due to the C_3-methine groups. According to Karplus' equation[9] these results indicate that both $C_{(3)}$–H and $C_{(4)}$–H in the molecule of VII are in the axial conformation. This ether was also obtained by treating III and IV with boron trifluoride etherate, as is shown in Table 2.

The Course of Formation. Under the same conditions (Experiments 1 and 7), although I and II showed a nearly equal conversion, an appreciable difference was observed in the relative yields of the hydrocarbons, alcohols, ethers, and residues (polymers): the yields of the monoterpene alcohols and the ethers were higher in the case of I, whereas the monoterpene hydrocarbons and the residue (polymer) were obtained in higher yields from II (*cf.* Table 1).

All the monoterpene hydrocarbons identified in the present investigation can be explained as being formed by the deprotonation of the carbonium ions listed in Scheme 1, A, B, C, and D, which may be produced from I and II in the presence of boron trifluoride etherate, and the formation of all the monoterpene alcohols is attributable to the coupling of these cations and the hydroxyl anions.

Of the ethers, the III, V, and VI characterized in the reaction of I and the III and IV characterized in the reaction of II may be formed by a combination between these carbonium ions and the mother alcohol, I or II; besides, VII, as has been mentioned above, is

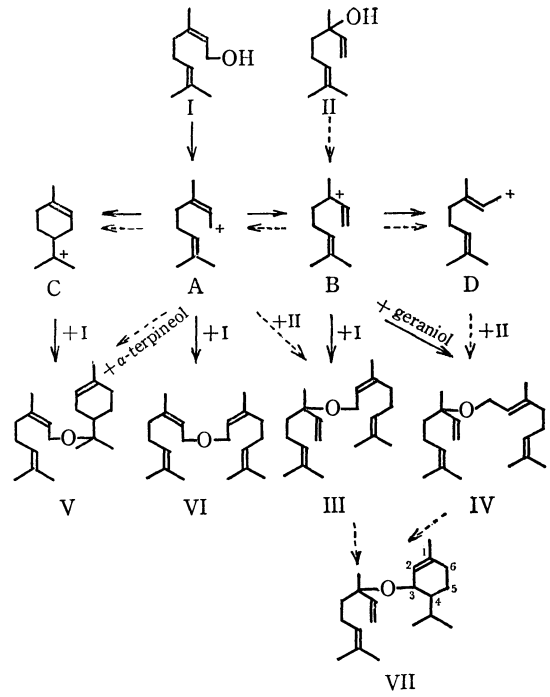

Scheme 1.

attributable to the cyclization of III and IV. Regarding the formation of IV in the reaction of I and that of V in the reaction of II, the contribution of geraniol and α-terpineol, which are produced in large amounts in these reactions, may be supposed.

Experimental

Apparatus. The IR spectra were taken either in liquid film or a CCl_4 solution, and the NMR spectra, on a 60 MHz spectrometer in a $CDCl_3$ solution, using TMS as the internal reference. The mass spectra were measured by means of a Hitachi RMS-4 spectrometer under these operating conditions: 80 eV, ionization-chamber voltage; 80 μA, total emission; 1800 eV, ion-accelerating voltage, and 200 °C, ionization-chamber temperature. The combined glc-mass analyses were carried out on a Shimadzu-LKB 9000 gas chromatograph, and the mass spectrometer, in connection with a 3 mm×3 m glass tube packed with Carbowax 20 M (10%) on Diasolid (60—80 mesh) under a 5 °C/min temperature program from 50 °C to 120 °C; 70 eV, ionization voltage; 3500 eV, ion-accelerating voltage and 200 °C, ionization temperature. The glc was carried out on a FID-type apparatus in connection with stainless-steel column (3 mm×3 m) packed with Carbowax 6000 (10%) on Diasolid (60—80 mesh), DEGS (10%), on Shimalite W (60—80 mesh) and Silicone SE-30 (10%) on Uniport B (60—80 mesh) under the 20 ml/min flow rate of a N_2 carrier.

Materials. Commercial nerol and *l*-linalool were used after repeated fractional distillation. They each showed one peak in glc with DEGS- and Carbowax 6000-packed columns, and the IR spectra of these materials coincided with authentic ones.[10] Nerol: bp 109 °C/10 mmHg, n_D^{20} 1.4630, $[\alpha]_D^{20}\pm0°$ ($CHCl_3$); linalool: bp 70 °C/4 mmHg, n_D^{25} 1.4650, $[\alpha]_D^{16}-19.7°$ ($CHCl_3$), phenylurethane, mp 63—64 °C.

A chemical-grade reagent of $BF_3\cdot Et_2O$ (BF_3 47%) was used without any purification.

Reaction of Nerol (I) and l-Linalool (II) with $BF_3\cdot Et_2O$.

To each 10 g portion of I and II, the amount of $BF_3 \cdot Et_2O$ listed in Table 1 was added, drop by drop. The mixture was then allowed to react under several temperatures for periods from 24 hr to 72 hr. The reacted mixtures were shaken with a saturated aqueous solution of sodium carbonate to decompose the remaining $BF_3 \cdot Et_2O$, washed with water, dried over anhydrous sodium sulfate, and fractionated under reduced pressure to separate two fractions (bp 60—90 °C/4 mmHg and 90—120 °C/4 mmHg).

Characterization of Monoterpene Compounds. Each low-boiling fraction (bp 60—90 °C/4 mmHg) separated from the reacted mixtures of I and II was eluted over a silica gel column with *n*-hexane and then ethyl acetate to separate it further into two hydrocarbon and alcohol portions. The hydrocarbon portions from I and II, both showing eight peaks in glc with a Carbowax 6000-packed column, was gas-chromatographed by admixing them with authentic samples and subjected to combined glc-mass analysis; they were thus identified as myrcene, β-ocimene X, β-ocimene Y, α-terpinene, γ-terpinene, dipentene, *p*-cymene, and terpinolene.[11] The IR spectra of these compounds which were taken after the isolation by preparative glc showed good agreement with those of authentic samples.

The alcohol portions from I and II each showed three peaks other than the peak of unreacted alcohol in glc with DEGS. By comparison with authentic samples through glc, and by taking the IR spectra of isolated individual components, the components were identified as linalool, α-terpineol, and geraniol in the case of I and as α-terpineol, $[\alpha]_D^{20}+31.0°$, nerol, and geraniol in the case of II. α-Terpineol phenylurethane (mp 112—113 °C) and geraniol phenylurethane (mp 123.5—124.0 °C) were also prepared.

Characterization of Dimeric Products from Nerol (I). The high-boiling fractions (bp 90—120 °C/4 mmHg) from reaction mixtures of I showed the existence of four compounds in tlc carried out with silica gel and benzene and in glc with Silicone SE-30- and Carbowax 20M-packed columns at 200 °C. By elution over a silica gel column with benzene, the compounds were isolated.

dl-*Linaloyl Neryl Ether (III).* The compound showing a peak of t_R 8.7 on the SE-30 was isolated as the most quickly-moving colorless, viscous oil in the elution chromatography with benzene. n_D^{17} 1.4714. $[\alpha]_D^{17}\pm0°$ ($CHCl_3$), $C_{20}H_{34}O$ (M^+ 290). $\nu_{max}^{CCl_4}$ cm^{-1}: 3080, 930, 1645 ($CH_2=CH-$), 1673, 840 ($-CH=\underline{C}-$), 1118, 1098, 1048, 1039 (C–O–C). $\delta_{ppm}^{CDCl_3}$: 1.27 (3H, s, $C\underline{H}_3-\underline{C}-O$), 1.60 (6H, br. s, $C\underline{H}_3-\underline{C}=\underline{C}-$), 1.67 (6H, br. s, $C\underline{H}_3-\underline{C}=\underline{C}-$), 1.72 (3H, d, $J=1$ Hz, $C\underline{H}_3-\underline{C}=\underline{C}-$), 3.80 (2H, d, $J=7$ Hz, $-\underline{C}=CH-C\underline{H}_2-O-$), 4.90—5.97 (5H, m, $C\underline{H}_2=C\underline{H}-$ and $-C\underline{H}=\underline{C}-$). Mass: *m/e* 41(80%), 69(base), 71(21), 81(67), 93(36), 95(36), 101(34), 121(11), 123(9), 136(18), 137(21), 153(6), 154(7), 247(2, $M^+-C_3H_7$), 290 (1, M^+, $C_{20}H_{34}O$).

Catalytic Hydrogenation of III: Compound III (200 mg) was hydrogenated over platinum oxide (20 mg) in acetic acid (6 ml) to give an octahydro derivative as a colorless oil in a good yield. $\nu_{max4}^{CCl_4}$ cm^{-1}: 1381, 1366 ($CH_3-\underline{C}H-CH_3$), 1149, 1072 (C–O–C). $\delta_{ppm}^{CDCl_3}$: 0.90 (15H, d, $J=6$ Hz, $C\underline{H}_3-\underline{C}H-$), 1.10 (3H, s, $C\underline{H}_3-\underline{C}-O-$), 3.30 (2H, t, $J=6$ Hz, $-\underline{C}-O-C\underline{H}_2-CH_2-$). The spectra were superimposable on those of the tetrahydrolinaloyl tetrahydroneryl ether synthesized in the following section.

Synthesis of Tetrahydrolinaloyl Tetrahydroneryl Ether. Tetrahydronerol (3 g) was dissolved in a mixture of hydrobromic (48%, 10 g) and concentrated sulfuric acids (3 g), and the solution was refluxed for 6 hr. The reacted mixture, after being cooled to room temperature, was successively washed with water, a 10% aqueous solution of sodium bicarbonate, and water, dried over sodium sulfate, and fractionated under ordinary pressure. The tetrahydroneryl (tetrahydrogeranyl) bromide was thus obtained as a colorless oil (bp 222—223 °C) in a yield of 60%. $\nu_{max}^{CCl_4}$ 4 cm^{-1}: 1391, 1374 ($CH_3-\underline{C}H-CH_3$). $\delta_{ppm}^{CDCl_3}$: 0.85 (9H, d, $J=6$ Hz, $C\underline{H}_3-\underline{C}H-$), 1.21 (8H, br.s, $-C\underline{H}_2-$), 3.42 (2H, t, $J=7$ Hz, $-CH_2-C\underline{H}_2-Br$).

dl-Tetrahydrolinalool (1 g) was refluxed with metallic sodium (0.3 g) in dried ether (10 ml) for 18 hr. After the unreacted sodium had been filtered off, the tetrahydroneryl bromide (0.5 g) prepared above was added to the filtrate; the mixture was then refluxed again for 18 hr. The mixture thus reacted was washed with water, dried over anhydrous sodium sulfate, and fractionated under reduced pressure to give tetrahydrolinaloyl tetrahydroneryl ether as a colorless oil in a 10% yield. n_D^{18} 1.4850, $[\alpha]_D^{20}\pm0°$ ($CHCl_3$). ν_{max}^{liq} cm^{-1}: 1381, 1366 ($CH_3-\underline{C}H-CH_3$), 1149, 1072 (C–O–C). $\delta_{ppm}^{CDCl_3}$: 0.89 (15H, d, $J=6$ Hz, $C\underline{H}_3-\underline{C}H-$), 1.10 (3H, s, $C\underline{H}_3-\underline{C}-O-$), 3.30 (2H, t, $J=6$ Hz, $-\underline{C}-O-C\underline{H}_2-CH_2-$).

dl-*Neryl α-Terpenyl Ether (V).* The compound, t_R 10.5 on the SE-30, was isolated as a colorless oil by elution chromatography with benzene. n_D^{17} 1.4809, $[\alpha]_D^{20}\pm0°$ ($CHCl_3$), $C_{20}H_{34}O$ (M^+ 290). $\nu_{max}^{CCl_4}$ cm^{-1}: 1381, 1369 ($CH_3-\underline{C}H-CH_3$), 1162, 1141, 1056, 1040 (C–O–C), 1675, 830 ($-\underline{C}=CH-$). $\delta_{ppm}^{CDCl_3}$: 1.13 (6H, s, $(C\underline{H}_3)_2-\underline{C}-O-$),1.60 (3H, br. s, $C\underline{H}_3-\underline{C}=CH-$), 1.67 (6H, br. s, $C\underline{H}_3-\underline{C}=CH-$), 1.72 (3H, d, $J=1$ Hz, $C\underline{H}_3-\underline{C}=CH-$), 3.87 (2H, d, $J=7$ Hz, $-\underline{C}=CH-C\underline{H}_2-O-$), 5.30 (3H, m, $-C\underline{H}=\underline{C}-$). Mass: *m/e* 41(53%), 69(68), 81(base), 83(20), 93(27), 95(53), 107(7), 109(4), 117(38), 119(34), 121(14), 136(36), 137(51), 154(9), 272(2, M^+-H_2O), 290 (1, M^+, $C_{20}H_{34}O$).

Catalytic Hydrogenation of V: Compound V (250 mg) was subjected to catalytic hydrogenation over platinum oxide (30 mg) in acetic acid (7 ml) to give a hexahydro derivative as a colorless oil in a good yield. $\nu_{max}^{CCl_4}$ cm^{-1}: 1383, 1368 ($CH_3-\underline{C}H-CH_3$ and $CH_3-\underline{C}-CH_3$), 1173, 1150, 1121, 1070 (C–O–C). $\delta_{ppm}^{CDCl_3}$: 0.86 (12H, d, $J=6$ Hz, $C\underline{H}_3-\underline{C}H-$), 1.08 (6H, s, $(C\underline{H}_3)_2-\underline{C}-O-$), 3.31 (2H, t, $J=6$ Hz, $-\underline{C}-O-C\underline{H}_2-CH_2-$). Mass: *m/e* 39(5%), 41(22), 43(48), 55(34), 57(80), 59(40), 69(22), 71(78), 81(10), 85(65), 99(17), 123(7), 139(9), 140(7), 141(38), 142(6), 199(base), 211(4), 281(4, M^+-CH_3), 296(2, M^+, $C_{20}H_{40}O$). The spectra were in good agreement with those of the tetrahydroneryl dihydro-α-terpenyl ether to be synthesized in the following section.

Synthesis of Tetrahydroneryl Dihydro-α-terpenyl Ether. Dihydro-α-terpineol (1 g) was refluxed with metallic sodium (0.3 g) in dried ether (10 ml) for 18 hr. After the unreacted sodium had then been filtered off, the tetrahydroneryl bromide (0.5 g) prepared in the above section was added to the filtrate, the mixture being refluxed for 18 hr. The reacted mixture was afterwards treated by a usual procedure to give tetrahydroneryl dihydro-α-terpenyl ether as a colorless oil in a yield of 15%. $\nu_{max}^{CCl_4}$ cm^{-1}: 1382, 1368 ($CH_3-\underline{C}H-CH_3$), 1173, 1150, 1121, 1070 (C–O–C). $\delta_{ppm}^{CDCl_3}$: 0.86 (12H, d, $J=6$ Hz, $C\underline{H}_3-\underline{C}H-C\underline{H}_3$), 1.08 (6H, s, $(C\underline{H}_3)_2-\underline{C}-O-$), 3.31 (2H, t, $J=6$ Hz, $-\underline{C}-O-C\underline{H}_2-CH_2-$). Mass:

m/e 41(22%). 43(48), 55(34), 57(80), 59(40), 69(22), 71(78), 81(20), 85(65), 123(7), 139(9), 141(38), 199(base), 281(4), 296(2, M^+, $C_{20}H_{40}O$).

Dineryl Ether (VI). The compound, t_R 11.8 on the SE-30, was isolated as the last colorless oil in the elution chromatography of the dimeric fraction of I. n_D^{17} 1.4771; $C_{20}H_{34}O$ (M^+ 290). $\nu_{max}^{CCl_4}$ cm^{-1}: 1672, 835 (-C=CH-), 1100, 1068 (C-O-C). $\delta_{ppm}^{CDCl_3}$: 1.60 (6H, br. s, CH_3-C=CH-), 1.67 and 1.72 (each 6H, d, J=1 Hz, CH_3-C=CH-), 4.03 (4H, d, J=7 Hz, -C=CH-CH_2-O-), 5.30 (4H, m, -CH=C-). Mass: *m/e* 41(96%), 69(base), 81(72), 83(27), 93(49), 95(36), 107(12), 117(45), 119(45), 121(14), 123(13), 135(13), 136(28), 137(21), 154(12), 290(1, M^+, $C_{20}H_{34}O$).

Catalytic Hydrogenation of VI: Compound VI (200 mg) was hydrogenated over a platinum oxide catalyst (20 mg) in acetic acid (6 ml) to give an octahydroether in a good yield. ν_{max}^{liq} cm^{-1}: 1390, 1383, 1371 (CH_3-CH-CH_3), 1119 (C-O-C). $\delta_{max}^{CDCl_3}$: 0.85 (18H, d, J=6 Hz, CH_3-CH-), 3.40 (4H, t, J=6 Hz, -CH_2-CH_2-O-). Mass: *m/e* 39 (19%), 41(62), 43(base), 55(50), 57(52), 69(37), 70(31), 71(30), 83(24), 85(18), 97(15), 140(10), 141(6), 163(6), 298(1, M^+, $C_{20}H_{42}O$). The spectra were superimposable upon those of the ditetrahydroneryl ether to be synthesized in the following section.

Synthesis of Ditetrahydroneryl Ether. Tetrahydroneryl bromide (1 g) was added to a dried ether solution of sodium tetrahydronerolate which had been prepared from tetrahydronerol and metallic sodium, the mixture being refluxed for 18 hr. The ditetrahydroneryl ether was thus obtained as a colorless oil in a 12% yield. ν_{max}^{liq} cm^{-1}: 1390, 1383, 1371 (CH_3-CH-CH_3), 1119 (C-O-C). $\delta_{ppm}^{CDCl_3}$: 0.85 (18H, d, J=6 Hz, CH_3-CH-), 3.40 (4H, t, J=6 Hz, -CH_2-CH_2-O-). Mass: *m/e* 39(19%), 41(62), 43(base), 55(50), 57(52), 69(37), 70(31), 71(30), 83(24), 85(18), 97(15), 140(10), 141(6), 298(1, M^+, $C_{20}H_{42}O$).

Characterization of Dimeric Products from l-Linalool (II). The high-boiling fraction (bp 90—120 °C/4 mmHg) from each reaction product of II showed the existence of four compounds in the tlc carried out with silica gel and benzene and in the glc carried out with the Silicone SE-30- and Carbowax 20 M-packed columns at 200 °C. These compounds were isolated by being eluted over a silica gel column with benzene and were characterized as is shown below.

l-Geranyl Linaloyl Ether (IV). The colorless oil, t_R 9.5, was isolated as the secondary eluted compound from the dimeric fraction of II by silica gel column chromatography with benzene. n_D^{15} 1.4834, $[\alpha]_D^{18}$ −16.7° ($CHCl_3$); $C_{20}H_{34}O$ (M^+ 290, Rast's mol. wt. 293). ν_{max}^{liq} cm^{-1}: 1670, 830 (-C=CH-), 1000, 917 (CH_2=CH-), 1108, 1050 (C-O-C). $\delta_{max}^{CDCl_3}$: 1.28 (3H, s, CH_3-C-O-), 1.60, 1.68 (15H, br. s, CH_3-C=CH-), 3.82 (2H, d, J=6 Hz, -CH_2-O-C-), 4.95—5.95 (6H, m, CH_2=CH- and -CH=C-). Mass: *m/e* 41 (62%), 55(21), 69(base), 81(50), 93(32), 95(29), 109(10), 121(14), 123(17), 137(22), 153(26), 290(2, M^+, $C_{20}H_{34}O$). These spectra were coincident with those of geranyl linaloyl ether.[1)]

Catalytic Hydrogenation of IV: Compound IV (100 mg) was hydrogenated over a platinum oxide catalyst (10 mg) to give an octahydro derivative as a colorless oil in a good yield. ν_{max}^{liq} cm^{-1}: 1381, 1366 (CH_3-CH-CH_3), 1149, 1072 (C-O-C). $\delta_{max}^{CDCl_3}$: 0.90 (15H, d, J=6 Hz, CH_3-CH-), 1.10 (3H, s, CH_3-C-O-), 3.30 (2H, t, J=6 Hz, -C-O-CH_2-CH_2-). These spectra were coincident with those of tetrahydrogeranyl tetrahydrolinaloyl ether synthesized as will be shown below.

Synthesis of dl-*Tetrahydrogeranyl Tetrahydrolinaloyl Ether.* Tetrahydrogeranyl bromide (1.0 g) and sodium *dl*-tetrahydrolinaloolate (1 g) were treated according to the above-mentioned procedure to give tetrahydrogeranyl tetrahydrolinaloyl ether in a 10% yield. n_D^{18} 1.4850; $[\alpha]_D^{20}$ ±0° ($CHCl_3$). ν_{max}^{liq} cm^{-1}: 1381, 1366 (CH_3-CH-CH_3), 1149, 1072 (C-O-C). $\delta_{max}^{CDCl_3}$: 0.89 (15H, d, J=6 Hz, CH_3-CH-), 1.10 (3H, s, CH_3-C-O-), 3.30 (2H, t, J=6 Hz, -C-O-CH_2-CH_2-).

l-Linaloyl Piperityl Ether (VII). The compound, t_R 11.2, was isolated as the most slowly-moving component by the elution chromatography of the dimeric fractions of II. n_D^{18} 1.4871; $[\alpha]_D^{18}$ −38.3° ($CHCl_3$), $C_{20}H_{34}O$ (M^+ 290, Rast's mol. wt. 286). ν_{max}^{liq} cm^{-1}: 3080, 1650, 991, 918 (CH_2=CH-), 1680, 835 (-C=CH-), 1388, 1371 (CH_3-CH-CH_3), 1148, 1118, 1108, 1085 (C-O-C). $\delta_{ppm}^{CDCl_3}$: 1.11, 1.16 (each 3H, d, J=6 Hz, CH_3-CH-), 1.28 (3H, s, CH_3-C-O-), 1.60, 1.68 (6H and 3H, each br. s, CH_3-C=CH-), 2.00 (4H, br. s, -CH_2-C=C-), 3.95 (1H, d, J=7 Hz, -O-CH-CH=C-), 4.95 (1H, q, J_{AB}=2 Hz, J_{BX}=10 Hz), 5.15 (1H, q, J_{AB}=2 Hz, J_{AX}=18 Hz), 5.95 (1H, q, J_{AX}=18 Hz, J_{BX}=10 Hz), 5.08 (2H, m, -CH=C-). Mass: *m/e* 41(56%), 43(23), 55(17), 69(base), 71(6), 80(7), 81(34), 93(20), 95(26), 107(12), 109(8), 121(11), 123(31), 137(14, $C_{10}H_{17}$), 275(2, M^+-CH_3), 290(2, M^+, $C_{20}H_{34}O$).

Dihydro Derivative of VII: When VII (150 mg) was submitted to catalytic hydrogenation over platinum oxide (20 mg) in methanol (6 ml), one molar equivalent of hydrogen was taken up. The reacted mixture was treated according to a usual procedure to obtain a dihydro derivative as an oil. ν_{max}^{liq} cm^{-1}: 1660, 835 (-C=CH-), 1385, 1376 (CH_3-CH-CH_3), 1140, 1024 (C-O-C). $\delta_{ppm}^{CDCl_3}$: 0.90 (3H, t, J=6 Hz, CH_3-CH_2-), 1.10 (3H, s, CH_3-C-O-), 1.11, 1.16 (each 3H, d, J=6 Hz, CH_3-CH-), 1.60, 1.68 (6H and 3H, br. s, CH_3-C=CH-), 2.00 (4H, br. s, -CH_2-CH=C-), 3.95 (1H, d, J=7 Hz, -C-O-CH-CH=C-), 5.08 (2H, m, -CH=C-).

Hexahydro Derivative of VII: The dihydro derivative of VII (120 mg) was again submitted to catalytic hydrogenation over platinum oxide (10 mg) in the same methanol solvent (7 ml) at room temperature; the hexahydro derivative was thus obtained. On the other hand, VII (300 mg) was also hydrogenated over platinum oxide (30 mg) by using acetic acid instead of methanol as a solvent at room temperature to give the same hexahydro derivative. ν_{max}^{liq} cm^{-1}: 1384, 1375 (CH_3-CH-CH_3), 1131, 1020 (C-O-C). $\delta_{ppm}^{CDCl_3}$: 0.85 (9H, d, J=6 Hz, CH_3-CH-), 1.11, 1.61 (each 3H, d, J=6 Hz, CH_3-CH-CH_3), 3.40 (1H, t, J=6 Hz, -O-CH-CH_2-), 1.10 (3H, s, CH_3-C-O-). Mass: *m/e* 41(33%), 43(40), 55(48), 69(40), 70(base), 71(43), 81(15), 83(43), 95(18), 97(22), 109(20), 111(19), 123(27), 126(19), 137(14), 139(6),

153(10), 238(28), 267(55, $C_{18}H_{35}O$), 281(16, M^+-CH_3, $C_{19}H_{37}O$), no molecular ion.

Ether Cleavage of the Hexahydro Derivative of VII with Hydroiodic Acid: Hexahydro derivative (200 mg) was refluxed with hydroiodic acid ($d=1.7$, 1 ml) for 10 min. The reaction product extracted from the reacted mixture was eluted over a silica gel column with *n*-hexane to separate a nonhydrocarbon portion as a colorless oil showing a peak at t_R 10.3 in glc with Silicone SE-30; 5% yield. n_D^{20} 1.5088. $\nu_{max}^{CCl_4}$ cm^{-1}: 1389, 1380, 1360, 1171. $\delta_{ppm}^{CDCl_3}$: 0.82, 0.92 (9H, d, $J=6$ Hz, $C\underline{H}_3$-CH-), 4.09 (1H, dt, $J=3$, 10 Hz, $-CH_2-C\underline{H}-I$). Mass: *m/e* 41(50%), 43(45), 55(70), 69(65), 83(base), 95(10), 97(12), 127(3, I^+), 139 (40, $C_{10}H_{19}$), 266 (1, M^+, $C_{10}H_{19}I$). These IR, NMR, and mass spectra were all superimposable on those of menthyl iodide which had been prepared by heating a mixture of menthol (2.0 g), red phosphorus (0.1 g), and resublimed iodide (1.0 g) at 150 °C for 2 hr.

Ether Cleavage of the Hexahydro Derivative of VII with Acetic Anhydride and $BF_3.Et_2O$: Hexahydro derivative (100 mg) was treated with acetic anhydride (0.2 ml) and $BF_3\cdot Et_2O$ (0.02 ml) in dried ether (1 ml) at room temperature for 48 hr. The reaction product separated according to a usual manner was chromatographed over silica gel with *n*-hexane and then a mixture of *n*-hexane and ethyl acetate (95 : 5) to separate an oxygen-containing compound as a colorless oil showing a peak at t_R 5.5 in glc with Silicone SE-30 in a yield of 5%. $\nu_{max}^{CCl_4}$ cm^{-1}: 1735, 1245, 1125 (-CO-OCH_3), 1389, 1371 (CH_3-CH-CH_3). $\delta_{ppm}^{CDCl_3}$: 0.80, 0.89 (9H, d, $J=6$ Hz, $C\underline{H}_3$-CH-$C\underline{H}_3$, $C\underline{H}_3$-CH-), 4.70 (1H, dt, $J=4$, 10 Hz, $-C\underline{H}-OCOCH_3$), 2.00 (3H, s, $-OCOC\underline{H}_3$). Mass: *m/e* 41(42%), 43(base), 55(22), 67(18), 81(27), 95(31), 109(5), 123(11), 138(19, M^+-CH_3COOH), 198 (trace, M^+). The IR, NMR, and mass spectra were respectively superimposable on those of a synthetic sample of *l*-menthyl acetate.

Conversion of III and IV by $BF_3\cdot Et_2O$. The III ether (200 mg) was dissolved in dried ether (1 ml) and mixed with 0.02 ml of $BF_3\cdot Et_2O$. On the other hand, IV (300 mg) was dissolved in dried ether (1.5 ml) and mixed with 0.03 ml of $BF_3\cdot Et_2O$. After the two mixtures had been allowed to stand at room temperature for 18 hr, a small amount of water was added to each of the reacted mixture to decompose the excess reagent. The reacted mixtures thus treated were then gaschromatographed on the DEGS separation column to determine their compositions; *cf.* Table 2. In these cases, the characteristics of the monoterpene hydrocarbons were assumed based on the retention times, while the monoterpene alcohols, linalool, α-terpineol, nerol, and geraniol, were tentatively identified by comparing the retention times with those of authentic samples. Linaloyl piperityl ether, after being isolated by preparative glc, was identified through a determination of the IR, NMR, and mass spectra.

The author wishes to express her sincere gratitude to Professor Shûichi Hayashi and Assistant Professor Mitsuru Nakayama, of Hiroshima University, for their kind guidance and discussion during this work.

References

1) K. Nagai, *Chem. Pharm. Bull.*, **18**, 2123 (1970).
2) K. Nagai, M. Nakayama, A. Matsuo, S. Eguchi, and S. Hayashi, This Bulletin, **47**, 1193 (1974).
3) K. Nagai, *J. Sci. Hiroshima Univ., Ser. A*, **38**, 141 (1974).
4) D. V. Banthorpe, P. A. Boullier, and W. D. Fordham, *J. Chem. Soc. Perkin I*, **1974**, 1637.
5) P. Valenzuela and O. Cori, *Tetrahedron Lett.*, **1967**, 3089; B. M. Mitzner, S. Lemberg, and E. T. Theimer, *Can. J. Chem.*, **44**, 1090 (1966); T. Matuura, *J. Sci. Hiroshima Univ., Ser. A*, **8**, 303 (1930), **13**, 275 (1944).
6) M. Shakaguchi, A. Hirakata, and H. Yamada, *The Koryo*, No. 102, 42 (1972).
7) A. R. Surrey, "Name Reaction of Organic Chemistry," Academic, Press, New York, N. Y. (1954), p. 169.
8) Y. Yukawa and S. Itō, "Spectral Atlas of Terpenes and the Related Compounds," Hirokawa Publishing Company, Tokyo (1973), pp. 152, 108, 84.
9) F. A. Anet, *Can. J. Chem.*, **39**, 789 (1961).
10) B. M. Mitzner, V. J. Mancini, S. Lemberg, and E. T. Theimer, *Appl. Spectroscopy*, **22**, 38 (1968).
11) R. Ryhage and E. von Sydow, *Acta Chem. Scand.*, **17**, 2025 (1963).

The Synthesis of 11-(2′-Dimethylaminoethyl)-5-methyl-5,11-dihydrodibenzo[*b*,*e*][1,4]thiazepin and Related Compounds. Neurotropic and Psychotropic Agents

Ikuo UEDA* and Suminori UMIO

Research Laboratories, Fujisawa Pharmaceutical Co., Ltd., Kashima, Yodogawa-ku, Osaka 532

(Received January 6, 1975)

The synthesis of 11-(2′-dimethylaminoethyl)-5-methyl-5,11-dihydrodibenzo[*b*,*e*][1,4]thiazepin and related compounds is described. 11-Lithiolated 5-methyl-5,11-dihydrodibenzo[*b*,*e*][1,4]thiazepin (**18**) was employed as the key intermediate in the preparation of these compounds.

Morimoto had indicated, from his molecular orbital treatment using the Hückel approximation, that the dibenzo[*b*,*e*][1,4]thiazepin ring has approximately the same π-electron level as phenothiazine.[1] This result led the present authors to investigate the synthesis of 11-substituted dibenzo[*b*,*e*][1,4]thiazepin derivatives (**I**).

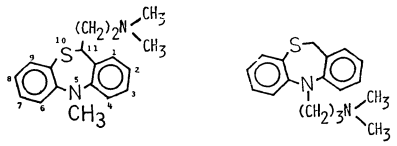

I **14e**

Chart 1.

In this paper, the authors will describe a synthesis of 11-substituted 5-methyl-5,11-dihydrodibenzo[*b*,*e*]-[1,4]thiazepin and related compounds which, in our animal studies, displayed an imipramine-like activity.[2]

Results and Discussion

The synthesis of Compound **I** was attempted by the following two methods. Method A involved the preparation of 11-substituted dihydrodibenzo[*b*,*e*][1,4]-thiazepins by the cyclization of α-substituted phenyl benzyl thioethers, while Method B involved the preparation of 5-methyl-11-substituted dibenzo[*b*,*e*][1,4]-thiazepins by the electrophilic substitution reaction of 5-methyl-5,11-dihydrodibenzo[*b*,*e*][1,4]thiazepin lithiolated(**18**) with alkyl halides and other reagents (Chart 2).

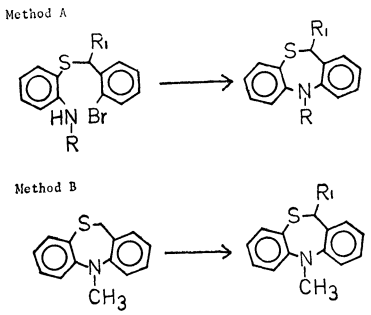

Chart 2.

The starting materials, α-substituted phenyl benzyl thioethers(**3**), were prepared by a patented procedure[3] or its modifications. The treatment of sodium thiophenolate with benzyl halides (**2**) in ethanol at room temperature or at the boiling point of the solvent used gave **3**, which was then allowed to react with 98% formic acid and with ethyl chloroformate to afford the **4** compounds in good yields. The catalytical hydrogenation of the Mannich base(**6**) with palladium carbon under atmospheric pressure gave an aminoalcohol(**9**). Compound **6** was reduced with sodium borohydride in methanol to give Compound **7**, which was then converted to benzyl chloride(**2d**) with thionyl chloride.

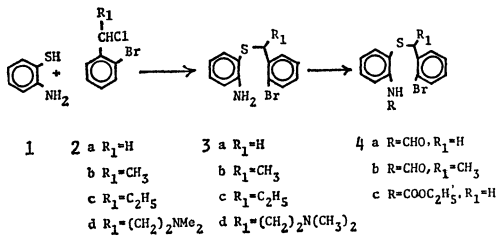

1 **2** a R_1=H, b R_1=CH_3, c R_1=C_2H_5, d R_1=$(CH_2)_2NMe_2$ **3** a R_1=H, b R_1=CH_3, c R_1=C_2H_5, d R_1=$(CH_2)_2N(CH_3)_2$ **4** a R=CHO, R_1=H, b R=CHO, R_1=CH_3, c R=$COOC_2H_5$, R_1=H

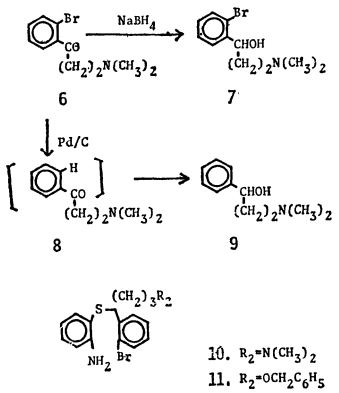

6 7 8 9

10. R_2=$N(CH_3)_2$
11. R_2=$OCH_2C_6H_5$

Chart 3.

The cyclization of **3a**, **b** and **4** at 120 to 140 °C in the presence of copper yielded 5,11-dihydrodibenzo-[*b*,*e*][1,4]thiazepins, **12** and **13**, in moderate yields, while the saponification of **13a**, **b** with an aqueous alcoholic sodium hydroxide solution gave Compound **12**. When R_1 in **3** was sterically bulky, such as a phenyl or dimethylaminoethyl group, either the starting material unchanged was recovered or resinous substances were formed. The alkylation of **12** with

* Abstracted from a portion of a Ph. D. Dissertation submitted by I. U. in March, 1974, to Osaka University.

sodium hydride and methyl iodide, allyl bromide, and dimethylaminoalkyl chloride[4] in DMF gave the corresponding 5-substituted 5,11-dihydrodibenzo[*b*,*e*]-[1,4]thiazepins(**14**) in moderate yields.

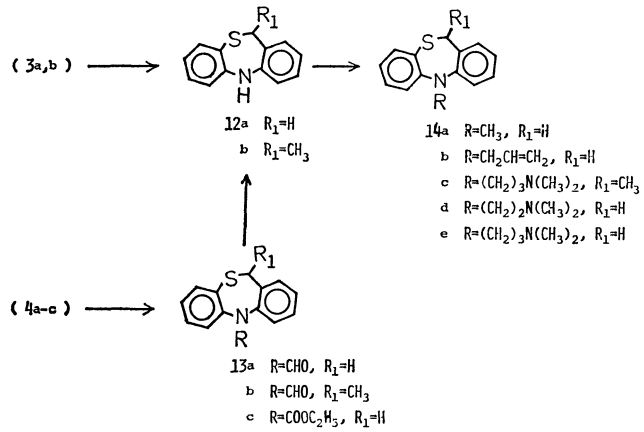

Chart 4.

It is known that compounds containing sulfur and/or nitrogen in the molecule are metalated at the carbon adjacent to the hetero atom by alkyl- or aryl-lithium to form organolithium compounds, which can then be used as synthetic intermediates.[5] The present authors employed this method for the preparation of 11-substituted dibenzo[*b*,*e*][1,4]thiazepin derivatives. In this case, the three sites shown by the a, b, and c arrows in Chart 5 are metalated with alkyl- or aryl-lithium.

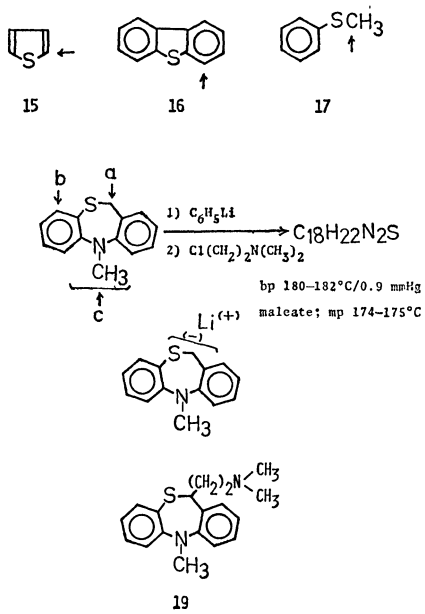

Chart 5.

The reaction of **14a** with phenyl lithium and dimethylaminoethyl chloride in ether afforded Compound **19** in a 62.4% yield. Evidence for the **19** structure was provided by the results of elementary analysis and by the spectral data. Compound **19** showed an emprical formula, $C_{18}H_{22}N_2S$, upon elementary analysis; its IR spectrum showed bands at 2800(tertiary amino group, NCH_3) and 700(condensed

Fig. 1. NMR spectrum of **19** in $CDCl_3$.

aromatic)cm^{-1}, and the NMR spectrum in deuteriochloroform exhibited signals at δ 2.17—2.50(4H, m, CH_2CH_2) 2.28(6H, s, $N(CH_3)_2$) and 3.25(3H, s, $N-CH_3$)ppm. A signal due to methine proton was observed at δ 4.29(1H, t, J=7.0 Hz, $C_{11}-H$)ppm. These findings show that the electrophlic substitution reaction occurred on the 11-position of **14a**. The structure of this product was, therefore, identified as 5-methyl-11-(2′-dimethylaminoethyl)-5,11-dihydrodibenzo[*b*,*e*][1,4]thiazepin (**19**).

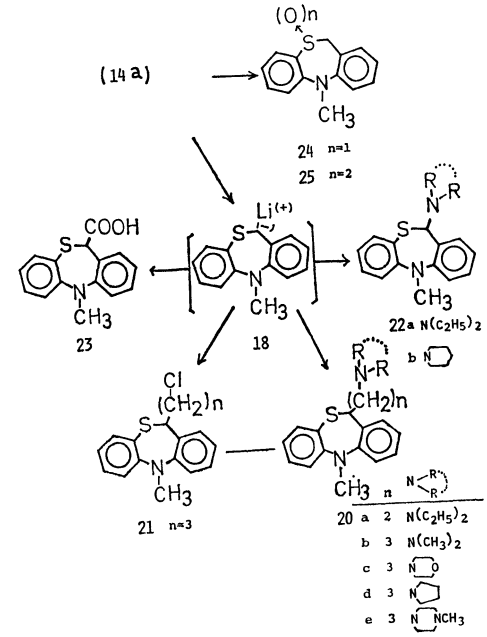

Chart 6.

The lithio derivative **18** was employed as a versatile intermediate for preparing 11-substituted 5,11-dihydrodibenzo[*b*,*e*][1,4]thiazepins; almost all the derivatives shown in Chart 6 were successfully prepared by this method. Thus, the reaction of **18** with carbon dioxide yielded 11-(5-methyl-5,11-dihydrodibenzo[*b*,*e*][1,4]thiazepin)carboxylic acid (**23**). The treatment of **18** with 1-bromo-3-chloropropane yielded a haloalkyl derivative(**21**), which was then allowed to react with 1-methylpiperazine to give **20e** in a moderate yield. It is hard to synthesize 11-amino compounds (**22**) by the usual method. However, **22** was prepared by this method in about a 20% yield. The reaction of **14a** with hydrogen peroxide in a mixed solvent of acetone and acetic

acid at room temperature or in a solution of acetone with refluxing led to 5-methyl-5,11-dihydrodibenzo-[b,e][1,4]thiazepin-10-oxide(**24**) or 5-methyl-5,11-dihydrodibenzo[b,e][1,4]thiazepin-10,10-dioxide (**25**).

Compound **19** and related compounds were shown to have an imipramine-like activity in experimental animals; **19** is the most valuable among these compounds.

Our pharmacological findings will be reported elsewhere in the near future.

Experimental

All the melting points are uncorrected. The IR spectra were taken with a Hitachi EPI-2 spectrometer. The NMR spectra were recorded by means of a Varian A-60 spectrometer in $CDCl_3$, using TMS as the internal standard.

The *o*-bromobenzylbromide was prepared by the bromination of *o*-bromotoluene by a previously reported procedure.[6] The *o*-bromo-1-chloroethylbenzene(**2b**)[7] (bp 98—105 °C/13 mmHg) and *o*-bromo-1-chloropropylbenzene(**2c**) (bp 100—110 °C/10 mmHg) were prepared by the reduction of *o*-bromoacetophenone and *o*-bromopropiophenone, and by the subsequent chlorination of the resulting substances.

*o-Bromo-3-dimethylaminopropiophenone (**6**).*[8] A mixture of *o*-bromoacetophenone (1.94 g), dimethylamine (10.7 g), paraformaldehyde (3.9 g), and conc. HCl (0.2 ml) in 15 ml of EtOH was refluxed for 2 hr on an oil bath and then cooled. The solid thus precipitated was filtered, washed with acetone, and recrystallized from a mixed solvent of acetone and MeOH to give **6** (2.10 g); mp 185—189 °C. Found: C, 45.20; H, 5.27; N, 4.66%. Calcd for $C_{11}H_{14}BrON \cdot HCl$: C, 45.15; H, 5.17; N, 4.79%.

*1-(o-Bromophenyl)-3-dimethylaminopropyl Alcohol (**7**).* To a solution of **6** (1.8 g) in 30 ml of MeOH, we added 5 ml of a 10% NaOH solution; $NaBH_4$ (500 mg) was then added in small portions, and the mixture was stirred for 2 hr at 50 °C. The solvent was then evaporated *in vacuo*. H_2O was added to the residue, and the aqueous layer was extracted with benzene. The benzene layer was dried over $MgSO_4$ and evaporated. The solid was recrystallized from a mixed solvent of benzene/petr. benzine to give **7** (1.3 g); mp 74—75 °C.

*1-o-Bromophenyl-3-dimethylaminopropyl Chloride (**2d**).* To a solution of **7** (1.0 g) in 30 ml of $CHCl_3$, $SOCl_2$ in $CHCl_3$ was added, drop by drop under cooling. The reaction mixture was stirred first at the same temperature for 30 min, and then at 50 °C for 2 hr, and subsequently cooled. The $CHCl_3$ was removed *in vacuo*, and the residue was recrystallized from acetone to give **2d** (0.8 g); mp 180.5—181 °C.

*1-Methyl-o-bromobenzyl-o'-aminophenylthioether (**3b**).* To NaOEt in an EtOH solution (prepared from Na (3.5 g) and abs. EtOH (80 ml)), then *o*-aminothiophenol (16.6 g) was added all at once. The mixture was stirred for 30 min. 1-Chloro-*o*-bromoethylbenzene **2b** (19.4 g) was added to this solution, and the mixture was refluxed for 2 hr. After the removal of the solvent, H_2O was added to the residue and the mixture was extracted with $CHCl_3$. The $CHCl_3$ layer was dried over $MgSO_4$ and evaporated. The oil thus obtained was distilled under reduced pressure. The fraction boiling at 169—172 °C/0.9 mmHg was collected to give **3b** (16.6 g; 60.6%). Found: C, 54.53; H, 4.41; N, 4.56; S, 10.70; Br, 25.79%. Calcd for $C_{14}H_{14}BrNS$: C, 54.55; H, 4.58; N, 4.54; S, 10.40; Br, 25.92%.

*1-Ethyl-o-bromobenzyl-o'-aminophenylthioether (**3c**).* In a similar manner, **3c**, a yellow viscous oil, was obtained in a 50% yield; bp 178—182 °C/0.55 mmHg. Found: C, 55.20; H, 4.78; N, 4.06; S, 10.20%. Calcd for $C_{15}H_{16}BrNS$: C, 55.91; H, 5.00; N, 4.35; S, 9.95%.

*N,N-Dimethyl-3-(o-bromophenyl)-3-(o'-aminophenylthio)-propylamine (**3d**).* To a solution of NaOEt in EtOH (EtOH; 100 ml, Na; 600 mg), *o*-aminothiophenol(1.0 g) and then 3.0 g of **2d** were added. The mixture was refluxed for 3 hr. A small amount of H_2O was then added to the reaction mixture, and the solvent was removed *in vacuo*. H_2O was added to the residue, and the mixture was extracted with $CHCl_3$. The $CHCl_3$ layer was dried over $MgSO_4$ and evaporated. An oil (3.9 g) was thus obtained; IR: ν_{max} (neat); 3400 and 3300 (primary amine), and 2800 cm^{-1} (tertiary amine). This oil was converted to an oxalate in a usual manner. The oxalate melted completely at 180 °C after having decomposed at 138—140 °C. Found: C, 50.04; H, 5.24; N, 6.27; S, 7.18; Br, 17.39%. Calcd for $C_{17}H_{21}N_2SBr \cdot C_2H_2O_4$: C, 50.12; H, 5.09; N, 6.15; S, 7.04; Br, 17.55%.

*o'-(N-Formylamino)phenyl-o-bromobenzylthioether (**4a**).*[4] A solution of **3a** (70 g) in 420 ml of 98% HCOOH was refluxed for 2 hr. The reaction mixture was then poured into ice water and extracted with $CHCl_3$. The $CHCl_3$ layer was washed with a 10% NaOH solution and H_2O, dried, and evaporated. The solid thus obtained was recrystallized from EtOH–cyclohexane to give 75 g of **4a**; mp 112—113 °C.

*o'-(N-Formylamino)phenyl-o-bromo-α-methylbenzyl thioether (**4b**)* was obtained in a 51.7% yield in a similar manner.

*o-Bromobenzyl-o'-(N-ethoxycarbonylamino)phenylthioether(**4c**).* To a solution of **3a** (2.9 g) in 5 ml of pyridine, we added $ClCOOC_2H_5$ (1.1 g) under cooling. Stirring was then continued for 2 hr. The mixture was allowed to stand overnight at room temperature, and then it was poured into water and extracted with ether; the ether layer was washed with H_2O and 10% HCl, dried over $MgSO_4$, and evaporated. The oil thus obtained was treated with EtOH to give a solid. The solid was recrystallized from aq. EtOH to give 1.5 g of **4c**, as colorless needles; mp 54–55 °C. Found: C, 52.72; H, 4.50; N, 3.97; S, 8.79; Br, 22.08%. Calcd for $C_{16}H_{16}NSO_2Br$: C, 52.47; H, 4.40; N, 3.82; S, 8.75; Br, 21.82%.

*5,11-Dihydrodibenzo[b,e][1,4]thiazepin (**12a**).* **3a** was prepared by Ullman reaction from *o*-bromophenyl-benzylthioether, which had itself been obtained by the reaction of *o*-aminothiophenol with *o*-bromobenzylbromide according to a patented procedure.[3]

A mixture of **3a** (100 g) and copper powder (10 g) in 1.01 of pyridine was stirred with refluxing at 110—115 °C in the presence of K_2CO_3(100 g) and then cooled. The solid was filtered off, and the filtrate was concentrated to one-third of the initial volume. The residue was poured into chilled 10% HCl, and the resulting semi-solid was extracted with ether. The ether layer was washed with H_2O, dried over $MgSO_4$, and evaporated. The residue was distilled under reduced pressure. The fraction boiling at 200—220 °C/0.4 mmHg was collected to give **12a** (80 g); mp 117—118 °C (lit, 121—122 °C).[3]

5-Formyl-5,11-dihydrodibenzo[b,e][*1,4*]*thiazepin (**13a**).*[4] A mixture of **4a** (70 g) and Cu powder (8.0 g) in 600 ml of pyridine was stirred with refluxing in the presence of K_2CO_3 (80 g). The solid was then filtered off, and the filtrate was concentrated *in vacuo*. The residue was poured into chilled dil. H_2SO_4, and extracted with $CHCl_3$. The $CHCl_3$ layer was washed with H_2O, dried, and evaporated to give **13a** (50 g); mp 123—124 °C.

5-Ethoxycarbonyl-5,11-dihydrodibenzo[b,e][*1,4*]*thiazepin (**13c**).* A mixture of **4c** (8.0 g), and K_2CO_3 (8.0 g) in 160 ml of pyridine was refluxed in the presence of Cu powder (0.8 g) for 4 hr. After the mixture had then been cooled, a solid was filtered off. The filtrate was poured into 20% H_2SO_4

Table 1. Preparation of 5-substituted dibenzo[*b,e*][1,4]thiazepin derivatives

	R	R_1	mp(bp)(°C)	Formula (Mol wt)	Analysis% Calcd (Found) C	H	N	S
14a	CH_3	H	93—94	$C_{14}H_{13}NS$ (227.25)	73.99 (78.91	5.77 5.73	6.16 6.05	14.08 14.15)
14b	$CH_2CH{=}CH_2$	H	104—104.5	$C_{16}H_{15}NS$ (253.29)	75.87 (75.77	5.97 6.17	5.53 5.43	12.67 12.44)
14c	$(CH_2)_3NMe_2$	CH_3	(187/0.6)[c]	$C_{19}H_{24}N_2S$ (312.40)			88.97 (88.87	10.24 10.24)
14d	$(CH_2)_2NMe_2$[a]	H	154—155[d]	$C_{17}H_{20}N_2S$ (284.32)	62.99 (63.03	6.04 6.11	7.00 7.01	7.99 8.61)[b]
14e	$(CH_2)_3NMe_2$[a]	H	133—134	$C_{18}H_{22}N_2S$ (298.32)	63.75 (63.65	6.32 6.53	6.67 6.53	7.72 7.76)[b]

a) P. Gailliot *et al.*, *Chem. Abstr.*, **55**, 19.972[d] (1961). b) Analysis of maleate is shown in Table 1. c) Maleate; mp. 153—155 °C (99% ethanol), Oxaleate; mp 139—143 °C (decomp.). d) Maleate.

and extracted with ether. The ether layer was washed with H_2O, dried, and evaporated. The solid thus obtained was recrystallized from 95% EtOH to give **13c** (4.2 g); mp 101.5—104 °C. NMR (δ); 1.23 (3H, t, J=7.0 Hz, $-CH_3$), 4.22 (2H, q, J=7.0 Hz, $-CH_2-$), 3.54 (1H, d, J=14 Hz, C_{11}–H), 4.88 (1H, d, J=14 Hz, C_{11}–H), 7.0—7.5 (8H, m, phenyl protons). Found: C, 65.46; H, 5.36; N, 5.17; S, 11.43%. Calcd for $C_{16}H_{15}NSO_2 \cdot 1/2H_2O$: C, 65.28: H, 5.49; N, 4.76; S, 10.89%.

Saponification of **13a** *with Alkaline Solution.* A solution of **13a** (50 g) and a 10% NaOH solution (110 ml) in 550 ml of 95% EtOH was refluxed for 2 hr. After the subsequent removal of the solvent *in vacuo*, the residue was poured into ice water and extracted with $CHCl_3$. The $CHCl_3$ layer was washed with H_2O, dried, and evaporated. The solid thus obtained was recrystallized from 99% EtOH to give **12a** (48 g); mp 120—121 °C.[4]

N-Formyl-11-methyl-5,11-dihydrodibenzo[b,e][*1,4*]*thiazepin* (***13b***): (mp 162—164 °C (from benzene-cyclohexane)) was obtained in a 75% yield by the Ullman reaction of **4b** at 110—115 °C. NMR (δ): 1.64 (3H, d, J=7.4 Hz, C_{11}–CH_3), 5.17 (1H, q, J=7.4 Hz, C_{11}–H), 7.0—8.0 (8H, m, phenyl protons). Found: C, 70.94; H, 5.04; N, 5.43; S, 12.74%. Calcd for $C_{15}H_{13}NSO$: C, 70.58; H, 5.13; N, 5.49; S, 12.80%.

11-Methyl-5,11-dihydrodibenzo[*b,e*][1,4]*thiazepin* (**12b**) (bp 190—200 °C (0.3 mmHg)) was obtained in a 50% yield by the saponification of **13b** with a 10% NaOH solution. NMR (δ): 1.51 (3H, d, J=7.5 Hz, C_{11}–CH_3), 4.33 (1H, q, J=7.5 Hz, C_{11}–H), 6.5—7.4 (8H, m, phenyl protons). Found: C, 73.71; H, 5.98; N, 6.09; S, 14.32%. Calcd for $C_{14}H_{13}NS$: C, 73.99; H, 5.77; N, 6.16; S, 14.08%.

5-Methyl-5,11-dihydrodibenzo[b,e][*1,4*]*thiazepin* (***14a***). To a suspension of NaH (50% mineral oil dispersion; 65 g) in a mixed solvent of toluene (500 ml) and DMF (500 ml), a solution of **12a** (200 g) in a mixed solvent of toluene (200 ml) and DMF (200 ml) was added, drop by drop. The mixture was then stirred for 2 hr at 50 °C, and a solution of CH_3I (283 g) in 200 ml of DMF was added. Stirring was continued for another 2 hr at 50 °C. After cooling, MeOH (100 ml) was added, drop by drop, to the reaction mixture to decompose the excess NaH. The mixture was then poured into ice water (1.0 l). The oil thus obtained was extracted with toluene. The toluene layer was washed with H_2O, dried, and evaporated *in vacuo*. The solid thus formed was recrystallized from *n*-hexane (2.0 l) to give **14a**; 117 g (87%). NMR (δ): 3.67 (3H, s, N–CH_3), 4.41 (2H, s, C_{11}–H), 6.5—7.5 (8H, m, phenyl protons).

Compounds **14d** and **14c**, prepared in a manner similar to those described above, are summarized in Table 1.

5-Methyl-5,11-dihydrodibenzo[b,e][*1,4*]*thiazepin-10-oxide* (***24***). To a solution of **14a** (22 g) in a mixed solvent of purified acetone (300 ml) and AcOH (300 ml), 30% H_2O_2 (20 g) was added, drop by drop, at a temperature below 25 °C; the reaction mixture was thereafter stirred for 25 hr at room temperature and poured into ice water (3.0 l). The solid thus precipitated was filtered off and recrystallized from MeOH to give **24**; 19.5 g (80%); mp 157 °C. NMR (δ): 3.44 (3H, s, N–CH_3), 4.30 and 4.55 (2H, d, J=12 Hz, C_{11}–H), 7.0—8.0 (8H, m, phenyl protons). Found: C, 69.69; H, 5.51; N, 5.78; S, 13.16%. Calcd for $C_{14}H_{13}NOS$: C, 69.13; H, 5.39; N, 5.76; S, 13.16%.

5-Methyl-5,11-dihydrodibenzo[b,e][*1,4*]*thiazepin-10,10-dioxide* ***25***. To a solution of **14a** (3.5 g) in 30 ml of purified aceton 30% H_2O_2 (3.0 g) was added, drop by drop; the reaction mixture was then refluxed for 3 hr. After the subsequent removal of the solvent, the residue was recrystallized from 99% EtOH to give **25**; 1.5 g (43.9%); mp 230—233 °C. NMR (δ): 3.37 (3H, s, N–CH_3), 4.86 (2H, s, C_{11}–H), 6.9–7.9 (8H, m, phenyl protons). Found: C, 65.09; H, 5.09; N, 5.19; S, 12.46%. Calcd for $C_{14}H_{13}NO_2S$: C, 64.80; H, 5.06; N, 5.40; S, 12.34%.

Preparation of Phenyllithium.[9] To a solution of bromobenzene (32 g, 0.204 mol) in 100 ml of abs. ether, we added Li metal (3.0 g, 0.43 mol) under a flow of nitrogen. Stirring was slowly started at room temperature, and the reaction begin. (The reaction mixture was heated up to ether reflux when the reaction was hard to initiate.) The reaction mixture was then refluxed for 30 min.

11-(2'-Dimethylaminoethyl)-5-methyl-5,11-dihydrodibenzo[b,e]-[*1,4*]*thiazepin* (***19***). To a solution of phenyllithium (prepared from bromobenzene (4.7 g) and Li metal (410 mg)), a solution of **14a** (6.1 g) in 80 ml of abs. ether was added, drop by drop, after which the mixture was stirred for 2—3 hr at room temperature. The color of the solution changed from gray to red- or black-brown. To the resulting solution we then added freshly distilled dimethylaminoethyl chloride (60 g). The mixture was stirred with refluxing for 5 hr and then cooled. The unchanged Li metal was removed, and the ether solution was washed with H_2O and extracted with HCl. The extract was made alkaline with a 10% NaOH solution under cooling. The oil thus obtained was extracted with $CHCl_3$, and the $CHCl_3$ layer was washed with H_2O, dried, and evaporated *in vacuo*. The residue was distilled under reduced pressure. A fraction boiling at 180—182 °C

Table 2. Preparation of 11-substituted-5-methyl-10,11-dihydrodibenzo[*b,e*][1,4]thiazepin derivatives

	n	$N\langle^{R}_{R}\rangle$	mp(bp)(°C)	Yield (%)	Formula (Mol wt)	Analysis(%) Cald(Found) C	H	N	S
20a	2	$N(C_2H_5)_2$	oil	58.2	$C_{20}H_{26}N_2S$	73.58	8.03	8.58	9.08
					(326.42)	(73.29	7.95	8.60	10.06)
20b	3	$N(CH_3)_2$	(200—230/0.5)	29.8	$C_{19}H_{24}N_2S$	73.04	7.44	8.94	10.24
					(312.40)	(72.42	7.74	8.87	9.10)
20c	3		(230—240/0.4—0.5)	71.5	$C_{21}H_{26}ON_2S$	71.14	7.39	7.90	9.05
					(354.43)	(71.40	7.45	3.15	9.10)
20d	3		(240—260/0.85)	26.6	$C_{21}H_{26}N_2S$	74.52	7.74	8.28	9.46
					(338.43)	(74.34	7.88	8.14	8.86)

(0.9 mmHg) was collected to give **19** of 5.0 g (62.4%). IR (ν) Nujol: 2800 (N-CH_3) and 700 (condensed aromatic) cm^{-1}, NMR (δ): 2.17—2.50 (4H, m, $-CH_2CH_2-$), 2.28 (6H, s, $N(CH_3)_2$, 3.25 (3H, s, N-CH_3), 4.29 (1H, t, J=7.0 Hz, C_{11}-H), 6.7—7.3 (8H, m, phenyl protons). Found: C, 72.30; H, 7.24; N, 9.56; S, 10.74%. Calcd for $C_{18}H_{22}N_2S$: C, 72.42; H, 7.43; N, 9.39; S, 10.72%.

The oil thus obtained was converted to maleate in a usual manner; mp 174—175 °C (decomp.) (from EtOH). Found: C, 63.28; H, 6.28; N, 6.59; S, 7.59%. Calcd for $C_{18}H_{22}N_2S \cdot C_4H_4O_4$: C, 63.75; H, 6.32; N, 6.72; S, 7.72%.

Compounds **20a—d**, prepared in a manner similar to that described above, are summarized in Table 2.

11-(4'-Methylpiperazinopropyl)-5-methyl-5,11-dihydrodibenzo[b,e][*1,4*]*thiazepin* (***20e***). To a reaction solution prepared by the reaction of **14a** (2.0 g) with phenyllithium, 1,3-propylene bromochloride (7.5 g) was added, after which the mixture was stirred with refluxing for 3 hr at 50 °C. After cooling, the ether layer was washed with H_2O, dried, and evaporated. Crude oil (2.0 g) was thus obtained.

A mixture of this crude oil and 1-methylpiperazine (20 ml) was heated at 120 °C for 7 hr with stirring. The reaction mixture was then poured into ice water and extracted with a 2 : 1 mixture of benzene and ether. The organic layer was extracted with 10% HCl, and the aqueous layer was made alkaline with a 10% NaOH solution. The oil thus obtained was extracted with $CHCl_3$, and the $CHCl_3$ layer was washed with H_2O, dried, and evaporated *in vacuo*. The oil in the AcOEt solution was chromatographed on alumina. The eluate was evaporated to give 1.1 g of a viscous oil which was distilled under reduced pressure. The fraction boiling at 240—260 °C (0.1—0.2 mmHg) was collected; 1.1 g of **20e**. The oil thus obtained was converted to maleate in a usual manner; mp 185—186 °C (decomp) (from 99% EtOH). Found: C, 60.05; H, 6.23; N, 7.05%. Calcd for $C_{22}H_{29}N_3S \cdot 2C_4H_4O_4$: C, 60.09; H, 6.21; N, 7.01%.

11-Diethylamino-5-methyl-5,11-dihydrodibenzo[b,e][*1,4*]*thiazepin* (***22a***). **18** was prepared from **14a** (2.3 g) and phenyllithium (prepared from bromobenzene (1.6 g) and Li metal (150 mg)) in abs. ether. To the resulting solution, we added a solution of diethylaminobromide[10] in abs. ether, after which the mixture was refluxed for 5 hr. After the removal of the unchanged Li, the ether solution was extracted with 10% HCl and the extract was made alkaline with a 10% NaOH solution under cooling. The oil thus obtained was extracted with $CHCl_3$, and the $CHCl_3$ layer was washed with H_2O, dried, and evaporated. The residue was distilled under reduced pressure. The fraction boiling at 200 °C (0.1 mmHg) was collected to give 0.5 g (16.8 %) of a yellow, viscous oil. Found: C, 71.94; H, 7.38; N, 9.28; S, 10.98%. Calcd for $C_{18}H_{22}N_2S$: C, 72.42; H, 7.43; N, 9.39; S, 10.73%.

11-Piperidino-5-methyl-5,11-dihydrodibenzo[*b,e*][*1,4*]*thiazepin* (***22b***) (bp 220—240 °C (0.3 mmHg)) was obtained in a 21.7% yield by the reaction of **14a** (6.1 g) lithiolated and *N*-chloropiperidine[10] in a manner similar to that described above. Found: C, 73.85; H, 7.23; N, 9.28; S, 10.43%. Calcd for $C_{19}H_{22}N_2S$: C, 73.51; H, 7.14; N, 9.02; S, 10.33%.

11-(5-Methyl-5,11-dihydrodibenzo[b,e][*1,4*]*thiazepin)-carboxylic Acid* (***23***). **18** was prepared by the reaction of **14a** with phenyllithium ((prepared from bromobenzene (3.0 g) and Li metal (300 mg)) in abs. ether. To the resulting solution we added, all at once, powdered dry ice (10 g) under cooling, after which the mixture was stirred with refluxing while CO_2 was passed through. The mixture was then poured into H_2O, and the ether layer was separated and extracted with a 10% $NaHCO_3$ solution. The aqueous layers were combined and made acid with 10% HCl. The oil obtained was extracted with $CHCl_3$ and the $CHCl_3$ layer was dried over $MgSO_4$ and evaporated *in vacuo*. The solid obtained was recrystallized from a mixed solvent of benzene and *n*-hexane, and then from benzene, to give 1.0 g, of **23**; mp 193—194 °C (decomp.). Found: C, 66.40; H, 4.99; N, 4.92; S, 11.57%. Calcd for $C_{15}H_{13}O_2NS$: C, 66.41; H, 4.83; N, 5.16; S, 11.79%.

The authors wish to thank H. Manabe for the spectra data and T. Ikeda and his associates for the microanalyses.

References

1) Y. Morimoto, Unpublished data.
2) Unpublished data.
3) P. Gailliot and F. Debarre, Fr. 1176115; *Chem. Abstr.*, **55**, 19972d (1961)
4) H. L. Yale, F. A. Sowinski, and J. Bernstein, U.S. 3188322; *Chem. Abstr.*, **63**, 8384h (1965).
5) H. Gilman and J. W. Morton Jr., "Organic Reactions," Vol. 8, ed. by R. Adams, John Wiley and Sons, Inc., New York and London (1954), p. 260. a) H. Gilman and R. L. Bebb, *J. Amer. Chem. Soc.*, **61**, 109 (1939); b) H. Gilman and F. J. Webb, *ibid.*, **62**, 987 (1940); c) H. Gilman and D. A. Shirley, *ibid.*, **71**, 1870 (1949).
6) D. F. Detar and L. A. Carpino, *J. Amer. Chem. Soc.*, **78**, 475 (1956).
7) C. S. Marvel and N. S. Moon, *ibid.*, **62**, 45 (1940).
8) T. Tsuji, T. Mizuma, and S. Toyoshima, *Chem. Pharm. Bull.*, **8**, 765 (1960).
9) M. Kotake (Ed.) "Jikken Kagaku Koza, Suppl.," Vol. 20, Maruzen, Tokyo (1963), p. 142.
10) a) G. H. Coleman, *J. Amer. Chem. Soc.*, **55**, 3001 (1933). b) G. H. Coleman. G. Nichols, and T. F. Martens, "Organic Syntheses," Coll. Vol. III, p. 159 (1955).

The Reaction of 2,4-Dehydrohomoadamantane: The Synthesis of Several 2-Mono- and 2,4-Di-substituted Homoadamantanes[1)]

Ryohei YAMAGUCHI, Takeo KATSUSHIMA, and Mituyosi KAWANISI

Department of Industrial Chemistry, Faculty of Engineering, Kyoto University, Yoshida, Sakyo-ku, Kyoto 606

(Received January 9, 1975)

The synthesis of several 2-mono- and 2,4-di-substituted homoadamantane derivatives is described. The photobromination of 2,4-dehydrohomoadamantane (I) at −78 °C gave *e,a*- and *e,e*-2,4-dibromohomoadamantanes (IIa and IIb). The treatment of a mixture of IIa and IIb with *t*-BuOK in HMPT gave *e*-2-bromohomoadamant-4-ene (IV) in an 84% yield. The methanolysis and hydrolysis of IV gave *e*-2-methoxyhomoadamant-4-ene (V) and *e*-2-hydroxyhomoadamant-4-ene (VI), with a retention of the configuration, in 90 and 99% yields respectively. The oxidation of VI with the CrO_3-pyridine complex gave homoadamant-4-en-2-one (VII) in a 94% yield. The reduction of VII with $LiAlH_4$ gave *a*-2-hydroxyhomoadamant-4-ene (VIII). The catalytic hydrogenations of VI, VII, and VIII gave *e*-2-hydroxyhomoadamantane (IX), homoadamantan-2-one (X), and *a*-2-hydroxyhomoadamantane (XI) respectively. The possibility that a homoallylic cation (XII) intervenes in the solvolysis of IV is proposed.

A large number of bridgehead-substituted (1- or 3-) homoadamantane derivatives (*cf.* Fig. 1) have been extensively studied.[2)] However, relatively speaking, there has been a remarkable absence from the chemical literature of references to the synthesis of bridge-substituted homoadamantane derivatives. Moreover, the few synthesized compounds have been restricted to those substituted only on the ethylene bridge (4- and/or 5-positions).[3)]

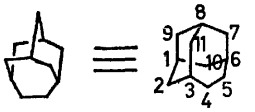

Fig. 1. Homoadamantane.

On the other hand, in the case of the adamantane system a good many bridge-substituted derivatives have been synthesized and studied.[2)] Particularly Udding *et al.* reported a very subtle synthesis of 2-mono- and 2,4-di-substituted adamantane derivatives by cleaving the cyclopropane ring of 2,4-dehydroadamantane with a variety of electrophilic reagents.[4)] We have ourselves previously reported the efficient synthesis of 2,4-dehydrohomoadamantane (I),[5)] a homologue of 2,4-dehydroadamantane. As a matter of cource, I might be a potential precursor of 2-mono- and 2,4-di-substituted homoadamantane derivatives. However, in comparison with the adamantane system there remain some difficulties; for example, an increase of one methylene carbon diminishes the high symmetry inherent to the adamantane system, causing a complex situation in the configurations of substituents in the homoadamantane system. In this paper we wish to report the first synthesis of several 2-mono- and 2,4-di-substituted homoadamantanes. The configurations of the substituents are tentatively named, as is shown in Scheme 1, after adamantane derivatives.[4)]

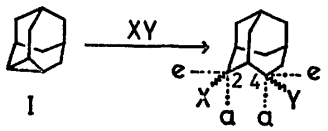

Scheme 1.

Results and Discussion

For cleaving the cyclopropane ring of I, we have chosen a radical-type reaction, *i.e.*, photobromination, taking account of the fact that an ionic reaction causes a skeletal alteration.[6)] Shea and Skell reported detailed studies of the photobromination of alkylcyclopropanes;[7)] we followed their procedures. When a solution of I and bromine in dichloromethane was irradiated at −78 °C for 5 min, a cleavage of the cyclopropane ring was observed, giving two dibromides (IIa and IIb, 52 : 48 by glc analysis) in an 82% yield, along with a small amount of monobromide. The structures of IIa and IIb were deduced to be 2,4-dibromohomoadamantanes on the basis of the following experimental results: (i) The reduction of IIa and IIb by tri-*n*-butyltin hydride gave homoadamantane (III), proving

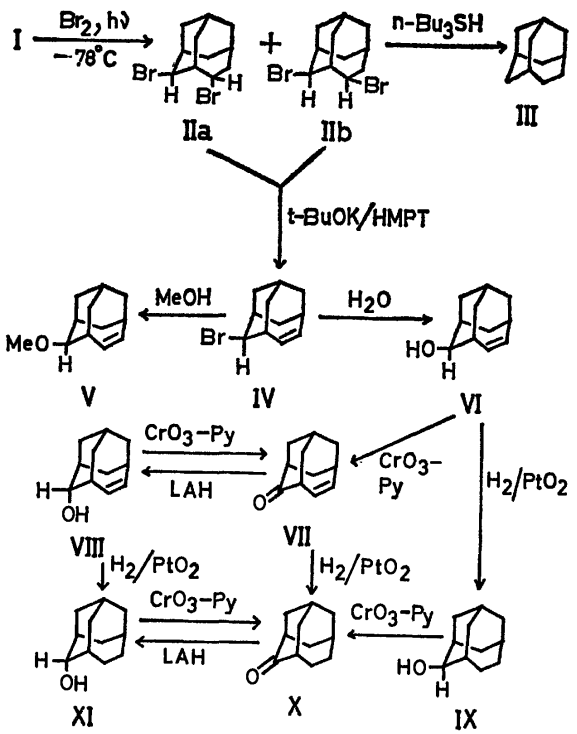

Scheme 2.

that IIa and IIb possess a homoadamantane skeleton. (ii) The treatment of IIa and IIb with a base could easily cause the elimination of one equivalent of hydrogen bromide to a sole compound (IV) (*vide infra*), indicating that one of the two bromine atoms is located on the ethylene bridge, and the other, on the methylene bridge.[8] (iii) As will be described later, the reaction of IV as well as the UV spectrum of homoadamant-4-en-2-one (VII) show that the substituents are obviously located at the 2- and 4-positions.

The treatment of a mixture of IIa and IIb with potassium *tert*-butoxide in hexamethylphosphoric triamide (HMPT) at 85—90 °C for 3 hr gave a sole product, 2-bromohomoadamant-4-ene (IV), in 80—90% yield. The above results indicate that the configuration of the bromine atom on the C-2 of IIa is identical with that of IIb. The PMR spectra of IIa, IIb, and IV are depicted in Fig. 2. As is shown in Fig. 2(c), the proton on the C-2 of IV does not couple with the adjacent bridge-head protons on the C-1 and C-3. The PMR studies using a shift reagent on 3-homoadamantanol established that the axial proton on the C-2 does not couple with the adjacent bridge-head proton, while the equatorial one does couple with the adjacent one, with a coupling constant of 4 Hz.[9] This report as well as the model investigation (FMM model) indicate that the proton on the C-2 must have the axial orientation. Thus, the structure of IV can be determined to be *e*-2-bromohomoadamant-4-ene.

The configurations at the C-4 positions of IIa and IIb were determined as follows. The difference between the chemical shift of the proton on the C-2 and that on the C-4 in IIa is larger than that in IIb, as is shown in Fig. 2(a) and 2(b). By analogy with the results for 2,4-dibromoadamantane,[10] we can deduce that IIa is *e,a*-2,4-dibromohomoadamantane and that IIb is *e,e*-2,4-dibromohomoadamantane.

The fact that the photobromination of I gives no *a,a*-2,4-dibromohomoadamantane is considered to be very similar to the case of 2,4-dehydroadamantane reported by Shea and Skell.[7,11] According to the mechanism suggested by them, the photobromination of I can proceed through the sequences shown in Scheme 3. It is of interest to note that the initial attack on the cyclopropane ring by the bromine atom is effected from the six-membered-ring side selectively. A larger steric requirement of the methylene hydrogen atoms on the C-5 than that of the methine hydrogen atom on the C-1 would inhibit the attack of the bromine atom from the seven-membered-ring side.

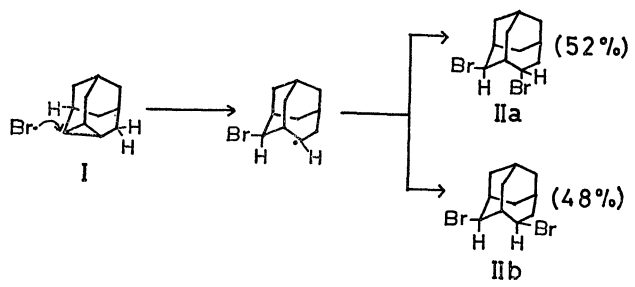

Scheme 3.

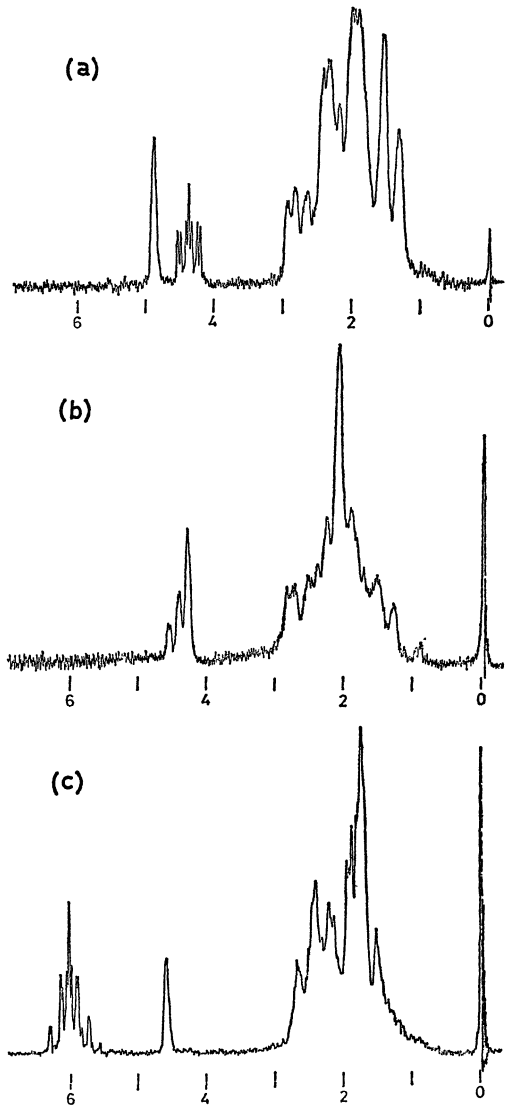

Fig. 2. PMR spectra of IIa, IIb, and IV.
(a): IIa, (b): IIb, and (c): IV.

The treatment of IV with methanol gave *e*-2-methoxyhomoadamant-4-ene (V) in a 90% yield, with a retention of the configuration. The configuration at the C-2 position of V was determined by PMR analysis in analogy with that of IV (see Experimental Section). When IV was hydrolyzed in 25% aqueous dioxane at the reflux temperature for 2 hr, *e*-2-hydroxyhomoadamant-4-ene (VI) was obtained in a 99% yield, again with a complete retention of the configuration. The oxidation of VI with a chromic anhydride–pyridine complex in dichloromethane gave homoadamant-4-en-2-one (VII) in a 94% yield. The UV spectrum of VII showed an n-π^* absorption at 300 nm (ε=127) (in EtOH); this suggests a homoconjugation between the carbonyl and the olefinic moieties.[12] The reduction of VII with lithium aluminum hydride in ether or sodium borohydride in ethanol gave *a*-2-hydroxyhomoadamant-4-ene (VIII) predominantly, along with a small amount of VI (VIII : VI=96 : 4 in the case of lithium aluminum hydride and 94 : 6 in the case of sodium borohydride, as determined by glc analysis). The PMR spectrum of VIII, shown in Fig. 3 (b),

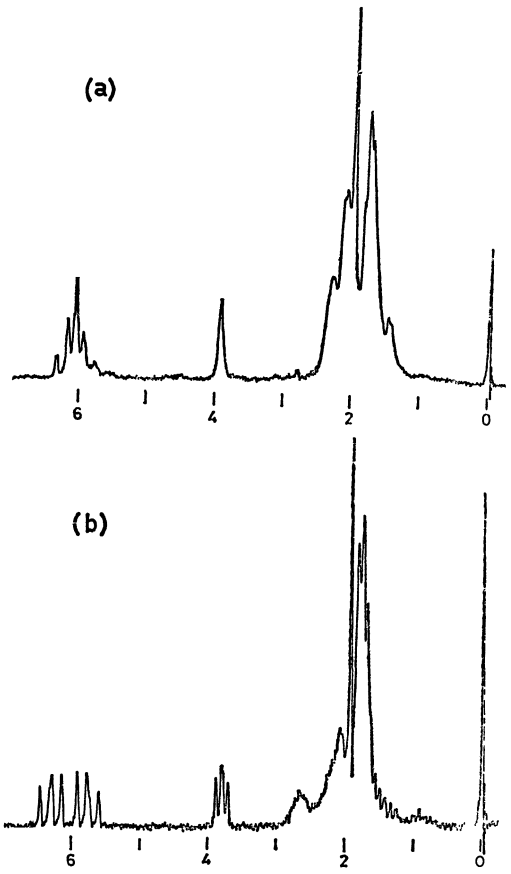

Fig. 3. PMR spectra of VI and VIII.
(a): VI, (b): VIII.

indicates that equatorial proton on the C-2 couples with the adjacent bridge-head protons with a coupling constant of *ca.* 4 Hz. The oxidation of VIII with a chromic anhydride–pyridine complex caused VIII to revert to VII, showing that no skeletal rearrangement took place during the above transformations.

The catalytic hydrogenations of VI, VII, and VIII utilizing platinum oxide in ethyl acetate gave the corresponding saturated compounds, *e*-2-hydroxyhomoadamantane (IX), homoadamantan-2-one (X), and *a*-2-hydroxyhomoadamantane (XI), in 98, 88, and 90% yields respectively. The oxidation of IX gave X. The reduction of X with lithium aluminum hydride in ether gave XI exclusively. The high stereoselectivities observed in the reductions of X as well as VII (*vide supra*) are similar to that observed in the reduction of bicyclo[3.3.1]nonan-2-one.[13] Moreover, it was confirmed that the Wolff-Kishner reduction of X gave the parent system, III. Thus, the above-mentioned transformations, depicted in Scheme 2, unequivocally confirm the structures of 2-mono- and 2,4-di-substituted homoadamantanes.

The complete retention of configuration at the C-2 position observed in the solvolysis of IV suggests the intervention of a homoallylic cation (XII).[14] In order to verify this possibility, we have solvolyzed IV in the presence of a buffer. When IV was hydrolyzed in 25% aqueous dioxane in the presence of sodium carbonate or potassium hydroxide, a new alcohol (XIII) was produced, along with a small amount of VI (XIII : VI=*ca.* 6 : 1 by glc analysis) (Scheme 4). The structure of XIII was deduced to be *e*-5-hydroxy-2,4-dehydrohomoadamantane on the basis of the following chemical and spectroscopic results: (i) The PMR spectrum of XIII had no signal due to the olefinic proton. (ii) The oxidation of XIII with the chromic anhydride–pyridine complex gave 2,4-dehydrohomoadamantane-5-one (XIV), which was then reduced by the Wolff-Kishner method to give I. (iii) A model investigation (FMM model) tells us that the axial proton on the C-5 of XIII must couple with the adjacent bridge-head protons, while the equatorial one does not, because the dihedral angle is nearly 90°. Since the PMR spectrum of XIII shows that the proton on the C-5 copules with the adjacent bridge-head protons with the coupling constant of *ca.* 6 Hz, XIII is determined to be *e*-5-hydroxy-2,4-dehydrohomoadamantane.

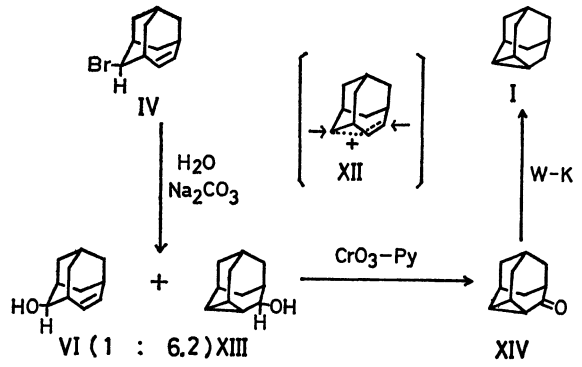

Scheme 4.

A complete understanding could, of course, be obtained by further precise experiments. However, the present results give powerful support to the notion that a homoallylic cation (XII) plays an important role in the solvolysis of IV.

Experimental

All the temperatures are uncorrected. The melting points were measured in a sealed tube in a liquid bath. The IR spectra were obtained on a Shimadzu IR-27 spectrometer. The UV spectra were recorded on a Hitachi EPS-2 spectrophotometer. The MS spectra were taken by using a Hitachi RMS-4 mass spectrometer. The PMR spectra were obtained on a Varian EM-360 spectrometer, TMS being chosen as the internal standard. The microanalyses were performed by Mrs. Kiyoko Fujimoto. No attempt has been made to maximize the yields of the reactions reported below.

2,4-Dihydrohomoadamantane (I). This compound was synthesized by the previously reported method.[5] A small contamination of homoadamant-4-ene can be easily removed by the treatment of the crude mixture with an appropriate amount of bromine in CH_2Cl_2, followed by column chromatography on silica gel eluted with *n*-hexane.

e,a-*2,4-Dibromohomoadamantane (IIa) and* e,e-*2,4-Dibromohomoadamantane (IIb).* A solution of I (1605 mg; 10.8 mmol) and Br_2 (0.54 ml, 1685 mg; 10.4 mmol) in 180 ml of CH_2Cl_2 was irradiated by means of a 300W medium-pressure mercury arc (soft glass filter) at −78 °C for 5 min. The reaction mixture was then warmed up to room temperature, washed successively with 10% aq. Na_2SO_3, aq. $NaHCO_3$, and brine, and dried (Na_2SO_4). The solvent was then

removed, and the residue (3008 mg) was chromatographed on silica gel (200 g). Elution by *n*-hexane gave first the unreacted starting material (208 mg) and then a monobromide of an unknown structure. Further elution by *n*-hexane gave IIa (187 mg), a mixture of IIa and IIb (2007 mg), and IIb (170 mg). The total yield of the dibromides, IIa and IIb (2364 mg), was 81.5%, calculated on the basis of the reacted I. The ratio of IIa to IIb was determined by glc analysis to be 52 : 48 (HVSG, 130 °C). IIa: mp 121—124 °C; IR (Nujol) 2950, 1460, 1380, 795, 720 cm^{-1}; PMR δ (CCl_4) 1.13—3.05 (broad complex m, 14H), 4.36 (d.d.d, 1H, J=2.8, 7.0, and 9.8 Hz), 4.89 (broad s, 1H); Found: C, 42.61; H, 5.26%. Calcd for $C_{11}H_{16}Br_2$: C, 42.88; H, 5.24%. IIb: mp 55—58 °C; IR (Nujol) 2950, 1460, 1380, 730 cm^{-1}; PMR δ (CCl_4) 1.07—3.05 (broad complex m, 14H), 4.41 (m, 2H); Found: C, 42.70; H, 5.27%. Calcd for $C_{11}H_{16}Br_2$: C, 42.88; H, 5.24%.

A mixture of IIa and IIb (115 mg; 0.37 mmol), *n*-Bu_3SnH (441 mg; 1.5 mmol), and benzene (2 ml) was refluxed under N_2 for 3 hr. The reaction mixture was then washed with brine and dried (Na_2SO_4). After the solvent had subsequently been removed, the residue was shown by glc analysis (PEG 20 M, 16 °C) to contain only one compound as a hydrocarbon component. This compound was isolated by preparative glc and determined to be homoadamantane (III) by comparison with the authentic sample [3b] (glc retention time, and MS and PMR spectra).

e-*2-Bromohomoadamant-4-ene (IV).* A solution of IIa and IIb (1668 mg; 5.42 mmol) and *t*-BuOK (705 mg; 6.29 mmol) in 17 ml of HMPT was heated at 85—88 °C for 3.5 hr under a nitrogen atmosphere. To the cooled reaction mixture we then added *n*-hexane, and the organic layer was repeatedly washed with brine and dried (Na_2SO_4). The solvent was then evaporated under reduced pressure, and the residue was sublimed (100—105 °C/10 mmHg) to give pure IV (1035 mg, 84.2%): mp 92—96 °C; MS: *m/e* 228 and 226 (M^+, 23 and 24%), 147 (100%); IR (Nujol) 2950, 1660 (weak), 1460, 1380, 1175, 790, 730, 695 cm^{-1}; PMR δ(CCl_4) 1.20—3.00 (broad complex m, 12H), 4.63 (broad s, 1H), 6.07 (m, 2H); Found: C, 58.40; H, 6.85%. Calcd for $C_{11}H_{15}Br$: C, 58.16; H, 6.66%.

The same treatment of pure IIa (126 mg; 0.41 mmol) with *t*-BuOK (74 mg; 0.66 mmol) in HMPT (3 ml) gave IV (82 mg, 88%).

The reaction was very sensitive to the reaction temperature, since IV was not very stable. When the temperature was higher, the resulting IV was converted to another compound, the structure of which was unknown. In our experiments, the yields were between 80 and 90%.

e-*2-Methoxyhomoadamant-4-ene (V).* A solution of IV (45 mg; 0.2 mmol) in 1 ml of methanol was heated at reflux for 5 hr. The reaction mixture was then concentrated under reduced pressure, and the residue was chromatographed on silica gel. Elution by *n*-hexane gave V (32 mg, 90%): bp 101—104 °C/22 mmHg; MS:*m/e* 178 (M^+, 100%); IR (neat) 2950, 1660 (weak), 1450, 1380, 1190, 1090, 945, 885, 735, 715 cm^{-1}; PMR δ (CCl_4) 1.10—2.57 (broad complex m, 12H) 3.20 (broad s, 1H), 3.26 (s, 3H), 6.00 (m, 2H); Found: C, 80.72; H, 10.39%. Calcd for $C_{12}H_{18}O$: C, 80.85; H, 10.18%.

e-*2-Hydroxyhomoadamant-4-ene (VI).* A solution of IV (449 mg; 1.98 mmol) in 20 ml of 25% aq. dioxane was heated at reflux for 2 hr. To the reaction mixture we then added aqueous $NaHCO_3$, and an organic material was extracted with CH_2Cl_2. The solution was washed with brine and dried (Na_2SO_4). The solvent was removed to give crude VI (322 mg, 99%): mp (from *n*-hexane) 226—229 °C; MS: *m/e* 164 (M^+, 96%), 91 (97%), 79 (100%); IR (Nujol) 3300, 2950, 1650 (weak), 1460, 1380, 1025, 710 cm^{-1}; PMR δ ($CDCl_3$) 1.10—2.70 (broad complex m, 12H), 2.01 (s, 1H, OH), 3.93 (broad s, 1H), 6.05 (m, 2H); Found: C, 80.34; H, 9.96%. Calcd for $C_{11}H_{16}O$: C, 80.44; H, 9.83%.

Homoadamant-4-en-2-one (VII). To a solution of pyridine (2.5 ml) in 12 ml of CH_2Cl_2, we gradually added CrO_3 (520 mg; 5.2 mmol). The solution was stirred at room temperature for 5 min, and then, to this solution, we added, drop by drop, a solution of VI (99 mg; 0.6 mmol) in 3.5 ml of CH_2Cl_2. The reaction mixture was stirred at room temperature for 2 hr and then washed successively 5% aqueous NaOH saturated with NaCl, 5% aqueous HCl (twice), aqueous $NaHCO_3$, and brine. The organic layer was dried (Na_2SO_4) and passed through a short alumina column. The solvent was removed to give crude VII (92 mg, 94%): mp (from *n*-hexane) 244—248 °C; MS: *m/e* 162 (M^+, 100%); IR (Nujol) 2950, 1710, 1650 (shoulder), 1460, 1380, 710 cm^{-1}; UV λ_{max} (EtOH) 300 nm (ε=127); PMR δ ($CDCl_3$) 1.63—3.23 (broad complex m, 12H), 6.10 (m, 2H); Found: C, 81.35; H, 8.88%. Calcd for $C_{11}H_{14}O$: C, 81.44; H, 8.70%.

a-*2-Hydroxyhomoadamant-4-ene (VIII).* To a suspention of $LiAlH_4$ (134 mg) in 10 ml of dry ether, we added, drop by drop, a solution of VII (120 mg; 0.74 mmol) in 10 ml of dry ether. The reaction mixture was then stirred at reflux temperature overnight. The usual work-up[15] and the removal of the solvent gave crude VIII, along with a small amount of VI (119 mg, 98%, VIII : VI=96 : 4 by glc analysis (PEG 20 M, 180 °C)). The crude material was chromatographed on alumina. Elution by a mixture of *n*-hexane and CH_2Cl_2 (7 : 3) gave pure VIII: mp 282—284 °C; MS: *m/e* 164 (M^+, 100%); IR (Nujol) 3300, 2950, 1665 (weak), 1460, 1380, 1060, 1040 cm^{-1}; PMR δ ($CDCl_3$) 1.20—2.90 (broad complex m, 12H), 1.92 (s, 1H, OH), 3.80 (d.d, 1H, J=4 and 4 Hz), 6.00 (m, 2H); Found: C, 80.25; H, 9.99%. Calcd for $C_{11}H_{16}O$: C, 80.44; H, 9.83%.

To a solution of VII (62 mg; 0.38 mmol) in 2 ml of EtOH, we added $NaBH_4$ (32 mg; 0.84 mmol), portion by portion, in an ice-bath. The reaction mixture was stirred at room temperature for 15 min, poured into water, and extracted with ether. The extract was washed with brine and dried (Na_2SO_4). The solvent was removed to give a crude product (59 mg, 93%; VIII : VI=94 : 6 by glc analysis).

The oxidation of VIII with the CrO_3-pyridine complex by the use of the procedure described above gave the starting material, VII, in a 97% yield.

e-*2-Hydroxyhomoadamantane (IX).* A solution of VI (32 mg; 0.2 mmol) and a small amount of PtO_2 in 2 ml of EtOAc was vigorously stirred under a hydrogen atmosphere. After 1 equivalent of H_2 had been absorbed, the PtO_2 was removed by filtration and the filtrate was evaporated under reduced pressure to give crude IX (31 mg, 98%): mp (from *n*-hexane) 257—260 °C; MS: *m/e* 148 (100%); IR (Nujol) 3300, 2950, 1460, 1380, 1030 cm^{-1}; PMR δ ($CDCl_3$) 1.00—2.30 (broad complex m, 16H), 2.00 (s, 1H, OH), 3.60 (broad s, 1H); Found: C, 79.27; H, 11.15%. Calcd for $C_{11}H_{18}O$: C, 79.46; H, 10.92%.

Homoadamantan-2-one (X). The procedure was essentially the same as that described above. The VII compound (102 mg; 0.63 mmol) gave X (92 mg, 88%): mp (from petroleum ether) 260—263 °C; MS: *m/e* 164 (M^+, 100%); IR (Nujol) 2950, 1720, 1460, 1380 cm^{-1}; PMR δ($CDCl_3$) 1.07—2.80 (broad complex m, 16H); Found: C, 80.24; H, 10.00%. Calcd for $C_{11}H_{16}O$: C, 80.44%; H, 9.83%.

The Wolff-Kishner reduction of X was conducted by the

use of the procedure described for the reduction of 2,4-dehydrohomoadamantan-5-one (XIV) (*vide infra*). The treatment of X (54 mg; 0.33 mmol) with KOH (368 mg) and 100% hydrazine hydrate (273 mg) in diethylene glycol (2 ml) gave homoadamantane (III) (35 mg, 71%), which was identical with an authentic sample[3b] (glc retention time, and MS and PMR spectra).

a-2-*Hydroxyhomoadamantane (XI).* This compound was prepared similarly from VIII in a 90% yield: mp (from *n*-hexane) >290 °C; MS: *m/e* 148 (100%); IR (Nujol) 3300, 2950, 1460, 1380, 1060, 1015 cm^{-1}; PMR $\delta(CDCl_3)$ 1.11—2.50 (broad complex m, 16H), 1.73 (s, 1H, OH), 3.83 (d.d, 1H, $J=5$ and 3.5 Hz); Found: C, 79.22; H, 11.13%. Calcd for $C_{11}H_{18}O$: C, 79.46; H, 10.92.

To oxidation of IX or XI by the CrO_3–pyridine complex gave a ketone, X. The reduction of X with $LiAlH_4$ in ether gave exclusively the axial epimer (XI). A PMR study showed the absence of IX.

e-*5-Hydroxy-2,4-dehydrohomoadamantane (XIII).* A solution of IV (322 mg; 1.4 mmol) and Na_2CO_3 (278 mg) in 10 ml of 25% aqueous dioxane was heated at reflux for 3 hr. The reaction mixture was then cooled, poured into water, and extracted with CH_2Cl_2. The extract was washed with brine and dried (Na_2SO_4). The subsequent removal of the solvent gave crude products (220 mg, 98%) which contained VI and XIII (1 : 6.2 by glc analysis; PEG 20 M, 160 °C). The separation of VI and XIII was effected by column chromatography on silica gel. Elution by *n*-hexane and ether (95 : 5) gave pure XIII (97 mg) and, subsequently, a mixture of VI and XIII (121 mg). The properties of XIII were as follows: mp (from *n*-hexane) 264—265 °C; MS: *m/e* 164 (M^+, 26%), 146 (100%); IR (Nujol) 3300, 2950, 1460, 1380, 1035 cm^{-1}; PMR $\delta(CDCl_3)$ 0.67—2.33 (broad complex m, 14H), 1.67 (s, 1H, OH), 4.40 (t, 1H, $J=6$ Hz); Found: C, 80.59; H, 9.98%. Calcd for $C_{11}H_{16}O$: C, 80.44; H, 9.83%.

When KOH was used in place of Na_2CO_3, the same products were obtained (VI : VIII = 1 : 6.9). When $AgClO_4$ was used, the reaction proceeded at room temperature but the product distribution was almost the same as has been described above (VI : XIII = 1 : 7.2).

2,4-*Dehydrohomoadamantan-5-one (XIV).* To a solution of pyridine (1.5 ml) in 7 ml of CH_2Cl_2, we gradually added CrO_3 (267 mg; 2.7 mmol). The solution was stirred at room temperature for 5 min, and then to this solution we added a solution of XIII (50 mg; 0.3 mmol) in 2 ml of CH_2Cl_2. The reaction mixture was stirred at room temperature for 2 hr and washed successively with 5% aqueous NaOH saturated with NaCl, 5% aqueous HCl (two times), 5% aqueous NaOH, and brine. The organic layer was dried (Na_2SO_4) and passed through a short alumina column. The solvent was removed to give crude XIV (44 mg, 90%): mp (from *n*-hexane) 238—241 °C; MS: *m/e* 162 (M^+, 100%); IR (Nujol) 2950, 1710, 1460, 1380 cm^{-1}; PMR $\delta(CDCl_3)$ 0.70—2.57 (broad complex m, 14H); Found: C, 81.38; H, 8.88%. Calcd for $C_{11}H_{14}O$: C, 81.44; H, 8.70%.

The Wolff-Kishner reduction of XIV was conducted following the procedure reported for the reduction of 8,9-dehydro-2-adamantanone.[16] A solution of XIV (31 mg; 0.19 mmol), KOH (208 mg), and 100% hydrazin hydrate (153 mg) in 1 ml of diethylene glycol was stirred at 110 °C for 30 min and subsequently at 180 °C for 3 hr. The material sublimed on the condenser was dissolved in petroleum ether (40—60 °C) and dried (Na_2SO_4). The subsequent removal of the solvent gave a sole product (21 mg, 75%), which was confirmed to be I by comparison with an authentic specimen (glc retention time, and MS and PMR spectra).

The UV maximum in $CHCl_3$ at 380 nm for the 2,4-dinitrophenylhydrazone of XIV was appropriate for a conjugated carbonyl function in comparison with the UV maximum in $CHCl_3$ at 371 nm for the 2,4-dinitrophenylhydrazone of 4-homoadamantanone.[17]

The 2,4-dinitrophenylhydrazone of XIV: mp (from EtOH) 184—185.5 °C; UV λ_{max} ($CHCl_3$) 380 nm; Found: C, 59.46; H, 5.26; N, 16.10%. Calcd for $C_{17}H_{18}O_4N_4$: C, 59.64; H, 5.30; N, 16.37%.

The 2,4-dinitrophenylhydrazone of 4-homoadamantanone: mp (from EtOH) 210—211 °C; UV λ_{max} ($CHCl_3$) 371 nm; Found: C, 59.18; H, 6.11; N, 16.36%. Calcd for $C_{17}H_{20}O_4N_4$: C, 59.29; H, 5.85; N, 16.27%.

The authors wish to thank Dr. Takeshi Imagawa for his helpful discussion.

References

1) Throughout this paper we have adopted trivial nomenclature for simplicity. The IUPAC names for 2,4-dehydrohomoadamantane and homoadamantane are tetracyclo[5.3.1.$0^{5,3}$.$0^{4,9}$]undecane and tricyclo[4.3.1.$1^{3,8}$]undecane, respectively.

2) For pertinent references; R. C. Fort, Jr. and P. v. R. Schleyer, *Chem. Rev.*, **64**, 277 (1964); R. C. Bingham and P. v. R. Schleyer, *Fortschr. Chem. Forsch.*, **18**, 1 (1971).

3) As to the methylene-bridge-substituted compounds, there is only one report, which is concerned with 2,7-disubstituted homoadamantanes; B. R. Vogt, *Tetrahedron Lett.*, **1968**, 1575. As to the ethylene-bridge-substituted compounds, see the following reports; (a) D. R. Kell and F. J. McQuillin, *Chem. Commun.*, **1970**, 599; K. Bott, *ibid.*, 1349 (1969); D. R. Kell and F. J. McQuilline, *J. Chem. Soc., Perkin Trans. I*, **1972**, 2100; K. Bott, *Ann. Chem.*, **766**, 51 (1972). (b) J. E. Nordlander, F. Y.-H. Wu, S. P. Jindal, and J. B. Hamilton, *J. Amer. Chem. Soc.*, **91**, 3962 (1969); P. v. R. Schleyer, E. Funke, and S. H. Liggero, *ibid.*, **91**, 3965 (1969). (c) I. Tabushi, Z. Yoshida, and N. Takahashi, *ibid.*, **92**, 6670 (1970); R. M. Black and G. B. Gill, *J. Chem. Soc., C*, **1970**, 671; J. L. M. A. Schlatmann, J. G. Korsloot, and J. Schut, *Tetrahedron*, **26**, 949 (1970); E. Bernaert, D. Danneels, M. Anteunis, and G. Verhegge, *ibid.*, **29**, 4127 (1973).

4) A. C. Udding, J. Strating, and H. Wynberg, *Tetrahedron Lett.*, **1968**, 1345.

5) The first synthesis; Z. Majerski, S. H. Liggero, and P. v. R. Schleyer, *Chem. Commun.*, **1970**, 949. Our results; R. Yamaguchi, T. Katsushima, T. Imagawa, and M. Kawanishi, *Synthetic Commun.*, **1974**, 83; R. Yamaguchi, T. Katsushima, and M. Kawanisi, This Bulletin, **47**, 2830 (1974).

6) An investigation concerned with the ionic cleavage of I is in progress in our laboratory, and it has been found that the homoadamantane skeleton was converted to other tricycloundecane system. The details will be the subject of further report.

7) K. J. Shea and P. S. Skell, *J. Amer. Chem. Soc.*, **95**, 6728 (1973).

8) According to the Bredt rule, it is highly probable that the bromine atom which locates on the methylene-bridge can not be eliminated to give an olefin. For example see E. Cuthbertson and D. D. MacNicol, *Tetrahedron Lett.*, **1974**, 2367.

9) H. Langhals and C. Rüchardt., *Chem. Ber.*, **107**, 1245 (1974).

10) F. W. v. Deursen and J. Bakker, *Tetrahedron*, **27**, 4593

(1971).

11) The ratio of *e,a*- and *e,e*-derivative in the photobromination of I was different from that of 2,4-dehydroadamantane (*e,a*-: *e,e*-=66 : 34).

12) For homoconjugation, see L. N. Ferguson, "The Modern Structural Theory of Organic Chemistry," Prentice-Hall, Inc., Princeton, N. J. (1963), p. 441 and 525.

13) (a) K. H. Baggaley, J. R. Dixon, J. M. Evans, and S. H. Graham, *Tetrahedron*, **23**, 299 (1967). (b) J. P. Schaefer, J. C. Lark, C. A. Flegal, and L. M. Honig, *J. Org. Chem.*, **32**, 1732 (1967).

14) Review: B. Capon, *Quart. Rev.*, **18**, 45 (1964); M. Hanack and H. J. Schneider, *Angew. Chem. Int. Ed. Engl.*, **6**, 666 (1967); H. G. Richey, "Carbonium Ions," Vol. 3, ed. by G. A. Olah and P. v. R. Schleyer, Wiley-Interscience, New York, N. Y. (1972), Chapter 25.

15) L. F. Fieser and M. Fieser, "Reagents for Organic Synthesis," Vol. 1, John Wiley & Sons, Inc., New York, N. Y. (1967). p. 581.

16) R. K. Murray, Jr. and K. A. Baliak, *J. Org. Chem.*, **38**, 2556 (1973).

17) J. E. Baldwin and W. D. Foglesong, *J. Amer. Chem. Soc.*, **90**, 4303 (1968).

The Photoreactions of 2,3-Dicyanobarrelene[1)]

Katsuhiro SAITO* and Toshio MUKAI

Department of Chemistry, Faculty of Science, Tohoku University, Aoba, Aramaki, Sendai 980

(Received January 21, 1975)

The direct irradiation of 2,3-dicyanobarrelene (II) provided 1,2-dicyanocyclooctatetraene (III). On the other hand, the acetone-sensitized photoreaction of II afforded semibullvalene derivatives (IV and V). Investigations of their NMR spectra clarified that IV completely degenerates, whereas V inclines to the favorable form of the valence isomers.

It is well known that the activation energy of the Cope rearrangement of the I system is very low.[2-9)] Recently, Hoffmann and Stohrer thoretically considered the substituent effects on such valence isomerizations and proposed a general rule for the prediction of the favorable isomers.[10)] However, the substituted derivatives possessing the I skeletone are not numerous, so the adequacy of the rule has not been proved sufficiently. Therefore, it seemed that it would be interesting to synthesize new derivatives of this system and to study their properties from the viewpoint of the substituent effects on the valence isomerizations. This study will be concerted with the photoreactions of 2,3-dicyanobarrelene (II),[11)] which is expected to give cyano-substituted semibullvalenes suitable for the study of the valence isomerizations.

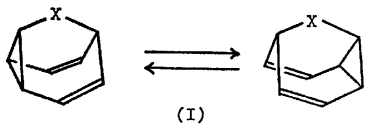

(I)

Fig. 1.

When a solution of II in *n*-hexane containing 10% of acetone was irradiated with a medium-pressure mercury lamp (Rayonet 300 nm) through a Pyrex filter, 1,2-dicyanocyclooctatetraene (III) was obtained in an almost quantitative yield. On the other hand, the irradiation of an acetone solution of II afforded 1,5-dicyanosemibullvalene (IV) and 3,4-dicyanosemibullvalene (V) in 4 and 56% yields respectively, in addition to 20% of III. As is well known in the photoreactions of barrelenes,[12)] the formation of semibullvalene derivatives (IV and V) may be ascribed to the acetone-sensitized reaction of II, although the cyclooctatetraene derivative (III) was also formed. It was also confirmed that IV and V are the primary photoproducts from II, because III did not afford IV and V upon irradiation under the same conditions.

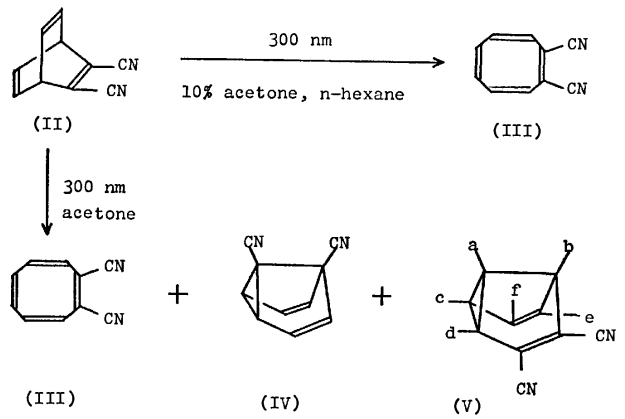

Fig. 2.

All the products, III, IV, and V, have the same molecular formula, $C_{10}H_6N_2$, and thier mass spectra exhibit the same molecular ion peak ($M^+=154$). The structures of the products were based on their spectral properties, shown below.

NMR (100 MHz, δ ppm): for III (in acetone-d_6), 6.2 (broad singlet 4H), 7.12 (broad singlet 2H); for IV (in $CDCl_3$), 4.78 (narrow multiplet 4H), 5.48 (narrow multiplet 2H); for V (in acetone-d_6), 3.45 (multiplet H_a), 3.72 (multiplet H_b), 4.32 (multiplet H_c), 4.55 (multiplet H_d), 5.26 (multiplet H_e), and 5.73 (multiplet H_f). Coupling constants in Hz; $J_{ab}=6.5$, $J_{ac}=4.0$, $J_{ad}=3.0$, $J_{be}=3.5$, $J_{cd}=3.0$, $J_{ce}=0.5$, $J_{cf}=3.5$, and $J_{ef}=4.0$.

UV (in methanol) nm (log ε): for III, 233 (4.31), 303 (2.79); for IV, 310 (2.31); for V, 310 (2.32).

IR (KBr): for III, 2226 cm^{-1}; for IV, 2240 cm^{-1}; for V, 2220 cm^{-1}.

The NMR spectrum of IV is very similar to that of 1,5-bis(trifluoromethyl)semibullvalene.[9)] The NMR spectrum of V is very complex, but the above data could be obtained using the double- and triple-resonance techniques.

The reaction mechanism for the formation of III can reasonably explained *via* a $2\pi+2\pi$-type intermediate (VI) which is derived from the singlet excited state.[12)] The formation of IV and V may be *via* a biradical intermediate (VII), which is an intermediate

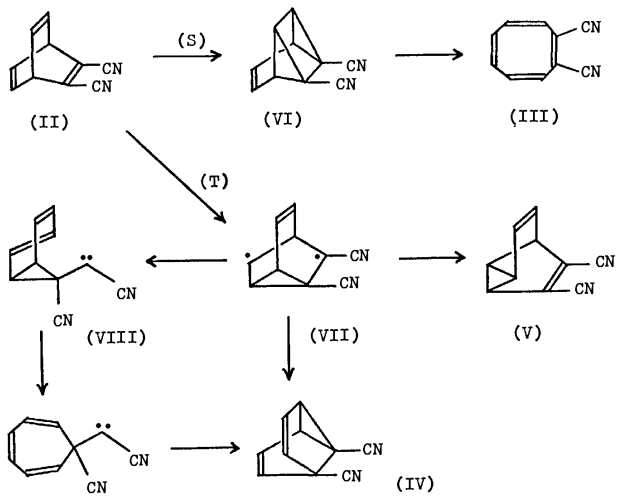

Fig. 3.

* Present address: Department of Chemistry, Nagoya Institute of Technology, Gokiso-cho, Showa-ku, Nagoya 466.

in di-π-methane rearrangements.[12] However, a path *via* a carbene intermediate (VIII) can not be eliminated for the formation of IV. The difference between the yields of IV and V can reasonably be explained by the stabilization ascribed to the formation of the double bond conjugated with two cyano groups.

Hoffmann and Stohrer pointed out that the symmetrically substituted semibullvalenes (possessing the same substituents at the positions which are symmetric with regard to the C_{2v}-axis or the mirror plane through C_3, C_7, and the center of the C_1–C_5 bond), should exist as degenerated valence isomers, except for an irrational compound (1,5-difluoro-2,4,6,8-tetracyanosemibullvalene).[10] That the NMR spectrum of IV shows two narrow multiplets with an area ratio of 2 : 1 implies that IV exists as a degenerated valence isomer; this fact coincides well with the prediction of Hoffmann *et al.*

According to the study of Hoffmann *et al.*,[10] the activation energies of the valence isomerizations of the symmetrically substituted semibullvalenes are sensitive toward substituents. In the case of the 1,5-dicyano derivative (IV), the activation energy may be expected to be considerably large and to be fixed more easily than those of other symmetric derivatives, bacause the stabilization effect of the cyano group operates more effectively on the reactant than on the transition state of the isomerization. From the above point of view, a low-temperature NMR study of IV was made, but the degenerated isomerization still occurs at low temperatures such as -100 °C, and no change was observed in the NMR spectrum.

3,4-Dicyanosemibullvalene (V) is likely to be fixed in the structure shown in Fig. 2. Hoffmann[13] and Günther[14] have proposed that an electron-withdrawing group attached to the C_1-position of a cyclopropane ring strengthens the C_2–C_3 bond and, instead, weakens the C_1–C_2 and C_1–C_3 bonds, whereas the electron-donating groups have the opposite effects. According to their proposition, when the substituent, R, in the structures in Fig. 4 are electron-withdrawing groups such as the cyano group, the C_2–C_8 bond of the structure (IX) weakens and, consequently, another valence isomer (X) should predominate. This is the case in our results. On the contrary, though, Liu and Krespan[9] have reported that 2,3-bis(trifluolomethyl)-semibullvalene, which has electron-withdrawing substituents at the same positions as V, is fixed in another structure, IX. Although this result seems to conflict with the above proposition, it can be reasonably explained as follows. The steric repulsion between the two trifluoromethyl groups which are located on a common plane in the X structure cause the shift of the isomerization to the IX structure, in which these two groups are in a twisted position. When the substituents are small, like the cyano group, the electronic effect dominates, whereas when the substituents become large, as the trifluoromethyl group, the steric effects seem to be predominant.

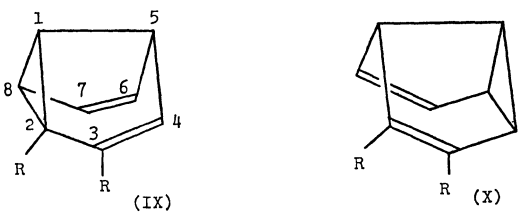

Fig. 4.

Experimental[15]

Direct Irradiation of 2,3-Dicyanobarrelene (II). A *n*-hexane solution of II containing 10% of acetone (100 mg/100 ml) was irradiated in a Pyrex vessel by means of a medium pressure mercury lamp (Rayonet 300 nm) for 2.5 hr. The subsequent evaporation of the solvent afforded a yellow crystalline product of III in a quantitative yield. III was recrystallized from methanol; mp 112 °C. Found: C, 77.72; H, 4.16; N, 18.35%. Calcd for $C_{10}H_6N_2$: C, 77.90; H, 3.92; N, 18.17%.

Acetone-sensitized Irradiation of 2,3-Dicyanobarrelene (II). An acetone solution of II (100 mg/100 ml) was irradiated in a Pyrex vessel by means of a medium pressure mercury lamp (Rayonet 300 nm) for 2.5 hr. After the subsequent removal of the solvent, an oily product (80 mg) was isolated by thin-layer chromatography (on silica gel, with benzene as the solvent). The NMR spectrum showed that this oil contained only III, IV, and V in a ratio of 25, 5, and 70; thus, the yields of III, IV, and V were calculated as 20, 4, and 56%, respectively. The distillation of this oil (85 °C, 0.02 mm/Hg) afforded an oily product, V. When the residue was separated by column chromatography using alumina, III was eluted with petroleum ether–benzene (3 : 7), and IV, with benzene. The recrystallization of IV from methanol afforded crystals with mp of 116 °C. Anal. for IV. Found: C, 77.94; H, 3.94; N, 18.17%. Calcd for $C_{10}H_6N_2$: C, 77.90; H, 3.92; N, 18.17%. Anal. for V. Found: C, 77.64; H, 3.90; N, 17.88%. Calcd for $C_{10}H_6N_2$: C, 77.90; H, 3.92; N, 18.17%.

References

1) Organic Photochemistry, XXXV. Part XXXIV: H. Tsuruta, M. Ogasawara, and T. Mukai, *Chem. Lett.*, **1974**, 887.
2) H. E. Zimmerman and G. L. Grunewald, *J. Amer. Chem. Soc.*, **88**, 183 (1966).
3) M. J. S. Dewar and W. W. Shoeller, *ibid.*, **93**, 1481 (1971).
4) H. E. Zimmerman and H. Iwamura, *ibid.*, **92**, 2015 (1970).
5) W. von E. Doering and W. R. Roth, *Tetrahedron*, **19**, 715 (1963).
6) G. Schröder, *Angew. Chem.*, **75**, 722 (1963).
7) R. Merenyi, J. F. M. Oth, and G. Schröder, *Chem. Ber.*, **97**, 3150 (1964).
8) H. Tsuruta, K. Kurabayashi, and T. Mukai, *Tetrahedron Lett.*, **1967**, 3775.
9) R. S. H. Liu and C. G. Krespan, *J. Org. Chem.*, **34**, 1271 (1969).
10) R. Hoffmann and W. D. Stohrer, *J. Amer. Chem. Soc.*, **93**, 6941 (1971).
11) E. Ciganek, *Tetrahedron Lett.*, **1967**, 3321.
12) H. E. Zimmerman, R. S. Givens, and R. M. Pagni, *J. Amer. Chem. Soc.*, **90**, 6096 (1968). *ibid.*, **91**, 3316 (1969).
13) R. Hoffmann, *Tetrahedron Lett.*, **1970**, 2907.
14) H. Günther, *ibid.*, **1970**, 5173.
15) All mp and bp were uncorrected. NMR spectra were measured by Varian-HA-100 spectrometer, and referred to TMS as an internal standard.

The Molecular and Crystal Structure of DL-3-Chloro-2,4-pentanediol

Shunsuke KURIBAYASHI

Government Industrial Research Institute, Osaka Midorigaoka, Ikeda 563

(Received March 17, 1975)

The crystal structure of DL-3-chloro-2,4-pentanediol has been determined by X-ray analysis. The crystal is triclinic, with dimensions of $a=6.573$, $b=8.991$, $c=6.243$ Å, $\alpha=80.18°$, $\beta=94.25°$, and $\gamma=102.87°$. The five carbon atoms have a TT conformation, and the two OH groups have intermolecular hydrogen bondings, whose distances are 2.75 Å and 2.80 Å respectively.

As in the case of 2,4-pentanediol,[1,2] 3-chloro-2,4-pentanediol is separated into two parts by elution chromatograph; one of the parts seems to be racemic, and the other, the *meso* form. However in the case of 3-chloro-2,4-pentanediol, synthesized by the hydrogenation of 3-chloro-2,4-pentanedione, the *meso* form is eluted faster than the racemic form when separated by an ion-exchanger chromatograph. The conformation, configuration, and hydrogen bonding of these compounds have been investigated by NMR and IR spectra.[3,4] The structure determination was undertaken by means of the X-ray method for the racemic form, which crystallizes at room temperature, in order to elucidate the conformation, configuration, and hydrogen bonding of the molecule, and to compare the results with those obtained by NMR and IR spectroscopy.

Experimental

The colorless prismatic crystals or platelets were obtained by the distillation of this substance under a pressure of 22 mmHg. The crystal used for the X-ray diffraction was a needle elongated along the c-axis; the crystal was cut into the cubic form to make its shape suitable for X-ray diffractometry. The crystallographic data are shown in Table 1. The cell dimensions were determined by the least-squares method using 15 reflections. The intensity data were collected by using a Rigaku four-circle diffractometer with Mo$K\alpha$ radiation, in the region from 2.5° to 55° for 2 θ. The experiment was carried out by the ω-2 θ technique. Out of 1637 possible independent reflections, 1329 non-zero data were collected. No absorption or extinction correction was made. The crystal density was measured by the flotation method.

TABLE 1. CRYSTAL DATA

$C_5H_{11}O_2Cl$	mol wt 138.6
$a=6.573(1)$ Å	mp 56—56.5 °C
$b=8.991(1)$ Å	$D_m=1.294$ g·cm^{-3}
$c=6.243(1)$ Å	$D_x=1.299$ g·cm^{-3}
$\alpha=80.18(1)°$	$Z=2$
$\beta=94.25(1)°$	Space group $P\bar{1}$
$\gamma=102.87(1)°$	
$V=354.22(7)$ Å^3	

Structure Determination

A sharpened Patterson map was synthesized, from which the co-ordinate of the Cl atom was then deduced. Successive structure factor calculations and Fourier syntheses revealed all of the remaining non-hydrogen atoms. On the basis of these atomic locations, least-squares refinements using isotropic temperature factors were carried out. After 5 cycles of refinements, the R factor was found to be 0.198 for the non-zero reflections. Anisotropic temperature factors were then introduced for all of the non-hydrogen atoms. After 6 cycles of refinements, the R factor was reduced to 0.079 for the non-zero reflections. At this stage of analysis, the difference Fourier map was computed; all of the hydrogen atoms were located in it, but the peaks thus obtained were not very sharp, so their locations, except for those which were attached to oxygen atoms, were replaced by the calculated values, assuming that the CH bond lengths are 1.09 Å and that the bond angles of the carbon atoms are kept tetrahedral. With these positional parameters, 6 more cycles of least-squares refinements were carried out. In these procedures, the positional and thermal parameters of the hydrogen atoms which are attached to carbon atoms were not varied, and the thermal parameters of all of the hydrogen atoms were assumed to be the same as the isotropic parameters of those of the atoms to which they are bonded. By these procedures, the R factor was reduced to 0.053. The weighting scheme used here was:

$$|F_0|<F_{min}: \quad w=0.2$$

$$F_{min}\leq|F_0|\leq F_{max}: \quad w=1.0$$

$$F_{max}<|F_0|: \quad w=F_{max}/|F_0|$$

where $F_{max}=20.0$ and $F_{min}=10.0$. The numerical calculations were carried out on a TOSBAC 3400-41 computer, using the program written by Tamaichi Ashida which is included in the UNICS program system.[5] The final atomic co-ordinates and temperature factors are shown in Tables 2 and 3. The

TABLE 2. ATOMIC CO-ORDINATES ALONG WITH THEIR ESTIMATED STANDARD DEVIATIONS

Atom	x/a	y/b	z/c
C (1)	−0.0833(5)	0.2952(4)	−0.2966(5)
C (2)	0.1208(4)	0.3494(2)	−0.1756(3)
C (3)	0.1702(3)	0.2272(2)	0.0100(3)
C (4)	0.3699(3)	0.2776(2)	0.1410(3)
C (5)	0.4229(5)	0.1493(4)	0.3136(5)
O (1)	0.2808(3)	0.3790(2)	−0.3263(2)
O (2)	0.3637(3)	0.4109(2)	0.2328(2)
Cl	−0.0439(1)	0.1708(1)	0.1895(1)
H(O_1)	0.392(6)	0.434(4)	−0.291(7)
H(O_2)	0.305(7)	0.389(4)	0.347(6)

Table 3. Temperature factors for every atom

The anisotropic parameters are represented by the form $\exp\{-(\beta_{11}h^2+\beta_{22}k^2+\beta_{33}l^2+2\beta_{12}hk+2\beta_{13}hl+2\beta_{23}kl)\times 10^{-4}\}$. Estimated standard deviations are shown in parentheses by cell edge for non-hydrogen atoms and in Å² for hydrogen atoms.

Atom	β_{11}	β_{22}	β_{33}	β_{12}	β_{13}	β_{23}
C (1)	317 (8)	227 (5)	282 (7)	15 (5)	−61 (6)	−44 (5)
C (2)	283 (6)	138 (3)	208 (5)	12 (3)	−5 (4)	−48 (3)
C (3)	242 (5)	122 (2)	198 (5)	−3 (3)	41 (4)	−38 (2)
C (4)	234 (5)	151 (3)	222 (5)	2 (3)	12 (4)	−29 (3)
C (5)	354 (9)	218 (5)	372 (10)	65 (5)	−19 (7)	21 (5)
O (1)	325 (5)	196 (3)	187 (3)	−60 (3)	26 (3)	−50 (2)
O (2)	313 (5)	153 (2)	197 (4)	−43 (2)	25 (3)	−50 (2)
Cl	278 (1)	210 (1)	273 (1)	−38 (1)	80 (1)	−49 (1)
$H(O_1)$	4.5 (8)					
$H(O_2)$	4.2 (8)					

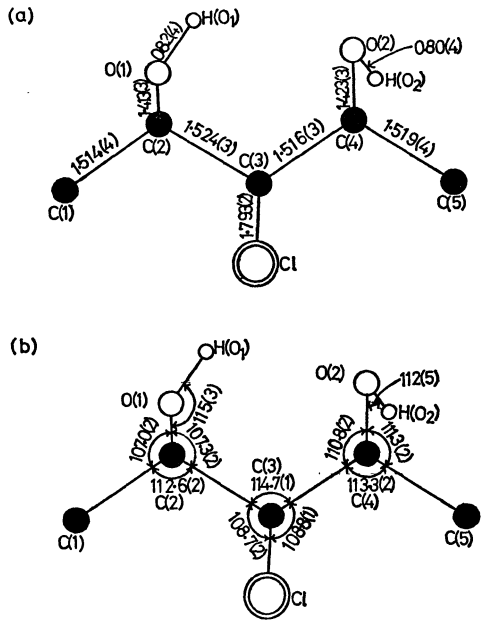

Fig. 1. The molecular shape, bond lengths (a), and angles (b), looking down through the direction perpendicular to the least square plane.

observed and calculated structure factors are listed in Table 4.*)

Results and Discussion

The bond lengths, bond angles, and the molecular shape are shown in Fig. 1. The bond lengths, ranging from 1.514 to 1.524 Å for C–C and from 1.413 to 1.423 Å for C–O, are not significantly different from the respective mean values of 1.519 and 1.418 Å. The OH bond lengths are 0.80 and 0.82 Å, a little shorter than the ordinary OH bond lengths. The C–C–C bond angles are systematically about 6° greater than the C–C–O bond angles. This fact has also been pointed out for other polyols.[6–10] The five carbon atoms are nearly on a plane, and they take a TT sequence. The equation of the least-squares plane through five carbon atoms is given by:

$$-0.6454x + 0.5489y + 0.7445z = 0.4262$$

with respect to the crystallographic axes. The deviations of five carbon atoms from the plane are shown in Table 5. The calculations were carried out using the program written by Tosio Sakurai.[5] The torsional angles, listed in Table 6 were calculated by means of the program written by Reikichi Iwamoto of our laboratory. In Figs. 2 and 3, the packing of the molecules looking down the c- and a-axes in the unit cell are shown. As is shown in these figures, the two oxygen atoms are hydrogen-bonded to each other. Each hydroxyl group forms two hydrogen bonds intermolecularly, one as donor and the other as acceptor. These two hydrogen-bond distances are 2.800 and 2.752 Å respectively. As is commonly observed, the spread of C–O–H angles at the donor oxygen atom of

Table 5. Deviations of five carbon atoms from the least-square plane

Atom	Deviations (Å)
C (1)	0.005
C (2)	−0.030
C (3)	0.020
C (4)	0.030
C (5)	−0.025

Table 6. Torsional angles

	Torsional angles
C (1)-C (2)-C (3)-C (4)	−178.19
C (2)-C (3)-C (4)-C (5)	−175.64
C (4)-C (3)-C (2)-O (1)	64.20
C (2)-C (3)-C (4)-O (2)	58.31
C (1)-C (2)-C (3)-Cl	−56.04
C (5)-C (4)-C (3)-Cl	62.30

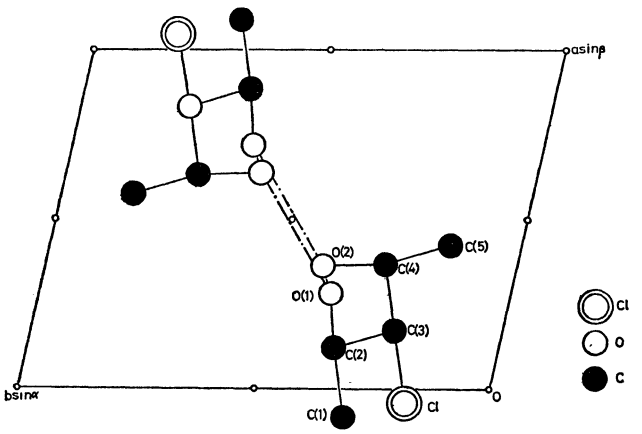

Fig. 2. The crystal structure of DL-3-chloro-2,4-pentanediol viewed down along the c-axis. Hydrogen bonds are shown by the chain lines.

* Table 4, which gives a complete list of the observed and the calculated structure factors, has been submitted to, and is kept by, the office of the Bulletin of the Chemical Society of Japan. (Document No. 7518).

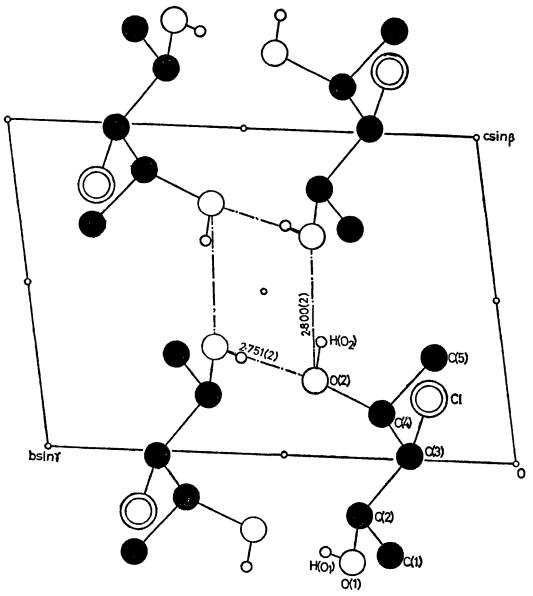

Fig. 3. The crystal structure of DL-3-chloro-2,4-pentanediol viewed down along the *a*-axis.

the hydrogen bond is less than those of H···O–C at the acceptor oxygen. The angles of the former are 112.5° and 115.4°, and of the latter, 124.0° and 137.9°. Surrounding the center of symmetry, four molecules are linked together by the hydrogen bonds. The shortest van der Waals contacts of C–C, C–O, C–Cl, O–O, and O–Cl are 3.52, 3.54, 3.60, 3.48, and 3.95 Å respectively.

As has been pointed out on the basis of NMR observation, the configuration of the molecule is proved to be the racemic form. From the IR spectra, measured in two concentrations, the conformations of racemic chloro-diol are thought to be mixtures of TT and TG, but in the crystalline state the conformations are TT only and all of the OH groups are linked together by intermolecular hydrogen bonds.

The author is indebted to Mr. Takahiko Kawaguchi and Professor Kaichi Sugita of Ritsumeikan University for supplying the sample and for giving him helpful advice.

References

1) M. Shiraki and E. Nagai, *Nippon Kagaku Zasshi*, **81**, 976 (1960).
2) E. Nagai, S. Kuribayashi, M. Shiraki, and M. Ukita, *J. Polym. Sci.*, **35**, 295 (1959).
3) T. Kawaguchi, Thesis of Master Degree. Ritsumeikan University (1969).
4) T. Kawaguchi, H. Takahashi, K. Sugita, and S. Kuribayashi, Lecture on spring annual meeting of the Chemical Society of Japan in 1969.
5) "The Universal Crystallographic Computation Program System (UNICS)," ed. by T. Sakurai, The Crystallographic Society of Japan, Tokyo (1967).
6) H. M. Berman and R. D. Rosenstein, *Acta Crystallogr.* **B24**, 435 (1968).
7) H. M. Berman, G. A. Jeffrey, and R. D. Rosenstein, *ibid.*, **B24**, 442 (1968).
8) H. S. Kim, G. A. Jeffrey, and R. D. Rosenstein, *ibid.*, **B24**, 1449 (1968).
9) H. S. Kim, G. A. Jeffrey, and R. D. Rosenstein, *ibid.*, **B25**, 2223 (1969).
10) N. Azarnia, G. A. Jeffrey, and M. S. Shen, *ibid.*, **B28**, 1007 (1972).

The Crystal and Molecular Structure of *cis*-2,2-Diphenyl-3,4-dichlorothietane

Shigekazu KUMAKURA and Toshiko KODAMA*

Department of Chemistry, Saitama University, 255 Shimo-okubo, Urawa 338

(Received July 1, 1974)

The crystal structure of *cis*-2,2-diphenyl-3,4-dichlorothietane has been determined from three-dimensional X-ray data collected by the photographic method. The compound forms monoclinic crystals with $a=9.94(1)$, $b=12.56(1)$, $c=12.96(1)$ Å, $\beta=120.66(8)°$, and $Z=4$ in the space group of $P2_1/c$. The structure has been refined by the block-diagonal least-squares method to a final R value of 0.10, based on 1578 observed reflections. The conformation of the C–Cl bonds with respect to the thietane ring is (3e4a), consistent with that in solution derived from the dipole moments. The thietane skeleton of the compound is puckered, with a dihedral angle of 151.1°. The two C–S distances are 1.81 Å and 1.89 Å, and the average distance between the C–Cl bonds is 1.785 Å. The C–S and C–Cl bond characters are discussed in terms of the CNDO/2 method. The intermolecular S···S contact of 3.32 Å is remarkably short; it may be explained as a consequence of an attractive interaction between the dipole moments of the molecules.

cis-2,2-Diphenyl-3,4-dichlorothietane (abbreviated hereafter as *cis*-DCTE) was synthesised by the cycloaddition of thiobenzophenone to *cis*-dichloroethylene.[1] A study of the dipole moment of a series of thietane derivatives including this compound has revealed an unusually large bond moment for the C_α–Cl bond in *cis*-DCTE.[2] This X-ray study was undertaken in order to establish the geometry of the thietane ring and to shed light on the bond character of the C_α–Cl bond.

Experimental

The crystals of *cis*-2,2-diphenyl-3,4-dichlorothietane grown from an *n*-hexane solution are colorless plates. The cell dimensions and the space group were determined from oscillation and Weissenberg photographs taken around the *b* and *a* axes, using Cu$K\alpha$ radiation ($\lambda=1.542$ Å). They are listed in Table 1, together with other crystal data.

Two specimens with dimensions of $0.05\times0.05\times0.30$ mm and $0.05\times0.06\times0.20$ mm were used for the collection of the intensity data around the *b* and *a* axes respectively. Equi-inclination Weissenberg photographs were taken for *h*0*l*—*h*9*l* and for 0*kl*—7*kl*. The intensities of 1578 reflections were estimated visually and were corrected for the usual Lorentz, polarization, and spot shape factors. The absorption effect was neglected in view of the small size of the specimen.

TABLE 1. CRYSTAL DATA

Monoclinic
$a=9.94(1)$ Å
$b=12.56(1)$ Å
$c=12.96(1)$ Å
$\beta=120.66(8)°$
$V=1392$ Å^3
Formula $C_{15}H_{12}Cl_2S$, F.W.$=295.13$
$D_x=1.408$ g/cm^3
$D_m=1.41$ g/cm^3
$Z=4$
$\mu=53.45$ cm^{-1} (Cu$K\alpha$)
Space group: $P2_1/c$
(Absent spectra: *h*0*l* when *l* is odd, and 0*k*0 when *k* is odd.)

* Present address: The Institute of Industrial Science, The University of Tokyo, Roppongi, Minato-ku, Tokyo 106.

Structure Analysis

The positions of the sulfur and chlorine atoms were deduced from a three-dimensional Patterson synthesis sharpened by a factor of $\exp(B\sin^2\theta/\lambda^2)$ ($B=3.0$ Å^2). The positions of the lighter atoms except for hydrogen were determined by the routine application of the heavy-atom method. Block-diagonal least-squares refinement using anisotropic temperature factors reduced the R value to 0.10. The positions of all the hydrogen atoms were given from the suitable geometry, but were not refined. The temperature factors for hydrogen were assumed to be isotropic, with the same values as those of the carbon atoms to which the hydrogen atoms are bonded. The following weighting scheme was employed for the least-squares refinement:

$$1.0 \text{ for } |F_o|\geq5.0$$

and

$$0.3 \text{ for } |F_o|<5.0.$$

The final difference map was flat within the range

TABLE 2. ATOMIC PARAMETERS

Positional parameters for the atoms in the asymmetric unit with their standard deviations ($\times10^4$).

	x/*a*	*y*/*b*	*z*/*c*
S	258(3)	932(2)	995(2)
Cl(1)	3647(3)	357(3)	2639(3)
Cl(2)	2500(4)	492(2)	4574(2)
C(2)	368(10)	1546(7)	2367(9)
C(3)	1073(11)	472(8)	3008(8)
C(4)	1660(12)	56(8)	2158(9)
C(11)	1494(11)	2539(7)	2827(8)
C(12)	2135(13)	2993(8)	2184(9)
C(13)	3073(13)	3897(9)	2603(10)
C(14)	3335(11)	4394(7)	3655(9)
C(15)	2707(11)	3966(8)	4294(9)
C(16)	1719(11)	3057(8)	3877(9)
C(21)	−1171(10)	1858(8)	2196(8)
C(22)	−2274(12)	2358(9)	1143(10)
C(23)	−3732(13)	2637(11)	953(13)
C(24)	−4082(11)	2390(9)	1844(12)
C(25)	−2971(14)	1885(11)	2910(13)
C(26)	−1519(12)	1594(10)	3113(10)

Thermal parameters.

The temperature factor ($\times 10^3$) is of the form:
$\exp[-2\pi^2(U_{11}a^{*2}h^2+U_{22}b^{*2}k^2+U_{33}c^{*2}l^2+2U_{12}a^*b^*hk+2U_{13}a^*c^*hl+2U_{23}b^*c^*kl)]$

	U_{11}	U_{22}	U_{33}	U_{12}	U_{13}	U_{23}
S	47	32	36	−3	50	−15
Cl(1)	48	58	97	18	87	14
Cl(2)	82	56	40	22	46	15
C(2)	28	34	59	12	56	16
C(3)	43	38	46	14	48	9
C(4)	53	38	46	23	54	0
C(11)	37	31	51	−15	62	3
C(12)	74	29	53	−43	93	−26
C(13)	61	51	77	−57	89	−3
C(14)	46	22	64	7	54	16
C(15)	46	41	47	4	41	−25
C(16)	38	38	56	−25	56	−25
C(21)	33	37	46	9	39	−14
C(22)	48	48	59	13	54	14
C(23)	43	77	99	53	32	46
C(24)	36	42	112	−19	74	−56
C(25)	59	87	105	−31	110	−46
C(26)	48	70	61	−51	82	−26

of ± 0.3 eÅ^{-3}. The final positional and thermal parameters are listed in Table 2. A list of the observed and calculated structure factors is preserved by the Chemical Society of Japan.[3]

The atomic scattering factors were taken from the International Tables for X-ray Crystallography.[4]

The calculations were carried out on a HITAC 5020E computer at the Computer Centre of the University of Tokyo and on a TOSBAC 3400 at Saitama University.

Description of the Structure and Discussion

The molecular conformation, bond lengths, bond angles, and their standard deviations are shown in Fig. 1, together with the atomic numbering scheme. The molecule is dissymmetric, and both enantiomorphs are present in the crystal.

The thietane ring is not planar. The dihedral angle (θ) between the planes, (C(2), C(3), C(4)) and (C(2), S, C(4)), is 151.1°. The C(2)–C(3)–C(4) angle and the average inner C–C–S angle are 98.1° and 87.8° respectively. The average distance of the C–C bonds in the ring is 1.565 Å. The C(2)–S of 1.89(1) Å is much longer than 1.812 Å, the mean of the 11 experimental values in the compounds containing the C–S single bonds.[5] Such lengthening has also been observed for the bonds of thietane rings in the following compounds: thietane itself (1.847(2) Å),[6] 2-isopropylidene-1,1,7,7,9,9-hexamethyl-3,5,10,11-tetrathiadispiro[3,1,3,2]undecane-8-thione (1.834(5) Å),[7] and *N*-(*p*-bromophenylcarbamoyl)thiamine anhydride (1.843(11) Å).[8] The longer bonds appear to be a common feature of such a strongly strained system. Thus, it might be unusual that the C(4)–S of 1.81(1) Å is much shorter than the C(2)–S. The C(4)–Cl of 1.78(1) Å is in agreement with the C(3)–Cl of 1.79(1) Å. This fact is in contrast to the unusually large bond moment of the C(4)–Cl.[9] In order to gain a better understanding of the C(4)–Cl and C(4)–S bond characters, a CNDO/2 calculation[10] was carried out for a model (*cis*-2,3-dichlorothietane) with skeletal dimensions assumed to be the same as those of *cis*-DCTE in the crystalline state. The lower electronic energy (−0.730 au) of the valence electrons for the C(2)–S bond of the model in comparison with that of C(4)–S (−0.660 au) may account for the shortening of the C(4)–S bond in *cis*-DCTE. A closer examination of the electronic energy matrix of the valence electrons reveals that this shortening may be attributed to increases in the π bond order and in the s character of the valence orbital of C(4). The atomic charge on Cl(1) in *cis*-DCTE is predicted to be slightly lower than that on Cl(2) (−0.121 e and −0.169 e for the respective atoms in the model), in contrast with the large value of the C(4)–Cl bond moment. The large C(4)–Cl bond dipole might be a consequence of additional contributions of the atomic polarization of component atoms in the molecule and the skeletal dipole due to the point-charge distribution. Here, it is noteworthy that a perturbation of the lowest vacant orbital to the ground-state electronic distribution could cause an increase in the ionic character of the C(2)–Cl bond (corresponding to the C(4)–Cl in *cis*-DCTE) and a decrease in that of the C(3)–Cl (corresponding to the C(3)–Cl) as a result of decreasing the electronic population in the lone pairs of sulfur.

Figure 1 shows that the conformation of *cis*-DCTE can be described as (3*e*4*a*). This conformation agrees

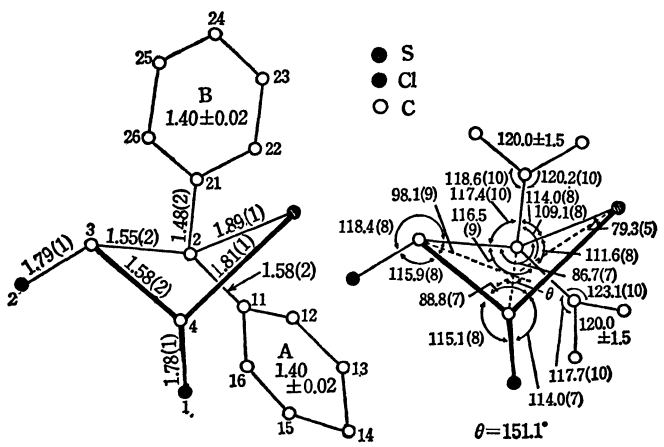

Fig. 1. Molecular geometry.

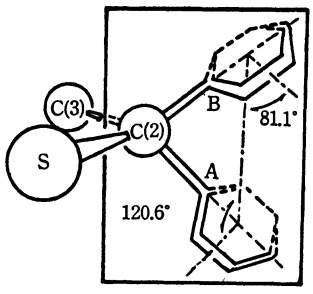

Fig. 2. Orientations of the phenyl groups.

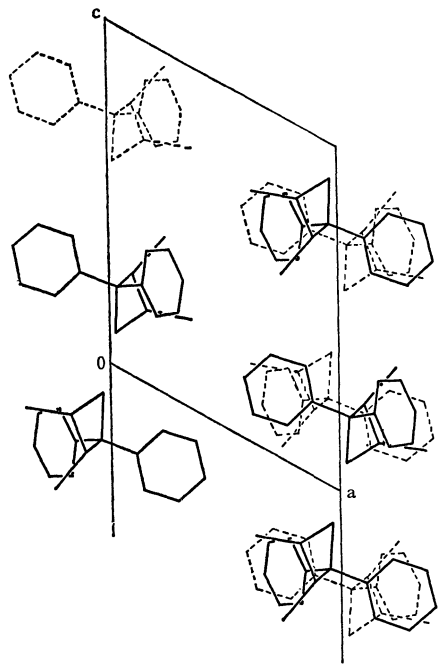

Fig. 3. Projection of the crystal structure of *cis*-DCTE viewed along the *b* axis.

Table 3. Closest intermolecular contacts

S···S^{i}	3.32 Å
S···C(15^{ii})	3.72
C(14)···C(26^{ii})	3.45
Cl(2)···C(13^{iii})	3.75

i=$-x$, $-y$, $-z$. ii=$-x$, $1/2+y$, $1/2-z$.
iii=x, $1/2-y$, $1/2+z$

with the results of the measurement of dipole moments in a benzene solution.

The phenyl groups, A and B, are practically planar. Their orientaions are shown in Fig. 2. The non-bonded distances of S···C(22), S···C(12), and Cl(2)···C(16) are 3.17, 3.10, and 3.33 Å respectively. Steric interactions between these non-bonded atoms play an important role in determining the orientations of the phenyl groups.

A projection of the crystal structure viewed along the *b* axis is presented in Fig. 3. The closest intermolecular contacts are listed in Table 3. They are normal except for that between S and S^{i}, which is significantly shorter than the usual contact of 3.70 Å.[11] The closest approach between the sulfur atoms is across a center of inversion. The dipole moments of the molecules involving these sulfurs are arranged in an antiparallel orientation. The dipole-dipole interaction energy was computed for the molecular pair related by a center of symmetry by rotating the component molecules around their respective centers of mass so as to alter their relative orientation and by placing the C–Cl and C–S bond moments on the centers of the corresponding bonds as a point dipole. The relative arrangement observed was found to be at the energy minimum, with a value of −5 kcal/mol. Therefore, the closest contact of the sulfur atoms might be explained as a consequence of attractive interaction between the molecular dipoles.

The authors are grateful to Dr. Atsuyoshi Ohno and Dr. Yutaka Ohnishi of the Sagami Chemical Research Center for kindly supplying the crystals of *cis*-DCTE and to Professor Takashi Shimozawa for his keen interest and valuable discussions. This research was supported in part by a Scientific Research Grant from the Ministry of Education, to which the authors' thanks are also due.

References and Notes

1) A. Ohno, Y. Ohnishi, and G. Tsuchihashi, *Tetrahedron Lett.*, **1969**, 161.
2) S. Kumakura, T. Shimozawa, Y. Ohnishi, and A. Ohno, *Tetrahedron*, **27**, 767 (1971).
3) The complete data of the F_o-F_c table are kept as a document at the office of the Bulletin of the Chemical Society of Japan. (Document No. 7519).
4) "International Tables for X-ray Crystallography," Vol. III, Kynoch Press, Birmingham (1962), p. 202.
5) E. G. Cox and G. A. Jeffrey, *Proc. Roy. Soc., Ser. A*, **207**, 110 (1951).
6) K. Karakida, K. Kuchitsu, and R. K. Bohn, *Chem. Lett.*, **1974**, 159.
7) C. D. Shirrell and D. E. Williams, *Acta Crystallogr.*, **B29**, 2128 (1973).
8) H. Nakai and H. Koyama, *J. Chem. Soc., Perkin II*, 248 (1972).
9) Another analysis of the dipole moments of *cis*- and *trans*-DCTE was carried out by using the molecular dimensions of the *cis*-compound observed in its crystalline state; there was only an insignificant deviation from the results previously obtained—*i.e.* $\mu(C_\alpha\text{–Cl})=1.9$ D and $\mu(C_\beta\text{–Cl})=1.3$ D.
10) A CNDO/2 calculation was carried out on a HITAC 8700/8800 computer at the Computer Centre of the University of Tokyo by using a published program (J. A. Pople and D. J. Beveridge, "Approximate Molecular Orbital Theory," McGraw-Hill, New York, 1970)) partly modified for the SP and SPD′ calculations (D. P. Santry, *J. Amer. Chem. Soc.*, **90**, 3309 (1968)). Only the SP calculation gives reasonable predictions with respect to the dipole moment and the conformation of the model. The calculated dipole moment of 2.19 D is in good agreement with the value of 2.16 D observed for *cis*-DCTE in a benzene solution.
11) L. Pauling, "The Nature of the Chemical Bond," 3rd ed., Cornell Univ. Press, Ithaca (1960).

A Study of the Molecular Compound between Inosine and Tryptophan

Yoshihisa SUZUKI, Kentaro HARA, and Tsuneo HIRAHARA

Central Research Laboratories, Ajinomoto Co., Inc., Suzuki-cho, Kawasaki 210

(Received November 7, 1974)

Equilibria have been determined at 30 °C for the inosine–L-tryptophan–water and inosine–D-tryptophan–water systems. They show the formation of a molecular compound, which was demonstrated in U.S. Patent 3532684, over a wide range of variable ratios of the two components, inosine and tryptophan. The influence of some organic solvents on the formation of the molecular compound was examined, and it was shown that the water molecule is significantly involved in the formation of the crystalline molecular compound, and that solvent interactions play an important role. Similar crystalline molecular compounds were not formed by chemically closely related substances; the high specificity of the interaction between inosine and tryptophan was confirmed.

In 1968 it was demonstrated for the first time by two of the present authors and by others in a Japanese patent[1] that equimolecular amounts of inosine and tryptophan form a crystalline molecular compound which is sparingly soluble in water. It has also been pointed out in several subsequent patents[2,3] that the molecular compound of L-tryptophan with inosine is less soluble than that of D-tryptophan, and that DL-tryptophan is optically resolved by conversion to the molecular compound. It was also demonstrated in a Japanese patent of 1973[4] that the biological production of L-tryptophan is greatly increased by the addition of inosine to the reaction system, probably because the tryptophan produced in the solution is continuously removed, thus forming a sparingly soluble molecular compound with inosine. These facts suggest a specific strong interaction between inosine and tryptophan in an aqueous solution.

L-Tryptophan is known to show a molecular interaction in an aqueous solution with some purine ribonucleosides, such as adenosine, guanosine, cytidine, uridine, and thymidine.[5–7] However, none of them have ever given any stable crystalline molecular compound. In frozen aqueous solutions, some of these purine ribonucleosides form aggregates[8,9] with tryptophan; these aggregates are supposed to be 1 : 1 complexes, even though there is no complex formation at room temperature.[10] Recently, the equilibrium constants and the thermodynamic parameters for the complex between inosine and L-tryptophan have been reported by Ibáñez *et al.*[11]

This paper will describe the equilibria for the inosine–L-tryptophan–water and inosine–D-tryptophan–water systems, the importance of the water of crystallization in the formation of the crystalline molecular compound, and attempts to prepare an analogous crystalline molecular compound.

Results and Discussion

Tables 1 and 2 show the composition data of the equilibria at 30 °C for the inosine–L-tryptophan–water and inosine–D-tryptophan–water systems respectively. They show experimental errors within ±0.04% and ±0.02% (absolute value) for inosine and tryptophan respectively. The composition data of the solution in the equilibria for these two systems are illustrated in Fig. 1 (the isothermal solubility curves), which clearly demonstrates the formation of the molecular compound over a wide range of the two components, inosine and tryptophan. The molecular compound is readily formed, with a steep decrease in the solubility when a small amount of one of the components is added to the other component in the solution.

A small difference is observed between the solubility curves of inosine related to L-tryptophan and that related to D-tryptophan, as is shown in Fig. 1. This is significant for the resolution of the racemic compound of tryptophan. Information has already been given in the patents[3] that the molecular compound of inosine

TABLE 1. COMPOSITION DATA OF THE EQUILIBRIUM FOR THE INOSINE–L-TRYPTOPHAN–WATER SYSTEM AT 30 °C

Run No.	Solution (Wt %)		Wet residue[c] (Wt %)		Solid phase[b]
	Ino.[a]	L-Trp	Ino.[a]	L-Trp	
1	3.10	0.00	—	—	I
2	3.07	0.02	35.8	1.31	I+L-T·I·3H$_2$O
3	2.99	0.05	—	—	I+L-T·I·3H$_2$O
4	2.22	0.02	54.6	36.2	L-T·I·3H$_2$O
5	1.05	0.06	55.5	35.7	L-T·I·3H$_2$O
6	0.27	0.24	53.8	36.5	L-T·I·3H$_2$O
7	0.16	1.12	50.1	41.3	L-T·I·3H$_2$O
8	0.07	1.43	12.3	25.0	L-T·I·3H$_2$O+L-T
9	0.10	1.46	33.4	60.1	L-T·I·3H$_2$O+L-T
10	0.00	1.42	—	—	L-T

a) Inosine. b) I: Inosine in the α-form.[13] L-T·I·3H$_2$O: Molecular compound, L-Trp·Inosine·3H$_2$O. L-T: L-Trp. c) Inosine+L-Tryptophan+Water=100%.

TABLE 2. COMPOSITION DATA OF THE EQUILIBRIUM FOR THE INOSINE–D-TRYPTOPHAN–WATER SYSTEM AT 30 °C

Run No.	Solution (Wt %)		Wet residue[c] (Wt %)		Solid phase[b]
	Ino.[a]	D-Trp	Ino.[a]	D-Trp	
1	3.10	0.00	—	—	I
11	3.24	0.07	57.6	38.1	I+D-T·I·H$_2$O
12	1.94	0.09	40.9	28.1	D-T·I·H$_2$O
13	0.49	0.27	32.0	24.4	D-T·I·H$_2$O
14	0.35	0.28	—	—	D-T·I·H$_2$O
15	0.23	0.55	53.8	41.9	D-T·I·H$_2$O
16	0.11	1.39	12.3	31.0	D-T·I·H$_2$O+D-T
10	0.00	1.42	—	—	(D-T)

a) Inosine. b) I: Inosine in the α-form.[13] D-T·I·H$_2$O: Molecular compound, D-Trp·Inosine·H$_2$O. D-T: D-Trp. c) Inosine+D-Tryptophan+Water=100%.

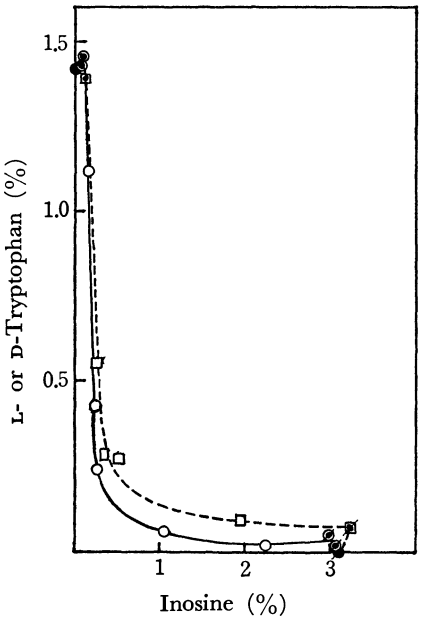

Fig. 1. An illustration of the composition of the solution phase in the equilibrium for the inosine-L-(or D-)tryptophan-water system at 30 °C.
The symbol marks of the solid phase are as follows:
○: L-Trp·Inosine·$3H_2O$ (molecular compound).
□: D-Trp·Inosine·H_2O (molecular compound).
●: L-Trp or D-Trp.
◐: Inosine (α-form).

with L-tryptophan is less soluble than that with D-tryptophan. The solubility difference of the curves in Fig. 1 is confirmed to be consistent with the above information over a wide region, even where the two components are not equimolar. Therefore, there is a possibility that the resolution of racemic tryptophan may be performed even when the amount of inosine is not equimolar.

It is known that racemic tryptophan is far less soluble than optically active ones. However, by the addition of a certain amount of inosine to the solution of racemic tryptophan, molecular compounds between inosine and optically active tryptophans were formed and precipitated because their solubilities are lower than the solubility of racemic tryptophan. The molecular compound of inosine with L-tryptophan was at first precipitated, leaving that of inosine with D-tryptophan in the solution.

It has been demonstrated[1,3] that the crystals of the molecular compound between inosine and L-tryptophan contain three molecules of water of crystallization, and that they lose two of them on heating in air, thus giving the monohydrate of the molecular compound. The experimental conditions used to obtain monohydrate from trihydrate were, for example, at 50 °C for 2 hr in air or at 110 °C for 40 min *in vacuo*.

It is found that the crystals of monohydrate thus obtained absorb moisture in air rapidly at first and gradually at the end, returning to original trihydrate in a few days. This process can be followed quantitatively by means of the X-ray powder diffraction spectra. Two strong peaks corresponding to the spacings of 7.63 Å and 6.33 Å are specific for the trihydrate, and two other strong peaks corresponding to the spacings of 7.25 Å and 6.92 Å are specific for the monohydrate. The change in the intensity of these four specific peaks reflects an increase and a decrease of these two forms in the crystals. However, when trihydrate crystals were very rapidly heated in air, it sometimes occurred that the X-ray diffraction spectra of trihydrate were unchanged even though the weight of the crystals was decreased by an amount as much as would correspond to two moles of water. This fact suggests that monohydrate crystals are sometimes able to retain the structure of original trihydrate crystals. Therefore, the two moles of water are likely to be nearly zeolitic water.

On the other hand, the crystals of the molecular compound between inosine and D-tryptophan were always obtained in monohydrate, and never in trihydrate. It is supposed that one mole of water in both molecular compounds is significantly involved in the formation of the molecular compound.

Trihydrate crystals of the molecular compound between inosine and L-tryptophan can be dried into anhydrous crystals by heating at 140 °C for 30 min *in vacuo*. The anhydrous crystals thus obtained also increased in weight because of the absorption of moisture when they were left in air. However, it was found that they never returned to being original hydrous crystals in air. Rather, they became amorphous.

The fact that one mole of water may play an important role in the formation of the crystalline molecular compound suggests the presence of solvent interaction in the intermolecular bonding between inosine and tryptophan. We examined the influence of several organic solvents on the trihydrate crystals of the molecular compound between inosine and L-tryptophan. Their crystals were practically insoluble; they remained unchanged in acetone, dioxane, tetrahydrofuran, and 1-butanol, while they were somewhat changed in appearance in methanol, ethanol, and 1-propanol. It was also confirmed by the X-ray method that the crystals of the trihydrate were partly changed into those of monohydrate in 85—95% (v/v) aqueous ethanol or aqueous 1-propanol, and that the crystals of L-tryptophan were found in the residue in addition to those of monohydrate in pure ethanol or pure 1-propanol. As was established in the patents,[3] the crystals added in methanol were changed into those of inosine. This last observation can be explained by the dissolution of the molecular compound, followed by the crystallization of inosine (leaving tryptophan in methanol).

It has been reported that the presence of ethanol destablizes the flavin–indole complexes.[12] The aggregates, which are supposed to be molecular complexes between nucleic acid derivatives and aromatic amino acids, in frozen aqueous solutions have been reported to be inhibited by the addition of organic solvents such as ethanol.[10] These destabilizing effects of the organic solvents on the molecular compounds demonstrate that solvent interactions play an important role in the formation of the molecular compound, especially in the present case when a water molecule is necessary to form the stable crystals.

Arcaya *et al.*[7] reported the interaction of L-aromatic amino acids including tryptophan with some ribonucleosides, and proposed a possible ring-ring-type interaction between an amino acid and nucleoside. This interaction is also possible in the present crystalline molecular compound between the imidazole ring in tryptophan and the purine ring in inosine. The fine hair-like appearance of the crystals of the molecular compound in this study suggests ring-ring vertical stacks with an alternative sequence of inosine and tryptophan. The growth of the linear vertical stacks would make for a long, slender crystal.

Besides such a ring-ring-type interaction based on the hydrophobic moiety in the molecule, the role of the hydrophilic moiety, such as the ribosyl or hydroxyl groups in the inosine molecule and the side-chain group in the tryptophan molecule, can never be disregarded in the formation of the crystalline molecular compound. Aiming to get some information about the role of such side chains, some compounds analogous to inosine and tryptophan were examined, and we attempted to make crystalline molecular compounds between them.

Several of the ribonucleosides illustrated in Fig. 2 were examined for interaction with L-tryptophan (**13**). Adenosine (**2**), guanosine (**3**), xantosine (**4**), hypoxanthine (**5**), and 9-β-D-ribopyranosyl hypoxanthine (**6**) all did not give any crystalline molecular compound

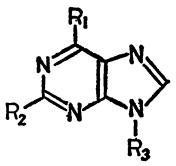

	R_1	R_2	R_3
1.	OH	H	β-D-Ribofuranose
2.	NH_2	H	β-D-Ribofuranose
3.	OH	NH_2	β-D-Ribofuranose
4.	OH	OH	β-D-Ribofuranose
5.	OH	H	H
6.	OH	H	β-D-Ribopyranose

Fig. 2. Purine ribonucleosides examined.

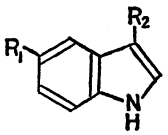

	R_1	R_2
7.	H	H
8.	COOH	H
9.	H	COOH
10.	H	CH_2COOH
11.	H	CH_2CH_2COOH
12.	H	$CH_2CH_2CH_2COOH$
13.	H	$CH_2CHCOOH$ NH_2
14.	H	$CH_2CHCOOH$ $NHCOCH_3$
15.	H	$CH_2CH_2NH_2$
16.	H	CH_2CH_2OH

Fig. 3. Indole derivatives examined.

except crystalline mixtures of two original components. It is of interest that the isomerization of the ribose moiety in inosine from the furanosyl form to the pyranosyl form inhibited the formation of the molecular compound. Some nucleosides, such as cytidine, uridine, and 5-amino-1-β-D-ribofuranosyl-4-imidazolecarboxamide, also gave negative results. Several indole derivatives illustrated in Fig. 3 were examined with inosine (**1**). Indole (**7**), indole-5-carboxylic acid (**8**), indole-β-carboxylic acid (**9**), β-indolyl acetic acid (**10**), β-indolyl propionic acid (**11**), β-indolyl butyric acid (**12**), acetyl-L-tryptophan (**14**), tryptamine (**15**), and tryptophol (**16**) all failed to give any crystalline molecular compound. It was thus confirmed that the interaction between inosine and tryptophan is highly specific.

Experimental

Materials and Equipment. The inosine (α-form),[13] guanosine, adenosine, 5-amino-1-β-D-ribofuranosyl-4-imidazolecarboxamide, hypoxanthine, L-tryptophan, and acetyl-L-tryptophan were obtained from the Ajinomoto Co., Inc. The 9-β-D-ribopyranosyl hypoxanthine was prepared according to the method of a previous paper.[14] The D-tryptophan was presented by Dr. Takekazu Akashi of the Ajinomoto Co., Inc. The other materials were commercially purchased. The X-ray (Cu$K\alpha$) powder diffraction data for the determination of crystal forms were obtained by means of a Rigaku-denki diffractometer.

Preparation of the Crystals of the Molecular Compounds. (1) The trihydrate crystals of the molecular compound between inosine and L-tryptophan were prepared according to the patents.[1] (2) The monohydrate crystals of the molecular compound between inosine and D-tryptophan were prepared by evaporating an equimolar aqueous solution of the two components to dryness *in vacuo*. The analytical data were coincident with those in the patents.[3]

Determination of Equilibria. *Procedure*: The equilibria were approached by dissolving the crystals in water at 30± 0.5 °C. The details in Table 1 show the results obtained by dissolving inosine (Run No. 1), by dissolving L-tryptophan (Run No. 10), by dissolving both inosine and L-tryptophan (Runs No. 3, 4, 5 and 7), by dissolving the molecular compound trihydrate of inosine with L-tryptophan (Run No. 6), by dissolving both inosine and the molecular compound trihydrate (Run No. 2), and by dissolving both L-tryptophan and the molecular compound trihydrate (Runs No. 8 and 9). The data in Table 2 show the results obtained by dissolving both inosine and D-tryptophan (Runs No. 13, 15 and 16), and by dissolving the molecular compound monohydrate of inosine with D-tryptophan in water (Run No. 14) or that in aqueous inosine solution (Run No. 12). It took 16 hr for the equilibrium to be reached by tumbling the bottles containing the mixture on a water bath at a constant temperature. The mixture in the bottles was quickly filtered in a chamber kept at 30 °C with a glass filter. The wet residues and the filtrates were sampled by weight, diluted to appropriate volumes, and submitted to analysis. *Analysis*: The composition data were determined by the measurement of the UV absorption of the samples in 0.1 M HCl at 250 nm and at 280 nm, which are the specific wavelengths giving the maximum absorption for inosine and tryptophan respectively. The UV absorbances of the two materials, inosine and tryptophan, had previously been measured under our experimental conditions; the molar extinction coefficients were obtained for inosine at 250 nm ($\varepsilon_{I\ 250}$, 11700) and at

280 nm ($\varepsilon_{I\ 280}$, 2450), and for tryptophan at 250 nm ($\varepsilon_{T\ 250}$, 1390) and at 280 nm ($\varepsilon_{T\ 280}$, 5620). The analytical data of the mixture of inosine and tryptophan were obtained by the use of the following two equations:

$$A_{250} = \varepsilon_{I\ 250}\frac{C_I \times 10^{-3}}{MW_I} + \varepsilon_{T\ 250}\frac{C_T \times 10^{-3}}{MW_T}$$

$$A_{280} = \varepsilon_{I\ 280}\frac{C_I \times 10^{-3}}{MW_I} + \varepsilon_{T\ 280}\frac{C_T \times 10^{-3}}{MW_T}$$

where A_{250} is the UV absorbance at 250 nm, A_{280} is that at 280 nm, C_I(mg/l) is the concentration of inosine, C_T(mg/l) is that of tryptophan, MW_I is the molecular weight of inosine (268), and MW_T is that of tryptophan (204). C_I and C_T were thus determined by the measurement of A_{250} and A_{280}. The confirmation of the crystalline form in the residues was performed by means of the X-ray powder diffraction method.[3]

Behavior of the Molecular Compound in Several Organic Solvents. Finely powdered trihydrate crystals of the molecular compound between inosine and L-tryptophan (0.5 g) were added to one of several organic solvents (10 ml). After the mixtures had been vigorously shaken, the undissolved crystals were observed with a microscope. Some of them were examined also by means of the X-ray method in order to determine the crystal form.

Attempts at the Preparation of the Analogous Crystalline Molecular Compound. One of the nucleosides and L-tryptophan, or one of the indole derivatives and inosine, were dissolved (in a molar ratio of 1 : 1) in water. Then the mixture was evaporated to dryness *in vacuo* in a desiccator. The resultant solid was examined by means of X-ray diffraction. When the solid is the mixture of the two original components, its spectra may be consistent with those of a mechanical mixture of them. If any molecular compound is present in the solid, though, its spectra may show novel and specific peaks.

References

1) Y. Suzuki, T. Hirahara, and T. Nakamura, Japan. Patent 43 29010 (1968).
2) Y. Suzuki, T. Akashi, and T. Nakamura, Japan. Patent 44 20983 (1969).
3) Y. Suzuki, T. Hirahara, T. Akashi, and T. Nakamura, Brit. Pat. 1180635 (1970); U.S. Pat. 3532684 (1970); West Ger. Offen. 1645977 (1970); Fr. Pat. 1601066 (1970).
4) H. Enei, H. Nakazawa, H. Matsui, S. Okumura, and H. Yamada, Japan. Patent Kokai 48 80785 (1973).
5) M. Pieber, C. Romero, C. Tirapegui, and J. C. Tohá, *Z. Naturforsh.* **24b**, 508 (1969).
6) M. Pieber, C. Romero, and J. C Tohá, *Arch. Biol. Med. Exp.* **6**, 58 (1969).
7) G. Arcaya, M. E. Pantoja, M. Pieber, C. Romero, and J. C. Tohá, *Z. Naturforsh.* **26b**, 1026 (1971).
8) C. Helene, *Biochem. Biophys. Res. Commun.*, **22**, 237 (1966).
9) C. Helene, R. Santus, and M. Ptak, *C. R. Acad. Sci. Ser. C*, **262**, 1349 (1966).
10) T. Montenay-Garestier and C. Helene, *Nature*, **217**, 844 (1968).
11) I. Ibáñez, M. Pieber, and J. C. Toha, *Z. Naturforsh. C*, **28**, 385 (1973).
12) J. F. Perira and G. Tollin, *Biochim. Biophys. Acta*, **143**, 79 (1967).
13) Y. Suzuki and N. Nagashima, This Bulletin, **43**, 1600 (1970).
14) Y. Suzuki, *ibid.*, **47**, 898 (1974).

Radiation Chemical Studies with Cyclotron Beams. IV. The Effect of Water in the Heavy-ion Radiolysis of Liquid Acetone

Masao MATSUI and Masashi IMAMURA

The Institute of Physical and Chemical Research, Wako, Saitama 351

(Received November 13, 1974)

A study was made of the effect of water on the LET dependence of the product yields for liquid acetone. Acetone containing 2 wt% water was subjected to irradiation by energetic ^{4}He, ^{12}C, and ^{14}N ions as well as by ^{60}Co γ rays at room temperature; the LET range was up to 80 eV Å^{-1}. A significant effect of water was observed above 50 eV Å^{-1}, where $G(H_2)$ and $G(CO)$ showed continuous increases with an increase in LET. For pure acetone, $G(H_2)$ and $G(CO)$ showed their peak values at 50 eV Å^{-1}, indicating a saturation of decomposition in the ionization track, as has been reported previously. The present results may be interpreted in terms of the hydrogen-bonded network formed by the addition of water; this will expand the reaction zone outside the track and result in increases in the product yields without any waste of excessive energy in the high-LET region.

Radiolysis with heavy ions which have very high LET values is an interesting and important subject in radiation chemistry. Since the track structure of heavy ions differes appreciably from that of low-LET radiations, chemical reactions characteristic of high-LET radiations may be expected. However, few experimental studies have been carried out[1] despite the relatively extensive development of theories of the interaction of heavy ions with matter.[2-4]

In a previous paper of this series,[5] we reported the characteristic features of the radiolysis of liquid aliphatic ketones (acetone, methyl ethyl ketone, and diethyl ketone) with energetic C and N ions over a wide LET range. The most significant results reported in the preceding paper were: (1) the amount of major gaseous products (H_2 and CO) formed per unit track length tend to be constant, independent of the amounts of energy absorbed in the high-LET region ($>$*ca.* 60 eV Å^{-1}), and (2) the ratios of $G(H_2)$ to $G(CO)$ increase steadily with an increase in LET.

The first result indicates that the decomposition of ketones takes place only within a track core with a constant radius above a critical LET; therefore, $G(H_2)$ and $G(CO)$ apparently begin to decrease above this LET. The excessive energy thus accumulated within the track core may be supposed to increase the temperature of the core and induce some chemical reactions with high activation energies.

The second result can be explained in terms of such a thermal-spike effect in the track core; we assumed the thermal decomposition of free radicals to account for the increases in $G(H_2)/G(CO)$ as well as $G(H_2)$ and $G(CO)$ themselves. We also assumed the formation of highly excited states of ketone molecules which give product distributions different from those in the radiolysis with low-LET radiations.

Since these results are specific for pure ketones, and since no similar results have been observed for other organic liquids in the LET region studied, we plan to carry out a series of experiments which will lend further support to the assumptions presented above. This paper will report on one of them, presenting the radiolysis results obtained with liquid acetone containing a small amount of water over a wide LET range.

The γ-radiolysis of acetone as well as of other ketones in a liquid phase has been studied,[6] and the effect of water on the γ-radiolysis yields from liquid acetone has been demonstrated; [7,8] the resulting increase in $G(H_2)$ has been explained on the basis of ion-molecule reactions.[7] We have found that a small amount of water exerts a significant effect on the LET dependence of the product yields from acetone in the high-LET region. This effect, not explicable on the same basis as that in the γ-radiolysis, will be discussed in terms of a hydrogen-bonded network formed in the solution on the basis of the assumptions presented in the preceding paper.[5]

Experimental

The experimental procedures were essentially the same as those described previously;[5,9,10] only the essential points will, then, be mentioned. Ions of ^{4}He, ^{12}C, and ^{14}N were accelerated with the 160-cm cyclotron at the Institute of Physical and Chemical Research. Their energies and LET (represented by the energy-loss parameter defined as[5] $z = 1/E\int_0^E(-dE/dx)dE$) were 18.9 MeV, 6.7 eV Å^{-1}, 30.0—66.4 MeV, 54.4—39.2 eV Å^{-1}, and 18.0—47.5 MeV, 80.0—62.4 eV Å^{-1}, for He, C, and N ions, respectively. Irradiation was carried out at an ambient temperature.

Reagent-grade acetone (Wako Pure Chem. Ind.) was dried and distilled before use;[5] the water was triply distilled. The gaseous products from radiolyzed acetone were Toepler-pumped and were subjected to gas-chromatographic analysis.

Results

All the experiments reported in this paper were carried out with acetone containing 2 wt% H_2O. No differences beyond the experimental erros in the product yield were found between solutions containing 2 and 5 wt% H_2O either for the γ-radiolysis or for the heavy-ion radiolysis.

Iodine was used as a free-radical scavenger for the γ and He-ion radiolyses; in the presence of iodide, one could obtain "molecular" yields, which may be regarded as the yields of the products formed inside radiation spurs or tracks.

In the C- and N-ion radiolyses, iodine was not used, since the yields of H_2 and CO in these cases are little affected by scavengers and, therefore, may be regarded as being practically equal to the molecular yields. In the present study, emphasis has been placed on the characteristic reactions taking place inside the densely

ionizing tracks formed with heavy ions of high LET.

Figure 1 shows the variations with the LET (given by z) of $G(H_2)$ and $G(CO)$ determined for acetone containing 2 wt% H_2O (solid lines); these yields were obtained using He, C, and N ions accelerated to various energies. In contrast to the previous results obtained with pure acetone (dotted lines), [5] no peaks of $G(H_2)$ and $G(CO)$ were observed with aqueous acetone. $G(H_2)$ and $G(CO)$, which are lower than the corresponding values for pure acetone in the low-LET region, increase steadily with an increase in LET, and in the high-LET region they become even higher.

For comparison with earlier results,[7,8] the effect of water in the γ-radiolysis was also studied. In the absence of iodine, 2 wt% H_2O increases the total yields of H_2, CO, CH_4, and C_2H_6, but exerts no effect on those of C_2H_2 and C_2H_4. The molecular yields of these products obtained with iodine added at 1.8×10^{-3} M are lower for H_2 and CO and higher for saturated hydrocarbons than those for pure acetone; the molecular yields of unsaturated hydrocarbons are, however, practically unaffected. The effects of water on the total yields, except for the case of CO, are in qualitative agreement with the results obtained by Barker and Noble,[7] who determined the yields with acetone containing 0.4 wt% H_2O.

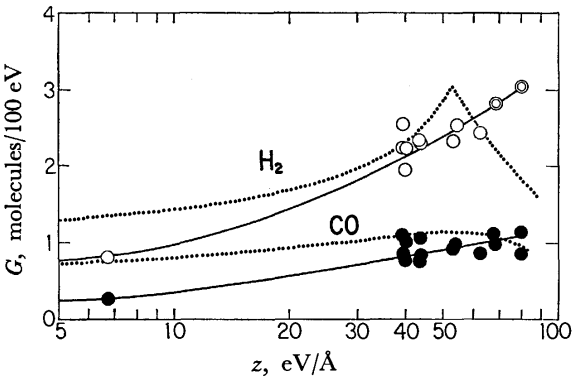

Fig. 1. LET dependence of $G(H_2)$ (○) and $G(CO)$ (●) for acetone containing 2 wt% H_2O.
LET dependence for pure acetone is shown by dotted lines for comparison (Ref. 5).

Discussion

Extensive studies of the primary processes in irradiated liquid acetone have been carried out by pulse radiolysis; they have revealed the formation of excited states[11-14] and molecular ions[11-19] in relatively high yields.

Electrons ejected by ionization attach to parent acetone molecules to form molecular anions; the total yield of the acetone cation and anion thus formed was determined and found to be approximately $G=1.5$.[13] Molecular anions will undergo recombination with cations to form excited states and neutral free radicals.

Earlier mass-spectrometric studies have shown that a rapid proton transfer does occur:[20,21]

$$(CH_3)_2CO^+ + (CH_3)_2CO \rightarrow (CH_3)_2COH^+ + CH_2COCH_3 \quad (1)$$

Sieck and Ausloos[19] suggested an important role of the ion-molecule reaction (1) as well as other reactions in liquid-phase radiolysis. However, in view of the fact that the transient absorptions of the acetone cation and anion are observable in the pulse radiolysis,[16,18] the rate constant of Reaction (1) may not necessarily be rapid in a condensed phase. Thus, there still remains an ambiguity concerning the ionic reactions taking place in liquid ketones.

A relatively high yield, $G=1.3\pm0.1$, has been reported for the excited states of acetone in a liquid phase; the excited states may be produced by direct excitation or by ion recombination.[14] Robinson and Rodgers[14] have also suggested, from their pulse-radiolysis study of acetone solutions, that the geminate recombination of ion pairs may produce excited states, too. In the radiolysis with heavy ions having high LET values, most of the initial ionic species are neutralized by the recombination inside densely ionizing tracks to form excited states.

In the γ-radiolysis of acetone, the effect of water on the product yields was explained by Barker and Noble[7] on the basis of the ion-molecule reaction (1). In fact, water is believed to react with the cation and anion of acetone molecules as follows:[16,18]

$$(CH_3)_2CO^+ + H_2O \rightarrow CH_3COCH_2 + H_3O^+ \quad (2)$$

$$(CH_3)_2CO^- + H_2O \rightarrow (CH_3)_2COH + OH^- \quad (3)$$

These reactions are probably responsible for the removal of the transient absorptions of the cation and anion by water; therefore, their rate constants must be higher than that of Reaction (1). However, since there is limited information available on the mechanism of ionic reactions taking place in the bulk, no further discussion can be made of the effect of water in the γ-radiolysis.

In the heavy-ion radiolysis, H_2 and CO are produced mostly inside the dense tracks and the ionic reactions are of less importance than in the γ-radiolysis. Water would interact with the excited states of the acetone molecules, which may be produced favorably in the heavy-ion radiolysis, as has been mentioned above.

It has been suggested that water may form a hydrogen-bonded network among acetone molecules, through which a rapid energy transfer may be expected to take place.[22] The significant effects of water on the product yields and their LET dependence in the heavy-ion radiolysis seem to be explainable in terms of the hydrogen-bonded network, as will be discussed below.

The previous results with pure ketones[5] indicate that, above the critical LET (50 eV $Å^{-1}$ for acetone), decomposition takes place only within the tracks of the limited radii. The excessive energy deposited in the tracks above the critical LET was assumed to cause the thermal decomposition of the free radicals with high activation energies, or to promote the formation of highly excited states of ketone molecules, resulting in more production of H_2 and CO. Under these conditions, however, some amounts of energy must be wasted not to form products, depending upon the amounts of energy deposited per unit track-length; therefore, the yields are reduced with an increase in LET, as is shown in Fig. 1 (dotted lines).

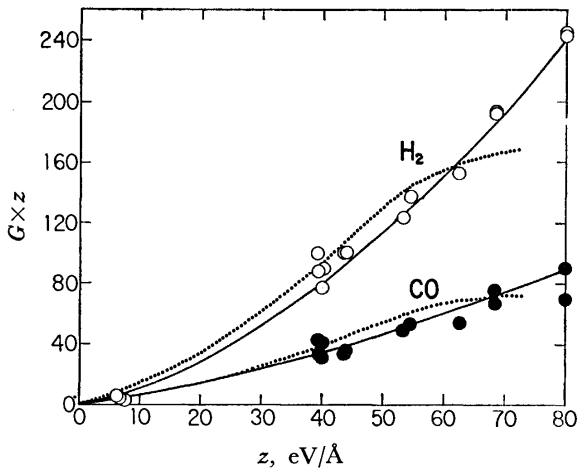

Fig. 2. Plots of Gz *vs.* z.
○, H_2; ●, CO. Dotted lines are for pure acetone (Ref. 5).

If the hydrogen-bonded network formed by water added to acetone could serve to transfer the excessive energy from the track outward the bulk, the reaction zone[23] in which acetone molecules can decompose would accordingly expand outside the track core.

Thus, the excessive energy, which would be wasted within the limited volume of the track in pure acetone at LET above 50 eV Å^{-1}, may be consumed efficiently and the yields may be expected to increase continuously with an increase in LET, as is shown in Fig. 1 (solid lines). In such expanding reaction zones, however, the occurrence of the thermal decomposition of free radicals or the formation of highly excited states will be more or less reduced, and the yields at LET below 50 eV Å^{-1} will be reduced compared with those for pure acetone. The experimental results are consistent with those expectations.

Figure 2 shows the plots of Gz *vs.* z, where Gz gives a measure of the number of molecules produced per 100 Å of track length. By comparing these plots (solid lines) with those for pure acetone (dotted lines),[5] one may see a steady expansion of the reaction zone with an increase in the LET; the plots for pure acetone show a saturation in the high-LET region.

The hydrogen-bonded network will also be operative to some extent in the radiolysis with low-LET radiations. The decreases in the molecular yields of H_2 and CO observed in the γ-radiolysis of aqueous acetone may be ascribed to the dissipation of energy from spurs to the bulk through the hydrogen-bonded network; the importance of this effect increases in liquid ketones with an increases in LET.

The authors wish to thank the members of the IPCR cyclotron operation group for their generous technical assistance throughout this study. The technical assistance of Miss Yuriko Moribe is also gratefully acknowledged.

References and Notes

1) See references cited in Ref. 5.
2) A. Mozumder, *Adv. Radiat. Chem.*, **1**, 1 (1969).
3) A. Mozumder, *J. Chem. Phys.*, **60**, 1145 (1974).
4) J. Fain, M. Monnin, and M. Montret, *Radiat. Res.*, **57**, 379 (1974).
5) M. Matsui and M. Imamura, This Bulletin, **47**, 1113 (1974).
6) Reviewed by J. Teply, *Radiat. Res. Rev.*, **1**, 361 (1969).
7) R. Barker and C. M. Noble, *J. Chem. Soc. A*, **1969**, 717.
8) J. Kucera, *Coll. Czech. Chem. Commun.*, **31**, 355 (1966).
9) M. Matsui, H. Seki, T. Karasawa, and M. Imamura, *J. Nucl. Sci. Tech.* (Tokyo), **7**, 97 (1970).
10) M. Imamura, M. Matsui, and T. Karasawa, This Bulletin, **43**, 2745 (1970).
11) S. Arai and L. M. Dorfman, *J. Phys. Chem.*, **69**, 2239 (1965).
12) M. A. J. Rodgers, *Trans. Faraday Soc.*, **67**, 1029 (1971).
13) S. Arai, A. Kira, and M. Imamura, *J. Chem. Phys.*, **54**, 5073 (1971).
14) A. J. Robinson and M. A. J. Rodgers, *J. Chem. Soc. Faraday I*, **69**, 2036 (1973).
15) E. Hayon, *J. Chem. Phys.*, **59**, 2353 (1970).
16) M. A. J. Rodgers, *J. Chem. Soc. Faraday Trans. I*, **68**, 1278 (1972).
17) S. A. Chaudhri and K.-D. Asmus, *J. Phys. Chem.*, **76**, 26 (1972).
18) S. Arai, M. Hoshino, and M. Imamura, *ibid.*, **79**, 702 (1975).
19) L. W. Sieck and P. Ausloos, *Radiat. Res.*, **52**, 47 (1972).
20) T. Shida and W. H. Hamill, *J. Amer. Chem. Soc.*, **88**, 3683 (1966).
21) M. S. B. Munson, *ibid.*, **87**, 5313 (1965).
22) N. Riehl, in "Energy Transfer in Radiation Processes," ed. G. O. Phillips, Elsevier, Amsterdam (1966), p. 95.
23) A track-core radius is given by the maximum impact parameter that can excite an electronic state (Ref. 2) and is considered to be constant for charged particiles of low energies although it expands with an increase in energy. (Refs. 2 and 3) We assumed here that a rapid transfer of energy from the track core may result in the formation of a reaction zone outside the core.

The Micelle Formation of Alkylammonium Chloride in 1-Propanol–Water and Acetone–Water Mixtures

Shigeyoshi MIYAGISHI

Department of Industrial Chemistry, Faculty of Technology, Kanazawa University, Kodatsuno, Kanazawa 920

(Received January 30, 1975)

The change in the critical micelle concentrations (CMC) of alkylammonium chlorides (C_{12}—C_{18}) and in the degree of the dissociation of the micelle (α) of dodecylammonium chloride was determined by adding 1-propanol and acetone to water. Both the CMC and the α increased with an additive concentration, each reaching a maximum at a certain concentration (critical composition of solvent for micelle formation, CCSM) and decreasing beyond the CCSM. The increment in the CMC was more influenced by the alkyl-chain length in the surfactant molecule in the presence of 1-propanol than in that of acetone. The effective coefficient of electrical energy (K_g) and the cohesive energy difference per methylene group between the micelle and the monomer states (ω) were calculated from the CMC and the α. The K_g values in both mixed solvents were constant beyond the respective CCSM. The value of ω was less in the presence of 1-propanol than in that of acetone.

It is well known that such factors as additives, temperature, alkyl-chain length, and polar group in a surfactant molecule give rise to considerable changes in the micelle formation.[1–4] Many investigations have been reported into the cooperative effects among these factors; for example, the effects of each alkyl-chain length in a surfactant and an added alcohol molecule,[5] the influence of the temperature[6] and of a change in the counterions[7,8] in the presence of the organic additives, and the effect of the organic additives on the CMC of the surfactant with different ethylene oxide chain lengths.[9,10] These investigations have suggested that the most significant factor in the micelle formation is the interaction between the water and the alkyl-chain in a surfactant molecule. However, there have been few reports about the effect of the alkyl-chain over a wide range of organic additive concentrations. In the present work, the micellar behavior of alkylammonium chlorides (C_{12}–C_{18}) in 1-propanol–water and acetone–water mixtures was studied over the additive concentration range from 0 to about 0.4 in the mole fraction.

Experimental

The alkylammonium chlorides were prepared from vacuum-distilled alkylamines in a manner described previously.[7] They were used after having been recristallized from ethanol-ether several times. The procedures for the measurements of the CMC and of the degree of dissociation of the micelle (α) have been reported previously.[7] The experiments were carried out at 35.0 °C.

Results and Discussion

The Influence of 1-Propanol on the Micelle Formation. The natural logarithms of the CMC in the four surfactant solutions are presented as a function of the mole fraction of 1-propanol in Fig. 1, while the degrees of dissociation of the dodecylammonium chloride micelle are plotted in Fig. 2. The CMC of dodecylammonium chloride (DAC) first decreased, passed through a minimum, and then increased steeply with the 1-propanol concentration until it reached a maximum value at a certain concentration. Similar behavior was observed with regard to the CMC of tetradecyl- (TAC), hexadecyl- (HAC), and octadecylammonium chloride (OAC), although the minimum gradually disappeared as the alkyl-chain length increased. The CMC-decreasing effect can be explained mainly in terms of the solubilization of an additive in a micelle,[5] while the CMC-increasing effect can be explained as being due to the solvent power of the mixture.[10,11] The minimum on the CMC-solvent composition curve is controlled by the competition of the above two effects.

The mole fraction of 1-propanol at which the CMC reaches its maximum— denoted as the critical composition of the solvent for micelle formation (CCSM)[11]

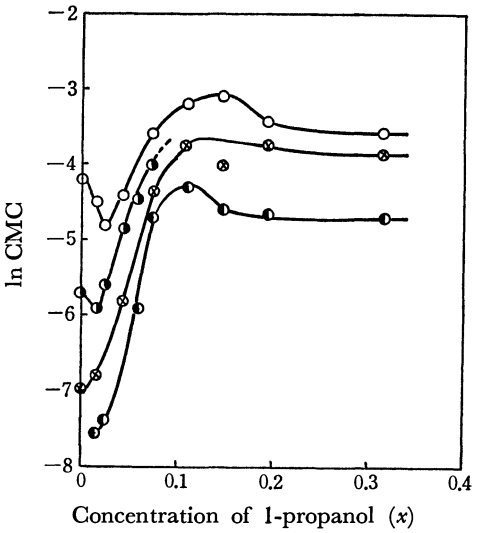

Fig. 1. The Effect of 1-propanol on CMC.
○: DAC, ◑: TAC, ⊗: HAC, ◐: OAC.

TABLE 1. THE CRITICAL COMPOSITIONS OF SOLVENT FOR THE MICELLE FORMATION

Surfactants	Mole fractions	
	1-Propanol	Acetone
D A C	0.12	0.10
H A C	0.12	0.11
O A C	0.11	0.15
S T S[a]	0.11	0.14
POE D E[b]	0.11	—

a) From Ref. 11. b) From Ref. 12.

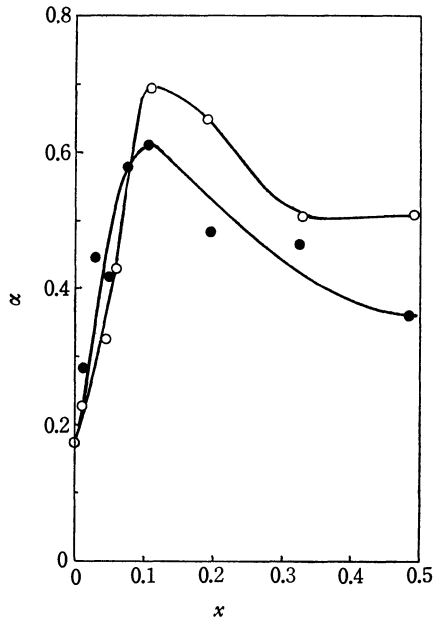

Fig. 2. The dependence of α on the additive concentration.
○: Acetone, ●: 1-Propanol.

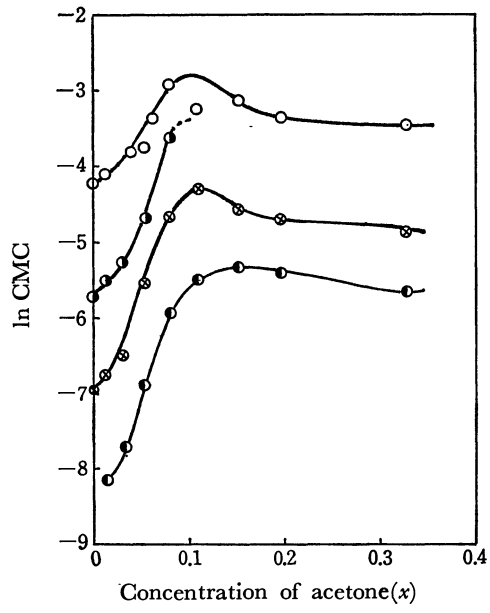

Fig. 3. The effect of acetone on CMC.
Symbols are identical with them in Fig. 1.

—is given in Table 1, together with the data for sodium tetradecyl sulfate (STS)[11] and polyoxyethylene dodecyl ether (POEDE).[12] The values of the CCSM were almost independent of the alkyl-chain length in the surfactant molecule and also of its head group. Also, the α increased with the 1-propanol concentration, reached a maximum at the same concentration as the CCSM, and decreased beyond it.

The Influence of Acetone on the Micelle Formation. The behavior of the alkylammonium chloride solutions containing acetone (Fig. 2, 3) was essentially the same as that of solutions in the presence of 1-propanol. However, both the solubilization effect and the solvent effect were less in the former mixed solvent than in the latter. There was no minimum in the values of the CMC as a function of the acetone concentration, and the increments in the CMC with acetone and the influence of the alkyl-chain length on their increments were less than in the presence of 1-propanol. The differences among the maximum CMC's of the alkylammonium chlorides were larger in the presence of acetone than in that of 1-propanol.

The CCSM in the acetone–water systems depended on the nature of the surfactants, but the values were scattered in the neighbourhood of 0.1—0.15. The heat of mixing in acetone–water systems has a minimum at 0.15,[13] and the viscosity and the tracer-diffusion coefficient of acetone have thier maximum and minimum, respectively, at about 0.2,[14,15] In the system of 1-propanol–water, the activity coefficient of 1-propanol changes rapidly in the neighbourhood of 0.1.[16] These authors, however, have avoided a detailed discussions concerning the structure change in the solutions. Any detailed discussion of the relation among these experimental facts must wait until details of the structure changes in the aqueous solutions become apparent. In the present paper, we will describe only the experimental fact; further investigation will be reported later.

In addition, it was found from the present experiment that the solubilities of these surfactants were less in acetone than in 1-propanol.

The Determination of K_g and ω. The CMC is expressed by this equation:[17]

$$\ln \mathrm{CMC} = -\frac{m\omega}{(1+K_g)kT} + \frac{K_g}{1+K_g}\ln\frac{2000\pi\sigma^2}{DNkT} + \frac{\ln(1000/Nv)-1}{1+K_g} \quad (1)$$

where m is the carbon number in a surfactant molecule, ω is the cohesive energy difference per methylene group between a micelle and a monomer states, K_g is the effective coefficient of the electrical energy, σ is the charge density, D is the dielectric constant of the solution, N is the Avogadro number, k is the Boltzmann constant, and T is the absolute temperature of the solution. As the second and the third terms on the right-hand side of this equation are almost independent of m,[17] the differentiation of Eq. (1) with respect to m gives the following equation:

$$\frac{\mathrm{d}\ln \mathrm{CMC}}{\mathrm{d}m} = -\frac{\omega}{(1+K_g)kT} \quad (2)$$

The values of $-\mathrm{d}\ln \mathrm{CMC}/\mathrm{d}m$ are plottedas functions of the additive concentrations in Fig. 4. It was found that $-\mathrm{d}\ln \mathrm{CMC}/\mathrm{d}m$ decreased rapidly with an increase in the concentration of the additives and reached constant values at the CCSM. The decreasing effect by the addition of 1-propanol was more than that by the acetone addition. In order to discuss these results in detail, we need to know the value of ω. We therefore attempted to determine K_g, and then ω was calculated from Eq. (2).

We define K_g as follows:

$$K_g = \phi/\phi_0 \quad (3)$$

where ϕ is the effective potential at the micelle surface

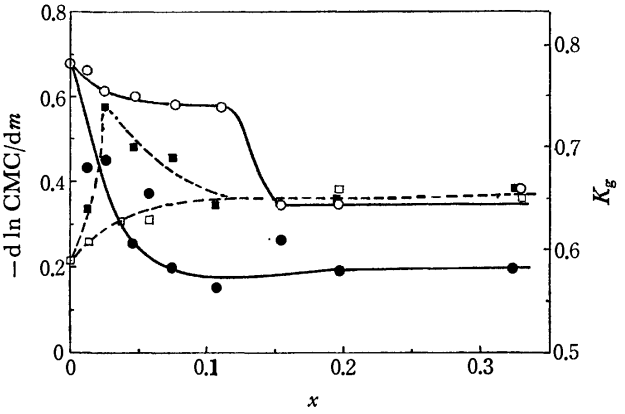

Fig. 4. The dependence of $-\mathrm{d}\ln\mathrm{CMC}/\mathrm{d}m$ and K_g on the additive concentrations.
○,□: Acetone, ●,■: 1-Propanol.
——: $-\mathrm{d}\ln\mathrm{CMC}/\mathrm{d}m$, ----: K_g.

and where ϕ_0 is the hypothetical potential when a counterion is not adsorbed on the micelle surface when the other conditions are constant. These potentials are given by the following two equations:

$$\phi = \frac{kT}{e}\ln\frac{2000\pi\sigma^2}{DNkTC_1} \tag{4-1}$$

$$\phi_0 = \frac{kT}{e}\ln\frac{2000\pi\sigma_0^2}{DNkTC_1} \tag{4-2}$$

where σ and σ_0 are the surface-charge densities of the micelle and of the hypothetical micelle, e is the electric elementary quantum, and C_i is the molarity of the couterion. By combining Eqs. (3) with (4—1) and (4—2), the following equation is obtained:

$$\frac{\varphi_0-\phi}{\phi} = \frac{1}{K_g} - 1 = \frac{2kT}{e\phi}\ln\frac{\sigma_0}{\sigma} \tag{5}$$

As σ/σ_0 is corresponds to α, Eq. (5) can be modified as follows:

$$K_g = \frac{e\phi/kT}{e\phi/kT - 2\ln\alpha} \tag{6}$$

On the other hand, according to a previous paper,[7] we have:

$$\frac{1-\alpha}{\alpha} = \frac{AMC_1}{1000}\exp(-\Delta G/kT) \tag{7}$$

where ΔG is the effective potential energy, M is the molecular weight of the solvent, and A is a constant. If ΔG can be given solely by an electrical term, we have the following equation:

$$\frac{\Delta G}{kT} = -\frac{e\phi'}{kT} = -\ln\frac{2000\pi\sigma'^2}{DNkTC_1} \tag{8}$$

where ϕ' and σ' are the potential and the charge density at a micelle surface in this case. Combining Eq. (7) with Eq. (8), we obtain:

$$\frac{e\phi'}{kT} = \ln\frac{1000}{AMC_1} + \ln\frac{1-\alpha}{\alpha} \tag{9}$$

As ϕ' is considered to be nearly equal to ϕ, the introduction of Eq. (9) into Eq. (6) gives the following equation:

$$K_g = \frac{\ln 1000/AMC_1 + \ln(1-\alpha)/\alpha}{\ln 1000/AMC_1 + \ln(1-\alpha)/\alpha^3} \tag{10}$$

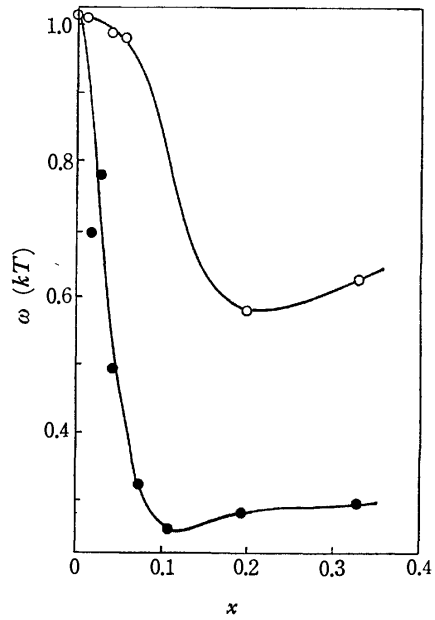

Fig. 5. The dependence of ω on the additive concentration.
○: Acetone, ●: 1-Propanol.

The concentration of the counterion, C_i, is equal to the CMC in the absence of an added electrolyte. Consequently, Eq. (10) becomes Eq. (11):

$$K_g = \frac{\ln(1-\alpha)/\alpha - \ln\mathrm{CMC} + \ln 1000/AM}{\ln(1-\alpha)/\alpha^3 - \ln\mathrm{CMC} + \ln 1000/AM} \tag{11}$$

The value of A is unknown, but it can be determined as follows. According to many papers published, ω in an aqueous solution is given as 1.08 kT. The value of $-\mathrm{d}\ln\mathrm{CMC}/\mathrm{d}m$ in the absence of an organic additive is given as 0.68 from Fig. 4. We can then obtain 0.59 as K_g from these two values and Eq. (2). Introducing 15×10^{-3} M, 0.18, 0.59, and 18 for the CMC, α, K_g, and M respectively in the aqueous solution into Eq. (11) gives 121 as A. Then, Eq. (11) may be rewritten as follows:

$$K_g = \frac{\ln(1-\alpha)/\alpha - \ln\mathrm{CMC} + \ln 1000/121M}{\ln(1-\alpha)/\alpha^3 - \ln\mathrm{CMC} + \ln 1000/121M} \tag{12}$$

The values of K_g calculated from Eq. (12) are shown in Fig. 4. Beyond the CCSM, they were almost constant. The values of ω calculated from Eq. (2) by using K_g and $-\mathrm{d}\ln\mathrm{CMC}/\mathrm{d}m$ are plotted in Fig. 5, which shows that ω decreased more rapidly in the presence of 1-propanol than in that of acetone and that the final value in the former solution was about one-half of that in the latter solution. These results suggest that the hydrophobic interaction in these micelle formation was less on the addition of 1-propanol than on that of acetone. However, we must note that the factors attributable to the decrease in ω are probably complicated; not only the hydrophobic interaction but also other factors, for example, the solubility parameters of the mixed solvents,[18] must be considered.

Fianlly, let us mention that the value of α calculated from Botré's equation[19] is not correct. Indeed, the decrease in the surfactant-ion concentration has been

considered above CMC.[20,21] However, the results determined on the basis of α are not unlike, for the divergence seems not be large when the experimental error of the determination of α is taken into consideration. Therefore, we believe that the qualitative behavior described above remains valid.

The author is greatly indebted to Professor Ryohei Matuura of Kyushu University, Assistant Professor Keishiro Shirahama of Saga University and Assistant Professor Morie Nishida for their encouragement and useful advice.

References

1) K. Shinoda, T. Nakagawa, B. Tamamushi, and T. Isemura, "Colloidal Surfactants," Academic Press, New York (1963).
2) P. Mukerjee, *Advan. Colloid Interface Sci.*, **1**, 241 (1967).
3) D. C. Poland and H. A. Sheraga, *J. Phys. Chem.*, **69**, 2431 (1965); *ibid.*, 69, 4425 (1965); *J. Colloid Interface Sci.*, **21**, 273 (1966).
4) P. Mukerjee, K. J. Mysels, and P. Kapauan, *J. Phys. Chem.*, **71**, 4166 (1967); P. Mukerjee and A. Ray, *ibid.*, **67**, 190 (1963).
5) K. Shinoda, *J. Phys. Chem.*, **58**, 1136 (1954).
6) M. F. Emerson and A. Holtzer, *ibid.*, **71**, 3320 (1967); K. Shiraham, M. Hayashi, and R. Matuura, This Bulletin, **42**, 1206 (1969); *ibid.*, **42**, 2123 (1969); W. B. Gratzer and G. H. Beaven, *J. Phys. Chem.*, **73**, 2270 (1969); P. Becher and S. E. Trifletti, *J. Colloid Interface Sci.*, **43**, 485 (1973).
7) S. Miyagishi, This Bulletin, **47**, 2972 (1974).
8) M. J. Schick, *J. Phys. Chem.*, **68**, 3585 (1964).
9) J. M. Corkill, J. F. Goodman, S. P. Harrold, and J. R. Tate, *Trans. Faraday Soc.*, **63**, 240 (1967); C. McDonald, *J. Pharm. Pharmac.*, **22**, 148 (1970); *ibid.*, **22**, 774 (1970); N. Nishikido, Y. Moroi, H. Uehara, and R. Matuura, This Bulletin **47**, 2634 (1974).
10) P. Becher, "Nonionic Surfactants," ed. by M. J. Schick, Marcel Dekker, New York, N.Y. (1967), p. 505.
11) H. Uehara, M. Manabe, and R. Matuura, *Mem. Fac. Sci. Kyushu Univ.* C, **8**, 55 (1972).
12) H. Mizuno, K. Deguchi, and K. Meguro, The 25th Discussion of Colloid and Interface Chemistry, Fukuoka, Japan, Oct. 1972, Abstract, p. 80.
13) D. E. Nicholson, *J. Chem. Eng. Data*, **5**, 309 (1960).
14) D. W. McColl and D. C. Doublass, *J. Phys. Chem.*, **71**, 987 (1967).
15) D. K. Anderson, J. R. Hall, and A. L. Babb, *ibid.*, **62**, 404 (1958).
16) K. Kojima, H. Seki, and K. Watase, *Kagaku Kogaku*, **32**, 149 (1968).
17) K. Shinoda, This Bulletin, **26**, 101 (1953).
18) K. Shirahama and R. Matuura, *ibid.*, **38**, 373 (1965).
19) C. Botré, V. L. Crescenz, and A. Mele, *J. Phys. Chem.*, **63**, 650 (1959).
20) T. Sasaki, The 27th Discussion of Colloid and Interface Chemistry, Akita, Japan, Oct. 1974, Abstracts, p. 1.
21) K. Shirahama, This Bulletin, **47**, 3165 (1974).

Ultrasonic Absorption Mechanisms in Aqueous Solutions of Alcohols

Sadakatsu NISHIKAWA, Mitsuo MASHIMA, Michio MAEKAWA,* and Tatsuya YASUNAGA*

Department of Chemistry, Faculty of Science and Engineering, Saga University, Honjo-machi, Saga 840

**Department of Chemistry, Faculty of Science, Hiroshima University, Higashisenda-machi, Hiroshima 730*

(Received February 25, 1975)

Ultrasonic absorption measurements in aqueous solutions of *tert*-butyl and allyl alcohols were carried out in the frequency range of 4.5—220 MHz at 25 °C. Two relaxation processes were observed in aqueous solution of *tert*-butyl alcohol and a single one in that of allyl alcohol. The former relaxation mechanisms were revealed to be due to the perturbation of the equilibria expressed by $AB \underset{\nearrow B}{\nwarrow} A \rightleftharpoons 1/3A_3$ where A and B were alcohol and water molecule respectively. The latter mechanism was due to that expressed by $AB \rightleftharpoons A+B$. The rate constants for all these processes were determined from the concentration dependence of the relaxation frequencies. The water structure in aqueous solutions was discussed in terms of a hydrophobic interaction, and it was concluded that the hydrophobic interaction decreased in this sequence, *tert*-butyl, *n*-propyl and allyl alcohols.

The effects of alcohols upon the properties of water continue to be investigated,[1] since the explanation of biological reaction mechanisms is intimately connected with liquid water structure. To understand the structural characteristics of liquids on a molecular scale, the application of wave technique with ultrasonic vibrations seems to be most appropriate. Though Blandamer and Waddington[2] have reported the ultrasonic absorption spectra in aqueous solutions of some alcohols, no quantitative analyses of the excess absorptions have been done. In a previous paper[3], the present authors have measured the ultrasonic absorption in aqueous solution of *n*-propyl alcohol and clarified the excess absorption mechanisms in relation to water structure. It becomes desirable to understand the properties of aqueous solutions of other alcohols and to compare the results in the case of *n*-propyl alcohol with those of other ones.

For this purpose, *tert*-butyl and allyl alcohols have been chosen and the ultrasonic absorption mechanisms in these aqueous solutions will be elucidated in this paper.

Experimental

The *tert*-butyl and allyl alcohols were reagent-grade commercial products and were distilled once. The purities of these alcohols were verified by gas chromatography to be higher than 99.5%. Solutions were prepared with doubly distilled water and we.e made up to the desired concentrations by weight. The measurements of the ultrasonic absorption were made in the frequency range of 4.5—220 MHz, using an ultrasonic pulse technique previously described[3,4]. The sound velocities were measured at 1.92 MHz using a sing-around technique. The densities were measured by means of a standard pycnometer. All the measurements were made at 25 °C.

Results and Discussion

Figures 1 and 2 show the representative ultrasonic absorption spectra in aqueous solutions of *tert*-butyl and allyl alcohols respectively. In general, the sound absorption caused by the several relaxation processes can be described by the following equation:

$$\alpha/f^2 = \sum A_i/[1+(f/f_{ri})^2] + B \qquad (1)$$

where α is the absorption coefficient; f the frequency; f_{ri} the relaxation frequency for the i-th process, and A_i and B, constants. The absorption spectra in aqueous solution of *tert*-butyl alcohol show the characteristic behavior due to a single relaxation process in the concentration range of less than 2.61 M and that due to double relaxation processes in the concentration range of more than 2.99 M. On the other hand, the measurements of α/f^2 for aqueous solution of allyl alcohol can be described by the relation for a single relaxation through out the concentration range measured. In the case of the single relaxation spectrum, a trial-and-error procedure was used to obtain the ultrasonic parameters which provided the straight line of the plots of α/f^2 *vs.* $[1+(f/f_r)^2]^{-1}$. The double relaxation spectrum was analyzed by a nonlinear least-squares routine, employing a Toshiba 3400 computer. In Table 1, the obtained values of the

Table 1. Relaxation parameters, sound velocities and densitifs in aqueous solutions of *tert*-butyl and aliyl alcohols

C_a (M)	ρ (g ml^{-1})	c (m s^{-1})	f_{r1} (MHz)	f_{r2}	A_1 (10^{-17} s^2 cm^{-1})	A_2	B
2.03	0.9758	1611	87	—	104	—	49
2.28	0.9738	1610	75	—	288	—	57
2.43	0.9720	1608	69	—	507	—	35
2.49	0.9714	1607	62	—	564	—	90
2.61	0.9670	1600	62	—	639	—	121
2.99	0.9600	1570	52	4.4	962	903	184
3.35	0.9561	1550	52	5.0	1121	907	226
4.00	0.9465	1519	60	8.7	937	1145	221
5.01	0.9243	1544	74	9.3	640	1211	205
6.01	0.9005	1393	69	9.0	452	849	214
7.02	0.9741	1344	66	9.1	279	545	218
8.02	0.9527	1287	114	11.7	147	158	174
8.99	0.8273	1232	103	13.2	77	38	186
		(*tert*-butyl alcohol)					
4.03	0.9742	1584	90	—	58	—	59
4.19	0.9730	1581	90	—	68	—	61
4.69	0.9696	1570	85	—	113	—	75
5.24	0.9643	1553	80	—	134	—	94
5.97	0.9581	1532	80	—	146	—	103
6.50	0.9531	1517	80	—	149	—	103
7.01	0.9469	1498	85	—	134	—	101
7.99	0.9365	1466	85	—	100	—	99
8.73	0.9302	1442	90	—	99	—	77
9.47	0.9201	1420	100	—	82	—	70
10.1	0.9120	1399	110	—	66	—	60
		(allyl alcohol)					

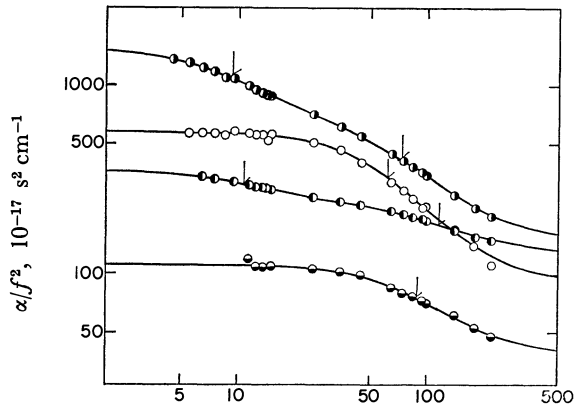

Fig. 1. Ultrasonic absorption spectra in aqueous solution of *tert*-butyl alcohol at 25 °C. The arrows show the relaxation frequencies.
◒: 2.03 M, ○: 2.61 M, ◑: 5.01 M, ◐: 8.02 M.

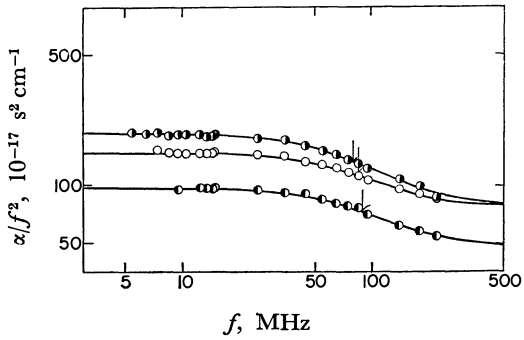

Fig. 2. Ultrasonic absorption spectra in aqueous solution of allyl alcohol.
◐: 4.19 M, ◑: 5.97 M, ○: 7.99 M.

ultrasonic parameters and the sound velocities are listed together with those of densities.

We have proposed that the excess absorptions in aqueous solution of *n*-propyl alcohol are due to the interaction between the alcohol and the water molecule, and the association and dissociation reaction of alcohol. Following this background, the excess absorption mechanisms in aqueous solutions of *tert*-butyl and allyl alcohols will be clarified. The model for the relaxation processes is as follows:

$$AB_m \underset{k_{21}}{\overset{k_{12}}{\rightleftarrows}} mB + A \underset{k_{32}}{\overset{k_{23}}{\rightleftarrows}} \frac{1}{n}A_n \tag{2}$$

where A is the molecule of alcohol; B that of water, and k_{ij}, the rate constant. The detailed derivations for the expressions of the relaxation frequency and the maximum excess absorption per wavelength have been described in a previous paper.[3] If the left reaction step proceeds much faster than the right one, the relaxation frequencies for each step are expressed by:

$$2\pi f_{r1} = 1/\tau_1 = k_{21}(m^2C_2^{m-1}C_3 + C_2^m) + k_{12} \tag{3}$$

$$2\pi f_{r2} = 1/\tau_2 = k_{32} + k_{23}n^2C_3^{n-1} - \frac{n^2k_{21}k_{23}C_2^mC_3^{n-1}}{k_{12}+k_{21}(m^2C_2^{m-1}C_3+C_2^m)} \tag{4}$$

where C_2 and C_3 are the equilibrium molar concentrations of the components, B and A, respectively, and τ_i the relaxation time. The maximum excess absorption per wavelength, μ_{maxi}, is given by the next equation;

$$\mu_{maxi} = \frac{1}{2}A_i f_{ri} c = (\pi\rho c^2\Gamma_i/RT)(\Delta V_i - \alpha_p^\infty \Delta H_i/\rho C_p^\infty)^2 \tag{5}$$

where ρ is density; c, the sound velocity; R, the gas constant; T, the absolute temperature; α_p^∞, the high-frequency limit of the thermal expansion coefficient; C_p^∞, the high-frequency limit of the constant pressure specific heat, and ΔV_i and ΔH_i, the parameters related to the volume and enthalpy changes associated with the reaction under consideration. The Γ_i terms for the reaction expressed by Eq. (2) are:

$$\Gamma_1 = \frac{1}{V}\left(\frac{1}{C_1}+\frac{m^2}{C_2}+\frac{1}{C_3}-\frac{m^2}{C_T}\right)^{-1} \tag{6}$$

$$\Gamma_2 = \frac{1}{V}\left[\frac{n}{C_3}(n-\tau_1 k_{21} n C_2^m)+\frac{n-1}{C_T}(n-1+\tau_1 k_{21} n C_2^m)+\frac{1}{C_4}\right]^{-1} \tag{7}$$

where C_4 is the equilibrium concentration of the component A_n and where $C_T = C_1+C_2+C_3+C_4$.

Let us first consider the excess absorption mechanisms in aqueous solution of *tert*-butyl alcohol. The excess absorption in the lower frequency range (4—14 MHz) is observed only in the concentration range of more than 2.61 M, while that in the higher frequency range (50—120 MHz) is always observed through out the concentration range measured. From these facts, the perturbation of the left equilibrium in Eq. (2) may be expected to be associated with the excess absorption mechanism in the higher frequency range. If a single water molecule interacts with a single alcohol one and if the concentration of the aggregate of alcohol, C_4, is small compared with the other components, Eq. (3) can be rewritten as:

$$2\pi f_{r1} = 1/\tau_1 = k_{21}\sqrt{(C_a-\beta C_w+K_{12})^2+4\beta C_w K_{12}} \tag{8}$$

where K_{12} is the equilibrium constant defined by $K_{12} = k_{12}/k_{21}$; β, the mole fraction of the water monomer, and C_a and C_w the analytical concentrations of alcohol and water respectively. The introduction of the parameter, β, means that, in aqueous solutions of alcohols, an equilibrium between the monomer and hydrogen-bonded cluster of water is established and that only monomeric water molecules participate in the alcohol water interaction. Therefore, the parameter, β, might indicate the stability of the water structure.

Using the values of f_{r1}, C_a and C_w, the parameters, β, K_{12} and k_{21}, were determined so as to obtain a best fit of the data to Eq. (8). Figure 3 shows the calculated values of the relaxation frequencies, f_{r1}, for aqueous solution of *tert*-butyl alcohol along with the experimental ones. One can also evaluate the concentration dependence of the maximum excess absorption per wavelength. As has been described previously, the μ_{max1} is approximately proportional to $\rho c^2\Gamma_1$. The calculated values of $\rho c^2\Gamma_1 V$ are shown by a solid line in Fig. 4 also with the experimental values of μ_{max1}. In this figure, both peaks appear at almost the same concentration and the tendencies of both are identical. These facts lead to the conclusion that the excess absorption mechanism of aqueous solution of *tert*-butyl

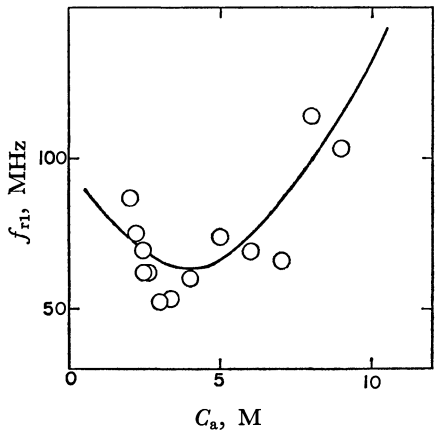

Fig. 3. Concentration dependence of the relaxation frequencies, f_{r1}, for aqueous solution of *tert*-butyl alcohol. The solid line indicates the calculated values.

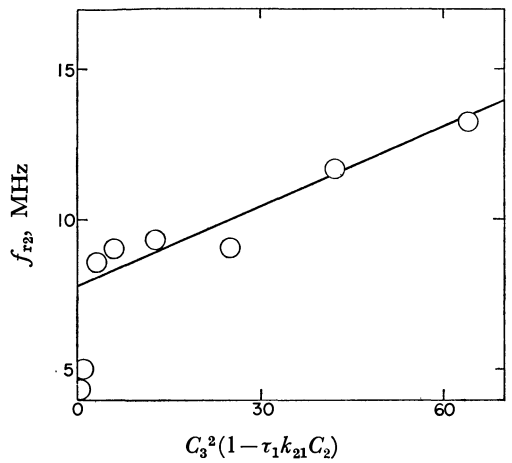

Fig. 5. The plots f_{r2} *vs.* $C_3^2(1-\tau_1 k_{21} C_2)$ for aqueous solution of *tert*-butyl alcohol at 25 °C.

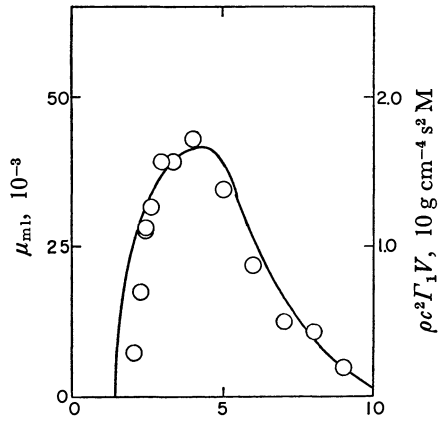

Fig. 4. The variations of μ_{max1} and $\rho c^2 \Gamma_1 V$ with the concentration of *tert*-butyl alcohol. The solid line represents the calculated values of $\rho c^2 \Gamma_1 V$. The circles are the experimental points of μ_{max1}.

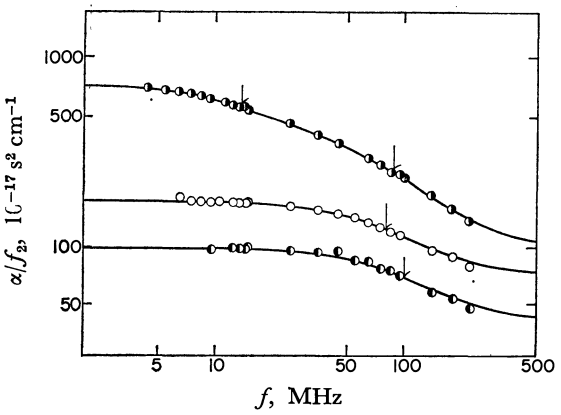

Fig. 6. Comparison of the ultrasonic absorption spectra in aqueous solution of *n*-propyl alcohol with that of allyl alcohol.
◑: 4.50 M, *n*-propyl alcohol, ○: 5.24 M, allyl alcohol, ◐: 4.19 M, allyl alcohol.

alcohol in the higher frequency range is attributed to the water alcohol interaction. Next, we will evaluate the excess absorption mechanism in the lower frequency range. Equation (4) is transformed to:

$$2\pi f_{r2} = 1/\tau_2 = n^2 k_{23} C_3^{n-1}(1-\tau_1 k_{21} C_2) + k_{32} \quad (9)$$

The aggregation number, n, was determined so as to obtain the straight line of the plots of f_{r2} *vs.* $C_3^{n-1}(1-\tau_1 k_{21} C_2)$, and from the slope and the intercept of this line the rate constants, k_{23} and k_{32}, were determined. Figure 5 shows the plots at $n=3$, where the best fit is obtained. The kinetic parameters obtained in this way are listed in Table 2. We also estimate the concentration dependence of the maximum excess absorption per wavelength for this reaction mechanism, but the value of $\rho c^2 \Gamma_2 V$ increases monotonically with the alcohol concentration.

Second, the excess absorption mechanism in aqueous solution of allyl alcohol, in which the excess absorption is not observed in the lower frequency range, will be clarified. In this solution, the association and dissociation reaction of alcohol may not be expected, about which we will discuss later. Therefore, it is sufficient to consider the perturbation of the left equilibrium as the excess absorption mechanism. For the sake of comparing the absorption spectra in aqueous solution of allyl alcohol with that of *n*-propyl alcohol, the spectra of the both solutions are shown in Fig. 6. As the behavior of the ultrasonic parameters in aqueous solution of allyl alcohol were close to those in aqueous solution of *tert*-butyl and *n*-propyl alcohols in the higher frequency range, the kinetic parameters for this mechanism in aqueous solution of allyl alcohol were also determined analogously to those obtained in the case of aqueous solution of *tert*-butyl alcohol. Figures 7 and 8 show the concentration dependence of the relaxation frequency and the maximum excess absorption per wavelength for aqueous solution of allyl alcohol. As may be seen in these figures, the calculated relaxation frequencies are very close to those of experimental values, and the position of the peak of the maximum excess absorption per wavelength appears at that of $\rho c^2 \Gamma_1 V$. These results make us conclude that the excess absorption mechanism in aqueous solution of allyl alcohol is due to the perturbation of the left equilibrium expressed by Eq. (2). The kinetic para-

Table 2. The reaction parameters and the stability of water structure in aqueous solutions of alcohols

Solute	k_{12} (s^{-1})	k_{21} ($M^{-1}s^{-1}$)	K_{12} (M)	k_{23} ($M^{-2}s^{-1}$)	k_{32} (s^{-1})	K_{23} (M^{-2})	β	ΔF_w (kcal)
n-Propyl alcohol[a]	1.6×10^8	6.2×10^7	2.6	2.2×10^5	6.9×10^7	0.0032	0.15	1.0
tert-Butyl alcohol	1.2×10^8	7.2×10^7	1.7	5.5×10^5	4.9×10^7	0.011	0.12	1.2
Allyl alcohol	1.5×10^8	6.3×10^7	2.4	—	—	—	0.19	0.82

a) Ref. 3.

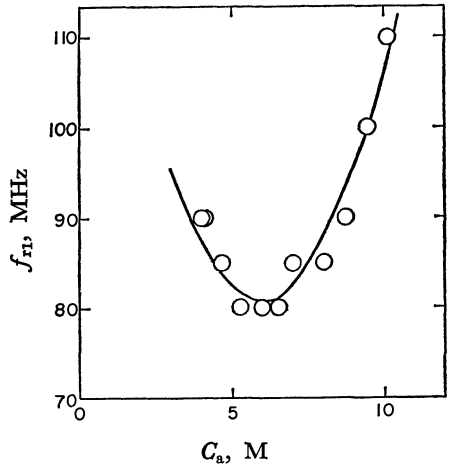

Fig. 7. Concentration dependence of the relaxation frequencies for aqueous solution of allyl alcohol.

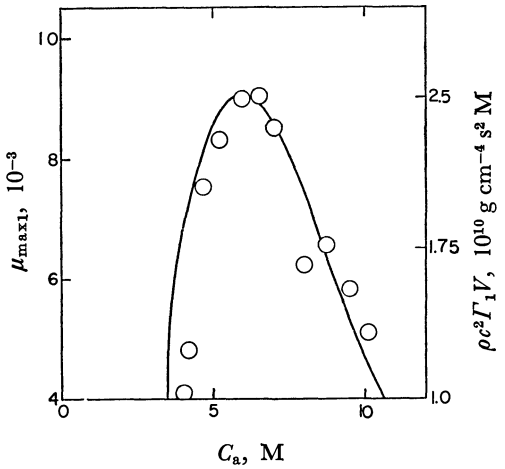

Fig. 8. The variations of μ_{max1} and $\rho c^2\Gamma_1 V$ with the concentration of allyl alcohol.

meters obtained are listed in Table 2. The parameter, β, can be related to the free energy difference between the hydrogen bonded and non-hydrogen bonded water by means of this equation; $\beta/(1-\beta)=\exp(-\Delta F_w/RT)$. In Table 2, the free energy difference in aqueous solutions of alcohols are also listed. Litovitz and his coworkers[5] have estimated the free energy difference in pure water to be 0.63 kcal at 25 °C utilizing the ultrasonic absorption technique. Therefore, the parameter, β, which is the mole fraction of monomeric water, is 0.26. Comparing this value with those obtained by the present investigation of aqueous solutions of alcohols, it is clear that all the alcohols studied here act as water structure promoters. The effect of the water structure promoter may be the result of a hydrophobic interaction. Recent investigations[6,7] of aqueous solutions of several alcohols have shown that even molecules which consist of relatively small hydrophobic groups have an ability of hydrophobic interaction. Especially, Shirahama and *et al.*[8] have found the decreasing effects of the critical micelle concentration in aqueous solutions of several alcohols and have reported that the more hydrophobic and the more concentrated the added alcohol, the more marked becomes the decrease in the critical micelle concentration. They have also shown that the hydrophobic interaction decreases in this sequence, *tert*-butyl, *n*-propyl and ethyl alcohols. The smaller the parameter, β, the more does the hydrophobic interaction increase. The results obtained in the present investigation are consistent with the above interpretation. It is well known that the presence of a double bond in a molecule weakens the hydrophobic interaction. If the aggregate of alcohol is formed by hydrophobic interaction in aqueous solutions, the absence of the excess absorption in the lower frequency range in aqueous solution of allyl alcohol can be well interpreted in terms of the decrease in the hydrophobic interaction.

In conclusion, the excess absorption mechanisms in aqueous solutions of alcohols investigated here may be attributed to the interaction of a single alcohol molecule and water molecule, and to the association and dissociation reaction of alcohol molecules. Furthermore, a decrease in the hydrophobic interaction of alcohol causes the aggregate of alcohol to disappear.

The authors wish to express their thanks to Dr. K. Shirahama in Saga University for his helpful discussions. They are also grateful to Dr. H. Yano in Daiichi College of Pharmaceutical Science for permitting them to use an ultrasonic absorption apparatus equipped in the 100—220 MHz frequency range. This work was partially supported by the Sakkokai Foundation.

References

1) H. L. Friedman and C. V. Krishnan, *J. Sol. Chem.*, **2**, 119 (1973).
2) M. J. Blandamer and D. Waddington, *Advan. Mol. Relaxation Processes*, **2**, 1 (1970).
3) S. Nishikawa, M. Mashima, and T. Yasunaga, This Bullitin, **48**, 661 (1975).
4) N. Tatsumoto, *J. Chem. Phys.*, **47**, 4561 (1967).
5) T. A. Litovitz and E. H. Carnevale, *J. Appl. Phys.*, **26**, 816 (1955).
6) C. Jolicoevr, E. Firkins, and P. Bernier, *J. Phys. Chem.*, **78**, 851 (1974).
7) M. M. Marciacq: Rousselot and M. Lucas, *ibid.*, **77**, 1056 (1973).
8) K. Shirahama and T. Kashiwabara, *J. Colloid Interfac. Sci.*, **36**, 65 (1971).

Group Interactions in Polyelectrolytes. X. The Amination Kinetics of Poly(vinyl haloacetals) and Related Compounds

Hiroshi KAWABE

The Institute of Physical and Chemical Research, Wako-shi, Saitama 351

(Received February 3, 1975)

Polyvinyl chloroacetal (PVCA) and polyvinyl bromoacetal (PVBA) were prepared from polyvinyl alcohol, whose acetal contents were close to the value expected on the basis of Flory's calculation for the intramolecular reaction between neighboring substituents. The amination of these polyvinyl haloacetals and polyvinyl chloroethyl ether with 2-aminobutanol and diethanolamine was investigated kinetically in dimethyl sulfoxide. The $\Delta G^{\ddagger}$ values in the amination of these polymers were much higher than that of chloromethylated polystyrene (CMPS) reported previously; this was because of their higher $\Delta H^{\ddagger}$ values. The lower $\Delta H^{\ddagger}$ of CMPS was ascribed to the resonance structure of the activation complex due to the phenyl substituent at the α-carbon of the chloromethyl group. This was ascertained by comparing the $\Delta H^{\ddagger}$ value in the amination of phenethyl chloride with that of benzyl chloride. The amination of PVBA was faster than that of PVCA as a result of the lower $\Delta H^{\ddagger}$ of the former.

The amination of haloacetalized polyvinyl alcohol has already been investigated for the purpose of improving vinylon fibers[1] and for the preparation of ion-exchange fibers.[2] The amination proceeded in a heterogeneous system, and the reaction was reported to be accompanied by cross-linking. The amination kinetics of polyvinyl haloacetal in a homogeneous system has not yet been studied, though. The present author has now prepared chloroacetal and bromoacetal of polyvinyl alcohol (PVA); their acetal contents are very close to the value calculated by Flory.[3] The amination of these polyvinyl haloacetals with diethanolamine or 2-aminobutanol in dimethyl sulfoxide (DMSO) has been found to proceed to nearly a 100% conversion in a homogeneous system.

The amination rate of polyvinyl bromoacetal (PVBA) was higher than that of polyvinyl chloroacetal (PVCA). The amination rates of these polyvinyl haloacetals are, however, much lower than that of chloromethylated polystyrene (CMPS), which was reported previously.[4,5] The present author has also investigated the amination of polyvinyl chloroethyl ether (PVCE) of a low molecular weight; the rate was only a little higher than that of PVCA. The higher amination rate of CMPS, as compared with PVBA, PVCA, and PVCE, may be ascribed to its resonance structure in the transition state. Then, the amination rate of benzyl chloride, which is a model of the structural unit of CMPS, has been compared with that of phenethyl chloride, which is considered to lack in resonance. Further, the amination rates of both benzyl chloride and cuminyl chloride with several amines have been measured in order to examine the propriety of the compounds as structural unit models of CMPS.

The amination rates of PVBA, PVCA, and phenethyl chloride with diethanolamine have been found to be a little lower than the corresponding amination rates with 2-aminobutanol. On the other hand, each amination of CMPS and benzyl chloride with diethanolamine was a little faster than that with 2-aminobutanol.[4,5] This reverse reactivity of the two aminoalcohols has been discussed with the aid of the amination data on PVCA and phenethyl chloride with several alkylamines, in addition to the published data on CMPS and benzyl chloride.

Experimental

Materials. The polyvinyl alcohols used were Gohsenols of Nihon Gosei Chem. Ind. Co., NH-18 (degree of hydrolysis: 99.0—100%; degree of polymerization, $\overline{P}$=over 1500) and KH-17 (degree of hydrolysis: 78.5—81.5%; $\overline{P}$=over 1500). The cuminyl chloride was prepared by treating cumen (0.4 mol) and chloromethyl ether (0.87 mol), with stanic chloride (0.096 mol) as the catalyst, in toluene at −10°C. The yield of the purified product (bp 110 °C/15 mmHg, $n^{21.5}$ 1.5224) was 52.6%. The 2-aminobutanol was prepared by the procedure described in a previous paper;[6] n^{20} 1.4529, $[\alpha]_D^{20}$ −10.23. The other chemicals and solvents were of a reagent grade and were distilled before use; they were proved to be pure by their refractive indices.

Preparation of Polyvinyl Haloacetals. To ethylene dichloride, which absorbed dry hydrogen chloride, we added PVA (equivalent to a 1% concentration) and chloroacetaldehyde diethyl acetal (equimolar to the hydroxyl group of PVA), after which the mixture was left for several days at 20 °C. The mixture was then poured into methanol to precipitate the polymer. The polymer was purified by reprecipitation with ethylene dichloride-methanol and by washing it thoroughly with methanol. The polyvinyl chloroacetal (PVCA) thus obtained was dried *in vacuo* at 40 °C. The content of acetal (E%) in the polymer was calculated from the content of chlorine (Cl%) in the polymer by means of:

$$E\% = 145.64 \times [\mathrm{Cl}\,\%]/(58.62-[\mathrm{Cl}\,\%]) \quad (1)$$

Polyvinyl bromoacetal (PVBA) was also prepared by the same procedure except that the reprecipitation was carried out with DMSO-methanol. The acetal content was calculated from the bromine content (Br%) in the polymer by means of:

$$E\% = 83.97 \times [\mathrm{Br}\,\%]/(76.15-[\mathrm{Br}\,\%]) \quad (2)$$

Preparation of Polyvinyl Chloroethyl Ether. To a solution of 2-chloroethyl vinyl ether (10.6 g) in diethyl ether (50 ml), we added, drop by drop, a solution of boron trifluoride etherate (0.15 g) in diethyl ether (50 ml), after which the mixture was kept for 200 min at 25 °C. The mixture was then washed with 5% aqueous sodium hydroxide and water. The ethereal solution was then dried with calcium chloride, and the diethyl ether was removed by the use of an evaporator. The molecular weight of the polyvinyl chloroethyl ether

(PVCE) thus obtained was 945 ($\bar{P}=9$). Found: C, 44.53; H, 6.56; Cl, 30.35%. Calcd for $(C_4H_7OCl)_n$: C, 45.08; H, 6.63; Cl, 33.27%.

Amination Kinetics Measurements. The amination rates of PVBA, PVCA, PVCE, phenethyl chloride, cuminyl chloride, and benzyl chloride were measured by the procedures described previously for the amination of CMPS and benzyl chloride.[4]

Results and Discussion

Haloacetalization of Polyvinyl Alcohol (PVA). Noma *et. al.*[7] reported that, in the chloroacetalization of PVA with chloroacetaldehyde diethyl acetal in ethylene dichloride containing hydrogen chloride, the fractional conversion, after repeated treatments, nearly reached the calculated maximum value of 0.8647 which was given by Flory for the intramolecular reaction between neighboring substituents of a polymer having the 1.3-structure.[3] In the present study, the chloroacetalization of PVA by Noma's procedure has been examined in an attempt to prepare the PVCA

Table 1. Chloroacetalization of PVA (NH-18) in dichloroethane at 20 °C[a]

HCl concn. M	Time day	Cl %	Acetal %
0.36	8	21.36	83.5
0.50	8	20.09	75.9
0.79	7	19.97	75.3
0.50	11	21.34	85.3
0.35	13	21.57	84.7
0.48	13	21.59	84.8
0.50	13	21.74	85.9
Calcd value (Flory)		21.83	86.47

a) Concentration of PVA: 1%.

Table 2. Bromoacetalization of PVA (NH-18) in dichloroethane at 20 °C[a]

HCl concn. M	Time day	Br %	Acetal %
0.42[b]	10	34.63	70.3
0.52	7	37.43	81.2
0.62[c]	7	37.01	79.7
0.50	7	38.85	87.5
0.50	10	38.34	85.1
0.50	13	38.14	84.2
Calcd value (Flory)		38.64	86.47

a) Concentration of PVA: 1%. b) Concentration of PVA: 0.56%. c) Room temp.

Table 3. Elementary analysis of chloroacetal and bromoacetal of PVA (NH-18)

Chloroacetal	C %	H %	Cl %	Acetal %
Found (PVCA)	49.03	6.38	21.74	85.9
Calcd (Flory)	49.01	6.36	21.83	86.47
Bromoacetal	**C %**	**H %**	**Br %**	**Acetal %**
Found (PVBA)	38.95	4.92	38.44	85.6
Calcd (Flory)	38.48	5.00	38.64	86.47

Table 4. Chloroacetalization of PVA in DMSO

PVA	Concn. %	HCl concn. M	Temp. °C	Time day	Acetal %
KH-17	1	0.25	Room	1	5.6
	1	0.50	Room	2	9.5
	1	0.50	Room	6	45.2
	1	1.00	30	1	11.2
	1	0.50	40	2	22.2
	2	0.50	40	1	24.6
	2	0.50	40	1	Gel
NH-18	2	0.50	30	8	33.8
	2	0.50	30	8	Gel

of maximum acetal content by only one treatment. The acetalization of PVA with bromoacetaldehyde diethyl acetal has also been investigated by means of the same procedure. The results are shown in Tables 1 and 2. The results of the elementary analysis of the haloacetals with the highest acetal content, which are shown in Table 3, indicate that the C, H, and halogen contents of each polymer are very close to the values calculated on the basis of the maximum conversion given by Flory.

In the above procedure, the reaction proceeded initially in a heterogeneous system, though the polymer was gradually swollen and finally dissolved in ethylene dichloride as the acetalization proceeded. The acetalization of PVA with chloroacetaldehyde diethyl acetal has also been investigated in DMSO; the results are summarized in Table 4. Although the reaction proceeded thoroughly in a homogeneous system, the acetal content of the product was low, and occasionally the gelation of the solution took place.

In the acetalization of PVA catalyzed by a proton, the probable mechanism of which is shown in the following scheme, the carbonium cation formed from the acetal may be subject to the nuclephilic attack by the oxygen of PVA to form the ether link, and the

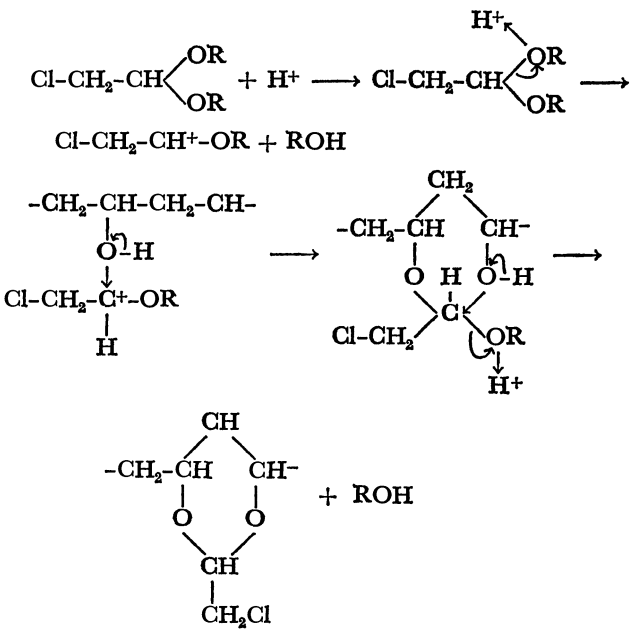

succeding reaction with the neighboring hydroxyl group in the same mechanism may result in the formation of the acetal ring. Since DMSO is a basic aprotic solvent and since cations are very likely to solvate in this solvent, the activation energy of the acetalization in DMSO is possibly enhanced by this solvation.

Amination of Polyvinyl Chloroacetal (PVCA). The amination kinetics of PVCA with 2-aminobutanol and diethanolamine in DMSO can be fully expressed by this second-order rate equation:

$$kt = \frac{1}{a-b}\ln\frac{b(a-x)}{a(b-x)} \quad (3)$$

where k is the rate constant, where a and b are the initial concentrations of the amine and halogen groups respectively, and where x is the concentration of halide ions formed after time, t.

During the amination of chloromethylated polystyrene (CMPS) with diethanolamine in DMSO, the second-order rate constant, computed on the basis of Eq. (3), decreased as the amination proceeded; this deceleration was ascribed to the steric obstruction in the transition state by the neighboring substituted group.[5] The lack of this steric obstruction in the amination of PVCA with diethanolamine, which is indicated by its ordinary kinetic behavior, can be explained by the fact that the distance between the reactive groups in PVCA is longer than that in CMPS.

Table 5. Amination of PVCA in DMSO[a,b,c]

Amine	Temp. °C	$k\times10^3$ l/mol min	E_a kcal/mol	log A[d]
2-Aminobutanol	90	0.740		
	100	1.57	19.6±0.2	8.68±0.09
	110	3.15		
	120	5.93		
Diethanolamine	90	0.470		
	100	0.953	18.9±0.1	8.06±0.05
	120	3.43		
	130	6.43		

a) PVCA was prepared from NH-18. b) Concentrations: a is about 0.757 M and b is about 0.038 M. c) Amination rates of PVCA prepared from KH-17 with diethanolamine were also measured to give the values, E_a of 18.9±0.7 and log A of 8.10±0.38. d) A is expressed by l/mol min.

Table 6. Amination of PVBA in DMSO[a,b]

Amine	Temp. °C	$k\times10^2$ l/mol min	E_a kcal/mol	log A[c]
2-Aminobutanol	70	0.977		
	80	1.91	16.8±0.1	8.70±0.06
	90	3.74		
	100	7.05		
Diethanolamine	79.9	1.12		
	85	1.49		
	90	2.08	16.5±0.2	8.26±0.12
	100	3.77		
	110	7.05		

a) PVBA was prepared from NH-18. b) Concentrations: a is about 0.36 and b is about 0.017 M. c) A is expressed by l/mol min.

The numerical values of k at different temperatures are tabulated in Table 5, together with the values of E_a, the activation energy, and A, the frequency factor expressed by l/mol min, both of which were computed by the least-squares method.

Amination of Polyvinyl Bromoacetal (PVBA). The amination kinetics of PVBA with 2-aminobutanol and diethanolamine also fit Eq. (3). The results of the amination are tabulated in Table 6. The amination rate of PVBA is about fifty times that of PVCA; this is a result of the lower E_a value of PVBA.

Amination of Polyvinyl Chloroethyl Ether (PVCE). The amination of PVCE with diethanolamine conformed to Eq. (3), and no deceleration was observed during the course of amination. Since the degree of polymerization of this polymer is very low ($\bar{P}=9$), and since its side chain is rather flexible, the steric obstruction between the reactive groups may be avoided by the free rotation in the main and side chains. The results of the kinetic measurements are shown in Table 7. The amination of PVCE is several times faster than that of PVCA.

Amination of Phenethyl Chloride. The amination rate of CMPS is much higher than those of PVCA, PVBA, and PVCE. In the comparison of the rate constants at 60 °C, for example, constants which are given by the extrapolation of the Arrhenious plots, the amination rate of CMPS is about ten thousand times that of PVCA. This large difference in their amination rates may be considered to originate in the stabilization of the transition state of CMPS because of its

Table 7. Amination of PVCE in DMSO[a]

Amine	Temp. °C	$k\times10^3$ l/mol min	E_a kcal/mol	log A[b]
Diethanolamine	60	0.370		
	70	0.797		
	80	1.73	18.2±0.2	8.52±0.11
	85	2.52		
	90	3.56		

a) Concentration: a is about 0.574 M and b is about 0.029 M. b) A is expressed by l/mol min.

Table 8. Amination of phenethyl chloride in DMSO

Amine	Temp. °C	$k\times10^2$ l/mol min	E_a kcal/mol	log A[c]
2-Aminobutanol[a]	90	0.882		
	100	1.70		
	110	3.05	16.9±0.1	8.13±0.07
	120	5.22		
	130	9.28		
Diethanolamine[b]	90	0.610		
	100	1.17		
	111	2.29	16.9±0.3	7.96±0.14
	120	3.50		
	130	6.30		

a) Concentration: a is about 0.400 M and b is about 0.040 M. b) Concentration: a is about 0.800 M and b is about 0.040 M. c) A is expressed by l/mol min.

TABLE 9. COMPARISON IN AMINATION RATES OF BENZYL CHLORIDE AND CUMINYL CHLORIDE[a)]

Amine	Solvent	Temp. °C	Chlodide	$k\times10^3$ l/mol min	k_{CC}/k_{BC}
Isobutyl	DMF	50	B C	9.97	
			C C	10.3	1.03
	Dioxane	90	B C	1.18	
			C C	1.23	1.04
s-Butyl	DMF	50	B C	3.79	
			C C	4.12	1.09
	Dioxane	90	B C	0.556	
			C C	0.583	1.05
2-Amino-butanol	DMF	50	B C	2.81	
			C C	3.03	1.08
Diethanol	DMF	40	B C	2.90	
			C C	3.17	1.09
Diethyl	DMF	30	B C	2.82	
			C C	3.22	1.14
Triethyl	DMF	50	B C	0.376	
			C C	0.490	1.30

a) In the table, BC represents for benzyl chloride and CC represents for cuminyl chloride.

resonance structure, associated with the phenyl substituent at the chloromethyl group. This conception has been examined by comparing the amination rate of benzyl chloride with that of phenethyl chloride, which has one methylene group between the phenyl group and the chloromethyl group. Table 8 lists the results of the amination of phenethyl chloride with 2-aminobutanol and diethanolamine. The amination rate of phenethyl chloride is considerably lower than that of benzyl chloride or CMPS; the former rate is almost comparable to those of the polymers without a phenyl group, as had been expected.

Amination of Cuminyl Chloride. In previous papers, benzyl chloride was chosen as a model of the structural unit of CMPS, and its amination rate was taken as a criterion. Another appropriate model of CMPS is cuminyl chloride, *p*-isopropyl chloromethyl benzene. The amination rates of cuminyl chloride with various amines have been measured; the rate constants are compared with those of benzyl chloride in Table 9. No significant difference is shown in the amination rate between the two chlorides in most cases. This result supports the propriety of benzyl chloride as a unit model of CMPS.

Amination of PVCA and Phenethyl Chlordie with Isobutylamine, s-Butylamine, and Diethylamine. As is shown in Tables 5, 6, and 8, the amination rates of PVCA, PVBA, and phenethyl chloride with 2-aminobutanol in DMSO are higher than the corresponding rates with diethanolamine. In the amination of CMPS and benzyl chloride in dimethyl formamide (DMF) and DMSO, however, the published data[4,5)] show that the amination rate with diethanolamine is higher than the rate with 2-aminobutanol. This difference in the reactivities of the two aminoalcohols is due to the difference in their enthalpy and entropy of activation, as will be discussed in the following section.

It will serve as a reference to examine the reactivities of some alkylamines in the amination of PVCA and phenethyl chloride and compare it with that in the amination of CMPS and benzyl chloride. In view of the data shown in Table 10, the reactivities of the amines decrease in the following order:

isobutyl>*s*-butyl>diethyl (PVCA; DMSO)
isobutyl>*s*-butyl≈diethyl (phenethyl chloride; DMSO)

TABLE 10. AMINATION OF PHENETYL CHLORIDE AND PVCA WITH ALKYLAMINES IN DMSO

Chloride	Amine	Temp. °C	k l/mol min
Phenethyl	Isobutyl	90	3.35×10^{-2}
	s-Butyl	90	1.09
	Diethyl	90	1.15
PVCA	Isobutyl	90	1.81×10^{-3}
		110	6.70
	s-Butyl	110	3.35
	Diethyl	110	2.29

On the other hand, in the amination of CMPS and benzyl chloride, the following order is given by the present author's previously published data.[5,8,9)]

diethyl>isobutyl>*s*-butyl (CMPS; DMF)
diethyl≈isobutyl>*s*-butyl (benzyl chloride; DMF)
isobutyl>*s*-butyl (CMPS, benzyl chloride; dioxane)

The order anticipated from the basicity of the amines is this: diethyl>isobutyl≈*s*-butyl, while the order anticipated from the steric hindrance in the transition state is: isobutyl>*s*-butyl>diethyl. Actually, the results indicate that isobutyl>*s*-butyl in all the cases; however, the reactivity of diethylamine is higher for CMPS and benzyl chloride and lower for PVCA and phenethyl chloride. The steric effect can be expected to be more significant for PVCA and phenethyl chloride than for CMPS and benzyl chloride, since the transition states in the amination of the former two are less polar and tighter than those of the latter two. The resonance in the transition states of the latter two, due to the phenyl substituent attached to the chloromethyl group, is thought to make their structures more polar and looser.

Activation Parameters. The activation parameters ($\Delta H^{\ddagger}$, $\Delta S^{\ddagger}$ and $\Delta G^{\ddagger}$) in the amination of PVCA, PVBA, PVCE, and phenethyl chloride are calculated and summarized in Table 11, in which the parameters of CMPS and benzyl chloride are also listed for comparison. The $\Delta G^{\ddagger}$ values of CMPS and benzyl chloride are much lower than those of the other polymers and phenethyl chloride. This difference in $\Delta G^{\ddagger}$ is due to the difference in $\Delta H^{\ddagger}$. In the amination of CMPS and benzyl chloride, the positive charge on the α-carbon of the chloromethyl group in the transition state can be delocalized because of the π-electrons of the phenyl group, and this resonance may lower the enthalpy of activation to a large extent.

The lower reactivity of PVCA than PVBA is contrary to expectation in view of the inductive effect of the halogen group. The lower $\Delta G^{\ddagger}$ of PVBA is due to the lower $\Delta H^{\ddagger}$. This difference in $\Delta H^{\ddagger}$ is considered

Table 11. Activation parameters of the aminations[a)]

Amine	Halide	Temp. °C	$\Delta H^{\ddagger}$ kcal/mol	$\Delta S^{\ddagger}$ e. u.	$\Delta G^{\ddagger}$ kcal/mol
2-Amino-	PVBA	100	16.1±0.1	−29.3±0.3	27.0
butanol	PVCA	100	18.9±0.2	−29.4±0.4	29.8
	PC	100	16.2±0.1	−31.9±0.3	28.1
	BC	25	11.9	−34.4	22.2
	CMPS	25	11.6	−36.2	22.4
Diethanol-	PVCE	100	17.5±0.2	−30.1±0.5	28.7
amine	PVBA	100	15.8±0.2	−31.3±0.6	27.5
	PVCA	100	18.2±0.1	−32.2±0.2	30.0
	PC	100	16.2±0.3	−32.7±0.7	28.4
	BC	25	11.2	−35.0	21.6
	CMPS	25	11.2	−35.4	21.7

a) In the table, BC and PC represent for benzyl chloride and phenethyl chloride respectively.

to reflect mainly the difference in bond energy between the α-carbon and the leaving halogen group. The effect of solvation on the leaving halogen group may be minor in such a dipolar aprotic solvent as DMSO, unlike protic solvents, though the solvation resulting from the mutual polalization may be stronger for bromide ions than chloride ions.

As is shown in Table 11, the $\Delta G^{\ddagger}$ of the amination with diethanolamine is lower than that with 2-aminobutanol for CMPS and benzyl chloride, and *vice versa* for PVBA, PVCA and phenethyl chloride. The $\Delta H^{\ddagger}$ of the amination with diethanolamine is lower than that with 2-aminobutanol not only for CMPS and benzyl chloride, but also for PVCA and PVBA. Further, the higher $\Delta G^{\ddagger}$ of the amination of PVCA and PVBA with diethanolamine can be ascribed to the lower $\Delta S^{\ddagger}$ of the amination with diethanolamine. In view of the basicity of the aminoalcohols, the amination rate with 2-aminobutanol can be expected to be higher than that with diethanolamine. The lower $\Delta H^{\ddagger}$ of the amination with diethanolamine may, then, be ascribed to a certain stabilizing factor in the transition state. A possible factor is the hydrogen bonding between the hydroxyl group of aminoalcohol and the leaving chlorine group, which is considered to be more significant in the amination with diethanolamine. The lower $\Delta S^{\ddagger}$ values in the amination of PVCA and PVBA with diethanolamine than the corresponding values with 2-aminobutanol can be explained in terms of such a steric fatcor as has been discussed in the preceding section. Since the transition state in the amination of the halide without a phenyl substituent at the α-carbon lacks the resonance effect, and since its structure is considered to be tighter than that with the phenyl group, the former may be more susceptible to the steric effect. Therefore, the reverse reactivity of 2-aminobutanol and diethanolamine in the amination of CMPS and polyvinyl haloacetals can be referred to the same steric effect which brings about the reverse reactivity of *s*-butylamine and diethylamine in the amination of CMPS and PVCA.

The author wishes to express his thanks to Dr. Masaya Yanagita for his valuable discussions. He is also grateful to Mr. Tsutomu Watabiki, Mr. Masaaki Kodera, and Mrs. Midori Shiraishi for thier helpful assistance in preparing the polymer and in carrying out the measurements.

References

1) I. Sakurada, A. Yamamoto, and Y. Sakaguchi, *Kobunshi Tenbo*, Coll. Vol. 6, Kobunshi Kagaku Kankokai Press, Kyoto (1952), p. 58.
2) Y. Motozato, H. Egawa I. Nagata, and N. Nakanishi., *Kogyo Kagaku Zasshi*, **60**, 472 (1957).
3) P. J. Flory, *J. Amer. Chem. Soc.*, **61**, 1518 (1939).
4) H. Kawabe and M. Yanagita, This Bulletin, **46**, 38 (1973).
5) H. Kawabe, *ibid.*, **47**, 2936 (1974).
6) H. Kawabe and M. Yanagita, *ibid.*, **44**, 896 (1971).
7) K. Noma, T. Kō, and T. Tsuneda, *Kobunshi Kagaku*, **6**, 439 (1949).
8) H. Kawabe and M. Yanagita, This Bulletin, **46**, 3267 (1973).
9) H. Kawabe, *ibid.*, **47**, 163 (1975).

Group Interactions in Polyelectrolytes. XI. The Kinetics of *N*-Methylation of Poly(ethyleneimine)

Hiroshi KAWABE

The Institute of Physical and Chemical Research, Wako-shi, Saitama 351

(Received March 6, 1975)

The *N*-methylation of polyethyleneimine (PEI) of low and high molecular weights as well as that of diethylenetriamine was investigated kinetically in 50% aqueous ethanol; during the procedure we observed deceleration due to the electrostatic effect of the neighboring charged groups. The rate equation was derived for the *N*-methylation of PEI, which proceeded in three steps with a marked deceleration beyond quarter-conversion and also beyond half-conversion. In the second and third steps of the *N*-methylation of PEI, additional energies equivalent to the electrostatic free energies due to the one and the two nearest-neighboring charged groups were required respectively, in addition to the intrinsic activation energy of the first step.

The amination of chloromethylated polystyrene with a large excess of primary and secondary amines was investigated kinetically in several organic solvents in order to establish that most of the amination with primary amines conformed to the ordinary second-order kinetics; however, the rate constant of the amination with secondary amines decreased as the amination proceeded.[1,2] Since no electrical charge forms on the polymer in this amination, the deceleration during the amination with secondary amine was ascribed to the steric obstruction by the neighboring substituted groups. On the other hand, a deceleration due to the electrostatic effect of the charge on the polymer was observed during the quarternization of the aminated chloromethylated polystyrene in 50% aqueous DMF.[2] Such a deceleration was also found in the quarternization of poly-4-vinyl pyridine with *n*-butyl bromide in tetramethyl sulfone or propyrene carbonate.[3] In these Menschutkin reactions of the polyamines, the deceleration was marked beyond half-conversion, and the reactions were treated kinetically as they proceeded in two steps. Although the *N*-methylation of ethylenediamine (EDA) with methyl iodide in water was not a Menschutkin reaction, the deceleration due to the electrostatic effect was also observed and the reaction could be described by the same kinetics as the quarternization of the aminated chloromethylated polystyrene.[4]

The *N*-methylation of diethylenetriamine (DETA), which has three amino groups, in 50% aqueous ethanol has been found to decelerate in three steps. Further, the *N*-methylation of polyethyleneimine (PEI), which has many amino groups, in 50% aqueous ethanol has also been found to proceed in three steps. These *N*-methylations have been investigated kinetically in the present study.

Experimental

Polyethyleneimine. Polyethyleneimine of a low molecular weight (PEI-L) was prepared by the cationic polymerization of ethyleneimine in dilute hydrochloric acid; the acid was removed by passing the reaction mixture through a column of Amberlite IRA-400 in the hydroxide form. The effluent was concentrated by the use of an evaporator and then lyophilized. Since this polymer was almost entirely absorbed in a column of Amberlite IRC-50 in the hydrogen form, its molecular weight was estimated to be relatively low.

Polyethyleneimine of a high molecular weight (PEI-H) was supplied by courtesy of the Nihon Shokubai Chem. Ind. Co. in a state of an aqueous solution (P-1000). The P-1000 was diluted and passed through a Dowex-50 (X-8, H-form) column and then through a Dowex-2 (X-8, OH-form) column, after which the effluent was concentrated and lyophilized.

Reagents. Commercial anhydrous ethylamine, ethylenediamine (EDA), and diethylenetriamine (DETA) of a reagent grade were treated with solid sodium hydroxide and distilled. Other organic solvents and reagents were also distilled before use. They were proved to be pure by their refractive indices. Deionized, decarbonized water was used throughout.

Kinetic Measurements. The procedure used for the kinetic measurements in the *N*-methylation of DETA and PEI was almost the same as that used for EDA.[4] The temperature of a reaction mixture, composed of an amine, methyl iodide, and a solvent, was maintained at 30±0.1 °C.

Conductometric Titration. Aqueous solutions of ethylamine, EDA, DETA, and PEI-L (0.010—0.016 amino group equivalent/l) were titrated with 0.1 M hydrochloric acid at 25+0.02 °C, and the conductivity measurements were made with the use of a Yanagimoto MY-7-type conductivity measuring set at 800 c.p.s.

Results

N-*Methylation of Diethylenetriamine (DETA).* In the *N*-methylation of DETA with methyl iodide in 50% aqueous ethanol, the second-order rate constant (k), computed on the basis of Eq. (1), decreased as the reaction proceeded:

$$kt = \frac{1}{a-b}\ln\frac{b(a-x)}{a(b-x)} \equiv \overline{kt} \qquad (1)$$

where a and b are the initial concentrations of the methyl iodide and the amino group respectively, and where x is the concentration of hydrogen iodide formed after time t. The course of the *N*-methylation is shown in Fig. 1, where β $(=x/b)$ is the fractional conversion and where $\overline{kt}$ represents the right-hand term of Eq. (1). The white circles in the figure represent the observed values of β, and the black circles, the values of $\overline{kt}$. The plot of $\overline{kt}$ *vs.* t could be represented approximately by three straight lines which intersect each other at $\beta\approx0.4$ and $\beta\approx0.65$. The apparent rate constants given by the slopes of these lines ($k_n' = \Delta\overline{kt}/\Delta t$) were:

$$k_1' = 5.66\times10^{-2},\quad k_2' = 2.03\times10^{-2}$$
$$k_3' = 8.83\times10^{-4}\ \text{l/mol min}$$

Although such reactions of compounds with two

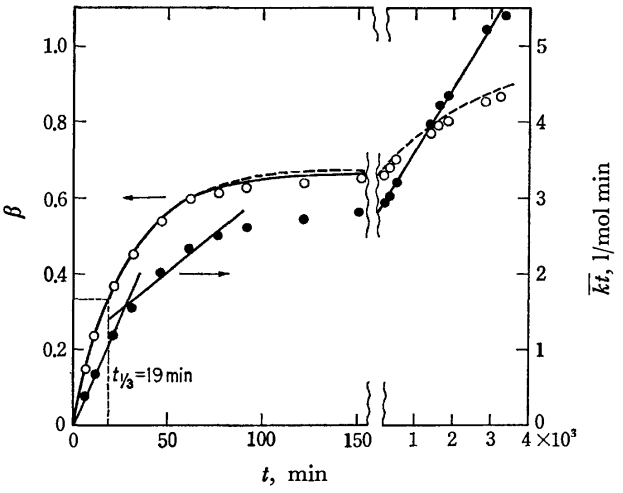

Fig. 1. *N*-Methylation of DETA with methyl iodide in 50% aq. ethanol at 30 °C. (a=0.3922, b=0.0362 mol/l)
—— Curve I, calculated on the basis of Eq. (5)
---- Curve II, calculated on the basis of Eq. (6).

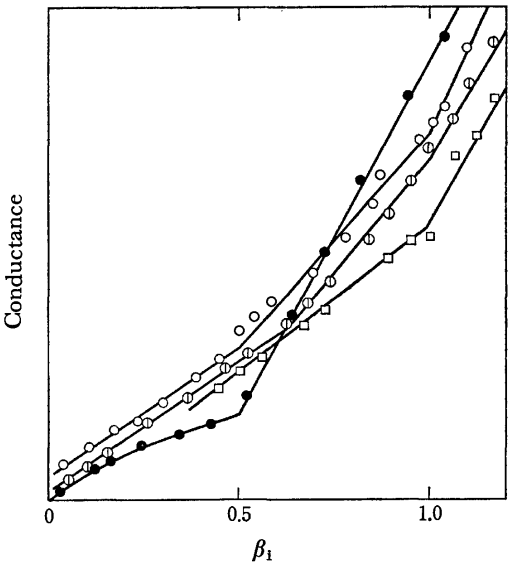

Fig. 2. Conductometric titration of PEI-L(●), DETA-(◑), EDA(○), and ethylamine(□) with hydrochloric acid.

reactive groups as the *N*-methylation of ethylenediamine (EDA)[4] and the alkaline hydrolysis of dimethyl succinate[5] could be treated as two-step reactions which decelerate markedly beyond $\beta=1/2$, the *N*-methylation of DETA, which has three reactive groups, may be treated as a three-step reaction which decelerates markedly at $\beta=1/3$ and $\beta=2/3$. The rate equation of this reaction is the same as that of the alkaline hydrolysis of triethyl citrate,[5] and the rate constants are given by:

$$k_1 = \frac{1}{[(3-2k_2/k_1)a-b]t} \ln \frac{1-\alpha}{1-(3-2k_2/k_1)\beta} \tag{2}$$

$$k_2 = \frac{\ln \dfrac{1-[3(2-k_3/k_2)/(4-k_3/k_2)\chi_1/b]}{1-[3(2-k_3/k_2)/(4-k_3/k_2)\beta]} \times \dfrac{1-\alpha}{1-\chi_1/a}}{[(2-k_3/k_2)a-(4-k_3/k_2)b/3](t-\tau_1)} \tag{3}$$

$$k_3 = (kt-C)/t \tag{4}$$

$$C = \ln[(1-\chi_2/a)/(1-\chi_2/b)] - k_2(a-b)\tau_2$$

where $\alpha=x/a$ and $\beta=x/b$; τ_1 is the time when the concentration of the first changed group (x_1) reaches approximately $b/3$, and χ_1 is the value of x at that time. C in Eq. (4) is a constant in a given reaction system. The calculated values of these constants were:

$k_1 = 6.08\times10^{-2}$, $k_2 = 4.77\times10^{-2}$,

$k_3 = 8.83\times10^{-4}$ l/mol min.

Further, when $a \gg b$, the course of this reaction can be calculated on the basis of the following two equations in the given ranges of β.
In the range of $\beta=0$—$2/3$:

$$\beta = \frac{2}{3} - \frac{3k_1-4k_2}{3(3k_1-2k_2)} e^{-3k_1at} - \frac{k_1}{3k_1-2k_2} e^{-2k_2at} \tag{5}$$

In the range of $\beta=1/3$—1:

$$\beta = 1 - \frac{2(k_2-k_3)}{3(2k_2-k_3)} e^{-2k_2a(t-t_{1/3})} - \frac{2k_2}{3(2k_2-k_3)} e^{-k_3a(t-t_{1/3})} \tag{6}$$

where $t_{1/3}$ is the value of t when $\beta=1/3$. The plot of β against t calculated on the basis of Eq. (5) is represented by the solid line (Curve I) in Fig. 1, from which $t_{1/3}$ is determined to be 19 min. The plot of Eq. (6) is represented by the broken line (Curve II) in the figure. The observed values represented by the white circles fall substantially on Curves I and II.

N-Methylation of Polyethyleneimine (PEI). Shepherd and Kitchener[6] reported that, although the pH titration curve of PEI of a relatively low molecular weight (number of monomeric units, n=35—40) could be described according to Katchalsky's theory[7] as a polybase with an intrinsic pK_0 value of 10 in a certain range of degree of ionization (β_1) (β_1=0.3—0.5), the titration curve deviated greatly from the theory in the $\beta_1>0.5$ range because of the intense electrostatic interaction due to two near-neighboring charged groups.

Figure 2 shows the results of conductometric titration of PEI-L (PEI of low molecular weight) with hydrochloric acid, in which a distinct inflexion point appears at β_1=0.5. The figure also shows the results for EDA and DETA, the inflexion points for which appear at β_1=0.5 and β_1=0.65 respectively, in addition to the points at β_1=1.0. For ethylamine, which has a single amino group, a distinct point appears only at β_1=1.0. These results for EDA and DETA are in accordance with the results of the *N*-methylation of the amines. The pH titration and the conductometric titration of PEI with a large molecular weight ($n\approx700$) were reported by Saber and Shams,[8] who found inflection points of the titration curves at β_1=0.6.

In view of the above-mentioned facts, the *N*-methylation of PEI is expected to decelerate markedly beyond $\beta=1/2$. On the other hand, it was found that the alkaline hydrolysis of polymethyl acrylate in 29% aqueous acetone decelerates at $\beta=1/4$, $1/2$, and $3/4$.[5,9] In the present study, PEI of low and high molecular weights (PEI-L and PEI-H) was *N*-methylated with methyl iodide, first in water; the results are shown in Fig. 3. The rate of the *N*-methylation becomes

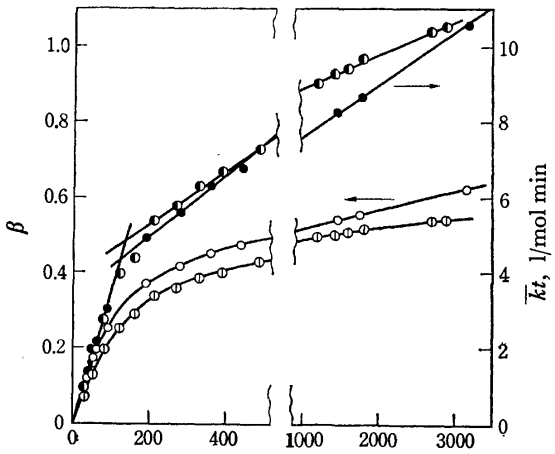

Fig. 3. *N*-Methylation of PEI with methyl iodide in water at 30 °C.
(PEI-L, $a=0.0831$, $b=0.0277$ mol/l; PEI-H, $a=0.984$, $b=0.0171$ mol/l)
◑,◐: PEI-L, ○,●: PEI-H.

very slow beyond half-conversion, as is to be expected; however, the plots of $\overline{kt}$ *vs.* t in the figure indicate additional intersecting points at $\beta=0.25$—0.3.

In the *N*-methylation of PEI in water, the complete kinetic measurements beyond $\beta=0.5$ were practically difficult because of its very slow rate; the solubility of methyl iodide in water was low, and its concentration was low. Therefore, PEI was also *N*-methylated in 50% aqueous ethanol; when the concentration of methyl iodide was increased, the *N*-methylation proceeded nearly to completion. The results are shown in Figs. 4 and 5, where white and black circles represent the observed values of β and $\overline{kt}$ respectively. The plot of $\overline{kt}$ *vs.* t is represented approximately by three straight lines which intersect each other nearly at $\beta=1/4$ and $\beta=1/2$. The plot in the range of $\beta=0.5$—0.85 is a straight line showing no inflection point, though an intersecting point at nearly $\beta=3/4$ in addition to those at $\beta=1/4$ and $1/2$ was observed in the case of the alkaline hydrolysis of polymethyl acrylate.

The numerical values of k_n' obtained as the slopes of the $\overline{kt}$ *vs.* t plots in Figs. 3, 4, and 5 are tabulated in Table 1. The values of k_n' are almost the same for PEI-L and PEI-H both in water and in 50% aqueous ethanol. This fact suggests, first, that the magnitude of the electrostatic effect of neighboring charged groups on the reactivity of amino groups of PEI at a given β value is almost independent of the molecular weight

Table 1. Rate constant k_n', l/mol min, in the *N*-methylation of PEI with methyl iodide at 30 °C

Solvent	Water		50% aq. Ethanol	
PEI	PEI-L	PEI-H	PEI-L	PEI-H
$k_1'\times10^2$	3.45	3.48	3.18	3.28
$k_2'\times10^3$	6.09	7.80	5.70	5.40
$k_3'\times10^4$	(8.10)[a]	(13.6)[a]	6.96	12.8

a) ( ) shows less acurate measurements.

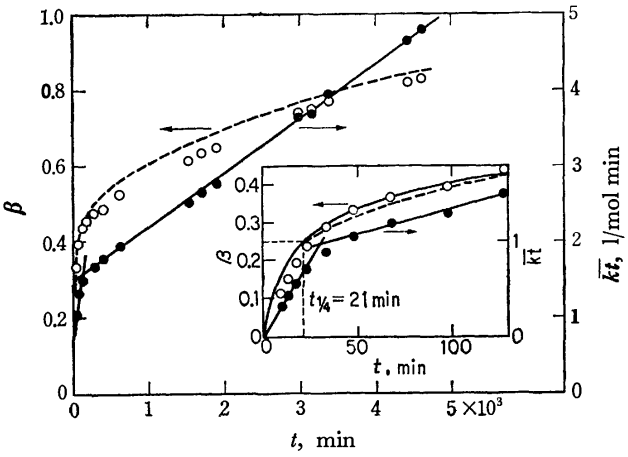

Fig. 4. *N*-Methylation of PEI-L with methyl iodide in 50% aq. ethanol at 30 °C. ($a=0.3922$, $b=0.0398$ mol/l)
—— Curve I, calculated on the basis of Eq. (12)
---- Curve II, calculated on the basis of Eq. (17).

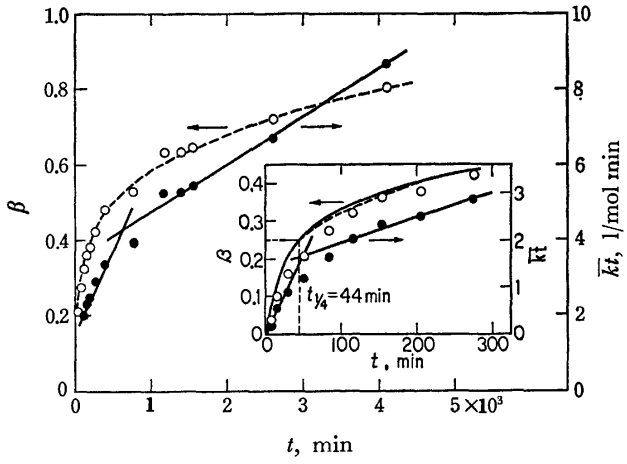

Fig. 5. *N*-Methylation of PEI-H with methyl iodide in 50% aq. ethanol at 30 °C. ($a=0.1976$, $b=0.0205$ mol/l)
—— Curve I, calculated on the basis of Eq. (12)
---- Curve II, calculated on the basis of Eq. (17).

of PEI. Second, a limited number of neighboring charged groups affect the reactivity, because the *N*-methylation of PEI as well as EDA and DETA is composed of a limited number of steps. Third, the dielectric constant of the microscopic environment surrounding the reactive groups is almost the same for the *N*-methylation both in water and in 50% aqueous ethanol.

Discussion

Kinetics of the N-*Methylation of PEI.* Since the *N*-methylation of PEI, unlike that of DETA, decelerates at $\beta=1/4$ and $\beta=1/2$, a somewhat different kinetic treatment is needed if we are to describe the former. In the following model compound composed of four reactive groups, the reactivity of X_2Y_2 is assumed to be the same as that of X_3Y namely $k_3=k_4$, since the reactivity of amino groups of PEI did not change in the $\beta>1/2$ range.

$$Y_4 \xrightarrow{k_1} X_1Y_3 \xrightarrow{k_2} X_2Y_2 \xrightarrow{k_3} X_3Y \xrightarrow[(=k_3)]{k_4} X_4$$

$$\mu_0 \qquad \mu_1 \qquad \mu_2 \qquad \mu_3 \qquad \mu_4$$

where X and Y represent the changed and unchanged groups respectively and where μ_0 and μ_n, represent the concentrations of the unchanged compound (Y_4) and the partially-changed one (X_nY_{4-n}), n groups of which have been changed at time t. These concentrations are given by the following:

$$\left.\begin{aligned}\mu_0 &= M - x_1 = (b/4) - x_1\\ \mu_n &= x_n - x_{n+1}\end{aligned}\right\} \tag{7}$$

where M is the initial concentration of the compound ($M=\sum_{n=0}^{4}\mu_n$) and where x_n is the concentration of the nth changed group at time t ($x=\sum_{n=1}^{4}x_n$).

The over-all rate of this reaction is given by the equation:

$$dx/dt = \sum_{n=1}^{4} dx_n/dt = (a-x)\sum_{n=1}^{4}(4-n+1)k_n\mu_{n-1} \tag{8}$$

The rate constants of this reaction, k_n, are given by the following equations on the assumption that $\sigma=4$ and $k_3=k_4$ (k_σ) in Eq. (6) of Ref. 5:

$$k_1 = \frac{1}{[(4-3k_2/k_1)a-3b/4]t}\ln\frac{1-\alpha}{1-(16/3-4k_2/k_1)\beta} \tag{9}$$

$$k_2 = \frac{\ln\dfrac{1-[2(3-2k_3/k_2)/(3-k_3/k_2)\chi/b]}{1-[2(3-2k_3/k_2)/(3-k_3/k_2)]\beta}\times\dfrac{1-\alpha}{1-\chi_1/a}}{[(3-2k_3/k_2)a-(3-k_3/k_2)b/2](t-\tau_1)} \tag{10}$$

$$k_3 = (\bar{k}t-C)/t \tag{11}$$

where C is a constant in a given reaction system; τ_1 is a time when $x_1=b/4$, and χ_1, a value of x at that time.

When $a \gg b$, on the assumption that the rate is substantially controlled by k_1 and k_2 in a range of $\beta=0$—$1/2$, β as a function of t is given by Eq. (12), which is the same equation as Eq. (3) in Ref. 9:

$$\beta = 1/2 - \frac{2k_1-3k_2}{2(4k_1-3k_2)}e^{-4k_1at} - \frac{k_1}{4k_1-3k_2}e^{-3k_2at} \tag{12}$$

In the range of $\beta=1/4$—1, the rate is given by Eq. (13), assuming that it is controlled by k_2 and k_3 ($=k_4$):

$$dx/dt = a[3k_2\mu_1+k_3(2\mu_2+\mu_3)] \tag{13}$$

On the assumption that $x_1=b/4$ and then $x=b/4+x_2+(x_3+x_4)$, μ_n is given by the following:

$$\left.\begin{aligned}&\mu_1 = x_1 - x_2 = b/4 - x_2\\ &\mu_2 = x_2 - x_3,\quad \mu_3 = x_3 - x_4\\ &2\mu_2 + \mu_3 = 2x_2 - (x_3+x_4) = b/4 + 3x_2 - x\end{aligned}\right\} \tag{14}$$

The combination of Eqs. (13) and (14) yields:

$$dx_2/dt = 3ka\mu_1 = 3k_2a(b/4-x_2) \tag{15}$$

$$dx/dt = a[(3k_2+k_3)b/4-3(k_2-k_3)x_2-k_3x] \tag{16}$$

By integrating Eqs. (15) and (16) we obtain:

$$\beta = 1 - \frac{3(k_2-k_3)}{4(3k_2-k_3)}e^{-3k_2a(t-t_{1/4})} - \frac{3k_2}{2(3k_2-k_3)}e^{-3k_3a(t-t_{1/4})} \tag{17}$$

where $t_{1/4}$ is the time when $\beta=1/4$. The over-all course of the reaction may be described by a combination of Eqs. (12) and (17).

Table 2. Rate constant k_n, l/mol min, in the *N*-methylation of PEI, DETA, and EDA with methyl iodide at 30 °C

Solvent / Amine	50% aq. Ethanol			Water
	PEI-L	PEI-H	DETA	EDA
$k_1\times10^2$	6.25	6.07	6.08	6.12
$k_2\times10^3$	9.00	9.15	47.7	13.0
$k_3\times10^4$	6.96	12.8	8.83	
k_2/k_1	0.14	0.15	0.78	0.21
k_3/k_1	0.011	0.021	0.015	

Table 3. Electrostatic free energies, kcal/mol, in the *N*-methylation of PEI, DETA, and EDA at 30 °C

Amine	PEI-L	PEI-H	DETA	EDA
$(\Delta G_{el}^{\neq})_2$	1.2	1.1	0.2	0.9
$(\Delta G_{el}^{\neq})_3$	2.7	2.3	2.6	

In Table 2 are tabulated the numerical values of k_n in the *N*-methylation of PEI-L and PEI-H in 50% aqueous ethanol, together with those in the *N*-methylation of DETA and EDA. The plots of β *vs.* t in the *N*-methylation of PEI, which are computed on the basis of Eq. (12), are the solid lines (Curve I) in Figs. 4 and 5, from which $t_{1/4}$ is determined to be 21 min for PEI-L and 44 min for PEI-H. The plots computed on the basis of Eq. (17) are represented by the broken lines (Curve II). The observed values represented by the white circles in the figures fall substantially on the curves; this suggests that the assumption used in the derivation of the rate equations is reasonable.

Electrostatic Interaction between Neighboring Groups in the N-*Methylation of PEI.* Since almost the same values of k_1 were obtained for PEI-L, PEI-H, DETA, and EDA, k_1 is taken to reflect the intrinsic reactivity of the amino group. The k_2 values of PEI are close to that of EDA, but different from that of DETA. However, the values of k_3 are almost the same for PEI-L, PEI-H, and DETA. The electrostatic free energies in these reactions, $(\Delta G_{el}^{\neq})_n$, are given by:

$$(\Delta G_{el}^{\neq})_n = RT\ln(k_0/k_n) \tag{18}$$

where k_0 is the intrinsic rate constant, $k_0=k_1$. The numerical values of $(\Delta G_{el}^{\neq})_n$ are shown in Table 3.

When the electrostatic interactions are assumed to be operative among only a few neighboring groups, $(\Delta G_{el}^{\neq})_n$ may be represented by:

$$(\Delta G_{el}^{\neq})_n = (Ne^2/D)\sum_i Z_i\bar{r_i} \tag{19}$$

where N is the Avogadro number: e, the unit of electrical charge; D, the dielectric constant ($D=81$); Z_i, the number of the electrical charge in the ith groups apart from the reactive group, and $\bar{r_i}$, the average distance between the reactive group and the ith group.

By setting the distance between the nitrogen atoms of EDA at 3.7 Å, $(\Delta G_{el}^{\neq})_2$ is calculated on the basis of Eq. (19) to be 1.1 kcal/mol, which is close to the value given in Table 3 calculated on the basis of Eq. (18).

However, the $(\Delta G_{el}^{\neq})_2$ value of DETA given in Table 3 is rather smaller than that given on the basis of Eq. (19), 0.6 kcal/mol, which is calculated by setting the distance between the end nitrogen atoms of the amine at 7.4 Å. The $(\Delta G_{el}^{\neq})_3$ of DETA is calculated to be 2.2 kcal/mol on the basis of Eq. (19) by assuming that the reactive group is affected electrostatically by the charges on the two end nitrogen atoms; this value is close to that given in Table 3. These results suggest that, in the *N*-methylation of polyethylene polyamine as well as DETA, the electrostatic contribution of the charge on the second-neighboring amino group is rather small, probably because the distance between these groups is so long that the effect of the second neighbors is cancelled by their counter ions. This can explain partly why the kinetic scheme of the *N*-methylation of PEI is somewhat different from that of the alkaline hydrolysis of polymethyl acrylate, in which the effect of the second-neighbors is distinct. The $(\Delta G_{el}^{\neq})_2$ value of PEI, which is close to that of EDA, is equivalent to the electrostatic free energy due to one first-neighboring charged group. The $(\Delta G_{el}^{\neq})_3$ of PEI, which is close to that of DETA, is equivelent to the electrostatic free energy due to two first-neighbors.

PEI, which is obtained by cationic polymerization, has a branched structure; the analysis of PEI indicates that approximately a quarter of all the amino groups are tertiary amino groups which correspond to branching points.[10] Consequently, in comparison with polymethyl acrylate, which has a linear structure, the structure of PEI is rather complex; however, the kinetics of the *N*-methylation of PEI has revealed that a limited number of neighboring groups interact electrostatically. In the *N*-methylation of PEI, composed of three steps, the first step is principally controlled by the intrinsic free energy of activation; however, the second step requires an additional free energy equivalent to the electrostatic effect of one nearest-neighboring group, and the third step requires an additional free energy equivalent to the effect due to two nearest-neighbors.

If the tertiary amino group of PEI, whose fraction is about 1/4, is finally *N*-methylated among all the species of amino groups, the reaction in the final stage will be accompanied by a larger $\Delta G_{el}^{\neq}$, because the tertiary group is apparently surrounded by three first-neighboring groups. Since the probability of this case is 1/4, and since its fractional contribution to the *N*-methylation of the total amino groups is 1/16, the deceleration due to this kind of interaction is significant, probably in the $\beta > 0.9$ range (at most). Actually, no such deceleration was observed, at least not in the range of measurements up to $\beta = 0.85$.

The author wishes to express his thanks to Dr. Masaya Yanagita for his valuable discussions. He is also grateful to Mrs. Midori Shiraishi for her helpful assistance in carrying out the kinetic measurements.

References

1) H. Kawabe and M. Yanagita, This Bulletin, **46**, 3627 (1973).
2) H. Kawabe, *ibid*, **47**, 2936 (1974).
3) R. M. Fuoss, M. Watanabe, and R. D. Coleman, *J. Polym. Sci.*, **43**, 5, (1960).
4) H. Kawabe and M. Yanagita, This Bulletin, **41**, 1518 (1968).
5) H. Kawabe and M. Yanagita, *ibid*, **42**, 3109 (1969).
6) E. J. Shepherd and J. A. Kitchener, *J. Chem. Soc.*, **1956**, 2448.
7) A. Katchalsky, N. Shavit, and H. Eisenberg, *J. Polym. Sci.*, **13**, 69 (1954).
8) T. M. H. Saber and A. M. Shams El Din, *J. Electroanal. Chem.*, **20**, 311 (1969).
9) H. Kawabe and M. Yanagita, This Bulletin, **44**, 310, (1971).
10) C. R. Dick and G. E. Ham, *J. Macromol. Sci.-Chem.*, **A4**(6), 1301 (1970).

The Partial Molal Volumes of Normal Chain Alcohols in Water-Ethanol Mixtures at 25 °C

Masahiro MANABE and Masaharu KODA

Department of Technical Chemistry, Niihama Technical College, Niihama, Ehime 792

(Received April 4, 1975)

The partial molal volumes ($\overline{V}^0$) of *n*-alcohols (R_mOH, $m=1-7$) at an infinitely dilute concentration in water-ethanol mixtures of various compositions have been determined by means of dilatometry. The $\overline{V}^0$ value does not depend on the concentration of the solute alcohol within the region studied in any composition of the solvent mixtures. The excess volume, the difference between $\overline{V}^0$ and the molal volume (V^0), is negative and is at a minimum in water-rich mixtures (<16 wt% ethanol) for all of the alcohols studied. On the other hand, in the moderate composition range the excess volumes for R_4OH and higher alcohols are positive and reach a maximum distinct from the disappearance of the maximum for R_3OH and lower alcohols. The volumetric contribution of a methylene group ($\overline{V}^{me}$) to $\overline{V}^0$ was separately evaluated. From the results, a linear relation was found between $\overline{V}^0$ and the alkyl chain length of the alcohols in the mixtures of 0—8 and 55—100 wt% ethanol, while in the mixtures the relationship was rather quadratic. Such volumetric behavior was discussed on the basis of the structural properties of the water-ethanol mixtures.

It is well known that a substance with alkyl groups such as surfactants or tetraalkylammonium halides shows anomalous behavior in the water-rich region of water-organic solvents (cosolvent) mixtures. For example, the critical micelle concentration (CMC)[1-3] and the Krafft point[4] of surfactants decrease with an increase in the content of such cosolvents as lower alcohols. Some of the phenomena can be interpreted on the basis of the structure-making effect of water, (hydrophobic interaction) upon the addition of the cosolvent. In more cosolvent-rich aqueous mixtures, however, the CMC increases, *via* a minimum, with the cosolvent content[5] and the micelle formation can not be detected at any specific composition of the mixture,[6,7] Ralston and Hoerr[8] investigated the solubility of dodecylammonium chloride in water-ethanol mixtures at various temperatures and found a maximum of solubility in a moderate composition range of the mixed solvent (*ca.* 40—80 wt% ethanol). Such a maximum solubility was attributed to the micelle formation.[9] Lee and Hyne[10] reported, after a study of the partial molal volume of tetraalkylammonium chlorides in water-ethanol mixtures, that the partial molal volumes of the cation showed a minimum at the 0.1 mol fraction of ethanol as well as a maximum at the 0.3 mol fraction, while that of the anion showed a minimum at the 0.3 mol fraction. These results were interpreted in terms of the structure of the solvent. A knowledge of the volumetric properties of model compounds, such as *n*-alcohols in water-cosolvent mixtures, will help us to understand the behavior of amphipathic compounds in the mixtures, mainly in relation to the structural effect of the mixtures. No systematic study of a homologous series over a complete concentration range of water-cosolvent mixrures has ever been reported.

In this study, we have determined the partial molal volume of *n*-alcohols, a typical homologous series, in water-ethanol mixtures by means of dilatometry, which is capable of determining the partial molal volume of a higher alcohol at a much lower concentration than it possible with the density method. We have attempted to see how the partial molal volume of *n*-alcohols and the contribution of a methylene group to it vary with the composition of the mixed solvent.

Experimental

A series of *n*-alcohols with 1—7 carbon atoms (R_mOH) was used in the present work. The lower alcohols ($m=1-4$) were distilled after refluxion over C_aO, while the higher alcohols were distilled under atomspheric or reduced pressures. They were confirmed to be pure by gas-liquid chromatography. The water used as the solvent was obtained by the distillation of water deionized with ion-exchange resin.

The dilatometer used for the measurement of the partial molal volumes of solute alcohols in water-ethanol mixtures is shown in Fig. 1. It consists of a glass bulb with a capacity of 120—200 ml, equipped with a magnetic roter coated with Teflon, a vertical uniform capillary (1.8 mm internal diameter), and an injection aperture which is sealed with a silicone rubber fixed with a metal fitting. The capillary was calibrated exactly with mercury. The dilatometer was filled with a mixed solvent of a given composition through a polyethylene tube fine and long enough to reach the bulb under pressure reduced by means of an aspirator to remove any dissolved air.[11] In each run, about 30 mg of R_mOH (weighing 1/100 mg) was injected through the injection aperture into the dilatometer by means of a microsyringe

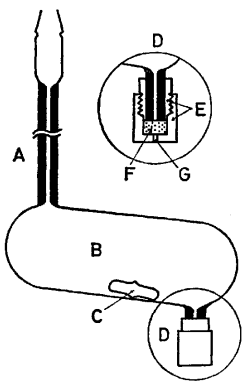

Fig. 1. Schematic diagram of dilatometer and its injection.
A: uniform capillary, 20 cm long and 1.8 mm internal diameter. B: grass bulb, capacity of 120—200 ml. C: magnetic roter. D: injection. E: metal fitting. F: silicone rubber. G: injection aperture.

TABLE 1. PARTIAL MOLAL VOLUMES OF *n*-ALCOHOLS IN WATER-ETHANOL MIXTURES AT 25 °C

Ethanol content (wt%)	Chain length						
	1	2	3	4	5	6	7
0	38.00	54.92	70.40	86.12	101.8_1	117.5_6	133.4_3
4	37.56	54.09	69.49	85.01	100.4_8	115.9_7	131.3_9
8	37.30	53.32	68.65	83.99	99.40	114.7_9	130.1_6
12	37.12	52.85	68.18	83.69	99.29	115.1_3	131.1_9
16	36.96	52.62	67.89	83.87	100.1_1	116.5_2	133.1_8
20	37.30	53.12	68.82	85.51	102.4_6	119.9_0	137.5_5
25	37.68	53.70	70.04	87.30	105.1_4	123.9_4	142.8_8
30	37.75	54.27	71.35	89.30	108.1_8	128.1_0	148.4_4
35	38.13	55.06	72.66	91.01	110.3_0	130.1_0	150.1_7
40	38.53	55.77	73.48	92.14	111.7_5	131.3_8	151.2_3
45	38.63	56.08	74.17	92.99	111.9_8	131.0_9	150.3_0
55	39.01	56.64	74.94	93.46	111.9_2	130.3_1	148.6_2
70	39.44	57.34	75.18	93.00	110.8_5	128.4_9	146.1_5
90	40.15	58.20	75.18	92.12	109.2_0	126.1_5	143.2_0
100	40.20	58.34	75.13	91.75	108.4_0	124.9_1	141.5_3
0[a]	38.05	54.97	70.20	85.77	101.92		
$\bar{V}^{\circ}$ [b]	40.74	58.69	75.38	92.07	108.76	125.46	142.15

a) Data from Ref. 14 (20 °C) b) The molal volumes of pure alcohols calculated from Eq. (1) except for R_1OH and the value of R_1OH was taken from Ref. 17.

five times successively. After each of the injections, the solution was stirred with a magnetic stirrer until the dissolution was complete.

The height of the meniscus of the solution in the capillary was read to 0.01 mm with a cathetometer. The partial molal volume of the solute alcohol could be calculated from the difference in the height of the meniscus and the quantity of alcohol added. The final concentration of the solute alcohol in any mixed solvent was far lower than its solubility in water.[12] The measurement was carried out at least two runs for each system. The standard deviations of these partial molal volumes were about 0.5% of their mean values.

All of the measurements were made at 25 °C in a water thermostat, the temperature of which was carefully controlled at ±0.001 °C.

Results and Discussion

Concentration Dependence of the Partial Molal Volume. No appreciable change in the partial molal volume of solute alcohol with its concentration was found within the limits of experimental error during one run in any water-ethanol mixture. Some illustrative examples for R_6OH are shown in Fig. 2. Franks and Smith[13] suggested that in the absence of solute-solute interactions, the apparent molal volume had no concentration dependence in the region of infinite dilution. The present measurements were carried out at very low concentrations, lower than 1 g/l. The mean value of the partial molal volumes of alcohols determined in water is in good agreement with the published values[14] obtained by extrapolating the density data to an infinite dilution. Therefore, the mean value can be regarded as the partial molal volume ($\bar{V}^0$) of the solute alcohol in an infinitely diluted solution; it is shown in Table 1.

Ethanol-Content Dependence of the Partial Molal Volume. It is well known that many physicochemical properties show anomalous behavior in a predominantly aqueous

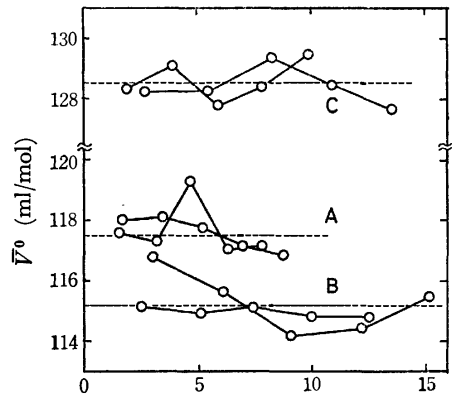

Fig. 2. Concentration dependence of $\bar{V}^0$ for R_6OH in water-ethanol mixtures. Experimental value (○), mean value (----). Ethanol content in wt%; A: 0, B: 12, C: 70.

composition range of water-lower alcohols binary systems.[15] Such behavior has generally been interpreted in terms of a structure-making effect, which continues up to a certain concentration of alcohol. The concentration dependence of the intensities of the X-ray diffraction band for water-cosolvent mixtures directly reveals the structural property; the high-intensity peak in a dilute aqueous solution of ethanol confirms the concept of a structure-making effect, and for the water-dioxane system the intensities falling below those calculated on the basis of additivity suggest a water-structure-breaking effect of dioxane.[16] The first derivatives of the viscosity-concentration curve, $d\eta/dC$, for the water-ethanol system increase to a maximum as the ethanol concentration increases; this fact suggests a structure-making effect. In the water-dioxane system, $d\eta/dC$ decreases with an increase

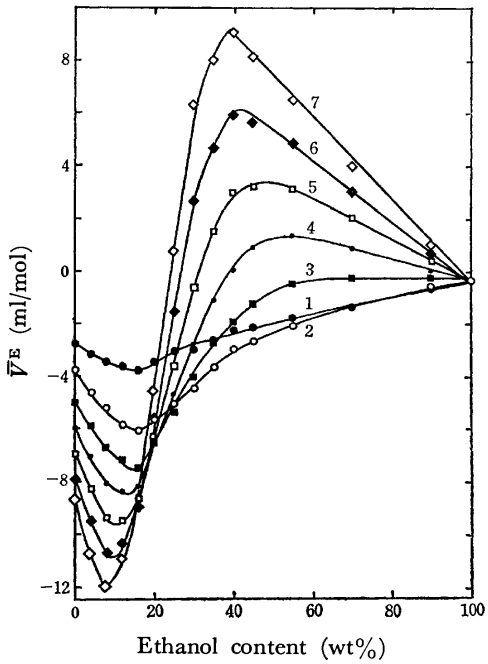

Fig. 3. The $\overline{V}^E$ values as a function of ethanol content in water-ethanol mixtures. The numbers indecate chain length of *n*-alcohols.

in the dioxane concentration, exhibition a structure-breaking effect, as has been pointed out by Franks.[5] The feature of the concentration dependence of the intensity of the X-ray diffraction band is in accordance with the dependence of the $d\eta/dC$ in both systems on the structural effect.

A comparison of the $\overline{V}^0$ values with each other and with V^0, a molal volume in the pure state for alcohols, makes it possible to calculate the excess molal volume ($\overline{V}^E$) from this definition, $\overline{V}^E=\overline{V}^0-V^0$, where V^0 is given by

$$V^0 = 16.69m + 25.30 \quad (m=2-7) \tag{1}$$

except for R_1OH. The two constants in this equation were determined by using the densities of pure alcohols reported in the literature.[17-19] The plots of $\overline{V}^E$ *vs.* the compositions of the water-ethanol mixtures are given in Fig. 3. The $\overline{V}^0$ values of R_2OH in the water–ethanol binary system are in good agreement with those obtained from the densities of the mixture.[20] The concentration dependence of $\overline{V}^E$ for R_2OH shows two distinct features. One is a negative dependence observed at lower ethanol concentrations (<16 wt% ethanol), and the other is a positive dependence observed at higher concentrations. The concentration at which the partial molal volume of R_2OH reaches its minimum is roughly compatible with that at which the intensity peak of the X-ray diffraction and the maximum of $d\eta/dC$ appear. Therefore, it may be concluded that the negative concentration dependence of $\overline{V}^E$ on R_2OH reflects a structure-making tendency, and the positive dependence of $\overline{V}^E$, a structure-breaking one. On the other hand, for the water-doxane system no such negative dependence of $\overline{V}^E$ on dioxane appears; only a positive one appears and the excess volume reaches positive values.[21] This may be attributed to the structure-breaking effect of dioxane.

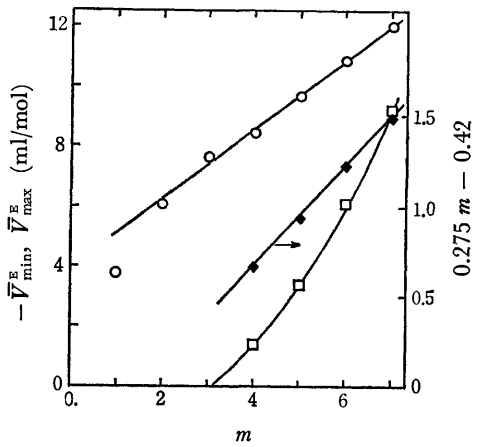

Fig. 4. Chain length dependence of $\overline{V}^E_{min}$ and $\overline{V}^E_{max}$.
○: $\overline{V}^E_{min}$, □: $\overline{V}^E_{max}$, ◆: $(\overline{V}^E_{max}+1.36)/m$,
——: $0.275\,m-0.42$, in Eq. (5).

Hardly no anomalous volumetric behavior for three-component systems has yet been reported.[10] In the present study, the system includes a very small quantity of the third component (*n*-alcohol), so that the interaction between solute molecules is negligible, judging from the independence of $\overline{V}^0$ of the solute concentration, as is shown in Fig. 2. Therefore, it may be considered that the added alcohol behaves volumetrically as a probe for the structuredness of a mixed solvent itself. As is shown in Fig. 3, the $\overline{V}^E$ values for all of the *n*-alcohols studied here are negative in the water-rich mixtures and decrease with an increase in the ethanol content (<16 wt% ethanol). This can be explained as follows: the solute alcohol is accommodated well in cavities which are formed with water molecules upon the addition of a small amount of ethanol in water, and the process of accommodation requires less space for the solute alcohol, leading to a decrease in the partial molal volume.

At a certain composition of ethanol, that at which the $\overline{V}^E$ value attains its minimum, the structuredness of the water–ethanol mixtures also reaches a maximum (8—16 wt% ethanol). The minimum value of $\overline{V}^E$, denoted by $\overline{V}^E_{min}$, exhibits a linear relation with the chain length of alcohols except for R_1OH, as is shown in Fig. 4. This relation may be expressed as:

$$\overline{V}^E_{min} = -1.17m - 3.86 \quad (m=2-7) \tag{2}$$

This relation may be converted into the following one for $\overline{V}^0_{min}$ by considering both Eq. (1) and the difinition of $\overline{V}^E$.

$$\overline{V}^0_{min} = 15.52m + 21.44 \quad (m=2-7) \tag{3}$$

where $\overline{V}^0_{min}$ is the minimum partial molal volume of a solute alcohol. This linear relation suggests that, at the specific composition of the mixed solvent where $\overline{V}^E$ reaches its minimum, the dissolved state of each methylene group is the same as that for the solute alcohol and the group occupies the cavities formed with water molecules in the same way. In other words, at the specific solvent composition the methylene groups may be dissolved into the corresponding state.

In the mixtures with moderate compositions of ethanol (8—55 wt%), the $\overline{V}^E$ value of the solute alcohol

increases with an increase in the ethanol content, while the value for R_4OH and higher alcohols becomes positive and reaches a maximum, denoted by $\overline{V}^E_{max}$, though the value for R_3OH and lower alcohols increases monotonously *i.e.*, $\overline{V}^E_{max}$ disappears, as is shown in Fig. 3. The increases in $\overline{V}^E$ for all of the alcohols with an increase in the ethanol content may contribute to the structure-breaking tendency of the solvent mixtures as the ethanol content increases. Such a volumetric behavior that $\overline{V}^E$ becomes positive and reaches a maximum value has not previously been known for any binary systems of water-lower alcohol mixtures. It may be due to the fact that higher alcohols are not sufficiently miscible with water. If a long-chain compound could be dissolved in water up to relatively high concentrations, such a volumetric behavior might appear even in the binary system, just as is seen in the water-dioxane binary system.[21] The appearance of $\overline{V}^E_{max}$ in the present ternary system means that the water–ethanol mixture at the composition corresponding to $\overline{V}^E_{max}$ has, essentially, a closer-packed structure around the solute alcohol molecule than any other mixture and pure ethanol. That is, the dissolution of the solute requires a maximum expansion of the solvent to accommodate the solute, with a consequent minimum free volume and $\overline{V}^E_{max}$ becomes higher as the size of the solute molecule increases. The plots of $\overline{V}^E_{max}$ against the chain length of alcohol are also shown in Fig. 4. The curve is concave upward, distinct from the linear relation between $\overline{V}^E_{min}$ and m, it may be expressed as in the following relation by the method of least squares in the second order:

$$\overline{V}^E_{max} = 0.275m^2 - 0.42m - 1.36 \quad (m=4-7) \tag{4}$$

This equation can then be rewritten as follows:

$$(\overline{V}^E_{max} + 1.36)/m = 0.275m - 0.42 \quad (m=4-7) \tag{5}$$

The value of the left-hand side falls on the straight line obtained from the right-hand-side values, as is shown in Fig. 4. When $\overline{V}^E_{max}=0$, $m=3.1$ from the equation; this value of m indicates the shortest chain length for $\overline{V}^E_{max}$ to appear, that is, for R_3OH and lower alcohols, the maximum of $\overline{V}^E$ does not appear. This finding does not conflict with the results shown in Fig. 3. That $\overline{V}^E_{max}$ is equal to zero means that the environment of the solute alcohol in the mixed solvent having a close-packed structure is volumetrically the same as that in pure ethanol, as is apparent from the definition of $\overline{V}^E$.

At a higher content of ethanol, the $\overline{V}^E$ values for all of the alcohols converge toward zero in pure ethanol with an increase in the ethanol content, as is shown in Fig. 3. This suggests that the properties of the water–ethanol mixtures come close to that of pure ethanol as the ethanol content increases. The fact that the $\overline{V}^E$ values for all of the alcohols in pure ethanol are equal to zero means that the mixing of any alcohol and ethanol is volumetrically ideal.

The compositions of the solvent at which $\overline{V}^E$ reaches its minimum and its maximum shift toward a lower ethanol content with an increase in the chain length of alcohols higher than R_3OH. In addition, the longer the alkyl chain length the larger $\overline{V}^E$ becomes.

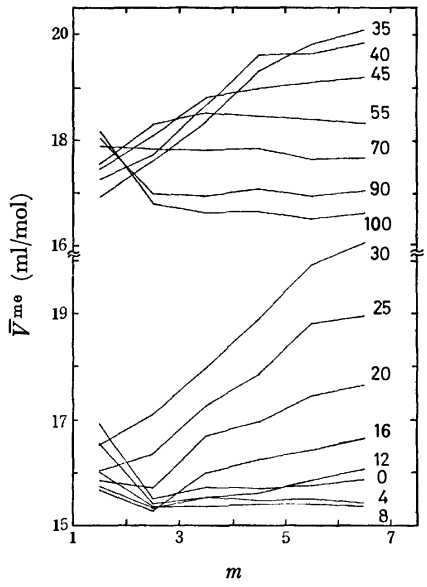

Fig. 5. Chain length dependence of $\overline{V}^{me}$ for *n*-alcohol. The numbers indecate the ethanol content in wt% in water-ethanol mixtures.

Such behavior can be discussed on the basis of the difinite volumetric contribution of the methylene group to the $\overline{V}^0$ of the solute alcohols.

Contribution of the Methylene Group to the Partial Molal Volume. The difference in $\overline{V}^0$ between two successive homologous alcohols is taken as the volumetric contribution of a methylene group ($\overline{V}^{me}$) to $\overline{V}^0$. Here, we will denote the contribution of the methylene group of a definite couple as $\overline{V}^{me}$ $(m, m+1)$, if necessary. The $\overline{V}^{me}$ value is plotted against the chain length, m, in Fig. 5; the features of the figure may be summarized as follows:

(I) $\overline{V}^{me}$ is independent of m in the mixtures at compositions lower than that at which $\overline{V}^E$ reaches its minimum (0—8 wt%).

(II) The increment in $\overline{V}^{me}$ is nearly linear with an increase in the chain length in the mixtures of 12—35 wt%.

(III) In the much more ethanol-rich region (40—100 wt%), $\overline{V}^{me}$ tends to be nearly constant with the methylene groups apart from the hydroxyl group in the alcohol molecule. The contribution of the methylene group obtained for both R_1OH and R_2OH, $\overline{V}^{me}$ (1, 2), is anomalous in the water or ethanol-rich mixtures compared with the moderate-content region. It is well known that various properties of *n*-alcohols usually have a linear dependence on the chain length. This is the case for $\overline{V}^{me}$ in water-rich and ethanol-rich mixtures, as is shown in Fig. 5. However, it is obvious from (II) that, in the mixtures with moderate compositions (12—35 wt%), $\overline{V}^0$ is the quadratic or the higher-order function of the chain length of the solute alcohol. In other words, even the methylene groups apart from the hydroxyl group in the alcohol molecule may be affected by the latter group. Therefore, the volumetric behavior of the alcohols in these mixtures is complex.

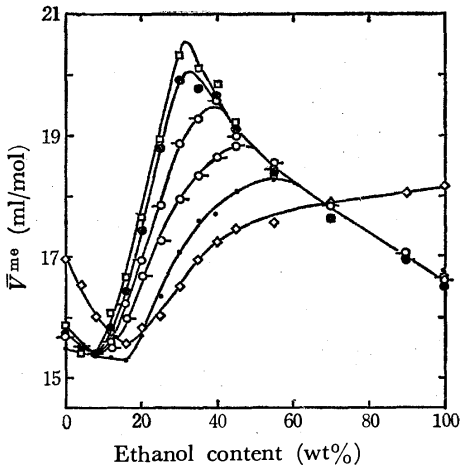

Fig. 6. The $\bar{V}^{me}$ values as a function of ethanol content in water-ethanol mixtures.
◇: (1,2), •: (2,3), ○-: (3,4), -○: (4,5),
●: (5,6), □: (6,7)
The numbers in parentheses indicate chain length of *n*-alcohols.

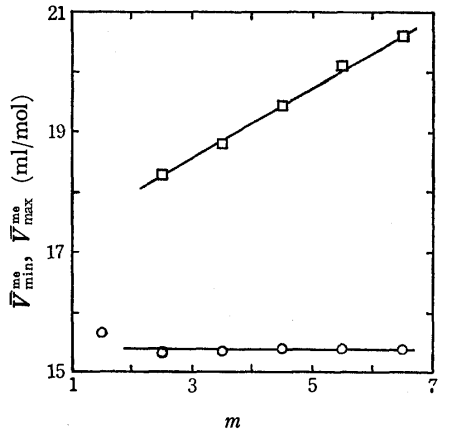

Fig. 7. Chain length depencence of $\bar{V}^{me}_{min}$ and $\bar{V}^{me}_{max}$.
○: $\bar{V}^{me}_{min}$, □: $\bar{V}^{me}_{max}$.

Figure 6 shows the relation between $\bar{V}^{me}$ and the ethanol content in the water-ethanol mixtures. The gross features of the curves are similar to those of the curves in Fig. 3; that is, the curve of $\bar{V}^{E}$ (1, 2) exhibits a minimum but no maximum and other curves in either case. It may be noted that the curve for $\bar{V}^{me}$ (2, 3) exhibits a maximum, although the curves for $\bar{V}^{E}$ of R_2OH and R_3OH exhibit no maximum in Fig. 3. The s-type curves except for that corresponding to lower alcohols gather to become a single line in the water and the ethanol-rich region, as may be seen from (I) and (II).

We denote the minimum and maximum of $\bar{V}^{me}$ in Fig. 6 as $\bar{V}^{me}_{min}$ and $\bar{V}^{me}_{max}$ respectively; then, $\bar{V}^{me}_{min}$ (1, 2) means $\bar{V}^{me}_{min}$ for the definite couple of R_1OH and R_2OH. The chain-length dependence of these values is shown in Fig. 7. It may be found from this figure that $\bar{V}^{me}_{min}$ is constant, 15.35 ml/mol, except for $\bar{V}^{me}_{min}$ (1, 2); this value is a little smaller than $d\bar{V}^{o}_{min}/dm$, 15.52 ml/mol, in Eq. (3). The ethanol content at which $\bar{V}^{me}_{min}$ appears is the same (8 wt%) for methylene groups further apart from the hydroxyl group. These features are different from the monotonous decrease in the ethanol content, during which $\bar{V}^{E}_{min}$ appears with an increase in the chain length, as is shown in Fig. 2. The chain-length dependence of $\bar{V}^{me}_{max}$ gives a linear relation;

$$\bar{V}^{me}_{max} = 0.58m + 16.83 \quad (m=2-7) \tag{6}$$

which is also shown in Fig. 7. The feature that the ethanol content of the mixture at which $\bar{V}^{me}_{max}$ appears decreases with the methylene group more apart from the hydroxyl group of the alcohol molecule is similar to that for $\bar{V}^{E}_{max}$ in Fig. 3. The appearance of $\bar{V}^{me}_{min}$ and $\bar{V}^{me}_{max}$ in the mixture must result from the structural effect of the mixture.

The authors wish to thank Professor Ryohei Matuura of Kyushu University and Assistant Professor Keishiro Shirahama of Saga University for their helpful discussions and advice.

References

1) K. Shinoda, T. Nakagaki, B. Tamamushi, and T. Isemura, "Colloidal Surfactants," Academic Press Inc., New York, N.Y. (1963), p. 69.
2) B. D. Flockhart, *J. Colloid Interface Sci.*, **12**, 557 (1957).
3) N. Nishikido, Y. Moroi, H. Uehara, and R. Matuura, This Bulletin, **47**, 2634 (1974).
4) K. Shirahama, M. Hayashi, and R. Matuura, *ibid.*, **42**, 1206 (1969).
5) F. Franks, "Physico-Chemical Processes in Mixed Aqueous Solvents," Heinemann Educational Books Ltd., London (1969), p. 50.
6) P. Becher, *J. Colloid Interface Sci.*, **20**, 728 (1965).
7) K. Deguchi, T. Mizuno, and K. Meguro, *ibid.*, **48**, 474 (1974).
8) A. W. Ralston and C. W. Hoerr, *J. Amer. Chem. Soc.*, **68**, 851 (1946).
9) K. Shirahama and R. Matuura, This Bulletin, **38**, 373 (1965).
10) L. Lee and J. B. Hyne, *Can. J. Chem.*, **46**, 2333 (1968).
11) G. Wada and S. Umeda, This Bulletin, **35**, 646 (1962).
12) K. Kinoshita, H. Ishikawa, and K. Shinoda, *ibid.*, **31**, 1081 (1958).
13) F. Franks and H. T. Smith, *Trans. Faraday Soc.*, **64**, 2962 (1968).
14) M. E. Friedman and H. A. Scheraga, *J. Phys. Chem.*, **69**, 3795 (1965).
15) F. Franks and D. I. G. Ives, *Quart. Rev.*, **20**, 1 (1966).
16) K. A. Covington and P. Jones, "Hydrogen-Bond Solvent Systems," Taylor & Francis Ltd. London (1968), p. 39.
17) "International Critical Table," McGrow-Hill Book Co. Inc., New York, N. Y. (1928), Vol. III.
18) "Bussei Josuu," Maruzen Publising Co., Tokyo (1971), Vol. 9 and (1972), Vol. 10.
19) J. A. Riddick and E. E. Toops, "Organic Solvents," Interscience Publishers, Ltd., London (1955).
20) Ref. 17) Vol. III, p. 116.
21) G. N. Malcolm and J. S. Rowlinson, *Trans. Fraaday Soc.*, **53**, 921 (1957).

Dufour Effect in Gases

A. BOUSHEHRI and S. AFRASHTEHFAR
Department of Chemistry, Pahlavi University, Shiraz, Iran
(Received December 6, 1974)

A study of the Dufour effect was made for five different gas mixtures: H_2–N_2, H_2–O_2, H_2–N_2O, He–N_2O and He–O_2. Measurements were made at 25 °C under 700 Torr. The values of the thermal diffusion factor were calculated for the above mixtures from the experimental data on the basis of the thermodynamics of irreversible processes.

The diffusion thermoeffect is perhaps the least investigated of the transport properties of gases. It involves the measurement of the transient temperature gradient which results from an initial concentration gradient as interdiffusion takes place. It is, of course, closely related to the inverse phenomenon of thermal diffusion. In this work five different gas mixtures are investigated. No previous measurements of the diffusion thermoeffect are known to have been made for H_2–N_2O, He–N_2O, and He–O_2 mixtures.

The effect was originally discovered by Dufour[1] in 1872, but not understood, until after its rediscovery by Clusius and Waldmann[2] in 1942. Rastogi and Madan[3] have recently studied the Dufour effect using a two-bulb interdiffusion apparatus with appropriately located thermocouples similar to the one used in the present work. Sawford *et al.*[4] and Mason *et al.*[5] have studied several aspects of the phenomenon in gases. A study of the temperature dependence of the diffusion thermoeffect was made by Boushehri.[6]

The Chapman-Enskog kinetic theory of this effect is well-known,[7,8] and provides a means of obtaining the thermal diffusion factor (α) from observations of the temperature difference as a function of time. The thermal diffusion factor was obtained very conveniently from the observation of the maximum temperature only. This maximum temperature difference occurs shortly after interdiffusion of the gases begins and there is thus no need to determine the temperature difference as a function of time which would be necessary if the Chapman-Enskog kinetic theory were used to calculate the thermal diffusion factor.

Theoretical Consideration

Our starting point is the well-known equation for the entropy production per unit volume (σ) in a motionless fluid of uniform density in which diffusion of matter and transfer of energy both occur[9]:

$$\sigma = J_{u,x}\frac{d}{dx}\left(\frac{1}{T}\right) - \sum_i J_{i,x}\frac{d}{dx}(\mu_i/T) \qquad (1)$$

where $J_{u,x}$ and $J_{i,x}$ are the energy flux density and mass flux density of component i in the x-direction (the "flux density" is defined as the amount of energy or mass crossing unit area perpendicular to the direction of flow—the x-axis-per unit of time); μ_i is the chemical potential per unit mass, and T is the absolute temperature. Equation (1) expresses the general idea that rate of production of entropy can be written as the algebraic sum of the product of "fluxes" and "forces" ($\sigma = J_k X_k$, where J_k has the form of a flux density and X_k—the thermodyanamic "force" has the general nature of a gradient).

It is convenient to write the entropy production in a different form. To do this, we begin with the relation:

$$d(\mu_i/T)/dx = (1/T)(d\mu_i/dx)_T - (H_i/T^2)(dT/dx)$$

where the specific enthalpy of component i is given by the Gibbs-Helmholtz equation:

$$H_i = -T^2[\partial(\mu_i/T)/\partial T]_p$$

We also introduce a new flux defined by

$$J_q = J_{u,x} - \sum H_i J_{i,x},$$

and Eq. (1) may then be written in the form:

$$\sigma = -\frac{J_q}{T^2}\frac{dT}{dx} - \sum \frac{J_i d\mu_i}{T dx} \qquad (2)$$

where J_i is an abbreviation for $J_{i,x}$. For a two-component system (i=1,2), Eq. (2) becomes

$$\sigma = -\frac{J_q}{T^2}\frac{dT}{dx} - \frac{J_1}{T}\frac{d\mu_1}{dx} - \frac{J_2}{T}\frac{d\mu_2}{dx} \qquad (3)$$

In this system, the two flows are not independent, since $J_1+J_2=0$. If we now use the Gibbs-Duhem equation,

$$C_1(d\mu_1/dx) + C_2(d\mu_2/dx) = 0$$

at constant temperature and pressure, Eq. (3) may be written as

$$\sigma = -\frac{J_q}{T^2}\frac{dT}{dx} - \frac{J_1}{C_2 T}\left(\frac{\partial \mu_1}{\partial C_1}\right)_{T,p}\frac{dC_1}{dx} \qquad (4)$$

where C_1 and C_2 are the mass fractions of components 1 and 2 respectively. Using the notation of Ref. 8, the mass fraction C_1 is related to the more familiar mole fraction n_{10} by

$$C_1 = \frac{n_{10}M_1}{n_{10}M + n_{20}M_2} \quad \text{and} \quad n_{10} = \frac{(C_1/M_1)}{(C_1/M_1)+(C_2/M_2)}$$

where M_1 and M_2 are the molar masses.

According to the linear thermodynamics of irreversible processes,[9] we may now write the phenomenological equations for the fluxes in terms of the thermodynamic forces:

$$J_q = -\frac{L_{qq}}{T^2}\frac{dT}{dx} - L_{q1}\frac{(\partial\mu_1/\partial C_1)}{C_2 T}\frac{dC_1}{dx} \qquad (5)$$

$$J_1 = -\frac{L_{1q}}{T^2}\frac{dT}{dx} - L_{11}\frac{(\partial\mu_1/\partial C_1)}{C_2 T}\frac{dC_1}{dx} \qquad (6)$$

In Eqs. (5) and (6), the forces and fluxes have been chosen from the expression(4) for the entropy production. The L's are the phenomenological coefficients. Although Truesdell has shown[10] that one cannot assume the validity of the Onsager reciprocal relations in general situations, it seems that we are justified

in doing so here.[11] Thus,

$$L_{1q} = L_{q1} \tag{7}$$

The phenomenological equations, when heat conduction and diffusion are considered separately, become

$$J_q = -\frac{L_{qq}}{T^2}\frac{dT}{dx}$$

$$J_1 = -\frac{L_{11}(\partial\mu_1/\partial C_1)}{C_2 T}\frac{dC_1}{dx}$$

These equations may be compared with Fourier's law for heat conduction [$J_q=-\lambda(dT/dx)$] and Fick's law for diffusion [$J_1=-\rho D_{12}(dC_1/dx)$] to yield expressions for the heat conductivity(λ) and diffusivity (D_{12}) coefficients:

$$\lambda = L_{qq}/T^2 \tag{8}$$

$$D_{12} = \frac{L_{11}(\partial\mu_1/\partial C_1)}{\rho C_2 T} \tag{9}$$

where ρ is the total mass density ($\rho=\rho_1+\rho_2$). We can also obtain a relationship involving the thermal diffusion factor by considering Eq. (6) [with $J_1=0$ in the stationary state] in conjunction with the difinition[7,8] [$(dC_1/dx)=-\alpha C_1 C_2 T^{-1}(dT/dx)$] of the thermal diffusion factor, α. Thus,

$$L_{1q} = L_{11}(\partial\mu_1/\partial C_1)_{T,p} C_1\alpha \tag{10}$$

We are now in a position to consider the Dufour effect. Suppose two gases (labelled with subscripts 1 and 2), initially at the same temperature, diffuse into each other. Equation (5), with the help of Eqs. (7), (8), and (9), then becomes:

$$J_q = -\lambda\frac{dT}{dx} - \rho_1\left(\frac{\partial\mu_1}{\partial C_1}\right)_{T,p} D_{12}\alpha\left(\frac{dC_1}{dx}\right) \tag{11}$$

From the difinition of J_q, it is apparent that it reduces to J_u in the limit when J_i approaches zero. By the conservation of energy, in the absence of convection, we have

$$\rho C_p\left(\frac{\partial T}{\partial t}\right) = -\frac{dJ_q}{dx}$$

where C_p is the constant pressure heat capacity of the mixture and $(\partial T/\partial t)$ is the variation of the temperature with time. Putting Eq. (11) into this equation, we obtain

$$\rho C_p\left(\frac{\partial T}{\partial t}\right) = \frac{d}{dx}\left[\lambda\frac{dT}{dx} + \rho_1\left(\frac{\partial\mu_1}{\partial C_1}\right)_{T,p} D_{12}\alpha\frac{dC_1}{dx}\right]$$

At the maximum temperature difference, ΔT_{max}, $(\partial T/\partial t)=0$. This condition holds in general when

$$\lambda\frac{dT}{dx} + \rho_1\left(\frac{\partial\mu_1}{\partial C_1}\right)_{T,p} D_{12}\alpha\frac{dC_1}{dx} = K \tag{12}$$

where K is a constant which depends on the geometry of the diffusion apparatus (in particular, the position of the thermocouples) and must be determined experimentally. It is possible to leave $K=0$ as Rastogi and Madan[3] did, but this is not the most general case.

Equation (12) can be put into a form suitable for calculating the thermal diffusion factor, α, from the maximum temperature difference, ΔT_{max}. We shall assume that the gases which interdiffuse are ideal, in so far as the expression for the chemical potential is concerned:

$$\mu_1 = \mu_1^\circ(T) + \frac{RT}{M_1}\ln\left[P(C_1/M_1)/(C_1/M_1+C_2/M_2)\right] \tag{13}$$

where μ_1° (T) is equal to a constant which is a function of temperature alone.

This equation may be substituted into Eq. (12) to give:

$$\lambda\frac{\Delta T}{\Delta x} + \frac{\rho_1 RTD_{12}\alpha}{C_1[M_1-C_1(M_1-M_2)]}\frac{\Delta C_1}{\Delta x} = K \tag{14}$$

where we have replaced differentials by finite changes, since the effect under consideration is very small (ΔT is written here in place of ΔT_{max}, and ΔT_{max} is usually less than 0.5 °C). Δx is the distance between the thermocouples.

Experimental

The apparatus used in the diffusion thermoeffect measurements was similar to that of Boushehri.[6] The apparatus consisted of two double-walled glass bulbs (50-ml capacity each) with a five junction thermocouple in each. The distance between the thermocouples (Δx) was 18.5 cm. The bulbs were connected *via* a stopcock having a bore of 8 mm in diameter. All runs were made at 25 °C under 700 Torr. The annular space between the double walls of the bulbs was evacuated to minimize heat loss. The maximum temperature difference between the thermocouples was obtained after the stopcock connecting the half cells was opened and interdiffusion was allowed to occur. The gases were supplied by the Fluka company and were used without further purification, since the results were not expected to be sensitive to small impurities. The minimum purity was at least 99.9%. The calculations were carried out at the Computer Center of Pahlavi University using the IBM 370 model 135.

Results and Discussion

Measurements were made at 25 °C and 700 Torr. It was observed that the temperature of the half-cell containing the lighter component always rose. The values of maximum temperature difference, $(\Delta T)_{max}$, are given in Table 1. No measurements of $(\Delta T)_{max}$ other than pure gases were carried out.

Equation (14) can be used to obtain α from ΔT_{max} provided that ΔC_1 is known together with the heat conductivity (λ), density (ρ_1) and diffusion coefficient (D_{12}). The apparatus constant K is usually eliminated by using a relative method, *i.e.* by performing the experiment with a pair of gases of known α. By knowing the time (typically a few seconds after initiating the diffusion process) at which ΔT reaches its

Table 1. Dufour effect in gaseous systems at 25 °C and 700 Torr

Systems	$(\Delta T)_{max}$ (in °C)	Warm side
$H_2 + N_2$	0.17	Hydrogen
$H_2 + O_2$	0.14	Hydrogen
$H_2 + N_2O$	0.25	Hydrogen
$He + N_2O$	0.19	Helium
$He + O_2$	0.11	Helium

Table 2. Thermal diffusion factors for gas mixtures

Systems	α, from Equation (14)	α, from Equation (8.2—50) of Ref. 13	α, from thermal diffusion measurements
$H_2 + N_2$	0.35	0.348	0.35
$H_2 + O_2$	0.45	0.332	0.33[a]
$H_2 + N_2O$	0.40	0.312	0.48[b]
$He + N_2O$	0.36	0.391	—
$He + O_2$	0.34	0.386	—

a) The value of α for H_2+O_2 was estimated using Fig. 3 of Nain and Saxena.[14] b) The value of α, for H_2+N_2O was estimated using Table 1 of El Nadi and Faragi for mean temperature 368 K.[15]

maximum value after the start of the experiment, Fick's second law of diffusion[12] can be used to obtain ΔC_1, assuming that D_{12} is known for the gases concerned. For λ and ρ_1, the values for the pure component were used, since typical values of ΔC_1 were little different from unity. The apparatus constant K was calculated to be 2.72×10^{-5} by setting the value of α equal to 0.35 for hydrogen–nitrogen mixture.[12] Since the apparatus geometry remained the same in all experiments, this value of K was used in estimating α for the other systems. These are shown in Table 2. It may be noted that the Dufour effect gives the value of α at specific temperature which is in one respect an advantage compared to the thermal diffusion measurements. The values of thermal diffusion factors for equimolar mixtures obtained from Eq. (8.2—50) of the treatise of Hirschfelder *et al.*[13] with those obtained directly from thermal diffusion measurements are also given in Table 2. The values of α obtained from irreversible thermodynamics of the Dufour effects are subject to several sources of error such as convective mixing effects in our experiments or to the use of pure component values of λ and ρ_1 in Eq. (14). Since diffusion apparatus is employed (with only the addition of an appropriately placed thermocouples), it seems that this approach could provide information on both the diffusion coefficient and the thermal diffusion factor in the same series of experiments.

The authors thank Dr. J. Soulati for the loan of some items of the apparatus, the Ministry of Higher Education Research Foundation, and the Department of Chemistry of Pahlavi University for the research facilities. One of us (S.A.), acknowledges a Research Scholarship he has received from the Graduate School during his graduate studies.

References

1) L. Dufour, *J. Chem. Soc.*, **26**, 835 (1873).
2) K. Clusius and L. Waldmann, *Naturwissenschaften*, **30**, 135 (1942).
3) R. P. Rastogi and G. L. Madan, *Trans. Faraday Soc.*, **62**, 3325 (1966).
4) B. L. Sawford, T. H. Spurling, and D. S. Thurley, *Aust. J. Chem.*, **23**, 1311 (1970).
5) E. A. Mason, L. Miller, and T. H. Spurling, *J. Chem. Phys.*, **47**, 1669 (1967).
6) A. Boushehri, *J. Chem. Eng. Data*, **19**, 313 (1974).
7) S. Chapman and T. G. Cowling, "The Mathematical Theory of Non-uniform Gases," 2nd ed., Cambridge Press, London (1952).
8) K. E. Grew and T. L. Ibbs, "Thermal Diffusion in Gases," Cambridge Press, London (1952).
9) S. R. de Groot and J. Mazur, "Non-Equilibrim Thermodynamics," North Holland Publishing Co., Amsterdam (1962).
10) C. Truesdell, "Rational Thermodynamics," McGraw-Hill Book Co., New York (1969).
11) I. Müller, *Arch. Rational Mech. Anal.*, **31**, 255 (1968).
12) W. Jost, "Diffusion in Solids, Liquids and Gases," Academic Press Inc., New York (1960).
13) J. O. Hirschfelder, C. F. Curtiss, and R. B. Bird, "Molecular Theory of Gases and Liquids," 2nd ed., John Wiley and Sons, New York (1964).
14) V. P. S. Nain and S. C. Saxena, *J. Chem. Phys.*, **51**, 1541 (1969).
15) M. El Nadi and N. Faragi, *J. Chim. Phys.*, **58**, 296 (1961).

Non-isothermal Studies of Adduct Molecules of Metallic Halides with Oxo-Compounds in Solid State. I.

N. Ray CHAUDHURI, S. MITRA, and G. K. PATHAK

Inorganic Chemistry Laboratory, Indian Association for the Cultivation of Science, Calcutta 700032, India

(Received August 23, 1974)

Non-isothermal studies of some adduct molecules of metallic halides with dioxane as the type $MX_2 \cdot y$(dioxane) in solid state, where M=Mn(II), Co(II), Ni(II), Cu(II), Zn(II) or Cd(II), X=Cl^- or Br^- and y=0.5—2, were carried out with a Derivatograph. These inorganic adduct molecules lose dioxane molecule in single or multiple steps on heating. Thermally stable intermediate products were isolated and characterised by elemental analysis and IR spectra. The activation energy for each step of decomposition of the adduct was evaluated from the analysis of TG, DTG and DTA curves. Enthalpy change was evaluated from the DTA peak area and the order of reaction was found to be unity for each step of decomposition. Thermal stability of the adducts was discussed.

The preparation and characterisation of inorganic adduct molecule with dioxane have been done by several groups of workers.[1–17] Recently, Barnes and Duncan[18,19] carried out thermal decomposition of dioxane adducts of some metal halides. They investigated the thermal properties of the adducts by thermogravimetry, differential enthalpic analyses *etc.*, but not by the simultaneous measurements of TG, DTG and DTA, and they did not evaluate activation energy and order of reaction for each step of decomposition of the dioxane adducts. The present work deals with thermal decomposition of several known and unknown dioxane adducts of some metal halides. The evaluation of activation energy for the decomposition of adducts was worked out simultaneously from TG, DTG and DTA curves. In addition to the evaluation of activation energy of decomposition, the present paper deals with the evaluation of order of reaction (n) and ΔH from DTA peak area. It also shows the effect on the change of cation and anion on the thermal properties of dioxane adducts.

Experimental

For the preparation of dioxane adducts of metal halides anhydrous dioxane in excess was added to the finely powdered anhydrous metal halides and the mixture was stirred for 24—48 hr under dry conditions. The mixture was kept in desiccator for slow evaporation of the excess dioxane. All the adducts were characterized by elemental analysis. The dioxane used was sufficiently purified and dried according to the standard procedure.[20]

The following adducts of metal halides were prepared:
1. $MnCl_2 \cdot 1D$ 2. $MnBr_2 \cdot 2D$ 3. $CoCl_2 \cdot 0.5D$ 4. $CoBr_2 \cdot 2D$
5. $NiCl_2 \cdot 1.5D$ 6. $NiBr_2 \cdot 2D$ 7. $NiBr_2 \cdot 1D$ 8. $CuCl_2 \cdot 0.75D$
9. $CuBr_2 \cdot 2D$ 10. $ZnBr_2 \cdot 1D$ 11. $CdCl_2 \cdot 0.5D$ 12. $CdBr_2 \cdot 1D$
where D denotes dioxane molecule.

A Paulik-Paulik-Erdey type MOM Derivatograph was used for thermal analysis. The particle size of the sample was within 150—200 mesh. Heating rate was about 1.5 °C/min. The volume of the sample in each case was same. Platinum crucible was used for thermal analysis. All these experiments were conducted in static air.

Results

The dioxane adducts of $MnCl_2$, $CoCl_2$, $NiCl_2$, $NiBr_2$, $CuCl_2$, $ZnBr_2$, $CdCl_2$, and $CdBr_2$ lose all dioxane molecules in a single step which is evident from their respective TG, DTG and DTA curves (Figs. 1—4). The adduct $MnBr_2 \cdot 2D$ loses dioxane molecule in two distinct steps forming stable $MnBr_2 \cdot 1D$ as an intermediate. $CoBr_2 \cdot 2D$ loses dioxane molecules in three steps, *i.e.*,

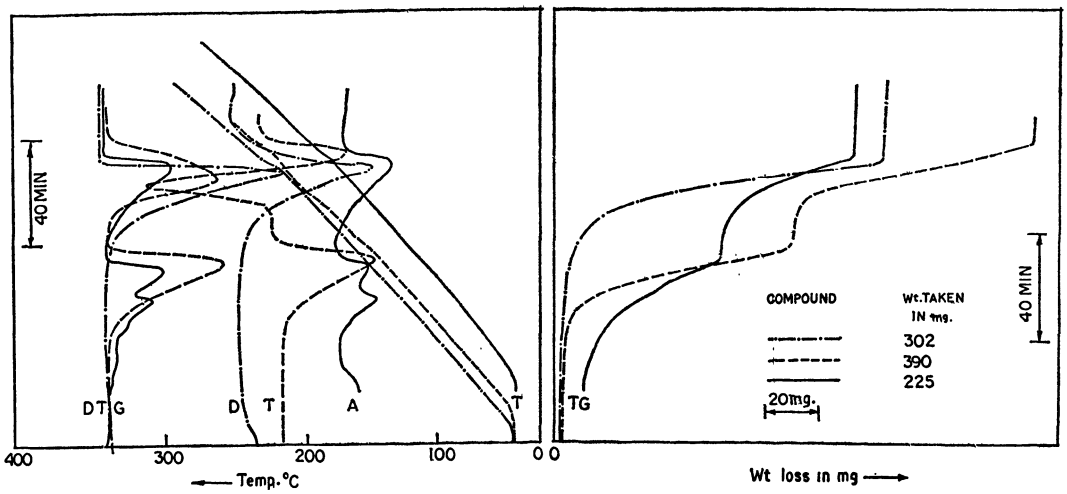

Fig. 1. The derivatograms for $MnCl_2 \cdot 1D$ (—·—·—), $MnBr_2 \cdot 2D$ (— — — —) and $CoBr_2 \cdot 2D$ (————).

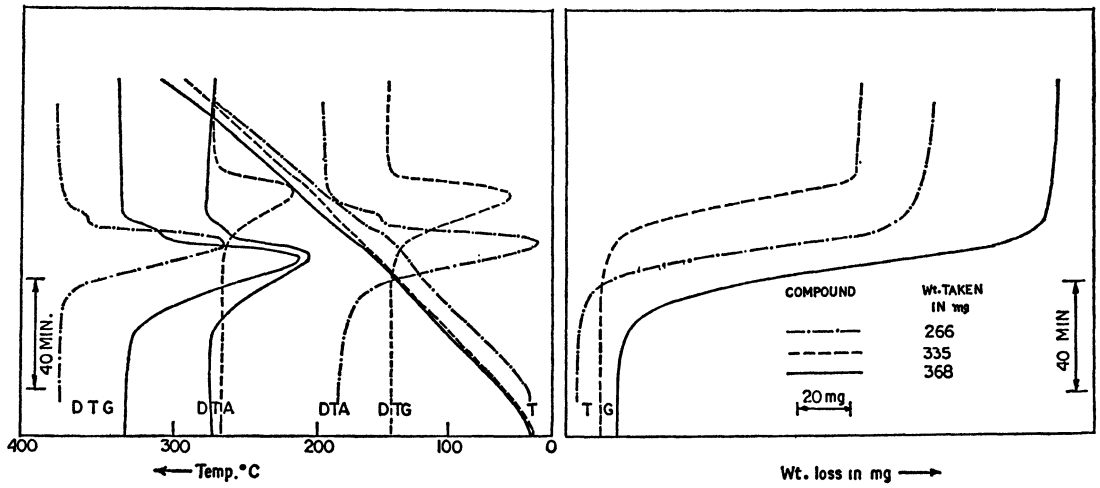

Fig. 2. The derivatograms for $NiCl_2 \cdot 1.5D$ (—·—·—), $NiBr_2 \cdot 1D$ (— — —) and $NiBr_2 \cdot 2D$ (———).

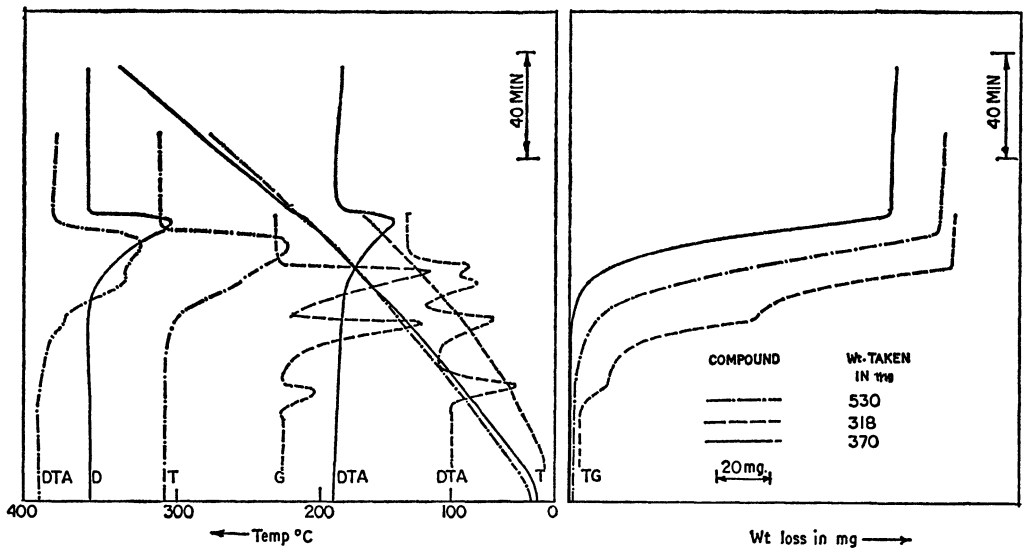

Fig. 3. The derivatograms for $CoCl_2 \cdot 0.5D$ (—·—·—), $CuBr_2 \cdot 2D$ (— — —) and $CuCl_2 \cdot 0.75D$ (———).

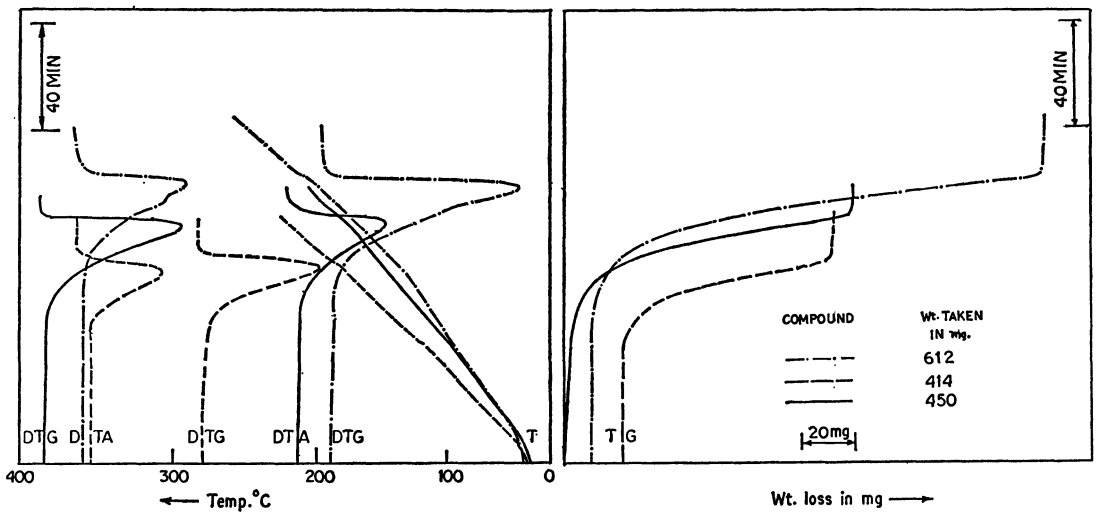

Fig. 4. The derivatograms for $ZnBr_2 \cdot 1D$ (—·—·—), $CdCl_2 \cdot 0.5D$ (— — —) and $CdBr_2 \cdot 1D$ (———).

$$CoBr_2\cdot 2D \xrightarrow{-0.5D} CoBr_2\cdot 1.5D \xrightarrow{-0.5D}$$

$$CoBr_2\cdot 1D \xrightarrow{-1D} CoBr_2$$

The first decomposition product $CoBr_2\cdot 1.5D$ is very unstable and second one is stable which is evident from its derivatogram (Fig. 1). Whereas, $CuBr_2\cdot 2D$ loses dioxane molecules in three steps, *i.e.*,

$$CuBr_2\cdot 2D \xrightarrow{-0.2D} CuBr_2\cdot 1.8D \xrightarrow{-0.8D}$$

$$CuBr_2\cdot 1D \xrightarrow{-1D} CuBr_2$$

All the intermediate products are unstable. DTA curve for the decomposition process of $CuBr_2\cdot 1D \rightarrow CuBr_2$ (Fig. 3) shows two overlapped endotherms. Whereas, its DTG curve indicates a single step of decomposition.

The decomposition of the adducts shows endotherm, except for tha of $MnBr_2\cdot 1D$ which shows an exotherm just followed by an endotherm in DTA curve. Temperature ranges of decomposition and the DTG peak temperatures for the adducts are listed in the second and third columns in Table 1, respectively.

Enthalpy change for each step of decomposition of the adducts was evaluated by the method of Sano[21,22] using copper sulfate pentahydrate as the standard and the values are tabulated in the last column in Table 1. When the two DTA peaks were too much overlapped with each other, the ΔH values were evaluated from the overall area of the DTA peaks concerned.

The activation energy for each step of decomposition of the adduct molecules was evaluated from the analysis of TG curves using Freeman and Carroll's[23] equation:

$$\frac{E_a}{2.3R}\Delta T^{-1}\Big/\Delta \log W_r = -n + \Delta \log \frac{dw}{dt}\Big/\Delta \log W_r,$$

where E_a is activation energy, n is order of reaction, T is absolute temperature, t is time, dw/dt is rate of weight loss with time, R is gas constant and W_r is weight loss at completion of reaction minus weight loss upto time t. The values are given in Table 1 and the corresponding curves are shown in Figs. 5 and 6. The order of reaction for each step of decomposition is unity.

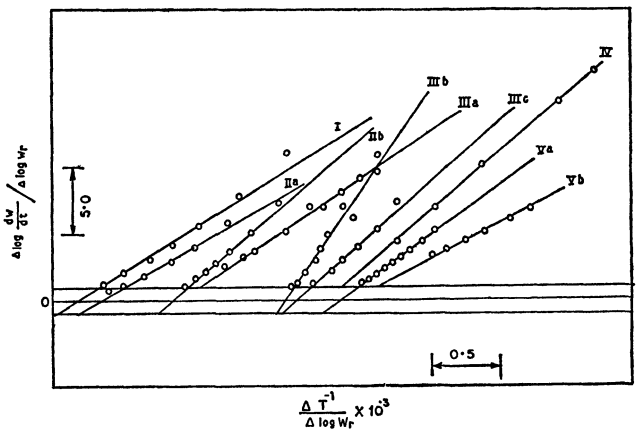

Fig. 5. Plots of $\Delta\log(dw/dt)/\Delta\log W_r$ *vs.* $\Delta T^{-1}/\Delta\log W_r \times 10^3$ from TG for the decomposition of $MnCl_2\cdot 1D \rightarrow MnCl_2$(I), $MnBr_2\cdot 2D \rightarrow MnBr_2\cdot 1D$(IIa), $MnBr_2\cdot 1D \rightarrow MnBr_2$(IIb), $CoBr_2\cdot 2D \rightarrow CoBr_2\cdot 1.5D$(IIIa), $CoBr_2\cdot 1.5D \rightarrow CoBr_2\cdot 1D$(IIIb), $CoBr_2\cdot 1D \rightarrow CoBr_2$ (IIIc), $NiCl_2\cdot 1.5D \rightarrow NiCl_2$(IV), $NiBr_2\cdot 1D \rightarrow NiBr_2$ (Va) and $NiBr_2\cdot 2D \rightarrow NiBr_2$(Vb).

Table 1. Thermal parameters for the decomposition of adduct molecules of some metallic halides with dioxane

	Decomposition reaction	Temp. range °C	DTG peak temp. °C	Activation energy E_a kcal/mol			Enthalpy change ΔH kcal/mol
				TG	DTG	DTA	
1.	$MnCl_2\cdot 1D \longrightarrow MnCl_2$	147.5—226	216	28.75	33.73	32.85	24.03
2a.	$MnBr_2\cdot 2D \longrightarrow MnBr_2\cdot 1D$	90 —155	142.5	26.83	28.75	28.75	12.51
b.	$MnBr_2\cdot 1D \longrightarrow MnBr_2$	170 —235	212	38.33	38.33	b)	b)
3.	$CoCl_2\cdot 0.5D \longrightarrow CoCl_2$	124.5—200	192	28.75	28.75	c)	20.59
4a.	$CoBr_2\cdot 2D \longrightarrow CoBr_2\cdot 1.5D$	30 — 80	83	30.60	c)	c)	20.74[a]
b.	$CoBr_2\cdot 1.5D \longrightarrow CoBr_2\cdot 1D$	84 —110	105	69.00	c)	c)	
c.	$CoBr_2\cdot 1D \longrightarrow CoBr_2$	128 —185	178	39.42	39.42	39.42	18.15
5.	$NiCl_2\cdot 1.5D \longrightarrow NiCl_2$	89 —205	144.5	34.50	34.50	34.50	32.86
6.	$NiBr_2\cdot 2D \longrightarrow NiBr_2$	84 —195	157.5	23.00	25.10	25.10	12.61
7.	$NiBr_2\cdot 1D \longrightarrow NiBr_2$	147.5—220	204	32.85	39.40	38.90	12.36
8.	$CuCl_2\cdot 0.75D \longrightarrow CuCl_2$	132 —217	209	31.50	31.50	31.50	7.76
9a.	$CuBr_2\cdot 2D \longrightarrow CuBr_2\cdot 1.8D$	36 — 50	50	c)	c)	c)	47.57
b.	$CuBr_2\cdot 1.8D \longrightarrow CuBr_2\cdot 1D$	55 — 93	89	34.50	38.30	38.30	14.16
c.	$CuBr_2\cdot 1D \longrightarrow CuBr_2$	93 —130	126	38.14	38.14	III	11.33
10.	$ZnBr_2\cdot 1D \longrightarrow ZnBr_2$	112 —224	200	26.20	26.20	26.20	11.73
11.	$CdCl_2\cdot 0.5D \longrightarrow CdCl_2$	120 —190	177	57.50	57.50	57.50	13.54
12.	$CdBr_2\cdot 1D \longrightarrow CdBr_2$	120 —185	177	30.66	30.66	30.66	16.24

a) Indicates overall enthalpy change. b) Activation energy and enthalpy change from DTA curve could not be evaluated due to irregular nature of the DTA peaks. c) Evaluation of activation energy was not possible due to much overlapping of the curves with each other.

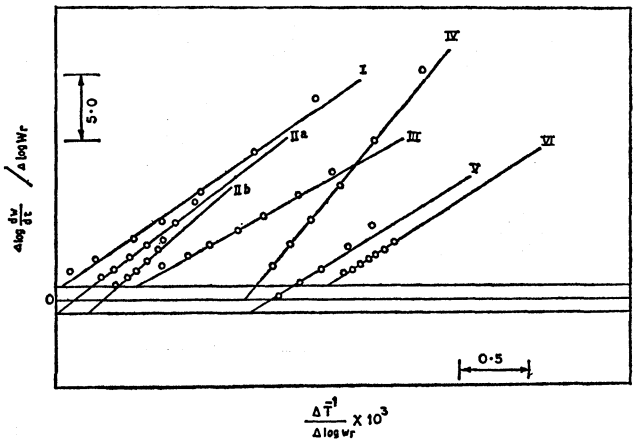

Fig. 6. Plots of $\Delta\log(dw/dt)/\Delta\log W_r$ *vs.* $\Delta T^{-1}/\Delta\log W_r \times 10^3$ from TG for the decomposition of $CuCl_2\cdot 0.75D \rightarrow CuCl_2$(I), $CuBr_2\cdot 1.8D \rightarrow CuBr_2\cdot 1D$(IIa), $CuBr_2\cdot 1D \rightarrow CuBr_2$(IIb), $ZnBr_2\cdot 1D \rightarrow ZnBr_2$(III), $CdCl_2\cdot 0.5D \rightarrow CdCl_2$(IV), $CdBr_2\cdot 1D \rightarrow CdBr_2$(V) and $CoCl_2\cdot 0.5D \rightarrow CoCl_2$(VI).

Activation energy for each step of decomposition was determined from the analysis of DTG curve using the method of Dave and Chopra.[24]

$$k = \frac{\left(\frac{A}{N_0}\right)^{n-1}\left(-\frac{dx}{dt}\right)}{(A-a)^n}$$

where N_0 is number of mol of sample at time t at which the DTG peak begins to appear, A and a are the total peak area and the area swept out till the time t, respectively, dx/dt is the displacement of the DTG curve from the base line and n is the order of reaction. The determination of order of reaction by this method is a trial and error process which amounts to calculating the rate constants corresponding to different values of n and finding out the best fitting curve for the Arrhenius plot which gives the value of n. In our work we found that by putting the value of the order of reaction $n=1$ (calculated from TG curve), we got the best fitting Arrhenius plot in all the cases. As a result

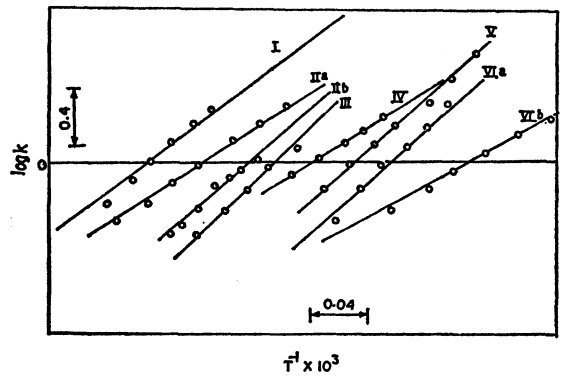

Fig. 7. Arrhenius plots, $\log k$ *vs.* $T^{-1}\times 10^3$, from DTG for the decomposition of $MnCl_2\cdot 1D \rightarrow MnCl_2$(I), $MnBr_2\cdot 2D \rightarrow MnBr_2\cdot 1D$(IIa), $MnBr_2\cdot 1D \rightarrow MnBr_2$(IIb), $CoBr_2\cdot 1D \rightarrow CoBr_2$(III), $CoCl_2\cdot 0.5D \rightarrow CoCl_2$(IV), $NiCl_2\cdot 1.5D \rightarrow NiCl_2$(V), $NiBr_2\cdot 1D \rightarrow NiBr_2$(VIa) and $NiBr_2\cdot 2D \rightarrow NiBr_2$(VIb).

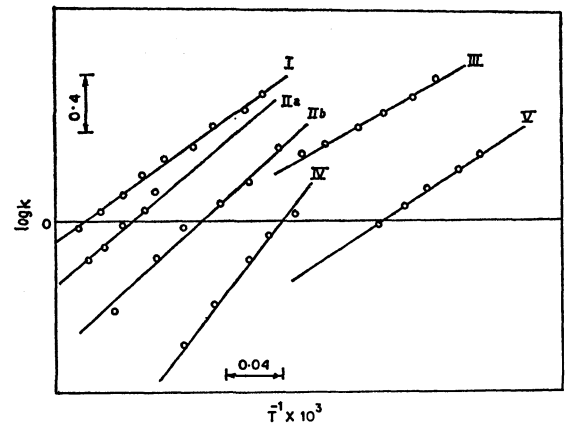

Fig. 8. Arrhenius plots, $\log k$ *vs.* $T^{-1}\times 10^3$, from DTG for the decomposition of $CuCl_2\cdot 0.75D \rightarrow CuCl_2$(I), $CuBr_2\cdot 1.8D \rightarrow CuBr_2\cdot 1D$(IIa), $CuBr_2\cdot 1D \rightarrow CuBr_2$(IIb), $ZnBr_2\cdot 1D \rightarrow ZnBr_2$(III), $CdCl_2\cdot 0.5D \rightarrow CdCl_2$(IV) and $CdBr_2\cdot 1D \rightarrow CdBr_2$(V).

we did not have to use the laborious trial and error method of Dave and Chopra. The values of the activation energies are given in Table 1 and the curves are shown in Figs. 7 and 8. We could not determine the activation energy by this method in some cases where the curves are too much overlapped.

Activation energy for each step of decomposition was also determined from the analysis of DTA curves using Brochardt equation[25] for first order reaction

$$k = \frac{C_p\frac{d\Delta T}{dt} + K\Delta T}{K(A-a) - C_p\Delta T}$$

where k is rate constant for the reaction, A is total DTA area, C_p is total heat capacity, K is cell constant, a is area at time t, $d\Delta T/dt$ expresses slope of the DTA curve at time t, ΔT is the displacement of the DTA curve from the base line at time t. As quantities $C_p\, d\Delta T/dt$ and $C_p\Delta T$ are, in general, small, the equa-

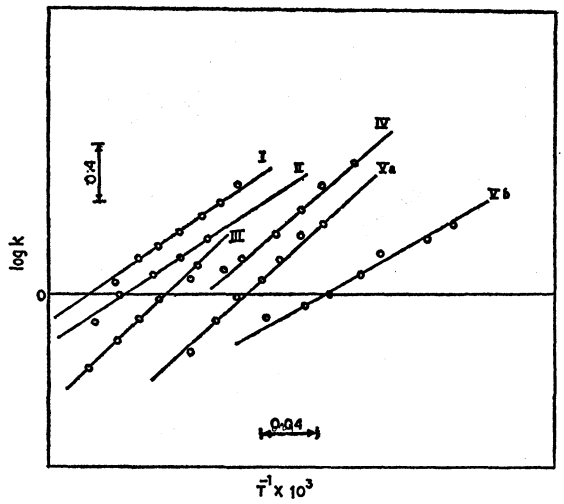

Fig. 9. Arrhenius plots, $\log k$ *vs.* $T^{-1}\times 10^3$, from DTA for the decomposition of $MnCl_2\cdot 1D \rightarrow MnCl_2$(I), $MnBr_2\cdot 2D \rightarrow MnBr_2\cdot 1D$(II), $CoBr_2\cdot 1D \rightarrow CoBr_2$(III), $NiCl_2\cdot 1.5D \rightarrow NiCl_2$(IV), $NiBr_2\cdot 1D \rightarrow NiBr_2$(Va) and $NiBr_2\cdot 2D \rightarrow NiBr_2$(Vb).

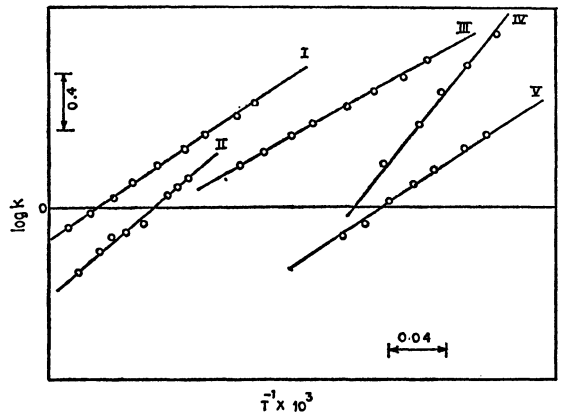

Fig. 10. Arrhenius plots, $\log k$ *vs.* $T^{-1} \times 10^3$, from DTA for the decomposition of $CuCl_2 \cdot 0.75D \rightarrow CuCl_2$(I), $CuBr_2 \cdot 1.8D \rightarrow CuBr_2 \cdot 1D$(II), $ZnBr_2 \cdot 1D \rightarrow ZnBr_2$-(III), $CdCl_2 \cdot 0.5D \rightarrow CdCl_2$(IV) and $CdBr_2 \cdot 1D \rightarrow CdBr_2$(V).

tion reduces to $k = \Delta T/(A-a)$. From the plot of $\log k$ *vs.* T^{-1} activation energy can easily be evaluated. The values are tabulated in Table 1 and the curves are shown in Figs. 9 and 10. Here also we could not determine the activation energy in some cases for too much overlapping of the DTA curves.

IR spectra of the adducts were taken to ensure the presence of dioxane molecule in the adducts.

Discussion

According to the observations by Barnes and Duncan[19] the adduct $MnBr_2 \cdot 2D$ loses all dioxane molecules in single step showing two overlapped endotherm. They could not isolate the intermediate product of composition $MnBr_2 \cdot 1D$. Whereas, we observed well-resolved DTA peaks for the two decomposition steps of $MnBr_2 \cdot 2D$ to $MnBr_2 \cdot 1D$ and of $MnBr_2 \cdot 1D$ to $MnBr_2$, the former showing an endotherm and the latter showing an exotherm followed by an endotherm in the DTA curve (Fig. 1). But the corresponding TG and DTG curves for the decomposition of $MnBr_2 \cdot 1D$ to $MnBr_2$ do not show any intermediate step. Earlier, dioxane adduct of $CoCl_2$ was known as $CoCl_2 \cdot 1D$. On the contrary, we isolated the adduct as $CoCl_2 \cdot 0.5D$ alone. The existence of $CoBr_2 \cdot 1.5D$, though not stable, was not pointed out earlier.[19] We isolated the adduct of $NiCl_2$ as $NiCl_2 \cdot 1.5D$, whereas, the composition of the adduct of the same salt was reported earlier[19] as $NiCl_2 \cdot 1D$. We could not isolate $NiBr_2 \cdot 1D$ from the thermal decomposition of $NiBr_2 \cdot 2D$ but isolated the same by keeping $NiBr_2 \cdot 2D$ in a vacuum desiccator for a long time. In case of $CuCl_2$ we repeatedly isolated the adduct $CuCl_2 \cdot 0.75D$ alone and never obtained 3 $CuCl_2 \cdot 2D$ and $CuCl_2 \cdot 2D$ reported earlier.[18] Whereas, dioxane adduct of $CuBr_2$ was reported by the same workers[19] as 3 $CuBr_2 \cdot 2D$ which showed single step of thermal decomposition. But we isolated the adduct as $CuBr_2 \cdot 2D$. In literature[1,19] two dioxane adducts such as $CdCl_2 \cdot 0.5D$ and $CdCl_2 \cdot 1D$ were reported. We could not isolate $CdCl_2 \cdot 1D$. The thermal decomposition of $CdCl_2 \cdot 1D$ reported earlier[19] did not show the existence of $CdCl_2 \cdot 0.5D$ from TG at any temperature.

The partial disagreement in our observations with those of the aforementioned works is possibly due to the difference in experimental conditions employed. Particular mention may be made of the wide difference of heating rate, *i.e.*, 8—10 °C/min used in the earlier works[19] compared to that of 1.5 °C/min used in our experiments.

DTG peak temperature for a series of adducts of the type $MBr_2(dioxane)_2$, where M is Mn(II), Co(II), Ni(II) or Cu(II), increases in the order: Cu(II) <Co(II) <Mn(II) <Ni(II) and for a series of adducts of the type MX_2dioxane, where M is Mn(II), Co(II), Ni(II), Cu(II), Zn(II) or Cd(II) and X is Cl^- or Br^-, increases in the order Cu(II) <Cd(II) <Co(II) <Zn(II) <Ni(II) <Mn(II). A similar order was found in the case of the decomposition of some pyridine 1-oxide coordination compounds.[26] Of the dioxane adducts of the halides of bivalent transition metal ion like Mn(II), Co(II), Ni(II) or Cu(II), the Mn(II) compound is thermally most stable. Among these metal ions Mn(II) is the hardest acceptor and oxygen donors like dioxane are hard donors. Naturally, dioxane will form the strongest donor acceptor bond with Mn(II) which is the hardest acceptor of the above series and the highest energy will be required to rupture the Mn(II)–dioxane bond.

It was observed that dioxane adduct of metal bromide is thermally less stable than the corresponding adduct of metal chloride. The value of enthalpy change for the decomposition of $CuBr_2 \cdot 1.8D \rightarrow CuBr_2 \cdot 1D$ is smaller than that for the first step of decomposition $CuBr_2 \cdot 2D \rightarrow CuBr_2 \cdot 1.8D$, though, in general, the latter step of decomposition gives larger ΔH value than the earlier step. It is noticed that the value of enthalpy change ranges from 7 to 47.5 kcal/mol.

Activation energies evaluated from TG, DTA and DTG do not differ much from each other, which shows that all the methods used for the evaluation of activation energies are standard. The differences in the activation energies of decomposition between the adducts do not show any systematic relationships with the kind or the nature of either cation (*i.e.*, the electronic configuration of the metal ion) or the anion.

In general, DTA curve shows endotherm for the decomposition of the similar type of adducts. This is seen in the decomposition of all the adducts except the decomposition of $MnBr_2 \cdot 1D \rightarrow MnBr_2$. Its nature of DTA and the corresponding TG and DTG curves possibly indicates some kinds of structural rearrangement at the beginning of the decomposition. The evolution of heat due to this rearrangement probably overcomes the endothermic effect due to decomposition at the beginning. This may explain the exotherm observed in the DTA curve.

The authors wish to express their hearty thanks to Dr. S.P. Ghosh, Research Officer of this laboratory for his kind discussion.

References

1) Sr. R. Juhasz and L. F. Yntema, *J. Amer. Chem. Soc.*, **62**, 3522 (1940).

2) P. M. Hamilton, R. Mcbeth, W. Bekebrede, and H. H. Sisler, *ibid.*, **75**, 2881 (1953).
3) A. E. Comyns and H. J. Lucas, *ibid.*, **76**, 1019 (1954).
4) R. F. Rolsten and H. H. Sisler, *ibid.*, **79**, 1068 (1957).
5) P. A. Mccusker, T. J. Lane, and S. M. S. Kennard, *ibid.*, **81**, 2974 (1959).
6) P. J. Kendra and D. B. Powell, *J. Chem. Soc.*, **1960**, 5105.
7) G. Vicentini, M. Perrier, and E. Giesbrecht, *Chem. Ber.*, **94**, 1153 (1961).
8) G. Vicentini, M. Perrier, W. G. R. DeCamargo, and J. M. V. Coutinho, *ibid.*, **94**, 1063 (1961).
9) M. Perrier, E. Giesbrecht, W. G. R. DeCamargo, and G. Vicentini, *ibid.*, **95**, 257 (1962).
10) A. M. Golub, O. O. Pisakaro'va, and L. D. Bogats'ka, *Fiz. ta Khim.*, **1**, 78 (1961).
11) G. Vicentini, J. V. Valarelli, M. Perrier, and E. Giesbrecht, *J. Inorg. Nucl. Chem.*, **24**, 1351 (1962).
12) E. Giesbrecht, W. G. R. DeCamargo, G. Vicentini, and M. Perrier, *ibid.*, **24**, 381 (1962).
13) G. Vicentini, M. Perrier, and E. Giesbrecht, *ibid.*, **26**, 2207 (1964).
14) B. E. Bridgland, G. W. A. Fowles, and R. A. Walton, *ibid.*, **27**, 383 (1965).
15) T. Gruhn and M. Gorman, *ibid.*, **27**, 482 (1965).
16) G. W. A. Fowles, D. A. Rice, and R. A. Walton, *J. Chem. Soc., A*, **1968**, 1842.
17) R. C. Maheshwari, S. K. Suri, and V. Ramakrishna, *Ind. J. Chem.*, **11**, 1196 (1973).
18) J. C. Barnes, *J. Inorg. Nucl. Chem.*, **31**, 95 (1969).
19) J. C. Barnes and C. S. Duncan, *J. Chem. Soc., A*, **1970**, 1442; **1972**, 923.
20) L. F. Fieser, "Experiments in Organic Chemistry," Second Ed., D. C. Heath and Co., Boston (1969), p. 368.
21) K. Sano, *Sci. Rep. Tohoku. Imp. Univ. 1st Ser.*, **24**, 719 (1936).
22) R. Tsuchiya, Y. Kaji, A. Uehara, and E. Kyuno, This Bulletin, **42**, 1881 (1969).
23) E. S. Freeman and B. Carroll, *J. Phys. Chem.*, **62**, 394 (1958).
24) N. G. Dave and S. K. Chopra, *Z. Phys. Chem.*, **48**, 257 (1966).
25) H. J. Brochardt and F. Daniels, *J. Amer. Chem. Soc.*, **79**, 41 (1957).
26) A. J. Pappas, F. A. Osterman, Jr., and H. B. Powell, *Inorg. Chem.*, **9**, 2695 (1970).

NOTES

BULLETIN OF THE CHEMICAL SOCIETY OF JAPAN, VOL. 48(8), 2381—2382 (1975)

The Proof of a Triplet Ground State in the *N,N'*-Di-*t*-butyl-*m*-phenylenebinitroxide Biradical

Kazuo MUKAI, Hiroshi NAGAI, and Kazuhiko ISHIZU*

Department of Chemistry, Faculty of Science, Ehime University, Matsuyama 790

(Received January 30, 1975)

Synopsis. The magnetic susceptibility of the *N,N'*-di-*t*-butyl-*m*-phenylenebinitroxide biradical has been measured in the temperature range from 60 to 300 K. The susceptibility follows the Curie-Weiss law, with a paramagnetic Curie constant of 0.90±0.04 K·emu/mol and a Weiss constant of −19±2 K. This susceptibility suggests that the ground state of the biradical is a triplet and that an intramolecular pure triplet approximation, $2J \gg kT$, is reliable in the temperature region below 300 K. The negative Weiss constant is due to the negative exchange interaction, $J'<0$, between the triplets.

Recently, Calder *et al.*[1] have succeeded in the synthesis of *N,N'*-di-*t*-butyl-*m*-phenylenebinitroxide, which is a fairly stable nitroxide biradical, as is shown in Fig. 1. The biradical has π-conjugated monoradical halves linked by a central phenylene π bridge, so the magnitude of the intramolecular spin-spin interaction in the biradical can be expected to be greater than those in σ-bridged nitroxide biradicals.[2,3] Actually, they observed a large ESR zero-field splitting in rigid media, indicating the existence of the triplet state in the biradical. They also proposed that the triplet is the ground state, from a study of the temperature dependence of the ESR signal intensity measured in the solid-state matrix. It is not very clear, however, from the above-mentioned results whether or not the observed triplet state is the ground state; there remains the possibility that they observed an excited triplet state which is thermally populated at that temperature; this would be true if the exchange interaction with a negative value, J, were smaller than the thermal excitation.

In order to clarify the level scheme of the spin system of the biradical, the magnetic susceptibility of the solid nitroxide biradial has been measured in the temperature range between 60 and 300 K.

In recent years, several stable π-conjugated bi- or tri-radicals, in which monoradical parts are linked with each other at the *meta*-position of a central phenyl group, have been prepared.[4-9] The existence of a triplet or quartet state in these radicals is also confirmed by ESR measurements in rigid media at 77 K.[6-11] However, the properties of the ground state in these radicals have not been fully established, except in the cases of a few radicals.[4,12] Studies of the temperature dependence of the static magnetic susceptibility are essential if we are to investigate the level scheme of the spin systems of these polyradicals.

* To whom correspondence should be addressed.

Experimental

The biradical was prepared by the method of Calder *et al.*[1] An orange crystalline compound (mp 67—69 °C) (lit, 68—70 °C) was obtained by the oxidation with silver oxide of the corresponding dihydroxylamine in purified chloroform and by subsequent rapid recrystallization from *n*-hexane in a dry-ice–acetone bath.

The susceptibility measurements were carried out with a Shimadzu-type MB-2 magnetic torsion balance, equipped with a low-temperature cryostat. The temperatures were measured using an AuCo-Cu thermocouple. Manganese Tutton salt was used for the calibration of the thermometers and the field gradient.

Results and Discussion

The inverse molar susceptibilities obtained for the nitroxide biradical are shown in Fig. 1 as a function of the temperature. The data have been corrected for the diamagnetic contribution of $\chi_{dia} = -0.17 \times 10^{-3}$ emu/mol calculated by Pascal's method. The susceptibility follows the Curie-Weiss law, with a Curie constant of 0.90±0.04 K·emu/mol and a Weiss constant of −19±2 K.

Calder *et al.*[1] have observed ESR spectra due to

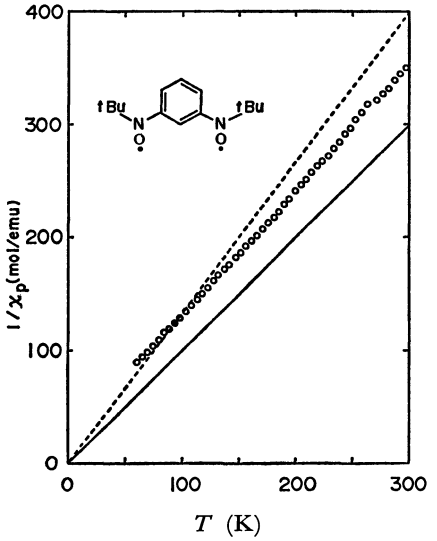

Fig. 1. Inverse molar susceptibility of *N,N'*-di-*t*-butyl-*m*-phenylenebinitroxide biradical *vs.* temperature. Solid and broken lines represent the Curie laws with Curie constants of 1.00 and 0.75 K·emu/mol, respectively.

transitions between the triplet states of the biradical in glassy media, as has been mentioned above. Therefore, the present susceptibility should be interpreted, in a first approach, by the singlet-triplet equilibrium (ST) model, in which the molar susceptibility is given by the following expression:

$$\chi_m = 2N_0g^2\beta^2/\{kT[3+\exp(-2J/kT)]\},$$

where the symbols have their usual meanings. At the high temperature limit, $|2J| \ll kT$, the susceptibility follows the Curie law and the Curie constant is 0.75 K·emu/mol from the above equation, regardless of the sign of the J parameter. This susceptibility corresponds to that of the noninteracting spin 1/2 particles. On the other hand, at the low-temperature limit, $|2J| \gg kT$, the Curie constant is 1.00 K·emu/mol for the positive J parameter. The positive exchange interaction requires the presence of the triplet ground state. This intramolecular triplet can behave as a pure triplet at low temperatures, because the exchange-interaction energy is much greater than the thermal excitation energy. If the J parameter is negative, the susceptibility falls off rapidly to zero after passing through its maximum at $T_{max} = -1.25\ J/k$. Accordingly, the Curie law does not hold in this temperature region.

Our experimental results show that the susceptibility of the biradical follows the Curie-Weiss law, with a Curie constant of 0.90 K·emu/mol in the temperature region below 300 K. This value is larger than the Curie constant of 0.75 K·emu/mol for noninteracting spin 1/2 particles, and is rather close to that of 1.0 K·emu/mol for pure triplet ($S=1$) ones. The discrepancy between the observed and calculated Curie constants for the pure triplet is probably due to the following two reasons: (i) the nitroxide biradical is not very stable and gradually changes to its diamagnetic aminoquinone imine *N*-oxide form by means of spontaneous topochemical change,[1] and (ii) the existence of a small amount of a monoradical impurity has been observed at the ESR spectra in a rigid solution at 77 K as a central singlet between the absorptions due to zero-field splitting.[1] These facts may explain the decrease in the Curie constant. The observed negative Weiss constant ($\theta = -19$ K) is due to the negative exchange interaction, $J' < 0$, between the triplets. All these results are very similar to those for *m*-phenylene-bis-verdazyl, whose magnetic susceptibility has also been explained as a contribution from its pure triplet ground state.[12]

References

1) A. Calder, A. R. Forrester, P. G. James, and G. R. Luckhurst, *J. Amer. Chem. Soc.*, **91**, 3724 (1969).
2) A. Nakajima, H. Ohya-Nishiguchi, and Y. Deguchi, This Bulletin, **44**, 2120 (1971). Other references are therein.
3) A. Nakajima, *ibid.*, **46**, 1129 (1973).
4) R. Kuhn, F. A. Neugebauer, and H. Trischmann, *Monatsh. Chem.*, **97**, 525 (1966).
5) G. Schmauss, H. Baumgartel, and H. Zimmermann, *Angew. Chem.*, **77**, 619 (1965); *Angew. Chem. Int. Ed. Engl.*, **4**, 596 (1965).
6) G. Kothe, K. H. Denkel, and W. Sümmermann, *Angew. Chem.*, **82**, 935 (1970); *Angew. Chem. Int. Ed. Engl.*, **9**, 906 (1970).
7) G. Kothe, C. Nowak, K. H. Denkel, E. Ohmes, and H. Zimmermann, *Angew. Chem.*, **82**, 521 (1970); *Angew. Chem. Int. Ed. Engl.*, **9**, 520 (1970).
8) G. Kothe, E. Ohmes, J. Brickmann, and H. Zimmerman, *Angew. Chem.*, **83**, 1015 (1971), *Angew. Chem. Int. Ed. Engl.*, **10**, 938 (1971).
9) A. Rassat and H. U. Sieveking, *Angew. Chem.*, **84**, 353 (1972).
10) K. Mukai, N. Azuma, H. Shikata, and K. Ishizu, This Bulletin, **43**, 3958 (1970).
11) P. Kopf, K. Morokuma, and R. Kreilick, *J. Chem. Phys.*, **54**, 105 (1971).
12) N. Azuma, K. Ishizu, and K. Mukai, *ibid.*, **61**, 2294 (1974).

BULLETIN OF THE CHEMICAL SOCIETY OF JAPAN, VOL. 48(8), 2383—2384 (1975)

The γ-Radiolysis of Liquid Nitrogen Containing Methane

Yona SIDERER* and Shin SATO

Department of Applied Physics, Tokyo Institute of Technology, Ookayama, Meguro-ku, Tokyo 152

(Received February 22, 1975)

Synopsis. The γ-radiolysis of the liquid nitrogen–methane system has been investigated. As products, hydrogen cyanide, ethane, and the basic compounds were observed. The G(HCN) attained was 0.08 at higher concentrations of methane, while the G(basic compounds) was found to be in the order of 0.5. In order to explain these results, different precursors for the HCN and the basic compounds are considered.

Methane is the simplest hydrocarbon. Therefore, if γ-radiolysis is carried out with a system of liquid nitrogen containing a small amount of methane, the number of different products will be limited. In a study of the gas-phase γ-radiolysis of the nitrogen–methane system,[1] it has been reported that hydrogen cyanide is the only nitrogen-containing product. Also, in an investigation of the reaction of the active nitrogen with methane,[2] the main nitrogen-containing product has been found to be hydrogen cyanide.

At the temperature of liquid nitrogen, no reaction with an activation energy higher than a few kcal mol^{-1} will occur. Therefore, if the formation of hydrogen cyanide is accompanied by a complicated rearrangement, which is usually postulated in the gas-phase reactions of nitrogen atoms with hydrocarbons,[3] these reactions will be inhibited in the liquid nitrogen; *i.e.*, only the association reaction and the strong exothermic reaction will occur.

With these expectations in mind, we have carried out the γ-radiolysis of liquid nitrogen containing methane.

Experimental

The methane used was supplied by the Takachiho Shoji Co. Nitrogen gas of a high purity was purchased from the Nihon Sanso Co. and was used after being bubbled through sulfuric acid. The hydrogen cyanide used for identification was synthesized from potassium cyanide and sulfuric acid. The Nessler reagent was obtained from Wako Pure Chemical Industries, Ltd.; sulfuric acid (95%) from the Yotsuhata Co., Ltd., and potassium carbonate, from the Junsei Pure Chemical Co., Ltd.

The experimental procedure was almost the same as that reported previously.[4] A 10-ml portion of liquid nitrogen containing a known amount of methane was irradiated by ^{60}Co γ-rays at a dose rate of 3.21×10^{19} eV/g hr. After evacuating the nitrogen at 77 K, we analyzed the remains by using a gas chromatograph (DOP column) and by using Conway's method.[4] The gas-chromatographic analysis showed the presence of hydrogen cyanide and ethane, while Conway's method revealed the presence of a comparatively large amount of the basic compounds in the product.

* Present address: Weizmann Institute of Science, Department of Biochemistry, Rehovot, Israel.

Results

Figure 1 shows the G-values of hydrogen cyanide and ethane obtained as functions of the concentration of methane. At methane concentrations higher than 3×10^{-3} mol l^{-1}, the increase in G(HCN) with an increase in the concentration of methane is much smaller than that in $G(C_2H_6)$. Table 1 summarizes the G-values of the basic compounds measured by Conway's method. Although the data are scattered, they may be enough to show that the G(basic compounds) is in the order of 0.5. One experiment was carried out using hydrogen in place of methane. This result suggests that the basic compounds obtained with methane are not products of the reaction of nitrogen atoms with the hydrogen eventually formed in the system.

Discussion

Since the C-H bond strength of methane (101 kcal

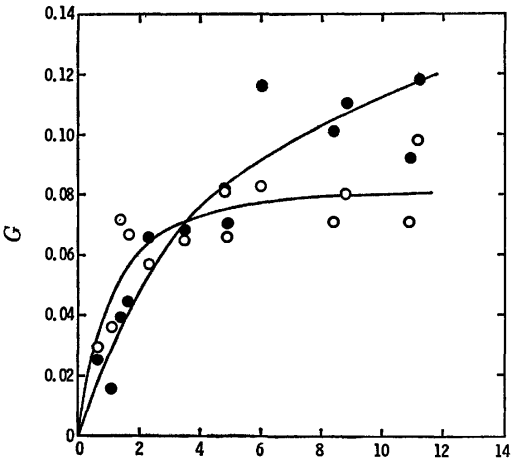

Fig. 1. The G-values of hydrogen cyanide (○) and ethane (●) as a function of the concentration of methane.

TABLE 1. THE G-VALUES OF AMMONIA MEASURED PHOTOMETRICALLY AFTER TREATING THE PRODUCT BY THE CONWAY METHOD AND USING NESSLER REAGENT

CH_4 (10^{-3} mol l^{-1})	H_2 (10^{-3} mol l^{-1})	$G(NH_3)$
0.56		0.44
1.29		0.36
2.01		0.60
2.83		0.51
3.57		0.41
	4.86	0.074

mol^{-1}) is much larger than the bond strength of N-H (86 kcal mol^{-1}),[5] the endothermic reaction:

$$CH_4 + N \longrightarrow NH + CH_3 \quad (1)$$

will not occur in the present system. The initiating reaction, therefore, must be the decomposition of methane in the collision of the excited nitrogen molecules with a long life (N_2^* $^3\Sigma_u^+$):

$$CH_4 + N_2^* \longrightarrow CH_3 + H + N_2 \quad (2)$$

In the gas-phase reaction, the following reaction:

$$CH_3 + N \longrightarrow HCN + H_2 \quad (3)$$

has often been assumed to occur; however, as was shown in the Results section, hydrogen cyanide is not the only nitrogen-containing product in the present experiment. Moreover, this reaction is not a spin-allowed one. A more plausible reaction in the present system is as follows:

$$CH_3 + N \longrightarrow CH_3N: \quad (4)$$

The intermediate, CH_3N:, may isomerize into methylene imine either in the liquid nitrogen or in the course of the warming up to room temperature.

It is known that methylene imine is not a stable compound at room temperature and that it polymerizes into a polymer. In fact, the mass-spectrometric analysis of the product showed the presence of a polymer, although it could not be identified. If Reaction (4) is a unique reaction between nitrogen atoms and methyl radicals, the formation of hydrogen cyanide cannot be explained. Another possible mechanism is as follows:

$$CH_3 + N \longrightarrow H_2CN + H \quad (5)$$

$$H_2CN + CH_3 \longrightarrow HCN + CH_4 \quad (6)$$

Reaction (6) was proposed by Safrany and Jaster in the investigation of the reaction of active nitrogen.[5] However, this reaction mechanism is not applicable to the present system. As has been shown in Fig. 1, the methane-concentration dependence of $G(HCN)$ is much smaller than that of $G(C_2H_6)$. If Reactions (5) and (6) are operative, the yield of hydrogen cyanide should be increased with the increase in the concentration of methyl radicals, which will itself increase with the concentration of methane.

As a possible source of hydrogen cyanide, let us consider the excited state of nitrogen atoms, ^2D, 2.38 eV above the ground state, ^4S. Even in the active nitrogen, the presence of the excited atoms ^2D has been reported, although the concentration is much less than that of the ground state.[3]

A tentative reaction mechanism to explain the present experimental results may be summarized as follows:

$$N_2 \begin{cases} \xrightarrow{\sim\sim} 2\,N\ (^4S),\ (^2D) \\ \xrightarrow{\sim\sim} N_2^*\ (^3\Sigma_u^+) \end{cases}$$

$$N_2^* + CH_4 \longrightarrow N_2 + CH_3 + H$$

$$CH_3 + N\ (^2D) \longrightarrow HCN + H_2$$

$$CH_3 + N\ (^4S) \longrightarrow CH_3N:$$

$$CH_3N: \longrightarrow \text{products}$$

(Conway's method)

$$\text{products} \longrightarrow NH_3 + \text{residue}$$

$$CH_3 + CH_3 \longrightarrow C_2H_6$$

$$(H + N \longrightarrow NH \cdots\cdots\rightarrow NH_3)$$

Further investigations are being made with a different approach.

This research was partially supported by a UNESCO Fellowship to Y.S.

References

1) A. T. Podkhalyuzin, A. E. Trishkin, and I. V. Vereshchinskii, *Khimiya Visokikh Energii*, **3**, 401 (1969). T. Oka, T. Shindo, and S. Sato, This Bulletin, **44**, 2274 (1971).

2) H. G. Evans, G. R. Freeman, and C. A. Winkler, *Can. J. Chem.*, **34**, 1271 (1956).

3) B. Brocklehurst and K. R Jennings, "Progress in Reaction Kinetics," Vol. 4, ed. by G. Porter, Pergamon Press, Oxford (1967), p. 1.

4) K. Ishizaki and S. Sato, This Bulletin, **47**, 2597 (1974).

5) D. R. Safrany, "Progress in Reaction Kinetics," Vol. 6, ed. by K. R. Jennings and R. B. Cundall, Pergamon Press, Oxford (1971), p. 1.

BULLETIN OF THE CHEMICAL SOCIETY OF JAPAN, VOL. 48(8), 2385—2386 (1975)

Energy Difference between Rotational Isomers of 1,2-Dibromoethane

Jiro HIRAISHI and Takako SHINODA

National Chemical Laboratory for Industry, Honmachi, Shibuya-ku, Tokyo 151

(Received March 27, 1975)

Synopsis. The energy difference between the rotational isomers of 1,2-dibromoethane in the liquid state was determined to be 910±80 cal/mol on the basis of the relative intensity of the Raman band at 660 cm^{-1} (*trans* form) to that at 551 cm^{-1} (*gauche* form) in the temperature range from 24.5 to 105.1 °C.

The energy difference ($\Delta E=E_g-E_t$) between the *trans* and *gauche* forms of 1,2-dibromoethane in the liquid state has been determined by many investigators.[1-7] The values reported are in the range from 650 to 1000 cal/mol. Fujiyama and Shimanouchi observed the ratio of the intensity of the Raman band at 660 cm^{-1} of the *trans* form (I_t) and that of the band at 551 cm^{-1} of the *gauche* form (I_g) in the liquid state and concluded that $\ln(I_t/I_g)$ was not proportional to $1/T$ (T represents the absolute temperature at the measurement).[5] Recently a cryostat was constructed in our laboratory for the measurement of the Raman spectra in the temperature range from 150 °C to liquid helium temperature.[8] By use of the apparatus we re-examined the energy difference of 1,2-dibromoethane in the liquid state in order to ascertain the non-linear relation between $\ln(I_t/I_g)$ and $1/T$.

The Raman spectra were measured with the use of a Raman spectrometer, Kawaguchi Electric Works Ltd. model RL-62. The exciting light was 488.0 nm line of the Ar^+ laser, NEC model GLG 2003. The power of the exciting light was kept constant during the measurement by use of the light feed back system for the GLG 2003 laser made by Kawaguchi Electric Works Ltd. The spectrum between 500 and 750 cm^{-1} was recorded at 24.5, 34.9, 45.0, 55.2, 65.0, 75.2, 84.9, 95.1, and 105.1 °C. The spectrum at room temperature is given in Fig. 1. The weak band at 583 cm^{-1} is the CBr stretching vibration band of b species of the *gauche* form. The bands at 660 and 551 cm^{-1} were used for obtaining the energy difference. The temperature was measured within an accuracy of about 0.03 K with the use of a chlomel p-constantan thermocouple, the calibration of which was given elsewhere.[9] The drift of the temperature was less than 0.2 K during a measurement. The spectra were recorded five times for the measurement at each temperature. Five copies were made for each recording with the use of Fuji Xerox 1000 and weighed the area of each band. 25 data of I_t/I_g were obtained for the measurement at each temperature. The standard deviation of the 25 data was in the range from 1.0 to 3.5% of the averaged value.

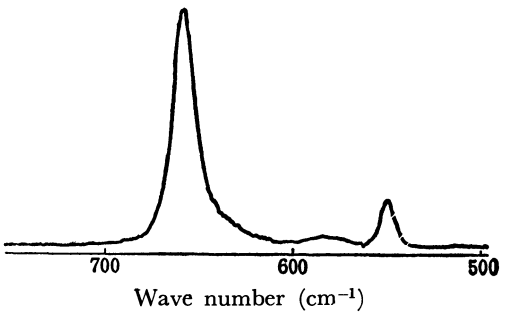

Fig. 1. The Raman spectra of 1,2-dibromoethane in the liquid state at room temperature.

Figure 2 illustrates the values of $\ln(I_t/I_g)$ against $1/T$, which indicates that $\ln(I_t/I_g)$ linearly depends on $1/T$. As the scattering intensity of the Stokes line[10] is proportional to $(1-e^{-h\nu/kT})^{-1}$, the temperature dependence of I_t/I_g can be expressed by the following equations:

$$\partial/\partial(1/T)[\ln(I_t/I_g)] = \Delta E/k + f(T)$$

$$f(T) = e^{-h\nu_g/kT}(h\nu_g/k)/(1-e^{-h\nu_g/kT}) - e^{-h\nu_t/kT}(h\nu_t/k)/(1-e^{-h\nu_t/kT})$$

where ν_t and ν_g represent the vibrational frequencies of the *trans* and *gauche* forms used for the determination of ΔE. The apparent value of ΔE directly obtained from Fig. 2 is 955±80 cal/mol. When $f(T)$ is taken into consideration, the value of ΔE decreases by 38 cal/mol at 24.5 °C and by 54 cal/mol at 105.1 °C. Consequently, the value of ΔE is determined to be 910±80 cal/mol.

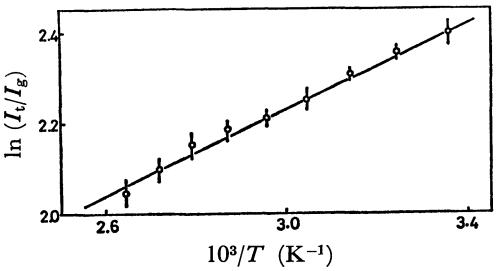

Fig. 2. Linearity between $\ln(I_t/I_g)$ and $1/T$.

As temperature range of the present study is wider and the measurement of temperature is more accurate than other vibrational spectroscopic measurements, we believe the present result is most reliable among them. I_t/I_g depends on the choice of the base line and also on the method of the separation of two bands ovelapping each other. As Fig. 1 shows, the two bands do not overlap each other so much and the base line is easily determined in this case. On estimating the error in I_t/I_g in Fig. 2, such systematic errors are not taken into account, which do not exceed 5%.

References

1) Y. Morino, S. Mizushima, K. Kuratani, and M. Katayama, *J. Chem. Phys.*, **18**, 754 (1950).

2) D. H. Rank, R. E. Kagarise, and D. W. E. Axford, *ibid.*, **17**, 1354 (1954).
3) I. Watanabe, I. Miyagawa, and Y. Morino, *Rept. Radiation Chem. Res. Inst. (Tokyo Univ.)*, **3**, 25 (1948).
4) K. Kuratani, T. Miyazawa, and S. Mizushima, *J. Chem. Phys.*, **21**, 1411 (1953).
5) T. Fujiyama and T. Shimanouchi, Symposium on Molecular Structure, Sendai (1972), 5C25.
6) K. Tanabe, *Spectrochim. Acta*, **28A**, 407 (1972).
7) R. J. Abraham and G. Gatti, *J. Chem. Soc., B*, **1969**, 961.
8) J. Hiraishi and T. Shinoda, This Bulletin, in press.
9) H. Enokido, T. Shinoda, and Y. Mashiko, This Bulletin, **44**, 108 (1971).
10) G. Placzek, "Rayleigh-Streuung und Raman Effekt," Handbuch der Radiologie, Heft 6, Teil 2, 71 (1934).

BULLETIN OF THE CHEMICAL SOCIETY OF JAPAN, VOL. 48(8), 2387—2388 (1975)

Gas-chromatographic Behavior of C_1, C_2, and C_3-Halocarbons Containing Iodine

Yoshihiro MAKIDE, Takefumi FUKUMIZU, and Takeshi TOMINAGA

Department of Chemistry, Faculty of Science, The University of Tokyo, Bunkyo-ku, Tokyo 113

(Received April 18, 1975)

Synopsis. The regularity of the specific retention volume (V_g) in gas chromatography was investigated on a number of C_1, C_2, and C_3 halocarbons containing iodine. The log V_g value was found to correlate with the number of halogen and carbon atoms in the molecule.

Although the gas-chromatographic behavior of a number of C_1 and C_2 carbon mixed halides containing F, Cl, and Br has been investigated,[1,2] no extensive work has been reported on carbon mixed halides containing iodine. The object of this article is to report on our recent study of the regularity in the specific retention volume of C_1, C_2, and C_3 mixed halocarbons containing iodine in addition to F, Cl, and Br.

Experimental

Materials. Twelve kinds of iodine-containing halocarbons were used in the present work. Of these, CF_2ClI, $CFCl_2I$, CF_2BrI, C_2F_4ClI, $C_2F_3Cl_2I$, C_3F_6ClI, and C_3F_6BrI were prepared by the γ-irradiation of mixtures of adequate halocarbons and iodine.[3] CF_3I, C_2F_5I, C_2F_4BrI, $C_2F_4I_2$, $C_2F_3Cl_2I$, and C_3F_7I were purchased from PCR, Inc., USA. The other halocarbons containing no iodine and used in this work were obtained as has been described previously.[2]

Determination of Retention Volume. The retention times of the halocarbons on a Silicone DC 550 column (20 wt% coated on acid-washed Chromosorb W80-100 mesh, 3 mm i.d. × 5 m long) were measured at constant temperatures between 40 and 100 °C by using a gas chromatograph equipped with a thermal conductivity detector. The carrier gas was He, at the flow rate of 15 ml/min. The gas-chromatographic data were expressed in terms of the specific retention volume (V_g), normalized from the measured retention time.

Results and Discussion

The logarithm of the specific retention volume of each halocarbon measured between 40 and 100 °C was linearly related to the reciprocal of the absolute temperature of the column; thus, the heat of vaporization from the solution in the Silicone DC 550 stationary phase remained constant over this range of column temperature. Furthermore, the heats of vaporization calculated for all the halocarbons from the slopes of the log $V_g - 1/T$ curves were correlated almost linearly with the logarithms of the specific retention volumes at any temperature.

Figure 1 reveals the correlation of the logarithm of the specific retention volume with the halogen composition for C_2-halocarbons.[4] The observed retention volumes of the C_2-halocarbons containing iodine (filled circles in Fig. 1) were plotted nearly at the lattice positions of the network for $C_2F_{6-x-y-z}Cl_xBr_yI_z$. Such results have also been obtained for the halocarbons containing no iodine,[1,2] which are

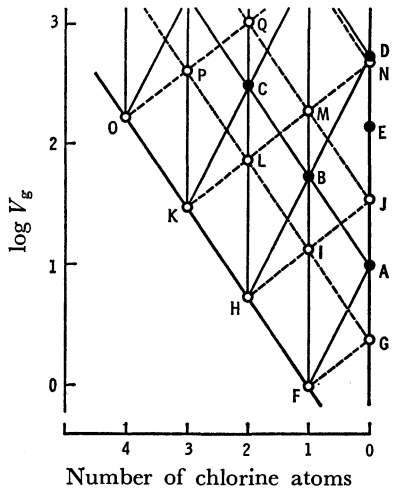

Fig. 1. Correlation between the logarithm of the specific retention volume on a Silicone DC 550 column (60 °C) and the halogen composition of C_2-halocarbons.
(A): C_2F_5I, (B): C_2F_4ClI, (C): $C_2F_3Cl_2I$, (D): $C_2F_4I_2$, (E): C_2F_4BrI, (F): C_2F_5Cl, (G): C_2F_5Br, (H): $C_2F_4Cl_2$, (I): C_2F_4ClBr, (J): $C_2F_4Br_2$, (K): $C_2F_3Cl_3$, (L): $C_2F_3Cl_2Br$, (M): $C_2F_3ClBr_2$, (N): $C_2F_3Br_3$, (O): $C_2F_2Cl_4$, (P): $C_2F_2Cl_3Br$, (Q): $C_2F_2Cl_2Br_2$.

represented by open circles in Fig. 1. A detailed examination of the additivity of log V_g with respect to the halogen composition indicates that, upon halogen substitution, the log V_g value is changed by a magnitude characteristic of the substitution: +0.76 by Cl-for-F, +1.17 by Br-for-F, and +1.76 by I-for-F (on a Silicone DC 550 column at 60 °C). The magnitude of the change in log V_g for the same type of halogen substitution was found to be identical irrespective of the number of carbon atoms in the molecule. Accordingly, the log V_g value of the halocarbons, $C_nF_{2n+2-x-y-z}Cl_xBr_yI_z$ (n=1, 2, and 3) on Silicone DC 550 at 60 °C, can be calculated as follows:

$$\log V_g = \alpha_n + 0.76x + 1.17y + 1.76z$$

where α_n is equal to −0.94, −0.80, and −0.61 for n=1, 2, and 3 (*i.e.*, C_1, C_2, and C_3) respectively.[5]

Figure 2 illustrates three-dimensionally the additivity of the log V_g values of all the C_2-halocarbons with respect to the number of F, Cl, Br, and I in the molecule. The log V_g value is expressed as the height from the ground plane. The four vertices of the larger tetrahedron correspond to C_2F_6, C_2Cl_6, C_2Br_6, and C_2I_6, while each edge includes C_2-halocarbons containing two kinds of halogens (*e.g.*, $C_2F_{6-x}Cl_x$ along the C_2F_6–C_2Cl_6 edge). C_2-halocarbons containing three kinds of halogens are located at the lattice positions on the surfaces of the tetrahedron except

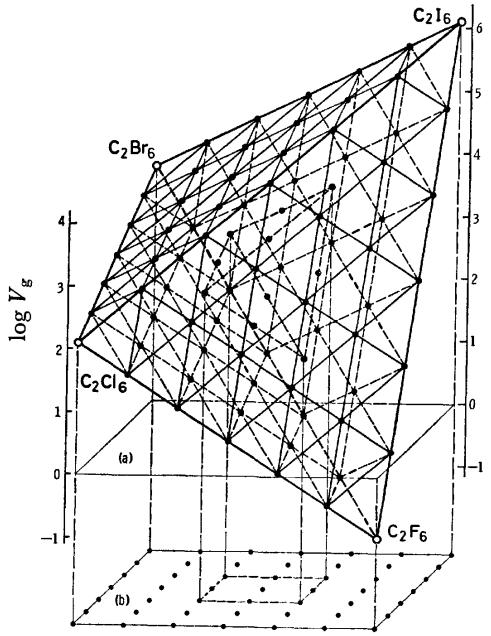

Fig. 2. Three dimensional diagram of the correlation between the logarithm of the specific retention volume and the halogen composition of $C_2F_{6-x-y-z}Cl_xBr_yI_z$.
(a): ground plane at log $V_g=0$.
(b): projection on a horizontal plane.

on the edges, while those which contain four kinds of halogens (*i.e.*, fluorochlorobromoiodocarbons) should be found along the edges of a smaller tetrahedron located inside (at the center) of the larger tetrahedron. The three-dimensional correlation diagram appears to be of analytical importance, since the order of elution or the relative difficulty of elution from a gas-chromatographic column can be predicted graphically for all the halocarbons. Such a correlation and relative order among these compounds can be retained at any temperature, although the absolute value of log V_g will be changed. Therefore, we may choose adequate column conditions for these compounds by

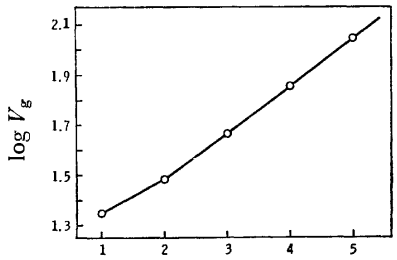

Fig. 3. Correlation between the logarithm of the specific retention volume and the number of carbon atoms in the series $C_nF_{2n-1}Cl_3$.

referring to the correlation diagram even if the log V_g—$1/T$ curves for all the compounds are not available.

In order to examine the dependence of log V_g on the number of carbon atoms, a series of $C_nF_{2n-1}Cl_3$ halocarbons (*i.e.*, $CFCl_3$, $C_2F_3Cl_3$, $C_3F_5Cl_3$, $C_4F_7Cl_3$, and $C_5F_9Cl_3$) are illustrated in Fig. 3. The log V_g value tends to increase with the number of carbon atoms, and the log V_g *vs.* carbon number curve apparently approaches a straight line as the number of carbon atoms increases. All other series of halocarbons C_nX_{2n+2} show similar behavior.

The present authors wish to thank Professor Nobufusa Saito for his encouragement and support.

References

1) T. Tominaga, R. Iwata, and Y. Makide, *Chem. Lett.*, **1973**, 485.
2) R. Iwata, Y. Makide, and T. Tominaga, This Bulletin, **47**, 3071 (1974).
3) Details will be published shortly.
4) Very similar correlation diagrams were also obtained for C_1 and C_3-halocarbons. The same type of halogen substitution gave the identical slope in diagrams of C_1, C_2, and C_3-halocarbons.
5) Namely, α_n corresponds to the log V_g value for C_nF_{2n+2} ($n=1$, 2, and 3).

BULLETIN OF THE CHEMICAL SOCIETY OF JAPAN, VOL. 48(8), 2389—2390 (1975)

Effects of HMPA in the Kharasch Type Reaction of Allylic Halides

Yoshihiro OHBE and Tsutomu MATSUDA

Department of Organic Synthesis, Faculty of Engineering, Kyushu University, Hakozaki, Higashi-ku, Fukuoka 812

(Received December 17, 1974)

Synopsis. Addition of HMPA was found to bring about an increase of cross-coupling products in the transition metal catalyzed reaction of allylic chlorides (allyl, crotyl, and methallyl) with Grignard reagents, the effect being most significant in copper (II) chloride catalyzed reactions.

In previous papers[1,2] it was shown that the Kharasch type reaction of an allylic halide with a Grignard reagent catalyzed by a transition metal halide resulted in the formation of a product mixture which could be understood by considering the following three processes (routes i, ii and iii), relative importance of the routes depending on the nature of an intermediate organometallic species and the structure of the Grignard reagent.

$$RMgX + MX_n \longrightarrow$$

$$\underset{\mathbf{A}}{R_nM} \longrightarrow R\text{-}R,\ R(-H),\ R(+H)$$

$$\underset{\mathbf{A}}{R_nM} \longrightarrow M^\circ$$

$$M^\circ + R'CH{=}CH\text{-}CH_2X \longrightarrow \underset{\mathbf{B}}{(R'\text{-}CH{=}CH\text{-}CH_2\text{-})_2M}$$

$$\mathbf{B} \xrightarrow{\text{i) } R''\underset{\displaystyle H}{C}HCH_2MgX} R'CH{=}CH\text{-}\underset{\displaystyle H}{C}H_2 + R''CH{=}CH_2$$

$$\mathbf{B} \xrightarrow{\text{ii) } RMgX} R'\text{-}CH{=}CH\text{-}CH_2\text{-}R$$

$$\mathbf{B} \xrightarrow{\text{iii) } R'\text{-}CH{=}CH\text{-}CH_2\text{-}X} (R'\text{-}CH{=}CH\text{-}CH_2\text{-})_2$$

and its isomers

Our previous studies were concerned mainly with the structure and behavior of the allylic metal intermediate (**B**).

The reactivity of a Grignard reagent can be considered as an important factor affecting the distribution of the products from allylic halide. The presence of an additive of strongly dative nature such as HMPA causes a considerable change in the reactions of Grignard reagents.[3]

We have examined the effect of HMPA in the Kharasch type reaction of allylic halides with the intention of increasing the selectivity of the reaction for obtaining cross-coupling products (route ii) by increasing nucleophilic activity of Grignard reagents.[4]

Results and Discussion

Table 1 shows the results obtained in the nickel (II) chloride catalyzed reactions of three typical allylic halides in the presence of two equivalents of HMPA to Grignard reagents, together with those without HMPA.

The effect of HMPA varies considerably with the type of halide. The product distribution from crotyl chloride was not influenced materially by the addition of HMPA except for a small increase in cross-coupling products. On the other hand, in the reaction with allyl chloride, a considerable decrease in the hydrogen transfer process (route i, formation of R(−H) and allyl (+H)) occurred accompanied by an increase in the cross-coupling product as well as R–R and homo-coupling products. A similar trend was observed with methallyl chloride to a lesser extent. The use of tetramethylethylenediamine (TMED) or dimethoxyethane (DME) produced a similar effect to that observed with HMPA, but resulted in a decrease in the total yield of products from methallyl chloride.

Dependence of the effect of HMPA on the type of catalyst was examined with methallyl chloride. The results are summarized in Table 2.

The use of one equivalent of HMPA in the presence of copper (II) chloride was found to be most effective for increasing the selectivity towards the cross-coupling process. The addition of HMPA seems to influence not only the reactivity of the Grignard reagents but also that of alkylmetal (**A**) and/or allylic metal intermediate (**B**).

It was found[5] that in the nickel(II) salt catalyzed

TABLE 1. EFFECT OF ADDITIVES IN THE NICKEL(II) CATALYZED REACTION OF ALLYLIC HALIDES[a]

R-MgBr	*n*-Bu-	Et-	*n*-Pr-		
Allylic chloride(Ally-Cl)	Allyl-	Crotyl-	Methallyl-		
Additive	HMPA	HMPA	HMPA	TMEDA	DME
R(+H)	4(1)	29(23)	10(28)	34	19
R(−H)	37(81)	62(69)	34(60)	4	1
Ally(+H)	38(70)	8(8)	30(61)	3	1
R-R	18(7)	10(16)	20(t)	16	5
Cross-coupling(R-Ally)	21(3)	15(t)	28(8)	16	6
Homo-coupling[$(Ally)_2$]	19(3)	43(47)	15(12)	15	10

a) Values(%) are based on the theoretical amount; t: trace amount; ( ): yields without the additive. Two molar equivalents of the additives to Grignard reagent were used.

Table 2. Effect of HMPA in the reaction of *n*-propylmagnesium bromide (R-MgBr) with methallyl chloride(Ally-Cl)[a]

MX_n	Non	$NiCl_2$	$CoCl_2$	$FeCl_3$	$CuCl_2$		
HMPA(×0.05 mol)	Non	2	2	2	2	1	0.5
R(+H)		10	10(28)	8(30)	48(12)	17(39)	11	23
R(−H)	t	9	36(60)	36(63)	6(71)	3(55)	3	19
Ally(+H)		0	30(61)	33(61)	1(46)	t (33)	t	5
R-R	0	7	20(t)	22(t)	15(t)	19(t)	4	2
Cross-coupling(Ally-R)	2	10	28(8)	27(7)	34(13)	53(12)	68	36
Homo-coupling[$(Ally)_2$]	1	2	15(12)	16(12)	16(30)	6(55)	6	28

a) Values(%) are based on the theoretical amount; t: trace amount; ( ): yields without the additive.

Table 3. Effect of HMPA in the copper(II) chloride catalyzed reactions of 2-cycloalkenyl bromide (Cyclo-Br)[a]

Cyclo-Br	Cyclo-C_6H_9		Cyclo-C_5H_7	
R-MgX	MeMgI	*i*-PrMgBr	MeMgI	*i*-PrMgBr
R(+H)	10(10)[12]	28(25)[18]	12(14)[10]	26(24)[20]
R(−H)	—(—)[—]	16(26)[21]	—(—)[—]	28(30)[22]
R-R	0(0)[0]	t (1)[4]	0(0)[0]	t (1)[5]
Cycloalkane	7(1)[7]	7(11)[8]	3(1)[4]	5(12)[6]
Cycloalkene	5(4)[3]	6(14)[4]	2(2)[4]	5(15)[4]
Cross-coupling(Cyclo-R)	88(86)[78]	52(47)[47]	80(89)[83]	55(50)[52]
Homo-coupling[$(Cyclo)_2$]	0(1)[0]	t (0)[t]	0(t)[0]	0(0)[0]

a) Values(%) are based on the theoretical amount; t: trace amount; ( ): yields without the additive.
[ ]: Results in the absence of both catalyst and HMPA.

reaction of allyl chloride with *n*-butylmagnesium bromide, the addition of triethylphosphine or use of bis(triethylphosphine)nickel bromide gave rise to a considerable increase in *n*-octane (R–R, 40 and 56%) and the homo-coupling product (12 and 59%, respectively), but scarcely influenced the yield of the cross-coupling product. The fact that a decrease in the amount of HMPA to a half equivalent, still in a large excess over the catalyst (0.02 molar equivalent), resulted in a decrease in the effect of HMPA would help exclude the possibility. However, in an uncatalyzed reaction, HMPA acts to increase to some extent both the radical process (formation of R(—H) and R(+H)) and Wurtz type coupling.

The increase of the cross-coupling products throughout the catalyzed reactions can be rationalized by assuming that HMPA acts principally to increase nucleophilic activity of alkyl groups of the Grignard reagents, but does not influence β-hydrogen transfer (route ii). The effect of HMPA was hardly seen in the reactions of 2-cyclopentenyl- and 2-cyclohexenyl bromide (Table 3) which are known to produce preferentially cross-coupling products even without catalyst.

However, it is noticeable that the presence of HMPA serves to suppress the formation of cycloalkane and cycloalkene in the reactions with isopropylmagnesium bromide which is liable to cause β-hydrogen transfer (route i).

Experimental

Materials. Commercial organic halides (*n*-BuBr, EtBr, *n*-PrBr, *i*-PrBr, allyl-Cl, crotyl-Cl and methallyl-Cl) and additives (HMPA, TMEDA, and DME) were purified by distillation.

2-Cyclohexenyl bromide and 2-cyclopentenyl bromide were prepared by bromination of the corresponding cycloalkene by *N*-bromosuccinimide in CCl_4.

Reaction Procedure. A mixture of a Grignard reagent (0.05 mol) and an additive (0.1 mol) in ether was added to a suspension of a catalytic amount (0.25 mmol) of metallic halide in anhydrous ether under nitrogen. The mixture was stirred until the evolution of gas ceased (reaction A).

To the resulting solution, an equivalent amount of allylic halide (0.05 mol) in ether was added with vigorous stirring.

The mixture was then heated under reflux until the evolution of gas stopped (reaction B). The mixture was hydrolyzed in the usual manner. For crotyl chloride[1,2] and 2-cycloalkenyl bromide, the products were analyzed by gas chromatography with a 2 m column packed with Silicone 703 (20%)-Celite 545. For allyl chloride[1,2] and methallyl chloride, the ethereal solution containing an internal standard (cyclohexene) was directly injected onto a Golay column HB 2000, 45 m.

2-Methyl-1-hexene(R-Ally) and 2,5-dimethyl-1,5-hexadiene ($Ally_2$) were produced from methallyl chloride and 3-alkylcycloalkenes(R-Cyclo), respectively. 3-(2′-Cycloalkenyl)-cycloalkenes($Cyclo_2$) were formed from the 2-cycloalkenyl bromides. They were identified by comparison with authentic specimens obtained by the Wurtz coupling. No other isomers and products were detected. The composition of gaseous products obtained in reactions A and B was determined with a silica gel column (2 m) for methane and ethane, and a benzyl ether column (40%, 6 m) for other gaseous hydrocarbons.

References

1) Y. Ohbe and T. Matsuda, *Tetrahedron*, **29**, 2989 (1973).
2) Y. Ohbe and T. Matsuda, *ibid.*, **30**, 2669 (1974).
3) H. O. House and W. F. Fisher, *J. Org. Chem.*, **33**, 949 (1968).
4) H. F. Ebel and B. O. Wagner, *Chem. Ber.*, **104**, 320 (1971).
5) Y. Ohbe, K. Doi, and T. Matsuda, *Nippon Kagaku Kaishi*, **1974**, 193.

BULLETIN OF THE CHEMICAL SOCIETY OF JAPAN, VOL. 48(8), 2391—2392 (1975)

The Synthesis of Flemichapparin-A and Its Derivatives

Shigetoshi YAMADA, Futara ONO, Takao KATAGIRI,* and Juntaro TANAKA*

Department of Industrial Chemistry, Junior College of Technology, Shizuoka University, Hamamatsu 432

**Department of Synthetic Chemistry, Faculty of Engineering, Shizuoka University, Hamamatsu 432*

(Received January 23, 1975)

Synopsis. Some chromenochalcones including Flemichapparin-A were synthesized in 53—63% yields from 6-acetyl-5,8-dihydroxy-2,2-dimethylchlomene and benzaldehydes.

Some chromenochalcones are naturally occurring compounds[1] and are expected to have some biological activities. Recently some papers on the synthesis of these compounds have appeared.[2]

The present authors have studied the synthesis of chromenochalcones, especially those which contain the isoprene skeleton in part.[3] These compounds contained Flemichapparin-A which was recently isolated from *Flemingia Chappar* Ham (Leguminosae). In this paper, we wish to report on these studies.

6-Acetyl-5,8-dihydroxy-2,2-dimethylchromene [IV] was obtained by the reaction of 2,4,5-trihydroxyacetophenone [III] with β-methylcrotonaldehyde [II] in pyridine.

The Claisen-Schmidt condensation of IV with various benzaldehydes (benzaldehyde, 2,4-dimethoxybenzaldehyde, 3,4-dimethoxybenzaldehyde and 4-methoxybenzaldehyde) gave chromenochalcones in 53—63% yields. Among these compounds, the data of I agreed with those of Flemichapparin-A.[1-c,2-d]

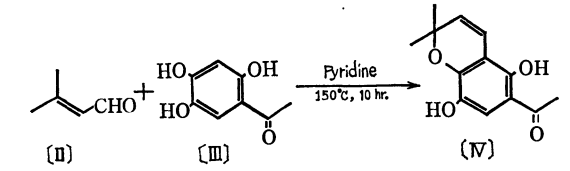

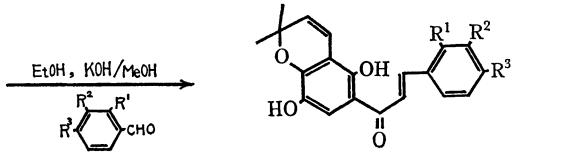

	R^1	R^2	R^3
[I]	H	H	H
[V]	OCH_3	H	OCH_3
[VI]	H	OCH_3	OCH_3
[VII]	H	H	OCH_3

Experimental

6-Acetyl-5,8-dihydroxy-2,2-dimethylchromene [IV]. β-Methylcrotonaldehyde (II, bp 39—40 °C/15 mmHg, 8.4 g, 0.1 mol) and 2,4,5-trihydroxyacetophenone (III, mp 198—200 °C, 8.4 g, 0.05 mol) were dissolved in pyridine (4.0 g, 0.05 mol) and were then heated with stirring at 150 °C for 10 hr. The reaction mixture was evaporated, and the residue was chromatographed on silica-gel. The fraction eluted by benzene afforded 6-acetyl-5,8-dihydroxy-2,2-dimethylchromene (IV, 58% yield) as yellow needles.

Mp 153—154 °C (recryst. from petroleum ether); IR (cm^{-1}, KBr disk): 3400 (-OH), 1640 (C=O), 1250 (-C-O-C-), 870 (penta substn. benzene); PMR (δ, $CDCl_3$): 1.50 (6H, s, $-C(CH_3)_2$), 2.49 (3H, s, $-COCH_3$), 5.28 (1H, broad s, -OH), 5.53 (1H, d, J=10.0 Hz, 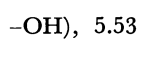), 6.70 (1H, d, J=10.0 Hz, 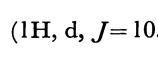), 7.09 (1H, s, aromatic H), 12.60 (1H, s, -OH). Found C, 66.77; H, 6.03%. Calcd for $C_{13}H_{14}O_4$: C, 66.65; H, 6.02%.

Chromenochalcones. A solution of IV (234 mg, 0.001 mol) and benzaldehydes (0.001 mol) in ethanol (4 ml) was added, under cooling under nitrogen, to 2 g of KOH in methanol (4 ml). After the reaction mixture had then stood at room temperature for 3—5 days, dilution, acidification (with 5 ml of 0.1 M-HCl), extraction with ether, and chromatography on silica-gel eluted by *n*-hexane–AcOEt (95 : 5 v/v) afforded chromenochalcones, which were identified by means of IR, PMR, and elemental analysis.

2′,5′-Dihydroxy-3′,4′(5″,6″)2″,2″-dimethyl-α-pyranochalcone (I). Yield, 53%; mp 190—192 °C (orange plates). IR (cm^{-1}, KBr disk): 3400 (-OH), 1640 (C=O), 1240 (-C-O-C-), 970 (*trans* RHC=CHR), 760 (*cis* RHC-CHR). PMR (δ, $CDCl_3$): 1.54 (6H, s, $-C(CH_3)_2$), 5.60 (1H, d, J=10.0 Hz, 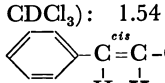), 6.78(1H, d, 10.0 Hz, 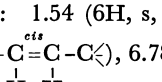), 7.20—7.70 (7H, m), 7.48 (1H, d, J=15.5 Hz, 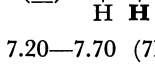), 7.90 (1H, d, J=15.5 Hz, 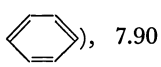), 13.37 (1H, s, -OH). Found C, 74.18; H, 5.86%. Calcd for $C_{20}H_{18}O_4$: C, 74.52; H, 5.63%. The mp and PMR data agreed with that on Flemichapparin-A in the literature.[1-c] (lit,[1-c] mp 191—192 °C; PMR (δ, $CDCl_3$); 1.50, 5.58, 6.76, 7.20—8.00, 13.60).

2′,5′-Dihydroxy-2,4-dimethoxy-3′,4′(5″,6″)2″,2″-dimethyl-α-pyranochalcone (V). Yield, 63%, mp 214—215 °C (yellow plates). IR (cm^{-1}, KBr disk): 3400 (-OH), 1640 (C=O), 1365 ($-OCH_3$), 1235, 1030 (-C-O-C-), 930 (*trans* RHC=CHR), 730 (*cis* RHC=CHR). PMR (δ, $CDCl_3$): 1.50 (6H, s, $-C(CH_3)_2$), 3.86 (6H, s, $-OCH_3$), 5.58 (1H, d, J=10.0 Hz, 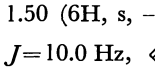), 6.45 (1H, s, -OH), 6.77 (1H, d, J=10.0 Hz, 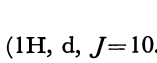), 6.50—7.50 (4H, m), 7.50(1H, d, J=15.5 Hz, 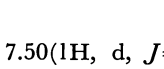), 8.12 (1H, d, J=15.5 Hz, 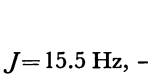), 13.60 (1H, s, -OH). Found C, 69.08; H, 5.68%. Calcd for $C_{22}H_{22}O_6$: C, 69.10; H, 5.80%.

2′,5′-Dihydroxy-3,4-dimethoxy-3′,4′(5″,6″)2″,2″-dimethyl-α-

pyranochalcone (VI). Yield, 54%, mp 192—193 °C (orange plates). IR (cm^{-1}, KBr disk): 3400 (-OH), 1640 (C=O), 1360, 1170 ($-OCH_3$), 1240, 1030 (-C-O-C-), 930 (*trans* RHC=CHR), 730 (*cis* RHC=CHR). PMR (δ, $CDCl_3$): 1.50 (6H, s, $-C(CH_3)_2$), 3.92 (6H, s, $-OCH_3$), 5.58 (1H, d, J=10.0 Hz, 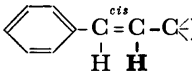), 6.77 (1H, d, J=10.0 Hz, 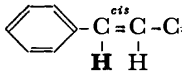), 6.95 (1H, s, -OH), 7.10—8.00 (4H, m), 7.25 (1H, d, J=15.5 Hz, 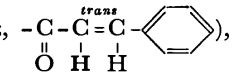), 7.60 (1H, d, J=15.5 Hz, 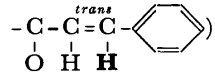), 13.47 (1H,s, -OH). Found C, 69.07; H, 5.78%. Calcd for $C_{22}H_{22}O_6$: C, 69.10; H, 5.80%.

2',5'-Dihydroxy-4-methoxy-3',4'(5'',6'')2'',2''-dimethyl-α-pyranochalcone (VII). Yield, 59%; mp 196—197 °C (orange plates). IR (cm^{-1}, KBr disk): 3400 (-OH), 1640 (C=O), 1360, 1170 ($-OCH_3$), 1240, 1030 (-C-O-C-), 930 (*trans* RHC=CHR), 730 (*cis* RHC=CHR). PMR (δ, $CDCl_3$): 1.50 (6H, s, $-C(CH_3)_2$), 3.92 (3H, s, $-OCH_3$), 5.60 (1H, d, J=10.0 Hz, 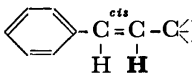), 6.79 (1H, d, J=10.0 Hz, 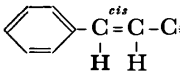), 7.00 (1H, s, -OH), 7.10—7.70 (5H, m), 7.60 (1H, d, J=15.5 Hz, 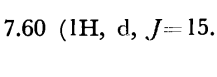), 8.20 (1H, d, J=15.5 Hz, 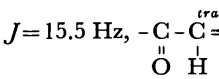), 13.48 (1H, s, -OH). Found C, 71.59; H, 5.84%. Calcd for $C_{21}H_{20}O_5$: C, 71.58; H, 5.72%.

References

1) a) B. S. Bajawa, P. L. Khanna, and T. R. Seshadri, *Curr. Sci.*, **41**, 814 (1972). b) G. Cardillo, L. Merlini, and R. Mondelli, *Tetrahedron*, **24**, 497 (1968). c) G. Cardillo, A. Gennaro, L. Merlini, G. Nasini, and S. Servi, *Tetrahedron Lett.*, **1970**, 4367. d) S. K. Mukerjee, P. Sharma, and T. R. Seshadri, *Indian J. Chem.*, **10**, 585 (1972).

2) a) G. Cardillo and L. Merlini, *Tetrahedron*, **24**, 4825 (1968). b) W. M. Bandaranayake, L. Crombie, and T. R. Whiting, *Chem. Commum.*, **1969**, 58. c) S. K. Mukerjee, P. Sharma, and T. R. Seshadri, *Indian J. Chem.*, **11**, 985 (1973). d) N. Adityachaudhury, D. Ghosh, A. Chaudhury, and C. L. Kirtania, *J. Indian Chem. Soc.*, **50**, 363 (1973).

3) a) Presented at 26th Annual Meeting of the Chemical Society of Japan, Tokyo, April, 1972, Preprint Vol. III, p. 1639 (1972). b) Presented at the Meeting of the Chemical Society of Japan (Tokai branch), Preprint, p. 191 (1973).

BULLETIN OF THE CHEMICAL SOCIETY OF JAPAN, VOL. 48(8), 2393—2394 (1975)

Photolysis of Aromatic Oxime Esters. Finding of Aromatic Substitution by Diphenylmethyleneimino Radicals

Hiroyuki OHTA and Katsumi TOKUMARU

Department of Chemistry, Faculty of Science, The University of Tokyo, Hongo, Bunkyo-ku, Tokyo 113

(Received February 5, 1975)

Synopsis. Diphenylmethyleneimino radicals, $Ph_2C{=}N\cdot$, generated from photolysis of benzophenoxime benzoates undergo aromatic substitution on benzene as well as dimerization into azine. On the other hand, phenylmethyleneimino radicals, $PhCH{=}N\cdot$, generated from photolysis of benzaldoxime benzoate are oxidized to benzonitrile in preference to dimerization.

Recently increasing interest has been paid to photochemical behaviour of carbon-nitrogen double bond.[1] Our interest in free radicals containing carbon-nitrogen double bond moiety[2] led us to investigate generation and behaviours of imino radicals by conducting photolysis of aromatic oxime esters in benzene. Previously, Okada, Kawanisi and Nozaki reported that irradiation of aromatic ketoxime benzoates afforded the corresponding ketazines probably through combination of the intermediate ketimino radicals but benzaldoxime benzoate did not afford benzaldazine.[3] Vermes and Beugelmans reported that the irradiation of steroidal oxime esters gave their parent oximes and ketones.[4] We now add new findings to photochemistry of benzophenoxime benzoates and benzaldoxime benzoate in benzene to show that the ketimino radicals undergo, in addition to their dimerization into the ketazine, nuclear substitution on benzene, whereas the aldimino radicals are oxidized to benzonitrile in preference to their dimerization into benzaldazine.

Results and Discussion

Benzophenoxime benzoate (Ia), *p*-methoxybenzoate (Ib), *p*-chlorobenzoate(Ic) and benzaldoxime benzoate(II) were photolyzed in benzene with a 400 W high pressure mercury lamp through Pyrex wall under nitrogen or oxygen without any added sensitizer or with benzophenone or naphthalene. The volatile products were determined as summarized in Table 1.

Photolysis of Ia gave, along with benzophenone azine(III) (20%), benzophenone, biphenyl, phenyl benzoate, benzoic acid and *N*-(diphenylmethylene)-aniline(IVa). The presence of oxygen in the photolysis remarkably increased the yields of benzophenone and phenyl benzoate accompanied by decrease of the yields of IVa and biphenyl. These products are understood to arise from diphenylmethyleneimino radicals (V) or benzoxyl radicals generated by photochemical homolysis of nitrogen-oxygen linkage of Ia.

$$Ph_2C{=}NOCOAr\ (I) \xrightarrow{h\nu} Ph_2C{=}N\cdot\ (V) + ArCO_2\cdot$$

Ar: a, C_6H_5; b, *p*-$CH_3OC_6H_4$; c, *p*-ClC_6H_4

The resulting benzoxyl radicals undergo the established reactions. Thus, they undergo aromatic substitution induced by oxygen to afford phenyl benzoate[5] or decarboxylation into phenyl radicals which substitute

TABLE 1. VOLATILE PRODUCTS FROM THE IRRADIATION OF BENZOPHENOXIME BENZOATE(Ia), *p*-METHOXYBENZOATE(Ib), *p*-CHLOROBENZOATE(Ic) AND BENZALDOXIME BENZOATE(II) IN BENZENE AT ROOM TEMPERATURE WITH A HIGH PRESSURE MERCURY LAMP

Ester[a]	Products (%)					
	Ph_2CO	ArPh[e]	$ArCO_2Ph$[e]	$PhCO_2H$	PhCR=NPh[f]	PhCN
Ia	27	14	10	g	6.4	
Ia[b]	89	1.2	60	g	0.6	
Ia[c]	g	22	15	g	16	
Ia[d]	21	14	10	g	6.5	
Ib	14	16	3	g	9	
Ib[c]	g	22	3	g	23	
Ic	g	13	g	g	8	
Ic[c]	g	20	g	g	25	
Ic[d]	g	14	g	g	5	
II		9.7	3	23	trace	40
II[b]		0.8	33	19	g	62
II[c]		17	g	g	g	28
II[d]		8	1	26	2	50

a) Under nitrogen except b) in 0.025 M. b) Under oxygen atmosphere. c) Benzophenone was added (0.025 M). d) Naphthalene was added (0.025 M). e) Ar: C_6H_5, *p*-$CH_3OC_6H_4$, *p*-ClC_6H_4 and C_6H_5 for Ia, Ib, Ic and II, respectively. f) R: Ph and H for I and II, respectively. g) Not determined.

on benzene to give biphenyl and its yield is reduced under oxygen due to the consumption of phenyl radicals by oxygen.[6]

$$PhCO_2\cdot + C_6H_6 \rightleftharpoons PhCO_2C_6H_6\cdot \xrightarrow{O_2} PhCO_2C_6H_5$$

On the other hand, the imino radicals, V, arising from I either dimerize into the azine, III, or substitute on benzene to afford IVa, or give benzophenone.

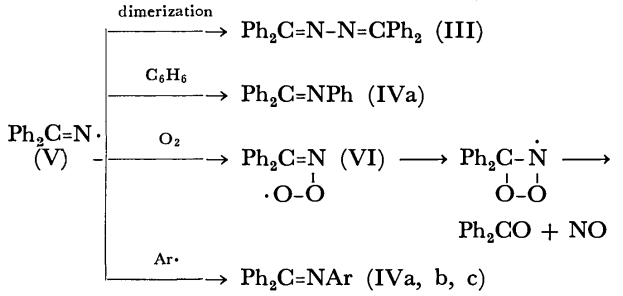

In view that vinylic radicals react with oxygen resulting in the oxidative cleavage of their unsaturated bonds,[7] it is reasonable to suppose that an imino radical combines with an oxygen molecule to give peroxy radical (VI), which would undergo intramolecular addition followed by decomposition to give benzophenone and nitric oxide, though detection of nitric oxide was not attempted.[8] Formation of benzophenone in the irradiation under nitrogen could be attributable to either reaction of the imino radical with oxygen eventually present or hydrolysis of the resulting benzophenone imine benzoate[3] with water adventitiously present or possible rearrangement of Ia into oxaziridine followed by its cleavage.[4]

Production of the imine, IVa, from Ia is mostly ascribed to substitution of the imino radical on benzene not to recombination between the imino and phenyl radicals both generated from Ia, since irradiation of Ib and Ic in benzene also gave IVa along with negligible amount of *N*-(*p*-methoxyphenyl)imine(IVb) and *N*-(*p*-chlorophenyl)imine(IVc), respectively. So, it is clear that the geminate reaction between the imino radical and aryl radical arisen from I does not effectively take place.

In the irradiation of I, the presence of naphthalene, which was attempted to be used as a sensitizer, did not affect the products formation. However, use of benzophenone remarkably increased the yield of IVa and moderately increased the yield of biphenyl; thus, aromatic substitutions by the imino radicals and phenyl radicals seem to be promoted by the presence of benzophenone. This fact is not attributable to the action of benzophenone molecules in their ground state on cyclohexadienyl-type radicals resulting from the addition of the imino radicals or phenyl radicals on benzene molecules, since a control experiment showed that the presence of benzophenone in thermal decomposition of dibenzoyl peroxide in benzene did not increase the yield of biphenyl. Therefore, benzophenone in the excited state seems to be responsible for this effect.

Irradiation of II is now shown to afford benzonitrile as a main product. Production of biphenyl, benzoic acid together with the effect of oxygen to increase the yield of phenyl benzoate shows that II is also photolyzed through N–O bond cleavage like I. An observed effect of oxygen to promote the production of benzonitrile suggests that benzonitrile results from phenylmethyleneimino radicals(VII) through their hydrogen atom transfer with other radicals or oxygen molecules.[9]

$$PhCH{=}N\cdot\ (VII) + R\cdot \longrightarrow PhCN + RH$$

R·: $PhCO_2\cdot$, Ph· or O_2 *etc.*

A possibility that irradiation of II would give benzaldazine and its subsequent photolysis would give benzonitrile seems to be excluded on the basis that irradiation of II did not afford stilbene which would be produced from photolysis of benzaldazine.[9]

Experimental

Benzophenoxime benzoate (Ia), *p*-methoxybenzoate (Ib), *p*-chlorobenzoate (Ic) and benzaldoxime benzoate (II) were prepared according to literature.[10,11] Irradiation was carried out for 0.025 M benzene solution (400 ml) with a 400 W Riko high pressure mercury lamp. The reaction mixture was shaken with aqueous sodium hydrogen carbonate to extract benzoic acid and the remaining solution was used for product analysis. In vpc analysis with a Hitachi K53 gas chromatograph, benzonitrile and benzaldehyde were determined with a 4 m series of columns of silicone and polyethyleneglycol sebaciate at 160 °C, and biphenyl, benzophenone, phenyl benzoate and IVa were determined with a 6 m or 4 m column of silicone at 240 °C. Production of benzophenone azine was confirmed by its separation through column chromatography over silica gel.

References

1) As reviews, a) G. Wettermark, "Chemistry of Carbon-Nitrogen Double Bond," ed. by S. Patai, John Wiley, New York (1970), Chapter 12. b) H. Ohta and K. Tokumaru, *Yuki Gosei Kagaku Kyokaishi*, **30**, 1006 (1972). c) A. Padwa, M. Dharan, J. Smolanoff, and S. I. Wetmore, Jr., *Pure Appl. Chem.*, **33**, 269 (1973); d) K. Tokumaru, *Kagaku*, **29**, 68 (1974).

2) H. Ohta and K. Tokumaru, *Chem. Commun.*, **1970**, 1601; *Chem. Ind.*, **1971**, 1301; *Chem. Lett.*, **1974**, 1403.

3) T. Okada, M. Kawanisi, and H. Nozaki, This Bulletin, **42**, 2981 (1969).

4) J. P. Vermes and R. Beugelmans, *Tetrahedron Lett.*, **1969**, 2091; R. Beugelmans and J. P. Vermes, *Bull. Soc. Chim. France*, **1970**, 342.

5) T. Nakata, K. Tokumaru, and O. Simamura, *Tetrahedron Lett.*, **1967**, 3303.

6) K. Tokumaru, K. Horie, and O. Simamura, *Tetrahedron*, **21**, 867 (1965).

7) K. Tokumaru, *Chem. Ind.*, **1969**, 291; N, Wada and K. Tokumaru, This Bulletin, **45**, 2787 (1972).

8) For the production of benzophenone under oxygen, a possibility that under the reaction condition the resulting azine would suffer sensitized oxygenation to give a cyclic peroxide (G. Rio and J. Berthelot, *Bull. Soc. Chim. France*, **1970**, 1509) followed by its decomposition into benzophenone and nitrogen may not be excluded.

9) R. W. Binkley, *J. Org. Chem.*, **34**, 931, 2072, 3218 (1969).

10) O. L. Brady and G. P. Mc Hugh, *J. Chem. Soc.*, **1925**, 2421.

11) A. W. Chapman and C. C. Howis, *ibid.*, **1933**, 806.

BULLETIN OF THE CHEMICAL SOCIETY OF JAPAN, VOL. 48(8), 2395—2396 (1975)

A Convenient Synthesis of 2,3-Benzotropone from α-Tetralone by Ring-expansion

Masaru SATO, Takashi TANAKA, Josuke TSUNETSUGU, and Seiji EBINE

Department of Chemistry, Faculty of Science and Engineering, Saitama University, Urawa, Saitama 338

(Received February 6, 1975)

Synopsis. 2,3-Benzotropone (**1**) has conveniently been prepared from easily available α-tetralone (**2**) in good overall yield by the following successive reactions: dihalocarbene addition to enol-ether (**3**) derived from **2**, ring-expansion of the adduct (**4**) to halobenzocycloheptadienone (**5**), and dehydrohalogenation of **5** giving **1**.

2,3-Benzotropone (**1**) is synthesized from 2,3-benzosuberone *via* 7,7-dibromo-2,3-benzosuberone.[1] We now report an alternate method of synthesizing **1** from easily available α-tetralone (**2**) by ring-expansion by modification of Birch and co-workers' synthetic method for monocyclic tropone[2] and nezukone[3] from six-membered ring compounds.

α-Tetralone (**2**) was converted with ethyl orthoformate in the presence of an acid catalyst into 1-ethoxy-3,4-dihydronaphthalene (**3**) in excellent yield [IR(neat), 1636 cm^{-1} for olefinic double bond; NMR (CCl_4), δ 5.33 (t, 1H) for an olefinic proton, 4.32 (q, 2H) and 1.83 (t, 3H) for ethyl protons]. The enol-ether (**3**) reacted with dihalocarbene by Makosza's method[4,5] to give adducts (**4a**, X=Br and **4b**, X=Cl) in good yields (IR and NMR spectra showed the absence of olefinic structure). **4a** was treated with aqueous silver tetrafluoroborate in ethanol at room temperature overnight to give 7-bromo-2,3-benzocyclohepta-2,6-dien-1-one (**5a**)[1] in 79% yield. On the other hand, **4b** did not react at room temperature but reacted with silver tetrafluoroborate under reflux for 45 min in ethanol to give chloro-ketone (**5b**) (31% yield) and **1** (3% yield) along with recovery of the starting material (43%). On Birch and co-workers' synthesis of monocyclic tropones,[2,3] the corresponding seven-membered cyclic dienones were not isolated. The compounds **5a** and **5b** were dehydrohalogenated by the method of Holysz[6] to give **1** in 91 and 86% yields, respectively. Thus, the reaction sequence, **2**—**3**—**4a**—**5a**—**1**, can serve a convenient route for preparing **1** (45% over-all yield).

Reaction of **4a** and **4b** with silver tetrafluoroborate under reflux in ethanol and chromatographic separation of the reaction mixture gave **1** directly in 41 and 35% yields respectively, which also constitutes an additional convenient route to **1**.

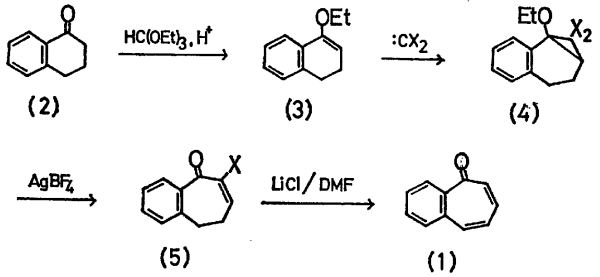

a: X=Br, b: X=Cl

Experimental

*1-Ethoxy-3,4-dihydronaphthalene (**3**).* To a solution of α-tetralone (**2**) (20 g, 0.137 mol) and ethyl orthoformate (27.2 ml, 0.164 mol) in anhydrous alcohol (20 ml) was added a few drops of concentrated sulfuric acid. After refluxing for 30 min under nitrogen atmosphere, the solution was allowed to stand for 2 days at room temperature. The reaction mixture was basified with sodium ethoxide, and then evaporated under reduced pressure. The residue was chromatographed on alumina with elution of benzene to give 1-ethoxy-3,4-dihydronaphthalene (**3**) (20.2 g, 84.7%) as a colorless liquid, bp 100—101 °C/2 mmHg. Found: C, 82.86; H, 7.93%. Calcd for $C_{12}H_{14}O$: C, 82.77; H, 8.10%. IR(neat): 1636, 1250 and 1065 cm^{-1}; NMR(CCl_4): δ 1.83 (t, 3H, J=7 Hz), 2.52—2.90 (m, 2H), 3.07—3.33 (m. 2H), 4.32 (q, 2H, J=7 Hz), 5.33 (t, 1H, J=4.5 Hz), 7.40—7.7 (m, 3H) and 7.83—8.05 (m, 1H).

*Dibromocarbene Adduct (**4a**).* To a mixture of **3** (6.87 g, 0.04 mol), bromoform (7.0 ml, 0.08 mol) and triethylbenzylammonium chloride (0.15 g) was added 50% aqueous sodium hydroxide (14 ml) and the solution was stirred at 40 °C for 3 hr. The resulting solution was diluted with water and extracted with dichloromethane. The extract, after washing with water and drying over sodium sulfate, was evaporated and the residual oil was chromatographed on alumina with elution of benzene-hexane (1 : 1). The dibromocarbene adduct (**4a**) was obtained as a nearly colorless oil (10.2 g, 75%), which solidified on standing in a refrigerator. Recrystallization from ethanol gave colorless crystals, mp 61—62 °C. Found: C, 45.26; H, 4.38%. Calcd for $C_{13}H_{14}Br_2O$: C, 45.12; H, 4.08%. IR (KBr): 1053 cm^{-1}; NMR (CCl_4): δ 1.20 (t, 3H, J=7 Hz), 1.86—2.45 (m, 3H), 2.45—2.94 (m, 2H), 3.46 (q, 2H, J=7 Hz), 6.91—7.45 (m, 3H) and 7.52—7.81 (m, 1H).

*Dichlorocarbene Adduct (**4b**).* A mixture of **3** (3.5 g, 0.02 mol), chloroform (2.4 ml, 0.03 mol), 50% aqueous sodium hydroxide (3.8 ml) and triethylbenzylammonium chloride (170 mg) was stirred for 4 hr at 45 °C. The mixture was diluted with water, extracted with dichloromethane, the extract was dried over sodium sulfate, and evaporated. The residual oil was chromatographed on alumina to give the adduct (**4b**) (4.03 g, 78%) as a nearly colorless liquid, bp 118 °C/3.5 mmHg. IR (neat): 1061 and 895 cm^{-1}; NMR (CCl_4): δ 1.17 (t, 3H, J=7 Hz), 1.90—2.50 (m, 3H), 2.50—2.87 (m, 2H), 3.42 (q, 2H, J=7 Hz), 6.90—7.40 (m, 3H) and 7.50—7.70 (m, 1H). Found: C, 60.94; H, 5.46%. Calcd for $C_{13}H_{14}Cl_2O$: C, 60.72; H, 5.49%.

*Treatment of **4a** with Silver Tetrafluoroborate.* To a solution of silver tetrafluoroborate prepared from silver oxide (5.0 g, 0.022 mol), 42% fluoroboric acid (40 ml) and ethanol (80 ml) was added the dibromocarbene adduct (**4a**) (7.0 g, 0.020 mol), and the mixture was stirred at room temperature for 16 hr. The reaction mixture was poured into saturated aqueous sodium chloride to give a precipitate which was filtered and washed with dichloromethane thoroughly. The filtrate and the washings were combined and extracted with

dichloromethane. The extract was washed with aqueous sodium bicarbonate and with water, then dried over sodium sulfate, and evaporated. The residue was chromatographed on silica gel to give the starting substance (0.22 g, 3.1%), 7-bromo-2,3-benzocyclohepta-2,6-dien-1-one[1] (**5a**) (3.80 g, 79.4%), and an unknown oil A (0.52 g, ν_{CO} 1679 cm^{-1}). **5a** solidified on standing in refrigerator and recrystallized from ethanol to give pale yellow crystals, mp 39—40 °C.

When the same reaction was performed under refluxing for 2 hr, there resulted **5a** (0.19 g, 4%), **1** (1.28 g, 41%), an unknown oil B (0.50 g, ν_{CO} 1677 and 1713 cm^{-1}) and an unknown oil C (0.28 g, ν_{CO} 1728 cm^{-1}).

*Treatment of **4b** with Silver Tetrafluoroborate.* A solution of **3b** (1.80 g, 7 mmol) in ethanol (15 ml) was added to a solution of silver tetrafluoroborate prepared from silver oxide (1.85 g, 8 mmol) and 42% fluoroboric acid (15 ml), and the mixture was gently refluxed on a water bath for 45 min. After the same work-up as described in **4a**, the starting material (0.78 g, 43%), the chloro ketone (**5b**) (0.43 g, 31%) and **1** (0.05 g, 3%) were obtained. **5b** was a pale yellow oil. Found: C, 68.77; H, 4.60%. Calcd for $C_{11}H_9ClO$: C, 68.58;, H, 4.70%. IR (neat): 1661 (vs), 1613 and 1600 cm^{-1}. NMR (CCl_4): δ 2.47—2.80 (m, 2H), 2.90—3.18 (m, 2H), 7.0—7.5 (m, 4H) and 7.5—7.8 (m, 1H).

The 4 hr's refluxing of the solution of **4b** (1.56 g, 6 mmol), silver oxide (2.1 g, 9 mmol), 42% fluoroboric acid (16 ml) and ethanol (16 ml) gave **1** (0.33 g, 35%) and an unknown oil C (0.13 g).

*Dehydrobromination of **5a**.* A solution of **5a** (805 mg, 3.4 mmol), lithium chloride (4.2 g) in dimethylformamide (50 ml) and benzene (15 ml) was heated under nitrogen atmosphere. After the benzene was removed azeotropically (30 min), the solution was refluxed for one hr. It was poured into water and extracted with benzene. The extract was washed with water, dried over sodium sulfate, and evaporated. The residual oil was chromatographed on silica gel with benzene–ether eluent to give **1** (480 mg, 91%).

*Dehydrochlorination of **5b**.* Refluxing of a solution of **5b** (0.38 g, 2 mmol) and lithium chloride (2.5 g, 0.06 mol) in dimethylformamide (30 ml) for 2 hr under similar conditions followed by the same work-up as above gave **1** (0.27 g, 86%).

References

1) E. W. Collington and G. Jones, *J. Chem. Soc. C*, **1969**, 1656.
2) A. J. Birch and J. M. H. Graves, *Proc. Chem. Soc.*, **1962**, 282.
3) A. J. Birch and R. Keeton, *J. Chem. Soc. C*, **1968**, 109.
4) M. Mokosza and W. Wawryniewcz, *Tetrahedron Lett.*, **1969**, 4659.
5) M. Makosza and M. Fedorynski, *Synth. Commun.*, **1973**, 305.
6) R. P. Holysz, *J. Amer. Chem. Soc.*, **75**, 4432 (1953).

BULLETIN OF THE CHEMICAL SOCIETY OF JAPAN, VOL. 48(8), 2397—2398 (1975)

N-Alkyldiarylamines from 3-Alkyl-3-aryl-1-(2-carboxyphenyl)triazenes

Jyuzo NAKAYAMA, Masayuki YOSHIDA, and Osamu SIMAMURA

Department of Chemistry, Faculty of Science, Tokyo University, Hongo, Tokyo 113

(Received December 24, 1974)

Synopsis. Heating 3-alkyl-3-aryl-1-(2-carboxyphenyl)triazenes in organic media afforded *N*-alkyldiarylamines in good yields, thus providing a useful synthetic route to this type of amines.

We have shown that 3-substituted 1-(2-carboxyphenyl)triazenes (I) are decomposed in boiling chlorobenzene in the presence of 2,3,4,5-tetraphenylcyclopentadienone to afford 1,2,3,4-tetraphenylnaphthalene, a benzyne adduct, in good yields,[1] while in the absence of the cyclopentadienone 1-(2-carboxyphenyl)-3,3-dimethyltriazene (I; $R^1=R^2=CH_3$) gave *N*,*N*-dimethylaniline (32%) and *N*-methyldiphenylamine (37%) the, products suggestive of the benzyne reaction with dimethylamine and *N*,*N*-dimethylaniline, respectively, in view of the work by Lepley and his co-workers.[2] Furthermore, heating 1-(2-carboxyphenyl)-3-methyl-3-phenyltriazene (Ia; $R^1=CH_3$, $R^2=C_6H_5$) gave *N*-methyldiphenylamine in 72% yield as the sole product. We, therefore, examined the formation of *N*-alkyldiarylamines (II) from 3-alkyl-3-aryl-1-(2-carboxyphenyl)triazenes (I) as a new synthetic route.

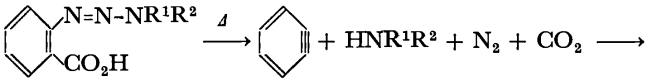

(I)

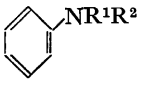

(II)

The triazenes (I) listed in Table 1 were prepared in excellent yields by diazotization of anthranilic acid by means of sodium nitrite and hydrochloric acid followed by treatment with potassium acetate and *N*-alkylarylamines. With *N*-*sec*-butylaniline and *N*-ethyl-1-aminonaphthalene, however, the azo-coupling reaction took place under the same reaction conditions, affording 4-(*sec*-butylamino)-2′-carboxyazobenzene (III) and 1-(2-carboxyphenylazo)-4-ethylaminonaphthalene (IV), respectively. Weakly basic amines such as diphenylamine and *N*-methyl-4-nitroaniline did not yield any amount of the expected triazenes (I).

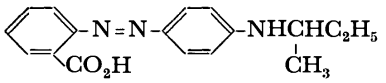

(III)

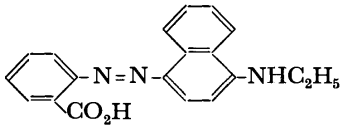

(IV)

Decomposition of the triazenes (I) by heating in organic solvent under reflux gave *N*-alkyldiarylamines (II), and the results are summarized in Table 2. Generally, the yields of *N*-alkyldiarylamines (II) are satisfactory, but 1-(2-carboxyphenyl)-3-phenyltriazene[3] (I; $R^1=H$, $R^2=C_6H_5$) yielded, on being decomposed in boiling chlorobenzene, a mixture of chlorobiphenyls (69%), but no diphenylamine. Evidently, it decomposed homolytically in chlorobenzene to generate phenyl radicals, presumably *via* a diazocarboxylate (V).

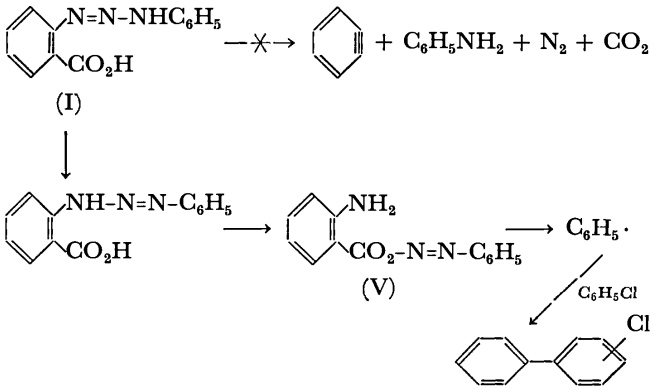

(I)

(V)

Table 1. 3-Alkyl-3-aryl-1-(2-carboxyphenyl)triazenes (I)

Compound	R^1	R^2	Mp (°C)	Yield (%)	Formula		Elementary analysis (%) C	H	N
Ia	CH_3	C_6H_5	137 (dec)	96	$C_{14}H_{13}N_3O_2$	Found	66.12	4.89	16.73
						Calcd	65.87	5.13	16.46
Ib	C_2H_5	C_6H_5	118 (dec)	93	$C_{15}H_{17}N_3O_2$	Found	67.06	5.51	15.31
						Calcd	66.90	5.61	15.61
Ic	*n*-C_4H_9	C_6H_5	72— 73 (dec)	94	$C_{17}H_{19}N_3O_2$	Found	68.43	6.40	14.34
						Calcd	68.66	6.44	14.13
Id	$C_6H_5CH_2$	C_6H_5	135—136 (dec)	85	$C_{20}H_{17}N_3O_2$	Found	72.45	5.09	12.98
						Calcd	72.49	5.17	12.68
Ie	C_2H_5	*p*-$CH_3C_6H_4$	124—125 (dec)	93	$C_{16}H_{17}N_3O_2$	Found	67.95	6.05	14.62
						Calcd	67.82	6.05	14.83
If	$C_6H_5CH_2$	*p*-ClC_6H_4	152 (dec)	68	$C_{20}H_{16}ClN_3O_2$	Found	65.92	4.49	11.20
						Calcd	65.67	4.41	11.49

Table 2. *N*-Alykyldiarylamines (II) from the triazenes (I)

Compound	Reaction Conditions[a]	II ($PhNR^1R^2$)			
		R^1	R^2	Yield (%)[b]	Bp (°C/mmHg) or [mp (°C)]
Ia	PhCl, refl., 5 hr	CH_3	C_6H_5	72	122—124/2[c]
Ib	PhCl, refl., 5 hr	C_2H_5	C_6H_5	63	127—129/2[d]
	$PhCH_3$, refl., 8 hr			68	
Ic	Xylene, refl., 5 hr	*n*-C_4H_9	C_6H_5	64	145—147/2[e]
Id	Xylene, refl., 4 hr	$C_6H_5CH_2$	C_6H_5	56	[86— 87][f]
Ie	PhCl, refl., 5 hr	C_2H_5	*p*-$CH_3C_6H_4$	77	106—108/0.4
If	PhCl, refl., 9 hr	$C_6H_5CH_2$	*p*-ClC_6H_4	63	[97— 97.5]

a) Refl. stands for heated under reflux. b) By weighing the isolated material. c) 175/31 (Ref. 4). d) 150/13 (Ref. 4). e) 164/11 (Ref. 4). f) [87] (Ref. 5).

Thus, generally the triazenes (I) are prepared easily from diazotized anthranilic acid and appropriate *N*-alkylarylamines in excellent yields and decompose at moderate temperatures to give satisfactory yields of the amines (II); accordingly the present method provides a useful synthetic route to the amines (II), which are otherwise prepared by the alkylation of diarylamines.[4-6]

Experimental

3-Alkyl-3-aryl-1-(2-carboxyphenyl)triazenes (I). Anthranilic acid (13.7 g, 0.1 mol) was dissolved in a mixture of 200 ml of methanol and 25 ml of concentrated hydrochloric acid and diazotized by addition of a solution of sodium nitrite (6.9 g, 0.1 mol) in 15 ml of water at 0—5 °C. To the resulting diazonium solution were added 200 g of crushed ice, 20 g of powdered potassium acetate (0.2 mol), and an appropriate *N*-alkylarylamine (0.1 mol). The mixture was stirred for 1 hr at 0—5 °C and then for 30 min at room temperature. 3-Alkyl-3-aryl-1-(2-carboxyphenyl)triazene (I) was precipitated by adding 200 ml of water, collected, washed with water and recrystallized from benzene or ethanol.

4-(sec-Butylamino)-2'-carboxyazobenzene (III) and 1-(2-carboxyphenylazo)-4-ethylaminonaphthalene (IV). These azo-compounds (III and IV) were obtained when *N-sec*-butylaniline and *N*-ethyl-1-aminonaphthalene were used in the preparation of triazoles (I).

Compound III (Found: C, 68.44; H, 6.37; N, 14.42%. Calcd for $C_{17}H_{19}N_3O_2$: C, 68.66; H, 6.44; N, 14.13%), mp 156 °C, ν_{max} (KBr) 3370 (N-H), 2800—2300 (O-H), 1715 (C=O), and 828 (*p*-disubstituted benzene ring) cm^{-1}.

Compound IV (Found: C, 71.41; H, 5.47; N, 12.98%. Calcd for $C_{19}H_{17}N_2O_2$: C, 71.45; H, 5.37; M, 13.16%), mp 185—187 °C, ν_{max} (KBr) 3330 (N-H) and 1700 (C=O) cm^{-1}.

N-Alkyldiarylamines (II). A triazene (I, 10 g) was heated under reflux in 200 ml of solvent for several hr. On cooling, the reaction mixture was washed successively with 1 M sodium hydroxide, 1 M hydrochloric acid, and water and dried over anhydrous sodium sulfate. The solvent was removed under reduced pressure and the residue was purified by distillation or recrystallization. Elementary analyses and spectral data for new *N*-alkyldiarylamines (II, $PhNR^1R^2$) are shown below.

Compound IIe ($R^1=C_2H_5$, $R^2=p$-$CH_3C_6H_4$) (Found: C, 84.96; H, 7.87; N, 6.86%. Calcd for $C_{15}H_{17}N$: C, 85.26; H, 8.11; N, 6.63%), bp 106—108 °C/0.4 mmHg; NMR ($CDCl_3$) δ 1.15 (t, 3H), 2.15 (s, 3H), 3.66 (q, 2H), and 6.5—7.3 (m, 9H).

Compound IIf ($R^1=C_6H_5CH_2$, $R^2=p$-ClC_6H_4) (Found: C, 77.72;, H, 5.74; N, 4.90%. Calcd for $C_{19}H_{16}ClN$: C, 77.68; H, 5.49; N, 4.77%), mp 97—97.5 °C; NMR (CCl_4) δ 1.15 (t, 3H), 2.15 (s, 3H), 3.66 (q. 2H), and 6.5—7.3 (m, 9H).

Decomposition of 1-(2-carboxyphenyl)-3-phenyltriazene (I; $R^1=H$, $R^2=C_6H_5$) in chlorobenzene. A solution of the triazene (I, 0.62 g) in 50 ml of chlorobenzene was heated under reflux for 2 hr. The reaction mixture was washed successively with 1 M hydrochloric acid, 1 M sodium hydroxide, and water, and dried over anhydrous sodium sulfate. After removal of chlorobenzene under reduced pressure, the brown oily residue was subjected to column chromatography on silica gel. Elution with benzene afforded 0.29 g of chlorobiphenyl (69%), consisting of the *ortho* (55%) and a mixture (45%) of the *meta* and *para* isomers, as revealed by vpc analysis.

References

1) J. Nakayama, O. Simamura, and M. Yoshida, *Chem. Commun.*, **1970**, 1222.
2) A. R. Lepley, A. G. Giumanini, A. B. Giumanini, and W. A. Khan, *J. Org. Chem.*, **31**, 2051 (1966).
3) P. Grammaticakis, *Bull. Chim. Soc. Fr.*, **1957**, 139.
4) A. Skita, F. Keil, and H. Havemann, *Ber.*, **66**, 1400 (1933).
5) R. Meldola, *Ber.*, **14**, 1385 (1881).
6) E. Lippmann and F. Flissner, *Monatsh.*, **4**, 788 (1883).

BULLETIN OF THE CHEMICAL SOCIETY OF JAPAN, VOL. 48(8), 2399—2400 (1975)

Light Induced Hydrogen Isotope Exchange between Terephthalonitrile and Thiols

Masayuki YOSHIDA, Hirochika SAKURAGI, Itaru TANAKA, Katsumi TOKUMARU, and Naotake MORIKAWA*

Department of Chemistry, Faculty of Science, The University of Tokyo, Bunkyo-ku, Tokyo 113

**Radioisotope Centre, The University of Tokyo, Bunkyo-ku, Tokyo 113*

(Received April 17, 1975)

Synopsis. Interaction of an excited singlet state of terephthalonitrile with thiol is shown to be responsible for the title reaction on the basis of higher reactivity of terephthalonitrile relative to benzene and efficient quenching of fluorescene from terephthalonitrile by thiols.

We have shown that irradiation of mixtures of aromatic compounds and propanethiol tritiated at the S-H bond causes tritium uptake by the aromatic nucleus with distributions different from the results of substitutions by hydrogen ions and atoms.[1] In addition the rate of nuclear tritiation relative to benzene (k_{rel}) was found to be fairly high in benzonitrile and methyl benzoate (k_{rel}: 254 and 421, respectively). On the basis of these observations, the mechanism was proposed as involving a reaction of an excited aromatic molecule with propanethiol. The present paper describes the identification of light-induced hydrogen exchange reaction of terephthalonitrile with thiols and the determination of the excited state participating in the reaction.

When a solution of terephthalonitrile in benzene was irradiated with a high pressure mercury arc lamp under nitrogen atmosphere in the presence of *n*-pentanethiol-*d*, incorporation of deuterium occurs to an extent of 22% in the nucleus of terephthalonitrile recovered. With tritium labelled *n*-pentanethiol, tritiation took place in both the nuclei of terephthalonitrile and benzene, the relative rate of tritiation of terephthalonitrile (k_{rel}) being 3.8×10^3 and 4.1×10^3 (per C-H bond) in duplicate runs. The marked enhancement of the relative rate by introduction of one more cyano substituent into benzonitrile argues against that tritium atoms generated by photolysis of thiols contribute mainly to the exchange,[2] and involvement of an excited terephthalonitrile in the nuclear tritiation process is suspected. In this connection it is of interest to study on quenching of the excited singlet states of aromatic compounds by thiols.

TABLE 1. QUENCHING OF FLUORESCENCE FROM AROMATIC COMPOUNDS BY *n*-OCTANETHIOL IN AERATED BENZENE

Aromatic compound	$k_q\tau_s$, M^{-1}
Naphthalene	0.37
Anisole	9.38
Benzonitrile	36.7
Phthalonitrile	34.6
Isophthalonitrile	43.0
Terephthalonitrile	68.1

TABLE 2. QUENCHING OF TEREPHTHALONITRILE FLUORESCENCE BY THIOLS IN AERATED BENZENE

Thiol	$k_q\tau_s$, M^{-1}
n-Propanethiol	63.0
n-Pentanethiol	62.2
3-Methylbutanethiol	51.4
1-Methylbutanethiol	46.3
n-Octanethiol	68.1

The fluorescence of aromatic compounds, such as benzonitrile and phthalonitriles, in benzene was quenched by the addition of *n*-octanethiol. Stern-Volmer plots of the reciprocal of relative fluorescence intensities against *n*-octanethiol concentrations were obtained for aromatic compounds; the slopes of these plots ($k_q\tau_s$) are presented in Table 1, where k_q is the rate constant for quenching of the excited singlet state of an aromatic compound by *n*-octanethiol and τ_s is the singlet lifetime of that aromatic compound. Similarly, the slopes ($k_q\tau_s$) obtained from the quenching of terephthalonitrile fluorescence by several thiols are given in Table 2.

It is notable, from Tables, that the slope ($k_q\tau_s$) is pronounced in benzonitrile and phthalonitriles in accord with their high rate of the tritiation reaction, while it is only slightly affected with respect to the structure of thiols. From the quenching of terephthalonitrile fluorescence by oxygen ($k_q\tau_s$: 289 M^{-1}) the terephthalonitrile singlet lifetime under air (τ_s) was obtained to be 1.3×10^{-8} s by assuming that the quenching rate by oxygen[3] is diffusion-controlled (1.5×10^{10} M^{-1} s^{-1}).[4] As the observed slope ($k_q\tau_s$) for terephthalonitrile is 68.1 M^{-1}, this leads to an estimate for k_q of 5.2×10^9 M^{-1} s^{-1}, which is higher than k_q of naphthalene, 2×10^7 M^{-1} s^{-1}, obtained from $k_q\tau_s$ of 0.37 M^{-1} and τ_s (aerated) of 1.5×10^{-8} s.[5] The result shows that *n*-octanethiol is an effective quencher of the excited singlet state of terephthalonitrile with the quenching rate constant near to the diffusion controlled one.

In order to examine a possibility that the triplet state of terephthalonitrile would interact with thiols, attempts have been made to observe the effect of *n*-pentanethiol on the triplet lifetime (τ_T) of terephthalonitrile. A convenient way of determining τ_T in solution at room temperature has often been to apply flash spectroscopy, but such a method was not applicable due to a failure in observing T-T absorption of the triplet state in the case of terephthalonitrile. A rewarding approach results from the measurement of the terephthalonitrile phosphorescence lifetime in EPA at 77 K, in which τ_T (1.6 s) is unaffected in the presence of high concentration of *n*-pentanethiol (1.1 M).

Thus, the tritiation from the triplet state appears to be improbable.

From all these results it is conceivable that interaction of the singlet excited terephthalonitrile with the ground state thiol is responsible to induce the hydrogen isotope exchange.

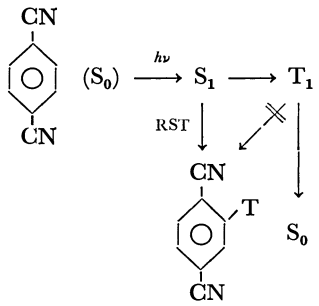

Experimental

Deuterium Exchange with Terephthalonitrile. A mixture of terephthalonitrile (1.57 mmol) and *n*-pentanethiol-*d* (16.5 mmol) in 30 ml of benzene was irradiated under nitrogen atomosphere for 20 hr with a 400 W high pressure mercury arc lamp. After removal of benzene and the thiol under reduced pressure, the residue was subjected to dry chromatography on silica gel. Elution with benzene gave 20 mg of the dinitrile. Deuterium included in the dinitrile was determined from its NMR spectrum in $CDCl_3$ using 1,4-dimethoxybenzene as an internal standard, reference being made to that of the authentic sample.

Tritium Exchange with Terephthalonitrile. A mixture of tritiated *n*-pentanethiol (0.992 mmol, 2.35×10^{12} dpm/mmol) and terephthalonitrile (0.499 mmol) in 10 ml of benzene was placed in a Pyrex tube, degassed by the usual chill and thaw cycles, and irradiated for 10 hr with a 1 kW high pressure mercury arc lamp using a merry-go-round photochemical reactor (RIKO Rotary Photochemical Reactor, Model RH 400-10W). After the irradiation, *n*-pentanethiol was removed by washing with aqueous sodium hydroxide and water. The amount of the dinitrile in the mixture (95 and 85% of the starting dinitrile for duplicate runs) was estimated by vpc on a 2 m column containing 10% XF 1150 on Chromosorb P at 200 °C. Benzene was recovered from the mixture by fractional distillation. To the residue 500 mg of the non-radioactive dinitrile was added and the combined dinitrile was purified by means of recrystallization until reproducible specific activities were obtained. The benzene distillate was washed further with aqueous basic hydrogen peroxide to remove traces of the radioactive thiol and submitted to tritium assay. Tritium activity was measured with a Packard Tri-Carb liquid scintillation spectrometer Model 3380. Each sample was counted for a period sufficient to reduce the randam error to 1% or less.

Quenching Studies. Fluorescence and phosphorescence spectra were recorded on a Hitachi fluorescence spectrophotometer MPF-2A.

References

1) H. Takiguchi, K. G. Yoshida, H. Ouchi, M. Yoshida, N. Morikawa, and O. Simamura, *Chem. Lett.*, **1974**, 593.

2) W. A. Pryor, T. H. Lin, J. P. Stanley, and R. W. Henderson, *J. Amer. Chem. Soc.*, **95**, 6993 (1973).

3) S. L. Murov, "Handbook of Photochemistry," Marcel Dekker, Inc., New York, N.Y. (1973), p. 55.

4) I. B. Berlman, "Handbook of Fluorescence Spectra of Aromatic Molecules," 2nd Ed., Academic Press, New York, N.Y. (1971), p. 58.

5) *Idem, ibid.*, p. 330.

BULLETIN OF THE CHEMICAL SOCIETY OF JAPAN, VOL. 48(8), 2401—2402 (1975)

Synthesis of Acyl Derivatives of β-Lysine for Peptide Synthesis

Tateaki WAKAMIYA, Hiroshi URATANI, Tadashi TESHIMA, and Tetsuo SHIBA

Department of Chemistry, Faculty of Science, Osaka University, Toyonaka, Osaka 560

(Received May 17, 1975)

Synopsis. Dibenzyloxycarbonyl- and di-*t*-butyloxycarbonyl-L-β-lysine were synthesized from corresponding diacyl-L-ornithine by modified Arndt-Eistert reaction involving diazoketone preparation *via* the mixed carbonic carboxylic anhydride. These diacyl-β-lysine derivatives are required for total- or semi-syntheses of peptide antibiotics, tuberactinomycins or streptothricins.

β-Lysine had been first found as a naturally occurring amino acid in the hydrolyzate of viomycin,[1] and thereafter isolated from streptolin,[2] streptothricin,[3] and similar antibiotics. In our recent studies on tuberculostatic peptide, tuberactinomycins, the presence of this amino acid was confirmed in tuberactinomycin B, *i.e.* viomycin, and also in tuberactinomycin O.[4]

Synthesis of the amino acid had been achieved by van Tamelen *et al.* for the purpose of a determination of its chemical structure.[2,3] In their method, N^{α},N^{δ}-diphthalyl-L-ornithine was elongated by Arndt-Eistert reaction and then hydrolyzed to 3,6-diaminohexanoic acid, *i.e.* β-lysine. In the course of this reaction, two amino groups had to be blocked with phthalyl group for the complete protection against a possible change with the acid chloride reagent which was used in the preparation of the diazoketone. On the other hand, benzyloxycarbonyl or *t*-butyloxycarbonyl group is preferable from a standpoint of the peptide synthesis where easily removable protecting groups are required. If the use of the acid chloride can be avoided by application of the mixed carbonic carboxylic anhydride method for the preparation of acylaminodiazoketone as in the case of simple diazoketones,[5] those alkyloxycarbonyl type protections may be employed instead of phthalyl group. Actually, Penke *et al.* synthesized several diazoketones from benzyloxycarbonyl or *t*-butyloxycarbonyl amino acid using the mixed anhydride method or dicyclohexylcarbodiimide method.[6] More recently, Ondetti *et al.* prepared *t*-butyloxycarbonyl derivative of 3-amino-4-phenylbutyric acid by Arndt-Eistert reaction employing the mixed anhydride method from *t*-butyloxycarbonylphenylalanine. This derivative had been further used to a synthesis of the β-amino acid peptide.[7] In the present paper, $N^{\beta},N^{\varepsilon}$-dibenzyloxycarbonyl- and $N^{\beta},N^{\varepsilon}$-di-*t*-butyloxycarbonyl-L-β-lysine were synthesized based on the same principle of combination of the protecting group and the mixed anhydride method (Scheme 1). These compounds are important starting materials for synthetic studies of tuberactinomycins and streptothricins containing β-lysine residues.

N^{α},N^{δ}-Dibenzyloxycarbonyl-L-ornithine (Ia) and N^{α},N^{δ}-di-*t*-butyloxycarbonyl-L-ornithine (Ib) were first converted to their ethoxycarbonic anhydrides in the presence of *N*-methylmorpholine or triethylamine. The mixed anhydrides were immediately allowed to react with diazomethane for the preparation of diazoketones(II). Following Wolff rearrangement in methanol gave acyl-β-lysine methyl esters (III) as crystals, which were successfully saponified to their acid derivatives (IV).

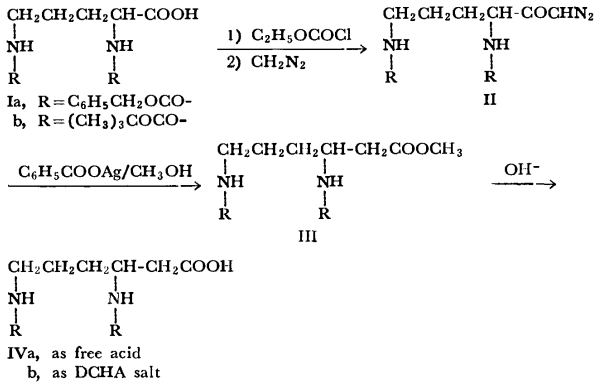

Scheme 1.

Preparation of such diacyl-β-lysine opened a way to the semi-synthesis of tuberactinomycin analogues. Thus, as reported in our recent study, dialkyloxycarbonyl-L-β-lysine 1-succinimidyl esters were coupled with tuberactinamine N, a cyclic peptide moiety isolated from tuberactinomycin N by selective liberation of the branched γ-hydroxy-β-lysine with acid treatment, and then diacyl groups were removed under mild conditions.[8] Synthetic tuberactinomycin O thus obtained was identical with natural compound in all respects. Consequently, dibenzyloxycarbonyl- or di-*t*-butyloxycarbonyl-L-β-lysine newly prepared *via* modified Arndt-Eistert reaction from the corresponding diacyl-L-ornithine proved to be very useful derivatives for syntheses of its peptides.

Experimental

All melting points are uncorrected. The specific rotations were measured with a Perkin-Elmer 141 polarimeter.

$N^{\beta},N^{\varepsilon}$-Dibenzyloxycarbonyl-L-β-lysine Methyl Ester (IIIa). N^{α},N^{δ}-Dibenzyloxycarbonyl-L-ornithine[9] (4.00 g, 0.01 mol) was dissolved in 200 ml of ethyl acetate and the solution was cooled on ice-salt bath. To a cold solution, *N*-methylmorpholine (1.11 g, 0.011 mol) and ethyl chloroformate (1.20 g, 0.011 mol) were added under stirring. After 3 hr, precipitated amine hydrochloride was rapidly filtered off in the cold. Then diazomethane in ether was added to the filtrate and stirred at 0 °C overnight. Excess diazomethane was removed by warming at 50 °C and thereafter the reaction mixture was evaporated *in vacuo*. Oily diazoketone* thus

* When oily product was stored in refrigerator, diazoketone was crystallized. Recrystallization from ethyl acetate and *n*-hexane gave pale yellow needles, mp 79—80 °C or 93—94 °C (polymorphism). Found: C, 62.20; H, 5.70; N, 13.12%. Calcd for $C_{22}H_{24}O_5N_4$: C, 62.25; H, 5.70; N, 13.20%. Since the diazoketone was generally unstable, oily product was immediately used for next Wolff rearrangement.

obtained was dissolved in 80 ml of methanol, and silver benzoate (0.50 g, 0.002 mol) in 5 ml of triethylamine was added. The mixture was stirred overnight in the dark and then concentrated *in vacuo*. The residue was dissolved in ethyl acetate and insoluble material was filtered off. The filtrate was washed with saturated sodium hydrogencarbonate solution, saturated sodium chloride solution, 1 M hydrochloric acid, and then finally saturated sodium chloride solution to neutral. Organic layer was dried over anhydrous sodium sulfate and evaporated *in vacuo*. Crystalline residue was recrystallized from ethyl acetate and *n*-hexane, yield 3.64 g (85%), mp 105—107 °C, $[\alpha]_D^{15}$ −5.0° (*c* 0.3, dimethylformamide).

Found: C, 64.38; H, 6.59; N, 6.58%. Calcd for $C_{23}H_{28}O_6N_2$: C, 64.47; H, 6.59; N, 6.54%.

N^{β},N^{ε}-*Di*-t-*butyloxycarbonyl*-L-*β-lysine Methyl Ester (IIIb).* N^{α},N^{δ}-Di-*t*-butyloxycarbonyl-L-ornithine(Ib)** was derived to IIIb in a similar way *via* its diazoketone (IIb)*** except the use of citric acid solution in place of hydrochloric acid for washing. Methyl ester (IIIb) was obtained in a 86% yield, mp 60—61 °C, $[\alpha]_D^{25}$ −5.8° (*c* 1, dimethylformamide).

Found: C, 56.47; H, 8.89; N, 7.80%. Calcd for $C_{17}H_{32}O_6N_2$: C, 56.64; H, 8.95; N, 7.77%.

N^{β},N^{ε}-*Dibenzyloxycarbonyl*-L-*β-lysine (IVa).* Methyl ester IIIa (0.86 g, 2 mmol) was dissolved in a small amount of dioxane and 1.5 ml of 1.5 M aqueous sodium hydroxide was added. After stirring at 0 °C for 30 min and then at room temperature for 1 hr, the reaction mixture was diluted with water, and extracted with ethyl acetate. Aqueous layer was acidified with 1 M hydrochloric acid and extracted with ethyl acetate. Organic layer was washed with saturated sodium chloride solution to neutral and dried over anhydrous sodium sulfate. The extract was concentrated *in vacuo* to give IVa, which was recrystallized from ethyl acetate, in a yield of 0.68 g (82%), mp 155 °C, $[\alpha]_D^{15}$ +1.0° (*c* 1, dimethyl formamide).

Found: C, 63.79; H, 6.36; N, 6.78%. Calcd for $C_{22}H_{26}O_6N_2$: C, 63.75; H, 6.32; N, 6.76%.

N^{β},N^{ε}-*Di*-t-*butyloxycarbonyl*-L-*β-lysine (IVb).* Corresponding methyl ester IIIb (0.90 g, 2.5 mmol) was dissolved in 3 ml of methanol and 2 ml of 1.5 M aqueous sodium hydroxide was added. The reaction mixture was treated as in the preparation of IIIa except use of citric acid for acidification. Oily product was crystallized as dicyclohexylammonium salt which was recrystallized from ether and *n*-hexane, 1.18 g (89%), mp 106—107 °C, $[\alpha]_D^{25}$ −3.5° (*c* 1, 95% ethanol)

Found: C, 62.93; H, 10.19; N, 7.73%. Calcd for $C_{28}H_{53}O_6N_3 \cdot 1/2\ H_2O$: C, 62.65; H, 10.14; N, 7.83%.

** N^{α},N^{δ}-Di-*t*-butyloxycarbonyl-L-ornithine was prepared by acylation of L-ornithine hydrochloride with *t*-butyl azidoformate[10] or *t*-butyl 4,6-dimethylpyrimidyl-2-thiol carbonate[11] in the usual manner, and the yield was 77% and 87%, respectively. Mp 120—121 °C, $[\alpha]_D^{20}$ −6.0° (*c* 1, dimethylformamide). Found: C, 54.23; H, 8.49; N, 8.34%. Calcd for $C_{15}H_{28}O_6N_2$: C, 54.20; H, 8.49; N, 8.43%.

*** Diazoketon (IIb) crystallized as well as in the case of IIa. It was recrystallized from ethyl acetate and *n*-hexane. Mp 114—115 °C, $[\alpha]_D^{23}$ −43.1° (*c* 1, dimethylformamide). Found: C, 53.71; H, 7.92; N, 15.66%. Calcd for $C_{16}H_{28}O_5N_4$: C, 53.91; H, 7.92; N, 15.72%.

References

1) T. H. Haskell, S. A. Fusari, R. P. Frohardt, and Q. R. Bartz, *J. Amer. Chem. Soc.*, **74**, 599 (1952).

2) E. E. van Tamelen and E. E. Smissman, *ibid.*, **74**, 3717 (1952); **75**, 2031 (1953).

3) H. E. Carter, W. R. Hearn, E. M. Lansford, Jr., A. C. Page, Jr., N. P. Salzman, D. Shapiro, and W. R. Taylor, *ibid.*, **74**, 3704 (1952).

4) a) H. Yoshioka, T. Aoki, H. Goko, K. Nakatsu, T. Noda, H. Sakakibara, T. Take, A. Nagata, J. Abe, T. Wakamiya, T. Shiba, and T. Kaneko, *Tetrahedron Lett.*, **1971**, 2043; b) R. Izumi, T. Noda, T. Ando, T. Take, and A. Nagata, *J. Antibiot.* (Tokyo), **25**, 201 (1972); c) T. Noda, T. Take, A. Nagata, T. Wakamiya, and T. Shiba, *ibid.*, **25**, 427 (1972).

5) D. S. Tarbell, and J. A. Price, *J. Org. Chem.*, **22**, 245 (1957).

6) B. Penke, J. Czombos, L. Balaspiri, J. Petres, and K. Kovacs, *Helv. Chim. Acta*, **53**, 1057 (1970).

7) M. A. Ondetti, J. Pluščec, E. R. Weaver, N. Williams, E. E. Sabo, and O. Kocy, "Chemistry and Biology of Peptides (Proc. of The 3rd American Peptide Symposium)," Ann Arbor Science Publishers Inc., Ann Arbor (1972), p. 525.

8) T. Wakamiya and T. Shiba, *J. Antibiot.* (Tokyo) **28**, 292 (1975).

9) a) R. L. M. Synge, *Biochem. J.*, **42**, 99 (1948); b) J. I. Harris and T. S. Work, *ibid.*, **46**, 582 (1950).

10) R. Schwyzer, P. Sieber, and H. Kappeler, *Helv. Chim. Acta*, **42**, 2622 (1959).

11) T. Nagasawa, K. Kuroiwa, K. Narita, and Y. Isowa, This Bulletin, **46**, 1269 (1973).

BULLETIN OF THE CHEMICAL SOCIETY OF JAPAN, VOL. 48(8), 2403—2404 (1975)

Di-*tert*-butyl Thioketone

Atsuyoshi OHNO, Kaoru NAKAMURA, Yukio NAKAZIMA, and Shinzaburo OKA
Institute for Chemical Research, Kyoto University, Uji, Kyoto-fu 611

(Received April 12, 1975)

Synopsis. Di-*tert*-butyl thioketone, a new aliphatic thioketone, has been prepared and its IR and UV spectral properties are studied.

Chemistry of thiocarbonyl compounds has been described on the bases of information mostly obtained from studies on aromatic thioketones, thionesters, and thioamides,[1] where the thiocarbonyl group is more or less resonance-participated by substituents. Information obtained from these compounds, therefore, may not be universal for the thiocarbonyl group and, before the description on the chemistry of thiocarbonyl compounds is generalized, it is desirable to study the chemistry of aliphatic thioketones.

Aliphatic thioketones, however, have been the subject of little attention, because they are, generally, unstable. Namely, they are quite sensitive to air and, when possible, tautomerization to the corresponding enethiol is very fast.[1,2]

In this article, we wish to report synthesis and spectral properties of di-*tert*-butyl thioketone, **1**.

General procedure to synthesize an aliphatic thioketone employs acid-catalyzed reaction of the corresponding ketal with hydrogen sulfide or, less frequently, the reaction of a ketone with phosphorous pentasulfide.[1,2a] However, these procedures cannot be applied to the present system because of its inertness to S_N2-type reactions as well as difficulty to obtain the starting materials themselves.

Results and Discussion

Preparation. The thioketone, **1**, was prepared from sodium salt of di-*tert*-butyl ketimine, **2**[3] and carbon disulfide after Ahmed and Lwowski.[4] Since the intermediate, **3**, is stable enough to be dissolved in water,

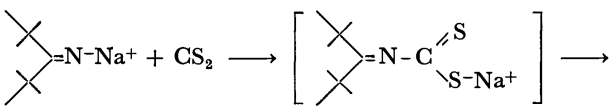

2 **3**

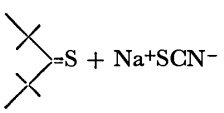

1

excess carbon disulfide and other organic impurities can be extracted with ether from the water layer before **3** decomposes to the final product. This procedure is more effective than fractional distillation to obtain **1** in high purity. That is, it is difficult to obtain the product in purity of higher than 97% after twice extractions and repeated fractional distillations, whereas repeated extractions (more than several times) until the water layer becomes colorless makes it possible to improve the purity as high as 99.9% by single fractional distillation. The purity was determined by vpc.

Although the overall yield of the reaction product is 34%, the yield of the thioketone by the addition of carbon disulfide to **2** can be calculated to be about 80%, since the yield of the latter compound is reported to be 43%.[3] The reaction temperature should be kept below −10 °C during the addition of carbon disulfide in order to improve the yield of the thioketone.

Detailed procedure will be described in Experimental Section.

Spectra. IR spectrum of **1** has an absorption at 1115 cm^{-1} due to $\nu_{C=S}$. The corresponding oxygen analog shows the absorption at 1686 cm^{-1} for $\nu_{C=O}$.[5] The ratio, $\nu_{C=O}/\nu_{C=S}$, is 1.52. Thioacetone, isopropyl methyl thioketone, and diisopropyl thioketone, exibit their $\nu_{C=S}$ at 1269, 1250, and 1240 cm^{-1}, respectively,[6] and their corresponding oxygen analogs show their $\nu_{C=O}$ at 1719,[7] 1719,[7] and 1716 cm^{-1},[5] respectively. The ratios, $\nu_{C=O}/\nu_{C=S}$, for these pairs are 1.35—1.38. The value for pairs of aromatic thioketones and ketones also falls in this range.[8] Thus, the frequency of the >C=S stretching vibration in **1** is extraordinally shifted toward the value as low as those of thioamides (1140± 80 cm^{-1}),[9] where the thiocarbonyl group has large single-bond character.[10]

Absorption maxima in electronic spectra of **1** are listed in Table 1 together with those of other aliphatic thioketones so far reported.[11]

As has been recognized from the IR spectrum, the energy level of the C–S π-orbital in **1** is much higher than those of other thioketones, whereas the absorption maximum for the π-π^* transition of this thioketone appears at normal position. This fact indicates that the energy level of the C-S π^*-orbital in **1** is lifted up as high as that of the π-orbital. On the other hand, the energy for the n-π^* transition of **1** is much lower (1300 cm^{-1}) than those of other thioketones, which indicates that the energy level of the n-orbital is more lifted up than the π^*-orbital in this thioketone. This is an unusual phenomenon in the sense that the energy level of a π^*-orbital is more affected than that of an n-orbital by electronic nature of substituents in ketones[12] and thioketones.[13] Present results may suggest larger steric effect of *tert*-butyl groups in **1** than that in di-*tert*-butyl ketone.

The results, consequently, may be best interpreted by allotting the largest contribution of the canonical structure **1b** for the structure of **1**.[14]

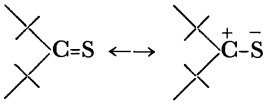

1a **1b**

Table 1. Electronic spectra of aliphatic thioketones

Thioketone	Solvent[a]	n → σ		π → π*		n → π*	
		λ_{max}, nm	ε	λ_{max}, nm	ε	λ_{max}, nm	ε
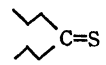	E	313	5000	231	6200	492	7.9
	C	215	5100	230	6300	503	8.9
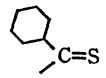	E	214	5600	236	7400	492	9.1
	C	215	5900	236	7900	508	10.0
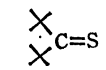	E	—	—	237	7900	536	8.9
	C	—	—	237	7800	539	9.8
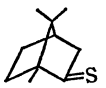	E	210	3700	246	11000	481	10.5
	C	214	4200	244	11000	493	12.3
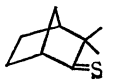	E	212	3500	243	12000	479	10.7
	C	215	4000	240	10000	488	11.0

a) E, Ethanol: C, Cyclohexane.

Experimental

*Preparation of Di-*tert*-butyl Thioketone (1).* A suspension of 7 g (0.3 mol) of finely divided sodium metal in 50 ml of petroleum ether was stirred under an atmosphere of nitrogen, while 16.6 g (0.2 mol) of pivalonitrile was added to this suspension over a period of 1 hr. The temperature was kept between 25 and 30 °C. The mixture was stirred for additional 15 min and was filtered under an atmosphere of nitrogen to remove unreacted sodium. The filtrate was cooled with an ice-salt bath and stirred, while 10 ml of carbon disulfide was added dropwise over a period of 1 hr. When carbon disulfide is added dropwise to the solution of **2**, the yellow color of the solution turned from dark to pale. Stirring was continued for additional 2 hr at room temperature, then 150 ml of water was added and the mixture was washed with ether (80 ml×5). The water layer was stood overnight at room temperature, whereas di-*tert*-butyl thioketone appeared as a red oil, which was separated from the water layer and the latter was extracted with ether. The red oil and the extract were combined and dried over calcium chloride. Distillation gave the thioketone (5.4 g) in 34% yield; bp 70.5—71.5 °C (18 Torr). NMR $\delta_{CCl_4}^{TMS}$ 1.43 (singlet).

Found: C, 67.85; H, 11.42; S, 20.50%. Calcd for $C_9H_{18}S$: C, 68.28; H, 11.46; S, 20.25%.

The purity of **1** was determined by vpc on Hitachi Perkin-Elmer F6 instrument (Golay column BDS 45 m, 80 °C, FID). The peak-area for **1** was compared to that of an unknown impurity contaminating.

Spectroscopy. The IR spectrum was recorded on Hitachi EPI-S2 with 2.5% CCl_4 solution. The electronic spectra were recorded on Shimadzu UV-200.

References

1) (a) E. Compaigne, "Thiones," in "The Chemistry of the Carbonyl Group," ed. by S. Patai, Interscience, New York, N.Y. (1966); (b) A. Ohno, "Thiones," in "Organic Chemistry of Sulfur," ed. by S. Oae, Plenum, London, in press.

2) (a) J. Morgenstern and R. Mayer, *J. Prak. Chem.*, **34**, 116 (1966); (b) R. Mayer, J. Morgenstern, and J. Fabian, *Angew. Chem. Int. Ed., Engl.*, **4**, 277 (1964).

3) H. D. Hartzler, *J. Amer. Chem. Soc.*, **93**, 4527 (1971).

4) (a) R. Ahmed and W. Lwowski, *Org. Prep. Proc. Int.*, **3**, 135 (1971); (b) R. Ahmed and W. Lwowski, *Tetrahedron Lett.*, **1969**, 3611.

5) P. D. Bartlett and M. Stiles, *J. Amer. Chem. Soc.*, **77**, 2806 (1955).

6) C. Andrieu, M. Demuynck, and Y. Mollier, *C. R. Acad. Sci., Paris, Ser. A*, **265B**, 127 (1967).

7) L. J. Bellamy and R. L. Williams, *J. Chem. Soc.*, **1957**, 4294.

8) O. Korver, J. U. Veenland, and Th. J. De Boer, *Rec. Trav. Chim. Pays-Bas*, **84**, 310 (1965).

9) E. Spinner, *J. Org. Chem.*, **23**, 2037 (1958).

10) J. Newman, Jr. and L. B. Young, *J. Phys. Chem.*, **69**, 2570 (1965).

11) J. Fabian and R. Mayer, *Spectrochim. Acta*, **20**, 299 (1964).

12) S. Nagakura, This Bulletin, **25**, 164 (1952).

13) O. Korver, J. U. Veenland, and Th. J. De Boer, *Rec. Trav. Chim. Pays-Bas*, **84**, 289 (1965).

14) Preliminary result from INDO-MO calculation supports the conclusion.

ESR Studies of Phenoxyl Radicals Produced by the PbO_2 Oxidation of Hindered Polyphenols. III. *p*- and *m*-Phenylene-bisgalvinoxyls, Stable Triplets

Kazuo MUKAI

Department of Chemistry, Faculty of Science, Ehime University, Matsuyama 790

(Received February 10, 1975)

PbO_2 oxidation of two hindered polyphenols produced, in turn, primary, secondary, and ternary radicals. The ternary radicals are π-conjugated biradicals; the structures of the radicals were assigned to be *p*- and *m*-phenylenebisgalvinoxyls. Both zero field splitting parameters and hyperfine splitting constants were determined from ESR spectra.

PbO_2 oxidation of 4-substituted 2,6-di-*t*-butylphenols in organic solvents produces the corresponding phenoxyl radicals, which are known as "hindered phenoxyls". The magnetic properties of these phenoxyls in solution have been extensively studied with the aid of the electron spin resonance (ESR) spectra.[1]

The galvinoxyl radical is a well known stable phenoxyl radical, which can be separated as a pure solid with 100% radical concentration.[2-4] This radical shows some anomalous magnetic properties in the solid state.[4,5] Phenylgalvinoxyl (I-S) (see Fig. 1(a)) has an electronic structure similar to galvinoxyl, and exhibits a stability approaching that of galvinoxyl.[6] These radicals can be prepared from their diphenylmethane precursors, 3,3',5,5'-Tetra-*t*-butyl-4,4'-dihidroxydiphenylmethane and 3,3',5,5'-Tetra-*t*-butyl-4,4'-dihydroxydiphenylphenylmethane (phenol (I)), by their PbO_2 oxidation in 2-MeTHF under vacuum or nitrogen gas.

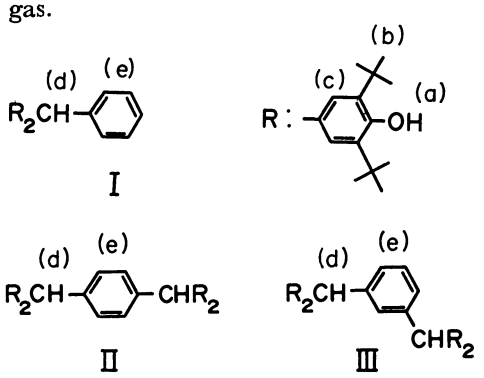

We have prepared two other *para*- and *meta*-phenylenebis(diphenylmethane) precursors (phenols (II) and (III)) which are related to phenol (I), and have succeeded in synthesizing the corresponding π-conjugated biradicals, *para*- and *meta*-phenylenebisgalvinoxyls (II-T) and (III-T) (see Figs. 1(b) and (c)).

The study of interelectronic interactions in organic π-conjugated biradicals has been of interest in recent years. However, the number of the stable π-conjugated biradicals reported are very limited: only about ten, as far as we know, including three of the phenoxyls.[7-9]

Experimental

3,3',5,5'-Tetra-t-butyl-4,4'-dihydroxydiphenylphenylmethane (phenol (I)). Phenol (I) was prepared according to the procedure used by Coffield *et al.*[10] 2,6-di-*t*-butylphenol (0.1 mol, 20.6 g) and benzaldehyde (0.1 mol, 10.6 g) were dissolved in 20 ml of ethanol in a three-necked flask, and a solution of KOH (6.6 g in 15 ml of ethanol) was added gradually under an atmosphere of nitrogen. The deep green solution was stirred overnight at 20 °C, and the solids were filtered out. The crude product was then taken up in ether to remove the potassium benzoate. Removal of the ether left a white crystalline solid, and this was recrystallized twice from ethanol, mp 164.0—164.5 °C (lit, mp 161—163 °C); UV spectrum (λ_{max}=278 nm, log ε=3.54, λ_{max}=286 nm, log ε=3.53 in *n*-hexane); NMR spectrum ($H^a\delta$=4.92 ppm (2), H^b 1.39 (36), H^c 6.80 (4), H^d 5.26 (1), H^e 6.98, 7.06, 7.16, 7.23 (total 5); δ in CCl_4 with TMS as internal standard).

para-Phenylene-bis(3,3',5,5'-Tetra-t-butyl-4,4'-dihydroxydiphenylmethane) (phenol (II)). 2,6-Di-*t*-butylphenol (15.2 g, 0.074 mol) and terephthalaldehyde (5.0 g, 0.037 mol) were dissolved under an atmosphere of nitrogen in 33 ml of ethanol under stirring, and a solution of KOH (4.8 g in 10 ml of ethanol) was added slowly. The color of the reaction mixture changed gradually from yellow to green at 30 °C. The reaction was continued overnight at 30 °C, and finally some white solids were precipitated in the viscous deep blue reaction mixture. The solids were filtered off and washed with ethanol. Then they were taken up in ethyl ether, washed with water, and dried over anhydrous sodium sulfate. After removal of the ethyl ether, the white solids were recrystallized first from benzene, second from *p*-xylene, and finally washed twice with acetone, mp 290—292 °C; Found: C, 83.07; H, 10.09%. Calcd for $C_{64}H_{90}O_4$: C, 83.24; H, 9.82%; UV spectrum (λ_{max}=278 nm, log ε=3.97, 284 nm; log ε=3.93 in tetrahydrofuran); NMR spectrum ($H^a\delta$=4.87 ppm (4), H^b 1.33 (72), H^c 6.80 (8), H^d 5.21 (2), H^e 6.94 (4); δ in CCl_4 with TMS as internal standard).

meta-Phenylene-bis(3,3',5,5'-Tetra-t-butyl-4,4'-dihydroxydiphenylmethane) (phenol (III)). Phenol (III) was synthesized by condensation of 2,6-di-*t*-butylphenol with isophthalaldehyde in KOH–ethanol solution under an atmosphere of nitrogen at 35 °C, following a method similar to that used with phenol (II). The reaction was continued for three days under stirring. The white solids obtained were recrystallized first from ethanol and second from methanol–acetone, giving white silky needles, mp 223.0—224.0 °C; Found: C, 83.06; H, 10.10%. Calcd for $C_{64}H_{90}O_4$: C, 83.24; H, 9.82%. UV spectrum (λ_{max} =277nm, log ε=3.82; 285 nm, log ε=3.80 in *n*-hexane); NMR spectrum (H^a δ=4.86 ppm (4), H^b 1.31 (72), H^c 6.73 (8), H^d 5.20 (2), H^e 6.84, 6.98, 7.07, 7.14 (total 4); δ in CCl_4 with TMS as internal standard).

Measurements. All the ESR measurements were carried out using a JES-ME-3X spectrometer equipped with a Takeda-Riken microwave frequency counter. ESR hyperfine splittings and *g*-values were measured relative to those of $(KSO_3)_2$-

Table 1. Hyperfine splittings (in G), fine structures (D) (in G), and g-values of phenoxyl radicals

Radical	Primary (P)			Secondary (S)		Ternary (T)		
	a_β^H	a_m^H	g-value	a_m^H	g-value	a_m^H	g-value	D
I	8.44	1.71	2.0044_4	1.34	2.0044_0	—	—	—
II	8.53	1.67	2.0044_3	1.34	2.0044_3	0.69	2.0044_5	20.0
III	8.74	1.68	2.0044_4	1.33	2.0044_2	0.69	2.0044_3	26.1

NO ($a^N=13.05\pm0.03$ G; $g=2.0054$[11]).

The NMR spectra were taken on a JEOLCO 4H-100 (100 MHz) nmr spectrometer.

Magnetic susceptibility measurements were carried out using a Shimadzu MB-2 type magnetic torsion balance.

Results and Discussion

An initial slight oxidation of the phenols (I)—(III) with PbO_2 in 2-MeTHF in a sealed, degassed system gives ESR spectra consisting of a doublet-triplet splitting. We assign the spectra to primary phenoxyl radicals (I-P), (II-P), and (III-P) formed from the parent phenols by abstraction of a phenolic hydrogen atom. The large doublet splittings in the primary radicals are clearly due to the *para* methylene group and the triplet splittings are explained by the *meta* hydrogens. The values of hyperfine splittings are listed in Table 1.

The spectrum due to radical (I-P) changes rapidly with time. Almost as soon as it was observed, a further quintet due to a secondary radical (I-S) was seen growing in the center of the spectrum, and this, after further oxidation, dominated the spectrum. The phenols (II) and (III) show similar behavior. The structure of the secondary radical (I-S), named phenylgalvinoxyl, is shown in Fig. 1(a); those from phenols (II) and (III) are analogous to those from phenol (I). The spectrum of (I-S) is shown in Fig. 2(a). The quintet splitting of the secondary radicals ($a^H=1.33$—1.34 G)[12] may be explained by four equivalently interacting hydrogens in the *meta* position.*

Phenylgalvinoxyl (I-S) is very stable and appears to be capable of existing for many days in 2-MeTHF in the absence of oxygen. The spectrum remains unchanged upon further oxidation. On the other hand, in the case of phenols (II) and (III), as the oxidation process proceeds, the five-line well resolved spectra of the secondary monoradicals begin to overlap with each other; finally, these are completely altered to a nine-line spectra with an equivalent splitting distance, as

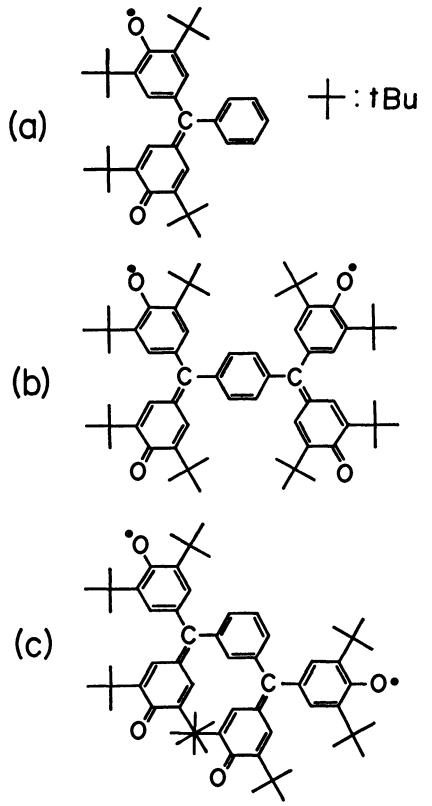

Fig. 1. Molecular structures of phenoxyl radicals. (a) Phenylgalvinoxyl (I-S). (b) *para*-Phenylenebisgalvinoxyl (II-T). (c) *meta*-Phenylenebisgalvinoxyl (III-T).

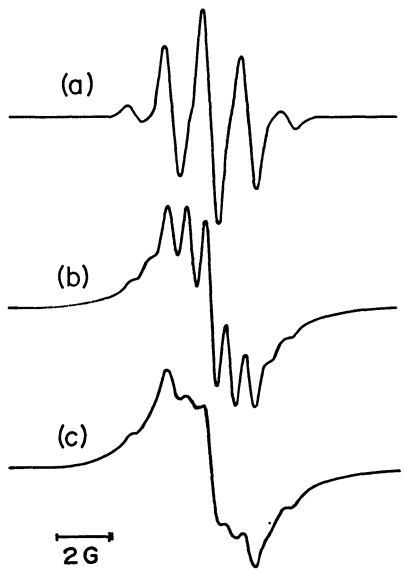

Fig. 2(a). First-derivative ESR spectrum observed for the monoradicals, (I-S), (II-S), and (III-S), produced by the PbO_2 oxidation of phenols (I-III) in 2-MeTHF.

Fig. 2(b) and (c). ESR spectra observed for the biradicals, (II-T) and (III-T), produced by the further oxidation of (II-S) and (III-S) in 2-MeTHF.

* In a recent ENDOR investigation, two kinds of hyperfine splittings due to *meta* ring protons are observed at −80 °C for this radical ($a^H_{m\text{-}1}=1.363$ G, $a^H_{m\text{-}2}=1.282$ G). T. Yamamoto, M. Kohno, T. Miyamae, K. Mukai, and K. Ishizu, *Chem. Lett.*, **1972**, 681.

shown in Fig. 2(b) and (c). These spectra, which consist of nine considerably overlapped lines, were unchanged at the lowest concentration at which they could be detected. Thus, they are thought to be due to the eight *meta* ring protons of phenoxyl biradicals, *p*- and *m*-phenylenebisgalvinoxyls ((II-T), a_m=0.69 G; (III-T), a_m=0.69 G). The structures of these biradicals are shown in Figs. 1(b) and (c).

When the solution containing the biradicals (II-T) and (III-T) is frozen into a rigid glass (77 K), one can observe some dipolar splittings, as are shown in Fig. 3(a) and (b). These spectra at 77 K can be interpreted on the basis of a randomly-oriented set of triplets with axial symmetry; thus the values of the dipolar splitting, D, are 20.0 G for the biradical (II-T) and 26.1 G for the biradical (III-T), as one half of the outer two lines' splitting.

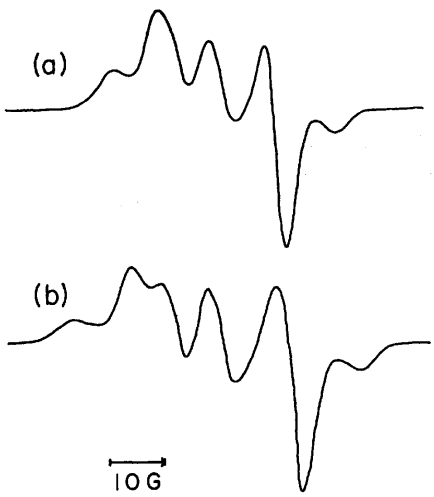

Fig. 3(a). ESR spectrum of the biradical (II-T) in 2-MeTHF at 77 K.
Fig. 3(b). ESR spectrum of the biradical (III-T) in 2-MeTHF at 77 K.

These small splittings may be explained by the large separation between the two galvinoxyl rings and the small unpaired spin density on the centered phenylene ring and the two carbon atoms bonded to the ring.**

The observed increase in the splitting constants, D(III-T)>D(II-T), is consistent with the structure. Using a model of two-point dipoles, that is, the relation $D=(3/2)g\mu_B r^{-3}$, the average interelectronic distances in the biradicals (II-T) and (III-T) are calculated to be 11.2 Å and 10.2 Å, respectively. The relative intensity of the central singlet varied with the samples, that is, with the radical concentration of the samples. A zero-field splitting of D=110 G has been reported for the bisgalvinoxyl biradical.[8] The calculated average interelectronic distance, using a model of two point dipoles, is about 6.3 Å. The comparison of the average interelectronic distances of 6.3 Å for bisgalvinoxyl and 11.2 Å for *p*-phenylenebisgalvinoxyl indicates that the two point dipole model is still acceptable for bisgalvinoxyl, because the length of the centered-phenylene ring is about 4.3 Å.

The ESR results for a 2-MeTHF solution of the secondary radicals (I—III-S) obtained from phenol (I—III) at room temperature consist of a five-line, well-resolved (a_m^H=1.33—1.34 G) spectra. On the other hand, the ESR measurements of the two phenoxyl biradicals in a rigid solution at 77 K indicate that a triplet state exists in these radicals. If there is a strong scalar exchange interaction, J, between the two electrons such that $J \gg a_m^H$, the spectrum will consist of 9 lines separated by $a_m^H/2$, corresponding to an interaction with 8 equivalent protons.[13] In fact, the ESR spectra of the phenoxyl biradicals (II-T) and (III-T) in 2-MeTHF show nine lines of equivalent hyperfine splittings (a_m^H=0.69 G), respectively. The poorer resolution in the biradical (III-T) with respect to the biradical (II-T) may be due to a larger dipolar interaction in the former. These circumstances are very similar to those of verdazyl[14-16] and tetrazolinyl[17] biradicals, which have a π-electron system related to that of *p*- and *m*-phenylenebisgalvinoxyl radicals; each of them has π-conjugated monoradical halves linked by *para* and *meta* positions of a central phenylene π-bridge, and shows comparatively small zero-field splittings (about 38—53 G).

Recent studies of magnetic susceptibilities of *p*- and *m*-phenylenebisverdazyl biradicals have showed the presence of a triplet ground state (S=1) in these biradicals.[18] The intramolecular positive exchange integrals, J/k, of these biradicals are much greater than 300 K. The magnetic susceptibility of Yang's biradical, known as a stable phenoxyl radical and possessing three-fold symmetry, follows the Curie-Weiss law with a paramagnetic Curie constant of 1.0 K·emu/mol and a Weiss constant of −4 K.[19] This susceptibility also suggests that an intramolecular pure triplet approximation is reliable in the temperature region below 300 K. On the other hand, the results of the paramagnetic shift of the bisgalvinoxyl show that this radical has a singlet ground state with a negative exchange integral of 93 K.[20] The comparison of the electronic structures in *para* and *meta* phenylenebisverdazyls and bisgalvinoxyls and the smaller dipole-dipole interaction in the latter suggest a smaller exchange interaction in the latter.

Phenyl-galvinoxyl is rather stable and Ley *et al.*[6] succeeded in isolating it as a solid with an 85% spin concentration. In an attempt to clarify the level scheme of the spin system of these biradicals, preliminary experiments were performed for making the biradical solids of (II-T) and (III-T) by the PbO_2 oxidation in THF and in ethyl ether, respectively, under nitrogen gas, following the method of Kharasch and Joshi.[2] Spin concentrations were obtained from the results of the paramagnetic susceptibility measurements at room temperature, after correcting for the diamagnetic contribution calculated by the Pascal method. The values were 64% for (II-T) and 68% for (III-T) as S=1/2, N=2N_0, assuming the Curie law. These low observed concentrations are probably due to both

** The orbital containing the unpaired electron of phenyl-galvinoxyl has, at least in the Hückel approximation, a node in the phenyl ring. Ref. C. Besev, A. Lund, T. Vänngård, and R. Håkansson, *Acta Chem. Scand.*, **17**, 2281 (1963).

diamagnetic and monoradical impurities in the individual samples, since it is difficult to oxidize these hindered polyphenols until the final biradicals, owing to their insolubility in ordinary solvents. In addition, these radicals are not as stable as galvinoxyl. Despite the low concentrations, at least the presence of two unpaired electrons per molecule has been confirmed for these radicals from the susceptibility measurements.

We wish to thank Professor Kazuhiko Ishizu and Professor Yasuo Deguchi for their helpful discussions. We also wish to express our gratitude to Mr. L. R. deAlvare for his kind help in preparing the manuscript. We are grateful to Mr. Taizi Itoh for the synthesis of phenol (III).

References

1) See, for example, A. R. Forrester, J. M. Hay, and R. H. Thomson "Organic Chemistry of Stable Free Radicals," Academic Press, London and New York, Chapter 7, (1968).
2) M. S. Kharasch and B. S. Joshi, *J. Org. Chem.*, **22**, 1435 (1957).
3) G. M. Coppinger, *J. Amer. Chem. Soc.*, **79**, 501 (1957).
4) K. Mukai, This Bulletin, **42**, 40 (1969).
5) K. Kosaki, H. Suga, S. Seki, K. Mukai, and Y. Deguchi, *ibid.*, **42**, 1525 (1969).
6) K. Ley, E. Müller, and K. Scheffler, *Angew. Chem.*, **70**, 74 (1958).
7) N. C. Yang and A. J. Castro, *J. Amer. Chem. Soc.*, **82**, 6208 (1960).
8) E. A. Chandross, *ibid.*, **86**, 1263 (1964).
9) G. Kothe, C. Nowak, K. H. Denkel, E. Ohmes, and H. Zimmermann, *Angew. Chem.*, **82**, 521 (1970). *Angew. Chem. Internat. Edit. Engl.*, **9**, 520 (1970).
10) T. H. Coffield, A. H. Filbey, G. G. Ecke, and A. J. Kolka, *J. Amer. Chem. Soc.*, **79**, 5019 (1957).
11) J. J. Windle and A. K. Wiersma, *J. Chem. Phys.*, **39**, 1139 (1963).
12) E. Müller, K. Ley, K. Scheffler, and R. Mayer, *Chem. Ber.*, **91**, 2682 (1958).
13) C. P. Slichter, *Phys. Rev.*, **99**, 479 (1955).
14) P. H. H. Fischer, *Tetrahedron*, **23**, 1939 (1967).
15) K. Mukai, N. Azuma, H. Shikata, and K. Ishizu, This Bulletin, **43**, 3958 (1970).
16) P. Kopf, K. Morokuma, and R. Kreilick, *J. Chem. Phys.*, **54**, 105 (1971).
17) N. Azuma, K. Mukai, and K. Ishizu, This Bulletin, **43**, 3960 (1970).
18) N. Azuma, K. Ishizu, and K. Mukai, *J. Chem. Phys.*, **61**, 2294 (1974).
19) K. Mukai, K. Ishizu, and Y. Deguchi, *J. Phys Soc. Japan*, **27**, 783 (1969).
20) P. W. Kopf and R. W. Kreilick, *J. Amer. Chem. Soc.*, **91**, 6569 (1969).

The Structure of the Cyclodextrin Complex. I. The Crystal and Molecular Structure of the α-Cyclodextrin-*p*-Iodoaniline Complex

Kazuaki HARATA

Research Institute for Polymers and Textiles, Sawatari 4, Kanagawa-ku, Yokohama 221

(Received February 17, 1975)

The crystal structure of the α-cyclodextrin–*p*-iodoaniline complex [$(C_6H_{10}O_5)_6 \cdot C_6H_6NI \cdot 3H_2O$] has been determined by the X-ray method. The space group is $P2_12_12_1$ with unit cell dimensions of $a=13.659(2)$, $b=15.413(3)$, and $c=24.486(5)$ Å. The structure was solved by the heavy-atom method and refined by least-squares techniques. The final *R*-value was 0.072. The *p*-iodoaniline molecule is included in the cavity with its axis coincident with the axis of α-cyclodextrin; the iodobenzene group is situated in the cavity, while the amino group sticks out from the cavity. The shortest contact between the α-cyclodextrin molecule and the "guest" *p*-iodoaniline molecule is 3.25 Å, indicating that the latter is rigidly fixed in the cavity of the former. The distances between the amino group and the hydroxyl group are greater than 4.0 Å; this fact well explains why the catalytic ability of α-cyclodextrin is low in the hydrolysis of *para*-substituted phenyl esters.

Cyclodextrins, which are cyclic α-1,4-linked D-glucose oligomers, form a number of inclusion compounds both in crystalline states and in an aqueous solution with a variety of "guest" molecules,[1-3] such as paraffins, alkyl halides, halogens, and aromatic compounds. X-Ray analyses of the α-cyclodextrin complex with potassium acetate,[4] iodine,[5] and water[6] have proved that the "guest" molecule is included in the cavity of α-cyclodextrin.

Cyclodextrins catalyze the hydrolysis of phenyl esters.[7] Bender and his co-workers suggested[8] that the hydrolysis occurs when the phenyl group is bound in the cavity of cyclodextrins and that the relative rates of reactions are controled by the stereo-specific complexing ability. The evidence for the formation of the inclusion compounds with aromatic molecules has been obtained from NMR,[9] kinetic,[10] and X-ray[2] studies, but the geometry of inclusion is yet unknown. The present paper will deal with the detailed crystal and molecular structure of the α-cyclodextrin–*p*-iodoaniline-(α-CDx-*p*-IAN) complex. A short communication has already been published.[11]

Experimental

Crystals of the α-CDx–*p*-IAN complex were prepared by mixing of a hot aqueous solution containing 10% α-CDx with *p*-IAN. They are colorless prisms elongated along the a-axis. The space group was determined by an inspection of the Weissenberg and oscillation photographs. The density was measured by the flotation method in a mixture of carbon tetrachloride and tetrabromoethane. The unit cell parameters and intensities were measured on a Rigaku AFC four-circle diffractometer with a specimen with dimensions of $0.2\times0.4\times0.7$ mm, using a graphite monochromatized Mo*K*α radiation ($\lambda=0.70926$ Å) and the ω-scanning mode. During the data collection the crystal turned blue, but no significant intensity change in the standard reflections was observed. 5007 independent reflections were obtained up to 50° in 2θ. No correction was made for absorption and extinction. The crystal data are shown in Table 1.

Table 1. Crystal data

$(C_6H_{10}O_5)_6 \cdot C_6H_6NI \cdot 3H_2O$	
Molecular weight	1245.9
Crystal system	Orthorhombic
Space group	$P2_12_12_1$
Z	4
Cell dimensions	$a=13.659(2)$Å
	$b=15.413(3)$
	$c=24.436(5)$
Cell volume	5144.4 Å^3
Density	$D_o=1.602$ g·cm^{-3}
	$D_x=1.610$

Determination and Refinement of the Structure

The crystal structure of the α-CDx-*p*-IAN complex was solved by the heavy-atom method using 1171 reflections with $2\theta\leqq30°$. The position of the iodine atom was deduced from a Patterson synthesis. An outline of the structure of the complex was obtained

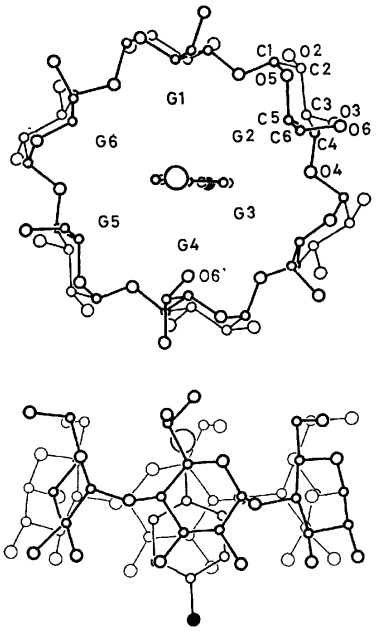

Fig. 1. Structure of the α-cyclodextrin–*p*-iodoaniline complex. The circles, in order of decreasing size, represent iodine, oxygen, and carbon atoms, and the black dots indicate nitrogen atoms.

TABLE 2. ATOMIC COORDINATES AND ANISOTROPIC TEMPERATURE FACTORS ($\times 10^4$) WITH STANDARD DEVIATIONS

The temperature factor expression used was $\exp[-(h^2B_{11}+k^2B_{22}+l^2B_{33}+hkB_{12}+klB_{23}+lhb_{31})]$.

	x	y	z	B_{11}	B_{22}	B_{33}	B_{12}	B_{23}	B_{31}
G1C(1)	1536(10)	−600(9)	6875(6)	34(8)	38(7)	15(3)	2(13)	7(7)	1(8)
G1C(2)	1319(11)	−1335(10)	6500(5)	51(10)	47(8)	7(2)	−28(15)	3(7)	0(8)
G1C(3)	1946(12)	−1252(8)	5978(6)	66(11)	18(5)	13(3)	9(13)	17(6)	2(9)
G1C(4)	1774(10)	−363(9)	5711(5)	31(8)	37(7)	10(2)	1(12)	9(7)	−1(7)
G1C(5)	1980(11)	374(8)	6156(6)	56(10)	26(6)	11(2)	7(12)	5(7)	−5(9)
G1C(6)	1743(15)	1281(10)	5938(6)	121(17)	36(7)	12(3)	14(19)	19(8)	3(12)
G10(2)	1578(9)	−2123(6)	6782(4)	91(9)	30(5)	12(2)	−45(11)	9(5)	−14(7)
G10(3)	1621(8)	−1913(6)	5603(4)	67(7)	25(4)	12(2)	−34(10)	1(5)	−3(6)
G10(4)	2440(6)	−274(6)	5288(3)	26(5)	36(4)	9(2)	−1(8)	11(5)	−6(5)
G10(5)	1366(8)	213(7)	6620(4)	60(7)	49(5)	10(2)	50(11)	9(5)	4(6)
G10(6)	773(11)	1325(8)	5712(5)	128(12)	63(7)	18(2)	103(16)	24(7)	11(9)
G2C(1)	2083(11)	−33(10)	4765(6)	44(9)	42(7)	11(3)	−1(14)	9(7)	1(8)
G2C(2)	2367(10)	−753(10)	4368(5)	32(8)	45(8)	11(2)	−16(14)	8(7)	−4(8)
G2C(3)	3483(10)	−869(9)	4346(5)	41(8)	23(5)	12(2)	−5(13)	−9(7)	3(7)
G2C(4)	3917(9)	40(8)	4212(5)	20(7)	23(6)	12(2)	1(10)	8(6)	3(7)
G2C(5)	3578(9)	737(8)	4604(6)	25(7)	25(6)	19(3)	3(11)	−5(7)	11(8)
G2C(6)	3909(14)	1643(9)	4434(7)	76(13)	19(6)	28(4)	−15(15)	11(8)	−2(12)
G20(2)	1960(7)	−1565(6)	4548(4)	44(6)	36(5)	10(2)	−16(9)	4(5)	1(5)
G20(3)	3754(7)	−1435(6)	3919(4)	53(7)	24(4)	17(2)	4(9)	−4(5)	1(6)
G20(4)	4952(8)	−78(5)	4291(3)	29(5)	34(4)	7(1)	10(11)	5(4)	1(6)
G20(5)	2519(7)	760(5)	4595(4)	48(6)	21(4)	14(2)	24(8)	15(4)	7(6)
G20(6)	3797(9)	1776(7)	3854(6)	82(9)	47(6)	32(3)	17(13)	41(8)	30(10)
G3C(1)	5647(9)	137(9)	3862(6)	32(8)	37(6)	11(2)	8(12)	4(7)	11(8)
G3C(2)	6276(9)	−672(8)	3776(5)	40(8)	40(7)	6(2)	−9(12)	5(7)	8(8)
G3C(3)	6791(8)	−879(9)	4279(5)	22(7)	35(6)	8(2)	−13(12)	13(7)	2(6)
G3C(4)	7338(9)	−118(9)	4531(5)	19(7)	43(7)	10(2)	2(12)	−1(7)	8(7)
G3C(5)	6727(11)	719(9)	4545(5)	59(10)	33(7)	8(2)	−10(14)	−1(6)	−2(8)
G3C(6)	7284(13)	1526(10)	4621(6)	67(11)	37(7)	13(3)	−22(16)	0(8)	−5(10)
G30(2)	5678(7)	−1370(6)	3580(4)	46(6)	36(5)	11(2)	4(9)	−16(5)	−4(5)
G30(3)	7495(7)	−1583(6)	4224(4)	43(6)	32(4)	13(2)	16(9)	−11(5)	8(6)
G30(4)	7590(6)	−360(6)	5081(3)	28(6)	37(5)	5(1)	−1(8)	7(4)	−3(4)
G30(5)	6219(7)	836(6)	4037(3)	40(6)	25(4)	11(2)	1(9)	10(4)	5(5)
G30(6)	8113(8)	1601(8)	4272(5)	54(7)	54(6)	21(2)	−32(12)	15(7)	5(7)
G4C(1)	8546(10)	−207(9)	5270(5)	29(8)	36(7)	12(3)	5(12)	−1(7)	2(8)
G4C(2)	8901(10)	−1014(10)	5566(5)	39(8)	48(8)	9(2)	19(14)	−5(8)	11(7)
G4C(3)	8273(10)	−1180(8)	6079(5)	34(8)	25(6)	14(3)	8(11)	−15(6)	1(7)
G4C(4)	8330(10)	−388(9)	6433(5)	41(9)	31(6)	10(2)	−2(12)	7(7)	−3(8)
G4C(5)	7946(11)	389(9)	6111(5)	55(10)	35(7)	11(3)	−3(13)	−24(7)	8(8)
G4C(6)	8055(15)	1266(9)	6436(9)	117(16)	23(6)	14(3)	−27(17)	2(7)	−20(12)
G40(2)	8834(7)	−1741(7)	5190(4)	49(7)	48(5)	9(2)	34(10)	−12(5)	0(6)
G40(3)	8700(8)	−1892(6)	6368(4)	60(7)	38(5)	13(2)	29(10)	−8(5)	−1(6)
G40(4)	7672(6)	−564(5)	6879(3)	31(5)	22(4)	7(1)	−8(7)	−1(4)	10(5)
G40(5)	8569(7)	512(6)	5631(4)	45(6)	36(5)	13(2)	−37(9)	3(5)	2(6)
G40(6)	9154(21)	1421(16)	6488(10)	66(20)	26(12)	10(5)	−56(27)	0(13)	−11(16)
G40(6′)	7438(13)	1914(11)	6121(6)	69(12)	52(9)	13(3)	−10(18)	0(9)	12(11)
G5C(1)	7994(10)	−412(8)	7419(5)	38(8)	19(6)	14(3)	−9(11)	−12(6)	−13(8)
G5C(2)	7739(10)	−1213(8)	7761(5)	35(8)	31(6)	8(2)	13(12)	1(6)	−8(7)
G5C(3)	6646(10)	−1327(7)	7791(5)	48(9)	30(6)	7(2)	17(13)	6(6)	1(8)
G5C(4)	6136(10)	−516(8)	7964(5)	36(8)	25(6)	10(2)	−7(11)	1(6)	−3(7)
G5C(5)	6433(10)	250(10)	7607(6)	33(8)	45(8)	14(3)	12(14)	−7(8)	16(8)
G5C(6)	6064(12)	1138(9)	7810(6)	57(10)	26(6)	15(3)	14(13)	−9(7)	−7(9)
G50(2)	8231(8)	−1943(6)	7534(4)	53(7)	30(5)	14(2)	30(9)	−2(5)	13(6)
G50(3)	6413(8)	−2034(6)	8170(4)	62(7)	33(5)	15(2)	3(10)	11(5)	14(7)
G50(4)	5118(7)	−656(5)	7881(3)	34(6)	36(4)	10(1)	9(10)	−9(4)	10(6)
G50(5)	7520(7)	330(6)	7643(3)	50(6)	25(4)	7(1)	−17(9)	−6(4)	0(5)
G50(6)	6146(8)	1196(7)	8399(4)	61(8)	47(6)	20(2)	15(11)	−31(6)	−11(7)
G6C(1)	4431(10)	−490(9)	8310(5)	41(9)	37(7)	7(2)	1(13)	−4(7)	−6(7)
G6C(2)	3778(11)	−1272(8)	8336(5)	50(9)	22(5)	8(2)	12(12)	10(6)	−3(8)
G6C(3)	3302(10)	−1415(9)	7779(6)	41(9)	28(6)	14(3)	−11(13)	1(7)	13(8)
G6C(4)	2774(10)	−566(8)	7613(5)	42(9)	29(6)	7(2)	10(12)	6(6)	16(7)
G6C(5)	3409(10)	259(8)	7647(5)	37(8)	15(5)	10(2)	7(11)	2(6)	10(7)
G6C(6)	2836(12)	1085(9)	7605(6)	60(11)	29(7)	17(3)	20(14)	−3(7)	12(9)
G60(2)	4312(8)	−2014(6)	8490(4)	64(8)	25(4)	19(2)	0(10)	17(5)	−1(7)
G60(3)	2587(8)	−2080(6)	7808(4)	53(7)	26(4)	20(2)	−25(10)	4(5)	1(7)
G60(4)	2537(6)	−666(6)	7052(3)	35(5)	32(4)	8(1)	−1(8)	4(4)	11(5)
G60(5)	3889(7)	272(6)	8190(3)	47(6)	29(4)	11(2)	21(9)	−6(5)	6(5)
G60(6)	1932(9)	1042(7)	7890(5)	79(8)	34(5)	22(2)	42(12)	−5(6)	1(8)
BC(1)	5045(13)	−438(7)	6080(5)	48(8)	27(5)	15(3)	−13(16)	−4(6)	−6(10)
BC(2)	5013(14)	−977(8)	6527(5)	64(9)	32(6)	12(2)	−24(20)	−1(7)	−18(11)
BC(3)	5007(14)	−1876(8)	6436(5)	65(10)	41(6)	8(2)	27(20)	−2(6)	−5(11)
BC(4)	5089(11)	−2198(7)	5896(5)	34(8)	28(5)	10(2)	−29(14)	1(5)	−10(9)
BC(5)	5121(12)	−1622(9)	5494(6)	50(10)	45(7)	11(2)	8(17)	−4(7)	9(10)
BC(6)	5111(11)	−736(8)	5552(5)	46(9)	33(6)	10(2)	1(15)	−3(6)	9(9)
I	4987(1)	924(1)	6209(0)	86(1)	35(0)	20(0)	−6(1)	−1(1)	−2(1)
N	5155(9)	−3103(6)	5794(4)	41(8)	27(4)	10(2)	−16(11)	−4(5)	−2(7)
WO(1)	5009(12)	−999(8)	2501(5)	79(8)	84(7)	21(2)	−29(21)	17(7)	−24(9)
WO(2)	4949(11)	−1499(9)	9632(5)	72(9)	99(9)	23(3)	−3(20)	0(8)	−14(11)
WO(3)	95(29)	−1900(24)	7870(13)	74(24)	105(23)	28(7)	−50(52)	−33(22)	4(28)
WO(3′)	9701(18)	−2620(14)	8260(9)	101(21)	62(12)	32(6)	−17(26)	−19(14)	−29(17)

from an electron density map calculated with the phases based on the iodine atom; the positions of the *p*-IAN molecule and six glucose residues were located, but the least-squares refinement of the atomic parameters was unsuccessful. The positions and orientations of the *p*-IAN molecule and six glucose residues except O(6) atoms were refined by the block-diagonal rigid-body least-squares technique.[4] The O(6) atoms and water molecules were found on a difference-Fourier map. The refinement was continued by the block-diagonal least-squares method. In these refinements, two of the oxygen atoms, G4O(6) and WO(3), were found to be disordered. The occupancies were estimated by assuming that the magnitude of the isotropic thermal factor of an occupant is the same as that of the other. They are 0.35, 0.65, 0.60, and 0.40 for G4O(6), G4O(6′), WO(3), and WO(3′) respectively. The final *R*-value was 0.072. The weighting schemes are as follows: $w=0.0$ for $F_o<3\sigma(F)$, and $w=1.0$ for $F_o\geq 3\sigma(F)$. The anomalous dispersion terms were ignored. The atomic scattering factors were taken from the "International Tables for X-ray Crystallography."[12] The atomic coordinates and the anisotropic temperature factors are listed in Table 2. The observed and calculated structure factors are listed in Table 4.[13] The computation was done on a HITAC 8450 computer in this Institute.[14]

Results and Discussion

Conformation of Glucose Residues. The structure of the α-CDx–*p*-IAN complex is illustrated in Fig. 1 with the absolute configuration corresponding to D-glucose. The average bond distances and angles in the glucose residues are normal (Fig. 2), varying in the ranges of ±0.05 Å and ±3° respectively (Table 3[13]). The valence angles of the α-1,4-linking oxygen atoms are 119—121°. These rather large angles are commonly observed in the α-CDx complexes: 118.8—119.4° in the potassium acetate complex, 116—122° in the iodine complex, and 116.2—119.4° in the water complex. In di-saccharides, α,α-trehalose[15] and β-maltose[16] give 115.8° and 117.2° respectively.

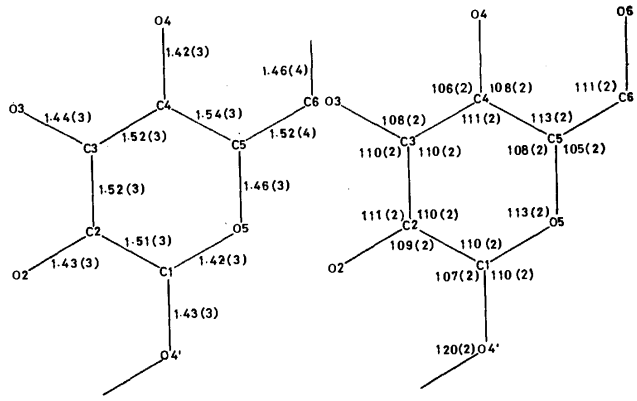

Fig. 2. Average bond distances and angles for the D-glucose residues with standard deviations.

Each glucose residue has the C1-chair conformation. The conformation angles around the pyranose ring vary from 45° to 66°. This range is similar to that found in the α-CDx–iodine complex (45—66°),[5] although it is rather wider than that of 52—66° in the α-CDx-potassium acetate complex,[4] that of 49—65° in the α-CDx-water complex,[6] and those found in di- and tri-saccharides.[15,17,18] In the G4 residue, the primary hydroxyl group takes two orientations: G4O(6) and G4O(6′). The former corresponds to a *gauche-gauche* conformation, and the latter to a *gauche-trans* conformation (Table 5). A similar disorder of the O(6) atom has been found in 1-kestose.[18] Both of those conformations have been found in the α-CDx-water complex, but in the α-CDx-potassium acetate complex the *gauche-gauche* conformation is not found because of the molecular packing and hydrogen bonds.

The macro-cyclic conformation of the α-CDx ring is described by the conformation angles including C(1)-O(4*)-C(4*) linkages. The C(1)-O(4*)-C(4*)-C(3*) and C(1)-O(4*)-C(4*)-C(5*) conformation angles are 123—132° and 104—115° respectively, while in the α-CDx-water complex they are 116.6—170.4° and

Table 5. Selected conformation angles (ϕ/°)

The angle was measured between projections of bonds *h–i* and *j–k* along the bond *i–j*. An asterisk (*) denotes the atom in the adjacent glucose residue.

h *i* *j* *k*	G1	G2	G3	G4	G5	G6
C(1)–C(2)–C(3)–C(4)	−56	−54	−52	−57	−51	−55
C(2)–C(3)–C(4)–C(5)	55	54	47	60	53	51
C(3)–C(4)–C(5)–O(5)	−56	−57	−45	−62	−57	−50
C(4)–C(5)–O(5)–C(1)	61	61	53	63	64	55
C(5)–O(5)–C(1)–C(2)	−63	−63	−61	−60	−64	−63
O(5)–C(1)–C(2)–C(3)	58	60	58	57	56	62
O(4*)–C(1)–C(2)–O(2)	54	59	64	57	61	64
O(2)–C(2)–C(3)–O(3)	70	69	65	66	65	66
O(3)–C(3)–C(4)–O(4)	−71	−71	−70	−68	−68	−73
O(4)–C(4)–C(5)–C(6)	68	73	79	71	72	77
O(5)–C(5)–C(6)–O(6)	−67	−76	−74	−76	−76	−80
O(5)–C(5)–C(6)–O(6′)	—	—	—	51	—	—
C(4)–C(5)–C(6)–O(6)	52	43	48	66	40	39
C(4)–C(5)–C(6)–O(6′)	—	—	—	−167	—	—
O(5)–C(1)–O(4*)–C(4*)	104	120	114	105	108	107
C(2)–C(1)–O(4*)–C(4*)	−134	−121	−127	−135	−132	−132
C(1)–O(4*)–C(4*)–C(3*)	123	129	126	134	132	129
C(1)–O(4*)–C(4*)–C(5*)	−115	−114	−115	−104	−112	−112

Table 6. Least-squares planes and deviations of atoms from the plane (d/Å)

(1) *p*-Iodoaniline

$0.9977X+0.0209Y+0.0648Z+7.8202=0$

BC(1)	0.009	BC(5)	−0.017
BC(2)	0.023	BC(6)	0.009
BC(3)	−0.031	N	0.031
BC(4)	−0.021	I	−0.003

(2) Six O(4) atoms

$0.0052X+0.9984Y+0.1020Z+0.8866=0$

G1O(4)	0.028	G4O(4)	0.018
G2O(4)	0.097	G5O(4)	0.108
G3O(4)	−0.119	G6O(4)	−0.132

Table 7. Selected intramolecular distances (d/Å)

(1) Between glucose residues			
G1O(3)–G2O(2)	2.68	G4O(3)–G5O(2)	2.92
G2O(3)–G3O(2)	2.76	G5O(3)–G6O(2)	2.98
G3O(3)–G4O(2)	3.00	G6O(3)–G1O(2)	2.87
(2) Between *p*-iodoaniline and glucose residues			
G1O(4)–BC(6)	3.78	G4O(4)–BC(2)	3.78
G2C(3)–BC(5)	3.72	G4O(6′)–I	3.70
G2O(4)–BC(6)	3.25	G5C(3)–BC(2)	3.85
G2O(4)–BC(5)	3.73	G5C(5)–BC(2)	3.78
G2C(3)–BC(6)	3.70	G5O(4)–BC(3)	4.00
G3C(3)–BC(5)	3.83	G5C(5)–BC(2)	3.99
G3C(3)–BC(6)	3.84	G5O(4)–BC(2)	3.35
G5C(5)–BC(6)	4.00	G5C(4)–BC(2)	3.90
G3O(4)–BC(6)	3.63	G6C(3)–BC(2)	3.91

69.3—129.7° respectively. This suggests that the α-CDx ring becomes more symmetrical when a bulky group is included. The six O(4) atoms are near the least-squares plane as is shown in Table 6. The r.m.s. displacement of the atoms from the plane is 0.10 Å, compared to that of 0.13 Å in the α-CDx-iodine complex. The distance between the O(2) and O(3) atoms of adjacent glucose residues corresponds to the acceptable one for the hydrogen bond (Table 7).

Structure of p-*Iodoaniline.* The bond distances and angles of *p*-IAN are shown in Fig. 3. The I–C(1) distrance is in agreement with that of 2.09 Å found in *o*-iodobenzonitrile.[19] The N–C(4) distance is longer than that of 1.371 Å in *N,N*-dimethyl-*p*-nitroaniline[20] and that of 1.358 Å in *p*-nitroaniline.[21] The planarity of *p*-IAN is good, as is shown in Table 6.

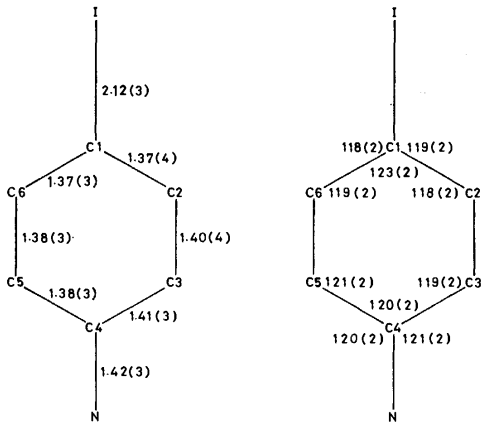

Fig. 3. Bond distances and angles with standard deviations in *p*-iodoaniline.

Geometry of Inclusion. As is shown in Fig. 1, the *p*-IAN molecule is included in the cavity of α-CDx, although the amino group sticks out. This suggests that the cavity is hydrophobic in nature and that α-CDx binds the hydrophobic portion of *p*-IAN. Selected intramolecular distances in the complex are shown in Table 7. The shortest interatomic distance of 3.25 Å, which is the distance between G2O(4) and BC(6), suggests that the "guest" molecule is rigidly fixed in the cavity. The iodine atom and G4O(6′) are in van der Waals contact. The amino nitrogen atom

TABLE 8. INTERMOLECULAR DISTANCES LESS THAN 3.0 Å AND ANGLES

The letters in parentheses denote the symmetry operations.

Distances (d/Å)			Angles (φ/°)	
G1O(2)–G3O(2)	(g)	2.77	G1C(2)–G1O(2)–G3O(2)	116
G1O(3)–G3O(3)	(g)	2.64	G1O(3)–G3O(3)–G3C(3)	109
G1O(6)–G4O(6)	(b)	2.92	G1C(6)–G1O(6)–G4O(6)	117
G1O(6)–WO(2)	(c)	2.83	G1C(6)–G1O(6)–WO(2)	136
G2O(2)–N	(g)	2.66	G2C(2)–G2O(2)–N	115
G2O(3)–G4O(3)	(h)	2.67	G2O(3)–G4O(3)–G4C(3)	128
G2O(3)–G6O(6)	(c)	2.75	G2C(3)–G2O(3)–G6O(6)	117
G2O(6)–WO(3)	(c)	2.85	G2C(6)–G2O(6)–WO(3)	141
G2O(6)–WO(3′)	(d)	2.83	G2C(6)–G2O(6)–WO(3′)	119
G2O(6)–G4O(6)	(i)	2.94	G2C(6)–G2O(6)–G4O(6)	113
G2O(6)–G4O(6′)	(i)	2.74	G2C(6)–G2O(6)–G4O(6′)	98
G3O(2)–WO(1)		2.85	G3C(2)–G3O(2)–WO(1)	110
G3O(3)–G5O(6)	(d)	2.81	G3C(3)–G3O(3)–G5O(6)	111
G3O(6)–WO(2)	(d)	2.80	G3C(6)–G3O(6)–WO(2)	124
G3O(6)–G5O(3)	(d)	2.85	G3O(6)–G5O(3)–G5C(3)	111
G4O(6)–WO(1)	(f)	2.80	G4C(6)–G4O(6)–WO(1)	116
G5O(2)–WO(3)	(a)	2.68	G5C(2)–G5O(2)–WO(3)	107
G5O(2)–WO(3′)		2.88	G5C(2)–G5O(2)–WO(3′)	112
G5O(6)–N	(j)	2.67	G5C(6)–G5O(6)–N	119
WO(1)–WO(3′)	(g)	2.86		
G6O(6)–WO(1)	(e)	2.82	G6C(6)–G6O(6)–WO(1)	99

Symmetry code	Symmetry operator		
	x,	y,	z
a	$1+x$,	y,	z
b	$-1+x$,	y,	z
c	$1/2-x$,	$-y$,	$-1/2+z$
d	$3/2-x$,	$-y$,	$-1/2+z$
e	$1/2-x$,	$-y$,	$1/2+z$
f	$3/2-x$,	$-y$,	$1/2+z$
g	$-1/2+x$,	$-1/2-y$	$1-z$
h	$1/2+x$,	$-1/2-y$,	$1-z$
i	$-1/2+x$,	$1/2-y$,	$1-z$
j	$1-x$,	$1/2+y$,	$3/2-z$

is apart more than 4.0 Å from any atom in α-CDx.

Crystal Structure. The crystal structure is shown in Figs. 4 and 5. The packing scheme of α-CDx is depicted in Fig. 6. Molecular layers composed of α-CDx are stacked along the b-axis in the crystal. The cavities of α-CDx do not form continuous channels which are found in the α-CDx-potassium acetate complex, since adjacent layers are each slipped by about half a molecule along the c-axis. The *p*-IAN molecule is so bulky that the amino group sticks out from the open end of the cavity. In the iodine and water complexes, the "guest" molecule is enclosed in the cavity, both ends of which are closed by the adjacent α-CDx molecules.

Intermolecular distances of less than 3.0 Å are shown in Table 8. Although the hydrogen atoms are not located, O···O and O···N distances less than 3.0 Å are taken as hydrogen bonds since the C-O···O and C-O···N angles are in the usual range for hydrogen bonds. The hydrogen-bonding network is formed in the crystal. The nitrogen atom forms hydrogen bonds with G2O(2) and G5O(6) in the adjacent layer. WO-(1) forms hydrogen bonds with G4O(6), G3O(2), G6O(6), and WO(3), while both WO(3) and WO(3′) are hydrogen-bonded to G2O(6) and G5O(2). WO-(2), which is separated from the other water molecules, is hydrogen-bonded to G3O(6) and G1O(6).

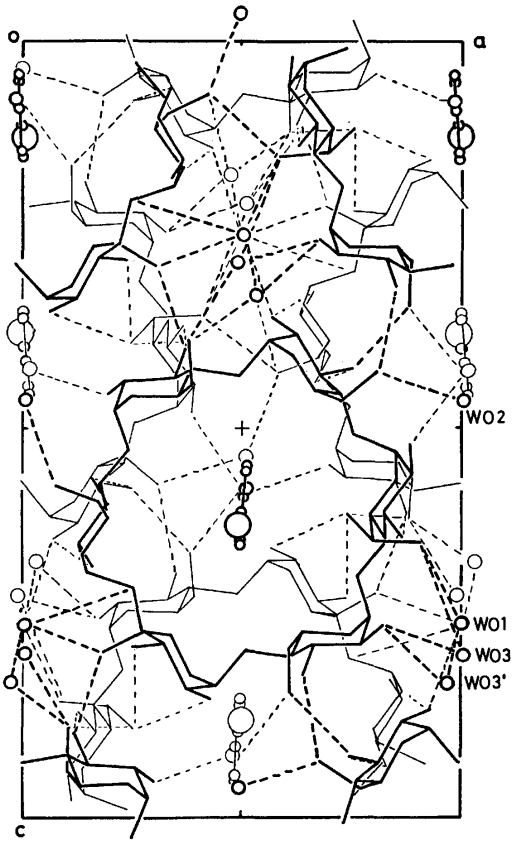

Fig. 4. Crystal structure viewed along the b-axis. Atoms represented by circles are those in *p*-iodoaniline and water molecules, and dashed lines indicate intermolecular distances less than 3.1 Å.

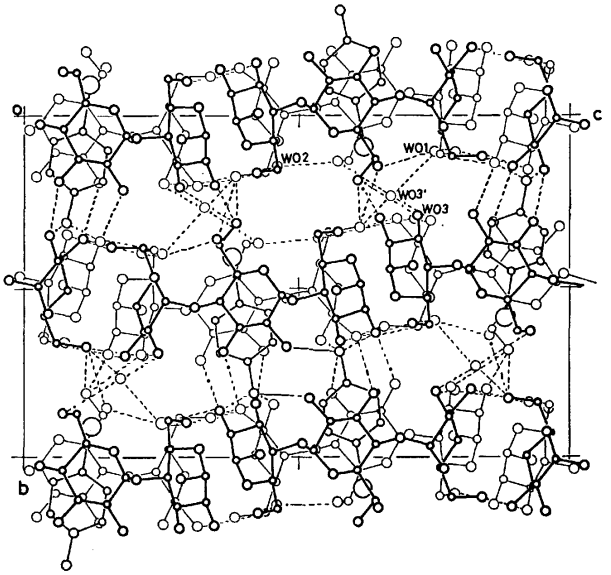

Fig. 5. Crystal structure viewed along the a-axis. Dashed lines indicate intermolecular distances less than 3.1 Å.

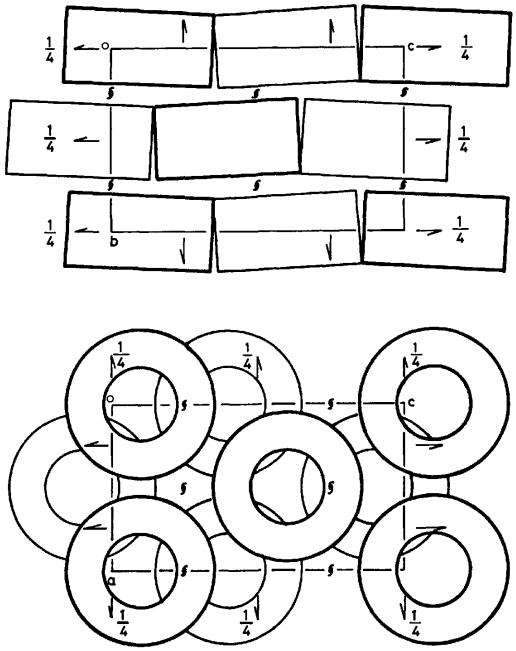

Fig. 6. The packing shemes of α-CDx in the crystal.

Between the layers, G1O(2), G1O(3), and G2O(3) form hydrogen bonds with G3O(2), G3O(3), and G4O(3) respectively.

Catalytic Property of α-Cyclodextrin. The cyclodextrin-catalyzed reactions have been interpreted in terms of the formation of inclusion compounds as intermediates. In the α-CDx-water complex, two of the primary hydroxyl groups of α-CDx have the *gauche-trans* conformation and form hydrogen bonds with water molecules in the cavity. In an aqueous solution, α-CDx seems to have a similar structure.[6] The cavity of α-CDx will release the water molecules when a "guest" molecule is included. Furthermore, the α-CDx ring will become more symmetrical and the *gauche-trans* conformation may turn to the *gauche-gauche* conformation, as in the iodine and *p*-IAN complexes.

It has been proved that the secondary hydroxyl group of α-CDx are catalytically reactive in the hydrolysis of substituted phenyl esters, and that the relative rates of the hydrolysis of *meta*-substituted phenyl esters are about 10^2 times faster than that of *para*-substituted phenyl esters. The structure of the α-CDx-*p*-IAN complex suggests that the hydrolysis of *para*-substituted phenyl esters will hardly occur if a substrate is included in the same manner as that of the *p*-IAN complex, since the distance between the secondary hydroxyl groups of α-CDx and the amino group of *p*-IAN is greater than 4.0 Å. On the other hand, *meta*-substituted phenyl esters must be in close contact with the secondary hydroxyl groups, judging from the inspection of molecular models, so the reaction will occur readily.

The author wishes to thank Professor J. Tanaka and Dr. H. Uedaira for their useful discussion.

References

1) J. A. Thoma and L. Stewart, "Starch: Chemistry and Technology," Vol. I, ed. by R. L. Whistler and E. F. Pashall, Academic Press, New York (1965), p. 209—249.
2) J. A. Hamilton, L. K. Steinrauf, and R. L. Van Etten, *Acta Crystallogr.*, **B24**, 1560 (1968).
3) R. K. McMullan, W. Saenger, J. Fayos, and D. Mootz, *Carbohyd. Res.*, **31**, 37 (1973).
4) A. Hybl, R. E. Rundle, and D. E. Williams, *J. Amer. Chem. Soc.*, **87**, 2779 (1965).
5) R. K. McMullan, W. Saenger, J. Fayos, and D. Mootz, *Carbohyd. Res.*, **31**, 211 (1973).
6) P. C. Manor and W. Saenger, *J. Amer. Chem. Soc.*, **96**, 3630 (1974).
7) W. D. Griffiths and M. L. Bender, "Advances in Catalysis," **23**, 209 (1973).
8) M. L. Bender, R. L. Van Etten, G. A. Clowes, and J. F. Sebastian, *J. Amer. Chem. Soc.*, **88**, 2318 (1966).
9) P. V. Demarco and A. L. Thakker, *Chem. Commun.*, **1970**, 2.
10) F. Cramer, W. Saenger, and H.-Ch. Spatz, *J. Amer. Chem. Soc.*, **89**, 14 (1967).
11) K. Harata and H. Uedaira, *Nature*, **253**, 190 (1975).
12) "International Tables for X-ray Crystallography," Vol. III, Birmingham: Kynoch Press (1965), p. 201.
13) Tables 3 and 4 have been submitted to, and kept by the office of The Chemical Society of Japan, 1–5 Kanda-Surugadai, Chiyoda-ku, Tokyo 101, as Document No. 7521.
14) The block-diagonal least-squares program HBLS IV (T. Ashida, 1967) was modified by the author.
15) G. C. Broun, D. C. Rother, B. Berking, C. A. Beevers, R. O. Gould, and R. Simpson, *Acta Crystallogr.*, **B28**, 3145 (1972).
16) G. J. Quigley, A. Sarco, and R. H. Marchessault, *J. Amer. Chem. Soc.*, **92**, 5834 (1970).
17) D. C. Rother, *Acta Crystallogr.*, **B28**, 425 (1972).
18) G. A. Jeffrey and Y. J. Park, *ibid.*, **B28**, 257 (1972).
19) S. Lam and D. Britton, *ibid.*, **B30**, 1119 (1974).
20) T. C. M. Mak and J. Trotter, *ibid.*, **18**, 68 (1965).
21) K. N. Trueblood, F. Goldish, and J. Donohue, *ibid.*, **14**, 1009 (1961).

The Crystal Structure of a Hofmann-en Type Pyrrole Clathrate, *catena*-μ-Ethylenediaminecadmium(II) *catena*-Tetra-μ-cyanonickelate(II)-Pyrrole (1/2)

Toschitake IWAMOTO and Mamoru KIYOKI

Department of Chemistry, College of General Education, The University of Tokyo, Komaba, Meguro, Tokyo 153

(Received April 24, 1975)

The crystal structure of the titled pyrrole clathrate $Cd(NH_2CH_2CH_2NH_2)Ni(CN)_4\cdot 2C_4H_5N$ has been determined from three-dimensional X-ray data collected by counter techniques. The clathrate crystallizes in the orthorhombic space group Pmmm with $a=7.618(3)$, $b=7.641(10)$, $c=7.861(4)$ Å, $Z=1$, $D_m=1.69$ g cm^{-3}, and $D_x=1.70$ g cm^{-3}. The structure has been refined by the full-matrix least-squares procedure to a conventional R index (on F) of 0.057 for 462 observed reflections. The metal complex host-framework has a three-dimensional infinite cage structure where the ambident ethylenediamine molecules span Cd atoms at the corners of unit cell along the [001] direction and the ambident cyanide ions make infinite two-dimensional networks parallel to (001) by spanning the Cd atoms with the Ni atom at (1/2, 1/2, 0). The two crystallographically independent pyrrole molecules are enclathrated in the molecular spaces of the cages in the host-framework. The statistical dispositions observed for en and pyrrol molecules can be interpreted in terms of motional behavior of these molecules in the crystal.

The crystal structures of the Hofmann type and analogous clathrates have been determined only for those of the benzene guest[1–7] except a Hofmann type biphenyl clathrate $Ni(NH_3)_2Ni(CN)_4\cdot 2C_{12}H_{10}$,[8] in spite that various polar molecules such as pyrrole, thiophene or aniline can be the guest.[9] With respect to the guest benzene molecule, the reorientational motion about its sixfold axis has been observed for Hofmann type clathrates above 140 K by wide-line PMR.[10] The atomic coordinates of the carbons in the crystal have been determined as the potential minima during the reorientational motion by single crystal X-ray analysis. It is a matter of interest how the polar molecules are arranged in the molecular spaces. The molecular electric dipole moments will play an important role in determining the arrangements of the polar molecules in the crystal. For the first attempt at the crystal structure analysis of the polar-guest clathrate of these types, a Hofmann-en type pyrrole clathrate $Cd(en)Ni(CN)_4\cdot 2C_4H_5N$ (en=$NH_2CH_2CH_2NH_2$) was taken up, since pyrrole has a large dipole moment (1.80 D) and since the structure of the Hofmann-en type benzene clathrate $Cd(en)Ni(CN)_4\cdot 2C_6H_6$ had already been determined.[3] The structural features of the pyrrole clathrate will be discussed in comparison with those of the benzene clathrate.

Experimental

The crystals of $Cd(en)Ni(CN)_4\cdot 2C_4H_5N$ were prepared by the method previously reported.[11] An approximately equidimensional crystal of $0.1\times 0.1\times 0.1$ mm in size was sealed in a thin-walled glass capillary (0.1 mmϕ) with a small amount of liquid pyrrole. Preliminary Weissenberg photographs suggested a tetragonal symmetry of the crystal and the cell-dimensions $a=7.62$ and $c=7.86$ Å, supporting the previous results obtained from the powder diffraction pattern.[11] Before intensity collection, however, the unit cell dimensions and the intensity distribution were reexamined on a Rigaku four-circle automated diffractometer,[12] and it was revealed that the crystal is orthorhombic with $a=7.618(3)$, $b=7.641(10)$ and $c=7.861(4)$ Å, the values being determined by the least-squares calculations with eight 2θ values in the range 20—40°, for Cu$K\bar{\alpha}$ radiation. The intensity data were collected with Cu$K\bar{\alpha}$ radiation monochromated by a graphite crystal ($\lambda=1.5418$ Å) using $2\theta-\theta$ scanning technique for 462 independent reflections with 2θ less than 120°. All the reflections had the non-zero intensities; 31 reflections had the values comparable with or less than three times the standard deviations. Three standard reflections were remeasured every 50 reflections; no significant variation in the intensities was observed. The Lp correction was applied, but no corrections for absorption and extinction were made. The density was measured by flotaion method in bromoform-xylene mixture.

Crystal data are:

$Cd(NH_2CH_2CH_2NH_2)Ni(CN)_4\cdot 2C_4H_5N$, M.W.=469.38

Orthorhombic, D_{2h}^1-Pmmm, $a=7.618(3)$, $b=7.641(10)$, $c=7.861(4)$ Å, $Z=1$. $D_m=1.69$, $D_x=1.70$ g·cm^{-3}. No systematic absence. $\mu(Cu K\bar{\alpha})=109.6$ cm^{-1}.

Structure Refinement

All the calculations were carried out on a HITAC 8800/8700 computer at the Computation Center of this University. The programs used were those in UNICS[13] and BLAN-2.[14] The atomic scattering factors used were those listed in the usual tabulation[15] for C and N, and those from Cromer and Waber[16] for Cd and Ni. In the least-squares calculations the quantity minimized was $\sum w(||F_o|-|F_c||)^2$ with $w=1/[\sigma(F_o)]^2$. The reliability indices of conventional $R_1=\sum w(||F_o|-|F_c||)/\sum|F_o|$ and $R_2=\sum w(||F_o|-|F_c||)^2/\sum|F_o|^2$ were defined in order to check the results of refinement. All the 462 observed reflections were used in the calculations.

Because of no systematic absence of the reflections, the possible space groups are P222, Pmm2 and Pmmm. Since the unit cell contains only a formula unit of $Cd(en)Ni(CN)_4\cdot 2C_4H_5N$, most of the atoms should lie on the special positions. From the three-dimensional Patterson synthesis, the Cd and the Ni atoms were placed at the positions 0,0,0 and 1/2,1/2,0, respectively. The centrosymmetric space group Pmmm was assumed prior to the other two non-centrosymmetric ones. The Fourier map phased with the heavy atoms gave clear peaks due to cyanide C and N atoms on the (001) plane, and the more diffused peaks due to en-C and -N atoms along the twofold axis parallel to [001]

Table 2. The bond lengths, interatomic distances less than 3.0 Å, and bond angles

Cd–N(1)	2.40(1) Å	Cd–N(2)	2.25(3) Å
Ni–C(1)	1.87(1)	C(1)–N(1)	1.12(2)
N(2)–C(2)	1.19(4)	C(2)–C(2′)	1.38(3)
N(3)–C(3)	1.43(8)	N(4)–C(5)	1.37(8)
C(3)–C(4)	1.49(11)	C(5)–C(6)	1.42(13)
C(4)–C(4′)	1.27(11)	C(6)–C(6′)	1.37(11)
N(3)–C(4)	2.36(10)	N(4)–C(6)	2.24(11)
C(3)–C(3′)	2.27(8)	C(5)–C(5′)	2.26(10)
C(3)–C(4′)	2.26(10)	C(5)–C(6′)	2.27(12)
Cd–N(1)–C(1)	180(1)°	N(1)–C(1)–Ni	180(1)°
Cd–N(2)–C(2)	139(3)	N(2)–C(2)–C(2′)	153(2)
N(3)–C(3)–C(4)	108(5)	N(4)–C(5)–C(6)	107(6)
C(3)–C(4)–C(4′)	109(7)	C(5)–C(6)–C(6′)	108(8)
C(3)–N(3)–C(3′)	105(6)	C(5)–N(4)–C(5′)	111(5)
N(2)–Cd–C(2)	14(1)		

Key to symmetry operations: C(2) at ((0,0,z), C(2′) at (0,0,$\bar{z}$); C(3) at (½,y,z), C(3′) at (½,y,z); C(4) at (½,y,z), C(4′) at (½,$\bar{y}$,z); C(5) at (x,½,z), C(5′) at ($\bar{x}$,½,z); C(6) at (x,½,z), C(6′) at ($\bar{x}$.½,z).

square-planar $Ni(CN)_4$ into a doublet, 2155 and 2146 cm^{-1} in the benzene, and 2154 and 2145 cm^{-1} in the pyrrole clathrates. In the orthorhombic D_{2h}^1-Pmmm unit cell of the latter, the Ni atom locates at the D_{2h} site, 1/2,1/2,0. The correlation among the molecular (effective) D_{4h}, the site D_{2h} and the crystal D_{2h} groups makes the degenerate E_u mode split into a B_{2u} and a B_{3u} modes. Although this interpretation cannot be directly applied to the benzene clathrate with the tetragonal C_{4h}^1-P4/m space group, the similar doublet structure suggests that the effective site symmetry of the Ni atom is lowered from tetragonal to orthorhombic probably owing to the reorientation of en molecules.

There are two crystallographically independent pyrrole molecules in the unit cell. The aromatic plane of one molecule is vertical to the (010) plane, and that of the other is vertcial to the (100) plane; the twofold axes of the molecules are parallel to [001]. Each pyrrole molecule is statistcially distributed with an equal probability in two orientations which are related one another by the mirror plane perpendicular to [001]. There are fairly large differences between the bond lengths and angles in the two independent molecules, but the differences are not significant in view of the large estimated standard deviations. The shapes of molecules appear to be elongated along the twofold axis and compressed along the direction vertical to the axis in comparison with the structure estimated by microwave spectroscopy.[18] In the molecular spaces, the reorientational motions of pyrrole molecules may occur, which are similar to that observed in a Hofmann type pyrrole clathrate $Cd(NH_3)_2Ni(CN)_4 \cdot 2C_4H_5N$ by wide-line PMR.[10] The large estimated standard deviations of atomic coordinates and the considerably large temperature factors support the motional behavior of the pyrrole molecules. Therefore, the atomic coordinates should be interpreted to be the postions of potential minima during their reorietnational motions, by which the directions of molecular dipoles are statistically in parallel and anti-parallel along the [001] direction.

The authors' thanks are due to Professor Niro Matsuura at this College for his kind support to this work.

References

1) J. H. Rayner and H. M. Powell, *J. Chem. Soc.*, **1952**, 319.
2) Y. Sasaki, This Bulletin, **42**, 2412 (1969).
3) T. Miyoshi, T. Iwamoto, and Y. Sasaki, *Inorg. Chim. Acta*, **6**, 59 (1972).
4) T. Miyoshi, T. Iwamoto, and Y. Sasaki, *ibid.*, **7**, 97 (1973).
5) T. Iwamoto, *Chem. Lett.*, **1973**, 723.
6) R. Kuroda, *Inorg. Nucl. Chem. Lett.*, **9**, 13 (1974).
7) R. Kuroda and Y. Sasaki, *Acta Crystallogr.*, **B30**, 687 (1974).
8) T. Iwamoto, T. Miyoshi, and Y. Sasaki, *ibid.*, **B30**, 292 (1974).
9) T. Iwamoto, T. Nakano, M. Morita, T. Miyoshi, T. Miyamoto, and Y. Sasaki, *Inorg. Chim. Acta*, **2**, 313 (1968); T. Iwamoto, M. Kiyoki, Y. Ohtsu, and Y. Takeshige, submitted to This Bulletin.
10) T. Miyamoto, T. Iwamoto, and Y. Sasaki, *J. Mol. Spectrosc.*, **33**, 244 (1970).
11) T. Iwamoto and Y. Ohtsu, *Chem. Lett.*, **1972**, 463.
12) The authors' thanks are due to Mrs. Midori Goto at National Chemical Laboratory for Industry for her kind help in the intensity data collection.
13) The Universal Crystallographic Computation Program System (UNICS), ed. by T. Sakurai, Crystallographic Society of Japan, Tokyo (1967).
14) The program for block-diagonal least-squares calculation and Fourier synthesis revised from HBLSIV in UNICS by Mr. T. Nishikawa, M. Sc., at the Department of Chemistry, Faculty of Science of this University. The authors' thanks are due to his kind permission to use this program under the auspices of Professor Yukiyoshi Sasaki.
15) International Tables for X-ray Crystallography, Vol. III, Kynoch Press, Birmingham, p. 202 (1968).
16) D. T. Cromer and J. T. Waber, *Acta Crystallogr.*, **18**, 104 (1965).
17) The table of the structure-factors is kept as Document No. 7522 at the Chemical Society of Japan.
18) B. Bak, D. Christensen, L. Hansen, and J. R. Andersen, *J. Chem. Phys.*, **24**, 720 (1956).

C-S Stretching Vibrations and Molecular Conformations of Isobutyl Methyl Sulfide and Related Alkyl Sulfides

Norimasa NOGAMI,* Hiromu SUGETA, and Tatsuo MIYAZAWA[1)]

* *Department of Chemistry, Faculty of Science, The University of Tokyo, Hongo, Bunkyo-ku, Tokyo 113*
Institute for Protein Research, Osaka University, Yamada-kami, Suita, Osaka 565

(Received May 16, 1975)

The Raman and infrared spectra of isobutyl methyl sulfide and related alkyl sulfides were measured. The Raman spectra of the liquid, unannealed solid, and annealed solid of isobutyl methyl sulfide were compared and skeletal normal vibrations of possible rotational isomers were treated. Three rotational isomers were found to coexist in the liquid state whereas only one isomer was observed in the annealed solid. The energy differences among the three rotational isomers were measured. The correlations between the CH_2–S stretching frequencies and molecular conformations were established, in common, for the molecules of isobutyl methyl sulfide, methyl propyl sulfide and ethyl methyl sulfide.

In our previous studies,[2,3)] Raman and infrared spectra of a series of dialkyl disulfides were analysed. The S–S and C-S stretching frequencies of the $\rangle C\text{-}CH_2\text{-}S\text{-}S\text{-}CH_2\text{-}C\langle$ group were found to depend upon the internal rotation about the CH_2-S and C-CH_2 bonds, respectively. The correlation for S-S stretching vibrations is useful for studying conformations of cystine groups of proteins in aqueous solution. On the other hand, C-S bonds are involved in methionine groups as well as in cystine groups of proteins. Accordingly, the molecule of methyl propyl sulfide was taken up as a model of the methionine group.[4)] New correlations were found between C-S stretching frequencies and the internal rotation about the C-CH_2 and CH_2-S bonds of the $\rangle C\text{-}CH_2\text{-}S\text{-}CH_3$ group. The Raman lines due to C-S stretching vibrations are now useful for studying conformations of methionine groups of proteins in aqueous solution.

In the present study, the Raman and infrared spectra of isobutyl methyl sulfide $CH_3\text{-}\underset{\displaystyle CH_3}{\underset{|}{CH}}\text{-}CH_2\text{-}S\text{-}CH_3$ were analysed. This molecule possibly serves as a model of *S*-methylcystein,

$$NH_3^+\text{-}\underset{\displaystyle COO^-}{\underset{|}{CH}}\text{-}CH_2\text{-}S\text{-}CH_3$$

The correlations for the C-S stretching frequencies of isobutyl methyl sulfide were compared with those of ethyl methyl sulfide, methyl propyl sulfide and isopropyl methyl sulfide.

Experimental

Isobutyl methyl sulfide, methyl propyl sulfide, and isopropyl methyl sulfide were prepared from methyl iodide and sodium salts of corresponding thiols. Ethyl methyl sulfide was obtained from commercial sources. All these samples were purified by distillation.

Raman spectra were recorded with a JEOL Raman Spectrometer (Model JRS-02AS) with an argon-ion laser (514.5 and 488.0 nm). Infrared spectra were recorded with a Hitachi EPI-G3 Infrared Spectrophotometer. The temperature of the sample in the low temperature cell for Raman scattering was measured with a copper-constantan thermocouple.

Normal Coordinate Treatment

As an aid for analysing the vibrational spectra in the low frequency region, normal vibrations were treated for the possible rotational isomers of isobutyl methyl sulfide. Methyl, methylene and methine groups were treated as single dynamic units. The structural parameters used in the calculation were the bond lengths of r(C-S)=1.81 Å and r(C-C)=1.54 Å, bond angles of ϕ(C-S-C)=98.67° and the tetrahedral angles for carbon atoms. The dihedral angles were 180° and ±60° for the *trans* (T) and *gauche* (G, G′) forms, respectively. The force constants of the Urey-Bradley type were transferred from related molecules (Table 1).

Table 1. Force constants[a)]

K(CH_3–S)	2.8	H(C–S–C)	0.16[b)]
K(CH_2–S)	2.3	H(C-C-S)	0.15
K(C–C)	3.6	H(C–C–C)	0.25
F(C–S–C)	0.21[b)]	Y(C–S)	0.05
F(C–C–S)	0.47	Y(C–C)	0.07
F(C–C–C)	0.33		

a) K(stretching) and F(repulsion), in unit of mdyn/Å; H(bending) in unit of mdyn/Å·rad²; and Y(internal-rotation) in unit of mdyn·Å/rad². This set was used previously.[4)] b) These were transferred from dimethyl sulfide.[7)] Others were from dialkyl disulfide (Sugeta, Go, and Miyazawa).

Isobutyl Methyl Sulfide

The Raman spectra of isobutyl methyl sulfide in the 850—150 cm^{-1} region are shown in Fig. 1. The top spectrum (Liquid) was observed for the liquid state. The second spectrum (Solid-1) was observed after freezing the sample rapidly. This solid sample was then annealed and the third spectrum (Solid-2) was observed.

Possible rotational isomers of isobutyl methyl sulfide are shown in Fig. 2. The conformations of the X$\rangle$C-CH_2-S– group are denoted with the atom located at the *trans* site (X) with respect to the sulfur atom. Thus, P_C and P_H refer to the conformations with carbon and hydrogen atoms, respectively, at the site X. The internal rotation about the CH_2-S bond is denoted by

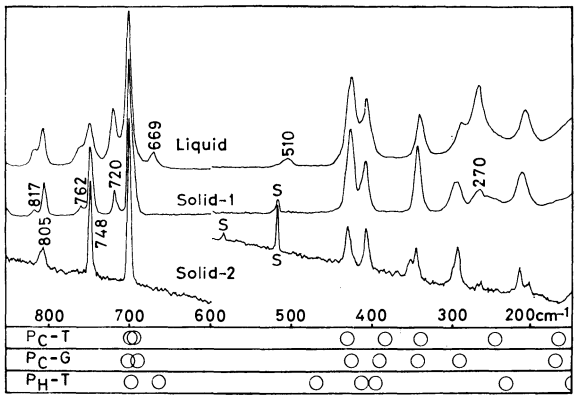

Fig. 1. The Raman spectra of the liquid (Liquid, at 300 K), unannealed solid (Solid-1, at 120 K), and annealed solid (Solid-2, at 120 K) samples of isobutyl methyl sulfide. Calculated frequencies are given with open circles. Spontaneous emission lines of the laser plasma are indicated as S.

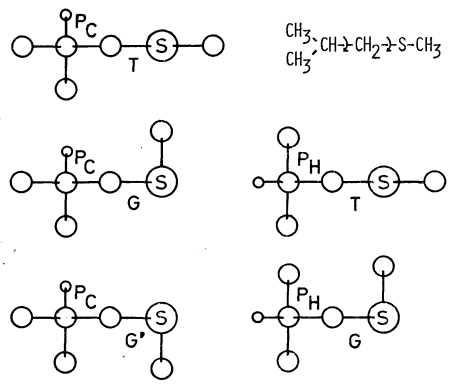

Fig. 2. Possible conformations of isobutyl methyl sulfide. Arrangements of sulfur and carbon atoms and methine hydrogen atom are given.

T (*trans*), G (right-handed *gauche*) and G′ (left handed *gauche*).

For each rotational isomer of isobutyl methyl sulfide, two C–S stretching vibrations are expected to appear in the region of 800—600 cm^{-1}. In fact, two strong Raman lines were observed at 748 and 701 cm^{-1} for Solid-2, indicating the presence of only one rotational isomer (to be called A hereafter). All the Raman lines of the isomer A were also observed in the spectrum of Solid-1, together with two additional lines at 762 and 720 cm^{-1}. These Raman lines are assigned to the C–S stretching vibrations of the second isomer (B), providing the evidence for the coexistence of two rotational isomers in the unannealed solid sample. All the Raman lines of the isomers A and B were also observed in the spectrum of the liquid state. The additional Raman line of the liquid at 669 cm^{-1} is assigned to the C–S stretching vibration of the third isomer (C).

The three rotational isomers (A, B, and C) are possibly the more stable ones among the five isomers shown in Fig. 2. The two isomers, P_C-G′ and P_H-G, are considered to be less stable because of strong steric repulsion between the terminal methyl groups. Accordingly the other isomers, P_C-T, P_C-G, and P_H-T, are expected to correspond to the three isomers experimentally observed in the Raman scattering.

It has been established that the C–Cl[6] and C–S[2] stretching frequencies of the P_H form are lower than those of the P_C form. The Raman line of the isomer C at 669 cm^{-1} is clearly due to the P_H-form. Furthermore, the Raman line of the isomer C at 510 cm^{-1} closely corresponds to the frequency (~470 cm^{-1}) calculated for the P_H-T isomer (Fig. 1). The vibrational frequencies calculated for the P_C-T and P_C-G forms in the 300 cm^{-1} region correspond to the Raman lines at 270 cm^{-1} (the isomer B) and at 299 cm^{-1} (the isomer A), respectively (Fig. 1). Thus, the isomers A, B, and C are now identified as the P_C-G, P_C-T, and P_H-T forms, respectively.

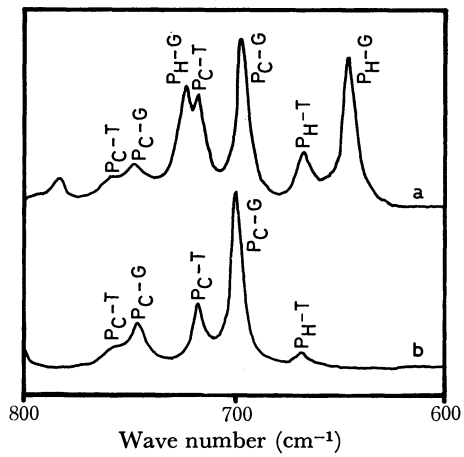

Fig. 3. Assignments of the Raman lines of methyl propyl sulfide (a) and isobutyl methyl sulfide (b) in the liquid state.

TABLE 2. OBSERVED FREQUENCIES (cm^{-1}), RELATIVE INTENSITIES,[a] AND VIBRATIONAL ASSIGNMENTS OF ISOBUTYL METHYL SULFIDE

Liquid		Solid-1	Solid-2	Assignments
Infrared	Raman	Raman	Raman	
	212m	215w	205vw 218w	skel. def.
	269 s	270w	—	skel. def. (P_C-T)
	292m	299w	297m	skel. def. (P_C-G)
	345m	347 s	349m 357w	skel. def.
408w	412 s	413 s	412m	skel. def.
427vw	431 s	431 s	434m	skel. def.
—	510vw	—	—	skel. def. (P_H-T)
670w	669m	—	—	CH_2–S str. (P_H-T)
700 s	701vs	700vs	701vs	C–S sym. str. (P_C-G)
718m	720 s	720m	—	CH_3–S str. (P_C-T)
748 s	745 s	748vs	748vs	C–S asym. str. (P_C-G)
758w	757m	762w	—	CH_2–S str. (P_C-T)
803 s	805 s	805m	805m	CH_2 rock. (P_C-G)
813w	815m	817w	—	CH_2 rock. (P_C-T)
849 s	851w	850w	851w	
862w	—	—	—	

a) vs: very strong, s: strong, m: medium, w: weak, vw: very weak.

The vibrational assignments of the infrared and Raman frequencies of isobutyl methyl sulfide are listed in Table 2. The Raman lines due to the C-S stretching vibrations of isobutyl methyl sulfide and methyl propyl sulfide[4] are compared in Fig. 3. The assignments to molecular conformations of these two sulfides correspond to each other case surprisingly well. It may be noted that, for the molecule of methyl propyl sulfide, the rotational isomers P_H-G and P_H-G′ are possible. However, the isomer P_H-G′ is considered to be much less stable because of strong steric repulsion between the terminal methyl groups. On the other hand, the isomer P_H-G is expected to be more stable and, in fact, the Raman lines due to this isomer were observed as shown in Fig. 3.

Energy Difference. The relative intensities of the Raman lines at 669 cm^{-1} (P_H-T), 720 cm^{-1} (P_C-T), and 701 cm^{-1} (P_C-G) were measured over the temperature range from 180 to 290 K. The P_C-G isomer was found to be most stable. The energy difference between the P_C-T and P_C-G isomers is 0.2 ± 0.1 kcal/mol and the energy difference between the P_H-T and P_C-G isomers is 0.8 ± 0.1 kcal/mol, in the liquid state.

C-S Stretching Frequencies of Alkyl Sulfides

For each of the P_C-G, P_C-T, and P_H-G forms of isobutyl methyl sulfide and methyl propyl sulfide, two Raman lines due to C-S stretching vibrations were observed as shown in Fig. 3. For the P_H-T form, however, only one Raman line due to the C-S stretching vibration was observed and the other Raman line was missing.

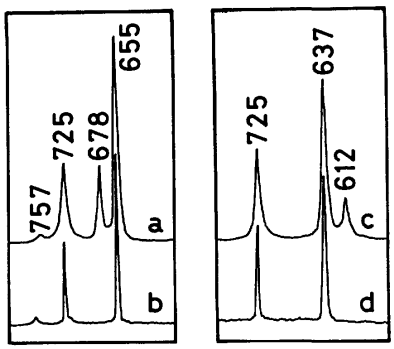

Fig. 4. The Raman spectra of the liquid (a) and annealed solid (b) of ethyl methyl sulfide and of the liquid (c) and annealed solid (d) of isopropyl methyl sulfide.

For studying the C-S stretching vibrations of the P_H-T form, Raman spectra were also measured of the liquid and annealed solid of ethyl methyl sulfide (Fig. 4).[7] The assignments of observed Raman lines to molecular conformations may be done with reference to the correlations found for the molecule of isobutyl methyl sulfide and methyl propyl sulfide. Thus the Raman lines of the annealed solid of ethyl methyl sulfide at 725 and 655 cm^{-1} may be assigned to the C-S stretching vibrations of the P_H-G form while the Raman line of the liquid at 678 cm^{-1} may be assigned to the P_H-T form.[8] The temperature dependence of the intensities of these three Raman lines suggests that the missing Raman line of the P_H-T form is overlapped by the Raman line of the P_H-G form at 725 cm^{-1}. This frequency is nearly equal to the average value (716 cm^{-1}) of the two CH_3-S stretching frequencies of dimethyl sulfide (antisymmetric: 741 cm^{-1}, symmetric: 691 cm^{-1}).[5] Accordingly the Raman line of ethyl methyl sulfide at 725 cm^{-1} is assigned to the CH_3-S stretching vibration. Similarly, the Raman line of methyl *tert*-butyl sulfide at 722 cm^{-1} is assigned to the CH_3-S stretching vibration.[12]

The CH_3-S stretching vibration was also studied for the molecule of isopropyl methyl sulfide. The Raman spectra of the liquid and annealed solid were observed, as shown in Fig. 4.[10] The Raman lines at 725 and 637 cm^{-1} have been assigned to the C_1 isomer and the line at 612 cm^{-1} to the C_S isomer.[11-13] The missing Raman line of the C_S isomer is now considered to be overlapped by the Raman line (at 725 cm^{-1}) due to the CH_3-S stretching vibration of the C_1 isomer.

Table 3. Characteristic C-S stretching frequencies (cm^{-1}) of alkyl sulfides

Molecule	Conformation				
	P_C-T	P_C-G	P_H-T	P_H-G	Mode
H, H, H: C-CH_2-S-CH_3	—	—	~725	725	S-CH_3
	—	—	678	655	CH_2-S
H, H, CH_3: C-CH_2-S-CH_3	719	(697)	~720	724	S-CH_3
	760	(746)	667	645	CH_2-S
H, CH_3, CH_3: C-CH_2-S-CH_3	720	(699)	~720	—	S-CH_3
	755	(743)	669	—	CH_2-S

The present analyses of the Raman spectra of isobutyl methyl sulfide and related alkyl sulfide lead to the conclusion that the CH_3-S stretching vibration is observed around 725 cm^{-1}, fairly independent of the changes in molecular conformations (except for the P_C-G form, see Table 3). On the other hand, the CH_2-S stretching frequencies are sensitive to the changes in molecular conformations. For the molecule of methyl propyl sulfide, the CH_2-S stretching frequencies are 645 (P_H-G), 667 (P_H-T), and 760 cm^{-1} (P_C-T). For the exceptional case of the P_C-G isomer, CH_3-S and S-CH_2 stretching modes are hybridized to yield normal vibrations at 746 cm^{-1} (pseudo-asymmetric) and 697 cm^{-1} (pseudo-symmetric). The average value (722 cm^{-1}) of these frequencies is, in fact, nearly equal to the 'intrinsic' frequency (725 cm^{-1}) of the CH_3-S stretching vibration.

References

1) To whom correspondences may be addressed; present address: Department of Biophysics and Biochemistry, Faculty of Science, The University of Tokyo, Hongo, Bunkyo-ku, Tokyo 113.

2) H. Sugeta, A. Go, and T. Miyazawa, *Chem. Lett.*, **1972**, 83.

3) H. Sugeta, A. Go, and T. Miyazawa, This Bulletin, **46**,

3407 (1973).

4) N. Nogami, H. Sugeta, and T. Miyazawa, *Chem. Lett.*, **1975**, 147.

5) Y. Shiro, M. Osaku, M. Hayashi, and H. Murata, This Bulletin, **43**, 609 (1970).

6) S. Mizushima, T. Shimanouchi, K. Nakamura, M. Hayashi, and S. Tsuchiya, *J. Chem. Phys.*, **26**, 970 (1957).

7) Previous studies on ethyl methyl sulfide include M. Hayashi, *Nippon Kagaku Zasshi*, **77**, 1692 (1956); **78**, 627 (1957); M. Osaku, Y. Shiro, and H. Murata, This Bulletin, **45**, 954 (1972); **46**, 1399 (1973), see also reference 4.

8) The weak Raman line at 757 cm^{-1} is assigned to the CH_2 rocking vibration, since the corresponding strong band was observed in the infrared spectrum.

9) D. W. Scott, W. D. Good, S. S. Todd, J. F. Messerly, W. T. Berg, I. A. Hossenlopp, J. L. Lacina, Ann Osborn, and J. P. McCullough, *J. Chem. Phys.*, **36**, 406 (1962).

10) The Raman line previously reported[11] at 659 cm^{-1} was not observed in the present study.

11) J. P. McCullough, H. L. Finke, J. F. Messerly, R. E. Pennington, I. A. Hossenlopp, and G. Waddington, *J. Amer. Chem. Soc.*, **77**, 6119 (1955).

12) D. W. Scott and M. Z. El-Sabban, *J. Mol. Spectrosc.*, **30**, 317 (1969).

13) M. Osaku, Y. Shiro, and H. Murata, This Bulletin, **45**, 3480 (1972).

Photoelectron Spectroscopic Study of Skew Compounds. III. *N,N'*-Dimethylhydrazine, Dimethyl Peroxide, and Dimethyl Disulfide[1]

Katsumi KIMURA and Kazuteru OSAFUNE[2]

Physical Chemistry Laboratory, Institute of Applied Electricity, Hokkaido University, Sapporo 060

(Received May 16, 1975)

He I photoelectron spectra of $CH_3HNNHCH_3$, $(CH_3)_2O_2$, and $(CH_3)_2S_2$ have been measured and the spectra below 18 eV have been resolved into nine ionization bands corresponding to p-type localized molecular orbitals. Orbital assignments of the resulting vertical ionization energies have been carried out with CNDO/2 calculations in which orbital energies were calculated as a function of the dihedral angle in the region 0—180 °. The separation of the nonbonding photoelectron bands suggests that $CH_3HNNHCH_3$ exists in outer-inner skew form, whereas $(CH_3)_2O_2$ is in *trans* form. The sum rule consideration previously proposed by the present authors has been applied to the compounds studied here. The total sum of the vertical ionization energies in the p-type region for each compound has been well reproduced in terms of appropriate empirical parameters based on the photoelectron spectra of simple molecules. The effects of methyl substitution on the ionization-energy total sums for N_2H_4, H_2O_2, and H_2S_2 have been found to be very similar to those for ethane and ethylene.

Previously, on the basis of Walsh-type diagrams, the present authors have studied the He I photoelectron spectra of the simplest skew compounds, hydrazine[3] and hydrogen peroxide.[4] From these photoelectron studies,[3,4] it was indicated that the whole of the spectra may be interpreted in terms of possible dihedral angles through semi-empirical calculations and that the splittings of the ionization bands corresponding to the nonbonding orbitals largely depend on the dihedral angles.[5] In the present work, we have extended our photoelectron study to symmetric methyl-disubstituted skew compounds, $CH_3HNNHCH_3$, CH_3OOCH_3, and CH_3SSCH_3, to analyze their full He I spectra.

A high-resolution photoelectron spectroscopy using He I (584 Å) line is now well known as a powerful method to study valence orbital structure.[6] Recently, dependences of the dihedral angle on nonbonding splittings in skew compounds including alkyl hydrazines,[7,8] disulfides,[9-11] and peroxides[12] have been received much attention in molecular photoelectron spectroscopy. Recently, Rademacher[7] and Nelsen *et al.*[8] have studied photoelectron nonbonding splittings for a variety of alkyl hydrazines; Wagner and Bock[9] and Baker *et al.*[10] for several alkyl disulfides; Colton and Rabalais[11] for S_2Cl_2, S_2Br_2, and $(CH_3)_2S_2$; and Batich and Adam[12] for mono- and di-*tert*-butyl peroxide. Earlier He I photoelectron works of $CH_3HNNHCH_3$ and $(CH_3)_2S_2$ were carried out by Dewar *et al.*[13] and Frost *et al.*,[14] respectively, using a retarding grid technique. Kroto and Suffolk[15] have recently reported a high-resolution He I spectrum of $(CH_3)_2S_2$. Most of these authors[7-15] have also carried out semi-empirical SCF MO calculations to interpret the photoelectron spectra. Very recently, Davies[16] has carried out *ab initio* calculations for H_2O_2 and H_2S_2 to interpret the available photoelectron data. Apart from the theoretical studies associated with photoelectron spectra, many other theoretical treatments for simple skew compounds have been carried out to study angular dependences of electron density, total energy, transition energy, nonbonding interaction, rotational barrier, *etc.*[17,18]

Conformation of $CH_3HNNHCH_3$, $(CH_3)_2O_2$, and $(CH_3)_2S_2$ have been studied by several workers.[19-21] Aston *et al.*[19] suggested for $CH_3HNNHCH_3$ that its entropy data may be interpreted with either a single outer-inner skew form or a 70%: 30% mixture of the outer-outer and outer-inner skew forms which are shown schematically in Fig. 1. A recent infrared and Raman study by During and Harris[20] indicated that $CH_3HNNHCH_3$ in the liquid phase consists of a mixture of *gauche* forms. For $(CH_3)_2S_2$, an experimental value of 84°42′ for the dihedral angle was obtained by Sutter *et al.*[21] using a microwave technique. There are no available data for the dihedral angle for $(CH_3)_2O_2$.

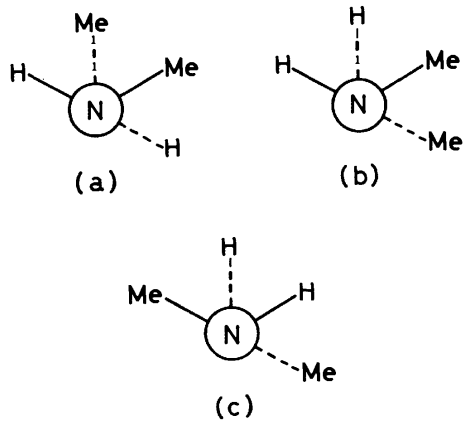

Fig. 1. *Gauche* forms of $CH_3HNNHCH_3$: (a) inner-inner form, (b) outer-inner form, (c) outer-outer form.

Under these circumstances, we considered it interesting to obtain conformational information from He I photoelectron spectra for the skew compounds studied here. From previous He I photoelectron studies of several series of aliphatic organic compounds, Kimura *et al.*[22] have indicated that the total sum of vertical ionization energies in the p-type region for each molecule may be reproduced in terms of vertical ionization energies of simple molecules. Therefore, such a sum rule consideration may be interesting for the compounds studied.

Experimental

Measurements of He I photoelectron spectra were carried out with the high-resolution photoelectron spectrometer used previously.[22] Calibration of the ionization energy scale was carried out using known ionization energies of Xe as an internal standard.[23] Gaseous samples were introduced through a vacuum glass line with a teflon needle valve. No metal tube was used to avoid decomposition.

sym-Dimethylhydrazine was librated from commercial dihydrochloride salt in aqueous alkaline solution, and then was dehydrated by barium oxide and finally distilled in vacuum. Dimethyl peroxide was prepared from dimethyl sulfate and hydrogen peroxide according to the method described by Hanst and Calvert[24] and purified by distillation in vacuum. Commercial dimethyl disulfide was purified by distillation in vacuum.

Theoretical Calculations

We carried out SCF MO calculations for $CH_3HNNHCH_3$, $(CH_3)_2O_2$, $(CH_3)_2S_2$, and H_2S_2, using the CNDO/2 method with the same parameterization as in the original paper.[25] The geometrical parameters used were taken from available structural studies,[26-28] which are summarized in Table 1. The CNDO/2 calculations of $(CH_3)_2O_2$, $(CH_3)_2S_2$, and H_2S_2 were performed for various dihedral angles from 0 to 180° with an interval of 10°. For $CH_3HNNHCH_3$, the calculations were carried out for the following conformations: 1) *cis* form, C_2; 2) *trans* form, C_2; 3) inner-inner skew form, C_2; 4) outer-inner skew form, C_1; and 5) outer-outer skew form, C_2. We used a FACOM-230/60 digital computer at the Computing Center of Hokkaido University.

Table 1. Geometrical parameters

$CH_3HNNHCH_3$[26]	$(CH_3)_2O_2$[27]
$r_{NN}=1.45$ Å	$r_{OO}=1.475$ Å
$r_{NC}=1.47$ Å	$r_{OC}=1.445$ Å
$r_{NH}=1.04$ Å	$r_{CH}=1.09$ Å
$r_{CH}=1.09$ Å	$\angle OOC=105°$
$\angle NNC=110°$	$\angle OCH=109°28'$

$(CH_3)_2S_2$[21]	H_2S_2[28b]
$r_{SS}=2.038$ Å	$r_{SS}=2.055$ Å
$r_{SC}=1.810$ Å	$r_{SH}=1.352$ Å
$r_{CH}=1.09$ Å	$\angle SSH=91°57'$
$\angle SSC=102°48'$	
$\angle SCH=109°28'$	

Results

The He I photoelectron spectra of $CH_3HNNHCH_3$, $(CH_3)_2O_2$, and $(CH_3)_2S_2$ are illustrated in Figs. 2—4, respectively. According to our previous photoelectron studies of various series of aliphatic compounds,[22] all the photoelectron bands due to p-type localized molecular orbitals (LO's) are located below about 18 eV. The same situation may also occur for the compounds studied. As done previously,[22] in the present work, the resolution of the photoelectron spectra into individual bands was carried out on the basis of 1) spectral shape (maxima and shoulders), 2) the number of p-type LO's, and 3) the sum rule consideration. The numbers of p- and s-type LO's for several related compounds are summarized in Table 2, from which it is seen that there are five p-type LO's in N_2H_4, H_2O_2, and H_2S_2 and nine in the methyl-disubstituted compounds. The p-type bands in the photoelectron spectra

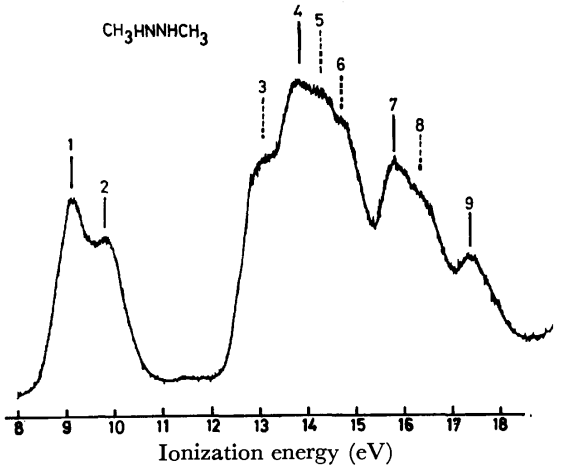

Fig. 2. He I photoelectron spectrum of $CH_3HNNHCH_3$.

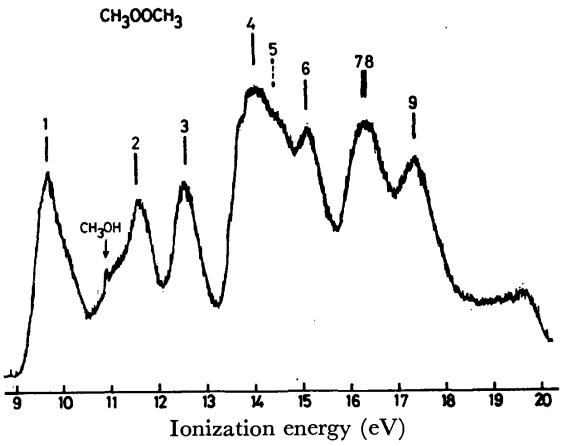

Fig. 3. He I photoelectron spectrum of $(CH_3)_2O_2$.

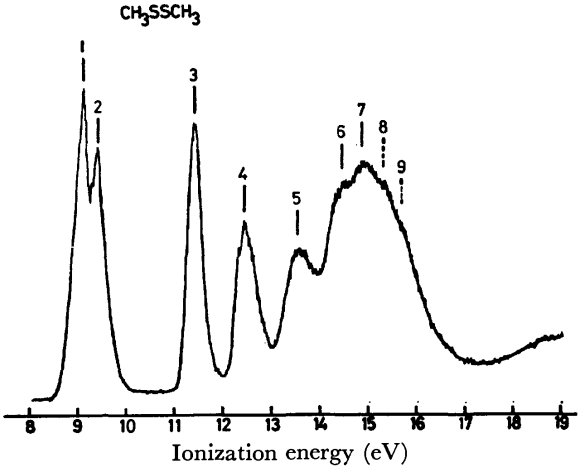

Fig. 4. He I photoelectron spectrum of $(CH_3)_2S_2$.

Table 2. Numbers of p- and s-type LO's[a]

	p-type LO's[b]						s-type LO's		
	n_X	σ_{XX}	σ_{XC}	σ_X'	π_{CH_3}	N_P	s_X	s_C	N_S
N_2H_4	2	1		2		5	2		2
H_2O_2	2	1		2		5	2		2
H_2S_2	2	1		2		5	2		2
$CH_3HNNHCH_3$	2	1	2		4	9	2	2	4
$(CH_3)_2O_2$	2	1	2		4	9	2	2	4
$(CH_3)_2S_2$	2	1	2		4	9	2	2	4

a) X=N, O, and S. N_P and N_S represent the total numbers of p- and s-type LO's respectively. b) σ_X' represents σ_{NH_2}, σ_{OH}, and σ_{SH} when X=N, O, and S, respectively.

Table 3. Vertical ionization energies obtained from the He I photoelectron spectrum and MO assignments based on CNDO/2 calculations for $CH_3HNNHCH_3$

	Vertical IE (eV)	MO assignment (CNDO/2) (outer-inner form)		
		Symmetry	Character	Energy (eV)[a]
I_1	9.02	a	n_N^+	−9.19
I_2	9.69	b	n_N^-	−9.80
I_3	13.0_0	a	σ_{NN}	−11.92
I_4	13.70	b	σ_{NC}^-	−13.92
I_5	14.2_0	a	σ_{NC}^+	−14.94
I_6	14.6_0	b	π_{CH_3}	−15.37
I_7	15.70	a	π_{CH_3}	−18.21
I_8	16.3_0	b	π_{CH_3}	−19.48
I_9	17.27	a	π_{CH_3}	−21.03

a) Reduced by 4 eV.

Table 4. Vertical ionization energies obtained from the He I photoelectron spectra of $(CH_3)_2O_2$ and $(CH_3)_2S_2$ and orbital assignments deduced mainly from CNDO/2 calculations[a]

	$(CH_3)_2O_2$			$(CH_3)_2S_2$		
	Vertical IE (eV)	MO assignment[b] $\phi=180°$ Sym.	Character	Vertical IE (eV)	MO assignment $\phi=84°42'$ Sym.	Character
I_1	9.71	b_g	n_O^-	8.96	a	n_S^+
I_2	11.61	a_u	n_O^+	9.26	b	n_S^-
I_3	12.58	a_g	σ_{OO}	11.26	a	σ_{SS}
I_4	14.02	a_g	σ_{OC}^+	12.31	b	σ_{SC}^-
I_5	14.4_5	b_u	π_{CH_3}	13.42	a	σ_{SC}^+
I_6	15.08	b_g	π_{CH_3}	14.3_5	b	π_{CH_3}
I_7	16.3_0	b_u	σ_{OC}^-	14.7_5	a	π_{CH_3}
I_8	16.3_0	a_g	π_{CH_3}	15.1_5	b	π_{CH_3}
I_9	17.34	a_u	π_{CH_3}	15.5_5	a	π_{CH_3}

a) For orbital energies of the CNDO/2 calculations, see the diagrams in Fig. 5. b) The assignments for the second and third photoelectron bands are based on the consideration of the nonbonding splitting.

in Figs. 2—4 are indicated by solid and broken lines, the numbering of ionization bands being also shown. The vertical ionization energies thus obtained for $CH_3HNNHCH_3$ are summarized in Table 3 together with the MO assignments obtained from the CNDO/2 calculations, while the vertical ionization energies of $(CH_3)_2O_2$ and $(CH_3)_2S_2$ are shown in Table 4.

The Walsh-type diagrams[29] based on the CNDO/2 calculations for $(CH_3)_2O_2$ and $(CH_3)_2S_2$ are illustrated in Fig. 5, in which the calculated orbital energies are plotted against the dihedral angle.

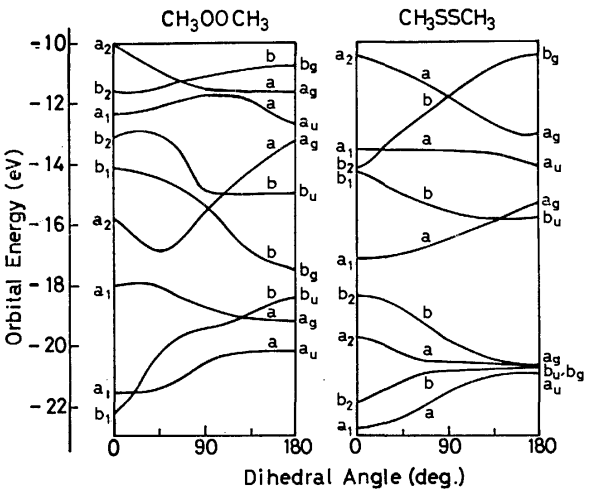

Fig. 5. Walsh-type orbital energy diagrams for $(CH_3)_2O_2$ and $(CH_3)_2S_2$, constructed on the basis of CNDO/2 calculations. (Energies for $(CH_3)_2O_2$ were reduced by 4 eV.)

Discussion

First we review the valence orbital structure of the simple skew compounds, N_2H_4, H_2O_2, and H_2S_2, using the available He I photoelectron spectra[3,4,9b] shown in Fig. 6 as well as Walsh-type orbital energy diagrams shown in Fig. 7, in which the diagrams of N_2H_4 and H_2O_2 were previously reported[3,4] and that of H_2S_2 was obtained from the present CNDO/2 calculations. It is seen that the orbital diagrams in Fig. 7 have the

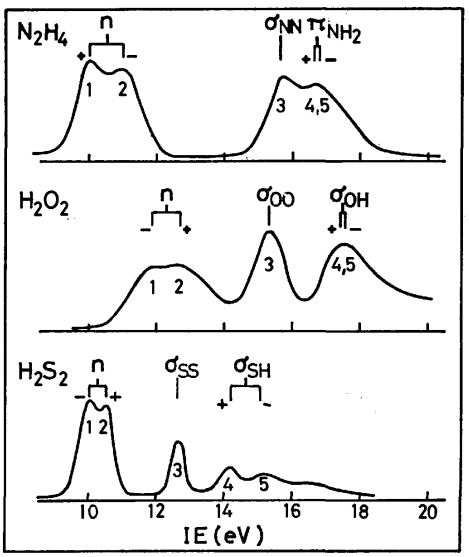

Fig. 6. Schematic drawing for the He I photoelectron spectra of N_2H_4, H_2O_2, and H_2S_2 reported in Refs. 3, 4, and 9b, respectively.

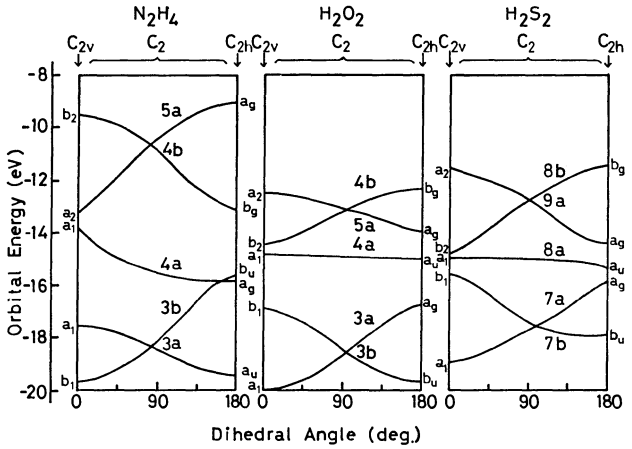

Fig. 7. Walsh-type orbital energy diagrams for N_2H_4, H_2O_2, and H_2S_2, constructed on the basis of CNDO/2 calculations. (Energies were reduced by 4 eV.)

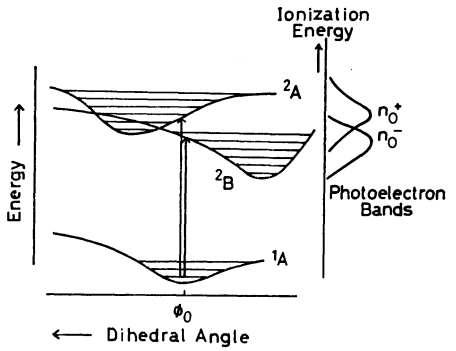

Fig. 8. Schematic drawing that explains the broadening of the nonbonding photoelectron bands of H_2O_2, using the potential curves of the ground and the ionic states expressed as a function of the dihedral angle. (ϕ_0 represents the equilibrium skew angle of the ground state molecule.)

following characteristics. 1) The two highest curves due to the $\pm$ combinations of the nonbonding orbitals cross each other at about 90°, the splitting being closely associated with the dihedral angle. Such angular dependences of the nonbonding orbital splitting have previously been reported by Yonezawa *et al.*[17] 2) The third curves due mainly to the N–N, O–O, and S–S bonds are quite insensitive to the dihedral angle. 3) The fourth and fifth curves also cross each other at about 90°.

Since experimental dihedral angles of 90—120° have been reported for N_2H_4, H_2O_2, and H_2S_2 from structural analysis studies,[30] it is seen from the Walsh-type diagrams in Fig. 7 that the orbital orderings are N_2H_4 [3a, 3b, 4a, 4b, and 5a], H_2O_2 [3b, 3a, 4a, 5a, and 4b], and H_2S_2 [7b, 7a, 8a, 9a, and 8b]. The difference in the orbital symmetry between N_2H_4 and H_2O_2 are due to the relative orientation of the nonbonding orbitals with respect to the C_2 axis. The recent *ab initio* calculations of Davies[16] gave rise to slightly different assignments that the above order of the 3b and 3a levels in H_2O_2 and that of the 7b and 7a levels in H_2S_2 are reversed. It should be mentioned that the experimental nonbonding splittings of N_2H_4, H_2O_2, and H_2S_2 (0.73,[3] 1.00,[4] and 0.27 eV,[9b] respectively) may be approximately reproduced by the CNDO/2 calculations using the available dihedral angles.

The photoelectron nonbonding bands in Fig. 6 are structureless and much broader compared with usual sharp nonbonding bands of aliphatic alcohols and amines.[6] It may be pointed out that the broadening of the nonbonding bands of the skew compounds may be interpreted in terms of differences in geometry between the ground and the ionized states. Since the original study by Walsh,[19] many workers have published qualitative and quantitative MO studies[31] using Walsh diagrams. Combining a ground-state orbital correlation diagram with the Walsh rule, we may qualitatively predict changes in geometry between the ground state and its ionized states. Now let us take H_2O_2 as an example. Ionization of an electron from the 4b orbital whose energy decreases with increasing dihedral angle (Fig. 7) gives rise to the ionized state ^2B which has a potential minimum at a smaller angle than the equilibrium ground-state dihedral angle (ϕ_0). The potential curves of the ground and the ionized states are schematically illustrated as a function of the dihedral angle in Fig. 8. On the other hand, in the case of the ionization from the 5a orbital, a reverse situation may occur, the orbital energy increasing with the dihedral angle (see Fig. 7). Therefore, the resulting potential curve (^2A) should have a minimum at a larger angle than ϕ_0 as shown in Fig. 8. The broadening of the nonbonding bands strongly suggests that the ^2B and ^2A ionized states are quite different in the equilibrium dihedral angle from the ground state.

N,N′-*Dimethylhydrazine.* The full photoelectron spectrum of $CH_3HNNHCH_3$ (Fig. 2) and its interpretation is reported here for the first time, although experimental nonbonding splittings for many alkyl hydrazines including $CH_3HNNHCH_3$ have previously been reported by Rademacher[7] and Nelsen *et al.*[8] There are only slight differences in vertical ionization energies between the literature values[7,8] and ours for the first two photoelectron bands which may be attributed to the nitrogen nonbonding orbitals.

As shown in Fig. 1, there may be three possible *gauche* configurations (inner-inner, outer-inner, and outer-outer forms). The present CNDO/2 calculations yielded nonbonding splittings of 2.72, 1.89, 0.62, 0.61, and 0.05 eV for *cis*, *trans*, inner-inner, outer-inner, and outer-outer forms, respectively. Our experimental nonbonding splitting was 0.67 eV which is close to the calculated splittings of the inner-inner and outer-inner forms, but largely differs from those of the *cis*, *trans*, and outer-outer forms. A possibility of inner-inner form may also be ruled out because of a steric interaction of the two methyl groups. Therefore, from the consideration of the nonbonding splitting, outer-inner skew form seems to be most plausible for $CH_3HNNHCH_3$.

An early electron diffraction study by Beamer[26] indicated that its experimental results are unfavorable to the *cis* configuration. Aston *et al.*[19] could rationalize the entropy data of $CH_3HNNHCH_3$ in terms of either

a single outer-inner (*gauche*) form or a 70%: 30% mixture of the outer-outer and outer-inner forms, respectively. The infrared and Raman study by During and Harris[20] also suggested that the molecule has more than a single form in its liquid and gaseous state. However, in the present study, the photoelectron spectrum may be interpreted in terms of only a single outer-inner form. This is supported by a very recent gas-phase electron diffraction study by Kuchitsu *et al.*[32]

The CNDO/2 results of $CH_3HNNHCH_3$ for the outer-inner form are summarized in Table 3, main orbital characters being also shown. For higher photoelectron bands, the present CNDO/2 calculations of $CH_3HNNHCH_3$ suggest that 1) the third band is of σ_{NN}, 2) the fourth and the fifth band are due to the $\pm$ combinations of the σ_{NC} orbitals, and 3) the last four bands are due to the methyl pseudo π orbitals.

Dimethyl Peroxide. For $(CH_3)_2O_2$ there are no available He I photoelectron spectra for comparison. This compound slightly decomposes at room temperature, the major products being methanol and carbon monoxide whose first vertical ionization energies are 10.91 eV[22d] and 14.01 eV,[6] respectively. The shoulder appearing at 10.9 eV in the spectrum may be due to a small amount of the decomposed methanol.

From the spectral shape as well as the number of p-type LO's we concluded that the spectrum below 18 eV in Fig. 3 consists of the nine p-type bands. The first three bands are well separated from one another. The CNDO/2 calculations indicated that the total energy becomes minimum at $\phi=180°$, where the nonbonding splitting amounts to 1.91 eV. This value is in good agreement with the experimental separation between the first and the second band, 11.61—9.71= 1.90 eV (Table 4). On the basis of the nonbonding splitting consideration, we tentatively propose that $(CH_3)_2O_2$ has a planar *trans* form in the gaseous phase. A similar situation was reported to occur for di-*tert*-butyl peroxide by Batich and Adam.[12]

The MO assignments of $(CH_3)_2O_2$ obtained by the CNDO/2 calculations are summarized in Table 4, in which the assignments for the second and the third photoelectron band are based on the consideration of the nonbonding splitting. The CNDO/2 calculations of $(CH_3)_2O_2$ in *trans* form indicated that the σ_{OO} level lies between the two nonbonding levels. This assignment may probably be incorrect, although the calculations gave rise to the reasonable nonbonding splitting, 0.91 eV. As shown in Table 4, we therefore concluded that the third photoelectron band to the σ_{OO} orbital.

Dimethyl Disulfide. The spectrum of $(CH_3)_2S_2$ in Fig. 4 is essentially the same as those previously reported by Kroto and Suffolk,[15] by Wagner and Bock,[9b] and by Colton and Rabalais.[11] However, our spectrum obtained here clearly shows the sixth band (appearing as a bump at 14.4 eV) which has not been pointed out by other workers, and also shows two slight shoulders at about 15.5 eV (indicated by broken lines in Fig. 4). On the basis of the number of p-type LO's in this compound, there should exist nine p-type ionization bands below 16 eV, therefore four ionization bands being located in the 14—16 eV range.

As has already been pointed out,[9b,11,15] the first and the second band of $(CH_3)_2S_2$ are due to the $\pm$ combinations of the sulfur nonbonding orbitals. The experimental nonbonding splitting (9.26—8.96=0.30 eV) was reproduced at dihedral angles of 84° and 98° in the present CNDO/2 calculations which showed that the total energy becomes minimum at 84°. It is interesting to see that this angle is very close to that (84°42′) determined by a microwave study by Sutter *et al.*[21] The MO symmetries and characters based on the CNDO/2 calculations (at $\phi=84°42'$) are summarized in Table 4. These MO symmetries are consistent with those reported by Wagner and Bock[9b] and Colton and Rabalais.[11]

According to the CNDO/2 calculations, the third inner orbital is of σ_{SS} in character and very insensitive to the variation of the dihedral angle (see Fig. 7). It may be pointed out here that the upper part of the correlation diagram of $(CH_3)_2S_2$ resembles those of H_2O_2, H_2S_2, and N_2H_4, but largely differs from that of $(CH_3)_2O_2$. This difference may be explained in terms of a difference in size between the sulfur 3p and oxygen 2p orbitals. In a photoelectron study by Sweigart and Turner,[33] it has been pointed out in oxygen- and sulfur-containing heterocyclic compounds that orbital interaction between sulfur nonbonding orbitals is mainly through-space interaction, whereas that between oxygen nonbonding orbitals is through bond dominant. Therefore, the difference in the pattern of the orbital energy diagrams between $(CH_3)_2O_2$ and $(CH_3)_2S_2$ in Fig. 5 may be attributed to the differences in the nonbonding orbital interactions.

Sum Rule Consideration. Using the experimental vertical ionization energies, we obtained the sum (T) over all the p-type bands in each compound by

$$T_{\text{expt.}} = \sum_i(-I_i) \qquad (1)$$

The results are summarized in Table 5, being plotted against the number (m) of substituted methyl groups

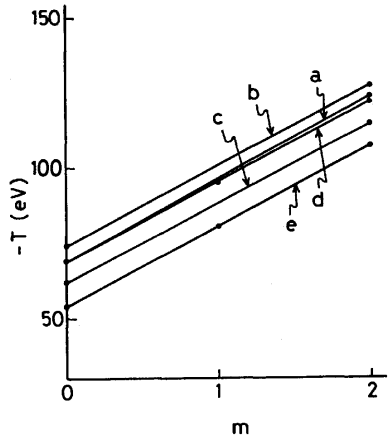

Fig. 9. Plots of the total sums of experimental vertical ionization energies *versus* the number of methyl groups for several series: (a) RHNNHR′, (b) ROOR′, (c) RSSR′, (d) RH_2CCH_2R', and (e) RHC=CHR′, where R=R′=H at $m=0$; R=H and R′=CH_3 at $m=1$; and R=R′=CH_3 at $m=2$.

TABLE 5. COMPARISON OF THE EXPERIMENTAL AND CALCULATED VALUES (in eV) ON THE PARTIAL SUM (P) AND THE TOTAL SUM (T) IN THE SUM RULE CONSIDERATION USING p-TYPE LO's

(I's)→(p-type LO's)	Expt.	Calcd.
$N_2H_4(C_2)$[a]	$T=-69.5$	-69.5[d]
$(I_1, I_3, I_5)\rightarrow a(n_N, \sigma_{NN}, \pi_{NH_2})$	$P=-42.2$	-42.2
$(I_2, I_4)\rightarrow b(n_N, \pi_{NH_2})$	$P=-27.3$	-27.3
$H_2O_2(C_2)$[b]	$T=-74.5$	-74.5[d]
$(I_2, I_3, I_5)\rightarrow a(n_O, \sigma_{OO}, \sigma_{OH})$	$P=-45.5$	-45.3
$(I_1, I_4)\rightarrow b(n_O, \sigma_{OH})$	$P=-29.1$	-29.2
$H_2S_2(C_2)$[c]	$T=-62.1$	-62.1[d]
$(I_1, I_3, I_5)\rightarrow a(n_S, \sigma_{SS}, \sigma_{SH})$	$P=-37.7$	-37.3
$(I_2, I_4)\rightarrow b(n_S, \sigma_{SH})$	$P=-24.4$	-24.8
$CH_3HNNHCH_3$ (C_1)	$T=-123.5$	-124.0
$(I_1, I_2, I_3, \cdots I_9)\rightarrow(2n_N, \sigma_{NN}, 2\sigma_{NC}, 4\pi_{CH_3})$		
$(CH_3)_2O_2(C_{2h})$	$T=-127.4$	-128.9
$(I_1, I_2, I_6, I_9)\rightarrow$Out-of plane $(2n_O, 2\pi_{CH_3})$	$P=-53.7$	-53.8
$(I_3, I_4, I_5, I_7, I_8)\rightarrow$In-plane $(\sigma_{OC}, 2\sigma_{OC}, 2\pi_{CH_3})$	$P=-73.7$	-75.1
$(CH_3)_2S_2(C_2)$	$T=-114.9$	-115.5
$(I_1, I_3, I_5, I_7, I_9)\rightarrow a(n_S, \sigma_{SS}, \sigma_{SC}, 2\pi_{CH_3})$	$P=-63.9$	-64.0
$(I_2, I_4, I_6, I_8)\rightarrow b(n_S, \sigma_{SC}, 2\pi_{CH_3})$	$P=-51.0$	-51.5

a) The I_i's were taken from Ref. 3: $I_1=9.91$, $I_2=10.61$, $I_3=15.61$, $I_4=I_5=16.66$ in eV units. b) The I_i's were taken from Ref. 4: $I_1=11.69$, $I_2=12.69$, $I_3=15.33$, $I_4=I_5=17.4$ in eV units. c) The I_i's were taken from Ref. 9b: $I_1=10.01$, $I_2=10.28$, $I_3=(12.6)$, $I_4=(14.1)$, $I_5=(15.1)$ in eV, where the values in parentheses were estimated from the reported photoelectron spectrum. d) Assumed to be equal to the experimental value.

in Fig. 9. Lines a, b, and c in Fig. 9 are drawn through the plots for the hydrazines, peroxides, and disulfides, respectively, to show variations in the total sum with m. Similar plots (lines d and e) are also shown in Fig. 9 for the methyl-substituted compounds of ethane and ethylene, clearly indicating linear relationships between T and m.[34] Previously, we have reported such linear tendencies for several series of methyl-, chloro-, and bromo-substituted compounds.[22f,g] We may point out here that, as seen from Fig. 9, lines a, b, and c are almost parallel to one another as well as to lines d and e. These experimental results indicate that the methyl-substitution effects of T for the hydrazines, peroxides, and disulfides are very similar to those for the alkanes and alkenes. The difference in T in each methyl substitution is estimated to be 27.0 eV in the hydrazines, 26.4 eV in the peroxides, 26.5 eV in the disulfides, while it is 26.0 eV in the alkanes and 26.8 eV in the alkenes.[22g]

As shown previously,[22] the total sum may be expressed approximately with the sum of empirical orbital energies (ε_i) over all the p-type LO's. The total sums for N_2H_4, H_2O_2, and H_2S_2 may be expressed by

$$T_{calc.} = 2\varepsilon(n_X) + \varepsilon(\sigma_{XX}) + 2\varepsilon(\sigma_X') \quad (2)$$

where X=N, O, and S, and σ_X' represents π_{NH_2}, σ_{OH}, and σ_{SH}, respectively. For $CH_3HNNHCH_3$, $(CH_3)_2O_2$, and $(CH_3)_2S_2$, the total sum may be given by

TABLE 6. EMPIRICAL ENERGIES (eV) USED FOR LOCALIZED MOLECULAR ORBITALS (LO's) IN THE SUM RULE CONSIDERATIONS

$\varepsilon(n_N)=-10.88$	$\varepsilon(\sigma_{NN})=-14.90$
$\varepsilon(n_O)=-12.61$	$\varepsilon(\sigma_{OO})=-16.10$
$\varepsilon(n_S)=-10.48$	$\varepsilon(\sigma_{SS})=-12.31$
$\varepsilon(\sigma_{NC})=-14.42$	$\varepsilon(\pi_{NH_2})=-16.40$
$\varepsilon(\sigma_{OC})=-15.19$	$\varepsilon(\sigma_{OH})=-16.60$
$\varepsilon(\sigma_{SC})=-12.42$	$\varepsilon(\sigma_{SH})=-14.30$
	$\varepsilon(\pi_{CH_3})=-14.30$

$$T_{calc.} = 2\varepsilon(n_X) + \varepsilon(\sigma_{XX}) + 2\varepsilon(\sigma_{XC}) + 4\varepsilon(\pi_{CH_3}) \quad (3)$$

With Eqs. (2) and (3), we estimated the total sums using the empirical energies ε_i given in Table 6, the resulting $T_{calc.}$ being also included in Table 5. All the ε values in Table 6 were previously used in the sum rule considerations of alkyl amines,[22d] alcohols,[22d] and thioalcohols,[35] except the $\varepsilon(\sigma_{XX})$'s which were determined so as to reproduce the experimental total sums of the parent compounds. As can be seen from Table 5, it is interesting to note that the experimental total sums for $CH_3HNNHCH_3$, $(CH_3)_2O_2$, and $(CH_3)_2S_2$ are reproduced in terms of the empirical LO energies with errors of 0.5, 1.5, and 0.6 eV, respectively.

Since N_2H_4, H_2O_2, H_2S_2, and $(CH_3)_2S_2$ are of molecular symmetry C_2, the LO's may be divided into two symmetry groups a and b. Therefore, the partial sums, P, belonging to these symmetry species were also calculated, as shown in Table 5. For $(CH_3)_2O_2$ which is proposed here to have C_{2h} symmetry, the LO's may be divided into the out-of-plane and in-plane ones, the resulting partial sums being also shown in Table 5. On the other hand, the experimental partial sums were obtained by appropriate combinations of I_i's on the basis of the MO assignments described before (Tables 3 and 4). Although no orbital interactions were taken into account for each set of equivalent LO's, a considerably good agreement is generally obtained between the experimental and theoretical partial sums as shown in Table 5.

Finally, we may point out the following point in connection with the sum rule considerations. Koopmans' theorem[36] was assumed for selecting the ε_i's from the photoelectron data of the simple molecules. However, if we consider each empirical value (in Table 6) without a negative sign as a hypothetical ionization energy, which is due to the ionization of an electron from the original unperturbed LO, then the present sum rule consideration may be thought as an additivity rule of ionization energy, independent of Koopmans' theorem.

The authors wish to thank Dr. S. Katsumata in this laboratory for his helpful discussion.

References

1) For Parts I and II, see Refs. 3 and 4, respectively.
2) Present address: Goverment Research Institute of Industry, Tosu-shi, Saga-ken.
3) K. Osafune, S. Katsumata, and K. Kimura, *Chem. Phys. Lett.*, **19**, 369 (1973).

4) K. Osafune and K. Kimura, *ibid.*, **25**, 47 (1974).
5) The dihedral angle of X–Y–Y–X type molecule is defined as the angle formed between the two X–Y–Y planes.
6) D. W. Turner, C. Baker, A. D. Baker, and C. R. Brundle, "Molecular Photoelectron Spectroscopy," Wiley, New York (1969).
7) P. Rademacher, *Angew. Chem. Int. Ed. Engl.*, **12**, 408 (1973).
8) S. F. Nelsen and J. M. Buschek, *J. Amer. Chem. Soc.*, **95**, 2011 (1973); S. F. Nelsen, J. M. Buschek, and J. P. Hintz, *ibid.*, **95**, 2013 (1973); S. F. Nelsen and J. M. Buschek, *ibid.*, **96**, 2392 (1974).
9) a) H. Bock and G. Wagner, *Angew. Chem. Int. Ed. Engl.*, **11**, 150 (1972). b) G. Wagner and H. Bock, *Chem. Ber.*, **107**, 68 (1974).
10) A. D. Baker, M. Brisk, and M. Gellender, *J. Electron Spectrosc.*, **3**, 227 (1974).
11) R. J. Colton and J. W. Rabalais, *ibid.*, **3**, 345 (1974).
12) C. Batich and W. Adam, *Tetrahedron Lett.*, **1974**, 1467.
13) N. Boder, M. J. S. Dewar, W. B. Jennings, and S. D. Worley, *Tetrahedron*, **26**, 4109 (1970).
14) W. R. Cullen, D. C. Frost, and D. A. Vroom, *Inorg. Chem.*, **8**, 1803 (1969).
15) H. W. Kroto and R. J. Suffolk, *Chem. Phys. Lett.*, **15**, 545 (1972).
16) D. W. Davies, *ibid.*, **28**, 520 (1974).
17) a) H. Yamabe, H. Kato, and T. Yonezawa, This Bulletin, **44**, 22 (1971). b) H. Yamabe, H. Kato, and T. Yonezawa, *ibid.*, **44**, 604 (1971).
18) Many theoretical works cited in Refs. 3, 4, 16, and 17.
19) J. G. Aston, G. J. Janz, and K. E. Russell, *J. Amer. Chem. Soc.*, **73**, 1943 (1951).
20) J. R. During and W. C. Harris, *J. Chem. Phys.*, **55**, 1735 (1971).
21) D. Sutter, H. Dreizler, and H. D. Rudolph, *Z. Naturforsch.*, **20A**, 1676 (1965).
22) a) K. Kimura, S. Katsumata, Y. Achiba, H. Matsumoto, and S. Nagakura, This Bulletin, **46**, 373 (1973). b) S. Katsumata and K. Kimura, *ibid.*, **46**, 1342 (1973). c) T. Yamazaki, S. Katsumata, and K. Kimura, *J. Electron Spectrosc.*, **2**, 335 (1973). d) S. Katsumata, T. Iwai, and K. Kimura, This Bulletin, **46**, 3391 (1973). e) K. Kimura, S. Katsumata, T. Yamazaki, and H. Wakabayashi, *J. Electron Spectrosc.*, **6**, 41 (1975). f) S. Katsumata and K. Kimura, *ibid.*, **6**, 309 (1975). g) T. Yamazaki and K. Kimura, This Bulletin, **48**, 1602 (1975). h) K. Kimura and K. Osafune, *Mol. Phys.*, **29**, 1073 (1975).
23) K. Kimura, T. Yamazaki, and K. Osafune, *J. Electron Spectrosc.*, **6**, 391 (1975).
24) P. L. Hanst and G. Calvert, *J. Phys. Chem.*, **63**, 104 (1959).
25) a) M. S. Gordon and J. A. Pople, *J. Chem. Phys.*, **49**, 4643 (1968). b) J. A. Pople and D. L. Beveridge, "Approximate Molecular Orbital Theory," McGraw-Hill, N. Y. (1970).
26) W. H. Beamer, *J. Amer. Chem. Soc.*, **70**, 2979 (1948).
27) W. Shand, "Tables of Interatomic Distances," Burlington House, London (1958), M138.
28) a) G. Winnewisser, M. Winnewisser, and W. Gordy, *J. Chem. Phys.*, **49**, 3465 (1968). b) M. Winnewisser and J. Haase, *Z. Naturforsch.*, **23A**, 56 (1968).
29) A. D. Walsh, *J. Chem. Soc.*, **1953**, 2260.
30) $\phi(N_2H_4)=90$—$95°$, A. Yamaguchi, I. Ichishima, T. Shimanouchi, and S. Mizushima, *Spectrochim. Acta*, **16**, 1471 (1960); $\phi(N_2H_4)=90°2'$, Y. Abe, Y. Abe, and S. Kojima, *J. Phys. Soc. Japan*, **18**, 1843 (1963); $\phi(H_2O_2)=111°30'$, R. H. Hunt, R. A. Leacock, C. W. Peters, and K. T. Hecht, *J. Chem. Phys.*, **42**, 1931 (1965); $\phi(H_2O_2)=120°1'\pm15'$, W. C. Oeleke and W. Gordy, *ibid.*, **51**, 5336 (1969); $\phi(H_2S_2)=90°36'\pm3'$ (Ref. 28a) and $90°37'\pm3'$ (Ref. 28b).
31) For instance, B. M. Gimarc, *J. Amer. Chem. Soc.*, **92**, 266 (1970); **93**, 593, 815 (1971); C. A. Coulson and B. M. Deb, *Int. J. Quant. Chem.*, **5**, 411 (1971); L. C. Allen, *Theoret. Chim. Acta*, **24**, 117 (1972); G. W. Schnuelle and R. G. Parr, *J. Amer. Chem. Soc.*, **94**, 8974 (1972).
32) K. Kohata, T. Fukuyama, and K. Kuchitsu, Abstracts of Annual Meeting of Chemical Society of Japan (1975), Vol. I, p. 111.
33) D. A. Sweigart and D. W. Turner, *J. Amer. Chem. Soc.*, **94**, 5599 (1972).
34) The experimental total sums obtainable from available ionization energies are −68.9 (ethane), −95.2 (*n*-propane), −121.24 (*n*-butane), −53.9 (ethylene), −80.8 (propene), −107.4 (*cis*-butene), and −107.8 (*trans*-butene).
35) Unpublished results in our laboratory.
36) T. Koopmans, *Physica*, **1**, 104 (1934).

The Infrared Dichroism and Molecular Orientation of Modifying Reagents, L-β-Phenyllactic Acid and L-β-Phenyl-α-alanine, in Thin Films on Nickel Metal Surfaces

Aritada HATTA and Wataru SUËTAKA

Laboratory of Interface Science of Metals, Faculty of Engineering, Tohoku University, Aramaki Aoba, Sendai 980

(Received September 17, 1974)

The infrared absorption spectra of thin films of modifying reagents, L-β-phenyllactic acid and L-β-phenyl-α-alanine, formed on nickel metal plates were measured by the high-sensitivity reflection method. From the infrared dichroism in the reflection spectra, the molecular orientations in the thin films were deduced. The C=O and alcoholic O–H bonds of L-β-phenyllactic acid are oriented nearly vertical to the metal surface, whereas the carboxyl O–H bond and the benzene ring are parallel to the surface. The benzene ring and the C–N bond in L-β-phenyl-α-alanine are oriented nearly parallel to the metal surface, while the O···O axis of the carboxylate group is inclined to the surface.

Infrared spectroscopy has been extensively applied to the study of surface phenomena. For example, the adsorption of gaseous molecules on metal surfaces has been often investigated by employing transmission methods.[1] On the other hand, the method of reflection using a beam polarized parallel to the plane of incidence at high incident angles (the high-sensitivity reflection method) has facilitated the spectral investigation of surface phenomena on bulk metal surfaces because of its high sensitivity, which, in turn, results from the enhanced intensity of the oscillating electric field normal to the reflecting metal surface.[2] The spectrum of thin film on a metal mirror obtained by this method is a faithful reproduction of the absorption spectrum if the film is isotropic and consists of organic compounds.[3] When the film is anisotropic, the reflection spectrum shows infrared dichroism, and the relative intensities of the infrared bands can be used to deduce the molecular orientation in the film.[4] Because of these advantages, the high-sensitivity reflection method has been successfully used in the investigations of the chemisorption on clean metal surfaces,[5,6] the polymorphism[7] and molecular orientation[8] in thin films on metal surface, and the oxidation and corrosion inhibition of metals.[9]

In recent years, a new type of asymmetric synthesis has been studied by Izumi and his co-workers using a Raney nickel catalyst modified by certain optically active compounds.[10] They have found that the hydrogenation of methylacetoacetate over Raney nickel modified with optically active hydroxy or amino acids affords a definite optical isomer of methyl-β-hydroxybutyrate, its identity depending upon the optical activity of the compound used as the modifying reagent.[10] While the mechanism is still uncertain, it is worth noting that the effective modifying reagents available for such an asymmetric reduction are limited to optically active acids in which a OH or NH_2 group is attached at the asymmetric carbon atom. Therefore, it seems most likely that the geometry of the modifying reagent adsorbed on the Raney nickel catalyst plays an important role in the determination of the optical isomer of the reduction product. Hence, a particular interest is focused on the molecular orientation of modifying reagents on the Raney nickel catalyst.

The epitaxial growth of an organic crystal occurs on a single crystal when the organic molecule is adsorbed strongly on the crystal, and the molecular orientation in the overgrowing crystal correponds to the state of the adsorbed molecule.[11] Tanabe and Uyeda investigated the thin film of L-β-phenyl-α-alanine, formed from an aqueous solution on nickel film, by electron microscopy and diffraction, and suggested that this molecule is in a certain state of oriented adsorption at the interface.[12] However, they could not determine the orientation of the molecules because the crystal structure of L-β-phenyl-α-alanine was unknown.

The present study was undertaken in the hope of making clear the orientations of the modifying reagents, L-β-phenyllactic acid and L-β-phenyl-α-alanine, in thin crystal films formed on nickel surfaces, using the high-sensitivity reflection technique.

Experimental

The infrared spectra were taken by means of a JASCO model IR-G spectrophotometer equipped with a JASCO PR-1 assembly designed for use in a single-beam reflection operation.[4] In this method, however, the weak absorptions are subjected to interference from atmospheric water vapor. This problem was solved by the combined use of signal averaging and back-ground elimination procedures.[5] The calculations were performed on a JEOL model JEC-5 spectrum computer. The modifying reagents of L-β-phenyllactic acid and L-β-phenyl-α-alanine were prepared and supplied by the Institute for Protein Research, Osaka University, and were used without further purification. In the present study, an electrolytical nickel (99.9% purity) plate was used as substrate and mirror. To obtain a high reflectivity, the nickel plate was polished with silicon carbide and chromium oxide to reduce its roughness to a minimum. After having been treated with a 20% NaOH solution at 80 °C and having been rinsed in distilled water, the nickel plate was immersed into a 0.5% aqueous solution of a modifying reagent. The sample of the modified nickel plate was dried in air and was then subjected to the reflection measurement. A thin film of fine crystallites of the reagent was formed on the metal substrate upon the evaporation of the water.

Results and Discussion

L-β-Phenyllactic Acid. The absorption spectrum of this compound, $C_6H_5CH_2CH(OH)COOH$, in the randomly oriented state and the assignment of the absorp-

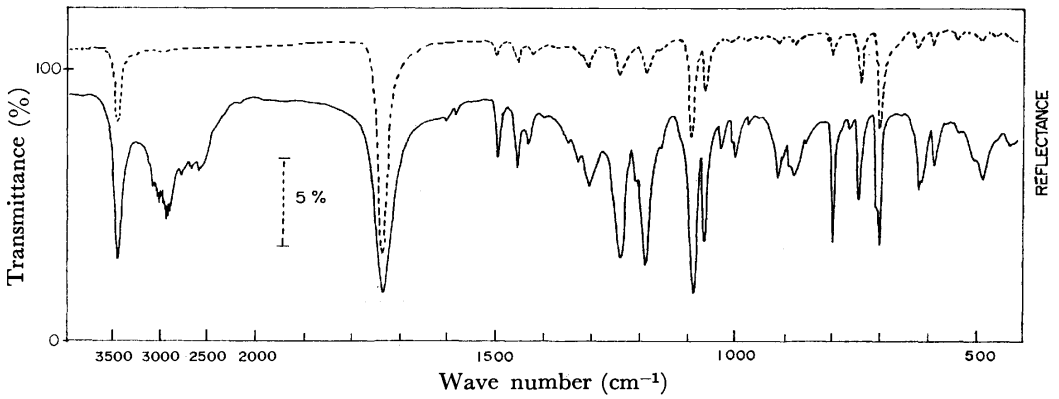

Fig. 1. Infrared absorption spectra of L-β-phenyllactic acid.
——: Transmission spectrum of powdered crystal (KBr disk).
·····: High sensitivity reflection spectrum of the thin film formed on nickel metal surface.

tion bands must be available if its reflection spectrum is to be discussed. For this purpose, the transmission spectrum of L-β-phenyllactic acid (PLA) was measured by the KBr disk method in the region of 400—4000 cm^{-1}. The spectrum thus obtained is shown in Fig. 1. The assignment, to be described below, is mainly based on comparison with the spectra of such related compounds as the sodium salt and *O*-deuterated compound of PLA, and DL-mandelic acid, its sodium salt, and its *O*-deuterated compound. The most important vibrational bands of PLA and its sodium salt are collected in Table 1. PLA shows a strong absorption at 3450 cm^{-1} and two broader absorptions centered around 2920 and 2570 cm^{-1}, all of which shifted to lower frequencies upon deuteration, as is shown in Table 1; these can be assigned to O-H stretching vibrations. The sodium salt of PLA shows a strong band at 3400 cm^{-1} and a weaker band at 3150 cm^{-1}, while no other band appears over the lower O-H stretching region. Therefore, the strong band at 3450 cm^{-1} observed with PLA is evidently due to the alcoholic O–H stretching, and the remaining broad bands in the lower-frequency region, to the carboxyl O-H stretchings. The strong absorption band observed at 1725 cm^{-1} can easily be assigned to the C=O stretching. The weak and narrow bands at 1500 and 1453 cm^{-1} of PLA are observed also for DL-mandelic acid and other related compounds, so these bands are assigned to the in-plane skeletal deformation of the benzene ring. The strong bands observed in the 1050—1300 cm^{-1} region are attributable to the C–O-H fragments. From the vibrational character, these bands involve the interacting in-plane deformation vibration of the C-O–H angle and the stretching one of the C–O bond, giving rise to two bands.[13] In PLA, there are two pairs of deuteration-sensitive bands, at 1245 and 1197, and at 1093 and 1070 cm^{-1}. The former pair disappears upon the change from –COOH to –COONa, while the latter shows no appreciable change. Therefore, we assigned the two bands at 1245 and 1197 cm^{-1} to the vibrations of the carboxylic C–O–H group, and the other pair, to alcoholic C-O–H. The intense bands at 708 (sh) and 700 cm^{-1} are assigned to the CH out-of-plane deformation or the skeletal deformation vibration of the benzene ring. These assignments are mainly based on the fact that the bands remain unshifted on the deuterations of O-H groups. The spectrum of mandelic acid changed with the deuteration and salt formation in the same manner as in the case of PLA, supporting the above-mentioned assignment.

Table 1. Infrared frequencies (cm^{-1}) and assignments of L-β-phenyllactic acid and its sodium salt (KBr disk)

$C_6H_5CH_2$-CHCOOH (OH)		$C_6H_5CH_2$-CHCOO$^-$Na$^+$ (OH)		Assignments
3450 (2540)	s	3400 (2500)	s	alcoholic O–H str.
		3150 (2320)	w	
2920 (2200)	m			carboxyl O–H str.
2570 (2030)	w			
1725	s			C=O str.
		1597	sh	COO^- antisym. str.
		1580	s	
1500	w	1497	w	phenyl ring def.
1453	w	1455	sh	phenyl ring def.
		1402	m	COO^- sym. str.
1245 (1085)	s			carboxyl C–O–H
1197 (1054)	s			
1093 (935)	s	1090 (932)	sh	alcoholic C–O–H
1070 (917)	m	1080	s	
708	sh			phenyl C–H out-of-plane def.
700	s	700	s	

s: strong, m: medium, w: weak, sh: shoulder.
Values in parentheses correspond to the peaks of *O*-deuterated compounds.

The high-sensitivity reflection spectrum of the thin PLA film formed on a nickel metal surface is shown in Fig. 1. The absorption bands of the thin film appear at essentially the same frequencies as in the transmission spectrum of the bulk crystals. However, differences in relative intensities are noticed between the thin film and the bulk crystals. Because no new band appeared in the reflection spectrum, the thin film probably did not contain any compound other than PLA in any appreciable quantity. The spectral change, therefore, can be interpreted in terms of a molecular orientation in the thin film, as has been discussed in previous papers.[4,5,8] In the high-sensitivity reflection method employed in the present work, the oscillating electric vector of radiation in the vicinity of the reflecting

surface is practically polarized normal to that surface.[2] Therefore, any spectral change in the band intensities can reveal information about the direction of the transition moments of the molecule; moreover, if the molecular structure in the solid phase is known, the molecular orientation as a whole may also be obtained. On the basis of the assignments mentioned above, the orientation of PLA to the nickel metal surface can be determined by comparing the thin film spectrum with the bulk one. In the thin film spectrum shown in Fig. 1, it can clearly be seen that the O-H stretching band of the carboxyl group almost disappears, while the alcoholic O–H stretching band appears strong. The bands arising from the C–O stretching and C-O–H in-plane deformation vibrations of the carboxyl group appear at almost the same frequencies as that in the bulk spectrum. In addition, it is quite likely that the carboxyl O–H group is hydrogen-bonded in crystalline phases. Therefore, the disappearance of the carboxyl O-H stretching band can not be ascribed to the dissociation of the hydrogen bond between carboxyl groups. These facts indicate that the carboxyl O-H bond is aligned nearly parallel to the nickel substrates, while the alcoholic O–H bond is not. On the other hand, the band due to the C=O stretching vibration of the carboxyl group has the highest absorption intensity in the thin film spectra; hence, the transition moment and, therefore, the C=O bond are considered to be perpendicular to the nickel metal surface. Accordingly, the molecule is probably oriented in such a way that the plane containing a carbon and two oxygen atoms of the carboxyl group is perpendicular to the nickel metal surface.

Another marked difference between the bulk and the thin film crystal is seen in the bands of the 1050—1300 cm^{-1} region due to the vibrations of the carboxyl and alcoholic C–O-H groups; *i.e.*, the bands arising from the former group lose much of their intensity in the thin film, while the bands of the latter are unchanged. In view of the fact that the C-O-H bands represent the interacting C–O stretching and in-plane O–H deformation vibrations, the observed results support the different alignments for the carboxyl and alcoholic O-H bonds mentioned above.

On the other hand, the crystal structure of *p*-bromo-L-*β*-phenyllactic acid was investigated by Kakudo *et al.*; the molecular conformation in the crystal is shown in Fig. 2.[14] Therefore, the determination of the molecular orientation as a whole can most conveniently be performed by assuming that the molecular conformation of *p*-bromo-L-*β*-phenyllactic acid is applicable to the

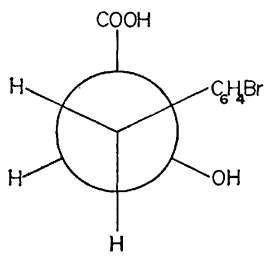

Fig. 2. Molecular conformation of *p*-bromo-L-*β*-phenyllactic acid, as viewed along the C_β—C_α bond.[14]

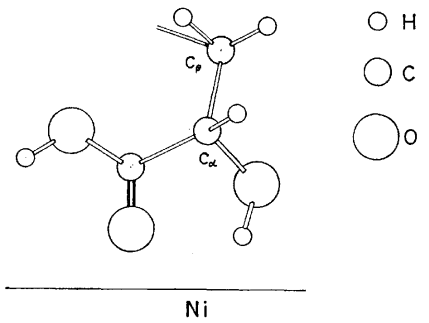

Fig. 3. Molecular orientation in thin L-*β*-phenyllactic acid crystal formed on nickel metal surface. The phenyl group is omitted from the figure.

case of PLA. The derived orientational model for thin PLA in crystal is shown in Fig. 3. In the thin film spectrum, the band at 700 cm^{-1} assigned to the CH out-of-plane deformation or skeletal deformation of the benzene ring remains as a strong band, while the bands assigned to the in-plane skeletal deformation of the benzene ring observed at 1453 and 1500 cm^{-1} decrease in relative intensity. These observations indicate that the plane of the benzene ring is aligned rather parallel to the nickel substrate.

The thickness of the films formed by the procedure described above is estimated from the band intensity in the reflection spectra to be a few hundred angstroms. The reflection spectra of films with such a thickness scarcely provide any direct information about the species chemisorbed on the nickel surface. However, the orientation of molecules in a thin film is governed by the orientation of the species which are adsorbed strongly on the substrate surface and which act as the nuclei of crystal growth.[11] The orientation of the PLA molecule in the film may, therefore, correspond to that of species strongly adsorbed on the nickel surface and playing an important role in the above-mentioned catalytic hydrogenation.

L-β-Phenyl-α-alanine. It is well known that L-*β*-phenyl-α-alanine exists in a crystal as a zwitter ion such as

$$C_6H_5CH_2\text{-}\underset{\displaystyle NH_3^+}{\underset{|}{CH}}\text{-}COO^-$$

As a result, it has the absorptions of an ionized carboxyl group and an NH_3^+ ion. Therefore, the important part of these characteristic bands can be expected to appear between 1400 and 1700 cm^{-1}, by analogy with other amino acids.[15] Figure 4 shows the transmission spectra of L-*β*-phenyl-α-alanine and its *N*-deuterated species, obtained by the KBr disk method in the region from 1400 to 1700 cm^{-1}. The strong three bands at 1500, 1565, and 1628 cm^{-1}, which disappear on *N*-deuteration, as is shown in Fig. 4, may be regarded as the bands due to the vibrations of the NH_3^+ group. The bands at 1410 and 1602 cm^{-1}, which remain unchanged on *N*-deuteration, can be assigned to the CO_2^- symmetric and anti-symmetric stretching vibrations respectively. The bands at 1500 and 1628 cm^{-1} can be assigned to the NH_3^+ symmetric deformation and degenerate deformation respectively by referring

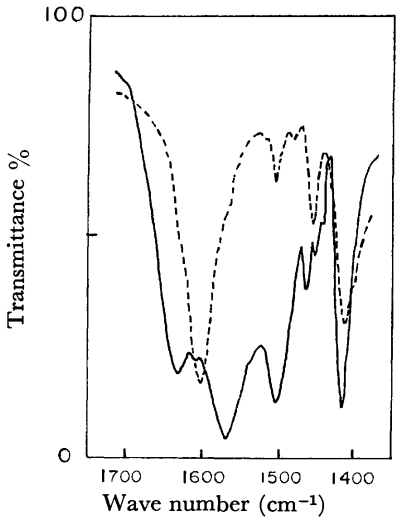

Fig. 4. Transmission spectra of L-β-phenyl-α-alanine (solid line) and its *N*-deuterated species (broken line).

to the assignments for DL-β-phenyl-α-alanine.[16] However, there is a marked difference between the spectrum of L-β-phenyl-α-alanine and that of DL-β-phenyl-α-alanine; the 1565 cm^{-1} band is present only in the former. This band is also observed with D-β-phenyl-α-alanine. According to Tsuboi *et al.*,[15] it is most likely that this band arises from the breaking down of the C_{3v} symmetry of the NH_3^+ group. Except for the 1565 cm^{-1} band, the spectrum of L-β-phenyl-α-alanine is identical with the spectrum of the DL-form, apart from slight shifts; hence, no further descriptions of it will be given.

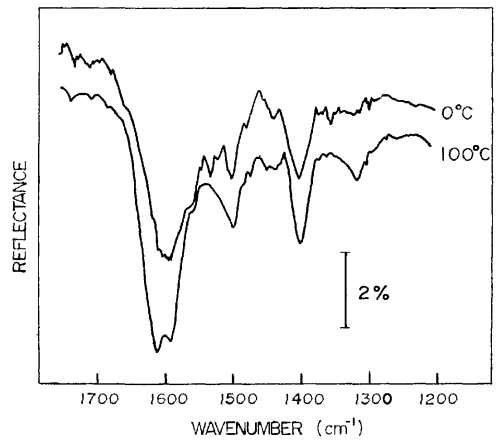

Fig. 5. High sensitivity reflection spectra of thin L-β-phenyl-α-alanine crystals formed on nickel metal surfaces. The temperature refers to the modifying temperature at which the sample was prepared.

Figure 5 shows the high-sensitivity reflection spectrum of the thin L-β-phenyl-α-alanine (L-phenylalanine) film formed on nickel metal surfaces at different modifying temperatures. The spectrum of the thin film is compared with that of the non-oriented sample obtained by using the KBr technique, as in the case of PLA. The thin film spectra show infrared dichroism, which is caused by the preferred orientation in the film; they correspond well to the results obtained by electron-optical methods.[12] The most remarkable feature is the weakness of the NH_3^+ band at 1565 cm^{-1} in the thin film spectra, irrespective of the modifying temperature. This change in intensity may be ascribed to the orientation of the NH_3^+ group, for another NH_3^+ deformation band appears at about 1610 cm^{-1} in the thin film. Another striking difference between the thin film and bulk crystals is seen in Fig. 5; the band at 1500 cm^{-1} due to the symmetric deformation of the NH_3^+ group remarkably decreases in intensity. This may be attributed to the molecular orientation in the thin L-phenylalanine crystal. In view of the fact that the vibrational mode of the NH_3^+ symmetric deformation has a transition moment along the C–N bond, it may be concluded that the C–N bond lies nearly parallel to the nickel substrate.

The most important bands yet to be discussed are those of the CO_2^- stretching vibrations appearing at 1400 and 1600 cm^{-1} in the thin films. It can be seen from Figs. 4 and 5 that the intensity of the band due to the CO_2^- symmetric stretching relative to that of the CO_2^- anti-symmetric stretching decreases with the change from the bulk crystals to the thin film. Considerations of these vibrational modes and the corresponding changing dipole moments provide a possible orientation for the CO_2^- group.

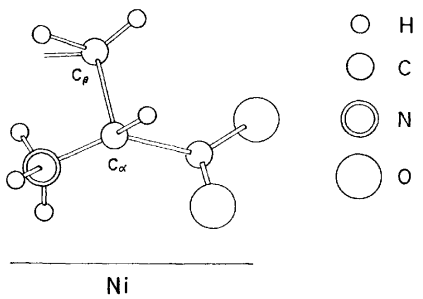

Fig. 6. Molecular orientation of thin L-β-phenyl-α-alanine film formed on nickel metal surface. The phenyl group is omitted from the figure.

No remarkable spectral change is found in the region below 1400 cm^{-1} except for the intensified bands at 700 and 740 cm^{-1}. Since these bands represent the out-of-plane deformations of the benzene ring, the above-mentioned results show the parallel orientation of the benzene ring to the nickel surface. Consequently, the most probable orientation is proposed by assuming that the molecular conformation obtained by X-ray work[14] is valid even for the thin film of the L-phenylalanine. The orientation model of the L-phenylalanine molecule in the thin film crystal is shown in Fig. 6. The aspect of the orientation is compatible with that obtained for α-alanine, so far as the common fragment is concerned,[12,17] suggesting that the nature of interaction between the molecule and nickel substrate is the same for both compounds.

The optical activity of the reaction product of catalytic hydrogenation changes with a change in the modifying temperature.[10] This change may be caused by the change in the posture of the modifying reagent on the nickel surface. The relative intensities of the bands

at 1322 and 1610 cm^{-1} in the thin-film spectra change with the modifying temperature, as can be seen in Fig. 5. This change may be attributed to the different molecular orientations in the films and may correspond to the change in the orientation of the species strongly adsorbed on the nickel surface. However, the results obtained are not sufficiently accurate, partly because of the interference from absorptions due to water vapor, to enable us to discuss the change in the orientation of the surface species with the temperature; any discussion must, therefore, be postponed until further information is available.

The authors wish to express their thanks to Professor Yoshiharu Izumi, Institute for Protein Research, Osaka University, for his kind supply of materials, and also to Dr. Tadao Harada for his useful suggestions.

References

1) L. H. Little, "Infrared Spectra of Adsorbed Species," Academic Press, London (1966).
2) W. Suëtaka, *Sci. Rept. Tohoku Univ., Ser, A.* **18**, Suppl., 129 (1966); R. G. Greenler, *J. Chem. Phys.*, **44**, 310 (1966).
3) W. Suëtaka, *Bunko Kenkyu*, **18**, 187 (1969); S. Tanaka, *Kinzoku Hyomen Gijutsu*, **23**, 308 (1972).
4) W. Suëtaka, This Bulletin, **40**, 2077 (1967).
5) M. Ito and W. Suëtaka, *J. Phys. Chem.*, **79**, 1190 (1975).
6) H. C. Eckstrom, G. G. Possley, S. E. Hannum, and W. H. Smith, *J. Chem. Phys.*, **52**, 5435 (1970); H. G. Tompkins and R. G. Greenler, *Surface Sci.*, **28**, 194 (1971); J. T. Yates, Jr., and D. A. King, *ibid.*, **30**, 601 (1972); M. L. Kottke, R. G. Greenler, and H. G. Tompkins, *ibid.*, **32**, 231 (1972); J. Pritchard, *J. Vac. Sci. Tech.*, **9**, 895 (1972); I. Ratajczykowa, *ibid.*, **48**, 549 (1975).
7) K. Suzuki, A. Hatta, and W. Suëtaka, *Chem. Lett.*, **1973**, 189.
8) S. F. Francis and A. H. Ellison, *J. Opt. Soc. Amer.*, **49**, 131 (1959); W. Suëtaka, *Bunko Kenkyu*, **16**, 219 (1968).
9) G. W. Poling, *J. Electrochem. Soc.*, **114**, 1209 (1967), **116**, 958 (1969); W. Suëtaka, *Nippon Kinzoku Gakkaishi*, **32**, 301 (1968); N. Morito, and W. Suëtaka, *ibid.*, **36**, 1131 (1972).
10) See for example, Y. Izumi, *Yuki Gosei Kagaku Kyokai Shi*, **25**, 1013 (1967).
11) M. Ashida, A. Hamada, and T. Watanabe, This Bulletin, **45**, 2312 (1972); N. Uyeda, Y. Murata, T. Kobayashi, and E. Suito, *J. Cryst. Growth*, **26**, 267 (1974).
12) K. Tanabe and N. Uyeda, *Bull. Inst. Chem. Res., Kyoto Univ.*, **52**, 616 (1974).
13) L. J. Bellamy, "The Infrared Spectra of Complex Molecules," 2nd Ed., Methuen, London (1958).
14) Kakudo *et al.*, private communication.
15) M. Tsuboi, T. Takenishi, and A. Nakamura, *Spectrochim. Acta*, **19**, 271 (1963).
16) Y. Inomata, T. Inomata, T. Moriwaki, and J. L. Walter, *ibid.*, **29A**, 1933 (1973).
17) A. Hatta, Y. Moriya, and W. Suëtaka, Preprints of the 29th Annual Meeting of the Chemical Society of Japan, Vol. 1, p. 681 (1973).

Studies of Fragment Ion Distribution and Reaction by the Use of a Charge Spectrometer. VII. Fragmentation of Aliphatic Thiol Ions Produced by Charge Exchange with Positive Ions

Kenji YOSHIHARA, Masanao KOBAYASHI, Shigeru IKUTA, and Takanobu SHIOKAWA
Department of Chemistry, Faculty of Science, Tohoku University, Aoba, Sendai 980
(Received December 11, 1974)

Fragmentation of molecular ions of methanethiol, ethanethiol, two kinds of propanethiols, and four kinds of butanethiols formed by charge exchange with positive ions has been studied using a tandem mass spectrometer. The results are compared with those of the corresponding alcohols obtained by Lindholm and coworkers, and similarities and differences between both series of ions are pointed out. The effect of the structure of the molecule on fragmentation is discussed. The fragment ions derived from primary scission are predicted on the basis of the EHMO calculation.

No report has yet been published on fragmentation of thiol ions formed by charge exchange with positive ions, whereas the phenomena were intensively studied with alcohols by Lindholm and coworkers.[1-4] We have been interested in the breakdown phenomena of methanol[5] and methylamine[6] after charge exchange. It is an important problem to understand what mechanisms are involved in the fragmentation of a series of compounds RX, where R is an alkyl group and X is a substituent. Although it would be interesting to elucidate the fragmentation processes of these compounds, previous authors have not studied them systematically. The effects of the size and structure of R, for example, have not been well understood so far.

In this report we have studied fragmentation mechanisms in a series of alkyl thiol ions, RSH^+, formed by charge exchange with positive ions, and found somewhat different behavior between thiols and alcohols. In the studies of electron impact mass spectroscopy, similarities between both series of compounds are usually emphasized, though the abundance of the parent peaks is different.[7] The differences of behavior of the fragmentation between both series of compounds have been made clear by observations using charge exchange reactions, where the energy transfered to the molecular ions is well defined.

Experimental

All the reagents, guaranteed by gas chromatographic analysis, were purchased from the Tokyo Kasei Co. Their purities were re-checked by gas chromatograph before use. The reagents were as follows: methanethiol CH_3SH, ethanethiol C_2H_5SH, 1-propanethiol $CH_3(CH_2)_2SH$, 2-propanethiol $CH_3CH(SH)CH_3$, 1-butanethiol $CH_3(CH_2)_3SH$, 2-methyl-1-propanethiol $(CH_3)_2CHCH_2SH$, 1-methyl-1-propanethiol $CH_3CH_2CH(SH)CH_3$, and 2-methyl-2-propanethiol $(CH_3)_3C$-SH.

Primary ions for the charge exchange reactions were $C_6H_6^+$, H_2S^+, $C_2H_2^+$, Xe^+, Kr^+, Ar^+, Xc^{2+}, Kr^{2+}, Ne^+, Ar^{2+}, and He^+; the source materials were of the high purity reported in the previous studies.[5,6,8-10]

A tandem mass spectrometer of the perpendicular type used here was described in the previous report.[11]

The pressure of the reaction chamber was kept below 6×10^{-6} Torr to avoid secondary reactions with other molecules.

Results

Methanethiol: The appearance potential of methanethiol is 9.44 eV,[12] and the parent ion is produced by the elimination of one of the lone-pair electrons located at the sulfur atom. The fragmentation of methanethiol is shown in Fig. 1. The following processes take place with an increase in excitation energy:

$$CH_3SH \longrightarrow CH_3SH^+ \quad (1)$$

$$CH_3SH^+ \longrightarrow CH_3S^+ + H \quad (2)$$

$$CH_3S^+ \longrightarrow CHS^+ + H_2 \quad (3)$$

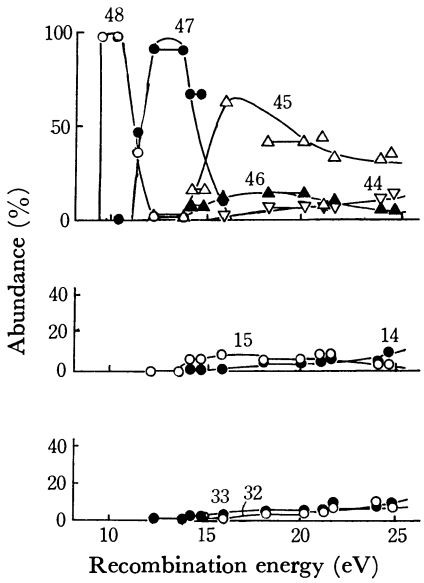

Fig. 1. Breakdown graph of CH_3SH.
m/e 48: CH_3SH^+, 47: CH_3S^+, 46: CH_2S^+, 45: CHS^+, 44: CS^+, 33: SH^+, 32: S^+, 15: CH_3^+, 14: CH_2^+.

These processes are similar to those in the case of methanol except that the elimination of one hydrogen occurs mainly in the S–H bond instead of in the C–H bonds. Rupture of the C–S bond occurs in such a manner that the abundance of CH_3^+ is higher than that of SH^+. S^+ is also produced in several percents in the higher energy region. For the appearance of the S^+ ion, rupture of both the C–S and S–H bonds must occur. It is clear that the S^+ ion is not derived from SH^+, judging from the breakdown curves in Fig.

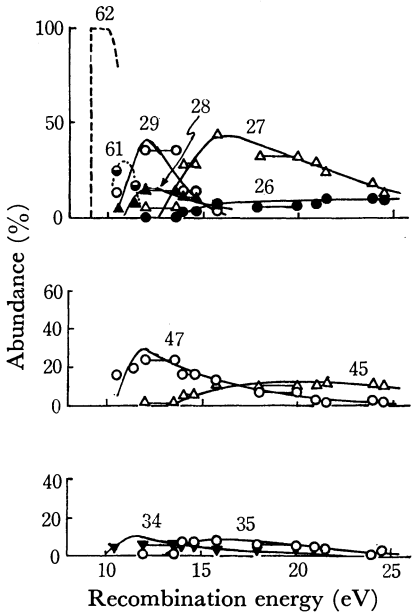

Fig. 2. Breakdown graph of C_2H_5SH.
m/e 62: $C_2H_5SH^+$, 61: $C_2H_5S^+$, 47: CH_2SH^+, 45: CHS^+, 35:SH_3^+, 34: SH_2^+, 29: $C_2H_5^+$, 28: $C_2H_4^+$, 27: $C_2H_3^+$, 26: $C_2H_2^+$.

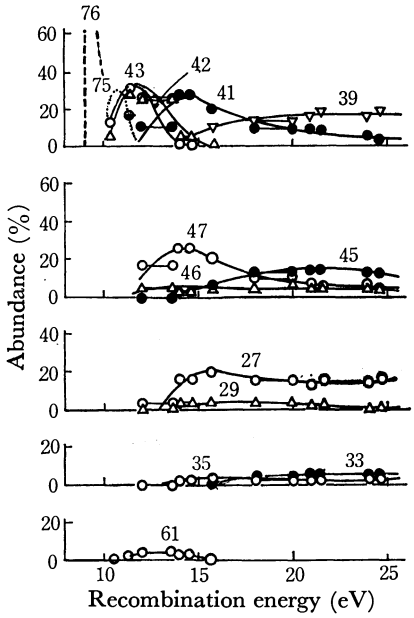

Fig. 3. Breakdown graph of 1-propanethiol.
m/e 76: $C_3H_7SH^+$, 75: $C_3H_7S^+$, 61: $C_2H_4SH^+$, 47: CH_2SH^+, 46: CH_2S^+, 45: CHS^+, 43: $C_3H_7^+$, 42: $C_3H_6^+$, 41: $C_3H_5^+$, 39: $C_3H_3^+$, 35: SH_3^+, 33: SH^+, 29: $C_2H_5^+$, 27: $C_2H_3^+$.

1. Therefore, the remaining possibility is as follows:

$$CH_3S^+ \longrightarrow CH_3 + S^+ \quad (4)$$

The tendency of the breakdown curves in Fig. 1 supports CH_3S^+ as the major precursor of S^+.

Ethanethiol: The fragmentation of ethanethiol is shown in Fig. 2.

The major processes in the breakdown phenomena of the parent ion are (i) rupture of the C–C bond and (ii) that of the C–S bond.

In the C–C bond rupture the following processes are observed:

$$C_2H_5SH^+ \longrightarrow CH_2SH^+ + CH_3 \quad (5)$$

$$CH_2SH^+ \longrightarrow CHS^+ + H_2 \quad (6)$$

In place of CH_2SH^+ in Reaction 5 the CH_3^+ ion whose abundance is a few percent at maximum is formed by the process:

$$C_2H_5SH^+ \longrightarrow CH_2SH + CH_3^+ \quad (7)$$

In the C–S bond rupture the following processes occur predominantly:

$$C_2H_5SH^+ \longrightarrow C_2H_5^+ + SH \quad (8)$$

$$C_2H_5^+ \longrightarrow C_2H_3^+ + H_2 \quad (9)$$

Besides these processes, hydrogen sulfide elimination from the parent ion occurs as follows:

$$C_2H_5SH^+ \longrightarrow C_2H_4^+ + H_2S \quad (10)$$

The relationship between energy and abundance in Fig. 2 clearly shows that the $C_2H_4^+$ ion is not derived from $C_2H_5^+$.

A small amount of SH_3^+ ion appears in the breakdown graph. This species is probably formed by the process:

$$C_2H_5SH^+ \longrightarrow C_2H_3 + SH_3^+ \quad (11)$$

SH_3^+ has an isoelectronic structure with PH_3 and shows high stability in the mediam energy region (15—20 eV).

1-Propanethiol: The breakdown graph of 1-propanethiol is shown in Fig. 3. (i) Rupture of the C–S bond and (ii) that of the C–C bonds are observed.

In the C–S bond rupture the following processes occur as energy increases:

$$C_3H_7SH^+ \longrightarrow C_3H_7^+ + SH \quad (12)$$

$$C_3H_7^+ \longrightarrow C_3H_5^+ + H_2 \quad (13)$$

$$C_3H_5^+ \longrightarrow C_3H_3^+ + H_2 \quad (14)$$

Elimination of hydrogen sulfide occurs in the low energy region in the same manner as Reaction 10.

$$C_3H_7SH^+ \longrightarrow C_3H_6^+ + H_2S \quad (15)$$

The mechanism of formation of the ion $C_2H_3^+$ is not clear, but the following processes are reasonable, judging from the energy relation in the figure:

$$C_3H_6^+ \longrightarrow C_2H_3^+ + CH_3 \quad (16)$$

$$C_3H_7^+ \longrightarrow C_2H_3^+ + CH_4 \quad (17)$$

The formation of SH_3^+ seen in Fig. 3 may be due to the rearrangement of $C_3H_7SH^+$ followed by decomposition:

$$C_3H_7SH^+ \longrightarrow [C_3H_5SH_3^+] \longrightarrow C_3H_5 + SH_3^+ \quad (18)$$

The probability of scission of the C(α)–C(β) bond is higher than that of the C(β)–C(γ) bond. A similar observation has been made in the case of 1-propanol.[3)]

$$C_3H_7SH^+ \longrightarrow CH_2SH^+ + C_2H_5 \quad (19)$$

$$C_3H_7SH^+ \longrightarrow C_2H_4SH^+ + CH_3 \quad (20)$$

As the energy increases CH_2SH^+ decomposes into a hydrogen molecule and CHS^+.

$$CH_2SH^+ \longrightarrow CHS^+ + H_2 \quad (21)$$

2-Propanethiol: The mass spectroscopic patterns obtained by electron impact[13)] show distinct differences in the cases of 1-propanethiol and 2-propanethiol. Posi-

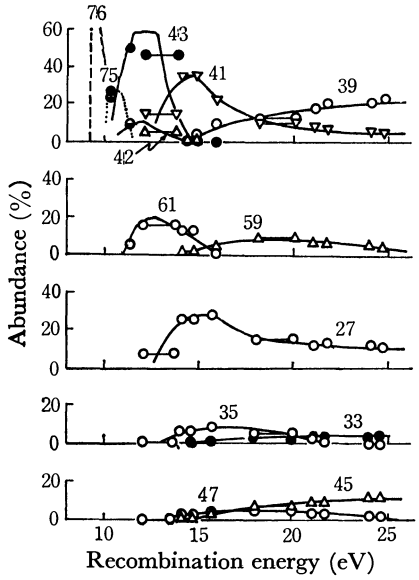

Fig. 4. Breakdown graph of 2-propanethiol.
m/e 76: $C_3H_7SH^+$, 75: $C_3H_7S^+$, 61: $C_2H_4SH^+$, 59: $C_2H_3S^+$, 47: CH_2SH^+, 45: CHS^+, 43: $C_3H_7^+$, 42: $C_3H_6^+$, 41: $C_3H_5^+$, 39: $C_3H_3^+$, 35: SH_3^+, 33: SH^+, 27: $C_2H_3^+$.

tive ion impact using a tandem mass spectrometer is often more useful to understand the fragmentation mechanisms than electron impact is.

The fragmentation of 2-propanethiol is shown in Fig. 4. In the case of the C–S rupture the following process takes place to give $CH_3CHCH_3^+$:

$$i\text{-}C_3H_7SH^+ \longrightarrow CH_3CHCH_3^+ + SH \quad (22)$$

As energy increases the ion $CH_3CHCH_3^+$ decomposes by the following processes:

$$CH_3CHCH_3^+ \longrightarrow C_2H_3^+ + CH_4 \quad (23)$$

$$CH_3CHCH_3^+ \longrightarrow C_3H_5^+ + H_2 \quad (24)$$

$$C_3H_5^+ \longrightarrow C_3H_3^+ + H_2 \quad (25)$$

The rearrangement product SH_3^+ is more abundant in 2-propanethiol (about 10% at maximum) than in 1-propanethiol (4% at maximum). This fact clearly shows that the hydrogen atoms attached to the β carbons are involved in the rearrangement reaction, and it is likely that the probability of the rearrangement depends on the number of the hydrogen atoms available.

In the case of the C–C bond rupture the following reaction occurs:

$$(CH_3)_2CHSH^+ \longrightarrow C_2H_4SH^+ + CH_3 \quad (26)$$

As the energy increases this $C_2H_4SH^+$ ion seems to decompose by the following processes:

$$C_2H_4SH^+ \longrightarrow C_2H_3^+ + H_2S \quad (27)$$

$$C_2H_4SH^+ \longrightarrow SH_3^+ + C_2H_2 \quad (28)$$

*1-Butanethiol (*n*-Butyl Mercaptan)*: The fragmentation of 1-butanethiol is shown in Fig. 5. In the case of the C–S bond rupture the hydrogen sulfide elimination process,

$$C_4H_9SH^+ \longrightarrow C_4H_8^+ + H_2S \quad (29)$$

occurs as well as the following process,

$$C_4H_9SH^+ \longrightarrow C_4H_9^+ + SH \quad (30)$$

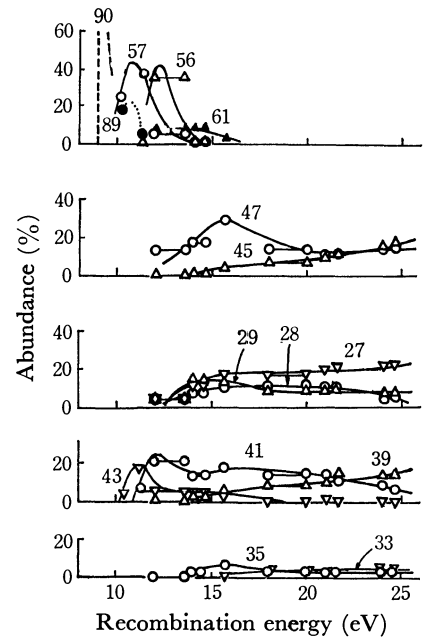

Fig. 5. Breakdown graph of 1-butanethiol.
m/e 90: $C_4H_9SH^+$, 89: $C_4H_9S^+$, 57: $C_4H_9^+$, 56: $C_4H_8^+$, 47: CH_2SH^+, 45: CHS^+, 43: $C_3H_7^+$, 41: $C_3H_5^+$, 39: $C_3H_3^+$, 35: SH_3^+, 33: SH^+, 29: $C_2H_5^+$, 28: $C_2H_4^+$, 27: $C_2H_3^+$.

$C_3H_7^+$ and $C_2H_5^+$ are probably produced by the direct scission of the C–C bonds from the parent ion; the molecular orbital calculation in Table 2 shows the presence of these ions as the primary scission products from the parents.

$$C_4H_9SH^+ \longrightarrow C_3H_7^+ + CH_2SH \quad (31)$$

$$C_4H_9SH^+ \longrightarrow C_2H_5^+ + C_2H_4SH \quad (32)$$

An alternative path for the formation of the ion $C_2H_5^+$ is $C_4H_9^+ \rightarrow C_2H_5^+ + C_2H_4$. The energy relationship in Fig. 5 shows that this process is possible. Formation of the $C_3H_3^+$ or $C_2H_3^+$ ions in the median and higher energy region in the figure will be explained by successive elimination of hydrogen molecules or by rupture of the C–C bonds in $C_4H_8^+$ *etc.*

The formation of $C_2H_4SH^+$ and CH_2SH^+ occurs by the following process:

$$C_4H_9SH^+ \longrightarrow C_2H_4SH^+ + C_2H_5 \quad (33)$$

$$C_4H_9SH^+ \longrightarrow CH_2SH^+ + C_3H_7 \quad (34)$$

2-Methyl-1-propanethiol (Isobutyl Mercaptan): The breakdown graph of this substance is shown in Fig. 6. The formation of $C_4H_8^+$ and $C_4H_9^+$ by the processes shown in Reactions 29 and 30 appears clearly in the figure. Besides these species, $C_3H_7^+$ in Reaction 31 and its degradation product ions, $C_3H_5^+$ and $C_3H_3^+$, appear also. The ion $C_2H_5^+$ or $C_2H_3^+$ may be a secondary or tertiary product due to a rearrangement of hydrogen atoms on the carbon skeleton. CH_2SH^+ in Reaction 34 is also detectable in this case.

*1-Methyl-1-propanethiol (*sec*-Butyl Mercaptan)*: Figure 7 shows the fragmentation of the substance. In this case formation of $C_4H_8^+$ by hydrogen sulfide elimination from the parent ion is a rather small possibility, and the ion $C_4H_9^+$ appears to be important. It is

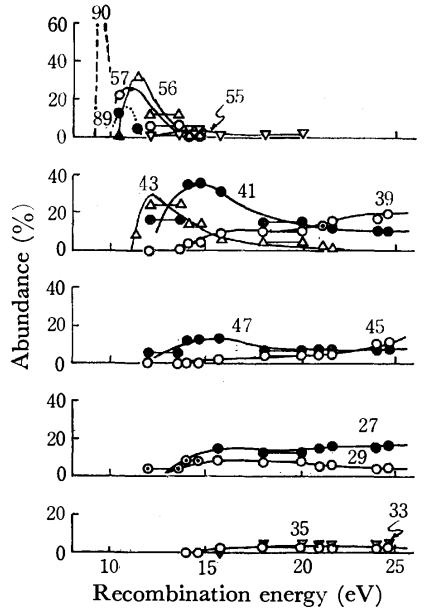

Fig. 6. Breakdown graph of 2-methyl-1-propanethiol. *m/e* 90: $C_4H_9SH^+$, 89: $C_4H_9S^+$, 57: $C_4H_9^+$, 56: $C_4H_8^+$, 55: $C_4H_7^+$, 47: CH_2SH^+, 45: CHS^+, 43: $C_3H_7^+$, 41: $C_3H_5^+$, 39: $C_3H_3^+$, 35: SH_3^+, 33: SH^+, 29: $C_2H_5^+$, 27: $C_2H_3^+$.

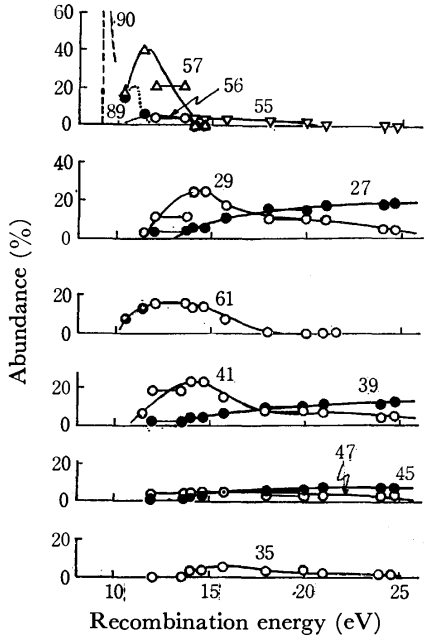

Fig. 7. Breakdown graph of 1-methyl-1-propanethiol. *m/e* 90: $C_4H_9SH^+$, 89: $C_4H_9S^+$, 61: $C_2H_4SH^+$, 57: $C_4H_9^+$, 56: $C_4H_8^+$, 55: $C_4H_7^+$, 47: CH_2SH^+, 45: CHS^+, 41: $C_3H_5^+$, 39: $C_3H_3^+$, 35: SH_3^+, 29: $C_2H_5^+$, 27: $C_2H_3^+$.

interesting to see that $C_2H_4SH^+$ is prominent in the lower energy region (10—15 eV). The ion $C_2H_5^+$ is produced probably by direct scission from the parent ion. $C_3H_5^+$ is produced not as a degradation product from $C_3H_7^+$, but as a product which is derived probably from $C_4H_9^+$ by elimination of CH_4.

$$C_4H_9SH^+ \xrightarrow{-SH} C_4H_9^+ \xrightarrow{-CH_4} C_3H_5^+ \qquad (35)$$

2-Methyl-2-propanethiol (tert-Butyl Mercaptan): Figure

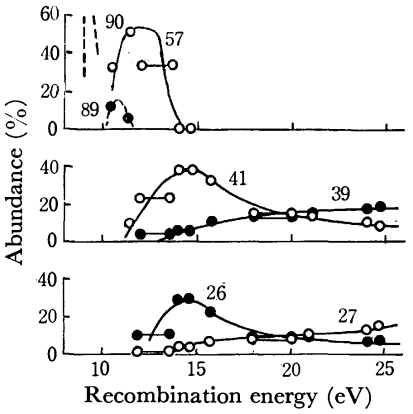

Fig. 8. Breakdown graph of 2-methyl-2-propanethiol. *m/e* 90: $C_4H_9SH^+$, 89: $C_4H_9S^+$, 57: $C_4H_9^+$, 41: $C_3H_5^+$, 39: $C_3H_3^+$, 29: $C_2H_5^+$, 27: $C_2H_3^+$.

8 shows the breakdown curves for this substance. The processes which are prominent for this substance involve formation of the $C_4H_9^+$ and $C_3H_5^+$ ions as in Reaction 35. Besides these, the ion $C_2H_5^+$ appears as a fragmentation product from $C_4H_9^+$ after rearrangement of the hydrogen atoms. In this case formation of $C_4H_8^+$ by elimination of hydrogen sulfide is only a slight possibility.

Discussion

The comparison of the present results of fragmentation in CH_3SH, C_2H_5SH, and 1-C_3H_7SH with those in CH_3OH, C_2H_5OH, and 1-C_3H_7OH obtained by Lindholm and coworkers[1-3] is summarized in Table 1. Only the main processes are listed in the table.

In methanethiol the main processes of hydrogen elimination are similar to those in methanol.[2,5] However, the SH^+ and S^+ ions are observed in methanethiol, whereas almost no OH^+ and O^+ ions are observed in methanol. The presence of SH^+ and the absence of OH^+ reflect the difference of bond strength between C–S and C-O. The bond energy of C-S (~70 kcal/mol) is larger than that of C-O (~90 kcal/mol).[14] The major precursor of the S^+ ion is not SH^+ but CH_3S^+, judging from the energy relation in Fig. 1.

In ethanethiol the fragmentation processes are rather different from those in ethanol. Hydrogen elimination is less important in ethanethiol than in ethanol. Elimination of hydrogen sulfide can be observed in ethanethiol, whereas almost no elimination of water is observed in ethanol. Formation of CH_2OH^+ in ethanol is much more important than that of CH_2SH^+ in ethanethiol, probably owing to the difference of stability between them. The rupture of the C-S bond occurs more easily than that of the C-O bond does.

In propanethiol hydrogen elimination from the parent ion is less important than in propanol. Hydrogen sulfide elimination from the parent ion $C_3H_7SH^+$ is prominent, but water elimination from $C_3H_7OH^+$ giving $C_3H_6^+$ is much more prominent than hydrogen sulfide elimination. The rupture of the C–S bond giving $C_3H_7^+$ is easier than that of the C–O bond, owing to the difference of the bond strength between them.

TABLE 1. COMPARISON OF FRAGMENTATION BY CHARGE EXCHANGE WITH POSITIVE IONS BETWEEN THIOLS AND ALCOHOLS

	Thiol	Alcohol
Methane	$CH_3SH^+ \xrightarrow{-H} CH_3S^+$ $CH_3S^+ \xrightarrow{-H_2} CHS^+$ $CH_3SH^+ \rightarrow CH_3^+ + SH^+$ $CH_3SH^+ \rightarrow S^+ + CH_3$	$CH_3OH^+ \xrightarrow{-H} CH_2OH^+$ $CH_2OH^+ \xrightarrow{-H_2} CHO^+$ $CH_3OH^+ \rightarrow CH_3^+ + OH$
Ethane	$C_2H_5SH^+ \xrightarrow{-H} CH_3CH_2S^+$ $CH_3CH_2S^+ \xrightarrow{-CH_3} CH_2SH^+ \xrightarrow{-H_2} CHS^+$ $C_2H_5SH^+ \xrightarrow{-SH} C_2H_5^+ \xrightarrow{-H_2} C_2H_3^+$ $C_2H_5SH^+ \xrightarrow{-H_2S} C_2H_4^+$	$C_2H_5OH \xrightarrow{-H} CH_3CHOH^+$ $CH_3CHOH^+ \xrightarrow{-CH_3} CH_2OH^+ \xrightarrow{-H_2} CHO^+$ $C_2H_5OH \xrightarrow{-OH} C_2H_5^+ \xrightarrow{-H_2} C_2H_3^+$
Propane	$C_3H_7SH^+ \xrightarrow{-H} C_3H_7S^+$ $C_3H_7S^+ \xrightarrow{-C_2H_5} CH_2SH^+ \xrightarrow{-H_2} CHS^+$ $C_3H_7SH^+ \xrightarrow{-SH} C_3H_7^+ \xrightarrow{-H_2} C_3H_5^+ \xrightarrow{-H_2} C_3H_3^+$ $C_3H_7SH^+ \xrightarrow{-H_2S} C_3H_6^+$	$C_3H_7OH^+ \xrightarrow{-H} C_3H_6OH^+$ $C_3H_6OH^+ \xrightarrow{-C_2H_5} CH_2OH^+ \xrightarrow{-H_2} CHO^+$ $C_3H_7OH^+ \xrightarrow{-OH} C_3H_7^+$ etc. $C_3H_7OH^+ \xrightarrow{-H_2O} C_3H_6^+$

⟹ important (>40%) ⟶ moderately important (40—20%) ⋯⋯→ less important (<20%)

Formation of CH_2SH^+ is less prominent than that of CH_2OH^+.

In the case of ethanol, for example, Koch and Lindholm[1] discussed the suggestion that the ionized oxygen atom has a valency of three and has a tendency towards formation of a double bond between C and O^+. Owing to this tendency, the other bonds of the carbon atom are weakened. They considered the following three resonant structures:

$$\left.\begin{array}{ll} \text{(a)} & CH_3-CH_2-\overset{+}{O}-H \\ \text{(b)} & -CH_3\ CH_2=\overset{+}{O}-H \\ \text{(c)} & CH_3-\underset{H}{CH}=\overset{+}{O}-H \end{array}\right\} \quad (36)$$

A similar consideration can apply to the cases of the higher alcohols and also to the cases of the corresponding thiols. Stabilization through an electron-releasing conjugative effect is well known to occur in the following manner:

$$H_2C=\overset{+}{\underset{\cdot\cdot}{X}}-H \longleftrightarrow H_2\overset{+}{C}-\underset{\cdot\cdot}{\overset{\cdot\cdot}{X}}-H \quad (37)$$

$$H_3\overset{\ominus}{\underset{\cdot\cdot}{C}}-CH=\overset{\oplus}{\underset{\cdot\cdot}{X}}-H \longleftrightarrow CH_2=\underset{H}{CH}-\underset{\cdot\cdot}{\overset{\cdot\cdot}{X}}-H \quad (38)$$

where X is O or S. As the π-bonding between C2p and S3p is weaker than that between C2p and O2p, rupture of the C-S bond occurs more easily than that of the C–O bond does. This tendency is pronounced in Table 1. The ions CH_2OH^+ and CH_3CHOH^+ (or $CH_3CH_2CHOH^+$) are remarkable compared to the ions $C_2H_5^+$ and $C_3H_7^+$, which are produced by the C-O rupture in the cases of ethanol and 1-propanol. On the other hand, the ions CH_2SH^+ and CH_3CHSH^+ (or $CH_3CH_2CHSH^+$) are not more abundant than $C_2H_5^+$ and $C_3H_7^+$ in the cases of ethanethiol and 1-propanethiol.

Hydrogen sulfide or water elimination from the molecular ions occurs easily in the larger thiols or alcohols. This process seems to proceed through the intermediate $R\text{-}SH_2^+$ or $R\text{–}OH_2^+$, which probably weakens the double bond formation between R-S or R-O in Reaction 36 (a) and (b) and therefore results in the rupture of the bond R-S or R–O in the lower energy region.

For the compounds larger than *n*-propyl, the apparent similarity is more pronounced for thiols and alcohols.[7] Increase of the length of the carbon chain causes a larger contribution of the alkyl group which is common to thiols and alcohols. This makes the fragmentation pattern similar for larger thiols and alcohols. However, the larger cross section of the sulfur atom in thiols for charge exchange or electron impact compared with that of oxygen in alcohols makes the parent ion more prominent in thiols. This fact will be confirmed by the study using a double mass spectrometer cross section measurement.[15]

Next, let us consider the effect of the structure of the compound. Methyl elimination from 2-propanethiol (SH: secondary position) giving C_2H_4SH is remarkable, whereas that from 1-propanethiol has only a small probability. For 2-propanethiol the following resonance forms should be considered in the same manner as Reaction 36:

$$\left.\begin{array}{ll} \text{(a)} & CH_3-CH(CH_3)-\overset{+}{S}-H \\ \text{(b)} & -CH_3\ CH(CH_3)=\overset{+}{S}-H \\ \text{(c)} & CH_3-\underset{CH_3}{CH}=\overset{+}{S}-H \end{array}\right\} \quad (39)$$

As (b) and (c) are the same expression, only the res-

onance between (a) and (b) can be taken in account here. Thus it is easily understood why methyl elimination from the molecular ion is highly probable in 2-propanethiol. On the other hand, it is obvious that 1-propanethiol loses its methyl group by a different mechanism. The ionic species $CH_2=\overset{+}{S}-H$ is known to be more abundantly produced than $CH_3CH=\overset{+}{S}-H$ on electron impact of 1-propanethiol. Generally the β-cleavage is easier than the γ-cleavage for sulfur-containing ions.[16] The same tendency is more pronounced for the case of electron impact mass patterns in 1- and 2-propanols.[17]

The difference of the mass patterns between 1-(primary) and 2-(secondary) butanethiols can be understood in principle in the same manner as stated above. The prominent ions CH_2SH^+ in 1-butanethiol and $C_2H_4SH^+$ in 2-butanethiol and formed through the resonance containing the C=S double bond.

Fragmentation of the tertiary compound of butyl mercaptan is entirely different from the other butyl mercaptan. It is initiated by rupture of the labile C-S bond. Not only hydrogen migration but also rearrangement of the carbon structure are involved in the decomposition processes.

In previous papers,[18-20] we have studied the possibility of direct fragmentation of the molecular ions from their electronically excited states. We found that this is true for various systems, by comparing the experimental results with those obtained by calculation. As calculation of methanethiol has been done in the other paper[21] submitted in this bulletin, only the results of the calculation for two kinds of propanethiols and four kinds of butanethiols are shown here. According to the Extended Hückel Molecular Orbital (EHMO) method the energy levels and eigenvectors of the molecular orbitals are calculated, and the main characters of the MO's are determined on the basis of these calculated eigenvectors. When an electron is ejected from a certain molecular orbital by charge exchange, the bond corresponding to the molecular orbital is subjected to scission, resulting in formation of various fragment ions. The energy levels, the main characters, and the product ions expected are shown in Tables 2 and 3 for propanethiols and for butanethiols, respectively. The tendency of appearance of the ions is in good agreement with the experimental results in Figs. 3 and 4 for propanethiols, and the same is true

Table 2. Calculated MO energy, calculated MO assignment, and fragment ions for 1-propanethiol and 2-propanethiol

	Calculated MO energy (eV)	Main character	Produced ions
1-Propanethiol	10.39	n(S)	76
	11.53	n(S) σ(SH)	76, 75
	13.03	$\sigma(C_1S)$ $\sigma(C_1C_2)$ $\sigma(C_2C_3)$	43, 42, 47 or 29, 61
	13.29	$\pi(CH_2)$	
	13.55	$\sigma(C_1C_2)$	47 or 29
2-Propanethiol	10.38	n(S)	76
	11.45	n(S) σ(SH)	76, 75
	13.13	$\sigma(C_2S)$	43 or 42
	13.26	$\sigma(C_1C_2)$ $\sigma(C_2C_3)$	61

Table 3. Calculated MO energy, calculated MO assignment, and fragment ions for various butanethiols

	Calculated MO energy (eV)	Main character	Produced ions
1-Butanethiol	10.40	n(S)	90
	11.52	σ(SH) $\sigma(C_1S)$	89, 57 or 56
	12.75	$\sigma(C_1S)$ $\sigma(C_2C_3)$	57 or 56, 61 or 29
	13.24	$\pi(CH_2)$	
	13.47	$\sigma(C_1C_2)$	47 or 43
2-Methyl-1-propanethiol	10.36	n(S)	90
	11.44	σ(SH) $\sigma(C_1S)$	89, 57 or 56
	12.95	$\sigma(C_1C_2)$	43 or 47
	13.10	$\sigma(C_2C_m)$	
1-Methyl-1-propanethiol	10.37	n(S)	90
	11.35	n(S) σ(SH) $\sigma(C_1S)$	89, 57 or 56
	12.87	$\sigma(C_1C_2)$ $\pi(CH_2)$	61 or 29
	13.09	$\sigma(C_1S)$ $\pi(CH_2)$	57 or 56
2-Methyl-2-propanethiol	10.36	n(S)	90
	11.45	n(S) σ(SH)	90, 89
	13.01	$\sigma(C_2S)$	57

C_m: C in 2-methyl group.

for butanethiols (see Figs. 5—8). It is likely that there is direct scission, which will give the various fragment ions shown in Tables 2 and 3. Even if all of the fragment ions are not derived from the direct scission of the molecular ions, at least some parts of these ions are considered to be formed by the scission from the electronically excited molecular ions. As the fragmentation processes in the higher energy region are profoundly influenced by the secondary scission, it is obvious that the calculation performed above cannot apply to the processes in the higher energy region.

From Table 2, it is shown that fragmentation in 2-propanethiol is simpler than that in 1-propanethiol; this tendency is in agreement with that obtained in the experimental results (Figs. 3 and 4). Similarly, from Table 3 fragmentation of 2-methyl-2-propanethiol (tertiary compound) is expected to be simpler than that of any other compounds of butanethiol. This tendency is in agreement with that obtained by the experiments in Figs. 5—8.

It is noteworthy that this kind of study using a double mass spectrometer can supply information about ion-molecule reactions involving the excited parent ions; it is especially useful to obtain the energy-abundance relation among the fragment ions.

The authors thank Mr. Hiraga for his cooperation throughout this work.

References

1) H. Van Koch and E. Lindholm, *Arkiv Fysik*, **19**, 123 (1961).
2) P. Wilmenius and E. Lindholm, *ibid.*, **21**, 97 (1962).
3) E. Pettersson, *ibid.*, **25**, 181 (1963).
4) E. Lindholm and P. Wilmenius, *Arkiv Kemi*, **20**, 255 (1963).
5) T. Nagatani, K. Yoshihara, and T. Shiokawa, This Bulletin, **46**, 1450 (1973).
6) T. Nagatani, K. Yoshihara, and T. Shiokawa, *ibid.*, **46**, 1306 (1973).
7) For example see K. Biemann, "Mass Spectroscopy: Organic Chemical Applications," p. 100, McGraw-Hill Book Co., New York (1962).
8) T. Nagatani, K. Yoshihara, and T. Shiokawa, This Bulletin, **46**, 1628 (1973).
9) T. Nagatani, K. Yoshihara, and T. Shiokawa, *ibid.*, **46**, 2721 (1973).
10) S. Ikuta, K. Yoshihara, and T. Shiokawa, *ibid.*, **46**, 3648 (1973).
11) T. Shiokawa, K. Yoshihara, M. Yagi, T. Omori, H. Kaji, M. Hiraga, T. Nagatani, and Y. Takita, *Mass Spectroscopy*, **18**, 1230 (1970).
12) J. L. Franklin, J. G. Dillard, H. M. Rosenstock, J. T. Herron, K. Draxland, and F. H. Field, "Ionization Potentials, Appearance Potentials, and Heat of Formation of Gaseous Positive Ions," NSRDS-NBS-26, National Bureau of Standards, U.S., Washington, D.C., (1969).
13) American Petroleum Institute Research Project 44. Catalogue of Mass Spectral Data, Carnegie Institute of Technology, Pittsburgh (1953).
14) V. I. Vendeneyev, L. V. Gurvich, V. N. Kondrat'yev, V. A. Medvedev, and Ye. L. Frankevich, "Bond Energies, Ionization Potentials and Electron Affinities," Edward Arnold, London (1966), p. 63, 64.
15) K. Yoshihara, J. C. Abbé, and J. M. Paulus, to be published.
16) E. J. Levy and W. A. Stahl, *Anal. Chem.*, **33**, 707 (1961).
17) R. A. Friedel, J. L. Shultz, and A. C. Sharkey, Jr., *ibid.*, **28**, 926 (1956).
18) S. Ikuta, K. Yoshihara, and T. Shiokawa, *Mass Spectroscopy*, **22**, 233 (1974).
19) S. Ikuta, K. Yoshihara, and T. Shiokawa, *ibid.*, **22**, 239 (1974).
20) S. Ikuta, K. Yoshihara, and T. Shiokawa, *ibid.*, **22**, 245 (1974).
21) S. Ikuta, K. Yoshihara, and T. Shiokawa, This Bulletin, **48**, 2134 (1975).

The Role of Solvents in the Dimerization of the 2,3-Dichloro-5,6-dicyano-*p*-benzoquinone Anion Radical

Akihiko YAMAGISHI

Department of Chemistry, Faculty of Science, Hokkaido University, Sapporo 060

(Received January 6. 1975)

The reversible dimerization of the anion radical of 2,3-dichloro-5,6-dicyano-*p*-benzoquinone (DDQ) has been studied in water, acetonitrile (MeCN), and other organic solvents. The analysis of the thermodynamic parameters of dimerization equilibria reveals that a large negative entropy term plays a primary role in determining the equilibrium constants. The temperature-jump measurement shows that the forward rate constant in water containing 5.8 M urea is nearly a diffusion controlled one, $(1\pm0.5)\times10^8$ M^{-1} s^{-1} at -6 °C. In MeCN–water mixtures, the backward reaction rate increases with the square of the MeCN concentration. This result suggests that a dimer is effectively decomposed by the successive attacks of the two MeCN molecules.

Since the theoretical work by Hausser and Murrell, the dimerization phenomena of ion radicals have been investigated extensively.[1-6] The main attention has been focused on the interaction between unpaired electrons. In this context, the dimerization in solution was compared to the stacking of ion radicals in the crystalline state.[4]

In the present work, the dimerization phenomena is taken up from a slightly different view-point: that is, the role of solvents played in the dimerization equilibria of ion radicals. Since the attractive force in a dimer arises from the charge-transfer interaction between two fragments, it must be a short-range force.[7] Thus the slight disturbance by solvent molecules on the geometrical structure of a dimer will cause a serious effect on the interaction of unpaired electrons, and accordingly on the stability of a dimer. In this sense the role of solvents in dimerization equilibria will be completely different from that in the ion-pair formation of a simple salt. In the latter case, the dielectric continuum theory has proved to be successful in interpreting the solvent effect on the ion-pair formation.[8] In the dimerization of ion radicals, however, more specific descriptions of solvents and solvation structures are needed in order to interpret the solvent effects on the dimerization equilibria. Until now, no systematic study on this topic has been carried out except for a few examples,[2,9] probably because the ion radicals dimerize only under extreme conditions such as low temperature, or oxygen-free conditions, or concentrated acidic media.[2-6]

In this paper, the study of the dimerization of the 2,3-dichloro-5,6-dicyano-*p*-benzoquinone anion radical (DDQ^-) is presented. DDQ^- dimerizes at room temperature in all solvents used. It is relatively stable in solution under air, although the stability depends on solvents and counter cations. The thermodynamic parameters of dimerization are obtained spectrophotometrically. The rate of dimerization is measured by a temperature-jump apparatus. From both the equilibrium and the rate data, the role of solvents in a dimerization reaction has been made clear, particularly from the view-point of the molecular processes involving radicals and solvent molecules. Some solvents are found to form a rigid solvation structure with a dimer, whereas others effectively decompose such a structure.

Experimental

The sodium (Na^+) and the tetraethylammonium (NEt_4^+) salts of DDQ were obtained by reducing DDQ with NaI and MEt_4I in acetonitrile (MeCN) respectively. MeCN, methanol (MeOH), and ethanol (EtOH) were purified as described elsewhere.[10] Acetone (Me_2CO), dimethylformamide (DMF), tetrahydrofuran (THF), and dimethoxyethane (DME) were distilled once. Water was deionized and distilled once. Tetra-*n*-propylammonium perchlorate (NPr_4ClO_4) was prepared by the reaction of NPr_4OH with $HClO_4$ in water. $NaClO_4$ of a C.P. grade was used after being dried at 130 °C.

The absorption spectra were measured with a Hitachi model EPS-3T spectrophotometer. In MeCN, Me_2CO and DMF, both Na^+DDQ^- and $NEt_4^+DDQ^-$ are stable enough for the precise spectroscopic measurements. In THF and DME, $NEt_4^+DDQ^-$ is found more stable than Na^+DDQ^-, although both salts decompose gradually. In EtOH, MeOH, and H_2O, both $NEt_4^+DDQ^-$ and Na^+DDQ^- decompose in the order of $H_2O>MeOH>EtOH$, which is inevitable even in a vacuum. The equilibrium measurements in such solvents as cause the decomposition of M^+DDQ^- were performed by reading the absorbances at the dimer and the monomer band repeatedly within several seconds. Here we assumed that the decomposition products of DDQ^- do not affect the dimerization equilibria. The extinction coefficients of DDQ^- monomer ε_M in these solvents were determined from the absorbance when the 0.1 ml of the MeCN stock solution of $NEt_4^+DDQ^-$ (*ca.* 10^{-3} M) was dissolved into the 2.0 ml of each solvent. ε_M was calculated from the known ε_M in MeCN (6.3×10^3 at 594 nm), assuming that the presence of a small amount of MeCN does not affect the magnitude of ε_M in each solvent. The extinction coefficients of DDQ^- dimer ε_D in all solvents except H_2O are assumed to be equal to that in MeCN. The details in determining ε_D in MeCN and water are described in the results.

The conductivity was measured with a Yanagimoto model MY-7 conductivity outfit. The temperature of a cell was maintained at 20 °C by circulating water. In THF, the concentration of $NEt_4^+DDQ^-$ was measured simultaneously by absorption spectra.

The rate was measured with a Union Giken temperature-jump apparatus. This appearatus instantly raises *ca.* 2 ml sample solution by 20—30 kV discharge through a co-axial cable. The cable has a length of 200 m, 0.02 μF capacitance, and 75 Ω characteristic impedance. The rise time of temperature was determined by observing the rate of a protonation reaction of phenolphthalein in H_2O at various ionic strength adjusted by NaCl. The temperature rise is attained within 2 μs when a sample solution has a conductivity higher

than $10^{-3}cm^{-1}\Omega^{-1}$. For the MeCN system, NPr_4ClO_4 is used as a conducting electrolyte. The reaction was monitored by the change of the transmittance at the dimer band near 710 nm. The amount of DDQ^- electrolyzed at discharge was concluded to be negligible since the concentration change was less than 5% after several times of discharge. The temperature of a sample solution was maintained by circulating EtOH cooled by liquid nitrogen. The temperature was measured by a thermocouple just before discharge. For the MeCN–water system, the sample solution was prepared by mixing a H_2O solvent containing 0.1 M NaCl and 6.0 M urea with the MeCN stock solution of $NEt_4^+DDQ^-$, both of which were pre-cooled at the desired temperature. The measurement was done about 3 minutes after preparing the solution. Thus, the concentration uncertainty of DDQ^- was estimated to be within 10%.

Results

Dimerization Equilibria in Various Solvents. A new absorption peak appears at 710 nm when Na^+DDQ^- is dissolved in MeCN to the concentration higher than 10^{-3} M (Fig. 1). In the concentration range of Na^+-

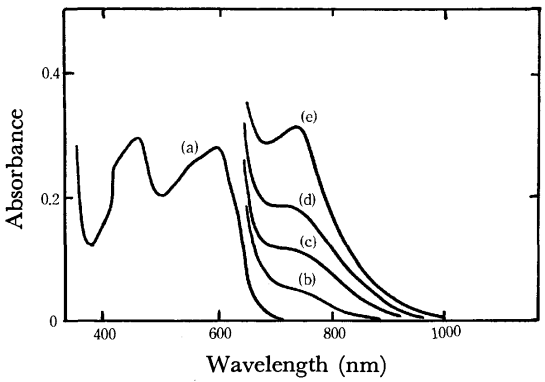

Fig. 1. The visible spectra of Na^+DDQ^- in MeCN at various concentrations: a) 4.5×10^{-5}, b) 1.9×10^{-3}, c) 2.9×10^{-3}, d) 3.7×10^{-3} and e) 4.6×10^{-3} M at 15 °C.

DDQ^- from 1×10^{-3} to 5×10^{-3} M, the absorbance at 710 nm increases exactly in proportion to the square of the concentration of Na^+DDQ^-. This phenomena is compared with the facts that the anion radicals of chloranil and *p*-benzoquinone dimerize in ethanol at low temperature, showing a new peak at 670 and 585 nm, respectively.[3,4] Assuming the dimer formation for DDQ^- ion,

$$2DDQ^- \rightleftarrows (DDQ^-)_2;\ K \qquad (1)$$

the absorbance at 710 nm, A_{710}, is related to the concentration of Na^+DDQ^-, C, as follows:

$$K = [(DDQ^-)_2]/[DDQ^-]^2 = A_{710}/\varepsilon_D(1-\alpha)^2C^2 \qquad (2)$$

where ε_D is a molar extinction coefficient of a dimer at 710 nm and α a degree of association. In deriving this relation, Na^+DDQ^- is assumed to dissociate completely in MeCN. This point is stated later in more detail. A_{710} would not increase linearly with C^2, since α becomes larger as C increases. The observation that A_{710} is exactly proportional to C^2 within an experimental error implies that K in the present system is too small to detect the variation of α with C. In this case, Eq. (2) reduces to

$$K = A_{710}/\varepsilon_D C^2, \qquad (3)$$
$$\varepsilon_D K = (1.7\pm0.2)\times10^4\ M^{-2} \text{ at } 15°C.$$

In order to obtain both K and ε_D, we first estimate ε_D in the following ways: (i) Assuming no absorption of a dimer at 594 nm where a monomer has an absorption peak, the decrease of the monomer band caused by dimerization is related to the dimer band absorption as below:

$$\Delta A_{594}/A_{710} = -2\varepsilon_M/\varepsilon_D \qquad (4)$$

where ε_M is a molar extinction coefficient of a monomer at 594 nm, 6.3×10^3. (ii) The addition of NPr_4ClO_4 is found to increase the absorption at 710 nm, giving no influence to the spectral shape of a monomer band. This effect is interpreted as the displacement of the equilibrium (1) to the righthand side due to the presence of the ionic atmosphere of NPr_4^+ ions. Therefore, the decrease of the absorbance at 594 nm when NPr_4ClO_4 is added into the MeCN solution is related to the increase of the absorbance at 710 nm as follows:

$$\Delta A_{594}/\Delta A_{710} = -2\varepsilon_M/\varepsilon_D. \qquad (5)$$

From relation (4), $\varepsilon_M/\varepsilon_D$ is obtained to be 1.0 ± 0.2, leading to $\varepsilon_D=(6.3\pm1)\times10^3$. From the difference spectrum of the sample solution containing 2.2×10^{-3} M $NEt_4^+DDQ^-$ and 0.123 M NPr_4ClO_4 with the solution of 2.2×10^{-3} M $NEt_4^+DDQ^-$ as reference, $\Delta A_{594}/\Delta A_{710}$ is obtained to be -2.4 ± 0.4, resulting in $\varepsilon_D=(7.2\pm2)\times10^3$. Thus the average value of ε_D is estimated to be $(7\pm1)\times10^3$ at 710 nm. Using this value, K is determined to be $2.5\pm0.5\ M^{-1}$ at 15 °C.

Similar new peaks around 710 nm are also observed, using DMF, Me_2CO, THF, DME, EtOH, and H_2O as solvents. In these solvents except for H_2O, K is calculated using the same ε_D value as obtained for MeCN and the proportional constant of A_{710} against C^2 in each solvent. For water, the K which is calculated in this way, is so large that we doubt the validity of the assumption that ε_D in H_2O is of the same magnitude as in MeCN. Thus ε_D in H_2O is determined independently by methods (i), additionally (iii) from the temperature-jump signals at the monomer and the dimer bands (Figs. 10 and 11). ε_D in H_2O is determined to be (i) $(2.5\pm0.8)\times10^4$ and (iii) $(2.4\pm0.8)\times10^4$. Taking the average of these values, ε_D is estimated to be $(2.5\pm1)\times10^4$. The large uncertainty for ε_D in H_2O arises from the gradual decomposition of DDQ^- in H_2O. In the temperature region of 0—30 °C, a straight line is obtained by plotting $\log K$ *versus* the reciprocal of absolute temperature for all solvents, from which the enthalpy and the entropy changes in reaction (1) are determined. They are given in Table 1.

It is likely that DDQ^- forms an ion-pair with a positive ion in solvents with small dielectric constants. Therefore, the conductivity of Na^+DDQ^- and NEt_4^+-DDQ^- is measured in MeCN and THF. The results are shown in Fig. 2.

$$M^+DDQ^- \rightleftarrows M^+ + DDQ^-;\ K_d \qquad (6)$$

In MeCN, the molar conductivity, λ, of M^+DDQ^- (M^+=Na^+, NEt_4^+) is almost constant with the change

TABLE 1. THE THERMODYNAMIC PARAMETERS OF THE DIMERIZATION EQUILIBRIUM OF $NEt_4^+DDQ^-$ IN VARIOUS SOLVENTS
λ denotes an absorption peak of a dimer.

Solvent	K(10 °C)/ M^{-1}	ΔH/ kcal·M^{-1}	ΔS/e.u.	λ/nm
MeCN	3.7	−9.7±1.0	−29±3	710
DMF	1.4	−7.0±0.2	−24±2	710
Me_2CO	1.1	−7.2±0.2	−25±2	720
THF	17	−3.0±0.2	−4.9±2	710
DME	13	−3.3±0.5	−6.5±2	710
EtOH	5.2	−5.0±1.0	−14±3	715
MeOH	5.0	−3.7±1.0	−11±4	712
H_2O	1300	−8.8±1.0	−17±2	712

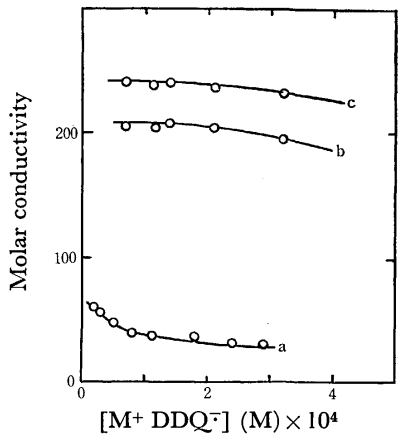

Fig. 2. The electric conductivity of M^+ DDQ^- in MeCN and THF at 20 °C. a) $NEt_4^+DDQ^-$ in THF, b) Na^+ DDQ^- in MeCN and c) NEt_4^+ DDQ^- in MeCN.

of the concentration. Thus, it is concluded that in MeCN, M^+DDQ^- dissociates completely to the free ions. Under this conclusion the limiting molar conductivity, λ_∞, of DDQ^- is estimated to be 150, since λ_∞ for Na^+ and NEt_4^+ are reported to be 70 and 86 respectively.[11] In other solvents whose dielectric constants are similar to that of MeCN, M^+DDQ^- is considered to dissociate completely. On the other hand, $NEt_4^+DDQ^-$ forms an ion pair at least partially in THF, because λ in THF is about 10% of that in MeCN, and increases as the decrease of the concentration. The approximate value of K_d is estimated by the equation

$$K_d = C\lambda^2/\lambda_\infty^2, \quad (7)$$

where λ_∞ is determined by extrapolating the straight line of λ *versus* $\sqrt{C}$ to the infinite dilution. K_d is determined to be about 10^{-5} M at 20 °C. This means that more than 90% of $NEt_4^+DDQ^-$ is ion-paired at $C=10^{-3}$ M. Thus, the dimerization equilibrium of NEt_4^+-DDQ^- in THF is almost expressed by the following equation:

$$2NEt_4^+DDQ^- \rightleftharpoons (NEt_4^+DDQ^-)_2 \quad (8)$$

The dimerization in DME is also considered to take place between two $NEt_4^+DDQ^-$s.

It is likely that DDQ^- is hydrogen-bonded on the oxygen atoms with the protonic solvents like EtOH, MeOH, and H_2O. The electronic spectra of NEt_4^+-

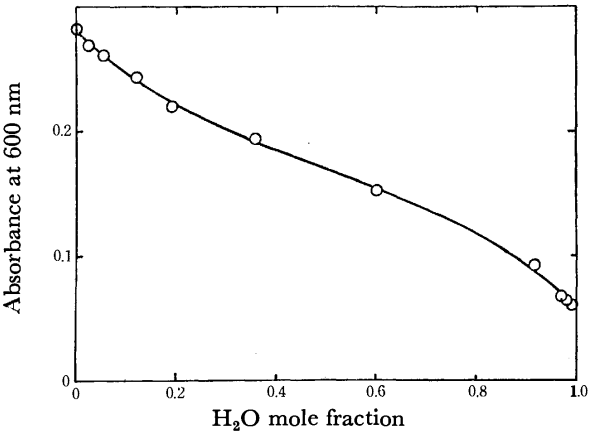

Fig. 3. The change of the absorbance of DDQ^- at 600 nm with the mole fraction of H_2O in an MeCN–H_2O mixed solvent. $[NEt_4^+DDQ^-]$ 4.6×10^{-5} M.

DDQ^- monomer depend on solvents and solvent composition. The absorption peak at 594 nm in MeCN displaces to the shorter wavelength when the salt is dissolved in alcohols or water. The qualitative feature of this phenomena is displayed by plotting the change of absorbance at 600 nm, A_{600}, against the mole fraction of H_2O (Fig. 3). The general trend of A_{600} with H_2O mole fraction well corresponds to the change of the ^{13}C coupling constant for *p*-benzoquinone anion radical (Q^-) in MeCN-H_2O mixtures recently observed by Stone and Maki.[12] In these investigations the change of the hyperfine coupling constants of carbon-13 is attributed to the specific solvation of Q^- by both MeCN and H_2O molecules. In the low concentration region of H_2O, Q^- is solvated by two MeCN molecules. In the medium concentration region of H_2O, Q^- is solvated by one MeCN and one H_2O molecule. In the high concentration region of H_2O, Q^- is solvated by two H_2O molecules. Therefore, it is concluded that in the present system there exists a competition between H_2O and MeCN for solvating DDQ^- ions although no theoretical basis for the solvent effect on the electronic spectra of DDQ^- is available at present. Contrary to the DDQ^- monomer, the absorption peak of a dimer is little affected by the solvents as given in Table 1. However, the remarkably large equilibrium constant in H_2O may clearly be related to the hydrogen-bonding property of water. This will be treated from the kinetic point of view in a later section.

The Effect of Cations on the Dimerization Equilibria. The presence of counter ions affects the dimerization equilibria remarkably. In Fig. 4, the increase of the absorbance at 710 nm is shown when $NaClO_4$, NEt_4ClO_4, and NPr_4ClO_4 are added. Although the ion-pairing of M^+DDQ^- is neglected in MeCN in the concentration range below 10^{-3} M, DDQ^- and $(DDQ^-)_2$ probably form ion-pairs with cations in the high concentration of cation. In case of $NaClO_4$, this is confirmed from the change of electronic spectra of a DDQ^- monomer and a dimer when a large amount of $NaClO_4$ is present (Figs. 5 and 6). The absorption of a dimer becomes broader as $NaClO_4$ is added, although the peak position is little altered. In case of a mono-

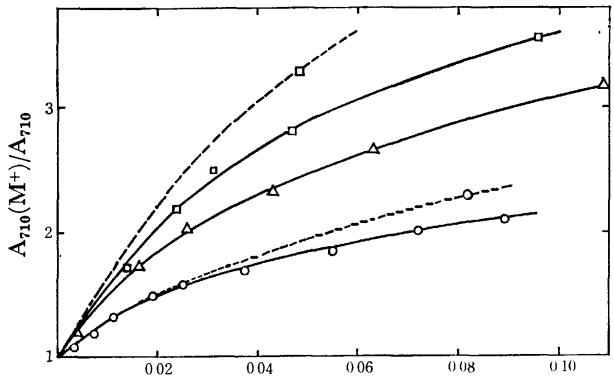

Fig. 4. The increase of the absorbance at 710 nm with the addition of various salts at 10 °C; $NaClO_4$ (□), NEt_4ClO_4 (△) and NPr_4ClO_4 (○). The dotted lines are a curve corrected against the concentration of free ions. The ordinate is taken as the ratio of the absorbace in the presence of salts, A_{710} (M^+), to that in the absence of salts, A_{710}.

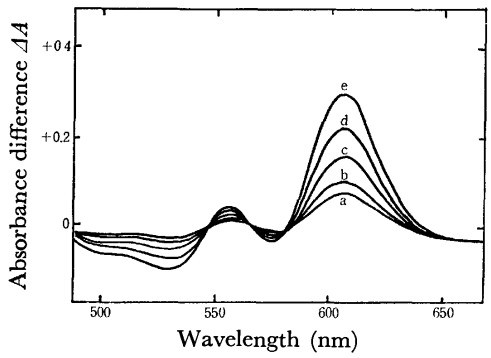

Fig. 5. The difference spectra of DDQ^- monomer at the high concentration of $NaClO_4$ at 10 °C. The sample solution contains [Na^+DDQ^-] 2.5×10^{-4} M, the reference [Na^+DDQ^-] 2.5×10^{-4} M and [$NaClO_4$] 0.047 M (a), 0.089 M (b), 0.16 M (c), 0.30 M (d) and 0.46 M (e).

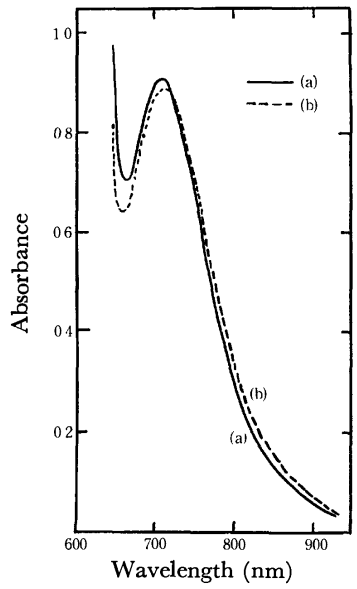

Fig. 6. The effect of $NaClO_4$ on the spectra of DDQ^- dimer. (a) [Na^+DDQ^-] 5.6×10^{-3} M (b) [Na^+DDQ^-] 2.8×10^{-3} M and [$NaClO_4$] 0.214 M.

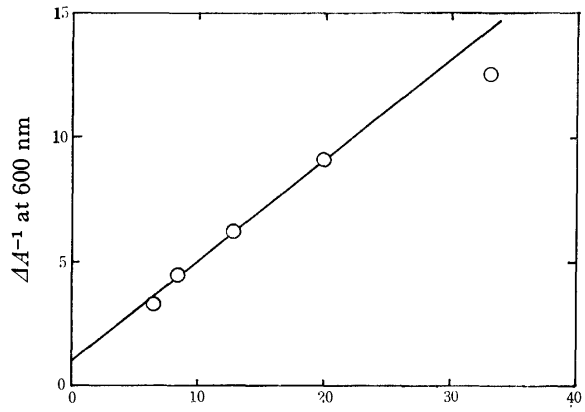

Fig. 7. The dependence of the absorbance change at 600 nm of DDQ^- monomer on the concentration of free Na^+ ion.

mer, the presence of the isosbestic points at 581, 565, and 547 nm in Fig. 5 implies that a free DDQ^- ion converts to another species, which is most likely to be a 1:1 ion-pair between Na^+ and DDQ^-. If this is correct, the change of absorbance ΔA in Fig. 5 is related to the free Na^+ concentration, $[Na^+]_f$ as follows:

$$\frac{1}{\Delta A}=\frac{1}{C(\varepsilon_1-\varepsilon_2)}\left(\frac{K_d}{[Na^+]_f}+1\right) \quad (9)$$

where C is the total concentration of M^+DDQ^-, and ε_1, ε_2 the extinction coefficients of DDQ^- and Na^+-DDQ^-, respectively. $[Na^+]_f$ is calculated from the conductivity results under the assumption that λ is directly proportional to the degree of the dissociation of $NaClO_4$. In Fig. 7, ΔA^{-1} at 600 nm is plotted against the reciprocal of $[Na^+]_f$. The straight line obtained from this plot confirms the formation of a 1:1 ion-pair between DDQ^- and Na^+. From the intrecept and the slope of the straight line, K_d is determined to be 0.40 M at 10 °C. On the other hand, NPr_4ClO_4 enhances the dimerization, although it gives no effect on the electronic spectra of DDQ^- monomer. This effect may be ascribed to the role of the ionic atmosphere of NPr_4^+ ions as stated previously.

Therefore, in the system containing a large amount of $NaClO_4$, the following equilibria are considered to exist:

$$DDQ^- + Na^+ \rightleftharpoons Na^+DDQ^-; \quad K_d \quad (6)$$

$$2DDQ^- \rightleftharpoons (DDQ^-)_2; \quad K \quad (1)$$

$$(DDQ^-)_2 + Na^+ \rightleftharpoons Na^+(DDQ^-)_2; \quad K_1 \quad (10)$$

$$Na^+(DDQ^-)_2 + Na^+ \rightleftharpoons (Na^+DDQ^-)_2; \quad K_2 \quad (11)$$

The absorbance at 710 nm is expressed as a function of the total concentration of Na^+DDQ^-, and the concentration of free Na^+ ion as follows:

$$A_{710}(Na^+) = (\varepsilon_D K+\varepsilon_3 KK_1[Na^+]_f+\varepsilon_4 KK_1K_2[Na^+]_f^2) \times(1+K_d^{-1}[Na^+]_f)^{-2}\cdot C^2 \quad (12)$$

where ε_3 and ε_4 are the molar extinction coefficient of $Na^+(DDQ^-)_2$ and $(Na^+DDQ^-)_2$, respectively. K_d, K, K_1, and K_2 are all dependent on ionic strength through the interaction of the ionic atmosphere of Na^+ ions with DDQ^- or $(DDQ^-)_2$. As a first approximation ε_3

and ε_4 are assumed equal to ε_D. The dependence of the equilibrium constant K on ionic strength can be eliminated by taking the ratio of the absorbance in the presence of $NaClO_4$, $A_{710}(Na^+)$, to that in the presence of the same amount of free NPr_4^+, $A_{710}(NPr_4^+)$, because in the latter system, only the reaction (1) takes place.

$$A_{710}(Na^+)/A_{710}(NPr_4^+) = (1+K_1[M^+]_f+K_1K_2[M^+]_f^2) \times (1+K_d^{-1}[M^+]_f)^{-2} \quad (13)$$

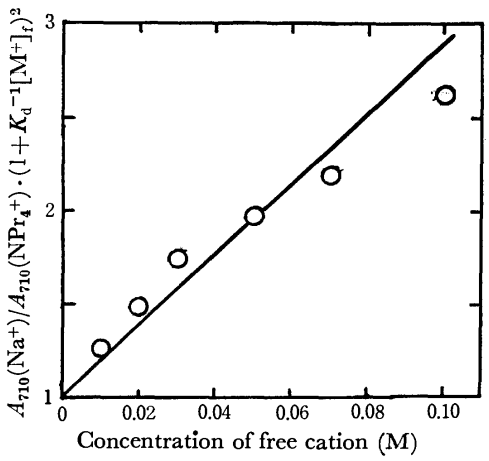

Fig. 8. The plot of A_{710} $(Na^+)/A_{710}$ $(NPr_4^+)\cdot(1+K_d^{-1}$ $[M^+]_f)^2$ against $[M^+]_f$ at 10 °C.

In Fig. 8 $A_{710}(Na^+)/A_{710}(NPr_4^+)\cdot(1+K_d^{-1}[M^+]_f)^2$ is plotted against $[M^+]_f$. All points are roughly on a straight line with a slope of 30 M^{-1}. Thus, it is concluded that in this concentration range of Na^+, there exists no appreciable amount of $(Na^+DDQ^-)_2$. The dimerization constant between Na^+DDQ^- and DDQ^-,

$$Na^+DDQ^- + DDQ^- \rightleftarrows Na^+(DDQ^-)_2;\ \tilde{K} \quad (14)$$

is expressed as

$$\tilde{K} = KK_1K_d.$$

Since K_1=30 M^{-1} and K_d=0.40 M, $\tilde{K}$=12 K at 10 °C, that is, the presence of Na^+ ion enhances the dimerization of DDQ^- by 12 times. The temperature dependence of the apparent dimerization constant gives that the apparent enthalpy change $-\Delta H$ decreases from 9.0±1.0 to 6.5±1.0 kcal M^{-1} as $[NaClO_4]$ increases from 0 to 1.14 M. This implies that the increase of the dimerization constant with the increase of Na^+ arises from the decrease of $-\Delta S$, but not from the increase of $-\Delta H$. This fact coincides with the small $-\Delta S$ observed in both THF and DME in which the dimerization occurs between ion-paired DDQ^- ions. As a result it is concluded that the entropy change for the dimerization becomes less negative, when the charge of anion radicals is screened by the counter cation. It may be probable that the large negative entropy change accompanied with dimerization is attributed to the freezing of solvent molecules due to the stronger solvation of a dimer than monomer ions. The neutralization of the charge of a dimer by a counter cation should result in the decrease of the solvating capacity of a dimer.

Kinetic Measurements. In order to look into the significance of the remarkably large dimerization constant in H_2O, the rates of dimerization in MeCN, H_2O, and MeCN-H_2O systems were measured by the temperature-jump method. Since the dimerization reaction of DDQ^- ions is largely exothermic, the equilibrium (1) displaces to the leftward at the sudden rise of temperature. In Fig. 9, the increase of the transmittance at 710 nm (dimer band) with time is shown for the MeCN solution of $NEt_4^+DDQ^-$ at −15 °C. The pseudo first-order rate constant k_{obsd} obtained from the signal is related to the forward and the backward rate constants of dimerization, $\vec{k}$ and $\overleftarrow{k}$, respectively, by Eq. (15):

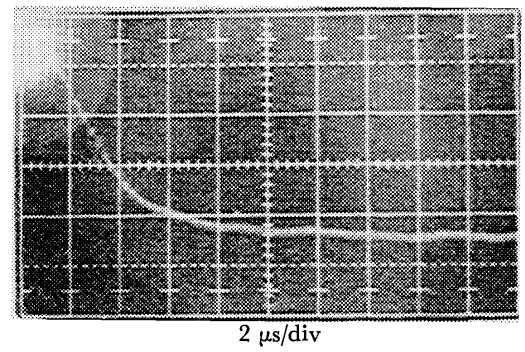

Fig. 9. The temperature-jump signal for the MeCN solution of $NEt_4^+DDQ^-$ at −15 °C. $[NEt_4^+DDQ^-]$ 5×10^{-3} M and $[NPr_4ClO_4]$ 2×10^{-2} M. Wavelength 710 nm.

$$k_{obsd} = 4\vec{k}[DDQ^-] + \overleftarrow{k} \quad (15)$$

Under the conditions of K=18.5 M^{-1} at −15 °C, and $[DDQ^-]\cong10^{-3}$ M, the first term in Eq. (15) is neglected. That is,

$$k_{obsd} = \overleftarrow{k}. \quad (16)$$

k_{obsd} is obtained to be 5×10^5 s^{-1} at −15 °C. However, the half-life time in Fig. 9 is almost equal to the minimum time for temperature-rise, 1.4 μs. Thus k_{obsd} is not related to $\overleftarrow{k}$ as in Eq. (16), instead it gives the lower limit of $\overleftarrow{k}$.

$$\overleftarrow{k} \geq 5\times10^5\ s^{-1} \text{ at } -15°C$$

Although the temperature of a sample solution is lowered down to −23 °C, no variation of k_{obsd} is observed. The lower limit of $\vec{k}$ is thus determined to be

$$\vec{k} = K\overleftarrow{k} \geq 2\times10^7\ M^{-1}\cdot s^{-1} \text{ at } -23°C,$$

since K at −23 °C is about 32 M^{-1}.

When H_2O containing 5.8 M urea and 1.8 M MeCN is used as a solvent, the k_{obsd} obtained at −6.0 °C is apparently smaller than the rate of the temperature-rise (Figs. 10 and 11). As expected from Eq. (15), k_{obsd} increases linearly as the increase of the concentration of free DDQ^- (Fig. 12). The slope and the intercept of the straight line in Fig. 12 give the values of $4\vec{k}$ and $\overleftarrow{k}$ respectively. Thus we obtain

$$\vec{k} = (1\pm0.5)\times10^8\ M^{-1}\cdot s^{-1}$$

$$\overleftarrow{k} = (3\pm2)\times10^4\ s^{-1} \text{ at } -6°C.$$

and $K=\vec{k}/\overleftarrow{k}=(3\pm2)\times10^3$ M^{-1}. K agrees with the

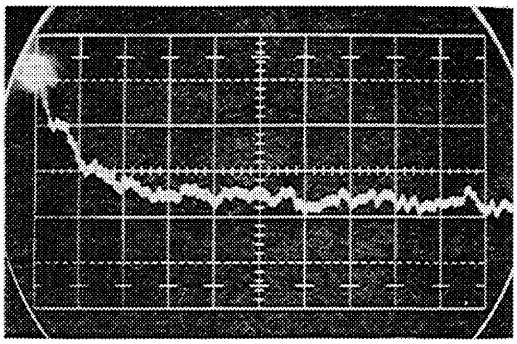

10 μs/div.

Fig. 10. The temperature-jump signal for the H_2O solution of $NEt_4^+DDQ^-$ at −6 °C. [DDQ^-] 2.0×10^{-4} M. [Urea] 5.8 M. [MeCN] 1.8 M. [NaCl] 0.1 M. Wavelength 700 nm.

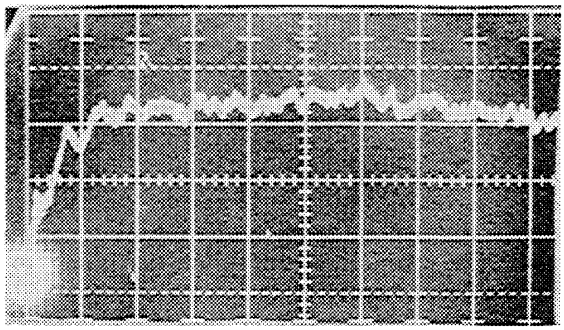

10 μs/div.

Fig. 11. The temperature-jump signal for the H_2O solution of $NEt_4^+DDQ^-$ at −6 °C. [DDQ^-] 3.4×10^{-4} M. [Urea] 5.8 M. [MeCN] 1.8 M. [NaCl] 0.1 M. Wavelength 530 nm.

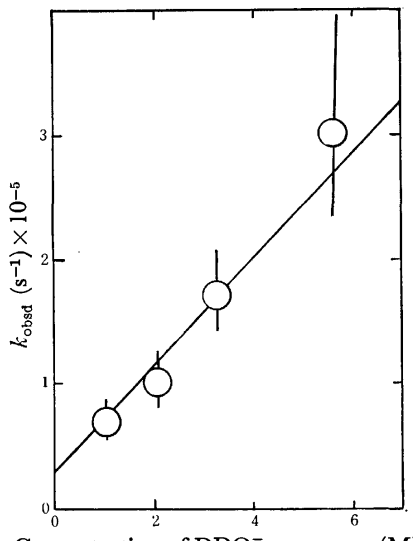

Fig. 12. The dependence of k_{obsd} on the concentration of free DDQ^- ion in H_2O (5.8 M urea and 1.8 M MeCN) at −6 °C.

value extrapolated from the equilibrium measurement at 0—15 °C, $K=(2\pm1)\times10^3\ M^{-1}$ at −6 °C.[13] Comparing the rate data in MeCN with those in H_2O, it is concluded that the large difference of the dimerization constants between these two solvents lies in the large difference of the decomposition rate constants of a dimer.

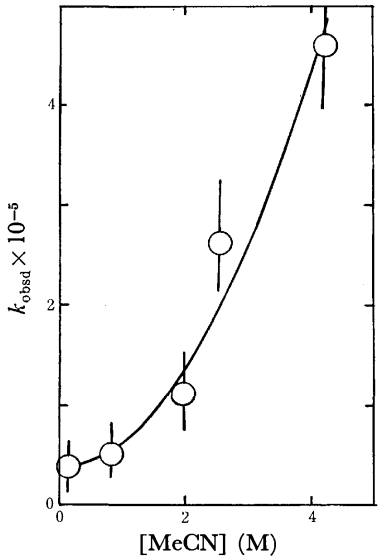

Fig. 13. The dependence of k_{obsd} on the concentration of MeCN in an MeCN/H_2O mixed solvent at −6 °C. [NEt_4DDQ^-] = $(1.5-3.0)\times10^{-4}$ M. [Urea] 5.8—4.8 M. [NaCl] 0.1—0.08 M.

In Fig. 13 is shown the effect of MeCN on k_{obsd} in an MeCN-H_2O mixed solvent. k_{obsd} increases superlinearly with the MeCN concentration. The dependence of k_{obsd} on the MeCN concentration is expressed approximately as

$$k_{obsd} = k_1 + k_2[MeCN]^2. \quad (17)$$

The forward reaction rate is considered to be independent of the solvent composition from the results obtained for pure MeCN and pure H_2O solvents. Thus, the backward rate constant is expressed from Eq. (17) as below.

$$\overleftarrow{k} = k_W + k_M[MeCN]^2 \quad (18)$$

k_W is the backward reaction rate in pure H_2O, while k_M, $(2.5\pm0.6)\times10^4\ M^{-2}\ s^{-1}$ (—6 °C), corresponds to the path where a dimer is decomposed by the attacks of MeCN molecules.

Discussion

From Table 1, it is quite clear that an entropy term plays an important role in determining the dimerization constants.[9] The order of $-\Delta H$ does not follow the order of the dimerization constants. In discussing the variation of the entropy change with solvents, it is instructive to divide ΔS into three parts according to their origins.

$$\Delta S = \Delta S_1 + \Delta S_2 + \Delta S_3 \quad (19)$$

ΔS_1 is an entropy change of the solvent molecules in the region where the solvent is considered to be a dielectric continuum and is polarized in proportion to the electrostatic field due to ion radicals. ΔS_2 is an entropy change of the solvent molecules in that region which constitues the solvation shell of the ion radicals. ΔS_3 is an entropy change accompanied with the loss

of degrees of freedom of motion of ion radicals due to dimerization. ΔS_3 is considered to be almost constant for all solvents, since a dimer always gives an absosrption peak around 710 nm, indicating that the geometry of a dimer is similar in all solvents.

ΔS_1 is estimated in the electrostatic way. The free energy of solvation of an ion of radius a and charge e is

$$\Delta F_I = -\left(1-\frac{1}{D}\right)\frac{e^2}{2a},$$

where D is a dielectric constant of a solvent. Thus, the change of free energy of solvation for the reaction of dimerization (1) is

$$\Delta F_I = -\frac{1}{2}\left(1-\frac{1}{D}\right)\left(\frac{4e^2}{r_D}-\frac{e^2}{r_M}\right),$$

where r_D and r_M are the radius of a dimer and a monomer respectively. The entropy change of dimerization is thus,

$$\Delta S_I = -\frac{\partial \Delta F_I}{\partial T} = \frac{\partial D}{D^2 \partial T}\left(\frac{2e^2}{r_D}-\frac{e^2}{r_M}\right) \qquad (20)$$

Since $\partial D/\partial T$ is negative, negative ΔS_I is obtained for the case of $r_D < 2r_M$, that is, the case that the effective radius of radicals contracts in dimerization. Taking $r_M = 4$ Å, $r_D = 6$ Å as typical values, the calculated value of ΔS_I in each solvent is given in Table 2. For MeCN, DMF, and Me_2CO, the experimentally observed ΔS is much larger than was predicted from Eq. (20). This implies that in these solvents, ΔS_2 or ΔS_3 contributes a great deal to the entropy change. Since MeCN, DMF, and Me_2CO are known as strong anion solvating solvents[14] it is concluded from the present results that at least a dimer is specifically solvated by MeCN solvent.

TABLE 2. THE ELECTROSTATIC ENTROPY CHANGE ΔS_1 OF DIMERIZATION REACTION CALCULATED USING Eq. (20).

Solvent	Dielectric constant at 15 °C	ΔS_1/e.u.
MeCN	38.3	−2.8
DMF	38.42	−2.8
Me_2CO	20.0	−6.6
EtOH	25.7	−5.8
MeOH	34.7	−4.7
H_2O	82.0	−1.5
THF	7.77	−17 (for Eq. (1))
		0 (for Eq. (8))

In THF and DME, both ΔH and ΔS are a little negative. As stated in the previous section, DDQ^- associates with a counter cation and the dimerization mostly occurs between ion-paired DDQ^- ions. Therefore, the less negative ΔS arises from the weak solvation of solvent molecules with the neutral ion-pair. ΔS_I is, of course, zero in these solvents. If ΔS_I and ΔS_2 are both zero, the observed ΔS corresponds to ΔS_3, which contains the loss of degrees of freedom of translation and rotations of monomer ions and the gain of degrees of freedom of vibrations of a dimer.

In EtOH, MeOH, and H_2O, both ΔH and ΔS are moderately negative. As stated previously, it is certain that these protic solvents form hydrogen-bonds with the oxygen atoms of DDQ^- ions. It is interesting to see how the hydrogen-bonding property affects the dimerization equilibria. As the results in Table 1 show, H_2O gives the largest $-\Delta H$ among these protonic solvents. Since ΔH and ΔS are the difference between two monomers and a dimer, the hydrogen bonding property seems to affect monomers and a dimer equally in EtOH and MeOH, resulting in the small value of the dimerization constants. On the other hand, H_2O favours the dimer side drastically by making ΔH largely negative. If some speculation can be permitted at this stage, these results indicate the structure of two water molecules acting as bridges between two DDQ^- ions, since H_2O is unique in having two protons in one molecule.[15]

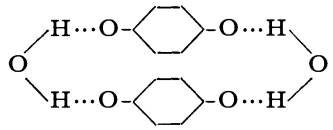

The rate data shows the large difference of the dimerization constant between MeCN and H_2O lies in the large difference of the decomposition rates between these two solvents. In order to see the meaning of the forward rate constant in H_2O, the diffusion controlled reaction rate constant is calculated according to the equation given below:[16]

$$k = \frac{4\pi e^2 N D_f (N/1000)}{DRT[\exp(e^2N/DRTr_M)-1]} \qquad (21)$$

where N is Avogadro's number, D_f the diffusion coefficient of a particle, D the dielectric constant of a medium and R the gas constant. r_M represents the diameter of a monomer which is assumed to be a sphere. Putting in the reasonable values of $D_f = 1\times10^{-5}$ cm^2 s^{-1}, and $r_M = 4\times10^{-8}$ cm, we obtain at −6 °C,

$$k(\text{calcd}) = 1.0\times10^8 \text{ M}^{-1}s^{-1}$$

k(calcd) is about one order larger than the observed $\vec{k}$. Considering that k(calcd) involves a large uncertainty in estimating D_f and r_M, it is concluded that the forward rate of dimerization in H_2O is nearly a diffusion controlled one.[17] This result implies that no decrease of entropy which would make the rate slower than k_{calcd} takes place until two DDQ^- ions come into contact with each other. When two DDQ^- ions approach each other within few angstroms, the charge-transfer interaction is considered to begin to operate.[7] This final process will result in the decrease of entropy observed in the equilibrium measurements. Thus these results support the previous conclusion from the equilibrium measurements that the large negative entropy arises from the specific solvation of a dimer ΔS_2 but not from the macroscopic entropy change of ΔS_1 or ΔS_3.

The reverse reaction rate is found to increase with the square of the MeCN concentration. This fact suggests that the main path of the decomposition of a dimer in relatively high concentration range of MeCN is the successive attacks of two MeCN molecules toward the dimer solvated by H_2O molecules.

$$(DDQ^{\cdot-})_2 + MeCN \rightleftarrows (DDQ^{\cdot-})_2(MeCN) \quad (22)$$

$$(DDQ^{\cdot-})_2(MeCN) + MeCN \rightleftarrows 2(DDQ^{\cdot-})(MeCN) \quad (23)$$

Here reaction (23) is considered to be rate-determining. In the above scheme, $(DDQ^{\cdot-})(MeCN)$ is introduced from the result of Fig. 3, which indicates that in the H_2O mole fraction range of 0.2—0.8, the main species of $DDQ^{\cdot-}$ is the one solvated by one MeCN molecule. The reactions (21) and (22) coincide with the previous postulate that $(DDQ^{\cdot-})_2$ ion combines with two H_2O molecules as bridges between two $DDQ^{\cdot-}$ ions. Thus the decomposition of $DDQ^{\cdot-}$ dimer is caused by the displacement of two solvated H_2O molecules by MeCN molecules.

In this way, the large solvent effect on the dimerization equilibria is understood as due to the molecular processes involving ion radicals and solvent molecules.

The author appreciates Prof. Masatoshi Fujimoto for his continuous encouragement and also thanks Dr. Mitsuyuki Soma, Mr. Mutsuo Yamada, Mr. Fumiyuki Watanabe, and Mrs. Michiyo Yamagishi for their kind advice. This work was supported by the Ministry of Education.

References

1) K. H. Hausser and J. N. Murrell, *J. Chem. Phys.*, **27**, 500 (1957).
2) R. H. Boyd and W. D. Phillips, *ibid.*, **43**, 2927 (1965).
3) K. Kimura, H. Yamada, and H. Tsubomura, *ibid.*, **48**, 440 (1968).
4) N. Sakai, I. Shirotani, and S. Minomura, This Bulletin, **44**, 675 (1971).
5) T. Yamazaki and K. Kimura, *ibid.*, **44**, 298 (1971).
6) S. Nakayama and K. Suzuki, *ibid.*, **46**, 3695 (1973).
7) T. Ota, T. Kunii, H. Kuroda, and H. Akamatsu, Paper presented at 24th Annual Meeting of the Chemical Socitey of Japan, Osaka, April, 1971.
8) M. Szwarc, *Makromol. Chem.*, **89**, 44 (1965).
9) A. Nakane, T. Sakata, and H. Tsubomura, Paper presented at 26th Annual Meeting of the Chemical Society of Japan, Tokyo, April, 1972.
10) A. Yamagishi and M. Sakamoto, This Bulletin, **47**, 2152 (1974).
11) P. Walden and E. J. Birr, *Z. Phys. Chem.*, **144**, 269 (1929).
12) E. W. Stone and A. H. Maki, *J. Amer. Chem. Soc.*, **87**, 454 (1965).
13) The presence of 6.0 M urea decreases K by 20%. This may arise from the increase of viscosity which reduces the forward rate constant. The increase of the dielectric constant due to urea is considered to have little effect on the equilibrium constant.
14) A. J. Parker, *Quart. Rev.*, **16**, 163 (1962).
15) It is interesting to compare the present results with the observation by S. Hiroma and H. Kuroda that the charge transfer interaction between chloranil anion radicals in potassium chloranil crystal is enhanced when the crystal absorbs a small amount of water. (Paper presented at the 26th Annual Meeting of the Chemical Society of Japan, Tokyo, April, 1972.)
16) A. A. Frost and R. G. Pearson, "Kinetics and Mechanism," John Wiley and Sons, New York (1961), p. 271.
17) A. Yamagishi, Y. Iida, and M. Fujimoto, This Bulletin, **45**, 3482 (1972).

The Photo-oxygenation Reactions of Diethyl Ether, *p*-Phenylenediamine, and *N,N*-Dimethylaniline

Kojiro MAEDA, Akihiro NAKANE,* and Hiroshi TSUBOMURA

Department of Chemistry, Faculty of Engineering Science, Osaka University, Toyonaka, Osaka 560

(Received February 3, 1975)

The products of photo-oxygenation reactions of ethyl-ether, *p*-phenylenediamine, and dimethylaniline were studied quantitatively and some radical intermediates were found by ESR measurements. The following quantum yields of the main products of these reactions were obtained: ethyl acetate (for ethyl ether), 0.49; *p*-benzoquinonediimine (for *p*-phenylenediamine), 0.01. As a possible reaction mechanism of the photo-oxygenation reactions of ethyl ether and *p*-phenylenediamine, it is proposed that at least part of the reaction is initiated by the charge transfer from the organic molecule to oxygen, followed by rapid proton detachment, yielding such radicals as EtO-$\dot{C}HCH_3$ and $\dot{N}HC_6H_4NH_2$ respectively.

In a previous paper, we have studied the photochemical reaction of the triethylamine–O_2 system under irradiation in the region of the charge transfer (CT) band.[1] By use of ESR spectroscopy and chemical analysis of the reaction products, the possible reaction mechanisms leading to various reaction products were speculated upon. This paper will present the results of similar studies of the photo-oxygenation of ethyl ether and some aromatic amines.

Experimental

Materials. Reagent grade diethyl ether was dried overnight with potassium chloride, and fractionally distilled through a Widmer column with Na-K amalgam. Reagent grade *p*-phenylenediamine (PPD) was purified by recrystallization from benzene and sublimed. *N,N*-Dimethylaniline (DMA) was dried with sodium hydroxide, vacuum distilled and preserved in a vacuum desiccator. Isopentane, *n*-heptane, and methylcyclohexane were purified by passing them through silica gel columns and then were distilled. Dioxane was dehydrated with sodium wire and then distilled.

ESR Measurements. The ESR measurements were made using a JES-ME-2X spectrometer of Japan Electron-Optics Laboratory Co. in the X-band. The magnetic field was measured by use of the proton magnetic resonance signal. The solution was put into a quartz capillary cell (5 mmϕ). After oxygen gas or air was bubbled into the cell, each sample was irradiated with a Ushio 500 W high pressure mercury lamp through Toshiba glass filters which transmit the light in the region of the CT band.

Analysis of the Photo-oxygenation Products. The reaction products were analyzed by the gas-chromatographic, chemical, IR, and UV techniques.

The analysis of peroxide was made by use of an electrochemical method suggested by Brewer and Milford.[2] The cathode was fine platinum and mercury was used as the anode. The polarizing potential was about 0.3 V and 0.2% KI aq. was used as the working solution.

The quantum yields of the reaction products were obtained with the aid of chemical actinometry using potassium ferrioxalate. A modified method of Hatchard and Parker[3] was used to prepare the actionometer solution. The irradiation was done through the reaction cell into the actinometer solution so that the light transmitted through the former was absorbed completely by the latter. The number of photons absorbed in the reaction cell was calculated as the difference between the number of photons absorbed in the actinometer with and without the presence of the reaction cell.

* Present address: Toray Co. Ltd., Minato-ku, Nagoya.

Results

The O_2-Ether System. No ESR signal was detected by the irradiation, at room temperature, of ether saturated with oxygen or of solutions of ether–O_2 in isopentane, *n*-heptane, and methylcyclohexane. When O_2-saturated ether at 1 atm was irradiated at 77 K with a UV-D25 filter (280—350 nm) for 3 min, a prominent quartet signal with a hyperfine coupling constant (hfs) of 26 G was obtained. This signal may be assigned to either the ethyl or the methyl radical. The former is more probable because of the high hyperfine coupling constant.[4,5] A similar result was obtained even when a mixture of methylcyclohexane and ether (in the vol. ratio of 1 : 1) was used as a solvent (Fig. 1(A)). When the input of the microwave power was raised up to about 100 mW, the quartet signal observed in the ether–O_2 system disappeared owing to saturation. On standing at 77 K, the ESR signal most likely assignable to an alkylperoxy radical appeared and became stronger

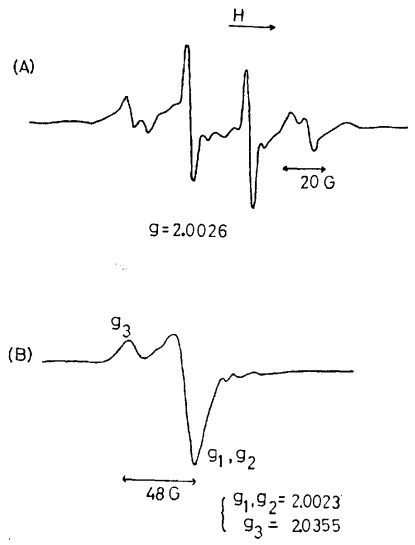

Fig. 1. ESR spectra of the species produced by the UV-irradiation of ether–O_2 at 77 K (A), followed by warming in the dark (B).

with time. When the sample cell was taken out from liquid nitrogen for several seconds and dipped in again, a different ESR signal with large anisotropic *g*-factor was obtained, as shown in Fig. 1(B). In isopentane, softer than methylcyclohexane at 77 K, an ESR spectrum quite similar to the latter one was observed from the beginning. Upon warming the matrix, the intensity decreased without any change in the spectral shape.

The reaction products were identified by comparison of the retention times of the gas chromatograms, using PEG-6000 as the column packing, with those of the pure products expected. The yields of the reaction products were determined by comparison of the areas under the gas-chromatographic peaks, with benzene used as an internal standard. Then, from the photon intensity measured by chemical actinometry, the quantum yields of the products were calculated; these are shown in Table 1.

Table 1. The quantum yields for the products of ethyl ether photo-oxygenation

Products	Quantum yield
Ethyl acetate	0.49
Ethyl formate	0.23
Acetaldehyde	0.17
Ethanol and/or[a] methanol	0.43

a) We were unable to separate ethanol and methanol in the gas-chromatogram.

The O_2-p-Phenylenediamine-Cyclohexane System. It is known that PPD in water or alcohol is thermally oxidized at room temperature to produce gradually the brown precipitate of Bandrowski's base.[6] When the cyclohexane or dioxane solution of PPD, more stable than the protic solutions, was irradiated in the region of the absorption band of PPD with bubbling oxygen, it turned to red. No change was observed when the same experiment was done in the deoxygenated state.

The spectrum of 9.54×10^{-5} M cyclohexane solution of PPD saturated with O_2 was shown in Fig. 2, together with the products of irradiation through a UV-D25 filter. The products were separated by thin layer chromatography and elution chromatography, the developing solvent being an acetone (1): benzene (1) solution, and were analyzed by IR, UV, and chemical techniques. The material which absorbs at about 380 nm was identified to be 4,4'-diaminoazobenzene (DAAB) by comparing its IR and UV spectrum with those of the synthesized DAAB. The two absorption bands at about 260 nm are assigned to *p*-benzoquinonediimine from the identity in the UV spectrum with the synthesized material.[7,8] Because of its high reactivity, we could not separate it from the reaction products. The shoulder at 470 nm agrees with the first band of Bandrowski's base,[9] and can most probably be assigned to it. 1.30×10^{-6} M peroxide was produced when a 1.27×10^{-4} M cyclohexane solution of PPD was irradiated.

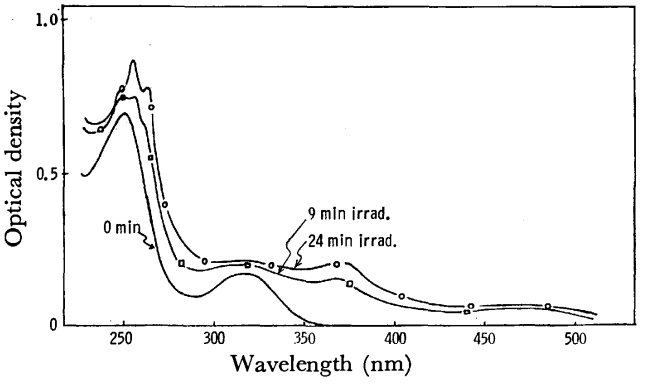

Fig. 2. Electronic spectral change of PPD in cyclohexane saturated with O_2 by the irradiation through a UV-D25 glass filter.

Each of the quantum yields for the reaction products was derived from the peak intensity of the UV absorption spectrum: *p*-benzoquinonediimine 0.01, DAAB 0.003, Bandrowski's base 0.002.

No ESR signal was detected for the dioxane solution irradiated at room temperature. But a weak broad singlet signal with the *g*-value of 2.016 was detected in cyclohexane irradiated at room temperature.

In the case of the cyclohexane solution at 77 K a broad singlet ESR spectrum was obtained. A similar spectrum was obtained for the dioxane solution. The *g*-values were 2.0050 and 2.0036, respectively. The broad singlet ESR bands became stronger with the irradiation time, without change in the shape. As the matrix was warmed, the signal intensity decreased.

The O_2–Dimethylaniline System. The ESR spectrum obtained for this system irradiated through a UV-39 filter at 77 K was a broad singlet. For the case of O_2-saturated DMA at room temperature, the *g*-value was 2.0065, and for the case of DMA (1): cyclohexane (1) at room temperature, the *g*-value was 2.0048. Although it is impossible to determine the species relevant to the ESR signal which appeared by the irradiation at room temperature, it seems reasonable to assign it to *N*-methylanilino radical, because of the fairly large *g*-value and the circumstances of its appearance.

When oxygen gas was bubbled into DMA, it turned to yellow owing to the CT absorption with O_2.[10] The reaction products were analyzed by gas chromatography using PEG 6000+KOH as column packing. No product was identified except for *N*-methylaniline. Its quantum yield could not be obtained because of the poor yield. *N*-Methylaniline was also obtained by the irradiation of deaerated DMA.

Discussion

The Ether-O_2 System. The results obtained indicate that the reaction mechanism in this system is rather similar to that for the triethylamine-O_2 system studied by us.[1] The formation of ethyl (or, less probably, methyl) radical is observed by the ESR studied at 77 K. Upon warming, the ethyl (methyl) radical and possibly a small quantity of some other radicals produced become mobile, and either react with oxygen to form peroxy radicals or abstract hydrogen atoms from ether. Our observed experimental results showed that the peroxy radicals were gradually pro-

duced in the ether–O_2 system irradiated at 77 K even if the temperature was kept at 77 K. The formation of ethyl, and possibly other radicals, can be explained by assuming the photo-excitation of the metastable singlet CT state or $EtO\dot{C}HCH_3$ formed by hydrogen abstraction from ether. The over-all scheme for the formation of the main reaction products can be shown by the following equations:

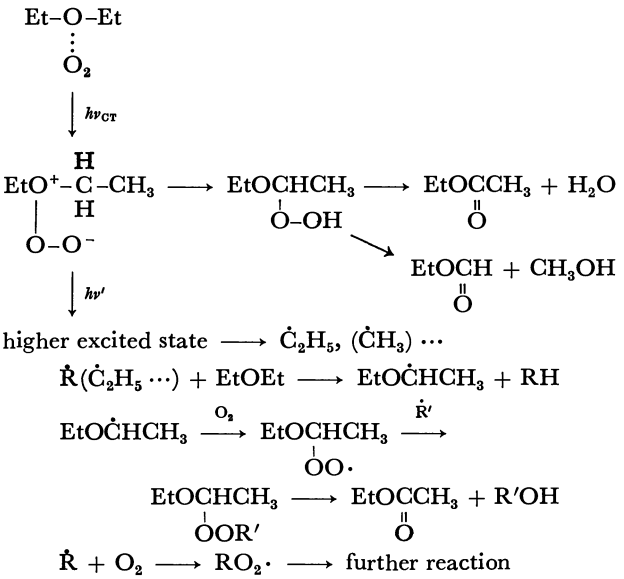

It might be worthwhile to note that no photodissociation of ether took place when deaerated ether was irradiated in the region of the CT absorption. Of course, reabsorption processes for the various radicals and other intermediates formed undoubtedly take place, which make the overall mechanism more complicated and harder to interpret.

The p-*Phenylenediamine–O_2 System.* The ESR signal detected in the irradiated cyclohexane solution at room temperature is attributable to the peroxy radical, but whether it is the hydroperoxy radical or alkylperoxy radical has not yet been proved. In view of the reaction products, it is more likely to assign it to the hydroperoxy radical. The ESR signal observed by irradiation at 77 K is most likely due to *p*-aminoanilino radical, in view of the *g*-value and the reaction products.

From the result described above, the reaction path might be as follows:

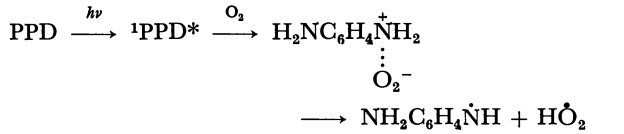

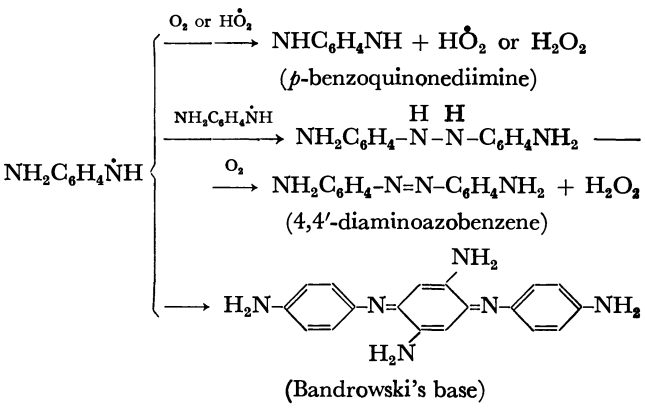

(Bandrowski's base)

The reaction path to lead to Bandrowski's base has not been clarified. But the studies of the dark reactions made in our laboratory between PPD and electron acceptors, *e.g.* *p*-benzoquinone, and the reactions between PPD^+ cations and other amines or PPD itself, indicated the formation of indamine-type compounds ($H_2N-C_6H_4-N=C_6H_4=NH_2^+$), Bandrowski's base, and, in certain cases, diazocompounds, $NH_2-C_6H_4-N=N-C_6H_4NH_2$.[6] Therefore, it seems very probable that both such thermal reactions and the photo-oxygenation reactions described in this paper pass through the PPD^+ cation, which, by subsequent proton transfer, forms the radical of the type $H_2N-C_6H_4-\dot{N}H$.

The authors thank Prof. Keiji Kuwata (Osaka University) and Prof. Yuzaburo Fujita (Tokyo University) for their valuable advice on the interpretation of the ESR spectra.

References

1) H. Tsubomura, T. Yagishita, and H. Toi, This Bulletin, **46**, 3051 (1973).
2) A. W. Brewer and J. R. Milford, *Proc. Roy. Soc. A*, **256**, 470 (1960).
3) Calvert and Pitts, "Photochemistry," John Wiley & Sons, Inc., N. Y. (1966), p. 783.
4) P. B. Ayscough and C. Thomson, *Trans. Faraday Soc.*, **58**, 1477 (1962).
5) K. Kuwata, Y. Kotake, K. Inada, and M. Ono, *J. Phys. Chem.*, **76**, 2061 (1972).
6) T. Sakata, H. Tsubomura, *et al.*, unpublished results.
7) J. F. Corbett, *J. Chem. Soc. B*, **1969**, 207.
8) J. F. Corbett, *ibid.*, **1969**, 213.
9) J. F. Corbett, *ibid.*, **1969**, 818.
10) H. Tsubomura and R. S. Mulliken, *J. Amer. Chem. Soc.*, **82**, 5966 (1960).

Solvent Effect of Methanol on the Rate of Formation Reaction of Monochloroiron(III) Complex in Aqueous Solution

Goro WADA and Yaeko KOBAYASHI

Department of Chemistry, Nara Women's University, Nara 630

(Received February 14, 1975)

The rate constants of the formation reaction of $FeCl^{2+}$ complex from Fe(III) and Cl^- ion were measured in water–methanol mixed solvents by use of a stopped-flow spectrophotometer. The apparent rate constant k is dependent upon the acid concentration of the medium, indicating that the reaction can proceed through two parallel paths, $Fe^{3+}+Cl^-$ (k_1) and $Fe(OH)^{2+}+Cl^-$ (k_H). Both k_1 and k_H increase with the increase in the mole fraction of methanol in the medium, x_M. Since k_H is much larger and is consequently much more accurately determined than k_1, considerations were mainly made on the nature of k_H. According to the dependence of k_H on the dielectric constant of the medium, it was found that the activation free energy of the $Fe(OH)^{2+}+Cl^-$ reaction consists of the electrical and non-electrical parts and that the dimension of the activated complex corresponds approximately to the distance of the outer-sphere approach between the reacting species. These facts are therefore in favor of an outer-sphere mechanism in the anation reactions of iron(III) by simple anions.

Many investigations have been done on the kinetics of fast formation reactions of transition metal complexes with various anions since the introduction of the flow method into the field of kinetic measurements;[1] in particular, the reaction of iron(III) with chloride ion, $Fe(III)+Cl^- \rightarrow Fe(III)Cl$, in aqueous solution was one of the earliest studied among the formation reactions of iron(III) complexes.[2]

The reaction is known to be dependent upon acid concentration and to proceed through two parallel steps of $Fe^{3+}+Cl^-$ and $FeOH^{2+}+Cl^-$, the latter being much faster than the former. Since the reaction occurs between ions of opposite signs, it may be supposed to be affected by the change of dielectric constant of the solvent. In order to prove this effect, mixed solvents of methanol and water were adopted; the reaction mechanism has been discussed in the present research.

Experimental

Materials. Iron(III) perchlorate was prepared by dissolving pure iron wire in perchloric acid, followed by oxidation with hydrogen peroxide. Methanol was purified by ordinary distillation of commercial methanol of S. P. grade under atmospheric pressure. Sodium chloride and sodium perchlorate were twice recrystallized from aqueous solution.

Determinations of Equilibrium Constants. The hydrolysis constant of Fe^{3+}, $K_H=[FeOH^{2+}][H^+]/[Fe^{3+}]$, the association constant between Fe^{3+} and ClO_4^-, $K_a=[Fe^{3+}\cdot ClO_4^-]/[Fe^{3+}][ClO_4^-]$, and the formation constant of $FeCl^{2+}$ complex, $K_1=[FeCl^{2+}]/[Fe^{3+}][Cl^-]$ at various mole fractions of methanol, x_M, were determined spectrophotometrically by use of a Hitachi-Perkin-Elmer UV-VIS spectrophotometer Model 139. The ionic strength of the solutions was adjusted with sodium perchlorate.

Kinetic Measurements. The measurements of the rate constants were performed by use of a Yanagimoto stopped-flow spectrophotometer SPS-1. Since the strict regulation of the reaction temperature was impossible in the present apparatus, the rate constants at desired temperatures were obtained by a graphical interpolation from those measured at temperatures close to the desired. The signals drawn on the memoriscope were photographed and analyzed.

Results and Discussion

Hydrolysis Constants of Fe^{3+}. When some of Fe^{3+}_{aq} is hydrolyzed to give $Fe(OH)^{2+}$ in slightly acid solution, the following relationship holds at total iron(III) concentration [Fe(III)]:

$$\frac{[Fe(III)]}{A_H} = \frac{1}{\varepsilon_H} + \frac{[H^+]}{\varepsilon_H K_H} \quad (1)$$

where A_H and ε_H represent the optical absorbance due to $Fe(OH)^{2+}$ ($A_H=\varepsilon_H[FeOH^{2+}]$), and the molar absorptivity of $Fe(OH)^{2+}$, respectively. From a linear relationship of $[Fe(III)]/A_H$ *vs.* $[H^+]$, ε_H and K_H can be obtained. At first, since A_H is not known yet, the total absorbance A and the total acid concentration $[HClO_4]$ are used in place of A_H and $[H^+]$ in Eq. (1), respectively. From the rough linearity, an approximate K_H is obtained, and therefore an approximate $[H^+]$ and A_H. The method of successive approximations gives the final value of K_H. The observation was performed at $[Fe(III)]=2\times10^{-4}$ M, $[HClO_4]=4\times10^{-3}$—9×10^{-3} M, $\mu=0.5$ M, 25 °C, and wavelength 350 nm. A typical case of the linear relationship of Eq. (1) at $x_M=0.395$ is shown in Fig. 1 and the values of K_H at various methanol concentrations are listed in Table 1, among which those for $x_M=0.15$—0.25 are

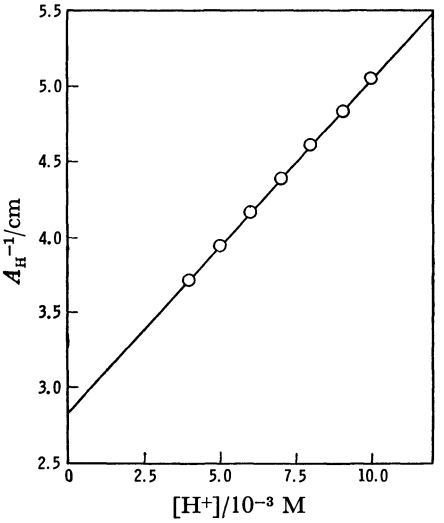

Fig. 1. Linear relationship between A_H^{-1} and $[H^+]$ at $[Fe(III)]=2\times10^{-4}$ M, $x_M=0.395$, $\mu=0.5$ M, 25 °C, and 350 nm.

reproduced from our previous literature.[3]

There exists the apparent feature that K_H increases with increasing methanol concentration; this is reasonable in view of the decrease in dielectric constant of the mixed solvent as the methanol concentration increases.

Ionic Association Between Fe^{3+} and ClO_4^-. When the perchloric acid concentration is relatively high in the mixed solvent, the phenomenon of ion-pair formation between Fe^{3+} and ClO_4^- ions has to be taken into account in the course of determination of the formation constant K_1, as will be described in the next section.[3]

The apparent molar absorptivity of the solution containing Fe^{3+} and perchloric acid, ε, may be expressed as follows:

$$\varepsilon = \frac{\varepsilon_0 + \varepsilon_H K_H/[H^+] + \varepsilon_a K_a[ClO_4^-]}{1 + K_H/[H^+] + K_a[ClO_4^-]} \quad (2)$$

where ε_0 and ε_a represent the molar absorptivity of Fe^{3+}_{aq} ion and the ion-pair $Fe^{3+}\cdot ClO_4^-$, respectively. Since K_a is very small, $K_a[ClO_4^-]$ is negligible compared to unity. When the acidity of the solution is high enough, $[FeOH^{2+}]$ may be negligibly small and, therefore, Eq. (2) is reduced to the following simple expression at a suitable wavelength:

$$\varepsilon = \varepsilon_0 + \varepsilon_a K_a[HClO_4] \quad (3)$$

The observations were performed at $[Fe(III)] = 1.0\times10^{-2}$ or 2.0×10^{-2} M and $[HClO_4] = 2.40$—3.60 M at a wavelength of 350 nm. The linear relationships of ε against $[HClO_4]$ are shown in Fig. 2, from whose slopes $\varepsilon_a K_a$ are obtained as listed in Table 1 at various x_M's. The values of $\varepsilon_a K_a$ will be necessary in the calculation of K_1.

Formation Constants of $FeCl^{2+}$. When Cl^- ion is added to the mixed solution containing iron(III) and perchloric acid, there occurs an additional complex formation between iron(III) and Cl^- ion. If the species of the complex formed is only $FeCl^{2+}$, Eq. (2) can be modified as follows:

$$\varepsilon = \frac{\varepsilon_0 + \varepsilon_H K_H/[H^+] + \varepsilon_a K_a[ClO_4^-] + \varepsilon_1 K_1[Cl^-]}{1 + K_H/[H^+] + K_a[ClO_4^-] + K_1[Cl^-]}$$

where ε_1 is the molar absorptivity of $FeCl^{2+}$.

By adopting reasonable approximations, as has been done above, the following equation can be derived at $[HClO_4] = 3.0$ M:

$$\varepsilon = \varepsilon_1 - \frac{\varepsilon - \varepsilon_0 - \varepsilon_a K_a[HClO_4]}{K_1[Cl^-]} \quad (4)$$

The linear relationship between ε and $(\varepsilon - \varepsilon_0 - \varepsilon_a K_a[HClO_4])/[Cl^-]$ was proved at $[Fe(III)] = (1-2)\times10^{-3}$ M, $[NaCl] = (1-5)\times10^{-3}$ M, and wavelength 350 nm. From the intercept and the slope of the straight line, ε_1 and K_1 are obtained. Since the concentration of free Cl^- ion, $[Cl^-]$, was not known at first, the total concentration of Cl^- ion, $[Cl]$, was used instead and the successive approximation yielded the final values of ε_1 and K_1. An example of the linearity of Eq. (4) is shown in Fig. 3 and the values of K_1 at various x_M are listed in Table 1. The values of K_1 are recognized to grow larger as the concentration of methanol becomes higher, as is expected from a viewpoint of the dielectric constants of mixed solvents.

Table 1. Hydrolysis constant, K_H, formation constant of $FeCl^{2+}$, K_1, and constant of ionic association for $Fe^{3+}\cdot ClO_4^-$, $\varepsilon_a K_a$, at different methanol concentrations, x_M, at 25 °C

x_M	K_H M	$\varepsilon_a K_a$ $M^{-2}\,cm^{-1}$	K_1 M^{-1}
0	1.65×10^{-3}	—	4.0
0.15	4.8×10^{-3}	3.33	2.6×10
0.20	6.2×10^{-3}	5.56	4.3×10
0.25	8.7×10^{-3}	7.06	5.0×10
0.395	1.38×10^{-2}	10.94	1.13×10^2
0.443	1.56×10^{-2}	12.57	1.37×10^2
0.519	1.90×10^{-2}	12.50	1.44×10^2

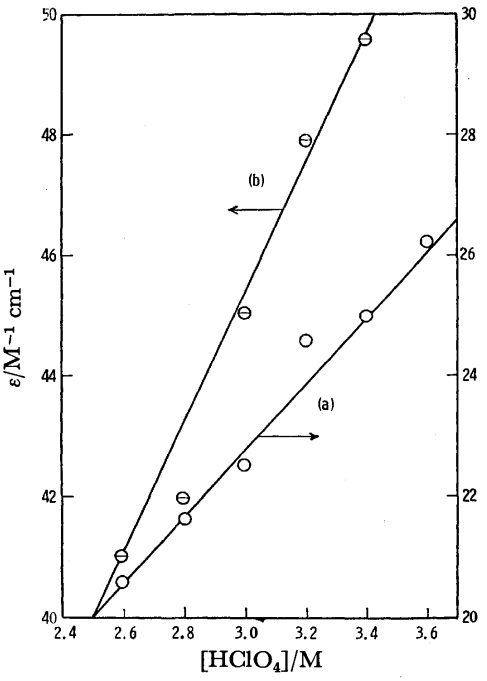

Fig. 2. Linear relationship between ε and $[HClO_4]$ at 25 °C and 350 nm. (a) $[Fe(III)] = 2.0\times10^{-2}$ M, $x_M = 0.2$; (b) $[Fe(III)] = 1.0\times10^{-2}$ M, $x_M = 0.935$.

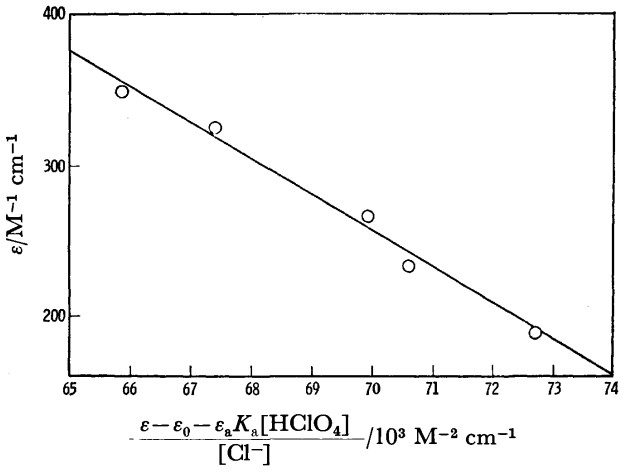

Fig. 3. Linear relationship between ε and $(\varepsilon - \varepsilon_0 - \varepsilon_a K_a[HClO_4])/[Cl^-]$ at $[Fe(III)] = 2\times10^{-3}$ M, $[HClO_4]$ 3.0 M, $x_M = 0.20$, 25 °C, and 350 nm.

Rate Measurements. In the wavelength range of 300—400 nm, $FeCl^{2+}$ species exhibits an absorption peak at 350 nm, while species other than $FeCl^{2+}$ absorb light very little as compared to $FeCl^{2+}$. Therefore, the observations of the rate constants, k, were carried out at this wavelength; the observed transmittance of the reaction solution decreased as the reaction proceeded. The initial concentrations of the dissolved species were as follows: $[Fe(III)]=(1.5—2.0)\times10^{-2}$ M, $[NaCl]=(1.5—2.0)\times10^{-2}$ M, and $[HClO_4]=(1.25—8.00)\times10^{-1}$ M. The occurrence of $FeCl_2^+$ and higher complexes was negligible.

Although the acid concentration is pretty high under the present circumstances, the $Fe(OH)^{2+}$ as a reactant and the $Fe(OH)Cl^+$ as a product must be taken into account in addition to Fe^{3+} and $FeCl^{2+}$ respectively. Then the following quantities are defined, the suffix e standing for the quantity at infinite time, namely at equilibrium:

$$[Fe] = [Fe^{3+}] + [FeOH^{2+}]$$

$$[FeCl] = [FeCl^{2+}] + [Fe(OH)Cl^+]$$

$$Q_1 = \frac{[FeCl]_e}{[Fe]_e[Cl^-]_e}$$

And the apparent reaction rate may be expressed by

$$\frac{d[FeCl]}{dt} = k[Fe][Cl^-] - k'[FeCl] \qquad (5)$$

where k and k' are the apparent forward and backward rate constants respectively. Since $Q_1=k/k'$ and $[Cl^-]=[FeCl]_e+[Cl^-]_e-[FeCl]$ and since $[Fe]$ is approximately equal to $[Fe]_e$ at a later reaction time close to equilibrium, the following rate equation may be obtained:

$$\frac{d[FeCl]}{dt} = k\left\{[Fe]_e+\frac{1}{Q_1}\right\}\{[FeCl]_e-[FeCl]\} \qquad (6)$$

By integrating Eq. (6), the following correlation may be established:

$$-\ln\frac{[FeCl]_e-[FeCl]}{[FeCl]_e-[FeCl]_0} = k\left\{[Fe]_e+\frac{1}{Q_1}\right\}t \qquad (7)$$

The suffix 0 indicates the quantity at zero time of integration, but not at the true initial time of the reaction, because the stopped-flow apparatus does not record the initial quantity but begins to record some time after the initiation of the reaction. The quantity $([FeCl]_e-[FeCl])/([FeCl]_e-[FeCl]_0)$ is equal to $(A_e-A)/(A_e-A_0)$, which is easily obtained from the observations. The value of Q_1 is considered to be approximately equal to K_1. Examples of the linear relationships of Eq. (7) are drawn in Fig. 4 at $x_M=0.25$. From the linearities are obtained the apparent rate constants, k.

Acid Dependence of k. When the values of k at different acid concentrations at a constant x_M and temperature are plotted against $[H^+]^{-1}$, a straight line is obtained, as shown in Fig. 5. Taking this fact into account, the following reaction scheme is available:

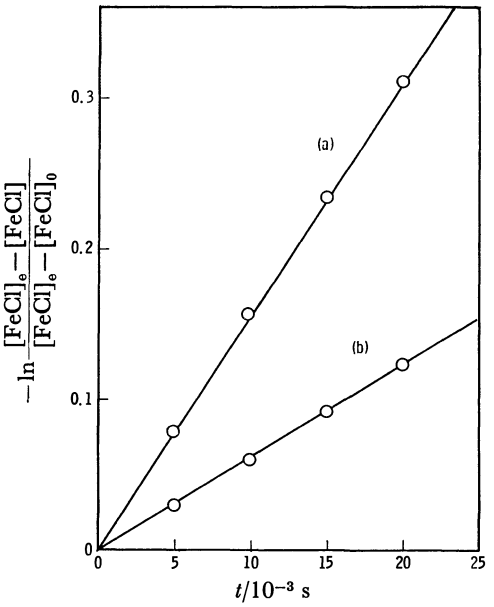

Fig. 4. Linear relationship between $-\ln([FeCl]_e-[FeCl])/([FeCl]_e-[FeCl]_0)$ and t at $F[e(III)]=[NaCl]=0.015$ M, $\mu=1.0$ M, $x_M=0.25$, and 350 nm. (a) $[HClO_4]=0.5$ M, 25.2 °C; (b) $[HClO_4]=0.8$ M, 22.5 °C.

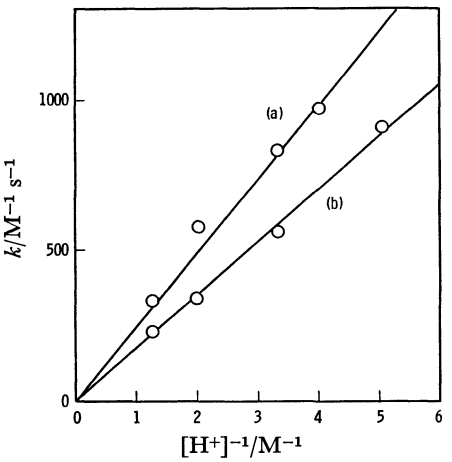

Fig. 5. Plot of k *vs.* $[H^+]^{-1}$ at $\mu=1.0$ M and 25 °C. (a) $x_M=0.25$; (b) $x_M=0.20$.

$$\begin{array}{ccc} Fe^{3+} + Cl^- & \underset{k_1'}{\overset{k_1}{\rightleftharpoons}} & FeCl^{2+} \\ {\scriptstyle H^+}\uparrow\downarrow{\scriptstyle -H^+} & & {\scriptstyle H^+}\uparrow\downarrow{\scriptstyle -H^+} \\ Fe(OH)^{2+} + Cl^- & \underset{k_H'}{\overset{k_H}{\rightleftharpoons}} & Fe(OH)Cl^+ \end{array} \qquad (8)$$

Therefore, k is represented by

$$k = \frac{k_1+k_HK_H/[H^+]}{1+K_H/[H^+]} \qquad (9)$$

on the assumption that the rates of protonation and deprotonation are much larger than those of the ligand substitution under consideration. When the acid concentration is high enough, the denominator of Eq. (9) can be regarded as nearly equal to unity and thus the linear relationship between k and $[H^+]^{-1}$ in Fig. 5 becomes clear.

TABLE 2. RATE CONSTANTS AT 25 °C AND ACTIVATION PARAMETERS AT DIFFERENT METHANOL CONCENTRATIONS

x_M	D^{-1}	k_1 $M^{-1}s^{-1}$	k_1' s^{-1}	k_H $M^{-1}s^{-1}$	$\Delta H_H^{*}+\Delta H_H^{\circ}$ kcal·mol^{-1}	$\Delta S_H^{*}+\Delta S_H^{\circ}$ cal·K^{-1}mol^{-1}	ΔG_{el}^{*} kcal·mol^{-1}	ΔG_0^{*} kcal·mol^{-1}
0	1.26×10^{-2}	7	2	1.2×10^{4}	19	13	−1.59	13.6
0.15	1.46×10^{-2}	9	0.4	2.6×10^{4}	20	18	−1.85	13.5
0.20	1.54×10^{-2}	2	0.05	2.8×10^{4}	21	22	−1.95	13.5
0.25	1.64×10^{-2}	6	0.1	2.8×10^{4}	—	—	−2.07	13.6
0.395	1.92×10^{-2}	21	0.2	6.3×10^{4}	24	34	−2.42	13.6
0.443	2.02×10^{-2}	30	0.2	7.6×10^{4}	—	—	−2.55	13.5
0.519	2.14×10^{-2}	30	0.3	1.00×10^{5}	23	33	−2.70	13.5

From the intercepts and the slopes of the straight lines expressed by Eq. (9), k_1 and k_H are calculated; these are listed in Table 2, along with the reverse rate constant k_1' calculated from $k_1/k_1'=K_1$. The values of k_1 and k_H in pure water agree well with those in the literature.[2] Although k_1 and k_1' are subjected to experimental errors to some extent, they still exhibit the trend that k_1 grows larger at higher x_M, while k_1' remains almost constant throughout the whole x_M range investigated. On the other hand, k_H is obtained more accurately than k_1, showing that k_H is approximately 10^3 larger than k_1 and that the higher the x_M, the larger the k_H value.

If we represent the hydrolysis equilibrium constant between the products in Scheme 8 as $K_{1H}=[Fe(OH)Cl^+][H^+]/[FeCl^{2+}]$, the following relation is given:

$$\frac{k_H}{k_H'}=\frac{K_{1H}}{K_H}\cdot\frac{k_1}{k_1'} \tag{10}$$

Since K_{1H} is supposed to be smaller than K_H on the basis of their electric charges, $(k_H/k_1)<(k_H'/k_1')$ is deduced, indicating that the hydrolyzed species is more favored in the backward reaction than in the forward.

Activation Parameters. A fact that both k_1 and k_H increase as x_M increases or the dielectric constant, D, of the mixed solvent decreases is consistent with an electrostatic expectation. According to Amis' equation,[4]

$$\ln k_H=\ln k_H^{\circ}-\frac{Z_AZ_Be^2}{kTrD} \tag{11}$$

$\ln k_H$ should show a linear relationship with respect to D^{-1} at constant temperature, where Z_A and Z_B stand for the numbers of electric charges on $Fe(OH)^{2+}$ and Cl^- ions respectively, e is the elementary electric charge, r is the distance between the two ions in the activated state, k is Boltzmann's constant, and k_H° is a rate constant which implies a rate constant at infinite dielectric constant. Figure 6 represents the relationship of $\ln k_H$ *vs.* the reciprocal dielectric constant of the mixed solvent, with a fine linearity from whose slope $r=$ 5.34 Å is obtained.

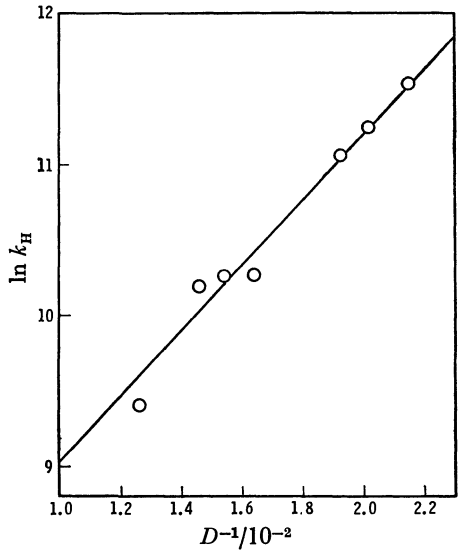

Fig. 6. Plot of $\ln k_H$ *vs.* D^{-1} at $\mu=1.0$ M and 25 °C.

When the values of radii $r(Fe^{3+})=0.67$ Å, and $r(Cl^-)=1.81$ Å, and of diameter $d(H_2O)=3.0$ Å are used, $r(Fe^{3+})+r(Cl^-)+d(H_2O)$ is equal to 5.5 Å, which is very close to the experimental result. Thus, the dimension of the activated complex is reasonable for a structure $[OH^-$–Fe^{3+}–H_2O–$Cl^-]$ which supports the outer-sphere mechanism of the reaction, and also indicates that a probable mixed solvation of methanol molecules in the coordination sheath of the complex at rather high x_M is independent of the reaction rate. This may be a proof of the reaction mechanism not only for the Fe(III)–Cl^- system[1,5] but for other similar systems such as Fe(III)–N_3^- [6] and Fe(III)–SCN^-.[7]

Temperature dependence of k_HK_H was measured; their Arrhenius plots against T^{-1} offer the activation parameters for the reaction in each solvent. Since the temperature dependence of K_H was not measured separately, $(\Delta H_H^{*}+\Delta H_H^{\circ})$ and $(\Delta S_H^{*}+\Delta S_H^{\circ})$ are the sum of the activated and the standard enthalpies and entropies for the reaction $Fe(OH)^{2+}+Cl^-\rightarrow Fe(OH)Cl^+$, respectively; the values are listed in Table 2. According to the values in Table 2, $(\Delta H_H^{*}+\Delta H_H^{\circ})$ exhibits a linear relationship with $(\Delta S_H^{*}+\Delta S_H^{\circ})$, as is

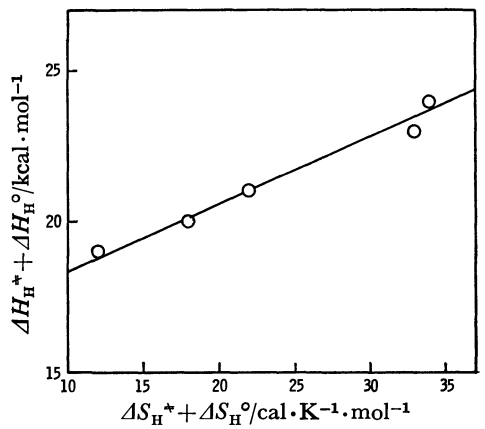

Fig. 7. Compensation relationship between $(\Delta H_H^{*}+\Delta H_H^{\circ})$ and $(\Delta S_H^{*}+\Delta S_H^{\circ})$.

shown in Fig. 7. This points out the occurrence of a compensation effect with an isokinetic temperature of 225 K, which is −48 °C.

The establishment of the linearity by Eq. (11) indicates that the free energy of activation ΔG_H^* consists of the electric part ΔG_{el}^* and the non-electrical one ΔG_O^*, the latter being indifferent to the composition of the solvent.

$$\Delta G_H^* = \Delta G_{el}^* + \Delta G_o^* \quad (12)$$

Since $\Delta G_{el}^* = NZ_AZ_Be^2/rD$ according to Eq. (11) where N is Avogadro's number, and $\Delta G_H^* = RT(\ln(kT/h) - \ln k_H)$, ΔG_O^* is also easily calculated. The results of this calculation are shown in Table 2. As a matter of course, ΔG_O^* is constant with a mean value of 13.5 kcal/mol. ΔG_{el}^* is related to the free energy change due to the approach of the two reacting ions as close as the distance of the activated complex in the dielectric medium and ΔG_O^* to that caused by the atomic and electronic configuration in the activated complex.

References

1) D. J. Hewkin and R. H. Prince, *Coord. Chem. Rev.*, **5**, 45 (1970).
2) R. E. Connick and C. P. Coppel, *J. Amer. Chem. Soc.*, **81**, 6389 (1959).
3) G. Wada and A. Endo, This Bulletin, **45**, 1073 (1972).
4) E. S. Amis and V. K. LaMer, *J. Amer. Chem. Soc.*, **61**, 905 (1939).
5) T. Yasunaga and S. Harada, This Bulletin, **42**, 2165 (1969).
6) D. Seewald and N. Sutin, *Inorg. Chem.*, **2**, 643 (1963).
7) S. Funahashi, S. Adachi, and M. Tanaka, This Bulletin, **46**, 479 (1973).

Circular Dichroism Spectra of *Unsym-cis(O)* Isomers of (L-Alaninate-*N*-monoacetato)(diethylenetriamine)cobalt(III) Complexes

Ken-ichi OKAMOTO,* Jinsai HIDAKA,** and Yoichi SHIMURA

Department of Chemistry, Faculty of Science, Osaka University, Toyonaka, Osaka 560

(Received May 10, 1975)

A couple of diastereomers, *ΔΔΛ-R(N)-L(C)* and *ΔΛΛ-R(N)-L(C)*, of *unsym-cis(O)*-(L-alaninate-*N*-monoacetato)(diethylenetriamine)cobalt(III)(1+) complex was prepared and characterized from the circular dichroism spectra, which presented an example for the additivity between the circular dichroism contributions due to the configurational (*ΔΔΛ* and *ΔΛΛ*) and the vicinal (*R(N)*+L(*C*)) chiralities.

In a previous paper[1] circular dichroism (CD) spectrum was reported for a *cis(O)*-[Co(L-alama)$(NH_3)_3$]$^+$ complex, where L-alama denotes L-alaninate-*N*-monoacetate(2-), which is an *O,N,O*-tridentate ligand. The present paper deals with the corresponding diethylenetriamine (dien) complex, *cis(O)*-[Co(L-alama)(dien)]$^+$. In a [Co(*O,N,O*-tridentato)(dien)]$^+$ type complex, four configurational isomers are possible as is seen in Fig. 1, neglecting the chirality which is produced by two meridionally coordinated non-planar tridentate ligands. In the *trans(O)* form the *O,N,O*-tridentate ligand spans in a meridional set of coordination sites, and in the remaining three *cis(O)* forms in a face of octahedron. Legg and Cooke[2] prepared all three geometrical isomers, *trans(O)*(a), *sym-cis(O)*(b), and racemic *unsym-cis(O)*(c+d), of [Co(ida)(dien)]$^+$, where ida is a simple *O,N,O*-tridentate ligand iminodiacetate(2−). Recently Yoshikawa *et al.*[3] reported optical resolution of the *unsym-cis(O)*-[Co(ida)(dien)]$^+$ by SE-sephadex column chromatography using an eluant containing tartar emetic.

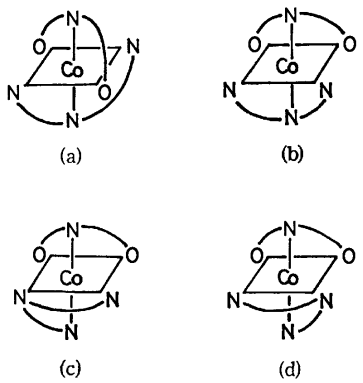

Fig. 1. Four possible isomers for a [Co(*O,N,O*-tridentato)(dien)]$^+$ type complex: (a) *trans(O)*, (b) *sym-cis(O)*, (c) *ΔΛΛ-unsym-cis(O)*, and (d) *ΔΔΛ-unsym-cis(O)*.

Since the ligand L-alama contains an asymmetric carbon atom, the isomers of cobalt(III) complex formed have two or more chiral centers, namely each one of asymmetric carbon (L) and nitrogen (*R* or *S*) atom, and in the case of *unsym-cis(O)* isomer a configurational chirality (*ΔΛΛ* or *ΔΛΛ*).[4] Thus the *unsym-cis(O)*-[Co(L-alama)(dien)]$^+$ complex offers a useful couple of diastereomers for examination of additivity of the configurational and vicinal CD.

The present paper is concerned mainly to the *cis(O)* isomers, especially *unsym-cis(O)*, and the *trans(O)* isomers are only briefly mentioned, because the stereochemistry of *trans(O)* isomers is rather complicated by possible existence of a new kind of chirality, which is produced by two meridionally coordinated non-planar tridentate ligands as in a established case of the optically resolved *mer*-[Co$(dien)_2$]$^{3+}$ complex.[5] Heretofore none of the *trans(O)* isomers of [Co(*O,N,O*-tridentato)(dien)]$^+$ type complexes have been optically resolved.

Experimental

Preparations. *(1)* Unsym-cis*(O)-(Diethylenetriamine)-(iminodiacetato)cobalt(III) Perchlorate Monohydrate*, unsym-cis*(O)-[Co(ida)(dien)]*$ClO_4 \cdot H_2O$: This was prepared by a modified method of Legg and Cooke.[2] To a suspension of 5.4 g of [$CoCl_3$(dien)][6] in 100 cm^3 of water was added a solution of 5.1 g of silver nitrate in 20 cm^3 of water. After the precipitated silver chloride was filtered off, to the filtrate was added a solution of 2.7 g of iminodiacetic acid which was neutralized in advance with potassium hydroxide. To the resulting mixture was added 3 g of charcoal and the mixture was constantly stirred at about 60 °C for three hours. After the reaction mixture had been cooled to room temperature, the charcoal was removed by filtration. The filtrate was poured into a column (35 mm × 500 mm) containing strong-acid cation exchange resin (Dowex 50 W × 8, 200—400 mesh, sodium form). After the column had been swept with water, the adsorbed band was eluted with 0.1 M aqueous solution of sodium perchlorate at a rate of 2.5 cm^3 per min. Three red bands were eluted. It had been already assigned from pmr spectra by Legg and Cooke that the first eluate contained *trans(O)* isomer, the second *sym-cis(O)* and the third *unsym-cis(O)*. So the third eluate was concentrated in a vacuum evaporator and a large amount of ethanol was added to the concentrated solution. The appeared complex was collected by filtration and recrystallized from a small amount of water by adding ethanol. The pure crystals were washed with ethanol and dried in air. Found: C, 23.76; H, 4.86; N, 13.69%. Calcd for [Co(ida)(dien)]$ClO_4 \cdot H_2O = C_8H_{18}N_4O_8ClCo \cdot H_2O$: C, 23.39; H, 4.91; N, 13.64%.

(2) $(+)_{589}$-Unsym-cis*(O)-(diethylenetriamine)(iminodiacetato)cobalt(III) chloride monohydrate*, $(+)_{589}$-unsym-cis*(O)-[Co(ida)(dien)]*$Cl \cdot H_2O$: Racemic *unsym-cis(O)*-[Co(ida)(dien)]$ClO_4 \cdot H_2O$ (0.84 g) was dissolved in an appropriate amount of water. The solution was poured into a column containing strong-base anion exchange resin (Dowex 1 × 8, 200—400 mesh, chloride form) and the column was eluted with water. Silver acetate (0.34 g) was added to the eluate

* Present address: Shimadzu Seisakusho LTD (Sanjo Works), Nishioji Sanjo, Nakagyoku, Kyoto 604.

** Present address: Department of Chemistry, The University of Tsukuba, Ibaraki 300-31.

and the silver chloride resulted was filtered off. The filtrate was concentrated in a vacuum evaporator. A solution of 0.40 g of $(+)_{589}$-Na[Co(ox)$_2$(en)]·4H$_2$O[7] in a minimum amount of water was added to the concentrated solution. The mixture was concentrated by stream of air at room temperature and then kept in a refrigerator. The less soluble diastereomer deposited as violet crystals, and they were collected by filtration and recrystallized from 15 cm^3 of warm water (40 °C). The pure diastereomer was washed with ethanol and dried in air. Yield: 0.31 g. Found: C, 26.18; H, 5.09; N, 12.94%. Calcd for *unsym-cis(O)*-[Co(ida)(dien)]·$(+)_{589}$-[Co(ox)$_2$(en)]·3H$_2$O=C$_{14}$H$_{26}$N$_6$O$_{12}$Co$_2$·3H$_2$O: C, 26.18; H, 5.02; N, 13.08%.

An aqueous solution of the diastereomer was poured into a column (Dowex 1×8, 200—400 mesh, chloride form) and was eluted with water. The eluate was concentrated in a vaccum evaporator and an appropriate amount of ethanol was added to the concentrated solution to obtain the optically active complex, $(+)_{589}$-*unsym-cis(O)*-[Co(ida)(dien)]Cl·H$_2$O, which was washed with ethanol and dried in air. Found: C, 26.28; H, 6.09; N, 15.14%. Calcd for $(+)_{589}$-*unsym-cis(O)*-[Co(ida)(dien)]Cl·H$_2$O=C$_8$H$_{18}$N$_4$O$_4$ClCo·H$_2$O: C, 26.35; H, 6.08; N, 15.36%.

(3) Isomers of (L-Alaninate-N-monoacetato)(diethylenetriamine)-cobalt(III) perchlorate, [Co(L-alama)(dien)]ClO$_4$: These isomers were prepared by a similar procedure to that for (**1**) using L-alamaH$_2$·HCl·1/4H$_2$O[8] instead of idaH$_2$. The prepared isomers were separated by using a cation exchange column (30 mm×1300 mm) in a similar manner to that described in (1). Six red bands were eluted and they were numbered (i), (ii), ……, and (vi) in the order of elution. The yields for the isomers (v) and (vi) were very low. It was confirmed by the measurement of absorption spectra that the isomer (i) is a *trans(O)* isomer and the isomers (ii)—(vi) *cis(O)*. The eluates were separately concentrated in a vacuum evaporator and a large amount of ethanol was added to each of the concentrated solutions. The desired complex was collected by filtration and recrystallized from a small amount of water by adding ethanol and then dried in air. The isomer (v) was not obtained as solid salt because of its low yield, and some other isomers were contaminated with a small amount of sodium perchlorate as shown in the following analytical data. Found for isomer (i): C, 22.36; H, 4.50; N, 11.82%. Calcd for [Co(L-alama)(dien)]ClO$_4$·1/2H$_2$O·1/2NaClO$_4$=C$_9$H$_{20}$N$_4$O$_8$ClCo·1/2H$_2$O·1/2NaClO$_4$: C, 22.67; H, 4.44; N, 11.75%. Found for isomer (ii): C, 25.92; H, 5.13; N, 13.53%. Calcd for [Co(L-alama)(dien)]ClO$_4$·1/2H$_2$O=C$_9$H$_{20}$N$_4$O$_8$ClCo·1/2H$_2$O: C, 26.01; H, 5.09; N, 13.48%. Found for isomer (iii): C, 25.35; H, 4.91; N, 13.34%. Calcd for [Co(L-alama)(dien)]ClO$_4$·1/4H$_2$O·1/10NaClO$_4$=C$_9$H$_{20}$N$_4$O$_8$ClCo·1/4H$_2$O·1/10NaClO$_4$: C, 25.53; H, 4.88; N, 13.23%. Found for isomer (iv): C, 26.31; H, 5.00; N, 13.52%. Calcd for [Co (L-alama) (dien)] ClO$_4$·1/4H$_2$O=C$_9$H$_{20}$N$_4$O$_8$ClCo·1/4H$_2$O: C, 26.29; H, 5.03; N, 13.63%. Found for isomer (vi): C, 26.22; H, 5.03; N, 13.60%. Calcd for [Co(L-alama)(dien)] ClO$_4$·1/4H$_2$O=C$_9$H$_{20}$N$_4$O$_8$ClCo·1/4H$_2$O: C, 26.29; H, 5.03; N, 13.63%.

(4) Isomers of (Diethylenetriamine)(L-prolinate-N-monoacetato)-cobalt(III) Perchlorate, [Co(L-proma)(dien)]ClO$_4$: The isomers were prepared and separated by a similar procedure to that described in (**1**) using L-promaH$_2$[8] instead of idaH$_2$. Two red bands were eluted; the absorption spectra indicated that the first eluate contained *trans(O)* isomer, and the second *cis(O)*. The first eluate was concentrated to dryness in a vacuum evaporator and then the sodium perchlorate in the residue was extracted with a large amount of ethanol. The desired complex was filtered and recrystallized from a small amount of water by adding ethanol. The second eluate was also concentrated in a vacuum evaporator and a large amount of ethanol was added to the concentrated solution. The obtained complex was filtered and recrystallized from a small amount of water by adding ethanol. Both the pure complexes were washed with ethanol and dried in air. Found for the *trans(O)* complex: C, 30.20; H, 5.19; N, 12.76%. Calcd for [Co(L-proma)(dien)]ClO$_4$·1/4H$_2$O=C$_{11}$H$_{22}$N$_4$O$_8$ClCo·1/4H$_2$O: C, 30.22; H, 5.19; N, 12.81%. Found for the *cis(O)* complex: C, 30.28; H, 5.13; N, 12.90%. Calcd for [Co(L-proma)-(dien)]ClO$_4$=C$_{11}$H$_{22}$N$_4$O$_8$ClCo: C, 30.53; H, 5.13; N, 12.95%.

Measurements. The electronic absorption spectra were measured by a Beckman DU spectrophotometer and a Shimadzu spectrophotometer UV-200. The CD spectra were recorded with a Jasco Model J-10 or J-20 spectropolarimeter with the CD attachment, or with a Roussel-Jouan Dichrograph. All the measurements were made in aqueous solutions at room temperature.

Results and Discussion

Visible and near ultraviolet absorption data of the present [Co^{III}(N)$_4$(O)$_2$] type complexes are shown in Table 1 and the typical absorption curves of a *cis-trans* couple are in Fig. 2. The isomers obtained are divided into two groups on the splitting pattern of the first absorption band. An isomer of the first group has a

Table 1. Absorption maxima of the [Co(*O,N,O*-tridentato)(dien)]$^+$ complexes
(wave numbers are given in 10^3 cm^{-1})

Complex ion	σ_{max}(logε_{max})	
	I band	II band
unsym-cis(O)-[Co(ida)(dien)]$^+$	19.6(2.04)	28.2(2.11)
cis(O)-[Co(L-alama)(dien)]$^+$		
isomer ii, *sym-cis(O)*	20.5(1.87)	28.7(1.96)
isomer iii, *unsym-cis(O)*-R	19.3(2.05)	28.1(2.14)
isomer iv, *unsym-cis(O)*-R	19.4(2.06)	28.1(2.17)
isomer v, *cis(O)*	20.6(—)	28.7(—)
isomer vi, *cis(O)*	19.7(2.03)	28.1(2.12)
sym-cis(O)-R-[Co(L-proma)(dien)]$^+$	19.9(1.92)	28.4(1.99)
trans (O)-[Co(ida)(dien)]$^+$[2]	19.6(2.24)	27.8(2.28)
trans(O)-[Co(L-alama)(dien)]$^+$	19.9(2.28)	28.0(2.27)
trans(O)-R-[Co(L-proma)(dien)]$^+$	19.9(2.24)	27.4(2.31)

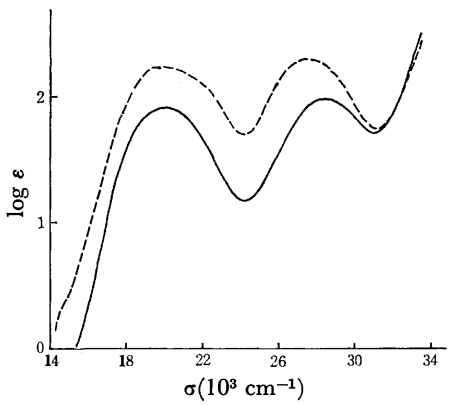

Fig. 2. Absorption curves of *cis(O)*-[Co(L-proma)-(dien)]$^+$ (——) and *trans(O)*-[Co(L-proma)(dien)]$^+$ (----).

shoulder at higher energy side of the major peak, and the second group only a symmetrical major peak (Fig. 2). It is concluded, therefore, that an isomer of the first group has a *trans*(*O*) structure and that the second group a *cis*(*O*). It is worthwhile to note that the first absorption bands of the *trans*(*O*) isomers of this type complexes are more intense than those of the *cis*(*O*) ones; $\log \varepsilon_{max}$ values are in a range of 2.24—2.28 for *trans*(*O*), while 1.87—2.06 for *cis*(*O*) (Table 1). The second absorption bands are also in the same trend, $\log \varepsilon_{max}$=2.27—2.31 for *trans*(*O*), while 1.96—2.17 for *cis*(*O*).

In the [Co(L-alama)(dien)]$^+$ and [Co(L-proma)-(dien)]$^+$ complexes, both the *cis*(*O*) and *trans*(*O*) isomers were obtained. Thus the L-alama and L-proma ligands take both the facial and meridional coordinations in the present dien complexes, in contrast to the corresponding triammine complexes, in which only the facial coordination occurred for both the ligands.[1]

In the preparation of [Co(L-proma)(dien)]$^+$ complex, each one of *trans*(*O*) and *cis*(*O*) isomers was obtained. A molecular model examination shows that the formation of *unsym-cis*(*O*) isomers is almost impossible because of the repulsion between the pyrrolidine ring of the L-proma ligand and the ethylenediamine moiety of the dien ligand. It is assigned, therefore, that the *cis*(*O*) isomer obtained takes *sym-cis*(*O*) configuration. As for the configuration of the coordinated asymmetric nitrogen atom, the L-proma ligand takes only *R* configuration stereospecifically.[9] Thus the two isomers obtained for the L-proma ligand are *trans*(*O*)-*R* and *sym-cis*(*O*)-*R* isomers.

One *trans*(*O*) and five *cis*(*O*) isomers were isolated for the [Co(L-alama)(dien)]$^+$ complex. Of the five *cis*(*O*) isomers the fifth eluate (isomer v) could not be examined by elemental analysis because of its extremely low yield, and then only the absorption spectrum was measured. Isomer vi was obtained in a lower yield than the earlier three isomers ii, iii, and iv. We have already found that for the coordinated asymmetric nitrogen atom of the L-alama ligand the *R* configuration is preferred to the *S* one; namely a repulsion exists in the L-alama ligand having the *S* asymmetric nitrogen atom, between the L-alaninate methyl group and a proton of the *N*-acetate chelate ring of the same ligand.[8] Therefore, the predominant isomers ii, iii, and iv may be assigned to *R* configuration and the poorly yielded isomers v and vi to *S*. From the consideration of the CD curves (see below), it is concluded that the isomers iii and iv take actually *R* structure, but ambiguities remain to the nitrogen configurations of the isomers ii, v, and vi.

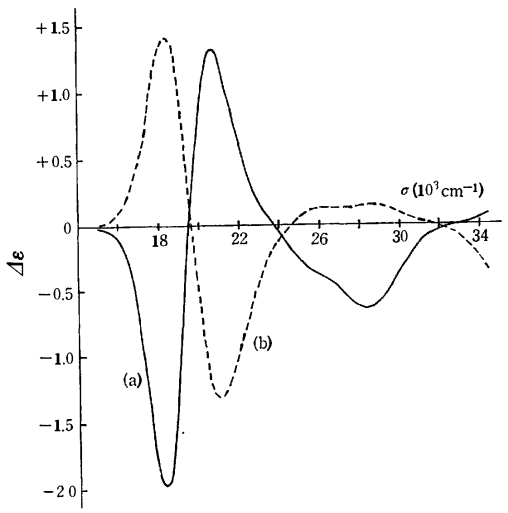

Fig. 3. CD curves of, (a) *ΔΛΛ-unsym-cis*(*O*)-*R*-[Co(L-alama)(dien)]$^+$ and (b) *ΔΔΛ-unsym-cis*(*O*)-*R*-[Co(L-alama)(dien)]$^+$.

Table 2. CD Data of the *cis*(*O*)-[Co(*O*,*N*,*O*-tridentato)(dien)]$^+$ complexes (wave numbers are given in 10^3 cm^{-1})

Complex ion	$\sigma_{ext}(\Delta\varepsilon_{ext})$ I band	$\sigma_{ext}(\Delta\varepsilon_{ext})$ II band
$(+)_{589}$-*Δ-unsym-cis*(*O*)-[Co(ida)(dien)]$^-$	18.5(+1.57) 21.1(−1.16)	28.6(+0.28)
unsym-cis(*O*)-*R*-[Co(L-alama)-(dien)]$^+$		
isomer iv, *ΔΔΛ*	18.4(+1.42) 21.2(−1.30)	28.7(+0.16)
isomer iii, *ΔΛΛ*	18.4(−1.97) 20.8(+1.34)	28.5(−0.63)
cis(*O*)-*R*-[Co(L-alama)-$(NH_3)_3$]$^+$ [1]	18.1(−0.17) 19.8(+0.12) 21.9(−0.17)	28.4(−0.22)
sym-cis(*O*)-*R*-[Co(L-proma)-(dien)]$^+$	18.1(−0.05) 20.0(+0.37) 22.6(−0.07)	28.3(−0.34)
cis(*O*)-*R*-[Co(L-proma)-$(NH_3)_3$]$^+$ [1]	17.9(−0.30) 19.9(+1.04)	28.1(−0.46)
sym-cis(*O*)-[Co(L-alama)(dien)]$^+$		
isomer ii	18.3(+0.02) 21.5(−0.38)	26.8(−0.14)

The CD data of *cis*(*O*) isomers are collected in Table 2. Of the three predominant *cis*(*O*) isomers of the L-alama complex, the isomer ii has much weaker CD intensity than the other two, iii and iv. The CD curve of isomer iii is almost a mirror image to that of the isomer iv as is seen in Fig. 3. These facts show that the isomer ii is *sym-cis*(*O*) type, while the isomers iii and iv *unsym-cis*(*O*).

If the configurational and vicinal CD are separable, the following additivity formulas are derived for the two *unsym-cis*(*O*)-*R* isomers as in other similar cases studied previously,[1,8]

$$\Delta\varepsilon(\Delta\Delta\Lambda) = \Delta + R(N) + \text{L}(C)$$
$$\Delta\varepsilon(\Delta\Lambda\Lambda) = \Lambda + R(N) + \text{L}(C)$$

where $\Delta\varepsilon(\Delta\Delta\Lambda)$ and $\Delta\varepsilon(\Delta\Lambda\Lambda)$ are the CD of the isomer *ΔΔΛ* and *ΔΛΛ*, Δ and Λ the configurational contributions of Δ and Λ chiralities, $R(N)$ and L(C) the vicinal contributions of *R*-nitrogen and L-carbon chiralities, respectively. Since $\Delta = -\Lambda$, we have

$$\Delta = 1/2\times\{\Delta\varepsilon(\Delta\Delta\Lambda) - \Delta\varepsilon(\Delta\Lambda\Lambda)\}$$
$$\Lambda = 1/2\times\{\Delta\varepsilon(\Delta\Lambda\Lambda) - \Delta\varepsilon(\Delta\Delta\Lambda)\}$$
$$R(N) + \text{L}(C) = 1/2\times\{\Delta\varepsilon(\Delta\Delta\Lambda) + \Delta\varepsilon(\Delta\Lambda\Lambda)\}$$

The partial contribution curves calculated under an assumption that the isomers iii and iv are *ΔΛΛ-R* and *ΔΔΛ-R*, respectively, are shown in Fig. 4. The cal-

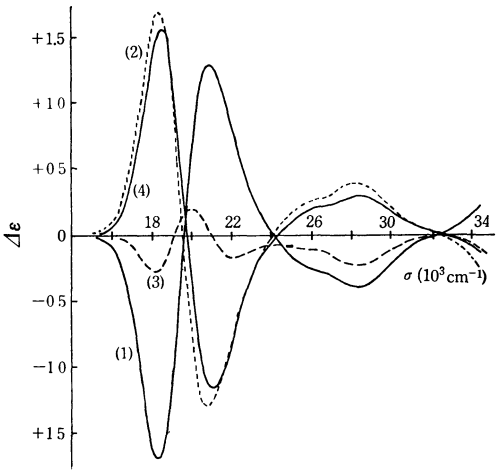

Fig. 4. CD curve analysis of *cis(O)*-[Co(L-alama)-(dien)]$^+$ complex: (1) *Δ* confirguational curve, $1/2\times\{\Delta\varepsilon(\text{iii})-\Delta\varepsilon(\text{iv})\}$; (2) *Δ* configurational curve, $1/2\times\{\Delta\varepsilon(\text{iv})-\Delta\varepsilon(\text{iii})\}$; (3) $\{R(N)+\text{L}(C)\}$ vicinal curve, $1/2\times\{\Delta\varepsilon(\text{iii})+\Delta\varepsilon(\text{iv})\}$; and (4) observed CD curve of $(+)_{589}$-*unsym-cis(O)*-[Co(ida)(dien)]$^+$.

culated *Δ* configurational curve shows a positive and a negative CD band from lower energy side in the first absorption band region and agrees well with the observed CD curve of $(+)_{589}$-*unsym-cis(O)*-[Co(ida)-(dien)]$^+$, which has been assigned to *ΔΔΔ* configuration by previous authors.[3] Since the higher energy component of the first absorption band of the *cis(O)*-$[Co(N)_4(O)_2]^+$ type complex is related to the $E(D_{4h})$ parentage, the above assignment is along the line of a

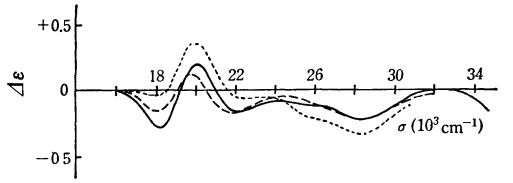

Fig. 5. CD curves of *cis(O)*-*R*-[Co(L-alama)$(NH_3)_3$]$^+$ (——)[1], *sym-cis(O)*-*R*-[Co(L-proma)(dien)]$^+$ (……), and vicinal effect curve of *unsym-cis(O)*-*R*-[Co(L-alama)-(dien)]$^+$ (——).

normal CD sign pattern for the first absorption band components.[10]

The calculated vicinal contribution $R(N)+\text{L}(C)$ for the *unsym-cis(O)*-*R*-[Co(L-alama)(dien)]$^+$ diastereomers coincides well with the observed CD curve of *cis(O)*-*R*-[Co(L-alama)$(NH_3)_3$]$^+$ complex[1] (Fig. 5). In conclusion, the additivity rule is well applicable to the present complexes to separate the configurational and vicinal CD curves, and the CD curve analysis (Figs. 4 and 5) established the configurations of the two *unsym-cis(O)* isomers of [Co(L-alama)(dien)]$^+$; namely the isomer iii has *ΔΛΛ-R* configuration and the isomer iv *ΔΔΛ-R*. The observed CD curve of the *cis(O)*-*R*-[Co(L-proma)(dien)]$^+$ is also similar to the vicinal curves of L-alama complexes (Fig. 5). This shows that the *cis(O)*-*R*-[Co(L-proma)(dien)]$^+$ complex has actually the *sym-cis(O)* structure as predicted from molecular model consideration. The *sym-cis(O)*-[Co(L-alama)-(dien)]$^+$ complex (isomer ii) shows somewhat different CD (Table 2), and the asymmetric nitrogen configuration of this isomer is not clear at present.

References

1) K. Okamoto, J. Hidaka, and Y. Shimura, This Bulletin, **46**, 3134 (1973).
2) J. L. Legg and D. W. Cooke, *Inorg. Chem.*, **5**, 594 (1966).
3) Y. Yoshikawa, A. Kondo, and K. Yamasaki, Abstract of 23rd symposium on Coordination Chemistry (Japan), p. 117 (1973).
4) The absolute configurations *ΔΔΛ* and *ΔΛΛ* are assigned according to the IUPAC "Nomenclature of Inorganic Chemistry," 2nd ed., p. 75 (1971).
5) F. R. Keene and G. H. Searle, *Inorg. Chem.*, **11**, 148 (1972); Y. Yoshikawa and K. Yamasaki, This Bulletin, **45**, 179 (1972).
6) P. H. Crayton, *Inorg. Synth.*, **7**, 207 (1963).
7) F. P. Dwyer, I. K. Reid, and F. L. Garvan, *J. Amer. Chem. Soc.*, **83**, 1285 (1961).
8) K. Okamoto, J. Hidaka, and Y. Shimura, This Bulletin, **44**, 1601 (1971).
9) K. Okamoto, J. Hidaka, and Y. Shimura, *ibid.*, **46**, 475 (1973).
10) K. Igi and B. E. Douglas, *Inorg. Chem.*, **13**, 425 (1974).

Preparation and Some Properties of Triorganosiloxy Derivatives of Cyclopentadienyl Titanium

Hideo SUZUKI and Toshio TAKIGUCHI

Department of Synthetic Chemistry, Faculty of Technology, Gunma University, Kiryu, Gunma 376

(Received September 5, 1974)

Several triorganosiloxy derivatives of cyclopentadienyl titanium were synthesized by the reactions of dicyclopentadienyl titanium dichloride or cyclopentadienyltitanium trichloride with triorganosilanols or their sodium salts. The products obtained include π-$Cp_2TiClOSiMe_3$, π-$CpTi(OSiMe_3)_3$, π-$CpTi(OSiMe_2Ph)_3$, π-$CpTi(OSiPh_2Me)_3$, π-$CpTi(OSiPh_3)_3$, π-$CpTi(OSiPh_3)_2Cl$ and π-$CpTi(OSiPh_3)Cl_2$. Some correlations were found to exist between the substituents on silicon atoms and cyclopentadienyl ring protons in NMR spectra and the Ti–O–Si bond absorptions in IR spectra. The chemical stabilities of the Ti–O–Si bonding in the products were dependent on the nature of the organic groups attached to the silicon atoms. The chemical resistance of the products against hydrolytic cleavage was regularly increased with successive replacement of methyl groups by phenyl groups.

In succession to our previous paper[1] dealing with preparation of some siloxy derivatives of cyclopentadienyl titanium, several new compounds in the series listed in Table 1 were obtained by analogous procedures. Most products were crystalline masses with moderate stability.

The NMR spectral investigations of the derivatives indicated that there are some correlations between the proton chemical shifts of cyclopentadienyl ring protons and the nature of the substituents on silicon.

The products generally reacted both with gaseous hydrogen chloride and with acetyl chloride, leaving the cyclopentadienyl groups intact and substituting the chlorine atoms for the siloxy groups, thus yielding partially triorganosiloxy-substituted cyclopentadienyltitanium chlorides.

The hydrolysis of the products was investigated by examining the relative intensities of the absorption bands due to the Si–O–Ti bond. It was found that the hydrolytic stability increased with successive replacement of methyl groups on silicon by phenyl groups.

No indication of any formation of ferrocene was obtained from the reaction between iron(II) chloride and the products.

Experimental

Triorganosilanols: Trimethylsilanol, bp, 98—99 °C, n_D^{20}, 1.3890, was prepared by hydrolysis of trimethylfluorosilane with 2 M-NaOH. Dimethylphenylsilanol, diphenylmethylsilanol, and triphenylsilanol were prepared by the method[2] reported previously.

Triorganosiloxy Derivatives of Cyclopentadienyl Titanium: A tetrahydrofuran (THF) solution of a silanol was added dropwise to a THF solution containing a theoretical amount of dicyclopentadienyltitanium dichloride or cyclopentadienyltitanium trichloride at room temperature under stirring and nitrogen atmosphere for about 30 min. At this point a THF solution of triethylamine (20% excess) was added to the mixture, which was stirred for another 10 hr. The precipitated triethylamine hydrochloride was then filtered off, and the filtrate was concentrated to give the triorganosiloxy derivative as a crude product. Purification either by distillation or by recrystallization from *n*-hexane gave the pure samples listed in Tables 1 and 2.

Reactivities: Some reactions of compounds I—VIII with gaseous hydrogen chloride, acetyl chloride, aqueous solution of sodium hydroxide, and ferrous chloride were investigated by means of NMR and IR spectral measurements.

Reaction with Gaseous Hydrogen Chloride: Dry hydrogen chlo-

TABLE 1. PHYSICAL PROPERTIES AND ELEMENTAL ANALYSIS OF PRODUCTS

	Compound	Mp (°C) bp (°C/mmHg)	Y%	Analytical data (%) Found (Calcd) C	H	Si	Ti	Mol wt Found (Calcd)
I	π-$Cp_2TiCl(OSiMe_3)$	104—105	40	51.85 (51.59)	6.34 (6.33)	9.1 (9.2)	16.9 (15.9)	318 (313)
II	π-$Cp_2TiCl(OSiMe_2Ph)$[a]	97—98.5						
III	π-$Cp_2TiCl(OSiPh_2Me)$[a]	160—161.5						
IV	π-$Cp_2TiCl(OSiPh_3)$	199.5—200.5	40	69.39 (69.00)	5.46 (5.16)	6.0 (5.8)	9.3 (9.8)	500 (489)
V	π-$CpTi(OSiMe_3)_3$	(71/0.15)	40	43.73 (44.42)	8.96 (8.43)	21.3 (22.0)	13.7 (12.6)	368 (380)
VI	π-$CpTi(OSiMe_2Ph)_3$	[b]	30	61.81 (60.77)	6.25 (6.88)	16.0 (17.1)	9.5 (8.6)	593 (557)
VII	π-$CpTi(OSiPh_2Me)_3$	114—115	60	69.85 (70.19)	6.05 (5.89)	10.7 (11.1)	6.3 (6.4)	728 (752)
VIII	π-$CpTi(OSiPh_3)_3$	204.5—205.2	70	75.08 (75.45)	5.69 (5.37)	9.4 (9.9)	5.5 (5.0)	955 (939)

a) Cited from our previous paper[1] b) Undistillable liquid

Table 2. NMR and IR spectral data

	NMR (τ, 6% in $CDCl_3$)		IR (cm^{-1}, 2 mmol% in CS_2)	
	Cp	Me	Ti–O–Si	=CH(π-Cp)
I	3.71	9.92	939	807
II	3.74	9.66	940	808
III	3.76	9.38	945	810
IV	3.76		951	814
V	3.70	9.94	908	803
VI	3.81	9.71	910	810
VII	3.94	9.47	910	810
VIII	4.03		915	816

Table 3. Reaction of the compounds with gaseous hydrogen chloride

Sample	Product	NMR (τ)	Ratio[a]
I—IV	π-Cp_2TiCl_2	3.40	100
V	π-$CpTiCl_3$	2.95	100
VI	π-$CpTiCl_3$	2.95	100
VII	π-$CpTi(OSiPh_2Me)Cl_2$[b]	3.45	80
VIII	π-$CpTi(OSiPh_3)_2Cl$	3.84	80
	π-$CpTi(OSiPh_3)Cl_2$	3.51	11

a) Ratio of ring proton converted from the original compounds to the products. b) Not fully identified.

ride was introduced for 2 hr into a boiling solution of 0.2 mmol of a sample in 100 ml of benzene, and volatile materials were removed by evaporation *in vacuo*. The solid residue was then dissolved in $CDCl_3$ and studied spectroscopically. The results are listed in Table 3.

The two partially substituted products from VIII were prepared independently by the following reaction:

$$CpTiCl_3 + 2Ph_3SiONa \xrightarrow[PhCH_3]{} CpTi(OSiPh_3)_2Cl + CpTi(OSiPh_3)Cl_2$$

The product obtained are as follows; the numerals represent respectively mp (°C), yield (%), C%, H%, Cl%, Si%, Ti% [Calcd], NMR (π-Cp, τ in $CDCl_3$) and IR (TiOSi, cm^{-1} in CS_2):

$CpTi(OSiPh_3)_2Cl$: 168—170, 50, 71.15 [70.56], 5.45[5.04], 5.6[5.1], 7.7[8.0], 7.2[6.9], 3.83, 904.

$CpTi(OSiPh_3)Cl_2$: 118—119, 10, 59.88[60.01], 4.50[4.28], 14.7[15.6], 5.9[6.1], 10.6[10.2], 3.50, 938.

On NMR spectra of π-$CpTi(OSiMe_{3-n}Ph_n)_3$ in Table 2 and π-$CpTi(OSiPh_3)_nCl_{3-n}$, it is shown that an increase of the number of phenyl groups leads to a shift of the cyclopentadienyl signal toward high field. This is believed to be due mainly to the diamagnetic anisotropy from phenyl groups and to the electron accepting properties of chlorine atoms. These results are in line with the observations of Beachell and Butter, who reported a detailed study of NMR spectra of titanocene sandwich compounds.[3]

Reaction with Acetyl Chloride: To a solution of 0.1 mmol of a sample in $CDCl_3$ was added 0.1 mmol (for I—IV) or 0.42 mmol (for V—VIII) of acetyl chloride and the mixture was heated at 45 °C for 2 hr. It was then submitted to NMR spectral investigations. The results are shown in Table 4.

Hydrolysis with Aqueous Sodium Hydroxide Solution: A solution of 0.2 mmol of a sample in 8 ml of THF was divided into four portions A, B, C, and D. The last three samples (B, C, and D) were treated with the reagents shown below in order to learn their stabilities towards hydrolytic cleavage.

Table 4. Reaction of the compounds with acetyl chloride

Sample	AcCl ($\times$0.1 mmol)	Product	NMR (τ)	Ratio (%)[a]
I	1.4	π-Cp_2TiCl_2	3.40	100
II	1.4	π-Cp_2TiCl_2	3.40	90
III	1.4	π-Cp_2TiCl_2	3.40	41
IV	1.4	π-Cp_2TiCl_2	3.40	39
V	4.2	π-$CpTi(OSiMe_3)Cl_2$[b]	3.25	90
VI	4.2	π-$CpTi(OSiMe_2Ph)Cl_2$[b]	3.38	90
VII	4.2	π-$CpTi(OSiPh_2Me)_2Cl$[b]	3.75	72
VIII	4.2	π-$CpTi(OSiPh_3)_2Cl$	3.81	46

a), b) The same as in Table 3.

Run	Reagent	Temp.
B	0.1 M-NaOH	r.t.
C	H_2O	70°C
D	0.1 M-NaOH	70°C

After 2 hr, each solution was evaporated *in vacuo* and the residue was dissolved in 2 ml of carbon disulfide to give a sample for IR spectral investigations. The intensities of the Ti-O-Si bond absorption of each sample relative to the intensity of the original sample A are shown in Table 5.

Table 5. Reaction of the compounds with water and aqueous sodium hydroxide solution

Sample	Reagent (μl)	Absorption intensity ratio in IR on TiOSi (A=100)	
I[a]	20	60(B)	15(C,D)
II[a]	20	90(B)	30(C,D)
III[a]	50	65(B)	30(C,D)
	[20]	[100(B)]	[35(C,D)]
IV[a]	50	80(B)	35(C,D)
V	20	35(B)	15(C,D)
VI	20	75(B)	35(C) 25(D)
VII	50	100(B.C)	90(D)
	[20]	[100(B.C)]	[95(D)]
VIII	50	100(B.C.D)	

a) When these samples were treated, besides the absorption band at about 945 cm^{-1}, a band centered at 920 cm^{-1} due to disproportionation appeared; its intensity was I>II>III>IV and in the order of D>C>B with respect to the treatment conditions. NMR spectra investigations indicated formation of π-Cp_2TiCl_2, particularly in run C.

Attempted reaction with Iron(II) Chloride: Attempted reactions of compounds I—VIII with iron(II) chloride prepared from iron(III) trichloride and iron powder in THF did not lead to any formation of ferrocene; this seems to be attributed both to the rather unionic property of the cyclopentadienyltitanium bond and to the steric effect of the triorganiosiloxy groups.

References

1) T. Takiguchi and H. Suzuki, This Bulletin, **41**, 2810 (1968).
2) T. Takiguchi, *J. Amer. Chem. Soc.*, **81**, 2359 (1959).
3) H. C. Beachell and S. A. Butter, *Inorg. Chem.*, **4**, 1133 (1965).

The Synthesis of 1,3-Thiazine-2,4-dithiones by the Reaction of Carbon Disulfide with Cyclic Ketones or Their Ketimines

Motomu MURAOKA, Tatsuo YAMAMOTO, and Tatsuo TAKESHIMA*

Department of Chemistry, Faculty of Science, Josai University, Keyaki-dai, Sakado, Saitama 350-02

** Department of Chemistry, Faculty of Science, Chiba University, Yayoi-cho, Chiba-shi 280*

(Received November 8, 1974)

Cyclohexanone, 4-methylcyclohexanone, and phloroglucinol, when treated with carbon disulfide in the presence of triethylamine and aqueous ammonia, gave the respective 3,1-benzothiazine-2(1*H*),4-dithiones. Glutazines and 2-iminocyclopentanedithiocarboxylic acid underwent this reaction without ammonia.

We have previously shown that cyclohexanone, in the presence of sodium amide, reacts with carbon disulfide to give a small amount of 5,6,7,8-tetrahydro-3,1-benzothiazine-2(1*H*),4-dithione in addition to the major product, 5,6,7,8-tetrahydro-spiro[2*H*-3,1-benzothiazine-2,1'-cyclohexane]-4(1*H*)-thione.[1]

Concerning 1,3-thiazine-2,4-dithiones, there have also been a few reports.[2-4]

We wish now to report a method of preparing the thiazinedithiones, involving the treatment of ketones or ketimines with carbon disulfide, in the presence of triethylamine, and also aqueous ammonia if needed.

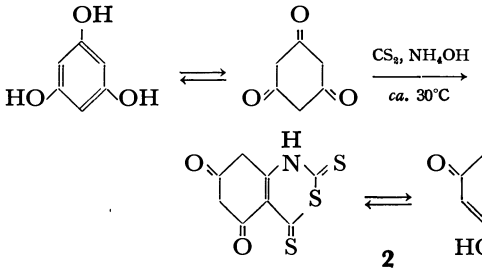

2

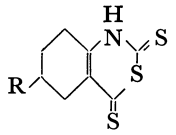

1a, R=H
1b, R=Me

2a, $R^1=R^2=Me$, $R^3=H$
2b, $R^1=R^2=R^3=Me$
2c, $R^1=COCH_3$, $R^2=R^3=H$

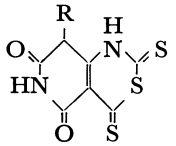

3a, R=H
3b, R=Me
3c, R=Et

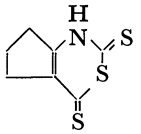

4

Cyclohexanone, 4-methylcyclohexanone, phloroglucinol, glutazine, and 3-substituted glutazines, in this reaction, afforded the expected thiazinedithiones or their tautomers—**1a**, **1b**, **2**, and **3a**—**c**, in yields ranging from 16 to 85%. Other ketones were reluctant to undergo this reaction. 2-Iminocyclopentanedithiocarboxylic acid,[5] on treatment with carbon disulfide and triethylamine, naturally gave 1,5,6,7-tetrahydrocyclopenta[*d*][1,3]thiazine-2,4-dithione (**4**), but 3-substituted 2-iminocyclopentanedithiocarboxylic acids did not undergo this reaction.

The structures were identified on the basis of their IR, UV, NMR, and mass spectra, together with elemental analyses and chemical reactions. Structure **2** was assigned on the basis of the following spectral data. The IR spectrum had an imino group band near 3260 cm^{-1}. The mass spectrum had the parent peak together with the most intense one, which corresponds to the elimination of the mercapto group from the molecular ion. On methylation or acetylation, the imino group band disappeared from both the IR and NMR spectra. Instead, the two doublets due to the two protons at 6- and 8-C of Compound **2** turned into two double doublets in the NMR spectrum of the acetyl derivative of this compound because of the restricted rotation of the acetyl group (in hexadeuteroacetone). These facts, together with the slightly broadened singlet corresponding to *ca.* two protons at τ −3.17 in the NMR spectrum of **2** (in heptadeuterodimethylformamide), led us to assign this structure: 1,7-dihydro-5-hydroxy-4-mercapto-7-oxo-3,1-benzothiazine-2-thione.

Experimental

The melting points, the appearances, the solvent of recrystallization, and the results of elemental analyses are all listed in Table 1.

*5,6,7,8-Tetrahydro-3,1-benzothiazine-2(1H),4-dithione (**1a**).* To a mixture of cyclohexanone (20 g), triethylamine (60 g), and aqueous 28% ammonia (40 ml), carbon disulfide (38 g) was added dropwise under cooling to 10 °C and vigorous stirring. The stirring was then continued for an additional 20 hr. A fairly viscous reaction mixture was acidified with dilute hydrochloric acid at 0 °C, and then a small quantity of ethanol was added to the red viscous oil which was thus separated. The red crystalline solid was dissolved in aqueous 28% ammonia to remove the insoluble material,[6] after which the solution was acidified again to give **1a** (11 g, 26%), which showed no depression of melting point on admixture with an authentic specimen[1] of **1a**.

*5,6,7,8-Tetrahydro-6-methyl-3,1-benzothiazine-2(1H),4-dithione (**1b**).* The preparation was the same as that described above (16%).[7] IR (KBr): 3120, 1590, and 1505 cm^{-1}. NMR [$(CD_3)_2SO$]: τ 6.56 (br, 1H), *ca.* 7.4 (m, 4H,) *ca.* 8.2 (m, 3H), and 8.97 ppm (d, 3H).

*5,6,7,8-Tetrahydro-5,7-dioxo-3,1-benzothiazine-2(1H),4-dithione (**2**).* A mixture of phloroglucinol dihydrate (5 g), carbon disulfide (12 g), triethylamine (1.5 g), and aqueous 28% ammonia (16 ml) was stirred for 50 hr at 32 °C. The yellow crystals which were then collected and washed with ether were dissolved in water, and the solution was acidified with

Table 1. Properties of thiazinedithiones

Compound	Mp (°C)	Appearance[a]	Recrystal from	Molecular formula	Calcd (%) C	H	N	S	Found (%) C	H	N	S
1b	214—215[b]	Red p	CH_3COCH_3-H_2O	$C_9H_{11}NS_3$	47.12	4.83	6.11	41.93	46.95	4.76	6.06	42.02
2	>300	Yellow n	Dioxane-H_2O	$C_8H_5NO_2S_3$	39.49	2.07	5.76	39.53	39.43	2.08	5.79	39.46
2a	153	Yellow n	CH_3OH	$C_{10}H_9NO_2S_3$	44.26	3.35	5.16	35.44	43.97	3.23	5.18	35.22
2b	71	Yellow n	DMF-H_2O	$C_{11}H_{11}NO_2S_3$	46.29	3.89	4.91	33.70	46.02	3.81	4.79	33.75
2c	199	Yellow n	DMF-H_2O	$C_{10}H_7NO_3S_3$	42.09	2.47	4.91	33.69	42.30	2.63	5.08	33.51
3a	>300	Yellow n	DMF	$C_7H_4N_2O_2S_3$	34.41	1.65	11.47	39.36	34.16	1.81	11.46	39.38
3b	>300	Yellow n	DMF	$C_8H_6N_2O_2S_3$	37.19	2.34	10.84	37.23	37.11	2.41	10.56	37.35
3c	>300	Yellow n	DMF	$C_9H_8N_2O_2S_3$	39.69	2.96	10.28	35.32	39.61	2.99	9.99	35.33
4	243—244[b]	Orange p	CH_3COCH_3-H_2O	$C_7H_7NS_3$	41.76	3.50	6.96	47.78	41.99	3.46	6.68	47.97

a) Plates and needles are abbreviated as p and n respectively. b) Decomposition point.

Table 2. Preparation[a] of **3a**—**c** and **4**

	Reactant	Reaction Conditions	Yield (%)
5,6,7,8-Tetrahydro-5,7-dioxopyrido[4,3-*d*]-[1,3]thiazine-2(1*H*),4-dithione (**3a**)	Glutazine[b]	Room temp 24 hr in DMF	60
5,6,7,8-Tetrahydro-8-methyl-5,7-dioxopyrido-[4,3-*d*][1,3]thiazine-2(1*H*),4-dithione (**3b**)	3-Methylglutazine	Room temp 24 hr in DMF	81
8-Ethyl-5,6,7,8-tetrahydro-5,7-dioxopyrido-[4,3-*d*][1,3]thiazine-2(1*H*),4-dithione (**3c**)	3-Ethylglutazine	Room temp 24 hr in DMF	85
1,5,6,7-Tetrahydrocyclopenta[*d*][1,3]thiazine-2,4-dithione (**4**)	2-Iminocyclopentanedithio-carboxylic acid	Room temp 16 hr in DMF	89

a) These compounds were isolated by the acidification of the respective reaction mixtures diluted with water.
b) Glutazine and the 3-substituted glutazines were prepared after Thorpe's method (*J. Chem. Soc.*, **85**, 1726 (1904)).

Table 3. IR and NMR[a] spectra of **3a**—**c** and **4**

Compound	cm^{-1} (KBr)	τ ppm in CD_3SOCD_3
3a	3070, 2915b, 2820b, 1650, 1615, 1575, 1537	4.43 (s, 1H), 4.67 (b, 1H), 7.06 (s, 1H), 7.18 (s, 1H)
3b	3310, 1635, 1605, 1550	−2.00 (br s, 1H), −1.80 (b, 1H), 6.62 (b, 1H), 8.07 (s, 3H) (further, 6.87 (q, 6H), 8.80 (t, 9H))
3c	3150, 1635, 1605, 1550	−0.13 (br s, 1H), 0.17 (b, 1H), 6.60 (b, 1H), 7.43 (q, 2H), 9.07 (t, 3H) (further, 6.87 (q, 6H), 8.83 (t, 9H))
4	3120, 1598, 1515	6.50 (b, 1H), 7.09 (t, 2H), 7.22 (t, 2H), 8.00 (m, 2H)

a) The NMR spectra of **3a**—**c** were obtained by the following conditions: **3a**; in CD_3SOCD_3-C_5D_5N (3: 1), **3b** and **3c**; as triethylammonium salt. (**3a**—**c** Were hardly soluble in most organic solvents and were denatured in dimethyl sulfoxide.)

dilute hydrochloric acid at 0 °C to give **2** (1.7 g, 23%). IR (KBr): 3260br, 1631, 1599, and 1532 cm^{-1}. NMR [$(CD_3)_2NCDO$] τ −3.17 and −3.10 (slightly br s, and br, >2H), 3.23 (d, J=2.4 Hz, 1H), 3.67 ppm (d, J=2.4 Hz, 1H). MS *m/e*: 243, 210, 178, 161, and 117.

Methylation of **2**. By methylation with diazomethane in a usual manner, a mixture of dimethyl and the trimethyl derivative of **2** was obtained. The hot solution which dissolved the mixture in methanol was cooled to separate out the dimethyl derivative of **2** (**2a**, 6%) [IR (KBr): 1620, 1574, and 1536 cm^{-1}; NMR (CF_3COOH): τ 3.11 (s, 2H), 5.91 (s, 3H), and 6.98 ppm (s, 3H); MS *m/e*: 271 and 224]. The solvent was evaporated from the mother liquor of **2a** to give the trimethyl derivative of **2** (**2b**, 28%).

Acetyl Derivative of **2**. To a solution of 2 (1 g) in pyridine, acetyl chloride (0.5 g) was added at 0 °C, after which the mixture was refluxed for 3 hr at 60 °C. The subsequent addition of water to the reaction mixture separated the acetyl derivative of **2** (**2c**) (0.8 g, 68%). IR (KBr): 1778, 1625, and 1530 cm^{-1}. NMR (CD_3COCD_3): τ 3.16 (dd, J=2.4 Hz, 1H), 3.52 (dd, J=2.4 Hz, 1H), 6.98 (s, 1H), 7.13 (s, 1H), and 7.66 ppm (s, 3H).

References

1) T. Takeshima, T. Hayashi, M. Muraoka, and T. Matsuoka, *J. Org. Chem.*, **32**, 980 (1967).
2) P. Papini and G. Auzzi, *Gazz. Chim. Ital.*, **96**, 430 (1966).
3) R. Gompper, B. Wetzel, and W. Elser, *Tetrahedron Lett.*, **1968**, 5519.
4) T. Takeshima, T. Miyauchi, N. Fukada, S. Koshizawa, and M. Muraoka, *J. Chem. Soc., C*, **1973**, 1009.
5) T. Takeshima, M. Yokoyama, T. Imamoto, M. Akano, and H. Asada, *J. Org. Chem.*, **34**, 730 (1969).
6) This material was spiro[2*H*-3,1-benzothiazine-2,1′-cyclohexane]-4(1*H*)-thione, mp 197—198 °C (lit,[1] 197—198 °C).
7) Spiro[2*H*-3,1-benzothiazine-2,1′-(4′-methylcyclohexane)]-4(1*H*)-thione was also obtained, mp 194—194.5 °C (lit,[1] 194—195 °C).

The Carbonyliron Complexes of Some Chlorocarbons

Takefumi MATSUKURA, Koichi MANO, and Akira FUJINO

Research Institute for Atomic Energy, Osaka City University, Sugimoto-cho, Sumiyoshi-ku, Osaka 558

(Received December 16, 1974)

The (tetracarbonyl)iron complexes of perchloro-(3,4-dimethylenecyclobutene) and perchlorofulvene, and the (tricarbonyl)iron complex of the former chlorocarbon were synthesized. The structural evidences for those complexes were given on the basis of the DSC, their chemical behaviors, and the UV, IR and other spectral data. Particularly, their mass-, NQR- and ^{13}C-NMR-spectra were discussed in detail by comparing them with those of the substrate chlorocarbons.

Little has been reported on the carbonyliron complexes with chlorocarbons as organic ligand. The thermochemical stabilities of a number of $L \cdot Fe(CO)_4$ type complexes (L: substituted ethylene) were discussed from the MO theoretical point of view by correlating their V-[1] or D/A- values[2] respectively with the ν_{CO} frequencies or the force constants in IR spectroscopy. However, the highly retarded chemical reactivity of conjugated polyenic chlorocarbons may have been a barrier to promote the work in this field; for instance, tetrachloroethylene, the simplest olefinic chlorocarbon, reacts with nonacarbonyl diiron under ordinary conditions to give the complex, but only in 0.1% yield,[3] reflecting a severe effect of perchloro-substitution. To our present knowledge, no carbonyliron compounds complexed with other chlorocarbon have appeared in the literature.

We examined the reactions between pentacarbonyl iron or nonacarbonyl diiron and three cyclic C_6Cl_6 chlorocarbons; *i.e.*, perchloro-(3,4-dimethylenecyclobutene) (**1**), -fulvene (**2**) and -benzene. Two kinds of complexes with the types of $L \cdot Fe(CO)_4$ and $L \cdot Fe(CO)_3$ were obtained from **1**, whereas only the one with the former type from **2**. Perchlorobenzene did not react with the reagents at all.

This paper describes the syntheses and some degradative reactions of those complexes, and discusses their structures mainly in terms of the IR-, mass-, NQR- and ^{13}C-NMR spectral data.

Results and Discussion

Syntheses and Degradative Reactions of Carbonyliron Complexes with Chlorocarbon Ligand. The chlorocarbon **1** reacted with nonacarbonyl diiron under the conditions specified in the experimental to furnish a complex (**3**), $C_6Cl_6Fe(CO)_4$ (mp 47.0 °C and decomp. *ca.* 76 °C, from the DSC). The oxidative degradation with Fe(III) or Ce(IV) smoothly liberated **1**. The thermal decomposition near 65 °C also proved the liberation of **1**, but there was no indication that dodecacarbonyl triiron formed through the trimerization of the component. The UV absorption for **3** were: $\lambda_{max}^{n\text{-hexane}}$ 230 (4.43), 287 (4.30) nm (log ε).

The second complex (**4**), $C_6Cl_6Fe(CO)_3$ (mp and dp: 90.5 and 105 °C, respectively, by DSC) was obtained by refluxing **3** in *n*-hexane with the inevitable production of **1**. The pyrolytic or oxidative liberation of **1** was essentially parallel to the above. Very drastic change in the UV spectrum ($\lambda_{max}^{n\text{-hexane}}$ 215 (4.36), 260_{sh} (3.99), 310_{sh} (3.70) and 386 (3.39); nm (log ε)) was observed in **4**. The only characteristically different behavior of **4** was the byproduction of a ketone (**5**) (mp 117 °C), C_7Cl_6O in the pyrolysis. The structure of perchloro-(bicyclo[3.2.0]hepta-1,5-diene-3-one) (**5a**) or its 1,6-diene alternative (**5b**) was assigned to **5** mainly on the basis of the UV spectral data.

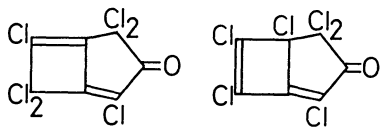

5a **5b**

The complex **4** was also produced by heating **1** and pentacarbonyl iron in a sealed tube at 85 °C, but in a poor yield.

The chlorocarbon **2** afforded in the analogous way the complex (**6**), $C_6Cl_6Fe(CO)_4$, through the reaction with nonacarbonyl diiron. The liberation of the substrate by either pyrolysis or the oxidative degradation was also confirmed. The observed mp by DSC was 72 °C. Interestingly, the exothermic degradation pattern of **6** suggested a two step successive loss of carbon monoxide, one at 84.5 °C, and the rest three at 93.5 °C.

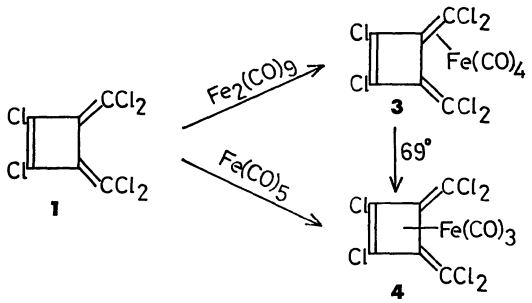

1 **3** **4**

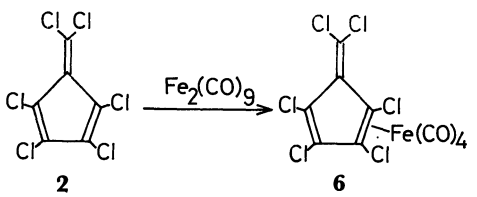

2 **6**

Further attempt was made to prepare the complex of h^4-type starting with **6** by the pyrolysis in *n*-hexane. Unfortunatelly, however, the product was too unstable

to be well caracterized; even very careful purification by chromatography near 0 °C resulted in failure in isolating the complex pure enough for succeeding analysis.

No formation of binuclear complex were observed in all the reactions of this work.

*IR Spectra** It was expected from the calculated HOMOs (by EHT) and the observed $\pi\rightarrow\pi^*$ energies of the chlorocarbons (−10.38 and 5.14 eV for **1** and −10.49 and 4.13 eV for **2**, respectively), that their interaction with $Fe(CO)_4$ (ionization potential: 7.0 eV[4]) would be much more advantageous for the complex formation than those in this case of dichloroethylenes (*e.g.*, for *trans*-isomer: HOMO −9.72 eV, $\pi\rightarrow\pi^*$ 6.49 eV[2]). There would be an effective stabilization in the total energy due to the back-donative bond formation.

The IR spectra of **3** gave rise to four very strong ν_{CO} bands at 2120, 2075, 2060 and 2035 cm^{-1}, indicative of the contribution of this back-donation from the central atom to the ligand, as well as of the equatorial position[5] of the latter in a trigonal bipyramidal structure. The band with the highest wave number and the lowest intensity due to A_1 asymmetric stretching vibration fell into the range between that for C_2Cl_4–$Fe(CO)_4$ (2134 cm^{-1}, the highest ever reported)[3] and those for 1,2-dichloroethylene-complexes (2106 cm^{-1})[2]. The $\nu_{C=C}$ bands corresponding to the free double bonds were at 1652 and 1595 cm^{-1}. An additional very weak band at 1375 cm^{-1} was detected by the special examination with a thick perchlorobutadiene mull; this should correspond to the double bond coordinated by the central atom. There have been no reports that describe such a drastic $\nu_{C=C}$ shift, but the $\Delta\nu_{C=C}$ value of *ca.* 170 cm^{-1} was within the acceptable range.[5]

The observed ν_{CO} bands of **4** were 2105 (vs) and 2065 (vs and broad) cm^{-1}, typical for diene–(tricarbonyl)iron complex.[6] The highest band was 52 cm^{-1} higher than the corresponding one of butadiene-$Fe(CO)_3$,[7] and will be the highest of all on reports as for the h^4-type complexes except some with cationic ligand.[8] Two strong $\nu_{C=C}$ bands with almost equal intensity were observed; the one at 1676 cm^{-1} for the free double bond and the other at 1375 cm^{-1} for the metal-coordinated.

The ν_{CO} bands (2120, 2070, 2065 and 2040 cm^{-1}, all vs) of **6** were almost the same as those for **3**. Therefore, the position of the organic ligand in the complex was assigned also to be equatorial in a trigonal bipyramidal structure, and the back-donation was nearly of the same extent. The $\nu_{C=C}$ bands appeared as two peaks (1570 and 1530 cm^{-1}, both s) splitted from the single broad one (1568 cm^{-1}, s) in **2**, and interestingly in this case, no band for the shifted $\nu_{C=C}$ was observed in the region 1500—1300 cm^{-1} even with a highly concentrated perchlorobutadiene solution.

Mass Spectra. The relative abundances are listed in Table 1 only for the main fragments including metal and/or C_6-skeleton from **1**, **2**, **3**, **4** and **6**. The distributions for the species less than C_5 were in all cases rather random and did not seem so informative. The successive loss of chlorine atom below *m/e* 282 in the cracking pattern was typically observed for all.

* Measured in C_2Cl_4 solution unless otherwise noted.

Table 1. Relative abundance in the mass spectra of **1**, **2**, **3**, **4** and **6**

m/e[a]	Ions	**1**	**2**[b]	**3**[c]	**4**	**6**
422	$C_6Cl_6\ Fe(CO)_x^+$ (x=3−0)	—	—	8	9	0
394				10	10	0
366				11	8	0
338				23	21	0
282	$C_6Cl_6^+$	77	100 (100)	42	5	100
247	$C_6Cl_5^+$	100	40 (39)	63	12	63
212	$C_6Cl_4^+$	33	21 (23)	100	100	30
177	$C_6Cl_3^+$	11	7	53	40	21
168	$Fe(CO)_4^+$	—	—	7	0	2
142	$C_6Cl_2^+$	23	17	84	67	49
140	$Fe(CO)_3^+$	—	—	9	0	0
126	$FeCl_2^+$	—	—	5	5	0
112	$Fe(CO)_2^+$	—	—	15	3	0
107	C_6Cl^+	11	10	28	20	54
91	$FeCl^+$	—	—	25	32	6
84	$Fe(CO)^+$	—	—	25	9	21

a) The *m/e*s are arranged monoisotopically, but their relative abundances are of all isotopic variants. b) Values in parentheses are from Ref. 9. c) Very poor production for *m/e* 450 (x=4).

However, some special comments can be made on the following points.

1) The cracking patterns are markedly different between **1** and **2** only in terms of the ratios of the relative abundance ($C_6Cl_6^+/C_6Cl_5^+$), although the distributions of other ions C_6Cl_x (x=3 or less) are essentially the same. Since the data for **2** meet well those reported by Meyerson *et al.*,[9] we suspect their suggestion that the cationized **1** would be the most possible intermediate fragment of perchloro-(1,2-dimethylenecyclobutane).

2) It was observed that the complex formation from **1** makes the fragmentation to C_6Cl_x (x=5 or less) dominant. This trend is rather common between **3** and **4**, and can be explained by the dominant elimination of FeCl or $FeCl_2$ from $C_6Cl_6Fe^+$ (*m/e* 338); the former elimination was evidenced by the relatively high abundance of the ion (*m/e* 91). The very small value for $C_6Cl_6^+$ from **4** seems to be related with the increased value for $FeCl^+$ ion, and further with the stability of L-Fe linkage in **4**.

3) On the other hand, **6** degradates under the same conditions quite differently; no $C_6Cl_6Fe(CO)_x^+$ fragments (x=4−0) were observed, and corresponding to this, the relative abundance of $FeCl^+$ was very small. The first fission of the L-Fe bond by electron impact must be the most essential fragmentation process in this case.

NQR Spectra. The NQR was particularly useful when, as our case, the direct comparison of the data between the ligand- and substrate-chlorocarbon is possible. The resonance lines for **1**, **3** and **4** are shown in Fig. 1, where the numerical figures indicate the values obtained by extrapolating the temperature dependence curve to 0 K for simpler and more precise

representation. It was generally experienced that the complex formation causes the intensification of the signals so effectively that the strong lines do appear even at room temperature. In all cases the number of crystallographically inequivalent chlorine atoms were found to be six.

It can be seen in Fig. 1 that some systematic frequency shifts exist through complex formation from **1**. The middle two lines for **3** near 37.5 MHz probably correspond to the two of four lines for **1** in the 38.0 MHz region which have already been assigned to the chlorine atoms at the exocyclic methylene carbons in the molecule.[10] Hence, the carbonyl iron-group presumably makes the π-bond with one of these double bond moieties, lowering the resonance frequencies for the chlorines attached to C_3', or C_4' of **1**. Another feature of the spectrum for **3** was the shifts of one of the two lines near 36.5 MHz assigned to the ring chlorines[10] to the higher frequency region, either because of the crystal field effect,** or as the result of some minor spatial interaction with one of the axial carbonyl groups. These interpretations may constitute the most principal reason for giving the structure of *acde*-tetracarbonyl-*b*-{1-1'-η-perchloro-(3,4-dimethylenecyclobutene)} iron finally to **3**.

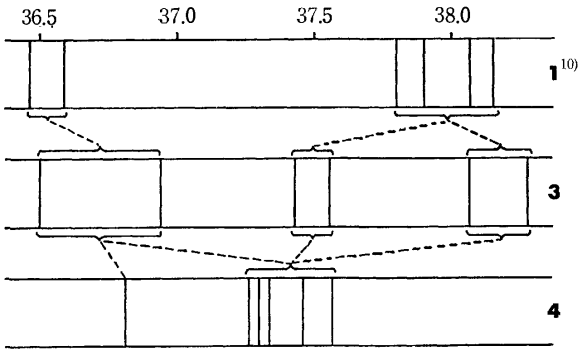

Fig. 1. NQR lines for **1**, **3**, and **4**.

In the resonance line pattern for **4**, the rest two lines with the highest frequency values also shifted downward joining together with the middle two for **3**. This suggests that the carbonyl iron interacts with both of the exocyclic double bonds of the ligand. In the 37.5 MHz region were observed actually five lines, one of which is obviously assigned to the chlorine atom on the four-membered ring. The upward shift is perhaps attributed to the spatial effect of the carbonyl group, deviating to some extent from the σ_v of the ligand, and hence, resulting in the lack of C_s symmetry of the complex molecule as a whole. The lowering of the resonance frequency caused by metal coordination is due to the releasing of the Cl-p_x electron through pi-conjugation according to the equation:[12]

$$fq \propto (N_x+N_y)/2 - N_z,$$

where N_x, N_y and N_z are the 3p AO population of a chlorine atom in x-, y- and z(C-Cl)-direction, respec-

** The frequency shifts seem more than those due to the crystal field effect which has been estimated to be less than 500 KHz in ordinary cases.[11]

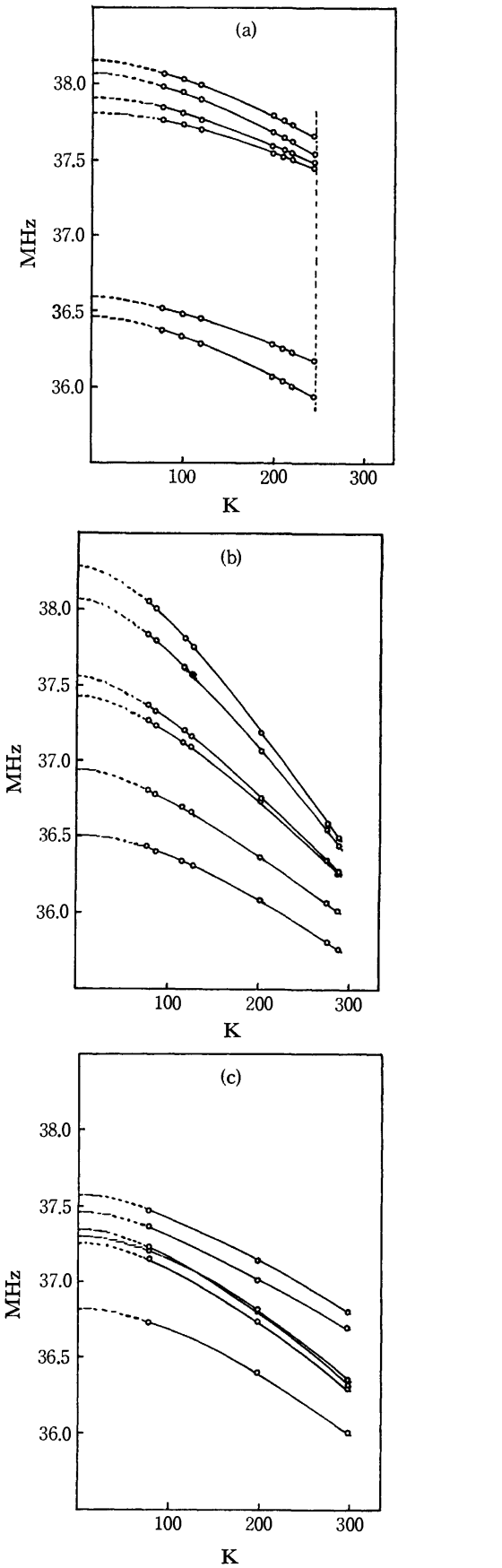

Fig. 2. Temperature dependences of NQR lines for **1**, **3**, and **4**. The vertical broken line in 2(a) indicates the fade-out temperature

tively. Thus, the structure of tricarbonyl-{1'-2'-η-perchloro-(3,4-dimethylenecyclobutene)}iron was assigned to **4**, although its stereochemical configuration has remained unsolved.

In order to see more detailed profile of the complexes in terms of the thermal molecular motion in crystals, the temperature dependence of those NQR lines were examined (Table 2 and Fig. 2). The fade-out of all six signals for **1** at 250 K or so (Fig. 2a) and the survival of the six strong ones for both **3** and **4** even at room temperature (Fig. 2b and 2c) may be a reflection of the situation that the complex formation is sensitively related to some restricted thermal molecular motion. The most salient feature among the Figs. 2a—c is the extraordinarily large temperature gradients of the curves in Fig. 2b for the signals ν_1 and ν_2 assigned to the chlorines at the exocyclic double bond moiety free from the coordination. The high steepness of the curves suggests that those two chlorines both become more affected locally than others by the thermal motion of the nearest carbonyl group as the temperature rises. This interpretation is also helpful for understanding the existence of the valence isomerization in **3**, about which a comment will be given later. The curves for **4** are all as easy as those for **1** making a clear contrast to that for **3**.

Table 2. Temperature dependence of NQR lines (MHz)

	Temp. (K)	ν_1	ν_2	ν_3	ν_4	ν_4	ν_6
3	0	38.28	38.07	37.56	37.43	36.94	36.50
	78	38.052	37.829	37.362	37.257	36.800	36.426
	200	37.190	37.070	36.760	36.732	36.350	36.090
	286	36.504	36.439	36.264	36.247	36.011	35.758
4	0	37.57	37.46	37.34	37.30	37.26	36.81
	78	37.461	37.362	37.223	37.198	37.145	36.733
	198	37.146	37.048	36.812	36.802	36.740	36.410
	298	36.803	36.705	36.366	36.324	36.308	36.042
6	0	38.21	38.07	37.80	37.63	37.60	36.41
	78	38.150	37.988	37.742	37.555	37.533	36.341
	198	37.939	37.639	37.478	37.239	37.200	36.027
	298	37.683	37.247	37.093	36.883	36.825	35.689

Figure 3 shows the resonance lines for **2** and **6**. Some published informations on the structural problem for **2** are available; *e.g.*, the phase transition between the ordered and the disordered forms studied by X-ray analysis,[13] two mutually different NQR assignments,[10,14] *etc.* Even on these backround, however, it appeared very difficult to find some systematic shift of the lines in this case. The slopes of the temperature dependence (Table 2 and Fig. 5) are somewhat easier than those for **2** and **4**.

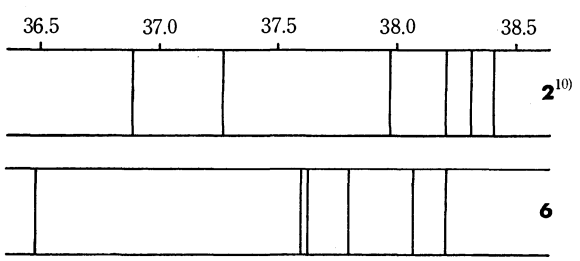

Fig. 3. NQR lines for **2** and **6**.

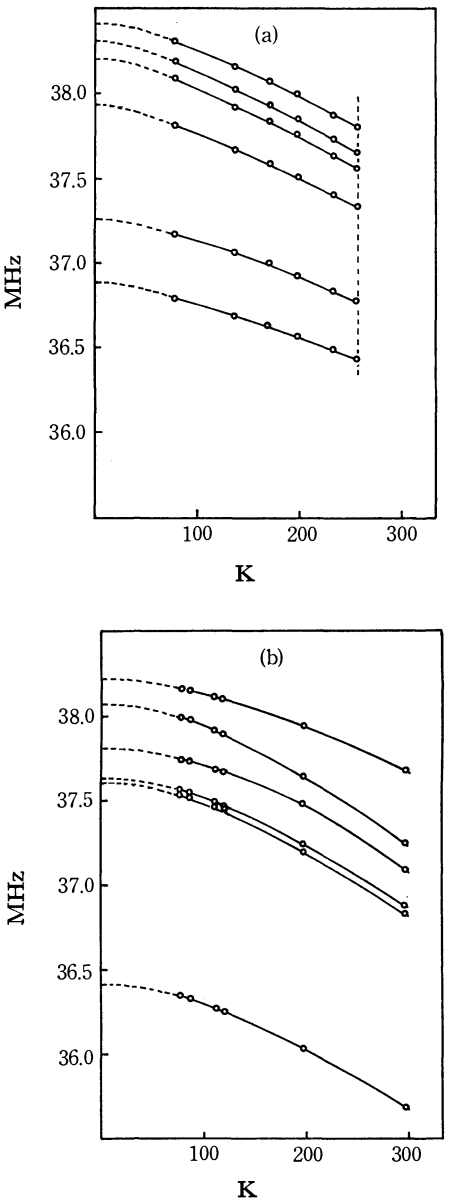

Fig. 4. Temperature dependences of NQR lines for **2** and **6**. The vertical broken line in 4(a) indicates the fade-out temperature.

The possible existence of phase transitions in those complexes were examined by means of DSC technique covering the low temperature range down to −160 °C. The observation of the inoccurence of such transition appeares parallel to our findings that the complex formation makes the molecular motion more restricted.

^{13}C-NMR Spectra. The ^{13}C-NMR spectra were taken for all the complexes and the substrate chlorocarbons. The FT-NMR measurement was accompanied by some technical difficulty because of the unstability of the complexes in solution, and, in addition, because of the extraordinarily long relaxation time of the excited species. However, successful results were obtained under

the conditions specified in Table 3.

The reported data for ^{13}C-NMR of the carbonyliron complexes with hydrocarbon ligand inform, although they are very few, of a surprisingly large upfield shift for the signal related to the olefinic carbon coordinated by metal. In the case of butadiene–$Fe(CO)_3$ complex, a pair of highly shifted signals, 35.8 and 80.8 ppm downfield from TMS was reported.[15] In our results, the signals in the 65—80 ppm region can be assigned also to the carbons coordinated by the iron metal. The absorption of the carbonyl-C in the complexes **3** and **6** are both very broad and splitted into two parts particularly in the former. The main reason for this broadening would presumably be either a very long relaxation of the carbonyl-C or the mutual transposition of the four carbonyls with an appropriately slow rate. Especially interesting was the appearence of only three signals in the complex **3**, which should give the six for ligand carbons, if the structure discussed in the preceding section is correct. The possibility that the carbonyliron positions at the double bond in the four-membered ring of **1** was certainly excluded from consideration on the basis of our present NQR interpretation. The most possible and rational explanation is the rapid degenerate rearrangement of **3** in the *d*-chloroform solution as shown below.*** The fluctional transposition of the bond between the iron and the C=C moiety may be related to the characteristically steeper temperature dependence curves in Fig. 2b. Some analogous examples have been dealt with in the carbonyliron complexes of allene,[17] cyclooctatetraene,[18] *etc.* The signal for the carbonyl-C of **4** was a sharp singlet and differed from those of **3** and **6**. No extraordinary upfield shifts for the olefinic carbons were observed in this case. This would be an exception with the potential significance that the h^4-type complex formation with chlorocarbon does not affect the absorption of the ligand so much as does the similar coordination in the hydrocarbon-complexes.

The observation of seven signals in total for **6** (six for the olefinic-C and one for the carbonyl-C) explained the coordination of the central atom at 1,2- C=C bond of **2**. If the C=C bond at 5,5′ is coordinated, the number of signals for the ligand would be four. Thus, the structure of *acde*-tetracarbonyl-*b*-{1-2-η-perchloro-(5-methylenecyclopentadiene)}iron was assigned to **6**.

TABLE 3. ^{13}C-NMR CHEMICAL SHIFTS FOR **1, 2, 3, 4** AND **6** (ppm downfield from TMS)

Compound	Carbonyl-C	Olefinic-C
1†		136.15, 131.66, 109.84
3	202.68, 202.41	139.39, 117.88, 73.91
4	199.23	149.23, 116.97, 105.98
2†		136.58, 130.87, 130.27 117.42
6	201.70	146.11, 142.61, 126.11 115.99, 76.27, 68.57

Solvent: C_6D_6 for **4** and $CDCl_3$ for others. Temperature: 0—10 °C for **3**, **4** and **6**; 40—50 °C for **1** and **2**. Approx. concentration: 2.5 g/5 ml (sample/solvent) for **3**, **4** and **6**; 1.5 g/5 ml for **1** and **2**. Pulse width: 1μs. Pulse interval: 1.4 s. † See also Ref. 16.

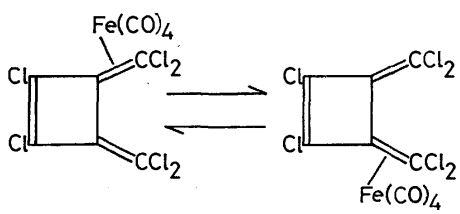

*** An attempted measurement at the temperature lower than −40 °C was technically unsuccessful.

Experimental

The preparations and purifications of the complexes were all carried out under the atmosphere of nitrogen and with sufficiently deaerated solvent. Especially, the low temperature chromatography at 2—10 °C (on sillicic acid, Mallinkrodt, 100 mesh) was applied for the isolation.

The spectrometers used were JASCO-DS-402-G for IR, Hitachi EPS-2U for UV, Decca for NQR, JEOL-JMS D-100 and Hitachi RMU-6E for MS and Varian XL-100 for ^{13}C-NMR. For the NQR measurement a special rf-coil was designed for detecting signals with high sensitivity and a grid-dipmeter (Delica, Mita Musen Kenkyusho KK.) for checking the proper absorption frequencies were used. The DSC data were obtained by Rigaku DSC-8001.

acde-Tetracarbonyl-b-{*1-1′-η-perchloro-(3,4-dimethylenecyclobutene)*}*iron (3)*. An *n*-hexane solution (200 ml) of perchloro-(3,4-dimethylenecyclobutene) (**1**) (4.0 g, 14 mmol) was stirred with nonacarbonyl diiron (6.2 g, 17 mmol) suspended in it, and gentle warming was applied until the temperature rose to 42 °C in 15 min, while the yellow suspension gradually changed to dark brown in color. The almost clear solution was obtained after 10 min keeping at 42—43 °C. The dark red solution obtained after cooling to room temperature and filtration through Hyflo Super-Cel (John-Manville) afforded, on removal of the solvent under reduced pressure below 30 °C, the crude crystals of the complex (**3**), which were purified by chromatography with *n*-hexane solution. The first fraction was composed of the recovered **1** (1.5 g). The lemon yellow crystals (4.3 g, 68%) of **3** were obtained as the second, and recrystallized from *n*-pentane at −78 °C. Found: C, 26.66; Cl, 47.31%. Calcd for $C_{10}Cl_6FeO_4$: C, 26.50; Cl, 46.99%.

Tricarbonyl{*1′-2′-η-perchloro-(3,4-dimethylenecyclobutene)*}*iron (4)*. The complex **3** (1.0 g, 2.2 mmol) was dissolved in *n*-hexane (65 ml) and the solution was heated under stirring so mildly that the solution started to reflux after 45 min. Being kept for several min under refluxing, the solution was cooled, filtered and chromatographed. The recovered **1** as the first fraction weighed 260 mg. The yellow crystals (150 mg) obtained as the second were recrystallized from *n*-pentane. Found: C, 25.35; Cl, 50.73%. Calcd for $C_9Cl_6FeO_3$: C, 25.42; Cl, 50.14%.

acde-Tetracarbonyl-b-{*1-2-η-perchloro-(5-methylenecyclopentadiene)*}*iron (6)*. To the solution of perchlorofulvene (**2**) (3.0 g, 10.5 mmol) in *n*-hexane (300 ml) was added nonacarbonyl diiron (3.9 g, 10.7 mmol) and the mixture was under stirring warmed gently for 1 hr until the temperature reached 40 °C, when the suspension of carbonyl iron disappeared within several min. The solution was cooled to room temperature and filtered through a glass filter. The regular work-up afforded the recovered **2** (0.4 g) and the orange

crystals of the complex (**6**) (2.0 g, 48%), which were recrystallized from *n*-pentane at −78 °C. Found: C, 26.67; Cl, 46.94%. Calcd for $C_{10}Cl_6FeO_4$: C, 26.50; Cl, 46.99%.

Pyrolyses of the Complexes 3 and 6 to the Original Chlorocarbons. The pyrolyses of **3** (64 mg) and **6** (74 mg) were carried out in the test tubes respectively at 65—66 °C for 2 min and at 85 °C for 10 min. The partial production of **1** was confirmed by the IR spectrum in the former case and that of **2** (24 mg) by the isolation of the latter.

A Typical Example among the Oxidative Degradations of the Complexes 3—6 by Cerric Ammonium Nitrate. The solution of **6** (340 mg) in acetone (30 ml) was stirred with cerric ammonium nitrate ($Ce(NO_3)_4 \cdot 2NH_4NO_3 \cdot xH_2O$, Kishida Kagaku KK.) (400 mg) at room temperature for 15 min. The solution was then concentrated under diminished pressure and poured onto water. From the carbon tetrachloride extract, **2** (140 mg, 65%) was isolated.

Pyrolytic Formation of the Carbonylated Product, Ketone (5) from the Complex 4. The complex **4** (2.57 g) was heated without solvent very carefully to 110 °C in a flask (100 cc) equipped with a condenser. The decomposition started at 116 °C so violently that some powdery amorphous product blew up through the condenser to the top. The *n*-hexane-soluble part (400 mg) was chromatographically purified. Beside a small amount of the recovered **1**, the yellow crystals of the ketone (**5**) (60 mg) were obtained. Found: C, 27.08; Cl, 67.35%. Calcd for C_7Cl_6O: C, 26.84; Cl, 68.05%. UV: $\lambda_{max}^{n\text{-hexane}}$ 228 (3.81), 259 (4.55), 267 (4.56), 302 (4.00), 315 (4.24), 330 (4.35) and 348 (4.42); nm (log ε). IR: ν_{max}^{Nujol} 1770 (CO), 1560 and 1495 (C=C) (cm^{-1}).

The authors are indebted to Prof. M. Nakagawa, Prof. Y. Odaira, Dr. K. Sonogashira and Dr. T. Atake of Osaka University, respectively for the ^{13}C-NMR, mass- and IR measurements. They are also grateful to Mr. J. Goda of Osaka City University for the elemental analyses, and to Dr. K. Nishimoto of the same University for his helpful discussion.

References

1) E. Koerner von Gustorf, M. C. Henry, and D. G. McAdoo, *Ann.*, **707**, 192 (1967).
2) E. W. Grevels and E. Koerner von Gustorf, *Ann.*, **1973**, 1821.
3) R. Fields, G. L. Godwin, and R. N. Haszeldine, *J. Organometal. Chem.*, **26**, (1970), C 70.
4) D. R. Bidinosti and N. S. McIntyre, *Can. J. Chem.*, **45**, 641 (1967).
5) M. Herberhold, "Metal π-Complexes," Vol. 2, Part 1. Elsevier Publishing Co., New York, N.Y. (1972), p. 325.
6) F. G. A. Stone and R. West (Editors), "Advances in Organometallic Chemistry," Vol. 1, Academic Press, New York, N.Y. (1964), p. 11.
7) K. Mack, *Helv. Chim. Acta*, **45**, 1847 (1962).
8) J. E. Mahler, D. A. K. Jones, and R. Pettit, *J. Amer. Chem. Soc.*, **86**, 3589 (1964).
9) S. Meyerson and E. K. Fields, *J. Chem. Soc. B*, **1966**, 1001.
10) M. Hashimoto and K. Mano, This Bulletin, **45**, 706 (1972).
11) E. A. C. Lucken: Nuclear Quadrupole Coupling Constants, Academic Press Inc., New York (N.Y.), (1969), p. 149.
12) T. P. Das and E. L. Hahn, "Nuclear Quadrupole Resonance Spectroscopy," Solid State Phys., Supplement 1. Academic Press Inc., New York, N.Y. (1958), p. 139.
13) K. Mano, F. Takusagawa, M. Hinamoto, and Y. Kushi, *Chem. Lett.*, **1973**, 1083.
14) I. Agranat, M. Hayek, and D. Gill, This Bulletin, **46**, 1575 (1973).
15) H. L. Retkofsky, E. N. Frankel, and H. S. Gutowsky, *J. Amer. Chem. Soc.*, **88**, 2710 (1966).
16) G. E. Hawks, R. A. Smith, and J. D. Roberts, *J. Org. Chem.*, **39**, 1276 (1974).
17) R. Ben-Shoshan and R. Pettit, *J. Amer. Chem. Soc.*, **89**, 2231 (1967).
18) C. E. Keller, G. F. Emerson, and R. Pettit, *ibid.*, **87**, 1388 (1965).

Monomer-Isomerization Polymerization. XIV. Monomer-Isomerization Polymerization of 4-Methyl-2-pentene with Ziegler-Natta Catalyst

Takayuki Otsu, Kiyoshi Endo, Hiroharu Nagahama, and Akihiko Shimizu

Department of Applied Chemistry, Faculty of Engineering, Osaka City University, Sugimoto-cho, Sumiyoshi-ku, Osaka 558

(Received January 6, 1975)

4-Methyl-2-pentene (4M2P) was found to polymerize in the presence of $TiCl_3$–$Al(C_2H_5)_3$ catalyst, and to yield a high molecular weight isotactic homopolymer of 4-methyl-1-pentene (4M1P). From the fact that the isomerizations from 4M2P to its positional isomers were also observed, it was concluded that this polymerization was induced by a monomer-isomerization polymerization mechanism, *i.e.* 4M2P isomerized first to 4M1P, which then homopolymerized. The rates of both polymerization and isomerization were affected by the Al/Ti molar ratio of catalyst system, and by the addition of transition metal compounds such as nickel acetylacetonate [Ni(acac)$_2$]. It was concluded that the maximum rates were observed at Al/Ti = 3 and Ni/Ti = 0.2 in molar ratio.

It has been well known that internal olefins do not polymerize to give high polymers in the presence of any catalysts, including Ziegler-Natta catalyst. Several years ago, however, it was found that some linear internal olefins such as 2-butene, 2-pentene, and 2-hexene polymerize with $TiCl_3$-$Al(C_2H_5)_3$ (Al/Ti$\geq$2) catalysts to give high molecular weight polymers, if allowed to react for a long time at 80 °C.[1-5]

Interestingly, the polymers thus obtained were confirmed to be homopolymers consisting of the corresponding 1-olefin units. In accordance with the observation that the isomerization from the starting 2-olefin to the 1-olefin occurs simultaneously during reaction, it was concluded that these 2-olefins isomerize first to the corresponding 1-olefins, which then homopolymerize. Since this kind of polymerization gives a new route for polymer synthesis, we have proposed that this polymerization proceeds *via* a monomer-isomerization polymerization mechanism.

These monomer-isomerization polymerizations have also been extended to the other higher internal olefins, such as 2-heptene, 3-heptene, and 2-octene.[6] In general, the monomer-isomerization polymerization involves two independent reaction steps: isomerization to the most polymerizable 1-olefin and polymerization of this 1-olefin. Accordingly, the total rate of polymerization is determined by both the rate of isomerization to 1-olefin and its concentration in an equilibrium olefin mixture. Since such a concentration in linear internal olefins is generally higher than that in branched ones, it is usually expected that the former olefins are more favorable to the monomer-isomerization polymerization than are the latter olefins.

However, it was found recently that some branched internal olefins, 4M2P, underwent monomer-isomerization polymerization in the presence of $TiCl_3$–$Al(C_2H_5)_3$ catalyst to give the homopolymer of 4M2P. The present paper describes the results of these monomer-isomerization polymerizations of 4M2P.

Experimental

Materials. 4M2P and 4M1P were purified through a fractional distillation of commercial grade samples. Purities of both monomers determined by gas chromatography were above 99.9%; here the *cis* and *trans* isomers could not be separated.

Triethylaluminum (Ethyl Corp.), titanium trichloride (Stauffer Chem.), and transition metal chelates of acetylacetonate (acac) such as Ni(acac)$_2$ and Co(acac)$_2$ (Dotite reagent) were used without further purification. Solvents were purified by ordinary methods.

Polymerization Procedure. Most polymerizations were carried out in a sealed glass tube with shaking in a thermostat for a given time. The charging of the required reagents into the tube and its sealing under vacuum were performed by methods described in the previous paper.[3] After polymerization the tube was opened and the unreacted olefin monomer was recovered by distillation in order to analyze the isomer distribution by means of gas chromatography, in which a bis(2-methoxyethyl) adipate column was used at 17 °C. The residue of the tube was then poured into a large amount of methanol containing hydrochloric acid to precipitate the polymer formed. The polymer yield was calculated from the weight of the dry polymer obtained. In these polymerizations, the polymer yield was dependent on the conditions of catalyst preparation, and seemed to contain $\pm$2% error.

Characterization of the Polymers. The structure of the resulting polymers was checked by infrared spectroscopy of their thin films. The isotacticity of the polymers was determined by the weight of the hot *n*-hexane-insoluble polymer.[7] The intrinsic viscosity ([η]) was determined from a viscosity measurement of the dilute decaline solution at 130 °C with an Ubbelohde viscometer. The number-average molecular weight ($\bar{M}_n$) was calculated from the following equation:[7]

$$[\eta] = 1.95\times10^{-4}\bar{M}_n^{0.75}$$

Results and Discussion

Polymerization and Isomerization of 4M2P with $TiCl_3$–$Al(C_2H_5)_3$ Catalyst. The results of polymerization and isomerization of 4M2P with $TiCl_3$-$Al(C_2H_5)_3$ catalyst in *p*-xylene or *n*-heptane are summarized in Table 1. As can be seen from this table, the yields of polymers in both solvents increase as a function of polymerization time, and those in *n*-heptane are somewhat higher than in *p*-xylene. Upon comparing these results with those of 4M1P under similar conditions, as shown in Table 2, the polymerization of 4M2P was found to proceed with a much slower rate.

Figure 1 shows the infrared spectra of the polymers obtained from 4M2P and 4M1P with the $TiCl_3$–$Al(C_2H_5)_3$ catalyst. From this figure, the infrared spectra of both polymers are quite identical. It is clear therefore that the polymers obtained from 4M2P and 4M1P

Table 1. Monomer-isomerization polymerization of 4-methyl-2-pentene with $TiCl_3$–$Al(C_2H_5)_3$ catalyst at 80 °C[a]

Solvent	Time (hr)	Yield (%)	Composition of methylpentenes recovered after polymerization, %[b]				
			2MP	4MIP	4M2P	2M2P	2M1P
p-Xylene	5	3.6	0.2	0.3	98.8	0.7	0.0
p-Xylene	10	5.4	0.2	0.2	98.5	1.1	0.0
p-Xylene	20	7.6	0.7	0.6	96.5	2.2	0.0
p-Xylene	45	11.8	1.2	0.5	95.1	3.2	0.0
p-Xylene	60	16.7	0.5	0.4	94.1	5.0	trace
n-Heptane	5	5.2	1.5	0.5	93.1	4.6	0.3
n-Heptane	10	10.6	1.8	0.5	88.7	8.3	0.7
n-Heptane	20	15.9	2.5	0.4	84.5	11.5	1.1
n-Heptane	45	16.5	2.3	0.5	83.5	13.1	0.6
n-Heptane	60	20.4	0.6	0.6	91.2	6.8	0.6
				0.5[c]	3.7[c]	82.6[c]	13.2[c]

a) Polymerization conditions: $[TiCl_3]=117$ mmol/l, [4M2P]=2.7 mol/l, Al/Ti=3.0 in molar ratio. b) Determined by gas chromatography of the unreacted monomer mixture recovered after polymerization. c) Equilibrated concentrations calculated from free energies of formation of the isomer.

Table 2. Polymerization of 4-methyl-1-pentene with $TiCl_3$–$Al(C_2H_5)_3$ catalyst in *p*-xylene[a]

Al/Ti molar ratio	Time (hr)	Temp. (°C)	Polymer Yield (%)
0.5	0.07	80	100
1.0	0.07	80	100
2.0	0.07	80	100
3.0	1.00	30	94.8

a) Polymerization conditions: $[TiCl_3]=117$ mmol/l, [4M1P]=3.0 mol/l.

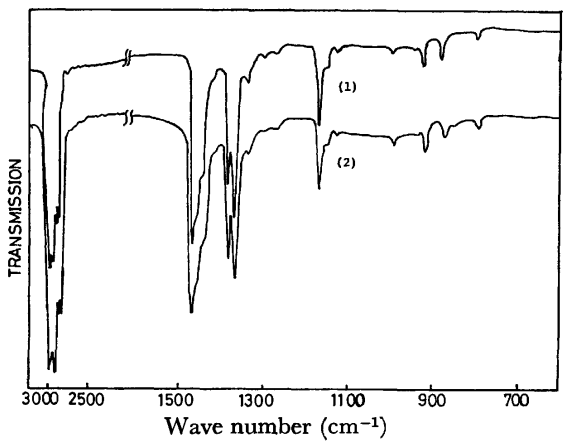

Fig. 1. Infrared spectra of polymers with $TiCl_3$–$Al(C_2H_5)_3$ catalyst (1) obtained from 4M1P, (2) obtained from 4M2P (film).

consist of the same recurring unit, 4M1P. Like the polymers obtained from 4M1P with Ziegler-Natta catalyst, the polymers from 4M2P are observed to contain isotactic polymers which have molecular weights of 4—11.5×10^4 (Table 3), and melt at 213 °C.

Table 3. Some properties of the polymers obtained from 4M2P with $TiCl_3$–$Al(C_2H_5)_3$ catalyst in *p*-xylene at 80 °C for 60 hr[a]

Al/Ti molar ratio	Ni/Ti molar ratio	Yield (%)	Solvent extraction		$[\eta]$ (dl/g)	$\bar{M}_n$ ($\times10^{-4}$)
			n-hexane soluble (%)	*n*-hexane insoluble (%)		
2.0	0.15	35.6	73.5	26.5	1.21	11.45
2.0	0.20	35.9	56.8	43.2	—	—
2.0	0.0	24.4	61.7[b]	38.3	—	—
3.0	0.0	27.5	56.9[b]	43.1	0.68	3.89

a) Polymerization conditions: $[TiCl_3]=117$ mmol/l, [4M2P]=2.7 mol/l. b) [4M2P]=3.0 mol/l.

As is also shown in Table 1, the isomerizations of 4M2P to its positional isomers are observed to proceed with a time in proportion to the polymer yield. In *n*-heptane, 2-methyl-1-pentene (2M1P) isomer was found during polymerization of 4M2P, but only a trace of this isomer was observed in *p*-xylene. Contrary to the results of the polymerization of 2-butene to poly-1-butene, the observed isomer distributions are seen to approach with a very slow rate to those in an equilibrium olefin mixture. However, it is obvious from Table 1 that the rate of isomerization to 4M1P, which is the most polymerizable isomer, is much greater than that to 2-methyl-2-pentene (2M2P), which is the most stable isomer.

Accordingly these results strongly indicate that 4M2P undergoes monomer-isomerization polymerization to give high molecular weight isotactic poly (4M1P), *i.e.* 4M2P isomerizes to 4M1P prior to polymerization and then this olefin homopolymerizes. In this case, it is interesting that 4M2P and 2M2P serve only as a diluent, and the high molecular weight homopolymer of 4M1P is obtained, although the observed concentration of 4M1P isomerized from 4M2P is as low as 0.5%. This result can be expected from the fact that the isomerization to 4M1P is sufficiently fast to replenish the consumed 4M1P.

The monomer-isomerization polymerization of 4M2P is expressed by the following reaction scheme:

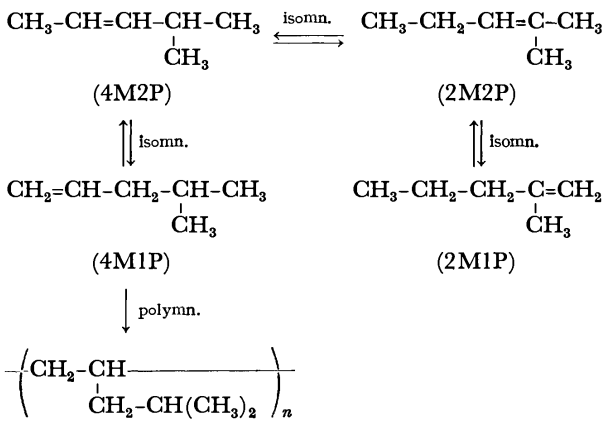

More recently it has been found that both 2M2P and 2M1P also undergo the monomer-isomerization polymerization with a very slow rate to give poly (4M1P).

Table 4. Effect of Al/Ti molar ratio on monomer-isomerization polymerization of 4-methyl-2-pentene with $TiCl_3$–$Al(C_2H_5)_3$ catalyst in *p*-xylene at 80 °C for 60 hr[a]

Al/Ti molar ratio	Yield (%)	Composition of methylpentenes recovered after polymerization, %[b]				
		2MP	4M1P	4M2P	2M2P	2M1P
0.25	0.0	1.1	0.1	98.1	0.7	0.0
0.5	trace	trace	trace	99.9	trace	0.0
1.0	10.6	0.2	0.2	92.3	7.0	0.3
2.0	24.4	0.8	0.4	91.3	7.0	0.5
3.0	27.5	0.4	0.1	84.8	14.1	0.6
3.5	33.1	0.5	0.2	87.7	11.4	0.2
4.0	17.6	1.2	0.8	89.7	8.0	0.3
5.0	10.2	2.5	2.1	86.0	9.0	0.4

a) $[TiCl_3]=117$ mmol/l, $[4M2P]=3.0$ mol/l. b) Determinaed by gas chromatography.

Table 5. Effect of isomerization catalyst (MeX) on the monomer-isomerization polymerization of 4-methyl-2-pentene with $TiCl_3$–$Al(C_2H_5)_3$ catalyst at 80 °C in *p*-xylene; Al/Ti=3.0 in molar ratio

MeX	$TiCl_3$ (mmol/l)	Monomer (mol/l)	Me/Ti molar ratio	Time (hr)	Yield (%)
None	70	4.0	0	96.5	11.0
$Ni(acac)_2$	70	4.0	0.5	96.5	6.4
$Co(acac)_2$	70	4.0	0.5	96.5	4.0
$Mn(acac)_2$	70	4.0	0.5	96.5	trace
None	105	3.0	0	100.0	24.6
$Ni(acac)_2$	105	3.0	0.5	100.0	14.4
$Fe(acac)_3$	105	3.0	0.5	100.0	5.9
$Co(acac)_3$	105	3.0	0.5	100.0	trace

Effect of Al/Ti Molar Ratios on Monomer-Isomerization Polymerization of 4M2P. In the monomer-isomerization polymerization of 2-butene with $TiCl_3$-$Al(C_2H_5)_3$ catalyst, it was found that the rate of polymerization was affected by the Al/Ti molar ratios used. A similar result was also reported in the polymerization of 4M1P with $TiCl_3$-$Al(C_2H_5)_3$ catalyst in which the rate went through a maximum at the Al/Ti molar ratio of 3.0.[8]

To check this point, the effects of Al/Ti molar ratio on the monomer-isomerization polymerization of 4M2P were investigated. The results are shown in Table 4, from which it is found that the maximum rates of both polymerization and isomerization are observed at a molar ratio Al/Ti of about 3.0—3.5. This finding is in agreement with that observed in the polymerization of 4M1P.[8]

From Table 4, at the Al/Ti molar ratio lower than 1.0, neither polymerization nor isomerization occured. The polymers obtained at the Al/Ti molar ratios higher than 1.0 were found to consist of poly (4M1P).

Effect of Metal Acetylacetonates [$Me(acac)_x$] on Monomer-Isomerization Polymerization of 4M2P. Since, in monomer-isomerization polymerization of 2-olefin, the isomerization to 1-olefin must occur before its polymerization,[4] the addition of isomerization catalyst is expected to accelerate this polymerizarion. As is shown in Table 5, however, the polymerizations of 4M2P slowed down in the presence of $Me(acac)_x$ in which the Me/Ti molar ratio was kept constant at 0.5. This observation is different from the observed accelerating effect on the monomer-isomerization polymerization of 2-butene.[4]

Table 6. Effect of $Ni(acac)_2$ on the monomer-isomerization polymerization of 4-methyl-2-penetene with $TiCl_3$–$Al(C_2H_5)_3$–$Ni(acac)_2$ catalyst at 80 °C in *p*-xylene for 60 hr[a]

Ni/Ti molar ratio	Yield (%)	Composition of methylpentenes recovered after polymerization, %[b]				
		2MP	4M1P	4M2P	2M2P	2M1P
0	18.5	0.9	0.5	92.0	6.3	0.3
0.06	20.9	1.9	1.2	89.3	7.0	0.6
0.15	35.6	1.4	0.8	68.2	26.8	2.8
0.20	35.9	—	—	—	—	—
0.30	18.6	1.3	2.3	70.9	22.3	3.2
0.40	3.5	0.7	4.5	78.6	13.9	2.3
0.50	1.0	0.5	2.8	75.0	16.7	5.0
Ni/Al=1/8	0.0	0.2	4.7	85.0	7.9	2.2

a) Polymerization conditions: $[TiCl_3]=117$ mmol/l, $[4M2P]=2.7$ mol/l, Al/Ti=2.0 in molar ratio. b) Determied by gas chromatography. c) In the absence of $TiCl_3$.

To test further the effect of $Me(acac)_2$, the polymerization and isomerization of 4M2P with $TiCl_3$–$Al(C_2H_5)_3$ (Al/Ti=2) catalyst in the presence of various Ni/Ti molar ratios of $Ni(acac)_2$ were investigated. The results are shown in Table 6. It is found that the rates of both polymerization and isomerization are dependent on the Ni/Ti molar ratio added, and their maximum rates are observed at an Ni/Ti molar ratio of about 0.15—0.2.

This observation seems to originate from the fact that $Ni(acac)_2$ behaves as both activator and deactivator of active sites for polymerization of 4M1P and isomerization from 4M2P to 4M1P, because $TiCl_3$ and $Ni(acac)_2$ react competitively with $Al(C_2H_5)_3$ in the catalyst system. Accordingly, it is found that at the molar ratio Ni/Ti of 0.5, the active sites for polymerization are destoroyed.

References

1) A. Shimizu, T. Otsu, and M. Imoto, *J. Polym. Sci.*, **B, 3**, 449 (1965).
2) A. Shimizu, T. Otsu, and M. Imoto, *ibid.*, **B, 3**, 1031 (1965).
3) T. Otsu, A. Shimizu, and M. Imoto, *ibid.*, **A-1, 4**, 1579 (1966).
4) T. Otsu, A. Shimizu, and M. Imoto, *ibid.*, **A-1, 7**, 3111 (1969).
5) J. P. Kennedy and T. Otsu, *Adv. Polym. Sci.*, **7**, 369 (1970).
6) T. Otsu, H. Nagahama, and K. Endo, *J. Polym. Sci.*, **B, 10**, 601 (1972).
7) S. Tani, F. Harada, and A. Nakajima, *Polym. J.*, **5**, 86 (1973).
8) Y. Atarashi, *Kobunshi Kagaku*, **21**, 264 (1964).

Optical Activity and Absolute Configuration of 2,3 : 6,7-Dibenzobicyclo[3.3.1]nona-2,6-diene Derivatives

Hitoshi TATEMITSU, Fumio OGURA, Yasuhiro NAKAGAWA, Masazumi NAKAGAWA, Koichiro NAEMURA,* and Masao NAKAZAKI*

Department of Chemistry, Faculty of Science, Osaka University, Toyonaka, Osaka 560

* *Department of Synthetic Chemistry, Faculty of Engineering Science, Osaka University, Toyonaka, Osaka 560*

(Received January 8, 1975)

2,3 : 6,7-Dibenzobicyclo[3.3.1]nona-2,6-diene-4,8-diol was synthesized and resolved *via* (−)-menthoxyacetate. Several kinds of optically active derivatives with the same absolute configuration were prepared from the (−)-diol and their chiroptical properties were recorded. The absolute configuration of this series of compounds was determined to be 1*R*, 5*R* by a chemical correlation with (*R*)-(−)-3-phenylbutanoic acid *via* (−)-1,3-diphenylglutaric acid and (−)-2,4-diphenylpentane.

A part of the present authors (members of Faculty of Science) has studied the relationship between structure and chiroptical properties of various triptycene derivatives[1] and related compounds.[2] The absolute configuration of optically active 2,5-dimethoxy-7- or 8-substituted or 2,7-disubstituted triptycenes[1] and 1,5-disubstituted 9,10-dihydro-9,10-etheno- and ethanoanthracenes[2] have been studied by either or both X-ray analyses and chemical correlations. However, exciton theoretical analyses of their CD spectra led to antipodal absolute configurations.[2,3]

The group of title compounds, 2,3: 6,7-dibenzobicyclo[3.3.1]nona-2,6-diene (XII) and its derivatives, having fairly rigid and well-defined strainless cage structure, can be regarded as one of the most appropriate dissymmetric compounds for the study of relationship between structure and optical activity.

The other authors (members of Faculty of Engineering Science) have studied on the stereochemistry of cage compounds such as twistane and related compounds,[4] and have been interested in the preparation of 2,3: 6,7-dibenzobicyclo[3.3.1]nona-2,6-diene (XII) as a precursor of optically active dibenzotwistane.

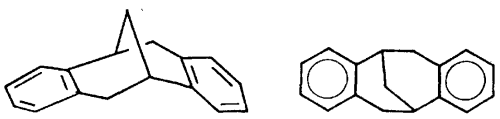

XII

The present paper deals with the synthesis, optical resolution and determination of absolute configuration by chemical means of dibenzobicyclononadiene (XII) and its derivatives.

Results and Discussion

Synthesis and Optical Resolution. The route of synthesis which followed a reported method[5] with considerable modification was outlined in Scheme 1. 1,3-Diphenylglutaronitrile (I) was prepared as a mixture of racemic and *meso* forms by the reaction of phenylacetonitrile with methylene iodide and powdered sodium hydroxide. The mixture of I was converted into a mixture of (±)- and *meso*-1,3-diphenylglutaric acids by an alkaline hydrolysis. (±)- and *meso*-1,3-Diphenylglutaric acids could be separated by repeated fractional

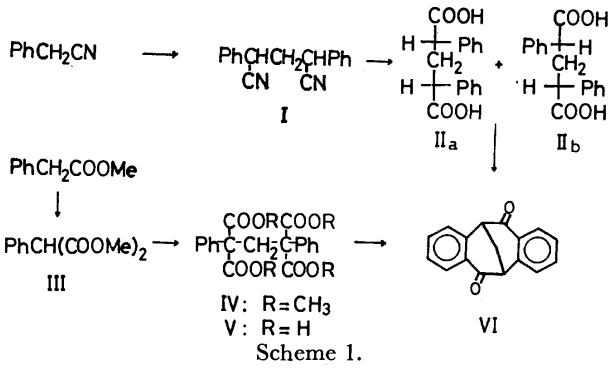

Scheme 1.

recrystallization from chloroform–ligroin and acetic acid. The higher-melting isomer (mp 191—192 °C) could be resolved in optical antipodes *via* quinine salt,[6] thus confirming racemic configuration (IIb). Consequently, the lower-melting isomer (mp 171.5—171.7 °C) was assigned to *meso* form (IIa). These assignments are found to be consistent with the NMR spectroscopic property of IIa and IIb. On irradiation of methine protons, triplet of methylene protons in the spectrum

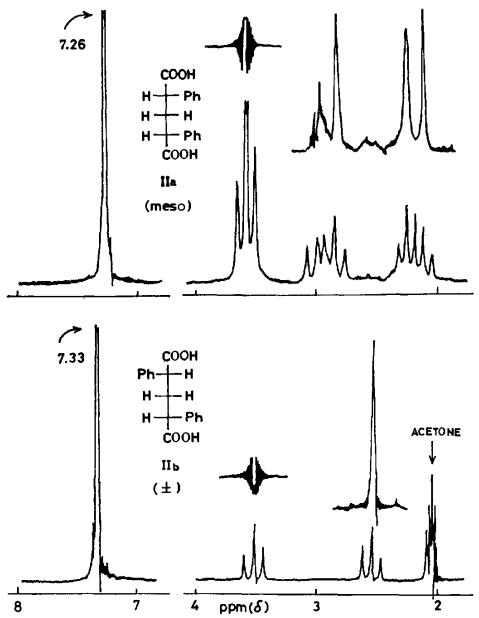

Fig. 1. 100 MHz NMR spectra of *meso*- and (±)-1,3-diphenylglutaric acids (IIa in $CDCl_3$ and IIb in acetone-d_6).

of higher-melting isomer collapsed to a singlet and multiplet of methylene protons of lower-melting isomer changed to double doublets (Fig. 1). These results indicate that the methylene protons in the higher-melting and in the lower-melting isomers situate in a magnetiacally equivalent and in an unequivalent environments, respectively. Consequently, the higher-melting isomer has a C_2 axis of symmetry passing through the methylene carbon, that is characteristic of racemic form (IIb), and the lower-melting isomer has a mirror symmetry of *meso* form (IIa). Both forms of 1,3-diphenylglutaric acid were converted into cyclic diketone (VI) with concentrated sulfuric acid. Diastereomeric mixture of the acids obtained by alkaline hydrolysis of a mixture of diastereomers of nitrile could be cyclized to the diketone (VI) directly without purification or fractionation under the same reaction conditions.

The same diketone (VI) could be prepared from methyl phenylacetate in a moderate yield *via* methyl phenylmalonate (III), methyl 1,3-diphenyl-1,1,3,3-tetracarboxylate (IV) and its hydrolysis product. The hydrolyzate consisting of mainly V was treated with polyphosphoric acid to give diketone (VI). From the diketone (VI) an identical glycol was obtained stereospecifically either by catalytic hydrogenation over platinum oxide catalyst or by reduction with lithium aluminum hydride in tetrahydrofuran. As shown in Scheme 2, three isomeric structures (VIIa,b,c) are possible in the glycol. But the formation of VIIb is excluded on the basis of NMR spectrum of the glycol and its diacetate which is prepared by a direct acetylation of the reduction product without any fractionation. The diacetate (VIII) shows doublet (J=6 Hz, 2H) at τ 3.73 (carbinyl protons) and a sharp singlet (6H) at τ 7.78 (methyl protons of acetyl groups). Therefore, the most probable structure seemed to be the one (VIIa) in which hydrogen atoms are delivered from the sterically less hindered, methano-bridge, side to generate two pseudo-axial hydroxyl groups. The inference was confirmed by the X-ray crystal structure analysis carried out on a single crystal of (+)-bis-*p*-bromobenzoate of (−)-glycol.[2)]

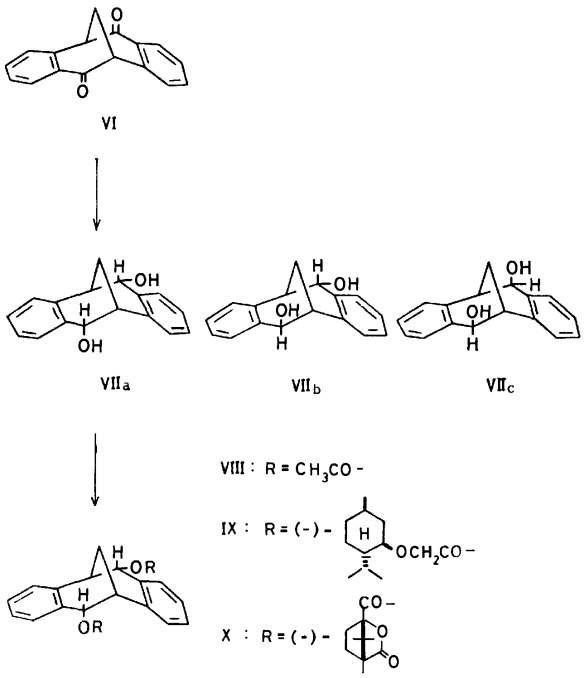

Scheme 2.

The optical resolution was carried out with (—)-methoxyacetyl chloride. Crude menthoxyacetate prepared from (±)-glycol (VIIa) and the chloride in pyridine was fractionally recrystallized eleven times from benzene-ethanol to give optically pure ester of (−)-enantiomer. The process of resolution could be traced by both polarimetry and IR spectroscopy. Optically pure menthoxyacetate was hydrolyzed by ethanolic potassium hydroxide to obtain optically pure (−)-glycol (VIIa). Attempts of optical resolution *via* camphanate showed poor reproducibility and the highest optical purity of (—)-glycol (VIIa) was 79.8%.

Starting from (—)-glycol (VIIa) several optically active derivatives with an identical configuration were prepared (Scheme 3). (—)-Glycol (VIIa) was oxidized by chromium trioxide-pyridine complex or by chromium trioxide in acetic acid to yield (+)-diketone (VI). The Clemmensen reduction of (+)-diketone (VI) yielded (—)-hydrocarbon (XII) in 33% yield. The same hydrocarbon was obtained quantitatively by lithium aluminum hydride reduction of (−)-dichloride

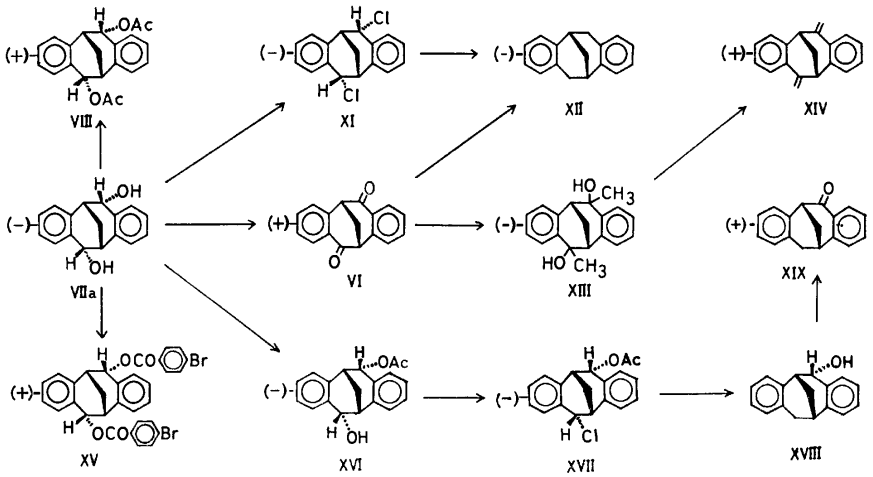

Scheme 3.

(XI) in tetrahydrofuran which is prepared from (−)-glycol (VIIa) by the usual method. The reaction of (+)-diketone (VI) with methylmagnesium iodide yielded (−)-*tert*-glycol (XIII). The configuration of carbinyl carbons could not be decided yet, but the Grignard reagent probably attacked from the side of methano-bridge to give pseudo-axial hydroxyl groups just as in the case of reduction of diketone (VI). Dehydration of (−)-*tert*-glycol (XIII) with phosphoryl chloride in pyridine gave (+)-diene (XIV) with styrene type chromophores. (−)-Glycol (VIIa) was converted into (+)-diacetate (VIII) and (+)-bis-*p*-bromobenzoate (XV) with acetic anhydride and *p*-bromobenzoyl chloride in pyridine, respectively. A single crystal of (+)-XV was submitted to the X-ray crystal structure analysis. (−)-Glycol (VIIa) was converted into (−)-monoacetate (XVI) with acetic anhydride in pyridine under a milder condition. (−)-Monoacetate (XVI) was treated with thionyl chloride in benzene to yield (−)-chloro-acetate (XVII). Lithium aluminum hydride reduction of (−)-XVII in tetrahydrofuran yielded alcohol (XVIII) which was oxidized without purification to (+)-monoketone (XIX) by the Jones reagent.

Absolute Configuration and Optical Activity. The absolute configurations of the compounds of dibenzobicyclo[3.3.1]nonadiene series were determined by chemical correlation with (*R*)-(−)-3-phenylbutanoic acid (XX).[7] The route was outlined in Scheme 4. (−)-1,3-Diphenylglutaric acid (IIb) was converted into (+)-diketone (VI) on dehydrative cyclization with concentrated sulfuric acid at 85 °C. (−)-2,4-Diphenylpentane-1,5-diol (XXIVb) was obtained by lithium aluminum hydride reduction of (−)-diphenylglutaric acid (IIb). Bis-methanesulfonate of (−)-XXIVb was reduced with lithium aluminum hydride in refluxing tetrahydrofuran to yield (−)-2,4-diphenylpentane (XXIIIb). *meso*-2,4-Diphenylpentane (XXIIIa) was obtained with essentially the same sequence of reactions from *meso*-1,3-diphenylglutaric acid (IIa). On the other hand, (*R*)-(−)-3-phenylbutanoic acid (XX) was converted into acid chloride and treated with diphenyl cadmium to give (*R*)-(−)-3-phenylbutyrophenone (XXI). The reaction of methylenetriphenylphosphorane with (*R*)-(−)-XXI gave (*R*)-(−)-2,4-diphenyl-1-pentene (XXII). Catalytic hydrogenation of (*R*)-(−)-XXII over the Adams catalyst yielded almost equimolar mixture of *meso*- and (*R*)-(−)-2,4-diphenylpentane (XXIIIa and XXIIIb) which were analyzed and identified by NMR spectroscopy.

(−)-2,4-Diphenylpentane obtained from (−)-1,3-diphenylglutaric acid (IIb) showed an identical CD spectrum with that of the mixture of XXIIIa and (*R*)-(−)-XXIIIb obtained from (*R*)-(−)-XX after correction of optical purity.

From the combined results of the above-mentioned sequence of reactions, it can be clearly concluded that all of optically active compounds shown in Scheme 4 have (*R*)-absolute configuration. The conclusion was consistent with the result of X-ray analysis carried out on a single crystal of (+)-2,3: 6,7-dibenzobicyclo[3.3.1]-nona-2,6-diene-4,8-diol-bis-*p*-bromobenzoate (XV).[8]

(+)-Diketone (VI) showed a strong positive CD band with well-developed fine structure in the longest wavelength region and a beautiful positive-negative couplet in 37000—44000 cm^{-1} region (Fig. 2). The longest wavelength band can be assigned to n→π^* transition of conjugated ketone on the basis of solvent effect and a considerably large anisotropic factor (Table 1). The strong couplet centered at near 40000 cm^{-1} was attri-

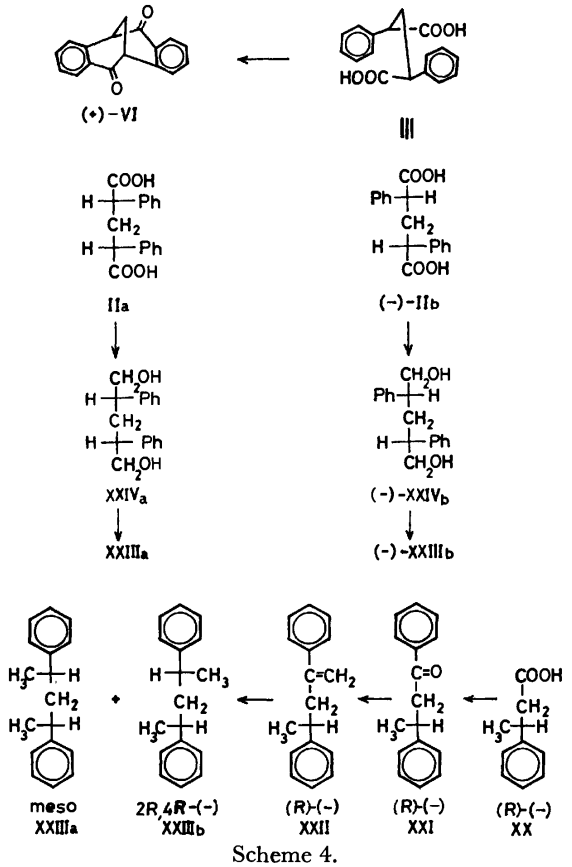

Scheme 4.

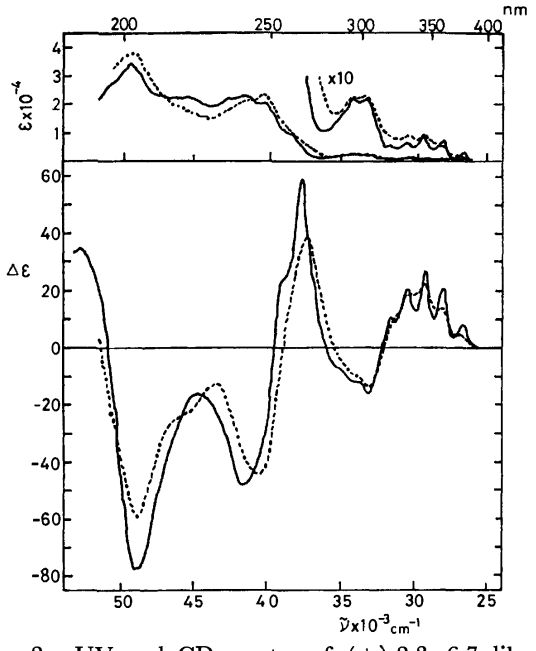

Fig. 2. UV and CD spectra of (+)-2,3 : 6,7-dibenzobicyclo[3.3.1]nona-2,6-diene-4,8-dione (VI) in cyclohexane (——) and in 99% ethanol (·····).

Table 1. UV spectra of VI and CD spectra of (+)-VI, (−)-VIIa, (−)-XII and (+)-XIV

UV spectra of VI

Solvent	λ_{max} in nm (ε) * Shoulder
Ethanol	372*(200), 355(580), 340(900), 329(880), 300(2290), 293*(2230), 249(23410), 243(21930), 207*(31720), 203.5(38060)
Cyclohexane	376(310), 358(740), 342(940), 328(740), 315(540), 301(2250), 292(2190), 260*(9760) 249(20780), 241(22640), 236(22100), 221*(22140), 203(34420), 197*(26550)

CD spectra

Compound	Solvent	λ_{max} in nm ($\Delta\varepsilon$) * Shoulder
(+)-VI	Cyclohexane	377*(+7.9), 375(+8.2), 357(+20.2), 342(+26.5), 328.5(+20.2), 316.5 (+10.0), 302(−15.9), 292.5(−11.5), 280(−3.2), 265.5(+58.6), 257* (+23.8), 248*(−36.0), 241(−48.2), 204(−77.6), 190(+34.8)
	Ethanol	372(+4.7), 354(+13.7), 340(+22.1), 329(+19.1), 318*(+9.7), 302 (−13.3), 290*(−8.0), 268(+38.4), 246(−44.2), 222*(−21.3), 205(−58.9)
(−)-VIIa	Ethanol	272(+0.36), 264(−0.51), 257*(−0.42), 251*(−0.31), 219*(−31.35), 205 (−86.01), 195(+22.30)
(−)-XII	Isooctane	273(+2.7), 266(+2.6), 260(+1.6), 254*(+0.9), 246*(+0.4), 226(−0.8), 222(+2.5), 218 (−8.6), 214 (−9.0), 197(−82.1)
(+)-XIV	Isooctane	299(+1.9), 291(+2.3), 260*(+65.1), 245(+83.2), 227*(−62.7), 216 (−152.4), 203(−78.6)
	Ethanol	298(+1.8), 290*(+2.2), 247(+66.0), 227*(−51.4), 215(−127.3), 205* (−78.2)

buted to an exciton couplet due to the interaction of two conjugated phenyl ketone chromophores. This compound (VI) is unique in the sense that it might be regarded as an α,β- and β,γ-unsaturated ketones at the same time. In applying the octant rule, a different conclusion came out by considering which of α,β- or β,γ-unsaturation contributed stronger to the observed optical activity.[9] It is easily shown by the Dreiding molecular model that molecular framework of this ketone (VI) brings about closely similar spatial disposition of carbonyl and phenyl groups as those in dimethylbenzsuberone and related typical β,γ-unsaturated ketone (Fig. 3).[10] Observed highly positive rotational strength of n→π^* transition is consistent with 1*R*,5*R* absolute configuration for (+)-diketone (VI) (Fig. 3). On the other hand, if the diketone (VI) is considered to be an α,β-unsaturated ketone, a small negative n→π^* Cotton effect may be expected for the above 1*R*,5*R* configuration on the ground of fairly good coplanarity of phenyl-carbonyl grouping[11] being the

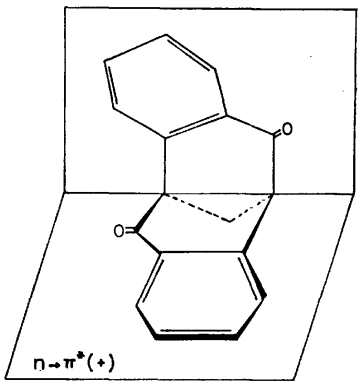

Fig. 3. Octant projection of (+)-1*R*,5*R*-2,3 : 6,7-dibenzobicyclo[3.3.1]nona-2,6-diene-4,8-dione (VI) as regarded as a β,γ-unsaturated ketone.

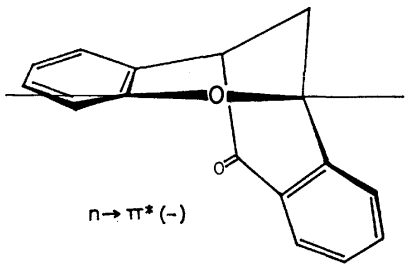

Fig. 4. Octant projection of (+)-1*R*,5*R*-2,3 : 6,7-dibenzobicyclo[3.3.1]nona-2,6-diene-4,8-dione (VI) as regarded as an α,β-unsaturated ketone.

dihedral angle of distortion less than 10 degrees as estimated from the Dreiding model (Fig. 4). We concluded that the contribution of β,γ-unsaturation is predominant and that of α,β-unsaturation is negligibly small in this ketone (VI).

With regard to the couplet in the $^1B_{1u}$ type $\pi\rightarrow\pi^*$ absorption region of (+)-diketone (VI), we assumed an exciton coupling of C_2 symmetry and the same 1*R*,5*R* configuration as shown in Fig. 5 could be deduced.

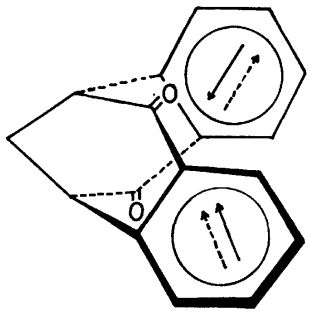

Fig. 5. Exciton coupling of $^1B_{1u}$ band of (+)-1*R*,5*R*-2,3: 6,7-dibenzobicyclo[3.3.1]nona-2,6-diene-4,8-dione (VI).

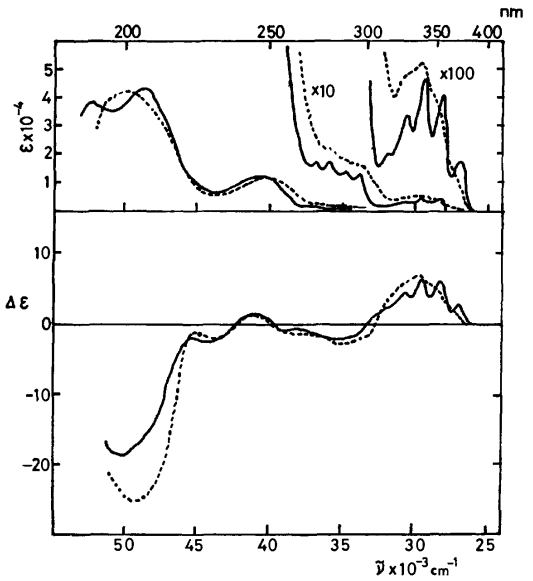

Fig. 6. UV and CD spectra of (+)-2,3 : 6,7-dibenzobicyclo[3.3.1]nona-2,6-diene-4-one (XIX) in cyclohexane (——) and in 99% ethanol (……).

The positive and negative bands can be assigned to transitions from ground to excited states with A and B symmetry, respectively, based on usual calculations. These assignments are consistent with intensity relationship of the corresponding isotropic absorption band and the absence of a CD couplet in the n→π* band region of (+)-monoketone (XIX) (Fig. 6). In the region of $^1B_{2u}$ type absorption, the situation is not so clear. A small positive-negative couplet is similarly anticipated for the same 1*R*,5*R* absolute configuration. Observed result seems to be consistent with this prediction, if we consider that long wavelength positive band is significantly overlapped with n→π* carbonyl band (*cf.*, solvent effect, Table 1 and Fig. 2). Combining the above-stated consistent results, we concluded that (+)-diketone (VI) has 1*R*,5*R* absolute configuration.

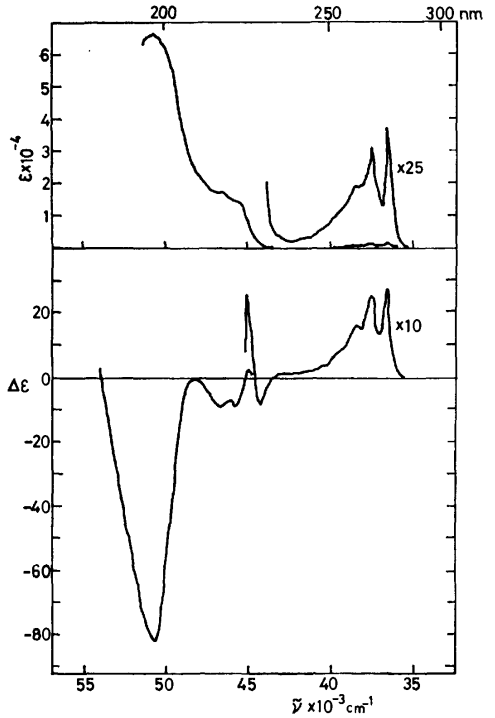

Fig. 7. UV and CD spectra of (−)-2,3 : 6,7-dibenzobicyclo[3.3.1]nona-2,6-diene (XII) in isooctane.

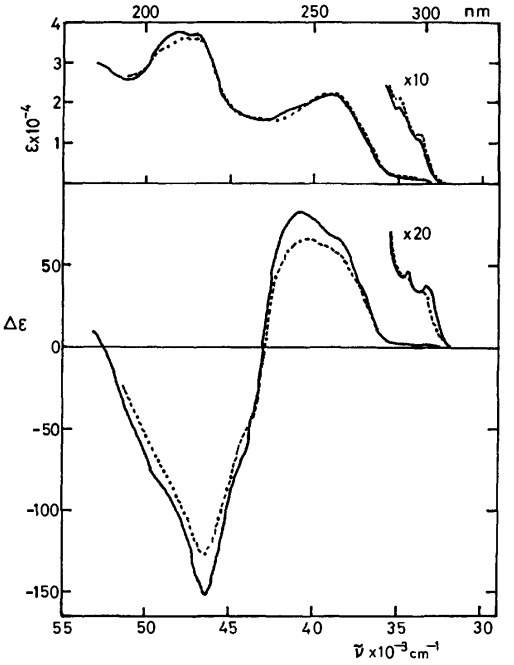

Fig. 8. UV and CD spectra of (+)-4,8-bis(methylene)-2,3 : 6,7-dibenzobicyclo[3.3.1]nona-2,6-diene (XIV) in isooctane (——) and in 99% ethanol (……).

The CD and electronic spectra of (−)-hydrocarbon (XII) are shown in Fig. 7. Complexity of the spectra might result from significant overlap of $^1B_{1u}$ and two degenerate $^1E_{1u}$ type bands and low absorption intensity of $^1B_{2u}$ band.

(+)-Diene (XIV) with styrene type chromophores showed a very interesting CD spectrum. In the π→π* spectral region, no couplet pattern could be observed (Fig. 8) in sharp contrast with (+)-diketone (VI). It is difficult to give a definite explanation, but one possible reason is that the direction of polarization of conjugation band of the styrene chromophore and position of its transition moments are considerably different from those of phenyl alkyl ketone.[12]

Experimental

The melting points were measured on a Mettler FP2 apparatus and a Shimadzu Kohfler micro hot stage, and are uncorrected. Purified and anhydrous solvents were used, unless otherwise stated. The IR spectra were obtained on a Hitachi EPI-2, EPI-G3 or a JASCO DS-301 spectrometers, electronic spectra on a Hitachi EPS-3T and a Zeiss PMQIIM4QIIId spectrometers, NMR spectra in deuteriochloroform, unless otherwise stated, on a Varian XL-100 or A-60D spectrometer using TMS as an internal standard and given in δ-unit. The optical rotations were obtained on a Yanagimoto ORD-185 spectropolarimeter or a Union Giken High Precision Polarimeter PM-71 or a JASCO DIP-SL polarimeter at 20 °C, unless otherwise stated. CD spectra were obtained on a JASCO J-20 spectrometer. Shoulders and inflections are denoted by an asterisk.

1,3-Diphenylglutaronitrile (I). Phenylacetonitrile (93.6 g, 0.799 mol), methylene iodide (107.2 g, 0.400 mol) and powdered sodium hydroxide (32.0 g, 0.800 mol) were mixed and heated to 165—170 °C for 30 min under stirring. Cooled mixture was diluted with water and extracted with ether. Combined organic layer was washed with water and concentrated undre reduced pressure. After volatile material had been removed by steam distillation (distillate, *ca.* 6 l), the residue was extracted with ether and dried over sodium sulfate. A black oil (66.1 g) obtained on concentration of the extract under reduced pressure was chromatographed on alumina (650 g) and fractions eluted with benzene (total 3.3 l) and benzene–ether (1: 1, total 1.5 l) were combined and concentrated under reduced pressure. The oily residue was crystallized from ethanol. Repeated recrystallization from the same solvent yielded analytically pure I as orange yellow crystals, mp 64.9—65.6 °C, IR (nujol mull): 2250 ($\nu_{C\equiv N}$) cm^{-1}, NMR (CCl_4): 7.33 (s, 10H, aromatic), 4.03, 3.63 (both t, J=8 Hz, 2H, methine), 2.33 (m, 2H, methylene).

The crude nitrile obtained by chromatography could be used directly for further reaction.

1,3-Diphenylglutaric Acid (II). Crude acid (II) obtained by an alkaline hydrolysis of the nitrile (I)[4] was converted into diethyl ester (see below). The purified ester was refluxed with 10% ethanolic potassium hydroxide. Colorless oil obtained on working up the reaction mixture crystallized gradually on standing, mp 147.5—163 °C (a mixture of *meso*- and *rac*-isomers), IR (Nujol mull): 1710 ($\nu_{C=O}$) cm^{-1}.

Diethyl 1,3-Diphenylglutarate. Crude carboxylic acid (II, 14.42 g) was refluxed with ethanol (100 ml) and concentrated sulfuric acid (5 ml). The reaction mixture was worked up as usual and the oily residue was distilled under reduced pressure to give pure ester, faintly yellow liquid (10.85 g, 62.8%), bp 182—186 °C/133 Pa, IR (neat): 1740, 1730 ($\nu_{C=O}$) cm^{-1}, NMR: 7.25, 7.23 (both s, 10H, aromatic), 3.88—4.33 (m, 4H, methylene of ethyl), 3.33—3.68 (m, 2H, methine), 2.58 (m, 2H, methylene), 1.17, 1.13 (both t, J=7 Hz, 6H, methyl).

meso- *and* rac-*1,3-Diphenylglutaric Acids (IIa and IIb).* Crude crystals of the acid mixture (29.7 g) were recrystallized from chloroform–ligroin. Crystals obtained (4.68 g) were recrystallized further three times from the same mixed solvent to yield colorless needles of pure racemate (IIb, 3.2 g), mp 191—192 °C, IR (Nujol mull): 1710*, 1690 ($\nu_{C=O}$) cm^{-1}, NMR (CD_3COCD_3): 7.26 (s, 10H, aromatic), 3.50 (t, of d, J=7 Hz and 1 Hz, methine), 2.52 (t, of d, J=7 Hz and 1 Hz, methylene).

Found: C, 71.70; H, 5.68%. Calcd for $C_{17}H_{16}O_4$: C, 71.82; H, 5.61%.

Crude crystals obtained by drying up the initial mother liquor *in vacuo* were recrystallized from 50% aqueous acetic acid. First crop of crystals enriched in racemate was removed by filtration. Water was added to the hot mother liquor till the mixture became 20% aqueous acetic acid solution. Precipitates obtained on cooling the mixture were recrystallized eight times from 20% aqueous acetic acid to yield pure *meso*-isomer (IIa, 1.224 g), mp 171.5—171.7 °C, IR (Nujol mull): 1710, 1700 ($\nu_{C=O}$) cm^{-1}, NMR: 7.26 (s, 10H, aromatic), 3.57 (dd, 2H, methine), 3.07—2.76 (q, 1H, methylene), 2.31—2.04 (q, 1H, methylene).

Found: C, 71.89; H, 5.66%. Calcd for $C_{17}H_{18}O_4$: C, 71.82; H, 5.67%.

Optical Resolution of rac-*1,3-Diphenylglutaric Acid (IIb).* The racemic acid (IIb, 1.204 g) dissolved in 99% ethanol (20 ml) was mixed with a 99% ethanol solution of quinine (1.374 g in 10 ml) and stood overnight at room temperature. Colorless crystals (1.578 g) deposited were collected and dried *in vacuo*, mp 215—219 °C. The mother liquor and washings were combined and concentrated under reduced pressure to give colorless residue (1.161 g).

The crystalline salt was decomposed by 3 M hydrochloric acid and extracted with ether. The extract was worked up in the usual way and concentrated under reduced pressure to yield (+)-acid (0.471 g, $[\alpha]_D$ +70.72 ° (*c* 0.2828, 99% EtOH). Enantiomeric (−)-acid (0.7068 g, $[\alpha]_D$ −48.16 ° (*c* 0.2824, 99% EtOH)) was obtained from the residue of mother liquor by the same procedure.

The quinine salt was found thermally unstable and seemed to be difficult to fractionate diastereomers by the usual recrystallization. Optically pure salt could be obtained by repetition of formation and decomposition of the quinine salt for six times at room temperature. The extent of resolution was checked by polarimetry of acid obtained from each mother liquor.

Optically pure salt (0.814 g), mp 219—223 °C (dec.), consisted of two molecules of quinine per a molecule of (+)-acid and contained one molecule of ethanol as a solvent of crystallization.

Found: C, 71.21; H, 7.21; N, 5.54%. Calcd for $C_{61}H_{76}N_4O_{10}$: C, 71.46; H, 7.47; N, 5.47%.

Optically pure (+)-1,3-diphenylglutaric acid (IIb, 0.238 g) was obtained from this salt, mp 197—198.5 °C (from chloroform–*n*-hexane), $[\alpha]_D$ +95.8 °, $[\alpha]_{546}$ +114.8 °, $[\alpha]_{436}$ +204.2 ° $[\alpha]_{405}$ +260.1 °, $[\alpha]_{365}$ +375.7 ° (*c* 0.179, 99% EtOH).

Found: C, 71.85; H, 5.66%. Calcd for $C_{17}H_{16}O_4$: C, 71.82; H, 5.67%.

Tetramethyl 1,3-Diphenylpropane-1,1,3,3-tetracarboxylate (IV). To a mixture of methanol (150 ml) and sodium methoxide (60 g) was added successively methyl phenyl acetate (150 g) and dimethyl oxalate (118 g). The mixture was allowed to stand overnight. After refluxing for 2 hr under stirring, the mixture was decomposed with water and hydrochloric acid, and extracted with ether. Combined extracts, after washing with water and drying over magnesium sulfate, were concentrated to remove solvent and volatile material. The oily residue was distilled under reduced pressure to yield dimethyl phenylmalonate (III. 178.4 g), bp 159—163 °C/3325 Pa. A mixture of dimethyl phenylmalonate (147.8 g) and methylene iodide (96.0 g) was added dropwise to a stirred solution of sodium methoxide (41 g) in methanol (180 ml), and the mixture was refluxed for 32 hr. Cooled reaction mixture was poured into water and extracted with ether. The extract, after washing and drying over calcium chloride, was concentrated, and the residue was distilled under reduced pressure to give pure tetraester (III, 67.3 g), bp 178—180 °C/133 Pa.

Found: C, 64.05; H, 5.72%. Calcd for $C_{23}H_{24}O_8$: C, 64.48; H, 5.65%.

2,3: 6,7-Dibenzobicyclo[3.3.1]nona-2,6-diene-4,8-dione (VI). From the Mixture of Racemic and Meso Forms: To 1,3-diphenylglutaronitrile (I, 40.0 g) dissolved in 99% ethanol (450 ml) was added a solution of potassium hydroxide (120 g) in water (330 ml) and the mixture was heated to 70 °C for 8 hr. The reaction mixture was mixed with water (550 ml) and washed with ether. Aqueous layer was acidified with concentrated hydrochloric acid and extracted with ethyl acetate. The extract was washed with brine and dried over sodium sulfate. Crude mixture of (±)- and *meso*-1,3-diphenylgluratic acids was obtained as a yellow oil on evaporating the solvent under reduced pressure. The mixture of acids (46.2 g) was dissolved in concentrated sulfuric acid and heated to 85 °C for 30 min. The reaction mixture was poured onto ice and extracted with benzene. The extract was washed with 3% aqueous potassium hydroxide and water successively and dried over sodium sulfate. On evaporating the solvent *in vacuo* was obtained colorless solid (24.3 g), which was recrystallized twice from

methanol to yield pure diketone (VI) as colorless needles, mp 147.7—147.8 °C, IR (Nujol mull): 1680 ($\nu_{C=O}$) cm^{-1}, NMR: 8.17—7.82 (m, 2H, aromatic protons adjacent to carbonyl group), 7.55—7.15 (m, 6H, aromatic), 4.01 (t, J= 3 Hz, 2H, bridgehead), 2.98 (t, J=3 Hz, 2H, methylene bridge).

Found: C, 81.99; H, 4.82%. Calcd for $C_{17}H_{12}O_2$: C, 82.24; H, 4.87%.

From Racemic and Optically Active Forms (IIb): By essentially the same cyclization procedure, identical (±)-diketone (VI) was obtained from (±)-IIb in 84% yield. The (−)-acid (IIb, 0.1411 g, $[\alpha]_D$ −48.2 ° (*c* 0.2824, 99% EtOH), optical purity 50.4%) yielded (+)-diketone (VI, 0.1054 g, $[\alpha]_D$ +139.5 ° (*c* 0.02108, 99% EtOH) by the same reaction conditions. Optical purity of the (+)-diketone (VI), estimated from the values of ORD peaks and troughs, was *ca.* 45%. A minor extent of racemization seemed to occur during the course of ring closure reaction.

From meso *Form (IIa)*: The *meso*-acid (IIa) yielded the identical (±)-diketone (VI) in 77% yield under the same reaction conditions.

From Tetramethyl Ester (IV): Tetramethyl ester (IV, 14.2 g) was mixed with 5% alcoholic potassium hydroxide and refluxed for 2 hr. The mixture was diluted with water and neutral material was removed by extraction with ether. Aqueous layer was acidified with hydrochloric acid and extracted with ether. The extract was washed with water and dried over magnesium sulfate. A partly crystallized residue (V, 5.0 g) obtained on evaporating the solvent under reduced pressure was mixed with polyphosphoric acid (150 g) and heated to 100 °C under stirring for 2 hr. The reaction mixture was poured onto ice water and extracted with ether. Organic layer was washed with 5% aqueous sodium carbonate and water, and dried over magnesium sulfate. Crystalline residue obtained by evaporating the solvent *in vacuo* was recrystallized from benzene–ligroin to yield the same (±)-diketone (VI).

2,3: 6,7-Dibenzobicyclo[3.3.1]nona-2,6-diene-4,8-diol (VIIa). By Lithium Aluminum Hydride Reduction: The diketone (VI, 0.5 g) in tetrahydrofuran (8 ml) was added under stirring to an ice-cooled suspension of lithium aluminum hydride (0.63 g) in the same solvent (16 ml). After stirring for further 1 hr under ice-cooling, the reaction mixture was worked up in the usual way, and extracted with ether. The extract was washed successively with water, aqueous potassium carbonate and saturated sodium chloride, and dried over sulfate. Evaporation of the solvent under reduced pressure yielded the crude glycol (VIIa), mp 225 °C (with sublimation), IR (Nujol mull): 3280 (broad), 3550, 3575 (ν_{O-H}) cm^{-1}.

Found: C, 80.66; H, 6.35%. Calcd for $C_{17}H_{16}O_2$: C, 80.92; H, 6.39%.

By Catalytic Reduction: The diketone (VI, 0.1228 g) in ethyl acetate (10 ml) was catalytically reduced over the Adams catalyst, yielding identical glycol (VIIa) in quantitative yield.

4,8-Diacetoxy-2,3: 6,7-dibenzobicyclo[3.3.1]nona-2,6-diene (VIII). Crude glycol (VIIa, 0.2081 g) dissolved in pyridine (3 ml) was mixed with acetic anhydride (4 ml) and heated to 90 °C for 5.5 hr. The reaction mixture was worked up in the usual way to give colorless solid (0.2247 g) which showed single spot on a silica gel TLC plate developed with benzene or benzene–ether. The solid was recrystallized from benzene–methanol to give colorless needles of VIII, mp 220.9—221.6 °C, IR (Nujol mull): 1730 ($\nu_{C=O}$) cm^{-1}, NMR: 7.32—6.87 (m, 8H, aromatic), 6.27 (d, J=6 Hz, 2H, methine), 3.55 (q, 2H, bridgehead), 2.43 (t, J=3.5 Hz, 2H, methylene), 2.22 (s, 6H, methyl).

Found: C, 74.97; H, 5.96%. Calcd. for $C_{21}H_{20}O_4$: C, 74.98; H, 5.99%.

Optical Resolution of 2,3: 6,7-Dibenzobicyclo[3.3.1]nona-2,6-diene-4,8-diol (VIIi). Via *Bis-(−)-menthoxyacetate (IX)*: (−)-Menthoxyacetyl chloride (2.18 g) was added to a stirred solution of (±)-glycol (VIIa, 1.00 g, 3.96 mmol) in pyridine (8 ml). After stirring overnight at room temperature, the mixture was poured into water and extracted with benzene. The extract was washed successively with 2 M hydrochloric acid, aqueous potassium carbonate and saturated aqueous sodium chloride, and dried over sodium sulfate. A brown solid obtained on evaporating the solvent under reduced pressure was chromatographed on silica gel (30 g). Elution with benzene–ether (4: 1) yielded light yellow solid (2.32 g), mp 179.7—189.4 °C, (Nujol mull): 1760, 1740 ($\nu_{C=O}$) cm^{-1}.

The crude bis-(−)-menthoxyacetate was recrystallized eleven times from benzene–ethanol (1: 1) to give an optically pure enantiomer as colorless needles (0.25 g), mp 215.7—216.3 °C, IR (Nujol mull): 1750 ($\nu_{C=O}$) cm^{-1}, ORD: $[\alpha]_D$ −41.4 °, $[\alpha]_{546}$ −49.7 °, $[\alpha]_{405}$ −119.4 ° (*c* 0.313, dioxane).

Found: C, 76.45; H, 8.74%. Calcd for $C_{41}H_{56}O_6$: C, 76.36; H, 8.75%.

Optically pure IX (0.217 g) thus obtained was dissolved in benzene and mixed with ethanolic potassium hydroxide (0.09 g in 5 ml). After the mixture had been refluxed for 2 hr, water was added. Precipitate formed, after being washed with water, was recrystallized from benzene to give optically pure (−)-glycol (VIIa), mp 189.5—189.8 °C, IR (Nujol mull): 3390 (ν_{O-H}) cm^{-1}, ORD: $[\alpha]_D$ −84.9 °, $[\alpha]_{546}$ −101.4 °, $[\alpha]_{500}$ −132 °, $[\alpha]_{450}$ −185 °, $[\alpha]_{436}$ −204 ° (*c* 0.4065, 99% EtOH), $[\alpha]_{405}$ −261 °, $[\alpha]_{350}$ −487 °, $[\alpha]_{320}$ −771 °, $[\alpha]_{250}$ −5400 °, $[\alpha]_{230}$ −19150 ° (*c* 0.2185, 99% EtOH), UV: $\lambda_{max}^{99\%EtOH}$ (ε) 272 (320), 269(360), 264(470), 275*(390), 255*(280), 249*(230), 244*(150), 215*(17300), 199(59100) nm, CD: see Table 1.

Via *Bis-(−)-camphanate (X)*: The crystals (0.4183 g) obtained from (±)-glycol (VIIa, 0.1754 g), (−)-camphanyl chloride (0.375 g) and pyridine (5 ml) were recrystallized five times from benzene–ligroin to give (+)-bis-camphanate (32 mg) with constant rotation, colorless needles, mp 281—285 °C, $[\alpha]_D$ +38.9 ° (*c* 0.4834, dioxane).

Found: C, 72.55; H, 6.59%. Calcd for $C_{27}H_{40}O_8$: C 72.53; H, 6.58%.

(−)-Glycol (VIIa, mp 187.9—188.3 °C (from benzene), $[\alpha]_{350}$ −388.5 ° (*c* 0.02059, 99% EtOH), optical purity 79.8%) was obtained on alkaline hydrolysis of the (+)-bis(−)-camphanate (X) with constant optical rotation.

(+)-4,8-Diacetoxy-2,3: 6,7-dibenzobicyclo[3.3.1]nona-2,6-diene (VIII). (−)-Glycol (VIIa,104.4 mg) was acetylated with acetic anhydride (2 ml) and pyridine (1.5 ml) on heating to 90 °C for 5.5 hr. The reaction mixture was worked up in the same way as racemate to give colorless crystals (129.3 mg) of (+)-VIII, which showed identical NMR spectrum and the same tlc-*Rf* value with those of the racemate. The crystals were recrystallized from methanol to give pure (+)-VIII, colorless needles, mp 242.6—243.0 °C, IR (Nujol mull): 1730 ($\nu_{C=O}$) cm^{-1}, ORD: $[\alpha]_D$ +10.7 °, $[\alpha]_{474}\approx$O °, $[\alpha]_{436}$ −12.4 °, $[\alpha]_{405}$ −31.4 °, $[\alpha]_{365}$ −83.0 ° (*c* 0.541, dioxane).

Found: C, 74.82; H, 6.03%. Calcd for $C_{21}H_{20}O_4$: C, 74.98; H, 5.99%.

(+)-2,3: 6,7-Dibenzobicyclo[3.3.1]nona-2,6-diene-4,8-dione (VI). Chromium trioxide (0.1 g) in acetic acid (1 ml) was added under stirring to an ice-cooled solution of (−)-VIIa (20.1 mg) in acetone (3 ml) and acetic acid (0.5 ml). After stirring for further 19 hr at room temperature, the mixture was worked up in the usual manner. Light brown solid (13.4 mg) obtained was dissolved in benzene

and passed through a short column of silica gel (1.5 g). The material obtained from the filtrate was recrystallized from ligroin to give (+)-VI, colorless needles, mp 194.—194.5 °C, IR (Nujol mull): 1685 ($\nu_{C=O}$) cm^{-1}, ORD: $[\alpha]_D$ +343 °, $[\alpha]_{546}$ +419 °, $[\alpha]_{436}$ +1370 °, $[\alpha]_{405}$ +2570 °, $[\alpha]_{372}$ +9140 °, $[\alpha]_{355}$ +12600 °, $[\alpha]_{341}$ +7480 °, $[\alpha]_{320}$ −9340 °*, $[\alpha]_{316}$ −23700 °*, $[\alpha]_{306}$ −29100 °, $[\alpha]_{274}$ +14600 °, $[\alpha]_{253}$ −77200 ° (*c* 0.0198, 99% EtOH), UV and CD: see Table 1.

Found: C, 82.23; H, 4.90%. Calcd for $C_{17}H_{12}O_2$: C, 82.24; H, 4.87%.

(−)-4,8-Dichloro-2,3 : 6,7-dibenzobicyclo[3.3.1]nona-2,6-diene (XI). (−)-Glycol (VIIa, 117.8 mg) in benzene (10 ml) was refluxed with thionyl chloride (1.3 ml) for 17.5 hr. The reaction mixture was treated in the usual way, and faintly yellow oil obtained on evaporating the solvent under reduced pressure was dissolved in benzene and passed through a short column of silica gel. Colorless oil (140.9 mg) obtained from the filtrate was crystallized from methanol to give pure (−)-XI, colorless leaflets, mp 130.4—132.1 °C, NMR (CCl_4): 7.30—7.10 (m, 8H, aromatic), 4.96 (d, J=2 Hz, 2H, methine), 3.52 (m, 2H, bridgehead), 2.55 (t, J=3 Hz, 2H, methylene), ORD (at 25 °C): $[\alpha]_{365}$ −428 °, $[\alpha]_{276}$ −2420 °, $[\alpha]_{271}$ −391 °* $[\alpha]_{250}$ −6770 ° (*c* 0.02148, 99% EtOH), UV: $\lambda_{max}^{99\%EtOH}$ (ε) 278(450), 273*(540), 270(580), 266*(560), 261*(500), 211.5 (26700), 206(25800), 202*(28100), 195(41700) nm, CD: $\lambda_{max}^{99\%EtOH}$ ($\Delta\varepsilon$) 278(−2.96), 270(−3.18), 264*(−1.88), 234 (+24.2), 218(+32.3), 198.5(−68.3) nm.

Found: C, 70.81; H, 4.91; Cl, 24.65%. Calcd for $C_{17}H_{14}Cl_2$: C, 70.60; H, 4.88; Cl, 24.52%.

Racemate was obtained as colorless needles, mp 173.4—174.2 °C (from methanol).

(−)-2,3: 6,7-Dibenzobicyclo[3.3.1]nona-2,6-diene (XII).

From (−)-Dichloride (XI): (−)-Dichloride (XI, 267 mg) in tetrahydrofuran (5 ml) was added to a stirred suspension of lithium aluminum hydride (0.37 g) in the same solvent (12 ml), and the mixture was refluxed for 24 hr. The reaction mixture was worked up in the usual manner. Light yellow oil obtained was dissolved in carbon tetrachloride–benzene (1: 1) and passed through a short column of silica gel (14 g). Colorless oil (180.9 mg) obtained from the filtrate was crystallized from methanol to yield (−)-XII, colorless needles, mp 100.8—102.2 °C, NMR: 7.28—6.85 (m, 8H, aromatic), 3.52—2.55 (m, 6H, methine and methylene), 2.92 (t, J=3 Hz, 2H, methano-bridge), ORD: $[\alpha]_D$ −247 °, $[\alpha]_{404}$ −635 °, $[\alpha]_{365}$ −900 °, $[\alpha]_{282}$ −2010 °, $[\alpha]_{268}$ −987 ° (*c* 0.02188, isooctane), UV: $\lambda_{max}^{isooctane}$ (ε) 273(1480), 266(1230), 262(790), 260(770), 258*(740), 252*(430), 246*(230), 219(14450), 214(17200), 196(66100) nm, CD: see Table 1.

Found: C, 92.40; H, 7.28%. Calcd for $C_{17}H_{16}$: C, 92.68; H, 7.32%.

Racemate: mp 71.7—73.5 °C.

By the Clemmensen Reduction of (±)-VI: A mixture of (±)-diketone (VI, 218 mg), toluene (3 ml), concentrated hydrochloric acid (1.75 ml), water (0.75 ml) and granulated zinc (1.2 g) activated with mercuric chloride and diluted hydrochloric acid was refluxed for 24 hr under stirring. The reaction mixture was worked up in the usual way to yield light yellow oil. The oil in carbon tetrachloride was passed through a short column of alumina and silica gel, successively. Colorless oil (64.3 mg) obtained from the filtrate was crystallized from 99% ethanol to give pure (±)-XII, colorless plates, mp 72.1—73.5 °C, which showed identical IR and NMR spectra with those of (±)-XII obtained from (±)-VIIa.

Found: C, 92.55; H, 7.43%. Calcd for $C_{17}H_{16}$: C, 92.68; H, 7.32%.

(−)-4,8-Dihydroxy-4,8-dimethyl-2,3 : 6,7-dibenzobicyclo[3.3.1]nona-2,6-diene (XIII). To an ice-cooled solution of methylmagnesium iodide (magnesium 0.9 g, methyl iodide 5.5 g and ether 30 ml) a solution of (+)-VI (511.3 mg) in tetrahydrofuran (25 ml) was added under stirring. After 1.5 hr, the mixture was refluxed for 5 hr. Brown oil (584.4 mg) obtained on treatment of the reaction mixture in the usual manner was dissolved in benzene and passed through a short column of silica gel (3 g). Colorless solid obtained from benzene and benzene–ether eluates was recrystallized once from benzene and twice from petroleum ether to give pure (−)-XIII, mp 115.1—116.0 °C, IR (Nujol mull): 3750, 3480 (ν_{O-H}) cm^{-1}, NMR: 7.65—7.05 (m, 8H, aromatic), 3.04 (t, J=3 Hz, 2H, bridgehead), 2.57 (t, J=3 Hz, 2H, methylene), 1.65 (s, 6H, methyl), 1.63 (s, 2H, OH), ORD (at 25 °C): $[\alpha]_{365}$ −349 °, $[\alpha]_{300}$ −1040 °, $[\alpha]_{260}$ −3010 ° (*c* 0.020645, 99% EtOH), UV: $\lambda_{max}^{99\%EtOH}$ (ε) 272(240), 268(200), 262.5 (400), 275.4*(330), 252*(250), 245*(150), 218*(15050), 214* (17900), 196.5(69400) nm, CD: $\lambda_{max}^{99\%EtOH}$ ($\Delta\varepsilon$) 274(+0.05), 271.5(−0.07), 265(−0.12), 256(−0.16), 251(−0.16), 216 (−35.3), 203(−85.6) nm.

Found: C, 81.27; H, 7.20%. Calcd for $C_{19}H_{20}O_2$: C, 81.39; H, 7.19%.

Racemate was prepared similarly and recrystallized twice from benzene–ligroin, mp 165.5—166.2 °C, IR (Nujol mull): 3570 (ν_{O-H}) cm^{-1}.

When just two equivalents of the Grignard reagent was added to (±)-VI, only 44.3% of (±)-XIII was obtained and a ketoalcohol, 4-hydroxy-4-methyl-2,3 : 6,7-dibenzobicyclo-[3.3.1]nona-2,6-dine-8-one, was isolated in 37.6% yield. The ketoalcohol was recrystallized three times from acetone to yield pure crystals, which contained a molecule of acetone as a solvent of crystallization, IR (Nujol mull): 3460 (ν_{O-H}), 1690, 1683 ($\nu_{C=O}$), 1712 ($\nu_{C=O}$, acetone) cm^{-1}, NMR: 7.85 (m, J_o= 7 Hz, J_m=3 Hz, J_p=1.5 Hz, 1H, aromatic *ortho* to carbonyl), 7.58—7.03 (m, 7H, other aromatic), 3.78 (t, J=3 Hz, 1H. bridgehead vicinal to hydroxyl), 3.28 (t, J=3 Hz, 1H, bridgehead vicinal to carbonyl), 2.66 (t, J=3 Hz, 2H, methylene), 2.09 (s, 6H, acetone), 1.98 (s, 1H, OH), 1.75 (s, 3H, methyl),

Found: C, 78.37; H, 6.85%. Calcd for $C_{18}H_{16}O_2 \cdot C_3H_6O$: C, 78.23; H, 6.88%.

(+)-4,8-Bis(methylene)-2,3 : 6,7-dibenzobicyclo[3.3.1]nona-2,6-diene (XIV). (−)-Dimethyl glycol (XIII, 467.4 mg) in pyridine (6 ml) was heated to 50—65 °C with phosphoryl chloride (1.8 ml) for 1.5 hr. The reaction mixture was worked up in the usual way. A benzene solution of light yellow oil obtained on evaporating the solvent under reduced pressure was passed through a short column of silica gel (7.5 g) to yield colorless crystals (231.1 mg) which were recrystallized from methanol to give pure (+)-XIV, colorless needles, mp 124.2—124.6 °C, IR (Nujol mull): 1620 ($\nu_{C=C}$) cm^{-1} NMR: 7.70—6.95 (m, 8H, aromatic), 5.44 (d, J=0.5 Hz, 2H, olefin *syn* to benzene), 5.25 (d, J=0.5 Hz, 2H, olefin *anti* to benzene), 3.88 (t, J=3 Hz, 2H, bridgehead), 2.32 (t, J=3 Hz, 2H, methylene), ORD (at 25 °C): $[\alpha]_D$ +392 °, $[\alpha]_{546}$ +703 °, $[\alpha]_{405}$ +1460 °, $[\alpha]_{365}$ +2390 °, $[\alpha]_{330}$ +4410 ° (*c* 0.01964, 99% EtOH), UV: $\lambda_{max}^{99\%EtOH}$ (ε) 296.5(1210), 286.5 (2130), 258(22100), 251*(21000), 230*(16000), 213.5(35650), 209(36000) nm, $\lambda_{max}^{isoctane}$(ε) 296.5(1130), 286.5(1930), 266* (16200), 258.5(22100), 251*(21000), 230*(16100), 213.5 (37200), 208.5(37900), 192*(27400) nm, CD: see Table 1.

Found: C, 93.20; H, 6.62%. Calcd for $C_{19}H_{16}$: C, 93.40; H, 6.60%.

Racemate: mp 81.2—81.5 °C (from *n*-pentane).

(+)-2,3 :6, 7-Dibenzobicyclo[3.3.1]nona-2, 6-diene-4,8-diol-bis-p-bromobenzoate (XV). To a stirred solution of (−)-VIIa (0.5 g) in pyridine (7 ml) *p*-bromobenzoyl chloride (0.5 g) was added at room temperature and the mixture was heated to 60 °C under stirring for 20 hr. The reaction mixture was

worked up in the usual way. A viscous oil (0.45 g) obtained was dissolved in benzene and chromatographed twice on silica gel (34 g each) very carefully. Colorless solid obtained from the benzene eluates was recrystallized from methanol to give (+)-XV, mp 212.7—213.7 °C, IR (Nujol mull): 1720 ($\nu_{C=O}$) cm^{-1}, NMR: 7.97 (d, J=8.4 Hz, 4H, *ortho* protons of *p*-bromobenzoyl groups), 7.34—6.88 (m, 8H, other aromatic protons), 6.60 (d, J=6 Hz, 2H, methine), 3.70 (q, 2H, bridgehead), 2.58 (t, J=3 Hz, 2H, methylene), ORD: $[\alpha]_D$ +192 °, $[\alpha]_{546}$ +231 °, $[\alpha]_{436}$ +424 °, $[\alpha]_{405}$ +532 °, $[\alpha]_{365}$ +753 ° (*c* 0.587, acetone), UV: $\lambda_{max}^{cyclohexane}$ (ε) 283(1410), 271* (3630), 255*(31000), 247(41200), 218*(23800), 200(116500) nm, CD: $\lambda_{max}^{cyclohexane}$ ($\Delta\varepsilon$) 287(+0.24), 284(−0.40), 278* (+2.25), 255(+46.8), 235(−3.04), 212(−63.9) nm.

Found: C, 60.44; H, 3.58; Br, 25.79%. Calcd for $C_{31}H_{22}O_4Br_2$: C, 60.21; H, 3.59; Br, 25.85%.

Single crystals of (+)-XV for the X-ray crystallographic analysis were prepared on standing an acetone solution (200 mg in 25 ml) in a loosely stoppered ground joint flask for three months in a dark place.

When the above-mentioned procedure was applied to (±)-VIIa, the (±)-diester (XV) was obtained only in 51% yield and mono-*p*-bromobenzoate was isolated in 40,6% yield.

(±)-Bis-*p*-bromobenzoate (XV): colorless needles, mp 233.7—234.4 °C (from methanol), IR (Nujol mull): 1714 ($\nu_{C=O}$) cm^{-1}.

(±)-Mono-*p*-bromobenzoate: colorless rods, mp 163.0—163.5 °C, IR (Nujol mull): 3310 (ν_{O-H}), 1728, 1718 ($\nu_{C=O}$) cm^{-1}, NMR (CCl_4): 7.79 (d, J=8.4 Hz, 2H, *ortho* protons of *p*-bromobenzoyl group), 7.46 (d, J=8.4 Hz, 2H, *meta* protons of *p*-bromobenzoyl group), 7.50—6.70 (m, 8H, other aromatic protons), 6.40 (d, J=6 Hz, 1H, methine of ester), 4.89 (q, 1H, methine of alcohol), 3.52 (m, 1H, bridgehead near to ester), 3.27 (m, 1H, bridgehead near to alcohol), 2.43 (broad s, 2H, methylene), 1.46 (d, J=12 Hz, 1H, OH, disappeared on addition of D_2O). Found: C, 66.01; H, 4.44; Br, 18.22%. Calcd for $C_{24}H_{19}O_3Br$: C, 66.22; H, 4.40; Br, 18.36%.

(−)-2,3 : 6,7-Dibenzobicyclo[3.3.1]nona-2,6-diene-4,8-diol-monoacetate (XVI). (−)-Diol (VIIa, 3.61 g, $[\alpha]_D^{25}$ −85.2 ° (*c* 0.9240, $CHCl_3$), $[\alpha]_D^{25}$ −48.3 ° (*c* 0.4968, 99% EtOH), optical purity 56.9%) in pyridine was mixed with acetic anhydride (1.46 g) under ice-cooling. The mixture was stirred for further 2 hr at the same temperature and allowed to stand overnight at room temperature. The reaction mixture was worked up in the usual manner. Crystals of recovered (−)-diol (VIIa, 0.563 g) deposited on concentrating the extract were removed by filtration, and the filtrate was chromatographed on alumina (70 g). Recrystallization from ether of the crystals obtained from benzene eluates yielded (+)-diacetate (VIII, 0.850 g), mp 211.0—213.0 °C, $[\alpha]_D^{25}$ +25 ° (*c* 0.2469, $CHCl_3$), Found: C, 74.74; H, 5.90%.

Crystals (1.59 g) obtained from ether–methanol (95:5) eluates were recrystallized from ether to give (−)-monoacetate, mp 129.0—133.0 °C, $[\alpha]_D^{25}$ −27.7 ° (*c* 0.5340, $CHCl_3$).

Found: C, 77.53; H, 6.16%. Calcd for $C_{19}H_{18}O_3$: C, 77.42; H, 6.14%.

(+)-2,3: 6,7-Dibenzobicyclo[3.3.1]nona-2,6-diene-4-one (XIX). A mixture of (−)-monoacetate (XVI, 1.40 g), thionyl chloride (18 ml) and benzene (120 ml) was refluxed for 17 hr. The reaction mixture was worked up in the usual way and the residue obtained on evaporating the benzene extract *in vacuo* was purified by crystallization from *n*-hexane to yield (−)-8-chloro-4-acetate (XVII), mp 139.0—144.0 °C, $[\alpha]_D^{22}$ −31.0 ° (*c* 0.4974, $CHCl_3$), Found: C, 73.06; H, 5.38; Cl, 11.30%. Calcd for $C_{19}H_{17}O_2Cl$: C, 72.95; H, 5.48; Cl, 11.33%.

(−)-Chloride (XVII, 0.850 g) in tetrahydrofuran (10 ml) was added dropwise to a stirred suspension of lithium aluminum hydride (1.2 g) in the same solvent (60 ml). After the mixture had been refluxed for 24 hr, the reaction mixture was treated in the usual manner and the solvent was removed *in vacuo*. Crude alcohol (XVIII) thus obtained was submitted to oxidation without further purification. To an ice-cooled solution of crude XVIII in acetone (40 ml) was added the Jones reagent dropwise under stirring till red color of the reagent persisted for a while. The mixture was stirred for further 30 min at the same temperature and then mixed with water. Ethereal extract, after being washed and dried, was concentrated *in vacuo*, and the residue dissolved in benzene was passed through a short column of silica gel (15 g). Colorless crystals (440 mg) obtained from benzene eluates were recrystallized from benzene–*n*-hexane to give pure (+)-XIX, mp 112—114 °C, $[\alpha]_D^{22}$ +27.5 ° (*c* 0.2479, $CHCl_3$), UV: $\lambda_{max}^{99\%EtOH}$ (ε) 370*(93.5), 350*(380), 337.5(523), 326*(483), 297*(1620), 290*(1730), 278(2210), 253(11900), 201(41800) nm, $\lambda_{max}^{cyclohexame}$ (ε) 374*(164), 371(176), 355.5(410), 340(464), 326(343), 315(204), 297(1400), 287(1420), 278.5(1790), 271 (1710), 251*(11000), 247(11600), 214*(26900), 206(43050), 191.5(37900), 190(38600) nm, CD (corrected for 100% optical purity): $\lambda_{max}^{99\%EtOH}$ ($\Delta\varepsilon$) 370*(+1.50), 352.5*(+5.10), 338.5(+6.93), 327*(+6.18), 315*(+3.85), 303*(−1.50), 283(−1.96), 276*(−1.72), 260*(−1.02), 245*(+1.11), 243 (+1.21), 229(−1.71), 203.5(−25.0) nm, $\lambda_{max}^{cyclohexane}$ ($\Delta\varepsilon$) 384* (+0.05), 380*(+0.20), 377*(+1.53), 371(+2.99), 354.5 (+6.29), 339.5(+6.65), 325.5(+4.64), 315(+2.58), 303* (+0.904), 298*(+0.86), 275(−1.17), 358(−0.63), 244 (+1.31), 225(−2.61), 199(−18.5) nm.

Found: C, 86.89; H, 5.92%. Calcd. for $C_{17}H_{14}O$: C, 87.15; H, 6.02%.

(R)-(−)-3-Phenylbutanoic Acid (XX). (±)-XX, bp 134—136 °C/800 Pa, was prepared by the reaction of benzene with crotonic acid in the presence of anhydrous aluminum chloride.[13] Optical resolution was carried out with (+)-α-phenylethylamine[14] to yield (*R*)-(−)-XX, $[\alpha]_D$ −52.0 ° (*c* 0.042, benzene).

(R)-(−)-3-Phenylbutylphenone (XXI). (*R*)-(−)-XX (3.61 g) was converted into acid chloride with thionyl chloride in ether. A solution of the acid chloride in benzene (50 ml) was added under ice-cooling and stirring to a benzene solution of diphenylcadmium (*ca.* 80 ml), which was prepared from phenylmagnesium bromide (magnesium 0.61 g, bromobenzene 2.6 ml, and ether 20 ml) and anhydrous cadmium chloride (2.5 g suspended in 50 ml of ether). After being refluxed for 3 hr, the reaction mixture was worked up in the usual way. Organic layer and benzene extracts, after being washed and dried, were evaporated under reduced pressure. Viscous brown oil (3.4 g) thus obtained was found to be contanimated with considerable amount of ethyl 3-phenylbutyrate. The crude product (1.3 g) in 99% ethanol (10 ml) was mixed with potassium hydroxide (0.7 g in ethanol 20 ml and water 5 ml) and the mixture was allowed to stand at room temperature overnight. After evaporating the solvent under reduced pressure, the mixture was diluted with water and extracted with benzene. The extract was washed with 5% aqueous sodium hydrogencarbonate, and dried over sodium sulfate. (*R*)-(−)-XX (0.381 g) was recovered from the aqueous layer and sodium hydrogencarbonate washings on acidification. Light yellow oil (0.7311 g) obtained from benzene extract was carefully purified by repeated chromatography on silica gel and alumina. (*R*)-(−)-Ketone (XXI) was obtained as a colorless oil, IR (neat): 1683 ($\nu_{C=O}$) cm^{-1} NMR: 8.0—7.8 (m, 2H, *ortho* protons of benzoyl group), 7.55—7.17 (m, 8H, other aromatic protons), 3.73—3.08 (m, 3H, methylene and methine), 1.31 (d, J=6.6 Hz, 3H, methyl), UV: $\lambda_{max}^{isooctane}$ (ε) 358*(24.5), 355*(26.0), 341*(47.3), 328*(62.5), 319(64.7),

287(724), 279(938), 277.5*(933), 273(891), 268.5(945), 264.7(919), 261*(946), 249*(8480), 240(13300), 205.5* (26900), 200.5(38100), 191.2(67500), 190(69000) nm, ORD: $[\alpha]_D$ −14.8°, $[\alpha]_{546}$ −19.0°, $[\alpha]_{436}$ −49.7°, $[\alpha]_{405}$ −79.5°, $[\alpha]_{367.5}$ −240.6°, $[\alpha]_{353}$ −335.1°, $[\alpha]_{339.5}$ −249° (*c* 1.1972, CCl_4), $[\alpha]_D$ +0.66°, $[\alpha]_{546}$ ≈0°, $[\alpha]_{436}$ −16.6°, $[\alpha]_{405}$ −40.8°, $[\alpha]_{370}$ −170.8°, $[\alpha]_{355}$ −262.7°, $[\alpha]_{340.5}$ −183.9°, $[\alpha]_{335.5}$ ≈0°, $[\alpha]_{322}$ +96.9°, $[\alpha]_{317}$ +303.8° (*c* 0.609, hexane), CD: $\lambda_{max}^{isooctane}$ ($\Delta\varepsilon$) 371 (−0.0628), 354.5 (−0.204), 340(−0.325), 327.5(−0.339), 316(−0.266), 306* (−0.174), 295*(−0.0876), 287(−0.116), 279.5(−0.0916), 268(−0.174), 261(−0.171), 252(−0.494), 219 (+2.24), 201.5(+8.76) nm.

Found: C, 85.36; H, 7.18%. Calcd for $C_{15}H_{16}O$: C, 85.68; H, 7.19%.

Racemate was obtained by the same procedure in 71% yield which was recrystallized from methanol to give pure (±)-XXI, colorless leaflets, mp 70.8—71.5 °C, IR (KBr disk): 1680 ($\nu_{C=O}$), 760, 705 (δ_{CH}, monosubstituted benzene) cm^{-1}. In this case contamination with the ethyl ester was not so serious that (±)-XXI could be easily purified by chromatography on silica gel and recrystallization.

(R)-(−)-2,4-Diphenyl-1-pentane (XXII). Triphenylmethylphosphonium bromide (1.761 g) suspended in ether (30 ml) was converted into triphenylphosphinmethylene with *n*-butyllithium (3 ml of 1.65 M hexane solution).[15] (−)-Ketone (XXI, 0.774 g) in ether (70 ml) was added over 5-min period to the stirred solution of the Wittig reagent and the mixture was refluxed for 11.5 hr under stirring. Solid deposited on cooling the reaction mixture was filtered and washed thoroughly with ether. The filtrate and washings were combined and dried over sodium sulfate. Colorless oil (1.120 g) obtained on evaporating the solvent under reduced pressure was dissolved in *n*-hexane and carefully chromatographed on silica gel (40 g). Evaporation of *n*-hexane eluates gave (−)-XXII, colorless oil (0.519 g, 67.6%), IR (neat): 890 ($\delta_{=CH}$ out of plane) cm^{-1}, NMR: 7.47—7.0 (m, 8H, aromatic), 5.21 (d, J=1.6 Hz, 1H, olefinic proton *cis* to phenyl), 4.97 (m, 1H, olefinic proton *trans* to phenyl), 3.07—2.52 (m, 3H, methylene and methine), 2.87 (d, J=6.5 Hz, 3H, methyl), UV: $\lambda_{max}^{isooctane}$ (ε) 290* (77.2), 268.5 (1270), 264(2130), 240(9170), 217*(12300), 206(27000), 191.5(67640), 190(68500) nm, ORD: $[\alpha]_D$ −68.1°, $[\alpha]_{546}$ −83.1°, $[\alpha]_{436}$ −156.9°, $[\alpha]_{405}$ −196.6°, $[\alpha]_{365}$ −279.4° (*c* 1.354, *n*-hexane), CD: $\lambda_{max}^{isooctane}$ ($\Delta\varepsilon$) 271.5(−0.121), 267.5(+0.102), 264(−0.160), 235(−3.21), 210(+5.37), 192 (−39.2) nm.

Found: C, 91.90; H, 8.29%. Calcd for $C_{17}H_{18}$: C, 91.84; H, 8.16%.

A small amount of (−)-ketone (XXI, 0.131 g, 16.9%) was recovered from benzene eluate.

(R)-(−)- and meso*-2,4-Diphenylpentane (XXIIIb and XXIIIa)* Hydrogenation of (*R*)-(−)-2,4-diphenyl-1-pentene (XXII, 0.422 g) in benzene (50 ml) and ethyl acetate (50 ml) over the Adams catalyst (48 mg) yielded colorless oil (0.407 g). The material in *n*-hexane was chromatographed on silica gel. Ratio of *meso*-(XXIIIa) and (−)-isomers (XXIIIb) could be estimated to be 50.7% and 49.3%, respectively, by the intensities of methyl signals in their NMR spectra of purified reduction product, UV: $\lambda_{max}^{isooctane}$ (ε) 268(330), 264.3(346), 261 (436), 259(443), 254.5*(370), 253.5(377), 248.5(279), 243* (194), 238*(140), 217*(10000), 213*(14300), 209(17600), 205*(17500), 193(89000), 191.8(97500), 190(91800) nm, ORD: $[\alpha]_D$ −39.4°, $[\alpha]_{546}$ −49.1°, $[\alpha]_{436}$ −84.4°, $[\alpha]_{405}$ −105.2°, $[\alpha]_{365}$ −150.4° (*c* 0.5140, isooctane), CD: $\lambda_{max}^{isooctane}$ ($\Delta\varepsilon$) 271(−0.0162), 268(+0.0117), 266*(−0.0208), 263.5 (−0.0483), 257(−0.0616), 251(−0.0485), 245*(−0.0350), 239*(−0.0266), 217(−4.59) nm.

Found: C, 91.28; H, 9.00%. Calcd for $C_{17}H_{20}$: C, 91.01; H, 8.99%.

(−)-2,4-Diphenylpentane-1,5-diol (XXIVb). (−)-1,3-Diphenylglutaric acid (IIb, 0.548 g, $[\alpha]_D$ −44.1° (*c* 0.295, 99% EtOH), optical purity 46%) in tetrahydrofuran (30 ml) was added to a stirred suspension of lithium aluminum hydride (0.1464 g) in the same solvent (20 ml), and the mixture was refluxed for 5 hr. The reaction mixture was worked up in the usual manner and extracted with ether. After washing and drying, the extract was concentrated under reduced pressure. Colorless oil (0.462 g) thus obtained was crystallized from benzene to give pure (−)-XXIVb, mp 72—90 °C, IR (neat): 3350 (very broad, ν_{O-H}) cm^{-1}, NMR: 7.40—6.83 (m, 10H, aromatic), 3.45 (d, J=6.2 Hz, 4H, $C\underline{H}_2OH$), 2.68—1.77 (m, 4H, methylene and methine), 2.13 (s, 2H, OH), ORD: $[\alpha]_D$ −39.1°, $[\alpha]_{546}$ −45.1°, $[\alpha]_{436}$ −80.9°, $[\alpha]_{405}$ −99.7°, $[\alpha]_{365}$ −135.3° (*c* 0.8432, 99% EtOH).

Found: C, 79.12; H, 7.85%. Calcd for $C_{17}H_{20}O_2$: C, 79.65; H, 7.86%.

meso*-2,4-Diphenylpentane-1,5-diol (XXIVa).* Reduction of *meso*-1,3-diphenylglutaric acid (IIa, 0.514 g) according to the same procedure used for (−)-isomer (IIb) gave *meso*-diol (XXIVa) in a quantitative yield which was recrystallized from benzene–ligroin to give pure material, mp 116.7—117.3 °C, IR (Nujol mull): 3250, 3170* (ν_{O-H}) cm^{-1}, NMR: 7.50—7.00 (m, 10H, aromatic), 3.73 (d, J=6.6 Hz, 4H, $C\underline{H}_2OH$), 3.07—1.58 (m, 4H, methylene and methine), 1.74 (s, 2H, OH).

Found: C, 79.52; H, 7.86%. Calcd for $C_{17}H_{20}O_2$: C, 79.65; H, 7.86%.

(−)-2,4-Diphenylpentane (XXIIIb). To an ice-cooled and stirred solution of (−)-diol (XXIVb, 0.406 g, optical purity, max. 46%) in pyridine (10 ml) was added dropwise methanesulfonyl chloride (1.0 g). The mixture was stirred for further 4 hr at room temperature and then allowed to stand overnight in a refrigerator. Treatment of the reaction mixture in the usual way gave bis-methanesulfonate (0.625 g) as light brown oil. A solution of the mesylate in tetrahydrofuran (30 ml) was added to a suspension of lithium aluminum hydride (1.0 g) in the same solvent (25 ml) and the mixture was refluxed for 12 hr. The reaction mixture was worked up in the usual manner to yield crude (−)-XXIIIb, faintly yellow oil (0.300 g). A *n*-hexane solution of the crude (−)-XXIIIb was chromatographed on silica gel (20 g), yielding pure (−)-XXIIIb, colorless oil, NMR: 7.47—6.96 (m, 10H, aromatic), 2.83—2.24 (sextet, 2H, methane), 1.96—1.72 (m, 2H, methylene), 1.14 (d, J=7 Hz, 6H, methyl), UV: $\lambda_{max}^{isooctane}$ (ε) 268(372), 264(361), 261.2(473), 259(458), 255(391), 253.5 (391), 249(287), 243*(188), 237*(115), 217*(10300), 213* (14600), 209(17700), 205*(17400), 193(82300), 191.5(86800), 190(87100) nm, ORD: $[\alpha]_D$ −34.7°, $[\alpha]_{546}$ −42.3°, $[\alpha]_{436}$ −73.4°, $[\alpha]_{405}$ −91.9°, $[\alpha]_{365}$ −124.6° (*c* 0.5740, isooctane), CD: $\lambda_{max}^{isooctane}$ ($\Delta\varepsilon$) 271 (−0.0164), 268(+0.0126), 266* (−0.0203), 263.5(−0.0580), 257(−0.0696), 251(−0.0464), 245*(−0.0261), 239*(−0.0145), 217(−6.19) nm.

Found: C, 91.03; H, 9.09%. Calcd for $C_{17}H_{20}$: C, 91.01; H, 8.99%.

meso*-2,4-Diphenylpentane (XXIIIa).* *meso*-Diol (XXIVa, 0.255 g) was converted into *meso*-bis-mesylate (0.396 g) by the reaction with methanesulfonyl chloride (0.274 g) in pyridine (5 ml) performed under the same reaction condition used for the (−)-diol (XXIVb). The *meso*-bis-mesylate was reduced by lithium aluminum hydride (0.9 g) in tetrahydrofuran. Purification of crude product (0.204 g) in *n*-hexane by chromatography on silica gel (25 g) yielded *meso*-XXIIIa, colorless oil, NMR: 7.46—6.98 (m, 10H, aromatic), 2.96—2.37

(sextet, 2H, methine), 2.21—1.48 (m, 2H, aromatic), 2.21—1.48 (m, 2H, methylene), 1.21 (d, J=6.7 Hz, 6H, methyl), UV: $\lambda_{max}^{isooctane}$ (ε) 268 (312), 264.5(330), 261.1(416), 259 (432), 255*(356), 253.5(359), 248.8(256), 244*(167), 238* (103), 217(10400), 213*(14200), 209(17400), 205*(17200), 193(87300), 192(95700), 190(94000), 188.5(69200) nm.

Found: C, 90.86; H, 8.95%. Calcd for $C_{17}H_{20}$: C, 91.01; H, 8.99%.

References

1) Optically Active Triptycenes. I–VII; Part VII, M. Hashimoto, Y. Shimizu, F. Ogura, and M. Nakagawa, This Bulletin, **47**, 1761 (1974). References are given therein.

2) J. Tanaka, C. Katayama, F. Ogura, H. Tatemitsu, and M. Nakagawa, *Chem. Commun.*, **1973**, 21; Y. Shimizu, H. Tatemitsu, F. Ogura, and M. Nakagawa, *ibid.*, **1973**, 22; H. Tatemitsu, F. Ogura, and M. Nakagawa, This Bulletin, **46**, 915 (1973).

3) J. Tanaka, K. Ozeki-Minakata, F. Ogura, and M. Nakagawa, *Spectrochim. Acta*, **29A**, 877 (1973).

4) H. W. Whitlock, Jr., *J. Amer. Chem. Soc.*, **84**, 3412 (1962); K. Adachi, K. Naemura, and M. Nakazaki, *Tetrahedron Lett.*, **1968**, 5467.

5) N. Zelinski and M. Feldmann, *Chem. Ber.*, **22**, 3289 (1889); H. Stetter and A. Reischl, *ibid.*, **93**, 791 (1960).

6) Different assignments were given without any experimental evidence; Y. Ito, *Nippon Kagaku Zasshi*, **83**, 195 (1962).

7) V. Prelog and H. Scherer, *Helv. Chim. Acta*, **42**, 2227 (1959); G. Sorlin and G. Bergson, *Ark. Kem.*, **29**, 593 (1968).

8) T. Kaneda, C. Katayama, and J. Tanaka, to be submitted to This Bulletin.

9) K. Mislow, M. Brzechffa, H. W. Gschwend, and R. T. Puckett, *J. Amer. Chem. Soc.*, **95**, 621 (1973).

10) A. Moscowitz, K. Mislow, M. A. W. Glass, and C. Djerassi, *J. Amer. Chem. Soc.*, **84**, 1945 (1962).

11) G. Snatzke, "Optical Rotatory Dispersion and Circular Dichroism in Organic Chemistry," Heyden and Son, London (1967), p. 208.

12) S. F. Mason and G. W. Vane, *Tetrahedron Lett.*, **1965**, 1593.

13) C. S. Marvel, J. Dec, and H. J. Cook, Jr., *J. Amer. Chem. Soc.*, **62**, 3499 (1940).

14) A-M. Weidler and G. Bergson, *Acta Chem. Scand.*, **18**, 1484 (1964).

15) G. Wittig and U. Schoellkopf, "Organic Syntheses," Coll. Vol. V, p. 751 (1973).

Metal Phosphinylides and Phosphinothioylides. IV.[1] Reactions with Tetrahydrofuran

Koshiro GODA, Masaaki YOSHIFUJI, Renji OKAZAKI, and Naoki INAMOTO
Department of Chemistry, Faculty of Science, The University of Tokyo, Hongo, Tokyo 113
(Received January 14, 1975)

Diphenylphosphinic (**1**) and diphenylphosphinothioic chlorides (**2**) were allowed to react in tetrahydrofuran (THF) in the presence of metal or metal salts at 120—150 °C. In the cases of lithium and magnesium, $[Ph_2PX]^-$ (X=O, S) thus formed attacked the α-carbon of THF to give ring-opening products, which were produced by deoxygenation, sulfurization, and reaction with **1** and **2**. In the cases of iron, copper, and their salts, *O*-4-chlorobutyl diphenylphosphinate (**12**) and diphenylphosphinothioate (**13**) were obtained in a homolytic fashion. The formation mechanisms have been discussed.

In a previous paper,[2] it was reported that reactions of $[Ph_2PX]$ M (X=O, S; M=Li, FeCl) with *p*-benzoquinone gave different type compounds, depending on the metals employed. The reactions show anionic and homolytic characters in the cases of M=Li and FeCl, respectively.

It is known that lithium dimethylphosphide (Me_2PLi) reacts rapidly with tetrahydrofuran (THF) to give 4-hydroxybutyldimethylphosphine by a nucleophilic attack on the α-carbon atom of THF.[3]

In order to clarify this difference still more, reactions of diphenylphosphinic (**1**) and diphenylphosphinothioic chlorides (**2**) with THF were carried out in the presence of several metals or metal salts.

The reaction of diphenylphosphinic chloride (**1**) with lithium in THF at 150 °C gave 29% of diphenylphosphine oxide (**3**), 3% of tetraphenyldiphosphine dioxide (**4**), and a trace amount of 4-substituted butyldiphenylphosphine oxide (**5**). The structure of **5** is unknown because of difficulties of purification but it is considered to be **8** (see below) mainly from the spectral data. A similar reaction of diphenylphosphinothioic chloride (**2**) gave 13% of **3**, 46% of tetramethylene bis(diphenylphosphinodithioate) (**6**), and 16% of *S,S*-tetramethylene diphenylphosphinothioate diphenylphosphinodithioate (**7**). The formation of **3** indicates the occurrence of desulfurization during the reaction.[4]

$$\underset{\mathbf{1}}{Ph_2P(O)Cl} + Li + THF \longrightarrow \underset{\mathbf{3}}{Ph_2P(O)H} + \underset{\mathbf{4}}{Ph_2P(O)\text{-}P(O)Ph_2} + \underset{\mathbf{5}}{Ph_2P(O)(CH_2)_4Y}$$

$$\underset{\mathbf{2}}{Ph_2P(S)Cl} + Li + THF \longrightarrow \underset{\mathbf{3}}{Ph_2P(O)H} + \underset{\mathbf{6}}{Ph_2P(S)S(CH_2)_4SP(S)Ph_2} + \underset{\mathbf{7}}{Ph_2P(S)S(CH_2)_4SP(O)Ph_2}$$

Reaction of **1** with magnesium in THF at 150 °C gave 21% of 1,4-bis(diphenylphosphino)butane 1,4-dioxide (**8**) and a trace amount of **5**. A similar reaction of **2** gave 6% of diphenylphosphinic acid, 21% of diphenylphosphinodithioic acid (**9**), a trace of tetraphenyldiphosphine disulfide (**10**), and 18% of *O,S*-tetramethylene diphenylphosphinothioate diphenylphosphinodithioate (**11**). The formation of diphenylphosphinic acid and **9** also indicates the occurrence of desulfurization during the reaction.

$$\mathbf{1} + Mg + THF \longrightarrow \underset{\mathbf{8}}{Ph_2P(O)(CH_2)_4P(O)Ph_2} + \mathbf{5}$$

$$\mathbf{2} + Mg + THF \longrightarrow Ph_2P(O)OH + \underset{\mathbf{9}}{Ph_2P(S)SH} + \underset{\mathbf{10}}{Ph_2P(S)P(S)Ph_2} + \underset{\mathbf{11}}{Ph_2P(S)S(CH_2)_4OP(S)Ph_2}$$

Reactions of **1** and **2** in the presence of a catalytic amount of iron, copper, cuprous chloride, and oxide in THF at 150 °C gave *O*-4-chlorobutyl diphenylphosphinate (**12**) and diphenylphosphinothioate (**13**). In some cases, 1 : 2 product (**14**) was also obtained. These products are quite different from those in the cases with lithium and magnesium. The results are summarized in Table 1.

$$\mathbf{1}\text{ or }\mathbf{2} + \text{M or MA} + THF \longrightarrow \underset{\mathbf{12}\ X=O;\ \mathbf{13}\ X=S}{Ph_2P(X)O(CH_2)_4Cl} + \underset{\mathbf{14}}{Ph_2P(X)[O(CH_2)_4]_2Cl}$$

M=Fe, Cu; MA=Cu_2Cl_2, Cu_2O

a, X=O; b, X=S

Table 1. Yields of **12**, **13**, and **14** (at 150 °C)

1 or 2	M or MA	12 (%)	13 (%)	14 (%)
1	Fe	22	—	—
	Cu	36	—	—
	Cu_2Cl_2	23	—	4
	Cu_2O	18	—	—
2	Fe	—	27	10
	Cu	—	28	5
	Cu_2Cl_2	—	46	—
	Cu_2O	—	59	—

In order to obtain some information on the formation mechanism of **12** and **13**, **1** and **2** were allowed to react in THF in the presence of a catalytic amount of various metals and metal salts at 120 °C for 6 hr; the yields of **12** and **13** were determined by gas chromatography (glc). The results are shown in Table 2.

As seen in Table 2, copper and the salts are favorable over iron and the salts as catalyst. Moreover, Friedel-Crafts catalysts such as ferric and aluminum chlorides are not so good, except for zinc chloride.

Table 2. Yields of **12** and **13** (at 120 °C for 6 hr)

Cat.	**12** (%)	**13** (%)
none	—	—
Cu	37	8
Cu_2Cl_2	34	25
$(i\text{-PrO})_3P \cdot CuCl$	39	16
$CuCl_2$	57	28
Fe	15	4
$FeSO_4$	7	<1
$FeCl_3$	5	<1
$ZnCl_2$	36	9
$AlCl_3$	2	<1

These facts suggest that the reactions in the presence of copper, copper salts, iron, and ferrous salts proceed in a homolytic fashion, because it has been known that the reactions of cuprous and ferrous salts with carbon tetrachloride,[5] sulfonyl chlorides,[6] and *N*-chloroamines[7] generate trichloromethyl, sulfonyl, and amino radicals, respectively.

Thus, the formations of **12**, **13**, and **14** are reasonably explained as follows:

$$Ph_2P(X)Cl + M \longrightarrow Ph_2\dot{P}(X) + M^+Cl^-$$

$$Ph_2\dot{P}(X) + \square O \longrightarrow \square \overset{+}{O}\text{-}\overset{\cdot\cdot}{\underset{\cdot\cdot}{P}}(X)Ph_2 \longrightarrow$$

$$Ph_2P(X)O(CH_2)_4\cdot \xrightarrow{MCl} Ph_2P(X)O(CH_2)_4Cl \quad \mathbf{12, 13}$$

$$Ph_2P(X)O(CH_2)_4\cdot \xrightarrow{M^+} Ph_2P(X)O(CH_2)_4^+ \xrightarrow{THF} \square \overset{+}{O}\text{-}(CH_2)_4OP(X)Ph_2 \xrightarrow{Cl^-}$$

$$Cl(CH_2)_4O(CH_2)_4OP(X)Ph_2 \quad \mathbf{14}$$

Since neither addition nor polymerization occurred in the presence of acrylonitrile, styrene, vinyl acetate, and dienes under the same conditions, it is considered that the reactions are homolytic but that free radicals are not produced in these reactions.

In the above mechanisms, the second step is analogous to the reactions of alcohols with $Ph_2P\cdot$[8] and $Ph_2P(S)\cdot$ radicals.[9]

In the presence of Friedel-Crafts catalysts, the formation of **12**, **13**, and **14** is explained as follows:

$$Ph_2P(X)Cl + MCl_n \longrightarrow Ph_2P(X)^+ MCl_{n+1}^- \xrightarrow{THF}$$

$$\square \overset{+}{O}\text{-}P(X)Ph_2 \longrightarrow {}^+(CH_2)_4OP(X)Ph \xrightarrow{THF\ Cl^-} \mathbf{14}$$

$$\downarrow Cl^-$$

12 or **13**

In the cases with lithium and magnesium, the formation of products is explicable by anionic mechanisms as follows:

$$[Ph_2PO]^- + \mathbf{1} \xrightarrow{(a)} Ph_2P(O)\text{-}OPPh_2 \xrightarrow{\Delta} Ph_2P(O)P(O)Ph_2$$

$$\uparrow [O] \quad \mathbf{4}$$

$$2[Ph_2PO]^- \xrightarrow{(b)} Ph_2P(O)O^- + Ph_2P^- \xrightarrow{1} Ph_2P\text{-}P(O)Ph_2$$

$$[Ph_2PO]^- + THF \longrightarrow Ph_2P(O)(CH_2)_4O^- \xrightarrow[(c)]{[Ph_2PO]^-}$$

$$Ph_2P(O)(CH_2)_4^- \xrightarrow{1} Ph_2P(O)(CH_2)_4P(O)Ph_2 \quad \mathbf{8}$$

$$\downarrow$$

$$Ph_2P(O)(CH_2)_4Y \quad \mathbf{5}$$

$$2[Ph_2PS]^- \xrightarrow{(d)} Ph_2P^- + Ph_2P(S)S^- \quad \mathbf{9}$$

$$[Ph_2PS]^- \xrightarrow[(e)]{2} Ph_2P(S)P(S)Ph_2 \quad \mathbf{10}$$

$$\downarrow THF$$

$$Ph_2PS(CH_2)_4O^- \xrightarrow{2} Ph_2P(S)S(CH_2)_4OP(S)Ph_2 \quad \mathbf{11}$$

$$\downarrow [Ph_2PS]^- \ (f)$$

$$Ph_2PS(CH_2)_4^- \xrightarrow{2} Ph_2PS(CH_2)_4SPPh_2$$

$$2 \swarrow \quad [O] \downarrow 2$$

$$Ph_2P(S)S(CH_2)_4SP(S)Ph_2 \quad \mathbf{6} \qquad Ph_2P(S)S(CH_2)_4SP(O)Ph_2 \quad \mathbf{7}$$

The steps (a) and (e) have been discussed in a previous paper.[9] The steps (c) and (f) are deoxygenation by trivalent phosphorus.[2] The steps (b) and (d) are disproportionation involving oxygen and sulfur atoms.

Experimental

All melting and boiling points are uncorrected. The IR spectra were recorded on a Hitachi EPI-G2 spectrophotometer. NMR spectra were measured with Hitachi R-24 and R-20B spectrometers using TMS as an internal standard, and MS spectra were determined with a Hitachi RMU-6L mass spectrometer. All reactions were carried out under nitrogen in a sealed tube.

Materials. Diphenylphosphinic[10] (**1**) and diphenylphosphinothioic chlorides[11] (**2**) were prepared by the reported methods.

Reaction with 1 and Lithium. A mixture of 1.83 g (7.7 mmol) of **1** and 70 mg (10 mg-atom) of lithium metal in 5 ml of THF was heated for 24 hr at 150 °C. The reaction mixture was poured into water and extracted with chloroform. After removal of the solvent from the dried extracts, ether was added to the residue. From the solution, **3** (0.457 g, 29%) was obtained (identified by IR and NMR). The insoluble part was purified by dry column chromatography (DCC) on an alumina column with acetone to give 49 mg (3%) of **4**, which was identified by IR,[9] and a small amount of **5**, which was difficult to purify. IR (neat): 3300 (br), 1185, and 1120 cm^{-1}; NMR ($CDCl_3$): δ 1.3—1.8(m), 1.8—2.7(m), 3.2—3.8(m), and 7.2—8.0(m).

Reaction with 2 and Lithium. A mixture of 1.52 g (6 mmol) of **2** and 55 mg (7.9 mg-atom) of lithium metal in 5 ml of THF was allowed to react and treated similarly. Ether was added to the residue to crystallize 0.354 g (26%) of diphenylphosphinothioic anhydride[9] (by IR). The ether solution

was treated by DCC on silica gel with ethyl acetate to separate oily fractions. One of the fractions was identified with **3** (0.152 g, 13%) by IR but was difficult to purify. The other fractions were treated again by DCC with ether to give crystalline and oily materials. The crystals (**6**) were recrystallized from *n*-hexane–dichloromethane, yield 0.304 g (46%), mp 91—92 °C. NMR ($CDCl_3$): δ 1.60 (m, 4H, $2CH_2$), 2.85 (dd, J_{PSCH} 13.2, J_{HCCH} 6.6 Hz, 4H, 2-SCH_2), and 7.30—8.15 (m, 20H, 4Ph); Mass: *m/e* 554 (M^+) and 217 (Ph_2PS^+, 100%).

Found: C, 61.33; H, 5.19%. Calcd for $C_{28}H_{28}P_2S_4$: C, 60.63; H, 5.09%.

The oily product (**7**) was 0.128 g (16%) and also difficult to purify. IR (neat): 1197 (P=O), 1100 (P–Ph), 655, and 530 cm^{-1} (P=S); NMR ($CDCl_3$): δ 1.6 (m, 4H, $2CH_2$), 2.6—2.9 (m, 4H, 2-SCH_2), and 6.3—7.1 (m, 20H, 4Ph); Mass: *m/e* 538 (M^+).

*Reaction with **1** and Magnesium.* A mixture of 1.45 g (6.1 mmol) of **1** and 0.134 g (5.5 mg-atom) of magnesium in 5 ml of THF was heated under the same conditions. The reaction mixture was poured into water and neutralized with 2 M hydrochloric acid to give precipitates. The aqueous solution was extracted with chloroform. Evaporation of the dried extracts gave a considerable amount (0.70 g, 53%) of diphenylphosphinic acid, which was removed by filtration of the alcoholic solution through an alumina column. The eluate was purified by DCC on a silica gel column with ether to give crystalline material (**8**), which was recrystallized from 95% ethanol, mp 264—266 °C, yield 0.198 g (21%); IR (KBr): 1185 (P=O) and 1120 cm^{-1} (P–Ph); NMR ($CDCl_3$): δ 1.5—2.0 (m, 4H, $2CH_2$), 2.0—2.5 (m, 4H, $2CH_2$), and 7.3—8.0 (m, 20H, 4Ph); Mass: *m/e* 458 (M^+).

Found: C, 73.61; H, 5.90%. Calcd for $C_{28}H_{28}O_2P_2$: C, 73.35; H, 6.16%.

*Reaction with **2** and Magnesium.* A mixture of 1.70 g (6.7 mmol) of **2** and 0.162 g (6.7 mg-atom) of magnesium in 5 ml of THF was heated similarly. After removal of unchanged magnesium (91 mg), the reaction mixture was decomposed with 30% aqueous ammonium chloride, extracted with chloroform, and the extracts were dried with anhydrous magnesium sulfate. The concentration gave crystals. The crystalline part was subjected to DCC on silica gel with chloroform to give 0.180 g (21%) of **9** and 10 mg of **10**, which were identified by IR. A similar treatment of the filtrate gave 83 mg (6%) of diphenylphosphinic acid and 0.209 g (18%) of **11**, mp 72—73 °C (from ether); IR (KBr): 1100 (P–Ph), 1020 (C–O), 945 (P–O), 660, and 545 cm^{-1} (P=S); NMR ($CDCl_3$): δ 1.75 (m, 4H, $2CH_2$), 2.95 (m, J_{PSCH} 13.8 Hz, 2H, SCH_2), 3.95 (m, J_{POCH} 7.8 Hz, 2H, OCH_2), and 7.20—8.15 (m, 20H, 4Ph); Mass: *m/e* 538 (M^+). However, the analytically pure sample could not be obtained because it was difficult to make the separation of a trace of impurity.

*Reaction with **1** and Iron.* A mixture of 1.43 g (6.0 mmol) of **1** and 31 mg (0.56 mg-atom) of reduced iron powder in 5 ml of THF was heated similarly. The resulting precipitates (iron diphenylphosphinate) was filtered off, and the filtrate was treated by DCC with ether to give 0.414 g (22%) of **12** as oil; IR (neat): 1220 (P=O), 1135 (P–C), 1030 (C–O), and 970 cm^{-1} (P–O); NMR ($CDCl_3$): δ 1.9 (m, 4H, $2CH_2$), 3.53 (m, 2H, CH_2Cl), 4.05 (m, J_{POCH} 15.6 Hz, 2H, OCH_2), and 7.35—8.0 (m, 10H, 2Ph).

Found: C, 62.14; H, 5.80; Cl, 11.23%. Calcd for $C_{16}H_{18}O_2ClP$: C, 62.24; H, 5.83; Cl, 11.51%.

*Reaction with **2** and Iron.* A mixture of 1.67 g (6.6 mmol) of **2** and 53 mg (0.96 mg-atom) of reduced iron powder in 5 ml of THF was heated similarly. A similar treatment gave 0.575 g (27%) of **13**, bp 117 °C/0.05 mmHg, and 0.268 g (10%) of **14b**, which was difficult to purify.

13: IR (neat): 1120 (P–C), 1030 (C–O), 960 (P–O), 640, and 520 cm^{-1} (P=S); NMR ($CDCl_3$): δ 1.83 (m, 4H, $2CH_2$), 3.43 (m, 2H, CH_2Cl), 3.98 (m, J_{POCH} 8.4 Hz, 2H, OCH_2), and 7.25—8.05 (m, 10H, 2Ph).

Found: C, 59.29; H, 5.30; Cl, 11.48; S, 10.14%. Calcd for $C_{16}H_{18}ClOPS$: C, 59.17; H, 5.59; Cl, 10.91; S, 9.87%.

14b: IR (neat): 1435 (P–C), 640, and 520 cm^{-1} (P=S); NMR ($CDCl_3$): δ 1.73 (m, 8H, $4CH_2$), 3.40 (m, 6H, $3CH_2$), 4.03 (m, J_{POCH} 7.8 Hz, 2H, OCH_2), and 7.3—8.1 (m, 10H, 2Ph).

Found: C, 61.33; H, 6.51%. Calcd for $C_{20}H_{26}ClO_2PS$: C, 60.52; H, 6.56%.

*Copper and Cuprous Salts-catalyzed Reactions with **1** and **2**.* A mixture of **1** or **2** (about 6 mmol) and catalyst (about 0.5 mmol/mmol of one Cu atom) in 5 ml of THF was heated for 24 hr at 150 °C. The reaction mixture was filtered and the filtrate was treated by DCC to separate the reaction products (**12**, **13**, and **14**). The results are summarized in Table 1.

14a: oil: IR (neat); 1435 (C–P), 1215 (P=O), 1135 (P–Ph), and 995 cm^{-1} (P–O).

Found: C, 63.01; H, 7.13; Cl, 9.30%. Calcd for $C_{20}H_{26}ClO_3P$: C. 63.07; H, 6.83; Cl, 9.36%.

*Reactions with **1** and **2** in the Presence of Various Catalysts.* A mixture of **1** or **2** (about 6 mmol) and catalyst (about 0.1 mmol) in about 6.3 g of THF was heated at 120 °C for 6 hr. The reaction mixture was treated with methanol, concentrated, and determined by gas chromatography (column: H 523 on Diasolid at 210 °C). The results are summarized in Table 2.

This work was supported by a grant-in-aid from the Ministry of Education.

References

1) For Part III see: M. Yoshifuji, H. Gomi, and N. Inamoto, This Bulletin, **47**, 2905 (1974).
2) K. Goda, H. Gomi, M. Yoshifuji, and N. Inamoto, *ibid.*, **47**, 2453 (1974).
3) R. E. Goldsberry, D. E. Lewis, and K. Cohn, *J. Organometal. Chem.*, **15**, 491 (1968).
4) T. Emoto, H. Gomi, M. Yoshifuji, R. Okazaki, and N. Inamoto, This Bulletin, **47**, 2449 (1974).
5) M. Asscher and D. Vofsi, *J. Chem. Soc.*, **1963**, 1887, 3921.
6) M. Asscher and D. Vofsi, *ibid.*, **1964**, 4962.
7) F. Minisci and R. Galli, *Tetrahedron Lett.*, **1964**, 167, 3197.
8) R. S. Davidson, R. A. Sheldon, and S. Trippett, *J. Chem. Soc. C*, **1966**, 722.
9) T. Emoto, R. Okazaki, and N. Inamoto, This Bulletin, **46**, 898 (1973).
10) W. A. Higgins, P. W. Vogel, and W. G. Craig, *J. Amer. Chem. Soc.*, **77**, 1864 (1955).
11) L. Maier, *Helv. Chim. Acta*, **47**, 120 (1964).

Hydrogenolyses of Halo-9,9′: 9′,9″-terfluorenyls with the Raney Nickel Catalyst

Masahiro MINABE and Kazuo SUZUKI

Department of Industrial Chemistry, Faculty of Technology, Utsunomiya University, Ishii-cho, Utsunomiya 321-31

(Received January 14, 1975)

2,7-Di- and 2- halo-9,9′ : 9′,9″-terfluorenyls were treated with the Raney nickel catalyst to give 9,9′: 9′,9″-terfluorenyl isomers (mp 293 °C (dec) (I) and mp 257 °C (dec) (II)), fluorene (III), 9,9′-bifluorenyl (IV), halofluorene, and/or 1,2,3,4,4a,9a-hexahydrofluorene (V). The conformation around the C_9–$C_{9'}$ –$C_{9''}$ single bonds of these halo-9,9′: 9′,9″-terfluorenyls were concluded to be *s-cis, s-cis*, identical with those of the parent hydrocarbon I. These assignments were confirmed by hydrogenolyzing 9,9″-dideuterio-2,7-dihalo-9,9′ : 9′,9″-terfluorenyls. The chemical shifts of the 9- and 9″-methine protons in these haloterfluorenyls were explained in terms of the torsional conformations of the molecules.

The conformations of the two stereoisomers for 9,9′: 9′,9″-terfluorenyls (mp 293 °C (dec) (I) and mp 257 °C (dec) (II)) were proposed to be *s-cis, s-cis* and *s-cis, s-trans* respectively, based on the restriction of rotation around the C_9–$C_{9'}$–$C_{9''}$ single bonds.[1] These isomers were obtained simultaneously by the Michael reaction[2] of 9,9′-bifluorenylidene with fluorene (III) and by other reactions.[3]

I was converted into II by treatment with the Raney nickel catalyst (R-Ni), while II gave 9,9′-bifluorenyl (IV), III, and 1,2,3,4,4a,9a-hexahydrofluorene (V) under the same reaction conditions.[2] On the contrary, II was isomerized to I by a reaction with potassium permanganate, triton B, or other reagents.[4]

Halo-9,9′: 9′,9″-terfluorenyls were obtained in the absence of their stereoisomers by the Michael addition[5] of the corresponding fluorene to 9,9′-bifluorenylidene, by the reaction[5a-c] of the corresponding 9-lithiofluorene with 9-bromo-9,9′-bifluorenyl, and by other reactions.[6]

The present paper will describe the treatment of several halo-9,9′: 9′,9″-terfluorenyls with R-Ni; the experiments were undertaken in order to relate the conformations of these haloterfluorenyls to the conformation of I or II. In addition, 2- and 2,7-di-halofluorene and some related compounds were treated with R-Ni.

TABLE 1. HYDROGENOLYSES OF HALO-9, 9′: 9′, 9″-TERFLUORENYLS OVER RANEY NICKEL CATALYST

Reactant	React. condns. R-Ni g	Et_3N g	Time hr	Products (mol%) Monohaloterfluorenyl	I	II	Reactant recovered mol%
2,7-F_2-[a]	20	0.6	3		22		12
2-F-[b]	10	0.6	1.5		6	29	5
2,7-Cl_2-	10	0.6	1.5	76			5
2,7-Cl_2-	10	0.6	3	45	14	4	3
2,7-Cl_2-	20	0.6	3	30	17	15	5
2-Cl-	10	0.6	1.5 (Room Temp.)				95
2-Cl-	5	0.6	1.5		37	7	37
2-Cl-	10	0.6	1.5		21	43	11
2,7-Br_2-	10	0.6	1.5	55	31		4
2,7-Br_2-	10	0.6	3	33	41	7	trace
2,7-Br_2-[c]	20	1.2	3	2	68	11	
2-Br-[c]	10	0.6	1.5		75	5	
2′,7′-Br_2-	10	0.6	3	49	26	3	6
2,7-I_2-	20	0.6	3		93		
2-I-	10	0.6	1.5		86	3	

a) In addition, 2,7-difluoro-9,9′-bifluorenyl (15%) was isolated. b) 2-Fluoro-9,9′-bifluorenyl (44%) was additionally obtained. c) Further, a small amount of IV was isolated.

Results and Discussion

The 2,7-di- and 2-halo-9,9′: 9′,9″-terfluorenyls were treated with R-Ni at 60 °C in toluene under a dry atmosphere, as is shown in Table 1.

2,7-Diiodo-9,9′: 9′,9″-terfluorenyl[5d] produced I in a good yield, along with small quantities of III and V. Similarly, the 2-iodo analog[5d] afforded I as the main product, accompanied by small amounts of II, III, and V. 2′,7′-Dibromo-9,9′: 9′,9″-terfluorenyl[5a] gave 2′-bromo-9,9′: 9′,9″-terfluorenyl,[5e] I, II, 2-bromofluorene, III, and V.

The hydrogenolysis of 2,7-dibromo-9,9′: 9′,9″-terfluorenyl[5a] yielded 2-bromo-9,9′: 9′,9″-terfluorenyl,[6] I, II, III, IV, V, and 2-bromo- and 2,7-dibromo-fluorene. The 2-bromo-9,9′: 9′,9″-terfluorenyl separated from the products was further treated with R-Ni to produce I, II, III, IV, and V. The corresponding chloro derivatives[5c] gave results similar to those of the bromo analogs.

2,7-Dichloro-9,9″-dideuterio-9,9′: 9′,9″-terfluorenyl afforded 2-chloro-9,9′ : 9′,9″-terfluorenyl, I, and II. The deuterium contents in 2,7-dichloroterfluorenyl, 2-chloroterfluorenyl, and I were of the same order: the deuterium was held at C-9 in II, but was exchanged with hydrogen at C-9″. Further, two deuterium atoms were held in I and 2-bromoterfluorenyl, which had been obtained by the treatment of 2,7-dibromo (and -iodo)-9,9″-dideuterio-9,9′: 9′,9″-terfluorenyl with R-Ni.

Accordingly, the conformations of these halo-9,9′:-9′,9″-terfluorenyls may be concluded to be identical with that of I, *i.e. s-cis, s-cis* around the central $C_{9-9'-9''}$ single bonds.

Thus, the hydrogenolysis of the aromatic carbon-halogen bonds in 2,7-dihalo-9,9′: 9′,9″-terfluorenyls occurs to form I without affecting the conformation at C-9 and C-9″ over R-Ni. For example, the reaction of 2,7-dichloro-9,9′: 9′,9″-terfluorenyl with R-Ni proceeds *via* 2-chloro-9,9′: 9′,9″-terfluorenyl to give I, which then isomerizes to II with an inversion of the conformation,[1] as is shown in Scheme 1. Small amounts of III, IV,

2,7-dichloro-, and 2-chloro-fluorene are formed by the reductive cleavage of the central $C_{9-9'}$ and/or $C_{9'-9''}$ bonds of terfluorenyls, and III is reduced to V.[2]

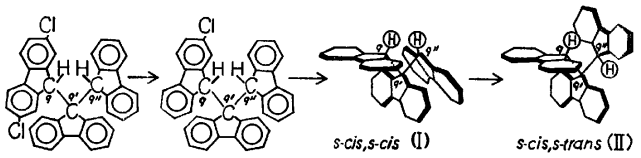

Scheme 1.

In general, in the dehalogenation of organic compounds by catalytic hydrogenation, the order of reactivity is: iodine>bromine>chlorine. The halide ions thus formed inhibit the halogen-hydrogen exchange.[7] In the hydrogenolysis of iodo derivatives, the further reaction of the I thus formed seems to be inhibited by the poisoning action of the iodine ion produced. On the other hand, the isomerization of I to II may follow the hydrogenolysis in the cases of chloro and bromo derivatives.

2,7-Difluoro-9,9': 9',9''-terfluorenyl[5b] gave I, 2,7-difluoro-9,9'-bifluorenyl (15% yield), 2,7-difluorofluorene, III, and V. Further, 2-fluoro-9,9': 9',9''-terfluorenyl[5b] afforded 2-fluoro-9,9'-bifluorenyl (44% yield), I, II, 2-fluorofluorene, III, and V by the same treatment.

The formations of 2,7-di- and 2-fluoro-9,9'-bifluorenyl indicate more resistance of the carbon-fluorine bond toward the hydrogenolysis, which may be attributed to the lesser polarizability of the carbon-fluorine bond and to its relatively weak affinity for the catalyst. The conformations of both fluoro-9,9': 9',9''-terfluorenyls can be identified as *s-cis*, *s-cis*, by analogy with other halo derivatives.

The hydrogenolysis of IV gave III and V, and 9,9'-bifluorenylidene yielded III, IV, and V.[8] 2,7-Di- and 2-halofluorene were treated with R-Ni to give III and V, as Table 2 shows. The tendency of these hydrogenations is similar to that of halo-9,9': 9',9''-terfluorenyls.

TABLE 2. HYDROGENOLYSES OF HALOFLUORENES WITH RANEY NICKEL CATALYST

Fluorene	Components of reaction mixture (mol%)							
	15 min[a]				60 min[a]			
	V	III	2-Halofluorene	2,7-Dihalofluorene	V	III	2-Halofluorene	2,7-Dihalofluorene
Fluorene	40	60			51	49		
2-F-	22	9	69		31	15	54	
2-Cl-	28	27	45		41	33	26	
2-Br-	16	40	44		29	45	26	
2-I-	17	47	36		25	46	29	
2,7-F_2-	12	0	1	87	16	1	0	83
2,7-Cl_2-	13	13	23	51	18	17	22	43
2,7-Br_2-	16	17	15	52	21	23	16	40
2,7-I_2-	20	23	14	43	20	26	20	34

a) Reaction time.

TABLE 3. THE CHEMICAL SHIFTS OF THE 9- AND 9''-METHINE PROTONS IN HALO-9,9': 9',9''-TERFLUORENYLS

9,9': 9',9''-Terfluorenyl	Chemical shift (δ) ppm	
	9-Hydrogen	9''-Hydrogen
I[1]	5.36	5.36
II[1]	5.36	4.61
2',7'-Br_2-	5.14	5.14
2,7-F_2-	5.14	5.14
2,7-Cl_2-	5.14	5.21
2,7-Br_2-	5.14	5.23
2,7-I_2-	5.11	5.26
2-F-	5.22	5.22
2-Cl-	5.22	5.26
2-Br-	5.20	5.26
2-I-	5.16	5.25

Table 3 shows the chemical shifts of the 9- and 9''-methine protons in halo-9,9': 9',9''-terfluorenyls.

The conformations of these halo-9,9': 9',9''-terfluorenyls are presumed to be *s-cis*, *s-cis* forms at the ground state, by analogy with the parent hydrocarbon, I.[1,2] However, the actual halomolecules are torsional conformers about the $C_{9-9'}$ and $C_{9'-9''}$ sp^3-sp^3 bonds, so that the 9- and 9''-fluorenyl rings are both twisted out from the 9'-fluorenylidene plane to release the strain within the range of the restricted degree, in the same way as with *o,o'*-substituted biphenyl. For example, *s-cis*, *s-cis*-2',7'-dibromo-9,9': 9',9''-terfluorenyl (A) may be sketched as (B) in Scheme 2.

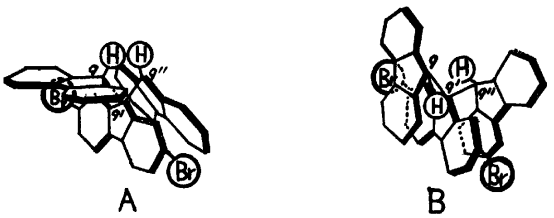

Scheme 2.

In addition, the equal torsion of each 9- and 9''-fluorenyl plane with respect to the central dibromo-9'-fluorenylidene may be more increased than in the case of I as a result of the greater steric repulsion by the bulky dibromo-9'-fluorenylidene group. Thus, two 9- and 9''-methine protons in 2',7'-dibromoterfluorenyl are located in the shielding zone of the π electron cloud on the central 9'-fluorenylidene ring, which shifts the signal to a higher field (5.14 ppm).

However, the 9- and 9''-methine proton should be oriented differently in 2-halo- and 2,7-dihalo-9,9': 9',9''-terfluorenyls because of the different degrees of torsional and repulsive effects of the 9- and 9''-fluorenyl groups with respect to the central 9'-fluorenylidene ring. The spatial situation of the 2,7-dibromo-9-fluorenyl plane with regard to 9'-fluorenylidene in 2,7-dibromoterfluorenyl may be similar to that of the 2',7'-dibromo analog: therefore, the 9-methine proton on the 2,7-dibromo derivative appears at 5.14 ppm. At the 9''-fluorenyl group in 2,7-dibromoterfluorenyl, the degree of twisting and repulsion is probably less than that of the 2',7'-dibromo system. Thus, the 9''-methine proton

signal is observed between those of the 9-methine protons of the 2,7-dibromo system and I.

Experimental

All the melting points are uncorrected. The compounds were confirmed by mixed-melting-point determinations and by a comparison of their IR spectra with those of authentic samples.

The melting points of the deuterio-compounds in this series are identical with those of the parent compounds.

The gc analyses were run with a JGC-1100FP gas chromatograph (Japan Electron Optics Lab. Co., Ltd.), using a 1 m Sus-27 column containing 3% Silicone DC QF-1 on Chromosorb WAW (60—80 mesh). Nitrogen gas, used as a carrier, was made to flow through at an inlet pressure of 1.0 kg/cm^2; the injector and detector temperatures were maintained at 290 and 265 °C respectively. The column temperature was 95 °C (for III and fluorofluorene), 125 °C (for chloro-derivatives), and 140 °C (for bromo- and iodo-analogies). The content of each component was calculated from the average value of five chromatograms.

The IR spectra were obtained as KBr pellets (4000—400 cm^{-1}) or as suspensions in hexachlorobutadiene (3000—2800 cm^{-1}) using a IR-G spectrophotometer (Japan Spectroscopic Co., Ltd.).

The mass spectra were recorded on a RMU-6E apparatus (Hitachi, Ltd.) by means of the direct-inlet system. The chamber voltage, total emission, and target current were maintained at 80 V, 80 μA, and 23 μA respectively. The sample was evaporated at 170 °C. The number of the deuterium in the compounds was calculated from the average value of five spectra.

The NMR spectra were measured by means of a JNM-C60-HL spectrometer (JEOL) in benzene-d_6, using TMS as the internal reference.

Treatment of 2,7-Dibromo-9,9′: 9′,9″-terfluorenyl with R-Ni. Typical Procedure: A solution of 2.00 g (3 mmol) of 2,7-dibromo-9,9′: 9′,9″-terfluorenyl and 0.6 g of triethylamine in 110 ml of toluene was stirred with 10 g of R-Ni (W-4) at 60 °C for 1.5 hr. The reaction mixture was then filtered, and the catalyst was extracted with four 40-ml portions of toluene. All the toluene solution was then evaporated under reduced pressure. The residue was extracted with a 30-ml portion of boiling ethanol: the insoluble parts were recrystallized from ethyl acetate to give 0.46 g (31%) of I (mp 291—293 °C (dec)), 0.89 g of 2-bromo-9,9′: 9′,9″-terfluorenyl (mp 252—253 °C (dec)), and 0.07 g (4%) of the starting material (mp 286—287 °C (dec)).

Upon standing, the alcohol extract gave 0.06 g (total 0.95 g, 55%) of 2-bromo-9,9′: 9′,9″-terfluorenyl (mp 252—254 °C (dec)). The mother liquor was evaporated to dryness, and the residue was sublimed *in vacuo* at 180 °C. The sublimate (0.01 g) proved by means of gas chromatography to be a mixture of V (*ca.* 2.6 mg), III (*ca.* 5.7 mg), 2-bromo- (*ca.* 0.8 mg), and 2,7-dibromo-fluorene (*ca.* 0.9 mg).

Hydrogenolyses of 9,9′-Bifluorenyl (IV) and 9,9′-Bifluorenylidene. A solution of 1.32 g (4 mmol) of IV and 0.3 g of triethylamine in 110 ml of toluene was refluxed with 10.0 g of R-Ni for 3 hr.

Upon treatment in a manner similar to that described above, the residue was recrystallized from 50 ml of ethyl acetate to afford 0.69 g of IV (mp 242—243 °C). The mother liquor was evaporated to dryness, and the residue was extracted with petroleum ether. The insoluble parts yielded IV (0.02 g; total 0.71 g, 54%); mp 242—244 °C. The extract was analyzed by means of gc; the presence of 0.17 g (13%) of III and 0.33 g (24%) of V was thus confirmed.

9,9′-Bifluorenylidene (1.32 g, 4 mmol) was submitted in the same way as above: 0.85 g (64%) of IV, 0.10 g (7%) of III, and 0.35 g (25%) of V were obtained.

Hydrogenolyses of Halofluorenes. A solution of 2.5 mmol of the substrate in 15 ml of toluene was refluxed with 2.0 g of R-Ni. After each time interval, a small amount of the reaction mixture was taken out and the supernatant was examined by means of gc.

Synthesis of 2-Bromo-9,9″-dideuterio-9,9′: 9′,9″-terfluorenyl. Typical Procedure: 2-Bromo-9,9-dideuteriofluorene was prepared in a 93% yield by the method of Cram and Kollmeyer.[9] The extent of deuterium incorporation was 97%, as determined by means of the NMR spectrum.

A solution of 1.64 g of 9,9′-bifluorenylidene, 1.35 g of 2-bromo-9,9-dideuteriofluorene, and a 1-ml portion of D_2O containing 0.3 g of sodium carbonate in 14 ml of dry pyridine was placed in a sealed tube and heated at 97—100 °C for 50 hr. Upon an usual treatment,[5a] the reaction mixture afforded 0.82 g (44% yield) of 2-bromo-9,9″-dideuterio-9,9′: 9′,9″-terfluorenyl. The deuterium incorporation was calculated by means of the mass spectrum to be as follows: d_0, 1%; d_1, 12%; d_2, 87%.

Treatments of 2,7-Dihalo-9,9″-dideuterio-9,9′: 9′,9″-terfluorenyls with R-Ni. Some deuterio-compounds were treated with R-Ni in a manner analogous to those used for the parent haloterfluorenyls. The deuterium contents of the substrates and products were determined by means of the mass spectra to be as follows:

a): 2,7-Dichloro-9,9′: 9′,9″-terfluorenyl (d_0, 1%; d_1, 12%; d_2, 87%) gave a 2-chloro analog (d_0, 1%; d_1, 12%; d_2, 87%), I (d_0, 2%; d_1, 13%; d_2, 85%), and II (d_0, 12%; d_1, 88%; d_2, 0%).

b): 2,7-Dibromo derivative (d_0, 0%; d_1, 13%; d_2, 87%) yielded 2-bromo-9,9′: 9′,9″-terfluorenyl (d_0, 0%; d_1, 14%; d_2, 86%) and I (d_0, 0%; d_1, 18%; d_2, 82%).

c): I (d_0, 0%; d_1, 22%; d_2, 78%) was obtained from 2,7-diiodo-9,9′: 9′,9″-terfluorenyl (d_0, 1%; d_1, 22%; d_2, 77%).

References

1) K. Suzuki and M. Minabe, *Tetrahedron Lett.*, **1974**, 1541.

2) M. Minabe and K. Suzuki, *J. Org. Chem.*, **40**, 1298 (1975).

3) K. Suzuki, *Nippon Kagaku Zasshi*, **70**, 189 (1949); S. Kajigaeshi, *ibid.*, **82**, 1397, 1712 (1961); **83**, 191 (1962); K. Suzuki and S. Kajigaeshi, This Bulletin, **35**, 408 (1962).

4) M. Minabe and K. Suzuki, *ibid.*, **48**, 1480 (1975).

5) For examples: a) K. Suzuki, M. Minabe, M. Fujimoto, and N. Nohara, *ibid.*, **42**, 1609 (1969); b) M. Minabe, A. Tanaka, M. Wakui, and K. Suzuki, *ibid.*, **44**, 1614 (1971); c) M. Minabe and K. Suzuki, *ibid.*, **48**, 586 (1975); d) M. Minabe and K. Suzuki, *ibid.*, **45**, 3196 (1972); e) K. Suzuki and M. Fujimoto, *ibid.*, **37**, 1833 (1964); f) K. Suzuki, *Nippon Kagaku Zasshi*, **72**, 825, 827 (1951); **75**, 711, 714, 793, 795 (1954).

6) For example: S. Kajigaeshi, *ibid.*, **83**, 102 (1962).

7) J. N. Pattison and Ed. F. Degering, *J. Amer. Chem. Soc.*, **73**, 611 (1951); K. Isogai, *Nippon Kagaku Zasshi*, **81**, 792 (1960).

8) A. Schönberg, K.-H. Brosowski, and E. Singer, *Chem. Ber.*, **95**, 2984 (1962).

9) D. J. Cram and W. D. Kollmeyer, *J. Amer. Chem. Soc.*, **90**, 1791 (1968).

The Facile Syntheses of Aldehydes and Aldehydic Acids from Carboxylic Acid Anhydrides Using Disodium Tetracarbonylferrate (—II)

Yoshihisa WATANABE, Masakazu YAMASHITA, Take-aki MITSUDO, Mineo IGAMI, and Yoshinobu TAKEGAMI

Department of Hydrocarbon Chemistry, Faculty of Engineering, Kyoto University, Sakyo-ku, Kyoto 606

(Received February 6, 1975)

Disodium tetracarbonylferrate reacts readily with aliphatic and aromatic carboxylic acid anhydrides under mild conditions; the corresponding aldehydes are formed in high yields by quenching the reaction solution with acetic acid. Intermolecular anhydrides give aldehydes and acids, and intramolecular ones give aldehydic acids. The reaction mechanism *via* acylcarbonylferrates is assumed.

Disodium tetracarbonylferrate has been shown to be an inexpensive, versatile and selective reagent converting alkyl halides, tosylates, and acid halides into aldehydes, carboxylic acid derivatives, and ketones in high yields.[1-4] On the other hand, though aldehydes are known to be derived from various carboxylic acid derivatives such as acid chlorides, imide chlorides, thioesters, hydrazides, and nitriles,[5] there have been only a few reports describing the reduction of carboxylic acid anhydrides to aldehydes.[6,7] These reactions can be applied mainly to aliphatic acid anhydrides and are of no practical use because of the low yields of the products or of their prolonged reaction times. We now report the facile syntheses of aldehydes and aldehydic acids from carboxylic acid anhydrides in good yields using the ferrate. The preliminary report of this work was published elsewhere.[8]

Results and Discussion

Carboxylic acid anhydrides react readily with disodium tetracarbonylferrate [I] in dry tetrahydrofuran (THF) at room temperature under argon atmosphere to give reduced products, *i.e.* aldehydes or aldehydic acid, after quenching the reaction mixture with acetic acid. Intermolecular acid anhydrides give aldehydes and acids, and intramolecular ones give aldehydic acids in excellent yields.

$$(RCO)_2O \xrightarrow[\text{ii) } H^+]{\text{i) } Na_2Fe(CO)_4} RCHO + RCOOH$$

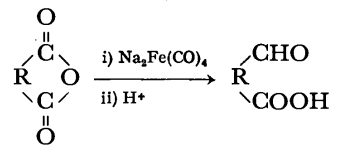

The reaction is completed in less than 20 minutes with a color change from pale yellow to dark red. The results of this reaction are shown in Table 1. This reaction can be applied to a wide variety of anhydrides, not only to aliphatic but also to aromatic ones; α,β-unsaturated carboxylic anhydrides such as maleic anhydride were not, however, reduced to the corresponding aldehydes.

The scheme of this reaction is reasonably considered as follows. One of the carbonyl groups of the anhydride is attacked nucleophilically by the ferrate to give an acyltetracarbonylferrate [II] and carboxylate, which are protonated to aldehyde and acid, as shown in Eq. (1), by quenching the reaction mixture with acetic acid. These reactions were monitored by infrared spectra. The absorption band at 1780 cm^{-1} due to the stretching vibration of the terminal carbonyls of the ferrate[9] disappeared as soon as anhydrides were added and two new bands at 1890 cm^{-1} and 1550—1600 cm^{-1} appeared. The former is attributed to the terminal carbonyls and the latter to the acyl group of [II].[10] In addition, the bands characteristic of carboxylates appeared. At this point the absorption bands of carbonyls of the anhydrides were not observed. These results support the scheme described above.

$$(RCO)_2O + [Fe(CO)_4]^{2-} \longrightarrow [RCO\text{-}Fe(CO)_4]^- + RCOO^- \longrightarrow RCHO + RCOOH \quad (1)$$

([II])

In the reaction of mixed carboxylic anhydrides, two ways for the nucleophilic attack of the ferrate to the two carbonyl groups of the anhydride are possible and thus the formation of two different aldehydes can be expected (Eq. (2)).

Table 1. Reduction of carboxylic acid anhydride using disodium tetracarbonylferrate

No.	Anhydride	Product	Yield (%)[a]
1	Propionic	Propionaldehyde	90[b]
2	*n*-Butyric	*n*-Butyraldehyde	61[b]
3	Isobutyric	Isobutyraldehyde	41[d]
4	*n*-Valeric	*n*-Valeraldehyde	67[b]
5	*n*-Caproic	*n*-Capronaldehyde	60[b]
6	Benzoic	Benzaldehyde	73[b]
7	*p*-Toluic	*p*-Tolualdehyde	75[b]
8	Succinic	Succinaldehydic acid	81[d]
9	Glutaric	Glutaraldehydic acid	60[c]
10	Phthalic	Phthalaldehydic acid	61[c]
11	Tetrachlorophthalic	Tetrachlorophthal-aldehydic acid	83[c]
12	1,8-Naphthalic	1,8-Naphthaldehydic acid	75[c]

a) (mol of product/mol of anhydride) × 100. b) Yields were determined by glpc. c) Isolated yields. d) Isolated yields as 2,4-DNP.

$$R^1\text{-}CO\text{-}O\text{-}CO\text{-}R^2 \xrightarrow[\text{ii) } H^+]{\text{i) } [Fe(CO)_4]^{2-}} \begin{matrix} R^1CHO + R^2COOH \\ \text{or} \\ R^1COOH + R^2CHO \end{matrix} \quad (2)$$

Several mixed anhydrides were allowed to react with the ferrate and the structural effects of anhydrides in this reaction were investigated. To make the comparison of the effects easy, benzoic acid was employed as one of the acids used as components of the anhydride. The results obtained are listed in Table 2.

Table 2. Reaction of mixed anhydrides with disodium tetracarbonylferrate in THF[a]

No.	$R^1C(=O)O(C=O)R^2$ R^1	R^2	Ratio[b] R^1CHO	R^2CHO
13	CH_3	C_6H_5	64	36
14	CH_3CH_2	C_6H_5	44	56
15	$(CH_3)_2CH$	C_6H_5	30	70
16	$CH_3(CH_2)_6$	C_6H_5	31	69
17	*p*-$CH_3C_6H_4$	C_6H_5	48	52
18	*m*-$CH_3C_6H_4$	C_6H_5	43	57
19	*p*-$CH_3OC_6H_4$	C_6H_5	32	68
20	*p*-ClC_6H_4	C_6H_5	55	45
21	*o*-$CH_3C_6H_4$	C_6H_5	21	79
22	*o*-ClC_6H_4	C_6H_5	18	82
23	*o*-$CH_3OC_6H_4$	C_6H_5	61	39
24	*o*-$CH_3OC_6H_4$	*p*-$CH_3C_6H_4$	61	39
25	*o*-$CH_3OC_6H_4$	*p*-ClC_6H_4	59	41

a) At 25 °C for 20 min. b) Total yields of aldehydes are 60—80% in all cases.

In the reaction of benzoic aliphatic carboxylic anhydride (Exps. 13—16), the proportion of aliphatic aldehydes to benzaldehyde decreases as the alkyl groups become bulky, showing that the nucleophilic attack of the ferrate appears to be sterically affected.

In the series of benzoic substituted benzoic anhydrides (Exps. 17—23), different substituents such as Cl–, CH_3–, and CH_3O– have different effects on the reaction and distribution of the products. When the substituents are located at *meta* and *para* positions, the distribution of aldehydes is affected by their electron donating-withdrawing property: that is, an electron withdrawing group, Cl-, seems to favor the formation of substituted benzaldehyde but electron-donating groups, CH_3- and CH_3O-, are unfavorable for such formation. This shows that the nucleophilic attack is affected by the electron density on the carbon of carbonyl group of the anhydrides. In the cases in which the substituents are located at an *ortho* position, the Cl- and CH_3- groups have steric hindrance effects and disturb considerably the formation of substituted benzaldehydes. But the CH_3O– group has no such effects but on the contrary promotes the formation of *o*-anisaldehyde (Exps. 23—25). The effect of *o*-CH_3O–, quite different from that of *o*-Cl and *o*-CH_3, may be due to some interaction between the methoxy group and ion-paired disodium tetracarbonylferrate.[11]

Experimental

The carboxylic acid anhydrides shown in Table 1 were all commercial products except for *p*-toluic anhydride. The other anhydrides were prepared in the usual manner from sodium carboxylates and acid chlorides in THF or in benzene. Disodium tetracarbonylferrate, $Na_2Fe(CO)_4$, was prepared according to the method described in the literature.[2] Iron pentacarbonyl was a commercial product and used without further purification.

General Procedure for the Reaction of Intermolecular Carboxylic Anhydrides with $Na_2Fe(CO)_4$. To 11 mmol of disodium tetracarbonylferrate in THF (50 ml), 11 mmol of acid anhydride in THF (10 ml) was added with stirring at room temperature under argon atmosphere. Twenty minutes later, the reaction mixture was treated with glacial acetic acid (1.2 ml) and stirred for an additional five minutes. Then it was poured into 50 ml of water and extracted with 20 ml of pentane and 20 ml of ethyl ether, and the organic extract was submitted to glpc analysis. The aldehydes were identified by comparison of the retention time of glpc with those of authentic samples and yields were determined using internal standards.

General Procedure for the Reaction of Intramolecular Carboxylic Anhydrides with $Na_2Fe(CO)_4$. In 60 ml of THF, 11 mmol of disodium tetracarbonylferrate and carboxylic acid anhydride was allowed to react according to the above procedure. After quenching with 1.2 ml of glacial acetic acid, the reaction solvent was distilled off under a reduced pressure, and the residue was extracted with 0.5 M NaOH aqueous solution (50 ml) and filtered. The filtrate was acidified and extracted with three portions of ether (70 ml). After drying over sodium sulfate, the organic layer was evaporated and the residue was purified by recrystallization or converted into 2,4-dinitrophenylhydrazone. The products were identified by NMR, IR, elemental analyses, and by comparison with literature data or with authentic samples.

The authors would like to thank Mr. Hideo Fujiwara for his assistance in experiments.

References

1) M. P. Cooke, Jr., *J. Amer. Chem. Soc.*, **92**, 6080 (1970).
2) Y. Watanabe, T. Mitsudo, M. Tanaka, K. Yamamoto, T. Okajima, andY. Takegami, This Bulletin, **44**, 2569 (1971).
3) J. P. Collman, S. R. Winter, and D. R. Clark, *J. Amer. Chem. Soc.*, **94**, 1788 (1972).
4) J. P. Collman, S. R. Winter, and R. G. Komoto, *ibid.*, **95**, 249 (1973).
5) R C. Fuson, "The Chemistry of the Carbonyl Group," ed. by S. Patai, Interscience Publishers, New York, N. Y. (1966), p. 211.
6) H. Wakamatsu, J. Furukawa, and N. Yamakami, This Bulletin, **44**, 288 (1971).
7) H. Musso and K. Figge, *Chem. Ber.*, **95**, 1844 (1962).
8) Y. Watanabe, M. Yamashita, T. Mitsudo, M. Tanaka, and Y. Takegami, *Tetrahedron Lett.*, **1973**, 3535.
9) W. F. Edgell, J. Huff, J. Thomas, H. Lehman, C. Angell, and G. Asato, *J. Amer. Chem. Soc.*, **82**, 1254 (1960).
10) W. O. Siegel and J. P. Collman, *ibid.*, **94**, 2516 (1972).
11) J. P. Collman, J. N. Cawse, and J. I. Brauman, *ibid.*, **94**, 5905 (1972).

α,β-Unsaturated Carboxylic Acid Derivatives. VIII. The Synthesis and Reaction of Esters *N*-Acyl-*N*-bromo-α-dehydroamino Acid[1)]

Chung-gi SHIN, Katsumi NANJO, Takashi NISHINO, Yoshiaki SATO, and Juji YOSHIMURA*

Laboratory of Organic Chemistry, Faculty of Technology, Kanagawa University, Rokkakubashi, Kanagawa-ku, Yokohama 221

* *Laboratory of Chemistry for Natural Products, Faculty of Science, Tokyo Institute of Technology, Ōokayama, Meguro-ku, Tokyo 152*

(Received February 14, 1975)

The addition of bromine to *t*-butyl 2-(*N*-acylamino)-2-alkenoate (**3**) was accompanied by the elimination of hydrogen bromide and the decomposition of the ester group to give 2-(*N*-acylamino)-3-bromo-2-alkenoic acid, while the bromination of **3** with NBS gave the corresponding *N*-bromo derivative (**7**), whose bromine atom gradually migrates to give *t*-butyl 2-(*N*-acylamino)-3-bromo-2-alkenoate. The substitution of the bromine of **7** with nucleophiles gave, successively, the corresponding *N*-methoxy, *N*-benzyloxy and *N*-cyano derivatives, while that with sodium azide gave the corresponding migration products. The structures of the new compounds were assigned.

In previous papers, we reported the new syntheses of alkyl 2-(*N*-acylamino)-2-alkenoate (**3**) by the condensation of alkyl 2-oxoalkanoate with chloroacetamide[2)] or chloroacetonitrile[3)] and by the elimination of acetic acid from alkyl 2-(*O*-acetyl-*N*-acyl-hydroxyamino)alkanoate, which had itself been derived by the acetylation of alkyl 2-hydroxyaminoalkanoate (**1**) or alkyl 2-(*N*-acyl-hydroxyamino)alkanoate (**2**).[4,5)]

Because of the possible synthetic utility of the *N*-bromo derivative of **3** in the preparation of α-dehydrohydroxyamino acids, cyclic hydroxamic acids such as mycelianamide,[6)] and other similar substances, the facile synthesis of *t*-butyl 2-(*N*-bromoacetamido)-2-alkenoate (**7**) was pursued, and it was briefly communicated that the bromination of **3** with bromine or *N*-bromosuccinimide (NBS) gave 2-(*N*-acylamino)-3-bromo-2-alkenoic acids (**5**) or **7** respectively.[7)] However, no available method of synthesizing **7** or **5** has ever been reported, except for the preparation of β-halo-*sec*- and -*tert*-enamines.[8–10)]

In the present paper, we wish to report the syntheses of **5** and **7** in detail, together with the replacement of the bromine atom of **7** with nucleophiles. A few substitutions were accompanied by the rearrangement of substituents, and the structures of the products were assigned by means of IR and NMR spectroscopies.

Results and Discussion

Bromination of 1 and 3. Attempts at the addition of bromine to ethyl 2-(*N*-acylamino)-2-alkenoate (**3**; R^1=Et) in chloroform and the subsequent elimination of hydrogen bromide under several experimental conditions were unsuccessful, except for the direct conversion of **3a,c,d** (R=CH_3, R^1=*t*-Bu: **a**; X=CH_3, **c**; X=OC_2H_5, **d**; X=Phthalyliminomethyl) into 2-(*N*-acylamino)-3-bromo-2-butenoic acid (**6a,c,d**) in an about 50% yield at room temperature for 2 days. Besides, it was found that the treatment of ethyl 2-hydroxyaminobutanoate (**1e**) with bromoacetyl bromide in benzene in the absence of an alkali such as pyridine at room temperature gave ethyl 3-bromo-2-bromoacetamido-2-butenoate (**5e**) directly, though the yield was low. It was deduced that the formation of ethyl 2-bromoacetamido-2-butenoate (**3e**; R=CH_3, R^1=C_2H_5, X=CH_2Br) *via* the corresponding hydroxamic acid ester (**2e**)[5)] was followed by the addition of bromine formed oxidatively from hydrogen bromide, and by the elimination of hydrogen bromide to afford **5e**. On the other hand, the reaction of **3** with bromine proceeded similarly through the addition of bromine and the elimination of hydrogen bromide to give **5**, which was subsequently converted into **6**.

On the other hand, the treatment of *t*-butyl 2-acetamido-2-alkenoate (**3a,b**: **b**; R=C_2H_5, R^1=*t*-Bu, X=CH_3) with NBS in tetrachloromethane at room temperature for 30 min gave **7a,b** as an unstable oily product in quantitative yield. It was found that the bromine on the nitrogen atom of **7a,b** gradually migrated at room temperature for 2 days to give **5a,b** as colorless crystals in about a 70% yield. The **5a,b** compound was composed of *E*- and *Z*-isomers, which were purely separated by chromatography on a silica gel column using benzene–ethyl acetate (5: 1 V/V). However, the unambiguous assignment of the geometric configuration of the products was difficult from only the spectroscopic data listed in Table 2.

The yields, the physical constants, and the spectral data of **5** and **7** are summarized in Tables 1 and 2 respectively.

Reactions of 7 with Nucleophiles. The treatment of **7a,b** with sodium methoxide in methanol at room temperature for 2 hr afforded *t*-butyl 2-(*N*-acetyl-*O*-methyl-hydroxyamino)-2-alkenoate (**8a,b**). Moreover, in a similar manner, compound **7a,b** reacted with sodium benzyloxide in benzyl alcohol to give the expected *t*-butyl 2-(*N*-acetyl-*O*-benzyl-hydroxyamino)-2-alkenoate (**9a,b**). On the other hand, the reaction of **7a,b** with sodium cyanide in dimethyl formamide also occurred at room temperature for 2 hr to give *t*-butyl 2-(*N*-cyanoacetamido)-2-alkenoate (**10a,b**). It was found that the products obtained were more stable than **7a,b** and that the methoxy, benzyloxy, and cyano groups on the nitrogen atom do not migrate to the carbon atom in the β-position.

On the other hand, the treatment of **7a,b** with sodium azide in dimethyl formamide at room temperature for 2 hr unexpectedly gave the *t*-butyl 2-acetamido-3-azido-2-alkenoate (**12a,b**) as a colorless syrup or as needles in a good yield. In this case, the expected *N*-substituted compound (**11a,b**) could not be isolated. However,

the preparation of **12** by the reaction of **5** with sodium azide was unsuccessful. Consequently, it was deduced that the direct formation of **12** from **7** proceeded through the rearrangement reaction of the intermediate, **11a,b**.

All of the new compounds were obtained as syrups; some of them gradually crystallized in considerably good yields after purification on a silica gel column using benzene–ethyl acetate.

The structures of all the new compounds were characterized spectroscopically and gave satisfactory results in elemental analysis. From the NMR spectra, the vinyl proton signals of **7**, **8**, **9**, and **10** showed peaks in the δ 4.12—5.01 region as quartets or triplets, while the NH proton signals of **5** and **12** showed their peaks in the δ 6.86—8.35 region as broad singlets. On the other hand, the disappearance of the NH absorption band in the IR spectrum of **3** indicates the formation of **7**, while the appearance of the NH band in the region 3150—3340 cm^{-1} seems to support the formation of

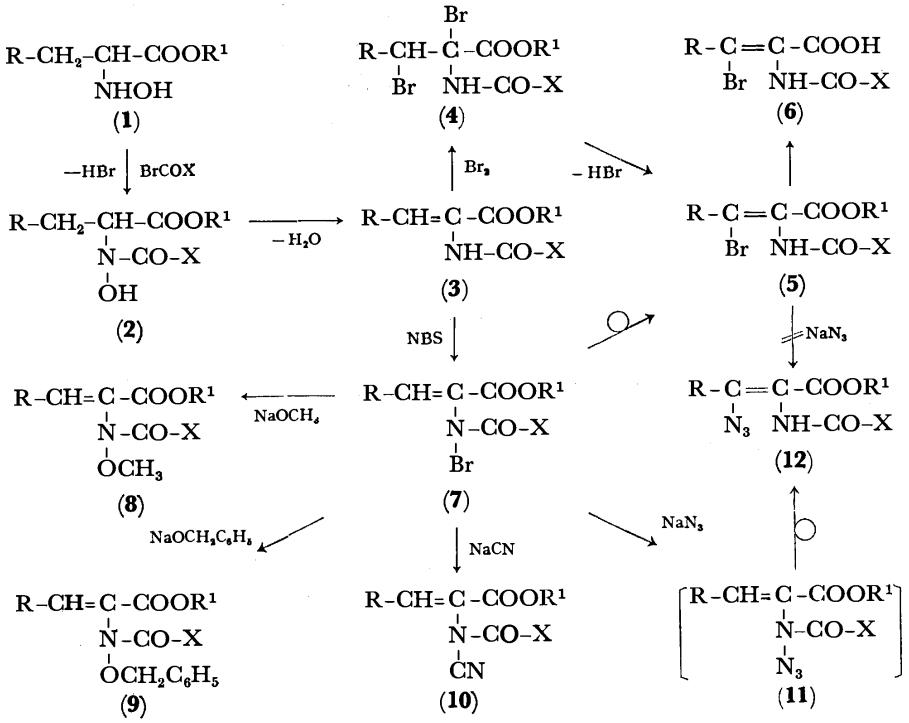

a; R=CH_3, R^1=*t*-Bu, X=CH_3, **b**; R=C_2H_5, R^1=*t*-Bu, X=CH_3,
c; R=CH_3, R^1=*t*-Bu, X=OC_2H_5, **d**; R=CH_3, R^1=*t*-Bu, X=Phthalyliminomethyl,
e; R=CH_3, R^1=Et, X=CH_2Br

Scheme 1.

TABLE 1. *t*-BUTYL 2-(*N*-SUBSTITUTED-ACETAMIDO)-2-ALKENOATES $\left(\begin{matrix} \text{R-CH=C-COOBu-}t \\ \text{N-COCH}_3 \\ \text{X} \end{matrix}\right)$

Compd. No.	X	Yield (%)	mp °C	Formula	Found (Calcd), % C	H	N	IR spectrum, cm^{-1} in KBr CN	COO	C=O	C=C	NMR spectrum,[d] β-H, δ
7a	Br	100	syrup[a]						1740	1720	1680	5.01
7b	Br	100	syrup[a]						1740	1725	1680	4.80
8a	OCH_3	96	syrup	$C_{11}H_{19}NO_4$	57.58 (57.62	8.12 8.35	6.43 6.11)		1745	1670		4.44
8b	OCH_3	66	syrup	$C_{12}H_{21}NO_4$	59.55 (59.24	8.85 8.70	6.02 5.76)		1740	1665		4.12
9a	$OCH_2C_6H_5$	72	58—59[b]	$C_{17}H_{23}NO_4$	66.83 (66.86	7.63 7.59	4.58 4.58)		1740	1670		4.53
9b	$OCH_2C_6H_5$	60	67—68[b]	$C_{18}H_{25}NO_4$	68.11 (67.69	7.92 7.89	4.30 4.39)		1740	1670		4.32
10a	CN	94	53—54[c]	$C_{11}H_{16}N_2O_3$	58.73 (58.91	7.04 7.19	12.31 12.49)	2240	1760	1660		4.98
10b	CN	99	syrup	$C_{12}H_{18}N_2O_3$	60.50 (60.48	7.72 7.61	11.58 11.76)	2240	1755	1660		4.66

a) Pale yellow syrup, structure of which was confirmed by means of IR and NMR spectra and conversion into following compounds. b) Colorless prisms from petroleum ether. c) Colorless tablets from petroleum ether.
d) Measured in $CDCl_3$.

TABLE 2. *t*-BUTYL 3-SUBSTITUTED-2-ACETAMIDO-2-ALKENOATES $\left(\begin{matrix}R\text{–}C=C\text{–}COOBu\text{-}t\\ \quad\ |\quad\ \ |\\ \quad X\quad NHCOCH_3\end{matrix}\right)$

Compd No.	X	Yield (%)	Mp °C	Formula	Found (Calcd), % C	H	N	IR spectrum, cm^{-1} in KBr NH	N_3	COO	C=O	C=C	NMR spectrum,[d] NH, δ
5a (*E*+*Z*)	Br	54	138—139[a]	$C_{10}H_{16}NO_3Br$	43.58 (43.18	5.80 5.80	5.06 5.04)	3340		1715	1680	1645	7.06
	Br	36	101.5—102.5[a]	$C_{10}H_{16}NO_3Br$	43.09 (43.18	5.88 5.80	4.93 5.04)	3340		1715	1685	1640	7.94
5b (*E*+*Z*)	Br	45	84—87[b]	$C_{11}H_{18}NO_3Br$	45.44 (45.22	6.31 6.21	4.79 4.79)	3270		1725	1670	1635	7.16
	Br	18	suyrp	$C_{11}H_{18}NO_3Br$			5.13 (4.79)	3270		1730	1680	1630	8.35
12a	N_3	92	104[c]	$C_{10}H_{16}N_4O_3$	50.07 (49.99	6.71 6.71	23.32 23.32)	3150	2110	1720	1640		6.86
12b	N_3	85	94[a]	$C_{11}H_{18}N_4O_3$	51.88 (51.95	7.02 7.14	21.98 22.03)	3150	2100	1720	1640		7.06

a) Colorless needles from di-*n*-butyl ether. b) Colorless fibrous from di-*n*-butyl ether. c) Colorless fibrous from tetrachloromethane. d) Measured in $CDCl_3$.

5 and **12**. From either the presence or absence of the vinyl or NH proton respectively, the structures of the above compounds were confirmed.

The above rearrangement reaction, which seems to be an intramolecular anionic 1,3-shift, and the configurational assignment of the products are now under investigation.

Experimental

All the melting points are uncorrected. The IR spectra were recorded with a Hitachi EPI-S2 Spectrometer. The NMR spectra were measured with a JNM-4H-100 Spectrometer (Japan Electron Optics Laboratory Co., Ltd.), using tetramethyl silane as the internal standard.

Materials. Compounds **1e** and **3a**, **b**, **c**, **d** were prepared by a method previously reported.[4]

Reaction of 3 with Bromine A solution of bromine (0.078 mol) in chloroform (20 ml) was stirred drop by drop, into a solution of *t*-butyl 2-acetamido-2-butenoate (**3a**: 0.078 mol) in chloroform (15 ml) below 0 °C. The reaction solution was then allowed to stand at room temperature for 2 days. The colorless crystals which had thus been separated out were collected and recrystallized from acetone to give colorless tablets, which were identified as 3-bromo-2-acetamido-2-butenoic acid (**6a**); yield, 58.8%; mp 150 °C (decomp). IR (KBr): 3300, 1720, 1645, 1630 cm^{-1}.

Found: C, 32.86; H, 3.60; N, 6.37%. Calcd for $C_6H_8NO_3Br$: C, 32.50; H, 3.60; N, 6.37%.

In a similar manner, the treatment of an equimolar amount of *t*-butyl 2-(*N*-ethoxycarbonylamino)-2-butenoate (**3c**) with bromine in chloroform gave 3-bromo-2-(*N*-ethoxycarbonylamino)-2-butenoic acid (**6c**) as colorless needles; those needles were recrystallized from chloroform; yield, 59.3%; mp 154—156.5 °C (decomp). IR (KBr): 3260, 1700, 1630 cm^{-1}.

Found: C, 33.58; H, 3.98; N, 5.58%. Calcd for $C_7H_{10}NO_4Br$: C, 33.35; H, 3.97; N, 5.56%.

In a similar manner, the treatment of an equimolar amount of *t*-butyl 2-(*N*-phthaloylglycylamino)-2-butenoate (**3d**) with bromine in glacial acetic acid gave a residual reddish syrup after the removal of the excess acetic acid under reduced pressure. When a small quantity of ethanol was added to the residue, crude crystals were gradually separated out. The crystals were collected and recrystallized from glacial acetic acid to give colorless needles, which were identified as 3-bromo-2-(*N*-phthaloylglycylamino)-2-butenoic acid (**6d**); yield, 37.8 %; mp 188 °C (decomp). IR (KBr): 3260, 1735, 1680, 1630 cm^{-1}.

Found: C, 45.82; H, 3.10; N, 7.68%. Calcd for $C_{14}H_{11}N_2O_5Br$: C, 45.80; H, 3.00; N, 7.63%.

Reaction of 1e with Bromoacetyl Bromide. To a solution of ethyl 2-hydroxyaminobutanoate (**1e**: 0.027 mol) in dry benzene (20 ml), we stirred bromoacetyl bromide (0.033 mol), drop by drop at room temperature. Then the reaction solution was heated at 70—80 °C for 30 min. After cooling to room temperature, the insoluble substance which had been separated out was filtered off, and the filtrate was evaporated under reduced pressure. The residual reddish oil was purified on a silica gel column using benzene–methanol (40: 1 v/v). After the removal of the solvent, the crystals which had been separated out were collected and recrystallized from di-*n*-butyl ether to give colorless needles, which were identified as ethyl 3-bromo-2-bromoacetamido-2-butenoate (**5e**); yield, 6.7%; mp 118—119 °C. IR (KBr): 3250, 1730, 1660, 1535 cm^{-1}.

Found: C, 29.60; H, 3.40; N, 4.26%. Calcd for $C_8H_{11}NO_3Br_2$: C, 29.20; H, 3.35; N, 4.26%.

Reaction of 3 with NBS. Into a solution of **3a** (0.020 mol) in tetrachloromethane (20 ml), we stirred NBS (0.021 mol), portion by portion at room temperature. After stirring for 30 min, the succinimide which had thus been separated out was filtered off, and the filtrate was evaporated under reduced pressure to give pale yellow syrup in a quantitative yield. This syrup was identified as *t*-butyl 2-(*N*-bromoacetamido)-2-2-butenoate (**7a**).

In a similar manner, *t*-butyl 2-(*N*-bromoacetamido)-2-pentenoate (**7b**) was also obtained in a quantitative yield starting from the reaction of an equimolar amount of *t*-butyl 2-acetamido-2-pentenoate (**3b**) and NBS.

Rearrangement Reaction of 7. When **7a** (0.07 mol) was allowed to stand at room temperature for 2 days, the syrup gradually crystallized to give colorless crystals, which were composed of *E*- and *Z*-isomers. The geometric isomers were separated purely by chromatography on a silica gel column using benzene–ethyl acetate (5: 1 v/v). After the removal of the solvent under reduced pressure, *t*-butyl 3-bromo-2-acetamido-2-butenoate (**5a***E* and **5a***Z*) was obtained.

In a similar manner, *t*-butyl 3-bromo-2-acetamido-2-pentenoate (**5bE** and **5bZ**) was also obtained in a pure state by starting from **7b** through the migration of bromine atom (Table 2).

Reaction of 7 with Sodium Methoxide. After treating **7a**

(0.0151 mol) with sodium methoxide (made from sodium (0.018 mol) and methanol (30 ml)), with stirring, at room temperature for 2 hr, the reaction solution was concentrated under reduced pressure. The residual yellow syrup was dissolved in benzene (30 ml), and then the solution was washed with water twice. The benzene layer was dried over anhydrous magnesium sulfate and then evaporated under reduced pressure. The residual pale yellow syrup was purified on a silica gel column using benzene–ethyl acetate (50: 1 v/v). The effluent was then condensed under reduced pressure to give a colorless syrup, which was identified as *t*-butyl 2-(*N*-acetyl-*O*-methyl-hydroxyamino)-2-butenoate (**8a**).

In a similar manner, *t*-butyl 2-(*N*-acetyl-*O*-methyl-hydroxyamino)-2-pentenoate (**8b**) was also obtained starting from the reaction of **7b** and sodium methoxide.

Reaction of 7 with Sodium Benzyloxide. After treating **7a** (0.0151 mol) with sodium benzyloxide (made from sodium (0.018 mol) and benzyl alcohol (30 ml)), with stirring, at room temperature for 2 hr, the reaction solution was concentrated under reduced pressure. The residual yellow syrup was dissolved with benzene (30 ml), and then the solution was washed with water three times. The benzene layer was dried over anhydrous magnesium sulfate and then evaporated under reduced pressure to give a pale yellow syrup, which was subsequently purified on a silica gel column using benzene–ethyl acetate (50: 1 v/v). The effluent was evaporated under reduced pressure to give a colorless syrup, which was identified as *t*-butyl 2-(*N*-acetyl-*O*-benzyl-hydroxyamino)-2-butenoate (**9a**).

In a similar manner, *t*-butyl 2-(*N*-acetyl-*O*-benzyl-hydroxyamino)-2-pentenoate (**9b**) was also obtained starting from the reaction of **7b** and sodium benzyloxide.

Reaction of 7 with Sodium Cyanide. Into a solution of **7a** (0.010 mol) in dimethyl formamide (25 ml), sodium cyanide (0.013 mol) was stirred portion by portion at room temperature. After stirring for 2 hr, the reaction solution was poured into ice water (30 ml) and then extracted with benzene three times. The benzene extracts were washed with water twice, dried over anhydrous magnesium sulfate, and finally evaporated under reduced pressure. The residual yellow syrup thus obtained gradually crystallized to give colorless crystals, which were identified as *t*-butyl 2-(*N*-cyanoacetamido)-2-butenoate (**10a**).

In a similar manner, *t*-butyl 2-(*N*-cyanoacetamido)-2-pentenoate (**10b**) was also obtained as a syrup; the syrup was subsequently purified on a silica gel column using benzene–ethyl acetate (50: 1 v/v), starting from the reaction of **7b** with sodium cyanide.

Reaction of 7 with Sodium Azide. Into a solution of **7a** (0.010 mol) in dimethyl formamide (25 ml), sodium azide (0.013 mol) was stirred portion by portion at room temperature. After stirring for 2 hr, the reaction solution was poured into ice water (30 ml) and then extracted with benzene three times. The benzene extracts were washed with water twice, dried over anhydrous magnesium sulfate, and finally evaporated to give a yellow syrup. Purification on a silica gel column using benzene–ethyl acetate (10: 1 v/v) and the evaporation of the effluent solvent under reduced pressure gave a pale yellow syrup, which gradually crystallized and which was identified as *t*-butyl 3-azido-2-acetamido-2-butenoate (**12a**).

In a similar manner, *t*-butyl 3-azido-2-acetamido-2-pentenoate (**12b**) was also obtained as a syrup, starting from the reaction of **7b** with sodium azide.

The authors are grateful to the Ministry of Education of Japan for its financial assistance.

References

1) Part VII: C. Shin, Y. Yonezawa, Y. Sekine, and J. Yoshimura, This Bulletin, **48**, 1317 (1975).
2) C. Shin, M. Fujii, and J. Yoshimura, *Tetrahedron Lett.*, **1971**, 2499; C. Shin, K. Sato, A. Ohtsuka, K. Mikami, and J. Yoshimura, This Bulletin, **46**, 3876 (1973).
3) C. Shin, M. Masaki, and M. Ohta, *ibid.*, **42**, 191 (1968).
4) C. Shin, K. Nanjo, E. Ando, and J. Yoshimura, *ibid.*, **47**, 3109 (1974).
5) C. Shin, K. Nanjo, and J. Yoshimura, *Chem. Lett.*, **1973**, 1039.
6) W. K. Anslow and H. Raistrick, *Biochem. J.*, **25**, 39 (1931).
7) C. Shin, K. Nanjo, and J. Yoshimura, *Tetrahedron Lett.*, **1974**, 521.
8) S. J. Huang and M. T. Lessard, *J. Org. Chem.*, **35**, 1204 (1970).
9) H. Ahlbrecht and T. Reiner, *Tetrahedron Lett.*, **1971**, 4901.
10) L. Duhamel, P. Duhamel, and J.-M. Poirier, *ibid.*, **1973**, 4237.

Substituent Effect on the Anomeric Effect in 1,3,5-Trithiane Derivatives

Michinori Ōki, Toshiyuki Endo, and Tadashi Sugawara
Department of Chemistry, Faculty of Science, The University of Tokyo, Tokyo 113
(Received April 30, 1975)

Anomeric effect in a series of 2-alkylthio- and 2-arylthio-1,3,5-trithianes has been studied by PMR spectroscopy to investigate the substituent effect on the anomeric effect. A remarkable steric effect is found in 2-*t*-butylthio-1,3,5-trithiane: the equatorial conformer is slightly favored over the axial one. The electron-withdrawing substituent in 2-arylthio-1,3,5-trithiane enhanced the anomeric effect. The origin of the steric and electric-electronic effect has been discussed on the ground of conformational analysis.

Anomeric effect[1] has drawn attention of many investigators and, to date, various factors affecting the anomeric effect have been discussed. In contrast to the *A* values[2] of the methoxy (0.55) and the chloro (0.53) groups in cyclohexane series, the axial forms of the methoxy and the chloro groups in pyranose rings are favored over the equatorial form by 1.5[3] and 2.7 kcal/mol,[4] respectively. Pierson and Runquist have reported that the magnitude of the anomeric effect is linearly related with the Taft σ^* values of the substituents.[5] Thus the electric-electronic effect of the substituent is important in determining the extent of the anomeric effect. The enhanced axial preference of benzoates over the acetates of pyranosides may be taken as another example of this effect.[6]

In contrast to the large electric-electronic effect, the steric effect is considered to be of minor importance. The axial form of the 2-alkoxyoxanes is present to the extent of 0.77, 0.76, 0.75 and 0.70 in terms of molar fractions for methoxy, ethoxy, isopropoxy, and *t*-butoxy compounds, respectively.[7] The similar trend is also observed in alkyl tri-*O*-benzoyl-β-D-ribopyranosides.[8] The 2-alkylthiooxanes, where alkyl may be methyl, ethyl, isopropyl or *t*-butyl, give practically the same free energy difference for a given equatorial-axial pair irrespective of the size of the alkyl group.[9] Indeed, comparison of the electric-electronic effects for various substituents was possible by assuming little steric effect of the substituted alkyl part of various RO groups.[5]

We have been interested in anomeric effect in 1,3,5-trithiane series for some time and have found that the phenylthio group exerts the stronger effect than the methylthio group: the enthalpy difference is found to be 1.3 kcal/mol in favor of the axial form for 2-phenylthio-1,3,5-trithiane in chloroform-*d*–carbon disulfide, whereas the difference is only 0.9 kcal/mol for 2-methylthio-1,3,5-trithiane.[10]

Trithiane represents a series different from those of cyclohexane and oxane. Since the bond length within the ring is one of the important factors in determining the 1,3-diaxial interaction and the steric effect exerted by the 1,3-diaxial interaction opposes the electric-electronic effect,[11] the longer C–S bond and a little flatter conformation of the trithiane ring should produce different extent of the substituent effect for a given substituent. It was felt that a systematic study would lend help in understanding the substituent effect on the anomeric effect in 1,3,5-trithianes. In addition, this kind of study may reveal the extent of the steric effect which has been neglected in the past studies.

This paper describes the results of a study on the electric-electronic effect in a series of 2-arylthio-1,3,5-trithianes and discusses the steric effect which is found in 2-*t*-butylthio-1,3,5-trithiane.

Results and Discussion

Steric Effects. It may be assumed that changing the alkyl group in 2-alkylthio-1,3,5-trithianes affects only the size of the substituent, to a good approximation, because ionization constants of alkanethiols are known to be relatively unaffected by the change of alkyl groups.[12] Thus 2-alkylthio-1,3,5-trithianes were synthesized by alkanethiolysis of 2-benzoyloxy-1,3,5-trithiane and their conformational equilibria were studied.

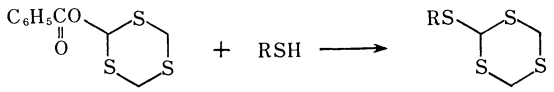

1: R=CH_3 **2**: R=C_2H_5
3: R=$(CH_3)_2CH$ **4**: R=$(CH_3)_3C$

PMR spectra of **1**, **2**, and **3** at room temperature show almost the same chemical shift differences, *ca.* 0.9 ppm, for the ring methylene protons (see Table 1 and Fig. 1), whereas that of **4** shows a smaller chemical shift difference. As these compounds exist as a mixture of ring-inversion isomers at room temperature, the observed chemical shift differences must be the averaged values of the individual isomers. Then almost the same chemical shift differences for compounds **1**—**3** mean that the population ratios of the equatorial and axial isomers are almost the same for these compounds, if the chemical shifts of each proton (δ_a and δ_e) are equal. The last assumption seems to be valid because the molecules are similar and the main moieties which affect the chemical shifts are equal.

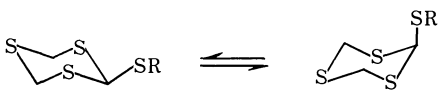

Further support for the above assumption must be obtained by analyzing the population ratio in more detail. PMR spectra of these compounds at low temperatures gave two sets of signals due to ring protons and the methine proton at 2-position, respectively, as reported for the case of compound **1**.[10] These signals are assigned by taking the anisotropy effect of the C–S

Table 1. Chemical shift differences ($\Delta\delta$) between two ring methylene protons of 2-alkylthio-1,3,5-trithiane at various temperatures and equilibrium contasnts (K=a/e) in $CDCl_3$–CS_2 (1: 1 v/v)

Compound							
	T °C	61	49	39	26	17.5	−83
1	$\Delta\delta$ ppm	0.84	0.86	0.88	0.92	0.94	a 1.56 e 0.46
	K	1.8	1.9	2.0	2.2	2.3	3.5[a]
	T °C	61	49	39	31	15	−83
2	$\Delta\delta$ ppm	0.84	0.88	0.90	0.92	0.97	a 1.55 e 0.47
	K	1.9	2.0	2.1	2.2	2.5	4.9[a]
	T °C	61	49		31	15	−83
3	$\Delta\delta$ ppm	0.80	0.84		0.89	0.98	a 1.56 e 0.47
	K	1.7	1.8		2.0	2.5	7.0[a]
	T °C	61	49	39		15	−83
4	$\Delta\delta$ ppm	0.26	0.25	0.24		0.23	a 1.55 e 0.54
	K	0.62	0.61	0.60		0.58	0.5[a]

a) Obtained by direct integration (±0.3).

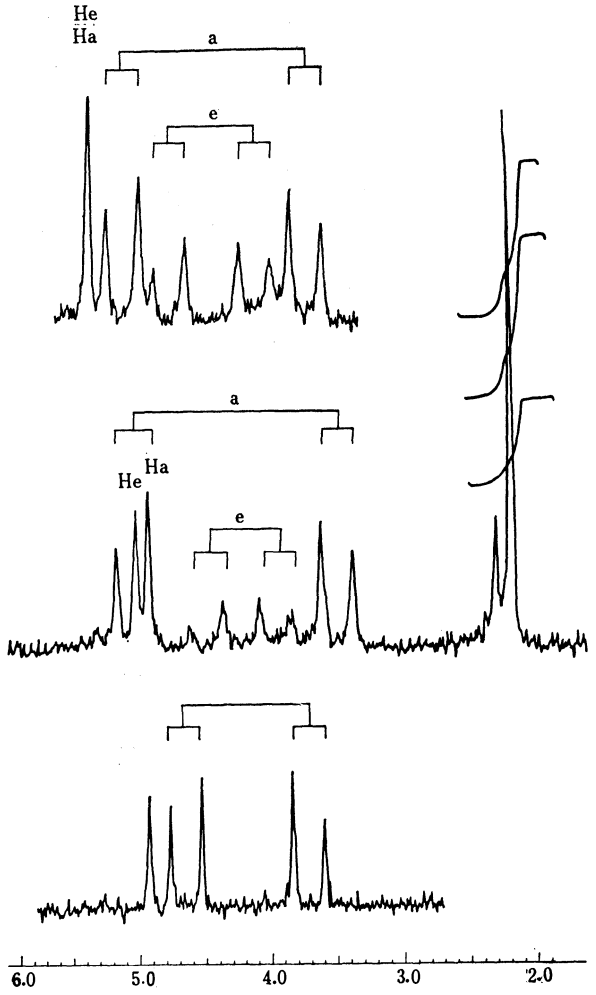

Fig. 1. PMR spectra of 2-methylthio-1,3,5-trithiane at 34 °C in $CDCl_3$–CS_2 (bottom), at −83 °C in $CDCl_3$–CS_2 (middle), and at −83 °C in $CDCl_3$–acetone-d_6 (1: 1 v/v) (top).

bond into consideration. If the C–S bond at 2-position is axially oriented, it should give the large deshielding effect to the axial protons at 4- and 6-positions. Thus the axial conformer will give a larger chemical shift difference between the equatorial and axial protons than that of 1,3,5-trithiane itself. On the other hand, the axial protons of the substituent-equatorial conformer suffer the small shielding effect from the C–S bond of the substituent to cause little change in the chemical shift difference of the AB protons from the corresponding ones in 1,3,5-trithiane.

Thus the AB protons showing the chemical shift difference of *ca.* 1.6 ppm can be assigned to the axial conformer and those with *ca.* 0.5 ppm difference to the equatorial conformer. This assignment is supported by a fact that the population of a conformer assigned to the equatorial form increases in the more polar media. Namely, the ratios of two conformers become *ca.* 1.1 in acetone-d_6 for compounds **1**—**3**, the conformer of larger chemical shift separation for the methylene being slightly favored. Compound **4** even failed to show any signals due to the conformer of larger separation of the methylene signals under the similar conditions. This solvent effect is accepted as the characteristics in anomeric equilibria and must be the result arising from the fact that the equatorial conformer is more polar than the axial.

Comparison of the peak intensities at −83 °C reveals that axial conformers are favored in the cases of **1** through **3**, whereas the equatorial conformer prevails in **4** (see Table 1). Using these chemical shifts, we may calculate the populations of the conformers at above the coalescence temperatures by the following equation.

$$\Delta\delta = N_a\Delta\delta_a + N_e\Delta\delta_e$$

where N_a and N_e are the molar fractions of axial and equatorial conformers, respectively, and $\Delta\delta$, $\Delta\delta_a$, and $\Delta\delta_e$ are the observed chemical shift difference at above the coalescence temperature, that of the axial conformer, and that of the equatorial conformer, respectively. Then the study on temperature dependence of the equilibria affords thermodynamic parameters as shown in Table 2.

Table 2. Thermodynamic parameters for the equilibrium (a⇌e) of 2-alkylthio-1,3,5-trithiane

Compound	ΔG kcal/mol (±0.05)	ΔH kcal/mol (±0.1)	ΔS e.u. (±0.2)
1	0.44	0.9	1.5
2	0.48	1.1	2.1
3	0.46	1.3	2.8
4	−0.33	−0.12	0.6

Inspection of the data in Table 2 indicates that, while the axial conformer of **1**—**3** is more stable than the equatorial conformer by about 0.5 kcal/mol, the equatorial conformer is slightly preferred over the axial in the case of **4**. This striking contrast must be caused by combination of steric and electric-electronic effect. Although the electric-electronic effect may arise as a result of preference or rejection of one or more confor-

mers as a secondary effect, it may be considered to be almost the same for the series of compounds, to the first approximation, due to the fact that they are all 2-alkylthio-1,3,5-trithianes. Then the steric effect becomes the prime importance. We shall forcus the discussion on the steric effect and then extend to the electric-electronic effect later.

Among the axial conformers, three rotamers, a_1, a_2, and a_3, may be considered. The polarity of these compounds are equal.

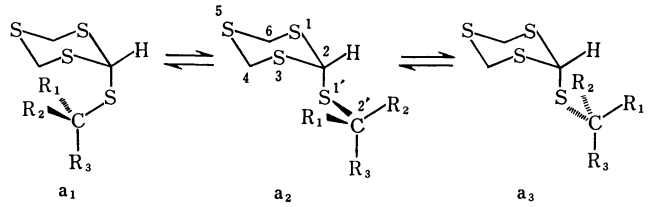

a_1 a_2 a_3

From the steric grounds, however, a_1 will be eliminated because of the severe steric effect between the *S*-alkyl group and the ring. This effect will be operative irrespective to the size of the alkyl group. In conformations of a_2 and a_3, there are two diaxial interactions if the C_2–S_1'–C_2, bonds are considered as a part of the chair ring: in a_2 conformation, C_2–S_3 and C_2'–R_1 bonds are in this relation and the relation between C_2–H and the C_2'–R_2 bonds is another case. Similarly the relation of C_2–S_1 and C_2'–R_2 bonds and that of C_2–H and C_2'–R_1 bonds are also diaxial in a_3. If the alkyl in alkylthio groups bears two hydrogens, the effect of these 1,3-diaxial interaction may be minimized by taking an appropriate conformation. Namely, the conformations a_2 and a_3 will be most stable when R_1 and R_2 are hydrogens in the case of **2**. When the alkyl group is an isopropyl, the increase in the 1,3-diaxial interaction is unavoidable. However, the severe interaction may be avoided by taking the a_2 conformation in which the C_2–H and C_2'–CH_3 bonds interact in 1,3-diaxial manner and C_2–S_3 and C_2'–H bonds interact similarly. A similar conformation is possible for a_3 also. Accordingly, it is possible for the isopropyl group in **3** to take a conformation in which repulsive force is not much higher than the corresponding methyl or ethyl compounds: in the latter two compounds also, the C–S/C–H interaction is unavoidable.

The situation of the *t*-butyl compound **4** is different from those of other alkylthio compounds. Since all the hydrogens of 2′-carbon are substituted by methyls, 1,3-diaxial interactions of the C–CH_3/C–S type become inevitable.*) The axial conformation of **4** is thus drastically destabilized as compared with other cases.

Now comparison of the energy levels of equatorial conformers becomes necessary. From the stand point of the steric effect, there seem to be some differences in the stability of the three forms, e_1, e_2, and e_3. In e_1 conformation, there are two 1,3-diaxial interactions of

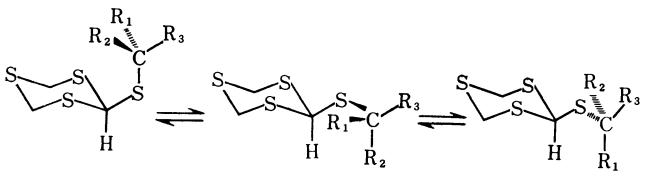

e_1 e_2 e_3

the C–S/C–R type, whereas the 1,3-diaxial interactions are C–S/C–R and C–H/C–R types in e_2 and e_3. If the alkyl is either the methyl or the ethyl, the destabilization of the e_1 form due to 1,3-diaxial interaction may not become severe by taking an appropriate conformation. The e_1 form of **3** is destabilized because at least one C–S/C–C diaxial interaction is unavoidable, although this destabilization may be lessened by rotating the isopropyl group about the S_1'–C_2 bond. On the other hand, the e_1 conformation of **4** is definitely unstable due to the presence of two C–S/C–C diaxial interactions. e_2 and e_3 conformations of **1**, **2**, and **3** are neither specially stabilized nor destabilized on the steric ground, if they are compared with another conformation e_1, because they will have only C–S/C–H and C–H/C–H interactions in **1** and **2** or C–H/C–C and C–S/C–H interactions in **3** in favorable conformations. The e_2 and e_3 conformations of **4** involve C–S/C–C and C–H/C–C interactions which are less severe than the 1,3-interactions in the e_1 form.

On the electric grounds, e_1 form is most favored because the dipole formed by the substituent partly compensates that of the ring, whereas in the other forms (e_2 and e_3), the dipole made by the substituent is nearly parallel to that of the ring. At the same time, both lone pairs of electrons on the sulfur atom of the substituent are anti-parallel to the C–S bonds of the ring in e_1 conformation. This conformation is favorable for stabilization by the resonance effect.[11d]

Summarizing the steric effect and the electric-electronic effect of the equatorial forms, we may conclude that the e_1 form predominates in compounds **1**—**3**,**) whereas e_2 and e_3 forms predominate in compound **4**. Then the discussion on the stability of axial and equatorial conformers is reduced to comparison of stabilities of $a_2(a_3)$ and e_1 in the cases of **1**—**3**, whereas it is comparison of the stabilities of $a_2(a_3)$ and $e_2(e_3)$ in the case of **4**.

In the a_2 and a_3 conformations of **1** and **2**, the 1,3-diaxial interactions are C–H/C–S and C–H/C–H types, whereas those are two C–H/C–S types in e_1 conforma-

* The methyl axial-conformation is less stable than the methyl-equatorial conformation by 2.4 kcal/mol in the 1,3,5-trithiane system, as studied by equilibration of *cis* and *trans* forms of 2,4,6-trimethyl-1,3,5-trithiane. M. Fukunaga, Ph. D. thesis, The University of Tokyo, 1972.

** This assumption is supported by a fact that the chemical shift of the axial 2-proton in these compounds is in a higher field than that of the equatorial. This phenomenon is contrary to the general consideration of the C–S bond anisotropy and has been attributed to the anisotropy effect of the C–S bond of the substituent in conformation e_1.[10] Similar situation occurs in 1,3-dioxane series also. The results of NOE experiment on *r*-2-methoxy-*t*-4,*t*-6-dimethyl-1,3-dioxane have been interpreted by assuming a conformation in which the methyl group in the methoxy lies nearly above the methine proton at 2-position, whereas the methoxy-methyl group of *r*-2-methoxy-*c*-4,*c*-6-dimethyl-1,3-dioxane seems to be away from the methine proton.[13]

tions of **1** and **2**. Thus a_2 and a_3 conformations of **1** and **2** are slightly favored over the e_1 form from the stand point of the steric effect in addition to the electric and electronic effects which are discussed frequently in explaining the anomeric effect. In the isopropyl compound **3**, a_2 and a_3 forms possess 1,3-interactions of C–H/C–S and C–H/C–C types, whereas e_1 has C–H/C–S and C–C/C–S types. Thus the steric effect favors the axial form in this compound. Combination of these steric, electric, and electronic factors seems to result the observed near coincidence of the difference in the stabilities of the equatorial and axial conformations.

e_2 and e_3 forms of compound **4** are disfavored from the stand point of the electric and the electronic factors and they have the steric effect due to the presence of C–C/C–S and C–H/C–C interactions. On the other hand, a_2 and a_3 forms have the same 1,3-diaxial interactions of C–S/C–C and C–H/C–C types with the e_2 and e_3 forms, although they are favored from the electric and electronic effects. The observed result that the equatorial form is more stable than the axial by about 0.12 kcal/mol may indicate that the contribution of the electronic and electric effect is considered to amount about this magnitude.

The results presented above make the striking contrast to the anomeric effect in the oxane series in a sense that the bulkiness of the alkoxy group has little effect on the distribution of the anomers.[7-9] This contrast may be attributed to the presence of heteroatoms on both sides of the electronegative substituent for the following reasons.

Since only one oxygen atom is present in the ring of oxane, the direction of dipole of the ring is not axial to the ring but is tilted. On electric grounds, this segregates two stable rotamers in oxane series, which are equivalent in trithianes. The energy levels of a_2' and a_3' of 2-alkoxyoxanes are different because two dipoles spearheaded by oxygens in a_3' are almost anti-parallel whereas those in a_2' have a definite value. Indeed, the calculated dipole moment and the observed are compared to draw a conclusion that the conformation of 2-alkoxyoxane can be taken as a_3' to the first approximation.[14]

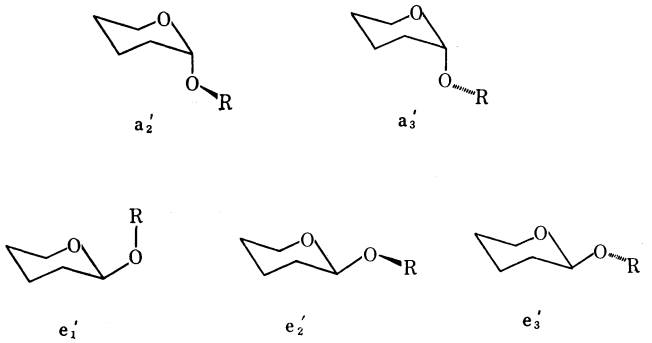

Likewise, the conformation e_2' can be taken unstable. The equatorial form can be considered to be a mixture of e_1' and e_3' from the electric factor. Since the steric factor is unfavorable in e_1', however, the e_3' form will prevail in the equatorial conformations to the first approximation.

Quantum mechanical calculation has been carried out for the conformations of methanediol as a model for the anomeric center in the pyranose.[15] The results indicate that the axial conformer has a sharp minimum at a_3' form, whereas the equatorial has two equivalent minima corresponding to conformations e_2' and e_3' with somewhat lessened O_1–C_2–O_{sub}–C_{sub} dihedral angle of 35°. This calculation is consistent with the consideration of molecular dipoles presented above.

We may now compare the stabilities of a_3' and e_3' of 2-*t*-butoxyoxane. Since there are 1,3-diaxial interactions of C–H/C–C and C–O/C–C types in both forms, the steric factor is almost equal. This will make the electric-electronic factor important to cause the preference of the axial form. The preference of the axial forms to the similar degree in *t*-butoxyoxane, compared with other alkoxyoxanes, is not surprising, because the steric factors in axial a_3' and equatorial e_3' forms of these compounds can be similar also.

Electric and Electronic Effects. The electric and electronic factors may be varied, by the introduction of various arylthio groups, without significant alteration of the steric effect. Thus a series of 2-arylthio-1,3,5-trithianes have been prepared by arenethiolysis of 2-benzoyloxy-1,3,5-trithiane.

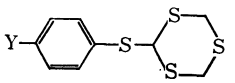

5: X=OCH_3 **6**: X=H
7: X=Cl **8**: X=NO_2

The equilibrium constants and thermodynamic parameters were obtained as described earlier and are tabulated in Tables 3 and 4.

The results indicate that the higher is the electronegativity of the *para*-substituent, the more the axial conformer is preferred. When the free energy differences between the axial and the equatorial conformers of each compound were divided into enthalpy and entropy terms (Table 4), it has become clear that the tendency in the conformational equilibria is the result of enthalpy

Table 3. Chemical shift differences ($\Delta\delta$) between two ring methylene protons of 2-arylthio-1,3,5-trithiane at various temperatures and equilibrium constants (K=a/e) in $CDCl_3$–CS_2 (1: 1 v/v)

Compound						
	T °C	63	49	33		−83
5	$\Delta\delta$ ppm	0.80	0.84	0.88		a 1.61 e 0.48
	K	1.6	1.7	1.9		5.0[a]
	T °C	63	49	33	15	−83
6	$\Delta\delta$ ppm	0.84	0.88	0.92	0.99	a 1.60 e 0.49
	K	1.8	1.9	2.1	2.4	8.2[a]
	T °C	63	49	29		−83
7	$\Delta\delta$ ppm	0.83	0.86	0.92		a 1.55 e 0.49
	K	1.8	1.9	2.2		8.2[a]
	T °C	63	49	29		−83
8	$\Delta\delta$ ppm	0.84	0.88	0.94		a 1.46 e 0.52
	K	2.2	2.4	2.8		[b]

a) Obtained by direct integration (±0.3). b) Not measured because of the poor solubility.

Table 4. Thermodynamic parameters for the equilibrium (a⇌e) of 2-arylthio-1,3,5-trithiane

Compound	ΔG kcal/mol (±0.05)	ΔH kcal/mol (±0.1)	ΔS e.u. (±0.2)
5	0.39	1.1	2.6
6	0.48	1.3	2.6
7	0.48	1.3	2.6
8	0.61	1.5	2.8

change rather than the entropy change. This result is the affirmation for the significance of the electric and electronic factors on the anomeric effect in this series.

Interpretation of the observed tendency from the stand point of the dipole-dipole interaction involves some obscureness. Estimation of the contribution of the aryl group to the dipole moment of the whole molecule is rather complicated. Putting an electronegative aryl group instead of an alkyl in the substituent of the axial form will increase the component of the dipole which is anti-parallel to the component of the trithiane ring. Thus the axial conformations seem to be stabilized more in arylthio compounds with electronegative substituents. On the other hand, in e_1 conformation of arylthiotrithianes with electronegative substituents, the dipole moment of the molecule will increase to some extent, whereas those of e_2 and e_3 conformations will decrease. Thus populations of e_2 and e_3 forms increase. These factors make it difficult to estimate the electric factor quantitatively. Although the discussion given above tends to favor the axial forms to enhance the anomeric effect, separation of the electric effect from the electronic is not possible at present.

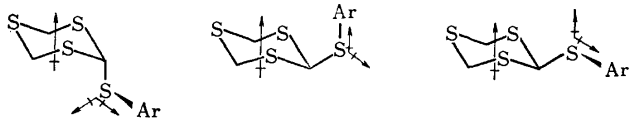

a_2 e_1 e_2

The observed results seem to be interpreted best by consideration of the resonance effect. As the electronegativity increases, the polarity of the C_2-S_1′ increases to facilitate the donation of the lone pair electrons on sulfur atoms (S_1 and S_3). In valence bond description, hydrids of ionic structures (9b and 9c) can be

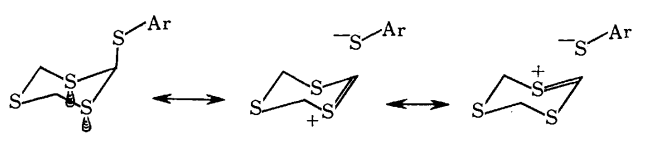

9a 9b 9c

considered in an axial conformer, because orbitals of lone pair electrons of the ring sulfur and that of the C_2-S_1′ bond are anti-parallel. The contribution of 9b and 9c becomes larger as the electronegativity of the aryl group increases, thus stabilizing the axial form. The anomeric effect becomes stronger in these cases. pK_a values of arenethiols are in accord with the consideration: pK_a's of *para*-substituted benzenethiols, as measured in 20% water-ethanol at 20 °C are *p*-methoxy 7.06, hydrogen 6.81, and *p*-chloro 6.53.[16] pK_a of *p*-nitrobenzenethiol has been measured in methanol as 8.4 when that of benzenethiol was 10.9.[17]

Hoffmann and coworkers proposed MO interpretation of the anomeric effect.[11c] According to the theory, the interaction takes place between the low-lying antibonding orbital of a polar bond and p-type orbital of the hetero atom to lower the latter level. Consequently the total energy of the molecule is lowered. This type of interaction occurs to a greater extent if the antibonding orbital is lower and the substituent is axial. The high electronegativity corresponds to the low antibonding orbital and the axial substituent means the better overlap of the orbitals concerned. The results presented here, therefore, give an experimental support to the MO interpretation.

Experimental

PMR Measurement. The PMR spectra were recorded on a Hitachi R 20B spectrometer equipped with a temperature variation accessory. Temperature was read by the chemical shift difference of methyl and hydroxy protons of methanol at the low temperature and those of ethylene glycol at room temperature or above.

Solvents. As the polarity of solvents was found to have a critical influence upon the anomeric equilibria, the solvent for measurements was picked up from a stock mixture of solvents ($CDCl_3$–CS_2 1: 1 v/v) in order to unify experimental conditions.

2-Methylthio-1,3,5-trithiane (1), mp 94—95 °C, was prepared from 2-benzoyloxy-1,3,5-trithiane and methanethiol as reported previously.[10]

2-Ethylthio-1,3,5-trithiane (2). A solution of 2 g (9 mmol) of 2-benzoyloxy-1,3,5-trithiane and 2 g (32 mmol) of ethanethiol in 30 ml of chloroform was heated for 3 hr in a reaction vessel equipped with a dry ice condenser. Benzoic acid produced during the reaction was removed by passing the solution through a potassium carbonate layer and the solvent was evaporated to give crude products (95%). This was purified by chromatography on neutral alumina. Elution with hexane–benzene (1: 1) afforded the desired product, mp 47—48 °C. Found: C, 30.56; H, 5.36; S, 64.27%. Calcd for $C_5H_{10}S_4$: C, 30.27; H, 5.08; S, 64.65%. PMR ($CDCl_3$, δ): 1.30 (t, 3H), 2.66 (q, 2H), 3.67 and 4.68 (q, J=14 Hz, 4H), 5.00 (s, 1H).

2-Isopropylthio-1,3,5-trithiane (3), mp 52—53 °C, was prepared from 2-benzoyloxy-1,3,5-trithiane and 2-propanethiol as described above. The crude product was purified by chromatography. Found: C, 34.18; H, 5.96; S, 60.15%. Calcd for $C_6H_{12}S_4$: C, 33.93; H, 5.70; S, 60.38%. PMR ($CDCl_3$, δ): 1.41 (d, 6H), 3.05 (sep, 1H), 3.69 and 4.70 (q, J=14 Hz, 4H), 5.04 (s, 1H).

2-t-Butylthio-1,3,5-trithiane (4), mp 94—95 °C, was prepared from 2-benzoyloxy-1,3,5-trithiane and 2-methyl-2-propanethiol. The crude product was purified by chromatography. Found: C, 37.21; H, 6.19%. Calcd for $C_7H_{14}S_4$: C, 37.13; H, 6.23%. PMR ($CDCl_3$, δ): 1.44 (s, 9H), 4.16 and 4.34 (q, J=14 Hz, 4H), 5.07 (s, 1H).

2-(p-Methoxyphenylthio)-1,3,5-trithiane (5), mp 129—131 °C, was prepared from 2-benzoyloxy-1,3,5-trithiane and *p*-methoxybenzenethiol.[18] The crude product was purified by chromatography. Found: C, 43.65; H, 4.28; S, 45.94%.

Calcd for $C_{10}H_{12}OS_4$: C, 43.45; H, 4.38; S, 46.39%. PMR ($CDCl_3$, δ): 3.80 (s, 3H), 3.82 and 4.68 (q, $J=14$ Hz, 4H) 5.18 (s, 1H), 6.83 and 7.50 (q, $J=8.4$ Hz, 4H).

2-Phenylthio-1,3,5-trithiane (6), mp 123.0—123.5 °C, was prepared from 2-benzoyloxy-1,3,5-trithiane and benzenethiol as reported previously.[10]

2-(p-Chlorophenylthio)-1,3,5-trithiane (7), mp 126—129 °C, was prepared from 2-benzoyloxy-1,3,5-trithiane and *p*-chlorobenzenethiol[18] and the desired product crystallized on standing. The product was purified by recrystallization from benzene. Found: C, 38.63; H, 3.15; Cl, 12.82; S, 45.44%. Calcd for $C_9H_9ClS_4$: C, 38.49; H, 2.23; Cl, 12.62; S, 45.66%. PMR ($CDCl_3$, δ): 3.83 and 4.72 (q, $J=14$ Hz, 4H), 5.31 (s, 1H), 7.33 and 7.45 (q, $J=9$ Hz, 4H).

2-(p-Nitrophenylthio)-1,3,5-trithiane (8), mp 174—175 °C, was prepared from 2-benzoyloxy-1,3,5-trithiane and *p*-nitrobenzenethiol[19] and the desired product crystallized on standing. The product was purified by recrystallization from benzene. Found: C, 37.25; H, 3.01; N, 4.74; S, 44.05%. Calcd for $C_9H_9NO_2S_4$: C, 37.00; H, 3.11; N, 4.81; S, 44.01%. PMR ($CDCl_3$, δ): 3.82 and 4.66 (q, $J=14$ Hz, 4H), 5.50 (s, 1H), 7.55 and 8.16 (q, $J=8.4$ Hz, 4H).

References

1) R. U. Lemieux, R. K. Kulling, H. J. Bernstein, and W. G. Schneider, *J. Amer. Chem. Soc.*, **80**, 6098 (1958).

2) F. R. Jensen, C. H. Bushweller, and B. H. Beck, *ibid.*, **91**, 344 (1969).

3) C. B. Anderson and D. T. Sepp, *Tetrahedron*, **24**, 1707 (1968).

4) C. B. Anderson, *J. Org. Chem.*, **32**, 607 (1967).

5) G. O. Pierson and O. A. Runquist, *ibid.*, **33**, 2572 (1968).

6) P. L. Durette and D. Horton, *Adv. Carbohyd. Chem. Biochem.*, **26**, 49 (1971).

7) E. L. Eliel and C. A. Giza, *J. Org. Chem.*, **33**, 3754 (1968).

8) P. L. Durette and D. Horton, *Carbohyd. Res.*, **18**, 289 (1971).

9) A. J. de Hoog and E. Havinga, *Rec. Trav. Chim.*, **89**, 972 (1970).

10) M. Ōki, T. Sugawara, and H. Iwamura, This Bulletin, **47**, 2457 (1974).

11) a) J. T. Edward, *Chem. & Ind.* (London), **1955**, 1102: b) R. O. Hutchins, L. D. Kopp, and E. L. Eliel, *J. Amer. Chem. Soc.*, **80**, 7174 (1968): c) S. David, J. O. Eisenstein, W. J. Hehre, L. Salem, and R. Hoffmann, *ibid.*, **95**, 3806 (1973): d) L. Radom, W. J. Hehre, and J. A. Pople, *ibid.*, **94**, 2371 (1972).

12) H. L. Loy and D. M. Himmelblau, *J. Phys. Chem.*, **65**, 264 (1961).

13) E. L. Eliel and F. Nader, *J. Amer. Chem. Soc.*, **91**, 536 (1969).

14) R. U. Lemieux, A. A. Pavia, J. C. Martin, and K. A. Watanabe, *Can. J. Chem.*, **47**, 4427 (1969): R. U. Lemieux and S. Koto, *Tetrahedron*, **30**, 1933 (1974).

15) G. A. Jeffrey, J. A. Pople, and L. Radom, *Carbohyd. Res.*, **25**, 117 (1972).

16) G. Chuchani and A. Frohlich, *J. Chem. Soc., B*, **1971**, 1471.

17) B. W. Clare, D. Cook, E. C. F. Ko, Y. C. Mac, and A. J. Parker, *J. Amer. Chem. Soc.*, **88**, 1911 (1966).

18) D. S. Tarbell and D. F. Fukushima, "Organic Synthesis," Coll. Vol. 3, p. 809 (1955).

19) L. B. Sebrell and C. E. Boord, *J. Amer. Chem. Soc.*, **45**, 2401 (1923).

Chemical Studies on Tuberactinomycin. IX.[1] Nuclear Magnetic Resonance Studies on Tuberactinomycins and Tuberactinamine N[2]

Tateaki WAKAMIYA and Tetsuo SHIBA

Department of Chemistry, Faculty of Science, Osaka University, Toyonaka, Osaka 560

(Received May 12, 1975)

Conformational analyses of peptide antibiotics tuberactinomycins were performed by NMR spectroscopy of 100 MHz. Studies on temperature dependence and deuterium exchange in amide proton resonances revealed the presence of an intramolecular hydrogen bond participated with α-amide proton of the guanidino amino acid residue in the cyclic part of each molecule. The same result was obtained in tuberactinamine N, which is the cyclopeptide moiety without amino acid side chain in tuberactinomycins N and O. The common rigid structure fixed by hydrogen bonding in the cyclic part seems to be a requisite for the exhibition of microbial activity in tuberactinomycin family.

The total chemical structures of antituberculous peptides tuberactinomycins A, B, N, and O, which were isolated from *Streptomyces griseoverticillatus* var. *tuberacticus*, were determined in our previous investigations as shown in Fig. 1.[3-8] The steric structure of tuberactinomycin O, one of the four congeners, was established by means of X-ray analysis.[4] Subsequently, Bycroft *et al.* studied on X-ray analysis of viomycin (tuberactinomycin B), applying our informations on tuberactinomycin O that the monohydrochloride-dihydrobromide of the antibiotic is adequate to crystallographic investigation.[9] From these studies, the presence of an intramolecular hydrogen bond between the α-amide proton of the guanidino amino acid residue, *i.e.*, capreomycidine (Cpd) or tuberactidine (Tbd), and the carbonyl oxygen of the serine residue (Ser(1)) neighboring the diaminopropionic acid (Dpr) residue was found in tuberactinomycin O and viomycin. This intramolecular hydrogen bond seems to be very important from the viewpoint of a relationship between the conformations of tuberactinomycins and their antimicrobial activities.

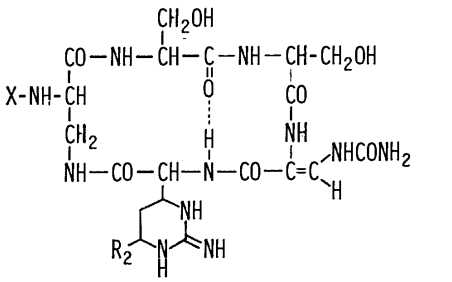

X = $CH_2CH_2CH(NH_2)$–$CH(R_1)$–$CH_2(NH_2)CO$–

Tuberactinomycins		
A	R_1=OH,	R_2=OH
B	R_1=H,	R_2=OH
N	R_1=OH,	R_2=H
O	R_1=H,	R_2=H
Tuberactinamine N	X=H,	R_2=H

Fig. 1. Chemical structures of tuberactinomycins and tuberactinamine N.

For studies on the structure of cyclic peptide, particularly related to the intramolecular hydrogen bond, NMR is known to be highly informational. In fact, many NMR studies on biologically active cyclopeptides, *e.g.*, gramicidin S,[10] oxytocin,[11] lysine vasopressin,[11d-e,12] and stendomycin,[13] have been reported. In the present investigation, the steric conformations of four tuberactinomycins in solutions were analyzed by their NMR spectra of 100 MHz. Furthermore, we recently succeeded in isolating a cyclic peptide moiety called tuberactinamine N (Fig. 1) common to molecules of tuberactinomycins N and O by selective liberation of γ-hydroxy-β-lysine residue from tuberactinomycin N with acid treatment.[1] Tuberactinamine N was found to possess comparable antibacterial activities to those of the mother molecule against several strains of tubercule bacilli.[1] NMR study on four tuberactinomycins and one tuberactinamine indicated clearly the presence of the same intramolecular hydrogen bond in all compounds.

From the results these conformational analyses in solutions referring to the crystal structures of tuberactinomycins O and B, we assumed that the conformation of the cyclic peptide, particularly the presence of the intramolecular hydrogen bond in the cyclic part, may reflect to the biological activities of those antibiotics as a requisite.

Experimental

Spectra were recorded on a Varian Associates XL-100-15 spectrometer equipped with a Varian VFT-100 (620/L) computer. Sample solutions were measured in tubes of 5 mm o.d. and the temperature was normally kept at 37 °C. The spectra were taken with internal H^2 lock method, thus in the case of H_2O solution 20% of DMSO-d_6 being added. Chemical shifts were obtained by δ value (ppm) from DSS in aqueous media and from TMS in DMSO-d_6 solution. Proton double resonances were carried out with frequency-sweep decouplings.

Materials. The samples of tuberactinomycins A, N, and O were prepared as trihydrochloride, whereas tuberactinomycin B (viomycin) was crystallized as monohydrochloride–dihydrobromide. Tuberactinamine N dihydrochloride was obtained by the selective cleavage of γ-hydroxy-β-lysine residue from tuberactinomycin N with concentrated hydrochloric acid according to the mechanism of *N,O*-acyl migration reaction.[1] Sample concentrations in NMR measurements were 15% in D_2O (also in the case of D_2O+TFA), 10% in H_2O (pH 2.5), and 4% in DMSO-d_6.

Results and Discussion

Spectral Assignments. In the PMR spectra of tuberactinomycins in D_2O solution, some α-methine protons were concealed by HOD signal. However, on addition with trifluoroacetic acid to the solution, those protons manifested themselves entirely with the shift of HOD signal to a lower field by about 0.7 ppm. This effect enabled decoupling experiments, and thereby spectral assignments covering all protons became feasible. Since the differences in the chemical structures of tuberactinomycin family are only limited to the degree of hydroxylation at R_1 and R_2 as shown in Fig. 1, the patterns of the corresponding signals in their spectra show close resemblances to each other. Thorough comparisons in spectra of four tuberactinomycins and one tuberactinamine were very profitable for the complete assignments of all signals. Especially a relatively simple spectrum of tuberactinamine N (Fig. 2) without the branched amino acid residue gave many key informations for assignments in tuberactinomycins (Fig. 3).

In the molecule of tuberactinamine N, there are five methylene groups of three types, *i.e.*, –C–CH_2–C–, –NH–CH_2–C–, and –C–CH_2–OH. Of these groups, γ-methylene protons in six-membered pyrimidine ring of Cpd appeared at around δ 1.8 and 2.1 as non-equivalent multiplets. A multiplet of δ-methylene protons of Cpd were resonated at δ 3.32 that corresponds to normal position for –NH–CH_2–C– type methylene. On the contrary, one of two β-methylene protons of Dpr showed normal chemical shift at δ 3.30, while the another appeared at an anomalous downfield of δ 4.12 as a quartet. This assignment was confirmed by the decoupling experiment in which an irradiation at δ 3.30 caused the quartet at δ 4.12 to collapse to a doublet and *vice versa*, accompanying concurrent decoupling with α-methine proton of Dpr at δ 4.40. Such large difference between two chemical shifts of non-equivalent β-methylene protons of Dpr seems to be ascribed to an environmental difference which comes from the situation that the peptide backbone in the cyclic moiety may be fixed in a definite conformation and prohibited from free rotation.

β-Methylene protons of two serine residues showed also significant differences in their chemical shifts. One residue Ser(1) connected with Dpr appeared at δ 3.95 as a doublet coupled with a triplet at δ 4.84, while the other Ser(2) adjacent to 3-ureidodehydroalanine (Uda) residue showed double-doublets at δ 3.90 and 4.20, respectively. Thess different situations indicate that some neighboring effect may act on the latter group causing a magnetic non-equivalency of two protons likely as in the case of β-methylene of Dpr.

Although the region from δ 4.0 to 4.5 was somewhat complicated by overlapping of five protons, the decoupling study and the comparison of coupling constants enabled the complete assignment. Two quartets at δ 4.12 and 4.20 were already assigned to one of β-methylene protons of Dpr and Ser(2), respectively. A quartet centered at δ 4.32 can be assigned to α-methine proton of Ser(2) as this has the same coupling constant (J=5 Hz) with a quartet at δ 4.20. An irradiation of a quartet centered at δ 4.40 caused a multiplet at δ 3.30 to collapse to a single peak, thereby this quartet was assigned to α-methine proton of Dpr. A multiplet at

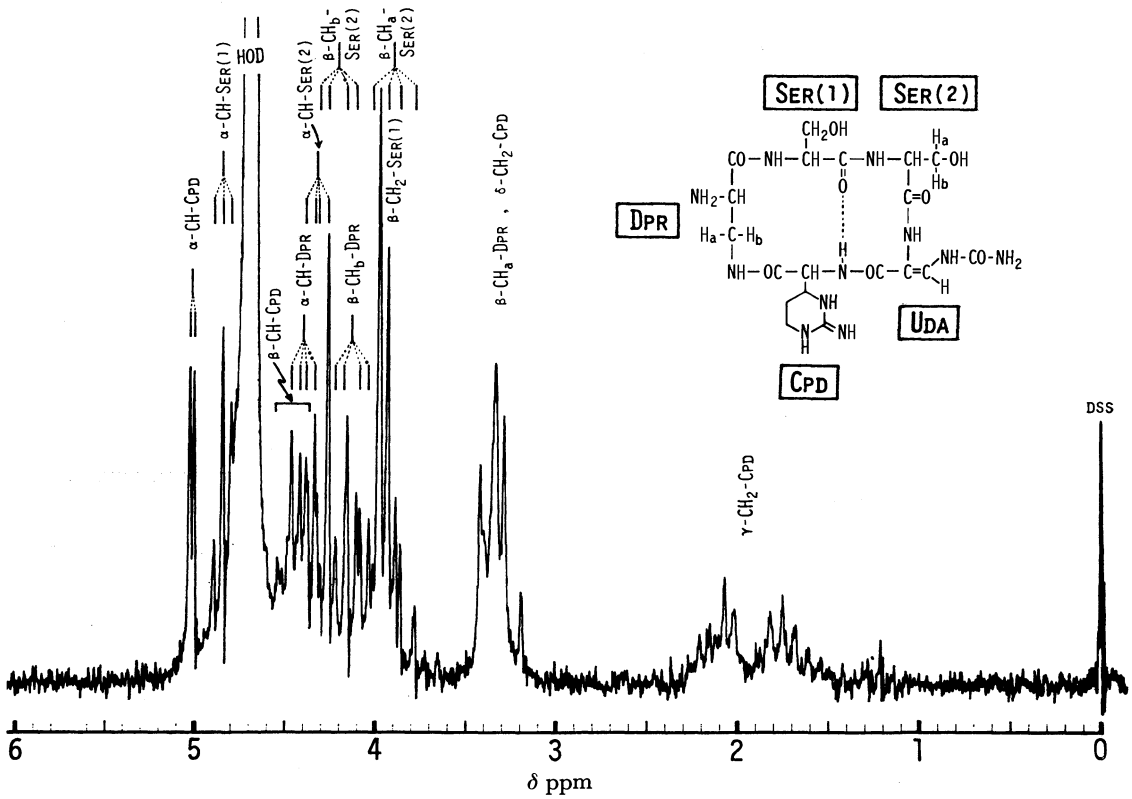

Fig. 2. NMR spectrum of tuberactinamine N in high-field region in D_2O.

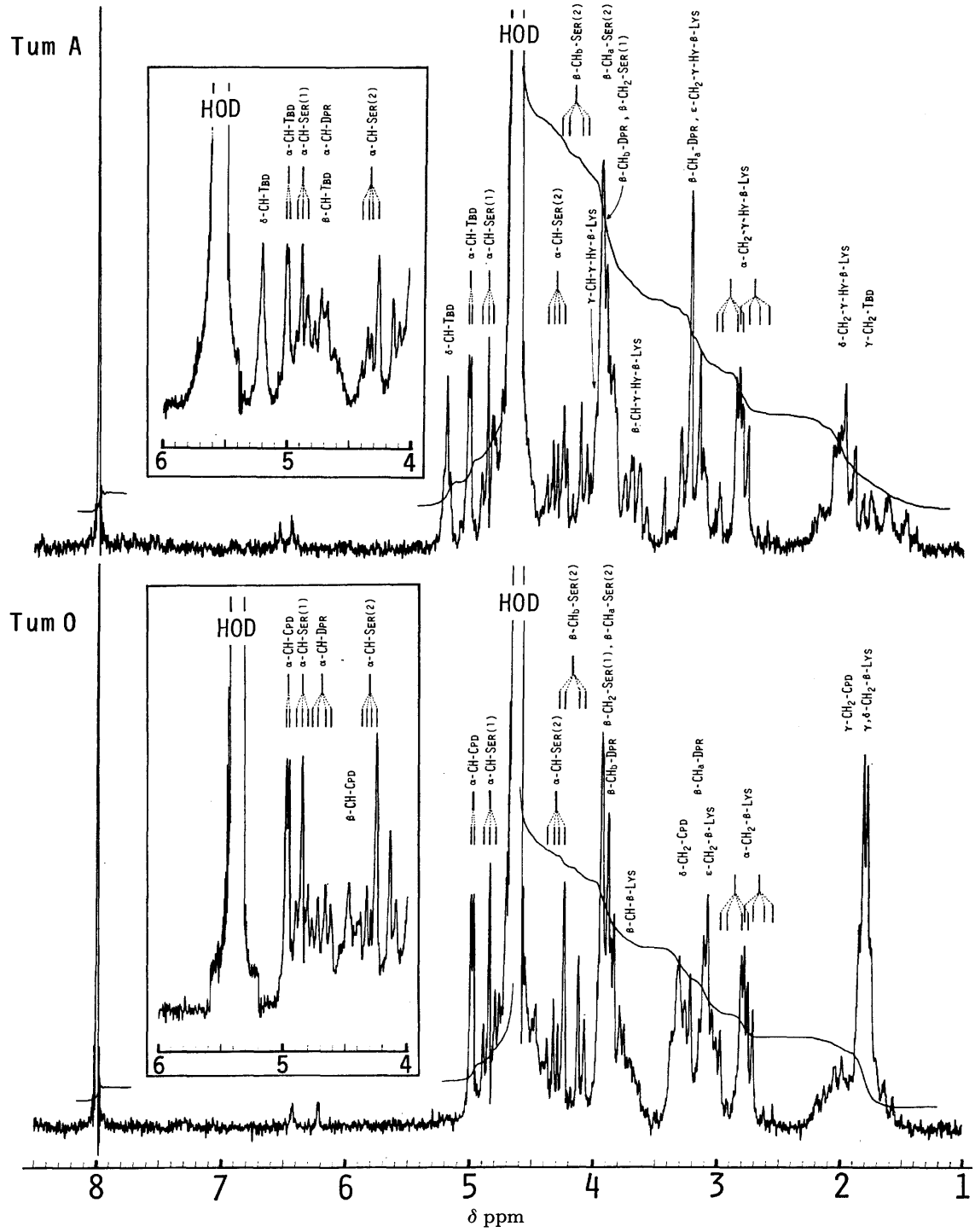

Fig. 3. NMR spectra of tuberactinomycins (Tum) A and O in D_2O. Figures in squares indicate the parts of spectra in D_2O+TFA.

δ 4.35 to 4.55 was collapsed by an irradiation of methylene protons at Cpd at δ 1.80 and 2.10. Reversely, an irradiation at δ 4.45 caused not only a change of Cpd γ-methylene as mentioned above but also of doublet at δ 5.01 of Cpd α-proton both to singlets. Thus the multiplet centered at δ 4.45 was determined to be due to β-methine proton of Cpd. A triplet at δ 4.84 and a doublet at 5.01 were necessarily assigned to α-methine protons of Ser(1) and Cpd, respectively as mentioned above already. Finally, a sharp peak at δ 8.04 was due to an olefinic proton of Uda, –C=CH-NHCONH$_2$.

Since the molecules of tuberactinomycins N and O are built up by joinings of γ-hydroxy-β-lysine and β-lysine respectively into the free α-amino group of Dpr in tuberactinamine N, simple comparisons of their spectra with that of tuberactinamine N are good enough for their assignments. However, by the effect of joining of β-amino acid with α-amino group of Dpr in tuberactinomycin N or O, the signal of the α-methine of the

TABLE 1. CHEMICAL SHIFTS OF TUBERACTINOMYCINS AND TUBERACTINAMINE N IN D_2O

		Tuberactinomycins				Tuberactinamine N
		A	B	N	O	
β-Lys	α-CH_2		2.66(1H, dd)		2.65(1H, dd)	
			2.86(1H, dd)		2.85(1H, dd)	
	β-CH		3.7 (1H, m)		3.7 (1H, m)	
	γ-CH_2		1.8 (2H, m)		1.8 (2H, m)	
	δ-CH_2		1.8 (2H, m)		1.8 (2H, m)	
	ε-CH_2		3.08(2H, m)		3.07(2H, m)	
γ-Hy-β-Lys	α-CH_2	2.72(1H, dd)		2.68(1H, dd)		
		2.92(1H, dd)		2.89(1H, dd)		
	β-CH	3.7 (1H, m)		3.7 (1H, m)		
	γ-CH	3.95(1H)		3.9 (1H)		
	δ-CH_2	1.95(2H, m)		1.95(2H, m)		
	ε-CH_2	3.22(2H, t)		3.20(2H, t)		
Dpr	α-CH	4.7 (1H)[a]	4.7 (1H)[a]	4.73(1H, q)[a]	4.70(1H, q)[a]	4.40(1H, q)
	β-CH_2	3.2 (1H)	3.1 (1H)	3.2 (1H)	3.1—3.3(1H)	3.30(1H)
		3.95(1H)	3.85(1H)	3.9 (1H)	3.9 (1H)	4.12(1H, q)
Ser(1)	α-CH	4.86(2H, t)	4.85(1H, t)	4.84(1H, t)	4.85(1H, t)	4.84(1H, t)
	β-CH_2	3.95(2H)	3.9 (2H)	3.9 (2H)	3.9 (2H)	3.95(2H, d)
Ser(2)	α-CH	4.32(1H, q)	4.31(1H, q)	4.31(1H, q)	4.30(1H, q)	4.32(1H, q)
	β-CH_2	3.95(1H)	3.9 (1H)	3.9 (1H)	3.9 (1H)	3.90(1H, dd)
		4.17(1H, dd)	4.15(1H, dd)	4.16(1H, dd)	4.18(1H, dd)	4.20(1H, dd)
Uda	β-CH	8.00(1H, s)	8.00(1H, s)	7.99(1H, s)	8.00(1H, s)	8.04(1H, s)
Cpd	α-CH			4.97(1H, d)	4.98(1H, d)	5.01(1H, d)
	β-CH			4.5 (1H, m)[a]	4.5 (1H, m)[a]	4.45(1H, m)
	γ-CH_2			1.4—2.2(2H)	1.5—2.3(2H)	1.8 (1H, m)
						2.1 (1H, m)
	δ-CH_2			3.2 (2H)	3.30(2H, m)	3.32(2H, m)
Tbd	α-CH	5.00(1H, d)	5.01(1H, d)			
	β-CH	4.7 (1H)[a]	4.7 (1H)[a]			
	γ-CH_2	1.4—2.2(2H)	1.5—2.2(2H)			
	δ-CH	5.19(1H)	5.19(1H)			

Abbreviations; s: singlet, d: doublet, dd: double-doublet, q: quartet. a) Chemical shifts in D_2O+TFA.

latter amino acid shifted to a lower field possibly due to the decrease of electron density on its α-carbon atom.

Tuberactinomycins A and B are only distinct from N and O in terms of replacement of capreomycidine with tuberactidine. Only this difference is reflected on their spectra so that a dull singlet attributed to methine proton of δ-carbon atom of Tbd at δ 5.19 appeared in place of the corresponding δ-methylene protons of Cpd at about δ 3.3. The other minor change recognized in spectra was a slightly lower shift of β-methine proton of Tbd compared to that of Cpd owing to the substitution of hydroxyl group at δ-carbon atom. Thus, all protons attached to carbon atom in four tuberactinomycins were successfully assigned as shown in Table 1.

Next, the amide proton resonances in water at pH 2.5 were studied to obtain the informations on a backbone stereochemistry of tuberactinamine and tuberactinomycins in solutions. (Figs. 4 and 5). Tuberactinamine N in H_2O solution at 30 °C (Fig. 4) shows a triplet at δ 8.3 which could be assigned to β-NH of Dpr from its coupling mode. A doublet at δ 9.4 has the same coupling constant (J=12 Hz) to that of a doublet at δ 8.0, which is ascribed to olefinic proton of Uda, and an irradiation on one of the either peaks caused the partner to collapse to a singlet. Therefore, the lower peak was determined to be an amide proton of the ureido group attached to olefinic carbon atom. A singlet at δ 8.95 was assigned to α-NH of Uda from its chemical shift. A highest doublet at δ 7.75 (J=10 Hz) at 30 °C moved to δ 7.68 at 60 °C which was successfully decoupled by an irradiation of a peak centered at δ 4.95 (dd, J=4, 10 Hz) of α-CH of Cpd on a shoulder of H_2O signal. Therefore, the signal of δ 7.75 could be determined as α-NH of Cpd. Two doublets at δ 9.5 and δ 8.8 belong to α-amide protons of two serine residues. The lower doublet was assigned to α-NH of Ser(2) and the higher one to that of Ser(1). The three single peaks corresponding to each two protons at δ 7.4, 6.2, and 6.5 were assigned to two ring NH, *exo* NH_2 protons in guanidino group of Cpd, and primary amide protons in ureido group of Uda, respectively. The lowest signal of them was separated to two peaks with a rise in temperature from 30 °C to 60 °C.

In the spectra of tuberactinomycins A, B, N, and O (Fig. 5), α-NH of Dpr newly appeared in the slightly higher field than that of Ser(1). In the case of tuberactinamine N, the protonated α-amino proton resonance of Dpr could not be observed perhaps due to overlapping with that of water. Except this feature, both spectral patterns of tuberactinomycins N and O were substantially identical with that of tuberactinamine N. On the other hand, in the spectra of tuberactinomycins A and B, all

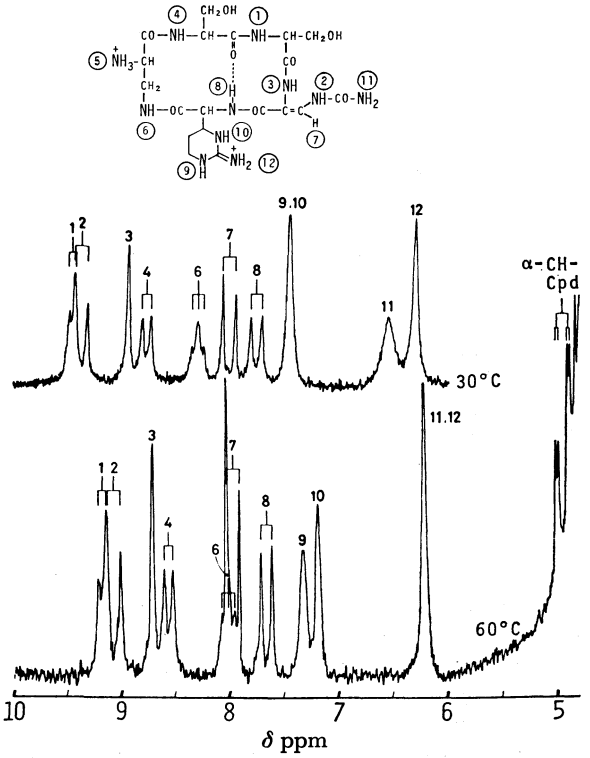

Fig. 4. NMR spectra of tuberactinamine N in low-field region in H_2O at pH 2.5.

of the guanidino proton resonances of Tbd shifted to the lower field compared with those of Cpd in the molecules of another three cyclic peptides. These shifts seem to be apparently effected by the influence of δ-hydroxyl group in Tbd. Especially, δ-NH resonance of Tbd markedly shifted to the downfield and its temperature dependence is relatively small compared with that of β-NH resonance in the same group. This tendency can serve for differentiation of two NH resonances in Cpd ring. Similarly *exo* amino proton as protonated form in Cpd or Tbd was differentiated from a primary amide proton of Uda by a smaller temperature dependence.

In addition to the experiments in H_2O solution, we also studied on spectra in DMSO-d_6 solution. In the spectrum of tuberactinamine N (Fig. 6), the complicated feature in α-methine proton region may be arised from the additional coupling with amide protons. However, the chemical shifts of them were substantially similar to those in D_2O solution. The relation between methine proton and amide proton region was examined by decoupling method on two Ser residues. Thus, an irradiation at the signal of Ser(2) α-CH of δ 4.1 caused the lowest doublet of δ 9.2 to collapse to a singlet. On the other hand, an irradiation at that of Ser(1) α-CH of δ 4.7 forced two doublets at δ 8.6 and 7.5 to collapse to a singlet. From this result, the former doublet can be assigned to that of Ser(1) α-NH, the latter to Cpd α-NH due to the concurrent decoupling with α-CH of Cpd near δ 4.7. The study in DMSO-d_6 solution has consequently supported the assignments of two serine α-NH protons in H_2O solution.

Temperature Dependence. Temperature dependence

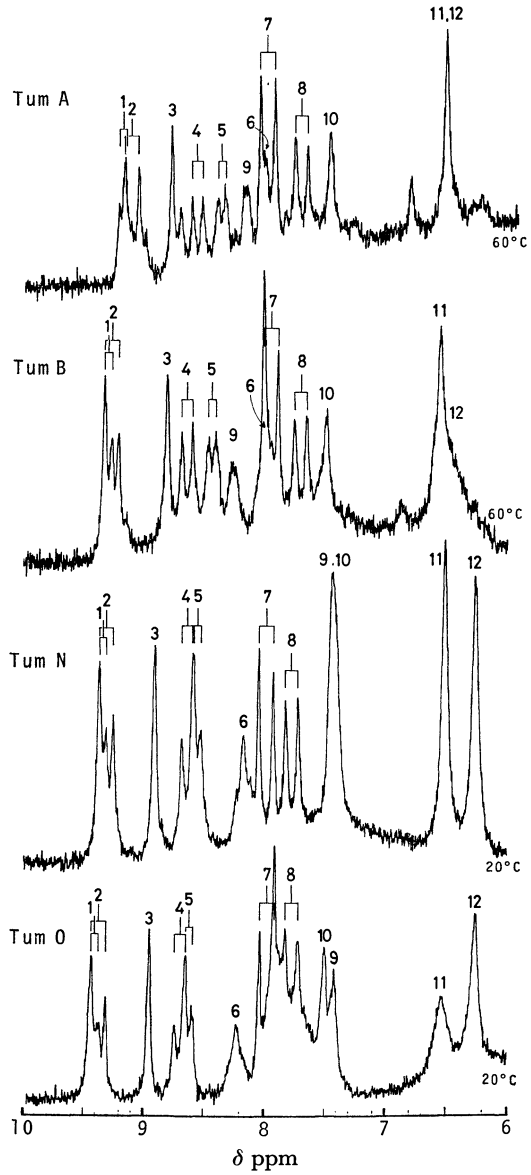

Fig. 5. NMR spectra of tuberactinomycins (Tum) A, B, N, and O in low-field region in H_2O at pH 2.5.

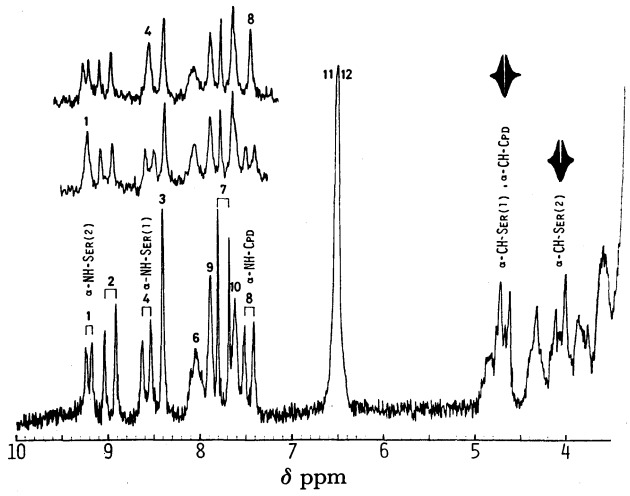

Fig. 6. A part of NMR spectrum of tuberactinamine N in DMSO-d_6.

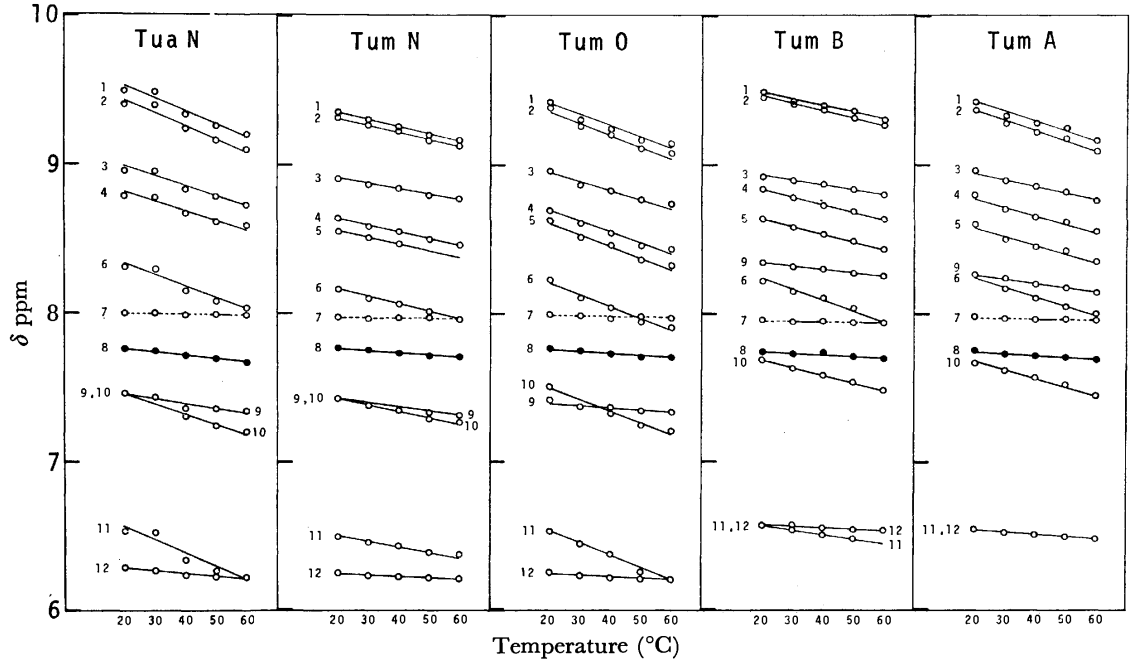

Fig. 7. Temperature dependence of chemical shifts of tuberactinomycins (Tum) and tuberactinamine (Tua) N in low-field region in H_2O at pH 2.5.
○···○ olefinic proton; ●—● α-amide proton of guanidino amino acids; ○—○ other amide and amino protons.

diagram of the lowfield proton resonances in H_2O solution at pH 2.5 of all compounds was given in Fig. 7. Each proton was numbered in order of increasing magnetic field, its assignment being described above. Of these protons, protons **7**, **8**, **9** and **12** showed small temperature coefficients, whereas the other protons shifted markedly to higher field with rise in temperature. Consequently, it appeared that protons **8**, **9**, and **12**, except olefinic proton **7**, were concerned more or less to either intra- or intermolecular hydrogen bond. Especially, the participation of proton **8** corresponding to Cpd or Tbd α-NH is important for comparison of the ring conformations in solutions and crystals. It should be noted that the similar result was obtained in tuberactinamine N which corresponds to the cyclic moiety of the natural peptides.

Deuterium Exchange. Deuterium exchange rates of NH resonances of tuberactinamine N in DMSO-d_6 containing 5% D_2O by volume were studied. Within 15 min after addition of D_2O, all of the resonances except protons **7** and **8** disappeared by exchange with deuteriums. Since the olefinic proton **7** can be excluded from the consideration, it is concluded that the resonance **8** corresponding to Cpd α-NH shows particularly slow exchange rate among NH protons. This proton was not replaced completely by deuteron after 2 hr and its signal remained to some extent even after allowing to stand overnight. The similar tendencies of the corresponding resonances were observed in each spectrum of four tuberactinomycins.

Consequently, it was revealed that only the α-amide proton **8** of Cpd and Tbd formed a fairly protected hydrogen bond in all compounds, while the two protons **9** and **12** may be located in somewhat crowded environment though not participating in the definite hydrogen bond. A carbonyl group as the partner to α-amide proton **8** could not be clarified unambiguously from only the above experiments. However, an intramolecular hydrogen bond was ascertained in crystals of tuberactinomycins O and B (viomycin) between the amide proton of guanidino amino acids and the carbonyl group of Ser(1) as mentioned before. In addition to this fact, taking into account a general information that many cyclic peptides form a stable β-turn structure involving the intramolecular hydrogen bond of ten membered ring, Ser(1) residue is unequivocally chosen as carbonyl partner in these cases. Furthermore the participation of Ser(1) residue in hydrogen bond made possible to understand the significant difference between the resonances of α-methine protons in two serine residues. Thus, the electron density on carbon atom of Ser(1) CO is forced to be lower by the formation of the hydrogen bond. Thereby the protons on atoms linked to Ser(1) CO, *i.e.*, Ser(1) α-CH and Ser(2) α-NH, have to show diamagnetic shift to the lower field.

The backbone conformation of cyclic moiety in crystals of tuberactinomycin O was shown in Fig. 8. The ring part in the molecule was fixed in a definite conformation with the intramolecular hydrogen bond. On the assumption that the conformation in D_2O or H_2O is the same in principle to that in crystals, one can elucidate all the observations consistently. Furthermore, the rigid conformation of tuberactinomycin O in crystals afforded useful informations for side chains in two serine residues. Thus, β-methylene group of Ser(1) was situated in the lateral direction to a nearly lined backbone chain "wall," and thereby the side chain is possible to rotate freely. On the other hand, the β-

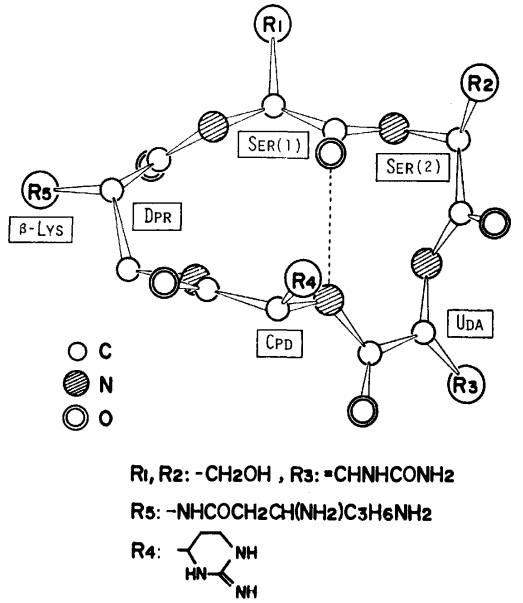

R1, R2: -CH2OH , R3: =CHNHCONH2

R5: -NHCOCH2CH(NH2)C3H6NH2

R4:

Fig. 8. Backbone conformation of tuberactinomycin O in crystals.

methylene group of Ser(2) was located just on the upper position to the "wall" and consequently a free rotation must be prevented by steric interaction with its own carbonyl group. These magnetically different environments of both side chains made a discrimination between coupling patterns of α- and β-protons. β-Methylene protons in Ser(1) must be coupled to doublet and α-methine proton to triplet, while the both corresponding protons in Ser(2) should appear as double-doublet of ABX type as in fact. The result of this consideration seems to be consistent with the supposition that the conformations of tuberactinamine and tuberactinomycins in solution are almost the same to that in crystals. Furthermore, this conclusion was supported by the following two facts: 1) there are little changes recognized in all α-CH–NH coupling constants at several temperatures in all compounds tested: 2) most of the dihedral angles in the backbone skeleton calculated from NMR spectra in tuberactinomycin O are substantially comparable to those from the result by X-ray analysis.

Recently, Viglino *et al.* reported a NMR study of viomycin, *i.e.*, tuberactinomycin B itself.[14] However, their assignments for some NH resonances did not agree with our results. According to them the lowest signal of singlet mode in acid solution was assigned to Uda α-NH resonance from the comparison of its chemical shift with that of conjugated ureide NH, *i.e.*, –C=CH–NHCONH$_2$. Moreover, another singlet corresponding to our Uda α-NH in tuberactinomycins had been deduced to *exo* imino proton of Tbd in their paper. The guanidino moiety in acid solution must be regarded as protonated form $\begin{matrix}-NH\\-NH\end{matrix}\!\!>\!\overset{+}{C}\!-NH_2$ but not as $\begin{matrix}-NH\\-NH\end{matrix}\!\!>\!C=$ NH. Consequently, their assignment of Ser(2) α-NH in viomycin was also inconsistent with our result for tuberactinomycins.

From our studies on NMR spectra of tuberactinomycins as mentioned above, some important conclusions were drawn: 1) a strong intramolecular hydrogen bond may serve to maintain a stable and fixed conformation in ring moiety based on β-turn structure in solutions as well as in crystals; 2) such a stable and rigid conformation is common to each antibiotics in tuberactinomycin family; 3) a cyclic peptide moiety, tuberactinamine N, possesses the same conformation with the intramolecular hydrogen bond as those in tuberactinomycin molecules. These results concerning the specific conformation may not be unrelated to the exhibition of antibiotic activities since all of five cyclic peptides showed the comparable antitubercular activities. For the purpose of further investigation on the relationship between conformations of tuberactinomycins and their biological activities, studies on hydrogenated derivatives or synthetic analogues of tuberactinomycins are now in progress.

The authors are deeply indebted to Professor Yoshimasa Kyogoku, Institute for Protein Research, Osaka University, for invaluable discussions. We also wish to express our appreciations to The Research Laboratories, Toyo Jozo Co., Ltd. for the supply of the samples of tuberactinomycins.

References

1) Part VIII. T. Wakamiya and T. Shiba, *J. Antibiot.*, **28**, 292 (1975).
2) Presented at the 12th Symposium on Peptide Chemistry, Kyoto, 1974, p. 135.
3) T. Wakamiya, T. Shiba, T. Kaneko, H. Sakakibara, T. Take, and J. Abe, *Tetrahedron Lett.*, **1970**, 3497.
4) H. Yoshioka, T. Aoki, H. Goko, K. Nakatsu, T. Noda, H. Sakakibara, T. Take, A. Nagata, J. Abe, T. Wakamiya, T. Shiba, and T. Kaneko, *ibid.*, **1971**, 2043.
5) T. Noda, T. Take, A. Nagata, T. Wakamiya, and T. Shiba, *J. Antibiot.*, **25**, 427 (1972).
6) T. Wakamiya, T. Shiba, and T. Kaneko, This Bulletin, **45**, 3668 (1972).
7) T. Wakamiya, T. Shiba, T. Kaneko, H. Sakakibara, T. Noda, and T. Take, *ibid.*, **46**, 949 (1973).
8) T. Wakamiya and T. Shiba, *J. Antibiot.*, **27**, 900 (1974).
9) B. W. Bycroft, *Chem. Commun.*, **1972**, 660.
10) a) A. Stern, W. Gibbons, and L. C. Craig, *Proc. Nat. Acad. Sci. U. S.*, **61**, 734 (1968); b) F. Conti, *Nature* (London), **221**, 777 (1969); c) M. Ohnishi and D. W. Urry, *Biochem. Biophys. Res. Commun.*, **36**, 194 (1969); d) T. P. Pitner and D. W. Urry, *J. Amer. Chem. Soc.*, **94**, 1399 (1972).
11) a) L. F. Johnson, I. L. Schwartz, and R. Walter, *Proc. Nat. Acad. Sci. U. S.*, **64**, 1269 (1969); b) D. W. Urry and R. Walter, *ibid.*, **68**, 956 (1971); c) R. Walter, R. T. Havran, I. L. Schwartz, and L. F. Johnson, "Proc. Tenth Eur. Peptide Symp., 1969," ed. by E. Scoffone, North-Holland Publ. Co., Amsterdam, (1971), P. 255; d) J. D. Glickson, D. W. Urry, and R. Walter, *Proc. Nat. Acad. Sci. U. S.*, **69**, 2566 (1972); e) R. Walter and J. D. Glickson, *ibid.*, **70**, 1199 (1973).
12) R. Walter, J. D. Glickson, I. L. Schwartz, R. T. Havran, J. Meienhofer, and D. W. Urry, *ibid.*, **69**, 1920 (1972).
13) T. P. Pitner and D. W. Urry, *Biochemistry*, **11**, 4132 (1972).
14) P. Viglino, C. Franconi, A. Lai, E. Brosio, and F. Conti, *Org. Magnetic Resonance*, **4**, 237 (1972).

Racemization Catalyst for Amino Acid. IV* Enantiomer Differentiating Racemization with (*S*)-2′-Nitro-5-nitroso-6,6′-dimethylbiphenyl-2-ol

Kazuhiro HIROTA

Division of Organic Chemistry, Institute for Protein Research, Osaka University, Suita, Osaka 565

(Received June 12, 1975)

The racemizations of both enantiomers of alanine were carried out with (*S*)-2′-nitro-5-nitroso-6,6′-dimethylbiphenyl-2-ol (**1**) in the presence of cupric ion. In time course studies, the apparent half-life of D-alanine is longer than that of L-alanine. Such an enantiomer differentiating ability is explained by a mechanism involving a reactive product formed from the preferred conformation of the diastereomeric cupric complexes, consisting of **1** and D- or L-alanine, respectively. Synthesis of **1** *via* the resolution of 2′-nitro-6,6′-dimethylbiphenyl-2-amine is also presented.

Amino acid racemases are known to catalyze the racemization of both D- and L-amino acids.[1] Studies of the enantiomer diferentiating ability of the racemases are particularly interesting, for they could provide significant stereochemical information regarding the formation of enzyme-substrate complex.

Lambert *et al.*[2] investigated the rate of racemization of alanine with racemase and found that the initial racemization rate for L-alanine is faster than that for D-alanine and that the kinetic parameters of the reaction, which would reflect the stereochemical properties of the enzyme-substrate complex, differ significantly between D- and L-alanine, regardless of the invariability of thermodynamic parameters.

Apart from the enzymatic studies, we have attempted to prepare a synthetic racemization catalyst with a chiral structure, assuming that if there are stereochemical interactions between substrate and catalyst during the reaction process, analogous to the enzyme-substrate complex in enzymatic system, the chiral catalyst should exhibit an enantiomer differentiation against the chiral substrate.

Thus, (*S*)-2′-nitro-5-nitroso-6,6′-dimethylbiphenyl-2-ol (**1**), which contains 4-nitrosophenol structure in the hindered biphenyl, has been synthesized and its enantiomer differentiating ability toward D- and L-alanine has been confirmed.[3]

The mechanism of racemization of alanine with 4-nitrosophenol derivatives has also been presented on the basis of kinetic and stereochemical studies.[4] The proposed reaction pathways are as follows:

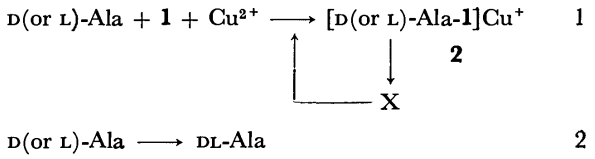

Ala: Alanine. X: Unidentified compound.

That is, 4-nitrosophenol derivatives are decomposed into an unidentified compound (X) *via* the cupric complex (**2**) consisting of 4-nitrosophenol and alanine, the resulting X then catalyzes both reactions 1 and 2. The induced period was regarded as the time necessary to accumulate sufficient concentration of X through the decomposition of **2**, according to the reaction mechanism shown in reaction 1.

Thus, the time course of the reaction, which shows a sigmoid curve and also the effect of steric bulk of substituents surrounding the hydroxyl group of the catalyst on the induced period of the reaction, is explained by this mechanism. In the present paper, the origin of an enantiomer differentiation in the racemization process with **1** is discussed from the view point that the racemization proceeds *via* the mechanism shown in reactions 1 and 2.

Results and Discussion

Racemizations of D- and L-alanine were carried out in the presence of **1** and cupric ion. The resulting time

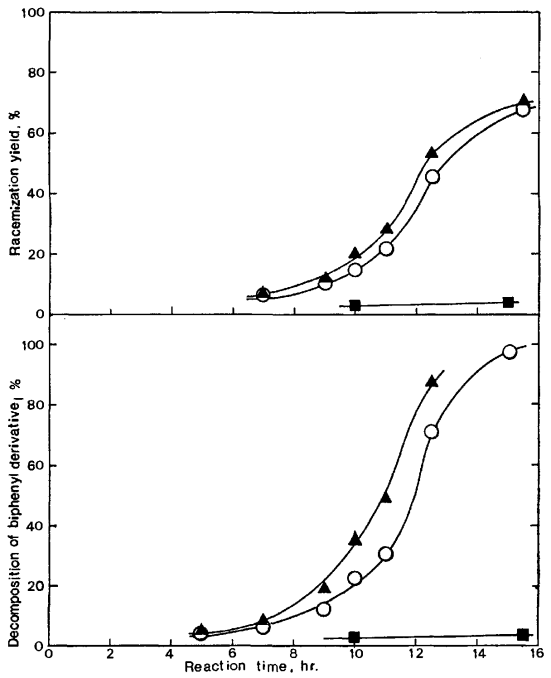

Fig. 1. The reaction mixture (0.5 ml) containing 0.5 mmol D- or L-alanine, 0.05 mmol $CuSO_4 \cdot 5H_2O$, and 0.0125 mmol the above biphenyl derivative in 0.025 M borate buffer (pH, 10.4 at 50 °C).
○: Reaction with D-alanine, ▲: Reaction with L-alanine, ■: Reaction with D-alanine in the absence of the biphenyl.

* Presented at the 30th Annual Meeting of the Chemical Society of Japan, Osaka, April, 1974.

courses of racemization and those of the decomposition of catalysts used exhibit sigmoid curves consisting of the induced period, the acceleration and maximum rate periods, and final stage, as shown in Fig. 1.

Actually the apparent racemization half-life of D-alanine is found to be longer than that of L-alanine as the result of the enantiomer differentiating ability of **1**. However the difference of half-life does not correspond to the difference in rate constants of reaction as was found in the enzymatic reaction, but solely depends on the difference in the induced period.

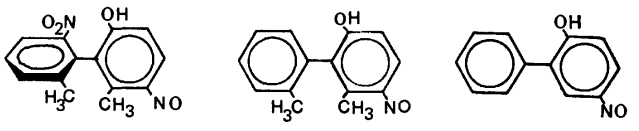

1 **3** **4**

In order to make clear the relationship between the apparent half-life of racemization and the structure of the catalyst, the racemization of alanine and decomposition of the catalyst used were further studied with two representative catalysts (**3** and **4**) whose structures closely resemble that of **1** (Fig. 2). In all cases, the time courses of the reactions show similar sigmoid curves, differing however, in the length of the induced period. The apparent half-lives of racemization, and as well the lengths of the induced period, are in the order; **1**>**3**≫**4**.

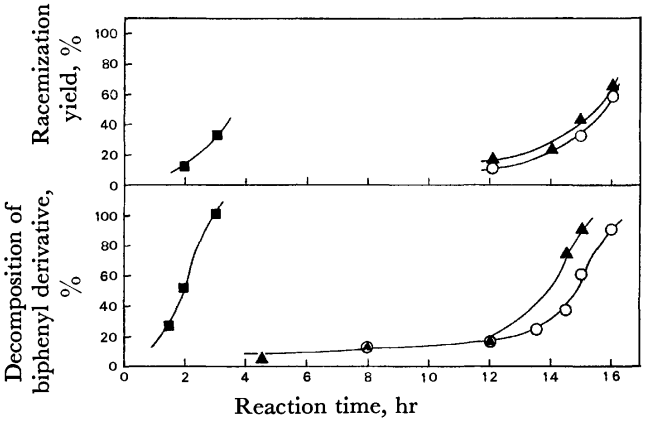

Fig. 2. The reaction mixture (0.5 ml) containing 0.5 mmol D-alanine, 0.05 mmol $CuSO_4 \cdot 5H_2O$ and 0.0125 mmol biphenyl derivatives in 0.025 M borate buffer (pH, 10.4 at 50 °C).
■: with **4**. ▲: with **3**. ○: with **1**.

The good correlation of time course between racemizations of alanine and decompositions of 4-nitrosophenol derivatives implies that both racemization and decomposition proceed though the same intermediate consisting of 4-nitrosophenol derivatives, alanine and cupric ion as shown in **2**.

Taking into account the steric effects on the induced period, it is reasonable that the rate of formation of X is directly related to the equilibrium concentration of **2** which reflects steric effects of substituents of 4-nitrosophenol derivatives in the reaction system. Thus, the direct correlation between the induced period and the structure of **2** was made clear.[4]

The same concept can be used to explain the enantiomer differentiating ability of **1**. The different effects of D-alanine and L-alanine in the decomposition of **1** could be ascribed to the equilibrium concentrations of D-alanine-**1**-cupric complex (D-**1**-Cu) and L-alanine-**1**-cupric complex (L-**1**-Cu) since this complex is an intermediate in the decomposition of **1**. As D-**1**-Cu and L-**1**-Cu are diastereomers, the concentration of D-**1**-Cu should be different from that of L-**1**-Cu.

The apparent half-life of D-alanine is longer than that of L-alanine is also explained by the stereochemical aspects of intermediate, **2**. Actually the results are found to correspond well with predictions using the stereo model as follows: Two types of stereo models, **5** and **6**, can be proposed for L-**1**-Cu. Structure **6**, however, has much less stereo interaction between the chiral center of alanine and the biphenyl ring of **1** than structure **5**. Accordingly structure **5** must make a larger contribution to the enantiomer differentiation of **1**. Structure **7** is the corresponding version of structure **5** for D-**1**-Cu. The steric hindrance between the α-methyl group of alanine and the 2′-nitro group of **1** in **5** is less than in **7**. Hence the concentration of X would be higher for L-**1**-Cu rather than for D-**1**-Cu, resulting in shorter half-life of racemization for L-alanine than for D-alanine.

Although it is not possible to speculate on the mechanism of enantiomer differentiating ability of alanine racemase with the results obtained from **1** because of the decomposition of **1** during the reaction, the enantiomer differentiating process in the formation of enzyme-substrate complex was considered to be well simulated by the complexes **5** and **7**.

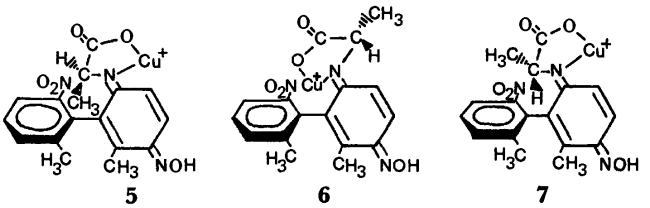

5 **6** **7**

The simulation of enantiomer differentiating racemization in the enzymatic systems with synthetic catalysts will be more feasible when the stable catalysts with a chiral structure are available. Efforts along this line are continuing.

Experimental

Melting points are uncorrected. IR spectra were determined on a Shimadzu 27-G spectrometer. NMR spectra were obtained on a Hitachi R-24 spectrometer with TMS as an internal standard.

2′-Nitro-6,6′-dimethylbiphenyl-2-amine (8). 2,2′-Dinitro-6,6′-dimethylbiphenyl[5] was reduced with sodium sulfide nonahydrate to get 2′-nitro-6,6′-dimethylbiphenyl-2-amine according to Sako's procedure.[6]

(S)-2′-nitro-6,6′-dimethylbiphenyl-2-amine (9). L-Cysteic acid monohydrate[7] (10 g) was dissolved in water (70 ml) with warming and then the solution (75 °C) was added dropwise to

a solution of **8** (12 g) in ethanol (550 ml) previously heated to the same temperature. The mixture was allowed to stand at room temperature for three hours to precipitate a white salt and chilled with ice-water for an hour. This salt was filtered by suction, washed with 90% ethanol (50 ml) and dried at 60 °C to give a white powder (11 g). It was boiled with 90% ethanol (1100 ml) and the excess L-cysteic acid which remained insoluble was filtered off. After standing at room temperature for several hours, the salt began to precipitate as a white powder and then the solution was kept in the refrigerator overnight. The precipitated salt was collected on a filter, washed with 90% ethanol and dried at 60 °C. In the successive recrystallizations, the following procedure was used in order to minimize the total volume of solvent; the salt was again dissolved in the minimum amount of boiling ethanol (80 ml) and then boiling absolute ethanol was added until the final concentration of ethanol was 90%. The yellow solution was allowed to stand overnight in the refrigerator. The white precipitate was filtered by suction and dried at 60 °C. The above recrystallization procedure was repeated four or five times. The color of the solution, during this repeated recrystallization, changed from reddish yellow to pale yellow and also the crystalline state of the salt changed from powder to white needles. Although the course of the recrystallization could be roughly monitored by observations of the above phenomena, it was accurately** followed by decomposition of the salt and measureing the optical rotation value of **9**. The salt was decomposed with 2 M sodium hydroxide to give yellow crystals, which were extracted with ether. The ether solution was washed with water and dried over sodium sulfate. After the evaporation of the ether, the residue started to crystallize almost immediately on cooling. Its specific rotation was measured on the dried sample, and the recrystallization was discontinued when there was essentially no further changes in rotation. After the resolution was complete, **9** liberated from the L-cysteic acid was recrystallized from petroleum ether to afford lustrous yellow crystals (1.8 g) in 30% yield: mp 108—109 °C (lit,[8] 108.3—109.0 °C); $[\alpha]_D$ −74° (*c* 1.0, ethanol), $[\alpha]_D$ −185° (*c* 1.0, 0.2 M HCl) (lit,[8] $[\alpha]_D$ −74.6° (*c* 1.0, 95% ethanol), $[\alpha]_D$ −187° (*c* 0.92, 0.2 M HCl)).

(S)-2-nitro-6,6′-dimethylbiphenyl-2-ol (10). **10** was prepared by the method of Angelletti,[9] but with a greatly improved yield. To a solution of 25% sulfuric acid (70 ml) was added the fine powder of **9** (1.20 g) with vigorous stirring and the diazotization performed at 0—5 °C with a solution of sodium nitrite (0.38 g) in water (1.0 ml). The resulting yellow solution was poured dropwise into continuously boiling water (20 ml) in over ten minutes. During this time, reaction took place with vigorous foaming of nitrogen and brown pitch-like material separated. After cooling, the mixture was made alkaline with 2 M sodium hydroxide and the insoluble brown materials was filtered off by suction. The filtrate was acidified with dilute sulfuric acid solution and the liberated oil was extracted with ethyl acetate. The extract was washed with water, dried over anhydrous sodium sulfate and the solvent was evaporated to give a dark colored syrupy oil containing **10**. The purification was carried out *via* acetylation as follows: The above syrupy oil was gently refluxed with acetic anhydride (5.0 ml) for forty minutes. After removal of the excess acetic anhydride under reduced pressure, the residue was dissolved in ether and the insoluble matter was filtered off. The filtrate was then washed with water, dried with anhydrous sodium sulfate, and the ether was distilled off. The brown residue was dissolved in hot ethanol (20 ml) and decolorized with charcoal.

After removal of the solvent, the residue was recrystallized from 50% ethanol to afford acetylated **10**: mp 77—78 °C, $[\alpha]_D$ +270° (*c* 1.0, ethanol), Found: C, 67.70; H, 5.04; N, 4.85%. Calcd for $C_{16}H_{15}NO_4$: C, 67.36; H, 5.30; N, 4.91%. IR(KBr): 1763 cm^{-1} (C=O) and 1530 cm^{-1} (NO_2).

The acetylated **10** (400 mg) was stirred rapidly with 2 M sodium hydroxide (30 ml) at 70—80 °C for an hour. After acidification of the reaction mixture with 2 M hydrochloric acid, the liberated oily matter was extracted with ethyl acetate (10 ml). After washing with water of the solvent, the mixture was dried over anhydrous sodium sulfate and was evaporated. The crystalline residue was recrystallized from cyclohexane to afford white crystals (0.5 g) in 41% yield from **9**: mp 109—110 °C $[\alpha]_D$ +60.0° (*c* 1.0, ethanol), Found: C, 68.55; H, 5.39; N, 5.63%. Calcd for $C_{14}H_{13}NO_3$: C, 69.12; H, 5.76; N, 5.39%. IR (KBr): 3450 cm^{-1} (OH) and 1523 cm^{-1} (NO_2).

(S)-2′-Nitro-5-nitroso-6,6′-dimethylbiphenyl-2-ol (1). **1** was prepared by the nitrosation of **10** according to the procedure described in a previous paper.[4] mp 205—208 °C, $[\alpha]_D$ −12.0 ° (*c* 1.0, ethanol), Found: C, 61.65; H, 4.22; N, 10.04%. Calcd for $C_{14}H_{12}N_2O_4$: C, 61.76; H, 4.44; N, 10.29%. IR ($CHCl_3$): 2550 cm^{-1} (OH). NMR (CD_3COCD_3): 12.5 ppm (OH), 1.96 and 2.22 ppm (CH_3).

5-Nitroso-6,6′-dimethylbiphenyl-2-ol (3). 2-Amino-6,6′-dimethylbiphenyl (4.0 g)[8] which was prepared from **8** was added to 20% sulfuric acid (50 ml) and diazotized by adding sodium nitrite (1.6 g) in water (10 ml) at 0—5 °C. The mixture was poured into boiling water (200 ml) and the resulting pitch-like material was separated by decantation of the solvent. It was stirred with 2 M sodium hydroxide (100 ml) and the insoluble material was filtered. After acidification of the filtrate with 4 M hydrochloric acid, the mixture was extracted with ether. The extract was washed with water, dried over anhydrous sodium sulfate and the solvent evaporated to afford 6,6′-dimethylbiphenyl-2-ol. The crude product was dissolved in 95% acetic acid and a solution of sodium nitrite (1.0 g) in water (30 ml) was added dropwise with stirring at 0—5 °C. The resulting brown precipitate was collected on a filter, washed with 60% acetic acid and recrystallized from 50% ethanol to afford yellow crystals (1.2 g) in 25% yield: mp 199—200 °C, Found: C, 74.47; H, 5.66; N, 6.01%. Calcd for $C_{14}H_{13}NO_2$: C, 73.99; H, 5.77; N, 6.16%.

5-Nitrosobiphenyl-2-ol (4). Biphenyl-2-ol was treated with sodium nitrite in acetic acid by the method described in the preparation of **1**. The precipitate from the reaction mixture was recrystallized from 30% ethanol to afford yellow crystals in 16% yield: mp 169—171 °C (lit,[10] mp 170—172 °C) Found: C, 72.63; H, 4.49; N, 6.84%. Calcd for $C_{12}H_9NO_2$: C, 72.35; H, 4.55; N, 7.03%.

Racemization Reaction. An aqueous solution of D- or L-alanine (0.5 mmol), cupric sulfate pentahydrate (0.05 mmol), and one of the biphenyl derivatives (0.0125 mmol) was made. The pH was adjusted to 10.4 (at 50 °C) with 1 M sodium hydroxide and diluted to a total volume of 0.25 ml. After dilution with 0.05 M borate buffer (0.25 ml, pH 10.4 at 50 °C), the mixture was shaken at 50 °C in a sealed tube. At specific time intervals the reaction was stopped by the addition of 6 M hydrochloric acid (0.25 ml).

Determination of the Ratio of D- and L-Alanine and the Recovery of Biphenyl Derivatives. The ratio of D- and L-alanine in the reaction mixture was determined by gas chromatography after conversion to *l*-menthyl D- and L-trifluoroacetylalaninates by the method described previously.[4] Careful measurements, compared with the calibrated curve, indicate an estimated

** Following the optical rotation of the salt itself could not be used as a criterion of purity due to a constant contamination of the salt with the L-cysteic acid during the procedure.

error of $\pm 0.5\%$. Biphenyl derivatives were determined spectrophotometrically after separation from reaction mixtures by thin layer chromatography according to the previously outlined procedure.[4]

The author wishes to express his thanks to Prof. Yoshiharu Izumi and Dr. Akira Tai for their continual guidance and encouragement. He also wishes to thank Prof. Shunji Kato for his valuable discussion.

References

1) K. Soda, J. Yorifuji, and K. Ogata, *Biochem. Biophys. Acta*, **146**, 606 (1967).
2) M. P. Lambert, F. C. Neuhaus, *J. Bacteriol.*, **110**, 978 (1972).
3) K. Hirota and Y. Izumi, This Bulletin, **41**, 2287 (1971).
4) K. Hirota, H. Koizumi, Y. Hironaka, and Y. Izumi, *ibid.*, to be published.
5) G. Wittig and O. Stichnoth, *Ber.*, **68**, 928 (1935).
6) S. Sako, This Bulletin, **9**, 396 (1934).
7) H. T. Clarke, "Organic Syntheses," Coll. Vol. 3, p. 226, (1955).
8) J. T. Melillo and K. Mislow, *J. Org. Chem.*, **30**, 2149 (1965).
9) A. Angelletti, *Gazz. Chim. Ital.*, **61**, 832 (1931).
10) W. Borsche, *Ann.*, **312**, 211 (1900).

Eine Ableitung aus der Hypothese über den Litheffekt

Tsuneo SUGA

Forschungslaboratorium der Konishiroku Photoindustrie AG, Hino-shi, Sakura-machi 1, Tokyo 191

(Eingegangen am 2. Juni 1975)

In früheren Arbeiten[1,2] wurde der Mechanismus der Lithentwicklung und die Hypothese über die Entstehung des Litheffekts diskutiert. Nach dieser Hypothese ist für einen bildscharfen Litheffekt eine richtige Balance zwischen der Entwickelbarkeit der stärker belichteten Bildkeime und der Oxydierbarkeit der schwächer belichteten wichtig. Damit wurde der gute Litheffekt der Chlorbromsilber-Emulsion mit hohem Chloridanteil und der Litheffekt der Bromjodsilber-Emulsion mit niedrigem Jodidanteil gut erklärt. In der vorliegenden Arbeit wurde eine steile Gradation einer Bromjodsilber-Emulsion aus der Ableitung der Hypothese versucht. Die steile Gradation der Bromjodsilber-Emulsion, die man in Gegenwart von Rhodanid im Entwickler an Stelle von Bromid erhielt, wurde der „Redox-Lith-Effekt" der Bromjodsilber-Emulsion genannt.[3]

In früheren Arbeiten[1,2] wies der Autor auf die Wichtigkeit des Oxydationseffekts der Oxydationsprodukte des Hydrochinons bei der Lithentwicklung sowie deren Beschleunigungseffekt hin. Außer den bereits zitierten Arbeiten,[2] die im Gegensatz zum Oxydationseffekt stehen, richtete neulich Austin[4] in der Revue über die Lithentwicklung auf den Oxydationseffekt wenig Aufmerksamkeit. Wie schon früher gezeigt wurde,[1] entsteht der Litheffekt aus einem Lithmaterial mit hohem Chlorsilberanteil und einem normalen Lithentwickler mit niedriger Konzentration von Sulfit. Einen guten Litheffekt erkennt man an der Grenzschärfe und der besonders steilen Gradation des zu hohen Schwärzungen ansteckend entwickelten Bildes. In der letzten Arbeit[2] wurde doch eine Oxydation der Entwicklungsbildkeime während der Induktionsperiode und noch früher[1] die Hypothese des Litheffekts vorgestellt. Nach der Hypothese ist für einen guten Litheffekt eine richtige Balance zwischen der Entwickelbarkeit der stärker belichteten Bildkeime und der Oxydierbarkeit der schwächer belichteten wichtig. Daher sind nicht alle Emulsionen dem guten Litheffekt zugänglich. Mit Hilfe der Hypothese ließ sich der gute Litheffekt der Chlorbromsilber-Emulsion sowie der schlechte der Bromjodsilber-Emulsion gut erklären.[1]

In der vorliegenden Arbeit wurde auf Grund der Hypothese versucht, einen bisher noch nicht erzielten steilen Effekt einer Bromjodsilber-Emulsion abzuleiten.

Experimentelles

Entwickler. Für die Entwicklung bei 20 °C dienten ein normaler Lithentwickler und dieser Lithentwickler mit 30 g/l Natriumsulfit. Die Entwickler enthielten Kaliumbromid oder Kaliumrhodanid unter der Konzentration von 0,02 mol/l.

Emulsion. Eine Bromjodsilber-Emulsion, die 1,5 mol% Jodsilber enthielt, und eine Chlorbromsilber-Emulsion, die 70 mol% Chlorsilber enthielt, wurden zum Versuch verwendet. Die feinkörnigen Emulsionen wurden schwefelsensibilisiert und dann auf eine Untelage gegossen. Einzelheiten der Rezepte und Versuchsdurchführung wurden schon gezeigt.[1]

Ergebnisse und Diskussion

Die Schwärzungskurven der an Halogensilberbestandteilen verschiedenen Emulsionen in Abb. 1 zeigten,

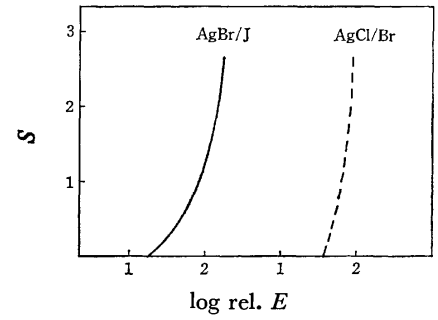

Abb. 1. Vergleich vom Litheffekt zwischen einer Chlorbromsilber-Emulsion (----) und einer Bromjodsilber-Emulsion (——) im normalen Lithentwickler, in 3 min. entwickelt.

daß die Chlorbromsilber-Emulsion einen bildscharfen Litheffekt, während die Bromjodsilber-Emulsion einen schlechten, mit einem langen Fuß auf der Schwärzungskurve darstellte.

Bei der Oxydation der Silberteilchen in der bromid- oder rhodanidhaltigen Chinonlösung wurde ein klarer Unterschied zwischen zwei Salzen schon früher mitgeteilt.[1] Dabei zeigte das erstere eine größere Wirkung als das letztere. Dies kann man aus dem Silberpotential rechnerisch voraussehen, weil die aus der Nernstschen Gleichung elektrochemisch mit den Werten der Löslichkeitsprodukte berechneten Silberpotentiale E_{Ag} gegen Normalwasserstoffelektrode bei 20 °C

$$E_{Ag}(0{,}02 \text{ mol KBr}) = 0{,}177 \text{ V}$$

$$E_{Ag}(0{,}02 \text{ mol KSCN}) = 0{,}201 \text{ V}$$

sind.

Das Verhalten der Bromjodsilber-Emulsion im bromid- oder rhodanidhaltigen Hydrochinon-Entwickler wird in den Abbildungen 2 und 3 dargestellt. Bei der Sulfit-Hydrochinon-Entwicklung in den Abbildungen 2 und 3a zeigte Rhodanid, verglichen mit Bromid, eine größere Entwickelbarkeit und eine steilere Gradation, als die gleichen Ergebnisse in gewöhnlichen Entwicklern.[5,6] In Abb. 3a wurde jedoch nichts vom einen Litheffekt bemerkt, weil Sulfit den Oxydationseffekt vernichten kann.

Die Erklärung des schlechten Litheffekts der Bromjodsilber-Emulsion wurde schon früher wie folgt vorgestellt.[1] Ihre latenten Bildkeime, verglichen mit

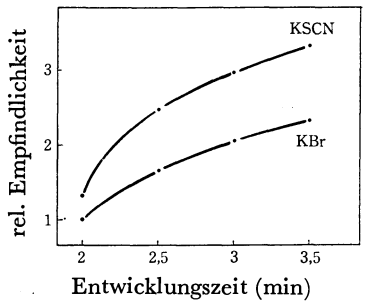

Abb. 2. Abhängigkeit der relativen Empfindlichkeit einer Bromjodsilber-Emulsion von der Entwicklungszeit in einem Sulfit-Hydrochinon-Entwickler, der KBr oder KSCN unter der Konzentration von 0,02 mol/l enthält.

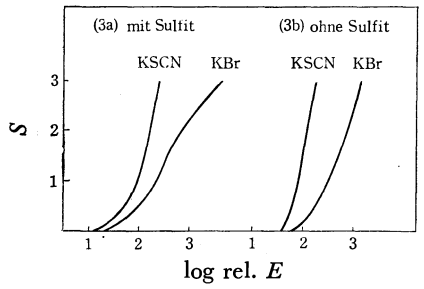

Abb. 3. Vergleich der Schwärzungskurven einer in 3 min entwickelten Bromjodsilber-Emulsion in einem Hydrochinon-Entwickler mit 30 g/l Natriumsulfit (Abb. 3a) und ohne Natriumsulfit (Abb. 3b). Die Entwickler enthalten KBr oder KSCN unter der Konzentration von 0,02 mol/l.

denen der Chlorbromsilber-Emulsion, sind an der schwächer belichteten Stelle leicht oxydierbar, und an der stärker belichteten langsam entwickelbar. Unter der Annahme der Hypothese sollte ein besserer Litheffekt der Bromjodsilber-Emulsion erhalten werden, wenn man die Oxydierbarkeit milder und die Entwickelbarkeit beschleunigender machen könnte. Aus obigen Ergebnissen folgert, daß Rhodanid dafür gelten kann. Mit anderen Worten, im Lithentwickler, in dem der Oxydationseffekt für wichtig gehalten wird, läßt wahrscheinlich Rhodanid den Oxydationseffekt an den schwächer belichteten Keimen milder und die Entwicklung der stärker belichteten beschleunigender machen. Mit dieser Absicht wurde Kaliumrhodanid an Stelle von Kaliumbromid dem Lithentwickler hinzugefügt. Dieser erwartungsvolle Versuch bewies in Abb. 3b eine sehr steile Gradation der Bromjodsilber-Emulsion. Abb.3b schildert einen Vergleich der Schwärzungskurven der im rhodanid- oder bromidhaltigen Lithentwickler behandelten Bromjodsilber-Emulsion.

In einer Rhodanid-Lösung tritt die chemische Umwandlung des Bromsilbers durch Rhodanid in Rhodansilber ein, wenn die Bedingung zwischen dem Löslichkeitsprodukt L und der Konzentration von Anionen [ ] auf die folgende Formel lautet.

$$L_{AgBr}/[Br^-] > L_{AgSCN}/[SCN^-]$$

Bei der Konzentration der SCN^--Ionen von 0,02 mol/l tritt die Umwandlung bei weniger als 0,007 mol/l Br^--Ionen rechnerisch ein. Die Messungen von Jaenicke[7] zeigten, daß das eingesetzte Rhodansilber in der Lösung von Rhodanid unter Komplexbildung als $[Ag(SCN)_2]^-$ aufgelöst wird. Klein[8] beobachtete auch die Komplexbildung mit der Konzentration des Rhodanids von 0,01 mol/l als $[Ag(SCN)_2]^-$, deren Komplexkonstante $1{,}67 \times 10^8$ bei 25 °C lagen. Daher wird angenommen, daß sich die Konzentration der Ag^+-Ionen in der Umgebung der Körner, als die aus dem Löslichkeitsprodukt berechnete, vielmehr steigen kann. Die Verminderung des Oxydationseffekts sowie die Vermehrung des Beschleunigungseffekts und die Möglichkeit[6] zur physikalischen Entwicklung, die durch Komplexbildung verursacht werden kann, scheint zusammenspielend eine günstige Wirkung zum steilen Effekt hervorzubringen.

Eine Deutung von Austin[4] lautet neulich, daß in der Lithentwicklung zwei Elementarprozesse eine große Rolle spielen. Nämlich, der Prozeß der Induktionsperiode und der von der katalytischen Beschleunigung der Oxydationsprodukte abhängige Prozeß. Wie schon erläutert wurde,[2] ist eine einheitliche Deutung des katalytischen Entwicklungsbeschleunigens für die Erklärung der Lithentwicklung nicht ausreichend.

Nach unserer Meinung ist zudem der Oxydationseffekt ein wichtiges Element bei der Lithentwicklung, besonders zu Beginn der Entwicklung. Der Oxydationseffekt, der von der oxydativen Hemmung der Entwicklung bis zum oxydativen Abbau der latenten Bildkeime führen kann, übt eine hindernde Wirkung auf die sichtbare Silberabscheidung aus.[2] Die Induktionsperiode ist eine eigentümliche Erscheinung der Lithentwicklung, welcher bei Abwesenheit von Sulfit der Oxydationseffekt in hohem Grad zugrunde liegen kann. Zum Beispiel verringerte Sulfit den Oxydationseffekt, so daß es eine kürzere Induktionsperiode[1,9] und keinen Litheffekt[1] verursachte. Mit der steigenden Konzentration von Bromid bei der Lithentwicklung, erniedrigt sich das Redoxpotential der latenten Bildkeime, um von der Oxydationsprodukte und H^+-Ionen oxydativ beeinflußt werden zu können, so daß sich dadurch die Induktionsperiode stark verlängern kann.[1]

Auf Grund der früher vorgeschlagenen Hypothese über den Litheffekt,[1] in welcher der Oxydationseffekt für wichtig gehalten wurde, ist hier der bisher noch nicht erzielte steile Effekt der Bromjodsilber-Emulsion durch eine Deutung der Redox-Vorgänge abgeleitet worden. Daher wurde dieser neue steile Effekt der „Redox-Lith-Effekt" der Bromjodsilber-Emulsion genannt, wie in dem Internationalen Kongreß der fotografischen Wissenschaften 1974 in Dresden berichtet wurde.[3]

Herrn Prof. Dr. K. Honda von der Universität Tokio für das Interesse und Ermuntern, Herrn Prof. Dr. W. Jaenicke von der Universität Erlangen-Nürnberg für die wertvolle Diskussion mit Unterstützung der Hypothese, Herren Prof. Emeritus Dr. S. Kikuchi von der Universität Tokio und Dr. F. Dietz von der Universität Leipzig für die freundlichen Worte beim ICPS 1974, Herren Prof. Dr. H. Irie von der Universität Chiba und Prof. Dr. T. Miyagawa von Tokyo College

of Photography für das Interesse an meinen Arbeiten, Herren Dr. Y. Wakabayashi und Dr. Y. Kuwabara von der Konishiroku Photoindustrie AG, Herrn Prof. Emeritus Dr. T. Somiya von der Universität Tokio für das stetige freundliche Wort zur Ermunterung, möchte ich herzlichst danken.

Literatur

1) T. Suga, Dieses Bulletin, **45**, 3464 (1972).
2) T. Suga, Dieses Bulletin, **47**, 2463 (1974).
3) T. Suga, *Int. Congr. Photogr. Sci., Dresden*, 3—39 (1974).
4) M. Austin, *J. Photogr. Sci.*, **22**, 293 (1974).
5) T. H. James und W. Vanselow, *Photogr. Eng.*, **7**, 90 (1956).
6) H. M. Smith und C. A. Callari, *Photogr. Sci. Eng.*, **19**, 130 (1975).
7) W. Jaenicke, *Z. Elektrochem.*, **57**, 843 (1953).
8) E. Klein, *Photogr. Korresp.*, **92**, 139 (1956).
9) T. L. Beaupre, R. R. Jasper, D. A. Turbide, und M. T. Williams, *Photogr. Sci. Eng.*, **18**, 535 (1974).

Crystal and Molecular Structure of Potassium Acetylacetonate Hemihydrate

Shuzo SHIBATA, Shigeki ONUMA, Yukinori MATSUI, and Shoichi MOTEGI

Department of Chemistry, Shizuoka University, Oya, Shizuoka 422

(Received August 14, 1974)

The crystal structure of potassium acetylacetonate hemihydrate, $KC_5H_7O_2 \cdot 1/2H_2O$, has been determined by X-ray diffraction method. Crystals are triclinic with space group $P\bar{1}$, $a=10.86$, $b=8.74$, $c=7.45$ Å, $\alpha=90.5$, $\beta=95.8$, $\gamma=91.9°$, and $Z=4$. The final R value was 0.109 for 1589 visually estimated reflection data. Each potassium ion is surrounded by seven oxygen atoms, at distances of 2.65 to 3.05 Å, six of which belong to four acetylacetone anions and the rest is a water molecule. The bond lengths and angles of the acetylacetone anion are very similar to those of acetylacetone groups in heavy metal chelates, but differ from those of the free molecule of acetylacetone.

A number of crystal-structure determination of transition metal complexes of acetylacetone[1-6] revealed that the chelate ring is nearly planar and the molecular dimension of the ring is almost independent of the kind of the metal atom. It is, therefore, particularly interesting to compare the structure of a free acetylacetone anion with that of acetylacetone coordinated to heavy metals. The crystal structure of potassium acetylacetonate hemihydrate, $KC_5H_7O_2 \cdot 1/2H_2O$ (hereafter denoted as PAH), is described in this paper.

Experimental

The samples of PAH were prepared by mixing hot alcoholic solution of potassium hydroxide and 2,4-pentanedione,[7] and single crystals were obtained in the form of rods. They are hygroscopic; the specimens were sealed in thin-walled glass capillary tubes. The crystal was found to be triclinic from Weissenberg photographs. The unit cell dimensions were determined on the basis of the high-angle reflections on Weissenberg photographs taken with Cu$K\alpha$ radiation ($\lambda=1.5418$ Å) as follows: $a=10.86\pm0.01$, $b=8.74\pm0.02$, $c=7.45\pm0.02$ Å, $\alpha=90.5\pm0.4$, $\beta=95.8\pm0.4$, and $\gamma=91.9\pm0.4°$. They were calibrated by using the reference lines of sodium chloride ($a=5.6396$ Å). The measured density was 1.40 g cm^{-3} (flotation method in carbon tetrachloride and cyclohexane), while the calculated one was 1.39 g cm^{-3} for $Z=4$. The intensities were recorded on multiple-film equi-inclination Weissenberg photographs with Cu$K\alpha$ radiation. Intensities of the layers $hk0$–$hk4$ were collected and estimated visually. The absolute scale of the structure amplitudes for each layer was obtained at a later stage by correlating with the calculated ones. In total, 1590 reflections were observed. Corrections for Lorentz and polarization effects were applied in the usual way. Correction for absorption was neglected. The space group $P\bar{1}$ was assumed at the outset and confirmed in the course of refinement.

Structure Determination

The structure analysis was initiated on the basis of the two-dimensional heavy-atom method. The x and y coordinates of two independent potassium ions were deduced from a Patterson projection onto the (001) plane; they were overlapped in the Fourier projection on this plane. Iterative Fourier and difference-Fourier syntheses refined the x and y coordinates of K, O and C atoms. The results suggested that the acetylacetone groups are almost planar and parallel to the (001) plane. The z coordinates of the atoms were guessed from a packing consideration. With the trial and error method, all the atoms in the two planar anions and the oxygen

Table 1. Positional and thermal parameters[a] with their estimated standard deviations ($\times 10^4$)

	x	y	z	B_{11}	B_{22}	B_{33}	B_{12}	B_{13}	B_{23}
K(1)	4915(3)	1931(3)	80(5)	60(2)	73(3)	90(11)	1(4)	1(7)	−26(8)
O(11)	3292(8)	3137(10)	2294(15)	57(8)	95(13)	196(36)	11(16)	−23(24)	−14(30)
O(12)	3691(8)	−132(10)	2477(15)	48(8)	95(13)	176(34)	−3(15)	0(23)	3(29)
C(11)	1235(15)	3825(19)	1145(30)	91(17)	146(27)	371(73)	106(34)	−97(52)	−35(64)
C(12)	2209(11)	2687(14)	1763(21)	55(11)	92(18)	98(49)	12(22)	−10(32)	−86(40)
C(13)	1816(12)	1101(16)	1601(23)	49(11)	138(22)	131(52)	21(25)	15(34)	−18(47)
C(14)	2548(11)	−165(14)	1963(22)	50(11)	78(17)	153(51)	−8(21)	10(32)	−17(40)
C(15)	1930(14)	−1760(17)	1654(28)	80(15)	103(21)	334(67)	−90(29)	30(46)	−64(55)
K(2)	4909(3)	1939(3)	4941(5)	62(2)	76(4)	103(11)	3(5)	−9(7)	−5(8)
O(21)	6379(8)	15(10)	2528(15)	55(8)	94(13)	190(35)	10(16)	−28(24)	−44(30)
O(22)	6424(9)	3310(10)	2664(15)	80(9)	97(13)	126(34)	27(17)	−29(25)	−80(29)
C(21)	8303(15)	−1129(17)	3405(28)	93(16)	114(22)	296(66)	100(31)	−28(47)	−40(55)
C(22)	7516(11)	243(15)	3060(20)	53(11)	111(19)	40(46)	23(23)	−4(30)	−23(40)
C(23)	8081(11)	1687(15)	3456(23)	45(11)	111(20)	184(54)	−30(23)	−8(34)	−54(46)
C(24)	7520(11)	3101(15)	3237(23)	48(11)	93(18)	186(54)	−38(22)	4(34)	−24(44)
C(25)	8334(19)	4474(19)	3960(35)	137(23)	113(25)	560(91)	−164(39)	40(69)	−172(73)
O(w)	4909(9)	5734(10)	2489(15)	95(10)	91(13)	116(34)	25(18)	29(26)	−31(29)

a) Thermal factors refer to the expresion $\exp[-(B_{11}h^2+B_{22}k^2+B_{33}l^2+B_{12}hk+B_{13}hl+B_{23}kl)]$.

TABLE 2. OBSERVED AND CALCULATED STRUCTURE FACTORS ($\times 10$)
Asterisks indicate reflections with $w=0.5$, otherwise $w=1.0$.

H FO FC	H FO FC	H FO FC	H FO FC	H FO FC	H FO FC	H FO FC	H FO FC
K,L= 0 0	5 178 162	6 53 -15	5* 0 34	K,L= 3 1	6* 31 8	9 106 -85	-12* 0 29	-4 330 284
2 99 -72	6 148-152	K,L= 10 0	6* 0 2	-9* 50 -53	7* 31 -30	10 139 124	-11* 0 -16	-3 342-302
3 684-755	7 183-191	-6 103 113	7 55 57	-8 64 64	K,L= -8 2	11 81 -85	-10 78 -67	-2 326 281
4 385 397	8 61 63	-5 132-139	8 64 -63	-7* 0 -16	-9 78 112	12 121 116	-9 94 74	-1 319-264
5 294-240	9 190 181	-4 78 86	9 60 69	-6* 0 -10	-8 112-126	K,L= -3 2	-8 98 -66	0 299 277
6 608 572	10 135-118	-3 102 -99	K,L= -2 1	-5 109-126	-7 109 113	-13 53 78	-7* 23 -16	1 250-207
7 629-543	11* 0 20	-2 135 132	-8* 50 35	-4 67 66	-6 106-128	-12 112-125	-6 141 132	2 313 283
8 372 352	12 61 -62	-1 165-171	-7 66 -77	-3* 0 -15	-5 78 95	-11 67 71	-5 94 -91	3 297-290
9 228-205	K,L= 5 0	0 164 171	-6 72 -67	-2 202 176	-4 116-123	-10* 0 -20	-4 155 138	4 211 190
10 103 84	-12 55 55	1 106-110	-5* 47 -42	-1 90-108	-3 187 194	-9 202 198	-3 329-277	5 288-320
11 69 -55	-11 56 -67	2 72 64	-4 180 199	0 209 229	-2 146-128	-8 322-321	-2 396 321	6 248 261
12 135 127	-10 146 136	3 83 -78	-3 67 -80	1 184-164	-1 136 120	-7 266 250	-1 178 -99	7* 0 -45
13 119-115	-9 220-211	4 98 109	-2 273 274	2 93 -98	0 225-206	-6 326-303	0 52 -34	8 79 83
K,L= 1 0	-8 267 264	5 63 -61	-1 73 -38	3 85 -93	1 199 181	-5 377 365	1 464-452	9 112-111
-13* 0 32	-7 264-241	K,L= 11 0	0 310-298	4 79 78	2 146-129	-4 183-171	2 440 429	10 81 74
-12 98 -75	-6 281 275	-2 58 71	1 154-128	5* 0 23	3 143 139	-3 56 -1	3 252-227	11 117-119
-11 146 133	-5 302-284	-1 54 -55	2 213 244	6 109 120	4 132-132	-2 330-273	4 531 526	K,L= 6 2
-10 73 -17	-4 308 272	0 82 100	3 237-250	7 97-115	5 78 87	-1 745 651	5 442-393	-11* 45 -46
-9 80 -64	-3 384-370	1 66 -70	4 206 221	8* 0 -14	6 81 -84	0 757-765	6 135 136	-10* 50 49
-8* 33 9	-2 445 409	2* 49 41	5* 48 -48	9 56 61	7 108 95	1 661 679	7 141-140	-9* 0 -21
-7* 0 -3	-1 477-463	K,L= -8 1	6* 0 15	K,L= 4 1	8 93 -90	2 132-148	8 125 94	-8 61 -74
-6 175-139	0 494 460	-3* 49 -52	7 78 81	-8* 50 -60	9 91 110	3 65 -36	9 176-162	-7* 0 -6
-5 185 165	1 449-405	-2* 0 -16	8 57 -47	-7* 0 45	K,L= -7 2	4 331-303	10 227 250	-6 95 92
-4 69 60	2 413 404	-1 75 75	9 124-128	-6* 0 7	-10* 12 24	5 171 169	11 144-141	-5 97 -70
-3 117 73	3 331-292	0* 0 -9	10 91 95	-5 113 124	-9* 15 19	6 122-114	12 66 73	-4 283 238
-2 145-125	4 298 273	1 54 45	K,L= -1 1	-4* 18 -20	-8 53 -55	7 394 395	13 95-108	-3 372-342
-1 238-241	5 244-238	2 68 -60	-12* 40 46	-3 108-118	-7 125 132	8 284-269	K,L= 2 2	-2 167 144
0 397 531	6 138 116	3* 0 -24	-11* 0 -1	-2 64 -51	-6 102 -98	9* 0 -8	-13 88 101	-1 85 61
1 219-211	7 218-220	4* 26 31	-10 66 -83	-1 182 188	-5* 0 4	10* 0 -3	-12 125-137	0* 0 21
2 183-157	8 254 258	5* 0 -6	-9* 46 35	0 248-264	-4 123-103	11 105 86	-11* 0 45	1 278-257
3 192-189	9 122-115	6 60 -57	-8* 46 55	1 71 65	-3 157 151	12* 42 -43	-10 93 -90	2 291 270
4 137 124	10 88 85	7 64 73	-7 116-102	2 140 133	-2* 0 13	K,L= -2 2	-9 296 303	3 273-254
5 67 58	11 70 -68	K,L= -7 1	-6 103 102	3* 0 10	-1 134 127	-13* 41 40	-8 287-293	4 279 299
6 268 246	K,L= 6 0	-3 53 56	-5* 49 50	4 66 -44	0 440-400	-12* 0 19	-7 287 273	5 163-170
7 376-313	-11 91 82	-2* 49 -40	-4 60 -42	5* 0 8	1 195 191	-11* 0 -25	-6 386-370	6 94 85
8 239 214	-10* 12 -36	-1* 35 -50	-3 108 129	6 97 -96	2 75 -60	-10 100 -94	-5 313 315	7 111-115
9 184-166	-9* 0 21	0 58 52	-2 351-403	7 107 106	3 239 239	-9 179 155	-4 297-294	8 94 -93
10* 18 31	-8 66 69	1 72 -59	-1 163-183	8* 0 7	4 185-186	-8 170-156	-3 393 351	9 129-115
11* 35 -26	-7 138-137	2* 0 6	0 372 471	9 61 -59	5 96 87	-7 155 150	-2 535-472	10 170 172
12 134 126	-6* 0 -19	3* 37 40	1 65 85	K,L= 5 1	6 138-128	-6 163-161	-1 658 580	K,L= 7 2
13 106 -98	-5* 0 13	4* 0 8	2 177-233	-10* 49 -44	7 142 150	-5 199 209	0 665-559	-11* 49 75
K,L= 2 0	-4* 0 3	5* 38 -34	3 137 117	-9* 0 31	8 143-168	-4 253-237	1 601 575	-10 111-128
-13 108 113	-3 166 149	6* 26 41	4* 0 -15	-8 71 97	9 137 151	-3 350 317	2 454-430	-9 124 150
-12 107-111	-2* 0 20	K,L= -6 1	5 61 47	-7 65 -78	10 85 -99	-2 436-406	3 278 295	-8 146-182
-11 179 166	-1 360-319	-9* 44 -44	6* 0 -4	-6* 40 47	K,L= -6 2	-1 463 483	4 262-268	-7 125 147
-10 290-295	0 395 349	-8* 51 42	7 81 -68	-5* 38 -44	-11 97-126	0 562-562	5 171 163	-6 77 -76
-9 156 141	1 155-148	-7* 38 57	8 56 -55	-4 115-117	-10 118 125	1 560 587	6 107-101	-5 224 239
-8 85 -49	2* 17 -10	-6* 0 -1	9 60 54	-3 65 53	-9 129-125	2 527-492	7 180 153	-4 232-233
-7 328 289	3 57 -54	-5 65 -69	10* 42 24	-2 100 103	-8 108 103	3 237 254	8 244-253	-3* 0 -5
-6 319-298	4 95 92	-4* 0 4	K,L= 0 1	-1 90 -81	-7 84 -85	4 281-315	9 184 177	-2 242-230
-5 335 329	5 134-106	-3 68 -74	-12 57 -41	0 140 150	-6 127 133	5 346 353	10* 0 8	-1 397 427
-4 538-569	6 195 207	-2 120 122	-11* 0 35	1 135-144	-5 182-183	6 185-179	11* 0 0	0 150-132
-3 462 506	7 190-207	-1* 16 -9	-10* 47 54	2* 0 -1	-4 247 232	7 333 338	12* 31 -38	1 134 94
-2 381-403	8 150 139	0 76 -77	-9* 0 -21	3 63 55	-3 358-320	8 402-393	K,L= 3 2	2 219-221
-1 317 316	9 118-117	1* 0 18	-8* 0 -36	4* 29 35	-2 345 309	9 154 132	-13* 47 48	3 94 78
0 264-262	10* 44 66	2 98 101	-7* 50 47	5 94-102	-1 148-144	10 88 -93	-12 103 -96	4* 0 -9
1 306 288	11* 20 -34	3* 0 -33	-6 84 -73	6* 46 33	0 60 -41	11 142 130	-11* 20 -24	5 113 107
2 294-277	K,L= 7 0	4* 0 -9	-5* 0 0	7* 0 6	1* 48 -37	12 80 -84	-10 78 69	6 118-122
3 339 322	-11 80 108	5 59 -70	-4* 0 -12	8* 0 33	2 260 288	13 82 96	-9 222 213	7 109 107
4 303-276	-10 54 -80	K,L= -5 1	-3* 37 18	9 62 -57	3 243-221	K,L= -1 2	-8 308-302	8 81 -78
5 236 223	-9* 13 57	-9* 48 55	-2* 43 61	K,L= 6 1	4 199 146	-13* 29 -42	-7 129 107	K,L= 8 2
6 216-183	-8 90 -82	-8* 0 -2	1* 0 -3	-3 95 97	5 197-196	-12 91 111	-6 306-304	-9 81 80
7 119 102	-7 115 100	-7* 18 -19	2* 0 2	-2* 42 -44	6* 0 25	-11 202-217	-5 392 341	-8 86 -92
8* 10 6	-6 171-191	-6 85 -78	3* 0 3	-1 88 -87	7* 44 55	-10 200 191	-4 122 95	-7 79 90
9 98 -72	-5 191 195	-5 86 87	4* 29 -22	0* 50 57	8* 0 10	-9 166-164	-3* 42 14	-6 85 -98
10* 25 -48	-4* 25 -34	-4* 0 24	5 76 -73	1 84 71	9* 0 -8	-8 122 122	-2 481-413	-5 110 113
11 151 120	-3 214 203	-3 55 -42	6 70 57	2 86 -93	10 70 66	-7 87 -79	-1 658 651	-4 130-126
12* 0 -18	-2 295-288	-2 61 -59	7* 51 -66	3* 31 12	11 63 -53	-6 362 310	0 877-844	-3 132 116
13* 0 1	-1 118 -96	-1 121 130	8* 22 45	4 72 -71	K,L= -5 2	-5 452-419	1 527 514	-2 159-147
K,L= 3 0	0* 0 40	0 102 -95	9 79 75	K,L= 7 1	-12* 49 73	-4 311 277	2* 48 -49	-1 203 199
-13 57 48	1 268 264	1 147 134	10* 0 -11	-3 66 -39	-11 76 -78	-3 512-516	3 163 148	0 163-151
-12* 0 -3	2 124-108	2 71 -65	11 62 -66	-2* 32 -21	-10 117 121	-2 638 611	4 334-327	1 162 157
-11 54 62	3* 20 28	3 125-115	K,L= 1 1	-1 72 53	-9 63 -75	-1 213-157	5 199 184	2 204-206
-10 243-230	4 164-172	4* 37 41	-9 90 -83	0 79 -81	-8* 0 43	1 344-289	6 266-256	3 141 153
-9 145 133	5 78 90	5* 0 12	-8* 21 -5	1* 0 -1	-7 159-158	2 368 340	7 442 458	4 88-114
-8 160 137	6* 24 45	6* 18 -35	-7* 0 19	2 65 65	-6 199 215	3 68 -56	8 247-249	5 103 106
-7 84 72	7* 0 -23	7 111 125	-6 80 66	K,L= 8 1	-5 210-210	4 158 182	9* 0 52	6 102-108
-6 317-300	8* 9 13	8* 0 -30	-5* 0 1	-7 57 -73	-4 269 245	5 271-250	10 110-118	7 135 151
-5 104 109	9* 49 17	9* 36 -45	-4 54 26	-6* 0 32	-3 295-260	6 87 70	11 110 115	8 130-150
-4 458-500	10 78 -78	K,L= -4 1	-3 218-234	-5* 0 18	-2 346 286	7* 0 -30	12 76 -76	K,L= 9 2
-3 755 907	K,L= 8 0	-9* 46 47	-2 233 284	-4* 46 -54	-1 316-263	8 105 -95	K,L= 4 2	-5 77 -62
-2 596-431	-9 63 58	-8* 18 39	-1 227 236	-3* 0 -9	0 315 246	9 158 137	-13* 32 -82	-4 81 96
-1 137 112	-8 79 -79	-7 76 -88	0 414-425	-2* 0 42	1 256-243	10* 0 23	-12 78 95	-3* 30 -52
0 192 -47	-7 109 111	-6* 45 50	1 156-172	-1* 0 0	2 280 225	11 62 -34	-11 131-150	-2* 0 -19
1 199 217	-6 144-157	-5 66 -56	2 146 203	0 82 66	3 330-310	12* 0 -23	-10 90 102	-1 86 75
2 680-760	-5 168 163	-4 73 54	3 113 -85	1 58 -58	4 296 285	13* 0 11	-9* 0 -12	0 80 -86
3 752 875	-4 183-175	-3 89 90	4 131 129	K,L= 9 1	5 234-222	K,L= 0 2	-8 93 94	1* 42 28
4 465-485	-3 219 209	-2 82 -75	5* 35 25	-3 53 60	6 259 238	-13* 0 -18	-7 213-221	2* 0 15
5 331 318	-2 224-212	-1 139-129	6 117 -96	3 59 71	7 158-143	-12 109 98	-6 173 156	3* 0 -12
6 362-366	-1 179 165	0 216 225	7 113 123	K,L=-10 2	8 84 80	-11 164-177	-5 121-114	4* 0 -37
7 162 150	0 211-203	1 194-183	8* 17 -46	-5 54 -74	9 87 -92	-10 198 180	-4 320 275	5 63 69
8 75 -53	1 265 258	2 80 -85	9 80 -93	-4 68 86	10 122 121	-9 205-164	-3 265-209	6 70 -39
9 282 274	2 200-184	3 83 88	10* 50 48	-3 106-132	11 141-155	-8 83 77	-2 82 86	7 76 85

Table 2. (continued)

H FO FC	H FO FC	H FO FC	H FO FC	H FO FC	H FO FC	H FO FC	H FO FC
10 288-278	3 188 187	4 107 116	11* 35 28	-2 116 150	K,L= -4 2	-7* 28 -3	-1 118 -82
11 139 128	4 222-236	5* 0 2	K,L= 2 1	-1 93-102	-12 69 -82	-6 341 275	0 199-155
12 119-116	5 194 198	6* 0 8	-10 124-143	0 59 67	-11 62 63	-5 520-474	1 62 -32
13 89 104	6 167-177	7 75-100	-9 78 58	1 70 -90	-10 80 75	-4 289 257	2 275 274
K,L= 4 0	7 131 129	8* 0 -13	-8 62 64	2 93 116	-9* 0 16	-3 815-875	3 91 62
-12 53 58	8 84 -71	9* 18 44	-7* 20 -21	3 116-146	-8 253-263	-2 8551138	4* 0 -9
-11* 43 -49	9 92 101	K,L= -3 1	-6* 0 9	4 91 113	-7 126 113	-1 466 464	5 178-182
-10* 0 46	K,L= 9 0	-11* 34 41	-5 70 84	5* 48 -74	-6 76 77	1 550-883	6 133-122
-9 197-187	-8* 50 59	-9* 42 -41	-4 214-204	K,L= -9 2	-5 165 147	2 419 545	7 268 268
-8 211 213	-7 56 -59	-8* 45 -60	-3 251 285	-7 66 64	-4* 17 -12	3 454-454	8* 0 -49
-7* 0 -36	-6 73 75	-7 100 109	-2 327-329	-6 69 -75	-3 324-275	4 691 690	9 55 -43
-6* 0 0	-5* 25 -13	-6* 42 -30	-1 179-170	-5 57 65	-2* 0 13	5 414-387	10 77 -56
-5 145-154	-4 60 -44	-5 61 61	0 191 187	-4* 37 -25	-1 53 40	6 100 106	11 76 61
-4 122 67	-3* 43 30	-4 108-108	1 252 221	-3* 0 -18	0* 0 -1	7 96 -61	K,L= 5 2
-3 141 85	-2 65 38	-3 55 -58	2 59 -75	-2* 0 -4	1 110 79	8 146 112	-12 100 115
-2 199 163	-1 103 -76	-2 66 -53	3 199 213	-1 62 50	2 218 183	9 203-179	-11 108-123
-1 224-166	0 98 74	-1 227 194	4 174-183	0 86 -75	3 245-229	10 234 220	-10 105 111
0 165 147	1* 44 -14	0 103-135	5 69 -70	1 83 73	4 94 74	11 137-140	-9 83 -90
1 311-259	2 87 -69	1 238 236	6* 0 -41	2* 20 -5	5 195-184	12* 26 44	-8 120 118
2 287-226	3 91 78	2 65 -56	7 71 58	3 66 -66	6 267 279	13 75 -83	-7 142-154
3 229 223	4* 38 -49	3* 38 23	8* 0 -1	4 74 73	7 124-112	K,L= 1 2	-6 188 189
4 134 124	5* 0 16	4 168-179	9* 38 40	5* 34 -22	8* 0 -17	-13* 0 36	-5 281-262
5* 27 34	3 117 109	-8* 0 28	4 67 57	-7* 38 -32	2* 50 -22	2 121 119	-2 354-271
6* 43 -42	4 93 -74	-7 56 -41	5 55 48	-6* 41 -48	3 98 -86	3 94 -69	-1 286 249
K,L= -8 3	5* 0 16	-6* 0 -1	6 126-132	-5* 0 48	4 110 96	4 107 -90	0 190-153
-4* 30 -40	6 110-130	-5* 0 -16	7* 37 43	-4* 0 1	5 58 39	5 81 59	1 187 152
-3* 0 20	7 82 83	-4 54 31	K,L= 4 3	-3 123 118	6* 0 -13	6* 39 -74	2 251-219
-2 54 43	11 58 59	-3 68 66	-10* 0 -4	-2 187-178	7 150-150	7* 18 12	3 177 154
-1* 0 -4	K,L= -3 3	2* 0 15	-9* 32 -44	-1* 0 -15	8 114 140	8 120 112	4 176-165
0* 0 5	-12* 39 43	3* 43 -36	-8* 46 62	0* 0 26	9 52 -61	9* 0 -7	5 239 228
1 74 -55	-10* 43 -46	4* 0 -7	-6 100 93	1 170 151	10 91 79	10 104 -78	6 180-175
2* 0 7	-8 56 55	5* 41 24	-5 109-108	2 98-104	K,L= -3 4	11* 38 38	7* 18 21
3* 43 35	-7* 43 -24	6* 0 -32	-4* 0 2	3* 36 46	-12 75 -82	K,L= 0 4	8 59 64
4* 52 -41	-6* 0 31	7 71 66	-3* 0 -10	4 126-128	-11 170 179	-13 61 -90	9* 17 36
5* 0 5	-5 77 -65	8* 43 49	-2 115 97	5 120 149	-10 159-179	-12* 0 55	10 92 -82
6* 49 46	-4* 31 -11	9 91 -81	-1 277-256	6 104-116	-9 85 101	-11* 23 -56	K,L= 3 4
K,L= -7 3	-3* 35 23	K,L= 1 3	0 216 222	7 82 77	-8 122-132	-10 84 84	-11 152 166
-4* 45 49	-2* 51 48	-10 62 -60	1* 0 2	8 53 -51	-7 187 190	-9 159-168	-10 73 -82
-3 72 -75	-1 74 -58	-9 62 61	2* 23 32	K,L= -6 4	-6 145-166	-8 310 317	-9 70 -51
-2* 32 25	0 167 143	-8* 0 -6	3 100 -78	-10 54 61	-5 209 219	-7 308-310	-8 100 -91
-1* 0 -14	1* 47 -60	-7 84 71	4* 0 17	-9 89 -86	-4 392-431	-6 220 226	-7 113 110
0* 0 -14	2* 47 -41	-6 74 -78	5 89 -82	-8 104 120	-3 482 504	-5 430-406	-6* 17 8
1* 0 8	3 106 -81	-5* 0 28	6 152 149	-7 120-140	-2 346-322	-4 346 310	-5 233 230
2 72 52	4* 13 33	-4 120-130	7 90 -89	-6 118 130	-1 192 157	-3 140 79	-4 475-448
3* 46 -43	5* 50 41	-3 319 288	K,L= 5 3	-5 120-113	0 80 -49	-2 369 450	-3 397 374
K,L= -6 3	12* 43 -40	-2 162-130	-10 56 54	-4 83 74	1 221 192	1 280-368	-2 283-253
-7* 31 -42	K,L= -2 3	-1 247-181	-8* 45 -60	-3* 0 -16	2 441-449	2 399 463	-1 96 48
-6* 0 -15	-10* 31 26	0* 37 18	-6 80 -70	-2* 36 30	3 264 299	3 238-253	0 90 -52
-5* 0 -12	-8 54 -31	1 177 181	-5* 21 -22	-1 192-176	4 201-211	4 157 160	1 405 367
-4* 0 7	-7* 42 -26	2 121-140	-4 106 97	0 251 251	5 290 312	5 302-289	2 456-457
-3 66 59	-6 66 56	3 156 169	-3* 0 -6	1 104 -86	6 92 -93	6 380 375	3 309 314
-2* 0 -31	-5* 49 43	4 135-119	-2* 19 -26	2* 0 1	7 103 -71	7 325-326	4 340-362
-1 67 -65	-4* 21 -32	5* 13 32	-1 98 76	3* 45 -41	8 83 -81	8 231 228	5 341 365
0 89 96	-3 66 93	6 64 63	0 136-120	4* 18 -37	9 152 160	9 117-114	6 110-101
1* 0 0	-2 96 -82	7 72 -79	1* 51 48	5* 18 18	10* 48 -68	10 57 62	7* 42 57
2* 0 -13	-1 130-151	8 65 -59	2 53 33	6 80 77	11* 46 29	11 135-119	8 222-216
3 66 -55	0 110 98	9 99 88	3 55 -53	7* 47 -55	K,L= -2 4	12 79 92	9 214 192
4* 0 6	1* 39 15	K,L= 2 3	K,L= 6 3	8* 51 44	-12 63 -53	K,L= 1 4	10 151-136
5* 0 13	2 100-107	-11 64 -69	-8* 43 -52	K,L= -5 4	-11* 31 37	-13* 41 46	11 150 136
6* 0 26	3 156 176	-10 88 88	-5 82 59	-10* 34 49	-10* 0 0	-12 69 -84	K,L= 4 4
7* 43 -41	4 78 -57	-9* 16 19	-4* 0 21	-9 125-133	-9* 0 -1	-11* 23 53	-10 96 108
K,L= -5 3	5* 0 37	-8* 15 -29	-3 67 -62	-8 121 151	-8* 0 -24	-10* 0 -16	-9 118-145
-10* 41 42	6* 43 35	-7* 0 19	-2 80 -64	-7 107-112	-7 75 65	-9* 0 3	-8* 26 66
-9* 0 -17	7 114-121	-6* 18 -41	-1 97 95	-6 130 142	-6 92 -93	-8* 0 -8	-7* 26 -47
-8* 38 -40	8* 0 -23	-5* 12 -33	0* 0 -7	-5 174-186	-5 141 129	-7* 34 52	-6 133 123
-7* 0 -15	9 105 102	-4 152 146	K,L= 8 3	-4 188 195	-4 175-157	-6* 31 -61	-5 65 -72
-6 82 63	K,L= -1 3	-3 278-236	1 82 22	-3 193-204	-3 206 180	-5* 0 25	-4* 0 9
-5* 0 2	-11* 52 -46	-2 52 32	K,L= -9 4	-2 256 237	-2 209-215	-4* 12 -17	-3 83 -58
-4* 47 -37	-10 78 69	-1 230 183	-4 58 -51	-1 266-258	-1 219 197	-3 126 92	-2 67 49
-3* 0 10	-9* 45 -32	0* 42 -29	-3 62 55	0 288 291	0 158-150	-2* 25 -36	-1 184-152
-2* 39 37	-8* 0 -18	1* 0 12	-2* 29 -34	1 338-332	1 175 157	-1 239-228	0 200 167
-1 66 -54	-7 72 52	2 68 53	-1* 0 -2	2 272 257	2 303-287	0 128 127	1 164 77
0 96 75	-6* 0 22	3 154-136	0* 51 49	3 208-217	3 296 306	1* 8 13	2* 0 -16
1 117 -94	-5* 31 -32	4* 33 -29	1 55 -45	4 245 246	4 201-206	2 181 178	3 84 -80
2* 0 -17	-4* 37 56	5* 52 31	2* 0 -1	5 171-167	5 274 309	3 92 -69	4 152-140
3 88 65	-3 327-340	6* 0 -10	3* 27 29	6 143 154	6 255-265	4 61 -36	5 125 120
4* 0 -28	-2 226 185	7 56 49	K,L= -8 4	7 187-208	7* 0 48	5 132-110	6 120 109
5* 0 9	-1 218 203	8* 0 10	-7 83 90	8 194 196	8 121-109	6 178 141	7 69 -71
6 82 83	0* 0 -20	9* 0 9	-6 125-135	9 163-155	9 189 194	7 190-185	8 97 -97
7 62 -75	1 165-167	10* 51 -43	-5 141 163	10 74 68	10 130-140	8 204 186	9 77 74
K,L= -4 3	2 151 170	K,L= 3 3	-4 112-114	K,L= -4 4	11 132 128	9* 25 -47	K,L= 5 4
-12* 37 -34	3 117-134	-10* 0 -17	-3 131 147	-11 100 100	K,L= -1 4	10* 0 38	-11 69 -76
-10* 0 13	4 121 118	-9* 46 38	-2 184-210	-10 134-148	-10 59 66	11 112-105	-10 101 122
-8 72 -65	5 124-107	-8* 0 -24	-1 137 153	-9* 0 -24	-9 112-111	K,L= 2 4	-9 126-160
-7 78 80	6* 0 -9	-6* 28 -32	0 111-120	-8 72 56	-8 207 207	-12 90-113	-8 142 181
-6 89 -84	7* 35 -30	-5* 50 46	1 141 158	-7 106 100	-7 181-172	-11 171 202	-7 176-208
-5 118 109	8 122 110	-4* 34 4	2 134-152	-6* 0 -18	-6 85 66	-10 118-130	-6 201 218
-4 54 -56	9* 45 -46	-3 65 58	3 115 122	-5 70 -51	-5 177-162	-9 93 92	-5 214-225
-3* 25 -22	10* 0 28	-2 56 -40	4 140-135	-4 152-135	-4 155 131	-8 171-167	-4 239 231
-2 59 -43	11* 38 -21	-1 132 114	5 131 138	-3 132 119	-3 103 84	-7 185 173	-3 296-250
-1 192 181	K,L= 0 3	0 179-159	6 103-112	-2* 0 -7	-2* 50 36	-6 207-181	-2 326 275
0 265-253	-12 52 35	1 61 -57	7 95 96	-1* 15 -28	-1 263-289	-5 265 260	-1 307-286
1 120 101	-10* 0 -35	2* 19 -19	K,L= -7 4	0 170 144	0 159 170	-4 366-334	0 352 353
2* 23 23	-9* 0 7	3 87 78	-8* 27 30	1 109 -80	1* 10 -5	-3 356 322	1 306-308

atom of water molecule could be located at approximately $z=1/4$, and two potassium ions at $z=0$ and 1/2, respectively.

Seven iterations of the block-diagonal least-squares refinement with isotropic thermal factors reduced the R value to 0.151. Then, anisotropic thermal factors were introduced, and the refinement was continued until all the parameter shifts became less than one tenth the estimated standard deviations. The final R value was 0.109 for nonzero reflections. A quantity $\sum w(|F_o|-|F_c|)^2$ was minimized, with $w=1.0$ if $F_o > 5.0$ and $w=0.5$ otherwise. All the data including zero reflections were used in the calculation with the exception of the reflection 100, which seemed to be seriously suffering from secondary extinction effect. The atomic scattering factors for a potassium ion, neutral oxygen and carbon atoms were taken from Ref. 8. The final positional and thermal parameters are listed in Table 1. Numbering of atoms is shown in Fig. 1. The observed and calculated structure factors are given in Table 2.

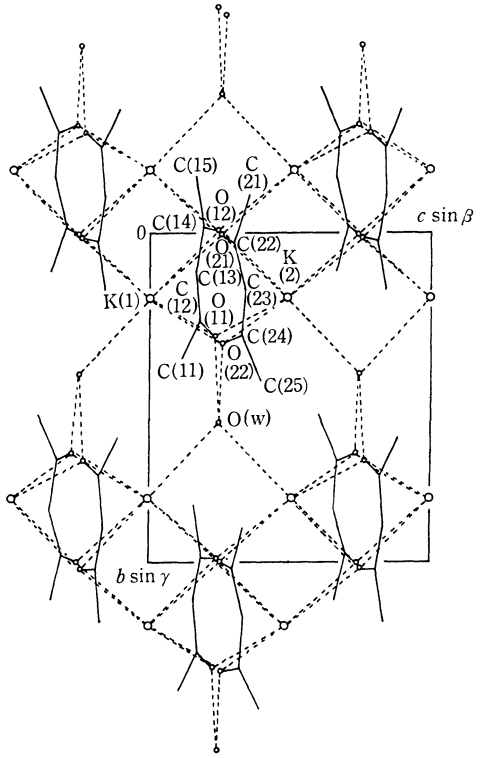

Fig. 1. Projection of the molecular skeleton along the a-axis. Solid lines indicate the acetylacetone framework and broken lines indicate the potassium-oxygen and oxygen-oxygen interactions. The numbering of the atoms refers to that in Table 1.

The space group assignment was finally checked by the distribution of the structure amplitudes.[9] The ratio of $\overline{F^2}/\overline{F}^2$ was found to be 0.631, while the theoretical values for centric and acentric distributions are 0.637 and 0.785, respectively. An $N(z)$ test[10] was also applied and indicated clearly the presence of a center of symmetry in agreement with the assigned space group.

Most of the calculations were carried out by using the UNICS programs[11] on a HITAC 8800 computer at the Computer Center of the University of Tokyo.

Results and Discussion

The crystal structure of PAH is shown in Fig. 1. Each potassium ion is surrounded by seven oxygen atoms, six of which belong to four different acetylacetone anions and the rest is a water molecule. The potassium-oxygen distances are in the range of 2.65 to 3.05 Å, as shown in Table 3.

The structures of several crystals including potassium ions in various coordination numbers were reported.

Table 3. Distances (d/Å) and angles (φ/°) with their estimated standard deviations shown in parentheses

The superscripts indicating the equivalent positions are shown at the right side of the bottom.

O(11)–C(12)	1.25(2)	C(12)–C(13)	1.44(2)	O(11)–C(12)–C(11)	121(2)
O(12)–C(14)	1.26(2)	C(13)–C(14)	1.40(2)	O(21)–C(22)–C(21)	118(1)
O(21)–C(22)	1.27(2)	C(22)–C(23)	1.40(2)	O(12)–C(14)–C(15)	116(2)
O(22)–C(24)	1.24(2)	C(23)–C(24)	1.40(2)	O(22)–C(24)–C(25)	119(2)
				C(12)–C(13)–C(14)	127(2)
C(11)–C(12)	1.52(3)	O(11)–O(12)	2.91(2)	C(22)–C(23)–C(24)	126(2)
C(14)–C(15)	1.53(3)	O(21)–O(22)	2.88(2)	C(11)–C(12)–C(13)	116(2)
C(21)–C(22)	1.50(3)	O(11)–O(22)	3.39(2)	C(21)–C(22)–C(23)	117(2)
C(24)–C(25)	1.53(3)	O(12)–O(21)	2.92(2)	C(13)–C(14)–C(15)	118(2)
				C(23)–C(24)–C(25)	115(2)
K(1)–O(11)	2.76(1)	K(2)–O(11)	2.75(1)	O(11)–C(12)–C(13)	124(2)
K(1)–O(12)	2.93(1)	K(2)–O(12)	2.77(1)	O(21)–C(22)–C(23)	125(2)
K(1)–O(21)	2.88(1)	K(2)–O(21)	3.05(1)	O(12)–C(14)–C(13)	126(2)
K(1)–O(22)	2.65(1)	K(2)–O(22)	2.74(1)	O(22)–C(24)–C(23)	126(2)
K(1)–O(12^{i})	3.01(1)	K(2)–O(12^{ii})	2.85(1)		
K(1)–O(21^{i})	2.81(1)	K(2)–O(21^{iii})	2.98(1)	none	x, y, z
K(1)–O(w^{iii})	2.83(1)	K(2)–O(w^{iv})	2.77(1)	i	$1-x$, $-y$, $-z$
				ii	$1-x$, $-y$, $1-z$
O(w)–O(11)	2.82(1)	K(1)–K(1^{i})	3.388(7)	iii	$1-x$, $1-y$, $-z$
O(w)–O(22)	2.72(1)	K(1)–K(2)	3.622(5)	iv	$1-x$, $1-y$, $1-z$
O(w)–K(1^{iii})	2.83(1)	K(2)–K(2^{ii})	3.403(7)	v	x, $-1+y$, z
O(w)–K(2^{iv})	2.77(1)				

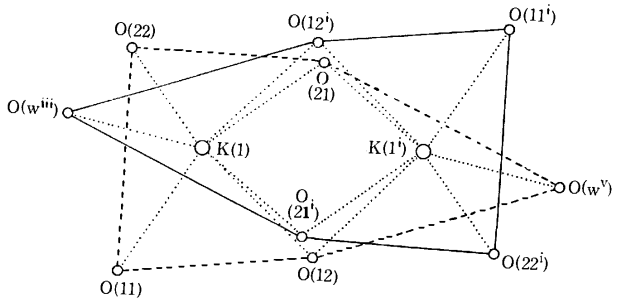

Fig. 2. Two distorted pentagons sandwiching two potassium ions.
The pentagons are shown by the solid and broken lines. The potassium ion interacts with seven oxygen atoms, as shown by dotted lines.

In potassium hydrogen bis(homophthalate),[12] the potassium ion is surrounded by four oxygen atoms at 2.76—2.80 Å. In potassium hexaiodatogermanate (IV),[13] there are two potassium ions in a tube of 18 oxygen atoms and each potassium ion is surrounded by nine oxygen atoms at 2.70—2.98 Å. In potassium hydrogen methylsuccinate,[14] the potassium ion is surrounded by a distorted tetrahedron of oxygen atoms at 2.705 to 2.763 Å and also by four oxygen atoms at longer distances of 2.956—3.085 Å. The observed K-O lengths for PAH are reasonable in comparison with these values.

The irregular seven-fold coordination of PAH can also be described, as a sandwich of two K^+ ions between two distorted pentagons shown in Fig. 2. The equation of the pentagonal plane through O(11), O(12), O(21), O(22) and O(w^{v}) is given in Table 4. The distance between the pentagonal plane is 3.7 Å. There is the crystallographically independent K^+ ion pair K(2)-K(2^{ii}), which takes the same arrangement as the K(1)-K(1^{i}) shown in Fig. 2. The distance of their pairs is about 3.4 Å.

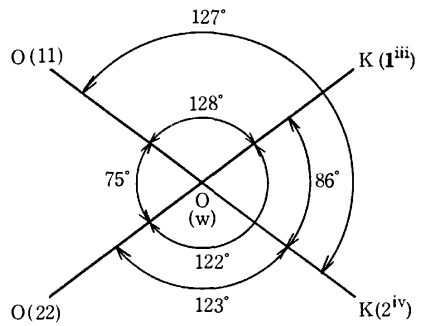

Fig. 3. Distorted tetrahedral environment of the water molecule.

The distorted tetrahedral environment of the water molecule consists of two K^+ ions and two oxygen atoms, as shown in Fig. 3. The distances of the OH···O hydrogen bonds are 2.82 and 2.72 Å. The mean values of intermolecular methyl-methyl and methyl-methylene carbon distances are 4.0 and 3.8 Å, respectively.

The mean values of bond lengths and angles in the acetylacetone anion are shown in Fig. 4. They are nearly equal to the corresponding mean values in heavy metal chelates of acetylacetone, as shown in Table 5. The skeleton of the acetylacetone anion in PAH is also nearly planar (Table 4) because of π-electron delocalization, though the methyl carbon atoms [C(11) and C(25)] are significantly out of the plane as seen in the case of the heavy metal chelates. These facts seem to suggest, though not conclusive, that the bonding between the ligand and metal atoms in heavy metal chelates of acetylacetone is rather ionic as in PAH.

Recently the molecular structure of acetylacetone was determined by gas electron diffraction.[15] It is of interest to note that the structure of the enol form, as shown in Table 5, is considerably different from the structure of acetylacetone in both PAH and the heavy metal chelates, where a heavy metal atom replaces the hydrogen atom. The greater C=O distance and the smaller CC_cC angle in the enolic acetylacetone can be

TABLE 4. EQUATIONS OF THE LEAST-SQUARES PLANES AND THE DEVIATIONS OF ATOMS FROM THE PLANES [IN SQUARE BRACKETS] (d/Å)[a]

A) Planes of the acetylacetone skeleton OCCCO
$-0.3141\,u+0.0046\,v+0.9494\,w-0.5497=0$
[O(11), 0.009; O(12), −0.007; C(11), −0.123; C(12), −0.010; C(13), 0.000; C(14), 0.008; C(15), −0.012]
$0.3433\,u+0.0382\,v-0.9384\,w-0.5664=0$
[O(21), −0.022; O(22), 0.007; C(21), 0.021; C(22), 0.024; C(23), −0.004; C(24), −0.007; C(25), −0.181]

B) Pentagonal oxygen plane
$-0.0484\,u+0.0009\,v+0.9988\,w-1.5947=0$
[O(11), −0.059; O(12), 0.054; O(21), −0.050; O(22), 0.052; O(w^{v}), −0.005; K(1), −1.792; K(2), 1.824; K(1^{i}), 1.923; K(2^{ii}), 1.899]

a) u, v, and w are the orthogonal coordinates (Å) defined by $u=ax\sin\gamma+cz(\cos\beta-\cos\alpha\cos\gamma)/\sin\gamma$, $v=ax\cos\gamma+by+cz\cos\alpha$, $w=czE/\sin\gamma$, $E=(1-\cos^2\alpha-\cos^2\beta-\cos^2\gamma+2\cos\alpha\cos\beta\cos\gamma)^{1/2}$.

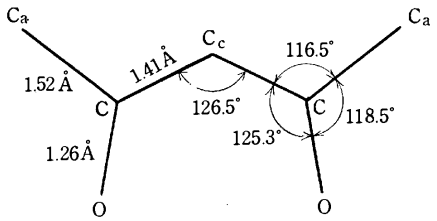

Fig. 4. Mean values of bond lengths and angles in an acetylacetone anion in PAH.

TABLE 5. COMPARISON OF SOME PARAMETERS OF ACETYLACETONE GROUPS

	PAH[a]	M(acac)$_n$[1]	acac[14]
C=O	1.26 Å	1.28 Å	1.315 Å
C–C_c	1.41	1.40	1.416
C–C_a	1.52	1.52	1.497
O···O	2.90	2.7—3.0	2.381
OCC_c	125.3°	125.3°	120.0°
OCC_a	118.5	115.7	120.0
CC_cC	126.5	124.5	118.0

a) Present study.

attributed to strong interaction between the oxygen and the hydrogen atoms by the intramolecular hydrogen bond and thus to π-electron delocalization through the six-membered ring.

References

1) E. C. Lingafelter, *Coord. Chem. Rev.*, **1**, 151 (1966).
2) G. J. Bullen, R. Mason, and P. Pauling, *Inorg. Chem*,. **4**, 456 (1965).
3) F. A. Cotton and R. C. Elder, *ibid.*, **4**, 1145 (1965).
4) M. J. Bennett, F. A. Cotton, and R. Eiss, *Acta Crystallogr.*, **B24**, 904 (1968).
5) B. Morosin, *ibid.*, **22**, 315 (1967).
6) S. Onuma and S. Shibata, This Bulletin, **43**, 2395 (1970).
7) L. F. Hatch and G. Sutherland, *J. Org. Chem.*, **12**, 249 (1948)
8) "International Tables for X-ray Crystallography," Vol. III, Kynoch Press, Birmingham (1962), p. 202.
9) M. M. Woolfson, "An Introduction to X-ray Crystallography," Cambridge University Press, London(1970), p. 239.
10) E. R. Howells, D. C. Phillips, and D. Rogers, *Acta Crystallogr.*, **3**, 210 (1950).
11) "The Universal Crystallographic Computing System (I)," The Crystallographic Society of Japan, Tokyo (1967).
12) M. P. Gupta and D. S. Dubey, *Acta Crystallogr.*, **B28**, 2677 (1972).
13) F. Schellhaas, H. Hartl, and R. Frydrych, *ibid.*, **B28**, 2834 (1972).
14) Y. Schouwstra, *ibid.*, **B28**, 2217 (1972).
15) A. H. Lowrey, C. George, P. D'Antonio, and J. Karle, *J. Amer. Chem. Soc.*, **93**, 6399 (1971).

Induced Circular Dichroism of Benzyl Chromophores Bound to Helical Polypeptides

Hiroyuki NOMORI, Nobuaki TSUCHIHASHI,* Shoji TAKAGI, and Masahiro HATANO
Chemical Research Institute of Non-Aqueous Solutions, Tohoku University, Katahira, Sendai 980

(Received November 20, 1974)

Extrinsic optical activity was observed for symmetric side chain chromophores in helical polypeptides. Poly-β-benzyl-L-aspartate, poly-β-*p*-nitrobenzyl-L-aspartate and poly-γ-*p*-nitrobenzyl-L-glutamate gave induced circular dichroism in the wavelength regions corresponding to the absorption bands of the benzyl and the *p*-nitrobenzyl chromophores of the side chains in their dilute solutions. Moreover, poly-γ-benzyl-D-glutamate gave induced circular dichroism due to the benzyl chromophore in its concentrated solutions which formed a liquid crystalline phase. The extrinsic optical activity thus observed was explained as the consequence of the loss of the rotational freedom of the chromophores relative to the α-helical structure and to the cholesteric helical structure of the polypeptides.

Blout and Stryer[1] reported that extrinsic optical activity is induced in the wavelength region corresponding to the absorption band of acridine orange (AO) or acriflavine when the dye molecule becomes bound to the α-helical poly-α,L-glutamic acid (PLGA) molecule or to nucleic acids. Recently, we made more intimate investigation into the optical activity of AO bound to the carboxylate group of the side chain of PLGA in the neutral and the alkaline pH regions.[2,3]

On the other hand, it has been found that poly-γ-(1-naphthylmethyl)-L-glutamate[4] and poly-γ-(β-*N*-carbazolylethyl)-D-glutamate[5] also exhibit some circular dichroism (CD) bands in the wavelength regions corresponding to the absorption bands of their side chain chromophores when the polypeptides are dissolved in helix solvents at low concentrations, such as 10^{-3} mol of the peptide residue/l.

Loucheux and Duflot[6] reported that the nitrobenzyl chromophore in α-helical PLGA exhibits a CD band at 295 nm which they assigned to the n-π^* transition of the nitrobenzyl group. They offered for the origin of the extrinsic optical activity of the symmetric chromophore of the side chain in the α-heical polypeptide the following three mechanisms, (i) strong chromophore-chromophore interactions; in this case, the α-helix served only to hold constant the relative geometry between neighboring chromophores, (ii) local interactions between the chromophore and the dissymmetric field of the α-helix and (iii) the perturbation to the chromophore by the dissymmetric field of the chiral carbon in the peptide residue.

In our recent investigation[7] concerning the optical activity of D-phenylglycine in comparison with that of L-phenylalanine, we indicated that the perturbation by the dissymmetric field of the chiral carbon to the transition of the phenyl group in an asymmetric molecule decreases abruptly as the rotational freedom of the phenyl chromophore is increased by increase in the chiral carbon to phenyl chromophore distance, and that the perturbation is expected to be only trivial for the chromophore separated by more than four atoms from the chiral carbon atom. The perturbation by the chiral carbon to which the side chain is attached should therefore have a very small contribution to the induced circular dichroism of the benzyl chromophores bound to the α-helical polypeptides studied in this paper, unless limitation of the rotation of the chromophore is caused by some origin.

In the present paper, the extrinsic optical activity of the benzyl chromophores bound to the helical polypeptides is examined and this optical activity is correlated to the rotational freedom of the chromophore.

Experimental

Materials. Poly-β-benzyl-L-aspartate (PBLA) and poly-γ-benzyl-D-glutamate (PBDG) were prepared by the conventional polymerization of the *N*-carboxyanhydrides of the parent amino acids. Unless otherwise noted, the degrees of polymerization of these polymers were 170 and 1320, respectively. Poly-β-*p*-nitrobenzyl-L-aspartate (PNO_2BLA) and poly-γ-*p*-nitrobenzyl-L-glutamate (PNO_2BLG) were prepared by the method reported by Ledger and Stewart.[8] Ethylene chlorohydrin and tetrachloroethane were purified by ordinary methods. The other solvents were spectral grade ones and were used without further purification.

Methods. The infrared (IR) spectra were measured by a Hitachi EPI-S_2 infrared spectrometer. The cell for observation consisted of two NaCl plates separated by a 30 μm lead spacer, and the polymer solution was inserted between the plates. The absorption spectra, the CD spectra and the optical rotatory dispersion (ORD) curves were observed for the concentrated polymer solution held between two quartz plates spaced by a suitable aluminum foil. In the case of the dilute solution, a usual optical quartz cell was used. The absorption spectra were recorded on a Hitachi EPS-3T spectrometer. The CD and the ORD measurements were carried out by a JASCO J-20A dichrograph and a J-15 spectropolarimeter, respectively.

Results and Discussion

Extrinsic Optical Activity of Benzyl and p-*Nitrobenzyl Chromophores Bound to Helical Polypeptides in Dilute Solutions.* Poly-γ-*p*-nitrobenzyl-L-glutamate shows a definite negative CD band in the neighborhood of 275 nm. The CD spectrum is shown in Fig. 1. In spite of the existence of the anomalous dispersion around 275 nm in its ORD curve, we can obtain Moffitt's b_0 of −540 from the fairly linear Moffitt plot in the longer

* Faculty of Engineering, Tohoku University, Aramaki, Sendai 980

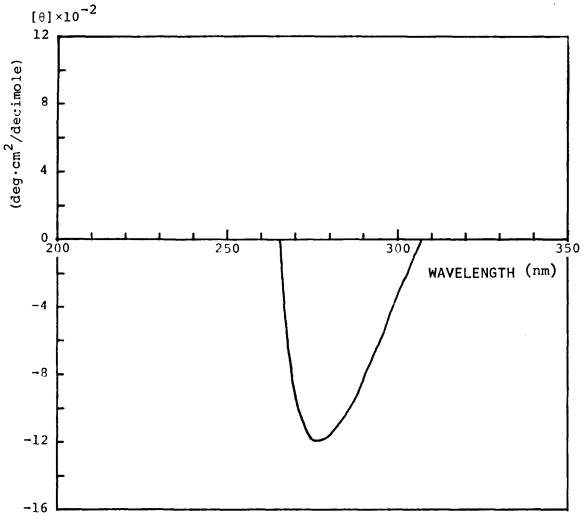

Fig. 1. CD spectrum of PNO_2BLG in *N,N*-dimethylformamide ($\Delta\varepsilon/\varepsilon = -3.8\times10^{-5}$ at 275 nm).

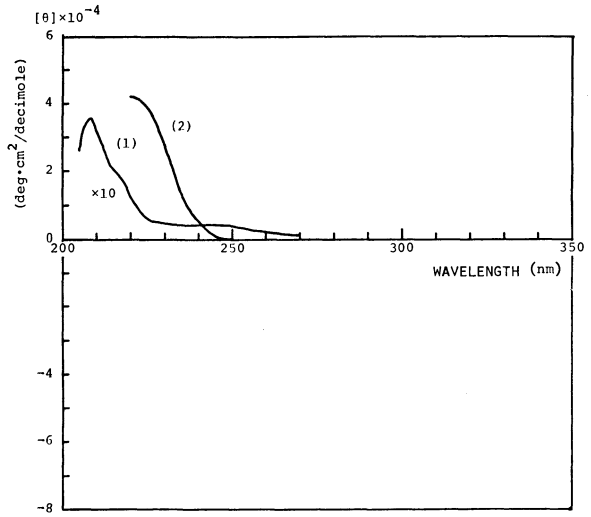

Fig. 2. CD spectra of (1) NO_2BLG in water and (2) PBDG (DP=165) in ethylene chlorohydrin; "$\times10$" denotes that the spectrum is magnified 10 times longitudinally.

wavelength region than 390 nm indicating the right-handed α-helical structure. As is shown in Fig. 2, we cannot detect any CD band in the wavelength region longer than 260 nm for γ-*p*-nitrobenzyl-L-glutamate and PBDG at low concentrations, such as 10^{-3} mol of glutamyl residue/l.

From these, it is deduced that the introduction of the nitro group into the side chain benzyl group of the polyglutamate intensifies the interaction between side chain groups leading to the increase of the probability of their definite orientation relative to the polypeptide main chain. This unexpected loss of the rotational freedom of the side chain chromophore causes interaction between the transition dipole moment of the nitrobenzyl chromophore and that in the α-helix main chain, and is the very reason why circular dichroism appears in the absorption region of the nitrobenzyl chromophore despite the distance between the chromophore and the polypeptide main chain.

Goodman *et al.*[9-11] reported that the nitrobenzyl group in PNO_2BLA forms a rigid side chain helix around the α-helix of the polypeptide main chain, but that the nitrobenzyl group in PNO_2BLG is not in a dissymmetric field and can rotate freely. Our above-mentioned observation of the circular dichroism or the anomalous optical rotatory dispersion ascribed to the aromatic chromophore is attained by the development of the J-20A dichrograph with a low noise-high output amplifier. Loucheux and Duflot reported that the CD spectrum of the copolymer of L-glutamic acid with *p*-nitrobenzyl-L-glutamate shows a positive peak at 296 nm in an aqueous solution at pH 4.5.[6] It is interesting that the incorporation of small amount of the γ-*p*-nitrobenzyl-L-glutamate unit into poly-L-glutamic acid results in a circular dichroism which differs both in the sign and the wavelength of the maximum from those in the homopolymer of γ-*p*-nitrobenzyl-L-glutamate.

The dilute solution of poly-β-benzyl-L-aspartate in chloroform or dichloromethane gives a weak but undoubted CD band centered at 252 nm, as is shown in Fig. 3. A large positive CD band appearing at 222 nm, means that PBLA exists in the left-handed α-helical structure.[12,13] We also observed the optical rotatory dispersion of the same chloroform solution of PBLA as is shown in Fig. 4 in comparison with that of the left-handed α-helical structure of PBDG. The feature is very similar to that reported by Blout and coworkers,[13] and shows an anomalous dispersion giving a negative Cotton effect in the absorption region of the benzyl chromophore. The extrinsic optical activity observed here is due, in similar manner to the case of PNO_2BLG, to the definite orientation of the benzyl chromophore relative to the main chain α-helix, which is brought about by the interaction between benzyl residues of PBLA whereas we have not detected any circular dichroism for the benzyl group of β-benzyl-L-aspartate. More crowded arrangement of the benzyl group in PBLA around the main chain α-helix because of the lack of one methylene group in the side chain leads to the increase in the interaction between benzyl

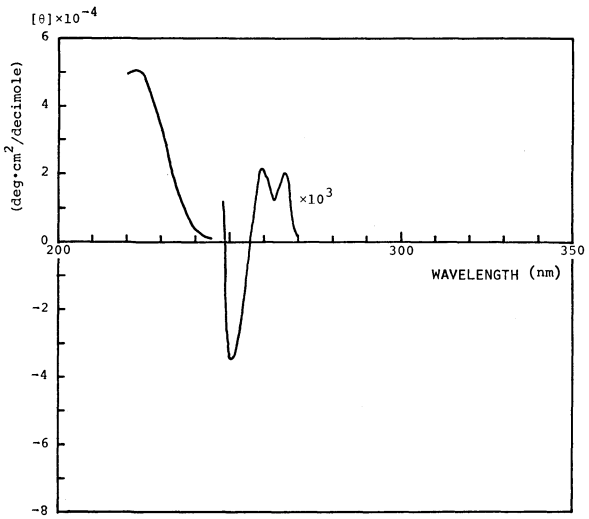

Fig. 3. CD spectrum of PBLA in chloroform ($\Delta\varepsilon/\varepsilon = -6.2\times10^{-5}$ at 252 nm); "$\times10^3$" denotes that the spectrum is magnified 10^3 times longitudinally.

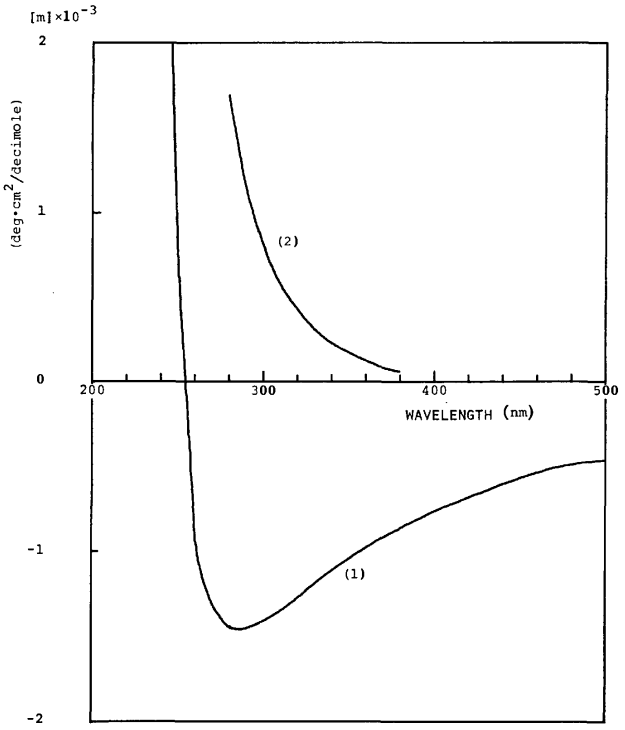

Fig. 4. ORD curves of (1) PBLA in chloroform and (2) PBDG in dichloromethane (0.018 mole of glutamyl residue/l).

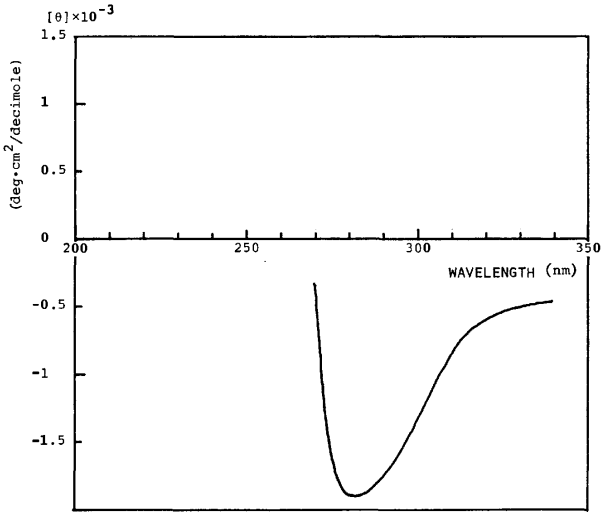

Fig. 5. CD spectrum of PNO_2BLA in *N,N*-dimethylformamide ($\Delta\varepsilon/\varepsilon = -6.9\times10^{-5}$ at 280 nm).

chromophores of PBLA, giving rise to the circular dichroism detected in PBLA while such is not the case for PBDG.

In Fig. 5 the CD spectrum of PNO_2BLA is shown. No circular dichroism is detectable in the wavelength region longer than 250 nm for β-*p*-nitrobenzyl-L-aspartate. The CD band of PNO_2BLA around 290 nm is also ascribed to its benzyl chromophore. The α-helical structure of PNO_2BLA in *N,N*-dimethylformamide has been ascertained by Goodman *et al.*[9] The molar ellipticity $[\theta]_{280}$ of PNO_2BLA is much larger than $[\theta]_{275}$ of PNO_2BLG. This again reflects the fact that the side chain in the polyaspartate is constrained in its orientation as a result of their shorter side chain length than that of the polyglutamate by one methylene group. It is remarkable that the absolute value of the optical anisotropy factor $\Delta\varepsilon/\varepsilon$ is only slightly larger in PNO_2BLA than in PBLA. The α-helical sense of PBLA is opposite to that of PNO_2BLA, so this difference in $\Delta\varepsilon/\varepsilon$ cannot be correlated in a straightforward way to the difference in the magnitude of the interaction between side chain aromatic chromophores.

It must be noticed that the size of the interaction between side chain chromophores of the above-mentioned polypeptides is no more than necessary to align the chromophores around the definite orientation relative to the main chain helices of the polypeptides and is not so strong as to cause strong chromophore-chromophore interactions mentioned in mechanism (i) by Loucheux and Duflot resulting in the Davydov splitting of the CD band.

Induced Circular Dichroism of Benzyl Chromophores Bound to Helical Polypeptides in Concentrated Solutions.

PBLG in α-helical conformation forms a cholesteric liquid crystal in its concentrated solutions (10—50 wt% of the polymer).[14] A chirality is caused by the existence of a unidirectional twist on the array of a set of equispaced parallel planes in which α-helical axes lie, nevertheless the solution forms an isotropic domain as a whole because of the random orientation of the axes of the cholesteric helix in the macroscopic domain. The extrinsic optical activity due to the side chain benzyl group is expected to occur in such a concentrated PBL(D)G solution since a regularly ordered array of the side chain chromophore may exist in such a phase.

In the concentration range of PBDG less than 0.1 mol of glutamyl residue/l in dichloromethane, no evidence of the occurrence of the higher order structure can be detected. ORD curves for such a concentration range (Fig. 4) show monotonic patterns as is encountered for the usual polypeptide solution having the α-helical structure. There is no Cotton effect observed in the wavelength region longer than 250 nm, and we get reasonable b_0 values around +650 from the good linearity of the Moffitt plot in the range of 280 nm—350 nm.

When the concentration is raised over 0.4 mol of glutamyl residue/l, it is found from the microscopic examination that the cholesteric liquid crystalline phase is formed in the system. For this system, the ORD curve, giving an anomalous dispersion near 255 nm, is quite different from those for less concentrated systems (Fig. 6), and it cannot be decided from this ORD curve whether or not the α-helical structure is retained since the Moffitt plot no longer gives a straight line and does not give a definite b_0. On the other hand, IR mesurements indicate that the α-helical structure is retained up to the concentration of 0.75 mol of glutamyl residue/l since the IR bands (amide I and amide II bands) which are ascribed to the α-helical structure appear at 1650 cm^{-1} and at 1550 cm^{-1} and a band at 1690 cm^{-1} due to the non-hydrogen bonded carbonyl group is absent.[15]

As expected from the remarkable concentration

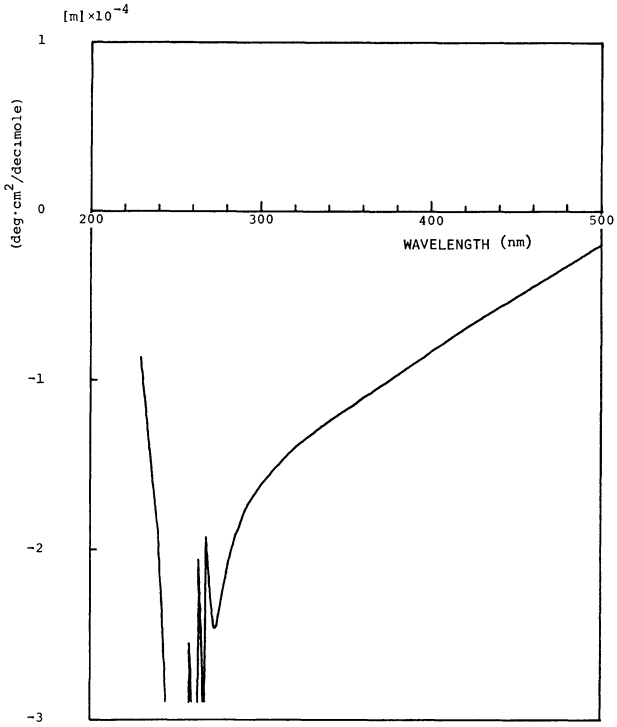

Fig. 6. ORD curve of concentrated PBDG solution in dichloromethane (0.74 mol of glutamyl residue/l).

dependence of the ORD curve, a CD band near 255 nm really appears at higher concentrations than 0.4 mol of glutamyl residue/l in dichloromethane. The cholesteric phase is also formed when PBDG is dissolved in other helix solvents such as dichloroethane and tetrachloroethane, giving similar CD bands near 255 nm, but the signs of the CD bands in these solvents are opposite to that in dichloromethane. The observed CD spectra are shown in Fig. 7. On the other hand, it has been confirmed by the polarizing microscopic observation that the nematic liquid crystalline phase of PBDG is formed when this polypeptide is dissolved in the solvent mixture of dichloromethane and dioxane (4: 1 in volume). No CD band around 255 nm appears in this nematic phase.

Extremely condensed phase is realized locally around closed-packed α-helices lying in parallel equispaced planes making up the cholesteric helix, and thus the benzyl chromophore attached to the α-helix is imposed to take a definite arrangement relative to this plane. This, in turn, means that the side chain benzyl chromophore assumes a definite orientation relative to the cholesteric helix. We can deduce, through the analogous way to that in the case of the dilute solution of PNO_2-BLG, that the extrinsic optical activity induced to the aromatic chromophore originates from the interaction between the aromatic chromophore of the polypeptide and the "helix." The solvent dependence of the sign of the Cotton effect of the benzyl chromophore of PBDG in the cholesteric liquid crystalline phase can probably be explained by the solvent dependency of the sense of the cholesteric helix reported by Robinson.[14]

No extrinsic optical activity can be observed for PBDG existing in the nematic liquid crystalline phase, while the benzyl chromophore of PBDG in such a

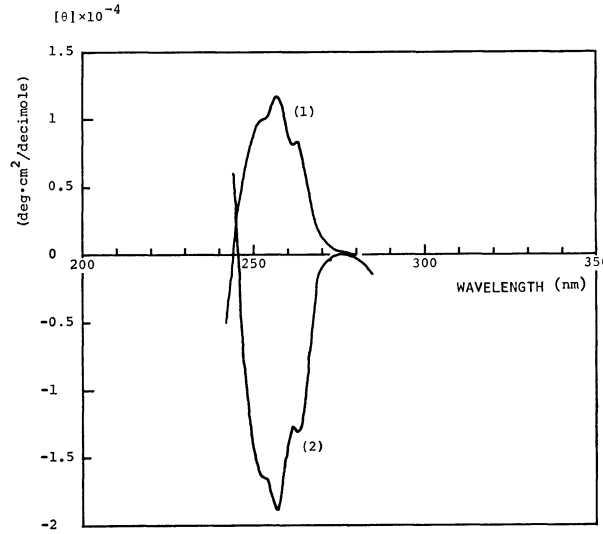

Fig. 7. CD spectra of PBDG in (1) dichloromethane (0.48 mol of glutamyl residue/l, $\Delta\varepsilon/\varepsilon = +0.014$ at 256 nm) and (2) tetrachloroethane (0.46 mol of glutamyl residue/l, $\Delta\varepsilon/\varepsilon = -0.022$ at 256 nm).

phase can be regarded as fixed in its orientation relative to the α-helix in the closed-packed structure as well as in the cholesteric phase and an extrinsic optical activity is expected to appear due to the dissymmetric field of the α-helical structure. To explain this fact, it might be necessary to assume that there exist enantiomeric arrangements of the benzyl chromophore subsisting simultaneously in the closed-packed plane of the nematic structure. This probably prevents the closed-packed plane of the nematic structure from arranging in a helical sense to form a cholesteric helical structure.

Again, as in the dilute solution of the polypeptide, there exists no Davydov pair of CD bands here, and so the benzyl chromophore of PBDG in the cholesteric liquid crystalline phase is not so closely stacked as to produce the interaction between electric transition moments in benzyl chromophores.

The optical anisotropy factor $\Delta\varepsilon/\varepsilon$ is 1.4×10^{-2} for this case, and this value is surprisingly large compared to those for PBLA, PNO_2BLA and PNO_2BLG in the dilute solutions which are -6.2×10^{-5}, -6.9×10^{-5}, and -3.8×10^{-5}, respectively. This fact is indicative that the dissymmetric field for the first case cannot be sought in the same origin as for the rest. This also supports the idea that the extrinsic optical activity of PBDG in its concentrated solutions should not be attributed to the α-helical structure of the polypeptide, but to the helical structure of the cholesteric liquid crystalline phase.

Conclusion

The dissymmetric field for the present case comes from two origins, namely the α-helical structure of the polypeptide and the cholesteric helical structure in the liquid crystalline phase of the polypeptide. The extrinsic optical activity appears when the benzyl chromophore loses its freedom of rotation to be oriented more rigidly relative to this dissymmetric field. PBLA has one less methylene group in its side chain than PBDG, realizing

more crowded arrangement of the benzyl group around the main chain α-helix. This leads to the definite orientation of the benzyl chromophore relative to the α-helix, giving rise to the extrinsic optical activity in the dilute solution of PBLA. The introduction of the nitro group into the benzyl chromophore increases the bulkiness of the side chain and the magnitude of the electrostatic interaction between side chains. This increase results in the enhancement of the probability of a definte orientation of the benzyl chromophore of PNO_2BLG relative to the α-helix of PNO_2BLG in its dilute solution or in the inversion of the left-handed α-helical sence of PBLA to the right-handed one of PNO_2BLA in the dilute solution. The benzyl chromophore of PBDG in its concentrated solution forming the cholesteric liquid crystalline phase takes a definite orientation in the closed-packed structure in the parallel equispaced planes making up the cholesteric helix.

We wish to thank Professor Akiyoshi Wada of the University of Tokyo for helpful discussions and encouragement.

References

1) E. R. Blout and L. Stryer, *J. Amer. Chem. Soc.*, **83**, 1411 (1961).
2) M. Hatano, M. Yoneyama, and Y. Sato, *Biopolymers*, **12**, 895 (1973).
3) Y. Sato and M. Hatano, This Bulletin, **46**, 3339 (1973).
4) M. Hatano, T. Enomoto, I. Ito, and M. Yoneyama, *ibid.*, **46**, 3698 (1973).
5) H. Nomori, T. Enomoto, and M. Hatano, *Chem. Lett.*, **1975**, 391.
6) M. H. Loucheux and C. Duflot, *Biopolymers*, **12**, 121 (1973).
7) S. Takagi, H. Nomori, and M. Hatano, *Chem. Lett.*, **1974**, 611.
8) R. Ledger and F. H. C. Stewart, *Aust. J. Chem.*, **18**, 1477 (1965).
9) M. Goodman, A. M. Felix, C. M. Deber, and A. R. Brause, *Biopolymers*, Symposia No. 1, 409 (1964).
10) D. F. Bradley, M. Goodman, A. Felix, and R. Records, *Biopolymers*, **4**, 607 (1966).
11) C. Taniolo, M. L. Falxa, and M. Goodman, *ibid.*, **6**, 1579 (1968).
12) E. R. Blout and R. H. Karlson, *J. Amer. Chem. Soc.*, **80**, 1259 (1958).
13) R. H. Karlson, K. S. Norland, G. D. Fasman, and E. R. Blout, *ibid.* **82**, 2268 (1960).
14) C. Robinson, *Mol. Cryst.*, **1**, 467 (1966) and references cited therein.
15) "Poly-α-Amino Acids," ed. by G. D. Fasman, Marcel Dekker, Inc., New York (1967), Chapter 2.

The Spectroscopic Study on the Dimerization of Pyridine Derivatives on the Surfaces of MgO, CaO and SrO

Tokio IIZUKA and Kozo TANABE

Department of Chemistry, Faculty of Science, Hokkaido University, Sapporo 060

(Received June 2, 1975)

The adsorption and dimerization of pyridine derivatives on MgO, CaO, and SrO were studied by ESR and visible absorption spectrometries. Adsorbed pyridine on the oxides was found to give an ESR signal of five lines and 580 nm absorption spectrum which were attributed to dipyridyl anion radical. The deuterium isotope effects for the formation of dipyridyl anion radicals were observed on MgO and CaO, but not on strong basic oxide, SrO. Methylpyridines adsorbed on MgO gave the same species as pyridine by the irradiation of light (λ>370 nm). From these facts, the surface intermediates for the dimerization reaction were discussed. When the adsorbed species were exposed to oxygen molecule, the dipyridyl anion radicals faded away and the ESR spectra attributed to the O_2^- ion were observed.

Alkaline earth metal oxides as solid base catalysts have recently been found to show a remarkable activity and interesting selectivity for the isomerization of olefins,[1] the alkylation of phenol with methanol,[2] the conversion of benzaldehyde into benzyl benzoate,[3] *etc.* On the other hand, the formation and stabilization of negative radical ions of aromatic nitro compounds on the surfaces of MgO[4] and CaO[5] by electron transfer process are well known.

In the present work, the formation of dipyridyl anion radical by the dimerization of pyridine derivatives adsorbed on MgO, CaO, and SrO was found by ESR and visible absorption spectroscopies, and their adsorbed states were discussed.

Experimental

Magnesium oxide used in this investigation was prepared from $Mg(OH)_2$, guaranteed reagent of Kanto Chemical Co., Inc., by evacuation at different temperatures for 1 hr. Calcium and strontium oxides were from the carbonates of Merck guaranteed reagents by evacuation at 700—900 °C for 1 hr. Pyridine and α, β, γ-methylpyridines were guaranteed reagents of Wako Pure Chemical Co., Inc., distilled in a vacuum and degassed by repeating a freezing-thawing cycle several times and dried by molecular sieve. Pentadeuteropyridine was purchased from Merck Co. and purified by the same method as in pyridine derivatives.

Adsorptions were done under the vapor pressures at room temperature in a vacuum system.

A JEOL ESR spectrometer operating with 100 kHz field modulation was employed to obtain the ESR spectra. The visible absorption spectra were recorded with Shimadzu MPS-50L spectrometer by using the *in situ* quartz cell in which the pressed wafer of $Mg(OH)_2$ powder was fixed. These spectra were recorded at 20 °C.

Light irradiation was done through the pyrex glass filter by Toshiba SHL-100UH-2 ultra high pressure mercury lamp.

Results

ESR Spectra of Adsorbed Pyridine. When pyridine was introduced to MgO, CaO, and SrO evacuated at high temperature, the color of the oxide surfaces turned to purple instantly, and broad unsymmetrical ESR signals were observed as shown in Fig. 1. On MgO surface, several numbers of splittings were observed, but

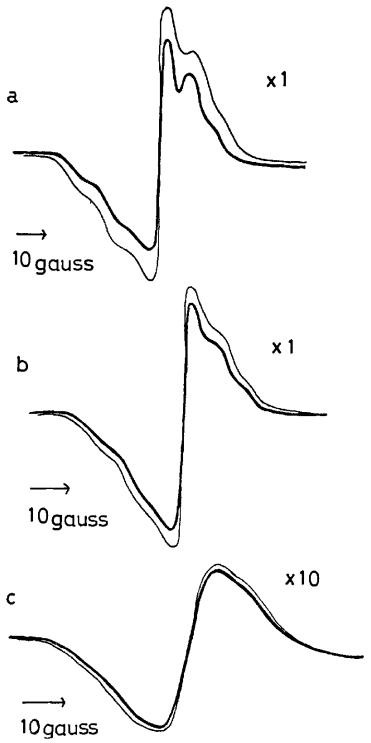

Fig. 1. ESR spectra of pyridine adsorbed on oxides. a. MgO evacuated at 600 °C, b. CaO evacuated at 700 °C, c. SrO evacuated at 900 °C, heavy line: 2 min after adsorption, weak line: 10 min after adsorption.

those splittings were obscure on CaO or SrO surface. As shown in Fig. 2, after pentadeuteropyridine (C_5D_5N) instead of pyridine adsorbed on these oxides, the sharp five splitted lines developed in the cases of MgO and CaO, but on SrO, the splitting was not clear.

From the dependence of signal shape on the microwave power change, those signals were thought to be due to one paramagnetic species, and concluded to be hyperfine structure of two equivalent ^{14}N. The hyperfine coupling constants were 8.2 for MgO, 7.4 for CaO, and 7.2 gauss for SrO.

The change of the spin concentration with adsorption time was shown in Fig. 3. On MgO surface, the broader and stronger signal was obserbed on pyridine adsorption than on the adsorption of pentadeuteropy-

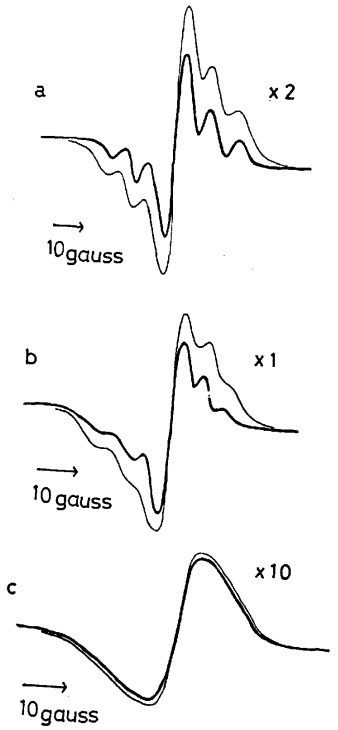

Fig. 2. ESR spectra of pentadeuteropyridine adsorbed on oxides. a. MgO evacuated at 600 °C, b. CaO evacuated at 700 °C, c. SrO evacuated at 900 °C, heavy line: 2 min after adsorption, weak line: 10 min after adsorption.

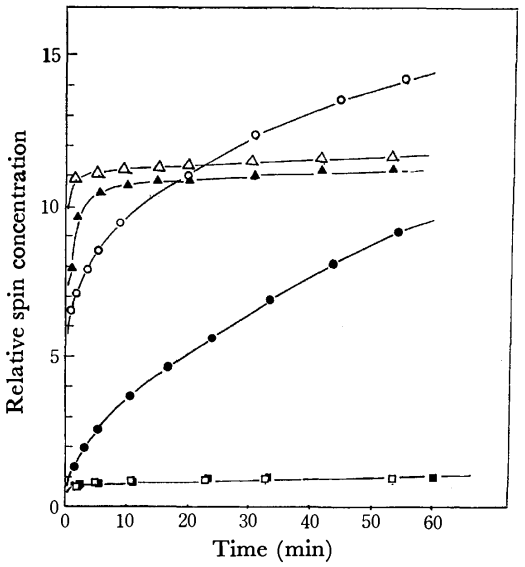

Fig. 3. Adsorption time dependence of spin concentration. ○: pyridine on MgO (evacuated at 600 °C), ●: deuteropyridine on MgO (600 °C), △: pyridine on CaO (700 °C), ▲: deuteropyridine on CaO (700 °C), □: pyridine on SrO (900 °C), ■: deuteropyridine on SrO (900 °C).

ridine. Those signals increased their intensity with adsorption time, but the shapes of two signals were very different as shown in Figs. 1 and 2.

On CaO surface, the differences in the intensity and the shape of those signals were obvious at the initial stage of the adsorption, but almost the same spectrum was observed after 20 min adsorption.

In the case of SrO, no difference was observed in the shape of spectra and spin concentration.

The Visible Spectra of Pyridine Adsorbed on MgO. The visible spectra of pyridine adsorbed on evacuated MgO were shown in Fig. 4. Those spectra had three absorption bands at 380, 470, and 580 nm.

In the reduction of pyridine by alkali metal, it is known that the formed 4,4′-dipyridyl anion radical shows the absorption at 381 and 570 nm.[6]

On MgO evacuated at high temperature, only the 580 nm band decreased remarkably. The change in 580 nm band intensity with evacuation temperature was shown in Fig. 5. It had very close correlation with the change in ESR spin density with evacuation temperature change. These facts suggest the formation of dipyridyl anion radical on MgO.

Actually, the UV spectrum of the extracted ethanol solution of adsorbed species on MgO coincided with that of 4,4′-dipyridyl.

The Visible and ESR Spectra of Methylpyridine Adsorbed on MgO. When methylpyridine adsorbed on MgO, the surface showed yellow color, but gave no ESR signal. The visible spectra of those adsorbed species

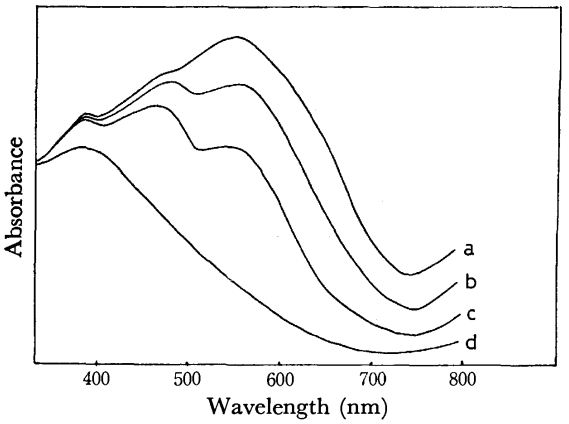

Fig. 4. Visible absorption spectra of pyridine adsorbed on MgO. a. evacuated at 600 °C, b. evacuated at 800 °C, c. evacuated at 1000 °C, d. exposed to oxygen gas.

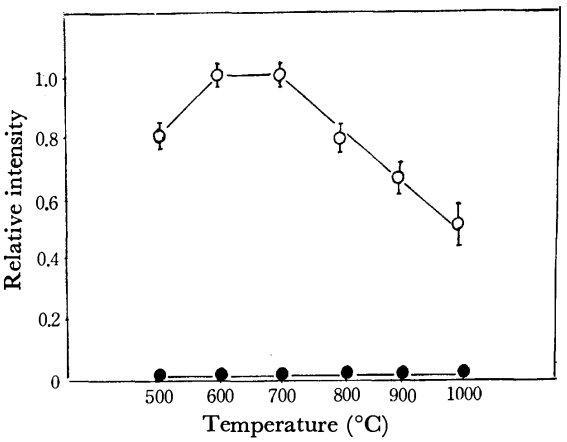

Fig. 5. Calcination temperature dependence of 580 nm band on MgO. ○: evaculated *in vacuo*, ●: heated in air.

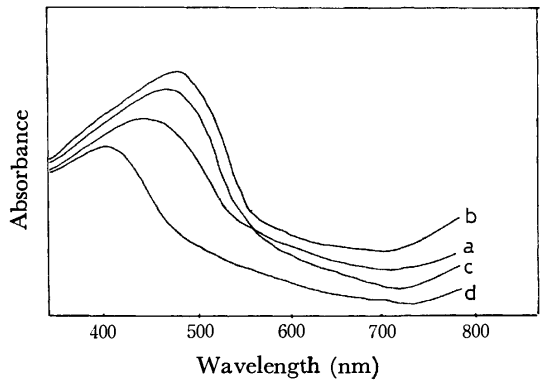

Fig. 6. Visible absorption spectra of methylpyridines adsorbed on MgO evacuated at 600 °C. a. γ-methylpyridine, b. β-methylpyridine, c. α-methylpyridine, d. exposed to oxygen gas.

are shown in Fig. 6. On any adsorbed species, only 470 nm band was observed. After the exposure to O_2 gas, this 470 nm band diminished immediately. When the methylpyridines adsorbed on MgO which showed no ESR signal were irradiated by light (λ>370 nm), those yellow surfaces turned to purple and the intense ESR signals analogous to that in pyridine adsorption were observed.

The ESR Spectra of the Adsorbed Pyridine Derivatives Exposed to Oxygen Gas. When the pyridine adsorbed on MgO was exposed to O_2 gas, the purple color and the ESR spectrum of dipyridyl anion radical disappeared and the new broad unsymmetrical ESR spectrum with g-values at g_1=2.076 and 2.060, g_2=2.008, g_3=2.001 was observed at room temperature. Those g values and the shape of this spectrum agreed well with those of the adsorbed O_2^- radical on ultraviolet irradiated MgO.[7]

On CaO surface, axial symmetrical signal with $g_{//}$= 2.082, $g_\perp$=2.005 was observed after exposure to O_2 gas. Though O_2^- ion adsorbed on CaO has never been reported, this signal would be also concluded to this ion. The O_2^- ion on SrO was not observed in spite of the disappearance of radical anion by exposure to O_2 gas. In the case of the methylpyridine adsorbed on MgO which gave no ESR signal, ESR signal of O_2^- ion appeared after the introduction of O_2 gas.

Discussion

The analysis of the ESR spectra with sharp hyperfine structure of adsorbed pentadeuteropyridine provides many informations about the electronic states of adsorbed ions, structural changes due to adsorption, and interaction with the surface. The signals shown in Fig. 2 having five line pattern are essentially due to the anisotropic interaction of the free spin of two nitrogen nuclei with each nuclear spin of unity. The Hamiltonian for this type of radical can be written in the form,

$$\mathcal{H} = \beta \cdot s \cdot \tilde{g} \cdot H + s \cdot \tilde{A} \cdot I,$$

where $\tilde{g}$, $\tilde{A}$ are tensors respectively. For axial symmetry such as an electron delocalized into a nitrogen 2p orbital, the observed hyperfine interaction α can be written as

$$\alpha^2 = [A^2 + 2AB(3\cos^2\theta - 1) + B^2(3\cos^2\theta - 1)],$$

Where A is the isotropic interaction and B is a traceless anisotropic term. If the radical is tumbling rapidly, the anisotropic interactions vanish and α becomes to A. In rigid adsorbed system, the observed hyperfine splittings can be attributed to the A and B terms, the hyperfine coupling $A+2B$ parallel to the p-orbital direction ($A_{//}$), and $A-B$ perpendicular to the p-orbital direction ($A_\perp$).

It is reasonable to consider that the outer four lines are parallel hyperfine, and the central line is the remaining parallel feature on which all the perpendicular components are overlapping.[8] Although a value for $(A+2B)$ has been measured, we must either measure $(A-B)$ or A independently to obtain values for A and B. Since the central line shows no resolution of $(A-B)$, some limiting values of A and B can be calculated assuming that $(A-B)<1/2\Delta H_{pp}$. These values (gauss) are shown in Table 1.

Table 1.

Oxide	$(A+2B)$	ΔH_{pp}	$g_{//}$	$g_\perp$	A	B	$A_{iso}N$
MgO	8.2	4.0	2.0022	2.0030	4.08	2.08	—
CaO	7.4	4.2	2.0022	2.0026	3.81	1.81	—
SrO	≃7.2	≃12	2.002	2.003	≃3.8	≃1.8	—
Solution[9]	—	—	—	—	—	—	3.64

Although the values of A and B are limiting values estimated from the equation,

$$A - B = \frac{1}{2}\Delta H_{pp}$$

so large error would not be involved, since the values of ΔH_{pp} are very small. The fact that the A value of dipyridyl on MgO is slightly larger than those of CaO and SrO is due to the difference in the ionic power or Lewis acidity of Mg^{2+}, Ca^{2+} and Sr^{2+} ions. Since the A value of the adsorbed species are almost comparable to the isotropic hyperfine coupling constant of γ,γ'-dipyridyl anion radical in solution[9] (A_{iso} N=3.64 G), the dipyridyl negative ion on the surface is not so polarized by the crystal field.

The values of A and B for the isotropic and anisotropic interactions of the nitrogen atom can be used to obtain the s and p character of the orbital of the unpaired elcetron, since those can be written:

$$A_N = a_{2s}^2 A_0,$$
$$B_N = a_{2p}^2 B_0,$$

where a_{2s}^2 and a_{2p}^2 are the populations of the nitrogen 2s and 2p orbitals. If the values of A_0=550 gauss and B_0=17.2 gauss are used for the nitrogen atom,[10] the spin population value are shown in Table 2.

There is no difference in the spectra between adsorbed pyridine and pentadeuteropyridine (C_5D_5N) on oxides, but pyridine adsorption gives larger spin density and broader spectrum than deuteropyridine adsorption on MgO. The broadening of the spectrum in this case would be caused by the dipole-dipole interaction of the

Table 2.

Oxide	a_{2s}^2	a_{2p}^2	a_{2p}^2/a_{2s}^2
MgO	0.0072	0.12	17
CaO	0.0069	0.105	15
SrO	≃0.0069	≃0.105	≃15

free spins adjoining very closely. Thus the spin density affected the shape of the spectrum. The difference in the spin density and the shape of the spectrum by the isotope labelling is evident on MgO, and this shows the isotope effect on abstraction of hydrogen or deuterium to form dipyridyl on the oxide. In the case of the adsorption on CaO, the evident isotope effect was observed in the initial stage of the adsorption, but in 20 min after the adsorption, the shape of the spectrum and the spin density became almost the same in the adsorption of pyridine or deuteropyridine. In this case, the cause of the spectrum broadening is apparently due to the increase in the spin density. On the other hand, there is no difference in the shape and spin density of adsorbed species on SrO by the isotope labelling. Since the order of the basic strength is MgO<CaO<SrO,[11] it is clear that the isotope effect becomes smaller with the increase of the basic strength, suggesting that surface oxide anion (O^{2-}) abstracts H^+ or D^+ from pyridine in the rate-determining step of the formation of dipyridyl.

The irradiation effect of light on the formation of the anion radical of phenazine on MgO was observed by Seshadri and Petrakis.[8] The anion radical formation of dipyridyl from pyridine proceeded even in dark, but the anion radical was not formed by the adsorption of methyl substituted pyridines without light irradiation. It is interesting to note that it is not necessary for the formation of the anion radical of methylpyridine dimer to irradiate with so high energy of light (λ<370 nm).

These facts suggest that both the electron transfer and H^+ abstraction are required to form dipyridyl anion radical from pyridine derivatives on alkaline earth oxides. The following scheme is proposed.

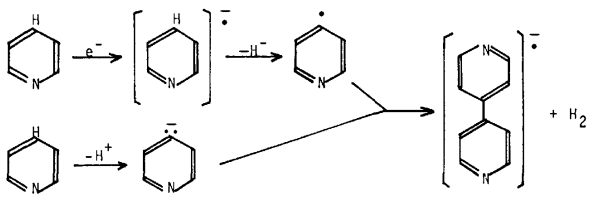

The electron transfer site on MgO was supposed to be the weakly coordinated O^{2-} ion of the surface by Che *et al.*[4b] In our scheme, the abstraction of H^+ on O^{2-} is also required. It is assured by the presence of the evident isotope effects. The abstraction of H^+ would proceed probably even on the more stabilized O^{2-} in the normal lattice than the low coordinated O^{2-} which possess electron donating ability.

On the surface of SrO, the amount of the formed dipyridyl anion radical was very small, but the isotope effect which was probably due to the abstraction of H^+ by surface O^{2-} ion was not observed.

When the adsorbed dipyridyl anion radical was exposed to oxygen gas, the anion diminished and the O_2^- ion was formed. Since the direct electron transfer to oxygen molecule on nonirradiated MgO was not observed, the expected reaction was $R^- + O_2 \rightarrow R + O_2^-$.

In the case of the exposure to O_2 gas of methylpyridine adsorbed on MgO which gave no ESR signal, the formation of O_2^- ion was also observed. From this fact, it is concluded that the adsorbed methylpyridines forms partially charge transfer complex with surface O^{2-} ion. Light facilitates this charge transfer enough to form dipyridyl derivatives through the anion radical.

References

1) H. Hattori, N. Yoshii, and K. Tanabe, Int. Congr. Catal., 5th Prepr. No. 10, Palm Beach, 1972.
2) T. Nishizaki and K. Tanabe, *Shokubai*, **15**, 94 (1973).
3) K. Tanabe and K. Saito, *J. Catal.*, **35**, 247 (1974).
4) a) A. J. Tench and R. L. Nelson, *Trans. Faraday Soc.*, **63**, 2254 (1967); b) M. Che, C. Naccache, and B. Imelik, *J. Catal.*, **24**, 328 (1972).
5) T. Iizuka, H. Hattori, Y. Ohno, J. Sohma, and K. Tanabe, *J. Catal.*, **22**, 130 (1971).
6) C. D. Schmulbach, C. C. Hinckley, and David Wasmund, *J. Amer. Chem. Soc.*, **90**, 6600 (1968).
7) J. H. Lunsford and J. P. Jane, *J. Chem. Phys.*, **46**, 1487 (1966).
8) K. S. Seshadri and L. Petrakis, *J. Phys. Chem.*, **74**, 1317 (1970).
9) A. Carrington and J. D. Santos-Veiga, *Mol. Phys.*, **5**, 21 (1962).
10) J. R. Morton, *Chem. Rev.*, **64**, 453 (1964).
11) K. Tanabe and Y. Fukuda, *React. Kinet. and Cat. Letters*, **1**, 21 (1974).

Relative Determination of the Soret Coefficients of Electrolytes. V

Toshio IKEDA, Yoshihiro TAKATSUKA, and Takeshi WATANABE
Department of Chemistry, Faculty of Science, Shizuoka University, 836 Ohya, Shizuoka 422
(Received December 23, 1974)

The Soret coefficients of aqueous solutions of some transition metal chlorides were determined by use of combined thermocells. The following values (in 10^{-3} K^{-1}) were obtained in 0.005 M solutions at 25 °C: −7.01 for $MnCl_2$, −4.61 for $CoCl_2$, −2.67 for $NiCl_2$, and −3.43 for $CuCl_2$. It was concluded that ion paramagnetism does not affect thermal diffusion.

The combined thermocell method[1,2] was proved to be as useful as the most sensitive conductometric method improved by Snowdon and Turner[3] in yielding reasonable values for the Soret coefficients of a number of electrolytes. However, only a few data are reliable for the Soret coefficients so far reported of divalent salts.[2,4] Accurate Soret data are required for a great number of divalent salts. In the present work, the Soret coefficients of a series of the transition metal chlorides, MCl_2, in aqueous solutions were determined by the combined thermocell method, special interest being taken to see whether paramagnetic ions of these salts have any influence upon thermal diffusion. Combined thermocells (a cell system of a back to back combination of two thermocells consisting of common electrodes and different electrolytes without liquid junctions) of the following type were used:

$$\underset{T}{\text{Hg–HgCl}},\ \text{LiCl}(m),\ \underset{T+\Delta T}{\text{HgCl–Hg–HgCl}},\ \text{MCl}_2\left(\frac{m}{2}\right),\ \underset{T}{\text{HgCl–Hg}} \qquad (1)$$

where the concentrations of the chloride ions in the left and right halves of the cell are taken to be equivalent to each other. Lithium chloride was taken as a standard since it shows a very slight Soret effect. The Soret coefficient, σ^{MCl_2}, for MCl_2 can be calculated in terms of the σ^{LiCl} for LiCl from the resulting initial thermoelectric power, $(dE/dT)_0$, of the cell (1) by using the following approximate equation,[2] ignoring terms of the transported entropies of the chloride ion:

$$\sigma^{MCl_2} = [4t^{LiCl}_{Li^+}B^{LiCl}\sigma^{LiCl} + 2F(dE/dT)_0/RT]/3t^{MCl_2}_{M^{2+}}B^{MCl_2} \qquad (2)$$

where t is the ionic transport number of ionic species indicated by the subscripts in the solution phases indicated by the superscripts. B is defined by

$$B = (1+d\ln\gamma_{\pm}/d\ln m)_{T,P}$$

where $\gamma_{\pm}$ is the mean activity coefficient in the molality scale at a molality m, F, R, T and P having their usual meanings.

Results and Discussion

All the solutions of four transition metal chlorides, $MnCl_2$, $CoCl_2$, $NiCl_2$, and $CuCl_2$, were prepared by guaranteed reagent grade chemicals (99.8% purity, Wakō Pure Chemical Industries, Ltd.) and adjusted to a concentration of 0.01 mol dm^{-3} with respect to the chloride ions. Experimental equipments and methods are entirely the same as those reported.[2] The range of

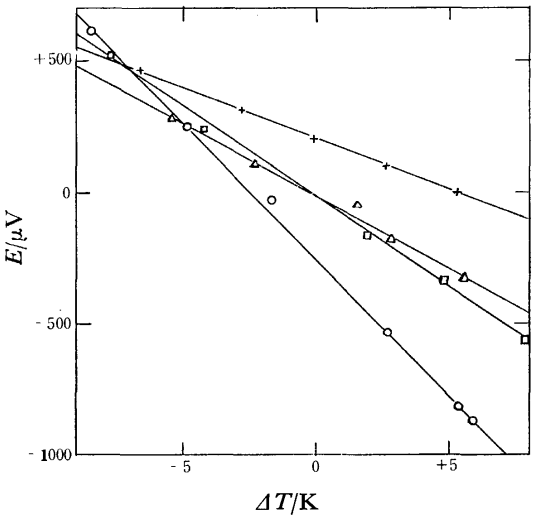

Fig. 1. Emf-plots of the combined thermocells (1) against temperature differences, ΔT: ○ for $MnCl_2$, □ for $CoCl_2$, + for $NiCl_2$, △ for $CuCl_2$.

ΔT was about 10 K around a mean temperature 25 °C, while the temperature T on the terminal electroldes was kept constant at 25 °C.

Some typical results are shown in Fig. 1. The values of the resulting initial thermoelectric power, $(dE/dT)_0$, averaged over 10—20 observations, are given in Table 1. The values of $(dE/dT)_0$ observed in the present work are accompanied by fluctuations several times larger than those ever seen in a similar work. The reason is not clear. The Soret coefficients found for the transition metal chlorides are relatively large for their small cation sizes as compared with those of the alkali and alkaline earth chlorides[2,4] which yield cations of a relatively large size. This is the reverse of the general tendency of the Soret coefficients known since the larger (the smaller) the cation size, the larger (the smaller) the Soret coefficients, and hence the stronger the ion hydration, the weaker the Soret effect. This rule seems to hold roughly so far as the elements of the same family are concerned. On the other hand, all the salts studied here are paramagnetic, and in fact the manganese chloride, which has the highest magnetic moment, showed the most predominant Soret effect, and so paramagnetism seems to have some influence on the Soret coefficient. However, this assumption might not be appropriate, since the Soret coefficients we found are not always parallel with the magnetic moments because of the one exception of cupric chloride which showed a considerable Soret effect despite the fact that the

TABLE 1. SORET COEFFICIENTS, σ, AND THE MOLAR HEATS OF TRANSFER, Q_m OF SOME TRAN ITION METAL CHLORIDES AT 0.005 M AND 25 °C

Chloride	m / mol kg^{-1}	t_+ [a]	B [b]	$(dE/dT)_0$ / μV K^{-1}	$-10^3\sigma$ / K^{-1}	Q_m / cal mol^{-1}
LiCl	0.01004	0.3289	0.969	—	(−0.01)[c]	−4
$MnCl_2$	0.00502	0.4120	0.906	−101.0±7.2	7.0_1	3340
$CoCl_2$	0.00498	0.4143	0.906	−64.4±5.7	4.6_1	2210
$NiCl_2$	0.00497	0.4143	0.908	−38.8±4.8	2.6_7	1280
$CuCl_2$	0.00501	0.4231	0.894	−50.1±5.3	3.4_3	1620

a) Estimated from the limiting ionic conductances. b) Graphical determination using the data obtained from Landolt-Boernstein, "Physikalische Chemische Tabellen," Erg. Bd. II (1931) and III (1936). c) The standard Snowdon and Turner's value (*Trans. Faraday Soc.*, **56**, 1409 (1960)) adjusted to the 25 °C.

magnetic moment is the smallest in this family. Thus it seems that ion paramagnetism does not affect the thermal diffusion.

References

1) Part IV: T. Ikeda and Y. Yamamoto, This Bulletin, **47**, 838 (1974).
2) T. Ikeda, H. Ohe, and S. Kawamura, *ibid.*, **41**, 2858 (1968).
3) P. N. Snowdon and J. C. R. Turner, *Trans. Faraday Soc.*, **56**, 1409 (1960).
4) A. D. Payton and J. C. R. Turner, *ibid.*, **58**, 55 (1962).

Proton Magnetic Resonance in Some Triarylaminium Salt Free Radicals

Toshio YOSHIOKA, Kohji WATANABE,* and Hiroaki OHYA-NISHIGUCHI
Department of Chemistry, Faculty of Science, Kyoto University, Sakyo-ku, Kyoto 606
**The Institute for Chemical Research, Kyoto University, Uji 611*
(Received January 6, 1975)

The static magnetic susceptibilities from 77 to 300 K and the proton NMR spectra from 1.5 to 77 K have been measured on powder samples of tris-*p*-chlorophenylaminium perchlorate and chloroantimonate, and tris-*p*-tolylaminium perchlorate and chloroantimonate. The Weiss constants have been determined to be −2.0, −40, −0.5, and −10 K respectively. A broad maximum which indicates an antiferromagnetic interaction has been observed in the electron susceptibilities of the chloroantimonates obtained from the paramagnetic shift. The magnetic behavior is interpreted assuming the linear-chain model. On the other hand, the perchlorates obeyed the Curie-Weiss law down to 1.5 K. The isotropic hyperfine coupling constants of these four aminium salts have been estimated from the proton NMR spectra, from which the cations of these crystalline aminium salts can be expected to have similar configurations.

The magnetic properties of the stable organic free radicals have been intensively investigated. A deviation from the Curie-Weiss law and a broad maximum in the susceptibilities of some ion-radical salts have been observed above the temperature of liquid nitrogen.[1] The anomalous behavior arises from the strong interaction between adjacent radicals and has been interpreted in terms of an exchange-coupled pair model or a linear-chain model. The mechanism of such a strong interaction is considered to be the charge-transfer stabilization. In the case of neutral organic radicals, an anomalous paramagnetism has often been found in the sufficiently low-temperature region and explained on the basis of a regular or alternating Heisenberg linear-chain model.[2,3] The mechanism of such a weak interaction is attributable to the overlap of $p_z\pi$-orbitals occupied by the unpaired electrons.

The series of *para*-substituted triarylaminium salts is reasonably stable in air and can be kept in the solid state for some time. Paramagnetic resonance absorption has been observed in these salts, and linewidth measurements have been reported for powder samples, together with the *g*-values.[4] However, the magnetic properties of these salts have never been studied except for the preliminary susceptibility measurements of three salts.[5] We would like to report on the magnetic behavior of four aminium salts, tris-*p*-chlorophenylaminium perchlorate and chloroantimonate (TCA·ClO_4 and TCA·$SbCl_5$), and tris-*p*-tolylaminium perchlorate and chloroantimonate (TTA·ClO_4 and TTA·$SbCl_5$), in the wide temperature range from 1.7 to 300 K. The two aminium cations, TCA and TTA, have the molecular structures shown in Fig. 1. A comparison of the infrared spectra of several tris-*p*-tolylaminium salts with those of triarylmethyl salts indicates that their cations have similar propeller-like configurations.[6] The triarylaminium radical cations are stabilized by the delocalization of the unpaired electron on the three rings.[7] Therefore, a large paramagnetic shift can be expected in the proton NMR of these salts. The proton NMR spectrum with two partially resolved lines for the TCA·ClO_4 salt have been studied at 77 K by Brown *et al.*[8] Since the paramagnetic shift is proportional to the product of the static magnetic susceptibility of the unpaired electron times the hyperfine constant, information concerning the electron susceptibility from the microscopic point of view, as well as the sign and magnitude of the hyperfine constant in the solid state, can be obtained from the nuclear magnetic resonance. The static susceptibility measurements of the four triarylaminium salts have been carried out in the high-temperature range from 77 to 300 K. The proton resonance spectra of these salts have been measured in the low-temperature range from 1.5 to 77 K in order to obtain the temperature dependence of the electron susceptibility and the hyperfine constants in the solid state. This is because some impurity effects at low temperatures encountered often in the static susceptibilities can be excluded in the case of the electron susceptibilities.

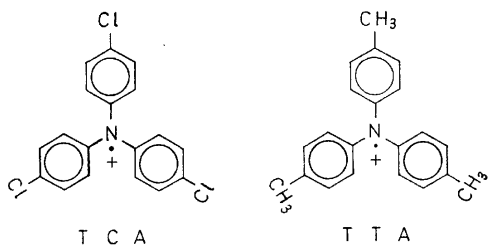

Fig. 1. The molecular structures of the triarylaminium cations, TCA and TTA.

Experimental

The tris-*p*-chlorophenylamine and tris-*p*-tolylamine were prepared by the method of Walter and were purified a few times through recrystallization. The TCA·ClO_4 and TTA·ClO_4 were prepared by the oxidation of the corresponding amine with silver perchlorate and iodine in ether by following the procedure of Walter.[9] The melting points were found to agree well with the values in the literature, and the results of the elementary analysis of the carbon, hydrogen, and nitrogen of each sample corresponded closely to the calculated values. The TCA·$SbCl_5$ was prepared by the following procedure. To a solution of the corresponding amine in chloroform, we added a chloroform solution of $SbCl_5$. A deep blue crystalline product with a metallic luster was obtained from the solution by cooling; it was then washed with chloroform and ether. This salt was found to be the most stable of the four salts. It melts sharply with decomposition at 195—196 °C. Found: C, 32.59; H, 2.09; N, 2.19; Cl, 44.35%. Calcd for $C_{18}H_{12}NCl_8Sb$: C, 33.38; H, 1.89; N, 2.16; Cl, 43.79%. The TTA·$SbCl_5$ was obtained accord-

ing to the method of Wieland,[10] mp 114—115 °C. Found: C, 42.79; H, 3.60; N, 2.29; Cl, 30.28%. Calcd for $C_{21}H_{21}NCl_5Sb$: C, 43.01; H, 3.61; N, 2.39; Cl, 30.23%.

The magnetic susceptibility measurements from 77 to 300 K were done, by means of a magnetic torsion balance described elsewhere,[11] on powder samples of about 50—100 mg in a field of 8.8 KG. The temperature was determined using a calibrated AuCo-Cu thermocouple. Manganese Tutton salt was used for the calibration of the thermometer as well as the product of the magnitude times the gradient of the magnetic field. The ESR spectra were observed at room temperature by using an X-band spectrometer PE3X of JEOLCO. The magnetic field was calibrated by the hyperfine splittings of Mn^{2+} doped in MgO. The proton NMR measurements were carried out using a Pound-Watkins-type spectrometer and a Robinson-type spectrometer at 20.0 and 35.0 MHz respectively, with an 80 Hz field modulation and a field sweep. The magnetic field was calibrated by means of the proton absorption of H_2O. A conventional cryostat was used, and the temperatures were determined using an Allen-Bradly carbon resistor calibrated against the vapor pressures of liquid helium, hydrogen, and nitrogen.

Results and Discussion

The diamagnetic correction was made using Pascal's constants. The value of the diamagnetic susceptibility for $SbCl_5^-$ was taken to be -1.24×10^{-4} cgs emu/mol, following Kainer and Hausser.[12] The paramagnetic susceptibilities of the four salts follow the Curie-Weiss law in the high-temperature range from 77 to 300 K. The values of the Curie constant and the Weiss constant were determined by plotting the inverse paramagnetic susceptibility against the temperature, and then the radical concentration was estimated from the Curie constant. The chloroantimonates have relatively large negative Weiss constants, indicating the presence of an antiferromagnetic exchange interaction between the unpaired electrons, while the perchlorates have small negative Weiss constants. The diamagnetic susceptibility, the Curie constant, the Weiss constant, and the radical concentration for each salt are summarized in Table 1.

Table 1. Results from susceptibility measurements

Compound	Diamagnetic susceptibility 10^{-6} (cgs emu/mol)	Curie constant (K·cgs emu/mol)	Weiss constant (K)	Radical concentration (%)
TCA·ClO_4	−246	0.358	-2.0 ± 0.5[a]	95
TCA·$SbCl_5$	−336	0.329	-40 ± 10	87
TTA·ClO_4	−230	0.281	-0.5 ± 0.2[a]	75
TTA·$SbCl_5$	−320	0.354	-10 ± 2	94

a) The values estimated from the paramagnetic shift in the low-temperature region.

The ESR absorption spectrum for each sample, as measured at room temperature, show a symmetrical single line. The linewidth, which was taken to be the peak-to-peak linewidth of the first derivative of the absorption spectrum, and the g-value are shown in Table 2. The ESR data indicate that each aminium salt is a monopositive cation radical salt.

Table 2. Results from ESR measurements

Compound	Linewidth (Gauss)	g-value
TCA·ClO_4[a]	4.6	2.0045
TCA·$SbCl_5$	4.0	2.0042
TTA·ClO_4[a]	2.3	2.0029
TTA·$SbCl_5$	1.4	2.0029

a) Ref. 4.

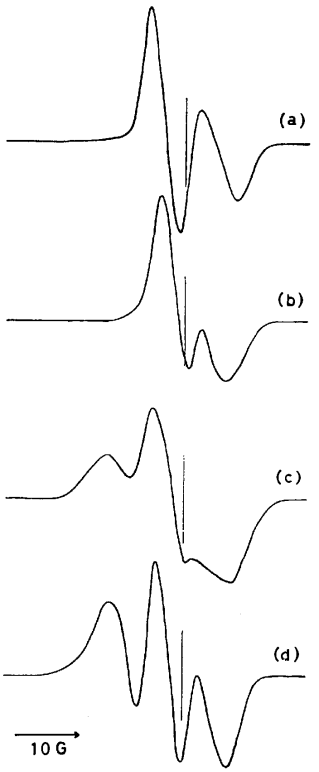

Fig. 2. Proton magnetic resonance absorption derivative curves (a) of TCA·ClO_4, (b) of TCA·$SbCl_5$, (c) TTA·ClO_4, (d) of TTA·$SbCl_5$, measured at 35.0 MHz, 77 K. The vertical lines show the free-proton position.

The 77 K proton resonance spectra of powder samples of the four salts measured at 35.0 MHz are shown in Fig. 2. The spectrum for TCA·ClO_4 agrees well with the results reported by Brown *et al.*[8] The spin Hamiltonian for a free radical in which one proton interacts with one unpaired electron can be described by the following equation:

$$\mathcal{H} = -g_N\beta_N\boldsymbol{H}\cdot\boldsymbol{I} + a_H\boldsymbol{S}\cdot\boldsymbol{I} + \boldsymbol{S}\cdot\boldsymbol{D}\cdot\boldsymbol{I} \quad (1)$$

The meanings of the symbols have been described in a previous paper.[13] In the paramagnetic state, the proton sees only a time-averaged local field proportional to the mean value, $\langle S_z\rangle$, of the electron spin component because of the exchange interaction between the unpaired electrons. In polycrystalline samples, the third term of Eq. (1), which is due to the electron-nuclear dipolar interaction, produces a distribution of the proton resonance shift and broadens the proton resonance, but it does not shift the resonance center of gravity signifi-

cantly.[8,13] In polycrystalline samples, therefore, the proton-resonance-signal shift from the free-proton position to a higher field can be approximately described by the following equation:

$$\Delta H = -a_H \chi H / g\beta g_N \beta_N \quad (2)$$

Thus, ΔH is proportional to the isotropic hyperfine coupling constant, the static susceptibility, χ, and the resonance frequency. Further, the more the resonance line is shifted, the broader the linewidth becomes because of the third term of Eq. (1). The isotropic hyperfine constant, a_H, of a proton attached to a carbon atom is related to the π-electron spin density on the carbon atom by the so-called McConnell relation, $a_H = Q\rho$.[14,15] The Q value for aromatic C–H fragment has been semiempirically determined as $Q(CH) = -22.5$ G. In the proton resonance of TCA·ClO_4 and TCA·$SbCl_5$ measured at 77 K, the upper-field line and the lower-field line are attributable to the *ortho* protons attached to the carbon atoms with positive spin densities, and to the *meta* protons attached to the carbon atoms with negative spin densities, respectively, following the results of Brown *et al.*[8] The fact that the two lines for TCA·ClO_4 are shifted from the free-proton position more than those for TCA·$SbCl_5$ can be ascribed to the difference in the magnitude of the magnetic susceptibility, for TCA·$SbCl_5$ has a much larger negative Weiss constant than TCA·ClO_4. One upper-field line and two lower-field lines have been observed in the spectra of TTA·ClO_4 and TTA·$SbCl_5$. The proton hyperfine coupling constant of a methyl group attached to an aromatic carbon atom is related to the π-electron spin density of the carbon atom. In this case, the Q value has been empirically estimated to be +27.2 G. Therfore, the line with the largest lower-field shift is attributable to the protons of the methyl groups attached to the carbon atoms with positive spin densities situated at the *para* positions. The upper-field line and the other lower-field line can be assigned to the *ortho* protons and to the *meta* protons respectively. The spectrum for TTA·ClO_4 apparently includes an unshifted line arising from the diamagnetic impurities due to the radical decomposition, as will be shown below.

On the basis of the assignment of the polycrystalline NMR spectra, the isotropic hyperfine constants in the crystalline state have been evaluated by using the susceptibility results. The results are tabulated in Table 3, together with the ESR results in solution.[7] The a_H values of TCA radical salts do not agree with those in solution. The disagreement may be due to the inadequacy of the ESR simulation or to some other effect. From the results, the unpaired electron distribution on the three aryl groups can be expected to be equal to each other, even in the crystalline state. Probably, the crystalline aminium salts have similar D_3 propeller-like configurations, as is to be expected from the infrared spectra.[6] The three protons of the methyl group have identical isotropic hyperfine constants; this suggests that the methyl group rotates freely about the C–C bond in solution and even in the crystalline state at 77 K. Further, the proton NMR data indicate that the paramagnetism of the chloroantimonates observed in the susceptibility measurements arises from the aminium cation, and that the antimony pentachloride in the salts has a diamagnetic formula. Kainer and Hausser have suggested the formula of $(SbCl_4^- + SbCl_6^-)/2$ for the complexes of diphenylamine derivatives.[12]

When the temperature was lowered from 77 K, the paramagnetic shift of the perchlorates increased con-

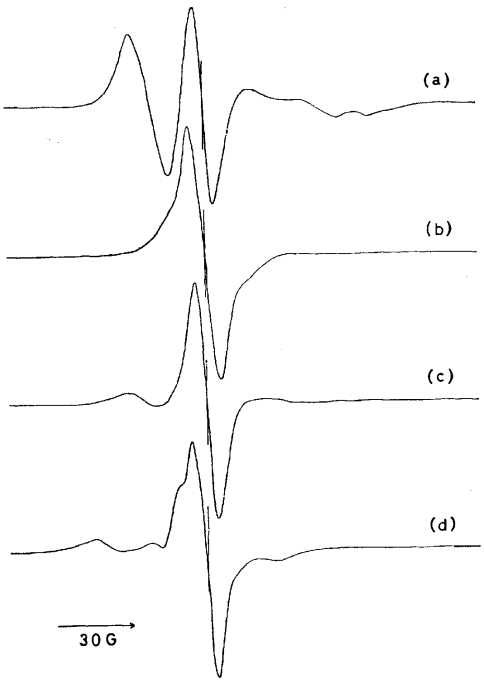

Fig. 3. Proton magnetic resonance absorption derivative curves (a) of TCA·ClO_4, (c) of TTA·ClO_4, measured at 20.0 MHz, 4.2 K, and (b) of TCA·$SbCl_5$, (d) of TTA·$SbCl_5$, measured, at 35.0 MHz, 4.2 K. The vertical lines show the free-proton position.

Table 3. Isotropic hyperfine constants obtained by the NMR spectra in the crystalline state and the ESR spectra in solution

Compound	a_N (Gauss)	a_O (Gauss)	a_m (Gauss)	a_{CH_3} (Gauss)
TCA·ClO_4[a]	—	−2.16	+1.27	—
TCA·$SbCl_5$	—	−2.35±0.15	+1.23±0.10	—
TCA (solution)[b]	9.56	1.12	0.56	—
TTA·ClO_4	—	−2.01±0.15	+1.04±0.10	+4.28±0.30
TTA·$SbCl_5$	——	−2.23±0.15	+0.96±0.10	+4.16±0.30
TTA (solution)[b]	9.45	2.06	1.03	3.89

a) Ref. 8, b) Ref. 7.

tinuously down to 1.5 K, following the Curie-Weiss law. By plotting the reciprocal of the paramagnetic shift *vs.* the temperature, the Weiss constants of TCA·ClO_4 and TTA·ClO_4 were determined to be −2.0 and −0.5 K respectively. The 4.2 K spectra measured at 20 MHz are shown in Figs. 3(a) and (c). The broadening of the shifted lines is due to the existence of an anisotropic hyperfine coupling coming from the third term of Eq. (1), which could lead to an asymmetric line shape for our polycrystalline samples. In the spectrum of TTA·ClO_4, only the absorption line of the *meta* protons shifted to the lower field can be detected; the lines of the *ortho* and methyl protons broaden out to the upper field and the lower field respectively. In addition to the shifted lines, an unshifted line was observed. In the measurements of TCA·ClO_4 after a month, we observed an increase in the intensity of the unshifted line, compared with that of the shifted lines. As the radical is not so stable and gradually decomposed, the diamagnetic impurities due to the radical decomposition are probably responsible for the unshifted line. The weak signal of the protons arising from the background is also attributable to the unshifted line.

A broad maximum in the paramagnetic shift of TCA·$SbCl_5$, which indicates an antiferromagnetic interaction, has been observed at about 40 K. The 4.2 K spectrum measured at 35.0 MHz shows an asymmetrical line at the free-proton position, as is shown in Fig. 3(b). However, a quantitative treatment is difficult since the magnitude of the shift is not very large.

The temperature dependence of the relative electron susceptibility of TTA·$SbCl_5$ obtained from the paramagnetic shift is illustrated in Fig. 4. In the spectra, the paramagnetic shift was defined as the distance between the free-proton position and some shifted lines which was proportional to the resonance frequency. When the temperature was lowered from 15 K, the paramagnetic shift deviated from the Curie-Weiss law and reached a broad maximum at 6.0 K. The 4.2 K spectrum measured at 35.0 MHz is shown in Fig. 3(d). The absorption line of *meta* protons was observed as the shoulder of the unshifted line arising from the radical decomposition. The absorption due to the methyl protons involves two lines at least, for the methyl protons are no longer equivalent at 4.2 K. This means that the methyl group is either completely locked or rotates rather slowly.[16] When the temperature is lowered from 4.2 K, the shifted line becomes so broad that the paramagnetic shift can not be estimated below 3.0 K.

The data of the paramagnetic shift can be interpreted by means of the one-dimensional Heisenberg model based on Bonner and Fisher's calculation,[17] rather than by means of the well-known pair model. The kT_m/J ratio is 1.282 for the one-dimensional Heisenberg model, where T_m is the temperature at which the susceptibility reaches its maximum value and where J is the exchange coupling constant. The J value for TTA·$SbCl_5$ is estimated to be −4.7 K from the T_m value obtained experimentally. In Fig. 4, the relative electron susceptibility obtained from the paramagnetic shift is compared

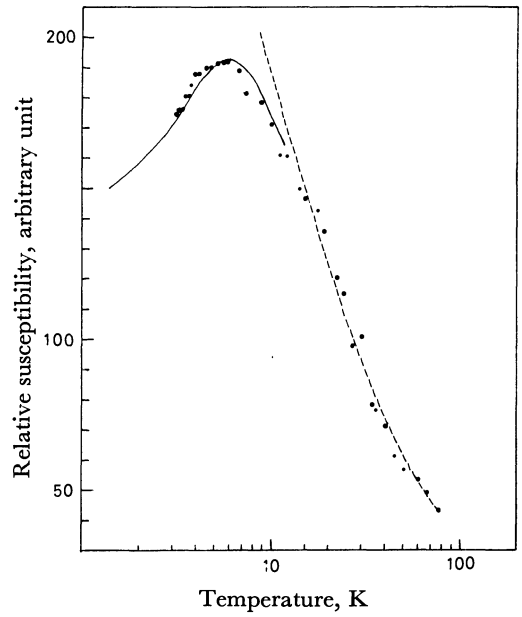

Fig. 4. The relative susceptibility of TTA·$SbCl_5$ obtained from the paramagnetic shift as a function of temperature. The solid line is the theoretical curve for one-dimentional Heisenberg model of $J=-4.7$ K, which is fitted at the temperature T_m. The dashed line represents the curve for the Curie-Weiss law, with the Weiss constant $\theta=-10$ K.

with the theoretical curve for the one-dimensional Heisenberg model of $J=-4.7$ K, which is fitted at the temperature of T_m. The broadening of the shifted lines below 4.2 K can no longer be explained by the third term of Eq. (1). Their behavior is perhaps attributable to an increase in the correlation time of the exchange motion because of the short-range magnetic ordering below the temperature of the susceptibility maximum.[18] Taking the results for the neutral organic radicals into account,[2,3] the mechanism of such a week interaction may be considered to be due to the overlap of π-orbitals occupied by the unpaired electron rather than to the charge-transfer stabilization. Although the interpretation, in which it is assumed that the cation radicals form chain-like arrays of molecules, is tentative, for lack of data on the crystal structure, the data of the paramagnetic shift are consistent with the linear Heisenberg antiferromagnetic exchange model.

On the other hand, the perchlorates exhibit a very small exchange interaction. The crystal structure of triphenylmethyl perchorate has been determined, and it has been reported that the carbonium ion is propeller-shaped, with a three-coplanar central bond, and that triphenylmethyl tetrafluoroborate is isomorphous with the perchlorate.[19] Provided that the aminium perchlorates have a crystal structure similar to that of triphenylmethyl perchlorate, they may be expected to form a three-dimensionally interacting spin-system rather than a one- or two-dimensionally interacting spin-system. Therefore, it is possible that the aminium perchlorates go into a three-dimensionally ordered antiferromagnetic state if the temperature is lowered below 1.5 K.

The authors are much obliged to Professor Yasuo Deguchi for his continuous encouragement throughout this work.

References

1) H. Nishiguchi, This Bulletin, **40**, 1587 (1967); Y. Sato, M. Kinoshita, M. Sano, and H. Akamatsu, *ibid.*, **40**, 2539 (1967); **42**, 3051 (1969); J. Tanaka, M. Inoue, M. Mizuno, and K. Horai, *ibid.*, **43**, 1998 (1970); D. B. Chesnut and W. D. Phillips, *J. Chem. Phys.*, **35**, 1002 (1961).

2) J. Yamauchi, This Bulletin, **44**, 2301 (1971).

3) W. Duffy, Jr., and D. L. Standburg, *J. Chem. Phys.*, **46**, 456 (1967).

4) R. I. Walter, R. S. Codrington, A. F. D'Adamo, and H. C. Torrey, *ibid.*, **25**, 319 (1956).

5) K. H. Hausser and H. Kainer, *Z. Naturforsch.*, **9a**, 783 (1954).

6) W. Otting and H. Kainer, *Chem. Ber.*, **87**, 1205 (1954); D. W. A. Sharp, *J. Chem. Soc.*, **1957**, 4804.

7) E. T. Seo, R. F. Nelson, J. M. Fritsch, L. S. Marcoux, D. W. Leedy, R. N. Adams, *J. Amer. Chem. Soc.*, **88**, 3498 (1966).

8) T. H. Brown, D. H. Anderson, and H. S. Gutowsky, *J. Chem. Phys.*, **33**, 720 (1960).

9) R. I. Walter, *J. Amer. Chem. Soc.*, **77**, 5999 (1955).

10) H. Wieland, *Ber.*, **40**, 4260 (1907).

11) M. Mekata, *J. Phys. Soc. Japan*, **17**, 796 (1962).

12) H. Kainer and K. H. Hausser, *Chem. Ber.*, **86**, 1563 (1953).

13) T. Yoshioka, H. Ohya-Nishiguchi, and Y. Deguchi, This Bulletin, **47**, 430 (1974).

14) H. M. McConell and H. H. Dearman, *J. Chem. Phys.*, **28**, 51 (1958).

15) H. M. McConnell and D. B. Chesnut, *J. Chem. Phys.*, **28**, 107 (1958); **27**, 984 (1957).

16) A. Horshield, J. R. Morton, and D. H. Whiffen, *Mol. Phys.*, **4**, 425 (1961).

17) J. C. Bonner and M. E. Fisher, *Phys. Rev.*, **135**, A640 (1961).

18) M. E. Anderson, R. S. Rhodes, and G. E. Pake, *J. Chem. Phys.*, **35**, 1527 (1961); K. Uchino, J. Yamauchi, H. Ohya-Nishiguchi, and Y. Deguchi, This Bulletin, **47**, 285 (1974).

19) A. H. Gomes de Mesquite, C. H. MacGillavry, and K. Eriks, *Acta Crystallogr.*, **18**, 437 (1965).

Studies of the Solvent Dyeing of Poly(ethylene terephthalate) with Disperse Dyes from Trichloroethylene and Isooctane

Zenzo MORITA, Shinji HIRAOKA,* Toshiyasu YAMAMORI, and Hiromi MOTOMURA

Department of Textiles and Polymer Science, Faculty of Engineering, Tokyo University of Agriculture and Technology, Koganei, Tokyo 184

(Received February 8, 1975)

The diffusion of 1,4-dihydroxyanthraquinone and C. I. Disperse Orange 3 in poly(ethylene terephthalate) (PET) from the trichloroethylene (TRI) and isooctance (ISO) dyebath was investigated by the method of the cylindrical film-roll. The stability of PET in TRI and ISO at high temperatures was also examined. The degradation of PET by solvents was in the following order: water>TRI>tetrachloroethylene (TCE) and ISO. The diffusion coefficients of Orange 3 from various solvents at 90 °C were in the order: TRI>TCE>water>ISO. The activation energy of diffusion from ISO was much larger than that from TRI, the latter being nearly identical to that from TCE. The Arrhenius plots of the diffusion coefficients in PET indicated some transitions. The glass transition temperature of PET in TRI was lower than that in TCE. The diffusion coefficient and the surface concentration of Orange 3 from ISO were increased by the addition of water, while those from TRI were not changed within the range of experimental error.

Solvent dyeing with disperse dyes from ISO has been studied by Schuler,[1] that from *n*-octane, by Kojima,[2] and that from TRI, by Parkins and Hall recently.[3,4] A bimodal relation between the effects of the solvents on PET and the solubility parameter, δ, has also been observed.[5,6] According to Ribnick *et al.*, the bimodal relation suggests that the specific groups of PET molecules interact differently with two types of solvents. One maximum, near $\delta=10$, is due to the interaction between the solvent and the hydrophobic group of PET, while the other one, near $\delta=12$, is due to that between the solvent and the hydrophilic ester group of PET. The difference between the solubility parameters of TCE and TRI is small, while that between the dyeing characteristics of these solvents is large.

There are also large differences in the diffusion coefficients of the disperse dyes from the solvents used in the present study, though all the solvents have a hydrophobic character. The diffusion coefficients from TRI and TCE are larger than that from water, though that from ISO is smaller.

The addition of water to the ISO and TCE dyebath has given rise to an increase in the diffusion coefficients and the equilibrium adsorption of the disperse dyes.[1,7] The addition of water to the TRI dyebath, however, has not yet been reported.

In the present paper, we wish to examine the diffusion of disperse dyes in PET from the TRI and ISO dyebath and the effect of water added to the solvent dyebath by means of the cylindrical film-roll method. The results and the transition phenomena of the PET-TRI system will be discussed and compared with those of the PET–water and PET–TCE systems reported earlier.[8,9]

Experimental

Materials. Biaxially oriented PET films (Mylar C-25. du Pont), TRI (commercial grade—Toa Gosei Kagaku Kogyo Co., Ltd.), and ISO (reagent grade) were used. 1,4-Dihydroxyanthraquinone (reagent grade) and C. I. Disperse Orange 3 recrystallized from ethanol were used as penetrants.

* Present address: Fuji Spinning Co., Ltd., 2-3 Nihonbashi-Ningyo-cho, Chuo-ku, Tokyo 103, Japan.

Stability of PET in TRI and ISO. The film was wound on a stainless steel rod ($\phi=1$ cm) in TRI or ISO so that there were no bubbles between the consecutive film layers, and the film end was fixed. The film-roll was then treated by TRI or ISO in the same dyeing bottle as before under definite conditions.[9] After drying, the viscosities of the PET films treated were measured by means of a Cannon-Fenske viscosimeter at 20 °C in the same manner as before.[9]

Diffusion. The biaxially oriented PET film treated by water at 160 °C for 1 hr was wound on glass tubing ($\phi=1$ cm) in the experiment with a glass diffusion bottle or on a stainless steel rod in the ISO system above 135 °C with a high-pressure diffusion bottle, in the same solvents as in the dyeing. The diffusion experiments were carried out in the same manner as before under the conditions shown in Tables 1—3.[9] The experiments above or near the boiling point of the dyeing solvent were done under pressure using a high-pressure diffusion bottle.

Before beginning the diffusion experiment, the diffusion bottle was inserted into a thermostat set at a given temperature to dissolve the water, if necessary, and then the dye for a long time (*cf.* Table 3). After that, a film-roll was immersed in the bottle. In the case of a high-pressure diffusion bottle, a test tube in which a given weight of the dye and a little of the dyeing solvent had been added and a film-roll were placed in the bottle in which the dyeing solvent was put. The bottle was kept at a given temperature for a prescribed time to dissolve the dye in the test tube and was then quickly turned upside down several times in order to mix completely the solution in the test tube with the dyeing solvent. The time when the solution began mixing was regarded as the initial time of diffusion. After diffusion and drying, the optical densities of the dyed film were measured by means of a Shimadzu MPS-50L recording spectrophotometer at the wavelength of maximum absorption. The concentration of dyes on the film was confirmed to obey Beer's law under the present experimental conditions.

The diffusion coefficients and surface concentrations were calculated by the Sekido-Matsui method from the concentration profile obtained experimentally.[10]

Results and Discussion

The Effect of Solvent on PET. The solution viscosities of PET treated by TRI and ISO are shown in Fig. 1. The treatment of PET with ISO at 180 °C for

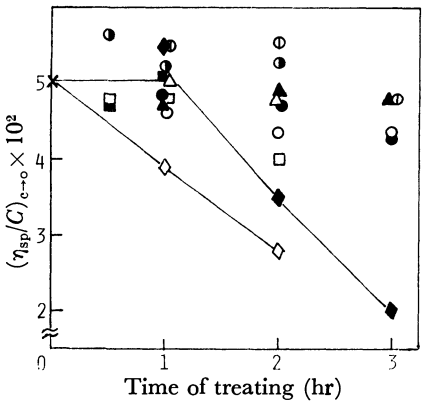

Fig. 1. Change of viscosity by treating with some solvents at high temperature (*m*-cresol: phenol=1: 1 (wt), 20 °C).

Solvent	140 °C	160 °C	180 °C
ISO	○	△	□
TRI	●	▲	■
TCE[9]	—	◐	◑
H_2O[8]	—	◆	◇
no treatment	×		

2 hr and with TRI at 180 °C for 1 hr brought about almost no change in the viscosity. However, during the treatment of PET with TRI at 180 °C for 2 hr, the TRI turned brownish and smelled offensively, and the film-roll could not be opened. No coloration of TRI was observed below 160 °C. On the other hand, the treatment of PET with water at 160 °C for more than 1 hr brings about a profound decrease in the viscosity.[8] That with TCE at 180 °C for less that 2 hr produces no change in the viscosity, but there is the decomposition of TCE above 180 °C, and the film-roll of PET treaed with TCE even at 200 °C for 1 hr could be opened.[9] Therefore, the degradation (in molecular weight) of PET by the solvents is in the following order: water>TRI>TCE and ISO. The order of TCE and ISO could not be determined by viscometry.

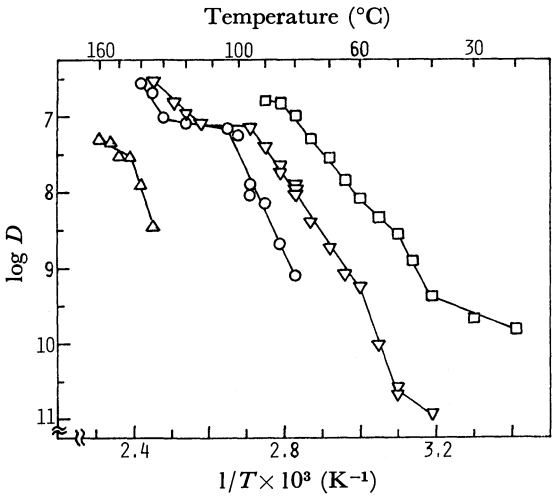

Fig. 2. Arrhenius plot of the diffusion coefficient (cm^2/min) of dye in PET from the solvent dyebath.
△: quinizarine from ISO, ○: C. I. Disperse Violet 8 from TCE,[9] ▽: Violet 1 from TCE,[9] □: Orange 3 from TRI.

Table 1. The diffusion and adsorption of C. I. disperse orange 3 from the solvent dyebath

Solvent	Temp. (°C)	Dyebath (g dye/ 100 ml solvent)	Diffusion time (min)	D (cm^2/min)	C_0 (g dye/ kg PET)
TRI	20	0.2	15710	1.51×10^{-10}	4.62
TRI	30	0.4	8487	2.19×10^{-10}	8.05
TRI	40	0.1	5800	4.22×10^{-10}	4.28
TRI	45	0.4	1440	1.26×10^{-9}	7.30
TRI	50	0.3	1080	2.92×10^{-9}	5.62
TRI	55	0.4	600	4.52×10^{-9}	6.00
TRI	60	0.3	480	8.09×10^{-9}	5.09
TRI	65	0.3	300	1.41×10^{-8}	4.67
TRI	70	0.4	90	2.78×10^{-8}	5.12
TRI	70	0.2	120	3.34×10^{-8}	2.18
TRI	75	0.4	100	5.11×10^{-8}	4.72
TRI	80	0.4	60	1.04×10^{-7}	4.85
TRI	85	0.4	30	1.60×10^{-7}	4.00
TRI	90	0.4	20	1.59×10^{-7}	3.34
TCE	90	0.2	120	6.52×10^{-8}	3.63
H_2O	90	0.3[a]	11355	3.83×10^{-10}	12.6
ISO	90	0.2	12870	3.07×10^{-11}	6.47

a) saturated solution

Table 2. The diffusion and adsorption of 1,4-dihydroxyanthraquinone from the ISO dyebath

Temperature (°C)	Diffusion time (min)	D (cm^2/min)	C_0 (g dye/ kg PET)
135	420	3.54×10^{-9}	39.3
140	300	1.26×10^{-8}	31.6
145	240	2.97×10^{-8}	27.5
150	180	3.05×10^{-8}	26.3
155	90	4.70×10^{-8}	22.2
160	77	4.88×10^{-8}	21.2

Diffusion from the TRI and ISO Dyebath. The diffusion coefficients, D, and the surface concentrations, C_0, of Orange 3 and 1,4-dihydroxyantraquinone from the TRI and ISO dyebath are shown in Tables 1 and 2 and in Fig. 2 as the Arrhenius plots. It is well known that the diffusion of penetrants in a polymer correlates with the intrinsic mobility of polymer molecules.[11] However, in the case of the diffusion in a polymer which is in a swelling equilibrium with a solvent, such as in dyeing, it also correlates with the swelling or plasticization of the polymer by the solvent.[8,9,12] The diffusion coefficients of Orange 3 from various solvents at 90 °C were in the order: TRI>TCE>water>ISO (Table 1). This order, therefore, is considered to be due to the plasticization effect of the solvents on PET or to the solvent-polymer interaction.

Orange 3 is one of the few kinds of dyes which can be dyed from various solvents. In the case using the ISO dyebath, the diffusion of even a small penetrant may be difficult below 100 °C. The activation energies for the diffusion of Orange 3 from the TRI dyebath and that of quinizarine from the ISO one were 30 (60—85 °C) and 80 kcal/mol (135—145 °C) respectively. That from ISO was very much larger than that from TRI, the

latter being nearly identical with that from TCE.[9]

The surface concentrations from the TRI and ISO dyebaths, shown in Tables 1 and 2, decreased with an increase in the temperature.

Transition Phenomena. A transition region was found above 145 °C in the Arrhenius plots of the diffusion coefficient from ISO (Fig. 2). In those from TRI, it was considered that there were three transitions—above 85 °C, between 50 and 60 °C (a shoulder), and below 40 °C. According to Ribnick, the glass-transition temperature, T_g, of PET has been reduced to a lower temperature by TRI than by TCE.[6] In a previous paper, a transition point at 60 °C and two transition regions between 95 and 110 °C and below 50 °C have been observed in the diffusion of C.I. Disperse Violet 1 from the TCE dyebath (*cf.* Fig. 2).[9] In comparison with the case from the TCE dyebath, it can be concluded that the transition region below 40 °C is the T_g of PET swollen by TRI, though the upper limit of T_g is reduced to 40 °C. A transition region between 50 and 60 °C, appearing as a shoulder in Fig. 2, may correspond to the transition at 60 °C from the TCE dyebath, though the lower limit is reduced to 50 °C.

The transition correlated with the maximum crystallization rate of PET[13] was observed as a trasition region above 145 °C in the diffusion in PET from the ISO dyebath and as a transition region above 85 °C in that from the TRI one. It has been observed as a transition region between 125 and 145 °C in water[8] and as one between 95 and 130 °C in TCE.[9] The lower limit of this transition in ISO was higher than that in water and TCE, while that in TRI was lower. Therefore, ISO has no capability to affect the properties of PET, the transitions in PET-ISO system being considered to be nearly identical with those of PET in the dry state. On the other hand, TRI has a more profound effect on PET than do water and TCE.

TABLE 3. DYEING OF C. I. DISPERSE ORANGE 3 FROM THE TRI AND ISO DYEBATH (0.2 g dye/100 ml solvent) IN ADDITION WITH WATER

Dyebath		Diffusion time (min)	D (cm²/min)	C_0 (g dye/kg PET)
Solvent (Temp.)	Water added (ml)			
TRI (70°C)	0	120—150	3.34×10^{-8}	2.18
	0.1	120—150	3.33×10^{-8}	2.38
	0.3	120—150	3.58×10^{-8}	2.30
	0.5	120—150	3.45×10^{-8}	2.20
	1.0	120—150	3.47×10^{-8}	2.36
ISO (90°C)	0	12870	3.07×10^{-11}	6.47
	0.1	12860	3.50×10^{-11}	10.5
	0.3	12860	3.75×10^{-11}	9.20
	0.5	12865	3.84×10^{-11}	9.41

Standing times in the TRI system for dissolving water and dye added were about 1 and 1—2 days, respectively. Those in the ISO system were 28 and 20 hrs, respectively. Glass-stoppered diffusion bottles were used to keep the dyebath from evaporation.

Mean values were shown in the diffusion coefficient and surface concentration of the TRI system.

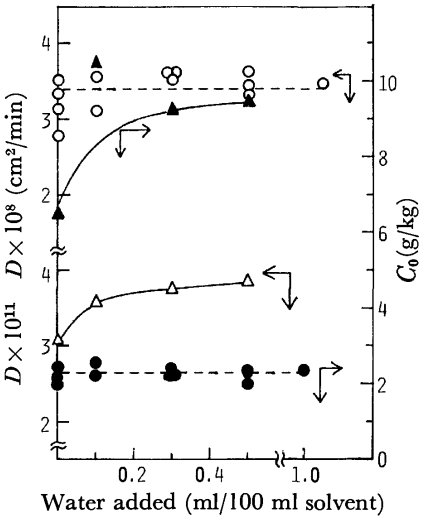

Fig. 3. The diffusion coefficients D and surface concentration C_0 of C. I. Disperse Orange 3 when water was added to the solvent dyebath (0.2 g dye/100 ml solvent).

Dyebath	D	C_0
ISO (at 90 °C)	△	▲
TRI (at 70 °C)	○	●

The Effect of Water Added to the Solvent Dyebath. The effect of the addition of water to the ISO dyebath on the diffusion and adsorption of Orange 3 at 90 °C is shown in Fig. 3 and Table 3. The solubility of water in ISO can be estimated from the data reported by Englin *et al.* to be about 0.3 wt% at 90 °C.[14] The diffusion coefficients and surface concentrations of Orange 3 from ISO increased with an increase in the addition of water to the dyebath. On the other hand, it has been observed that the water added to the TCE dyebath has the capability of accelerating the diffusion of disperse dyes.[7] In the solvent dyeing of nylon 6, the diffusion of C. I. Disperse Violet 1 from the TCE dyebath has been slower than that from the aqueous one.[15] The water added to the TCE dyebath, however, has accelerated the diffusion in nylon. These facts show that the water added to the TCE and ISO dyebath promotes the diffusion of disperse dyes in PET and nylon.

In order to elucidate these phenomena, the effect of the addition of water on diffusion and adsorption from the TRI dyebath has been examined. The solubility of water in TRI at 90 °C can be estimated from McGovern's data to be 0.15 g water/100 g TRI.[16] The results in Fig. 3, however, show that the diffusion coefficients and the surface concentrations of Orange 3 did not change within the range of experimental error when water was added to the TRI dyebath. It may be considered that, as TRI with an active hydrogen atom is adsorbed on both the hydrophilic and hydrophobic groups of PET and the water added to the TRI dyebath on the former, the adsorption of water brings about a decrease in that of TRI as a result of their competition. In the TRI system, therefore, there may be no addition effect of water. The effect of the addition of water to the TCE dyebath on the diffusion and adsorption of some disperse dyes in PET is more complicated than

that investigated in the present study; it is currently under investigation.

The authors should like to thank Prof. Kiichiro Sakaoku for his helpful discussions. Acknowledgements are also due to Nippon Kayaku Co., Ltd. for its staff's assistance in the preparation of this paper.

References

1) M. Schuler, *Text. Res. J.*, **27**, 352 (1957).
2) H. Kojima, *Kogyo Kagaku Zasshi*, **70**, 183 (1969).
3) W. S. Parkins and D. M. Hall, *Tex. Res. J.*, **43**, 115, (1973).
4) W. S. Parkins and D. M. Hall, "Textile Solvent Technology—Update '73," American Association of Textile Chemists and Colorists, p. 49 (1973).
5) W. R. Moore and R. P. Sheldon, *Polym.*, **2**, 315 (1961).
6) A. S. Ribnick and H.-D. Weigmann, *Text. Res. J.*, **43**, 316 (1973).
7) K. Gebert, *Melliand Textilber.*, **52**, 710 (1971); *J. Soc. Dyers Colour.*, **87**, 509 (1971)
8) Z. Morita, K. Koyama, and T. Iijima, *Nippon Kagaku Kaishi*, **1972**, 1522.
9) Z. Morita, R. Kobayashi, K. Uchimura, and H. Motomura, *J. Appl. Polym. Sci.*, **19**, 1095 (1975).
10) M. Sekido and K. Matsui, *Sen-i Gakkaishi*, **20**, 778 (1964).
11) J. Crank and G. S. Park, "Diffusion in Polymers," Academic Press, London (1968).
12) R. E. Pattle and P. J. A. Smith, *Trans. Faraday Soc.*, **62**, 1776 (1966).
13) N. D. Scott, *Polym.*, **1**, 114 (1960).
14) B. A. Englin, A. F. Plate, V. M. Tugolukov, and M. A. Pryanishnikova, *Khim. i Technol. Topliv. i Masel*, **10**, 42 (1965); *Chem. Abstr.*, **63**, 14608 (1965).
15) Z. Morita, K. Uchimura, and H. Motomura, This Bulletin, **48**, 1081 (1975).
16) E. W. McGovern, *Ind. Eng. Chem.*, **35**, 1230 (1943).

The Enthalpy of Vitreous Beryllium Fluoride

Seiichi TAMURA and Toshio YOKOKAWA
Department of Chemistry, Faculty of Science, Hokkaido University, Sapporo 060
(Received February 12, 1975)

The enthalpy increments of beryllium fluoride were measured by the drop method in the glassy and liquid states from 450 to 914 K. The other thermodynamic functions were also calculated. The estimated configurational entropy of the supercooled liquid showed its temperature dependence to be small compared with those of nearly all other glass-forming liquids. The theory of Adam and Gibbs was applied to explain both the present enthalpy data and the Arrhenius viscosity behaviour over an unusually wide temperature range. The similarity between beryllium fluoride and silicon dioxide was also shown with respect to the heat capacities of the glassy and supercooled liquid states.

Beryllium fluoride has been considered to be the low-temperature model of silicon dioxide. Similarities between them are observed in many respects, for instance, in the crystal structure, the structure of the vitreous state, and the low-temperature heat capacities.

On the other hand, silicon dioxide differs from nearly all other glass-forming liquids, which exhibit marked and rather abrupt increases in their heat capacities from the glassy to the liquid state. Since this glass transition occurs in most liquids at a viscosity of approximately 10^{13} poise, it should be realized around 1430 K for silicon dioxide.[1,2] The best calorimetric data on vitreous silicon dioxide indicate the heat capacity to show a smooth and monotonous temperature dependence in this temperature region.[3,4] As for beryllium fluoride, the glass transition temperature can be expected from the viscosity data to be about 580 K.[5,6] However, the enthalpy increments or the heat capacities of the vitreous beryllium fluoride have not yet been measured in this temperature region because of the spontaneous devitrification.[7,8]

Recently, the rates of crystallization were measured in our laboratory for vitreous samples of beryllium fluoride which had various different thermal histories.[9] The results showed that the glass which has been prepared by quenching, as in the previous calorimetric study described above, certainly crystallizes abruptly, but that when the glass or, more correctly, the supercooled liquid has not been brought to room temperature, it does not crystallize, not even at the most appropriate temperature for crystallization, *i.e.*, 740 K, in the case of beryllium fluoride, within the time scale of the calorimetric experiments (say, one or two hours). This is related to the nucleation process. Therefore the enthalpy of the vitreous sample can be measured in the temperature region that the previous work could not cover. The purpose of the present work is to measure the enthalpy increments and to calculate the other thermodynamic functions of vitreous beryllium fluoride in the temperature range in which the glass transition may be observed. Further, the enthalpies of the glasses at 298.15 K were measured by solution calorimetry in order to detect any effect of the heat treatments. The results of the enthalpy of the vitreous state are compared with those for silicon dioxide and other glass-forming substances.

Experimental

Materials. The beryllium fluoride used for this study was prepared from a commercial beryllium fluoride (Mitsuwa Kagaku Co., Ltd.) which was approximately 99.5 moles per cent pure. The sample was heated at about 380 K, and then the remaining water was removed by gradually raising the temperature to about 900 K over a 2-day period. The above preparation was performed in a nitrogen atmosphere. All the containers were made of platinum tubes 8 mm in diameter, 45 mm in height, and 0.2 mm thick (2 to 2.5 g). Samples of 1.5 to 2.5 g were loaded into the sample containers, after which the tops of the containers were sealed by arc-welding in a glove-box filled with nitrogen.

Drop Calorimetry. The calorimeter used for this study was a high-temperature calorimeter of the Calvet type described previously.[10] The assembly of the apparatus for the present work is identical to that used in the previous work[8] except that the thermostat maintained at 298.15 K is now replaced by an electric furnace and that liquid mercury is used instead of coarse silver powder in the calorimeter cells. The electric furnace is shown in Fig. 1. The samples were held at the A position to be maintained at 903 K and then taken down to the B position to be maintained at the measuring temperature, T, in the electric furnace. It took 40 to 70 min for the samples to achieve the thermal equilibrium, and the average cooling rates ranged from 10 to 40 K min^{-1}. Then the samples were dropped into the calorimetric receiver at room temperature. The measureing temperatures ranged from 450 to 914 K. The temperatures were measured with a calibrated chromel–alumel thermocouple in terms of IPTS-68. The energy equivalent of this calorimeter was determined by the drop method, using a calorimetric standard, synthetic sapphire, provided by the National Bureau of Standards. As a preliminary check on the accuracy of the calorimetric systems, the enthalpy increments of gold were measured at several temperatures in the temperature range of the main measurements. The enthalpy results did not deviate more than ± 0.6 per cent from the values in Kelley's table, and so the calorimetric system was assumed to be working satisfactorily.

Solution Calorimetry. The calorimeter used was of a CM-502 model micro-calorimeter (LESCA, Ltd.). Two types of glassy samples were used in this solution calorimetry. One was "quenched glass" which had been prepared by heating the sample at various temperatures above the melting point, and by then dropping it into a silver crucible at room temperature for rapid cooling. The other was "slowly cooled glass" which had been cooled slowly from 903 K to several temperatures below the melting point and then quenched in the same manner as in the drop-calorimetry experiment.

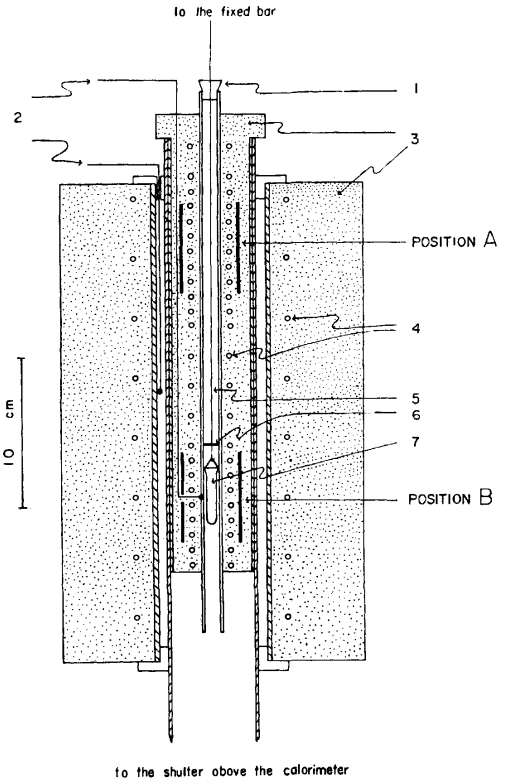

Fig. 1. Furnace assembly.
1: Cap with a pinhole, 2: thermocouples, to the temperature controllers, 3: asbestos, 4: heaters, 5: nichrom wire, 6: radiation shield fixed to nichrom wire, 7: platinum sample container.

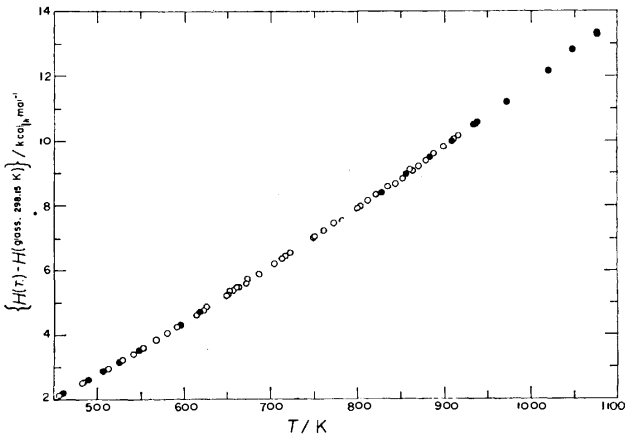

Fig. 2. Enthalpy increments of beryllium fluoride
○: Present work, ●: our previous work (Ref. 8).

These samples (about 0.5 g) were crushed to the grain sizes in order to dissolve them easily in the solvent which contained 47 g of sodium acetate in one liter of 0.1M acetic acid solution. Calorimetric calibration was performed electrically by means of the heater in the calorimeter.

Results

The results obtained by the drop method, including the data of the glass and liquid, are listed in Table 1 and are depicted in part in Fig. 2. These enthalpy increments are referred to the enthalpy of glass at 298.15 K, H (glass, 298.15 K). However, because of their very nature, the enthalpies of the glasses at room temperature might differ from each other according to the temperatures before dropping. This point was not cleared up in the previous work by Taylor and Gardner.[7] The heat of solution measurements were carried out in order to ascertain whether H (glass, 298.15 K) varies from one sample to the other. The results of the measurements are given in Table 2. From the results, the enthalpy differences, H (glass, 298.15 K) $-H$ (α-q-BeF_2, 298.15 K), in all runs appeared to have a nearly constant value, (1070 ± 60) $cal_{th}\,mol^{-1}$.* This value is in good agreement with what had been obtained by the transposed-temperature drop calorimetry where the glassy sample was prepared by quenching the melt from 903 K.[8] The investigation by the X-ray diffraction method also did not reveal any difference between the X-ray diffraction halos of glassy samples with different thermal histories. Furthermore, in order to ascertain whether the crystallization was completely prevented and whether a particular experimental value of the enthalpy suffered from the heat effect of premelting or pretransition, the so-called Shomate plot[11] was applied to the enthalpy increments, which included the present results as well as those of the glass below 630 K and the liquid from the melting point to 1083 K obtained previously.[8] The Shomate plot gives a straight line, as is depicted in Fig. 3. No crystallization effect exceeding the experimental error could be detected by this plot. Further, since any glass transition is accompanied by a heat-capacity increase around the glass-transition temperature, this plot will be bent around this temperature. A tentative plot with the increase of 0.4 $cal_{th}\,K^{-1}\,mol^{-1}$ at 580 K for this system shows a clearly distinguishable bending at this temperature; this is in contrast with the fact. Therefore, no distinction between glass and supercooled liquid is appreciable in the present system. The least-squares treatment gives the following equation

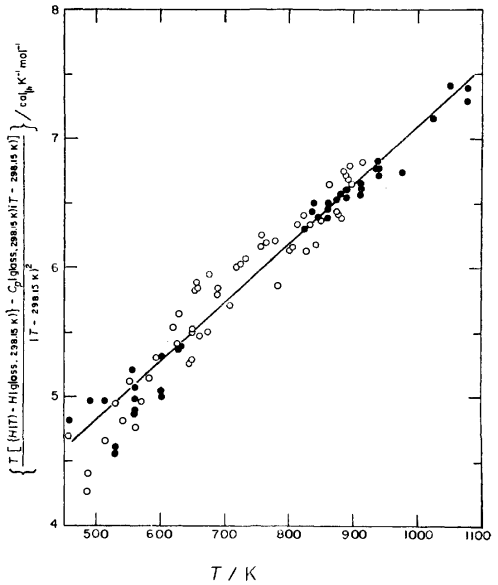

Fig. 3. Shomate plot of enthalpy increments.
○: Present work, ●: our previous work (Ref. 8).
The value of C_p (glass, 298.15 K) is cited from Ref. 7.

* Throughout this paper $cal_{th}=4.184$ J.

TABLE 1. EXPERIMENTAL VALUES OF $\{H°(T)-H°(298.15\ K)\}$ FOR BERYLLIUM FLUORIDE

Figures in parenthesis after temperature denote the number of measurements and the values in column 3 are those calculated from Eq. (1).

$\delta=\{H°(T)-H°(298.15\ K)\}$ (calc.) $-\{H°(T)-H°(298.15\ K)\}$ (expt)

$cal_{th}=4.184\ J$

T/K	$H°(T)-H°$ (glass, 298.15 K)/$cal_{th}\ mol^{-1}$ expt	calcd	δ/$cal_{th}\ mol^{-1}$
455.1	2119.7	2101.2	−18.5
456.6	2151.9	2123.4	−28.5
482.7	2494.1	2513.9	+19.8
484.6	2531.6	2542.7	+11.1
488.3	2631.8	2599.0	−32.8
502.9	2868.0	2823.1	−44.9
510.0	2959.8	2933.1	−26.7
511.0	2970.6	2948.7	−21.9
511.4	2948.2	2954.9	+ 6.7
526.1	3194.8	3185.1	− 9.7
527.0 (3)	3169.4	3199.3	+29.9
528.1	3227.9	3216.7	−11.2
539.8	3391.8	3402.3	+10.5
549.2	3570.5	3552.6	−17.9
553.6	3648.3	3623.4	−24.9
556.3	3675.9	3666.9	− 9.0
556.5	3667.2	3670.1	+ 2.9
557.5	3672.1	3686.3	+14.2
557.7	3671.5	3689.5	+18.0
558.8	3676.0	3707.3	+31.3
567.7	3837.5	3851.7	+14.2
579.7	4048.0	4047.8	− 0.2
591.1	4249.9	4235.7	−14.2
599.1 (3)	4335.0	4368.4	+33.5
600.1	4356.1	4385.1	+29.0
600.4	4354.1	4390.1	+36.0
602.1 (2)	4322.7	4418.4	+95.7
602.5	4376.7	4425.1	+48.4
602.8	4350.9	4430.1	+79.2
617.8	4714.1	4681.5	−32.6
624.0	4792.5	4786.1	− 6.4
626.1	4866.9	4821.6	−45.3
626.8 (2)	4832.3	4833.5	+ 1.2
645.1	5102.7	5145.2	+42.5
646.6	5178.2	5170.9	− 7.3
647.8	5193.4	5191.5	− 1.9
648.3	5150.9	5200.1	+49.2
648.7	5282.7	5207.0	−75.7
649.5	5292.3	5220.7	−71.6
652.8	5349.2	5277.4	−71.8
656.4	5397.9	5339.5	−58.4
660.5 (2)	5428.6	5410.3	−18.3
671.2	5572.3	5595.8	+23.5
672.0	5680.1	5609.8	−70.3
686.1	5883.3	5856.2	−27.1
686.6	5895.5	5864.9	−30.6
705.2	6174.9	6193.1	+18.2
716.4	6439.6	6392.2	−47.4
723.2	6556.6	6513.8	−42.8
728.0	6643.7	6599.8	−43.9
752.2	7112.4	7036.9	−75.5
753.4	7102.9	7058.7	−44.2
761.1	7244.2	7199.0	−45.2
773.5	7458.6	7426.1	−32.5
783.9	7524.0	7617.7	+93.7
793.5	7762.0	7795.3	+33.3
794.1	7809.2	7806.5	− 2.7
801.1	7909.7	7936.6	+26.9
803.3	7953.3	7977.5	+24.2
806.0	7972.5	8027.9	+55.4
807.4 (2)	8017.3	8054.0	+36.7
812.1	8164.8	8141.9	−22.9
818.4	8312.5	8260.0	−52.5
821.0	8343.9	8308.8	−35.1
823.0 (3)	8370.5	8346.4	−24.1
823.7	8374.7	8359.6	−15.1
824.2	8355.0	8369.0	+14.0
829.0	8376.3	8459.4	+83.1
832.1	8511.8	8517.9	+ 6.1
833.5 (2)	8580.0	8544.4	−35.6
836.6 (2)	8633.6	8603.0	−30.6
836.7	8600.4	8604.9	+ 4.5
836.9	8654.8	8608.7	−46.1
837.4	8632.0	8618.2	−13.8
837.9 (6)	8634.5	8627.7	− 6.8
838.6 (2)	8642.1	8640.9	− 1.2
839.1 (2)	8643.9	8650.4	+ 6.5
843.8	8648.0	8739.6	+91.6
846.9 (4)	8790.3	8798.5	+ 8.2
853.2	8881.0	8918.5	+37.5
859.5 (2)	9020.2	9038.8	+18.6
860.0 (2)	9035.8	9048.4	+12.6
860.3 (2)	9086.5	9054.1	−32.4
860.8	9136.4	9063.7	−72.7
861.3	9131.2	9073.2	−58.0
869.7	9219.3	9234.3	+15.0
871.6	9247.3	9270.9	+23.6
872.9 (8)	9278.2	9295.9	+17.7
873.1 (2)	9276.7	9299.7	+23.0
874.9	9288.2	9334.4	+46.2
878.8 (4)	9399.6	9409.5	+ 9.9
882.8	9407.2	9486.8	+79.6
883.0	9560.4	9490.6	−69.8
886.8	9616.7	9564.2	−52.5
888.8	9633.5	9602.9	−30.6
890.7 (2)	9641.5	9639.7	− 1.8
891.5 (2)	9676.8	9655.2	−21.6
891.7	9648.0	9659.1	+11.1
892.1	9738.1	9666.9	−71.2
892.8	9708.7	9680.5	−28.8
899.3	9803.6	9806.8	+ 3.2
909.5 (5)	9997.4	10005.8	+ 8.4
910.5 (3)	9987.2	10025.3	+38.1
910.9	9994.6	10033.2	+38.6
913.9	10141.3	10091.9	−49.4
936.1 (2)	10541.0	10528.8	−12.2
937.1	10532.8	10548.6	+15.8
937.3	10538.2	10552.5	+14.3
938.0 (4)	10552.4	10566.4	+14.0
973.1	11179.5	11266.0	+86.5
1021.6	12269.2	12249.3	−19.9
1048.9	12927.0	12811.1	−115.9
1076.4 (2)	13380.9	13383.1	+ 2.2

Table 2. Heat of solution ΔH_s of beryllium fluoride at 298.15 K[a]

T is the temperature at which the glass is maintained. $cal_{th}=4.184$ J

T / K	ΔH_s / cal_{th} mol^{-1}
quenched galss	
853.5	4645.8
853.5	4623.4
904.3	4644.1
958.1	4639.0
998.2	4573.8
998.2	4602.6
1063.1	4654.0
1133.1	4610.2
slowly cooled galss	
573.5	4635.4
675.3	4587.0
770.4	4613.5
crystal (α-quartz form)	
	3576.5
	3550.2
	3540.0

a) As for the solution, see the text.

for these enthalpy increments of the glassy through liquid beryllium fluoride:

$$\{H(T)-H(\text{glass, 298.15K})\}/(\text{cal}_{th}\ \text{mol}^{-1}) = (13.452\pm0.936)\times(T/\text{K}) + (3.6314\pm0.4260)\times10^{-3}(T/\text{K})^2 + (4.1861\pm1.5849)\times10^5(\text{K}/T) - (5692.5\pm674.7) \quad (450\text{K}<T<1083\text{K}) \quad (1)$$

Table 3. Thermodynamic functions of beryllium fluoride ($cal_{th}=4.184$ J)

T / K	$H^\circ(T)-H^\circ(\alpha\text{-q}, 298.15\ \text{K})$[a] / cal_{th} mol^{-1}	C_p° / cal_{th} K^{-1} mol^{-1}	S° / cal_{th} K^{-1} mol^{-1}	$-\{G^\circ(T)-H^\circ(\alpha\text{-q}, 298.15\ \text{K})\}/T$ / cal_{th} K^{-1} mol^{-1}
Glassy through liquid state				
450	3161	14.65	19.87	12.84
500	3913	15.41	21.45	13.62
550	4700	16.06	22.95	14.41
600	5518	16.65	24.38	15.18
650	6364	17.18	25.73	15.94
700	7236	17.68	27.02	16.68
750	8132	18.15	28.26	17.41
800	9051	18.61	29.44	18.13
823(m.p.)	9481	18.81	29.97[b]	18.45
850	9992	19.05	30.58	18.83
900	10955	19.47	31.69	19.51
950	11939	19.89	32.75	20.18
1000	12944	20.30	33.78	20.84
1050	13969	20.70	34.78	21.48
1100	15014	21.10	35.75	22.10

a) $H^\circ(\text{glass, 298.15 K})-H^\circ$ (α-q, 298.15 K) = 1135 cal_{th} mol^{-1} from Ref. 8 is used. b) estimated from the entropy of β-quartz form of BeF_2 at the melting point[8] and the present enthalpy data of the liquid.

The standard deviation is 39 cal_{th}mol^{-1}. The enthalpy increments calculated from Eq. (1) and the deviations are listed in Table 1. Some thermodynamic functions were derived from Eq. (1) with well-known equations; they are tabulated in Table 3. Fig. 4 shows the derived heat capacities as well as those of other phases.

Discussion

The present experimental results indicate two interesting facts: (1) the glass transition was not observed, and (2) the heat capacity and the temperature dependence of the entropy of the supercooled liquid are quite similar to those of the crystal. Figure 5 illustrates the entropies of the crystalline, glassy, and liquid forms as functions of the temperature. Here the entropy of fusion, ΔS_f°, was quoted from our previous work,[8] while the residual entropy of the glass at 0 K, S_{res}°, was quoted from Ref. 12. The heat capacity data of the crystal and glass at low temperatures were also quoted from the literature.[7,13] For a closer examination, the data of the residual entropy, the entropy of fusion, and the heat-capacity differences between the liquid and glassy states of various glass-forming liquids are tabulated in Table 4. The first column shows the heat-capacity differences between the liquid and glassy states as a basis for a later discussion of the glass transition. The second column is the value of $\Delta C_p/n$, where n is the number of beads defined as the smallest molecular units, whose movements may change the molecular configuration.[14] Though it is a concept devised for chain polymers, it is tentatively set at 2 for beryllium fluoride. The fact

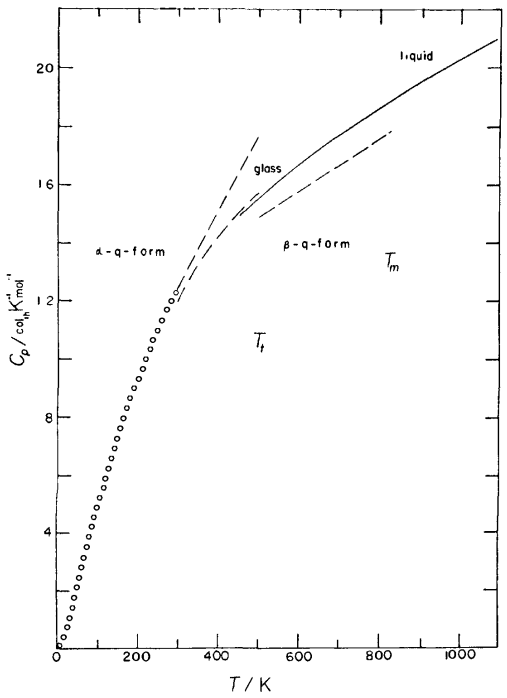

Fig. 4. Heat capacities of beryllium fluoride.
○: α-quartz form, by adiabatic calorimetry (Ref. 7),
— · —: α-quartz form, by drop calorimetry (Ref. 7),
—··—: glassy state, by drop calorimetry (Ref. 7),
------: β-quartz form, our previous work (Ref. 8),
———: glassy through liquid state, Present work.

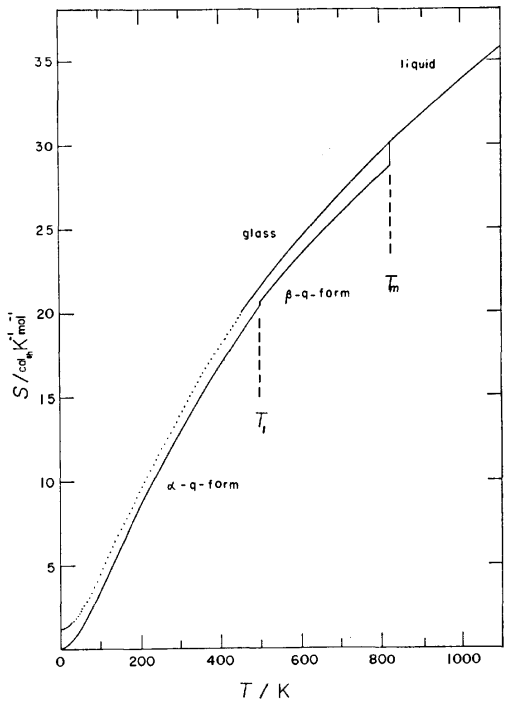

Fig. 5. Entropies of beryllium fluoride.
·····: have not been measured.

that the heat capacity of the supercooled liquid of beryllium fluoride is quite similar to that of the crystal is reflected in the similarity of the entropy trends, as may be seen in Fig. 5. ΔS_f° (T_m) is kept nearly constant down to S_{res}° at 0 K. These facts seem to be closely related to the viscosity-temperature curve of this system.

As is well known, the viscosities of liquids in a temperature range considerably above their melting points obey a two-parameter Arrhenius equation of this form:

$$\eta = A \exp(E_\eta/RT) \tag{2}$$

where η is the viscosity, A is a constant, R is the gas constant, and E_η is the activation energy of the viscous flow. However, this equation is not applicable to the group of liquids with high viscosities or to the supercooled liquids with a glass-forming tendency. For these liquids, Fulcher[15] and Tammann and Hesse[16] found an empirical equation of the form:

$$\eta = B \exp\{C/(T-T_0)\} \tag{3}$$

where B, C, and T_0 are constants.

Meanwhile, according to Adam and Gibbs,[17] the temperature dependence of such transport properties as viscosity is given by an equation of this form:

$$\eta = D \exp(\Delta\mu s_c^*/kTS(T)^{config}) \tag{4}$$

where D is a temperature-independent factor, k is Boltzmann's constant, $\Delta\mu$ is the potential energy barrier impending over the cooperative rearrangement, s_c^* is the critical configurational entropy, and $S(T)^{config}$ is the configurational entropy of liquids. Since the temperature dependence of $\Delta\mu$ is so small as to be safely neglected,[17] the above equation explicitly explains the temperature dependence of the viscosity (Eqs. 2 and 3) in terms of the configurational entropy of the glass-forming liquids. From the standpoint of the modern lattice theory of the liquid state,[18,19] any thermodynamic function of the supercooled liquid may be separated into two terms: vibrational and configurational. Thus, the entropy of the liquid, $S(T)^{liq}$, is given by $S(T)^{liq} = S(T)^{vib} + S(T)^{config}$, and since $S(T)^{vib}$ is approximately equal to the entropy of the crystal, $S(T)^{cryst}$, at the same temperature, the following equation is obtained:

$$S(T)^{config} \approx S(T)^{liq} - S(T)^{cryst} \equiv \Delta S_f(T) \tag{5}$$

It is very interesting to note that Kishimoto, Suga and Seki compared the T_0 (dynamic) in Eq. 3 with the T_2 (static) estimated in their study and found a consistency between these values.[20] Here T_2 is the temperature, as proposed by Gibbs and DiMarzio,[21] at which the configurational entropy, $S(T_2)^{config}$, of a liquid would vanish *via* a second-order thermodynamic transition if it were possible to cool the liquid in a metastable equilibrium state to T_2.

On the other hand, beryllium fluoride is also different from nearly all other glass-forming liquids in that the viscosity shows Arrhenius behaviour over a wide range of more than 10 orders of magnitude, as is shown in Fig. 6.[5,6] This behaviour is analogous to that of silicon dioxide.[1,2] This unusual viscosity behaviour of beryllium fluoride can be understood when the configura-

TABLE 4. HEAT CAPACITIES AND ENTROPIES OF GLASS-FORMING LIQUIDS

	ΔC_p° [a] / cal$_{th}$ K^{-1} mol^{-1}	$\Delta C_p^\circ/n$ [b] / cal$_{th}$ K^{-1} mol^{-1}	$\Delta S_f^\circ(T_m)$ / cal$_{th}$ K^{-1} mol^{-1}	S_{res}°(gl, 0 K) / cal$_{th}$ K^{-1} mol^{-1} obsd	S_{res}°(gl, 0 K) / cal$_{th}$ K^{-1} mol^{-1} calcd	$\Delta S_f^\circ(T_m)/S_{res}^\circ$ (gl, 0 K)
BeF_2	0.93	0.47	1.33	—	1.08[12]	1.25
SiO_2	2.1[24]	1.1	1.25[25]	0.9[26]	1.04[12]	1.20
Se	3.5[27]	3.5	3.1[29]	0.94[28]	0.78[12]	3.9_7
	3.3[28]	3.3		0.86[28]		
				0.66[30]		
B_2O_3	1.66[31]	0.55	7.3_3[32]	—	—	—
Isopentane	16.8[33]	4.2	10.9[33]	3.3_0[33]	—	3.3_0
Isopropylbenzene	15.9[20]	4.0	9.9[20]	2.8_7[20]	—	3.44

a) $\Delta C_p^\circ \equiv C_p^\circ(1, T_g) - C_p^\circ(gl, T_g)$ The values of $C_p^\circ(1, T_m) - C_p^\circ(c, T_m)$, and $C_p^\circ(gl, T_m) - C_p^\circ(c, T_m)$ are used for BeF_2 and SiO_2 respectively since $C_p^\circ(1, T_g) - C_p^\circ(gl, T_g)$ has not yet been obtained. The state symbols are l, liquid form; gl, glassy form; c, crystal form. b) n is the number of beads proposed by Wunderlich.[14]

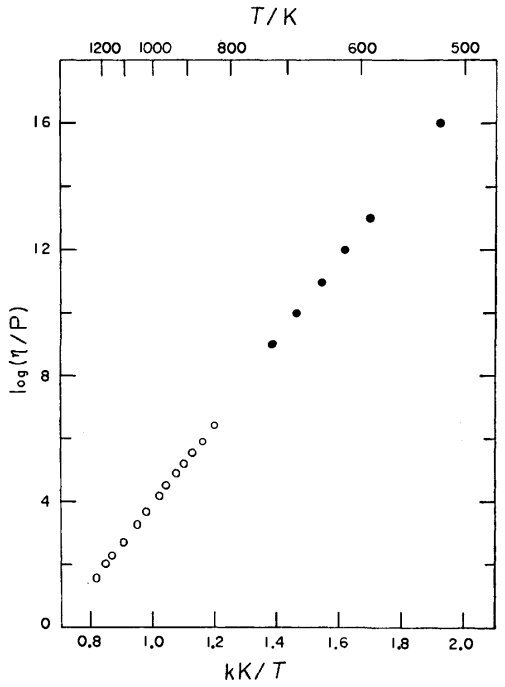

Fig. 6. Arrhenius plot of viscosity.
○: cited from Ref. 5, ●: cited from Ref. 6.

tional entropy of a liquid is independent of the temperature, as in the present work (see ΔC_p in Table 4); then Eq. 4 turns into Eq. 2. In other words, it is very difficult to estimate T_2 because $S(T)^{\text{config}}$ shows little temperature-dependence. If T_2 were estimated, it might be quite low. It is also difficult to estimate T_g because the entropy of fusion is small, comparable with the residual entropy. The small entropy of fusion implies that the structure of the liquid is not very different from that of the crystal. Thus, any heat-capacity increase at the glass-transition temperature would be negligibly small.

In conclusion, the present data, if coupled with the heat of fusion and the unusual viscosity behaviour, suggest that the structures of the crystal, glass, and liquid states are similar to each other. This is consistent with the similarities of their spectroscopic data.[22,23] No distinction between glass and the supercooled liquid of beryllium fluoride is appreciable in the present work.

References

1) E. H. Fontana and W. A. Plummer, *Phys. Chem. Glasses*, **7**, 139 (1966).
2) R. Bruckner, *Glastech. Ber.*, **37**, 413 (1964).
3) J. C. Southard, *J. Amer. Chem. Soc.*, **63**, 3142 (1941).
4) E. H. Egan, Jr., Z. T. Wakefield, and K. L. Elmore, *ibid.*, **72**, 2418 (1950).
5) C. T. Moynihan and S. Cantor, *J. Chem. Phys.*, **48**, 115 (1968).
6) S. V. Nemilov, *Fiz. Tverd. Tela*, **6**, 1375 (1964) and references cited therein.
7) A. R. Taylor, Jr., and T. E. Gardner, U. S. Bur. Mines Rept. Invest. No. 6664 (1965).
8) S. Tamura, T. Yokokawa, and K. Niwa, *J. Chem. Thermodynamics*. **7**, 633 (1975).
9) to be published.
10) T. Maekawa, T. Yokokawa, and K. Niwa, *J. Chem. Thermodynamics*, **3**, 143 (1971).
11) C. H. Shomate, *J. Phys. Chem.*, **58**, 368 (1954).
12) I. Gutzov, *Z. Phys. Chem.*, **221**, 153 (1962).
13) A. J. Leadbetter and K. E. Wycherley, *Phys. Chem. Glasses*, **12**, 41 (1971).
14) B. Wunderlich, *J. Phys. Chem.*, **64**, 1052 (1960).
15) G. S. Fulcher, *J. Amer. Ceram. Soc.*, **8**, 339 (1925).
16) G. Tammann and W. Hesse, *Z. Anorg. Allgem. Chem.*, **156**, 245 (1926).
17) G. Adam and J. H. Gibbs, *J. Chem. Phys.*, **43**, 139 (1965).
18) T. L. Hill, "Statistical Mechanics," McGraw-Hill, New York (1956).
19) S. Glasstone, K. J. Laidler, and H. Eyring, "The Theory of Rate Processes," McGraw-Hill, New York (1941).
20) K. Kishimoto, H. Suga, and S. Seki, This Bulletin, **46**, 3020 (1973).
21) J. H. Gibbs and E. A. DiMarzio, *J. Chem. Phys.*, **28**, 373 (1958).
22) A. H. Narten, *J. Phys. Chem.*, **56**, 1905 (1972).
23) A. S. Quist, J. B. Bates, and G. E. Boyd, *Spectrochimica Acta*, **28A**, 1103 (1972).
24) K. K. Kelley, U. S. Bur. Mines Bull. No. 584 (1960).
25) J. L. Holm, O. J. Kleppa, and E. F. Westrum, Jr., *Geochimica et Cosmochimica Acta*, **31**, 2289 (1967).
26) F. Simon and F. Lange, *Z. Phys.*, **38**, 227 (1926).
27) G. Tammann and H. Elsner v. Gronow, *Z. Anorg. Allgem. Chem.*, **192**, 193 (1930).
28) S. S. Chang and A. B. Bestul, *J. Chem. Thermodynamics*, **6**, 325 (1974).
29) O. Kubaschewski, *Z. Electrochem.*, **54**, 275 (1950).
30) C. T. Anderson, *J. Amer. Chem. Soc.*, **59**, 1036 (1937).
31) S. B. Thomas and G. S. Parks, *J. Phys. Chem.*, **35**, 2091 (1931).
32) J. C. Southard, *J. Amer. Chem. Soc.*, **63**, 3147 (1941).
33) M. Sugisaki, K. Adachi, H. Suga, and S. Seki, This Bulletin, 41, 593 (1968).

A Photoconductivity Study of Trapped Ionic Species in γ-Irradiated Ethylcyclohexane Glass at 77 K

Noriyuki KATO, Kenji FUEKI, and Zen-ichiro KURI
Department of Synthetic Chemistry, Nagoya University, Chikusa-ku, Nagoya 464
(Received February 27, 1975)

A photoconductivity study has been made of trapped ionic species in γ-irradiated ethylcyclohexane glass at 77 K. The photocurrent peak initially increases with an increase in the dose, reaches a maximum, and then decreases with a further increase in the dose. The experimental results indicate that the photocurrent *vs.* dose curve is probably affected by the radiolysis products. The photocurrents of γ-irradiated ethylcyclohexane–cyclopentane and 3-methylpentane glasses were also measured in the presence of biphenyl. It has been observed that electrons can be transferred almost reversibly between the biphenyl molecules and solvent traps. An analysis of the experimental data shows that only a very small fraction of the trapped electrons are responsible for the observed photoconductivity. A procedure is developed for estimating the lifetime of mobile electrons in glassy matrices.

Since the investigation of ionic processes became one of the main subjects in radiation chemistry, a great many efforts have been made to investigate the properties of trapped ionic species in glassy matrices by the techniques of ESR and optical absorption spectroscopy.

Electrical conductivity techniques have, on the other hand, been used mostly in the radiolysis of liquids. They are particularly useful, since even those ionic species can be measured which are not observable by means of ESR and optical absorption spectroscopy. In previous studies, photoconductivity studies have brought information on the energy levels of trapped electrons in the glassy matrices of MTHF,[1] 3-methylhexane,[2] and alkaline ice,[3] while thermal conductivity studies have been made on the thermal behavior of trapped ionic species in the glassy matrices of 3-methylpentane,[4,5] and of TEA[6] after γ-irradiation. The present paper will report on the photoconductivity of trapped ionic species in glassy hydrocarbon matrices.

Experimental

Materials and Sample Preparation. The ethylcyclohexane (ECH), cyclopentane (CP), and biphenyl were Tokyo Kagaku Seiki standard pure and were used as received. The Aldrich 3-methylpentane (3MP) was purified by passing it through an activated silica gel column.

The sample preparation was carried out by distilling the proper solvent, dried over calcium hydride *in vacuo*, into a conductivity cell.

Photoconductivity Apparatus. The photoconductivity cell is of a rectangular type with suprasil windows, as is shown in Fig. 1a. The electrodes of stainless steel mesh are separated from each other with a quartz ring spacer 1 mm thick.

The electric circuit is shown schematically in Fig. 1b. A series of 90 V dry batteries were used as the voltage supply. The electric current was measured with a Toa Electronics Ltd. PM-18C electrometer and recorded with a Toa Electronics Ltd. EPR-2T recorder. The lower limit of the measurable current value was of the order of 10^{-12} A.

The light sources for photobleaching were a Toshiba 500 W lamp for the IR region and a Toshiba medium-pressure mercury lamp for the UV region.

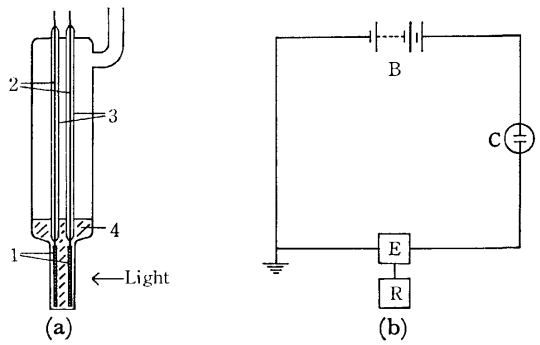

Fig. 1. (a) Schematic view of the conductivity cell: (1) stainless mesh electrode; (2) tungsten rod; (3) glass shield; (4) preparated sample.
(b) Electrical circuit: (B) applied voltage source; (C) cell; (E) electrometer; (R) recorder.

Results and Discussion

Photoconductivity of ECH Glasses. A typical photocurrent profile of the γ-irradiated and IR bleached ECH glass at 77 K is shown in Fig. 2. The photocurrent

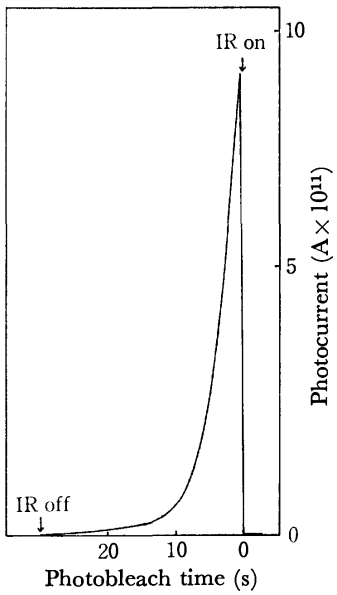

Fig. 2. Typical photocurrent profile for γ-irradiated (2×10^{19} eV/g) ECH glass at 77 K with an applied electric field of 4.5 kV/cm.

rises instantaneously within the response time of the apparatus and decays at a rate which differs slightly from one hydrocarbon matrix to another. The magnitude of the photocurrent per cm^2 is given by the following equation;

$$I = en\mu\tau E \quad (1)$$

where e is the electronic change, n is the number density of current carriers photoexited into the conduction band per second, μ is the mobility of the current carriers, τ is the average lifetime of the carriers, and E is the applied field. Since μ and τ are normaly independent of the applied field, Eq. (1) indicates that the photocurrent is linearly proportional to the applied field; this is called Ohm's law. The observed voltage-dependence of the initial photocurrent on the ECH glass was almost linearly proportional to the applied field up to 5.4×10^3 V/cm. The measurement of the photocurrent was carried out in this ohmic region.

Dose Dependence of the Photocurrent. The dose dependence of trapped electrons in γ-irradiated hydrocarbon glasses at 77 K has been previously investigated by ESR[7] and IR[8] absorption techniques. Those studies indicate that the yields of trapped electrons reach a maximum at a dose of from 1 to 2 Mrads.

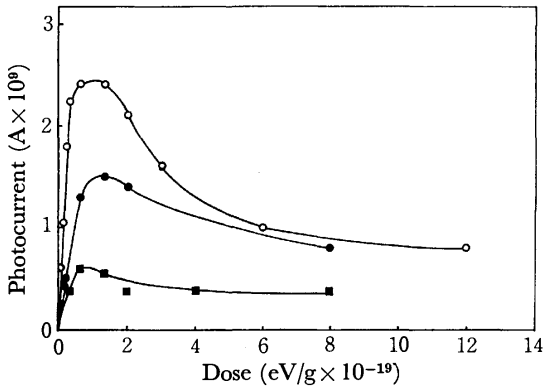

Fig. 3. Dose dependence of initial photocurrent for ECH glass at 77 K: ○, fresh sample; ●, the same sample preirradiated with a dose of 2.57×10^{20} eV/g; ■, the same sample preirradiated with a dose of 3.81×10^{20} eV/g.

The photocurrent peak *vs.* dose curves on ECH glasses at 77 K are shown in Fig. 3. The curves show two characteristic dose dependences: (a) they have a maximum value at a dose of about 0.1 Mrad, much lower than the 1 Mrad reported for 3 MP;[7] (b) they suffer from the effect of preirradiation, *i.e.*, the photocurrents diminish in intensity each time a sample is repeatedly melted, freezed, and irradiated after the previous experiment. The (b) result indicates the influence of some impurities formed by the γ-irradiation. This may be supported by the following experiment. The photocurrent-dose curve for ECH glass containing 0.04% biphenyl is shown in Fig. 4.[12] This curve is close in the shape and magnitude of the current to those for samples preirradiated with high doses (Fig. 3). The plateau of the current in an ECH-biphenyl system starts at about the same dose as that at the maximum current in pure

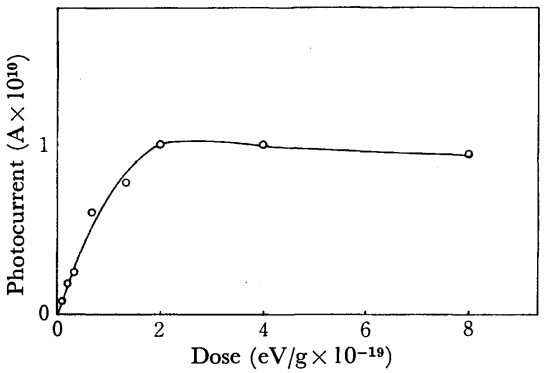

Fig. 4. Dose dependence of initial photocurrent for ECH glass containing 0.04% biphenyl at 77 K.

ECH, as is shown in Fig. 3. However, the impurities formed by radiolysis are yet unknown. Treatment with concentrated sulfuric acid could not eliminate them.

The appearance of the photocurrent maximum mentioned in the (a) result is at present a well-known phenomenon except that the dose at the maximum is much lower than that in the literature.[7,8] The decrease in the yield of trapped electrons with an increase in the dose has been interpreted in terms of the reactions of trapped electrons with trapped positive ions and radicals.[7] The (a) result may be explained by this hypothesis, but the influence of molecular products other than radicals and ionic species may also be significant, because the value of the maximum current is lowered every time the γ-irradiation is repeated.

The photocurrent profile in Fig. 2 may be represented as follows Eq. (1);

$$A = \int I dt = n_t e\mu\tau E = n_t e w \quad (2)$$

where A is the area under the photocurrent curve, n_t ($=\int n dt$) is the total number of electrons per unit of volume released by bleaching, and w is the average distance of carrier movement.

The electrons contribute to the photocurrent when they are trapped far from parent ions where the Coulomb potential is very weak. Then, n_t can be expressed as follows;

$$n_t = G_{fl}^{p}\frac{D}{100}V \quad (3)$$

where G_{fl}^{p} is the yield per 100 eV of the electrons mentioned above, D is the dose (eV/g), and V is the volume between the electrodes.

In the region of a linear current-dose relation for the fresh sample (Fig. 3), the following numerical relation was obtained from Eqs. (2) and (3), with V taken as 0.1 cm^3 and D as 5×10^{18} eV/g;

$$5.7\times10^{-9} = G_{fl}^{p}\times0.8\times10^{-3}\times w \quad (4)$$

If all of the free electrons are assumed to travel over the distance between the electrodes, w becomes 0.1 cm and G_{fl}^{p} is calculated as 7.1×10^{-5}. It should be noted that this value is at the lower limit for G_{fl}^{p}.

By further putting μ=0.1 $cm^2/V\cdot s$[9] and $E=4.5\times10^3$ V/cm into $\mu\tau E=w$, τ is obtained as 2.2×10^{-4} s. However, flash photobleaching is necessary for the

measurement of the precise value of τ, which will be carried out in a subsequent work.

Photoconductivity of Hydrocarbon Glasses in the Presence of Biphehyl. ECH glass has some cracks at 77 K, but an ECH-cyclopentane (CP) mixture (50 : 50 in volume) forms a very transparent glass. However, the photocurrent shows the same value as that for pure ECH.

ECH-CP glass containing 0.04% biphenyl yields both trapped electrons and biphenyl anions under γ-irradiation.

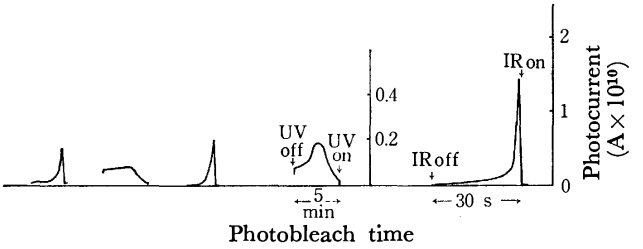

Fig. 5. Photocurrent profile for ECH–CP (50: 50 in volume) glass containing 0.04% biphenyl illuminated alternately with IR and UV light.

The photoconductivity profile of the sample illuminated alternately with IR light with $\lambda>900$ nm and UV light with $\lambda<340$ nm is shown in Fig. 5. The profile indicates that electrons can be transferred back and forth between the matrix and biphenyl molecules with little loss due to neutralization with positive ions. 3MP glass containing 0.04% biphenyl illuminated alternately with IR light and UV light showed the same photocurrent profile as the ECH–CP glass containing 0.04% biphenyl in Fig. 5. The results are the same as those found for MTHF[10] and 3MP[11] glasses spectroscopically.

The number of electrons photobleached is almost equal in each bleaching cycle except for the first cycle. The decrease in the photocurrent in the first cycle is presumably to be attributed to the recombination of electrons with positive ions in the neighborhood. The following relation may be deduced from Eq. (2);

$$\frac{A_2}{A_1} = \frac{n_t e\mu\tau_2 E}{n_t e\mu\tau_1 E} \qquad (5)$$

where the subscripts 1 and 2 stand for the bleached electrons from the solvent traps and those from the biphenyl anions respectively.

The A_2/A_1 ratio obtained from the bleaching profile is equal to the ratio of the lifetimes of the electrons, τ_2/τ_1, in the conduction state; it is 1.1×10^2.

The value of 1.1×10^2 for τ_2/τ_1 implies that the electrons detached from biphenyl anions have a mean free path, $\bar{l}$, 1.1×10^2 times as large as that for the electrons from the solvent traps, since the lifetime is represented as $\tau=\bar{l}/\mu E$. It is conceivable that this difference in lifetime is due to the difference between the average energy of electrons optically released from the biphenyl anions and that of electrons released from the solvent traps.

Photoconductivity due to Carbanions. As has been stated above, only a very small fraction of the trapped electrons are responsible for the observed photoconductivity. A major fraction of them may be captured by impurities and/or radicals and neutralized by cations. As is the case with the biphenyl anions in the above section, electrons can be photoionized from carbanions by UV light shorter than 340 nm, as is shown in Fig. 6. Such a phenomenon has already been seen by Willard *et al.* on 3MP and 3EP glass by means of optical absorption spectroscopy.[7]

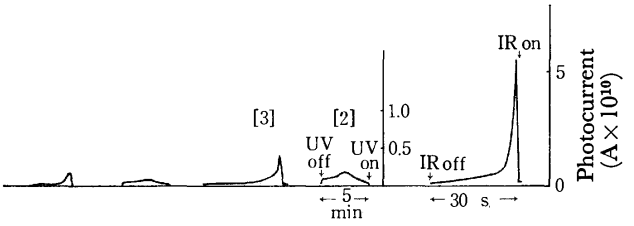

Fig. 6. Photocurrent profile for ECH–CP (50: 50 in volume) illuminated alternately with IR and UV light.

The photocurrent areas, [2] and [3], in Fig. 6 are almost equal. This might idicate that the solvent radicals have nearly the same trapping rate for mobile electrons as the solvent traps under the present experimental conditions.

References

1) T. Huang, I. Eisele, D. P. Lin, and L. Kevan, *J. Chem. Phys.*, **56**, 4702 (1972).
2) T. Huang and L. Kevan, *J. Amer. Chem. Soc.*, **95**, 3122 (1973).
3) I. Eisele and L. Kevan, *J. Chem. Phys.*, **53**, 1867 (1970).
4) B. Wiseall and J. E. Willard, *ibid.*, **46**, 4387 (1967).
5) I. Kosa Somogyi and J. Balog, "Radiation Chemistry," Advances in Chemistry Series 82, Vol. II, ed. by E. J. Hart, American Chemical Society, Washington, D. C., (1968), p. 291.
6) A. K. Munjal and L. Kevan, *J. Phys. Chem.*, **76**, 2781 (1972).
7) A. Ekstrom, R. Suenram, and J. E. Willard, *ibid.*, **74**, 1888 (1970).
8) A. Ekstrom and J. E. Willard, *ibid.*, **72**, 4599 (1968).
9) Y. Maruyama and K. Funabashi, *J. Chem. Phys.*, **56**, 2342 (1972).
10) P. J. Dyne and O. A. Miller, *Can. J. Chem.*, **43**, 2696 (1965).
11) J. B. Gallivan and W. H. Hamill, *J. Chem. Phys.*, **44**, 1279 (1966).
12) The concentration of biphenyl is given in units of weight percent.

Dielectric Relaxation in Substituted Benzaldehydes

B. SINGH and J. K. VIJ
Department of Physics, Punjabi University, Patiala-147002, India
(Received December 23, 1974)

The measurements of the relative permittivity at frequencies of 1 MHz and 9.274 GHz and of the refractive index at sodium D-line have been carried out at 30 °C for *o*-chlorobenzaldehyde (A), *m*-chlorobenzaldehyde (B), *p*-chlorobenzaldehyde (C), *o*-nitrobenzaldehyde (D), *m*-nitrobenzaldehyde (E), and *p*-nitrobenzaldehyde (F), in dilute solutions of benzene, cyclohexane, carbon tetrachloride, *p*-dioxane and Nujol. The dielectric relaxation times for the overall rotation and the electric dipole moments for these molecules have been calculated. These results have been used to calculate the dipole moment for the internal rotations, possibly of the CHO-group, in the molecule. The results are analyzed in terms of the solute-solvent interactions for these molecules. The bonding between the hydrogen atom of the aldehyde group and the oxygen atom of the dioxane molecule seems to be fairly weak. The comparative behavior of the chlorobenzaldehydes and the nitrobenzaldehydes has also been discussed.

In the past decade, attempts have been made to detect intramolecular rotations of the polar group in the organic molecules by using the dielectric dispersion techniques.[1,2] Several interesting results have been obtained especially when one of the hydrogen atoms of the benzene ring is replaced by any of the groups namely, -OH, $-OCH_3$, $-NH_2$, $-CH_2Cl$. In some cases, the results have led to the quantitative interpretations about the mechanisms of the intramolecular rotations. Measurements have been made on a particular molecule over several decades of frequency. The results have been analyzed using either the Cole-Cole[3] plot or the Scaife's polarizability[4] plot in terms of the molecular relaxation time, τ_1, the intramolecular relaxation time, τ_2, and their respective contributions to the observed dielectric dispersion.

Recently,[5,6] an attempt has been made to analyze the data in terms of two arbitrary dielectric relaxation times defined by the equations given below:

$$\tau(1) = \frac{a''}{w(a'-a_\infty)} \tag{1}$$

$$\tau(2) = \frac{a_0-a'}{wa''} \tag{2}$$

where w is the pulsatance, a_0, a', a'', a_∞ are defined in linear range by the equations,

$$\left.\begin{aligned} \varepsilon &= \varepsilon_1 + a_0 w_2, \\ \varepsilon' &= \varepsilon_1' + a' w_2, \\ \varepsilon'' &= a'' w_2, \\ \varepsilon_\infty &= \varepsilon_{1\infty} + a_\infty w_2. \end{aligned}\right\} \tag{3}$$

Subscript 1 refers to the pure solvent, 2 to the solute and the subscript ∞ refers to the values of the relative permittivity at infinite frequency. w_2 is the weight fraction of the solute. The analysis reported in the paper[6] has shown that $\tau(1)$ is dependent on τ_1,τ_2 and on the relative contribution of τ_2 to the observed dielectric loss, C_2. It has also been shown that for certain cases, $\tau(2)$ leads to τ_1. It has also been proved[7] that $\tau(1)$ is approximately equal to the dielectric relaxation time, $\tau_{G.K.}$, determined using the Gopala Krishna method.[8] It follows, therefore, that $\tau_{G.K.}$ depends on τ_1,τ_2 and C_2. As a consequence the value of $\tau_{G.K.}$ provides only with an indication of the presence of the intramolecular rotations in the molecule. The presence of these rotations is concluded only when $\tau(2)$ and $\tau_{G.K.}$ differ significantly from each other.

The following parameters, however, are introduced to quantify these rotations. First we calculate $\tau(2)$ using Eq. (2) and then we calculate a_∞ from Eq. (1) on the assumption that $\tau(1)$ is equal to $\tau(2)$. Then the parameter a_∞ would correspond to those rotations of the molecule to which the value of $\tau(2)$ corresponds. For simplification, this parameter is designated as a_{∞_2}. Now the parameter governing the slope of a_∞ *versus* concentration curve is differentiated from a_{∞_2} and is designated as a_{∞_1}. The difference between a_{∞_2} and a_{∞_1} is suggested to provide us with the magnitude of the residual dipole moment taking part in the internal rotations of the molecule.

To our knowledge, no systematic work on the measurements of the substituted benzaldehydes is available in literature. However, the values of $\tau_{G.K.}$ are reported[9] for some of the molecules in *p*-xylene solution. In this paper, we report the results of the measurements on the *o*-, *m*- and *p*-chlorobenzaldehydes and of the nitrobenzaldehydes in the dilute solutions of benzene, cyclohexane, carbon tetrachloride, *p*-dioxane and Nujol at the temperature of 30 °C. These measurements are of relevance because the results can help in advancing the understanding of the dielectric relaxation mechanism of the methoxy compounds which are being studied in Professor Walker's laboratory.[10] A methoxy or an aldehyde group when attached to the benzene ring should have similar dielectric relaxation mechanisms. The paper also deals with examining the possibility of detecting the solute-solvent interactions of the aldehydes with the solvent molecules. This is important particularly when the carbonyl groups are known to have interactions with the π-orbital electrons of the benzene molecule.

Materials and the Dielectric Measurements

The name and the specifications of the materials, as given by the manufactures, are given in parentheses of the particular sample.

1. *o*-chlorobenzaldehyde (Fluka A.G., purum).
2. *m*-chlorobenzaldehyde (Koch Light, pure grade).
3. *p*-chlorobenzaldehyde (Koch Light, pure grade).
4. *o*-nitrobenzaldehyde (Koch Light, puriss).

5. *m*-nitrobenzaldehyde (B.D.H., L. R.).
6. *p*-nitrobenzaldehyde (Koch Light, pure grade).

The materials mentioned above, with the exception of the *m*-nitrobenzaldehyde, were used without further purification. *m*-Nitrobenzaldehyde was crystallised in methanol and was thereafter vacuum-dried to remove traces of the solvent. The materials with serial number 3—6 were checked for their melting points. The refractive indices for the materials 1 and 2 were measured. For the cases studied, the agreement between the measured value and its literature value was good.

The solvents namely benzene, cyclohexane, carbon tetrachloride, *p*-dioxane and Nujol were of the same purity specifications as already given.[11] These solvents were treated similarly for further purification. The measurements of the relative permittivity at the frequency of 9.274 GHz and of the refractive index at wavelength of the sodium D-line were made in the same way as already described.[11,12] The relative permittivity measurements at frequency of 1 MHz were taken using the dielectrometer based on the principle of heterodyne beat method.[13] This piece of equipment was assembled to the same specifications as already reported in the paper by one of the authors (JKV). The Rohde and Schwarz[14] two terminal dielectric cell (Type KMF BN 5721) was used. The capacitance between the inner and the outer electrode is measured to be 37.09 pF. Both the terminals of the dielectric cell are properly screened from each other.

Results

The values of a_0, a', a'', of the so called slopes, defined by Eq. (3), are given in Table. a_D is defined as given below:

$$n_D^2 = n_{1D}^2 + a_D w_2.$$

These slopes have been determined by fitting the appropriate data of the appropriate equation using the multiple regression program on the IBM 360/44 digital computer. The standard errors of estimate, as obtained, are given with their coefficients. An examination, of the coefficients and of their standard deviations, indicates that the errors in a_0, a', a'' and a_D are of the order of 2%, 3%, 4% and 5%, respectively. Bearing in mind that the total number of observations in each case is only 7 and also taking into account the errors involved in the measurement of a particular parameter, one leads to the conclusion that Eq. (3) are valid within the experimental range of the solute concentration in dilute solutions. The range of the solute concentration by weight is approximately 7% of the solvent in each case.

The experimental data is analyzed by determining $\tau(2)$. Hereinafter this parameter would be denoted as the dielectric relaxation time for the overall rotations,

TABLE 1. VALUES OF a_0 (SLOPE OF ε *versus* CONCENTRATION CURVE) a' (SLOPE OF ε' *versus* CONCENTRATION CURVE), a'' (SLOPE OF ε'' *versus* CONCENTRATION CURVE) AND a_D (SLOPE OF n_D^2 *versus* CONCENTRATION CURVE)

Medium	a_0	a'	a''	a_D
		o-Chlorobenzaldehyde		
Benzene	7.306±0.160	4.508±0.083	2.451±0.075	0.142±0.006
Cyclohexane	5.858±0.082	3.888±0.124	1.876±0.059	0.243±0.003
Carbon tetrachloride	12.466±0.169	6.374±0.125	4.889±0.098	0.449±0.009
p-Dioxane	8.768±0.161	3.564±0.072	3.380±0.092	0.346±0.007
Nujol	5.763±0.160	2.448±0.063	1.810±0.060	0.169±0.073
		m-Chlorobenzaldehyde		
Benzene	5.638±0.130	3.448±0.049	2.118±0.068	0.158±0.001
Cyclohexane	4.820±0.002	3.096±0.040	1.670±0.050	0.220±0.059
Carbon tetrachloride	10.640±0.212	4.414±0.168	3.200±0.141	0.393±0.013
p-Dioxane	6.504±0.192	2.564±0.043	2.240±0.010	0.352±0.006
Nujol	5.265±0.003	1.435±0.040	1.03 ±0.045	0.155±0.003
		p-Chlorobenzaldehyde		
Benzene	3.522±0.057	1.920±0.05	0.913±0.029	0.164±0.001
p-Dioxane	3.937±0.038	1.890±0.06	1.430±0.040	0.361±0.007
		o-Nitrobenzaldehyde		
Benzene	14.320±0.195	7.100±0.180	5.200±0.120	0.200±0.010
Cyclohexane	10.080±0.200	6.676±0.200	3.789±0.072	0.231±0.012
Carbon tetrachloride	22.599±0.184	10.258±0.132	9.137±0.178	0.451±0.012
p-Dioxane	17.151±0.144	4.895±0.150	5.350±0.150	0.348±0.008
		m-Nitrobenzaldehyde		
Benzene	8.944±0.146	4.030±0.060	3.268±0.065	0.174±0.006
Carbon tetrachloride	15.802±0.176	6.211±0.123	5.622±0.139	0.461±0.011
p-Dioxane	10.615±0.175	3.071±0.037	3.441±0.063	0.394±0.007
		p-Nitrobenzaldehyde		
Benzene	4.559±0.003	2.281±0.102	1.206±0.055	0.174±0.006
p-Dioxane	5.771±0.003	2.065±0.032	1.811±0.051	0.393±0.005

τ. For reasons given in the introduction, this value of τ is plugged into Eq. (1) to calculate a_{∞_2}. Equation (1) is written as

$$a_{\infty_2} = a' - \frac{a''}{w\tau} \tag{4}$$

Under these conditions, the physical significance of a_{∞_2} is that it is the slope of the relative permittivity when plotted against concentration. The relative permittivity values are measured at frequency such that the electric dipole taking part in the molecular rotations ceases to follow the alternations of the field. In other words, for frequencies higher than this limit, only the dipole moment for the internal rotations can contribute to the dielectric loss in the liquid.

Now the magnitude of the dipole moment involved in the internal rotations is calculated as follows.

The parameter a_0 in the modified Higasi's equation[15] is replaced by the parameter a_{∞_2}, determined as outlined above. Higasi's equation for the dipole moment of the internal rotations is written as:

$$\mu_{\text{int.rot.}} = B\sqrt{(a_{\infty_2} - a_{\infty_1})}, \tag{5}$$

where

$$B = \frac{1}{2(\varepsilon_1+2)}\sqrt{\frac{27kTM_2}{\pi N_A d_1}}$$

and ε_1 is the relative permittivity of the solvent, k is the Boltzmann constant, T is the absolute temperature of the material, N_A is the Avogadro's number and d_1 is the density of the solvent.

The parameter a_{∞_1} is calculated from the parameter a_D by the equation

$$a_{\infty_1} = a_D + \Delta a_D$$

whereas Δa_D is calculated using the following equation suggested by Higasi *et al.*[16]

$$\frac{\Delta P_E}{P_E} = \frac{3a_D}{(\bar{n}_{2D}^2+2)(\bar{n}_{2D}^2-1)}$$

on putting

$$\frac{\Delta P_E}{P_E} = 0.05$$

where

$$\bar{n}_{2D}^2 = n_{1D}^2 + a_D$$

The subscript 1 refers to the solvent and 2 refers to the solute.

The electric dipole moment of these molecules in the dilute solutions of the non-polar solvents is calculated using the modified Higasi's equation[15] given below:

$$\mu = B\sqrt{(a_0 - a_{\infty_1})} \tag{6}$$

where the constant B is the same as in Eq. (5).

Discussion

The experimental dipole moment for *p*-chlorobenzaldehyde as shown in Table 2 agrees well with its literature value. There does not seem to be any literature value available for *o*-chloro- and *m*-chlorobenzaldehydes based on measuring the static relative permittivity in solutions. There seems to be a constant difference of 0.2 D in the moments for *o*- and *m*-nitrobenzaldehydes when compared to their literature values, a point worth noting. An experimental error of this magnitude seems to be unlikely.

The dielectric relaxation times for *o*-nitrobenzaldehyde and *p*-nitrobenzaldehyde in *p*-xylene and for *o*-chlrobenzaldehyde in *p*-dioxane have been determined by Mehrotra and Saxena[9] at a temperature of 22 °C, using the Gopala Krishna (G.K.) method.[8] The method adopted over here is different, for reasons already stated. The viscosity of *p*-xylene when compared to benzene is within 1%. A comparison of the τ values in the two solvents determined by the same method is therefore of interest. By using the G.K. method, our data yields the $\tau_{\text{G.K.}}$ values for *o*-nitrobenzaldehyde and for *p*-nitrobenzaldehyde in benzene solution as 14.1 ps and 10.8 ps respectively. On the basis of the standard errors of estimates in the parameters a_0, a', a'', and a_D, given in Table 1, the standard error in the estimate of the τ values is 10%. The agreement in the τ values is reasonably good when a temperature difference of 8 °C and a change in the nature of the solvent is considered. The τ value for *o*-chlorobenzaldehyde is 19.2 ps/30 °C when compared to its literature value of 16.6 ps/22 °C. Obviously, there is no explanation for the disagreement. The authors have not quoted the accuracy in their determination of the τ value.

The remarks made in the previous section lead us to the conclusion that the τ values given in Table 2 correspond either to those for the overall rotation or to that of the longest relaxation time of the molecule. The results also indicate that these molecules have a higher frequency dipolar absorption. This is evidenced by a large difference between the a_{∞_2} and the a_{∞_1} values, given in Table 2. The difference between the a_{∞_2} and a_{∞_1} values has also been thought of in terms of the dipole moment for the internal rotations ($\mu_{\text{int.rot}}$) of these molecules. From the structural considerations of these molecules alone, one would not expect any moment for the internal rotations for the chlorobenzene or the nitrobenzene molecules. This is because rotations of the chloro or the nitro group along their respective bonds to the carbon atom of the molecules do not give rise to a change in the direction of the dipole moment. But the situation is, however, different when the -CHO group is attached to the benzene ring. The dipole makes an angle of 55° with the C-C bond. The rotations of the -CHO group along the C-C bond of these molecules as shown

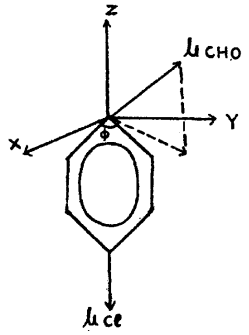

Fig. 1. *p*-Chlorobenzaldehyde.

Table 2. Calculated values of the dielectric relaxation time for overall rotation, the electric dipole moment and the dipole moment for internal rotations

Medium	$\tau(=\tau_{(2)})\times 10^{12}$ s		Dipole moments μ (D)		a_{∞_2}	a_{∞_1}	$(a_{\infty_2}-a_{\infty_1})$	$\mu_{\text{int.rot.}}$ (D)
	Expt. value	Lit. value	Experiment	Literature				
			o-Chlorobenzaldehyde					
Benzene	18.5	—	3.09	—	2.09	0.342	1.748	1.55
Cyclohexane	16.7	—	3.02	—	1.73	0.427	1.303	1.51
Carbon tetrachloride	21.5	—	3.04	—	2.47	0.687	1.783	1.17
p-Dioxane	26.4	16.6[9),a)]	3.14	—	1.37	0.543	0.827	0.99
Nujol	33.8	—	2.83	—	1.54	0.358	1.182	1.30
			m-Chlorobenzaldehyde					
Benzene	18.0	—	2.69	—	1.41	0.360	1.050	1.20
Cyclohexane	17.8	—	2.73	—	1.48	0.402	1.078	1.35
Carbon tetrachloride	33.4	—	2.78	—	2.76	0.620	2.140	1.29
p-Dioxane	30.2	—	2.67	—	1.29	0.550	0.740	0.94
Nujol	63.9	—	2.59	—	1.15	0.349	0.804	1.06
			p-Chlorobenzaldehyde					
Benzene	30.2	—	2.08	2.05[19)]	1.40	0.369	1.031	1.19
p-Dioxane	24.6	—	2.01	—	0.89	0.561	0.329	0.63
			o-Nitrobenzaldehyde					
Benzene	23.8	14.9[9),a)]	4.44	4.26[20)],	3.36	0.412	2.943	2.04
Cyclohexane	17.7	—	4.32	4.30[17)]	2.95	0.391	2.559	2.20
Carbon tetrachloride	23.2	—	4.26	—	3.49	0.721	2.769	1.52
p-Dioxane	39.5	—	4.62	4.35[20)]	2.52	0.545	1.975	1.60
			m-Nitrobenzaldehyde					
Benzene	25.8	—	3.55	3.32[20)]	1.86	0.381	1.479	1.60
Carbon tetrachloride	29.3	—	3.54	—	2.92	0.701	1.919	1.36
p-Dioxane	37.6	—	3.59	3.39[20)]	1.50	0.596	0.904	1.08
			p-Nitrobenzaldehyde					
Benzene	32.4	12.3[9),a)]	2.43	2.40[21)] 2.43[19)], 2.47[20)]	1.643	0.381	1.262	1.34
p-Dioxane	35.2	—	2.53	2.65[20)]	1.176	0.599	0.577	0.85

a) These literature values are for τ in *p*-xylene solvent and are calculated using the Gopala Krishna method.

in Fig. 1, can be depicted by resolving the dipole moment, in three components along the Cartesian axes. The problem is illustrated by considering the case of *p*-chlorobenzaldehyde as shown in Fig. 1.

Let θ be the angle between the μ_{CHO} and the C–C bond and ϕ be the angle that the projection of μ_{CHO} on the X–Y plane, makes with the x-axis.

$$\mu_x = \mu_{CHO} \sin\theta \cos\phi$$
$$\mu_y = \mu_{CHO} \sin\theta \sin\phi$$
$$\mu_z = \mu_{CHO} \cos\theta - \mu_{C-Cl}$$

On the basis of free rotations of the groups, the total dipole moment and the dipole moment for internal rotations in these molecules can, therefore, be written as

$$\mu = (\mu_{CHO}^2 + \mu_{C-Cl}^2 - 2\mu_{CHO}\cdot\mu_{C-Cl}\cdot\cos\theta)^{1/2}$$
$$\mu_{\text{int.rot.}} = \mu_{CHO} \sin\theta$$

The determined values of $\mu_{\text{int. rot.}}$ are nearly consistent with the model. However, the difference is that the angle θ comes out to be of the order of 45 °C. There are several approximations made in calculating the resultant dipole moment of the molecule. One of them is that an addition of another group to the benzaldehyde molecule leads to a change in the angle which the dipole of the –CHO group makes with the C–C bond. Secondly, the magnitude of the group moment of the –CHO group changes with an addition of another polar group to the molecule due to the phenomenon of mesomerism. It may be desirable to mention here that the dipole moment studies of the nitrobenzaldehydes[17)] reveal that the dipole of the –CHO group makes an angle of 36.5° with the C–C bond.

The dependence of the magnitude of $\mu_{\text{int. rot}}$ on the solvent can be interpreted in terms of its interactions with the –CHO group. A lower value possibly indicates hindrances to free rotations of the –CHO group. One notices that the values of the $\mu_{\text{int. rot.}}$ in cyclohexane, particularly for *o*-chlorobenzaldehyde and *o*-nitrobenzaldehyde, are higher when compared to other solvents. Therefore there is a possibility of the interaction of the remaining solvents with the benzaldehyde group. These observations are extended further by considering a plot of log τ *versus* log η, shown in Fig. 2, for these molecules. Firstly, one

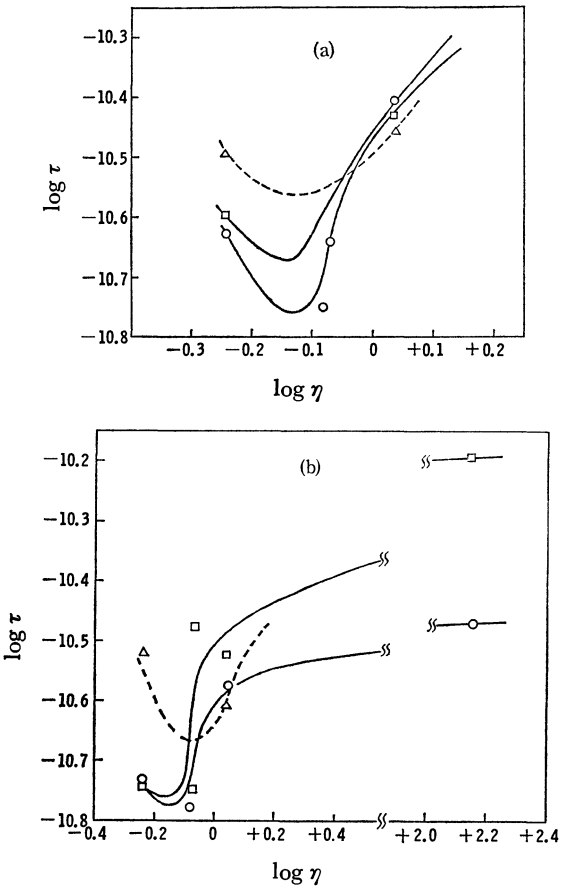

Fig. 2. Plot of $\log \tau$ *vs.* $\log \eta$.
(a) ○: *o*-Nitrobenzaldehyde, □: *m*-nitrobenzaldehyde, △: *p*-nitrobenzaldehyde.
(b) ○: *o*-Chlorobenzaldehyde, □: *m*-chlorobenzaldehyde, △: *p*-chlorobenzaldehyde.

notices that the τ values for the molecules increase from the *o*- to *p*-substituents through the *m*-position for both the chlorobenzaldehydes and nitrobenzaldehydes. Secondly, the τ values for the isomers of the nitrobenzaldehyde are larger than the corresponding isomer of the chlorobenzaldehyde. This trend is repeated by nearly all the solvents. The first observation is in line with our ealier studies[11] on the chloroanilines, and is thought of arising due to the shape of the molecule. Possibly, this indicates that the greater the departure from the spherical shape, the longer is the dielectric relaxation time for the molecule. In the case of the *p*-substituent the molecule is elongated in comparison with the *o*- and *m*-substituents and therefore the dielectric relaxation time appears to increase in the following order, *o*-, *m*-, and *p*-substituent. The second observation can be explained on the basis of the molecular volumes. The molecular volume for the nitrobenzaldehydes is approximately 20% higher than the value for the chlorobenzaldehydes.

One of the interesting features of these studies is that the dielectric relaxation time in benzene, τ_B, for the molecules under study seems to be larger than anticipated because of the low viscosity of benzene when compared with the values in other solvents. It is suggested that these molecules could be undergoing an interaction with the benzene molecules. The effect seems to be independent of the isomer and appears to be a result of the aldehyde group only. There is a possibility of transfer of π-electrons from the benzene ring to the C=O bond resulting to the formation of a complex. This could account for the increase in the dielectric relaxation time of the molecules in benzene and in a decrease of the dipole moment for the internal rotations of the –CHO group. Similarly, the dielectric relaxation times in carbon tetrachloride for the three molecules A, B and D, are larger by about 30% of the τ values of these molecules in cyclohexane. The viscosity of carbon tetrachloride over cyclohexane is only 3% greater. The anomalous behavior of the carbon tetrachloride follows a general trend exhibited by a number of molecules. This is thought of being due to the 'sticky' nature of the carbon tetrachloride which arises possibly from the fairly large short range forces between the molecules of the solute and of the carbon tetrachloride. The effect is further evidenced by comparatively small magnitude of the dipole moment for internal rotations of the –CHO group in carbon tetrachloride. The dielectric relaxation times in *p*-dioxane when compared to those in other solvents are expected on the basis of its viscosity alone. There is no great difference in the total dipole moment values of the molecules in dioxane and in benzene. These observations are in contrast to those already reported on anilines.[13,18] One would have normally expected a hydrogen bonding between the hydrogen atom of the –CHO group and the oxygen atom of the dioxane molecule. The findings suggest that such a bonding, if at all there, is fairly weak. Possibly, the oxygen atom of the –CHO group does not allow formation of the intermolecular bond. It is suggested that a qualitative experimental study of these system should be made in order to verify these predictions.

The work was financed by the Department of Atomic Energy, Government of India, to which the authors are thankful. The authors are grateful to Professor B.S. Sood, for administering the research project. One of the authors (B. Singh) is thankful to Mr. I. Krishan for his help in the measurements.

References

1) K. Higasi, "Dielectric Relaxation and Molecular Structure," Monograph Series of the Research Institute of Applied Electricity, No. 9 Hokkaido University, Sapporo, Japan (1961).
2) C. P. Smyth, "Molecular Relaxation Processes," Chemical Society Publication, No. 20, Academic Press, London (1966).
3) K. S. Cole and R. H. Cole, *J. Chem. Phys.*, **9**, 341 (1941).
4) B. K. P. Scaife, *Proc. Phys. Soc.*, **81**, 124 (1963).
5) K. Higasi, Y. Koga, and M. Nakamura, This Bulletin, **44**, 988 (1971).
6) J. K. Vij, I. Krishan, and K. K. Srivastava, *ibid.*, **46**, 17 (1973).
7) J. K. Vij and K. K. Srivastava, *Trans. Faraday Soc.*, **66**, 1087 (1970).
8) K. V. Gopala Krishna, *ibid.*, **53**, 767 (1957).

9) N. K. Mehrotra and M. C. Saxena, *Indian J. Pure Appl. Phys.*, **5**, 69 (1967).
10) A. Morita, private communication.
11) K. K. Srivastava and J. K. Vij, This Bulletin, **43**, 2307 (1970).
12) The measurements at frequency of 9.274 GHz were made in the laboratory of Dr. K. K. Srivastava, at the Panjab University, Chandigarh, India.
13) J. K. Vij and K. K. Srivastava, *Indian J. Pure Appl. Phys.*, **7**, 391 (1969).
14) Instruction manual 'Dielectric Bridge' for capacitors, Type VKB BN3520, Rohde and Schwarz Company, Germany.
15) K. Higasi, *Oyo Denki Kenkyusho Iho*, **4**, 231 (1952).
16) K. Higasi, K. Chitoku, and S. Ogata, *ibid.*, **18**, 147 (1966)
17) K. E. Calderbank and R. J. W. Le.Fe'vre, *J. Chem. Soc.*, **1949**, 1462.
18) K. Chitoku and K. Higasi, This Bulletin, **39**, 2160 (1966).
19) D. I. Coomber and J. R. Partington, *J. Chem. Soc.*, **1938**, 1444.
20) A. E. Lutskii, V. T. Alekseeva and B. P. Kondratenko, *Zhur. Fiz. Chim.*, **35**, 1706 (1961).
21) J. W. Williams, *J. Amer. Chem. Soc.*, **50**, 2350 (1928).

The Crystal Structure of Monoaquobis(1,10-phenanthroline)-copper(II) Nitrate, $[Cu(H_2O)(phen)_2](NO_3)_2$

Hisayoshi NAKAI* and Yoshito DEGUCHI

Department of Chemistry, Faculty of Science, Osaka City University, Sugimoto-cho, Sumiyoshi-ku, Osaka 558

(Received February 28, 1975)

The crystal structure of the title compound has been determined from three-dimensional X-ray data collected on Weissenberg photographs, using Cu$K\alpha$ radiation. The intensities were estimated visually with a standard scale. The structure was solved by the heavy-atom method and refined by the least-squares method. The final R value was 0.118 for 1835 observed reflections. The space group is C2/c, with $a=22.58(2)$, $b=7.23(1)$, $c=16.58(2)$ Å, $\beta=123.6(1)°$, and $Z=4$. The crystal is composed of $[Cu(H_2O)(phen)_2]^{2+}$ cations with C_2-symmetry and NO_3^- anions. The copper atom is surrounded by four nitrogen atoms of the two phenanthroline ligands (average Cu–N=2.01 Å) and a water-oxygen atom (Cu–O=2.18 Å) in a distorted trigonal-bipyramidal arrangement. One oxygen atom and two nitrogen atoms of two different phenanthroline ligands are coplanar with the central copper atom, and lines linking the copper atom with each of the axial nitrogen atoms make angles of about 10°, with the normal to the basal N–N–O plane. The electronic reflectance spectrum of this complex shows a characteristic band at about 12.5×10^3 cm^{-1}, which is analogous to that of $[CuI(bipy)_2]I$.

It is well known that 1,10-phenanthroline (=phen) forms a number of bis-phenanthroline copper (II) complexes with the general formula $Cu(phen)_2X_2\cdot nH_2O$.[1] In this case, however, the two phenanthroline molecules can not assume a square-coplanar arrangement about the copper atom because of the steric repulsions between the hydrogen atoms on the 2- and 9-carbon atoms of one molecule and the corresponding ones in the other.[2] Several investigations[3–5] have been made of the coordination geometry of these complexes, but the detailed structure has not yet been established. Jørgensen,[3] and James *et al.*,[4] have independently suggested, from their spectral studies, that the bis-phenanthroline copper(II) complexes take a *cis*-octahedral configuration in an aqueous solution. On the other hand, Faye[5] used the elementary ligand-field theory to interpret the absorption spectra of those complexes in an acetone medium, and concluded that they probably have a trigonal bipyramidal structure.

One of the present authors (H. N.) has been attempting the crystal structure analyses of bis-bipyridine and bis-phenanthroline copper(II) complexes.[6,7] This paper will describe the crystal structure of $Cu(phen)_2(NO_3)_2\cdot H_2O$.

Experimental

The green crystals of $Cu(phen)_2(NO_3)_2\cdot H_2O$ were easily prepared by adding a methanol solution of 1,10-phenanthroline (20 mmol in 30 cm^3 of the solvent) to an aqueous solution of cupric nitrate (10 mmol in 30 cm^3 of water), and were recrystallized from a water–methanol mixture. Found: C, 50.80; H, 3.27; N, 14.34%. Calcd for $Cu(phen)_2(NO_3)_2\cdot H_2O$: C, 50.93; H, 3.21; N, 14.85%.

The crystal symmetry was determined from preliminary Weissenberg photographs, which showed a Laue symmetry of 2/m and systematic absences of hkl for $h+k=2n+1$ and of $h0l$ for $l=2n+1$. Hence, the space group is C2/c or Cc. The centro-symmetric choice, C2/c, was initially taken on the basis of intensity statistics;[8] it was subsequently verified by the successful refinements of the derived structure. Cu$K\alpha$ radiation ($\lambda=1.5418$ Å) was used throughout the diffraction study. The lattice parameters were obtained by the least-squares refinement of the data from the higher-angle reflections of the $h0l$ and $hk0$ Weissenberg photographs, on which aluminium powder lines were superimposed for calibration. The density was measured by the flotation technique using a mixture of benzene and bromoform. The crystal data are listed in Table 1.

Table 1. Crystal data

$[Cu(H_2O)(phen)_2](NO_3)_2$
F.W.=566.0
Monoclinic
$a=22.58(2)$ Å
$b=7.23(1)$
$c=16.59(2)$
$\beta=123.6(1)°$
$V=2256$ Å^3
$Z=4$
$D_x=1.66$ g·cm^{-3}
$D_m=1.65$ g·cm^{-3}
$\mu=20.9$ cm^{-1} (for Cu$K\alpha$)
Space group: C2/c

The intensity data of $h0l$ to $h4l$ and $hk0$ to $hk8$ were collected by the multiple-film equi-inclination technique from two cylindrically shaped crystals with approximate dimensions of $0.2\times0.2\times0.8$ mm. The intensities of 2102 independent reflections were visually estimated by comparison with a standard scale; 267 of them were too weak to be measured and so were assumed to be zero. After the intensity data has been corrected for Lorentz-polarization, spot-extension, and absorption effects, the structure factors were placed on a common arbitrary scale by the least-squares method.

The reflectance spectrum of this compound was also measured, using a Hitachi 139 spectrophotometer fitted with a standard reflectance attachment.

Structure Determination

As described above, the space group of this compound is C2/c, and the number of the complex molecules in the unit cell is four. Therefore, the copper and oxygen

* Address correspondence to present address: Department of Chemistry, Hyogo College of Medicine, Mukogawa-cho, Nishinomiya-shi, Hyogo 663.

Table 2. The atomic coordinates, thermal parameters and their estimated standard deviations ($\times 10^4$)

The thermal parameters are of the form

$$T=\exp\{-(\beta_{11}\times h^2+\beta_{22}\times k^2+\beta_{33}\times l^2+\beta_{12}\times h\times k+\beta_{13}\times h\times l+\beta_{23}\times k\times l)\}.$$

Atom	x	y	z	β_{11}	β_{22}	β_{33}	β_{12}	β_{13}	β_{23}
Cu	5000	4001(3)	2500	14(1)	136(5)	23(1)	0	21(1)	0
O(4)	5000	7017(16)	2500	28(4)	101(27)	74(9)	0	50(10)	0
N(1)	4027(4)	4218(12)	2235(5)	14(2)	120(17)	25(4)	3(10)	20(4)	−5(14)
N(2)	5242(4)	3031(11)	3798(5)	14(2)	92(16)	20(3)	12(9)	19(4)	16(13)
C(1)	3428(5)	4850(16)	1425(7)	17(3)	139(22)	37(5)	20(13)	22(6)	20(20)
C(2)	2803(5)	5140(16)	1422(8)	15(3)	148(23)	41(6)	5(13)	23(6)	2(21)
C(3)	2791(5)	4819(16)	2204(8)	17(3)	146(23)	42(6)	−12(13)	28(7)	−20(21)
C(4)	3416(5)	4095(15)	3056(6)	15(2)	114(19)	32(5)	−8(12)	27(6)	−13(18)
C(5)	3450(5)	3649(16)	3910(7)	23(3)	144(24)	43(6)	−20(14)	44(7)	−9(20)
C(6)	4063(6)	2978(17)	4714(7)	27(3)	154(25)	41(6)	−14(15)	48(8)	−16(21)
C(7)	4686(5)	2745(15)	4692(7)	21(3)	123(21)	29(5)	−24(13)	31(6)	−8(18)
C(8)	5336(6)	2086(16)	5507(7)	27(3)	130(23)	32(5)	−13(15)	31(7)	6(19)
C(9)	5906(6)	1882(16)	5416(7)	24(3)	116(22)	33(5)	3(14)	21(7)	8(19)
C(10)	5848(5)	2366(15)	4557(6)	17(3)	117(21)	26(4)	5(12)	14(6)	11(17)
C(11)	4667(4)	3191(13)	3861(6)	14(2)	74(17)	20(4)	−1(10)	17(5)	4(15)
C(12)	4020(4)	3835(14)	3028(6)	13(2)	97(19)	24(4)	−9(11)	17(5)	−8(16)
N(3)	3428(5)	9638(13)	1586(6)	24(3)	153(21)	39(5)	−12(12)	38(6)	−35(17)
O(1)	3564(6)	9481(18)	2393(7)	58(5)	398(38)	49(5)	−10(22)	61(9)	−16(24)
O(2)	2872(6)	10495(18)	1025(9)	41(4)	368(37)	100(9)	−33(20)	54(10)	−72(30)
O(3)	3776(7)	9008(18)	1254(9)	74(6)	313(32)	123(10)	−89(24)	152(14)	−91(31)

atoms in the complex cation $[Cu(H_2O)(phen)_2]^{2+}$ must be situated at a special position, and the two phenanthroline ligands as well as the two nitrate ions are equivalent.

The position of the copper atom was readily determined from a three-dimensional Patterson map, which lies on the two-fold axis. The Fourier synthesis phased with the Cu atom gave positions of about a half of the lighter atoms; the remaining non-hydrogen atoms were obtained from the subsequent Fourier and difference Fourier maps. The structure was refined by the block-diagonal least-squares method, using the HBLS-IV program.[9] The weighting scheme used was:

$$w = 0.2 \text{ when } F_0 = 0$$

and

$$w = 1.0 \text{ when } F_0 > 0.$$

The atomic scattering curves were taken from the International Tables for X-ray Crystallography, Vol. III,[10] the real part of the anomalous dispersion correction ($\Delta f'=-2.1$) being applied for the neutral copper atom. Three cycles of refinements with anisotropic thermal parameters for the copper atom and isotropic for the remainder reduced the R value to 0.15 for 1835 non-zero reflections. A further two cycles of refinements with anisotropic thermal parameters for all the non-hydrogen atoms improved the R value to 0.118. In the last cycle of the calculations, the shift in any parameter was less than one-tenth of its estimated standard deviation. The final atomic coordinates and temperature factors are listed in Table 2. A comparison of the observed and calculated structure factors is given in Table 3**.

** Table 3 has been deposited at the Office of the Chemical Society of Japan, Document No. 7520.

Results and Discussion

The crystal consists of the $[Cu(H_2O)(phen)_2]^{2+}$ cations and the nitrate anions. Figure 1 shows the b-axis projection of the crystal structure. The bond lengths and bond angles, with their estimated standard deviations, are given in Table 4.

Figure 2 shows a schematic drawing of the complex cation $[Cu(H_2O)(phen)_2]^{2+}$, where only two nitrogen atoms of each phenanthroline ligand are shown. As is shown in Fig. 2, the complex cation has a two-fold axis passing through the oxygen atom O(4) of the coordi-

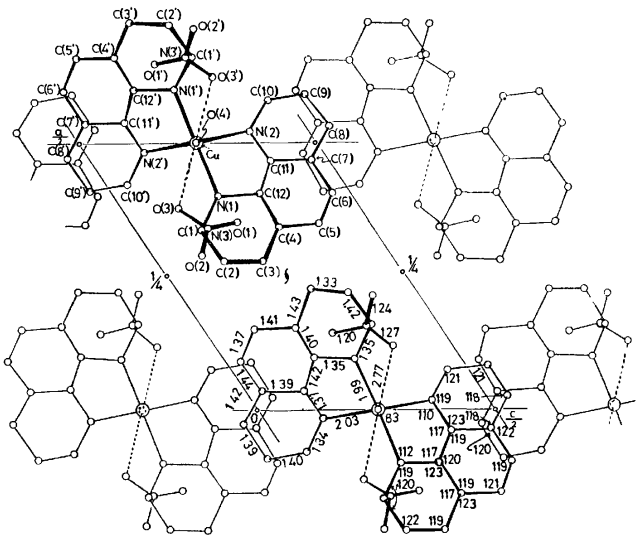

Fig. 1. The b-axis projection of the structure of $[Cu(H_2O)(phen)_2](NO_3)_2$.

Table 4. Bond distances and angles with their estimated standard deviations in parentheses[a)]

Distances (d/Å)	
Cu–N(1)=1.99(1)	C(6)–C(7)=1.44(2)
Cu–N(2)=2.03(1)	C(7)–C(8)=1.42(2)
Cu–O(4)=2.18(1)	C(8)–C(9)=1.39(2)
N(1)–C(1)=1.35(2)	C(9)–C(10)=1.40(2)
N(1)–C(12)=1.35(1)	C(11)–C(12)=1.42(1)
N(2)–C(11)=1.37(1)	C(7)–C(11)=1.39(1)
N(2)–C(10)=1.34(1)	C(4)–C(12)=1.40(2)
C(1)–C(2)=1.42(2)	N(3)–O(1)=1.20(2)
C(2)–C(3)=1.33(2)	N(3)–O(2)=1.24(2)
C(3)–C(4)=1.43(2)	N(3)–O(3)=1.27(2)
C(4)–C(5)=1.42(2)	
C(5)–C(6)=1.37(2)	O(3)···O(4)=2.77(2)
Angles[b)] (φ/°)	
N(1)–Cu–N(2)=83.0(4)	C(1)–C(2)–C(3)=122(1)
N(1)–Cu–N(2′)=100.1(4)	C(2)–C(3)–C(4)=119(1)
N(1)–Cu–N(1′)=171.0(4)	C(3)–C(4)–C(5)=123(1)
N(2)–Cu–N(2′)=139.6(4)	C(3)–C(4)–C(12)=117(1)
O(4)–Cu–N(1)=85.5(4)	C(5)–C(4)–C(12)=119(1)
O(4)–Cu–N(2)=110.0(4)	C(4)–C(5)–C(6)=121(1)
Cu–N(1)–C(12)=112.0(7)	C(4)–C(12)–C(11)=120(1)
Cu–N(2)–C(11)=110.0(7)	C(5)–C(6)–C(7)=119(1)
C(1)–N(1)–C(12)=119(1)	C(6)–C(7)–C(8)=122(1)
C(10)–N(2)–C(11)=119(1)	C(6)–C(7)–C(11)=120(1)
N(1)–C(1)–C(2)=120(1)	C(7)–C(11)–C(12)=119(1)
N(1)–C(12)–C(4)=123(1)	C(7)–C(8)–C(9)=118(1)
N(1)–C(12)–C(11)=117(1)	C(8)–C(7)–C(11)=118(1)
N(2)–C(10)–C(9)=121(1)	C(8)–C(9)–C(10)=121(1)
N(2)–C(11)–C(7)=123(1)	O(1)–N(3)–O(2)=114(1)
N(2)–C(11)–C(12)=117(1)	O(2)–N(3)–O(3)=118(1)
	O(1)–N(3)–O(3)=128(1)

a) Estimated standard deviations, shown in parentheses, are right-adjusted to the last digit of the preceding number. b) Atoms with primes are related by two-fold symmetry to the corresponding unprimed atoms (see Fig. 1 for labelling of atoms).

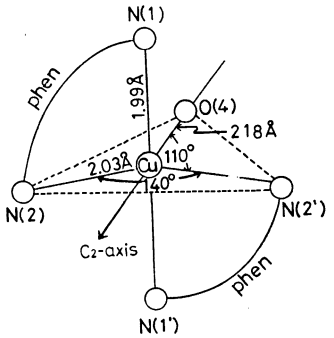

Fig. 2. A schematic drawing of the complex cation $[Cu(H_2O)(phen)_2]^{2+}$.

nated water molecule. The coordination geometry about the copper atom is a distorted trigonal bipyramid; the axial positions are occupied by N(1) and N(1′), while the Cu, N(2), N(2′), and O(4) atoms lie on the trigonal plane. The axial Cu–N bonds are 1.99 Å long and are slightly shorter than the equatorial Cu–N bonds (2.03 Å). The N(1)–Cu–O(4) angle is 85.5°; thus, the axial Cu–N bonds are not perpendicular to the trigonal plane. The angles between those axial bonds and that normal to the trigonal plane are about 10°. The angles of O(4)–Cu–N(2) and N(2)–Cu–N(2′) in the trigonal plane are 110.0 and 139.6° respectively. The N–Cu–N angles in chelate rings are 83.0°, normal for metal-phenanthroline complexes.[11–15] An analogous stereochemistry with the chromophore $[CuN_4O]$ has been found in $[Cu(NO_3)(bipy)_2]NO_3 \cdot H_2O$, where the bipy is the 2,2′-bipyridine molecule. Although these two complexes have such an analogous stereochemistry and both have the general formula of $Cu(chelate)_2(NO_3)_2 \cdot H_2O$ (chelate=phen or bipy), it must be noted that the coordinating group in the fifth position is different.

The phenanthroline ligands are planar within a maximum deviation of 0.04 Å (Table 5). The dihedral angle between the best planes of these two phenanthro-

Table 5. The deviations of the atoms from the least-squares plane

(X, Y, and Z are coordinates in Å along the a, b, and c* axes respectively)

Best plane through phenanthroline ligand			
$0.122X + 0.938Y + 0.324Z = 4.74$			
N(1)	0.02 Å	C(6)	0.02 Å
N(2)	−0.04	C(7)	0.01
C(1)	0.03	C(8)	0.00
C(2)	0.00	C(9)	0.01
C(3)	−0.04	C(10)	−0.01
C(4)	−0.01	C(11)	−0.01
C(5)	0.00	C(12)	0.01
Distance from the above plane			
Cu	−0.19 Å		
Best plane through nitrate anion			
$0.456X + 0.852Y + 0.256Z = 9.36$			
N(3)	−0.006 Å	O(1)	0.004 Å
O(2)	0.003	O(3)	0.004
Plane formed by Cu, N(1), and N(2)			
$0.006X + 0.930Y + 0.366Z = 4.01$			

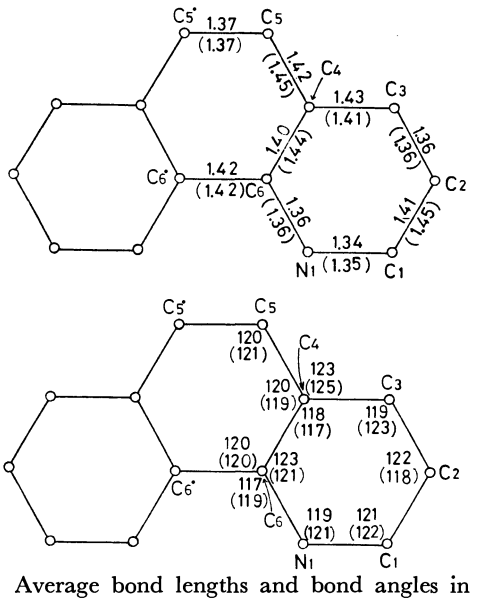

Fig. 3. Average bond lengths and bond angles in the phenanthroline ligand (values in parentheses are corresponding ones in $[Cu(phen)_3](ClO_4)_2$).

line ligands is about 40°. The bond lengths in the phenanthroline ligands range from 1.33 (2) to 1.44 (2) Å in C–C and from 1.34 (1) to 1.37 (1) Å in C–N (Fig. 1 and Table 4). Assuming that the phenanthroline ligand has a C_{2v}-symmetry, the average bond lengths and bond angles are as given in Fig. 3, where the values in parentheses are the corresponding ones in $[Cu(phen)_3](ClO_4)_2$.[11] As is shown in Fig. 3, the C(2)–C(3) and C(5)–C(5′) bond lengths are shorter than the others by 0.3—0.7 Å; the same trend has been observed in $[Cu(phen)_3](ClO_4)_2$. All the average bond lengths and angles are in good agreement with those in the $[Cu(phen)_3]^{2+}$ in view of the standard deviations.

The nitrate anions are planar (Table 5) and are linked to the water molecule in $[Cu(H_2O)(phen)_2]^{2+}$ by hydrogen bonds, which are indicated by the dotted lines in Fig. 1 (O(3)···O(4)=2.77 Å). This value is comparable to the $O(NO_3^-)\cdots O(H_2O)$ distance (2.79 Å) found in $Cu(NO_3)_2\cdot 5/2H_2O$.[16]

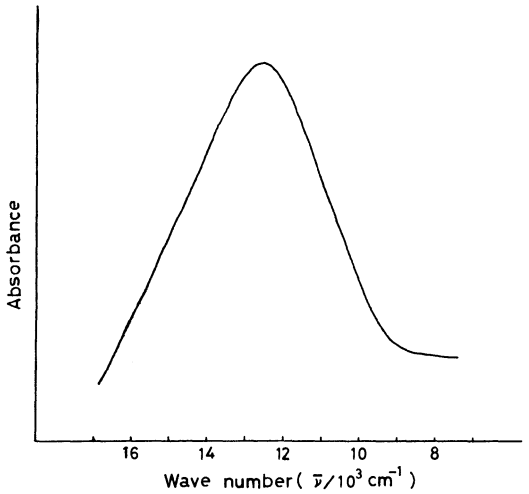

Fig. 4. Electronic reflectance spectrum of $[Cu(H_2O)(phen)_2](NO_3)_2$.

The electronic reflectance spectrum of this compound was also measured at room temperature (Fig. 4); it shows a single peak at 12.5×10^3 cm^{-1}. This is quite similar to those of $[CuI(bipy)_2]I$ and $[Cu(NH_3)(bipy)_2]X_2$ (X=ClO_4 or BF_4), but is clearly different from the spectrum of the trigonal-bipyramidal $[Cu(NO_3)(bipy)_2]^+$.[17] On examining the crystal structure of $[Cu(NO_3)(bipy)_2]NO_3\cdot H_2O$ in detail,[6] we can recognize, however, two more oxygen atoms at a distance of 2.8—3.0 Å from the copper atom.

The authors wish to express their thanks to Professor Hisao Kuroya and Dr. Shun'ichiro Ooi for their kind discussions throughout the present work.

References

1) C. M. Harris, T. N. Locker, and H. Waterman, *Nature*, **192**, 424 (1961).
2) F. P. Dwyer, H. A. Goodwin, and E. C. Gyarfas, *Austr. J. Chem.*, **16**, 544 (1963).
3) C. K. Jørgensen, *Acta Chem. Scand.*, **9**, 1362 (1955).
4) B. R. James, M. Parris, and R. J. P. Williams, *J. Chem. Soc.*, **1961**, 4630.
5) G. H. Faye, *Can. J. Chem.*, **44**, 2165 (1966).
6) H. Nakai, S. Ooi, and H. Kuroya, This Bulletin, **43**, 577 (1970).
7) H. Nakai, *ibid.*, **44**, 2412 (1971).
8) H. Lipson and W. Cochran, "The Determination of Crystal Structures," G. Bell and Sons, London, England (1957), pp. 32—41.
9) "The Universal Crystallographic Computing System (I)," Japanese Crystallographic Association (1967).
10) "International Tables for X-ray Crystallography," Vol. III, Kynoch Press, Birmingham (1962), p. 202.
11) O. P. Anderson, *J. Chem. Soc., Dalton*, **1973**, 1237.
12) P. S. Shetty and Q. Fernando, *J. Amer. Chem. Soc.*, **92**, 3964 (1970).
13) G. P. Khare and R. Eisenberg, *Inorg. Chem.*, **9**, 2211 (1970).
14) C. G. Pierpont and R. Eisenberg, *ibid.*, **9**, 2218 (1970).
15) K. R. Butler and M. R. Snow, *J. Chem. Soc., A*, **1971**, 565.
16) B. Morosin, *Acta Crystallogr.*, **B26**, 1203 (1970).
17) B. J. Hathaway, I. M. Procter, R. C. Slade, and A. A. G. Tomlinson, *J. Chem. Soc., A*, **1969**, 2219.

Ion-exchange Chromatographic Studies of the $[Co(N)_4(O)_2]^+$-type Complexes

Kazuhiro KOBAYASHI and Muraji SHIBATA

Department of Chemistry, Faculty of Science, Kanazawa University, Kanazawa 920

(Received March 20, 1975)

The following complexes of the $[Co(N)_4(O)_2]^+$ type have been prepared: $[Coox(tn)_2]^+$, *u-fac-*, *s-fac-*, and *mer*-$[Coox(NH_3)(dien)]^+$, *cis-* and *trans*-$[Coox(NH_3)_2(en)]^+$, *u-fac-* and *s-fac*-$[Co(ida)(NH_3)(en)]^+$, *fac*-$[Co(ida)(NH_3)_3]^+$, and *cis*(O)*trans*(N)*cis*(NH_3)-, *cis*(O)*cis*(N)*cis*(NH_3)-, and *cis*(O)*cis*(N)*trans*(NH_3)-$[Co(gly)_2(NH_3)_2]^+$. The geometrical structures have been determined on the basis of the PMR spectra, the absorption spectra, *etc.* Including these new complex species, twenty-six species of the $[Co(N)_4(O)_2]^+$ type have been investigated through ion-exchange chromatographic separation. The elution orders obtained have been discussed in connection with the geometrical configurations.

Recent years have seen a dramatic development in the application of ion-exchange chromatography to the preparation of isomeric complexes of cobalt(III), in particular that of isomeric complexes of the $[Co(N)_4(O)_2]^+$ type consisting of polydentate ligands. In contrast to such practical separations of the isomeric complexes, only a little attention has been focused on the relationship between the order of the chromatographic separation and the geometrical configuration; a few works[1] were, though, once undertaken in order to establish the elution order of such simple complexes as diacidotetraamminecobalt(III) ions. Very recently, a wide variety of cobalt(III) complexes were investigated by means of high-speed liquid chromatography.[2]

In the present work, experiments were designed, in the first place, to prepare some complexes of the $[Co(N)_4(O)_2]^+$ type in order to undertake the work systematically. All the complexes including the new ones were classified into several series according to their geometrical structures. Then the order of elution was determined among the complexes of each series. The comparison between the series was done by using suitable complexes as the markers.

Experimental

Preparations. The new complexes designed in this work were prepared by the methods to be described below.

a) Oxalatobis(trimethylenediamine)cobalt(III) Chloride, $[Coox(tn)_2]Cl$. To a suspension of 6.3 g (0.02 mol) of *trans*-$[CoCl_2(tn)_2]Cl$[3] in 20 ml of water, we added 3.7 g (0.02 mol) of potassium oxalate monohydrate, after which the mixture was stirred at 50 °C for 10 min. After an insoluble material had been removed by filtration, the filtrate was kept in a refrigerator overnight. The purple-red crystals thus deposited were filtered and washed with ethanol and ether. The yield was 3 g.

b) Oxalatoamminediethylenetriaminecobalt(III) Chloride, $[Coox(NH_3)(dien)]Cl$. Method 1: To a solution of 25 g (0.1 mol) of $K[Co(CO_3)_2(NH_3)_2]\cdot H_2O$[4] in 200 ml of water, we added 35.7 g of the solid material which had been isolated by saturating an aqueous diethylenetriamine with carbon dioxide; thereafter the mixture was stirred at room temperature for a day. To the resulting red solution oxalic acid was added until the solution showed a pH of *ca.* 3. The solution was again stirred at room temperature for a day. After the removal of insoluble white precipitates by filtration, the filtrate was found to be contain three geometrical isomers of the desired complex, their formation ratio being estimated to be *u-fac*: *s-fac*: *mer*=59: 6: 35 by means of ion-exchange chromatography (the symbols *s-* and *u-* indicate the structures with and without a plane of symmetry respectively).

Method 2: To a solution containing 0.7 g (0.005 mol) of ammonium oxalate in 50 ml of 2.8% aqueous ammonia, we added 1.3 g (0.005 mol) of *mer*-$[CoCl_3(dien)]$;[5] the mixture was then stirred at room temperature for 1.5 hr. The mixture contained mainly two geometrical isomers of the complex, their formation ratio being estimated to be *u-fac*: *mer*=8: 92.

c) Oxalatodiammineethylenediaminecobalt(III) Chloride, $[Coox(NH_3)_2(en)]Cl$. This complex was prepared from *trans*(NH_3)-$[CoCl_2(NH_3)_2(en)]Cl$.[6] A solution containing 3.0 g (0.015 mol) of the dichloro complex and 2.2 g (0.015 mol) of potassium oxalate monohydrate in 20 ml of water was warmed at 60 °C for 30 min. When the warm solution was allowed to stand at room temperature for some time, pink precipitates appeared. The substance was filtered and washed with ethanol and ether. The yield was 0.8 g. When the filtrate was kept in a refrigerator, red crystals were deposited, along with a small amount of the pink precipitates. The yield of this crude product was 1.2 g. The product was recrystallized twice from water. The pink complex was identified as the *cis*(NH_3) isomer, and the red one, as the *trans*(NH_3) isomer, from their absorption and PMR spectra.

d) Iminodiacetatoammineethylenediaminecobalt(III) Chloride, $[Co(ida)(NH_3)(en)]Cl$. To a green solution of tricarbonatocobaltate(III)[4] $(Co(NO_3)_2\cdot 6H_2O$, 0.1 mol scale) we added a mixture of 16 g (0.12 mol) of iminodiacetic acid and 20 ml of concd aqueous ammonia; the mixture was then stirred at 50 °C for 10 min. To the resulting blue solution we added 7.2 g (0.12 mol) of ethylenediamine and 1 g of activated charcoal. The mixture was stirred vigorously at room temperature for a day. After the charcoal had then been filtered off, the filtrate was acidified with aqueous perchloric acid until the solution showed a pH of *ca.* 3, and then again filtered to remove the precipitated material. The solution thus obtained contained *u-fac* and *s-fac* isomers in the formation ratio of 88: 12.

e) Iminodiacetatotriamminecobalt(III) Chloride, $[Co(ida)(NH_3)_3]Cl$. To a green solution of tricarbonatocobaltate (III)[4] $(Co(NO_3)_2\cdot 6H_2O$, 0.1 mol scale) we added a mixture of 16 g (0.12 mol) of iminodiacetic acid and 20 ml of concd aqueous ammonia, after which the whole was stirred at 50 °C to give a blue solution (*ca.* 10 min). Twenty ml of concd aqueous ammonia and 1 g of activated charcoal were then added to the solution, and the mixture was stirred again at 50 °C for 2 hr. After the charcoal has subsequently been removed by filtration, the deep red filtrate was neutralized with aqueous hydrochloric acid and then kept in a refrigerator overnight. The red crystals thus deposited were collected and washed with ethanol and ether. The yield was 10 g. This complex was characterized as the *fac* isomer on the basis of its spectral data.

f) Bis(glycinato)diamminecobalt(III) Chloride, $[Co(gly)_2(NH_3)_2]Cl$. This was readily prepared by modifying the method for the corresponding ethylenediamine complex $[Co(gly)_2(en)]Br$.[7] A solution of 10 g (0.042 mol) of cobalt(II) chloride hexahydrate in 10 ml of water was added to another solution containing 20 ml of concd aqueous ammonia and 6.4 g (0.085 mol) of glycine in 30 ml of water. After the addition of 10 g of lead dioxide, the solution was heated on a water-bath for 30 min. The reaction was completed by adding 10 more grams of lead dioxide and by then warming the solution for an hour. After having been cooled in a refrigerator overnight, the solution was filtered. The red solution thus obtained contained three *cis*(O) isomers; the formation ratio was found to be *cis*(O)*trans*(N)*cis*(NH_3): *cis*(O)*cis*(N)*cis*(NH_3): *cis*(O)*cis*(N)*trans*(NH_3)=46: 49: 5.

The other known complexes used in this work were as follows: $[CoCO_3(NH_3)_4]Cl$, $[CoCO_3(en)_2]Cl$, $[Coox(NH_3)_4]Cl$, $[Coox(en)_2]Cl$, $[Comal(NH_3)_4]NO_3$, $[Comal(en)_2]I$, α-$[Coox(trien)]Cl$, β-$[Coox(trien)]ClO_4$, $[Co(ida)(dien)]Cl$ and $[Co(gly)_2(en)]Cl$. They were all prepared according to the known methods.

Elution. The columns used in this work were those containing 100—200 mesh Dowex 50W- X 8 in sodium form (diameters, 2.0—7.0 cm; resin heights, 10—50 cm). The elutions were carried out with 0.3—0.4 M NaCl aqueous solutions at rates in the range of *ca.* 0.3—1.2 ml/min. The complexes were classified into several series, and the chromatographic separation was carried out with each series.

Resolution. The optical resolution of the *cis*(O)*trans*(N)*cis*(NH_3) isomer of the $[Co(gly)_2(NH_3)_2]^+$ complex was carried out successfully by means of ion-exchange chromatography; the complex dissolved with a small amount of water was charged on a column of Dowex 50W- X 8 resin (100—200 mesh, Na-form, 2.5×50 cm). When being eluted by an aqueous solution of sodium antimony $(+)_{589}$-tartrate (0.25 M) at the rate of 0.3 ml/min, a band adsorbed on the top of the column was clearly separated into two bands. The first band corresponded to the $(-)_{589}$-antipode, and the second band, to the $(+)_{589}$-antipode.

Measurements. The absorption spectra were measured with a Hitachi EPU-2A spectrometer. The circular dichroism spectrum (CD) was recorded on a JASCO Model ORD/UV-5 spectrometer with a CD attachment. The proton magnetic resonance spectra (PMR) were recorded on a JEOL JNM-PS-100 MNR spectrometer at about 22 °C, using D_2O or a mixture of D_2O and 30% D_2SO_4 as the solvent. The values of the chemical shifts were determined in relation to the sodium D_4-trimethylsilylpropionate (TMSP) used as an internal reference.

Results and Discussion

Characterization of Complexes. The results of the elemental analysis and numerical data of the absorption spectra for the new complexes are summarized in Table 1. The geometrical structures of these complexes were determined mainly on the basis of their absorption and PMR spectra. For convenience, the PMR spectra will be discussed in the succeeding section.

The possible geometrical forms regarding the present complexes are shown in Fig. 1: There are three isomers for the $[Coox(NH_3)(dien)]^+$ complex. Among those, the *u-fac* isomer was easily characterized by its PMR spectrum, but the *s-fac* and *mer* isomers were not by their PMR spectra. However, we have found that the preparation from the *mer*-$[CoCl_3(dien)]$ complex produced one isomer predominantly. Considering this fact, the *mer*-form was tentatively assigned to that isomer obtained in a predominant yield.

Two isomers may be expected for the $[Coox(NH_3)_2(en)]^+$ complex. The complexes obtained were characterized by comparing their PMR spectra.

Table 1. Elemental analyses and absorption spectral data

Complex	Found (calcd) %			ν_I		ν_{II}		ν_{CT}	
	C	H	N	$\bar{\nu}/10^3$ cm^{-1}	log ε	$\bar{\nu}/10^3$ cm^{-1}	log ε	$\bar{\nu}/10^3$ cm^{-1}	log ε
$[Coox(tn)_2]Cl\cdot H_2O$	27.87 (27.55)	6.66 (6.37)	16.02 (16.07)	19.5	1.93	27.9	2.23	41.1	4.43
u-fac-$[Coox(NH_3)(dien)]Cl\cdot H_2O$	22.84 (22.47)	6.04 (5.67)	17.21 (17.84)	19.9	2.12	28.2	2.24	44.2	4.35
s-fac-$[Coox(NH_3)(dien)]Cl$[a]	—	—	—	20.0	—	28.2	—	44.3	—
mer-$[Coox(NH_3)(dien)]Cl\cdot H_2O$	22.60 (22.47)	6.06 (5.67)	17.36 (17.48)	20.0	2.09	28.0	2.15	44.0	4.32
cis-$[Coox(NH_3)_2(en)]Cl\cdot 1/2H_2O$	17.24 (16.82)	5.50 (5.30)	19.47 (19.10)	19.8	2.03	28.1	2.17	44.7	4.34
trans-$[Coox(NH_3)_2(en)]Cl\cdot 2H_2O$	15.67 (15.37)	6.18 (5.81)	18.10 (17.92)	19.9	1.88	28.3	2.02	45.2	4.36
u-fac-$[Co(ida)(NH_3)(en)]Cl\cdot H_2O$	22.69 (22.47)	6.05 (5.67)	17.48 (17.48)	*ca.* 17.9 20.1	sh 1.88	28.4	2.01	47.2	4.41
s-fac-$[Co(ida)(NH_3)(en)]Cl\cdot H_2O$	22.84 (22.47)	6.05 (5.67)	17.05 (17.48)	19.4	2.07	28.1	2.13	48.4	4.35
fac-$[Co(ida)(NH_3)_3]Cl\cdot H_2O$	16.68 (16.31)	5.76 (5.49)	18.66 (19.02)	19.8	1.93	28.1	2.07	49.0	4.39
cis(O)*trans*(N)*cis*(NH_3)-$[Co(gly)_2(NH_3)_2]Cl$	17.54 (17.37)	5.33 (5.11)	20.22 (20.26)	20.1	1.95	28.2	2.13	49.0	4.35
cis(O)*cis*(N)*cis*(NH_3)-$[Co(gly)_2(NH_3)_2]Cl$	17.49 (17.37)	5.53 (5.11)	19.97 (20.26)	19 6	2.03	27.8	2.11	47.6	4.34
cis(O)*cis*(N)*trans*(NH_3)-$[Co(gly)_2(NH_3)_2]Cl$	17.43 (17.37)	5.27 (5.11)	19.81 (20.26)	19.7	2.00	28.4	1.75	47.4	4.36

a) Because of the poor yield, no elemental analysis was carried out.

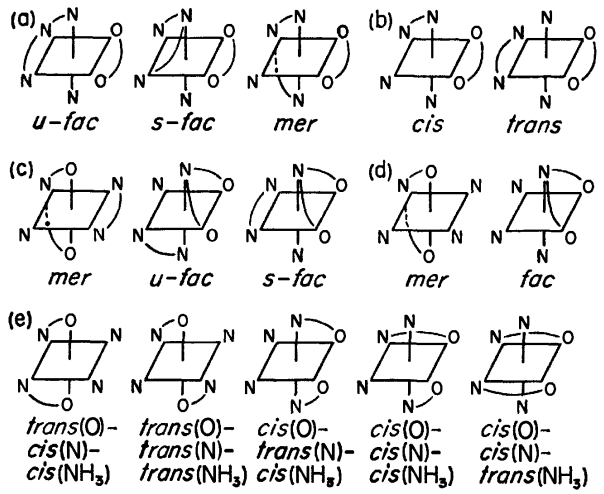

Fig. 1. Possible geometrical isomers.
(a) $[Coox(NH_3)(dien)]^+$ (b) $[Coox(NH_3)_2(en)]^+$
(c) $[Co(ida)(NH_3)(en)]^+$ (d) $[Co(ida)(NH_3)_3]^+$
(e) $[Co(gly)_2(NH_3)_2]^+$.

The $[Co(ida)(NH_3)(en)]^+$ complex can exist in three geometrical isomers. In the absorption spectrum of the *mer* isomer of the $[Co(ida)(NH_3)(en)]^+$ complex, a clear splitting of the first absorption band is to be expected from the *trans*(O) structure. In the spectrum of the known $[Co(ida)(dien)]^+$ complex,[8] the separation of the split of the first band is estimated to be about 2900 cm^{-1}. In the spectra of the present two compounds, no such remarkable separation is observed, as may be seen in Fig. 2. This suggests that both the compounds are of facial forms. It is well known that the ida chelating in the *mer*-position is very strained.[8,9] This suggests the preferential chelation of the ida in the facial configuration for the present compounds.

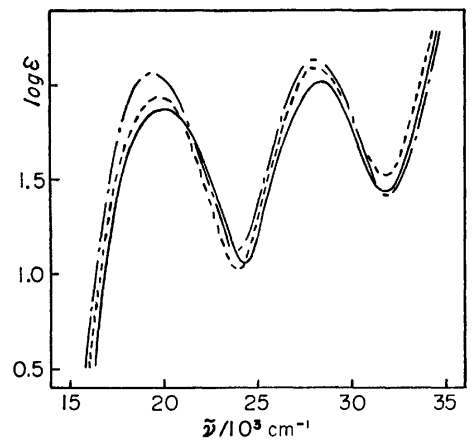

Fig. 2. Absorption spectra of iminodiacetato complexes.
———: *u-fac*-$[Co(ida)(NH_3)(en)]^+$
— · —: *s-fac*-$[Co(ida)(NH_3)(en)]^+$
------: *fac*-$[Co(ida)(NH_3)(en)]^+$.

With the $[Co(ida)(NH_3)_3]^+$ complex, two geometrical isomers can exist, but only one was actually obtained; it was identified as having the *fac* form on the basis of the absorption spectrum (Fig. 2).

Five geometrical isomers can exist for the $[Co(gly)_2(NH_3)_2]^+$ complex. Much as in the absorption spectra of the above ida complexes, the spectra of the three isomers show no splittings in their first absorption bands (Fig. 3); therefore, they may be regarded as the *cis*(O) isomers. With the related $[Co(gly)_2(en)]^+$ complex, its *trans*(O) isomer and *cis*(O) isomers were isolated,[7] but with the present diammine complex no *trans*(O) isomers were obtained. One of the three *cis*(O) isomers, *cis*(O)-*cis*(N)*cis*(NH_3), was easily assigned on the basis of its PMR spectrum. Of the other two isomers, the *cis*(O)-*trans*(N)*cis*(NH_3) isomer can be resolved into antipodes. In fact, the resolution was successful using a chromatographic method. Accordingly, the distinction between the resolvable *cis*(O)*trans*(N)*cis*(NH_3) isomer and the unresolvable *cis*(O)*cis*(N)*trans*(NH_3) isomer was made on the basis of such resolution experiments. The CD spectrum of the antipode eluted earlier is shown in Fig. 3. The spectrum shows a lower-energy negative component ($\Delta\varepsilon = -1.23$, 19300 cm^{-1}) and a higher-energy positive component ($\Delta\varepsilon = +0.41$, 22000 cm^{-1}) in the region of the first absorption band.

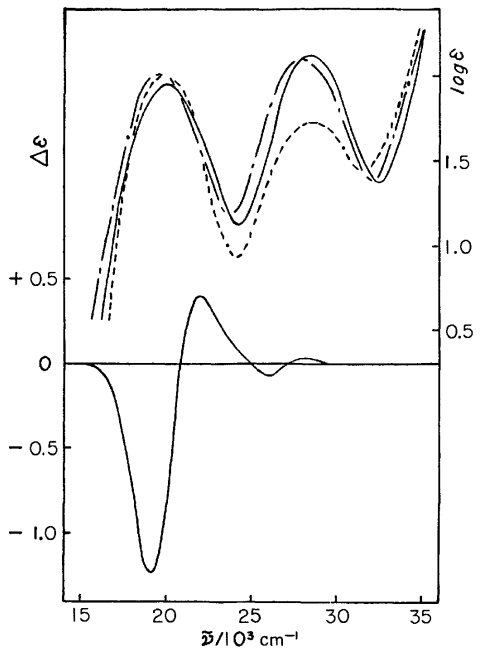

Fig. 3. Absorption and CD spectra of $[Co(gly)_2(NH_3)_2]^+$.
———: *cis*(O)*trans*(N)*cis*(NH_3)
— · —: *cis*(O)*cis*(N)*cis*(NH_3)
------: *cis*(O)*cis*(N)*trans*(NH_3).

PMR Spectra. *a)* *[Coox(NH$_3$)(dien)]Cl*: Figure 4 shows the PMR spectra of the three isomers. The spectrum of one of the two *fac* isomers shows a small peak at 6.78, two small peaks at 4.68 and 4.50, and a sharp peak at 3.63 ppm, with an integrated ratio of 1: 2: 2: 3. The spectrum of the other *fac* isomer exhibits a small peak at 6.9, a somewhat large peak at 4.94 and a sharp peak at 3.50 ppm, with a ratio of 1: 4: 3. The spectrum of the *mer* isomer exhibits a small peak at 6.27, a rather large peak at 4.90, and a sharp peak at 3.20 ppm, with a ratio of 1: 4: 3. From an inspection of the intensities, the peaks at 6.2—7.0 ppm are assignable to the NH proton resonances, the ones at 4.2—5.2 ppm, to the NH_2 proton resonances, and the ones at 3.1—3.7 ppm, to the NH_3

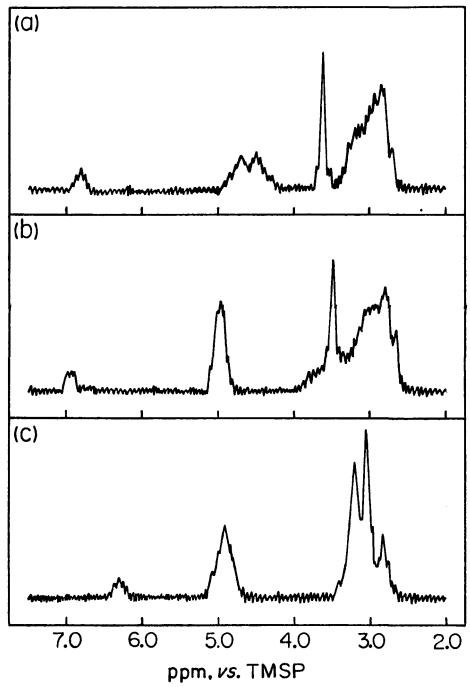

Fig. 4. PMR spectra of $[Coox(NH_3)(dien)]^+$.
(a) *u-fac* (b) *s-fac* (c) *mer* (D_2O–30% D_2SO_4).

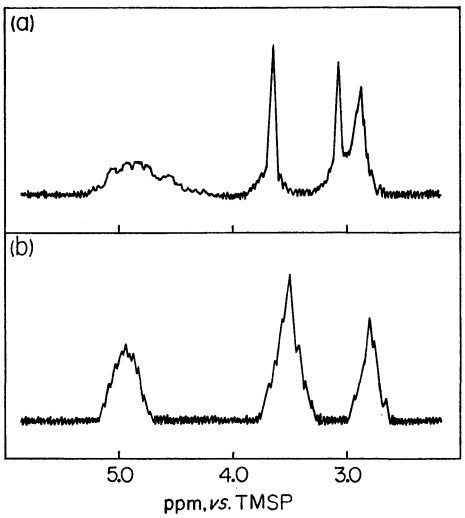

Fig. 5. PMR spectra of $[Coox(NH_3)_2(en)]^+$.
(a) *cis* (b) *trans* (D_2O–30% D_2SO_4).

proton resonances. The peaks due to the C_2H_4 groups appear at 2.6—3.4 ppm. On this basis, the *u-fac* configuration, with two non-equivalent NH_2 groups (Fig. 1), can be assigned to the complex whose spectrum shows the two peaks due to the NH_2 groups.

b) $[Coox(NH_3)_2(en)]Cl$: The PMR spectra of the two isomers are shown in Fig. 5. The spectrum of one of the two isomers shows a broad peak at 4.2—5.2 ppm, and two sharp peaks at 3.64 and 3.06 ppm, in which the integrated ratio is 4: 3: 3. The spectrum of the other isomer exhibits a broad peak at 4.94 and a sharp one at 3.51 ppm, with a ratio of 4: 6. From the intensities, the peaks at 4.2—5.2 ppm can be assigned to the NH_2 proton resonances, and those at 3.0—3.7 ppm, to the NH_3 proton resonances. The resonances due to the C_2H_4 groups appear at 2.5—3.0 ppm. The structures illustrated in Fig. 1 suggest that both the NH_2 and the NH_3 proton resonances split into two for the *cis*(NH_3) isomer. On this basis, the former complex is identified as the *cis*(NH_3) isomer. In the spectrum of the latter complex, each peak appears, in accord with the *trans*-(NH_3) structure.

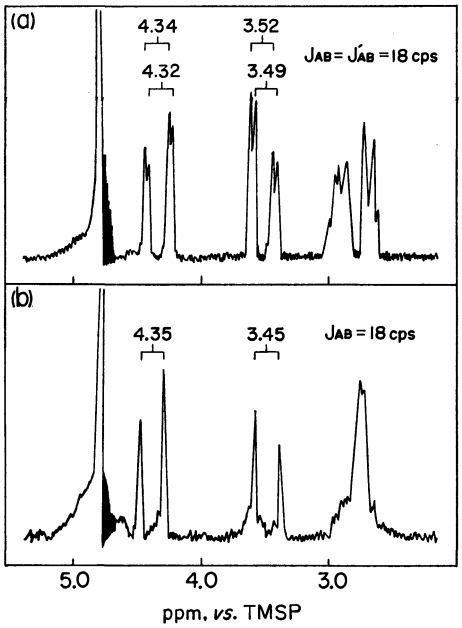

Fig. 6. PMR spectra of $[Co(ida)(NH_3)(en)]^+$.
(a) *u-fac* (b) *s-fac* (D_2O).

c) $[Co(ida)(NH_3)(en)]Cl$: The PMR spectra of the two isomers are shown in Fig. 6. The peaks due to the CH_2 proton resonances of the acetate rings of the ida appear at a lower field (3.3—4.5 ppm) than the C_2H_4 proton resonances of the en (2.6—3.0 ppm) because of the combined deshielding effects on the acetate protons from the carboxylate and amine groups.[8] When the geminal acetate protons are in magnetically different situations, the spectrum shows symmetrical AB quartets due to two spin-coupled protons. One of the two *fac* isomers exhibits two overlapping AB quartets, indicating that the two CH_2 groups are in slightly different environments, while the other isomer exhibits one quartet (Fig. 1). On this basis, the former complex is assigned to the *u-fac* isomer, and the latter, to the *s-fac* isomer.

In the spectrum of the *u-fac* isomer thus assigned, the

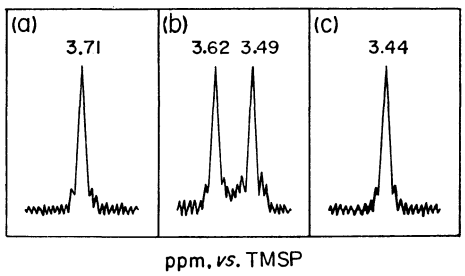

Fig. 7. PMR spectra of $[Co(gly)_2(NH_3)_2]^+$.
(a) *cis*(O)*trans*(N)*cis*(NH_3) (b) *cis*(O)*cis*(N)*cis*(NH_3)
(c) *cis*(O)*cis*(N)*trans*(NH_3) (D_2O).

C_2H_4 protons of the en give two complicated peaks because of the inequality of the two CH_2 groups, while in the spectrum of the *s-fac* isomer the C_2H_4 protons give a symmetrical peak because of the equality of the two CH_2 groups.

d) $[Co(gly)_2(NH_3)_2]Cl$: The PMR spectra of the three *cis*(O) isomers show only peaks due to the CH_2 protons of the glycinate rings (Fig. 7); one of the three isomers shows two peaks, at 3.62 and 3.49 ppm, indicating different situations of the CH_2 groups, while the other two isomers exhibit only one peak each, at 3.71 and 3.44 ppm respectively. On this basis, the *cis*(O)-*cis*(N)*cis*(NH_3) configuration can be assigned to the former one.

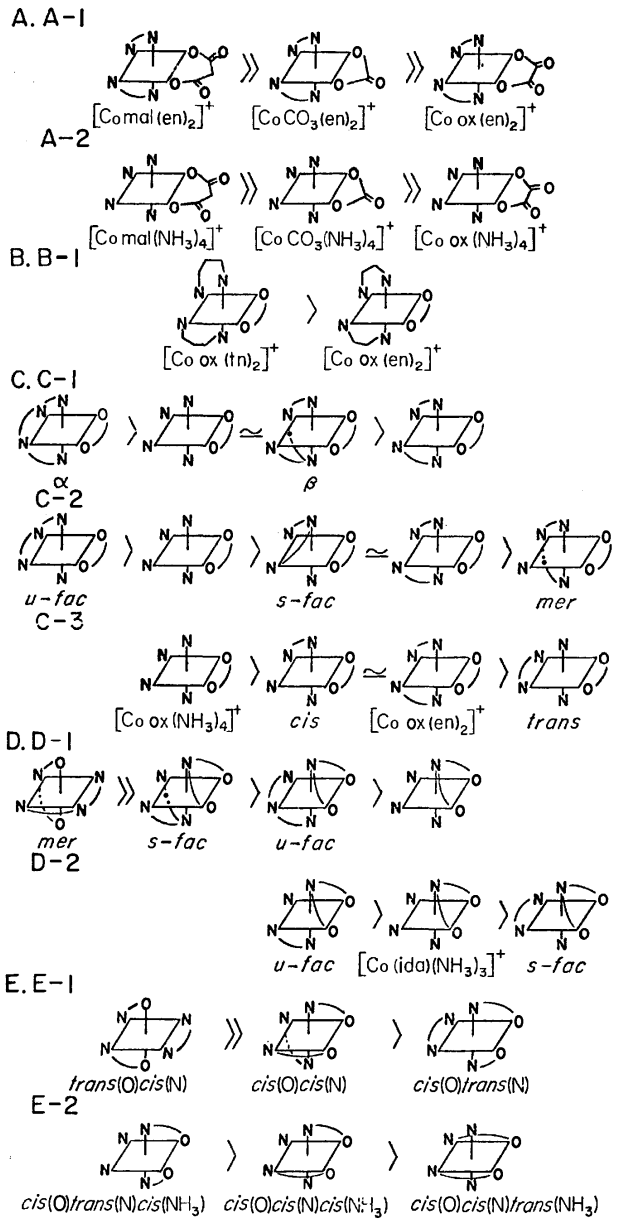

Fig. 8. Elution orders.
A. A-1: $[Co(O-O)(en)_2]^+$ A-2: $[Co(O-O)(NH_3)_4]^+$
B. B-1: $[Coox(diamine]_2]^+$
C. C-1: $[Coox(trien)]^+$ C-2: $[Coox(NH_3)(dien)]^+$
C-3: $[Coox(NH_3)_2(en)]^+$
D. D-1: $[Co(ida)(dien)]^+$ D-2: $[Co(ida)(NH_3)(en)]^+$
E. E-1: $[Co(gly)_2(en)]^+$ E-2: $[Co(gly)_2(NH_3)_2]^+$.

Elution Order. The elution orders were investigated with the series classified A—E. The results are summarized in Fig. 8, where the $>$notation indicates an earlier elution of a complex species written on the left side than that on the right side ($\gg$indicates a separation with a long distance, and$\simeq$means nearly the same order of elution).

In the A series, the carbonato, oxalato, and malonato complexes of a tetraammine type were compared. In the B series, the oxalato–ethylenediamine, and –trimethylenediamine complexes were compared. In the C series, the ox ligand was fixed and the other ligands were varied, being trien in the C-1, NH_3+dien in the C-2, and $2NH_3$+en in the C-3 series. In addition, the $[Coox(NH_3)_4]^+$ and $[Coox(en)_2]^+$ complexes were used as markers in order to compare the elution orders among the series. In the D series, the ida ligand was fixed and the other ligands were varied, being dien in the D-1 and NH_3+en in the D-2 series. In the E series, the *bis*-(glycinato)-en (E-1) and -diammine (E-2) complexes were examined.

In both the *bis*(ethylenediamine) and tetraammine complexes (A-1 and A-2), the elution order was found to be malonato$\gg$carbonato$\gg$oxalato. This fact indicates that such a variety of dicarboxylate ions makes the separation of the complexes may clear. In the B series, the elution order was found to be tn$>$en; the more bulky tn complex was eluted earlier. Between the two markers used in the C series, the $[Coox(en)_2]^+$, with two en chelate rings, was eluted later than the $[Coox(NH_3)_4]^+$, which has no such chelate rings, while the $[Coox(trien)]^+$, with three such chelate rings, was eluted faster than the $[Coox(en)_2]^+$.

In both D-1 and E-1, the *trans*(O) isomers, *mer*-$[Co(ida)(dien)]^+$ and *trans*(O)*cis*(N)-$[Co(gly)_2(en)]^+$, were eluted faster than the corresponding *cis*(O) isomers. The same results have previously been reported by other workers[7,8]; this order is in accordance with the general tendency found in the *cis* and *trans* isomers of the simple complexes.[1]

So far as the elution order of the *cis*(O) isomers is concerned, only a little discussion has been done; Legg and Cooke[8] stated that, in the $[Co(ida)(dien)]^+$ complex, the *u-fac* isomer was eluted later than the *s-fac* one because of more unsymmetrical charge distribution. This explanation is applicable to the present C-1 and D-1 series. However, in the C-2, C-3, D-2, and E series, their *cis*(O) isomers, in which more symmetrical change distributions are to be expected, were eluted later.

It is well known that a chelated dien ring situated in the *mer*-position is very distorted.[10] It is considered that, in the present C-2 series, the *mer* isomer is in such a strained configuration. In the D-1 series, the *u-fac* isomer is known to have a strained configuration because of steric repulsion between the amine substituent of the chelated ida and the $-CH_2-$ protons of the chelated dien.[8] In the D-2 series, the *s-fac* isomer may have the most strained structure for the same reason. Corresponding to these strained structures, the last eluted species in each series was the isomer mentioned above.

It is noticeable that a partial reverse in the elution orders between the E-1 and E-2 series was observed; the *cis*(O)*cis*(N) isomer was eluted faster than the *cis*(O)-*trans*(N) isomer in the E-1 series,[7] but the corresponding two isomers of the E-2 series were eluted in the reverse order.

References

1) M. Mori, M. Shibata, and J. Azami, *Nippon Kagaku Zasshi*, **76**, 1003 (1955); M. Mori, M. Shibata, and M. Nanasawa, This Bulletin, **29**, 947 (1956); M. Mori, M. Shibata, and K. Hori, *ibid.*, **34**, 1809 (1961).
2) Y. Yoshikawa, M. Kojima, M. Fujita, M. Iida, and H. Yamatera, *Chem. Lett.*, **1974**, 1163.
3) Y. Kojima, to be published.
4) M. Shibata, *Nippon Kagaku Zasshi*, **87**, 771 (1966).
5) P. H. Crayton and J. A. Mattern, *J. Inorg. Nucl. Chem.*, **13**, 248 (1960).
6) C. J. Hawkins, J. A. Stark, and C. L. Wong, *Aust. J. Chem.*, **25**, 273 (1972).
7) N. Matsuoka, J. Hidaka, and Y. Shimura, This Bulletin, **40**, 1868 (1967).
8) J. I. Legg and D. W. Cooke, *Inorg. Chem.*, **5**, 594 (1966).
9) J. Hidaka, Y. Shimura, and R. Tsuchida, This Bulletin, **35**, 75 (1962).
10) Y. Yoshikawa and K. Yamasaki, *ibid.*, **45**, 179 (1972).

Neutron-activation Analysis of Selenium, Osmium and Ruthenium in Rocks, Sediments and Biological Materials by Successive Distillations with Three Kinds of Strong Phosphoric Acid Reagents*

Kikuo TERADA, Ken MATSUMOTO, and Toshiyasu KIBA

Department of Chemistry, Faculty of Science, Kanazawa University, Kanazawa, Ishikawa 920

(Received May 22, 1975)

A new separation scheme is presented for the neutron-activation analysis of selenium, osmium and ruthenium in solid samples such as rocks, sediments and biological materials. A neutron-irradiated sample accompanying the carriers of the three elements was heated with the bromide-SPA reagent to 250 °C, whereupon selenium came out as gaseous selenium tetrabromide. The second distillation was performed by heating the residual sample with Ce(IV)-SPA reagent till 285 °C to separate osmium as osmium tetroxide gas. The last distillation of ruthenium as ruthenium tetroxide followed under heating the residue with the Cr(VI)-SPA reagent till 245 °C. Each distillate was absorbed in an appropriate absorbing solution from which selenium metal, osmium thiourea chromithiocyanato complex, and ruthenium metal were respectively recovered and they were submitted to γ-counting by means of a Ge(Li) detector coupled with a multi-channel pulse height analyzer. The chemical recoveries of the added carriers were found to be about 80% for selenium and above 90% for osmium and ruthenium.

Because of its excellent decomposing power against various insoluble solid samples, strong phosphoric acid(SPA) is very useful in chemical analysis to avoid tedious treatments for samples such as fusion with flux or dissolution by acids.[1] The SPA treatment of samples can be done in a closed system throughout the analysis, therefore losses of the elements upon the decomposition can be prevented, and the method might be most effectively employed in the activation analysis of various solid samples.

Previously[2] the present authors reported the chemical separation and determination of osmium and ruthenium in the neutron-irradiated samples such as rocks, sediments, and biological materials, where two kinds of strong phosphoric acid reagents, Ce(IV)-SPA and Cr(VI)-SPA, were employed successively. In spite of the excellent results for the separation of the two elements, it was found in the distillation of osmium tetroxide some radioactive nuclides were apt to be accompanied in the distillate: those were selenium, iodine, bromine, mercury and arsenic. Among them Se-75 had to be removed prior to the distillation of osmium because, if it came in the distillate, its photopeaks of 121.0 keV and 136.6 keV locate too close to distinguish from those of 129.4 keV and 139.0 keV of Os-191. In order to make the separation of selenium feasible in the same SPA medium, various reagent-SPA systems were examined, and finally ammonium bromide-SPA reagent has been found most preferable for the purpose.[3] By heating the sample with this ammonium bromide-SPA, selenium(IV) and (VI) can be evolved as selenium tetrabromide in gaseous state, while osmium and ruthenium are not affected at all. Accompaniment of arsenic, iodine, bromine, and mercury to the selenium tetrabromide distillate seemed unavoidable, but these do not interfere the radiochemical determination of selenium. Therefore, the distillation of selenium is well suited as the treatment preceeding the Ce(IV)-SPA treatment for osmium and the Cr(VI)-SPA treatment for ruthenium. Thus, three successive distillations for selenium by ammonium bromide-SPA, for osmium by Ce(IV)-SPA, and for ruthenium by Cr(VI)-SPA could finish the complete separation of the three elements taking only one specimen from the sample.

* Part of this work was done at the Research Reactor Institute, Kyoto University.

Experimental

Reagents. *Strong Phosphoric Acid (SPA)*: SPA was prepared from orthophosphoric acid of extra-pure reagent grade as described previously.[2,3]

Standard Selenium Solution (1 mg/ml): Anhydrous sodium selenite of guaranteed reagent grade was dissolved in 0.1 M hydrochloric acid, and the solution was standardized by iodimetric titration.

Osmium Standard Solution (2 mg/ml) and Ruthenium Standard Solution (2.5 mg/ml): Their trichlorides of guaranteed reagent grade were dissolved in 2 M hydrochloric acid, respectively. They were standardized gravimetrically as thiourea chromithiocyanato complex for osmium and as metal for ruthenium.

Radioactive Tracers: Se-75, Re-186 and Os-191 were prepared by irradiation of each pure metal of them in the KUR, Research Reactor Institute, Kyoto University. On the other hand, As-74, Br-82, Fe-59, Hg-203, I-131, Ir-192, Ru-106, Sb-124, and Sn-113, those purchased from the Radiochemical Centre (England), New England Nuclear Corp. (U.S.A.), Union Carbide Corp. (U.S.A.), Japan Atomic Energy Research Institute (Japan) and Dainabot RI Lab. (Japan). Tc-99 m was obtained by milking of Ultratechnecow which was purchased from Mallincrodt Chemical Works (U.S.A.). Other chemicals were of guaranteed reagent grade.

Apparatus. A well-type γ-ray scintillation counter, Kobe Kogyo Co., Model STL-200 and a 2-cm^3 Ge(Li) detector, ORTEC Model 8100-45 having a resolution of about 2.5 keV for the 1335-keV gamma-peak of Co-60 were used, being coupled with a 400 channel pulse-height analyser, TMC Model 401D, and a printer Model 500P, to determine the radioactivity.

The reaction vessel and the absorption tubes were all the same as those recommended in the previous report.[3]

Procedure. Each 0.5—1.0 g of the finely-ground rocks, sediments or biological materials was accurately weighed and sealed in a clean silica tube. For the standard, about 0.01 ml of 500-ppm standard selenium solution, 10-ppm standard osmium solution and 10-ppm standard ruthenium solution were placed in separate small silica tubes by microsyringe,

respectively, then weighed, dried and sealed. The samples and the standards were irradiated with a thermal neutron flux of 4.65×10^{13} n·cm^{-2}·sec^{-1} for 80 hr at Research Reactor Institute, Kyoto University.

After cooling for 4—5 days, the sample was transfered into the SPA reaction vessel together with non-radioactive carriers of the elements in question, *i.e.*, 10 mg of Se(IV), 4 mg of Os(III), and 10 mg of Ru(III).

About 30—40 g of SPA and about 0.1—0.2 g of ammonium bromide were added to the reaction vessel. The vessel was connected with the absorption tubes which contain each 10 ml of a 1: 1 v/v mixture of 0.3 M hydrochloric acid and 0.6 M perchloric acid. The air was sucked slowly from the last outlet tube with a pump and the reaction vessel was heated with an electric heater to start the reaction. Within 30—50 min the temperature of the contents in the vessel was raised to 250 °C. After the distillation, the heating was stopped and all the connections were disconnected. The absorbing solutions and washings were combined in an Erlenmeyer flask (100 ml), and the solution was made about 6 M in hydrochloric acid, heated on the water-bath, added with about 3 ml of 10% tin(II) chloride solution (in concentrated hydrochloric acid) and digested for 1 hr. The precipitate was filtered off on a previously weighed glass-fiber filter paper (Toyo Roshi, GB-60), washed successively, with 6 M hydrochloric acid, distilled water and ethyl alcohol, then dried at 110 °C and weighed. The final precipitate was wrapped in a "Mylor" film or paraffin-waxed paper and the 136.0 or 264.6 keV photopeaks of Se-75 (121 d) was counted with a Ge(Li) solid-state detector coupled with a 400 channel pulse-height analyser.

After the separation of selenium as described above, about 4 g of cerium(IV) sulfate was put into the reaction vessel which must be cooled to below 100 °C after the selenium distillation. The vessel must be cooled whenever the reagent is added, to make the dissolution of the reagent uniform in the SPA medium. The osmium was distilled by heating the reaction vessel to 285 °C within 30—40 min. The absorbing solution was 1: 1 v/v 2% thiourea and 2 M hydrochloric acid mixture. After distillation the absorbing solution and washings were transfered into a beaker (100 ml) to make the volume about 50 ml. One milliliter of 40% potassium chromithiocyanate solution[4] was added and the contents were stirred vigorously until precipitation was complete. The precipitate was filtered as described in the selenium determination, and washed several times with distilled water, dried at 105 °C for 1 hr, then weighed. Finally, the 129.4 keV photopeak of Os-191 (14.6 d) was counted as same as for selenium.

After the second distillation about 2 g of potassium dichromate (in 2 or 3 portions) was put into the vessel, in the same way for osmium. The ruthenium was distilled by heating the reaction vessel to 240 °C within 30—40 min. The absorbing solution was 1: 1 v/v 6 M hydrochloric acid and ethyl alcohol mixture. After distillation the absorbing solution and the washings were transfered into an Erlenmeyer flask (100 ml) and was diluted with distilled water to about 1 M in hydrochloric acid. About 1.3 g magnesium powder was put little by little into the flask to reduced Ru(III) to Ru(0), followed by heating to coagulate the precipitate on a water-bath. The excess of magnesium was dissolved by a drop-wise addition of concentrated hydrochloric acid to be required and the solution was heated gently. The ruthenium metal thus obtained was collected on a glass-fiber filter paper, and washed several times with hydrochloric acid, distilled water, ethyl alcohol and ethyl ether, successively. The precipitate was dried at room temperature for 2 hr under reduced pressure, and weighed. The 215.8 keV photopeak of Ru-97 (2.88 d) was counted with a Ge(Li) solid-state detector.

Nuclear Data

Naturally occurring selenium consists of six isotopes, Se-74(0.87%), Se-76(9.02%), Se-77(7.58%), Se-78 (23.52%), Se-80(49.82%) and Se-82(9.19%). Some of these isotopes give rise to radionuclides when subjected to the irradiation with thermal neutrons, these are as follows:

$$^{74}\mathrm{Se}(n,\gamma)^{75}\mathrm{Se} \xrightarrow[t=121\,\mathrm{d}]{\mathrm{EC}} {}^{75}\mathrm{As}$$

$$^{78}\mathrm{Se}(n,\gamma)^{79m}\mathrm{Se} \xrightarrow[t=3.91\,\mathrm{m}]{\mathrm{IT}} {}^{79}\mathrm{Se} \xrightarrow[t=6.5\times10^{4}\,\mathrm{y}]{\beta^-} {}^{79}\mathrm{Br}$$

$$^{80}\mathrm{Se}(n,\gamma)^{81m}\mathrm{Se} \xrightarrow[t=57\,\mathrm{m}]{\mathrm{IT}} {}^{81}\mathrm{Se} \xrightarrow[t=18\,\mathrm{m}]{\beta^-} {}^{81}\mathrm{Br}$$

$$^{82}\mathrm{Se}(n,\gamma)^{83}\mathrm{Se} \xrightarrow[t=23\,\mathrm{m}]{\beta^-} {}^{83}\mathrm{Br} \xrightarrow[t=2.40\,\mathrm{h}]{\beta^-} {}^{83}\mathrm{Kr}$$

Among them Se-75 is the most useful nuclide to estimate the total amount of selenium in the present study.

Osmium consists of seven isotopes, Os-184(0.01%), Os-186(1.59%), Os-187(1.64%), Os-188(13.3%), Os-189(16.1%), Os-190(26.4%) and Os-192(41.0%). The nuclear data are as follows:

$$^{184}\mathrm{Os}(n,\gamma)^{185}\mathrm{Os} \xrightarrow[t=94\,\mathrm{d}]{\mathrm{EC}} {}^{185}\mathrm{Re}$$

$$^{190}\mathrm{Os}(n,\gamma)^{191m}\mathrm{Os} \xrightarrow[t=14\,\mathrm{h}]{\mathrm{IT}} {}^{191}\mathrm{Os} \xrightarrow[t=15\,\mathrm{d}]{\beta^-} {}^{191}\mathrm{Ir}$$

$$^{192}\mathrm{Os}(n,\gamma)^{193}\mathrm{Os} \xrightarrow[t=31\,\mathrm{h}]{\beta^-} {}^{193}\mathrm{Ir}$$

Osmium was determined in terms of the nuclide Os-191-(15 d) in all cases, and in some cases in terms of the nuclide Os-185 (31 hr).

Naturally occurring ruthenium consists of seven isotopes: Ru-96(5.57%), Ru-98(1.91%), Ru-99(12.7%), Ru-100(12.0%), Ru-101(17.0%), Ru-102(31.5%) and Ru-104(18.5%). The production and the decay of the radionuclides are represented by the following sequences:

$$^{96}\mathrm{Ru}(n,\gamma)^{97}\mathrm{Ru} \xrightarrow[t=2.88\,\mathrm{d}]{\mathrm{EC}} {}^{97m}\mathrm{Tc}$$

$$\xrightarrow[t=91\,\mathrm{d}]{\mathrm{IT}} {}^{97}\mathrm{Tc} \xrightarrow[t=2.6\times10^{6}\,\mathrm{y}]{\mathrm{EC}} {}^{97}\mathrm{Mo}$$

$$^{102}\mathrm{Ru}(n,\gamma)^{103}\mathrm{Ru} \xrightarrow[t=39.8\,\mathrm{d}]{\beta^-} {}^{103m}\mathrm{Rh} \xrightarrow[t=57\,\mathrm{m}]{\mathrm{IT}} {}^{103}\mathrm{Rh}$$

$$^{104}\mathrm{Ru}(n,\gamma)^{105}\mathrm{Ru} \xrightarrow[t=4.5\,\mathrm{h}]{\beta^-} {}^{105m}\mathrm{Rh}$$

$$\xrightarrow[t=45\,\mathrm{s}]{\mathrm{IT}} {}^{105}\mathrm{Rh} \xrightarrow[t=36.5\,\mathrm{h}]{\beta^-} {}^{105}\mathrm{Pd}$$

Taking into consideration of possible interferences from the nuclear reactions: U(n,f)^{103}Ru, U(n,f)^{105}Ru and U(n,f)^{106}Ru, Ru-97 was used for the determination of ruthenium.

Results and Discussion

Distillation Recovery of Selenium. Various solid chlorides and bromides were tested for the SPA decom-

position and distillation, and the amount of selenium distilled was determined radiometrically in every cases. As the results, ammonium bromide was found the most useful for the purpose. The following reactions might take place simultaneously[5]:

$$H_2SeO_3 + 4HBr \longrightarrow SeBr_4 + 3H_2O$$

$$H_2SeO_4 + 2HBr \longrightarrow H_2SeO_3 + Br_2 + H_2O$$

Consequently, in the presence of bromide Se(IV) and Se(VI) can evolve themselves as gaseous selenium tetrabromide from a solid matrix such as rocks, sediments, and biological materials, by heating the samples with ammonium bromide in strong phosphoric acid. Under the condition, elemental selenium and selenide were not affected at all, however, these species could react with bromide after converting them to selenite state by adding 40—50 mg of potassium iodate in the SPA medium as reported previously.[3]

Ammonium bromide together with potassium iodate was found not to react with osmium and ruthenium, and their tetroxide did not appear at all in the absorbing solution as shown in Table 1 which exhibits also the recoveries of selenium, osmium and ruthenium at various temperatures of the SPA media. It is seen that selenium is completely distilled till the temperature reached about 250 °C.

Table 1. Recovery of selenium, osmium and ruthenium at various temperatures of the SPA medium

Reagent (g/30 g SPA)	Temp. °C	Recovery after distillation, %		
		Se	Os	Ru
NH_4Br (0.1) + KIO_3 (0.04)	220	83—85	0	0
	240	93—95	0	0
	250	98—99	0	0
	260	98—99	0	0
	270	94—96	0	0
$Ce(SO_4)_2$ (4)	210		60—70	0
	250		85—90	0
	280		98—99	0
	285		99	0
$K_2Cr_2O_7$ (2)	180			95
	210			99
	230			100
	240			100

Carriers added: Se(IV): 10 mg, Os(III): 4 mg
Ru(III): 10 mg.

Furthermore, the time taken to raise the temperature to 250 °C seemed affect the recovery of selenium tetrabromide. Too fast and too slow heating gave poor recovery of the element. The heating to 250 °C should be done for 30 to 50 min.

Next, various kinds of absorbing solutions were examined for quantitative trapping of the distilled selenium tetrabromide. A 1: 1 v/v mixture of 0.3 M hydrochloric acid and 0.6 M perchloric acid was found to give the best results.

Distillation Recovery of Osmium. The osmium should be oxidized to Os(VIII) and evolved as the tetroxide from the matrix. Spectrophotometric method with thiourea and radioisotopic tracer method were used to find a suitable reagent for the oxidation of osmium. The results show that osmium in various forms, *e.g.*, metal, sulfide, tetrahydroxide and tetroxide, could be distilled quantitatively by means of Ce(IV)-SPA. Ruthenium did not react with cerium(IV) sulfate and not evolve its tetroxide. This fact was explained by Rao's experiments for the formal redox potentials in phosphoric acid of increasing concentrations.[6] The results indicate that cerium(IV) sulfate behaves as a less powerful oxidant than potassium dichromate in SPA contrarily the order of their ordinary oxidation potentials in an aqueous solution. In Table 1, the recovery of osmium is given as a function of temperature. It is seen that the heating to 280 °C or more bring the quantitative recovery of osmium.

Osmium tetroxide evolved could be absorbed in alkaline solution or a mixture of 6 M hydrochloric acid and ethyl alcohol (1: 1 v/v), plus 1 ml of 10% thiourea solution.[2] But in the present study 2% thiourea and 2 M hydrochloric acid mixture (1: 1 v/v) was preferably employed as an absorbing solution for the convenience of the subsequent precipitation of $Os(NH_2 \cdot CS \cdot NH_2)$-$Cr(SCN)_6$. In the presence of ethyl alcohol in the absorbing solution no precipitate appears because the complex can be easily dissolved in ethyl alcohol. The chemical yield is generally 90—95%.

Distillation Recovery of Ruthenium. As described in the previous report[2] potassium dichromate was found the most suitable oxidizing reagent for ruthenium in SPA medium. Ruthenium can be distilled quantitatively by heating with Cr(VI)-SPA to 240 °C and absorbed in 1: 1 v/v mixture of 6 M hydrochloric acid and ethyl alcohol (Table 1).

The time required for completion of reaction was examined and the results showed that the chloride was the most easily decomposed, taking only about 5 min, but sulfide and metallic ruthenium were more resistant, since it took about 30 min to complete the distillation of ruthenium tetroxide.

Table 2. Distillation of various elements by SPA method

Element	Recovery, %		
	Br^--SPA (250 °C)	Ce(IV)-SPA (285 °C)	Cr(VI)-SPA (245 °C)
As(III)	>95	0— 2	0— 2
Br^-	>95	>95	>95
Cl^-	>95	>95	>95
Fe(III)	0	0	0
Hg(I, II)	>95	0—10	10—20
I^-	>95	>95	>95
Ir(IV)	0	0	0
Mn(II)	0	0	0
Os(III)	0	100	100
Re(VII)	0	0	0
Ru(III)	0	0	100
Sb(III, V)	~2	40—60	30—40
Se(IV, VI)	100	0	0
Sn(II, IV)	~3	0	0
Tc(VII)	0	10—20	10—20
Te(IV, VI)	~10	0	0

Behavior of Other Elements. Other elements giving their volatile bromides, oxides as well as volatile acids are believed to be released from their acidic solutions by heating.[7] Table 2 shows that more than 95% of As(III), Br^-, Cl^-, I^- (as hydrohalogenic acid), Hg(I, II), and a few per cent of Sb(III, V), Sn(II, IV) and Te(IV, VI) are driven off from Br^--SPA medium by heating. On the other hand, distillation of As(III) and Hg(I, II) do not exceed a few per cent and 20%, respectively, from Ce(IV)-SPA and Cr(VI)-SPA. In conclusion, not only selenium but other volatilizable elements are almost distilled off on the first Br^--SPA distillation, and hence they do not appear in the absorbing solutions of the second and third distillation with Ce(IV)-SPA and Cr(VI)-SPA. Thus osmium and ruthenium could be separated quantitatively without contaminations except some of technetium species which might be produced secondary from molybdenum [$^{98}Mo(n,\gamma)^{99}Mo \xrightarrow{\beta^-} {}^{99m}Tc(t=6.04\ hr)$ and $^{100}Mo(n,\gamma)$-$^{101}Mo \xrightarrow{\beta^-} {}^{101}Tc(t=14.0\ min)$]. In the present study the interferences by these nuclides were found to be neglible.

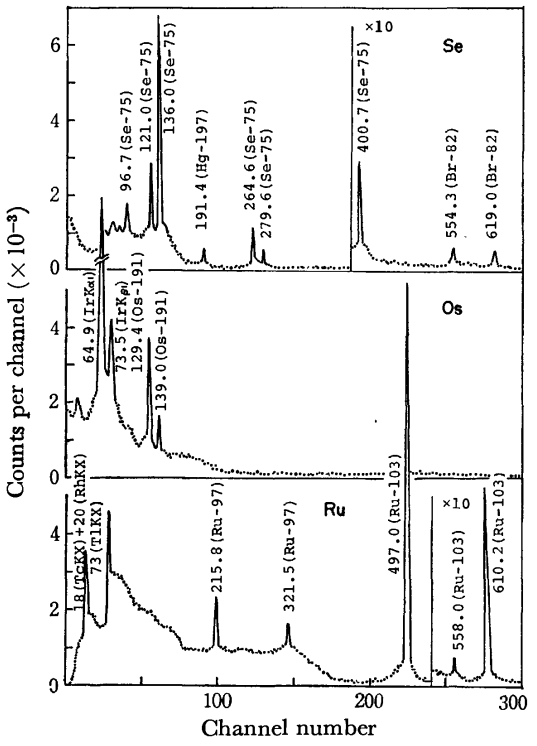

Fig. 1. Gamma-spectra of selenium-, osmium- and ruthenium-fractions after the separation by SPA method (Marine sediment, Japan Sea).

Successive Distillations for Selenium, Osmium and Ruthenium. Successive distillations were tried for marine sediment samples which were collected from the bottoms of Japan Sea, and of Pacific Ocean. One gram of the dried sample was irradiated and processed by the present method as described above, and the final counting samples were submitted to γ-counting. The typical γ-spectra of each fraction separated by the method are shown in Fig. 1. From these spectra, the selenium fraction after Br^--SPA treatment is seen to be contaminated with some of the other nuclides, mainly with Hg-197(65 hr) and Br-82(35.87 hr). However, these radionuclides do not interfere the determination of selenium. On the other hand, the osmium and ruthenium fractions after the Ce(IV)-SPA and then Cr(VI)-SPA treatment were not contaminated with any other radionuclides. In the γ-spectrum of the ruthenium fraction a large photopeak of 497.0 keV appear and it seems to be attributed to mainly Ru-103 produced by fission of uranium existing in the sediment sample. Fission product Ru complicates seriously the determination of ruthenium by the activation analysis. In several sediment samples, ruthenium was characterized by radiation from Ru-103 only and no Ru-97 component could be identified from γ-spectra. According to Gijbels,[8] when the U/Ru ratio is unity the error caused by simply measuring Ru-103 is *ca.* 12%. However, when U/Ru ratio is higher as in the case of marine sediments (10^3—10^4), the ruthenium determination *via* Ru-103 poses a significant problem. It is thus necessary to measure the Ru-97 activity to obtain the reliable results.

TABLE 3. SELENIUM, OSMIUM AND RUTHENIUM CONTENTS OF THE STANDARD ROCKS AND MARINE SEDIMENTS

	Se, ppb	Os, ppb	Ru, ppb
Standard rock			
JG-1 (5)	2.7±0.2	2.7±0.2	n.d.
JB-1 (5)	26 ±2	1.9±0.2	n.d.
Marine sediment			
0°00′00″ N 150°04′07″ E (3)	470	1.0	n.d.
0°48′08″ N 163°59′05″ E (3)	870	9.8	3.6
37°24′ N 132°03′ E (3)	2600	16	8.2
38°33′ N 131°01′ E (3)	910	17	4.3

Determination of Selenium, Osmium and Ruthenium in Rocks and Marine Sediments. The separation and determination of selenium, osmium and ruthenium in standard rock samples and marine sediments were tried by the proposed method. The results are shown in Table 3. Selenium and osmium contents in the standard rocks, JG-1 and JB-1 are the average of five determinations, respectively. Ruthenium was not identified in the present condition. The values for marine sediments are the average of three determinations, respectively. Some sediments were found to contain measurable amount of selenium, while osmium and ruthenium could not be determined, therefore these analytical results are omitted in the table.

The chemical recoveries of the added carriers were in the range 80—85%, 90—95% and 90—95% for selenium, osmium and ruthenium, respectively, within the error of ±10%. The time required for the completion of the radiochemical separation of a sample was about 3 hr.

It will be expected that the present SPA method is applicable for the simultaneous determination of selenium, arsenic, mercury, and bromide from a single

sample and the technique will be described elsewhere.

The authors are much indebted to the members of the Research Reactor Institute of Kyoto University for their help with the activation of the samples and radiochemical treatment. Support of a part of this work by the Ministry of Education is gratefully acknowledged.

References

1) T. Kiba, *Bunseki Kagaku*, **9**, 651 (1960).
2) T. Kiba, K. Terada, T. Kiba, and K. Suzuki, *Talanta*, **19**, 451 (1972).
3) K. Terada, T. Ooba, and T. Kiba, *ibid.*, **22**, 41 (1975).
4) J. W. Morgan, *Anal. Chim. Acta*, **32**, 8 (1965).
5) I. M. Kolthoff and P. J. Elving ed., "Treatise on Analytical Chemistry," Part II, Analytical Chemistry of the Elements, Vol. 7, Interscience Publishers, New York, N. Y. (1961), p. 147.
6) G. G. Rao, *Talanta*, **10**, 1251 (1963).
7) E. B. Sandell, "Colorimetric Determinations of Traces of Metals," 3rd. Ed., Interscience Publishers, New York, N. Y. (1959), p. 72.
8) R. Gijbels, *Talanta*, **18**, 587 (1971).

Mixed Ligand Copper(II) Complexes of Amino Acids and Related Compounds with Possible Ligand-Ligand Interactions

Osamu YAMAUCHI, Yasuo NAKAO, and Akitsugu NAKAHARA

Institute of Chemistry, College of General Education, Osaka University, Toyonaka, Osaka 560

(Received June 12, 1975)

Ternary systems composed of copper(II) and two ligands, each with an oppositely charged uncoordinated group in the side chain, have been investigated by synthetic and spectral methods. The absorption and circular dichroism(CD) spectra in the d-d region were measured at various pH values for the binary and ternary systems, $Cu(B)_2$ and Cu(A)(B), where A refers to ethylenediamine-*N*-monoacetic acid(EDMA), glycylglycine(Gly·Gly), glycyl-β-alanine(Gly·β-Ala), ethylenediamine(en), or glycine(Gly), and B to D- and L-arginine (D- and L-Arg), L-ornithine(L-Orn), L-lysine(L-Lys), L-alanine(L-Ala), or L-valine(L-Val), and the following complexes containing ligands with polar side chains were isolated as crystals: $[Cu(EDMA)(L\text{-}Arg)]ClO_4 \cdot H_2O$; $[Cu(EDMA)(L\text{-}Orn)]ClO_4 \cdot 1/2H_2O$; $[Cu(EDMA)(L\text{-}Lys)]ClO_4$; $[Cu(Gly\cdot Gly)(L\text{-}Arg)] \cdot 3/2H_2O$. From comparison of the CD magnitudes expressed in terms of the relative magnitude which assumes half the value for $Cu(B)_2$ as unity, the magnitude enhancements observed for the systems Cu(EDMA)(D- and L-Arg), Cu(EDMA)(L-Orn), Cu(EDMA)-(L-Lys), and Cu(Gly·β-Ala)(D- and L-Arg) in water and in 50% aqueous ethanol have been inferred to be due to the intramolecular electrostatic interactions between the charged groups in the side chains of ligands A and B.

Transition metal ions in the biological systems are most probably in the forms of various mixed complexes. Thus, the enzyme–metal–substrate complex, formed as an intermediate in the enzymatic reaction in the presence of a metal ion, is a kind of mixed ligand complex, and the reaction itself is regarded as a ligand-ligand interaction assisted by the cooperative action of the central metal ion. A well known example is the carboxypeptidase A–peptide complex whose crystal structure has been disclosed by X-ray analysis.[1] What appeared most interesting to us is that it has electrostatic or hydrogen bondings between the guanidinium group of arginine 145 of the enzyme and the carboxylate terminus of its substrate. Since such an interaction serves as a driving force for the enzyme-substrate complex formation, we considered it to be of fundamental importance to work out reasonable model systems based on the carboxypeptidase A-peptide complex and investigate, as a chemical counterpart of the enzymatic reactions, the possibilities of ligand-ligand interactions within mixed ligand complex molecules.

Studies have been reported for the stereoselective effects of the interactions between coordinated ligands in various cobalt(III) complexes, where, for example, the uncoordinated carboxylate group around the central atom interacts with the adjacent coordinated amino group through hydrogen bonding. Such interactions have been concluded to give rise to stereoselectivity in the formation of the diastereoisomers.[2–5] Wellman and Wong[6] observed favored formation of the L-histidinol-containing mixed ligand complexes of copper(II), whose circular dichroism(CD) spectra suggested the interaction between the imidazole group of L-histidinol and the amino group of the other ligand. Angelici *et al.*[7,8] reported the stereoselectivity exhibited by (*N*-carboxymethyl-L-valinato)copper(II) toward optically active amino acids and ascribed it to the interference between the amine hydrogens of the two ligands in the resulting complexes. However, mixed ligand systems involving explicit electrostatic interactions within a molecule have not been reported yet.

As an approach to the biological systems, we studied the properties of the mixed ligand copper(II) complexes of the type shown in Scheme 1 in expectation of intramolecular electrostatic ligand-ligand interactions that would occur between the oppositely charged, uncoordinated groups of the side chains of ligands A and B.

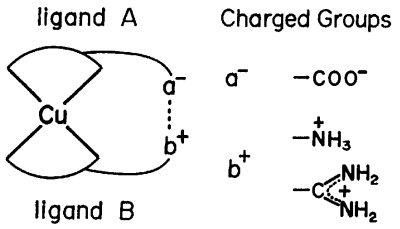

Scheme 1.

We selected for this purpose such pairs of A and B as would exhibit the mentioned interactions, as well as the pairs without possible interactions, and investigated isolation and absorption and CD spectral properties of the copper(II) complexes of type Cu(A)-(B), which are to be described in the following sections. For convenience, ethylenediamine-*N*-monoacetic acid (EDMA), glycylglycine(Gly·Gly), glycyl-β-alanine (Gly·β-Ala), ethylenediamine(en), and glycine(Gly) will be referred to as A ligands, and D- and L-arginine (D- and L-Arg), L-ornithine(L-Orn), L-lysine(L-Lys), L-alanine(L-Ala), and L-valine(L-Val) as B ligands.

Experimental

Materials. L-Arginine, L-ornithine hydrochloride, L-lysine dihydrochloride, and L-alanine were purchased from Nakarai Chemicals, Ltd., and L-valine and glycine from Wako Pure Chemical Industries, Ltd. D-Arginine hydrochloride was obtained from Fluka AG. Glycylglycine was obtained from Protein Research Foundation, Osaka, and glycyl-β-alanine was prepared according to the literature.[9] The dihydrochloride of EDMA was prepared by the method of Fujii *et al.*,[10] and the purity was checked by elemental analysis and potentiometric titration.

All the chemicals used were of reagent grade or of highest grade available.

Synthesis of Mixed Ligand Copper(II) Complexes. [*Cu(EDMA)(L-Arg)*]$ClO_4 \cdot H_2O$: EDMA dihydrochloride hydrate (1.05 g, 5 mmol), L-arginine (0.87 g, 5 mmol), and copper(II) perchlorate hexahydrate (1.85 g, 5 mmol) were mixed in water, and the pH of the resulting solution was adjusted to 8 with aqueous sodium hydroxide. The chloride ions were removed from the reaction mixture by passing it through a column of Amberlite IRA-400 in perchlorate form. The blue oily residue obtained after concentration *in vacuo* was mixed with methanol and kept at room temperature for a few days, when it gradually crystallized. Recrystallization from aqueous methanol–ethanol and drying *in vacuo* over silica gel gave deep blue crystals. Found: C, 25.40; H, 5.35; N, 17.80%. Calcd for $C_{10}H_{23}N_6O_8ClCu \cdot H_2O$: C, 25.43; H, 5.34; N, 17.79%.

[*Cu(EDMA)(L-Orn)*]$ClO_4 \cdot 1/2H_2O$: A neutralized solution (pH 7) of EDMA dihydrochloride hydrate (1.05 g, 5 mmol), L-ornithine hydrochloride (0.84 g, 5 mmol), and copper(II) chloride dihydrate (0.85 g, 5 mmol) in water was treated in the manner described above to give deep blue crystals. Found: C, 25.84; H, 5.22; N, 12.88%. Calcd for $C_9H_{21}N_4O_8ClCu \cdot 1/2H_2O$: C, 25.87; H, 5.22; N, 13.29%.

[*Cu(EDMA)(L-Lys)*]ClO_4: This was prepared in a similar manner from EDMA dihydrochloride hydrate (1.05 g, 5 mmol), L-lysine dihydrochloride (1.10 g, 5 mmol), and copper(II) chloride dihydrate (0.85 g, 5 mmol). The deep blue crystals were recrystallized from methanol–water and dried *in vacuo* over P_4O_{10} at 60 °C. Found: C, 28.18; H, 5.56; N, 12.77%. Calcd for $C_{10}H_{23}N_4O_8ClCu$: C, 28.17; H, 5.44; N, 13.14%.

[*Cu(Gly·Gly)(L-Arg)*]$\cdot 3/2H_2O$: An aqueous solution containing Gly·Gly (1.3 g, 10 mmol), L-arginine (1.7 g, 10 mmol), and copper(II) perchlorate hexahydrate (3.7 g, 10 mmol) was made alkaline (pH 10) with aqueous sodium hydroxide, stirred for 1 hr at room temperature, and filtered. Ethanol was added to the filtrate to give deep blue crystals, which were recrystallized from aqueous methanol-ethanol. Found: C, 30.41; H, 5.88; N, 21.28%. Calcd for $C_{10}H_{20}N_6O_5Cu \cdot 3/2H_2O$: C, 30.57; H, 5.60; N, 21.42%.

Measurements of Spectra. Absorption spectra were recorded on a Union Giken SM-401 High-Sensitivity recording spectrophotometer and CD spectra on a JASCO MOE-1 spectropolarimeter. The spectra were measured for most of the systems with Cu(II): A: B ratios of 1: 2: 0, 1: 0: 2, and 1: 1: 1 at various pH values in the ranges 350—750 nm (absorption spectra) and 350—800 nm (CD spectra). The measurements were made at a constant copper(II) concentration of 5.0×10^{-3} M in four different media: (i) water (ionic strength (μ) not adjusted (μ=variable)); (ii) water (μ=0.1 ($NaClO_4$)); (iii) water (μ=0.5 ($NaClO_4$)); (iv) 50% aqueous ethanol. The pH values of the solutions were roughly adjusted with aqueous sodium hydroxide and dilute perchloric acid and finally determined immediately after the spectral measurements. The values described are meter readings with no corrections for difference in the medium.

The above measurements were made at room temperature.

Results and Discussion

Synthesis of the Mixed Ligand Complexes. Out of the mixed ligand systems investigated, [Cu(EDMA)(L-Arg)]ClO_4, [Cu(EDMA)(L-Orn)]ClO_4, [Cu(EDMA)-(L-Lys)]ClO_4, and [Cu(Gly·Gly)(L-Arg)] have been isolated as crystals under the conditions employed. The pH of the reaction mixture was so adjusted as to keep the most basic group of the α-amino acid protonated.

Table 1. Absorption spectral data for binary systems $Cu(A)_2$ and $Cu(B)_2$ at various pH values (μ=0.1($NaClO_4$))

Ligand	pH	λ_{max} (nm)	ε
EDMA	4.1	668	72
	7.8	616	59
	10.8	616	59
Gly·Gly	4.5	651	43
	7.2	635	83
	8.8	624	83
	10.3	631	79
en	4.5	690	38
	7.1	546	62
	9.2	546	62
L-Arg	4.6	684	31
	7.0	622	54
	9.6	620	57
L-Orn	4.7	675	34
	6.8	623	53
	8.3	620	57
	10.1	632	64
	11.1	636	64
L-Lys	4.7	681	32
	7.0	619	54
	8.1	618	57
	10.1	618	58
	11.1	621	58
L-Ala	4.6	704	30
	7.1	622	52
	9.8	619	56
L-Val	4.7	687	32
	7.2	617	57
	10.0	616	58

The compositions of the isolated complexes indicate that each complex involves a ligand with a negatively charged uncoordinated group and a ligand with a positively charged one. The behavior of these particular systems may be correlated with the stereoselectivity reported for cobalt(III) complexes.[2-5] In the present cases, ligand-ligand interactions, which should be electrostatic in nature, are reasonably expected to occur between the charged groups of the side chains (Scheme 1).

Absorption Spectra. The absorption spectra in the d-d region were measured in water (μ=variable, 0.1, and 0.5) and in 50% aqueous ethanol at various pH values. The shifts of the absorption maxima of the binary and ternary systems due to the increase of ionic strength were small (*ca.* 2—4 nm toward shorter wavelength), and their intensities remained virtually constant at different ionic strengths except that they slightly increased in 50% aqueous ethanol. Table 1 shows the absorption spectral data for various binary systems at μ=0.1. The data for the ternary Cu(A)(B) systems at μ=variable are summarized in Table 2.

The absorption maxima of the ternary systems containing EDMA, Gly·Gly, Gly·β-Ala, or Gly as ligand A fall in the region 610—640 nm at pH>9 where Cu(A)(B) is expected to be the major complex species

TABLE 2. ABSORPTION SPECTRAL DATA FOR TERNARY SYSTEMS AT VARIOUS pH VALUES (μ=variable)

Ligand B	Ligand A: EDMA			Gly·Gly			Gly·β-Ala			en			Gly		
	pH	λ_{max} (nm)	ε	pH	λ_{max} (nm)	ε	pH	λ_{max} (nm)	ε	pH	λ_{max} (nm)	ε	pH	λ_{max} (nm)	ε
L-Arg	7.2	633	63	7.1	638	72	7.9	628	66	7.2	583	55	7.0	630	48
	8.3	620	62	10.1	635	75	10.2	616	65	10.3	584	57	9.2	627	51
	9.6	620	61												
D-Arg	7.3	632	62	7.2	638	72	9.9	618	65	9.6	580	57	7.2	630	48
	9.8	620	62	10.2	636	74							10.0	627	51
L-Orn	7.0	640	62	7.5	635	72	7.1	629	65	7.0	583	54	7.2	628	48
	10.3	623	64	10.1	628	77	8.1	626	66	10.2	591	58	9.2	632	53
	11.0	627	65	11.5	639	73	10.4	618	69	11.2	594	58			
L-Lys	7.1	639	64	7.2	637	73	7.7	628	70	7.1	582	55	7.0	630	47
	9.0	619	63	8.9	626	75	8.9	620	67	8.9	580	57	9.9	628	50
	10.1	619	64	10.5	627	76	10.5	613	66	10.3	583	57			
	11.4	622	64	11.4	636	76									
L-Ala	7.1	645	63	7.0	640	73	10.1	619	67	7.0	584	54	7.3	630	47
	10.3	620	62	10.3	634	73				10.2	584	56	10.0	627	50
L-Val	7.1	640	64	7.0	638	73	7.7	627	67	7.0	583	56	7.0	629	48
	10.2	617	64	10.2	632	72	10.1	619	66	10.2	583	59	9.8	624	51

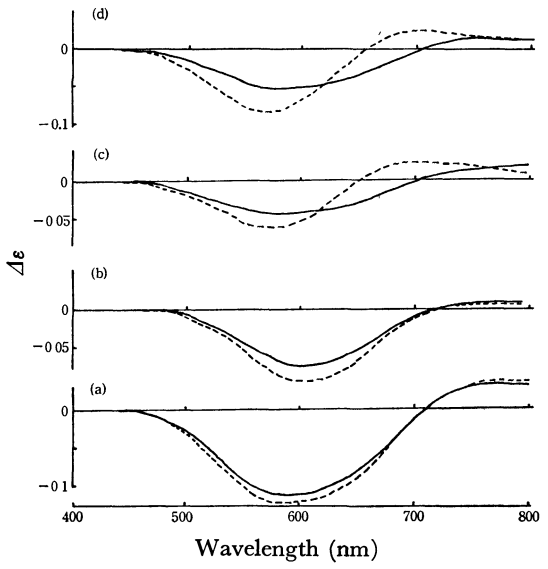

Fig. 1. Visible CD spectra of L-arginine-containing systems in water (μ=variable).
(a) Cu(L-Arg)$_2$: ——, pH 7.1; – – –, pH 9.2
(b) Cu(EDMA)(L-Arg): ——, pH 7.2; – – –, pH 8.3
(c) Cu(Gly·Gly)(L-Arg): ——, pH 7.1; – – –, pH 10.1
(d) Cu(Gly·β-Ala)(L-Arg): ——, pH 7.9; – – –, pH 10.2.

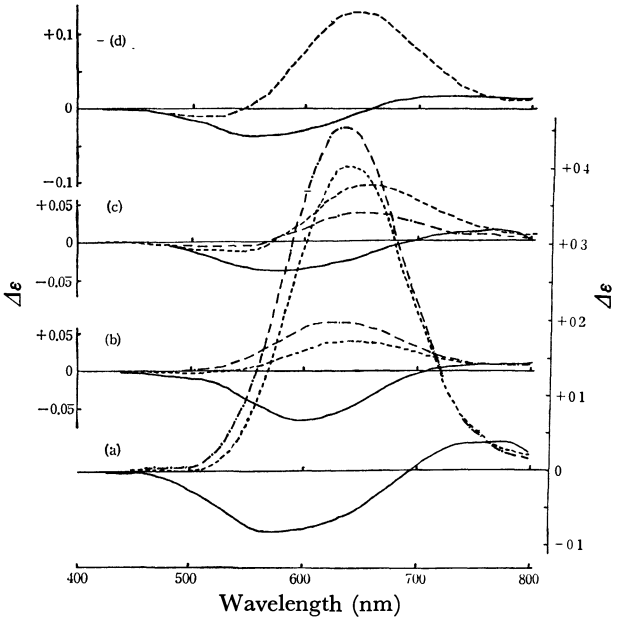

Fig. 2. Visible CD spectra of L-ornithine-containing systems in water (μ=variable).
(a) Cu(L-Orn)$_2$: ——, pH 7.1; – – –, pH 9.9; -·-·-, pH 10.8
(b) Cu(EDMA)(L-Orn): ——, pH 7.0; – – –, pH 10.3; ····, pH 11.0
(c) Cu(Gly·Gly)(L-Orn): ——, pH 7.5; – – –, pH 10.1; ····, pH 11.5
(d) Cu(Gly·β-Ala)(L-Orn): ——, pH 8.1; – – –, pH 10.4.

present. As we see from the data for Cu(A)(L-Orn) and Cu(A)(L-Lys), some of the spectra exhibit shifts to longer wavelengths at pH>10, probably due either to apical coordination by the δ- or ε-amino group or to formation of hydroxy complexes. This point will be referred to again in connection with the CD spectra.

CD Spectra. In the d-d spectral region, the binary and ternary systems containing optically active amino acids exhibited CD extrema due to the vicinal effect of the asymmetric carbon. Figs. 1 and 2 illustrate the spectra for the systems involving L-arginine and L-ornithine, respectively. The spectral data in water (μ=variable) at selected pH are listed in Table 3. Usually a negative extremum, which is shifted to longer wavelengths at μ=0.1 and 0.5, is observed in the region 570—610 nm with a weak positive peak at >700 nm.

TABLE 3. CD SPECTRAL DATA FOR BINARY AND TERNARY SYSTEMS (μ=variable)

Ligand B	Binary system Cu(B)$_2$			Ternary system Cu(EDMA)(B)			Ternary system Cu(Gly·Gly)(B)		
	pH	λ_{max} (nm)	$\Delta\varepsilon$	pH	λ_{max} (nm)	$\Delta\varepsilon$	pH	λ_{max} (nm)	$\Delta\varepsilon$
L-Arg[a)]	7.1	598	−0.11	7.2	606	−0.08	7.1	588	−0.04
		≃765	+0.03		>760	+0.01		>760	+0.01
	9.2	598	−0.12	8.3	606	−0.10	10.1	574	−0.06
		≃765	+0.03		>760	+0.01		700	+0.02
D-Arg	6.9	598	+0.12	7.3	610	+0.08	7.2	590	+0.04
		≃765	−0.03		>760	−0.02		≃755	−0.02
	10.1	598	+0.11	9.8	610	+0.10	10.2	574	+0.06
		≃765	−0.03		>760	−0.02		700	−0.02
L-Orn	7.1	575	−0.08	7.0	600	−0.07	7.5	570	−0.04
		≃760	+0.04		>740	+0.01		>760	+0.01
	9.9	632	+0.40	10.3	643	+0.04	10.1	654	+0.07
	10.8	630	+0.45	11.0	630	+0.06	11.5	650	+0.04
L-Lys	7.1	600	−0.11	7.1	607	−0.06	7.2	588	−0.05
		>750	+0.03		>750	+0.01		>780	+0.02
	9.4	600	−0.13	9.0	607	−0.09	8.9	578	−0.06
		>750	+0.03		>750	+0.01		740	+0.02
	10.8	600	−0.14	11.4	607	−0.09	11.4	578	−0.03
		>750	+0.03		>750	+0.01		≃740	+0.01
L-Ala	7.0	625	−0.07	7.1	610	−0.03	7.0	615	−0.03
		>760	+0.01		>760	+0.01			
	10.1	625	−0.08	10.3	610	−0.04	10.3	590	−0.05
		>760	+0.01		>760	+0.01		≃740	+0.02
L-Val	7.3	596	−0.28	7.1	612	−0.08	7.0	595	−0.10
		≃780	+0.05		≃780	+0.02		>760	+0.02
	9.8	596	−0.29	10.2	612	−0.12	10.2	587	−0.12
		≃780	+0.05		≃780	+0.03		752	+0.04

Ligand B	Ternary system Cu(Gly·β-Ala)(B)			Ternary system Cu(en)(B)			Ternary system Cu(Gly)(B)		
	pH	λ_{max} (nm)	$\Delta\varepsilon$	pH	λ_{max} (nm)	$\Delta\varepsilon$	pH	λ_{max} (nm)	$\Delta\varepsilon$
L-Arg[a)]	7.9	576	−0.05	7.2	596	−0.05	7.0	604	−0.06
		>750	+0.02		≃750	+0.01		>760	+0.02
	10.2	570	−0.08	10.3	596	−0.05	9.2	604	−0.07
		710	+0.02		≃750	+0.01		>760	+0.02
D-Arg	9.9	570	+0.08	9.6	595	+0.05	7.2	604	+0.06
		710	−0.02		≃750	−0.01		>760	−0.02
							10.0	604	+0.06
								>760	−0.02
L-Orn	7.1	580	−0.04	7.0	596	−0.04	7.2	600	−0.04
		>740	+0.01		>740	+0.01		>740	+0.01
	8.1	556	−0.04	10.2	616	+0.14	9.2	633	+0.11
		>720	+0.02	11.2	610	+0.15			
	10.4	503	−0.01						
		644	+0.13						
L-Lys	7.7	602	−0.05	7.1	595	−0.05	7.0	607	−0.06
		>740	+0.02		≃750	+0.01		>760	+0.02
	8.9	574	−0.06	8.9	595	−0.06	9.9	607	−0.07
		≃750	+0.02		≃750	+0.01		>760	+0.02
	10.5	573	−0.06	10.3	595	−0.06			
		710	+0.02		≃750	+0.01			
L-Ala	10.1	589	−0.05	7.0	614	−0.03	7.3	630	−0.04
		≃740	+0.01	10.2	614	−0.04	10.0	630	−0.04
L-Val	7.7	595	−0.12	7.0	580	−0.12	7.0	604	−0.13
		≃770	+0.02		≃770	+0.02		>760	+0.03
	10.2	580	−0.12	10.2	580	−0.13	9.8	604	−0.14
		≃750	+0.03		≃770	+0.02		>760	+0.03

a) The data (pH, λ_{max} (nm), $\Delta\varepsilon$) for Cu(EDMA)(L-Arg) at higher concentrations are as follows: (i) at 0.05 M, 8.2, 603, −0.11; (ii) at 0.1 M, 9.0, 604, −0.11.

The magnitudes of the negative peaks are small in acid solution (pH 3—5) and increase with pH up to their maximum at pH 9—10, which indicates the chelation by the amino acid is almost complete at this pH. That the CD spectra observed for the ternary systems are due primarily to Cu(A)(B) and not to the binary $Cu(B)_2$ is substantiated by the wavelengths of their extrema which are significantly different from those of the binary ones. Except for the L-ornithine series, the systems Cu(EDMA)(B), Cu(en)(B), and Cu(Gly)(B) at pH>7 have their peaks at 600—612, 580—616, and 600—630 nm, respectively, and the wavelengths do not shift greatly with pH. On the other hand, the systems with Gly·Gly or Gly·β-Ala as ligand A have negative bands around 570—600 nm, which are shifted to shorter wavelengths with the increase of pH. The behavior may be due to the deprotonation of the peptide NH group and the concomitant change of the donor atom from oxygen to nitrogen.

A sign inversion of the main peak was observed for $Cu(L\text{-}Orn)_2$ and every Cu(A)(L-Orn) system studied, and there appeared a positive peak in the region 610—650 nm at pH 9—10. The same spectral changes have been reported by Wellman *et al.*[11] and Wilson *et al.*[12] for the systems Cu(Gly)(L-Orn)[11,12] and Cu(en)-(L-Orn).[12] It was concluded from their studies that the change is due to apical coordination by the δ-amino group of L-ornithine in these systems. The present observation that the sign inversion coincides with the acid dissociation of the δ-amino group (pK_a=10.67[13]) supports their conclusion, and apical coordination by this group is inferred to occur in all the L-ornithine-containing systems studied. The shifts of the absorption maxima to longer wavelengths at high pH correspond with those observed for copper(II)–ammine complexes.[14] Apical coordination by the ε-amino group of L-lysine, if at all, seems to be negligible, because the absorption and CD spectral changes exhibited at pH 8—10 are small.

CD Magnitude and Intramolecular Ligand-Ligand Interaction. Of utmost interest is the fact that the CD magnitudes shown in Table 3 have a distinct trend which seems to reflect the differences in the environments where the amino acids are located. In order to make a clearer comparison of the magnitudes of the negative extrema in the region 570—620 nm, we tentatively expressed a series of magnitudes related to an amino acid in terms of the relative magnitude which assumes half the magnitude ($\Delta\varepsilon/2$) of the binary complex of that amino acid as unity. Table 4 displays the relative magnitudes calculated in this way for various systems in water (μ=variable) at pH as indicated. The values for L-ornithine series were calculated at pH 7 where its apical coordination does not take place appreciably. It is now apparent that the systems Cu(EDMA)(L-Arg), Cu(EDMA)(L-Orn), Cu(EDMA)(L-Lys), and Cu(Gly·β-Ala)(L-Arg) have significantly larger relative magnitudes than unity, while the others have values close to 1.

Although attempts have been made to interpret the CD spectral patterns of copper(II) complexes in the d-d region and to correlate them with the structures around copper(II),[15—22] it is still necessary to determine experimentally whether or not the relative CD magnitudes as defined above can be compared between different systems or, in other words, whether the additivity of the CD magnitude holds in complexes with differentcombinations of ligands. Tsangaris and Martin[23] reported the magnitude additivity observed for copper(II)–dipeptide complexes. In the present studies, the donor atoms of A ligands are two nitrogens(2N) or a nitrogen and an oxygen(1N1O), and simple additivity may not hold owing to the differences in the environments. However, we see from Table 4 that the relative magnitudes observed for the Cu(en)(B) and Cu(Gly)-(B) series, where the donor atoms are 2 N and 1N1O, respectively, are 0.8—1.1 irrespective of B ligands.[24] Also, the ternary systems containing L-alanine or L-valine as B have magnitudes of 0.8—1.2 for all combinations with A. These results clearly indicate that the relative CD magnitude is approximately equal to 1 and accordingly additive unless both ligand A and ligand B have respectively a negatively charged and a positively charged group in their side chain. In addition, we may infer from this that the mode of coordination of the simple α-amino acids in the ternary systems studied is the same as in the binary systems. As α-amino acids are effective bidentate ligands, the carboxylate group of EDMA, Gly·Gly, or Gly·β-Ala are probably dis-

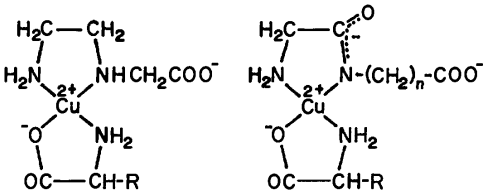

Cu(EDMA)(B) Ia

Cu(Gly·Gly)(B) (n=1)
Cu(Gly·β-Ala)(B) (n=2) Ib

TABLE 4. RELATIVE CD MAGNITUDES IN WATER (μ=variable)[a]

Ligand B	$Cu(B)_2$	Cu(EDMA)(B)	Cu(Gly·Gly)(B)	Cu(Gly·β-Ala)(B)	Cu(en)(B)	Cu(Gly)(B)
L-Arg	1.0(9.2)[b]	1.6(9.6)	1.0(10.1)	1.4(10.2)	0.8(10.3)	1.1(9.2)
D-Arg	1.0(10.1)	1.8(9.8)	1.1(10.1)	1.5(9.9)	1.0(9.6)	1.0(10.0)
L-Orn	1.0(7.1)	1.6(7.0)	0.9(7.5)	1.0(7.1)	0.9(7.0)	1.0(7.2)
L-Lys	1.0(9.4)	1.5(9.0)	1.0(8.9)	0.9(8.9)	1.0(8.9)	1.0(9.9)
L-Ala	1.0(10.1)	0.9(10.3)	1.1(10.3)	1.2(10.1)	1.0(10.1)	1.1(10.0)
L-Val	1.0(9.8)	0.8(10.2)	0.8(10.2)	0.8(10.2)	0.9(10.2)	1.0(9.8)

a) Relative CD magnitude is the magnitude relative to $\Delta\varepsilon/2$ of $Cu(B)_2$ as unity. b) Numerals in parentheses refer to the pH values where the comparison was made.

placed from the tetragonal plane upon formation of Cu(A)(B) (**1a** and **1b**).

Considering that the magnitude enhancement is observed only for the combination of A and B with oppositely charged side chains and that the CD measurements have been performed at a copper(II) concentration of 5.0×10^{-3}M, we may take the enhancement as an indication of the presence of an intramolecular ligand-ligand interaction which adds to rigidity of the complex. The enhancement of the CD magnitude and the sign inversion have been reported for the Cu(bipyridyl)(L-amino acid) systems,[25] which are quite different in nature from the present ones.

Molecular models for Cu(EDMA)(L-Arg), Cu(EDMA)(L-Orn), and Cu(EDMA)(L-Lys) corroborate the favorable steric requirements for the assumed intramolecular hydrogen bonds as shown for Cu(EDMA)(L-Arg) (**2**). According to this structure, the imino nitrogen of EDMA can be asymmetric if it is fixed around copper(II) by hydrogen bonding. For the systems without charged pairs, such as Cu(en)(L-Orn) (**3**) and Cu(EDMA)(L-Ala) (**4**), no intramolecular hydrogen bonding is possible, and the observed CD magnitudes are expectedly close to **1**.

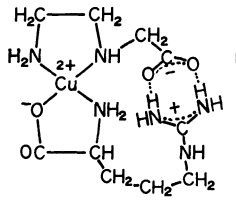

Cu(EDMA)(L-Arg)

2

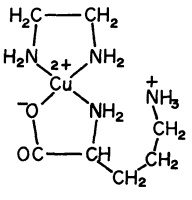

Cu(en)(L-Orn)

3

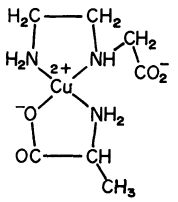

Cu(EDMA)(L-Ala)

4

As regards the Cu(Gly·Gly)(B) and Cu(Gly·β-Ala)(B) systems except Cu(Gly·β-Ala)(L-Arg), the relative magnitudes are 0.8—1.2 and apparently contradictory to the ligand-ligand bondings as are expected from the molecular models of the structures like **5**. Table 3 indicates that in the peptide series the positive peak found at >700 nm is shifted to shorter wavelength with the increase of pH, probably inducing the cancellation of the two Gaussian curves with signs opposite to each other. This may explain the unexpectedly small relative magnitudes. Space-filling models do not reveal explicitly the stereochemical difference between Cu(Gly·Gly)(L-Arg) and Cu(Gly·β-Ala)(L-Arg) of

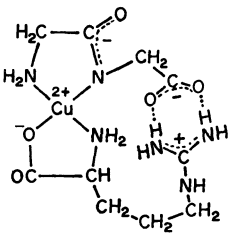

Cu(Gly·Gly)(L-Arg)

5

which the latter has a significantly larger magnitude of 1.5 than that of the former.

From the CD spectral behavior of Cu(EDMA)(D-Arg), the CD patterns for the other D-amino acid series are expected to be the same as those observed for the corresponding L-series with the signs inverted.

If the assumed electrostatic ligand-lagand bonding as illustrated in **2** and **5** is real and has influence on the CD spectra, the relative magnitude should then be affected by the ionic strength and the polarity of the solvent. The results of the spectral measurements in water at $\mu=0.1$ and 0.5 are compared with those at $\mu=$variable in Table 5, which discloses that the enhanced values for Cu(EDMA)(L-Arg), Cu(EDMA)(L-Orn), and Cu(EDMA)(L-Lys) at $\mu=$variable decrease to nearly normal values with the increase of ionic strength, while those for Cu(EDMA)(L-Ala), Cu(EDMA)(L-Val), and Cu(en)(B) remain unaffected. On the other hand, the data obtained in 50% aqueous ethanol indicate that the ionic strength-dependent values are further increased up to 2.1—2.7 by lowering the polarity of the solvent with ethanol. Interestingly, the CD patterns of Cu(EDMA)(L-Arg) at concentrations as high as 0.05 M (pH 8.2) and 0.1 M (pH 9.0) were the same as the pattern observed at 0.005 M (Table 3, footnote). This points to the fact that the molecular environment in the complex is not affected by the concentration of the solution in the range studied.

Taken together, the observations may provide evidence that there exists, at least in solution, an intramolecular electrostatic bonding in a certain pair of oppositely charged ligands constituting a mixed ligand copper(II) complex and that it affects the CD magnitude under favorable conditions.

We wish to acknowledge the helpful comments and

Table 5. Relative CD magnitudes in various media at pH 7—10

Ligand B	Cu(EDMA)(B)				Cu(Gly·Gly)(B)[a]				Cu(en)(B)			
	water, μ			50% aq. ethanol	water, μ			50% aq. ethanol	water, μ			50% aq. ethanol
	var.	0.1	0.5		var.	0.1	0.5		var.	0.1	0.5	
L-Arg	1.6	1.3	1.2	2.7	1.0	0.9	1.0	1.2	0.8	0.9	0.9	1.0
L-Orn	1.6	1.4	1.1	2.6	0.9	0.8	0.9	0.9	0.9	0.8	0.7	0.9
L-Lys	1.5	1.2	1.1	2.1	1.0	0.9	1.0	1.1	1.0	1.0	0.9	1.1
L-Ala	0.9	1.1	—[b]	—	1.1	1.1	—	—	1.0	1.0	—	—
L-Val	0.8	0.8	—	0.9	0.8	0.8	—	1.0	0.9	0.9	—	1.0

a) The values for Cu(Gly·β-Ala)(B) in 50% aqueous ethanol are as follows: L-Arg, 2.3; L-Orn, 0.9; L-Lys, 1.2.
b) Not measured.

discussions by Professor Jinsai Hidaka of Tsukuba University and Professor Takaji Yasui of Kochi University. We are also indebted to Mr. Takeshi Sakurai and Miss Atsuko Yamashita for technical assistance and to Miss Taeko Dei for elemental analysis. This work was supported in part by a grant from the Ministry of Education, to which our thanks are due.

References

1) W. N. Lipscomb, G. N. Reeke, Jr., J. A. Hartsuck, F. A. Quiocho, and P. H. Bethge, *Phil. Trans. Roy. Soc.*, **B257**, 177 (1970); W. N. Lipscomb, *Accounts Chem. Res.*, **3**, 81 (1970).
2) J. H. Dunlop, R. D. Gillard, N. C. Payne, and G. B. Robertson, *Chem. Commun.*, **1966**, 874.
3) T. Yasui, J. Hidaka, and Y. Shimura, This Bulletin, **39**, 2417 (1966).
4) R. D. Gillard, R. Maskill, and A. Pasini, *J. Chem. Soc., A*, **1971**, 2268.
5) M. Takeuchi and M. Shibata, This Bulletin, **47**, 2797 (1974) and their papers cited therein.
6) K. M. Wellman and B.-K. Wong, *Chem. Commun.*, **1969**, 1213.
7) B. E. Leach and R. J. Angelici, *J. Amer. Chem. Soc.*, **91**, **1969**, 6296.
8) R. V. Snyder and R. J. Angelici, *J. Inorg. Nucl. Chem.*, **35**, 523 (1973).
9) H. T. Hanson and E. L. Smith, *J. Biol. Chem.*, **175**, 833 (1948).
10) Y. Fujii, E. Kyuno, and R. Tsuchiya, This Bulletin, **43**, 786 (1970).
11) K. M. Wellman, T. G. Mecca, W. Mungall, and C. R. Hare, *J. Amer. Chem. Soc.*, **90**, 805 (1968).
12) E. W. Wilson, Jr., M. H. Kasperian, and R. B. Martin, *ibid.*, **92**, 5365 (1970).
13) L. G. Sillén and A. E. Martell, "Stability Constants of Metal Ion Complexes," Special Publication No. 17, The Chemical Society, London (1964).
14) B. J. Hathaway and A. A. G. Tomlinson, *Coord. Chem. Rev.*, **5**, 1 (1970).
15) T. Yasui, J. Hidaka, and Y. Shimura, *J. Amer. Chem. Soc.*, **87**, 2762 (1965).
16) T. Yasui, This Bulletin, **38**, 1746 (1965).
17) K. M. Wellman, S. Bogdansky, C. Piontek, C. R. Hare, and M. Mathieson, *Inorg. Chem.*, **8**, 1025 (1969).
18) C. J. Hawkins and C. L. Wong, *Aust. J. Chem.*, **23**, 2237 (1970).
19) R. D. Gillard and S. H. Laurie, *J. Chem. Soc., A*, **1970**, 59.
20) T. Murakami and M. Hatano, This Bulletin, **46**, 3116 (1973).
21) C. J. Hawkins, "Absolute Configuration of Metal Complexes," Wiley-Interscience, New York (1971), p. 148.
22) R. B. Martin, "Metal Ions in Biological Systems," Vol. 1, ed. by H. Sigel, Marcel Dekker, Inc., New York (1974), p. 129.
23) J. M. Tsangaris and R. B. Martin, *J. Amer. Chem. Soc.*, **92**, 4255 (1970).
24) The results agree well with the values described in Ref. 12 for L-alanine, L-ornithine, and L-lysine as B.
25) R. B. Martin and R. Prados, *J. Inorg. Nucl. Chem.*, **36**, 1665 (1974).

The Acid-catalyzed Reaction of Cycloalkanones with Formaldehyde

Fukumi HIRANO and Shoji WAKABAYASHI

Department of Chemistry, Faculty of Science, Okayama College of Science, Okayama 700

(Received January 14, 1975)

The acid-catalyzed reactions of several cycloalkanones, such as cyclopentanone (**1a**), 2-methylcyclopentanone (**1b**), cyclohexanone (**1c**), 2-methylcyclohexanone (**1d**), and 2-isopropyl-5-methylcyclohexanone (**1e**), with formaldehyde were investigated. These reactions involved an aldol condensation analogous to the Prins reaction, and they afforded methylol derivatives and cyclic ethers. It was found that the formation of the products is strongly influenced by the skeletal structure and by the substituent on the cycloalkanones. That is, **1a**, **1c**, and **1d** gave mainly 1,3-dioxanes, while **1b** and **1e** formed only methylol derivatives. The reaction of cycloalkanone enol esters with formaldehyde was also studied.

The base-catalyzed reaction of cycloalkanones with formaldehyde has already been studied by many workers.[1-4] However, only a few papers have been reported on the acid-catalyzed reaction. For example, Olsen[5] has shown that cyclohexanone in sulfuric acid gave mono- and *bis*-1,3-dioxanes. Lumma[6] has recently reported the formation of methylol derivatives in the reaction of 2-methylcyclohexanone in trifluoroacetic acid. However, the details of the products have not been described.

In this investigation, the reaction of cycloalkanones and their enol esters with formaldehyde in the presence of an acid-catalyst was examined in considering the effects of the skeletal structure and of the substituents on the cycloalkanones.

Results and Discussion

These reactions were mainly carried out in a mixture of acetic acid and acetic anhydride in the presence of phosphoric acid.

The reaction of cyclopentanone (**1a**) with formaldehyde gave 2-hydroxymethylcyclopentanone (**2a**), the acetate (**2'a**), 2-[(acetoxymethoxy)methyl]cyclopentanone (**4'a**), and 2,4,8,10-tetraoxatricyclo[4.4.3.0^{1,6}]tridecane (**6a**) as the main products.

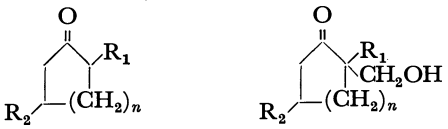

1

2 **2'** the acetate

a; $n=1$, $R_1=R_2=H$
b; $n=1$, $R_1=CH_3$, $R_2=H$
c; $n=2$, $R_1=R_2=H$
d; $n=2$, $R_1=CH_3$, $R_2=H$
e; $n=2$, $R_1=CH(CH_3)_2$, $R_2=CH_3$

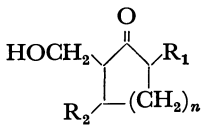

3 **3'** the acetate

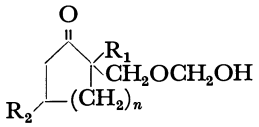

4 **4'** the acetate

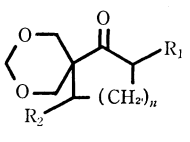

5

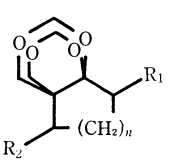

6

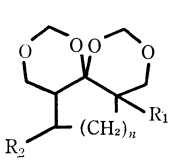

7

Scheme 1.

TABLE 1. REACTANTS AND PRODUCTS IN THE ACID-CATALYZED REACTION OF CYCLOALKANONES WITH FORMALDEHYDE

Reactants	Products
1a	**2a, 2'a, 4'a, 6a**
1b	**2b, 2'b, 3b, 3'b**
1c	**2c, 2'c, 4'c, 5c, 6c, 7c**
1d	**2d, 2'd, 3'd, 4'd, 6d, 7d**
1e	**2e, 2'e, 3e, 3'e**

The reaction of 2-methylcyclopentanone (**1b**) with formaldehyde yielded 2-hydroxymethyl-2-methylcyclopentanone (**2b**), the acetate (**2'b**), 5-hydroxymethyl-2-methylcyclopentanone (**3b**), and the acetate (**3'b**) mainly. In this reaction, no formation of a bis-1,3-dioxane, such as **6a**, was detected.

The reaction of cyclohexanone (**1c**) with formaldehyde afforded 2-hydroxymethylcyclohexanone (**2c**), the acetate (**2'c**), 2-[(acetoxymethoxy) methyl] cyclohexanone (**4'c**), 2,4-dioxa-7-oxospiro[5.5]undecane (**5c**), 2,4,8,10-tetraoxatricyclo[4.4.4.0^{1,6}]tetradecane (**6c**), and 2,4,12,-14-tetraoxatricyclo[8.4.0.0^{1,6}]tetradecane (**7c**) mainly.

Similarly, the reaction of 2-methylcyclohexanone (**1d**) gave 6-methyl-2,4,12,14-tetraoxatricyclo[8.4.0.0^{1,6}]-tetradecane (**7d**), along with small amounts of 2-hydroxymethyl-2-methylcyclohexanone (**2d**), the acetate (**2'd**), 6-acetoxymethyl-2-methylcyclohexanone (**3'd**), 2-[(acetoxymethoxy)methyl]-2-methylcyclohexanone (**4'd**), and 11-methyl-2,4,8,10-tetraoxatricyclo[4.4.-4.0^{1,6}]tetradecane (**6d**).

The reaction of 2-isopropyl-5-methylcyclohexanone (**1e**) with formaldehyde gave 2-hydroxymethyl-2-isopropyl-5-methylcyclohexanone (**2e**), the acetate (**2'e**) 6-hydroxymethyl-2-isopropyl-5-methylcyclohexanone (**3e**), and the acetate (**3'e**) as the main products. Methylol derivatives (**2e** and **3e**) when heated to 160—210 °C decomposed to **1e** and formaldehyde. A similar treatment of the acetates (**2'e** and **3'e**) yielded 2-isopropyl-5-methyl-1-cyclohexenyl acetate and formaldehyde.

The methanolysis of bis-1,3-dioxanes (**6c** and **7d**) gave the methylol compounds, (**2c** and **2d** respectively).

The spectral data of these products are summarized in Tables 2 and 3.

TABLE 2. SPECTRAL DATA OF METHYLOL DERIVATIVES

Compd.	IR, cm^{-1} a)	NMR (δ, in CCl_4)
2a	3450, 1730, 1250	1.5—2.5(m, 7H), 3.6—3.8(m, $-\dot{C}HCH_2$ OH, 2H), 4.14(s, 1H)
2'a	1730, 1230	1.5—2.4(m, 7H), 1.98(s, 3H), 4.0—4.3(m, $-\dot{C}HCH_2OAc$, 2H)
2b	3500, 1735, 1030	1.08(s, 3H), 1.5—2.7(m, 6H), 2.90(s, 1H), 3.2—3.8(m, $-\dot{C}CH_2OH$, 2H)
2'b	1735, 1230, 1160, 1070, 1030	1.02(s, 3H), 1.5—2.5(m, 6H), 2.00(s, 3H), 4.00(s, $-\dot{C}CH_2OAc$, 2H)
2c	3500, 1700, 1020	1.0—2.7(m, 9H), 3.20(broad s, 1H), 3.2—3.9(m, $-\dot{C}HCH_2OH$, 2H)
2'c	1740, 1710, 1230	1.0—2.7(m, 9H), 2.04(s, 3H), 3.9—4.3(m, $-\dot{C}HCH_2OAc$, 2H)
2d	3400, 1700, 1125, 1040	1.12(s, 3H), 1.5—2.7(broad, 8H), 2.86(s, 1H), 3.43(s, $-\dot{C}CH_2OH$, 2H)
2'd	1735, 1705, 1235, 1125, 1035	1.10(s, 3H), 1.6—2.6(broad, 8H), 1.99(s, 3H), 4.03(AB-q centered at 4.03, J=11 Hz, $-\dot{C}CH_2OAc$, 2H)
2e	3500, 1700, 1040, 1020	0.8—1.1(m, $-CH_3$, 9H), 1.7—2.7(m, 8H), 3.02(s, 1H), 3.62(AB-q centered at 3.62, J=12 Hz, $-\dot{C}CH_2OH$, 2H)
2'e	1740, 1700, 1230, 1030	0.7—1.2(m, $-CH_3$, 9H), 1.5—2.5(m, 8H), 2.00(s, 3H), 4.20(AB-q centered at 4.20, J=12 Hz, $-\dot{C}CH_2OAc$, 2H)
3b	3500, 1740, 1040	0.97(d, J=3.0 Hz, 3H), 1.5—2.8(m, 6H), 3.5—3.8(m, $-\dot{C}HCH_2OH$, 2H), 4.02(s, 1H)
3'b	1740, 1735, 1235, 1160, 1095, 1030	0.98(d, J=3.0 Hz, 3H), 1.5—2.7(m, 6H), 1.92(s, 3H), 3.8—4.1(m, $-\dot{C}H-CH_2OAc$, 2H)
3'd	1740, 1715, 1235, 1130, 1035	1.00(d, J=3.0 Hz, 3H), 1.4—2.7(m, 8H), 1.98(s, 3H), 3.4—4.5(m, $-\dot{C}H-CH_2OAc$, 2H)
3e	3500, 1700, 1220, 1060, 1020	0.7—1.1(m, $-CH_3$, 9H), 1.5—2.5(m, 8H), 2.92(s, 1H), 3.40(q, centered at 3.40, J=12 Hz, $-\dot{C}HCH_2OH$, 2H)
3'e b)	1740, 1700, 1230, 1030	0.7—1.2(m, $-CH_3$, 9H), 1.4—2.5(m, 8H), 1.98(s, 3H), 4.12(q, centered at 4.12, J=12 Hz, $-\dot{C}HCH_2OAc$, 2H)

a) Neat liquid film. b) IR spectrum was determined in Nujol.

TABLE 3. SPECTRAL DATA OF ETHER DERIVATIVES

Compd.	IR, cm^{-1}	NMR (δ, in CCl_4)
4'a	1745, 1730, 1220, 1110	1.5—2.4(m, 7H), 2.06(s, 3H), 3.6—3.9(m, $-\dot{C}HCH_2O-$, 2H), 5.15(s, $-OCH_2O-$, 2H)
4'c	2780, 1740, 1710, 1215, 1160	1.0—2.7(m, 9H), 2.07(s, 3H), 3 3—3.7(m, $-\dot{C}HCH_2O-$, 2H), 5.25(s, $-OCH_2O-$, 2H)
4'd	1735, 1710, 1230, 1155, 1120, 1030	1.05(s, 3H), 1.7—2.5(m, 8H), 2.10(s, 3H), 3.65(AB-q, centered at 3.65, J=9.8 Hz, $-\dot{C}CH_2O-$, 2H), 5.25(s, $-OCH_2O-$, 2H)
5c	2770, 1710, 1160, 1030	1.5—2.4(m, 8H), 3.78(s, $-CH_2O-$, 4H), 4.62(AB-q centered at 4.62, J=6.0 Hz, $-OCH_2O-$, 2H)
6a	2780, 1145, 1130, 1090	1.5—2.3(m, 6H), 3.54(AB-q centered at 3.54, J=11 Hz, $-CH_2O-$, 4H), 4.82(AB-q centered at 4.82, J=5.6 Hz, $-OCH_2O-$, 4H)
6c	2780, 1170, 1080	1.3—2.1(broad, 8H), 3.3—4.3(broad, $-CH_2O-$, 4H), 4.94(AB-q centered at 4.94, J=5.5 Hz, $-OCH_2O-$, 4H)
6d	2800, 1170, 1090, 1040, 980	0.82(d, J=6.2 Hz, 3H), 1.0—2.6(m, 7H), 3.43(AB-q centered at 3.43, J=11 Hz, $-CH_2O-$, 2H), 3.67(AB-q, J=11 Hz, $-CH_2O-$, 2H), 4.80(s, $-OCH_2O-$, 2H), 4.82(AB-q, J=5.6 Hz, $-OCH_2O-$, 2H)
7c	2800, 1160, 1070	1.0—2.6(m, 8H), 3.2—4.3(m, $-CH_2O-$, 4H), 4.5—5.1(m, $-OCH_2O-$, 4H)
7d	2790, 1165, 1095, 985	0.84(s, 3H), 1.1—2.7(m, 7H), 2.9—3.9(m, $-CH_2O-$, 4H), 4.78(AB-q centered at 4.78, J=5.7 Hz, $-OCH_2O-$, 2H), 4.81(AB-q, J=5.7 Hz, $-OCH_2O-$, 2H)

Effect of the Skeletal Structure. The reaction products in the condensation of **1a** and of **1c** with formaldehyde were compared. The reaction of **1c** afforded a spiro-type 1,3-dioxane (**5c**), along with a bis-1,3-dioxane (**6c**), in good yields. On the contrary, in the case of **1a**, the yield of bis-1,3-dioxane was remarkably less than that in the case of **1c**, and a spiro-type 1,3-dioxane was not formed at all. These

results indicate that the formation of a 1,3-dioxane ring involving the adjacent two carbon atoms of cyclopentane and that of a spiro-type 1,3-dioxane involving the α-carbon atom to the carbonyl group of cyclopentanone are attended with various difficulties, because of the consequent internal strain and the steric hindrance respectively.

Effect of the Substituent. In the reaction of **1d**, which has the methyl group in the α-position to the carbonyl group, with formaldehyde, bis-1,3-dioxane (**7d**) was produced in a greater yield than in the case of **1c**, but no spiro-type 1,3-dioxane such as **5c** was formed. On the other hand, the α-substituted cyclopentanone (**1b**) did not give any 1,3-dioxane derivatives. Moreover, the reaction of **1e**, with a bulky substituent such as an isopropyl group, also did not give 1,3-dioxanes at all. These results suggest that a methyl or isopropyl substituent attached at the α-position of cycloalkanones plays an important role in the formation of the 1,3-dioxane ring, in combination with the effect of the skeletal structure.

Effect of the Reaction Temperature. In all cases, the reactions carried out at temperatures between 40 and 60 °C provided products in good yields. At temperatures below 30 °C, these reactions scarcely proceeded at all. Above 90 °C, the reaction mixture gave a large amount of a polymer, along with the other products which could be isolated with difficulty from the reaction mixture.

Effect of the Catalyst. The effects of catalyst in these reactions were examined using several inorganic and organic acids, and also such Lewis acids as zinc chloride. Phosphoric acid and *p*-toluene sulfonic acid were found to be most effective catalysts. The use of hydrochloric acid, sulfuric acid, and *d*-10-camphorsulfonic acid gave rise to the polymerization of reactants, resulting in the formation of the products in lower yields. Lewis acids had little catalytic effect. The effect in the reaction of **1d** with formaldehyde is shown in Fig. 1 as an example.

Effect of the Solvent. It was found that the ratio and constitutions of the products are largely dependent on the solvents employed. The results shown in Tables 4

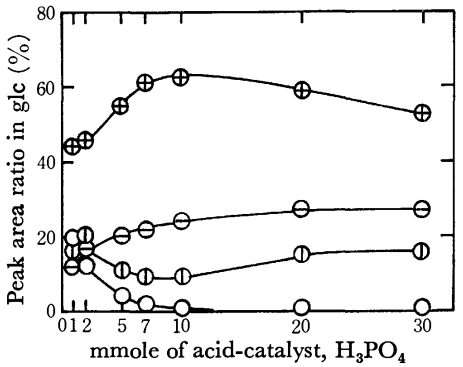

Fig. 1. Effect of supported amount of acid-catalyst, H_3PO_4 in the reaction of **1d** with formaldehyde Reaction conditions: Reactants, **1d** 10 mmol; $(CH_2O)_n$ 30 mmol; Solvent, AcOH 10 ml; Reaction temperature, 60 °C; Time, 15 hr.
○: **2d**; ⊖: **2'd**; ◐: **6d**; ⊕: **7d**

Table 4. Solvent effect of the various aliphatic acids in the reaction of **1d** with formaldehyde

Reactant (mmol)		Solvent (ml)	Peak area ratio in glc (%)			
1d	$(CH_2O)_n$		**2d**	**6d**	**7d**	others
10.0	30.0	HCOOH(10)	5.7	9.0	55.2	30.1
10.0	30.0	AcOH(10)	2.6	8.6	62.5	26.3
10.0	30.0	Ac_2O(10)	20.6	12.0	33.5	33.9
10.0	30.0	Ac_2O–AcOH (5—15)	8.4	18.1	42.5	31.0
10.0	30.0	C_2H_5COOH (10)	3.1	8.8	62.5	25.6
10.0	30.0	*n*-C_3H_7COOH (10)	4.6	22.5	43.0	29.9

Reaction conditions: Catalyst, H_3PO_4 10.0 mmol; Reaction temperature, 60 °C; Time, 15 hr.

Table 5. Solvent effect in the reaction of **1b** with formaldehyde

Reactant (mmol)		Solvent (mmol)	Catalyst (mmol)	Time (hr)	Peak area ratio in glc (%)	
1b	$(CH_2O)_n$				**2b**+**2'b**	**3b**+**3'b**
25.0	75.0	AcOH(125)	4.2	10	28	72
25.0	75.0	Ac_2O(125)	3.8	10	92	8
25.0	75.0	AcOH–Ac_2O (125—25)	2.6	21.5	21	79
25.0	75.0	*n*-Hex–Ac_2O (125—25)	5.2	7.5	14	86
25.0	75.0	EtOH–Ac_2O (125—25)	6.4	10	47	53
25.0	75.0	AcOEt–Ac_2O (125—25)	6.4	8.5	11	89
25.0	75.0	C_6H_6–Ac_2O (125—25)	4.2	7	9	91

Reaction conditions: Reaction temperature, 70 °C; Catalyst, PTS.

and 5 indicate that the reaction is affected markedly by the character of the solvents. Especially, the use of aliphatic alcohol caused a remarkable reduction in the yields of the products. When the reaction was carried out in halogen-substituted alkanes under reflux, the only products were 1,3-dioxanes. The reaction proceeded hardly at all in the same solvents at a lower temperature. In acetonitrile, lower aliphatic acids, and ethers, the reaction gave 1,3-dioxanes mainly.

Reaction of Cycloalkanone Enol Esters with Formaldehyde. The acid-catalyzed reaction of cycloalkanone enol esters (acetates and propionates) with formaldehyde was investigated under the same reaction conditions as those used for cycloalkanones. The reactions of cycloalkanones and of its enol esters with formaldehyde afforded quite similar products, but in the latter reaction the yields of 1,3-dioxanes increased remarkably. Especially, the reaction of the enol esters of cycloalkanones (**1c** and **1d**) with formaldehyde led preferentially to the formation of 1,3-dioxanes, even under milder reaction conditions. Therefore, it may be considered that the 1,3-dioxane derivatives are produced through the enolization of cycloalkanone, followed by a mechanism analogous to the Prins reaction.

Experimental

All the melting points are uncorrected. The IR spectra were measured with a JASCO Model IR-G spectrometer. The NMR spectra were recorded on a JEOL LMN-MH-60 II spectrometer (60 MHz) in CCl_4, using TMS as an internal standard.

Materials. *2-Methylcyclopentanone (**1b**)* was prepared by the method of van Rysselberge[7] from adipic acid. bp 138.0—138.5 °C; d_4^{25} 0.9127; n_D^{25} 1.4330. *2-Isopropyl-5-methylcyclohexanone (**1e**)* was prepared by the oxidation of 2-isopropyl-5-methylcyclohexanol with sodium bichromate,[8] bp 66—67 °C/4 mmHg; d_4^{25} 0.8950; n_D^{25} 1.4499; α_D^{25} −26.62 °. The other cycloalkanones, solvents, and catalysts were commercial materials.

The enol acetates of cycloalkanones were prepared by the method of Goodman *et al.*[9] *1-Cyclopentenyl acetate*: bp 47—49 °C/15 mmHg; d_4^{25} 1.0115; n_D^{25} 1.4480. *2-Methyl-1-cyclopentenyl acetate*: bp 62.5—63.0 °C/9 mmHg; d_4^{25} 0.9864; n_D^{25} 1.4476. *1-Cyclohexenyl acetate*: bp 178—179 °C; d_4^{25} 1.0082; n_D^{25} 1.4547. *2-Methyl-1-cyclohexenyl acetate*: bp 67—68 °C/14 mmHg; d_4^{25} 0.9901; n_D^{25} 1.4568. *2-Isopropyl-5-methyl-1-cyclohexenyl acetate*: bp 88—90 °C/3 mmHg; d_4^{25} 0.9465; n_D^{25} 1.4550; α_D^{25} +66.35 °.

The enol propionates of cycloalkanones (**1c** and **1d**) were prepared by the method described in the literature.[10] *1-Cyclohexenyl propionate*: bp 194—195 °C; d_4^{25} 0.9783; n_D^{25} 1.4548. *2-Methyl-1-cyclohexenyl propionate*: bp 73—75 °C/3 mmHg; d_4^{25} 0.9649; n_D^{25} 1.4539.

*Reaction of Cycloalkanones (**1a—1e**) with Formaldehyde.* To a mixture of paraformaldehyde (0.30 mol), acetic anhydride (0.10 mol), glacial acetic acid (1.00 mol), 85% phosphoric acid (0.05 mol), and cycloalkanone (0.10 mol) was added in several portions, under moderate cooling, after which the mixture was stirred at 40 or 60 °C for 10 or 15 hr. The reaction mixture was poured into cold water (30 ml), neutralized with 5% sodium carbonate, and then extracted with ether. After the ether had been evaporated, the residual oil was subjected to fractional distillation under reduced pressure. From these fractions, the individual products were isolated by preparative glpc using a DEGSP column at 160 °C.

The reaction of the enol ester of cycloalkanone with formaldehyde was carried out similarly.

The structures of the products were identified on the basis of the elemental analysis, and the MS, IR, and the NMR spectra. Tables 2 and 3 show some pertinent spectral data on the products.

*2-Hydroxymethylcyclopentanone (**2a**)*: Bp 95—96 °C/10 mmHg (lit,[11] 104 °C/13 mmHg); d_4^{25} 1.0823; n_D^{25} 1.4629; MR: 29.042. Calcd for $C_6H_{10}O_2$: 29.244. MS: *m/e* 114 (M^+).

Found: C, 63.10; H, 9.00%. Calcd for $C_6H_{10}O_2$: C, 63.13; H, 8.83%.

*2-Acetoxymethylcyclopentanone (**2'a**)*: Bp 100—102 °C/10 mmHg (lit,[11] 120—121 °C/15 mmHg); d_4^{25} 1.0886; n_D^{25} 1.4502; MR: 38.570. Calcd for $C_8H_{12}O_3$: 38.609. EV: 359. Calcd 359.3.

Found: C, 61.54; H, 7.94%. Calcd for $C_8H_{12}O_3$: C, 61.52; H, 7.75%.

*2-[(Acetoxymethoxy)methyl]cyclopentanone (**4'a**)*: Bp 109—110 °C/5 mmHg; d_4^{25} 1.1136; n_D^{25} 1.4513; MR: 45.046. Calcd for $C_9H_{14}O_4$: 44.870. EV: 296. Calcd: 301.3. MS: *m/e* 186 (M^+).

Found: C, 57.91; H, 7.49%. Calcd for $C_9H_{14}O_4$: C, 58.05; H, 7.58%.

*2,4,8,10-Tetraoxatricyclo[4.4.3.0^{1,6}]tridecane (**6a**)*: Bp 102—102.5 °C/10 mmHg: d_4^{25} 1.1920; n_D^{25} 1.4741. MR: 43.907. Calcd for $C_9H_{14}O_4$: 43.734. MS: *m/e* 186 (M^+).

Found: C, 58.02; H, 7.61%. Calcd for $C_9H_{14}O_4$: C, 58.05; H, 7.58%.

*2-Hydroxymethyl-2-methylcyclopentanone (**2b**)*: n_D^{25} 1.4677 (lit,[12] n_D^{20} 1.4681).

Found: C, 65.54; H, 9.45%. Calcd for $C_7H_{12}O_2$: C, 65.59; H, 9.44%.

*2-Acetoxymethyl-2-methylcyclopentanone (**2'b**)*: Bp 194—195 °C*; d_4^{25} 1.0558; n_D^{25} 1.4485. MR: 43.196. Calcd for $C_9H_{14}O_3$: 43.277. EV: 327. Calcd: 329.7.

Found: C, 63.50; H, 8.23%. Calcd for $C_9H_{14}O_3$: C, 63.51; H, 8.29%.

*5-Hydroxymethyl-2-methylcyclopentanone (**3b**)*:

Found: C, 65.52; H, 9.40%. Calcd for $C_7H_{12}O_2$: C, 65.59; H, 9.44%.

*5-Acetoxymethyl-2-methylcyclopentanone (**3'b**)*: Bp 206—207 °C*; d_4^{25} 1.1080; n_D^{25} 1.4692. MR: 42.794. Calcd for $C_9H_{14}O_3$: 43.277. EV: 322. Calcd: 329.7.

Found: C, 63.48; H, 8.34%. Calcd for $C_9H_{14}O_3$: C, 63.51; H, 8.29%.

*2-Hydroxymethylcyclohexanone (**2c**)*: d_4^{25} 1.0660; n_D^{25} 1.4735 (lit,[13] n_D^{11} 1.4780). MR: 33.759. Calcd for $C_7H_{12}O_2$: 33.862. MS: *m/e* 128 (M^+).

Found: C, 65.70; H, 9.43%. Calcd for $C_7H_{12}O_2$: C, 65.59; H, 9.44%.

*2-Acetoxymethylcyclohexanone (**2'c**)*: n_D^{25} 1.4628 (lit,[14] n_D^{20} 1.4632). EV: 321. Calcd for $C_9H_{14}O_3$: 330.0. MS: *m/e* 170 (M^+).

Found: C, 63.51; H, 8.32%. Calcd for $C_9H_{14}O_3$: C, 63.51; H, 8.29%.

*2-[(Acetoxymethoxy)methyl]cyclohexanone (**4'c**)*: d_4^{25} 1.1466; n_D^{25} 1.4818. MR: 49.768. Calcd for $C_{10}H_{16}O_4$: 49.488. EV: 283. Calcd: 280.2. MS: *m/e* 200 (M^+).

Found: C, 60.02; H, 8.22%. Calcd for $C_{10}H_{16}O_4$: C, 59.98; H, 8.05%.

*2,4-Dioxa-7-oxospiro[5.5]undecane (**5c**)*: d_4^{25} 1.1532; n_D^{25} 1.4848. MR: 42.284. Calcd for $C_9H_{14}O_3$: 42.659. MS: *m/e* 170 (M^+).

Found: C, 63.32; H, 8.13%. Calcd for $C_9H_{14}O_3$: C, 63.51; H, 8.29%.

*2,4,8,10-Tetraoxatricyclo[4.4.4.0^{1,6}]tetradecane (**6c**)*: d_4^{25} 1.1720; n_D^{25} 1.4852. MR: 48.981. Calcd for $C_{10}H_{16}O_4$: 48.352. Mp 86.5—87.0 °C (from *i*-C_3H_7OH). MS: *m/e* 200 (M^+).

Found: C, 59.92; H, 8.23%. Calcd for $C_{10}H_{16}O_4$: C, 59.98; H, 8.05%.

*Methanolysis of Bis-1,3-dioxane (**6c**)*: A solution of **6c** (25 mmol) in methanol (10 ml) was refluxed with two drops of conc. sulfuric acid for 15 hr, and then the solvent was evaporated. The residual mixture was extracted with ether, and the extract was washed with water, dried, and evaporated. The distillation of the residue gave a methylol derivative (**2c**) including a small amount of cyclohexanone (**1c**).

*2,4,12,14-Tetraoxatricyclo[8.4.0.0^{1,6}]tetradecane (**7c**)*: Mp 59—60 °C (from *i*-C_3H_7OH).

Found: C, 59.84; H, 8.18%. Calcd for $C_{10}H_{16}O_4$: C, 59.98; H, 8.05%.

*2-Hydroxymethyl-2-methylcyclohexanone(**2d**)*: Bp 85.0—85.5 °C/3 mmHg (lit,[13] 107—108 °C/11 mmHg); d_4^{25} 1.0310; n_D^{25} 1.4702. MR: 38.492. Calcd for $C_8H_{14}O_2$: 38.470. MS: *m/e* 142 (M^+).

Found: C, 67.23; H, 9.98%. Calcd for $C_8H_{14}O_2$: C, 67.57; H, 9.93%.

*2-Acetoxymethyl-2-methylcyclohexanone (**2'd**)*: Bp 103—104 °C/3 mmHg; d_4^{25} 1.0600; n_D^{25} 1.4598. MR: 47.585. Calcd for $C_{10}H_{16}O_3$: 47.845. EV: 304. Calcd: 304.6. MS: *m/e* 184 (M^+).

Found: C, 64.87; H, 8.93%. Calcd for $C_{10}H_{16}O_3$: C,

* Measured by a capillary method.

65.19; H, 8.75%.

The saponification of the acetate (**2'd**) did not produce the methylol (**2d**), but a polymer with a glass-like gloss.

6-Acetoxymethyl-2-methylcyclohexanone (3'd): d_4^{25} 1.0540; n_D^{25} 1.4602. MR: 47.891. Calcd for $C_{10}H_{16}O_3$: 47.845. EV: 302. Calcd: 304.6.

Found: C, 65.37; H, 8.68%. Calcd for $C_{10}H_{16}O_3$: C, 65.19; H, 8.75%.

2-Methyl-2-[(acetoxymethoxy)methyl]cyclohexanone (4'd): d_4^{25} 1.0971; n_D^{25} 1.4661. MR: 54.097. Calcd for $C_{11}H_{18}O_4$: 54.106. EV: 252. Calcd: 261.9.

Found: C, 61.64; H, 8.38%. Calcd for $C_{11}H_{18}O_4$: C, 61.66; H, 8.47%.

11-Methyl-2,4,8,10-tetraoxatricyclo[4.4.4.0^{1,6}]tetradecane (6d): d_4^{25} 1.1410; n_D^{25} 1.4762. MR: 52.980. Calcd for $C_{11}H_{18}O_4$: 52970. Mp 74—75 °C (from *i*-C_3H_7OH).

Found: C, 61.73; H, 8.54%. Calcd for $C_{11}H_{18}O_4$: C, 61.66; H, 8.47%.

6-Methyl-2,4,12,14-tetraoxatricyclo[8.4.0.0^{1,6}]tetradecane (7d): Bp 104.5—105.0 °C/3 mmHg; d_4^{25} 1.1464; n_D^{25} 1.4818. MR: 53.262. Calcd for $C_{11}H_{18}O_4$: 52.970. Mp 79—80 °C (from *i*-C_3H_7OH). MS: *m/e* 214 (M^+).

Found: C, 61.58; H, 8.53%. Calcd for $C_{11}H_{18}O_4$: C, 61.66; H, 8.47%.

Methanolysis of Bis-1,3-dioxane (7d): By the use of the procedures described for the methanolysis of **6c**, **7d** was treated with methanol to afford a methylol derivative (**2d**) including a small amount of 2-methylcyclohexanone (**1d**).

2-Hydroxymethyl-2-isopropyl-5-methylcyclohexanone (2e):

Found: C, 71.63; H, 10.92%. Calcd for $C_{11}H_{20}O_2$: C, 71.69; H, 10.94%.

2-Acetoxymethyl-2-isopropyl-5-methylcyclohexanone (2'e): Bp 130—131 °C/2 mmHg; d_4^{25} 1.0182; n_D^{25} 1.4635. MR: 61.276. Calcd for $C_{13}H_{22}O_3$: 61.699. EV: 243. Calcd: 247.9. MS: *m/e* 226 (M^+).

Found: C, 68.80; H, 9.99%. Calcd for $C_{13}H_{22}O_3$: C, 68.99; H, 9.80%.

6-Hydroxymethyl-2-isopropyl-5-methylcyclohexanone (3e):

Found: C, 71.62; H, 11.03%. Calcd for $C_{11}H_{20}O_2$: C, 71.69; H, 10.94%.

6-Acetoxymethyl-2-isopropyl-5-methylcyclohexanone (3'e): Bp 138—139 °C/2 mmHg; mp 39—40 °C (from *i*-C_3H_7OH). EV: 242. Calcd for $C_{13}H_{22}O_3$: 247.9. MS: *m/e* 226 (M^+).

Found: C, 69.02; H, 9.87%. Calcd for $C_{13}H_{22}O_3$: C, 68.99; H, 9.80%.

References

1) C. Mannich and W. Brose, *Chem. Ber.*, **56**, 833 (1923).

2) H. Gault and J. Skoda, *Bull. Soc. Chim. Fr.*, **13**, 308 (1946). H. Gault and E. Steckel, *C. R. Acad. Sci. Paris*, **207**, 475 (1938).

3) J. Colonge, *Bull. Soc. Chim. Fr.*, **1955**, 250.

4) F. Beke and K. Wick, *Ger. pat.*,1085520. *Chem. Abstr.*, **55**, 19827 (1961).

5) S. Olsen, *Acta Chim. Scand.*, **7**, 1364 (1953).

6) W. C. Lumma Jr. and O. H. Ma, *J. Org. Chem.*, **35**, 2391 (1970).

7) von Rysselberge, *Bull. Acad. Belgigue*, **12**, 171. *Bull. Soc. Chim. Belg.*, **35**, 315.

8) E. Beckmann, *Ann.*, **250**, 325 (1889).

9) L. Goodmann, A. Benitz, C. D. Anderson, and B. R. Baker, *J. Amer. Chem. Soc.*, **80**, 6587 (1958).

10) C. Mannich and Hăncu, *Ber.*, **41**, 567 (1908).

11) H. Gault and J. Skoda, *Bull. Soc. Chim. Fr.*, **13**, 316 (1946).

12) A. Eschenmoser and A. Frey, *Helv. Chim. Acta*, **35**, 1660 (1952).

13) J. Colonge, J. Dreux, and H. Delplace, *Bull. Soc. Chim. Fr.*, **1956**, 1635.

14) N. V. Elagina, N. S. Martinkova, and B. A. Kazanskiĭ, *Zh. Obsh. Khim.*, **29**, 4011 (1959).

α,β-Unsaturated Carboxylic Acid Derivatives. IX. The Cyclization of α-(*N*-Acyl-hydroxyamino) Acid Esters with Ammonia or Hydroxylamine[1]

Chung-gi SHIN, Katsumi NANJO, Masaki KATO, and Juji YOSHIMURA*

Laboratory of Organic Chemistry, Faculty of Technology, Kanagawa University, Rokkakubashi, Kanagawa-ku, Yokohama 221

**Laboratory of Chemistry for Natural Products, Faculty of Science, Tokyo Institute of Technology, Ōkayama, Meguro-ku, Tokyo 152*

(Received February 17, 1975)

A new type of cyclization reaction of α-(*N*-acyl-hydroxyamino) acid esters to imidazolidine-4-one derivatives and the synthesis of several 2,5-piperazinedione derivatives are described. The treatment of β-methoxy-α-(*N*-chloroacetyl- or *N*-phthaloylglycyl-hydroxyamino) acid esters with ammonia gave 2-carbamoyl-2-(1-methoxy)alkyl- or aralkyl-imidazolidine-4-ones, while a similar cyclization of α-(*N*-haloacetylamino) or α-(*N*-haloacyl-hydroxyamino) acid esters with ammonia or hydroxylamine gave 2,5-piperazinedione, 1-hydroxy-2,5-piperazinedione or 1,4-dihydroxy-2,5-piperazinedione derivatives. The difference in the formation mechanisms between the imidazolidine-4-one and 2,5-piperazinedione and their structural assignment were discussed.

In previous papers, we have reported that the cyclization of newly synthesized ethyl α-(*N*-chloroacetylamino)-α-alkenoate (**8**)[2] with alcoholic ammonia generally gave 3-alkylidene- or 3-arylidene-2,5-piperazinediones,[3] while a similar cyclization of ethyl β-methoxy-α-(*N*-chloroacetyl- or *N*-phthaloylglycyl-hydroxyamino)alkanoates (**4**) with ammonia afforded 2-carbamoyl-2-(1-methoxy)alkyl-imidazolidine-4-ones (**10**).[4] However, it was later found that the same cyclization of the *O*-acetyl derivative of **4d** (**5d**; ethyl 2-(*O*-acetyl-*N*-chloroacetyl-hydroxyamino)-3-methoxy-3-phenylpropanoate)[5] gave the normal cyclization products, 3-(1,1-dialkoxy)benzyl-2,5-piperazinediones (**15** and **16**).

In this paper, we wish to report in detail on the conversion of **4** into **10**, and on the difference in the mode of cyclization between **4** and **5**. Moreover, it has been confirmed that the cyclization of ethyl 2-(*N*-bromoacetyl-hydroxyamino)-3-phenylpropanoate (**3d**), which has no methoxy group in the alkyl moiety, with ammonia and hydroxylamine gives the corresponding 1-hydroxy and 1,4-dihydroxy-2,5-piperazinediones (**17** and **18**), as reported by Cook and Slater.[6]

Results and Discussion

As the starting materials, ethyl α-(*N*-haloacetyl-hydroxyamino)-β-phenylpropanoate (**3d**; X=Cl and X=Br) and **4** (X=phthalylimino: **a**; R=C_2H_5, **b**; R=*n*-C_3H_7, **c**; R=*i*-C_3H_7, **d**; R=C_6H_5. X=Cl: **d**; R=C_6H_5) were synthesized by the acylation of ethyl α-hydroxyaminoalkanoate (**1**) or ethyl α-hydroxyamino-β-methoxyalkanoate (**2**)[7] with haloacetyl halide or phthaloylglycyl chloride respectively.

When an ethanol solution of **4** was saturated with ammonia at room temperature, an unexpected compound, **10** was obtained in a 23—51% yield. The structure of **10** was confirmed by elementary analysis, by the spectral data, and by the acetylation of **10**. The infrared spectrum showed the absorption bands of the amide and cyclic imino groups in the 3180—3360 region and that of the carbonyl groups in the 1665—1700 cm^{-1} region. The acetylation of **10** with acetic anhydride under reflux afforded 2-carbamoyl-1,3-diacetyl-2-(1-methoxy)alkyl-imidazolidine-4-one (**11**) in a good yield.

A similar treatment of ethyl 2-(*N*-chloroacetyl-hydroxyamino)-3-phenylpropanoate (**3d**; X=Cl) with ammonia yielded 3-benzylidene-2,5-piperazinedione (**12**) in a 30% yield, instead of the expected **17** or 2-benzyl-2-carbamoyl-imidazolidine-4-one. On the other hand, the same reaction of the **5** obtained by the acetylation of **4** with acetic anhydride[2] with methanolic or ethanolic ammonia gave 3-(1,1-dimethoxy) (**15**)- or 3-(1-ethoxy-1-methoxy)benzyl-2,5-piperazinedione (**16**) respectively, though the yields were poor.

In a previous paper,[5] we have reported that the treatment of **5** with alkali in benzene gave ethyl 2-(*N*-chloroacetylamino)-3-methoxy-3-phenyl-2-propenoate (**9**) *via* the corresponding imino derivative (**7**). Consequently, the formation of **15** and **16** indicates that ethyl 2-(*N*-chloroacetylamino)-3,3-dimethoxy (**13**)- or 3-ethoxy-3-methoxy-3-phenylpropanoate (**14**) is formed by the addition of alcohols to **9** and that it subsequently cyclizes to give **15** or **16** respectively. In fact, the treatment of **5** with methanol or ethanol in the presence of 3 M-potassium hydroxide at room temperature gave **13** or **14** respectively in a good yield. When the cyclization of the **13** or **14** isolated with alcoholic ammonia was performed at room temperature, the expected **15** or **16** was also obtained in a good yield.

From the above facts, it seems that the cyclization reaction of the β-methoxy compound (**4**) may proceed through an imino intermediate (**7**→**7′**) formed by the dehydration of **4** to give **10**, while, in the case of **3**, the corresponding imino intermediate (**6**) readily isomerizes to the tautomeric enamine (**8**→**8′**)[8] and then cyclizes to give **12**. It may be deduced that **7** is more stable, because of the influence of the methoxy group in the 3-position, than **6**, the prototropy of which readily takes place from the carbon in the 3-position to the nitrogen atom. Furthermore, on the other hand, it may be postulated that the difference in the reaction products between **4** and **5** depends upon their relative rate of dehydration from **4** and the elimination of acetic acid from **5**.[5] It may safely be concluded that the structures of the products in these cyclization are determined by the relative rate of elimination (**3,4**→

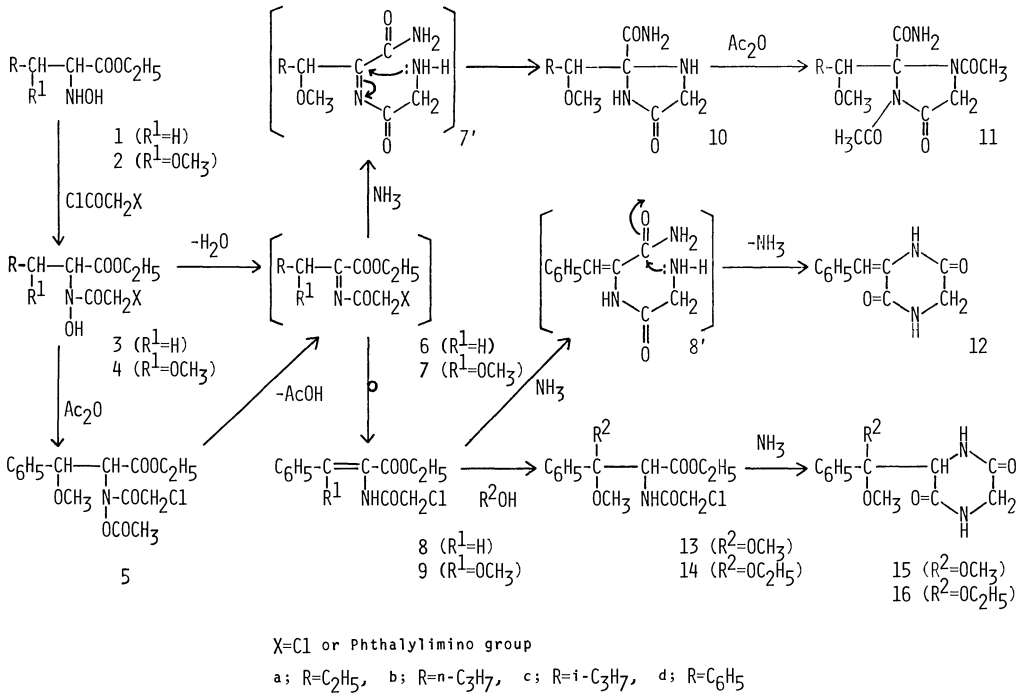

Scheme 1.

6,7 and **5**→**7**), the substitution of the halogen atom (X) with ammonia (X→NH_2), and the addition of alcohol to enamine (**8** and **9**). If the substitution of the halogen atom is faster than the elimination of water, as in the case of **4**, the newly formed amino group easily attacks the electron-deficient imino carbon to give a five-membered imidazolidine derivative. Even though the isomerization from **6** or **7** into **8** and **9** proceeds smoothly, **15** and **16** will be produced when the addition of alcohols to enamines (**8** and **9**) proceeds readily.

The infrared spectra of **13** and **14** showed the absorption band of NH at 3380 and the carbonyl group at 1700 cm^{-1}, while that of **15** and **16** showed them at 3080 and 3200 and in the 1680—1695 and 1660—1670 cm^{-1} regions, essentially as in ordinary 2,5-piperazinedione derivatives.

The physical constants, the yield, and the spectral data of the **10** and **11** and of **12**, **15**, and **16** obtained above are summarized in Tables 1 and 2 respectively.

When a solution of **3d** (X=Br) in ethanol was

Table 1. 2-Carbamoylimidazolidine-4-one derivatives (**10** and **11**)

Compd.	Yield (%)	Mp (°C)	Formula	Found, %			Calcd, %			IR spectrum, cm^{-1}, in KBr
				C	H	N	C	H	N	
10a	48	185—186	$C_8H_{15}N_3O_3$	47.80	7.66	21.00	47.75	7.51	20.88	3240, 3200, 1700
10b	31	192—194	$C_9H_{17}N_3O_3$	50.29	8.09	19.28	50.22	7.96	19.52	3350, 3180, 1690
10c	23	181—182	$C_9H_{17}N_3O_3$	49.98	8.22	19.74	50.22	7.96	19.52	3350, 3180, 1670
10d	51[a]	190—191	$C_{12}H_{15}N_3O_3$	57.88	6.06	16.59	57.82	6.07	16.86	3360, 3180, 1665
11a	75	169—170	$C_{12}H_{19}N_3O_5$	50.10	6.54	14.90	50.52	6.71	14.73	3410, 3250, 1705, 1690, 1570
11c	82	138—140	$C_{13}H_{21}N_3O_5$	51.97	6.93	14.08	52.16	7.07	14.08	3400, 3300, 1715, 1665, 1510
11d	95	191—193	$C_{16}H_{19}N_3O_5$	57.61	5.63	12.90	57.65	5.75	12.61	3425, 3225, 1670, 1665, 1545

a) Compound **10d** was also obtained in 46% yield from **4d** (X=Cl).

Table 2. 3-Benzylidene- and 3-benzyl-2,5-piperazinedione derivatives

Compd.	Yield (%)	Mp (°C)	Formula	Found, %			Calcd, %			IR spectrum, cm^{-1} in KBr
				C	H	N	C	H	N	
12	30	278—280[a]								
15	44	238—239	$C_{13}H_{16}N_2O_4$	58.98	6.51	10.32	59.08	6.10	10.60	3200, 3080, 1680, 1660
16	39	243—244	$C_{14}H_{18}N_2O_4$	60.43	6.43	10.05	60.42	6.52	10.07	3200, 3080, 1695, 1670
17	54	247—248	$C_{11}H_{12}N_2O_3$	59.94	5.54	12.88	59.99	5.49	12.72	3150, 3060 1650
18	70	250—251	$C_{11}H_{12}N_2O_4$	55.69	5.14	11.80	55.93	5.12	11.86	3075, 2870, 1660
19	84	134—136	$C_{13}H_{14}N_2O_4$	59.63	5.20	10.32	57.53	5.38	10.68	3200, 1800, 1700, 1680
20	72	165—167.5	$C_{15}H_{16}N_2O_6$	56.33	4.99	8.66	56.25	5.04	8.75	1810, 1790, 1710

a) Ref. 3.

saturated with ammonia at room temperature, according to the Cook and Slater method,[6] Compound **17** was obtained, while the reaction with hydroxylamine gave **18** in a good yield. However, as has been mentioned above, Compound **17** and **18** could not be derived from **3d** (X=Cl).

From the above results and from facts previously reported,[6] it is evident that **3d** (X=Cl) reacts with ammonia to give **12** after dehydration into **6**, whereas **3d** (X=Br) cyclizes without the dehydration to give **17** and **18**. These results indicate the difference in the reactivity of chlorine and bromine atoms with ammonia or hydroxylamine.

Compounds **17** and **18** gave a deep violet coloration with methanolic ferric chloride, indicating the presence of the cyclic hydroxamino-acid structure. Moreover, for the purposes of the structural assignment, **17** or **18** was treated with excess acetyl chloride under reflux to give 3-benzyl-4-acetoxy (**19**)- or 3-benzyl-1,4-diacetoxy-2,5-piperazinedione (**20**) respectively, in a good yield; the characteristic coloration with the ferric chloride was not found. The attempted conversion of **17** or **19** into **12** by the dehydration or the elimination of acetic acid in methanolic ammonia *via* the pyrazine derivative was unsuccessful.

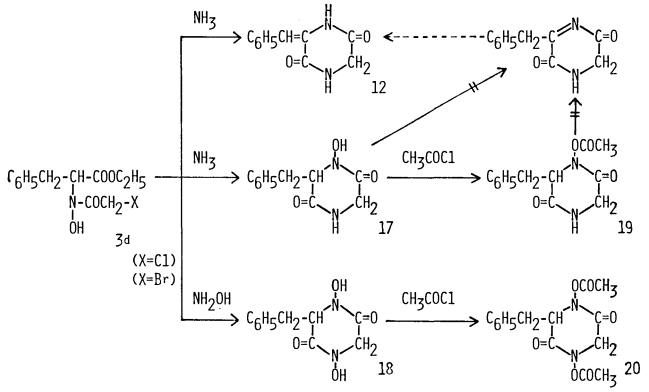

Scheme 2.

Experimental

All the melting points are uncorrected. The IR spectra were recorded with a Hitachi EPI-S2 Spectrometer. The NMR spectra were measured with a JNM-4H-100 Spectrometer (Japan Electron Optics Laboratory Co., Ltd.), using tetramethyl silane as the internal standard.

Materials. The ethyl 2-hydroxyamino-3-phenylpropanoate (**1d**)[5] and ethyl α-hydroxyamino-β-methoxyalkanoate (**2**)[7] were prepared by the methods previously reported.

Ethyl α-(N-Haloacetyl-hydroxyamino)-β-phenylpropanoate (3d). Into a solution of **1d** (0.027 mol) and pyridine (0.027 mol) in dry benzene (40 ml), we stirred, drop by drop, a solution of acetyl chloride or bromide (0.027 mol) in dry benzene (15 ml) at room temperature. After stirring for 3 hr, the resulting solution was washed successively with water, an aqueous solution of sodium hydrogencarbonate, 3 M-hydrochloric acid, and then finally with water. The benzene layer was dried over anhydrous magnesium sulfate and then evaporated. The reddish residual syrup was purified by chromatography on a silica gel column using benzene–ethyl acetate (X=Cl; 10: 1 or X=Br; 20: 1 in v/v) and the effluent solvent was evaporated under reduced pressure to give a pale yellow syrup (**3d**; X=Br) or colorless crystals (**3d**; X=Cl), which were then recrystallized from benzene–petroleum ether to give colorless needles. Ethyl 2-(*N*-chloroacetyl-hydroxyamino)-3-phenylpropanoate: yield, 41%; mp 64—65 °C. IR (KBr): 3200, 1730, 1640 cm^{-1}. NMR ($CDCl_3$): δ 7.54 (1H, bs, OH), 7.33 (5H, s, aromatic H), 5.42 (1H, t, J=8.2 Hz, $-CH_2-\underline{C}H-$), 4.23 (2H, s, $-COCH_2-$), 3.22 (2H, d, J=8.2 Hz, $-\underline{C}H_2-CH-$). Found: C, 54.79; H, 5.67; N, 4.85%. Calcd for $C_{13}H_{16}NO_4Cl$: C, 54.64; H, 5.65; N, 4.90%. Ethyl 2-(*N*-bromoacetyl-hydroxyamino)-3-phenylpropanoate: yield, 46%. IR (KBr): 3200, 1730, 1620 cm^{-1}. Found: C, 47.58; H, 5.02; N, 4.11%. Calcd for $C_{13}H_{16}NO_4Br$: C, 47.29; H, 4.89; N, 4.24%.

Ethyl α-(N-Chloroacetyl- or Phthaloylglycyl-hydroxyamino)-β-methoxyalkanoate (4). Compound **4** was prepared by the methods previously reported.[5,7] Ethyl 2-(*N*-chloroacetyl-hydroxyamino)-3-methoxy-3-phenylpropanoate (**4d**; X=Cl); colorless needles from benzene–petroleum ether; yield, 58%; mp 108—109°C. IR (KBr): 3100, 1740, 1640 cm^{-1}. NMR ($CDCl_3$): δ 7.40 (1H, s, OH), 7.27 (5H, s, aromatic H), 5.35 (1H, d, J=7.0 Hz, $-\underline{C}H-OCH_3$), 4.88 (1H, d, J=7.0 Hz, $-\underline{C}H-N-$), 4.22 (2H, s, $-COCH_2-$). Found: C, 53.10; H, 5.73; N, 4.30%. Calcd for $C_{14}H_{18}NO_5Cl$: C, 53.25; H, 5.71; N, 4.44%.

2-Carbamoyl-2-(1-methoxy)alkyl-imidazolidine-4-ones (10). When a solution of **4a**—**d** (0.02 mol) in ethanol (20 ml) was saturated with dry gaseous ammonia under cooling and then allowed to stand overnight at room temperature, colorless crystals were separated out. The crystals were collected and washed with methanol twice. Recrystallization from methanol gave **10a**—**d** as colorless needles. The melting points of all the new compounds decomposed.

In an analogous manner, **4d** (X=Cl) also reacted with ammonia to give **10d** (Table 1).

2-Carbamoyl-1,3-diacetyl-2-(1-methoxy)alkyl-imidazolidine-4-ones (11). A suspension of **10a**, **c**, **d** (0.002 mol) in acetic anhydride (4 ml) was heated at 120—130 °C until the crystals dissolved. The reaction solution was then concentrated under reduced pressure to dryness, giving a crystalline residue. The crystalline product was collected and recrystallized from boiling water to give **11a**, **c**, and **d** as colorless prisms (Table 1).

Ethyl α-(N-Chloroacetylamino)-β,β-dialkoxy-β-phenylpropanoate (13 and 14). To a solution of **5d** (0.005 mol, an unstable syrup, which was assigned by means of the IR spectrum (the $OCOCH_3$ band appeared at 1800 cm^{-1}) and which had no coloration with methanolic ferric chloride, derived by the reaction of **4d** (X=Cl) with excess acetic anhydride by a method previously reported[5]) in methanol (20 ml), with stirring, we added, drop by drop, a solution of potassium hydroxide (0.23 g) in methanol (10 ml) at room temperature. After continuous stirring for a day, the reaction solution was poured into benzene (20 ml) and washed with 3M-hydrochloric acid twice and with water. The benzene layer was dried over anhydrous magnesium sulfate and then evaporated under reduced pressure. The residual syrup thus obtained gradually crystallized. The crystalline product was collected and recrystallized from di-*n*-butyl ether to give **13** as colorless prisms; yield, 58%; mp 92—94 °C. IR (KBr): 3380, 1740, 1700, 1505 cm^{-1}. Found: C, 54.62; H, 6.06; N, 4.38%. Calcd for $C_{15}H_{20}NO_5Cl$: C, 54.64; H, 6.11; N, 4.25%.

In an analogous manner, Compound **14** was also obtained as a colorless syrup by the reaction of **5d** with ethanol, its structure was confirmed by means of the IR spectrum and by its conversion into **16**. Yield, 75%. IR (KBr): 3380, 1740, 1700, 1505 cm^{-1}.

Reaction of 13 or 14 with Ammonia. A solution of **13** (0.005 mol) in ethanol (20 ml) was saturated with dry gaseous

ammonia under cooling. When the resultant solution was allowed to stand at room temperature, a crystalline substance was precipitated. The ethanol was evaporated under reduced pressure, and the residual crystals were collected and washed successively with water and with ethanol. Subsequent recrystallization from glacial acetic acid gave **15** as colorless needles.

In an analogous manner, Compound **14** also reacted with ammonia to give **16** as colorless needles from acetic acid.

*Reaction of **4d** (X=Cl) with Ammonia.* A solution of **4d** (0.005 mol) in ethanol (20 ml) was saturated with dry gaseous ammonia under cooling. When the resultant solution was allowed to stand at room temperature for a day, colorless crystals were precipitated. The crystals were collected, washed with ethanol, and then recrystallized from glacial acetic acid to give **16** as colorless needles. The product was identical, in melting point and IR spectrum, with the sample obtained from **14**. Yield, 28%.

*Reaction of **3d** (X=Cl) with Ammonia.* When a solution of **3d** (0.005 mol) in ethanol (20 ml) was saturated with dry gaseous ammonia under cooling and then allowed to stand overnight at room temperature, colorless crystals were separated out. These crystals were collected and washed successively with water and with ethanol. Subsequent recrystallization from glacial acetic acid gave **12**. The product was identical, in melting point and IR spectrum, with the sample obtained by the method previously reported.[2]

*Reaction of **3d** (X=Br) with Ammonia.* A solution of **3d** (0.005 mol) in ethanol (30 ml) was saturated with dry gaseous ammonia under cooling. When the resultant solution was allowed to stand at room temperature overnight at room temperature, a crystalline product was precipitated. The precipitates were collected and washed with ethanol. The ethanol filtrate was condensed under reduced pressure to give a colorless powder, which was consistent with the first crystals obtained. Subsequent recrystallization from methanol gave **17** as colorless needles.

*Acetylation of **17** with Acetyl Chloride.* A mixture of **17** (0.001 mol) and acetyl chloride (3 ml) was refluxed at *ca.* 80 °C for 30 min until the crystals dissolved. The reaction solution was concentrated under reduced pressure to give a crystalline residue, which was collected and then washed with dry benzene twice. Recrystallization from benzene gave **19** as colorless needles. NMR ($CDCl_3$): δ 7.02—7.38 (6H, m, aromatic H and NH), 4.49 (1H, t, J=3.7 Hz, $-CH_2-\underline{C}\underline{H}-$), 3.23 (2H, d, J=3.7 Hz, $-C\underline{H}_2-CH-$), 2.58, 3.07 (2H, AB q, J=17.5 Hz, $-C\underline{H}_2-NH-$), 2.25 (3H, s, $-OCOCH_3$).

*Reaction of **3d** (X=Br) with Hydroxylamine.* A solution of **3d** (0.0066 mol) and hydroxylamine (made from hydroxylamine hydrochloride (0.6 g) and sodium (1.8 g)) in ethanol (150 ml) was refluxed for 3 hr. The reaction solution was then concentrated under reduced pressure. The residual syrup was dissolved in water (10 ml), and the aqueous solution was acidified with 3M-hydrochloric acid and then allowed to stand overnight in a refrigerator. The colorless crystals which were then separated out were collected and washed successively with water and ethyl ether. Recrystallization from ethyl acetate gave **18** as colorless tablets.

*Acetylation of **18** with Acetyl Chloride.* A mixture of **18** (0.001 mol) and acetyl chloride (3 ml) was refluxed at *ca.* 80 °C for 1 hr. After the removal of an insoluble substance, the reaction solution was condensed under reduced pressure to give a crystalline residue. The crystalline product was collected, washed with petroleum ether, and then recrystallized from benzene–petroleum ether to give **20** as colorless prisms. NMR ($CDCl_3$): δ 7.10—7.45 (5H, m, aromatic H), 4.67 (1H, t, J=4.0 Hz, $-CH_2-\underline{C}\underline{H}-$), 3.33 (2H, d, J=4.0 Hz, $-C\underline{H}_2-CH-$), 3.21, 3.93 (2H, AB q, J=16.0 Hz, $-CH_2-N-$), 2.21, 2.28 (6H, two s, $-OCOCH_3$).

References

1) Part VIII: C. Shin, K. Nanjo, T. Nishino, Y. Sato, and J. Yoshimura, This Bulletin, **48**, 2492 (1975).

2) C. Shin, M. Fujii, and J. Yoshimura, *Tetrahedron Lett.*, **1971**, 2499.

3) C. Shin, K. Sato, A. Ohtsuka, K. Mikami, and J. Yoshimura, This Bulletin, **46**, 3876 (1973).

4) C. Shin, K. Nanjo, and J. Yoshimura, *Chem. Lett.*, **1973**, 1039.

5) C. Shin, K. Nanjo, E. Ando, and J. Yoshimura, This Bulletin, **47**, 3109 (1974).

6) A. H. Cook and C. A. Slater, *J. Chem. Soc., C*, **1956**, 4130.

7) C. Shin, M. Masaki, and M. Ohta, This Bulletin, **43**, 3219 (1970).

8) C. Shin, M. Masaki, and M. Ohta, *ibid.*, **44**, 1654 (1971).

Syntheses of Photosensitive Poly(amino acids)

Masato NANASAWA and Hiroyoshi KAMOGAWA
Faculty of Engineering, Yamanashi University, Tadeka, Kofu 400

(Received February 28, 1975)

New poly(amino acids)(L-glutamic acid, L-tyrosine and L-lysine) containing photosensitive acryloyl, methacryloyl, and cinnamoyl groups in their side chains were synthesized from the corresponding amino acid NCAs. Their photosensitivities under UV irradiation were also investigated as to kind of functional group and the skeleton portion of the poly(amino acids). As regards the effect of the former, the sensitivities were in the order: acryloyl≃methacryloyl>cinnamoyl; as regards the effect of the latter, the sensitivities were in the order: poly-glutamate>poly-lysine>poly-tyrosine.

Many basic studies of the syntheses and properties of poly (amino acids) have been reported. Furthermore, these polymers have been used as synthetic fibers with characterstics similar to those of natural polypeptide fibers, leather, and surface-coating agents, and have also been utilized as models for natural peptides in the field of biochemistry. In recent years, some functinal polymers containing the naphthalene,[1] carbazole,[2] and cinnamyl[3] groups at the γ-position of poly-glutamate, and photochromic groups[4] at the ω-position of poly-tyrosine have been synthesized with the intention of keeping the steric regularities of poly(amino acids). This paper will describe the syntheses of characteristic photo resins carrying photosensitive groups at the ω-positions of the side chains of the poly(amino acids) in the light of the properties of poly(amino acid) films, which possess a high vapor permeability and thermal stability and which are edible.

The polymers were derived from the following L-amino acid derivatives previously synthesized: γ-acryloyloxyethyl-L-glutamate (**1a**), γ-methacryloyloxyethyl-L-glutamate (**2a**), γ-cinnamoyloxyethyl-L-glutamate (**3a**), *O*-acryloyl-L-tyrosine (**4a**), *O*-methacryloyl-L-tyrosine (**5a**), *O*-cinnamoyl-L-tyrosine (**6a**), ε-*N*-acryloyl-L-lysine (**7a**), ε-*N*-methacryloyl-L-lysine (**8a**), and ε-*N*-cinnamoyl-L-lysine (**9a**). These derivatives were transformed into the corresponding amino acid *N*-carboanhydrides by treatment with phosgene, followed by polymerization with tertiary amine in dichloromethane. The routes of the syntheses were as follows:

$$\mathrm{RCOOCH_2CH_2OH} + \text{L-glutamic acid} \xrightarrow{H_2SO_4}$$

$$(\mathbf{1a}\text{—}\mathbf{3a}) \xrightarrow{COCl_2} \text{NCA } (\mathbf{1b}\text{—}\mathbf{3b}) \xrightarrow{Bu_3N}$$

$$\left[\mathrm{RCOOCH_2CH_2OOC(CH_2)_2CH}\begin{matrix}\diagup\mathrm{CO}\\ \diagdown\mathrm{NH}\end{matrix}\right]_n \quad (\mathbf{1c}\text{—}\mathbf{3c})$$

$$\mathrm{RCO}\diagdown \\ \quad \mathrm{O} + \text{O-Na-L-tyrosine-Cu} \longrightarrow (\mathbf{4a}\text{—}\mathbf{6a})\text{-Cu} \\ \mathrm{RCO}\diagup$$

$$\xrightarrow{H_2S} (\mathbf{4a}\text{—}\mathbf{6a}) \xrightarrow{COCl_2} \text{NCA } (\mathbf{4b}\text{—}\mathbf{6b}) \xrightarrow{Bu_3N}$$

$$\left[\mathrm{RCOO}\text{-}\langle\bigcirc\rangle\text{-}\mathrm{CH_2CH}\begin{matrix}\diagup\mathrm{CO}\\ \diagdown\mathrm{NH}\end{matrix}\right]_n \quad (\mathbf{4c}\text{—}\mathbf{6c})$$

$$\mathrm{RCO}\diagdown \\ \quad \mathrm{O} + \text{L-lysine-Cu} \longrightarrow (\mathbf{7a}\text{—}\mathbf{9a})\text{-Cu} \\ \mathrm{RCO}\diagup$$

$$\xrightarrow{H_2S} (\mathbf{7a}\text{—}\mathbf{9a}) \xrightarrow{COCl_2} \text{NCA } (\mathbf{7b}\text{—}\mathbf{9b}) \xrightarrow{Bu_3N}$$

$$\left[\mathrm{RCONH(CH_2)_4CH}\begin{matrix}\diagup\mathrm{CO}\\ \diagdown\mathrm{NH}\end{matrix}\right]_n \quad (\mathbf{7c}\text{—}\mathbf{9c})$$

R; CH_2=CH- (**1**, **4**, **7**), CH_2=C(CH$_3$)- (**2**, **5**, **8**), -CH=CH- (**3**, **6**, **9**)

The films made of the resulting photosensitive poly(amino acids) were crosslinked by irradiation from a UV lamp, the solubilities of the films being compared as to the kind of functional group and amino acid.

Experimental

The IR spectra were measured on a Hitachi EPI-G spectrophotometer. The elemental analyses were carried out by the use of a Perkin-Elmer 240 apparatus. The melting points were measured by a capillary method and were not corrected. The double-bond contents of the polymers were determined by the pyridine-sulfate dibromide method.[5] Materials of a reagent grade were used without further purification; all the solvent were of the highest purity commercially available and were used after dehydration over a molecular sieve.

γ-Acryloyl(methacryloyl)oxyethyl-L-glutamate (1a, 2a). Into a mixture of 8.5 g (58 mM) of L-glutamic acid, 25 ml (232 mM) of 2-hydroxyethyl acrylate, and 0.2 g of hydroquinone, concentrated sulfuric acid was dropped with stirring at 25 °C until the mixture was in solution. After then standing for five days, the reaction mixture was vigorously stirred into 200 ml of ether. The ether layer was discarded, the remaining viscous crude ester-sulfate being washed once with ether and dissolved in 150 ml of ethanol. The solution was then neutralized with *n*-tributylamine. The crude ester was isolated by filtration, washed with ethanol, and dried *in vacuo*. The product was then dissolved in 50 ml of water and then stored in a refrigerator overnight. The remaining L-glutamic acid thus crystallized was filtered; the filtrate was precipitated into a large quantity of ethanol, and then dried *in vacuo*. **1a**: Yield, 52.6%. Mp 145—147 °C. Found: C, 47.95; H, 6.39; N, 5.71%. Calcd for $C_{10}H_{15}NO_6$: C, 48.98; H, 6.12; N, 5.71%. **2a**: Yield, 55.6%. Mp 152 °C. Found: C, 49.80; H, 6.89; N, 5.67%. Calcd for $C_{11}H_{17}NO_6$: C, 50.88; H, 6.56; N, 5.40%.

γ-Cinnamoyloxyethyl-L-glutamate (3a). 2-Hydroxyethyl-cinnamate was prepared from cinnamic acid and ethyleneglycol in the presence of *p*-toluenesulfonic acid; bp 130—131 °C/0.5 mmHg (lit,[6] 186—189 °C/10 mmHg). A mixture of 3.53 g (24 mM) of L-glutamic acid, 23 g (120 mM) of 2-

hydroxyethylcinnamate, and 4 ml of conc. sulfuric acid was stirred at 90 °C for 10 min. After then standing for two days at 25 °C, the reaction mixture was warmed up to 40 °C over a 4 hr period and then vigorously stirred into 100 ml of ether. The ether layer was discarded, and the remaining viscous crude ester-sulfate was washed with ether and dissolved in 50 ml of water. The solution was then neutralized with dil. aqueous ammonia and cooled in a refrigerator overnight. The ester thus crystallized was filtered, washed with cold water, and dried *in vacuo*. Yield, 10.2%. Mp 167—168 °C. Found: C, 59.27; H, 5.85; N, 4.13%. Calcd for $C_{16}H_{19}NO_6$: C, 59.81; H, 5.91; N, 4.36%.

O-*Acryloyl(methacryloyl)*-L-*tyrosine (4a, 5a)*. Acrylic (methacrylic) anhydride was prepared from the corresponding acid with triethylamine and phosgene by a conventional method.[7] Compounds **4a** and **5a** were prepared from acid anhydrides and L-tyrosine Cu-complex as in the case of the preparation of *O*-acetyl-L-tyrosine in an alkali solution.[8] **4a**: Yield, 67.5%. Mp 211—214 °C (dec.). Found: C, 61.38; H, 5.94; N, 5.48%. Calcd for $C_{12}H_{13}NO_4$: C, 61.21; H, 5.53; N, 5.95%. **5a**: Yield, 56.7%. Mp 228—230 °C (dec.). Found: C, 62.62; H, 6.09; N, 5.65%. Calcd for $C_{13}H_{15}NO_4$: C, 62.58; H, 6.02; N, 5.62%.

O-*Cinnamoyl*-L-*tyrosine (6a)*. L-Tyrosine (4.5 g, 25 mM) was dissolved in 50 ml of 1 M sodium hydroxide, followed by the addition of 3.43 g (10% excess) of cupric sulfate. The solution was stirred at 60 °C for 30 min, then cooled to 30 °C and filtered. To the filtrate, 13.92 g (50 mM) of cinnamic anhydride in 100 ml of DMF was added dropwise. The mixture was stirred at 50 °C for 3 hr, and then cooled to room temperature, filtered, and washed with water. The *O*-cinnamoyl-L-tyrosine-Cu thus obtained was washed with hot benzene. The finely powdered **6a**-Cu was decomposed with hydrogen sulfide in 0.5 M hydrochloric acid, followed by filtration. The filtrate was neutralized with dil. aqueous ammonia and cooled overnight. The product thus crystallized was isolated by filtration, washed with cold water and then with ethanol, and dried *in vacuo*. Yield, 57.0%. Mp 238—241 °C (dec.). Found: C, 69.32; H, 5.51; N, 4.50%. Calcd for $C_{18}H_{17}NO_4$: C, 69.38; H, 5.46; N, 4.50%.

ε-N-*Acryloyl (methacryloyl)*-L-*lysine (7a, 8a)*. L-Lysine-Cu (4.63 g, 13 mM) was suspended in 80% THF containing 2.82 g (30 mM) of sodium acrylate; 3.93 g (31.2 mM) of acrylic anhydride was then added dropwise to the mixture in an ice bath. The mixture was stirred in an ice bath for 2 hr, then stirred at 25 °C overnight and refluxed for 4 hr. The product (**7a**-Cu) was isolated by filtration and washed with cold water. The **7a**-Cu and **8a**-Cu thus obtained were decomposed with hydrogen sulfide in 50 ml of water and then filtered. The filtrates were concentrated *in vacuo* below 50 °C. The residues were recrystallized from 90% ethanol. **7a**: Yield, 45.8%. Mp 213—216 °C (dec.). Found: C, 53.99; H, 7.95; N, 13.72%. Calcd for $C_9H_{16}N_2O_3$: C, 53.92; H, 7.99; N, 13.98%. **8a**: Yield, 42.6%. Mp 218—225 °C (dec.). Found: C, 55.66; H, 8.49; N, 13.98%. Calcd for $C_{10}H_{18}N_2O_3$: C, 55.98; H, 8.40; N, 13.07%.

ε-N-*Cinnamoyl*-L-*lysine (9a)*. The molar ratio of L-lysine-Cu, cinnamic anhydride, and sodium cinnamate was equal to that of the above preparation. A mixture of the three compounds in 100 ml of 80% THF was refluxed for 12 hr with stirring, filtered while still hot, and washed with water. The **9a**-Cu thus obtained was decomposed with hydrogen sulfide in 100 ml of warm 0.5 M hydrochloric acid, and then filtered. The filtrate was neutralized with dil. aqueous ammonia and cooled in a refrigerator. The resulting solid was isolated by filtration, washed with cold water, and dried *in vacuo*. Yield, 38.5%. Mp 225—228 °C (dec.). Found: C, 65.31; H, 7.29; Calcd for $C_{15}H_{20}N_2O_3$: C, 65.31; H, 7.24; N, 10.13%.

Preparation of NCA and Polymerization. A dry and finely powdered amino acid derivative (4 mM) was suspended in 25 ml of abs. THF and stirred at 50—55 °C. A 12 mM portion of phosgene (30% in carbon tetrachloride) was then added dropwise to the mixture, and the mixture was stirred at that temperature for 1 hr. The unreacted phosgene was taken off by passing through dry nitrogen gas. The reaction mixture was concentrated to a 2—3 ml volume *in vacuo*, followed by precipitation into dry petroleum-ether cooled in a dry ice methanol bath. The crude amino acid NCA thus obtained was subjected to chromatographic purification with 10 g of a molecular sieve (type 3A) column[9] in dichloromethane. The NCA solution was then concentrated to 5 ml and precipitated into petroleum ether. NCA (2 mM) was dissolved in 15 ml of dichloromethane to afford a 2—3% (wt/vol) solution, which was then polymerized with 0.4 mM of dry *n*-tributylamine at 25 °C with stirring. The solution was stirred for 3 hr, allowed to stand for three days, and then precipitated into ether to isolate a solid polymer. Polymer films were made from dichloromethane solution on cover glass plates so as to afford 30—35 mg of the polymer (by weight), left overnight, and then dried *in vacuo* for 2 hr. The polymer films were crosslinked upon irradiation for 15 min by the use of a mercury lamp (Toshiba SHL 100UV-2) placed at a distance of 15 cm; the films crosslinked being immersed in chloroform overnight; they were then dried *in vacuo* for 2 hr to determine their weight loss.

Results and Discussion

Syntheses of ω-Derivatives of L-*Amino Acid*. Ester (**1a**—**3a**) were synthesized using sulfuric acid as the esterification catalyst. The yield of **3a** was lower than those of the others (**1a** and **2a**) because of the gelation of the reaction mixture at room temperature. When the reaction is prolonged at 90 °C, the ester and double bond of 2-hydroxyethyl cinnamate might be broken. With other acidic catalysts such as *p*-toluenesulfonic acid, however, the yield was very little, so, for this direct esterification, the method with sulfuric acid was adopted. The IR spectra indicated the NH-bond at 3350 cm^{-1}, $COO^-NH_4^+$ at 2600—3200 cm^{-1}, the C=O band of the ester at 1740 cm^{-1}, NH_4^+ at 1610 cm^{-1}, COO^- at 1590 cm^{-1} and the double bond of the corresponding ester at 900—1000 cm^{-1}. Compounds **1a** and **2a** were soluble in water and 50% ethanol; **3a** was slightly soluble in hot water and hot ethanol. *O*-Acetyl-L-tyrosine was directly prepared from L-tyrosine and acetyl chloride without the protection of the α-amino group of the former.[10] In this experiment, however, drastic conditions are unsuitable since double bonds are present in the reaction mixture and should be affected by the reaction; the direct use of acid chloride would cause low yield. In the synthesis of **6a**, the reaction mixture gradually turned brown, presumably due to the decomposition of a certain amount of the Cu-complex. The IR spectra indicated the phenyl group of tyrosine at 1900 and 840—850 cm^{-1} besides the absorption noted above. Compounds **4a** and **5a** were freely soluble in water and were slightly soluble in hot ethanol. Compound **6a** was slightly soluble only in hot water, but its hydrochloride was freely soluble in water

and ethanol. ε-*N*-Derivatives of L-lysine were prepared by the so-called aminolysis of L-lysine with the methyl ester in conc. aqueous ammonia.[11] With an acrylic or methacrylic ester, however, the possibilities of the formation of α-derivatives of L-lysine and the occurrence of a Michael reaction are present, so aminolysis is not suitable. The yield of the product prepared with L-lysine-Cu and acid anhydride in an aqueous solution was about 20% lower than those of tyrosine derivatives (**4a**—**6a**). Sodium salt was used to prevent the decomposition of the Cu-complex under basic conditions,[12] although a long reaction time at a high temperature as in the case of the preparation of **9a** caused a certain amount of decomposition. The IR spectra indicated amide I at 1650 and amide II at 1510 cm^{-1}, besides the absorption of amino acid and the double bond noted above. Compounds **7a** and **8a** were soluble only in water; **9a** was slightly soluble in hot water.

Syntheses of Polymer from ω-Derivatives of Amino Acid. Amino acid *N*-carboanhydrides (NCA) were prepared by a general method with phosgene from the corresponding ω-derivatives of amino acid, and were purified by reprecipitation and by column chromatography carried out with a 3A sieve. The chlorine contents and the purity were not determined. The NCAs (**1b**—**3b**) were poorly crystallized because of the presence of two ester bonds; they melted between 55 and 70 °C and were soluble in conventional organic solvents except petroleum ether. The solubility in dichloromethane was decreased in the order of the *O*-derivatives of tyrosine NCA and the ε-*N*-derivatives of lysine NCA. The melting points of the NCAs were about 100 °C lower than those of the preceding amino acid ω-derivatives: **4b**, 98 °C; **5b**, 111 °C; **6b**, 118 °C; **7b**, 98—100 °C; **8b**, 110—115 °C; **9b**, 120—123 °C. The IR spectra in dichloromethane indicated the absorption of NCA at 1860—1870 and 1790 cm^{-1} besides the absorption of the functional groups in the ω-position and the double bonds described above. Amino-acid NCAs, even without drying, were polymerized with *n*-tributylamine in dichloromethane. When the solubility of NCA in dichloromethane was low, an α-helix solvent such as DMF was added until cleanness was reached. Table 1 shows the results of the analysis of the polymer thus prepared. The values of the double-bond content less than 100% may be accounted for by the some precipitates were formed during the pyridine-sulfate-dibromide titrations of the polymer solutions in dichloroacetic acid (DCA), thereby causing errors in analysis due to heterogeneity. The degrees of polymerization were low in the case of the polymers carrying sterically large cinnamoyl groups at the ω-position. The solubility in an α-helix solvent was large when polymers contained two ester groups as in the case of **1c**—**3c**, and decreased in the order of substituted poly-lysine and poly-tyrosine. The IR spectra indicated NH at 3280 cm^{-1}, the ester at 1720—1740 cm^{-1}, amide I and amide II at 1650 and 1530 cm^{-1} respectively (**7c**—**9c** overlapped), and the double bonds in the side chains at 900—1000 cm^{-1}. Table 2 shows the results obtained in the crosslinking experiments effected for polymer films. To compare the effect of the kind of sensitizer, the weightloss by solvent extraction was determined for **2c**; none, 74.8%; methylene blue, 66.1%; 1% chlorophyll, 67.0%; 1% methylene blue and 5% benzoyl peroxide (BPO), 14.0% and 1% chlorophyll and 5% BPO, 4.3%. The last combination was used for the crosslinking experiments shown in Table 2. As regards the effects of functional groups in polymers, the degree of crossliking was in the order: acryloyl≃methacryloyl>cinnamoyl. No differences in effect were observed between the acryloyl and the methacryloyl groups. The photodimerizable cinnamoyl groups caused a very low degree of crosslinking, presumably because of steric hindrance.

TABLE 1. THE RESULTS OF ANALYSIS OF PLOY(AMINO ACID) ω-DERIVATIVES

Polymer No.	Yield[a] %	$[\eta]$[b] dl/g	Double bond[c]	Elemental analysis Found (Calcd), % C	H	N	Solubility[d] Soluble	Insoluble
1c	53.7	0.302	81.2	51.53 (52.86)	6.02 (5.72)	6.26 (6.16)	DCA, DCM, DMF, THF, CF, warm EtOH, AC	Et_2O, W
2c	55.7	0.313	88.9	54.26 (54.77)	6.47 (6.22)	5.95 (5.81)	DCA, DCM, DMF, THF, CF, warm EtOH, AC	Et_2O, W
3c	50.2	0.204	94.0	64.48 (63.36)	6.07 (5.61)	4.40 (4.62)	DCA, DCM, DMF, CF, warm EtOH	MeOH, Et_2O, W
4c	45.0	0.280	79.0	66.84 (66.26)	5.78 (5.06)	5.86 (6.44)	DCA, warm DCM, DMF, CF	EtOH, MeOH, Et_2O, AC, W
5c	42.1	0.359	87.7	67.23 (67.44)	5.67 (5.62)	6.17 (6.05)	DCA, warm DCM, CMF, CF	EtOH, MeOH, Et_2O, AC, W
6c	38.8	0.178	77.7	74.41 (73.32)	5.33 (5.12)	4.11 (4.79)	DCA, DCM, DMF, CF, warm AC	MeOH, Et_2O, W
7c	57.3	0.292	83.2	60.91 (59.24)	7.61 (7.68)	14.72 (15.35)	DCA, DCM, DMF, CF slightly EtOH, AC	MeOH, Et_2O, W
8c	72.0	0.235	91.2	61.83 (61.13)	8.29 (8.15)	14.05 (14.26)	DCA, DCM, DMF, CF slightly EtOH, AC	MeOH, Et_2O, W
9c	38.7	0.208	81.0	70.39 (69.66)	6.96 (6.79)	10.10 (10.84)	DCA, DCM, DMF, CF, warm EtOH, AC	MeOH, Et_2O, W

a) Based on amino acid ω-derivatives. b) **1c**—**3c** in DMF at 25 °C, **4c**—**9c** in DCA at 25 °C. c) mol % based on theory by the method of pyridine-sulfate-dibromide. d) Determined woithut drying of polymers, DCM, dichloromethane; CF, chloroform; AC, acetone; W, water.

Table 2. Crosslinking of polymer films[a,b]

Polymer	Sensitizer None	Present[c] I	Present[c] II	Appearance[d]
1c	64.5	2.4	2.7	Swelling
2c	74.8	4.3	10.9	Swelling
3c	74.7	24.8		Swelling
4c	73.5	46.8	29.3	Swelling
5c	59.2	28.5	9.7	Swelling
6c	90.1	83.1	83.5	Almost dissolved
7c	68.8	11.6	26.3	Swelling
8c	61.6	28.1	39.1	Swelling
9c	86.1	69.8	66.8	Almost dissolved

a) 15 min-irradiation at 15 cm from Hg lamp. b) Weight loss % due to the immersion in $CHCl_3$ overnight after irradiation. c) 1% chlorophyll and 5% BPO based on polymer. I, weightloss in $CHCl_3$; II, after immersion in $CHCl_3$ (I), weightloss in DCA determined in the same manner as in I. d) For the irradiated polymer films containing the sensitizers.

As regards the effect of the skeleton portion of poly amino acid, the degree of crosslinking was in the order: poly-glutamate>poly-lysine>poly-tyrosine. The substituted poly-tyrosine have a sterically large phenyl groups adjacent to the ester group, thereby causing a low extent of crosslinking; while poly-glutamates carrying photosensitive functional groups at the ends of long flexible side chains were crosslinked to a large extent.

This work was supported in part by a grant from the Alumni Association of Yamanashi University.

References

1) M. Hatano, T. Enomoto, I. Ito, and M. Yoneyama, This Bulletin, **46**, 3639 (1973).
2) H. Nomori, T. Enomoto, and M. Hatano, *Chem. Lett.*, **1975**, 391.
3) Y. Kodama, A. Ueno, K. Takeda, K. Uno, and Y. Iwakura, *J. Polym. Sci. Polym. Lett. Ed.*, **12**, 715 (1974).
4) P. H. Vandewyer and G. Smets, *J. Polym. Sci. A-1*, **8**, 2361 (1970).
5) Product manual N-70 of Rohm & Haas Company (1959), p. 46.
6) Beilstein, "Handbuch der Organishen Chemie, Erste Erganz," Vol. 9, p. 231.
7) T. K. Brotherton, J. Smith, Jr., and J. W. Lynn, *J. Org. Chem.*, **26**, 1283 (1961).
8) K. Schlogl, F. Wessely, and E. Wawersich, *Monatsh.*, **84**, 705 (1953).
9) S. Ishida and T. Ooizumi, Japan, 20181 (1968).
10) H. Bretschneider, *Monatsh.*, **81**, 647 (1950).
11) J. Yamamoto, M. Naruse, and H. Yasui, Japan, 29647 (1970).
12) As regards related procedure, confer S. R. Sandler and W. Karo, "Organic Functional Group Preparation," Vol. I, Academic Press Inc., New York (1968), p. 282.

Restricted Rotation Involving the Tetrahedral Carbon. XVI. Isolation of Stable Rotamers about an sp^3-sp^3 Carbon Bond[1,2]

Gaku YAMAMOTO, Mikio NAKAMURA, and Michinori ŌKI

Department of Chemistry, Faculty of Science, The University of Tokyo, Bunkyo-ku, Tokyo 113

(Received June 5, 1975)

Both antiperiplanar and synclinal rotamers resulted from the restricted rotation about a C–C single bond between the bridgehead *t*-alkyl group and the skeleton of 9-(1,1-dimethyl-2-phenylethyl)-11-methoxycarbonyl-9,10-dihydro-9,10-ethenoanthracene-12-carboxylic acid are isolated. Optical resolution of the synclinal rotamer is successfully performed by way of the mono-(−)-menthyl esters and a pair of enantiomers of the acid, $[\alpha]_D^{32} \pm 24.7°$, are isolated as stable entities. Activation energy for the interconversion between the rotamers of dimethyl esters is found to be 33.2 kcal/mol with a frequency factor of $10^{13.3}$ s^{-1}.

Isolation of stereoisomers originated from the restricted rotation about a single bond, *i.e.*, atropisomerism,*[3] has been one of the challenging problems for organic chemists. In substituted biphenyl and styrene derivatives, in which both of the two carbon atoms constructing the bond in quenstion is sp^2 hybridized, plenty of examples of realization of atropisomerism have been reported[4] with the first example of optical resolution of 6,6′-dinitrodiphenic acid as far back as 1922.[5]

As for the bond between two sp^3 hybridized carbon atoms, the situation is quite different. It had long been believed that the rotation about a saturated carbon bond is completely free, and it was not until 1949 that the concept of the energy barrier to rotation about the C–C bond in ethane with the staggered forms as the most stable conformations was definitely established.[6] Since then many investigations have been performed on the internal rotation in ethane derivatives making use of infrared and microwave spectroscopies as well as thermodynamic methods. Toward the end of 1950s nuclear magnetic resonance spectroscopy, especially so-called dynamic NMR, became available to this area of investigation and a vast number of reports have appeared since then. Several review articles have been published.[7]

At the outset of this investigation, all the compounds yet examined by DNMR had an energy barrier to rotation of less than 20 kcal/mol and no example had been recorded in which the rotation was still slow on the NMR time scale at the highest temperature attained. In order that the atropisomerism is realized at room temperature, the energy barrier to rotation about the bond in question should be higher than 23 kcal/mol assuming the mean lifetime of 1 hr at 25 °C and the frequency factor of 10^{13} s^{-1}.**

The energy barrier to internal rotation of a *t*-butyl group attached to a flexible residue could not exceed 12 kcal/mol,[10] but when a *t*-butyl group is attached to the bridgehead position of a rigid framework, the barrier rises considerably. First of such cases was reported by Brewer *et al.* in an ethenonaphthalene derivative **1**.[11] Although the authors did not give the

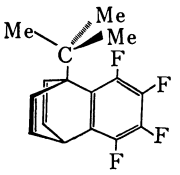

1

definite value, the energy barrier of about 20 kcal/mol is estimated, based on the chemical shift (*ca.* 0.2 ppm) and the coalescence temperature (between 120 °C and 180 °C). In one of the preceding papers of this series, a 9-*t*-butyl-9,10-dihydroethenoanthracene derivative **2** has been shown to exist in a staggered conformation shown by the Newman projection **3** and to have an extraordinarily high barrier to rotation about the axis bond (more than 25 kcal/mol), from the observation that the methyl signals of the *t*-butyl group remained 2:1 doublet even at 180 °C without any indication of line broadening.[12]

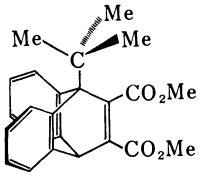

2

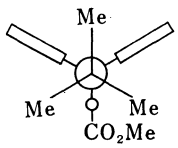

3

If one of the methyls of the *t*-butyl group of **2** is replaced by a suitable group X of similar bulkiness, the resulting three staggered conformations **4**, **5a**, and **5b** should exist as atropisomers, which are stable at room temperature.

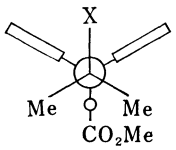

4: *ap*

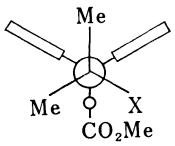

5a: *P-sc*

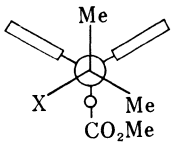

5b: *M-sc*

* We confine the discussion in this article only to carbon-carbon single bonds.

** Realization of atropisomerism at low temperatures does not necessarily require the high barrier to rotation. Certain compounds are known to be conformationally pure in the crystalline state. Crystals of *gauche* and *trans* conformations of 1,1,2,2-tetrabromoethane were independently obtained depending on the way of crystallization.[8] The equatorial conformer of chlorocyclohexane was purely isolated not only in the crystalline state but also in solution at −150 °C.[9] In these compounds the energy barrier is lower than 15 kcal/mol and naturally the conformational equilibrium is immediately attained in solution at room temperature.

Table 1. PMR data of the atropisomers **7** and **8**[a]

Protons	*ap*-Isomer (**7**)		*sc*-Isomer (**8**)	
	$CDCl_3$	C_6D_6	$CDCl_3$	C_6D_6
C–Me	1.78 (6H, s)	1.90 (6H, s)	1.83 (6H, br, s)[b]	1.83 (3H, s) 1.97 (3H, s)
O–Me	3.65 (3H, s) 3.72 (3H, s)	3.25 (3H, s) 3.39 (3H, s)	3.72 (3H, s) 3.75 (3H, s)	3.28 (3H, s) 3.43 (3H, s)
CH_2	3.75 (2H, s)	3.70 (2H, s)	3.64 (2H, q: J_{AB}=13.8 Hz, δ_{AB}=18.1 Hz)	3.90 (2H, q: J_{AB}=14.4 Hz, δ_{AB}=4.9 Hz)
10-H	5.57 (1H, s)	5.70 (1H, s)	5.56 (1H, s)	5.69 (1H, s)
aromatic[c]	6.9—7.6(11H, m)	6.7—7.5(11H, m)	6.7—7.6(11H, m)	6.6—7.6(11H, m)
peri	8.0 (2H, m)	8.0 (2H, m)	7.7 (1H, m) 8.0 (1H, m)	7.7 (1H, m) 8.0 (1H, m)

a) Obtained for *ca.* 10% (w/v) solution at 34 °C and 60 MHz, and given in ppm relative to internal tetramethylsilane. b) Appearent singlet with a half width of 2.1 Hz, suggesting the overlap of two slightly shifted singlets. c) Excluding the *peri*-protons.

We report here the successful manifestation of this prediction in a case where X is a benzyl group in the following sequence of procedures***: stereoselective synthesis of the antiperiplanar or meso form (**4**), isomerization of **4** to the equilibrium mixture of the atropisomers, isolation of the racemic synclinal form (**5a** and **5b**), and optical resolution of the *sc*-form† through mono-(−)-menthyl ester of the acid.

Enantiomeric atropisomerism, or optical activity due to the restricted rotation, involving an sp^3-sp^3 carbon bond is completely unprecedented, although realization of diastereomeric atropisomerism has been claimed by several groups of investigators without "convincing" evidence.[14]

Results and Discussion

Stereoselective Synthesis of the Antiperiplanar Isomer. 9-(1,1-Dimethyl-2-phenylethyl)anthracene (**6**) was synthesized by treatment of 1,1-dimethyl-2-phenylethylmagnesium chloride with anthrone followed by dehydration with phosphorus pentoxide.

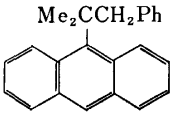

6

Heating **6** with dimethyl acetylenedicarboxylate in toluene under reflux for 5 hr gave colorless needles, mp 200—201 °C, in a spectral yield of *ca.* 85%. PMR data (Table 1) as well as those of MS and elemental analysis of the product clearly showed that it was a 1:1 Diels-Alder adduct with 9,10-dihydro-9,10-ethenoanthracene skeleton. The benzylic methylene as well as the geminal dimethyl groups appeared as a singlet and the *peri*-protons (protons at 1- and 8-positions of the skeleton), which appeared at δ *ca.* 8.0 separated from the other aromatic protons (δ 6.9—7.6), showed a two-proton multiplet indicating the magnetic equivalence of the two *peri*-protons. Although these NMR features could be understood assuming that the internal rotation of the bridgehead *t*-alkyl group were fast on the NMR time scale, such an interpretation is not consistent with the slow rotation of the *t*-butyl group in compound **2**. The most reasonable interpretation will be that the product has the antiperiplanar conformation (**7**) and the rotation about the axis bond is hindered at room temperature.

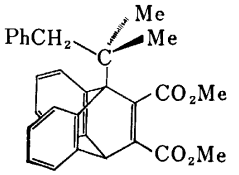

7

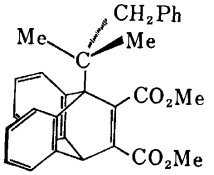

8

Careful inspection of the reaction mixture by PMR revealed the existence of *ca.* 15% of another product, spectral properties of which were consistent with the other atropisomer of the synclinal conformation (**8**).†† Separation of **8** from the reaction mixture seemed laborious and time consuming because of the small quantity and the similar chromatographic behavior as that of **7**. Thus the isolation and characterization of **8** was performed by another way described in the next section. No other products than these two were identified in the reaction mixture. The selective formation of the *ap*-isomer (**7**) in the Diels-Alder reaction is not the result of thermodynamic control as is shown later and therefore must be the result of kinetic origin. This means that the approach of the dienophile from the opposite direction to the benzyl group is favored. Since the *peri*-protons to the *t*-alkyl group in **6** give PMR signals at δ 8.0 in contrast to those in 9-*t*-butylanthracene (δ 8.4), the *peri*-protons in **6** are considered to be within the shielding cone of the benzyl-phenyl group. Although this does not necessarily mean that the conformation is fixed in such a form, the population of the folded conformation (**9**)

*** The benzyl group was chosen because of the synthetic convenience.

† Nomenclature of conformations used here is in accord with that proposed by Cahn, Ingold and Prelog.[13]

†† One of the enantiomers, the *P*-*sc* form, is illustrated.

must, at least, be significant. In conformation **9**, the attack of the dienophile from the benzyl side may effectively be blocked. This type of stereoselectivity has been observed in the Diels-Alder reaction between 9-*t*-alkylanthracenes and dienophiles such as dimethyl acetylenedicarboxylate[15] and benzynes.[16]

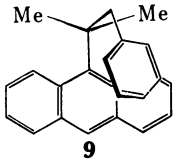

9

Equilibration of the Rotamers and Isolation of the Synclinal Isomer. The *ap*-isomer (**7**) was thermally quite stable at room temperature both in solution and in the crystalline state. Upon heating in chlorobenzene at 150 °C, however, **7** gradually isomerized to give an equilibrium mixture in which **7** and an isomerization product existed in a ratio of 1 : 3. The major component was isolated as colorless granules, mp 149—151 °C, upon chromatography on silica gel and was concluded to be the *sc*-atropisomer (**8**) from the data of PMR (Table 1) together with those of MS and elemental analysis. Two singlets for *gem*-methyls, an AB quartet for the methylene and the nonequivalent *peri*-protons suggested the chiral structure of the compound and are consistent with **8**. And these spectral features of **8** are the same as those of the minor product in the Diels-Alder reaction.

Reversible nature of the interconversion of these two atropisomers was confirmed by the equilibration experiment starting from the *sc*-isomer: upon heating in chlorobenzene at 150 °C, **8** afforded the same equilibrium mixture as that attained from the *ap*-isomer (**7**).

Kinetics of the equilibration and thermodynamics of the equilibrium are described in later section in some detail.

Optical Resolution of the Synclinal Isomer. Treatment of the synclinal dimethyl ester **8** with alcoholic potassium hydroxide afforded an isoluble crystalline mass which upon acidification gave a monocarboxylic acid. The acid was shown by PMR to have retained the synclinal conformation regarding the axis bond. Although no definite conclusion has yet been available as to which of the two methoxycarbonyl groups was hydrolyzed, structure **10** was tentatively assigned from the consideration of steric effects on hydrolysis.†††

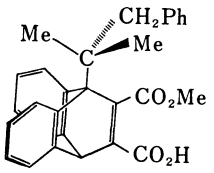

10

Attempts to obtain crystalline salts of **10** with alkaloid bases such as strychnine, quinine, cinchonine, and brucine gave no successful results. Thus resolution of **10** by way of the ester with a chiral alcohol was attempted. The racemic carboxylic acid **10** was converted to the corresponding acid chloride and treated with (−)-menthol to afford *ca.* 1 : 1 mixture of two diastereomeric (−)-menthyl esters **11** and **12** as an oil. Upon dissolution of the oil in hexane, one of the diastereomers (tentatively named as **A**) selectively crystallized out, leaving *ca.* 1 : 5 mixture of **A** and the other diastereomer (named as **B**) in the mother liquor. The glass obtained

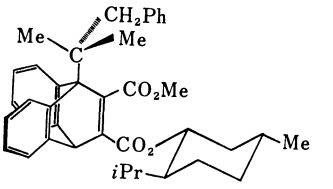

11

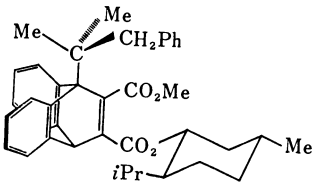

12

upon evaporation of the mother liquor resisted crystallization, andvarious attempts to isolate pure **B** were unsuccessful.

Alkaline hydrolysis of the distereomerically pure **A** gave a crystalline monocarboxylic acid, $[\alpha]_D^{32}$ −24.6°, whose PMR spectrum was identical with that of the racemic acid. The obtained acid ((−)-**10**) showed poorer solubility (for example in benzene) than (±)-**10**, and the IR spectrum of (−)-**10** in Nujol mull was essentially the same as that of the racemic acid. These observations suggested that (±)-**10** formed a conglomerate rather than a racemate or a racemic solid solution. The fact that the specific rotation of (−)-**10** did not change by further recrystallization together with the observations mentioned above suggested that (−)-**10** was obtained optically pure.

Similar saponification of the glassy mixture (1 : 5) of **A** and **B** afforded another crystalline carboxylic acid, $[\alpha]_D^{32}$ +24.8°, which showed the same PMR and IR spectra as those of (±)-**10**. The poorer solubility of (+)-**10** compared to the racemic acid seemed to help to isolate the pure dextrorotatory form.

Equilibration and Its Kinetics. Interconversion of the atropisomers is most reasonably assumed to occur through the rotation about the axis bond, although possibility of alternative mechanisms such as retro-Diels-Alder reaction and bond fission-recombination mechanisms involving biradical or zwitterionic intermediates could not be definitely eliminated. Thus kinetics of equilibration of the *ap*-isomer (**7**) was studied using PMR in order to obtain the energy barrier to interconversion between the atropisomers (**7** and **8**).

TABLE 2. KINETIC DATA OF EQUILIBRATION OF THE *ap*-ISOMER (**7**)[a]

$ap \underset{k_{-1}}{\overset{k_1}{\rightleftarrows}} sc$: $K = k_1/k_{-1}$

Temperature (°C)	k_1 (s^{-1})	τ (hr)	K
111	2.5×10^{-6}	114	3.0
126	1.1×10^{-5}	24	3.0
138	3.7×10^{-5}	7.5	3.0
152	1.6×10^{-4}	1.7	3.0

a) Measured in *ca.* 10% solution in chlorobenzene.

††† The remaining methoxycarbonyl group severely resisted hydrolysis.

Detailed method is described in the experimental section. First order rate constants k_1 (*ap*→*sc*) and equilibrium constants K were obtained at four temperatures in the range of 111—152 °C and shown in Table 2 along with the mean lifetime τ.

Arrhenius and Eyring plots of k_1's gave the good linear relationship and thermodynamic parameters were obtained as shown in Table 3.‡ Extrapolation of the data gives the mean lifetime of 18 days at 100 °C, 7 months at 80 °C, and 2600 years at 25 °C.

Table 3. Thermodynamic parameters of equilibration of the *ap*-isomer (**7**)

$E_a = 33.2$ kcal/mol	$\Delta H^{\ddagger} = 32.4$ kcal/mol
$\log A = 13.3$	$\Delta S^{\ddagger} = -0.4$ eu

Kinetics of the equilibration starting from the *sc*-isomer (**8**) was studied at 138 °C, and gave the rate constant k^{-1} of 1.1×10^{-5} s^{-1} and hence k_1 ($= K \times k^{-1}$) of 3.3×10^{-5} s^{-1} which agreed well with $k_1 = 3.7 \times 10^{-5}$ s^{-1} obtained from the forward reaction.

Ratio of *sc*- to *ap*-isomers at equilibrium remained constant at 3.0 throughout the temperature range examined. This means that there is little enthalpy difference between the isomers and the entropy term is in favor of the *sc*-isomer by 2.2 eu due to entropy of mixing and some other factors.

The barrier obtained here represents the third highest barrier to rotation about an sp^3-sp^3 carbon bond yet reported, following 37.7 kcal/mol for 9,10-bis(1-cyano-1-methylethyl)triptycene (**13**)[17] and 33.6 kcal/mol for 2,3-dichloro-9-(1,1-dimethyl-2-phenylethyl)-triptycene (**14**).[16]

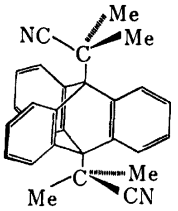

13

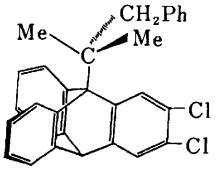

14

Experimental

Melting points were uncorrected. PMR spectra were recorded on a Hitachi R-20B spectrometer at 60 MHz and 34 °C, and tetramethylsilane was used as an internal reference. Mass spectra were measured on a Hitachi RMU-6L mass spectrometer, IR spectra on a Hitachi EPI-G2 grating spectrophotometer, and optical rotations on a JASCO DIP-SL automatic polarimeter using a 10 mm quartz cell.

9-(1,1-Dimethyl-2-phneylethyl)anthracene (6). To a chilled Grignard reagent prepared from 67.5 g (0.4 mol) of 1,1-dimethyl-2-phenylethyl chloride according to the procedure of Brown *et al.*[19] was added 19.4 g (0.1 mol) of anthrone powder in small portions during the course of 1 hr. The reaction mixture was allowed to stand overnight at room temperature and decomposed with a saturated aqueous solution of ammonium chloride. The ethereal solution was evaporated and heated *in vacuo* at 100 °C to remove low boiling substances. The residual oil, mainly composed of 9-(1,1-dimethyl-2-phenylethyl)-9-hydroxy-9,10-dihydroanthracene‡‡ and anthrone, was dissolved in 200 ml of carbon tetrachloride and heated under reflux for 5 hr in the presence of 30 g of phosphorus pentoxide. The carbon tetrachloride solution was filtered and evaporated. The residue was chromatographed through alumina column with the use of hexane containing 5% of benzene as an eluent to give **6** as pale yellow fluorescent crystals, mp 125—127 °C, in 15% yield. (Found: C, 93.04; H, 7.32%. Calcd for $C_{24}H_{22}$: C, 92.86; H, 7.14%). PMR (CCl_4): δ 1.74 (6H, s), 3.68 (2H, s), 7.01 (5H, s), and 6.9—8.2 (9H, m). The presence of mineral acids easily induced the decomposition of **6** into anthracene and (2-methyl-1-propenyl)benzene.‡‡‡

ap-9-(1,1-Dimethyl-2-phenylethyl)-11,12-bis(methoxycarbonyl)-9,10-dihydro-9,10-ethenoanthracene (7). A mixture of 2.80 g (9 mmol) of the anthracene **6** and 2 ml of dimethyl acetylenedicarboxylate in 30 ml of toluene was heated under reflux for 5 hr. Recrystallization of the product from chloroform–methanol gave 2.79 g (70%) of colorless needles, mp 200—201 °C. (Found: C, 79.78; H, 6.18%. Calcd for $C_{30}H_{28}O_4$: C, 79.62; H, 6.24%). MS (*m/e*): 452 (M^+, 1.5), 361 (61), 301 (44), 273 (68), 260 (33), 243 (50), 242 (48), 241 (33), 203 (33), 202 (39), and 91 (100).* IR (Nujol): 1735 and 1715 cm^{-1}.

(±)-sc-9-(1,1-Dimethyl-2-phenylethyl)-11,12-bis(methoxycarbonyl)-9,10-dihydro-9,10-ethenoanthracene (8). The *ap*-isomer **7** was heated at 150 °C for 10 hr in *o*-dichlorobenzene. After evaporation of the solvent, the equilibrated mixture was chromatographed on silica gel (Wakogel C-200) and eluted with benzene. Although the separation was poor, the *sc*-isomer was eluted slightly faster than the *ap*-isomer and repeated chromatographic operation of the fractions containing both of the two isomer enabled us to isolate **8**. Recrystallization of **8** from methanol gave colorless granules, mp 149—151 °C. (Found: C, 79.54; H, 6.42%. Calcd for $C_{30}H_{28}O_4$: C, 79.62; H, 6.24%). MS (*m/e*): 452 (M^+) (Essentially the same fragmentation pattern as that of the *ap*-isomer was obtained). IR (Nujol): 1742 and 1725 cm^{-1}. Recrystallization of **8** from solvents containing benzene or chloroform resulted in the inclusion of the solvent into the crystals.

(±)-sc-9-(1,1-Dimethyl-2-phenylethyl)-11-methoxycarbonyl-9,10-dihydro-9,10-ethenoanthracene-12-carboxylic acid (10). A solution of 420 mg (0.93 mmol) of the dimethyl ester **8** in 20 ml of ethanol was mixed with a solution of 200 mg of potassium hydroxide in 10 ml of ethanol and allowed to stand overnight at room temperature. The resulted crystalline mass was collected by filtration, acidified with dilute hydrochloric acid, and extracted with ether. The ethereal solution, upon evaporation of the solvent followed by recrystallization from chloroform–carbon tetrachloride, afforded 298 mg (73%) of white crystals, mp 188—190 °C (dec.). Found: C, 79.13; H, 5.69%. Calcd for $C_{29}H_{26}O_4$: C, 79.43; H, 5.98%. PMR ($CDCl_3$): δ 1.84 (6H, br s), 3.63 (2H, q, $J_{AB} = 14.8$,

‡ The parameters obtained here correspond to the pathway through the anticlinal transition state. Information on the synperiplanar transition state would be obtained by the study of racemization behavior of the optically active *sc*-isomer, which is left for future study.

‡‡ This alcohol was not isolated but its formation was recognized by the PMR spectrum (CCl_4) of the reaction mixture: δ 0.62 (6H, s), 2.60 (2H, s), and 3.82 (2H, q: $J_{AB} = 19$, $\delta_{AB} = 24$ Hz).

‡‡‡ The acid-catalyzed decomposition of 9-*t*-butylanthracene to anthracene and isobutylene was reported.[19]

* Fragmentation peaks with the intensity of more than 30% are cited.

δ_{AB}=16.7 Hz), 3.72 (3H, s), 5.55 (1H, s), 6.8—8.1 (13H, m), and 11.7 (1H, br s); (C_6H_6): δ 1.82 (3H, s), 1.97 (3H, s), 3.39 (3H, s), 3.90 (2H, br s), and 5.68 (1H, s). IR (Nujol): 1735 and 1685 cm^{-1}.

ap-9-(1, 1-Dimethyl-2-phenylethyl)-11-methoxycarbonyl-9, 10-dihydro-9, 10-ethenoanthracene-12-carboxylic acid, mp 223—225 °C (dec.), was similarly prepared from the *ap* diester (**7**). Found: C, 79.77; H, 6.32%. Calcd for $C_{29}H_{26}O_4$: C, 79.43; H, 5.98%. PMR ($CDCl_3$): δ 1.76 (6H, s), 3.63 (3H, s), 3.72 (2H, s), 5.52 (1H, s), 6.9—8.1 (13H, m), *ca.* 8.1 (1H, br s). IR (Nujol): 1735 and 1675 cm^{-1}.

(−)-Menthyl esters of the carboxylic acid ***10***. A solution of 710 mg (1.6 mmol) of the carboxylic acid **10** and 0.5 ml of thionyl chloride in 50 ml of benzene was heated under reflux for 1 hr in the presence of a catalytic amount of pyridine. Complete convertion of **10** to the corresponding acid chloride was checked by PMR of the reaction mixture: δ 1.77 and 1.88 (*gem*-Me_2), 3.30 (OMe), 3.78 (q, J_{AB}=14, δ_{AB}=8.5 Hz, CH_2Ph), and 5.69 (bridgehead). The reaction mixture was evaporated and the residual oil, without purification, was heated with 500 mg of (−)-menthol in 50 ml of pyridine at 100 °C for 2 hr. Evaporation of the solvent followed by chromatography on silica gel with benzene afforded a glass, which was shown to be *ca.* 1: 1 mixture of two diastereomeric esters by PMR. One of the diastereomers (Diastereomer **A**) crystallized out upon dissolution of the glass in hexane. Recrystallization from tetrahydrofuran–methanol gave 133 mg (15%) of colorless granules, mp 199—200 °C. $[\alpha]_D^{25}$ −77.0° (c=5.7, $CHCl_3$). PMR (C_6H_6): δ 1.84 and 2.02 (*gem*-Me_2), 3.51 (OMe), 3.87 (q, J_{AB}=14.1, δ_{AB}=9.1 Hz, CH_2Ph), and 5.87 (bridgehead). MS (*m/e*): 576 (M^+). IR (Nujol): 1735 and 1715 cm^{-1}.

Evaporation of the mother liquor gave a glass which was found by PMR to be *ca.* 1: 5 mixture of **A** and the other diastereomer (**B**). The latter showed the following PMR signals (C_6H_6): δ 1.87 and 1.96 (*gem*-Me_2), 3.51 (OMe), 3.98 (br s, CH_2Ph), and 5.87 (bridgehead).

(−)-sc-9-(1, 1-Dimethyl-2-phenylethyl)-11-methoxycarbonyl-9, 10-dihydro-9, 10-ethenoanthracene-12-carboxylic acid. A solution of 330 mg (0.57 mmol) of Diastereomer **A** in 20 ml of ethanol containing 200 mg of potassium hydroxide was heated at 60 °C for 3 hr and allowed to stand overnight at room temperature. The solution was evaporated *in vacuo* and the residue was acidified with dilute hydrochloric acid and extracted with chloroform. The chloroform solution was dried over magnesium sulfate and evaporated. The resulting solid mass was washed twice with small amounts of benzene to remove (−)-menthol. Recrystallization from chloroform–benzene gave 210 mg (84%) of colorless crystals, mp 188—190 °C (dec.). $[\alpha]_D^{32}$ −24.6 ° (c=2.4, $CHCl_3$). Found: C, 79.25; H, 6.08%. Calcd for $C_{29}H_{26}O_4$: C, 79.43; H, 5.98%.

(+)sc-(1, 1-Dimethyl-2-phenylethyl)-11-methoxycarbonyl-9, 10-dihydro-9, 10-ethenoanthracene-12-carboxylic acid. Similar treatment of 182 mg of the glassy mixture (1: 5) of **A** and **B** with potassium hydroxide followed by recrystallization from chloroform–benzene afforded 58 mg of colorless crystals, $[\alpha]_D^{32}$ +24.8° (c=1.2, $CHCl_3$).

Kinetics. A solution of the *ap*-isomer (**7**) in chlorobenzene (*ca.* 10% (w/v)) was sealed in a PMR sample tube and dipped in a boiling solvent bath. At appropriate intervals the sample tube was taken out from the bath and rapidly cooled to room temperature. The PMR spectrum was measured at 34 °C. Careful integration of methyl signals of the methoxycarbonyl groups of the *ap*- and *sc*-isomers afforded the relative population of both isomers.

The rate law for a first order reversible reaction is given[20] by

$$\log\left[1-\left(1+\frac{1}{K}\right)\frac{x}{a}\right] = -\frac{k_1}{2.303}\left(1+\frac{1}{K}\right)t$$

where a is the initial concentration of the *ap*-isomer, x the quantity of the *sc*-isomer formed at time t, and K the equilibrium constant [*sc*]/[*ap*]. The left side of the equation was calculated from the PMR integration data and the plot against t gave a good straight line, the slope of which afforded the rate constant k_1. This procedure was performed at four temperatures using the following solvents as a bath: toluene (111 °C), diethyl carbonate (126 °C), *p*-xylene (138 °C), and cumene (152 °C).

Thermodynamic parameters were obtained from the least square analysis of the following equations:

$$\log k_1 = \log A - \frac{E_a}{4.576}\cdot\frac{1}{T} \quad \text{(Arrhenius plot)}$$

$$\log\frac{k_1}{T} = \left(\frac{\Delta S^{\ddagger}}{4.576}+10.319\right) - \frac{\Delta H^{\ddagger}}{4.576}\cdot\frac{1}{T} \quad \text{(Eyring plot)}$$

References

1) The preceding paper: M. Nakamura and M. Ōki, This Bulletin, **48**, 2106 (1975).

2) Presented in part as a preliminary form: M. Ōki and G. Yamamoto, *Chem. Lett.*, **1972**, 45.

3) E. L. Eliel, "Stereochemistry of Carbon Compounds," McGraw Hill, New York (1962), pp. 156—178.

4) R. Adams and H. C. Yuan, *Chem. Rev.*, **12**, 261 (1933).

5) G. H. Christie and J. Kenner, *J. Chem. Soc.*, **121**, 614 (1922).

6) J. D. Kemp and K. S. Pitzer, *J. Chem. Phys.*, **4**, 749 (1936); L. G. Smith, *ibid.*, **17**, 139 (1949).

7) See for example: E. B. Wilson, *Adv. Chem. Phys.*, **2**, 367 (1959); J. P. Lowe, *Progress Phys. Org. Chem.*, **6**, 1 (1968). As to DNMR, see for example: G. Binsch, *Top. Stereochem.*, **3**, 97 (1968); I. O. Sutherland, *Annu. Rep. NMR Spectrosc.*, **4**, 71 (1971).

8) R. E. Kagarise, *J. Chem. Phys.*, **24**, 300 (1956).

9) F. R. Jensen and C. H. Bushweller, *J. Amer. Chem. Soc.*, **91**, 3223 (1969).

10) C. H. Bushweller, S. Hoogasian, and W. G. Anderson, *Tetrahedron Lett.*, **1974**, 547; C. H. Bushweller, G. U. Rao, W. G. Anderson, and P. E. Stevenson, *J. Amer. Chem. Soc.*, **94**, 4743 (1972); C. H. Bushweller and W. G. Anderson, *Tetrahedron Lett.*, **1972**, 1811; J. E. Anderson and H. Pearson, *ibid.*, **1972**, 2779; *Idem.*, *J. Chem. Soc., B*, **1971**, 1209; B. L. Hawkins, W. Bremser, S. Borcic, and J. D. Roberts, *J. Amer. Chem. Soc.*, **93**, 4472 (1971); W. E. Heyd and C. A. Cupas, *ibid.*, **93**, 6086 (1971); F. A. L. Anet, M. St. Jacques and G. N. Chmurny *ibid.*, **90**, 5243 (1968).

11) J. P. N. Brewer, H. Heaney, and B. A. Marples, *Chem. Commun.*, **1967**, 27.

12) M. Ōki and M. Suda, This Bulletin, **44**, 1876 (1971).

13) R. S. Kahn, C. K. Ingold, and V. Prelog, *Angew. Chem. Int. Ed. Engl.*, **5**, 386 (1966).

14) a) G. Wittig, G. Koenig, and K. Clauss, *Ann.*, **593**, 127 (1955); b) F. Kohen, R. A. Mallory, and I. Scheer, *Chem. Commun.*, **1969** 580; c) K. Suzuki and M. Minabe, *Tetrahedron Lett.*, **1974**, 1541.

15) G. Yamamoto and M. Ōki, *Chem. Lett.*, **1974**, 65.

16) *Idem.*, *ibid.*, **1974**, 713.

17) H. Iwamura, *ibid.*, **1973**, 232.

18) W. G. Brown, C. J. Mighton, and M. Senkus, *J. Org. Chem.*, **3**, 62 (1938).

19) R. C. Parish and L. M. Stock, *ibid.*, **31**, 4265 (1966).

20) K. S. Wiberg, "Physical Organic Chemistry," John Wiley and Sons, New York (1964), pp. 326—327.

NOTES

BULLETIN OF THE CHEMICAL SOCIETY OF JAPAN, VOL. 48 (9), 2597—2598 (1975)

Degradation of Polyacrylamide Molecules in Aqueous Solutions by High-speed Stirring

Waichi NAGASHIRO, Teruo TSUNODA, Makoto TANAKA, and Mitsuru OIKAWA
Central Research Laboratory, Hitachi Ltd., Kokubunji, Tokyo 185

(Received January 21, 1975)

Synopsis. The viscosity of polyacrylamide aqueous solutions decreases as a result of high-speed stirring, due possibly to the degradation of the molecules.

It has been observed that the viscosity of the polyacrylamide (PAM) solution decreased with increased high-speed stirring time. This decrease is assumed to be due to a change in the dissolved state and/or the degradation of the PAM molecules. It was experimentally found that the molecular weight decreased, implying that the PAM molecules were degradated.

Experimental

PAM solutions were placed in a type M (Tokushu Kika) Homo-Mixer and subjected to high-speed stirring for various periods of time. Care was taken that the blades were immersed to the same level in the liquid in each case in order to ensure identical stirring conditions. The viscosities of these solutions were then measured by a type B viscometer (Tokyo Keiki).

The intrinsic viscosities $[\eta]$ (reduced viscosity at zero concentration) were obtained by extrapolating the measured values for a 0.1—1.0 g/dl concentration. The molecular weights M were calculated from the intrinsic viscosities by using the Staudinger equation, $[\eta]=KM^{\alpha}$. The constants K and α in the equation are given, for PAM in water at 25 °C, as 0.631×10^{-4} and 0.8, respectively.[1)]

Results and Discussion

The high-speed stirring effect on the viscosity of PAM solutions is shown in Fig. 1. The figure indicates that the viscosities of the solutions decrease initially, and then saturate as the stirring time is increased. The saturated values depend on the stirring speed.

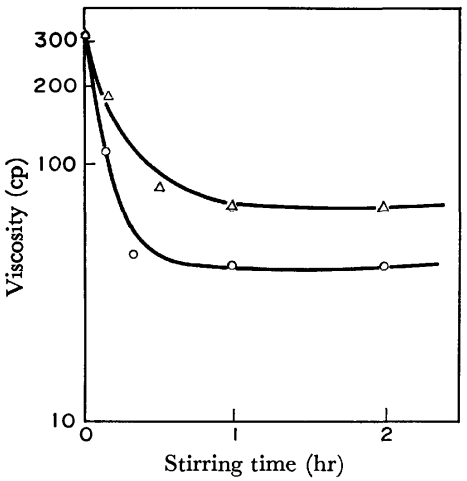

Fig. 1. Viscosity decrease of PAM solutions by high-speed stirring at 25 °C.
(—○—: 7000 rpm, —△—: 4000 rpm)

Two assumptions were made to explain this phenomenon. One is that the dissolved state of PAM solutions changes due to stirring. From various investigations, however, this assumption was found to be invalid.

The other assumption is that the PAM molecules degradate by high-speed stirring. Figure 2 shows the graph of reduced viscosity η_{sp}/C against the concentration C for PAM solutions at various stirring speeds. Here, these solutions are three days after stirring was completed. The figure shows the linear relationship between η_{sp}/C and C as well as the decrease in $[\eta]$ as the stirring speed is increased. The molecular weight cal-

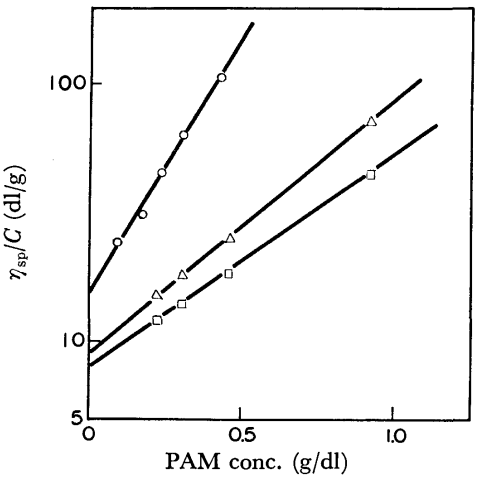

Fig. 2. Reduced viscosity η_{sp}/C of PAM solutions for stirring time at 25 °C.
(—○—: no stirring, —△—: 4000 rpm 1 hr stirring
—□—: 7000 rpm 1 hr stirring)

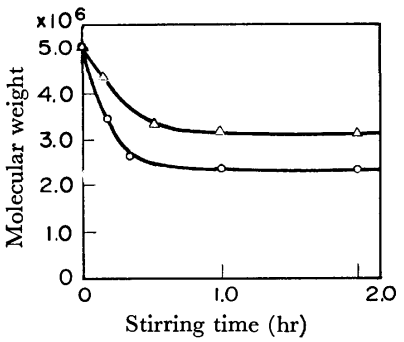

Fig. 3. Molecular weight decrease of PAM by high-speed stirring.
(—○—: 7000 rpm, —△—: 4000 rpm)

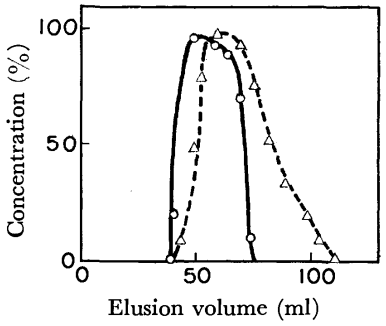

Fig. 4. GPC elusion curve of PAM solution.
(—○—: before stirring, ---△---after stirring)

culated from $[\eta]$, with respect to the stirring time, is given in Fig, 3. The figure shows that the molecular weight reduced to about a half of the initial value after stirring at 7000 rpm at 25 °C. The distribution of molecular sizes measured by gel permeation chromatography (GPC) is shown in Fig. 4. It is evident from the figure that the molecular size of PAM was reduced after stirring. It can be concluded that the decrease in the viscosity of the PAM solution by high-speed stirring is due to degradation of the PAM molecules.

The degradation mechanism of vinyl polymer has been widely described. Our degradation results for PAM molecules can be explained by employing the formula given by Jellinek,[2]

$$dB_i/dt = k(P_i - 1)n_i \quad \text{for } P_i > P_1$$
$$dB_i/dt = 0 \quad \text{for } P_i \leqq P_1$$

where B_i is the number of shear degradation, P_i is the degree of polymerization, P_i is the limiting degree of polymerization, n_i is the number of molecules, k is the rate constant, and t is the time. The solution of Jellinek's equation, together with the experimental results, are shown in Fig. 5. The agreement is good, indicating the applicability of Jellinek's theory.

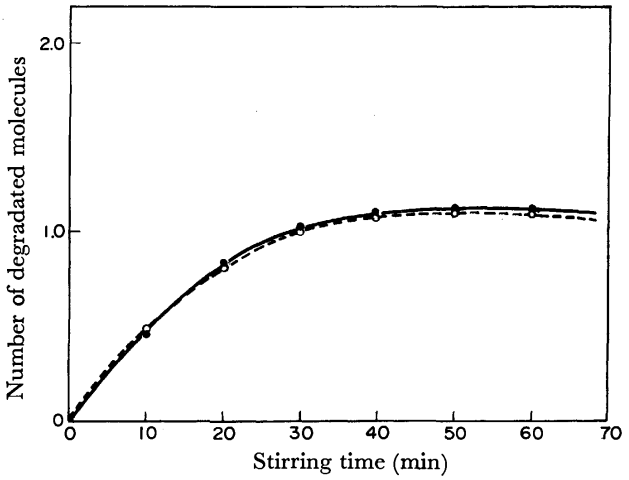

Fig. 5. Relation between the number of degradated molecules and stirring time.
(—●—: Experiment, ---○---: Calculated)

References

1) W. Scholtan, *Makromol. Chem.*, **14**, 168 (1954).
2) H. H. G. Jellinek and G. White, *J. Polym. Sci.*, **6**, 745 (1951).

BULLETIN OF THE CHEMICAL SOCIETY OF JAPAN, VOL. 48 (9), 2599—2600 (1975)

Measurement of Singlet-Triplet Absorption Spectrum of Pyridazine by a Sensitized-Phosphorescence Excitation Method

Kohzaburo YAMAMOTO, Takeshi TAKEMURA, and Hiroaki BABA

Division of Chemistry, Research Institute of Applied Electricity, Hokkaido University, Sapporo 060

(Received March 5, 1975)

Synopsis. The $S_0 \rightarrow T$ absorption spectrum of pyridazine was measured by means of sensitized-phosphorescence excitation in EPA rigid-glass solution at 77 K. Its intensity was found to be much lower than that of the corresponding spectrum of pyrazine.

The phosphorescence of pyridazine has not been observed as yet, although its intersystem-crossing quantum yield is of the same order of magnitude as the yields of strongly phosphorescent pyrazine and pyrimidine.[1] It may be presumed that a slow rate of radiative decay of the triplet state, compard with its radiationless decay, is responsible for the non-phosphorescent property of pyridazine.

Hochstrasser and Marzzacco[2] measured $S_0 \rightarrow T$ absorption of pyridazine crystal at 4.2 K, where S_0 and T denote the ground singlet and excited triplet states respectively, and they evaluated the rate constant for the radiative triplet decay (k_p). According to their results, the k_p value for pyridazine is of the same order of magnitude as those for pyrazine and pyrimidine, and the 0–0 band of the $S_0 \rightarrow T$ absorption of pyridazine is located at 412.5 nm. Recently, however, Innes *et al.*[3] reported that pyridazine vapor gives $S_0 \rightarrow T$ absorption with the 0–0 band at 445 nm.

In the present study, the $S_0 \rightarrow T$ absorption of pyridazine in rigid-glass solution was measured by a method based on sensitized-phosphorescence excitation (SPE). In the SPE method, a triplet energy donor and an acceptor are used. Only the donor molecule is excited, and an excitation spectrum is obtained by monitoring the sensitized phosphorescence emitted from the acceptor triplet produced by triplet-triplet energy transfer. The SPE spectrum thus obtained corresponds to the donor absorption spectrum. Note that the SPE spectrum can be measured even when the donor gives no phosphorescence, and that the SPE method has a high sensitivity compared with the absorption method. In this study pyridazine was used as energy donor and naphthalene-d_8 as acceptor.

Experimental

Pyridazine (Nakarai Chemical Co.) was carefully purified by repeated vacuum distillation. Pyrazine (Nakarai Chemical Co.) and naphthalene-d_8 (E. Merck Co.) were purified by vacuum sublimation. EPA (5: 5: 2 parts by volume of ethyl ether, isopentane, and ethyl alcohol) was used as solvent. The acceptor concentration was fixed, while the donor concentration was widely changed. All the sample solutions were degassed by repeated freeze-thaw cycles.

The SPE spectra were measured at 77 K with a high-resolution, high-sensitivity emission spectrophotometer equipped with a photon-counting detector and a phosphoroscope. The SPE spectra were corrected for the spectral intensity of the light source and monochromator system.[4]

The quantum yield of the donor triplet is either equal to or less than unity according as the donor molecule is photoexcited in the wavelength region of $S_0 \rightarrow T$ or $S_0 \rightarrow S$ absorption; in the latter case the yield is identical with the intersystem-crossing yield. Allowance was made for this difference in quantum yield[5] to obtain the SPE spectrum which, throughout the two wavelength regions, has an intensity proportional to the absorption intensity represented by the molar extinction coefficient (ε). The intensity of the excitation spectrum at a certain wavelength in the $S_0 \rightarrow S$ absorption region was then equated to the ε value at that wavelength to convert the excitation spectrum to the absorption spectrum.

Results and Discussion

In order to confirm the validity of the present method, we first observed the SPE spectrum for a system of pyrazine (donor) and naphthalene-d_8 (acceptor). The resulting absorption spectrum of pyrazine is compared in Fig. 1 with the absorption spectrum derived from the usual phosphorescence excitation (PE) spectrum which was measured with pyrazine alone. The two spectra are in good agreement with each other.

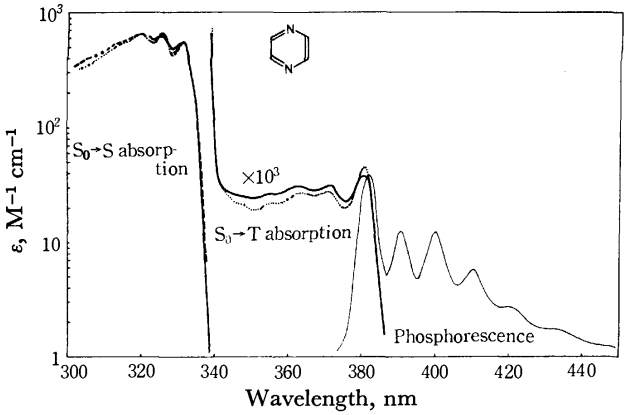

Fig. 1. Absorption and phosphorescence spectra of pyrazine in EPA at 77 K. Solid and dotted lines depict the absorption spectra derived from SPE and PE spectra, respectively. Broken line shows the usual $S_0 \rightarrow S$ absorption spectrum. Scale of intensity in the phosphorescence spectrum is linear.

An example of the SPE spectrum obtained for the system of pyridazine and naphthalene-d_8 is given in Fig. 2 with solid lines (a). The PE spectrum which was measured under the same conditions (except for the absence of pyridazine) as in the measurement of the SPE spectrum (a) is also shown in Fig. 2 with dotted lines (b). The PE spectrum (b) ranging from 385 to 470 nm corresponds to the $S_0 \rightarrow T$ absorption of naphthalene-d_8. Comparison of the spectra (a) and (b) shows

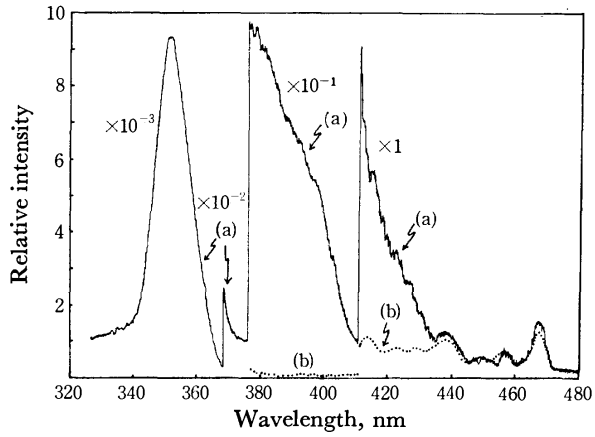

Fig. 2. Uncorrected chart of SPE and PE spectra.
(a) SPE spectrum of 0.1 M pyridazine and 0.06 M naphthalene-d_8 pair in EPA at 77 K; (b) PE spectrum of naphthalene-d_8 under the same conditions.

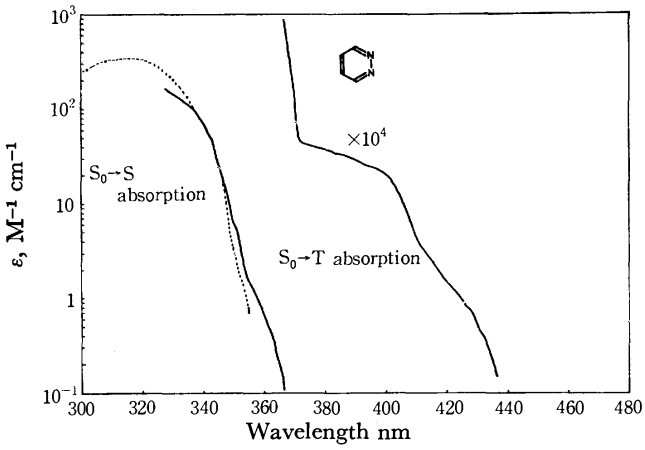

Fig. 3. Absorption spectrum of pyridazine in EPA at 77 K. Solid line, spectrum obtained by the SPE method; broken line, the usual $S_0 \rightarrow S$ absorption spectrum.

that the SPE spectrum between 435 and 470 nm originates actually from the direct $S_0 \rightarrow T$ excitation of naphthalene-d_8. Subtraction of the spectrum (b) from the spectrum (a) yields the true SPE spectrum, which in turn leads to the absorption spectrum of pyridazine through the procedure described before; the results are shown in Fig. 3.

In Fig. 3 the absorption occurring in a region of 370—440 nm can be assigned to an $S_0 \rightarrow T$ transition. Alternatively, one may imagine that it consists of two transitions which are to be called $S_0 \rightarrow T_1$ and $\rightarrow T_2$ in order of increasing energy. Theoretically, $^1A_1 \rightarrow {}^3B_1(n, \pi^*)$ and $^1A_1 \rightarrow {}^3A_2(n, \pi^*)$ transitions are possible for the C_{2v} pyridazine molecule.[2,3] The $S_0 \rightarrow T_1$ transition may then be related to the 445 nm absorption reported by Innes *et al.*,[3] and the $S_0 \rightarrow T_2$ to the 412.5 nm absorption by Hochstrasser and Marzzacco.[2] The values of ε_{max} for the $S_0 \rightarrow T_1$ and $\rightarrow T_2$ transitions are about 5×10^{-5} and 2×10^{-3} M^{-1} cm^{-1}, respectively. In either case the ε_{max} value is much smaller than the corresponding value for pyrazine (3×10^{-2} M^{-1} cm^{-1} from Fig. 1).[6] If, in this way, the $S_0 \rightarrow T$ absorption of pyridazine involves two transitions, the phosphorescence must originate from the lower triplet state, T_1. Then, it follows from the intensity of the $S_0 \rightarrow T_1$ absorption that k_p of pyridazine is as small as 0.16 s^{-1}. It may be noted that k_p of pyrazine is estimated to be 110 s^{-1} from its $S_0 \rightarrow T$ absorption intensity.

The lack of phosphorescence in pyridazine may thus be attributed, at least in part, to the fact that its lowest excited triplet has a relatively small k_p value.

References

1) T. Takemura, K. Yamamoto, I. Yamazaki, and H. Baba, This Bulletin, **45**, 1639 (1972).

2) R. M. Hochstrasser and C. Marzzacco, *J. Chem. Phys.*, **46**, 4155 (1967).

3) K. K. Innes, W. C. Tincher, and E. F. Pearson, *J. Mol. Spectrosc.*, **36**, 114 (1970).

4) H. Baba, L. Goodman, and P. C. Valenti, *J. Amer. Chem. Soc.*, **88**, 5410 (1966).

5) The intersystem crossing quantum yield, Φ_{ISC} used is 0.33 for pyrazine and 0.2 for pyridazine in EPA at 77 K. The former value was determined from our unpublished work by the same method as used in Ref. 1. The latter is taken from Ref. 1. These values are equal to the ones reported by Cohen and Goodman (*J. Chem. Phys.*, **46**, 713 (1967)).

6) L. Goodman and M. Kasha, *J. Mol. Spectrosc.*, **2**, 58 (1958).

BULLETIN OF THE CHEMICAL SOCIETY OF JAPAN, VOL. 48 (9), 2601—2602 (1975)

Kinetics of Reduction of Mercury(II) Chloride to Mercury(I) Chloride Induced by the Decomposition of Trioxalatocobaltate(III) in Acid Aqueous Solutions

Toshiro SATO and Masaru KIMURA*

Department of Applied Chemistry, Yamagata University, Yonezawa 992

**Department of Chemistry, Nara Women's University, Nara 630*

(Received May 15, 1975)

Synopsis. The decomposition reaction of trioxalatocobaltate(III) complex in the presence of mercury(II) chloride in acid medium induces the reduction of the latter to mercury(I) chloride (calomel). The results are accounted for by a sequence of a chain reaction which is initiated by the intramolecular redox decomposition of trioxalatocobaltate(III). The formation rate of mercury(I) chloride is expressed as half order with respect to the concentrations of oxalic acid, mercury(II) chloride, and trioxalatocobaltate(III). Mechanisms and kinetics are presented to account for these facts.

The light-initiated reduction of mercury (II) chloride by oxalate in a neutral medium has long been known as Eder's reaction after its discovery.[1] The photochemical reactions of this reaction have been studied by many investigators. Recently, Kimura *et al.*[2] have reported that the slow addition of a trace of a strong oxidizing agent to dilute oxalic acid solutions in dilute sulfuric acid causes the formation of free radicals which can bring about the reduction of mercury (II) chloride to mercury (I) chloride, and also reported briefly that a similar reaction occurs upon the thermal decomposition of trioxalatocobaltate (III) complex in an acid medium. In the present paper, the kinetics of the reduction of mercury (II) chloride to mercury (I) chloride according to the decomposition reaction of trioxalatocobaltate (III) is studied in the acid aqueous solutions.

Experimental

The potassium trioxalatocobaltate(III) was prepared following the directions of Sörensen.[3] All chemicals were of the guaranteed reagent grade. Pure nitrogen gas was bubbled through the reaction mixture. All experiments were carried out in the dark at a given temperature. The amount of mercury(I) chloride formed was determined by weighing after filtering through a glass-sintered crucible, washing, and drying at 80 °C. In order to compare conveniently the amount of mercury(I) chloride with the concentrations of the other species such as oxalic acid, mercury(II) chloride, and so forth, the amount of mercury(I) chloride formed is expressed as molarity which refers to the volume of the reaction mixture. After removal of mercury(I) chloride by filtration, concentrations of trioxalatocobaltate(III) in the filtrates were determined by means of the absorption spectra at 600 nm.

Results and Discussion

The relative efficiency of trioxalatocobaltate (III) in initiating the reaction increases with increasing concentrations of oxalic acid and mercury (II) chloride. Table 1 illustrates this effect over the range 0—0.4 M in oxalic acid, in 0.1 and 0.2 M in mercury (II) chloride at varying the reaction time. The concentration of trioxalatocobaltate (III) decreases in accordance with the first order expression, $-d[Co(C_2O_4)_3^{3-}]/dt=k_0[Co(C_2O_4)_3^{3-}]$ which is the same as that reported in the previous paper.[4] Concentrations of trioxalatocobaltate (III) decomposed are also listed in Table 1. The temperature effect on the formation of mercury (I) chloride was investigated in an initial composition of 0.1 M in oxalic acid, 0.1 M in mercury (II) chloride, and 10^{-3} M in potassium trioxalatocobaltate (III). The data obtained at various temperatures are listed in Table 2. Similarly as in Table 1, the concentrations of trioxalatocobaltate (III) decomposed were determined. But the data are omitted in Table 2. In all the instances, the amount of mercury (I) chloride formed was many times greater than that of trioxalatocobaltate (III) decomposed.

TABLE 1. FORMATION OF MERCURY(I) CHLORIDE INDUCED UPON DECOMPOSITION OF TRIOXALATOCOBALTATE(III)[a]

Oxalic acid M (added)	Reaction time in hr									
	0.5	1	2	3	4	0.5	1	2	3	4
	$[Hg_2Cl_2]_{formed}\times10^3$, M					$[Co(C_2O_4)_3^{3-}]_{decomposed}\times10^4$, M				
0		0.25	0.7	0.82			3.6	5.8	7.2	
0.01		2.6	4.2	4.6	5.8		3.4	5.5	7.2	7.7
0.1	5.2	8.5	12.1	16.0	16.5	1.4	2.4	4.2	6.4	7.4
0.1[b]	8.9	13.0	21	25	29	1.0	2.7	4.9	6.6	7.2
0.2		10.3					2.4			
0.4		11.2					2.4			

a) Initial solutions 1.0×10^{-3} M in potassium trioxalatocobaltate(III), 0.1 M in mercury(II) chloride, 0.1 M in sulfuric acid, and the varied concentrations of oxalic acid. Solution saturated with nitrogen gas; Dark; 40 °C. b) As in a) except 0.2 M in mercury(II) chloride.

* To whom correspondence should be addressed.

Table 2. Temperature dependence on the formation of mercury(I) chloride[a)]

Temp., °C	Reaction time, hr			
	1	2	3	4
	$[Hg_2Cl_2]_{formed} \times 10^3$, M			
25	0.74	2.3	3.4	
30	2.1	4.7	4.9	7.9
35	4.6	7.5	10.3	12.0
40	8.5	12.1	16.0	16.5

a) Initial solutions 1.0×10^{-3}M in potassium trioxalatocobaltate(III), 0.1 M in oxalic acid, 0.1 M in mercury (II) chloride, and 0.1 M in sulfuric acid; The other conditions are the same as in Table 1.

Therefore, a chain reaction must occur. The initiation reaction is probably the intra-molecular redox decomposition of trioxalatocobaltate (III).[4)]

$$Co(C_2O_4)_3^{3-} \longrightarrow Co(II) + 2C_2O_4^{2-} + CO_2 + CO_2^{\cdot-} \quad (1)$$

$$Co(C_2O_4)_3^{3-} + H^+ \longrightarrow Co(II) + 2C_2O_4^{2-} + H^+ + CO_2 + CO_2^{\cdot-} \quad (2)$$

The radical which is formed in the above reactions may be either $CO_2^{\cdot-}$ or $C_2O_4^{\cdot-}$. An approximate theoretical calculation[5)] indicates that the latter radical is more stable, but the two forms do not appear to be distinguishable on the basis of kinetic or spectroscopic evidence.[6)] Conveniently we write $CO_2^{\cdot-}$ in this paper. In this paper, in which all the experiments were carried out in acid media, considerations must be taken of the protonated and dissociated forms of the anion species. According to the data by Fojtik *et al.*,[7)] the acid dissociation constant for the reaction $HCO_2^{\cdot} \rightleftarrows CO_2^{\cdot-} + H^+$ is $pK_a = 3.9$. Therefore, in 0.1 M sulfuric acid solutions such as in Tables 1 and 2, a predominant species of radicals is assumed to be $HCO_2^{\cdot}$. By a similar calculation for the protonated and dissociated forms of oxalate, $H_2C_2O_4$ is assumed as a predominant species. Consequently, in subsequent equations $HCO_2^{\cdot}$ and $H_2C_2O_4$ are written rather than $CO_2^{\cdot}$ and $C_2O_4^{2-}$.

Following after the initiation reactions (1) and (2), reactions, (3), (4), and (5) constitute a chain reaction.

$$HgCl_2 + HCO_2^{\cdot} \longrightarrow Hg(I) + H^+ + 2Cl^- + CO_2 \quad (3)$$

$$H_2C_2O_4 + Hg(I) \longrightarrow Hg + HCO_2^{\cdot} + CO_2 + H^+ \quad (4)$$

$$HgCl_2 + Hg \longrightarrow Hg_2Cl_2 \quad (5)$$

Termination presumably occurs mainly *via*

$$Hg(I) + HCO_2^{\cdot} \longrightarrow Hg + CO_2 + H^+ \quad (6)$$

Assumption of the steady state concentrations for HCO_2, Hg (I), and Hg, together with the assumption that the chain is long, leads to the following equation.

$$[Hg_2Cl_2]_{formed} = \sqrt{\frac{k_0 k_3 k_4 [HgCl_2][H_2C_2O_4][Co(C_2O_4)_3^{3-}]}{2k_6}}\ \tau \quad (7)$$

where k_0 indicates an overall decomposition-rate constant of trioxalatocobaltate (III), k_n, the rate constant of reaction (n), and τ, the reaction time. When the initial concentrations of oxalic acid and mercury (II) chloride are much larger than the concentrations of mercury (I) formed, the former concentrations remain approximately constant during the reaction time. Under these circumstances, Eq. (7) predicts a linear relation between $[Hg_2Cl_2]_{formed}/[Co(C_2O_4)_3^{3-}]^{1/2}$ and τ. This relation was found experimentally at all the experiments. Several examples obtained at the various temperatures are given in Fig. 1. The slopes of the straight lines in Fig. 1 correspond to the apparent-overall rate constants, *i.e.*, $k_{app} = \{k_0 k_3 k_4/(2k_6)\}^{1/2}$. From Arrhenius plots with respect to k_{app} and k_0, activation energies for the overall and initiation reactions were determined to be $E_{app} = 28$ kcal/mol, and $E_0 = 39$ kcal/mol, respectively. From the relation between the overall rate constant and the rate constants for the separate steps in the reaction scheme, the activation energy of the overall reaction constitutes a function with the activation energies for the separate steps in reaction, *i.e.*, $2E_{app} = E_0 + E_3 + E_4 - E_6$. If the activation energy for the termination reaction (6) is assumed to be negligibly small, the activation energy for the chain propagation steps is calculated to be $E_3 + E_4 = 17$ kcal/mol.

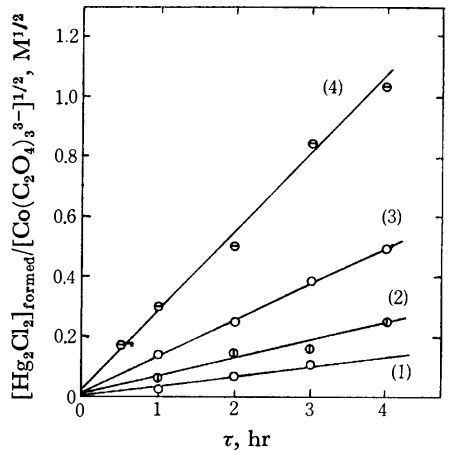

Fig. 1. Plot of $[Hg_2Cl_2]_{formed}/[Co(C_2O_4)_3^{3-}]^{1/2}$ *vs.* τ. Conditions as in Table 2. Temperatures are 25 °C (1), 30 °C (2), 35 °C (3), and 40 °C (4).

The authors acknowledge the Japanese Ministry of Education for the financial support.

References

1) J. M. Eder, *Ber.*, **13**, 166 (1880).
2) M. Kimura, I. M. Kolthoff, and E. J. Meehan, *J. Phys. Chem.*, **77**, 1262 (1973).
3) S. P. L. Sörensen, *Z. Anorg. Allg. Chem.*, **11**, 1 (1896).
4) M. Kimura and T. Sato, This Bulletin, **46**, 471 (1973).
5) Z. Simon, *Rev. Roumaine Chim.*, **14**, 705 (1964).
6) G. D. Cooper and B. A. deGraff, *J. Phys. Chem.*, **75**, 2897 (1971).
7) A. Fojtik, G. Czapski, and A. Henglein, *J. Phys. Chem.*, **74**, 3204 (1970).

BULLETIN OF THE CHEMICAL SOCIETY OF JAPAN, VOL. 48 (9), 2603—2604 (1975)

Note on the Preparation and Catalytic Properties of Dichlorotris[tris(*p*-methoxyphenyl)phosphine]ruthenium

Shigeo NISHIMURA, Osamu YUMOTO, Kiyoshi TSUNEDA,* and Hiromu MORI*

Department of Industrial Chemistry, Tokyo University of Agriculture and Technology, Koganei, Tokyo 184
**Chemical Research Laboratory, Teikoku Hormone Manufacturing Co., Ltd., Shimosakunobe, Kawasaki 213*

(Received October 14, 1974)

Synopsis. The procedure for the preparation of $RuCl_2[(p\text{-}MeOC_6H_4)_3P]_3$ was improved, resulting in a higher catalytic activity. The complex was thirteen and five times as active as $RuCl_2(Ph_3P)_3$ in the hydrogenation of 1,4-androstadiene-3,17-dione (I) and 4-androstene-3,17-dione (II), respectively, indicating that the methoxy complex is more selective for formation of II in the consecutive hydrogenation pathway of I.

In the preceding paper,[1] it was shown that the catalytic activity of dichlorotris(triarylphosphine)-ruthenium was enhanced by *p*-methoxy and *p*-methyl groups and reduced by *p*-fluoro group when the complex was used in the presence of an optimal amount of triethylamine. During this study it has been noticed that the complex with *p*-methoxy substituent prepared by the same procedure as for the preparation of dichlorotris-(triphenylphosphine)ruthenium[2] was often of different color and showed different catalytic activity depending on preparation. Since tris(*p*-methoxyphenyl)phosphine is much less soluble in ethanol than triphenylphosphine, it seemed that the amount of ethanol used (120 ml for 1 g of $RuCl_3 \cdot 3H_2O$ and 6 molar equivalents of the phosphine) would be too small for the preparation of the methoxy complex. The complex formed in this amount of ethanol might be contaminated with free phosphine or its hydrochloride, which would be harmful to the catalytic activity of the resulting complex.[3] From this point of view the ruthenium complex was prepared using a larger amount of ethanol and the precipitate filtered off before the reaction mixture was cooled to room temperature.[4] By this simple improvement, however, the catalytic activity of the complex was greatly increased. A rather long refluxing time (*ca.* 6 hr) was also favorable for the catalytic activity. The *p*-methoxy complex thus prepared gave satisfactory C, H, and Cl analyses corresponding to the formula $RuCl_2[(MeOC_6H_4)_3P]_3$. Application of this improvement to the preparation of the *p*-methyl complex resulted in only a moderate increase in catalytic activity and no increase in the case of the complex without substituent, as might be expected from the higher solubilities of the corresponding phosphines in ethanol. For the same reason it is advisable to use a lesser amount of ethanol for the preparation of the complex with tris(*p*-fluorophenyl)phosphine because of its much higher solubility in ethanol.

Stoichiometrically the amount of triarylphosphine required for the preparation of the ruthenium complex must be 4.5 molar equivalents if the reaction occurs by the equation:

$$RuCl_3 + \frac{9}{2}Ar_3P + \frac{1}{2}H_2O \longrightarrow RuCl_2(Ar_3P)_3 + \frac{1}{2}Ar_3P{=}O + Ar_3P \cdot HCl$$

The complexes prepared with use of 5 molar equivalents of the phosphine, however, were slightly less active than those obtained with 6 molar equivalents. Blum and Becker[5] prepared triarylphosphine ruthenium complexes by refluxing ruthenium chloride and triarylphosphine in methanol. We also prepared the complexes according to their procedure, but the resulting complexes were less active than those obtained in ethanol by the improved procedure. They describe the colors of the methoxy and methyl complexes as apparently the same, but those of our preparations are definitely different from each other (dark brown for the methoxy complex and brown for the methyl complex).

In Table 1 are summarized the results of the hydrogenation of 1,4-androstadiene-3,17-dione (I) and 4-androstene-3,17-dione (II), using the complexes obtained

TABLE 1. HYDROGENATION OF 1,4-ANDROSTADIENE-3,17-DIONE (I) AND 4-ANDROSTENE-3,17-DIONE (II) WITH DICHLOROTRIS(TRIARYLPHOSPHINE)RUTHENIUM[a]

Compound	Catalyst X in $RuCl_2[(p\text{-}XC_6H_4)_3P]_3$	Reac. time (min)	Composition of reac. mixture (mol%)			$10^4 k_x$[c] (s^{-1})	k_x/k_H[c]
			I	II	III[b]		
I	OMe	20	3.7	90.0	6.3	27.5	13.1
I	Me	40	6.8	87.1	6.1	11.2	5.3
I	H	180	10.3	85.8	3.9	2.1	1.0
II	OMe	360	—	86.9	13.1	0.065	5.0
II	H	490	—	96.1	3.9	0.013	1.0

a) The compound (500 mg) was hydrogenated in 10 ml benzene in the presence of 0.026 mmol of the ruthenium complex and 0.034 mmol of triethylamine at 50 °C under a hydrogen pressure of 100 kg/cm². b) 5α- and 5β-androstane-3,17-dione. c) k_x and k_H denote the pseudo-first-order rate constants for the hydrogenations catalyzed by the ruthenium complexes with *p*-substituent X and with no substituent, respectively.

by the improved procedure. Pseudo-first-order rate constants were calculated by assuming that the rate of hydrogenation is first-order in the concentration of I and II.[6] It is seen that the catalytic activity of dichlorotris(triphenylphosphine)ruthenium is enhanced definitely more by the *p*-methoxy substituent than by the *p*-methyl to such an extent as would be expected from its substituent constant in the Hammett equation.

The *p*-methoxy complex is only five times as active as the complex with triphenylphosphine in the hydrogenation of II compared to thirteen times in the hydrogenation of I. Thus the ratio of the rate of hydrogenation of I to that of II is much greater for the *p*-methoxy complex. Accordingly, the *p*-methoxy complex will be more selective than the triphenylphosphine complex for formation of II in the consecutive hydrogenation pathway: I→II→saturated ketones. On the other hand, the amount of the saturated ketone formed directly from I[1,2] appears slightly increased with the methoxy complex. Therefore it is recommended to use the highly active methoxy complex at a lower temperature (*e.g.* 30 °C) to obtain a high yield of II by hydrogenation of I.

Experimental

Preparation of Dichlorotris[tris(p-methoxyphenyl)phosphine]ruthenium. A mixture of 0.425 g of $RuCl_3 \cdot 3H_2O$ (obtained from the Nippon Engelhard Co.), 3.43 g of tris(*p*-methoxyphenyl)phosphine (6 molar equivalents) and 80 ml ethanol was refluxed for 6 hr under the atmosphere of nitrogen. The crystals were filtered off before the reaction mixture was cooled to room temperature, and washed with ethanol and then with a small amount of ether. The yield was 1.83 g (92%) (Found: C, 61.37; H, 5.14; Cl, 5.96%. Calcd for $C_{63}H_{63}Cl_2O_9P_3Ru$: C, 61.56; H, 5.18; Cl, 5.77%). The same procedure is also applicable to the preparation of $RuCl_2[(p\text{-}MeC_6H_4)_3P]_3$ and results in a slightly lower yield.

The authors are grateful to the Mitsubishi Chemical Industries Co. for the analysis of chlorine.

References

1) S. Nishimura, T. Ichino, A. Akimoto, and K. Tsuneda, This Bulletin, **46**, 279 (1973).
2) S. Nishimura and K. Tsuneda, This Bulletin, **42**, 852 (1969).
3) P. S. Hallman, B. R. McGarvey, and G. Wilkinson, *J. Chem. Soc., A*, **1968**, 3143.
4) *Cf.* J. A. Osborn, A. H. Jardine, J. F. Young, and G. Wilkinson, *J. Chem. Soc. A*, **1966**, 1711.
5) J. Blum and Y. Becker, *J. Chem. Soc., Perkin II*, **1972**, 982.
6) It was confirmed that the rate of hydrogenation of I over the *p*-methoxy complex obeys first-order kinetics in concentration of I in the experiments employing a smaller amount of the complex.

BULLETIN OF THE CHEMICAL SOCIETY OF JAPAN, VOL. 48 (9), 2605—2606 (1975)

The Reaction of 1,2,4,5-Tetrazines with 2-Phenyl-1-azirine. The Synthesis of 2*H*-1,2,4-Triazepine Derivatives

Masahiko TAKAHASHI, Norimoto SUZUKI, and Yoshihiko IGARI

Department of Industrial Chemistry, Faculty of Engineering, Ibaraki University, Hitachi, Ibaraki 316

(Received December 19, 1974)

Synopsis. The Reaction of 3,6-disubstituted 1,2,4,5-tetrazines (**1a**—**c**) with 2-phenyl-1-azirine (**2**) afforded 3,7-disubstituted 6-phenyl-2*H*-1,2,4-triazepines (**5a**—**c**) in good yields.

The thermal and photochemical reactions of 1-azirines have been extensively investigated in recent years. Some examples of the Diels-Alder reaction of 1-azirines with cyclic dienes have been reported to yield cycloadducts or their ring-expanded products. The reaction of 1-azirines with cyclopentadienones[1,2] gives strained cycloadducts, which undergo a loss of carbon monooxide to yield azanorcaradienes, followed by ring enlargement to form 3*H*-azepine derivatives. The reaction of the benzo analogue of cyclopentadienones[3] has also been reported to form condensed azepine derivatives. The reaction of diphenylisobenzofuran[4,5] has been reported to yield cycloadducts and to be subjected to subsequent ring expansion to isoquinoline and azanorcarane derivatives.

The reaction of 1,2,4,5-tetrazines with cyclopropenes is a simple and convenient diene synthesis of substituted 5*H*-1,2-diazepines.[6] A similar reaction of 1,2,4,5-tetrazine with 1-azirine suggests a useful method for the synthesis of 1,2,4-triazepines. As an extension of our studies of the synthesis of triazepine derivatives,[7] we examined this reaction. Recently, Anderson *et al.*[8] and Johnson *et al.*[9] have reported that the same cycloaddition reaction gives 2*H*-1,2,4-triazepines. We wish to report our independent results[10] on the sunthesis of 2*H*-1,2,4-triazepines.

A toluene solution of 3,6-diphenyl-1,2,4,5-tetrazine (**1a**) and 2-phenyl-1-azirine (**2**) was refluxed for 26 hr. A product was obtained in a 58% yield as orange needles. The IR spectrum of the product showed a NH absorption at 3320 cm^{-1} and a C=N absorption at 1635 cm^{-1}. The mass spectrum of the product showed the following significant peaks: *m/e* 323 (M^+, 41%), 322 (M^+-1, 52%), 296 (M^+-HCN, 42%), 220 (M^+-PhCN, 100%), and 178 ($PhC{\equiv}CPh^+$, 19%). From the above data and the elemental analysis, the structure of the product was considered not to be triazanorcaradiene (**3a**) or its [3,3]sigmatropically rearranged product (**4a**), but rather the 2*H*-1,2,4-triazepine derivative (**5a**) or its 1*H* isomer (**6**), which seemed to be the result of the [1,5]sigmatropical shift of the C-5 hydrogen of **4a**. However, it was thought that **6** was more unstable than **5a** because of the sterical crowding of the C-6 and C-7 phenyl groups. Similar examples have been described in the case of the isomerization of 2*H*-azepines to 3*H*-azepines.[1,2] The possibility of the 4*H*-1,2,4-triazepine structure (**7**) is small, because **7** seemed to be the product of the 1,5-hydrogen shift of **6**. The signal of the vinyl proton resonance is probably contained in the region of aromatic protons at δ7.0—8.1 ppm, as is observed in the case of azepines.[1,2] Although 5*H*-1,2-diazepine derivatives were thermally isomerized into diazabicyclo [3,2,0]heptadiene,[6] another possibility of a bicyclic structure (**8**) of the present product was eliminated on the basis of the absence of bridgehead methine proton resonance at *ca.* δ 3.1—4.1 ppm such as observed for the photoisomers of azepines and oxepines.[11] The results cited above indicate that the structure of the product is probably 3,6,7-triphenyl-2*H*-1,2,4-triazepine, **5a**. Other derivatives, **5b** and **5c**, were similarly obtained in good yields.

The reaction **5a** with benzoyl chloride afforded a bezoate (**5d**) in a 35% yield. The IR spectrum of **5d** showed no NH absorption, but it did show a C=O absorption at 1685 cm^{-1}. Although the parent peak at *m/e* 427 was not observed in the mass spectrum, the other peaks were analogous to those of **5a**.

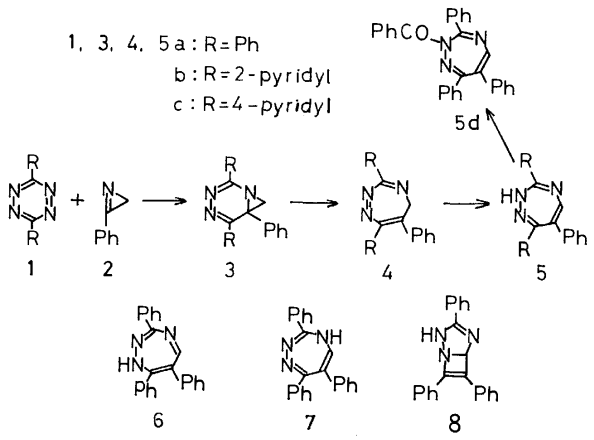

Experimental

All the melting points are uncorrected. The IR, UV, and NMR spectra were measured with a JASCO Model IRA-2 spectrometer, a Shimadzu Model MPS-501 spectrometer, and a Hitachi Model R-20 spectrometer respectively. A Shimadzu Model UM-3B apparatus was used for the elemental analysis.

3,6,7-Triphenyl-2H-1,2,4-triazepine (5a). A mixture of 0.80 g (3.4 mmol) of 3,6-diphenyl-1,2,4,5-tetrazine[12], **1a**, and 0.90 g (7.7 mmol) of **2**[13] in 60 ml of toluene was refluxed for 26 hr. After the subsequent concentration of the solution *in vacuo* and cooling, the resulting precipitates were filtered to afford 0.65 g (58% yield) of **5a**. It was recrystallized from ethanol to give orange needles; mp 208—210 °C. Found: C, 81.43; H, 5.24%. Calcd for $C_{22}H_{17}N_3$: C, 81.71; H, 5.30%. IR (KBr): 3320, 3050, 3020, 1635 cm^{-1}. UV λ_{max}^{MeOH} nm (log ε): 234 (4.59), 271 (4.67), 360 sh (3.50). NMR (DMSO-d_6): δ 7.00—8.10 (m, aromatic and olefinic H). Mass *m/e* (%): 323 (41), 322 (52), 297 (10), 296 (42), 295 (18), 221 (18), 220 (100), 219 (20), 191 (17), 189 (17), 178 (19), 165 (17),

118 (8.3), 104 (11), 90 (13), 77 (17).

*3,7-Bis(2-pyridyl)-6-phenyl-2*H-*1,2,4-triazepine (5b).* A mixture of 2.58 g (11 mmol) of 3,6-bis(2-pyridyl)-1,2,4,5-tetrazine,[14] **1b**, and 2.11 g (18 mmol) of **2** in 140 ml of toluene was refluxed for 16 hr. A treatment of the mixture similar to that described for **5a** afforded 2.25 g (63% yield) of **5b**. It was recrystallized from methanol to give orange needles; mp 190—192 °C. Found: C, 73.97; H, 4.62%. Calcd for $C_{20}H_{15}N_5$: C, 73.83; H, 4.65%. IR (KBr): 3330 (NH), 3042, 1640 (C=N) cm^{-1}. UV λ_{max}^{MeOH} nm (log ε): 232 (4.21), 281 (4.34), 383 sh (3.34). NMR ($CDCl_3$): δ 6.90—8.70 (aromatic and olefinic H).

*3,7-Bis(4-pyridyl)-6-phenyl-2*H-*1,2,4-triazepine (5c).* A mixture of 710 mg (3.0 mmol) of 3,6-bis(4-pyridyl)-1,2,4,5-tetrazine,[15] **1c**, and 420 mg (4.2 mmol) of **2** was refluxed for 20 hr. After the evaporation of the solvent *in vacuo*, the solid residue was washed with a small amount of methanol to afford 812 mg (83% yield) of **5c**. It was recrystallized from methanol to give orange needles; mp 218—219 °C. Found: C, 73.27; H, 4.58%. Calcd for $C_{20}H_{15}N_5$: C, 73.83; H, 4.65%. IR (KBr): 3320 (NH), 3050, 3020, 1626 (C=N) cm^{-1}. UV λ_{max}^{MeOH} nm (log ε): 232 (4.44), 268 (4.42). 385 sh (3.07).

*2-Benzoyl-3,6,7-triphenyl-2*H-*1,2,4-triazepine (5d).* A solution of 407 mg (1.3 mmol) of **5a** and 247 mg (1.8 mmol) of benzoyl chloride in 10 ml of tetrahydrofuran was refluxed for 21 hr. The solvent was removed *in vacuo* to give an oily residue, which was then dissolved into 10 ml of methanol and crystallized by cooling. The precipitates were filtered to afford 190 mg (35% yield) of **5d**. It was recrystallized from the mixed solvent of benzene and methanol to give white needles; mp 145—146 °C. Found: C, 81.55; H, 4.99%. Calcd for $C_{29}H_{21}ON_3$: C, 81.48; H, 4.95%. IR (KBr): 3040, 3020, 1685, 1595 cm^{-1}. UV λ_{max}^{MeOH} nm (log ε): 228 (4.58), 282 sh (4.02). NMR ($CDCl_3$): δ 7.20—8.60 (m, aromatic and olefinic H). Mass *m/e* (%): 323 (43), 322 (6.3), 296 (6.3), 295 (8.0), 221 (3.6), 220 (2.7), 219 (3.6), 191 (8.0), 189 (13), 165 (5.4), 105 (100), 77 (72).

The authors wish to express their thanks to Dr. Masatoshi Hirayama for the NMR measurements and to the Sankyo Co., Ltd., for the mass measurements.

References

1) D. J. Anderson and A. Hassner, *J. Amer. Chem. Soc.*, **93**, 4339 (1971).
2) V. Nair, *J. Org. Chem.*, **37**, 802 (1972).
3) A. Hassner and D. J. Anderson, *J. Amer. Chem. Soc.*, **94**, 8225 (1972).
4) V. Nair, *J. Org. Chem.*, **37**, 2508 (1972).
5) A. Hassner and D. J. Anderson, *ibid.*, **39**, 2031 (1974).
6) M. A. Battiste and T. J. Barton, *Tetrahedron Lett.*, **1967**, 1227.
7) M. Takahashi, S. Onizawa, and T. Satoh, This Bulletin, **47**, 2724 (1974).
8) D. J. Anderson and A. Hassner, *Chem. Commun.*, **1974**, 45.
9) G. C. Johnson and R. H. Levin, *Tetrahedron Lett.*, **1974**, 2303.
10) Presented in part at the 30th Spring Annual Meeting of the Chemical Society of Japan, Osaka, April 1, 1974.
11) L. A. Paquette and J. H. Barret, *J. Amer. Chem. Soc.*, **88**, 1718 (1966).
12) K. Nakahara and M. Ohta, *Nippon Kagaku Zasshi*, **77**, 388 (1956).
13) A. G. Hortmann, D. A. Robertson, and B. K. Gillard, *J. Org. Chem.*, **37**, 322 (1972).
14) W. A. Butte and F. H. Case, *ibid.*, **26**, 4690 (1961).
15) F. Dallacker, *Monatsh. Chem.*, **91**, 294 (1960).

BULLETIN OF THE CHEMICAL SOCIETY OF JAPAN, VOL. 48 (9), 2607—2608 (1975)

Friedel-Crafts Reaction of 1,3,5-Trialkylbenzenes with Sulfur Monochloride and *N*-Chlorodimethylamine

Masaaki YOSHIFUJI, Susumu TANAKA, and Naoki INAMOTO

Department of Chemistry, Faculty of Science, The University of Tokyo, Hongo, Tokyo 113

(Received January 14, 1975)

Synopsis. The reaction of sulfur monochloride gave 2,4,6-tri-*t*-butylchlorobenzene (**3**) from 1,3,5-tri-*t*-butylbenzene (**1**), but gave the corresponding sulfide and disulfide from mesitylene (**2**). The reaction of *N*-chlorodimethylamine gave **3**, 2-chloro-3,5-di-*t*-butyltoluene and 2,4,6-trimethylchlorobenzene from **1**, 3,5-di-*t*-butyltoluene and **2**, respectively. The reaction of *N*-chlorodimethylamine with benzene gave chlorobenzene or *N,N*-dimethylaniline in 1-nitropropane or nitromethane.

The Friedel-Crafts reaction of sulfur monochloride gives diphenyl sulfide from benzene,[1] and diaryl sulfide and disulfide from substituted benzene.[2] Similarly, *N*-chlorodimethylamine gives *N,N*-dimethylanilines in reactions with benzene and substituted benzenes.[3] We have found that the Friedel-Crafts reaction of 1,3,5-tri-*t*-butylbenzene (**1**) with phosphorus trichloride gave an abnormal product, *t*-butyl-3,5-di-*t*-butylphenylphosphinic chloride.[4]

Therefore, the Friedel-Crafts reaction of 1,3,5-tri alkylbenzenes with sulfur monochloride or *N*-chlorodimethylamine was investigated.

Reaction with Sulfur Monochloride in the Dark. In the case of **1**, 2,4,6-tri-butylchlorobenzene (**3**) was always obtained (Table 1). Use of aluminum chloride as a catalyst gave a yellow tarry material and the yield of **3** was lower than when iron powder was used. The reaction of mesitylene (**2**) in the presence of iron powder at 0 °C gave a mixture or dimesityl sulfide (**4**) and disulfide (**5**); their yields were 64 and 15%, respectively, by gas chromatography (glc).

Reaction with N-*Chloromethylamine.* Compounds **1**,**2**, and 3,5-di-*t*-butyltoluene (**6**) were allowed to react in the presence of anhydrous aluminum chloride in nitromethane, nitrobenzene, or 1-nitropropane as solvents. Reaction with **1** gave always **3** (Table 2). The best result was obtained in 1-nitropropane by use of five molar amounts of *N*-chlorodimethylamine (Run 4). This method is applicable to the preparation of **3**, because **3** has been prepared from **1** through nitration, reduction, diazotization, and then Sandmeyer reaction.[5]

The reaction of **2** with five molar amounts of *N*-chlorodimethylamine in nitropropane at room temperature gave 60%[1] of 2,4,6-trimethylchlorobenzene (**7**), a trace of 2,4-dichloromesitylene (**8**), and 3% of 3,3′-dichloro-2,4,6,2′,4′,6′-hexamethylbiphenyl (**9**). A similar reaction of **6** at 60 °C gave 65% of 2-chloro-3,5-di-*t*-butyltoluene (**10**).

The reaction of **2** in nitromethane gave **7** (38%), bimesityl (**11**, 4%), and 2,4,6-trimethylbenzonitrile (**12**, 2.6%). The nitrile (**12**) was also obtained from the Friedel-Crafts reaction of **2** with nitromethane.[6]

Since **2** gave chloride (**7**), the reaction with benzene[3] was re-examined. The reaction in 1-nitropropane gave only chlorobenzene, but the reaction in nitromethane gave *N,N*-dimethylaniline. This difference is very interesting, but the reason for it is still obscure.

Table 1. Friedel-Crafts reaction of **1** with S_2Cl_2 in CS_2

1 (mmol)	S_2Cl_2 (mmol)	Cat.	(mmol)	Temp.	Time (hr)	**3** (%)
40	44	Fe	0.23	r.t.	6.0	57,[a] 12[b]
17	25	Fe	0.42	0 °C then r.t.	7.5 24	76,[c] 16[b]
20	25	$AlCl_3$	3.2	0 °C	5.8	39,[a] 10[b]

a) Determined by NMR. b) Isolated yields.
c) Contained a trace of sulfur.

Experimental

All boiling and melting points are uncorrected. All reactions were carried out under nitrogen.

Materials. 1,3,5-Tri-*t*-butylbenzene (**1**)[7] (mp 73—74.5 °C), 3,5-di-*t*-butyltoluene (**6**)[8] (mp 29.5—31 °C), and *N*-chlorodimethylamine[3] (bp 43—44 °C) were prepared by the reported methods.

Reaction of **1** *with Sulfur Monochloride (***13***).* A typical procedure is described below. To a stirred mixture of **1** (9.91 g, 40 mmol) and iron powder (13 mg, 0.23 mg-atom) in CS_2 (10 ml) was added dropwise **13** (5.9 g, 44 mmol) in CS_2 (5 ml) over 1.5 hr, and the mixture was stirred for an additional 4.5 hr. The reaction mixture was poured into water and extracted with ether and then CH_2Cl_2. The combined extracts were washed with water and dried with $MgSO_4$. After evaporation of solvent, ether was added to the residue to leave sulfur (1.65 g, 51.5 mg-atom). The filtrate was evaporated to leave 9.21 g as a residue, which was recrystallized three times from MeOH to give 1.31 g (12%)

Table 2. Reactions of **1** with *N*-chlorodimethylamine

Run	**1** (mmol)	$AlCl_3$ (mmol)	Me_2NCl (mmol)	Solvent	(mmol)	Temp. (°C)	Time (hr)	**3** (%)
1	20	19	15	$MeNO_2$	200	80	4	35,[a] 7.4[b]
2	20	16	15	$PhNO_2$	161	80	4	24,[a] 8[b]
3	20	16	15	$PrNO_2$	201	80	4	35,[a] 27[b]
4	20	23	100	$PrNO_2$	201	65—70	1	79[b]

a) Determined by NMR. b) Isolated yield.

of **3**, mp 156.5—160 °C (lit,[5] 162 °C).

Reaction of ***2*** *with* ***13***. To a stirred mixture of **2** (30.2 g, 252 mmol) and iron powder (20.5 mg, 0.37 mg-atom) was added dropwise **13** (3.38 g, 25 mmol) in CS_2 (3 ml) over 1.5 hr at 0 °C. The mixture was stirred at room temperature for one day. After a similar treatment, distillation gave 5.4 g of a yellowish brown substance, bp 174 °C/3 mmHg, which was fractionally recrystallized five times from EtOH to give 1.1 g (15%) of **5**, mp 123.5 °C (lit,[9] 123—124 °C), and 1.0 g (15%) of **4**, mp 90—91 °C (lit,[10] 91—92 °C). The yields of **4** and **5** were estimated to be 64 and 15% by glc.

Reaction of ***1*** *with* N-*Chlorodimethylamine (****14****)*. To a stirred solution of **1** (5.01 g, 20 mmol) in 1-nitropropane (13.5 ml) was added $AlCl_3$ (3.0 g, 22.5 mmol) and then **14** (7.96 g, 100 mmol) in 1-nitropropane (4.5 ml) dropwise at 0 °C. The mixture was stirred at 65—70 °C for 1 hr and poured into ice-water. The reaction mixture was made alkaline with aq. NaOH and extracted with CH_2Cl_2. After drying, distillation *in vacuo* gave crude **3** (5.62 g, 98%), mp 153—156 °C, which was recrystallized from MeOH, mp 161—162 °C, yield 4.50 g (79%).

Reaction of ***2*** *with* ***14***. *a) In 1-Nitropropane*: To a stirred mixture of **2** (4.84 g, 40 mmol), 1-nitropropane (3.58 g), and $AlCl_3$ (5.5 g, 41 mmol) was added dropwise **14** (15.9 g, 200 mmol) at 0 °C. The mixture was stirred at room temperature for 3 hr. After a similar treatment, distillation under vacuum gave **7** (3.73 g, 60%), bp 39—40 °C/1 mmHg (lit,[11] 51—52 °C/1.5 mmHg). The residue was chromatographed on silica gel with *n*-hexane to give 35 mg (0.5%) of **8**, mp 58.3—59.8 °C (lit,[12] 59 °C), and 180 mg (3%) of **9**, mp 131.1—131.9 °C (lit,[13] 130—131.5 °C).

b) In Nitromethane: A mixture of **2** (9.62 g, 80 mmol), $AlCl_3$ (4.0 g, 30 mmol), **14** (1.59 g, 20 mmol), and nitromethane (4.88 g) was stirred for 5 hr at 80 °C. After a similar treatment, distillation under vacuum recovered **2** (3.53 g, 37%). The residue was chromatographed on silica gel. Elution with *n*-hexane gave 1.18 g (38%) of **7** and 207 mg (4%) of **11**, mp 101.5—102 °C (from EtOH) (lit,[14] 101—102 °C). Elution with CCl_4 gave 308 mg (2.6% based on **2** used) of **12**, mp 48—48.5 °C (from EtOH) (lit,[15] 50—52 °C); IR (KBr): 2200 cm^{-1}.

Reaction of ***6*** *with* ***14***. A mixture of **6** (3.39 g, 16.6 mmol), **14** (6.43 g, 81 mmol), $AlCl_3$ (2.2 g, 16.5 mmol), and 1-nitropropane (14.3 g) was stirred for 3 hr at 60 °C. After a similar treatment, the residue of the distillation was chromatographed on silica gel with *n*-hexane to give 2.57 g (65%) of **10**, bp 113 °C/2.5 mmHg. NMR (CCl_4): δ 1.30 (s, 9H, *t*-Bu), 1.50 (s, 9H, *t*-Bu), 2.36 (s, 3H, Me), 6.99—7.05 (d, J_{HCCCH} 3 Hz, 1H, Ar-H), and 7.20—7.26 (d, J_{HCCCH} 3 Hz, 1H, Ar-H). Found: C, 75.39; H, 9.68; Cl, 15.09%. Calcd for $C_{15}H_{23}Cl$: C, 75.45; H, 9.71; Cl, 14.85%.

Reaction of Benzene with ***14***. A solution of benzene (6.26 g, 80 mmol) in 1-nitropropane (7.15 g), $AlCl_3$ (4.0 g, 30 mmol), and then **14** (1.58 g, 20 mmol) were mixed under stirring at −10 °C, and stirred at 80 °C for 5 hr. The reaction mixture was treated similarly. *N,N*-Dimethylaniline could not be detected by glc. After drying, the distillation gave 701 mg (31%) of chlorobenzene, bp 130—133 °C.

A mixture of benzene (5.27 g, 67.5 mmol), $AlCl_3$ (3.3 g, 24.7 mmol), nitromethane (4.08 g), and **14** (1.38 g, 17.4 mmol) was stirred for 5 hr at 80 °C; a similar treatment gave 625 mg (30%) of *N,N*-dimethylaniline, bp 40 °C/1.8 mmHg.

References

1) W. W. Hartman, L. A. Smith, and J. B. Dickey, "Organic Syntheses," Coll. Vol. 2, p. 242 (1943).
2) T. Fujisawa, N. Ohtsuka, T. Kobori, and G. Tsuchihashi, *Tetrahedron Lett.*, **1968**, 4533.
3) H. Bock and K.-L. Kompa, *Chem. Ber.*, **99**, 1347 (1966).
4) M. Yoshifuji, I. Fujishima, R. Okazaki, and N. Inamoto, *Chem. Ind.* (London), **1970**, 625; M. Yoshifuji, R. Okazaki, and N. Inamoto, *J. Chem. Soc., Perkin I*, **1972**, 559.
5) J. Rigaudy and J. C. Verniéres, *Compt. Rend.*, **261**, 5516 (1965).
6) M. Yoshifuji, S. Tanaka, and N. Inamoto, *Chem. Lett.*, **1974**, 1245.
7) D. E. Pearson and C. A. Buehler, *Synthesis*, **1971**, 455.
8) J. Geuze, C. Ruinard, J. Saeterbroek, P. E. Verkade, and B. M. Wepster, *Rec. Trav. Chim. Pays-Bas*, **75**, 301 (1956).
9) C.-H. Wang and S. G. Cohen, *J. Amer. Chem. Soc.*, **79**, 1924 (1957).
10) W. E. Truce and O. L. Norman, *ibid.*, **75**, 6023 (1953).
11) E. T. McBee and R. E. Leech, *Ind. Eng. Chem.*, **39**, 393 (1947).
12) R. Fittig and S. Hoogewerff, *Ann.*, **150**, 327 (1869).
13) P. Kovacic and C. Wu, *J. Org. Chem.*, **26**, 759 (1961).
14) I. I. Lapkin, *Zh. Obshch. Khim.*, **16**, 721 (1946); *Chem. Abstr.*, **41**, 1218 (1947).
15) R. C. Fuson and J. J. Denton, *J. Amer. Chem. Soc.*, **63**, 654 (1941).

BULLETIN OF THE CHEMICAL SOCIETY OF JAPAN, VOL. 48 (9), 2609—2610 (1975)

Iodotrimethylpivalophenones and Iodotetramethylpivalophenones. Preparation and Properties[1)]

Hitomi SUZUKI, Katsuro ISHIZAKI, and Terukiyo HANAFUSA

Department of Chemistry, Faculty of Science, Hiroshima University, Higashi-sendamachi, Hiroshima 730

(Received June 16, 1975)

Synopsis. Three isomeric iodotrimethylpivalophenones and iodotetramethylpivalophenones have been prepared from the corresponding polymethylbenzenes by using the Perrier procedure of the Friedel-Crafts acylation, followed by the iodination of the resulting ketones with iodine-periodic acid dihydrate. Attempts to convert some of these hindered iodoketones to bis(pivaloyl)polymethylbenzenes *via* the Grignard reagent have failed.

In the course of our work on the non-conventional electrophilic substitution of polyalkylaromatics, some bis(pivaloyl)polymethylbenzenes are required. Several hindered aromatic ketones such as acetomesitylene, acetodurene, and acetoisodurene have been known to allow further acylation due to the lack of the coplanarity between acyl group and aromatic ring.[2)] Similar attempts to convert hindered polymethylpivalophenones to bis(pivaloyl)polymethylbenzenes, however, did not afford the desired diketones but led to the extensive deacylation, giving the complicated mixture of hydrocarbons and polymeric substances. No evidence has been obtained of the diketone formation.

As an alternative approach to the diketones, the reaction of the Grignard reagent from bromopolymethylpivalophenones with pivaloyl chloride appeared to be attractive, since 3-bromo-2,4,6-trimethylpivalophenone had been reported by Pinkus and coworkers to yield the Grignard reagent with a keto carbonyl function intact.[3)] We repeated their work and found the reaction to be slow and incomplete. Consequently, it was thought desirable to replace the bromo compound by the iodo one for the preparation of the Grignard reagent. This note describes the preparation and some properties of iodotrimethylpivalophenones and iodotetramethylpivalophenones.

Direct nuclear iodination of alkyl aryl ketones has apparently not been described to date probably because of the high propensity of the alkyl ketone moiety to react with attacking species as well as the deactivating effect of acyl group upon the aromatic ring. Iodine-periodic acid dihydrate as an iodinating agent was found to provide a simple direct route to some iodopolymethylacylophenones.[4)] Trimethylpivalophenones were readily iodinated with the above reagent to give the monoiodo derivatives in an average isolated yield of over

TABLE 1. PHYSICAL PROPERTIES OF SOME MONOIODOTRIMETHYLPIVALOPHENONES AND MONOIODOTETRAMETHYLPIVALOPHENONES

Compound	Mp (°C)	Yield (%)	^{1}H NMR spectra (δ)		IR spectra[b)] (cm^{-1})	Elementary analysis (%)			
			CH_3[a)]	Aromatic H		Found		Calcd	
						C	H	C	H
5-Iodo-2,3,4-trimethylpivalophenone	107—109	83	1.24 (3) 2.08 (1) 2.29 (1) 2.49 (1)	7.45	978, 1092, 1205, 1283, 1693,	50.63	5.81	50.92	5.80
3-Iodo-2,4,5-trimethylpivalophenone	85—86	89	1.24 (3) 2.30 (1) 2.35 (1) 2.48 (1)	6.85	891, 1092, 1178, 1274, 1697	51.10	5.83	50.92	5.80
3-Iodo-2,4,6-trimethylpivalophenone	52—53	88	1.23 (3) 2.14 (1) 2.32 (1) 2.44 (1)	6.93	932, 1160, 1696	50.71	5.82	50.92	5.80
6-Iodo-2,3,4,5-tetramethylpivalophenone	114—116	85	1.34 (3) 2.15 (1) 2.17 (1) 2.32 (1) 2.49 (1)	—	888, 933, 1689	52.08	6.23	52.34	6.15
5-Iodo-2,3,4,6-tetramethylpivalophenone	92—94	94	1.23 (3) 2.08 (1) 2.31 (2) 2.57 (2)	—	907, 1086, 1198, 1695	52.20	6.36	52.34	6.15
4-Iodo-2,3,5,6-tetramethylpivalophenone	133—134	93	1.23 (3) 2.16 (2) 2.49 (2)	—	960, 1091, 1680	51.93	6.15	52.34	6.15

a) Numerals in parentheses refer to the number of methyl groups. b) Principal peaks in the region, 650—1300 and 1500—2000 cm^{-1}.

80%, with the ease of iodination decreasing in the order 2,4,6->2,3,4->2,4,5-. 2,3,4-Trimethylpivalophenone gave 5-iodo-2,3,4-trimethylpivalophenone, and 2,4,5-trimethylpivalophenone gave 3-iodo-2,4,5-trimethylpivalophenone as the only product. As expectedly, the *meta* position to the acyl group was preferred to *ortho* position. The position occupied by iodine atom in these systems was established by the comparison of their ^{1}H NMR spectra with those of the parent ketones.

Iodination of tetramethylpivalophenones proceeded with much ease. Of three isomeric ketones, 2,3,4,6-tetramethylpivalophenone was the most reactive, followed by 2,3,5,6-tetramethylpivalophenone and 2,3,4,5-tetramethylpivalophenone. Infrared and ^{1}H NMR spectral inspection of the crude reaction product had no indication of displacement of acyl group by iodine atom nor substitution on alkyl side-chain.

All the iodotrimethylpivalophenones and iodotetramethylpivalophenones obtained are well crystallized solids melting between 85 and 134 °C. They are moderately or readily soluble in light petroleum, benzene, carbon tetrachloride, chloroform, and hot ethanol, and are only slightly soluble in cold methanol. Yields, physical constants, and analytical data are given in Table 1.

The Grignard reagents were prepared from 5-iodo-2,3,4,6-tetramethylpivalophenone and 4-iodo-2,3,5,6-tetramethylpivalophenone, respectively, and treated with an excess of pivaloyl chloride. Ordinary work-up followed by chromatography on alumina, however, gave the parent tetramethylpivalophenones as the major product. Thick-layer chromatography of the product mixture gave some amounts of two other products, and none of these proved to be the expected bis(pivaloyl)-tetramethylbenzenes.

Experimental

All mp's are uncorrected. ^{1}H NMR measurements were made with a Varian T-60 spectrometer in deuteriochloroform solutions against internal TMS. Infrared spectra were determined in Nujol mulls on a Hitachi 215 spectrophotometer. Trimethylpivalophenones and tetramethylpivalophenones were prepared from the corresponding polymethylbenzenes by using the Perrier procedure of the Friedel-Crafts acylation.[5]

Procedure for the Preparation of Iodopolymethylpivalophenones. The general procedure is illustrated below by the reaction of 2,3,4,6-tetramethylpivalophenone.[6]

5-Iodo-2,3,4,6-tetramethylpivalophenone. A mixture of 2,3,4,6-tetramethylpivalophenone (6.45 g), iodine (3.0 g), periodic acid dihydrate (1.35 g), and 80% acetic acid (40 ml) containing several drops of concentrated sulfuric acid was kept with stirring at 70—80 °C for about 1 hr until the color of iodine disappeared. After cooling water was added, and the crystalline deposit was collected by filtration and passed over a short alumina column with light petroleum. From the eluate the iodo compound was obtained as colorless prisms, mp 92—94 °C (from methanol). Yield, 9.52 g (94%).

Attempted Conversion of Iodotetramethylpivalophenones to Bis-(pivaloyl)tetramethylbenzenes. To a solution of 5-iodo-2,3,-4,6-tetramethylpivalophenone or 4-iodo-2,3,5,6-tetramethylpivalophenone (3.38 g) in dry ether (50 ml) were added magnesium powder (0.24 g) and a small crystal of iodine, and the mixture was stirred magnetically in a tightly stoppered vessel placed in a polythene bag containing silica gel desiccant until the metal had almost disappeared. This required several days. The Grignard reagent was then added at one time to a solution of fresh pivaloyl chloride (6.0 g) in the same solvent (20 ml). After mild reaction had ceased, the mixture was hydrolyzed by pouring it into a slurry of crushed ice and hydrochloric acid. The ether layer was separated and washed with aqueous sodium hydrogencarbonate and water. The ethereal solution was dried over anhydrous sodium sulfate and evaporated to leave a light yellow oil, which on standing partly solidified to a crystalline mass. The solid product (*ca.* 1.4 g) was identified as the parent tetramethylpivalophenone by comparison with the authentic sample. Preparative thick-layer chromatography of the oily part gave three minor components. They were found to be unchanged starting material, aliphatic ketone, and alcohol of yet unidentified structure, respectively. None of the expected diketones could be isolated.

Expenses for this work were defrayed by grants from the Ministry of Education and the Saneyoshi Scientific Foundation.

References

1) The Reaction of Polysubstituted Aromatics. Part XLIII; Part XLII: H. Suzuki, H. Yoneda, and T. Hanafusa, This Bulletin, **48**, 2116 (1975).

2) L. I. Smith and C. Guss, *J. Amer. Chem. Soc.*, **59**, 804 (1937).

3) A. G. Pinkus, J. I. Riggs, Jr., and S. M. Broughton, *ibid.*, **90**, 5043 (1968).

4) H. Suzuki, "Organic Syntheses," Vol. 51, p. 94 (1971). The title ketones are not accessible by the Friedel-Crafts synthesis from iodopolymethylbenzenes, pivaloyl chloride, and aluminum chloride, since decarbonylation of the chloride as well as disproportionation of iodoalkylaromatics readily take place.

5) P. H. Gore, "Friedel-Crafts and Related Reactions," Vol. III, ed. by G. A. Olah, Interscience, New York (1964), Part I, p. 4; H, Suzuki, H. Wada, K. Maruyama, and R. Goto, This Bulletin, **39**, 1201 (1966).

6) New compound. Mp 35—38 °C; bp 133—135 °C/6 mmHg. ^{1}H NMR: δ 1.23 (s, 3H), 2.10 (s, 3H), 2.13 (s, 3H), 2.24 (s, 3H), and 6.84 ppm (s, aromatic H). Prolonged, slow pivaloylation of isodurene leads to the formation of appreciable amounts of 2,3,5,6-tetramethylpivalophenone.

BULLETIN OF THE CHEMICAL SOCIETY OF JAPAN, VOL. 48 (9), 2611—2612 (1975)

Smiles-Type Rearrangement of *N*-(*trans*-Styrylsulfonyl) and *N*-(4-Phenyl-1,3-butadienylsulfonyl)thioureas and Isothioureas

Kiyoshi HASEGAWA, Syuzi HIROOKA, and Tadashi SASAKI*

Department of Industrial Chemistry, Faculty of Engineering, Toyama University, Takaoka-shi 933
**Institute of Applied Organic Chemistry, Faculty of Engineering, Nagoya University, Furo-cho, Chikusa-ku, Nagoya 464*

(Received April 28, 1975)

Synopsis. Treatment of *N*-(*trans*-styrylsulfonyl)- (**1**) and *N*-(4-phenyl-1,3-butadienylsulfonyl)-*N'*-methylthiourea (**2**), and the corresponding *S*-methylisothioureas (**6** and **7**), with strong base afforded the Smiles-type and Michael-type products. Effects of substituents at C-2 and nucleophiles on the products are discussed.

We recently reported that treatment of *N*-(2,2-diarylvinylsulfonyl)thioureas,[1] isoureas,[2] isothioureas[2] and *N*-(*trans*-*p*-nitrostyrylsulfonyl)thiourea[1] with base affords Smiles-type products. Matier and Comer[3] described that base-treatment of *N*-(*trans*-styrylsulfonyl)-amidines yields Michael-type and Smiles-type products. These rearrangements are facilitated by electron-withdrawing *para* substituents on the aromatic rings. However, effects of substituents at C-2 and nucleophiles on the products are not well known. This paper describes these effects by base-treatment of 2-substituted vinylsulfonylthioureas **1**—**3** and isothioureas **6** and **7**.

Results and Discussion

In contrast to known base-catalyzed Michael cycloaddition of *N*-(*trans*-styrylsulfonyl)thioureas[4] (**1**), -isothioureas[5] (**6**) and *N*-(4-phenyl-1,3-butadienylsulfonyl)-thioureas[6] (**2**), treatment of **1** and **2** with strong base (ten equiv. of 10M NaOH) in some solvents for 3 hr at 80 °C gave Smiles-type products, *N*-methyl-*S*-(*trans*-styryl)- (**4**) and *N*-methyl-*S*-(4-phenyl-1,3-butadienyl)-isothioureas (**5**), respectively (Table 1). No Michael cycloadducts were obtained because

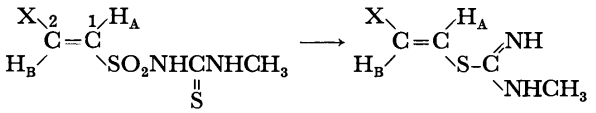

1: X=*p*-R¹C₆H₄ **4**: X=*p*-R¹C₆H₄
2: X=C₆H₅CH=CH **5**: X=C₆H₅CH=CH

they were split into **1** and **2** in the strongly basic media (pH>13.30).[4] Similar treatment of *N*-(2-methyl-*trans*-styrylsulfonyl)-*N'*-methylthiourea (**3**) and *N*-(*trans*-styrylsulfonyl)-*N'*-methylurea afforded no rearranged products. The IR spectra of **4** and **5** exhibited absorption bands at 3450—3150 (NH) and 1615 (C=N) cm⁻¹.

Smiles-type rearrangement of **6** requires more vigorous reaction conditions than those of *N*-(2,2-diarylvinylsulfonyl)- and *N*-(4-phenyl-1,3-butadienylsulfonyl)-*N'*, *S*-dimethylisothioureas (**7**). Treatment of **6** with ten equiv. of aqueous 10M NaOH in DMF for 3 hr at 75 °C gave *N*-(*trans*-styryl)-*N*-methylureas (**12**) and 4-methyl-5-aryl-2,3,5,6-tetrahydro-3-oxo-1,2,4-thiadiazine-1,1-dioxides[5] (**15**) (Tables 1 and 2). Similar treatment of **7** gave the corresponding urea (**13**) and *N*-(4-phenyl-1,3-butadienylsulfonyl)-*N'*-methyurea (**16**). The Michael cycloadduct of

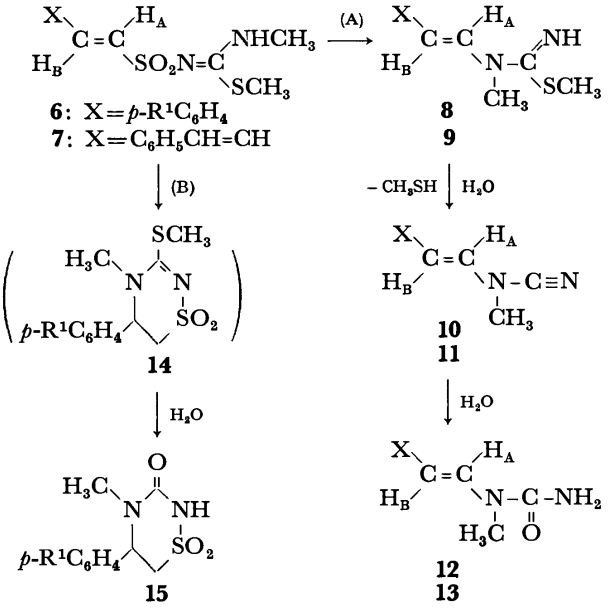

6: X=*p*-R¹C₆H₄ **8**
7: X=C₆H₅CH=CH **9**
14 **10**
11
15 **12**
13

7 was not obtained because of stabilization of Smiles-type intermediary carbanion.[1-3] The structures of **12**, **13**, **15**, and **16** were determined on the basis of analytical and spectral data (1650 and 1600 (C=O) cm⁻¹).

The formation of **12** and **13** would proceed through a Smiles rearrangement path (**A**) and that of **15** through a Michael cycloaddition path (**B**). Rearrangement path (A) is similar to that of *N*-(2,2-diarylvinylsulfonyl)-*N'*,*S*-dimethylisothioureas.[2] Attempts to obtain the intermediary new isothioureas **8** and **9**, and the new cyanamides **10** and **11** were unsuccessful due to their easy hydrolysis to **12** and **13** under the reaction conditions used. Under moderate reaction conditions (1N NaOH, 45 °C, 4 hr), **7** gave **9** (3%, IR: 1615 (C=N) cm⁻¹) and **11** (7%, IR: 2220 (C≡N) cm⁻¹) as yellow oils after column chromatography on silica gel, but, satisfactory analytical data were not obtained.

Tables 1 and 2 show that the rearrangements of the thioureas and isothioureas are favored by electron-withdrawing substituents on the aromatic ring, by the styryl group at C-2 and by solvents of high polarity.

Possible mechanisms for the formation of the isothioureas, **4**, **5**, **8**, and **9**, are analogous to those for the rearrangements of *N*-(2,2-diarylvinylsulfonyl)thioureas,[1] isothioureas[2] and *N*-(*trans*-styrylsulfonyl)amidines.[3] The presence of the styryl group at C-2 would stabilize the cinnamyl carbanion by resonance more than the

Table 1. List of rearranged products

Compd.	X	Yield (%) solvent			Mp (°C)	Found (%)				Calcd (%)			
		DMF	Acetone	Dioxane		C	H	N	S	C	H	N	S
4a[a]	*p*-$NO_2C_6H_4$	>95[b]			181—182	50.73	4.52	17.75	13.69	50.63	4.67	17.72	13.49
4b	*p*-BrC_6H_4	91	90	79	174—175	44.48	3.79	10.50		44.31	4.09	10.33	
4c	*p*-ClC_6H_4	70	67	39	171—172	53.10	4.87	12.39	13.89	52.97	4.89	12.36	14.14
4d	C_6H_5	21	7	0	149—150	62.76	6.24	14.52	16.61	62.48	6.29	14.58	16.65
4e	*p*-$CH_3C_6H_4$	6	2	0	161—162	64.29	7.09	13.83		64.06	6.84	13.58	
5	C_6H_5CH=CH	67			180—181	66.15	6.71	12.73		66.03	6.94	12.83	
12a	*p*-BrC_6H_4	65			209—211	47.24	4.57	11.02		47.08	4.35	10.98	
12b	*p*-ClC_6H_4	46			197—198	57.22	5.36	13.15		57.01	5.26	13.30	
12c	C_6H_5	18			191—193	67.87	6.72	15.81		68.16	6.86	15.90	
13	C_6H_5CH=CH	42			193—195	71.26	6.72	14.03		71.26	6.98	13.85	

a) Mp and analytical data were already given in the previous paper.[1] b) Compound **4a** was obtained in a yield more than 95% after 30 min.

Table 2. Product distribution from the base treatment of **6** and **7**

X	Yield (%)		Yield (%)	
	12	**13**	**15**	**16**
p-BrC_6H_4	65		trace	
p-ClC_6H_4	46		4	
C_6H_5	18		56	
p-$CH_3C_6H_4$	trace		68	
C_6H_5CH=CH		42		10

phenyl group. Introduction of electron-releasing methyl group at C-2 would descrease benzyl carbanion, stability, and no rearrangement could occur.

Experimental

Spectral data are given only for a representative of each class.

*Base-treatment of **1** and **2**.* The isothioureas **4** and **5** were prepared by a method similar to the base-treatment of *N*-(2,2-diarylvinylsulfonyl)thioureas[1] and recrystallized from methanol. **4d**: IR (KBr); 3420, 3280, and 3170 (NH), 1615 (C=N) cm^{-1}. NMR (DMSO-d_6) δ: 3.50 (s, 3, CH_3), 6.25 (d, 1, H_A), 8.53 (d, 1, H_B), J_{AB}=15.0 Hz, 7.30—7.70 (m, 5, C_6H_5), 7.90 (broad, 1, $\underline{NH}CH_3$) and 8.34 (broad, 1, NH). MS *m/e*: 192 (M^+). **5**: IR (KBr); 3400, 3260, and 3140 (NH), 1610 (C=N) and 1580 (C=C) cm^{-1}. MS *m/e*: 218 (M^+).

*Base-treatment of **6** and **7**.* The sulfonylthioureas **6** and **7** were treated with ten equiv. of aqueous 10M NaOH in DMF for 3 hr at 75 °C and the mixtures were poured into water and filtered to give **12** and **13**, respectively, which were recrystallized from chloroform. **12b**: IR (KBr): 3360 and 3180 (NH), 1650 and 1600 (C=O) cm^{-1}. NMR (DMSO-d_6) δ: 3.07 (s, 3, CH_3), 5.70 (d, 1, H_A), 7.72 (d, 1, H_B), J_{AB}=15.0 Hz, 6.65 (s, 2, NH_2) and 7.30 (s, 4, C_6H_4). MS *m/e*: 210 (M^+). Acidification of the filtrate gave **15b** (4%, R^1=Cl), which was recrystallized from methanol, mp 235—237 °C (236—238 °C[5]).

13: IR (KBr): 3350 and 3170 (NH), 1650 and 1600 (C=O) cm^{-1}. MS *m/e*: 202 (M^+). Acidification of the filtrate gave **16** which was recrystallized from benzene–petroleum ether, mp 188—190 °C. IR (KBr): 3340 (NH), 1655 (C=O), 1335 and 1145 (SO_2) cm^{-1}. MS *m/e*: 266 (M^+). Found: C, 54.14; H, 5.38; N, 10.41%. Calcd for $C_{12}H_{14}N_2O_3S$: C, 54.13; H, 5.30; N, 10.52%.

References

1) K. Hasegawa, S. Hirooka, and T. Sasaki, This Bulletin, **48**, 1513 (1975).
2) K. Hasegawa, S. Hirooka, T. Sasaki, Y. Mizukami, T. Yamamoto, J. Ishikawa, and H. Shinno, *Nippon Kagaku Kaishi*, **1975**, 1035.
3) W. L. Matier and W. T. Comer, *J. Org. Chem.*, **39**, 3080 (1974).
4) K. Hasegawa and S. Hirooka, This Bulletin, **45**, 525 (1972).
5) K. Hasegawa and S. Hirooka, *ibid.*, **45**, 1893 (1972).
6) K. Hasegawa, S. Hirooka, T. Sasaki, S. Ikeda, and K. Hashimoto, *Nippon Kagaku Kaishi*, **1975**, 1028.

Studies of Surface Modification of Solids. III. Reaction of Silica with Trifluoroethanol

Kazuo Tsutsumi, Haruo Emori, and Hiroshi Takahashi

Institute of Industrial Science, The University of Tokyo, Roppongi, Minato-ku, Tokyo 106

(Received August 19, 1974)

The esterification of silica was performed by reactions with 2,2,2-trifluoroethanol vapor and ethanol vapor with and without basic catalysts, such as ammonia and pyridine. The esterification with ethanol was referred to as the control. The extents of the esterifications were observed by means of infrared spectroscopy. The reactivity of the silica with trifluoroethanol was higher than that with ethanol. This is presumably because trifluoroethanol is more acidic than ethanol. The esterification was accelerated by the addition of ammonia as a base catalyst. For example, in the reaction of the silica with trifluoroethanol of 10.7 Torr at 30 °C for 3 hr, 35% of the surface silanols were esterified without any catalyst, while with the ammonia (0.2 Torr) catalyst, 98% of them was esterified. This suggests that the extraction of the proton from the hydroxyl groups of alcohol by NH_3 contributes to the esterification. The addition of pyridine influenced the reaction rate as well, but the esterification itself was disturbed by the addition of excess pyridine, because pyridine was adsorbed strongly on the surface silanol and its heterocyclic ring prevented the alcohols from adsorption. It is supposed that the physical adsorption of trifluoroethanol on the surface silanol is necessary in the first stage of the esterification. The esterified silica became hydrophobic, and it was hydrolyzed in the presence of water.

The surfaces of such metal oxides as silica and alumina are covered with hydroxyl groups, which are known to influence the adsorption properties of the surface.[1] As is well known, the hydrophilicity of silica surface originates from the silanol groups and is lost upon the esterification of the silanol groups with alcohol:[2]

$$\gtrdot\text{Si-OH} + \text{ROH} \longrightarrow \gtrdot\text{Si-O-R} + \text{H}_2\text{O} \qquad (1)$$

Hair *et al.* showed that silica treated with an ammonium fluoride solution had, in part, surface fluorine instead of silanol, and that its surface became hydrophobic. The activity of the Brönsted acid of the surface silanol was enhanced by the electronegativity of an adjacent fluorine atom, and the silica was endowed with a high catalytic activity for the cracking of cumene:[3]

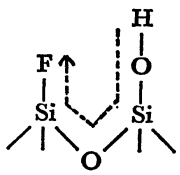

In this study, the adsorption and the reaction of 2,2,2-trifluoroethanol on the silica surface were investigated by means of infrared spectroscopy. The silica used in this experiment was preheated in an electric furnace at a high temperature in advance of the esterification. By this treatment, variously reactive OH groups other than the so-called "free OH groups" or "isolated OH groups" were removed from the surface.

The rate of the reaction of 2,2,2-trifluoroethanol vapor with silica in the presence of a catalyst vapor was investigated. The reactivity of the chlorinated silica was also studied. The esterification with ethanol was also referred to.

Experimental

Aerosil-380 (Japan Aerosil Co., Ltd.) was used as the sample of silica. It was heated at 800 °C in an electric furnace under air prior to use. By this thermal pretreatment, all the molecular water and mutually-hydrogen-bonded hydroxyl groups were removde from the silica surface. In consequence, the silica surface was covered only with the isolated silanol groups and the siloxane-type groups. The trifluoroethanol, ethanol, and water were purified by repeated vacuum distillation.

The spectroscopic work was performed in a quartz cell fitted with NaCl windows[4], the cell was set in a Hitachi-EPI G3-type infrared spectrometer. The silica sample was pressed into an orbicular wafer about 10 mg/cm^2 thick. The sample was then set in a cell and heated *in vacuo* to any desired temperature. After the cell has then been cooled to room temperature under *vacuo*, the spectrum was observed. The silica was evacuated at 30 °C under 10^{-5} Torr in the cell prior to any reaction. The adsorption and the reaction studies were carried out in the same cell at various temperatures and pressures. In order to obtain the adsorption isotherm, the gaseous reactant was introduced into the cell at various pressures, and the extinction of the isolated silanols was measured at various stages during the adsorption and the reaction.

The hydroxyl group of surface silanol was exchanged also with chlorine by the use of thionyl chloride ($SOCl_2$).[5] The silica wafer pretreated in the electric furnace at 800 °C was put into $SOCl_2$ and refluxed for a total period of 14 days. The chlorinated silica was transferred quickly into the cell of the spectrometer so as not to be hydrolyzed, and then evacuated at 30 °C prior to the reaction with the reagent:

$$\gtrdot\text{Si-OH} + \text{SOCl}_2 \longrightarrow \gtrdot\text{Si-Cl} + \text{HCl} + \text{SO}_2 \qquad (2)$$

Results and Discussion

Isolated OH Groups of Silica. The heat treatment of silica at 800 °C in the electric furnace resulted in the change of the spectra shown in Fig. 1.

The absorption bands of water molecules (3500 cm^{-1}) and hydrogen-bonded hydroxyl group (3650 cm^{-1}) disappeared, and only the band of the isolated hydroxyl groups (3750 cm^{-1}) remained. The silica surface was ultimately covered with the isolated silanol and the siloxane linkages.

In the infrared spectra of silica after the reaction with trifluoroethanol, the OH stretching vibration of the silanol groups decreased and the CH_2 stretching (3000—2800 cm^{-1}), the CH_2 bending (1470 cm^{-1}), the CH_2 twisting (1440 cm^{-1}), the overtone of the CF_3

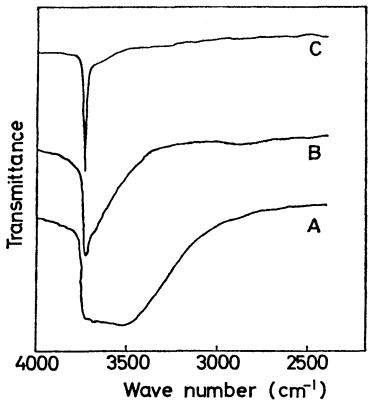

Fig. 1. Infraed spectra of silica after various treatments.
A: evacuation at 30 °C
B: evacuation at 400 °C
C: evacuation at 30 °C after heat treatment in electric furnace at 800 °C

asymmetric deformation (1360 cm^{-1}), and the CF_3 asymmetric stretching (1310 cm^{-1}) vibrations appeared (*cf.* Fig. 2).[6] The spectra indicate that the esterification occurs on the silanol according to the following equation:

$$\geqslant Si\text{-}OH + CF_3CH_2OH \longrightarrow \geqslant Si\text{-}O\text{-}CH_2\text{-}CF_3 + H_2O \quad (3)$$

The 3750 cm^{-1} band remained after the esterification. The complete esterification of all the silanols could not be attained.

The rate of the esterification of the silica with trifluoroethanol was analyzed by measuring the diminishing rate of the absorbance of the 3750 cm^{-1} band due to the isolated silanol. Since the physically absorbed alcohol has previously been desorbed by the evacuation, the diminishing rate of the 3750 cm^{-1} band corresponded to the rate of the reaction. The degree of coverage (θ) by physical adsorption at the reaction temperatures was measured by taking the spectra of the silica with the residual gas present in the cell, while the reaction was still going on. One example of the determination of the surface coverage (θ) from the infrared spectra is given in Fig. 3 for illustration. From this figure, the surface coverage (θ) of ethanol to the silanol group under the conditions of an ethanol pressure of 20 Torr at 30 °C was determined. In this figure, θ is the ratio of $\overline{OB}$ to $\overline{AB}$. The $\overline{OB}$ absorbance at the reaction time of 18 min was interpolated from the values of the absorbances at the reaction times of 10 min and 20 min respectively.

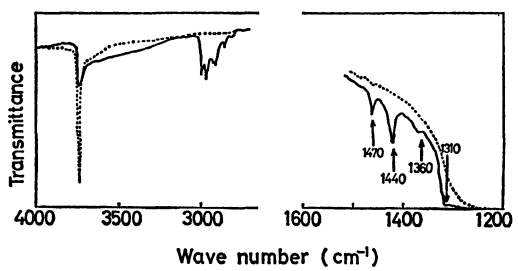

Fig. 2. Esterification of silica with trifluoroethanol (25.0 Torr).
Reaction period: 8 hr, Reaction temperature: 60 °C.
Solid line: infrared spectrum after the esterification and the successive evacuation of the residual vapor of trifluoroethanol. Broken line: infrared spectrum of original silica.

The absorbance $\overline{AB}$ was obtained by deducting $\overline{OA}$ from $\overline{OB}$. By the same manner, the values of the surface coverage of trifluoroethanol under the various conditions were determined.[7] The ratio of the extinction with the residual gas present to the interpolated value gives the fraction of hydroxyl groups not covered by physically absorbed molecules, *i.e.*, $1-\theta$. In this case, it was supposed that the fraction was independent of the degree of esterification. By the calculations of this method, the reactivity of the silica with trifluoroethanol or ethanol was investigated. The rate of the esterification with trifluoroethanol is faster than that with ethanol (*cf.* Fig. 7, Curves A and B). The hydroxylic proton of alcohol takes part in the esterification reaction, and the rate of the reaction must be controlled by the ease of the proton release. Because of the inductive effect of the electronegative fluorine atoms bonded directly to the α-carbon, trifluoroethanol releases the proton more easily than ethanol. From this point of view, the difference in the reactivities of the two alcohols seems reasonable.

Heat of Adsorption. In view of the fact that the reaction of the silica with trifluoroethanol goes on slowly at high temperatures, the esterification may be considered to take place when there is physically adsorbed alcohol on the surface silanol. As is shown in Fig. 4, the quantity of physically adsorbed alcohol

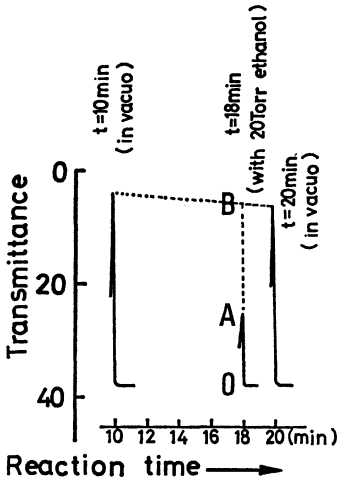

Fig. 3. Change of 3750 cm^{-1} -OH band of silica taken during the course of reaction at 30 °C, illustrating spectra used for determining the fraction of freely vibrating hydroxyl groups covered by physically adsorbed ethanol.

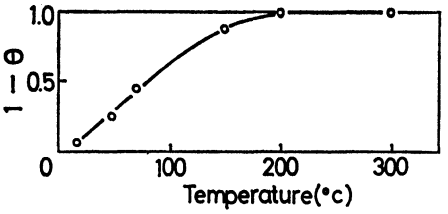

Fig. 4. Change of surface coverage of trifluoroethanol with temperature (trifluoroethanol pressure: 17.0 Torr).

Table 1. Isosteric heats of adsorption of trifluoroethanol on silica

Surface coverage (θ)	ΔH (kcal/mol)
0.1	8.0
0.2	7.0
0.3	6.4
0.4	6.8

on the surface silanol decreases with the rise in the temperature. By determining spectroscopically the amount of coverage on the freely-vibrating OH groups of the silica, it is possible to obtain the isotherms for the adsorption on these groups, independent of the adsorption at any other sites. The fraction of coverage (θ) was thus decided at various temperatures and pressures, from which the isosteric heats of the physical adsorption of trifluoroethanol on the free hydroxyl groups of the silica were derived. Some typical adsorption isotherms determined at various temperatures are given in Fig. 5. The slope of the plot relating log P to $1/T$ is proportional to the isosteric heat of adsorption, according to Clausius-Clapeyron's equation. Same typical plots are given in Fig. 6. The heats calculated from these plots are given in Table 1.

Esterification Catalyzed by Ammonia. An acid or base catalyst is normally used in the esterification.[8] Therefore, the catalytic effects of NH_3 and pyridine on the esterification were examined. In the presence of NH_3, the rate of the esterification with trifluoroethanol increased remarkably (*cf.* Fig. 7, Curves B and E). The reaction of the silica with ethanol in

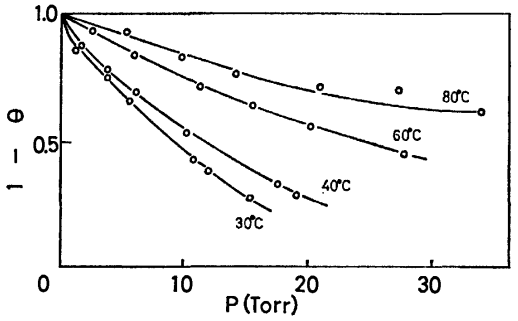

Fig. 5. Adsorption isotherms of trifluoroethanol interacted with the free hydroxyl groups on silica.

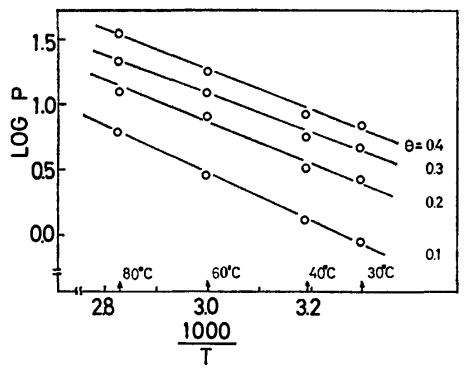

Fig. 6. Examples of the relations between log P and $1/T$ for the adsorption isotherms of trifluoroethanol on Aerosil-380.

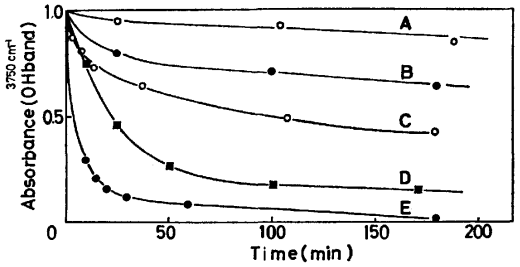

Fig. 7. Esterification rate at 30 °C under various conditions.
A: ethanol [7.0 Torr]
B: trifluoroethanol [11.3 Torr]
C: ethanol [7.8 Torr] and ammonia [0.2 Torr]
D: trifluornethanol [11.2 Torr] and pyridine [0.3 Torr]
E: trifluoroethanol [10.8 Torr] and ammonia [0.2 Torr]

place of trifluoroethanol was found to be accelerated by the NH_3 catalyst (Fig. 7, Curves A and C).

The mechanism of the esterification catalyzed by NH_3 can be explained as follows. In the first stage, the alcohol molecule is adsorbed on the silanol, and then ammonia containing lone-pair electrons forms a hydrogen bond with the hydroxylic proton of alcohol. On the basis of the hypothesis, the model of the adsorption of these molecules may be written as in the picture below. The reaction is completed by the formation of the ester and water. Since the ability of NH_3 to draw out the hydroxylic proton of alcohol is proportional to the acidity of alcohol, the catalytic action of NH_3 on the esterification with trifluoroethanol is more effective than on that with ethanol. No reaction between trifluoroethanol and NH_3 occurred without the silica. It is certain that NH_3 adsorbs directly on the isolated silanol. This problem will be discussed in the next paragraph.

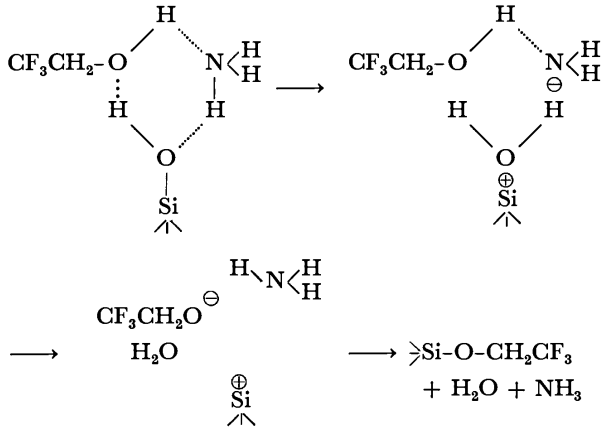

Esterification Catalyzed by Pyridine. When pyridine was used as the catalyst, the esterification of the silica with trifluoroethanol was accelerated (*cf.* Fig. 7, Curves B and D). Since pyridine could not be completely desorbed by the evacuation at 30 °C, the effect on the esterification rate of the fraction of hydroxyl groups covered by the strongly adsorbed pyridine (θ=0.07) was considered in Curve D of Fig. 7. However, the catalytic effect of pyridine was not so remarkable as that of NH_3. It is noticeable that an excess of

Table 2. Heats of adsorption on silica

Absorbate	$\Delta H^{a)}$ (kcal/mol)	$\Delta H^{b)}$ (kcal/mol)[c]
Trifluoroethanol	7.1±0.9[a]	6.2
Ammonia	8.9±0.2[b]	9.8
Pyridine	10.8±1.0[b]	10.6

a) Obtained from Table 1. b) After Hertl and Hair.[7] c) Calculated from frequency shift by using Eq. (4).

pyridine lowers the esterification rate. This means that pyridine strongly adsorbed on the isolated silanol retards the adsorption of alcohol on it.

In Table 2, the heats of the adsorption of trifluoroethanol, NH_3, and pyridine on the isolated silanol are shown. The heat of adsorption ($\Delta H^{a)}$) is obtained by measuring the isosteric heat of adsorption in the freely vibrating hydroxyl group.[8] In the case of trifluoroethanol, the heat of adsorption ($\Delta H^{a)}$) was calculated from the data of the adsorption isotherm, as is shown in Figs. 5 and 6 by using Clausius-Clapeyron's equation. When physical adsorption takes place on the surface of the silica, it is observed that the band in the infrared spectrum attributable to the freely vibrating hydroxyl group is perturbed to lower frequencies. The heat of adsorption ($\Delta H^{b)}$) is a function of the frequency shift.

This was given by this equation:[9]

$$\Delta H^{b)} = 0.455\ (\Delta\nu\ \mathrm{cm^{-1}})^{1/2} - 2.3. \qquad (4)$$

In this equation, $\Delta\nu$ means the frequency shift of the OH stretching vibration. As is shown in Table 2, the strength of the adsorption of these molecules on the isolates silanol is in the order of: pyridine>ammonia>trifluoroethanol. The hydrogen bonding between the hydroxylic proton of the silanol and pyridine is very strong. A test showed that pyridine completely covered the surface silanols at the pressure of 4 Torr, for instance, whereas ammonia could not cover all the silanols even at 80 Torr. The infrared spectrum of the ammonia adsorbed on the silica is shown in Fig. 8. The disappearance of the isolated hydroxyl bands (3750 cm^{-1}) is accompanied by the appearance of two new bands, at 3400 and 3320 cm^{-1}. These two bands can be attributed to the asymmetric and symmetric N–H stretching vibrations. The OH vibration is shifted by about 700 cm^{-1} and is observed as a very

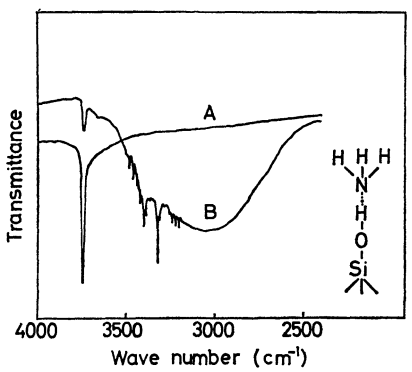

Fig. 8. Infrared spectrum of adsorbed ammonia.
A: Silica
B: Silica with ammonia (82.0 Torr)

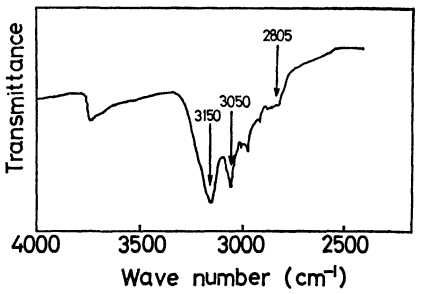

Fig. 9. Infrared spectrum of the chlorinated silica after the treatments of the esteification with trifluoroethanol in the presence of ammonia at 30 °C. (Indicated bands are assigned to ammonium chloride)

broad absorption band at about 3050 cm^{-1}. Since the intensity of the absorption band at 3750 cm^{-1} can be restored by the evacuation at 30 °C, ammonia seems to be adsorbed physically on the surface silanol.

The pyridine adsorbed on the silanol could not be removed entirely by evacuation at room temperature. When the isolated silanols are completely covered by pyridine, the esterification of the silica with trifluoroethanol is unfavorable because of the steric hindrance of the heterocyclic ring of pyridine.

Esterification of the Chlorinated Silica. The chlorination of silica was evidenced by the appearance of the infrared absorption band due to NH_4Cl molecules when the $SOCl_2$-treated silica was exposed to ammonia (*cf.* Fig. 9).[10] However, no infrared absorption bands attributable to Si–Cl bands were recognized. The reaction of the chlorinated silica with trifluoroethanol formed so few esters that they could not be observed by infrared spectroscopy. This might be because of the strengthening of the acidity of the residual silanol after about 60% of the surface OH groups has been replaced by chlorine atoms.

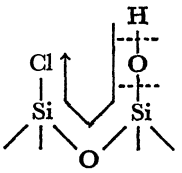

As a consequence, it became difficult to split the silicon atom from the oxygen which is necessary for the esterification. In the presence of NH_3 (0.8 Torr) as the catalyst, the esterification of the chlorinated silica with trifluoroethanol of 33.1 Torr at 30 °C for 25 min reached 80% of the surface OH groups.

Hydrolysis and Pyrolysis of the Esterified Silica. The nature of the silica surface was modified by treatment with trifluoroethanol and became very hydrophobic. For instance, when the modified silica wafer was immersed in water, it first floated on the surface of the water. However, the wafer floating on the water surface then began to sink very slowly. The change in the affinity of the esterified silica with water may be elucidated by the hydrolysis of the ester. As the ester (Si–O–CH_2–CF_2) possesses an oxygen atom between the silicon and the carbon atoms, it has a tendency to be hydrolyzed. The absorption of the OH stretching vibration of trifluoroethanol and that

of the water molecules appeared in the infrared spectrum of the esterified silica in the presence of water vapor. The spectrum obtained after the evacuation showed an increase in the isolated hydroxyl groups and a decrease in the $-CH_2-CF_3$ groups. When the esterified silica was placed in water vapor of 15 Torr at 30 °C for one hr, it was found that 26% of the ester was hydrolyzed. Moreover, samples which had been kept in water for one day were completely hydrolyzed. At the same time, the siloxane linkages were opened.

$$\geqslant Si\text{-}O\text{-}CH_2CF_3 + H_2O \longrightarrow \geqslant Si\text{-}OH + CF_3CH_2OH \quad (5)$$

The surface species of the esterified silica were stable up to about 200 °C. However, they were decomposed by evacuation above 300 °C.

References

1) H. P. Boehm, *Adv. Catal.*, **16**, 179 (1966). H. Utsugi *et al.*, *Nippon Kagaku Kaishi*, **1972**, 1007.
2) K. Tsutsumi and H. Takahashi, *ibid.*, **1972**, 1800. H. Utsugi *et al.*, *ibid.*, **1972**, 1557.
3) I. D. Chapman and M. L. Hair, *J. Catal.*, **2**, 145 (1963).
4) K. Tsutsumi, T. Ida, and H. Takahashi, This Bulletin, to be published.
5) M. Forman, *Trans. Faraday Soc.*, **57**, 2000 (1961).
6) A. J. Barnes, H. E. Hallam, and D. Jones, *Proc. Roy. Soc., Ser. A*, **335**, 97 (1973).
7) W. Hertl, *J. Phys. Chem.*, **72**, 1248 (1968).
8) R. C. Azrak and C. L. Angell, *ibid.*, **77**, 3048 (1973).
9) W. Hertl and M. L. Hair, *ibid.*, **72**, 4676 (1968).
10) R. S. McDonald, *ibid.*, **62**, 1168 (1958).

The Ligation of Phosphine Derivatives and the Oxygen-binding Properties of the Cobalt Mesoporphyrin IX Dimethyl Ester in Toluene

Teruo TAKAYANAGI, Haruhiko YAMAMOTO, and Takao KWAN

Faculty of Pharmaceutical Sciences, University of Tokyo, Hongo, Bunkyo-ku, Tokyo 113

(Received November 5, 1974)

The coordination of phosphine derivatives and some other bases to the cobalt mesoporphyrin IX dimethyl ester in toluene has been spectrophotometrically investigated. The coordination equilibrium constants were determined for each base, and found to be of this sequence (25 °C) : $P(C_4H_9)_3 \gg P(OCH_3)_3 > P(C_6H_5)_3 > S(CH_3)_2 > As(C_6H_5)_3$. The reversible oxygenation of the penta-coordinate complexes formed as above was investigated at lower temperatures (−20——80 °C): the corresponding equilibrium constants were found to be in the following sequence (−80 °C): $P(C_4H_9)_3 > P(OCH_3)_3 > S(CH_3)_2 > P(C_6H_5)_3 > As(C_6H_5)_3$. These relations were discussed in terms of the σ-donating ability of a ligand coordinated *trans* to oxygen.

The reversible oxygenation of cobalt porphyrin has been the subject of considerable interest in recent years. EPR spectral evidence for the reversible oxygen uptake by the penta-coordinate cobalt porphyrins in a frozen organic solution at the temperature of liquid nitrogen has already been presented.[1,2] The success in the replacement of iron by cobalt in hemoglobin and myoglobin[3] particularly stimulated investigations of the amine-ligation and oxygen-binding properties of cobalt porphyrins.[4-6]

In the present work we investigated the effects of such axial ligand as $P(C_6H_5)_3$, $P(C_4H_9)_3$, $P(OCH_3)_3$, $As(C_6H_5)_3$, and $S(CH_3)_2$ on the reversible oxygenation of cobalt porphyrins. Among these bases, phosphine, phosphite, and arsine derivatives are usually considered to have not only σ-donor but also π-acceptor properties. Particularly, triphenylphosphine, a good π-acceptor, is very frequently used in the field of organometallic chemistry to stabilize the low-valent state of metal complexes. It would be interesting, therefore, to compare the effects of the ligation of phosphine derivatives on the oxygenation of cobalt porphyrins with those of the amine ligation.

In this report, we will present thermodynamic data on the ligation and oxygenation of the cobalt mesoporphyrin IX dimethyl ester in toluene solutions. The bonding properties of phosphine derivatives as well as the effect of the bases coordinated *trans* to oxygen on the oxygen-binding ability will be discussed in comparison with those of unsaturated amines.

During the course of the present work, Wayland *et al.*[7-9] reported EPR studies of tetraphenylporphyrincobalt(II) coordinated with PR_3 or $(POR)_3$, and their dioxygen complexes. The results of the EPR measurements of our cobalt porphyrin system completely agreed with those reported by these authors. Therefore, the results of our EPR measurements will be omitted.

Experimental

Materials. The mesoporphyrin IX dimethyl ester (Sigma Chemical Co.) was used without further purification. The Co(II) mesoporphyrin IX dimethyl ester (CoP) was prepared according to the established method.[10] Reagent-grade toluene was purified by the usual method and used as the solvent. The trimethylphosphite and dimethylsulfide were also distilled *in vacuo* prior to use. All the other chemicals were of a reagent grade and were used without special pretreatment.

Measurements. The coordination equilibria of CoP were measured by means of a spectrophotometric titration procedure (Hitachi spectrophotometer EPS-3T). Aliquots of a ligand solution (1—10^{-3} M in toluene) were added to 3.6 ml of a toluene solution of CoP (*ca.* 5×10^{-6} M) from a calibrated micro syringe (Terumo MS 10). The absorption spectra in the range from 350 to 400 nm were recorded after each addition of the ligand solution. The equilibrium constants of coordination (K) were derived from the changes in the absorbance at 394 nm. The constants were found to be independent of the wavelengths. Dilution corrections were kept small, and good isosbestic points were obtained. The cell temperature was controlled to ±0.2 °C in the 10—30 °C range by the use of Haake's thermostat, type "F." The temperature was measured by means of an inserted copper-constantan thermocouple.

The oxygenations were carried out in an optical cell mounted in a Pyrex Dewar. For a typical measurement, a 4-ml portion of a toluene solution containing CoP (10^{-5}—10^{-6} M) and a ligand (10^{-1}—10^{-4} M) was placed in the cell and nitrogen gas was bubbled in from a cylinder. The oxygenation temperature (−20——80 °C) was controlled by introducing cold nitrogen gas purged from the liquid-nitrogen container into the Pyrex Dewar mounted in the sample compartment of the spectrophotometer; it was kept constant within ±0.5 °C. The temperature was measured by the thermocouple attached to the outside of the sample cell.

Oxygen and nitrogen from cylinders were mixed by means of a mixing apparatus equipped with two calibrated flowmeters, and a mixture of a given composition was introduced into the solution of penta-coordinate CoP complexes. Complete spectra from 340 to 500 nm were recorded after each equilibration.

Determination of the Equilibrium Constant. The equilibrium constant, K, of the ligation of CoP, as expressed by:

$$\mathrm{CoP} + \mathrm{L} \overset{K}{\rightleftharpoons} \mathrm{CoPL} \qquad (1)$$

was determined graphically by spectrophotometric titration without direct measurements of the extinction coefficients of the complexes, using the Ketelaar method,[11] as is shown below:

$$\frac{1}{A_0 - A} = \frac{1}{K(\varepsilon_{\mathrm{CoP}} - \varepsilon_{\mathrm{CoPL}})[\mathrm{CoP}]_t[\mathrm{L}]_t} + \frac{1}{(\varepsilon_{\mathrm{CoP}} - \varepsilon_{\mathrm{CoPL}})[\mathrm{CoP}]_t} \qquad (2)$$

where

A_0: absorbance of the starting solution ([L]=0)

A: absorbance of the solution containing ligand ($[L]_t$)
ε_{CoP}, ε_{CoPL}: molar extinction coefficients of CoP, CoPL
$[CoP]_t$: molar concentration of the total CoP($[CoP]_t = [CoP] + [CoPL]$)
$[L]_t$: molar concentration of the total ligand ($[L]_t = [L] + [CoPL]$)

By plotting $1/(A_0 - A)$ against $1/[L]_t$, a straight line should be obtained. From the intercept and the slope of the straight line, K can be derived. In the concentration range of the ligand studied, hexa-coordinate complexes, $CoPL_2$, were not formed, which is in accordance with the results of EPR studies.[7]

The equilibrium constant, K_{O_2}, of the reversible oxygenation of the penta-coordinate CoP expressed by:

$$CoPL + O_2 \overset{K_{O_2}}{\rightleftharpoons} CoPL \cdot O_2 \qquad (3)$$

can be derived similarly to K from the plot of $1/(A_0 - A)$ against $1/P_{O_2}$:

$$\frac{1}{A_0 - A} = \frac{1}{K_{O_2}(\varepsilon_{CoPL} - \varepsilon_{CoPL \cdot O_2})[CoPL]_t} \frac{1}{P_{O_2}} + \frac{1}{(\varepsilon_{CoPL} - \varepsilon_{CoPL \cdot O_2})[CoPL]_t} \qquad (4)$$

The oxygenation equilibria were measured at appropriate intervals between −25 and −80 °C. When K_{O_2} was small (L=$P(C_6H_5)_3$ and $As(C_6H_5)_3$), oxygenation was investigated only near −80 °C.

Results

Ligand Binding. Figure 1 shows typical ligand-titration spectra obtained when $P(C_4H_9)_3$ was added, step by step, to a CoP solution at 11.8 °C. It is apparent from the figure that the absorbance in the Soret region (~397 nm) gradually decreases with the increase in the concentration of $P(C_4H_9)_3$ and that the spectral change is well characterized by isosbestic points. The addition of the other ligands to the CoP solution was found to cause similar changes in the Soret region. No appreciable shift was observed in the Soret band, however.

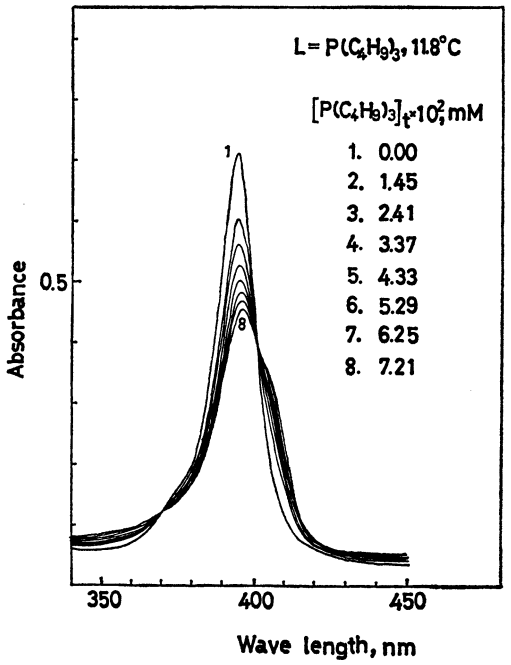

Fig. 1. The spectrophotometric titration spectrum for the determination of K at 11.8 °C for L=$P(C_4H_9)_3$. Spectrum 1 is that of 5.5×10^{-6} M Co mesoporphyrin IX dimethyl ester and 2−8 are at concentration of tri-*n*-butylphosphine added: 1.45, 2.41, 3.37, 4.33, 5.29, 6.25 and 7.21×10^{-5} M, respectively.

Figure 2 shows the plots of $1/(A_0 - A)$ (394 nm) against $1/[L]_t$ at 11.8, 15.3, and 20.5 °C respectively. Straight lines were obtained in the plots, indicating that Eq. (2) is valid. Ligand titrations were further performed with $P(OCH_3)_3$, $P(C_6H_5)_3$, $S(CH_3)_2$, and $As(C_6H_5)_3$; all were found to give rise to a similar relation. The equilibrium constant, K, of the reaction (1) was then calculated for each ligand at various temperatures. The results are summarized in Fig. 3 as well as in the third column of Table 1, where the

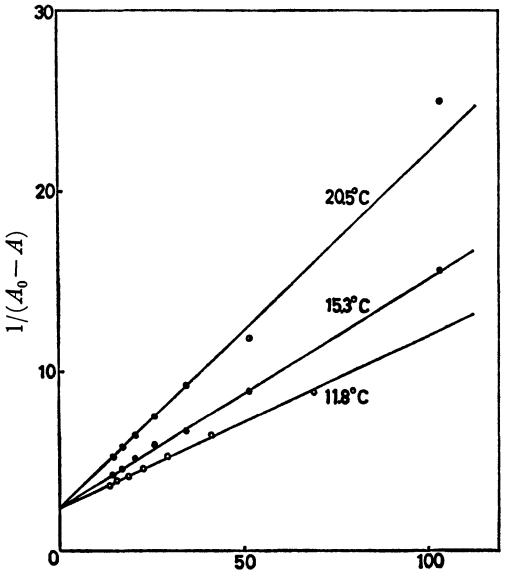

Fig. 2. $1/(A_0 - A)$ as a function of the reciprocal tri-*n*-butylphosphine molar concentration added, $1/[P(C_4H_9)_3]_t$ for three temperatures.
○ 11.8 °C, ● 15.3 °C, ◑ 20.5 °C

Table 1. Thermodynamic data for equilibrium,

$$CoP + L \overset{K}{\rightleftharpoons} CoP \cdot L$$

L	Temp., °C	K, M^{-1}	ΔG, kcal/mol	ΔH, kcal/mol	ΔS, e.u.
$P(C_6H_5)_3$	9.3	62.3	−2.3		
	16.0	41.8	−2.1	−7.0	−17
	26.0	30.4	−2.0		
$P(C_4H_9)_3$	11.8	24.2×10^3	−5.7		
	15.3	18.6×10^3	−5.6	−13.3	−27
	20.5	12.1×10^3	−5.5		
$P(OCH_3)_3$	16.9	63.1	−2.4		
	19.6	58.9	−2.4	−6.9	−15
	25.4	45.1	−2.3		
$S(CH_2)_2$	11.0	33.8	−2.0		
	21.5	24.9	−1.9	−4.5	− 9
	26.0	22.5	−1.9		
$As(C_6H_5)_3$	15.3	4.7	−0.9		
	20.6	4.6	−0.9	−5.2	−15
	24.9	3.5	−0.7		

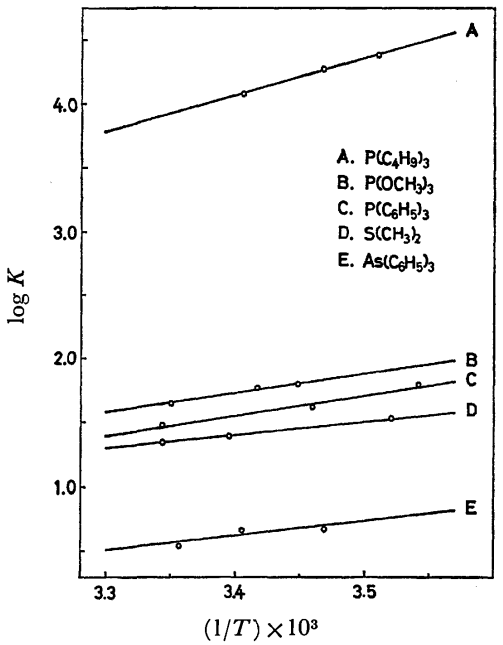

Fig. 3. The van't Hoff plots of K for L=$P(C_4H_9)_3$ (A), $P(OCH_3)_3$ (B), $P(C_6H_5)_3$ (C), $S(CH_3)_2$ (D) and $As(C_6H_5)_3$ (E).

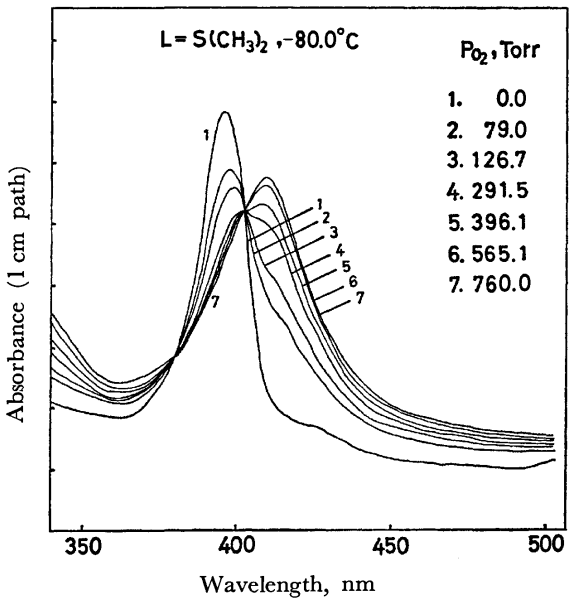

Fig. 4. The spectrophotometric titration for the determination of K_{O_2} at −80.0 °C for L=$S(CH_3)_2$. Spectrum 1 is that of 1 : 1 complex between cobalt mesoporphyron IX dimethyl ester and dimethylsulfide and 2—7 are at partial pressure of oxygen: 79.0, 126.7, 291.5, 396.1, 565.1 and 760.0 Torr, respectively.

corresponding thermodynamic quantities are also presented in the last three columns.

In the range of 9—26 °C, the coordination capability of the ligands was qualitatively given by:

$$P(C_4H_9)_3 \gg P(OCH_3)_3 > P(C_6H_5)_3 > S(CH_3)_2 > As(C_6H_5)_3$$

Oxygen Binding. Figure 4 shows the spectral changes in CoPL under various oxygen partial pressures from 0 to 760 Torr at −80 °C (L=$S(CH_3)_2$). The CoP

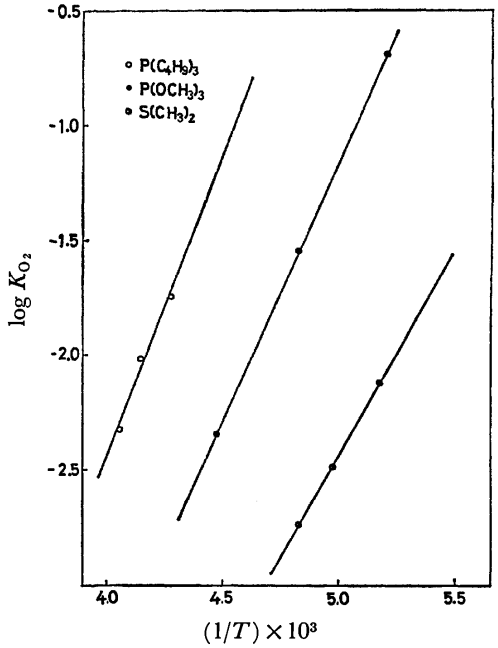

Fig. 5. The van't Hoff plots of K_{O_2} for L=$P(C_4H_9)_3$ (○), $P(OCH_3)_3$ (●) and $S(CH_3)_2$ (◑).

TABLE 2. THERMODYNAMIC DATA FOR REACTION,

$$CoP\cdot L + O_2 \overset{K_{O_2}}{\rightleftharpoons} CoP\cdot L\cdot O_2$$

L	Temp., °C	K_{O_2}, $Torr^{-1}$	ΔH, kcal/mol	$\Delta S^{a)}$, eu
$P(C_6H_5)_3$	−82.0	$(3.8\pm0.1)\times10^{-3}$	—	—
$P(C_4H_9)_3$	−26.5	$(4.7\pm0.5)\times10^{-3}$	−11.8	−59
	−32.0	$(9.6\pm0.6)\times10^{-3}$		
	−39.5	$(18.0\pm2.0)\times10^{-3}$		
$P(OCH_3)_3$	−49.5	$(4.5\pm1.1)\times10^{-3}$	−10.3	−57
	−66.0	$(28.4\pm1.5)\times10^{-3}$		
	−81.0	$(203.4\pm20.0)\times10^{-3}$		
$S(CH_3)_2$	−66.0	$(1.8\pm0.8)\times10^{-3}$	−8.1	−52
	−72.0	$(3.3\pm0.2)\times10^{-3}$		
	−80.0	$(7.6\pm0.4)\times10^{-3}$		
$As(C_6H_5)_3$	−79.0	$(1.5\pm0.2)\times10^{-3}$	—	—

a) Standard State of 1 Torr O_2.

coordinated with the other ligands gave spectral changes similar to those in the case of $S(CH_3)_2$; the absorption peak of the penta-coordinate complex (deoxy form) decreased, step by step, upon oxygenation, while another absorption peak originating from the oxygenated form appeared in the longer-wavelength region. The spectral change was reversible with respect to the ambient oxygen pressure; the original spectrum was restored when nitrogen gas was bubbled into the CoPL solution.

Among the ligands studied, the oxygenation reached a saturation under 760 Torr at −80 °C with $P(C_4H_9)_3$ or $P(OCH_3)_3$ while only a partial oxygenation was observed with $P(C_6H_5)_3$, $S(CH_3)_2$, or $As(C_6H_5)_3$, even at −80 °C. Figure 5 shows the van't Hoff plots of K_{O_2}. The K_{O_2} values as well as the related thermodynamic parameters are presented in Table 2.

In the temperature range studied (−20 °C——80 °C), the K_{O_2} values for CoPL decreased in the following

order of ligands coordinated *trans* to oxygen:

$P(C_4H_9)_3 > P(OCH_3)_3 > S(CH_3)_2 > P(C_6H_5)_3 > As(C_6H_5)_3$

This order was parallel with that of the ligation capability of L except $S(CH_3)_2$ and $P(C_6H_5)_3$ were reversed. Despite the large difference in the value of K for $P(C_4H_9)_3$ ($\log K = 4.08$ at 20 °C) and $P(OCH_3)_3$ ($\log K = 1.77$ at 20 °C), the K_{O_2} values for $P(C_4H_9)_3$ ($\log K_{O_2} = -1.2$ at −50 °C) and $P(OCH_3)_3$ ($\log K_{O_2} = -2.3$ at −50 °C) were not very different from one another, suggesting that K and K_{O_2} are not determined by common factors alone.

Discussion

Ligand Binding: The importance of σ-bonding properties between ligand and metal ion has previously been recognized. Recently, it has been suggested that the π-bonding properties are also important for unsaturated amines to form a cobalt-oxygen adduct.[5,6] The importance of π-bonding properties has been well accepted for the derivatives of phosphine, leading to the stabilization of low-valent organometallic complexes.[12] Here, we shall comparatively discuss the bonding properties of unsaturated amines, phosphorous, and arsenic bases on the basis of their ligation equilibria to CoP.

We first presume that the pK_a of the conjugate acid is a measure of the σ-donor property of a base. Unfortunately, the pK_a of phosphorous and arsenic bases is little known. From the literature[13] we adopt 8.43 and 2.73 respectively as the pK_a values of $P(C_4H_9)_3$ and $P(C_6H_5)_3$. The pK_a of $P(OCH_3)_3$ was estimated to be about 3.5. The estimation was carried out on the basis of the linear relationship observed between the half-neutralization potential and pK_a for a series of tertiary phosphorous bases.[13,14] The pK_a of $As(C_6H_5)_3$ must be very low. We presumed it to be 0.0 ± 0.5 on the basis of the results of a potentiometric titration of periodic-group V_a triaryls.[15]

The log K values given in Table 1 were then plotted against the pK_a estimated as above for each base in Fig. 6a, together with the corresponding plots for unsaturated amines due to Stynes *et al.*[6] As is shown in Fig. 6a, unsaturated amines were found to stabilize their complexes more strongly than phosphorous and arsenic bases at the same pK_a, while fairly good straight lines were obtained between log K and pK_a for the two base groups. Especially, it should be noticed that the slope of the straight line ($\partial \log K / \partial pK_a$) was greater for the phosphorous and arsenic bases (0.4) than for the amines (0.1). The greater dependence of log K on pK_a must mean that the σ-donor properties of the ligand predominantly control the stability of the complex.

The ligand binding to CoP may generally be associated not only with the donation of electrons from the ligand to the cobalt atom (σ-bonding), but also with the interaction of the d-orbitals of cobalt with the π^* and/or π-orbitals of the ligand (π-bonding). Thus, it follows from Fig. 6a that unsaturated amines participate in their binding to CoP *via* the π-interacting properties more significantly than do the phosphorous and arsenic bases.

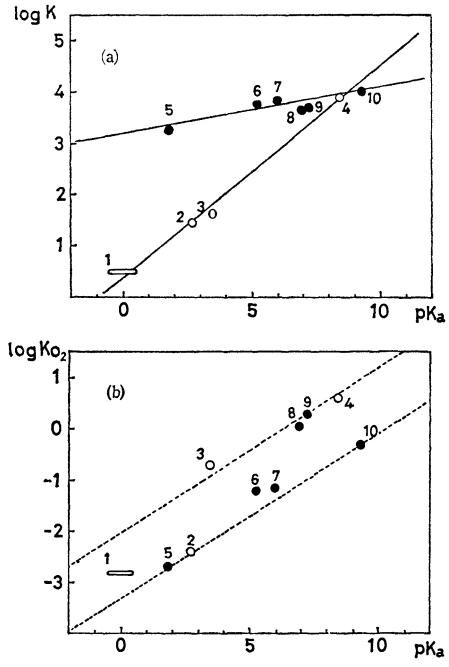

Fig. 6. The plots of pK_a of ligands against log K(a) or log K_{O_2}(b).
Open circles: $As(C_6H_5)_3$(1), $P(C_6H_5)_3$(2), $P(OCH_3)_3$ (3), $P(C_4H_9)_3$(4) Solid circles: 4-CN-pyridine(5), pyridine(6), 4-*t*-Bu-pyridine(7), imidazole(8), 1-Me-imidazole(9), 4-NH_2-pyridine(10).

Contrary to expectation, the π-bonding properties of phosphorous and arsenic bases appeared to be weaker than those of unsaturated amines. It seems that this can be explained by such factors as the contraction of the orbitals of the cobalt ion (divalent and low spin) and the expansion of the orbitals of the phosphorous atom as compared with those of the nitrogen atom. This explanation is not inconsistent with the thermodynamic observations that the binding of unsaturated amines to CoP is accompanied by larger heats and smaller entropy changes when compared with those of the phosphorous and arsenic bases.

Oxygen Binding. In the same way as in the case of ligand binding to CoP, the log K_{O_2} values were plotted against the pK_a of the ligands. The results are shown in Fig. 6b. It is apparent from Fig. 6b that the oxygen-binding properties of the complexes are promoted by larger pK_a values of the ligands, just as in the case of ligand binding, although the linear relation is only approximate. Nevertheless, it is interesting to note that the slope of the straight line for phosphorous and arsenic bases was roughly identical with that for pyridine bases, in contrast with the case for the ligand binding. In other words, the oxygen-binding properties of CoPL, in which L is the amine, seem to depend more strongly on the pK_a of L than does their ligation to CoP, suggesting that the σ-donating properties of L are important for the oxygen binding.

According to the molecular orbital model proposed by Wayland *et al.*,[8] the cobalt-oxygen binding is

considered to be principally a covalent bonding of the singly occupied cobalt(II), d_{z^2}, and the signly occupied oxygen σ-orbital that results from the splitting the π^* degeneracy: also, a ligand molecule, L, elevates in proportion to the donating ability of L, the d_{z^2} cobalt and stabilizes the cobalt-oxygen bond. The low π^*-orbital energy of oxygen will tend to localize the covalent σ pair on oxygen, causing a decline in the cobalt-oxygen $d\pi$—$p\pi$ bonding. In consequence, the π-bonding properties of L are considered to contribute to only a little to the cobalt-oxygen bonding.

The poor relationship between $\log K_{O_2}$ and pK_a may indicate that the ligands coordinated *trans* to oxygen also control oxygen-binding not only by σ-donating ability but also with other factors such as π-donating ability and/or the degree of polarization induced upon oxygenation.

We wish to thank Dr. A. Kuboyama, National Chemical Laboratory for Industry, Tokyo for our use of Haake's thermostat, type "F".

References

1) K. Yamamoto and T. Kwan, *J. Catal.*, **18**, 354 (1970).
2) F. A. Walker, *J. Amer. Chem. Soc.*, **92**, 4235 (1970).
3) B. M. Hoffman and D. H. Petering, *Proc. Nat. Acad. Sci.*, **67**, 637 (1970).
4) H. C. Stynes and J. A. Ibers, *J. Amer. Chem. Soc.*, **94**, 1559 (1972).
5) F. A. Walker, *ibid.*, **95**, 1154 (1973).
6) D. V. Stynes, H. C. Stynes, B. R. James, and J. A. Ibers, *ibid.*, **95**, 1796 (1973).
7) B. B. Wayland and M. E. Abd-Elmageed, *Chem. Commun.*, **1974**, 61.
8) B. B. Wayland, J. V. Minkiewicz, and M. E. Abd-Elmageed, *J. Amer. Chem. Soc.*, **96**, 2795 (1974).
9) B. B. Wayland and M. E. Abd-Elmageed, *ibid.*, **96**, 4809 (1974).
10) J. E. Falk, "Prophyrins and Metalloporphyrine," Elsevier, New York, N.Y. (1964), p. 139.
11) J. A. A. Ketelaar, C. van de Stlope, A. Goudsmit, and W. Dzcubas, *Rec. Trav. Chim.*, **71**, 1104 (1952).
12) J. F. Nixon, *Adv. Inorg. Radiochem.*, **13**, 363 (1970).
13) C. A. Streuli, *Anal. Chem.*, **32**, 985 (1960).
14) E. M. Thorsteinson and F. Basolo, *J. Amer. Chem. Soc.*, **88**, 3929 (1966), Ref. 16.
15) O. W. Kolling and E. A. Mawdsley, *Inorg. Chem.*, **9**, 408 (1970).

Photoconductivity of Vinyl Polymers with Large Pendant π-Electron Systems. I. Poly-9-vinylacridine

Saburo MORIWAKI,* Ken-ichi OKAMOTO,** Shigekazu KUSABAYASHI, and Hiroshi MIKAWA

Department of Applied Chemistry, Faculty of Engineering, Osaka University, Yamadakami, Suita, Osaka 565

***Department of Chemical Engineering, Faculty of Engineering, Yamaguchi University, Ube, Yamaguchi 755*

(Received November 25, 1974)

The dark- and photo-conductivities of poly-9-vinylacridine (PVAcr) were investigated in comparison with those of poly-*N*-vinylcarbazole (PVCz). The dark current was ohmic over the whole voltage region studied up to 150000 V/cm. The photocurrent showed a linear dependence on the applied voltage even in fairly high applied fields up to 130000 V/cm and a spectral dependence corresponding antibatically to the absorption spectrum. The magnitude of the photocurrent with positive electrode illumination (i_{ph}^{+}) was only 1.5—2 times larger than that with negative electrode illumination (i_{ph}^{-}), the behavior differing entirely from that in a PVCz film. The magnitude of the photocurrent of PVAcr was smaller than that of PVCz by several times for i_{ph}^{-} and by a hundred times for i_{ph}^{+}. The poor photoconductivity of PVAcr was attributed both to the high concentration of the excimer-forming site acting as an effective exciton trap and to the poor electron-donating character.

The electrical conductivity of vinylpolymers with pendant π-electron systems has been extensively investigated.[1–10] Most investigations have been done with poly-*N*-vinylcarbazole (PVCz), being used as the material for electrophotography. The large photoconductivity of PVCz is attributed both to the good efficiency of the carrier generation through the field-assisted thermal dissociation of an exciplex formed between an excited carbazolyl group and some electron-accepting impurity, and to the ease of the carrier migration through the overlap of π-orbitals of neighboring carbazolyl groups in one polymer chain.[10] In other words, it is due to the presence of the short-range electronic interaction (such as the electron exchange interaction) between neighboring carbazolyl groups in one polymer chain, which are bulky and have a fairly low ionization potential. This has been confirmed by the fact that the photoconductivity of PVCz is much superior to that of poly-*N*-carbazolylethylvinylether where carbazolyl groups are connected far apart from the skeletal chain and the short-range electronic interaction between neighboring carbazolyl groups is very weak.[11]

On the basis of investigation on both the UV spectra of a series of the vinylpolymers[12] and their NMR spectra,[13] it has been found that the vinylpolymers with large pendant π-electron systems such as poly-9-vinylacridine (PVAcr) and poly-1-vinylpyrene have also some electronic interactions between neighboring pendant chromophores in one polymer chain even in solution in a manner similar to the case of PVCz. It is, therefore, very important to investigate the photoconductivity of these polymers in comparison with that of PVCz in order to obtain information on the factors determining the photoconductivity of the vinylpolymers. This paper deals with the steady-state photoconductivity of PVAcr in a sandwich-type cell.

Experimental

PVAcr was prepared by anionic polymerization of the monomer with Na-naphthalene complex at room temperature,[14] and reprecipitated three times from chloroform (containing 1% ethanol) solution with *n*-hexane. The average molecular weight of the polymer thus prepared was determined to be 20000 with use of a membrane osmometer.

Thin films (15 or 9 μm thick) of the polymer undoped and doped with 0.5 mol% of *p*-chloranil (CA) were made on nesa-coated quartz plates from the chloroform solution. Semitransparent gold main and guard electrodes were evaporated on the film to prepare a sandwich-type cell. The cell was used for the electrical conductivity measurements without exposure to the air after the evaporation of the metal electrodes. Measurements were carried out by the DC method in a vacuum (10^{-7}—10^{-8} Torr) or in the air. A 500 W xenon lamp monochromatized by a grating monochromator was used as a light source.[10]

Results and Discussion

Dark Conductivity. PVAcr showed an ohmic dark current (specific conductivity at 60 °C, $\sigma_{60}=3\times10^{-19}\,\Omega^{-1}\,cm^{-1}$ in a high vacuum) over the whole voltage region up to 150000 V/cm. The activation energy of the dark current was 1.0 eV. The behavior differs from that in PVCz films which show a nonohmic dark current attributable to either Poole-Frenkel[2] or Richardson-Schottkey effects.[1] With doping of CA, the dark current increased by several times but the activation energy hardly varied at all.

Photoconductivity. The photocurrent showed two types of response curves (Fig. 1). Illumination with the weakly-absorbed light ($\lambda>400$ nm) induced a photocurrent of Type A, while the illumination with the strongly-absorbed light ($\lambda\leq400$ nm) induced that of Type B. The photoresponse curve of Type B seems to be attributable to the effect of space charges built up by the illumination with the strongly-absorbed light.[15] The results were obtained for the steady-state value of the photocurrent.

The voltage dependence of the photocurrent is shown in Fig. 2. The photocurrents in the films, undoped and doped with CA, were proportional to the applied voltage in the fields lower than 70000 V/cm. The superlinear dependence of photocurrent on the applied voltage, regarded as an important character of the photoconductivity of PVCz,[10] was exceptionally observed for the photocurrent induced with the light

* Present address: Yokkaichi Division, Mitsubishi Petrochemical Co., Ltd., Toho-cho 1, Yokkaichi, Mie 510.

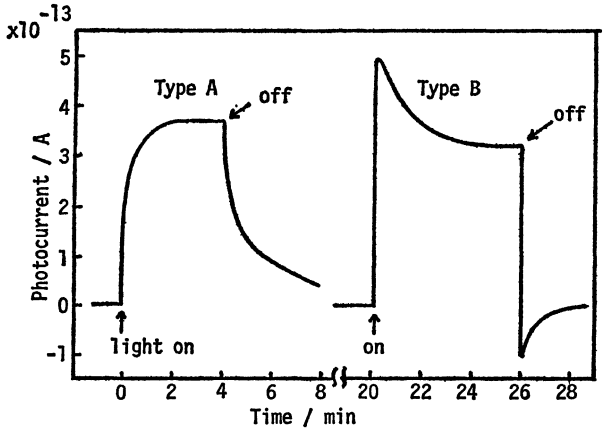

Fig. 1. Representative photoresponse curves in a PVAcr sandwich-type cell.

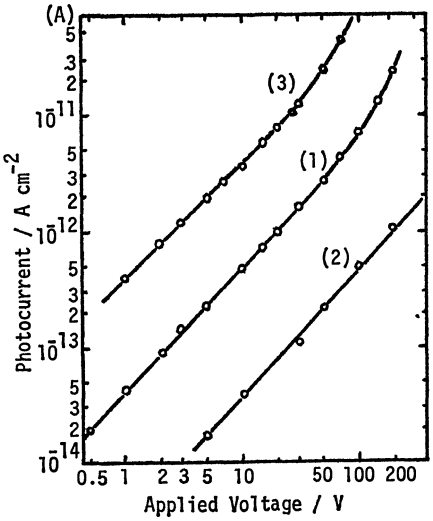

Fig. 2. Voltage dependence of photocurrent with positive electrode illumination in a PVAcr sandwich-type cell in a high vacuum.
(1) an undoped film, 15 μm thick, 410 nm.
(2) an undoped film, 15 μm thick, 350 nm.
(3) a film doped with 0.5 mol% of CA, 9 μm thick, 410 nm.

of 410 nm in fields higher than 70000 V/cm. The voltage at which the superlinearity appeared was larger for PVAcr than for PVCz by 10 times.

The photocurrent was always proportional to the light intensity (10^{12}—10^{14} photon/cm^2 s) regardless of doping of CA.

Plots of logarithm of the photocurrent *vs.* $1/T$ gave a straight line over the whole temperature range (20—130 °C). The activation energy of the photocurrent was 0.18±0.03 eV at 360—410 nm under 35000V/cm and varied little with doping of CA. The value is nearly equal to that for PVCz.

The spectral dependence of the photocurrent is shown in Fig. 3. It was obtained by normalizing the observed photocurrent values to a constant light intensity, 2×10^{13} photon/cm^2 s. It was not affected by the polarity of the illuminated electrode, applied voltage, ambient oxygen and doping of CA. The photocurrent peaks appeared at 410 and 290 nm

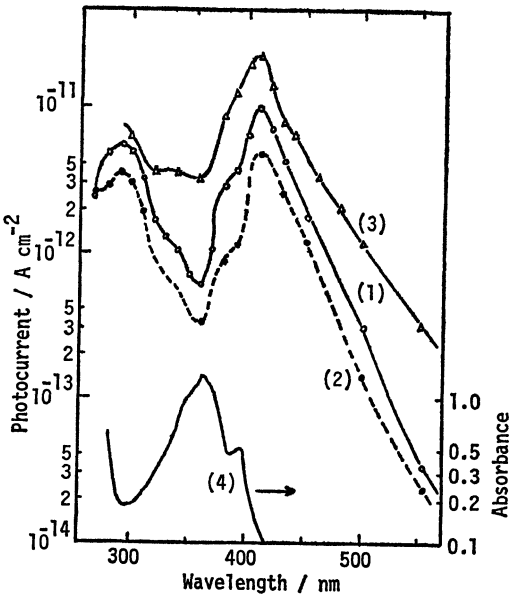

Fig. 3. Spectral dependence of photocurrent with positive electrode illumination in a PVAcr sandwich-type cell under an applied field of 33000 V/cm at a light intensity of 2×10^{13} photon/cm^2 s.
(1) an undoped film, 15 μm thick, in a high vacuum.
(2) an undoped film, 15 μm thick, in the air.
(3) a film doped with 0.5 mol% of CA, 9 μm thick, in a high vacuum.
(4) absorption spectrum of an undoped film (0.5 μm thick).

corresponding to the wavelength of the absorption edge of the ^1L_a band and the absorption minimum between the ^1L_a and ^1B_a bands, respectively. The photocurrent minimum appeared at 360 nm corresponding to the wavelength of the absorption maximum of the ^1L_a band. The spectral dependence, thus, corresponded antibatically to the absorption spectrum.

In general, for a film thick enough to absorb the light almost completely, the type of spectral dependence mentioned above appears when the carrier generation in the bulk is predominant, while the other type of spectral dependence of the photocurrent corresponding symbatically to the absorption spectrum appears when the surface carrier generation is predominant. In a PVAcr film, the latter type was not observed even under 70000 V/cm, and the photocurrent with positive electrode illumination (i_{ph}^+) was larger than that with negative electrode illumination (i_{ph}^-) only by 1.5—2 times in magnitude. These results are quite different from those for PVCz; in a PVCz film under an applied field higher than 7000 V/cm, i_{ph}^+ showed the latter type of spectral dependence, being much larger than i_{ph}^- in magnitude (*e.g.*, 20—100 times at 35000 V/cm).[10] From Fig. 4 which shows a comparison of the photocurrents observed for PVAcr and PVCz films under the same experimental condition, we see that the magnitude of the photocurrent of PVCz is larger than that of PVAcr by several times for i_{ph}^- and by a hundred times for i_{ph}^+. Judging from these results and the absence of the superlinearity of the photocurrent on applied voltage in a PVAcr film, the surface carrier generation does not seem to be predominant in

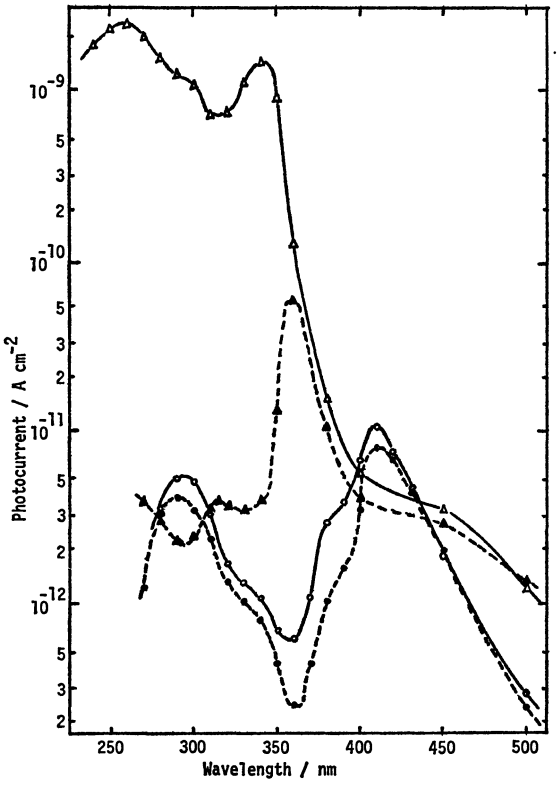

Fig. 4. A comparison of the magnitudes of the photocurrents between PVAcr and PVCz.
The photocurrents were measured in sandwich-type cells (15 μm thick) under an applied field of 33000 V/cm at 2×10^{13} photon/s in a high vacuum of 10^{-7} Torr at 20 °C.
(—○—): PVAcr, positive electrode illumination,
(--●--): PVAcr, negative electrode illumination,
(—△—): PVCz, positive electrode illumination,
(--▲--): PVCz, negative electrode illumination.

a PVAcr film even under a fairly high applied field (130000 V/cm), although it has been considered to be a predominant carrier generation process in a PVCz film.

With doping of CA, the photocurrent increased over the whole wavelength region by 2—3 times with no distinct change in the spectral dependence. No new photocurrent peak was found in the charge-transfer absorption region. This is not surprising, since the charge-transfer absorption band (λ_{max}=535 nm in $CHCl_3$ solution) could hardly be found in the film (9 μm thick) doped with 0.5 mol% of CA. A film doped heavily with CA could not be used for the electrical measurements, since it easily cracked.

Although PVAcr is not considered to be inferior to PVCz as regards the electronic interaction between neighboring pendant groups in one polymer chain on the basis of their UV and NMR spectra,[12] the photoconductivity of PVAcr is greatly inferior to that of PVCz. In a PVCz film, the surface carrier generation through an exciplex formed between a singlet exciton and some electron-accepting impurity has been considered to be predominant even under a fairly low applied field. In a PVAcr film, however, such a surface carrier generation does not seem to be predominant even under a fairly high applied field. This is a reason for the poor photoconductivity of PVAcr.

A singlet exciton migrates efficiently in a polymer film and the migration is strongly affected by the inherent trapping site such as the excimer-forming site.[16] PVAcr shows exclusively excimer fluorescence not only in solid but also in a solution with no monomeric fluorescence.[17] This is probably due to the high concentration of the excimer-forming site. In this case, a singlet exciton is considered to cover only a small number of acridine rings during its life time, because its migration is limited by the excimer-forming site. As one of the most conceivable carrier generation process in an undoped PVAcr film, we can assume the field-assisted thermal dissociation of an exciplex ($(D^{\delta+}\cdots A^{\delta-})^*$) formed between a singlet exciton (D^*) and some electron-accepting impurity (A) to the ion radicals (D^+ and A^-), as is the case with PVCz[10]

$$D^* + A \longrightarrow (D^{\delta+}\cdots A^{\delta-})^* \longrightarrow D^+ + A^- \qquad (1)$$

However, the efficiency of this carrier generation might be poor for a PVAcr film because of the limitation of the exciton migration. The situation is the same as for the other extrinsic carrier generation mechanisms such as the interaction between the electrode and a singlet (or triplet) exciton. The high concentration of the excimer-forming site, therefore, may be the main cause for the poor photoconductivity of PVAcr.

In general, the efficiency of extrinsic or intrinsic photo-carrier generation increases with an increase in the electron-donating character of the aromatic rings. The situation is the same as for the carrier generation due to the dissociation of an exciplex (Eq. 1), because of an increase in the degree of charge-transfer in the exciplex state, $(D^{\delta+}\cdots A^{\delta-})^*$, with the electron-donating character. Another reason for the poor photoconductivity of PVAcr may be the poor electron-donating character of PVAcr; the first ionization potential has been determined to be 7.88 eV for PVAcr and 7.43 eV for PVCz, from the energy of the first charge-transfer absorption in chloroform solution.[18]

From the viewpoint of intensity of the electronic interaction between neighboring pendant chromophores in one polymer chain examined by the UV, CT, and NMR spectra,[12,13,18] the carrier mignation may be assumed to be as easy in a PVAcr film as in a PVCz film. The poor photoconductivity of PVAcr is, therefore, attributable mainly to the poor efficiency of carrier generation, although it remains ambiguous whether the excimer-forming site acts as an effective carrier trapping site.

The discussion mentioned above reconfirmed that the good photoconductivity of PVCz is due to both the comparatively low ionization potential of the carbazolyl groups and the low concentration of the excimer-forming sites in the polymer, in spite of the presence of the short-range electronic interactions between neighboring pendant carbazolyl groups.

References

1) P. J. Reucroft, S. K. Ghosh, and D. Keever, *J. Polym. Sci.*, **A-2**, **10**, 2305 (1972); *Phys. Rev.*, **B 8**, 803 (1973).

2) K. Okamoto, S. Kusabayashi, and H. Mikawa, This Bulletin, **46**, 1953 (1973).
3) J. E. Carnes, and P. J. Warter, Jr., *Phys. Rev.*, **B 5**, 1557 (1972).
4) R. C. Hughes, *J. Chem. Phys.*, **58**, 2212 (1973).
5) C. F. Hackett, *ibid.*, **55**, 3178 (1971).
6) G. Pfister, M. Abkiwitz, and D. J. Williams, *ibid.*, **57**, 2979 (1972).
7) P. J. Melz, *ibid.*, **57**, 1694 (1972).
8) W. D. Gill, *J. Appl. Phys.*, **43**, 5033 (1972).
9) J. Mort, *Phys. Rev.*, **B 5**, 3329 (1972). I. Chen, R. L. Emerald, and J. Mort, *J. Appl. Phys.*, **44**, 3490 (1973).
10) K. Okamoto, S. Kusabayashi, and H. Mikawa, This Bulletin, **46**, 1948, 2324, 2883, 2613 (1973), and references therein.
11) K. Okamoto, A. Itaya, and S. Kusabayashi, *Polym. J.*, in press.
12) K. Okamoto, A. Itaya, and S. Kusabayashi, *Chem. Lett.*, **1974**, 1167.
13) K. Okamoto, S. Kusabayashi, M. Yokoyama, K. Kato, and H. Mikawa, "Electrophotography," ed. by D. R. White, Society of Photographic Scientists and Engineers, Washington (1974), p. 152.
14) S. Moriwaki, S. Kusabayashi, and H. Mikawa, *Chem. Commun.*, **1971**, 607.
15) Analysis of the photocurrent of Type B has been tried successfully for thermally-treated polyacrylonitrile; H. Sasabe, 22nd Symposium on Macromolecules, Nov., 1973 (Tokyo), Preprint I-411.
16) W. Klöpffer, *J. Chem. Phys.*, **50**, 2337 (1969). R. C. Powell, *ibid.*, **55**, 1871 (1971). K. Okamoto, A Yano, S. Kusabayashi, and H. Mikawa, This Bulletin, **47**, 749 (1974).
17) M. Yokoyama, T. Tamamura, T. Nakano, and H. Mikawa, *Chem. Lett.*, **1972**, 499.
18) K. Okamoto, M. Ozeki, A. Itaya, S. Kusabayashi, and H. Mikawa, This Bulletin, **48**, 1362 (1975).

ESR and ENDOR Studies of Hindered Internal Rotation of Higher Alkyl Groups in 4,4′-Dialkylbiphenyl Anion Radicals

Fujito NEMOTO, Fumio SHIMODA, and Kazuhiko ISHIZU

Department of Chemistry, Faculty of Science, Ehime University, Bunkyo-cho, Matsuyama 790

(Received January 13, 1975)

ESR and ENDOR spectra were obtained for the anion radicals of 4,4′-diisopropylbiphenyl, 4,4′-dicyclohexylbiphenyl and 4,4′-dicyclopentylbiphenyl. Both the β- and γ-proton coupling constants of the alkyl groups were precisely determined. The temperature dependence of the β-proton splittings of the alkyl groups were investigated. According to the Heller-McConnell relationship for hyperconjugation, $a_i^\beta=(B_0+B_2\cos^2\theta)\rho_i^\pi$, the positive temperature dependence of the alkyl β-proton splitting was adequately interpreted utilizing a revised model with restricted rotation. The rotational potential barrier and the energy difference of the two equilibrium states obtained were 1.2 and 0.5, 1.2 and 0.6, and 1.2 and 0.6 kcal/mol for the 4,4′-diisopropyl-, 4,4′-dicyclohexyl-, and 4,4′-dicyclopentylbiphenyl anions, respectively. The energy difference of the non-bonding interatomic interaction was calculated in terms of the Lennard-Jones 6—12 potential. Excellent agreement is found between the experimentally-determined value of the potential barrier and that calculated theoretically. ENDOR observations carried out for 4,4′-dicyclohexyl- and 4,4′-dicyclopentylbiphenyl anion radicals in solution demonstrated that γ-protons revealed two different hyperfine coupling constants. These hyperfine coupling constants were assigned to the stereochemically different γ-protons. The ratio of these γ-protons splittings suggest that hyperconjugation plays an important role in producing a spin density of the γ-protons as has been proposed for explanations of the β-proton splittings.

Restricted rotation of the alkyl groups has been extensively studied by ESR for a number of aromatic radicals.

Rotational potentials of the alkyl groups have been proposed from the analysis of the magnitudes of the β-proton coupling constants, and their temperature dependence has often been discussed based on the McConnell-Heller relationship with the aid of Boltzmann statistics.

In this work, ESR and ENDOR techniques were applied to the study of the anion radicals of 4,4′-diisopropylbiphenyl, 4,4′-dicyclopentylbiphenyl, and 4,4′-dicyclohexylbiphenyl.

Analysis of the ESR spectra, which contains complicated hyperfine structure due to the extra γ-proton splitting, was greatly simplified by ENDOR measurement, and the β-proton coupling constants of the alkyl groups and their temperature dependence were accurately determined. The temperature dependence of the β-proton splitting was theoretically investigated based on the revised model of restricted rotation. A new potential function, which has a double minimum, has been proposed,[1] and the energy barriers were calculated in terms of the rotational wave functions expanded in a Fourier series.

The potential barrier height and corresponding energy difference between the two equilibrium states were estimated by comparing the observed temperature dependence with that calculated theoretically.

On the other hand, the energy difference of the non-bonding interaction between the isopropyl group and the neighboring aromatic protons was calculated on the basis of a Lennard-Jones 6—12 potential. The maximum repulsion energy between the isopropyl and the ring protons thus calculated justified the value of the potential barrier determined experimentally.

In addition to the studies of the temperature dependence of the β-proton splittings, the dependence of γ-proton splitting was also investigated using ENDOR. A large difference between the hyperfine splitting of the two γ-protons, which have stereochemically distinct conformations, was clearly detected for the cycloalkyls. The magnitude of the γ-proton splitting is reasonably understandable under the assumption that a direct hyperconjugation is also the dominant mechanism producing the spin density of the γ-protons.

Experimental

The 4,4′-dialkylated biphenyls were prepared from the coupling of *para*-alkyl phenyl magnesium bromide in the presence of anhydrous cobaltous chloride, according to the following process.[2]

0.068 mol of freshly distilled *para*-alkyl bromobenzene was dissolved in about 30 ml of dry tetrahydrofuran (THF) and was added to magnesium chips (0.074 mol) mixed in a like amount of dry THF. To ensure the absence of any unreacted bromo-compound, the Grignard solution was refluxed for 3 hr. After reaction, the solution was dropped into a mixture of 0.05 mol of anhydrous cobaltous chloride and 0.05 mol of ethylbromide in about 30 ml of THF, and the mixture was refluxed for 4 hr. The organic product was extracted with ether. After the removal of the solvent, the residue was recrystallized from ethyl alcohol.

The materials thus obtained were all purified by silica-gel chromatography, using *n*-hexane as the solvent.

The physical constants of the white crystalline solids are listed below.

		λ_{max} nm(ε)
4,4′-diisopropylbiphenyl	mp 64.8 °C	
	UV(Hexane)	256.5 (29400)
4,4′-dicyclohexylbiphenyl	mp 204 °C	
	UV(Hexane)	258 (21300)
4,4′-dicyclopentylbiphenyl	mp 144—146 °C	
	UV(Hexane)	259.5 (22400)

The anion radicals were prepared in a solution of dimethoxyethane (DME) by reduction with potassium and sodium metal. The ESR spectra were measured in the temperature range from +20 °C to −90 °C using a Japan Electron Optics (JEOL) JES-ME-3X type spectrometer equipped with 100 kHz magnetic field modulation.

The ENDOR spectra were measured in the temperature

range from −90 °C to −50 °C using a JEOL ES-EDXI type spectrometer operating with 80 Hz magnetic field modulation.

About 150 W of continuous radio waves, frequency modulated at 6.5 kHz, were present in the cavity for NMR excitation.[3]

The magnetic field was calibrated using a perylene cation radical prepared in concentrated sulfuric acid.

Results

The ENDOR spectra of the 4,4′-diisopropylbiphenyl anion, the reference compound of the cycloalkyl derivatives, are shown in Fig. 1.

By comparison with the ENDOR signal of the biphenyl anion,[17] the signal at 14.50, 17.15 and 17.64 MHz can be assigned to the splitting due to the *meta*-, the alkyl β-, and the *ortho*-protons respectively. In addition, the splittings due to the γ-protons are recorded in the vicinity of the free proton frequency.

With elevation of the temperature, it is observed that the signals of alkyl β-protons designated by the dotted line in the figure show a higher frequency shift, that is, the positive temperature dependence of the alkyl β-protons is thus fairly well demonstrated as is in previous ESR observations.[4] The temperature dependence of the β-proton splitting of the isopropyl has been theoretically treated in terms of the restricted rotation of the alkyl group. The calculation of the β-proton splitting as a function of temperature has already been carried out with the proposed adequate potential function in a previous paper.[1]

The ENDOR spectra of the 4,4′-dicyclopentylbiphenyl anion, shown in Fig. 2, can easily be analyzed with reference to the hyperfine splittings of the 4,4′-diisopropylbiphenyl anion. Of particular interest is the fact that γ-protons of the cyclopentyl give rise to two different hyperfine splittings, although the isopropyl γ-proton produces only one hyperfine splitting. Observation of the two different γ-splittings for the cycloalkyls may be attributed to the fact that methylene groups are tightly locked in the cycloalkyl groups, while the methyl group in isopropyl undergoes free rotation.

Computer calculation of the ESR line intensities based on the hyperfine coupling constants determined by the present ENDOR measurements are in excellent agreement with the observed line intensities as shown in Fig. 3.

The ENDOR spectra of the cyclohexylbiphenyl anions (Fig. 4) are very similar to those of the cyclopentyl anions, where the equatorial and the axial γ-proton splittings are also highly resolved.

In Fig. 5, the slopes of the plots are compared for the cycloalkyls and isopropyls. A slight increase of the slope noted for cycloalkyls suggests that some modifications of the rotational function occur. A detailed analysis of the rotational potential function will be discussed in the following section.

The proton coupling constants of each derivative thus determined are summarized in Table 1.

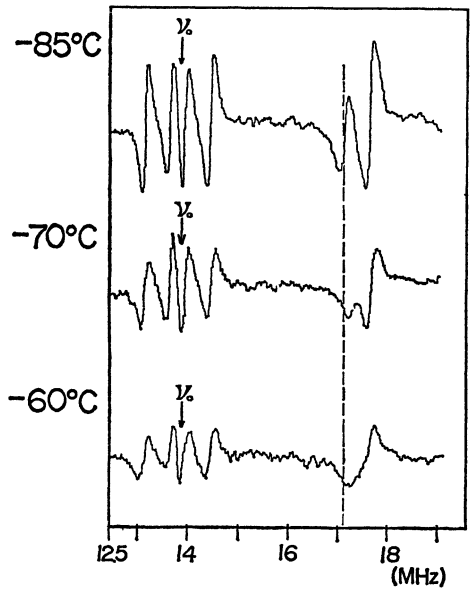

Fig. 1. ENDOR spectra of the system 4,4′-diisopropylbiphenyl-DME-K.

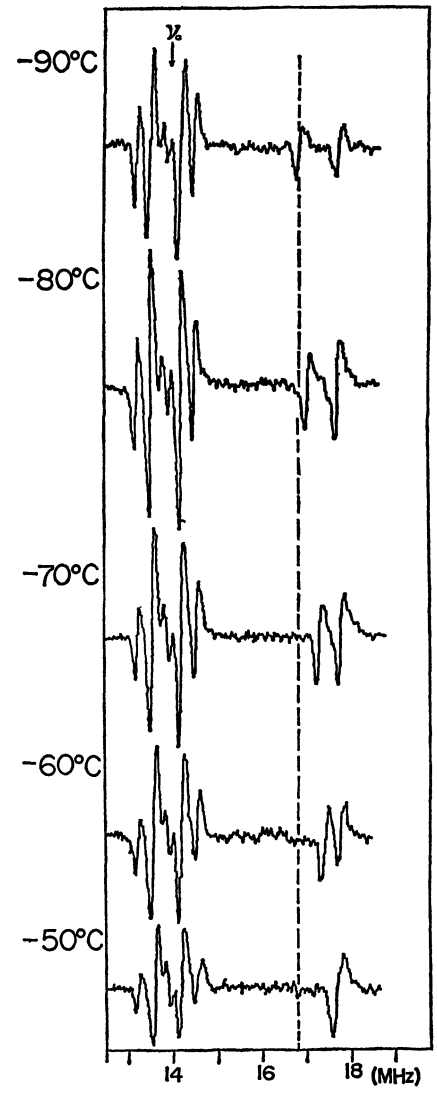

Fig. 2. ENDOR spectra of the system 4,4′-dicyclopenthylbiphenyl-DME-K.

Table 1. Proton coupling constants of the 4,4'-dialkylbiphenyl anion radicals (G)

	a_2^H	a_3^H	a_4^β	$a_4^{\gamma 1}$	$a_4^{\gamma 2}$	$a_4^\beta/a_4^{CH_3}$
p,p'-Bitolyl[4]	2.66	0.51	5.63	—	—	—
4,4'-Diisopropyl	2.70	0.46	2.35	0.10	—	0.417
4,4'-Dicyclohexyl	2.70	0.44	2.21	0.24	0.80	0.393
4,4'-Dicyclopentyl	2.72	0.45	2.20	0.24	0.90	0.391

The observed temperature is −85 °C.

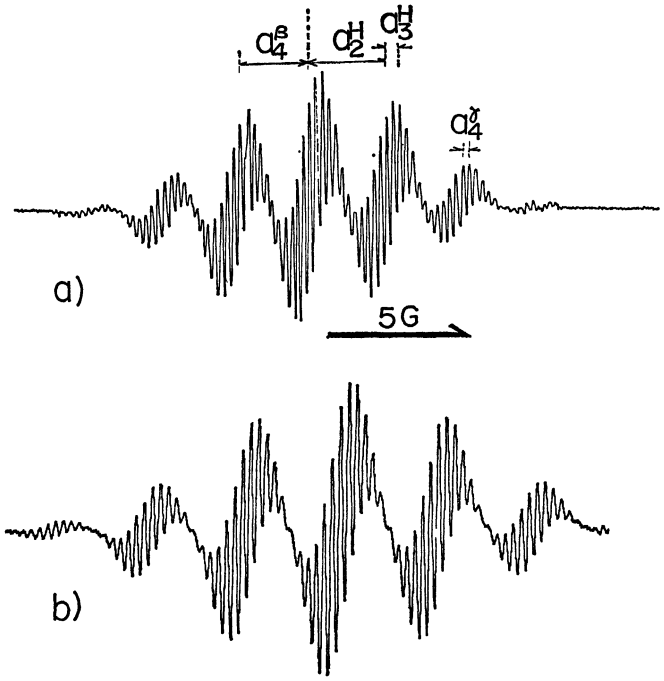

Fig. 3(a). ESR spectrum of the system 4,4'-dicyclopenthylbiphenyl-DME-K at −60 °C. (b). A part of simulated spectrum of (a).

Discussion

Alkyl β-Proton. The magnitude of the β-proton splitting can often be calculated using the following equations:

$$a_4^\beta = \langle Q(\theta)\rangle \rho_4^\pi \tag{1}$$

and

$$Q(\theta) = B_0 + B_2 \cos^2\theta \tag{2}$$

where B_0 and B_2 are empirical parameters, ρ_4^π is the spin density at the *para*-position and θ is the angle between the axis of the $2p_z$ orbital and the aliphatic C–H bond of the alkyl group, both projected on the plane perpendicular to the bond between the methylene carbon of the alkyl and the aromatic carbon.

$\langle Q(\theta)\rangle$ is the quantum mechanical average of $\cos^2\theta$ over the appropriate rotational wave functions $\psi_i(\theta)$. The β-proton splitting as a function of temperature was calculated based on Eqs. (1) and (2), with the aid of Boltzmann statistics.[6]

$$a_4^\beta = B\rho_4^\pi \langle \cos^2\theta\rangle, \qquad \theta = \alpha + \theta_0 \tag{3}$$

$$\langle \cos^2\theta\rangle = \frac{\sum_{i=0}^{\infty} \langle \psi_i(\alpha)\,|\cos^2(\alpha+\theta_0)|\,\psi_i(\alpha)\rangle e^{-E_i/kT}}{\sum_{i=0}^{\infty} e^{-E_i/kT}} \tag{4}$$

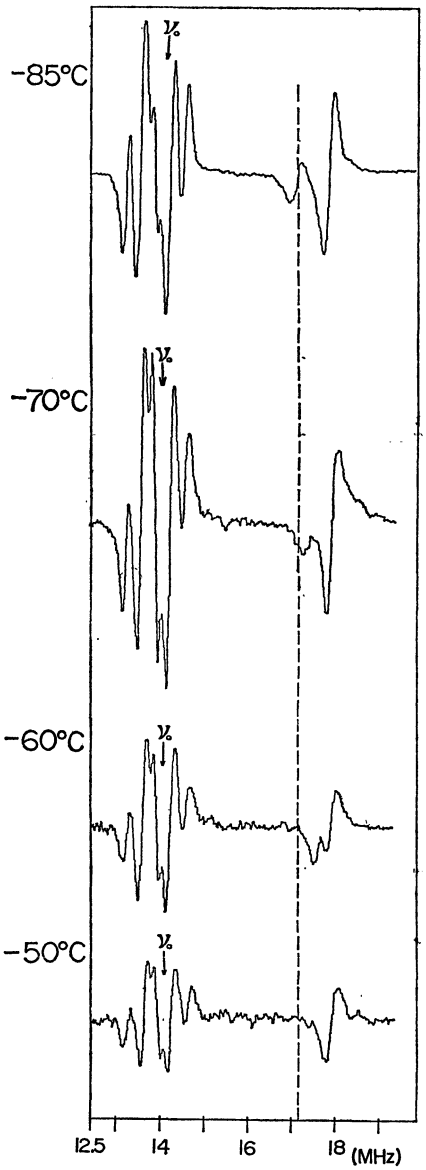

Fig. 4. ENDOR spectra of the system 4,4'-dicyclohexylbiphenyl-DME-K.

The contribution of B_0 was neglected in Eq. (2) and the value of $B\rho_4^\pi$ was estimated from the methyl proton splitting of the 4,4'-dimethylbiphenyl anion radical assuming free rotation of the methyl group, with $B\rho_4^\pi$ being 2×5.6 G.[4,8]

In Eq. (4), the wave function $\psi_i(\alpha)$ and the eigenvalue E_i are obtained by solving the following equation:

$$-\left(\frac{\hbar^2}{2I}\right)\left(\frac{d^2\psi_i}{d\alpha^2}\right) + [V(\alpha) - E_i]\psi_i = 0 \tag{5}$$

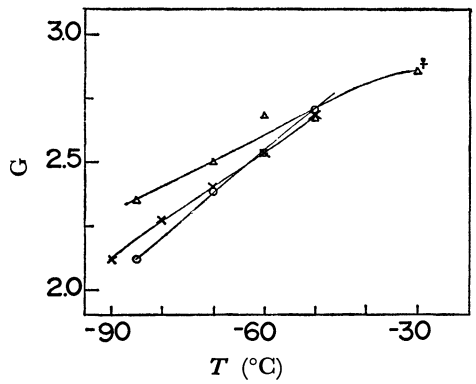

Fig. 5. Temperature dependence of the hyperfine coupling constants for the alkyl β-protons measured by ENDOR.
△; 4,4′-diisopropylbiphenyl, ○; 4,4′-dicyclohexylbiphenyl, ×; 4,4′-dicyclopentylbiphenyl, ♀; ESR data.[4]

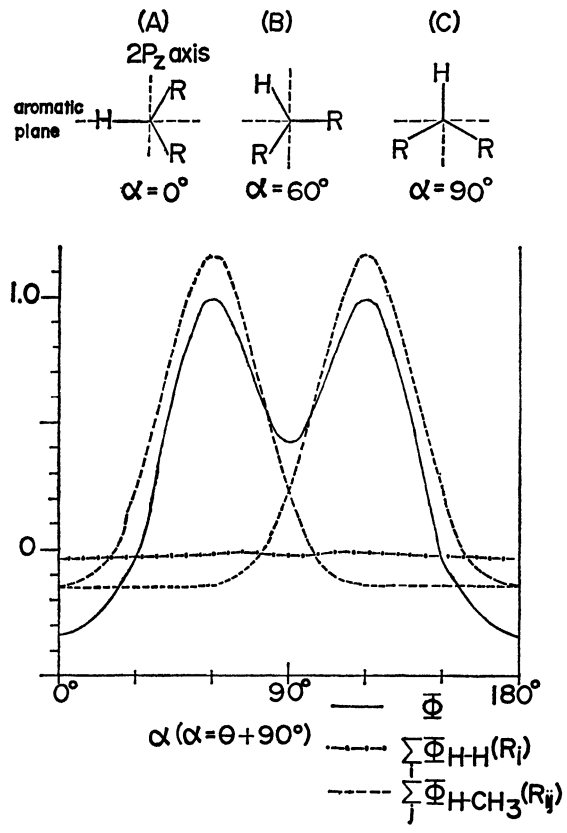

Fig. 6. Conformations of the 4,4′-diisopropylbiphenyl anion and non-bonded interaction energies between the rotating isopropyl and ring *meta* protons as a function of α.

where the moment of inertia I of the molecular fragment ϕ–R can be calculated to be 0.70×10^{-38} g·cm^2 for 4,4′-diisopropylbiphenyl, 1.90×10^{-38} g·cm^2 for 4,4′-dicyclohexylbiphenyl and 1.60×10^{-38} g·cm^2 for 4,4′-dicyclopentylbiphenyl assuming that a prefered rotation of the residual group occurs about the longer axis of the 4,4′-dialkylbiphenyl molecules.

Before solving Eq. (5) numerically, we must know the valid rotational potentials $V(\alpha)$ of the alkyl groups. For 4,4′-diisopropylbiphenyl, restricted rotation of the isopropyl group has already been discussed and the appropriate potential function obtained is illustrated in Fig. 6, as reported in a previous publication.[1] Since the principal steric repulsions occur between the γ-methyl and *meta* C–H groups of the biphenyl ring for 4,4′-diisopropylbiphenyl, and between the γ-methylene and *meta* C–H groups for the 4,4′-dicycloalkylbiphenyls, the rotational potential structures should be essentially the same in both cases. From the above considerations, the rotational potential barrier $V(\alpha)$ of each isopropyl, cyclohexyl and cyclopentyl group was approximated by:

$$V(\alpha) = V_0 \sum_{i=0}^{3} a_i \cos 2i\alpha \tag{6}$$

$$a_0 = \frac{1}{18}\left(\frac{9V_m}{V_0}+4\right),\quad a_1 = \frac{4}{9},\quad a_2 = \frac{2}{9},$$

$$a_3 = \frac{1}{18}\left(8-\frac{9V_m}{V_0}\right)$$

where V_0 and V_m are the potential energy differences between the lowest potential at state [A] and the highest potential at state [B] and that between the lowest potential at state [A] and the medium value at state [C], respectively, as is illustrated in Fig. 6. At the most stable conformation [A], the β-hydrogen of these alkyl groups is in the plane of the aromatic ring and the dihedral angle of the β-proton, θ_0 in Eq. (3), is equal to $\pi/2$. The Hamiltonian matrix $\langle i|\mathscr{H}|j\rangle$ was diagonalized by expanding the wave function in a Fourier series.

$$\psi_i(\alpha) = \sum_{j=0}^{\infty} (C_{ij}\sin j\alpha + D_{ij}\cos j\alpha) \tag{7}$$

We have calculated the temperature dependence of $\langle\cos^2\theta\rangle$ as a function of V_0 and V_m for three 4,4′-dialkylbiphenyls. For example, $\langle\cos^2\theta\rangle$ calculated for 4,4′-diisopropylbiphenyl in the temperature range

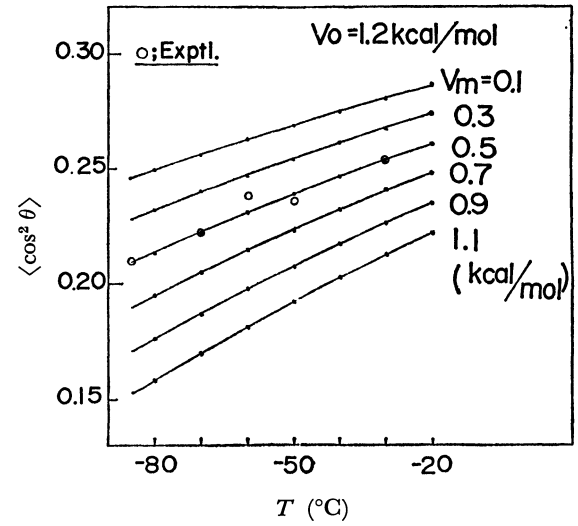

Fig. 7. Theoretical temperature dependence of $\langle\cos^2\theta\rangle$ for rotating isopropyl.
Numerical calculations were carried out taking the energy difference between the two minima, V_m, as the variable parameter, where the maximum barrier of the potential, V_0, was fixed to be 1.2 kcal/mol everywhere.

from −80 °C to −20 °C for various values of V_0 and V_m are shown in Fig. 7.

The best agreement between the calculated and experimental temperature dependences of $\langle\cos^2\theta\rangle$ is obtained with $V_0=1.2$, $V_m=0.5$, $V_0=1.2$, $V_m=0.6$ and $V_0=1.2$, $V_m=0.6$ kcal/mol for 4,4′-diisopropyl, 4,4′-dicyclohexyl and 4,4′-dicyclopentyl biphenyl.

Calculation of the Repulsive Potential Energies between the Isopropyl and the Aromatic Protons. In a previous publication,[8] calculation of the energy of the non-bonding interaction has been reported for the rotating ethyl group in the 4,4′-diethylbiphenyl, and it was found a simple calculation of the non-bonding interaction was in excellent agreement with the value determined experimentally. The interactions between the counter-cation and the radical anions had been disregarded everywhere, because it was known from conductivity measurements,[9] NMR shift observation[10] and studies of the temperature dependence of the ENDOR intersities of several alkylated biphenyl anions[11] that the radical anions may exist as solvent separated ion-pairs and may act freely under the present experimental circumstances.

In the present studies, similar calculations of the non-bonded interaction between rotating alkyl and aromatic protons are applied to the 4,4′-diisopropyl derivative using the following approximations.

[1] The methyl groups in the isopropyl are treated as a rare gas atom of Kr, since the methyl group is thought to be rapidly rotating in comparison with the motion of the isopropyl group, and not only is it non-polar in nature, but also its spherical size as given by the van der Waals radius are almost the same as those of the Kr atom.

[2] Two kinds of interatomic interactions were considered in the present calculations. The first is the interaction between the ring-*meta* protons and the alkyl β-proton, $\Phi_{H_m\text{-}H_\beta}$. The second is the interaction between the ring-*meta* protons and the methyl groups, $\Phi_{H_m\text{-}CH_3}$. All other interactions are neglected.

The total interatomic potential was calculated from a summation of the energy of interacting pairs, and each interatomic interaction was estimated using the Lennard-Jones 6—12 potential function, thus

$$\Phi_{H_m\text{-}H_\beta}(R_i) = A_{H\text{-}H}/R_i^{12} - B_{H\text{-}H}/R_i^6 \quad (8)$$

and

$$\Phi_{H_m\text{-}CH_3}(R_{ij}) = A_{H\text{-}Kr}/R_{ij}^{12} - B_{H\text{-}Kr}/R_{ij}^6 \quad (9)$$

where R_i is the interatomic distance between the ring-*meta* proton and the alkyl β-proton and R_{ij} is that between the ring-*meta* proton and the methyl group. As shown in Fig. 8, R_i and R_{ij} were calculated as functions of the rotation angle of the alkyl (α) by taking the bond angle of the tetrahedral carbons to be 109°29′ and that of the ring carbons to be 120°. The bond distances between the carbon and hydrogen atoms were estimated to be 1.09 Å everywhere, and carbon-carbon distance to be 1.52 Å for the aliphatic group, 1.45 Å for the alkyl carbon-ring carbon separation, and 1.40 Å for the aromatic ring.[12] The numerical values of parameters $A_{H\text{-}H}$, $B_{H\text{-}H}$, $A_{H\text{-}Kr}$, and $B_{H\text{-}Kr}$ in the Lennard-Jones 6—12 potential have already been established by Yasuda[13] and Oobatake.[14]

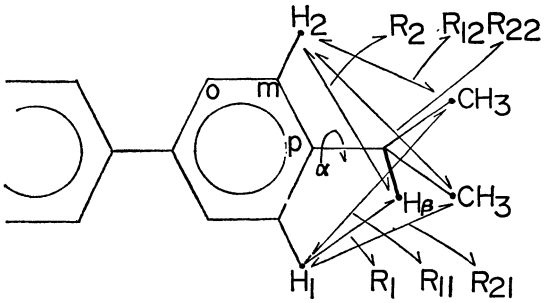

Fig. 8. Scheme of the distance R_{ij} and R_I between ring *meta* protons and methyl groups in the isopropyl and between ring *meta* protons and isopropyl β-proton.

We have already used these values to calculate of the potential barrier height of the rotating ethyl group in 4,4′-diethylbiphenyl[8] and the calculated value was in excellent agreement with the value obtained from the measurement of the temperature dependence of the β-proton splittings, using the following parameters:[13]

$$A_{H\text{-}H} = 4.7\times10^2 \text{ kcal}\cdot\text{Å}^{12}/\text{mol},$$
$$B_{H\text{-}H} = 9.2 \text{ kcal}\cdot\text{Å}^6/\text{mol}$$
$$A_{H\text{-}Kr} = 3.3\times10^4 \text{ kcal}\cdot\text{Å}^{12}/\text{mol},$$
$$B_{H\text{-}Kr} = 1.2\times10^2 \text{ kcal}\cdot\text{Å}^6/\text{mol}.$$

The interatomic potential energy Φ is given by

$$\Phi = \sum_{i=1}^{2}\Phi_{H_m\text{-}H_\beta}(R_i) + \sum_{i,j=1}^{2}\Phi_{H_m\text{-}CH_3}(R_{ij}) \quad (10)$$

In Fig. 6, we give the plot of the interatomic potential energy as a function of the rotating angle (α) of the alkyl group.

The maximum repulsion energy thus calculated was 1.4 kcal/mol when a methyl group is fixed on the aromatic ring [state (B)], while the configuration [A], in which the β-proton is in the plane of the aromatic ring, is found to be the most stable. The potential height (V_m) calculated for the configuration [C], in which the β-hydrogen is parallel with the axis of the $2p_z$ ring carbon, was 0.7 kcal/mol.

The potential function of the isopropyl thus calculated, assuming the non-bonded interatomic interaction, shows not only a double minimum but also is in satisfactory agreement with the value obtained from the measurement of the temperature dependence of the β-proton splittings.

In conclusion, the rotation of the isopropyl, cyclohexyl and cyclopentyl groups may be more or less restricted in the potential as given in Fig. 6, which have the maximum repulsion energy of ~1.2 kcal/mol, this value being slightly above the thermal activation energy at 300 K.

From these considerations, it can be said, at room temperature the isopropyl, cyclohexyl and cyclopentyl groups in para alkylated biphenyl retain fairly large degrees of freedom of rotation affected by the thermal activation, in contrast to the tight restriction of rotation of the alkyls as seen in the space-filling molecular-models.

Alkyl γ-Proton Splitting. The difference in the magnitude of the γ-proton hyperfine coupling of the cycloalkyls may be attributed to the stereochemically different γ-protons, and this offers a useful test to determine whether direct hyperconjugation is the dominant mechanism producing the spin density at these protons, as already reported by Adams *et al.*[7] In cyclohexyls, the axial and equatorial γ-protons remain stereochemically equivalent in pairs against restricted rotation of the cyclohexyl group in the rotational potential, where we assign the larger coupling (240 mG at −85 °C) to the equatorial protons, and the smaller one to the axial protons.

In Fig. 9, it is seen that the equatorial γ-proton splitting of the cyclohexyl decreases with elevation of the temperature, but the other axial γ-proton splittings exhibit only minor increases or remain constant. The similar temperature dependence of the cyclohexyl of the phenoxyl radical has already been reported,[7] and the importance of hyperconjugation of the γ-methylene group has been noted.

Hyperconjugation with a $2p_z$-orbital gives a spin density contribution at the γ-proton of the form

$$a_4^{\gamma} = (A_\gamma + B_\gamma \cos^2\theta)\rho_4^{\pi}. \qquad (11)$$

For a γ-proton, θ is the usual dihedral angle and A_γ and B_γ are empirical constants defined in the same ways as is done for β-protons. The major exchange interaction may be expected between a γ-proton and an unpaired electron in a $2p_z$-orbital on the adjacent ring carbon atoms. The interactions attributed to the other ring carbons were all neglected because the spin density of the ring *meta* carbon is about 1/10 of that of the ring *para* carbon,[15] and the distance between the γ-proton and ring *ortho* carbon is too great.

In the 4,4′-dicyclohexylbiphenyl anion, the axial and equatorial protons move on the same circle during rotations of alkyls about the C_p–C_α bond, and we can write

$$a_4^{\gamma e} = A_{\gamma e} + B_\gamma \cos^2(\theta + \theta_e^0) \qquad (12)$$

and

$$a_4^{\gamma a} = A_{\gamma a} + B_\gamma \cos^2(\theta + \theta_a^0) \qquad (13)$$

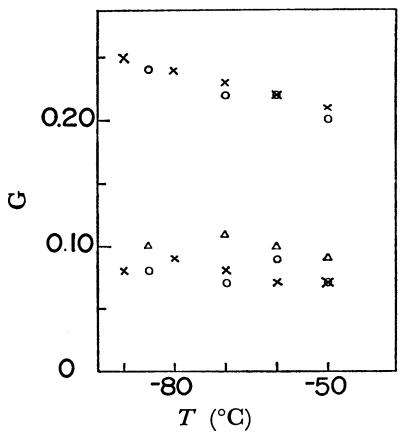

Fig. 9. Temperature dependence of the hyperfine coupling constants for the alkyl γ-protons measured by ENDOR.
△; 4,4′-Diisopropylbiphenyl, ○; 4,4′-dicyclohexylbiphenyl,, ×; 4,4′-dicyclopenthylbiphenyl.

where θ_e^0 and θ_a^0 are the equilibrium dihedral angles of the equatorial and axial protons, respectively. θ_e^0 and θ_a^0 were calculated to be 5°35′ and 54°25′ by taking the aliphatic C–H bond length to be 1.10 Å and the alicyclic C–C bond length to be 1.52 Å.[12]

A qualitative explanation of the $a_4^{\gamma e}/a_4^{\gamma a}$ ratio can be made assuming that the alkyl β-proton exchanges rapidly between state [A] and state [C] as shown in Fig. 6, and the contribution of the other state [B] is negligible. The ratio (n_A/n_C) of the populations at state [A] to that at state [C] is estimated using

$$n_A/n_C = \exp(V_m/kT) \qquad n_A + n_c = 1 \qquad (14)$$

where V_m is the energy difference between state [A] and state [C], 0.6 kcal/mol. At −85 °C, the values of n_A and n_C are estimated to be 0.87 and 0.17, respectively, and therefore the ratio $a_4^{\gamma e}/a_4^{\gamma a}$ can be calculated assuming the $|A_{\gamma e}|$ and $|A_{\gamma a}| \ll B_\gamma$, that is, that

$$\frac{a_4^{\gamma e}}{a_4^{\gamma a}} = \frac{n_A\langle\cos^2 5°35'\rangle + n_C\langle\cos^2 95°35'\rangle}{n_A\langle\cos^2 54°25'\rangle + n_C\langle\cos^2 144°25'\rangle} = 2.1. \qquad (15)$$

The calculated value of $a_4^{\gamma e}/a_4^{\gamma a}$ is nearly the same as the experimental value of 3.0.

In the case of the 4,4′-dicyclopentylbiphenyl anion, the equilibrium dihedral angles θ_0^{e1} for the pseudo-axial γ-protons and those for the equatorial γ-protons θ_0^{e2} have almost the same value, 21°, but two γ-protons in the methylene group do not move on the same circle during rotation about the C_4–C_α bond. This means that each γ-proton is separated from the ring C_4 carbon by the distinct distance of 1.51 abd 2.97 Å, respectively. Since B_γ in Eq. (11) should be represented by the exchange integral between the C_γ–H_γ bond and the $2p_z$-orbital on C_4 as discussed by McLachlan,[16] it will be a function of the distance between the $2p_z$-orbital on C_4 and the γ-proton, which is on the plane perpendicular to the nodal plane of the $2p_z$-atomic orbital. We can, therefore, assign the larger coupling to the proton taking a position closer to the ring C_4 carbon atom at a distance of 1.51 Å and that for the smaller one at a distance of 2.97 Å.

In view of the above discussion, it is seen that different hyperfine couplings observed for cyclohexyl γ-protons are attributed to the difference in the averaged value of $\cos^2\theta$. On the other hand, in cyclopentyl γ-protons, the different B_γ values produce nonequivalent γ-proton splittings.

The authors wish to thank Dr. K. Mukai for his useful discussions throughout the course of this work.

The numerical calculations were carried out on the FACOM 230-75 at the Data Processing Center, Kyoto University.

References

1) F. Nemoto, F. Shimoda, and K. Ishizu, *Chem. Lett.*, **1974**, 639.
2) M. S. Kharasch and E. K. Frelds, *J. Amer. Chem. Soc.*, **63**, 2316 (1941).
3) T. Yamamoto, K. Sato, and T. Miyamae, *Japan. J. Appl. Phys.*, **11**, 1508 (1972).
4) K. Ishizu, K. Mukai, H. Hasegawa, K. Kubo, H.

Nishiguchi, and Y. Deguchi, This Bulletin, **42**, 2808 (1969).
5) C. Heller and H. M. McConnell, *J. Chem. Phys.*, **32**, 1535 (1960).
6) E. W. Stone and A. H. Maki, *ibid.*, **37**, 1326 (1962).
7) R. F. Adams and N. M. Atherton, *Mol. Phys.*, **17**, 673 (1967).
8) F. Nemoto and K. Ishizu, *J. Phys. Chem.*, in press.
9) P. Chang, R. V. Slates, and M. Szwarc, *ibid.*, **70**, 3180 (1966).
10) G. W. Canters and E. de Boer, *Mol. Phys.*, **26**, 1185 (1973).
11) To be published.
12) L. Pauling, "The Nature of the Chemical Bond," 3rd Edition, Cornell University Press, Ithaca, N.Y. (1960), p. 260.
13) H. Yasuda, *Prog. Theor. Phys.*, **45**, 1361 (1971).
14) M. Oobatake and T. Ooi, *ibid.*, **48**, 2132 (1972).
15) K. Ishizu, M. Ohuchi, F. Nemoto, and M. Suga, This Bulletin, **46**, 2932 (1973).
16) A. D. McLachlan, *Mol. Phys.*, **1**, 233 (1958).
17) R. Biehl, K. P. Dinse, and K. Mobis. *Chem. Phys. Lett.*, **10**, 605 (1971).

Monolayers and Built-up Films of *N,N'*-Disubstituted Dithiooxamide Cu(II) Coordination Compounds*

Asahi SUZUKI, Kuwako OHKAWA, Seiichi KANDA, Masanori EMOTO**, and Shunichi WATARI***

Department of Applied Chemistry, Faculty of Engineering, Tokushima University, Minamijosanjima, Tokushima 770

(Received February 10, 1975)

N,N'-Disubstituted dithiooxamide-Cu(II) as compound semiconductors prepared by the usual method have been liable to be an isomeric mixture of coordination polymers. Syntheses of the stereospecific coordination polymers were attempted by an interfacial technique. The dithiooxamides with two hydrophobic substituents, R's, on nitrogen atoms of a ligand molecule could be spread on a water surface to form the monomolecular film, where its possible structure is *cis* isomers of the ligands. Some coordination compounds, *i.e.* the stereospecific coordination polymers, between the *cis* isomers and Cu^{2+} ions were found to be produced at the air-water interface by employing the substrate solution containing Cu^{2+} ions. This was established by the surface pressure *vs.* area measurements for their ligand molecules with $C_6H_5CH_2$–, C_6H_{11}–, $C_{12}H_{25}$–, and $C_{12}H_{25}OCOCH_2$– as hydrophobic substituents, and by the effects of various spreading solvents, pH in substrate solutions and temperatures on their monolayers. Furthermore, built-up films of these polymers were examined for thickness.

N,N'-Disubstituted dithiooxamide–Cu(II) complex (R-DTOA-Cu) have been studied as a series of organic or metal-organic semiconductors.[1] In our study the coordination polymers were prepared by "bulk method," that is, a simple mixing of the solutions of the both components. From their chemical compositions and the properties, a two-dimensional polymeric structure has been proposed for the compounds,[2] although a linear chain structure had been proposed before.[3] However, the preparation of R-DTOA–Cu by the "bulk method" might result in the isomeric mixtures called type A because of a rotational isomerism around the central carbon-carbon bond of the ligands themselves (Fig. 1a) and the coordination isomerism in the compounds as a whole (Fig. 2). Actually all of the black precipitates show a few diffused hallows for each compound in their X-ray diffraction patterns by the powder method.[2], The discussions on electric, magnetic, and other properties, which are more or less related to the stereostructure of the molecules, would be restricted because of the isomeric irregularity.[4]

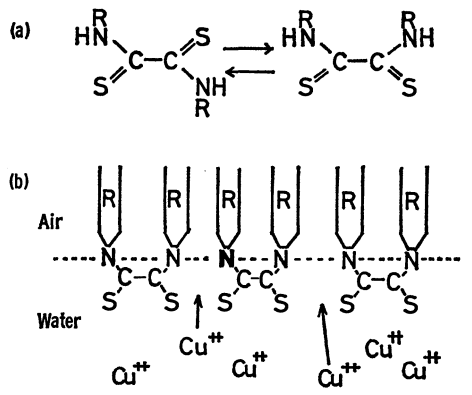

Fig. 1a. Expected rotational isomerism of the ligands.
1b. A schematic mechanism of the stereospecific synthesis of the type B compounds.

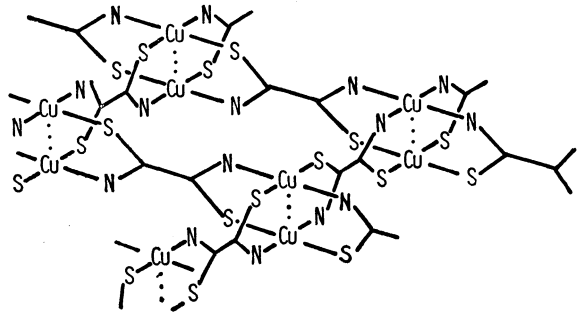

Fig. 2. Non-stereospecific two-dimensional net-work model with dimer structures of copper acetate type. For simplicity, substituents on nitrogen atoms are omitted.

For the solution of the ambiguity, the stereospecific synthesis of the polymers has been attempted by the "monolayer method" in which the ligands with the two hydrophobic substituents on the nitrogen atoms are spread on an aqueous subphase containing cupric ions (Fig. 1b) and the resultant products are called type B. The reaction yields of the type B compounds of $C_6H_5CH_2$–, C_6H_{11}–, and $C_{12}H_{25}$–DTOA-Cu seem to be more or less qualitative.[4],† On the other hand the coordination of a new ligand, dodecyl ester of $HOOCCH_2$-DTOA-H_2, with Cu^{2+} ions at the air/water interface seems to be quantitative as shown in this study, and the monomolecular film is stable. As a result, the molecular structures of the type B compounds are confirmed, and some properties of the coming built-up films might be interpreted in relation to this molecular structure.

Experimental

Materials. *N,N'*-Disubstituted dithiooxamides, RNH–C(S)–C(S)–NHR, in which the R's were $C_6H_5CH_2$– (benzyl), C_6H_{11}– (cyclohexyl), and $C_{12}H_{25}$–(dodecyl), were from the

* Parts of this study were presented at the 15th ICCC. 1973, in Moscow. III, Fri. 61.

** Present address: Scientific Investigation Research Laboratory, Tokushima Prefectural Police H.Q.

*** Present address: Miura Co., Ltd., Matsuyama, Ehime.

† The preliminary study of diffraction patterns by the X-ray powder method and the presumption about the crystallinity mentioned in the previous paper (Ref. 4, pp. 91, 95) need supplemental experiments and more carefull consideration on the data.

Mallinckrodt Chemical Works, and was recrystallized from ethanol. Dodecyl ester of *N,N'*-carboxymethyl dithiooxamide, $C_{12}H_{25}OC(O)CH_2NHC(S)C(S)NHCH_2C(O)OC_{12}H_{25}$, was prepared from dodecyl alcohol and *N,N'*-bis(carboxymethyl)-dithiooxamide in the presence of a acid catalyst, H_2SO_4. The crude ester was recrystallized from acetone, mp 101 °C (uncorrected). Cupric sulfate (Special Grade Reagent, Wako Pure Chemical Industries, Ltd.) was heated for 2 hr at 350 °C in a furnace to diminish the surface active contaminations. The organic solvents (Special Grade, Wako P.C.I., Ltd.) were distilled twice. Water used for the subphase was distilled in a copper distillatory first and in a glass vessel next. Solid substrates, glass and quartz plates, were cleaned by a ultrasonic method with help of detergent followed by a treatment with hot cleaning solution ($Na_2Cr_2O_7$ in concd H_2SO_4). For the purpose of uniform deposition of the complex monolayer, each solid substrate was coated with three monolayers of Fe-stearate under the surface pressure of 29 dyn/cm.

Procedure. About 2 mg of the ligand was dissolved in 10 ml of the binary mixed solvents composed of ethanol, propanol, benzene, or hexane as shown in Figs. 3—6. The solution was spread from an Alfa micrometersyringe on water or aqueous solution in a conventional Langmuir trough ($60\times13.5\times1$ cm^3). The surface pressure (π) was measured by a automatic recording systems as a function of the surface area (A) using the hanging plate method.[5] Unless otherwise specified, the measurements were carried out at a room temperature (15—25 °C). In examining the temperature effects on complex monolayer, the temperature of the subphase was regulated at the selected values in the range of 20 to 5 °C by thermoelectric modules attached at the bottom of the trough.

Complex monolayers were transferred onto a solid substrate by the Langmuir-Blodgett method as follows. The Langmuir trough was divided into three sections for the "transfer method."[6] The ligand solution was spread on an aqueous cupric solution in the first section and was allowed to stand for 30—60 min for the complete coordination reaction. The obtained complex monolayer was transferred to the water surface in the second section for washing the non-reacted Cu^{2+} ions adsorbed beneath the complex monolayer. Furthermore the monolayer was transferred to the third section filled with pure water, where the built-up procedure was carried out. It was made by an automatic equipment with a certain speed. During the procedure, the surface pressure of monolayer was kept constant by the piston oil. The pressure of piston oil was adjusted by changing the mixing ratio of ethylmyristate and liquid paraffin. The conditions for the preparation are shown in Table 1.

Table 1. Conditions of the preparation of the built-up films of R-DTOA-Cu

R	Spreading solvent	Spreading pressure (dyn/cm)
C_6H_{11}-	benzene : ethanol = 1 : 4	15
$C_6H_5CH_2$-	benzene : ethanol : hexane = 1 : 4 : 5	19
$C_{12}H_{25}$-	benzene : ethanol = 1 : 4	15
$C_{12}H_{25}OCOCH_2$-	benzene : hexane = 2 : 3	19

Results and Discussion

Monolayer. The spread monolayers of the ligands or the complexes on an aqueous subphase were studied in order to find the structure of the molecule at the interface and the optimum conditions for the preparation of built-up films. The mechanisms of spreading of the ligand and of the coordination reactions at an air/water interface are presumed as follows. The molecules of dithiooxamides having both hydrophilic and lipophilic parts would be oriented at the surface by surface free energy, forming a monolayer. Due to internal rotation around the central carbon-carbon bond of the ligand molecule the *trans*-form, which is more stable in crystal and probably in solution,[7] is isomerized to the *cis*-form.

Equilibrium between the *trans*- and the *cis*-form of a ligand molecule at an air/water interface was studied as a first approximation by an equation, $-RT\ln([cis]/[trans]) = -RT\ln K = \Delta F^\circ = \Delta F_1 + \Delta F_2$, where K denotes the equilibrium constant; $\Delta F^\circ = F^\circ(cis) - F^\circ(trans)$, standard free-energy change in the reaction concerned; ΔF_1, the free energy change originated from an internal rotation of the isolated molecules; ΔF_2, that originated from the transfer of a hydrophobic substituent R from the water phase to the air phase. As an example, in case of R = $C_{12}H_{25}$–, the ΔF_1 was evaluated to be +1.5 kcal/mol by the measurement of the temperature variation of absorption intensities in an infrared region.[8] The ΔF_2 per $-CH_2-$ group have been estimated to be −(0.8—0.9) kcal/mol in a linear hydrocarbon chain, therefore, $\Delta F_2 = -(0.8—0.9)\times12 = -10$ kcal/mol.[9] Then the ΔF° is −(8—9) kcal/mol, and $K = [cis]/[trans]$ at the interface is greater than 10^5 approximately. Also in the case of ligands with other hydrophobic substituents, $C_6H_5CH_2$–, C_6H_{11}–, and $C_{12}H_{25}OCOCH_2$–, analogous results are expected. In conclusion virtually all the ligand molecules are expected to take the *cis*-form at the air/water interface.††

Figure 3 shows the π-A isotherms obtained for the monolayers of ligands on distilled water at a room temperature (15—25 °C). The ligands having a pair of long hydrocarbon chains as the substituents, $C_{12}H_{25}$–

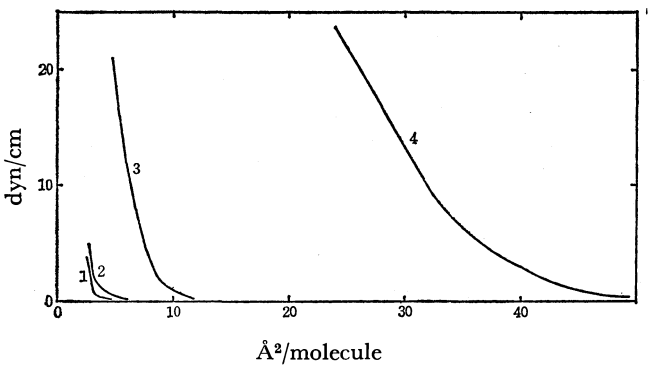

Fig. 3. Surface pressure *vs.* molecular area curves for R-DTOA-H_2 spread on pure water. Substituent, R, and spreading solvent with mixing ratio is as follows: 1) $C_6H_5CH_2$- (benzene 1, ethanol 4), 2) C_6H_{11}- (butanol 1, hexane 4), 3) $C_{12}H_{25}$- (ethanol 4, benzene 1), 4) $C_{12}H_{25}OCOCH_2$- (benzene 1, ethanol 1).

†† The more extensive study on the *cis-trans* isomerization of the ligand molecules are now in progress, and will be published elsewhere.

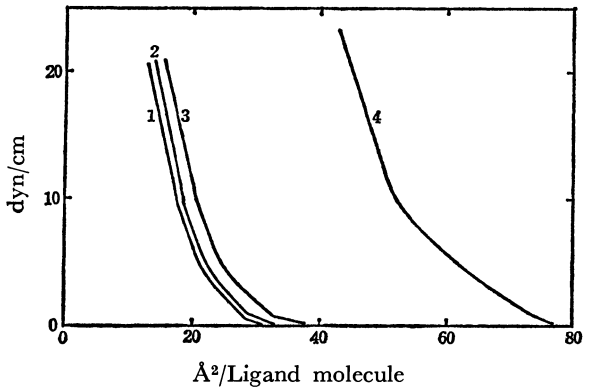

Fig. 4. Surface pressure *vs.* molecular area curves for R-DTOA-H_2 spread on 0.005 M $CuSO_4$ aqueous solution. Substituent, R, and spreading solvent with mixing ratio are as follows: 1) $C_{12}H_{25}$- (buthanol 1, hexane 4), 2) $C_6H_5CH_2$- (buthanol 1, hexane 4), 3) C_6H_{11}- (benzene 1, hexane 4), 4) $C_{12}H_{25}OCOCH_2$- (benzene 2, hexane 3).

or $C_{12}H_{25}OCOCH_2$–DTOA–H_2, form monolayers on water, whereas the others, $C_6H_5CH_2$– and C_6H_{11}–DTOA–H_2, hardly spread over a water surface due to their poor hydrophobicity; the latters might be dissolved in the subphase owing to the fair solubilities of 0.14 and 0.12 g per 100 ml of water at 25 °C, respectively.[10] The limitting areas (A_0) estimated by extrapolation of the surface pressure to zero were 7 and 38 Å²/molecule for $C_{12}H_{25}$– and $C_{12}H_{25}OCOCH_2$–DTOA–H_2, respectively. As the molecule has two hydrophobic substituents on both ends, A_0 values of the ligands should be larger than twice the value of the cross-section of a hydrocarbon linear chain, 20 Å²/chain.[11] Data for the ester is reasonable but that for another is smaller than expected; the small A_0 can be attributed to pile-up of the ligand molecules on water due to the hydrophile-lipophile unbalance and/or the dissolution owing to the solubility of 0.06 g per 100 ml of water at 25 °C.[10]

Figure 4 shows the π-A isotherms of ligands spread on 5×10^{-3} M $CuSO_4$ aqueous solutions. In this case, $C_6H_5CH_2$– and C_6H_{11}–DTOA–H_2 exhibit detectable surface pressures due to a decrease in solubility with formation of a copper compound. The complexes of the type A of these two ligands are insoluble in water though the two ligands are slightly soluble in water as mentioned previously. The A_0 values were evaluated as 25, 22, 22, and 56 A²/molecule for C_6H_{11}–, $C_6H_5CH_2$–, $C_{12}H_{25}$–, and $C_{12}H_{25}OCOCH_2$–DTOA–Cu, respectively. The former three values are smaller than that expected.

To obtain the conditions giving a reasonable limitting area, the concentration of Cu^{2+} ion, the compression speed, the spreading solvents, and the pH of the subphase were examined.††† As an example, the changes in the π-A isotherms of C_6H_{11}–DTOA–Cu complex are shown in Fig. 5a, b, c, d. In Fig. 5a, the π-A isotherms are shown as a function of Cu^{2+} ion concentration from 5×10^{-5} to 5×10^{-2} M. On the subphases of extreme cupric ion concentrations, 5×10^{-5} and 5×10^{-2} M, the results showed poor reproducibility and were found in ranges shown by the pairs of dashed and dotted lines. On the moderate concentrations, 5×10^{-4} and 5×10^{-3} M, reproducible π-A curves were obtained for both concentrations. The π-A curves observed with the various compression speeds are shown in Fig. 5b. The selected speeds were in a range of 0.33—2 cm/min (0.11—0.67 Å²/molecule·min). The A_0 did not remarkably depend on the compression speed except for the highest one, 2 cm/min.

The mixtures of benzene–hexane, chloroform–hexane, 1-pentanol–heptane, 2-pentanol–heptane, or propanol–hexane were used as the spreading solvent, the mixing ratios were 1 : 4 by volume in most cases, and the results are shown in Fig. 5c. The character of the π-A curves was not changed essentially and only displacements of the π-A curves were observed. The effect of pH of subphases was examined by adjusting pH to the values from 2.9 to 10.2 with use of hydrochloric acid or sodium hydroxide. The results found on 5×10^{-3} M $CuSO_4$ aqueous solution are shown in Fig. 5d. In the acid region, the π-A relation was not remarkably affected by the pH, whereas in the alkali region A_0 was decreased with increasing pH. The effect of pH may be attributed to the decreasing concentrations of hydrated cupric

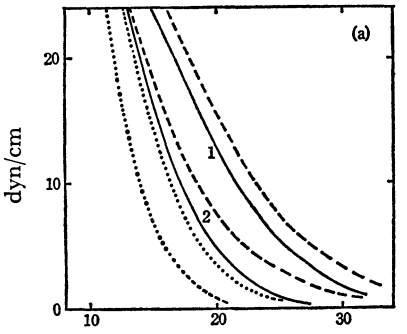

Fig. 5a. The effect of $CuSO_4$ concentration on π *vs.* A curve for C_6H_{11}-DTOA-Cu monolayer. Solid line 1) 5×10^{-3} M $CuSO_4$, Solid line 2) 5×10^{-4} M $CuSO_4$, Dotted lines) 5×10^{-5} M $CuSO_4$, Dashed lines) 5×10^{-2} M $CuSO_4$. Spreading solvent: benzene 1, hexane 4.

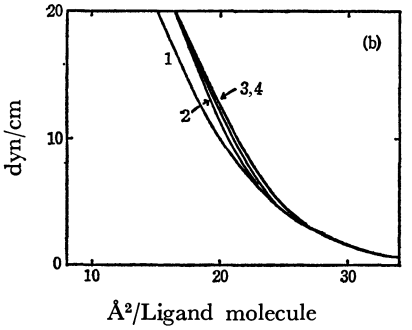

Fig. 5b. π *vs.* A curves with various compression speeds on a unit of Å²/molecule·min: 1) 0.67, 2) 0.33, 3) 0.22, 4) 0.11. The film substance is C_6H_{11}-DTOA-Cu on 5×10^{-3} M $CuSO_4$ aq. Spreading solvent: benzene 1, hexane 4.

††† This experiment was mainly operated by Mr. Watari.

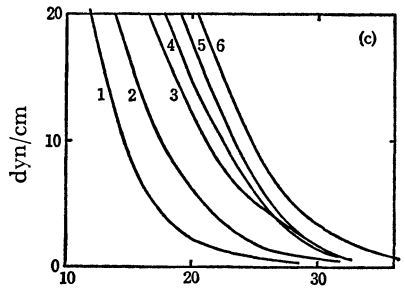

Fig. 5c. The effect of spreading solvents on π *vs.* A relation for C_6H_{11}-DTOA-Cu on 5×10^{-3} M $CuSO_4$ aq. The components and the mixing ratios: 1) benzene and hexane, 1 : 1, 2) chloroform and hexane, 1 : 1, 3) benzene and hexane, 1 : 4, 4) 1-pentanol and heptane, 1 : 4, 5) 2-pentanol and heptane, 1 : 4, 6) propanol and hexane, 1 : 4.

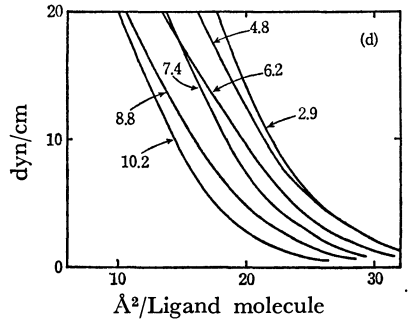

Fig. 5d. The effect of pH of the subphase on π *vs.* A for C_6H_{11}-DTOA-Cu on 5×10^{-3} M $CuSO_4$. pH of the subphases are indicated in the figure. Spreading solvent: benzene 1, hexane 4.

ions, $Cu(H_2O)_{4-6}^{2+}$, as Stickland discussed.[12]

The presented results so far for the monolayer of C_6H_{11}–DTOA–Cu indicate that the limitting area was rather small, in the range of 15 to 29 Å²/molecule. Even 30 Å²/molecule is still smaller than that expected for two hydrophobic substituents on the ligand molecule in the *cis*-form. This phenomenon could be caused from the dissolution of unreacting ligand molecules into water or the stacking of the copper complex which might be too hydrophobic to form a monomolecular film. A similar reasoning may be applicable to the monolayers of $C_6H_5CH_2$– and $C_{12}H_{25}$–DTOA–Cu complexes. The A_0's for $C_{12}H_{25}OCOCH_2$–DTOA–H_2 on pure water and on the cupric aqueous solution, 38 and 56 Å²/molecule, respectively, were reproducible, and the former is reasonably related to twice the limitting area of single chain fatty acids, therefore the quantitative formation of monolayer of the ester ligand in the *cis*-form was confirmed.

The effect of temperature on the π-A curves of $C_{12}H_{25}OCOCH_2$–DTOA–Cu on a 5×10^{-3} M $CuSO_4$ solution is shown in Fig. 6.‡ By the measurements at lower temperature, 5 and 10 °C, two kinds of limiting areas, A_0^α and A_0^β in a larger (α) and a smaller (β) area region as shown in Fig. 6, were obtained. At a higher temperature A_0^α was not established clearly

‡ This operation was done mainly by Mr. Emoto.

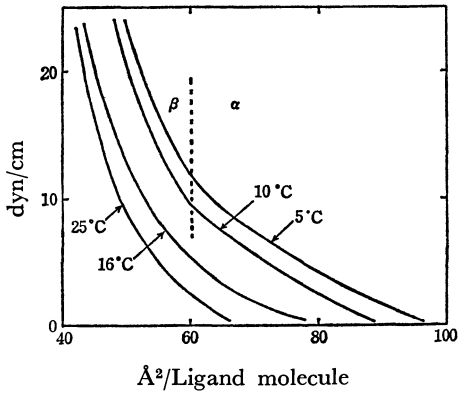

Fig. 6. The effect of temperature on π *vs.* A relation for $C_{12}H_{25}OCOCH_2$–DTOA–Cu on 5×10^{-3} M $CuSO_4$. Spreading solvent: benzene 2, hexane 3.

because of the disappearance of the α-region of the curves; the α-region might be attributed to the formation of the island structure. The A_0^β at each temperature were evaluated as follows: 52 Å² (25 °C), 56 Å² (16 °C), 60 Å² (10 °C), 64 Å² (5 °C). Contrary to the general relation between A and T, the A_0^β decreases with an increase in temperature. This unusual tendency can be explained by the slower dissolution of the unreacted ligand molecule at a lower temperature into the aqueous phase before the completion of the coordination reaction with cupric ions at a water surface. This implies that the dissolution of the ligand, even in such a slightly soluble one, should be responsible for the smaller apparent A_0 than the true value, and the same should be more probable for the more soluble other ligands. The true value of the limiting area for the ester ligand complex presumed experimentally by extrapolation might be about 65 Å² or more; this value is acceptable one if all the ligand molecules added on the water surface are assumed to exist there as the *cis* isomer and combine with cupric ions in a certain manner.

In the previous paper[4] we proposed the 'copper-acetate' type model which was a two-dimensional network for the compounds obtained by both the "bulk" and "monolayer" methods, namely the type A and B compounds. However this model is now obviously catastrophic as a model for the type B compounds by the following reasons: 1) by the calculation from the bond lengths it is concluded that this model requires only 30 Å² at most for a R–DTOA–Cu structure unit, but it is much smaller than above mentioned 65 Å², 2) 30 Å² for this model does not satisfy a condition to accomodate two hydrocarbon chains which is required in the B compounds, though the requirement is not needed in the A compounds. For the solution to the difficulty, a new model, named 'improved' model shown in Fig. 7, is proposed, and in this case a calculated area per R–DTOA–Cu unit is 60—70 Å² which agrees nicely with the observed limitting area for $C_{12}H_{25}OCOCH_2$–DTOA–Cu compound. For the type B compounds with other substituents R, we are not able to derive a suitable model from their small limitting areas experimentally obtained (22—25 Å²), however the 'improved' model

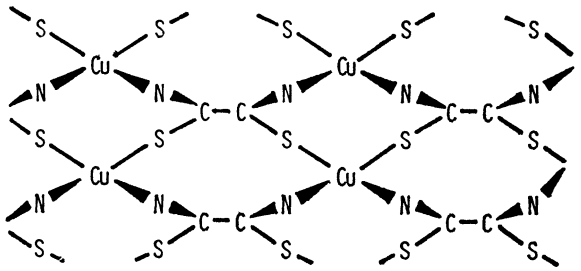

Fig. 7. "Improved model," the proposed molecular model of the stereospecific dithiooxamide copper coordination polymers.
Unevenness of its plane is indicated by a arrowhead affixed to a nitrogen atom.

can be also adopted to them with a certain confidence.

Built-up films. The complex monolayer was transferred from the water surface to the solid substrate by repeated dipping and withdrawing processes, the Langmuir and Blodgett method.[13] The coating of glass or quartz slides with Fe-stearate monolayers was effective for the tight fixation of the complex monolayers.

The uniform built-up films of Y type[13] of $C_{12}H_{25}$-$OCOCH_2$–DTOA–Cu complex were obtained but the other complexes, C_6H_{11}–, $C_6H_5CH_2$–, and $C_{12}H_{25}$–DTOA–Cu, were not uniformly transferred on to the solid substrates. With latters, defects in the surface of the multilayers were often appeared and could not be recovered.

The optical density of $C_{12}H_{25}OCOCH_2$–DTOA–Cu multilayers on quartz plates was measured in the visible and the ultraviolet region. The optical density was linearly increased with the number of films transferred. It means that transfer ratio from the water surface is the same for each monolayer. The absorption maximum was observed at 380 nm for $C_{12}H_{25}OCOCH_2$–DTOA–Cu compound.

The thickness of the built-up films estimated by observing the colors by reflected skylight is listed in Table 2. The relationship between the wavelength, λ, and the thickness of film, d, is given by an equation for an interface:

$$4d(n_2^2 - n_1^2 \sin^2\beta)^{1/2} = (2m-1)\lambda$$

where n_1 and n_2 are the refractive indexes of films and air, respectively, β is the incident angle measured and m is an integer.[14] The refractive index of the films was assumed to be $n_1=1.5$. The estimated value of thickness of a layer is reasonably explained by considering the molecular model of the compound.

Table 2. The thickness of a layer of $C_{12}H_{25}OCOCH_2$–DTOA–Cu estimated from the colors of reflection from the built-up films

Number of layers	Color	Thickness of a layer (Å)
40	yellow	22.3
50	reddish yellow	19.3
62	violet	20.5
72	green	21.7

The electric resistance of the built-up films was measured and will be published elsewhere.

Part of this research was supported by a Grant-in-aid for Scientific Research from the Ministry of Education. The dithiooxamides were donated by the Mallinckrodt Chemical Works, for which we express our appreciation.

References

1) B. A. Bolt, "Organic Semiconducting Polymers," ed. by J. E. Katon, Marcel Dekker, New York (1968), Chapter 4.
2) S. Kanda, *Nippon Kagaku Zasshi*, **83**, 560 (1962)., S. Kanda, K. Ito, and T. Nogaito, *J. Polym. Sci., Part C*, **17**, 151 (1967).
3) K. A. Jensen, *Z. Anorg. Chem.*, **252**, 227 (1944). R. V. G. Evans and C. S. Gibson, *J. Chem. Soc.*, **1949**, 431. R. N. Hurd, G. DeLaMater, G. C. McEleheny, and L. V. Peiffer, *J. Amer. Chem. Soc.*, **82**, 4454 (1960).
4) S. Kanda, A. Suzuki, and K. Ohkawa, *Ind. Eng. Chem. Prod. Res. Develop.*, **12**, 88 (1973).
5) A. Suzuki, S. Ikeda, and T. Isemura, *Ann. Rep. Biol. Work, Osaka Univ.*, **15**, 83 (1967).
6) T. Yamashita and H. B. Bull, *J. Colloid Interface Sci.*, **27**, 19 (1968). P. Fromheltz, *Biophys. Acta*, **225**, 382 (1971).
7) P. J. Wheatley, *J. Chem. Soc.*, **1965**, 396.
8) S. Son, S. Kanda, A. Suzuki, and K. Ohkawa, Presented at the 28th National Meeting of the Chem. Soc. Japan (Tokyo), 4Q47 (1973).
9) R. S. Hansen, F. A. Miller, and S. D. Christian, *J. Chem. Phys.*, **59**, 391 (1955).
10) Dithiooxamide Information Bulletin, page 3, Mallinckrodt Chem. Works.
11) I. Langmuir, *J. Amer. Chem. Soc.*, **39**, 1848 (1917), reviewed in G. L. Gaines, Jr., "Insoluble Monolayers at Liquid-Gas Interface," Interscience, New York (1966).
12) F. G. W. Stickland, *J. Colloid Interface Sci.*, **40**, 142 (1972); *ibid.*, **42**, 96 (1973).
13) K. B. Blodgett, *J. Amer. Chem. Soc.*, **56**, 495 (1934); *ibid.*, **57**, 1007 (1935).
14) M. Born and E. Wolf, "Principles of Optics," 4th Ed. Pergamon Press, Oxford (1970), p. 281.

^{13}C Nuclear Magnetic Resonance Studies of the Hindered Internal Rotation and the Molecular Association of *N,N*-Dimethylacetamide

Isao ANDO, Naomi JINNO, and Atsuo NISHIOKA

Department of Polymer Chemistry, Tokyo Institute of Technology, Ookayama, Meguro-ku, Tokyo 152

(Received February 12, 1975)

The concentration and temperature dependences of the ^{13}C chemical shifts of *N,N*-dimethylacetamide (DMA) in CCl_4, H_2O, and H_2SO_4 solutions were measured by means of a ^{13}C FT-NMR spectrometer at 25.15 MHz. From the temperature dependence of the chemical-shift difference between the *cis*- and *trans*-NCH_3 carbons, the activation energy, E_a, for the hindered internal rotation about the C–N bond was obtained to be 10—17.5 kcal/mol; it was also found to be *ca.* 10 kcal/mol at an infinite dilution in a CCl_4 solution. The chemical shift of each carbon in the DMA molecule was calculated using Pople's expression under the average excitation-energy approximation by means of the CNDO/2 method. The calculated finding that each carbon in DMA appears in the order of carbonyl, *trans*-NCH_3, *cis*-NCH_3, and acetyl carbons from the low field agrees with the order assigned by McFarlane. Further, as for the molecular association in neat liquid, various models are discussed on the basis of quantum-chemical calculations, and a model is proposed which has antiparallel oriented carbonyl groups in associated states of the molecules of more than two. The observed differences between the chemical shifts of the carbonyl carbons at dilutions in CCl_4 and H_2O solutions, and between those in CCl_4 and H_2SO_4 solutions, are found to agree well with the results calculated using the model in which the DMA molecules at dilutions in CCl_4, H_2O, and H_2SO_4 exist as monomer, hydrogen-bonded DMA with H_2O, and protonated DMA respectively.

Since the first NMR study of the hindered internal rotation of the C–N bond in amide compounds was carried out by Gutowsky *et al.*,[1] many studies have been concerned with the activation energy, E_a, for the hindered internal rotation and the molecular association[2] of amide compounds through the proton chemical shift, the line shape, and the spin-lattice relaxation time. Recently a quantum-chemical study of the hindered internal rotation has been done,[3] and some interesting results have been obtained. However, the mechanisms of the molecular association have scarcely been studied at all theoretically from the viewpoint of the chemical shift, even though this approach is very interesting. From the viewpoint of the chemical shift, the proton-decoupled carbon-13 (^{13}C) NMR spectra have greater advantages than ^1H NMR because of their simplicity. In addition, the ^{13}C chemical shift can be treated theoretically by the molecular orbital method, and the observed and calculated ^{13}C chemical shifts can be compared quantitatively with each other. Therefore, these results may be of use in obtaining information on the molecular association mechanism. In this paper, we will seek to compare the observed and calculated chemical shifts of the *N,N*-dimethylacetamide (DMA) molecule, which does not form a hydrogen bond itself and which may be a much-favored dipolar model. We will be concerned with the amide-amide associate, the hydrogen-bonded amide, and the protonated amide, which correspond to the behavior in neat liquid, H_2O, and H_2SO_4 solutions respectively, and with the monomer amide, which corresponds to the behavior at an infinite dilution in CCl_4.

Experimental

Materials. The DMA, CCl_4, and H_2SO_4 were obtained from the Tokyo Kasei Co., while the H_2O was distilled.

Measurements. High-resolution natural-abundance pulsed ^{13}C FT-NMR spectra were obtained at 25.15 MHz using a Japan Electron Optics Laboratory JNM PS-100 spectrometer equipped with the PFT-100 Fourier transform system, a JEC-6 spectrum computer, a ^2D field-frequency lock, and a noise-modulated proton-decoupling system. The core memory of the computer is 12K words, and the memory of the magnetic drum used is 8K words. The length of each word is 16 bits. The observed free induction decay (FID) was sampled in 8192 points. The pulse-recycle time was chosen as 60 s, considering the *N*-methyl carbon spin-lattice relaxation time, T_1, of 14 s. However, when only the measurement of the chemical shift was required, the recycle time of 30 s was used. The FID signal was observed after a 90° pulse with a width of 20 μs.

The activation energy for the hindered internal rotation was estimated for the N–CH_3 carbon signals by the peak-separation method.[1] The temperature range of the measurements was 22.5—100 °C. The concentration range of the solution measured was 2—100%. An accumulation of 20 or 500 scans was necessary for a 100 or 2% solution respectively, but when the NCH_3 carbon signals become broad at 60 °C, the accumulations were about 2—3 times greater.

Theoretical Calculation

The magnetic shielding constant, σ_A, of any specified carbon atom, A, in a molecule can be approximately estimated by means of the sum of the following diamagnetic and paramagnetic terms:[4]

$$\sigma_A = \sigma_A^{dia} + \sigma_A^{para} \quad (1)$$

where σ_A^{dia} and σ_A^{para} are the diamagnetic and paramagnetic contributions respectively.

The approximate value of σ_A^{dia} is given as:[6]

$$\sigma_A^{dia} = 4.45\,Z^*q \quad (2)$$

where:

$$Z^* = 3.25 - 0.35\,(q-4) \quad (3)$$

in which q is the total electron density around the carbon atom, and Z^*, the "effective nuclear charge" estimated according to Slater's rule.

The paramagnetic term is estimated according to Pople's theory,[4] with the average excitation-energy (ΔE) approximation as follows:

$$\sigma_A^{para} = -(e^2\hbar^2/2m^2c^2\Delta E)\ \langle r^{-3}\rangle_{2p} \sum_{B(=A)} Q_{AB} \quad (4)$$

where:

$$Q_{AB} = \frac{4}{3}\delta_{AB}(P_{x_Ax_B}+P_{y_Ay_B}+P_{z_Az_B}) - \frac{2}{3}(P_{y_Ay_B}P_{z_Az_B}+P_{z_Az_B}P_{x_Ax_B}+P_{x_Ax_B}P_{y_Ay_B}) + \frac{2}{3}(P_{y_Az_B}P_{z_Ay_B}+P_{z_Ax_B}P_{x_Az_B}+P_{x_Ay_B}P_{y_Ax_B})$$

$$\langle r^{-3}\rangle_{2p} = \frac{1}{24a_0^3}(3.25-0.35(q-4))^3 \quad (6)$$

In these formulae, $\sum_{B(=A)}$ is a summation over all the atoms; $\langle r^{-3}\rangle_{2p}$; δ_{AB}, the Kronecker symbol; a_0, the Bohr radius, and $P_{x_Ax_B}$, the element of the bond-order matrix for the $2p_x$ atomic orbitals on the A and B atoms.

σ_A^{dia} and σ_A^{para} were estimated by the CNDO/2 method.[5] The bond lengths and bond angles used in a DMA molecule are shown in Table 1.

Table 1. The used bond lengths and bond angles of *N,N*-dimethylacetamide[a]

Bond lengths (Å)		Bond angles (°)	
C-C	1.54	C-C-H	109.5
C-N	1.32	N-C-H	109.5
C=O	1.24	C-C=O	120
C-H	1.09	N-C=O	120
		C-N-C	127

a) All the data were taken from standard bond lengths and bond angles in Ref. 5 except that the bond angles of C-C=O, N-C=O and C-N-C were taken from Ref. 7.

Results and Discussion

CCl_4 Solution. Concentration Dependence: Each carbon signal in the ^{13}C NMR spectrum of DMA in the CCl_4 solution appears in the order of carbonyl, *trans*-NCH_3, *cis*-NCH_3, and acetyl carbons from the low field, based on the assignment by McFarlane[8], where their positions appear at −73.90, 59.58, 62.67 and 66.26 ppm respectively (relative to CCl_4) in a 20% v/v CCl_4 solution at 30 °C. His assignment agrees with the calculated results for each carbon in the molecule, as will be described below.

Next, let us discuss the concentration dependence of the chemical shift for each carbon. The concentration dependences of the carbonyl carbon at 30, 60, and 80 °C are shown in Fig. 1. This carbon shows a considerable concentration dependence and shifts to a low field with an increase in the concentration of DMA. The chemical-shift change from an infinite dilution to an 80% solution is about 1.5 ppm. On the other hand, the concentration dependences of the chemical shifts for the other carbons are small, as is shown in Fig. 2. These concentration dependences do not show any large change upon a variation in the temperature except for the $COCH_3$ carbon. Further, the chemical-shift difference between the *trans*- and *cis*-NCH_3 carbons is found to increase by

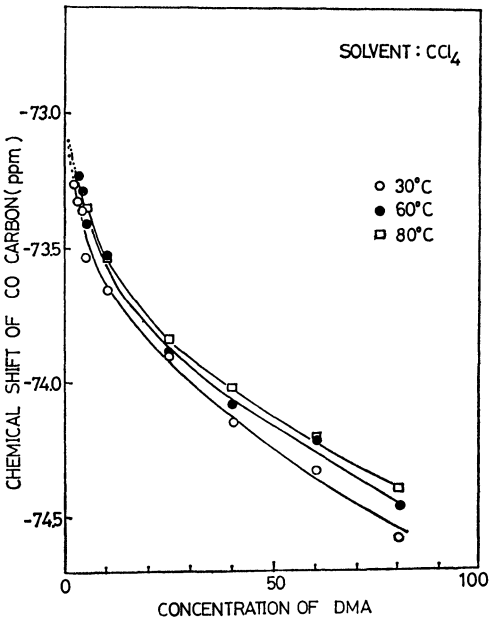

Fig. 1. Concentration dependence of the ^{13}C chemical shift of carbonyl carbon in CCl_4 solution.

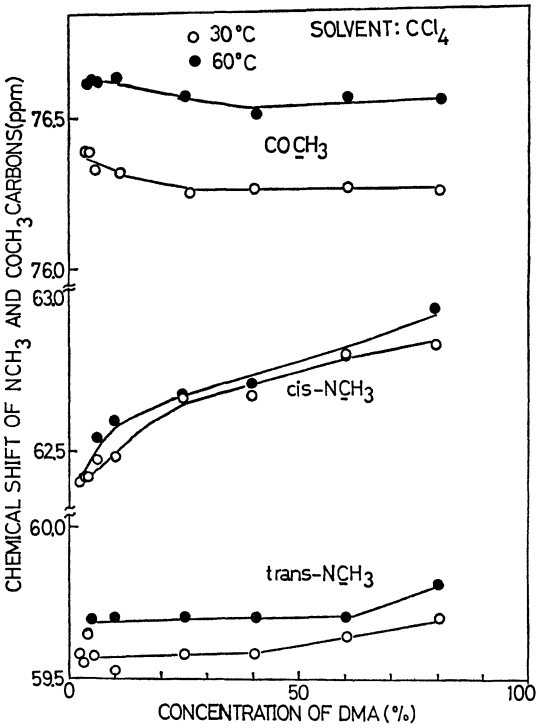

Fig. 2. Concentration dependence of the ^{13}C chemical shifts of *trans*-NCH_3 and acetyl carbons in CCl_4 solution.

about 0.3 ppm with the variation in the concentration from a 2% solution to neat liquid with an increase in the concentration, as is shown in Fig. 3. This indicates that the value of E_a increases with an increase in the concentration of DMA. A rapid increase within the range from zero to 20% corresponds well to the rapid decrease in the carbonyl carbon's shift, which suggests that the solution structure changes rapidly in this concentration range and that it may be

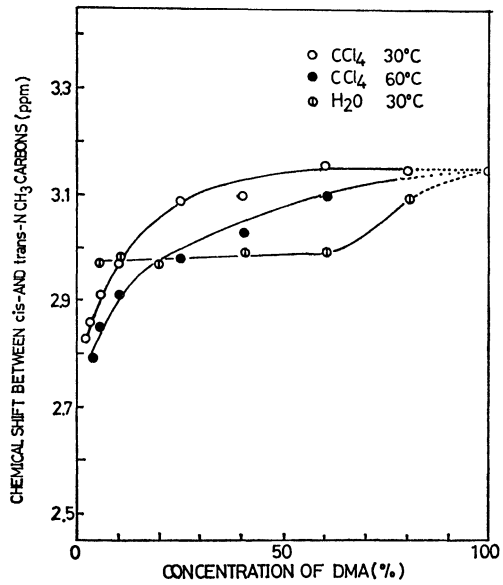

Fig. 3. Concentration dependence of the ^{13}C chemical shifts of *cis*-NCH_3 and *trans*-NCH_3 carbons in CCl_4 and H_2O solution.

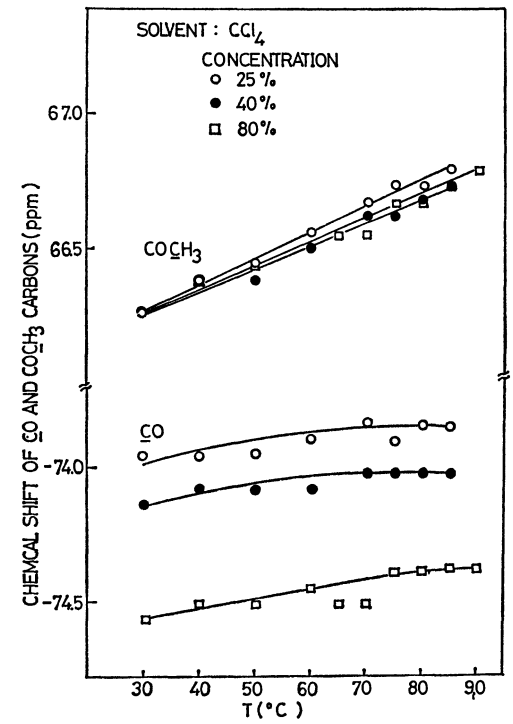

Fig. 4. Temperature dependence of the ^{13}C chemical shifts of carbonyl and acetyl carbons in CCl_4 solution.

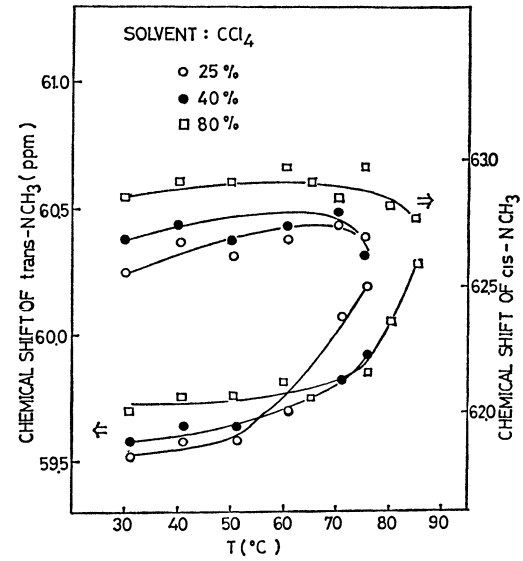

Fig. 5. Temperature dependence of the ^{13}C chemical shifts of *cis*-NCH_3 and *trans*-NCH_3 carbons in CCl_4 solution.

qualitatively interpreted in terms of an association model as well as the results of a similar study by means of ^{1}H NMR.[2h] Also, Sato *et al.*[21] have reported that the slopes of linear plots of the ^{1}H relaxation rate, $1/T_1$, against the concentration differ considerably from each other on both sides of concentration of about 3 mol/l, which corresponds to the above-mentioned concentration; these slopes have been qualitatively interpreted in terms of association.

Rabinovitz *et al.*[2h] have reported regarding the change in the ^{1}H chemical shift observed with the concentration of *N,N*-dimethylformamide in CCl_4 that a more satisfactory explanation lies in the contribution of the direct dimer shielding described in a monomer-dimer equilibrium. Therefore, it is considered that, in the monomer-dimer equilibrium, the monomer state increases with a decrease in the concentration. It is likely that the behavior of DMA in the CCl_4 solution may be described as in a monomer-dimer equilibrium. Thus, the value extrapolated using the data of low concentrations (we define this the value at an infinite dilution) may correspond to the value in a monomer state. The chemical-shift difference between the *trans*- and *cis*-NCH_3 carbons at an infinite dilution is obtained to be about 2.75 ppm, but it may possibly give a somewhat larger value than the true value at an infinite dilution because the present experiment was not done below the concentration of 2%. This value is used to compare with the calculated value.

Temperature Dependence: Next, the temperature dependences of each group in DMA at various concentrations are discussed in the temperature range from 30 to 90 °C. First, the results of the carbonyl and acetyl carbons are shown in Fig. 4. The carbonyl carbon shifts slightly by *ca.* 0.1 ppm at a high field with an increase in the temperature from 30 to 90 °C, whereas the acetyl carbon shifts linearly by *ca.* 0.5 ppm at a high field with an increase in the temperature. The former changes are smaller than those caused by the concentration. Thus, it may be predicted that the influence of the association caused by the variation in the concentration is larger than that caused by the variation in the temperature. As is shown in Fig. 5, the temperature dependence of the *cis*-NCH_3 carbon is slight, but that of the *trans*-NCH_3 carbon shifts greatly at a high field above 50 °C. Therefore, the chemical-shift difference between the two carbons decreases considerably at high temperatures. This is due to the internal rotation about the C–N bond in DMA.

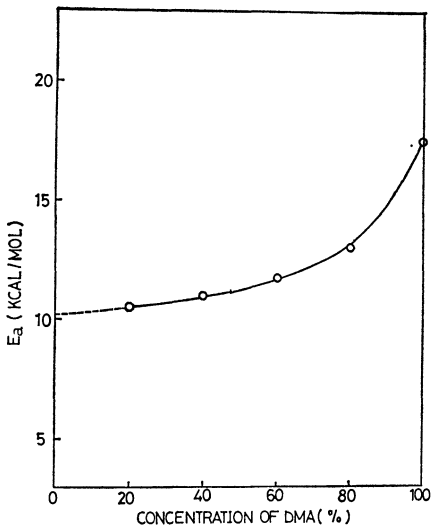

Fig. 6. Concentration dependence of activation energy E_a for the hindered internal rotation about the C–N bond in CCl_4 solution.

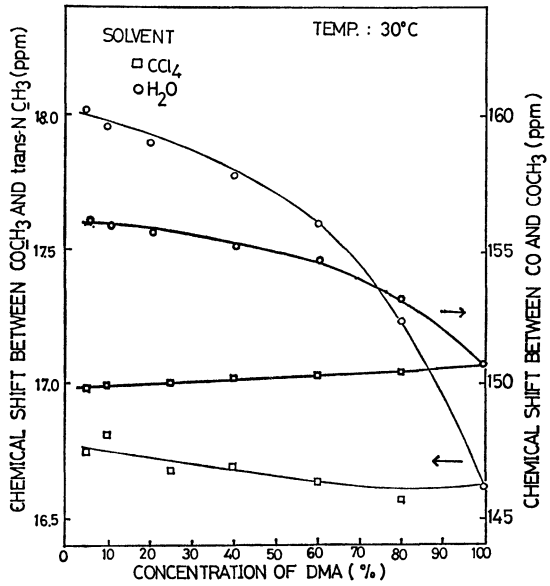

Fig. 7. Concentration dependence of the ^{13}C chemical-shift differences between carbonyl and acetyl carbons, and between *trans*-NCH_3 and acetyl carbons in CCl_4 and H_2O solutions.

From these data, the activation energies of the hindered internal rotation about the C–N bond at various contributions were obtained; they are shown in Fig. 6. The value in a neat liquid was obtained 17.5 kcal/mol, which agrees well with the value of 18.1 kcal/mol obtained from the study of ^1H NMR by Newman *et al.*[2d] Further, the value at an infinite dilution in CCl_4 is given as about 10 kcal/mol. The larger value of E_a in a neat liquid than in the CCl_4 solution may be qualitatively interpreted in terms of the association.

H_2O Solution. Concentration Dependence: The concentration dependence of the chemical-shift difference between the carbonyl and acetyl carbons in H_2O solution was found to be larger than in the CCl_4 solution, as is shown in Fig. 7. This may mainly be due to the existence of the hydrogen bond in the case of the former, while the latter case has no such bond. At an infinite dilution the difference between the two cases is about 6 ppm. On the other hand, the chemical-shift difference between the acetyl and *trans*-NCH_3 carbons in the H_2O solution was found to decrease rapidly, contrary to the case in the CCl_4 solution, as is shown in Fig. 7. Remembering that the chemical shift of the NCH_3 carbon depends hardly at all upon the concentration, this tendency shows that the acetyl carbon shifts to a low field through the formation of a hydrogen bond in an aqueous solution. At an infinite dilution in CCl_4 and H_2O solutions, the difference between the two values becomes about 1.2 ppm; this may be due to an indirect interaction through the formation of a hydrogen bond between the carbonyl group and H_2O. It is well-known that the carbonyl carbon shifts to a low field as a result of the formation of a hydrogen bond; the results shown in Fig. 7 are consistent with this.

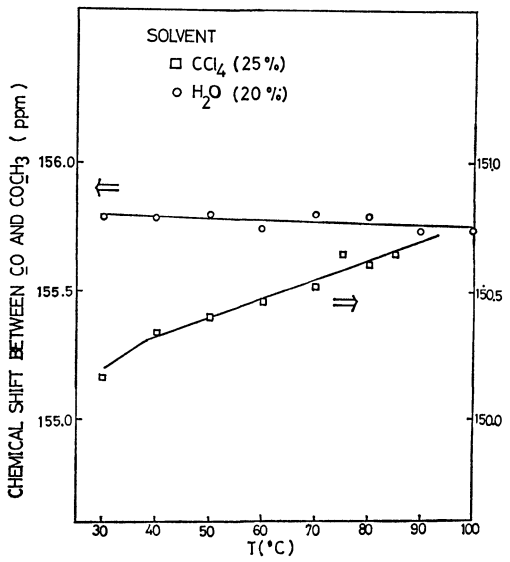

Fig. 8. Temperature dependence of the ^{13}C chemical-shift difference between carbonyl and acetyl carbons in CCl_4 and H_2O solution.

Temperature Dependence: The results of the temperature dependence of each carbon in this system are shown in Figs. 8 and 9. As may be seen from Fig. 8, the chemical-shift difference between the acetyl and carbonyl carbons in an aqueous solution is almost constant from 30 to 100°C, contrary to the case of the CCl_4 solution. This shows that probably the hydrogen bond with the H_2O molecule is stronger than the interaction between the DMA molecules and is more stable in this range of temperatures. Figure 9 shows the temperature dependence of the chemical-shift difference between the *trans*- and *cis*-NCH_3 carbons at various concentrations in an aqueous solution. These chemical-shift differences decrease with a decrease in the concentration below 60 °C. The hydrogen bonds between DMA and H_2O molecules are formed at low concentrations with the internal rotation about the C–N bond, being somewhat hindered, but at higher

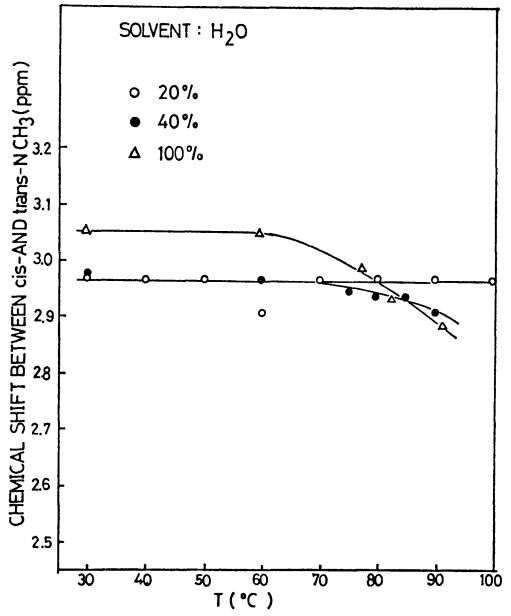

Fig. 9. Temperature dependence of the ^{13}C chemical-shift difference between *cis*-NCH_3 and *trans*-NCH_3 carbons in H_2O solution.

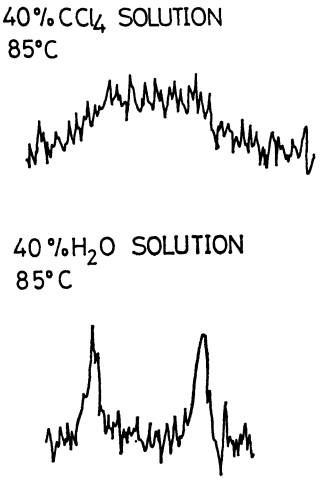

Fig. 10. ^{13}C NMR signals of NCH_3 carbons in CCl_4 and H_2O solution.

concentrations the interaction among DMA molecules becomes effective and, therefore, the rotation about the C–N bond becomes more hindered than in aqueous solutions of low concentrations. Generally, the hydrogen bond may be stronger than the interaction among the DMA molecules. The N–CH_3 carbon signals at 85 °C in 40% CCl_4 and H_2O solutions are shown in Fig. 10. From this it is clear that the rotation about the C–N bond in the H_2O solution is more hindered than in the case of the CCl_4 solution at the same concentration.

H_2SO_4 Solution. Concentration Dependence: The concentration dependence of the chemical shifts of each carbon in DMA is shown in Fig. 11. It is found particularly that the dependence of the carbonyl carbon is somewhat larger than that of the other carbons and that the carbonyl carbon shifts to a low field with a decrease in the concentration. This

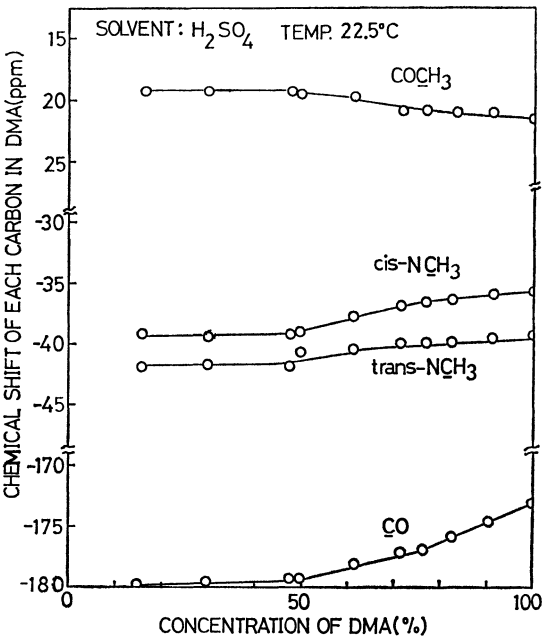

Fig. 11. Concentration dependence of the ^{13}C chemical-shifts of each carbon of *N,N*-dimethylacetamide in H_2SO_4 solution (relative to TMS).

may be due to the formation of protonated DMA molecules at the site of the carbonyl group in the H_2SO_4 solution. Further, the dependence of the *cis*-NCH_3 carbon slightly greater than that of the *trans*-NCH_3 carbon, and these carbons shift to a low field with a decrease in the concentration, contrary to the behavior of the acetyl carbon. These tendencies differ considerably from those of the aqueous solution. Therefore, it may be suggested that the influence of the protonation on the electronic state of DMA differs from that in the case of the hydrogen bond. (This tendency appears in the calculated electron-density distribution, as will be described below.)

Next, the concentration dependence of the nuclear Overhauser enhancement (NOE)[9] of the intensity of

Table 2. Concentration dependence of the enhancement of the carbonyl carbon due to ^1H decoupling in H_2SO_4 solution at 25 °C

Concentration of H_2SO_4 (% v/v)	Ratio of intensity of carbonyl carbon to TMS[a)]
0	1.85
9	1.74
16.7	1.76
23	1.70
28.5	1.83
37.5	1.99
50	3.17
58	3.21
70	3.16
85	3.02

a) Tetramethylsilane is contained as the standard signal (as external reference) to obtain the magnitude of the enhancement due to ^1H decoupling.

Table 3. Chemical shift of monomer *N,N*-dimethylacetamide by average excitation energy method using CNDO/2 method (ppm)

	σ_{dia}	σ_{para}	σ_t
$CO_3\underline{C}H_3$	58.68	−376.80	−318.12
cis-$N\underline{C}H_3$	56.54	−404.43	−347.89
trans-$N\underline{C}H_3$	56.26	−408.47	−352.21
$\underline{C}O$	54.77	−537.73	−480.96

The used value of average excitation energy is 5.69 eV.

the carbonyl carbon signal by the ^1H decoupling is shown in Table 2 to facilitate further study of the nature of the protonation. The enhancement increases rapidly in a 50% solution and the enhancement becomes constant. It may be considered that, when the ratio of the number of DMA's to that of protons is 1 : 1, the enhancement is at its maximum, and that even in high concentrations of H_2SO_4 the full protonation is maintained.

The observed behavior of DMA molecules in various solutions has been described above. We will now discuss this behavior theoretically.

Theoretical Considerations. We have described in a section that the DMA molecule at an infinite dilution in the CCl_4 solution can be considered as in a monomeric state. First, let us discuss this. The results of the calculated chemical shifts as a monomer DMA molecule are shown in Table 3, where, as the average excitation energy, ΔE, the value of 5.69 eV (maximum absorption of amide[10]; 208 nm) obtained by ultraviolet absorption spectroscopy, is adopted. The chemical shift of each carbon is found to be dominated mainly by the paramagnetic term. Each carbon appears in the order of acetyl, *cis*-NCH_3, *trans*-NCH_3, and carbonyl carbons; this order coincides with that of the experimental results. Also, the quantitative agreement between the two sets of results is good. Thus, the present results support McFarlane's statement that the ^{13}C resonance of the methyl group *cis* to the carbonyl group is at a higher field than that which is *trans*. As for these carbons, the observed and calculated chemical-shift differences between the two carbons are 3.09 ppm and 5.32 ppm respectively. Although the latter gives a somewhat larger value than the former, it seems natural to consider the chemical-shift difference between *trans*- and *cis*-NCH_3 carbons as being due to the contribution of the paramagnetic term; this is contrary to McFarlane's suggestion[8] that the principal contribution to this difference arises from an intramolecular electric field due to the carbonyl group.

In the neat liquid the DMA molecule has been suggested, on the basis of experimental results, to exist as the self-association state. We will now proceed to discuss its association based on the quantum-chemical calculation of the conformational energy and the ^{13}C chemical shift, and the experimental data. As has been described in the introduction, several models for the self-association of DMA molecules are possible. In Fig. 12 some models are shown, where (a) is the model of the cyclic structure proposed by Woodbrey

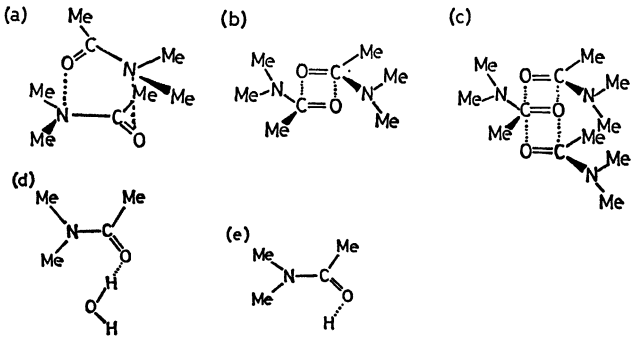

Fig. 12. Some association models (a), (b), (c), and Hydrogen-bonded (d) and protonated (e) DMA models.

et al.[2c] and Newman *et al.*,[2d] and where (b) and (c) are the dimer and trimer of an antiparallel orientation respectively, extending Saito's[12] model proposed for the acetone molecule, *etc.* to the case of the DMA molecule. For these models, the total energies were calculated by the CNDO/2 method; the results are shown in Table 4. The dimerization model (a) becomes unstable, but the (b) and (c) models become stable. The (a) model is unstable by 1.8 kcal/mol (the distance between the N and O atoms is 3 Å). The stabilization energies for the (b) and (c) models are 2.8 and 5.11 kcal/mol respectively (the distance between the C and O atoms is 3 Å). Thus, as the form of the association the (b) and (c) models may be suggested to be more appropriate than the (a) model. The total electron-density distributions of the monomer, dimer, and trimer models are shown in Table 5. As is shown in the (a) model, both N and O atoms have negative charges; therefore, this model may become unstable as a result of the electrostatic repulsion between these atoms. In the (b) and (c) models, however, the C and O atoms have positive and negative charges respectively; therefore, these models become stable as a result of electrostatic attraction between the atoms. As for the (b) model, the dependences of the total energy and the stabilization energy on the distance between the C and O atoms were calculated; the results are shown in Table 6, where the distances of 2.5,3 and 3.5 Å were used. In all of these distances, the formation of dimerization is stable; the stabilization energy at 3 Å is the largest, 2.8 kcal/mol.

Table 4. Total energies of various models in *N,N*-dimethylacetamide calculated by CNDO/2 method

Model	Total energy (eV)	Stabilization energy (eV)	Stabilization energy (kcal/mol)
Monomer	−1776.31104		
Dimer[a]			
(a) Model[b]	−3552.55607	0.06601	1.80
(b) Model[c]	−3552.72559	−0.10351	−2.82

a) These models correspond to those shown in Fig. 15. b) The distance between N and O atoms is 3 Å. c) The distance between C and O atoms is 3 Å.

TABLE 5. ELECTRON DENSITY DISTRIBUTIONS OF VARIOUS MODELS IN *N,N*-DIMETHYLACETAMIDE CALCULATED BY CNDO/2 METHOD

Atom		Monomer	(a)[a]	(b)[b]	(c)model[c]		DMA···H_2O	DMA···H
					Central	External		
O_1		6.351	6.370	6.372	6.374	6.374	6.374	6.161
N_2		5.152	5.140	5.142	5.143	5.139	5.134	5.032
C_3	CO	3.649	3.642	3.637	3.633	3.634	3.624	3.585
C_4	*trans*-NCH$_3$	3.813	3.815	3.814	3.815	3.813	3.818	3.871
C_5	COCH$_3$	4.103	4.105	4.105	4.108	4.104	4.107	4.118
C_6	*cis*-NCH$_3$	3.846	3.853	3.847	3.848	3.848	3.851	3.903
H_7	*trans*-NCH$_3$	1.042	1.041	1.044	1.044	1.045	1.036	0.969
H_8		1.045	1.035	1.036	1.039	1.038	1.041	0.996
H_9		1.045	1.049	1.048	1.039	1.038	1.041	0.996
H_{10}	*cis*-NCH$_3$	1.031	1.029	1.031	1.031	1.032	1.025	0.960
H_{11}		1.017	1.021	1.018	1.020	1.017	1.014	0.975
H_{12}		1.017	1.015	1.021	1.020	1.021	1.014	0.975
H_{13}	COCH$_3$	0.958	0.955	0.957	0.955	0.958	0.953	0.904
H_{14}		0.966	0.964	0.959	0.962	0.958	0.956	0.906
H_{15}		0.966	0.969	0.970	0.962	0.958	0.956	0.906

These models correspond to those shown in Fig. 12. The terms "Central" and "External" correspond to the central and external *N,N*-dimethylacetamides in trimer.
a) The distance between N and O atoms is 3 Å. b), c) The distance between C and O atoms is 3 Å. d) H_7, H_{10}, and H_{13} are *trans* position relative to OC–N bond respectively.

TABLE 6. DEPENDENCE OF TOTAL ENERGY OF DIMER (b) AND TRIMER (c) MODELS IN *N,N*-DIMETHYLACETAMIDE ON DISTANCE BETWEEN C AND O ATOMS CALCULATED BY CNDO/2 METHOD

	Distance (Å)		
	2.5	3.0	3.5
Dimer			
Total energy (eV)	−3552.6799	−3552.7256	−3552.6402
Stabilization energy (kcal/mol)	−1.57	−2.82	−0.49
Trimer			
Total energy (eV)	−5329.0162	−5329.1213	−5328.9616
Stabilization energy (kcal/mol)	−2.26	−5.11	−0.53

Next, let us consider the trimer model. The dependences of the total energies and stabilization energies upon the distance between the DMA molecules at trimeric state are shown in Table 6. Just as in the case of the dimer model, the formation of the trimer is stable, and the stabilization energy at 3 Å becomes the largest value, 5.11 kcal/mol, twice the value in the dimer model. It may be suggested that the DMA molecules in a neat liquid are preferable polymerized in the antiparallel oriented form.

In order to obtain more detailed information about the associated form, let us consider the dipole moment briefly. The dipole moments calculated for various models are shown in Table 7, together with the observed results. The calculated values of the monomer and the (c) model agree well with the observed value. The (a) and (b) models have no dipole moment. Thus, in the odd *n*-mer model it is clear that the *n*-mer has a definite dipole moment. The experimental results cannot be interpreted by the dimer model; therefore, an equilibrium among the various *n*-mers, including the monomer, must exist in the neat liquid or the CCl_4 solution at high concentrations.

Next, let us discuss the value of *n* in terms of the stabilization energy. The results in Fig. 6 show that the energy difference between the hindered rotational energies at an infinite dilution in the CCl_4 solution and in the neat liquid is about 7.5 kcal/mol; this difference may be considered to be the energy due to the change from monomer to *n*-mer. As is shown in Table 6, the stacking between the DMA molecules corresponds to a stabilization energy of about 2—2.5 kcal/mol, one third of the value of 7.5 kcal/mol obtained above. Therefore, the value of *n* is about 4. Accordingly, the DMA molecule may be supposed roughly to exist in a tetramer in the neat liquid, though this is not conclusive.

Further, let us discuss the chemical shift as a continuation of the above description of the chemical shift of the monomer DMA molecule. First, we will treat the concentration dependence of the chemical shift in the CCl_4 solution on the basis of the theoretical results. As is shown in Fig. 1, the chemical shift of the carbonyl carbon shifts to a lower field with an increase in the concentration and shifts about 1.5 ppm in the range from an infinite dilution to a neat liquid. The calculated chemical shift, σ_t, of the carbonyl carbon of the monomer, which corresponds to the molecular structure at an infinite dilution, is −480.36 ppm (Table 3); the σ_t's of the dimer and the trimer, which have been suggested to exist at the neat liquid, are −483.14 ppm and −483.87 ppm for the central DMA and −483.38 ppm for the outside DMA in the trimer, as is shown in Tables 8 and 9 (in this case,

Table 7. Dipole moment of *N,N*-dimethylacetamide calculaed by CNDO/2 methoed and observed (D.U.)

Monomer	(a)model	(b)model	(c)model	DMA···H_2O	DMA···H	Obsd[a]
3.22	0.0	0.0	3.39	5.44	6.99	3.79

In (b) and (c) models the distance between C and O atoms is 3 Å.
a) Observed at 30 °C in benzene (Ref. 11).

Table 8. Dependence of chemical shift of dimer (b)model in *N,N*-dimethylacetamide on distance between C and O atoms by average excitation energy method using CNDO/2 method. σ_t (ppm)

	Distance (Å)		
	2.5	3.0	3.5
$CO\underline{C}H_3$	−317.62	−318.02	−318.13
cis-$N\underline{C}H_3$	−347.49	−348.01	−348.54
trans-$N\underline{C}H_3$	−351.99	−352.05	−352.10
$\underline{C}O$	−484.68	−483.14	−482.05

The used value of average excitation energy is 5.69 eV.

Table 9. Chemical shift of trimer (c)model in *N,N*-dimethylacetamide calculated by average excitation energy using CNDO/2 method. σ_t (ppm)

	Central[a]	External[a]
$CO\underline{C}H_3$	−317.75	−318.10
cis-$N\underline{C}H_3$	−348.07	−347.97
trans-$N\underline{C}H_3$	−351.73	−352.19
$\underline{C}O$	−483.87	−483.38

a) The terms "Central" and External" correspond to the central and external *N,N*-dimethylacetamide in trimer model.
The used value of average excitation energy is 5.69 eV.
The distance between C and O atoms is 3 Å.

the distance between the DMA molecules is 3 Å). From this, the carbonyl carbon is found to shift about 2 ppm to a lower field upon the formation of the dimer and the trimer. Therefore, this result agrees well with the observed one. The observed chemical shifts of the acetyl, *cis*-NCH_3, and *trans*-NCH_3 carbons did not depend as greatly on the concentration as in the case of the carbonyl carbon. On the other hand, the calculated chemical shifts of these carbons in the monomer, dimer, and trimer differ almost not at all from each other; this agrees with the observed results.

Next, let us concern ourselves with the behavior of DMA in the H_2O and H_2SO_4 solutions in terms of the chemical-shift calculation in addition to the above observed results. de Jeu[13] has suggested a reasonable model for the molecular structure of the acetone molecule in the corresponding solution based on his study of ^1H, ^{13}C, and ^{17}O NMR. We have adopted his model for the molecular structure of DMA which have a carbonyl group like the acetone molecule in their solutions. These corresponding models are shown in Fig. 12. The hydrogen-bonded >C=O···H–O–H amide–solvent associate (d) and protonated >C=O ···H associate (e) are formed in the H_2O and H_2SO_4 solutions respectively. Here, the ∠ >C=O···H and ∠H–O–H bond angles are set at 120° and 105° respectively, while the O–H bond length is set at 1.05 Å. The distances between the oxygen of the carbonyl group and the hydrogen atom for the cases of >C=O···H–O–H and >C=O···H are 1.34 Å and 0.985 Å respectively.[13] The electron-density distributions of these models are shown in Table 5. The protonated DMA shows a very high charge separation, as a whole, compared with the other structures. Correspondingly, as is shown in Table 7, the dipole moment is larger than that of the other structure. However, in the DMA···H_2O structure, although the charge separation does not change compared with the monomer, the dipole moment is relatively large because of the association with H_2O. If these results are confirmed experimentally, it will give important information about the DMA association in solution. Further, let us discuss the chemical shifts of these models. The carbonyl carbon is sensitively influenced by the formation of a hydrogen bond and by protonation. The difference between the carbonyl carbons at infinite dilutions in the CCl_4 and H_2O solutions is found to be about 6 ppm, as is shown in Fig. 7. These structures correspond to the monomer and the structure (d) shown in Fig. 12. From Tables 3 and 10, the corresponding calculated chemical-shift difference is found to be about 6 ppm (=487.18—480.96 ppm). This agrees well with the observed results. Also, as for the NCH_3 carbons, the observed results agree with the calculated result that the *trans*- and *cis*-NCH_3 carbons in the H_2O solution shift at a higher fileld than in the CCl_4 solution. These results suggest that the association model described above for the structure of the DMA molecule in the H_2O solution is a plausible model.

Table 10. Chemical shift of model hydrogen-bonded and protonated model in *N,N*-dimethylacet amide calculated by average excitation energy method using CNDO/2 method. σ_t (ppm)

	DMA···H_2O	DMA···H
$CO\underline{C}H_3$	−317.93	−319.07
cis-$N\underline{C}H_3$	−347.19	−340.23
trans-$N\underline{C}H_3$	−351.42	−344.06
$\underline{C}O$	−487.18	−497.05

The used value of average excitation energy is 5.69 eV.

Next, let us concern ourselves with the chemical shift of DMA in the H_2SO_4 solution. As expected for the electron-density distribution of this model, the calculated chemical shift of the carbonyl carbon occurs at a lower field than that of the hydrogen-bonded model and appears at a field lower by about 16 ppm

than that of the monomer model. However, the observed chemical shift of the carbonyl carbon at an infinite dilution in the H_2SO_4 solution appears at a field lower by only about 5 ppm than that at an infinite dilution in the CCl_4 solution; this value is smaller than the value obtained in the case of the hydrogen-bonded DMA with H_2O. Further, the calculated chemical shifts of the other carbons do not agree with the observed results. As the causes of these disagreements, the following reasons may be noted. i) the present model is not always appropriate, ii) the ΔE approximation for this case is gross, and so on. It will be necessary to study this problem in more detail in order to obtain exact information about the protonated DMA molecule.

References

1) H. S. Gutowsky and D. H. Holm, *J. Chem. Phys.*, **25**, 1228 (1956).

2) For example; (a) G. Fraenkel and C. Franconi, *J. Amer. Chem. Soc.*, **88**, 4478 (1960); (b) M. T. Rogers and J. C. Woodbrey, *J. Phys. Chem.*, **66**, 540 (1962); (c) J. C. Woodbrey and M. T. Rogers, *J. Amer. Chem. Soc.*, **84**, 13 (1962); (d) R. C. Newman, Jr. and L. B. Young, *J. Phys. Chem.*, **69**, 2570 (1965); (e) L. A. LaPlanche, H. B. Thompson, and M. T. Rogers, *ibid.*, **69**, 1482 (1965); (f) A. G. Whittaker and S. Siegel, *J. Chem. Phys.*, **42**, 3320 (1965); (g) R. C. Neuman, Jr., D. N. Roark, and V. Jonas, *J. Amer Chem.. Soc.*, **89**, 3412 (1967); (h) M. Rabinovitz and A. Pines, *ibid.*, **91**, 1585 (1969); (i) R. C. Neuman, Jr., W. R. Woolfeuden, and V. Jonas, *J. Phys. Chem.*, **73**, 3117 (1969); (j) A. Calzolari, F. Conti, and C. Franconi, *J. Chem. Soc., B*, **1970**, 555; (k) R. C. Neuman, Jr., and V. Jonas, *J. Phys. Chem.*, **75**, 3532, 3550 (1971); (l) K. Sato and A. Nishioka, This Bulletin **44**, 52, 2931 (1971); (m) T. Drankenberg, K. Dahlqvist, and S. Forsen, *J. Phys. Chem.*, **76**, 2178 (1972); (n) H. Akiyama, F. Furuya, and K. Ouch., Reprints of the 12th NMR Symposium, Hiroshima (1973), pp. 217, 220; (o) As general review; G. Binsch, *Topics Stereochem.*, **3**, 97 (1968); W. E. Stewart and T. H. Siddall, III, *Chem. Rev.*, **70**, 517 (1970); H. Kessler, *Angew. Chem.*, **82**, 237 (1970).

3) For example; (a) J. F. Yam, F. A. Momany, R. Hoffmann, and H. A. Scherage, *J. Phys. Chem.*, **74**, 420 (1970); (b) see Ref. 2 (1).

4) J. A. Pople, *Mol. Phys.*, **7**, 301 (1964).

5) J. A. Pople and D. L. Beveridge, "Approximate Molecular Orbital Theory," McGraw-Hill Book Co., New York (1970), p. 111.

6) T. Yonezawa, I. Morishima, and H. Kato, This Bulletin, **39**, 1398 (1966).

7) C. C. Costain and J. M. M. Dowling., *J. Chem. Phys.*, **32**, 158 (1960).

8) W. McFarlane, *Chem. Commun.*, **1970**, 418.

9) G. C. Levy and G. L. Nelson, "Carbon-13 Nuclear Magnetic Resonance for Organic Chemists," Wiley-Interscience, New York (1972), p. 33.

10) R. M. Silverstein, "Spectrometric Identification of Organic Compounds", John Wiley & Sons, New York (1964), p. 98.

11) W. D. Kumler and C. W. Porter, *J. Amer. Chem. Soc.*, **56**, 2549 (1934).

12) H. Saito, Y. Tanaka, S. Nagata, and K. Nukada, *Can. J. Chem.*, **51**, 2118 (1973).

13) W. H. de Jeu, *J. Phys. Chem.*, **74**, 822 (1970).

The Crystal and Molecular Structure of Versicolorin C, A Metabolite of *Aspergillus versicolor*

Keiichi FUKUYAMA, Tomitake TSUKIHARA, Yukiteru KATSUBE, Takashi HAMASAKI,* and Yuichi HATSUDA*

Faculty of Engineering, Tottori University, Koyama, Tottori 680

(Received February 24, 1975)

The crystal structure of versicolorin C, $C_{18}H_{12}O_7$, has been determined by the X-ray diffraction method. The crystals are monoclinic, with the space group $P2_1/a$, and with four molecules in a unit cell with dimensions of $a=24.918(7)$, $b=7.922(3)$, $c=7.003(3)$ Å, and $\beta=92.85(4)°$. The structure was refined by the least-squares method to $R=0.053$ for 1693 non-zero reflections. There are two intramolecular hydrogen bonds. A pair of molecules related by a center of symmetry forms a dimer by means of intermolecular hydrogen bonds.

Aspergillus versicolor (Vuillemin) Tiraboschi and *Aspergillus flavus* Link ex Fries produce a variety of compounds which contain a tetrahydrofuranofuran or a dihydrofuranofuran moiety. Versicolorin C, containing a tetrahydrofuranofuran moiety, was isolated as a metabolite of *Aspergillus versicolor*.[1] The crystal structures of several compounds containing a dihydrofuranofuran moiety have been determined in our laboratory. The structural investigation of the title compound is of interest in connection with the metabolites containing a dihydrofuranofuran moiety; these metabolites are believed to be toxic to animals.[2] The crystal and molecular structure of aflatoxin B_2, which has a tetrahydrofuranofuran moiety, was described in detail by van Soest *et al.*[3] As few X-ray analysis have, however, been done on the compounds involving a tetrahydrofuranofuran moiety, it seems worth carrying out the X-ray analysis of versicolorin C in order to obtain additional information about the dimensions of this moiety. Another point of interest in this analysis is to confirm the structural formula (shown below) proposed on the basis of the chemical

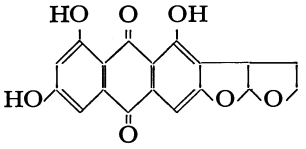

and spectroscopic methods.[1] This investigation has been undertaken as part of a series of systematic studies of the structures of the metabolites of the genus *Aspergillus*.[4-6]

Experimental

Versicolorin C, crystallized from an acetone solution in the form of orange red plates elongated along the b-axis. The crystal data and experimental conditions are summarized in Table 1. The intensities were collected on a Rigaku Denki computer-controlled four-circle diffractometer with a scintillation counter equipped with a pulse-height analyser. Attenuators were inserted when the maximum counting rate exceeded 8000 cps. The background was measured for 8 sec at both the start and end points of the scan range. Out of 2024 independent reflections measured up to $\sin\theta/\lambda=0.562$, 1696 reflections had a non-zero intensity. No significant variation in the intensities of the three reference reflections were observed during the data-collection process. The intensities were corrected for the Lorentz and polarization factors, but not for the absorption.

TABLE 1. CRYSTAL DATA AND EXPERIMENTAL CONDITIONS OF VERSICOLORIN C

Molecular formula	$C_{18}H_{12}O_7$
Molecular weight	340.3
Crystal system	monoclinic
Space group	$P2_1/a$
$a=24.918(7)$, $b=7.922(3)$, $c=7.003(3)$ Å	
$\beta=92.85(4)°$	
$V=1381$ Å^3	
$D_c=1.637$ g cm^{-3} (for $Z=4$)	
$\mu(\mathrm{Cu}K\alpha)=11.0$ cm^{-1}	
Crystal size	*ca.* $0.05\times0.10\times0.15$ mm
Radiation	Ni-filtered Cu$K\alpha$
Scan technique	ω-2θ
Scan speed (ω)	2° min^{-1}
Scan range (ω)	$1.0°+0.15°\tan\theta$

Structure Determination and Refinement

The orientation and location of the anthraquinone skeleton was determined by an interpretation of a three-dimensional Patterson map. A three-dimensional Fourier synthesis computed with the signs due to the skeleton revealed all the remaining non-hydrogen atoms. The atomic coordinates and isotropic temperature factors were refined by a block-diagonal least-squares method. By introducing anisotropic temperature factors for the non-hydrogen atoms in the refinement, the R value was reduced to 0.081. Three intense reflections, 220, 221, and 321, were rejected from the subsequent calculations. The positions of the hydrogen atoms were determined by a difference Fourier synthesis computed at this stage. The final refinement was made by including the positional parameters and isotropic temperature factors of the hydrogen atoms, using the following weighting scheme: $w=0.0$ for $F_o=0$, $w=1.0$ for $0<F_o\leqq40$, and $w=1.0/(1.0+0.467(F_o-40))$ for $40<F_o$. The final R value was 0.053 for 1693 non-zero reflections. The final atomic parameters are listed in Table 2. A list of observed and calculated structure factors is preserved by the Chemical Society of Japan (Document No. 7517).

The atomic scattering factors were taken from the International Tables for X-ray Crystallography.[7] The computations were performed on a TOSBAC 3400

* Faculty of Agriculture, Tottori University, Koyama, Tottori 680.

TABLE 2(a). FINAL ATOMIC PARAMETERS AND e.s.d.'s ($\times 10^4$) FOR NON-HYDROGEN ATOMS
The anisotropic temperature factors are of the form: $\exp(-\beta_{11}h^2-\beta_{22}k^2-\beta_{33}l^2-\beta_{12}hk-\beta_{13}hl-\beta_{23}kl)$

	x	y	z	β_{11}	β_{22}	β_{33}	β_{12}	β_{13}	β_{23}
C (1)	1476(1)	5043(4)	6822(4)	12(1)	155(6)	158(7)	3(3)	3(3)	−21(11)
C (2)	969(1)	4567(4)	7381(4)	13(1)	122(6)	150(6)	6(3)	12(3)	−8(10)
C (3)	622(1)	3679(4)	6106(4)	11(1)	128(6)	149(6)	12(3)	7(3)	15(10)
C (4)	83(1)	3210(4)	6633(4)	12(1)	127(6)	154(6)	11(3)	10(3)	11(10)
C (5)	−268(1)	2285(4)	5316(4)	11(1)	119(5)	147(6)	10(3)	0(3)	34(10)
C (6)	−789(1)	1758(4)	5780(4)	12(1)	148(6)	161(7)	12(3)	15(3)	16(11)
C (7)	−1115(1)	849(4)	4501(4)	11(1)	149(6)	195(7)	10(3)	4(3)	37(11)
C (8)	−935(1)	436(4)	2721(4)	12(1)	145(6)	186(7)	8(3)	−11(3)	19(11)
C (9)	−422(1)	928(4)	2204(4)	13(1)	145(6)	172(7)	7(3)	−1(3)	7(11)
C (10)	−96(1)	1812(4)	3488(4)	12(1)	119(6)	160(7)	10(3)	8(3)	34(10)
C (11)	460(1)	2233(4)	2948(4)	14(1)	122(6)	143(6)	10(3)	5(3)	30(10)
C (12)	802(1)	3251(4)	4274(4)	12(1)	122(6)	143(6)	7(3)	14(3)	10(10)
C (13)	1302(1)	3756(4)	3695(4)	13(1)	166(6)	163(7)	−4(3)	14(3)	−7(11)
C (14)	1617(1)	4673(4)	4985(4)	12(1)	172(7)	180(7)	−2(3)	19(3)	17(12)
C (15)	2326(1)	6214(5)	6294(5)	15(1)	187(7)	209(8)	−13(3)	3(3)	31(13)
C (16)	2693(1)	4169(6)	8244(5)	18(1)	262(9)	209(8)	23(4)	7(4)	81(14)
C (17)	2238(1)	4865(5)	9352(5)	15(1)	241(8)	191(8)	0(4)	−2(3)	−10(14)
C (18)	1920(1)	5959(5)	7875(5)	13(1)	174(7)	200(7)	−1(3)	6(3)	−48(12)
O (1)	842(1)	5003(3)	9166(3)	15(1)	203(5)	148(5)	−2(2)	14(2)	−76(8)
O (2)	−79(1)	3660(3)	8240(3)	14(1)	225(5)	144(5)	4(2)	23(2)	−75(8)
O (3)	−988(1)	2138(3)	7496(3)	14(1)	221(5)	184(5)	−7(2)	29(2)	−52(8)
O (4)	−1271(1)	−442(3)	1508(3)	14(1)	232(5)	204(5)	−11(2)	−6(2)	−73(9)
O (5)	624(1)	1713(3)	1428(3)	16(1)	200(5)	155(5)	−9(2)	25(2)	−76(8)
O (6)	2111(1)	5310(3)	4601(3)	14(1)	222(5)	200(5)	−25(2)	20(2)	−20(9)
O (7)	2806(1)	5503(4)	6921(3)	12(1)	320(6)	235(6)	−5(3)	8(2)	78(10)

TABLE 2(b). FINAL POSITIONAL PARAMETERS ($\times 10^3$) AND ISOTROPIC TEMPERATURE FACTORS (Å^2)

	x	y	z	B
H (1)	52(2)	447(6)	939(6)	6.4(12)
H (2)	−74(2)	270(5)	820(5)	4.6(16)
H (3)	−148(1)	47(4)	490(4)	1.7(7)
H (4)	−110(2)	−83(5)	48(5)	4.6(10)
H (5)	−30(1)	66(5)	88(5)	3.4(9)
H (6)	139(1)	343(5)	231(5)	3.1(8)
H (7)	238(1)	748(5)	585(5)	3.2(8)
H (8)	257(1)	303(5)	748(5)	4.0(9)
H (9)	306(2)	402(5)	914(5)	4.5(10)
H (10)	240(2)	552(6)	1044(6)	5.1(11)
H (11)	201(1)	386(4)	977(4)	2.2(7)
H (12)	181(1)	707(5)	846(5)	3.0(8)

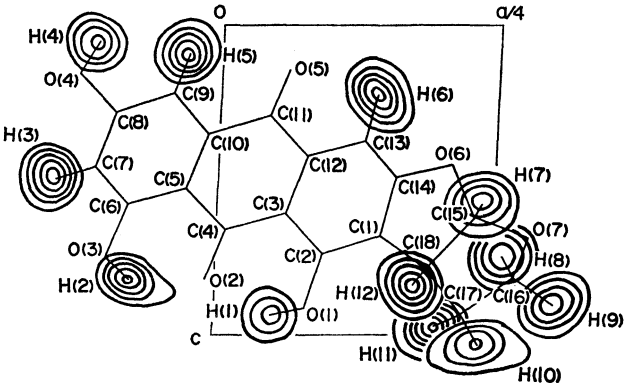

Fig. 1. The difference electron density map of versicolorin C. The contours are at equally spaced intervals on an arbitrary scale.

computer at the Tottori University Computing Center and on a NEAC 2200-N700 computer at the Computation Center of Osaka University.

Results and Discussion

The structural formula of versicolorin C has been confirmed by this X-ray analysis. The difference-electron-density map and the numbering of atoms are shown in Fig. 1, which indicates the presence of two intramolecular hydrogen bonds, O(1)–H(1)···O(2) and O(3)–H(2)···O(2). The bond lengths and angles are shown in Fig. 2 and Table 3. In the quinonoid group, the lengths of the C(3)–C(4) and C(4)–C(5) bonds are shorter than those of the C(10)–C(11) and C(11)–C(12) bonds, and the length of the C(4)–O(2) bond is longer than that of the C(11)–O(5) bond. Such a lack of equivalence of bond lengths in the quinonoid group implies that the double-bond character at the C(11)–O(5) bond in the $\begin{matrix}C(10)\\C(12)\end{matrix}\!\!>$C(11)=O(5) system is greater than that at the C(4)–O(2) bond in the $\begin{matrix}C(3)\\C(5)\end{matrix}\!\!>$C(4)=O(2) system. These features are also found in averufin[5] and *N,N'*-diphenyl-1,8-diaminoanthraquinone.[8] As is shown in Table 4,

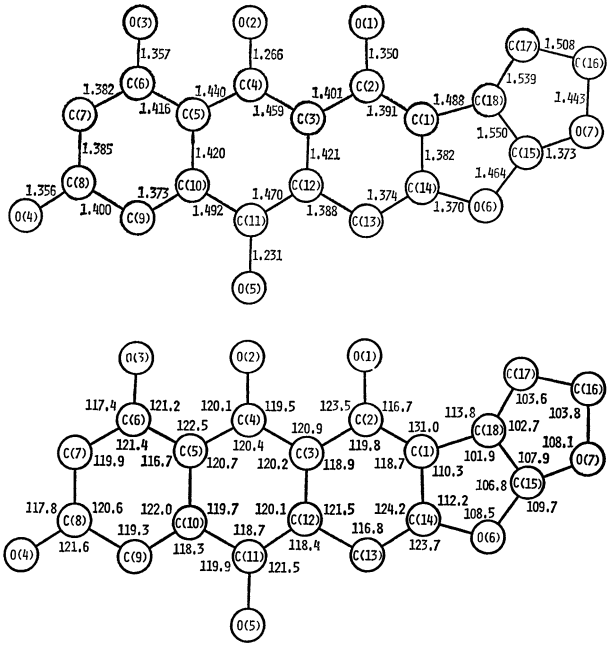

Fig. 2. The bond lengths (Å) and angles (°). The mean estimated standard deviations for the bond lengths and angles are about 0.004 Å and 0.3°, respectively.

TABLE 3. BOND LENGTHS AND ANGLES INVOLVING HYDROGEN ATOMS

The mean estimated standard deviations of the bond lengths and angles are 0.04 Å and 2°, respectively. Broken lines indicate hydrogen bonds.

(a) Bond lengths (Å)			
O(1)-H(1)	0.93	O(2)···H(1)	1.78
O(3)-H(2)	0.89	O(2)···H(2)	1.81
C(7)-H(3)	1.01	O(4)-H(4)	0.91
O(5)[a]···H(4)	1.96	C(9)-H(5)	1.02
C(13)-H(6)	1.04	C(15)-H(7)	1.06
C(16)-H(8)	1.08	C(16)-H(9)	1.09
C(17)-H(10)	0.99	C(17)-H(11)	1.03
C(18)-H(12)	1.02		
(b) Bond angles (°)			
C(2)-O(1)-H(1)	107	O(1)-H(1)···O(2)	143
C(4)-O(2)···H(1)	102	O(6)-O(3)-H(2)	109
O(3)-H(2)···O(2)	146	C(4)-O(2)···H(2)	101
H(2)···O(2)···H(1)	154	C(6)-C(7)-H(3)	119
C(8)-C(7)-H(3)	121	C(8)-O(4)-H(4)	111
O(4)-H(4)···O(5)[a]	171	C(11)[a]-O(5)[a]···H(4)	162
C(8)-C(9)-H(5)	120	C(10)-C(9)-H(5)	121
C(12)-C(13)-H(6)	115	C(14)-C(13)-H(6)	128
C(18)-C(15)-H(7)	116	O(6)-C(15)-H(7)	106
O(7)-C(15)-H(7)	111	C(17)-C(16)-H(8)	111
O(7)-C(16)-H(8)	110	C(17)-C(16)-H(9)	112
O(7)-C(16)-H(9)	105	H(8)-C(16)-H(9)	113
C(16)-C(17)-H(10)	107	C(18)-C(17)-H(10)	114
C(16)-C(17)-H(11)	108	C(18)-C(17)-H(11)	110
H(11)-C(17)-H(10)	113	C(1)-C(18)-H(12)	114
C(15)-C(18)-H(12)	112	C(17)-C(18)-H(12)	111

a) $-x, -y, -z$

the dimensions of the tetrahydrofuranofuran moiety in versicolorin C are in good agreement with those of the moiety in aflatoxin B_2.[3] Among the three C(sp^3)–O bonds in the tetrahydrofuranofuran moiety, the length of the C(15)–O(7) bond (1.373 Å) is significantly shorter than the others (1.464 and 1.443 Å), and

TABLE 4. COMPARISON OF THE BOND LENGTHS AND ANGLES IN THE TETRAHYDROFURANOFURAN MOIETY OF VERSICOLORIN C AND THOSE OF AFLATOXIN B_2

Standard deviations are given in parentheses.

(a) Bond lengths (Å)	versicolorin C	aflatoxin B_2
C(1)-C(14)	1.382(5)	1.382(3)
C(1)-C(18)	1.488(5)	1.504(3)
C(14)-O(6)	1.370(4)	1.359(3)
C(15)-C(18)	1.550(5)	1.553(4)
C(15)-O(6)	1.464(5)	1.465(3)
C(15)-O(7)	1.373(5)	1.385(5)
C(16)-C(17)	1.508(6)	1.513(6)
C(16)-O(7)	1.443(5)	1.434(5)
C(17)-C(18)	1.539(5)	1.523(5)
(b) Bond angles (°)	**versicolorin C**	**aflatoxin B_2**
C(2)-C(1)-C(18)	131.0(3)	132.2(3)
C(14)-C(1)-C(18)	110.3(3)	110.5(2)
C(1)-C(14)-O(6)	112.2(3)	112.5(2)
C(13)-C(14)-O(6)	123.7(3)	122.4(3)
C(18)-C(15)-O(6)	106.8(3)	107.3(2)
C(18)-C(15)-O(7)	107.9(3)	107.7(5)
O(6)-C(15)-O(7)	109.7(3)	110.0(5)
C(17)-C(16)-O(7)	103.8(3)	103.9(6)
C(16)-C(17)-C(18)	103.6(3)	103.1(5)
C(1)-C(18)-C(15)	101.9(3)	101.0(3)
C(1)-C(18)-C(17)	113.8(3)	115.4(3)
C(15)-C(18)-C(17)	102.7(3)	102.9(4)
C(14)-O(6)-C(15)	108.5(3)	107.3(3)
C(15)-O(7)-C(16)	108.1(3)	108.6(4)

TABLE 5. DEVIATIONS OF ATOMS FROM EACH PLANE (Å)

(a) Plane through anthraquinone-skeleton with O(1), O(3), and O(4) atoms			
C(1)	0.003	C(2)	0.025
C(3)	0.007	C(4)	−0.013
C(5)	−0.020	C(6)	0.001
C(7)	0.014	C(8)	0.006
C(9)	−0.011	C(10)	−0.006
C(11)	0.058	C(12)	−0.004
C(13)	−0.056	C(14)	−0.082
O(1)	0.065	O(2)	−0.058
O(3)	−0.002	O(4)	0.006
O(5)	0.174	C(15)[a]	−0.182
C(18)[a]	0.032	O(6)[a]	−0.180
(b) Plane through the terminal five-membered ring			
C(15)	0.030	C(17)	0.017
C(18)	−0.027	O(7)	−0.021
C(16)[a]	0.525		

a) Not included in the least-squares calculation.

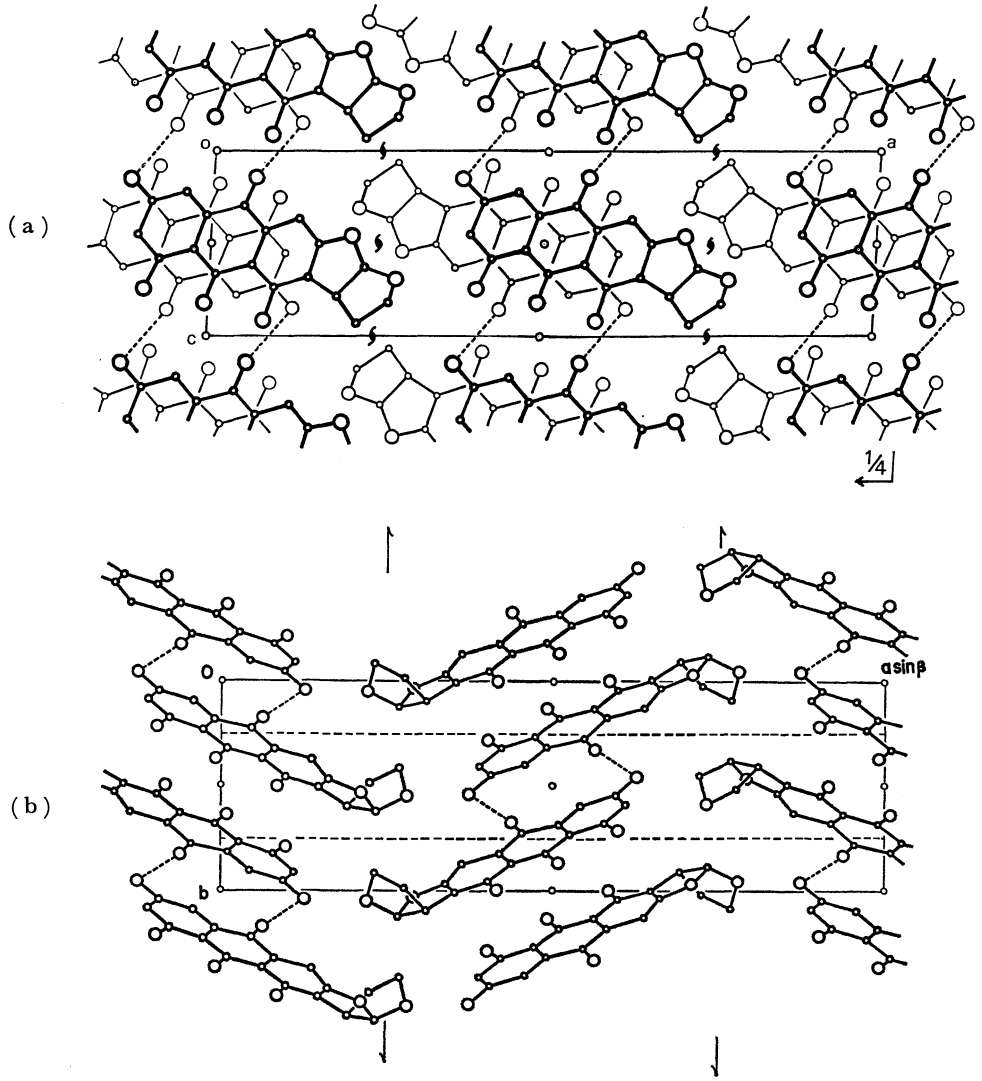

Fig. 3. The crystal structure of versicolorin C; (a) viewed along the b-axis, (b) viewed along the c-axis. Broken lines indicate intermolecular hydrogen bonds.

among the three $C(sp^3)$–$C(sp^3)$ bonds in the moiety, the length of the C(16)–C(17) bond (1.508 Å) is slightly shorter than the others (1.539 and 1.550 Å).

The least-squares planes through the anthraquinone skeleton with the O(1), O(3), and O(4) atoms and through the terminal five-membered ring except the C(16) atom are represented by these equations:

$$0.3501X - 0.8582Y + 0.3754Z = -0.4366,$$

and

$$0.2722X + 0.8409Y + 0.4678Z = 7.7470$$

respectively, where $X=ax+cz\cos\beta$, $Y=by$, and $Z=cz\sin\beta$. The dihedral angle between the above planes is 63.2°, compared with that of 62.8° in aflatoxin B_2.[3] The deviations of the atoms from these planes are listed in Table 5, which indicates that the anthraquinone skeleton is slightly twisted along the longitudinal axis of the molecule and that the terminal five-membered ring is puckered at the C(16) atom.

The crystal structure is shown in Fig. 3. A pair of molecules related by a center of symmetry are linked together by intermolecular hydrogen bonds, O(4)–H(4)···O(5) (2.857 Å), to form a dimer. The parallel dimers are held together by van der Waals

Table 6. Intermolecular distances (Å) less than 3.5 Å

C (8)···O (5)^{i}	3.488	C (9)···O (5)^{i}	3.313
O (5)···O (4)^{i}	2.857[a)]	C (13)···O (1)^{ii}	3.462
O (5)···O (1)^{ii}	3.112	O (5)···O (2)^{ii}	3.169
C (2)···O (4)^{iii}	3.434	C (3)···C (8)^{iii}	3.441
C (3)···O (4)^{iii}	3.422	C (4)···C (9)^{iii}	3.472
C (5)···C (9)^{iii}	3.486	C (5)···C (10)^{iii}	3.462
C (6)···O (5)^{iii}	3.387	C (6)···C (11)^{iii}	3.374
C (11)···C (7)^{iii}	3.395	C (12)···C (7)^{iii}	3.439
O (3)···O (5)^{iii}	3.260	C (1)···C (7)^{iv}	3.489
C (5)···C (3)^{iv}	3.451	C (11)···O (2)^{iv}	3.478
C (12)···O (2)^{iv}	3.467	C (13)···O (3)^{iv}	3.439
C (14)···O (3)^{iv}	3.403	C (13)···O (7)^{v}	3.444
O (7)···C (7)^{vi}	3.420		

Symmetry code: i) $-x$, $-y$, $-z$ ii) x, y, $-1+z$ iii) $-x$, $-y$, $1-z$ iv) $-x$, $1-y$, $1-z$ v) $1/2-x$, $-1/2+y$, $1-z$ vi) $1/2+x$, $1/2-y$, z
a) Hydrogen bond

forces to stack in the direction of the b-axis; the interplanar distances are 3.39 and 3.40 Å. The intermolecular distances for the non-hydrogen atoms shorter than 3.5 Å are listed in Table 6, which indicates the absence of any abnormally short contact.

The authors wish to thank Professor Tamaichi Ashida of Nagoya University for his permission to use the block-diagonal least-squares program and the staff of the Institute for Protein Research of Osaka University for the use of the diffractometer.

References

1) T. Hamasaki, Y. Hatsuda, N. Terashima, and M. Renbutsu, *Agr. Biol. Chem.*, **29**, 696 (1965).
2) A. Ciegler, E. B. Lillehoj, R. E. Peterson, and H. H. Hall, *Appl. Microbiol.*, **14**, 934 (1966).
3) T. C. van Soest and A. F. Peerdeman, *Acta Crystallogr.*, **B26**, 1956 (1970).
4) N. Tanaka, Y. Katsube, Y. Hatsuda, T. Hamasaki, and M. Ishida, This Bulletin, **43**, 3635 (1970).
5) Y. Katsube, T. Tsukihara, N. Tanaka, K. Ando, T. Hamasaki, and Y. Hatsuda, *ibid.*, **45**, 2091 (1972).
6) K. Fukuyama, T. Tsukihara, Y. Katsube, T. Hamasaki, Y. Hatsuda, N. Tanaka, T. Ashida, and M. Kakudo, *ibid.*, **48**, 1639 (1975).
7) "International Tables for X-ray Crystallography," Vol. III, Kynoch Press, Birmingham (1962), p. 202.
8) M. Bailey and C. J. Brown, *Acta Crystallogr.*, **22**, 493 (1967).

Temperature Effects on the Electronic Spectra of 2-Methyl-1-aceanthrenone

Satoshi HIRAYAMA

Faculty of Textile Science, Kyoto Technical University, Matsugasaki, Sakyo-ku, Kyoto 606

(Received February 27, 1975)

The absorption, fluorescence, and excitation spectra of 2-methyl-1-aceanthrenone (I) were investigated in several solvents in the temperature range of 77—298 K. The results show that the hydrogen-bonded (fluorescent) and non-hydrogen-bonded (very weakly fluorescent) molecules of I coexist in ethanol to a comparable extent. This is the reason why its absorption spectra are very broad in alcoholic solvents. With a decrease in the temperature, the apparent fluorescence quantum yield in ethanol at first rises to a maximum (0.37) at 197 K and then decreases. Below *ca.* 113 K, a new fluorescence band due to the non-hydrogen-bonded molecule appears. In 2-methyltetrahydrofuran (MTHF), the temperature dependence of the fluorescence quantum yield of I is significant only at low temperatures. The yield varies monotonously from 0.014 at 132 K to 0.30 at 77 K. A behavior intermediate between those in ethanol and in MTHF is observed in EPA. The rise and fall of the fluorescence quantum yield in ethanol or in EPA may be interpreted in terms of the temperature-dependent concentration change in the hydrogen-bonded molecule. From the results in MTHF, the maximum rate constant of the intersystem crossing between the $S_{1\pi\pi^*}$ and $T_{n\pi^*}$ states is estimated to be of the order of 10^{13} s^{-1}.

The way to interprete the electronic spectra of 9-anthracenecarboxaldehyde (9-CHO-A), which is distinguished from the other 9-carbonyl derivatives of anthracene by its high photochemical reactivity, is not unique,[1,2] because the diffuse nature of the electronic spectra makes impossible any accurate location of electronic states. This ambiguity has often led to very different interpretations of experimental results.[3–5] Recently, however, the present author has noted that a comparison of the electronic spectra of 9-CHO-A with those of 2-methyl-1-aceanthrenone (I), which is very similar in molecular structure to 9-CHO-A but which shows well-defined electronic spectra in all of the non-hydrogen-bonded, hydrogen-bonded, and cation forms, has made it possible to elucidate the electronic nature of the excited states of 9-CHO-A.[6]

Although such a comparison is successful in some points, as has previously shown,[6] the spectroscopic data on I and 9-CHO-A have never been adequate enough. In this paper, therefore, prominent, newly found temperature effects on the electronic spectra and the fluorescence quantum yields of I will be reported. The results obtained will not only confirm the author's earlier interpretation as to the electronic nature of the excited states of 9-CHO-A and I,[6] but will also add important experimental facts on the radiationless transition processes of 9-carbonylanthracenes.[6–11] Furthermore, compound I may be expected to serve as a model compound in interpreting unestablished spectroscopic properties of the compounds whose carbonyl groups are co-planar or almost co-planar with the parent aromatic rings.[12] For instance, the present results will point out, as may be seen below, that the interpretation of the spectroscopic properties of pyrene-3-aldehyde (3-CHO-P) and 9-CHO-A given by Förster *et al.*[1] should be re-examined.

Experimental

Materials. Compound I, obtained as one of the main photo-products of 9-α-bromopropionylanthracene,[9] was purified by column chromatography and was then sublimated twice *in vacuo*. The 9-methylanthracene (9-Me-A) was synthesized according to the well-known method[13] and recrystallized from ethanol. The 9,10-diphenylanthracene (9,10-diph-A) was obtained from the Nakarai Chem. Co., Ltd., and was used as received.

Among the solvents employed for the spectroscopic measurements, *n*-hexane and ethanol were of a spectro grade. Acetonitrile (ACN), dimethylformamide (DMF), 2-methyltetrahydrofuran (MTHF), methylenedichloride (MDC), triethylamine (TEA), isopentane (IP), methylcyclohexane (MCH), and diethyl ether were of a guaranteed grade from the Nakarai Chem. Co., Ltd., and were distilled carefully before use.

Optical Measurements. The absorption spectra were taken on a Hitachi Dual-Beam Spectrophotometer 124. For low temperature measurements, a rectangular quartz cell ($1\times1\times5$ cm, with a glass pipe 30 cm long attached on the top of the cell to facilitate handling and evacuation), each corner of which was well-fused in order to avoid cracking due to sudden cooling or warming, was held by a block made of brass, and the whole was put into a transparent Dewar vessel. The same type of cell and Dewar vessel as described above was used as a reference-cell combination. Only the sample-cell combination was cooled.

The excitation and fluorescence spectra were recorded on a Shimadzu Corrected Spectrofluorophotometer, RF 502, whose spectral characteristics have been described elsewhere.[6] For measurements at low temperatures, a Dewar vessel and a sample cell described previously[6] were employed. Correction for the spectral response of its particular cell arrangement was carried out by using a quinine bisulfate solution (5×10^{-5} M in 0.5 M sulfuric acid[14]) and an ethanol solution of anthracene as standard solutions for the fluorescence and excitation spectral measurements respectively.

In every case, the temperature of the sample was controlled by boiling liquid nitrogen using a power resister and allowing cold nitrogen gas to enter the Dewar vessel. The temperature was monitored through a thermocouple immersed in the sample cell and was recorded on a Yokogawa recorder, Type 3046. After thermal equilibrium had been reached, all the measurements were performed.

Determination of the Fluorescence Quantum Yields. In order to determine the fluorescence quantum yields as a function of the temperature, it is necessary to correct for the absorbance change with the temperature, so the absorption spectra of I were measured in MTHF, ethanol, and EPA (ether, isopentane and ethanol 5 : 5 : 2 by volume) at various temperatures. Thus, a calibration curve of the absorbance change as a function of the temperature was obtained for each solvent. A similar correction was made at 77 K for 9-Me-A,[15] which was used as a fluorescence-quantum-yield

standard of the unit yield at 77 K. The excitation of the fluorescence was performed at the 0–0 band of the $^1L_b \leftarrow {}^1A$ transition of I[6] (370 nm, band pass, 5 nm), since this band showed little spectral shift upon a decrease in the temperature.

A comparison of the areas of the corrected fluorescence spectra of I taken at various temperatures with that of 9-Me-A obtained at 77 K gave the relative fluorescence quantum yields of I at the corresponding temperatures. In correcting the relative fluorescence quantum yield, allowance was not made for variation in the refractive indices of the solvents with the temperature, since appropriate data were not available.

The relative fluorescence quantum yields of I in various solvents at room temperature were determined in a similar manner except that 9,10-diph-A was used as the fluorescence quantum-yield standard of the unit yield.[15] The change in the refractive index with the solvent was taken into account in this case.[17]

Since oxygen did not affect the present results, all these experiments were carried out without degassing. The fluorescence intensity was always measured in a dilute solution ($2—3\times10^{-5}$ M).

Results

Figure 1 shows the temperature dependence of the absorption spectra of I in ethanol. A small peak at 418 nm seen at room temperature gradually sharpened as the temperature was decreased and eventually became the main absorption band, with a peak at 425 nm at 77 K. Corresponding to this, a shoulder at 425 nm at room temperature came to form a small but clearly resolved band with a peak at 433 nm. The position of the latter band agreed approximately with the 0–0 absorption band observed for the hydrogen-bonded molecule of I formed in *n*-hexane containing a small amount of trichloroacetic acid (abbreviated as IH hereafter).[6]

In non-polar solvents, such as MCH or IP, and aprotic polar solvents, such as MTHF, however, no peak corresponding to the one at 433 nm was found at any temperature. Consequently, the small absorption peak at 433 nm found in ethanol at low temperatures can be attributed to a hydrogen-bonded molecule.

From the (g) spectrum, approximately 5—10% of I is seen to exist in a hydrogen-bonded form, even at 77 K, if the hydrogen-bonded molecule of I in ethanol is assumed to have a molar extinction coefficient of a magnitude similar to that of IH.

Figure 2 shows the effect of the temperature on the fluorescence spectra of I in ethanol. At first the spectrum was diffuse, but it gradually became structured with a decrease in the temperature. At tem-

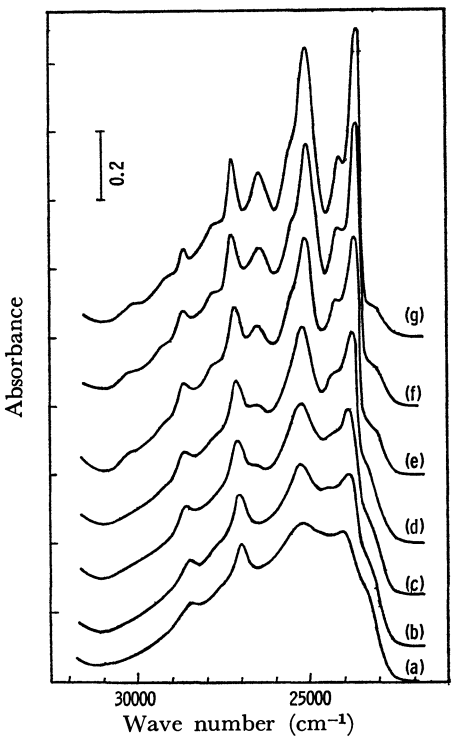

Fig. 1. Temperature effect on the absorption spectra of I (6.0×10^{-5} M) in ethanol.
(a) 290 K, (b) 250 K, (c) 233 K, (d) 190 K, (e) 160 K, (f) 125 K, (g) 77 K.
For the sake of clarity, the base line (right-hand side) of each spectrum is shifted by an appropriate amount of absorbance. The small peaks at 433 nm seen clearly in (e)—(g) are due to the hydrogen-bonded molecule of I. The decrease in the absorbance at 433 nm with a decrease in the temperature can be verified by a comparison of (d)—(g).

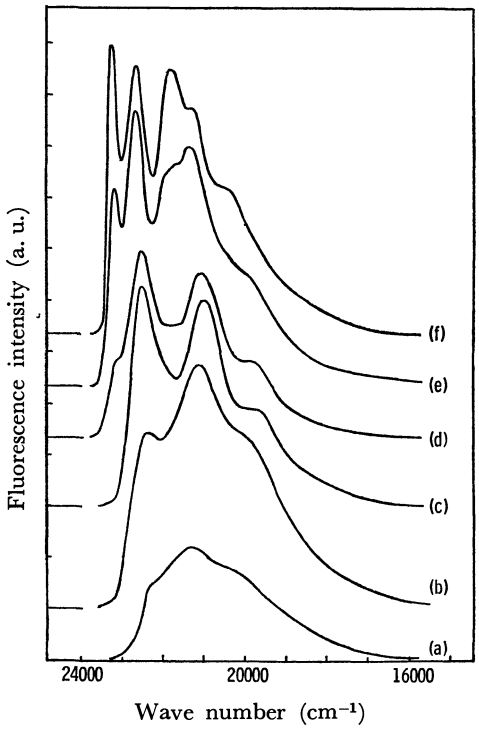

Fig. 2. Temperature effect on the fluorescence spectra of I (*ca.* 3×10^{-5} M) in ethanol.
(a) 256 K, (b) 185 K, (c) 134 K, (d) 103 K, (e) 89 K, (f) 77 K.
The excitation wavelength was 370 nm (band pass, 5 nm). The base line of emission intensity for each spectrum is shown by the solid line on the left-hand side. The fluorescence intensity of each spectrum is not parallel with the fluorescence quantum yield (for the exact value, see Fig. 5). Below *ca.* 110 K a new fluorescence band due to the non-hydrogen-bonded molecule appears on the shorter-wavelength side.

peratures near 134 K, the observed fluorescence spectrum closely resembles that of IH observed at room temperature.[6] It should be noted that the temperature effect on the shift of the fluorescence 0–0 band frequency (or the fluorescence-maximum frequency) is relatively small, reflecting a rigid molecular structure of I.[1] At temperatures below *ca.* 110 K, a new fluorescence band began to grow on the shorter-wavelength side; at 77 K this band surpassed the band at the longer wavelength.

The excitation spectra of the fluorescence of I in ethanol were also observed under similar conditions; the results are displayed in Fig. 3. In comparison with the absorption spectra shown in Fig. 1, it is quite evident that the main absorbing species is not the emitting species. The excitation spectra at low temperatures above *ca.* 110 K agreed well with those of IH, indicating that fluorescence is emitted by the hydrogen-bonded molecule. Below *ca.* 100 K, however, the excitation spectra changed significantly with the wavelength where fluorescence is observed, since, at these temperatures, two kinds of fluorescence are observable with a comparable intensity.

In Fig. 4 the fluorescence spectra of I in MTHF at low temperatures are shown. Contrary to the case in ethanol, the fluorescence spectrum in MTHF consists of only one component, which corresponds well to the component observed on the shorter-wavelength side in ethanol at very low temperatures. Evidently, the fluorescence observed in MTHF is due to a non-hydrogen-bonded molecule of I, so, of the two fluorescence components in ethanol, the one on the shorter-wavelength side can be attributed to the non-hydrogen-bonded molecule.

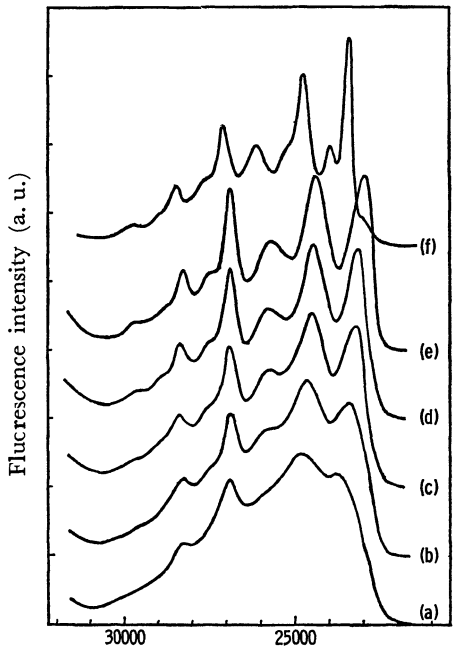

Fig. 3. Temperature effect on the excitation spectra of I (*ca.* 3×10^{-5} M) in ethanol.
(a) 290 K, (b) 236 K, (c) 185 K, (d) 148 K, (e) 106 K, (f) 77 K.
The fluorescence intensity was observed at 470 nm (the approximate fluorescence maximum of the hydrogen-bonded molecule of I) except in the case of (f), where the measurement was made at 460 nm (the approximate fluorescence maximum of the non-hydrogen-bonded molecule of I). In comparison with Fig. 1, it is evident that, except for 77 K, the excitation spectra do not accord with the absorption spectra. The coincidence of the spectra at 77 K is fortuitous.

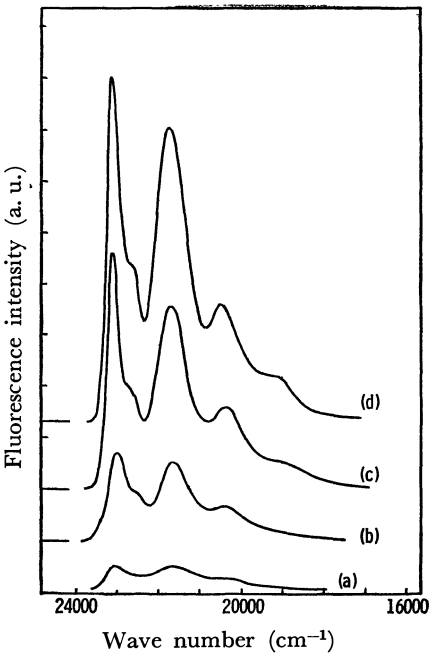

Fig. 4. Temperature effect on the fluorescence spectra of I (*ca.* 2×10^{-5} M) in MTHF.
(a) 128 K, (b) 111 K, (c) 98 K, (d) 92 K.
The excitation wavelength was 370 nm (band pass, 5 nm). The base line of the emission intensity for each spectrum is shown by the solid line on the left-hand side. The fluorescence intensity is not parallel with the fluorescence quantum yield (for the exact value, see Fig. 5). Below 92 K the fluorescence spectra are almost the same in shape.

In non-polar solvents such as MCH and IP, only a very weak fluorescence was observed. The fluorescence spectra in these solvents at 77 K were unresolved and shifted greatly to the red (λ_{max}=480 nm). In a frozen matrix of these solvents, diffuse emission spectra are frequently observed, probably because either of educed microcrystals or aggregated molecules of solutes. However, the absorption spectra of I observed in a mixed solvent of MCH and IP (3 : 1 by volume, abbreviated as MCHIP) down to temperatures as low as 77 K revealed that, at such a low concentration ($2-3\times10^{-5}$ M) as was used for the fluorescence measurements, the eduction of the solute was minute; hence, most of the solute must be dissolved homogeneously. Therefore, it may be presumed that the red-shifted weak emission observed in MCH or IP is due to educed microcrystals and that the temperature effect on the fluorescence yield of I is not appreciable in these non-polar solvents. The reason for this will be considered in a later section.

In Fig. 5 the temperature dependences of the fluores-

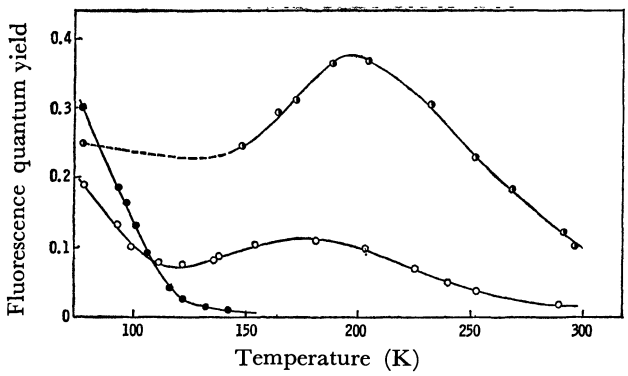

Fig. 5. Temperature dependence of the fluorescence quantum yields of I in ethanol, EPA, and MTHF.
—◑—: ethanol, —○—: EPA, —●—: MTHF.
Between 150 and 77 K a precise determination of the quantum yields in ethanol was difficult because of its unhomogeneous glassing.

cence yields of I in three media are depicted. In ethanol and EPA, the hydrogen-bonded and non-hydrogen-bonded molecules should coexist, so the obtained fluorescence yields in these media are sums of the apparent fluorescence yields from the two species. In MTHF, only at very low temperatures, the fluorescence became appreciable and the fluorescence quantum yield increased monotonously with a decrease in the temperature.

The behavior seen in EPA is intermediate between those in ethanol and in MTHF. The once-decreased fluorescence quantum yield begins rapidly to increase again near 113 K. Below this temperature, there was almost no fluorescence exhibited by the hydrogen-bonded molecule, and at 77 K no evidence for the existence of the hydrogen-bonded molecule was found in any of the absorption, excitation, and fluorescence spectra. Hence, the second increase in the apparent yield is attributable to the increase in the fluorescence quantum yield of the non-hydrogen-bonded molecule. This difference in temperature dependence between that in ethanol and that in EPA seems to reflect a difference in the hydrogen-bonding ability of these media toward I at low temperatures.

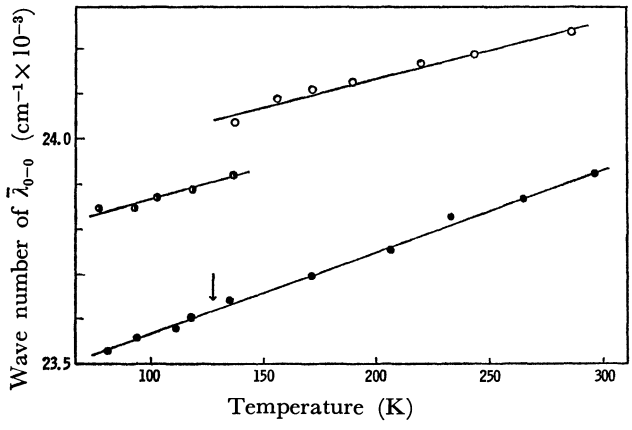

Fig. 6. Temperature-induced red shifts of the 0–0 absorption bands of $^1L_a \leftarrow {}^1A$ in MCHIP and MTHF.
—◑—: MCHIP, —○—: MCHIP, —●—: MTHF.
In MCHIP, the red shift of the 0–0 absorption band, and a large spectral change in shape were both observed as is shown in Fig. 7.

In Fig. 6 the frequencies of the 0–0 bands of the $^1L_a \leftarrow {}^1A$ transition observed in MTHF and MCHIP are plotted against the temperature. The red shift in MTHF is monotonous. In MCHIP not only the red shift but also the inversion of the absorption intensity was observed, as is represented in Fig. 7. As the temperature was lowered, a new band appeared on the longer-wavelength side of the band which was temporarily assigned as a 0–0 band at room temperature. A further decrease in the temperature inverted the absorption intensities of these two bands. In Fig. 6, therefore, the two frequencies of these two bands are plotted against the temperature. In either case, however, the magnitude of the red shift observed on cooling to 77 K is greater in MTHF than in MCHIP. Moreover, the value of $\bar{\lambda}_{0-0}$ in MTHF at the temperature where the fluorescence quantum yield of I begins to increase (indicated by the arrow in Fig. 6) is still smaller than the smallest $\bar{\lambda}_{0-0}$ (at 77 K) in MCHIP. These two facts are worth mentioning when we note that the lowering of the excited singlet-state energy is

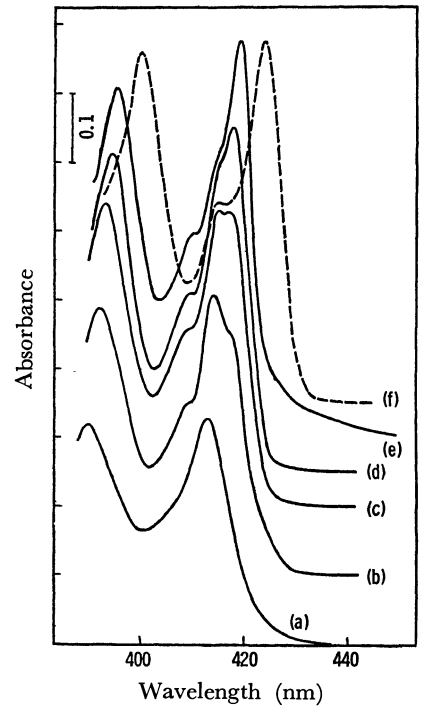

Fig. 7. Temperature effect on the absorption spectra of I (3.3×10^{-5} M) in MCHIP.
(a) 286 K, (b) 188 K, (c) 156 K, (d) 138 K, (e) 77 K, (f) 77 K (in EPA).
For the sake of clarity, the base line of each spectrum is shifted by an appropriate amount of absorbance. For comparison, the absorption spectrum in EPA (the broken line) is also shown. The broad tail seen for (e) is indicative of the existence of the educed microcrystals of I, which may be responsible for a broad weak fluorescence in this medium at 77 K. The other vibrational bands which belong to the ^1L_a or ^1L_b band did not show any marked change in shape as the temperature is lowered.

Table 1. Fluorescence quantum yields of I in various solvents

Solvent	Quantum yield[a]	Fluorescence maximum[b] ($10^{-3} \times cm^{-1}$)
n-Hexane	<0.002	22.22
TEA	<0.002[c]	—
MDC	0.016	21.65
MTHF	0.006 (0.30)[d]	21.88
DMF	0.011	21.60
ACN	0.016	21.74
EPA	0.017 (0.19)[d]	21.65
Ethanol	0.12 (0.25)[d]	21.37
n-Hexane + a small amount of trichloroacetic acid	0.78[e]	21.28[e]

a) Values at *ca.* 18 °C with reference to 9,10-diph-A. For further details, see text. b) Data on the absorption spectra of I are given in Ref. 6. c) A strong fluorescence similar to the one in MTHF at 77 K was also observed in this solvent at 77 K. The 0-0 absorption band shifted much more to the red, compared with those in the other non-polar solvents. d) The quantum yields at 77 K, with reference to 9-Me-A. e) The values for IH.

indispensable for the appearance of the strong fluorescence of I, as will be discussed later.

Relative fluorescence quantum yields of I obtained in various solvents at room temperature are collected in Table 1. It is evident from Table 1 tends to show fluorescence activation.[1] The comparatively high fluorescence quantum yield in ethanol is due to the coexisting hydrogen-bonded molecule.

Discussion

Temperature Effects on the Electronic Spectra. As is shown in Fig. 1, it is evident that, in ethanol at least, two forms of I, *i.e.*, the hydrogen-bonded and the non-hydrogen-bonded molecules, exist to a comparable extent. Thus, the present author's earlier supposition[6] that the diffuse absorption spectra of I in ethanol and acetic acid must be partly due to the coexistence of the two species has been confirmed experimentally. It is the rigid molecular structure of I that makes such experimental confirmation feasible.

In contrast to the rather rapid sharpening in the shape of the absorption and excitation spectra, the fluorescence spectra become structured less rapidly with a decrease in the temperature. On the other hand, the fluorescence spectra of IH are considerably structured, even at room temperature. From these facts, it may be inferred that the hydrogen-bonded molecule of I in ethanol does not have a definite composition and structure, but rather a loose structure composed of several solvent molecules which may be deformable upon photo-excitation.[18] Such a structure is appropriate to explain the absence of the hydrogen-bonded molecule in EPA at 77 K, in contrast to the case in ethanol.

The temperature effect on the absorption spectra of I in non-hydrogen-atom-donating polar solvents is merely a red shift. The magnitude of the red shift of I in MTHF between room temperature and 77 K (400 cm^{-1}) is larger than the corresponding values for 9-Me-A (240 cm^{-1}) and 9-propionylanthracene (9-CH_3CH_2CO-A, 200 cm^{-1}). (The latter compound shows an analogous temperature effect on the fluorescence intensity at temperatures near 77 K.) This is indicative of the greater increase in the dipole moment of the excited singlet state of I, compared with those of 9-Me-A and 9-CH_3CH_2CO-A, and also compatible with the great increase in the basicity of the carbonyl group of I at the first excited singlet state.[6]

The cause of the anomalous temperature effect seen in the absorption spectrum of I in MCHIP is not yet clear. Dissolved oxygen and moisture did not affect the spectrum. A trace amount of impurities, if any, cannot explain such a large spectral change. Since the spectra observed at temperatures below *ca.* 140 K are quite close to those in MTHF except for the larger red shift in the latter solvent, the anomalous spectrum change may be related to a structural change in I, probably occurring in the slightly strained five-membered ring. Such a structural change brought about by lowering the temperature will affect the transition moments, resulting in the reversal of the absorption intensities.[19]

Temperature Effects on the Fluorescence Quantum Yields. Since fluorescence in ethanol is emitted almost entirely from the hydrogen-bonded molecule except at very low temperatures, the rise or fall of the apparent fluorescence yield seen above 113 K must be determined by the variation in the fluorescence quantum yield of the hydrogen-bonded molecule and/or the variation in its concentration with the temperature. Since the fluorescence quantum yield of IH was determined to be close to unity (0.78), if a value with a similar magnitude is adopted for the fluorescence quantum yield of the hydrogen bonded molecule in ethanol[20] its temperature-induced increase, if any, will be too small to account for the initial three-fold increase in the apparent fluorescence quantum yield.

On the other hand, the heat of formation of IH was calculated as -12.6 kcal mol^{-1} from the temperature dependence of its formation constant. Therefore, for the hydrogen-bonded molecule formed in ethanol, we can also expect at least a negative value for its heat of formation, though it may plausibly be larger than -12.6 because of the stronger interactions between ethanol molecules compared with those of *n*-hexane, in which the heat of formation of IH was determined. Moreover, as has been calculated from the 0–0 band frequencies of the absorption and fluorescence spectra by the use of the Förster cycle, the hydrogen-bond formation constant, K, in ethanol is larger at the first excited singlet state than at the ground state. The difference in log K for the excited singlet state between at 298 and 200 K is calculated to be greater than 0.5, corresponding to more than a three-fold increase in the concentration of the electronically excited hydrogen-bonded molecule on cooling to 200 K, if the hydrogen-bonding at the excited state is completely accomplished. Hence, the initial increase in

the apparent fluorescence yield shown in Fig. 4 can most reasonably be interpreted in terms of the increase in the concentrations of the hydrogen-bonded molecules both at the ground and first excited singlet states.

At temperatures near the melting point of ethanol, however, the interactions of solvent molecules themselves come to predominate over interactions between I and ethanol molecules. As a result of this, a gradual decrease in the concentration of the hydrogen-bonded molecules, and hence a fall in the apparent fluorescence quantum yield shown in Fig. 4, are brought about. Although it may be difficult to verify quantitatively the initial increase in the concentration of the hydrogen-bonded molecule at the ground state from the absorption spectra shown in Fig. 1, the decrease in its concentration below *ca.* 190 K is definitely indicated by the absorption spectra.

In EPA, as is shown in Fig. 2 in Ref. 6, no evidence for the existence of the hydrogen-bonded molecule of I could be obtained at 77 K, indicating a prohibition of the hydrogen-bond formation at very low temperatures.[22]

A similar phenomenon, *i.e.*, the appearance of a maximum in fluorescence quantum yields when the temperature is varied, has previously been noted for 3-CHO-P by Förster *et al.*[1] It was inferred by these authors that the $\pi\rightarrow\pi^*$ and $n\rightarrow\pi^*$ excited singlet states ($S_{\pi\pi^*}$ and $S_{n\pi^*}$ respectively) are close-lying in this molecule and that a decrease in the temperature brings about a level inversion between fluorescent $S_{\pi\pi^*}$ and non-fluorescent $S_{n\pi^*}$ states, which is responsible for the rise and fall in the fluorescence quantum yield of 3-CHO-P as a function of the temperature. Although this concept is now widely accepted,[21] strong evidence supporting their proposition has not yet been obtained. Particularly, the location of the $S_{n\pi^*}$ state has not yet been established experimentally. Considering the analogous spectroscopic behavior found in three compounds—I, 9-CHO-A, and 3-CHO-P,[1,6,23] the interpretation given in the present paper for the temperature dependence of the fluorescence quantum yield of I seems also applicable to the case of 3-CHO-P.[23] In this sense, the proposition given by Förster *et al.* should be re-examined, though the complex electronic spectra of 3-CHO-P may prevent the drawing of a definite conclusion.

Mechanism of the Intersystem Crossing. Based on the facts that a high radiative electronic transition probability is expected for I because of its large molar extinction coefficient[9b] and that I does not suffer any significant photochemical reactions which affect the excitation energy dissipation processes,[6] the very low fluorescence quantum yield inherent in I must be interpreted in terms of the existence of an efficient intersystem crossing process. In the other non-fluorescent 9-carbonylanthracenes, a similar circumstance has already been met with, and the two main factors which determine the efficiency of the intersystem crossing process have previously been proposed by the present author and his co-workers.[9] One is the relative positions of the $S_{1\pi\pi^*}$ and $T_{n\pi^*}$ states, between which the intersystem crossing process is supposed to be dominant, while the other is the degree of the prohibition of the rotational motion of the carbonyl group upon photo-excitation.

Since the lowest excited singlet state of I is undoubtedly $S_{1\pi\pi^*}$, as has been discussed in Ref. 6, and since a significant structural change of I upon photo-excitation is unexpected in view of its structure, the temperature and solvent effects on the fluorescence quantum yield of I can be interpreted most reasonably in terms of these effects on the position of the $S_{1\pi\pi^*}$ state relative to that of the $T_{n\pi^*}$ state, which is expected to lie in the close vicinity of the $S_{1\pi\pi^*}$ state.[24] If the energy of the $S_{1\pi\pi^*}$ state is lowered relative to that of the $T_{n\pi^*}$ state by some cause, fluorescence will come to be emitted. In this sense, it is noteworthy that the red shift of $\bar{\lambda}_{0-0}$ with a decrease in the temperature is larger in MTHF than in non-polar solvents, where temperature-induced fluorescence enhancement was not observed. In the former solvent, moreover, the energy of the $T_{n\pi^*}$ state must be higher than those in non-polar solvents. The increase in the energy of the $T_{n\pi^*}$ state will add to the energy gap between $S_{1\pi\pi^*}$ and $T_{n\pi^*}$ state by that amount. This is the reason for the presence of a rather strong fluorescence in MTHF at very low temperatures.

It will be instructive to apply our reasoning to the case of IH. The energy of the $S_{1\pi\pi^*}$ state of IH is lower by 630 cm^{-1} than that of I in *n*-hexane, while the $T_{n\pi^*}$ state of IH is expected to shift greatly in the higher-energy direction on account of the lowering of the energy of the n-orbital of oxygen. Because of these effects, the energy gap between the $S_{1\pi\pi^*}$ and $T_{n\pi^*}$ states of IH is far greater than the corresponding gap of the non-hydrogen-bonded molecule in polar solvents. As a result, the fluorescence quantum yield of IH is considered to take a high value, close to unity.

Analysis of the Temperature Dependence of the Fluorescence Quantum Yield. When the external quenching of the fluorescence is absent, the following three processes are considered to determine the fluorescence quantum yield of I: the radiative process, the temperature-independent intersystem crossing process, probably from the $S_{1\pi\pi^*}$ state to the $T_{2\pi\pi^*}$ state, and the temperature-dependent intersystem crossing process from the $S_{1\pi\pi^*}$ state to the $T_{n\pi^*}$ state. We will represent the rate constants of these processes by k_f, k_{is}, and k'_{is} with the activation energy of E_a respectively. Then the fluorescence quantum yield, $\phi_f(T)$, at the temperature, T K, can be given by Eq. (1):

$$\phi_f(T) = \frac{k_f}{k_f + k_{is} + k'_{is}\exp(-E_a/RT)} \tag{1}$$

where k_f is assumed to be independent of the temperature and where the rate constant of the internal conversion from the $S_{1\pi\pi^*}$ state is assumed to be negligibly small, as is frequently done for anthracene derivatives.[25]

Equation (1) can also be rewritten as:

$$\ln\left(\frac{1}{\phi_f(T)} - 1 - \frac{k_{is}}{k_f}\right) = \ln\frac{k'_{is}}{k_f} - \frac{E_a}{RT} \tag{2}$$

The results in MTHF were analyzed by the use of Eq. (2). Since the value of k_{is}/k_f is not known in

our case, by putting an appropriate value of k_{is}/k_f into Eq. (2) the left-hand side of Eq. (2) was plotted against $1/T$. When $k_{is}/k_f=2.2$, the most satisfactory straight line, with a correlation coefficient of 0.998, was obtained. From the slope of the line, the activation energy was calculated as 780 cm^{-1}. From the intercept, assuming $k_f=10^8\ s^{-1}$, $k'_{is}\simeq 10^{13}\ s^{-1}$ was also obtained. Then the limiting maximum fluorescence quantum yield calculated from these values becomes 0.313, very close to that found at 77 K in MTHF.[26]

The very large value of k'_{is}, which is not unreasonably high for the rate constant of a transition between two excited states of different electronic natures, explains the very low fluorescence quantum yield of I, particularly in non-polar solvents. If a similar value can be adopted for the corresponding process of the other 9-carbonylanthracenes, its magnitude will be large enough to account for the absence of fluorescence in these compounds at the ambient temperature.[7-11]

References

1) K. Bredereck, Th. Förster, and H. G. Oesterlin, "Molecular Luminescence of Organic Materials," ed. by H. Kallmann and G. M. Spruch, Wiley, New York (1962), p. 164.

2) R. N. Nurumukhametov, *Opt. Spectrosc.*, **23**, 209 (1967).

3) J. F. Young and S. G. Schulman, *Talanta*, **20**, 399 (1973).

4) P. Suppan, *Tetrahedron Lett.*, **1971**, 4469.

5) D. A. Warwick and C. H. J. Wells, *ibid.*, **1969**, 4955.

6) S. Hirayama, This Bulletin, **48**, 1127 (1975).

7) T. Matsumoto, M. Sato, and S. Hirayama, *Chem. Phys. Lett.*, **13**, 13 (1972).

8) T. Matsumoto, M. Sato, and S. Hirayama, *ibid.*, **18**, 563 (1973).

9) (a) T. Matsumoto, M. Sato, and S. Hirayama, *ibid.*, **27**, 237 (1974). (b) T. Matsumoto, M. Sato, and S. Hirayama, This Bulletin, **48**, 1659 (1975).

10) S. Hirayama, *Rev. Phys. Chem. Japan*, **42**, 49 (1972).

11) T. Matsumoto, M. Sato, and S. Hirayama, This Bulletin, **47**, 358 (1974).

12) P. Bentley, J. F. McKeller, and G. O. Phillips, *J. Chem. Soc., Perkin II*, **1974**, 523.

13) A. Sieglitz and R. Marx, *Ber.*, **56**, 1619 (1923).

14) W. H. Melhuish, *J. Phys. Chem.*, **64**, 762 (1960).

15) E. C. Lim, J. D. Laposa, and J. M. H. Yu, *J. Mol. Spectrosc.*, **19**, 412 (1966). 9-Me-A was suitable as a fluorescence-quantum-yield standard at 77 K because it had a sharp absorption peak similar to that of I at the excitation wavelength.

16) (a) I. B. Berlman, "Handbook of Fluorescence Spectra of Aromatic Molecules," Academic Press, New York (1965), p. 130. (b) I. B. Berlman, *Chem. Phys. Lett.*, **21**, 344 (1973).

17) J. A. Riddick and W. B. Bunger, "Techniques of Chemistry," Vol. II, ed. by A. Weissberger, Wiley-Interscience, New York (1970).

18) Since a stronger interaction between I and ethanol molecules was expected in non-polar solvents, the temperature effect on the absorption spectrum of I was investigated in IP containing 1—10% ethanol down to temperatures as low as 163 K. However, no marked spectral change indicative of a considerable amount of the hydrogen-bonded molecule was observed.

19) Such a structural change is assumed to be already occurring in MTHF.

20) To assume a high value for the fluorescence quantum yield of the hydrogen-bonded molecule in ethanol is reasonable when we take into account the apparent fluorescence quantum yield of 0.37 at 197 K, where the amount of the hydrogen-bonded molecule is estimated as 20—25%.

21) C. A. Parker, "Photoluminescence of Solutions," Elsevier Publishing Company, New York (1968), pp. 376, 433.

22) To confirm whether or not this suppression of the hydrogen-bond formation in polar solvents at low temperatures is general, the temperature effects on the concentration change of IH were studied in MCHIP (trichloroacetic acid 1.4×10^{-3} M) and EPA (trichloroacetic acid *ca.* 0.2 M). In the former medium, as expected, the concentration of IH increased continuously with a decrease in the temperature, until almost all the molecules of I had been transformed into IH (and IH_n; $1:n$ complex). In the latter, however, in spite of the much higher concentration of trichloroacetic acid, the concentration of IH was low and decreased slightly at low temperatures with a decrease in the temperature. The amount of IH formed in other polar solvents, such as ACN, DMF, and MTHF, was also minute.

23) P. Kröning, *Z. Naturforsch.*, **29a**, 804 (1974). Kröning has reported in the above paper that the monomer fluorescence quantum yield of 3-CHO-P in polar media depends considerably on the excitation wavelength, increasing steeply in the long-wave tail of the first absorption band. This phenomenon can also be interpreted in terms of the coexistence of a hydrogen-bonded (fluorescent) molecule and a non-hydrogen-bonded (non-fluorescent) molecule, without trusting to the concept of a dynamic model or local heating, as Kröning did. In fact, he found that the absorption and excitation spectra of 3-CHO-P in hydroxylic media did not accord with each other, implying the existence of two different species.

24) D. A. Warwick and C. H. J. Wells, *Tetrahedron Lett.*, **1968**, 4401.

25) J. B. Birks, "Photophysics of Aromatic Molecules," Interscience, London (1968).

26) It is not correct to employ the values of these rate constants in order to calculate the fluorescence quantum yields near room temperature, because such a single equation as Eq. (1) will not hold over a wide temperature range.

Photosensitized Decomposition of Trioxalatocobaltate (III) Ion by Organic Triplet Sensitizers

Shukichi SAKURABA, Akio KAKUTA, and Ryoka MATSUSHIMA

Department of Industrial Chemisty, Faculty of Engineering, Shizuoka University, Hamamatsu 432

(Received February 27, 1975)

Sensitized decomposition of the trioxalatocobaltate(III) ion was studied in deoxygenated aqueous solution at room temperature, using biacetyl as an n-π^* triplet sensitizer and 9-carboxyanthracene as a π-π^* triplet sensitizer. In the presence of one of these sensitizers the photodecomposition rate of the complex was increased, and the plot of the reciprocal of the sensitization quantum yield as a function of the concentration of the complex gave a straight line for each sensitization system. On the other hand, the complex quenched the phosphorescence without affecting the fluorescence of the sensitizers, indicating a triplet energy transfer mechanism. A photokinetic treatment of the data for both the sensitized photolysis and the quenching process gave a result in line with proposed mechanism for bimolecular triplet energy transfer.

The behavior of the photoproduced radical intermediates has extensively been studied for the photolysis of trioxalate complex ions of Co(III), Fe(III) and Mn(III),[1] but not the nature of the primary excited states, $*M(ox)_3^{3-}$.[2]

Sensitization and quenching methods are useful for identifying excited states whose lifetimes are very short. Thus, triplet sensitizers have been powerful tools for determining chemically reactive excited states of transition metal complexes, *e.g.*, Co(III)[3] and Cr(III).[4] In the present paper we report the results on the sensitized photodecomposition of $Co(ox)_3^{3-}$, using biacetyl as an n-π^* triplet donor and 9-carboxyanthracene as a π-π^* triplet donor.

Experimental

$K_3[Co(ox)_3^{3-}]\cdot 3H_2O$ and $K_3[Cr(ox)_3^{3-}]\cdot 3H_2O$ were prepared from the corresponding chlorides and potassium oxalate,[5,6] and were crystallized thrice. Biacetyl, 9-carboxyanthracene and organic solvents (guaranteed grade, Nakarai Chem.) were used without further purification. Water was distilled over potassium permanganate after passing through ion-exchange resins.

The light source was a 500 W high pressure mercury lamp with an attachment for obtaining a parallel light beam (Ushio Electric). Monochromatic light (366, 405 or 436 nm) was obtained by means of an interference filter or a suitable combination of glass filters. Absorption and emission measurements were carried out with a Hitachi 124-Spectrophotometer and a Hitachi 204-Fluorescence Spectrophotometer, respectively. For measurements of the emission of the sensitizers, the solutions were bubbled with purified nitrogen until there was no further increase in the phosphorescence intensity (*i.e.*, 40—60 min), and were kept air-tight with liquid paraffin and paraffin film.

Sample solutions to be photolyzed were mostly buffered at pH 3.9 with sodium acetate-acetic acid, and were irradiated at 20 °C, after deoxygenation with purified nitrogen followed by sealing. Concentrations of the Co(II) and the ox^{2-} ions formed were determined by reported methods.[7,8] Quantum yields were measured by the usual method.[9,10]

Results and Discussion

Direct Photolysis. Preliminary examination on the direct photolysis of $Co(ox)_3^{3-}$ under conditions similar to those of the sensitized photolysis showed that the molar ratios of Co(II) and ox^{2-} to the consumption of the complex, $-\Delta$[Co(III)], were independent of the extent of the reaction and the wavelength. The molar ratio, $[ox^{2-}]/[Co(II)]$ near 2.5, agreed with the mechanism previously proposed,[2] though the molar ratios of Co(II) and ox^{2-} to $-\Delta$[Co(III)] were rather small. The quantum yields of the Co(III) consumption for direct photolysis, under conditions similar to those for sensitized photolysis, depended on the temperature as well as the excitation wavelength. This indicates that the charge transfer state is the reactive state (even when the ligand field state is initially reached).[1b] The effect of the dissolved oxygen on the quantum yields was negligible for direct photolysis with light of 366 nm, while significant oxygen quenching was found for sensitized photolysis.

Biacetyl-Sensitized Photolysis. In the presence of 0.2 M biacetyl as an n-π^* sensitizer, $Co(ox)_3^{3-}$ in the concentration range 2.5×10^{-3} —1.5×10^{-4} (buffered at pH 3.9) was irradiated with a monochromatic light 366 nm at 20 °C, after deoxygenation. Under such conditions the complex absorbs the light directly up to 20% of the intensity (I_a) absorbed by the system. The number of the light quanta absorbed by the sensitizer, I_s, was estimated in proportion, *i.e.*, $I_s = I_a\varepsilon_s C_s/\sum_i \varepsilon_i C_i$. The quantum yields ($\phi$) of biacetyl-sensitized decomposition of the complex at its various concentration were determined, where photodecomposition of the complex due to its direct absorption was eliminated by calculation. The plot of $1/\phi$ as a function of 1/[Co(III)] gives a straight line with a slope, $1/K\phi_{11m}=2.1\times10^{-3}$ M and an intercept, $1/\phi_{11m}=7.6$ (Fig. 1).

9-Carboxyanthracene-Sensitized Photolysis. The quantum yields of the photosensitized decomposition of $Co(ox)_3^{3-}$ by 9-carboxyanthracene as a π-π^* sensitizer were measured at various initial concentrations of the complex in 30% aqueous acetone. The plot of $1/\phi$ as a function of 1/[Co(III)] gives a straight line with a slope, $1/K\phi_{11m}=1.28\times10^{-2}$ M, and an intercept, $1/\phi_{11m}=7.6$ (Fig. 1).

Oxygen Effect on the Sensitized Photolysis. The rate of Co(II) formation in the sensitized photolysis was depressed by the dissolved oxygen both for biacetyl- and 9-carboxyanthracene-sensitized photolyses. No significant effect was found for the rate of the direct

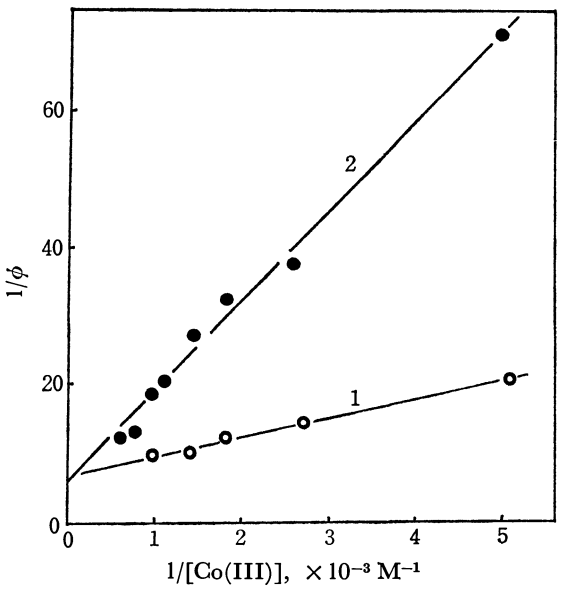

Fig. 1. Plot of $1/\phi$ *vs.* 1/[Co(III)] for organic triplet-sensitized decomposition of $Co(ox)_3^{3-}$. (1) Solvent: water (pH 3.9), sensitizer: biacetyl 0.04 M, $\lambda(h\nu)$: 366 nm. (2) Solvent: 30% aqueous acetone (pH 3.9), sensitizer: 9-carboxyanthracene 5×10^{-4} M, $\lambda(h\nu)$: 366 nm.

photodecomposition of the complex (10^{-3} M) under similar conditions. The results suggest that a bimolecular energy transfer mechanism of triplet states is involved but that the lifetime of the triplet state of the complex is too short (namely $\tau_0<10^{-9}$ s) to be significantly intercepted by the dissolved oxygen.

Quenching of the Sensitizer Emission by Complex. For clarification of the energy transfer mechanism of the sensitized reactions, quenching of the fluorescence and phosphorescence of the sensitizers by the complex were investigated. In deoxygenated aqueous solutions, $Co(ox)_3^{3-}$ quenched the phosphorescence of biacetyl without significant effect on the fluorescence.

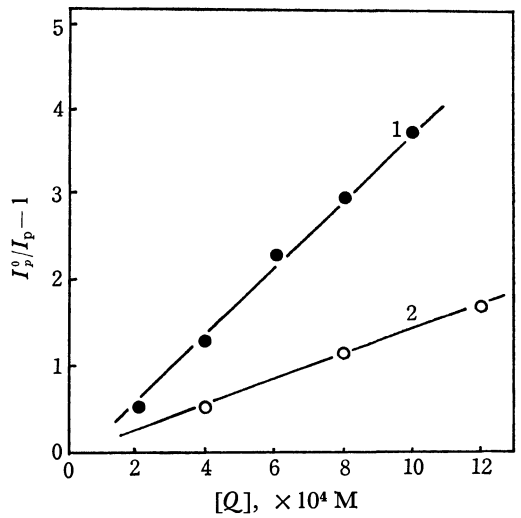

Fig. 2. Stern-Volmer plots for the quenching of biacetyl phosphosescence (512 nm peak) by (1) $Co(ox)_3^{3-}$ and (2) $Cr(ox)_3^{3-}$. Biacetyl: 0.04 M, λ(excitation): 366 nm.

The Stern-Volmer plot is given in Fig. 2. This indicates that the n-π^* triplet state is effective in the photosensitized decomposition of the complex. Form the quenching constants and the phosphorescence lifetime of biacetyl in solution at room temperature in the absence of the quenchers, $\tau_0=2.3\times10^{-4}$ s,[11] the bimolecular quenching rate constants are estimated to be $k_5=1.7\times10^7$ M^{-1} s^{-1} for $Co(ox)_3^{3-}$ and 1.0×10^7 M^{-1} s^{-1} for $Cr(ox)_3^{3-}$.

The emission of 9-carboxyanthracene in a deoxygenated aqueous alcohol solution at room temperature was only slightly affected by $Co(ox)_3^{3-}$, while in an aerated solution the emission was entirely unquenched. This implies that the energy transfer occurs from the triplet state (presumably π-π^*) of 9-carboxyanthracene.

Kinetic Analysis. A kinetic analysis of the energy transfer process for the photosensitized decomposition of $Co(ox)_3^{3-}$ will be given below.

Since the fluorescence of either biacetyl or 9-carboxyanthracene is not quenched by the complex, participation of the excited singlet states of the sensitizers is excluded. The excited singlet state of the complex is also excluded on the basis of the spin conservation rule for bimolecular energy transfer processes.[12] Direct chemical interactions between the complex and the excited state biacetyl, such as hydrogen abstraction or charge transfer, seem to be unimportant.[4b,c]

The following scheme can be assumed.

$$S + h\nu \xrightarrow{I_s} {}^1S^* \xrightarrow{\phi_{st}} {}^3S^* \quad (1)$$

$${}^3S^* \xrightarrow{k_2} S + h\nu' \quad (2)$$

$${}^3S^* \xrightarrow{k_3} S + \text{heat} \quad (3)$$

$${}^3S^* \xrightarrow{k_4,\,O_2} S + {}^1O_2^* \text{ (or } O_2+\text{heat)} \quad (4)$$

$${}^3S^* + C \xrightarrow{k_5} S + {}^3C^* \quad (5)$$

$${}^3C^* \xrightarrow{k_6} C + \text{heat} \quad (6)$$

$${}^3C^* \xrightarrow{\phi_c} Co(II) + \text{other products} \quad (7)^{2)}$$

Here, S and C are sensitizer and $Co(ox)_3^{3-}$, respectively. I_s is the light quanta absorbed by the sensitizer per unit time per unit volume, ϕ_{st} is the quantum yield of triplet formation from $^1S^*$, and ϕ_c is the quantum yield of Co(II) formation from $^3C^*$. Process (4) is included since a trace of the dissolved oxygen might be contained even after careful deoxygenation.

Since the lifetime of the triplet state of the complex $^3C^*$ seems to be short, and the bimolecular quenching rate constant k_5 is relatively small, one may assume that the unimolecular processes (6) and (7) of the complex are fast compared to (5). The steady state assumption for $^3S^*$ and $^3C^*$ leads to the following equation for the quantum yield of Co(II) formation in the sensitized reaction.

$$\frac{1}{\phi} = \frac{1}{\phi_{11m}}\left(1+\frac{1}{K[C]}\right) \quad (8)$$

$$\phi = \phi_c + \phi_{st} \quad (9)$$

$$K = k_5\tau_0 \quad (10)$$

Table 1. Rate parameters for the photosensitized decomposition of $Co(ox)_3^{3-}$ by biacetyl and 9-carboxyanthracene.

Sensitizer	ϕ_{1lm} [a]	ϕ_{st}	ϕ_c	K [b], M^{-1}	K_q, M^{-1} [c]
Biacetyl	0.13	0.99[14]	0.13	3.5×10^3	3.9×10^3
9-Carboxyanthracene	0.13	0.7—1[d]	0.13—0.19[d]	5.7×10^2	

a) From Eq. (8) and Fig. 1. b) Reciprocal of the slope of the plot of $1/\phi$ *vs.* 1/[C]. c) Quenching constant of the complex for the quenching of sensitizer phosphorscence. d) Though ϕ_{st} of 9-carboxyanthracene was not available, it is assumed to be close to unity (and hence ϕ_c to be close to 0.13), since it has been reported that the presence of the carboxyl group singificantly increases the rate of S-T intersystem crossing of aromatic hydrocarbons (*e.g.*, *J. Amer. Chem. Soc.*, **93**, 6396 (1971)).

where, $\tau_0=1/(k_2+k_3+k_4[O_2])$ is the lifetime of the triplet state of the sensitizer in the absence of the quencher (complex).

The experimental results in Fig. 1 agree with Eq. (8), supporting the assumed scheme. From the intercept and the slope of the plot of $1/\phi$ *vs.* 1/[C], ϕ_c is derived by substituting ϕ_{1lm} and ϕ_{st} into Eq. (9). These values are also given in Table 1, together with the quenching constant K_q for the quenching of the phosphorescence of biacetyl by $Co(ox)_3^{3-}$. K_q is the slope of the Stern-Volmer plot (Fig. 2) which has the following form

$$I_p^0/I_p = 1 + K_q[C] \quad (11)$$

where I_p^0 and I_p are the phosphorescence intensities of biacetyl in the absence and presence of the complex, respectively, and

$$K_q = k_5\tau_0 \quad (12)$$

From Eqs. (10) and (12), K and K_q (which were obtained from independent measurements) should be equal. The agreement of K with K_q in Table 1 might support the assumed scheme.

The upper limit of the sensitized photodecomposition quantum yield, ϕ_{1lm}, is 0.13 which is in the range of the direct photodecomposition quantum yields at its d-d band. The rate constant k_5 is a measure of the efficiency of the triplet energy transfer from the sensitizer to the complex. Though no report was found for the lifetime of 9-carboxyanthracene, it could be assumed that the π-π^* triplet lifetime is greater than the n-π^* triplet lifetime (*e.g.*, τ_0 of anthracene in solution at 20 °C is 0.026—0.035 s,[15] which is greater than that of biacetyl by two orders of manitude). Thus, the bimolecular rate constant k_5 for the triplet sensitized photolysis with 9-carboxyanthracene (as a π-π^* triplet sensitizer) is assumed to be smaller than that with biacetyl (as an n-π^* triplet sensitizer).

References

1) (a) C. A. Parker and C. G. Hatchard, *J. Phys. Chem.*, **63**, 22 (1959); (b) D. R. Eaton and S. R. Swart, *ibid.*, **72**, 400 (1968); (c) V. Balzani and V. Carassiti, "Photochemistry of Coordination Compounds," Academic Press, London, pp. 221—224.

2) (a) J. B. Copestake and N. Uri, *Proc. Roy. Soc., Ser. A*, **228**, 252 (1955); (b) G. B. Porter, J. G. W. Doering, and S. Karanka, *J. Amer. Chem. Soc.*, **84**, 4027 (1962).

3) (a) A. Vogler and A. W. Adamson, *ibid.*, **90**, 5943 (1968); (b) G. B. Porter, *ibid.*, **91**, 3989 (1969); (c) M. A. Scandola, F. Scandola, and V. Carassiti, *Mol. Photochem.*, **1**, 403 (1969); (d) M. A. Scandola and F. Scandola, *J. Amer. Chem. Soc.*, **92**, 7278 (1970); (e) M. A. Scandola and F. Scandola, *ibid.*, **94**, 1805 (1972).

4) (a) D. J. Binet, E. L. Goldberg, and L. S. Forster, *J. Phys. Chem.*, **72**, 3017 (1968); (b) E. Zinato, P. Tulli, and P. Riccieri, *ibid.*, **75**, 3504 (1971); (c) V. Balzani, M. T. Gandolfi, and L. Moggi, *J. Amer. Chem. Soc.*, **93**, 339 (1971).

5) T. Ito, K. Inamura, H. Kobayashi, A. Nakahara, Y. Shinmura, K. Yamazaki, and S. Yamada, "Zikken Kagaku Koza," Vol. II, Maruzen, Tokyo (1956), p. 37.

6) J. C. Bailar and E. M. Jones, "Inorganic Syntheses," Vol. I, ed. by H. S. Booth McGraw-Hill, New York, N.Y. (1939), pp. 35—38.

7) (a) N. Shinotsuka and S. Kikuchi, *Nippon Kagaku Zasshi*, **87**, 97 (1966); (b) J. Aggett and A. L. Odell, *J. Chem. Soc., Ser. A*, **1968**, 1415.

8) D. A. Britton and J. C. Guyon, *Anal. Chim. Acta*, **44**, 397 (1969).

9) M. Koizumi, S. Shida, S. Kato, N. Mataga, and M. Imamura, "Zikken Kagaku Koza," Vol. 6, Maruzen, Tokyo (1956), pp. 282—286.

10) (a) C. A. Parker, *Proc. Roy. Soc.*, **A220**, 104 (1953); (b) J. C. Calvert and J. N. Pitts, "Photochemistry," Wiley, New York, N. Y. (1966), pp. 738—786.

11) H. L. G. Backstorm and K. Sandros, *Acta Chem. Scand.*, **12**, 823 (1958).

12) Ref. 10 (b), pp. 88—92.

13) (a) M. A. El-sayed, *J. Chem. Phys.*, **38**, 2834 (1963); (b) N. J. Torro, "Molecular Photochemistry," W. A. Benjamin, New York, N. Y. (1967), p. 86.

14) S. T. Spees and A. W. Adamson, *Inorg. Chem.*, **1**, 531 (1962).

15) D. Phillips, "Photochemistry," Vol. 3, ed. by Chemical Society, Burlington House, London (1972), p. 146.

Photochemistry in the Adsorbed Layer. V. Effects of Surface Pretreatments upon the Photolysis of Adsorbed 2-Pentanone

Masakazu ANPO, Toshiaki WADA, and Yutaka KUBOKAWA

Department of Applied Chemistry, College of Engineering, University of Osaka Prefecture, Mozu-Umemachi, Sakai, Osaka 591

(Received March 7, 1975)

The effects of surface pretreatment upon the photolysis as well as the absorption and phosphorescence spectra of 2-pentanone adsorbed on porous Vycor glass have been investigated. The rate of propane formation (Norrish type I reaction) passes through a maximum and then decreases at higher degassing temperatures, while that of ethylene formation (Norrish type II reaction) decreases with increasing degassing temperature. Simultaneously, the phosphorescence intensity increases while the blue shift of the (n,π^*) band decreases. This suggests that with a rise in degassing temperature the triplet lifetime increases while the surface polarity decreases. Thus, the decrease in the rate of ethylene formation is attributed to destabilization of the 1,4-biradicals formed by the intramolecular hydrogen abstraction, and the decrease in the rate of propane formation to the decrease in the lifetime of the *n*-propyl radicals, the hydrogen abstraction efficiency, and the probability of α-cleavage.

Photolysis as well as absorption and phosphorescence spectra of acetone, methyl ethyl ketone, and 2-pentanone adsorbed on porous Vycor glass have been investigated recently.[1] It was shown that acetone most strongly hydrogen bonded to the surface OH groups exhibits the most efficient radiationless deactivation. It was found that in the photolysis of adsorbed 2-pentanone Norrish type I reaction occurs to a larger extent than that in the gas phase photolysis.[2]

It is well-known that the concentration of surface OH groups and their reactivity markedly change after surface pretreatment such as heat[3] or fluoridation pretreatment.[4] It is expected therefore that the interaction of alkyl ketones with the surface OH groups would be seriously affected by such surface treatment. We have investigated the effects of surface pretreatment upon the photochemistry of adsorbed 2-pentanone in order to obtain information on the nature and reactivity of the excited states.

Experimental

Details of the apparatus, procedures, and materials were described previously.[1] A conventional vacuum system was used in conjunction with a special quartz cell capable of studying the spectra and photolyses in the adsorbed layer. The specimen of porous Vycor glass which had been heated in oxygen to remove carbonaceous impurities was introduced into the cell and degassed at temperatures 100—800 °C for 7 hr. After 2-pentanone had been adsorbed on the specimen, photolysis was carried out using an ultra high pressure mercury lamp without filter. The amount of 2-pentanone adsorbed was 2.19×10^{-5} mol/g. The BET surface area[5] of the specimen remained unchanged until 500 °C, decreasing at higher temperatures from 160 m^2/g at 500 °C to 140 m^2/g at 700 °C. In the case of NH_4F pretreatment, the specimen was dried at 100 °C and then degassed at 800 °C for 7 hr. After such treatment the BET surface area was reduced to about 60% of its initial value. The IR spectra after the treatment indicate that about 60—65% of the surface OH groups was removed.

Results

Effects of Degassing Temperature upon Absorption and Phosphorescence Spectra. Figure 1 shows the blue shifts of the (n, π^*) transition of adsorbed 2-pentanone and methyl ethyl ketone against the degassing temperature. It is seen that the magnitude of the blue shift decreases with a rise in degassing temperature. It is well-known that the (n, π^*) transition of the ketones is blue shifted in polar solvents due to hydrogen bonding, its magnitude increasing with the polarity of the solvent.[6] Since alkyl ketones are adsorbed on porous Vycor glass by hydrogen bonding between the surface OH groups and C=O groups of the ketone, such a decrease in the blue shift with increasing degassing temperature is attributable to a decrease in the polarity of the surface OH groups. The change in the number of surface OH groups/g with degassing temperature obtained by Low and Ramasubramanian[3] is given in Fig. 2. A similar relative change in the number of OH groups with the degassing temperature was obtained with our specimen from the intensity measurements of the band at 3750 cm^{-1}. This suggests that the surface polarity decreases with decreasing

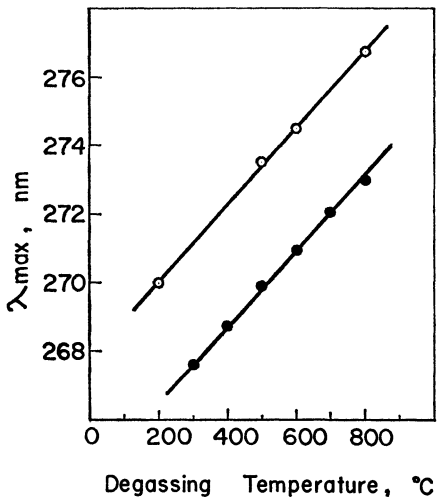

Fig. 1. Effect of degassing temperature upon the (n, π^*) transition of the ketones adsorbed. The amounts of adsorbed methyl ethyl ketone and 2-pentanone were 2.37×10^{-5} mol/g and 2.10×10^{-5} mol/g, respectively. ●, methyl ethyl ketone; ○, 2-pentanone.

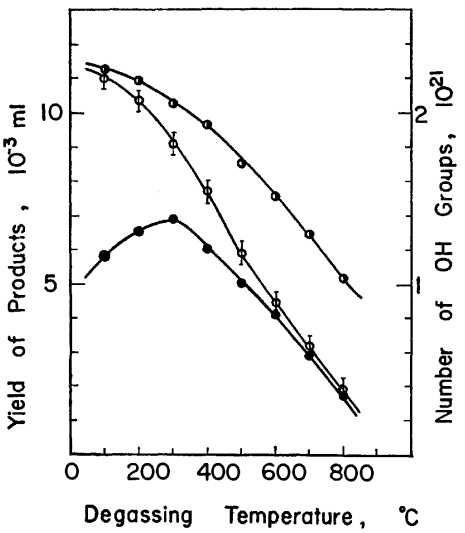

Fig. 2. Effect of degassing temperature upon the yield of products from the 2-pentanone photolysis. Amounts of adsorbed 2-pentanone was 2.19×10^{-5} mol/g. Irradiation time, 20 minutes; Temperature, 25 °C. Φ, the number of OH groups/g; ◑, ethylene; ●, propane.

TABLE 1. EFFECT OF DEGASSING TEMPERATURE UPON THE PHOSPHORESCENCE INTENSITY OF 2-PENTANONE ADSORBED

Temperature °C	Amount adsorbed 10^{-5} mol/g	Phosphoresence max. nm	Relative intensity
300	7.01	445±5	1.00
500	7.01	450±5	1.23
700	7.01	455±5	1.70
300	20.1	445±5	1.00
700	20.1	455±5	1.68

concentration of the surface OH groups.

A similar behavior has been reported by Glass and Ross[7] who found that the heat of adsorption of hydrogen sulfide adsorbed on silica gels by hydrogen bonding decreased with increasing degassing temperature, *i.e.*, with decreasing concentration of the surface OH groups.

Table 1 shows the effect of the degassing temperature upon the phosphorescence spectra of adsorbed 2-pentanone, its intensity increasing with increasing degassing temperature. Taking into account the fact that there was no change in the relative intensity of the absorption spectra with a rise in degassing temperature, such a decrease in the phosphorescence intensity is attributable to a decrease in the population of the excited triplet ketone molecules.[8] The more blue shifted, *i.e.*, the more strongly hydrogen bonded a ketone molecule is, the more efficient radiationless deactivation becomes.[1] Thus, the decrease in the concentration of the triplet molecules is attributable to the increase in the radiationless deactivation efficiency.

Effect of Surface Pretreatment upon Type I and II Reactions. The major gaseous products in the photolysis of adsorbed 2-pentanone are ethylene (type II) and propane (type I).[1] The effect of degassing temperature upon the rates of type I and II reactions is shown in Fig. 2. With increasing degassing temperature the rate of type II reaction decreases while the rate of type I reaction passes through a maximum and then decreases at higher degassing temperatures.

TABLE 2. EFFECT OF SURFACE PRETREATMENTS UPON THE PHOTOLYSIS OF 2-PENTANONE ADSORBED

Condition of pretreatment[a]	Yield of propane 10^{-2} ml/hr	Yield of ethylene 10^{-2} ml/hr	Value of propane/ethylene
No-treatment	0.88	2.00	0.44
NH_4F solution	2.09	2.01	1.04

a) The specimens were degassed at 800 °C. Amount of 2-pentanone adsorbed was 1.43—1.70 mol/g. Minor products; CO, CH_4, C_2H_6, C_6H_{12}. CH_3COCH_3 was not determined.

The results of the NH_4F treatment are given in Table 2. Taking into account a decrease in the surface area after the treatment, it is concluded that both type II and type I reactions are enhanced after the treatment, its extent being larger for the latter than for the former. According to the work of Chapman and Hair,[4] after NH_4F pretreatment the surface consists of silanol groups (Si-OH) and F atom attached to Si atoms on the surface. Owing to the electronegativity of F atoms, the weakening of the O-H bond takes place, resulting in the increase in surface acidity or surface polarity. Thus, essentially the same trend was observed for both experiments, suggesting a significant role of the polarity of the surface OH groups in determining the rates of product formation.

Discussion

Type II Reaction. Type II reactions of alkyl ketones having γ-hydrogen atoms have been investigated by many workers.[9-12] According to Yang and Elliot[9] who investigated the type II reaction of the optically active ketone, 5-methyl-2-heptanone, there seems to be no doubt that the reaction proceeds *via* 1,4-biradicals formed by the intramolecular hydrogen abstraction.

Wagner found that the type II reaction is enhanced in polar solvents in comparison with in nonpolar solvents.[10] The quantum yield of the residual singlet reaction, however, which remains after addition of sufficient amounts of diene to quench all the excited triplet ketone molecules, is the same in all solvents.[10,13] This suggests that polar solvents should increase the efficiency of type II reactions from the alkyl ketone excited triplet state. This effect has been attributed by Wagner to a decreased probability for return of the γ-hydrogen in the 1,4-biradical, formed by the intramolecular hydrogen abstraction in the excited triplet states, due to hydrogen bonding between the polar solvent and the hydroxyl group of the biradical.

The ethylene formation from adsorbed 2-pentanone decreases with increasing degassing temperature. The surface polarity or acidity decreases with increasing

degassing temperature. The following tentative conclusion may be drawn: In the photolysis of adsorbed 2-pentanone only the ethylene formation from the triplet excited states would be affected by the change in the degassing temperature. The decrease in ethylene formation with increasing degassing temperature is associated with the decrease in surface polarity which results in destabilization of the 1,4-biradicals. The photolysis of the absorbed 2-pentanone may be represented by the following scheme:

$$P + h\nu \longrightarrow {}^1P \quad (1)$$

$${}^1P \xrightarrow{k_{isc}} {}^3P \quad (isc)$$

$${}^1P \xrightarrow{k_2} P + \text{heat} \quad (2)$$

$${}^1P \xrightarrow{k_3} P + h\nu' \quad (3)$$

$${}^3P \xrightarrow{k_4} \dot{C}_3H_7 + \dot{C}OCH_3 \quad (4)$$

$${}^3P \xrightarrow{k_5} \dot{C}H_2CH_2CH_2\text{-}\underset{\underset{H}{|}}{\overset{\overset{O}{|}}{\dot{C}}}\text{-}CH_3 \quad (5)$$

$${}^3P \xrightarrow{k_6} P + \text{heat} \quad (6)$$

$${}^3P \xrightarrow{k_7} P + h\nu'' \quad (7)$$

$$\dot{C}H_2CH_2CH_2\text{-}\underset{\underset{H}{|}}{\overset{\overset{O}{|}}{\dot{C}}}\text{-}CH_3 \xrightarrow{k_8} C_2H_4 + CH_3\overset{\overset{O}{\|}}{C}\text{-}CH_3 \quad (8)$$

$$\dot{C}H_2CH_2CH_2\text{-}\underset{\underset{H}{|}}{\overset{\overset{O}{|}}{\dot{C}}}\text{-}CH_3 \xrightarrow{k_9} P + \text{heat} \quad (9)$$

(Reaction Scheme 1)

Reaction 9 is the radiationless deactivation process which proceeds *via* a return of γ-hydrogen in the 1,4-biradical. Using the steady state approximation in the excited states, the rate of type II reaction can be represented by

$$\text{Rate}_{(C_2H_4)} = \left(\frac{k_5}{k_4+k_5+k_6+k_7}\right)\left(\frac{k_8}{k_8+k_9}\right)I_p\Phi_{isc} \quad (I)$$

where I_p is the rate of light absorption by molecule P and Φ_{isc} the efficiency of the intersystem crossing.

With increasing degassing temperature the 1,4-biradical lifetime τ_b, *i.e.*, $(k_8+k_9)^{-1}$ decreases owing to an increase in k_9. The phosphorescence measurements suggest that the triplet lifetime τ_t, *i.e.*, $(k_4+k_5+k_6+k_7)^{-1}$ increases with increasing degassing temperature. The magnitude of the decrease in the biradical lifetime would be larger than that of the increase in the triplet lifetime, since the rate of ethylene formation decreases with increasing degassing temperature.

Type I Reaction. The rate of propane formation can be represented as follows: In addition to scheme 1 the following reactions are included;

$$\dot{C}_3H_7 + [H] \xrightarrow{k_{10}} C_3H_8 \quad (10)$$

$$[\dot{C}_3H_7 + \dot{C}OCH_3]_{ads} \xrightarrow{k_{11}} \text{Recombination or Disproportionation Products} \quad (11)$$

$$R_{(C_3H_8)} = k_{10}[H][\dot{C}_3H_7] = \left(\frac{k_4}{k_4+k_5+k_6+k_7}\right)\left(\frac{k_{10}[H]}{k_{10}[H]+k_{11}[\dot{C}OCH_3]}\right)I_p\Phi_{isc} \quad (II)$$

The rate of propane formation is determined by hydrogen abstraction efficiency, $k_{10}[H]$, as well as the steady state concentration of the propyl radicals. In the photolysis of acetone-d_6 adsorbed on porous Vycor glass the methane formed contained 55% of CD_3H at the amount adsorbed of 2×10^{-5} mol/g.[14] This suggests that in the case of the photolysis of adsorbed 2-pentanone the hydrogen abstraction from the surface OH groups would contribute considerably to the overall propane formation at least in the range of the small amounts adsorbed. Accordingly, the hydrogen abstraction efficiency $k_{10}[H]$ would decrease with increasing degassing temperature owing to the decrease in the concentration of the surface OH groups.

The steady state concentration of the propyl radicals is determined by the propyl radical and triplet 2-pentanone lifetime as well as by the k_4 value (Eq. (II)). The change in the radical lifetime with degassing temperature can be determined by the effect of oxygen pressure upon the propane formation,[15] by means of the Stern-Volmer relationship

$$\frac{Q_0}{Q} = 1 + \tau_r k_s[O_2]$$

where τ_r is the radical lifetime and k_s the scavenging rate constant with oxygen. Q and Q_0 are the rates of propane formation in the presence and absence, respectively, of oxygen. Assuming that the value of k_s scarcely changes with degassing temperature, the change in the radical lifetime with degassing temperature is obtained from the Stern-Volmer plots. The lifetime of propyl radicals decreases with increasing degassing temperature (Fig. 3). Remem-

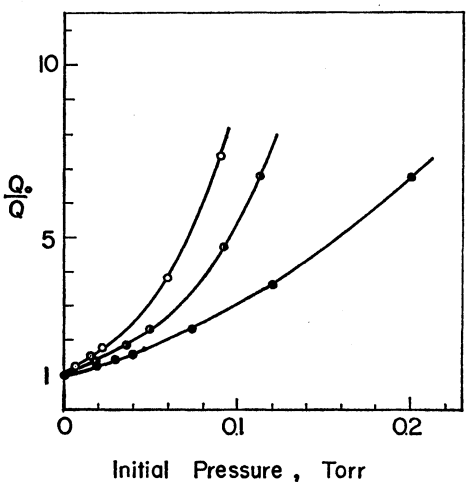

Fig. 3. Stern-Volmer plot for scavenging of the propane formation with oxygen. ○, pretreated at 300 °C; ◑, pretreated at 500 °C; ●, pretreated at 700 °C.

bering that the hydrogen abstraction efficiency $k_{10}[H]$ decreases with increasing degassing temperature, it is concluded that the increase of $(k_{10}[H]+k_{11}[\dot{C}OCH_3])$ and the decrease of $k_{10}[H]$ occurs simultaneously. This suggests that the contribution of $k_{10}[H]$ to the value of $(k_{10}[H]+k_{11}[\dot{C}OCH_3])$ is rather small. In other words, the lifetime of the propyl radicals is determined mainly by the value of $k_{11}[\dot{C}OCH_3]$, which refers to the reaction of *n*-propyl-acetyl radical pairs such as the recombination and disproportionation reactions.[16] Such an increase in the value of $k_{11}[\dot{C}OCH_3]$ with increasing degassing temperature would be expected since the magnitude of k_{11} depends upon the surface mobility of the radicals, which will increase with decreasing strength of the interaction between the radicals and the surface OH groups. The weak interaction of the radicals with the Vycor glass surface pretreated at a higher temperature was also studied by Garbutt and Gesser by means of ESR technique.[17]

Such a decrease in the strength of the interaction between the radicals and the surface with increasing degassing temperature suggests the decrease in stabilization of the radicals formed in the primary process, which would be expected to result in a decreased probability of α-cleavage, *i.e.*, a decreased k_4 value. It is concluded that the decrease in the propane formation with increasing degassing temperature is attributable to a decreased probability of α-cleavage as well as the decrease in the radical lifetime and the hydrogen abstraction efficiency. In the temperature range where no decrease in these values occurs it is expected that the propane formation increases with increasing degassing temperature owing to the increase in the lifetime of the triplet excited ketone molecules. It appears that such a situation is realized in the temperature range below 300 °C. Thus, a maximum in the propane formation is explicable.

References

1) Y. Kubokawa and M. Anpo, *J. Phys. Chem.*, **78**, 2442 (1974). M. Anpo and Y. Kubokawa, *ibid.*, **78**, 2446 (1974).

2) P. Ausloos and E. Murad, *J. Amer. Chem. Soc.*, **80**, 5929 (1958). F. S. Wettack and W. A. Noyes, Jr., *ibid.*, **90**, 3901 (1968).

3) M. J. D. Low and N. Ramasubramanian, *J. Phys. Chem.*, **71**, 730 (1967).

4) I. D. Chapman and M. L. Hair, *J. Catal.*, **2**, 145 (1963); *Trans. Faraday Soc.*, **61**, 1507 (1965).

5) S. Brunauer, P. H. Emmett, and E. Teller, *J. Amer. Chem. Soc.*, **60**, 309 (1938).

6) A. Bulasubramanian and C. N. R. Rao, *Spectrochim. Acta.*, **18**, 1337 (1962). H. H. Jaffé and Milton Orchin, "Theory and Application of Ultraviolet Spectroscopy," Wiley, New York (1962), p. 173.

7) R. W. Glass and R. A. Ross, *J. Phys. Chem.*, **77**, 2571 (1973).

8) D. M. Hercules, "Fluorescence and Phosphorescence Analysis," Wiley, New York (1966), p. 169.

9) N. C. Yang and S. P. Elliot, *J. Amer. Chem. Soc.*, **91**, 7550 (1969).

10) P. J. Wagner, *Tetrahedron Lett.*, **1968**, 5385; **1967**, 1753; *J. Amer. Chem. Soc.*, **89**, 5898 (1967).

11) J. C. Dalton and N. J. Turro, *Ann. Rev. Phys. Chem.*, **21**, 499 (1970).

12) H. E. O'Neal, R. G. Miller, and E. Gunderson, *J. Amer. Chem. Soc.*, **96**, 3351 (1974).

13) J. A. Barltrop and J. D. Coyle, *Tetrahedron Lett.*, **1968**, 3235.

14) M. Anpo, S. Hirohashi, and Y. Kubokawa, This Bulletin, **48**, 985 (1975).

15) In general, the decrease in propane formation by oxygen arises from the quenching of the triplet excited states as well as of the radicals. The Stern-Volmer plots were found to be non-linear (Fig. 3). It was confirmed,[1] however, that in the pressure range below 10^{-1} Torr the radical scavenging is the predominant process.

16) Reaction of $\dot{C}_3H_7+\dot{C}OCH_3\rightarrow C_3H_7COCH_3$ and reaction of $\dot{C}_3H_7+\dot{C}OCH_3\rightarrow C_3H_8+CH_2CO$ (or $\dot{C}_3H_7+\dot{C}OCH_3\rightarrow C_3H_6+CH_3COH$) take place. Some evidence supporting the disproportionation reaction has been given.[14]

17) G. B. Garbutt and H. D. Gesser, *Can. J. Chem.*, **48**, 2685 (1970).

A Conformational Study of the NO_x(x=1 or 2)-catalyzed Isomerization of *cis*-2-Butene Using the INDO-UHF Method

Katsutoshi OHKUBO, Hiromichi IKEBE, and Masahide OKADA

Department of Synthetic Chemistry, Faculty of Engineering, Kumamoto University, Kurokami, Kumamoto 860

(Received March 12, 1975)

The NO_x(x=1 or 2)-catalyzed isomerization of *cis*-2-butene was investigated by means of the INDO-UHF theory, with a particular view to the energetic and conformational aspects of the reaction. The NO_2-addition process to form the intermediate radical (R_1) had no appreciable activation barrier, although the NO_2-fission process from the intermediate radical (R_2) had the C–NO_2 dissociation energy of 44.6 kcal/mol. Some characteristic features of the stretched C–C bond in the intermediate radical (R_1) were; (1) r_{CC}=1.45 Å, which was roughly equal to the value (1.481 Å) in *cis*-2-butene at the transition state of its thermal isomerization; (2) a pseudo π-conjugation with a small π-character (about 13% of E^R_{CC}) in comparison with that (about 29% of E^R_{CC}) in *cis*-2-butene, and (3) approximately the same magnitude of the hfsc value (34.40—34.47 G) for the sp^2-hydrid carbon as that (experimental value of 39.07 G) for the said atom in the ethyl radical. The calculated internal-rotation barrier of the intermediate radical (R_1) around the C–C bond (1.75—3.01 kcal/mol in the two rotating directions) was smaller than that (around 4 kcal/mol) obtained from the thermodynamic estimations. The energetically most stable or unstable rotamer was found in the staggered or the eclipsed configuration respectively; a hydrogen-bonding effect on the stabilization was observed in staggered configuration, although a remarkable effect of the homoconjugation or the repulsive interaction of unpaired and lone-paired electrons can be disregarded in the present internal-rotamer.

The isomerization about the C=C double bond of olefin with free-radical catalysts, especially with NO_x (x=1 or 2), has currently received considerable attention in connection with olefin consumption in photochemical smog. In regard to the gas-phase *cis*-2-butene isomerization catalyzed by NO_x(x=1 or 2), Cundall[1] and Pitts *et al.*[2] have performed kinetic investigations of the gas-phase isomerization mechamism, and the mechanism may now be postulated qualitatively to be as follows:

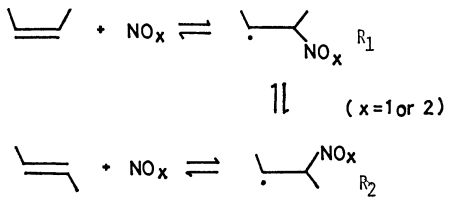

In the above reaction paths, the NO_x catalyst actually diminishes the activation energy of the reaction fro 62.8 kcal/mol[3] in the thermal isomerization to 26.2 kcal/mol in the case of NO[1] or 12.1±0.3 kcal/mol in the case of NO_2.[2] It has also been established with respect to the olefin isomerization that the reaction is catalyzed by such free radicals as I,[4,5] S,[6] HS,[7] and RS.[8] The isomerization mechanism, however, is still open to question on a molecular level in view of the fact that the energetics of the reaction paths have been studied only by means of thermodynamic estimations.

On the other hand, semi-empirical calculations have recently been carried out on the thermal *cis-trans* isomerization of such olefins as 2-butene and 2-pentene with a particular view to the activation barrier of the reaction.[9] For 2-butene, there was a considerable agreement of the calculated activation energy of 56.4 kcal/mol[9] with the experimental value, 62.8 kcal/mol.[3] However, there is no literature dealing with the free-radical catalyzed isomerization of olefins on the basis of the MO theory.

In this paper, we wish to report the application of the INDO-UHF method[10] to a conformational study of the energetics of the NO_x-catalyzed isomerization of *cis*-2-butene. The specific objectives of this study are: (1) to elucidate the mode of the interaction between the NO_x catalyst and *cis*-2-butene, (2) to provide information about the conformations of the intermediate radicals (R_1 and R_2), and (3) to discuss quantitatively the process of the internal rotation of the R_1 radical.

Method of Calculation

The following three systems were mainly investigated in this work: (a) the interacting system of NO_x (x=1 or 2) and *cis*-2-butene, involving the NO_x-addition process; (b) the intermediate radicals (R_1 and R_2), and (c) the internal rotation of the intermediate radical (R_1), augmented by the NO_x-fission process from the R_2 radical.

All the calculations on the above systems were performed by means of a semi-empirical INDO-UHF method[10] which is relatively reliable for bond angles, but less so for bond lengths.[11] The integrations and parametrizations involved in the above method will not be repeated here, because they have been described in detail in Ref. 10.

The geometries of *cis*-2-butene (r_{CC}=1.34 Å in the double bond; r_{CC}=1.54 Å in the single bond; r_{CH}=1.06 Å; ∠C=C–C=∠C=C–H=120°; ∠HCH=∠CCH=109°28′) and NO_2 (r_{NO}=1.188 Å; ∠ONO=134.1°) were obtained from a standard compendium,[12] while the bond length of NO (r_{NO}=1.159 Å) in NO was obtained as an optimum one by the INDO-UHF calculation. With regard to the optimum rotation angle of the two methyl groups in *cis*-2-butene, the INDO calculations gave the best configuration as III, which has minimum electron and nuclear repulsions, among the following three possible configurations:

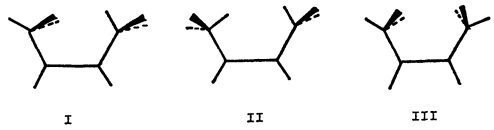

The bond index of E_{AB} for the A–B bond, which is defined as the energy contribution of the A–B bond to the total energy of a molecule, was evaluated by means of a method of energy partitioning:[13,14]

$$E_{AB} = E^{R}_{AB} + E^{V}_{AB} + E^{J}_{AB} + E^{K}_{AB} + E^{N}_{AB}$$

where each energy term has the usual significance described in Refs. 13 and 14.

Results and Discussion

Interaction of the NO_x (x=1 or 2) Catalyst and cis-2-*Butene.* The ground state of NO_x(x=1 or 2) has a doublet-spin multiplicity and, hence, a free-radical character. Therefore, the SOMO (singly-occupied MO) of the NO_x, which expands predominantly around the nitrogen atom in the direction of the z-axis in Fig. 1, plays an important role in the interaction with the HOMO (highest-occupied MO) and LUMO (lowest-unoccupied MO) of *cis*-2-butene (π and π^* orbitals on the C=C double bond respectively). The interaction is favored under the maximum overlappings between the above frontier orbitals of the two reactants. In the modes of the interaction shown in Fig. 1, the bridge-type interaction was discarded because of the following reasons:

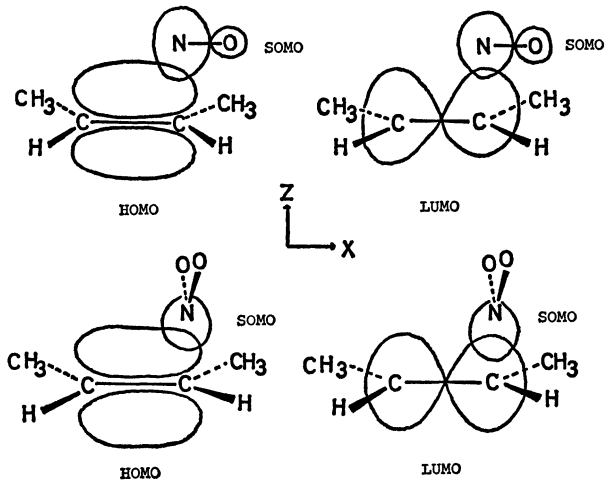

Fig. 1. Schematic representations of the modes of interaction between NO_x and *cis*-2-butene.

(a) the SOMO of the NO_x and the LUMO of *cis*-2-butene overlap unfavorably in the bridge structure; (b) the nearly equivalent rates of the exchange and isomerization reactions in such a system of di-iodoethylene and free-radical iodine atoms obviates the bridge structure,[15] even though the EPR spectroscopy of the system of *cis*-2-butene and hydrogen bromide is positive for the bridge structure,[16] and (c) the conformation of the intermediate radical formed in the isomerization of *cis*-2-butene by the sulfhydroyl radical does not favor the bridge structure.[7] In this respect,

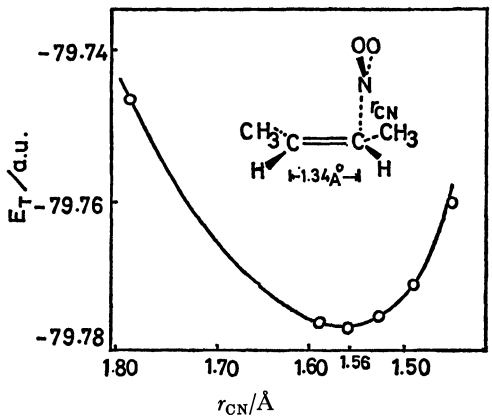

Fig. 2. Total energy of the system between NO_2 and *cis*-2-butene as a function of r_{CN}.

the present INDO-UHF calculation indicates that the two possible interacting structures mentioned above cannot be distinguished from each other only by the total energy and the overlap population[17] (0.002 at r_{CN}=3.0 Å) of the C–N bond.

Next, let us discuss the energetic aspect of the interaction system of the NO_x and *cis*-2-butene, taking NO_2 as an example. So long as the C=C double bond of *cis*-2-butene is kept constant, the NO_2 catalyst approaches *cis*-2-butene, by the least motion, in the direction of the carbon p_z-orbital expansion. As can be seen from Fig. 2, the total energy (E_T) of the above interacting system as a function of r_{CN} indicates a monotoneous stabilization of the system until r_{CN}= 1.56 Å, which is longer than the usual C–N bond length (1.47 Å[12]). With the approach of NO_2 to *cis*-2-butene, the electrons of the π-orbital of the latter flow into the former (predominantly into the two oxygen atoms) with an appreciable electron back-donation from NO_2 to the p_z-orbital of the remote carbon (not in CH_3 group) through the π-conjugation

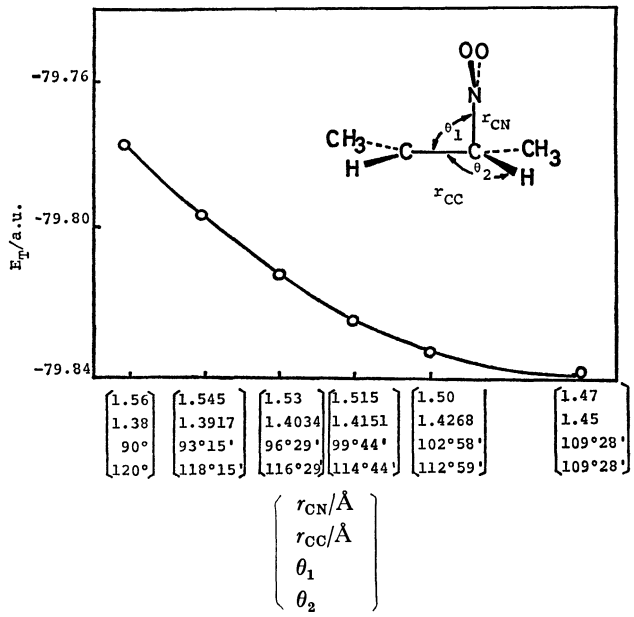

Fig. 3. Total energy for the NO_2-addition process.

of the C=C bond. Further interaction within r_{CN}= 1.56 Å will require a stretching of the C=C bond and a change in the sp^2 hybridization of the carbon atom. We will, therefore, try to simulate the NO_2-addition process by changing the carbon hybridization=sp^2 -sp^3, r_{CN}=1.56—1.47 Å, and r_{CC}=1.34—1.45 Å (see below), with the residual part retaining its equilibrium geometries. As Fig. 3 indicates, the process has no appreciable activation barrier, although the activation energy of 12.1±0.3 kcal/mol was given for the above NO_2-addition process by Pitts *et al.*[2] The discrepancy between the INDO-UHF calculation and the experiment may be caused by the present incomplete MO-simulation; the exclusion of geometry optimizations (except for r_{CN}) in the process gave only the stabilization energy of 103.8 kcal/mol, a value which was obtained from the difference in the total energies between the intermediate radical (R_1) and the two reactants isolated.

Conformation of the Intermediate Radicals. It is necessary first to interpret the r_{CC} value of 1.45 Å for the intermediate radical (R_1) used for the MO-simulation mentioned above. Plots of the total energies (E_T) for the radical (R_1) *vs.* r_{CC} in Fig. 4 indicate that r_{CC}=1.45 Å gives the energetically most stable radical (R_1: x=1 or 2). This C–C bond length is slightly longer than that (1.430 Å[18]) of the ethylene cation, but shorter than that (1.484 Å[18]) of the ethyl cation or that (1.516 Å[18]) of the ethyl radical. Interestingly, the r_{CC} value of 1.45 Å is roughly in harmony with that (1.481 Å[9]) of 2-butene at the transition state in its thermal isomerization.

Next, we will discuss the rotation of NO_x(x=1 or 2) around the C–N bond in the intermediate radical (R_1). The rotation barrier of the C–NO ring was evaluated to be 4.08 kcal/mol, while that of the C–NO_2 ring was 1.82 kcal/mol. The former value is markedly larger than that in the methyl rotation of *cis*-2-butene (0.75 kcal/mol[19]) or of ethane (2.88 kcal/mol[20]), while the latter value of 1.82 kcal/mol is approximately of the same magnitude as the methyl rotation in *trans*-2-butene (1.95 kcal/mol[21]). At any rate, the C–NO_x (x=1 or 2) ring has indeed a restriction in rotation because its rotation barrier is essentially large as compared with the free-rotation barrier (0.6 kcal/mol at room temperature). It should be stressed here that the NO_x rotation around the C–N bond does not appreciably change the C–C bond length (1.45 Å) over 0.02 Å in the intermediate radical (R_1), because r_{CC}=1.43 or 1.47 Å makes the radical (R_1) unstable at any rotation angle in comparison with the stability of the radical (R_1) at r_{CC}=1.45 Å. The energetically most stable intermediate radical (R_1) has the following conformation:

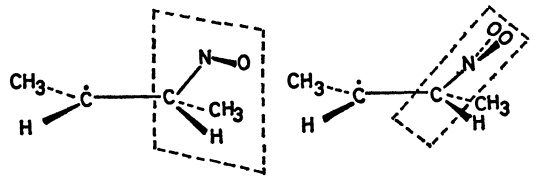

R_1 (x=1) R_1 (x=2)

The most stable intermediate radical (R_1)

In the R_1 (x=1), the bond axes of N–O and C–H are on the same plane, and the bond angle of C–N–O is 118°, smaller by 2° than that of nitrosomethane[22]. In the R_1 (x=2), the O–O axis is perpendicular to the C–C bond axis. It is of interest here to discuss how the NO_x (x=1 or 2) rotation around the C–N bond changes the total energy and the energy-contribution terms of the radical (R_1). In Table 1, we list the total energy (E_T), and the attraction (E_I) and repulsion (E_{II} and E_N) terms as functions of some clockwise-rotation angles (θ). As can be seen form Table 1, the repulsions decrease monotonously until the R_1 takes its most stable conformation (θ=240° for NO and θ=90° for NO_2), with a normal augmentation of the attraction. It may be deduced, therefore, that the least repulsion, rather than the attraction, makes

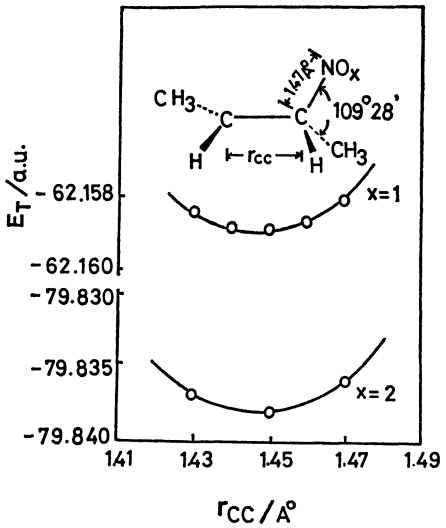

Fig. 4. Total energies of intermediate radical (R_1) as a fuction of r_{CC} (angle of C–N–O in R_1(x=1) =125°: taken from *p*-iodonitrosobenzene in M. S. Webster, *J. Chem. Phys.*, **24**, 555 (1956)).

Table 1. Total energies and their energy contributions in the NO_x(x=1 or 2)-rotation around the C–N bond of the intermediate radical (R_1)
(Values are in a.u. unit)

	R_1(x=1)			
θ	0° a)	120°	180°	240°
E_T	−62.150	−62.154	−62.151	−62.157
E_N	132.638	132.292	130.868	130.231
E_I	−357.653	−356.949	−354.075	−352.780
E_{II}	162.865	162.503	161.056	160.392
	R_1(x=2)			
θ	0° a)	45°	90°	120°
E_T	−79.836	−79.837	−79.838	−79.835
E_N	179.857	179.743	179.544	179.693
E_I	−480.906	−480.655	−480.245	−480.563
E_{II}	221.213	221.075	220.863	221.036

a) At this angle, the oxygen atom is on the C–C bond axis.

Table 2. Bond energies for the C–C bond of intermediate radical (R_1)
(Values are in a. u. unit)

	$R_1(x=1)$	$R_1(x=2)$	*cis*-2-Butene
E_{CC}	−1.161	−1.161	−2.062
E^R_{CC}	−1.249	−1.249	−1.696
s-s	−0.171	−0.173	−0.236
s-p_x	−0.583	−0.585	−0.682
p_x-p_x	−0.330	−0.327	−0.292
p_z-p_z	−0.107	−0.105	−0.398
p_y-p_y	−0.058	−0.059	−0.088
σ-total	−1.084	−1.085	−1.210
π-total	−0.165	−0.164	−0.486
E^V_{CC}	−11.081	−11.019	−12.213
E^J_{CC}	5.516	5.455	5.886
E^K_{CC}	−0.187	−0.186	−0.358
E^N_{CC}	5.840	5.839	6.318

the conformation of the R_1 shown above stable. This stabilization of a rotamer is sometimes caused by the aid of hydrogen bonding,[23] the *gauche* effect,[23–26] and the interaction effect of lone-paired electrons.[27] In this respect, the hydrogen bonding seems to be expected in the hydrogen and oxygen atoms on the same plane of the R_1 ($x=1$). However, the negative overlap population does not favor such a stabilization effect.

Now, let us extend the discussion to some characteristic features of the intermediate radical (R_1), paying particular attention to the C–C bond-nature and the hfsc (hyperfine splitting constant) of the sp^2-hybrid carbon. In Table 2 we list the E_{CC} and its contribution terms, together with those for *cis*-2-butene. The weakening of the C–C bond strength by the NO_x addition is well reflected in the relatively small E_{CC} and E^R_{CC} values in comparison with those in *cis*-2-butene. Interestingly, the electrostatic interaction ($E^V_{CC}+E^J_{CC}+E^N_{CC}$) becomes more repulsive in the intermediate radical (0.275 a.u.) than in *cis*-2-butene (−0.009 a.u.). This is attributable mainly to the fact that the exchange energy (E^K_{CC}) of the R_1 cannot overcompensate for the repulsion because of the diminution of the π-conjugation in the radical. It is noteworthy with respect to the π-conjugation that a weak π-conjugation (about 13% of E^R_{CC}) in the radical (R_1), as compared with that (about 29% of E^R_{CC}) in *cis*-2-butene, is possible by the aid of the following pseudo π-orbital:

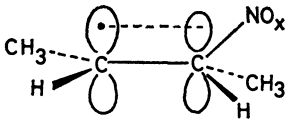

Pseudo π-orbital of intermediate radical (R_1)

The pseudo π-orbital is also supported by the positive bond-order between the p_z-orbitals of the two carbon atoms (0.302 for R_1 ($x=1$) and 0.309 for R_1 ($x=2$)). In this case, the SOMO of R_1 ($x=1$ or 2) is strongly localized by the p_z-orbital of the sp^2-hybrid carbon (spin density=0.830 for R_1 ($x=1$) or 0.828 for R_1 ($x=2$)), and the interaction of this electron-unpaired p_z-orbital and the lone-pair orbitals on the oxygen atom seems to be favorably avoided in the optimum conformation of the intermediate radical (R_1). As to the hfsc values of the sp^2-hybrid carbon in the R_1, the calculated hfsc values, (+)34.47 G for R_1 ($x=1$) and (+)34.40 G for R_1 ($x=2$), are approximately of the same magnitude as that ((+)39.07 G[28]) obtained experimentally for the sp^2-hybrid carbon in ethyl radical.

Internal Rotation of the Intermediate Radical. The intermediate radical (R_1) is transformed to the R_2 radical *via* its internal rotation around the C–C bond in two directions, *i.e.*, the clockwise and counter-clockwise rotations shown in Fig. 5. As can be seen from Fig. 5, the clockwise rotation has the energetically most stable rotamer at $\theta\simeq60°$, with the most favorable attraction (E_I), while the other rotation has the energetically best conformation at $\phi\simeq120°$, with the least repulsions ($E_{II}+E_N$). These energetically stable conformers correspond to the staggered configurations, while the most unstable ones ($\theta=150°$ and $\theta=30°$) correspond to the eclipsed configurations (see Fig. 6). As may be seen from Fig. 6, the steric repulsion of the two methyl groups seems to destabilize the rotamer, even though the size of this repulsion, 0.4 kcal/mol,[2] is relatively small. We should also discuss the stabilization effects of homoconjugation and hydrogen bonding in the rotamer and the destabilization effect of the repulsive interaction between the unpaired and lone-paired electrons. In an eclipsed configuration ($\theta=90°$), the following coplanar conformation, obtained by the NO_x ($x=1$ or 2) rotation around the C–N bond, seems to be stabilized by the aid of the homoconjugation and the hydrogen bonding.

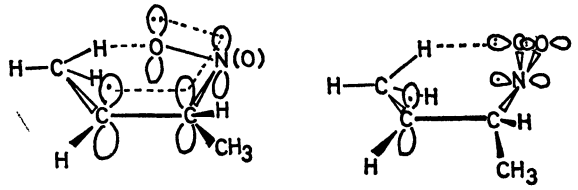

Homoconjugation and hydrogen bonding in the intermediate-radical rotamer

However, the NO_x rotation caused only electron and nuclear repulsions (augmented by the repulsion of the unpaired and lone-paired electrons), which overcome the above stabilization effects. On the other hand, the hydrogen bonding can be expected for the staggered configuration ($\theta=60°$) with a relative small interaction between the unpaired and lone-paired electrons.

Some remarks should be made with regard to the conformation of the rotamer. No change in the C–C bond length (1.45 Å) over ±0.02 Å was observed during the internal rotation of the intermediate radical (R_1), because the E_T values at $r_{CC}=1.43$ or 1.47 Å for the staggered and eclipsed conformers indicated the energetically destabilization of the rotamer. In addition, the fission of the NO_x from the intermediate radical (R_1) during the internal rotation cannot be expected in view of the fact that, at any rotation angle, the rotamer (R_1) was always more stable than the

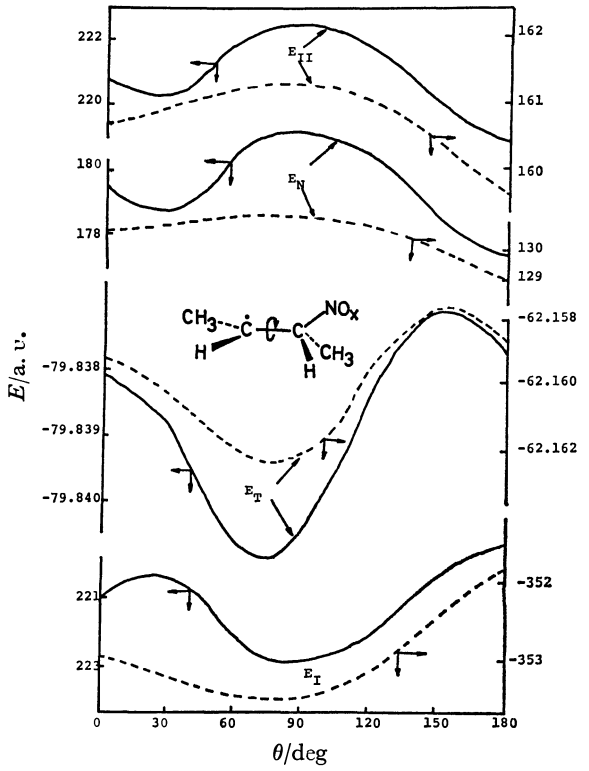

(a) Clockwise rotation

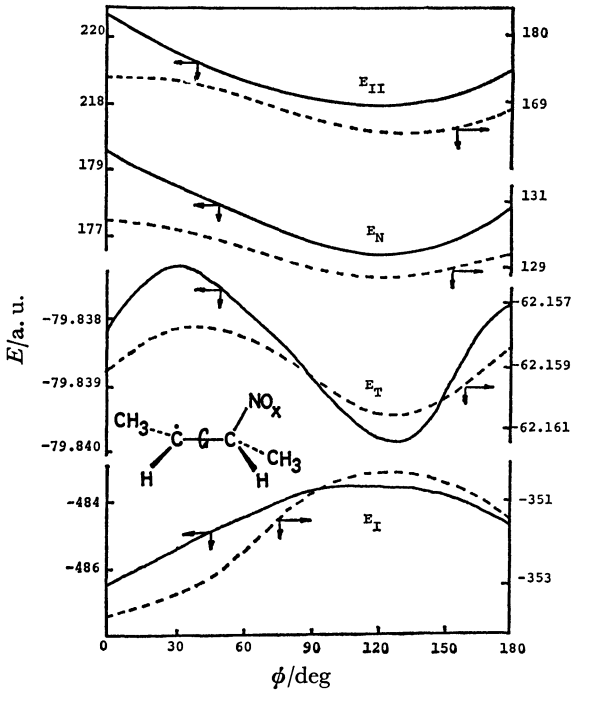

(b) Counter-clockwise rotation

Fig. 5. Energies for the internal rotation of radical (R_1) as a function of the rotation angle (solid and dotted curves: R_1 ($x=2$) and R_1 ($x=1$) respectively).

system of the isolated NO_x and the isolated rotamer of *cis*-2-butene ($r_{CC}=1.45$ Å was used).

Now, let us discuss the activation barrier of the internal rotation of the radical (R_1). The clockwise-rotation barriers were calculated to be 3.01 kcal/mol for

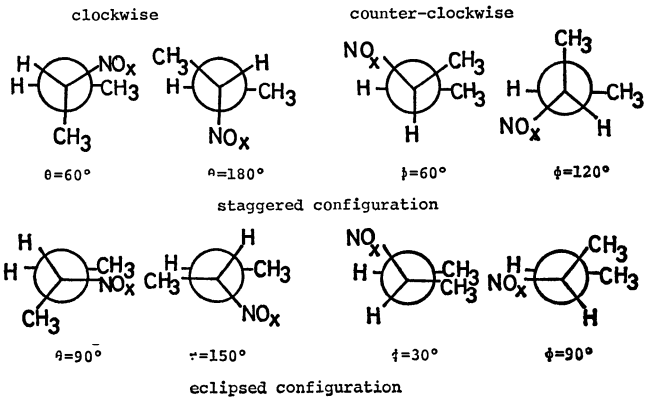

Fig. 6. Staggered and eclipsed configurations of the radical (R_1).

the R_1 ($x=1$) and 2.70 kcal/mol for the R_1 ($x=2$), while the counter-clockwise rotation-barriers were smaller, 1.82 kcal/mol for the former and 1.75 kcal/mol for the latter. The rotation barriers obtained from the present INDO-UHF calculations are relatively small as compared with those obtained from the thermodynamic estimations, 4.2 kcal/mol[29] for the R_1 ($x=1$) and 4±0.5 kcal/mol[2] for the R_1 ($x=2$). At any rate, it can be said that the NO_x ($x=1$ or 2) catalyst seems to depress extremely the activation barrier of the thermal internal-rotation of *cis*-2-butene, 62.8 kcal/mol.[3]

With regard to the intermediate radical (R_2) formed by the internal rotation of the R_1 radical, the R_2 radical is less stable by 0.36 kcal/mol ($x=1$) or 0.50 kcal/mol ($x=2$) than the R_1 radical. However, the electronic properties of the R_2 radical are not so very different from the R_1 radical in terms of the C–C and C–N bond energies ($E_{CC}=-1.158$ a.u. and $E_{CN}=-0.943$ a.u.), the spin density of the unpaired-electron orbital, and the hfsc value of the sp^2-hybrid carbon.

Finally, let us mention briefly the NO_x-fission process in the intermediate radical (R_2), taking the NO_2-fission as an example. The process was simulated much as in the case of the NO_2-addition process by changing $r_{CN}=1.47$—1.56 Å, $r_{CC}=1.45$—1.34 Å, and the hybridization of the carbon binding to NO_2= sp^3—sp^2. The monotoneous destabilization of the E_T values for the above simulated NO_2-fission process brought about a dissociation energy of 44.6 kcal/mol, a value of approximately the same magnitude as the experimental dissociation energy of the C–NO_2 bond, 60 kcal/mol.[2]

The calculations were carried out on a FACOM 230-75 at the Data Processing Center of Kyushu University.

References

1) R. B. Cundall, *Prog. React. Kinet.*, **2**, 165 (1964).

2) J. L. Sprung, H. Akimot, and J. N. Pitts, Jr., *J. Amer. Chem. Soc.*, **93**, 4358 (1971); H. Akimoto, J. L. Sprung, and J. N. Pitts, Jr., *ibid.*, **94**, 4850 (1972); J. L. Sprung, H. Akimoto, and J. N. Pitts, Jr., *ibid.*, **96**, 6549 (1974).

3) S. W. Benson and H. E. O'Neal, "Kinetic Data on Gas Phase Unimolecular Reactions," NSRDS-NBS21, U.S. Government Printing Office, Washington, D. C. (1970),

p. 351.
4) M. H. Back and R. J. Cvetanovic, *Can. J. Chem.*, **41**, 1396 (1963).
5) S. W. Benson, K. W. Egger, and D. M. Golden, *J. Amer. Chem. Soc.*, **87**, 468 (1965).
6) M. W. Schmidt and E. K. C. Lee, *J. Chem. Phys.*, **51**, 2024 (1969).
7) K. Sugimoto, W. Ando, and S. Oae, This Bulletin, **38**, 224 (1965).
8) D. M. Graham, R. L. Mieville, and C. Sivertz, *Can. J. Chem.*, **42**, 2239 (1964).
9) T. Beringhelli, A Gavezzotti, and M. Simonetta, *J. Mol. Struct.*, **12**, 333 (1972).
10) J. A. Pople and D. L. Beveridge, "Approximate Molecular Orbital Theory," McGraw-Hill, New York, N.Y. (1970).
11) M. D. Newton, W. A. Lathan, W. J. Hehre, and J. A. Pople, *J. Chem. Phys.*, **52**, 4064 (1970); see also Ref. 10.
12) "Tables of Interatomic Distances," ed. by L. E. Sutton, The Chemical Society, London, Special Publications No. 11 (1958) and No. 18 (1965).
13) M. S. Gordon, *J. Amer. Chem. Soc.*, **91**, 3122 (1969).
14) H. Fischer and H. Kollmar, *Theor. Chim. Acta*, **16**, 163 (1970).
15) S. W. Benson, D. M. Golden, and K. W. Egger, *J. Chem. Phys.*, **42**, 4265 (1965).
16) P. I. Abell and L. H. Piette, *J. Amer. Chem. Soc.*, **84**, 916 (1962).
17) R. S. Mulliken, *ibid.*, **23**, 1833, 1841 (1955). The overlap population for the bridge-type structure was given as the sum of that for the two C–N bonds.
18) W. A. Lathan, W. J. Hehre, and J. A. Pople, *J. Amer. Chem. Soc.*, **93**, 808 (1971).
19) R. A. Beudet, *J. Chem. Phys.*, **40**, 2705 (1964).
20) K. S. Pitzer, *Discuss. Faraday Soc.*, **10**, 66 (1951).
21) M. S. Newman, "Steric Effects in Organic Chemistry," Wiley, New York (1956), p. 56.
22) K. L. McEwen, *J. Chem. Phys.*, **34**, 547 (1961).
23) For instance, P. J. Krueger and H. D. Mettee, *Can. J. Chem.*, **42**, 326 (1964).
24) S. Wolfe, *Accounts Chem. Res.*, **5**, 102 (1972).
25) S. Wolfe, A. Rauk, L. M. Tel, and I. G. Csizmadia, *J. Chem. Soc., B*, **1971**, 136.
26) S. Wolfe, L. M. Tel, W. J. Haines, M. A. Robb, and I. G. Csizmadia, *J. Amer. Chem. Soc.*, **95**, 4863 (1073).
27) P. J. Krueger, J. Jan, and H. Wieser, *J. Mol. Struct.*, **5**, 375 (1970).
28) R. W. Fessenden, *J. Phys. Chem.*, **71**, 74 (1967).
29) R. B. Cundall and T. F. Palmer, "Actes du Deuxieme Congres International de Catal, se Paris," Editions Technip (1961), p. 573.

A Formulation of Chemical Kinetics in Micellar Solutions

Keishiro SHIRAHAMA

Department of Chemistry, Faculty of Science and Engineering, Saga University, Saga 840

(Received March 19, 1975)

Reaction kinetics in the presence of micelles is formulated on the basis of a microheterogeneous reaction in accordance with a current model of micellar catalysis. The necessary molecular parameters are the radius of the hydrocarbon core of a spherical micelle, the thickness of a reaction surface layer, the surface and zeta potentials, and a distribution coefficient of a hydrophobic substrate. The derived expression was applied to the hydrolysis reaction of methylorthobenzoate in the presence of sodium dodecylsufate micelle to describe reaction properties such as a rate-surfactant concentration profile, inhibition by added electrolyte, and activation energy. The micellar effect on the reaction rate was explained by a simple concentration effect of the reactants; the stabilization of the transition state by the micellar surface potential need not be taken into consideration. Inhibition of the orthoester hydrolysis by a cationic surfactant is also predicted.

The last decade has witnessed a remarkable development in studying chemical reactions in surfactant solutions,[1-3] wherein 5- to 1000-fold acceleration of rates as well as inhibitions of various magnitudes have been reported. Most reactions are analyzed by a chemism formula akin to the Michaelis-Menten equation to obtain a rate constant at the micellar phase k_m, and one at the bulk phase k_b, separately. However, no attempt has been made to look into the physical and chemical significances of k_m, except for a few works.[4-7]

In this communication a model that has been proposed by organic chemists will be formulated and analyzed on the basis of a microheterogeneous reaction in order to give insights into the nature of micellar catalysis.

Theoretical

Now let us define $v(\boldsymbol{r})$, which may be called the "reaction density,"

$$v(\boldsymbol{r}) = k(\boldsymbol{r})C_A(\boldsymbol{r})C_B(\boldsymbol{r}) \quad (1)$$

In this equation, which is apparently that of a second order reaction, $v(\boldsymbol{r})$ is a reaction rate in an elementary volume $d\boldsymbol{u}$, $k(\boldsymbol{r})$ is a rate constant, and $C_A(\boldsymbol{r})$ and $C_B(\boldsymbol{r})$ are the concentrations of reactants A and B in the volume. It should be noted that they are all expressed as a function of the coordinate $\boldsymbol{r}$. A reaction rate in an entire reaction vessel is obtained by integrating Eq. (1) over the vessel

$$dn/dt = \int_V v(\boldsymbol{r})d\boldsymbol{u} \quad (2)$$

More specifically, consider that there are N micelles in the reaction vessel, each micelle being equivalent, and that the micellar concentration is too dilute for any two micelles to approach each other. Then this system is approximated by an assembly which consists of N subsystems, where in a subsystem it is supposed that a micelle is located at the center. The subsystem satisfies $(4/3)\pi\rho^3 = V/N$, ρ being the radius of the spherical subsystem. A reaction rate in the subsystem is expressed as

$$I = 4\pi\int_0^\rho x^2 k(x)C_A(x)C_B(x)dx \quad (3)$$

where x is the distance from the center of a spherical micelle which is very likely at concentrations not far above a critical micelle concentration (CMC). It can be further assumed that reactant A is a hydrophobic substrate, and reactant B an ionic species, without losing generality too much. Concentration profiles of these reactants around a micelle are illustrated in Fig. 1, where R is the radius of the hydrocarbon core of a micelle, and s the thickness of a surface layer around a micelle. This surface layer is presumed to be the reaction site which contains the so-called Stern layer and extends up to a plane of shear. Reactant A is partitioned in the micellar phase because of its hydrophobicity, and $C_A(x)$ decreases across the surface layer down to the bulk concentration C_{Ab}. Reactant B is concentrated around micelles by the Coulombic force if the charge is opposite to that of the micelle. The ionic reactant scarcely penetrates into the hydrocarbon core of a micelle, and, beyond the surface layer, is distributed in a diffused double layer down to the bulk concentration C_{Bb}. Then Eq. (3) is integrated in two regions: $R \leqq x \leqq R+s$, and $R+s \leqq x \leqq \rho$, respectively.

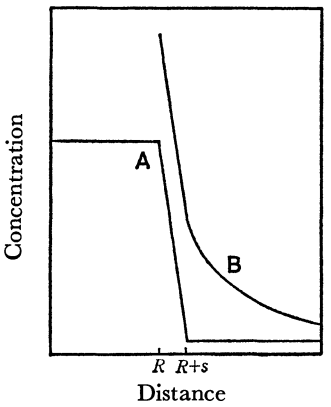

Fig. 1. Schematic representation of concentration profile around a micelle. A: a hydrophobic reactant, B: an ionic reactant.

Zeroth Approximation. It is assumed that $k(x) = k_s$, $C_A(x) = C_{As}$, and $C_B(x) = C_{Bs}$ in the surface layer, and $k(x) = k_b$, $C_A(x) = C_{Ab}$, and $C_B(x) = C_{Bb}$ in the outer layer. Then one obtains

$$I = 4\pi k_s C_{As}C_{Bs}\int_R^{R+s} x^2dx + 4\pi k_b C_{Ab}C_{Bb}\int_{R+s}^{\rho} x^2dx$$
$$= V_s k_s C_{As}C_{Bs} + V_b k_b C_{Ab}C_{Bb} \quad (4)$$

In Eq. (4), V_s and V_b are volumes of the surface and

bulk phases in a subsystem, respectively. Converting Eq. (4) into a conventional rate equation in a concentration scale, one has

$$dC/dt = (1/V)(dn/dt) = I/V_{sub} = IN/V$$
$$= \phi_s k_s C_{As} C_{Bs} + \phi_b k_b C_{Ab} C_{Bb} \quad (5)$$

where $V_{sub}=(4/3)\pi\rho^3$, and $\phi_i=NV_i/V$ is the volume fraction indicated by the respective subscript. Equation (5) is somewhat similar to equations previously reported,[4,5] but is not identical. The surface layer concentrations appearing in Eq. (5) are expressed in terms of the corresponding bulk concentrations by using the distribution coefficients K_A and K_B,

$$K_A = C_{Am}/C_{Ab} = C_{As}/C_{Ab} \quad (6)$$

where C_{Am} is a concentration of A in the micellar phase. The second identity, *i.e.*, $C_{Am}=C_{As}$ is a result of the zeroth approximation, and

$$K_B = C_{Bs}/C_{Bb} = \exp(-e\psi_0/kT) \quad (7)$$

where ψ_0 is a surface potential of a micelle. Equation (5) becomes

$$dC/dt = (\phi_s k_s K_A K_B + \phi_b k_b) C_{Ab} C_{Bb} \quad (8)$$

This equation can be expressed by the analytical concentrations of the reactants, C_A and C_B.

$$dC/dt = (\phi_s k_s K_A K_B + \phi_b k_b) C_A C_C/(\phi_m K_A + \phi_b) \quad (9)$$

where the following relations were used:

$$VC_A = (V_m C_{Am} + V_b C_{Ab}) N \quad (10)$$

and

$$C_B = C_{Bb} \quad (11)$$

In Eq. (10), V_m is a volume of the micellar region and C_{Am} a concentration of substrate A there. Equation (11) holds for a buffered species, although there is an argument suggesting the difficulty in estimating the concentration at the micellar surface.[8] Comparing Eq. (9) with the experimental expression, $v=k_2 C_A C_B$, one obtains

$$k_2 = [(\phi_s f K_A K_B + \phi_b)/(\phi_m K_A + \phi_b)] k_b \quad (12)$$

where $k_s=fk_b$ is introduced, and f implies an intrinsic micellar effect taken relative to k_b.

First Approximation. At this stage, it is assumed, based on a more realistic model, that the concentrations of the reactants decrease linearly in the surface layer, *i.e.*,

$$C_A(x) = C_{Am}[1-(K_A-1)(x-R)/K_A s] \quad (13)$$

and

$$C_B(x) = C_{Bm}[1-[1-\exp(-(\zeta-\psi_0)/kT)](x-R)/s] \quad (14)$$

In Eq. (14), the zeta potential ζ was used to denote the concentration of reactant B at $x=R+s$, or the plane of shear. Substituting Eqs. (13) and (14) into Eq. (3) for the surface layer part I_s, one has

$$I_s = 4\pi f k_b C_{Am} C_{Bm}$$
$$\times \int_R^{R+s} x^2[1-(K_A-1)(x-R)/K_A s]$$
$$\times [1-[1-\exp(-e(\zeta-\psi_0)/kT)(x-R)/s]dx \quad (15)$$

Comparing Eq. (15) with Eq. (4), one can understand that the integral in Eq. (15) corresponds to the volume of the surface layer, and it may be called the effective volume of the surface layer V_{es}. Replacing ϕ_s in Eq. (12) with $\phi_{es}=NV_{es}/V$, an effective volume fraction of the surface layer, one has

$$k_2 = k_b(\phi_{es} f K_A K_B + 1)/(\phi_m K_A + 1) \quad (16)$$

where $\phi_b=1$ was used in accordance with an assumption of very dilute micellar concentration. Equation (16) has many more detailed physicochemical contents than does the formally similar equation.[2]

Application to MOB–SDS System. Now our discussion will be confined to the hydrolysis kinetics of methylorthobenzoate (MOB) in sodium dodecylsulfate (SDS) solution, for the kinetic studies on MOB in aqueous and in SDS solutions have been fully described,[1,3,10] and since SDS is one of the most explored surfactants, the necessary molecular parameters are available.[1-3,11] First, the rate enhancement k_2/k_b at 0.01 M SDS in micellar form will be estimated according to Eq. (16). The necessary parameters are listed in Table 1. Prior to the numerical calculation, the parameters are briefly examined. Dougherty and Berg have recently reported the distribution coefficient of MOB between the micelle and the bulk phases by the ultrafiltration method.[12] The value they obtained varies with the substrate concentration, but at the concentration in the kinetic experiment (about 5×10^{-5} M), $K=1.4\times10^4$ (MOB mol fraction in micelle/MOB mol fraction in the bulk), which is converted to $K_A=C_{Am}/C_{Ab}$ [(mol of solubilized MOB/micellar volume)/(mol of MOB in the bulk/l of water)] by using the molar volume of SDS micelle=0.3 l/mol, which is between the partial molar volume of SDS micelle, 0.25 l/mol,[13] and a calculated micellar volume with a radius=$R+s$ and aggregation number of a micelle=70, 0.33 l/mol. The value of K_B, or exp $(-e\psi_0/kT)$ is taken from that calculated by Stigter and Mysels using a modified Gouy-Chapman potential, which differs by only a few milivolts from the spherical potential.[9,14] There may be various factors affecting f. The factor f should have a form $f=\exp(-\Delta G^{\neq}/RT)$, where $\Delta G^{\neq}$ is an activation free energy representing the relative stabilizations of the transition state by the hydrophobic interaction, the orientation effect, and electrostatic effects including the Coulombic as well as dipole-field interactions. For the moment $f=1$ is assumed, although there is an opinion stressing the electrostatic stabilization of the transition state,[3,15] *i.e.*, $f>1$; this is an overestimation, as will be shown later. Equation (16) gives $k_2/k_b=103$, which is com-

Table 1. Parameters to calculate the micellar effect on reaction kinetics

Quantity		Unit	Ref.
Radius of hydrocarbon core, R	16.6	Å	11
Thickness of the surface layer, s	4.4	Å	11
Surface potential (0.01 M), ψ_0	−178	mV	9, 14
(0.03 M),	−161	mV	9, 14
(0.05 M),	−150	mV	9, 14
Zeta potential, $\zeta=\psi_0/2$		mV	9, 14
Distribution coefficient of MOB, K_A	833	(M/M)	12
Aggregation number of a micelle	70		11

parable to a 69-fold enhancement experimentally obtained for MOB–SDS system at 25 °C.[15] Many aspects of the micellar effects on the kinetics will be explained on the basis of Eq. (16)

Inhibition of Rate Enhancement by Added Electrolyte A marked dependence of the rate on the added electrolyte can be analyzed in the following manner. Under the condition, $\phi_{es}K_A f\exp(-e\psi_0/kT) \gg 1$ at a constant micelle concentration, Eq (16) becomes

$$k_2/k_b = \phi_{es}K_A f\exp(-e\psi_0/kT) \times \text{constant} \quad (17)$$

Taking the logarithm of Eq. (17), and assuming $\phi_{es}=$ constant because it varies by less than 1% even if ψ_0 is changed from 170 to 130 mV as a result of numerical calculation, one obtains

$$\ln(k_2/k_b) = -\nu\Phi_0 + \text{constant} \quad (18)$$

where ν expresses an electrostatic effect arising from terms other than K_B, possibly from $f=\exp(-\Delta G^{\neq}/RT)$, and $\Phi_0=e\psi_0/kT$ is a reduced surface potential, which can be approximated by a simplified Gouy-Chapman potential under the pertinent condition, $|\psi_0|>100$ mV,[16]

$$\Phi_0 = \ln C_t + \text{constant} \quad (19)$$

In Eq. (19), C_t is the total counterion concentration. Combining Eq. (18) with Eq. (19), one has

$$\log(k_2/k_b) = -\nu \log C_t + \text{constant} \quad (20)$$

In Fig. 2, $\log(k_2/k_b)$ is plotted against $\log C_t$, where the kinetic data are those of Dunlap and Cordes,[15] and $C_t=cmc+$buffer concentration (0.01 M)+added salt concentration C_a. Before interpreting the features appearing in Fig. 2, it should be noted that *cmc* is remarkably diminished by the added electrolyte, and this tendency becomes approximately saturated when the added salt concentration is as much as, *e.g.*, 0.1 M.[17] Dunlap and Cordes have performed their measurement at a constant total SDS concentration of 0.01 M, and therefore the micellar concentration increases with increasing added electrolyte concentration; the fraction of micellized SDS is about 0.5 at $C_a=0$, and about 0.85 at $C_a=0.1$ M. So in accordance with the assumption of constant micellar concentration, it is the slope at the high concentration region of added electrolyte that is significant, because the micellar concentration remains nearly constant in this region of C_a. As seen in Fig. 2, the slope in the region is unity, $\nu=1$, which implies that there is no electrostatic effect other than $K_B=\exp(-\Phi_0)$ in Eq. (17). If there were any other electrostatic effect such as the stabilization of transition state,[3,15,18] a value of $\nu>1$ should be expected: in other words, $\Delta G^{\neq}$ should contain a Φ_0 term. Therefore it is considered that the carbonium ion at the transition state is stabilized by the surface potential to the same degree as the protonated MOB, a reactant of the rate-determining step, is, because of the proximity of the protonated MOB and the carbonium ion-like transition state on a reaction coordinate.[10] Thus it may be concluded that the micellar effect on MOB hydrolysis is mainly, if not solely, ascribed to the concentration effect due to the hydrophobic interaction with a micelle as well as to the electrostatic attraction of the proton.

Activation Energy. Another subsidiary piece of evidence that supports the absence of electrostatic stabilization of the transition state is obtained by examining the activation energy. The Arrhenius plot gives the activation energy in the presence of micelles, $E_m^{\neq}=11$ kcal/mol, which is about 4.5 kcal/mol smaller than the one in the absence of micelles, $E_b^{\neq}$.[10] Strictly speaking, $\Delta E^{\neq}=E_m^{\neq}-E_b^{\neq}$ arises from the temperature dependences of K_A, $K_B=\exp(-\Phi_0)$, and f, but the main part of it is certainly occupied by $\Phi_0 kT=-4$ kcal/mol ($\psi_0=-170$ mV), for the temperature dependence of the hydrophobic interaction is very small.[19] There would be no possibility for the f-factor to contribute another Φ_0 term originating from the electrostatic stabilization of the transition state to the activation energy, unless a fortuitous cancellation between the K_A and f terms occurs.

Rate-Surfactant Concentration Profile. It has been well known that there is a tri-phasic feature in the rate-surfactant concentration profile, which can be reproduced by Eq. (16), as shown in Fig. 3. It should be noted that a curve with a slight and broad maximum can be obtained only when a ψ_0 that decreases with increasing counterion concentration is employed: ψ_0 was varied from -172 mV at [M]= 0.005 M to -165 mV at [M]=0.065 M, where [M] denotes the SDS concentration in micellar form.

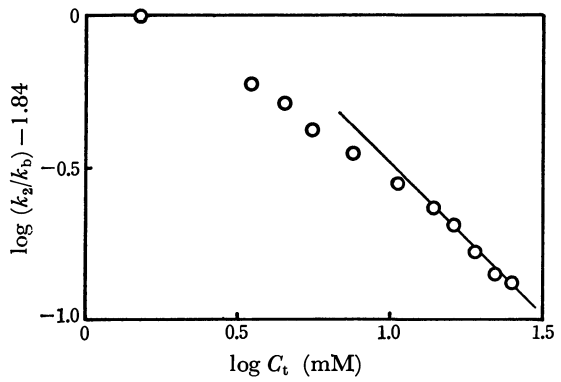

Fig. 2. Effect of added electrolyte on rate enhancement.

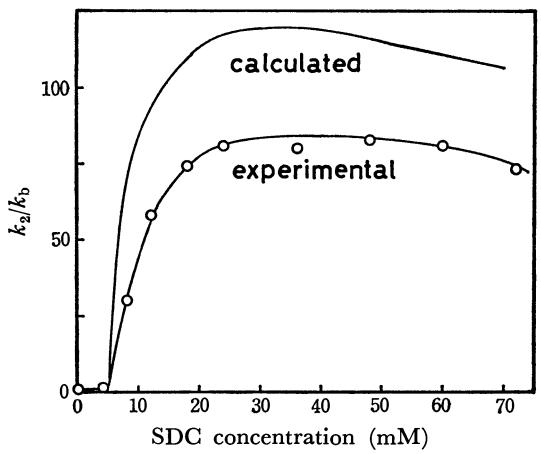

Fig. 3. Rate-SDS concentrationprofile. The experimental data from Ref. 15.

Discussion

Now let us examine the factors which are contributing to rate enhancement by means of Eq. (16). The term ϕ_{es} is numerically expressed as 0.054 [M], where [M] is a micellar concentration in SDS mol/l, and roughly evaluated by (the total SDS concentration —*cmc*), although there is some difficulty in estimating [M].[20] The numerical factor, 0.054 is an effective volume of the surface layer per one SDS molecule in l/mol. So, at [M]=0.01 M, for example, ϕ_{es}= 0.00054. Multiplied by K_A, $\phi_{es}K_A$=0.453, which is too small to explain the observed rate enhancement. Further multiplied by $K_B=\exp(-\Phi_0)$=840, $\phi_{es}K_AK_B$=380, which is divided by $(\phi_m K_A+1)$=3.52 to give 103-fold enhancement, an expected magnitude. There is a systematic discrepancy between the observed and the calculated rates, as seen in Fig. 3. A value of f=0.7 would give striking coincidence, but a deviation from unity of this size might be insignificant in view of the simplicity of the fundamental model and the consequent uncertainty in the molecular parameters. Here again it may be inferred that a simple concentration effect is the most important factor, and effects specific to micelles would be, if present, of secondary importance. In order to simulate the curve in Fig. 3, it was necessary that 15% of micellar concentration, in addition to the *cmc* and the buffer concentration, be taken as the total counterion concentration C_t: in other words, about 15% of the counterion of a micelle is shared among other micelles.

Inhibition of MOB Hydrolysis by Cationic Surfactant. Although our discussion heretofore has been restricted to the MOB–SDS system, the inhibition of MOB hydrolysis by a cationic surfactant should be briefly referred to. Hydrolysis of MOB is inhibited about 3-fold in the presence of 0.04 M cetyltrimethylammonium bromide.[21] This inhibition can be interpreted in terms of Eq. (16), in which the $\phi_{es}K_A f \exp(-\Phi_0)$ term is neglected because $\exp(-\Phi_0) \ll 1$ in this case.

$$k_2/k_b = 1/(\phi_m K_A + 1) \quad (21)$$

Equation (21) predicts about 10-fold inhibition when $\phi_m=0.3\times0.04=0.012$ and K_A=800, as a rough estimate, are substituted. Thus the inhibition is explained by the fact that MOB is localized in a micellar region by the hydrophobic interaction, while the protons are expelled out of there by the Coulombic repulsion.

The author thanks Dr. Y. Moroi of Kyushu University for his interest and discussions.

References

1) E. H. Cordes and R. B. Dunlap, *Accounts Chem. Res.*, **2**, 329 (1969).
2) E. J. Fendler and J. H. Fendler, *Advan. Phys. Org. Chem.*, **8**, 271 (1970).
3) E. H. Cordes, Ed., "Reaction Kinetics in Micelles," Plenum Publishing Co., New York, N. Y. (1972).
4) P. Heitmann, *European J. Biochem.*, **5**, 305 (1968).
5) A. K. Yatsimirski, K. Martinek, and I. V. Berezin, *Tetrahedron*, **27**, 2855 (1971).
6) S. J. Dougherty and J. C. Berg, *J. Colloid Interface Sci.*, **49**, 135 (1974).
7) C. Gitler and A. Ochoa-Solano, *J. Amer. Chem. Soc.*, **90**, 5004 (1968).
8) C. A. Bunton and B. Wolfe, *ibid.*, **95**, 3742 (1973).
9) D. Stigter and K. J. Mysels, *J. Phys. Chem.*, **59**, 45 (1955).
10) H. G. Bull, K. Koehler, T. C. Pletcher, J. Ortiz, and E. H. Cordes, *J. Amer. Chem. Soc.*, **93**, 3002 (1971).
11) D. Stigter, *J. Colloid Interface Sci.*, **23**, 379 (1967); *ibid.*, **47**, 473 (1974).
12) S. J. Dougherty and J. C. Berg, *ibid.*, **48**, 110 (1974).
13) C. Tanford, Y. Nozaki, J. A. Reynolds, and S. Makino, *Biochemistry*, **13**, 2369 (1974).
14) J. T. Davies and E. K. Rideal, "Interfacial Phenomena," Academic Press, New York, N. Y. (1961), p. 146.
15) R. B. Dunlap and E. H. Cordes, *J. Amer. Chem. Soc.*, **90**, 4395 (1968).
16) P. 76 in Ref. 14.
17) M. F. Emerson and A. Holtzer, *J. Phys. Chem.*, **71**, 1898 (1967).
18) R. B. Dunlap and E. H. Cordes, *ibid.*, **73**, 361 (1969).
19) G. Nemethy and H. A. Scheraga, *ibid.*, **66**, 1773 (1962).
20) K. Shirahama, This Bulletin, **47**, 3165 (1974).
21) M. T. A. Behme, J. G. Fullington, R. Noel, and E. H. Cordes, *J. Amer. Chem. Soc.*, **87**, 266 (1965).

Refinement of the Crystal Structure of Sodium Hexahydroxoantimonate(V), $NaSb(OH)_6$

Takeshi Asai

Institute of Scientific and Industrial Research, Osaka University, Yamada-kami, Suita, 565

(Received March 31, 1975)

The crystal structure of sodium hexahydroxoantimonate (V), $NaSb(OH)_6$, has been refined. The previous structure given by Schrewelius was confirmed, but the positional parameters of oxygen atoms were shifted significantly. Both antimony and sodium atoms are surrounded by six oxygen atoms octahedrally. The interatomic distances are: Sb-O=1.972—1.999 Å (mean 1.98 Å), O-O=2.758—2.834 Å (2.80 Å) for an SbO_6 octahedron, Na-O=2.375—2.406 Å (2.39 Å) and O-O=3.229—3.526 Å (3.38Å) for an NaO_6 octahedron. Two types of sequences of hydrogen bonds were recognized. They were compared with the sequences of hydrogen bonds in $In(OH)_3$ and $MnSn(OH)_6$.

In the course of our NMR studies on the metal hydroxides, $In(OH)_3$, $MgSn(OH)_6$ and $NaSb(OH)_6$, accurate structural information was needed on these compounds. The crystal structure of $In(OH)_3$,[1] and that of $MnSn(OH)_6$,[2] which is isomorphous with $MgSn(OH)_6$,[3,4] have already been analyzed with single crystal X-ray diffraction data. On the other hand, the crystal structure of $NaSb(OH)_6$ was derived from powder X-ray diffraction intensities[5,6] with accordingly poor accuracy. The analysis resulted in an OH group free from hydrogen bonding and another with a very short OH···O distance (2.55 Å).

Experimental

The compound was obtained by slow evaporation of a dilute aqueous solution containing $KSb(OH)_6$ and NaCl in the molar ratio of 2 : 1. The crystals thus obtained were enclosed with one (001) and eight {111} faces.

The space group and lattice constants[5,6] were confirmed from Weissenberg and precession photographs. Crystallographic data obtained in this study are given in Table 1.

The intensity data were collected using a Rigaku automatic four-circle diffractometer with a scintillation counter and the Mo$K\alpha$ radiation. A total of 821 reflections in two octants, among which 465 reflections were independent, were measured within $\sin\theta/\lambda$ of 0.60 Å^{-1}. Ninety-six reflections with $|F_o|$ values less than 2σ, twice the estimated standard deviations based on the counting statistics, were assumed to have zero amplitudes. The whole reflections were corrected for Lorentz and polarization effects, but not for absorption nor extinction effects (μR=0.55).

Table 1. Crystallographic data

$NaSb(OH)_6$,	F. W. 246.8
Tetragonal	
a=8.029(2),	c=7.894(3) Å
U=508.9Å^3,	Z=4
D_m = 3.20 g·cm^{-3} [5]	
D_x=3.22 g·cm^{-3}	
Systematic absences:	$hk0$ with $h+k=2n+1$
	$00l$ with $l=2n+1$
Space group $P4_2/n$ (No. 86)	

From a three-dimensional Patterson synthesis, approximate positional parameters for all non-hydrogen atoms were obtained. They were refined by a block-diagonal least-squares method firstly with isotropic thermal factors and then with anisotropic ones. The final residual R was 0.063. A trial to find hydrogen positions in the difference Fourier maps was unsuccessful. The weighting scheme was; w= 1 for $|F_o|\neq 0$, and w=0 for $|F_o|=0$. Reflections of 020 and 002 were omitted in the refinement because they were seriously affected by extinction. The atomic scattering amplitudes for Sb^{5+}, Na^+ and O^- with anomalous dispersion corrections were taken from Ref. 7. All calculations were performed on a NEAC 2200/700 computer at the Computer Center, Osaka University, using UNICS programs RSSFR-5, HBLS-V and RSDA-4 with some modifications. The final parameters are given in Table 2. The final observed and calculated structure factors are listed in Table 3.

Discussion

The crystal structure is projected in Fig. 1. Interatomic distances and angles are shown in Fig. 2. The structure is in general the same as that given by Schrewelius.[6] The oxygen atoms, however, were significantly shifted (0.13—0.69 Å); as a result, his short OH···O distance (2.55 Å) increased to a normal distance of 2.859 Å, while his longer O···O distance (4.51 Å) decreased to 3.149 Å. The antimony atom is surrounded by six oxygen atoms. This coordination polyhedron is a nearly regular octahedron with the mean interatomic distances of 1.98 Å for Sb-O and 2.80 Å for O-O. The sodium ion is surrounded by six oxygen atoms belonging to six different

Table 2. Final positional and thermal parameters ($\times 10^4$) with their e.s.d.'s in parentheses

Thermal factors are of the form $T=\exp[-(h^2B_{11}+\cdots+klB_{23})]$.

Atom	x	y	z	B_{11}	B_{22}	B_{33}	B_{12}	B_{13}	B_{23}
Na	7500	7500	7500	45(9)	49(9)	57(8)	−8(14)	18(16)	−10(15)
Sb	2500	2500	2500	22(1)	15(1)	24(1)	−3(2)	4(2)	5(2)
O(1)	1942(8)	274(8)	3482(8)	63(11)	35(10)	26(10)	−14(17)	4(18)	−11(17)
O(2)	292(8)	3320(8)	3228(9)	35(10)	51(10)	39(10)	10(17)	7(18)	54(17)
O(3)	1605(8)	1815(7)	281(8)	48(10)	13(9)	22(9)	6(16)	−22(17)	−9(16)

Table 3. Final observed and calculated structure factors, $|F_o|$ and $|F_c|$

K Fo Fc	K Fo Fc	K Fo Fc	K Fo Fc	K Fo Fc	K Fo Fc	K Fo Fc	K Fo Fc	K Fo Fc
H,L= 0,0	7 6 6	6 8 5	6 5 4	2 31 27	H,L= 8,3	4 0 2	H,L= 4,5	2 7 5	1 8 7
2 210 225	8 0 2	7 9 9	7 0 1	3 115 113	1 17 15	5 5 4	1 7 5	3 8 10	2 15 16
4 184 182	9 11 11		8 7 4	4 11 12	2 8 10	6 7 8	2 7 4	4 0 1	3 0 5
6 88 89		H,L= 7,1		5 105 106	3 0 2	7 6 6	3 8 5	5 0 2	4 10 13
8 88 89	H,L= 1,1	1 67 68	H,L= 4,2	6 16 14	4 8 2		4 12 13	6 0 4	5 0 10
	1 159 160	2 0 1	1 27 23	7 89 89		H,L= 6,4	5 0 2		
H,L= 1,0	2 7 5	3 84 83	2 155 156	8 10 8	H,L= 9,3	1 20 19	6 8 3	H,L= 4,6	H,L= 5,7
1 7 4	3 156 155	4 7 7	3 25 25	9 65 68	1 67 70	2 105 103	7 0 1	1 11 12	1 77 77
3 18 14	4 7 3	5 72 72	4 131 131			3 0 0		2 110 113	2 7 6
5 8 8	5 127 126	6 0 2	5 8 6	H,L= 2,3	H,L= 0,4	4 104 104	H,L= 5,5	3 0 6	3 55 54
7 5 8	6 5 4		6 102 101	1 47 42	0 162 162	5 7 2	1 74 76	4 103 102	4 0 3
9 0 3	7 72 72	H,L= 8,1	7 8 5	2 18 16	1 20 19	6 91 92	2 0 1	5 7 6	
	8 6 4	1 6 4	8 93 94	3 11 10	2 172 181		3 64 63	6 100 102	H,L= 6,7
H,L= 2,0	9 75 76	2 0 3		4 5 3	3 20 17	H,L= 7,4	4 4 6		1 7 4
2 149 151		3 16 16	H,L= 5,2	5 22 20	4 124 125	1 0 2	5 86 88	H,L= 5,6	2 7 4
4 193 199	H,L= 2,1	4 0 1	1 15 15	6 6 9	5 10 9	2 10 9	6 7 6	1 0 4	
6 114 110	1 0 1	5 0 0	2 17 15	7 25 27	6 114 113	3 9 8		2 8 10	H,L= 0,8
8 117 115	2 0 1		3 13 14	8 0 0	7 6 4	4 8 2	H,L= 6,5	3 7 7	0 94 94
	3 53 49	H,L= 9,1	4 17 15		8 92 89	5 0 1	1 5 6	4 0 0	1 0 0
H,L= 3,0	4 7 5	1 85 84	5 0 6	H,L= 3,3			2 0 2	5 0 6	2 102 101
1 32 26	5 0 2	2 7 8	6 9 8	1 113 113	H,L= 1,4	H,L= 8,4	3 14 13		3 13 11
3 40 36	6 0 5	3 69 69	7 12 10	2 8 8	1 6 1	1 10 11	4 6 6	H,L= 6,6	4 89 88
5 6 4	7 7 5			3 108 106	2 17 13	2 88 88	5 7 2	1 0 1	5 8 6
7 9 12	8 0 1	H,L= 0,2	H,L= 6,2	4 0 2	3 0 2	3 7 3		2 87 84	
9 13 16	9 13 14	0 178 209	1 22 20	5 95 97	4 0 1		H,L= 7,5	3 7 3	H,L= 1,8
		1 19 14	2 137 138	6 0 2	5 0 3	H,L= 0,5	1 81 81	4 79 77	1 5 7
H,L= 4,0	H,L= 3,1	2 158 162	3 6 4	7 82 82	6 6 3	1 0 2	2 0 1		2 15 16
2 160 157	1 74 62	3 40 35	4 107 106	8 7 3	7 7 8	2 13 13	3 72 75	H,L= 7,6	3 0 7
4 142 141	2 21 17	4 182 185	5 7 6		8 14 15	3 32 31	4 0 1	1 7 3	4 14 15
6 95 91	3 109 107	5 20 17	6 91 90	H,L= 4,3		4 6 6		2 15 14	
8 99 101	4 21 21	6 135 137	7 9 9	1 7 7	H,L= 2,4	5 11 8	H,L= 8,5		H,L= 2,8
	5 86 82	7 7 5		2 12 14	1 32 29	6 0 4	1 0 3	H,L= 0,7	1 7 2
H,L= 5,0	6 26 26	8 106 107	H,L= 7,2	3 9 10	2 171 181	7 0 0		1 6 8	2 101 99
1 17 17	7 87 87	9 6 4	1 9 10	4 0 2	3 21 20	8 8 6	H,L= 0,6	2 6 8	3 8 6
3 21 20	8 7 7		2 7 2	5 16 15	4 115 113		0 81 82	3 6 5	4 82 79
5 8 8	9 76 78	H,L= 1,2	3 0 0	6 0 0	5 8 4	H,L= 1,5	1 6 8	4 0 3	
7 0 1		1 24 20	4 9 9	7 8 7	6 105 103	1 111 113	2 125 127	5 7 9	H,L= 3,8
	H,L= 4,1	2 28 24	5 7 3	8 7 8	7 7 5	2 0 2	3 0 8	6 7 3	1 0 1
H,L= 6,0	1 12 10	3 17 16	6 12 12		8 77 76	3 87 81	4 109 108		2 0 6
2 143 146	2 18 18	4 27 25		H,L= 5,3		4 4 1	5 8 8	H,L= 1,7	3 8 9
4 134 139	3 4 3	5 5 2	H,L= 8,2	1 103 104	H,L= 3,4	5 61 58	6 119 117	1 67 67	4 0 2
6 117 119	4 6 3	6 11 8	1 9 12	2 7 2	1 15 13	6 9 7	7 0 1	2 0 3	
	5 12 11	7 0 0	2 101 101	3 90 88	2 13 10	7 73 72		3 73 71	H,L= 4,8
H,L= 7,0	6 0 0	8 6 2	3 6 7	4 23 23	3 25 25	8 0 1	H,L= 1,6	4 6 2	1 13 12
1 6 4	7 0 3	9 0 0	4 75 74	5 77 77	4 18 18		1 0 0	5 74 75	2 87 87
3 10 10	8 8 8			6 18 18	5 12 11	H,L= 2,5	2 13 10	6 0 0	3 9 7
5 0 1		H,L= 2,2	H,L= 9,2	7 67 68	6 0 2	1 7 7	3 0 3		
	H,L= 5,1	1 29 24	1 13 13		7 7 4	2 14 12	4 14 14	H,L= 2,7	H,L= 5,8
H,L= 8,0	1 111 107	2 154 150	2 0 3	H,L= 6,3	8 8 8	3 13 12	5 10 4	1 0 0	1 8 12
2 107 102	2 9 10	3 30 24		1 24 24		4 14 15	6 0 7	2 9 8	
4 82 83	3 129 132	4 180 188	H,L= 0,3	2 0 0	H,L= 4,4	5 5 2	7 10 7	3 14 16	H,L= 0,9
	4 4 3	5 18 16	1 68 57	3 11 10	1 0 2	6 0 4		4 10 7	1 7 8
H,L= 9,0	5 77 76	6 138 140	2 11 13	4 5 5	2 136 136	7 0 6	H,L= 2,6	5 0 0	2 0 11
1 0 2	6 8 7	7 0 0	3 0 2	5 10 10	3 20 20		1 18 21	6 0 5	
3 11 11	7 77 78	8 113 114	4 10 7	6 10 3	4 122 122	H,L= 3,5	2 137 139		H,L= 1,9
	8 8 1	9 0 5	5 32 30		5 10 12	1 126 130	3 7 6	H,L= 3,7	1 78 79
H,L= 0,1			6 0 1	H,L= 7,3	6 113 112	2 0 0	4 95 91	1 95 97	2 8 5
1 0 1	H,L= 6,1	H,L= 3,2	7 0 1	1 89 88	7 0 2	3 94 94	5 6 2	2 5 7	
2 0 0	1 8 8	1 28 24	8 0 1	2 8 0		4 5 6	6 101 101	3 78 78	H,L= 2,9
3 73 62	2 5 5	2 24 19	9 0 4	3 75 75	H,L= 5,4	5 86 86	7 11 7	4 0 6	1 0 7
4 8 7	3 18 17	3 22 20		4 15 15	1 5 3	6 17 14		5 79 80	2 14 12
5 5 3	4 5 7	4 15 14	H,L= 1,3	5 67 66	2 25 25	7 64 64	H,L= 3,6		
6 6 3	5 0 0	5 13 15	1 109 106		3 8 9		1 0 4	H,L= 4,7	

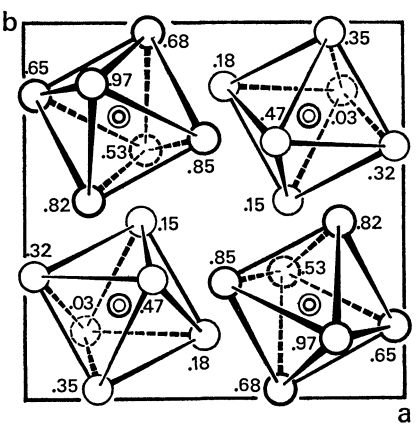

Fig. 1. The crystal structure of $NaSb(OH)_6$ projected along the [001] axis. Numbers attached to the oxygen atoms are their z-parameters.

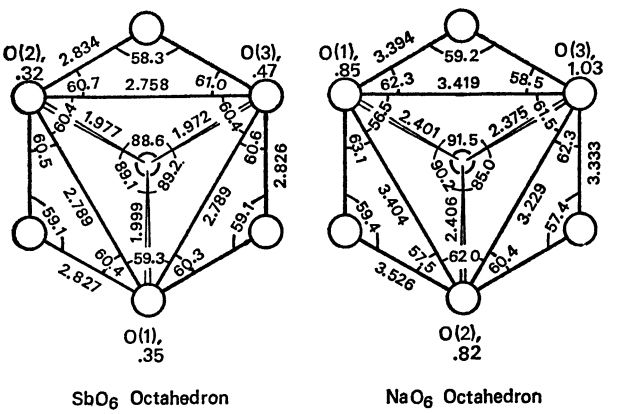

Fig. 2. Interatomic distances (l/Å) and angles (ϕ/°) for SbO_6 and NaO_6 octahedra. The e. s. d.'s are ±0.009 Å and ±0.2°, respectively. The metal atoms are situated on the center of inversion, Sb at (1/4, 1/4, 1/4) and Na at (3/4, 3/4, 3/4). Numbers attached to the oxygen atoms are their z-parameters.

SbO_6 octahedra. The coordination polyhedron is also octahedral, but the distortion is greater than that of the SbO_6 octahedron. The interatomic distances are 2.375—2.406 Å (mean 2.39 Å) for Na–O and 3.229—3.526 Å (mean 3.38 Å) for O–O.

Interatomic distances of O···O which can be associated with hydrogen bonding are given in Table 4. The table shows that all OH groups are hydrogen-bonded[8], and the OH group free from hydrogen bonding in the Schrewelius' analysis is eliminated. These hydrogen bonds extend in the whole crystal. The sequences of hydrogen bonding in $In(OH)_3$, $MnSn(OH)_6$ and $NaSb(OH)_6$ are compared schematically in Fig. 3. Squares of four hydrogen-bonded OH's

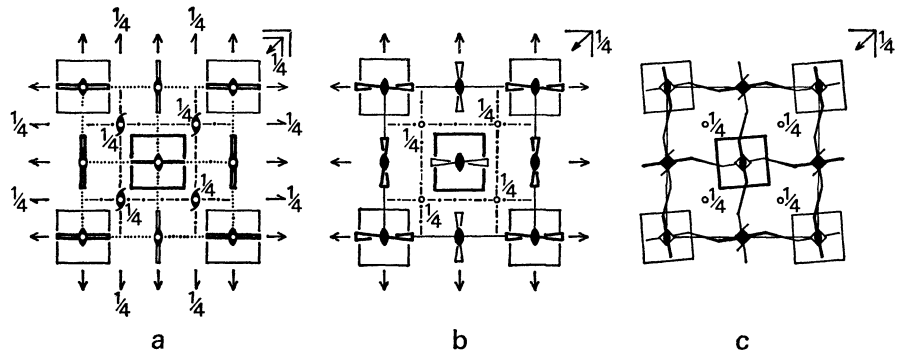

Fig. 3. Schematic sequences of hydrogen bonding viewed along the [001] axis; (a) $In(OH)_3$, (b) $MnSn(OH)_6$ and (c) $NaSb(OH)_6$. The squares at $z \simeq 0$ are shown in thin lines and those at $z \simeq 1/2$ in heavy lines. Vertical mirror planes in $In(OH)_3$ are shown in dotted lines, while the other symmetry elements are shown after the usual fashion.

Table 4. Interatomic distances associated with the hydrogen bonding

The e.s.d.'s are ±0.009 Å

$O(1)^{i}\cdots O(2)^{iv}$	2.859 Å
$O(1)^{i}\cdots O(1)^{ii}$	3.149
$O(2)^{i}\cdots O(2)^{v}$	2.738
$O(3)^{i}\cdots O(3)^{iii}$	2.787

Superscripts in this table and in the text mean the following symmetry operations to the positional parameters given in Table 2.

i	$1/2-x$,	$1/2-y$,	$1/2-z$
ii	$1/2+x$,	$1/2+y$,	$1/2-z$
iii	$1/2+y$,	$1/2-x$,	$1/2+z$
iv	$1/2-y$,	$1/2+x$,	$-1/2+z$
v	$1/2+x$,	$-1/2+y$,	$1/2-z$
vi	$3/2-y$,	$1/2+x$,	$1/2+z$

are found in $In(OH)_3$ and $MnSn(OH)_6$. Each edge of these squares affords two sites for a hydrogen atom, yielding a statistical structure of hydrogen atoms.[1,2,9] A similar hydrogen-bonded square of O(3)'s is found also in $NaSb(OH)_6$. At the same time, however, hydrogen-bonded chains of the type $\cdots O(2)^{iv}\cdots O(1)^{i}\cdots O(1)^{ii}\cdots O(2)^{iii}\cdots O(2)^{vi}\cdots$ are running along the a and b axes. These chains are found only in $NaSb(OH)_6$ among these compounds; therefore the chain structure of the hydrogen bond is a characteristic feature of this compound. Considering the symmetry, hydrogen atoms in $NaSb(OH)_6$ may also take a statistical structure.

Appearance of the chain sequences of hydrogen bonding in $NaSb(OH)_6$ can be explained well if we consider the differences in the bond nature in these $AB(OH)_6$ compounds. In $In(OH)_3$ the lattice is constructed with equivalent $In(OH)_6$ octahedra through sharing their corners, while in $NaSb(OH)_6$ it is constructed with Na^+ and $Sb(OH)_6^-$ ions. The more ionic character in $NaSb(OH)_6$ will allow an anion to take a different orientation from that of $In(OH)_6$ octahedra, yielding a distortion of $Na(OH)_6$ octahedra. The distortion in $NaSb(OH)_6$ is such that the interatomic distances of O(1)'s in the same square become longer and the distance of $O(1)\cdots O(1)^{ii}$ between the adjacent squares becomes shorter; thus a hydrogen-bonded chain is formed. A similar trend is also seen in $MnSn(OH)_6$. However, the difference between the ionic radii of Mn^{2+} and Sn^{4+} cations is much smaller than that between those of Na^+ and Sb^{5+} cations in $NaSb(OH)_6$. This means that $Sb(OH)_6^-$ octahedra must rotate much more than $Sn(OH)_6^{2-}$ octahedra in order for the lattice to accomodate A^{n+} cations in the interstices of $B(OH)_6^{n-}$ anions. Therefore, the hydrogen-bonded squares in $MnSn(OH)_6$ experience only a little distortion, while two thirds of the squares in $NaSb(OH)_6$ are forced to break and to recombine into chains.

The author is grateful to Messrs. S. Matsumoto and S. Wakano for their assistance in experiments.

References

1) A. N. Christensen, N. C. Broch, O. von Heidenstam, and Å. Nilsson, *Acta Chem. Scand.*, **21**, 1046 (1967).

2) A. N. Christensen and R. G. Hazell, *ibid.*, **23**, 1219 (1969).

3) H. Strunz and B. Contag, *Acta Crystallogr.*, **13**, 601 (1960).

4) G. T. Faust and W. T. Schaller, *Z. Kristallogr., Kristallgeom., Kristallphys., Kristallchem.*, **134**, 116 (1971).

5) J. Beintema, *Rec. Trav. Chim. Pays-Bas*, **56**, 931 (1939).

6) N. Schrewelius, *Z. Anorg. Allg. Chem.*, **238**, 241 (1938).

7) "International Tables for X-Ray Crystallography," Vol. 4, ed. by J. A. Ibers and W. C. Hamilton, Kynoch Press, Birmingham, England (1974).

8) This statement does not mean that a hydrogen atom is located just on the line connecting two oxygen atoms. In fact, it must deviate slightly from the line in order to avoid closer contact than the van der Waals one. See, Refs. 1 and 9.

9) C. Cohen-Addad, *Bull. Soc. Fr. Mineral. Cristallogr.*, **91**, 315 (1968).

The Photobleaching of Trapped Electrons and the Electron Capture of Radicals in γ-Irradiated Hydrocarbon Matrices at 77 K

Yo-ichi Ishikawa, Ko-ichi Oka, and Shin Sato

Department of Applied Physics, Tokyo Institute of Technology, Ookayama, Meguro-ku, Tokyo 152

(Received April 2, 1975)

The rate of the photobleaching of the trapped electrons in the 3-methylhexane and methylcyclohexane matrices at 77 K was measured by means of ESR as a function of the concentration of the 3-methylhexyl or methylcyclohexyl radicals present in the matrices. The quantum yield of the photobleaching at the wavelength of 1300 nm increased with the increase in the radical concentration. The stable products such as olefins formed during the γ-irradiation did not affect the quantum efficiency. These results support the suggestion made by Willard *et al.* that the 3-methylhexyl and methylcyclohexyl radicals capture the electrons released from the trapping sites by the irradiation of the infrared light. A comparison showed that the radicals are comparable with sulfur hexafluoride in electron capture.

The γ-irradiation of hydrocarbon glasses produces trapped electrons, radicals, and cations.[1] The increase in the radical concentration is approximately linear during the first 4×10^{20} eV g^{-1}. After *ca.* 2×10^{21} eV g^{-1} of continuous irradiation, the yield of radicals reaches a steady state.[2] On the other hand, the yield of trapped electrons has its maximum value at the point where the yield of radicals becomes saturated, and it drops to zero when the yield of radicals reaches the steady state.[3]

After complete bleaching with IR light, the irradiation of UV light at 375 nm can regenerate the trapped electrons.[4–7] This experiment suggests the following reversible reaction;

$$R + e_t^- \underset{UV}{\overset{IR}{\rightleftharpoons}} R^-$$

although the reformed trapped electrons are much fewer than originally. In the pulse radiolysis of a solution of alkali metal cations in tetrahydrofuran, the rate constant of the reaction between tetrahydrofuran radicals and mobile electrons has been reported to be 6×10^{10} mol^{-1} s^{-1}.[8]

The present study attempted to measure the rate of the electron capture of the radicals produced in the γ-irradiated, glassy 3-methylhexane (3-MHX) and methylcyclohexane (MCH) matrices. If this rate is very large, the electron capture by radicals has to be taken into account in the interpretation of the dose dependence of the formation of trapped electrons, as Willard *et al.* have mentioned.[4]

Experimental

The details of the ESR instrument, the method for the purification of 3-MHX, the set-up for photobleaching, and the actinometry of the IR light were reported in a previous paper.[9]

The MCH, purchased from the Tokyo Kasei Kogyo Co., Ltd., was degassed by freeze-thaw cycles and stored with sodium-potassium alloy. The 1-pentene, supplied by Tokyo Kasei Kogyo, was used without further purification.

A constant volume of hydrocarbons, 0.32 ml for 3-MHX and 0.25 ml for MCH, was sealed in a Suprasil quartz tube in a mercury-free vacuum system. The γ-irradiation of the samples was done at a dose rate of $0.53—0.44\times10^6$ R hr^{-1} at 77 K in the dark.

In order to obtain various concentrations of the matrix radicals, we used the following technique. The sample is γ-irradiated for various intervals, 5—150 min; we can thus obtain the trapped electrons and the 3-methylhexyl or methylcyclohexyl radicals. When this sample is irradiated with IR and visible light from a tungsten lamp (375 W) for an appropriate time interval, the trapped electrons disappear and only the matrix radicals remain. In some cases, a medium-pressure mercury lamp was used without any filter to bleach radical anions completely. This sample is again γ-irradiated for 5 min in the case of 3-MHX and for 30 min in the case of MCH. Then, we can obtain trapped electrons in the matrix, together with various concentrations of matrix radicals.

Results

Radical Concentration. For the estimation of the concentration of the trapped electrons in the 3-MHX and MCH glassy matrices, we assumed $G(e_t^-)=0.87$ for 3-MHX and 0.38 for MCH.[10] The concentration of the radicals was estimated by comparing the integrated areas of the spectrum of the radicals with those of standard samples (DPPH and Ultramarine blue). Values of G(3-MHX radicals)$=4.3\pm0.5$ and G(MCH radicals)$=4.0\pm0.5$ were obtained. When the concentration of the trapped electrons is measured by ESR, attention has to be paid to the saturation effect. Therefore, we made a calibration curve and measured the ESR spectra, usually at a constant low power of microwaves, 0.08 mW.

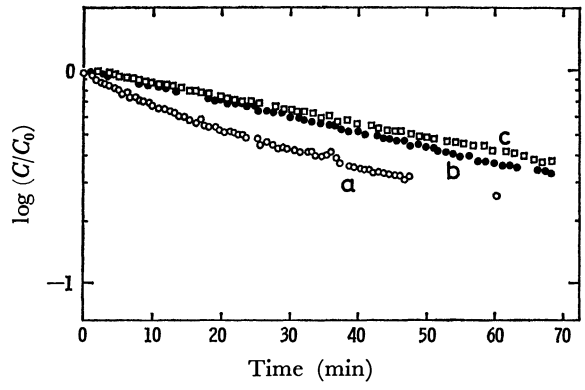

Fig. 1. Semilogarithmic plot for the decay of trapped electrons in the γ-irradiated 3-MHX glass during photobleaching at 1300 nm. The γ-irradiation dose were a) 0.27, b) 4.8, and c) 6.4×10^{19} eV g^{-1}.

Photobleaching in the Case of 3-MHX. Figure 1 shows a typical decay plot for the trapped electrons in the 3-MHX matrix during the irradiation of the IR light at 1300 nm. Apparently the decay rate is larger for a smaller initial amount of the trapped electrons. However, this is due to the non-uniformity of the light intensity in the sample tube.[9] When the concentration of the trapped electrons is high, the light absorption in the tube is not homogeneous and the apparent decay rate decreases, although the quantum yield for the decay is not affected. The details have been discussed in the previous paper.[9] Consequently, in order to study the effect of the radicals on the decay rate, we have to start with a low concentration of trapped electrons in the presence of various concentrations of the radicals.

In order to check the effect of radicals on the microwave-power-saturation phenomenon of the trapped electrons' spectrum, we made four samples containing various concentrations of the radicals in the matrix. The procedure for the preparation was described in the experimental section. Then, these samples were γ-irradiated with a constant dose of 2.57×10^{18} eV g^{-1}, and the yields of the trapped electrons were measured. Figure 2 shows the results. Here, each plot was obtained by extrapolating the microwave power to zero. The microwave-power-saturation character for the trapped electrons in 3-MHX is shown in Fig. 3. As we used the ESR instrument under fast and non-adiabatic conditions,[11] the saturation factor, Z, may be given by the following equation:[12]

$$Z = (1+2\gamma H_1^2 T_1/\pi H_m)^{-1}$$

Here, γ is the gyromagnetic ratio, H_1 is the component of the rotating magnetic field perpendicular to the direction of the external magnetic field, T_1 is the spin-lattice relaxation time, and H_m is the width of

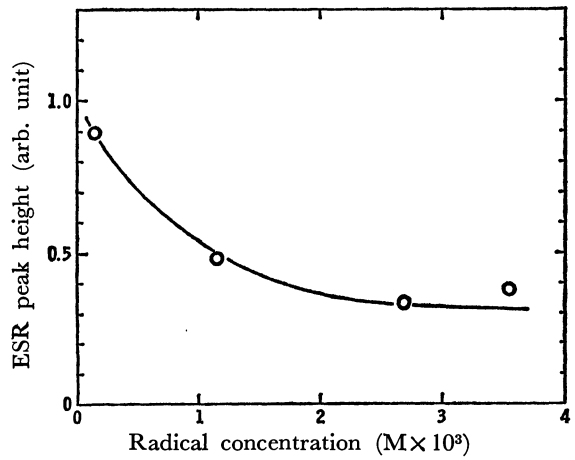

Fig. 2. The yield of trapped electrons in the γ-irradiated 3-MHX glass in the presence of various concentrations of radicals. The γ-irradiation dose for the production of trapped electrons was 0.26×10^{19} eV g^{-1}.

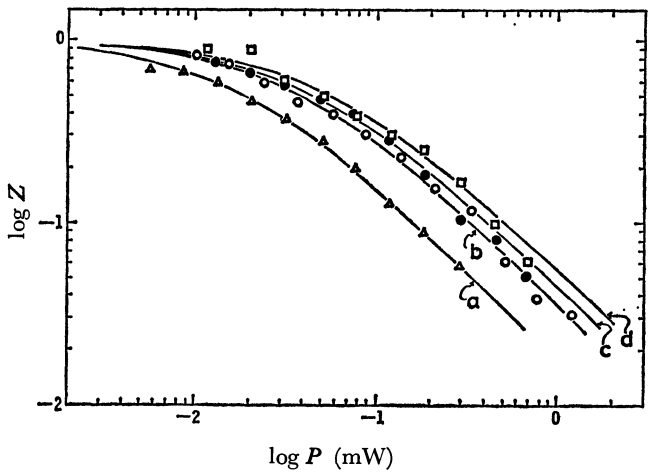

Fig. 3. Experimental values and theoretical curves for microwave-power saturation of trapped electrons in the 3-MHX glass at 77 K. P is microwave power in mW. The radical concentrations are a) 0.14, b) 1.2, c) 2.7, and d) 3.5×10^{-3} mol l^{-1}.

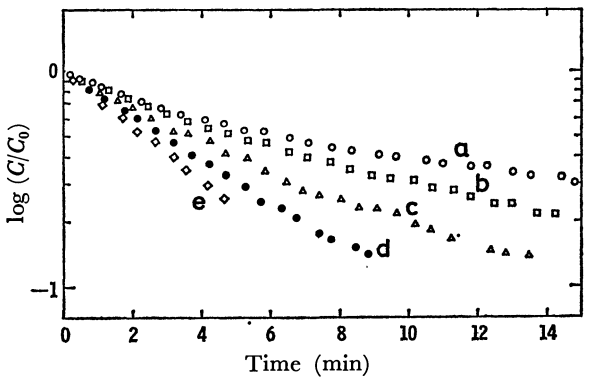

Fig. 4. Semilogarithmic plot for the decay of trapped electrons in the γ-irradiated 3-MHX during photobleaching at 1300 nm. The radical concentrations are a) 0.15, b) 1.2, c) 1.8, d) 2.9, and e) 3.7×10^{-3} mol l^{-1}.

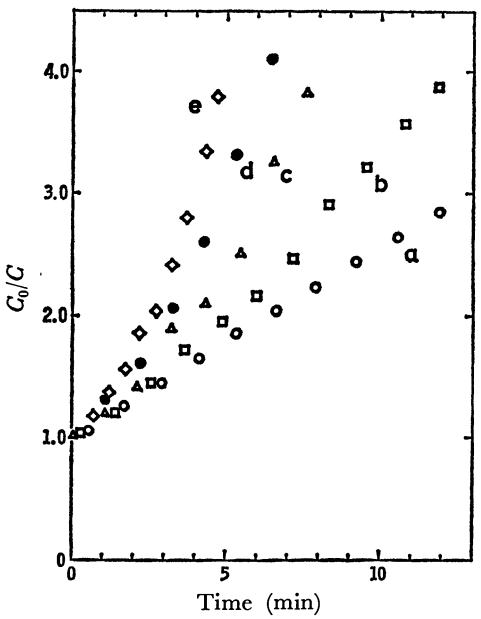

Fig. 5. The second-order decay plot for the trapped electrons in the γ-irradiated 3-MHX. The radical concentrations are a) 0.15, b) 1.2, c) 1.8, d) 2.9, and e) 3.7×10^{-3} mol l^{-1}.

the modulating magnetic field. As Fig. 3 shows, the experimental values coincide with the theoretical curves.

The results of the decay of the trapped electrons during photobleaching with various 3-MHX radical concentrations are shown in Fig. 4. Figure 5 is the second-order decay plot of the same results. Obviously the decay rate increases with the increase in the radical concentration. Moreover, when the radical concentration is small, the decay rate is of the second-order, and as the concentration increases, the decay rate becomes first-order.

In order to check the effect of the stable compounds produced by the pre-irradiation, the decay rate was measured by using samples which had been annealed to room temperature after the pre-irradiation (Fig. 6). The decay rate decreased slightly with the pre-irradiation. The stable products are some olefins and paraffins, and perhaps only olefins affect the decay rate of trapped electrons. Figure 7 shows the decay rate of the trapped electrons in the 3-MHX matrix in the presence of various concentrations of 1-pentene. These results show that the stable products do not make the decay of trapped electrons fast, but, rather, make it a little slow.

In order to obtain a completely neutralized system, we used the UV light from a mercury medium-pressure

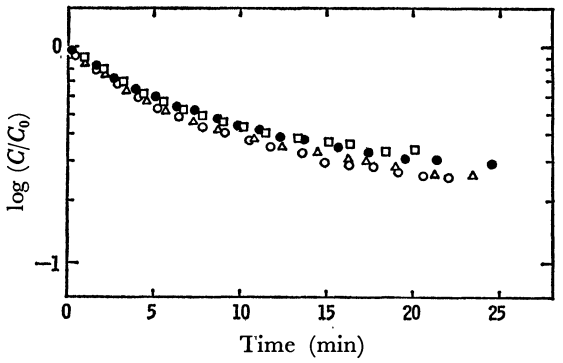

Fig. 6. Effect of thermal annealing on the decay of the trapped electrons by photobleaching. The dose for the production of trapped electrons is 0.27×10^{19} eV g^{-1} after annealing. The dose of the initial γ-irradiation are 0 (○), 2.2 (△), 5.2 (●), and 6.8 $\times10^{19}$ eV g^{-1} (□).

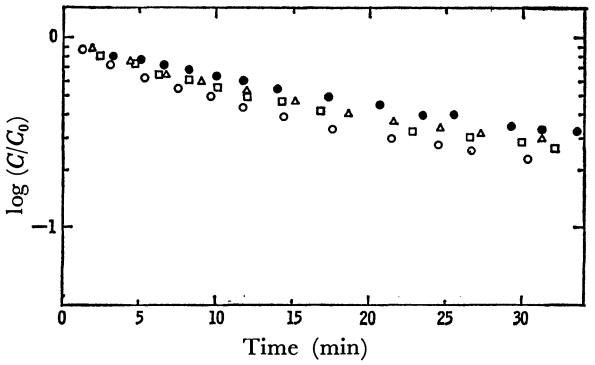

Fig. 7. The effect of the addition of 1-pentene on the decay of the trapped electrons by photobleaching. The concentrations of 1-pentene are 0(○), 5×10^{-3} (□), 6×10^{-2} (△), and 1.1×10^{-1} mol l^{-1} (●).

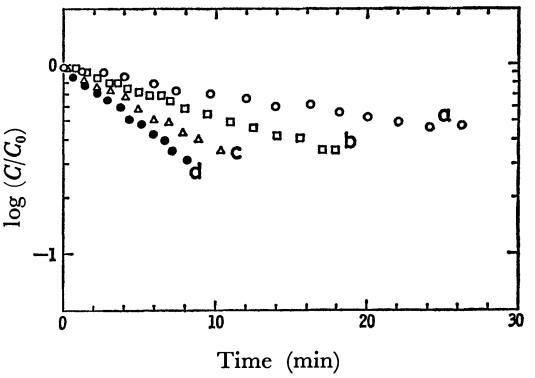

Fig. 8. The effect of UV photobleach on the decay of the trapped electrons by photobleaching at 1300 nm. The radical concentrations are a) 0.13, b) 1.7, c) 2.5, and d) 3.4×10^{-3} mol l^{-1}.

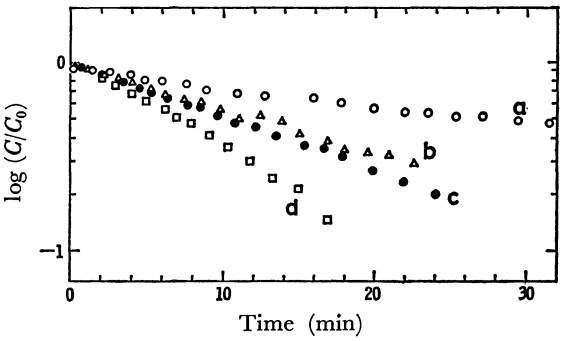

Fig. 9. Semilogarithmic plot for the decay of trapped electrons in the γ-irradiated MCH during photobleaching at 1300 nm. The dose for the production of the trapped electrons is 1.37×10^{19} eV g^{-1}. The radical concentrations are a) 0.84, b) 2.5, c) 3.3, and d) 4.1×10^{-3} mol l^{-1}.

lamp in addition to bleaching with the tungsten lamp. If all the matrix cations do not recombine with electrons by photobleaching with the tungsten lamp, the decay rate depends not only on the concentration of the radicals, but also on that of matrix cations. Irradiation with both the tungsten and the medium-pressure mercury lamps will make all the electrons recombine with cations. The peak of the absorption of the 3-methylpentyl radical anions has been reported to be at 375 nm.[4] The 3-MHX radical anions have a similar absorption spectrum. Figure 8 shows the decay curves for the trapped electrons, along with the samples thus obtained. The results are the same as those shown in Fig. 4. That is, in the present experiment, the electrons photobleached with the tungsten lamp seem to recombine completely with cations.

Photobleaching in the Case of MCH. The results are shown in Fig. 9. There was a small difference in the electron-scavenging ability, but the general tendency was almost the same between the 3-MHX and MCH matrices.

Discussion

We may draw the following conclusions from the experimental results: 1) In the matrices γ-irradiated

at 77 K, there is something which can capture the electrons released from trapping sites by the irradiation of IR light. 2) From the experiments of the thermal annealing and the addition of 1-pentene, the stable products cannot be the cause of the electron capture. 3) From the experiment of UV bleaching, the matrix cations also are not the cause of the change in the decay rate. Finally, we may conclude that the matrix radicals can capture the electrons released from the trapping sites by the irradiation of IR light.

Under a constant illumination of the IR light, the decay rate of the trapped electrons may be expressed in this form:

$$-\frac{\mathrm{d}(\log C)}{\mathrm{d}t} = \varepsilon\Phi I\bar{Q} \qquad \text{(I)}$$

Here, C denotes the concentration of the trapped electrons; ε, the molar extinction coefficient; Φ, the quantum yield by which the released electrons react with substances in the matrix and do not give the trapped electrons any more, and I, the light intensity. $\bar{Q}$ is a correction factor depending upon the optical density of the substance which absorbs the light and upon the shape of the sample tube. The details of the calculation for $\bar{Q}$ and the actinometry have been reported in the previous paper.[9] By using $\varepsilon_{3\text{-MHX}} = 2.04\times10^4$ cm^{-1} l mol^{-1} and $\varepsilon_{\text{MCH}} = 2.40\times10^4$ cm^{-1} l mol^{-1} at 1300 nm,[13] we have calculated the quantum efficiency as a function of the relative concentration of the trapped electrons. The results for 3-MHX are summarized in Fig. 10.

When the trapped electrons are released from the trapping sites by the illumination of IR light, they undergo the following three reactions: 1) Recombination with the parent cations. Since the electrons ejected by γ-irradiation are trapped around their parent cations, there should be a certain distribution for the position of the trapped electrons from their parent cations. When they are released, the electrons trapped close to their parent cations will react faster than those trapped distantly. 2) Retrapping by the trapping sites. 3) Reactions with the radicals in the matrix. The trapping sites and the radicals may be distributed homogeneously in the matrix.

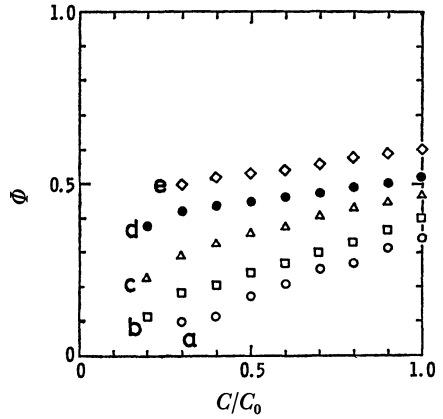

Fig. 10. The relation between the quantum yield Φ and the relative amount of the trapped electrons in the 3-MHX glass. The radical concentrations are a) 0.15, b) 1.2, c) 1.8, d) 2.9, and e) 3.7×10^{-3} mol l^{-1}.

The reaction mechanism under consideration may be described as follows:

$$\mathrm{M} \rightsquigarrow \mathrm{M}^+, \mathrm{R}, \mathrm{e_t}^- \qquad (1)$$

$$\mathrm{e_t}^- + h\nu \xrightarrow{\sigma} \mathrm{e_m}^- \qquad (2)$$

$$\mathrm{e_m}^- + \mathrm{T.S.} \longrightarrow \mathrm{e_t}^- \qquad (3)$$

$$\mathrm{e_m}^- + \mathrm{M}^+ \longrightarrow \mathrm{M} \qquad (4)$$

$$\mathrm{e_m}^- + \mathrm{R} \longrightarrow \mathrm{R}^- \qquad (5)$$

where M is the matrix molecule; R, the matrix radical; $\mathrm{e_m}^-$, the mobile electron, and T.S., the trapping site. σ is the quantum efficiency for the photo-liberation of trapped electrons from the trapping sites. The quantum yield for the photobleaching, then, may be equated in this form:

$$\Phi = \sigma\frac{k_4W + k_5[\mathrm{R}]}{k_3S_t + k_4W + k_5[\mathrm{R}]} \qquad \text{(II)}$$

Here, W is a function depending on the concentration of the cations and on the distribution of the trapped electrons. S_t is the concentration of trapping sites. With the progress of photobleaching, the spatial distribution of the trapped electrons will be changed. Consequently, W is also a function of the irradiation time.

From Eq. (II), assuming $\sigma=1$,[9] we can obtain the following equation:

$$\frac{1}{1/\Phi_i - 1} = \frac{k_4W_i}{k_3S_t} + \frac{k_5}{k_3S_t}[\mathrm{R}] \qquad \text{(III)}$$

Here, the subscript, i, attached to Φ and W means $t=0$. The left-hand side of Eq. (III) is plotted in Fig. 11 as a function of the concentration of matrix radicals. From the slopes of these plots, we could obtain:

$$k_5/k_3S_t = (0.29\pm0.06)\times10^3 \text{ mol}^{-1}\text{ l}$$

for 3-MHX and

$$k_5/k_3S_t = (0.14\pm0.06)\times10^3 \text{ mol}^{-1}\text{ l}$$

for MCH.

When sulfur hexafluoride was used as an electron scavenger in 3-MHX,[9] the following ratio was reported:

$$k_6/k_3S_t = 1.2\times10^3 \text{ mol}^{-1}\text{ l}$$

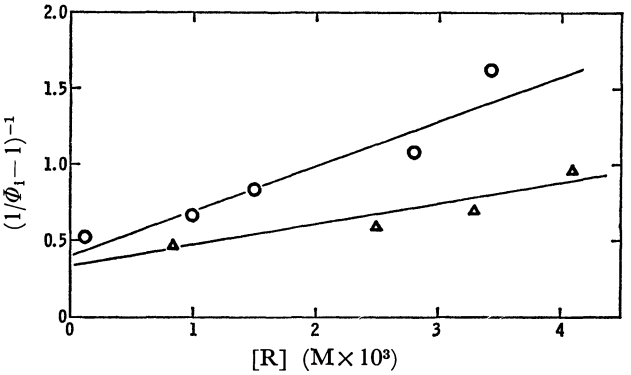

Fig. 11. The relation between $1/(1/\Phi_i - 1)$ and the radical concentration [R]. ○ for 3-MHX and △ for MCH.

Here, k_6 is the rate constant of the reaction:

$$e_m^- + SF_6 \longrightarrow SF_6^- \quad (6)$$

These values suggest that the radicals under consideration have an ability comparable with sulfur hexafluoride in the electron capture in the glassy hydrocarbon at 77 K.

References

1) H. Yoshida, T. Shiga, and M. Irie, *J. Chem. Phys.*, **52**, 4960 (1970).
2) D. P. Lin and J. E. Willard, *J. Phys. Chem.*, **78**, 2233 (1974).
3) J. Zimbrick and L. Kevan, *J. Amer. Chem. Soc.*, **89**, 2483 (1967).
4) A. Ekstrom, R. Suenram, and J. E. Willard, *J. Phys. Chem.*, **74**, 1888 (1970).
5) J. E. Willard, *Int. J. Radiat. Phys. Chem.*, **4**, 405 (1972).
6) D. P. Lin and J. E. Willard, *J. Phys. Chem.*, **78**, 1135 (1974).
7) J. E. Willard, *Int. J. Radiat. Phys. Chem.*, **6**, 325 (1974).
8) G. A. Salmon, W. A. Seddon, and J. W. Fletcher, *Can. J. Chem.*, **52**, 3259 (1974).
9) K. Oka, H. Yamazaki, and Y. Hatano, This Bulletin, **48**, 1107 (1975).
10) J. Lin, K. Tsuji, and F. Williams, *J. Amer. Chem. Soc.*, **90**, 2766 (1968).
11) K. Oka, H. Yamazaki, and S. Shida, This Bulletin, **46**, 2347 (1973).
12) M. Weger, *Bell. System Tech. J.*, **39**, 1013 (1960).
13) This value was estimated assuming that the value for the molar extinction coefficient of the trapped electrons in the 3-methylpentane matrix at 1700 nm is 3.0×10^4 cm^{-1} $1\ mol^{-1}$. J. B. Gallivan and W. H. Hamill, *J. Chem. Phys.*, **49**, 1279 (1966).

Distribution of Trapped Electron-Cation Distance in γ-Irradiated 2-Methyltetrahydrofuran Glassy Matrix

Tsuneki ICHIKAWA, Hiroshi YOSHIDA, and Koichiro HAYASHI*

Faculty of Engineering, Hokkaido University, Kita-ku, Sapporo 060

(Received April 2, 1975)

An approach was presented to elucidate the distribution of trapped electron-cation distance from isothermal decay of the trapped electron by numerically solving the Smoluchowski equation and was applied to the observed isothermal decay of trapped electron at 92.2—95.0 K in 2-methyltetrahydrofuran glass irradiated by γ-rays at 77 K. The distribution curve (the probability density of finding initially the electron at the distance r) thus obtained was close to a Gaussian function.

One of the important features of radiation chemistry in condensed media is in spatial inhomogeneity of the formation of primary active entities such as electrons, ions and free radicals. It is generally accepted that the distance of an electron from its counterpart cation is smaller than average distance between pairs of the electron and the cation, and that the charge recombination process occurs mostly as an isolated event (spur reaction in liquid media). The electron-cation distance when the electron is trapped or solvated is dependent upon the kinetic energy of the secondary electron, the energy loss process and trapping or solvation process in condensed media. Distribution of the electron-cation distance was studied in liquid media by means of electron scavenge method[1-3] and electrical conductivity measurements,[4-6] and some analytical expressions were given for it. However, it is difficult to study the distribution in glassy matrices. Only average distance between the trapped electron and its counterpart cation has been estimated from the effect of electron scavenger upon the yield of the trapped electron[7-9] and also from paramagnetic relaxation measurements of the trapped electron.[10-13]

Recently we studied the isothermal decay of the trapped electron in 2-methyltetrahydrofuran (MTHF) glassy matrix irradiated by γ-rays at 77 K and found that the time profile of the decay at several temperatures above 92 K was independent of either radiation dose or temperature, if the time scale was corrected with an Arrhenius factor.[14] The results indicate that the electron is trapped close to its counterpart cation and suggest that its decay is determined solely by the electron-cation distance. This leads to the point that the time profile of the decay is correlated to the distribution of the distance and, therefore, the analysis of the decay curve may give a new approach to elucidate the distribution of the distance in glassy matrices.

The principal aim of the present paper is in reexamining the time profile of the isothermal decay of the trapped electron in MTHF glassy matrix previously reported[14] in order to show the possibility of elucidating the distribution of the distance on the basis of the Smoluchowski equation which describes the migration of electron in the matrix.

Theoretical Background

Assuming that (1) the electron migrates in the matrix as a classical particle, (2) it is formed in pairing with a cation, and (3) the mean free path of the electron is much smaller than the migration path traveled before charge recombination, the migration of the electron is regarded as the diffusion under the spherical Coulombic field due to the cation. In such circumstances, the time profile of the electron decay can be correlated with the distribution of the distance between the electron and the cation by the well known Smoluchowski equation,[15]

$$\frac{1}{D}\frac{\partial W(r,t)}{\partial t}=\frac{\partial^2 W(r,t)}{\partial r^2}+\left(\frac{2}{r}+\frac{r_c}{r^2}\right)\frac{\partial W(r,t)}{\partial t}, \tag{1}$$

where r is the distance, t time, D diffusion coefficient, $W(r,t)$ the probability density of finding the electron at r and at t, and $r_c(=e^2/\varepsilon kT)$ the Onsager length. Since the electron is presumed to disappear only in recombining with the cation, a boundary condition of the differential equation is given as

$$[W(r,t)]_{r=r_0}=0 \tag{2}$$

where r_0 is so-called recombination radius. The initial distribution is given by $W(r,0)$. On the other hand, the time profile of the electron decay, $P(t)$, is given by the spatial integration of $W(r,t)$ as

$$P(t)=\int_{r_0}^{\infty} W(r,t)4\pi r^2 dr \tag{3}$$

and $dP(t)/dt$ is given by the rate of electron flow across the spherical surface of reaction radius,

$$\frac{dP(t)}{dt}=-4\pi r_0^2 D\left[\frac{\partial W(r,t)}{\partial r}\right]_{r=r_0}. \tag{4}$$

The aim of the present study is in the derivation of $W(r,t)$ from the given $P(t)$ corresponding to the observed time profile of the electron decay. This turns out to solve Eq. (1) under the boundary conditions (2) and (4), but Eq. (1) is generally unable to be solved analytically. Several approximation methods have been invented and used, which encompass the prescribed diffusion method,[16,17] the Laplace transformation method[18] and perturbation methods.[19,20] These methods, however, are not useful for the present aim, because they derive $W(r,t)$ from a given $W(r,0)$ but not from a given $P(t)$.

One of modifications of the Smoluchowski equation is the Nernst-Einstein relationship, where the diffusion term in Eq. (1) is completely neglected.[21] On this basis, one can readily derive the initial distribution from the time profile of the electron decay:

$$W(r,0)=-\left[\frac{dP(t)}{dt}\right]_{t=t'} \tag{5}$$

* Present address: The Institute of Scientific and Industrial Research, Osaka University, Suita, Osaka 565.

where

$$t' = \frac{r^3 - r_0^3}{3Dr_C}.$$

In this case however, the calculated distribution is not very accurate because of the neglect of the diffusion term.[22]

More accurate distribution is expected to be derived by taking the diffusion term into account. This can be achieved by expanding the time profile of the observed electron decay into the Dirichlet series,

$$P(t) = \sum a_i \exp(-k_i t), \tag{6}$$

and by transforming the probability density as

$$W(r, t) = \sum R_i(r) \exp(-k_i t). \tag{7}$$

Thus the Smoluchowski equation can be transformed into ordinary differential equation:

$$\frac{d^2R_i(r)}{dr^2} + \left(\frac{2}{r} + \frac{r_C}{r^2}\right)\frac{dR_i(r)}{dr} + \frac{k_i}{D}R_i(r) = 0. \tag{8}$$

The boundary conditions of the above equation,

$$[R_i(r)]_{r=r_0} = 0 \tag{9}$$

and

$$\left[\frac{dR_i(r)}{dr}\right]_{r=r_0} = \frac{k_i a_i}{4\pi r_0^2 D} \tag{10}$$

are obtained also by transforming Eqs. (2) and (4). Equation (8) is solved, for example, by Runge-Kutta-Gill method and the initial distribution of the distance between the trapped electron and the cation is to be obtained numerically.

Observed Isothermal Decay

According to our recent study,[14] the electron trapped in the γ-irradiated MTHF glassy matrix decay rapidly in following a pseudo-first order reaction (independent of the radiation dose and the initial concentration of the electrons), when the glassy matrix is warmed to temperature higher than 92 K. This strongly suggests that an electron is trapped close to its counterpart cation and that no spatial overlapping occurs between the electron-cation pairs.

The time profile of the electron decay in the temperature range 92.2—95.0 K was observed by electron spin resonance method, and found to be superimposable on each other if the time scale was corrected by the half-life of the electrons at each temperature (the corrected time is real time devided by the half-life, $\tau = t/t_{1/2}$). The dependence of $t_{1/2}$ upon temperature followed the Arrhenius relation, which gave an activation energy of 0.8 eV in the temperature range examined. This large activation energy indicates that the charge recombination results from the migration of electron in the matrix at temperatures close to its liquifying temperature. On the other hand, the activation energy becomes smaller and approaches to zero by lowering temperature, which is consistent with the view that the charge recombination is caused essentially by quantum mechanical tunnelling of electron from its trap to the cation at low temperature.[23,24]

Quantum efficiency of photobleaching trapped electron was examined for γ-irradiated MTHF matrix at 77 K and found to be much smaller than unity.[7] This indicates that the electron photoliberated from its trap does not recombine at once with the cation, but undergoes several detrap-retrap cycles before the charge recombination. This retrapping efficiency is most probably higher at higher temperature because of the ease of reorientation of the matrix molecules to solvate the electron.

These two facts, the large activation energy and the small quantum efficiency, indicate that the lifetime of electron at elevated temperature is determined by the migration path length travelled by the electron before charge recombination and, therefore, by the number of thermal activation process (trap-detrap process). It turns out that the temperature independent time profile of the electron decay is directly correlated to the distribution of the electron-cation distance before the glassy matrix is warmed. The observed time profile of the decay to be analyzed in the following chapter is taken from the previous paper[14] and shown in Fig. 1 with open circles.

Calculation and Results

Because the diffusion coefficient D is temperature dependent, the time profile of the electron decay to be obtained from a given distribution of the electron-cation distance based on Eq. (1) is necessarily temperature dependent. However, the fundamental Smoluchowski equation is readily transformed by using the corrected diffusion coefficient

$$D_0 = Dt_{1/2} \tag{11}$$

into

$$\frac{1}{D_0}\frac{\partial W(r, \tau)}{\partial \tau} = \frac{\partial^2 W(r, \tau)}{\partial r^2} + \left(\frac{2}{r} + \frac{r_C}{r^2}\right)\frac{\partial W(r, \tau)}{\partial r}. \tag{12}$$

This differential equation gives temperature independent correlation between the distribution of the distance and the time profile of the electron decay, if the latter is plotted in the corrected time scale ($\tau = t/t_{1/2}$) and if D_0 is temperature independent. This is really the case as observed previously.[14] The temperature independent corrected diffusion coefficient implies that the migration of the electron is thermal activation process and it is controlled by thermal detrapping of electron (or thermal collapse of electron trap). The value of r_C is regarded as constant in a narrow range of temperature.

Starting from Eq. (12), Eqs. (6), (7), (8) and (10) are rewritten as follows:

$$P(\tau) = \sum a_i \exp(-k_i \tau), \tag{13}$$

$$W(r, \tau) = \sum R_i(r) \exp(-k_i \tau), \tag{14}$$

$$\frac{d^2R_i(r)}{dr^2} + \left(\frac{2}{r} + \frac{r_C}{r^2}\right)\frac{dR_i(r)}{dr} + \frac{k_i}{D_0}R_i(r) = 0 \tag{15}$$

and

$$\left[\frac{dR_i(r)}{dr}\right]_{r=r_0} = \frac{k_i a_i}{4\pi r_0^2 D_0}. \tag{16}$$

The observed time profile of the electron decay (shown in Fig. 1) was graphically analyzed and expanded

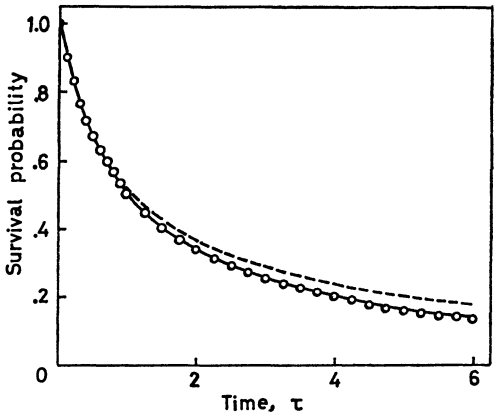

Fig. 1. Time profile of the decay of trapped electron in γ-irradiated MTHF glassy matrix (O) observed at about 93 K, (solid line) computed from the initial distribution of electron-cation distance given by open (for $r \leq 40$ Å) and filled circles (for $r \geq 40$ Å) in Fig. 2, and (dashed curve) computed from the initial distribution of the distance given by the dashed curve in Fig. 2 based on Eq. (15).

by the Dirichlet series

$$P(\tau) = 0.34 \exp(-0.15\tau) + 0.46 \exp(-0.90\tau) + 0.20 \exp(-2.85\tau). \quad (17)$$

In order to calculate numerically the initial distribution $W(r,\tau)$ from the observed $P(\tau)$ based on the differential equation (15) and the boundary conditions (9) and (16), the numerical values of r_0, r_c and D_0 should be known. The Onsager length r_c at 93 K was estimated to be 624 Å from the dielectric constant of the glassy matrix, 2.88.[25] The reaction radius r_0 was taken to be 10 Å rather arbitrarily, but the ambiguity in r_0 affects little the calculated initial distribution, because the migration of electron toward the cation is fast in its vicinity. Although there is no means to estimate the diffusion coefficient D and, therefore, the corrected diffusion coefficient D_0, the latter was arbitrarily taken to be 66 Å^2. This value gave the average initial distance between the trapped electron and the cation of about 50 Å, which seems plausible for accounting for the previous results of paramagnetic relaxation of the trapped electron in the MTHF glassy matrix.[10]

The calculated initial distribution of the distance is shown by the solid curve in Fig. 2. The oscillatory feature at large r resulted from the essential fact that the boundary value problem is not well-posed for the parabolic partial differential equation such as Eq. (12). It turns out that small errors inevitably included in the observed boundary condition (the decay curve, especially at large τ) deteriorate the calculated initial distribution of the distance at large r. If one ignores the unrealistic oscillation, the distribution curve is approximated, as shown by open and filled circles in Fig. 2, by

$$W(r, 0) = 2.5 \times 10^{-6} \exp(-r^2/1600) \quad \text{for } r_0 < r \leq 40\text{Å} \quad (18)$$

and

$$W(r, 0) = 11.5 \times 10^{-6} \exp(-r/16) \quad \text{for } r \geq 40\text{Å} \quad (19)$$

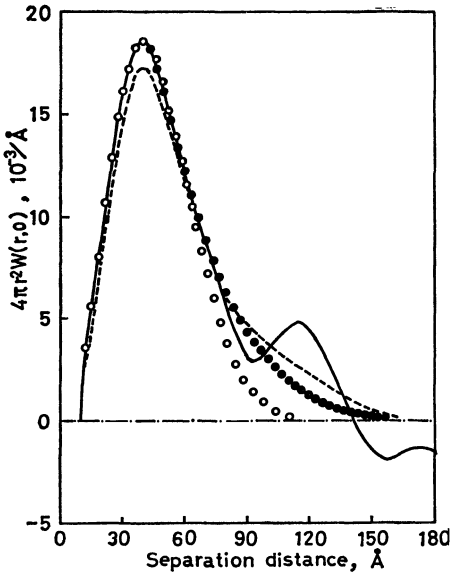

Fig. 2. Initial distribution of electron-cation distance in γ-irradiated MTHF glassy matrix derived from the time profile of electron decay shown by open circles in Fig. 1, (solid curve) on the basis of the Smoluchowski equation (15) and (dashed curve) on the basis of the Nernst-Einstein approximation (Eq. (5)). Open circles and filled ones show the smoothed distribution curve given by Eqs. (18) and (19), respectively. For $r > 40$ Å, the filled circles express the distribution better.

where r is measured in Å unit. Although the curve is not expressed by a single function, its whole shape is rather close to the Gaussian function. In order to check the validity of smoothing the oscillatory feature and that of the relationships (18) and (19), the time profile of the electron decay was reconstructed from them by using the finite difference approximation based on the Smoluchowski equation (12) (see Appendix). The result is shown by the solid curve in Fig. 1. It agrees very well with the observed time profile from which the initial distribution of the distance was derived.

Discussion

It has been shown above that the initial distribution of the distance of the trapped electron from its counterpart cation in the glassy matrix can be derived, on the basis of the Smoluchowski equation describing the behavior of electron under the spherical Coulombic field, by observing the isothermal decay of the trapped electron. The same approach may be applicable also to study the distance between solvated electron and its counterpart cation in liquid media, if the complete time profile of the prompt decay of the solvated electron becomes available by the pulse radiolysis experiments with time resolution high enough.

From mathematical point of view, the present procedure of deriving the initial distribution of the distance from the time profile of the electron decay is the translation of a boundary condition of the

Smoluchowski equation into its initial condition. The scavenger method for studying the distribution[3] is essentially one of the modification of the present method: in the scavenger method the time profile of the electron decay was obtained indirectly from the Laplace transformation of the scavenging curve.[26] However, this method presumes that electron can react with scavenger only after the thermalization (or solvation). The initial distribution of the distance was also derived from the field dependence of electric conductivity during irradiation. In this case, the probability of escaping geminate recombination and of contributing to the conductivity decreases with decreasing electron-cation distance. Therefore, this method is suitable to study the distribution only at large r. Contrary, the present method gives reliable information for small r but not for large r, because the later part of the electron decay is experimentally less accurate, which is translated into the distribution at large r.

The most direct correlation between the electron decay and the distribution of the distance is given by the Nernst-Einstein approximation (relationships (5) and (6), where t, t' and D should be replaced by τ, τ' and D_0 to analyze the decay data in Fig. 1). According to this approximation, the observed electron decay shown in Fig. 1 gave straightforwards the distribution curve shown by the dashed line in Fig. 2. The neglect of the diffusion term in the Smoluchowski equation caused a small but apparent depression of the curve for small r. Such tendency should become enhanced and the diffusion term cannot be ignored, if the distribution is very sharp and if the initial distance is as large as the Onsager length. The dashed line in Fig. 1 shows the time profile of the electron decay reconstructed from the distribution given by the dashed curve in Fig. 2 by means of the finite difference approximation based on the Smoluchowski equation (12). Here also, the contribution of the diffusion term is apparently seen from the deviation of the dashed line from the solid line.

The half-life, $t_{1/2}$, of the trapped electron was found to be temperature dependent with an activation energy of 0.8 eV (19 kcal/mol) and a pre-exponential factor of 1×10^{-42} s in the temperature range 92.2—95.0 K.[14] Based on Eq. (11) and the presumed value of 66 Å^2 for D_0 (see the preceding section), the diffusion coefficient, D, is calculated to be 10^{-7} cm^2 s^{-1} in this temperature range within the framework of the present procedure. On the other hand, Huang and Kevan measured the drift mobility of 0.055 cm^2 V^{-1} s^{-1} at 77 K for electrons photoliberated from their trap in γ-irradiated MTHF glassy matrix.[27] Assuming that the well known relationship, $\mu/D=e/kT$, between the mobility and the diffusion coefficient is valid for these electrons, we can obtain the diffusion coefficient of 3.6×10^{-4} cm^2 s^{-1}.

A big difference in the diffusion coefficient may be attributed to the difference in the mechanism of electron transport. The measurement of the drift mobility dealt with the electrons photoliberated into conduction state, which seem to have reached the collecting electrode without suffering retrapping in the matrix.[27] The electrons in the present investigation are mobilized by thermal detrapping probably due to thermal collapse of the trapping site and they seem to be more or less solvated during their migration. Therefore, it is reasonable that their diffusion coefficient is much smaller than that for the electrons in conduction state. If the big diffusion coefficient, 3.6×10^{-4} cm^2 s^{-1}, is used in deriving D_0 on trial, the observed isothermal decay of Eq. (17) gives an initial average distance between the trapped electron and its counterpart cation of more than 10^6 Å, which is unrealistically too big.

A drawback in the present approach is in the lack of the available numerical data on the diffusion coefficient D, measurements of which are highly desirable.

All numerical computations in this investigation were made by using facilities of the Computing Center of Hokkaido University.

Appendix

The Smoluchowski equation (12) is solved straightforward to give the solution $W(r,\tau)$, if the initial condition $W(r,0)$ as well as the bounday condition is given. The finite difference approximation is one of the most appropriate method to solve the equation numerically. The difference equation corresponding to the differential equation (12) is

$$W_{m,n+1} = W_{m,n} + \frac{D_0K}{H^2}(W_{m+1,n}-2W_{m,n}+W_{m-1,n}) + \frac{D_0K}{2H}\left\{\frac{2}{r_0+mH}+\frac{r_C}{(r_0+mH)^2}\right\}(W_{m+1,n}-W_{m-1,n}) \quad \text{(A1)}$$

where $W_{m,n}=W(r,\tau)$, $r=r_0+mH$ and $\tau=nK$. The time profile of the electron decay $P(\tau)=P_n$ is given as

$$P_n = \sum_{i=0}^{M} 4\pi(r_0+iH)^2HW_{i,n}. \quad \text{(A2)}$$

The upper limit of summation, M, should be so large that $4\pi(r_0+MH)^2W_{M,n}$ is vanishingly small. P_n was computed consecutively under the given initial condition $W_{m,0}$ and the boundary condition $W_{0,n}$, $W_{M,n}=0$. In the calculation, the parameters were taken as small as $H=0.6$ Å and $K=0.002$ and as large as $M=500$, which were tested to be small or large enough for the good approximate solution to be obtained.

References

1) S. Sato, This Bulletin, **41**, 304 (1968).
2) S. Sato and T. Oka, *ibid.*, **44**, 856 (1971).
3) G. C. Abell and K. Funabashi, *J. Chem. Phys.*, **58**, 1079 (1973).
4) W. F. Schmidt and A. O. Allen, *J. Phys. Chem.*, **72**, 3730 (1968).
5) J. -P. Dodelet, P. G. Fuoch, and G. R. Freeman, *Can. J. Chem.*, **50**, 1617 (1972).
6) J. -P. Dodelet, K. Shinsaka, U. Kortsch, and G. R. Freeman, *J. Chem. Phys.*, **59**, 2376, (1973).
7) P. J. Dyne and A. O. Miller, *Can. J. Chem.*, **43**, 2696 (1965).
8) W. A. Seddon and D. R. Smith, *ibid.*, **45**, 3083 (1967).
9) H. Hase and L. Kevan, *J. Phys. Chem.*, **74**, 3358 (1970).
10) D. R. Smith and J. J. Pieroni, *Can. J. Chem.* **43**, 876 (1965).
11) J. Zimbrick and L. Kevan, *J. Chem. Phys.*, **47**, 2364 (1967).

12) H. Hase and L. Kevan, *ibid.*, **52**, 3183 (1970).
13) D. P. Lin and L. Kevan, *ibid.*, **55**, 2629 (1971).
14) T. Ichikawa, H. Yoshida, and K. Hayashi, This Bulletin, **46**, 812 (1973).
15) M. Smoluchowski, *Ann. Phys.*, **21**, 756 (1906).
16) A. Mozumder, *J. Chem. Phys.*, **48**, 1659 (1968).
17) A. Mozumder, *ibid.*, **55**, 3020 (1971).
18) G. C. Abell, A. Mozumder, and J. L. Magee, *ibid.*, **56**, 5422 (1972).
19) H. Yamazaki and K. Shinsaka, This Bulletin, **43**, 2713 (1970).
20) G. C. Abell and A. Mozumder, *J. Chem. Phys.*, **56**, 4079 (1972).
21) F. Williams, *J. Amer. Chem. Soc.*, **86**, 3954 (1964).
22) P. K. Ludwig, *J. Chem. Phys.*, **10**, 1787 (1969).
23) J. R. Miller, *ibid.*, **56**, 5173 (1972).
24) K. I. Zamariev, R. F. Khairontdinov, A. J. Mikhailov, and V. I. Goldanskii, *Dokl. Akad. Nauk USSR*, **199**, 640 (1971).
25) K. F. Baverstock and P. J. Dyne, *Can. J. Chem.*, **48**, 2182 (1970).
26) A. Mozumder, *J. Chem. Phys.*, **55**, 3026 (1971).
27) L. Kevan, *Int. J. Radat. Phys. Chem.*, **6**, 297 (1974).

Quantitative Estimates of π-Contact-term Contributions to the Lanthanide-induced Paramagnetic ^{1}H Shifts in Aniline and *m*-Toluidine

Masatoshi HIRAYAMA, Michihiko SATO, Makoto TAKEUCHI, and Makoto SAITO

Department of Chemistry, Faculty of Science, Ibaraki University, 2-1-1 Bunkyo, Mito 310

(Received April 4, 1975)

The paramagnetic proton chemical shifts induced by a series of Ln(FOD)$_3$(Ln=Pr, Eu, Dy, Ho, Er, and Yb) were observed for aniline and *m*-toluidine in CCl_4. In an attempt to separate the pseudo-contact(pcs) and contact shift(cs) contributions, the spin-density distributions of the π-cation radicals or the Ni(AcAc)$_2$-induced shifts were used for the cs pattern in a molecule, as well as the geometric factors for the pcs pattern. The appropriate regions of the two geometric parameters were determined by the computer-search method for the least-squares fits of the observed to the calculated shifts. Thus, the intramolecular average value of the ratio of cs-to-pcs contributions was evaluated. The variation in this ratio with an Ln ion corresponds relatively well to that of the theoretical ratio, $|\langle S_z\rangle/|\delta|$, where $\langle S_z\rangle$ has been calculated by Golding *et al.* and where δ is the relative pcs predicted by Bleaney *et al.*

There have been a number of reports showing that the contribution of the contact shift(cs) to the lanthanide-induced shifts(LIS's) may be considerable for protons as well as for ^{13}C and ^{31}P. However, most of the discussions of cs contributions have been qualitative.[1] It has recently been reported in studies of the temperature dependence of LIS's that the term proportional to $1/T$ can be separated from the term depending on $1/T^2$ on the basis of Bleaney's theory[2] and that it leads to the cs contribution for all the complexes except for those of Eu^{3+} and Sm^{3+}.[3] With a correction for the temperature effect on the equilibrium between an Ln complex(Ln=lanthanide metal) and a substrate, this method may be valuable for the determination of the cs contribution. On the other hand, the determination of the molecular structure and the conformation analysis due to the use of LIS have been made in terms of a computer search for the best fit of the calculated geometric factors to the observed paramagentic shifts.[4] These searches are based on the fact that a true pattern of pseudo-contact shifts(pcs) can be calculated if a ligand molecule includes several or more nuclei having only pcs almost entirely. Therefore, these searches are limited to the σ-compounds, in which there is a cs contribution only in some atoms close to a coordinating atom. In such a molecule, the σ-cs contribution can be calculated as the difference between the observed shift and pcs.[5] However, for aromatic molecules with cs at almost all atoms, the above procedure cannot be applied, and a relative cs(a cs pattern) in a molecule is required for a quantitative separation of the two contributions. Three possible sources of cs pattern are: (1) Gd(III)-induced shifts,[6] (2) Ni(AcAc)$_2$-induced shifts(NIS's), and (3) a theoretically estimated pattern. While (1) may not be used for ^{1}H because of the long T_1 of the electron spin,[7] an attempt has been made to use (2)[8] or (3). The results from (3) seem to be unsatisfactory.[9]

In a previous paper,[10] our procedure for estimating the cs contribution has been outlined. This report will describe in detail an attempt at separation by using the cs patterns obtained from a π-spin density distribution of a cation radical and NIS for both aniline and *m*-toluidine. In the present study, the agreement factor, *R*,[11] between the observed and calculated shifts was satisfactorily small for the adducts with all the Ln(FOD)$_3$* substances used here. In order to check the validity of our procedure for the separation of the two contributions, the relative cs contribution thus evaluated was compared to the $\langle S_z\rangle$ value reported by Golding *et al.*[12] for the six Ln chelates studied here, and a comparatively good correspondence was thus obtained. The separated pcs contribution led to a good linear relation to the relative value of Bleaney's pcs.[2]

Experimental

Aniline and *m*-toluidine were purified by vacuum distillation from zinc dust and were dried over barium oxide in the dark. CCl_4(Spectro grade) was used as the solvent without further purification. The Ln(FOD)$_3$ complexes were prepared according to the method of Springer, Jr., Meek and Sievers,[13] except for the Pr, Eu, and Yb complexes, which were obtained commercially. Particular care was taken for all the substrates used to ensure anhydrous conditions, since the observed shifts are very sensitive to traces of moisture. The solutions were *ca.* 0.5 M in the substrates. The amount of Ln(FOD)$_3$ or Ni(AcAc)$_2$ was continuously varied up to a Ln(FOD)$_3$- or Ni(AcAc)$_2$-substrate molar ratio of about 0.2. The NMR spectra were recorded with a Hitachi R-20A spectrometer at 60 MHz at a probe temperature of 34 °C, operating in the frequency-swept mode, using TMS as the internal standard.

Results and Discussion

In many lanthanide shift experiments, it has become customary to consider only one step of equilibrium with a sufficiently rapid exchange:

$$L + A \rightleftharpoons LA \qquad K_1 = \frac{[LA]}{[A]\cdot[L]} \qquad (1)$$

and to use the shift characteristic of a 1 : 1 adduct (δ_1) obtained from the linear extrapolation of $[L_0]/[A_0]=R_L$ to 1, on the basis of the idea that the observed shift is approximately equal to $R_L\cdot\delta_1$ if $R_L \ll 1$ and $K_1 \gg 1$, where A and L are a substrate and an Ln chelate respectively, and where $[L_0]$ and $[A_0]$ are the total concentrations of L and A. However, it was recently found in low-temperature experiments that two mole-

* FOD = 1,1,1,2,2,3,3-heptafluoro-7,7-dimethyl octane-4,6-dione.

cules of $(CH_3)_2SO$ coordinate to $Eu(FOD)_3$ in CD_2Cl_2.[14] Also, considering a second equilibrium for the *n*-hexyl amine–$Eu(FOD)_3$ system in $CDCl_3$,

$$LA + A \rightleftharpoons LA_2 \qquad K_2 = \frac{[LA_2]}{[LA][A]} \tag{2}$$

an attempt has been made to determine K_1, K_2, δ_1, and the shift characteristic of a 1 : 2 adduct (δ_2) from the least-squares fits.[15]

In the present investigation, δ_2 is assumed to be approximately equal to δ_1 in magnitude;[16] consequently, if $K_1 \gg 1$ and $R_L \ll 1$, the observed LIS (S) is formulated as Eq. (3):

$$S = \delta_1 \cdot R_L \frac{1+2K_2\cdot[A_0]}{1+K_2\cdot[A_0]} \tag{3}$$

K_1 may be expected to be sufficiently large. Actually, we obtained an apparent linearity between the observed shifts and R_L at sufficiently low values of R_L in all the systems investigated in this work. The shift value

Table 1. The observed lanthanide-induced shifts and the separation of calculated shifts to cs and pcs contributions for aniline[a]

	Position	Pr S_{obsd}[b]	Pr S_{calcd}[c] S_{pcs}	Pr S_{calcd}[c] S_{cs}	Eu S_{obsd}[b]	Eu S_{calcd}[c] S_{pcs}	Eu S_{calcd}[c] S_{cs}	Dy S_{obsd}	Dy S_{calcd}[c] S_{pcs}	Dy S_{calcd}[c] S_{cs}
NH_2	2	22.33	21.88	0.40	−16.07	−14.58	−1.48	185.0	185.55	−0.94
			21.92	0.43		−14.44	−1.59		186.43	−1.00
	3	6.90	7.06	−0.15	−4.00	−4.56	0.56	62.3	62.03	0.36
			7.07	−0.17		−4.66	0.65		61.81	0.41
	4	5.97	5.53	0.45	−5.23	−3.55	−1.69	47.8	48.95	−1.08
			5.54	0.43		−3.65	−1.59		48.70	−1.00
	χ	46—50°			43—47°			49—54°		
		46—50°			45—50°			49—54°		
	A	1729±69			−1157±47			14576±578		
		1732±69			−1146±51			14559±599		
	B	0.398±0.017[e]		d)	−1.480±0.031[e]		d)	−0.920±0.182[e]		d)
		0.428±0.020			−1.589±0.026			−0.993±0.140		
	$\frac{\sum\|S_{cs}\|}{\sum\|S_{pcs}\|}$	0.024±0.001			0.137±0.003			0.007±0.002		
		0.026±0.001			0.146±0.003			0.007±0.001		

	Position	Ho S_{obsd}	Ho S_{calcd}[c] S_{pcs}	Ho S_{calcd}[c] S_{cs}	Er S_{obsd}	Er S_{calcd}[c] S_{pcs}	Er S_{calcd}[c] S_{cs}	Yb S_{obsd}	Yb S_{calcd}[c] S_{pcs}	Yb S_{calcd}[c] S_{cs}
NH_2	2	60.84	61.78	−1.09	−49.14	−47.31	−1.72	−30.83	−30.48	−0.40
			62.06	−1.16		−47.20	−1.85		−30.33	−0.43
	3	20.31	19.93	0.41	−14.60	−15.27	0.65	−9.69	−9.83	0.15
			19.82	0.47		−15.37	0.76		−9.88	0.18
	4	14.35	15.61	−1.24	−13.89	−11.96	−1.96	−8.17	−7.70	−0.46
			15.50	−1.16		−12.07	−1.85		−7.75	−0.43
	χ	46—49°			46—50°			46—50°		
		45—49°			47—51°			47—51°		
	A	4900±175			−3739±149			−2409±96		
		4911±195			−3724±149			−2394±96		
	B	−1.077±0.062[e]		d)	−1.716±0.039[e]		d)	−0.403±0.025[e]		d)
		−1.156±0.066			−1.841±0.051			−0.430±0.025		
	$\frac{\sum\|S_{cs}\|}{\sum\|S_{pcs}\|}$	0.023±0.001			0.048±0.001			0.018±0.001		
		0.024±0.001			0.052±0.001			0.019±0.001		

a) All the S values are given in ppm. The observed shifts were corrected for CFS's observed with $La(FOD)_3$. The values in the second line are those calculated by using NIS as R_{cs}. Negative signs designate shifts to lower field. b) The data reported by M. Kainosho *et al.*, 12th NMR Symposium, 1973, Abstract, p. 107. c) The values giving rise to the minimum of R with $r_N = 2.7$ Å. d) The regions of some quantities on the restriction of R to less than 1% with a range of 2.6—2.8 Å for r_N. e) The sign of B coincides with that of the electron spin introduced into the ligand molecule.

TABLE 2. THE OBSERVED LANTHANIDE-INDUCED SHIFTS AND THE SEPARATION OF CALCULATED SHIFTS TO CS AND PCS CONTRIBUTIONS FOR *m*-TOLUIDINE[a)]

Position	Pr S_{obsd}	Pr S_{calcd}[b)] S_{pcs}	Pr S_{calcd}[b)] S_{cs}	Eu S_{obsd}	Eu S_{calcd}[b)] S_{pcs}	Eu S_{calcd}[b)] S_{cs}	Dy S_{obsd}	Dy S_{calcd}[b)] S_{pcs}	Dy S_{calcd}[b)] S_{cs}
2	25.63	25.08	0.21	−15.53	−13.86	−1.32	227.2	222.50	−2.70
		25.14	0.19		−13.75	−1.38		224.26	−3.08
4	6.97	6.02	0.24	−5.17	−3.32	−1.50	59.6	56.89	−3.08
		6.03	0.19		−3.39	−1.38		56.68	−3.08
5	8.29	7.75	−0.08	−3.92	−4.28	0.49	80.2	72.47	1.00
		7.77	−0.08		−4.35	0.56		72.35	1.24
6	25.14	25.08	0.20	−14.83	−13.86	−1.29	214.4	222.50	−2.63
		25.14	0.19		−13.75	−1.38		224.26	−3.08
CH_3	4.27	4.81	0.08	−2.94	−2.66	−0.53	39.4	46.37	−1.08
		4.82	0.07		−2.73	−0.49		46.05	−1.09
χ	42—46°			42—46°			46—52°		
	42—46°			43—49°			46—52°		
A	1994±74			1102±43			17576±797		
	1999±76		e)	1090±53		e)	17873±1076		f)
B	0.220±0.067[c)]			−1.322±0.015[c)]			−2.660±0.716[c)]		
	0.193±0.053			−1.387±0.016			−3.284±0.673		
$\frac{\Sigma\lvert S_{cs}\rvert}{\Sigma\lvert S_{pcs}\rvert}$	0.013±0.004			0.135±0.001			0.017±0.005		
	0.010±0.002			0.138±0.000$_5$			0.020±0.004		

Position	Ho S_{obsd}	Ho S_{calcd}[b)] S_{pcs}	Ho S_{calcd}[b)] S_{cs}	Er S_{obsd}	Er S_{calcd}[b)] S_{pcs}	Er S_{calcd}[b)] S_{cs}	Yb S_{obsd}	Yb S_{calcd}[b)] S_{pcs}	Yb S_{calcd}[b)] S_{cs}
2	97.5	96.97	−2.99	−59.2	−57.55	−1.67	−35.03	−34.58	−0.07
		96.85	−3.40		−57.34	−1.71		−34.62	−0.05
4	22.5	24.75	−3.40	−17.6	−14.55	−1.90	−8.56	−8.05	−0.08
		24.76	−3.40		−14.66	−1.71		−8.05	−0.05
5	34.5	31.53	1.10	−18.8	−18.57	0.62	−10.82	−10.43	0.03
		31.55	1.37		−18.68	0.69		−10.44	0.02
6	90.0	96.79	−2.91	−59.2	−57.55	−1.63	−34.39	−34.58	−0.07
		96.85	−3.40		−57.34	−1.71		−34.62	−0.05
CH_3	17.5	20.17	−1.20	−11.4	−11.82	−0.67	−5.92	−6.38	−0.03
		20.19	−1.20		−11.95	−0.60		−6.39	−0.02
χ	47—52°			45—52°			39—45°		
	46—52°			45—53°			39—45°		
A	7613±307			4533±223			2760±129		
	7645±340		f)	4529±243		d)	2763±132		d)
B	−3.035±0.265[c)]			−1.674±0.189[c)]			−0.078±0.149[c)]		
	−3.382±0.323			−1.729±0.167			−0.062±0.133		
$\frac{\Sigma\lvert S_{cs}\rvert}{\Sigma\lvert S_{pcs}\rvert}$	0.044±0.004			0.040±0.005			0.004±0.004		
	0.047±0.005			0.041±0.004			0.004±0.004		

a), b), and c): See Footnotes a), c), and e) in Table 1, respectively. d) Values on the restriction of R to less than 3%. e) Values on the restriction of R to less than 3.5%. f) Values on the restriction of R to less than 4.5%.

obtained from the linear extrapolation of R_L to 1 is $\delta_1(1+2K_2[A_0])/(1+K_2[A_0])$; K_2 value is required in estimating the magnitude of δ_1. However, since the relative shift values are adequate for the estimation of the intramolecular ratio of the cs and pcs contributions, we used $\delta_1(1+2K_2[A_0])/(1+K_2[A_0])$ as S_{obs}. The S_{obs} values were corrected for the diamagnetic shifts due to complex formation (CFS's),[1e)] by using shifts induced by $La(FOD)_3$ in CCl_4; they are listed in Tables 1 and 2 for aniline and *m*-toluidine respectively,

with Ln(FOD)$_3$ (Ln=Pr, Eu, Dy, Ho, Er, and Yb). It has been presumed that the geometry of such an adduct does not vary widely with an Ln ion. From this point of view, the variation in the S_{obs} ratios with an Ln ion seen in Tables 1 and 2 clearly shows the existence of a cs contribution.

Our procedure for separating the two contributions is as follows: At first, the calculated shift is taken as $S_{cal}=S_{pcs}+S_{cs}=A\cdot R_{pcs}+B\cdot R_{cs}$, where R_{pcs} is the geometric factor; R_{cs}, the cs relative to the 2 position, and A and B, the proportionarity constants. With the R_{pcs} and R_{cs} patterns in a molecule obtained by appropriate methods, the A and B values are determined by the least-squares technique and lead to S_{cal}. In order to assess the correspondence between S_{cal} and S_{obs}, the agreement factor, R,[11] is used as a good criterion. The dependence of R on the two geometric parameters χ and r_N (Fig. 1) required for determining R_{pcs} is conveniently displayed using contour lines on a map projection. Appropriate combinations of χ and r_N values are chosen, based on the mode of minimizing the R values in the contour plot, and on the validity of the molecular structure. From the amounts of S_{cs} and S_{pcs} corresponding to these values, the average intramolecular cs contribution to the pcs contribution, $\Sigma|S_{cs}|/\Sigma|S_{pcs}|$, is calculated. Here, if $K_2[A_0]\gg 1$, $S_{cs}/2$ and $S_{pcs}/2$ are the separated shifts corresponding to the δ_1 value.

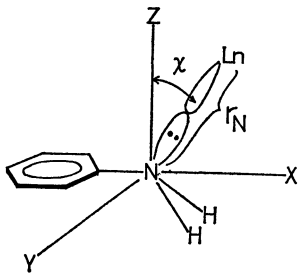

Fig. 1. Geometric parameters in the aniline adduct of Ln(FOD)$_3$.

McConnell-Robertson's equation[19] for axial symmetry was used in evaluating R_{pcs}, because, for such an adduct of the lanthanide chelate, this relation has been successfully used to interpret the dipolar shifts. Thus, the geometric factors were calculated with varying amounts of two geometric parameters, χ and r_N in the chemically reasonable ranges of 20—60°[20] and 2.0—4.0 Å respectively (Fig. 1). Here, since the Ln–N vector was assumed to be co-linear with a principal magnetic axis,[21] the rotation about the N–Ln bond did not need to be considered. The effect of rotation about the N–C bond was not introduced into the pcs calculations, because the N-lone pair orbital could be expected to conjugate with the π-MO of the ring to a great extent. For CH_3 protons, R_{pcs} was averaged over those values calculated for each 10° of rotation about the C–CH_3 bond.

Since the spin induced into the N-lone pair orbital may be expected to be delocalized predominantly through the π-bonds,[22] an approximate π-spin density distribution obtained by McLachlan's method[23] was used for the calculation of R_{cs}. There are four possible R_{cs} patterns occurring from the α- and β-spins in the highest occupied π-MO [h.o(α) and h.o(β)] and from the α- and β-spins in the lowest vacant π-MO [l.v(α) and l.v(β)]. It was found from a preliminary comparison of S_{obs} and S_{cal} that only the R_{cs} due to the h.o is effective in correcting the R_{pcs} pattern. This corresponds well to the fact that the h.o is symmetric to the molecular axis and can interact strongly with an AO of the metal ion. Furthermore, this preliminary testing suggested that the electron spin introduced into the h.o has a sign opposite to that of some Ln ions. For example, the h.o(β) is particularly excellent in explaining the observed relation, $|S(\beta H)|<|S(\gamma H)|$, for the aniline adduct of Eu(FOD)$_3$. Then, an intramolecular R_{cs} pattern was calculated from the π-spin density distribution of the cation radical[24] (ρ_c^π) of each substrate and was applied to all the Ln complexes (Table 3). The map projection of R for the aniline adduct is very similar in mode for all the Ln ions used here and does not reveal a single smooth minimum in R, an example with Eu(FOD)$_3$ being shown in Fig. 2(a). However, a very deep valley in R passes through a structurally favorable region in the map and, besides, varies in shape almost not at all with an Ln ion. This suggests that the π-approximation for R_{cs} is valid; further, that there seems to be no large variation in the geometry of an adduct with an Ln ion. Also, with the R_{cs} due to NIS's (Table 3), contour plots were produced for all the Ln ions, which are very similar in pattern to one another and, further, to those formed with ρ_c^π and which include sufficiently small values of R. The map projection prepared from the Ho(FOD)$_3$-induced shifts is shown in Fig. 2(b). This leads us to conclude that the amount of S_{cs} may by considerably smaller than that of S_{pcs}. Then, by reference to the N–Ln distance in the Eu(DPM)$_3$-(Pyridine)$_2$ crystal, 2.65 Å,[25] the range of 2.6—2.8 Å was adopted as a reasonable one, and by restricting the limit of R to 1%, a reasonable area on the map was determined (Fig. 2). A possible range of $\Sigma|S_{cs}|/\Sigma|S_{pcs}|$ corresponding to this area was then evaluated, where $\Sigma|S_{cs}|/\Sigma|S_{pcs}|$ is the average value of the cs contribution relative to that of pcs in a molecule.

Table 3. The intramolecular relative cs[a]

Compound	Position	$R_{cs}(\rho_c^\pi)$[b]	R_{cs}(NIS)[c]
Aniline	2	1.000	1.000
	3	−0.377	−0.410
	4	1.139	1.000
m-Toluidine	2	1.000	1.000
	4	1.138	1.000
	5	−0.370	−0.402
	6	0.974	1.000
	CH_3	0.401	0.354

a) See Tables 1 and 2 on the positions. b) ρ_c^π represents the spin density distribution of α spin in the h. o (h. o(α)). Q_{CH}^H and $Q_{CCH_3}^H$ were taken as −24.0 and 27.0 gauss, respectively. c) NIS's were observed in our laboratory, but are essentially those reported in Ref. 22.

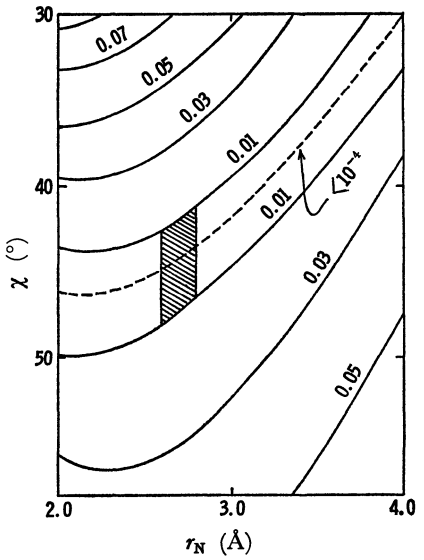

(a)

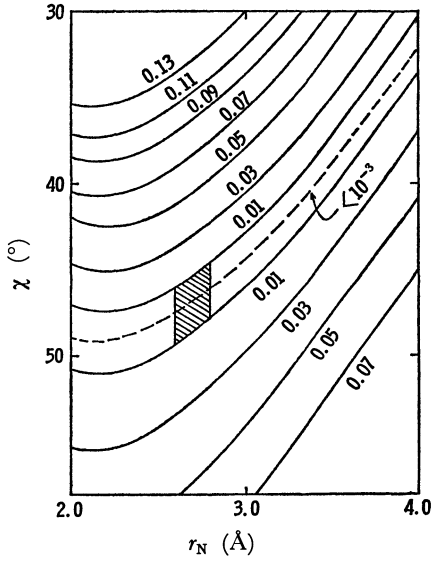

(b)

Fig. 2. Contour plots of R for the aniline adduct of $Eu(FOD)_3$ calculated by using ρ_c^π as R_{cs} (a), and of $Ho(FOD)_3$ calculated by using NIS as R_{cs} (b). Shaded parts indicate those chosen to determine a possible range of the magnitudes of S_{cs}.

The results with all the $Ln(FOD)_3$ substances are shown in Table 1, along with the ranges of χ, where the magnitudes of S_{cs} and S_{pcs} are those giving rise to the minimum of R with r_N=2.7 Å. In all the systems, the agreement between S_{obs} and S_{cal} is sufficiently good and the χ values fall within the range of 40—55°. When the limit of R can be extended to the 5% level, with the range of r_N held constant, the corresponding region of χ is fairly much expanded, but $\Sigma|S_{cs}|/\Sigma|S_{pcs}|$ does not vary so widely, except with $Dy(FOD)_3$.

Next, in order to check the above results, on the assumption of the K_2 being independent of the Ln ion, attempts were made at examining the relation of the A value to the relative pcs by Bleaney *et al.*[2] and that of the B value to $\langle S_z \rangle$ by Golding *et al.*[12] As

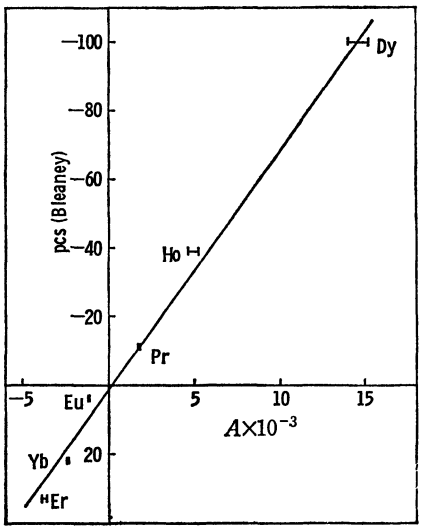

Fig. 3. Comparisons of A values for aniline (Table 1) to Bleaney's relative pcs, where A values were calculated by using ρ_c^π as R_{cs}. This figure is almost equal to that obtained with NIS as R_{cs}.

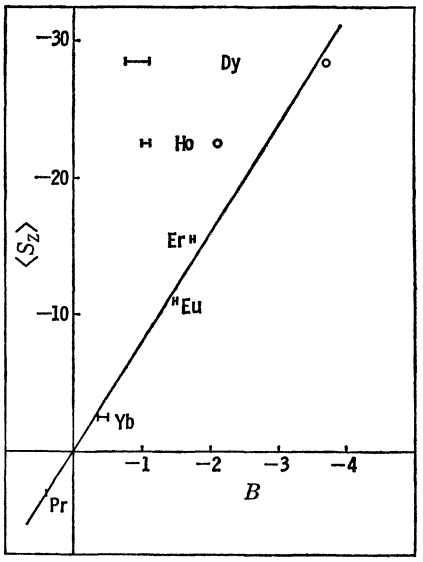

Fig. 4. Comparisons of B values for aniline (Table 1) to Golding's $\langle S_z \rangle$, where B values were calculated by using ρ_c^π as R_{cs}. This figure is similar in pattern to that with NIS as R_{cs}. (See the text) The circles show B values obtained from the expansion of allowed limit of R to 0.07.
○ (Dy): r_N=2.7 Å, χ=35°, R=0.07
○ (Ho): r_N=2.4 Å, χ=34°, R=0.07

is shown in Fig. 3, the linearity for the former is fairly good, consequently, one may consider that the above assumption regarding K_2 is acceptable. For the latter comparison, a good correspondence was obtained, as may be seen from Fig. 4, except for the values with Ho and $Dy(FOD)_3$. If a large expansion of the limit of R to 0.07 is allowable, and if the resulting decrease in χ to about 35° is not particularly noticable, for these two chelates the values of B calculated by using ρ_c^π can be improved to some extent, as may be seen

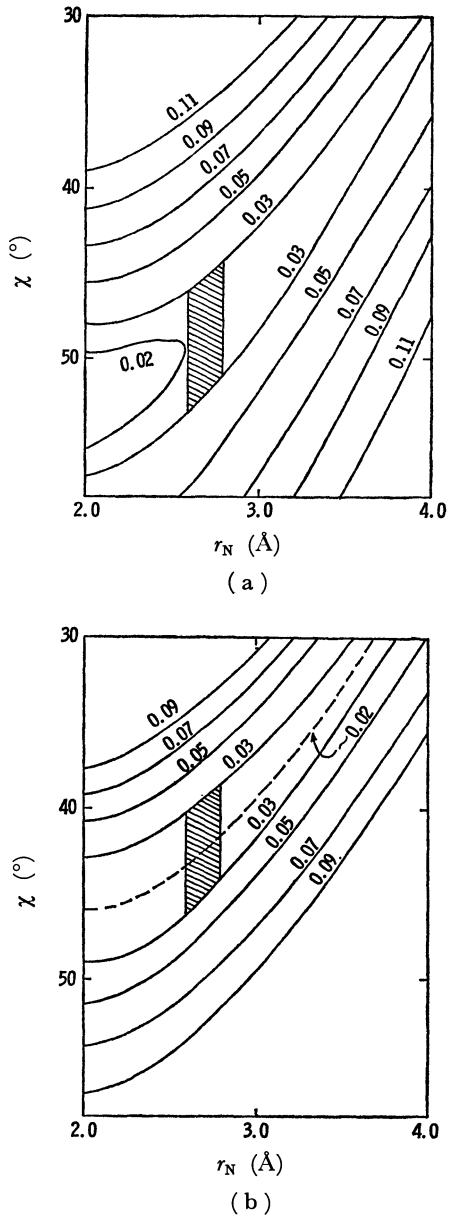

Fig. 5. Contour plots of R for the m-toluidine adduct of Eu(FOD)$_3$ calculated by using ρ_c^π as R_{cs} (a), and of Yb(FOD)$_3$ calculated by using NIS as R_{cs} (b). Shaded parts indicate those chosen to determine a possible range of the magnitudes of S_{cs}.

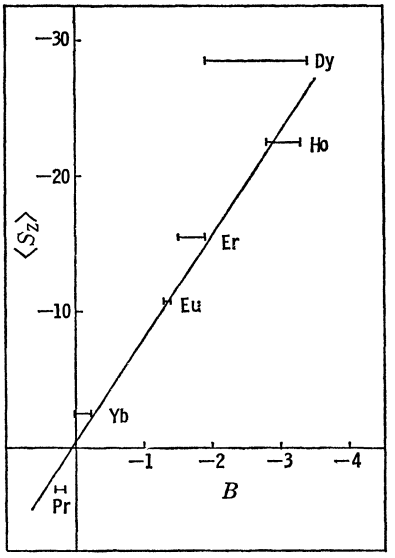

Fig. 6. Comparisons of B values for m-toluidine (Table 2) to Golding's $\langle S_z \rangle$, where B values were calculated by using ρ_c^π as R_{cs}. This figure is almost equal to that with NIS as R_{cs}.

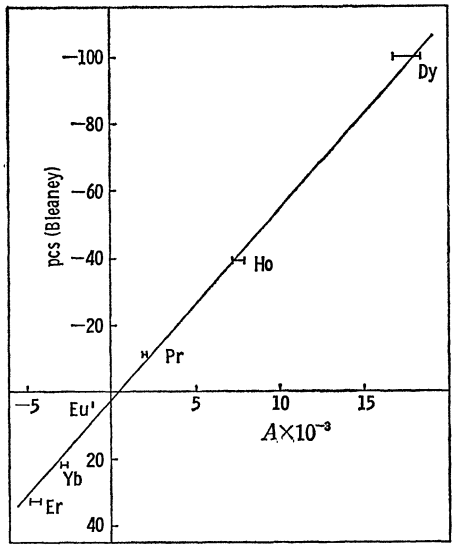

Fig. 7. Comparisons of A values for m-toluidine (Table 2) to Bleaney's relative pcs, where A values were calculated by using ρ_c^π as R_{cs}. This figure is almost equal to that with NIS as R_{cs}.

from Fig. 4, but those due to NIS's cannot be largely altered under such conditions.

The same treatments of m-toluidine adducts of Ln(FOD)$_3$ using the R_{cs} values from both ρ_c^π and NIS led to satisfactorily small values of R, though not with a valley in R so steep as in aniline, in the contour plot. We then discussed with setting the limit of R at a level between 3.0 and 4.5%. Some examples of the contour plots are shown in Fig. 5. The linear relation of the cs term to $\langle S_z \rangle$ is better than that in aniline, as is shown in Fig. 6, as is that of the pcs term to Bleaney's theoretical one (Fig. 7). Furthermore, the $\Sigma|S_{cs}|/\Sigma|S_{pcs}|$ ratios are compared with the theoretical ratios of $|\langle S_z \rangle|/|\text{pcs}|$ (Bleaney) in Fig. 8. The results for aniline are inferior to those for m-toluidine, corresponding to the comparison made separately for cs and pcs.

Thus, it may be considered that the present attempt has been roughly successful in determining the intramolecular ratio of cs and pcs contributions. However, these results may be fairly much affected by the combined inaccuracies introduced by the several assumptions and approximations included. In order to make a more accurate estimate of the cs contribution, the following investigations are in progress: (1) the variation in the angle between the Ln–N vector and the principal magnetic axis in the adduct is introduced to the computer program, and the rotation about the

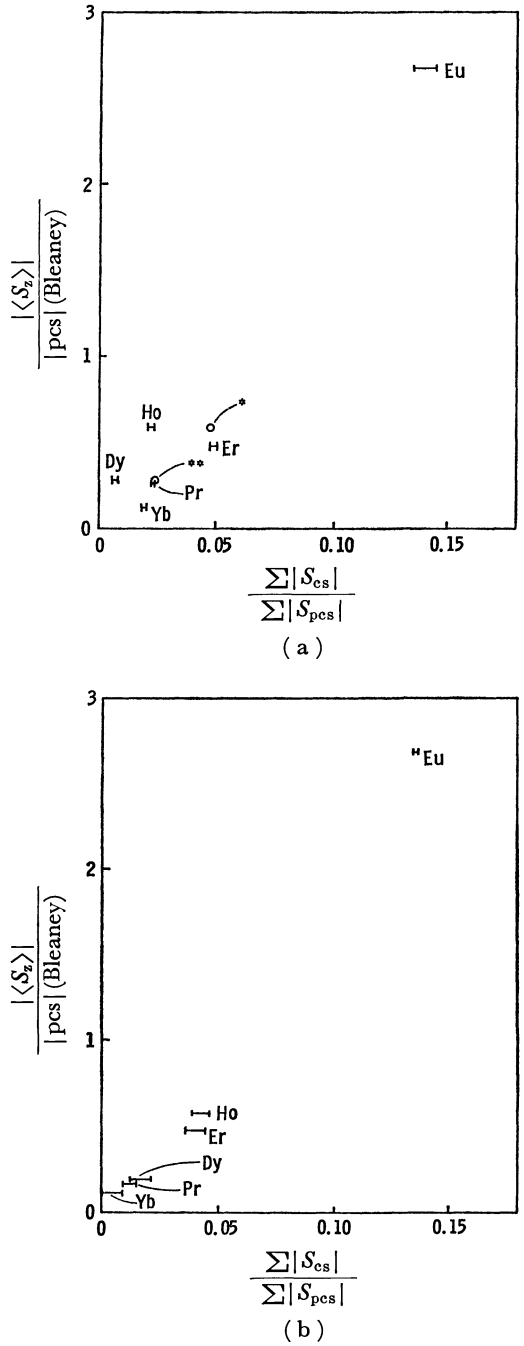

Fig. 8. Plots of $\sum|S_{cs}|/\sum|S_{pcs}|$ *vs.* $|\langle S_z\rangle|/|\mathrm{pcs}|$ (Bleaney).
(a) For the aniline adduct with ρ_c^π as R_{cs}.
*: Corresponding to ○ (Ho) in Fig. 4.
**: Corresponding to ○ (Dy) in Fig. 4.
(b) For the *m*-toluidine adduct with ρ_c^π as R_{cs}.

Ln–N vector is simultaneously accounted for; (2) the amount of δ_2 is separated from that of δ_1 by the least-squares curve fitting for the observed shifts, and (3) a σ-cs term is added to the R_{cs} pattern.

References

1) a) J. Briggs, F. A. Hart, and G. P. Moss, *Chem. Commun.*, **1970**, 1506. b) J. Briggs, F. A. Hart, G. P. Moss, and E. W. Randall, *ibid.*, **1971**, 364. c) M. Kainosho, K. Ajisaka, and K. Tori, *Chem. Lett.*, **1972**, 1061. d) K. Tori, Y. Yoshimura, M. Kainosho, and K. Ajisaka, *Tetrahedron Lett.*, **1973**, 1573. e) K. Tori, Y. Yoshimura, M. Kainosho, and K. Ajisaka, *ibid.*, **1973**, 3127. f) K. Ajisaka, M. Kainosho, H. Shigemoto, K. Tori, Z. W. Wolkowski, and Y. Yoshimura, *Chem. Lett.*, **1973**, 1205, g) R. J. Cushley, D. R. Anderson, and S. R. Lipsky, *Chem. Commun.*, **1972**, 636. h) B. F. G. Johnson, J. Lewis, P. McArdle, and J. R. Norton, *ibid.*, **1972**, 535.

2) B. Bleaney, C. M. Dobson, B. A. Levine, R. B. Martin, R. J. P. Williams, and A. V. Xavier, *ibid.*, **1972**, 791.

3) A. M. Grotens, J. J. M. Backus, and E. de Boer, *Tetrahedron Lett.*, **1973**, 4343; G. A. Elgavish and J. Reuben, *J. Magn. Resonance*, **16**, 360 (1974).

4) F. Inagaki, S. Takahashi, M. Tasumi, and T. Miyazawa, This Bulletin, **48**, 853 (1975); F. Inagaki, S. Takahashi, M. Tasumi, and T. Miyazawa, *ibid.*, **48**, 1590 (1975).

5) a) G. E. Hawkes, C. Marzin, S. R. Johns, and J. D. Roberts, *J. Amer. Chem. Soc.*, **95**, 1661 (1973). b) C. M. Dobson, R. J. P. Williams, and A. V. Xaxier, *J. Chem. Soc., Dalton*, **1973**, 2662. c) O. A. Gansow, P. A. Loeffler, R. E. Davis, M. R. Willcott, III, and R. E. Lenkinski, *J. Amer. Chem. Soc.*, **95**, 3389 and 3390 (1973).

6) G. N. La Mar and J. W. Faller, *ibid.*, **95**, 3817 (1973).

7) K. Ajisaka and M. Kainosho, 13th NMR Symposium, 1974, Abstract, p. 30; A. A. Chalmers and K. G. R. Pachler, *J. Chem. Soc., Perkin II*, **1974**, 748.

8) S. Amiya and R. Chujo, 12th NMR Symposium, 1973, Abstract, p. 91.

9) H. Huber and C. Pascual, *Helv. Chim. Acta*, **54**, 913 (1971); M. Hirayama, E. Edakawa, and Y. Hanyu, *Chem. Commun.*, **1972**, 1343; M. Hirayama and Y. Hanyu, This Bulletin, **46**, 2687 (1973).

10) M. Hirayama and M. Sato, *Chem. Lett.*, **1974**, 725.

11) M. R. Willcott, III, R. E. Lenkinski, and R. E. Davis, *J. Amer. Chem. Soc.*, **94**, 1742 (1972).

12) R. M. Golding and M. P. Halton, *Aust. J. Chem.*, **25**, 2577 (1972).

13) C. S. Springer, Jr., D. W. Meek, and R. E. Sievers, *Inorg. Chem.*, **6**, 1105 (1967).

14) D. F. Evans and M. Waytt, *Chem. Commun.*, **1972**, 312.

15) F. Inagaki, M. Tasumi, and T. Miyazawa, This Bulletin, **48**, 1427 (1975).

16) As this work was in progress, it was reported by Shapiro *et al.* that δ_2 is fairly smaller than δ_1 in the cyclohexanone- and cyclohexanol-Eu(FOD)$_3$ systems in CCl_4.[17] The combination of this finding and that of the *n*-hexyl amine-Eu(FOD)$_3$ system in $CDCl_3$[15] indicates that both the difference in magnitude between δ_1 and δ_2 in each position in the molecule and the difference in the intramolecular ratio of δ_2 from that of δ_1 vary considerably with the substrate. Consequently, it may be considered that our present findings regarding cs contributions, as described in the last part in the text, are not very reliable. However, if K_2 is large, the shift value obtained from the linear extrapolation of the initial slope, R_L, to 1.0 is approximately two times δ_2, as was indicated by Shapiro *et al.*[18] From this point of view, the cs contributions estimated here are possibly those on δ_2, if the K_2 can be expected to be as large as that ($\sim$14) in the *n*-hexyl amine-Eu(FOD)$_3$ system dealt with in Ref. 15.

17) M. D. Johnston, Jr., B. L. Shapiro, M. J. Shapiro, T. W. Proulx, A. D. Godwin, and H. L. Pearce, *J. Amer. Chem. Soc.*, **97**, 542 (1975).

18) B. L. Shapiro and M. D. Johnston, Jr., *ibid.*, **94**, 8185 (1972).

19) H. M. McConnell and R. E. Robertson, *J. Chem. Phys.*, **29**, 1361 (1958).

20) The calculation of R while varying χ from 0° to 90°

using a suitable range of r_N values showed that only the region of 20—60° in χ is needed for all the Ln ions. This suggests that the χ is slightly larger than that in the $Ni(AcAc)_2$- or $Co(AcAc)_2$-aniline adduct,[22] probably because of the steric hindrance and a different complexation.

21) The shift study on the $Eu(DPM)_3$-3-picoline system by Cramer *et al.* at low temperatures has shown that, when the $(3\cos^2\theta-1)/r^3$ term for axial symmetry is used in the calculation of dipolar shifts at room temperature, the effect of restricted rotation about the Eu–N bond should be accounted for, since the Eu–N vector may not accord with the magnetic axis. However, since the angle between the Eu–N vector and the effective magnetic axis may be expected to be very small,[5a] we roughly regard this angle as zero in the present study. See R. E. Cramer and R. Dubois, *Chem. Commun.*, **1973**, 939.

22) T. Yonezawa, I. Morishima, Y. Akana, and K. Fukuta, This Bulletin, **43**, 379 (1970).

23) A. D. McLachlan, *Mol. Phys.*, **3**, 233 (1960).

24) The values for MO parameters used were those reported by Yonezawa *et al.*,[22] and the λ value in McLachlan's equation was taken as 1.2. Although a decrease in β_{NC} corresponding to an increase in χ was introduced into the MO calculation, the pattern of contour plot was almost insensitive to the variation in β_{NC}. Therefore, β_{NC}/β was kept at 0.6.

25) R. E. Cramer and K. Seff, *Chem. Commun.*, **1972**, 400.

Interpretation of Shake-up Satellites in the X-Ray Photoelectron Spectra of Small Hydride Molecules by One-Center-Expansion *ab initio* Calculation with Equivalent-Core Approximation

Takashi Fujikawa, Tomoo Aoyama, Toshiaki Ohta, and Haruo Kuroda

Department of Chemistry, Faculty of Science, University of Tokyo, Hongo, Tokyo 113

(Received April 14, 1975)

One-center-expansion *ab initio* calculations with STO basis set were carried out on H_2O, NH_3, CH_4 and BH_3, to estimate the energies and probabilities of shake-up processes accompanying the photoionization of a core level. A method based on equivalent-core approximation and that based on configuration interaction procedure were applied to obtain wave functions of core-hole ions. It is shown that the calculations by the former method yield very satisfactory results, not only for the core ionization potential, but also for the energies and intensities of shake-up satellites.

Recent development of X-ray photoelectron spectroscopy of gaseous molecules has revealed that core-electron peaks of X-ray photoelectron spectra are often accompanied by satellite bands arising from the two-electron process where a secondary excitation (shake-up) or ejection (shake-off) of an outer shell electron takes place simultaneously with the ionization of a core level.[1-5] These phenomena are of great theoretical interest since they are closely related to the relaxation accompanied with the ejection of a core electron.

Several authors[4-9] have attempted to calculate the energies and intensities of shake-up satellites on the basis of sudden approximation[10,11] where the secondary excitation (or ejection) of an outer-shell electron is treated as arising from the sudden perturbation of potential due to the removal of a core electron. On the core-hole states of small first-row molecules, Aarons *et al.*[4] carried out an *ab initio* unrestricted Hartree-Fock (UHF) calculation with Gaussian basis set, and calculated shake-up satellites of these molecules, with reasonable success. Another type of approach was done by Guest *et al.*[7] and, more recently, by Wood.[8] These authors treated the relaxed core-hole state with a configuration interaction (CI) procedure using molecular orbitals obtained by *ab initio* SCF-MO calculations on the neutral molecules. For relatively complex molecules, semi-empirical molecular orbital methods incorporated with equivalent-core approximation have been applied to calculate the energies and intensities of shake-up satellites, and found to give reasonable results.[5,6] Equivalent-core approximation[12] has been known to be a useful tool for calculating core ionization potentials. In effect, Adams and Clark[13,14] have shown that an *ab initio* calculation combined with this approximation can provide satisfactory predictions of core ionization potential. Hitherto, however, no attempt has been done to use this approximation in calculating shake-up transitions by *ab initio* molecular orbital methods.

In the present study, we carried out *ab initio* calculations by one-center-expansion method on the neutral molecules and core-hole ions of small hydrides of first-row atoms, using equivalent-core approximation, and calculated the energies and intensities of the shake-up satellites accompanying the core-electron peaks in their X-ray photoelectron spectra. The results obtained by core-hole CI method will be also given for the sake of comparison.

Methods of Calculation

According to the sudden approximation, the probability of the transition which yields the final core-hole state $\Psi_f(2n-1)$ is given by,[10,11]

$$P_f = |\langle \Psi_f(2n-1)|\Phi_0(2n-1)\rangle|^2 \quad (1)$$

where $\Phi_0(2n-1)$ is the core-hole wave function in which all molecular orbitals have been frozen as they are in the neutral molecule.[15] We may construct the ground-state wave function $\Phi_G(2n)$ of a neutral molecule from the one-electron molecular orbitals $\{\phi_i\}$.[16]

$$\Phi_G(2n) = |\phi_1\bar{\phi}_1\phi_2\bar{\phi}_2\cdots\phi_n\bar{\phi}_n| \quad (2)$$

Then, $\Phi_0(2n-1)$ can be written as follows by taking ϕ_1 as the ionizing core orbital;

$$\Phi_0(2n-1) = |\bar{\phi}_1\phi_2\bar{\phi}_2\cdots\phi_n\bar{\phi}_n| \quad (3)$$

In the present study, we obtained the one-electron molecular orbitals through one-center-expansion (OCE) *ab initio* calculation with Slater-type-orbital (STO) basis set. This method has been successfully applied by Hartmann *et al.*[17] to calculate the ground-state properties of various hydride molecules. We used 25 STO basis functions except in the case of H_2O where 19 basis functions were used; the zeta values of the used STO bases are given in Table 1.

In order to obtain the final-state wave function, we used two different methods; the equivalent-core approximation method and the core-hole CI method.

(a) Equivalent-Core Approximation (ECA) Method. In the equivalent-core approximation, it is assumed that, when a core electron is removed from an atom, the outer-shell electrons adjust themselves as if the nuclear charge of the ionized atom has increased by one unit.[13] This means that, in the case of CH_4, one can get the valence-electron orbitals of the core-hole ion by performing a calculation on the N^+H_4 system, in which the molecular geometry has been taken the same as that of CH_4 molecule, instead of directly calculating on the core-hole ion, C^*+H_4.[18] Thus, we carried out calculations on the equivalent-core models, C^+H_3, N^+H_4, O^+H_3 and F^+H_2, to obtain the relaxed valence-electron orbitals of the core-hole ions, B^*+H_3, C^*+H_4, N^*+H_3 and O^*+H_2, respectively.

In each case, the zeta values of the first five STO basis functions only were replaced with those corresponding to the change of the nuclear charge as shown in Table 1.

By using the relaxed one-electron orbitals $\{\phi_i\}$, the wave functions of the ground and excited configurations of a core-hole ion can be expressed as follows;

$$\Psi_0(2n-1) = |\bar{\phi}_1\phi_2\bar{\phi}_2\cdots\phi_n\bar{\phi}_n| \quad (4)$$

$$\Psi_{i\to j}(2n-1) = |\bar{\phi}_1\phi_2\bar{\phi}_2\cdots\bar{\phi}_{i-1}\phi_j\bar{\phi}_i\phi_{i+1}\cdots\phi_n\bar{\phi}_n| \quad (5)$$

where the core orbital ϕ_1 is assumed to be the same as ϕ_1 by adopting the frozen-core approximation. Then, the probabilities of the transition to Ψ_0 and that to $\Psi_{i\to j}$ are given as follows according to Eq. (1);[19]

$$P_0 = |\mathbf{S}_0|^4, \qquad P_{i\to j} = |\mathbf{S}_0|^2|\mathbf{S}_{i\to j}|^2 \quad (6)$$

where

$$\mathbf{S}_0 = \begin{vmatrix} \langle\phi_2 & \phi_2\rangle\cdots\cdots\langle\phi_2 & \phi_n\rangle \\ \vdots & \ddots & \vdots \\ \langle\phi_n & \phi_2\rangle\cdots\cdots\langle\phi_n & \phi_n\rangle \end{vmatrix}$$

and

$$\mathbf{S}_{i\to j} = \begin{vmatrix} \langle\phi_2 & \phi_2\rangle\cdots\cdots\langle\phi_2 & \phi_n\rangle \\ \vdots & \ddots & \vdots \\ \langle\phi_{i-1} & \phi_2\rangle\cdots\cdots\langle\phi_{i-1} & \phi_n\rangle \\ \langle\phi_j & \phi_2\rangle\cdots\cdots\langle\phi_j & \phi_n\rangle \\ \langle\phi_{i+1} & \phi_2\rangle\cdots\cdots\langle\phi_{i+1} & \phi_n\rangle \\ \vdots & \ddots & \vdots \\ \langle\phi_n & \phi_2\rangle\cdots\cdots\langle\phi_n & \phi_n\rangle \end{vmatrix} \begin{matrix} \\ \\ \\ \\ \\ \\ \\ \end{matrix} \begin{matrix} \\ \\ \\ \\ \\ \\ <i \end{matrix}$$

The relative probability of shake-up, $\bar{P}_{i\to j}=P_{i\to j}/P_0$, is given as,

$$\bar{P}_{i\to j} = |\mathbf{S}_{i\to j}|^2/|\mathbf{S}_0|^2 \quad (7)$$

For the excited states of each core-hole ion, we carried out a configuration interaction calculation, extensively taking into account singly-excited configurations. Then, the relative probability of the shake-up process which yields the k-th excited state of the core-hole ion, was obtained by the following relation by using the weight $(w^k_{i\to j})$ of each configuration;[20]

$$\bar{P}_k = \sum_{i\to j} w^k_{i\to j}\bar{P}_{i\to j} \quad (8)$$

The total probability of shake-up (P_{up}) and that of shake-off (P_{off}) are given as follows;

$$P_{\mathrm{up}} = \sum_k \bar{P}_k \cdot P_0 \quad (9)$$

$$P_{\mathrm{off}} = 1 - (P_0 + P_{\mathrm{up}}) \quad (10)$$

The procedure proposed by Adams and Clark[13] was used to estimate the core ionization potentials from the calculations by ECA method.[21]

(b) Core-hole CI (CH-CI) Method. In the core-hole CI procedure, a wave function of a relaxed core-hole ion is described as follows;

for the ground state,

$$\Psi_0(2n-1) = a^0_0\Phi_0(2n-1) + \sum_{(i\to j)} a^0_{i\to j}\Phi_{i\to j}(2n-1) \quad (11)$$

and, for the k-th excited state,

$$\Psi_k(2n-1) = a^k_0\Phi_0(2n-1) + \sum a^k_{i\to j}\Phi_{i\to j}(2n-1) \quad (12)$$

where Φ_0 and $\Phi_{i\to j}$ are the frozen-orbital wave functions of core-hole configurations and a^k_0 and $a^k_{i\to j}$ are the coefficients. Then, the probabilities of the transitions to Ψ_0 $(2n-1)$ and to Ψ_k $(2n-1)$, can be given as,

$$P_0 = |a^0_0|^2 \quad (13)$$

$$P_k = |a^k_0|^2 \qquad \text{thus} \quad \bar{P}_k = |a^k_0|^2/|a^0_0|^2 \quad (14)$$

Therefore, the energies and probabilities of shake-up transitions are obtainable through the diagonalization of CI matrix. The core ionization potential can be calculated by the following formula,

$$I_p(\mathrm{core}) = \langle\Psi_0(2n-1)|H(2n-1)|\Psi_0(2n-1)\rangle - \langle\Phi_G(2n)|H(2n)|\Phi_G(2n)\rangle \quad (15)$$

We carried out the calculations described above, using the frozen-orbital wave functions constructed from the one-electron molecular orbitals which have been obtained by the one-center-expansion *ab initio* calculations on the neutral molecules with the STO basis sets given in Table 1.

All computations were performed with HITAC 8700/8800 at the computer center of the University of Tokyo, by using the programs written by ourselves. In the present calculations, we used the observed molecular geometries of free hydrides molecules, except in the case of BH_3.

Results and Discussion

In Tables 2(a)—(d), we show the orbital energies obtained by the present calculations of the neutral molecules of H_2O, NH_3, CH_4 and BH_3. As for the virtual orbitals, we have given there only three or four lower-energy ones, omitting all others of higher energies. On these molecules, *ab initio* LCAO calculations with Gaussian basis set have been carried out by other authors,[22-24] the results of which are shown in the same table for the sake of comparison.

The ionization potentials of the molecular orbitals of H_2O, NH_3 and CH_4 have been experimentally determined by use of photoelectron spectroscopy.[25-27] These experimental values are also given in Tables 2(a)—(c). We can see that the experimental ionization potentials are smaller than the values expected from the calculated orbital energies according to Koopmans' theorem. The discrepancy is especially significant in the case of the ionization potentials of core levels. As it is known, this discrepancy is mainly associated with the electronic relaxation of core-hole state.

The values of the core ionization potential which we have calculated by CH-CI method and by ECA method

Table 1. Zeta values of STO bases

(a) H_2O

Neutral molecule (19 basis)			Equivalent-core model (19 basis)		
n	l	zeta	n	l	zeta
1	0	7.6579	1	0	8.6501
2	0	2.2458	2	0	2.5638
2	1	2.2266	2	1	2.5500
3	0	2.2000	3	0	2.3500
3	1	2.1000	3	1	2.2500
3	2	1.9000	3	2	1.9000
4	0	2.2000	4	0	2.2000
4	1	1.7000	4	1	1.7000
5	0	2.2000	5	0	2.2000

(b) NH_3

Neutral molecule (25 basis)			Equivalent-core model (25 basis)		
n	l	zeta	n	l	zeta
1	0	6.6651	1	0	7.6579
2	0	1.9237	2	0	2.2458
2	1	1.9170	2	1	2.2266
3	0	1.9000	3	0	2.0500
3	1	1.8500	3	1	2.0000
3	2	1.8000	3	2	1.8000
4	0	1.9000	4	0	1.9000
4	1	1.8000	4	1	1.8000
4	3	2.0000	4	3	2.0000

(c) CH_4

Neutral molecule (25 basis)			Equivalent-core model (25 basis)		
n	l	zeta	n	l	zeta
1	0	5.6727	1	0	6.6651
2	0	1.6083	2	0	1.9237
2	1	1.5679	2	1	1.9170
3	0	1.6000	3	0	1.6000
3	1	1.5600	3	1	1.5600
3	2	1.4500	3	2	1.4500
4	0	1.5400	4	0	1.5400
4	1	1.5000	4	1	1.5000
4	3	1.6000	4	3	1.6000

(d) BH_3

Neutral molecule (25 basis)			Equivalent-core model (25 basis)		
n	l	zeta	n	l	zeta
1	0	4.6795	1	0	5.6727
2	0	1.2881	2	0	1.6083
2	1	1.2107	2	1	1.5679
3	0	1.2680	3	0	1.2680
3	1	1.1800	3	1	1.1900
3	2	1.2600	3	2	1.2600
4	0	1.2400	4	0	1.2400
4	1	1.1700	4	1	1.1700
4	3	1.4900	4	3	1.4900

Table 2. Calculated orbital energies of neutral molecules of H_2O, NH_3, CH_4 and BH_3

(a) H_2O

Orbital	Orbital energy (eV) (calcd)		I_p (eV)[25] (obsd)
	Present study	Neumann and Moskowitz[22]	
$4a_1$	15.08		
$2b_2$	13.40		
$3a_1$	7.72		
$1b_1$	−13.34	−13.80	12.6
$2a_1$	−15.15	−15.84	14.7
$1b_2$	−18.59	−19.56	18.4
$1a_1$	−36.76	−36.79	32.2
core	−561.50	−559.40	539.7

(b) NH_3

Orbital	Orbital energy (eV)		I_p (eV) (obsd)
	Present study	Palke and Lipscomb[23]	
3e	23.37		
$4a_1$	18.10		
2e	16.32		
$3a_1$	10.19	15.90	
$2a_1$	−11.13	−9.96	10.16[26]
1e	−15.92	−15.85	14.8[26]
$1a_1$	−30.59	−29.97	
core	−422.34	−422.38	405.6[2]

(c) CH_4

Orbital	Orbital energy (eV)		I_p (eV) (obsd)
	Present study	Clementi and Routh[24]	
$2t_2$	12.57		
$3a_1$	7.57		
$1t_2$	−13.53	−14.81	13[25]
$1a_1$	−25.18	−25.71	23[25]
core	−304.14	−305.17	290.8[27]

(d) BH_3

Orbital	Orbital energy (eV)	
	Present study	Clementi and Routh
2e′	6.476	
$1a_1'$	4.753	
$1a_2''$	1.436	
1e′	−12.41	−13.888
$1a_1'$	−18.76	−19.398
core	−206.71	−208.96

according to the procedures given in the preceding section, are given in Table 3, together with the results obtained of the probability of one-electron process (P_0), and the total probabilities of shake-up (P_{up}) and shake-off (P_{off}) processes. We see that, while both CH-CI and ECA methods yield reasonable values of core ionization potential, the agreement with observa-

TABLE 3. CALCULATED VALUES OF I_p(core), P_0, P_{up} AND P_{off}

	OCE		CNDO/2 (ECA)	Aarons *et al.*[4] UHF	Obsd
	CH-CI	ECA			
H_2O					
I_p[eV]	542.0	540.1		539.7	539.7[28]
P_0[%]	80.8	74.7	87.6	79.2	
P_{up}[%]	19.2	10.9	5.9	18.8	
P_{off}[%]	—	14.4	6.5	2.0	
NH_3					
I_p[eV]	409.1	407.7		405.6	405.6[25]
P_0[%]	79.6	74.4	87.6	77.8	
P_{up}[%]	20.4	10.5	5.9	19.7	
P_{off}[%]	—	15.1	6.5	2.5	
CH_4					
I_p[eV]	294.1	288.0		291.1	290.8[25]
P_0[%]	81.2	74.1	87.0	77.1	
P_{up}[%]	18.8	11.1	6.1	20.4	
P_{off}[%]	—	14.8	6.9	2.5	
BH_3					
I_p[eV]	200.3	192.4			
P_0[%]	80.8	72.1	89.3		
P_{up}[%]	19.2	13.3	5.1		
P_{off}[%]	—	14.6	5.6		

tion is much better in the cases when ECA method has been used.

The P_0 values by CH-CI method are generally larger as compared with those by ECA method. Probably, this is due to the neglect of shake-off configurations in the present CH-CI calculation. Incidentally, the P_0 values obtained by Aarons *et al.*[4] through their UHF calculations on the same molecules fall in between our values by CH-CI method and those by ECA method. It may be worthwhile to compare the above P_0 values with those by the CNDO/2 calculation with equivalent-core approximation, since the last method has been conveniently used for more complex molecules. The values which we have obtained by this method are given in Table 3. We note that the CNDO/2 calculations yielded P_0 values considerably larger than those by *ab initio* calculations. Seemingly, this is reflecting the situation that the virtual orbitals which appear in CNDO/2 calculations, are quite limited as compared with those in *ab initio* calculations.

The energies and relative intensities of shake-up satellites obtained from the present calculations are summarized in Table 4. First of all, we note that CH-CI method has given unreasonably large values for the energies of shake-up transitions. The same conclusion has been reported by Guest *et al.*,[7] who have carried out an *ab initio* calculation by core-hole CI method on similar molecules. Recently it was pointed out by Wood[8] that a good result is obtainable if the effect of valence-orbital relaxation is taken into account in a core-hole CI method.

On the other hand, our results by ECA method seem to be quite reasonable when they are compared with the reported experimental data. Recently, Siegbahn[28] observed the satellite bands accompanying the Ols peak of the X-ray photoelectron spectrum of H_2O, with a high resolution technique employing monochromatized X-ray as the stimulating radiation. The satellite spectrum reported by Siegbahn is reproduced in Fig. 1, where the shake-up transitions predicted from our calculations by ECA method are indicated as vertical lines. The calculated results are

TABLE 4. ENERGIES OF SHAKE-UP SATELLITES OF THE CORE-ELECTRON PEAKS FOR H_2O, NH_3, CH_4 AND BH_3[a]

Transition	Calculation		UHF[4]	Observation[4,28]
	Present study CH-CI	ECA		
H_2O(O1s)				
$2a_1 \rightarrow 3a_1$	40.59(0.54)	17.92(0.44)	17.8(3.1)	~15(shoulder)
$1b_1 \rightarrow 2b_1$	43.92(4.82)	23.98(3.11)	23.8(8.1)	~24(17)
$2a_1 \rightarrow 4a_1$	47.43(4.41)	24.93(2.77)		
$1b_2 \rightarrow 2b_2$	59.74(4.73)	33.22(2.76)		
NH_3(N1s)				
$2a_1 \rightarrow 3a_1$	29.81(0.47)	14.18(0.74)		(~13)
$2a_1 \rightarrow 4a_1$	36.16(8.53)	22.38(3.11)	21.1(14.1)	~22(8)
$1e \rightarrow 2e$	37.74(10.04)	23.02(5.15)		
$1e \rightarrow 3e$		30.20(0.03)		~30(weak)
$1a_1 \rightarrow 3a_1$	50.03(2.46)	39.22(2.64)		
CH_4(C1s)				
$1t_2 \rightarrow 2t_2$	29.02(13.03)	17.49(8.06)	18.8(18.4)	~18(18)
$1a_1 \rightarrow 2a_1$	37.61(3.64)	31.17(3.34)		~30(3)
$1t_2 \rightarrow 3t_2$	50.55(4.09)	20.51(0.26)		
BH_3(B1s)				
$1e' \rightarrow 2e'$	20.9(8.22)	15.49(5.82)		
$1a_1' \rightarrow 2a_1'$	33.1(2.33)	23.55(4.38)		
$1e' \rightarrow 3e'$	24.6(4.26)	17.16(1.16)		

a) Relative intensities are listed in the parentheses.

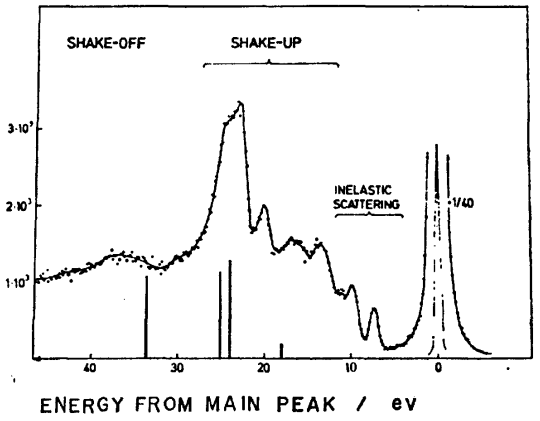

Fig. 1. Satellite bands of the Ols peak of H_2O (Siegbahn, Ref. 28). The shake-up bands predicted by the present study are shown by vertical lines.

quite satisfactory as regards the prediction of main shake-up band. In the observed spectrum, the main shake-up band is at about 24 eV from the Ols peak with an indication that it is composed of more than one components. This is in good agreement with our calculation which predicts two strong shake-up bands, at 23.98 eV ($1b_1 \rightarrow 2b_1$) and at 24.93 eV ($2a_1 \rightarrow 4a_1$). However, there is a problem concerning the interpretation of the weak satellite bands observed at lower energies. In the observed spectrum, there are three weak bands in the 11—22 eV region, their maxima being at about 13, 17 and 20 eV, respectively. All of them have been attributed by Siegbahn[28] to shake-up processes. On the other hand, our calculation predicts only one shake-up band at 17.92 eV ($2a_1 \rightarrow 3a_1$). A similar conclusion has been given by Aarons *et al.*,[4] who obtained also only one shake-up transition at 17.8 eV by UHF calculation. Seemingly, it is rather hard to explain why there are three shake-up bands in the 11—22 eV region. Siegbahn[28] attributed a broad maximum observed at about 33 eV to shake-off process. In effect, this is the energy region where we can expect a shake-off satellite. However, it should be noted also that our calculation predicts a relatively strong shake-up band at 33.22 eV ($1b_2 \rightarrow 2b_2$). Thus, there is a possibility that the 33 eV band in the observed spectrum is, at least partly, associated with a shake-up process.

For NH_3, our calculation predicts two relatively strong shake-up bands at 22.38 and 23.02 eV, which are associated with $2a_1 \rightarrow 4a_1$ and $1e \rightarrow 2e$ transitions, respectively. This is in agreement with the observation reported by Aarons *et al.*,[4] who found that the main satellite band accompanying the N1s peak of NH_3 is in the 18—25 eV region with a maximum at about 22 eV. According to our calculation, we should expect a weak shake-up band at about 14 eV. Unfortunately, however, it is difficult to judge from the reported data if there is any band corresponding to the predicted one or not.

In the case of CH_4, a relatively strong shake-up transition ($1t_2 \rightarrow 2t_2$) is predicted at 17.49 eV and a weak one ($1a_1 \rightarrow 2a_1$) at 31.17 eV. According to Aarons *et al.*,[4] the C1s spectrum of CH_4 exhibits a strong shake-up satellite at 18.1 eV, and a weak one at about 30 eV. Although they observed a weak band at about 26 eV, they attributed it to shake-off process. Seemingly, the observed spectrum is consistent with the results of our calculation.

As described above, our calculation by equivalent-core approximation (ECA) method yielded quite satisfactory results not only for the core ionization potentials, but also for the energies and intensities of shake-up satellites. On the other hand, calculations by core-hole CI(CH-CI) method failed to predict the energies of shake-up transitions correctly, while it gave reasonably good results as regards the core ionization potentials. Although we could improve the core-hole CI method by taking into account the relaxation of valence-electron orbitals as it has been proposed by Wood,[8] the equivalent core approximation method seems to have much advantage because good results are obtainable through a relatively simple computation, and, seemingly, this method can be a convenient tool for the interpretation of X-ray photoelectron spectra of molecules.

References

1) U. Gelius, C. J. Allan, D. A. Allison, H. Siegbahn, and K. Siegbahn, *Chem. Phys. Lett.*, **11**, 224 (1971).
2) C. J. Allan, U. Gelius, D. A. Allison, G. Johansson, H. Siegbahn, and K. Siegbahn, *J. Electron Spectrosc.*, **1**, 131 (1972/73).
3) R. W. Shaw, Jr. and T. D. Thomas, *Chem. Phys. Lett.*, **14**, 121 (1972).
4) L. J. Aarons, M. Barber, M. F. Guest, I. H. Hillier, and J. H. McCartney, *Mol. Phys.*, **26**, 1247 (1973).
5) T. Ohta, T. Fujikawa, and H. Kuroda, *Chem. Phys. Lett.*, **32**, 369 (1975).
6) L. J. Aarons, M. F. Guest, and I. H. Hillier, *J. Chem. Soc., Faraday, II*, **68**, 1866 (1972).
7) M. F. Guest, I. H. Hillier, V. R. Sanders, and M. H. Wood, *Proc. Roy. Soc., Ser. A*, **333**, 201 (1973).
8) M. H. Wood, *Chem. Phys.*, **5**, 471 (1974).
9) P. S. Bagus, M. Schrenk, D. W. Davis, and D. A. Shirley, *Phys. Rev.*, **A9**, 1090 (1974).
10) T. Åberg, *Phys. Rev.*, **156**, 35 (1967).
11) R. Manne and T. Åberg, *Chem. Phys. Lett.*, **7**, 282 (1970).
12) D. W. Shaw and T. D. Thomas, *ibid.*, **22**, 127 (1973).
13) D. B. Adams and D. T. Clark, *Theor. Chim. Acta* (Berl.), **31**, 171 (1973).
14) D. B. Adams and D. T. Clark, *J. Electron Spectrosc.*, **2**, 201 (1973).
15) The probabilities that the system will make the corresponding transition after the removal of a core electron.
16) Here, assumed a closed shell for the ground state.
17) H. Hartmann, L. Papula, and W. Strehl, *Theor. Chim. Acta*, **17**, 131 (1970); *ibid.*, **19**, 155 (1970).
18) $C^{**}H_4$ represents the state that an electron has been removed from the core orbital (Cls) of the carbon atom of CH_4.
19) The effect of this approximation on the estimation of probability is almost negligible since $\langle \phi_1 / \phi_l \rangle \doteqdot 0 (l=2, 3, \cdots\cdots)$ and $\langle \phi_1 | \phi_1 \rangle$ is nearly equal to 1 from the calculation by use of Slater's rule.
20) Strictly speaking, $P_k = |\langle \sum_{i \rightarrow j} C^k_{i \rightarrow j} \psi_{i \rightarrow j} | \Phi_0 \rangle|^2$

$$= \sum_{(i\to j)} |C^k_{i\to j}|^2 |\langle\psi_{i\to j}|\Phi_0\rangle|^2 + 2\sum_{(i\to j)}\sum_{(l\to m)} C^k_{i\to j}C^k_{l\to m}\langle\psi_{i\to j}|\Phi_0\rangle \times\langle\psi^k_{l\to m}|\Phi_0\rangle$$

where $C^k_{i\to j}$ is the coefficient of the $(i\to j)$ excitation configuration of the k-th excited state.

However, since the second sum of the above equation was negligibly small in most cases, P_k can be expressed as follows,

$$P_k = \sum_{(i\to j)} |C^k_{i\to j}|^2 |\langle\psi_{i\to j}|\Phi_0\rangle|^2$$

On the other hand, P_0 is reasonably assumed to be $|\langle\psi_0|\Phi_0\rangle|^2$.

Thus, we obtain Eq. (8).

21) For example, the ionization potential of the Ols level of H_2O is estimated as follows;

$I_p(\text{Ols};H_2O) = E(H_2F^+) - E(H_2O) + E(O^{*7+}) - E(F^{7+}) - \delta_0$

where $E(H_2O)$ and $E(H_2F^+)$ are the total energies calculated of H_2O and the equivalent-core model (H_2F^+) of the core-hole ion, respectively. $E(O^{*7+})$ and $E(F^{7+})$ were also obtained by calculation. For the correction term δ_0, we assumed the values proposed by Adams and Clark.[12)]

22) D. Neumann and J. W. Moskowitz, *J. Chem. Phys.*, **49**, 2056 (1968).

23) W. E. Palke and W. N. Lipscomb, *J. Amer. Chem. Soc.*, **88**, 2384 (1966).

24) E. Clementi and A. Routh, *Int. J. Quant. Chem.*, **6**, 525 (1972).

25) K. Siegbahn, C. Nordling, G. Johansson, J. Hedman, P. F. Heden, K. Hamrin, U. Gelius, T. Bergmark, L. O. Werme, R. Manne, and Y. Baer, "ESCA applied to Free Molecules," North-Holland, Amsterdam (1969).

26) D. W. Turner, C. Baker, A. D. Baker and C. R. Brundle, "Molecular Photoelectron Spectroscopy," John Wiley & Sons, N.Y. (1970).

27) U. Gelius and K. Siegbahn, *J. Electron Spectrosc.*, **3**, 423 (1973).

28) K. Siegbahn, *ibid.*, **5**, 1 (1974).

The Steric Effects of Alkyl Groups on the N-H Stretching Vibrations and the Rotational Isomerism of Alkylureas

Yoshiyuki MIDO and Tamotsu GOHDA

Department of Chemistry, Faculty of Science, Kobe University, Nada, Kobe 657

(Received April 14, 1975)

The free N-H stretching vibrations of various trialkylureas, R_2UR', in dilute solutions were studied in order to resolve our questions concerning the rotational isomerism of dialkylureas. In the infrared spectrum of R_2UR', where R is isopropyl or cyclohexyl, an additional N-H band appears on the higher-frequency side of the *trans* N-H band. It was also observed that the larger the effective size of the R' group on R_2UR' is, the stronger the intensity of the additional band becomes. It was concluded, in connection with the rotational isomerism of dialkylureas, that the additional band arises from a form in which the N-H group is out of the skeletal plane.

In our previous studies of mono- and dialkylureas,[1-4] it was shown that *N,N'*-dialkylureas (*RUR'*) in solution take the configuration with the *trans-trans* relation between the C=O group and the two N-H groups; this was contrary to the interpretation by Rao *et al.*[5] However, the infrared spectrum of *sym*-di-*t*-butylurea (*s*-D*t*BU) showed a very weak N-H stretching band (3469 cm^{-1}) in addition to the *trans* N-H stretching band (3437 cm^{-1}); this suggested that the coexistence of a certain additional isomer arises as a result of the steric hindrance between the bulky alkyl group and the C=O group.[1] If this isomer, coexisting with the dominant *trans-trans* isomer, is assumed to be in the *trans-cis* configuration, the substitution of another bulky group for either of the two imino hydrogen atoms on *RUR'* having bulky groups will stabilize the *trans* form further for the following reasons.

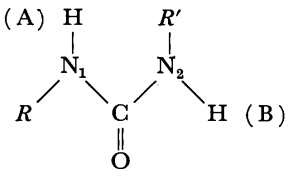

trans-cis

The substitution of the bulky group at the A site may decrease the amount of the *cis* form about the C-N_2 axis by virtue of the steric hindrance between the substituted group and the R' group. On the other hand, the substitution at the B site does not change the *trans* form about the C-N_1 axis. Accordingly, in the spectra of trialkylureas with bulky groups, the band corresponding to the 3469 cm^{-1} band of *s*-D*t*BU is expected to be weak or absent, if the above assumption is correct.

Thus, in the present study, the N-H stretching vibrations of various trialkylureas, $R_2NCONHR'$ (R_2UR'), were investigated in order to examine whether or not the 3469 cm^{-1} band of *s*-D*t*BU arises from the *cis* form and to establish the relationships between the configurations and the N-H stretching frequencies of R_2UR'.

Experimental

Various R_2UR' substances were prepared by adding the corresponding alkylisocyanate to some dialkylamines. These crude samples were purified by repeated recrystallizations from suitable solvents, and the purified samples were identified by elementary analysis. Solvents for spectroscopy were used.

The infrared measurements were made with a Hitachi EPI-2G Infrared Grating Spectrophotometer. Samples were examined as 0.02 M solutions using 5-mm (3 μm region) and 0.5-mm cells (6 μm region). The recording conditions of the spectra were the same as in the previous study.[1]

Results and Discussion

The N-H Stretching Bands. The infrared spectra of R_2UR' in solutions will exhibit only one free N-H stretching band, if rotational isomerism is not taken into account, since R_2UR' substances have only one N-H bond. However, as is shown in Table 1 and Fig. 1, where the observed free N-H stretching bands are summarized, the spectra of ten R_2UR' derivatives (five D*i*PU*R'* and five DcHU*R'*) exhibited two free N-H bands (we will conventionally denote this type of R_2UR' as R_2UR'-II), and the spectra of the other R_2UR' derivatives showed one free N-H band (R_2UR'-I). Also, cHMUR'-type compounds, examined for comparison, exhibited only one N-H band (see the bottom of Table 1). Among the three kinds of solutions studied, the CS_2 solution showed most prominently the two N-H bands of R_2UR'-II.

From the comparisons of the band positions, the lower-frequency band of R_2UR'-II, as well as only one band of R_2UR'-I and cHMUR', is assigned to the N-H stretching vibration arising from the configuration with the *trans* relation between the N-H and C=O groups.

These N-H bands—the band of R_2UR'-I and the lower band of R_2UR'-II—appear at the positions characteristic of the substituent, R', attached to the N-H bond. Such correlations between the N-H stretching frequencies and the type of R' group correspond to the similar correlations obtained previously for the *trans* N-H stretching frequencies of *RUR'*,[1-4] although the N-H frequencies of R_2UR' are higher by ~20 cm^{-1} than those of the *trans* bands of *RUR'*.

On the other hand, the spectra of R_2UR'-II showed another free N-H band observed at the higher-(approximately 20 cm^{-1}) frequency side of the *trans* N-H band. As may be seen from Table 1, the appearance of the two free N-H bands is dependent upon the bulkiness of the R groups on R_2UR' but not on that

TABLE 1. THE N-H STRETCHING FREQUENCIES (cm^{-1}) OF $R_2NCONHR'$

R_2	Solvent	R' M (methyl)	E (ethyl)	*i*P (isopropyl)	cH (cyclohexyl)	*t*B (*t*-butyl)
DM (dimethyl)	$HCCl_3$	3489	3471	3460	3457	3467
	CCl_4	3483	3470	3460	3455	3460
	CS_2	3475	3466	3452	3453	3456
DE (diethyl)	$HCCl_3$		3471	3459	3458	3466
	CCl_4	———	3474	3459	3460	3461
	CS_2		3466	3453	3454	3457
DP (di-*n*-propyl)	$HCCl_3$	3489		3458	3459	3466
	CCl_4	3484	———	3460	3460	3461
	CS_2	3476		3454	3456	3457
D*i*P (di-*i*-propyl)	$HCCl_3$	3505 3491	3493 sh	3483 3464	3481 3462	3482 sh
	CCl_4	3498 3479	3490 sh	3479 3458	3480 3460	3482 3455
	CS_2	3494 3472	3484 3464	3478 3452	3477 3454	3480 3452
DB (di-*n*-butyl)	$HCCl_3$				3458	3466
	CCl_4	———	———	———	3459	3462
	CS_2				3455	3459
D*i*B (di-*i*-butyl)	$HCCl_3$	3489		3459	3466	3468
	CCl_4	3483	———	3460	3462	3462
	CS_2	3476		3459	3458	3461
DcH (di-cyclohexyl)	$HCCl_3$	3505 3489	3490 sh	3481 sh	3479 sh	3485 3463
	CCl_4	3495 3481	3487 sh	3478 3460	3477 sh	3478 3455
	CS_2	3492 3472	3482 3464	3477 3454	3474 3454	3478 3451
cHM (cyclohexyl, methyl,)	$HCCl_3$	3486		3461		3461
	CCl_4	3484	———	3461	———	3462
	CS_2	3474		3452		3457

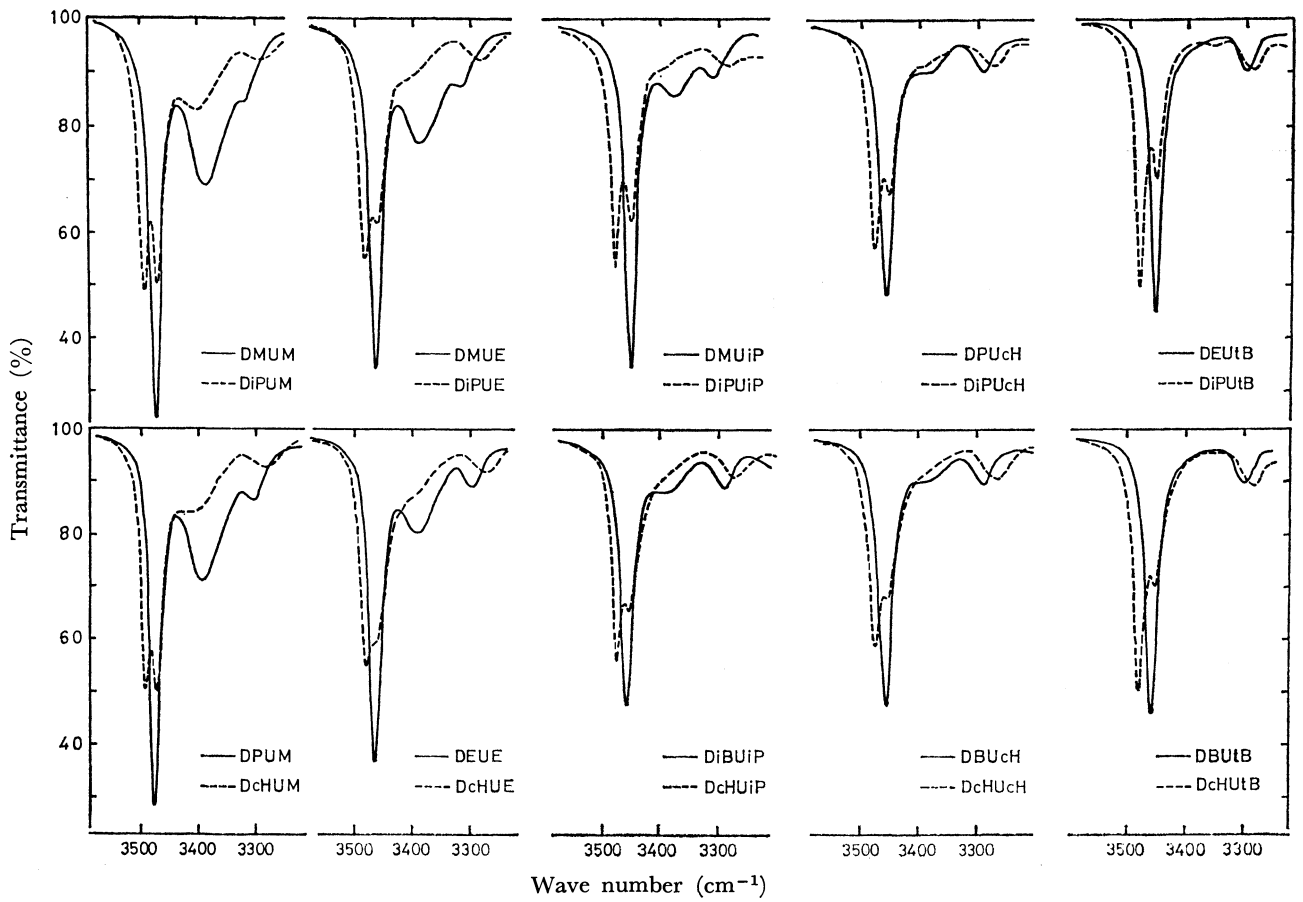

Fig. 1. The free N-H stretching absorption bands of various R_2UR' in CS_2 (0.02 M).

of the R' group. Even cHMUtB, with the C_6H_{11}–$\overset{CH_3}{\overset{|}{N}}$– group of a sterically medium size, exhibited only one N-H band.

Examining the band intensities of R_2UR' in Fig. 1, one can understand easily that the higher N-H band appears at the expense of the intensity of the *trans* N-H band (the lower band). Therefore, the higher band may be concluded to originate from a certain rotational isomer which is mainly caused by the steric hindrance of the R groups and the C=O group, and that this band corresponds to the very weak band at 3469 cm^{-1} of *s*-DtBU in CCl_4.

On the assumption that the 3469 cm^{-1} band of *s*-DtBU arises from the *cis* form in the *trans-cis* configuration, consider the substitution of another bulky group for either of the two imino hydrogen atoms on RUR' with the *trans-cis* configuration.

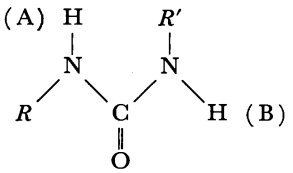

trans-cis

If the hydrogen atom at the A site is substituted for a bulky group, the steric hindrance between the substituent and the R' group may be more serious than that between the C=O and the R' groups in the case of the *trans* form. Accordingly, this substitution will favor the *trans* configuration. On the other hand, another substitution at the B site leaves the *trans* configuration. Thus, if the weak 3469 cm^{-1} band of *s*-DtBU arises from the *cis* form, the corresponding band of trialkylureas with bulky groups may be expected to be weak or absent.

Let us consider *N*-cyclohexyl-*N'*-*t*-butylurea (cHUtB) and *N*-dicyclohexyl-*N'*-*t*-butylurea (DcHUtB) as examples. We have previously reported that the spectrum of cHUtB in $CHCl_3$ shows a weak band at 3471 cm^{-1} corresponding to the 3469 cm^{-1} band of *s*-DtBU.[4] In the spectrum of DcHUtB in Fig. 1, the corresponding band appears strongly at 3478 cm^{-1} and is even stronger than the *trans* N-H band at 3451 cm^{-1}, contrary to the expectation based on the above assumption. These observations clearly indicate that the coexisting rotational isomer of *s*-DtBU in solution is not in the *trans-trans* configuration.

All the spectra of DiPUR' and DcHUR' examined in this study have a band corresponding to the 3478 cm^{-1} band of DcHUtB. As has been mentioned above, this band appears when two R groups on R_2UR' are isopropyl or cyclohexyl groups, either of which is bulkier than the other groups. Unfortunately, no R_2UR' with the bulkiest R group, *t*-butyl, could be examined.

It is quite evident from Fig. 1 that the bulkier the effective size of the R' group on R_2UR'-II is, the stronger the intensity of this band becomes at the expense of that of the *trans* N-H band. This indicates that probably the steric hindrance between the R' and the

Table 2. The C=O (Amide I) stretching frequencies of $R_2NCONHR'$ (0.02 mol/l in CCl_4)

R_2	R' = M	E	*i*P	cH	*t*B
DM	1668	1667	1665	1667	1672
DE	———	1660	1658 1651	1659 1651	1665
DP	1663	———	1659 1652	1659 1652	1665
D*i*P	1659 1640	1659 1651	1658 1652 1638	1658 1652 1645	1659 1654
DB	———	———	———	1658 1651	1663
D*i*B	1663	———	1658 1651	1659 1652	1664
DcH	1658 1652 1649	1658 1652 1644	1658 1651 1645	1658 1651 1640	1658 1653
cHM	1660 1654	———	1659 1654	———	1661

Table 3. The C=O (Amide I) and C-N (Amide II) stretching frequencies of $R_2NCONHR'$ (0.02 mol/l in $CHCl_3$)

R_2	R' = M		E		*i*P			cH			*t*B	
	I[a]	II[a]	I	II	I	II		I	II		I	II
DM	1642	1533	1640	1524	1640	1520		1633	1513		1641	1520
DE	———		1633	1518	1630	1510		1632	1510		1634	1513
DP	1638	1525	———		1630	1510		1630	1509		1633	1514
D*i*P	1623	1516	1624	1513	1620	1510	1502	1621	1512	1505	1623	1511
DB	———		———		———			1628	1508		1633	1513
D*iB*	1639	1525	———		1628	1509		1629	1512		1635	1512
DcH	1622	1515	1620	1514	1619	1510	1505	1620	1512	1505	1642	1625 1512
cHM	1632	1520	———		1625	1510		———			1634	1512

a) I : C=O stretch (Amide I), II : C-N stretch (Amide II).

C=O groups plays an important role in determining the amount of the coexisting rotational isomer.

As for the associated N–H band of all the R_2UR' substances on the lower-frequency side of the *trans* N–H band, it may be seen that the bulkier the effective size of substituents is, the weaker the intensity of this band becomes.

From the above discussion, it may be concluded that the serious steric hindrance prevents the two R groups from leaving the skeletal plane, and that, at the same time, this effect makes the N–H bond out-of-plane, but cannot convert the N–H bond into the *cis* position. That is, the 3469 cm^{-1} band of *s*-D*t*BU arises from a form in which the N–H group is out-of-plane owing to the steric hindrance (we will call this form the *out* form hereinafter), and the rotational isomers with the *trans-trans* (dominant) and probably *out-out* configurations may coexist in solutions of *s*-D*t*BU.

In the case of R_2UR'-II, it may be seen that the amount of the coexisting *out* configuration increases with the bulkiness of the effective size of the R' group; R_2UM-II=50%, R_2UE-II=55%, R_2U*i*P-II≈R_2UcH-II=60%, and R_2U*t*B-II=65%.

The C=O and C–N Stretching Band. The C=O stretching frequencies of R_2UR' in CCl_4 and $CHCl_3$ are shown in Tables 2 and 3 respectively. The frequencies of R_2UR' in CCl_4 are higher by 24—38 cm^{-1} than those in $CHCl_3$; this indicates that the hydrogen bonding between the proton of $CHCl_3$ and the C=O group is formed in the $CHCl_3$ solution.

The C=O stretching frequencies of R_2UR' in the same solvent are similar, though those of DMUR' are somewhat higher in either solvent. However, it should be noted that the main C=O stretching band of R_2UR'-II appears at a frequency lower than that of R_2UR'-I by ~10 cm^{-1} and has a few prominences, as is shown in Fig. 2.

The C–N stretching bands of some R_2UR'-II substances in $CHCl_3$ appear at a frequency lower than those of R_2UR'-I, and others have an additional band (Table 3).

This work was supported by a grant from the Ministry of Education.

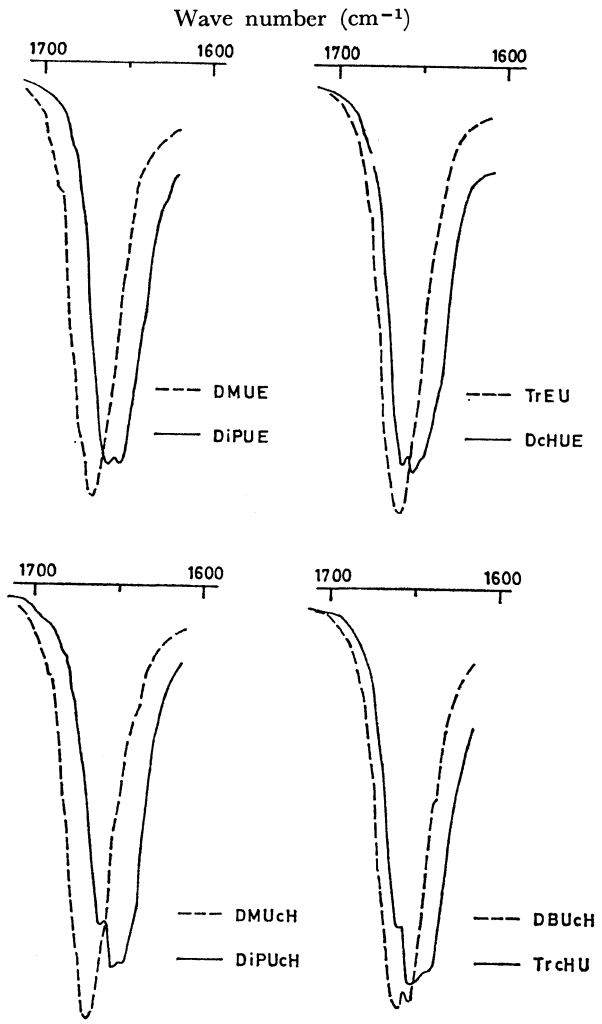

Fig. 2. The C=O stretching absorption bands of some R_2UR' in CCl_4 (0.02 M).

References

1) Y. Mido, *Spectrochim. Acta*, **29A**, 1 (1973).
2) Y. Mido, *ibid.*, **29A**, 431 (1973).
3) Y. Mido, This Bulletin, **47**, 1833 (1974).
4) Y. Mido, *Spectrochim. Acta*, to be published.
5) C. N. R. Rao, G. C. Chaturvedi, and R. K. Gosavi, *J. Mol. Spectrosc.*, **28**, 526 (1968).

Ion Association of Some 2 : 2 Electrolytes in Water at 25 °C. I. Studies of Magnesium, Calcium, Manganese, and Tris(1,10-phenanthroline)-ruthenium(II) Sulfate Solutions with a Vapor-Pressure Osmometer*

Haruhiko YOKOYAMA** and Hideo YAMATERA

Department of Chemistry, Faculty of Science, Nagoya University, Chikusa-ku, Nagoya, 464

(Received April 18, 1975)

The osmotic coefficients of aqueous solutions of magnesium, calcium, manganese, and tris(1,10-phenanthroline)ruthenium(II) sulfates were measured at 25 °C by means of a vapor-pressure osmometer. Then the ion-association constants of these electrolytes were obtained as a function of the closest distance of approach of ions from the measured osmotic coefficients as well as from the available conductivity and cryoscopy data. The *best* values of the closest distance of approach and the ion-association constant (given in Table 6) were estimated with the help of theories of ion association. The formation of triple-ions and quadrupoles and the hydration of ions are also discussed in connection with the ion-association constant.

In a previous paper,[1] we re-examined the Debye-Hückel theory[2] of strong electrolyte solutions and especially discussed ion association from the theoretical point of view. It was shown that the observed deviations from the Debye-Hückel theory could be explained without referring to ion association, but at the same time it was reported that the concept of ion association is a practical and useful convention to complement the Debye-Hückel theory. This convention can be justified at least for symmetrical strong electrolytes, irrespective of whether or not ion-pairs are actual well-defined entities.

The existing data of ion-association constants are not sufficient for comparison with our theoretical expression of ion-association constants.[1] Except in a few cases,[3-7] the literature gives only one set of values of the ion-association constant (K) and the closest distance of approach of ions (a). However, the K value to be obtained from the analysis of experimental results must be influenced by the choice of the value of a.[3-7] The theoretical expression of the ion-association constant also shows a dependence of K on a, but in a different way. Thus, it is of interest to obtain ion-association constants as a function of a and to discuss what are the *best* values of the ion-association constant and the closest distance of approach. As will be described below, we measured the osmotic coefficients of aqueous solutions of some 2 : 2 electrolytes by means of a vapor-pressure osmometer. Assuming ideal Debye-Hückel behavior of the free ions, the ion-association constants were obtained with several values of a from analyses with and without taking triple-ion formation, quadrupole formation, and ion hydration into account. Ion-association constants were also obtained as functions of a by the recalculation of the available cryoscopy and conductivity data.[3,6,8-13] These results will be shown and discussed in connection with the theories of ion association.[1,14,15]

Experimental

The osmotic coefficients of the electrolyte solutions were measured by vapor-pressure osmometry (vpo). This method has been described by many authors.[16] Thus, a brief explanation of the apparatus and the procedure will suffice.

A Hitachi Perkin-Elmer 115 molecular-weight apparatus was used in the experiment. It has a cell surrounded by double thermostats. The cell is equipped with two thermistors covered with glass, on which liquids are dropped. The thermistors are connected with a bridge circuit, which is balanced when both thermistor tops are covered with a solvent in equilibrium with its vapor. When the solvent on one of the thermistors is replaced by a solution, the solvent vapor condenses into the solution and liberates the heat of condensation. The temperature of the solution increases until an equilibrium is reached. The change in temperature is detected by the thermistor and shown as a change in the electrical resistance, ΔR. The value of ΔR is dependent on the concentration (molality), m, and the molal osmotic coefficient, ϕ, of the solute, and can be fitted to a power series of the form:

$$\Delta R = s_1(\nu m\phi) + s_2(\nu m\phi)^2 + s_3(\nu m\phi)^3 + s_4(\nu m\phi)^4 \quad (1)$$

where ν is the number of moles of ions formed from one mole of the electrolyte (for nonelectrolyte, $\nu=1$) and where s_1, s_2, s_3, and s_4 are the coefficients to be determined experimentally. We used glucose as the standard material and measured the values of ΔR on its aqueous solutions with concentrations from 0.005 to 0.18 mol kg^{-1}. Assuming $\phi=1$ for glucose in water at 25.0 °C, we obtained $s_1=4925$, $s_2=-998.7$, $s_3=13050$, and $s_4=-47920$ by the method of least-squares. The observed values of ΔR for various solutions were put into Eq. (1), and the osmotic coefficients (ϕ) were evaluated. We measured the osmotic coefficients (ϕ) of sodium chloride and obtained the approximate expression:

$$1-\phi = 0.2963m^{1/2} + 0.1036m - 1.306m^{3/2}$$

The values of ϕ predicted by this equation at several concentrations up to 0.1 mol kg^{-1} agreed with the values from e.m.f. measurements[17] within the range of experimental error. This shows that the assumption of $\phi=1$ for glucose solutions is adequate.

Materials. A reagent-grade glucose (anhydride) was used as the standard material after having been dried at about 80 °C and then kept over silica gel. A reagent-grade sodium chloride was recrystallized by concentrating its aqueous solution, and was then dried at about 600 °C. A

* Presented in part at the 24th Annual Meeting of the Chemical Society of Japan, Osaka, April, 1971; published in part in *Chem. Lett.*, **1973**, 337.

** Present address: Department of Chemistry, Yokohama City University, 4646 Mutsuura-cho, Kanazawa-ku, Yokohama, 236.

TABLE 1. OSMOTIC COEFFICIENTS ϕ OF SOME 2 : 2 ELECTROLYTES MEASURED WITH A VAPOR-PRESSURE OSMOMETER AT 25.0 °C

$MgSO_4$		$CaSO_4$		$MnSO_4$		$[Ru(phen)_3]SO_4$	
m (mol kg^{-1})	ϕ	m (mol kg^{-1})	ϕ	m (mol kg^{-1})	ϕ	m (mol kg^{-1})	ϕ
0.005036	0.800±0.008	0.002990	0.816±0.012	0.008371	0.744±0.005	0.008542	0.829±0.005
0.01485	0.722±0.004	0.004438	0.809±0.009	0.01662	0.695±0.003	0.01675	0.806±0.003
0.02021	0.700±0.003	0.005943	0.773±0.007	0.02549	0.664±0.003	0.02498	0.775±0.003
0.02473	0.686±0.003	0.007465	0.763±0.006	0.03346	0.646±0.003	0.03300	0.760±0.002
0.03050	0.672±0.002	0.008923	0.745±0.005	0.04187	0.632±0.002	0.04079	0.744±0.002
0.03464	0.664±0.002	0.01044	0.736±0.004	0.05108	0.619±0.002	0.05040	0.727±0.002
0.03948	0.655±0.002	0.01187	0.721±0.004	0.05858	0.609±0.002	0.05868	0.716±0.002
0.04455	0.648±0.002	0.01334	0.729±0.004	0.06786	0.599±0.002	0.06763	0.705±0.002
0.04961	0.638±0.002	0.01491	0.709±0.004	0.07549	0.594±0.002	0.07635	0.699±0.002
0.05984	0.629±0.002			0.08432	0.584±0.002	0.08536	0.687±0.002
0.07903	0.610±0.002			0.1006	0.569±0.002		
0.09945	0.596±0.002			0.1264	0.557±0.002		
0.1490	0.573±0.002						

reagent-grade magnesium sulfate was recrystallized as the hydrate, $MgSO_4 \cdot 7H_2O$, from its aqueous solution below 48 °C and then air-dried at room temperature. Its composition was confirmed by gravimetric analyses of magnesium as magnesium pyrophosphate and of sulfate as barium sulfate. The calcium sulfate used was dihydrate of reagent grade. The number of water of crystallization was confirmed by the dehydration at about 700 °C and by the titration of the calcium ion with ethylenediaminetetraacetic acid. A stock solution of manganese sulfate was prepared by the use of a recrystallized reagent-grade hydrate. Its concentration was determined by gravimetric analysis of sulfate. Tris(1,10-phenanthroline)ruthenium(II) sulfate hydrate, $[Ru(phen)_3]SO_4 \cdot 7H_2O$, was prepared in a manner similar to that described by Dwyer.[18] The complex was synthesized by adding sodium hypophosphite as a reducing agent to a solution containing ruthenium chloride and 1,10-phenanthroline; the iodide was obtained by precipitation from the solution. Sulfate of this complex was prepared by the double decomposition of the iodide and silver sulfate, and was purified by repeated precipitations with acetone from alcoholic solutions and by a final recrystallization from an aqueous solution. It was dried over silica gel for a few days until it reached a constant weight. The number of the water of crystallization was determined to be seven—directly by the Karl-Fischer method and by the spectrophotometric analysis of HDO in a D_2O solution of the salt,[19] and indirectly by the gravimetric analysis of sulfate.

Results and Discussion

The ΔR values were measured for some 2 : 2 electrolytes in aqueous solutions at 25.0±0.03 °C. The osmotic coefficients (ϕ) were calculated from ΔR with Eq. (1) and are shown in Table 1.*** The measured ϕ values are plotted against the molal concentration of the solute, m, in Fig. 1 for $MgSO_4$ and in Fig. 2 for $CaSO_4$, together with the results from cryosocopic measurements.[3,6] These figures also give the ϕ *vs.* m curves predicted by the Debye-Hückel theory[2] with a few values assumed for the closest distance of approach of ions, a. None of the theoretical curves fits the experimental results. For any reasonable value of a, the experimental ϕ values are lower than the values predicted by the Debye-Hückel theory. A decrease in ϕ is usually considered to result from ion association.[3-6] According to this usual convention, we shall assume an ion-association equilibrium and shall estimate the ion-association constants on the basis of an analysis of the experimental ϕ values.

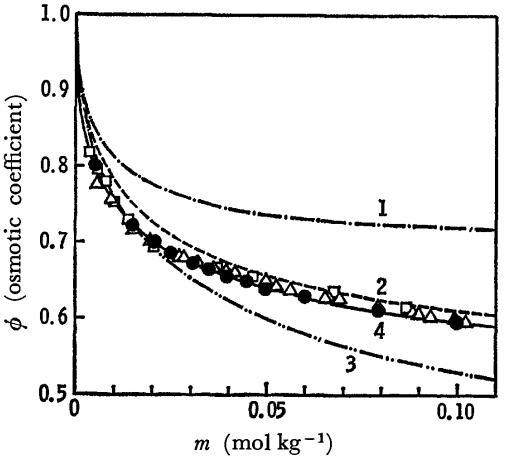

Fig. 1. Osmotic coefficients of $MgSO_4$ solutions. ●, present work at 25.0°C (vpo). △, Brown and Prue[3] at 0 °C (cryoscopy). □, Isono[6] at 0 °C (cryoscopy). Curves 1 (—·—), 2 (----), and 3 (—··—) are theoretical curves due to the Debye-Hückel theory with a=6.0, 4.0, and 3.0 Å, respectively. Curve 4 (——) is calculated with the K and K_t values in Table 2 (25.0 °C); each set of the K and K_t values gives the essentially same curve.

The ion-association equilibrium for a symmetrical electrolyte is expressed by:

$$\begin{array}{lccc} & M + A & \rightleftharpoons & MA \\ \text{concentration} & m(1-\alpha) \quad m(1-\alpha) & & m\alpha \end{array} \qquad (2)$$

*** The values of ϕ obtained for $MgSO_4$ and $MnSO_4$ around 0.1 mol kg^{-1} are, respectively, 1.6% and 3.0% smaller than those obtained by Robinson and Jones,[20] who made isopiestic vapor-pressure measurements.

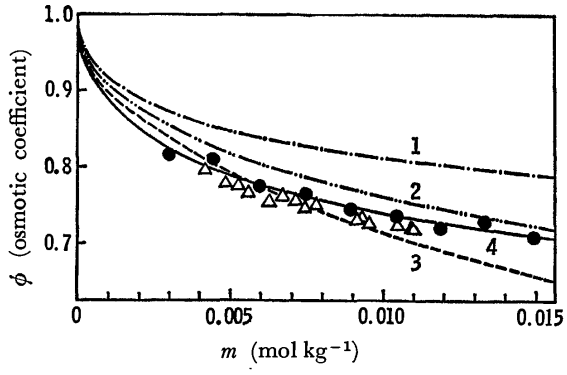

Fig. 2. Osmotic coefficients of $CaSO_4$ solutions.
●, present work at 25.0 °C (vpo). △, Brown and Prue[3] at 0 °C (cryoscopy). Curves 1 (—·—), 2 (—··—), and 3 (----) are theoretical curves due to the Debye-Hückel theory with a=6.0, 3.0, and 1.0 Å, respectively. Curve 4 (——) is calculated with the K and K_t values in Table 2 (25.0 °C); each set of the K and K_t values gives the essentially same curve.

where m denotes the molality of the electrolyte and where α is the degree of association defined by:

$$\alpha = \frac{[MA]}{m}$$

The brackets indicate the concentration of a given species. The ions, M and A, having the z_1e and z_2e charges respectively ($z_1=-z_2=z>0$), are usually considered as *free* ions in the sense that the Debye-Hückel theory can be applied to them. On the other hand, the ion-pair, MA, is presumed to behave like a non-electrolyte in dilute solutions. Therefore, the ϕ of an electrolyte solution is related to α as follows:

$$\phi = (1-\alpha)\phi_{DH} + \frac{\alpha}{2} \tag{3}$$

or

$$\alpha = \frac{\phi_{DH}-\phi}{\phi_{DH}-0.5}$$

where ϕ_{DH} is the molal osmotic coefficient expected by the Debye-Hückel theory and is given by:

$$\phi_{DH} = 1 - \frac{z^2\kappa s}{6}\sigma(\kappa a) \tag{4}$$

with the definition of the function $\sigma(x)$:

$$\sigma(x) = \frac{3}{x^3}\left[(1+x) - 2\ln(1+x) - \frac{1}{1+x}\right]$$

In Eq. (4), a is the closest distance of approach of ions, and s is a parameter equal to $e^2/\varepsilon kT$, whose value is 7.157 Å† in water at 25.0 °C with the dielectric constant (ε) of 78.30$_3$. The parameter κ is the so-called "reciprocal thickness of the ionic atomsphere" and is defined by:

$$\kappa^2 = \frac{8\pi N}{1000}z^2 s m(1-\alpha) \tag{5}$$

where N is the Avogadro number and where $m(1-\alpha)$ represents the concentration of the free ion on the molality scale. The molality can be used in place of the molar concentration, since the difference between the two values is less than the experimental error in dilute solutions up to about 0.1 mol kg^{-1}.

The values of α, κ, and ϕ_{DH} were calculated by successive approximations in the following way. The value of κ was calculated by using Eq. (5), with α=0 provisionally. The value of ϕ_{DH} was evaluated with Eq. (4), and then the value of α, with Eq. (3). This value of α was in turn put into Eq. (5) in order to recalculate the value of κ. With this κ value, the values of ϕ_{DH} and α were recalculated in the same way as before. After several cycles of the successive approximation, the parameter values were fixed. The final value of α was used for the calculation of the ion-association constant, K, with the expression:

$$K = \frac{\alpha}{(1-\alpha)^2 m\gamma_M\gamma_A}$$

where γ_M and γ_A are the activity coefficients of the free ions, M and A respectively, and are given by:

$$\ln\gamma_M = \ln\gamma_A = -\frac{z^2\kappa s}{2(1+\kappa a)} \tag{6}$$

The activity coefficient of the MA ion-pair was regarded as unity.

The ion-association constants of some 2 : 2 electrolytes were calculated with several a values assumed. The results for $MgSO_4$, $CaSO_4$, $MnSO_4$, and $[Ru(phen)_3]SO_4$ are shown in Figs. 3 to 6 respectively. Apparent linear relationships were observed between log K and m up to about 0.05 mol kg^{-1}; extrapolation to m=0 gave different log K values, depending on the a values.

In each figure for $MgSO_4$, $CaSO_4$, and $MnSO_4$, there seems to be a specific a value at which the log K value is apparently independent of the concentration, *i.e.*, a=4.2 Å for $MgSO_4$, about 4 Å for $CaSO_4$, and 3.8 Å for $MnSO_4$. However, such a situation may be incidental, since the log K values for $MgSO_4$ and $MnSO_4$ are no longer constant at concentrations higher than 0.06 mol kg^{-1}. The concentration de-

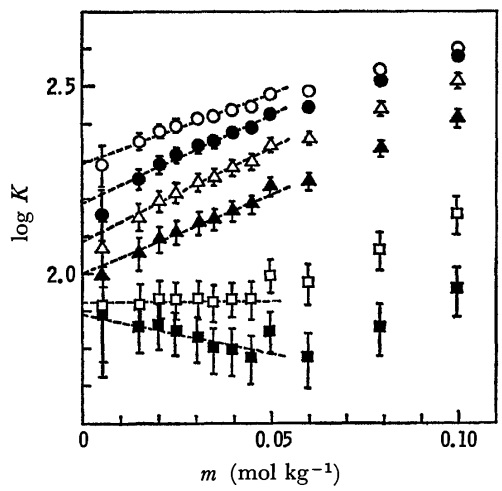

Fig. 3. log K values of $MgSO_4$. The assumed a values are 14.3 Å (○), 8.0 Å (●), 6.0 Å (△), 5.0 Å (▲), 4.2 Å (□), and 4.0 Å (■).

† 1 Å=10^{-10} m

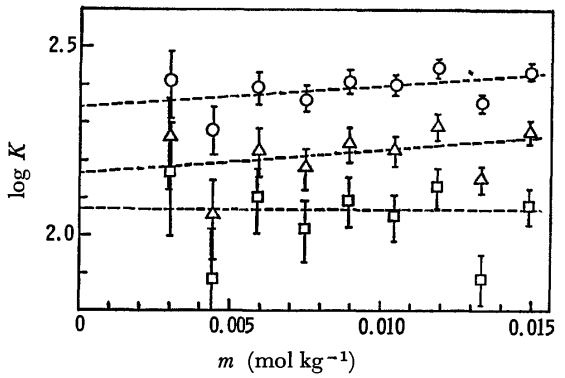

Fig. 4. log K values of $CaSO_4$. The assumed a values are 14.3 Å (○), 6.0 Å (△), and 4.0 Å (□).

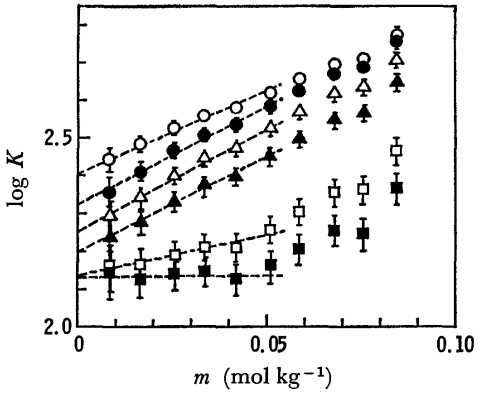

Fig. 5. log K values of $MnSO_4$. The assumed a values are 14.3 Å (○), 8.0 Å (●), 6.0 Å (△), 5.0 Å (▲), 4.0 Å (□), and 3.8 Å (■).

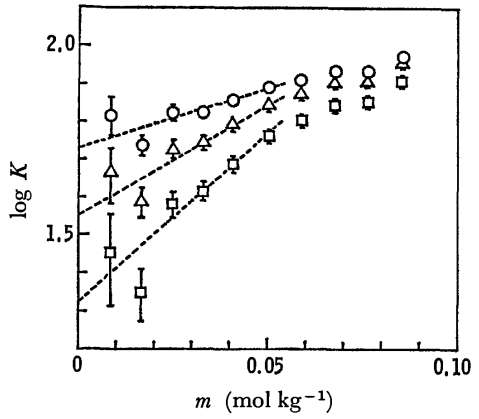

Fig. 6. log K values of $[Ru(phen)_3]SO_4$. The assumed a values are 14.3 Å (○), 11.0 Å (△), and 9.0 Å (□).

pendence of the ion-association constant may be attributed to the effects of other ion-ion interactions and ion hydration disregarded in the analysis. Below, we shall take the triple-ion formation into consideration in order to obtain better ion-association constants.

Triple-Ion Formation. When an ion approaches an ion-pair, the electrostatic interaction between the charge and the dipole will cause the formation of a so-called "triple-ion." There are two possible equilibria for the formation of a triple-ion:

$$MA + M \rightleftharpoons M_2A$$

$$MA + A \rightleftharpoons MA_2$$

Assuming an equal formation constant for the M_2A and MA_2 triple-ions, one can express the concentration of each species as follows:

$$[M] = [A] = m[1-\alpha(1+3\beta)]$$

$$[MA] = m\alpha$$

$$[M_2A] = [MA_2] = m\alpha\beta$$

where β is the parameter defined by:

$$\beta = \frac{[M_2A]}{[MA]} = \frac{[MA_2]}{[MA]}$$

Thus, the formation constant for the triple-ions, K_t, is expressed by:

$$K_t = \frac{[M_2A]\gamma_{M_2A}}{[MA][M]\gamma_M} = \frac{[MA_2]\gamma_{MA_2}}{[MA][A]\gamma_A} = \frac{\beta}{[1-\alpha(1+3\beta)]m} \quad (7)$$

where γ_{M_2A} and γ_{MA_2} are the activity coefficients of M_2A and MA_2 and are assumed to be equal to γ_M and γ_A respectively.

With the above assumptions, the osmotic coefficient of the electrolyte can be expressed by:

$$\phi = [1-\alpha(1+2\beta)]\phi_{DH} + \frac{\alpha}{2} \quad (8)$$

where

$$\phi_{DH} = 1 - \frac{z^2\kappa s}{6}\sigma(\kappa a) \quad (9)$$

Eq. (9) is apparently the same as Eq. (4), but here the parameter κ is given by:

$$\kappa^2 = \frac{8\pi N}{1000}z^2 s m[1-\alpha(1+2\beta)] \quad (10)$$

Assuming the value of K_t for a given a value and using Eqs. (7) to (10), the values of α, β, κ and ϕ_{DH} were calculated by successive approximations. With the α and β values thus obtained, the ion-association constant, K, was calculated according to the expression:

$$K = \frac{\alpha}{[1-\alpha(1+3\beta)]^2 m\gamma_M\gamma_A}$$

The value of K was thus obtained at each concentration, and then the K values were averaged. The osmotic coefficient was calculated for each concentration with the averaged value of K and used for the calculation of the standard deviation, σ_ϕ, defined by:

$$\sigma_\phi = \sqrt{\frac{\sum_{i=1}^{n}(\phi_{calcd,i}-\phi_{obsd,i})^2}{n-2}}$$

where n is the total number of points of the run and where ϕ_{obsd} and ϕ_{calcd} are the observed and calculated osmotic coefficients respectively. The σ_ϕ value was obtained as a function of K_t for a given a value. The K_t value giving the minimum value of σ_ϕ was regarded as the *best* value of K_t.

The K value was calculated at each concentration with the K_t value obtained above and was plotted against m. Fig. 7 shows the results for magnesium sulfate, assuming a few a values. For each value of a, the log K value shows a very good constancy up to about 0.1 mol kg^{-1}. In the same figure, the corresponding previous plots are reproduced from Fig. 3

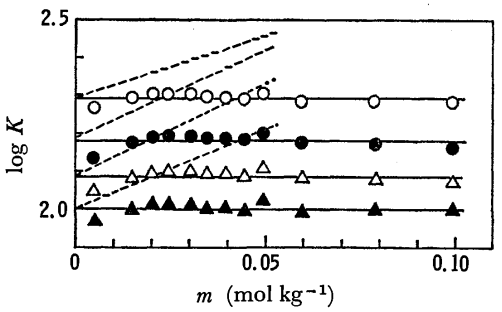

Fig. 7 Constant log K values of $MgSO_4$ obtained with the assumption of appropriate K_t values. (See the columm h=0 of Table 2.) a=14.3 Å (○), 8.0 Å (●), 6.0 Å (△), and 5.0 Å (▲).

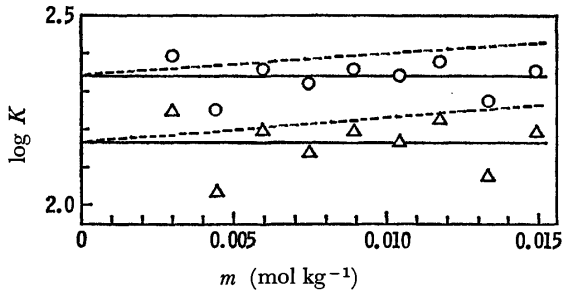

Fig. 8. Constant log K values of $CaSO_4$ with the assumption of appropriate K_t values. (See the column h=0 of Table 2.) a=14.3 Å (○) and 6.0 Å (△).

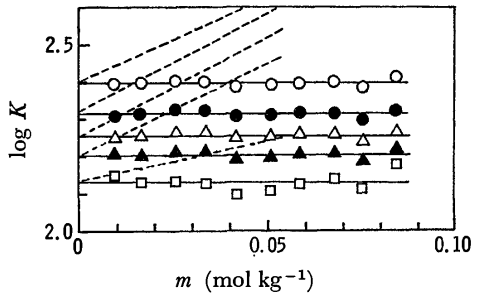

Fig. 9. Constant log K values of $MnSO_4$ with the assumption of appropriate K_t values. (See the columm h=0 of Table 2.) a=14.3 Å (○), 8.0 Å (●), 6.0 Å (△), 5.0 Å (▲), and 4.0 Å (□).

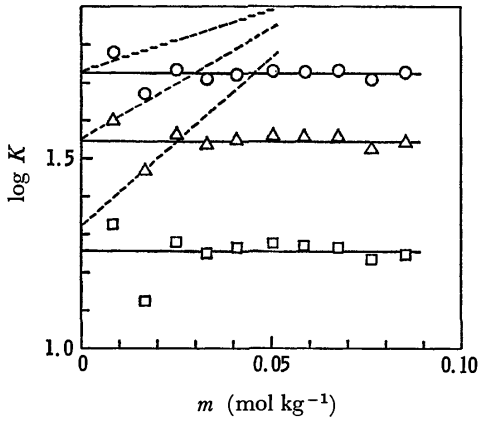

Fig. 10. Constant log K values of $[Ru(phen)_3]SO_4$ with the assumption of appropriate K_t values. (See the columm h=0 of Table 2.) a=14.3 Å (○), 11.0 Å (△), and 9.0 Å (□).

in broken lines. The constant value of log K obtained here for each of the given a values is in fairly good agreement with the value obtained by extrapolation to m=0 in the previous plot. This shows that a good enough estimation of the ion-association constant K can be made without taking the triple-ion formation into account. The same discussion also applies to Figs. 8 to 10 for the other electrolytes.

Hydration. The ion hydration causes a decrease in the concentration of the water as solvent. This decrease is equal to hm, where h represents the hydration parameter given by:

$$h = \frac{h_M[M]+h_A[A]+h_{MA}[MA]+h_{M_2A}[M_2A]+h_{MA_2}[MA_2]}{m}$$

$$= (h_M+h_A)[1-\alpha(1+3\beta)]+h_{MA}\alpha+(h_{M_2A}+h_{MA_2})\alpha\beta \quad (11)$$

where h_M, h_A, h_{MA}, h_{M_2A}, and h_{MA_2} are the hydration numbers of the M, A, MA, M_2A, and MA_2 species respectively. If the ion hydration is allowed for, the molality of the solute, m', can be expressed by:

$$m' = \frac{55.51}{55.51-hm}m = \frac{m}{1-0.0180hm}$$

and the expression for the osmotic coefficient ϕ becomes:

$$\phi = \frac{1}{1-0.0180hm}\left\{[1-\alpha(1+3\beta)]\phi_{DH}+\frac{\alpha}{2}\right\}$$

where ϕ_{DH} is given by Eq. (9). The ion-association constant, K, and the triple-ion formation constant, K_t, are expressed by:

$$K = \frac{\alpha}{[1-\alpha(1+3\beta)]^2 m'\gamma_M\gamma_A}$$

and

$$K_t = \frac{\beta}{[1-\alpha(1+3\beta)]m'}$$

If the value of the parameter h is given, the K and K_t values can be calculated by the procedure described before. Since it is difficult to estimate the hydration numbers, h_{MA}, h_{M_2A}, and h_{MA_2}, involved in the parameter h [Eq. (11)], for convenience we shall consider two extreme cases in order to learn how far the ion hydration affects the estimation of the K and K_t values.

Case (A): The hydration numbers of the ion-pair and the triple-ions are simply equal to the sums of the hydration numbers of the constituent ions.

$$h_{MA} = h_M + h_A = h_0$$
$$h_{M_2A} = 2h_M + h_A \quad (12)$$
$$h_{MA_2} = h_M + 2h_A$$

where the parameter h_0 can be determined by the measurement of the hydration number in very dilute solutions. By using Eq. (12), the parameter h in Eq. (11) is expressed by:

$$h = h_0$$

Case (B): The hydration number of the ion-pair is equal to zero and the sum of the hydration numbers of the M_2A and MA_2 triple-ions is equal to h_M+h_A:

$$h_{MA} = 0$$
$$h_{M_2A} + h_{MA_2} = h_M + h_A = h_0$$

Thus, the expression for h becomes:

$$h = h_0[1-\alpha(1+2\beta)]$$

Tentatively taking $h_0=15$,†† the ion-association constants were calculated for the two cases, (A) and (B). The case of $MgSO_4$ with $a=6.0$ Å will be taken as an example. The K_t values giving the minimum values of σ_ϕ are 3.1 and 2.7 mol^{-1} kg for (A) and (B) respectively. These K_t values are slightly greater than the value, 2.2 mol^{-1} kg, which was obtained by disregarding the ion hydration. However, the K values remained unchanged at 121 ± 5 mol^{-1} kg. The log K value for $MgSO_4$ with $a=6.0$ Å is plotted against m in Fig. 11, where the overlapping solid marks of different kinds show the unchanged K values. The log K values obtained by disregarding the triple-ion formation ($K_t=0$) are also plotted in Fig. 11. In each case, an apparent linear relationship is observed between log K and m up to about 0.05 mol kg^{-1}. The slopes are different from one another, indicating different K_t values. However, extrapolations of the lines to $m=0$ give the same intercept, showing the same log K value.

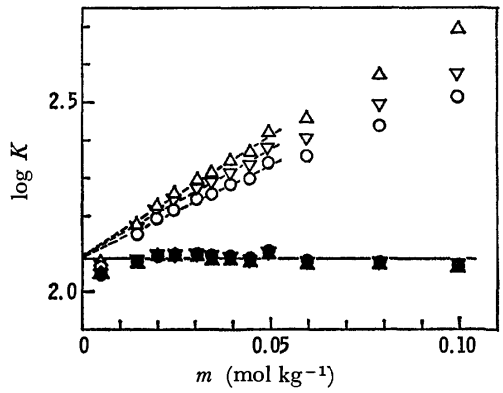

Fig. 11. log K values for $MgSO_4$ with $a=6$ Å allowing for hydration of ions.
○ and ●: $h=0$, reproduced from Figs. 3 and 7, respectively. △ and ▲: $h_0=15$, case (A). ▽ and ▼: $h_0=15$, case (B). $K_t=0$ (○, △, ▽), 2.2 (●), 3.1 (▲), and 2.7 (▼) mol^{-1} kg were assumed.

The consideration of the triple-ion formation and the ion hydration resulted in no appreciable change in the ion-association constant K from that obtained by the extrapolation of the log K *vs.* m plots in Figs. 3 to 6, where the triple-ion formation and the ion hydration were ignored. When the triple-ion formation and the ion hydration were allowed for, the value of K was practically constant up to about 0.1 mol kg^{-1}. On the other hand, the value of K_t was slightly dependent on the estimation of the hydration numbers of the ions. Table 2 gives the K values for a variety of a values, together with the K_t values. Each set of the values of a, K, and K_t can reproduce the observed osmotic coefficients within the range of experimental error. This is shown in Figs. 1 and 2. In each of the figures, the best-fitting curves for different a values coalesce into a curve (the solid line).

Fuoss and Kraus[22] have proposed a theory of the triple-ion formation. Their theory predicts K_t values of 2.6 mol^{-1} kg at $a=8.2$ Å and 3.3 mol^{-1} kg at $a=5.7$ Å for 2 : 2 electrolytes in aqueous solutions at 25 °C. These are close to the values obtained in the present work (Table 2).

Gardner and Glueckauf[5] have obtained K and K_t values for some 2 : 2 electrolytes by a reanalysis of the cryoscopic data given by Brown an Prue.[3] The manner of the analysis of the data was different from that described in the present paper. We also reanalyzed the same and other cryoscopic data[3,6] for $MgSO_4$ and $CaSO_4$ in the manner followed in the analysis of the vpo data. The results are shown in Table 3. For $a=9.25$ Å, Gardner and Glueckauf obtained $K_t=2.6$ mol^{-1} kg and $K=158$ mol^{-1} kg for $MgSO_4$ and $K_t=2.7$ mol^{-1} kg and $K=234$ mol^{-1} kg for $CaSO_4$. Their result for $CaSO_4$ is appreciably different from that given in Table 3, whereas for $MgSO_4$ the results are close to each other and also to the result of our vpo experiment (25 °C).

TABLE 2. K AND K_t VALUES OF SOME 2 : 2 ELECTROLYTES DETERMINED BY THE VAPOR-PRESSURE OSMOMETRIC MEASUREMENTS AT 25.0 °C

a (Å)	$MgSO_4$				$CaSO_4$				$MnSO_4$				$[Ru(phen)_3]SO_4$			
	K (mol^{-1} kg)	K_t (mol^{-1} kg)			K (mol^{-1} kg)	K_t (mol^{-1} kg)			K (mol^{-1} kg)	K_t (mol^{-1} kg)			K (mol^{-1} kg)	K_t (mol^{-1} kg)		
		$h=0$	$h_0=15$ (B)[a]	$h_0=15$ (A)[a]		$h=0$	$h_0=15$ (B)	$h_0=15$ (A)		$h=0$	$h_0=15$ (B)	$h_0=15$ (A)		$h=0$	$h_0=15$ (B)	$h_0=15$ (A)
4.0	72±8	0	0.7	0.9	118±27	0	0	0	136±8	0.7	1.2	1.5				
5.0	100±3	1.5	2.1	2.4	135±25	1.4	1.8	2.1	159±5	1.9	2.3	2.7				
6.0	121±5	2.2	2.7	3.1	147±24	2.8	3.3	3.5	178±4	2.5	3.0	3.5				
7.0	137±6	2.5	3.0	3.5	159±24	3.6	4.0	4.3	192±4	2.9	3.4	4.0				
8.0	150±7	2.6	3.1	3.7	169±24	4.0	4.4	4.7	204±5	3.1	3.6	4.3	7±2	20	20	21
10.0	169±7	2.7	3.1	3.9	188±24	4.2	4.6	5.0	222±5	3.4	3.8	4.6	28±3	5.1	5.9	6.5
12.0	183±6	2.6	3.1	3.9	204±24	4.1	4.4	4.8	235±6	3.4	3.9	4.8	42±3	3.2	3.7	4.3
14.3[b]	194±6	2.5	2.9	3.8	219±24	3.6	3.9	4.3	246±8	3.4	3.8	4.8	53±4	2.2	2.6	3.1

a) See the text (p. 2712). b) The critical distance of ion association at 25 °C in Bjerrum's theory.[14]

†† The literature gives various values of the hydration number of the electrolyte.[21] The average value of h_0 for $MgSO_4$ is probably about 15.

Table 3. K and K_t values determined by the reanalysis of the cryoscopic data up to 0.1 mol kg^{-1} at 0 °C

a (Å)	$MgSO_4$ (Brown and Prue[3]) K (mol^{-1} kg)	K_t (mol^{-1} kg) $h=0$	$h_0=15$ (B)[a]	$h_0=15$ (A)[a]	$MgSO_4$ (Isono[6]) K (mol^{-1} kg)	K_t (mol^{-1} kg) $h=0$	$h_0=15$ (B)	$h_0=15$ (A)	$CaSO_4$ (Brown and Prue[3]) K (mol^{-1} kg)	K_t (mol^{-1} kg) $h=0$	$h_0=15$ (B)	$h_0=15$ (A)
4.0	87±15	0	0.6	0.8	81±20	0	0.2	0.5	159±15	2.1	2.5	2.8
5.0	114±10	1.1	1.6	1.9	101±18	1.0	1.5	1.8	171±15	3.7	4.3	4.4
6.0	134±8	1.6	2.0	2.4	117±18	1.7	2.1	2.5	181±14	4.9	5.3	5.6
7.0	149±8	1.8	2.2	2.7	130±18	2.0	2.4	2.8	191±14	5.5	5.9	6.2
8.0	161±8	1.9	2.3	2.9	141±19	2.1	2.5	3.0	200±14	6.0	6.4	6.7
10.0	179±9	1.9	2.3	3.0	160±19	2.1	2.5	3.1	217±14	6.2	6.6	7.0
12.0	192±10	1.9	2.2	3.0	174±19	2.0	2.3	3.0	231±14	6.1	6.5	6.9
13.9[b]	201±11	1.8	2.1	3.0	184±19	1.8	2.2	2.8	243±14	5.9	6.2	6.6

a) See the text (p. 2712). b) The critical distance of ion association at 0 °C in Bjerrum's theory.[14]

Quadrupole Formation. In the preceding sections, the triple-ion formation constant, K_t, was estimated disregarding the quadrupole formation. We shall now discuss how the correction for quadrupole formation will affect the values of K and K_t to be obtained.

The equilibrium for the formation of a quadrupole $(MA)_2$ is expressed by:

$$MA + MA \rightleftharpoons (MA)_2$$

The formation constant, K_q, is given by:

$$K_q = \frac{[(MA)_2]}{[MA]^2} = \frac{\delta}{m\alpha}$$

where δ is the parameter defined by:

$$\delta = \frac{[(MA)_2]}{[MA]}$$

Then, the osmotic coefficient becomes:

$$\phi = \frac{1}{1-0.0180hm}\left\{[1-\alpha(1+2\beta+2\delta)]\phi_{DH}+\frac{\alpha(1+\delta)}{2}\right\}$$

The experimental data are not good enough to estimate the values of K_t and K_q at the same time. Thus, some relation between K_t and K_q values has to be assumed if one is to estimate them by the analysis of the experimental data.

Defining K' as:

$$K' = \frac{[(MA)_2]}{[M_2A][A]\gamma_{M_2A}\gamma_A} = \frac{[(MA)_2]}{[MA_2][M]\gamma_{MA_2}\gamma_M}$$

one obtains the relation:

$$\frac{K_q}{K_t} = \frac{K'}{K}$$

K' is the ion-association constant of a kind of 2 : 2 electrolyte and can be approximated by K. Then, K_q/K_t will have a value near unity. Assuming $K_q = K_t$, we obtained the K_t, K_q, and K values for $MgSO_4$ shown in Table 4. The ion-association constants (K) given here are slightly greater than the corresponding values shown in Table 2, but the change is within the range of experimental error except when large a values are assumed. The K_t values are appreciably smaller than those shown in Table 2. Thus, it was found that a correction for the quadrupole formation would make the K_t values smaller than the values shown in Table 2, but would affect the K values very little.

Table 4. K and K_t values of $MgSO_4$ obtained with the assumption of $K_q=K_t$ at 25.0 °C (vpo)

a (Å)	K (mol^{-1} kg)	K_q (=K_t) (mol^{-1} kg) $h=0$	$h_0=15$ (B)[a]	$h_0=15$ (A)[b]
4.0	72±9	0	0.6	0.8
5.0	102±3	1.2	1.6	1.9
6.0	126±6	1.5	1.8	2.1
7.0	144±8	1.5	1.8	2.1
8.0	159±9	1.4	1.7	2.1
10.0	182±10	1.3	1.5	1.8
12.0	197±10	1.1	1.3	1.6
14.3	210±9	1.0	1.1	1.5

a) $h=h_0[1-\alpha(1+2\beta+2\delta)]$; the assumption for the hydration number of the quadrupole is similar to that described in the paragraph following case (B) on p. 2712. b) $h=h_0$; a similar assumption to that described in the paragraph following case (A) on p. 2712.

Comparison with the Ion-Association Constants Obtained from Conductivity Experiments. The electric conductivity was mesaured for $MgSO_4$ solutions by Dunsmore and James[8] and Katayama,[9] for $CaSO_4$ solutions by Inada *et al.*,[10] and for $MnSO_4$ solutions by Hallada and Atkinson[11] and Petrucci *et al.*[12] Although no conductivity measurements were made of $[Ru(phen)_3]SO_4$ solutions, the electric conductivities of $[Fe(phen)_3]SO_4$ solutions were measured by Kubota and Yokoi.[13] They analyzed the conductivity data in order to obtain the values of the ion-association constant and the closest distance of approach. However, these results have to be revised before they can be compared with the results from vpo, since different authors used different theoretical equations for the analysis of the conductivity data.

For the reanalysis of the conductivity data, we used Fuoss-Hsia's equation[23] expanded by Fernández-

Prini.[24] This equation gives the equivalent conductivity, Λ, for an association system as follows:

$$\frac{\Lambda}{1-\alpha} = \Lambda_0 - S[c(1-\alpha)]^{1/2} + Ec(1-\alpha)\log[c(1-\alpha)] + J_1c(1-\alpha) - J_2[c(1-\alpha)]^{3/2} \quad (13)$$

where Λ_0 is the limiting equivalent conductivity, c is the concentration of the solute on the molar scale, and α is the degree of association. The latter is related to K by:

$$K = \frac{\alpha}{(1-\alpha)^2 c y_M y_A} \quad (14)$$

The parameters, J_1 and J_2, as well as the activity coefficients, y_M and y_A, of the free ions, M and A, are functions of the closest distance of approach of ions, a. Since measurements of the conductivity are usually made at concentrations well below 10^{-2} mol l^{-1}, c, y_M, and y_A on the molar concentration scale can be approximated by m, γ_M, and γ_A [Eq. (6)] on the molality scale respectively; the other interactions, such as triple-ion formation, described in the previous sections can be ignored.

With a given value of a and a roughly estimated value of Λ_0, K was calculated for each concentration by means of Eqs. (13) and (14). With the averaged K value, the electric conductivity at each concentration was calculated and then used to calculate the standard deviation, as defined by:

$$\sigma_\Lambda = \sqrt{\frac{\sum_{i=1}^{n}(\Lambda_{\mathrm{calcd},i} - \Lambda_{\mathrm{obsd},i})^2}{n-2}}$$

where n is the total number of points of the run and where Λ_{obsd} and Λ_{calcd} are, respectively, the observed and the calculated electric conductivity at each concentration. The averaged K value depended on the assumed Λ_0 value. The best-fitting values of K and Λ_0 for a given a value were determined by the minimization of the standard deviation, σ_Λ, and are listed in Table 5 as a function of a for each of the electrolytes. The log K values given in Table 5 show a tendency similar to that observed in Table 2 (results from vpo), and each of the K values has a magnitude similar to the corresponding one in Table 2.

Critical Discussion of the Minimum Standard Deviation as the Criterion of the Best *Values.* As a criterion of the *best* values, we used the minimum standard deviations of ϕ and Λ respectively for the determination of K and K_t from the vapor pressure osmometric measurements and for the determination of K and Λ_0 from the conductivity data. The rather sharp minima shown

Table 5. K and Λ_0 values of some 2 : 2 electrolytes determined by the reanalysis of the conductivity data at 25.0 °C with Fuoss-Hsia's equation[23,24]

a (Å)	$MgSO_4$[a] (Dunsmore and James[8])		$MgSO_4$[b] (Katayama[9])		$CaSO_4$[c] (Inada *et al.*[10])	
	K (mol^{-1} l)	Λ_0 (Ω^{-1} cm^2 mol^{-1})	K (mol^{-1} l)	Λ_0 (Ω^{-1} cm^2 mol^{-1})	K (mol^{-1} l)	Λ_0 (Ω^{-1} cm^2 mol^{-1})
3.0	59±5	132.43	23±12	131.25	62±13	139.39
4.0	83±4	132.63	63±10	132.05	86±12	139.54
5.0	103±3	132.77	92±6	132.50	105±12	139.66
6.0	119±3	132.88	115±4	132.82	121±12	139.75
7.0	133±2	132.96	133±3	133.02	135±12	139.82
8.0	146±2	133.02	148±2	133.15	147±12	139.86
10.0	167±2	133.10	169±2	133.25	167±12	139.93
12.0	183±2	133.11	182±3	133.15	184±12	139.95
14.3	197±2	133.08	188±6	132.86	198±12	139.92

a (Å)	$MnSO_4$[d] (Hallada and Atkinson[11])		$MnSO_4$[e] (Petrucci *et al.*[12])		$[Fe(phen)_3]SO_4$[f] (Kubota and Yokoi[13])	
	K (mol^{-1} l)	Λ_0 (Ω^{-1} cm^2 mol^{-1})	K (mol^{-1} l)	Λ_0 (Ω^{-1} cm^2 mol^{-1})	K (mol^{-1} l)	Λ_0 (Ω^{-1} cm^2 mol^{-1})
3.0	50±10	131.88	69±10	132.23		
4.0	90±6	132.50	106±6	132.84		
5.0	119±5	132.92	134±4	133.26		
6.0	142±5	133.21	155±2	133.55		
7.0	160±6	133.40	173±2	133.75		
8.0	175±7	133.53	188±2	133.89		
10.0	197±7	133.62	210±2	134.00	19±5	114.40
12.0	210±6	133.54	224±2	133.94	34±5	114.39
14.3	216±6	133.28	232±3	133.70	46±5	114.29

a) The calculations were made by the use of eleven data at the concentrations from 0.1634×10^{-3} up to 0.8846×10^{-3} mol l^{-1}. b) 10 data, $(0.2—3.0)\times10^{-3}$ mol l^{-1}. c) 10 data, $(0.1-1.0)\times10^{-3}$ mol l^{-1}. d) 9 data, $(0.2013—3.141)\times10^{-3}$ mol l^{-1}. e) 5 data, $(0.2758-2.235)\times10^{-3}$ mol l^{-1}. f) 17 data, $(0.1745-1.662)\times10^{-3}$ mol l^{-1}.

by the standard deviations, σ_ϕ and σ_Λ, for each given a value made the determination of the *best* parameter values possible. In most conductivity studies, however, where the minimization of σ_Λ has been used for the simultaneous determination of the values of three parameters, K, Λ_0, and a, the minimum standard deviation is not necessarily a good criterion of the *best* parameter values. The minimum values of σ_ϕ and σ_Λ we obtained for each fixed value of a are plotted against a in Figs. 12 and 13 respectively. In the latter, the

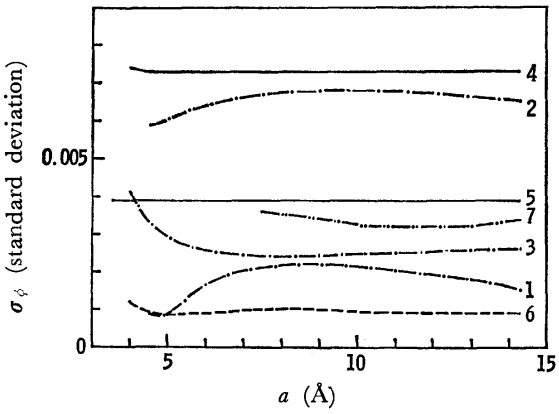

Fig. 12. The standard deviation σ_ϕ as a function of a. 1, 2, and 3: $MgSO_4$. 4 and 5: $CaSO_4$. 6: $MnSO_4$. 7: $[Ru(phen)_3]SO_4$. 1, 4, 6, and 7 are concerned with the vpo data, whereas the others with the cryoscopic data due to Isono[6] (2) and Brown and Prue[3] (3 and 5).

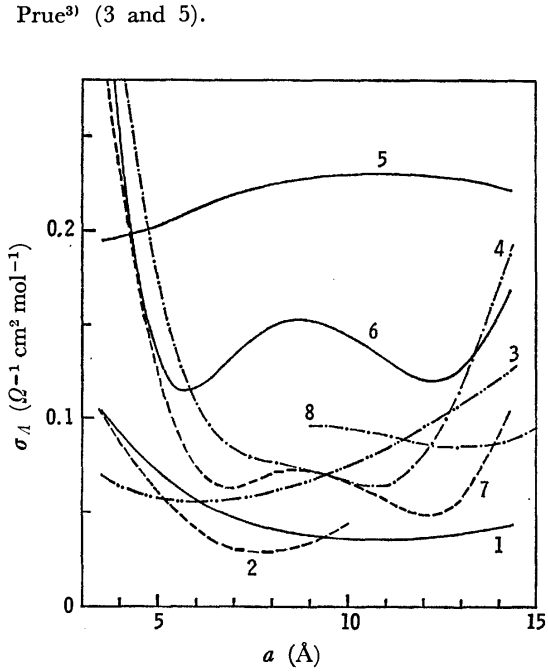

Fig. 13. The standard deviation σ_Λ as a function of a obtained from reanalysis of conductivity data. 1, 2, and 3: $MgSO_4$ (Dunsmore and James[8]). 4: $MgSO_4$ (Katayama[9]). 5: $CaSO_4$ (Inada *et al.*[10]). 6: $MnSO_4$ (Hallada and Atkinson[11]). 7: $MnSO_4$ (Petrucci *et al.*[12]). 8: $[Fe(phen)_3]SO_4$ (Kubota and Yokoi[13]). Fuoss-Hsia's equation[23,24] was used for the analysis of data, except for the cases of 2 and 3 where Fuoss-Onsager's[25] and Pitts's equation[26] were used, respectively.

results obtained for $MgSO_4$ by the use of Fuoss-Onsager's equation[25] and Pitt's equation[26] are also shown for comparison. In Fig. 13, some of the curves have two minima, while others have a shallow minimum. The a value giving the minimum σ_Λ depends not only on the experimental data, but also on the theoretical equations used for the analysis of the data. These facts imply that the minimum standard deviation cannot be a good basis for the determination of the *best a* value. Figure 12 gives hardly a clue for determining the *best a* value from the vpo data. Regarding the conductivity method, a similar discussion has also been made in detail by Hanna *et al.*[7,27] Thus, we shall try to estimate the *best a* and K values with the help of theories of ion association.[1,14,15]

Estimation of the Best *Values with the Help of Theories of Ion Association.* In a previous paper,[1] we made a refinement of the Debye-Hückel theory[2] on the basis of the purely electrostatic model and introduced a correction term into the Debye-Hückel expression for the chemical potential of a dissolved electrolyte. By connecting the correction term with the conventional concept of ion association, we derived the following expression for the ion-association constant:

$$K = \frac{8\pi N a^3}{1000} \sum_{n=1}^{\infty} \frac{b^{2n+2}}{(2n+2)!(2n-1)}$$

where b is Bjerrum's parameter as defined by $b=z^2e^2/\varepsilon kTa$. This equation gives the K value as a function of a. Since this theoretical K value decreases monotonously with the increase in a, and since the experimental K value increases with the increase in the assumed value of a, only one choice of a set of a and K values can satisfy both theory and experiment. Such sets of a and K values are given in Table 6. Each of the listed a values is somewhat greater than the sum of the crystallographic radii of the cation and the anion, r_M+r_A,††† and is plausible if hydration of the ions is taken into consideration. This can be taken as evidence for the validity of the theory.

††† The values of r_M+r_A given in Table 6 were estimated as follows. The crystallographic data of $CaSO_4\cdot 2H_2O$ and K_2SO_4[28] were used for the estimation of the radius, r_A, of the sulfate ion. Pauling's radius[29] of each cation was subtracted from the distance between the metal ion and the nearest oxygen atom of the neighboring sulfate ion; the difference, 1.3_8 Å, was obtained as the radius of the oxygen atom belonging to a sulfate ion. This oxygen radius was added to the bond length between the sulfur and the oxygen atom of a sulfate ion, 1.5_0 Å,[28,30] to obtain 2.8_8 Å as the value of r_A for the sulfate ion. Pauling's radii[29] were used as the r_M values for magnesium, calcium, and manganese ions. For $[Fe(phen)_3]^{2+}$, the data of X-ray diffraction[31] are available. They give 6.1_3 Å as the distance from the central iron atom to the most distant hydrogen atom of the coordinated 1,10-phenanthroline ligand. The r_M value of $[Fe(phen)_3]^{2+}$ was estimated as the sum of this distance, 6.1_3 Å, and the effective radius of the hydrogen atom, 0.9_5 Å, as estimated from the interatomic distance between the hydrogen atom of the ligand and the nearest oxygen atom of a tartratoantimonate ion given in the literature.[31] The r_M value for $[Ru(phen)_3]^{2+}$ was assumed to be equal to that for the iron-complex ion.

Table 6. The *best* values of a and K obtained with the help of the theoretical expression[1] for the ion-association constant (25 °C)

Electrolyte	$r_M + r_A$ (Å)	From vpo		From conductivity (recalcd)		
		a (Å)	K (mol^{-1} kg)	a (Å)	K (mol^{-1} l)	data
$MgSO_4$	3.5_3	5.4_6	110	5.4_4	111	[8]
				5.5_8	106	[9]
$CaSO_4$	3.8_7	$4{\cdot}9_2$	134	5.4_2	112	[10]
$MnSO_4$	3.6_8	4.6_4	151	5.1_4	123	[11]
				4.9_5	132	[12]
$[Ru(phen)_3]SO_4$	10.0	11.5_2	40			
$[Fe(phen)_3]SO_4$	10.0			12.3_8	36	[13]

Fuoss's theory[15] of ion association could be used in place of our theory. In that case, the results for $MgSO_4$, $CaSO_4$, and $MnSO_4$ are similar to those given in Table 6, but no value of a would simultaneously satisfy the theory and the experiment for $[Ru(phen)_3]SO_4$ and $[Fe(phen)_3]SO_4$. This disagreement between theory and experiment may substantiate our previous criticism[1] of Fuoss's theory of ion association.

Bjerrum's theory[14] could also be used to determine the values of the ion-association constant and the closest distance of approach of ions, but in a manner different from the above. Since his theory regards a cation and an anion within the critical distance q ($=z^2e^2/2\varepsilon kT$) of each other as forming an ion-pair, the substitution of q for a in the Debye-Hückel expression [Eqs. (4) and (9)] should give a K value consistent with Bjerrum's theory. Such K values are given at the bottoms of Tables 2 to 5, where the values of q (14.3 Å at 25 °C and 13.9 Å at 0 °C) are substituted for a. In Bjerrum's theory, the parameter a characteristic of each electrolyte is the closest distance of approach of the cation and the anion of an ion-pair, and the value can be calculated by the use of a relation between K and a. The values of a thus obtained from the vpo experimental results are 4.6_4 Å for $MgSO_4$, 4.3_6 Å for $CaSO_4$, 4.1_3 Å for $MnSO_4$, and 9.9_0 Å for $[Ru(phen)_3]SO_4$. These a values are smaller than those given in Table 6. Especially, the value, 9.9_0 Å, for $[Ru(phen)_3]SO_4$ is very close to the sum of the crystallographic radii of the cation and the anion, 10.0 Å. This could be taken as an indication of there being no appreciable hydration. However, in view of the fact that the salt is highly soluble in water and crystallizes as a hydrate with more than seven molecules of water, there seem to be water molecules intervening between the ions in aqueous solutions; thus, the a value of 9.9_0 Å is possibly too small. This may be caused by the unreasonable characteristic of Bjerrum's theory that the theoretical ion-association constants decrease rapidly to zero as the value of a approaches the critical distance, 14.3 Å.

The authors wish to thank the Ministry of Education for the financial support granted for this research. Thanks are also due to Nagoya University Computation Center for the use of a FACOM 230-60 computer.

References

1) H. Yokoyama and H. Yamatera, This Bulletin, **48**, 1770 (1975).
2) P. Debye and E. Hückel, *Phys. Z.*, **24**, 185 (1923).
3) P. G. M. Brown and J. E. Prue, *Proc. Roy. Soc. Ser A*, **232**, 320 (1955).
4) J. E. Prue, "Ionic Equilibria," Pergamon Press (1966).
5) A. W. Gardner and E. Glueckauf, *Proc. Roy. Soc, Ser. A*, **313**, 131 (1969).
6) T. Isono, *Sci. Pap. Inst. Phys. Chem. Res.*, **64**, 9 (1970).
7) E. M. Hanna, A. D. Pethybridge, and J. E. Prue, *Electrochim. Acta*, **16**, 677 (1971).
8) H. S. Dunsmore and J. C. James, *J. Chem. Soc.*, **1951**, 2925.
9) S. Katayama, This Bulletin, **46**, 106 (1973).
10) E. Inada, K. Shimizu, and J. Osugi, *Nippon Kagaku Zasshi*, **92**, 1096 (1971); *Rev. Phys. Chem. Japan*, **42**, 1 (1972).
11) C. J. Hallada and G. Atkinson, *J. Amer. Chem. Soc.*, **83**, 3759 (1961).
12) S. Petrucci, P. Hemmes, and M. Battistini, *ibid.*, **89**, 5552 (1967).
13) E. Kubota and M. Yokoi, private communication; presented at the 21st Conference on Coordination Chemistry of the Chemical Society of Japan, Nagoya, October, 1971.
14) N. Bjerrum, *Kgl. Danske Videnskab. Selskab.*, **7**, No. 9 (1926).
15) R. M. Fouss, *J. Amer. Chem. Soc.*, **80**, 5059 (1958).
16) A. P. Brady, H. Huff, and J. W. McBain, *J. Phys. Colloid Chem.*, **55**, 304 (1951); W. L. Masterton, *J. Phys. Chem.*, **71**, 2885 (1967); H. Nomura, M. Ando, and Y. Miyahara, *Nippon Kagaku Zasshi*, **90**, 1222 (1969); **91**, 840 (1970); I. Paligorić and I. J. Gal, *J. Chem. Soc. Faraday Trans. I*, **68**, 1093 (1972).
17) G. J. Janz and A. R. Gordon, *J. Amer. Chem. Soc.*, **65**, 218 (1943).
18) F. P. Dwyer, J. E. Humpoletz, and R. S. Nyholm, *J. Proc. Roy. Soc.* (N. S. Wales), **80**, 212 (1946).
19) H. Yamatera, M. Fujita, and S. Nagai, *Nippon Kagaku Zasshi*, **92**, 182 (1971).
20) R. A. Robinson and R. S. Jones, *J. Amer. Chem. Soc.*, **58**, 959 (1936).
21) J. F. Hinton and E. S. Amis, *Chem. Rev.*, **71**, 627 (1971).
22) R. M. Fuoss and C. A. Kraus, *J. Amer. Chem. Soc.*, **55**, 2387 (1933).
23) R. M. Fuoss and K. -L. Hsia, *Proc. Nat. Acad. Sci. U.S. A.*, **57**, 1550 (1967); **58**, 1818 (1968).
24) R. Fernández-Prini, *Trans. Faraday Soc.*, **65**, 3311 (1969).

25) R. M. Fuoss and L. Onsager, *J. Phys. Chem.*, **61**, 668 (1957).
26) E. Pitts, *Proc. Roy. Soc. Ser. A*, **217**, 43 (1953); R. Fernández-Prini and J. E. Prue, *Z. Phys. Chem.* (Leipzig), **228**, 373 (1965).
27) E. M. Hanna, A. D. Pethybridge, J. E. Prue, and D. J. Spiers, *J. Solution Chem.*, **3**, 563 (1974).
28) Gmelins Handbuch der Anorganischen Chemie, Syst. No. 28, Part B, p. 729 (1961); Syst. No. 22, p. 710 (1937).
29) L. Pauling, "The Nature of the Chemical Bond," 3rd ed., Cornell Univ. Press (1960), p. 514.
30) Gmelins Handbuch der Anorganischen Chemie, Syst. No. 9, Part B2, p. 636 (1960).
31) A. Zalkin, D. H. Templeton, and T. Ueki, *Inorg. Chem.*, **12**, 1641 (1973).

Ion Association of Some 2 : 2 Electrolytes in Water at 25° C. II. Spectrophotometric Studies of the Ion Association of Magnesium, Calcium, Manganese, Copper, and Zinc Sulfates*

Haruhiko YOKOYAMA** and Hideo YAMATERA

Department of Chemistry, Faculty of Science, Nagoya University, Chikusa-ku, Nagoya 464

(Received May 14, 1975)

Simple and mixed aqueous solutions of copper, magnesium, calcium, manganese, and zinc sulfates were spectrophotometrically studied in order to obtain the ion-association constants of the divalent metal ions with the sulfate ion. The ion-association constant of copper sulfate was obtained from the measured absorbances of copper sulfate solutions at 250 nm as a function of the closest distance of approach of ions. For the other metal sulfates which show a negligible absorption at 250 nm, absorbances were measured on the mixed solutions with copper sulfate, and the results were analyzed by the use of the results on copper sulfate in order to obtain the ion-association constants. The *best* values of the ion-association constant and the closest distance of approach were determined for each metal sulfate with the help of the theory of ion association. The results were compared with those obtained from the measurements of osmotic coefficients and electric conductivities. The numerical results are summarized in Table 6 of the text.

In previous papers,[1,2] we have developed a theory of ion association and have made use of it in the experimental determinations of the *best* values of ion-association constants and the closest distance of approach of ions. With the help of the theory, consistent and plausible results have been derived from vapor-pressure osmometry and conductivity measurements on 2 : 2 electrolyte solutions. In this connection, it is of interest to see if spectrophotometric studies give results consistent with the previous ones.

The absorption spectra of ion-pairs in the ultraviolet region have often been measured on solutions of metal complex salts such as hexamminecobalt(III) salts, and analyzed to obtain the ion-association constants.[3-6] The ion association of divalent ions has been observed between the Cu^{2+}, Hg^{2+}, $[CoCl(NH_3)_5]^{2+}$, and UO_2^{2+} cations and the SO_4^{2-} ion,[7-13] and between some metal cations such as Mg^{2+} and the $S_2O_3^{2-}$ ion.[14] These are considered to be special cases where spectrophotometry can be directly applied to the determination of the ion-association constant. In most electrolyte solutions, ion-pair formation causes no appreciable change in the absorption. However, even when no absorption change occurs, the ion-association constant can be indirectly determined by means of appropriate indicators.[15] For example, with the pH indicator, 2,4-dinitrophenol, the ion-association constant of $MgSO_4$ in 20% ethanol solutions has been measured by Bale *et al.*[16] This method with the pH indicator has the disadvantage, however, that the complex composition of the solution makes the analysis of the data difficult and introduces considerable uncertainty into the results.

In the present study, an attempt has been made to determine spectrophotometrically the ion-association constants of magnesium, calcium, manganese, and zinc sulfates, with copper sulfate as an indicator. Copper sulfate in aqueous solutions is known to show an intense ultraviolet absorption attributable to the formation of ion-pairs,[7-11] whereas the other four sulfates are nearly transparent in aqueous solutions and no ion-pair formation is detected spectrophotometrically. When copper sulfate is mixed with one of the four sulfates, the ion-association of the latter can be expected to be indirectly observed through the change in absorption due to copper sulfate ion-pairs. Although spectrophotometric studies of the ion association of copper sulfate have been made by several authors,[7-11] they are not sufficient for the purpose of the present investigation. Thus, a re-examination has also been made of the ion association in simple copper sulfate solutions.

Experimental

Materials. The copper perchlorate was prepared by dissolving basic copper carbonate in an aqueous solution containing an equivalent amount of perchloric acid. After the solution had then been concentrated on a water bath, the salt was crystallized with stirring at room temperature and recrystallized twice from its aqueous solution containing a very small amount of perchloric acid. The crystal was obtained as a hexahydrate after having been dried over phosphorus pentaoxide. Its composition was confirmed by the electrolytic analysis of the copper ion. A reagent-grade copper sulfate was recrystallized as a pentahydrate from its aqueous solution containing a very small amount of sulfuric acid; it was then air-dried at room temperature. Its composition was confirmed by the electrolytic analysis of the copper ion and by dehydration at about 220 °C. The magnesium and calcium sulfates used were prepared and analyzed according to the procedure described in the preceding paper.[2] The manganese sulfate used was a reagent-grade hydrate. The manganese concentration in its stock solution was determined by the titration of the manganese ion with EDTA.[17] The zinc sulfate used was a heptahydrate of reagent grade. The zinc concentration in its stock solution was determined by the titration of the zinc ion with EDTA.

Measurements. The absorption measurements were made at 250 nm with a Carl Zeiss PMQ II spectrophotometer equipped with a M4Q III monochromator, using 1-cm quartz

* Presented in part at the 24th Conference on Coordination Chemistry of the Chemical Society of Japan, Kanazawa, October, 1974.

** Present address: Department of Chemistry, Yokohama City University, 4646 Mutsuura-cho, Kanazawa-ku, Yokohama, 236.

cells. The slit width was 0.15 mm, resulting in a spectral-band width of 0.57 nm at 250 nm. The cells were maintained at 25.00±0.05 °C by the circulation of water from a thermostat to the cell holder.

Copper perchlorate solutions of 5.007×10^{-3} and 1.001×10^{-2} M were prepared by the dilution of a stock solution of 5.007×10^{-2} M copper perchlorate containing about 2×10^{-3} M perchloric acid to protect it against hydrolysis. Their absorbances, observed at 250 nm, were 0.0607 and 0.1218 respectively, which gave absorbances per mol l^{-1} of the copper ion of 12.12 and 12.16 respectively. These values are in agreement with each other within the range of experimental error; the average, 12.14, was used as the molar extinction coefficient of the free copper ions.

A stock solution of 1.000×10^{-2} M copper sulfate containing 1.01×10^{-4} M sulfuric acid was diluted with a 1.01×10^{-4} M sulfuric acid solution. Thereby, nine copper sulfate solutions with concentrations from 2×10^{-3} to 10^{-2} M at 10^{-3} M intervals were prepared; their absorbances were then measured.

A stock solution of 1.000×10^{-2} M magnesium sulfate containing 1.01×10^{-4} M sulfuric acid was mixed with the stock solution of copper sulfate, and with 1.01×10^{-4} M sulfuric acid when necessary, to make nine mixed electrolyte solutions. (The compositions of the solutions are shown in Table 3.) Similar mixed electrolyte solutions containing copper sulfate and another divalent metal sulfate were also prepared with calcium, manganese, and zinc sulfates in the same manner as in the case of magnesium sulfate. The absorbances of all the solutions were measured under the condition described above. Simple solutions containing no copper sulfate were also prepared by the dilution of the stock solutions, and their absorbances were measured as the blank values to be subtracted from the absorbances of the mixed electrolyte solutions. The blank values were nearly zero, or less than 0.001. All the solutions were prepared within an error of ±0.1% in concentration, and their transmittances were observed within an error of ±0.05%.

Results and Discussion

Determination of the Ion-Association Constant of Copper Sulfate. The observed absorbances (D) of aqueous copper sulfate solutions of various concentrations (c_M) containing 1.01×10^{-4} M H_2SO_4 are shown in Table 1, together with the absorbances per mol l^{-1} of copper sulfate (D/c_M). The corresponding values are also listed for copper perchlorate solutions containing about 2×10^{-3} M $HClO_4$. The D/c_M values of the copper sulfate solutions are very much greater than those of the copper perchlorate solutions and increase with the increase in the concentration. This phenomenon has usually been attributed to the ion association of the copper ion with the sulfate ion.[7-11] In the following, the absorption data will be analyzed in order to obtain the ion-association constant.

TABLE 1. ABSORBANCES OF AQUEOUS COPPER SULFATE SOLUTIONS CONTAINING 1.01×10^{-4} M H_2SO_4 AND OF AQUEOUS COPPER PERCHLORATE SOLUTIONS CONTAINING ABOUT 2×10^{-3} M $HClO_4$ (250 nm, 1-cm cells, 25.0 °C)

Electrolyte	$10^3\,c_M$ (mol l^{-1})	D	D/c_M (mol^{-1} l)
$CuSO_4$	2.000	0.0818±0.0003	40.9
	3.000	0.1426±0.0003	47.5
	4.000	0.2100±0.0004	52.5
	5.000	0.2824±0.0005	56.5
	6.000	0.3595±0.0005	59.9
	7.000	0.4395±0.0006	62.8
	8.000	0.5230±0.0008	65.6
	9.000	0.6083±0.0009	67.6
	10.000	0.6968±0.0011	69.7
$Cu(ClO_4)_2$	5.007	0.0607±0.0003	12.12
	10.01	0.1218±0.0003	12.16

The possible ion-association equilibria between ions in the solution are:

$$M + A \rightleftharpoons MA \quad (1)$$

$$H + A \rightleftharpoons HA \quad (2)$$

where M, A, H, HA, and MA represent Cu^{2+}, SO_4^{2-}, H^+, HSO_4^-, and $Cu^{2+}SO_4^{2-}$ respectively. Since the concentration of the sulfuric acid is as low as 1.01×10^{-4} M, the formation of the $Cu^{2+}HSO_4^-$ ion-pair was ignored. The formations of the $(Cu^{2+})_2SO_4^{2-}$ and $Cu^{2+}(SO_4^{2-})_2$ triple-ions and the $(Cu^{2+}SO_4^{2-})_2$ quadrupole were also ignored. According to a previous work,[2] this approximation is good enough for the present study, where the concentrations of the solutions are lower than 10^{-2} M. The formation constants, K_{MA} and K_{HA}, of $Cu^{2+}SO_4^{2-}$ and HSO_4^- respectively are given by:

$$K_{MA} = \frac{[MA]}{[M][A]y_M y_A} \quad (3)$$

$$K_{HA} = \frac{[HA]y_{HA}}{[H][A]y_H y_A} \quad (4)$$

where y_M, y_H, y_A, and y_{HA} are the activity coefficients of Cu^{2+}, H^+, SO_4^{2-}, and HSO_4^- respectively. The activity coefficient of the $Cu^{2+}SO_4^{2-}$ ion-pair was regarded as unity. The total concentrations of Cu^{2+}, SO_4^{2-}, and H^+, denoted by c_M, c_A, and c_H respectively, are related to the concentrations of the species existing in the solution as follows:

$$\left.\begin{aligned} c_M &= [M] + [MA] \\ c_A &= [A] + [MA] + [HA] \\ c_H &= [H] + [HA] \end{aligned}\right\} \quad (5)$$

The absorption observed at 250 nm can be attributed to the free Cu^{2+} ion and the $Cu^{2+}SO_4^{2-}$ ion-pair. Thus, the absorbance, D, of each solution can be expressed by:

$$\begin{aligned} D &= \varepsilon_M[M] + \varepsilon_{MA}[MA] \\ &= \varepsilon_M c_M + (\varepsilon_{MA}-\varepsilon_M)[MA] \end{aligned} \quad (6)$$

where ε_M and ε_{MA} are the molar extinction coefficients of Cu^{2+} and $Cu^{2+}SO_4^{2-}$ respectively. Using Eqs. (3), (5), and (6), one can derive the relation:

$$P = \frac{1}{\varepsilon_{MA}-\varepsilon_M}Q + \frac{1}{K_{MA}(\varepsilon_{MA}-\varepsilon_M)} \quad (7)$$

where P and Q are variables defined by:

$$\left.\begin{aligned} P &= \frac{(c_A-[HA])y_M y_A}{(D/c_M)-\varepsilon_M} \\ Q &= (c_M+c_A-[MA]-[HA])y_M y_A \end{aligned}\right\} \quad (8)$$

If K_{MA}, ε_M, and ε_{MA} are assumed to be constant under the present experimental conditions, a linear relationship can be expected between P and Q in Eq. (7). The parameters appearing in Eq. (8) were treated as follows.

The molar extinction coefficient of the free ion, ε_M, was assumed to be equal to the absorbance (per cm) per mol l^{-1} of copper perchlorate in dilute solutions. This assumption is justified, at least at 250 nm, since the copper perchlorate solutions at this wavelength obey Beer's law, as is shown in Table 1; however, this does not exclude the possibility that ion-pairs may be formed between copper ions and perchlorate ions. The concentration of the hydrogensulfate ion, [HA], is given by:

$$[HA] = \frac{R_1 - \sqrt{R_1^2 - 4c_H(c_A - [MA])}}{2} \quad (9)$$

where R_1 is a variable defined by:

$$R_1 = c_H + c_A - [MA] + \frac{1}{K_{HA}y_A}$$

These equations were derived from Eqs. (4) and (5) on the assumption that $y_{HA}=y_H$. This assumption is acceptable for the calculation of the P and Q values with Eq. (8), since, at the low acid concentration of $c_H=2.02\times10^{-4}$ M, [HA] is very low compared with c_A. The value of K_{HA} was taken from the literature.[18] The $\log K_{HA}$ value of 1.99 was obtained by many authors by means of various experimental methods. The activity coefficients, y_M and y_A, were expressed by the Debye-Hückel expression:[19]

$$\log y_M = \log y_A = -\frac{4A\sqrt{I}}{1+Ba\sqrt{I}} \quad (10)$$

where a is a parameter representing the closest distance of approach of ions (in Å†), where A and B are constants involving the absolute temperature and the dielectric constant of the solvent ($A=0.5115$ and $B=0.3291$ in aqueous solutions at 25.0 °C), and where I is the ionic strength given by:

$$I = 2(c_M + c_A - 2[MA] - [HA]) + \frac{1}{2}c_H \quad (11)$$

The values of P, Q, and K_{MA} were calculated by the method of successive approximations in the following way. Assuming $[MA]=[HA]=0$ provisionally, the ionic strength and then the activity coefficients were estimated for a given a value. By putting the values of these parameters into Eq. (8), the values of P and Q were calculated for each solution. Assuming a linear relationship between the P and Q values, the coefficient of the first term, $1/(\varepsilon_{MA}-\varepsilon_M)$, and the second term, $1/K_{MA}(\varepsilon_{MA}-\varepsilon_M)$, of the right-hand side of Eq. (7) were evaluated by the method of least squares; the value of K_{MA} was then obtained as the ratio between them. The K_{MA} value thus obtained was used for the calculation of the [MA], [HA], I, y_M, and y_A values by means of Eqs. (3)—(5) and (9)—(11); these values were in turn used for the recalculation of the values of P and Q. Then, by the use of these values, the value of K_{MA} was evaluated again in the same way as above. In order to obtain the final value of K_{MA}, such calculations were repeated several times until the values of $1/(\varepsilon_{MA}-\varepsilon_M)$ and $1/K_{MA}(\varepsilon_{MA}-\varepsilon_M)$ in Eq. (7) became constant within 0.05% of their respective values.

The resulting plot of P *vs.* Q is shown in Fig. 1 for each value of the parameter a. In Table 2, the values of K_{MA} and ε_{MA} are shown for the several a values assumed. Figure 2 gives the plot of $\log K_{MA}$ *vs.* a. For $a=10$ Å, the result in the present work, $K_{MA}=241$ mol^{-1} l, is in essential agreement with that obtained by Davies *et al.*[9] at 240 nm, $K_{MA}=250$ mol^{-1} l,

Table 2 also gives the standard deviation of D in percentage, σ_D (%), defined by:

$$\sigma_D(\%) = \sqrt{\frac{\sum_{i=1}^{n}[100(D_{obsd,i}-D_{calcd,i})/D_{calcd,i}]^2}{n-2}}$$

where $D_{obsd,i}$, and $D_{calcd,i}$, are the observed and calculated absorbances respectively for the i-th copper sul-

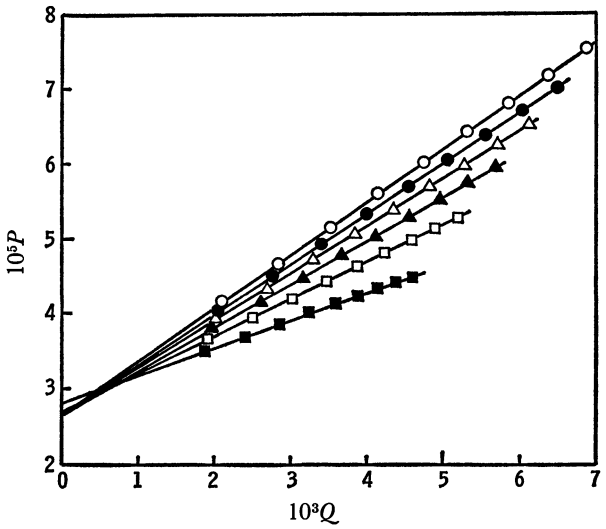

Fig. 1. Plots of P against Q. [For the definitions of P and Q, see Eq. (8).] The assumed a values are 14.3 Å (○), 12.0 Å (●), 10.0 Å (△), 8.0 Å (▲), 6.0 Å (□), and 4.0 Å (■).

TABLE 2. K_{MA} AND ε_{MA} VALUES OF COPPER SULFATE DERIVED FROM THE SPECTROPHOTOMETRIC MEASUREMENTS ON THE COPPER SULFATE SOLUTIONS AT 25.0 °C (with several a values assumed)

a (Å)	K_{MA} (mol^{-1} l)	ε_{MA} (cm^{-1} mol^{-1} l)	σ_D(%)
3.0	87±1	403	0.34
4.0	130±1	287	0.15
5.0	161±1	239	0.09
6.0	185±1	213	0.11
7.0	203±1	197	0.14
8.0	219±1	185	0.15
10.0	241±1	170	0.16
12.0	256±1	161	0.16
14.3[a]	269±1	153	0.14

a) The critical distance of ion association at 25 °C in Bjerrum's theory.[20]

† 1 Å$=10^{-10}$ m.

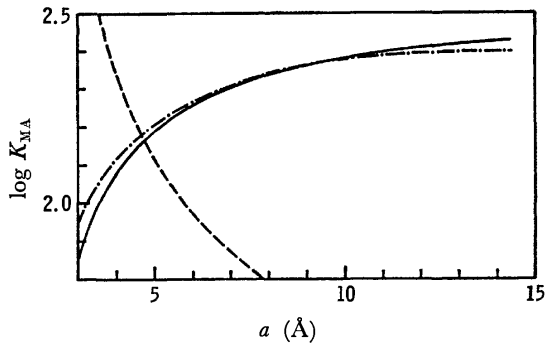

Fig. 2. $\log K_{MA}$ for $CuSO_4$ as a function of a.
(——): From spectrophotometry. (—·—): From conductivity measurements (recalculation of the data due to Owen and Gurry[29]). (----): Theoretical curve according to Eq. (20).

fate solution. The value of $D_{calcd,i}$ was calculated by means of Eq. (6), where the ε_{MA} value given in Table 2 was used together with the connected K_{MA} value from which the [MA] value was derived. As is shown in Table 2, the $\sigma_D(\%)$ values for the a values between 4 and 14.3 Å (Bjerrum's critical distance of ion association[20]) are as small as 0.09—0.16%. This shows that the observed absorbances are reproducible within the range of experimental error with each set of the a, K_{MA}, and ε_{MA} values. The value of a which gives the minimum $\sigma_D(\%)$ might be regarded as the *best* value. A minimum was actually found around a=5 Å. However, it is a shallow minimum; therefore, there is some uncertainty as to the *best* value of a.

Determination of the Ion-Association Constants of Magnesium, Calcium, Manganese, and Zinc Sulfates from Measurements of Mixed Electrolyte Solutions. The absorbances of the mixed $CuSO_4$–$MgSO_4$, $CuSO_4$–$CaSO_4$, $CuSO_4$–$MnSO_4$, and $CuSO_4$–$ZnSO_4$ solutions containing 1.01×10^{-4} M of H_2SO_4 are shown in Table 3. A comparison of Table 3 with Table 1 shows that the addition of a second divalent metal sulfate increases the absorbance of the solution. This increase in the absorbance is attributable to the increase in the concentration of the ion-pair, $Cu^{2+}SO_4^{2-}$, caused by the increase in the concentration of the sulfate ion. However, the quantity of free sulfate ions supplied by the second metal sulfate depends on the ion-association constant of the second metal ions with sulfate ions, if the concentrations of the second components are the same. In the following paragraphs, the ion-association constant of the second metal sulfate will be estimated on the basis of an analysis of the absorption data.

We shall discuss the mixed $CuSO_4$–$MgSO_4$ solutions as an example. The third ion-association equilibrium, Eq. (12), must be considered in addition to Eqs. (1) and (2) for copper sulfate solutions:

$$M' + A \rightleftharpoons M'A \tag{12}$$

where M' represents the Mg^{2+} ion and M'A, the $Mg^{2+}SO_4^{2-}$ ion-pair. The formation constant of the ion-pair, $K_{M'A}$, is expressed by:

$$K_{M'A} = \frac{[M'A]}{[M'][A]y_{M'}y_A} \tag{13}$$

Where $y_{M'}$ is the activity coefficient of the free magnesium ion. The activity coefficient of the $Mg^{2+}SO_4^{2-}$ ion-pair is regarded as unity. The total concentrations, c_M, c_H, $c_{M'}$, and c_A, are related to the concentrations of the species existing in the solution as follows:

$$\left.\begin{aligned} c_M &= [M] + [MA] \\ c_H &= [H] + [HA] \\ c_{M'} &= [M'] + [M'A] \\ c_A &= [A] + [MA] + [M'A] + [HA] \end{aligned}\right\} \tag{14}$$

The concentration of the $Cu^{2+}SO_4^{2-}$ ion-pair can be expressed by:

$$[MA] = \frac{D-\varepsilon_M c_M}{\varepsilon_{MA}-\varepsilon_M} \tag{15}$$

which was obtained by rewriting Eq. (6). Equation (6) can also be used for the mixed electrolyte solutions, since magnesium sulfate as well as the other second components give absorbances as small as 0.001 or less in solutions of $c_{M'}=10^{-2}$ M; the small absorbance has been allowed for in obtaining each D value given in Table 3. By combining Eqs. (3) and (14), one obtains:

$$[M'A] = c_A - [MA] - [HA] - \frac{[MA]}{(c_M-[MA])K_{MA}y_My_A} \tag{16}$$

The concentration [HA] is given by:

Table 3. Absorbances of mixed aqueous solutions of divalent metal sulfates containing 1.01×10^{-4} M H_2SO_4 (250 nm, 1-cm cells, 25.0 °C)

$10^3 c_M$ (mol l^{-1})	$10^3 c_{M'}$ (mol l^{-1})	$CuSO_4$-$MgSO_4$ D	$CuSO_4$-$CaSO_4$ D	$CuSO_4$-$MnSO_4$[a] D	$CuSO_4$-$ZnSO_4$ D
2.000	4.000	0.1226±0.0003	0.1218±0.0003	0.1224±0.0003	0.1217±0.0003
2.000	6.000	0.1342±0.0003	0.1331±0.0003	0.1341±0.0003	0.1336±0.0003
2.000	8.000	0.1442±0.0003	0.1424±0.0003	0.1432±0.0003	0.1432±0.0003
4.000	2.000	0.2421±0.0004	0.2424±0.0004	0.2428±0.0004	0.2414±0.0004
4.000	4.000	0.2669±0.0004	0.2650±0.0004	0.2656±0.0004	0.2635±0.0004
4.000	6.000	0.2862±0.0004	0.2829±0.00$_0$5	0.2840±0.0004	0.2838±0.0004
6.000	2.000	0.3962±0.0006	0.3964±0.0006	0.3964±0.0006	0.3959±0.0006
6.000	4.000	0.4249±0.0008	0.4237±0.0006	0.4241±0.0006	0.4224±0.0006
8.000	2.000	0.5625±0.0008	0.5622±0.0008	0.5630±0.0008	0.5613±0.0008

a) The concentrations of $MnSO_4$($c_{M'}$) in the $CuSO_4$-$MnSO_4$ solutions were slightly higher than given in the second column. In this case, read 2.044 for 2.000, 4.088 for 4.000, 6.132 for 6.000, and 8.176 for 8.000.

$$[HA] = \frac{R_2 - \sqrt{R_2^2 - 4c_H(c_A - [MA] - [M'A])}}{2} \quad (17)$$

where R_2 is a variable defined by:

$$R_2 = c_H + c_A - [MA] - [M'A] + \frac{1}{K_{HA}y_A}$$

Equation (17) was derived from Eqs. (4) and (14) by assuming $y_{HA}=y_H$ in the same manner as in the case of copper sulfate solutions.

Then, by the use of Eqs. (13)—(17), $K_{M'A}$ can be calculated if the values of K_{HA}, K_{MA}, ε_M, ε_{MA}, y_M, $y_{M'}$, and y_A are known. As has been mentioned above, $\log K_{HA}=1.99$ is given in the literature[18] and the value of ε_M has been experimentally determined to be 12.14 (Table 1). The values of K_{MA} and ε_{MA} have already been obtained as a function of a; they are listed in Table 2. By assuming that both copper and magnesium sulfates have the same a value, the activity coefficients of the free ions, y_M, $y_{M'}$, and y_A, are given by the Debye-Hückel theory[19] as follows:

$$\log y_M = \log y_{M'} = \log y_A = -\frac{4A\sqrt{I}}{1+Ba\sqrt{I}} \quad (18)$$

where the ionic strength, I, is given by:

$$I = 2(c_M + c_{M'} + c_A - 2[MA] - 2[M'A] - [HA]) + \frac{1}{2}c_H$$

The calculation of $K_{M'A}$ was done as follows. Assuming $[M'A]=[HA]=0$ provisionally, the ionic strength, I, and then the activity coefficients, y_M and y_A, were evaluated for a given a value. [MA] was calculated by the use of Eq. (15) with the corresponding ε_{MA} value for the given a value. By putting these values into the right-hand side of Eq. (16), the value of [M'A] was obtained, and then the value of [HA] was calculated by the use of Eq. (17). The values of [M'A] and [HA] thus obtained were used for the recalculation of I, y_M, and y_A, after which [M'A] and [HA] were re-evaluated in the same way. Such a procedure was repeated several times until both the [M'A] and [HA] values became constant within 0.05% of their respective values. The values of [M'A], [HA], and y_A thus obtained were then used to evaluate the ion-association constant, $K_{M'A}$, by means of Eqs. (13), (14), and (18). The values of $K_{M'A}$ were thus obtained for the solutions of each different composition, after which the $K_{M'A}$ values were averaged. In Table 4, the averaged $K_{M'A}$ value of $MgSO_4$ as well as those of the other sulfates are shown for the several a values assumed.

Table 4. $K_{M'A}$ values of some 2 : 2 electrolytes derived from the spectrophotometric measurements on the mixed electrolyte solutions at 25.0 °C (with several a values assumed)

a (Å)	$MgSO_4$ $K_{M'A}$ (mol^{-1} l)	$CaSO_4$ $K_{M'A}$ (mol^{-1} l)	$MnSO_4$ $K_{M'A}$ (mol^{-1} l)	$ZnSO_4$ $K_{M'A}$ (mol^{-1} l)
4.0	44±15	60±17	62±16	66±18
5.0	77±10	93±14	95±12	99±14
6.0	101±7	117±14	119±11	123±13
7.0	120±6	136±14	139±11	142±12
8.0	135±5	151±14	154±11	157±12
10.0	157±5	173±14	176±11	180±12
12.0	172±5	188±14	191±11	195±12
14.3	184±6	200±14	203±11	207±13

A comparison of Table 4 with Table 2 shows that the ion-association constants ($K_{M'A}$) of $MgSO_4$, $CaSO_4$, $MnSO_4$, and $ZnSO_4$ are considerably smaller than that of $CuSO_4$ (K_{MA}) at the same a value, and that, as the assumed a value increases, $K_{M'A}$ increases in parallel with K_{MA}, with the difference kept almost constant; *i.e.*, $K_{MA}-K_{M'A}=84$—86 for $MgSO_4$, 68—70 for $CaSO_4$, 65—68 for $MnSO_4$, and 61—64 for $ZnSO_4$.

These results were derived from the data on the mixed aqueous solutions of copper sulfate and a second metal sulfate in question, assuming that the a value for the latter was the same as that for copper sulfate. Therefore, the results obtained for the second metal sulfates (Table 4) may be different from those which would be obtained from the experiments on single electrolyte solutions. This problem will be examined below.

The activity coefficient of each ionic species is expressed by:

$$\log y_i = -\frac{4A\sqrt{I}}{1+Ba_i\sqrt{I}} \quad (19)$$

where the subscript i stands for the ionic species, whether M, M', or A. Rigorously speaking, the condition $a_i=a_j$ is required in order for Eq. (19) and a similar equation for j-ions to satisfy the thermodynamical relation:[21]

$$\frac{\partial(\log y_i)}{\partial c_j} = \frac{\partial(\log y_j)}{\partial c_i}$$

As an approximation, however, Eq. (19) will be used without the condition that $a_i=a_j$.

The main ionic species existing in the mixed $CuSO_4$–$MgSO_4$ solutions are Cu^{2+}, Mg^{2+}, and SO_4^{2-}. Since the sulfate ion is the predominant anionic species, the closest distance of approach of the copper ion in the mixed electrolyte solution, a_M, can be reasonably approximated by the a value in single copper sulfate solutions. The same argument applies to $a_{M'}$ for the magnesium ion. Considering the probability of a sulfate ion colliding with each of the metal cations, we assumed the equation:

$$a_A = \frac{a_M c_M + a_{M'} c_{M'}}{c_M + c_{M'}}$$

Then the activity coefficient of each ion was calculated by the use of Eq. (19). The K_{MA} and ε_{MA} values were so chosen from Table 2 as to correspond to the assumed a_M value. Then the experimental data was analyzed in the way described above, except that different a values and, accordingly, different activity coefficients were used for different ions instead of a common a and a common activity coefficient. The values of $K_{M'A}$ were thus obtained for various combinations of the values of a_M and $a_{M'}$.

In Fig. 3, the values of $K_{M'A}$ obtained for $MgSO_4$ are plotted against the values of $a_{M'}$, with several fixed a_M values. This figure also shows, for comparison, the plot of the results given in Table 4, which was

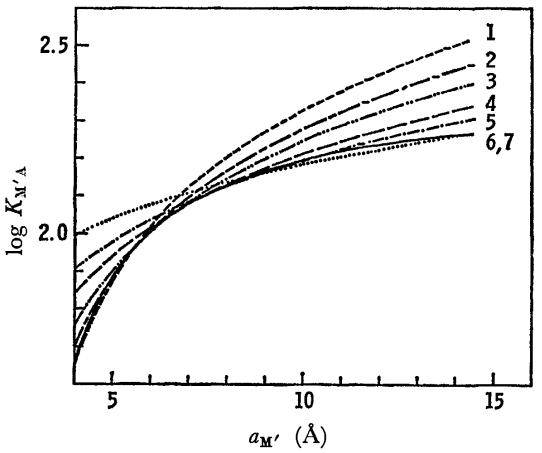

Fig. 3. log $K_{M'A}$ for $MgSO_4$ as a function of $a_{M'}$ with the assumption of several a_M values: a_M=4.0 Å [curve 1 (----)], 5.0 Å [curve 2 (— — —)], 6.0 Å [curve 3 (—··—)], 8.0 Å [curve 4 (— —)], 10.0 Å [curve 5 (—·—)], and 14.3 Å [curve 6 (·····)]. Curve 7 (——) is obtained with the assumption of $a_M=a_{M'}$ [Eq. (18)].

obtained above with the assumption that $a_M=a_{M'}$ ($=a_A$) [Eq. (18)]. The values of $K_{M'A}$ obtained with and without this assumption [Eq. (18)] are close to each other when the value of $a_{M'}$ is not very different from the value of a_M; for example, $a_{M'}$=3—7 Å for a_M=5 Å and $a_{M'}$=6.5—12 Å for a_M=10 Å. This condition is probably satisfied in view of the fact that the crystallographic radius of the magnesium ion is only slightly different from that of the copper ion (see Table 6). Thus, the $K_{M'A}$ values given in Table 4 for the special case of $a_M=a_{M'}$ approximate the $K_{M'A}$ values in the general case without the assumption that $a_M=a_{M'}$, if one reads $a_{M'}$ for a. In other words, the results obtained for $MgSO_4$ from experiments on the mixed electrolyte solutions with the assumption that $a_M=a_{M'}$ probably represent the results which would be obtained from experiments on single magnesium sulfate solutions. The same argument also applies to the cases of the other mixed electrolyte solutions investigated.

Comparison with the Vapor-Pressure Osmometry and the Conductivity Method. In the preceding paper,[2] the ion association of $MgSO_4$, $CaSO_4$, and $MnSO_4$ in aqueous solutions was studied with a vapor-pressure osmometer, and the ion-association constants were obtained. The ion-association constants of these electrolytes were also obtained by reanalyzing the literature values of the conductivity[22-26] by means of Fuoss-Hsia's equation[27] expanded by Fernández-Prini.[28] In connection with the present spectrophotometric studies, the conductivity data on aqueous $CuSO_4$ and $ZnSO_4$ solutions measured by Owen and Gurry[29] were reanalyzed in the same manner as in the previous work, and the ion-association constants were evaluated with various a values assumed. The results are shown in Table 5; the log K_{MA} for $CuSO_4$ is plotted against a in Fig. 2. In the range of a=3.0—14.3 Å, the ion-association constant of $CuSO_4$ derived from the conductivity data is not very different from that determined

TABLE 5. VALUES OF THE ION-ASSOCIATION CONSTANT K AND THE LIMITING EQUIVALENT CONDUCTIVITY Λ_0 DETERMINED BY THE REANALYSIS OF THE CONDUCTIVITY DATA[29] AT 25.0 °C WITH FUOSS-HSIA'S EQUATION[27,28] (with several a values assumed)

a (Å)	$CuSO_4$		$ZnSO_4$	
	K (mol^{-1} l)	Λ_0 (Ω^{-1} cm^2 mol^{-1})	K (mol^{-1} l)	Λ_0 (Ω^{-1} cm^2 mol^{-1})
3.0	70±12	131.15	44±11	130.46
4.0	119±7	132.40	92±6	131.68
5.0	154±4	133.18	127±3	132.46
6.0	181±2	133.71	153±1	132.98
7.0	202±1	134.04	173±2	133.32
8.0	218±1	134.25	189±2	133.50
10.0	239±1	134.33	210±2	133.58
12.0	249±2	134.10	220±1	133.35
14.3	250±5	133.50	221±5	132.74

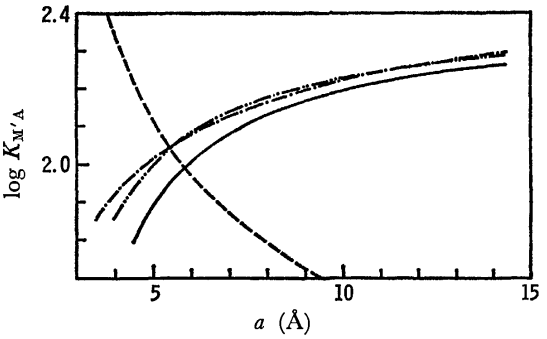

Fig. 4. log $K_{M'A}$ for $MgSO_4$ as a function of a. (——): From spectrophotometry. (—·—): From conductivity measurements (recalculation of the data due to Dunsmore and James[22]). (—··—): From vapor-pressure osmometry.[2] (— — —): Theoretical curve according to Eq. (20).

by the spectrophotometry (Table 2).

Figure 4 gives the plot of log $K_{M'A}$ *vs.* a for $MgSO_4$ as an example of the results obtained from the spectrophotometric studies of the mixed electrolyte solutions, together with those previously obtained from the vapor-pressure osmometric and conductivity studies of the single electrolyte solutions.[2] The spectrophotometric method gives slightly smaller ion-association constants than those given by the other methods.

In Fig. 5, the log K values (the subscripts, MA and M'A, are omitted) are plotted against the reciprocal of the crystallographic radii of the cations, with the assumption that a=6 Å. The log K values increase in the order: $MgSO_4<CaSO_4<MnSO_4<ZnSO_4<CuSO_4$. This order is the same as that obtained by the other methods. The same tendency was also obtained with the assumption that a=14.3 Å. Such a tendency in the magnitude of the ion-association constants seems to reflect some properties of the metal ions. In this connection, further discussions will be made in the next section.

Estimation of the Best *Value of a with the Help of the Theory of Ion Association.* In a previous work,[1]

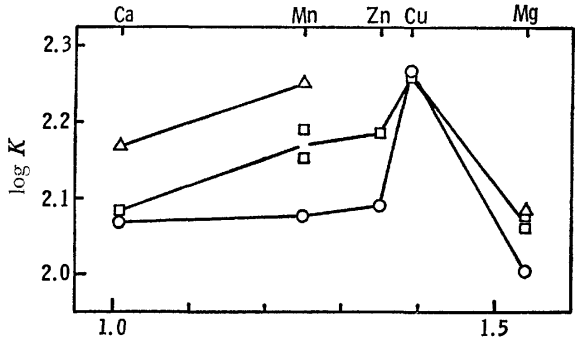

Fig. 5. log K values for divalent metal sulfates as a function of the reciprocal of crystallographic radius of the metal ion. (a=6 Å is assumed.) ○: From spectrophotometry. △: From vapor-pressure osmometry.[2] □: From conductivity measurements [recalculation of the data due to Dunsmore and James[22] ($MgSO_4$, upper), Katayama[23] ($MgSO_4$, lower), Inada *et al.*[24] ($CaSO_4$), Hallada and Atkinson[25] ($MnSO_4$, lower), Petrucci *et al.*[26] ($MnSO_4$, upper), and Owen and Gurry[29] ($CuSO_4$ and $ZnSO_4$)].

we derived an expression for the excess chemical potential of a symmetrical electrolyte in very dilute solutions. This expression has, in addition to the Debye-Hückel term, a supplementary term resulting from a more proper account of the energy of the interactions of ions existing near each other. Assuming that the contribution of ion association to the chemical potential of the electrolyte corresponds to this supplementary term, we obtained the expression for the ion-association constant:

$$K = \frac{8\pi Na^3}{1000} \sum_{n=1}^{\infty} \frac{b^{2n+2}}{(2n+2)!(2n-1)} \qquad (20)$$

where b is Bjerrum's parameter defined by $b=z^2e^2/\varepsilon kTa$. ε is the dielectric constant of the solvent, and ze is the absolute value of the charge of the ions. The log K *vs.* a curves obtained with the theoretical equation (20) are shown in Figs. 2 and 4 (broken curves) and there compared with the experimental curves. The point where the experimental curve cross the theoretical curve gives experimental a and K values consistent with the theory of ion association.[1]

The values of a and K for each electrolyte were obtained in this way; they are shown in Table 6. The magnitude of the ion-association constant increased with the decrease in a and with the decrease in the crystallographic radii of the metal ions except for the case of the magnesium ion. This general trend can be expected from electrostatic considerations. The small value of K and the large value of a for magnesium sulfate, in spite of the small crystallographic radii of the magnesium ion, can be attributed to the strong hydration of the magnesium ion.

The results given in Table 6 show that the differences between the a value of copper sulfate and those of the other electrolytes are much less than 2 Å. This satisfies the above-mentioned condition for the validity of the present treatment in deriving ion-association constants from the spectrophotometric data on the mixed electrolyte solutions.

The authors wish to thank the Ministry of Education for the financial support granted for this research. Thanks are also due to Nagoya University Computation Center for the use of a FACOM 230–60 computer.

References

1) H. Yokoyama and H. Yamatera, This Bulletin, **48**, 1770 (1975).
2) H. Yokoyama and H. Yamatera, *ibid.*, **48**, 2708 (1975).
3) M. G. Evans and G. H. Nancollas, *Trans. Faraday Soc.*, **49**, 363 (1953).
4) N. Tanaka, Y. Kobayashi, and M. Kamada, This Bulletin, **40**, 2839 (1967); N. Tanaka, H. Kaneko, T. Shirakashi, *Nippon Kagaku Zasshi*, **92**, 957 (1971).
5) L. Johansson, *Acta Chem. Scand.*, **27**, 1637, 2335 (1973).
6) H. Yokoyama and H. Yamatera, This Bulletin, **44**, 1725 (1971).
7) R. Näsänen, *Acta Chem. Scand.*, **3**, 179, 959 (1949).
8) W. D. Bale, E. W. Davies, and C. B. Monk, *Trans. Faraday Soc.*, **52**, 816 (1956).
9) W. G. Davies, R. J. Otter, and J. E. Prue, *Discuss. Faraday Soc.*, **24**, 103 (1957).

TABLE 6. THE *BEST* VALUES OF a AND K OBTAINED FROM SPECTROPHOTOMETRY (sp), VAPOR-PRESSURE OSMOMETRY (vpo), AND CONDUCTIVITY MEASUREMENTS (con), WITH THE HELP OF THE THEORETICAL EXPRESSION[1] FOR THE ION-ASSOCIATION CONSTANT (25.0 °C)

Electrolyte	r_M+r_A[a] (Å)	From sp		From vpo		From con (recalcd)		
		a (Å)	K (mol^{-1} l)	a (Å)	K (mol^{-1} kg)	a (Å)	K (mol^{-1} l)	data
$MgSO_4$	3.5_3	5.8_5	98	5.4_6	110	5.4_4	111	22)
						5.5_8	106	23)
$CaSO_4$	3.8_7	5.5_5	107	4.9_2	134	5.4_2	112	24)
$MnSO_4$	3.6_8	5.5_1	108	4.6_4	151	5.1_4	123	25)
						4.9_5	132	26)
$CuSO_4$	3.6_0	4.6_5	151			4.7_3	146	29)
$ZnSO_4$	3.6_2	5.4_4	111			5.0_3	128	29)

a) Sum of crystallographic radii of the metal ion (r_M) and the sulfate ion (r_A). (The values have been given in the preceding paper.[2])

10) R. A. Matheson, *J. Phys. Chem.*, **69**, 1537 (1965).
11) P. Hemmes and S. Petrucci, *ibid.*, **72**, 3986 (1968).
12) F. A. Posey and H. Taube, *J. Amer. Chem. Soc.*, **79**, 255 (1957).
13) E. W. Davies and C. B. Monk, *Trans. Faraday Soc.*, **53**, 442 (1957).
14) F. G. R. Gimblett and C. B. Monk, *ibid.*, **51**, 793 (1955).
15) C. B. Monk, "Electrolytic Dissociation," Academic Press (1961), p. 194.
16) W. D. Bale, E. W. Davies, D. B. Morgans, and C. B. Monk, *Discuss. Faraday Soc.*, **24**, 94 (1957).
17) H. Yamada, T. Maeda, and I. Kojima, *Anal. Chim. Acta*, **72**, 426 (1974).
18) A. E. Martell and L. G Sillén, "Stability Constants," The Chemical Society, London (1964) p. 232; "Stability Constants," Supplement No. 1, The Chemical Society, London (1971) p. 134.
19) P. Debye and E. Hückel, *Phys. Z.*, **24**, 185 (1923).
20) N. Bjerrum, *Kgl. Danske Videnskab. Selskab.*, **7**, No. 9 (1926).
21) R. A. Robinson and R. H. Stokes, "Electrolyte Solutions," Butterworths (1959), p. 435.
22) H. S. Dunsmore and J. C. James, *J. Chem. Soc.*, **1951**, 2925.
23) S. Katayama, This Bulletin, **46**, 106 (1973).
24) E. Inada, K. Shimizu, and J. Osugi, *Nippon Kagaku Zasshi*, **92**, 1096 (1971); *Rev. Phys. Chem. Japan*, **42**, 1 (1972).
25) C. J. Hallada and G. Atkinson, *J. Amer. Chem. Soc.*, **83**, 3759 (1961).
26) S. Petrucci, P. Hemmes, and M. Battistini, *ibid.*, **89**, 5552 (1967).
27) R. M. Fuoss and K. -L. Hsia, *Proc. Nat. Acad. Sci. U.S.A.*, **57**, 1550 (1967); **58**, 1818 (1968).
28) R. Fernândez-Prini, *Trans. Faraday Soc.*, **65**, 3311 (1969).
29) B. B. Owen and R. W. Gurry, *J. Amer. Chem. Soc.*, **60**, 3074 (1938).

The Formation and Collapse of Mixed Monolayers of 1-Hexadecanol and 1-Octadecanol with Interest in Evaporation Control of Water by Monolayers[1)]

Noriaki FUNASAKI and Masayuki NAKAGAKI*

Kyoto College of Pharmacy, Misasagi, Yamashina, Higashiyama-ku, Kyoto 607

**Faculty of Pharmaceutical Sciences, Kyoto University, Sakyo-ku, Kyoto 606*

(Received April 28, 1975)

Collapse pressure, equilibrium spreading pressure, and melting points of binary mixtures of hexadecanol and octadecanol were measured in order to study the phase equilibrium among a monolayer, a solid, and a liquid and to apply the result to evaporation control of water by monolayers. Collapse pressure and equilibrium spreading pressure of solid mixtures have a maximum at a given composition, while the equilibrium spreading pressure of a liquid mixture has not a maximum. Melting points have a minimum at a given composition. From thermodynamic analysis of these phase equilibriums, it was concluded that the mixed monolayer and liquid mixture were ideal solutions, while the solid mixture was a lattice-distorted solid solution. That is, when the two components of different molecular volumes form a solid solution, the solid solution has high energy due to the distortion of the crystal lattice and consequently, it becomes easier to spread and the mixed monolayer becomes more stable against collapse. From these results, the relations between the composition of solid solution and the surface pressure, composition, and specific evaporation resistance of the mixed monolayer in equilibrium with the solid solution, were obtained.

It is said that a dusting of powdered solids of the mixed hexadecanol and octadecanol appears to meet best the purpose of the evaporation control of water by monolayers.[2)] Therefore, the effectiveness of lowering the evaporation rate by these mixed monolayers[2,3)] and the temperature dependence of the equilibrium spreading pressure[4)] have been studied in detail. But the relation between the composition of the solid mixture and the evaporation resistance of the monolayer which is in equilibrium with the solid mixture has not yet been found. The authors have shown how to get the relation between the compositions of a mixed monolayer and a bulk mixture in equilibrium with each other.[5,6)] By applying this method to the binary system of hexadecanol and octadecanol, the relation between the composition of the solid mixture and the specific evaporation resistance of the mixed monolayer in equilibrium with the solid mixture was obtained.

Theoretical

Phase equilibriums among a monolayer, a solid, and a liquid of the hexadecanol-octadecanol system are summarized in Scheme 1. The following notations are used hereafter: x is mole fraction, V is molal volume, μ is chemical potential, F is surface pressure, A is molecular area, $\bar{A}$ is partial molecular area, ΔH_v is molal heat of evaporation, ΔH_m is molal heat of fusion, and n is mole number; the subscripts 1 and 2 indicate the components 1 and 2, the subscripts e and m mean equilibrium and melting, the superscripts m, s, and l mean monolayer, solid, and liquid, and the superscript o means pure substance or standard state. R, T, and N are gas constant, absolute temperature, and Avogadro's number, respectively.

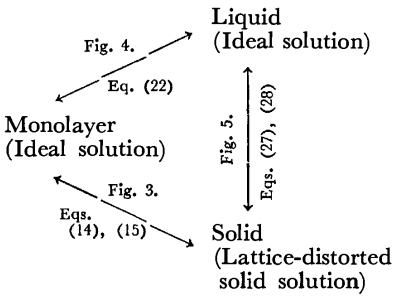

Scheme 1. Summarized relationship among three phases of a monolayer, a solid, and a liquid for the binary mixture of hexadecanol and octadecanol.

Equilibrium between a Monolayer and a Solid. It is known that the distortion energy of a crystal lattice due to the differences of size and shape of molecules contributes greatly to the heat of mixing of solids and, consequently, that it often makes the formation of a solid solution difficult.[7)] According to Scott,[7,8)] this distortion energy, ΔE_D, is given by the following equation:

$$\Delta E_D = \frac{2\delta_1\delta_2(V_1V_2)^{1/2}(V_1-V_2)^2}{x_1^sV_1^2+x_2^sV_2^2}x_1^sx_2^s, \quad (1)$$

where δ is the solubility parameter:

$$\delta = \left(\frac{\Delta H_v - RT}{V}\right)^{1/2}. \quad (2)$$

In order to simplify this equation, ω is defined as

$$\omega = 2\delta_1\delta_2(V_1V_2)^{1/2}(V_1-V_2)^2. \quad (3)$$

Assuming that the entropy of mixing ΔS and the enthalpy of mixing ΔH may be written as

$$\Delta S = -R(x_1^s \ln x_1^s + x_2^s \ln x_2^s) \quad (4)$$

and

$$\Delta H = \Delta E_D, \quad (5)$$

and from the definitions of Gibbs free energy G and chemical potential μ:

$$\Delta G = \Delta H - T\Delta S \quad (6)$$

and

$$\mu_1^s - \mu_1^{os} = \left[\frac{\partial(n_1+n_2)\Delta G}{\partial n_1}\right]_{T,P,n_2}, \quad (7)$$

we obtain μ_1^s for component 1:

$$\mu_1^s = \mu_1^{os} + RT\ln x_1^s + \frac{\omega(x_2^sV_2)^2}{(x_1^sV_1^2+x_2^sV_2^2)^2}. \quad (8)$$

Similarly, we obtain μ_2^s for component 2:

$$\mu_2^s = \mu_2^{0s} + RT\ln x_2^s + \frac{\omega(x_1^s V_1)^2}{(x_1^s V_1^2 + x_2^s V_2^2)^2}, \quad (9)$$

where μ^{os} is the chemical potential in the pure solid. Assuming that a mixed monolayer is considered as an ideal solution, in the equilibrium state of a monolayer and a solid, the following equations

$$\mu_1^{0s} + RT\ln x_1^s + \frac{\omega(x_2^s V_2)^2}{(x_1^s V_1^2 + x_2^s V_2^2)^2} = \mu_1^{0m} + RT\ln x_1^m + N\bar{F}A_1 \quad (10)$$

and

$$\mu_2^{0s} + RT\ln x_2^s + \frac{\omega(x_1^s V_1)^2}{(x_1^s V_1^2 + x_2^s V_2^2)^2} = \mu_2^{0m} + RT\ln x_2^m + N\bar{F}A_2 \quad (11)$$

can be established,[5,6] where μ^{om} is the standard chemical potential in the monolayer. For the one-component systems,

$$\mu_1^{0s} = \mu_1^{0m} + NF_{1e}A_{1e} \quad (12)$$

and

$$\mu_2^{0s} = \mu_2^{0m} + NF_{2e}A_{2e} \quad (13)$$

are derived from Eqs. (10) and (11). Substituting Eqs. (12) and (13) for Eqs. (10) and (11), we obtain the following equations:

$$RT\ln x_1^s + \frac{\omega(x_2^s V_2)^2}{(x_1^s V_1^2 + x_2^s V_2^2)^2} + NF_{1e}A_{1e} = RT\ln x_1^m + N\bar{F}A_1 \quad (14)$$

and

$$RT\ln x_2^s + \frac{\omega(x_1^s V_1)^2}{(x_1^s V_1^2 + x_2^s V_2^2)^2} + NF_{2e}A_{2e} = RT\ln x_2^m + N\bar{F}A_2. \quad (15)$$

Equilibrium between a Monolayer and a Liquid. Assuming that both the monolayer and the liquid are ideal solutions, in equilibrium with each other, the following equations

$$\mu_1^{01} + RT\ln x_1^l = \mu_1^{0m} + RT\ln x_1^m + N\bar{F}A_1 \quad (16)$$

and

$$\mu_2^{01} + RT\ln x_2^l = \mu_2^{0m} + RT\ln x_2^m + N\bar{F}A_2 \quad (17)$$

can be established.[5,6] For the one-component systems,

$$\mu_1^{01} = \mu_1^{0m} + NF_{1e}A_{1e} \quad (18)$$

and

$$\mu_2^{01} = \mu_2^{0m} + NF_{2e}A_{2e} \quad (19)$$

are derived from Eqs. (16) and (17). Substituting Eqs. (18) and (19) for Eqs. (16) and (17), we obtain the following equations:

$$RT\ln x_1^l + NF_{1e}A_{1e} = RT\ln x_1^m + N\bar{F}A_1 \quad (20)$$

and

$$RT\ln x_2^l + NF_{2e}A_{2e} = RT\ln x_2^m + N\bar{F}A_2. \quad (21)$$

Substituting Eqs. (20) and (21) for the following equation:

$$x_1^l + x_2^l = 1,$$

we obtain Eq. (22):

$$x_1^m e^{(F\bar{A}_1 - F_{1e}A_{1e}/kT)} + x_2^m e^{(F\bar{A}_2 - F_{2e}A_{2e}/kT)} = 1. \quad (22)$$

Equilibrium between a Solid and a Liquid. In the equilibrium state of a solid and a liquid, from Eqs. (10), (11), (16), and (17), we obtain Eqs. (23) and (24):

$$\mu_1^{0s} + RT\ln x_1^s + \frac{\omega(x_2^s V_2)^2}{(x_1^s V_1^2 + x_2^s V_2^2)^2} = \mu_1^{01} + RT\ln x_1^l \quad (23)$$

and

$$\mu_2^{0s} + RT\ln x_2^s + \frac{\omega(x_1^s V_1)^2}{(x_1^s V_1^2 + x_2^s V_2^2)^2} = \mu_2^{01} + RT\ln x_2^l. \quad (24)$$

Assuming that ΔC_p is independent of temperature, the following equations

$$\mu_1^{01} - \mu_1^{0s} = \Delta H_{1m}\left(1 - \frac{T}{T_{1m}}\right) - \Delta C_{1p}(T_{1m} - T) + T\Delta C_{1p}\ln\frac{T_{1m}}{T} \quad (25)$$

and

$$\mu_2^{01} - \mu_2^{0s} = \Delta H_{2m}\left(1 - \frac{T}{T_{2m}}\right) - \Delta C_{2p}(T_{2m} - T) + T\Delta C_{2p}\ln\frac{T_{2m}}{T} \quad (26)$$

are derived for the one-component systems.[9] Substituting Eqs. (25) and (26) for Eqs. (23) and (24), we obtain Eqs. (27) and (28):

$$\Delta H_{1m}\left(1 - \frac{T}{T_{1m}}\right) - \Delta C_{1p}(T_{1m} - T) + T\Delta C_{1p}\ln\frac{T_{1m}}{T} + RT\ln x_1^l = RT\ln x_1^s + \frac{\omega(x_2^s V_2)^2}{(x_1^s V_1^2 + x_2^s V_2^2)^2} \quad (27)$$

and

$$\Delta H_{2m}\left(1 - \frac{T}{T_{2m}}\right) - \Delta C_{2p}(T_{2m} - T) + T\Delta C_{2p}\ln\frac{T_{2m}}{T} + RT\ln x_2^l = RT\ln x_2^s + \frac{\omega(x_1^s V_1)^2}{(x_1^s V_1^2 + x_2^s V_2^2)^2}, \quad (28)$$

where ΔC_p is the differences in the molal heat capacities between the liquid and the solid.

Experimental

Materials. The 1-hexadecanol and 1-octadecanol used are supplied by Nihon Yushi Company. The composition of hexadecanol (abbreviated as $C_{16}OH$) was $C_{18}OH$ 0.6%, $C_{16}OH$ 99.0%, and $C_{14}OH$ 0.4% and that of octadecanol was $C_{20}OH$ 1.0%, $C_{18}OH$ 98.7%, and $C_{16}OH$ 0.3%. The melting points of hexadecanol and octadecanol were 50.0—50.5 °C (literature value[10,11] 49.3 °C) and 58.5—59.0 °C (literature value[10] 58.0 °C), respectively. The solid mixture was prepared by the methods of fusion and solution (*n*-hexane as solvent; details have been reported previously[5,6]) and used later than one month after the preparation. The water and *n*-hexane of analytical grade used were distilled twice.

Measurement of Surface Pressure. The surface pressure was measured at 20±0.1 °C using a surface trough equipped with a vertical-type surface balance described previously.[5,6] The pressure-area curve was drawn by measuring the surface pressure of the monolayer which had been compressed at nearly constant speed independently of the area and the composition of mixed monolayers. The equilibrium spreading pressure was determined as an unvaried surface pressure exerted after the solid mixture (prepared by the solution method) had been placed onto the aqueous surface. Details

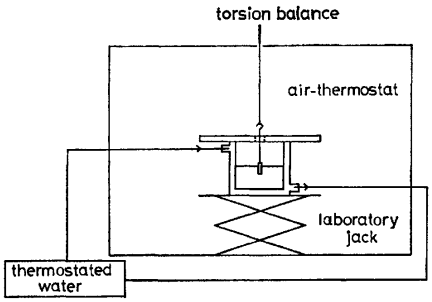

Fig. 1. The apparatus for measuring surface pressure at 65 °C.

have been described previously.[5,6]

The equilibrium spreading pressure at 65±0.2 °C was measured by means of the same surface balance in a thermostated glass cell (Fig. 1).

Measurement of Melting Points. The initial and final melting points of solid mixtures (prepared by the methods of solution and fusion) were measured with a Yanagimoto-melting point apparatus, SR-50, equipped with a polarization microscope.

Results

Collapse Pressure and Equilibrium Spreading Pressure. Figure 2 shows the pressure-area curve of a hexadecanol monolayer at 20 °C. The collapse pressure, F_c, was determined as the surface pressure unvaring with the area after the monolayer began to collapse. The collapse pressures of mixed monolayers of hexadecanol and octadecanol were likewise determined. The open circles in Fig. 3 show the relation between the collapse pressure and the mole fraction of hexadecanol in mixed monolayer, x_{16}^m. The closed circles in Fig. 3 show the relation between the equilibrium spreading pressure, F_e, and the mole fraction of hexadecanol in the solid mixture, x_{16}^s. The values of F_c and F_e have a maximum, at which F_c and F_e are 44.0 and x_{16}^m and x_{16}^s are 0.56 dyn/cm. The collapse pressure of hexadecanol, F_{16c}, was equal to the

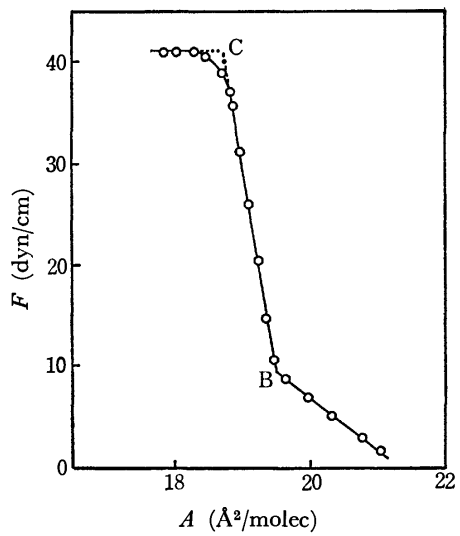

Fig. 2. The pressure-area curve of a hexadecanol monolayer at 20 °C.

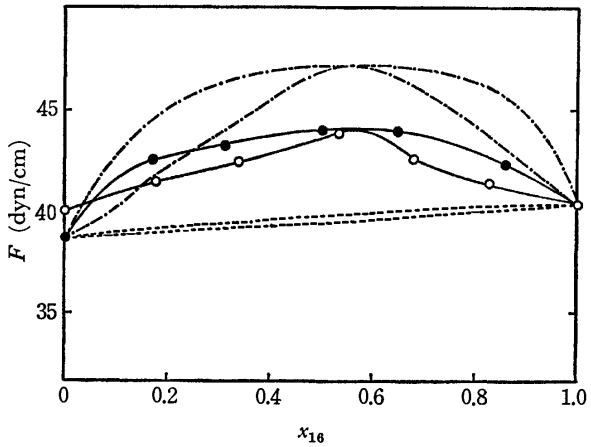

Fig. 3. Equilibrium spreading pressure and collapse pressure for the binary mixture of hexadecanol and octadecanol at 20 °C.
●: $F_e-x_{16}^s$, ○: $F_c-x_{16}^m$. —·— Curve calculated from the Eqs. (14) and (15). ---- Curve calculated from the Eqs. (32) and (33).

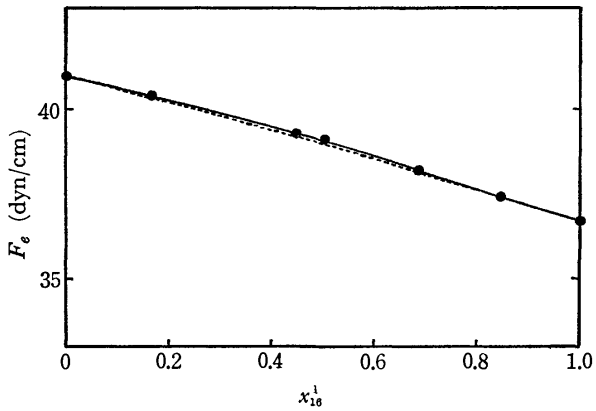

Fig. 4. Equilibrium spreading pressure for the binary system of hexadecanol and octadecanol at 65 °C.
●: $F_e-x_{16}^l$. ---- Curve calculated from the Eq. (22).

equilibrium spreading pressure, F_{16e}, while the collapse pressure of octadecanol, F_{18c}, was higher than the equilibrium spreading pressure, F_{18e}. This means that the octadecanol monolayer tends to be over-compressed. Therefore, it is suspected that the collapse pressure of octadecanol-rich mixed monolayer is also higher than the equilibrium value.

Since the value of the equilibrium spreading pressure varies greatly near the melting point,[4,11] the equilibrium spreading pressure of liquid was measured at 65 °C somewhat higher than the melting points of the mixtures. The closed circles in Fig. 4 show the relation between the equilibrium spreading pressure at 65 °C and the mole fraction of hexadecanol in the liquid mixture, x_{16}^l. In this case, it was found that the equilibrium spreading pressure did not have a maximum. The measurement of the collapse pressure at 65 °C was very hard because of the dissolution of the monolayers and the evaporation of the underlying water.

Phase Diagram of Solid-Liquid Equilibrium. The open and closed circles in Fig. 5 are initial and final

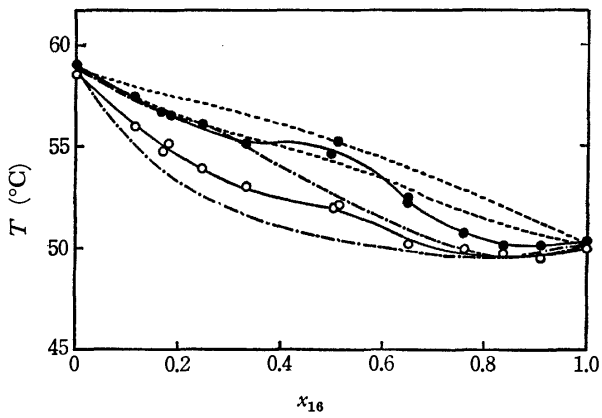

Fig. 5. The initial and final melting points for the binary system of hexadecanol and octadecanol.
○: Initial melting point, ●: final melting point.
—·— Curve calculated from the Eqs. (27) and (28).
----- Curve calculated from the Eqs. (27) and (28) with $\omega=0$.

melting points of the solid mixtures, respectively. It was found that mixtures of hexadecanol and octadecanol form a complete series of solid solutions and the melting points have a minimum near $x_{16}=0.84$.

Discussion

Phase Equilibriums among a Monolayer, a Solid, and a Liquid. Equilibrium between a Monolayer and a Solid: The numerical values of ΔH_v, V_1/V_2, F_e, A_e, and $\overline{A}$ are necessary for calculating x^m and x^s at a given surface pressure from Eqs. (14) and (15). From Figs. 2 and 3, we obtain $F_{16e}=40.8$ dyn/cm, $F_{18e}=38.7$ dyn/cm, $A_{16e}=18.70$ Å^2/molec, and $A_{18e}=18.76$ Å^2/molec. $\overline{A}$ was assumed to be equal to the molecular area, A, calculated from the state equation of the solid film using Fig. 2 (straight line BC):

$$A = -0.0265F + 19.78 \quad (\text{Å}^2/\text{molec}). \tag{29}$$

ΔH_v was calculated from the experimental results of Davies and Kybett:[12]

$$\Delta H_{16v} = 47.6 - 0.0642T \quad (\text{kcal/mol}) \tag{30}$$

and

$$\Delta H_{18v} = 52.8 - 0.0716T \quad (\text{kcal/mol}) \tag{31}$$

with $T=293.15$ K. For the ratio of molar volumes, V_{18}/V_{16}, 1.118, which is the value of supercooled liquid at 20 °C,[10] was used.

Substituting these numerical values and solving the simultaneous equation of Eqs. (14) and (15) numerically, we obtain x_{16}^m and x_{16}^s at a given surface pressure. These calculated results are shown by the chained lines in Fig. 3. In addition, assuming that the solid solution is ideal *viz.*, $\omega=0$, we obtain from Eqs. (14) and (15) the following equations:

$$x_1^m e^{(F\overline{A}_1-F_{1e}A_{1e})/kT} + x_2^m e^{(F\overline{A}_2-F_{2e}A_{2e})/kT} = 1 \tag{32}$$

and

$$x_1^s = x_1^m e^{(F\overline{A}_1-F_{1e}A_{1e})/kT}. \tag{33}$$

We can calculate x_{16}^m and x_{16}^s at a given surface pressure from Eqs. (32) and (33). These calculated results are shown by the dotted lines in Fig. 3. The values calculated as an ideal solid solution are very different from the experimental values, while the values calculated as a lattice-distorted solid solution explain the features of the experimental values well. It is, however, found that ΔE_D of Eq. (1) is slightly too large.

Equilibrium between a Monolayer and a Liquid: From the experimental results of Fig. 4, we obtain $F_{16e}=36.7$ dyn/cm and $F_{18e}=41.0$ dyn/cm. The values of A_{16e}, A_{18e}, $\overline{A}_{16}$, and $\overline{A}_{18}$ at 65 °C are set equal to 24.8 Å^2/molec, the value of which is extrapolated from the data of Boyd and Schubert.[11] Substituting these values in Eqs. (22) and (20), we can calculate x_{16}^m and x_{16}^l at a given surface pressure. This result is shown by the dotted line in Fig. 4 and is in close agreement with the experimental values.

Equilibrium between a Solid and a Liquid: T_{16m} and T_{18m} are 323.20 K and 331.70 K (our values). According to Davies,[12]

$$\Delta H_{16m} = 3.6 + 0.0316T \quad (\text{kcal/mol}),$$

$$\Delta H_{18m} = 5.7 + 0.0362T \quad (\text{kcal/mol}),$$

$$\Delta C_{16p} = 0.0316 \quad (\text{kcal/mol}\cdot\text{deg}),$$

and

$$\Delta C_{18p} = 0.0362 \quad (\text{kcal/mol}\cdot\text{deg}).$$

Substituting these values for Eqs. (27) and (28), we can solve these equations numerically as a simultaneous equation. These results are shown by the chained lines in Fig. 5. Moreover, the values which are calculated from Eqs. (27) and (28) with $\omega=0$, *viz.*, as ideal solid solution, are also shown by the dotted lines in Fig. 5. The experimental values are different from the dotted lines, while they have the same tendency as the chained lines. It is, however, found that ΔE_D of Eq. (1) is slightly too large.

From the above thermodynamic treatment of phase equilibriums among a monolayer, a solid, and a liquid for the binary system of hexadecanol and octadecanol, it is concluded that a monolayer and a liquid are ideal solutions and a solid is a lattice-distorted solution, as is shown in Scheme 1. In other words, when the two components consisting of different molecular volumes form a solid solutions, the solid solution has a high energy due to the distortion of the crystal lattice; consequently, it becomes easier to spread and easier to melt and the mixed monolayer becomes more stable against collapse. These are found from the comparison of the solid lines with the dotted lines in Figs. 3 and 5.

Application to Evaporation Control of Water by Monolayers. In view of the effectiveness of lowering evaporation rate, spreading rate, and economic reasons, it is said that dusting of powdered solids of the mixed hexadecanol and octadecanol appears to meet best the purpose of evaporation control of water by monolayers.[2]

If a horizontal line is drawn at a given surface pressure in Fig. 3, the intersections of this line with the curve of the equilibrium spreading pressure (drawn through closed circles) and with the curve of the collapse pressure (drawn through open circles) give the

mole fractions of hexadecanol in the solid solution and the mixed monolayer, respectively. Therefore, if the composition of the solid solution is given, the equilibrium spreading pressure and the composition of the mixed monolayer in equilibrium are determined.

The specific evaporation resistance of the mixed monolayer, representing the effectiveness of lowering evaporation rate, can be calculated as a function of the surface pressure and the composition of mixed monolayer from the following equations:[2,3]

$$\ln r = \frac{FA^{\ddagger}}{kT} + \frac{mE^{\ddagger}_{CH_2}}{RT} + \text{constant} \qquad (34)$$

and

$$\ln r = x_1^m \ln r_1 + x_2^m \ln r_2 . \qquad (35)$$

Figure 6 shows the relation between the specific resistance and the mole fraction of hexadecanol in solid solution calculated from the data of Fig. 3, using

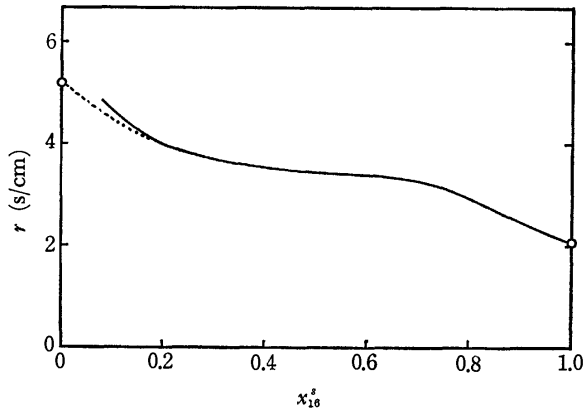

Fig. 6. The relation between the specific evaporation resistance and the mole fraction of hexadecanol in solid solution which is in equilibrium with the mixed monolayer of hexadecanol and octadecanol.

Eqs. (34) and (35). The mixed monolayer tends to be slightly overcompressed in the region where the mole fraction of octadecanol is large. It seems likely that the dotted line through the open circles represents the relation between r and x_{16}^s at equilibrium. As the result, it may be concluded that the lowering of the evaporation rate of water is expected to be more effective when a solid mixture contains more octadecanol. It is also seen from Fig. 6 that the effect remains almost unchanged when the solid mixture is varied over the compositions between 0.3 and 0.7.

References

1) Presented at the 28th Meeting of Chemical Society of Japan, April, 1973.
2) G. T. Barnes and V. K. LaMer, "Retardation of Evaporation by Monolayers," ed. by V. K. LaMer, Academic Press, New York, London (1962), pp. 9, 32.
3) V. K. LaMer, L. A. G. Aylmore, and T. W. Healy, *J. Phys. Chem.*, **67**, 2793 (1963).
4) J. H. Brooks and A. E. Alexander, "Retardation of Evaporation by Monolayers," ed. by V. K. LaMer, Academic Press, New York, London (1962), p. 245.
5) M. Nakagaki and N. Funasaki, This Bulletin, **47**, 2094 (1974).
6) M. Nakagaki and N. Funasaki, *ibid.*, **47**, 2482 (1974).
7) J. H. Hildebrand and R. L. Scott, "The Solubility of Nonelectrolytes," Dover, New York (1964), pp. 302—304.
8) R. L. Scott, *Phys. Rev.*, **78**, 317 (1950).
9) J. H. Hildebrand and R. L. Scott, "The Solubility of Nonelectrolytes," Dover, New York (1964), p. 270.
10) "Yushikagaku Binran," ed. by Japanese Oil Chemists' Society, 2nd Ed., Maruzen (1971), p. 126.
11) G. E. Boyd and J. Schubert, *J. Phys. Chem.*, **61**, 1271 (1957).
12) M. Davies and B. Kybett, *Trans. Faraday Soc.*, **61**, 1608 (1965).

The Raman Spectra and the Phase Transition of 1,2-Dibromoethane

Jiro HIRAISHI and Takako SHINODA

National Chemical Laboratory for Industry, Honmachi, Shibuya-ku, Tokyo 151

(Received May 13, 1975)

The lattice vibrations of 1,2-$C_2H_4Br_2$ and 1,2-$C_2D_4Br_2$ were measured by means of Raman spectroscopy. The temperature dependence of the frequencies and the half widths of the lattice vibrations indicates that the phase transition of the crystal is associated with the rotation of the molecule around the Br–Br axis.

The solids 1,2-dichloroethane and 1,2-dibromoethane, undergo a phase transition at 177 and 249.49 K, respectively.[1] According to the X ray diffraction studies by Lipscomb *et al.*,[2-4] the crystal of both the high (α-phase) and the low temperature phase (β-phase) of 1,2-dichloroethane is monoclinic and belongs to the space group C_{2h}^5-$P2_1/c$. A unit cell consists of two molecules. Ozora, Nakagawa, and Ito[5] studied the temperature dependence of the low frequency Raman bands of 1,2-dichloroethane and concluded that the phase transition is associated with the free rotation of the molecule about the Cl-Cl axis, which agrees with the result by Reeds and Lipscomb.[3]

On the other hand, the crystal structure and the nature of the phase transition of 1,2-dibromoethane have not been studied in detail. Pitzer[1] measured the heat capacity of the crystal and suggested that the structure of the α-phase of 1,2-dibromoethane was different from that of the β-phase. Reeds and Lipscomb[3] quoted the work by Meerman and stated that the β-phase of 1,2-dibromoethane has the same structure as that of the β-phase of 1,2-dichloroethane. In the present paper we report the temperature dependence of the low frequency Raman bands of 1,2-$C_2H_4Br_2$ and 1,2-$C_2D_4Br_2$ and discuss the nature of the phase transition of the crystal.

Experimental

A chemically pure grade reagent of 1,2-$C_2H_4Br_2$ obtained from Tokyo Kasei Co. Ltd. was further purified by means of a spinning band fractional distillation column made by Tokyo Kagaku Seiki Co. Ltd. 1,2-$C_2D_4Br_2$ purchased from Merk Darmstadt Germany was used for the measurement without further purification.

The Raman spectra were measured by use of a laser Raman spectrometer, Kawaguchi Electric Works model RL-62. The 514.5 nm line of a NEC argon ion laser model GLG2003 was used as an exciting source.

Figure 1 shows the cryostat designed in our laboratory for the measurement of the Raman spectra of liquid or solid samples in the range from liquid helium temperature to about 150 °C. About one litre of liquid helium can be contained in D. A thermal station C has an volume of about 100 ml. For measurements below 90 K the cryostat is covered by a glass vessel which contains liquid nitrogen. A sample cell, shown in Fig. 2, is made of quartz glass. The cell is hung by means of nylon cords within the adiabatic shield. The temperature was measured by use of a chlomel p-constantan thermocouple, the calibration of which was reported elsewhere.[6] A germanium resistance thermometer, which was calibrated by Cryocal. Inc., was used in the temperature range below 30 K. The temperature of the sample was held constant within ± 0.05 K during a measurement of a band.

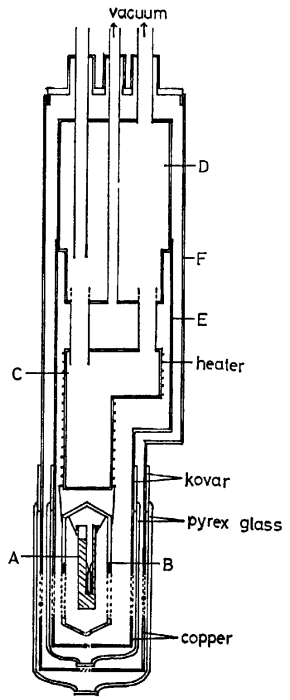

Fig. 1. A cross-section of the cryostat. A: sample vessel, B: adiabatic shield, C: thermal station, D: coolant container, E: inside jacket, and F: outside jacket.

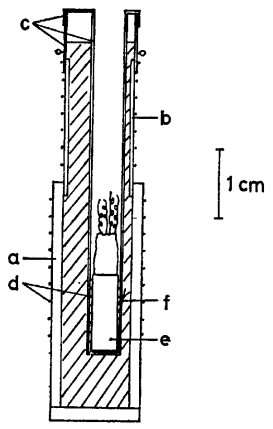

Fig. 2. A cross-section of the sample vessel. a: quartz glass, b: Kovar tube, c: silver-plated copper, d: manganin heater, e: germanium thermometer, and f: thermocouple.

Result and Discussions

Assignment of the Low Frequency Raman Bands of the β-Phase. Four bands at 27.7, 44.9, 56.9, and 126.5 cm^{-1} were observed for 1,2-$C_2H_4Br_2$ at 40.0 K in the frequency region below 150 cm^{-1}. 1,2-dibromoethane has two rotational isomers, the *trans* and *gauche* forms. As the molecule has a *trans* form in the crystalline state[7] and the lowest frequency[8] of the Raman active intramolecular vibrations of the *trans* form is 190 cm^{-1}, the bands observed below 150 cm^{-1} are definitely attributable to the lattice vibrations. According to Ozora, Nakagawa, and Ito,[5] the β-phase of 1,2-$C_2H_4Cl_2$ also exhibits four bands in the Raman spectra below 150 cm^{-1}. This result does not contradict the suggestion by Pitzer[1] that the crystal structure of the β-phase of 1,2-$C_2H_4Br_2$ is the same as that of the β-phase of 1,2-$C_2H_4Cl_2$.

Six rotational lattice vibrations ($3a_g+3b_g$) are expected to appear in the Raman spectrum of the β-phase. Ozora, Nakagawa, and Ito assigned the highest frequency band of the four of the β-phase of 1,2-$C_2H_4Cl_2$ to the rotational mode about the Cl-Cl axis. In order to confirm the assignments we also observed the Raman spectrum of 1,2-$C_2D_4Br_2$. The observed frequencies of 1,2-$C_2H_4Br_2$ and 1,2-$C_2D_4Br_2$ near 95 K are shown in Table 1. The transition temperature, T_c, of 1,2-$C_2D_4Br_2$ crystal was found to be about 256.0 K, from the total thermal analysis, by using the cryostat described above. As the T_c of 1,2-$C_2D_4Br_2$ is higher by about 6.5 K than that of 1,2-$C_2H_4Br_2$, the temperature for 1,2-$C_2D_4Br_2$ in Table 1 is a little higher than that for 1,2-$C_2H_4Br_2$. ν_D/ν_H and $I_D(A)/I_H(A)$ in the table represent the values of the ratios of the frequencies and the principal moment of inertia around the A axis, respectively, of 1,2-$C_2D_4Br_2$ to those of 1,2-$C_2H_4Br_2$. The values of the moment of inertia of the molecules were calculated by assuming that all of the valence angles were 109°28′ and the interatomic distances were $r_{CH}=r_{CD}=1.09$, $r_{CC}=1.54$, and $r_{CBr}=1.91$ Å.[9] The lowest frequency band observed at 27.7 cm^{-1} for 1,2-$C_2H_4Br_2$ at 40.0 K was not observed above 80 K, as the tail of the Rayleigh scattering band lapped over the band. The result of Table 1 indicates that the highest frequency band at approximately 120 cm^{-1} for 1,2-$C_2H_4Br_2$ or at approximately 100 cm^{-1} for 1,2-$C_2D_4Br_2$ should be assigned to the rotational lattice vibration about the C axis, that is, the Br-Br axis.

Temperature Dependence of the Raman Bands. Figure 3 shows the Raman spectra of the crystals at several temperatures. Below T_c three or four bands are observed for each crystal, while only one band was observed above T_c, although for the β-phase of 1,2-

Table 1. Observed frequencies near 95 K

$C_2H_4Br_2$ (93.6K)	43.6 cm^{-1}	55.4	121.4
$C_2D_4Br_2$ (96.5K)	43.1	54.9	99.0
ν_D/ν_H	0.989	0.991	0.815

$\sqrt{I_H(A)/I_D(A)}=0.996$, $\sqrt{I_H(B)/I_D(B)}=0.998$, $\sqrt{I_H(C)/I_D(C)}=0.815$

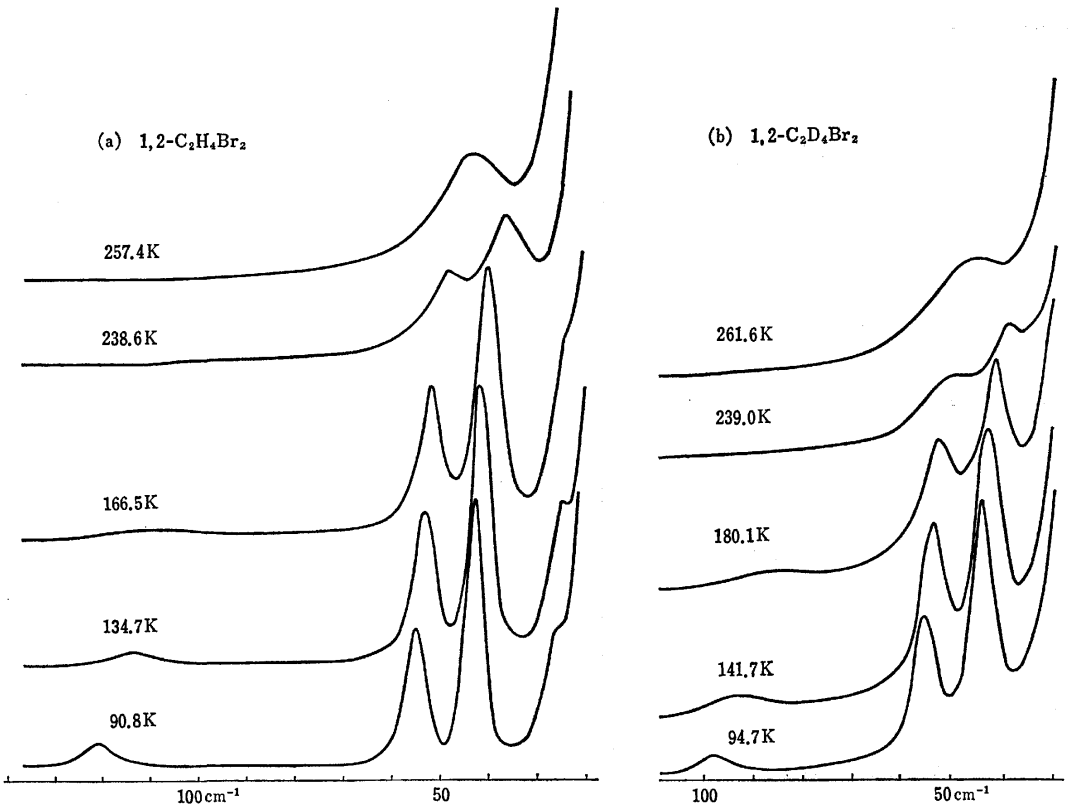

Fig. 3. The Raman spectra of (a) 1,2-$C_2H_4Br_2$ and (b) 1,2-$C_2D_4Br_2$ below 150 cm^{-1} at several temperatures.

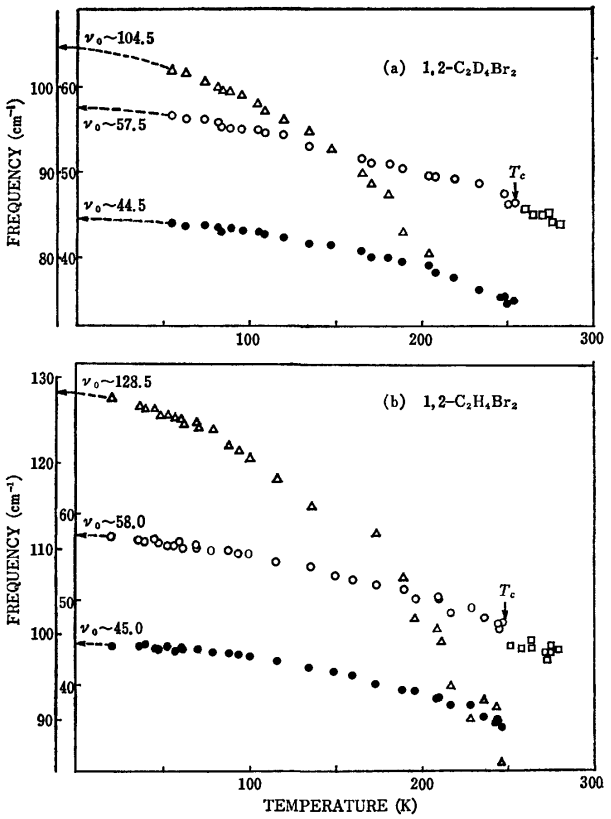

Fig. 4. The temperature dependence of the frequencies of the lattice vibrations.

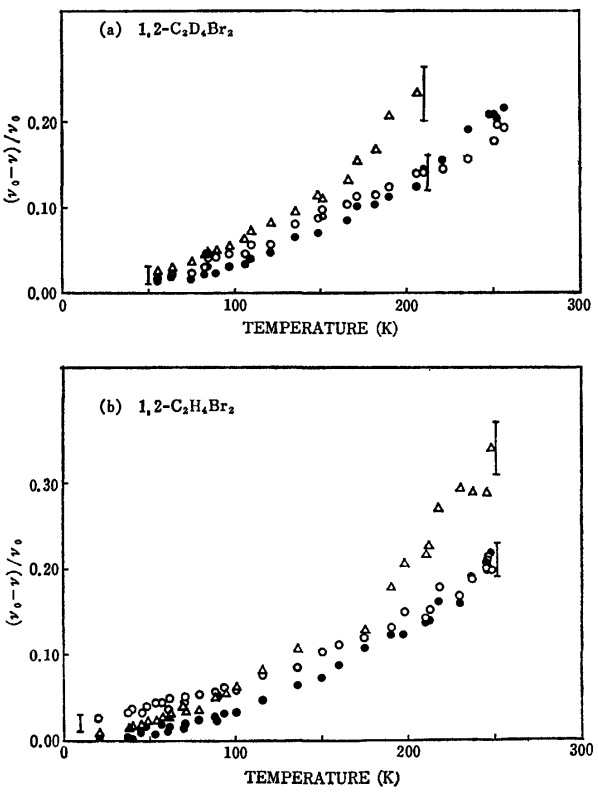

Fig. 5. The temperature dependence of $(\nu_0-\nu)/\nu_0$, where ν_0 represents the frequency obtained by extrapolation to 0 K (see text).

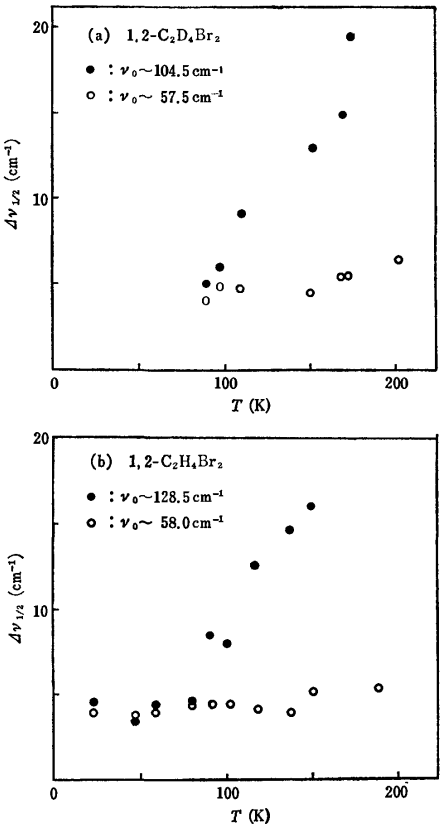

Fig. 6. The temperature dependence of the half width of the lattice vibrations.

dichloroethane two bands were reported.[5] The result may be explained in terms of a crystal structure of 1,2-dibromoethane different from that of 1,2-dichloroethane above T_c.

The widths and frequencies of lattice vibrations depend on temperature due to unharmonicity. Near T_c the crystal is expected to be very unharmonic. If there is a lattice vibration which is associated with the phase transition, the frequency of the vibration will depend on temperature much more than the other vibrations.[10] As Fig. 4 shows, the frequencies of the lattice vibrations of the crystals decreases as the temperature approaches T_c. By extrapolating the frequencies to the limit at 0 K, the values of ν_0 were estimated for each band; those are also given in Fig. 4. Figures 5 and 6 show the temperature dependence of $(\nu_0-\nu)/\nu_0$ and half width of each band. The lines in Figs. 5 and 6 represent the errors in the measurements. The frequencies of the rotational lattice vibrations about the Br–Br axis of the β-phase decrease and the half widths of the bands increases greatly with approaching Tc, as compared with the other rotational lattice vibrations. In other words, the rotational vibration about the Br-Br axis is more unharmonic than the others, which suggests that the phase transition of the crystal is associated with a rotational motion of the molecule around its Br-Br axis.

References

1) K. S. Pitzer, *J. Amer. Chem. Soc.*, **62**, 331 (1940).
2) M. E. Milberg and W. N. Lipscomb, *Acta Crystallogr.*,

4, 369 (1951).
3) T. B. Reeds and W. N. Lipscomb, *ibid.*, **6**, 45 (1953).
4) W. N. Lipscomb and F. E. Wang, *ibid.*, **14**, 1100 (1961).
5) A. Ozora, T. Nakagawa, and M. Ito, This Bulletin, **45**, 95 (1972).
6) H. Enokido, T. Shinoda, and Y. Mashiko, *ibid.*, **44**, 108 (1971).
7) S. Mizushima and Y. Morino, *Proc. Ind. Acad. Sci.*, **8**, 315 (1938).
8) T. Shimanouchi, Tables of Molecular Vibrational Frequencies Consolidated Vol. 1. NSRDS-NBS 39, United States Department of Commerce (1972).
9) L. E. Sutton, "Tables of Interatomic Distances and Configuration in Molecules and Ions," The Chemical Society, London (1958).
10) See references cited by P. M. A. Sherwood in "Vibrational Spectroscopy of Solids," Cambridge University Press (1972).

Photoelectron Spectroscopic Study of Skew Compounds. Methylhydrazine and Unsymmetrical Dimethylhydrazine

Katsumi KIMURA, Shunji KATSUMATA, and Kazuteru OSAFUNE[1)]

Physical Chemistry Laboratory, Institute of Applied Electricity, Hokkaido University, Sapporo 060

(Received June 28, 1975)

The He I photoelectron spectra of unsymmetric hydrazines CH_3HNNH_2 and $(CH_3)_2NNH_2$ have been measured and CNDO/2 calculations have been carried out, in which *gauche* (outer- and inner-skew) forms and *trans* form were taken into account for CH_3HNNH_2 and *gauche* and *trans* form for $(CH_3)_2NNH_2$. It has been found that nonbonding splittings in the photoelectron spectra are well reproduced by CNDO/2 calculations with *gauche* forms. The present results of conformation are supported by available conformational studies. The following conclusions have been obtained on orbital assignments of the photoelectron spectra: 1) The first and second bands are due to the methylated and unmethylated nitrogen lone pairs, respectively. 2) The third bands are attributed to the N–N bonding orbitals. 3) The rest of the photoelectron spectra up to 18 eV can be explained in terms of other p-type orbitals (C–N bonding, CH_3 pseudo π, and NH_2 pseudo π).

Previously, the He I photoelectron spectra of typical skew compounds, hydrazine[2)] and hydrogen peroxide,[3)] have been interpreted in terms of Walsh-type diagrams based on the CNDO/2 method. The separations of the first two photoelectron ionization bands due to nonbonding orbitals in these skew compounds have well been reproduced by CNDO/2 calculations at available dihedral angles. Recently, for a series of symmetrical dimethyl derivatives of hydrazine, hydrogen peroxide, and hydrogen disulfide, a similar analysis of He I photoelectron spectra[4)] suggested conformations that CH_3OOCH_3 has a *trans* planar form, while $CH_3HNNHCH_3$ and CH_3SSCH_3 are in *gauche* form. In connection with the previous studies,[2-4)] in the present work we have extended our photoelectron work to two kinds of unsymmetrical hydrazines in order to study nonbonding splittings as well as variations in inner valence orbitals with possible different conformations.

Nelsen and Buschek[5)] studied the nonbonding splittings of the photoelectron spectra of CH_3HNNH_2 and $(CH_3)_2NNH_2$ together with many other hydrazines, and indicated from INDO calculations that nonbonding splittings may be interpreted with a dihedral angle of 90°. Independently, Rademacher[6)] estimated the dihedral angles of various hydrazines by analyzing photoelectron nonbonding splittings. Bodar *et al.*[7)] earlier suggested in their He I photoelectron spectra of retarding-potential type for hydrazines that the nonbonding splitting reflects the skew angle.

From an entropy consideration, Janz and Russell[8)] indicated that the gaseous methylhydrazine exists predominantly as an outer-skew form. This compound can exist in either of two possible *gauche* conformations, "outer" or "inner" form. The *gauche* form with the methyl group farthest from the hydrogens of the amino group is called the outer form, while the other is known as the inner form.[8)] The outer form of methylhydrazine was later supported by an infrared and Raman study by Durig *et al.*[9)] For $(CH_3)_2NNH_2$ it was also indicated by Durig and Harris[10)] that the compound mainly exists in *gauche* rather than *trans* form.

Experimental

Measurements of He I photoelectron spectra were carried out with a high-resolution photoelectron spectrometer used previously.[2-4)] Calibration of the ionization energy scale was carried out using known ionization energies of Xe as an internal standard. Gaseous samples were introduced through a vacuum glass line with a teflon needle valve. The compounds studied are liberated from commercial hydrochloride salts in aqueous alkaline solution, and then were dehydrated by barium oxide and finally distilled in vacuum.

Results and Discussion

The He I photoelectron spectra obtained here for methylhydrazine and unsymmetrical dimethylhydrazine are shown by curves (a) and (b), respectively, in Fig. 1. Since the previous photoelectron works[11-14)] of various series of alkyl compounds have indicated that

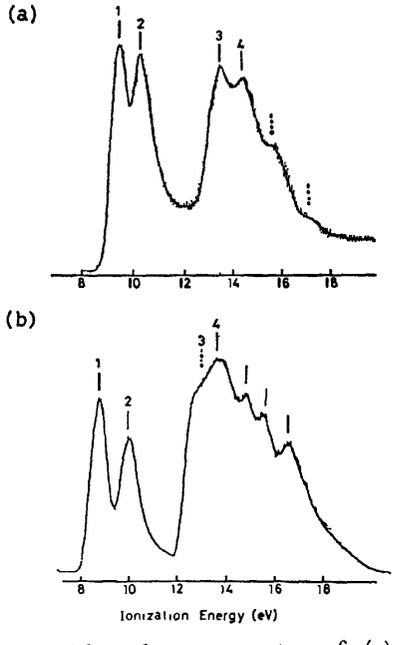

Fig. 1. He I Photoelectron spectra of (a) methylhydrazine and (b) unsymmetric dimethylhydrazine.

all photoelectron bands due to p-type localized molecular orbitals (LO's) are located below about 18 eV, the same situation may be expected to occur in the compounds studied. There are seven and nine p-type LO's in methylhydrazine and unsymmetrical dimethylhydrazine, respectively, the LO's being represented by n_N(nitrogen nonbonding), σ_{NN}(N-N bonding), σ_{CN} (C-N bonding), π_{NH_2}(NH_2 pseudo π), and π_{CH_3}(CH_3 pseudo π) orbitals. From the spectral shapes (maxima and shoulders) of the photoelectron spectra in Fig. 1, six and seven ionization bands can be identified in the region below about 18 eV. However, the remaining p-type bands are concealed under the photoelectron spectra in Fig. 1. The vertical ionization energies obtained from the photoelectron spectra in Fig. 1 are summarized in Table 1.

Table 1. Vertical ionization energies (eV) of methylhydrazine and unsymmetrical dimethylhydrazine

CH_3HNNH_2	
9.36, 10.28, 13.38, 14.32, 15.5[a], 17.1[a]	
$(CH_3)_2NNH_2$	
8.85, 10.07, 13.0[a], 13.50, 14.75, 15.40, 16.35	

a) Shoulder.

The first two vertical ionization energies slightly differ from those reported by Nelsen and Buschek (9.32 and 10.24 eV for CH_3HNNH_2; 8.88 and 10.13 eV for $(CH_3)_2NNH_2$),[5] but our separations (0.92 and 1.22 eV, respectively) are in good agreement with the reported ones (0.92 and 1.25 eV, respectively).[5] For higher ionization energies, there have been reported no high-resolution photoelectron data available for comparison.

In the present work, CNDO/2 calculations[15] were carried out for the outer, inner, and *trans* forms of methylhydrazine and for the *gauche* and *trans* forms of unsymmetrical dimethylhydrazine. Electron diffraction data of Beamer[16] were used for structural parameters. The calculated results of the p-type orbitals are illustrated in the energy level diagrams in Fig. 2, in which main characters are indicated in terms of the p-type LO's. (An ordinary 4 eV correction was made in the calculated energies.) The experimental levels based on Koopmans' theorem[17] are also compared with the calculated levels of the different conformations.

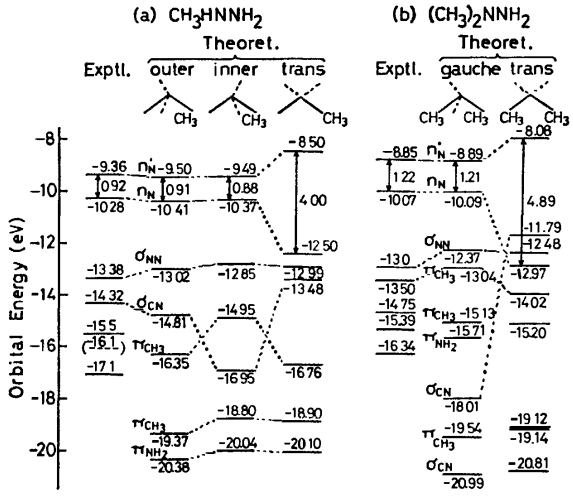

Fig. 2. Experimental and calculated (CNDO/2) energy levels for (a) methylhydrazine and (b) unsymmetric dimethylhydrazine.

Methylhydrazine. As can be seen from Fig. 2, the calculated nonbonding splittings of the outer and inner forms (0.91 and 0.88 eV, respectively) are close to the experimental one (0.92 eV), whereas the calculated splitting of the *trans* form (4.00 eV) is quite large. The comparison of the nonbonding splitting between experiment and theory therefore strongly suggests that this compound exists in the skew rather than *trans* form. This result of conformation is consistent with that of Nelsen and Buschek[5] who interpreted the nonbonding splittings of 21 hydrazines including methylhydrazine in terms of a dihedral angle of 90° using INDO calculations. According to the entropy considerations of Janz and Russell[9] and Durig *et al.*,[10] methylhydrazine mainly exists as an outer form. It would be very difficult to distinguish the outer and the inner form from each other from a photoelectron study.

The CNDO/2 results indicated that the outermost orbital is assigned to the methylated nitrogen lone pair. (Its energy level is represented by n_N' in Fig. 2.) The third and fourth photoelectron bands may correspond to the N–N and C–N bonding orbitals, respectively. It is interesting to note that the σ_{NN} level is almost independent of the dihedral angle. This tendency was previously pointed out in hydrazine.[2]

The fourth band at 14.32 eV may be due to the σ_{CN} LO, close to the 14.42-eV band of methylamine previously assigned to the σ_{CN} LO.[12] As mentioned before, there may be a concealed band in the methylhydrazine spectrum. The 15—18 eV spectrum in Fig. 1(a) should be associated with three p-type LO's (two π_{CH_3}'s and one π_{NH_2}). The position of the concealed band may be estimated on the basis of the photoelectron data of simple molecules. Using the empirical energy parameters previously proposed,[4] we have a value of —96.08 eV for the total energy sum over all the p-type LO's of methylhydrazine. On the other hand, the summation of the experimental vertical ionization energies shown in Table 1 gives rise to 79.9 eV. Therefore, the remaining photoelectron band is expected to appear around 16.1 eV (=96.0—79.9), the corresponding level being shown by a dotted line in Fig. 2. It may be concluded that the 15—18 eV spectrum consists of three ionization bands (two π_{CH_3} and one π_{NH_2}).

Unsymmetrical Dimethylhydrazine. The photoelectron nonbonding splitting again suggests that this compound may exist as a *gauche* rather than *trans* form. It is seen from Fig. 2 that the experimental nonbonding splitting (1.22 eV) is in excellent agreement with that of *gauche* form (1.21 eV). The nonbonding splitting of *trans* form (4.89 eV) is very large compared with that of *gauche* form. According

TABLE 2. COMPARISON OF NONBONDING SPLITTINGS (in eV) BETWEEN EXPERIMENT AND CALCULATION (CNDO/2)

	N_2H_4[2]	H_2O_2[3]	$(CH_3)_2O_2$[4]	CH_3HNNH_2	$(CH_3)_2NNH_2$	$CH_3HNNHCH_3$[4]	$(CH_3)_2S_2$[4]
Exptl.	0.73	1.00	1.90	0.92	1.22	0.67	0.30
CNDO/2	0.60	0.58	1.91	0.88, 0.91[b]	1.21	0.71	0.28
ϕ_0[a]	95°	111°30′	180°	90°	90°	90°	84°42′

a) The dihedral angle used in the CNDO/2 calculations. b) Inner and outer forms, respectively.

to the entropy study of Durig and Harris,[11] the compound exists predominantly as a *gauche* form.

The CNDO/2 calculations indicated that the third and fourth levels may correspond to the σ_{NN} and π_{CH_3} LO's, respectively. The third, 13.0-eV band due to the σ_{NN} LO is fairly close to the 13.38-eV band of methylhydrazine. The fourth, 13.50-eV band is considered to arise from the orbital interaction of two methyl groups.

The sum rule consideration mentioned above may help to estimate the remaining photoelectron bands. The total sum of LO energies is −124.68 eV. On the other hand, the sum of the experimental ionization energies given in Table 1 is 91.9 eV. A difference of 32.7 eV (=124.6—91.9 eV) suggests that there are two additional bands in the region 15—17 eV. In Fig. 2(b), it is not easy to correlate the experimental levels to the five deepest CNDO/2 levels of the *gauche* form which are shown by π_{CH_3}, π_{NH_2}, $\sigma_{CN(-)}$, π_{CH_3}, and $\sigma_{CN(+)}$ in this order. (These characters simply represent the largest contributions in the calculated MO's.) From our experiences,[11-14] however, the p-type LO's of this compound are considered to be $\sigma_{CN(-)}$ and $4\pi_{CH_3}$ instead of $\sigma_{CN(\pm)}$ and $3\pi_{CH_3}$, in addition to n_N', n_N, and π_{NH_2}. This conclusion was also supported by MINDO/2 calculations[18] which were also carried out in the present work. The MINDO/2 results of the *gauche* form showed that the five deepest levels mentioned above correspond to π_{CH_3}, π_{NH_2}, $\sigma_{CN(-)}$, π_{CH_3}, and π_{CH_3} in this order. The $\sigma_{CN(+)}$ orbital was indicated to give the first s-type one. (For methylhydrazine, the MINDO/2 calculations led to the same orbital assignments as the CNDO/2 calculations.) The MINDO/2 calculations were also found to give rise to somewhat smaller nonbonding splittings than the CNDO/2 calculations.

Potts *et al.*[19] indicated in their He II photoelectron spectra that s-type bands appear at 21.9 and 27.5 eV in methylamine, 20.6, 22.4, and 28.0 eV in dimethylamine, and 24.5 eV in hydrazine. The first s-type bands of the methylated hydrazines studied here are therefore expected to appear in the region 20—21 eV.

Table 2 summarizes experimental and calculated nonbonding splittings for the compounds so far studied in this laboratory. It is interesting to note that the experimental nonbonding splittings are well reproduced by CNDO/2 calculations with available skew angles.

References

1) Present address: Government Research Institute of Industry, Tosu-shi, Saga-ken.
2) K. Osafune, S. Katsumata, and K. Kimura, *Chem. Phys. Lett.*, **19**, 369 (1973).
3) K. Osafune and K. Kimura, *ibid.*, **25**, 47 (1974).
4) K. Kimura and K. Osafune, This Bulletin, **48**, 2421 (1975).
5) S. F. Nelsen and J. M. Buschek, *J. Amer. Chem. Soc.*, **95**, 2011 (1973).
6) P. Rademacher, *Angew. Chem. Int. Ed. Engl.*, **12**, 408 (1973).
7) N. Bodor, M. J. S. Dewar, W. B. Jennings, and S. O. Worley, *Tetrahedron*, **26**, 4109 (1970).
8) G. J. Janz and K. E. Russell, *J. Chem. Phys.*, **17**, 1352 (1949).
9) J. R. Durig, W. C. Harris, and D. W. Wertz, *ibid.*, **50**, 1449 (1969).
10) J. R. Durig and W. C. Harris, *ibid.*, **51**, 4457 (1969).
11) K. Kimura, S. Katsumata, Y. Achiba, H. Matsumoto, and S. Nagakura, This Bulletin, **46**, 373 (1973).
12) S. Katsumata, T. Iwai, and K. Kimura, *ibid.*, **46**, 3391 (1973).
13) K. Kimura, S. Katsumata, T. Yamazaki, and H. Wakabayashi, *J. Electron Spectrosc.*, **6**, 41 (1975).
14) K. Kimura and K. Osafune, *Mol. Phys.*, **29**, 1073 (1975).
15) J. A. Pople and D. L. Beveridge, "Approximate molecular orbital theory," McGraw-Hill, N. Y. (1970).
16) W. H. Beamer, *J. Amer. Chem. Soc.*, **70**, 2979 (1948).
17) T. Koopmans, *Physica*, **1**, 104 (1934).
18) M. J. S. Dewar and E. Haselbach, *J. Amer. Chem. Soc.*, **92**, 590 (1970).
19) A. W. Potts, T. A. Williams, and W. C. Price, *Discuss. Faraday Soc.*, **54**, 104 (1972).

Metachromasy. III.* Metachromatic Behavior of Trypaflavine in the Presence of Polyphosphates with Various Chain Lengths

Kiwamu YAMAOKA, Mineo TAKATSUKI, and Masaji MIURA
Faculty of Science, Hiroshima University, Higashisenda-machi, Hiroshima 730
(Received May 17, 1974)

The interaction of trypaflavine with sodium polyphosphate in aqueous solutions in the pH range 6—7 has been investigated by means of light absorption spectroscopy, conductometric titration and ultrafiltration. The metachromatic behavior of the bound dye was characterized in terms of hypso- and hypochromic effects in both visible and UV regions where no pronounced metachromasy band was observed. The effects were studied by varying the mixing ratio of polymer residue to dye, P/D, from 0.1 to 10000. They were found to be maximum in the P/D range 2–10. The effect of the chain length of polyphosphate on metachromasy was determined by use of fourteen refractionated samples with the degree of polymerization, $\bar{n}$, ranging from 8 to 158. No metachromasy appeared in samples with $\bar{n}<7$. It fully developed for those with $\bar{n}>20$, sharply depending on the chain length between 7 and 20. By conductometric titration and ultrafiltration, it was verified that the dye binds to the ionized phosphate almost at 1 : 1, and that the disappearance of metachromasy with the increase in P/D values or with the addition of salts results from two entirely different processes. The results were compared with the data for other dyes.

The physicochemical basis of metachromasy still remains to be clarified because of its extraordinary complexity.[1,2] However, it has become apparent that the metachromatic behavior of cationic dyes depends on the combination of the chemical structure of an individual dye with the conformation of a given polyelectrolyte having a specific functional group (binding site).[1,3,4] Studies of metachromasy have been directed to the interaction between biopolymers, DNA and RNA in particular, and various kinds of dyes whose structures are closely related, because of the practical application to selective staining of nucleic acids.[5–8] Such interaction is complicated due to the intricate structure of the biopolymers. Thus, in order to understand the mechanism involved in metachromasy, certain simpler polymeric models, one of which is polyphosphate, have been used.[9–12]

Metachromatic change of crystal violet (CV) occurs in the presence of sodium polyphosphate (NaPP).[1,2] The present work was undertaken with two objectives; to see whether the previous findings are confined to CV, a triphenylmethane dye, or whether they can also be observed with dyes of another class, such as cationic acridines, and also to provide basic data for a study on competitive binding to polyphosphate between two dyes of different classes.

As an acridine dye, trypaflavine (TF)—3,6-diamino-10-methylacridinium chloride—was chosen for the following reasons. The metachromatic behavior is close to that of proflavine — 3,6-diaminoacridinium chloride — but differs from that of acridine orange and its homologs, all of which have been known to interact with DNA.[3,13–15] Both TF and proflavine have been suggested to constitute a subgroup among the symmetrical 3,6-disubstituted acridines.[3,8] TF was also used together with CV in a study on competitive binding to DNA.[16] From the results obtained by means of absorption spectroscopy, conductometric titration and ultrafiltration, the metachromatic behavior of the NaPP–TF system has been compared with that of the NaPP–other related dye systems.

* Part II, Ref. 2.

Experimental

Materials. All NaPP samples are the same refractionated preparations as reported,[2] unless otherwise stated. TF in the chloride form (Chroma Gesellschaft, Schmidt & Co.) was used without further purification. The maximum molar extinction coefficient, ε, at 451 nm was found to be 42000 at 1.19×10^{-5} M.

Procedures and Measurements. Procedure for the preparation of stock solutions and polymer-dye mixtures has been reported.[2] The final concentration of TF was kept at 1.19×10^{-5} M, unless otherwise specified. Measurements of the absorption spectra and electric conductivity of NaPP-dye solutions were carried out with the precautions described previously.[2]

Ultrafiltration. In order to separate the unbound dye from the bound one in the NaPP-dye solution, a Millipore Sweenex ultrafiltration cell was used with the PSAC membrane which nominally retains molecular weights higher than 1000. Since the complete retention of a high molecular weight NaPP sample ($\bar{n}=216$) by the membrane was confirmed, this sample was used for the filtration experiments.

Results

UV and Visible Spectra of TF in the Presence of NaPP in Aqueous Solutions. The UV and visible absorption spectra of TF in the presence of a high molecular weight NaPP ($\bar{n}=216$) are shown in Fig. 1. The value of P/D as defined previously[2,17] was varied by adjusting the polymer concentration at a constant concentration of TF. The absorption maximum of TF at 451 nm was affected hypso- and hypochromically by the addition of NaPP up to P/D about unity, while the family of spectra showed two isosbestic points at 475 nm and 370 nm. The metachromatic behavior of the absorption maximum at 262.5 nm was similar to that of the 451 nm band, the isosbestic point being at 304 nm. As the P/D value increased from unity to approximately 3, the hypso- and hypochromic effects were enhanced in both UV and visible regions, no isosbestic point being observed. With the further increase in P/D value, the spectral trends reversed very slowly, three isosbestic points appearing

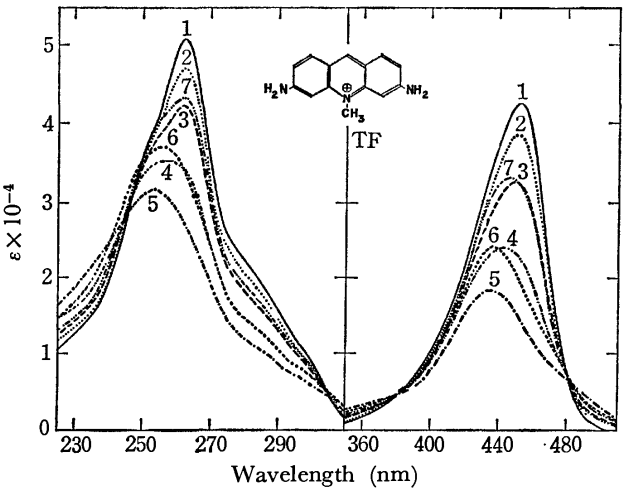

Fig. 1. Visible and UV spectra of TF in the presence of NaPP ($\bar{n}$=216) at various P/D values in aqueous solutions.
(1) pure TF (P/D=0) for comparison, (2) P/D=0.3, (3) P/D=0.5, (4) P/D=1.0, (5) P/D=3.0, (6) P/D =50, (7) P/D=850.

at 479, 374, and 307 nm. At exceedingly high P/D values, the overall spectra became almost the same as the spectrum of TF alone. It should be noted that, in contrast with the data on the NaPP-CV system,[1,2] no pronounced metachromasy band was observed for TF.

The effect of the chain length of NaPP on the UV and visible spectra of the NaPP–TF system is shown in Fig. 2. The P/D value was held at 3 (most appropriate for the metachromatic change of TF). The spectra are essentially the same as the spectrum of TF alone when the number-average degree of polymerization, $\bar{n}$, is less than 5. With an increase in the $\bar{n}$ of NaPP, the band intensity at 451 and 262.5 nm decreased, while the peak positions shifted towards the shorter wavelength. The decrease in intensity

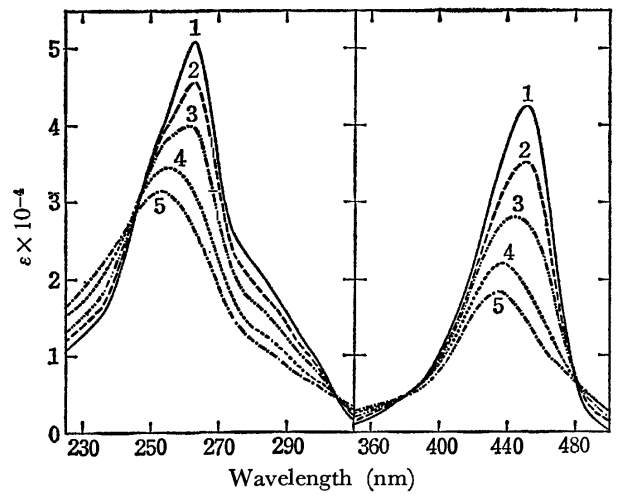

Fig. 2. Visible and UV spectra of TF in the presence of NaPP with various chain lengths at a P/D value of 3 in aqueous solutions.
(1) pure TF (P/D=0) for comparison, (2) $\bar{n}$=8, (3) $\bar{n}$=11, (4) $\bar{n}$=23, (5) $\bar{n}$=158.

occurred in a narrow region of $\bar{n}$ approximately between 7 and 20. Since the dependence of the metachromatic behavior of TF on P/D and $\bar{n}$ is characterized by hypso- and hypochromic effects, all the results are hereafter expressed in terms of both the molar extinction coefficients at 451 nm, ε_{451}, and at 262.5 nm, $\varepsilon_{262.5}$, and the wavelength shift from either the 451 or 262.5 nm maximum of TF, $\Delta\lambda=\lambda(\varepsilon_{max})-451$ or 262.5 nm. The results of the prominent shoulder at 285 nm are not included, because its change is similar to that of the 262.5 nm band.

Effect of the P/D on the Absorption of TF in the Presence of NaPP with Various Chain Lengths. In Figs. 3a and 3b, the molar extinction coefficient (open) and

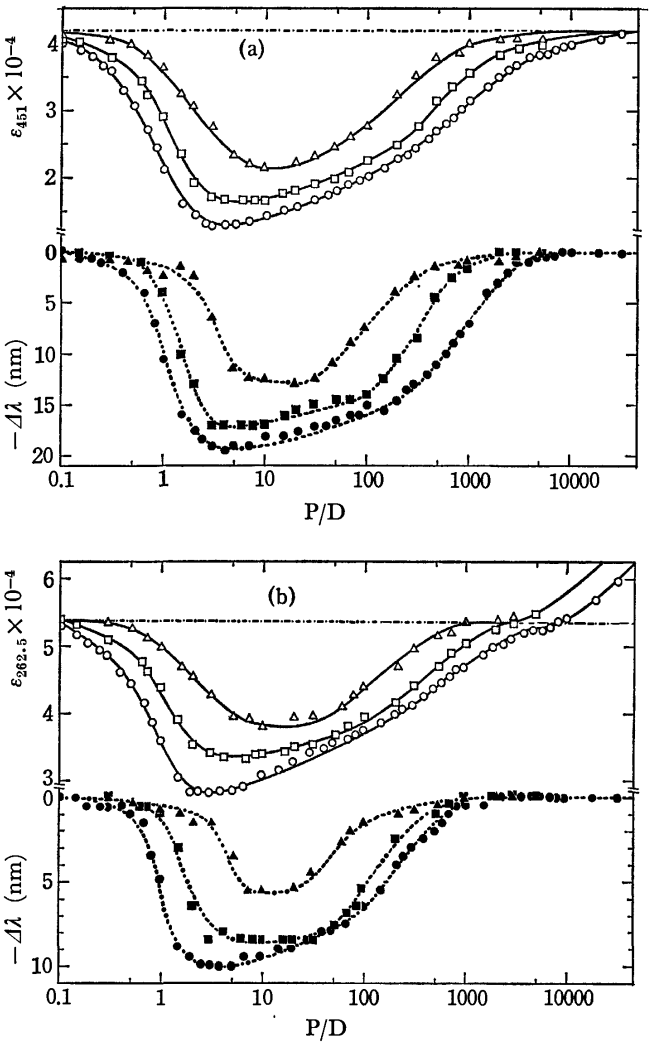

Fig. 3. The dependence of the hypo- and hypsochromisms of TF on the P/D value in the presence of NaPP with different chain lengths in the (a) visible and (b) UV regions.
Open symbols are the molar extinction coefficients of NaPP-TF at (a) 451 nm and (b) 262.5 nm (horizontal lines are those of TF alone), and filled ones are the wavelength shifts of the absorption maximum from (a) 451 nm and (b) 262.5 nm, defined as $\Delta\lambda\equiv\lambda(\varepsilon_{max})-451$ and 262.5 nm, respectively. -○- and -●- for $\bar{n}$=216, -□- and -■- for $\bar{n}$=24, -△- and -▲- for $\bar{n}$=11.

wavelength shift (filled) of TF are plotted against P/D in the presence of three NaPP samples which give rise to a small ($\bar{n}$=11), medium ($\bar{n}$=24), and large ($\bar{n}$=216) metachromatic change, respectively.[2] The intensity of the 451 and 262.5 nm bands became minimum and the corresponding wavelength shift maximum at a P/D value of approximately 7, 3, or 2 for each NaPP-TF system ($\bar{n}$=11, 24, or 216, respectively). The minimum value of ε at this P/D value depends on the chain length of the polymer.

The ε and band position of the NaPP–TF system approach those of TF alone at both extremely low and high values of P/D** (Figs. 3a and 3b). In order to see if the approach results from the dissociation of TF from the polymer site, filtration of an aqueous solution of TF in the presence of NaPP ($\bar{n}$=216) at a high P/D value of 1000, was carried out (*cf.* Experimental part). Three filtrates (3.0 ml each) were successively collected from the solution (total 15 ml). No filtrates showed the coloration of TF. In contrast, the filtrates from a NaPP–TF solution at a low P/D value of 0.6 all showed the spectrum of pure TF. It is obvious that TF is bound to the polymer site at very high P/D but partly liberated from it at low P/D.

Effect of the Chain Length of NaPP on the Absorption of NaPP–TF Solutions at Various Values of P/D. The effect of the chain length of NaPP on the metachromatic change of the NaPP–TF system is shown in Fig. 4, where the molar extinction coefficient and band shift are plotted against the chain length of NaPP. The P/D value chosen here is each responsible for a large (P/D=3), medium (P/D=30), and small (P/D=300) metachromatic change. The band intensity decrease and peak position shift toward the shorter wavelength occur in a narrow range of $\bar{n}$ between 7 and 20. Both ε and $\Delta\lambda$ leveled off, as the chain lengths of NaPP approach *ca.* 100 and over. The midpoints of those sigmoidal changes for the visible band are located at about $\bar{n}$=10 and 11 (P/D=3), $\bar{n}$=8 and 9 (P/D=30), and $\bar{n}$=11 and 19 (P/D=300), respectively (Fig. 4a). Similar changes are also noted for the UV band (Fig. 4b). It is evident that the metachromatic behavior of the TF bound to NaPP is affected by the chain length of the polymeric moiety and that the critical chain length is associated with oligomeric dimensions.

Influence of Small Ions on Metachromatic Changes. The small ions affect visible and UV bands of TF bound to NaPP ($\bar{n}$=154 and 24) at (a) P/D=3 and (b) P/D=30 (Figs. 5a and 5b). At each P/D value, the effect of the addition of sodium phosphates on the absorption spectra was negligible when the salt concentration was comparable with that of TF (10^{-5}—10^{-4} M). As the salt concentration was increased to 1×10^{-3} M, however, the effect became apparent: both ε and $\Delta\lambda$ changed hyper- and bathochromically relative to those of the low salt solution. At the exceedingly high salt concentration of the order of

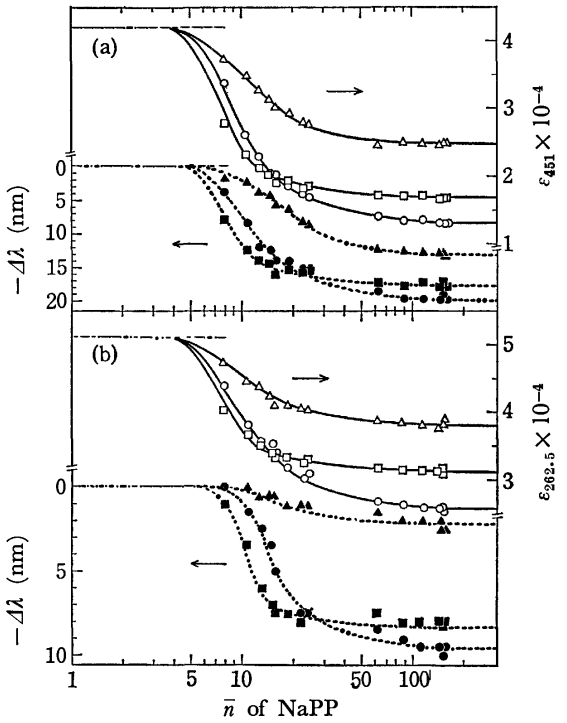

Fig. 4. The dependence of the hypo- and hypsochromisms of the NaPP-TF system on the chain lengths of NaPP at various P/D values in the (a) visible and (b) UV regions.
Open symbols are the molar extinction coefficients of NaPP-TF at (a) 451 nm and (b) 262.5 nm, and filled ones are the wavelength shifts of the absorption maximum in the presence of NaPP from (a) 451 nm and (b) 262.5 nm as defined in Fig. 3. -○- and -●- for P/D=3, -□- and -■- for P/D=30, -△- and -▲- for P/D=300.

10^{-2} M (about 1000 Na^+ ions per dye), the whole spectrum of the NaPP–TF solution was reduced to the spectrum of TF alone. In order to see if the dye is dissociated from the polymer site in the presence of the salt, ultrafiltration of an NaPP($\bar{n}$=216)–TF solution at the salt concentration and P/D of 1×10^{-2} M and 30 was carried out. Three colored filtrates (3.0 ml each) were successively collected from the NaPP-TF solution (16 ml initially). The visible spectrum of each filtrate was identical with that of free dye and that of the initial NaPP–TF solution within experimental error. The bound TF is evidently compelled to dissociate from the site in the presence of an excess of the small ions. In Figs. 5a and 5b, the midpoints of the sigmoidal changes of ε and $\Delta\lambda$ for the longer NaPP–TF solutions are displaced towards the higher salt concentrations. This indicates that more small ions are needed to dissociate the bound TF from the NaPP with a longer chain length.

Conductometric Titration of TF with NaPP in Aqueous Solutions. The results of conductometric titration of TF in aqueous solutions with three NaPP samples ($\bar{n}$=11, 24, and 154) are shown in Figs. 6a—6c. In the absence of TF the conductivity of the NaPP solution is proportional to the polymer concentration regardless of the chain length, although

** The $\varepsilon_{262.5}$ value, but not the band shift for the 262.5 nm band, exceeds that of TF at extremely high P/D. This is because polyphosphate absorbs light in this region.[18]

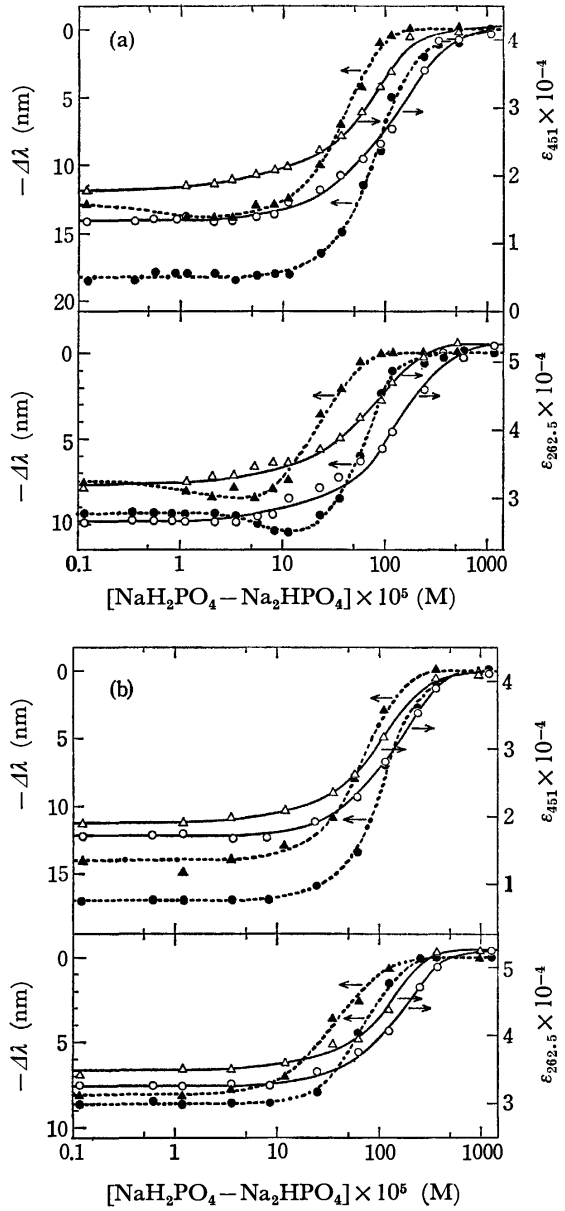

Fig. 5. The effect of sodium phosphates on the hypo- and hypsochromisms of TF in the presence of NaPP at two P/D values (a) P/D=3 and (b) P/D=30. Open symbols are the molar extinction coefficients of NaPP-TF at 451 nm (upper half) and 262.5 nm (lower half), and filled ones are the wavelength shifts of the absorption maximum from 451 nm (upper half) and 262.5 nm (lower half). -○- and -●- for NaPP with $\bar{n}=154$, -△- and -▲- for NaPP with $\bar{n}=24$.

the slope is less steep for the higher $\bar{n}$ sample. In the presence of TF, the conductivity of the titrated solution also increases linearly. However, a break occurs at a P/D value of about unity (1.2, 1.1, and 1.0) for each NaPP sample ($\bar{n}$=11, 24, and 154) as indicated by the intersection of two interpolated lines. Considering the fact that the deviation of the observed points from linearity results from the equilibrium between bound and unbound TF, the conductometric data seem to indicate that TF could be bound to the

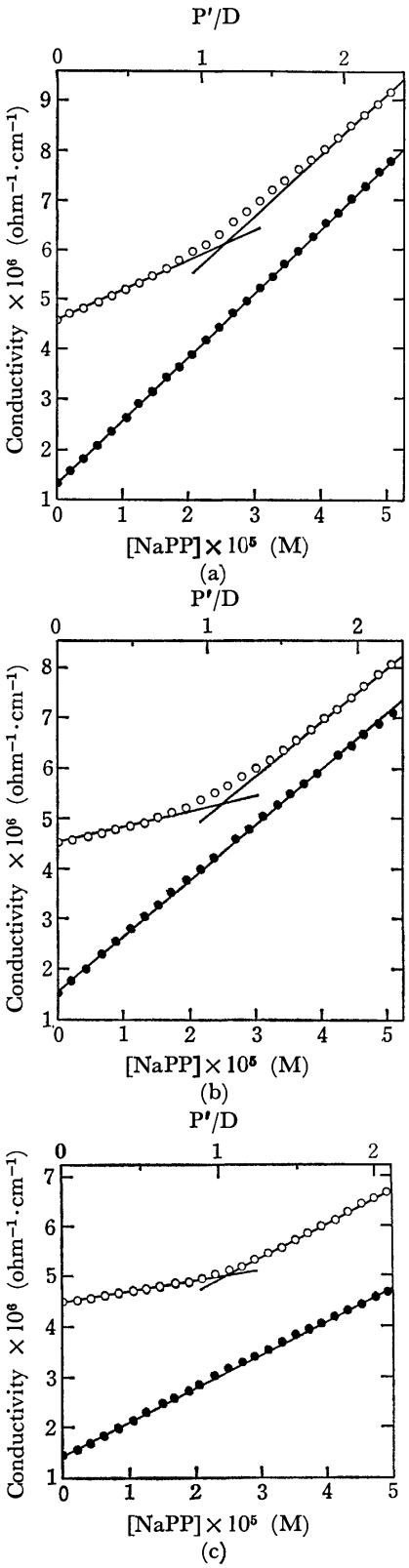

Fig. 6. Conductometric titration of TF with NaPP with various chain lengths (a) $\bar{n}=11$, (b) $\bar{n}=24$, and (c) $\bar{n}=154$.
-○- for the dye solution (the initial concentration of TF 2.26×10^{-5} M) titrated with NaPP and -●- for the blank solution titrated with NaPP for comparison. The concentration of NaPP is corrected for volume increase. P' is the concentration of the ionized group of the polymer and corrected as equal to $P(1+1/\bar{n})$ where P is the residue concentration.

ionized phosphate residue almost up to a one-to-one ratio regardless of the polymer chain length.

Discussion

Comparison of Metachromatic Behavior between TF and CV in the Presence of NaPP. The metachromatic behavior of the 451 nm band of the NaPP-TF system (Fig. 1) considerably differs qualitatively from that of the 592 nm band of the NaPP-CV system,[2] although many quantitative aspects are common to both TF and CV. The most striking difference is the appearance of a distinct metachromasy band at 506 nm in the bound CV. If such a band were also involved in the spectra of the bound TF, it would be very weak in intensity and exist in the wavelength region shorter than the 374—370 nm isosbestic point. (No apparent metachromasy band appears for either of these two dyes in the UV region). Difference is also noted for the variation of the peak positions in the presence of NaPP. The 451 nm band of TF steadily shifts hypsochromically as indicated by $\Delta\lambda$ (Figs. 1—3), whereas in the bound CV the original band at 592 nm, a shoulder at about 550 nm, and the new metachromasy band at 506 nm remain unshifted.[1,2]

Except for the differences described above, both TF and CV show the following common features. A long wavelength isosbestic point is noted at 479—475 nm for TF and at 637—639 nm for CV. The existence of such a point should imply that there is an absorption band in the wavelength region greater than that of the major band. A new long wavelength band has been observed in some triphenylmethane and acridine dyes in the solid state.[19] The P/D dependence of the metachromatic change of the two systems is also alike (Figs. 1 and 3 in Ref. 2; Figs. 1, 3a, and 3b in this article); for example, at very high and low P/D values, the absorbance of either system approaches that of the corresponding dye alone regardless of the polymer chain length. Another similarity is noted for the chain length dependence of the metachromatic change. For either dye the critical chain length of NaPP is rather short in terms of the number-average degree of polymerization. If the midpoint of the ε *vs.* $\bar{n}$ curves (Fig. 4) is taken to be a measure of the chain length dependence of metachromasy, the critical chain length is slightly shorter for TF ($\bar{n}=10$) than for CV ($\bar{n}=14$—16).[2]

For the NaPP sample whose $\bar{n}$ value is either 154, 24, or 11, a given P/D value of, say 310, signifies a polymer–dye solution containing on an average about two, thirteen, or twenty-eight polymer molecules per dye, respectively. The observed metachromatic change of TF in the solution is not abrupt but only gradual in the P/D range 100—1000 (Fig. 3). The result is best interpreted by assuming that the binding of TF to the polymer site is statistically random and essentially independent of the kind of site. If a preferential binding occurs to the dissociated secondary phosphate at the chain terminal of NaPP (only one terminal is fully dissociated at neutral pH),[20] the ε *vs.* P/D curve would show an abrupt change at a P/D value which nearly equals the $\bar{n}$ value of a given NaPP sample. Apparently this is not the case (Figs. 3a—3b). Thus, the present data on TF is not in accord with the notion that acridine orange is bound preferentially by the terminal doubly charged phosphates in the polynucleotide–acridine orange complexes.[21,22]

As observed for CV,[2] the binding of TF to NaPP is of electrostatic nature.[1,23] This is indicated from the results of the effect of small ions on metachromatic behavior (Figs. 5a and 5b) and conductometric titration (Figs. 6a—6c). It is clear from a comparison of Figs. 5a—5b with the result of the previous study on CV[2] that TF requires slightly more Na^+ ions than CV to dissociate from NaPP. The chemical structure of TF may be responsible for this result. Once bound to the polymer site, the quaternary ring nitrogen (the most probable binding locale) of TF may be shielded effectively from the small ions by two amino groups at the 3- and 6-positions, while the positively charged dimethylamino nitrogen of CV (a quaternary[24] or quinonoidal iminium ion[25]) could be exposed more to solvent and consequently susceptible to Na^+ ions.

Comparison of Metachromatic Behavior between Certain Acridine Dyes in the Presence of NaPP. Interaction with NaPP has been studied in some detail for acridine orange,[9–12] proflavine[9] and TF. The metachromatic behavior of the NaPP–proflavine system is very close to that of the NaPP-TF system. This is understandable considering the chemical structure of proflavine (protonated rather than methylated at the ring nitrogen but otherwise identical with TF). The spectral change of the visible band of the NaPP-acridine orange system differs from that of the NaPP–TF system; a broad, new band appears at 450 nm at the expense of the intensity of the principal 492 nm band as P/D values decrease.[10] This is somewhat analogous to the metachromatic behavior of the CV bound to NaPP.[2] Acridine orange possesses two dimethylamino groups, and proflavine or TF has two amino groups at the 3- and 6-positions, the pK values being 10.45, 9.65, and >12, respectively.[26] Thus, the difference and similarity of the observed metachromatic behavior should be sought from these two factors.

In spite of a qualitative variety of the spectral characteristics, the quantitative aspects of the metachromatic behavior of these acridine dyes are remarkable alike. The ε *vs.* P/D curves of acridine orange bound to NaPP indicate that the metachromatic change is maximum in the P/D range 2–20 (The Kurrol salt)[10] and 1—20 ($\bar{n}=110$),[11] and approximately 20—40 ($\bar{n}=9$)[10] and 10—40 ($\bar{n}=12$)[12] for unfractionated oligomeric samples. No metachromatic change was observed for the NaPP sample with $\bar{n}$ less than 5[10] or 3.[12] As P/D values increase to 10^4, the molar extinction coefficients of the bound dye approach the value of free acridine orange.[10] Since all the results compare favorably with the present data of the NaPP–TF system and the present work has established the fact that TF is totally bound to NaPP, acridine orange should also remain bound to NaPP even at exceedingly high P/D. The stoichiometry of the binding of the flat, symmetrical acridine dyes with substituents at

the 3- and 6-positions appears to be general for NaPP.

Closing Remarks. Together with the results with malachite green[1] and CV,[2] the present study of the interaction between NaPP and TF reveals the following. The metachromatic behavior depends on the chain length of NaPP, and the critical range of the degree of polymerization lies from 7 to 20. The dye is definitely bound to the polymer site at extremely high P/D values, irrespective of the appearance of the absorption spectra which do not appreciably differ from the free dye spectra. Although a closely resembling situation results from the addition of a great deal of the small ion to the NaPP-dye solution, the bound dye is compelled to dissociate from the polymer site because of the competition with the small ion. Thus, the resulting spectra are nearly the same in these two cases, but the underlying processes are proved to be different. It is thus concluded that the binding mode of each dye to NaPP is general and arises from complicated electrostatic interactions for which the positively charged nitrogen moiety of the dye is mostly responsible. The spectral behavior is remarkably characteristic of individual dyes, even though they belong to the same structural class.

References

1) K. Yamaoka, T. Suenaga, A. Fujita, and M. Miura, *J. Sci. Hiroshima Univ., Ser. A-II*, **34**, 1 (1970).

2) K. Yamaoka, M. Takatsuki, K. Yaguchi, and M. Miura, This Bulletin, **47**, 611 (1974).

3) K. Yamaoka, *Biopolymers*, **11**, 2537 (1972). Also references cited therein.

4) K. Yamaoka, *Chem. Lett.*, **1973**, 305.

5) L. Michaelis and S. Granick, *J. Amer. Chem. Soc.*, **67**, 1212 (1945).

6) L. Michaelis, *Cold Spring Harber Symposia Quant. Biol.*, **12**, 131 (1947).

7) G. Löber, *Photochem. Photobiol.*, **8**, 23 (1968).

8) G. Löber and G. Achtert, *Biopolymers*, 8, 595 (1969).

9) G. Weill and M. Calvin, *ibid.*, **1**, 401 (1963).

10) M. Miura and Y. Kubota, This Bulletin, **40**, 466 (1967).

11) V. Kleinwächter and J. Koudelka, *Biophysik*, **5**, 119 (1968).

12) B. L. van Duuren, in "Fluorescence and Phosphorescence Analysis," ed. by D. M. Hercules, John Wiley & Sons, New York, N. Y. (1966), p. 201.

13) H. G. Heilweil and Q. Van Winkle, *J. Phys. Chem.*, **59**, 939 (1955).

14) A. R. Peacocke and J. N. H. Skerrett, *Trans. Faraday Soc.*, **52**, 261 (1956).

15) R. K. Tubbs, W. E. Ditmars, Jr., and Q. Van Winkle, *J. Mol. Biol.*, **9**, 545 (1964).

16) C. L. Greenblatt, N. E. Sharpless, and K. Yamaoka, *Mol. Pharm.*, **6**, 649 (1970).

17) K. Yamaoka and R. A. Resnik, *J. Phys. Chem.*, **70**, 4051 (1966).

18) M. Bennoson and D. J. Williams, *ibid.*, **76**, 3673 (1972).

19) K. Yamaoka, Y. Matsuoka, and M. Miura, *ibid.*, **78**, 1040 (1974).

20) J. R. van Wazer and K. A. Holst, *J. Amer. Chem. Soc.*, **72**, 639 (1950).

21) R. F. Beers, Jr., D. D. Hendley, and R. F. Steiner, *Nature*, **182**, 242 (1958).

22) R. F. Steiner and R. F. Beers, Jr., *Arch. Biochem. Biophys.*, **81**, 75 (1959).

23) A. Levine and M. Schubert, *J. Amer. Chem. Soc.*, **74**, 91 (1952).

24) R. J. Goldacre and J. N. Phillips, *J. Chem. Soc.*, **1949**, 1724.

25) H. H. Freedman, in "Carbonium Ions", John Wiley & Sons, Inc., New York, N. Y. (1973), Vol. IV, Chapter 28, pp. 1501—1578.

26) A. Albert, "The Acridines", St. Martin's Press, New York, N. Y. (1966), pp. 170—171.

The Franck-Condon Factor of a Polyatomic Molecule. Its Method and Application to Acetylene and Dideuteroacetylene

Isao KANESAKA and Kiyoyasu KAWAI

Faculty of Literature and Science, Toyama University, Gofuku, Toyama 930

(Received December 24, 1974)

An advanced method for the calculation of the Franck-Condon factor is reported. It is realized on the assumption of the neglect of the zero-point motions except for the three normal coordinates whose vectors are three-dimensionally orthogonal to each other. The overlap integral is given by the Cartesian displacement coordinate system in order to consider precisely the molecular structures of the ground and excited states. This coordinate system does not cause any conflicts with the above assumption. Thus, the overlap integral is defined every nucleus with one- to three-dimensional formulae to satisfy sufficiently the Franck principle, which has been considered precisely only in the case of the diatomic molecule. The method is applied to acetylene and dideuteroacetylene with very good results. The intensity factors obtained are discussed, along with the effects of the force constants and anharmonicity.

There has generally been found a wide variation in the intensity of each band in the progression of the electronic spectra of a polyatomic molecule, whose structure of the excited state changes greatly from that of the ground state. It has been found, in a progression for the $\tilde{A}\leftarrow\tilde{X}$ band of acetylene,[1] that the relative intensities vary from 1 for $v=1$ up to 285 for $v=5$. In this case, in the molecular structure of the excited state the angle of CCH is 120.2° and the distances of the H-C and C=C bonds are 1.08 and 1.383 Å respectively. Thus, it is suitable for the study of the Franck-Condon principle of a polyatomic molecule.

Ingold and King[1] have calculated the Franck-Condon factor of the progression of acetylene by the method established by Craig,[2] assuming the CH groups to be compound atoms. However, they could not explain the observed intensity distribution. In their treatment, the internal coordinate of the excited state is related one-dimensionally to that of the ground state in spite of the bent-linear transition. This is probably the reason for their failure. Smith and Warsop[3] have also calculated the Franck-Condon factor of the progression of acetylene by the method of Ansbacher.[4] However, they too could not explain the observed spectra. Their treatment of the overlap integral is based on this equation:

$$R(v,0)=\int\phi_0''(d-Q')\phi_v'(Q')\mathrm{d}Q' \tag{1}$$

where Q' is the normal coordinate of the excited state, d represents the separation of the origin of the two corresponding coordinates, and ϕ_0'' and ϕ_v' are the vibrational wave functions of the ground and excited states respectively. That is, the relation:

$$Q''=d-Q' \tag{2}$$

is assumed. The approximation of Eq. (2) is very low,[5] and, furthermore, d has not been defined clearly by the molecular structures of the ground and excited states, but estimated from the accordance of the observed with the calculated relative intensities. Though it is easy to make the observed relative intensities accord with those calculated, the value of d obtained is deficient in reliability because of its low approximation.

However, it is easily found that Eq. (1) can be applied to the diatomic molecule as it is. That is, Eq. (1) is precise if the direction of the normal coordinate of the excited state coincides with that of the ground state. In this case, the difference in d in Eq. (1) or in a frequency parameter does not cause any difficulties. On the other hand, in a polyatomic molecule a normal coordinate of the ground state does not generally coincide with that of the excited state. Therefore, Eq. (1) does not fulfill the Franck principle. That is, the value of $\phi_0''(d-Q')\phi_v'(Q')$ in Eq. (1) is correct only at a point of intersection of the two coordinates and is estimated largely at the other points. Thus, more than one-dimensional formulae is needed to estimate the correct value of the latter points. In our treatment, the vertical transition is considered sufficiently.

Method

In a polyatomic molecule, the Franck-Condon factor is generally given by:

$$R_{v'v''}=\int\phi_v'\phi_v''\mathrm{d}\tau_v \tag{3}$$

where the total wave function is given by:

$$\phi_v=\phi_1(Q_1)\phi_2(Q_2)\cdots\phi_{3N-6}(Q_{3N-6}) \tag{4}$$

where the wave function $\phi_i(Q_i)$ is given by:

$$\phi_i(Q_i)=N_{v_i}\exp\{-(\alpha_i/2)Q_i^2\}H_{v_i}(\sqrt{\alpha_i}Q_i) \tag{5}$$

where N_v is a normalization constant, $\alpha_i=4\pi^2\nu_i/h$, and $H_v(\sqrt{\alpha_i}Q_i)$ is a Hermitte polynominal of the vth degree. We will here consider the means of Eq. (4) by following the discussion of Herzberg.[6]

If only one normal vibration is excited, the total eigen-function is given by:

$$\phi_v=NH_{v_1}(\sqrt{\alpha_1}Q_1)\exp\{-(\alpha_1/2)Q_1^2-(\alpha_2/2)Q_2^2-(\alpha_3/2)Q_3^2\cdots\} \tag{6}$$

If we neglect the zero-point motion of all the other normal vibrations, we have $\phi_v=\phi_1(Q_1)$. In this case, as found from the equation:

$$\mathbf{X}=\mathbf{LQ} \tag{7}$$

where $\mathbf{X}$ is a Cartesian displacement coordinate vector, and $\mathbf{Q}$ a normal coordinate vector, the dis-

placement components of all the nuclei are proportional to Q_1. Then, the wave function conjugated with X_N is given by:

$$\psi(X_N) = \psi(Q_1) \tag{8}$$

However, actually we can not neglect the zero-point motion of the other vibration. In this case, Eq. (6) does not simplify to $\psi_1(Q_1)$ and Eq. (7) does, in general, not lead to such a simple expression for the $\mathbf{Q}$.

Departing from the discussion of Herzberg, if we use Eq. (7) as an approximation, we find that we may use $\psi_i(Q_i)$ instead of Eq. (4) as a wave function of the excited state. On the other hand, for the ground state, if the jth normal vibration is considered, we have $\psi_j(Q_j)$. If the kth normal vibration is considered, we have $\psi_k(Q_k)$, and so on. This shows, thus, that Eq. (3) can be expressed by:

$$R(v, 0) = \sum_j \int \psi_{0j}''(Q_j'')\psi_v'(Q_i')\mathrm{d}Q_i' \tag{9}$$

or

$$R(v, 0) = \sum_j \int \psi_{0j}''(d-Q_i')\psi_v'(Q_i')\mathrm{d}Q_i' \tag{10}$$

Eq. (10) is essentially equal to Eq. (1). That is, the zero-point motions different from ψ_0'' are also neglected or averaged in Eq. (1).

If we use the Cartesian displacement coordinate of each nucleus related linearly with a normal coordinate, d in Eq. (10) is defined clearly as the distance between the equilibrium positions of the nuclei of the ground and excited states. Thus, we transform Eq. (10) into the formula defined by the Cartesian displacement coordinate.

We use the $\psi(X_N)$ of Eq. (8) to resolve Eq. (10). However, $\psi_i(X_N)$ is not normalized on all Cartesian displacement coordinates of the ith normal coordinate as it is. That is shown by the consideration that the $\int\psi_i^*(X_N)\psi_i(X_N)\mathrm{d}X_N$ of a light atom such as hydrogen is larger than that of a heavy atom such as carbon. According to the reciprocal, l_N, of the $\mathbf{L}$ matrix element, a normal coordinate is expressed by:

$$Q_i = \sum_N^{Mi} l_N X_N \tag{11}$$

From the property of a normal coordinate in our approximation, there are these relations:

$$Q_i = l_1X_1 = l_2X_2 = \cdots = l_{M_i}X_{M_i} \tag{12}$$

That is, it is found that the above normalization can be settled by multiplying $\int\psi_i^*(X_N)\psi_i(X_N)\mathrm{d}X_N$ by l_N/M_i. Then, $\sqrt{|l_N|/M_i}\psi_i(X_N)$ is reasonable as the function of Eq. (9) or (10) and for the dimension of the vibrational wave function as well.

From Eq. (11) the overlap integral is given by the summation of $R_N(v,0)$ on all the coordinates. $R_A(v,0)$ is defined for every atom, and these one- to three-dimensional formulae are given by:

$$R_A(v, 0)_x = \sum_i \int \sqrt{|l_{ix}''|/M_i''}\psi_{0i}''(d_x-X') \times \sqrt{|l_{x}'|M'}\psi_v'(X')\mathrm{d}X' \tag{13}$$

$$R_A(v, 0)_{xy} = 2\sqrt{M_i''M'}R_A(v, 0)_xR_A(v, 0)_y \tag{14}$$

$$R_A(v, 0)_{xyz} = 3M_i''M'R_A(v, 0)_xR_A(v, 0)_yR_A(v, 0)_z \tag{15}$$

where the summation is carried out for all the normal coordinates of the ground state in the case of the absorption spectra. Generally, the vibrational modes expressed by the Cartesian coordinate system are not independent of each other. However, it is easily found that Eq. (12) is realized in our approximation, as has been discussed above.

In our approximation, the $\psi_i(X)$ of the ith normal coordinate would be different from zero only along the line of the Cartesian displacement coordinate. Actually, $\psi_i(X)$ is not zero outside the line, but decreases in the direction perpendicular to this line. Therefore, it is found that Eq. (13) is a very low approximation in a case such as a bent-linear transition. That is, a factor should be multiplied to Eq. (13) to satisfy the Franck principle. In our treatment, $R_A(v,0)_y$ is the factor for $R_A(v,0)_x$. Thus though Eq. (14) is a two-dimensional formula, this means the one-dimensional overlap integral and Eq. (15) has also the same mean as Eq. (14). That is, though the zero-point motions of the same axis as $R_A(v,0)_x$ are neglected in Eq. (7), those of the other axes are considered sufficiently.

By using Eqs. (13)—(15), the overlap integral of Eq. (10) is given by:

$$R(v, 0) = \sum_A R_A(v, 0) \tag{16}$$

where the sign of each term of $R_A(v,0)$ is easily determined by the displacement vector of each nucleus of the excited state, because ψ'' considered is always positive. In the case of the bent-linear transition, it is clear that the potential of the one axis, y, of the excited state is the double minimum and is symmetrical about the other, x. Then, the overlap integral of the axis becomes either double or zero. It is also possible to replace the integral for y in Eq. (14) with z. Then, Eq. (16) is rewritten by:

$$R_L(v, 0) = 4R(v, 0) \tag{17}$$

The Cartesian displacement coordinate vector is related to the normal coordinate vector by Eq. (7) in every symmetry species. Then, the values of $\psi_v'(X_N)$ of the excited state are calculated by Eq. (8), and those of $\psi_{0i}''(d-X_N)$ of the ground state by the expression:

$$\psi_{0i}''(d-X_N) = \psi_{0i}''(Q_i'') \tag{18}$$

where Q_i'' is given by:

$$Q_i'' = (d-L_N'Q')/L_{N_i}'' \tag{19}$$

where L_N is the $\mathbf{L}$ matrix element. The calculation of such an integral as Eq. (13) is carried out by the numerical calculation of $\psi_{0i}''(d-X)\psi_v'(X)$ at various values of X. Thus, the $R(v,0)$ of Eq. (16) or (17) is calculated; the square of $R(v,0)$ or $R_L(v,0)$ gives the intensity factor.

Application

Acetylene. We applied our method to the progression (C progression) of the bending vibration (1049 $\mathrm{cm^{-1}}$) of the first-excited state, ^1A_u, of acetylene.

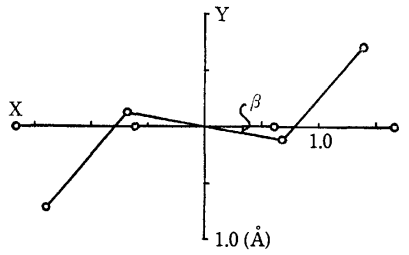

Fig. 1. The molecular structures of the ground and excited states of acetylene.

The absorption consists of a large number of very weak absorption bands, extending from 2400 to 2100 Å.[1,7] It has been determined, by an analysis of both the vibrational and rotational structures, that, in the excited state, acetylene is bent, taking the C_{2h} symmetry. The molecular structure of this excited state is shown in Fig. 1, along with that of the ground state, in which the bond lengths of the H-C and C≡C bonds are 1.064 and 1.201 Å[8] respectively. In our treatment, the principal axes of the ground and excited states should coincide as shown in Fig. 1. Thus, it is found that the relative equilibrium positions of the isomer differ considerably in the same Cartesian coordinate system, though their molecular structures are, of course, identical; we will describe dideutero-acetylene later. The intensities, expressed as the oscillator-strength, of the C progression have been measured from C_1 to C_5[1], where C_v represents the v–0 transition. They are shown in Table 1. All the fundamental frequencies of the A_g species of the excited state have been observed[1,7] at 1049, 1380, and 3000 cm^{-1}; they are assigned to the CCH bending, C=C, and C-H stretching vibrations respectively.

Table 1. The observed oscillator-strengths (f_v) and the relative intensities of C progression of acetylene

Band	C_1	C_2	C_3	C_4	C_5
$10^5 f_v$	0.0042	0.036	0.145	0.51	1.2
Relative intensities	1	8.57	34.5	121	285

The normal coordinate analysis was carried out by the computer program reported by Shimanouchi,[9] using the electronic computer, FACOM-45S, of Toyama University. The **L**S matrix obtained is expressed by:

$$\mathbf{S} = \mathbf{L}_S\mathbf{Q} \tag{20}$$

where **S** is the symmetry coordinate vector. From the $\mathbf{L}_S$ matrix, the **L** matrix is obtained by this expression:

$$\mathbf{L} = \mathbf{M}^{-1}\mathbf{B}_S\mathbf{G}\mathbf{L}_S \tag{21}$$

where the $\mathbf{M}^{-1}$ matrix consists of the reciprocal of the mass of the atom and where $\mathbf{B}_S$ and **G** are Wilson's $\mathbf{B}_S$ and **G** matrixes.[10] The **L** matrix (Set I) of Q_3' of the excited state is given in Table 2. The calculated frequencies agree completely with the observed ones. The force constants (Set I) are given in Table 3, where the H··C repulsive force constant was fixed in the least-squares adjustment. The fundamental frequencies of the ground state were quoted from a reference.[6] The **L** matrix of the ground state is also given in Table 2. The calculated frequencies agree with the observed ones. The force constants are also given in Table 3, where the interaction term between the CCH bending coordinates was taken into consideration. The calculation of Eq. (13) or Eq. (14) was carried out using the same computer mentioned above. In the summation of Eq. (14), there are two normal coordinates for y, with frequencies of 611.8(Π_g) and 729.1(Π_u) cm^{-1}, and three for x, with frequencies of 1973.8(Σ_g^+), 3287.0(Σ_u^+) and 3373.7(Σ_g^+) cm^{-1}.

It is interesting to compare the overlap integrals

Table 2. The **L** matrix of the excited and ground states of acetylene[a]

		Excited(A_g) Set I	Excited(A_g) Set II	
X_H	=	0.525	0.515	Q_3'
Y_H		0.283	0.261	
X_C		0.0715	0.0914	
Y_C		−0.0812	−0.0730	
Ground (Σ_g^+)				
X_H	=	0.639	0.302	Q_1
X_C		−0.0873	0.185	Q_2
Ground (Σ_u^+)				
X_H	=	0.679		Q_3
X_C		−0.0566		
Ground (Π_g)				
Y_H	=	−0.609		Q_4
Y_C		0.128		
Ground (Π_u)				
Y_H	=	−0.679		Q_5
Y_C		0.0566		

a) Given only for two atoms

Table 3. The force constants of the excited and ground states of acetylene

	Excited Set I	Excited Set II	Ground
K(C-H)	4.861	4.902	5.888
K(C≡C)[a]	6.348	6.223	15.660
H(HCC)	0.377	0.424	0.188
F(H···C)[b]	0.0905	0.0	—
I(HCC, HCC)	—	—	−0.0686

a) Triple bond for ground state. b) Fixed force constant (mdyn/Å).

TABLE 4. THE OVERLAP INTEGRALS FOR y OF ACETYLENE[a)]

v	$Q_4(\Pi_g)$		$Q_5(\Pi_u)$	
	$H/10^{-4}$	$C/10^{-2}$	$H/10^{-3}$	$C/10^{-6}$
0	0.0552	0.0484	0.0083	0.0007
1	0.121	0.107	0.0175	0.0048
2	0.217	0.187	0.0306	0.0230
3	0.350	0.293	0.0483	0.0886
4	0.529	0.422	0.0712	0.293
5	0.758	0.578	0.101	0.864

a) Twice as much as Eq. (13).

of two normal coordinates for y, because only one of them has been considered. The results of Eq. (13) for hydrogen and carbon atoms are given in Table 4, where Eq. (16) is applied. The largest value of $R_A(v,0)$ is the $R_C(v,0)$ of the carbon atom of Q_4. The $R_H(v,0)$ of the hydrogen atom of Q_4 is nearly equal to that of Q_5, and both are smaller than the $R_C(v,0)$ of Q_4. The $R_C(v, 0)$ of Q_5 is negligible. It should be noticed that their large discrepancies result from the differences in the **L** matrix elements given in Table 2.

The overlap integrals for x are given in Table 5, where the results of Q_3 are omitted because they are similar to those of Q_1. In this case, the $R_H(v, 0)$ values of Q_1 and Q_2 are much larger than those in Table 4. This results mainly from the small value of d_x, 0.287 Å. The $R_C(v, 0)$ of the carbon atom of Q_2 is quite large.

From the above results, we estimated the intensity factor in two manners: (I) using only one term of Eq. (14), and (II) using all the terms of Eq. (14). Though we could not always expect a very large term

TABLE 5. THE OVERLAP INTEGRALS FOR x OF ACETYLENE

v	$Q_1(\Sigma_g^+)$		$Q_2(\Sigma_g^+)$	
	$H/10^{-1}$	$C/10^{-3}$	$H/10^{-1}$	$C/10^{-1}$
0	0.0704	0.0003	0.0285	0.0216
1	0.209	0.0019	0.104	0.0422
2	0.415	0.0080	0.258	0.0666
3	0.645	0.0269	0.486	0.0937
4	0.818	0.0783	0.734	0.123
5	0.854	0.203	0.900	0.153

in Eq. (14), it is found in acetylene that ${}^{q_2}R_C(v,0)\cdot{}^{q_4}R_C(v,0)$ (Manner I) is much larger than the other terms. The intensity factors obtained are given in Table 6, where Eq. (17) is applied. The calculated relative intensities to C_1 are also given in Table 6. The accordances with the observed values are sufficiently satisfactory.[1)]

The oscillator-strength of the whole electronic transition is given by this relation:

$$f = f_v/R_L(v, 0)^2 \qquad (22)$$

where f_v is the observed oscillator-strength of the vth band. Then, the value of f obtained is 0.51 from v=5. This value is as large as that of an ordinary allowed electronic dipole transition.

Dideuteroacetylene. With dideuteroacetylene, in the transition to the ^1A_u state the spectra or the vibrational structures are generally similar to those of acetylene.[1,7)] That is, the C progression forms the main milestones of the spectra, with an interval of about 800 cm^{-1} between successive bands. However, the frequency intervals are so small that there is more overlapping of bands, and the band intensity is lower. Since the intensity of the C progression has not been measured, we calculate it only to compare the intensity factor of dideuteroacetylene with that of acetylene.

In this case, the equilibrium positions of the atoms of the excited state are obtained by taking β=16°40′ in Fig. 1. The fundamental frequencies of the A_g species have been reported to be at 844, 1310, and 2215 cm^{-1}. However, C_0 and C_1 have not been observed because of the low intensity, and we assumed 864 cm^{-1} as the CCD bending vibration. The normal coordinate analysis was carried out in the same manner as for acetylene. The calculated frequencies completely accord with the observed ones. The **L** matrix is given in Table 7, and the force constants in Table 8. The fundamental frequencies of the ground state are quoted from a reference.[6)] A good accordance of the observed frequencies with those calculated was obtained. The **L** matrix and the force constants are also given in Tables 7 and 8 respectively.

In the summation of Eq. (14), there are two normal coordinates for y, with frequencies at 505(Π_g) and 539.1(Π_u) cm^{-1}, and three for x, with frequencies at 2700.5(Σ_g^+), 2427.0(Σ_u^+) and 1762.4(Σ_g^+) cm^{-1}. In this instance, there are two cases of a large contribution to the overlap integral for y, while the other two

TABLE 6. THE INTENSITY FACTORS AND THE RELATIVE INTENSITIES OF ACETYLENE

v	Intensity factors/10^{-5}			Relative intensities		
	Manner I		Manner II	Manner I		Manner II
	Set I	Set II		Set I	Set II	
0	0.00022	0.00040	0.00027	0.053	0.049	0.049
1	0.00417	0.0081	0.0055	1	1	1
2	0.0321	0.0635	0.0458	7.70	7.85	8.36
3	0.155	0.304	0.234	37.1	37.6	42.7
4	0.550	1.02	0.850	132	126	155
5	1.59	2.75	2.37	382	340	433

Table 7. The **L** matrix of the excited and ground states of dideuteroacetylene[a)]

Excited (A_g)			
X_D		0.361	
Y_D	=	−0.183	Q_3'
X_C		0.0750	
Y_C		0.0935	
Ground (Σ_g^+)			
X_D	=	0.342 0.364	Q_1
X_C		−0.149 0.140	Q_2
Ground (Σ_u^+)			
X_D	=	0.463	Q_3
X_C		−0.0772	
Ground (Π_g)			
Y_D	=	−0.363	Q_4
Y_C		0.168	
Ground (Π_u)			
Y_D	=	−0.463	Q_5
Y_C		0.0772	

a) Given only for two atoms.

Table 8. The force constants of the excited and ground states of dideuteroacetylene

	Excited	Ground
K(C-D)	4.825	5.965
K(C≡C)[a)]	5.817	15.826
H(DCC)	0.423	0.179
F(D···C)[b)]	0.0905	—
I(DCC, DCC)	—	−0.0815

a) Triple bond for ground state. b) Fixed force constant (mdyn/Å).

are negligibly small. The large ones are the $R_C(v, 0)$ of Q_4 and the $R_D(v, 0)$ of the deuterium atom of Q_5. They are given in Table 9, where Eq. (16) is applied. As for x of Eq. (14), all the overlap integrals are of the same order; only the values of the carbon and deuterium atoms of Q_2 are given in Table 9. They are fully considered in the calculation of the intensity factor, which is given in Table 10, where Eq. (17) is applied. The intensities relative to C_2 are also given in Table 10. The intensity factors of dideuteroacetylene are to some extent larger than those of acetylene. Since the observed band intensity of dideuteroacetylene is lower than that of acetylene, it is considered that the oscillator-strength of dideuteroacetylene is smaller than that of acetylene.

Table 9. The overlap integral of dideuteroacetylene

v	$Q_5(\Pi_u)$[a)] $D/10^{-3}$	$Q_4\Pi(g)$[a)] $C/10^{-3}$	$Q_2(\Sigma_g^+)$ $D/10^{-4}$	$Q_2(\Sigma_g^+)$ $C/10^{-1}$
0	0.0129	0.0433	0.0062	0.0686
1	0.0242	0.101	0.0341	0.155
2	0.0392	0.186	0.110	0.260
3	0.0583	0.306	0.242	0.364
4	0.0817	0.467	0.403	0.454
5	0.111	0.670	0.520	0.529

a) Twice as much as Eq. (13).

Table 10. The intensity factors and the relative intensities of dideuteroacetylene

v	Intensity factors/10^{-5}	Relative intensities
0	0.00012	0.0030
1	0.00378	0.092
2	0.0412	1
3	0.241	5.85
4	0.940	22.8
5	2.74	66.6

Discussion

The above results would seem to justify our method. As has been seen in the above discussion, it may be said that in Eq. (14) the wave function of the excited state is defined by the two-dimensional formula. This naturally causes overlaps with the corresponding wave functions of the ground state. A one-dimensional model of the Franck-Condon integral, that is, an explanation of Eq. (13), is given in Fig. 2, where the

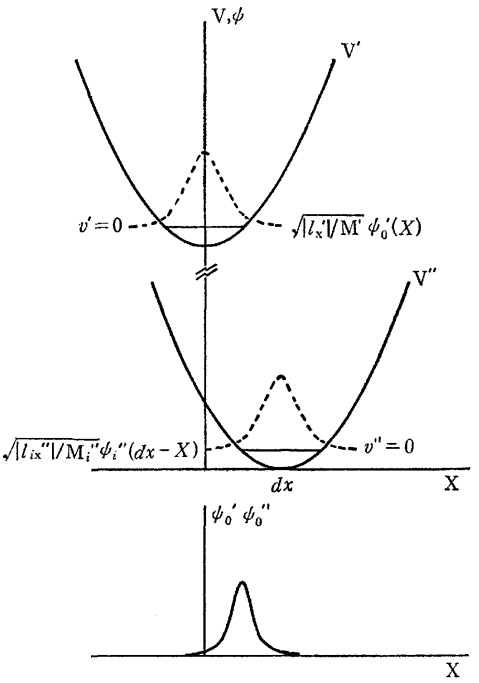

Fig. 2. One-dimensional model of the Franck-Condon integral for $R(0, 0)$.

$\psi_0''\psi_0'$ for $R(0,0)$ is also shown. The potential V' for y is similarly considered, though the V' for y is double minimum function, as has been described above. Actually V' and V'' are not generally on the same plane, as is shown in Fig. 2. That is, in the equilibrium position V' is on the plane separated by d_y perpendicular to the plane in Fig. 2. However, since the vertical transition in the Franck sense is the fundamental principle, V' and V'' should be on the same plane. In our treatment, the restriction is filled up by the overlap for y. The inverse consideration is realized. On the other hand, in Eq. (10) the above vertical transition could not be estimated precisely as it is.

The force constants of the ground state of acetylene agree satisfactorily with those of dideuteroacetylene. These values agree also with those given by Herzberg,[6] where the interaction term of the C–H with the C≡C bond is taken into consideration, *viz.*, I(C–H, C≡C)$=-0.037$ mdyn/Å in acetylene. The remaining differences are mainly due to the neglect of anharmonicity. The force constants of the excited state of acetylene are, to some extent, different from those of dideuteroacetylene. These differences may be caused mainly by using the same repulsive force constant in the isomer. Therefore, it is proper to use the other set of force constants to discuss the effect of force constants on the overlap integral; we do this for acetylene.

The new set (Set II) of the force constants of the excited state of acetylene is given in Table 3, where the repulsive force constant is assumed to be zero. The **L** matrix (Set II) of Q_3' is also given in Table 2. The intensity factors obtained by Manner I and the relative intensities are also given in Table 6. The intensity factors in Set II are, to some extent, larger than those in Set I, and the relative intensities are nearer to the observed ones. Thus, it is found that the small difference in the force constants does not have as much effect on the overlap integral.

Anharmonicity should be considered in the calculation of the overlap integral.[11] In a vibrational wave function of Morse oscillator, it is characteristic that there is asymmetry on the origin. This results in the differences of (1) the probability on both sides of the origin, and then (2) the distance from the origin at the same probability. To estimate the effect of (2) from the wave function of the harmonic oscillator, we assume this expression:

$$\alpha_v = 4\pi^2\nu_v/h \qquad (23)$$

where ν_v is the difference between the observed frequencies of the $v+1$ and vth bands.

The normal coordinate vector of Q_3' is shown in Fig. 3 by the broad solid arrow. It is generally considered that the nucleus in this phase responds to a smaller potential than in the inverse-phase. Therefore, in our assumption, the ν_v of the narrow solid arrow of the carbon atom decreases with an increase in v, and that of the broken arrow increases. In the case of the increase we assumed a regular increase of 15 cm^{-1}. The results obtained using Manner I

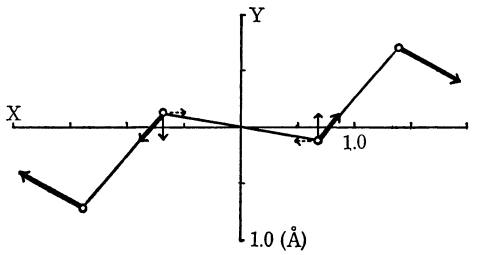

Fig. 3. The normal coordinate vector of Q_3' of the excited state of acetyleue. The vector for carbon atom is trebled.

TABLE 11. THE INTENSITY FACTORS AND THE RELATIVE INTENSITIES INVOLVING THE CONTRIBUTION OF ANHARMONICITY IN ACETYLENE

v	Intensity factors/10^{-5}	Relative intensities
0	0.00022	0.052
1	0.00424	1
2	0.0338	7.97
3	0.175	41.2
4	0.635	150
5	1.90	449

are given in Table 11. The intensity factors and the relative intensities are barely larger than those of Set I in Table 6. From Fig. 3, we can expect this to be a compensation for the increase and decrease in the overlap integrals of each coordinate. On the other hand, if the potential is the inverse of the above, results very similar to Set I in Table 6 are obtained; that is, complete compensations are found in this case. As a result, even if the precise wave function were used, a large change could not be expected in acetylene.

We wish to thank Dr. Y. Yasuda of the Faculty of Literature and Science of Toyama University for his valuable discussion of method.

References

1) C. K. Ingold and G. W. King, *J. Chem. Soc.*, **1953**, 2725.
2) D. P. Craig, *ibid.*, **1950**, 2146.
3) W. L. Smith and P. A. Warsop, *Trans. Faraday Soc.*, **64**, 1165 (1968).
4) F. Ansbacher, *Z. Naturforsch.*, **14a**, 889 (1959).
5) F. Duschinsky, *Acta Physicochim.*, **7**, 551 (1937).
6) G. Herzberg, "Infrared and Raman Spectra of Polyatomic Molecules," Van Nostrand, Princeton (1945).
7) C. K. Ingold and G. W. King, *J. Chem. Soc.*, **1953**, 2745.
8) B. D. Saksena, *J. Chem. Phys.*, **20**, 95 (1952).
9) T. Shimanouchi, "Computer Program for Normal Coordinate Treatment of Polyatomic Molecule," Tokyo University Press (1968).
10) E. B. Wilson, J. C. Decius and P. C. Cross, "Molecular Vibrations," McGraw-Hill, New York (1955).
11) T. Y. Chang and M. Karplus, *J. Chem. Phys.*, **52**, 783 (1970).

Soret Coefficients and Heat of Transport of Polyvalent Electrolytes in an Aqueous Solution

Masayasu SUGISAKI

Department of Nuclear Engineering, Faculty of Engineering, Kyushu University, Fukuoka 812

(Received February 7, 1975)

The Soret coefficients of aqueous electrolytes were measured by the conductometric method for salts of K_2SO_4, Na_2SO_4, $ZnSO_4$, and $CdSO_4$ in the concentration range from 0.001 to 0.01 M at 25 °C and 35 °C. The heats of transport were calculated from the Soret coefficients. The concentration dependence of the heat of transport was ascertained to be proportional to the square root of the ionic strength, and the slopes for Na_2SO_4 and K_2SO_4 salts at 25 °C were found to be larger than those reported by Snowdon and Turner. The temperature dependence of the heat of transport was examined based on the data at 25 °C and 35 °C. The heat capacities concerning the transported entropy were found to be negative for the four salts examined.

In the basic construction of irreversible thermodynamics, Onsager's reciprocal relation plays an important role. Its validity has been checked experimentally by several investigators[1] by studying a diffusion phenomenon of a ternary system. In this phenomenon, a cross effect is due to coupling between diffusion fluxes. The another cross effect was observed in coupling of a heat flux and a diffusion flux. In this case, the concept of the heat of transport was introduced by using Onsager's reciprocal relation. There are several molecular interpretations of the heat of transport concerning the thermal diffusion of an electrolytic aqueous solution. Eastman[2] interpreted the heat of transport in terms of the interaction between ion and solvent; to his mind, the positive and negative values of the heat of transport were related to structure-forming and structure-breaking ions respectively. On the other hand, Helfand and Kirkwood[3] interpreted the heat of transport as being due to the interaction between ions; they based their consideration on the non-equilibrium statistical mechanics. They could derive the concentration dependence of the heat of transport as proportional to the square root of the ionic strength. Agar[4] studied the interaction of the ion-solvent in a hydrodynamical approximation and also derived a similar concentration dependence. In order to unify these molecular interpretations, the data in the heat of transport of an ion in several different solvents may be very useful. The temperature dependence of the heat of transport may also be expected to give important information, because the change in temperature necessarily gives rise to a change in the thermal motion of the solvent. The purposes of the present work are, first, to construct a thermal diffusion cell which can be used for the aqueous and non-aqueous electrolytes; second, to measure the temperature dependence of the heats of transport of several aqueous electrolytes, and finally, to discover some thermodynamical properties useful for the theoretical development of the molecular interpretation of the heat of transport.

Experimental

Apparatus. The arrangement of the cell is shown in Fig. 1. The solution was placed in a central cylindrical hole, 20 mm in inside diameter and 10 mm in height, drilled vertically in a polycarbonate plate. The ends of the hole

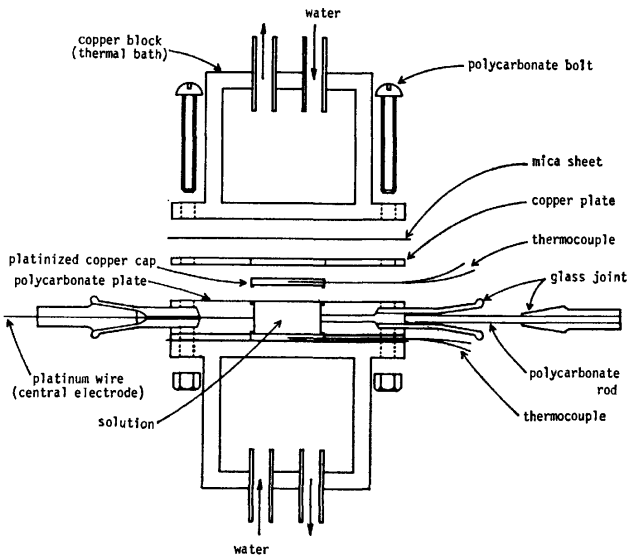

Fig. 1. Description of the cell.

are tightly covered by caps of platinized copper, which act as electrodes, secured with a small amount of epoxy resin adhesive. These platinized caps were faced to the copper blocks which were used as thermal baths, the temperature of each being maintained constant by circulating water from an external thermostat tank equipped with a mercury regulator. The temperature of each electrode was measured by means of a copper-constantan thermocouple embedded in the central part of the copper electrode. The cell was then filled, emptied, and washed out through a lateral hole, which had been closed by a polycarbonate rod during the measurement. The polycarbonate plate and the copper blocks were joined with four polycarbonate bolts. The total arrangement was especially designed to assure an uniform temperature distribution in the radial direction of a solution. This cell was set in an air thermostat and incorporated into an audio-frequency bridge with a Wagner earth operated between 900-1000 Hz/s. Thereading precision of the bridge was one part in 10^5.

Solution. Commercial extra pure salts were dried and weighed. The solution was prepared using conductivity water(specific resistance$> 10^6\ \Omega$ cm) purified by means of an ion-exchange resin column. The Na_2SO_4, $CdSO_4$, and $ZnSO_4$ were carefully dried in order to remove the water of crystallization completely.

Measurements. The concentration gradient in a solution induced by a thermal gradient was measured as a resistivity gradient of the solution. When the resistance of the

upper part of a solution is R'' and that of the lower part, R', the quantity, Y, was defined by this relation; $Y=(R'-R'')/(R'+R'')$. According to Agar and Turner[5], the Soret coefficient was calculated by means of the following relation;

$$Y_t - Y_0 = (bS\Delta T/4)[1-(32/\pi^3)\exp(-t/\theta)],$$
$$b = -[1+(\partial \ln \Lambda/\partial \ln C)].$$

Here, Y_0 and Y_t represent the initial value of Y and that at time t respectively and S the Soret coefficient; θ is called the relaxation time and is related to the interdiffusion coefficient by this equation; $\theta=a^2/(\pi^2 D)$. a is the height of the cell; D, the interdiffusion coefficient of a solution; Λ, the equivalent conductivity; C, the concentration of the solution, and ΔT, the temperature difference between the upper and lower ends of the solution. The measurements were performed as follows. First, the total cell was inversely set (*i.e.*, the lower-temperature side was upward, and the upper, downward), and the temperature gradient was applied in the solution by circulating water, the temperature of which was kept constant withinin ± 0.02 °C, into each thermal bath from the external thermostat tank. This state was held for about 1 hr to insure the stational temperature distribution in the cell. During this inverse setting the concentration gradient induced by ΔT was almost completely destroyed by the strong convective stream in the solution; the concentration of the solution was kept uniform in spite of the application of the temperature gradient. When the measurement was started, the direction of the cell was set normal by turning the cell (*i.e.*, the hot side was now up, and the cold, down); this instance was defined as time zero, t_0, and during the run of the thermal diffusion, Y_t was followed by means of the resistance bridge for a long time. The measurements were performed for the solutions of Na_2SO_4, K_2SO_4, $ZnSO_4$, and $CdSO_4$ in the concentration range from 0.001 to 0.01 M and at mean temperatures of 25 °C and 35 °C; the temperature difference, ΔT, applied across the solution was about 5 °C, which was determined within 0.01 °C for each thermal-diffusion run.

Results

Soret Coefficient. The Soret coefficient was determined from the slope of the curve of Y_t against exp$(-t/\theta)$, which is shown in the case of a 0.005 M solution of K_2SO_4 in Fig. 2. The interdiffusion coefficients, D, necessary for the calculation of the relaxation times, θ, are available in the literature at 25 °C and 35 °C for K_2SO_4[6] and at only 25 °C for Na_2SO_4.[7] Therefore for the analysis for Na_2SO_4 at 35 °C it was assumed that the D_{35}/D_{25} ratio is the same as the ratio for K_2SO_4. For the calculation of θ for $ZnSO_4$ and $CdSO_4$, the integrated interdiffusion coefficients were used; they were measured by the diaphragm-cell method for 0.01 M salt diffusing into water.[8]

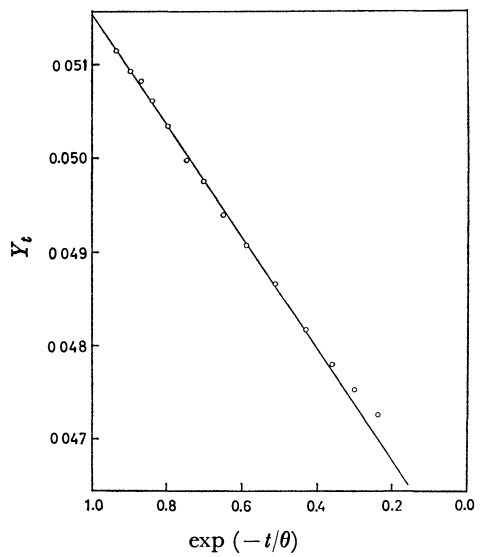

Fig. 2. The experimental plot of Y_t against exp $(-t/\theta)$ for the 0.005 M K_2SO_4 solution at 25 °C.

Table 1. Soret coefficients and heats of transport at 25 °C and 35 °C

Salt	Molality	25 °C $S\times 10^3$ (deg^{-1})	25 °C $\hat{Q}$ (kcal/mol)	35 °C $S\times 10^3$ (deg^{-1})	35 °C $\hat{Q}$ (kcal/mol)
Na_2SO_4	0.002	6.80	3.32	7.92	4.13
	0.005	6.07	2.87	6.83	3.45
	0.010	5.40	2.44	5.93	2.86
K_2SO_4	0.002	6.29	3.07	6.98	3.64
	0.005	5.33	2.52	6.50	3.28
	0.010	5.04	2.28	5.65	2.73
$ZnSO_4$	0.001	8.54	2.70	10.4	3.69
	0.010	8.30	1.98	9.39	2.40
$CdSO_4$	0.001	10.22	2.98	11.4	3.58
	0.010	8.22	2.12	8.90	2.46

Table 2. Some parameters used for the calculation of Soret coefficients

Salt	Molality	$-b$	$\left(1+\frac{\partial \ln \gamma}{\partial \ln m}\right)$	$D\times 10^5$ (cm^2/s) 25 °C	$D\times 10^5$ (cm^2/s) 35 °C
Na_2SO_4	0.002	0.951	0.921	1.159	1.508
	0.005	0.936	0.892	1.124	1.462
	0.010	0.926	0.853	1.093	1.422
K_2SO_4	0.002	0.959	0.921	1.406	1.829
	0.005	0.937	0.892	1.398	1.819
	0.010	0.923	0.853	1.369	1.781
$ZnSO_4$	0.001	0.897	0.895	0.789	1.27
	0.010	0.793	0.675	0.789	1.27
$CdSO_4$	0.001	0.875	0.830	0.701	1.26
	0.010	0.805	0.730	0.701	1.26

In some experiments the plot of Y_t against exp$(-t/\theta)$ showed a deviation from linearity at high values of exp$(-t/\theta)$. Since such lack of a linearity resulted from convective mixing,[5] the determination of the Soret coefficient was performed by using the linear relation at lower values of exp$(-t/\theta)$. The Soret coefficients thus obtained are summarized in Table 1, while the data which were necessary for the calculation summarized in Table 2.

Heat of Transport. The heat of transport is defined by irreversible thermodynamics[1] as:

$$\hat{Q} = RT^2(\nu_1+\nu_2)\left(1+\frac{\partial \ln \gamma}{\partial \ln m}\right)S.$$

Here, $\hat{Q}$ stands for the heat of transport; ν_1, and ν_2 the stoichiometric numbers of ions of Species 1 and 2 when the salt is dissociated in a solution; γ, the activity

coefficients, and m, the molality. For the calcultaion it is necessary to have the values of $(1+\partial\ln\gamma/\partial\ln m)$, which are available in the literature for all solutions at 25 °C.[9] The data at 25 °C cited in Table 2 were also used for the analysis at 35 °C, because the experimental results show that the temperature dependence of $(\partial\ln\gamma/\partial\ln m)$ is not very large. The obtained heats of transport are summarized in Table 1.

Disscussion

Calculation of the Soret Coefficient. In the present experiment a deviation from linearity was often observed in the plot of Y_t against exp $(-t/\theta)$ in the latter half of the thermal-diffusion run when θ was calculated by using the interdiffusion coefficient data. If θ was adjusted so that the linearity of the plot of Y_t against exp $(-t/\theta)$ held, its value tended to become smaller than that calculated from the isothermal interdiffusion data. Agar and Turner[5] and Sagert and Breck[10] observed similar situations and interpreted them as being due to the convective mixing. Since such convective interference could be considered to be very small in the earlier stage of the thermal diffusion run, where the concentration gradient induced by the temperature gradient has not yet become very large, the initial linear part of the plot of Y_t against exp $(-t/\theta)$ was adopted to calculate the Soret coefficients in Table 1.

The Soret coefficients and the heats of transport of the present three salts of K_2SO_4, Na_2SO_4, and $CdSO_4$ were measured at 25 °C by Snowdon and Turner[11]; their values agree with those of the present work in the range of concentrations near 0.002 M for K_2SO_4 and 0.01 M for Na_2SO_4, but the concentration dependences do not agree with each other (see Figs. 3 and 4). These discrepancies in the concentration dependence of $\hat{Q}$ may result from the unreliable estimation of the convective interference, since we could not determine unambiguously the instant from which the convective mixing began to have appreciable influence on the construction of the concentration gradient. In fact, the Soret coefficient varied in a range of about 5 per cent depending upon the method used to estimate the linearity of the plot of Y_t against exp $(-t/\theta)$. It should be noted, however, that the precision of the reproducibility of the measurement is within 1 per cent. Therefore, the values of the Soret coefficient and the heat of transport summarized in Table 1 may involve an ambiguity of only a few per cent. In the case of the $CdSO_4$ solution, the two sets of data agree with each other, as is shown in Fig. 5. This agreement is significant because the Soret coefficient of the dilute $CdSO_4$ solution obtained by the conductivity method has been ascertained to be smoothly related to that of a higher concentration measured by a optical method.[11]

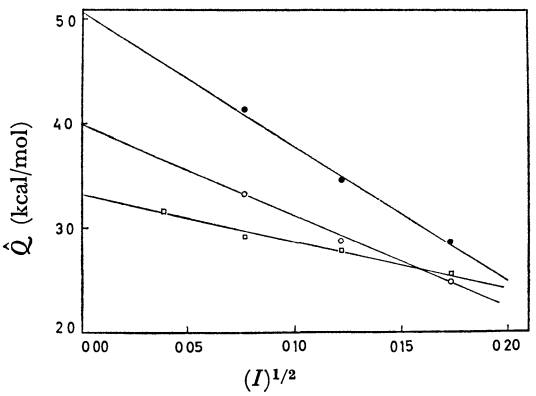

Fig. 3. The concentration dependence of the heat of transport of Na_2SO_4 solution at 25 °C and 35 °C. The open and filled circles represent the present work at 25 °C and 35 °C, respectively. The rectangles stand for the data of Snowdon and Turner at 25 °C.

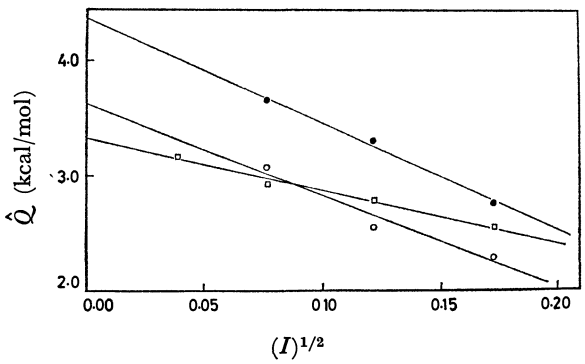

Fig. 4. The concentration dependence of the heat of transport of K_2SO_4 solution at 25 °C and 35 °C. The open and filled circles represent the present work at 25 °C and 35 °C, respectively. The rectangles stand for the data of Snowdon and Turner at 25 °C.

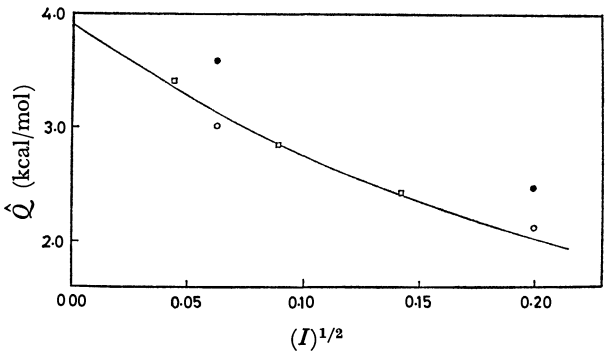

Fig. 5. The concentration dependence of the heat of transport of $CdSO_4$ solution at 25 °C and 35 °C. The open and filled circles represent the present work at 25 °C and 35 °C, respectively. The rectangles stand for the data of Snowdon and Turner at 25 °C.

Concentration Dependence of $\hat{Q}$. Agar[4] developed Eastman's idea of the molecular interpretation of $\hat{Q}$ and derived the concentration dependence of $\hat{Q}$ as proportional to the square root of the ionic strength. He could calculate the slope of the concentration dependence of $\hat{Q}$ at 25 °C in the dilute range for the 1 : 2 electrolyte as;

$$\hat{Q}_0 - \hat{Q} \approx 7500\sqrt{I}.$$

where $\hat{Q}_0$ is the value of $\hat{Q}$ at an infinite dilution, and I, the ionic strength.[4] The present results for the two alkali sulfates indicate that the $\hat{Q}_0-\hat{Q}$ varies from about $800\sqrt{I}$ for K_2SO_4 to about $900\sqrt{I}$ for Na_2SO_4. The slopes of the present results are larger than those reported by Snowdon and Turner[11] and are rather nearer to the above theoretical results. This agreement, however, must not be overestimated because of the crude approximation of the theory.

Temperature Dependence of $\hat{Q}$. The temperature dependence of $\hat{Q}$ has been studied by Alexander[12] and Agar[4] and some thermodynamical quantities has been defined. The transported entropy, $\bar{\bar{S}}$, was defined as;

$$\bar{\bar{S}} = \hat{S} + s.$$

where $\hat{S}$ stands for the entropy of transport, and s, partial molar entropy. $\hat{S}$ can be related to the heat of transport, $\hat{Q}$, by $\hat{S}=\hat{Q}/T$. The "heat capacities", $\hat{C}$ and $\bar{\bar{C}}$ were also defined as;

$$\hat{C} \equiv T(\partial\hat{S}/\partial T) = (\partial\hat{Q}/\partial T) - (\hat{Q}/T)$$

$$\bar{\bar{C}} \equiv T(\partial\bar{\bar{S}}/\partial T) = C + C_p.$$

where C_p represents the ordinary partial molar heat capacity at a constant pressure. $\bar{\bar{C}}$ can be calculated from the experimental results of the heat of transport at 25 °C and 35 °C. The C_p values for Na_2SO_4 and K_2SO_4 solutions are available in the literature.[13] The C_p values for $ZnSO_4$ and $CdSO_4$ solutions were calculated from the previously reported data of the heat capacity of the solution at 19 °C.[14,15] As the temperature dependence of the C_p of solution is not usually so large, using the data at 19 °C for the present analysis may not produce any significant error. The results are shown for the 0.01 M solution in Table 3, which shows that the values of $\bar{\bar{C}}$ are negative for all the present four salts. This result forms a striking contrast to the cases of many 1 : 1 salts summarized by Agar[4], in which the values of $\bar{\bar{C}}$ are all positive. The fact that the values of $\bar{\bar{C}}$ are positive in the cases of such alkali halides as NaCl and KCl suggests that the negative values of $\bar{\bar{C}}$ for Na_2SO_4 and K_2SO_4 may be attributed to the SO_4^{2-} ion. By summarizing many data, Tyrrell[16] showed that the contribution of the entropy of transport, $\hat{S}$, to the transported entropy, $\bar{\bar{S}}$, is relatively small as compared with the partial molar entropy, s, and that there is a good correlation between the transported entropies and the conventional partial molar standard ionic entropy except for the cases of H^+, OH^-, and SO_4^{2-}, which have larger transported entropies in spite of their small values of s relative to other cations and anions.

TABLE 3. "HEAT CAPACITIES", $\hat{C}$, C_p AND $\bar{\bar{C}}$ (cal/mol·K) FOR 0.01 M SOLUTION AT 25 °C

Salt	$\hat{C}$	C_p	$\bar{\bar{C}}$
Na_2SO_4	34.8	−42.2	−7.4
K_2SO_4	37.0	−54.7	−17.7
$ZnSO_4$	33.3	−55	−22
$CdSO_4$	36.8	−61	−24

These two exceptional aspects of the behavior of SO_4^{2-} ion may be explained in terms of the interaction between ion and solvent. The theory by Helfand and Kirkwood based on the non-equilibrium statistical mechanics may be so rigorous that it is difficult to include such a solvation effect of an ion in the theory. On the other hand, the interpretation originated by Eastman and developed by Agar, while it is phenomenological and less rigorous from the viewpoint of non-equilibrium statistical mechanics, yet has the merit of giving a simple insight into the physical significance of the approximation involved in the theory. Consequently, it would be better to examine the ion-ion contribution to the heat of transport as rigorously as possible by the theory of Helfand and Kirkwood, and to discuss the interaction between ion and solvent by the theory based on Eastman's idea: the heat of transport must be considered as a sum of those contributions.

The author would like to express his thanks to Professor Yasumichi Oishi for his useful advice in this work. Thanks are also due to Messrs. Hideyuki Moriyama, Munanori Tanemura, and Fumihiro Otsubo for their technical assistance.

References

1) D. D. Fitts, "Nonequilibrium Thermodynamics," McGraw-Hill Book Co., New York, 1962.
2) E. D. Eastman, *J. Amer. Chem. Soc.*, **50**, 283, 292 (1928).
3) E. Helfand and J. G. Kirkwood, *J. Chem. Phys.*, **32**, 857 (1960).
4) J. N. Agar, "Advances in Electrochemistry and Electrochemical Engineering," Electrochemistry, Vol. 3, ed. by P. Delahay, Interscience Publishers, New York, London, 1963, p. 31.
5) J. N. Agar and J. C. R. Turner, *Proc. Roy. Soc.* (London), **A255**, 307 (1960).
6) J. W. Mullin and A. W. Nienow, *J. Chem. Eng. Data*, **9**, 526 (1964).
7) H. S. Harned and C. A. Blake, Jr., *J. Amer. Chem. Soc.*, **73**, 2448 (1951).
8) M. Sugisaki, unpublished.
9) R. Parsons, "Handbook of Electrochemical Constants," Butterworths (1959).
10) N. H. Sagert and W. G. Breck, *Trans. Faraday Soc.*, **57**, 436 (1961).
11) P. N. Snowdon and J. C. R. Turner, *ibid.*, **56**, 1812 (1960).
12) K. F. Alexander, *Z. Physik. Chem.* (Leipzig), **203**, 181, 203, 213, 228, 357 (1954).
13) M. Randall and F. D. Rossini, *J. Amer. Chem. Soc.*, **51**, 323 (1929).
14) E. Cohen, W. D. Helderman, and A. L. Th. Moesveld, *Z. Physik. Chem.*, **112**, 135 (1924).
15) E. Cohen and A. L. Th. Moesveld, *ibid.*, **95**, 305 (1920).
16) H. J. V. Tyrrell, "Diffusion and Heat Flow in Liquids," Butterworths, London, 1961.

Activity Measurement and Colloid Chemical Studies of Aqueous Sodium Tetradecyl Sulfate Solutions

Masakatsu KOSHINUMA* and Tsunetaka SASAKI

Department of Chemistry, Faculty of Science, Tokyo Metropolitan University, Setagaya, Tokyo 158

(Received February 25, 1975)

A concentration cell using an ion-exchange semipermeable membrane as a septum for the measurement of the activities of ionic surfactants has been constructed, the method of measurement is here in described. The membranes used proved each to be exclusively permeable to one ion. The activities of both the tetradecyl sulfate ion (TS^-) and the counterion (Na^+) were determined. In the concentration region from 4.0×10^{-4} mol/l to CMC, $\log f_\pm = -(0.070 \log C + 0.283)$ held for the mean activity coefficient, $f_\pm$. The $f_\pm$ value at the CMC was found to be 0.81, considerably smaller than the value, 0.978, calculated by the Debye-Hückel equation taking account of the ionic size, 5.5 Å. Above the CMC the activity of the TS^- ion decreased, that of the Na^+ ion increased, and the mean activity slightly increased with the NaTS concentration. The Gibbs adsorption isotherm was applied for the adsorption of NaTS, using exclusively the observed data of the amount of adsorption, the surface tension, and the activities. A satisfactory agreement was obtained between the amount of adsorption observed and that calculated. The observed decrease in the surface tension above the CMC was confirmed by calculations using the Gibbs adsorption iostherm, the observed data of activity, and the amount of adsorption. The charged-phase separation model was verified as the mechanism of the micelle formation, and the degree of counterion attachment was calculated to be 0.81.

In order to elucidate various properties of the surfactants, such as the adsorption, the micelle formation, the solubilization, the dispersibility, the emulsification, and the detergency, the study of the activity of the aqueous surfactant solutions is important as a basis. However, there have been few such reports[1–5] because of the difficulty of measurement at the low concentrations where surfactants are generally used and of the inevitable error involved in the method of measurement. Amoung the various methods of measurements,[4–7] that of the electromotive force of a concentration cell with an ion-exchange membrane semipermeable to a surfactant anion has proved effective, and one of the present authors has previously applied this method to the study of sodium dodecylsulfate.[8] The activity measurement of the ionic surfactant requires those of both the surfactant ion and the counterion; in the case of the anionic surfactant, the counterion activity can be measured also by means of a pNa-responsive electrode.[8–10] The measurements of the activities of both ions by the concentration cells using anion and cation-exchange membranes are also possible.[1,2] In the present paper, the activities of both the surfactant anion and the counterion were measured for aqueous sodium tetradecyl sulfate solutions by the EMF measurement of the concentration cell with an ion-exchange membrane, which had been specially constructed to prolong the life of the membrane and to obtain reproducible results. The activity coefficients were calculated for sodium tetradecyl sulfate, which was selected as a surfactant for comparison with the sodium dodecyl sulfate (NaDS) already reported,[8] in order to study the effect of the change in the hydrophobic chain length on various properties of the aqueous solution.

The surface tension and the amount of adsorption were also measured by the Wilhelmy plate method and the radiotracer method respectively. From these results, the applicability of the Gibbs adsorption isotherm was examined with the results obtained below the CMC.[11–13] The mechanism of the micelle formation and the surface tension lowering above the CMC were also discussed. Moreover, the counterion attachment of the micelle was calculated and compared with that of NaDS.

Experimental

Materials. For the preparation of sodium tetradecyl sulfate (NaTS), 99% tetradecyl alcohol, obtained by fractional distillation and its purity checked by gas chromatography (apparatus : Yanagimoto GC G-3DH), was sulfated with chlorosulfonic acid and neutralized with an aqueous sodium hydroxide solution. The inorganic salts thus formed were removed, and the product was then recrystallized several times from ethanol. To remove the unreacted tetradecyl alcohol, extractions with ether were continued until the minimum in the surface tension *vs.* concentration curve disappeared. The tritium-labelled sodium tetradecyl sulfate used for the adsorption measurement was synthethesized much[14] as has previously been reported.[13] Deionized water was used for the EMF measurement, and thrice-distilled water, for the surface-tension and absorption measurements. The ion-exchange membranes used for the surfactant-ion and Na^+-ion activities were an anion exchanger, Neosepta AV-4T, and a cation exchanger, Neosepta CL-25T, both supplied by the Tokuyama Soda Co., Ltd.

Apparatus and Measurements. *Adsorption*: The amounts of adsorption were measured by means of a thin-window gas-flowing tube devised for soft β-ray radioactivity measurements.[15]

Surface Tension: The surface tension was measured by Wilhelmy's vertical plate method using a strain gauge as a transducer; the steady value recorded after 4 hr was regarded as an equilibrium value.[16] The error in the surface-tension measurement was ±0.05 dyne/cm for a glass plate 4 cm in perimeter.

Electromotive Force Measurement: The anion- and cation-exchange membranes used for the activity measurment were stored in an aqueous 0.5 M-NaCl solution. They were then rinsed with water and soaked in an aqueous 10.0×10^{-3}

* Present address: Laboratory of Chemistry, Faculty of Education, Chiba University, Chiba.

Saturated Calomel Electrode	1M-NH_4NO_3 2%-Agar Bridge	STS (C)	Membrane AV-4T or CL-25T	STS (C_0) 10 mM	1M-NH_4NO_3 2%-Agar Bridge	Saturated Calomel Electrode

Fig. 1. Surfactant concentration cell.

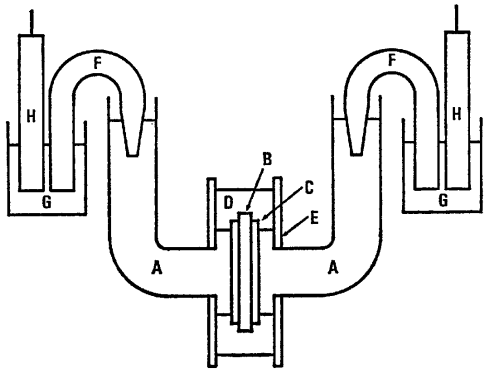

Fig. 2. Apparatus of surfactant concentration cell.
A: U-shaped glass cell with surfactant solution. B: Anion or cation exchange membrane. C: Silicone rubber washer. D: Low melting paraffin. E: Aluminum frame. F: 1 M-NH_4NO_3 agar bridge. G: Saturated KCl aqueous solution. H: Calomel electrode.

mol/l NaTS standard solution for two or three days in order to replace all of the exchangeable ions with TS^- or Na^+ ions. The membranes were then rinsed with deionized water and immediately fixed to the cells. The concentration cell shown in Fig. 1, which had been improved from a former one, was constructed as in illustratd in Fig. 2. In this figure, a U-shaped cell, A, with flanges held an ion-exchange membrane, B, with the aid of silicon rubber washers, C. They were tightly fixed between aluminum frames, E. Water evaporation from the open edge of the ion-exchange membranes, causing craks in the film and reducing the life of the membrane, was avoided by sealing the edge with low-melting-point paraffin, as is shown by D. A sample solution and the standard NaTS solution were introduced separately into the two chambers of A, one on either side of the membrane. The aqueous 10.0×10^{-3} mol/l NaTS solution was chosen as the standard solution because the change in the concentration of the standard solution in this region gave the relative insensitivity of the EMF. Each of the two calomel electrodes, H, was connected through 1 M-NH_4NO_3 agar bridges, F, to the solutions in A. Two-percent agar was used to prepare the bridges, and NH_4NO_3 was used to avoid the direct contact of NaTS with the KCl of the calomel, which would form insoluble potassium tetradecyl sulfate. Measurements of the EMF were made by using a high-impedance electrometer, Keithly model 610 C, with an input impedance of more than 10^{14} ohm, in an air-thermostated box at 32 ± 1 °C; the EMF was recorded on a recorder of the Riken Electronic Co., Ltd., model SP-5. Both the chambers of A were filled with the same aqueous 10.0×10^{-3} mol/l NaTS solution, and they were renewed several times until the asymmetry potential (E_{as}) became constant. Each chamber was rinsed several times with each solution to be measured before the setting of the cell. Then, the solution in one chamber of A was replaced by the NaTS solution to be measured; the recording of the potential was started about 20 min after the setting. A steady EMF, E_1, was usually obtained 20 min after the setting and kept constant for about 20 min, after which it gradually decreased. The E_{as} value was confirmed to be nearly constant during each measurment. The potential, E, of the concentration cell is obtained as:

$$E = E_1 - E_{as}$$

When not in use, both chambers of the cell, A, were filled with the standard solution and the cell was placed in a vessel saturated with the vapor of the standard solution in order to avoid any evaporation of the solution in the cell and any change in the membrane properties. The membrane thus protected could be used continuously for about two weeks before the renewal of the membrane.

Results and Discussion

Calculation of Activity. The EMF of the concentration cell using a membrane permeable to the TS^- ion is given according to Nernst's equation as follows:

$$E_{TS} = (\lambda_- - \lambda_+)(2.303\,RT/F)\log(a_{TS}/a_{O,TS}) \quad (1)$$

where λ_+ and λ_- are the transport numbers of the TS^- and Na^+ ions in the membrane respectively: a_{TS} and $a_{O,TS}$, the activities of the TS^- ion in the sample and the standard solutions respectively: F, the Faraday constant: R, the gas constant, and T, the absolute temperature. To determine the activity from Eq. (1), the values of λ_- and λ_+ must be estimated. The evaluation of $\lambda_- - \lambda_+$, usually made by referring to ions of known activities, is impossible in the present experiment because no activity coefficient data are available, but we have several reasons to believe that $\lambda_- - \lambda_+$ is close to unity. First, the differenciation of Eq. (1) with respect to log C gives:

$$dE_{TS}/d\log C = (\lambda_- - \lambda_+)(2.303\,RT/F)(d\log a_{TS}/d\log C) \quad (2)$$

where C is the concentration of NaTS. In Eq. (2), since $dE_{TS}/d\log C$ is found to be nearly equal to $2.303\,RT/F$ in the concentration range from 4.0×10^{-4} to 2.0×10^{-3} mol/l, Eq. (2) gives:

$$(\lambda_- - \lambda_+)\, d\log a_{TS}/d\log C = 1$$

Since $d\log a_{TS}/d\log C$ is considered to be not larger than unity for such dilute solutions as in the present experiment, $\lambda_- - \lambda_+$ is expected to be nearly equal or larger than unity. However, from the definition, $\lambda_- + \lambda_+ = 1$. In order to satisfy both of these requirements, $\lambda_- = 1$ and $\lambda_+ = 0$ must hold, so $\lambda_- - \lambda_+$ may reasonably be taken to be close to unity. Moreover, as will be discussed below the linearity of the extrapolation function down to low concentrations of the NaTS solution, as is shown in Fig. 3, and the agreement between the calculated and observed amounts of the NaTS adsorption (Fig. 6) also indicate that $\lambda_- - \lambda_+$ may safely be taken to be unity. Thus, Eq. (1) is reduced to:

$$E_{TS} = (2.303\,RT/F)\log(a_{TS}/a_{O,TS}) \quad (3)$$

According to similar reasoning and similar observed data, the conditions of $\lambda_- = 0$ and $\lambda_+ = 1$ also hold for the cation-exchange membrane in the concentration range from 3.0×10^{-4} to 2.0×10^{-3} mol/l, and the EMF of the Na^+-ion concentration cell is given by:

$$E_{Na} = -(2.303\,RT/F)\log(a_{Na}/a_{O,Na}) \quad (4)$$

where $a_{O,Na}$ is the activity of the Na^+ ion in the solution of the standard electrode.

Experimental results of the EMF *vs.* concentration curve are expressed by Eqs. (3) and (4). In order to calculate the values of $a_{O,TS}$ and $a_{O,Na}$, the following extrapolation function, E', is constructed:[17]

$$E'_{TS} = (2.303\,RT/F)\log C - E_{TS} \quad (5)$$

The substitution of Eq. (3) into Eq. (5) gives:

$$E'_{TS} = (2.303\,RT/F)(\log C - \log a_{TS} + \log a_{O,TS})$$
$$= (2.303\,RT/F)(-\log f_{TS} + \log a_{O,TS})$$

Since $f_{TS} = 1$ for $C = 0$, the value of E'_{TS} extrapolated to $C = 0$ gives:

$$E'_{TS,C=0} = (2.303\,RT/F)\log a_{O,TS}$$

from which $a_{O,TS}$ can be calculated. The activity, $a_{O,Na}$, is similarly calculated from the corresponding function, E'_{Na}. Figure 3 shows the E'_{TS} and E'_{Na} *vs.* $C^{1/2}$ plots and their extrapolation. The activities calculated, $a_{O,TS}$ and $a_{O,Na}$, are:

$$\log a_{O,TS} = -3.018 \text{ and } \log a_{O,Na} = -2.556$$

The a_{Na} and a_{TS} values calculated according to Eqs. (3) and (4) are shown in Fig. 4, together with the mean activity calculated by means of this definition:

$$a_\pm = (a_{TS}\cdot a_{Na})^{1/2} \quad (6)$$

The activity coefficient, $f_\pm$, calculated from the $a_\pm$ thus obtained was nearly unity at the concentration of 1.5×10^{-4} mol/l, and it gradually decreased with an increase in the concentration. In the concentration region from 4.0×10^{-4} to 2.0×10^{-3} mol/l (CMC),

$$\log f_\pm = -(0.070\log C + 0.283) \qquad C;\ \text{mol/l}$$

holds. It is noted that the mean activity coefficient at the CMC was found to be 0.81, considerably smaller than the value, 0.978, calculated according to the modified equation of Debye-Hückel using the mean ionic diameter of 5.5 Å.[18] Such a difference is similar to the cases of cetyltrimethylammonium bromide[19] and sodium dodecyl sulfate.[8] It may be explained by the effect of the long hydrophobic chain in the molecule, which is neglected in the Debye-Hückel equation, or by the so-called "premicelle" formation.[20]

Above the CMC the activity of the TS^- ion was found to decrease, while that of the Na^+ ion increased with an increase in the concentration of the surfactant. As a result, the mean activity is not constant, as has been stated,[21] but slightly increases, as in the case of sodium dodecyl sulfate.[8] It should be noticed that the linearity of the extrapolation functions, E'_{TS} and E'_{Na}, observed down to a low concentration, C, proves $\lambda_- - \lambda_+$ and $\lambda'_+ - \lambda'_-$ to be unity for the anion- and cation-exchange membranes. This is because, for instance, Eqs. (1), (3) and (5) give:

$$E'_{TS} = (2.303\,RT/F)\{(1-\Delta)\log C - \Delta\log f_{TS} + \log a_{O,TS}\}$$

where $\Delta = \lambda_- - \lambda_+$. This equation means that, for $\Delta \neq 1$, the $(1-\Delta)\log C$ term becomes infinity at $C = 0$: a marked deviation from the linearity may be expected as tending to zero, but the linear plots of E'_{TS} down to low C values may exclude such a possibility. A similar argument can be made for the cation-exchange membrane.

Application of the Gibbs Adsorption Isotherm. The Gibbs adsorption isotherm was used to calculate the amount of adsorption, putting only the observed data of surface tension and activities into the isotherm; the values were then compared with the observed amounts of adsorption for NaTS at the surface of an aqueous solution. The amount of adsorption was calculated according to the Gibbs adsorption isotherm:

$$\Gamma = -(1/2.303RT)(d\sigma/d\log C)/\{(d\log a_{TS}/d\log C) + (d\log a_{Na}/d\log C)\} \quad (7)$$

by putting the $d\log a_{TS}/d\log C$, $d\log a_{Na}/d\log C$, and $d\sigma/d\log C$ values, which were obtained from Fig. 4 and from the surface tension *vs.* $\log C$ plots in Fig. 5 respectively, into Eq. (7). Figure 6 shows the calculated value of Γ by a solid line and the observed value obtained by the radiotracer method, by circles. A

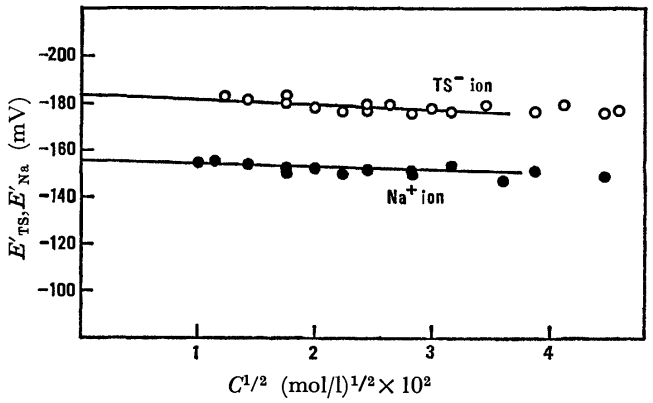

Fig. 3. Extrapolation of E'_{TS} and E'_{Na} function.
○: Extrapolation function (E'_{TS}) for TS^- ion.
●: Extrapolation function (E'_{Na}) for Na^+ ion.

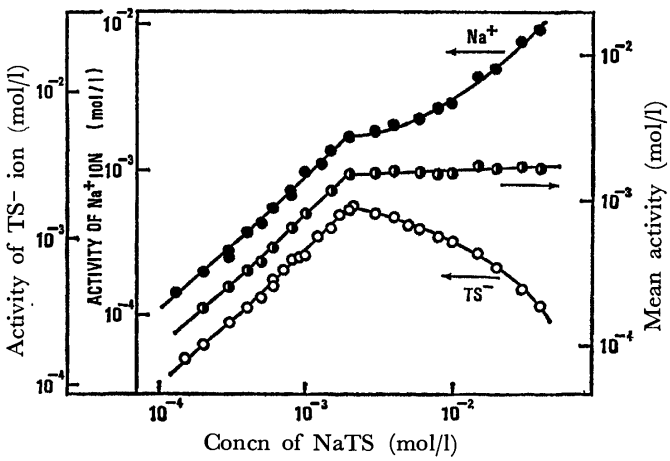

Fig. 4. Activities of TS^- ion, Na^+ ion and the mean activity *vs.* NaTS concentration.
○: TS^- ion activity. ●: Na^+ ion activity.
◑: Mean activity.

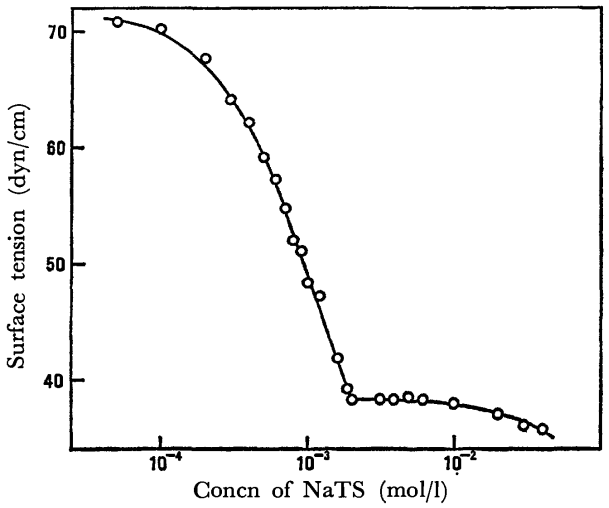

Fig. 5. Surface tension *vs.* NaTS concentration.

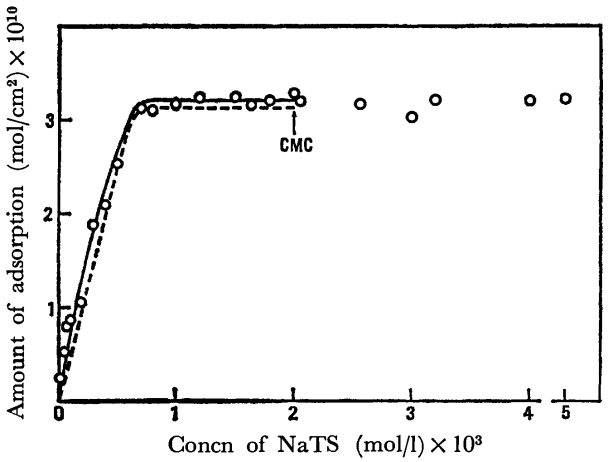

Fig. 6. Direct confirmation of the Gibbs adsorption isotherm.
○: Amount of adsorption observed. ——: Amount of adsorption calculated from activities data. ----: Amount of adsorption calculated assuming activity coefficient to be unity.

satisfactory agreement was obtained between them, and the saturate value of Γ was found to be 3.21×10^{-10} mol/cm². It should be noted that the agreement obtained here is another evidence that the $\lambda_- - \lambda_+$ value for the anion-exchange membrane is unity and that the $\lambda'_+ - \lambda'_-$ value for the cation-exchange membrane is also unity, since the introduction of $\lambda_- - \lambda_+$ and $\lambda'_+ - \lambda'_-$ values less than unity reduces the calculated Γ values according to:

$$\Gamma = -(1/2.303RT)(\mathrm{d}\sigma/\mathrm{d}\log C)/\{(\mathrm{d}\log a_{\mathrm{TS}}/(\lambda_- - \lambda_+)\mathrm{d}\log C + (\mathrm{d}\log a_{\mathrm{Na}}/(\lambda'_+ - \lambda'_-)\,\mathrm{d}\log C\}$$

from that calculated by Eq. (7), and this causes a disagreement between the calculated and the observed values. That the values of λ_- and λ'_+ are unity and the observed activity of NaTS are thus confirmed to be valid.

The value calculated assuming the activity coefficient to be unity is shown as a broken line in Fig. 6. The agreement between these values and the observed ones is not so good as in the case of Γ calculated in terms of the activity data, but the deviation is not very large. Thus, the assumption of $f_\pm = 1$ often made proves invalid in this case also.

Calculation of the Surface Tension above the CMC. As is shown in Fig. 5, the surface tension of the NaTS solution above the CMC is not constant, but gradually decreases with an increase in the concentration of the surfactant. It is worthwhile to confirm the validity of the observed a_{TS} and a_{Na} values by comparing the surface tension observed and that calculted from the Gibbs adsorption isotherm using these activity data and the observed Γ values above the CMC. For this purpose, the following equation is used:

$$\sigma = \sigma_{\mathrm{CMC}} - 2.303RT\Gamma_{\mathrm{CMC}}\{(\mathrm{d}\log a_{\mathrm{TS}} + \mathrm{d}\log a_{\mathrm{Na}})_C - (\mathrm{d}\log a_{\mathrm{TS}} + \mathrm{d}\log a_{\mathrm{Na}})_{\mathrm{CMC}}\} \quad (8)$$

which is obtained by the integration of the Gibbs adsorption isotherm:

$$\mathrm{d}\sigma = -2.303\,RT\Gamma(\mathrm{d}\log a_{\mathrm{TS}} + \mathrm{d}\log a_{\mathrm{Na}})$$

from the CMC up to the C concentration, taking account of the fact that the amount of adsorption observed above the CMC, Γ_{CMC}, was constant (3.21×10^{-10} mol/cm²), as is shown in Fig. 6. The surface tension calculated according to Eq. (8) is shown by circles in Fig. 7, where the observed value is indicated by a solid line. The agreement as a whole is good, just as in the case of sodium dodecyl sulfate.[8] Thus, the observed decrease in the surface tension, together with the observed a_{Na}, a_{TS} and $a_\pm$ values above the CMC may be comfirmed as valid. It is emphasized that the calculation of σ needs no assumption such as is necessary in the case of the calculation by the mass-action law.[22]

Micelle Formation and Degree of Counterion Attachment. As has been mentioned,[8] the mechanism of micelle formation by the mass-action law[22-24] gives:

$$a_{\mathrm{M}}/(a_{\mathrm{TS}})^p(a_{\mathrm{Na}})^q = K$$

or

$$p\log a_{\mathrm{TS}} + q\log a_{\mathrm{Na}} = \log a_{\mathrm{M}}/K \neq \text{const.} \quad (9)$$

where a_{M} denotes the activity of micelles composed of p TS^- ions and q Na^+ ions.

On the other hand, the phase-separation model[25]

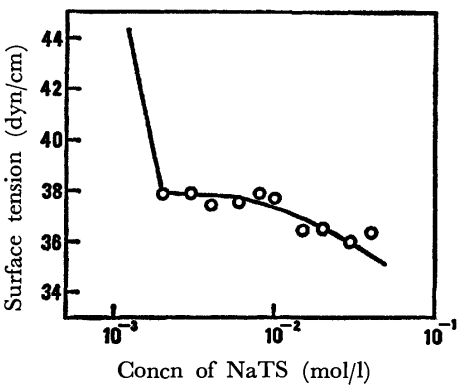

Fig. 7. Observed and calculated surface tension above CMC.
○: Surface tension calculated. ——: Surface tension observed.

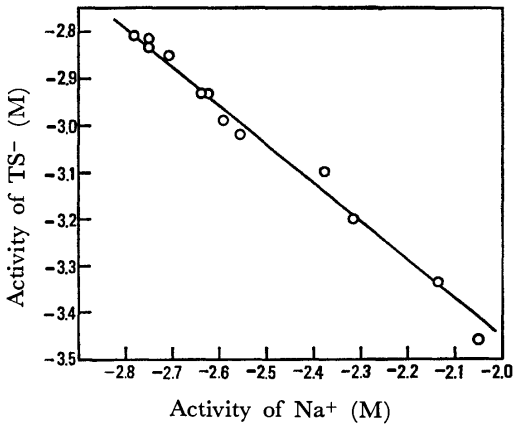

Fig. 8. $\log a_{TS}$ *vs.* $\log a_{Na}$ above CMC.

gives:

$$(a_{TS})^p(a_{Na})^q = a_M = \text{const.}$$

or

$$p \log a_{TS} + q \log a_{Na} = \text{const.} \quad (10)$$

where $p=q$ represents the uncharged-phase separation model, and $p \neq q$, the charged-phase separation model, respectively.

The plots of $\log a_{TS}$ against $\log a_{Na}$ are shown in Fig. 8. As is shown in the figure, a linear relation with $p \neq q$ is obtained; this proves that the charged-phase separation model is valid, just as in the case of sodium dodecyl sulfate.[8] The value of $p/q=0.81$ obtained as the degree of counterion attachment is somewhat larger than the latter. Though such a tendency is theoretically to be expected, it is significant that it is experimentally confirmed by reliable data. Similar results are also obtained in the system of NaTS in ethanol-water mixtures of various compositions, they will be reported in the following paper.

The gradual increase in $a_{\pm}$ with the surfactant concentration is expressed from Eqs. (6) and (10) with $p/q=0.81$ as:

$$a_{\pm} = K^{1/2}(a_{Na})^{0.095} \quad (11)$$

According to Eq. (11), $a_{\pm}$ slowly increases as a_{Na} increases, that is, with an increace in the concentration of the surfactant.

References

1) C. Botre, D. G. Hall, and R. V. Scowen, *Kolloid-z. Z. Polym.*, **250**, 900 (1972).
2) K. Shirahama, *ibid.*, **250**, 620 (1972).
3) C. Botre, F. De. Matiis, and M. Solinas, *J. Phys. Chem.*, **68**, 3624 (1964).
4) C. Gavach, *Proc. 5th. Int. Congr. Surf. Act. Sub.*, **2**, 859 (1968).
5) P. Ekwall, H. Eiken, and P. Stenius, *Acta Chem. Scand.*, **21**, 1639 (1967).
6) F. V. Vader, *Trans. Faraday Soc.*, **57**, 110 (1961).
7) W. V. Malik, S. I. Ahmad, and A. K. Jain, *Kolloid-z. Z. Polym.*, **218**, 155 (1967).
8) T. Sasaki, M. Hattori, J. Sasaki, and K. Nukina, submitted for publication in This Bulletin.
9) L. Shedlovsky, C. W. Jakob, and M. B. Epstein, *J. Phys. Chem.*, **67**, 2075 (1969).
10) I. Satake, T. Tahara, and R. Matuura, This Bulletin, **42**, 319 (1969).
11) B. A. Pethica, *Trans. Faraday Soc.*, **48**, 1052 (1952).
12) R. Matuura, H. Kimizuka, S. Miyamoto, and R. Shimozawa, This Bulletin, **31**, 532 (1958).
13) K. Tajima, M. Muramatsu, and T. Sasaki, *ibid.*, **43**, 1991 (1970). M. Muramatsu, K. Tajima, M. Iwahashi, and K. Nukina, *J. Colloid and Interface Sci.*, **43**, 499 (1973).
14) The detail will be reported in a near future.
15) M. Koshinuma and T. Sasaki, Abstract of the 9th annual meeting on radioisotopes in the physical sicence and industry.
p. 15p-II-3. The detail will be reported in a near future.
16) M. Koshinuma, A. Nakamura, T. Seimiya, and T. Sasaki, This Bulletin, **45**, 344 (1972).
17) R. A. Robinson and R. H. Stokes, "Electrolyte Solutions," Butterworths Pub. London (1959), p. 190.
18) G. D. Parfitt and A. L. Smith, *Trans. Faraday Soc.*, **61**, 2736 (1965).
19) A. I. Rusanov and V. V. Krotov, *Proc.* 6th *Int. Congr. Surf. Act. Sub.*, **2**, 795 (1972).
20) P. Mukerjee, K. J. Mysels, and C. I. Dulin, *J. Phys. Chem.*, **62**, 1390 (1958).
21) K. J. Mysels, P. Mukerjee, and Abu-Hamdiyyah, *ibid.*, **67**, 1943 (1963).
22) P. H. Elworthy and K. J. Mysels, *J. Colloid and Interface Sci.*, **21**, 331 (1962).
23) E. Matijevic and B. A. Pethica, *Trans. Faraday Soc.*, **54**, 587 (1958).
24) J. N. Phillips, *ibid.*, **51**, 561 (1955).
25) K. Shinoda and E. Hutchinson, *J. Phys. Chem.*, **66**, 577 (1962).

The Pressure Broadening of the Cadmium-resonance Line at 326.1 nm in Ammonia and Argon

Hironobu UMEMOTO, Shunzo YAMAMOTO, and Shin SATO

Department of Applied Physics, Tokyo Institute of Technology, Ookayama, Meguro-ku, Tokyo 152

(Received March 14, 1975)

The ratio of the collison-broadening cross-section of ammonia to that of argon for the cadmium-resonance line at 326.1 nm has been estimated to be 2.1 by comparing the experimental data of the transmission measurement with the theoretically calculated numerical table. The table shows the relation between the transmission of a resonance line passing through the system containing absorbing atoms and the ratio of the Lorentz half-breadth to the Doppler half-breadth at different values of two parameters; the optical density, and the ratio of the Doppler half-breadth of the emission line to that of the absorption line. This table may have universal importance for the study of the absorption of atomic spectra.

It is well known from experiments that atomic spectral lines have an observable breadth and are not so sharp as the simple quantum theory predicts. Such broadenings of spectral lines may be classified into four types: natural broadening, Doppler broadening, pressure broadening, and the broadening due to isotopes or hyperfine interaction. If a strong electric or magnetic field is present, the Stark and the Zeeman effects also have to be taken into account.

One of the most fundamental problems in the study of the reactions photosensitized by a certain atom is the quantitative estimation of the light intensity absorbed by the atoms. This quantity is seriously affected by the ratio of the Doppler half-breadth of the emission line to that of the absorption line. This ratio is denoted by α in the treatment of Zemansky.[1] If the optical density, $k_0(\nu_0)l$, at the maximum of the resonance line in the absence of pressure broadening is known, the intensity of the transmitted light is expressed as a function of the ratio of the Lorentz half-breadth to the Doppler half-breadth of the absorption line of the atoms in the system for a given value of α. Yang discussed this effect extensively in the particular case of mercury photosensitization.[2] Experimentally, such an effect has usually been avoided by using an appropriate actinometer or by diluting the system with a large amount of an inert gas which has a negligible quenching cross-section for the excited atoms under consideration.

In this investigation, we attacked two problems. One was the making of a numerical table of the relation between the transmission, T, and the ratio of the Lorentz half-breadth to the Doppler half-breadth at various values of α and $k_0(\nu_0)l$. This table has universal importance for the measurement of atomic spectra. The other was the determination of the collision-broadening cross-sections of ammonia and argon for the cadmium-resonance line at 326.1 nm by using the table obtained above.

Calculation

In order to discuss the pressure dependence of the transmission in terms of line broadening, it is necessary to know the shapes of the emission and absorption lines. Here, the emission line is taken to be a Doppler broadening:

$$E(\nu) = C\exp[-(\omega/\alpha)^2] \tag{1}$$

where C is a constant and where

$$\omega = 2(\nu-\nu_0)\sqrt{\ln 2}/\Delta\nu_D$$

$$\alpha = \Delta\nu_E/\Delta\nu_D$$

Here, $\Delta\nu_D$ denotes the Doppler half-breadth of the absorption line, while $\Delta\nu_E$ is that of the emission line. ν_0 is the frequency at the center of the emission line. The absorption coefficient is taken to be a type combining the Doppler broadening and the Lorentz broadening, ignoring natural broadening.[3]

$$k(\nu_0) = k_0(\nu_0)\frac{a}{\pi}\int_{-\infty}^{+\infty}\frac{\exp(-y^2)}{a^2+(\omega-y)^2}dy \tag{2}$$

where

$$a = \Delta\nu_L\sqrt{\ln 2}/\Delta\nu_D \tag{3}$$

$\Delta\nu_L$ is the half-breadth of the Lorentz broadening. $k_0(\nu_0)$ is the absorption coefficient at the maximum of the absorption line in the absence of the Lorentz broadening and may be estimated by means of the following equation.[3]

$$k_0(\nu_0) = \frac{\lambda_0^3 g_2 N}{8\pi^{3/2} g_1 \tau_0 v_0} \tag{4}$$

Here, λ_0 is the wavelength at the center of the absorption line, g_1 and g_2 are the degeneracies of the lower and upper levels, τ_0 is the lifetime, v_0 is the most probable velocity of the atoms, and N is the atomic density. Then, the transmission, T, is expressed as follows:

$$T = \frac{\int_{-\infty}^{+\infty}\exp[-(\omega/\alpha)^2]\exp\left[-k_0(\nu_0)l\frac{a}{\pi}\int_{-\infty}^{+\infty}\frac{\exp(-y^2)}{a^2+(\omega-y)^2}dy\right]d\omega}{\int_{-\infty}^{+\infty}\exp[-(\omega/\alpha)^2]d\omega} \tag{5}$$

The T values were calculated at various α, a, and $k_0(\nu_0)l$ values by using a Facom 230-75 computer. The evaluation of the numerator was carried out using Simpson's formula, with a mesh of 0.05, and the upper and lower limits of integral were taken to be ± 16. The denominator is equal to $1.7725\,\alpha$. The following is the range of parameters used for the calculations. α: 1.0~4.5, a: 0.05~7.0, and $k_0(\nu_0)l$: 0.001~99.999. A part of the results are shown in Figs. 1—4.

The general features of the calculated results may be summarized as follows:

i) The transmission, T, decreases with the increase in the optical density, $k_0(\nu_0)l$. This is a matter of course.

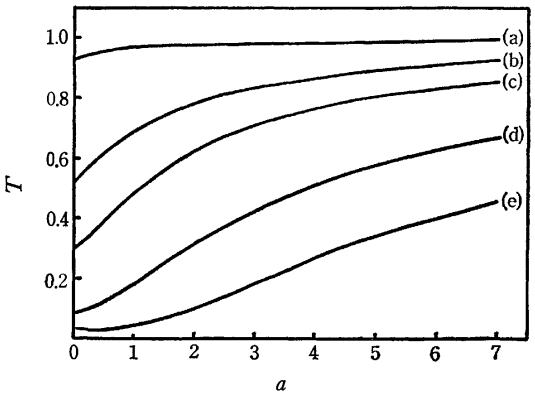

Fig. 1. Relation of the calculated transmission to the value of a with several values of optical density in the case of $\alpha=1$.
The optical density is equal to (a): 0.1, (b): 1.0, (c): 2.0, (d): 5.0, (e): 10.0.

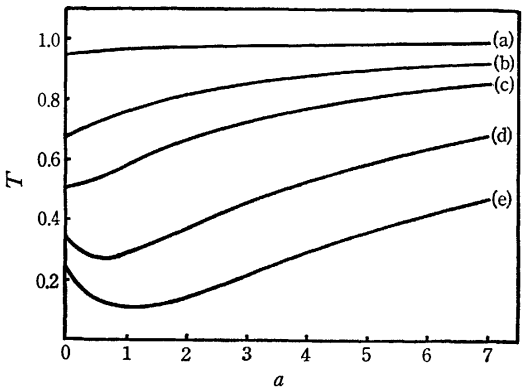

Fig. 2. Relation of the calculated transmission to the value of a with several values of optical density in the case of $\alpha=2$.
The optical density is equal to (a): 0.1, (b): 1.0, (c): 2.0, (d): 5.0, (e): 10.0.

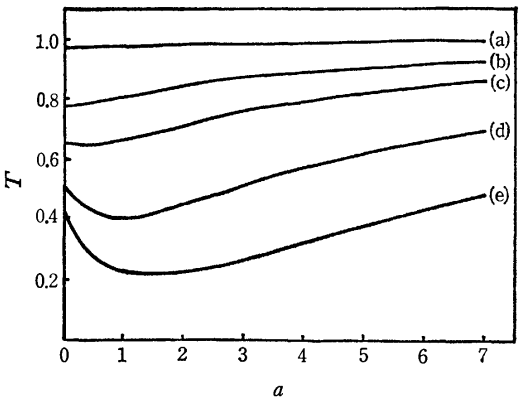

Fig. 3. Relation of the calculated transmission to the value of a with several values of optical density in the case of $\alpha=3$.
The optical density is equal to (a): 0.1, (b): 1.0, (c): 2.0, (d): 5.0, (e): 10.0.

ii) As the value of a is increased, the effect of α on the T value is reduced: *i.e.*, with the increase in the Lorentz broadening, the effect of the difference in Doppler broadening between emission and absorption lines is reduced.

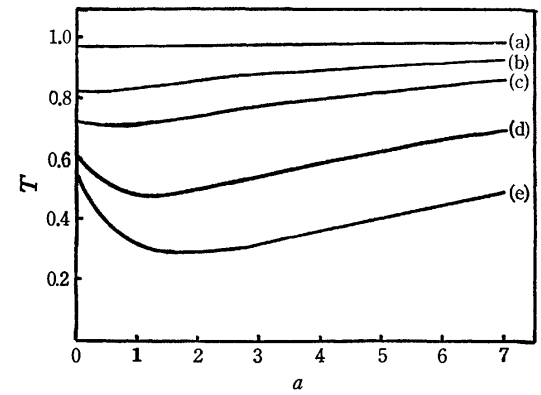

Fig. 4. Relation of the calculated transmission to the value of a with several values of optical density in the case of $\alpha=4$.
The optical density is equal to (a): 0.1, (b): 1.0, (c): 2.0, (d): 5.0, (e): 10.0.

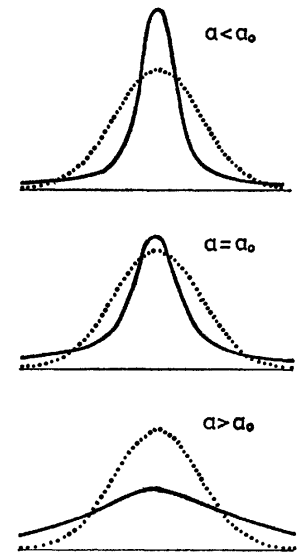

Fig. 5. The variation of the overlap between emission (dotted) and absorption (solid) lines with the increase of a. The maximum overlap is obtained at $a=a_0$.

iii) Similarly, as the α value is increased, the effect of a on the T value is reduced.

iv) On the other hand, with the increase in optical density, $k_0(\nu_0)l$, the effect of a on the T value is increased.

v) When both α and $k_0(\nu_0)l$ are large, T has a minimum at a certain value of a. This relation is qualitatively visualized in Fig. 5.

Measurements

The experimental apparatus was the same as that reported in a previous paper,[4] although the exciting resonance lamp was not used this time. The materials—cadmium, ammonia, and argon—were also the same as those described previously.[4] The furnace was maintained at 191±2 °C, while the cadmium reservoir was kept at 186±2 °C. The furnace for the resonance lamp was kept at 219±2 °C.

The results are shown in Fig. 6. The transmission n-

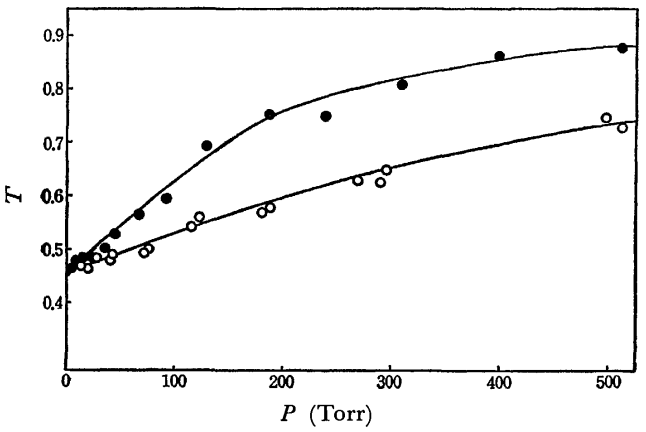

Fig. 6. The intensity of the transmitted light at 326.1 nm as a function of the pressure of argon (○) or ammonia (●).
The vapor pressure of cadmium is 1.48×10^{-4} Torr.

creased with the increase in the pressure of foreign gas. The rate of increase in ammonia was about twice that in argon. The transmission in the absence of any foreign gas, T_0, was 46.2±0.9%.

Discussion

Collision-broadening Cross-section. The $k_0(\nu_0)l$ value in the present experiment was calculated to be 2.3±0.3 by substituting the corresponding values into Eq. (4). However, this value cannot be used directly for the estimation of the collision-broadening cross-section because the presence of isotopes in natural cadmium metal has to be taken into account.

According to the work of Schüler and Westmeyer, the emission line at 326.1 nm of natural cadmium is split into three peaks.[5] Brix and Steudel demonstrated that the main peak observed by Schüler and Westmeyer is further split into three peaks.[6] Figure 7 shows the emission spectrum constructed according to the observations of Schüler and Westmeyer and those of Brix and Steudel, and by considering the Doppler broadening at 191 °C. From this figure, it may be assumed that natural cadmium consists of three imaginary isotopes, the propotions being 16 : 76 : 8.

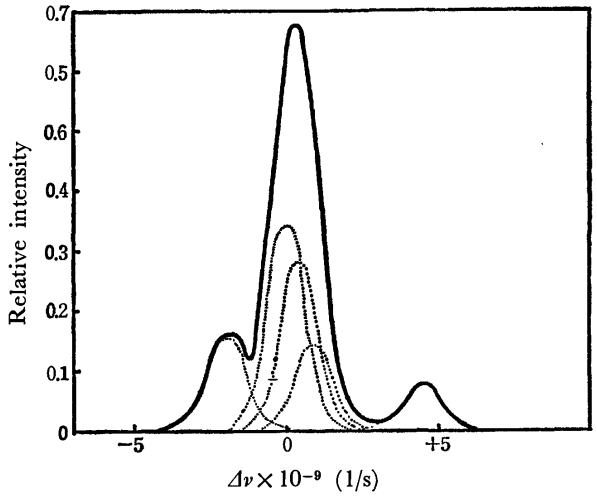

Fig. 7. Hyperfine structure of the cadmium resonance line at 326.1 nm with the Doppler broadening at 191 °C.

Unfortunately, the overlap between the two spectra due to the two imaginary isotopes (16 and 76%) is not small. In the following calculations, therefore, we assume two extreme cases. One is Case A, in which the three spectral lines are assumed not to overlap with each other at all. The other is Case B, in which the spectrum of the natural atom is assumed to consist of two separate spectra, the intensities of which are in the ratio of 92 : 8. Consequently, the true collision cross-sections of ammonia and argon will be in between the two values calculated in the two extreme cases.

In the absence of any foreign gas, the transmission, T_0, was 46.2%. The theoretical equation for this value is written as follows:

$$T_0 = \frac{\int_{-\infty}^{+\infty} \exp[-(\omega/\alpha)^2]\exp[-k_0(\nu_0)l\exp(-\omega^2)]d\omega}{\int_{-\infty}^{+\infty}\exp[-(\omega/\alpha)^2]d\omega} \quad (6)$$

The T_0 value was calculated by Horiguchi and Tsuchiya as a function of $k_0(\nu_0)l$ at different values of α.[7] This T_0 value can also be obtained from the figures shown in the previous section. Using these figures, we can estimate the α and $k_0(\nu_0)_c l$ values. Here, $k_0(\nu_0)_c l$ is the optical density corrected for the

Table 1. Calculated transmission in the absence of any foreign gas and the optical density corrected for the presence of isotopes

	3 components	2 components	α
T_0	46.2±3.5%		1.04
		46.2±3.2%	1.58
$k_0(\nu_0)_c l$	1.22	1.81	

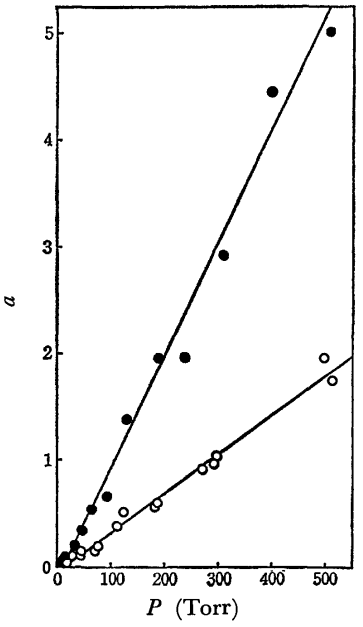

Fig. 8. The values of a as a function of the pressure of argon (○) or ammonia (●).

presence of isotopes; it may be used for the estimation of the collision-broadening cross-sections. The details of the calculation are shown in the Appendix. The results obtained are summarized in Table 1.

Once the α value and the corrected optical density are obtained, we can estimate, by using the numerical table, the value of a for each T value experimentally obtained. Thus, the a values are plotted in Fig. 8 as a function of the pressure of foreign gases. This figure is for Case A. A similar plot has also been obtained for Case B. The linear increase in the a value with the pressure is consistent with the Lorentz theory, which demands that

$$\Delta\nu_L = \frac{1}{\pi}\sigma^2 N(8\pi kT/\mu)^{1/2} \quad (7)$$

Here, σ^2 is the collision-broadening cross-section, N is the number of foreign gas molecules per cm^3, and μ is the reduced mass. Calculation by the least-squares method gives the values for σ^2. The results are listed in Table 2.

Table 2. Collision broadening cross sections (in Å^2) of argon and ammonia

	3 components	2 components
σ^2_{Ar}	49.0	72.9
σ^2_{NH3}	100.0	152.6
ratio	2.04	2.09

When we drew the spectrum shown in Fig. 7, we did not take into account any broadening other than the Doppler broadening at 191 °C. Since the resonance lamp was operated at 219 °C and contained about 3 Torr of argon as a carrier gas, the emission line should have been broadened more than that shown in Fig. 7. The α values estimated were 1.04 and 1.58 for Cases A and B respectively. These values correspond to the temperatures of 289 and 885 °C if the broadening is only due to the Doppler effect. Obviously, though, we have to consider the Stark effect in Case B. However, since we cannot estimate the broadening due to the Stark effect in the present experiment, we cannot tell which case is closer to the truth.

On the Dilution with Inert Gases. In the measurement of the quenching efficiency for excited atoms, inert gases have often been used as diluents so as to keep the broadening of the absorption line constant. In a previous paper,[4] we ourselves also used argon as a diluent gas in the measurement of the quenching efficiency of ammonia for the cadmium resonance line at 326.1 nm. One of the most severe conditions was: $k_0(\nu_0)l=0.71$ with 40 Torr of argon and 10 Torr of ammonia. The difference between the light intensity absorbed by this system and that absorbed by the system containing 50 Torr of argon without ammonia was estimated to be within 1%.

Generally speaking, the collision-broadening cross-section does not seem to depend greatly on the kind of molecule as compared with the quenching cross-section for excited atoms. Therefore, if a certain gas which has a negligible quenching cross-section for the excited atoms under consideration is found, we can probably use it as a diluent for keeping the broadening of absorption line constant.

The authors are indebted to Professor Soji Tsuchiya and Dr. Hiroyuki Horiguchi of Tokyo University for letting them use the Facom 230-75 computer and for their valuable discussions.

Appendix

The optical density for a separate spectrum, the proportion being denoted by x, is obviously $xk_0(\nu_0)l$. If the value of α is known, we can estimate the transmission, T_{ox}, for each spectrum by using the numerical table of T_0 against $k_0(\nu_0)l$. Such a relation is shown in Fig. 9. The total transmission is the average of these transmissions:

$$T_0 = \sum xT_{ox}$$

This value should be equal to the experimentally obtained value, 46.2%. Thus, the value of α was obtained by trial and error. By replacing the final value of α in Eq. (6), we can estimate the corrected optical density, $k_0(\nu_0)_c l$.

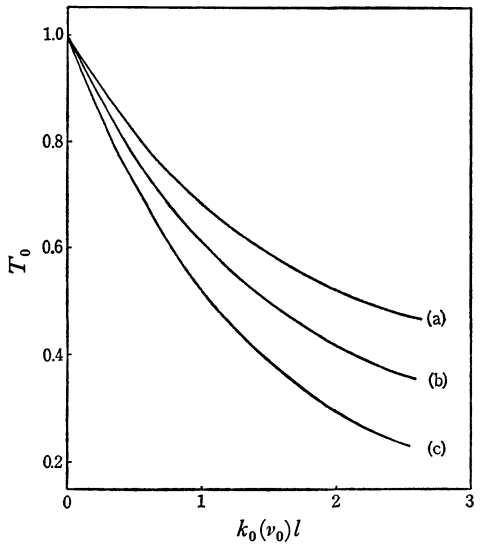

Fig. 9. Relation of the calculated transmission in the absence of any foreign gas to the optical density, $k_0(\nu_0)l$, with several values of α. (*a*): $\alpha=2.0$, (b): $\alpha=1.5$, (c): $\alpha=1.0$.

References

1) M. W. Zemansky, *Phys. Rev.*, **36**, 919 (1930).
2) K. Yang, *J. Amer. Chem. Soc.*, **86**, 3941 (1964).
3) A. C. G. Mitchell and M. W. Zemansky, "Resonance Radiation and Excited Atoms," The Cambridge University Press, Cambridge (1934).
4) S. Tsunashima, T. Toyono, and S. Sato, This Bulletin, **46**, 2654 (1973); M. Takaoka, S. Yamamoto, S. Tsunashima, and S. Sato, *Chem. Lett.*, **1974**, 343; S. Yamamoto, M. Takaoka, S. Tsunashima, and S. Sato, This Bulletin, **48**, 130 (1975); S. Yamamoto, S. Tsunashima, and S. Sato, *ibid.*, **48**, 1172 (1975); S. Yamamoto and S. Sato, *ibid.*, **48**, 1382 (1975); S. Yamamoto, K. Tanaka, and S. Sato, *ibid.*, **48**, 2172 (1975).
5) H. Schüler and H. Westmeyer, *Z. Phys.*, **82**, 685 (1933).
6) P. Brix and A. Steudel, *ibid.*, **128**, 260 (1950).
7) H. Horiguchi and S. Tsuchiya, This Bulletin, **44**, 1213 (1971).

A Study of Catalysis by Uranium Oxide and Its Mixed Catalysts. IX.[1] A Catalytic Reduction of Nitric Oxide with Carbon Monoxide

Fumio NOZAKI, Fumio MATSUKAWA, and Yoshikazu MANO

Department of Industrial Chemistry, Faculty of Engineering, Chiba University, Yayoi-cho, Chiba 280

(Received March 29, 1975)

The reduction of NO with CO over the uranium oxide catalyst and its mixed catalysts with alkali metal oxide or alkaline earth metal oxide has been investigated using conventional flow and pulse reactors at temperatures of 250 to 450 °C under atmospheric pressure. The activity of the uranium oxide catalyst without any additive was higher than that of the Fe_2O_3 catalyst, although it was inferior to that of the CuO-Cr_2O_3 catalyst. The addition of alkali metal oxide or alkaline earth metal oxide to uranium oxide, particularly in the case of Cs_2O or K_2O, was effective in enhancing the catalyst activity. The W/F-conversion curves revealed that the reduction of NO to N_2 proceeds consecutively, passing through N_2O as a gas-phase intermediate. The reaction rates were formulated as $r=kP_{CO}^{1.0}P_{NO}^{0.4}$. The kinetic study suggested a redox reaction sequence. The oxidation states of the catalysts were discussed on the basis of X-ray diffractograms.

The catalytic reduction of NO with CO, H_2 or NH_3 has recently been investigated very actively as part of a comprehensive study of air pollution control, and much useful information has been presented in both fundamental study and development research.[2] In spite of the considerable number of publications on the catalysts, however, few reports have been published about the uranium oxide catalyst. Our preliminary study has revealed that uranium oxide has a high activity for NO-CO reaction.

In this paper, we will describe the behavior of uranium oxide as a catalyst and the influence of the addition of alkali metal oxide or alkaline earth metal oxide upon the catalytic activity. In addition, the results of a kinetic study and details of the catalyst structure will be given.

Experimental

Catalyst Preparation. The uranium oxide catalyst without additive (to be subsequently referred to as the U catalyst) was prepared by the method described in a previous paper.[3] The mixed catalysts with alkali metal oxide or alkaline earth metal oxide were prepared by the wet mixing method: the prescribed amount of an aqueous solution of Cs_2CO_3, KOH, NaOH, $Ca(OH)_2$, or $Mg(OH)_2$ was added to the yellow precipitate $(NH_4)_2U_2O_7$, obtained from $UO_2(NO_3)_2$ by precipitation with NH_4OH. The respective slurries were followed by drying in an air oven at the temperature of 110 °C. The resulting paste-like solid masses were well-mixed by a knead-machine for 3 hr, and were then extruded to obtain the desired pellet size. (These mixed catalysts will subsequently be referred to as the U-Cs catalyst, the U-K catalyst, *etc.*) A series of catalysts containing a certain kind of metal oxide in different proportions was prepared by the same method. The compositions of the mixed catalysts were expressed by the atomic M/(U+M) ratio, where M represents the species of the metals added to the catalyst as an oxide. All the catalysts were calcined at 500 °C for 2 hr in a stream of air before use in the catalytic tests. After calcination, the U catalyst was green-black in color; all of the mixed catalysts with alkali metal oxide or alkaline earth metal oxide were tan-orange, although their chroma was somewhat different from one another, depending upon the catalyst composition. The specific surface areas of the catalysts were determined according to the BET method, using nitrogen as the adsorbate.

In order to characterize the U catalyst, three kinds of commercial catalysts were used; the CuO-Cr_2O_3 catalyst (Nissan-Kemetron, Inc., type G-22; CuO 42%, Cr_2O_3 40%, BaO 12%), the Pt-Al_2O_3 catalyst (Nippon-Engelhard, Inc., Pt 0.5%), and the Fe_2O_3 catalyst (Shell, Inc., type 105; Fe_2O_3 93%, Cr_2O_3 5%, K_2CO_3 2%). These catalysts were also calcined at 500 °C for 2 hr in a stream of air before use.

Apparatus and Analysis. Most of the catalytic-activity measurements were carried out on a conventional flow apparatus consisting of a 18 mmϕ glass reactor. The reactor contained a packed bed consisting of 1.0 g of the catalyst and small glass-beads in the ratio of 1 : 10 by volume, thereby improving the isothermal conditions during the course of reaction. Before the start of the experiments, the catalyst was heated in a stream of helium to 500 °C for 1 hr, and then cooled to the reaction temperature. A mixture of NO and CO was admitted into the reactor at a constant rate of flow. After we had ascertained that the flow system had attained a stationary state, we began to analyze the product stream. The reaction products and the reactor feed were introduced at regular time intervals into a gas-chromatographic unit consisting of a 0.5-m column of Porapak Q and a 1-m column of Molecular Sieve 13X. The columns were operated at room temperature, with helium as the carrier gas; a detector of a thermal-conductivity type was placed between the Porapak and Molecular Sieve columns. Such a procedure permitted a satisfactory analysis of the mixture consisting of N_2, N_2O, NO, CO, and CO_2, even with the injection of only one sampling.

Considering the stoichiometry of the reaction, the conversion of NO, x_{NO}, and the selectivity, S_{N_2}, for nitrogen formation were given by:

$$x_{NO} = \frac{N_2+N_2O}{N_2+N_2O+1/2\,NO} \quad (1)$$

$$S_{N_2} = \frac{N_2}{N_2+N_2O} \quad (2)$$

In order to elucidate the reaction mechanism, some of the experiments were carried out on a conventional pulse-reaction method, using helium as the carrier gas. The gas-chromatographic unit described above served as an analytical tool.

X-Ray Diffractograms of the Catalysts. X-Ray diffraction measurements were made for the purpose of qualitatively identifying the catalysts. The X-ray diffractograms of the powdered samples were obtained at room temperature by using Ni-filtered copper radiation (Rigaku Denki Co., Geigerflex D-3F spectrometer).

Results and Discussion

Activity of the U Catalyst and the Pressure-dependency of Reaction Rates. The change in the catalyst activity during the course of the reaction was practically negligible throughout the catalytic tests.

In Fig. 1, the activity and the selectivity of the U catalyst are compared with those of commercial catalysts. Figure 1 indicates that the catalytic activity decreases in this order: $CuO\text{-}Cr_2O_3 > U > Fe_2O_3 > Pt\text{-}Al_2O_3$; the $Pt\text{-}Al_2O_3$ catalyst does not begin to be active until much higher temperatures than the other catalysts, but, in such a case, the degree of reaction approches the level of 90%, the relative activity of the Pt catalyst is rather higher than those of the U and Fe_2O_3 catalysts. The selectivity, S_{N_2}, for nitrogen formation was inclined to increase with an increase in the reaction temperature in every catalyst. In the case of the U catalyst, the selectivity curve appears to have its minimum at temperatures near 300 °C. However, a steep dip as described in the literature[4,5] was not observed under the reaction conditions of this work.

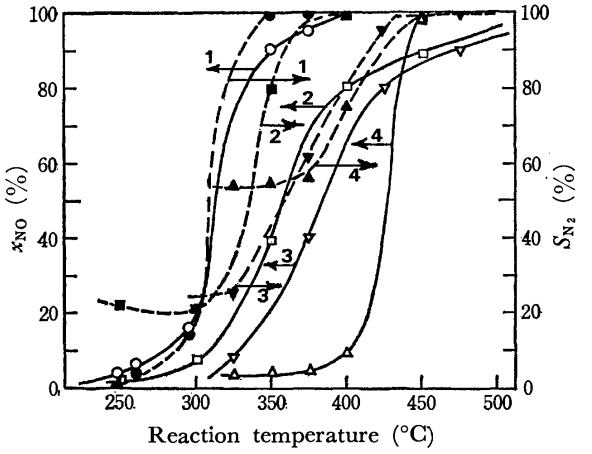

Fig. 1. Activities and selectivities of various catalysts.
1: $CuO\text{-}Cr_2O_3$, 2: U, 3: Fe_2O_3, 4: $Pt\text{-}Al_2O_3$.
Catalyst weight (W): 1.0 g, NO/CO feed ratio (m): 1.0, Flow rate of feed gas (F): 50 ml/min.

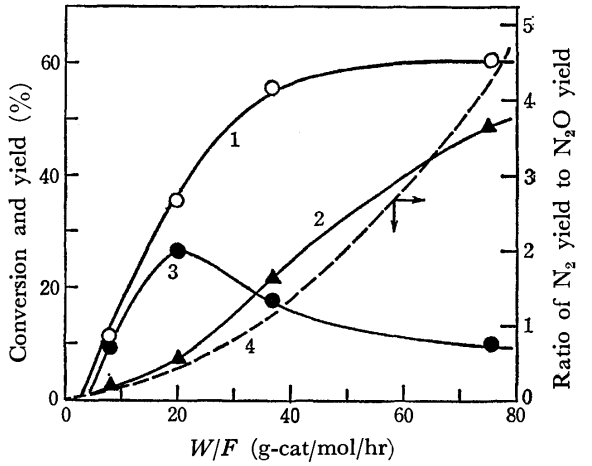

Fig. 2. Effects of W/F on the catalytic reaction.
1: x_{NO}, 2: N_2 yield ($=x_{NO} \times S_{N_2}$), 3: N_2O yield ($=x_{NO} - x_{NO} \cdot S_{N_2}$), 4: Ratio of N_2 yield to N_2O yield.
Reaction temperature (t): 310 °C, m: 1.0.

It must be noted that the U catalyst has a high activity for the NO–CO reaction; nevertheless, uranium oxide belongs to the class of heavy metal oxides which also includes MoO_3, V_2O_5, and WO_3. The MoO_3, V_2O_5, and WO_3 catalysts exhibited very little activity; the x_{NO} values were only a few %, even when the reaction temperature was raised to 500 °C. The fact that the activity of the U catalyst for the NO-CO reaction was exceptionally high for a heavy metal oxide catalyst was quite similar to the finding previously reported in the study of $CO\text{-}O_2$ reaction.[3]

Figure 2 shows the influence of W/F on the results of the reaction. The N_2O yield-W/F curve reaches a maximum. In addition, the curve of the ratio of the N_2 yield to the N_2O yield passes through the point of origin, as it increases with an increase in W/F. These facts suggest that the reduction of NO to N_2 proceeds consecutively, passing through N_2O as a gas-phase intermediate.

The rate measurements were conducted in a low range of W/F, in which one may assume the differential reactor. The reaction rate, r, can be obtained from the slopes of the linear relationship between $y_0 \cdot x_{NO}$ (y_0: mol-fraction of NO at the inlet of the reactor) and W/F. The dependence of the reaction rates on the partial pressure of NO or CO is illustrated in Fig. 3. It can be seen from Fig. 3 that the reaction rates are expressed by this equation:

$$r = kP_{CO}^{0.1}P_{NO}^{0.4} \quad (3)$$

where k is the reaction rate constant in mol/g-cat hr $atm^{1.4}$.

Influences of the Addition of Alkali Metal Oxide or Alkaline Earth Metal Oxide upon the Activity of the Uranium Oxide Catalyst. Temperature-conversion curves over the U–Cs catalysts containing cesium oxide in different proportions are shown in Fig. 4. Since the selectivity, S_{N_2}, for nitrogen formation showed a behavior similar to that in Fig. 1, the conversion datum alone is plotted in Fig. 4 as a function of the reaction temperature.

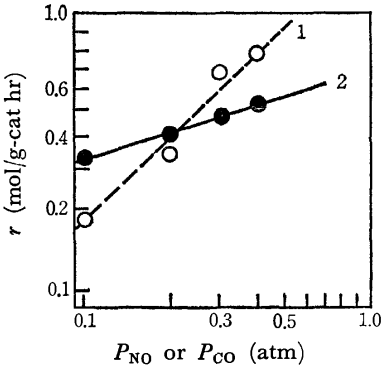

Fig. 3. Reaction rates as a function of NO or CO partial pressure.
1: Effect of CO partial pressure (P_{NO} was kept at constant pressure of 0.1 atm).
2: Effect of NO partial pressure (P_{CO} was kept at constant pressure of 0.1 atm).
Total pressure ($\pi = P_{CO} + P_{NO} + P_{He}$): 1 atm, t: 310 °C.

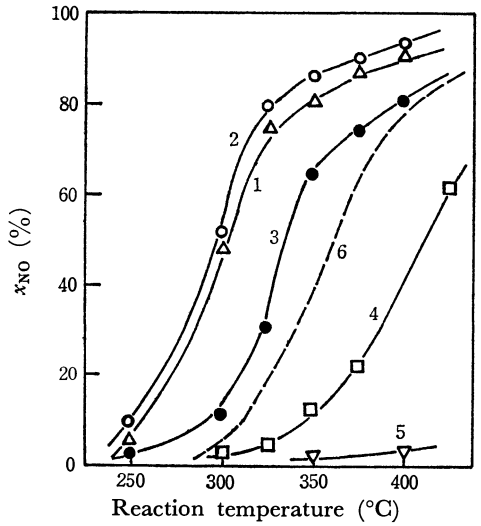

Fig. 4. Temperature-conversion curves over the catalysts containing Cs_2O in a different proportion.
Catalyst composition in atomic Cs/(U+Cs) ratio—1: 0.1, 2: 0.2, 3: 0.3, 4: 0.4, 5: 0.5, 6: 0.0 (U catalyst without Cs_2O).
Reaction conditions are the same as for Fig. 1.

Figure 4 indicates that the U–Cs catalysts with an adequate composition are much more active than the U catalyst without Cs_2O. In order to make a quantitative expression of the results, the rate constants, k_{flow}, were calculated according to a conventional manner for the ideal tubular flow reactor: at the point in the reactor where the conversion is x_{NO}, P_{NO} and P_{CO} may be written as $P_{NO}=P_{CO}=(1-x_{NO})/(2-0.5\,x_{NO})$ by taking into account the stoichiometry of the reaction and the feed NO/CO ratio of 1.0. Thus,

$$k_{flow}=\frac{y_0}{W/F}\int_0^x\frac{dx}{r}=\frac{0.5}{W/F}\int_0^{x_{NO}}\left(\frac{2-0.5x_{NO}}{1-x_{NO}}\right)^{1.4}dx_{NO} \quad (4)$$

From the series of conversion data shown in Fig. 4, the values of k_{flow} at 350 °C were evaluated by means of a graphical integral in Eq. (4) for each experimental point. The values are plotted in Fig. 5 as a function of the catalyst composition, together with the data relating to the BET surface area of the catalysts. Figure 5 shows that the catalyst activity increases with an increase in the atomic (Cs/U+Cs) ratio, passes through a maximum at about 0.2, and then almost disappears above 0.5. The k_{flow} value of the U–Cs catalyst with an atomic ratio of 0.2 was about five times that of the U catalyst without any additive. An increase in the activity upon the addition of Cs_2O was achieved in the range with a lower atomic Cs/U+Cs ratio than 0.3, and the further addition of (Cs_2O) resulted in a decrease in the activity. The correlation between the surface area of the catalysts and the composition of the catalysts leads us to the conclusion that the enhancing of activity attributable to Cs_2O addition is independent of the change in the surface area of the catalysts.

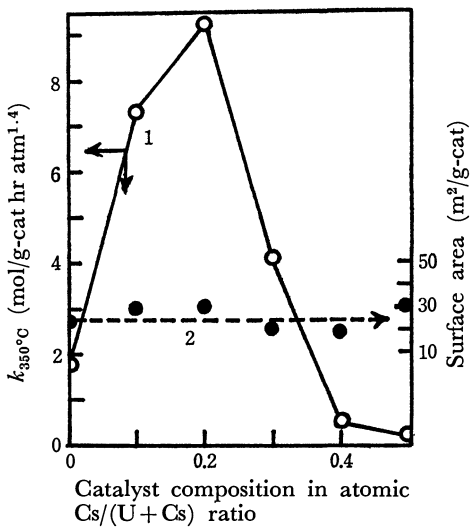

Fig. 5. Rate constant and surface area of U-Cs catalyst as a function of catalyst composition.
1: Rate constant *vs.* catalyst composition.
2: Surface area *vs.* catalyst composition.

The temperature-conversion curves over the other mixed catalysts are shown in Fig. 6. Figure 6 depicts that the addition of K_2O, Na_2O, CaO or MgO is in every cases effective in the modification of catalyst activity, although the influence of CaO and MgO upon the enhancing of activity is very slight. The effect of K_2O on activity was particularly noteworthy, by analogy with the Cs_2O addition. The modified catalysts with Cs_2O or K_2O added were superior in activity to the $CuO–Cr_2O_3$ catalyst, or at least to a catalyst of comparable magnitude. Thus, it appears established that the enhancing of the activity of the uranium oxide catalyst can be realized by the addition of small amounts of Cs_2O or K_2O, which are alkali metal oxides with lower electronegative properties.

A Plausible Reaction Mechanism. The results of an experiment in which the pulse-reaction method was employed to characterize the reduction and re-oxidation processes of the catalyst are shown in Figs. 7 and 8. Figure 7 suggests that the re-oxidation of

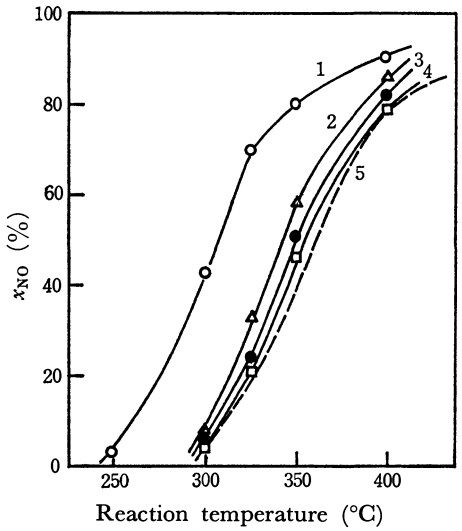

Fig. 6. Temperature-conversion curves over the catalysts containing various additives.
1: U-K, 2: U-Na, 3: U-Ca, 4: U-Mg, 5: U- without additive
Catalyst composition: M/(U+M)=0.2, Reaction conditions are the same as for Fig. 1.

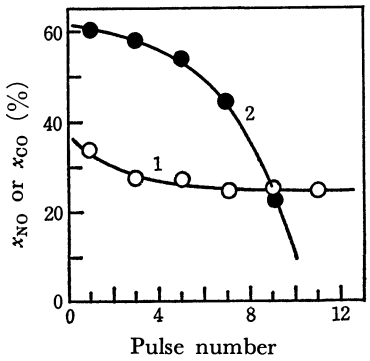

Fig. 7. Changes in conversion with repeated sample injections in pulse-reaction method.
1: Change in CO conversion, when CO pulses were injected to the fresh U catalyst.
2: Change in NO conversion, when NO pulses were injected to the reduced U catalyst.
W: 0.2 g, t: 350 °C, Pulse size: 0.5 ml, Helium flow rate as a carrier gas (F'): 20 ml/min.

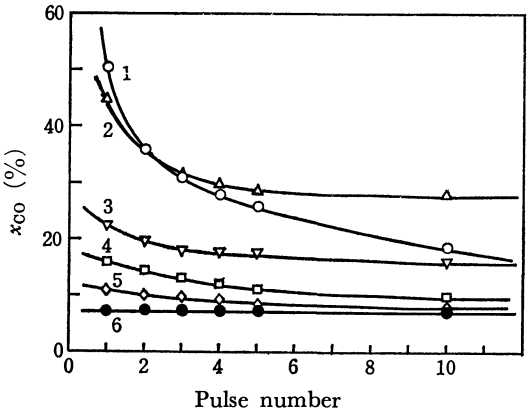

Fig. 8. Comparison of reduction rates in the catalysts with and without additive.
Catalyst—1: U-Cs, 2: U-K, 3: U-Na, 4: U-Ca, 5: U-Mg, 6: U-without additive.
Composition of the catalysts containing additive is 0.2 in atomic M/(U+M) ratio.
W: 0.1 g, t: 350 °C, Pulse size of CO: 0.8 ml, F': 30 ml/min.

the reduced catalyst with NO pulses takes place more rapidly than the reduction of the catalyst with CO pulses. Figure 8, in which the facilities and regularities in the reduction of various catalysts are compared to one another, indicates that the ease of reduction decreases in this order: U-Cs>U-K>U-Na>U-Ca>U-Mg>U; this order is in accord with that of the catalyst activity. On the basis of information obtained in Figs. 7 and 8, we have speculated on a mechanism for the NO–CO reaction featuring the following reduction-reoxidation sequence:

$$\text{CAT-O} + \text{CO} \xrightarrow{\text{A}} \text{CAT} + \text{CO}_2 \qquad (5)$$

$$\text{CAT} + \text{NO} \longrightarrow \text{CAT-O} + 1/2\text{N}_2 \qquad (6)$$

where CAT-O and CAT represent an active site on the catalyst and its site as reduced by CO respectively. Provided that the rate-limiting step in the redox sequence is a reduction process of the catalyst by CO, as is shown by Eq. (5), both the results of Fig. 7 and the kinetic orders of Eq. (3) are readily understandable.

In order to make the successive order of the reduction rates of various catalysts clearer, we have analyzed the conversion data of Fig. 8 by two methods. One of the methods is to calculate the rate constant from the values of x_{CO} at the first pulse, using the rate equation for a pulse-reaction system:[6]

$$k_{\text{pulse, CAT-O+CO}} = \frac{1}{273R\,W/F} \ln \frac{1}{1-x_{CO}} \qquad (7)$$

The other method is to determine the coefficient of the variation in the CO conversion at the initial stage; $(\Delta x_{CO}/\text{pulse number})_0$ was evaluated from the conversion data of the first and second pulses for each catalyst.

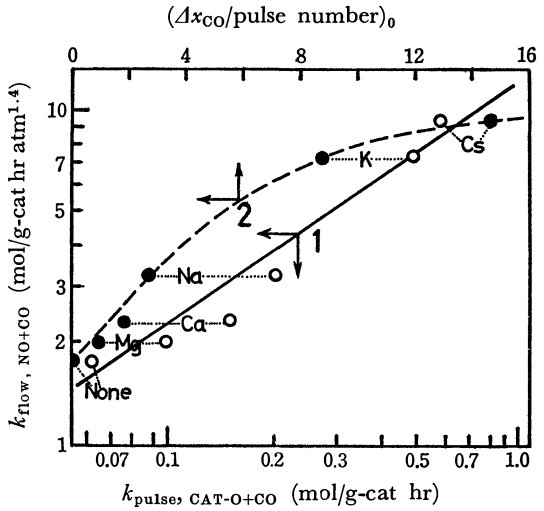

Fig. 9. Correlation between activity of the catalysts and reducibility of the catalysts.
1: $k_{\text{pulse, CAT-O+CO}}$ *vs.* $k_{\text{flow, NO+CO}}$.
2: $(\Delta x_{CO}/\text{pulse number})_0$ *vs.* $k_{\text{flow, NO+CO}}$.

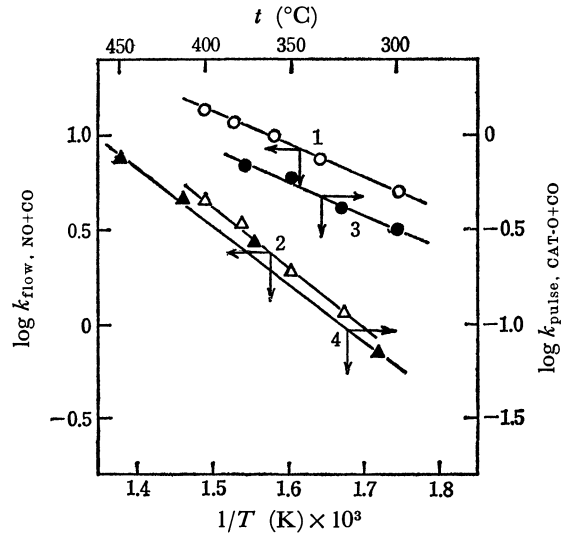

Fig. 10. Arrhenius plots for the rate constants.
1: Rate constants of NO-CO reaction over U-Cs catalyst in flow method, 2: Rate constant of NO-CO reaction over U catalyst in flow method, 3: Reduction rate constant of U-Cs catalyst in pulse method, 4: Reduction rate constant of U catalyst in pulse method.

In Fig. 9, the resulting two parameters by which the ease of reduction by CO is represented are correlated to k_{flow}. Figure 9 shows that there is a direct correlation between k_{flow} and the k_{pulse} parameter or $(\Delta x_{CO}/\text{pulse number})_0$.

Arrhenius plots of the rate constants for the U and U–Cs catalysts are illustrated in Fig. 10. Both log k_{flow} and log k_{pulse} are correlated to $1/T$ by straight lines. The apparent activation energy was found to be about 8 kcal/mol for the U–Cs catalyst and about 15 kcal/mol for the U catalyst. The finding to be emphasized here is that the activation energy observed in a flow-reaction method is entirely consistent with that of the reduction process of CAT-O by CO in a pulse-reaction method. This is suggestive of the redox mechanism which is expressed in the forms of Eqs. (5) and (6). However, a more detailed experiment, *e.g.*, tracer work labeled with an oxygen-18 isotope, is necessary to confirm the reaction mechanism. In this paper, it can only be said that all the experimental results have been interpreted satisfactorily on the basis of the redox mechanism.

X-Ray Diffractograms of the Catalysts. The X-ray diffractograms of the catalyst samples are shown in Fig. 11. Diagram 4, for the U catalyst, reveals that the sample consists mainly of U_3O_8. In contrast, Diagram 1, 2, and 3 for the catalysts containing Cs_2O, K_2O, and Na_2O respectively, show, without exception, that the definite peaks attributable to $UO_3 \cdot 2H_2O$ are present, together with minor peaks the assignment of which is unknown. The $UO_3 \cdot 2H_2O$ compound

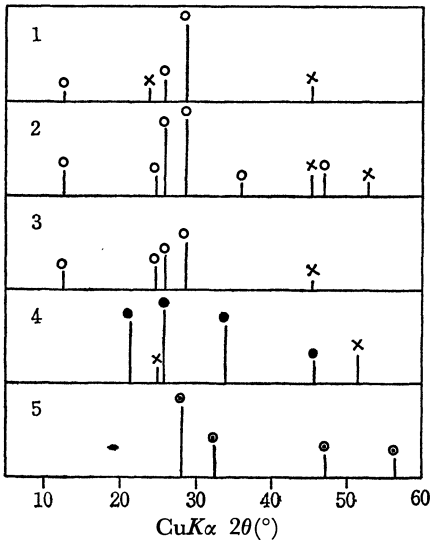

Fig. 11. X-ray diffractograms of the catalysts.
1: U-Cs catalyst (atomic Cs/(U+Cs) ratio: 0.2) before use for reaction, 2: U-K catalyst (atomic K/(U+K) ratio: 0.2) before use for reaction, 3: U-Na catalyst (atomic Na/(U+Na) ratio: 0.2) before use for reaction, 4: U catalyst before and after use for reaction, 5: U-Cs catalyst (atomic Cs/(U+Cs) ratio: 0.2) after use for reaction.
○: Peak attributable to $UO_3 \cdot 2H_2O$ (Ref. ASTM card 13—408), ●: Peak attributable to U_3O_8 (Ref. ASTM card 2-276), ⊙: Peak attributable to U_3O_7 (Ref. ASTM card 15—4), ×: Unknown peak for assignment.

results when UO_3 is allowed to stand in contact with air containing moisture; the hydrate is quickly reconverted into UO_3 by heating above 200 °C, as has previously been described.[7] The peaks attributable to $UO_3 \cdot 2H_2O$ were likewise observed in the catalysts containing CaO or MgO; however, in such cases the diffraction lines were weak in intensity.

Thus, it may be concluded that the addition of small amounts of alkali metal oxide or alkaline earth metal oxide can be used to elevate the oxidation state of U_3O_8 to UO_3. This can also readily be understood from the great difference in color between the U catalyst without any additive and the mixed catalysts; the former was green-black, characteristic of U_3O_8, whereas the latter was tan-orange, characteristic of UO_3.

The X-ray diffraction pattern of the U catalyst was entirely unchanged even after the catalyst had been used for the catalytic reaction. In contrast, the diffractogram of the U–Cs catalyst after having been used for the reaction (Diagram 5) was greatly different from Diagram 1, and the peaks were identified as belonging to those of U_3O_7. Therefore, one is forced to consider that, during the reaction, the oxidation state of uranium oxide is lower in the U–Cs catalyst than in the U catalyst. This fact is in conflict with the redox mechanism described in the previous section, because the oxidation state of the catalysts is considered to remain unaltered through the NO–CO reaction provided it proceeds *via* the sequence of Eqs. (5) and (6). This problem has not yet been completely elucidated, but it has been speculated that the U–Cs catalyst is more liable than the U catalyst to lead the formation of N_2O and that its use results in an excess of CO by unbalancing the redox reaction sequence of Eqs. (5) and (6), whereupon the reduction to the lower oxidation state takes place in the case of the U–Cs catalyst. However, a further investigation of the surface structure directly responsible for the catalytic reaction is required for a comprehensive understanding of the uranium oxide as a catalyst.

In the X-ray diffractograms of the catalysts containing alkali metal oxide or alkaline earth metal oxide, the peaks corresponding to the normal uranate and/or polyuranate structures were completely missing. The uranate K_2UO_4, which was prepared by a soaking method in a separate batch, showed only a very low activity in the NO–CO reaction.

References

1) Part VIII of this series: F. Nozaki and I. Inami, *Nippon Kagaku Kaishi*, **1974**, 1856.
2) For example, N. Todoh, *Shokubai*, **15**, 182 (1973); Y. Murata, *ibid.*, **16**, 99 (1974); E. Echigoya, H. Niiyama, and A. Ebitani, *Nippon Kagaku Kaishi*, **1974**, 222; A. Ebitani, H. Niiyama, and E. Echigoya, *ibid.*, **1974**, 1185.
3) F. Nozaki and K. Ohki, This Bulletin, **45**, 3473 (1972).
4) M. Shelef and K. Otto, *J. Catal.*, **10**, 408 (1968).
5) G. L. Bauerle, G. R. Service, and K. Nobe, *Ind. Eng. Chem. Prod. Res. Develop.*, **11**, 54 (1972).
6) D. W. Bassett and H. W. Habgood, *J. Phys. Chem.*, **64**, 769 (1960).
7) J. J. Katz and E. Rabinowitch, "Chemistry of Uranium," Dover Publication, New York, N.Y. (1961), p. 287.

Semi-empirical Localized MO Calculations of Saturated Carbocyclic and Heterocyclic Compounds

Gernot FRENKING, Hiroshi KATO,* Kimihiko HIRAO,** and Kenichi FUKUI

Department of Hydrocarbon Chemistry, Kyoto University, Sakyo-ku, Kyoto 606

**College of General Education, Nagoya University Chikusa-ku, Nagoya 464*

(Received April 1, 1975)

Localized MO calculations have been carried out by the "energy localization" method of Edmiston and Ruedenberg, based upon the INDO MO's, for 3-, 4-, and 5-membered cycloalkanes and their heterocycles containing one oxygen or nitrogen atom. Furthermore, LMO calculations were performed for the protonated three-membered heterocyclic compounds. The s-nature of the LMO's is discussed and correlated with the bond angle, the bond moment, the bond energy, and the bond polarity. Some LMO density maps are shown.

The usefulness of the localized molecular orbital (LMO) method has been pointed out by many authors.[1-7] Not only has the LMO method an advantage compared with the classical bond concept, but also the results which can be obtained by this method can be correlated directly with some physicochemical concepts or quantities, such as hybridization, the bond angle, and the bond moment.

In this paper, some physical and chemical properties of saturated cyclic compounds are investigated by the LMO method which was presented by Edmiston and Ruedenberg[1] based on the INDO method.[8] The compounds treated are saturated 3-, 4-, and 5-membered cycloalkanes and their heterocycles containing one oxygen or nitrogen atom. The LMO calculation for these compounds has not yet been made except for some LMO studies of three-membered heterocycles and some cycloalkanes.[5-7] Special attention is paid to the correlation between the degree of hybridization (s-nature of LMO's) in these compounds and the experimental quantities to be compared. The results of the bond polarity and the LMO charge maps are given.

Method and Details of Computation

The canonical MO's (CMO's) are obtained by the INDO method of Pople *et al.*,[8] and the LMO's, by the "energy localization" method of Edmiston and Ruedenberg.[1] In a later section, the LMO's total energy will be discussed by using the term "bond energy" presented by Parks and Parr.[2] The outline of the definition of "bond energy" may be briefly given as follows: the total energy by the LMO method, E_{el}, is given as the sum of the i-th LMO's energies, E_i's:[3]

$$E_{el} = \sum_i E_i$$

$$E_i = \langle i | F + H^c | i \rangle$$

where the summation, i, runs over all the occupied LMO's in the compound and where F and H^c denote the Fock and the core operators in the SCF Hamiltonian respectively.

The total energy, E_o, is taken as the sum of the bond energies, B_i's, where B_i belongs to the i-th two - or one-center LMO:

$$E_0 = E_{el} + E_n = \sum_i B_i$$

where:

$$B_i = E_i + E_{i\leftarrow n}$$

in which E_n is the total core repulsion energy and E_{in} is its i-th part.[2]

The geometries of the treated compounds are cited from the literature[9] if they exist. As to ethylene imine, the following values are assumed: C–N 1.488 Å; C–C 1.502 Å; C–H 1.08 Å; N–H 1.00 Å; ∠HCH 112°; as to the protonated ethylene oxide and imine, $O-H^+$ is taken as 0.96 Å and $N-H^+$ is 1.00 Å, and the bond angle between the newly formed $X-H^+$ bond (X=O, N) and the ring plane is assumed to be 56°, the other values remain unchanged. For the sake of simplicity, the rings of all the compounds, with the exception of cyclobutane, are assumed to be planar.

Results and Discussion

As a measure of the degree of localization of each LMO, Table 1 shows the sum of the squared AO-coefficients at the atoms which do not take part in the considered bond or lone pair. The values in Table 1 indicate the achievement of a high degree of localization (more than 90% in almost all LMO's); accordingly, some discussions in later sections based on the assumption of pure localization will be admissible.

In this section, the s-nature of the LMO's, the deviation of the bond angle and the bond energy, and so on, will be discussed.

s-Nature. Coulson and Moffitt[10] have pointed out the irregular degree of hybridization of small-membered cycloalkanes. In Table 2 our results are compared with the values of s% and the deviation of bond angle given by Coulson and Moffitt (C–M). The agreement between the two approaches is good. The reliability of the results by the LMO approach has also been examined by comparison between the observed $J_{C^{13}-H}$ coupling constant,[6,11a-c] and those estimated by means of the empirical formula: $J_{C-H} = 5 \times (\%s)$ cps.[11a] In Table 3 the agreement is excellent. Hence, this way of estimating the s-nature seems reasonable. The LMO's obtained by means of the INDO and *ab initio* methods have already been

** Present address: Department of Chemistry, the University of Alberta, Edmonton, Alberta, Canada.

Table 1. Deviation of localization

(bond A-B: $\sum c^2_{C\neq A\neq B}$; lone pair A: $\sum c^2_{B\neq A}$)

bond	X=O	X=NH	X=CH$_2$	X=O	X=NH	X=CH$_2$	X=O	X=NH	X=CH$_2$
X-C	0.022	0.020	—	0.007	0.007	—	0.010	0.006	—
X	0.016	0.019	—	0.013	0.019	—	0.019	0.021	—
C_1-C_2	0.002	0.004	0.016	0.005	0.005	0.007	0.005	0.005	0.006
C_2-C_3	—	—	—	—	—	—	0.013	0.011	—

Table 2. s-Nature of cycloalkanes and the deviation of bond angles ($\theta°$)

Molecule	s nature: Coulson-Moffitt [10] C-C	C-H	ours C-C	C-H	$\theta°$: C-M [10]	ours
$(CH_2)_3$	19.53	30.49	18.8	32.1	22°	28°55′
$(CH_2)_4$	23.59	26.39	24.6	27.8	9°	12°20′
$(CH_2)_5$	25.00	25.00	27.3	24.5	0°	2°30′

Table 3. NMR C-H Coupling (J_{CH}) and s nature

Molecule	J_{CH}[11b,18]	%s[a]	Calcd %s
$(CH_2)_3$	162	32	32.1
$(CH_2)_4$	136	27	27.8 (av.)
$(CH_2)_5$	131	26	24.5
$(CH_2)_2NH$	168	—	33.1 (166)
$(CH_2)_2O$	176	—	34.7 (174)

a) $J_{CH}=5\times(\%s)$ cps

compared by England and Gordon.[4] Our results in Table 2 are close to that of the *ab initio* LMO calculation of Newton *et al.*, which gives the deviation of the bond angle (C–C–C) as 28.4°, and the 22.9% s character in the CH bond and the 20.8% s character in the CC bond in cyclopropane.[5]

In Table 4, the values of the %s nature of various compounds are collected. From the data, it seems that there is a regular increase in s% in the CC and CX (X=N, O) bonds and the decrease in the CH and NH bonds and lone pairs with the increase in the ring size. The above tendency indicates that the 2s electrons which are highly localized in the CH bonds or the lone pairs of the small-membered ring compounds come to participate in the bonding of the CC or CX bonds with an increase in the ring size.

Since the s AO's energies are generally lower than the p AO's, a high degree of s character leads to a more stable bond. It is commonly known that a bond in the ring plane of small ring compounds is more liable to break than in the normal-size ones, and also that the CH-bond stretching frequencies become smaller with an increase in the ring size,[17] reflecting the decrease in the %s of the bond, as is shown in Table 5.

Table 4 also shows the s nature in each LMO of the protonated ethylene oxide and imine. The results reveal that the amount of %s increases at the hetero atom in the CX bond, while it decreases at the CX carbon and remains almost unchanged in the other parts, in comparison with the parent compound. Those results indicate that the change in the electronic structure by protonation is limited around the hetero

Table 4. %s Nature of each LMO

bond[a]	X=O	X=N	X=O	X=N	X=O	X=N	X=O	X=N
C_1-H_1[b]	35.5	34.1	34.7	33.1	31.1	29.4	28.6	27.1
C_1-H_2	34.8	34.1	34.7	33.9	31.1	30.1	28.6	27.8
C_2-H_3[b]	—	—	—	—	27.0	26.7	25.4	25.0
C_2-H_4	—	—	—	—	27.0	26.5	25.4	25.0
C_1-C_2	20.5	19.8	19.3	19.7	26.7	25.5	30.0	28.7
C_2-C_1	20.5	19.8	19.3	19.7	24.5	25.2	26.8	27.0
C_2-C_3	—	—	—	—	—	—	26.0	26.8
X-C	19.6	19.6	13.0	16.4	18.1	22.4	20.4	24.5
C-X	13.5	15.2	16.7	17.6	20.1	22.0	23.2	24.7
X(l.p.)	34.2	—	37.3	41.0	32.7	33.9	20.3	31.8
X-H	25.1	28.8	—	27.5	—	22.6	—	20.9

a) The numbers in the table refer to the one of the first atom of the bond. b) C-H bond on the same side of the molecular plane as N-H bond.

Table 5. The values of the highest C-H stretching frequencies[17]

[cm^{-1}]

X	Number of ring atoms		
	3	4	5
C	3078	2990	2964
O	3010	2996	2975
N	3060	—	2958

atom directly bonded to the proton.

Some attempts have previously been made to correlate the degree of hybridization to the bond angle.[12-16] We have estimated the bond angle by the vector sum of the coefficients of p AO's; the data are summarized in Table 6. The results are as follows: the bond angles in the ring plane decrease towards the tetrahedral angle with an increase in the ring size, and the deviation becomes smaller in all cases. The decrease in the bond angle is somewhat surprising and in contradiction to previous results. It indicates that there is not always a strict correlation between the hybridization and the bond angle.

Bond Energy. Parks and Parr pointed out that the additivity and the invariance of bond energy, as defined by them, hold under the assumptions that the neutral penetration term is negligible and that the bond is homopolar.[2] Hirao calculated the bond energy of various types of CH bonds with respect to hydrocarbons and pointed out that the bond energy parallels the degree of hybridization[3] and is nearly equal within the bonds of the same degree of hybridization.[19]

Table 7 lists the values of the bond energy, while their dependence on the ring size is plotted in Fig. 1. The invariance of the bond energy does not hold in these heterocyclic compounds, but the change due to the ring size is parallel to that of the s nature of the bonds or the lone pairs considered. That is, with an increase in the ring size, the energy of the CH bond and that of the lone pair become higher and those of the CC and CX bonds become lower. This tendency is roughly in accord with the values of s% in Table 3. It is interesting that the change in the CC bond energy between the three- and four-membered rings is most remarkable; this result reflects the large change in the degree of hydribization of their carbon atoms and can also be correlated to the stability of the ring.

Table 6. Deviation of bond angle. geometry

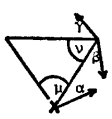
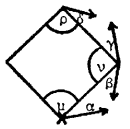
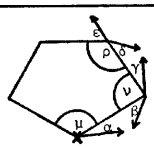

angle	X=O	X=NH	X=O	X=NH	X=O	X=NH
α	25°40′	28°	5°35′	7°50′	−3°30′	−1°45′
β	23°	25°30′	10°5′	11°45′	0°20′	1°15′
γ	33°10′	31°	12°	13°15′	0°	1°35′
δ	—	—	13°	12°10′	3°10′	2°30′
ε	—	—	—	—	4°	2°40′
l.p.[a]	62°35′	57°30′	59°	54°	57°15′	52°20′
μ	61°40′	59°40′	94°30′	94°30′	111°	111°
ν	59°10′	60°10′	88°40′	87°38′	109°5′	107°15′
ρ	—	—	88°10′	90°15′	105°25′	107°15′
N-H[b]	—	56°	—	56°	—	56°

a) l.p.=angle between lone-pair orbital and ring plane. b) N-H=angle between N-H bond and ring plane.

Table 7. Bond energies [eV]

bond	X=O	X=N	X=C	X=O	X=N	X=C	X=O	X=N	X=C
C_1-H_1[a]	−68.12	−67.41	−67.68	−67.56	−66.94	−67.19[b]	−66.81	−66.60	−66.74
C_1-H_2	−68.12	−67.66	−67.68	−67.56	−67.10	−67.19	−66.81	−66.74	−66.74
C_2-H_3[a]	−68.12	−67.41	−67.68	−67.79	−67.26	−67.19	−67.64	−67.16	−66.74
C_2-H_4	−68.12	−67.66	−67.68	−67.79	−67.17	−67.19	−67.64	−67.16	−66.74
C_1-C_2	−92.00	−92.64	−92.70	−95.38	−94.84	−94.48	−95.87	−95.59	−96.03
C_2-C_3	—	—	—	−95.38	−94.84	−94.48	−96.65	−96.07	−96.03
X-C	−134.42	−111.01	—	−134.73	−112.49	—	−136.28	−112.98	—
X	−150.18	−106.87	—	−149.31	−106.61	—	−148.84	−106.64	—
X-H	—	−88.19	—	—	−87.83	—	—	−87.35	—

a) C-H bond at the same side of ring plane as N-H. b) average value.

TABLE 8. CHARGE BOND MOMENTS FROM LMO'S [D]

bond	X=O	X=N	X=O	X=N	X=O	X=N	X=O	X=N
X-C	1.19	0.70	2.60	2.07	1.23	0.68	1.26	0.72
C-C	—	—	—	—	0.11	0.05	0.09	0.07

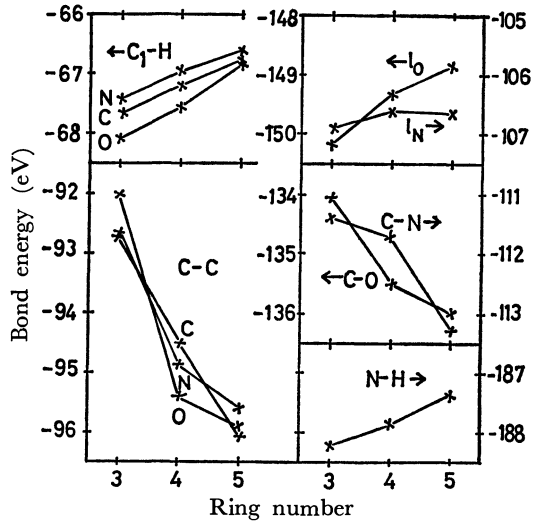

Fig. 1. Various bond energy *vs.* ring number.

Bond Polarity and Charge-density Contour Maps. The concept of bond polarity can be discussed directly by using the LMO results. Table 8 lists the values of the chargebond moment; μ_{AB}, which have been calculated by the following equation:

$$\mu_{AB} = 4.804\, R_m(Q_{Ai} - Q_{Bi})$$

$$Q_{Ai} = (2 \sum_{t}^{\text{on A}} C_{it}(\text{A})^2) - 1$$

where R_m is one half of the AB bond distance in units of Å and where the point of origin is the midpoint of the AB bond. Q_{Ai} is the atomic charge of the A atom in the i-th LMO, which is localized in the AB bond. C_{it} is the coefficient of the t-th AO of the A atom in the i-th LMO. The summation, t, runs over all the valence AO's of the atom A. The μ_{AB} value defined above is an approximated one. That is, this value neglects the contribution of atomic dipoles and the moments by the other parts. In spite of this approximation, the μ_{AB} values are well suited for discussing the bond polarity. It may be seen in Table 8 that the moments of the bonds of the same sort are nearly constant, and that the CX moment values are the largest (while being smaller in CN bonds than in CO bonds, as was expected), while the CC bond moments are very small. This result indicates that the polarity in the heterocycles is found only on the CX bond and that the effect of the hetero atom rapidly decreases with the distance. For reference, the AO coefficients of the LMO's in some five-membered rings are listed in Table 9; the values at the corresponding locations are nearly equal. The values of the C_2 atom in the C_1–C_2 and C_2–C_2, bonds

TABLE 9. THE AO COEFFICIENTS OF THE ATOMS IN LMO'S

	Atom	LMO	s	x	y	z
	O	l. p.±	0.54	0.0	−0.45	±0.70
		$OC_{1,1'}$	0.35	∓0.54	±0.42	0.0
	C_1	C_1O	0.31	−0.46	−0.31	0.0
		C_1C_2	0.38	−0.16	0.57	0.0
		C_1H	0.37	0.31	0.15	±0.47
	C_2	C_2C_1	0.37	0.19	−0.58	0.0
		$C_2C_{2'}$	0.36	−0.60	0.04	0.0
		C_2H	0.35	−0.22	0.29	±0.48
	N	l. p.	0.56	0.0	−0.50	−0.65
		NH	0.33	0.0	−0.35	0.55
		NC_1	0.37	0.52	0.38	0.03
	C_1	C_1N	0.33	−0.47	−0.34	0.01
		C_1C_2	0.38	−0.16	0.57	0.0
		C_1H	0.36	0.32	−0.13	±0.47
	C_2	C_2C_1	0.37	0.20	−0.57	0.0
		$C_2C_{2'}$	0.36	−0.60	0.03	0.0
		C_2H	0.35	0.22	0.29	±0.48
	C_2	$C_2C_{2'}$	0.37	−0.60	0.03	0.0
		C_2H	0.34	0.22	0.29	±0.49

can be taken as examples. This indicates the same trend as in the results of the bond moments.

Figures 2(a)–(c) show the LMO density maps for the bonds in the ring plane and the lone pairs of the 3-, 4-, and 5-membered cyclic ethers. The contour lines representing the densities smaller than 1.0 A eÅ^{-3} are omitted. The figures of the LMO-charge maps in the ring bond reveal a shift of the density maxima toward the interatomic lines with an increase in the ring size. Although they indicate a significant polarity of the CO bond, the considerable change in the hybridization (s nature) with a difference in ring size is not demonstrated. This holds true also for the lone pair LMO's. It is worth noticing that the CC bonds always show two maxima, whereas the CO bonds show only one maximum, which is shifted to the oxygen atom. The figures of the cyclic imines are omitted, since they exhibit a shape very similar to that of the cyclic ethers.

Figure 2(d) shows the LMO maps of the CC bond of cyclopropane. It clearly demonstrates that the maximum of the electron density lies outside the CC line. This tendency is reduced in larger ring compounds, as can be seen from the bond-angle data in Table 3.

Figure 2(e) shows the LMO maps of the ring bonds and the lone pair of protonated ethylene oxide. There is no significant change in the shape compared to that of the neutral compound. The change in the CO bond is interesting, since more of the LMO charge

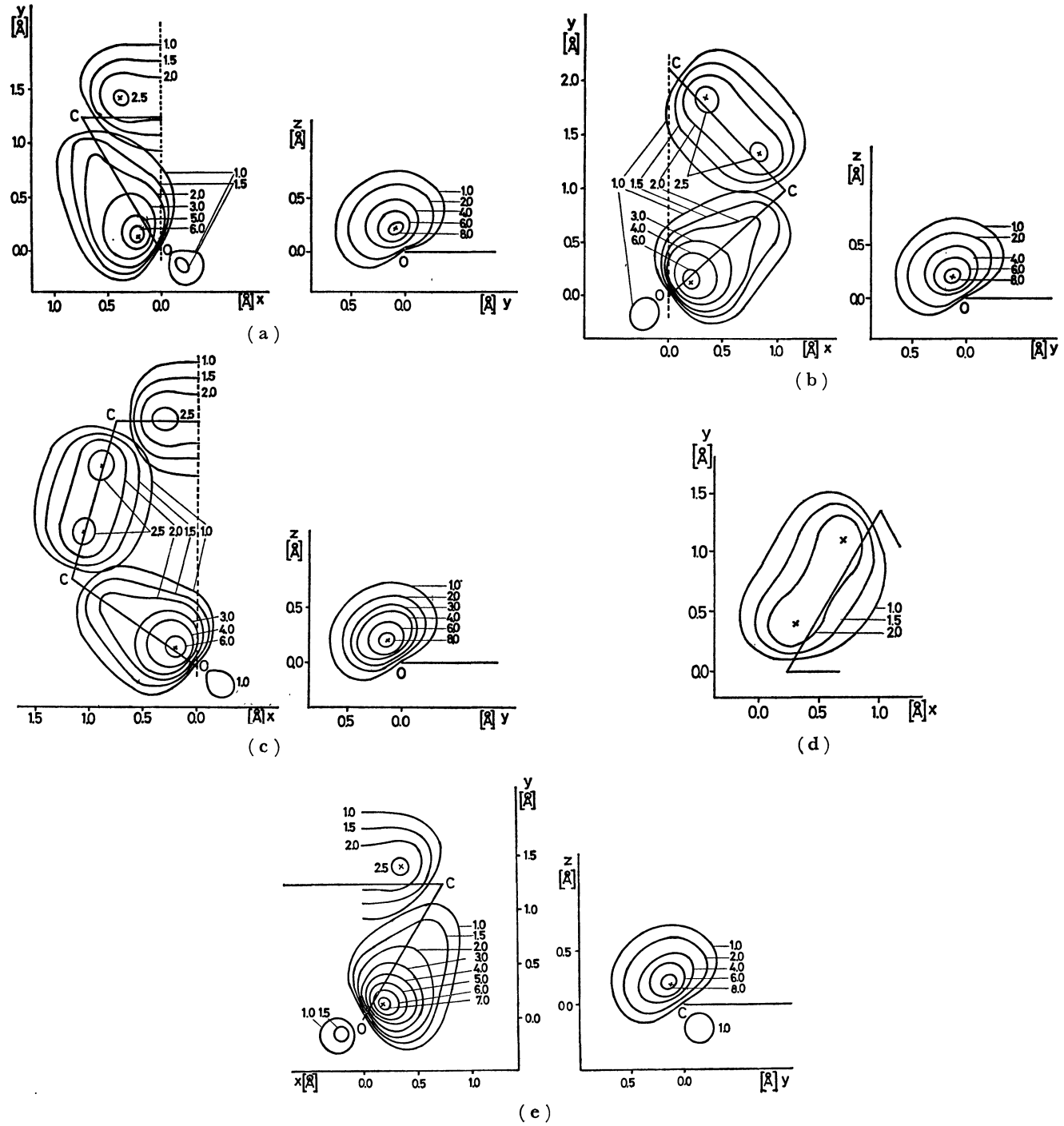

Fig. 2. LMO density maps for the ring bonds and lone pairs of ethylene oxide (a); trimethylene oxide (b); THF (c); C-C bond of cyclopropane (d); ring bonds and lone pair of protonated ethylene oxide (e). Maxima are denoted by a cross. The unit of density is $Å^{-3}$.

is shifted toward the oxygen atom, and the polarity of the CO bond becomes larger by the protonation. This trend agrees with the results of the charge-bond moment shown in Table 8.

It is interesting to visualize the characteristic features of the LMO's. We show the total-density maps of ethylene oxide and imine in Figures 3(a)–(d). The similarity between the LMO and the total-density pictures is not very clearly demonstrated. The CC bond still holds two maxima outside the ring. As to the CX bond, the maximum near the hetero atom in the LMO map is found to be the tail-off of a broad maximum nearly all around this atom. As going from the LMO picture to the total-electron-density picture, the special characteristics of the single and localized bonds given by the LMO's become more and more diffuse, as is to be expected. The differences between these two maps are produced mainly by the neglect of the overlap effect between the charges of the LMO's.

One of the authors (G.F.) is indebted to Mr. Tsutomu Minato for making available the computer programs. He also wishes to express his gratitude to the Japanese

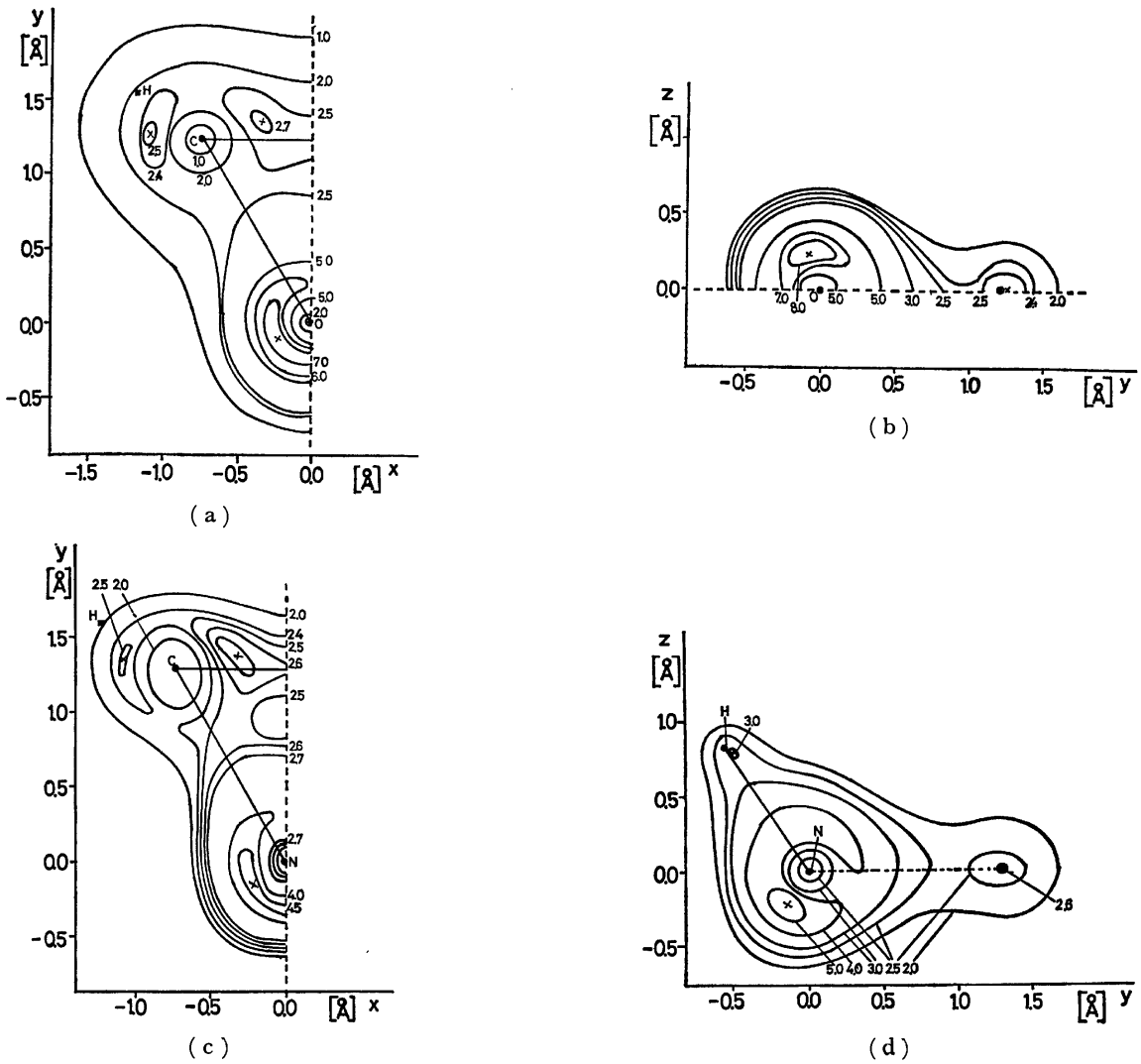

Fig. 3. Total electron density maps in the ring plane (x—y), and perpendicular plane (y—z) crossing the middle of the C-C bond and the heteroatom ethylene oxide (a), (b), and ethylene imine (c), (d); maxima are denoted by a cross (×); the position of the perpendicular C-C bond in the y—z map is denoted by a cross in a circle (⊗); the projected hydrogen position upon the x—y plane is assigned by a square (■); the ring plane in the y—z map is indicated by a dashed line.

Ministry of Education and the Deutscher Akademischer Austauschdienst for giving grants.

The authors wish to express their appreciation to the Data Processing Center of Kyoto University for its generous permission to use the FACOM 230-60 computer.

References

1) C. Edmiston and K. Ruedenberg, *Rev. Mod. Phys.*, **35**, 457 (1963).
2) J. M. Parks and R. G. Parr, *J. Chem. Phys.*, **28**, 335 (1958).
3) K. Hirao, *Chem. Phys. Lett.*, to be published.
4) W. England and M. S. Gordon, *J. Amer. Chem. Soc.*, **93**, 4649 (1971); **94**, 5168 (1972).
5) M. D. Newton, E. Switkes, and W. N. Lipscomb, *J. Chem. Phys.*, **53**, 2645 (1970).
6) C. Trindle and O. Sinanoglu, *J. Amer. Chem. Soc.*, **91**, 853 (1969).
7) R. Bonaccorsi, E. Scrocco, and J. Tomasi, *J. Chem. Phys.*, **52**, 5270 (1970).
8) J. A. Pople, D. L. Beveridge, and P. A. Dobosh, *ibid.*, **47**, 2026 (1967).
9) "Tables of Interatomic Distances," The Chemical Society, Spec. Publ. 11, London 1958. In case of cyclobutane, the puckering angle has been taken as 21°10′.
10) C. A. Coulson and W. E. Moffitt, *Phil. Mag.*, **40**, 1 (1949).
11) a) N. Muller and D. E. Pritchard, *J. Chem. Phys.*, **31**, 1425 (1959). b) G. C. Levy and G. L. Nelson, "^{13}C NMR for Organic Chemists," Wiley-Interscience, 1972. c) J. B. Stothers, "Carbon-13 NMR Spectroscopy," Academic Press, New York, London (1972), p. 270.
12) H. A. Bent, *Chem. Rev.*, **61**, 275 (1961).
13) C. S. Foote, *Tetrahedron Lett.* **9**, 579 (1963).
14) K. Mislow, *ibid.*, **22**, 1415 (1964).
15) C. A. Coulson and T. H. Goodwin, *J. Chem. Soc.*, **1962**, 2851; **1963**, 3161.
16) P. Kollman, *J. Amer. Chem. Soc.*, **96**, 4363 (1974).
17) Landolt-Boernstein: "Zahlenwerte und Funktionen aus Physik, Chemie, Astronomie, Geophysik und Technik," 6th edition, vol. 1, part 2, pp. 294—295, 287.
18) K. B. Wiberg, *Tetrahedron*, **24**, 1083 (1968).
19) While this paper was submitted for publication: W. von Niessen, *Theoret. Chim. Acta*, (Berl.) **38**, 9 (1975).

Ultra-thin Layer of Lipids in Polymer Film and Its Electric Properties. New Sorption Method to Prepare a Model Biomembrane System

Tadayoshi Yoshida, Shin-ichiro Ogura, and Masataka Okuyama

Department of Engineering Chemistry, Nagoya Institute of Technology, Showa-ku, Nagoya 466

(Received April 8, 1975)

The ultra-thin layer of glycerol α-*cis*-9-octadecenate (glycerol α-monooleate:GMO) could be formed by impregnating nitrocellulose (NC) film with GMO and by then filling microscopically the interstices of the network structure of NC with microdrops of GMO. The dielectric dispersion characteristic of this film was found to be similar to that observed for bimolecular films. In a concentrated KCl solution (100 mM), however, an anomalous dielectric dispersion phenomenon was observed below 10 kHz. The low-frequency dispersion was attributed to surface conductance along the planes of contact between the GMO microdrops and the NC network. The ultra-thin film of di(*cis*-9-octadecenyl)phosphate (dioleyl phosphate: DOPH) could also be formed by this method. When a constant DC voltage (50 mV) was applied across the film in a 20 mM KCl solution, the electric current through the whole system changed periodically.

In a previous paper, we have reported that a stable bilayer was formed from a mixture of 1-tetradecanol and tetradecanoic acid.[1] The mixed bilayer, however, was frequently broken at higher temperatures or pH's. This could be explained by the transformation of the precursor monolayer of tetradecanoic acid from the condensed to the expanded state. Therefore, the mixed bilayer cannot be used as a model system in which a transformation of the molecular conformation in the membrane takes place.

A recent study has reported that a membrane composed of a filter paper and lipid may be used as a model system accompanying a conformational change.[2] The thickness of the model membrane, however, is *ca.* 10^4 times that of living membranes.

In the present paper, we wish to introduce a new model system that satisfies the following requirements: (1) the aggregative change (or conformational change) of the molecules constituting the model system does not result in a rupture of the film itself, and (2) the thickness and electric resistance of the model system are comparable to those of living membranes. The present model system should be useful in elucidating the molecular mechanism of excitable living membranes.

Experimental

Materials. The glycerol α-monooleate (GMO, purity> 99%) used in this study was purchased from the Gasukuro Co., Ltd. The nitrocellulose (NC; nitrogen content, 11.07%; degree of polymerization, 300) was kindly given by the Daicel Co., Ltd., while the ethylcellulose (EC;ethoxyl content, 48%; 9.5 centipoises in a 5% toluene–ethanol solution (80 : 20) at 25 °C) was obtained from the Tokyo Kasei Co., Ltd. All the solvents used in this study were reagent-grade.

Preparation of the Ultra-thin Layer of GMO. The porous NC-film (thickness, 1000—2000 Å) was prepared by the following processes prior to the formation of the ultra-thin layer of GMO: (1) A clean glass slide wad dipped in an ethylacetate solution (10 ml) containing both NC (60 mg) and EC (60 mg). (2) When the slide was taken out from the ethylacetate solution, a thin liquid layer of the solution covered the slide. (3) The slide is allowed to stand at room temperature to remove the ethylacetate. (4) Next the slide was transferred into benzene to wash out the EC from the NC–EC mixed film. (5) After an hour, when the slide was taken out from the benzene, the porous NC-film was left on the glass slide. (6) Dipping one end of the slide in water, the porous NC-film peeled off spontaneously from the glass slide within 5 minutes and floated on the water surface.

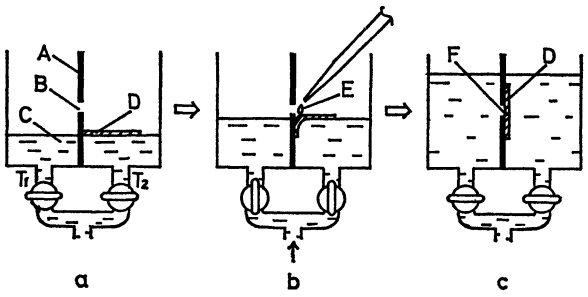

Fig. 1. Method of preparation of ultra-thin layer.
A: Teflon plate, B: Pore (0.5—1.0 mm in diameter), C: Aqueous solution, D: Porous NC-fllm, E: A drop of GMO/*n*-decane solution, F: Ultra-thin GMO-layer, T_1 and T_2: Tube.

The ultra-thin layer of GMO could be formed in the NC-film by the following procedures. (1) As is shown in Fig. 1a, two compartments of the same volume were separated by a Teflon plate (1 mm thick) with a small hole (0.5—1.0 mm in diameter) at the center. An aqueous KCl solution of the same volume was poured simultaneously into both compartments until the water surfaces were raised *ca.* 5 mm below the hole of the Teflon plate. The above-mentioned porous NC-film then floated on the water surface on the right-hand side. (2) An equal volume of the aqueous KCl solution was gradually added to both compartments through T_1 and T_2 with the two levels kept equal. In this procedure, the porous NC-film was gradually transferred to the surface of the Teflon plate as the water levels rose (see Fig. 1b). (3) When the water levels had been raised to *ca.* 1 mm below the hole of the Teflon plate, an aliquot (*ca.* 0.01 ml) of a GMO/*n*-decane solution was dropped on to the porous NC-film. The water levels were then gradually raised further until they reached *ca.* 5 mm above the hole (see Fig. 1c). In this procedure, the microdrops of GMO filled the pores of the NC-film and formed ultra-thin layers.

Measurement of Electric Properties. The electric capacitance of the whole system was measured by means of an AC bridge (Ando Electric Co., Ltd. Model TR-1C); the whole system consists of the ultra-thin GMO layer, the porous NC-film, and the adjacent aqueous solutions (see the first part of the Results and Discussion section). Measurments were carried out in the frequency range from 30 Hz to 3 MHz.

The constant potential (DC 50 mV) was applied between silver-silver chloride or platinized platinum electrodes in each compartment. The potential across the film was measured by means of an electrometer of a high-input impedance (Takeda Riken Industry Co., Ltd. Model TR-8651). The area of the film was estimated photographically. The temperature of the compartments was controlled to 20± 0.5 °C.

Results and Discussion

Our membrane system, prepared by impregnating GMO into the porous NC film, consisted of three phases; the ultra-thin GMO layer, the porous NC film, and the adjacent aqueous KCl solutions; the phases were connected in series with each other. However, the electric capacitance and resistance of the porous NC film (without GMO) in a 100 mM KCl solution were practically equal to those of an aqueous solution. Consequently. in view of the equivalent circuit, our system could be approximated by two phases: the ultra-thin GMO layer and the adjacent aqueous solution. On the other hand, a bilayer and its adjacent aqueous solution could also be approximated by two phases.[13] It is expected, therefore, that the characteristic of the dielectric dispersion of our new system is similar to that observed for the bilayer. The characteristic of the dielectric dispersion of our system in 10 mM KCl was nearly semicircular (Fig. 2). However, a marked deviation from the semicircular relation was observed below 300 Hz. The deviation became greater as the KCl solution was diluted. No such deviation was observed for bilayers.

The deviation in the low-frequency region may be attributed to the following difference in conductance between the bilayer and the thin GMO layer. In accordance with the suggestion of Hanai *et al.*,[3] the

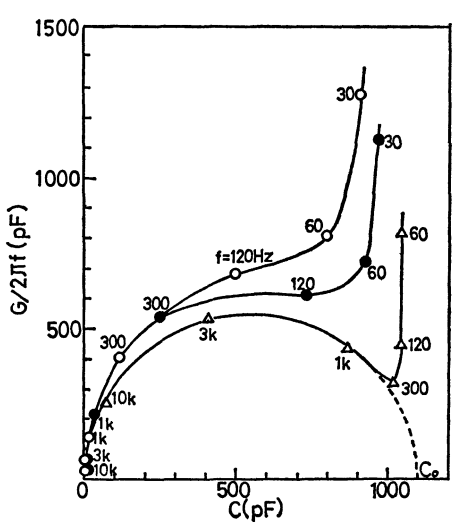

Fig. 2. Complex capacitance diagram of a whole system (aqueous solution+ultra-thin layer+porous NC-film) in three concentrations of KCl.
G: Conductance of a whole system, C: Capacitance of a whole system, f: Frequency Hz (the figures indicated with plots).
○: 0,05 mM, ●: 0,1 mM, △: 10 mM.

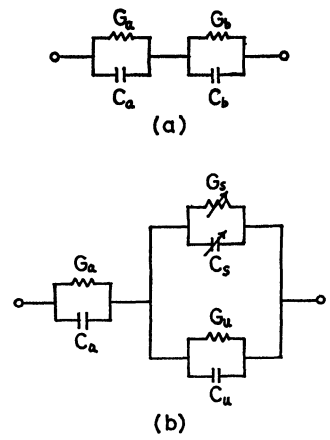

Fig. 3. Equivalent circuit.
(a): Bilayer system, (b): Our whole system.
Subscript a: Aqueous solution, b: Bilayer, s: Plane of contact between GMO microdrop and NC network, u: Ultra-thin layer.

bilayer and its adjacent aqueous solution can each be represented by a parallel combination of capacitance and conductance, connected in series with each other (Fig. 3a, C_b and G_b for the bilayer: C_a and G_a for the aqueous solution). In this electric circuit, the total conductance, G, and the capacitance, C, of the bilayer system are expressed by:

$$\frac{G}{2\pi f} = \frac{G_0}{2\pi f} + \frac{2\pi f\tau(C_0 - C_\infty)}{1+(2\pi f)^2\tau^2} \quad (1)$$

$$C = C_\infty + \frac{C_0 - C_\infty}{1+(2\pi f)^2\tau^2} \quad (2)$$

where f is the frequency, τ is $(C_a+C_b)/(G_a+G_b)$, G_0 is $G_aG_b/(G_a+G_b)$, C_0 is $(G_a^2C_b+G_b^2C_a)/(G_a+G_b)^2$, and C_∞ is $C_aC_b/(C_a+C_b)$. For the bilayer system, since G_b (*ca.* 10^{-8} ℧) $\ll G_a$(*ca.* 10^{-3} ℧) and C_b(*ca.* 10^3 pF) $\gg$ C_a (*ca.* 1 pF), the first term on the right hand side of Eq. (1) is negligibly small compared to the second term. Since the conductance of the thin GMO layer $G_u(10^{-4}$—10^{-5} ℧) $< G_a$ (*ca.* 10^{-3} ℧), the first term is not negligibly small in the low-frequency region. The first term is responsible for the deviation from the semicircular relation at low frequencies.

The combination of Eqs. (1) and (2) leads to Eq. (3):

$$G - G_0 = -\frac{1}{\tau}(C - C_0) \quad (3)$$

When G is plotted against C, therefore, a straight line should result. In fact, as is shown in Fig. 4, G and C for our system satisfied Eq. (3), which had been derived from the model of the two phases. Therefore, the capacitance of the thin GMO layer should be equal to the extrapolated value, C_0, at the low-frequency end of the semicircular curve (see Fig. 2). Assuming the thin GMO layer to be a parallel-plate condenser whose dielectric constant is 2, we find, from the above extrapolated value of C_0 (1100 pF, or 0.14 μF/cm²), that the thickness is *ca.* 150 Å, approximately 4 times that of the 1-tetradecanol bilayer.[1]

The G–C curve for our system in a 100 mM KCl solution departs from a straight line (Fig. 4). In

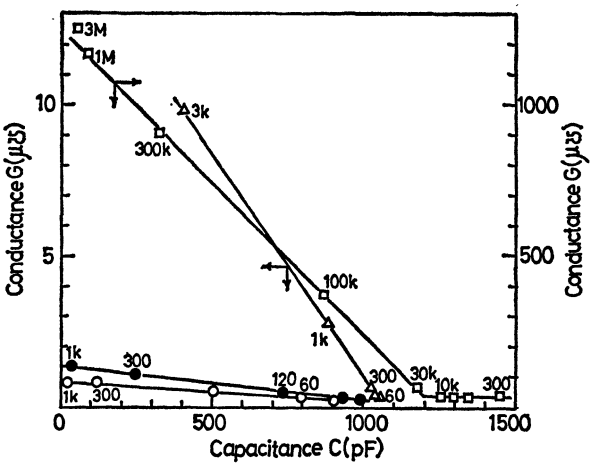

Fig. 4. Electric characteristic of a whole system.
The corresponding frequencies (Hz) are indicated beside some points.
Concentration of KCl solution, ○: 0.05 mM, ●: 0.1 mM, △: 10 mM, □: 100 mM.

the deviated region, below 10 kHz, the capacitance of the whole system increases with a decrease in the frequency, but the conductance is constant (30 μ℧, or 3.8×10^{-3} ℧/cm^2). This phenomenon at low frequencies was not observed for our system in 0.05 mM, 0.1 mM, or 10 mM KCl solutions. Since the area of the electrodes is *ca.* 100 times larger than that of the ultra-thin GMO layer, the diffusion impedance at the electrode surface is negligible. Therefore, it seemed that the above phenomenon is attributable to the property of the ultra-thin GMO-layer system itself.

When the following procedure was repeated after the formation of the ultra-thin GMO layer in the 100 mM KCl solution, the *G–C* charactristic was changed as is shown in Fig. 5. The water levels of both compartments were lowered simultaneously to *ca.* 5 mm below the hole of the Teflon plate. In this procedure, the ultra-thin GMO layer was exposed to air. Moreover, the water levels returned to the original state within one minute. The capacitance increased with the repeated exposures, and the break in the curve at low frequencies became obtuse, as is shown in Fig. 5. The increase in the capacitance should be attributed to the reduction of the GMO-layer thickness or to the quantity of GMO absorbed into the porous NC film. From the experimental results (Fig. 5) and the calculated thickness of the GMO layer (150 Å), it seemed reasonable to assume that the ultra-thin GMO layer was formed by filling the interstices of the network structure of NC with microdrops of GMO.

The form of the *G–C* curve was very similar to that observed for the suspensions of *Austerias* eggs by Cole *et al.*[4] They explained qualitatively the break in the *G–C* curve in the low-frequency region as being caused by the surface conductance at the egg–water interfaces. On the other hands, Coster[5] suggested that the double fixed-charge membrane model could account for the low-frequency dispersion. In both cases it was useful to introduce the concept of frequency-dependent elements [$C(f)$ and $G(f)$]. In our system, the surface conduction possibly occurred also at the interface of the GMO microdrop-NC network. According to Schwan *et al.*,[6] the surface conductance can be represented by a parallel combination of the capacitance, C_s, and the conductance, G_s, where C_s is inversely proportional to $\sqrt{f}$ and where G_s is proportional to $\sqrt{f}$ on the first approximation. Therefore, our system may be represented by the circuit shown in Fig. 3b. G_u and C_u indicate the conductance and the capacitance of the ultra-thin layer respectively. Curve (a) in Fig. 6 represents the calculated curve, using the equivalent circuit (Fig. 3b) with $C_a=10^{-12}$ F, $C_u=1.2\times10^{-9}$ F, $G_a=1.2\times10^{-3}$ ℧, $G_u=3\times10^{-5}$ ℧, $G_s=1.25\times10^{-8}\sqrt{f}$ ℧, $C_s=1.25\times10^{-8}/2\pi\sqrt{f}$ F. The above values of G_a and C_a correspond to those of the 100 mM KCl solution, while

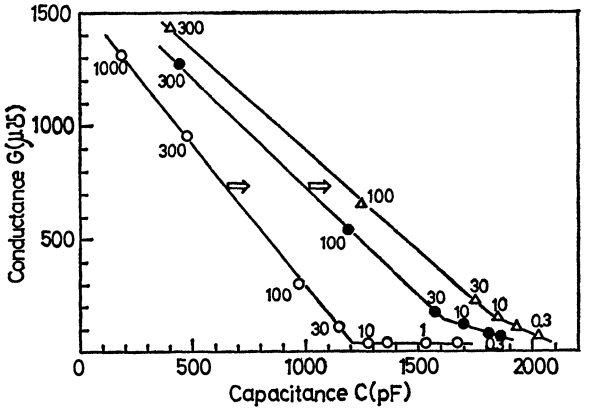

Fig. 5. Influence of up-and-down procedures of the water levels on *G–C* characteistic.
The corresponding frequencies (kHz) are given beside some points.
Concentration of KCl solution is 100 mM.
○: Initial characteristic, ●: After the first procedure, △: After the second procedure.

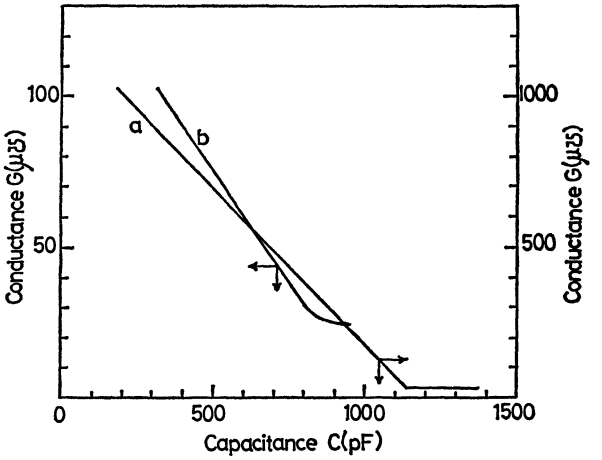

Fig. 6. Whole system characteristic, calculated from the equivalent circuit, Fig. 3(b).
Curve(a): With $C_a=10^{-12}$ F, $C_u=1.2\times10^{-9}$ F, $C_s=1.25\times10^{-8}/2\pi\sqrt{f}$ F, $G_a=1.2\times10^{-3}$ ℧, $G_u=3\times10^{-5}$ ℧, $G_s=1.25\times10^{-8}\sqrt{f}$ ℧.
Curve(b): With the same values of C_a, C_u, C_s, G_u, G_s as above, and with $G_a=1.7\times10^{-4}$ ℧.

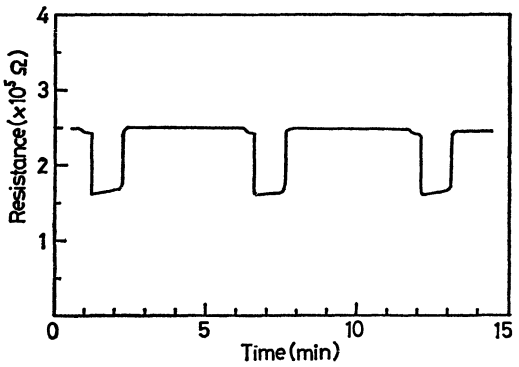

Fig. 7. Periodic change of the resistance of ultra-thin DOPH layer.

C_u is equal to the extrapolated value of C_0 at the low-frequency end of the semicircular curve in Fig. 2. Moreover, G_u is equal to the conductance at low frequencies (below 1 kHz). If we use $G_a = 1.7 \times 10^{-3}$ ℧ (the value for 10 mM KCl solution) instead of 1.2×10^{-3} ℧, Curve (b) in Fig. 6 is obtained. The bend of Curve (b) in the low-frequency region is not clear compared with Curve (a). In other words, the dilution of the KCl solution is accompanied by the disappearance of the bend in the *C–G* curve. These curves agree with the experimental results (Fig. 4)

The ultra-thin layer of dioleyl phosphate (DOPH) could also be prepared by a similar method. When a constant DC voltage (50 mV) was applied across the film in a 20 mM KCl solution, the electric current through the whole system changed periodically (Fig. 7).

Yoshida *et al.*[2] have reported that DOPH impregnated in filter paper changes its conformation discontinuously from oil droplets to bilayer films at a critical concentration of the adjacent solution and that this conformational change increases the conductance of the model membrane. On the other hand, according to Barry *et al.*,[7] the difference in transport number of ions between the membrane and the adjacent solution causes an increase in the salt concentration in the unstirred layer near the membrane surface.

In both studies, we presumed that the periodic phenomenon (Fig. 7) resulted from the following processes. If the ultra-thin layer of DOPH, as well as the ultra-thin layer of GMO, could be formed by filling the interstices of the network structure of NC with microdrops of DOPH, then the current must flow along the planes of contact between the DOPH microdrops and the NC network because of the high resistance of the DOPH microdrops. On the other hand, since DOPH possesses a negative charge, the transport number of positive ions at the planes of contact is greater than in the adjacent solution. This difference in transport number will result in an increase in the KCl concentration on one side of the thin layer-solution interfaces. If the DOPH in the NC film, as well as the DOPH in the filter paper, changes its conformation at a critical concentration of the adjacent solution, the conductance of our model membrane will increase discontinuously when the concentration at the thin layer-solution interface reaches a critical value. The periodic phenomenon (Fig. 7) disappeared in a 10 mM or 30 mM KCl solution. This fact suggests that the DOPH in the NC film changes its conformation when the concentration at the thin layer-solution interface reaches 20–30 mM. The increase in conductance is accompanied by the disappearance of the enhancement of the concentration at thin layer-solution interface. Consequently, the DOPH in the NC film returns from the transition state (bilayer) to the original state (microdrop) after *ca.* one minute (Fig. 7), and then the conductance of the whole system decreases to the original lower value. We assumed that the periodic phenomenon in Fig. 7 resulted from a repetition of the above processes. The periodic phenomenon was not observed for the ultra-thin GMO layer, which has no charged group. Therefore, it seems that the occurrence of the periodic phenomenon in Fig. 7 requires the presence of the charged group and of two conformational states of the molecule.

From the facts presented above, we may conclude that the ultra-thin layer consists of the microdrops of GMO (or DOPH) in the interstices of the network structure of NC and that the thickness of the ultra-thin layer is 150 Å.

The authors wish to thank Dr. Hirofumi Okabayashi of our laboratory for his valuable discussions. They also wish to thank Mr. Kazuo Kazikawa of the Daicel Co. for his kind supply of nitrocellulose.

A part of this research was supported by a Scientific Research Grant from the Ministry of Education.

References

1) M. Okuyama, T. Yoshida, T. Tanii, M. Kunugi, and I. Ishizaki, This Bulletin, **48**, 191 (1975).
2) M. Yoshida, N. Kamo, and Y. Kobatake, *J. Membrane Biol.*, **8**, 389 (1972).
3) T. Hanai, D. A. Haydon, and J. Taylor, *Proc. Roy. Soc., Ser. A*, **281**, 377 (1964).
4) K. S. Cole and R. H. Cole, *J. Gen. Physiol.*, **19**, 609 (1936).
5) H. G. L. Coster, *Biophys. J.*, **13**, 118 (1973).
6) H. P. Schwan, G. Schwarz, J. Maczuk, and H. Pauly, *J. Phys. Chem.*, **66**, 2626 (1962).
7) P. H. Barry and A. B. Hope, *Biophys. J.*, **9**, 700 (1969).

Molecular Reorientational Motion of the Benzene Molecule in a Mixture of Benzene with Carbon Tetrachloride by Raman Band Spape Analysis

Hiroyasu NOMURA and Yutaka MIYAHARA

Department of Chemical Engineering, Faculty of Engineering, Nagoya University, Chikusa-ku, Nagoya 464

(Received April 18, 1975)

The reorientational correlation times of the benzene molecule in mixtures of benzene with carbon tetrachloride were measured by the method of the Raman line shape analysis. The reorientational relaxation times τ_{OR} of C_6H_6 in solutions increased with increasing mole fraction of CCl_4. Information was also obtained on an intermolecular vibration-vibration energy transfer process which primarily affects the mean life time of the first excited vibrational state ν_2 (a_{1g}) in benzene in solutions.

Numerous investigations have been made to determine the nature of the interaction which affects the Raman spectra of molecules in solution. The measured linewidth of the Raman line provides new information about the mechanisms of intermolecular interaction in solutions.

The most accessible experimental quantity in studies of rotational molecular motion in liquids and/or solutions is the rotational correlation time τ. This value is the zero Fourier transform of the orientational time correlation function. Values of τ can be estimated from a variety of experimental techniques, for example Rayleigh-wing scattering and Raman line shape analysis.[1-4]

We estimated the reorientational correlation times of the benzene molecule in a mixture of benzene with carbon tetrachloride from the Raman line shape analysis. As a result, information has been obtained on an intermolecular vibration to vibration energy transfer process which primarily affects the mean life time of the first excited vibrational state $\nu_2(a_{1g})$ in benzene.

Experimental

We have used an argon ion laser (Coherent Radiation Co. Ltd. 2W) for the light source. The scattered light was analyzed with a double monochromator (JRS-Ul Laser Raman Spectrometer).

Raman theory and analysis

Analysis of the Raman line shape of the $\nu_2(a_{1g})$ fundamental in benzene yields information about the diffusion constant $D_\perp$. The theory has recently been summarized[5] and needs only a cursory introduction here. The mechanics of the data aquisition and analysis requires clarification, however.

All experiments were done using 90° scattering and linearly polarized incident light. With $I_\parallel(\omega)$ and $I_\perp(\omega)$ representing the strong and weak components of the scattered light, one can write

$$I_\parallel(\omega) = I_{isot}(\omega) + 4/3 I_{anis}(\omega) \quad (1)$$

$$I_\perp(\omega) = I_{anis}(\omega) \quad (2)$$

$$\rho_s = \frac{I_\perp(\omega)}{I_\parallel(\omega)} = \frac{I_{anis}(\omega)}{I_{isot}(\omega) + 4/3\, I_{anis}(\omega)} \quad (3)$$

where ρ_s is the depolarization ratio. $I_{isot}(\omega)$ represents the intrinsic vibrational line shape, whereas $I_{anis}(\omega)$ is a convolution of the vibrational line shape and the orientational spectrum. The problem is to separate the two accurately.

$I_{isot}(\omega)$ can be extracted directly from measurements of $I_\parallel(\omega)$ and $I_\perp(\omega)$. But since the depolarization ratio is very small for the band under consideration (ρ_s (991 cm^{-1}) = 0.00986±0.0005) the intrinsic vibration line shape $I_{isot}(\omega)$ and the measured line shapes $I_\parallel(\omega)$ can be considered to be the same without introducing significant errors ($I_{isot}(\omega) \simeq 0.991\ I_\parallel(\omega)$). Generally, however, the measured spectrum is a convolution of the true spectrum and the Gaussian slit function $S(\nu_i, \omega)$. One can write

$$I'_{anis}(\omega) = \int_{-\infty}^{\infty} I_{or}(\omega) I_{isot}(\omega) S(\nu_i, \omega) d\omega \quad (4)$$

and

$$I'_{isot}(\omega) = \int_{-\infty}^{\infty} I_{isot}(\omega) S(\nu_i, \omega) d\omega \quad (5)$$

where the primed and unprimed functions denote the measured and true shapes respectively. At first sight, it would appear that the order of convolution is not important and hence the slit function would cancel. This is not the case except when the line widths are very similar in magnitude. To obviate the large errors associated with this assumption, true line widths were determined directly as a function of slit width; a plot is shown in Fig. 1. For the 991 cm^{-1} line of benzene, $I_\parallel(\omega)$ can be determined directly by setting the slit 20 μ or less. In order to obtain

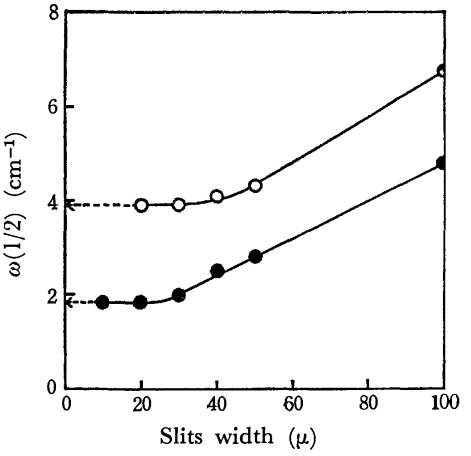

Fig. 1. Linewidth of $\nu_2(a_{1g})$ of C_6H_6 in carbon tetrachloride as a function of slit width. (37.6 mol% of benzene)
○: $\omega_{anis}(1/2)$, ●: $\omega_{isot}(1/2)$

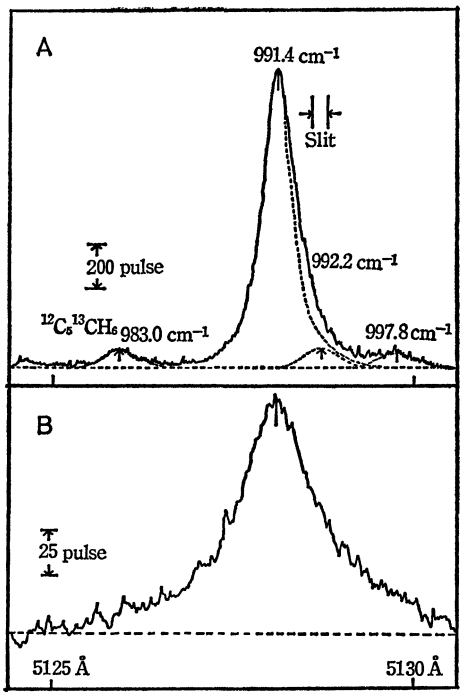

Fig. 2. A; Polarized Raman spectrum, $I_{\parallel}(\omega)$, of $\nu_2(a_{1g})$ of C_6H_6 (slit=20 μ×10 mm high, scan rate=0.5 Å/min), B; Depolarized spectrum $I_{\perp}(\omega)$(slit=25 μ×10 mm high, scan rate=0.5 Å/min) (20.0 mol% of benzene in mixtures).

$I_{isot}(\omega)$, $I_{\perp}(\omega)$ must be evaluated at the same slit width. Examples of measured $I_{\parallel}(\omega)$ and $I_{\perp}(\omega)$ are shown in Fig. 2. Errors arising from monochromator polarization response, beam convergence, light collection angles, analyzer light leak, ellipticity of the exciting light polarization, laser power fluctuations, and stray light have been minimized.

Implicit in the treatment of the data are the assumptions that $I_{isot}(\omega)$ and $I_{anis}(\omega)$ are Lorentzian and that vibrational and reorientational motions are not coupled. A test of these assumptions is shown in Fig. 3, in which $I_{isot}(\omega)$ and $I_{anis}(\omega)$, normalized to unit height, are displayed (pionts). The solid lines are calculated Lorentz functions based on the observed line width. Because $I_{anis}(\omega)$ is a convolution of

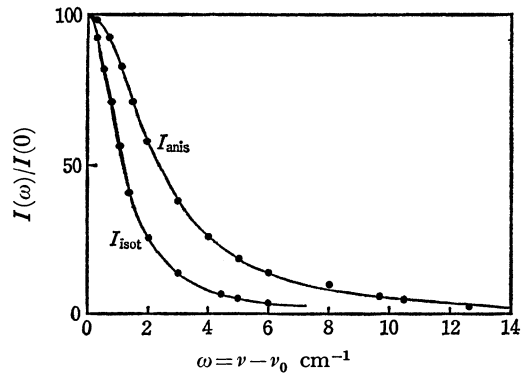

Fig. 3. Normalized line shapes of $I_{isot}(\omega)$(●) and $I_{anis}(\omega)$(○) of the $\nu_2(a_{1g})$ band of C_6H_6 in carbon tetrachloride (20.0 mol% of benzene).

$I_{isot}(\omega)$ with $I_{or}(\omega)$, the $I_{or}(\omega)$ is also Lorentzian. Accordingly,

$$\omega_{1/2}(\text{anis}) = \omega_{1/2}(\text{isot}) + \omega_{1/2}(\text{or}) \quad (6)$$

where the $\omega_1/_2$ terms are half widths. Furthermore, the reorientational correlation time is obtained as follows:

$$\tau^{-1}(\text{or}) = 2\pi c\omega_{1/2}(\text{or}) \quad (7)$$

where c is the velocity of light.

Results and Discussion

Before the measurements of the benzene–carbon tetrachloride solution were made, we measured the reorientational correlation time of pure liquid benzene together with a calibration of the Raman Spectrometer used. The values obtained by the excitation light of 4880 Å and 5145 Å wavelengths are summarized in Table 1. As is seen there, the reorientational correlation time τ from these values was in very good agreement with that obtained by Litovitz *et al.*[5] and also the values of $\omega_{1/2}$ (isot) were in good agreement with those of Griffith *et al.*[6] The line shapes of the 991 cm^{-1} Raman active fundamental of C_6H_6 are shown in Fig. 2(a). This line shape is also the same as that obtained by Griffith *et al.*[6] Several prominent features are observed. Important hot bands cause the observed bands to be skewed. The most interesting feature is that the hot band in C_6H_6 occurs on the high frequency side of ν_2. Additional Raman bands also occur in the far wings of the bands under study but they do not interfere significantly.

The dependence of the linewidth of the 991 cm^{-1} band on the mole fraction of CCl_4 is shown in Fig. 4. The reported linewidths are those obtained after

Table 1. Line width of $\nu_2(a_{1g})$ of C_6H_6 at various lights

	$\omega_{1/2}$(aniso)	$\omega_{1/2}$(isot)	$\omega_{1/2}$(or)
5145 Å	4.54 cm^{-1}	2.45 cm^{-1}	2.09 cm^{-1}
4880 Å	4.52 cm^{-1}	2.49 cm^{-1}	2.03 cm^{-1}
* Litovitz *et al.*[5]			2.0±0.5 cm^{-1}

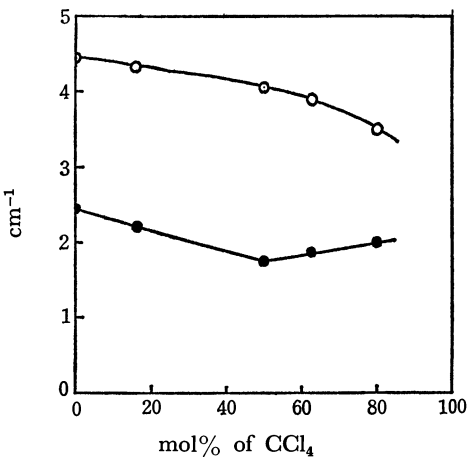

Fig. 4. Relationship between $\omega_{1/2}$(isot), $\omega_{1/2}$(anis) and the mole fraction of carbon tetrachloride.

graphical resolution of the over-all contour into the constituent $v=0\rightarrow1$ and hot band components. As is seen in Fig. 4, the $\omega_{1/2}$ (anis)'s decreased monotonously with increasing CCl_4 mole fraction. However, the $\omega_{1/2}$ (isot)'s decreased with increasing concentration of CCl_4 up to about the equimolar point and after this minimum point increased with increasing concentration of CCl_4.

Recently, the linewidths of the 991 cm^{-1} and 945 cm^{-1} bands for several mixtures of C_6H_6 and C_6D_6 were measured by Griffith *et al.*[6] They have explained their results as follows: the linewidth of the 954 cm^{-1} band of C_6D_6 is independent of the concentration, thereby supporting the initial supposition that the lack of close lying energy levels would preclude an intermolecular vibration to vibration energy transfer process from affecting the lifetime of the v'_2 state in that molecule. In C_6H_6, however, where two close lying energy levels are available, at 985 cm^{-1} and 970 cm^{-1}, the linewidth of the 991 cm^{-1} line is linearly dependent upon the concentration. As the C_6H_6 concentration decreases, the frequency of collisions between C_6H_6 molecules decreases to the same extent. If the life time of v_2 becomes longer by the mechanism for the energy dissipating process, the linewidth will be narrow and continue narrowing untill no more collisions between C_6H_6 molecules occur.

For the C_6H_6–CCl_4 mixtures, the energy dissipating process can be considered as the same mechanism. In CCl_4, there is a vibrational combination band of benzene near 991 cm^{-1} of $\nu_2(a_{1g})$; it is measured by infrared absorption spectra. We consider the following energy transfer mechanism:

$$C_6H_6(v_2') + CCl_4(v_2, v_3) \rightarrow C_6H_6(v_2) + CCl_4(v_2', v_3') + E\ (9\ cm^{-1})$$

But the linewidth broadenings by such collisions are smaller than those by C_6H_6–C_6H_6 collisions in solutions.

We consider the line broadening or narrowing mechanism of $\nu_2(a_{1g})$ of benzene in C_6H_6–CCl_4 mixtures to be that the line narrowing occurs due to the energy transfer by the collision process of C_6H_6–C_6H_6 upon increasing the mole fraction of CCl_4, but after the equimolar point the collisions between C_6H_6 and CCl_4 are predominant and then line broadening occurs due to the energy transfer in C_6H_6–CCl_4 collisions.

Following Griffith *et al.*,[6] we take the value of 1.62 cm^{-1} for the mean intrinsic linewidth of ν_2 in the absence of energy transfer collisions and we can obtain the reorientational relaxation time (τ) of C_6H_6 in solutions. We show the relationship between the τ (or) of C_6H_6 and the mole fraction of CCl_4 in Fig. 5. As is seen in Fig. 5, the τ (or) of C_6H_6 in solutions increased with increasing mole fraction of CCl_4. The reorientational relaxation times are related to the "micro-viscosity" of solution η_m as follows:

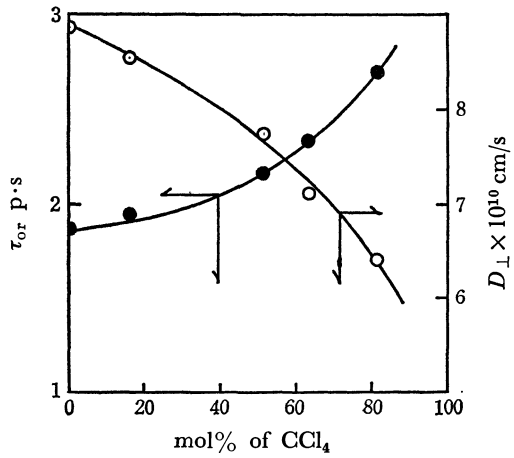

Fig. 5. Dependence of reorietntational correlation times with the mole fraction of carbon tetrachloride.

$$\tau_D = \frac{4\pi a^3}{kT}\eta_m \tag{8}$$

where a is the radius of the molecules in solution. Now assuming the micro-viscosity η_m to be equal to the viscosity η, τ_D/η should be constant. The value of τ_D/η at various mole fractions of CCl_4 is $2.96\pm0.20\times10^{-9}$ and independent of the mole fraction of CCl_4. The radius of the C_6H_6 molecules in solutions is found to be about 4.6 Å. This value is a very reasonable one.

References

1) S. Bratos and E. Marechal, *Phys. Rev.*, **A4**, 1078 (1971).
2) K. T. Gillen and J. E. Griffiths, *Chem. Phys. Lett.* **17**, 359 (1972).
3) J. E. Griffiths, *ibid.*, **21**, 354 (1973).
4) J. E. Griffiths, *J. Chem. Phys.*, **59**, 751 (1973).
5) F. J. Bartoli and T. A Litovitz, *ibid.*, **56**, 404, 413 (1972).
6) J. E. Griffiths, M. Clerc, and P. M. Rentzepis, *ibid.*, **60**, 3824 (1974).

Ion-Solvent Interaction of Tetraalkylammonium Ions in Dimethyl Sulphoxide from Electrolytic Conductivity Data

Jai Shanker JHA, Sudha SINGH, and Ram GOPAL
Chemistry Department, Lucknow University, Lucknow, U.P., India
(Received July 26, 1974)

Ion-solvent interaction of some tetraalkylammonium ions in dimethyl sulphoxide has been studied in this communication from the point of view of electrolytic conductivity and the derived Walden product. The R_4N^+ ions do not appear to interact strongly with this solvent; further, the salts examined appear to be completely dissociated in the concentration range studied here.

During the past few years, considerable interest has been shown to study the properties of the tetraalkylammonium ions (R_4N^+) in water and non-aqueous media.[1] Studies on R_4N^+–solvent interaction, using electrolytic conductivity data, in some solvents of high dielectric constant like *N*-methylformamide, *N*-methylacetamide and *N*-methylpropionamide, have been recently reported from this laboratory.[2,3] Dimethyl sulphoxide (DMSO) is an interesting solvent as it is highly polar[4] which would promote strong ion–solvent dipole interaction; it has no hydrogen bonding which distinguishes it from NMF, NMA and NMP. So it appears a little surprising that only a few studies, specially on electrolytic conductivity,[5–10] have been reported in this solvent. Electrolytic conductivities of some tetraalkylammonium halides and other salts in DMSO have been reported by Arrington and Griswold[11] at 25 °C; these studies appear to be rather sketchy, and a more detailed investigation appears very desirable. As the temperature dependence of electrolytic conductivity and the derived Walden product can be used to throw light on ion–solvent interaction, it is proposed to investigate the same in DMSO in this communication.

Experimental

DMSO (Fluka, purum) was purified by the method described in an earlier communication;[12] the purified sample was found to have conductivity $\approx 10^{-6}\Omega^{-1}\,cm^2$. Tetraalkylammonium salts (DPI, USA) were purified in the usual manner.[2] Solutions were prepared at 30 °C in a thermostat, and the concentration was corrected for the changes in volume at other temperatures from the corresponding densities which were also determined experimentally. The conductance of the solvent was taken into account while calculating the molar conductivities of the electrolytes. The conductance measurements were made with a suitably grounded Wheatstone Bridge and the cell was placed in a thermostat regulated to within ±0.01 °C in the lower temperature range and ±0.02 °C in the higher temperature range. The accuracy of measurements was checked by determining the electrolytic conductivity of some electrolytes of known conductivity.[5,11]

Results and Discussion

The plots of the molar conductivity Λ against the square root of concentration C, at different temperatures, are found to be almost straight lines. Such curves for 40 °C are given in Fig. 1. Extrapolation of the Λ *vs.* $\sqrt{C}$ curves to infinite dilution gives Λ_0-values* which are given in Table 1; from these values, the molar ionic conductivities of the R_4N^+ ions, *i.e.*, Λ_0^+, have been obtained by using the Λ_0^--values of the bromide ion, obtained from the cationic transport number of KBr[13] and its electrolytic conductivities at 25, 30, 40, and 50 °C. These data are recorded in Table 1.

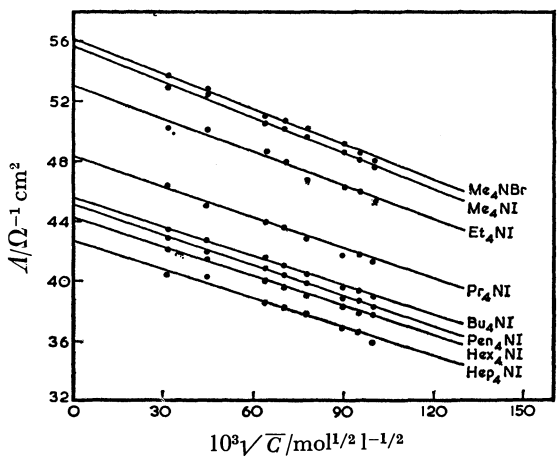

Fig. 1. Λ *vs.* $\sqrt{C}$ curves for R_4NX salt in DMSO at 40 °C.

From the Λ_0-values, the theoretical slope, S_T, of the Λ *vs.* $\sqrt{C}$ curves for different salts at 40 °C, was estimated and compared with the corresponding experimental slope, S, in Table 2. Values of the dielectric constant and viscosity, used for estimating S, are 43.97 and 1.508 $g\cdot m^{-1}\cdot s^{-1}$. respectively and have been obtained graphically from the data of Yao and Bennison.[8]

The fact that the plots of Λ *vs.* $\sqrt{C}$ gave straight lines indicates that, in dilute solution, these salts are completely ionized in DMSO. It may be noted from Table 2 that there is a good agreement between the experimental and theoretical slopes. Hence the Debye-Hückel-Onsager theory of conductivity of electrolytes in solution appears to be very closely applicable. It

* It may be mentioned that Arrington and Griswold[11] analyzed their conductivity data with the help of Fuoss-Onsager relation for unassociated electrolytes, namely,

$$\Lambda = \Lambda_0 - S\sqrt{C} + EC\log C + (J - F\Lambda_0)C$$

This analysis appears unnecessary since the electrolytic conductivity data of these workers give a reasonable straight-line Λ *vs.* $\sqrt{C}$ plot as 25 °C in different cases and this plot gives Λ_0-values in reasonable agreement with that obtained from the Fuoss-Onsager relation in most cases.

Table 1. The $\Lambda_0/\Omega^{-1}\,cm^2$ values of R_4NX salts, R_4N^+, Br^- and I^- ions at different temperatures

Salt or ion	Limiting conductivity at					
	30 °C	35 °C	40 °C	45 °C	50 °C	55 °C
Br^-	25.97	—	30.76	—	35.57	—
Me_4NBr	47.07	51.51	56.04	61.06	65.66	71.36
Me_4N^+	21.10	—	25.28	—	30.09	—
Me_4NI	46.82	51.32	55.72	60.23	64.88	69.70
I^-	25.72	—	30.44	—	34.79	—
Et_4NI	44.65	48.80	53.02	57.31	61.62	66.83
Et_4N^+	18.93	—	22.58	—	26.83	—
Pr_4NI	40.96	44.42	48.34	52.56	56.86	61.90
Pr_3N^+	15.24	—	17.90	—	22.02	—
Bu_4NI	38.51	41.85	45.57	49.49	53.51	57.83
Bu_4N^+	12.79	—	15.13	—	18.72	—
Pen_4NI	38.03	41.50	45.15	48.96	52.94	57.12
Pen_4N^+	12.31	—	14.71	—	18.15	—
Hex_4NI	37.05	40.58	44.23	48.06	51.98	56.10
Hex_4N^+	11.93	—	13.79	—	17.19	—
Hep_4NI	36.18	39.36	42.68	46.12	49.90	53.87
Hep_4N^+	10.46	—	12.94	—	15.11	—

Table 2. Onsager slope in DMSO at 40 °C

Salt	$S_T/\Omega^{-1}\,cm^2\cdot mol^{-1/2}\,l^{1/2}$	$S_E/\Omega^{-1}\,cm^2\cdot mol^{-1/2}\,l^{1/2}$	% Deviation $\frac{S_T-S_E}{S_T}\times 100$
Me_4NI	−74.59	−79.7	+6.85
Me_4NBr	−74.75	−77.9	+4.21
Et_4NI	−73.22	−74.2	+1.34
Pr_4NI	−70.84	−68.4	−3.44
Bu_4NI	−69.43	−65.7	−5.37
Pen_4NI	−69.22	−68.1	−1.62
Hex_4NI	−68.75	−65.8	−4.99
Hep_4NI	−67.96	−63.3	−6.85

may be mentioned that the studies on apparent molar volume of these salts in DMSO[12] appear to indicate appreciable ionic interaction at higher concentrations, but in dilute solutions, the salts appear to be completely dissociated.

The cationic Walden product, $\Lambda_0\eta^0$, of the R_4N^+ ions at different temperatures were obtained using the Λ_0-values** given in Table 1; viscosities used are: $\eta^0/g\cdot m^{-1}\,s^{-1}=1.908$(25 °C), 1.814(30 °C), 1.508 (40 °C), 1.275(50 °C). The $\Lambda_0\eta^{0+}$ *vs.* t plots are given in Fig. 2 for different R_4N^+ ions. It may be noted that the plots are straight lines with approximately zero slope, *i.e.*, $\Lambda_0\eta^0$ is almost independent of temperature. This shows that these ions neither promote nor break the structure of DMSO for the simple reason that no hydrogen-bonded structure is present originally in the pure solvent nor it can be formed. Electrostatic ion–solvent dipole interaction, if any, is not likely to be affected by a few degrees changes in temperature. It may be mentioned that similar conclusions have been arrived at for $(isoamyl)_3BuN^+$, Na^+, $B(Ph)_4^-$, ClO_4^-, SCN^-, and $CF_3SO_3^-$ ions.[8]

** Values of electrolytic conductivity at 25 °C used are those of Arrington and Griswold.[11]

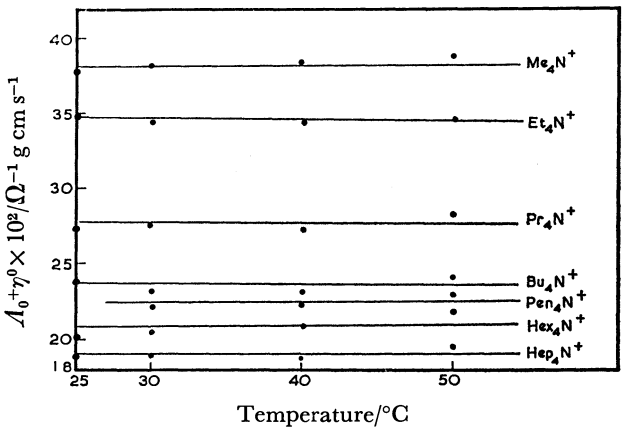

Fig. 2. Plot of $\Lambda_0\eta^0$ *vs.* temperature/°C in DMSO.

One of us (J.S.J.) is grateful to the Governments of Nepal and India for providing a research scholarship under Technical Co-operation Scheme of the Colombo Plan. Authors are thankful to the Society of the Sigma Xi of U.S.A. for the help in importing some of the chemicals from abroad.

References

1) R. L. Kay and D. F. Evans, *J. Phys. Chem.*, **70**, 2325 (1966); R. Gopal and M. A. Siddiqi, *ibid.*, **72**, 1814 (1968); *ibid.*, **73**, 3390 (1969); R. D. Singh P. P. Rastogi and R. Gopal, *Can. J. Chem.*, **46**, 3525 (1968). More references would be found in these articles.

2) R. D. Singh, P. P. Rastogi, and R. Gopal, *Can. J. Chem.*, **46**, 3525 (1968).

3) R. D. Singh and R. Gopal, This Bulletin, **45**, 2088 (1972).

4) "Dimethyl Sulphoxide, Technical Bulletin," Crown

Zellerbach Corporation, Chemical Products Division, Camas, Washington (1966), p. 14.
5) P. G. Sears, G. Lester, and L. R. Dawson, *J. Phys. Chem.*, **60**, 1433 (1956).
6) M. Schalfer and W. Schaffernicht, *Angew. Chem.*, **72**, 618 (1960).
7) A. D. Archer and R. P. H. Gasser, *Trans. Faraday Soc.*, **62**, 3451 (1966); J. S. Dunnett and R. P. H. Gasser, *ibid.*, **61**, 922 (1965).
8) Neng Ping Yao and D. N. Bennison, *J. Electrochem. Soc.*, **118**, 1097 (1971).
9) L. Strauss and G. Marx, *Z. Naturforsch.*, *A*, **28**, 543 (1973).
10) B. Bianchin and J. J. Delpuech, *Bull. Soc. Chim. Fr.*, **1**, 34 (1973).
11) D E. Arrington and E. Griswold, *J. Phys. Chem.*, **74**, 123 (1970).
12) R. Gopal, R. Kumar, and D. K. Agarwal, This Bulletin, **46**, 1973 (1973).
13) R. Gopal and J. S. Jha, *J. Phys. Chem.*, **78**, 2405 (1974).

Dielectric Relaxation Studies of Trihalogenated Esters in Different Solvents at Microwave Frequency

H. D. PUROHIT, H. S. SHARMA and A. D. VYAS

Microwave Laboratory, Department of Physics, University of Jodhpur, Jodhpur, India

(Received Jannary 21, 1975)

The dielectric permittivity ε' and dielectric loss ε'' have been measured at 9.83 GHz for the solutions of four trihalogenated esters in six non-polar solvents having wide range of viscosities at 35 °C. The static permittivity ε_0 at 1 MHz and high frequency limiting permittivity $\varepsilon_\infty = n_D^2$ have also been measured at 35 °C. The normalized plots of log τ *vs.* log η for these esters are linear for non-interacting solvents only. The anomalous behaviour of these solutes in other solvents has been explained in terms of solute-solvent interactions. The distribution parameter α, the free energies of activation ΔF_τ, ΔF_η and the dipole moment μ of these esters have also been reported.

The relaxation time of a polar molecule in a non-polar solvent can be determined from the measurement of dielectric permittivity and dielectric loss. The relaxation time at a constant temperature depends upon mass and structure of the solute molecule, the intermolecular forces, viscosity of the medium and the interaction between the molecules of the solute and the solvent. As to how this relaxation time depends upon the viscosity of the medium has been a matter of considerable interest. Debye[1] considered the molecule as a sphere embedded in a continuous viscous fluid. The familiar Debye-Stoke's equation may be expressed as

$$\tau = \frac{4\pi\eta a^3}{KT}$$

in which η is the viscosity of the liquid and 'a' is the radius of the polar spherical molecule. The value of the molecular radius evaluated from the measured values of relaxation time and viscosity was considerably lower than those calculated from other sources (*viz.* van der Waals radius, molecular weight and density) for most of the cases. To overcome this discrepancy a number of modifications[2,3] in Debye equation and empirical[4,5] relations have been suggested. On the basis of present theories[6–8] it is expected that the relation between log τ and log η should be linear. This has been verified by many workers[9–11] using single solvent whose viscosity was changed by varying the temperature. The dependence of relaxation time of a polar solute in different solvents having different viscosities was studied by some workers[12,13] in a small range of viscosities. They found that the relation between log τ and log η no longer remains linear.

In present investigations dielectric relaxation time studies of four trihalogenated esters have been carried out in different solvents having wide range of viscosities with a view to study the dependence of relaxation time on the viscosity of the solvents. The esters have been selected as they are unassociated liquids and relax predominantly by overall rotation. The discrepancies have been explained in terms of solute–solvent interaction. The investigations also include determination of distribution parameter α, the free energies of activation ΔF_τ, ΔF_η and the dipole moment μ of these esters in different solvents.

Method of Measurement and Analysis of Data. The dielectric permittivity ε' and dielectric loss ε'' of solutions at microwave frequency 9.83 GHz were determined by the measurement of wavelength in dielectric and standing wave ratio using a short circuited movable plunger by the method suggested by Heston *et al*[14] adapted for short circuited termination. The following expressions were used for calculation of ε' and ε''

$$\varepsilon' = \left(\frac{\lambda_0}{\lambda_c}\right)^2 + \left(\frac{\lambda_0}{\lambda_d}\right)^2$$

$$\varepsilon'' = \frac{2}{\pi}\left(\frac{\lambda_g}{\lambda_d}\right)\left(\frac{\lambda_0}{\lambda_d}\right)^2 \frac{d\rho}{dn}$$

where ρ stands for inverse standing wave ratio.

The heterodyne beat method was used for determining the static permittivity ε_0 and ε_∞ was taken as square of the refractive index which was measured by an Abbe's refractometer. The density of the solution was found out by a pycnometer. The viscosity of the solvent was determined by an Ostwald viscometer. All the measurements were made at 35 °C and the temperature was controlled within ±0.5 °C by a thermostat.

The solutes methyl trifluoroacetate (Purum), ethyl trifluoroacetate (Puriss) and ethyl trichloroacetate (Purum) were obtained from Mr. Fluka A.G., Switzerland. These substances were used without any further purification. Methyl trichloroacetate and *n*-propyl trichloroacetate were synthesized by the usual method of esterification using trichloroacetic acid and excess of methyl and *n*-propyl alcohol respectively. The boiling points, densities and refractive indices of the synthesized compounds were found to be in good agreement with the literature values.

Benzene AnalaR grade (B.D.H., India), carbon tetrachloride guaranteed reagent (E. Merck), *n*-heptane pure grade and cyclohexane AnalaR grade (Riedel, Hungary) were used after double distillation. *p*-Dioxane AnalaR grade (B.D.H., India) and decalin pure grade (Riedel, Germany) were used as such.

The dielectric relaxation time τ and the distribution parameter α were calculated by using Higasi's single frequency measurement method.[15] The expressions for τ and α are as under

$$\tau = \frac{1}{\omega}\left(\frac{A^2+B^2}{C^2}\right)^{1/2(1-\alpha)}$$

$$1-\alpha = \frac{2}{\pi}\tan^{-1}\frac{A}{B}$$

where

$$A = a''(a_0 - a_\infty)$$

$$B = (a_0 - a')(a' - a_\infty) - a''^2$$
$$C = (a' - a_\infty)^2 + a''^2$$

a_0, a', a'' and a_∞ are the slopes defined by the relations

$$\varepsilon_0 = \varepsilon_{10} + a_0 W_2$$
$$\varepsilon' = \varepsilon_1' + a' W_2$$
$$\varepsilon'' = a'' W_2$$
$$\varepsilon_\infty = \varepsilon_{1\infty} + a_\infty W_2$$

The polarization at infinite dilution $(P_2)_\infty$ was calculated with the help of Halverstadt and Kumler equation[16] as given below

$$(P_2)_\infty = \frac{3M_2 a_0 V_1}{(\varepsilon_1+2)^2} + M_2(\beta + V_1)\frac{\varepsilon_1 - 1}{\varepsilon_1 + 2}$$

where M_2 is the molecular weight of the solute and β is defined by $V_0 = V_1 + \beta W_2$. Where W_2 represents the weight fraction of the solute, ε_1 and V_1 are the static permittivity and specific volume of solvent and ε_0 and V_0 are the static permittivity and specific volume of the solution. With this value of $(P_2)_\infty$ and accepted bond refractivities the dipole moment was evaluated.

The free energies of activation for dielectric relaxation ΔF_τ and for viscous flow ΔF_η have been calculated using Eyring's equation.[17]

Results and Discussion

The values of d, ε_0, ε', ε'' and ε_∞ for five solutions of different concentrations of methyl trifluoroacetate, methyl trichloroacetate, ethyl trifluoroacetate and ethyl trichloroacetate in different solvents and *n*-propyl trichloroacetate in cyclohexane have been measured. The values of slopes a_0, a', a'' and a_∞ and β are recorded in Table 1. The values of τ, α and μ are given in Table 2(a) and 2(b).

It is evident from Table 2(a) that the relaxation time in each solvent increases with the increase in molecular size. This shows that relaxation time of the solute molecule is sensitive to molecular size. The large value of relaxation time for each of these molecules indicates that they relax predominantly by overall rotation.

Figure 1 gives the normalized plots of log τ *versus* log η for the above mentioned esters. The plots are linear for the solvents *n*-heptane, cyclohexane and decalin. In these solvents the relaxation time increases as the viscosity of the sovlent increases and the increase is in agremment with the relation $\tau = A\eta^x$ proposed

Table 1. Values of the slopes a_0, a', a'', a_∞ and β

Solvent	a_0	a'	a''	a_∞	β
	Methyl trifluoroacetate				
n-Heptane	3.10	2.66	0.80	−0.10	−0.60
Benzene	5.16	3.53	1.68	−0.34	−0.33
Cyclohexane	3.60	2.53	1.17	−0.20	−0.89
Carbon tetrachloride	9.20	6.66	3.00	−0.60	+0.22
p-Dioxane	6.83	4.75	2.80	−0.25	−0.19
Decalin	4.13	2.36	1.30	−0.14	−0.28
	Ethyl trifluoroacetate				
n-Heptane	3.80	3.30	1.20	−0.15	−0.55
Benzene	6.02	3.46	2.46	−0.46	−0.28
Cyclohexane	4.30	2.50	1.75	−0.26	−0.39
Carbon tetrachloride	10.13	4.88	4.50	−0.78	+0.24
p-Dioxane	8.00	4.16	3.00	−0.12	−0.17
Decalin	5.10	2.31	1.85	−0.17	−0.28
	Methyl trichloroacetate				
n-Heptane	2.24	2.00	0.64	+0.06	−0.80
Benzene	3.60	2.75	1.38	−0.06	−0.45
Cyclohexane	2.55	2.12	0.80	0.00	+0.61
Carbon tetrachloride	5.44	4.22	1.88	0.00	+0.45
p-Dioxane	4.50	3.00	1.50	+0.07	−0.28
Decalin	3.00	1.85	0.88	−0.05	−0.50
	Ethyl trichloroacetate				
n-Heptane	2.50	2.00	0.87	+0.08	−0.78
Benzene	3.88	2.11	1.70	−0.10	−0.42
Cyclohexane	2.93	1.89	1.02	0.00	−0.53
Carbon tetrachloride	6.53	3.53	2.20	0.00	+0.11
p-Dioxane	4.58	1.94	1.50	+0.06	−0.14
Decalin	3.45	1.33	1.13	−0.05	−0.38
	n-Propyl trichloroacetate				
Cyclohexane	3.00	1.80	0.90	0.03	−0.44

Table 2(a). The values of relaxation time and distribution parameter for trihalogenated esters in non-polar solvents

Solvent	Methyl trifluoroacetate		Methyl trichloroacetate		Ethyl trifluoroacetate		Ethyl trichloroacetate		*n*-Propyl trichloroacetate	
	τ(ps)	α	τ(ps)	α	τ(ps)	a	τ(ps)	α	τ(ps)	α
n-Heptane η=0.374 cp	4.3	0.14	4.7	0.04	6.5	0.04	6.8	0.07	—	—
Benzene η=0.520 cp	7.5	0.23	7.8	0.07	11.8	0.16	14.2	0.10	—	—
Cyclohexane η=0.750 cp	5.8	0.21	6.0	0.09	11.3	0.11	12.7	0.18	19.3	0.28
Carbon tetrachloride η=0.797 cp	6.9	0.20	7.3	0.11	14.2	0.10	16.6	0.22	—	—
p-Dioxane η=0.987 cp	9.3	0.09	9.4	0.20	15.2	0.19	21.9	0.24	—	—
Decalin η=1.831 cp	10.8	0.31	10.3	0.32	18.1	0.22	25.9	0.29	—	—

TABLE 2(b). THE VALUES OF DIPOLE MOMENT (in Debye) FOR TRIHALOGENATED ESTERS IN NON-POLAR SOLVENTS

Solvent	Methyl trifluoroacetate	Ethyl trifluoroacetate	Methyl trichloroacetate	Ethyl trichloroacetate	*n*-Propyl trichloroacetate
n-Heptane	2.48	2.88	2.33	2.60	—
Benzene	2.66	2.95	2.49	2.70	—
Cyclohexane	2.43	2.82	2.29	2.61	2.76
Carbon tetrachloride	2.64	2.90	2.28	2.63	—
p-Dioxane	2.79	3.19	2.58	2.78	—
Decalin	2.40	2.87	2.27	2.62	—

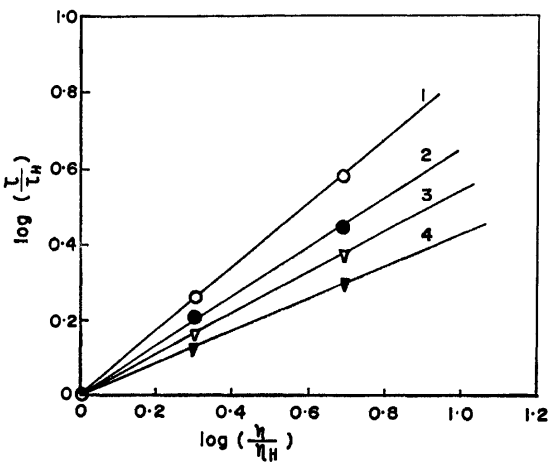

Fig. 1. The normalized plots of $\log \tau$ *vs.* $\log \eta$ for trihalogenated esters.
1: Ethyl trichloroacetate, 2: Ethyl trifluoroacetate, 3: Methyl trifluoroacetate, 4: Methyl trichloroacetate.

by Higasi.[6] Here x is a parameter less than unity. For spherical molecules x is very small and for non-spherical molecules x is nearly unity. The values of x obtained for these molecules lie between 0.50 and 0.85 hence these molecules are not spherical. Thus it may be concluded that the Higasi equation explains the dielectric behaviour of polar solutes in non-polar solvents of different viscosities provided the solvent molecules are inert to solute molecules.

The relaxation time for all these esters in benzene, *p*-dioxane and carbon tetrachloride shows an anomalous behaviour. The viscosity of benzene is less than that of cyclohexane whereas the relaxation time in benzene is more than that in cyclohexane. Similarly, although carbon tetrachloride and cyclohexane have nearly equal viscosity but the relaxation time in carbon tetrachloride is more than that in cyclohexane. The relaxation time in *p*-dioxane is quite large. Since the molecules have been studied in quasi-isolated state and as such the dipole-dipole interactions are negligible, this anomalous behaviour can be explained in terms of solute-solvent interactions. It is a well known fact that the ester molecule is a resonance hybrid in which carbonyl carbon assumes positive character. This positive character is further accentuated by the three electron attracting halogen atoms attached to the α carbon. This positive carbonyl carbon is liable to interact strongly with the oxygen lone-pair electrons in *p*-dioxane and π electrons of benzene ring forming complexes with these solvents resulting in large values of relaxation time. Though carbon tetrachloride is a symmetrical and non-polar molecule

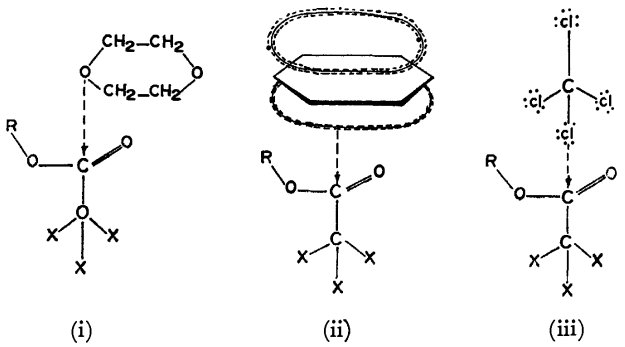

yet each chlorine atom in carbon tetrachloride has three lone pairs of electrons and it can function as electron donor. Hence there is a possibility of interaction between the positive carbonyl carbon of the ester with the solvent carbon tetrachloride. Apart from the solute-solvent interactions the sticky nature of carbon tetrachloride may also play a considerable role in increasing the relaxation time of the ester molecule.

The value of dipole moment of each solute in different non-interacting solvents Table 2(b) is almost the same. The small difference may possibly be due to the solvent effect. The dipole moment of ethyl trifluoroacetate and ethyl trichloroacetate is higher than that for methyl trifluoroacetate and methyl trichloroacetate in each solvent. This is a general trend expected for members of a homologous series,[18] the effect being more pronounced for the second member of the series. This increase in moment may be attributed to the induction effects but no quantitative explanation has been advanced so far.[19] The dipole moment values for all these esters in cyclohexane, benzene and *p*-dioxane enable us to study the solute–solvent interactions in greater details. The difference $(\mu_D - \mu_C)$ and $(\mu_B - \mu_C)$, where μ_D, μ_B and μ_C refer to dipole moment of these esters in *p*-dioxane, benzene and cyclohexane respectively, are listed in Table 3.

TABLE 3. $(\mu_D - \mu_C)$ AND $(\mu_B - \mu_C)$

Solute	$\mu_D - \mu_C$ (Debye)	$\mu_B - \mu_C$ (Debye)
Methyl trifluoroacetate	0.36	0.23
Ethyl trifluoroacetate	0.33	0.13
Methyl trichloroacetate	0.30	0.21
Ethyl trichloroacetate	0.17	0.09

Table 4. The values of free energies of activation ΔF_τ and ΔF_η for trihalogenated esters

Solvents	ΔF_τ kcal/mol				ΔF_η kcal/mol
	Methyl trifluoroacetate	Ethyl trifluoroacetate	Methyl trichloroacetate	Ethyl trichloroacetate	
n-Heptane	2.03	2.27	2.13	2.30	3.01
Benzene	2.36	2.63	2.38	2.75	3.19
Cyclohexane	2.21	2.61	2.22	2.68	3.25
Carbon tetrachloride	2.31	2.75	2.34	2.84	3.22
p-Dioxane	2.49	2.79	2.49	2.96	3.27
Decalin	2.58	2.89	2.55	3.11	4.01

The difference is appreciable for all these molecules which indicates strong solute–solvent interactions. The $(\mu_D-\mu_C)$ values are higher than $(\mu_B-\mu_C)$ values which shows that the interactions of these esters with *p*-dioxane are stronger than those with benzene. It is interesting to note that difference values for fluoro compounds is more than that for corresponding chloro compounds. This is probably due to more electron attracting character of fluorine atom than chlorine atom which makes the carbonyl carbon more positive in fluoro compunds in comparison to that in chloro compounds.

The finite value of distribution parameter α calculated for these esters suggests that in these esters there are two possible relaxation mechanisms of Debye type *i.e.* overall rotation and intramolecular rotations. It is not possible to resolve the two relaxation times from single frequency measurements. If measurements are made at a number of microwave frequencies and a graph is plotted between a' and $a''\omega$ two distinct straight lines are obtained from which τ_1 and τ_2 can be evaluated. The systematic increase of α with increase of viscosity may be interpreted in terms of the disparity in two relaxation mechanisms involved in the relaxation processes. Almost regular rise of α implies that molecular relaxation time increases with viscosity where as the intramolecular does not seem to increase very much with the viscosity of the medium. It is evident from Table 2(a) that the distribution parameter increases with increase in chain-length *i.e.* from methyl to *n*-propyl trichloro esters. This increase in distribution parameter with chain length can be attributed to the number of shapes which the molecule can acquire by twisting around C-C bonds.[19] However, in case of trifluoroacetates it is observed that the distribution parameter decreases with chain-length. It is probable that addition of each CH_2 group in trifluoro esters tends to make the molecule more and more symmetric about O=C-O and thereby decreasing distribution parameter as has been suggested by Rajyam and Murty.[20] This fact needs further verification. It is expected that *n*-propyl trifluoroacetate might have a much smaller value of α, but could not be verified in this laboratory due to non-availability of this compound.

The free energies of activation ΔF_τ and ΔF_η for dielectric relaxation and for viscous flow respectively are listed in Table 4. It is evident from the table that the free energy of activation for dielectric relaxation increases with increase in molecular size. The free energy of activation for viscous flow is greater than that for the dielectric relaxation process. This is in agreement with the fact that the process of viscous flow involves greater interference by neighbours than in the case of relaxation process, because the former takes place by both rotation as well as translation where as the latter involves rotation only.[21,22]

The authors are grateful to Professor Krishnaji, University of Allahabad, Allahabad and Dr. N. K. Mathur, Department of Chemistry of this University for many helpful discussions. They are also thankful to Professor A. N. Nigam for providing facilities for research. One of the authors (A.D.V.) is also thankful to U.G.C. for providing financial assistance.

References

1) P. Debye," Polar Molecules," Chemical Catalogue, New York (1929), Chapter 5.
2) F. Perrin, *J. Phys. Radium*, **5**, 497 (1934).
3) N. E. Hill, *Proc. Phys. Soc.*, **B 67**, 149 (1954).
4) E. Fischer, *Phys. Z.*, **40**, 645 (1939).
5) A. Aihara and M. Davies, *J. Colloid Sci.*, **11**, 671 (1956).
6) K. Chitoku and K. Higasi, This Bulletin, **36**, 1064 (1963).
7) Krishnaji and A. Man Singh, *Ind. J. Pure Appl. Phys.*, **2**, 176 (1964).
8) O. F. Kalman and C. P. Smyth, *J. Amer. Chem. Soc.*, **82**, 783 (1960).
9) B. Sinha, S. B. Roy, and G. S. Kastha, *Ind. J. Phys.*, **40**, 101 (1966).
10) J. Bhattacharya, B. Sinha, S. B. Roy, and G. S. Kastha, *ibid.*, **38**, 413 (1964).
11) D. H. Whiffen and H. W. Thompson, *Trans. Faraday Soc.*, **42A**, 122 (1946).
12) S. Chandra and D. Nath, This Bulletin, **43**, 1614 (1970).
13) G. P. Shrivastva, P. C. Mathur, and M. Krishna, *Can. J. Phys.*, **50**, 1449 (1972).
14) W. M. Heston, Jr., A. D. Franklin, E. J. Hennely, and C. P. Smyth, *J. Amer. Chem. Soc.*, **72**, 3443 (1950).
15) K. Higasi, This Bulletin, **39**, 2157 (1966).
16) I. F. Halverstadt and W. D. Kumler, *J. Amer. Chem. Soc.*, **64**, 2988 (1942).
17) S. Glasstone, K. J. Laidler, and H. Eyring, "The Theory of Rate Processes", McGraw-Hill, New York (1941), Chap. 9.
18) E. Bock, D. Iwacha, H. Hutton, and A. Queen, *Can. J. Chem.*, **46**, 1645 (1968).
19) C. P. Smyth, "Dielectric Behaviour and Structure," McGraw Hill Book Co., New York (1955), Chap. 4.
20) B. S. Rajyam and C. R. K. Murty, *Ind. J. Pure Appl. Phys.*, **12**, 697 (1974).
21) A. J. Petro and C. P. Smyth, *J. Amer. Chem. Soc.*, **79**, 6142 (1957).
22) Krishnaji and A. Man Singh, *J. Chem. Phys.*, **42**, 2503 (1965).

The Thermal Decomposition Reactions of Bivalent Metal Succinates in the Solid State

Hiroko YOKOBAYASHI, Kenzo NAGASE, and Kazuo MURAISHI*

College of General Education, Tohoku University, Kawauchi, Sendai 980

**Department of Chemistry, Faculty of Science, Yamagata University, Koshirokawa, Yamagata 990*

(Received January 25, 1975)

The thermal decomposition reactions of $MC_4H_4O_4$ (M : Mg(II), Co(II), Ni(II), Cu(II), Zn(II), and Pb(II)) in nitrogen or helium were investigated by means of TG-DTA, X-ray diffraction measurements, gas chromatography, and combustion analysis for carbon. The decomposition residues of the Mg and Zn salts were composed of the corresponding metal oxides and some carbon, while those of the Co, Ni, Cu, and Pb salts were composed of the corresponding metals and some carbon. H_2, O_2, CO, CO_2, H_2O, CH_4, C_2H_2, C_2H_4, $HCOOCH_3$, $HCOOC_2H_5$, $CH_3COOC_2H_5$, $C_2H_5COOC_2H_5$, and $(CH_2CO)_2O$ were identified as the gaseous decomposition products; the compositions of the gaseous mixtures varied a great deal with the metals. Possible reaction mechanisms were discussed mainly on the basis of the decomposition products.

The thermal decomposition reactions of metal formates and oxalates have been widely investigated. In the case of metal oxalates, the primary decomposition stages was divided in three types, forming (i) metal oxide and an equimolar mixture of CO and CO_2, (ii) metal and CO_2, and (iii) metal carbonate and CO.[1] The tendency to form either metal or metal oxide is consistent with the prediction on thermodynamic grounds of the Ellingham diagram.[2]

The thermal decomposition reactions of metal salts of carboxylic acids with high proportions of both hydrogen and carbon have also been investigated by many workers, but the reactions are not well established in terms either of decomposition product or mechanism. Limited to metal succinates, only fragmentary information is available in the literature.[3-5]

In the present study, the solid and gaseous decomposition products of the anhydrous succinates of Mg(II), Co(II), Ni(II), Cu(II), Zn(II), and Pb(II) will be determined in detail, and the reaction mechanisms of these salts will be discussed on the basis of the results obtained systematically.

Experimental

Materials. The metal succinates were prepared by dissolving the corresponding metal carbonates in an aqueous solution of succinic acid. The values of the elemental analyses of C and H agreed with the calculated values within $\pm 0.3\%$ for all the salts.

Measurements. The thermogravimetric(TG) and differential thermal analytic(DTA) curves were obtained with a Shinku Riko TGD-3000 apparatus at a heating rate of 10 °C/min. In each measurement, *ca.* 20 mg of powdered sample was placed in a platinum crucible. X-Ray diffraction measurements were carried out with a Toshiba ADG-101 diffractometer in a nitrogen atmosphere. Except for the cobalt samples, Cu$K\alpha$ radiation and a nickel filter were used. Fe$K\alpha$ radiation and a manganese filter were used for the cobalt samples.

The evolved gas curves were obtained by the conductometric technique at a heating rate of 10 °C/min in a helium atmosphere. The procedure was described in a previous paper.[6] Analyses of evolved gas were performed with a Shimadzu GC-1C gas chromatograph and a Shimadzu PYR-1A pyrolyzer. A column (2 meters long) packed with 60—80 mesh active carbon was used for the analysis of nonpolar gases, and a column (2 meters long) with 60—80 mesh Gaskuro Kogyo Chromosorb-101 was used for that of polar gases. The procedure was as follows: the temperature of the pyrolysis chamber was adjusted to the peak temperature on the evolved gas curves. *Circa* 3 mg of a powdered sample in a platinum boat was introduced into the pyrolysis chamber, and it was then maintained at that temperature for 3 min. By changing the two-way valve, helium carrier gas (60 ml/min) was routed through the pyrolysis chamber so that the evolved gases were carried out into the column which was maintained at a constant temperature. The column temperatures were 100 °C for active carbon and 60, 90, and 120 °C for Chromosorb-101. The retention times were as follows: active carbon column (at 100 °C): 0.5 (H_2), 0.9(O_2), 1.1(CO), 2.0(CH_4), 3.7(CO_2), 13.5(C_2H_2), and 19.8(C_2H_4) min. Chromosorb-101 column (at 120 °C):1.2(H_2O), 2.2($HCOOCH_3$), 5.2 ($HCOOC_2H_5$), 11.7 ($CH_3COOC_2H_5$), and 27.5($C_2H_5COOC_2H_5$). The assignments were checked by using columns coated with liquid paraffin or triacetin.

Results

The TG-DTA curves of the salts of Mg, Co, Ni, Cu, Zn, and Pb in a nitrogen atmosphere are given in Figs. 1 and 2. A weight-loss beginning at 25—62 °C for the salts of Mg, Co, Ni, and Cu corresponded to the removal of the water molecules contained in these salts. The anhydrous salts of Mg, Co, and Ni just after the dehydration were amorphous, and the anhydrous salts of Mg and Co recrystallized at 306 and 272 °C respectively, with a sharp exotherm on each DTA curve. The lead salt showed an endotherm at 160 °C on its DTA curve. The endothermic passage corresponded to the phase transition from tetragonal to cubic. The details of the thermal behavior before the decomposition of the anhydrous salts will be reported elsewhere.

The decomposition of the anhydrous salts began at 237—426 °C. The decomposition temperatures (t_i) which were determined by means of the initial weight-loss temperatures, varied a great deal with the metal as may be seen in Table 1. Except for the magnesium salt, the DTA peaks splits into two or more, suggesting that these salts decomposed through multiple steps. The infrared absorption measurements at several magnitudes of the decomposition showed no presence of solid intermediates in the course of the decomposi-

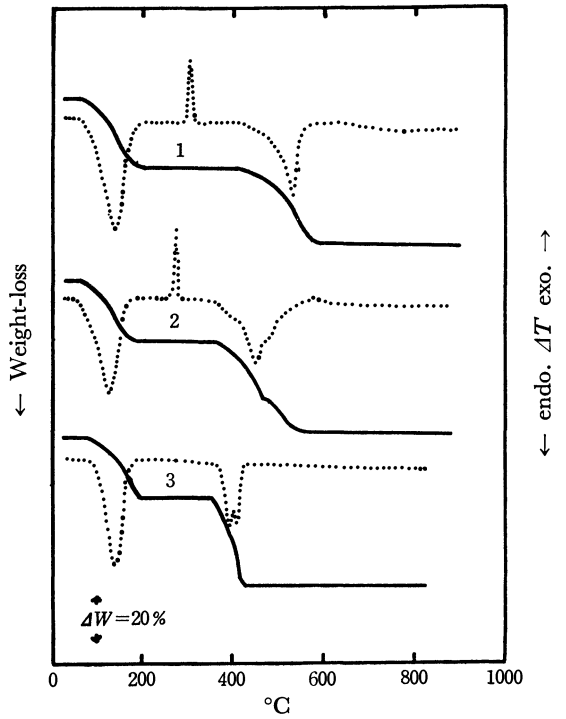

Fig. 1. TG-DTA curves of (1) $MgC_4H_4O_4 \cdot 4H_2O$, (2) $CoC_4H_4O_4 \cdot 4H_2O$, and (3) $NiC_4H_4O_4 \cdot 4H_2O$ in a nitrogen atmosphere: — indicates TG and ···, DTA.

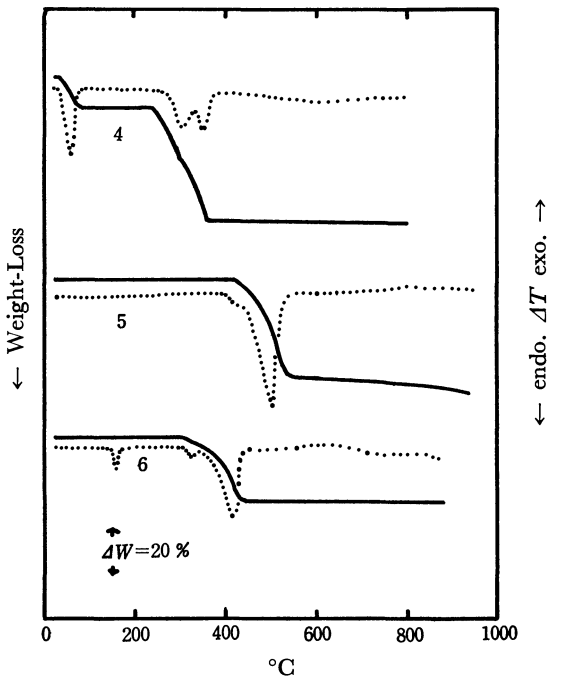

Fig. 2. TG-DTA curves of (4) $CuC_4H_4O_4 \cdot 2H_2O$, (5) $ZnC_4H_4O_4$, and (6) $PbC_4H_4O_4$ in a nitrogen atmosphere: — indicates TG and ···, DTA.

tion processes. Except for the salts of Mg, Zn, and Pb, however, the values of CO/CO_2 in the gaseous mixtures were greatly different between the primary and following steps. In the case of the copper salt, which decomposed in two steps, the CO/CO_2 ratio at the primary step was 2.3, while that at the secondary step was near zero. The salts of CO and Ni showed a similar tendency. On the other hand, the salts of Mg, Zn, and Pb predominantly evolved CO_2 over the decomposition processes.

The X-ray diffraction measurements confirmed that the final decomposition products for the salts of Co, Ni, Cu, and Pb were the metals, while those for the magnesium and zinc salts were the metal oxides. In the case of the zinc salt, however, the vaporization of zinc metal was observed above 600 °C, so no well-difined plateau for zinc oxides was seen on its TG curve, the reduction of zinc oxide probably taking place above that temperature. Although the product of the lead salt was identified as lead metal by the X-ray diffraction, it did not melt even well above the melting point of pure lead (327.3 °C). The lead metal obtained might be finely divided pyropholic lead metal, as indicated in the thermal decomposition of lead citrate[7] and tartarate.[8]

The decomposition residues for all the salts contained some carbon in addition to the metals or the metal oxides. The amount of carbon included was determined by combustion analysis (Table 1). There is possibility of the formation of the metal carbides, as has been reported in connection with the thermal decomposition of nickel malonate in a vacuum.[9] In the present work, however, no X-ray diffraction lines corresponding to the metal carbides were observed. The weight-losses (ΔW_{obsd}) agreed approximately with the values calculated (ΔW_{cald}) for the compositions which were evaluated from X-ray diffraction measurements and combustion analysis for carbon, as may be seen in Table 1.

The gas chromatograms of the salts of Mg, Co, and Cu are given in Figs. 3 and 4 as examples. They correspond to the evolved gases when the anhydrous salts were pyrolyzed at the final peak temperature of

Table 1. Initial decomposition temperatures (t_i), weight-losses (ΔW) and decomposition residues of the succinates, and heats of formation (ΔH_f°) of the metal oxides $M + 1/2O_2 \rightarrow MO$

Salt	t_i/°C	ΔW_{obsd}/%	ΔW_{calcd}[a]/%	Residue	ΔH_f°/kcal
$MgC_4H_4O_4 \cdot 4H_2O$	409	34.9	35.8	MgO+2.0C	−143.8
$CoC_4H_4O_4 \cdot 4H_2O$	356	39.3	40.2	Co+1.4C	−57.2
$NiC_4H_4O_4 \cdot 4H_2O$	351	39.6	39.7	Ni+1.5C	−58.4
$CuC_4H_4O_4 \cdot 2H_2O$	237	50.2	51.6	Cu+0.4C	−37.1
$ZnC_4H_4O_4$	426	42.9	41.9	ZnO+1.2C	−83.2
$PbC_4H_4O_4$	309	27.7	29.7	Pb+1.6C	−52.1[b]

a) The values calculated from the compositions in the the column of "Residue." b) Yellow form.

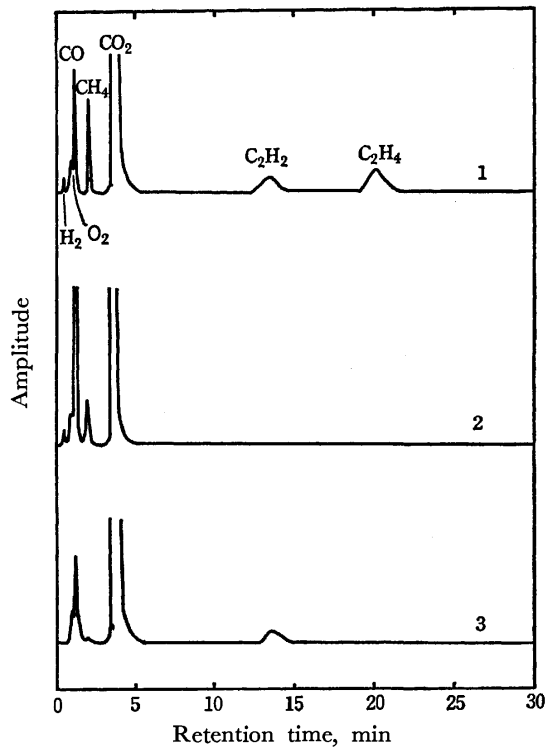

Fig. 3. Gas chromatograms of (1) $MgC_4H_4O_4$, (2) $CoC_4H_4O_4$, and (3) $CuC_4H_4O_4$, using an active carbon column.

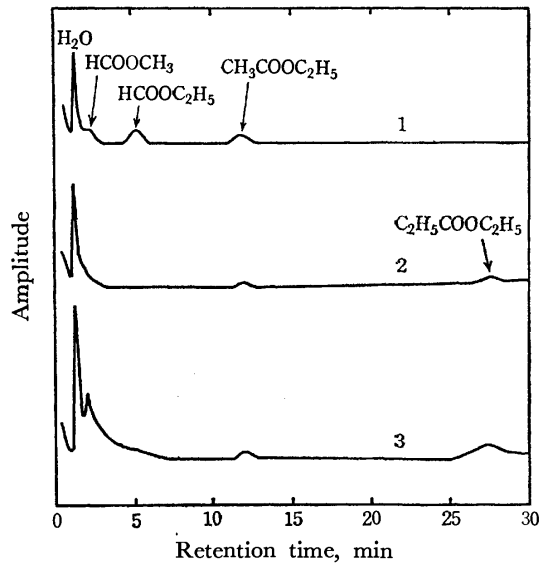

Fig. 4. Gas chromatograms of (1) $MgC_4H_4O_4$, (2) $CoC_4H_4O_4$, and $CuC_4H_4O_4$, using a Chromosorb-101 column.

each evolved gas curve. Although CO_2 predominated in the gaseous products for all the salts, the compositions of the gaseous mixtures varied considerably with the metals. The salts investigated could be divided in three groups. The magnesium and zinc salts, which gave similar chromatographic patterns, evolved hydrogen-rich compounds, such as H_2, CH_4, and C_2H_4, while the copper and lead salts in another group tended to evolve O_2, H_2O, $HCOOCH_3$, and C_2H_2. The latter gases are relatively oxygen-rich or hydrogen-poor compounds. Although H_2O and $HCOOCH_3$ were observed for all the salts, the latter salts were richer in them. The cobalt and nickel salts were intermediate between the two groups in the quantities of CH_4 and H_2O and were characterized as evolving a large amount of CO. All the salts gave succinic anhydride in addition to the gases shown in the gas chromatograms. Its formation was confirmed by infrared measurements.

Discussion

The values of t_i increased with the decrease in the heats of formation of metal oxide (ΔH_f°), as may be seen in Table 1, with the exception of the magnesium salt. The values of t_i for the salts of Co, Ni, Cu, and Pb, which gave the metals as decomposition residues, were correlated by a straight line with ΔH_f° (Fig. 5), suggesting that the decomposition of these salts may be initiated by electron transfer from a succinate anion to a metal cation, as has been indicated for metal oxalates and metal oxalato complexes.[10]

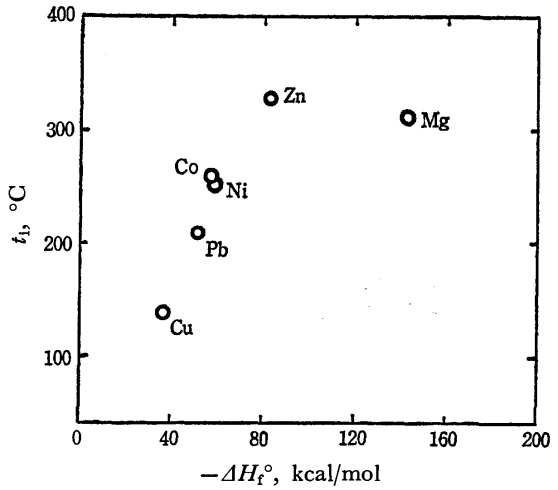

Fig. 5. Correlation of initial decomposition temperatures(t_i) of the anhydrous succinates with heats of formation(ΔH_f°) of the metal oxides.

The amounts of carbon in the decomposition residues are considered to correlate, to some extent, with ΔH_f°, since such secondary reaction as

$$MO + C \longrightarrow M + CO$$

or

$$MO + 1/2C \longrightarrow M + 1/2CO_2$$

are possible at the decomposition temperatures. In fact, the amount of carbon decreased with the increase in ΔH_f°, with a few exceptions (Table 1).

The amounts of H_2 and O_2 are also considered to correlate with ΔH_f° as a result of possible secondary reactions, such as

$$M + 1/2O_2 \longrightarrow MO$$

$$MO + H_2 \longrightarrow M + H_2O$$

In the case of the salt of Cu, which is thermodynamically most stable in the metallic state, the evolution of

H_2 was not observed. It is difficult to discuss the reaction schemes in detail, since the overall reactions might be composed of a number of elementary reactions whose contributions might vary with the reaction temperature, the decomposition pressure, and the extent of decomposition.

References

1) Y. A. Ugai, *Zhur. Obschei Khim.*, **24**, 1315 (1954).
2) H. J. T. Ellingham, *J. Soc. Chem. Ind.*, **63**, 125 (1944).
3) Le V. My, G. Perinet, and R. Lafont, *C. R. Acad. Sci., Paris, Ser. C*, **268**, 406 (1969).
4) B. Y. Andreev and B. P. Vesnovskii, *Kinet. Ketal*, **12**, 498 (1971).
5) V. P. Sevost'yanov and L. M. Dvornikova, *Zh. Neorg. Khim.*, **16**, 1812, (1971).
6) K. Nagase, This Bulletin, **46**, 144 (1973).
7) J. Charless, P. W. Kopf, and S. Toby, *J. Phys. Chem.*, **70**, 1478 (1966).
8) P. E. Yankwich and J. L. Copeland, *J. Amer. Chem. Soc.*, **79**, 2081 (1957).
9) K. A Jones, R. J. Acheson, B. R. Wheeler, and A. K. Galway, *J. Chem. Soc.*, **1968**, 1887.
10) K. Nagase, This Bulletin, **45**, 2166 (1972).

The Extraction Spectrophotometric Determination of Iron(III) with Eriochrome Cyanine R and Tridodecylethylammonium Bromide

Yoshio SHIJO

Department of Industrial Chemistry, Faculty of Engineering, University of Utsunomiya, Ishii-machi, Utsunomiya 321-31

(Received January 28, 1975)

A sensitive spectrophotometric procedure for the determination of iron(III) has been developed, utilizing the ternary complex system of iron-Eriochrome Cyanin R-Tridodecylethylammonium. The iron-Eriochrome Cyanin R chelate anion was extracted with tridodecylethylammonium bromide in xylene. The extracted species had an absorption maximum at 613 nm in the organic layer. The optimum pH range for the extraction was 5.8—6.5. Beer's law held for 0.2—2 μg of iron(III) in 5 ml of the organic layer. The molar absorptivity of the extracted species was 1.73×10^5 $cm^{-1}\cdot mol^{-1}\cdot l$ at 613 nm. The composition of the ternary complex was assumed to be $\{[Fe(HR)_3]^{6-}\}\cdot\{(R'-\overset{R''}{\overset{|}{N}}{}^{+}-R'')_6\}$. Lead, mercury, tin, chromium, beryllium, thorium, uranium, nitrate, iodide, thiocyanate, and perchlorate interfered with the determination of iron(III).

In the process of investigating the extraction of the metal chelate anion with tridodecylethylammonium bromide (abbreviated as TDEA) in the organic layer, we have recently described an extraction spectrophotometric method for scandium[1] and yttrium[2] as metal-Xylenol Orange chelate anions and for copper,[3] tin,[4] and aluminum[5] as metal-Pyrocatechol Violet chelate anions. These studies showed that the extracted ternary complex systems of [Metal-Ligand-TDEA] were very sensitive in their colour reactions. Eriochrome Cyanin R (abbreviated as ECR) forms water-soluble chelate anions with metal ions and has been used as a metallochromic indicator or as a colorimetric reagent for several metal ions. The interaction of metal-ECR chelate anions with quaternary ammonium salts such as cetyltrimethylammonium chloride had been applied to the spectrophotometric determination of aluminum,[6,8] beryllium,[7] iron,[8] and uranium[9]. The extraction of the metal-ECR chelate anions, however, had not been yet reported. In this paper, the fundamental conditions for the extraction spectrophotometric determination of iron (III) as the iron-ECR-TDEA ternary complex and the composition of the ternary complex extracted into xylene will be discussed. Further, the relation between highly sentitive colour reaction of the iron-ECR-CTMA complex in a micelle solution of CTMA and the extracted ternary complex of the iron-ECR-TDEA system will be described somewhat.

Experimental

Reagent. A 2.5×10^{-3} M iron(III) solution was prepared by dissolving a definite amount of ferric ammonium sulfate in 1 M hydrochloric acid. A working standard solution was prepared as needed by the dilution of the 2.5×10^{-3} M solution with deionized water to the desired concentration. Tokyo Kasei Eriochrome Cyanin R was purified following the purification method Chromazurol S.[10] 4 g of ECR were dissolved in 20 ml of deionized water, and the tetrabasic acid was precipitated by adding 20 ml of concentrated hydrochloric acid. The precipitate was filtered in a glass filter crucible, washed with a 1 : 1 hydrochloric acid solution, and dried in a vacuum over solid potassium hydroxide. The acid was reprecipitated from the solution, filtered, washed, and dried as has been described above. Further, the final product was dried to a constant weight over phosphorus pentoxide. Drying loss at 150 °C; 1.8%. Sulfur found by means of the combustion flask method; S, 6.63%, Calculated for $C_{23}H_{18}O_9S$; S, 6.81%. A 5×10^{-4} M ECR solution was prepared by dissolving the purified ECR in 0.001 M HNO_3 and by then adding 0.02% of urea. The TDEA was prepared by the reaction[11] of tridodecylamine with ethylbromide in an alcoholic solution. The salt was recrystallized from petroleum benzine. A 8×10^{-4} M TDEA solution was subsequently prepared by dissolving the above TDEA in xylene.

Apparatus. All the measurements of the absorbance were made with a Hitachi manual spectrophotometer, model Epu-2A. Matched 10-mm, 5-mm, and 2-mm absorption cells were used. The pH measurements were made with a Hitachi-Horiba model M-5 glass electrode pH meter.

Standard Procedure. Place up to 2 μg of iron(III) in a 100-ml separatory funnel and add a definite amount of 0.2 M hydrochloric acid. Add 2 ml of a 5×10^{-4} M ECR solution. Adjust the pH to 6 with a 2 ml portion of a 2 M sodium acetate buffer solution and dilute to 25 ml with deionized water. Add 5 ml of 8×10^{-4} M TDEA in xylene and extract for 2 min with vigorous shaking. After the phase have separated, draw off the aqueous layer and centrifuge the extract for 3 min at 3000 rpm. Transfer the extract into an absorption cell and measure the absorbance at 613 nm against the reagent blank obtained in the same way.

Results and Discussion

Absorption Spectra. The absorption spectra of the ternary complex extracted into xylene, of the iron (III)-ECR-CTMA complex in a micelle solution of CTMA, and of the iron(III)-ECR chelate anion in an aqueous solution are given in Fig. 1, along with that of the reagent blank. The iron(III)-ECR chelate anion had an absorption maximum at 560 nm in an aqueous solution. On the other hand, the absorption maximum of the ternary complex in xylene shifted to a longer wavelength, 613 nm, and the absorbance increased remarkably. The absorption characteristics of the iron(III)-ECR-CTMA complex in a micelle solution of CTMA were similar to those of the ternary complex. These results showed that the

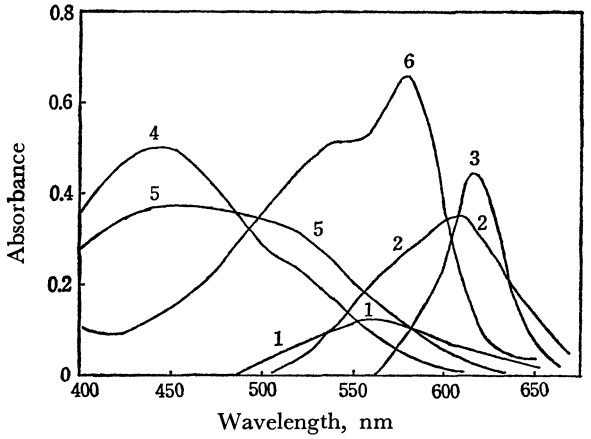

Fig. 1. Absorption spectra of the Fe-ECR-TDEA complex.
pH: 6, Volume of aq. layer $V_w=25$ ml, $[acetate]_w=0.16$ M, Volume of org. layer $V_0=5$ ml, 10 mm cell
(1) Fe-ECR in aq. soln. $[Fe]_w=2.5\times10^{-6}$ M
(2) Fe-ECR-CTMA in micelle soln. of CTMA $[Fe]_w=2.5\times10^{-6}$ M
(3) Fe-ECR-TDEA in xylene $[Fe]_o=2.5\times10^{-6}$ M.
(4) ECR in aq. soln. $[ECR]_w=3\times10^{-5}$ M
(5) ECR in micelle soln. of CTMA $[ECR]_w=3\times10^{-5}$ M
(6) ECR-TDEA in xylene $[ECR]_o=3\times10^{-5}$ M.

shift of the absorption maximum and the increase in the absorbance occurred in common with the action of long-chain quaternary ammonium salts to the iron(III)–ECR chelate anion, not only in a micelle solution of them. It was thought that the organic phases in the micelle and the extracted layer were related to the absorption characteristics of the ternary complex. The absorption maximum of ECR extracted with TDEA in xylene shifted to a longer wavelength.

Effect of pH. The effect of the pH of the aqueous phase on the absorbance was examined. The results are shown in Fig. 2. The maximum absorbance of the ternary complex was obtained at pH values from 5.8 to 6.5. The complex was extrated at considerably higher pH values, *viz.*, about 8, by the addition of glycine to the initial aqueous phase.

Organic Solvents. Several kinds of organic solvents were tested in order to achieve a quantitative extraction of iron (III). The ternary complex could be extracted into benzene, toluene, xylene, carbon tetrachloride, and *n*-buthyl acetate, but not into such polar solvents as *n*-butanol, methyl isobutyl ketone, and nitrobenzene. Xylene was chosen as the solvent.

The Effect of the ECR Concentration. The effect of the ECR concentration in the aqueous phase on the extraction of the ternary complex was examined by varying the ECR concentration, while the other variables were held constant. The absorbance of the extract was constant when the ECR in the initial aqueous phase was in the concentration range from 3.6×10^{-5} M to 4.4×10^{-5} M, as is shown in Fig. 3. The absorbance of the extract decreased suddenly upon the further addition of ECR. It was considered that a large quantity of ECR suppressed the extraction of the ternary complex, consuming the TDEA to form an ion pair with it.

The Effect of the TDEA Concentration. The effect of the concentration of TDEA in xylene on the absorbance of the ternary complex was examined. The absorbance of the extract was constant when the TDEA in xylene was in the concentration range from 7×10^{-4} M to 9×10^{-4} M, as is shown in Fig. 4. The absorbance of the extract gradually decreased upon the further addition of TDEA. However, the extraction of the ternary complex was carried out almost quantitatively in the concentration range of TDEA from 9×10^{-4} M to 1.5×10^{-3} M. The molar absorptivity of the ternary complex decreased when there was a large excess of TDEA in xylene.

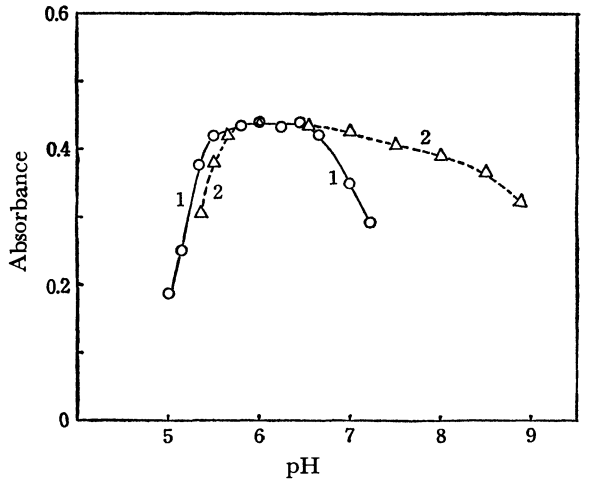

Fig. 2. Effect of pH on the extraction of the Fe-ECR-TDEA complex.
$V_w=25$ ml, $V_0=5$ ml, Fe: 0.7 μg, $[ECR]_w=4\times10^{-5}$ M, $[TDEA]_o=8\times10^{-4}$ M, $[acetate]_w=0.16$ M, 613 nm, 10 mm cell
(1) $[glycine]_w=0$
(2) $[glycine]_w=4\times10^{-2}$ M.

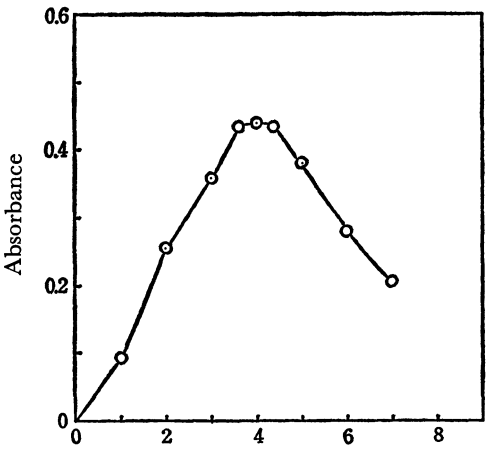

Fig. 3. Effect of the Eriochrome Cyanin R concentration in aqueous phase on the extraction of the Fe-ECR-TDEA complex.
pH: 6, $V_w=25$ ml, $V_0=5$ ml, Fe: 0.7 μg, $[TDEA]_o=8\times10^{-4}$ M, $[acetate]_w=0.16$ M, 613 nm, 10 mm cell.

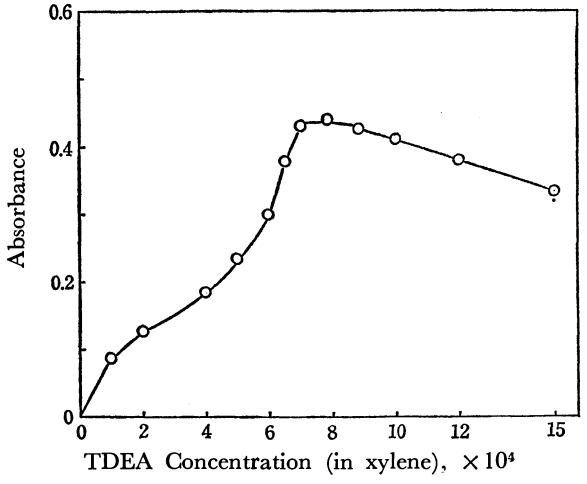

Fig. 4. Effect of tridodecylethylammonium bromide concentration in xylene on the extraction of the Fe-ECR-TDEA complex.
pH: 6, $V_w=25$ ml, $V_0=5$ ml, Fe: 0.7 μg, $[ECR]_w=4\times10^{-5}$ M, $[acetate]_w=0.16$ M, 613 nm, 10 mm cell.

Table 1. Determination of iron(III) in the presence of diverse ions

Ion	Amount added (mg)	Iron(III) found (μg)	Error
None	—	1.4	—
Ni^{2+}	0.1	1.3[a]	−0.1
Co^{2+}	0.1	1.3[a]	−0.1
Cu^{2+}	0.1	1.3[a]	−0.1
Cd^{2+}	0.1	1.4[a]	0
Zn^{2+}	0.1	1.4[a]	0
Pb^{2+}	0.1	1.1[a]	−0.3
Hg^{2+}	0.1	1.1[a]	−0.3
Bi^{3+}	0.1	1.4[a]	0
Mn^{2+}	0.1	1.4[a]	0
Sn(II)	0.1	1.0[b]	−0.4
Cr(III)	0.1	1.3[b]	−0.1
W(VI)	0.1	1.3[b]	−0.1
Mo(VI)	0.1	1.4[a]	0
V(V)	0.1	1.4[b]	0
Al^{3+}	0.1	1.5[b]	+0.1
Be^{2+}	0.1	1.6[b]	+0.2
Th^{4+}	0.1	1.1[b]	−0.3
Zr^{4+}	0.1	1.3[b]	−0.1
Mg^{2+}	0.1	1.4[a]	0
La^{3+}	0.1	1.4[a]	0
U(VI)	0.1	1.2[b]	−0.2
Cl^-	10	1.4[a]	0
NO_3^-	10	1.0[a]	−0.4
SO_4^-	10	1.5[a]	+0.1
I^-	10	−0.6[a]	−2.0
SCN^-	10	−1.0[a]	−2.4
$C_6H_5O_7^-$	10	0.1[a]	−1.3
F^-	10	1.5[a]	+0.1
ClO_4^-	10	−1.0[a]	−2.4
EDTA	10	−0.1[a]	−1.5

a) 1 ml of 1M glycine was added as masking agent. b) 1 ml of 1 M glycine, 1 ml of 30% hydrogen peroxide, and 1 ml of 1 M potassium fluoride were added as masking agents.

The Effect of the Shaking Time. The shaking time was varied from 10s to 10 min. The absorbance of the extract was constant for the shaking times from 30 s to 10 min. A shaking time of 2 min was, therefore, selected.

Extractability and Molar Absorptivity. The extractability of the ternary complex under the optimum conditions was determined by a repetition of the extraction procedure on the same aqueous layer. When a 25-ml portion of an aqueous layer containing 1.4 μg of iron(III) was shaken with 5 ml of xylene, 97% of the iron(III) was extracted by one extraction. The molar absorptivity of the ternary complex calculated by using the percentage extraction and the absorbance was 1.73×10^5 $cm^{-1}\cdot mol^{-1}\cdot l$.

Calibration Curve. A calibration curve for the determination of iron(III) was made under the optimum conditions. A good linear relationship was obtained over the concentration range from 0.2 to 2 μg of iron(III) per 5 ml of xylene.

The Effect of Diverse Ions. The effect of foreign ions on the determination of iron(III) under the addition of 1 ml of 1 M glycine, 1 ml of 30% hydrogen peroxide, and 1 ml of 1 M potassium fluoride as masking agents to the initial aqueous phase at pH 8 was examined. The results are summarized in Table 1. Lead, mercury, tin, beryllium, thorium, and uranium interfered considerably. Of the anions tested, nitrate, iodide, thiocyanate, and perchlorate interfered seriously, giving a negative error. Chelating agents such as EDTA also interfered.

The Composition of the Ternary Complex. The results of the continuous-variation method indicated

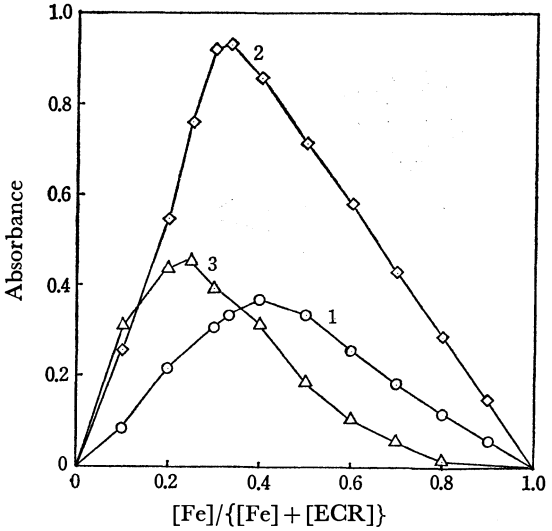

Fig. 5. Continuous variation method applied to the Fe-ECR-TDEA complex, the Fe-ECR-CTMA complex, and the Fe-ECR chelate.
pH: 6, $[acetate]_w=0.16$ M, 5 mm cell
(1) Fe-ECR chelate in aq. soln. $[Fe]_w+[ECR]_w=4\times10^{-6}$ M, 560 nm.
(2) Fe-ECR-CTMA cnmplex in micelle soln. of CTMA $[Fe]_w+[ECR]_w=4\times10^{-6}$ M,645 nm.
(3) Fe-ECR-TDEA complex in xylene $[Fe]_w+[ECR]_w=4\times10^{-6}$ M, $[TDEA]_o=8\times10^{-4}$ M, $[Glycine]_w=4\times10^{-2}$ M, 613 nm.

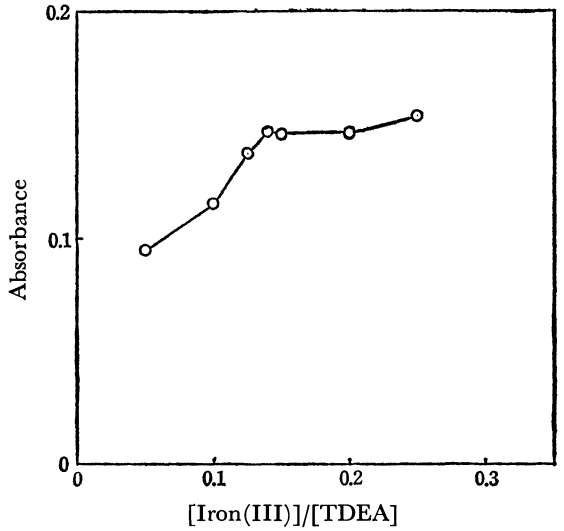

Fig. 6. Mole ratio method applied to the Fe-ECR-TDEA complex.
pH: 6, $[acetate]_w = 0.16$ M, $[ECR]_w = 4 \times 10^{-5}$ M, $[TDEA]_o = 8 \times 10^{-4}$ M, 600 nm, 2 mm cell.

that the molar ratios of iron(III) to ECR in the chelates were 1 : 1.5 in an aqueous solution, 1 : 2 in a micelle solution of CTMA, and 1 : 3 in the extracted species, as is shown in Fig. 5. The molar ratios of iron(III) to ECR increased in the micelle solution of CTMA and in the extracted species. It was thought that the increase in the combination ratio of ECR in the extracted species was due to the higher coordinated complex, it was more stable in the organic layer. The results of the mole-ratio method indicated that the molar ratio of iron(III) to TDEA in the extracted species was about 1 : 7, as is shown in Fig. 6. The bulk of ECR, however, existed as HR^{3-} [12] in the aqueous solution about pH 6, and the molar ratio of iron(III) to ECR in the extracted species was estimated to be 1 : 3. Therefore, the extracted species was assumed to be probably the ternary complex $\{[Fe(HR)_3]^{6-}\}\cdot\{(TDEA^+)_6\}$.

References

1) Y. Shijo, *Nippon Kagaku Kaishi*, **1974**, 889.
2) Y. Shijo, *Bunseki Kagaku*, **23**, 884 (1974).
3) Y. Shijo, This Bulletin, **47**, 1642 (1974).
4) Y. Shijo, *Nippon Kagaku Kaishi*, **1974**, 1658.
5) Y. Shijo, *ibid.*, **1974**, 1912.
6) Y. Shijo and T. Takeuchi, *Bunseki Kagaku*, **17**, 323 (1968).
7) H. Kohara, N. Ishibashi and K. Fukamachi, *ibid*, **17**, 1400 (1968).
8) Y. Shijo and T. Takeuchi, *ibid.*, **20**, 980 (1971).
9) M. Otomo and K. Kodama, *ibid*, **20**, 1581 (1971).
10) F. J. Langmyhr and K. S. Klausen, *Anal. Chim. Acta*, **29**, 149 (1963).
11) A. B. Scott and H. V. Tartar, *J. Amer. Chem. Soc.*, **65**, 692 (1943).
12) V. Suk and V. Miketukova, *Collect. Czech. Chem. Commun.*, **24**, 3629 (1959).

The Gas-chromatographic Determination of Selenium in Copper Metal and Copper Salts with 4-Nitro-*o*-phenylenediamine

Yasuaki SHIMOISHI*

Department of Chemistry, Faculty of Science, Okayama University, Tsushima, Okayama-shi, 700

(Received January 30, 1975)

The gas-chromatographic method using an electron-capture detector has a high sensitivity for the determination of selenium. Moreover, as the reaction of selenium(IV) with 4-nitro-*o*-phenylenediamine is scarcely disturbed by other elements, the chemical separation from the matrix element is not necessary. The direct determination of very small amounts of selenium in copper and copper salts has been investigated. A mixture of equal volumes of nitric acid, hydrochloric acid, and perchloric acid dissolves the copper sample and also oxidizes the selenium to the quadrivalent state quantitatively. No loss of selenium was observed upon this treatment. The proposed method can determine the selenium in copper samples in amounts as low as 0.005 μg/g.

Trace amounts of selenium are commonly present in metals and alloys. The selenium content in metals influences the mechanical strength. In some instances, small amounts of selenium are added in order to improve the property. The accurate determination of trace amounts of selenium in copper has become increasingly important in recent years. Various methods, such as the spectrophotometric method,[1,2] X-ray spectroscopy,[3] and the atomic-absorption method[4] are widely used. However, chemical separation[5-7] is usually necessary before one can analyze trace amounts of selenium.

The present author has recently proposed a far more sensitive method for determining selenium in sulfuric acid,[8] tellurium,[9] sea water,[10] and plant materials[11] by means of a gas chromatograph equipped with an electron-capture detector using 4-nitro-*o*-phenylenediamine. Cheng[1] has reported that copper is masked with EDTA in the determination of selenium using 3,3′-diaminobenzidine. However, the reaction of selenium(IV) with 4-nitro-*o*-phenylenediamine was not disturbed by a large amount of copper and selenium present in copper salts, and copper metal can be determined without any separation or masking. The present paper will describe the determination of very small amounts of selenium in copper metal and copper salts.

Experimental

Reagents. 4-Nitro-*o*-phenylenediamine dihydrochloride solution (1%): The reagent was purified by repeated recrystallizations of commercial 4-nitro-*o*-phenylenediamine from a hydrochloric-acid solution. One gram of the reagent was dissolved in 100 ml of 1 M hydrochloric acid. Selenium(IV) stock solution: A 704-mg portion of selenium dioxide was dissolved in 500 ml of distilled water. The concentration was determined gravimetrically as 0.98 mg/Se/ml. The working solutions were prepared by dilution. Oxidation mixture: Concentrated hydrochloric acid and nitric acid were mixed in equal volumes. This solution was prepared each time before use. The other reagents were of an analytical reagent grade.

Apparatus. A Shimadzu Model GC-3AE Gas Chromatograph equipped with an electron-capture detector was used. A glass column (1 m long, 4 mm bore) was packed with 15% SE-30 on 60—80 mesh Chromosorb W. The column and detector temperature was maintained at 200 °C. The nitrogen flow-rate was 36 ml/min. A Shimadzu Model 250A recorder was used at a chart speed of 5 mm/min.

Standard Procedure. Accurately weighed copper samples which have been cut into about 10-mg segments are placed in a 100 ml conical flask. Five ml of perchloric acid and 10 ml of the oxidation mixture are added, and the mixture is heated on a sand bath (200—230 °C) in a fume hood (this acid mixture is used for 1 g of copper or less). A vigorous oxidation reaction soon takes place, and a copious brown vapor is evolved. After a few minutes, the main reaction comes to an end. The solution is heated further until a white fume of perchloric acid is evolved. Then the conical flask is removed from the sand bath. After the precipitate has been redissolved with 10 ml of distilled water, the content is transferred into a 50-ml volumetric flask. The solution is diluted to the mark with distilled water. An aliquot containing 0.01—0.03 μg of selenium is transferred into a 100-ml separatory funnel containing 25 ml of 1 M hydrochloric acid which has previously been washed with toluene. A 2-ml portion of 1% 4-nitro-*o*-phenylenediamine is then added, and the solution is allowed to stand for 2 hr. Then, the 5-nitropiaselenol formed is extracted into 1 ml of toluene by shaking for 5 min and the toluene extract is washed with 2 ml of a 7.5 M hydrochloric acid solution. A 5-microliter portion of the toluene extract is injected into the gas chromatograph, and the peak height is measured.

The selenium content in copper salts is always less than that in copper metal. Consequently, in the case of copper salts, after the oxidation procedure all the contents are transferred into a 100-ml separatory funnel and washed with 1 ml of toluene. Then, the aqueous phase is transferred into another 100 ml separatory funnel. A 2-ml portion of 4-nitro-*o*-phenylenediamine is added. The following procedure is the same as that described above.

Results and Discussion

Oxidation of Selenium. Most of the selenium contained in copper metal is present in the form of selenium(II), since, on the electrolytic refining of copper, selenium can easily react with copper to form Cu_2Se. Clark[12] reported that, when a piece of thin copper film was dipped in a hydrochloric acid solution of selenite, the copper was coated with a black film of Cu_2Se. Therefore, the selenium in copper and copper salts must be oxidized to the quadrivalent state. Nitric acid is usually used in order to dissolve

* Present address: School for X-Ray Technicians, Faculty of Medicine, Okayama University, Shikatacho, Okayama-shi 700.

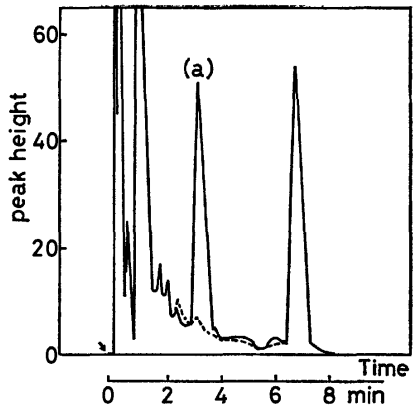

Fig. 1. Gas chromatogram of 5-nitropiaselenol.
—— 0.50 g copper powder (1.59 μg Se/g Cu)
---- blank
(a) 5-nitropiaselenol
Range 0.2 V.

and oxidize both copper and selenium. Gorsuch[13] suggested that there was not 100% recovery when a mixture of nitric acid and sulfuric acid was used for plant samples. The mixtures of nitric- and perchloric acid, hydrochloric- and nitric acid, and hydrochloric-, nitric- and perchloric acid were compared in terms of their efficiency in oxidizing selenium in both copper metal and copper salts. Only the last acid mixture can oxidize quantitatively the selenium in both samples. Thus, the mixture of hydrochloric-, nitric-, and perchloric acid was used for the dissolution of copper samples. The bromine-bromide redox buffer[8] in a sulfuric acid medium can also be used as a convenient oxidation reagent for copper salts. A gas chromatogram obtained with 500 mg of copper treated by the above-mentioned procedure is shown in Fig. 1.

Dissolution with the Mixture of Hydrochloric-, Nitric-, and Perchloric Acid. Usually, volatile compounds, such as $SeO_2 \cdot 2HCl$ and $SeOCl_2$, are formed during a dissolution in the presence of hydrochloric acid. These compounds must be responsible for the loss of selenium. In order to check whether or not there is any loss of selenium, the effects of the concentration of the oxidation mixture, the oxidation time, and the oxidation temperature were studied. As is shown in Fig. 2, the selenium in 0.5 g of copper metal could be oxidized quantitatively with more than 3 ml of the oxidation mixture in the presence of 5 ml of perchloric acid, and a good recovery was observed. If a smaller amount of the oxidation mixture is used, the back ground of the chromatogram becomes so high that the determination is not accurate. Therefore, 10 ml of the oxidation mixture and 5 ml of perchloric acid were used for the following experiments. If more than 1 g of copper metal is used for the determination, the procedure is disturbed by the deposition of the copper salt during the oxidation procedure. However, this trouble can be overcome by dissolving the precipitate with another 5 ml of perchloric acid.

The oxidation temperature was examined in the approximate range from 130 to 270 °C (sand-bath temperature). The maximum constant peak height was obtained in this region. As a longer oxidation time was needed at a lower oxidation temperature, the optimum oxidation temperature was in the approximate range from 200 to 230 °C. When the heating was continued at this temperature until the color of the solution turned pale blue, the selenium in the copper was oxidized to the quadrivalent state completely. Moreover, no selenium at the 0.1 μg level was lost by volatilization when heated for 20 min, after the evolution of white fumes of perchloric acid. Consequently, the heating was continued at about 230 °C until white fumes of perchloric acid were evolved. The whole oxidation procedure requires about 30 min.

Very small amounts of interfering substances in the distilled water used for dilution often disturb the determination, because the sensitivity of the electron-capture detector is extremely high for the unknown impurities as well as for 5-nitropiaselenol. Therefore, these interfering substances should be remove by washing with toluene. When the selenium content in copper metal is too high, the sample solution is diluted with a 1 M hydrochloric acid solution which has previously been washed with pure toluene. For the copper salts, the sample solution is washed directly with 1 ml of toluene after oxidation. Moreover, the reagent solution also contains small amounts of interfering substances; therefore, 1 ml of the toluene extract after the formation of 5-nitropiaselenol should be washed again with 2 ml of 7.5 M hydrochloric acid.

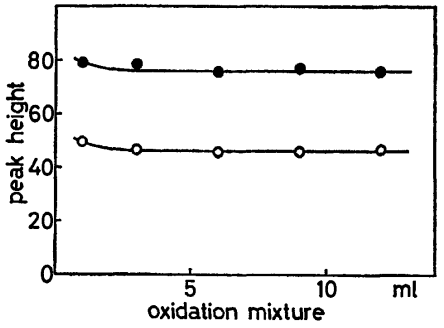

Fig. 2. Effect of volume of oxidation mixture in the presence of 5 ml of perchloric acid.
--○— 0.50 g copper power,
—●— 0.49 μg selenium(IV) + 0.50 g copper powder.

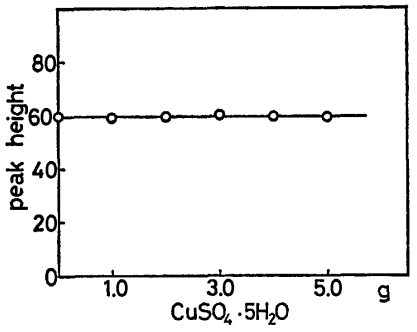

Fig. 3. Effect of copper matrix.
0.0196 μg selenium(IV) + $CuSO_4 \cdot 5H_2O$
No oxidation procedure.

Effect of the Copper Matrix. In order to check the influence of a large amount of copper ions upon the determination of selenium, 0.0196 μg Se(IV) was added to a copper-sulfate solution and determined. As is shown in Fig. 3, the selenium was recovered qunatitatively even in the presence of 5 g of $CuSO_4 \cdot 5H_2O$. Therefore, the masking or separation procedure is not necessary before the determination.

Effects of Foreign Ions. The effects of several foreign ions, such as Fe^{3+}, As^{3+}, and Pb^{2+}, were reported in the previous paper.[9] As is shown in Table 1, even if 10^3 times as many foreign ions are present, no effect is found. In particular, this method is scarcely effected by Mn^{2+} and V^{5+}. It seems that this method can be utilized for the direct determination of selenium in the presence of considerably large amounts of these elements.

Accuracy and Precision. The accuracy of the procedure was evaluated by recovery experiments using copper metal (powder). Recovery was established by dissovling the copper metal to which a known amount of selenium had been added, and by treating the samples as has been described. In all cases, theoretical recovery was obtained within the limits of experimental error (Table 2). The precision was evaluated using a copper metal (powder). The results are shown in Table 3.

Calibration Curve. The calibration curve was made with known amounts of selenous acid in a hydrochloric acid solution. The curve was coincident with that obtained from the same selenous acid by the oxidation procedure. Therefore, the curve obtained without the oxidation procedure is used for the determination. One of the calibration curves obtained at various sensitivities of the gas chromatograph is shown in Fig. 4. More than 0.005 μg of selenium can be determined.

Determination of Selenium in Copper metal and Copper Salts. Selenium can be determined successfully even in 0.1 g of copper metal or copper salts, because the ECD gas chromatograph is very sensitive to 5-nitropiaselenol. However, the values obtained in small-sample portions are dispersed widely; this implies that the distribution of the selenium is heterogeneous in copper metal and copper salts. Therefore, in many cases, 10 g or more is mixed well, and a small portion should be taken from the matrix for the determination. However, if copper powder is used, the value of the selenium content is proportional to the powder weight, because the selenium content in copper powder seems to be homogeneous. When 10 g of copper (99.999%) plate was cut into 10-mg segments, and 1—2 g of it was taken after mixing for the determination, the value obtained was reproducible. The peak height of selenium in the sample thus obtained is proportional to the sample weight, as is

Table 1. Effect of foreign ions

$$\frac{[X]}{[Se]} = 10^3$$

Foreign ion [X]	Added as	Se recovery (μg/g Cu)
None		1.59
Cd^{2+}	$Cd(NO_3)_2 \cdot 4H_2O$	1.62
Mn^{2+}	$Mn(NO_3)_2 \cdot 6H_2O$	1.56
Ni^{2+}	$Ni(NO_3)_2 \cdot 6H_2O$	1.55
Zn^{2+}	$Zn(NO_3)_2 \cdot 6H_2O$	1.67
Mg^{2+}	$Mg(NO_3)_2 \cdot 6H_2O$	1.58
Al^{3+}	$Al(NO_3)_3 \cdot 9H_2O$	1.57
Cr^{3+}	$Cr(NO_3)_3 \cdot 9H_2O$	1.57
Mo^{6+}	$(NH_4)_6Mo_7O_{24} \cdot 4H_2O$	1.58
V^{5+}	NH_4VO_3	1.58

Table 2. Recovery of selenium added to copper powder

Copper (g)	Added selenium (μg)	Selenium found (μg)	Selenium recovered (μg)	Recovery
0.500	None	0.0159		
None	0.0098	0.0100	0.0100	102
0.300	0.0098	0.0195	0.0100	102
0.300	0.0098	0.0192	0.0097	99
0.500	0.0098	0.0250	0.0091	93
0.500	0.0098	0.0255	0.0096	98

Observed value from one-fifth volume of solution oxidized.

Table 3. Reproducibility of selenium determination in copper powder

Copper (g)	Peak height	Selenium determined (μg/g Cu)
0.501	46.9	1.60
0.501	46.5	1.58
0.500	45.1	1.55
0.500	47.6	1.61
0.501	45.2	1.55
0.500	46.0	1.57
0.500	51.2	1.72
0.500	46.7	1.59
0.500	44.8	1·53
0.501	46.7	1.59
Mean		1.59
Std. dev.		±0.052
Coeff. of var.		3.3%

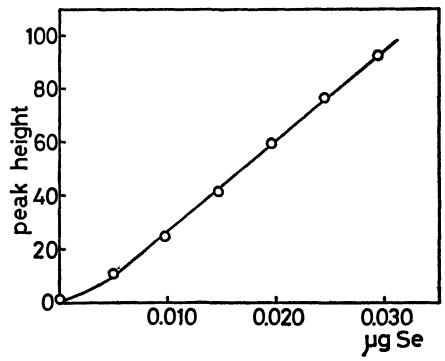

Fig. 4. Calibration curve.
No oxidation procedure.
Range 0.2 V.

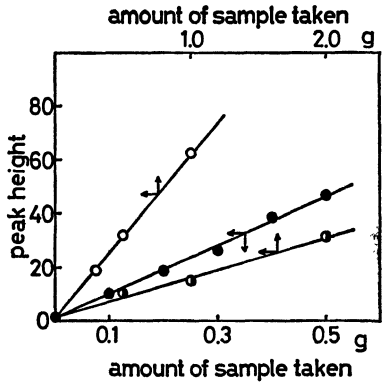

Fig. 5. Effect of amount of sample taken.
—○— $CuSO_4 \cdot 5H_2O$ extra pure (Range 0.4 V)
—●— copper 99% powder (Range 0.2 V)
—◑— copper 99.999% plate (Range 0.2 V).

shown in Fig. 5, and all the lines pass through the same point. The peak height of this point is in fair agreement with the blank value. This indicates that the oxidation is complete and that no loss of selenium occurs during the procedure.

The selenium in 1—2 g of copper metal was determined by the standard procedure; the results are shown in Table 4. The selenium in copper salts can also be determined by the standard procedure, as is shown in Table 5. The selenium in cupric sulfate seems to exist in the form of selenide, because it can not be determined without the oxidation procedure. On the other hand, the selenium in cupric nitrate and chloride may exist in the quadrivalent state, because it can be determined quantitatively without the oxidation procedure (Procedure C in Table 5). To copper metal or copper salts, a known amount (0.0098—0.49 μg) of selenium was added in the quadrivalent state, and the recovery was then examined. The results were satisfactory in all cases, within the limits of experimental error.

Table 4. Selenium content in copper metal

Material	Selenium content[a] $\times 10^{-5}$%
Copper 99% power	15.9±0.5
Copper 99.99% electrolytic (I)	8.1±0.9
Copper 99.99% electrolytic (II)	1.4±0.1
Copper 99.99% electrolytic (III)	1.9±0.2
Copper 99.999% plate	3.3±0.1
Copper sponge glanular for elementary analysis	5.0±0.5
Copper oxide wire for elementary analysis	2.6±0.3

a) The mean value of five mesurements.

The author wishes to thank Professor Kyoji Tôei for his encouragement and helpful discussions throughout the work and Mr. Taiichi Yamamoto (Dowa Mining Co., Ltd.) for supplying the electrolytic copper.

References

1) K. L. Cheng, *Chemist-analyst.*, **45**, 67 (1956).
2) T. Murakami and E. Ishii, *Kogyo Kagaku Zasshi*, **68**, 1865 (1965).
3) C. H. Albright, K. E. Burke, and M. M. Yarak, *Talanta*, **16**, 309 (1969).
4) W. Reichel and B. G. Bleakley, *Anal. Chem.*, **46**, 59 (1974).
5) P. Stantscheff, *Z. Anal. Chem.*, **233**, 404 (1968).
6) C. L. Luke, *Anal. Chem.*, **31**, 572 (1959).
7) E. Jackwerth, *Z. Anal. Chem.*, **235**, 235 (1968).
8) Y. Shimoishi and K. Tôei, *Talanta*, **17**, 165 (1970).
9) Y. Shimoishi, This Bulletin, **44**, 3370 (1971).
10) Y. Shimoishi, *Anal. Chim. Acta*, **64**, 465 (1973).
11) Y. Shimoishi, This Bulletin, **47**, 997 (1974).
12) L. M. Clark, *J. Chem. Soc.*, **130**, 2388 (1928).
13) T. T. Gorsuch, *Analyst*, **84**, 135 (1959).
14) Presented at the 35th Symposium on the Analytical Chemistry, Yonezawa, Japan, June 1974, Abstracts, P. B68.

Table 5. Selenium content in copper salts

Material	Selenium content: Analytical reagent grade, $\times 10^{-6}$%			Selenium content: Extra pure reagent $\times 10^{-6}$%		
	A	B	C	A	B	C
$CuSO_4 \cdot 5H_2O$	0.2	0.2	—	5.4±0.5	5.1±0.6	—
$Cu(NO_3)_2 \cdot 3H_2O$	0.7±0.5	0.6±0.08	0.8	1.7±0.1	—	1.7
				—	2.6±0.1	—
$CuCl_2 \cdot 2H_2O$	5.1±0.5	—	—	5.4±0.3	—	5.0
				—	6.2±0.2	—

The mean value of five measurements. A: Sample is oxidized with the oxidation mixture. B: Sample is oxidized with 0.1 M Br_2-Br^- redox buffer.[14] C: No oxidation procedure.

Isomerism of the Metal Complexes Containing Multidentate Ligands. VI. Geometric and Optical Isomers of the Tris(*meso*-2,3-butanediamine)-cobalt(III) Complex

Masaaki KOJIMA, Hiromi FUNAKI, Yuzo YOSHIKAWA, and Kazuo YAMASAKI
Department of Chemistry, Faculty of Science, Nagoya University, Chikusa-ku, Nagoya 464
(Received February 19, 1975)

The tris(*meso*-2,3-butanediamine)cobalt(III) complex was prepared, and four possible isomers, *mer*-Λ, *mer*-Δ, *facial*-Λ, and *facial*-Δ, were isolated by column chromatography on SP-Sephadex in the formation ratio of 1.4 : 1.4 : 1.0 : 1.0. The configurations and conformations of these isomers were proposed on the basis of the electronic, the circular dichorism, and the PMR spectra.

When unsymmetric bidentate ligands such as *R*-1,2-propanediamine(*R*-pn)[2] and 2-methyl-1,2-propanediamine(ibn)[3] coordinate to the cobalt(III) ion, geometric(*mer* and *facial*) isomers are formed by the positions of the methyl groups in addition to the optical isomers(Δ and Λ); they have been isolated and characterized. When a symmetric ligand with a *meso* structure like *meso*-2,3-butanediamine(mbn) coordinates, geometric isomers(*mer* and *facial*) are formed by the alignment of two asymmetric carbons(*R* and *S*) for each of the absolute configurations, Δ and Λ (Fig. 1). Theoretically eight(lel_3, $3lel_2ob$, $3lelob_2$, ob_3) and four (lel_3, lel_2ob, $lelob_2$, ob_3) energetically unique conformational isomers are expected for the *mer* and *facial* isomers respectively, but a rapid inversion of the chelate rings in solution will make only four isomers detectable: *mer*-Λ, *mer*-Δ, *facial*-Λ, and *facial*-Δ (Fig. 1).

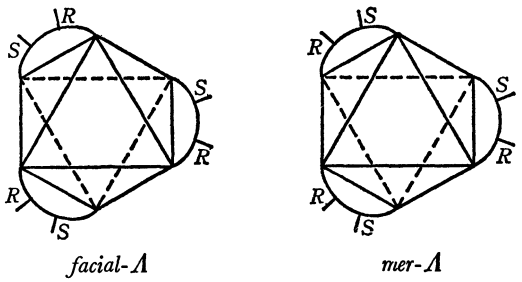

Fig. 1. Geometric isomers of Λ-$[Co(mbn)_3]^{3+}$.

The tris(*meso*-2,3-butanediamine)cobalt(III) complex was first studied by Woldbye,[4] but no geometric isomer was separated and only optical isomers with low optical activities were obtained. In the present paper the isolation of four possible isomers in a pure state and their characterization will be presented.

Experimental

Ligands. A mixture of *meso* and *racemic* 2,3-butanediamine was prepared by the reduction of dimethylglyoxime with Raney nickel in alkaline solution;[5] the isomers were then separated by the procedure of Dickey *et al.*[5]

Preparation of the Complex. *Meso*-2,3-butanediamine hydrochloride(1.3 g, 8.1 mmol) was dissolved in 5 ml of water, and the solution was adjusted to pH 8 by adding a concd. NaOH solution. To this solution, $[CoBr(NH_3)_5]Br_2$ (0.9 g, 2.3 mmol) and active charcoal (0.3 g) were added, after which the mixture was stirred for from one to three days at room temperature. The brown solution thus obtained was directly subjected to column chromatography on SP-Sephadex after the removal of charcoal.

Chromatographic Separation of the Isomers. On the top of the adsorbent layer of an SP-Sephadex column (ϕ 2.7 × 120 cm), the same SP-Sephadex, saturated in advance with a prepared solution containing about 0.4 mmol of the complex, was poured; the complex was subsequently eluted by a 0.18 M sodium $(+)_{589}$ tartratoantimonate(III) solution* at a rate of 0.75 ml per minute. The effluent was separated into fractions of 15 ml each, and the absorbance at 470 nm was plotted against the eluate volume (Fig. 2). Two separated peaks, A and B, were thus obtained, but as each peak seemed to be a mixture of enantiomers, the fractions were again adsorbed on SP-Sephadex after dilution with water, and subsequently eluted with a 0.20 M sodium $(+)_{589}$ tartrate solution. Figure 3 shows the elution curve of the fractions corresponding to the band A. Two separated peaks, A-1

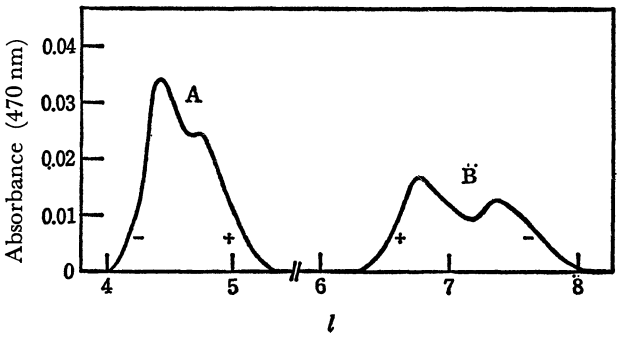

Fig. 2. Elution curve of the isomers of $[Co(mbn)_3]^{3+}$. Eluent: 0.18 M sodium $(+)_{589}$ tartratoantimonate-(III).

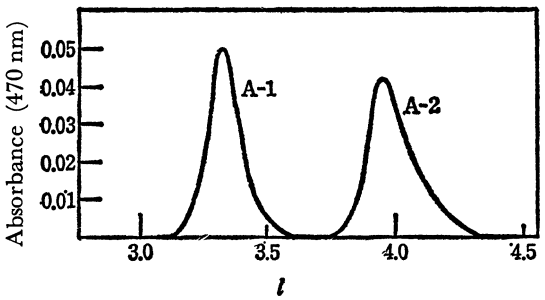

Fig. 3. Elution curve of the fractions corresponding to the band A of Fig. 2.
Eluent: 0.20 M sodium $(+)_{589}$ tartrate.

* The concentration was calculated on the basis of the formula: $[Sb_2(C_4H_2O_6)_2]^{2-}$.

and A-2, appeared. Two peaks similarly separated from the peak B were named B-1 and B-2, in the order of elution. Thus, four isomers, A-1, A-2, B-1, and B-2, were isolated. Found: A-1, C, 29.34; H, 8.56; N, 17.20%. A-2, C, 29.45; H, 8.66; N, 17.26%. B-1, C, 29.15; H, 8.63; N, 17.19%. B-2, C, 29.10; H, 8.96; N, 17.04%. Calcd for $[Co(mbn)_3]Cl_3 \cdot 3.5\ H_2O$ ($C_{12}H_{43}O_{3.5}N_6CoCl_3$): C, 29.25; H, 8.80; N, 17.05%.

Measurements. The electronic absorption(AB) and circular dichroism(CD) spectra were measured at 25 °C, as has been reported previously.[1] The 100 MHz PMR spectra were measured in D_2O by means of a JEOL JNM-MH-100 spectrometer. A small amount of a concd. NaOD-D_2O solution was added to deuterate the amine protons. DSS (sodium 2,2-dimethyl-2-silapentane-5-sulfonate) was used as the internal reference.

Results and Discussion

(1) *PMR Spectra.* Figures 4a and 4b show the PMR spectra of *N*-deuterated A-1 and B-1 isomers respectively. Although the ligand $ND_2CH(CH_3)CH(CH_3)ND_2$ in the *gauche* conformation can give rise to the eight-spin system of the $X_3AA'X'_3$ type, the spin-spin coupling constants $J_{XX'}$ and $J_{AX'}=J_{A'X}$ are considered to be approximately zero. For both isomers, the peaks at 1.1—1.4 ppm and 2.9—3.6 ppm were assigned to the methyl and methine protons respectively.

As the *facial* isomer has three equivalent chelate rings(Fig. 1), two doublet signals due to the axial and equatorial methyl protons are expected unless the chelate rings assume a symmetric envelope conformation. On the other hand, the *mer* isomer, which has no symmetry axis of rotation and which belongs to the point group C_1, should show more complicated methyl signals consisting of up to six doublets. Actually, the A-1 and B-1 isomers showed three and two methyl doublets respectively; the *mer* and *facial* forms were assigned to them.

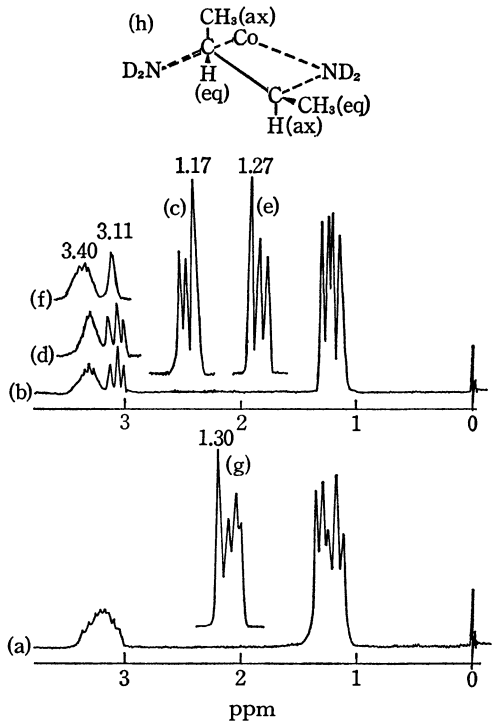

Fig. 4. 100 MHz PMR spectra of the isomers A-1 (a) and B-1 (b).
Double resonance spectra irradiated at $\delta=3.40$ ppm (c), 1.17 ppm (d), 3.11 ppm (e), and 1.27 ppm (f) of the isomer B-1. The methyl part of double resonance spectrum irradiated on the methine signal (3.15 ppm) of the isomer A-1 (g). δ-Conformation of the mbn chelate ring (h).

The methine proton signals of the *facial* isomer consist of two components, and the resonances centered at 3.11 ppm are considered as axial methine proton signals, by analogy with the methylene proton signals of $[Co(CN)_4(R\text{-pn})]^-$[6] and $[Co(pn)_3]^{3+}$.[7] The nuclear magnetic double-resonance technique was used to clarify the spin-spin coupling between methyl and methine protons(Figs. 4c—4g). For the *facial* isomer, irradiation at the methine signals (3.40 ppm) converted the methyl doublet(1.17 ppm, $J_{H\text{-}CH_3}=7$ Hz) into a sharp singlet(Fig. 4c), indicating that it originates from the axial methyl protons. Conversely, the irradiation of the doublet at 1.17 ppm made the methine signals (3.40 ppm) decouple to a still broad peak (Fig. 4d). This broadening is probably due to the spin-spin coupling between two methine protons and the strong scalar coupling with the Co-59 quadrupolar nucleus ($I=7/2$)[8] in the *gauche* conformation. Similarly, the methine signals centered at 3.11 ppm couple with the methyl protons (1.27 ppm, $J_{H\text{-}CH_3}=7$ Hz) (Figs. 4e and 4f); this doublet corresponds to the equatorial methyl group. These methyl protons have an additional bond removed from the central cobalt atom compared with the methine protons and are apparently not affected by the coupling with the Co-59 nucleus.[8]

As for the *mer* isomer, its spectrum is too complicated to be analyzed accurately. Irradiation at the methine signals (3.15 ppm) converted the lower methyl doublet (1.30 ppm) into a singlet (Fig. 4g).

It is to be noted that the $[Co(mbn)_3]^{3+}$ and $[Co(ibn)_3]^{3+}$ ions show chemichal-shift differences between the axial and equatorial methyl groups, whereas the $[Co(NH_3)_4(mbn)]^{3+}$ and $[Pt(mbn)_2]^{2+}$ ions[9] show none, giving only one sharp methyl doublet; in the latter complexes, the two methyl groups are indistinguishable upon rapid chelate ring inversion at room temperatures. However, the proton-decoupled ^{13}C-NMR spectrum of $[Co(en)_2(mbn)]^{3+}$ and $[Co(en)_2(ibn)]^{3+}$ shows two methyl signals[10] due to the axial and equatorial methyl groups. These facts indicate that the axial and equatorial methyl groups in tris(diamine)metal complexes are magnetically nonequivalent because of the unequal energy of the *lel* and *ob* conformations, even when chelate ring inversion is rapid. This chemical-shift difference[11] between axial and equatorial methyl protons was used for the conformational analysis. The difference in the B-1 (*facial*) isomer is 0.10 ppm (=1.27—1.17 ppm), slightly larger than that (0.07 ppm) of the *facial*-$[Co(ibn)_3]^{3+}$.[3] For *meso*-2,3-butanediamine-*N*,*N*,*N'*,*N'*-tetraacetatocobaltate(III), in which the diamine part is considered to be fixed in the *gauche*

Table 1. Absorption and circular dichroism spectra (in cm^{-1})

Isomer	First band		Second band		CT band	
	AB	CD	AB	CD	AB	CD
A-1 (*mer*-*Λ*)	21100(102)	20300(+2.92) 23400(−0.08)	29400(94)	28100(+0.32)	46900(24600)	45500(−34) 51800(+11)
A-2 (*mer*-*Δ*)	21100(102)	20300(−2.91) 23500(+0.08)	29400(94)	28100(−0.32)	46700(23600)	45500(+32) 52100(−10)
B-1 (*facial*-*Λ*)	21100(109)	20300(+3.28) 23400(−0.12)	29400(98)	28100(+0.36)	46900(24100)	45500(−32) 52400(+14)
B-2 (*facial*-*Δ*)	21100(106)	20300(−3.13) 23400(+0.12)	29400(96)	28100(−0.36)	46900(24700)	45700(+33) 52400(−13)

Molar extinction coefficients(ε) and $\Delta\varepsilon$ values are given in parentheses.

conformation, the chemical-shift difference has been reported to be 0.16 ppm.[12] These facts indicate that the B-1(*facial*) isomer in this case has chelate rings with non-symmetric gauche conformations.

It has been concluded for the *Λ*-$[Co(S\text{-pn})_3]^{3+}$ ion[8] that the ligands exist primarily in one conformation with the equatorial methyl group, and that the observed difference, 0.35 ppm, can be taken as the difference between the axial and equatorial methylene protons. If this result can be used to interpret the spectrum of the *facial*-*Λ*-$[Co(mbn)_3]^{3+}$ ion, the difference between the axial and equatorial methine protons, 0.29 ppm (=3.40—3.11), may suggest that the ligand mbn is primarily in the $\delta\delta\delta(lel_3)$ conformation (*cf.* (2)).

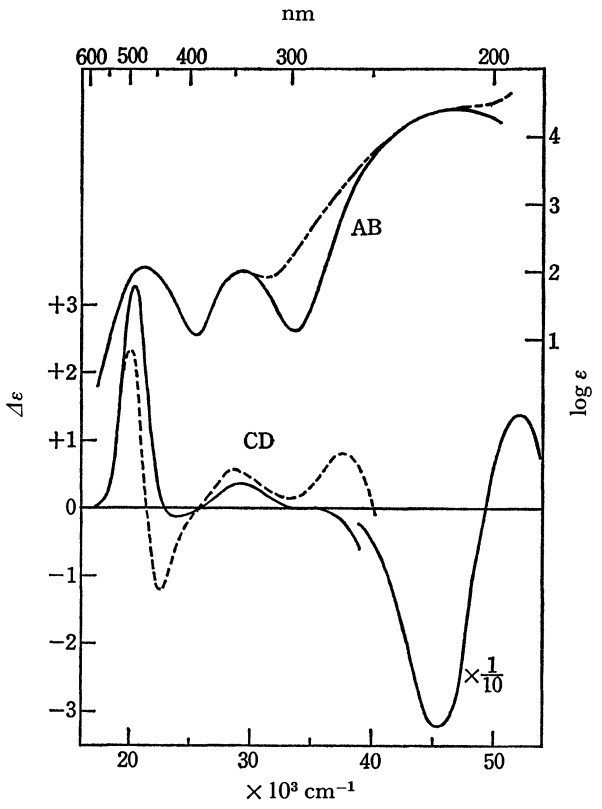

Fig. 5. AB and CD spectra of the isomer B-1(*facial*-*Λ*); —— in water, −−− and —— in 0.2 M Na_3PO_4 solution.

For the A-1(*mer*) isomer, the ligand seems to assume a more distorted conformation than for the B-1(*facial*) isomer, because: (a) the methine signals appear in a broad peak, (b) the *mer* isomer is energetically less stable than the *facial* isomer(*cf.* (3)), and (c) the A_2 component in the CD spectrum is weak(*cf.* (2)).

(2) *Absorption and Circular Dichroism Spectra.* The AB and CD spectral data are listed in Table 1. The rotations shown by the fractions corresponding to the four peaks, A-1, A-2, B-1, and B-2, are +, −, +, and − for 589 nm. The first absorption maxima of $[Co(mbn)_3]^{3+}$ (473 nm) and $[Co(ibn)_3]^{3+}$ [3] (480 nm) are in a lower energy region than that of the *Λ*-$[Co(R\text{-pn})_3]^{3+}$ ion (467 nm). The shift may be due to two methyl groups of the ligand, mbn or ibn, one of them being forced to be in the axial position regardless of the chelate ring (δ or λ).

The CD spectrum of the B-1 isomer resembles that of *Λ*-$[Co(en)_3]^{3+}$ in both the d-d and charge-transfer regions (Fig. 5). Thus, taking the PMR results into account, its absolute configuration can tentatively be determined to be *facial*-*Λ*. Similarly, the configurations of the isomers A-1, A-2, and B-2 are determined to be *mer*-*Λ*, *mer*-*Δ*, and *facial*-*Δ* respectively. The AB and CD spectra of two geometric isomers, *mer* and *facial*, are similar in shape, but the peak intensities of the former are slightly lower than those of the latter (Table 1).**

The negative CD component at 427 nm corresponding to the higher-energy band in the first absorption region is slightly weaker for the *mer* than the *facial* isomer (A-1). This peak is enhanced to the same intensity for both isomers in a 0.2 M sodium phosphate solution, and it is assigned to the $A_2(D_3)$ component. There is a general tendency for the A_2 com-

** A sample of $(+)_{589}[Co(mbn)_3]Br_3$ resolved by the fractional crystallization of the diastereoisomer with $(+)_{589}$ nitrocamphor[4] was kindly provided by Prof. F. Woldbye, which showed a small CD intensity with the constant value of $\Delta\varepsilon(20240\ cm^{-1})/\varepsilon(21200\ cm^{-1}) = 22.7\times10^{-4}$. Chromatographic separation revealed this to be a mixture of four isomers, *mer*-*Δ*, *mer*-*Λ*, *facial*-*Λ*, and *facial*-*Δ*, in the ratio 1.8 : 2.2 : 1.2 : 1.0; the composition explained the low optical activity previously reported,[4] *i.e.* the incomplete resolution.

ponent of the tris(diamine)cobalt(III) complexes to become weak as the chelate ring deviates from the *lel* conformation. The *mer* isomer has, therefore, a more distorted conformation than the *facial* isomer. In the above sodium phosphate solution, a new, weak CD peak appeared at 264 nm ($\Delta\varepsilon = +0.80$ for the *facial*-Λ isomer) as a result of the ion-pair formation, this peak is characteristic of the *lel* conformation.[13]

(3) *Formation Ratio.* If the relative abundance of geometric isomers is governed by statistics alone, the ratio of the *mer* isomer to the *facial* isomer should be 3 : 1; *i.e.*, 75% of the $[Co(mbn)_3]^{3+}$ formed should be the *mer* isomer. The actual formation ratio, as calculated from the area of the elution peaks and the extinction coefficients at 470 nm ,was A-1 : A-2 : B-1 : B-2=1.4 : 1.4 : 1.0 : 1.0; the formation of the B isomers (*facial*) was therefore more favored than the statistically calculated ratio. From the above data, the apparent free energies of the isomers at 300 K were calculated to be 0 for the *facial* isomer (B) and −0.2 kcal/mol for the *mer* isomer (A). An entropy contribution to the free energy from the 1 : 3 statistical weighting of the two configurations, *facial* and *mer*, must be taken into account. The calculated enthalpies and other entropy contributions give rise to relative energies of the following order: *facial* isomer = 0 and *mer* isomer = 0.5 kcal/mol. This value is in good agreement with the result, 0.7 kcal/mol, of the conformational analysis calculated by Niketic and Woldbye.[14]

(4) *Effects of the Eluents on the Separation Order of the Isomers.* As has been described above, when $(+)_{589}$ tartratoantimonate(III) was used as the first eluent, the isomers were eluted in the order: (A-2+A-1), (B-1+B-2) (Fig. 2), whereas with sodium $(+)_{589}$ tartrate as the eluent, four isomers were eluted in the order: (A-1+B-1), (A-2+B-2), and each peak, the mixture of the geometric isomers, was further separated by sodium $(+)_{589}$ tartratoantimonate(III). Thus, sodium $(+)_{589}$ tartratoantimonate(III) is effective in separating geometric isomers, whereas sodium $(+)_{589}$ tartrate in resolving optical isomers on an SP-Sephadex column. The geometric isomers of the $[Co(mbn)_3]^{3+}$ ion were completely separated by a 0.16 M sodium sulfate solution as well.

The X-ray determination of the absolute configuration of the *facial*-Λ-isomer is now under way in the laboratory of Professor Y. Saito, the University of Tokyo.

We are grateful to Professor F. Woldbye, the Technical University of Denmark, for providing the sample.

References

1) Part V was published in This Bulletin, **48**, 879 (1975).
2) M. Kojima, Y. Yoshikawa, and K. Yamasaki, *Inorg. Nucl. Chem. Lett.*, **9**, 689 (1973).
3) M. Kojima, Y. Yoshikawa, and K. Yamasaki, This Bulletin, **46**, 1687 (1973).
4) F. Woldbye, *Proc. Roy. Soc., Ser. A*, **297**, 79 (1967); "Studier over Optisk Aktivitet," Polyteknisk Forlag, Copenhagen (1969), p. 228.
5) F. H. Dickey, W. Fickett, and H. J. Lucas, *J. Amer. Chem. Soc.*, **81**, 4185 (1959).
6) S. Yano, H. Ito, Y. Koike, J. Fujita, and K. Saito, This Bulletin, **42**, 3184 (1969).
7) J. K. Beattie and L. H. Novak, *J. Amer. Chem. Soc.*, **93**, 620 (1971).
8) J. K. Beattie, *Inorg. Chem.*, **10**, 426 (1971).
9) S. Yano, H. Ito, Y. Koike, J. Fujita, and K. Saito, *Chem. Commun.*, **1969**, 460.
10) S. Bagger, O. Bang, and F. Woldbye, *Acta Chem. Scand.*, **27**, 2663 (1973).
11) J. K. Beattie, *Accounts Chem. Res.* **4**, 253 (1971).
12) R. J. Day and C. N. Reilley, *Anal. Chem.*, **37**, 1326 (1965).
13) S. F. Mason and B. J. Norman, *J. Chem. Soc., A*, **1966**, 307.
14) S. R. Niketic and F. Woldbye, *Acta Chem. Scand.*, **27**, 3811 (1973).

Derivatographic Studies on Transition Metal Complexes. XVI.[1] Thermal Chelation of Na[CoX(Hedta or Hpdta)] and [CoX(Hgly)en$_2$]X$_2$ (X=Cl$^-$ or Br$^-$) Type Complexes in Solid Phase[2]

Ryokichi Tsuchiya, Katsuhide Manzaki,* Shigeru Sekiya,** Akira Uehara, and Eishin Kyuno

Department of Chemistry, Faculty of Science, Kanazawa University, Kanazawa 920

(Received March 3, 1975)

Thermal chelation of the following two types of complexes in solid phase was investigated by means of derivatography: Na[CoX(Hedta or Hpdta)] and [CoX(Hgly)en$_2$]X$_2$ (X=Cl$^-$ or Br$^-$), where Hedta or Hpdta and Hgly designate quinquedentate ethylenediaminehydrogentetraacetate or propylenediaminehydrogentetraacetate ion and unidentate glycine molecule, respectively. The results show that all the complexes undergo characteristic thermal chelation through the dehydrohalogenation, giving an increase in ligand denticity from five to six in Na[CoX(Hedta or Hpdta)] and one to two in Na[CoX(Hgly)en$_2$]X$_2$. The reaction mechanism in the thermal chelation of each complex in solid phase was discussed in terms of the thermochemical data.

In some complexes where multidentate ligand coordinates to metal ion with its partial denticity, the potential multidenticity can be completely satisfied by further occupying the other coordination sites vacated by the escape of volatile molecule upon heating.

Such a change in which the increase of ligand denticity is involved is designated as "thermal chelation" in this paper. The situation may easily arise when the atom entering into the coordination site to form chelation in multidentate ligand resides near the escapable ligand such as H_2O or NH_3. As an example, Hertzenberg and Bailar found[3] that the unidentate sulfato complexes *cis*-[Co(SO$_4$)(H$_2$O)(NH$_3$)$_4$]X (X=ClO$_4^-$, BF$_4^-$ or 1/2PtCl$_6^{2-}$) are deaquated to form the bidentate sulfato complexes [Co(SO$_4$)(NH$_3$)$_4$]X at temperatures in the range 110—160 °C upon heating. Another example of the reaction was also reported on the quinquedentate EDTA complex [Cr(Hedta)(H$_2$O)] and on the terdentate NPDA (nitrilopropionicdiacetic acid) complex [Cr(OH)(Hnpda)(H$_2$O)$_2$]: the former was converted into sexidentate EDTA complex H[Cr(edta)] and the latter into quadridentate NPDA complex [Cr(npda)(H$_2$O)$_2$] with the increase of ligand denticity through deaquation by heating.[4]

In this paper, we deal with the thermal chelation of two additional types of complexes, Na[CoX(Hedta or Hpdta)] and [CoX(Hgly)en$_2$]X$_2$ (X=Cl$^-$ or Br$^-$), where Hedta, Hpdta and Hgly designate quinquedentate EDTA and PDTA and unidentate glycine molecule, respectively. These two types of thermal chelation are essentially distinguished from those mentioned above[3,4] with respect to the involvement of "dehydrohalogenation" in place of "dehydration".

Experimental

Preparation of Complexes. Both types of complexes used as the starting materials are characterized (Fig. 1), by the coordination of a halide ion and of quinquedentate diaminocarboxylate anion or unidentate amino acid molecule, the latter containing an uncoordinated -COOH group. They easily evolve the hydrogen halide formed from H$^+$ in -COOH and X$^-$ in the coordination sphere upon heating.

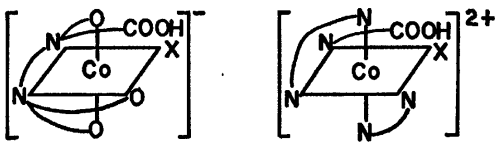

Na[CoX(Hedta or Hpdta)] [CoX(Hgly)en$_2$]X$_2$

Fig. 1. Structure of the complexes used.

Quinquedentate EDTA and PDTA Complexes: Na[CoCl(Hedta)]·2H$_2$O, Na[CoBr(Hedta)], Na[CoCl(Hpdta)]·2H$_2$O and Na[CoBr(Hpdta)]·1/2H$_2$O. They were prepared according to the procedures described in literature.[5-7]

Unidentate Glycine Complexes: [CoCl(Hgly)en$_2$]Cl$_2$ and [CoBr(Hgly)en$_2$]Br$_2$. They were synthesized by the method of Alexander and Busch[8] modified as folllows.

[CoCl(Hgly)en$_2$]Cl$_2$. *trans*-[CoCl$_2$en$_2$]Cl (2.9 g, 0.01 mol) and ethyl glycinate (1.4 g, 0.01 mol) were placed in a mortar together with water (3 ml) and diethylamine (1 ml). The mixture was triturated sufficiently to form red aggregates, which were suspended in ethanol and then collected by filtration.[9] To the ethyl glycinato complex (1 g, 0.003 mol) thus obtained was added 4 M hydrochloric acid (13 ml) to hydrolyze it and isopropyl alcohol (18 ml) was dropped into the resulting red solution, which was left to stand overnight in a refrigerator. Reddish voilet crystals were obtained and recrystallized from a minimum amount of hot water. Yield 0.5 g.

Found: C, 19.8; H, 6.2; N, 19.3%. Calcd for [Co(C$_6$H$_{21}$N$_5$O$_2$Cl)]Cl$_2$: C, 20.0; H, 5.9; N, 19.4%.

[CoBr(Hgly)en$_2$]Br$_2$. The complex was prepared by a procedure analogous to that for the above complex except that *trans*-[CoBr$_2$en$_2$]Br, triethylamine and 7 M hydrobromic acid solution were used in place of *trans*-[CoCl$_2$en$_2$]Cl, diethylamine and 4 M hydrochloric acid solution, respectively. Recrystallization was carried out from hydrobromic acid solution. From 1 g of the starting glycinato complex [CoBr(NH$_2$CH$_2$COOC$_2$H$_5$)en$_2$]Br$_2$ was obtained 0.2 g of the product.

Found: C, 14.7; H, 4.8; N, 13.9%. Calcd for [Co(C$_6$H$_{21}$N$_5$O$_2$Br)]Br$_2$: C, 14.6; H, 4.3; N, 14.2%.

Measurements. The thermal reactions of the complexes under non-isothermal conditions were observed with a MOM Derivatograph Typ-OD-102,[10] and those under isothermal conditions were measured with a Shimadzu

* Present address: Tōyō Kasei Kogyo Co. Ltd., Takasago, Hyogo 676.

** Present address: Sumitomo Kinzoku Kozan Co. Ltd. Ohme, Tokyo, 198.

TM-1A thermanobalance or an Abderhalden's apparatus. The IR and UV spectra of the samples obtained at the various heating steps were measured in Nujol-mull state with JASCO model IR-E and Hitachi EPS spectrophotometers.

Results and Discussion

In order to visually grasp the thermal chelation in EDTA, PDTA and glycine complexes, experimental results obtained with Na[CoBr(Hedta)] and [CoCl(Hgly)en_2]Cl_2 are given as the typical examples.

Derivatography. Figure 2 gives the derivatograms of Na[CoBr(Hedta)] and [CoCl(Hgly)en_2]Cl_2. The TG curve of Na[CoBr(Hedta)] shows that each half mole of HBr is evolved at 53—105 °C and at 105—145 °C, respectively, the DTA curve giving two endothermic peaks in the range corresponding to the evolution of each half mole of HBr. The original bluish violet color of the complex turned violet at the final stage of dehydrobromination.

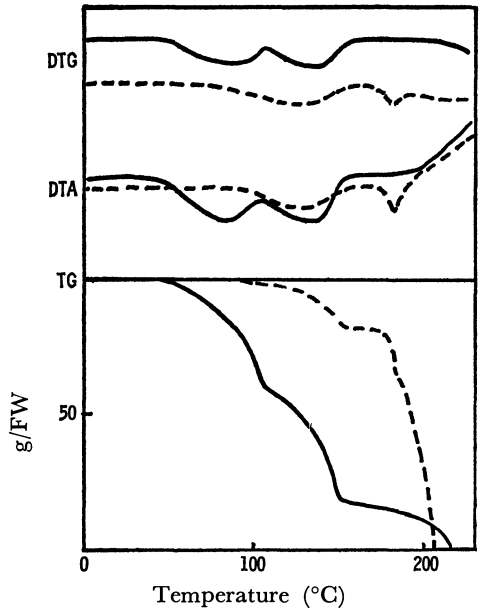

Fig. 2. Derivatograms of Na[CoBr(Hedta)](——) and [CoCl(Hgly)en_2]Cl_2(----).

In the case of [CoCl(Hgly)en_2]Cl_2, the complex releases at first a half mole of HCl at 75—150 °C and then decomposes rapidly at 175 °C as shown in its TG curve. However, a reflection and a small endothermic peak are observed in TG and DTA curves, respectively, at the point which gives the weight loss corresponding to the liberation of a further half mole of HCl. Although the formation of the stable intermediate product can not be confirmed distinctly, the color of the original complex turned orange red from reddish violet after complete dehydrobromination. The isothermal measurement also showed that the original complex brings about the complete dehydrobromination to form the bidentate glycinato-complex [Co(gly)en_2]Cl_2 upon heating at 150 °C for 10 hr.

IR Spectra. Figure 3 shows the changes of the ν_{CO} in Na[CoBr(Hedta)] and [CoCl(Hgly)en_2]-

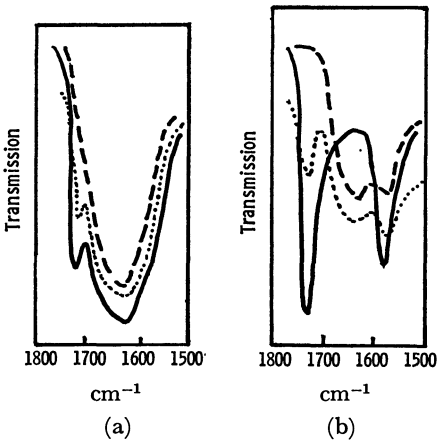

Fig. 3. (a) IR spectra of Na[CoBr(Hedta)](——) and its products obtained upon heating at 105 °C (·····) and at 145 °C (----).
(b) IR spectra of [CoCl(Hgly)en_2]Cl_2 (——) and its products obtained upon heating at 150 °C (·····) and upon heating isothermally at 150 °C for 10 hr (----).

Cl_2. Na[CoBr(Hedta)] gave a sharp band at 1730 cm^{-1} and a broad one at 1600—1700 cm^{-1} before heating, the former being assigned to $\nu_{C=O}$ of free carboxylic acid (–COOH) and the latter to that of the coordinated carboxylate group (–COO–Co).[11] The IR spectral pattern obtained in the sample heated at 105 °C does not essentially differ from that of the original one, the sharp band at 1730 cm^{-1} disappearing in the sample heated at 145 °C. This indicates that free carboxylic acid in the complex participated in coordination as a consequence of complete dehydrobromination, thermal chelation thus taking place. On the other hand, [CoCl(Hgly)en_2]Cl_2 still gave a sharp band at 1740 cm^{-1} due to the presence of free –COOH besides the band at 1580 cm^{-1} attributable to the δ_{NH_2} of glycinate ion. However, the sharp band disappeared in the sample isothermally heated at 150 °C for 10 hr, while a band due to the presence of –COO–Co appeared at 1600—1700 cm^{-1}. This suggests that the unidentate glycine complex was now converted into the bidentate glycinato-complex through complete dehydrochlorination, thermal chelation taking place.

Electronic Spectra. Figure 4 shows the electronic spectra of aqueous solutions of Na[CoBr(Hedta)], the complex heated at 145 °C and the reference complex Na[Co(edta)]·$2H_2O$ prepared by the method in literature.[12] The absorption maxima of Na[CoBr(Hedta)] heated at 145 °C appear in relatively higher frequency region as compared with those of the original complex Na[CoBr(Hedta)], and closely resemble those of the reference complex. This also indicates that the original complex was converted into Na[Co(edta)] by dehydrobromination accompanied by thermal chelation.

A similar change in electronic spectra is recognized in the case of [CoCl(Hgly)en_2]Cl_2 (Fig. 5); the complex heated isothermally at 150 °C for 10 hr gives essentially the same spectrum as that of the reference complex [Co(gly)en_2]Cl_2.[8]

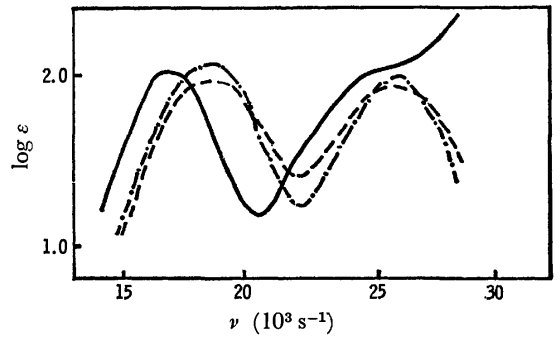

Fig. 4. Electronic spectra of Na[CoBr(Hedta)] (——), its product obtained upon heating at 145 °C (----) and the reference complex, Na[Co(edta)]·2H$_2$O (—·—).

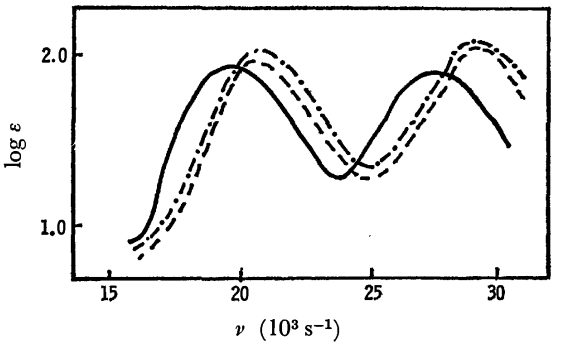

Fig. 5. Electronic spectra of [CoCl(Hgly)en$_2$]Cl$_2$ (——), its product obtained upon heating at 150 °C for 10 hr (----) and the reference complex, [Co(gly)en$_2$]Cl$_2$·H$_2$O (—·—).

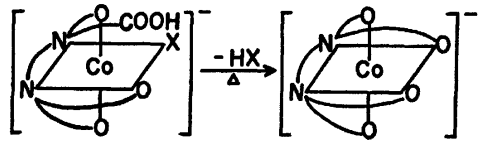

blue violet violet

(a) Na[CoX(Hedta or Hpdta)]

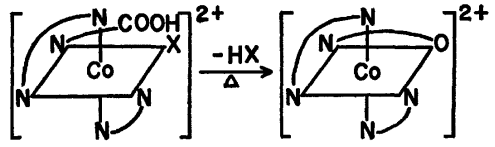

red violet orange red

(b) [CoX(Hgly)en$_2$]X$_2$

Fig. 6. Schemes of thermal chelation of Na[CoX(Hedta or Hpdta)] (a) and (CoX(Hgly)en$_2$]X$_2$ (b).

This is another evidence supporting the following conversion.

$$[CoCl(Hgly)en_2]Cl_2 \xrightarrow[\Delta]{} [Co(gly)en_2]Cl_2 + HCl$$

Measurement of magnetic susceptibilities showed that the cobalt ion in all the complexes remained as a tervalent state throughout the dehydrohalogenation process. The reaction seems to proceed according to the schemes shown in Fig. 6.

Thermochemical Data. Thermochemical data such as initiation temperatures, enthalpy changes (ΔH) and activation energies (E_a) were estimated in order to study the effect of kinds of ligands or counter ions on thermal chelation.

Na[CoX(Hedta or Hpdta)] Type Complexes. The enthalpy change of the reaction was estimated from the DTA peak area in the derivatograms and the activation energy from the slope of Arrhenius plots derived from the analysis of the DTA or DTG curve.[10] The numerical values of the thermochemical data are summarized in Table 1.

Table 1. Thermochemical data for thermal chelation of Na[CoX(Hedta or Hpdta)] type complexes

Complex		Init. Temp °C	ΔH kcal/mol	E_a kcal/mol
Na[CoCl(Hedta)]·2H$_2$O	1st	97	17.4	28.3
	2nd	103	17.0	57.0
Na[CoCl(Hpdta)]·2H$_2$O	1st	110	19.2	21.5
	2nd	181	18.3	116
Na[CoBr(Hedta)]	1st	53	26.4	29.2
	2nd	105	22.5	30.8
Na[CoBr(Hpdta)]·1/2H$_2$O	1st	92	20.8	40.8
	2nd	108	19.2	129

1st and 2nd denote the first (1/2 mol) and the second (1/2 mol) liberation steps, respectively, of the dehydrohalogenation.

The values of the enthalpy changes for the first and second dehydrohalogenation steps are approximately in the same order, but the value of the activation energy for the first step almost exceeds that for the second step in each complex. This suggests that the evolution of the first half mole of hydrogen halide and that of the second half mole of it proceed *via* different mechanisms though the details are still unknown.

The enthalpy changes for the bromo-complexes are relatively greater than those for the chloro-complexes and the same tendency is also recognized in the activation energies except for the second step of Na[CoCl(Hedta)]·2H$_2$O. This reflects the fact that thermal chelation of the bromo-complexes takes place with more difficulty than that of chloro-complexes. This can be understood in terms of data of the bond energies[13] as follows.

From the bond energies of O-H, 110.6, H-Cl, 103.2 and H-Br, 87.5 kcal mol^{-1}, the energy required for the bond rupture between O and H subtracted by the energy evolved in the bond formation between H and Br, ΔH=15.7 kcal mol^{-1}, is larger than the corresponding value concerning H and Cl, 7.4 kcal mol^{-1}. These two values are in line with those of the enthalpy changes in the thermal chelation of Na[CoBr(Hedta or Hpdta)] and Na[CoCl(Hedta or Hpdta)], respectively.

Comparison of the enthalpy changes and the avtivation energies for the EDTA-complexes with the corresponding data for the PDTA-complexes reveals

that the former complexes undergo thermal chelation more easily than the latter.

$[CoX(Hgly)en_2]X_2$ Type Complexes. Although the occurrence of thermal chelation could be confirmed by measurements of infrared and electronic spectra, no plateau distinctly indicating the formation of the intermediate products could be observed in the TG curve. Thus, no reliable thermal data were available from DTA and DTG peak analyses.

So far as the complexes $[CoX(Hgly)en_2]X_2$ are concerned, the activation energies for the thermal chelation were estimated by the isothermal measurement in the following manner. The sample was heated at each temperature of 140, 147, 152, and 164 °C for 150 min and the compositions of the products were determined spectrophotometrically. Since the absorbancies of the original complex $[CoCl(Hgly)en_2]Cl_2$ and the reference complex $[Co(gly)en_2]Cl_2 \cdot H_2O$ are 33.3 and 11.4 at 580 nm, and 62.5 and 106.4 at 484 nm, respectively, the composition of samples in each product by thermal chelation was calculated by means of the following simultaneous equations:

$$33.3x + 11.4y = D_{580}$$
$$62.6x + 106.4y = D_{484},$$

where x and y are the concentrations of the original complex and the complex formed by the thermal chelation, respectively, and D_{580} and D_{484} are the absorbancies at 580 and 484 nm, respectively. The chelation ratios, $[CoCl(Hgly)en_2]/[Co(gly)en_2]$ therefore, are given by $y/(x+y)$. Similar procedures were also employed for the bromo-complex. The rate constant k for thermal chelation was obtained by the chelation ratio. The activation energies were estimated from slope of the Arrhenius plots derived from the relationship of log k *vs.* $1/T$.

The values of 32.4 and 26.1 kcal mol^{-1} were obtained as the activation energies for the chloro- and the bromo-complexes, respectively. It might be said that the thermal chelation of the bromo-complex takes place more easily than that of the chloro-complex. This tendency is in contrast to that for the EDTA- and PDTA-complexes, the reason being not clear as yet.

References

1) Part XIV: R Tsuchiya, Y. Natsume, A. Uehara, and E. Kyuno, *Thermochimica Acta*, **12**, 147 (1975); Part XV: R. Tsuchiya, T. Ohoki, A. Uehara, and E. Kyuno, *ibid.*, **12**, 413 (1975).

2) Presented at the 24th Symposium on Coordination Compounds of the Chemical Society of Japan, Kanazawa, October, 1974.

3) E. P. Hertzenberg and J. C. Bailar, Jr., *Inorg. Chem.* **10**, 2377 (1971).

4) R. Tsuchiya, A. Uehara, and E. Kyuno, This Bulletin, **42**, 1886 (1969).

5) M. Mori, M. Shibata, E. Kyuno, and H. Nakajima, *ibid.*, **29**, 887 (1956).

6) M. L. Morris and D. H. Busch, *J. Amer. Chem. Soc.*, **78**, 5178 (1956).

7) F. P. Dwyer and F. L. Garvan, *ibid.*, **83**, 2610 (1961).

8) M. D. Alexander and D. H. Busch, *Inorg. Chem.*, **5**, 1590 (1966).

9) M. D. Alexander and D. H. Busch, *ibid.*, **5**, 602 (1966).

10) R. Tsuchiya, Y. Kaji, A. Uehara, and E. Kyuno, This Bulletin, **42**, 1881 (1969).

11) D. H. Busch and J. C. Bailar, Jr., *J. Amer. Chem. Soc.*, **75**, 4574 (1953).

12) H. Brintzinger, H. Thiele, and U. Müller, *Z. Anorg. Allgem. Chem.*, **251**, 285 (1943).

13) L. Pauling, "The Nature of the Chemical Bond," Cornell University Press (1959), p. 85.

The Decomposition of the Oxalato Complex of Manganese(IV) in Oxalate Buffer Solutions[1]

Takashi UEHIRO, Iwao TAMINAGA, and Yukichi YOSHINO

Department of Chemistry, College of General Education, The University of Tokyo, Meguro-ku, Tokyo 153

(Received March 6, 1975)

The spontaneous decomposition of the oxalato complex of manganese(IV), $[Mn_2^{IV}O_2(C_2O_4)_4]^{4-}$, in oxalate buffer solutions is investigated photometrically. It is found that the reaction proceeds in two steps, the first step being $[Mn_2^{IV}O_2(C_2O_4)_4]^{4-} \rightarrow [Mn^{III}(C_2O_4)_3]^{3-}$ and the second, $[Mn^{III}(C_2O_4)_3]^{3-} \rightarrow$ manganese(II) complexes. The experimental rate at pH 3.9 is written as:

$$\text{rate} = -d[Mn_2^{IV}]/dt$$
$$= \alpha[Mn^{III}] + \beta[Mn_2^{IV}]^{1/2}[Mn^{III}] + \gamma[Mn_2^{IV}]^{1/2},$$

where Mn_2^{IV} and Mn^{III} denote $[Mn_2^{IV}O_2(C_2O_4)_4]^{4-}$ and $[Mn^{III}(C_2O_4)_3]^{3-}$ respectively. Compared with α and β terms, the contribution of the γ term is much smaller. A mechanism involving the CO_2^- radical is postulated for the reaction.

In a previous paper[2] we reported that the oxalato complex of manganese(IV) has a dimeric structure and should be formulated as $K_4[Mn_2O_2(C_2O_4)_4]\cdot 4H_2O$. It was also pointed out that the complex in an oxalate buffer solution spontaneously decomposes to give manganese(II) complex *via* manganese(III).

Since little is known about the reaction of quadrivalent manganese in solution, we have carried out a systematic study of the decomposition reaction of the oxalate complex of manganese(IV) in oxalate buffer solutions. The present paper will describe the kinetics and mechanism of the reactions of this sort.

Experimental

Materials. Potassium di-μ-oxo-tetrakis(oxalato)dimanganate(IV) tetrahydrate, $K_4[Mn_2O_2(C_2O_4)_4]\cdot 4H_2O$, and potassium tris(oxalato)manganate(III), $K_3[Mn(C_2O_4)_3]\cdot 3H_2O$ (abbreviated hereafter in rate equations, *etc.* as Mn_2^{IV} and Mn^{III} respectively) were prepared by the method described in earlier papers.[2-4] The other chemicals were all of a reagent grade and were recrystallized from water when necessary. Ordinary distilled water was purified by repeated distillation. Pyrex and Hario H-32 glass vessels were used throughout the experiment.

Kinetic Runs. The reaction was followed with a Hitachi 124 spectrophotometer, with a Hitachi 056 recorder attached. The temperature of the cell was controlled by circulating water from a Haake thermostat. In each run, a sample solution was prepared by dissolving the solid complex in a 0.05—0.5 M $K_2C_2O_4$–$H_2C_2O_4$ (2 : 1) solution of the required temperature, and then a part of the solution was transferred quickly into a 10-mm quartz cell with a joint cap. The concentration of the sample was $1—10\times 10^{-3}$ M in total manganese. The wavelengths chosen were 643 nm for $[Mn^{IV}{}_2O_2(C_2O_4)_4]^{4-}$ and 520 nm for $[Mn^{III}(C_2O_4)_3]^{3-}$. When necessary, the buffer solution was deoxygenated by nitrogen or saturated with oxygen. It was ascertained that, under these conditions, the photochemical effect on the rate of decomposition of the complex was negligibly small.

Results and Discussion

As was described in the previous paper,[2] the quadrivalent manganese complex in an oxalate buffer solution exhibits an absorption maximum at 643 nm. As the decomposition of the complex proceeds, the absorbance at 643 nm decreases, and there appear three isosbestic points—at 490, 580, and 848 nm. Therefore, during this period, the quadrivalent manganese complex can be considered to change into its conjugate colored species. It was confirmed that the spectrum observed just before the disappearance of the isosbestic points coincides with that of the tris(oxalato)manganate(III) ion, with an absorption maximum at 520 nm. Hence, it is clear that the net reaction in the first period is the reduction of the quadrivalent manganese complex to a tervalent one, $[Mn^{III}(C_2O_4)_3]^{3-}$. Thus,

$$[Mn_2^{IV}O_2(C_2O_4)_4]^{4-} + 2HC_2O_4^- + H_2C_2O_4 \rightarrow 2[Mn^{III}(C_2O_4)_3]^{3-} + 2H_2O + 2CO_2$$

After the isosbestic points disappeared, the absorbance at 520 nm decreased more slowly. In the second period it is considered that the tris(oxalato)manganate (III) is reduced to give an oxalato complex of manganese(II) (probably $[Mn^{II}(C_2O_4)_2(H_2O)_2]^{2-}$). The overall reaction may, then, be written as follows:

$$2[Mn^{III}(C_2O_4)_3]^{3-} + 4H_2O \rightarrow 2[Mn^{II}(C_2O_4)_2(H_2O)_2]^{2-} + C_2O_4^{2-} + 2CO_2$$

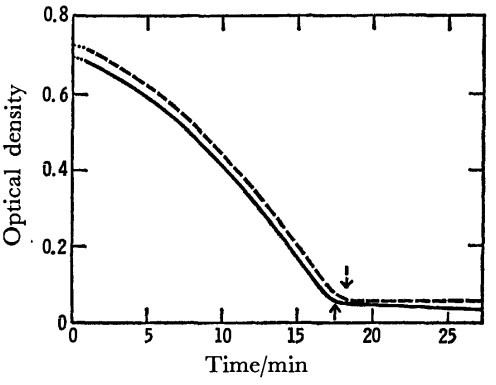

Fig. 1. Decomposition of $[Mn_2^{IV}O_2(C_2O_4)_4]^{4-}$ at 30 °C in oxalate solution (pH 3.9). Initial concentration= 2×10^{-3} M. λ=643 nm.
——: in the absence of O_2, ----: in the presence of O_2. Change from the first period to the second occurs at the points indicated by arrows.

Figure 1 shows a typical absorbancy-time curve for the oxalato complex of manganese(IV) at 30 °C in either the absence or presence of oxygen. As may be seen in Fig. 1, the effect of oxygen on the rate in the first period is very small, while, in the second, the dissolved oxygen depresses the rate strikingly, as has been reported in the case of the decomposition of the oxalato complexes of manganese(III).[5,6] The second period corresponds to the decomposition of the tervalent manganese complex. Thus, we will hereafter be concerned only with the first period of the reaction.

Since the reaction was started by dissolving a solid sample in an oxalate buffer solution, the initial-rate method was not applicable. The rate of decomposition at time t was evaluated by reading the slope of the optical density *vs.* time curve, as may be understood from the following relation:

$$\text{rate} = -\frac{d[Mn_2^{IV}]}{dt} = -\frac{d}{dt}\left(\frac{D-\varepsilon^{III}C_0}{\varepsilon^{IV}-2\varepsilon^{III}}\right) = -\frac{1}{\varepsilon^{IV}-2\varepsilon^{III}}\frac{dD}{dt}$$

where D denotes the optical density of the solution and C_0, the total concentration of $[Mn_2^{IV}O_2(C_2O_4)_4]^{4-}$ and $[Mn^{III}(C_2O_4)_3]^{3-}$. The ε^{IV} and ε^{III} are the molar extinction coefficients of $[Mn_2^{IV}O_2(C_2O_4)_4]^{4-}$ and $[Mn^{III}(C_2O_4)_3]^{3-}$ respectively (at 643 nm, $\varepsilon^{IV}=440$ and $\varepsilon^{III}=12$).

The Effect of the Concentration of the Complexes. The rates of decomposition of the oxalato complex of manganese(IV) in 0.05—0.5 M oxalate buffer solutions

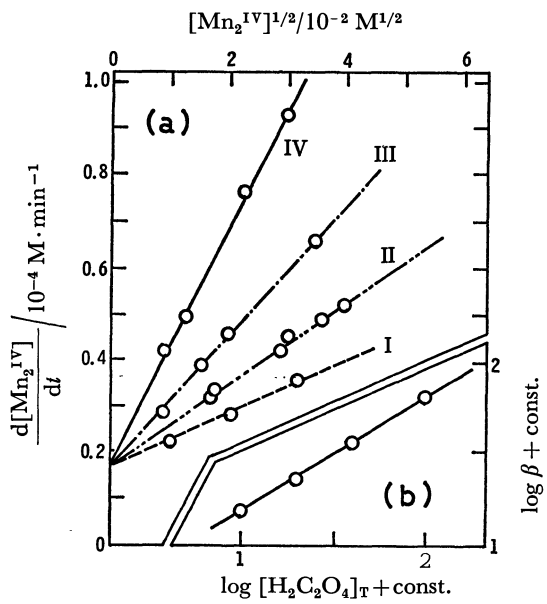

Fig. 2. Dependence of the decomposition rate of $[Mn_2^{IV}O_2(C_2O_4)_4]^{4-}$ on the concentration of $[Mn_2^{IV}O_2(C_2O_4)_4]^{4-}$ and buffer solution.
a) Plots of the rate at a definite concentration of $[Mn^{III}(C_2O_4)_3]^{3-}$ (3.5×10^{-3} M) *vs.* the square root of $[Mn_2^{IV}O_2(C_2O_4)_4]^{4-}$ concentration at 20 °C in the absence of oxygen. Buffer concentrations (pH 3.9): I, 0.05 M; II, 0.1 M; III, 0.2 M; IV, 0.5 M.
b) log-log plot between the rate constant β and buffer concentration.

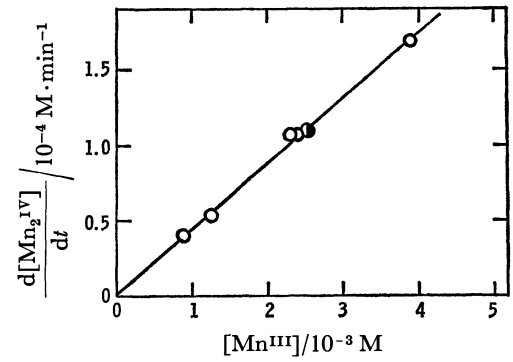

Fig. 3. Plots of the decomposition rate of $[Mn_2^{IV}O_2(C_2O_4)_4]^{4-}$ at a definite $[Mn_2^{IV}O_2(C_2O_4)_4]^{4-}$ concentration (1×10^{-3} M) *vs.* $[Mn^{III}(C_2O_4)_3]^{3-}$ concentration.
○: in the absence of O_2, ◑: in the presence of O_2.

(pH 3.9) were measured by varying the initial concentrations of the manganese(IV) and manganese(III) complexes. The plots of the rate at a definite concentration of the manganese(III) complex *versus* the square root of the concentration of the manganese(IV) complex give a straight line (Fig. 2). Thus, the rate at a definite concentration of the manganese(III) complex, v_{III}, may be expressed as:

$$v_{III} = a + b[Mn_2^{IV}]^{1/2} \quad (1)$$

The rate at a definite concentration of the manganese (IV) complex was plotted against the concentration of the manganese(III) complex (Fig. 3). The good straight-line relationship gives the rate, v_{IV}, as:

$$v_{IV} = c + d[Mn^{III}] \quad (2)$$

Figure 3 indicates that the value of c is very small.

The Rate Equation. By combining Eqs. (1) and (2), the following rate equation may be obtained:

$$\text{rate} = -\frac{d[Mn_2^{IV}]}{dt} = (1/2)\frac{d[Mn^{III}]}{dt} = \alpha[Mn^{III}] + \beta[Mn_2^{IV}]^{1/2}[Mn^{III}] + \gamma[Mn_2^{IV}]^{1/2} \quad (3)$$

where α, β, and γ are the apparent rate constants. From the experimental data obtained under various conditions, the values of α, β, and γ were evaluated (Table 1).

The solution of the manganese (IV) complex becomes turbid when the pH of the solution rises to *ca.* 4.5. On the other hand, $[Mn^{III}(C_2O_4)_3^{3-}]$ dissociates into $[Mn^{III}(C_2O_4)_2(H_2O)_2]^-$ in the lower pH region ($K=3.8\times10^{-3}$ at 0 °C), and it is impossible to vary the pH alone without varying the composition of the buffer. Therefore, a quantitative examination of the pH dependence of the rate was difficult to carry out. Qualitatively, the rate became slightly faster as the pH of the solution decreased.

The effect of the ionic strength was also examined by the use of Na_2SO_4, but in the range of 0.01—1.5, the ionic strength has no significant effect on the rate.

For the α term, it may be found from Fig. 2 that the rate is independent of the concentration of the buffer solutions (0.05—0.50 M). The activation energy, E_α, for the α term was calculated as 19.5 kcal/mol from the plot of log α *vs.* $1/T$.

Table 1. Apparent rate constants for decomposition of the oxalato complex of manganese(IV) in 0.1 M oxalate solution (pH 3.9) under N_2

Temperature (°C)	α (min^{-1})	β ($M^{-1/2}min^{-1}$)	γ ($M^{1/2}min$)	k_1[a] (min^{-1})
10	2.39×10^{-3}	1.1×10^{-2}	1.5×10^{-5}	
20	0.85×10^{-2}	2.74×10^{-2}	2.4×10^{-5}	0.84×10^{-2}
30	3.00×10^{-2}	3.91×10^{-2}	4.8×10^{-5}	3.01×10^{-2}
40	0.85×10^{-1}	4.56×10^{-2}	6.5×10^{-5}	

a) Rate constant for the decomposition of $[Mn(C_2O_4)_3]^{3-}$. The rate equation and mechanism for this reaction can be written as follows.[5-7]

$$-\frac{d[Mn^{III}]}{dt} = 2k_1[Mn^{III}]$$

$$Mn^{III} \xrightarrow{k_1} Mn(II) + CO_2^- + CO_2$$

$$Mn^{III} + CO_2^- \xrightarrow[fast]{} Mn(II) + CO_2$$

The behavior of the β term is rather complicated. It was found, in the 0.05—0.5 M buffer solutions of pH 3.9, that the order of the reaction is about 0.6 with respect to the buffer concentration (Fig. 2).

The Arrhenius plot of the β term did not give a straight line, but a curve which is convex upward. The apparent activation energy was estimated as *ca.* 5 kcal/mol at 30 °C and as *ca.* 13 kcal/mol at 15 °C.

The contribution of the γ term was very small. The experimental error inherent in the γ term is large, though, no detailed discussion can be given.

Reaction Mechanism. On the basis of the above observations, a plausible mechanism for the reaction involving the CO_2^- radical was proposed as follows:

$$Mn^{III} \xrightarrow{k_1} Mn(II) + CO_2^- + CO_2 \quad (1)$$

$$Mn^{III} + CO_2^- \xrightarrow{fast} Mn(II) + CO_2 \quad (2)$$

$$Mn^{IV} + CO_2^- \xrightarrow{fast} Mn(III) + CO_2 \quad (3)$$

$$Mn^{IV} + Mn(II) \xrightarrow{fast} 2Mn(III) \quad (4)$$

$$Mn_2^{IV} + ox \overset{K}{\rightleftharpoons} 2Mn^{IV} \quad (5)$$

$$Mn^{IV} + Mn(III) \xrightarrow{k_6} Mn(II) + Mn(III) + 2CO_2 \quad (6)$$

$$Mn^{IV} \xrightarrow{k_7} Mn(II) + 2CO_2 \quad (7)$$

In the above equations, the following abbreviations were used: Mn(III): any tervalent manganese complex which turns into Mn^{III} quickly; Mn(II): divalent manganese complex; Mn^{IV}: any mononuclear complex of quadrivalent manganese; ox: oxalate ion or its protonated species.

Reactions (1)-(4) in the above scheme seem to account reasonably for the α term of the rate equation. In the first step, $[Mn^{III}(C_2O_4)_3]^{3-}$ decomposes to produce Mn(II) and the CO_2^- radical (Reaction (1)). The Mn(II) or CO_2^- radical once produced successively reacts with Mn^{IV} or Mn^{III} very fast (Reactions (2)—(4)). This mechanism is supported by the following facts. The rate constant, α, is in good agreement with that of Reaction (1). Reactions (1) and (2) correspond to the mechanism widely accepted for the decomposition of $[Mn^{III}(C_2O_4)_3]^{3-}$, where Reaction (1) is the rate-determining step.[6,7] The activation energy for the α term also agrees with that of Reaction (1).[6] One piece of the experimental evidence for Reaction (4) is that we can titrate the manganese(IV) complex with the manganese(II) solution in an oxalate buffer; the formation of $[Mn^{III}(C_2O_4)_3]^{3-}$ is observed in the resultant solution. Reactions (1)—(4) indicate that, along with the decomposition of $[Mn^{III}(C_2O_4)_3]^{3-}$ according to Reaction (1), double the amount of Mn^{IV} changes into Mn(III). Accordingly, the rate equation for the α term is expressed as:

$$-d[Mn(IV)_T]/dt = -2d[Mn_2^{IV}]/dt$$
$$= 2\alpha[Mn^{III}] = 2k_1[Mn^{III}],$$

where $[Mn(IV)_T]$ denotes the total concentration of quadrivalent manganese; most of the species of quadrivalent manganese may be $[Mn_2^{IV}O_2(C_2O_4)_4]^{4-}$.

Reactions (5) and (6) correspond to the β term, which indicates that the reaction is half-order in Mn_2^{IV} and first-order in Mn^{III}. Such an order of a reaction might be explained by assuming a simple scheme involving a dimer-monomer equilibrium, that is:

$$Mn_2^{IV} \rightleftharpoons 2Mn^{IV}$$

$$Mn^{IV} + Mn(III) \longrightarrow Mn(II) + Mn(III) + 2CO_2$$

In this case, however, this simple mechanism cannot explain the buffer-concentration dependence of the rate. As has been mentioned earlier, the experimental order with respect to the buffer concentration is very close to 1/2. The scheme postulated above, Reactions (5) and (6), will account for this observation. If we assume that the (5) equilibrium is rapidly established, lying far to the left, and that Reaction (6) is slow, the rate equation for the β term may be written as:

$$-d[Mn_2^{IV}]/dt = k_6[Mn_2^{IV}]^{1/2}[Mn^{III}](K[ox])^{1/2}$$

in accord with the experimental requirements. Since we observed no significant effect of the ionic strength on the β term, it is presumed that Reactions (5) and (6) are not between charged species only, but between charged and neutral species.

As for the γ term, which corresponds to Reaction (7), the accurate determination of the rate constant was extremely difficult. We can only say that the value of the rate constant is significantly smaller than those of the α and β terms.

The oxygen effect on the decomposition rate of the oxalato complex of tervalent manganese has been explained by the formation of the $O_2CO_2^-$ (or HO_2-CO_2) radical, which is the product of the reaction between the CO_2^- (or HCO_2) radical and oxygen, O_2.[6-9] The $O_2CO_2^-$ or its derivative radical (*e.g.*, O_2^-) is known to be less active toward magnanese(III); moreover, it oxidizes manganese(II) to manganese(III). In contrast, manganese(IV), which is considered to be a stronger oxidant than manganese(III),[2] may be able to oxidize $O_2CO_2^-$ or O_2^-. That is why the decomposition rate in the first period was not affected by the dissolved oxygen, while in the second period the rate was strongly depressed.

In conclusion, the decomposition of the quadrivalent

manganese complex, di-μ-oxo-tetrakis(oxalato)dimanganate(IV), can be interpreted as an autocatalytic reaction, where Mn(III) and/or Mn(II) work as catalysts. The reaction proceeds mainly in two ways, one is the $Mn^{IV}+Mn(II)\rightarrow 2\,Mn(III)$ reaction, where Mn(II) is a decomposition product of the Mn(III). The other is a direct reaction between Mn^{IV} and Mn(III). That is to say, the oxalato complex of quadrivalent manganese is relatively stable, and its decomposition rate should be extremely slow in the absence of Mn(III) and/or Mn(II). It was actually observed that the optical density of 0.1 M buffer solution of a pure sample did not change for over 2 hr at 5 °C.

A part of the expenses of this study were defrayed by a Grant for Scientific Research of the Ministry of Education.

References

1) Presented at the 23rd Symposium on Coordination Chemistry, Fukuoka, October, 1973.
2) Y. Yoshino, I. Taminaga, M. Kokiso, and T. Uehiro, This Bulletin, **47**, 2787 (1974).
3) G. H. Cartledge and W. P. Ericks, *J. Amer. Chem. Soc.*, **58**, 2069 (1936).
4) G. H. Cartledge and W. P. Ericks, *ibid.*, **58**, 2061 (1936).
5) G. H. Cartledge and W. P. Ericks, *ibid.*, **58**, 2065 (1936).
6) H. Taube, *ibid.*, **70**, 1218 (1948).
7) J. W. Ladbury and C. F. Cullis, *Chem. Rev.*, **58**, 403 (1958).
8) I. M. Kolthoff, E. J. Meehan, and M. Kimura, *J. Phys. Chem.*, **75**, 3343 (1971).
9) M. Kimura, *ibid.*, **77**, 1265 (1973).

Kinetics of Multidentate Ligand-substitution Reactions. XVIII.* Substitution Reactions of Triethylenetetraaminehexaacetate (TTHA) with Nickel(II)–Dien, –EDMA, and –NTA Complexes

Mutsuo KODAMA

Department of Chemistry, College of General Education, Hirosaki University, Bunkyo, Hirosaki 036

(Received March 22, 1975)

The kinetics of the substitution reactions of TTHA with nickel(II) complexes of diethylenetriamine (Dien), ethylenediaminemonoacetate (EDMA), and nitrilotriacetate (NTA) were studied systematically by employing the polarographic technique. All the substitution reactions were found to have a common reaction mechanism. They were first-order with respect to TTHA and also first-order with respect to a 1 : 1-ratio nickel(II) complex of Dien, EDMA, or NTA. In all the substitution reactions, the rate constants for the reactions involving a completely-deprotonated TTHA anion were nearly identical to those for the corresponding DTPA (diethylenetriaminepentaacetate) reactions, suggesting that the TTHA reaction has the same reaction mechanism as the DTPA reaction. In the Dien system, the rate constant for the reaction of the quadrivalent TTHA anion is nearly identical to that of the quinquivalent TTHA anion, whereas, in the reactions of NTA and EDMA complexes, the reaction of the quadrivalent TTHA anion is drastically slower than that of the quinquivalent TTHA anion. These facts suggest that the proton transfer from the entering group to the leaving group plays an important role in determining the rate of the multidentate ligand-substitution reaction.

The present author has previously studied a series of substitution reactions involving metal(II)-aminopolycarboxylate complexes and has discussed their detailed reaction mechanism.[1–6] In this paper, he will also deal with the kinetics of the substitution reactions of TTHA with nickel(II) complexes of NTA, EDMA, and Dien as an extension of earlier investigations involving metal(II)-aminopolycarboxylate complexes, and will discuss the effect of the basicity of the ligand on the reaction rate. The substitution reactions of DTPA in acid and neutral media will also be studied, and their rates will be compared with those of the TTHA reaction.

Experimental

Reagents. The preparation and standardization of the nickel(II) nitrate solution were described in a previous paper.[1] Reagent-grade NTA and DTPA were recrystallized as their acid forms from their aqueous solutions. The way of purification of Dien used in this study was described in a previous paper.[2] The preparation and recrystallization of the acid forms of TTHA and EDMA were also given previously.[7,8] All the other chemicals used were of an analytical reagent grade and were used without further purification.

Apparatus and Experimental Procedures. The apparatus and experimental procedures employed were the same as those given previously.[9,10] In the EDMA system, no buffer reagent was used, because all the sample solutions always contained a large excess of uncomplexed EDMA and had a big enough buffer capacity over the entire pH range covered ($9.20<pH<10.50$, and $6.30<pH<7.65$). Phosphate ($6.00<pH<8.00$) and acetate ($4.60<pH<5.80$) buffers were used in the Dien and NTA systems respectively. All the kinetic measurements were conducted under experimental conditions in which all the reactions could be treated as pseudo first-order reactions. The rate of the substitution reaction was determined by measuring the change in the dissolution wave-height due to the uncomplexed TTHA or DTPA. The ionic strength of the sample solution was adjusted to 0.30 by adding an appropriate amount of potassium nitrate. The pseudo first-order rate constant, k_{ap}, was determined from the slope of the linear relation between log (i_0/i_t) and time, t.[1]

Results and Discussion

In this study, all the kinetic measurements were conducted under experimental conditions in which the 2 : 1 ratio nickel(II)-TTHA complex was not involved in the mixture of the reaction products. All reactions were run with several different reactant concentrations in order to determine the reaction order with respect to each reactant. Although the results will not be shown here, the rates for all the reactions studied were 1) exactly proportional to the total concentration of the nickel(II) ion, $[Ni(II)]_t$, 2) inversely proportional to $(1+K_2[X]_f/(\alpha_H)_X)$, and 3) proportional to the initial concentration of TTHA, $[TTHA]_l$, when the other experimental conditions are kept constant. These findings suggest that all the reactions studied in this paper are first-order with respect to the 1 : 1 ratio nickel(II) complex of Dien, EDMA, or NTA, and also first-order with respect to TTHA, corresponding to the following rate expression:

$$\text{Rate}=k_{ap}\cdot[TTHA]_l=k_f\cdot\frac{[Ni(II)]_t}{1+\dfrac{K_2}{(\alpha_H)_X}\cdot[X]_f}\cdot[TTHA]_l \qquad (1)$$

Here, $[X]_f$ means the concentration of uncomplexed Dien, EDMA, or NTA; K_2, the second successive formation constant of the nickel(II)–Dien, EDMA, or NTA complex, and $(\alpha_H)_X$, the (α_H) value of Dien, EDMA, or NTA, defined as $1+[H^+]/K_n+[H^+]^2/K_n\cdot K_{n-1}+\cdots+[H^+]^n/K_n\cdots K_1$, where K_i stands for the i-th deprotonation constant of H_nX^{n-m}. k_f in Eq. (1) is a function of the hydrogen-ion concentration.

Dien System. In the pH range from 8.80 to 10.00, the plot of $k_{ap}\cdot(\alpha_H)_Z\cdot(1+K_2[X]_f/(\alpha_H)_X)$ against

* Part XVII: M. Kodama, This Bulletin, **47**, 2200 (1974).

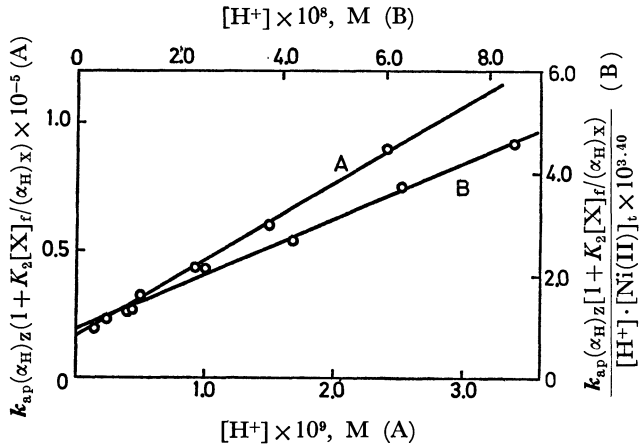

Fig. 1. The relation between $k_{ap}\cdot(\alpha_H)_Z\cdot(1+K_2[X]_f/(\alpha_H)_X)$ and the hydrogen-ion concentration, [H+], (A), and that between $k_{ap}\cdot(\alpha_H)_Z\cdot(1+K_2[X]_f/(\alpha_H)_X)/[H^+]$ and [H+] (B).
$\mu=0.30$, $[Ni(II)]_t=10.0$ mM
$[TTHA]_t=1.0$ mM
(A) Solution pH ranged from 8.80 to 10.00
25 °C, $[Dien]_f=100$ mM
(B) Solution pH ranged from 6.35 to 7.65
1.0 °C, $[Dien]_f=80$ mM

the hydrogen-ion concentration, [H+], invariably gave a straight line with an intercept of a finite value (25 °C). This indicates that the reaction proceeds through two simultaneous reaction pathways involving completely deprotonated and quinquivalent TTHA anions, Z^{6-} and HZ^{5-}. Here, $(\alpha_H)_Z$ is defined as $1+[H^+]/K_6+\cdots+[H^+]^6/K_6\cdot K_5\cdots K_1$, where K_i stands for the i-th dissociation constant of H_6Z. On the other hand, in the pH range from 6.35 to 7.65, the plot of $k_{ap}\cdot(\alpha_H)_Z\times(1+K_2[X]_f/(\alpha_H)_X)/[H^+]$ against [H+] gave a linear relation with an intercept of a finite value (1.0 °C) (Fig. 1). This fact suggests that the reaction in this pH range proceeds through two reaction pathways involving HZ^{5-} and H_2Z^{4-}. Furthermore, thermodynamic calculations using the reported equilibrium constants for the nickel(II)–TTHA and –Dien complexations reveal that the reaction product for the substitution reaction contains an appreciable amount of the protonated nickel(II)–TTHA complex, $NiHZ^{3-}$. Accordingly, the above findings lead to the conclusion that the reaction proceeds through two simultaneous reaction pathways, (3) and (4), in the pH range from 8.80 to 10.00 and in the pH range from 6.35 to 7.65 through (4) and (5), both reactions being preceded by the rapid dissociation of NiX_2^{2-2m} (2).

$$NiX_2^{2-2m} \rightleftharpoons NiX^{2-m} + X^{m-} \quad \text{rapid} \qquad (2)$$

$$NiX^{2-m} + \left\{\begin{array}{ll} Z^{6-} \overset{k_0}{\rightleftharpoons} NiZ^{4-} + X^{m-} & (3) \\ HZ^{5-} \overset{k_H}{\rightleftharpoons} NiHZ^{3-} + X^{m-} & (4) \\ H_2Z^{4-} \overset{k_{2H}}{\rightleftharpoons} NiHZ^{3-} + HX^{1-m} & (5) \end{array}\right\} \text{slow}$$

As in the case of the reaction of the nickel(II)–NTA complex with DTPA,[9] the rate constants, k_0, k_H, and k_{2H}, for the reaction of TTHA with the nickel(II)–Dien complex were determined from the intercepts and slopes of the linear relations in Fig. 1; they are listed in Table 1.

Table 1. Rate constants ($M^{-1}\,s^{-1}$, $\mu=0.30$)

	System	k_0	k_H	k_{2H}	Temp. °C
DTPA	NTA[9]	9.1×10^2	3.06×10^2	1.78	25
	EDMA[12]	1.4×10^3	2.58×10^2	—	25
		—	8.32×10^1	5.90×10^1	1.0
	Dieen[12]	7.2×10^5	9.80×10^4	—	25
		—	3.0×10^4	2.0×10^4	1.0
TTHA	NTA	2.8×10^3	9.65×10^2	1.06	25
	EDMA	4.3×10^3	2.86×10^3	4.36	25
	Dien	1.5×10^6	5.46×10^5	—	25
		—	2.7×10^4	3.0×10^3	1.0

EDMA System. In the EDMA system, all the kinetic measurements were conducted at 25 °C. in the pH range from 8.40 to 10.30, a straight line with an intercept of a finite value could be obtained by plotting $k_{ap}\cdot(\alpha_H)_Z\cdot(1+K_2[X]_f/(\alpha_H)_X\cdot)$ against [H+], whereas, in the pH range from 7.00 to 8.14, it could be obtained by plotting the $k_{ap}\cdot(\alpha_H)_Z\cdot(1+K_2[X]_f/(\alpha_H)_X)/[H^+]$ value against [H+]. Therefore, the reaction of the EDMA complex can be concluded to proceed through (3) and (4) in the former pH range and through (4) and (5) in the latter pH range. From the intercept and slope of the linear relation between $k_{ap}\cdot(\alpha_H)_Z\cdot(1+K_2[X]_f/(\alpha_H)_X)$ and [H+], the k_0 and k_H values were determined. The k_{2H} value was determined from the slope of the linear relation between $k_{ap}\cdot(\alpha_H)_Z\cdot(1+K_2[X]_f/(\alpha_H)_X)/[H^+]$ and [H+] obtained in the pH range from 7.00 to 8.14. They are also listed in Table 1. The k_H value estimated from the intercept of the linear relation at pH's lower than 8.14 agreed well with that estimated from the slope of the linear relation at pH's higher than 8.40. The influence of the phosphate buffer on the reaction rate was also investigated. No effect on the rate constant was observed that can be attributed to the buffer reagent.

NTA System. As in the case of the EDMA system, the reaction rates were determined at 25 °C. In the pH range from 8.46 to 9.50, the $k_{ap}\cdot(\alpha_H)_Z\cdot(1+K_2[X]_f/(\alpha_H)_X$ value gave a straight line with an intercept of a finite value when it was plotted against [H+], whereas, in the pH range from 4.50 to 5.70, the $k_{ap}\cdot(\alpha_H)_Z\cdot(1+K_2[X]_f/(\alpha_H)_X)/[H^+]^2$ gave a linear relation when it was plotted against [H+]. These facts indicate that the reaction proceeds through (3) and (4) in the range from 8.40 to 9.50, and through (5) and (6) in the pH range from 4.50 to 5.70.

$$NiX_2^{2-m} \rightleftharpoons NiX^{2-m} + X^{m-} \quad \text{rapid} \qquad (2)$$

$$NiX^{2-m} + H_3Z^{3-} \underset{\text{slow}}{\overset{k_{3H}}{\rightleftharpoons}} NiH_2Z^{2-} + HX^{1-m} \qquad (6)$$

The rate constants, k_0 and k_H, were determined from the intercept and slope of the linear relation between the $k_{ap}\cdot(\alpha_H)_Z\cdot(1+K_2\cdot[X]_f/(\alpha_H)_X)$ value and [H+], and the k_{2H} value from the intercept of the linear relation between $k_{ap}\cdot(\alpha_H)_Z\cdot(1+K_2\cdot[X]_f/(\alpha_H)_X)/[H^+]^2$ and [H+]. The calculation using the rate constant for

the proton-assisted dissociation of the 1 : 1 ratio nickel (II)–NTA complex determined by Kimura[11] reveals that, under the present experimental conditions, the contribution of the dissociation of the nickel(II)–NTA complex to the overall reaction rate is negligibly small. The k_H and k_{2H} values for the DTPA reactions with the nickel(II)–EDMA and –Dien complexes (1.0 °C) and with the nickel(II)–NTA complex (25 °C) were also determined by examining the effect of the solution's pH on the reaction rate. The rate constants for the DTPA reactions obtained are also listed in Table 1.

Previously, the present author determined the detailed reaction mechanism of DTPA reactions with the nickel(II)–NTA,[6] –EDMA,[3,12] and –Dien[3,12] complexes from a comparison of the observed rate constants. The substitution reaction of DTPA with the NTA complex was found to proceed through a glycinate reaction intermediate, where the leaving NTA anion and the entering DTPA anion are bonded to the nickel(II) ion through the glycinate and iminodiacetate chelate rings (glycinate reaction mechanism) respectively, while those with the nickel(II)–EDMA and –Dien complexes proceeded through an ethylenediamine reaction intermediate, in which the leaving EDMA or Dien anion and the entering DTPA anion are bonded to the nickel(II) ion through ethylenediamine (En) and glycinate (Gly) chelate rings respectively (ethylenediamine reaction mechanism). As is shown in Table 1, the k_0 values of the TTHA reactions are nearly identical to those of the corresponding DTPA reactions. This fact evidently suggests that the rates of the TTHA reaction with the NTA complex can be understood by assuming the glycinate reaction mechanism, and those with the EDMA and Dien complexes, by assuming the ethylenediamine reaction mechanism. Furthermore, the above fact indicates that, despite its large molecular size, the entering TTHA anion exerts practically no steric effect on the reaction rate. This can be cheifly ascribable to the free-bond rotation of the TTHA anion and the leaving ligand involved.

In the EDMA and NTA systems, the addition of the first proton to the TTHA anion, Z^{6-}, exerts little effect on the reaction rate, whereas the addition of the second proton to the TTHA anion remarkably diminishes the rate constant. In the Dien system, however, the second proton addition of the entering ligand causes only a small change in the reaction rate. Bohigian and Martell[13] have reported that the second protonation constant of the TTHA anion is nearly identical to its first protonation constant. This suggests that, in the quadrivalent TTHA anion, H_2Z^{4-}, two terminal nitrogen atoms are protonated. The present author has mentioned in his polarographic study of the zinc(II)–GEDTA (2,2′-ethylenedioxydi(ethylamine)-*N,N,N′N′*-tetraacetate) complex that the deprotonation of one of two terminal nitrogen atoms of the divalent GEDTA anion is required in its complexation reaction with the zinc(II) ion.[14] Similarly, in the reaction of the quadrivalent TTHA anion with the metal(II) complex ion, the deprotonation of one of the two terminal nitrogen atoms is also required. In the formation of the reaction intermediate of the multidentate ligand-substitution reaction, the protons of the entering ligand will be redistributed between it and the leaving ligand, depending on the relative basicity of their coordination sites. In the light of the structures of the reaction intermediates proposed, the free basic site of the leaving ligand, which can act as a proton acceptor in the NTA and EDMA systems, is the weakly basic carboxylate group, whereas that in the Dien system is the amino group. Therefore, in the latter system, the leaving group can accept the proton from the quadrivalent TTHA anion easily, and the ethylenediamine reaction intermediate is formed between the 1 : 1 ratio nickel(II)–Dien complex and H_2Z^{4-} without any difficulty. Thus, the second proton addition of the entering ligand, the TTHA anion, causes only a small change in the reaction rate. On the other hand, in the former systems, because of the weak basicity of the carboxylate group, the second protonation of the terminal nitrogen atom of the TTHA anion hinders the formation of the reaction intermediate and diminishes the rate constant remarkably. The rate constants obtained for the DTPA reactions listed in Table 1 also support the above explanation of the effect of the protonation of the entering ligand on the reaction rate.

References

1) M. Kodama, S. Karasawa, and T. Watanabe, This Bulletin, **44**, 1815 (1971).
2) M. Kodama, T. Sato, and S. Karasawa, *ibid.*, **45**, 2757 (1972).
3) M. Kodama, M. Hashimoto, and T. Watanabe, *ibid.*, **45**, 2761 (1972).
4) M. Kodama and K. Hagiya, *ibid.*, **46**, 3151 (1973).
5) M. Kodama, *ibid.*, **47**, 1430 (1974).
6) M. Kodama, *ibid.*, **47**, 2200 (1974).
7) A. Itoh and K. Ueno, *Japan Analyst*, **17**, 327 (1968).
8) Y. Fujii, E. Kyuno, and R. Tsuchiya, This Bulletin, **43**, 786 (1970).
9) M. Kodama, *ibid.*, **42**, 2532 (1969).
10) M. Kodama, *ibid.*, **47**, 1434 (1974).
11) M. Kimura, *Nippon Kagaku Zasshi*, **89**, 1209 (1967).
12) M. Kodama, Y. Fujii, and T. Ueda, This Bulletin, **43**, 2085 (1970).
13) T. A. Bohigian and A. E. Martell, *J. Inorg. Nucl. Chem.*, **26**, 3 (1964).
14) M. Kodama and N. Oyama, This Bulletin, **45**, 2169 (1972).

The Kinetics and Mechanisms of Reaction of Iodine with Bis(*N*,*N*-diethyldithiocarbamato)dimethyltin(IV) and Related Compounds

Hidetoshi KITA, Koji TANAKA, and Toshio TANAKA

Department of Applied Chemistry, Faculty of Engineering, Osaka University, Suita, Osaka 565

(Received March 25, 1975)

The reactions of $Me_2SnL(S_2CNEt_2)$ ($L=S_2CNEt_2$ (**1**) and I (**2**)) with iodine in cyclohexane were investigated employing a stopped-flow technique. The kinetic data indicate that the reaction in the presence of a large excess of **1** or **2** proceeds *via* a charge-transfer complex of $Me_2SnL(S_2CNEt_2)\cdot I_2$, which decomposes in the rate-determining step to yield $Me_2SnI(L)$ and unstable $I(S_2CNEt_2)$. This unstable intermediate reacts with the excess **1** or **2** to afford $Me_2SnI(L)$ and tetraethylthiuramdisulfide (**3**). The reaction of **1** with a large excess of I_2 was also kinetically studied to reveal the formation of the 1 : 2 complex, $Me_2Sn(S_2CNEt_2)_2\cdot 2I_2$, as an intermediate; this intermediate then undergoes a simultaneous degradation to afford Me_2SnI_2 and **3**. The transition state in the reaction is discussed.

Several reactions of dithiocarbamato-metal complexes with halogen have been reported thus far; bis(*N*,*N*-dialkyldithiocarbamato)zinc(II), -cadmium(II) and -mercury(II) react with X_2 (X=Cl, Br, I) in the mole ratio of 1 : 1 to give adducts between MX_2 (M=Zn, Cd, Hg) and tetraalkylthiuramdisulfide, $MX_2(R_4tds)$ ($R_4tds=[R_2NC(S)S\text{-}]_2$).[1] On the other hand, *N*,*N*-dialkyldithiocarbamato complexes of Cu(I),[2] Au(I)[2] and Ni(II)[1] oxidatively add X_2 to yield $MX_2(S_2CNR_2)$ (M=Cu, Au) and $NiX(S_2CNR_2)_3$ respectively. These reactions, however, have not been studied kinetically.

Recently, we have noticed that $Me_2Sn(S_2CNEt_2)_2$ and $Me_2SnI(S_2CNEt_2)$ react with I_2 to give $Me_2SnI(S_2CNEt_2)$ and Me_2SnI_2 respectively, together with tetraethylthiuramdisulfide. This paper will report on our kinetic and mechanistic studies of these reactions as well as that of $Me_2Sn(S_2CNEt_2)_2$ with an excess of I_2 in cyclohexane. The stability constant of the charge-transfer complex between tetraethylthiuramdisulfide and iodine is also obtained.

Experimental

Materials. Bis(*N*,*N*-diethyldithiocarbamato)dimethyltin(IV), $Me_2Sn(dtc)_2$ ($dtc=S_2CNEt_2$), was obtained as has been described in a previous paper.[3] *N*,*N*-Diethyldithiocarbamatodimethyliodotin(IV), $Me_2SnI(dtc)$, was prepared by the reaction of $Me_2SnCl(dtc)$ with a large excess of NaI in acetone in the manner described previously;[3] it was then recrystallized from ligroin; mp 124 °C. Found: C, 19.82; H, 4.04; N, 3.50%. Calcd for $C_7H_{16}NS_2ISn$: C, 19.84; H, 3.81; N, 3.31%.

Iodine was purified by sublimation five times. Commercially available tetraethylthiuramdisulfide, Et_4tds ($tds=\rangle NC(S)S\cdot SC(S)N\langle$), was recrystallized from ligroin; mp 70 °C. Cyclohexane used as a solvent in the kinetic experiments was purified in the usual manner.[4]

Reactions. (i) A solution of I_2 (1.02 mmol) in benzene (20 ml) was added to $Me_2Sn(dtc)_2$ (2.38 mmol) in the same solvent (20 ml) at room temperature. The solution was stirred for 30 min, and then evaporated to dryness under reduced pressure. The resulting solid was recrystallized from ligroin to afford white crystals of $Me_2SnI(dtc)$ (1.87 mmol). The filtrate after recrystallization was evaporated to dryness again to give Et_4tds (0.84 mmol).

(ii) A benzene solution (20 ml) containing I_2 (0.5 mmol) and $Me_2SnI(dtc)$ (1.9 mmol) was stirred for 1 hr at room temperature; the subsequent application of the procedure described above gave Me_2SnI_2 (0.6 mmol).

(iii) A benzene solution (20 ml) of $Me_2Sn(dtc)_2$ (2.3 mmol) was added to the excess of I_2 (4.5 mmol) in the same solvent (20 ml) at room temperature. The solution was then stirred for 3.5 hr, filtered, and evaporated to a small volume. The precipitate which appeared was collected by filtration and recrystallized from petroleum ether to afford $Me_2SnI(dtc)$ (0.3 mmol). The filtrate was evaporated to give a solid product, from which Me_2SnI_2 (1.5 mmol) was obtained.

Spectra. The electronic spectra were recorded on a Hitachi 124 spectrophotometer. The infrared spectra were measured in Nujol mulls on a Hitachi EPI-L spectrophotometer.

Kinetics. Kinetic experiments were carried out under pseudo-first-order conditions at 25 °C, using at least a ten-fold excess amount of either iodine or the tin compound. The rate of reaction was followed by monitoring the transmittance at a fixed wavelength in the electronic spectra of the reaction mixture, using a Union RA-1100 stopped-flow spectrophotometer equipped with a 1-cm quartz cell. The measurements were usually made over a period of 3 half-lives of the reaction. Pseudo-first-order rate constants, k_{obsd}, were obtained from the semi-logarithmic plots of $\ln(A_t-A_\infty)$ against time, where A_t and A_∞ are absorbances at a given wavelength at time t and at the end of the reaction respectively. Rapid scanning spectra were measured on a Union RA-1300 stopped-flow reaction analyzer in order to determine the wavelength of which the reaction could best be followed.

Results and Discussion

Stoichiometry of the Reaction. The reaction of I_2 with excess $Me_2Sn(dtc)_2$ rapidly proceeds to give $Me_2SnI(dtc)$ and Et_4tds in good yields. Iodine also reacts with $Me_2SnI(dtc)$ to afford Me_2SnI_2 and Et_4tds; this reaction is reversible. The forward and backward reactions require a few minutes and several days respectively to come to an equilibrium. Thus, the stoichiometry for the reaction of $Me_2Sn(dtc)_2$ with I_2 may be expressed as follows:

$$Me_2Sn(dtc)_2 + \frac{1}{2}I_2 \xrightarrow{\text{fast}} Me_2SnI(dtc) + \frac{1}{2}Et_4tds \quad (1)$$

$$Me_2SnI(dtc) + \frac{1}{2}I_2 \underset{\text{very slow}}{\overset{\text{slow}}{\rightleftharpoons}} Me_2SnI_2 + \frac{1}{2}Et_4tds \quad (2)$$

Stability Constant of the Charge-transfer Complex between I_2 and Et_4tds. By analogy with the formation of a stable charge-transfer complex between I_2 and

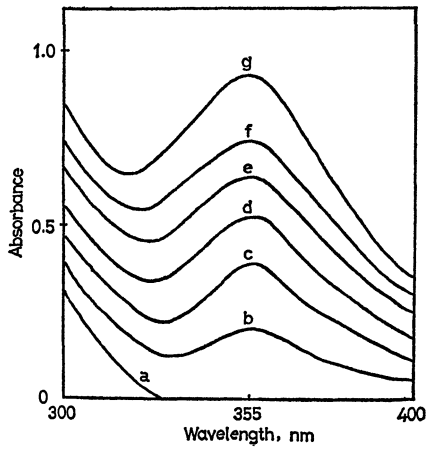

Fig. 1. Absorption spectra of Et_4tds in cyclohexane (1.0×10^{-4} M) containing varying amounts of I_2: (a) 0, (b) 1.0×10^{-3}, (c) 2.0×10^{-3}, (d) 3.0×10^{-3}, (e) 4.0×10^{-3}, (f) 5.0×10^{-3}, (g) 8.0×10^{-3} M (25 °C).

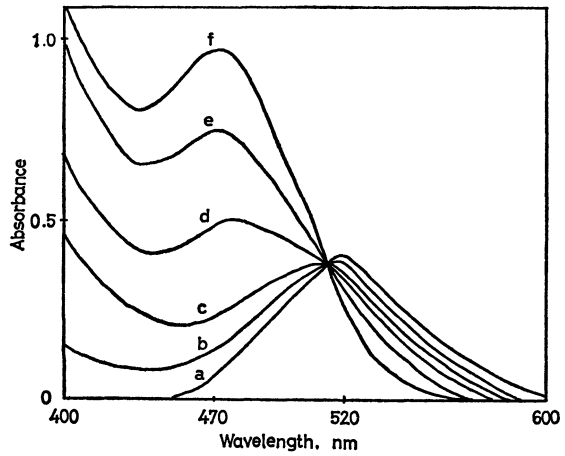

Fig. 2. Absorption spectra of I_2 in cyclohexane (8.0×10^{-4} M) containing varying amounts of Et_4tds: (a) 0, (b) 8.0×10^{-4}, (c) 1.6×10^{-3}, (d) 4.0×10^{-3}, (e) 8.0×10^{-3}, (f) 1.6×10^{-2} M (25 °C).

N-methylthioacetamide,[5] *N*-methylthiocarbamate[5] or other sulfur containing compounds,[5,6] I_2 may be expected to form a complex with Et_4tds, which is the reaction product between I_2 and $Me_2Sn(dtc)_2$ or $Me_2SnI(dtc)$. In accordance with this, cyclohexane solutions containing Et_4tds and I_2 exhibit an absorption at 355 nm, which is intensified with an increase in the amounts of I_2, as is shown in Fig. 1. Thus, the 355 nm band can unequivocally be assigned to the CT transition from Et_4tds to I_2. Figure 2 shows the electronic spectra of I_2 in cyclohexane containing varying amounts of Et_4tds. The 520 nm band due to I_2 is shifted to a short wavelength (470 nm) by adding Et_4tds, and an isosbestic point is observed at 515 nm. The continuous-variation method at 470 nm revealed that the composition of the CT complex is 1 : 1. Thus, the following equilibrium takes place in solution:

$$I_2 + Et_4tds \rightleftharpoons I_2\cdot Et_4tds \quad (3)$$

The equilibrium constant, as calculated from the absorbances at 470 nm ($\varepsilon_{max}=2.14\times10^3$) by means of the Rose-Drago equation,[7] was $K=3.75\ (\pm0.01)\times10^2$ in cyclohexane at 25 °C.

Reaction of I_2 with Excess $Me_2Sn(dtc)_2$ or $Me_2SnI(dtc)$. The rapid scanning spectra for the reaction of I_2 with excess $Me_2Sn(dtc)_2$ are depicted in Fig. 3, which reveals that a strong band appears at 386 nm immediately after mixing and that the band decays with a half-life of about 200 ms. An almost identical half-life of decay was found at the 520 nm band. The reaction of I_2 with excess $Me_2SnI(dtc)$ also showed the decay of the 386 nm band with a half-life of about 40 s. However, the CT band due to $I_2\cdot Et_4tds$ at 355 nm was not observed at all.

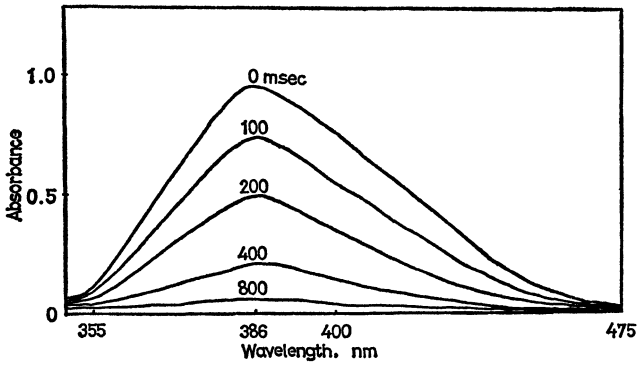

Fig. 3. The decay of the electronic spectrum after mixing I_2 (1.7×10^{-3} M) with $Me_2Sn(dtc)_2$ (3.0×10^{-2} M) in cyclohexane at 25 °C.

The rate of reaction was followed by measuring the transmittances at 386 and 520 nm of a solution right after the mixing of I_2 with excess $Me_2Sn(dtc)_2$. The Guggenheim plots showed a good linear relationship between $\ln(A_t-A_\infty)$ and the time. Thus, the reaction apparently obeys the first-order kinetics with respect to I_2. The apparent first-order rate constants, k_{obsd}, obtained at various concentrations of $Me_2Sn(dtc)_2$ are collected in Table 1.

Plots of the rate constants obtained from the decay of the transmittances at 386 and 520 nm against the concentration of $Me_2Sn(dtc)_2$ showed a good linearity, as may be seen in Fig. 4; this indicates that the reaction is first-order in both I_2 and $Me_2Sn(dtc)_2$.

Taking into account this result and the fact that I_2 can form CT complexes with various sulfur-containing compounds,[5,6] the band at 386 nm may be

Table 1. Apparent rate constants for the reactions of $Me_2Sn(dtc)_2$ with I_2 at various mole ratios in cyclohexane at 25 °C. $[I_2]=3.0\times10^{-4}$ M

[Sn]/[I_2]	10	20	30	40	50	60	80
k_{obsd} (386 nm)	0.263	0.527	0.846	1.08	1.32	1.57	2.24
k_{obsd} (520 nm)	0.268	0.555	0.761	1.02	1.32	1.63	2.16

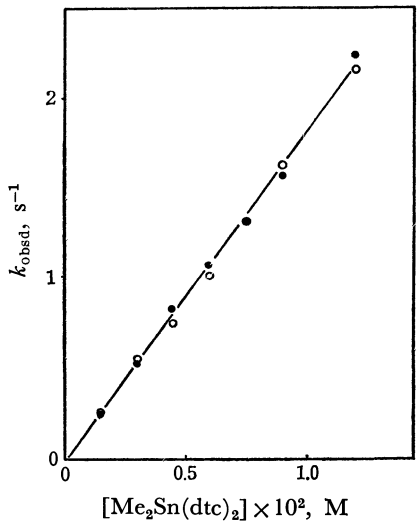

Fig. 4. Plots of the apparent rate constant against the $Me_2Sn(dtc)_2$ concentrations; ● 386 nm, ○ 520 nm.

assigned to the CT complex formed between I_2 and $Me_2Sn(dtc)_2$ in the initial process. The addition of Et_4tds to the reactant solution caused no appreciable decrease in the rate of reaction. Thus, the following pathways for the reaction may reasonably be suggested:

$$Me_2Sn(dtc)_2 + I_2 \overset{K_1}{\rightleftharpoons} Me_2Sn(dtc)_2 \cdot I_2 \quad (4)$$

$$Me_2Sn(dtc)_2 \cdot I_2 \overset{k_1}{\longrightarrow} Me_2SnI(dtc) + I(dtc) \quad (5)$$

$$I(dtc) + Me_2Sn(dtc)_2 \overset{fast}{\longrightarrow} Me_2SnI(dtc) + Et_4tds \quad (6)$$

Reaction (5) represents the rate-determining step, producing unstable I(dtc). Although there is no evidence for the formation of I(dtc) as an intermediate, a somewhat analogous species, ISCN, has been reported to exist in the following equilibrium:[8]

$$I^- + (SCN)_2 \rightleftharpoons I(SCN)_2^- \rightleftharpoons ISCN + SCN^- \quad (7)$$

It may be possible that the two molecules of I(dtc) produced in Eq. (5) react with each other to afford I_2 and Et_4tds, but this reaction dose not seem to occur, since no band was observed at 355 nm (due to $I_2 \cdot Et_4tds$) at all in the presence of excess $Me_2Sn(dtc)_2$. Instead, I(dtc) must react rapidly with excess $Me_2Sn(dtc)_2$ to give $Me_2SnI(dtc)$ and Et_4tds, as is shown in Eq. (6). According to this reaction scheme, k_{obsd} can be expressed by Eq. (8):

$$k_{obsd}^{(1)} = \frac{k_1K_1[Me_2Sn(dtc)_2]}{1+K_1[Me_2Sn(dtc)_2]} \quad (8)$$

If $K_1[Me_2Sn(dtc)_2]$ is negligibly small compared with unity, $k_{obsd}^{(1)}$ is reduced to $k_1K_1[Me_2Sn(dtc)_2]$. This expression is consistent with the plots of k_{obsd} against the concentration of $Me_2Sn(dtc)_2$ with a zero intercept (Fig. 4). Thus, k_1K_1 is obtained as 1.84×10^2 M^{-1} s^{-1}.

Kinetic experiments on the reaction of $Me_2SnI(dtc)$ with I_2 were carried out by monitoring the transmittance only at 386 nm, since there was no marked change in the transmittance at 520 nm in this system because of the low solubility of $Me_2SnI(dtc)$ in cyclohexane. The k_{obsd} values obtained at various concentrations of $Me_2SnI(dtc)$ are listed in Table 2, which shows the reaction to be first-order in both $Me_2SnI(dtc)$ and I_2.

Table 2. Apparent rate constants for the reaction of $Me_2SnI(dtc)$ with I_2 at various mole ratios in cyclohexane at 25 °C. $[I_2] = 3.3 \times 10^{-4}$ M

$[Sn]/[I_2]$	23	28	38	47
$k_{obsd} \times 10^2$ (386 nm)	1.10	1.24	1.59	2.08

By analogy with the $Me_2Sn(dtc)_2$–I_2 system, the following pathways may be postulated, where $k_2K_2 = 1.37$ M^{-1} s^{-1}:

$$Me_2SnI(dtc) + I_2 \overset{K_2}{\rightleftharpoons} Me_2SnI(dtc) \cdot I_2 \quad (9)$$

$$Me_2SnI(dtc) \cdot I_2 \overset{k_2}{\longrightarrow} Me_2SnI_2 + I(dtc) \quad (10)$$

$$I(dtc) + Me_2SnI(dtc) \overset{fast}{\longrightarrow} Me_2SnI_2 + Et_4tds \quad (11)$$

Since both K_1 and K_2 are unknown, k_1K_1 and k_2K_2 have been difficult to analyze quantitatively.

Reaction of $Me_2Sn(dtc)_2$ with Excess I_2. The rate of reaction was determined from the decay of the transmittance at 386 nm. A good linear relationship between the $\ln(A_t - A_\infty)$* and the time was observed, except for the final short period, in which the 355 nm band arising from the product of $I_2 \cdot Et_4tds$ is intensified and the tail of this band is overlapped with the 386 nm band. Plots of k_{obsd} *vs.* the square of I_2 concentrations gave a straight line in the presence of a large excess of I_2, while a significant deviation from it was observed in the presence of a small excess of I_2, as is shown in Fig. 5. These results may be interpreted by assuming the reaction pathways shown in Scheme 1.

One of the pathways involves the formation of the 1 : 2 adduct between $Me_2Sn(dtc)_2$ and I_2, which

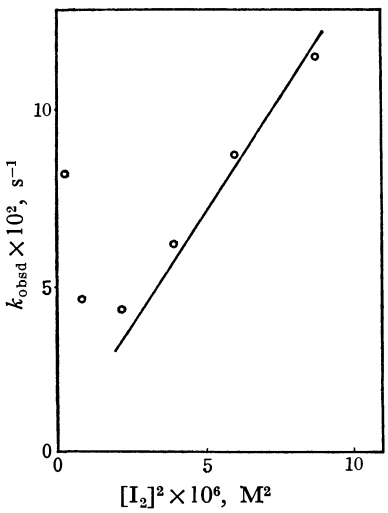

Fig. 5. Plots of the apparent rate constant against the square of the I_2 concentrations; $Me_2Sn(dtc)_2$ 5.1×10^{-4} M.

* Here, A_∞ was assumed to be zero.

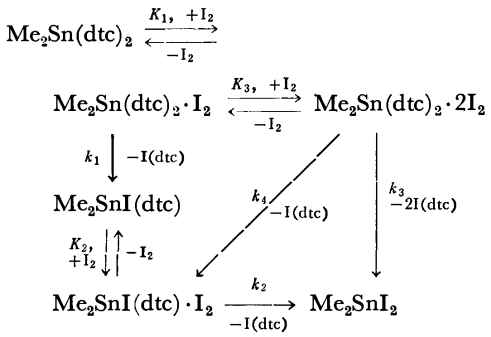

Scheme 1.

undergoes either consecutive (k_4 and k_2 in Scheme 1) or simultaneous (k_3) degradation to yield Me_2SnI_2 and $I_2 \cdot Et_4tds$. These processes can well explain the second-order dependence of the I_2 concentration. Taking into account the result that the reaction is much faster than that of I_2 with excess $Me_2SnI(dtc)$, the simultaneous degradation of the 1 : 2 adduct is preferable to the consecutive one. Another route is the successive formation of two 1 : 1 adducts, $Me_2Sn(dtc)_2 \cdot I_2$ and $Me_2SnI(dtc) \cdot I_2$, followed by degradation such as has been described above. This pathway leads us to the assumption that the reaction obeys the first-order kinetics in the I_2 concentration, because $k_1K_1 \gg k_2K_2$. It may, therefore, be assumed that, in the presence of a small excess of I_2, the processes *via* both the 1 : 1 and 1 : 2 adducts take place. Thus, in the presence of a large excess of I_2, the rate constant can be expressed by Eq. (12):

$$k^{(2)}_{obsd} = \frac{k_3K_1K_3[I_2]^2}{1+K_1K_3[I_2]^2} \qquad (12)$$

If $K_1K_3[I_2]^2$ is negligibly small compared with unity, one can obtain $k^{(2)}_{obsd}=k_3K_1K_3[I_2]^2$, which coincides with the experimental data, and $k_3K_1K_3=1.34\times 10^4\ M^{-2}\ s^{-1}$.

There are two possible mechanisms to form the unstable 1 : 2 adduct between $Me_2Sn(dtc)_2$ and I_2. One is a nucleophilic attack of two I_2 molecules on the tin atom. This is, however, not likely to occur, since no eight-coordination of tin is common. The other mechanism is an electrophilic attack of I_2 on the sulfur of separate dithiocarbamato ligands in a given complex, such as is shown in **a**. This can be assumed on the basis of the fact that I_2 forms CT complexes with various sulfur-containing compounds.[5,6]

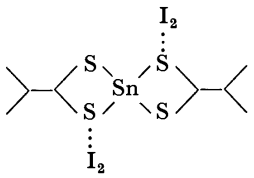

a

In conclusion, we propose that the reaction proceeds through a transition state involving a six-membered ring formed by the electrophilic attack of I_2 on the sulfur as follows: This mechanism predicts that the

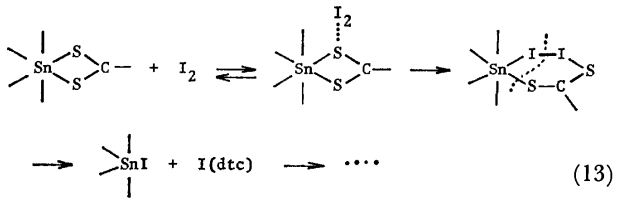

(13)

stronger Sn-S bond would be, the less reactive toward I_2. This is consistent with the present result that the rate of the reaction of $Me_2SnI(dtc)$ with I_2 is slower than that of $Me_2Sn(dtc)_2$, since the ν(Sn-S) frequency of $Me_2SnI(dtc)$ (393 cm^{-1}) is fairly higher than that of $Me_2Sn(dtc)_2$ (366 cm^{-1}).

The authors are grateful to the Ministry of Education for a Science Research Grant-in-aid. They are also indebted to Professor Shin-ichi Kawaguchi, Osaka City University, for letting them use the rapid-scan spectrophotometer.

References

1) H. C. Brinkhoff, J. A. Cras, J. J. Steggerda, and J. Willemse, *Rec. Trav. Chim. Pays-Bas*, **88**, 633 (1969).
2) D. Coucouvanis, *Progr. Inorg. Chem.*, **11**, 272 (1970).
3) M. Honda, M. Komura, Y. Kawasaki, T. Tanaka, and R. Okawara, *J. Inorg. Nucl. Chem.*, **30**, 3231 (1968).
4) J. A. Riddick and E. E. Toops, Jr., "Technique of Organic Chemistry," Vol. VII, 2nd Ed., ed. by A. Weissberger, Interscience Publishers, New York, N.Y. (1955), p. 307.
5) K. R. Bhaskar, S. N. Bhat, A. S. N. Murthy, and C. N. R. Rao, *Trans. Faraday Soc.*, **62**, 788 (1966).
6) G. Reichenbach, S. Santini, and U. Mazzucato, *J. Chem. Soc., Faraday I*, **69**, 143 (1973).
7) N. J. Rose and R. S. Drago, *J. Amer. Chem. Soc.*, **81**, 6138 (1959).
8) C. Long and D. A. Skoog, *Inorg. Chem.*, **5**, 206 (1966).

Metal Chelates of 9-Hydroxy-1-phenalenone

Yoichi DEMURA, Toshio KAWATO, Hajime KANATOMI, and Ichiro MURASE

Laboratory of Chemistry, College of General Education, Kyushu University, Ropponmatsu, Chuo-ku, Fukuoka 810

(Received April 11, 1975)

Metal chelates of 9-hydroxy-1-phenalenone(9-hydroxyperinaphthenone) have been prepared. Metal-ligand compositions were 1 : 2 for Cu(II), Ni(II), Co(II), Mn(II), Zn(II), Mg(II), UO_2(II), and Be(II) chelates and 1 : 3 for Fe(III) and Al(III) chelates. The structure of the Cu(II) chelate was determined to be square-planar by the spectral analogy to copper(II) acetylacetonate. The Ni(II), Co(II), Mn(II), Zn(II), and Mg(II) chelates were octahedral with further coordination of two moles of water. The structure determination dealt at first with the Ni(II) chelate by means of its electronic spectrum and magnetic property; the others were studied using the similarity of their X-ray diffraction diagrams to that of the Ni(II) chelate. The Fe(III) and Al(III) chelates were also octahedral and probably have D_3 symmetry. Infrared spectra were studied for the free ligand and the metal chelates and the assignment of the carbonyl and metal-oxygen stretching vibrations was discussed by comparison with those of metal acetylacetonates.

9-Hydroxy-1-phenalenone (abbreviated as HPNA), which was first synthesized by Laudon,[1] carries a hydroxyl group at a *peri* position to a carbonyl group and can be regarded as a cyclic analogue of an enol form of acetylacetone. Although metal chelates of acetylacetone have been studied extensively, those of HPNA have not been reported so far. The chemical behavior of HPNA is anomalous as a ketone or a phenol because the hydroxyl group is neither acetylated nor methylated and the carbonyl group affords no oxime or Schiff bases. This is assumed to be due to a very strong conjugated hydrogen bonding between the functional groups and it is evidenced by the fact that HPNA exhibits no absorption due to the OH stretching vibration and shows anomalous carbonyl stretching frequency in its infrared spectrum. In this respect the metal chelate formation of this compound as a bidentate ligand will be worth investigating. In this paper, we deal with the synthesis of the metal chelates and their structure determination and will discuss the infrared assignment of the carbonyl and metal-oxygen vibrations in comparison with those of metal acetylacetonates.

Experimental

Infrared absorption spectra were taken by a Koken Model DS-301 with NaCl prism for the 4000—700 cm^{-1} region and by a Hitachi EPI-G2 grating spectrophotometer for the 700—400 cm^{-1}. Electronic reflectance spectra were measured with a Hitachi EPS-3T spectrophotometer. NMR spectra were recorded at 60 MHz in $CDCl_3$ with a Hitachi Model R-24 spectrometer. The chemical shifts are quoted as τ values relative to TMS. X-Ray diffraction diagrams were obtained with a Rigakudenki Geigarflex and magnetic moments were measured by a Faraday method at room temperature.

9-Hydroxy-1-phenalenone(HPNA) was prepared according to the method of Laudon[1] and purified by vacuum sublimation followed by repeated recrystallization from methanol: yellow plates, mp 199—200 °C.

Metal Chelates were prepared by the following general procedure: one mol of HPNA was dissolved in hot ethanol and to this was added 1/2 mol of a divalent metal salt or 1/3 mol of a trivalent metal salt in minimum amount of dilute ethanol. The mixture was heated in a water bath for 30 min and the resulting precipitates were filtered after cooling and washed with ethanol. The crude metal chelates were recrystallized from butanol for those of Ni(II), Co(II), Mn(II), Zn(II), and Mg(II) or from pyridine for those of Cu(II), UO_2(II), Be(II), Al(III), and Fe(III), and dried *in vacuo* at room temperature. When the Ni(II) and Co(II) chelates were recrystallized from pyridine, the dipyridinate complexes were obtained. The metal salts employed in the reactions were acetates, except for beryllium nitrate, potassium alum, and ferric chloride hexahydrate. The sodium salt was prepared by adding excess sodium ethoxide in ethanol to the absolute ethanol solution of HPNA. The elemental analyses of these metal chelates are summarized in Table 1.

Results and Discussion

It has been found that 9-hydroxy-1-phenalenone (HPNA) showed fairly strong chelating tendencies, yielding chelates with a wide variety of metal ions. The elemental analyses revealed that the metal-ligand composition was 1 : 2 for the bivalent metal chelates and that they carried two moles of water, except for the Cu(II) and Be(II) chelates.

Because of their low solubility in ordinary organic solvents, the spectroscopic study of these metal chelates had to be done in the solid state. Figure 1 shows a reflectance spectrum of the Cu(II)-chelate, in which one can observe at least two and probably three d-d transition bands at 18.5×10^3, 15.6×10^3, and 14.5×10^3 cm^{-1}. The spectral pattern is similar to that obtained for bisacetylacetonatocopper(II),[2] whose structure has been established to be square-planar by X-ray crystallography.[3] It is obvious, therefore, that the Cu(II)-chelate has a similar square-planar structure.

The Ni(II) dihydrate complex was paramagnetic (μ_{eff}=3.48 B.M.) and the waters could be replaced by two pyridine molecules by recrystallization from the solvent; the dipyridinate complex was also

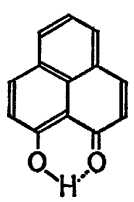

HPNA

Scheme 1.

Table 1. Elemental analyses of metal chelates of 9-hydroxy-1-phenalenone

Formula	C%		H%		M%	
	Calcd	Found	Calcd	Found	Calcd	Found
$C_{13}H_7O_2Na$	71.56	71.23	3.23	3.63	10.54	10.31
$C_{26}H_{14}O_4Cu$	68.79	69.17	3.11	3.39	14.00	13.81
$C_{26}H_{14}O_4Ni$	69.53	69.06	3.14	3.09	—	—
$C_{26}H_{14}O_4Ni\ 2H_2O$	64.37	64.13	3.74	3.93	12.10	11.90
$C_{26}H_{14}O_4Ni\ 2C_5H_5N$[a]	71.20	71.09	3.98	3.92	—	—
$C_{26}H_{14}O_4Co\ 2H_2O$	64.34	64.35	3.74	4.01	12.14	12.70
$C_{26}H_{14}O_4Co\ 2C_5H_5N$[b]	71.17	71.15	3.98	4.01	—	—
$C_{26}H_{14}O_4Zn\ 2H_2O$	63.50	63.43	3.69	3.74	13.29	13.62
$C_{26}H_{14}O_4Mn\ 2H_2O$	64.88	64.98	3.73	3.88	11.42	10.14
$C_{26}H_{14}O_4Mg\ 2H_2O$	69.28	69.03	4.03	4.01	5.39	5.93
$C_{26}H_{14}O_6U\ C_5H_5N$[c]	50.35	50.54	2.59	2.88	32.19	33.14
$C_{26}H_{14}O_4Be$	78.19	77.88	3.53	3.36	—	—
$C_{39}H_{21}O_6Al$	76.47	76.32	3.46	3.84	4.41	4.77
$C_{39}H_{21}O_6Fe$	73.03	72.82	3.30	3.57	8.71	8.40

a) Calcd N: 4.61, Found 4.68%. b) Calcd N: 4.61, Found 4.42%. c) Calcd N: 1.89, Found 1.65%.

paramagnetic (μ_{eff}=3.05 B.M.). The reflectance spectrum of the dihydrate complex as well as the dipyridinate complex exhibits d-d transitions around 8×10^3 and 18×10^3 cm^{-1} as seen in Fig. 1. It is due to a partial overlap with a tail-off from the π-π^* transition of the phenalenone ring that the absorption bands are not well defined. They are, however, essentially similar to those for octahedral Ni(II)-complexes such as bisacetylacetonatonickel(II) dihydrate and bis-salicylaldehydatonickel(II) dihydrate.[4] Judging from the magnetic and spectral evidence, an octahedral configuration is most probable for the Ni(II) dihydrate and dipyridinate complexes.

The water and pyridine molecules in the Ni(II)-complexes could be eliminated by heating at 150 °C *in vacuo*. The resulting anhydrous Ni(II)-chelate still showed an appreciable magnetic moment (μ_{eff}= 1.5 B.M.). This value is, however, too low to be reliable evidence for adopting a polymeric octahedral structure in which the planar unit is linked by sharing a lone pair of the oxygen atoms. This is probably due to contamination by the paramagnetic dihydrate complex species, because the crystals were fairly hygroscopic and the magnetic moment increased to 2.05 B.M. after standing in air for a while. The chelate which resulted from the dipyridinate complex was identical to the anhydrous one in its electronic spectral pattern, as seen in Fig. 1. The absorption due to the d-d transition, which appears at 15×10^3 cm^{-1} and is absent at lower frequencies, is normally associated with a square-planar configuration.[5]

For the structural determination of other bivalent metal chelates, X-ray powder diffraction diagrams were drawn for the dihydrate complexes of Co(II), Zn(II), Mn(II), and Mg(II), and compared with that of the Ni(II) dihydrate complex. As seen in Fig. 2, all patterns are identical; they are therefore isomorphous and the configurations are all similar to the Ni(II) dihydrate complex. Thus they are octahedral.

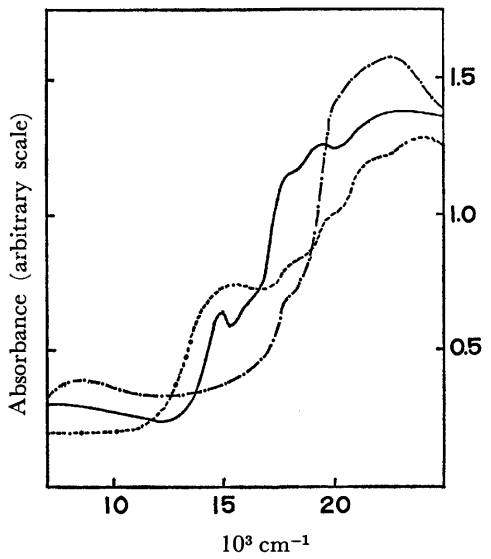

Fig. 1. Reflectance spectra of metal-chelates of HPNA: (----), Cu(II); (——), Ni(II); (—·—), Ni(II)·$2H_2O$.

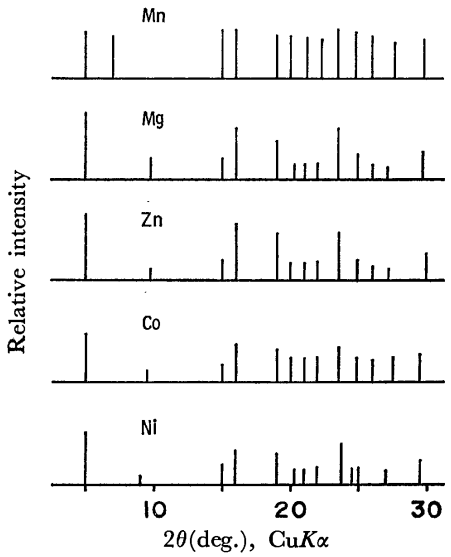

Fig. 2. X-ray powder diffraction diagrams of Mn(II), Mg(II), Zn(II), Co(II), and Ni(II) dihydrate complexes of HPNA.

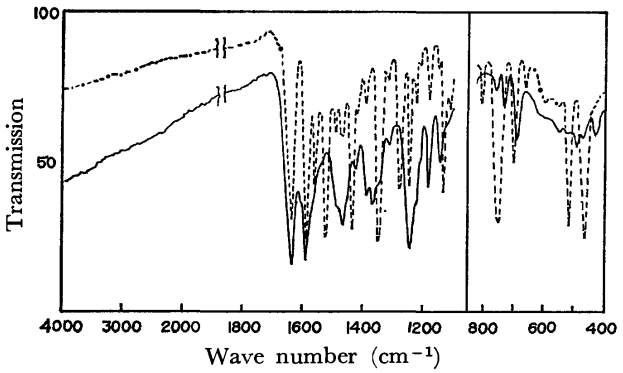

Fig. 3. IR spectra of HPNA (——) and Cu(II)-chelate (----); 4000—1900 cm^{-1} in hexachlorobutadiene, 1900—1100 cm^{-1} in Nujol, and 900—400 cm^{-1} in KBr.

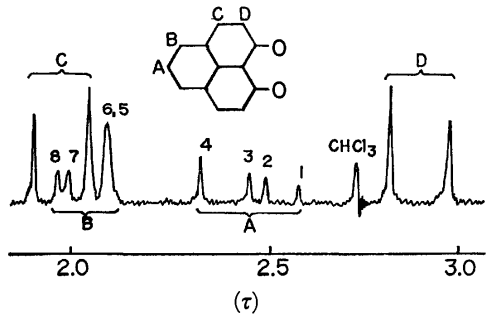

Fig. 4. PMR spectrum of HPNA in $CDCl_3$.

As has been revealed by the elemental analyses, the metal-ligand composition of the Fe(III) and Al-(III) chelates was 1 : 3; therefore, they undoubtedly take an octahedral configuration with coordination of three moles of the ligand.

The infrared absorption spectrum of HPNA shown in Fig. 3 exhibits no OH stretching band in the solid state or in benzene or chloroform. This implies the presence of a very strong intramolecular hydrogen bonding with the carbonyl oxygen. The PMR spectrum of the phenalenone ring protons is shown in Fig. 4, in which assignment of the peaks is also illustrated. The spectral pattern can be explained as an $AB_2CC'DD'$ system, providing no spin-spin coupling occurs between B and C protons ($J_{BC}=0$) and $\Delta\nu_{AB}/J_{AB}=2.7$.[6] This leads to two doublets for C(C') and D(D') protons, which appear at τ 2.02 and τ 2.92 respectively with $J_{CD}=10$ Hz. For the AB_2 system there are theoretically eight peaks, as numbered in the spectrum. Peaks 5 and 6 are not resolved in this instance. Consequently the molecule has a C_{2v} symmetry and the two carbon-oxygen bonds are equivalent so far as the PMR spectrum is concerned. The hydroxyl proton resonance appears at very low magnetic field (τ 5.90), which indicates the proton is located in a strong hydrogen bonding evironment.

In the carbonyl region of the IR spectrum the first and the second bands appear at 1637 and 1590 cm^{-1} with similar intensity. In general, the carbonyl frequency of aromatic ketones and quinones is lowered by 20—50 cm^{-1} by intramolecular hydrogen bonding, some examples of which are illustrated in Table 2. Judging from these facts, the PMR evidence, and comparison of the carbonyl vibration with that of phenalenone (1637 cm^{-1}), the band at 1590 cm^{-1} is tentatively assigned to the carbonyl band. The extremely low frequency for a carbonyl stretching vibration is assumed to be due to the high conjugation with the phenalenone ring associated with the intramolecular hydrogen bonding.

Upon metal chelate formation, the spectral patterns became sharp and new bands appeared, along with strengthening of some original bands, as illustrated for the Cu(II)-chelate in Fig. 3. The assignment of the principal absorption bands of the free ligand and the metal chelates are summarized in Table 3.

Nakamoto and Martell assigned the bands in the 1500 cm^{-1} region to the C=O vibration of the metal acetylacetonates from a calculation based on a normal coordinate analysis.[14,15] Providing the degree of the resonance of the metal chelate ring is proportional to the stability of the complex, the more the stability increases, the lower the C=O frequency will become. Although no simple relation existed between the C=O stretching frequency and the stability in a series of metal acetylacetonates, the band which was sensitive to the change in metal ions could be assigned to the C=O absorption. In the present case, the bond order of the carbonyl linkage is intrinsically decreased even in the free ligand by the resonance contribution through the phenalenone ring. In this respect the influence of metal chelate formation against the bond order is assumed to be negligible. Thus the band around 1500 cm^{-1} which was sensitive to the change in metal ions was chosen for the C=O absorption in a series of the metal chelates. The increasing order of the wave number is:

Cu(1525 cm^{-1}) < Ni(1531) < Co(1547) < Zn(1548) < Mg(1550)

TABLE 2. COMPARISON OF HYDROGEN-BONDED AND FREE CARBONYL FREQUENCIES (cm^{-1})

				Δ	Ref.
o-Hydroxyacetophenone	1648	Acetophenone	1691	43	7
1-Hydroxynaphthoquinone	1642	Naphthoquinone	1661	19	8
1-Hydroxy-4-methoxy-8-tetralone	1637	4-Methoxy-8-tetralone	1684	47	9
9-Hydroxy-10-acetylphenanthrene	1611	10-Acetylphenanthrene	1686	75	10
1-Hydroxyanthraquinone	1636	Anthraquinone	1673	37	11
Tropolone	1613	Tropone	1635	32	
	1548		1580	32	12
9-Hydroxy-1-phenalenone	1590	Phenalenone	1637	47	13

Table 3. Vibrational frequencies and band assignments of metal chelates of 9-hydroxy-1-phenalenone (cm^{-1})

Metal ion	C=O		C=O	C=O, C-H				Ring deform., M-O	
H	1637	1590	1590	1468	1372	—	1242	—	—
Na(I)	1634	1597	1558	1443	1357	—	1238	480	442
			1543						
Be(II)	1631	1585	1515	1437	1357	1285	1246	647	534
Mg(II)[a]	1642	1603	1558	1447	1357	1261	1244	494	460
			1550	1437					
Mn(II)[a]	1629	1585	1517	1420	1353	1259	1245	489	450
Co(II)[a]	1639	1600	1547	1437	1355	1266	1250	498	454
		1563		1427					
Ni(II)[a]	1634	1592	1531	1427	1353	1264	1247	504	454
		1563							
Cu(II)	1634	1587	1524	1433	1351	1271	1248	517	467
		1565							
Zn(II)[a]	1639	1597	1548	1439	1357	1261	1247	497	450
				1431					
Al(III)	1631	1590	1527	1447	1357	1276	1245	514	486
		1567		1435					
Fe(III)	1629	1585	1517	1420	1353	1266	1245	494	462
		1567							
UO_2(II)	1629	1587	1517	1415	1350	1260	1246	482	455
(2py)		1565				(905[b], 645[c])			

a) Dihydrate complexes. b) U=O stretching. c) U-Py?

The earlier work of Nakamoto and Martell has revealed that the bands near 400 cm^{-1} were due to a M–O stretching vibration for metal acetylacetonates.[14,15] The decreasing order of the vibration was the same as the stability order: Cu(455 cm^{-1})> Ni(452)>Co(422)≈Zn(422) for the bivalent metal chelates. Nakamoto and coworkers extended the observation of the IR spectra to a lower frequency region and confirmed the M–O stretching mode assignment by using a metal isotope technique.[16] The bands which showed a large isotope shift were 455.0 and 290.5 cm^{-1} for the ^{63}Cu chelate and 421.1 and 228.6 cm^{-1} for the ^{58}Ni chelate, and they were in agreement with the assignment based on a normal coordinate analysis, in which the latter bands were due to a pure M–O stretching vibration.[17] Although we could not use the isotope technique and did not cover the 200 cm^{-1} region, two metal sensitive bands were observed in 400—500 cm^{-1} in each metal chelate. Since the M–O stretching mode is similar to that of metal acetylacetonates, it can be inferred that the strength of the coordinate bond in each transition metal chelate is comparable to that of the corresponding metal acetylacetonate, providing the lower frequency band in Table 3 is taken as the M–O stretching vibration. The markedly different M–O frequency of the Be(II)-chelate will be attributed to the light mass of the beryllium atom and the short Be–O distance.

Conclusion

Judging from the IR and PMR evidence, HPNA is a highly conjugated and symmetrical molecule including the two carbon-oxygen bonds and there exists very strong hydrogen bonding between the two oxygen atoms. The Cu(II) and the anhydrous Ni(II) chelates are monomeric in the solid state and square-planar, while the dihydrate complexes of Mn(II), Ni(II), Co(II), Zn(II), and Mg(II) are octahedral. The two water molecules probably coordinate axially to the chelate plane, as pictured in Fig. 5. The Fe(III) and Al(III) chelates are octahedral and probably have D_3 symmetry like those of acetylacetonates. It is also concluded in the IR band assignment of the metal chelates that the first two bands in the double bond region are due to the skeletal C=C vibration of the phenalenone ring, because similar frequency bands are found in the free ligand and they do not move on metal chelate formation. Consequently, the second band at 1590 cm^{-1} in the free ligand is an overlap with the carbonyl stretching vibration.

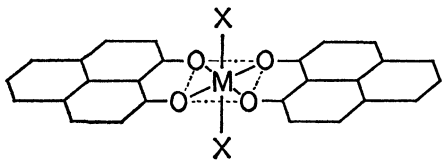

M: Cu (X: none); Ni (X: H_2O; Py); Co (X: H_2O; Py) Zn (X: H_2O); Mn (X: H_2O); Mg (X: H_2O)

Fig. 5. Probable structure of metal-chelates of HPNA.

References

1) J. D. Laudon and R. K. Razidan, *J. Chem. Soc.*, **1954**, 4299.
2) J. Ferguson, *J. Chem. Phys.*, **34**, 1609 (1961).

3) H. Koyama, Y. Saito, and H. Kuroya, *J. Inst. Polytech. Osaka City Univ.*, **C4**, 43 (1955).
4) G. Maki, *J. Chem. Phys.*, **29**, 162 (1958).
5) W. Manch and W. C. Fernelius, *J. Chem. Educ.*, **38**, 192 (1961).
6) J. D. Roberts, "An Introduction to the Analysis of Spin-Spin Splitting in High-Resolution Nuclear Magnetic Resonance Spectra," W. A. Benjamin, Inc., New York (1961), p. 70.
7) I. M. Hunsberger, *J. Amer. Chem. Soc.*, **72**, 5629 (1950).
8) T. Shoji, *Yakugaku Zasshi*, **79**, 1034 (1959).
9) T. Momose, Y. Ueda, and H. Yano, *Talanta*, **3**, 65 (1959).
10) I. M. Hunsberger, R. Ketcham, and H. G Gutowsky, *J. Amer. Chem. Soc.*, **74**, 4839 (1952).
11) M. St. C. Flett, *J. Chem. Soc.*, **1948**, 1441.
12) Y. Ikegami, This Bulletin, **35**, 967 (1962); S, Kinumaki, K. Aida, and U. Ikegami, *Sci. Rep. Res. Inst. Tohoku Univ.*, **A8**, 263 (1956).
13) For phenalenone, N. H. Cromwell, and G. V. Hudson, *J. Amer. Chem. Soc.*, **75**, 872 (1953).
14) K. Nakamoto and A. E. Martell, *J. Chem. Phys.*, **32**, 588 (1960)
15) K. Nakamoto, P. J. McCarthy, A. Ruby, and A. E. Martell, *J. Amer. Chem. Soc.*, **83**, 1066, 1272 (1961).
16) K. Nakamoto, C. Udovich, and J. Takemoto, *ibid.*, **92**, 3973 (1970).
17) M. Mikami, I. Nakagawa, and I. Shimanouchi, *Spectrochim. Acta*, **23A**, 1037 (1967).

The Polarographic Reduction of [Pd(oxine)$_2$] and [Pd(acac)$_2$] in a *N,N*-Dimethylformamide Solution

Michio HIROTA and Shizuo FUJIWARA

Department of Chemistry, Faculty of Science, The University of Tokyo, Hongo, Tokyo 113

(Received May 7, 1975)

Palladium(I) species were produced by the polarographic reduction of palladium(II)–oxinate and –acetylacetonate complexes in a *N,N*-dimethylformamide solution. These species were unstable and decomposed into electro-inactive species through an irreversible following chemical reaction. The rate constants were obtained from the fundamental and second harmonic AC polarograms, which were obtained at two different frequencies of the AC potential, 55.8 and 173.6 Hz, at 22.5 °C as 5.5 ± 1.0 s^{-1} for the oxinate complex and as 50 ± 10 s^{-1} for the acetylacetonate complex.

Many palladium(II) complexes are irreversibly reduced to a palladium amalgam at a dropping mercury electrode in an aqueous solution.[1] However, it has been found that Pd(I) is detected as a product of the following chemical reaction in the case of $[Pd(CN)_4]^{2-}$.[2]

Such a lower-valence state has been proven to be produced in an aprotic dipolar solvent by the polarographic reduction of bipyridine complexes of iron, cobalt, and other metal ions.[3,4] The palladium *o*-phenylenediamine complex can also exist as a low-valent species in an acetonitrile solution.[5] These results seem to suggest that the π-bonding nature between the central ion and the ligand stabilizes the lower-valence state and that Pd(I) may be observed in the polarographic reduction of the oxinate and acetylacetonate complexes of palladium.

In this study, the polarographic reduction of the palladium(II)–oxinate and –acetylacetonate complexes was studied in a *N, N*-dimethylformamide(DMF) solution. Low-valent species(Pd(I)) were detected as unstable intermediates. The life-times of the intermediates were obtained quantitatively by the fundamental and second harmonic AC polarography.

Experimental

Material. The palladium(II) complexes were prepared according to the usual method and were recrystallized. The DMF was treated with K_2CO_3 and distilled. The tetraethylammonium perchlorate (TEAP) was recrystallized five times from water.

Measurements. The DC polarogram was taken with a Yanagimoto Polarograph, Model P-8. The oscillo- and AC polarograms were taken with apparatuses constructed in this laboratory. The details of the measurements were the same as those given in previous papers.[6,7] An H-type cell was used with a reference electrode (saturated calomel electrode(SCE), Yanagimoto Model MRP). The flow rate of the mercury was 0.67 mg/s at the mercury column height of 40 cm in a 1 M KCl solution at an open circuit. All the measurements were carried out at (22.5 ± 0.5) °C. All the potentials were referred to the SCE.

The calculations of the simulation curves were based on the expanding plane model.[8,9] The following chemical reactions were assumed to be irreversible (See Results and Discussion). A computer simulation was performed with a HITAC 8700/8800 system, the Computer Center, the University of Tokyo, using the FORTRAN program of Smith.[8,9]

Results and Discussion

DC Polarography. The oxinate complex, [Pd(oxine)$_2$], was reduced through two waves (first at -1.39 V and second at -1.8 V). The first wave gave a diffusion controlled current. The second wave was very drawn out. The acetylacetonate complex, [Pd(acac)$_2$], was reduced through one wave at -1.17 V. This wave was also diffusion controlled and corresponded to the reduction of Pd(II) to a palladium amalgam.[10]

Oscillopolarography. The oscillopolarograms of these complexes are shown in Fig. 1-(A, B).

In the system of [Pd(oxine)$_2$]–0.5 M TEAP, the (1) and (5) waves correspond to the two waves of the DC polarogram. The (2) wave is the reoxidation wave of the reduced product of the (1) wave. This wave refers to the presence of the low-valent species. If the first reduced form is the palladium amalgam, it is difficult for the palladium to be reoxidized before the dissolution of mercury starts.[11] The (5) wave is irreversible. Hence, it is attributed to the reduction to the palladium amalgam. The (1), (2), and

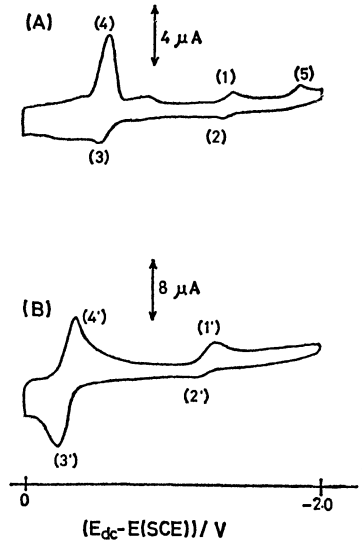

Fig. 1. The oscillopolarogram of Pd(II) complexes in N,N-dimethylformamide.
[TEAP]=0.5 M, sweep rate=34.8 V/s
h=40 cm, $T=(22.5\pm0.5)$ °C
(A) [Pd(oxine)$_2$]=0.27 mM
(B) [Pd(acac)$_2$]=1.28 mM.

(5) waves suggest that $[Pd(oxine)_2]$ is first reduced to the Pd(I) species and then to the amalgam.

In the system of $[Pd(acac)_2]$-0.5 M TEAP, the (1′) wave corresponds to the wave of the DC polarogram. The reoxidation wave (2′) suggests that a low-valent species (Pd(I) or Pd(0)) is present. The (3′) and (4′) waves did not appear when the sweep range was reduced so that the reduction of $[Pd(acac)_2]$ did not occur. Therefore, these waves are assumed probably to be due to the oxidation and reduction of mercury by the free acetylacetonate anion,[10] which has been liberated by the reduction of $[Pd(acac)_2]$.

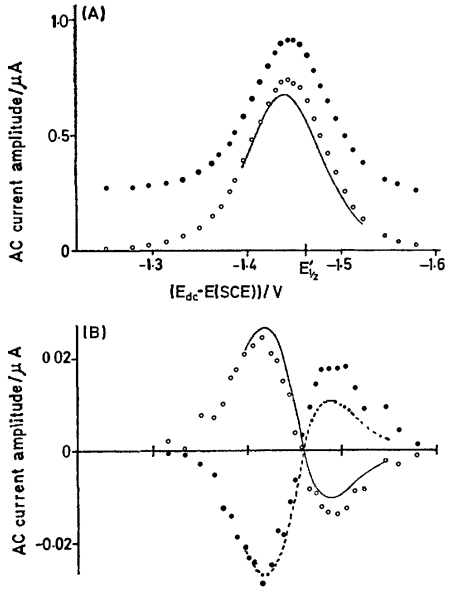

Fig. 2. The AC polarogram of $[Pd(oxine)_2]$.
$[Pd(oxine)_2]=0.50$ mM, $[TEAP]=0.5$ M
(A): Fundamental harmonic AC polarogram.
(B): Second harmonic AC polarogram.
○: In-phase component, ●: quadrature component.
Simulation curves;
—— in-phase component, --- quadrature component
$n=1$, frequency$=55.8$ Hz, $\Delta E=5$ mV, $D_o=D_r=1.28\times10^{-5}$ cm²/s, $k_s=\infty$, $k_f=5.5$/s, $A=0.015$ cm², $T=(22.5\pm0.5)$ °C.

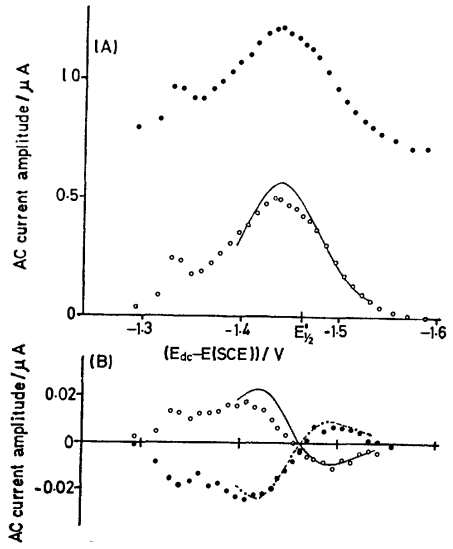

Fig. 3. The AC polarogram of $[Pd(oxine)_2]$.
$[Pd(oxine)_2]=0.24$ mM, $[TEAP]=0.5$ M
(A): Fundamental harmonic AC polarogram.
(B): Second harmonic AC polarogram.
○: In-phase component, ●: quadrature component.
Simulation curves;
—— in-phase component, --- quadrature component
same parameters as Fig. 2, except frequency$=173.6$ Hz.

In the system of $[Pd(oxine)_2]$-0.5 M TEAP, the (3) and (4) waves appeared only when the reduction of $[Pd(oxine)_2]$ occurred. When only the (1) wave appeared, these waves were also observed, but were as small as one-third of those in Fig. 1. These wave forms were different from the normal redox wave. This is probably because of the adsorption of the species which participate in the redox reaction of mercury by the oxinate anion.

AC Polarography. Figures 2 and 3 show the AC polarograms of $[Pd(oxine)_2]$ corresponding to the first wave of the DC polarogram. Though the phase angles of the fundamental and second harmonic AC polarograms were almost consistent with that of the reversible electrode reaction, the amplitudes were considerably smaller than that expected from the diffusion coefficient, which was calculated from the DC polarogram. The peak potential(E_p) of the fundamental harmonic AC polarogram was not equal to the zero-current potential (E_{min}) of the second harmonic AC polarogram. These features are typical of a reversible electrode reaction coupled with a following chemical reaction. As was seen in the preceding paragraph, the following chemical reaction was a decomposition reaction and was assumed to be irreversible. In the case of an irreversible following chemical reaction, the presence of the zero-current potential and the small cathodic peak height compared with the anodic one in the second harmonic AC polarogram indicate that the following chemical reaction is slow and so is inoperative in the AC polarographic sense. Figures 2 and 3 correspond to this case. This conclusion coincides with the fact that the cotangent of the phase angle of the second harmonic AC polarogram was almost equal to -1.[9] From the half-width of the fundamental harmonic AC polarogram, the number of electrons transferred(n) was found to be one. Therefore, the life-time of the Pd(I) species is assumed to be long in the AC polarographic sense. From the computer simulation, which was carried out at two frequencies, the rate constant of the following chemical reaction was estimated to be 5.5 ± 1.0 s^{-1}; *i.e.*, the life-time was about 0.18 s.

Figures 4 and 5 show the AC polarograms of $[Pd(acac)_2]$. In the fundamental harmonic AC polarogram, another small peak was observed at -1.65 V. These results seem to suggest that $[Pd(acac)_2]$ is also reduced through two steps. The observed second wave was irreversible; hence, it was attributed to the reduction to the amalgam. The Pd(I) species was also detected in this system. The two waves were so close together that the DC polarogram apparently showed only one wave. The first AC wave was also typical of an electrode reaction coupled with a following chemical reaction. When the rate constant of

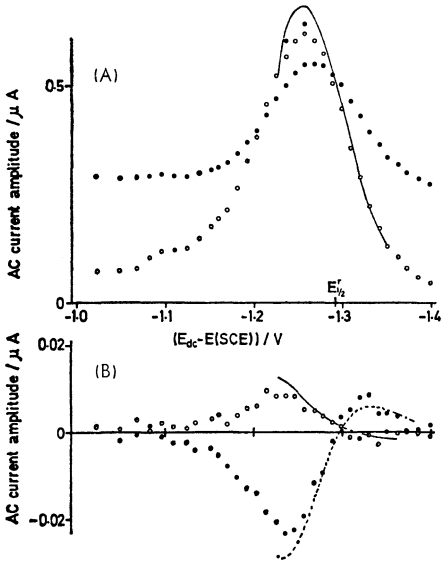

Fig. 4. The AC polarogram of [Pd(acac)$_2$].
[Pd(acac)$_2$]=1.12 mM, [TEAP]=0.5 M.
(A): Fundamental harmonic AC polarogram.
(B): Second harmonic AC polarogram.
○: In-phase component, ●: quadrature component.
Simulation curves;
—— in-phase component, --- quadrature component
n=1, frequency=55.8 Hz, ΔE=5 mV, $D_o=D_r=1.52\times10^{-5}$ cm^2/s, $k_s=7\times10^{-2}$ cm/s, α=0.50, k_f=50/s, A=0.015 cm^2, T=(22.5±0.5) °C.

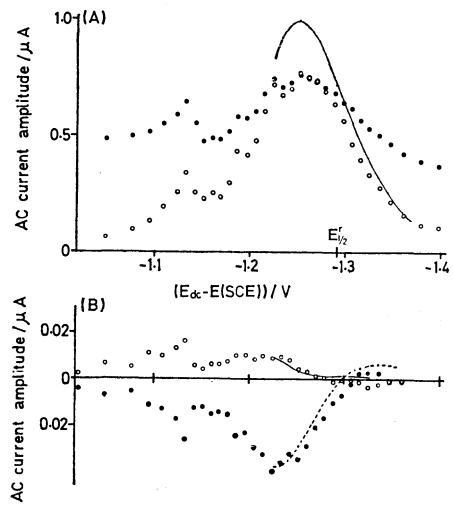

Fig. 5. The AC polarogram of [Pd(acac)$_2$].
[Pd(acac)$_2$]=1.06 mM, [TEAP]=0.5 M.
(A): Fundamental harmonic AC polarogram.
(B): Second harmonic AC polarogram.
○: In-phase component, ●: quadrature component.
Simulation curves;
—— in-phase component, --- quadrature component
same parameters as Fig. 4, except frequency=173.6 Hz.

the following chemical reaction increases and/or that of the charge transfer reaction decreases, the phase angle of the second harmonic AC polarogram deviates from the value of a reversible electrode reaction, and the cathodic peak of the second harmonic AC polarogram becomes remarkably small. The system of

Table 1. Polarographic data of Pd(II)-0.5 M TEAP System

	$E^r_{1/2}$ or Pd(II)/Pd(I) (*vs.* SCE)	k_s (α=0.5)	k_f of Pd(I)
[Pd(oxine)$_2$]	−1.46$_2$ V	>1 cm/s	(5.5±1.0)/s
[Pd(acac)$_2$]	−1.29$_2$ V	(0.07±0.03) cm/s	(50±10)/s

T=(22.5±0.5)°C, k_s; the standard rate constant of a charge transfer reaction, k_f; the rate constant of a following chemical reaction.

[Pd(acac)$_2$] corresponds to this case. From the computer simulation assuming an irreversible following chemical reaction and assuming that the transfer coefficient of the charge transfer reaction(α) was 0.5, it was found that n was 1 and that the rate constant of the following chemical reaction and the standard rate constant of the charge transfer reaction were 50± 10 s^{-1} and 0.07±0.03 cm/s respectively; *i.e.*, the lifetime of the Pd(I) species was about 0.020 s. The parameters of these complexes can be summarized as is shown in Table 1.

In conclusion, these complexes were first reduced to mono-valent species. These complexes may have the same configuration as the starting complexes. These mono-valent species were unstable, decomposed, and liberated the ligands. These mono-valent species were also reduced irreversibly to palladium amalgams, and liberated the ligands.

The k_s of the Pd(II)/Pd(I) couple was larger in the [Pd(oxine)$_2$] system than in the [Pd(acac)$_2$] system. The rate constant of the decomposition was slower in the [Pd(oxine)$_2$] system than in the [Pd(acac)$_2$] system. These results show that the bi-valent species is reduced to the mono-valent species more easily in the oxinate complex than in the acetylacetonate complex, and that the mono-valent species is more stabilized as the oxinate complex than as the acetylacetonate complex.

From the ESR study of γ-ray irradiated Pd(I) complexes,[12] the covalency of the palladium-ligand σ bond has been found larger in [Pd(I)(oxine)$_2$]$^-$ than in [Pd(I)(acac)$_2$]$^-$. Therefore, the stabilization of Pd(I) may be due to the delocalization of the highest occupied energy level of Pd(I) complexes.

The product of the decomposition reaction is unknown. However, from the second harmonic AC polarogram, the regeneration of Pd(II) species can not be considered.[13] As there seems to be no species which can stabilize the mono-valent species, the decomposition reaction may be the reduction to palladium metal. In both systems with the higher frequency of the AC potential, humps were observed in the second harmonic AC polarogram. These are probably due to the adsorption of the complex preceding the reduction. In the data analysis for the following chemical reaction, this effect was neglected. In the simulation program, the diffusion coefficients of the first reduced form and the product of the following chemical reaction are assumed to be equal to each other. This condition was not applicable in these systems. However, this discrepancy was as-

sumed not to be very serious. The effect of a spherical diffusion was also not considered.

References

1) M. Hirota, Y. Umezawa, M. Nakamura, and S. Fujiwara, *J. Inorg. Nucl. Chem.*, **33**, 2617 (1971).
2) M. Hirota and S. Fujiwara, *ibid.*, **35**, 3883 (1973).
3) N. Tanaka and Y. Sato, *Electrochim. Acta*, **13**, 333 (1968).
4) N. Tanaka and Y. Sato, This Bulletin, **41**, 1021, 2059 (1968).
5) A. L. Balch and R. H. Holm, *J. Amer. Chem. Soc.*, **88**, 5201 (1966).
6) T. Kugo, Y. Umezawa, and S. Fujiwara, *Chem. Instr.*, **2**, 189 (1969).
7) M. Hirota, Y. Umezawa, H. Kojima, and S. Fujiwara, This Bulletin, **47**, 2486 (1974).
8) T. G. McCord, H. L. Hung, and D. E. Smith, *J. Electroanal. Chem.*, **21**, 5 (1969).
9) T. G. McCord and D. E. Smith, *Anal. Chem.*, **41**, 1423 (1969).
10) R. W. Murray and L. K. Hiller, Jr. *ibid.*, **39**, 1221 (1967).
11) E. P. Parry and K. B. Oldham, *ibid.*, **40**, 1031 (1968).
12) M. Nakamura and S. Fujiwara, *J. Coord. Chem.*, **1**, 221 (1971).
13) K. R. Bullock and D. E. Smith, *Anal. Chem.*, **46**, 1567 (1974).

Reaction of Nickel Ion Fixed on the Ion Exchange Resin with 2-Thenoyltrifluoroacetone

Kunio OHZEKI, Tooru TAMURA, and Tomihito KAMBARA

Department of Chemistry, Faculty of Science, Hokkaido University, Sapporo 060

(Received June 7, 1975)

The reaction of nickel ions fixed on the ion exchange resin with 2-thenoyltrifluoroacetone was investigated in various organic solvents. In the presence of pyridine, nickel ions were quantitatively extracted from the resin into the organic phase in the form of the adducts of nickel(II) chelate with pyridine. The synergistic effect of a series of pyridine bases on the removal of the metal ions from the resin decreased in the order : pyridine> γ-picoline> β-picoline> α-picoline.

Several studies on the conversion of a metal ion fixed on the ion exchange resin to a chelate compound based on the ion exchange reaction in organic medium have been investigated in our laboratory. The authors have reported the quantitative removal of iron(III)[1] and copper(II)[2] ions fixed on Amberlyst 15 by acetylacetone with the aid of a small amount of pyridine–water mixture. In this work, the reaction of the nickel ions fixed on Amberlyst 15 with 2-thenoyltrifluoroacetone(Htta) was investigated in benzene, carbon tetrachloride, chloroform, and ethyl alcohol, and the effects of pyridine bases on the quantitative removal of the nickel ions were discussed.

Experimental

Apparatus and Reagents. Absorption measurements were carried out by the aid of a Shimadzu Spectronic 88 spectrophotometer and a Hitachi 356 two-wavelength double-beam spectrophotometer with 10 mm cells. A Hitachi 508 atomic absorption spectrophotometer was used for the nickel absorption measurement at 231.4 nm in air-acetylene flame. 2-thenoyltrifluoroacetone and β-picoline were obtained from Wako Chemical Inc. and used without further purification. Pyridine, α-picoline, γ-picoline, and all other materials used were of guaranteed grade.

Preparation of Nickel(II)-Form Resin. The resin used was sulfonic acid cation exchanger, Amberlyst 15, with a macroreticular structure. The commercially available Amberlyst 15 was crushed and shieved to a fraction of 60—80 mesh. The resin was converted to Ni(II)-form by treatment with 0.1 mol dm^{-3} solution of nickel nitrate. The resulting Ni(II)-form resin was washed with water until the washings showed no color reaction with dimethylglyoxime and dried over silica gel. The ratio of exchange capacity of nickel ion to proton was 0.996, and that the nickel ions are expected to be adsorbed on the resin in the form of Ni^{2+}. When the air dried Ni(II)-form was dried at 110 °C for 3 hours, the weight loss was found to be about 24%. The infrared spectrum of the resin showed the existence of a small amount of water. The water on the oven dried resin was determined by the method described in the previous paper[2] and it is supposed that two water molecules are coordinated to a nickel(II) ion on the resin, such as $(RSO_3)_2Ni\cdot 2H_2O$. In the following experiments, the air dried resin was used without oven drying.

Determination of Nickel Ions on the Ni(II)-Form Resin. The nickel ions on the air dried Ni(II)-form resin were eluted by 4 mol dm^{-3} hydrochloric acid solution and determined by EDTA titration. It was found that 2.95±0.02 meq of nickel ions were adsorbed onto 1.00 g of the air dried Ni(II)-form resin.

Reaction of Ni(II)-Form Resin. A portion of 5 ml of 0.1 mol dm^{-3} Htta in organic medium was poured onto the 25 mg of air dried Ni(II)-form resin in a test tube and varying amounts of pyridine and/or pyridine–water mixture were added. The mixture was shaken mechanically for 10 min at room temperature (around 19 °C) and for equilibrium study, it was allowed to stand for 24 hours with occasional shakings. After filtration, the resin was washed with ethyl alcohol and water. The nickel ions remaining on the resin were eluted by 4 mol dm^{-3} hydrochloric acid solution and determined by atomic absorption spectrophotometry.

Results and Discussion

Effect of Pyridine. Any portion of the nickel ions fixed on the resin could not be removed by Htta alone into organic medium. But the addition of a small amount of pyridine or pyridine–water mixture was highly effective, as Fig. 1 shows. Upon addition of pyridine to Htta solution in contact with the Ni(II)-form resin, green color was developed in the organic phase, indicating the formation of $Ni(tta)_2py_2$. More than 99% of nickel ions can be removed from the resin by the addition of the 30 : 1 to 100 : 1 pyridine–water mixture, where Htta dissolved in chloroform in 4—14% (v/v) is employed. The resin floated up to the surface of the solvent as the reaction proceeded.

Effect of Solvents. Figure 2 shows the effect of the solvents on the removal of nickel ions from the resin. More than 99% of the nickel ions are extracted into benzene and carbon tetrachloride by the

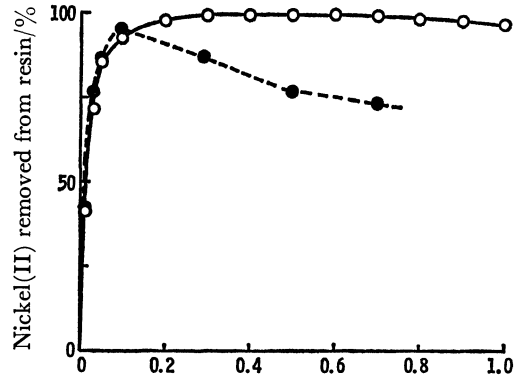

Fig. 1. Effect of the addition of pyridine (●), and pyridine-water (50 : 1) mixture (○) on the removal of nickel ions from the resin with 5 ml of 0.1 mol dm^{-3} Htta solution in chloroform.

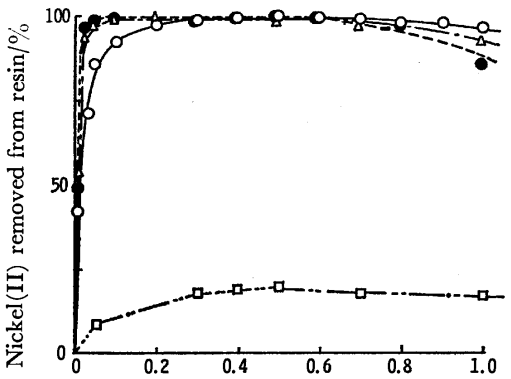

Fig. 2. Removal of nickel ions from the resin with 5 ml of 0.1 mol dm^{-3} Htta solution in various solvents. Ethyl alcohol (□), chloroform (○), benzene (△) and carbon tetrachloride (●).

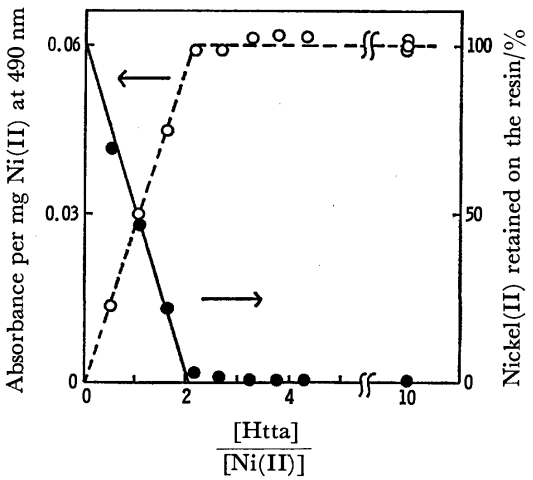

Fig. 3. Effect of Htta concentration in chloroform containing 1.14 mol dm^{-3} pyridine-water (50 : 1) mixture. The absorbance measurement of the organic extract (○), and nickel retained on the resin (●).

addition of pyridine as well as pyridine-water mixture. The poor extraction of nickel ions in ethyl alcohol is due to a probable interaction of the solvent and Htta.

Ion Exchange Extraction Constant. The composition of the complex in chloroform medium was determined by the mole ratio method. The nickel ions remaining on the resin were eluted by 4 mol dm^{-3} hydrochloric acid solution and determined by atomic absorption spectrophotometry and the absorbance of the solution was measured at 490 nm against chloroform. Consequently the composition of the Ni(II)-Htta complex was estimated to be Ni(II) : Htta=1 : 2 as shown by Fig. 3. It is reported that Ni(II)-Htta complex adds two moles of pyridine at high concentration of pyridine[3] and it is reosonable to expect that pyridinium ion is adsorbed on the resin instead of nickel ion[1]. Consequently the following ion exchange extraction equilibrium is proposed.

$$(RSO_3)_2Ni + 2\,Htta + 4\,py \rightleftharpoons 2\,RSO_3Hpy + Ni(tta)_2py_2 \quad (1)$$

where R denotes the resin matrix.

Now we can define the ion exchange extraction constant K_{ex}^{r} as

$$K_{ex}^{r} = \frac{[Ni(tta)_2py_2]_o[pyH^+]_r^2}{[Ni^{2+}]_r[Htta]_o^2[py]_o^4} \quad (2)$$

where the subscripts r and o denote the chemical species on the resin and in the organic phase, respectively. In this case, the distribution ratio of nickel is shown by

$$D = \frac{[Ni(tta)_2py_2]_o}{[Ni^{2+}]_r} \quad (3)$$

Introducing the ion exchange extraction constant shown by the Eq. (2) into the Eq. (3), one obtains.

$$\log D[py]_o^{-4} = \log K_{ex}^{r} + 2\log[Htta]_o[pyH^+]_r^{-1} \quad (4)$$

Consequently a plot of $\log D[py]_o^{-4}$ against $\log [Htta]_o[pyH^+]_r^{-1}$ should give a straight line of slope 2. The result is given in Fig. 4. The values of $\log K_{ex}^{r}$ obtained are 1.96 in chloroform, 4.81 in benzene, and 4.91 in carbon tetrachloride. In all calculations, the concentration of the species on the resin is expressed as mole per gram of Ni(II)-form resin.

Effect of Pyridine Bases. The relationship between the percentage of nickel ions removed from the resin and the shaking time was examined with various pyridine bases. It is found that picolines are less effective than pyridine and it takes several hours to remove more than 99% of nickel ions from the resin as Fig. 5 shows. The synergistic effect of the pyridine bases on the removal of the nickel ions from the resin decreased in the order of pyridine>γ-picoline>β-picoline>α-picoline. On the other hand, it is reported that the synergistic effect decreases in the order of γ-picoline>β-picoline>pyridine>α-picoline in the solvent extraction of nickel ions with Htta.[3] The disagreement of the results between ion exchange

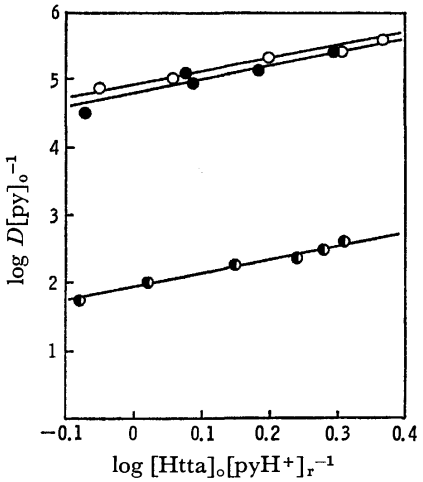

Fig. 4. Effect of ligand concentration on distribution ratio of nickel in the presence of pyridine.
Solution of Htta in carbon tetrachloride (○), benzene (●), and chloroform (◐).

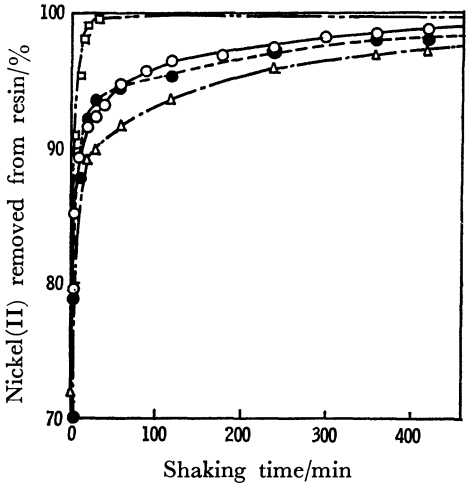

Fig. 5. Synergistic effect of the pyridine bases on the removal of nickel ions from the resin with 0.1 mol dm^{-3} Htta solution in benzene, containing 0.245 mol dm^{-3} of pyridine (□), γ-picoline (○), β-picoline (●), and α-picoline (△).

extraction and solvent extraction may be caused by the steric influence of the resin matrix with methyl group of the picolines.

Comparison of Chelating Reagents. The removal of nickel ions from the resin into benzene with benzoylacetone(Hba) was investigated in the presence of pyridine as the function of the shaking time as Fig. 6 shows. It is found that the reaction rate is much

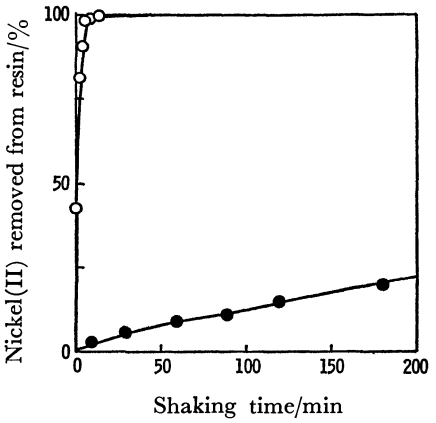

Fig. 6. Comparison of reaction rates.
Htta (○) and Hba (●) in benzene in the presence of pyridine.

slower in the case of Hba than Htta. This may be due to the difference in the acidity of the chelating reagents, Hba (pK_a=9.8), Htta (pK_a=5.7).

References

1) K. Ohzeki, M. Ikeuchi and T. Kambara, This Bulletin, **48**, 67 (1975).
2) T. Okamura, K. Ohzeki and T. Kambara, *ibid.*, **48**, 469 (1975).
3) H. Kawamoto and H. Akaiwa, *J. Inorg. Nucl. Chem.*, **31**, 1141 (1969).

An Electron Spin Resonance Study of Some Quadridentate Schiff Base Complexes of Copper(II)

David J. Cookson, Thomas D. Smith, and John R. Pilbrow*
Chemistry Department, Monash University, Clayton, Victoria, Australia 3168
**Physics Department, Monash University, Clayton, Victoria, Australlia 3168*
(Received June 16, 1975)

The X-band ESR spectra of a series of quadridentate Schiff base complexes of copper(II) have been examined in frozen xylene and chloroform solutions. Well resolved triplet state spectra were observed both at *g ca.* 2 and *g ca.* 4 due to dimeric forms of these complexes which exist in frozen solution. Magnetic and structural parameters have been determined by computer simulation of the triplet state spectra based on a lower than axial symmetry model for the copper(II) pair system.

The structural features of Schiff base compounds have been the subject of numerous investigations and more recently ESR spectroscopy has been used to study the dimeric forms of several copper(II) Schiff base complexes in frozen solution.[1-6] The application of a dipole-dipole coupled model to copper(II) dimers of low symmetry has enabled the ESR spectra to be analysed by computer simulation and has yielded values for the copper(II)-copper(II) separation, r, and the angle ξ (Fig. 1). In some cases it has been possible to compare structural data deduced from X-ray diffraction studies with similar information obtained from ESR spectra.[1,7]

Crystallographic studies on the dimeric forms of copper(II) Schiff bases indicate that the symmetry is monoclinic. However the host lattice relevant to the X-ray crystallographic studies is quite different from that involved in ESR measurements which are confined to isolated interacting pairs of copper(II) ions in solvent mixtures and it is possible that the stereochemistry of the dimers formed in solution may be dependent upon solvent effects.

Chikira and Isobe[2] concluded from computer simulations of the observed ESR lineshapes that the dimeric structure of bis(*N*-salicylidenemethylaminato)-copper(II), [Cu(MeSal)], in frozen toluene solution was similar to that found for the γ-form crystals as determined by X-ray methods. Furthermore it was found necessary to take into account the non-coincidence of the principal axes of the g tensor with those of the fine structure tensor in order to estimate such dimeric structures.[2]

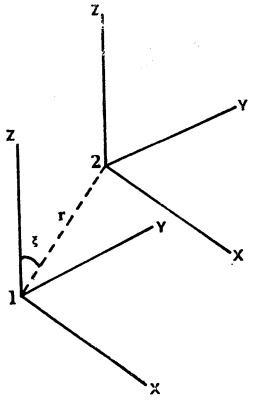

Fig. 1. Orientation of g tensor principal axes and internuclear axis for centrosymmetric metal ion dimers.

A more recent investigation by Chikira *et al.* involved a study of the triplet state ESR spectra due to the dimeric forms of the copper(II) complexes of some bidentate and quadridentate Schiff bases.[3] The spectra were analysed on the basis of the previously obtained results concerning the non-coincident g and fine structure tensors.[2] Their results indicated that the angles between the $g_{\parallel}$ axis and the copper-copper axis of the dimers of the quadridentate Schiff base complexes were considerably smaller than those of the bidentate ones. The lineshapes and the magnetic parameters of the bidentate Schiff base complexes were characterized by non-coaxial g and fine structure tensors whereas the quadridentate complexes were thought to show ESR spectra indicative of near coaxial g and fine structure tensors. It was concluded from this argument that the difference between the solid state and frozen solution dimeric structure of *N,N'*-ethylenebis-(salicylideneiminate)copper(II), [Cu(Salen)], was due to the fact that, in frozen solution the $g_{\parallel}$ axis almost coincides with the copper–copper axis.

These results are in direct conflict with the previously reported results of Toy *et al.*[1] who estimated the copper–copper distance and the angle between the $g_{\parallel}$ axis and the copper–copper axis for Cu(Salen) dimers in chloroform at 4.55±0.05 Å and 40±5° respectively. It was later claimed by Chikira *et al.* that the spectral patterns for the $\Delta Ms=\pm1$ transition of Cu(Salen) could not be reproduced by the use of such non-coincident g and spin-dipole interactions.[3] The magnetic and structural parameters determined by Toy *et al*[1]. were obtained by computer simulation of the low field ($\Delta Ms=\pm2$) components of the spectra only since, in all cases, the observation of the corresponding $\Delta Ms=\pm1$ spectrum at *g ca.* 2 proved difficult due to masking in

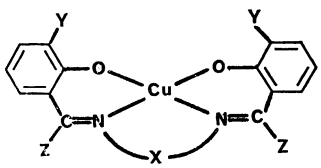

X = $\underset{\underset{CH_3}{|}}{CHCH_2}$ (pn), $(CH_2)_3$ (tn)
Y = H, OCH_3
Z = H, CH_3

Fig. 2. Structural formulae of copper(II) Schiff base complexes.

that region by a strong signal due to the monomer species. On the other hand, the parameters determined by Chikira *et al.*[3] were based on computer simulation of the $\Delta Ms=\pm1$ spectra only and no data relevant to the $\Delta Ms=\pm2$ transitions was presented.

The present investigation involves the determination of structural and magnetic parameters of a number of copper(II) Schiff base complexes which include *N,N'*-isopropylenebis(salicylideneiminato)copper(II), Cu(Salpn); *N,N'*-propylenebis(salicylideneiminato)copper(II), Cu(Saltn); *N,N'*-isopropylenebis(3-methoxysalicylideneiminato)copper(II), Cu(3MeO-Salpn); *N,N'*-propylenebis(3-methoxysalicylideneiminato)copper(II), Cu(3MeO-Saltn); *N,N'*-isopropylenebis(7,7'-dimethylsalicylideneiminato)copper(II), Cu(7,7'Me_2Salpn) and *N,N'*-propylenebis(7,7'-dimethylsalicylideneiminato)copper(II), Cu(7,7'Me_2Saltn). The structural formulae of these complexes are shown in Fig. 2.

The results obtained are based on computer simulation of both the $\Delta Ms=\pm1$ and $\Delta Ms=\pm2$ transitions in the ESR spectra due to the dimeric forms of the Schiff base complexes, and indicate that the *g* and fine structure tensors are in fact non-coincident.

Experimental

ESR spectra were recorded by means of a Varian E12 spectrometer. Cu(Salpn), Cu(Saltn), Cu(3MeO-Salpn) and Cu(3MeO-Saltn) were prepared by refluxing in ethanol the salicylaldehyde or 3MeO-salicylaldehyde complex of copper(II) with the appropriate diamine. Cu(7,7' Me_2Salpn) and Cu(7,7' Me_2Saltn) were prepared by refluxing in ethanol, copper(II) acetate, *o*-hydroxyacetophenone and the appropriate diamine.

In all cases the composition of the products was established by elemental analysis.

Results

Chikira *et al.*[3] calculated the magnetic parameters for a wide range of quadridentate Schiff base complexes, including Cu(Salpn), from the triplet state ESR spectra, at *g ca.* 2, arising from frozen toluene solutions of the complexes. However, even under these conditions, the ESR spectra included contributions from the doublet spectra due to monomeric forms of the Schiff bases.

Ideal conditions for computer simulation of triplet state ESR spectra arise when there is complete conversion to dimer and where the signals due to the $\Delta Ms=\pm1$ and $\Delta Ms=\pm2$ transitions are easily discerned and the resolution of their peaks is good enough to compare with computed lineshapes. A solvent which was found to provide these requirements was xylene. The ESR spectrum, at −140 °C, due to a xylene solution of Cu(Salpn) is shown in Fig. 3. Similar spectra were observed in the case of xylene solutions of Cu(Saltn), Cu(7,7' Me_2Salpn) and Cu(7,7' Me_2Saltn).

The ESR spectra of Cu(3MeO-Salpn) and 3MeO-Saltn) in xylene, at −140 °C, consisted of single broad lines, (approx. 150 gauss from peak to peak), indicative of the formation of aggregate forms of the Schiff bases under these conditions. The best circumstances for the observation of triplet state spectra were provided by chloroform, although monomer spectra of comparable intensity were also observed. The ESR spectrum, at −140 °C, due to a chloroform solution of Cu(3MeO-Salpn) is shown in Fig. 4. A chloroform solution of Cu(3MeO-Saltn) gave rise to a similar spectrum.

No triplet state spectra were obtained from chloroform solutions of the other Schiff bases although at sufficiently high concentrations (*ca.* 10^{-1} M), weak signals at *g ca.* 4 were observed due to small concentrations of dimer in solution. The ESR spectrum due to a solution of Cu(Saltn) in chloroform, at −140 °C, is shown in Fig. 5. The copper(II) Schiff base complexes are soluble in polar solvents such as ethanol and pyridine but under these circumstances triplet state ESR spectra are not observed.

It was found that Ni(Salpn) could readily be doped with Cu(Salpn) thus providing the conditions for diamagnetic dilution. The ESR spectrum at −140 °C due to Cu(Salpn) under these circumstances is shown in Fig. 6.

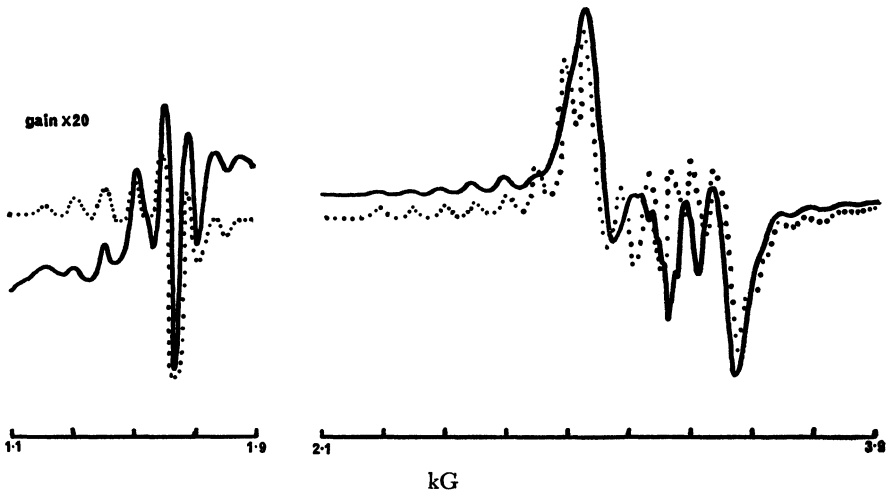

Fig. 3. X-Band ESR spectrum due to a xylene solution of Cu(Salpn) (1.0×10^{-2} M) at −140 °C; microwave frequency 9150 MHz. The dotted curves represent the computer simulation of the experimental spectrum using the parameters listed in Table 1. Baseline drift ignored in $\Delta Ms=\pm2$ spectrum.

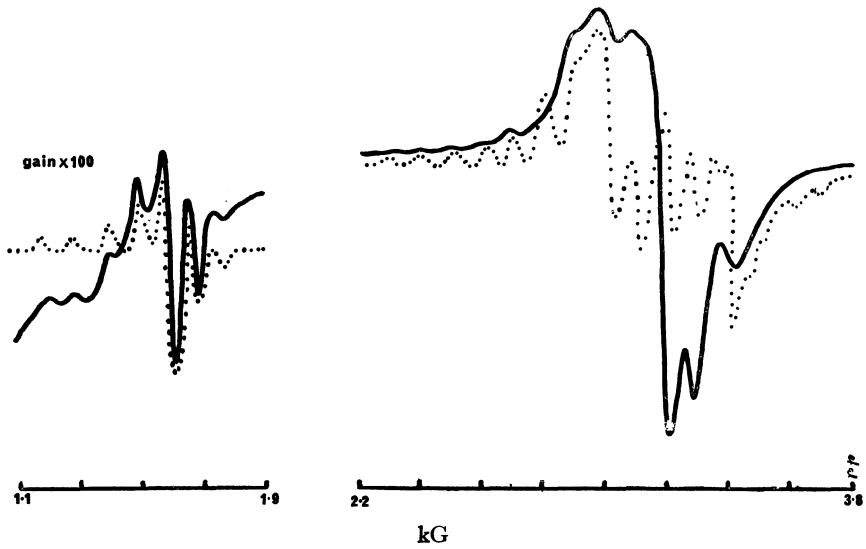

Fig. 4. X-Band ESR spectrum due to a chloroform solution of Cu(3MeO-Salpn) (3×10^{-3} M) at -140 °C; microwave frequency 9150 MHz. The dotted curves represent the computer simulation of the experimental spectrum using the parameters listed in Table 1. Baseline drift ignored in $\Delta Ms=\pm2$ spectrum.

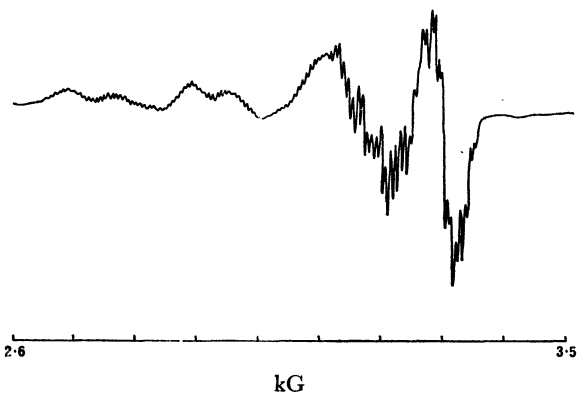

Fig. 5. X-Band ESR spectrum due to a chloroform solution of Cu(Saltn) (3×10^{-3} M) at -140 °C; microwave frequency 9150 MHz.

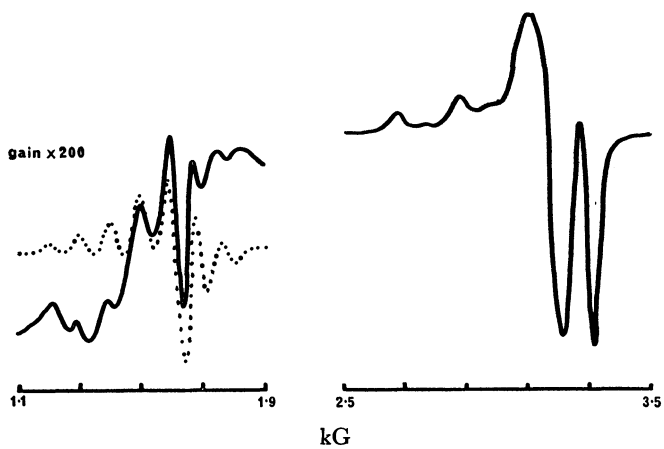

Fig. 6. X-Band ESR spectrum due to a powder sample of Cu(Salpn) doped into the corresponding nickel complex in a 1 : 9 ratio; microwave frequency 9150 MHz, temperature -140 °C. Baseline drift ignored in $\Delta Ms=\pm2$ spectrum.

Quantitative Treatment of Results and Discussion

Observation of the ESR spectrum, shown in Fig. 3, for a frozen xylene solution of Cu(Salpn) indicates that negligible amounts of monomeric species are present under these conditions.

The low field (*g ca.* 4) component of the spectrum is attributed to $\Delta Ms=\pm2$ transitions in the triplet state arising from magnetic dipole-dipole coupling of the copper(II) ions in a dimeric form of Cu(Salpn) while the signal at *g ca.* 2 is attributed to the corresponding $\Delta Ms=\pm1$ transition.

The intensity pattern of peaks in the $\Delta Ms=\pm2$ signal is indicative of a monoclinic arrangement of the copper(II) ions in the pair system[7] and the structural and magnetic parameters obtained by computer simulation of the experimental lineshape using this symmetry model are listed in Table 1.

Theoretical considerations involved in the computer simulation of an ESR spectrum using this model for the copper(II) pair system have been described previously.[7] The results of Chikira *et al.*[3] are in agreement with those of Lund and Hatfield.[6] who determined the magnetic parameters for a series of copper(II) dimers and concluded for Cu(Salen), that the principal axes of the *g* and fine structure tensors were coincident. However, as has been shown in a recent review,[8] Lund and Hatfield[6] omitted necessary terms in the Hamiltonian for lower than axial symmetry dimers and were therefore unable to reconcile their ESR results with known structural data. This has been discussed previously by two of the authors.[8] On the other hand Boyd *et al.*,[7] in examining many of the same systems in terms of a theoretical model which included all necessary terms for low symmetry dimers, did, in fact obtain very sensible agreement between X-ray and ESR structural parameters.

The effect of low symmetry on calculated spectra shows that the intensity pattern and field positions of

TABLE 1. MAGNETIC PARAMETERS FOR THE DIMERIC FORMS OF THE COPPER(II) SCHIFF BASES

Schiff base	Transition	r(Å)[a]	$g_{\parallel}$[b]	$g_{\perp}$[b]	$10^4 A_{\parallel}$[c] (cm^{-1})	$10^4 A_{\perp}$[c] (cm^{-1})	ξ[d]
Cu(Salpn)	$\Delta Ms=\pm1$	3.95	2.18	2.03	225	10	35
	$\Delta Ms=\pm2$	4.10	2.17	2.03	200	10	35
Cu(Saltn)	$\Delta Ms=\pm1$	3.95	2.18	2.03	225	10	35
	$\Delta Ms=\pm2$	4.20	2.17	2.02	200	10	35
Cu(3MeO-Salpn)	$\Delta Ms=\pm1$	4.00	2.17	2.04	220	10	35
	$\Delta Ms=\pm2$	4.00	2.17	2.04	200	5	35
Cu(3MeO-Saltn)	$\Delta Ms=\pm1$	4.05	2.18	2.04	230	10	35
	$\Delta Ms=\pm2$	4.00	2.17	2.04	200	5	35
Cu(7,7'Me_2Salpn)	$\Delta Ms=\pm1$	4.00	2.18	2.03	230	15	35
	$\Delta Ms=\pm2$	4.20	2.17	2.02	205	10	35
Cu(7,7'Me_2Saltn)	$\Delta Ms=\pm1$	3.95	2.17	2.03	225	10	35
	$\Delta Ms=\pm2$	4.20	2.17	2.02	210	10	35
10% Cu(Salpn) in Ni(Salpn)	$\Delta Ms=\pm2$	4.20	2.16	2.02	200	10	35

a) ±0.05. b) ±0.005. c) ±5. d) ±2.

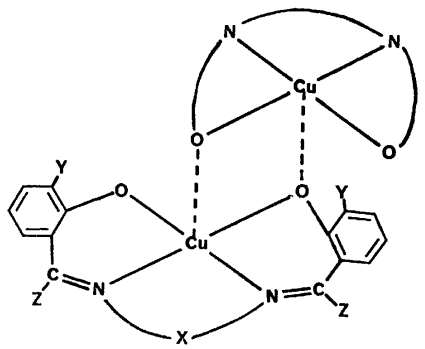

Fig. 7. Proposed structure for the dimeric forms of the copper(II) Schiff base complexes, present in frozen solution.

the lines in the low field ($\Delta Ms=\pm2$) region in particular, are affected considerably by variation in ξ.[7,8] This indicates the necessity of obtaining a well resolved low field spectrum before any conclusion about the symmetry of the copper(II) pair system can be made and unique set of structural and magnetic parameters determined.

The ESR spectrum due to a chloroform solution of Cu(3MeO-Salpn) at −140 °C is the result of the presence of a mixture of monomeric and dimeric species in solution. However the triplet state spectrum, due to the dimer, is still easily discerned at both *g ca.* 2 and *g ca.* 4 and the parameters obtained from computer simulation of this spectrum as well as that of Cu(3MeO-Saltn) in chloroform, are summarised in Table 1. A structure which meets the symmetry requirements as outlined in Table 1 is shown in Fig. 7 and involves a value of ξ of about 35°.

The ESR spectrum of Cu(Saltn) in $CHCl_3$ at −140 °C indicates the formation of a monomeric species only. The predominant feature of this spectrum, as well as those of Cu(Salpn), Cu(7,7' Me_2Salpn) and Cu(7,7'-Me_2Saltn) in chloroform, is the appearance of extra hyperfine splitting in addition to that due to copper. Each line is split into approximately fourteen additional lines although the exact number is difficult to ascertain because of a certain degree of overlap. The separation of the lines is 7 G. Interaction of the unpaired electron on copper with two equivalent nitrogen nuclei each having a nuclear spin of 1, would be expected to result in the splitting of each copper hyperfine line into five lines with intensity ratios 1 : 2 : 3 : 2 : 1, and spacing between adjacent lines of 14—15 G. It is possible therefore that the lineshape may be the result of either the superposition of two or more monomer spectra or, that interactions with atoms other than nitrogen are occurring.

The signal observed at *g ca.* 4 in the ESR spectrum due to Cu(Salpn) doped into Ni(Salpn) indicates the formation of a dimeric species under these conditions, although only in small concentrations. The lineshape of the low field component of the spectrum again points to a monoclinic symmetry of the copper(II) pair system and the calculated magnetic and structural parameters from this spectrum are listed in Table 1. It can be seen from the similarity of these parameters to those obtained from frozen solution measurements, that the structural features of the copper(II) Schiff base are unchanged despite the gross change in host lattice.

Chikira *et al.* have studied the equilibrium between monomeric and dimeric forms of the copper(II) Schiff bases and have estimated equilibrium constants for the conversion of monomer to dimer by comparing the spectral intensities of the two species.[3] Their calculations concerning the quadridentate Schiff base complexes indicated that the K values (K is the equilibrium constant for the reaction $2M \rightleftharpoons M_2$, where M is the monomer) were not changed by branching methyl groups at the ethylene bridge. Contrary to their results however we have shown that when the iminoic nitrogens are bridged by a timethylene group, as in Cu(Saltn), the distribution of dimer in solution is unaltered and readily detectable triplet state ESR spectra are observed. A similar situation arises when

there is a methyl group on the imine carbon in the Schiff bases derived from *o*-hydroxyacetophenone and, once again, increasing the size of the bridging group from two to three carbon atoms produced no noticeable effect on the ESR spectra of these complexes. No evidence for dimer formation involving the complex with a tetramethylene bridge could be detected due to the low solubility of this complex in common organic solvents.

The effect of substituents on the phenyl ring is more noticeable. The tendency to dimerise is greater in the substituted complexes as can be seen by comparing the ESR spectra of Cu(Saltn) and Cu(3MeO-Saltn) in frozen chloroform. In xylene or toluene the substituted complexes aggregate further whereas the unsubstituted complexes are essentially dimeric in these solvents. This result indicates that solvent effects also play an important part in the dimerization and polymerization of the copper(II) Schiff base complexes in frozen solution. In all cases association was more marked in xylene than in chloroform presumeably due to the greater solvating tendencies of the latter.

The Australian Research Grants Committee is thanked for a grant for the purchase of the Varian E-12 ESR Spectrometer. D.J.C. acknowledges receipt of a Commonwealth Post Graduate Award.

References

1) A. D. Toy, M. D. Hobday, P. D. W. Boyd, T. D. Smith, and J. R. Pilbrow, *J. Chem. Soc. Dalton*, **1973**, 1259.
2) M. Chikira and T. Isobe, This Bulletin, **45**, 3006, (1972).
3) M. Chikira, H. Yakoi, and T. Isobe, *ibid.*, **47**, 2208 (1974).
4) G. D. Simpson, G. O. Carlisle, and W. E. Hatfield, *J. Inorg. Nucl. Chem.*, **36**, 2257, (1974).
5) M. Chikira and T. Isobe, *Chem. Phys. Lett.*, **30**, 498, (1975).
6) T. Lund and W. E. Hatfield, *J. Chem. Phys.*, **59**, 885, (1973).
7) P. D. W. Boyd, A. D. Toy, and T. D. Smith, J. R. Pilbrow, *J. Chem. Soc., Dalton*, **1973**, 1549.
8) T. D. Smith and J. R. Pilbrow, *Coord. Chem. Rev.*, **13**, 173, (1974).

Non-isothermal Studies of Adduct Molecules of Metallic Halides with Oxo Compounds in Solid State. III.

N. Ray Chaudhuri and S. Mitra

Inorganic Chemistry Laboratory, Indian Association for the Cultivation of Science, Calcutta 700032, India

(Received December 23, 1974)

Non-isothermal studies of some adduct molecules of metallic halides with ethylene glycol dimethyl ether of the type $MX_2(EGDME)_y$ in solid state were carried out with a derivatograph, where M=Mn(II), Co(II), Ni(II), Cu(II) or Cd(II), X=Cl^- or Br^-, EGDME=ethylene glycol dimethyl ether and y=0.5—1. These adduct molecules lost ethylene glycol dimethyl ether in single or multiple steps upon heating. Thermally stable intermediate products were isolated and characterised by elemental analysis and IR spectral measurement. The activation energy for each step of decomposition of the adduct was evaluated from the analysis of TG, DTG and DTA curves of the respective derivatograms. Enthalpy change was evaluated from the DTA peak area and the order of reaction was found to be unity for each step of decomposition. Thermal parameters for the above adducts were compared with those for the corresponding type of adducts with oxo-compounds like dioxane or tetrahydrofuran.

Works on the adduct molecule with ethylene glycol dimethyl ether were carried out by several groups of workers,[1-11] but they only prepared and characterised some adduct molecules of metallic halides with ethylene glycol dimethyl ether. Ludwig and Schroer[12] carried out thermal decomposition of ethylene glycol dimethyl ether adducts of some metal halides. They investigated the thermal properties of the adducts by thermogravimetry and differential thermal analysis but not by the measurement of DTG, and they did not evaluate the activation energy, order of reaction and enthalpy change for each step of decomposition of the adducts. In continuation of our previous works[13,14] on dioxane and tetrahydrofuran, the present paper deals with thermal decomposition of ethylene glycol dimethyl ether adducts of some metal halides to evaluate the activation energy for decomposition of the adducts from the results by simultaneous TG, DTG, and DTA measurements as well as the order of reaction(n) from the TG curve and ΔH from the DTA peak area. This paper gives a comparative picture on the thermal properties of adducts similar in composition and a discussion on the thermal properties relating the other oxo-compounds studied earlier.[13,14]

Experimental

All the adducts were prepared by a method similar to that described previously[13,14] and characterised by elemental analysis and IR spectral measurement. The ethylene glycol dimethyl ether used was sufficiently purified according to the standard procedure.[8]

The following adducts of the metal halides were prepared

1. $MnCl_2 \cdot 0.5EGDME$
2. $MnBr_2 \cdot 1EGDME$
3. $CoCl_2 \cdot 0.5EGDME$
4. $CoBr_2 \cdot 1EGDME$
5. $NiCl_2 \cdot 1EGDME$
6. $NiBr_2 \cdot 1EGDME$
7. $CuCl_2 \cdot 0.5EGDME$
8. $CuBr_2 \cdot 1EGDME$
9. $CdCl_2 \cdot 1EGDME$
10. $CdBr_2 \cdot 1EGDME$

where EGDME represents ethylene glycol dimethyl ether.

A Paulik-Paulik-Erdey type MOM derivatograph was used for thermal analysis. The particle size of the sample was within 150—200 mesh. Heating rate was about 1.5 °C/min. The volume of the sample in each case was the same. Platinum crucible was used. All the experiments were conducted in static air.

Results

Adducts of $MnBr_2$, $NiBr_2$, $CuBr_2$, $CdCl_2$ and $CdBr_2$ with ethylene glycol dimethyl ether are similar in composition with one another and lose ethylene glycol dimethyl ether in a single step upon heating as indicated by their respective derivatogram in Figs. 1 and 2. A similar single step decomposition is observed in the adduct of $CuCl_2$ although its composition is not similar to that of the former adducts. The adducts of $MnCl_2$ and $CoCl_2$ are similar to one of $CuCl_2$ in composition and they lose ethylene glycol dimethyl ether on heating in different fashion (Fig. 3); *i.e.*, $MCl_2 \cdot 0.5EGDME \rightarrow MCl_2 \cdot 0.25EGDME$; $MCl_2 \cdot 0.25EGDME \rightarrow MCl_2$, where M=Mn(II) or Co(II). The adduct of $NiCl_2$ though it is similar to the adduct of $NiBr_2$ in composition loses ethylene glycol dimethyl ether upon heating in the following way as shown in Fig. 4; $NiCl_2 \cdot 1EGDME \rightarrow NiCl_2 \cdot 0.25EGDME \rightarrow NiCl_2$. The intermediate product *i.e.*, $NiCl_2 \cdot 0.25EGDME$ is not stable. The adduct of $CoBr_2$ which is similar in composition to the major number of adducts described earlier loses ethylene glycol dimethyl ether in multiple steps upon heating as shown in Fig. 4. None of these intermediate products are stable enough to be isolated. Its derivatogram indicates its decomposition in three steps and the intermediate products are very unusual in composition.

The decomposition of all the adducts shows endotherm. Temperature ranges of decomposition and the DTG peak temperatures for the adducts are listed in Table 1. Enthalpy change for each step of decomposition of the adducts was evaluated by the method of Sano[15] using copper sulfate pentahydrate as the standard. When the two DTA curves are too much overlapped with each other, the ΔH values are evaluated from the overall area of the DTA peaks concerned.

The activation energy for each step of decomposition of the adduct molecules was evaluated (Table 1) from the analysis of the TG curves using Freeman and Carroll's[16] equation. The plots of $\Delta\log(dw/dt)/\Delta\log W_r$ *vs.* $\Delta T^{-1}/\Delta\log W_r \times 10^3$ from TG curves are shown in Fig. 5. The order of reaction for each step of decomposition is found to be unity.

Activation energy for each step of decomposition was also evaluated from the analysis of the DTG curve

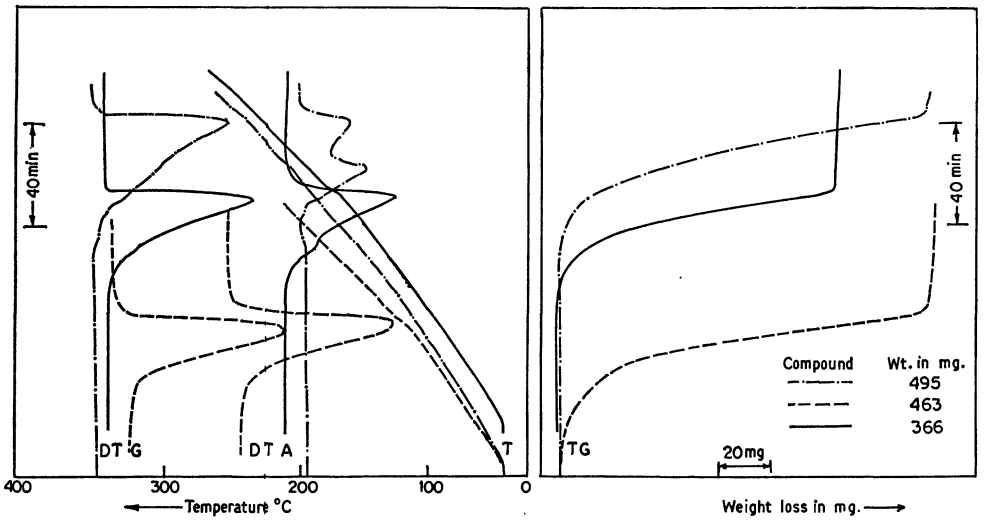

Fig. 1. Derivatograms for $CuBr_2 \cdot 1EGDME$ (-·--·-), $NiBr_2 \cdot 1EGDME$ (----) and $MnBr_2 \cdot 1EGDME$ (——).

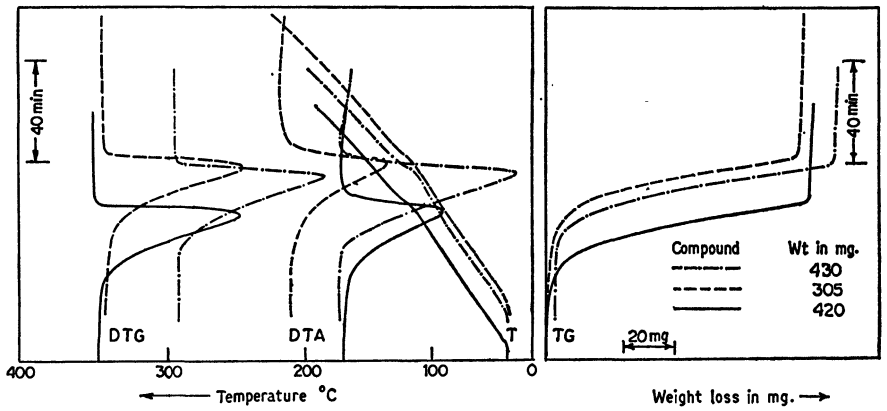

Fig. 2. Derivatograms for $CuCl_2 \cdot 0.5EGDME$ (-·--·-), $CdCl_2 \cdot 1EGDME$ (----) and $CdBr_2 \cdot 1EGDME$ (——).

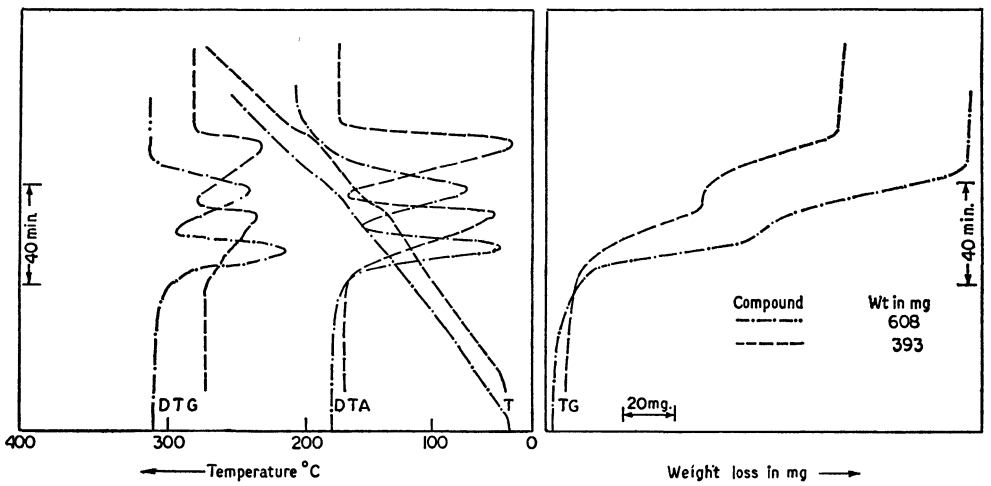

Fig. 3. Derivatograms for $MnCl_2 \cdot 0.5EGDME$ (-·--·-) and $CoCl_2 \cdot 0.5EGDME$ (----).

using the method of Dave and Chopra[17] and the method described in our earlier work[13] and also from the analysis of DTA curve using Brochardt's[18] equation for first order reaction (Table 1). The Arrhenius plots of log k *vs* $T^{-1} \times 10^3$ from DTG and DTA curves are shown in Figs. 6 and 7 respectively.

IR spectra of the adducts were taken to conform the presence of ethylene glycol dimethyl ether molecule in the adduct.

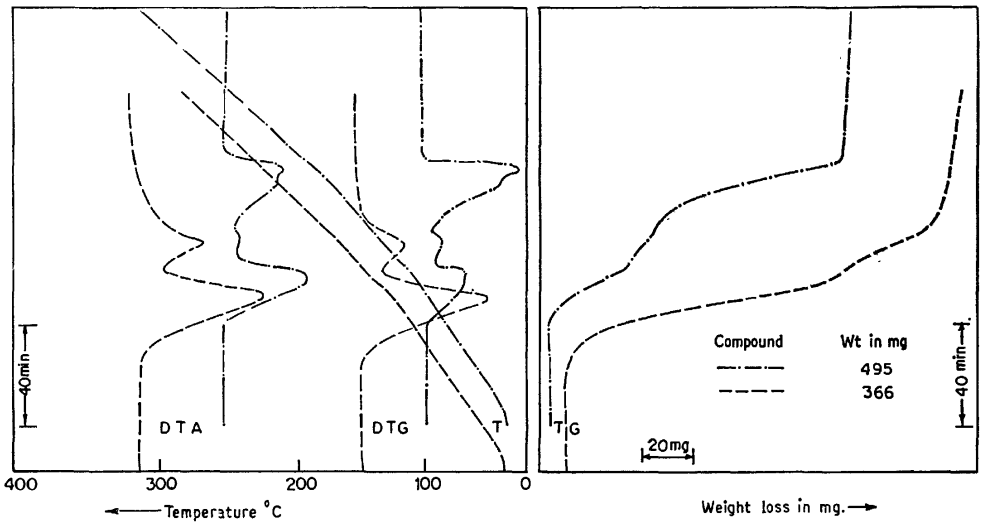

Fig. 4. Derivatograms for $CoBr_2 \cdot 1EGDME$ (-·-·-) and $NiCl_2 \cdot 1EGDME$ (----).

TABLE 1. THERMAL PARAMETERS FOR THE DECOMPOSITION OF ADDUCT MOLECULES OF SOME METALLIC HALIDES WITH ETHYLENE GLYCOL DIMETHYL ETHER

	Decomposition reaction	Temp. range °C	DTG peak temp. °C	Activation energy ΔE_a kcal/mol TG	DTG	DTA	Enthalpy change ΔH kcal/mol
Ia.	$MnCl_2 \cdot 0.5A \rightarrow MnCl_2 \cdot 0.25A$	85—140	135	27.1	a)	a)	46.0[b]
b.	$MnCl_2 \cdot 0.25A \rightarrow MnCl_2$	140—202	179	49.8	a)	a)	
II.	$MnBr_2 \cdot 1A \rightarrow MnBr_2$	107—175	169	33.5	33.5	33.5	19.5
IIIa.	$CoCl_2 \cdot 0.5A \rightarrow CoCl_2 \cdot 0.25A$	100—143	135	46.0	46.0	46.0	50.0
b.	$CoCl_2 \cdot 0.25A \rightarrow CoCl_2$	155—200	190	46.0	41.4	46.0	57.9
IVa.	$CoBr_2 \cdot 1A \rightarrow CoBr_2 \cdot 0.74A$	76—114	110	46.0	46.0	39.8	
a′.	$CoBr_2 \cdot 0.74A \rightarrow CoBr_2 \cdot 0.65A$	114—144	135	c)	c)	c)	32.0[b]
b.	$CoBr_2 \cdot 0.65A \rightarrow CoBr_2$	144—194	188	46.0	39.5	39.0	
Va.	$NiCl_2 \cdot 1A \rightarrow NiCl_2 \cdot 0.25A$	85—150	125	32.9	a)	a)	26.2[b]
b.	$NiCl_2 \cdot 0.25A \rightarrow NiCl_2$	150—209	167	126.5	a)	a)	
VI.	$NiBr_2 \cdot 1A \rightarrow NiBr_2$	65—131	110	23.0	29.2	29.2	28.9
VII.	$CuCl_2 \cdot 0.5A \rightarrow CuCl_2$	75—127	112	33.5	33.5	33.5	33.9
VIII.	$CuBr_2 \cdot 1A \rightarrow CuBr_2$	160—245	240	34.5	34.5	a)	24.8
IX.	$CdCl_2 \cdot 1A \rightarrow CdCl_2$	55—120	113	23.0	27.0	27.0	22.8
X.	$CdBr_2 \cdot 1A \rightarrow CdBr_2$	59—120	112	23.0	23.0	23.0	22.8

A Ethylene glycol dimethyl ether. a) Evaluation of activation energy not possible due to too much overlapping of the corresponding curves. b) Overall enthalpy change. c) Evaluation of activation energy and enthalpy change not possible due to very weak resolution of the curve.

Discussion

The adduct of $MnCl_2$ was known as $MnCl_2 \cdot 1EGDME$.[8] On repeated preparation we could not isolate an adduct of similar composition. Recently Hengge and Zimmermann[11] isolated the adduct of $MnCl_2$ like ours. Its composition and nature of thermal decomposition are similar to the corresponding adduct with tetrahydrofuran.[14] It is observed that thermal stability of $MnCl_2 \cdot 0.5EGDME$ is greater than the corresponding tetrahydrofuran adduct, whereas its intermediate product, $MnCl_2 \cdot 0.25EGDME$, is thermally less stable than the corresponding tetrahydrofuran adduct. It is also noted that values of activation energies for decomposition of $MnCl_2 \cdot 0.5EGDME \rightarrow MnCl_2 \cdot 0.25EGDME$ and $MnCl_2 \cdot 0.25EGDME \rightarrow MnCl_2$ are less than those for the corresponding tetrahydrofuran adduct.

The adduct of $MnBr_2$ is similar in composition to the corresponding adduct with tetrahydrofuran and dioxane we isolated.[13,14] The thermal stability of $MnBr_2 \cdot 1EGDME$ is higher than the corresponding adduct with tetrahydrofuran and less than the corresponding adduct with dioxane. The value of activation energy evaluated for the decomposition of $MnBr_2 \cdot 1EGDME \rightarrow MnBr_2$ is less than that for the corresponding adduct with dioxane.

The adduct of $CoCl_2$ was isolated as $CoCl_2 \cdot 1EGDME$.[12] Ludwick and Schroer[12] carried out its thermal decomposition and DTA study. In their studies the

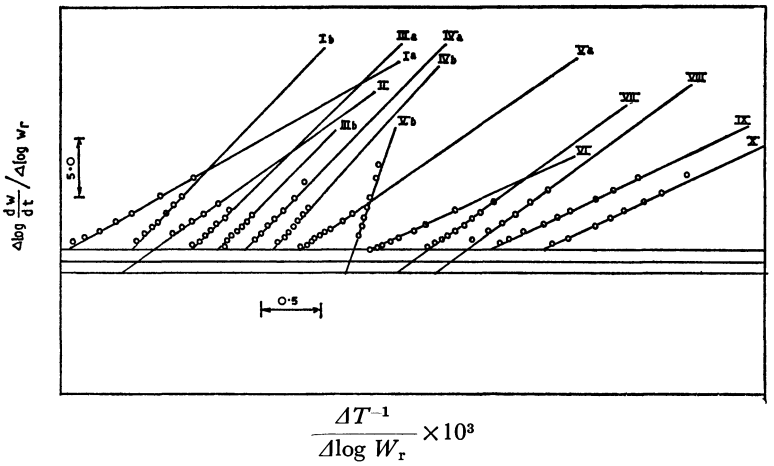

Fig. 5. Plots of $\Delta \log \frac{dw}{dt} / \Delta \log W_r$ *vs.* $\Delta T^{-1}/\Delta \log W_r \times 10^3$ from TG for the decomposition of $MnCl_2 \cdot 0.5$-EGDME → $MnCl_2 \cdot 0.25$EGDME (Ia), $MnCl_2 \cdot 0.25$EGDME → $MnCl_2$ (Ib), $MnBr_2 \cdot 1$EGDME → $MnBr_2$ (II), $CoCl_2 \cdot 0.5$EGDME → $CoCl_2 \cdot 0.25$EGDME (IIIa), $CoCl_2 \cdot 0.25$EGDME → $CoCl_2$ (IIIb), $CoBr_2 \cdot 1$EGDME → $CoBr_2 \cdot 0.74$EGDME (IVa), $CoBr_2 \cdot 0.65$EGDME → $CoBr_2$ (IVb), $NiCl_2 \cdot 1$EGDME → $NiCl_2 \cdot 0.25$EGDME (Va), $NiCl_2 \cdot 0.25$EGDME → $NiCl_2$ (Vb), $NiBr_2 \cdot 1$EGDME → $NiBr_2$ (VI), $CuCl_2 \cdot 0.5$EGDME → $CuCl_2$ (VII), $CuBr_2 \cdot 1$EGDME → $CuBr_2$ (VIII), $CdCl_2 \cdot 1$EGDME → $CdCl_2$ (IX) and $CdBr_2 \cdot 1$EGDME → $CdBr_2$ (X).

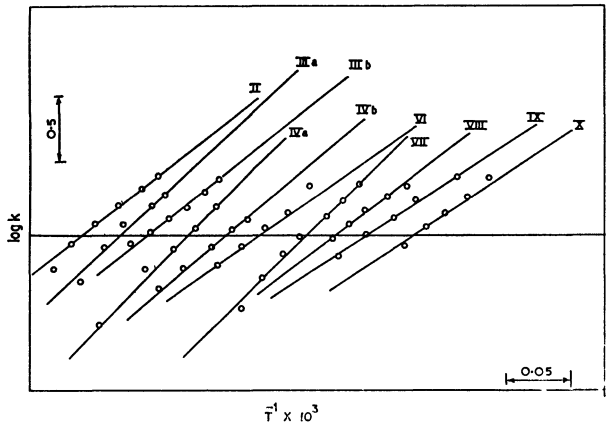

Fig. 6. Arrhenius plots of $\log k$ *vs.* $T^{-1} \times 10^3$, from DTG for the decomposition of $MnBr_2 \cdot 1$EGDME → $MnBr_2$(II), $CoCl_2 \cdot 0.5$EGDME→$CoCl_2 \cdot 0.25$EGDME (IIIa), $CoCl \cdot 0.25$EGDME → $CoCl_2$ (IIIb), $CoBr_2 \cdot 1$EGDME → $CoBr_2$. 0.74EGDME (IVa), $CoBr_2 \cdot 0.65$EGDME→$CoBr_2$ (IVb), $NiBr_2 \cdot 1$EGDME→$NiBr_2$ (VI), $CuCl_2 \cdot 0.5$ EGDME→$CuCl_2$ (VII), $CuBr_2 \cdot 1$EGDME→$CuBr_2$ (VIII), $CdCl_2 \cdot 1$EGDME→$CdCl_2$ (IX) and $CdBr_2 \cdot 1$EGDME→$CdBr_2$ (X).

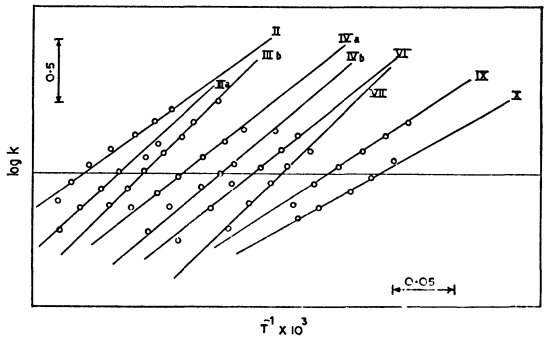

Fig. 7. Arrhenius plots of $\log k$ *vs.* T^{-1}, from DTA for the decomposition of $MnBr_2 \cdot 1$EGDME → $MnBr_2$ (II), $CoCl_2 \cdot 0.5$EGDME→$CoCl_2 \cdot 0.25$EGDME (IIIa), $CoCl_2 \cdot 0.25$EGDME→$CoCl_2$ (IIIb), $CoBr_2 \cdot 1$EGDME → $CoBr_2 \cdot 0.74$EGDME (IVa), $CoBr_2 \cdot 0.65$EGDME→ $CoBr_2$ (IVb), $NiBr_2 \cdot 1$EGDME → $NiBr_2$ (VI), $CuCl_2 \cdot 0.5$EGDME→$CuCl_2$ (VII), $CdCl_2 \cdot 1$EGDME→$CdCl_2$ (IX) and $CdBr_2 \cdot 1$EGDME → $CdBr_2$ (X).

existence of $CoCl_2 \cdot 0.5$EGDME was observed from the TG curve and the two overlapped endothermic peaks of the DTA curve. We could not isolate the adduct of the composition described above.[8,12] The adduct $CoCl_2 \cdot 5$EGDME we isolated is similar in composition to that of the adduct with tetrahydrofuran and dioxane, its nature of thermal decomposition being also similar to that of the adduct of $MnCl_2$ and the corresponding adduct with tetrahydrofuran. $CoCl_2 \cdot 0.5$D being similar to the corresponding adduct with ethylene glycol dimethyl ether in composition loses dioxane in a single step. The existence of $CoCl_2 \cdot 0.25$EGDME, $MnCl_2 \cdot 0.25$EGDME and corresponding adduct with THF is indicated by their respective derivatograms. The thermal stability of $CoCl_2 \cdot 0.5$EGDME is equal to the corresponding adduct of $MnCl_2$ and the activation energy for the decomposition of $CoCl_2 \cdot 0.5$EGDME→ $CoCl_2 \cdot 0.25$EGDME is greater than that for the decomposition of $MnCl_2 \cdot 0.5$EGDME→$MnCl_2 \cdot 0.25$-EGDME. On the other hand the thermal stability of $CoCl_2 \cdot 0.25$EGDME is higher than that of the corresponding adduct of $MnCl_2$. However, the thermal stability, activation energy and enthalpy change of this intermediate product are practically equal to that of tetrahydrofuran adduct.[14] The thermal stability of the adduct $CoCl_2 \cdot 0.5$EGDME is lower than the corresponding similar adduct with dioxane but greater than the corresponding tetrahydrofuran adduct. The activation energy for the first step of decomposition of $CoCl_2 \cdot 0.5$EGDME is higher in comparison to the corresponding similar adducts with dioxane and

tetrahydrofuran

The adduct $CoBr_2 \cdot 1EGDME$ we isolated is similar in composition to the adducts isolated by Fowles *et al.*[8] and Ludwig and Schroer.[12] DTA study of $CoBr_2 \cdot 1EGDME$[12] shows that the decomposition takes place in two steps and the intermediate product is very unstable. In our case the nature of decomposition is somewhat different. This is probably due to the very small rate of heating in comparison with that in the earlier work.[12] Though the intermediate products are unstable, we obtained three endothermic peaks in the DTA curve. The weight loss of the second step is very small. Though the composition of the adduct of $CoBr_2$ with ethylene glycol dimethyl ether is similar to that of the corresponding adduct with dioxane, the nature of thermal decomposition of the two differs. The adduct $CoBr_2 \cdot 1D$ loses dioxane in a single step. The thermal stability of $CoBr_2 \cdot 1D$ is lower than that of the corresponding adduct with ethylene glycol dimethyl ether. Activation energy is smaller in case of dioxane adduct.

The composition of the adduct of $NiCl_2$ we isolated differs from that of the corresponding adduct with dioxane and tetrahydrofuran.[13,14]

The adduct of $NiBr_2$ was isolated as $NiBr_2 \cdot 2EGDME$.[12] Its TG and DTA studies indicate multiple steps of decomposition. Ludwig and Schroer could not isolate the adduct as $NiBr_2 \cdot 1EGDME$ thermally. However, Ward[10] isolated the same recently. $NiBr_2 \cdot 1EGDME$ we isolated is similar in composition to the corresponding dioxane adduct[13] but not similar to the corresponding adduct with THF.[14] The nature of thermal decomposition of the adduct $NiBr_2 \cdot 1EGDME$ is similar to the corresponding dioxane adduct, $NiBr_2 \cdot 1D$. With respect to the thermal stability and activation energy of decomposition the ethylene glycol dimethyl ether adduct is less stable than the dioxane adduct in the case of $NiBr_2$.

The adduct $CuCl_2 \cdot 0.5EGDME$ we isolated was reported earlier.[8,12] Although the composition of the adduct of this salt with dioxane and tetrahydrofuran differs from this adduct, the nature of decomposition of this adduct and the adduct of dioxane is the same.

Ethylene glycol dimethyl ether adduct of $CuBr_2$ we isolated is similar in composition to the corresponding adduct with tetrahydrofuran. The dioxane adduct of similar composition is observed as an intermediate during the thermal decomposition of $CuBr_2 \cdot 2D$. Thermal stability and activation energy of $CuBr_2 \cdot 1EGDME$ are equal to those of the corresponding adduct with THF but the adduct $CuBr_2 \cdot 1EGDME$ is thermally more stable than the corresponding dioxane adduct.

Preparation and characterisation of the adduct of $CdCl_2$ and $CdBr_2$ with ethylene glycol dimethyl ether were carried out by Fowles *et al.*[8] We isolated the adducts of $CdCl_2$ and $CdBr_2$ as $CdCl_2 \cdot 1EGDME$ and $CdBr_2 \cdot 1EGDME$ which are similar in composition to their adducts and also similar to the corresponding adduct with tetrahydrofuran but not similar to the corresponding adduct with dioxane in the case of $CdCl_2$. Dioxane forms the adduct of $CdCl_2$ as $CdCl_2 \cdot 0.5D$. The nature of the decomposition of the adducts of both $CdCl_2$ and $CdBr_2$ with ethylene glycol dimethyl ether is similar to the adducts of other oxo-compounds such as tetrahydrofuran and dioxane.[13,14] The thermal stability and activation energy of the decomposition of $CdCl_2 \cdot 1EGDME$ are lower than those of the corresponding tetrahydrofuran adduct. The adduct $CdBr_2 \cdot 1EGDME$ is thermally less stable than the corresponding adduct with dioxane and more stable than that of adduct with tetrahydrofuran. The activation energy of decomposition of ethylene glycol dimethyl ether adduct of $CdBr_2$ is lower than that of the corresponding adduct with tetrahydrofuran or dioxane.

Thermal stability of the adducts of the type $MBr_2 \cdot 1EGDME$, where M=Mn(II), Co(II), Ni(II), Cu(II) and Cd(II) increase in the order: Cu>Mn>Cd>Ni=Co. The thermal stability, activation energy and enthalpy change of decomposition of $CdCl_2 \cdot 1EGDME$ and $CdBr_2 \cdot 1EGDME$ are nearly the same. Such similarities are not observed between the corresponding tetrahydrofuran adducts of $CdCl_2$ and $CdBr_2$.

In general the later step of decomposition gives larger ΔH value and activation energy than the earlier step. But such a tendency is not observed in the decomposition of all the adducts.

The authors wish to express their hearty thanks to Prof. P. C. Dutta of this Institute for his kind help in the work.

References

1) H. Meerwein, V. Hederich, and K. Wunderlich, *Arch. Pharm. Ber. Dtch. Pharmaz. Ges.*, **291**, 541 (1958).
2) E. L. Muetterties, *J. Amer. Chem. Soc.*, **82**, 1082 (1960).
3) F. Fairbrother, N. Flitcroft, and H. Prophet, *J. Less-Common Metals*, **2**, 49 (1960).
4) N. Ya. Turova, A. V. Novoselova, and K. N. Semenko, *Zh. Neorg. Khim.*, **5**, 1705 (1960).
5) G. W. A. Fowles, R. A. Hoodles, and R. A. Walton, *J. Chem. Soc.*, **1963**, 5873.
6) B. E. Bridgland, G. W. A. Fowles, and R. A. Walton, *J. Inorg. Nucl. Chem.*, **27**, 383 (1965).
7) H. P. Schroer and B. Heyn, *Z. Chem.*, **7**, 238 (1967).
8) G. W. A. Fowles, D. A. Rice, and R. A. Walton, *J. Inorg. Nucl. Chem.*, **31**, 3119 (1969).
9) L. R. Nylander and S. F. Pavkovic, *Inorg. Chem.*, **9**, 1959 (1970).
10) L. G. L. Ward, "Inorganic Syntheses," Vol 13, p. 154 (1971).
11) E. Hengge and H. Zimmermann, *Monatsh. Chem.*, **103**, 418 (1972).
12) W. Ludwig and H. P. Schroer, *Z. Anorg. Allg. Chem.*, **357**, 74 (1968).
13) N. Ray Chaudhuri, S. Mitra, and G. K. Pathak, This Bulletin, **48**, 2375 (1975).
14) N. Ray Chaudhuri and S. Mitra, This Bulletin, **48**, 2375 (1975).
15) K. Sano, *Sci. Rep. Tohoku Imp. Univ. 1st Ser.*, **24**, 719 (1936).
16) E. S. Freeman and B. Carroll, *J. Phys. Chem.*, **62**, 394 (1958).
17) N. G. Dave and S. K. Chopra, *Z. Phys. Chem.*, **48**, 257 (1966).
18) H. J. Brochardt and F. Daniels, *J. Amer. Chem. Soc.*, **79**, 41 (1957).

Synthesis of 2,3,6,7-Tetramethylnaphthalene from 2,3-Dimethylsuccinic Anhydride and *o*-Xylene

Yasuhiko Dozen and Masato Hatta

Government Industrial Research Institute, Osaka, Ikeda-shi, Osaka 563

(Received October 24, 1974)

2,3,6,7-Tetramethylnaphthalene (**7b**) was prepared from 2,3-dimethylsuccinic anhydride (**1**) and *o*-xylene in five steps, and the configurations of their intermediates were studied. The higher-melting isomer (*threo* form) of **1** gave higher-melting products in each step, while the lower-melting isomer (*erythro* form) of **1** gave lower-melting ones. The configurations of the intermediates were confirmed by the MNR spectral data of tetramethyltetralines (**6b**). Similar reactions were carried out with 3-benzoyl-2,3-dimethylpropionic acid (**2a**) in order to learn the configurations of the intermediates. 3-Aroyl-2,3-dimethylpropionic acids (**2**) gave 2,3-dimethyl-4-aryl-3-buten-4-oildes (**3**) upon heating with hydrochloric acid.

In the course of the investigation of thermally stable polyimide polymers derived from naphthalenetertacarboxylic acid anhydrides and aromatic diamines, we realized the necessity of a convenient method of synthesizing 2,3,6,7-naphthalenetetracarboxylic acid. The anhydride of this acid has been prepared by the dehydrogenation of 1,2,3,4,5,6,7,8-octahydronaphthalene-2,3,6,7-tetracarboxylic acid dianhydride[1-3] with bromine.[4,5] 2,3,6,7-Tetramethylnaphthalene, which is oxidizable to the tetracarboxylic acid, has been synthesized by Mosby[6] and Rieke *et al.*[7] but these procedures are inadequate for obtaining the acid in quantity. 4-Arylbutyric acids, which give rise to naphthalene derivatives by cyclization, have been prepared by the Clemmensen reduction of 3-aroylpropionic acids[8] or by catalytic hydrogenation over palladium in acetic acid.[9-11] A partial hydrogenation of 3-benzoylpropionic acid over palladium in alcoholic ammonia gives 4-phenylbutyrolactone.[12]

The present paper will deal with the synthesis of 2,3,6,7-tetramethylnaphthalene (**7b**) from 2,3-dimethylsuccinic anhydride (**1**) and *o*-xylene in five steps, as is shown in Scheme 1, where the *threo* isomer has been designated as an example. A mixture of the diastereoisomer of the starting material could be used for the synthesis of **7b**. When optically inactive *threo* **1** was used, the products of each step in Scheme 1 were of the *threo* form, with a retention of the configuration. Similarly, *erythro* **1** gave *erythro* products. Similar reactions with **2a** were carried out as an adjunct for the investigation of the configuration. The intermediates reported here are new compounds.

Results and Discussion

3-Aroyl-2,3-dimethylpropionic Acids (*2*). In the Friedel-Crafts reaction of **1** with benzene alone or with *o*-xylene in tetrachloroethane, the higher-melting isomer (*threo* form) of **1** gave predominantly the higher-melting isomer of **2a** or **b**. On the other hand, the lower-melting isomer (*erythro* form) of **1** gave the lower-melting isomer of **2a** or **b**. These results suggest that the configuration is retained in the reaction.[13] The NMR and IR spectral data of **2** are summarized in Table 1.

The *threo* **2a** was insoluble in carbon tetrachloride, whereas the *erythro* isomer was soluble. On the other hand, *threo* and *ertyhro* **2b** could not be separated into two diastereoisomers by solvent extraction; rather, they were characterized on the basis of the NMR spectra. The *threo* or *erythro* **2a** was converted to a mixture of nearly equal amounts of them in a strong alkaline solution, while in a weak alkaline solution only a small portion of *threo* **2a** was epimerized, as is shown in Table 2.

2,3-Dimethyl-4-aryl-3-buten-4-olides (*3*). On the Clemmensen reduction of *threo* **2a**, compounds **3a** (racemate) and **4a** (*threo* and *erythro* mixture) were obtained in a molar ratio of 37 : 63, while a mixture of *threo* and *erythro* **2b** (about 1 : 1) gave **3b** (racemate) and **4b** (*threo* and *erythro* mixture) in a 62 : 38 ratio. Refluxing a mixture of **2** and hydrochloric acid gave racemic **3**[14] (Table 3). The IR and NMR spectral data of **3** are shown in Table 4.

Table 1. NMR and IR data of 2

Compound		NMR (δ, ppm)								IR (in Nujol, cm^{-1})	
		2-CH_3	3-CH_3	Ar-CH_3	2-CH	3-CH	Ar-H	CO_2H	$CHCl_3$	ν_{CO}	δ_{Ar-H}
2a	*threo*[a]	1.16, 3H d, J=7 Hz	1.23, 3H d, J=7 Hz	—	2.84—3.14 1H, quint	3.61—3.91 1H, quint	7.35—7.95 5H, m	—	7.24 1H, s	1705 s 1680 s	699 s
	erythro[a]	1.18, 3H d, J=7 Hz	1.26, 3H d, J=7 Hz	—	2.84—3.14 1H, oct	3.61—3.91 1H, oct	7.36—7.99 5H, m	—	7.25 1H, s	1700 s 1674 s	699 s
2b	*threo*[b]	1.12, 3H d, J=7 Hz	1.19, 3H d, J=7 Hz	2.31 6H, s	2.79—3.10 1H, quint	3.62—3.90 1H, quint	7.09—7.65 3H, m	10.65 1H, s	—	1705 s 1676 s	882w 836w
	erythro[b]	1.16, 3H d, J=7 Hz	1.22, 3H d, J=7 Hz	2.31 6H, s	2.75—3.05 1H, oct	3.52—3.82 1H, oct	7.13—7.70 3H, quart	10.76 1H, s	—	1698 s 1673 s	885w 840w

a) NMR: in 2% $CDCl_3$. b) NMR: in 10% CCl_4.

Table 2. Epimerization of **2a** in aqueous alkaline solution

Reactant		Product, %		
Compound	Base	Yield	*threo*	*erythro*
threo	KOH	91	53	47
threo	Na_2CO_3	94	>91	<9
erythro	KOH	92	42	58

Table 3. Lactonization of **2** to **3** with hydrochloric acid

Reactant **2**	Recovered **2**, %	Product **3**, %
a *threo*	6	83
erythro	4	82
b *threo*	4	88

The aliphatic methyl hydrogen signal which appeared upfield in the NMR spectra of racemic **3a** and **b** has triplet bands, while that downfield has a sextet. The downfield signal was changed to a triplet by decoupling with the methine proton. The splitting into a triplet can not be explained at present.

An attempt to esterify the racemic **3b** with methanol in the presence of sulfuric acid failed, and the lactone was recovered. The Clemmensen reduction of racemic **3b** for 10 hr gave a mixture of *threo* and *erythro* **4b** in a 13.5% yield, and 76% of the racemic **3b** was recovered. The hydrolysis of racemic **3b** with potassium hydroxide in aqueous ethanol gave a mixture of the diastereoisomers of **2b**. A reddish color was observed at the initial stage of the hydrolysis, in analogy with angelicalactone.[15]

4-Aryl-2,3-dimethylbutyric Acids (*4*). On the catalytic hydrogenation with palladium on carbon in glacial acetic acid, the higher-melting isomers (*threo* form) of **2a** and **b** gave higher-melting ones of **4a** and **b** respectively, and the lower-melting isomers (*erythro* form) of **2a** and **b** were converted to the lower-melting ones of **4a** and **b**, as is shown in Table 5. The NMR and IR data are summarized in Table 6. It is interesting to note that the carbonyl band of *threo* **4** in the IR spectra appeared at a lower frequency than that of *erythro* ones.

Tetralones (*5*). The cyclization of the acid chloride of *threo* **4a** with anhydrous aluminum chloride in tetrachloroethane gave predominantly the higher-melting isomer of **5a**, while *erythro* **4a** and **b** gave

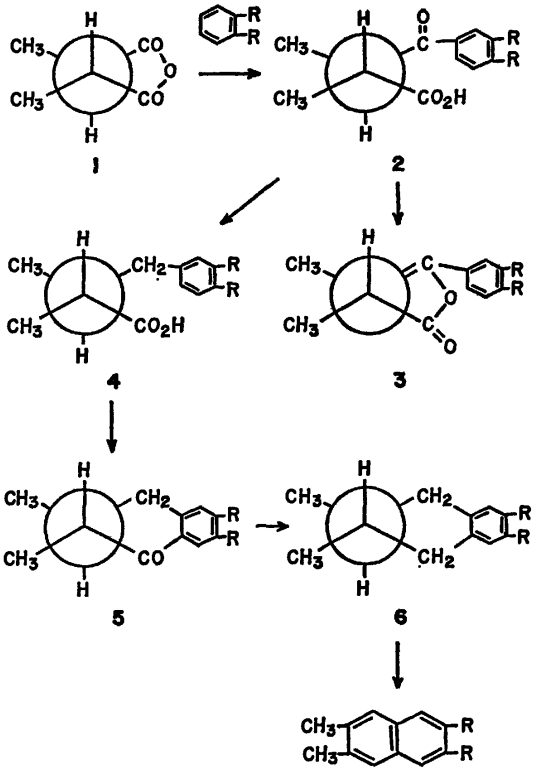

Scheme 1. *threo*-Isomer.

lower-melting ones of **5a** and **b** respectively, as is shown in Table 7. The cyclization of *threo* or *erythro* **4a** and **b** with polyphosphoric acid (PPA), on the other hand, gave a mixture of the diastereoisomers of **5a** and **b** respectively. The ratio of *threo* and *erythro* **5a** and **b** could be determined by fractional crystallization from petroleum ether or methanol. After heating the *erythro* **5b** with PPA at 115 °C for 1 hr, the recovered tetralone (mp 65—95 °C) was composed of a mixture of nearly equal amounts of the diastereoisomers of **5b**. These results suggest that the configuration is retained during the cyclization by the Friedel-Crafts reaction. It is assumed that the configuration is retained at the cyclization step with PPA, but the tetralone obtained is rapidly epimerized through the enolization catalyzed by the proton.

The NMR data of **5** are summarized in Table 8. The aliphatic methyl proton signals of *threo* and *erythro* **5** overlapped, but they could be distinguished from each other. The methylene and 3-methyl proton

Table 4. NMR and IR data of **3**

Compound	NMR (δ, ppm, in 10% CCl_4)					IR (cm^{-1})			
						ν_{CO}		$\nu_{C=C}$	
	3-CH_3	2-CH_3	2-CH	Ar-CH_3	Ar-H	In 5% CCl_4	Liquid	In 5% CC_4	Liquid
a	1.72, 3H, t	1.77, 3H, sextet	5.51, 1H, b	—	7.06—7.36, 5H, m	1762 s	1759 s	1689m	1691m, 1680m
b	1.76, 3H, t	1.83, 3H, sextet	5.39, 1H, b	2.24, 6H, s	6.80—7.08, 3H, quart	1760 s	1741 s [a]	1685m	1681m[a], 1673m[a]

a) In Nujol.

Table 5. Catalytic hydrogenation of **2** to **4**

Material, **2**	Product, **4** Yield, %	Mp or bp/mmHg	Material, **2**	Product, **4** Yield, %	Mp or bp/mmHg
a *threo*	92	mp 76.5—77.5 °C	**b** *threo*	99	mp 72.5—73.5 °C
erythro	81	bp 151 °C/4.5	*erythro*	85	mp 56—58 °C

Table 6. NMR and IR data of **4**

Compound	NMR (δ, ppm, in 10% CCl_4) 3-CH_3	2-CH_3	Ar-CH_3	CH and CH_2	Ar-H	CO_2H	IR (cm^{-1}, in Nujol or liquid film) ν_{CO}	δ_{Ar-H}
a *threo*	0.87, 3H d, J=6.5 Hz	1.16, 3H d, J=7 Hz	—	2.12—2.88, 4H, m	7.04—7.44 5H, m	11.84 1H, s	1694 s	727m, 694 s
erythro	0.90, 3H d, J=6.5 Hz	1.19, 3H d, J=7 Hz	—	2.08—2.52, 3H, m (3-C**H**, 4-CH_2) 2.76—2.95, 1H, quart (2-C**H**)	7.04—7.36 5H, m	11.70 1H, s	1705 s 1687 s	738m, 700 s
b *threo*	0.84, 3H d, J=6.5 Hz	1.12, 3H d, J=7 Hz	2.20 6H, s	2.2—2.7, 4H, m	6.82—7.04 3H, quart	11.93 1H, s	1696 sh 1687 s	887w, 820m
erythro	0.89, 3H d, J=6.5 Hz	1.19, 3H d, J=7 Hz	2.17 6H, s	2.13—2.56, 2H, m (4-CH_2) 2.68—2.84, 2H, quart (2-C**H**, 3-C**H**)	6.73—7.00 3H, quart	12.16 1H, s	1701 s	892w, 827w

Table 7. Cyclization of **4** to **5**

Material	Recovered **4**, %	Product (**5**) Yield, %	*threo* : *erythro*	
With $AlCl_3$ and acid chloride				
a *threo*	8	58	~100	
erythro[a]	4	93	b)	b)
b *erythro*	4	94	27	73
With PPA				
a *threo*	0	86	b)	b)
erythro[a]	0	80	b)	b)
b *threo*	0	96	49	51
erythro	0	96	48	52

a) Contaminated with 9% of *threo* isomer. b) Could not be isolated.

signals in **5** and **6** exhibited similar chemical shifts, whereas the 2-methyl proton signal of **5** was shifted to a lower field as compared with that of **6** (see Table 10) as a result of the deshielding by the carbonyl group. The lower-field shift of the signal of 8-H as compared with that of 5-H in **5b** may also be attributed to deshielding by the carbonyl group.

Tetralines (**6**). The catalytic hydrogenation of *threo* **5a** and **b** over palladium on carbon in glacial acetic acid at 70—80 °C gave predominantly higher-melting isomers of **6**, as is shown in Table 9. The ratios of the *threo* and *erythro* isomers were determined by means of the aliphatic methyl proton signals in the NMR spectra. The NMR spectral data of **6** summarized in Table 10 support the theory that the two methine protons in the higher-melting isomer are axial and hence the aliphatic methyl groups are equatorial, and that the methine protons in the lower-melting isomer are one axial and one equatorial.[16] Therefore, it may be concluded that the higher-melting isomers in each step have the *threo* (*trans*) configuration, while the lower-melting isomers have the *erythro* (*cis*) one.

2,3,6,7-Tetramethylnaphthalene (**7**) *and -Naphthalenetetracarboxylic Acid.* The diastereoisomer of **6a** and **b** was dehydrogenated with palladium on carbon at 300 °C to 2,3-dimethylnaphthalene and 2,3,6,7-tetramethylnaphthalene respectively. The tetra-

Table 8. NMR data of **5** (δ, ppm in 10% CCl_4)

Compound	3-CH_3	2-CH_3	CH	CH_2	Ar-CH_3	Ar-H
a *threo*	1.14, 3H d, J=7 Hz	1.20, 3H d, J=7 Hz	1.80—2.80 2H, m	2.56—3.05 2H, m	—	7.03—7.88, 4H, m
erythro[a]	0.95 d, J=7 Hz	1.12 d, J=7 Hz	1.75—3.10, m		—	7.02—7.86, m
b *threo*	1.15, 3H d, J=6.5 Hz	1.21, 3H d, J=6.5 Hz	1.76—2.20 2H, m	2.44—2.96 2H, m	2.27 6H, s	6.89, 1H s (5-H) 7.66, 1H s (8-H)
erythro[a]	0.95 d, J=7 Hz	1.14 d, J=7 Hz	1.96—3.08, m		2.28, s	6.97, s 7.76, s

a) Contaminated with *threo* isomer.

Table 9. Isomer ratio of reduction product (6)

Material (5)	Product (6) Yield, %	*threo* : *erythro*	
a *threo*	34	94	6
b *threo*	92	95	5

Table 10. NMR data of **6** (δ, ppm in 10% CCl_4)

Compound	Aliph-CH_3	Ar-CH_3	CH	CH_2	Ar-H
a *threo*	1.01, 6H d, J=6 Hz	—	1.24—1.65 2H, m	2.25—2.87 4H, m	6.90 4H, s
erythro[a)]	0.91 d, J=6.5 Hz	—	1.88—2.07 m	2.28—2.96 m	7.02 s
b *threo*	1.02, 6H d, J=6 Hz	2.12, 6H, s	1.14—1.57 2H, m	2.16—2.76 4H, oct	6.64 2H, s
erythro	0.88, 6H d, J=7 Hz	2.12, 6H, s	1.66—2.13 2H, quart	2.26—2.94 4H, oct	6.68 2H, s

a) A mixture of *erythro* and *threo* isomers (57 : 43).

methylnaphthalene was then oxidized to the corresponding naphthalenetetracarboxylic acid with aqueous sodium bichromate at 275 °C for 20 hr under an autogeneous pressure in the presence of pyridine to avoid the sublimation of hydrocarbon.

Experimental

All the melting points are uncorrected. The compounds described here are optically inactive. The IR spectra were recorded with a JASCO IR-G Spectrophotometer. The NMR spectra were measured with a JEOL JIM PS 100 apparatus (with TMS as the internal standard).

2,3-Dimethylsuccinic Anhydride (1). Diethyl 2-cyano-2,3-dimethylsuccinate[18,19)] was hydrolyzed with hydrochloric acid to give a mixture of *threo* and *erythro* 2,3-dimethylsuccinic acids. *erytho* (*cis*, *meso*) Acid was obtained by recrystallization from diluted hydrochloric acid[20)]; mp 205 °C (decompn.) (lit, mp 209 °C[20,21)]). The *threo* (*trans*, *racemic*) isomer was isolated from the original mother liquors by extraction with ether; mp 119 °C (lit, mp 127 °C,[20)] 129 °C,[21)] and 128—130 °C[22)]). These acids were then converted to the corresponding acid anhydrides (**1**) by treating them with acetyl chloride.[23)] *threo* **1**: bp 115—120 °C/8—10 mmHg, mp 81—82 °C (lit, mp 89 °C[21)]), NMR (δ, ppm) C**H** 2.68, m in 5% CCl_4, 2.78, m in 2% $CDCl_3$ (lit, 2.76 in $CDCl_3$[21)]) and CH_3 1.41, d, J=7 Hz in 5% CCl_4 1.46, d in 2% $CDCl_3$ (lit, 1.40 in $CDCl_3$[21)]). *erythro* **1**: bp 102—104 °C/7 mmHg, mp 36—37 °C (lit, mp 39—40 °C[20)]), NMR (δ) C**H** 3.18, m in 10% CCl_4, 3.24, m in 2% $CDCl_3$ (lit, 3.23 in $CDCl_3$[21)]) and CH_3 1.26, d, J=7.5 Hz in 10% CCl_4, 1.30, d in 2% $CDCl_3$ (lit, 1.30 in $CDCl_3$[21)]). These acid anhydrides (**1**) exhibited slightly lower melting points than the literature values, but they were NMR spectroscopically pure substances. Therefore, **1** was used in the subsequent reactions without further purification.

3-Aroyl-2,3-dimethylpropionic Acids (2). A mixture of *threo* **1** (24.0 g, 0.188 mol) and anhydrous aluminum chloride (50.5 g, 0.376 mol) in 200 ml of benzene was stirred for 0.5 hr in an ice-water bath, heated for 1 hr at 50 °C, and then poured into 200 ml of ice water containing 30 ml of concd. hydrochloric acid. The precipitate was filtered and washed with benzene. The solid was dissolved in sodium carbonate (8.0 g) in 200 ml of hot water, treated with active carbon, and then acidfied with hydrochloric acid to give 26.7 g of *threo* **2a**; mp 147—148 °C. The benzene solution was extracted with 7.0 g of sodium carbonate in 150 ml of water. The aqueous solution was acidified with hydrochloric acid, and the solid was recrystallized from 40 ml of carbon tetrachloride (treated with active carbon) to give 1.9 g of *threo* **2a**; mp 145—147 °C. The removal of the solvent gave 2.3 g of *erythro* **2a**; mp 69—80 °C. The total yield of **2a** was 28.6 g (79.6%), and the ratio of the *threo* and *erythro* isomers was 92.6 : 7.4. Pure *threo* **2a** was obtained by recrystallization from methanol; mp 148.5—149.5 °C. Found: C, 69.94; H, 6.98%. Calcd for $C_{12}H_{14}O_3$: C, 69.89; H, 6.84%.

A mixture of *erythro* **1** (26.0 g, 0.203 mol) and anhydrous aluminum chloride (54.5 g, 0.408 mol) in 200 ml of benzene was treated as above. The benzene solution was then extracted with 14.0 g of sodium carbonate in 200 ml of water. After the acidification of the aqueous solution, the separated oily material was extracted with ether. The subsequent removal of the solvent gave 37.8 g (90.4%) of *erythro* **2a**; mp 75—78 °C. Found: C, 69.67; H, 6.89%.

o-Xylene (16.6 g, 0.156 mol) was added to a solution of *threo* **1** (20.0 g, 0.156 mol) and anhydrous aluminum chloride (42.0 g, 0.315 mol) in 150 ml of tetrachloroethane chilled with an ice-water bath, after which the reaction mixture was treated as above. *threo* **2b** was obtained from the aqueous alkaline extract; 27.1 g (59.4%); mp 110—113 °C. Recrystallization from aqueous ethanol (1 : 1 vol) gave a pure sample; mp 116.5—117.5 °C. Found: C, 71.51; H, 7.56%. Calcd for $C_{14}H_{18}O_3$: C, 71.75; H, 7.74%.

From the reaction product of *o*-xylene and *erythro* **1**, pasty *erythro* **2b** was obtained in a 92.1% yield.

Epimerization of 2a. A mixture of 10.3 g of *threo* or *erythro* **2a**, 4.5 g of potassium hydroxide (or 3.8 g of sodium carbonate), and 100 ml of water was heated at 85 °C for 3 hr. The solution was then acidified with hydrochloric acid, filtered, and dried over soda lime under a vacuum. The solid was heated with 100 ml of carbon tetrachloride to separate the undissolved *threo* isomer. The *erythro* isomer was obtained from the mother liquors (Table 2).

Clemmensen Reduction of **2**. After the Clemmensen reduction of *threo* **2a** (40 g) for 10.5 hr, the product was extracted with benzene. The removal of benzene gave a pasty product; bp 157—160 °C/5 mmHg; 29.9 g. The distillate was added to aqueous sodium carbonate and extracted with benzene. Racemic **3a** was obtained from the benzene solution; bp 149 °C/4 mmHg; 8.3 g (29%). A mixture of *threo* and

erythro **4a** was obtained by the acidification of the aqueous solution; bp 143—144 °C/2.5 mmHg; 17.0 g (49%). The molar ratio of **3a** : **4a** was 33 : 67. Similarly, a mixture of *threo* and *erythro* **2b** was reduced for 12 hr to give **3b** (racemate) and **4b** (*threo* and *erythro* mixture) in a molar ratio of 62 : 38.

The racemic **3b** was recrystallized from methanol to give a pure sample; mp 66.5—67.5 °C. Found: C, 77.50; H, 7.51%. Calcd for $C_{14}H_{16}O_2$: C, 77.75; H, 7.46%.

Lactonization of **2** *to* **3**. A mixture of *threo* (or *erythro*) **2a** (16.0 g) 80 ml of concd. hydrochloric acid, and 20 ml of water was heated at 150 °C for 1 hr. The product was then treated as above to separate lactone (**3**) and ketonic acid (**2**)) Table 3).

Catalytic Hydrogenation of **2** *to* **4**. Compound (**2**) was hydrogenated to **4** with 5% Pd/C in glacial acetic acid at 60—80 °C for 1 hr under an initial pressure of hydrogen of 60—80 kg/cm² in an autoclave. The product, which was contaminated with 2–5% of ring-hydrogenated compound, was filtered and washed with methanol. After the removal of the solvent, the residue was recrystallized from petr. ether or distilled under a vacuum to give **4** (Table 5). *threo* **4a**: Found: C, 74.61; H, 8.51%. Calcd for $C_{12}H_{16}O_2$: C, 74.97; H, 8.39%. An analysis of NMR spectra of *erythro* **4a** showed it to contain 18% of the *threo* isomer. *threo* **4b**: Found: C, 76.07; H, 9.38%. Calcd for $C_{14}H_{20}O_2$: C, 76.32; H, 9.15%. *erythro* **4b**: Found: C, 75.96; H, 9.42%.

The catalytic hydrogenation of racemic **3** required a higher temperature (*ca.* 115 °C) than that of **2**, and the product was comtaminated with 20—40% of a ring-hydrogenated compound.

Cyclization of **4** *to* **5**. *A)*: A mixture of 15.0 g (0.078 mol) of *threo* or *erythro* **4**, 15 g of thionyl chloride, and 30 ml of benzene was heated in an oil bath at 90 °C for 2 hr. The excess thionyl chloride and solvent were then removed under reduced pressure. The resulting acid chloride, dissolved in 30 ml of tetrachloroethane, was added to 10.4 g of anhydrous aluminum chloride in 60 ml of tetrachloroethane chilled with an ice-water bath. Stirring was continued for 0.5 hr at this temperature and then for 1 hr at 60—70 °C. The product was subsequently treated in the usual manner. Fractional crystallization from methanol or petr. ether gave pure *threo* and *erythro* **5b** (Table 7). *threo* **5a** (mp 33.5—34.5 °C): Found: C, 82.49; H, 8.05%. Calcd for $C_{12}H_{14}O$: C, 82.72; H, 8.10%. *threo* **5b** (mp 112.5—113.0 °C): Found: C, 83.41; H, 9.11%. Calcd for $C_{14}H_{18}O$: C, 83.12; H, 8.97%. *erythro* **5b** (mp 51.5—52.5 °C): Found: C, 83.34; H. 9.12%.

B): *threo* or *erythro* **4** (10.0 g) was added to PPA (prepared from 50 ml of 85% phosphoric acid and 60 g of phosphorous pentoxide) at 120 °C. The mixture was stirred for 50 min at this temperature and then poured into 200 ml of ice water. The product was extracted with 100 ml of benzene, and the organic layer was washed with aqueous sodium hydroxide. After the removal of the solvent under reduced pressure, the residue was treated as above to give **5** (Table 7).

Catalytic Hydrogenation of **5** *to* **6**. *threo* **5b** (15.0 g, 0.075 mol) was hydrogenated to give 12.9 g of **6b** in glacial acetic acid (150 ml) in the presence of 5% Pd/C (0.7 g) at 70—80 °C for 1—2 hr under an initial pressure of 60 kg/cm². Subsequent recrystallization from methanol gave a pure sample (mp 104—105 °C); IR (Nujol), 856 cm^{-1} (aromatic one free hydrogen). Found: C, 89.55; H,11.03%. Calcd for $C_{14}H_{20}$: C, 89.29; H, 10.71%.

erythro **5b** was hydrogenated to give *erythro* **6b**, contaminated with the *threo* isomer, in a 93—98% yield. Fractional crystallization from petr. ether gave a pure sample; mp 51.5—52.5 °C.

threo **5a** (2.9 g) gave *threo* **6a**; mp 34—35 °C.

Dehydrogenation of **6** *to* **7**. *threo* **6b** (40.0 g) was dehydrogenated to **7b** in the presence of 3.3 g of 5% Pd/C and 10 ml of α-methylnaphthalene at 290—300 °C for 6 hr. The product was extracted with 500 ml of hot benzene and then filtered. The subsequent removal of the solvent gave 35.0 g (89%) of **7b**; mp 192—193.0 °C (from benzene) (lit, mp 191.2—191.8 °C[6] and 188—190 °C[7]). IR (Nujol): 894 cm^{-1} (aromatic one free hydrogen). NMR (δ. ppm in 2% CCl_4): 2.41 (12H, s, Ar-CH_3) (lit, $\tau=7.66$[7] and 7.64[24]) and 7.44 (4H, s, CH) (lit, $\tau=2.63$[7]).

Similarly, *erythro* **6b** gave **7b** in an 82.5% yield. *threo* **6a** gave **7a** in an 83% yield; mp 103.5—104.5 °C (from methanol).

Oxidation of **7b** *to 2,3,6,7-Naphthalenetetracarboxylic Acid.* A mixture of 9.2 g (0.05 mol) of **7b**, 75 g (0.25 mol) of dihydrate of sodium bichromate, 10 ml of pyridine, and 150 ml of water was stirred in an autoclave (300 ml) at 275 °C for 20 hr under autogeneous pressure (40—50 kg/cm²). The product was filtered while hot, and the filtrate was acidified with hydrochloric acid to give 10.1—11.2 g (67—74%) of 2,3,6,7-naphthalenetetracarboxylic acid. The tetramethyl ester had a mp of 184.0—185.0 °C (from 3 : 1 vol methanol/benzene) (lit, mp 181—183 °C[5]). IR (Nujol): ν_{co} 1734 cm^{-1} (lit[5], 1740 cm^{-1})

The authors would like to thank Mr. Jun Iyoda for his helpful determination and discussion of the decoupling of the NMR spectra.

References

1) K. Alder and O. Ackermann, *Ber.*, **87**, 1567 (1954).
2) A. T. Bromquist and J. A. Verdol, *J. Amer. Chem. Soc.*, **78**, 109 (1956).
3) H. N. Cripps, J. K. Williams, and W. H. Sharkey, *ibid.*, **81**, 2723 (1959).
4) W. Webster, U.S. Pat. 2912442 (1959).
5) W. Webster and W. H. Sharkey, *J. Org. Chem.*, **27**, 3354 (1962).
6) W. L. Mosby, *J. Amer. Chem. Soc.*, **75**, 3600 (1953).
7) R. D. Rieke, K. White, and E. McBride, *J. Org. Chem.*, **38**, 1430 (1973).
8) E. L. Martin, "Organic Reactions," Vol. 1 (1942), p. 115.
9) E. R. Alexander and A. Mudrak, *J. Amer. Chem. Soc.*, **72**, 3194 (1954).
10) D. J. Goldsmith, *J. Org. Chem.* **26**, 2078 (1961).
11) R. H. Baker and W. Jenkins, *J. Amer. Chem. Soc.*, **68**, 2102 (1946).
12) F. Knoop and H. Oesterlin, *Z. Physiol. Chem.*, **148**, 314 (1925); "Beilstein Handbuch der Organischen Chemie," Band 17, Ergänz, II, p. 340 (1952).
13) *Cf.* (*S*)(+)-2-Methylbutyroyl chloride gives (*S*)(+)-2-methylbutyrophenones by Friedel-Crafts reaction with substituted benzenes: (a). A. P. Desai, I. G. Vasi, and K. A. Thaker, *J. Indian Chem. Soc.*, **47**, 117 (1970), (b). O. Korver, *Tetrahedron*, **27**, 4643 (1971).
14) The cyclization of 3-benzoyl-2,3-diphenylpropionic acid to 2,3,4-triphenyl-3-buten-4-olide with sulfuric acid has been reported: H. M. Crawford, *J. Amer. Chem. Soc.*, **60**, 3078 (1938).
15) J. Thiele, R. Tischbein, and E. Lossow, *Ann. Chem.*, **319**, 184 (1901).
16) Two methylene proton signals of **6b** had octet of two AB type couplings. The observed J_{vic} of CH-CH_2 in *threo* **6b** is 10 Hz ($\delta=2.16$—2.24 ppm) and 5 Hz ($\delta=2.56$—2.76),

Effects of Solvents and Added Amines on the Selective Hydrogenation of 2-Naphthol over Urushibara Nickel and Cobalt Catalysts

Masatsugu KAJITANI, Yoshio WATANABE, Yutaka IIMURA, and Akira SUGIMORI

Department of Chemistry, Faculty of Science and Technology, Sophia University, Kioi-cho, Chiyoda-ku, Tokyo 102

(Received November 16, 1974)

The selective hydrogenation of 2-naphthol (NL) was investigated with Ni (U-Ni-B, U-Ni-A, and R-Ni) and Co (U-Co-B, U-Co-A, and R-Co) catalysts in various solvents at elevated temperatures and pressure (50 kg/cm²). U-Ni-B and U-Ni-A exhibited a high selectivity for the formation of 1,2,3,4-tetrahydro-2-naphthol (ac-TL), expecially in alcoholic solvents, while the hydrogenation with R-Ni in Et_2O, *i*-PrOH, and benzene solvents gave preferentially 5,6,7,8-tetrahydro-2-naphthol (ar-TL). The ar-TL formation over Ni catalysts decreased in the following order, irrespective of the catalysts. *i*-PrOH>EtOH>MeOH and Et_2O>benzene. However, the selectivity over Co catalyst was influenced to a lesser extent by the solvents. The addition of amines promoted the hydrogenation of NL to ar-TL in the following order: prim->*sec*->*tert*-amine in EtOH over Ni and Co catalysts. In general, Ni catalysts are more susceptible to the effects of solvents and added amines than Co catalysts.

The partial hydrogenation of 2-naphthol (NL) over nickel and cobalt catalysts gives predominantly either the alcohol 1,2,3,4-tetrahydro-2-naphthol (ac-TL) or the phenol 5,6,7,8-tetrahydro-2-naphthol (ar-TL). Musser and Adkins reported that R-Ni gave the alcohol (ac-TL, 55%), decahydro-2-naphthol (20%), and tetrahydronaphthalene (8%) at 140 °C and 100—200 kg/cm² of hydrogen pressure, and Cu-Cr oxide gave higher yields of the alcohol (ac-TL) than was obtained with R-Ni.[1] Stork found that the hydrogenation of 2-naphthol (NL) is influenced by the acidity of the solvent used, as shown below.[2]

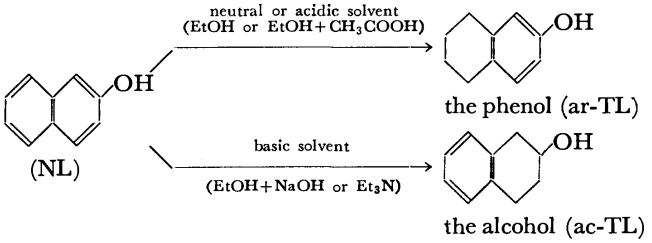

Adkins and Kusek reported that the use of R-Ni in EtOH gave ac-TL (*ca.* 10%) and ar-TL (*ca.* 80%), but the use of R-Ni in EtOH containing a small amount of NaOH or Et_3N gave ac-TL in more than 60% yield.[3]

Thus, the selective hydrogenation of 2-naphthol has been investigated mainly by changing the solvent acidity, while the solvent effect has been largely ignored.

In this study, the selective hydrogenation of 2-naphthol with Urushibara nickel, Urushibara cobalt, Raney nickel, and Raney cobalt catalysts in various neutral solvents and in ethanol containing various amines was investigated. The characteristic differences between Ni and Co catalysts, especially with respect to the effects of solvents and added amines, are discussed.

Experimental

Material and Solvents. 2-Naphthol (Wako Pure Chemical Industries, GR) was recrystallized from H_2O-EtOH (v/v=1/3). Solvents were purified according to the standard methods described in the literature.[4]

Commercial guaranteed reagent grade amines were used without further purification.

Catalysts. Urushibara nickel and cobalt catalysts were prepared by simplified methods.[5] R-Ni (W-7 type) and R-Co catalysts were prepared by the method of Adkins and Billica:[6] To a well-stirred solution of 2 g of sodium hydroxide in 10 ml of distilled water was added 2 g of Raney nickel or cobalt alloy (Al-Ni or Co, w/w=1/1) at such a rate as to maintain the temperature (for *ca.* 30 min) at 50± 2 °C. After the addition was completed the mixture was digested at 50 °C for an additional 50 min with gentle stirring. Ordinarily the W-7 R-Ni catalyst, after digestion, is washed with water three times by decantation, but the Raney catalysts were washed with distilled water until the washings were neutral to phenolphthalein.

When the solvents were immiscible with water, the catalysts were first washed with *i*-PrOH to remove the water and then with the solvent specified.

Each catalyst thus prepared contained about 1 g of Ni or Co metal. Urushibara nickel-cobalt catalyst (U-Ni, Co-B) contained 0.5 g of Ni and 0.5 g of Co.

Hydrogenation. 2-Naphthol (3.6 g; 0.025 mol) was hydrogenated with the catalyst in 25 ml of solvent at an elevated temperature under the initial hydrogen pressure of 50 kg/cm² in an autoclave (Nitto Hannoki; 100 ml) at an agitation rate of 450—500 rpm. The reaction temperature was raised from room temperature at the rate of 4±1 °C/min.

Analysis of Reaction Mixtures. After the reaction, the catalyst was filtered off, and the filtrate was analyzed by gas chromatography using the Yanagimoto GC 550T equipped with a column of 5% Silicone OV-17 on Uniport B (Gaschro Kogyo) (ϕ 3 mm×220 cm; glass column, column temp. 180 °C, carrier gas He; 7 ml/min).

Results and Discussion

Selectivity (S value). The main products obtained by the hydrogenation of 2-naphthol (NL) were 1,2,3,4- and 5,6,7,8-tetrahydro-2-naphthols (ac-TL and ar-TL). Since the sums of the yields of decahydro-2-naphthol and tetralin were less than about 5% in most cases, the selectivity in the hydrogenation of 2-naphthol is discussed with respect to the formation of tetralols (ac-TL and ar-TL). The selectivity (S) of the hydrogenation is expressed by

$$S = [\text{ar-TL}/(\text{ac-TL}+\text{ar-TL})] \times 100.$$

Solvent Dependence of Selectivity. The results of

the hydrogenation of 2-naphthol over Ni and Co catalysts prepared by various methods are shown in Tables 1 and 2.

The different selectivities of U-Ni-B, U-Ni-A, and R-Ni in the various solvents are more clearly seen in Fig. 1.

The selectivities over Ni catalysts changed over a wide range from 22% (U-Ni-B, MeOH) to 81% (R-Ni, *i*-PrOH or Et_2O) with the combinations of catalysts and solvents. In general, the hydrogenation

TABLE 1. SOLVENT EFFECTS ON THE SELECTIVITY OF THE HYDROGENATION OF 2-NAPHTHOL OVER Ni CATALYSTS

2-naphthol(NL): 0.025 mol, solvent: 25 ml, Ni content of catalysts: 1 g, Selectivity: $S=100\times$ ar-TL/(ar-TL+ac-TL).

Table 1-1. Hydrogenation over U-Ni-B

Solvent	React. Time (min)	React. Temp. (°C)	Recov. NL(%)	Selectivity (*S*)(%)
MeOH	60	80—114	43	22
EtOH	90	82—130	0[a]	34
EtOH	35	r.t.—140	0	38
i-PrOH+H_2O[b]	25	—96	21	33
i-PrOH	30	—94	43	43
i-PrOH	13	80—95	74	47
i-PrOH	7	130—152	13[c]	47
Cyclohexane	35	r.t.—96	22	35
Toluene	30	—114	0[d]	37
Toluene	22	—82	49	37
Benzene	30	—118	0	38
Benzene	24	—91	37	39
$(i\text{-Pr})_2O$	35	—100	8	39
THF	35	—136	56	40
THF	30	—104	90	46
Et_2O	40	—140	0[e]	42
Et_2O	30	—96	26	45
Et_2O	30	—100	40	47
Dioxane	30	—116	39	50
$(n\text{-Bu})_2O$	40	—110	68	54

a) Tetralin, 3%; Decalol, 4%. b) H_2O, 2 ml. c) Tetralin, 1%; Decalol, 9%. d) Tetralin, 0.4%; Decalol, 3%. e) Tetralin, 7%; Decalol, 11%.

TABLE 1-2. HYDROGENATION OVER U-Ni-A, ppt-Ni, AND R-Ni

Catalyst	Solvent	React. Time (min)	React. Temp. (°C)	Recov. NL (%)	Selectivity (*S*)(%)
U-Ni-A	MeOH	90	r.t.—152	79	28
	EtOH	30	—118	43	35
	i-PrOH	40	—150	20	44
	Benzene	20	—72	32	53
	$(i\text{-Pr})_2O$	35	—132	25	48
	Et_2O	25	—92	32	62
	$(n\text{-Bu})_2O$	30	—98	95	65
ppt-Ni	EtOH	90	—136	63	41
R-Ni	MeOH	23	—84	25	65
	EtOH	16	—58	20	67
	i-PrOH	17	—60	27	81
	Benzene	15	—53	45	75
	Et_2O	18	—65	43	81

Selectivity: $S=100\times$ **ar-TL**/(**ar-TL**+**ac-TL**) (%)

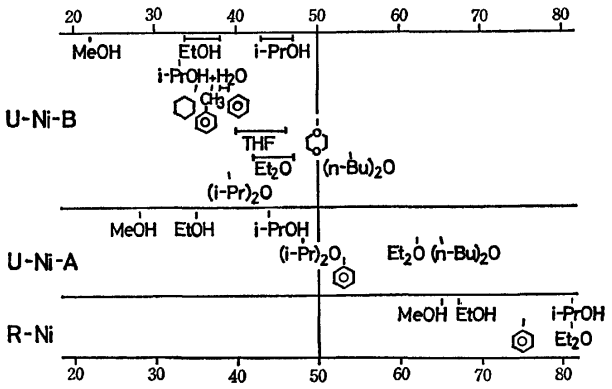

Fig. 1. Solvent effects on the selective hydrogenation of 2-naphthol over Ni catalysts.
ac-TL: 1,2,3,4-Tetrahydro-2-naphthol
ar-TL: 5,6,7,8-Tetrahydro-2-naphthol

of the phenol ring occurred preferentially over R-Ni and that of the benzene ring over U-Ni-B. The selectivity over U-Ni-A was intermediate between those over U-Ni-B and the R-Ni and *S* values over the catalyst were widely distributed with different solvents, as seen in Fig. 1.

Although the *S* values differed widely with the catalysts, the effects of the solvents with respect to *S* were similar, irrespective of the catalysts, as seen in Fig. 1. Thus, the ar-TL formation over Ni catalysts decreases in the following order: *i*-PrOH>EtOH> MeOH and Et_2O>benzene. The *S* values in ethers were generally greater than those in hydrocarbons.

The hydrogenation over U-Co-B was influenced to a lesser extent by the solvents used than that over U-Ni-B; all the *S* values over U-Co-B were about 50%, as seen in Table 2-1. U-Ni, Co-B catalyst exhibited a greater similarity to U-Ni-B than to U-Co-B. The selectivities by U-Co-A and R-Co catalysts

TABLE 2. SOLVENT EFFECTS ON THE SELECTIVITY OF THE HYDROGENATION OF 2-NAPHTHOL OVER Co CATALYSTS

2-naphthol(NL): 0.025 mol, solvent: 25 ml, Co content of catalysts: 1 g, Selectivity: $S=100\times$ ar-TL/(ar-TL+ac-TL).

Table 2-1. Hydrogenation over U-Co-B

Solvent	React. Time (min)	React. Temp. (°C)	Recov. NL (%)	Selectivity (*S*)(%)
Cyclohexane	35	r.t.—124	0	44
Benzene	40	—148	0	47
i-PrOH	40	—144	16	50
EtOH	42	—138	0	52
EtOH+H_2O[a]	30	—120	11	54
EtOH	120	110—130	16	55
EtOH	50	150—180	17	56
EtOH	60	80—118	8	57
MeOH	40	r.t.—152	37	56
Et_2O	4	—134	12	55
Dioxane	30	—126	65	56

a) EtOH, 20 ml; H_2O, 5 ml.

TABLE. 2-2. HYDROGENATION OVER U-Co-A, U-Ni, Co-B, AND R-Co

Catalyst	Solvent	React. Time (min)	React. Temp. (°C)	Recov. NL (%)	Selectivity (*S*)(%)
U-Co-A	Benzene	35	r.t.—142	41	47
	Et_2O	38	—162	34	46
	Et_2O	45	—164	0	49
	EtOH	30	—127	29	54
U-Ni, Co-B[a)]	EtOH	60	80—94	35	43
R-Co	Benzene	20	r.t.—73	3	46
	EtOH	25	—90	3	52
	Et_2O	35	—138	41	54

a) Ni, 0.5 g; Co, 0.5 g.

were practically similar to those by U-Co-B. Compared with Ni catalysts, Co catalysts were not very susceptible to the solvent effects on the selectivity.

It is widely recognized that a solvent containing oxygen atoms often acts as a catalyst poison, because of the strong affinity of the oxygen atom to the catalyst surface. Orito and Imai showed that the solvent effect is a critical factor in the hydrogenation of benzene and toluene over Ni catalysts; hydrocarbons are good solvents for rapid hydrogenation, but solvents containing oxygen atoms, particularly primary alcohols and dioxane, strongly restrain the hydrogenation.[7)]

In the hydrogenation of 2-naphthol over Ni catalysts, primary alcohols tended to suppress the hydrogenation of the unsubstituted benzene ring, whereas secondary alcohol, ether, and hydrocarbon solvents gave greater *S* values than the primary alcohols. However, it is still not clear why the selectivity of hydrogenation depends on the solvents or why the solvent effect of Ni catalyst differs from that of Co catalyst.

The selectivity may depend on the reaction temperature, the amount of hydrogen uptake, or the presence of H_2O. However, it was confirmed that the reaction temperature and the amount of hydrogen uptake influenced the selectivity to only a small extent (less than about 5%), as seen in Tables 1-1 and 2-1. In the hydrogenation over U-Ni-B in *i*-PrOH containing H_2O, added H_2O tends to promote the formation of ac-TL. The selectivity over U-Co-B was only slightly affectes by the addition of H_2O.

Effects of Added Amine on the Selectivities. The effects of added amine (the amount of amine added: 5 ml) on the hydrogenation in 20 ml of EtOH were investigated. The results with Ni and Co catalysts are shown in Tables 3 and 4, respectively.

It has so far been thought that amines promote the hydrogenation of NL to ac-TL. Stork[2)] and Adkins and Kusek[3)] reported that the addition of Et_3N in EtOH solution over R-Ni catalyst also promotes this reaction.

However, as shown in Tables 3 and 4, the effects of added amines on the selective hydrogenation depend on the nature of the amines: the primary amines tend to increase the yield of ar-TL. On the other hand, the addition of tertiary amines promoted slightly the formation of ac-TL with Ni catalysts and was of

TABLE 3. EFFECTS OF ADDED AMINES ON THE SELECTIVITY OF THE HYDROGENATION OF 2-NAPHTHOL OVER Ni CATALYSTS

2-naphthol(NL): 0.025 mol, solvent: EtOH 20 ml + amine 5 ml, Ni content of catalysts: 1 g, Selectivity: $S=100\times$ ar-TL/(ar-TL+ac-TL).

Catalyst	Amine	React. Time (min)	React. Temp. (°C)	Recov. NL (%)	Selectivity (*S*)(%)
U-Ni-B	Et_3N	30	r.t.—130	41	33
	O N-Et	35	—140	53	40
	Et_2NH	45	—152	40	41
	i-$PrNH_2$	40	—152	28	54
	n-$BuNH_2$	35	—158	75	70
R-Ni	Et_3N	15	—64	13	33
	O N-Et	25	—68	30	46
	Et_2NH	30	—77	12	34
	i-$PrNH_2$	30	—130	10	57
	n-$BuNH_2$	30	—120	54	64
	n-$BuNH_2$	30	—136	8	67

TABLE 4. EFFECTS OF ADDED AMINES ON THE SELECTIVITY OF THE HYDROGENATION OF 2-NAPHTHOL OVER Co CATALYSTS

2-naphthol(NL): 0.025 mol, solvent: EtOH 20 ml + amine 5 ml, Co content of catalysts: 1 g, Selectivity: $S=100\times$ ar-TL/(ar-TL+ac-TL).

Catalyst	Amine	React. Time (min)	React. Temp. (°C)	Recov. NL (%)	Selectivity (*S*)(%)
U-Co-B	Et_3N	35	r.t.—154	28	57
	O N-Et	40	—132	49	59
	Et_2NH	40	—148	49	62
	i-$PrNH_2$	45	—156	43	63
	n-$BuNH_2$	45	—180	0	65
R-Co	Et_3N	30	—120	21	55
	O N-Et	30	—120	21	52
	Et_2NH	25	—90	47	51
	i-$PrNH_2$	35	—106	14	59
	n-$BuNH_2$	70	—184	22	62

little effect in the case of Co catalysts. Thus, the selectivities (*S*) decreased in the following order: primary amine>secondary amine>tertiary amine.

Furthermore, it is noteworthy that the *S* values over Ni catalysts are influenced in a wide range by the addition of various amines, as compared with Co catalysts: *e.g.*, from 70% with *n*-$BuNH_2$ to 33% with Et_3N over U-Ni-B and from 65% with *n*-$BuNH_2$ to 57% with Et_3N over U-Co-B. Thus, concerning the amine effects, the characteristic differences between Ni and Co catalysts are similar to those of the solvent effects discussed above.

The rate of hydrogenation both over Ni and Co catalysts decreased with increasing selectivity (*S*). The effects of the amines to depress the rate of hydrogenation were in the following order: prim-amine> *sec*-amine> *tert*-amine. The order is parallel to that

of the adsorption strength of the amines.

Usually, it has been thought that hydrogenation of a phenol proceeds *via* an intermediate cyclohexanone, which in some cases can be isolated. Stork reported that palladium on charcoal in basic media (*N*-ethylmorpholine) can be used as a good catalyst for the hydrogenation of 2-naphthol to 2-tetralone.[8]

In the present work, however, the formation of 2-tetralone could not be observed, even when the hydrogenation was carried out in the presence of amine with Ni and Co catalysts, respectively. This may be plausible because the conversion of 2-tetralone to 2-tetralol (ac-TL) would be rapid over Ni and Co catalysts.

Stork has reported that the accelerating effects of Et_3N on the formation of ac-TL might be attributed to the shift of equilibrium toward the ketonic tautomer of 2-naphthol.[8] Though this idea may account for the effect of Et_3N, it does not explain how prim- or *sec*-amines promote the formation of ar-TL. Owing to lesser steric hindrance, prim- or *sec*-amines would be more strongly adsorbed onto the catalyst surface than tertiary amines.[4] The results obtained suggest that the presence of strongly adsorbed amines on the catalyst surface might inhibit the adsorption of the phenol ring more than that of the benzene ring of 2-naphthol.

References

1) D. M. Musser and H. Adkins, *J. Amer. Chem. Soc.*, **60**, 664 (1938).
2) G. Stork, *ibid.*, **69**, 576 (1947).
3) H. Adkins and G. Kusek, *ibid.*, **70**, 412 (1948).
4) Y. Orito and S, Kawachi, *Tokyo Kogyo Shikensho Hokoku*, **55**, 453 (1960).
5) S. Taira, This Bulletin, **34**, 1294 (1961).
6) H. Adkins and H. R. Billica, *J. Amer. Chem. Soc.*, **70**, 695 (1948).
7) Y. Orito and S. Imai, *Tokyo Kogyo Shikensho Hokoku*, **58**, 119 (1963).
8) G. Stork, *J. Amer. Chem. Soc.*, **68**, 2172 (1946).

Selective Homogeneous Hydrogenation of 3-Oxo-1,4-diene Steroids. III.[1] On the Formation of Saturated 5α-Ketone in the Hydrogenation Catalyzed by Dichlorotris(triphenylphosphine)ruthenium

Shigeo NISHIMURA, Tomio ICHINO, Akira AKIMOTO, Kiyoshi TSUNEDA,* and Hiromu MORI*

Department of Industrial Chemistry, Tokyo University of Agriculture and Technology, Koganei, Tokyo 184

**Chemical Research Laboratory, Teikoku Hormone Manufacturing Co., Ltd., Shimosakunobe, Kawasaki 213*

(Received December 5, 1974)

Hydrogenation of 1,4-androstadiene-2,17-dione (**1**) with $RuCl_2(Ph_3P)_3$ gives some saturated 5α-ketone together with 4-androstene-3,17-dione (**2**). The ratio of **2** to the saturated ketone formed increases almost in proportion to hydrogen pressure. The rate dependence upon hydrogen pressure has been shown to be first-order for formation of **2** and zero-order for formation of the saturated ketone. A mechanism which involves a 1,5-hydride shift at an intermediate species is proposed for the stereoselective formation of the 5α-ketone.

In previous papers,[1,2] it was shown that 1,4-androstadiene-3,17-dione (**1**) is hydrogenated selectively to 4-androstene-3,17-dione (**2**) with dichlorotris(triarylphosphine)rutheniums as catalysts. Although hydrogenation of **2** to saturated ketones (**3a** and **3b**) was very slow with the ruthenium complex some saturated 5α-ketone was found to arise directly from **1**.[2] This was in contrast to the hydrogenation catalyzed by chlorotris(triphenylphosphine)rhodium[3,4] where saturated ketones were all produced consecutively through **2**.[2]

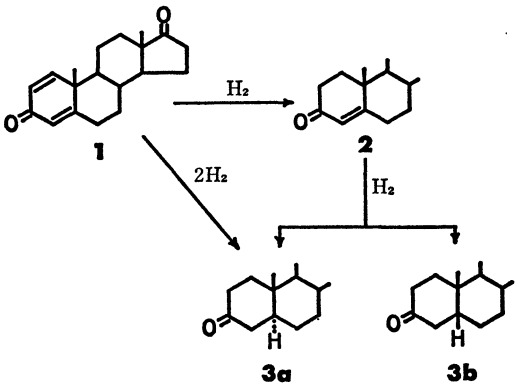

Scheme 1. Hydrogenation pathways of 1,4-androstadiene-3,17-dione (**1**).

This paper describes further studies which were undertaken to get an insight into the mechanism of formation of the saturated 5α-ketone in the ruthenium complex catalyzed hydrogenation.

Experimental

Material. 1,4-Androstadiene-3,17-dione (**1**) was obtained from the Kikkoman Shoyu Co. and used without further purification, mp 138—139 °C.

Catalyst. Dichlorotris(triphenylphosphine)ruthenium was prepared as described previously.[1]

Hydrogenation and Analysis of the Products. The hydrogenation apparatus and the method of analysis of the products were the same as those described previously.[1] **1** (500 mg) was hydrogenated with 50 mg of the ruthenium complex in 10 ml benzene at 50 °C under various hydrogen pressures. During each hydrogenation the hydrogen pressure was kept almost constant. The reaction time was varied from 505 min for the hydrogenation at the lowest pressure (2.2 kg/cm²) to 60 min for that at the highest pressure (101 kg/cm²). The conversion of **1** ranged from 16% to 42% by hydrogenations. The pseudo-first-order rate constants were calculated from the compositions of reaction mixtures employing the integrated form of Eq. (1).

Results

Figure 1 shows the effect of hydrogen pressure on the ratio of **2** to saturated ketone formed in the hydrogenation of **1** in benzene at 50 °C. Hydrogenation of **2** to saturated ketones **3a** and **3b** was extremely slow under these conditions and this ratio was, therefore, practically independent of the conversion of **1** at a given hydrogen pressure. As described previously,[2] the saturated ketone formed here is predominantly 5α-androstane-3,17-dione (**3a**) and this is also indicative that the saturated ketone was not formed through **2**, because hydrogenation of **2** gave an about 2 : 1 mixture of **3a** and **3b**. As is seen from Fig. 1, the ratio of **2** to the saturated ketone increases

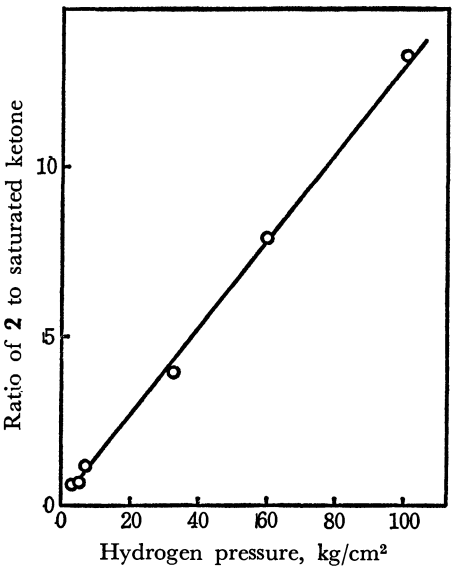

Fig. 1. Effect of hydrogen pressure on the ratio of 4-androstene-3,17-dione (**2**) to the saturated ketone formed in the hydrogenation of **1**. **1** (500 mg) was hydrogenated with 50 mg of $RuCl_2(Ph_3P)_3$ in 10 ml benzene at 50 °C. Each hydrogenation was performed at nearly constant pressure.

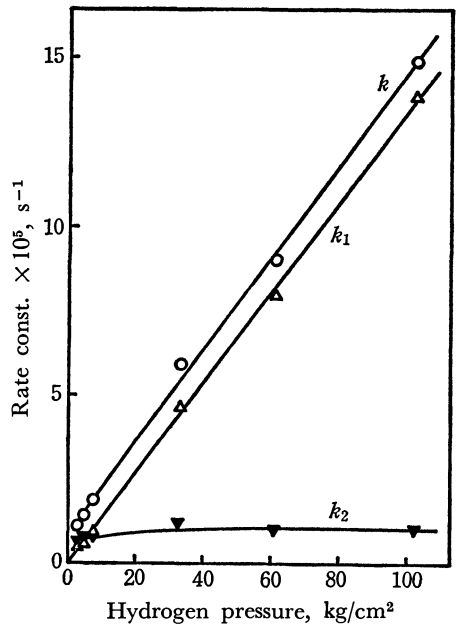

Fig. 2. Effects of hydrogen pressure on the conversion of **1**, the formation of **2** and the formation of saturated ketone. k, k_1, and k_2 are pseudo-first-order rate constants defined by Eq. (1). For experimental conditions, see the footnote of Fig. 1.

almost in proportion to the hydrogen pressure in a wide range of 2 to more than 100 kg/cm².

Figure 2 shows the effect of hydrogen pressure on a pseudo-first-order rate constant k defined by Eq. (1).[5] The rate constant k can be separated into the

$$-\frac{d[\mathbf{1}]}{dt} = k[\mathbf{1}] = (k_1+k_2)[\mathbf{1}] \quad (1)$$

two rate constants k_1 and k_2 for formation of **2** and the saturated ketone, respectively, from the results shown in Fig. 1. From the effects of hydrogen pressure on k_1 and k_2 thus obtained (Fig. 2), it is concluded that the rate of formation of **2** is first-order in hydrogen pressure while that of the saturated ketone is independent of hydrogen pressure. At low pressures, however, k_2 appears to decrease with decreasing hydrogen pressure.

From the plots of the log of the ratio **2**: saturated ketone *vs.* the reciprocal of reaction temperature

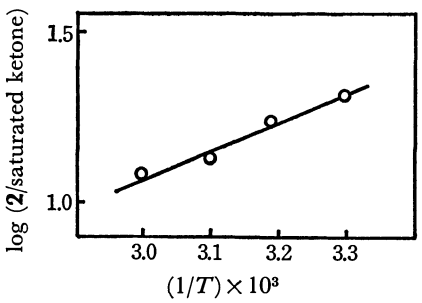

Fig. 3. Effect of reaction temperature on the ratio of **2** to the saturated ketone formed in the hydrogenation of **1**. **1** (500 mg) was hydrogenated with 50 mg of $RuCl_2(Ph_3P)_3$ in 10 ml benzene at 100 kg/cm² hydrogen pressure.

(Fig. 3), we know that the apparent activation energy for formation of saturated ketone is 3.8 kcal/mol higher than for formation of **2**. Thus a better selectivity for **2** is obtained in the hydrogenation at a low temperature.

Discussion

The active species in the hydrogenation catalyzed by dichlorotris(triphenylphosphine)ruthenium is considered to be the hydrido complex $RuClH(Ph_3P)_3$ formed by the hydrogenolysis of the dichloro complex.[6,7] The first step of the hydrogenation of **1**, therefore, will be the addition of the hydrido complex (abbreviated as RuH) to **1**, probably from the α-face.[4] Although the mode of addition of RuH to an α,β-unsaturated ketone is not certain, it might be presumed to occur in the following ways: *1,2* to the C_1–C_2 double bond to give **A** or *1,4* to give **B** as shown in Scheme 2.[8] If we assume that isomerization of **B** to **C** by a 1,5-hydride shift at the cyclic conjugated diene system would occur during the hydrogenation of **A** or **B**,[9] the stereoselective formation of saturated 5α-ketone **3a** could be accounted for because such hydride shifts would be expected to occur without difficulty between quasi-axial 1α and axial 5α positions, assisted by the cyclic conjugated system.[10] The observed zero-order dependence of the rate of formation of **3a** upon hydrogen pressure will not be in conflict with this mechanism if we assume that the hydride shift is rate-controlling in the course of hydrogenation leading to the formation of **3a**. The driving

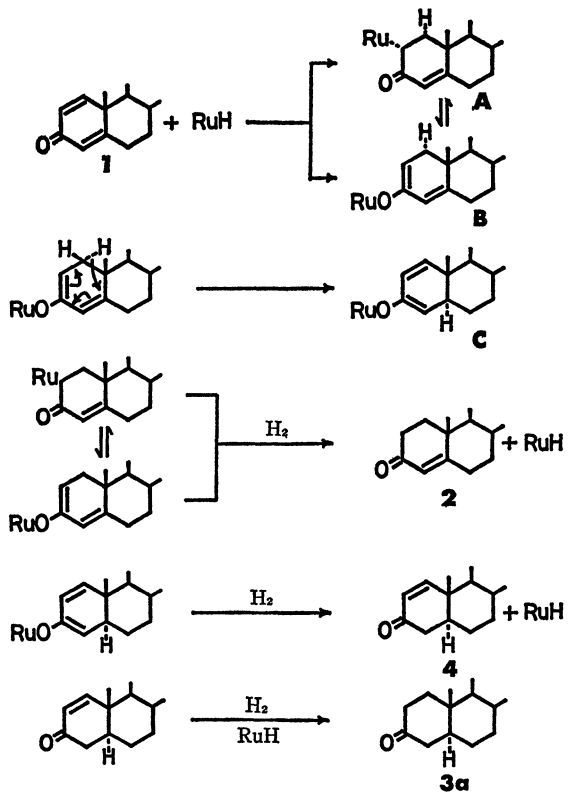

Scheme 2. A mechanism for formation of 4-androstene-3,17-dione (**2**) and saturated 5α-ketone (**3a**) in the ruthenium complex catalyzed hydrogenation of 1,4-androstadiene-3,17-dione (**1**).

force for the isomerization of **B** is presumed to be the decrease of electron density at the C-5 carbon atom, which would be caused by the coordination of the enolate anion to ruthenium.[11] The hydrogen chloride liberated by the hydrogenolysis of the dichloro ruthenium complex may contribute to this decrease of electron density by interacting with the triphenylphosphine ligand. The effect of the addition of triethylamine to depress the formation of the saturated ketone[1] may give a support for this consideration, because the degree of the depression caused by the addition of triethylamine was so great (from 10.5% to 1.7%), and such a great effect would be difficult to explain by an only twofold increase in the rate of hydrogenation with addition of the amine alone.

From the observed dependencies of the rates on hydrogen pressure, it seems that **C** and **4** are hydrogenated faster than those species which afford **2** on hydrogenation. It is suggested that **C** and **4**, which both have the 5α configuration, will be less hindered than **A** and **B** for the hydrogenation from the α-face, because the 5α species are in a flatter conformation regarding the rings A and B than the Δ^4 species such as **A** and **B**. This is supported by the fact that 5α-1-androstene-3,17-dione (**4**) is hydrogenated more easily than **1** with the ruthenium complex under comparable conditions.[12]

The authors are grateful to Professor J. A. Marshall of Northwestern University for his valuable suggestion concerning the 1,5-hydride shift.

References

1) Part II: S. Nishimura, T. Ichino, A. Akimoto, and K. Tsuneda, This Bulletin, **46**, 279 (1973).
2) S. Nishimura and K. Tsuneda, *ibid.*, **42**, 852 (1969).
3) A. J. Birch and K. A. M. Walker, *J. Chem. Soc., C*, **1966**, 1894.
4) C. Djerassi and J. Gutzwiller, *J. Amer. Chem. Soc.*, **88**, 4357 (1966).
5) The first-order kinetics in concentration of **1** which was obtained in the hydrogenation with added triethylamine[1] was confirmed to hold for the hydrogenation without the amine (unpublished results).
6) P. S. Hallman, B. R. McGarvey, and G. Wilkinson, *J. Chem. Soc., A*, **1968**, 3143.
7) D. Rose, J. O Gilbert, R. P. Richardson, and G. Wilkinson, *ibid.*, **1969**, 2610.
8) A similar mode of addition to α,β-unsaturated carbonyl compounds has been suggested by Goetz and Orchin in the cobalt hydrocarbonyl catalyzed hydrogenation [*J. Amer. Chem. Soc.*, **85**, 2782 (1963)]. Alternative reverse addition of RuH would be less probable because of an increased steric interaction between the Ru moiety and 9α-hydrogen in the resulting species.
9) For the preference of 1,5- over 1,3-hydrogen shift, see R. T. Morrison and R. N. Boyd, "Organic Chemistry," 3rd ed., Allyn and Bacon, Inc., New York (1973), p. 954.
10) The saturated 5α-ketone formed in the deuteration of **1** at about 40% conversion, on treatment with methanolic sodium hydroxide, gave 5α-ketone-d_2 as the predominant product. This result suggests that no exchange occurred at the C-6 carbon during the deuteration and excludes the mechanism involving the C-6 hydrogen, e.g., enolization of **1** prior to hydrogenation, which may well explain the stereospecific 5α-ketone formation.
11) For a coordination of a similar type, see H. W. Thompson and E. McPherson, *J. Amer. Chem. Soc.*, **96**, 6232 (1974).
12) **4** was completely hydrogenated to **3a**, compared with only 84% conversion of **1** under the same conditions (unpublished results; see also Ref. 2)

II→I, should proceed also concertedly through the bonding interaction between χ_4 and $\psi_1'^*$: in which χ_4 and χ_3 face the phase in the same direction, and χ_3 and χ_2 in the inverse direction. Orbital χ_1 which becomes vacant in II is always in the same, invariable phase. When the process I→II→I is concerted, it can be represented by the following scheme (Scheme 1).[13,14]

In the following concerted reaction of hexatriene which is considered to comprise a butadienic and an additional ethylenic system,

$$\begin{array}{l} CH_2{=}CH{-}CH{=}CH{-}CH{=}CH_2 \\ \qquad\qquad \text{III} \\ \quad \psi_1 \quad\quad \psi_2 \quad\quad \psi_3 \\ \quad \psi_1^* \quad\quad \psi_2^* \quad\quad \psi_3^* \\ \longrightarrow \overset{+}{C}H_2{-}CH{=}CH{-}\overset{-}{C}H{-}CH{=}CH_2 \\ \qquad\qquad \text{IV} \\ \qquad\quad \psi_1' \quad \chi_4 \quad\quad \psi_3 \\ \chi_1 \quad\quad \psi_1'^* \quad\quad\quad \psi_3^* \\ \longrightarrow \overset{+}{C}H_2{-}CH{=}CH{-}CH{=}CH{-}\overset{-}{C}H_2 \qquad (2) \\ \qquad\qquad \text{V} \\ \qquad\quad \psi_1' \quad\quad \psi_2' \quad\quad \chi_6 \\ \chi_1 \quad\quad \psi_1'^* \quad\quad \psi_2'^* \end{array}$$

the orbital representation of this process can be given as follows (Scheme 2):[15]

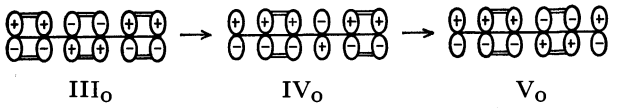

Scheme 2.

The first step, III→IV, is the same as that of I→II in Eq. 1, and the second step, IV→V, is equivalent to the reverse process, II→I, in Eq. 1. If these two steps(III→IV and IV→V) are included in one concerted process, *viz.*, the process III→V proceeds concertedly, the phase of χ_6 in V_o should be dependent upon that of χ_1 (or χ_2). Each elementary step in Eqs. 1 and 2 can be considered to be a sort of nucleophilic substitution analogous to S_N2 reaction. Thus, the conversion of III to V may be a sequential nucleophilic substitution process. The phase correlation of AO's in such concerted processes as shown above can be expected to hold also for σ-systems.

In general, from a non-cyclic system (S_α) with n-two-center MO's (σ and/or π, n=2,3,4,⋯) by sequential nucleophilic process, a new non-cyclic system (S_ω) can be obtained which is composed of an unoccupied nonbonding MO (χ_1) and an occupied nonbonding MO (χ_{2n}) in the two terminals, and of new ($n-1$)-two-center MO's between the two nonbonding MO's (*vide infra*). If this system forms a pericyclic system, the unoccupied orbital χ_1 should be situated in the position adjacent to the occupied orbital χ_{2n}. So long as the reaction proceeds concertedly, the phase of χ_{2n} is determind by that of χ_1. When the positive overlapping between χ_1 and χ_{2n} in S_ω is possible, an additional two-center bond is formed by χ_1 and χ_{2n}, making the pericyclic reaction allowable. On the other hand, when the overlapping between χ_1 and χ_{2n} is negative or antibonding, the two-center bond between the two terminals can not be formed, thus the reaction is forbidden.

$$\begin{array}{l} \qquad\qquad \text{Sequential Nucleophilic Process} \\ S_\alpha \longrightarrow S_\omega \\ \psi_1 \ \psi_2 \ \psi_3 \cdots\cdots \psi_n \qquad \psi_1' \ \psi_2' \cdots\cdots \psi'_{n-1} \ \chi_{2n} \\ \psi_1^* \ \psi_2^* \ \psi_3^* \cdots\cdots \psi_n^* \qquad \chi_1 \ \psi_1'^* \ \psi_2'^* \cdots\cdots \psi'_{n-1}{}^* \end{array}$$

χ_1, χ_{2n} in S_ω	Pericyclic Rection
Bonding	Allowable
Antibonding	Forbidden

The phase relationship (bonding or antibonding) between χ_1 and $\chi_{2\omega}$ in S_ω should change according to the number and the relative configuration of the two-center bonds included in the pericyclic system. For example, when II_o and V_o are shown in the cis-bent form, it can easily be predicted that the reaction butadiene→cyclobutene is conrotatory, and that the reaction hexatriene→cyclohexadiene is disrotatory (Fig. 2).

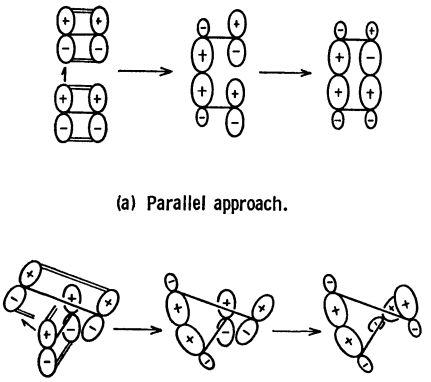

Fig. 1. Mutual cycloaddition of ethylenes.

The analysis of reaction based on this argument is well demonstrated by the examples in Fig. 1. The mutual cycloaddition of ethylene in parallel approach gives the antibonding interaction between the terminals in the final step, which indicates that the reaction is forbidden. On the other hand, the bonding interaction between the terminals can be obtained in orthogonal approach, which means that the reaction is allowable. Other examples of allowed reactions are given in Fig. 2.

When the reaction system contains an odd number of AO's as in the case of carbanion or carbonium ion, the following treatment is reasonable.

System Involving an Occupied Nonbonding MO. In the following reaction,

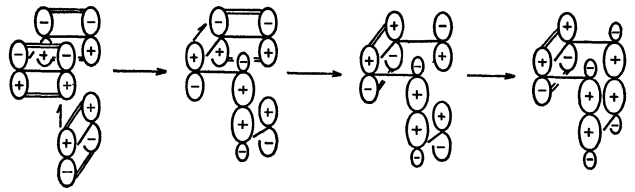

(a) Diels-Alder reaction.

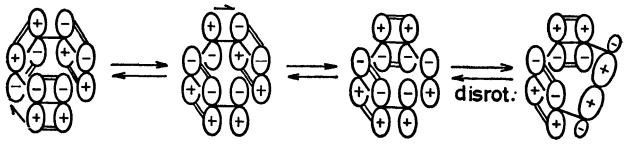

(b) Electrocyclic reaction (⟶ cyclization; ⟵ ring opening).

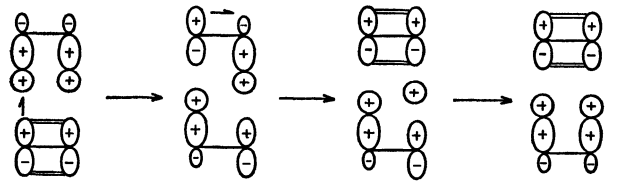

(c) Group transfer reaction ($CH_2=CH_2+CH_3-CH_3 \rightarrow CH_3-CH_3+CH_2=CH_2$).

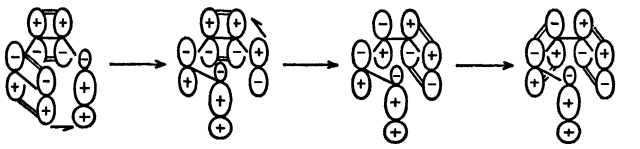

(d) Superfacial [1,5] shift of a hydrogen atom.

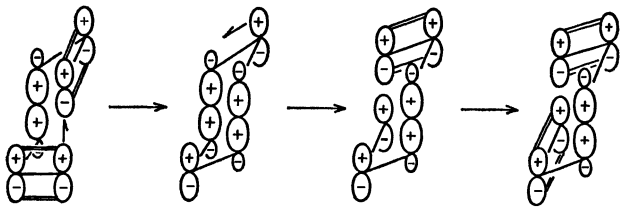

(e) Cope rearrangement (with chair-type transition state).

Fig. 2. Examples of allowed reaction.

$$\underset{\text{VI}}{\bar{C}H_2-CH=CH-CH=CH_2} \rightarrow \underset{\text{VII}}{CH_2=CH-\bar{C}H-CH=CH_2}$$

χ_0 $\quad$ ϕ_1 $\quad$ ϕ_2 $\quad$ ϕ_0' $\quad$ χ_2 $\quad$ ϕ_2

$\quad\quad$ ϕ_1^* $\quad$ ϕ_2^* $\quad\quad$ $\phi_0'^*$ $\quad\quad$ ϕ_2^*

$$\rightarrow \underset{\text{VIII}}{CH_2=CH-CH=CH-\bar{C}H_2} \qquad (3)$$

ϕ_0' $\quad$ ϕ_1' $\quad$ χ_4

$\phi_0'^*$ $\quad$ $\phi_1'^*$

the orbital-array representations of each step are given as follows (Scheme 3):

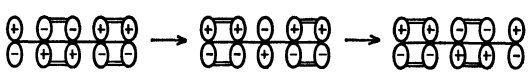

VI_o $\quad\quad$ VII_o $\quad\quad$ $VIII_o$

Scheme 3.

Since the two ethylenic π-systems and one negative center in VI are regarded as being independent of each other, the phase of AO's between these three systems can be taken arbitrarily. Similarly to Eqs. 1 and 2, reaction VI→VII is initiated through the interaction between χ_0 and ϕ_1^*, two new two-center bonds and an occupied nonbonding center at another terminal being obtained in VIII.

In general, by sequential nucleophilic process, from a noncyclic system (S_α) consisting of an occupied nonbonding MO(χ_0, the lone-pair center) at the beginning terminal and n-two-center MO's($n=1,2,3\cdots\cdots$),[16] a new system (S_ω) can be obtained which is composed of new n-two-center MO's and a new lone-pair center (χ_{2n}) at the end terminal.

$$S_\alpha \xrightarrow{\text{Sequential Nucleophilic Process}} S_\omega$$

χ_0 $\quad$ ϕ_1 $\quad$ ϕ_2 $\quad\cdots\cdots$ ϕ_n $\quad\quad$ ϕ_0' $\quad$ ϕ_1' $\quad\cdots\cdots$ ϕ'_{n-1} $\quad$ χ_{2n}

$\quad\quad$ ϕ_1^* $\quad$ $\phi_2^*\cdots\cdots$ ϕ_n^* $\quad\quad$ $\phi_0'^*$ $\quad$ $\phi_1'^*\cdots\cdots$ ϕ'^*_{n-1}

When this system forms a pericyclic system, the unoccupied orbital $\phi_0'^*(=\chi_0-\chi_1)$ is to be situated in the position adjacent to the occupied orbital χ_{2n}. So long as the reaction proceeds concertedly, the phase of χ_{2n} is determined by that of χ_0. Thus, if the positive overlapping between χ_{2n} and χ_0 in $\phi_0'^*$ is possible, χ_{2n} can interact with $\phi_0'^*$ in a bonding manner; in this case, this pericyclic reaction is allowable.

Alternatively, this type of reaction can be treated in the same way as that of systems with an even number of AO's by regarding χ_0 as a two-center MO with a ghost unoccupied AO. (*Cf. Participation of Lone-pair Orbital*).

System Involving an Unoccupied Nonbonding MO. In the following reaction,

$$\underset{\text{IX}}{CH_2=CH-\overset{+}{C}H-CH=CH_2} \rightarrow \underset{\text{X}}{\overset{+}{C}H_2-CH=CH-CH=CH_2}$$

ϕ_0 $\quad\quad$ ϕ_2 $\quad\quad$ ϕ_1 $\quad$ ϕ_2

ϕ_0^* $\quad$ χ_2 $\quad$ ϕ_2^* $\quad\quad$ χ_0 $\quad\quad$ ϕ_1^* $\quad$ ϕ_2^*

$$\rightarrow \underset{\text{XI}}{\overset{+}{C}H_2-\overset{+}{C}H-CH=CH-\bar{C}H} \qquad (4)$$

ϕ_1' $\quad$ χ_4

χ_0 $\quad$ χ_1 $\quad\quad$ $\phi_1'^*$

the orbital-array representations of each step can be given as follows (Scheme 4):

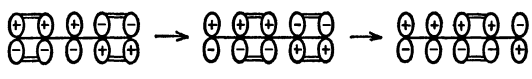

IX_o $\quad\quad$ X_o $\quad\quad$ XI_o

Scheme 4.

As in the case of I_o, III_o, and VI_o, the phase of AO's between three systems (two ethylenic π-systems and one nonbonding center) in IX_o can be taken arbitrarily. The phase of the unoccupied nonbonding MO is adjusted to that of ϕ_0 so that the bonding interaction may arise between them in the process $IX_o \rightarrow X_o$; the treatment corresponds to that of each elementary step in Scheme 1—3. The first nucleophilic process

(IX→X) is not of substitution, and the second process (X→XI) is equivalent to I→II in Eq. 1.

For this type of reaction system, the following general, schematic expression can be given:[16]

$$S_\alpha \xrightarrow{\text{Seq. Nuc. Process}} S_\alpha' \longrightarrow S_\omega$$

$$\psi_0 \quad \psi_2 \cdots \psi_n \qquad \psi_1 \ \psi_2 \cdots \psi_n \qquad \psi_1' \cdots \psi'_{n-1} \ \chi_{2n}$$
$$\psi_{0*} \ \chi_2 \ \psi_2^* \cdots \psi_n^* \quad \chi_0 \ \psi_1^* \ \psi_2^* \cdots \psi_n^* \quad \chi_0 \ \chi_1 \ \psi_1'^* \cdots \psi'^*_{n-1}$$

In the concerted process, the phase of χ_{2n} is determined by that of χ_0(or χ_1) in ψ_0 of $S_\alpha(\psi_0=\chi_0+\chi_1)$. Therefore, when the positive overlapping between χ_0 and χ_{2n} in S_ω is possible, the pericyclic reaction is allowable.[17]

Cheletropic Reactions. Cheletropic reactions are a specific type of pericyclic reaction. As an example, the addition reaction of singlet carbene to ethylene is discussed. The carbene species has two localized MO's; one is occupied sp^2 (σ orbital) and the other unoccupied p(p orbital).[18] In order to avoid introducing a qualified nucleophilic and electrophilic center into the reaction process, these two orbitals are dealt with as their combination in terms of LCMO. Thus, the new bonding and antibonding MO are given as follows:

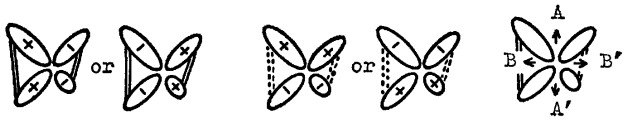

$\sigma+p \quad -(\sigma+p)$ Bonding MO $\qquad \sigma-p \quad -(\sigma-p)$ Antibonding MO

The bonding MO should be occupied, having its maximum extension in the direction of B; the antibonding MO should be unoccupied, having its maximum extension in the direction of A. Consequently, carbene species should direct side B toward the ethylene π system in its pseudo-nucleophilic(PN) approach to ethylene (*vide infra*), and side A toward the π system in its pseudo-electrophilic(PE) approach according to the HOMO-LUMO maximum overlapping principle.[19] In view of the fact that the extensions B-B' and A-A' can be considered alternatively to be the σ and the p MO of carbene, respectively, the merit of π approach of carbene in addition to olefin[20] can be interpreted easily.

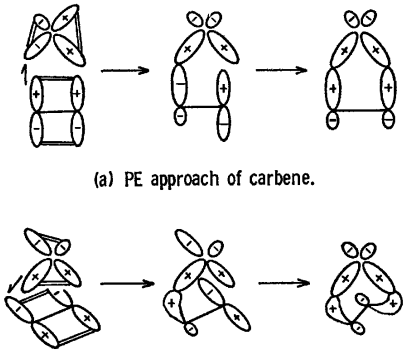

Fig. 3. Addition of carbene to ethylene.

Thus, the addition of singlet carbene to ethylene can be illustrated as in Fig. 3, in which the MO's of carbene can be treated in the same manner as that of olefinic π MO.[21] The process through PE approach of carbene to ethylene is allowed, while the reaction through PN approach is impossible because of steric reasons though the process is formally allowed. By this MO representation, it can be easily understood that carbene functions in an antarafacial manner in PE approach, namely in non-linear cheletropic reaction, and that it acts in a suprafacial fashion in PN approach, namely in linear cheletropic reaction.

Interpretation of Secondary Effects. The secondary conformational effects in concerted cyclo-addition or sigmatropic reactions have been interpreted in terms of the HOMO-LUMO[1,2] or the NHOMO-NLUMO interaction.[2] The present approach can also provide an analogous interpretation for the effects. As an example, the endo selectivity in the Diels-Alder reaction of two butadiene molecules is explained in the following way (Fig. 4). The reaction is represented by the process: from C_6 to C_1, from C_2 to C_3, and from C_4 to C_5(C_6→C_1; C_2→C_3; C_4→C_5, Route I). An alternative process, however, can proceed via [C_2→C_7; C_6→C_1, (Route II)] to afford a four-membered cyclic transition species. In this transition species, C_4 and C_5 are still interactive, so that it changes to the Diels-Alder adduct *via* [C_4→C_5; C_8→C_7; C_2→C_3,

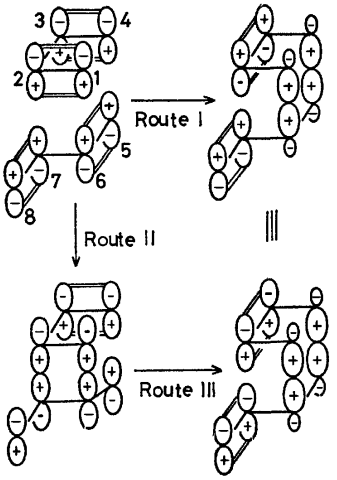

Fig. 4. Diels-Alder reaction of two butadiene molecules

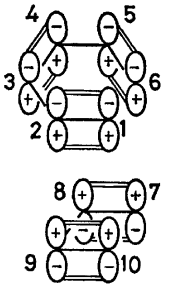

Fig. 5. MO representation of the endo approach of [4+6] cycloaddition between butadiene and hexatriene.

(Route III)]. That is to say, the MO bonding interaction, $C_2 \rightarrow C_7$ and $C_6 \rightarrow C_1$, may decrease the energy of the endo transition state, and promote the formation of cyclohexene ring. In contrast, in a [4+6] cyclo-addition (Fig. 5), an allowed process, $C_2 \rightarrow C_3$; $C_4 \rightarrow C_5$; $C_6 \rightarrow C_7$; $C_8 \rightarrow C_9$; $C_{10} \rightarrow C_1$, can be followed to give the [4+6] cyclo-adduct. However, an alternative process *via* $C_5 \rightarrow C_8$; $C_9 \rightarrow C_2$ is possible to give easily a six-membered cyclic transition species, in which the orbitals of C_1 and C_{10}, and of C_6 and C_7 become antibonding with each other, respectively. Consequently, the endo approach of the reactants may prevent the [4+6] cycloaddition. The preference of chair type transition state in the Cope rearrangement can be interpreted also in the same way.

Participation of Lone-pair Orbital to Pericyclic Systems. In nucleophilic non-cyclic concerted reactions with amines, the lone-pair orbital (n orbital) of nitrogen should function as the HOMO. When a hetero-atom such as nitrogen, oxygen, or halogen is contained in a pericyclic reaction system, its n orbital can also participate, at least formally, as a HOMO in the MO interaction.[22,23]

Isomerization of isoxazoline to *C*-acylaziridine[24] can be analyzed as an allowed [1,3] sigmatropic reaction with inversion at nitrogen. For this reaction, an alternative allowable process can be represented with participation of the nitrogen n orbital (Fig. 6), in which the configuration of nitrogen of the product is identical with that of the former process. By steric requirement, the latter process might be favorable. In this type of process, an n orbital should be regenerated with retention of orbital phase at the hetero-atom for allowed reactions (Fig. 6). By taking up the participation of 3p-n orbital of chlorine, a cyclic concerted scheme can be illustrated formally for S_Ni reaction of alkyl chlorosulfite.

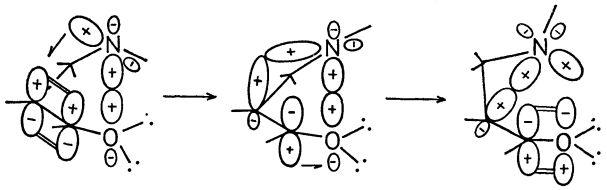

Fig. 6. Isomerization of isoxazoline to acylaziridine with participation of nitrogen lone-pair orbital.

Discussion

Pericyclic reactions in ground states can be followed by the present procedure (Fig. 2). The acutal reactions proceed neither stepwise nor via the so-called nucleophilic substitution scheme. However, according to Fukui, "a stepwise recognition of concerted reactions may be more reasonable than an attempt to understand each concerted multi-center reaction as a simultaneous change."[2] The feasiblity of stepwise recognition of concerted multi-center reactions might be related to the fact that delocalized MO's can be derived from localized MO's in terms of LCMO.[25] If a multi-center cyclic reaction proceeds concertedly, each consituent elementary step should be a concerted process(*vice versa*).

The orbital arrays of II_o, V_o, $VIII_o$, and XI_o are the same as those of the HOMO-LUMO interaction method(Scheme 1—4):

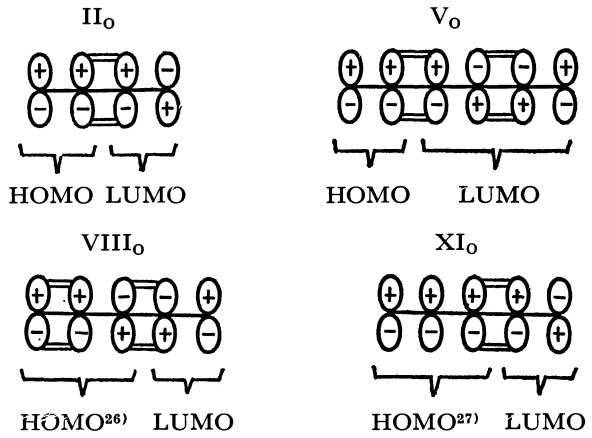

So far as the orbital phase alteration is concerned, the process through nucleophilic substitution scheme represents the delocalized LUMO: for example, in systems with an even number of AO's, the first nucleophilic process induces the localized HOMO to the localized LUMO, and the next and further processes will give the delocalized LUMO through the procedure corresponding to the LCMO method. This relationship can afford a theoretical ground to the present method.

Transformation between canonical forms of a conjugate system in classical molecular formula is to be taken as an intramolecular nucleophilic process. In Hückel systems, the two Kekulé formulas of [4N+2] annulene can be converted into each other by the present procedure, but not those of [4N] annulene; on the other hand, the principle should be the reverse in Möbius systems. This situation can give an alternative indirect reasoning for the present method in view of the aromaticity of transition state of pericyclic reactions in the Hückel-Möbius concept.[3,4]

Although the present method is somewhat roundabout, it can in a unified manner be applied also to the systems with low symmetry and to those in which the delocalized HOMO and LUMO can not easily be represented. This method is inapplicable to the systems with delocalized or three- or multi-center bonds. Since reaction systems are represented with localized MO's, the exact nature of molecules, especially of conjugate systems, can not be expressed. π and σ bonds are not differentiated from each other, and the analysis of reaction is carried out merely qualitatively. This method can not estimate the facility of reaction, but only whether a reaction can proceed concertedly or not.

For reactions in excited states, the present procedure does not afford any prediction, since it is based essentially on nucleophilic substitution process. Formally, however, a modification in which the antibonding representation is adopted for the initial nucleophilic center instead of the bonding one can give selection rules for reactions in excited states. This procedure corresponds to the SOMO-LUMO interaction scheme,[2]

but has no theoretical grounds within the scope of the present consideration based on nucleophilic processes.

References

1) R. B. Woodward and R. Hoffmann, *Angew. Chem.*, **81**, 797 (1969); *Angew. Chem., Int. Ed., (Engl.)*, **8**, 781 (1969); "The Conservation of Orbital Symmetry," Academic Press, New York (1969).

2) K. Fukui, *Accounts Chem. Res.*, **4**, 57 (1971).

3) H. Zimmerman, *ibid.*, **4**, 272 (1971).

4) M. J. S. Dewar, *Tetrahedron Suppl.*, **8**, 75 (1966).

5) H. Zimmerman, *Accounts Chem. Res.*, **5**, 393 (1972).

6) It has been shown by Fukui that a concerted multicenter reaction can be treated as a combination of two two-center interactions in the HOMO-LUMO interaction method. (See Ref. 2).

7) W. A. Goddard III, *J. Amer. Chem. Soc.*, **92**, 7520 (1970); **94**, 793 (1972).

8) This type of reaction has also been explained MO-theoretically. (See Ref. 2.)

9) E. S. Gould, "Mechanism and Structure in Organic Chemistry," Henry Holt and Co., New York (1960), p. 492.

10) S_N2 reactions treated MO-theoretically have been reported. *Cf.* (a) A. Streitwieser, Jr., "Molecular Orbital Theory for Organic Chemists," John Wiley & Sons, Inc., New York (1961), p. 367; (b) K. Fukui, "Modern Quantum Chemistry," Vol. I, ed. by O. Shinanoglŭ, Academic Press, New York (1965), p. 49.

11) The charge transfer from ϕ_1 to ϕ_2* will cause weakening of both bonds.

12) "The total stabilization energy (ΔW) of a chemically-interacting state in a reaction between two systems is given by Coulombic (E_Q), exchange (E_K), delocalization (D), and polarization(π) terms as follows:

$$\Delta W = E_Q - E_K - D - \pi$$

D is the stabilization energy due to the mixing in of the charge-transferred states; it works to promote the reaction. The last term is also the stabilization energy, but less important." *Cf.* K. Fukui and H. Fujimoto, This Bulletin, **41**, 1989(1968).

13) There is no orbital-phase relationship between ϕ_1 and ϕ_2 before the reaction. Once the reaction proceeds concertedly, the relationship develops throughout all orbitals that take part in reaction.

14) In general, two or more alternative representations of orbital arrays of the localized bonding MO are possibile for a conjugate system, each giving the same result. The orbital phase of the antibonding MO is so chosen that the bonding interaction may arise in the process analogous to nucleophilic substitution.

15) Three orbital representations are possible for the bonding level of III, each giving the same result(V_o).

16) It is possible in any system of this type to arrange the nonbonding center and two-center bonds in this manner.

17) $n=1,2,3,\cdots\cdots$. When $n=1$, χ_0 should be bonding to χ_2 in ϕ_1 of $S_{\alpha'}$ in the allowed reaction as a matter of course.

18) W. Kirmse, "Carbene Chemistry," 2nd Ed., Academic Press, New York (1971), p. 165.

19) As for this principle, see Ref. 2.

20) Ref. 18, p. 281.

21) Intra- and intermolecular insertion reactions of carbene also can be analyzed easily with the present MO representation.

22) The role of a localized vacant orbital such as the 2p orbital of boron has been pointed out by Fukui. *Cf.* K. Fukui, This Bulletin, **39**, 498 (1966).

23) The possibility of such participation of lone-pair orbital as well as low-lying unoccupied orbital of hetero-atom has been mentioned by Woodward and Hoffmann. *Cf.* Ref. 1.

24) I. Adachi, K. Harada, R. Miyazaki, and H. Kano, *Chem. Pharm. Bull.* (Tokyo), **22**, 61 (1974).

25) For example, the process III→V can be considered to be the delocalization process of a conjugate system.

26) Although this orbital array is not correct for the HOMO of allyl anion, it can be assigned to the HOMO for allyl anion due to the fact that this representation has nodal properties similar to that of the correct one.

27) HOMO of allyl cation.

Electroorganic Chemistry XVIII[1] Anodic Oxidation of Substituted Cyclopropanes

Tatsuya SHONO and Yoshihiro MATSUMURA

Department of Synthetic Chemistry, Faculty of Engineering, Kyoto University, Kyoto 606

(Received February 6, 1975)

The anodic oxidations of polyalkyl-substituted cyclopropanes (**1**—**3**) and spiro[2.n]alkanes (**4**—**6**) were carried out in methanol. Monomethoxyolefin and dimethoxy compound resulted from the selective cleavage at the most substituted carbon–carbon bond. The decrease in the oxidation potential brought about by the substitution of the one methyl group was observed to be about 0.3 V *vs.* SCE. The analysis of the products and oxidation potentials of the cyclopropanes suggested that the σ-electron transfer from cyclopropane to the anode may be the initiation process and that the stereochemistry at the surface of the solid electrode plays an important role in this anodic oxidation.

The electrochemical oxidation of a cyclopropane ring seems quite interesting because of its olefin-like character. In a previous study,[2] we have reported the first evidence that the carbon–carbon single bond in a cyclopropane ring could be anodically oxidized to yield ring-opened products which may be synthesized by other methods only with difficulty.

In the present study, we wish to report the effect of an alkyl substituent and some specific selectivity on the anodic ring cleavage of cyclopropanes.

Results

Product Study. The anodic oxidations of polyalkyl-subsituted cyclopropanes (**1**—**3**) and spiro[2.n]alkanes (**4**—**6**) were carried out in methanol containing tetraethylammonium *p*-toluenesulfonate (Et_4NOTs) as a supporting electrolyte (Eqs. (1) and (2)). Compounds **1**—**5** gave monomethoxy and dimethoxy products, which resulted from the cleavage of the most highly substituted carbon–carbon bond, although **3a** and **5a** were not isolated because of their further oxidation. Interestingly, spiropentane (**6**) was anodically stable.

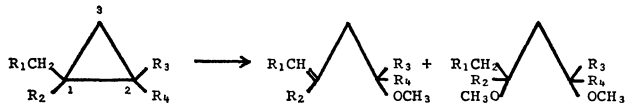

1:	$R_1=H$, $R_2=R_3=R_4=CH_3$	**1a**	**1b**
2:	$R_1=R_4=H$, $R_2=R_3=CH_3$	**2a**	**2b**
3:	$R_1=CH_3$, $R_2=CH_2CH_3$, $R_3=R_4=H$	**3a**	**3b**

(1)

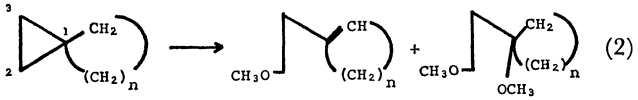

(2)

4:	$n=4$	**4a**	**4b**
5:	$n=2$	**5a**	**5b**
6:	$n=1$		

It is noticeable that in all of the unsaturated ethereal products (**1a**, **2a**), the unsaturated bond was formed in the direction of the side chain; further, products (**1a'**, **2a'**) which possess an unsaturated bond at the position corresponding to the cyclopropane 1,3-bond were completely lacking.

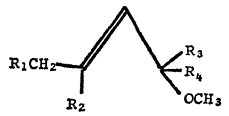

1a': $R_1=H$, $R_2=R_3=R_4=CH_3$
2a': $R_1=R_4=H$, $R_2=R_3=CH_3$

TABLE 1. PRODUCT YIELDS[a] AND CURRENT EFFICIENCIES OF ANODIC OXIDATIONS OF **1**—**5**

Cyclopropane	Product yields (%)		Current efficiencies (%)
	Monomethoxy	Dimethoxy	
1	**1a** (47)	**1b** (24)	71
2	**2a** (11)	**2b** (10)	21
3	**3a** (—)[b]	**3b** (12)	12
4	**4a** (1)	**4b** (5)	6
5	**5a** (—)[b]	**5b** (26)	26

a) Yields were calculated at the time when 2F/mol of electricity had been passed. b) The corresponding monomethoxy product could not be isolated.

All products were identified by spectroscopic and elemental analysis. Yields and current efficiences are shown in Table 1.

Oxidation Potential and Current–Potential Relationship. In order to evalute the effect of alkyl substituents on the oxidation potentials of cyclopropanes, they were measured in acetonitrile containing tetraethylammonium tetrafluoroborate as a supporting electrolyte. All cyclopropanes gave one oxidation wave, showing the lowering of the oxidation potential in proportion to the increase in the number of alkyl substituent. Table 2 lists the oxidation potentials of cyclopropanes together with those of the corresponding olefins.

The current–potential relationship was measured under the condition of the preparative oxidation of cyclopropane. As the number of alkyl substituents increases, the current–potential curve becomes more cathodic, indicating a lowering of the oxidation potential of the cyclopropane.

Acid-catalyzed Methanolysis of Cyclopropanes. It has been well known[3] that, owing to its olefin-like character, the cyclopropane ring may be able to be cleaved by the attack of an electrophile to yield ring-opened products. It seems interesting to compare

Table 2. Oxidation potentials[a] of cyclopropanes and olefins

Cyclopropane	+E (V *vs.* SCE)	Olefin	+E (V *vs.* SCE)
(**7**)	>2.5		
(**2**)	2.30		1.96
(**1**)	2.05		1.74
(**4**)	2.38		
(**8**)	2.40		2.26

a) Average of three measurements; solvent, CH_3CN; supporting electrolyte, Et_4NBF_4.

the mode of the anodic ring cleavage of cyclopropane with that observed in the acid-catalyzed methanolysis.

The reflux of a methanolic solution of **1** containing a catalytic amount of *p*-toluenesulfonic acid gave ring-opened products (**1c** and **1d**) as shown in Eq. (3). The similar treatment of compound **3** yielded **3c** and **3d** (Eq. (4)), and compound **4** gave **4c** and **4d** (Eq. (5)).

In contrast to the bond cleavage in the anodic oxidation, the 1,3-bond (compound **1**) or 1,2-bond (compounds **3** and **4**) was cleaved in the acidic methanolysis.

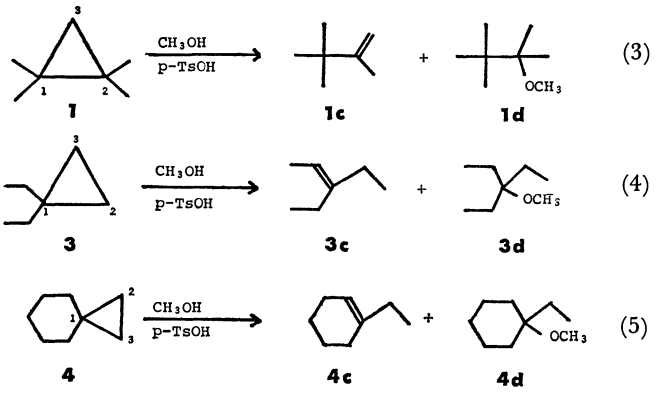

(3) (4) (5)

Discussion

Reaction Mechanism. As was pointed out in the previous study,[2] a direct σ-electron transfer from cyclopropane to the anode may be the initiation process of this anodic oxidation. The oxidation wave and the current–potential relationship support this proposal, which leads to the following reaction pathway (Scheme I):

In the anodic electron transfer from the cyclopropane σ-bond, the electron must be ejected from the most strained σ-bond, where the ionization potential would be the lowest. In the cation radical generated from **1**, the free rotation of the bond between C-1 and C-3 may be hindered owing to the steric restriction brought about by the surface of the solid electrode. This stereochemical hindrance may be the reason why the unsaturated ether of type **1a'** was not formed in the oxidation of **1**.

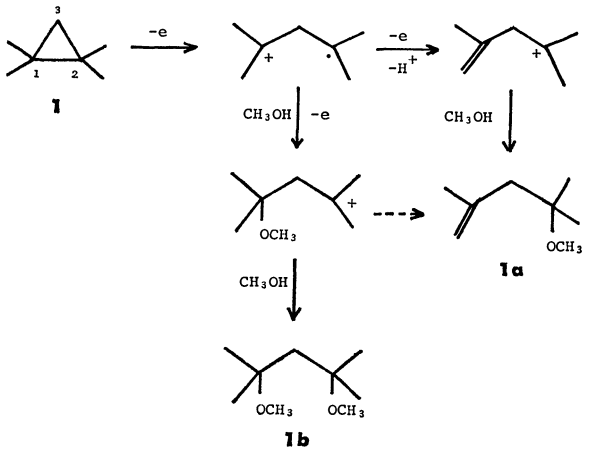

Scheme 1.

On the other hand, the attack of the proton in the acid catalyzed methanolysis occurs on the less hindered side, which is in disagreement with the selectivity of bond cleavage observed in the anodic reaction.

Oxidation Potential. The increase in the oxidation potential was observed in the order of **1**<**2**<**7**; this can be explained from the notion that the substitution of an alkyl group stabilizes the intermediate, whereas it increases the energy of the starting compound owing to the steric strain. The decrease in the oxidation potential brought about by the substitution of one methyl group was about 0.3 V *vs.* SCE (Table 2), and this amount is comparable to that which results from the substitution of an alkyl group into the olefinic system. In view of the strain energy, the oxidation of spiro[2.2]pentane (**6**) was expected to give a relatively high current efficiency. The disagreement of this prediction with the experimental observation may be explained by the instability of the intermediate.

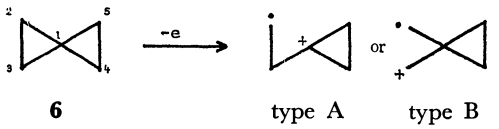

The intermediate of type A is analogous to a cyclopropyl cation, whose instability has been demonstrated by the solvolytic study.[4]

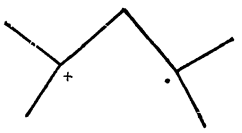

type C

Furthermore, the intermediate of type B may not be stabilized by the interaction with the neighboring cyclopropyl group since the direction of the vacant p-orbital of the cation may be orthogonal to the plane

of the cyclopropane ring if the C_1-C_3 bond is not able to rotate freely at the time when the electron transfer from the C_2–C_3 σ-bond takes place on the surface of the anode. The absence of such free rotation is supported by the fact that **1a** was the only unsaturated ether from the intermediate of type C.

Experimental

Materials. Compounds **1**,[5] **2**,[6] **3**,[7] **4**,[7] and **6**[8] were prepared by the reported methods. Compound **5** was prepared by the Simmons-Smith method[9] from methylenecyclobutane[10] and identified spectroscopically by comparison with an authentic sample[11] (yield 28%).

Preparative Electrolysis of Cyclopropane. General: Into a 100 ml electrolysis cell equipped with a magnetic stirrer and two carbon electrodes were poured a solution of 0.05 mol of cyclopropane and 0.01 mol of Et_4NOTs in 0.50 mol of methanol. The electrolysis was carried out under the constant potential condition until 2F/mol of electricity had been passed. The reaction mixture was poured into water, extracted with three portions of ether, dried on magnesium sulfate, filtered, and concentrated successively. The residue was distilled to give the oxidized products.

1,1,2,2,-Tetramethylcyclopropane (**1**) was electrolyzed at the anode potential of 1.45 V *vs.* SCE and gave 2,4-dimethyl-4-methoxy-1-pentene (**1a**) and 2,4-dimethyl-2,4-dimethoxypentane (**1b**) in 47.2 and 24.2% yields respectively after 2F/mol of electricity was passed. **1a**: IR 3070 (olefin), 2820 (ether), 1640 (olefin), 1075 cm^{-1} (ether); NMR (CCl_4) τ 5.4 (d, 2, $C\underline{H}_2$=), 6.85 (s, 3, $OC\underline{H}_3$), 7.85 (s, 2, $C\underline{H}_2$), 8.20 (s, 3, $CC\underline{H}_3$), 8.87 (s, 6, $C\underline{H}_3$); (Found: C, 74.95; H, 12.57%. Calcd for $C_8H_{16}O$: C, 74.94; H, 12.58%). **1b**: IR 2820, 1075 cm^{-1} (ether); NMR (CCl_4) τ 6.90 (s, 6, $OC\underline{H}_3$), 8.37 (s, 2, $C\underline{H}_2$), 8.80 (s, 12, $C\underline{H}_3$); (Found:, C, 67.04; H, 12.70%. Calcd for $C_9H_{20}O_2$: C, 67.45; H, 12.57%)

1,1,2-Trimethylcyclopropane (**2**) was electrolyzed at the anode potential of 1.6 V *vs.* SCE and yielded 2-methyl-4-methoxy-1-pentene (**2a**) (contaminated with a small amount of unknown products) and 2-methyl-2,4-dimethoxypentane (**2b**) in 10.7 and 9.9% yields respectively. **2b** was spectroscopically identified with the sample which was prepared by the methoxylation of hexylene glycol. **2a**: IR 3080, 1640 cm^{-1} (olefin); NMR (CCl_4) τ 5.30 (broad s, 2, $C\underline{H}_2$=), 6.85 (s, 3, $OC\underline{H}_3$), 6.6—7.0 (m, 1, $C\underline{H}$), 7.8 (d, 2, =C–$C\underline{H}_2$), 8.3 (s, 3, $C\underline{H}_3$), 8.9 (d, 3, $C\underline{H}_3$), mass spectrum parent peak, *m/e* 114. (Found: C, 73.79; H, 12.54. Calcd for $C_7H_{14}O$: C, 73.63; H, 12.36%). **2b**: IR 2840, 1090 cm^{-1} (ether); NMR (CCl_4) τ 6.6 (m, 1, $C\underline{H}$), 6.80 (s, 3, $OC\underline{H}_3$), 6.90 (s, 3, $OC\underline{H}_3$), 8.90 (s, 6, $C\underline{H}_3$), 8.95 (d, 3, $C\underline{H}_3$). (Found: C, 65.43; H, 12.68%. Calcd for $C_8H_{18}O_2$: C, 65.74; H, 12.41%).

1,1-Diethylcyclopropane (**3**) yielded 3-ethyl-1,3-dimethoxypentane (**3b**) in a 11.7% yield. **3b**: NMR (CCl_4) τ 6.65 (q, 2, $C\underline{H}_2$), 6.70 (s, 3, $OC\underline{H}_3$), 6.90 (s, 3, $OC\underline{H}_3$), 8.2—8.8 (m, 6, $C\underline{H}_2$), 9.20 (t, 6, $C\underline{H}_3$).

Spiro[2.5]octane (**4**) was electrolyzed at the anode potential of 2.30 V *vs.* SCE and yielded 1-(1-cyclohexenyl)-2-methoxyethane (**4a**) and 1-(1-methoxycyclohexyl)-2-methoxyethane (**4b**) in 1.1 and 4.8% yields respectively. 1,1-Dimethoxymethylcyclohexane was not detected; **4a**: IR 3050, 1630 (olefin), 2845, 1120 cm^{-1} (ether); NMR (CCl_4) τ 4.63 (broad s, 1, C=C$\underline{H}$), 6.70 (t, 2, $C\underline{H}_2O$), 6.75 (s, 3, $OC\underline{H}_3$), 7.7—8.7 (m, 10, $C\underline{H}_3$). mass spectrum parent peak, *m/e* 140. **4b**: IR 2840, 1115 cm^{-1} (ether); NMR (CCl_4) τ 6.7 (t, 2, $C\underline{H}_2$), 6.75 (s, 3, $OC\underline{H}_3$), 6.95 (s, 3, $OC\underline{H}_3$), 8.0—9.0 (m, 12, $C\underline{H}_2$). (Found: C, 71.58; H, 11.76%. Calcd for $C_{10}H_{20}O_0$: C, 77.09; H, 11.50%).

Spiro[2.3]hexane (**5**) was electrolyzed at the anode potential of 2.25 V *vs.* SCE and yielded 1-(1-methoxycyclobutyl)-2-methoxyethane (**5b**) in a 25% yield. **5b**: IR 2840, 1120 cm^{-1} (ether); NMR (CCl_4) τ 6.70 (t, 2, $C\underline{H}_2O$), 6.70 (s, 3, $OC\underline{H}_3$), 6.93 (s, 3, $OC\underline{H}_3$), 7.80—8.60 (m, 8, $C\underline{H}_2$), (Found: C, 66.33; H, 11.06%. Calcd for $C_8H_{16}O_2$: C, 66.63; H, 11.18%).

Spiro[2.2]pentane (**6**) yielded no detectable products.

Acid Catalyzed Methanolysis of Cyclopropane. General: A solution of 0.05 mol of cyclopropane in 0.50 mol of methanol containing 0.01 mol of *p*-toluenesulfonic acid was refluxed for one or two days.

After cooling, the solution was poured into water and extracted with ether. The ethereal layer was shaken with aqueous carbonate and water and dried on magnesium sulfate. After the magnesium sulfate was filtered and the ether was removed, the residue was distilled to give products.

1,1,2,2-Tetramethylcyclopropane (**1**) gave 2,3,3-trimethyl-1-butene (**1c**) and 2,3,3-trimethyl-2-methoxybutane (**1d**) in 6 and 60% yields respectively.

1c was identified spectroscopically by comparison with an authentic sample.[12] **1d**: IR 2840, 1080 cm^{-1} (ether); NMR (CCl_4) τ 6.85 (s, 3, $OC\underline{H}_3$), 8.90 (s, 6, $C\underline{H}_3$), 9.10 (s, 9, $C\underline{H}_3$). (Found: C, 73.98; H, 13.69%. Calcd for $C_8H_{18}O$: C, 73.78; H, 13.92%).

1,1-Diethylcyclopropane (**3**) yielded 3-ethyl-2-pentene (**3c**) and 3-ethyl-3-methoxypentane (**3d**) in 57 and 10% yields respectively. **3c**: IR 3020 cm^{-1} (shoulder, olefin); NMR (CCl_4) τ 4.85 (q, 1, C=C$\underline{H}$), 7.70—8.20 (m, 4, $C\underline{H}_2$), 8.4 (d, 3, $C\underline{H}_3$), 9.0 (double triplet, 6 $C\underline{H}_3$). Compound **3c** was also identified spectroscopically by comparison with an authentic sample.[13] **3d**: NMR (CCl_4) τ 6.97 (s, 3, $OC\underline{H}_3$), 8.40—8.80 (m, 6, $C\underline{H}_2$), 9.25 (t, 9, $C\underline{H}_3$).

Spiro[2.5]octane (**4**) yielded 1-ethylcyclohexane (**4c**) and 1-ethyl-1-methoxycyclohexane (**4d**) in 42 and 3% yields respectively. **4c**: IR 1630 cm^{-1} (olefin); NMR (CCl_4) τ 4.63 (broad s, 1, =C$\underline{H}$), 7.70—8.60 (m, 10, $C\underline{H}_2$), 9.00 (t, 3, $C\underline{H}_3$). **4c** was also identified spectroscopically by comparison with an authentic sample.[14] **4d**: IR 2840, 1080 cm^{-1} (ether); NMR (CCl_4) τ 6.97 (s, 3, $OC\underline{H}_3$), 8.10—8.80 (m, 12, $C\underline{H}_2$), 9.23 (t, 3, $C\underline{H}_3$); mass spectrum parent peak, *m/e* 142.

Oxidation Potential. The data were obtained at room temperature in dry acetonitril containing 0.1 M tetraethylammonium tetrafluoroborate[15] in a three-electrode polarography system (Yanako P8DP).

References

1) Part XVII in this series, T. Shono, A. Ikeda, and H. Omizu, to be published.

2) T. Shono, Y. Matsumura, and Y. Nakagawa, *J. Org. Chem.*, **36**, 1771 (1971).

3) R. J. Ouellette, R. D. Robins, and A. South, Jr., *J. Amer. Chem. Soc.*, **90**, 1619 (1968). O. A. Nesmeyanova, M. Y. Lukina, and B. A. Kazanskii, *Dokl. Akad. Nauk SSSR*, **153**, 357 (1963). *Chem. Abstr.*, **60**, 530 h (1964). M. Y. Lukina and O. A. Nesmeyanova, *ibid.*, **158**, 625 (1964). *Chem. Abstr.*, **16**, 15949d (1964).

4) J. A. Landgrebe and D. E. Applequist, *J. Amer. Chem. Soc.*, **86**, 1536 (1964).

5) R. G. Kelso, K. W. Greenlee, J. M. Derfer, and C. E. Boord, *J. Amer. Chem. Soc.*, **77**, 1751 (1955).

6) J. D. Bartleson, R. E. Burk, and H. P. Lankelms, *ibid.*, **68**, 2513 (1946).

7) R. W. Shortridge, R. A. Craig, K. W. Greenlee, J. M. Derfer, and C. E. Boord, *J. Amer. Chem. Soc.*, **70**, 946

(1948).
8) D. E. Applequist, G. E. Fanta, and B. W. Henrikson, *J. Org. Chem.*, **23**, 1715 (1958).
9) R. D. Smith and H. E Simmons, *Org. Syn.*, **41**, 72 (1961).
10) J. D. Roberts and C. W. Sauer, *J. Amer. Chem. Soc*,. **71**, 3925 (1949).
11) D. E. McGreer, *Can. J. Chem.*, **38**, 1938 (1960).
12) G. Edgar, G. Calingaert, and R. E. Marker, *J. Amer. Chem. Soc.*, **51**, 1483 (1929).
13) B. T. Brooks and I. Humphrey, *ibid.*, **40**, 835 (1918).
14) K. Auwers and Ph. Ellinger, *Ann. Chem.*, **387**, 221 (1912).
15) H. O. House, E. Feng, and N. P. Peet, *J. Org. Chem.*, **36**, 2371 (1971).

Oxidative Cleavage of Aromatic Methoxy Compounds with Photo-excited Aromatic Nitro Compounds[1-2]

Isao SAITO, Masaaki TAKAMI, and Teruo MATSUURA

Department of Synthetic Chemistry, Faculty of Engineering, Kyoto University, Kyoto 606

(Received February 10, 1975)

Photochemical addition of the aromatic nitro group with aromatic methoxy compounds leading to the cleavage of the aromatic ring was studied. The oxidative cleavage occurs selectively at 1,2-bond with respect to a methoxy group of methoxybenzenes and methoxynaphthalenes. Aromatic nitro compounds having the lowest π,π^* triplet are more effective to the oxidative ring cleavage of the methoxynaphthalenes than those having the lowest n,π^* triplet. A mechanism involving charge-transfer complex is proposed. The scope and limitation on the use of these photochemical reactions are discussed.

The photochemical addition of the aromatic nitro group to alkenes[3-4] and alkynes[3-5] has received considerable attention. Recent work by de Mayo and co-workers[4a] has shown that aromatic nitro compounds having the lowest $^3n,\pi^*$ state undergo photocycloaddition with alkenes to give 1,3,2-dioxazolidines which decompose readily at room temperature to yield two carbonyl fragments.

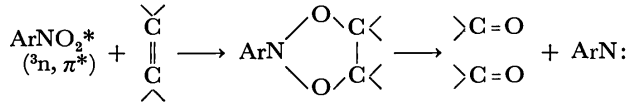

From our interest in the oxidative cleavage of aromatic nuclei in relation to the biological oxidation of aromatic compounds,[6] we investigated the photochemical reaction of aromatic nitro compounds with aromatic methoxy compounds. We now report that aromatic nitro compounds having either $^3n,\pi^*$ or $^3\pi,\pi^*$ state could react photochemically with aromatic methoxy compounds to yield ultimately 1,2-cleavage products, providing a useful method for the selective 1,2-cleavage of an aromatic ring. The scope and limitation on the use of this type of photochemical reactions are also discussed.

Results and Discussion

Photoreaction of Nitrobenzenes with Methoxybenzenes. We first examined the photochemical reaction of *m*-chloronitrobenzene (**1**) and nitrobenzene, known to have the lowest $^3n,\pi^*$ state,[3] in the presence of methoxybenzenes. A solution of **1** and a methoxybenzene in benzene was irradiated with a high pressure mercury lamp through a Pyrex glass under nitrogen atmosphere at room temperature. Products were separated from polymeric tars by column chromatography or distillation under reduced pressure, and their structures were assigned on the basis of spectral and chemical evidences. In a typical run, when a solution of **1** (0.086 M) and veratorole (**2a**) (0.516 M) in benzene was irradiated, dimethyl *trans,trans*-muconate (**3a**) was obtained in 8% yield (basid on reacted **1**) along with *m*-chloroaniline (**4**) (4%) and polymeric tars. Irradiation of a solution of **1** with 1,4-dimethoxybenzene (**2b**) gave the corresponding 1,2-cleavage product **3b** (14%) and **4** (7%). Similarly, irradiation of **1** in anisole (**2c**) gave **3c** (6%), phenol (5%) and 3,3'-dichloroazobenzene (**5**) (trace) (Table 1).

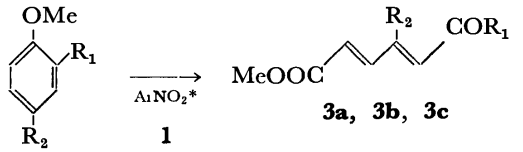

2a: R_1=OMe, R_2=H
2b: R_1=H, R_2=OMe
2c: $R_1=R_2$=H

3a, 3b, 3c + $ArNH_2$ + ArN=NAr
4 **5**
Ar=*m*-Cl-Ph-

The photoreaction of methoxybenzenes with nitrobenzene was found to proceed much less efficiently, but the products were essentially the same in both cases (Table 1). Although the yields of ring cleavage products (**3a**, **3b**, **3c**) are relatively low, it should be noted that the oxidative cleavage occurs selectively at 1,2-bond with respect to a methoxyl group.

Photoreaction of m-Chloronitrobenzene with Methoxynaphthalenes. Methoxynaphthalenes react much faster with photo-excited *m*-chloronitrobenzene to give the cleavage products in good yield than methoxybenzenes (Table 1). As an example, irradiation of 1,4-dimethoxynaphthalene (**6a**) (0.545×10^{-2} M) and **1** (0.673×10^{-2} M) in benzene gave the corresponding 1,2-cleavage product **7a** (70%), **4** (5%), **5** (13%) and *m*-chloroformanilide (**8**) (7%). The results of other methoxynaphthalenes (**6b**, **6c**) are given in Table 1.

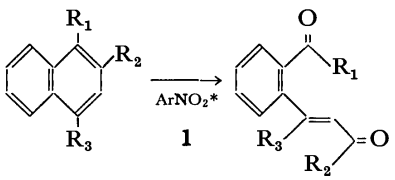

6a: $R_1=R_3$=OMe, R_2=H
6b: R_1=OMe, $R_2=R_3$=H
6c: $R_1=R_3$=H, R_2=OMe

7a, 7b, 7c + $ArNH_2$ + ArN=NAr + ArNHCHO
4 **5** **8**
Ar=*m*-Cl-Ph-

Although the fate of the reacted **1** in these reactions is complicated and appears to depend upon the starting methoxy aromatics, it is very probable that the azobenzene **5** and formanilide **8** result from the corresponding nitrene or its precursor, since the photoreaction of **1** without methoxy compounds gave neither **5** nor **8**, but only **4**.

Photoreaction of 1-Nitronaphthalene with Methoxynaph-

Table 1. Photoreaction of aromatic nitro compounds ($ArNO_2$) with aromatic methoxy compounds (ArOMe) in benzene

	ArOMe	$ArNO_2$	Products (yield)[b]			
1	**2a**	**1**	**3a** (8%)	**4** (4%)		
2	**2a**	Nitrobenzene[a]	**3a** (2%)	azobenzene (trace)		
3	**2b**	**1**	**3b** (14%)	**4** (7%)		
4	**2b**	Nitrobenzene[a]	**3b** (5%)	azobenzene (trace)		
5	**2c**[a]	**1**	**3c** (6%)	**5** (trace)	phenol (5%)	
6	**6a**	**1**	**7a** (70%)	**4** (5%)	**5** (13%)	**8** (7 %)
7	**6b**	**1**	**7b** (33%)	**4** (18%)	**5** (13%)	**8** (15%)
8	**6c**	**1**	**7c** (14%)	**4** (12%)	**5** (3%)	**8** (10%)
9	**6a**	**9**	**7a** (58%)	**10** (20%)	**11** (14%)	**12** (43%)
10	**6b**	**9**	**7b** (60%)	phthalic anhydride (14%)		
			11 (16%)	**12** (25%)		
11	**6c**	**9**	**7c** (28%)	**11** (trace)	**12** (4%)	

a) Used as solvent. b) Yields were based on reacted starting materials.

thalenes. It has been reported that 1-nitronaphthalene (**9**) or 2-nitrobiphenyl, which has the lowest $^3\pi,\pi^*$ state,[7-8] does not undergo cycloaddition with alkenes after prolonged irradiation.[4a] We have observed that photo-excited **9** is much more effective to the oxidative ring cleavage of the methoxynaphthalenes. When a solution of **9** (4.68×10^{-2} M) and **6a** (4.25×10^{-2} M) in benzene was irradiated, the reaction proceeded rapidly and **7a** (58%) was obtained along with dimethyl phthalate (**10**) (20%), 1-naphthylamine (**11**) (14%) and 1-formaminonaphthalene (**12**) (43%). Yields of **7a** (or **10**) and **11** (or **12**) were based on the reacted **6a** and **9**, respectively. The results are shown in Table 1. The photoreaction of **9** differs from that of **1** in the following respect; (1) The reaction of **9** proceeds much faster than that of **1**. (2) Considerable amounts of **10**, which results most likely from the 1,4-addition of **9** to **6a**, is obtained in the reaction of **9** with **6a**.

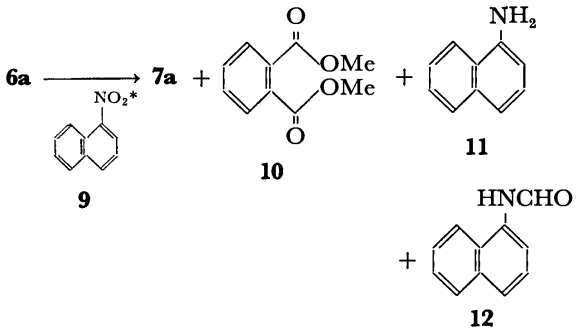

Mechanism of Reaction. Since 1,4-dimethoxynaphthalene (**6a**) showed the highest reactivity toward the photo-excited **9** and both **7a** and **10** were obtained in good yield, we examined the photoreaction of **9** with **6a** in some detail.

Solvent Effect

The rate of disappearance of **6a** is highly sensitive to solvent and temperature. At room temperature the photoreaction proceeds at an appreciable rate in benzene, ether, *n*-hexane and acetone, but much more slowly in more polar solvents such as methanol and acetonitrile (Table 2). When the reaction was carried out in ether solution at −78 °C, the rate of the reaction increased considerably as compared to that at room temperature, suggesting that an initially formed adduct collapses thermally to the starting compounds **6a** and **9**.

Table 2. Solvent effect on the rate of disappearance of **6a**

Solvent	Relative rate of disappearance of **6a**[a]
n-Hexane	0.8
Benzene	1.0
Ether	1.4
Acetone	0.2
Methanol	0.02
Acetonitrile	0.02

a) Solutions of **6a** (4.00×10^{-3} M) and **9** (5.80×10^{-3} M) in each solvent were irradiated simultaneously in a merry-go-round apparatus. The relative rate was determined by glc analysis at *ca.* 20% conversion of **6a**.

We also observed that the product ratio **10**/**7a** is sensitive to temperature, solvent, and degree of conversions of **6a**, the product ratio not being reproducible in some cases. However, the addition of a trace organic acid such as benzoic acid or acetic acid to the reaction system considerably changes the ratio. The presence of these acids completely inhibited the formation of **10**, and the 1,2-cleavage product **7a** was obtained almost exclusively (Table 3).

Table 3. Effects of acids on the product ratio **10**/**7a** in the photoreaction of **6a** with **9** in benzene

Product ratio	Acetic acid[a]		Benzoic acid[b]	
	None	2.33×10^{-2} M	None	6.85×10^{-3} M
10/**7a**[c]	0.48	0.03	0.63	0.02

a) [**6a**]=[**9**]=4.89×10^{-3} M. b) [**6a**]=[**9**]=5.55×10^{-3} M. c) The ratio was determined by glc analysis at *ca.* 50% conversion.

Excited State and Multiplicity

Questions concerning the mechanism of the reaction include those on the excited state and multiplicity of the nitro aromatics. In order to ascertain whether the lowest triplet state of **9** is involved in the reaction, we carried out quenching experiments. Quenching effects of piperylene and oxygen on the formation of **7a** and **10** in the reaction of **6a** with **9** are shown in Table 4.

Table 4. Quenching effects of piperylene and oxygen on the rate of formation of **7a** and **10**[a]

Quencher (equiv. mol)	Relative rate of formation	
	7a	**10**
0	1.0	1.0
100	0.55	0.52
300	0.34	0.37
O_2 (saturated)	0.65	0.68

a) [**6a**]=[**9**]=2.56×10^{-3} M.

The formation of **7a** and **10** was inhibited considerably by added piperylene. Considering the relatively high efficiency of the intersystem crossing of **9**,[9] it is very likely that the lowest triplet state (π,π^*) of **9** is involved in the reaction.

In order to elucidate the excited state of the nitro compound involved in the reaction, we examined the photochemical reaction of **6a** with various nitro compounds, whose lowest excited triplet states are well characterized, using a merry-go-round apparatus with light through Pyrex glass. Relative reactivity of the nitro compounds with respect to nitrobenzene as a standard (1.0) is given in Table 5. Although the relative reactivity indicates only the efficiency of the reaction for a preparative mean and does not mean the absolute quantum efficiency of the reaction, it is interesting to note that both an $^3n,\pi^*$ and a $^3\pi,\pi^*$ state of the nitro compounds could participate in the photoaddition and that the $^3\pi,\pi^*$ state seems to be more reactive than the $^3n,\pi^*$ state. Solvent effects on the reaction of **1** ($^3n,\pi^*$) and **9** ($^3n,\pi^*$) with **6a** are essentially the same, suggesting that the same mechanism operates in both cases (Table 6).

The photoreaction of **9** with **6a** could proceed at a moderate rate under irradiation with visible light at 435 nm or even at 545 nm. At this wavelength (545 nm) neither **9** nor **6a** absorbs the light. The results suggest a mechanism involving a charge-transfer complex. A new absorption band located at *ca.* 430 nm was observed in the electronic spectrum of a solution of **9** (0.05 M) and **6a** (0.05 M) in benzene (Fig. 1). However, no spectroscopic evidence for the formation of such ground state complex between **9** and **6b** or **6c** has been observed.

As a further indication for the charge-transfer complex mechanism, solutions of **9** in the presence of various aromatic methoxy compounds were irradiated simultaneously, and the relative rates of disappearance of the methoxy compounds were determined. The relative rates were obtained with respect to 1,4-dimethoxybenzene (**2a**) as a standard (1.0). The results are shown in Table 7. If a charge-transfer like transition state is involved in the reaction, then increase of electron availability in the methoxy aromatic system should be expected to increase the rate of reaction. The aromatic methoxy compounds with more powerful electron-donating properties are more reactive to photo-excited **9**. The result can best be explained by a donor-acceptor mechanism involving a charge-transfer complex, although an alternative mechanism involving an electrophillic attack of a short-lived triplet

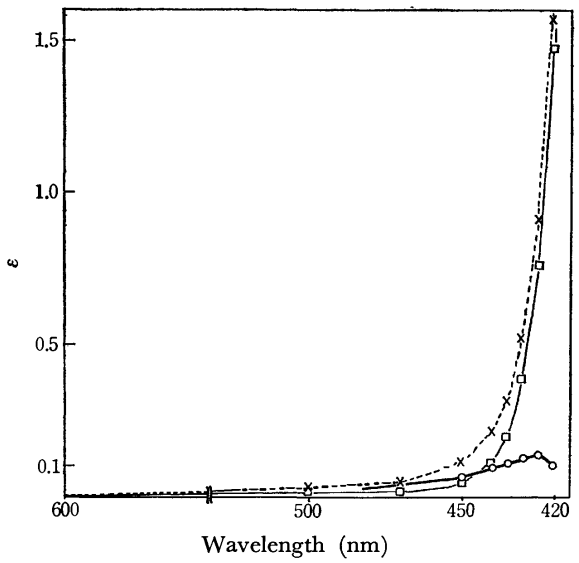

Fig. 1. The UV spectra of **9** and **6a** in benzene.
—□— **9** (0.05 M), --×-- **9** (0.05 M)+**6a** (0.05 M), —○— calculated absorption spectrum of a complex (**9**···**6a**).
In this region (600—420 nm) there is no absorption of **6a**.

Table 5. Photoreactivity of aromatic nitro compounds ($ArNO_2$) toward **6a**[a]

Lowest excited triplet state	n,π^*				π,π^*		
$ArNO_2$ (Ar=)	*m*-Cl-Ph-[7], **1**	*m*-CN-Ph[7],	Ph-[7],	*p*-MeO-Ph-[10],	1-Napht-[8], **9**	2-Napht-,[8]	3-Cl-1-Napht-[8]
Relative rate of disappearance of **6a**	0.8	1.0	1.0	1.3	7.7	10.8	6.1

a) Solution of an equimolar amount of a nitro compound ($ArNO_2$) and **6a** (5.0×10^{-3} M) in benzene was irradiated in a merry-go-round apparatus. The relative rate of disappearance of **6a** with respect to that of nitrobenzene (1.0) was determined by glc analysis.

Table 6. Solvent effects on the photoreactions of 1 and 9 with 6a in the presence of acid[a]

Solvent	$ArNO_2$ (Ar=)	
	m-Cl-Ph-(**1**) (n, π^*)	1-Napht-(**9**) (π, π^*)
Benzene	1.00	1.00
Methanol	0.16	0.02
Acetonitrile	0.25	0.02

a) Solutions containing $ArNO_2$ (2.78×10^{-3} M), **6a** (2.78×10^{-3} M) and benzoic acid (5.55×10^{-3} M) were irradiated simultaneously. The rate of disappearance of **6a** was determined by glc analysis.

Table 7. Relative reactivity of aromatic methoxy compounds (ArOMe) toward photo-excited 9

ArOMe	Rel. reactivity
1,4-Dimethoxybenzene (**2b**)	1.0
1,2,4,5-Tetramethoxybenzene	1.5
2-Methoxynaphthalene (**6c**)	2.6
1-Methoxynaphthalene (**6b**)	7.3
1,4-Dimethoxynaphalene (**6a**)	20.6

of **9** on the methoxy compound[4a] cannot be ruled out rigorously.

Reaction Sequence

The ultimate formation of two carbonyl fragments **7a** and **10** can be interpreted by a mechanism involving a thermal and prototropic equilibrium mixture of 1,2- (**13**) and 1,4-cycloadduct (**14**), formed *via* a triplet excited complex **15**. The excited complex **15**, a key intermediate in the mechanism, might be formed either by the excitation of the ground-state complex (435 nm) or by the interaction between $^3\pi, \pi^*$ state and ground state **6a**. The complex **15** thus formed could collapse to the cycloadducts **13** and **14** or decay to ground state **9** and **6a**. It may be considered that both of the processes have solvent dependence, the latter process becoming predominant in polar solvents such as methanol.

The 1,2-cycloadduct (**13**), a 1,3,2-dioxazolidine derivative, would thermally decompose to the corresponding carbonyl product **7a** with the elimination of an aryl nitrene. The 1,4-cycloadduct (**14**) could decompose photochemically[11] or thermally to yield **10**, acetylene and an aryl nitrene. In an attempt to isolate such cycloadducts, we carried out the photoreaction at low temperature. However, such intermediates were too unstable to be detected even at −78 °C. While the fate of the aryl nitrene is not fully elucidated, it could account satisfactorily for the formation of the corresponding azo[12] and amino[13] compounds. In order to confirm whether the aryl nitrene could be a precursor for the formamino compound (**8** or **12**), we examined the photochemical reaction of *m*-chlorophenyl azide with **6a** in benzene. However, the reaction only gave **5** (10%) and **4** (trace), no trace of the corresponding formanilide **8** being detected. This suggests that the formamino compound is formed by an unknown side reaction which still remains to be clarified (Scheme 1).

Scope and Limitation. We also examined the photoreaction of aromatic nitro compounds with several other aromatic compounds. These were methyl-, dimethylamino-[14] and hydroxy-substituted benzenes. The reactions of these compounds with photo-excited nitro compounds resulted in the hydrogen abstraction from these groups, no product resulting from the oxidative ring cleavage being observed (Scheme 2). However, 9,10-dimethoxyanthracene (**16**) was found to react smoothly with the photo-excited **1** to give similar types of products **17** (36%), **10** (14%), 9,10-anthraquinone (22%), **5** (5%) and **8** (26%).

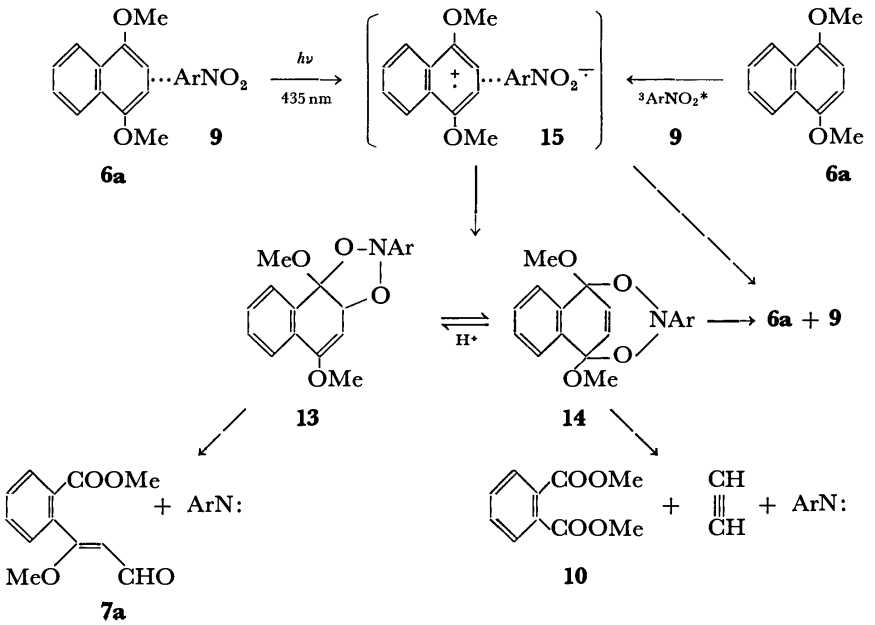

Scheme 1

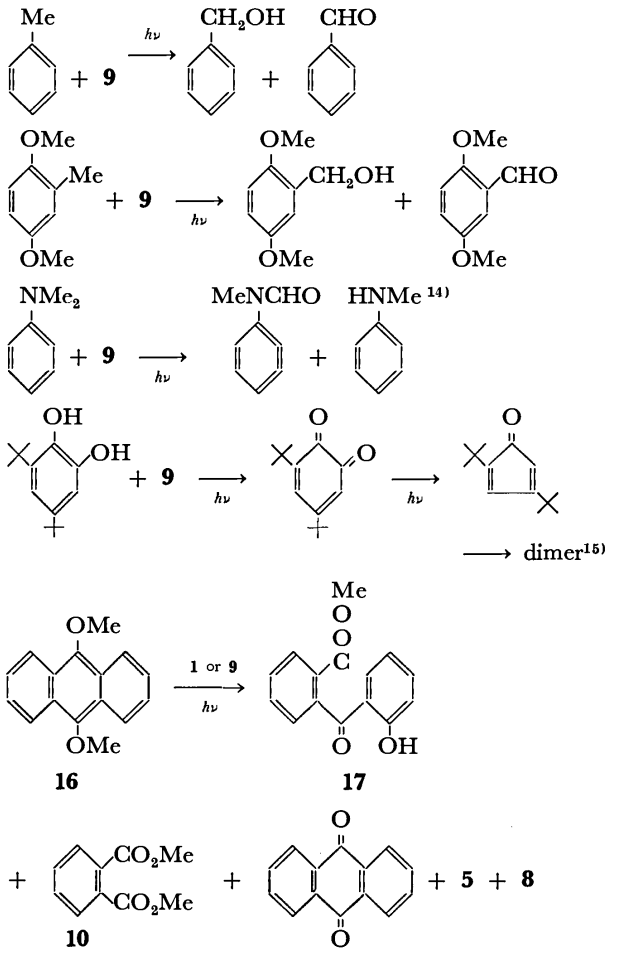

Scheme 2

Experimental

IR spectra were recorded on an IRA-1 spectrometer, NMR spectra on a Varian T-60 with TMS as an internal standard, and UV spectra on a Shimadzu UV-200. Light source was a high pressure mercury lamp (Ushio 400 W or 100 W) through Pyrex glass. Yields were based on reacted starting materials.

Photolysis of m-*Choronitrobenzene (**1**) with Veratrol (**2a**).* A solution of **1** (4.074 g, 25.9 mmol) and **2a** (21.381 g, 155 mmol) in 300 ml benzene was irradiated with a 400 W high pressure mercury lamp (Pyrex filter) under nitrogen atmosphere at room temperature for 35 hr. The resulting red brown solution was concentrated and the residue was distilled *in vacuo* to give the unreacted starting materials (19.71 g of **2a**, 3.05 g of **1**). Preparative glc (Silicon DC 550, 170 °C) of the residue gave *m*-chloroaniline (**4**) (0.041 g, 4%) and colorless crystals (mp 155—156 °C, 0.101 g, 8%) which was identical with an authentic sample of dimethyl *trans,trans*-muconate (**3a**).

*Photolysis of Veratrol (**2a**) in Nitrobenzene.* A solution of **2a** (1.00 g, 7.25 mmol) in 20 ml nitrobenzene was irradiated externally for 30 hr. After removal of the solvent, the residue was chromatographed on silica gel (52 g). Elution with PE-benzene (1 : 1) gave azobenzene (0.002 g). Elution with benzene gave unreacted **2a** (0.496 g). Elution with $CHCl_3$ and subsequent preparative glc (Silicon DC 550, 190 °C) yielded **3a** (0.020 g, 2%).

Photolysis of m-*Chloronitrobenzene (**1**) with 1,4-Dimethoxybenzene (**2b**).* A solution of **1** (4.0 g, 25.4 mmol) and **2b** (8.0 g, 58.0 mmol) in 300 ml benzene was irradiated for 24 hr under the same conditions. Unreacted starting materials (3.07 g of **1**, 6.412 g of **2b**) were removed by distillation *in vacuo*. Preparative glc (Silicon DC 550, 170 °C) of the residue gave **4** (0.086 g, 7%) and **3b** (0.22 g, 14%), mp 85—86 °C; IR (Nujol): 1725, 1660 cm^{-1}; UV (EtOH): 289 nm (ε 16000), 218 nm (ε 13800): NMR ($CDCl_3$); τ −0.10 (1H, d, J=6.0 Hz), 2.10 (1H, d, J=15 Hz), 3.40 (1H, d, J=15 Hz), 4.37 (1H, d, J=6 Hz), 6.17 (3H, s), 6.20 (3H, s); MS *m/e* 170 (M^+).

Found: C, 56.77; H, 6.08%. Calcd for $C_8H_{10}O_4$: C, 56.46; H, 5.90%.

*Photolysis of 1,4-Dimethoxybenzene (**2b**) in Nitrobenzene.* A solution of **2b** (4.03 g, 28.2 mmol) in nitrobenzene (82 g) was irradiated for 55 hr under the same conditions. After removal of the solvent, the residue (0.996 g) was chromatographed on a silica gel column (25 g). Elution with PE-benzene (1 : 1) gave azobenzene (0.005 g). Elution with benzene yielded unreacted **2b** (0.042 g). Further elution with $CHCl_3$ gave a black solid which on recrystallization from benzene-*n*-hexane gave **3b** (0.052 g, 5%). The remaining polymeric tars (0.81 g) was eluted with acetone.

Photolysis of m-*Chloronitrobenzene (**1**) in Anisole (**2c**).* A solution of **1** (1.497 g, 9.5 mmol) in 200 ml anisole was irradiated for 31 hr. After removal of the solvent, the residue was chromatographed on silica gel (100 g). Elution with PE-benzene (1 : 1) afforded red crystals of 3,3′-dichloroazobenzene (**5**) (mp 107 °C, 0.005 g). Further elution with the same solvent yielded unreacted **1** (0.695 g). Elution with benzene gave phenol (0.125 g, 5%). Elution with $CHCl_3$ gave a black mass which on crystallization from benzene-*n*-hexane yielded **3c** (0.147 g, 6%), mp 82 °C; IR (Nujol): 1730, 1675 cm^{-1}; NMR ($CDCl_3$): τ 0.33 (1H, d, J=8 Hz), 2.57 (1H, d d, J=12, J'=15 Hz), 2.84 (1H, d d, J=12, J'=15 Hz), 3.59 (1H, d d, J=8, J'=15 Hz), 3.71 (1H, d, J=8 Hz), 6.17 (3H, s). This compound was identical with an authentic sample.[16]

Photolysis of m-*Chloronitrobenzene (**1**) with 1,4-Dimethoxynaphthalene (**6a**).* A solution of **1** (0.53 g, 3.36 mmol) and **6a** (0.512 g, 2.72 mmol) in 500 ml benzene was irradiated for 22 hr. After removal of the solvent, the residue was chromatographed on silica gel (35 g). Elution with PE-benzene (1 : 1) gave **5** (0.031 g, 12.5%). Further elution with the same solvent gave a mixture of unreacted starting materials **1** (0.22 g) and **6a** (0.116 g). Eluiton with benzene yielded **4** (0.013 g, 5.2%). Elution with $CHCl_3$ and subsequent preparative glc (Silicon DC 550, 190 °C) gave *m*-chloroformanilide (**8**) (0.020 g, 6.6%) and **7a** (0.302 g, 69.5%), mp 43 °C; IR (Nujol): 1730, 1650, 1600 cm^{-1}; NMR ($CDCl_3$): τ 0.88 (1H, d, J=8 Hz), 2.00 (1H, m), 3.47 (2H, m), 3.63 (1H, m), 4.45 (1H, d, J=8 Hz), 6.17 (3H, s), 6.18 (3H, s); MS *m/e* 191 (M^+−CHO).

Found: C, 65.78; H, 5.36%. Calcd for $C_{12}H_{12}O_4$: C, 65.44; H, 5.49%.

Photolysis of m-*Chloronitrobenzene (**1**) with 1-Methoxynaphthalene (**6b**).* A solution of **1** (1.104 g, 7.02 mmol) and **6b** (1.014 g, 6.42 mmol) in 500 ml benzene was irradiated for 36 hr. After removal of the solvent, the residue was chromatographed on silica gel (40 g). Elution with PE-benzene (1 : 1) gave **5** (0.03 g, 12.6%) and unreacted starting materials **1** (0.797 g) and **6b** (0.761 g). Elution with benzene gave **4** (0.045 g, 18.1%). Elution with $CHCl_3$-benzene (1 : 1) yielded a black mass which on recrystallization from benzene-*n*-hexane gave colorless crystals of **7b** (0.123 g, 33.2%), mp 47 °C; IR (nujol): 1725, 1680 cm^{-1}; NMR ($CDCl_3$): τ 0.30 (1H, d, J=8 Hz), 1.62 (H, d, J=15 Hz), 2.04 (1H, d, J=7 Hz), 2.36 (1H, dd, J=7, J'=2 Hz), 2.49 (1H, m), 2.60 (1H, m), 3.52 (1H, dd, J=15, J'=8

Hz), 6.09 (3H, s); MS *m/e* 161 (M^+-CHO).

Found: C, 69.81; H, 5.41%. Calcd for $C_{11}H_{10}O_3$: C, 69.46; H, 5.30%. Elution with $CHCl_3$ gave **8** (0.046 g, 15%).

Photolysis of m-*Chloronitrobenzene (**1**) with 2-Methoxynaphthalene (**6c**).* A solution of **1** (0.750 g, 4.75 mmol) and **6c** (0.660 g, 4.18 mmol) in 500 ml benzene was irradiated for 47 hr. After removal of the solvent, the residue was chromatographed on silica gel (40 g). Elution with PE-benzene (1 : 1) gave **5** (0.005 g, 3%). Further elution with the same solvent gave a mixture of starting materials **1** (0.537 g) and **6c** (0.566 g). Elution with benzene yielded **4** (0.02 g, 12%). Elution with $CHCl_3$-benzene (1 : 1) and subsequent preparative glc (Silicon DC 550, 170 °C) yielded **7c** (0.035 g, 13.6%), mp 82 °C: IR (Nujol): 1730, 1605 cm^{-1}; NMR ($CDCl_3$): τ −0.27 (1H, s), 1.49 (1H, d, J=16 Hz), 2.14 (1H, m), 2.40 (3H, m), 3.36 (1H, d, J=16 Hz), 6.18 (3H, s); MS *m/e* 161 (M^+-CHO). This compound was prepared independently by esterification of the corresponding acid.[17] Elution with $CHCl_3$ and subsequent glc separation (Silicon DC 550, 170 °C) yielded **8** (0.042 g, 10%).

*Photolysis of 1-Nitronaphthalene (**9**) with 1,4-Dimethoxynaphthalene (**6a**).* A solution of **9** (0.405 g, 2.34 mmol) and **6a** (0.400 g, 2.12 mmol) in 50 ml benzene was irradiated with a 100 W high pressure mercury lamp for 12 hr. After removal of the solvent, the residue was chromatographed on silica gel (26 g). Elution with PE-benzene (1 : 1) gave a mixture of unreacted starting materials **6a** (0.059 g) and **9** (0.071 g). Benzene eluted 1-aminonaphthalene (**11**) (0.39 g, 14%) and dimethyl phthalate (**10**) (0.074 g, 20%). Elution with $CHCl_3$ and subsequent glc separation (Silicon DC 550, 200 °C) yielded **7a** (0.247 g, 58%) and 1-formaminonaphthalene (**12**) (0.141 g, 43%).

*Photolysis of 1-Nitronaphthalene (**9**) with 1-Methoxynaphthalene (**6b**).* A solution of **9** (0.552 g, 3.19 mmol) and **6b** (0.481 g, 3.04 mmol) in 500 ml benzene was irradiated for 13 hr. After removal of the solvent, the residue was chromatographed on silica gel (30 g). **6b** (0.104 g), **9** (0.163 g), **11** (0.044 g, 16%), **7b** (0.172 g, 60%), **12** (0.114 g. 25%) and phthalic anhydride (0.030 g, 14%) were obtained (Table 1).

*Photolysis of 1-Nitronaphthalene (**9**) with 2-Methoxynaphthalene (**6c**).* A solution of **9** (0.414 g, 2.39 mmol) and **6c** (0.475 g, 3.0 mmol) in 400 ml benzene was irradiated for 33 hr. Products were separated by column chromatography (silica gel, 30 g). **6c** (0.369 g), **9** (0.151 g), **7c** (0.036 g, 28%), **12** (0.015 g, 4%) and **11** (trace) were obtained (Table 1).

*Effects of Acids on the Product Ratio **10**/**7a**. Acetic acid*: A solution of **6a** (19.2 mg) and **9** (15.1 mg) in 18 ml benzene was divided into two parts, one of which contained 25 mg of acetic acid. These two solutions were irradiated simultaneously in a merry-go-round apparatus for 30 min. The product ratio **10**/**7a** was determined by glc analysis (Table 3). *Benzoic acid*: A solution of **6a** (22 mg) and **9** (17.3 mg) in 18 ml benzene was divided into two parts, one of which contained 15 mg of benzoic acid. The solutions were irradiated as descrived above. The result is shown in Table 3.

Quenching Experiments. Solutions containing **6a** (2.56×10^{-3} M), **9** (2.56×10^{-3} M) and varying amounts of piperylene in benzene was irradiated in a merry-go-round apparatus. The relative rates of formation of **7a** and **10** were determined by glc analysis (Table 4).

*Photolysis of 1-Nitronaphthalene (**9**) in Toluene.* A solution of **9** (0.080 g) in toluene (20 ml) was irradiated externally for 8 hr. After removal of the solvent, the residue was analyzed by glc and NMR. The results indicates that it contains benzaldehyde and benzyl alcohol (1 : 4). The products were separated by preparative glc and identified by IR.

*Photolysis of 1-Nitronaphthalene (**9**) with 2,5-Dimethoxytoluene.* A solution of 2,5-dimethoxytoluene (0.322 g, 2.12 mmol) and **9** (0.44 g, 2.54 mmol) in 600 ml benzene was irradiated for 31 hr. After removal of the solvent, the residue was analyzed by glc and tlc. Glc of the residue showed two peaks corresponding to 2,5-dimethoxybenzyl alcohol and 2,5-dimethoxybenzaldehyde (6 : 1). The products were identified by IR.

*Photolysis of 1-Nitronaphthalene (**9**) with* N,N-*Dimethylaniline.* A solution of *N,N*-dimethylaniline (0.140 g, 1.16 mmol) and **9** (0.200 g, 1.16 mmol) in 50 ml benzene was irradiated for 6 hr. The resulting yellow solution was concentrated and the residue was chromatographed on silica gel (11 g). Elution with PE-benzene (1 : 1) gave unreacted **9** (0.016 g). Further elution with the same solvent and subsequent glc separation yielded *N*-methylaniline (0.010 g, 8%), *N*-methylformanilide (0.053 g, 31%), and 1-aminonaphthalene (0.033 g, 37%). Elution with $CHCl_3$ gave formanilide (0.040 g, 23%).

*Photolysis of 1-Nitronaphthalene (**9**) with 3,5-di-*t*-Butylcatechol.* A solution of 3,5-di-*t*-butylcatechol (0.130 g, 0.59 mmol) and **9** (0.102 g, 0.59 mmol) in 70 ml benzene was irradiated for 25 hr. The resulting red brown solution was concentrated. Preparative glc of the residue yielded 2,4-di-*t*-butylcyclopentadienone dimer (0.070 g, 60%), which was identified by comparison of its IR spectrum with that of an authentic sample.[15]

*Photolysis of 9,10-Dimethoxyanthracene (**16**) with* m-*Chloronitrobenzene (**1**).* A solution of **16** (0.204 g. 0.86 mmol) and **1** (0.430 g, 2.73 mmol) in 250 ml benzene was irradiated for 39 hr. After removal of the solvent, the residue was chromatographed on silica gel (20 g). Elution with PE-benzene (1 : 1) gave **5** (0.005 g, 5%). Further elution gave a mixture of starting materials **16** (0.041 g) and **1** (0.311 g). Elution with benzene and subsequent preparative tlc yielded anthraquinone (0.035 g, 22%) and **17**[18] (0.70 g, 36%), which were identified by comparison of their IR spectra with those of authentic samples. Elution with $CHCl_3$-benzene (4 : 1) gave **10** (0.020 g, 14%). Elution with $CHCl_3$ yielded **8** (0.031 g, 26%).

This work was supported by a Grant-in-Aid for Scientific Research from the Ministry of Education.

References

1) Photoinduced Reactions. LXXXV

2) Preliminary communications; I. Saito, M. Takami, and T. Matsuura, *Chem. Lett.*, **1972**, 1195; I. Saito, M. Takami, and T. Matsuura, *Tetrahedron Lett.*, **1974**, 659.

3) For a review, see H. A. Morrison, "The Chemistry of the Nitro and Nitroso Groups," Part 1, ed. by H. Feuer, Interscience, New York, N. Y. (1969), p. 193.

4) a) J. L. Charlton, C. C. Liao, and P. de Mayo, *J. Amer. Chem. Soc.*, **93**, 2463 (1971) and references therein; b) G. Büchi and D. E. Ayer, *ibid.*, **78**, 689 (1969); c) J. S. Cridland and S. T. Reid, *Chem. Commun.*, **1969**, 125; d) P. Bouchet, C. Coquelet, J. Elquero, and R. Jacquier, *Tetrahedron Lett.*, **1973**, 891; J. T. Pinhey and E. Rizzardo, *ibid.*, **1973**, 4057.

5) a) M. L. Scheinbaum, *J. Org. Chem.*, **29**, 2200 (1964); b) J. A. Van Allan, S. Farid, G. A. Reynolds, and S. C. Chang, *ibid.*, **38**, 2834 (1973); c) C. C. Leznoff and R. J. Haward, *Canad. J. Chem.*, **49**, 3596 (1971).

6) a) I. Saito, N. Yoshimura, T. Arai, K. Omura, A. Nishinaga, and T. Matsuura, *Tetrahedron*, **28**, 5131 (1972); b) I. Saito, M. Imuta, and T. Matsuura, *ibid.*, **28**, 5307 (1972); c) I. Saito, S. Kato, and T. Matsuura, *Tetrahedron Lett.*, **1970**, 239.

7) a) W. Trotter and A. C. Testa, *J. Amer. Chem. Soc.*, **90**, 7044 (1968); b) R. Hurley and A. C. Testa, *ibid.*, **91**, 1946 (1969).

8) R. Rusakowicz and A. C. Testa, *Spectrochim. Acta*, **27** A, 787 (1970).

9) R. Hurley and A. C. Testa, *J. Amer. Chem. Soc.*, **90**, 1949 (1968).

10) R. L. Lestinger and R. R. Hantala, *Tetrahedron Lett.*, **1969**, 4205.

11) G. Rio and J. Berthelot, *Bull. Soc. Chim. Fr.*, **1970**, 1509; 2938.

12) A. Reiser, F. W. Willet, G. C. Terry, W. Willson, and R. Marley, *Trans. Faraday Soc.*, **64**, 3265 (1968).

13) P. A. S. Smith, "Nitrenes," Ed. N. Lwowasi, Interscience, New York, N. Y. (1970), p. 99.

14) M. Takami, I. Saito, and T. Matsuura, *Tetrahedron Lett.*, **1974**, 661.

15) R. C. Deselms and W. R. Schleigh, *Synthesis*, **1973**, 614.

16) A. Funke and P Karrer, *Helv. Chim. Acta*, **32**, 1016 (1949).

17) R. H. Wiley and P. H. Hobson, *J. Amer. Chem. Soc.*, **71**, 2429 (1949).

18) F. F. Blicke and O. J. Weinkauff, *ibid.*, **54**, 1450 (1932).

The Nucleophilic Photo-substitution Reaction of Anthraquinone Derivatives. II. The Mechanism of the Photoamination of Sodium 1-Amino-4-bromoanthraquinone-2-sulfonate

Haruo INOUE, Kenichi NAKAMURA, Seijiro KATÔ, and Mitsuhiko HIDA

Department of Industrial Chemistry, Faculty of Technology, Tokyo Metropolitan University, Setagaya-ku, Tokyo 158

(Received February 14, 1975)

The photoamination of sodium 1-amino-4-bromoanthraquinone-2-sulfonate (I) by ammonia or alkylamines in acrated 4 : 1 2-propanol–water was investigated. No effect on the reaction was observed by the addition of Rose Bengal as the addition of the triplet quenchers. The reciprocal of the quantum yield was proportional to the reciprocals of both the partial pressure of oxygen and the concentration of the amine. The peroxide was produced as the photoamination proceeded, and the simultaneous photodecomposition took place in a constant ratio to the photoamination. This reaction scheme for the photoamination of (I) was proposed: the exciplex was formed by the excited (I) (^{1}CT) and the ground-state oxygen, followed by the nucleophilic attack of the amine.

While many detailed studies have been made of the photochemical behavior of anthraquinone derivatives, especially the photoreduction by a hydrogen abstraction reaction in their excited $n\pi^*$ triplet states, few examples of the photosubstitution reaction of anthraquinones have been known.[1,2] However, recently many reports have been written on the photochlorination, the photoamination, and the photohydroxylation of anthraquinone derivatives.[3–15] Richards and his co-workers proposed an interesting reaction scheme for the photohydroxylation of 1-methoxyanthraquinone in which the reaction product was formed by the attack of a hydroxyl ion on the photochemically generated semiquinone radical anion. We also have found that the bromine atom of sodium 1-amino-4-bromoanthraquinone-2-sulfonate (I) is replaced by ammonia or alkylamines under the irradiation of visible light.[16] In a previous paper we reported that: 1) the presence of the oxygen molecule is essential for the photoamination of (I); 2) the effect of the addition of the oxidizer suggests that the dissolved oxygen does not act as a smiple oxidizing agent, but plays a more complicated role in the photoamination; 3) any reaction scheme including the photoreduction of (I) can be excluded; 4) the reaction is induced by the absorption of the light corresponding to the first absorption band of (I), and 5) the solvent effect suggests the presence of a polar intermediate in the reaction.[17] On taking account of the role of oxygen in the photoamination of (I), the following several reaction schemes are possible.

Scheme A: The oxygen molecule participates in the photoamination as a singlet oxygen.

Scheme B: The photoamination of (I) proceeds through some interaction between the excited (I) and the ground-state oxygen as follows.

a) The oxygen enhances the intersystem crossing between the lowest excited singlet and triplet states of (I). The latter state is assumed to be active in the photoamination

b) The photoamination proceeds through the exciplex between the excited (I) and the ground-state oxygen, such as:

$$AQ^* + O_2 \rightarrow [AQ^{\delta+} \cdots\cdots O_2^{\delta-}]$$

$$[AQ^{\delta+} \cdots\cdots O_2^{\delta-}] \rightarrow AQ + O_2$$

$$[AQ^{\delta+} \cdots\cdots O_2^{\delta-}] \xrightarrow{\text{Amine}} \text{Amination}$$

where AQ* denotes the excited (I).

In the present paper we will report the results obtained by photochemical studies of the photoamination of (I) and propose that the best reaction scheme is Scheme B-b), including the exciplex formation between (I) in its excited singlet state and the ground-state oxygen.

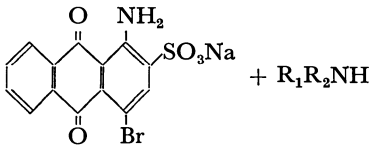

(I)

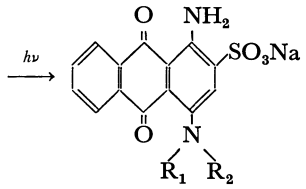

(II)

Experimental

The sodium 1-amino-4-bromoanthraquinone-2-sulfonate (I) and 2-propanol were purified as has been reported previously.[17] Shimadzu UV-200 spectrophotometer was used for the measurement of the visible and UV spectra. The quantum yield of the photoamination of (I) was determined by the use of a potassium ferrioxalate chemical actinometer according to the method recommended by Hatchard and Parker.[18] A quantitative analysis of the peroxide produced in the reaction system was carried out by the colorimetric iodide method.[19] The reaction mixture was irradiated by meas of a 500 W xenone lamp (USHIO UXL-500DXO) or a 100 W high-pressure mercury lamp (Eikosha) through the following filter system: a Toshiba interference filter KL-47 and a glass filter VY-45 were used for the monochromatic light (λ=468 nm) irradiation, soda glass for the irradiation of λ>300 nm, and a Toshiba glass filter VO-57 for the irradiation for λ>550 nm.

Results and Discussion

Effect of the Oxygen. If the singlet oxygen participates in the reaction of the photoamination of (I), a promotive effect can be expected upon the addition of Rose Bengal as a singlet oxygen sensitizer. Solutions of (I) (1.000×10^{-4} mol/l) and ammonia

Table 1. Effect of the addition of Rose Bengal on the photoamination of (I) by ammonia

[Rose Bengal] (mol/l)	Yield of the aminated product (%)[a]
0	31.0
5×10^{-6}	21.5

a) 15 min irradiation of $\lambda>300$ nm by Xe 500 W lamp.

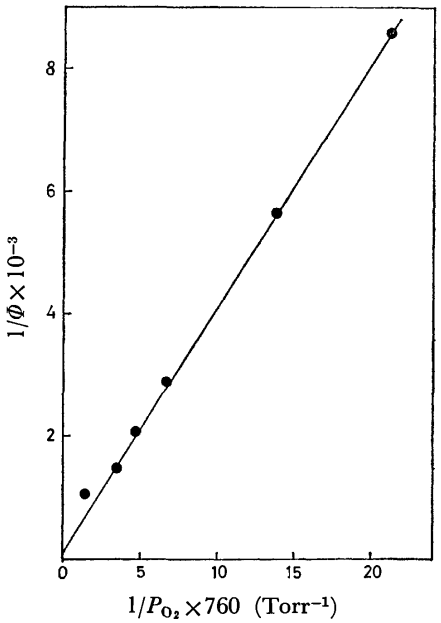

Fig. 1. Effect of the partial pressure of the oxygen on the quantum yield Φ of the photoamination of (I). [I]$\sim1.00\times10^{-4}$ mol/l, [NH_3]$\sim5.00\times10^{-2}$ mol/l in 4 : 1 2-propanol-water, irradiation of $\lambda=468$ nm.

(5.00×10^{-2} mol/l) in aerated 4 : 1 2-propanol–water with and without Rose Bengal (5.00×10^{-6} mol/l) were irradiated by the light of $\lambda>300$ nm or $\lambda>550$ nm. In the case of the irradiation of $\lambda>300$ nm, which excites both (I) and Rose Bengal, no promotive effect was observed upon the addition of Rose Bengal. The retardative results shown in Table 1 can be attributed to the inner-filter effect of Rose Bengal. Moreover, no amination was observed upon the irradiation of $\lambda>550$ nm, which excites only Rose Bengal. These results probably exclude the reaction scheme including the singlet-oxygen formation. Consequently, the other reaction scheme, including the interaction between the excited (I) and the ground-state oxygen, is probable. As is shown in Fig. 1, a plot of the reciprocal of the quantum yield of the photoamination of (I) *vs.* the reciprocal of the partial pressure of the oxygen in the reaction cell gave a good straight line. This strongly suggests that the photoamination proceeds through the collision process between the oxygen molecule and a transient intermediate such as the excited (I).

Formation of the Peroxide. The addition of acetic acid and a 20% aqueous solution of potassium iodide to the irradiated reaction mixture of (I) (1.00×10^{-4} mol/l) and ammonia (5.00×10^{-2} mol/l) in aerated 2-propanol–water increased the absorption intensity

Table 2. Peroxide formation during the photoamination

([I]$\sim1.00\times10^{-4}$ mol/l in 4 : 1 aerated 2-propanol-water)

Irradiation time[a] (min)	NH_3 (mol/l)	Yield of the aminated product (mol/l)	Peroxide in the reaction system (mol/l)
0	5.00×10^{-2}	0	0
7	5.00×10^{-2}	10.6×10^{-6}	2.34×10^{-6}
13	5.00×10^{-2}	29.5	7.8
30	5.00×10^{-2}	48.3	10.6
20	0	0	0

a) Irradiation of $\lambda>300$ nm by Xe 500 W lamp.

Table 3. Peroxide formation in the case of various amines

Amine	NH_3	CH_3NH_2	$C_2H_5NH_2$	n-$C_4H_9NH_2$
[Peroxide]$\times10^6$ (mol/l)	10.6	132	138	166
Conversion of I (%)	48.3	43.6	43.5	43.0

at 357 nm. The enhancement of the absorption intensity at 357 nm, which is characteristic of the triiodide ion, I_3^-, shows the formation of peroxide. Hence, the amount of peroxide produced in the reaction system was estimated by means of the difference in the absorption intensity at 357 nm between the irradiated and the unirradiated solutions, because the absorption intensity of the unirradiated reaction mixture is unchanged by the addition of acetic acid and a potassium iodide aqueous solution.[20] As is shown in Table 2, the peroxide was produced as the photoamination of (I) proceeded. When ammonia was absent, no photoamination could occur and the peroxide was not produced at all. These results indicate that the peroxide is formed in the course of the photoamination of (I). When alkylamines were used in place of ammonia, the peroxide was also produced in the same manner. The amounts of the peroxide produced in the reaction system in the case of various amines at nearly the same conversion of (I) are compared in Table 3. If a formation of the exciplex such as [$AQ^{\delta+}\cdots O_2^{\delta-}$] is assumed in the photoamination, it seems reasonable that the super oxide ion O_2^- and, consequently, the peroxide are produced as the reaction proceeds.

Effect of the Triplet Quencher. In order to clarify the multiplicity of the reactive excited state in the photoamination, the effect of the triplet quenchers on the reaction was studied. The solution of (I) (1.00×10^{-4} mol/l) and ammonia (5.00×10^{-2} mol/l) in aerated 4 : 1 2-propanol–water with or without a triplet quencher (*ca.* 10^{-2}—10^{-4} mol/l) such as naphthalene (E_T=60.9 kcal/mol), anthracene (E_T=42.0 kcal/mol), or naphthacene (E_T=29.3 kcal/mol), was irradiated by the monochromatic light of $\lambda=468$ nm which excites only (I). In no case was any quenching effect observed. Since it has been reported that anthraquinones have their $n\pi^*$ triplet states in *ca.* 62—3 kcal/mol and 1-aminoanthraquinone has

TABLE 4. THE VALUES OF THE RATIO OF THE INTERCEPT TO THE GRADIENT IN THE PLOT OF $1/\Phi$ *vs.* 1/[amine] ([I]$\sim 1.00\times10^{-4}$ mol/l in aerated 4 : 1 2-propanol-water, irradiation of $\lambda=468$ nm by Xe 500 W lamp)

Amine	CH_3NH_2	$C_2H_5NH_2$	$C_6H_5CH_2NH_2$	NH_3	n-$C_4H_9NH_2$	CH_2-$(CH_2)_4$-NH	$(n$-$C_4H_9)_2NH$
pK_a	10.62	10.63	9.34	9.21	10.43	11.22	11.25
Intercept / Gradient ($mol^{-1}\cdot l$)	89	72	75	68	51	43	42

its intramolecular CT triplet state between 47.1 kcal/mol and 42.1 kcal/mol[21], the above fact indicates that the excited singlet state of (I) is the active one in the photoamination. As has previously been reported, the amination is induced by the absorption of the light corresponding to the first absorption band, which inherently has an intramolecular CT nature. Thus, it may be concluded that the photoaminatuin of (I) proceeds through the lowest excited singlet CT state of (I) and that Scheme B-a), in which the lowest excited triplet state is the active one, can also be excluded.

Effect of the Concentration of the Amine. The effect of the concentration of the amine on the quantum yield of the photoamination was studied. A representative, good linear plot of the reciprocal of the concentration of ammonia against the reciprocal of the quantum yield is shown in Fig. 2. A similar relationship was also found in every alkylamine, such as methylamine, ethylamine, *n*-butylamine, benzylamine, di-*n*-butylamine, and piperidine. These results strongly suggest the presence of a collisional process between the amine and a transient intermediate in the course of the photoamination. The values of the intercept divided by the gradient in the plot of $1/\Phi$ *vs.* 1/[amine] and the value of pK_a of each amine are compared in Table 4.

Simultaneous Photodecomposition. As has been reported previously, the photoreaction of (I) with ammonia in an aerated 4 : 1 2-propanol–water mixture by the irradiation of the visible light gave only one colored product (II).[17] However, as is shown in Table 5, the conversion (%) of (I) was not equal to the yield (%) of (II) and the ratio of the yield to the conversion had an almost constant value of 0.62 during the course of the photoreaction,—that is, about 40% of the conversion of (I) was the yield of the other compound, which has no absorption band in the visible region. From the paper-chromatogram of the concentrated reaction mixture, a pale yellow, unknown compound was indeed isolated; it has no absorption band in the region of $\lambda>400$ nm. The pH measurement of the reaction system ([I]$\sim 1.00\times10^{-4}$ mol/l, [NH_3]$\sim 5.00\times10^{-2}$ mol/l in 4 : 1 2-propanol–water) indicated that the amount of OH^- did not exceed more than 1×10^{-4} mol/l. When the amine was absent, (I) and the reaction product (II) alone did not decompose at all upon the irradiation of visible light and only a slight photodecomposition occurred in the presence of OH^- (1×10^{-4} mol/l). Consequently, it may be concluded that the photoamination proceeds competitively with the photodecomposition of (I). Moreover, the fact that the ratio of the yield to the conversion has a constant value during the course of the photoamination strongly suggests that the photoamination and the simultaneous photodecomposition proceed through a common intermediate in a certain ratio. Similar phenomena

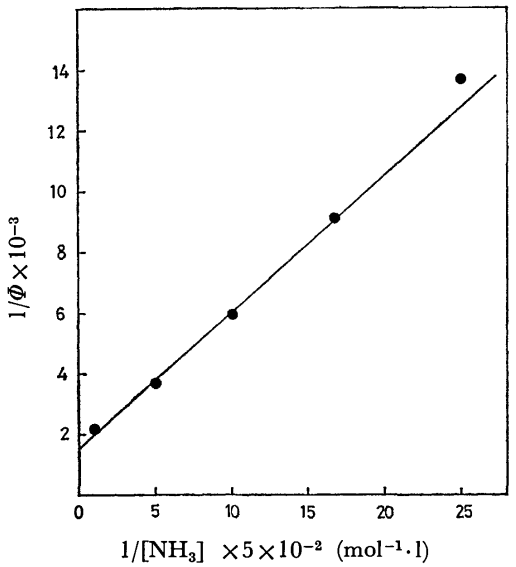

Fig. 2. Effect of the concentration of ammonia on the quantum yield Φ of the photoamination of (I). [I]$\sim 1.00\times10^{-4}$ mol/l in aerated 4 : 1 2-propanol-water, irradiation of $\lambda=468$ nm

TABLE 5. THE CONVERSION OF (I) AND THE YIELD OF (II) IN THE PHOTOAMINATION OF (I) BY AMMONIA ([I]$\sim 1.00\times10^{-4}$ mol/l, [NH_3]$\sim 5.00\times10^{-2}$ mol/l in aerated 4 : 1 2-propanol-water, irradiation of $\lambda>300$ nm by high pressure Hg lamp)

Irradiation time (h)	Conversion of I (%)	Yield of II (%)	Yield / Conversion
2	32.6	20.0	0.61
4	53.5	33.2	0.62
6	68.2	42.1	0.62
8	78.4	48.6	0.62

TABLE 6. THE RATIO OF THE YIELD OF (II) TO THE CONVERSION OF (I) IN THE PHOTOAMINATION OF (I) BY VARIOUS AMINES ([I]$\sim 1.00\times10^{-4}$ mol/l, [amine]$\sim 5.00\times10^{-2}$ mol/l in aerated 4 : 1 2-propanol-water)

Amine	NH_3	CH_3NH_2	$C_2H_5NH_2$	n-$C_4H_9NH_2$
Yield of (II) / Conversion of (I)	0.62	0.66	0.67	0.73

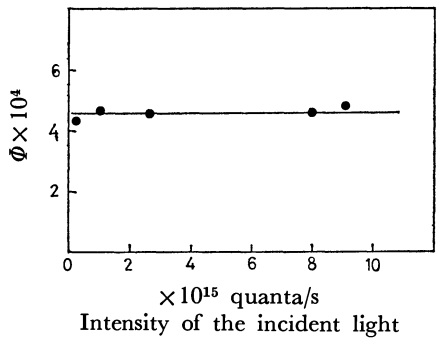

Fig. 3. Effect of the intensity of the incident light on the quantum yield Φ of the photoamination of (I). [I]~1.00×10^{-4} mol/l, [NH_3]~5.00×10^{-2} mol/l in aerated 4 : 1 2-propanol-water, irradiation of $\lambda=468$ nm.

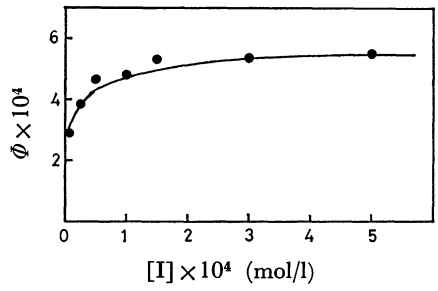

Fig. 4. Effect of the concentration of (I) on the quantum yield Φ of the photoamination of (I). [NH_3]~5.00×10^{-2} mol/l in aerated 4 : 1 2-propanol-water, irradiation of $\lambda=468$ nm.

were also observed in other amines; the various ratios of the yield to the conversion in the amines are compared in Table 6.

Effect of the Intensity of the Incident Light. As is shown in Fig. 3, the quantum yield was constant, independent of the intensity of the incident light. This clearly indicates that the photoamination of (I) requires only one photon and that any reaction scheme which requires two photon is invalid.

Effect of the Concentration of (I). Figure 4 shows that the quantum yield increased gradually with the increase in the concentration of (I). This suggests that the second molecule of (I) participates in the photoamination of (I). A linear relationship between $1/\Phi$ and $1/[I]$ was approximately obtained; the ratio of the intercept to the gradient in the plot was estimated to be about 10^5 mol$^{-1}\cdot$l. If the photoamination of (I) proceeds through the D-D scheme[22], which has been reported in the photofading of the xanthene dyes as Scheme C:

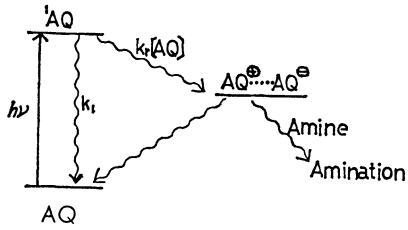

Scheme C

where k_1 denotes the deactivation rate constant of the excited (I) and k_r, the rate constant of the reaction between the excited (I) and the second (I), k_r/k_1 can be estimated as 10^5 mol$^{-1}\cdot$l. As k_r is smaller than the diffusion-controlled rate constant (10^{10} mol$^{-1}\cdot$l s^{-1}), k_1 should be smaller than 10^5 s^{-1}; that is, the excited (I) should have rather long lifetime of $\tau\gtrsim$ 0.01 ms. However, the actual lifetime of the excited (I) (^{1}CT) is much shorter than 0.01 ms; hence, the D-D scheme can also be excluded.

Reaction Mechanism of the Photoamination. The experimental results presented above exclude the reaction schemes of both A) and B-a), which was stated in the Introduction, and also Scheme C. Eventually, then, the following reaction scheme, B-b), for the mechanism of the photoamination of (I) including the CT interaction between (I) in its excited singlet state and the ground-state oxygen, comes to be the most probable one:

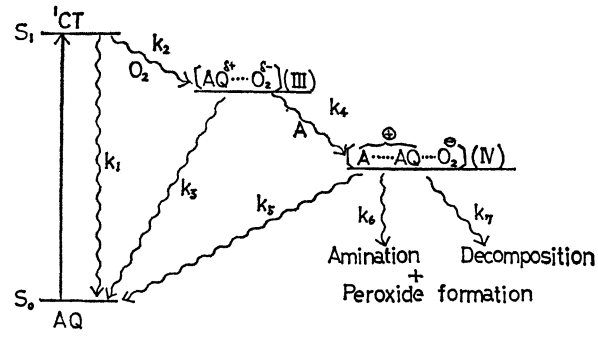

Reaction Scheme B-b)

In the above scheme, AQ and A denote (I) and the amine respectively. (I) in its lowest excited singlet CT state interacts with the ground-state oxygen to form the exciplex (III) (k_2). The exciplex (III) deactivates into (I) and the oxygen in the ground state (k_3) or is attacked by the amine to form the intermediate (IV) (k_4), in which a complete one-electron transfer from (I) to the oxygen molecule can occur. The deactivation (k_5), the amination (k_6), and the decomposition (k_7) take place from the intermediate (IV) at a constant ratio, along with the production of the superoxide ion, O_2^-, and the consequent formation of the peroxide. Hence, by applying the steady-state approximation for the respective intermediates, the quantum yield, Φ, of the photoamination of (I) is expressed as:

$$\Phi = C\cdot\left(\frac{k_2[O_2]}{k_1+k_2[O_2]}\right)\left(\frac{k_4[A]}{k_3+k_4[A]}\right)\left(\frac{k_6}{k_5+k_6+k_7}\right) \quad (1)$$

and the reciprocal of Φ is:

$$1/\Phi = 1/C\cdot\left(1+\frac{k_1}{k_2[O_2]}\right)\left(1+\frac{k_3}{k_4[A]}\right)\left(\frac{k_5+k_6+k_7}{k_6}\right) \quad (2)$$

where k_i denotes the rate constant of each process shown in the scheme and where C denotes the efficiency of the production of the aminated product (II) from the intermediate (IV). Linear relationships between $1/\Phi$ and both $1/[O_2]$ and 1/[amine] are found in Eq. (2). If Eq. (2) is rewritten as Eq. (2′), it is obvious that the efficiency of the formation of the exciplex,

$k_2[O_2]/(k_1+k_2[O_2])$, can be given by the product of the quantum yield, Φ, and the intercept (f) in the linear plot of $1/\Phi$ against $1/[O_2]$:

$$1/\Phi = f\cdot\left(1+\frac{k_1}{k_2[O_2]}\right) \quad (2')$$

When ammonia (5.00×10^{-2} mol/l) was used in aerated 4 : 1 2-propanol–water, the quantum yield of the photoamination Φ was 4.8×10^{-4} and the value of the intercept in Fig. 1 was 102. Consequently, the efficiency of the exciplex (III) formation in the aerated 4 : 1 2-propanol–water mixture should be 4.9×10^{-2}; that is, the small values of the quantum yield of the photoamination of (I) are mainly ascribable to the low efficiency of the exciplex (III) formation.

Equation (2) also shows that the ratio of the intercept to the gradient in the plot of $1/\Phi$ *vs.* 1/[amine] is equal to k_4/k_3. As k_3 is the rate constant of the deactivation process of the exciplex (III) and can reasonably be assumed to be independent of the variation in the amine, the values of k_4/k_3 compared in Table 4 are proportional to the rate constant of the reaction process between the exciplex (III) and the amine. The values of k_4/k_3 of the primary amines were roughly in the order of their basicities, but the secondary amines have smaller values of k_4/k_3 than those of the primary amines. Therefore, it seems that the order of the reactivity of each amine can be explained by the basicity and steric factors and it seems reasonable that a nucleophilic attack by the amine on the exciplex (III) takes place.

The amount of the peroxide produced in the case of the alkylamines is more than ten times larger than that in the case of ammonia (Table 3). One possible explanation for this result is as follows. In the case of ammonia used as a nucleophile, the super oxide ion, O_2^-, or the peroxide may be formed in the processes giving the amination and the decomposition products from an intermediate (IV). On the other hand, in the case of alkylamines used as a nucleophile the super oxide ion, O_2^-, or the peroxide may also be formed in the deactivation process of the intermediate (IV) by an electron transfer from the alkylamine to the oxygen, since alkylamines have much lower ionization potentials than does ammonia (NH_3: I_p=10.154 eV, CH_3NH_2 : I_p=8.97 eV, $C_2H_5NH_2$: I_p=8.86 eV, and n-$C_4H_9NH_2$: I_p=8.71 eV respectively).

The fate of the superoxide ion, O_2^-, produced in the course of the reaction is considered to be as follows: hydrogen peroxide is produced by the dismutation of $HO_2\cdot$, and the hydroperoxide is also produced as:

$$O_2^- + H^+ \rightleftharpoons HO_2\cdot \begin{cases} \nearrow\ 1/2\ H_2O_2 + 1/2\ O_2 \\ \xrightarrow[\text{Amine}]{}\ \text{Hydroperoxide} \end{cases}$$

The super oxide ion, O_2^-, may react with the amine to give the corresponding nitric oxide:[23]

$$R_1R_2NH + O_2^- \longrightarrow R_1R_2NO + OH^-.$$

Moreover, the super oxide ion, O_2^-, and $HO_2\cdot$ may participate in the decomposition process of (I) (k_7) in an oxidative manner. On the whole, the simultaneous formation of the peroxide with the photoamination can be reasonably explained, but a quantitative explanation is difficult at present.

It seems that the second molecule of (I) participates in the process after the formation of the intermediate (IV), though the role of the second molecule of (I) is not clear. The quantitative explanation of the peroxide formation and the role of the second molecule of (I) will lead to a complete elucidation of the mechanism after the formation of the intermediate (IV).

References

1) J. M. Bruce, *Quart. Rev.*, **21**, 405 (1967).
2) H. Inoue and M. Hida, *Yuki Gosei Kagaku Kyokai Shi*, **32**, 348 (1974).
3) G. O. Phillips, N. W. Worthington, J. F. Mckeller, and R. R. Sharpe, *J. Chem. Soc., A*, **1969**, 767.
4) A. V. El'tsov, O. P. Studzinskii, O. V. Kul'bitskaya, N. V. Ogal'tsova, and L. S. Efros, *Zh. Org. Khim.*, **6**, 638 (1970).
5) O. P. Studzinskii, N. I. Rtischev, and A. V. El'tsov, *ibid.*, **7**, 1272 (1971).
6) *Idem*, *ibid.*, **8**, 349, 774 (1972).
7) A. D. Broadbent and R. P. Newton, *Can. J. Chem.*, **50**, 381 (1972).
8) K. P. Clark and H. I. Stonehill, *J. Chem. Soc., Faraday II*, **1972**, 577, 1676.
9) N. I. Rtishchev, O. P. Studzinskii, and A. V. El'tsov, *Zh. Org. Khim.*, **8**, 349 (1972).
10) O. P. Studzinskii, N. I. Rtishchev, A. V. El'tsov, and A. V. Devekki, *ibid.*, **8**, 774 (1972).
11) L. A. Zvenigorodskaya, E. R. Zahks, L. S. Efros and A. V. El'tsov, *ibid.*, **8**, 1054 (1972).
12) J. Griffiths and C. Hawkins, *Chem. Commun.*, **1973**, 111.
13) G. G. Wubbels, D. M. Tollefsen, R. S. Meredith, and L. A. Herwald, *J. Amer. Chem. Soc.*, **95**, 3821 (1973).
14) A. V. El'tsov, O. P. Studzinskii and A. V. Devekki, *Zh. Org. Khim.*, **9**, 740, 847 (1973).
15) M. Ahmed, A. K. Davies, G. O. Phillips, and J. T. Richards, *J. Chem. Soc., Perkin II*, **1973**, 1386.
16) H. Inoue, T. D. Tuong, M. Hida, and T. Murata, *Chem. Commun.*, **1971**, 1347.
17) H. Inoue, T. D. Tuong, M. Hida, and T. Murata, This Bulletin, **46**, 1759 (1973).
18) C. G. Hatchard and C. A. Parker, *Proc. Roy. Soc.* (London), *A*, **235**, 518 (1956).
19) R. D. Mair and R. T. Hall, "Organic Peroxides", Vol. II, ed. by D. Swern, John Wiley & Sons, Inc., New York (1971), p. 621.
20) The absorption intensity of triiodide ion at 357 nm was calibrated by the solution of potasium iodide and the standardized aqueous hydrogen peroxide solution.
21) B. E. Hulme and his co-workers reported an efficient energy transfer from 1-aminoanthraquinone in its excited CT triplet state to anthracene in benzene. B. E. Hulme, E. J. Land, and G. O. Phillips, *J. Chem. Soc., Faraday, I*, **68**, 2003 (1972).
22) T. Ohno, S. Kato, and M. Koizumi, This Bulletin, **39**, 232 (1966).
23) R. Poupko and I. Rosenthal, *J. Phys. Chem.*, **77**, 1722 (1973).

Chemical Structure and Some Properties of Roseoflavin

Sabu KASAI, Retsu MIURA, and Kunio MATSUI

Division of Biology, Research Institute for Atomic Energy, Osaka City University, Sumiyoshi-ku, Osaka 558

(Received February 22, 1975)

Roseoflavin (I) is identified as 7-methyl-8-dimethylamino-10-(1'-D-ribityl)-isoalloxazine (IX) by comparing I with four diastereoisomers of 7-methyl-8-dimethylamino-10-D-*n*-pentitylisoalloxazine, which were synthesized from 2-dimethylamino-4-amino-toluene, D-pentoses, and violuric acid. The coincidence of chemical and physical properties—elemental analysis, UV-visible absorption spectrum, melting point, optical rotation, R_f value in thin layer chromatography, and NMR spectrum—of free and acetylated I with those of the free and acetylated IX, respectively, verified the identity. Some of the properties of I and acetylated I (pK_a, oxidation-reduction, absorption spectra, and extinction coefficients of various ionic species, and photosensitivity) are also described.

Recently many derivatives of riboflavin have been found to be consitituents of coenzymes. In most cases, 8-CH_3 of riboflavin is modified, for example, to >N-CH_2-,[1] -S-CH-,[2,3] or 8-CH_3 is substituted with an HO-group.[4] Otani *et al.*[5] isolated an antibacterial red pigment, roseoflavin (I), from a culture medium of a *Streptomyces* strain No. 768, and it was revealed that in I, 8-CH_3 of riboflavin is substituted with a $(CH_3)_2N$-group. In this report we describe the details of the determination of the chemical structure and some properties of I.

Results and Discussion

Properties of I. I forms dark reddish-brown fine needles, which are slightly soluble in water producing a grenadine red solution. The UV-visible absorption spectrum in water, shown in Fig. 1 (curve 1), is analogous to that of 8-hydroxyflavin[4] and dissimilar to that of riboflavin in water. I is not fluorescent in water in contrast with riboflavin and 8-hydroxyflavin. The results of mp, $[\alpha]_D$, and elemental analyses are shown in Table 1. The molecular weight is estimated to be 405 from the molecular ion peak in the mass spectrum. This value coincides with the molecular weight of $C_{18}H_{23}N_5O_6$.

As described in a previous communication,[6] I was oxidized with periodate forming 7-methyl-8-dimethylamino-10-formylmethylisoalloxazine $C_{15}H_{15}N_5O_3$. From this fact it is deduced that the 10-side chain should be tetrahydric pentityl chain. I was acetylated by the usual method with acetic anhydride producing tetraacetate (Ia).

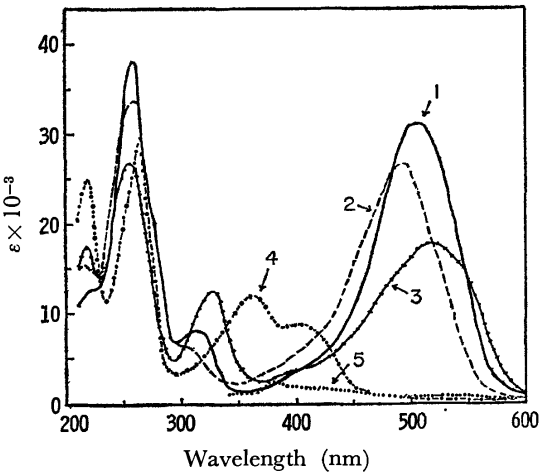

Fig. 1. UV-Visible absorption spectra of I and IX. Curve 1, I in water and IX at pH 6.99; curve 2, IX at pH 11.99; curve 3, IX at pH 0.60; curve 4, IX in 11 M HCl; curve 5, reduced IX in $Na_2S_2O_4$ solution (2.5 g/100 ml).

Properties of Ia. Ia was recrystallized from ethanol (dark reddish-brown fine needles). The results of mp, $[\alpha]_D$, and elemental analyses are shown in Table 1. The observed values coincide with those calculated for $C_{26}H_{31}N_5O_{10}$ which corresponds to a tetraacetyl compound. The molecular weight ob-

TABLE 1. MP, $[\alpha]_D$, AND ELEMENTAL ANALYSIS

Substance	mp °C	$[\alpha]_D$ in 0.1 M NaOH °	Molecular formula	Elemental analysis % Found C	H	N	Calculated C	H	N
I	274—276	−315	$C_{18}H_{23}N_5O_6 \cdot H_2O$	51.17	5.84	16.62			
IX	274—276	−320	$C_{18}H_{23}N_5O_6 \cdot H_2O$	51.83	5.88	16.44	51.06	5.95	16.54
X	282—284	+640	$C_{18}H_{23}N_5O_6 \cdot H_2O$	51.84	5.83	17.00			
XI	280—282	−470	$C_{18}H_{23}N_5O_6 \cdot 2H_2O$	48.66	6.15	15.77	48.97	6.17	15.87
XII	273—275	+295	$C_{18}H_{23}N_5O_6 \cdot 1.5H_2O$	50.08	6.08	16.15	49.99	6.07	16.20
		in $CHCl_3$							
Ia	279—280	+264	$C_{26}H_{31}N_5O_{10}$	54.12	5.51	12.09			
IXa	279—280	+260	$C_{26}H_{31}N_5O_{10}$	54.21	5.42	12.42			
Xa	258—259	−24	$C_{26}H_{31}N_5O_{10}$	53.77	5.36	12.75	54.44	5.45	12.21
XIa	250—253	+44	$C_{26}H_{31}N_5O_{10}$	54.12	5.40	12.75			
XIIa	255—256	−124	$C_{26}H_{31}N_5O_{10}$	53.68	5.68	12.33			

Table 2. The chemical shifts of assignable protons of Ia and synthesized isoalloxazine tetraacetates

Substance	Chemical shift of protons of CH_3						Aryl	
	Acetyl				7-	8αN-		
Ia	1.80	2.07	2.13	2.27	2.47	3.13	6.80	7.87
IXa	1.80	2.07	2.13	2.27	2.47	3.13	6.80	7.87
Xa	1.83	1.98	2.03	2.28	2.47	3.12	6.88	7.85
XIa	1.92	1.95	2.07	2.25	2.47	3.13	6.97	7.83
XIIa	1.77	2.05	2.05	2.23	2.48	3.12	6.80	7.85

Solvent, $CDCl_3$. The chemical shifts are expressed in ppm with tetramethylsilane as an internal standard.

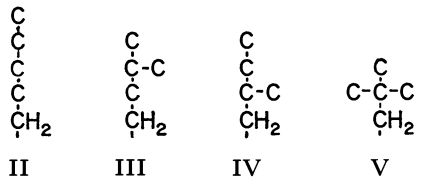

II III IV V

Scheme 1.

tained from mass spectrometry was 574, which coincide with the value calculated for the above compound. UV($CHCl_3$), λ_{max} (ε_{mM}): 260 (40.7), 500 nm (40.9).

The chemical shifts of the protons in Ia are shown in Table 2. Twelve protons were assigned to (CO–CH_3)$_4$, 3 to C–CH_3, 6 to N(CH_3)$_2$, 2 to the H linked to the aromatic nucleus, and one to acidic H. Seven unassignable protons were found in the range from 4.23 to 5.70 ppm. These results agree with the structure of 7-methyl-8-dimethylamino-10-*n*-pentityl-isoalloxazine tetraacetate. The NMR spectrum shows 4 different shifts for the protons of CO–CH_3 (the ratio of the intensity of the signals being 1 : 1 : 1 : 1). This suggests that the pentityl side chain is unbranched, because among the possible structures of the pentityl side chain (scheme 1), II satisfies three requirements: (1) optical activity, (2) the formation of a formylmethyl compound by oxidation with periodate and (3) the formation of tetraacetate having the characteristic NMR spectrum described above.

The *n*-pentityl structure is consistent with the peaks of the fragment ions in the mass spectrum of I. In addition to the peak of the molecular ion (*m/e* 405), small peaks for *m/e* of 388, 374, 344 and 314, and large peaks at 284, 271 and 270 were observed. They are assumed to be residual fragments deprived of –OH, $-CH_2OH$, $-(CHOH)_2-H$, $-(CHOH)_3-H$, $-(CHOH)_4-H$, $-CH_2-(CHOH)_4-H(+H)$ and $-CH_2-(CHOH)_4-H$, respectively.

*Synthesis of 7-methyl-8-dimethylamino-10-*n*-pentitylisoalloxazine and Its Tetraacetates.* *n*-Pentitylisoalloxazine has eight diastereoisomers. We synthesized four D-isomers and their tetraacetates for comparison with I and Ia. The process is shown in Scheme 2. VI[7] was condensed with D-ribose to VII, for which the structure was not confirmed, but is assumed to be ribopyranoside.[8] VII was reduced with H_2 in the presence of Raney nickel to VIII. As VII and VIII were too labile to be isolated in pure states, the reaction mixtures were subjected to succeeding steps as

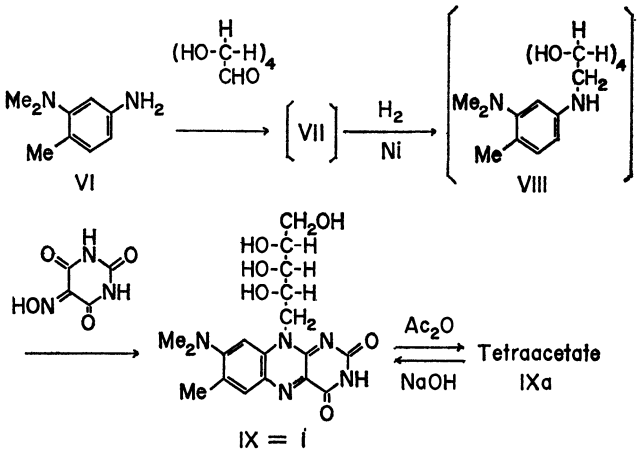

Scheme 2.

soon as possible without purification. VIII was condensed with violuric acid to isoalloxazine IX (Piloty's alloxazine synthesis[9]), which was purified through acetate, *i.e.*, IX was acetylated with acetic anhydride and pyridine producing tetraacetate (IXa), which was recrystallized from ethanol and hydrolyzed with 1 M NaOH forming IX.

Three other D-diastereoisomers and their tetraacetates, D-arabinityl- (X, Xa), D-xylityl- (XI, XIa), and D-lyxityl- (XII, XIIa), were synthesized in the same way as IX.

Comparison of I and Ia with Synthesized Isoalloxazines and Their Acetates. Of the four synthetic isoalloxazines (IX—XII) only IX coincides with I for all three properties (mp, $[\alpha]_D$, and elemental analyses) and of the four tetraacetates (IXa—XIIa) only IXa coincides with Ia (Table 1). Mixed examinations of the mp of I–IX and Ia–IXa also demonstrated the identities of I–IX and Ia–IXa.

For NMR (Table 2), the chemical shifts of protons of Ia coincide with those of IXa. For thin-layer chromatography, the R_f value of I (0.45) coincides with that of IX (0.45) and not with those of X, XI and XII (0.37, 0.24 and 0.29, respectively) (the solvent being acetone–water 9 : 1 by volume; Merck's Precoated TLC Plate Silica Gel 60F-245). UV-visible absorption spectrum of I in water was coincident with that of IX at a pH of 6.99 (neutral species, Fig. 1) and those in 6 M HCl and in 0.1 M NaOH (not shown in Fig. 1) also coincide with those of IX under the

same conditions. However, the differences in absorption spectra of the diastereoisomers of IX are so small that this does not provide definite proof of the identification of diastereoisomer.

Therefore, I was identified to be 7-methyl-8-dimethylamino-10-(1'-D-ribityl)-isoalloxazine (Scheme 2).

The identification of I as 7-methyl-8-dimethylamino-10-(1'-D-ribityl)-isoalloxazine using physicochemical methods was consistent with bacteriological data, *i.e.*, IX was antibacterially as active as I and more active than the other diastereoisomers.[10]

The mp of I recrystallized from water was 274—276 °C as described above. However, in a previous paper,[5] the authors reported that the mp of I was 276—278 °C. It was ascertained by repeated experimentation that this discrepancy was caused by the presence of water of crystallization, that is, the previous sample was dried over P_2O_5 *in vacuo* at 110 °C and the sample used in this paper was dried over $CaCl_2$ *in vacuo* at room temperature and contained one mole of water of crystallization.

Other Properties of I and IX. Some properties of I are analogous to those of riboflavin and 8-hydroxyflavin, *e.g.*, pK_a, reducibility-autoxidizability, and photosensitivity. pK_a was measured spectrophotometrically using IX. The observed values, 10.8 and 1.6, correspond to those of riboflavin, 10.2 and 1.7,[11] and of 8-hydroxyflavin, 11.5 and 0.7.[4] The absorption spectra of IX at pH 11.99, 6.99, and 0.60 (Fig. 1) show these for the anion, the neutral species, and the cation. When the solution was acidified to less than pH 0.1, the absorption spectrum changed even more (see, for example, absorption curve 4 (11 M HCl) shown in Fig. 1). Therefore, IX should have another $pK_a<0.1$, and in this range IX should be protonated doubly. The absorption properties are as follows: λ_{max} (ε_{mM}): (pH 6.99, neutral species) 225 sh (12.7), 259 (38.2), 275 sh (20.3), 314 (8.0), 505 nm (31.1); (pH 0.60, cation) 219 (17.3), 255 (26.6), 328 (12.5), 519 nm (17.8): (11 M HCl, divalent cation) 219 (24.8), 265 (29.4), 364 (12.1), 402 nm (8.8), (pH 11.99, anion) 215 (15.2), 259 (33.7), 308 (6.0), 492 nm (26.6).

I was reducible with sodium dithionite to a yellow substance, which was autoxidizable to the original form. During the reduction with dithionite, no color of the intermediate (semiquinone) was recognized in contrast with riboflavin. The visible absorption spectrum of the reduced form is shown in Fig. 1. The oxidation-reduction potential of I, E_{m7}, was estimated to be −0.466 V, while that of riboflavin to be −0.428 V (*vs.* SCE, 20 °C, by the polarographic method). These values indicate that I is more difficult to reduce than riboflavin.

I was photosensitive as is riboflavin. When an alkaline solution of I was illuminated, the solution turned yellow and fluoresced. Two of the photolytic products of I were identified as 7-methyl-8-methylamino-10-(1'-D-ribityl)-isoalloxazine (a demethylated compound) and 7-methyl-8-dimethylaminoalloxazine. The details have been published elsewhere.[12]

Some properties of I are qualitatively different from those of riboflavin, for example, the absorption spectra. The neutral species of I has only one absorption peak (505 nm) in the range from 350 to 600 nm, while riboflavin has two (375 and 445 nm). The cation of I has one peak (509 nm) similar to that of riboflavin (396 nm). However, the divalent cation of I (in 11 M HCl) has two peaks (364 and 402 nm). In fluorescence, I was different from riboflavin. The neutral species of I does not fluoresce in water and ethanol, while that of riboflavin is fluorescent. However, Ia is apparently green fluorescent in chloroform, at a λ_{max} (emission) of 534 nm (uncorrected), as is riboflavin tetraacetate. However, it is curious that I was not fluorescent while Ia was fluorescent, and moreover, that other 8-dialkylamino-isoalloxazine tetraacetates were not fluorescent in chloroform (from unpublished data). The λ_{max} for excitation of Ia was 494 nm, which does not coincide with the λ_{max} for absorption of Ia (500 nm). Therefore, it would be reasonable to assume that the Ia preparation was fluorescent because of some impurity (or impurities).

Otani[13] reported that I inhibited the growth of *Lactobacillus casei* by competing with riboflavin. I has similar and dissimilar properties to riboflavin—this could be the cause of the antibacterial activity of I.

Experimental

Materials and Methods. I from *Streptomyces* strain No. 768 was provided by Mr. Takatsu of Nissin Food Products Co., Ltd.[5] As necessary, it was recrystallized from water. 2-Dimethylamino-4-aminotoluene[7] (VI) was prepared from *N*-dimethyl-*o*-toluidine by nitration and reduction with $SnCl_2$.

Absorption spectra, extinction coefficients, and fluorescence emission spectra were measured with a Hitachi recording spectrophotometer EPS-2U, fluorescence excitation spectra with a Jasco spectrofluorometer FP-4, specific rotation with a Jasco recording spectropolarimeter J-20, proton NMR spectra with a JEOL NMR spectrometer C-60 HL (60 MHz) (by Dr. Kinoshita), mass spectra with a Hitachi mass spectrometer RM-50 (direct injection method), oxidation reduction potential with a Yanaco Polarograph P-8 (by Mr. Ichimura), and pH with a Corning digital pH meter model 109.

Roseoflavin Tetraacetate (Ia). I (85 mg) was suspended in pyridine (10 ml) and dissovled by adding acetic anhydride (2 ml). The mixture was left standing overnight at room temperature. After the addition of cold water (about 30 ml) with ice cooling, the reaction mixture was evaporated in a rotary evaporator. The product was recrystallized from ethanol five times. Yield, 60.7 mg, reddish dark brown fine needles with metallic luster. Mp, elemental analysis, $[\alpha]_D$, see Table 1; NMR, see Table 2.

Synthesis of Flavins. 7-Methyl-8-dimethylamino-10-(1'-D-ribityl)isoalloxazine (IX): D-Ribose (3.0 g) and 3.3 g of freshly distilled VI were suspended in 6 ml of absolute methanol. The suspension was refluxed to dissolve the materials, and after complete dissolution the reflux was further continued for 2 hr. Immediately after cooling, the reaction mixture was transferred into an autoclave and mixed with 8 g of freshly prepared Raney nickel. After hydrogenation at 100 °C at a pressure of 120 atm for 1 hr, the catalyst was removed by filtration. The solvent was removed in a rotary evaporator, and the residual syrup was again dissolved in

10 ml of methanol. The solution was poured into a hot solution of violuric acid (3.2 g in 50 ml of methanol). After reflux for 2 hr, the reaction mixture was chilled in a refrigerator overnight. The deposited crystals were filtered and washed with cold methanol. The filtrate, combined with washings, was evaporated and the residue was extracted with hot water. The second crop from the concentrated extract was recrystallized from water-methanol. The combined crystals (first and second crops) were further recrystallized from water. Yield, 4.4 g, 50%.

The purest material was obtained by hydrolysis of the recrystallized IXa (see following). IXa (3.0 g) was dissolved in 30 ml of 1 M NaOH, and after 10 min, the solution was neutralized with acetic acid (about 3 ml). The precipitates were filtered and washed with water. If necessary, it was recrystallized from water. Yield, 2.0 g, 90% of dark reddish-brown fine needles with metallic luster. Mp, elemental analysis, $[\alpha]_D$, see Table 1.

IX Tetraacetate (IXa): IX (2.0 g) dissolved in 20 ml of pyridine was mixed with 8 ml of acetic anhydride. After stirring at room temperature for several hours, the reaction mixture was evaporated to dyrness in a rotary evaporator. The residue was dissolved in chloroform, and washed with water. The chloroform layer was dried over anhydrous magnesium sulfate, and was then evaporated. The product was recrystallized from ethanol. Yield, 2.0 g, 74% of dark reddish-brown fine needles with metallic luster. Mp, elemetal analysis, $[\alpha]_D$, see Table 1; NMR, see Table 2.

7-Methyl-8-dimethylamino-10-(1'-D-arabinityl)-isoalloxazine(X): This compound was prepared from 3.0 g of D-arabinose, 3.3 g of VI, and 3.2 g of violuric acid (yield of crude preparation, 4.4 g, 50%), and purified through tetraacetate in the same way as IX. Yield, 2.0 g from 3.0 g of Xa, 90% of dark reddish-brown fine needles with metallic luster. Mp, elemental analysis, $[\alpha]_D$, see Table 1.

X Tetraacetate (Xa): This substance was prepared by acetylation of X in the same way as IXa. Yield, 2.0 g from 2.0 g of X, 74% of dark reddish-brown fine needles with metallic luster. Mp, elemental analysis, $[\alpha]_D$, see Table 1; NMR, see Table 2.

7-Methyl-8-dimethylamino-10-(1'-D-xylityl)-isoalloxazine (XI): This compound was prepared from 3.0 g of D-xylose, 3.3 g of VI, and 3.2 g of violuric acid (yield of crude preparation, 4.3 g, 48%), and purified through tetraacetate in the same way as IX. Yield, 2.0 g from 3.0 g of XIa, 87% of dark reddish-brown fine needles with metallic luster. Mp, elemental analysis, $[\alpha]_D$, see Table 1.

XI Tetraacetate (XIa): This compound was prepared by acetylation of XI in the same way as IXa. Yield, 1.9 g from 2.0 g of XI, 75% of dark reddish-brown fine needles with metallic luster. Mp, elemental analysis, $[\alpha]_D$, see Table 1: NMR, see Table 2.

7-Methyl-8-dimethylamino-10-(1'-D-lyxityl)-isoalloxazine (XII): This compound was prepared from 3.0 g of D-lyxose, 3.3 g of VI, and 3.2 g of violuric acid (yield of crude preparation, 4.6 g, 53%), and purified through tetraacetate in the same way as IX. Yield, 2.0 g from 3.0 g of XIIa, 88% of dark reddish-brown fine needles with metallic luster. Mp, elemental analysis, $[\alpha]_D$, see Table 1.

XII Tetraacetate (XIIa): This compound was prepared by acetylation of XII in the same way as IXa. Yield, 1.9 g from 2.0 g of XII, 75% of dark reddish-brown fine needles with metallic luster. Mp, elemental analysis, $[\alpha]_D$, see Table 1; NMR, see Table 2.

The authors thank Prof. S. Otani of Koshien University for encouragement, Mr. M. Takatsu of Nissin Food Products Co., Ltd. for the I, and Dr. Kinoshita and Mr. Ichimura of Osaka City University for the NMR spectra and polarographic measurements, respectively.

References

1) W. H. Walker, T. P. Singer, S. Ghisla, and P. Hemmerich, *Eur. J. Biochem.*, **26**, 279 (1972).
2) W. H. Walker, E. B. Kearney, R. Seng, and T. P. Singer, *Biochem. Biophys. Res. Commun.*, **44**, 287 (1971).
3) W. C. Kenney, P. Edmondson, R. Seng, and T. P. Singer, *Biochem. Biophys. Res. Commun.*, **52**, 434 (1973).
4) S. Ghisla and S. Mayhew, *J. Biol. Chem.*, **248**, 6568 (1973).
5) S. Otani, M. Takatsu, M. Nakano, S. Kasai, R. Miura, and K. Matsui, *J. Antibiotics*, **27**, 88 (1974).
6) R. Miura, K. Matsui, K. Hirotsu, A. Shimada, H. Takatsu, and S. Otani, *Chem. Commun.*, **1973**, 703.
7) F. Ullmann, M. Rozenband, B. Mühlhauser, and E. Grether, *Ber.*, **35**, 326 (1902).
8) G. P. Ellis and J. Honeyman, "Advances in Carbohydrate Chemistry," Vol. 10, ed. by M. L. Wolfrom and R. S. Tipson, Academic Press, New York, N. Y. (1955), p. 95.
9) O. Piloty, *Liebig's Ann. Chem.*, **333**, 22 (1904).
10) Personal communication from Mr. Takatsu. The details of the work will be reported in future by Takatsu.
11) R. Kuhn and G. Moruzzi, *Ber.*, **67**, 888 (1934).
12) K. Matsui and S. Kasai, "Flavins and Flavoproteins, Proceedings of the Fifth International Symposium on Flavins and Flavoproteins," ed. by T. P. Singer, in press.
13) S. Otani, "Flavins and Flavoproteins, Proceedings of the Fifth International Symposium on Flavins and Flavoproteins," ed. by T. P. Singer, in press.

The Role of Nucleophilic Solvents in the Acid-Catalyzed Cyclization of a Cross-Conjugated Cycloalkadienone

Ryoji NOYORI, Yasushi OHNISHI, and Masao KATÔ
Department of Chemistry, Nagoya University, Chikusa, Nagoya 464
(Received February 25, 1975)

In acetic acid or methanol containing a trace amount of H_2SO_4, 2,8-cyclononadienone cyclizes readily to give bicyclic ketones; the mechanism including the role of the nucleophilic media is discussed.

The acid-catalyzed cyclization of cross-conjugated dienones to produce cyclopentenones is known as the Nazarov cyclization.[1] Woodward and coworkers analyzed the reaction with *di*-1-cyclohexenyl ketone and concluded the transformation as occurring through conrotatory ring closure of the protonated dienone–hydroxypentadienyl cation resonance hybrid (Scheme 1).[2] As might be expected, common and medium-sized cycloalkadienones in an oxygen-protonated form are thermally stable, because the symmetry-allowed electrocyclization is sterically prohibited by the presence of a methylene chain which links the β and β' carbons. This paper describes an example where a combination of an acid and certain nucleophiles can facilitate the so far restricted cyclization of a medium-sized cyclic dienone.

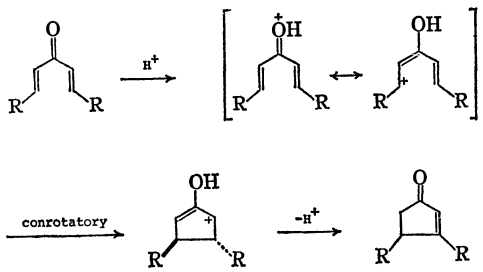

Scheme I.

2,8-Cyclononadienone (**1**) in 97% H_2SO_4 or FSO_3H exists in a protonated form as indicated by spectral data (NMR and UV)[3,4] and remains unchanged for an extended period below room temperature. The dienone is also inert in acetic acid below 30 °C. Remarkably, however, when a drop of H_2SO_4 was added to an acetic acid solution of **1**, spontaneous reaction took place at room temperature yielding the bicyclic enone **2** (25%) and the epimeric acetoxy ketones **3** and **4** (40% combined yield).

No reactions were observed when **1** was allowed to stand in methanol solution at room temperature. Again, rapid reaction was caused by the addition of a drop of H_2SO_4, and there was obtained a mixture of **2** (6%), the bicyclic methoxy ketones **5** and **6** (72%), and the monocyclic methoxy ketone **7** (7%). These products **2**—**7** were stable under the present reaction and workup conditions.

The reaction in methanol-*O*-*d* as solvent gave the deuterium-incorporated bicyclic products **8**—**10**. The mass spectral analysis showed that these consisted mainly (69—85%) of d_1 material and contained some d_0 and d_2 products. The NMR spectra indicated that the deuterium atoms are located specifically at position α to carbonyl group but randomly with respect to stereochemistry, the *exo* to *endo* ratio being approximately 1 : 1. Control experiments showed that **2** suffers protium-deuterium exchange to some extent under the present reaction conditions.

The observed reactions forming the bicyclic ketones are characteristic of the nine-membered dienone **1**. With seven-, eight-, and twelve-membered cross-conjugated dienones, only mixtures of monocyclic solvent-incorporated products were obtained.

Apparently the presence of both acidic and nucleophilic species is a necessary condition for promotion of the β,β' bond-forming reaction of **1**. Although

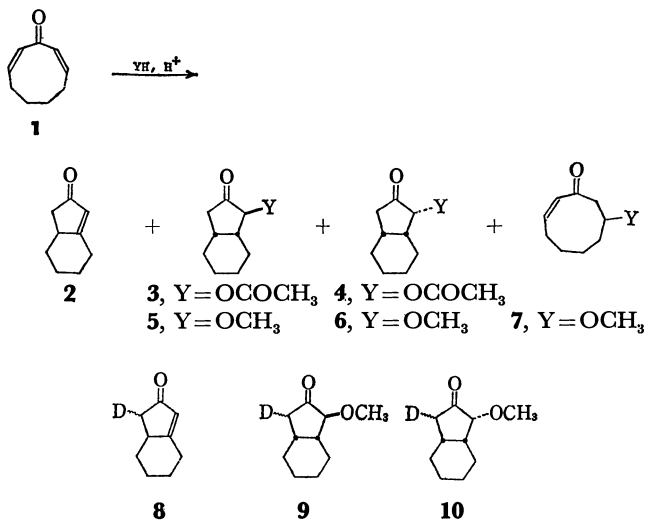

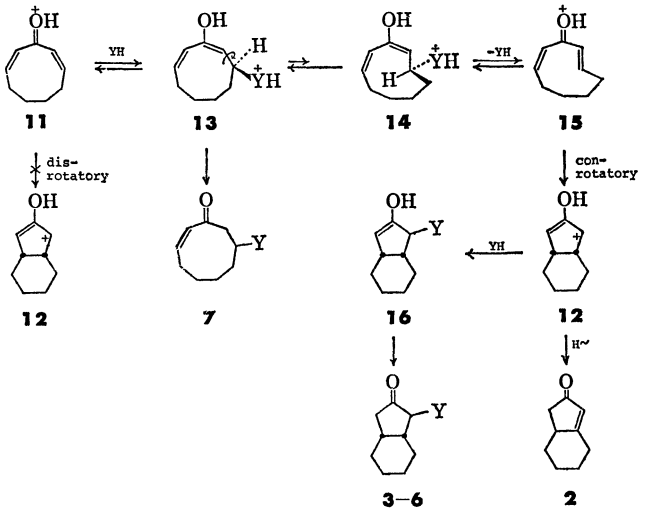

YH=CH_3COOH or CH_3OH

Scheme II.

there may be a variety of possible mechanisms conceivable, the most likely seems to be a pathway which involves solvent-assisted *cis-trans* isomerization of **1** in a key step as outlined in Scheme II. The protonated *cis, cis* dienone **11** cannot undergo unimolecular electrocyclizations; the disrotatory ring closure to the bicyclic hydroxyallyl cation **12** is symmetry-forbidden, while the alternative conrotatory cyclization to the *trans*-fused bicyclic system is unlikely due to the high strain energy involved in the transition state as indicated by molecular models. Reaction of **11** with the nucleophilic solvent YH at the electron-deficient β carbon produces the dienol adduct **13**.[5] Reketonization gives the monocyclic adduct **7**. If the conformational change, **13**→**14**, followed by elimination of YH occurs prior to ketonization, then the key intermediate, protonated *cis, trans* dienone **15**,[6] is formed, which in turn undergoes conrotatory ring closure to give **12**. Its proton reorganization affords the bicyclic enone **2**, while nucleophilic trapping with YH and subsequent ketonization produces the epimeric bicyclic solvent adducts **3**—**6**. Patterns of the deuterium incorporation observed for the reaction in methanol-*O-d* solvent are also consistent with the mechanism of Scheme II. The conformational change of type **13**→**14**, an essential process for the formation of the reactive *cis, trans* dienone, would be feasible only with the nine-membered dienone **1**; with the lower homologs, the form corresponding to **14** could hardly be accomodated in the conformational equilibrium. With twelve-membered dienones, the *cis-trans* isomerism in the protonated form also seems possible. Neither *cis, cis* nor *cis,trans* isomer, however, is strained enough to undergo the unimolecular electrocyclization to give bicyclic hydroxypentadienyl cations.

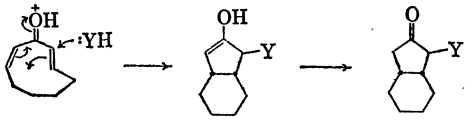

15 **16** **3—6**

Scheme III.

Photochemically generated *cis, trans*-2,8-cyclononadienone is known to undergo the cyclization in protic solvents with or without added Brönsted acids.[7] Under the present reaction conditions, **3**—**6** may also be derived *via* bimolecular reaction of **15** and YH as illustrated in Scheme III. An alternative mechanism involving direct, bimolecular reaction between the *cis,cis* dienone **11** and YH is unlikely to be operating, since it could not explain the profound ring-size effect on the reaction course.

Experimental

General. NMR spectra were taken in CCl_4 solution using a JEOLCO Model C-60 H instrument. IR spectra were obtained on a JASCO Model DS-402 G spectrometer. A Hitachi Model RMU-6C mass-spectrometer was used for mass spectral analysis. Gas-liquid partition chromatography (glpc) was done with a Yanagimoto Model G-8 chromatograph equipped with a 2-m column of 5% poly(ethylene glycol succinate) on Celite 545. Product ratio was determined using C_{12}—C_{16} hydrocarbons as internal standard. Thin-layer chromatography (tlc) was carried out on silica gel (E. Merck GF_{254} silica gel). 2,8-Cyclononadienone (**1**) was prepared by the method of Garbisch.[8]

Reaction of 2,8-Cyclononadienone (1) in Nucleophilic Solvents Containing H_2SO_4. A solution of **1** (492 mg, 3.64 mmol) in acetic acid (5 ml) containing one drop of 96% H_2SO_4 was stirred at room temperature for 20 min. The mixture was diluted with water, neutralized with sodium bicarbonate, and extracted with ether. The ethereal solution was washed with water, dried over $MgSO_4$, and concentrated *in vacuo* to give a crude oil (514 mg). Glpc analysis (150 °C) of the oil indicated the formation of bicyclo[4.3.0]non-6-en-8-one (**2**) (25% yield), *exo*-7-acetoxy-*cis*-bicyclo[4.3.0]nonan-8-one (**3**) and *endo*-7-acetoxy-*cis*-bicyclo[4.3.0]nonan-8-one (**4**) (5 : 2 ratio, 40% combined yield). Each compound was separated by preparative tlc (1 : 1 *n*-hexane-ether) and identified by comparison of the NMR and IR data with those of an authentic sample.[4,7]

Similarly, when a 10% methanol solution of **1** containing a trace amount of H_2SO_4 was allowed to stand for 20 min at room temperature, a mixture of the enone **2** and the methanol adducts was obtained. Glpc analysis (140 °C) of the crude product showed the formation of **2** (6%), *exo*-7-methoxy-*cis*-bicyclo[4.3.0]nonan-8-one (**5**) and *endo*-7-methoxy-*cis*-bicyclo[4.3.0]nonan-8-one (**6**) (5 : 2 ratio, 72%), and 8-methoxy-2-cyclononenone (**7**) (7%).[7] The identity of these compounds was established by comparison with authentic specimens.

Reaction of 1 in Methanol-O-d *Containing D_2SO_4.* The dienone **1** (129 mg, 0.96 mmol) was dissolved in methanol-*O-d* (1 ml, E. Merck, deuterium content >99%) containing a trace amount of 97% D_2SO_4 (E. Merck, deuterium content >99%). The resulting solution was stirred at room temperature for 20 min, diluted with dichloromethane (10 ml), and washed with water three times. The organic layer was dired by being passed through a short Na_2SO_4-silica gel column and concentrated *in vacuo* to leave a crude oil (156 mg), which contained the solvent adducts as the major components. In order to minimize loss of deuterium atom from the products, the reaction mixture was worked up as quick as possible. About 10 min were required for this work-up procedure. Preparative tlc with a 1 : 1 *n*-hexane-ether mixture (2 developments) afforded bicyclo-[4.3.0]non-6-en-8-one-9-*d* (**8**) (13 mg), *exo*-7-methoxy-*cis*-bicyclo[4.3.0]nonan-8-one-9-*d* (**9**) (73 mg), and *endo*-7-methoxy-*cis*-bicyclo[4.3.0]nonan-8-one-9-*d* (**10**) (56 mg). The deuterated derivative of **7** could not be isolated in a pure state. The structures were deduced from thier NMR spectra. The spectra taken in CCl_4 solution with the added $Eu(fod)_3$ shift reagent indicated that deuterium atom in these products was incorporated at the carbonyl α position, where the *exo* to *endo* ratio was approximately 1.0. The molecular ion peaks in the mass spectra appeared at *m/e* 137 for **8** and 169 for **9** and **10**. Comparison of the intensities with those of the neighboring peaks showed the extent of deuterium incorporation: **8** 15% d_0, 69% d_1, and 16% d_2; **9** 17% d_0, 82% d_1, and 1% d_2; **10** 13% d_0, 85% d_1, and 2% d_2. The enone **2** recovered after treatment with methanol-*O-d* containing D_2SO_4 at room temperature for 20 min contained deuterium atoms; 29% d_0, 54% d_1, and 17% d_2.

References

1) a) I. N. Nazarov, I. I. Zaretskaya, and T. I. Sorkina, *Zh. Obsh. Khim.*, **30**, 746 (1906); *Chem. Abstr.*, **55**, 524 h (1961); b) E. A. Braude and J. A. Coles, *J. Chem. Soc.*, **1952**,

1430; c) C. W. Shoppee and B. J. A. Cooke, *J. Chem. Soc., Perkin I*, **1972**, 2271; d) C. W. Shoppee and B. J. A. Cooke, *ibid.*, **1973**, 1026, 2197; e) S. Hirano, T. Hiyama, and H. Nozaki, *Tetrahedron Lett.*, **1974**, 1429.

2) a) R. B. Woodward and R. Hoffmann, *Angew. Chem.*, **81**, 797 (1969); b) D. Kurland, Ph. D. Thesis, Harvard University, Cambridge, Mass. (1967); c) R. Lehr, Ph. D. Thesis, Harvard University, Cambridge, Mass. (1968).

3) R. Noyori, Y. Ohnishi, and M. Katô, *J. Amer. Chem. Soc.*, **94**, 5105 (1972).

4) R. Noyori, Y. Ohnishi, and M. Katô, *J. Amer. Chem. Soc.*, **97**, 928 (1975).

5) For stable dienols in solution, see a) R. Noyori, H. Inoue, and M. Katô, *J. Amer. Chem. Soc.*, **92**, 6699 (1970); b) H. M. R. Hoffmann and E. A. Schmidt, *ibid.*, **94**, 1373 (1972).

6) For related *cis-trans* isomerizations of double bonds, see a) E. L. Eliel, "Stereochemistry of Carbon Compounds," McGraw-Hill, New York, N. Y. (1962), pp 341—346; b) K. Mackenzie, "The Chemistry of Alkenes," Vol. 2, ed. by J. Zabicky, Interscience, New York, N. Y. (1970), Chapter 3.

7) R. Noyori, Y. Ohnishi, and M. Katô, *Tetrahedron Lett.*, **1971**, 1515.

8) E. Garbisch, Jr., *J. Org. Chem.*, **30**, 2109 (1965).

New Syntheses of Fervenulin (1,3-Dimethyl-7-azalumazine) and Analogs

Fumio YONEDA and Tomohisa NAGAMATSU

Faculty of Pharmaceutical Sciences, Kumamoto University, Oe-honmachi, Kumamoto 862

(Received March 3, 1975)

A new, convenient method for the synthesis of fervenulin and its derivatives on the basis of the condensation of 6-amino-5-nitrosouracils and aldehyde hydrazones is described. A transformation of toxoflavins into fervenulins *via* 1-demethyltoxoflavins is also described. The alkylation of 1-demethyltoxoflavin with several alcohols in the presence of diethyl azodicarboxylate and triphenylphosphine gave the corresponding fervenulin homologs.

Fervenulin, an antibiotic having pyrimido[5,4-*e*]-*as*-triazine ring system, was first synthesized in 1958 by Pfleiderer and Schündehütte.[1] Since then there has been considerable interest in the synthesis and the reaction of pyrimido[5,4-*e*]-*as*-triazine derivatives.[2] This paper will describe a new, convenient method for the synthesis of fervenulin and its derivatives on the basis of the condensation of 6-amino-5-nitrosouracils and aldehyde hydrazones; additionally, we wish to describe a transformation of toxoflavins into fervenulins *via* 1-demethyltoxoflavins and the synthesis of homologs of fervenulin by the alkylation of 1-demethyltoxoflavin.[3]

Reaction of 6-Amino-5-nitrosouracils with Aldehyde Hydrazones

Stirring a suspension of 6-amino-1,3-dimethyl-5-nitrosouracil (**1**) in aprotic solvents, such as dimethylformamide or dimethyl sulfoxide, with an equimolar amount of 37% aqueous formaldehyde and hydrazine hydrate under cooling, followed by a mild refluxing of the mixture, resulted in the formation of fervenulin (**2a**) in about a 40% yield. The product was found by IR and elemental analysis to be identical with an authentic sample prepared by an alternative route.[1] Similarly, the heating of **1** with other aldehydes and hydrazine hydrate in dimethylformamide or dimethyl sulfoxide gave the corresponding 3-substituted fervenulins (6- substituted 1,3-dimethyl-7-azalumazines) (see Table 1).

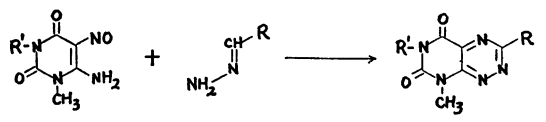

1 R′=CH$_3$ **2a-p** R′=CH$_3$
3 R′=H **4a,b** R′=H

Scheme 1.

The reaction essentially involves **1** and the aldehyde hydrazones, since aldehydes and hydrazine hydrate react immediately to give the hydrazones. In fact, the yields of the 3-substituted fervenulins increased when **1** was allowed to react with the aldehyde hydrazones.

6-Amino-1-methyl-5-nitrosouracil (**3**) also gave the corresponding 7-azalumazine derivatives by the condensation with aldehyde hydrazones. For instance, the heating of **3** with formaldehyde and benzaldehyde hydrazones in dimethylformamide gave 1-methyl-7-azalumazine (**4a**) and 1-methyl-6-phenyl-7-azalumazine (**4b**) respectively. These 7-azalumazines gave the corresponding fervenulins (**2a**, **b**) by treatment with methyl iodide in dimethylformamide in the presence of potassium carbonate.

It is interesting to note that the heating of 6-amino-5-nitrosouracils with aryl aldehyde 1,1-dimethylhydrazones (instead of aryl aldehyde hydrazones) in dimethylformamide gave 8-arylxanthines. This purine synthesis can be explained as is depicted in Scheme 2.[4]

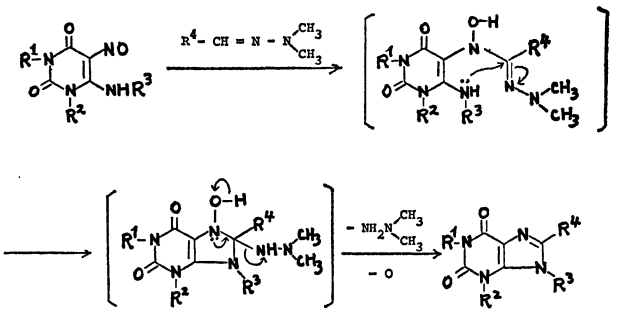

Scheme 2.

From the above facts, the reaction of the new fervenulin synthesis seems to proceed by the initial nucleophilic attack of the electron-rich-α-carbon of the hydrazones on the nitroso group of the uracils to form hydroxylamine intermediates, which are then converted into fervenulins by the elimination of the ammonia and water.

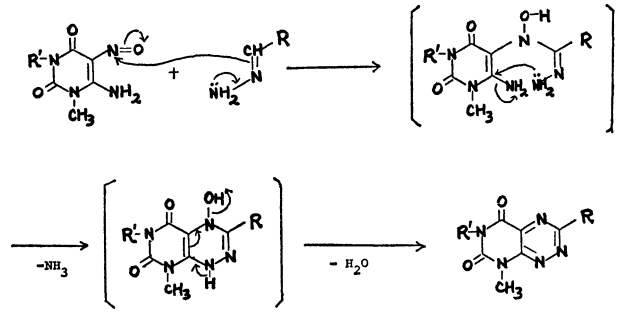

Scheme 3.

Another explanation of the mechanism would be initial transamination of the 6-amino-5-nitrosouracils by the aryl aldehyde hydrazones. It is possible that the previously formed 6-benzylidenehydrazino-5-nitrosouracils undergo intramolecular cyclization to give fervenulins. However, this mechanism seems unlikely, because the transamination of 6-amino-5-nitrosouracils with amines usually requires more drastic conditions

TABLE 1. SYNTHESIS OF FERVENULINS BY THE REACTION OF 6-AMINO-1,3-DIMETHYL-5-NITROSOURACIL (1) WITH ALDEHYDES AND HYDRAZINE HYDRATE

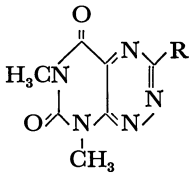

Aldehyde	3-Substituent (R) in product	Mp (°C)	Yield (%)	Formula	Analysis (%) Calcd (Found) C	H	N
Formaldehyde	Hydrogen (**2a**)[1]	175	40	$C_7H_7N_5O_2$	43.52 (43.23)	3.65 (3.60)	36.26 (35.98)
Benzaldehyde	Phenyl (**2b**)[2]	270	53	$C_{13}H_{11}N_5O_2$	57.98 (57.77)	4.12 (4.06)	26.01 (26.21)
4-Chlorobenzaldehyde	4-Chlorophenyl (**2c**)	280	62	$C_{13}H_{10}N_5O_2Cl$	51.41 (51.27)	3.32 (3.32)	23.06 (23.14)
3,4-Dichlorobenzaldehyde	3,4-Dichlorophenyl (**2d**)	249	67	$C_{13}H_9N_5O_2Cl_2$	46.17 (45.88)	2.68 (2.53)	20.71 (20.45)
4-Bromobenzaldehyde	4-Bromophenyl (**2e**)	303	48	$C_{13}H_{10}N_5O_2Br$	44.84 (44.78)	2.90 (2.93)	20.12 (20.02)
4-Nitrobenzaldehyde	4-Nitrophenyl (**2f**)[2]	323	62	$C_{13}H_{10}N_6O_4$	49.68 (49.44)	3.21 (3.20)	26.74 (26.38)
Salicylaldehyde	2-Hydroxyphenyl (**2g**)	282	85	$C_{13}H_{11}N_5O_3$	54.73 (54.87)	3.89 (3.69)	24.55 (24.53)
Anisaldehyde	4-Methoxyphenyl (**2h**)	268	78	$C_{14}H_{13}N_5O_3$	56.18 (56.22)	4.38 (4.37)	23.40 (23.33)
Veratraldehyde	3,4-Dimethoxyphenyl (**2i**)	305	58	$C_{15}H_{15}N_5O_4$	54.71 (54.39	4.59 (4.44)	21.27 (21.36)
Piperonal	3,4-Methylenedioxyphenyl (**2j**)	274	72	$C_{14}H_{11}N_5O_4$	53.67 (53.70)	3.54 (3.61)	22.36 (22.29)
4-Dimethylaminobenzaldehyde	4-Dimethylaminophenyl (**2k**)	>330	73	$C_{15}H_{16}N_6O_2$	57.68 (57.44)	5.16 (5.08)	26.91 (26.73)
Cinnamaldehyde	Styryl (**2l**)	263	45	$C_{15}H_{13}N_5O_2$	61.01 (60.89)	4.44 (4.42)	23.72 (23.82)
Picolinaldehyde	2-Pyridyl (**2m**)[2]	285	45	$C_{12}H_{10}N_6O_2$	53.33 (53.31)	3.73 (3.67)	31.10 (31.06)
Nicotinaldehyde	3-Pyridyl (**2n**)[2]	213	57	$C_{12}H_{10}N_6O_2$	53.33 (53.24)	3.73 (3.73)	31.10 (29.83)
Isonicotinaldehyde	4-Pyridyl (**2o**)[2]	262	47	$C_{12}H_{10}N_6O_2$	53.33 (53.38)	3.73 (3.77)	31.10 (31.46)
Thiophene-2-aldehyde	2-Thienyl (**2p**)	272	25	$C_{11}H_9N_5O_2S$	47.99 (47.83)	3.30 (3.32)	25.44 (25.27)

(*e.g.* fusion at a higher temperature in the presence of an acid catalyst).[5]

The Transformation of Toxoflavins into Fervenulins

Toxoflavin,[6,7] another antibiotic with pyrimido-[5,4-*e*]-*as*-triazine ring system, is isomeric with fervenulin. We are the first to have succeeded in the transformation of toxoflavin and its derivatives into fervenulin and its derivatives respectively. Heating toxoflavin (**5a**) under reflux with methyl iodide in dimethylformamide containing anhydrous potassium carbonate for 2 hr gave fervenulin (**2a**) in a moderate yield in a single step. Similarly, heating other toxoflavin derivatives with methyl iodide in dimethylformamide in the presence of potassium carbonate led to the formation of the corresponding 3-substituted fervenulins (Table 2).

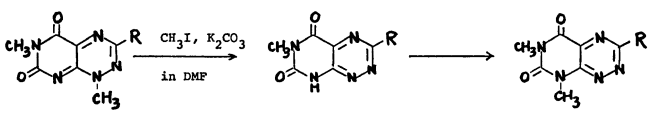

5a-c, i, n **6** **2a-c, i, n**

Scheme 4.

The reaction essentially involves the demethylation of the toxoflavins (**5**) to 1-demethyltoxoflavins (**6**), and the subsequent methylation of **6** with methyl iodide. Both heating **5** with excess methyl iodide in dimethylformamide in the absence of potassium carbonate, and heating **5** alone in dimethylformamide in

TABLE 2. CONVERSION OF TOXOFLAVINS INTO FERVENULINS

3-Substituent (R) of starting materials (Toxoflavins)	3-Substituent (R) of products (Fervenulins)	Yield (%)
Hydrogen (**5a**)	Hydrogen (**2a**)	35
Phenyl (**5b**)	Phenyl (**2b**)	52
4-Chlorophenyl (**5c**)	4-Chlorophenyl (**2c**)	61
3,4-Dimethoxyphenyl (**5i**)	3,4-Dimethoxyphenyl (**2i**)	57
3-Pyridyl (**5n**)	3-Pyridyl (**2n**)	66

the presence of potassium carbonate yielded only the corresponding **6** in almost quantitative yields.[8]

The Alkylation of 1-Dimethyltoxoflavins

Mistunobu *et al.*[9] have reported a convenient alkylation of phthalimide with alcohols in the presence of equimolar amounts diethyl azodicarboxylate (DAD) and triphenylphosphine. We have extended this reaction to the alkylation of **6**,[8] which was easily prepared by the demethylation of **5** with dimethylformamide.

Refluxing a mixture of 3-phenyl-1-demethyltoxoflavin (**6b**) and an alcohol in dioxane in the presence of DAD and triphenylphosphine gave the corresponding 1-alkyl-3-methyl-6-phenyl-7-azalumazines (Table 3). Some of these compounds were identified with the authentic samples prepared by the alkylation of **6b** with the corresponding alkyl halides. When **6b** and ethylene glycol were used in this reaction, 1-(2-hydroxyethyl)-3-methyl-6-phenyl-7-azalumazine (**7e**) was obtained.

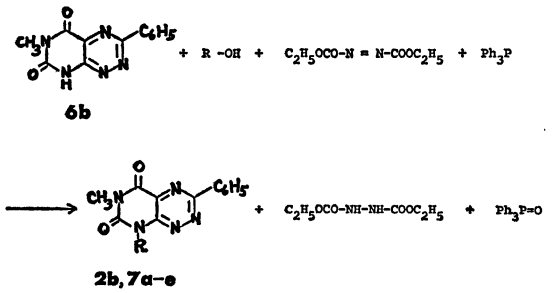

Scheme 5.

Experimental

The melting points were determined on a Yanagimoto Micro-melting Point apparatus and are uncorrected. The infrared spectra were determined on a Japan Spectroscopic Co., Ltd., spectrophotometer, Model IR-I A, from samples mulled in Nujol.

*Fervenulin (1,3-Dimethyl-7-azalumazine) (**2a**).* To a cooled suspension of 6-amino-1,3-dimethyl-5-nitrosouracil (**1**) (1.8 g, 0.01 mol) in DMF (50 ml), we added 37% formaldehyde (0.8 g, 0.01 mol) and 100% hydrazine hydrate (0.5 g, 0.01 mol). The mixture was stirred for about 10 min under cooling with ice water and then refluxed for 3 hr. After the solvent had been evaporated to dryness, the residue was extracted with chloroform. The chloroform extracts were evaporated, and the resulting residue was treated with 50% aqueous MeOH to cause the separation of 0.76 g (40%) of **2a** which was identical in all respects with an authentic sample.[1]

*3-Substituted Fervenulins (**2b-p**); General Procedure*: A mixture of **1** (0.01 mol), an aryl aldehyde (0.01 mol), and 100% hydrazine hydrate (0.01 mol) in DMF (50 ml) was refluxed for 3—5 hr. The reaction mixture was then evaporated to dryness, and the residue was diluted with EtOH in order to precipitate a crude product, which was recrystallized from EtOH to give the 3-arylfervenulin as yellow needles.

Sometimes a small amount of a by-product, the corresponding 8-aryltheophylline, was isolated from the mother liquor.

*7-Methyl-7-azalumazine (**4a**).* To a suspension of 6-amino-1-methyl-5-nitrosouracil (**3**) (2 g, 0.012 mol) in DMF (50 ml), we added 37% formaldehyde (0.96 g, 0.012 mol) and 100% hydrazine hydrate (0.6 g, 0.012 mol) under cooling in ice water with continuous stirring, after which the mixture was refluxed for 4 hr. The reaction mixture was then concentrated *in vacuo*, and the residue was diluted with EtOH to precipitate crystals, which were subsequently recrystallized from EtOH to give 1.25 g (58%) of pale brown crystals; mp>260 °C (decomp.). MS *m/e* 179 (M^+). Found: C, 40.20; H, 2.77; N, 38.87%. Calcd for $C_6H_5N_5O_2$: C, 40.23; H, 2.81; N, 39.10%.

*7-Methyl-6-phenyl-7-azalumazine (**4b**).* A mixture of **3** (2 g, 0.012 mol), benzaldehyde (1.25 g, 0.012 mol), and 100% hydrazine hydrate (0.6 g, 0.012 mol) in DMF (50 ml) was refluxed for 5 hr. After the DMF had been evaporated, the residue was treated with EtOH to precipitate crude **4b**, which was collected by filtration and recrystallized from

TABLE 3. PREPARATION OF 1-ALKYL-3-METHYL-6-PHENYL-7-AZALLMAZINES

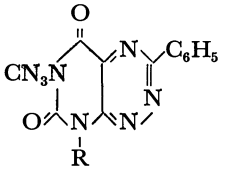

1-Alkyl (R)	Mp (°C)	Yield (%)	Appearance	Formula	Analysis (%) Calcd (Found) C	H	N
Methyl (**2b**)	270	51	yellow needles	$C_{13}H_{11}N_5O_2$	—	—	—
Ethyl (**7a**)	228	60	yellow prisms	$C_{14}H_{13}N_5O_2$	59.35(59.31)	4.63(4.70)	24.72(24.50)
n-Propyl (**7b**)	214	67	yellow needles	$C_{15}H_{15}N_5O_2$	60.59(60.57)	5.09(5.01)	23.56(23.60)
i-Propyl (**7c**)	226	76	yellow needles	$C_{15}H_{15}N_5O_2$	60.59(60.48)	5.09(5.08)	23.56(23.54)
Allyl (**7d**)	213	78	yellow needles	$C_{15}H_{13}N_5O_2$	61.01(61.09)	4.44(4.48)	23.72(23.79)
2-Hydroxyethyl (**7e**)	215	95	yellow prisms	$C_{14}H_{13}N_5O_3$	56.18(56.37)	4.38(4.36)	23.40(23.50)

DMF+EtOH to give 1.45 g (47%) of yellow crystals; mp> 280 °C (decomp.). MS *m/e* 255 (M^+). Found: C, 56.38; H, 3.67; N, 27.23%. Calcd for $C_{12}H_9N_5O_2$: C, 56.47; H, 3.55; N, 27.44%.

In the mother liquor, a trace of 3-methyl-8-phenylxanthine[10] was detected.

*Methylation of **4b** with Methyl Iodide.* A mixture of **4b** (0.5 g, 0.002 mol), CH_3I (1.4 g, 0.01 mol), and K_2CO_3 (0.7 g, 0.005 mol) in DMF (20 ml) was refluxed for 2 hr. The reaction mixture was then concentrated *in vacuo*, and the residue was diluted with H_2O to precipitate 0.3 g (56%) of 3-phenylfervenulin, which was found by IR to be identical with the **2b** prepared by the above method.

Conversion from Toxoflavins into Fervenulins; General Procedure: To a mixture of CH_3I (0.05 mol) and K_2CO_3 (0.01 mol) in DMF (50 ml), we added a toxoflavin (0.005 mol), after which the mixture was refluxed for 2—3 hr. After the solvent had been evaporated *in vacuo*, the resulting residue was diluted with H_2O to separate yellow crystals. Recrystallization from EtOH gave the corresponding fervenulin.

*Alkylation of 3-Phenyl-1-demethyltoxoflavin (**6b**) General Procedure:* To a suspension of **6b** (0.002 mol) and triphenylphosphine (0.03 mol) in dioxane (30 ml), we added diethyl azodicarboxylate (0.004 mol) and an alcohol (0.01—0.02 mol), after which the mixture was refluxed for 3 hr. The reaction mixture was then evaporated *in vacuo*, followed by dilution with benzene or EtOH to precipitate a crude sample, which was collected by filtration and recrystallized from EtOH to give the corresponding homologs of fervenulin (1-alkyl-3-methyl-7-azalumazines).

*Ethylation of **6b** with Ethyl Iodide.* A mixture of **6b** (1.5 g, 0.005 mol), C_2H_5I (3.9 g, 0.025 mol), and K_2CO_3 (3.5 g, 0.025 mol) in DMF (50 ml) was refluxed for 2 hr. After the insoluble material had been filtered off, the filtrate was concentrated to dryness *in vacuo* and the residue was diluted with H_2O to give crystals. Recrystallization from EtOH gave 1 g (71%) of 8-ethyl-3-methyl-6-phenyl-7-azalumazine (**7a**), which was found by IR and elemental analysis to be identical with the product prepared as has been described above.

References

1) W. Pfleiderer and K. H. Schündehütte, *Ann. Chem.*, **615**, 42 (1958).

2) For references to this ring system, see Blankenhorn and W. Pfleiderer, *Chem. Ber.*, **105**, 3334 (1972).

3) A part of this paper has been reported in preliminary form; see F. Yoneda, M. Kanahori, K. Ogiwara, and S. Nishigaki, *J. Heterocyclic Chem.*, **7**, 1443 (1970); F. Yoneda and T. Nagamatsu, *Tetrahedron Lett.*, **1973**, 1577.

4) F. Yoneda, K. Ogiwara, M. Kanahori, and S. Nishigaki, *Chem. Commun.*, **1970**, 1068.

5) H. Goldner, G. Dietz, and E. Carstens, *Ann. Chem.*, **691**, 142 (1966).

6) G. D. Daves, R. K. Robins, and C. C. Cheng, *J. Amer. Chem. Soc.*, **83**, 3904 (1961).

7) F. Yoneda, K. Shinomura, and S. Nishigaki, *Tetrahedron Lett.*, **1971**, 851.

8) F. Yoneda and T. Nagamatsu, *Chem. Pharm. Bull.* (Tokyo), **23**, 2001 (1975).

9) O. Mitsunobu, M. Wada, and T. Sano, *J. Amer. Chem. Soc.*, **94**, 679 (1972).

10) F. Yoneda, M. Higuchi, and T. Nagamatsu, *ibid.*, **96**, 5607 (1974).

Synthesis of [4-5,4′-5′-Bis(δ-Aminovaleric Acid)]-Gramicidin S[1]

Shōsuke SŌFUKU, Ichiro MURAMATSU, Kazuki OKADA, and Akira HAGITANI

Department of Chemistry, College of Science, Rikkyo (St. Paul's) University, Nishi-Ikebukuro, Tokyo 171

(Received March 26, 1975)

An analog of gramicidin S, [4-5,4′-5′-bis(δ-aminovaleric acid)]-gramicidin S, was synthesized, in which both of the two residues of D-Phe-L-Pro of gramicidin S (GS) were replaced with δ-aminovaleric acid residues (δAva). The spectra of optical rotatory dispersion (ORD) and circular dichroism (CD) of this analog suggest that its conformation in solution at room temperature is a random structure by comparison with that of GS. This analog has no antimicrobial activity. The linear peptide H-(Val-Orn-Leu-δAva-)$_2$-OH also has no activity and its ORD and CD are nearly the same as those exhibited by the random structure of the polypeptide. These results indicate the importance of the presence of D-Phe-L-Pro in GS for the maintenance of the specific conformation.

In order to investigate the contribution of amide bonds in peptides to their activity and conformation, we have synthesized analogs of gramicidine S (GS) containing δ-aminovaleric acid residue (δAva). In a previous paper,[1] it was reported that the synthetic analog, [δAva$^{4-5}$]-GS, had antimicrobial activity and showed a type of opitical rotatory dispersion (ORD) and circular dichroism (CD) spectra similar to that of GS. Proton magnetic resonance data[2] indicated that the secondary structure of this analog was similar to that of GS.

In this paper, we describe the synthesis of [δAva$^{4-5,4'-5'}$]-GS, in which both of the residues of D-Phe-L-Pro of GS were replaced with δAva, as well as the results of the antimicrobial assay and the ORD and CD measurements of this analog.

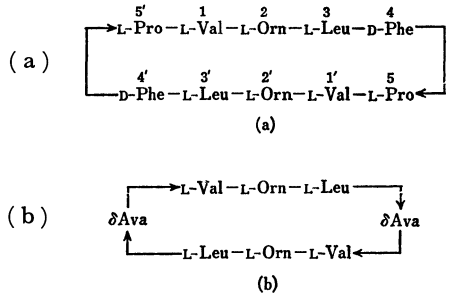

Fig. 1. Structures of gramicidin S (a), and [δAva$^{4-5,4'-5'}$]-GS (b).

The route of the synthesis of this analog is shown in Scheme 1. The synthesis of *p*-methoxybenzyloxycarbonyl-L-valyl-N^{δ}-benzyloxycarbonyl-L-ornithyl-L-leucyl-δ-aminovaleric acid hydrazide has been reported in the previous paper.[1] The azide derived from the hydrazide was coupled with IV. The resulting linear octapeptide (V) was used for cyclization reaction, which was carried out in the same manner as in the cyclization described in the previous paper. The cyclic peptide (VI) was obtained in 32% yield, which was inferior to that of the cyclization of the peptide containing one residue of δAva in the case of [δAva$^{4-5}$]-GS. This result might indicate that the yield of cyclization depends on whether the conformation of the active ester is such as to be favorable for the cyclization or not. [δAva$^{4-5,4'-5'}$]-GS diacetate (VII) was obtained by hydrogenolysis of the benzyloxycarbonyl groups on the ornithine residues of VI in the presence

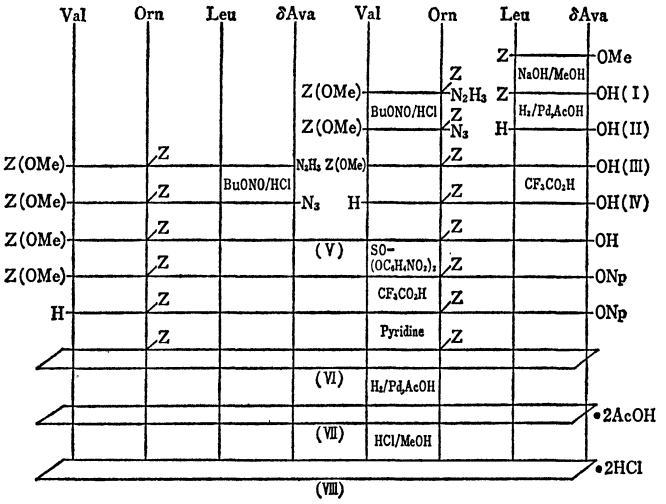

Scheme 1.

of acetic acid. VII was coupled with 1-dimethylaminonaphthalene-5-sulphonyl chloride (DNS-Cl).[3] After the hydrolysis of this DNS derivative, only N^{δ}-DNS-ornithine was detected in thin layer chromatography.[1] This result proves that VII has a cyclic form. The antimicrobial activity of this analog toward several microorganisms was tested for, but none could be found.

The related linear octapeptide, H-(Val-Orn-Leu-δAva-)$_2$-OH·3HCl (IX),[4] was prepared from V by hydrogenolysis of its N-protecting groups in the presence of hydrogen chloride. This peptide also did not exhibit any antimicrobial activity.

ORD and CD spectra of the cyclic peptide dihydrochloride (VIII) were measured. These spectra are different from those of GS and some of its biologically active analogs[1,5] as shown in Figs. 2 and 3. The minimum value of ORD of the analog (VIII) is observed at 208 nm, this represents a conspicuous difference from the spectrum of GS (232 nm). The CD spectrum of this peptide has a trough at 198 nm. In methanol also the trough of the CD at room temperature appeared at 199 nm.

ORD and CD spectra of the linear peptide (IX) in Figs. 2 and 3 show that it has a random structure.

Thus, the conformation of VIII in solution at room temperature is presumed to be a random structure,[6,7] while those of GS[8] and [δAva$^{4-5}$]-GS[1] are ordered.

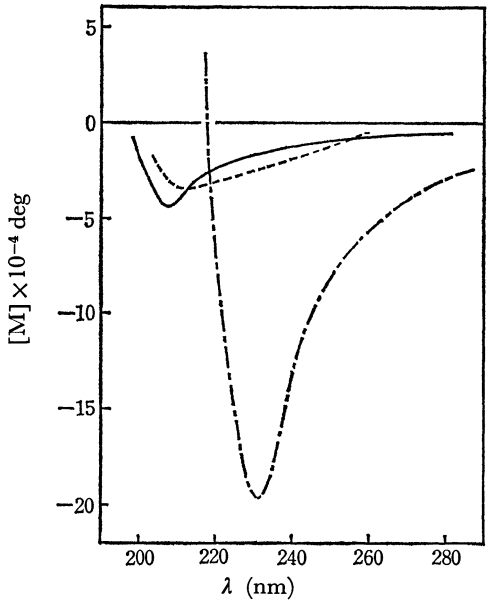

Fig. 2. Optical rotatory dispersion spectra of [δAva$^{4-5,4'-5'}$]-GS·2HCl (VIII), linear peptide (IX), and gramicidin S·2HCl (GS) in water; VIII (——), IX (----), and GS (———). Measurments were made using a 1 mm quartz cell at room temperature.

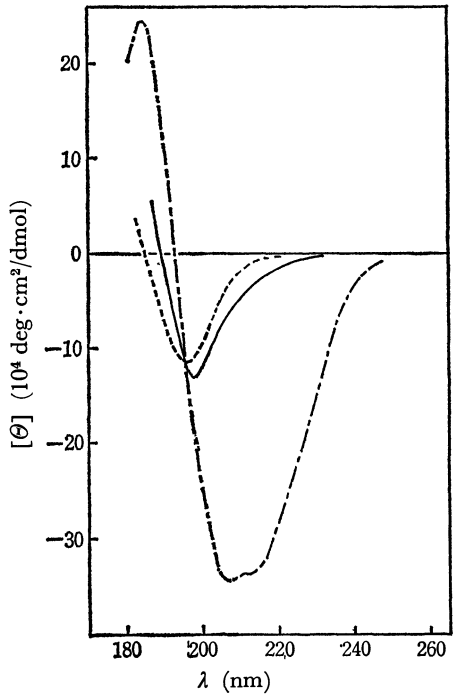

Fig. 3. Circular dichroism spectra of [δAva$^{4-5,4'-5'}$]-GS·2HCl (VIII), linear peptide (IX), and gramicidin S·2HCl (GS) in water; VIII (——), IX (----), and GS (———). Measurments were made using a 0.5 mm quartz cell at room temperature.

These results indicate that the cyclic structure of GS is retained not only by the formation of hydrogen bonds but also by the presence of D-phenylalanyl-L-prolyl residue in the β-turn.[9]

Experimental[10]

ORD and CD spectra were measured with a JASCO model J-20 spectrometer and represented by the values of molar optical rotation and molar ellipticity, respectively. The molecular weight was determined with a Hitachi molecular weight apparatus model 115, using methanol. Thin layer chromatography (tlc) was carried out on silica gel and the spot was detected with ninhydrin reagent. N-protected compounds were also detected with ninhydrin after deblocking with concd hydrobromic acid. The following solvent systems (V/V) were used in tlc: Solv. 1, $CHCl_3$–MeOH–AcOH (95 : 5 : 3); Solv. 2, $CHCl_3$–MeOH (9 : 1); Solv. 3, *n*-BuOH–AcOH–pyridine–H_2O (4 : 1 : 1 : 2); Solv. 4, *n*-BuOH–EtOH–concd NH_3 (6 : 1 : 3). Amino acid analyses were performed with a JEOL automatic amino acid analyzer, after hydrolyzing samples with 6 N HCl in evacuated sealed ampoules for 20 hr at 110 °C.

Benzyloxycarbonyl-L-leucyl-δ-aminovaleric Acid (I). Z-L-Leu-δAva-OMe (12.5 g, 33 mmol)[11] was saponified in methanol (90 ml) with 1 M NaOH (34 ml) at 38 °C for 2 hr. The reaction solution was acidified with 1 M HCl on cooling and evaporated *in vacuo*. The oily residue was dissolved in ethyl acetate and extracted with 5% sodium bicarbonate. This solution was acidified with 1 M HCl and extracted with ethyl acetate. The organic phase was dried over sodium sulfate and evaporated *in vacuo*. Upon recrystallization from ethyl acetate and *n*-hexane the product (10.18 g) was obtained in 84.6% yield. Mp 70—72 °C; $[\alpha]_D^{20.5}$ −15.4° (*c* 1.0, ethanol); tlc; R_f 0.42 (Solv. 1).

Found: C, 62.35; H, 7.80; N, 7.57%. Calcd for $C_{19}H_{28}N_2O_5$: C, 62.62; H, 7.74; N, 7.69%.

L-Leucyl-δ-aminovaleric Acid Acetate (II). I (4.38 g, 12 mmol) in ethanol (50 ml) and glacial acetic acid (2.5 ml) was hydrogenolyzed in the presence of palladium black for 4 hr. After removal of the catalyst and concentration of the filtrate *in vacuo*, an oily product was obtained in the theoretical yield.

p-Methoxybenzyloxycarboxyl-L-valyl-N$^\delta$-benzyloxycarbonyl-L-ornithyl-L-leucyl-δ-aminovaleric Acid(III). Z(OMe)-L-Val-L-Orn(δ-Z)-$NHNH_2$[11] (6.53 g, 12 mmol) was suspended in DMF (100 ml), followed by the addition of 1.81 M dry HCl in THF (26.51 ml) at −30 °C. After the addition of *n*-butyl nitrite[12] (1.45 ml) the reaction mixture was stirred at −20——30 °C for 15 min. To this azide solution, Et_3N (6.68 ml) and a solution of II(12 mmol) and Et_3N (1.67 ml) in DMF (20 ml) were added dropwise at −60 °C. The stirring was continued at −20 °C for 1.5 hr and at 0 °C for 2 days. After the addition of water (1 l) into the reaction mixture, the precipitate was filtered and washed with 5% citric acid and water. The crude product was recrystallized from DMF and ethyl ether. Yield, 6.24 g (70.1%); mp 177—180 °C; $[\alpha]_D^{24}$ −14.6° (*c* 1.0, DMF); tlc: R_f 0.72 (Solv. 2).

Found: C, 61.33; H, 7.56; N, 9.39%. Calcd for $C_{38}H_{55}N_5O_{10}$: C, 61.52; H, 7.47; N, 9.44%.

L-Valyl-N$^\delta$-benzyloxycarbonyl-L-ornithyl-L-leucyl-δ-aminovaleric Acid Trifluoroacetate(IV). III (5.94 g, 8.0 mmol) was dissolved in trifluoroacetic acid (30 ml) containing anisole (2.56 ml) in an ice-salt bath. After 20 min, the reaction solution was concentrated *in vacuo* at 0 °C. White crystals produced by trituration of the oily residue with ethyl ether were collected by filtration, and after drying weighed 5.30 g (95.8%). Mp 88—90 °C; $[\alpha]_D^{20}$ −17.0° (*c* 1.0, ethanol); tlc: R_f 0.8 (Sov. 3).

p-Methoxybenzyloxycarbonyl-L-valyl-N$^\delta$-benzyloxycarbonyl-L-

ornithyl-L-leucyl-δ-aminovaleryl-L-valyl-N$^{\delta}$-benzyloxycarbonyl-L-ornithyl-L-leucyl-δ-aminovaleric Acid (V). Z(OMe)-L-Val-L-Orn(δ-Z)-L-Leu-δAva-NHNH$_2$[1] (5.30 g, 7.0 mmol) and IV (4.92 g. 7.1 mmol) were subjected to the same treatment as was used for III. After the reaction mixture was stirred for 3 days at 0 °C, water was added to it. The resulting precipitate was separated by centrifugation and washed with 5% citric acid and water. Recrystallization of the dried crude product from DMF and ethyl ether gave 4.96 g (54.4%) of the pure product. Mp 254—257 °C (decomp.); $[\alpha]_D^{20}$ +17.7 °C (*c* 0.1, DMF); tlc: R_f 0.81 (Solv. 1).

Found:,C, 61.22; H, 7.66; N, 10.74%. Calcd for $C_{67}H_{100}N_{10}O_{16}$: C, 61.83; H, 7.74; N, 10.76%.

cyclo-L-*Valyl-N$^{\delta}$-benzyloxycarbonyl-L-ornithyl-L-leucyl-δ-aminovaleryl-L-valyl-N$^{\delta}$-benzyloxycarbonyl-L-ornithyl-L-leucyl-δ-aminovaleryl (VI).* The reaction of V (1.96 g, 1.5 mmol) and di-*p*-nitrophenyl sulfite (4.87 g, 15 mmol) in a mixture of DMF (200 ml) and pyridine (50 ml) at room temperature for 45 hr gave the *p*-nitrophenyl ester of V. In the same manner as described in Ref. 1, the removal of Z(OMe)-group of this ester and the cyclization (1.5×10^{-3} M in pyridine, at 58—60 °C) were carried out. After evaporation of the reaction solution and treatment through columns, Dowex-1 (OH^- form) and Dowex-50 (H^+ form), the effluent was concentrated to dryness *in vacuo* and a white crystalline product was obtained in 33.4% yield. It was recrystallized from aqueous methanol. Yield, 540 mg (32.2%); mp 209—210 °C; $[\alpha]_D^{20}$ −71.7° (*c* 0.3, methanol); tlc: R_f 0.35 (Solv. 1), 0.6 (Solv. 2); mol wt. Found: 1090 (Calcd for $C_{58}H_{90}N_{10}O_{12}$:1119).

Found: C, 61.68; H, 8.45; N, 12.22%. Calcd for $C_{58}H_{90}N_{10}O_{12}\cdot1/2\ H_2O$: C, 61.73; H, 8.13; N, 12.41%.

cyclo-L-*Valyl-L-ornithyl-L-leucyl-δ-aminovaleryl-L-valyl-L-ornithyl-L-leucyl-L-δ-aminovaleryl Diacetate (VII).* VI (400 mg, 0.36 mmol) was hydrogenolyzed in ethanol containing a few drops of glacial acetic acid in the presence of palladium black (0.5 g) for 2 hr. After removal of the catalyst, the filtrate was concentrated to an oily residue *in vacuo*. Its aqueous solution was filtered through active charcoal. The product was obtained by lyophilization of the filtrate. Yield, 220 mg (63.5%); mp 282—285 °C (decomp.); $[\alpha]_D^{26}$ −86.4° (*c* 0.22, ethanol); tlc: R_f 0.7 (Solv. 3), 0.4 (Solv. 4). Paper electrophoresis: migration distance −11.8 cm, *cf.* −11.0 cm for GS diacetate [HCOOH : AcOH : H_2O= 4 : 15 : 180 (pH 1.9), 600 V, 11.5—14.5 mA, 2 hr, Toyo No. 50 (15×40 cm)]. Amino acid ratios; Val, 0.96; Orn, 1.00; Leu, 1.14; δAva, 0.89.

Found: C, 57.33; H, 9.44; N, 14.14%. Calcd for $C_{46}H_{86}N_{10}O_{12}$: C, 56.88; H, 8.93; N, 14.42%.

cyclo-L-*Valyl-L-ornithyl-L-leucyl-δ-aminovaleryl-L-valyl-L-ornithyl-L-leucyl-δ-aminovaleryl Dihydrochloride (VIII).* The acetate (VII) was dissolved in excess dry methanolic hydrogen chloride (*ca.* 1M) at room temperature. After the solution had been evaporated *in vacuo*, the residue was lyophilized in water. The product was obtained in the theoretical yield. Mp 200—202 °C (decomp.); $[\alpha]_D^{28}$ −63.1 °C (*c* 0.15, ethanol).

Found: C, 50.62; H, 8.93; N, 13.60%. Calcd for $C_{62}H_{80}O_8N_{10}Cl_2\cdot4H_2O$: C, 50.64; H, 8.90; N, 14.06%.

L-*Valyl-L-ornithyl-L-leucyl-δ-aminovaleryl-L-valyl-L-ornithyl-L-leucyl-δ-aminovaleric Acid Trihydrochloride (IX).* V (1.0 g, 0.77 mmol) was hydrogenolyzed in DMF (120 ml) containing concd HCl (1.0 ml) in the presence of palladium black (610 mg) for 22 hr. After removal of the catalyst, the filtrate was concentrated to dryness *in vacuo*. The product was isolated from this crude preparation by countercurrent distribution (0.01 M HCl/*n*-butanol = 10/10 ml, ten transfers). The aqueous layers (No. 3—7) were concentrated to dryness *in vacuo*. The pure product was obtained by recrystallization from methanol and ethyl ether in 60.3% yield (470.3 mg). Mp 221—225 °C; $[\alpha]_D^{26}$ −44.3° (*c* 0.3, ethanol). Paper electrophoresis: migration distance −13.5 cm, *cf.* −10.8 cm for GS dihydrochloride (the same conditions in the case of VII). Amino acid ratios: Val, 0.86; Orn, 1.08; Leu, 1.07; αAva, 0.98.

Found: C, 49.58; H, 9.02; N, 14.17; Cl, 12.66%. Calcd for $C_{42}H_{83}N_{10}Cl_3\cdot H_2O\cdot1/2HCl$: C, 49.71; H, 8.49; N, 13.80; Cl, 12.22%.

Peptides VIII and IX did not exhibit antimicrobial activity toward the microorganisms *Bacillus subtilis, Staphylococcus aureus, Micrococcus flavus, and Sarcina lutea* in concentrations below 100 mcg/ml by the agar dilution method.

The authors are indebted to the members of the Research Laboratories of Toyo Jozo Co., for their elemental analyses and microbiological assays.

References

1) Part I of this series; S. Sōfuku, This Bulletin, **46**, 968 (1973).

2) H. Naganawa, T. Takita, I. Muramatsu, S. Sōfuku, and L. W. Cary, Proceedings of the 10th Symposium on Peptide Chemistry, Japan, 121 (1973).

3) G. Pataki, "Dünnschichtchromatographie in der Aminosäure- und Peptide-Chemie," Walter de Gruyter & Co., Berlin (1966), p. 167.

4) Abbreviations with no prefix show L-amino acid residue.

5) T. Kato, M. Waki, S. Matsuura, and N. Izumiya, *J. Biochem.* (Tokyo), **68**, 751 (1970).

6) E. R. Blout, I. Schmier, and N. S. Simmons *J. Amer. Chem. Soc.*, **84**, 3193 (1962).

7) R. Townend, T. F. Kumosinski, S. N. Timasheff, G. D. Fasman, and B. Davidson, *Biochem. Biophys. Res. Commun.*, **23**, 163 (1966).

8) A. Stern, W. A. Gibbons, and L. C. Craig, *Proc. Nat. Acad. Sci. U.S.*, **61**, 734 (1968).

9) D. W. Urry and M. Ohnishi; "Spectroscopic Approaches to Biomolecular Conformation," ed. by D. W. Urry, the American Medical Association, Chicago, Illinois (1970), p. 263.

10) The following abbreviations are from *J. Biol. Chem.*, **247**, 977 (1972): Z-, benzyloxycarbonyl; Z(OMe)- *p*-methoxybenzyloxycarbonyl; -ONp, *p*-nitrophenoxy; -OMe, methoxy. Other abbreviations: DMF, dimethylformamide; THF, tetrahydrofuran; Et_3N, triethylamine.

11) T. Kato, M. Kondo, M. Ohno. and N. Izumiya, This Bulletin, **38**, 1202 (1965).

12) W. A. Noyes, "Organic Syntheses," Coll. Vol. II, p. 108 (1943).

α,β-Unsaturated Carboxylic Acid Derivatives. X. The Synthesis and Reaction of α-Azido-diethoxyphosphinyl-α- and β-alkenes[1]

Chung-gi SHIN, Yasuchika YONEZAWA, Hiroshi SAKAMOTO, and Juji YOSHIMURA*

Laboratory of Organic Chemistry, Faculty of Technology, Kanagawa University, Rokkakubashi, Kanagawa-ku, Yokohama 221

**Laboratory of Chemistry for Natural Products, Faculty of Science, Tokyo Institute of Technology, Ōkayama, Meguro-ku, Tokyo 152*

(Received March 31, 1975)

α,β-Dibromo-β-diethoxyphosphinylalkane (**2**) was obtained as a stereo-isomeric mixture (erythro : threo= 50 : 50) by the bromination of β-diethoxyphosphinyl-α-alkene, composed of the *E*-isomer and the *Z*-isomer (50 : 50). It was found that the reaction of **2** with sodium azide proceeded stereoselectively to give only the *E*-isomer of α-bromo-β-diethoxyphosphinyl-α-alkene, which could then be converted into α-azido-β-diethoxyphosphinyl-α-alkene (**4**), and α-azido-β-diethoxyphosphinyl-β-alkene, whose configuration was determined by the coupling constants between the phosphorus atom and the vinyl protons. Moreover, the irradiation of **4** yielded a new type of β-diethoxyphosphinyl-α-alkene-α-imine, which later rearranged into the corresponding nitrile.

Although there have been fairly many reports on the synthesis and reaction of the saturated phosphinylalkane, only a little attention has been paid to the unsaturated phosphinyl derivative. We ourselves have reported the synthesis of β-diethoxyphosphinyl-α-alkene and ethyl β-diethoxyphosphinyl-α-alkenoate (**1**) by the reaction of α-nitro-α-alkene or ethyl α-nitro-α-alkenoate with triethyl phosphonate in one step.[2,3]

Because of the pharmacological and structural interest of phosphinyl-2*H*-azirene, aziridine,[4-6] or other phosphinyl derivatives,[7,8] the replacement of the dibromo derivative of **1** (**2**) with sodium azide and the photochemical transformation of the azido derivatives thus obtained will be examined in this paper.

Results and Discussion

*Reaction of **2** with Sodium Azide.* The addition of bromine to 2-diethoxyphosphinyl-1-butene (**1a**), 2-diethoxyphosphinyl-3-methyl-1-butene (**1b**), and ethyl 3-diethoxyphosphinyl-2-pentenoate (**1c**) in chloroform at room temperature for a day gave the corresponding dibromo derivatives, 1,2-dibromo-2-diethoxyphosphinylbutane (**2a**), 1,2-dibromo-2-diethoxyphosphinyl-3-methylbutane (**2b**), and ethyl 2,3-dibromo-2-diethoxyphoshpinyl-pentanoate (**2c**), in good yields.

The ratio of the geometric isomers (*E*-isomer : *Z*-isomer=50 : 50) in **1**, as determined from the intensity of the olefinic proton signals, was maintained in the diastereomers (*erythro* : *threo*=50 : 50) in **2**.

Since the dehydrobromination of **2a**, **b** with triethylamine scarcely proceeded at, all a solution of **2a** in dimethylformamide was treated with sodium azide with stirring at 40—45 °C for 24—35 hr to give 1-bromo-2-diethoxyphosphinyl-1-butene (**3a**) as the main product, together with a small amount of 1-azido-2-diethoxyphosphinyl-2-butene (**5a**). The similar treatment of **2b** gave 1-azido-2-diethoxyphosphinyl-3-methyl-2-butene (**5b**) as the main product, along with a small amount of 1-bromo-2-diethoxyphosphinyl-3-methyl-2-butene (**3b**). Compound **3a** was also obtained in a good yield by the reaction of **2a** with liquid ammonia in a sealed tube at room temperature for 2 days. The treatment of **3a** or **3b** with sodium azide with stirring at 50—55 °C for 45—50 hr gave 1-azido-2-diethoxyphosphinyl-1-butene (**4a**) or 1-azido-2-diethoxyphosphinyl-3-methyl-1-butene (**4b**) respectively in a good yield. On the contrary, the dehydrobromination of **2c** proceeded smoothly with triethylamine to give ethyl 2-bromo-3-diethoxyphosphinyl-2-pentenoate (**3c**); ethyl 2-azido-3-diethoxyphosphinyl-2-pentenoate (**4c**) could not be obtained. This fact may be attributed to the inactivity of the α-bromo atom of the α, β-unsaturated carboxylic ethyl ester. Compounds **3**, **4** and **5** were separated by distillation under reduced pressure or by chromatography on a silica-gel column, using benzene-acetone as the eluent. It is interesting that **3**, **4** and **5** are all composed of only one geometric isomer. The yields, physical constants, and spectral data are summarized in Tables 1 and 2.

The stereochemical assignment of **3**, **4** and **5** was made on the basis of elementary and spectroscopic analyses. The IR spectra of **3** and **4** showed a weak band of the carbon-carbon double bond in the 1575—1618 and 1610 cm^{-1} regions respectively, and strong bands of the diethoxyphosphinyl group in the 1240—1260 (≫P=O) and 1020—1025 (≫P-O-C) cm^{-1} regions, while that of **5** showed a band of the carbon-carbon double bond at 1625—1630, ≫P=O in the 1235—1250 region, and ≫P-O-C at 1025 cm^{-1}. The absorption pattern of **3**, **4** and **5** is essentially the same as that of the starting material (**1**) except for the characteristic strong azido band of **4** and **5** appearing in the 2100—2110 cm^{-1} region. The NMR spectra of **3**, **4** and **5** showed a vinyl hydrogen signal in the α- or γ-position with regard to the β-phosphorus atom in lower magnetic fields, and with smaller coupling constants ($J_{P,H}$=12.0—23.0 Hz), in comparison with those of the *E*-isomer ($J_{P,H}$=22.3—23.0 Hz) and the *Z*-isomer ($J_{P,H}$=48.0—59.0 Hz) of **1**[3] and others appearing in the literature.[9] From the above results, it may be deduced that the dehydrobromination of **2** proceeded stereoselectively to give only an *E*-isomer and that the configuration was retained in the subsequent substitution of the bromine atom of **3** with the azido group.

*Irradiation of **4a** and **5b**.* A solution of **4a** in cyclohexane was irradiated in a stream of nitrogen by means of an external high-pressure mercury lamp for

Table 1. The yields, boiling points and elementary analyses of **2**, **3**, **4**, and **5**

Compound	Yield (%)	bp °C/mmHg	Formula	Found (Calcd), %		
				C	H	N
2a	73.5	100—105/0.1	$C_8H_{17}O_3PBr_2$	27.18 (27.29	4.99 4.87)	
2b	70.5	105—109/0.42	$C_9H_{19}O_3PBr_2$	29.50 (29.53	5.67 5.23)	
2c	71.3	syrup[a]				
3a	61.6	67— 72/0.16	$C_8H_{16}O_3PBr$	35.13 (35.44	6.20 5.95)	
3b	9.2	65— 67/0.09	$C_9H_{18}O_3PBr$	37.95 (37.91	6.27 6.27)	
3c	30.0	syrup	$C_{10}H_{18}O_5PBr$	36.65 (36.49	5.90 5.51)	
4a	70.6	syrup	$C_8H_{16}N_3O_3P$	40.92 (41.20	7.15 6.92	18.40 18.02)
4b	62.5	syrup	$C_9H_{18}N_3O_3P$			17.23 (17.00)
5a	7.2	73— 77/0.25	$C_8H_{16}N_3O_3P$			18.34 (18.02)
5b	70.3	80— 85/0.25	$C_9H_{18}N_3O_3P$	43.75 (43.72	7.48 7.29	17.16 17.00)

a) Unstable syrup for distillation, the structure of which was confirmed by means of spectral data and the conversion into **3c**.

Table 2. Spectral data of **2**, **3**, **4**, and **5**

Compound	IR spectrum, cm^{-1} in KBr				NMR spectrum, δ in $CDCl_3$	
	N_3(s)[a]	C=C(w)[b]	P=O(s)	P-O-C(s)	α-H (γ-H)	$J_{P,H}$(Hz)
2a			1250,	1020	3.75—4.10 m[c]	
2b			1255,	1020	3.65—4.07 m	
2c			1255,	1020	4.70—4.97 m	
3a		1590,	1250,	1025	7.24 d[d]	15.0
3b		1575,	1250,	1025	7.24 d	15.0
3c		1618,	1260,	1020	(2.01 d)	12.0
4a	2100,	1610,	1250,	1025	7.18 d	14.0
4b	2100,	1595,	1240,	1025	7.28 d	19.0
5a	2110,	1630,	1250,	1025	4.40 d	23.0
5b	2110,	1625,	1235,	1025	4.95 d	

a) s=Strong. b) w=Weak. c) m=Multiplet. d) d=Doublet.

a day until the azido band at *ca.* 2100 cm^{-1} had disappeared at room temperature; the chromatographic separation of the resultant solution gave 2-diethoxyphosphinyl-1-butene-1-imine (**7a**) in a 30% yield and a small amount of 2-diethoxyphosphinyl-butanenitrile (**8a**), instead of the expected 1-ethyl-1-diethoxyphosphinyl-2*H*-azirene (**9**). Since the irradiation of the isolated **7a** gave **8a** in a 17% yield, it was concluded that **8a** was derived from **7a** by the 1,3-shift of hydrogen.[10] On the other hand, the irradiation of **5b** in cyclohexane in a stream of nitrogen by means of a high-pressure mercury lamp gave several kinds of products, none yielding the expected 2-diethoxyphosphinyl-3-methyl-2-butene-1-imine (**6b**). The structures of the products are now under investigation.

The IR spectrum of **7a** showed a characteristic strong band at 2070, and that of **8a** showed a weak nitrile band at 2250 cm^{-1}, causing the band at

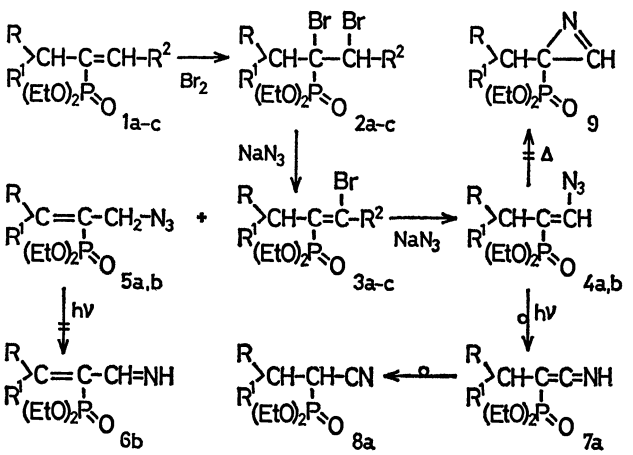

a; R=CH_3, R^1=R^2=H b; R=R^1=CH_3, R^2=H c; R=CH_3, R^1=H, R^2=COOEt

Scheme 1.

2070 cm^{-1} to disappear. On the other hand, the NMR spectrum of **7a** showed the imino proton signal at δ 4.80. These spectral data support the structures of **7** and **8**.

Experimental

All the boiling points are uncorrected. The IR spectra were recorded with a Hitachi EPI-S2 Spectrometer. The NMR spectra were measured with a JNM-4H-100 Spectrometer (Japan Electron Optics Laboratory Co., Ltd.), using tetramethylsilane as the internal standard.

Material. Compounds **1a—c** were prepared by the method previously reported.[3]

*Reaction of **1a** and **1b** with Bromine.* Into a solution of **1a** (19.2 g, 0.1 mol) in chloroform (70 ml), a solution of bromine (16 g, 0.1 mol) in chloroform (30 ml) was stirred portion by portion, at room temperature. The resultant solution was sealed tightly in a vessel (200 ml) and allowed to stand overnight at room temperature, and then the solution was concentrated. The residual oil was distilled under reduced pressure to give **2a** as a colorless oil.

In a similar manner, equimolar amounts of **1b** and bromine were reacted to give **2b** as a colorless oil after standing for 2 days.

*Reaction of **1c** with Bromine.* Into a solution of **1c** (7.5 g, 0.03 mol) in chloroform (30 ml), a solution of bromine (4.8 g, 0.03 mol) in chloroform (10 ml) was stirred at room temperature. After having been heated in a sealed tube at 100 °C for 12 hr, the reaction solution was concentrated. The residual syrup was purified on a silica-gel column, using benzene–acetone (10 : 1 V/V) as the eluent; the eluent solvent was then evaporated under reduced pressure to give **2c** as a colorless syrup which could not be distilled.

*Reaction of **2a** and **2b** with Sodium Azide.* Into a mixture of sodium azide (3.9 g, 0.06 mol) in dry dimethylformamide (50 ml), we stirred a solution of **2a** (7.04 g, 0.02 mol) in dimethylformamide (5 ml), portion by portion, at room temperature. After continuous stirring at 40 °C for 25 hr, the reaction solution was poured into ice water (300 ml), and then the aqueous solution was stirred for 1 hr. The solution was extracted well with benzene (100 ml) three times. The benzene extracts were washed with water twice, dried over anhydrous sodium sulfate, and then evaporated under reduced pressure to give a yellow oil. The purification of the oil on a silica-gel column, using benzene–ethyl ether (20 : 1 V/V) as the eluent, and the evaporation of the eluent solvent under reduced pressure gave **3a** from the first fraction and **5a** from the last fraction, both as colorless oils.

In a similar manner, Compound **2b** was reacted with sodium azide in dimethylformamide to give **3b** and **5b**.

*Reaction of **2a** with Liquid Ammonia.* Compound **2a** (7.04 g, 0.02 mol) was dissolved in liquid ammonia (15 ml), and then the solution was allowed to stand in a sealed tube at room temperature for 2 days. To the reaction solution, dry chloroform (20 ml) was then added. After the removal of the ammonium bromide deposited, the chloroform solution was concentrated. The residual oil was purified on a silica-gel column, using benzene–ethyl ether (20 : 1 V/V), to give **3a** as a colorless oil in a 67.5% yield.

*Reaction of **3a** and **3b** with Sodium Azide.* Into a mixture of sodium azide (6.5 g, 0.1 mol) in dry dimethylformamide (70 ml), a solution of **3a** (3.8 g, 0.014 mol) in dimethylformamide (5 ml) was stirred, portion by portion, at room temperature. After continuous stirring at 50 °C for 56 hr, the reaction solution was poured into ice water (300 ml), and then the aqueous solution was stirred for 1 hr. The solution was extracted well with benzene (100 ml) three times. The benzene extracts were washed with water twice, dried over anhydrous magnesium sulfate, and finally evaporated under reduced pressure to give a yellow syrup. Purification on a silica-gel column, using benzene–ethyl ether (10 : 1 V/V), and the evaporation of the eluent solvent under reduced pressure gave **4a** as a colorless syrup.

In a similar manner, Compound **4b** was obtained as a colorless syrup by the reaction of **3b** with sodium azide in dimethylformamide.

*Reaction of **2c** with Sodium Azide.* Into a mixture of sodium azide (3.9 g, 0.06 mol) in dry dimethylformamide (50 ml), we stirred, portion by portion, a solution of **2c** (8.2 g, 0.02 mol) in dimethylformamide (5 ml) at room temperature. After continuous stirring at room temperature for 15 hr, the reaction solution was poured into ice water (300 ml), and then the aqueous solution was stirred for 1 hr. The solution was extracted well with benzene (100 ml) three times. The benzene extracts were washed with water twice, dried over anhydrous magnesium sulfate, and then finally evaporated under reduced pressure to give a yellow syrup. The purification of the syrup on a silica-gel column, using benzene–acetone (7 : 1 V/V), and the evaporation of the eluent solvent under reduced pressure gave **3c** as a colorless syrup which could not be distilled.

*Irradiation of **4a**.* A solution of **4a** (2.0 g, 0.0086 mol) in cyclohexane (50 ml) was irradiated in a stream of nitrogen by means of a 500 W high-pressure mercury lamp at room temperature for 6 hr. After the removal of the solvent under reduced pressure, the residual syrup was purified on a silica-gel column, using carbon tetrachloride–acetone (5 : 1 V/V), and then the eluent solvent was evaporated to give **7a** in a 30% yield from the first fraction and **8a** in a 7% yield from the last fraction, both as colorless syrups. **7a**; IR (KBr disk): 2080 (C=C=N), 1635 (C=C), 1243 (P=O), and 1225 (P–O–C) cm^{-1}. NMR ($CDCl_3$): δ 4.80 (1H, broad s, NH) and 1.72—2.24 (2H, m, $CH_3\underline{CH_2}-C=$). The structure of **7a** was confirmed by means of the spectral data and by its conversion into **8a**. **8a**; IR (KBr disk): 2230 (C≡N), 1260 (P=O), and 1220 (P–O–C) cm^{-1}. NMR ($CDCl_3$): δ 2.70—3.14 (1H, m, $-CH_2\underline{CH}-C\equiv$).

Found: N, 6.58%. Calcd for $C_8H_{16}NO_3P$: N, 6.83%.

*Isomerization of **7a** to **8a**.* A solution of **7a** (0.2 g, 0.00086 mol) in dry tetrahydrofuran (30 ml) was irradiated in a stream of nitrogen by means of a 500 W high-pressure mercury lamp at room temperature for 10 hr. After the subsequent removal of the solvent under reduced pressure, the residual syrup was purified on a silica-gel column, using benzene–acetone (5 : 1 V/V), and then the solvent was evaporated under reduced pressure to give **8a** in a 17% yield.

The authors are grateful to the Ministry of Education, Japanese Government, for its financial support of this work.

References

1) Part IX: C. Shin, K. Nanjo, M. Kato, and J. Yoshimura, This Bulletin, **48**, 2584 (1975).

2) C. Shin, Y. Yonezawa, and J. Yoshimura, *ibid.*, **44**, 3488 (1971).

3) C. Shin, Y. Yonezawa, K. Katayama, and J. Yoshimura, *ibid.*, **46**, 1727 (1973).

4) S. Rengaraju and K. D. Berlin, *J. Org. Chem.*, **37**, 3304 (1972).
5) A. Hassner and J. E. Galle, *J. Amer. Chem. Soc.*, **92**, 3733 (1970).
6) T. Nishiwaki and T. Saito, *J. Chem. Soc., C*, **1971**, 3021.
7) J. S. Meek and J. S. Fowler, *J. Org. Chem.*, **33**, 985 (1968).
8) G. Pattenden and B. J. Walker, *J. Chem. Soc., C*, **1969**, 531.
9) A. M. Aguiar and D. Daigle, *J. Org. Chem.*, **30**, 2826, 3527 (1965).
10) K. Friedrich, *Angew. Chem.*, **79**, 980 (1967).

Aminocyclitols. 32. Synthesis of Inosadiamine-1,4[1]

Tetsuo SUAMI, Kinnichi TADANO, and Sumio HORIUCHI

Department of Applied Chemistry, Faculty of Engineering, Keio University, Hiyoshi, Yokohama 223

(Received April 15, 1975)

Three new inosadiamines have been prepared by nitromethane cyclization of dialdehyde, followed by catalytic hydrogenation. Their structures were established to be *scyllo*-1,4, *myo*-1,4, and *epi*-inosadiamine-3,6 by PMR spectra.

Nitromethane cyclization of dialdehydes is a well known and well studied reaction in a field of carbohydrate chemistry.[2] The first successful application of this reaction to a carbohydrate was accomplished by Sowden and Fischer[3] in 1944 and later Grosheintz and Fischer[4,5] extended this reaction to intramolecular cyclization to prepare nitrodeoxyinositols. These reactions were extensively studied by several investigators.[6–10]

In connection with the preceding paper of this series,[11] we have attempted to prepare an inosadiamine-1,4 by means of the nitromethane cyclization of dialdehydes. In the present article, we wish to report the synthesis of three new inosadiamines: *scyllo*-1,4, *myo*-1,4, and *epi*-inosadiamine-3,6.

The starting material: 1,4-di-*O*-acetyl-2,3-*O*-cyclohexylidene-(1,4/2,3,5-5)-acetamide-1,2,3,4-cyclopentanetetrol (**1**) was prepared by the method of Ahluwalia *et al.*[12] Mild hydrolysis of **1** in 80% aqueous acetic acid afforded 1,4-di-*O*-acetyl-(1,4/2,3,5)-5-acetamido-1,2,3,4-cyclopentanetetrol (**2**).[13] The 1,4-di-*O*-benzoyl derivative (**3**) was prepared by the analogous reaction process.

Compound **2** was oxidized by periodate in an aqueous solution to give 3-acetamido-2,4-di-*O*-acetyl-2-deoxy-*xylo*-pentodialdose (**4**) as a syrup. Compound **4** was treated with nitromethane under the presence of sodium methoxide. The product was hydrogenated in the presence of Raney nickel under a hydrogen atomosphere and subsequently acetylated. The product was fractionated by means of recrystallization and column chromatography to give three new hexaacetyl inosadiamines (**7**), (**8**) and (**9**) in 3.5, 39, and 1.3% yields, respectively.

In the case of the reactions starting from the di-*O*-benzoyl derivative **3**, the analogous results were obtained.

TABLE 1. CHEMICAL SHIFTS OF THE ACETYL METHYL PROTONS IN DMSO-d_6 (60 MHz) IN τ-VALUE

Compound		Acetoxy		Acetamido	
		ax.	eq.	ax.	eq.
7	*scyllo*-1,4		8.07(12H)		8.22(6H)
8	*myo*-1,4	7.82(3H)	8.05(3H)		8.20(3H)
			8.09(3H)		8.23(3H)
			8.10(3H)		
9	*epi*-3,6	7.88(6H)	8.13(6H)		8.17(3H)
					8.24(3H)

There are fourteen theoretically possible isomers in inosadiamine-1,4 and five ones are already described in the literatures.[14–17] The three inosadiamines obtained in the present experiment are not identical with any one of these known isomers. In the present reaction, three new chiral centers are introduced in the products and therefore, six isomers are conceivable. Among these six isomers, *muco*-3,6[16] and *chiro*-inosadiamine-1,4[15] are known isomers.

Compound **7** should be one of the remaining four unknown compounds. The PMR spectrum of **7** revealed a simple pattern of the signals due to the acetyl methyl protons and this was only compatible with hexaacetyl *scyllo*-inosadiamine-1,4.

The PMR spectrum of **8** revealed six sharp signals with a same intensity of three protons. The two signals at τ 8.20 and 8.23 are attributed to the two equatorial acetamido groups and the signal at τ 7.82 is due to an axial acetoxy group.[19] The other three signals are attributed to the equatorial acetoxy groups

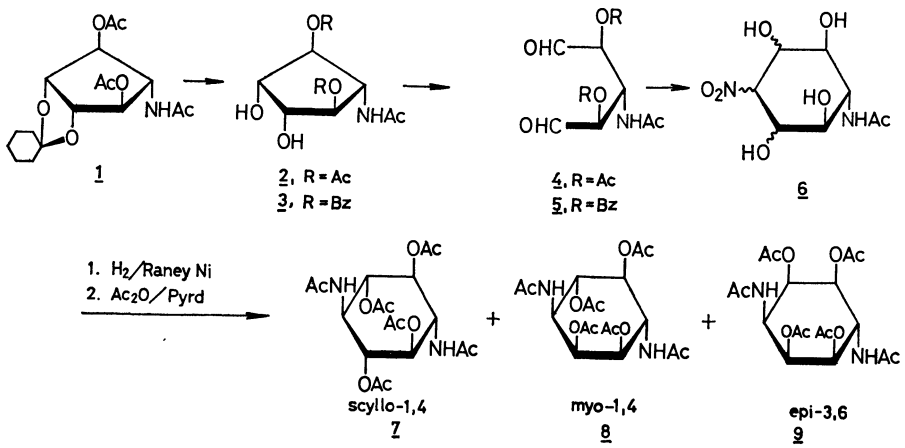

Scheme 1.

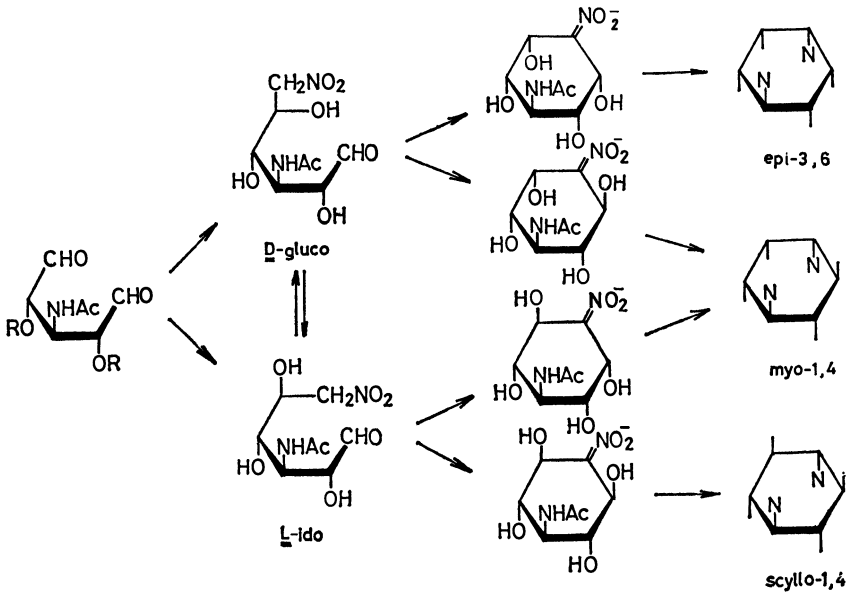

Scheme 2.

and therefore, **8** was assigned as hexaacetyl *myo*-inosadiamine-1,4.

Compound **9** showed four sharp signals in its PMR spectrum. The signal at τ 7.88 is attributed to the two axial acetoxy groups and the two signals at τ 8.17 and 8.24 are due to the two equatorial acetamido groups. Hence, **9** was assigned to be hexaacetyl *epi*-inosadiamine-3,6.

Besides the above described three inosadiamines, another minor product was detectable on tlc, but the structural assignment of this product was unsuccessful owing to a poor yield.

The reaction mechanism of nitromethane cyclization has been well studied by Kovar and Baer[6] using 6-deoxy-3-*O*-methyl-6-nitro-D-glucose and -L-idose. The present experiments are coincident with their results.[6]

In the present reaction, the initial step of the reaction is an addition reaction between nitromethane and one of the two aldehyde groups in **4** to give two diastereomers: D-*gluco* and L-*ido* type intermediates. The second step of the reaction is intramolecular cyclization of the intermediates to give *myo*-1,4 and *epi*-3,6 type compounds from the D-*gluco*, and *myo*-1,4 and *scyllo*-1,4 type compounds from the L-*ido* *via* corresponding nitronate salts.

Exeprimental

All melting points were determined in capillary tubes and are uncorrected. Solutions were evaporated under diminished pressure below 40 °C. Acetylation was carried out with acetic anhydride in pyridine. PMR spectra were measured at 60 MHz on a Varian A-60D in dimethyl sulfoxide-d_6 (DMSO-d_6) with reference to tetramethylsilane as an internal standard and the peak positions are given in τ values.

*3-Acetamido-2,4-di-*O*-acetyl-3-deoxy*-xylo-*pentodialdose* (**4**). 1,4-Di-*O*-acetyl-(1,4/2,3,5)-5-acetamido-1,2,3,4-cyclopentanetetrol (**2**) was prepared by the method of Suami *et al.*[13] from 1,4-di-*O*-acetyl-2,3-*O*-cyclohexylidene-(1,4/2,3,5)-5-acetamido-1,2,3,4-cyclopentanetetrol.[12] Compound **2** (6.0 g) was dissolved in cold water (60 ml) and sodium metaperiodate (5.13 g) was added to the solution under ice cooling with agitation. The solution was stirred overnight at room temperature and neutralized with sodium hydrogencarbonate. Methanol (60 ml) was added to the solution and the mixture was settled overnight in a refrigerator. The mixture was filtered and the filtrate was evaporated. The residue was extracted with a mixture of ethanol and ethyl acetate (1 : 1, v/v) and the extract was evaporated to give a crude product of **4** (6.7 g) as a pale yellow syrup. The product showed a positive Fehling test and a spot on tlc at R_f 0.3 in benzene–ethanol (5 : 1, v/v) solvent system.

*3-Acetamido-2,4-di-*O*-benzoyl-3-deoxy*-xylo-*pentodialdose* (**5**). 2,3-*O*-Cyclohexylidene-(1,4/2,3,5)-5-acetamide-1,2,3,4-cyclopentanetetrol[13] (1.37 g) was acylated with benzoyl chloride (1.8 ml) in pyridine (25 ml). After the mixture was agitated for 2 hr, the mixture was poured into ice cold water (600 ml) to give crystals. The crystals were collected by filtration to give 2.40 g (99%) of 1,4-di-*O*-benzoyl-2,3-*O*-cyclohexylidene-(1,4/2,3,5)-5-acetamide-1,2,3,4-cyclopentanetetrol, mp 187—188 °C.

Found: C, 67.92; H, 6.13; N, 2.77%. Calcd for $C_{27}H_{29}NO_7$: C, 67.63; H, 6.10; N, 2.92%.

The above described product (2.5 g) was heated in 80% aqueous acetic acid (70 ml) under reflux for 3 hr and the solution was evaporated to give a crystalline residue. The residue was recrystallized from a mixture of ethanol and ethyl acetate (1 : 5, v/v) to give 1.61 g (72%) of 1,4-di-*O*-benzoyl-(1,4/2,3,5)-5-acetamido-1,2,3,4-cyclopentanetetrol (**3**), mp 177—178 °C.

Found: C, 62.95; H, 5.41; N, 3.35%. Calcd for $C_{21}H_{21}NO_7$: C, 63.15; H, 5.30; N, 3.51%.

Compound **3** (7.64 g) was dissolved in ethanol (200 ml) and a solution of sodium metaperiodate (7.01 g) in cold water (300 ml) was added to the solution under ice cooling with agitation. After stirred overnight at room temperature, the mixture was neutralized with sodium hydrogencarbonate. The mixture was filtered and the filtrate was evaporated to give 7.14 g (94%) of **5** as a crude syrup. The product showed a positive Fehling test and a spot on tlc at R_f 0.7 in benzene–ethanol (5 : 1, v/v) system.

Nitromethane Cyclization of **4**. To a mixture of **4** (6.7 g), nitromethane (2.4 ml) and methanol (30 ml), 2.2 M methanolic sodium methoxide (20 ml)was added under ice cooling

with agitation. After settled overnight in a refrigerator, the reaction mixture was adjusted to pH 6 with glacial acetic acid and evaporated to give a brown residue (11.9 g).

Hexaacetyl scyllo-*Inosadiamine-1,4 (7).* The crude nitromethane cyclization product (11.9 g) was hydrogenated in water (25 ml) under the presence of Raney nickel T-4 catalyst[18] in 3.4 kg/cm^2 hydrogen atomosphere for 12 hr. After the catalyst was removed by filtration, the solution was evaporated to give a dark residue (11.5 g). The residue was acetylated overnight at room temperature to give a dark product. The product was recrystallized two times from ethanol to give 120 mg of **7**, mp above 290 °C. The mother liquor was evaporated and the residue was recrystallized from ethanol to give another crop of **7** (207 mg). Total yield was 327 mg (3.5% from **4**).

Found: C, 49.95; H, 6.03; N, 6.52%. Calcd for $C_{18}H_{26}N_2O_{10}$: C, 50.23; H, 6.09; N, 6.51%.

Hexaacetyl myo-*Inosadiamine-1,4 (8).* The ethanolic mother liquor of **7** was evaporated and the residue was recrystallized from a mixture of benzene and ethanol (5 : 1, v/v) to give 2.50 g of **8**. The mother liquor was evaporated and the residue was fractionated on a silica gel column (Wakogel C-300, 80 g, 30×400 mm) with benzene-ethanol (5 : 1, v/v) as an eluating solvent. The fractions which showed a single spot on tlc at R_f 0.28 in the same solvent system were collected and evaporated to give another crop of **8** (1.14 g). The product was recrystallized from ethanol to give 3.63 g (39% from **4**) of **8**, mp 258—259 °C.

Found: C, 50.39; H, 6.11; N, 6.47%. Calcd for $C_{18}H_{26}N_2O_{10}$: C, 50.23; H, 6.09; N, 6.51%.

Hexaacetyl epi-*Inosadiamine-3,6 (9).* Another product was obtained from the column chromatography by collecting the fractions which showed a single spot at R_f 0.26 on tlc in the same solvent. The product was recrystallized from a mixture of benzene and ethanol (5 : 1, v/v) to give 121 mg (1.3% from **4**) of **9**, mp 228—230 °C.

Found: C, 50.07; H, 6.05; N, 6.51%. Calcd for $C_{18}H_{26}N_2O_{10}$: C, 50.23; H, 6.09; N, 6.51%.

The mother liquor was evaporated and the residue was recrystallized repeatedly from a mixture of acetone, benzene and ethyl acetate (1 : 10 : 1, v/v) to give 5 mg of hexaacetyl inosadiamine, mp 278—280 °C. The product showed practically a single spot at R_f 0.20 on tlc in a benzene-ethanol (5 : 1, v/v) solvent system and gave a correct analysis for hexaacetyl inosadiamine (Found: C, 50.37, H, 6.26; N, 6.71%).

Nitromethane Cyclization of **5**. To a mixture of **5** (8.5 g), nitromethane (10 ml) and methanol (200 ml), 2.2 M methanolic sodium methoxide (30 ml) was added under ice cooling with agitation. The reaction mixture was worked up as described in the case of **4** to give compounds **7**, **8** and **9** in 4.1, 32 and 1.6% yields, respectively.

The authors express their sincere thanks to Mr. Saburo Nakada for his elementary analyses.

References

1) This work was presented in part at the 7th International Symposium on Carbohydrate Chemistry, Bratislava, Czechoslovakia, August 5, 1974.
2) H. H. Baer, "Advances in Carbohydrate Chemistry," Academic Press, New York (1969), Vol. 24, p. 67.
3) J. C. Sowden and H. O. L. Fischer, *J. Amer. Chem. Soc.*, **66**, 1312 (1944); J. C. Sowden, "Advances in Carbohydrate Chemistry," Academic Press, New York (1951), Vol. 6, p. 291.
4) J. M. Grosheintz and H. O. L. Fischer, *J. Amer. Chem. Soc.*, **70**, 1476 (1951).
5) ditto, *ibid.*, **70**, 1479 (1948).
6) J. Kovář and H. H. Baer, *Can. J. Chem.*, **51**, 2836 (1973).
7) F. W. Lichtenthaler, *Angew. Chem.*, **76**, 84 (1964).
8) A. C. Richardson and H. O. L. Fischer, *J. Amer. Chem. Soc.*, **83**, 1132 (1961).
9) M. L. Wolfrom, S. M. Olin, and W. J. Polglase, *J. Amer. Chem. Soc.*, **72**, 1724 (1950).
10) F. W. Lichtenthaler, *Angew. Chem.*, **75**, 93 (1963).
11) T. Suami, S. Ogawa, H. Uchino, and Y. Funaki, *J. Org. Chem.*, **40**, 456 (1975).
12) R. Ahluwalia, S. J. Angyal, and B. M. Luttrell, *Aust. J. Chem.*, **23**, 1819 (1970).
13) T. Suami, Y. Sakota, K. Tadano, and S. Nishiyama, This Bulletin, **44**, 2222 (1971).
14) *allo*-Inosadiamine-1,4: T. Suami, S. Ogawa, S. Oki, and H. Sato, *ibid.*, **47**, 138 (1974).
15) *chiro*-Inosadiamine-1,4: T. Suami, S. Ogawa, H. Uchino, and M. Uchida, *ibid.*, **46**, 2840 (1973).
16) *muco*-1,4-and *muco*-Inosadiamine-3,6: T. Suami, F. W. Lichtenthaler and S. Ogawa, *ibid.*, **40**, 1488 (1967).
17) *neo*-Inosadiamine-1,4: F. W. Lichtenthaler and H. O. L. Fischer, *J. Amer. Chem. Soc.*, **83**, 2005 (1961).
18) S. Nishimura, This Bulletin, **32**, 61 (1959).
19) F. W. Lichtenthaler and P. Emig, *Carbohyd. Res.*, **7**, 121 (1968).

The Hydroxyphenylation of Methylstyrenes with Phenylpalladium Chloride

Hiroshi HORINO and Naoto INOUE

Department of Chemistry, College of General Education, Tohoku University, Kawauchi, Sendai 980

(Received April 16, 1975)

The reaction of α- or β-methylstyrene with phenylpalladium chloride in aqueous acetone were studied. From *cis*- or *trans*-β-methylstyrene, a mixture of *erythro* and *threo* isomers of hydroxyphenylation products PhMeCHCHOHPh (VIa, VIb) and chlorophenylation products PhMeCHCHClPh (IVa, IVb) were obtained accompanying the phenylated olefins (I, II, and III). The main reaction product was the tertiary alcohol $PhCH_2C(OH)MePh$ (V). The reaction of α-methylstyrene with phenylpalladium chloride gave V exclusively. Phenylpalladium acetate and phenylpalladium bromide were used as phenylating agents. The yields of hydroxyphenylation products are in decreasing order: chloride > bromide > acetate.

Recently, Heck reported a new arylation of olefins with the reactive organopalladium compounds prepared *in situ* from organomercurials and palladium salts to give the arylated olefins.[1)]

When the Heck reaction was applied to some conjugated benzocycloalkenes with phenylpalladium chloride in protic solvents, the phenyl group and an anion part of the protic solvent were found to add to the olefins simultaneously (Oxyphenylation)[2a,b)] The formation of the oxyphenylation products was illustrated by solvolysis of the organopalladium intermediate in which *cis*-elimination of hydridopalladium moiety is prevented by the *cis* configuration between a vicinal phenyl group and the palladium atom.[2b)]

In order to study the general applicability of the oxyphenylation reaction and clarify the reason why the *trans* isomer is obtained exclusively in the reaction of conjugated benzocycloalkenes, we extended our studies to acyclic olefins conjugated to a benzene ring.

In this paper, we describe the reaction of styrene, α- and β-methylstyrene with phenylpalladium chloride in an aqueous acetone.

Results and Discussion

The reaction of *cis*-β-methylstyrene with an equivalent amount of phenylpalladium chloride gave a complicated mixture of products which produced seven peaks in its gas chromatogram. Identification of these compounds was carried out by gas chromatographic analyses (glc) and also isolation by elution column chromatography. They are numbered I, II, III, IV, V and VI in the order of their appearance in the gas chromatogram. (Table 1). Although compounds I and II were unable to be isolated due to their poor yield, they were determined by glc analysis to be *cis*-1,2-diphenyl-1-propene[3)] and 2,3-diphenyl-1-propene,[3)] respectively.

Column chromatography succeeded in isolating the other products. Three crystalline products III (mp 79 °C), IVa (mp 138 °C) and IVb (mp 44 °C) were obtained upon elution with *n*-hexane. Compound III was identified as *trans*-1,2-diphenyl-1-propene.[3)] Further elution with a mixture of benzene and *n*-hexane (1 : 1) produced crystals with a mp of 50 °C (V), whose IR spectrum showed the presence of a carbinol moiety at 3600—3500 cm^{-1} and 1100 cm^{-1}. The structure of V was determined to be 1,2-diphenylpropan-2-ol by comparison with an authentic sample.[5)]

Elution with benzene gave an oily substance VI having absorption bands at 3500—3300 cm^{-1} and 1030—1000 cm^{-1} (carbinol). However, the comparison of the NMR spectrum of VI with those of authentic samples[3)] indicate that VI is a mixture of *erythro*- and

Table 1. Hydroxyphenylation of methylstyrene with phenylpalladium complexes[a)]

Olefin[b)]	PhHgX	PdX_2	Yield[c)] (%)	Product ratio[c)] (%)					
				I	II	III	IV	V	VI
c-MS	PhHgCl	Li_2PdCl_4	83.9	0.8	1.3	33.6	5.4[d)]	40.4	22.8[f)]
t-MS	PhHgCl	Li_2PdCl_4	92.9	1.0	0.2	12.8	27.2[e)]	30.1	15.2[g)]
α-MS	PhHgCl	Li_2PdCl_4	83.8	3.6		4.5		91.9	
c-MS	PhHgBr	Li_2PdBr_4	69.8	9.0	22.5	33.1			11.3
t-MS	PhHgBr	Li_2PdBr_4	37.6	19.1	21.0	45.8		2.1	12.0
α-MS	PhHgBr	Li_2PdBr_4	57.6	1.2	21.0	12.8		64.9	
c-MS	PhHgOAc	$Pd(OAc)_2$	43.0	28.8	32.0	34.2			
t-MS	PhHgOAc	$Pd(OAc)_2$	57.0	9.1	13.5	65.1			
α-MS	PhHgOAc	$Pd(OAc)_2$	37.6	2.6	60.1	37.2			
Styrene	PhHgCl	Li_2PdCl_4	57.1	*t*-Stilbene (88.4)			1,2-Diphenylethanol (6.1)		

a) In a mixture of acetone and water (1 : 1) at 30 °C for 2 hr. b) *c*-MS; *cis*-β-methylstyrene. *t*-MS; *trans*-β-methylstyrene. α-MS; α-methylstyrene. c) Determined by glc analysis (PEG 20M, 180 °C) using α-methylstilbene as the external standard. d) As the decomposition of IVb occurred during glc analyses, the net yield of IV (17%) and the ratio of *erythro* to *threo* IVa/IVb (30/70) was determined independently by column chromatography. e) Only the *erythro* isomer IVa was detected. f) The ratio of *erythro* to *threo* isomer VIa/VIb (47/53) (NMR). g) VIa/VIb (34/66) (NMR).

threo-1,2-diphenylpropan-1-ol (VIa and VIb). The doublet peaks centered at 1.07 and 1.35 ppm were assigned to the methyl protons of VIa and VIb, respectively. The NMR spectrum shows that VI consists of VIa and VIb in a ratio of 47 : 53.

Both IVa and IVb showed the same gas chromatographic peak. The patterns of the NMR spectra of IVa and IVb were very similar to those of VIa and VIb, respectively, and their elemental analyses correspond to $C_{15}H_{15}Cl$. The treatment of VIb with thionyl chloride produced two chlorides which were found to be identical with IVa and IVb. Since the chemical shift of the methyl protons of the *erythro* isomer VIa is located at higher magnetic field than that of the *threo* isomer VIb, the doublet peak centered at 1.17 ppm for IVa and that of 1.54 ppm for IVb were assigned to the methyl protons of *erythro* and *threo*-1,2-diphenylpropyl chloride, respectively. This is the first example of chloride formation in the Heck reaction without cupric chloride. Attention should be called to the glc analysis (PEG 20 M, 180 °C) in which the *threo* chloride IVb decomposed to give olefines I (5.6%), II (4.4%) and III (76%). On the other hand, the *erythro* isomer IVa decomposed to III only in a 12% conversion with the recovery of IVa.

The product distribution in the reactions of *trans*-β-methylstyrene under the same conditions was different from that of *cis*-β-methylstyrene in the following points: 1) the amount of chloride IV from the *trans* olefin was considerably greater than that from the *cis* olefin, 2) only the *erythro* chloride IVa was isolated in the reaction with the *trans* olefin, and 3) the ratio of *erythro* alcohol VIa to the *threo* isomer VIb was determined to be 34 : 66, whereas the *cis* olefin gave a ratio of 47 : 53.

The reaction of α-methylstyrene with phenylpalladium chloride under the same conditions gave the tertiary alcohol V (91.9%) accompanying a small amount of olefins I and III. Styrene reacted with phenylpalladium chloride under the same conditions to give a mixture of *trans*-stilbene (88%) and 1,2-diphenylethanol[6] (6%).

Isolation of the chlorides IVa and IVb is based on the assumption that the hydroxyphenylated product, *e.g.*, the alcohols VIa and VIb, may be derived from IVa and IVb. With the view of confirming this possibility, the chlorides IVa and IVb were treated with a mixture of lithium chloropalladite and mercuric chloride in 50% aqueous acetone at 30 °C for 2 hr. The *threo* isomer IVb gave a mixture of VIa and VIb (34 : 66) with a conversion of 76.3%. On the other hand, the *erythro* isomer VIa was unchanged under the same conditions. This fact indicates that a part of the secondary alcohols VIa and VIb was formed *via* *threo*-1,2-diphenylpropyl chloride IVb.

Heck[1b] proposed step by step and stereospecific reaction mechanisms consisting of the *cis* addition of the phenylpalladium compound to the olefins and subsequent *cis* elimination of the hydridopalladium species. The phenylated olefins I, II and III were obtained in the reaction of *cis*-β-methylstyrene with phenylpalladium acetate. (PhPdOAc in place of PhPdCl in Fig. 1). However, II and III cannot arise from the direct *cis* elimination of hydridopalladium

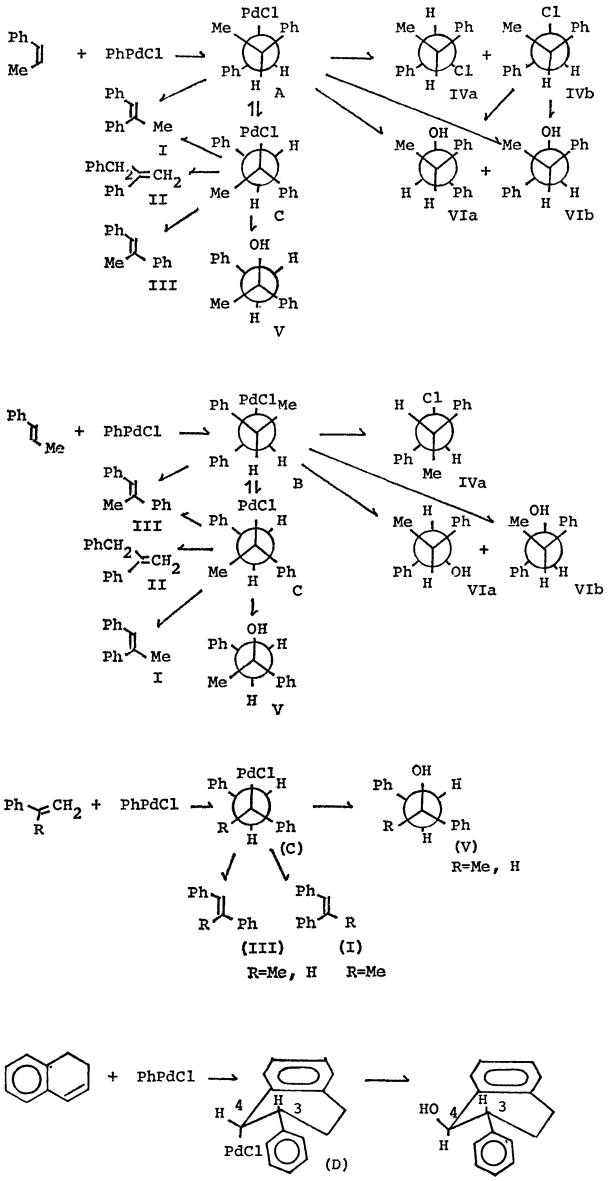

Fig. 1

acetate (HPdOAc) from the initially formed intermediate (A). To explain the formation of II and III, he proposed the formation of a rearranged intermediate (C) which is able to produce the olefins by the *cis* elimination of HPdOAc. The complex C was also used to illustrate the formation of the unexpected olefins I and II from *trans*-methylstyrene.

Henry[7] has studied the stereochemistry of the acetoxypalladation of cyclohexene. He suggested that the reaction intermediate, the *trans* acetoxypalladium compound, was decomposed by the chloride ion *via* the S_N1 mechanism to give the *trans* chloroacetate (with retention of configuration), while *cis* diacetate was produced by reaction with the acetate ion in S_N2 fashion (with inversion of configuration).[8]

Applying the mechanism proposed by Heck and Henry, our experimental results can be explained by the reaction scheme shown in Fig. 1. A *cis* addition of phenylpalladium chloride to *cis* and *trans*-β-methylstyrenes produced the organopalladium intermediates

A and B, respectively. Phenylated olefins I and III are formed by the *cis* elimination of HPdCl from A and B, respectively, while C explains the formation of II and III from *cis*-methylstyrene, or the production of I and II from the *trans* olefin. The secondary chlorides (IVa and IVb) and the secondary alcohols (VIa and VIb) are produced by S_N1-type substitution with the chloride ion and S_N1-type hydrolysis of A and B.

The ratio of *erythro* to *threo* IVa/IVb (30/70) from *cis*-methylstyrene shows that IVb is the main product in S_N1-type substitution of A with the chloride species. However, the failure to isolate IVb from *trans* methylstyrene may be attributed not only to the sensitivity of IVb to hydrolysis under the reaction conditions but also to the small quantity of IVb in this S_N1-type substitution of B. The retention of configuration tendency in the chloride formation is consistent with Henry's conclusion mentioned above. Also, unsuccessful isolation of the expected tertiary chloride from C may be due to its higher reactivity, even if it is produced.

The formation of the tertiary alcohol V from either A or B is unimaginable. The rearrangement of A and B to the tertiary intermediate C is necessary to explain the formation of V. In a protic solvent, the carbon-palladium bond of A, B and C may be somewhat ionic, since the carbon atom bearing the palladium atom is located at a benzylic position liable to solvolysis. On the assumption that the stability of A, B and C is based only on the structure of the benzylic carbon, the tertiary intermediate C is more favorable to the secondary A and B. If an equilibrium between A or B and C exists,[1b] the higher reactivity of C increases the amount of V at the expense of IV and VI. This is supported by the exclusive formation of V from α-methylstyrene. The yield of V is higher than VIa and VIb in the reaction of both *cis* and *trans* β-methylstyrenes.

In previous papers,[2] the authors reported that the oxyphenylation of conjugated benzocycloalkenes gave large quantities of the *trans* alcohols. The elimination of hydridopalladium species between C_3 and C_4 from D (Fig. 1) is difficult because of its *trans* configuration. The exclusive formation of the *trans* alcohol was interpreted on the basis of the prevention of *cis* S_N1-type attack at C_4 by *cis* phenyl group at C_3. However, the corresponding hydroxyphenylation products from methylstyrenes were a mixture of *erythro* and *threo* isomers (VIa and VIb). In the case of acyclic A or B, it is possible to rotate around the carbon-carbon bond of A or B to give the most favorable conformation for S_N1-type solvolysis. Therefore, S_N1-type substitution is rather general for the palladium intermediate in hydroxy- or oxyphenylation.

In order to examine the effect of a chloride ion, the reactions of methylstyrene with phenylpalladium acetate were carried out in the same conditions as in the case of phenylpalladium chloride. The glc and IR analyses of the reaction products indicate the absence of alcohols, but the phenylated olefins I, II and III were obtained in good yields (Table 1).

The reaction of methylstyrenes with phenylpalladium bromide in aqueous acetone gave predominantly phenylated olefins (I, II and III). A trace of the tertiary alcohol V in the reaction of β-methylstyrene suggests the characteristic distinction between bromide and chloride ions (Table 1). However, α-methylstyrene reacted with phenylpalladium bromide producing predominantly V. It is not clear why the ligands of the palladium complexes and the position of the methyl groups on the substrate play a significant role in controlling the direction and extent of the hydroxyphenylation.

Experimental

All melting points and boiling points are uncorrected. Glc analyses were performed using a Shimadzu GC 5A on a 2 m column packed with 5% PEG 20 M. IR and NMR spectra were measured with a Hitachi 215 grating infrared spectrometer by the KBr method, and with a Hitachi R22 in carbon tetrachloride or deuteriochloroform using TMS as the internal standard.

Materials. *cis*-β-Methylstyrene[9] and *trans*-β-methylstyrene[9] were synthesized by decarboxylation of α-methylcinnamic acid and by reduction with cinnamic chloride with lithium aluminum hydride. Styrene and α-methylstyrene of commercial grade were used for distillation before use. Phenylmercuric chloride was prepared by treating commercial phenylmercuric acetate with lithium chloride.

Standard Samples. According to the appropriate references, the following standard samples were synthesized, with which the reaction products were compared by glc analyses, mixed-melting-point tests and spectroscopic techniques.

cis-1,2-diphenyl-1-propene I, mp 46—48 °C (lit,[3] mp 47—48 °C; Found: C, 92.71; H, 7.32%); *trans*-1,2-diphenyl-1-propene III, mp 81—82 °C (lit, [3,5] mp 81—82 °C; Found: C, 92.85; H. 7.41%); 2,3-diphenyl-1-propene II, bp 113—114 °C/4 Torr (lit,[4] 140—143 °C under reduced pressure; Found: C, 92.62; H, 7.38%); *erythro*-1,2-diphenylpropan-1-ol VIa, mp 49—51 °C (lit,[3] mp 50—51 °C; Found: C, 84.20; H, 7.56%); *threo*-1,2-diphenylpropan-1-ol VIb, mp 27 °C (bp 136—137 °C/1—2 Torr. Reported as an oily substance[3]; Found: C, 84.88; H, 7.70%); *p*-nitrobenzoate of VIb, mp 142—143 °C (lit,[3] mp 143—144 °C; Found: C, 73.20; H, 5.42; N, 3.78%); 1,2-diphenylpropan-2-ol V, mp 50 °C (lit,[5] mp 50—51 °C; Found: C, 84.88; H. 7.65%).

erythro- *and* threo-*1,2-Diphenylpropyl Chloride IVa and IVb.* Thionyl chloride (0.72 g, 6 mmol) was added to a cooled solution of VIb (1.06 g, 5 mmol) in dry ether (20 ml) with stirring. The solution became turbid when pyridine (0.2 ml) was introduced. The reaction mixture was stirred for 30 min, and then refluxed for 2 hr. After evaporation of the solvent by suction, the residue was recrystallized from *n*-hexane to give 25 mg of VIa, mp 132—133 °C. Concentration of the mother liquor yielded 955 mg of IVb, mp 48—50 °C. Recrystallization of IVa and IVb was carried out from *n*-hexane and *n*-pentane, respectively. IVa, mp 138 °C. Found: C, 78.09; H, 6.53%. Calcd for $C_{15}H_{15}Cl$: C, 78.09; H, 6.55%. IVb, mp 55 °C. Found: C, 78.29; H, 6.75%. Calcd for $C_{15}H_{15}Cl$: C, 78.09; H, 6.55%.

General Procedure for the Reaction of Methylstyrenes with Phenylpalladium Chloride. To a solution of palladium chloride (1.78 g, 10 mmol) and lithium chloride (0.85 g, 20 mmol) in aqueous acetone (50%, 200 ml), the olefin (12 mmol) and then phenylmercuric chloride (3.13 g, 10 mmol) were added. The mixture was stirred for 2 hr at 30 °C, and then poured into a saturated solution of sodium chloride. The resulting oil was extracted with benzene, dried over

sodium sulfate, and then evaporated under reduced pressure. The residue was diluted with ether to provide a sample solution for glc analysis. After the solvent was replaced with *n*-hexane, the solution was chromatographed on a silica gel column (Wako gel C 200, 60 g). Each volume of these eluted fractions was maintained below 60 ml, some of which were analysed by glc and also checked by IR spectra. Elution with *n*-hexane gave crystals of III, IVb and IVa successively in the order of separation. No depression was observed in the mixed-melting-point tests of III, IVa and IVb with *trans*-1,2-diphenyl-1-propene, *erythro*- and *threo*-1,2-diphenylpropyl chloride, respectively. Evaporation of the benzene-*n*-hexane (1 : 1) eluent produced an oily substance, a part of which was distilled under reduced pressure to give crystals of V. This was identified to be 1,2-diphenylpropan-2-ol from a comparison of the mixed-melting-point test and IR spectrum with those of the authentic sample.[5] Elution with benzene produced another oily substance which, although it possessed a single peak in its gas chromatogram, was found to be a mixture of VIa and VIb from its NMR spectrum. Their structure was determined by comparison of their glc and NMR spectra with those of the standard samples. The ratio was confirmed by comparison of the area of the methyl protons in the NMR spectrum.

Reaction of Methylstyrenes with Phenylpalladium Bromide or Phenylpalladium Acetate. These experiments were carried out in a manner similar to that described above, except for the use of a bromide or an acetate for all anions in the reactions.

Reaction of Styrene with Phenylpalladium Chloride. To a solution of lithium chloropalladite (3 mmol) in a mixture of acetone and water (1 : 1), styrene (345 mg, 3.3 mmol) and phenylmercuric chloride (940 mg, 3 mmol) were added successively. The reaction mixture was treated in the same way as in the reaction of methyl-styrenes. By column chromatography on silica gel, *trans*-stilbene (225 mg) and 1,2-diphenylethanol (20 mg)[6] were eluted with *n*-hexane and benzene, respectively. They were identified by the mixed-melting-point test and the comparison of IR spectra with authentic samples.

Solvolysis of IVa and IVb. A solution of lithium chloropalladite (1 mmol) and mercuric chloride (270 mg, 1 mmol) in aqueous acetone (50%, 20 ml) was added to IVa or IVb (230 mg, 1 mmol), and stirred for 2 hr at 30 °C. The reaction mixture was diluted with an aqueous solution of sodium chloride and extracted with ether. The extract was analyzed by the glc method and then chromatographed on a silica gel column. A mixture of VIa and VIb (42 mg) was prepared and the recovery of IVb (166 mg) were performed, however, no alcohol formation was observed with the quantitative recovery of IVa from the glc and IR analyses of the solvolysis of IVa.

The authors wish to express their thanks to the Kawaken Fine Chemicals Co. Ltd., for its gift of palladium chloride.

References

1) a) R. F. Heck, *J. Amer. Chem. Soc.*, **90**, 5518 (1968). b) R. F. Heck, *ibid.*, **91**, 6707 (1969).

2) a) H. Horino and N. Inoue, This Bulletin, **44**, 3200 (1971). b) H. Horino, M. Arai, and N. Inoue, *ibid.*, **47**, 1683 (1974). c) M. Arai, K. Kabuto, H. Horino, and N. Inoue, *Chem. Lett.*, **1972**, 889.

3) D. J. Cram and F. A. A. Elhalez, *J. Amer. Chem. Soc.*, **74**, 5829 (1952). b) F. A. A. Elhalez and D. J. Cram, *ibid.*, **74**, 5846 (1952).

4) J. von Braun, J. Seeman, and A. Schutheiss, *Ber.*, **55**, 3808 (1922).

5) C. Hell, *Ber.*, **37**, 457 (1904).

6) W. Gerrad and J. Kenyon, *J. Chem. Soc.*, **1928**, 2564.

7) P. M. Henry and G. A. Ward, *J. Amer. Chem. Soc.*, **93**, 1494 (1971).

8) In the paper of Henry, a chloroacetate of the same configuration as the chloropalladium group of the reaction intermediate was explained to result from the S_N1 substitution by a chloride complexed to palladium.

9) W. R. R. Park and G. F. Wright, *J. Org. Chem.*, **19**, 1435 (1959).

Aromatic Solvent-induced Shift(ASIS). I. An Interpretation Based on the Dipole-Quadrupole Interaction[1)]

Kunio NIKKI, Naoya NAKAGAWA, and Yoshito TAKEUCHI*

The University of Electro-Communications, Chofu, Tokyo 182

**Department of Chemistry, College of General Education, University of Tokyo, Komaba, Meguro-ku, Tokyo 153*

(Received April 17, 1975)

Two general theoretical ways of estimating aromatic solvent-induced shifts(ASIS), which are based on the dipole (solute)-induced diple(solvent) interaction [(μ-μ')interaction] or the dipole(solute)-quadrupole(solvent) interaction [(μ-Q) interaction], are proposed. Solvent shifts can occur by means of the magnetic anisotropy of solvent molecules, which take specific orientations due to those electro-static interactions. As an example, we calculate the ASIS of a hypothetical spherical molecule, a model for camphor, with a dipole near the center and covered with protons, immersed in benzene. The estimated ASIS based on (μ-μ') interaction is much too small to account for the shifts normally observed, while those based on (μ-Q) interaction agree well with the observed ASIS in respect to both its magnitude and angular dependency (*e.g.*, the carbonyl plane rule). More specifically, the theoretical and experimental ASIS for methyl protons of camphor are compared.

It is well known that large chemical-shift differences are often incurred by the proton resonance of organic molecules if the medium is changed from a solvent such as cyclohexane or carbon tetrachloride to an aromatic solvent like benzene. This phenomenon is frequently referred to as the aromatic solvent-induced shift (ASIS).[2-5)]

Various explanations have been put forward to explain the ASIS. These have been based on a kind of hydrogen-bonding,[6)] the 1 : 1 complex formation between the solute and the solvent, particularly of the specifically oriented one,[7-9)] the dipole-induced dipole interaction,[10)] the time-averaged 1 : n cluster formation,[5)] *etc.* Several years ago one of the present authors suggested that the interaction between the permanent dipole of the solute and the permanent quadrupole of the aromatic solvent might cause ASIS.[12)] The purpose of this paper is to give quantitative evidence for this interaction.

Theoretical

It is noteworthy that ASIS are observed for those molecules having a permanent dipole. Hence, whatever the origin of the ASIS, the permanent dipole of the solute should be responsible for the solute-solvent interaction which causes the ASIS. There are various possible modes of electrostatic interaction between the solute and the solvent, in which the solute permanent dipole plays an important role. These modes are the dipole(solute)-dipole(solvent) interaction, the dipole(solute)-induced dipole(solvent) interaction [hereafter specified as the (μ-μ') interaction], the dipole(solute)-quadrupole(solvent) interaction [hereafter specified as the (μ-Q) interaction], and interactions of higher orders. The first will not be considered here since a benzene molecule has no permanent dipole; also, the last need not be taken into consideration, as their magnitude must be very small. Now, these two (μ-μ') and (μ-Q) interactions will be compared.

When molecules with a permanent dipole are dissolved in benzene, the orientation of benzene molecules surrounding a solute molecule is less random than that of pure benzene molecules; they take a specific orientation due to the electric field caused by the permanent dipole. The situation is best represented in Figs. 1a and 1b. As is indicated, the orientation is, as a whole, determined by the assumed interaction, (μ-μ') or (μ-Q), between the solute and the solvent. The ASIS should reflect the orientation involved. The calculation of the ASIS will be carried out in the following manners.

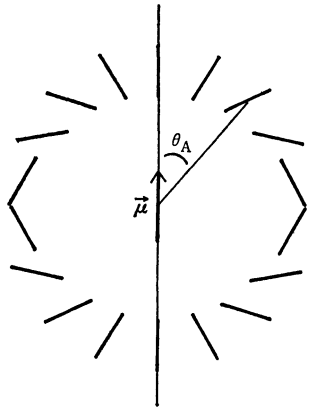

Fig. 1a. Orientation of benzene molecules in the least stable direction based on the (μ-μ') interaction. —— is a six-fold axis of symmetry of benzene.

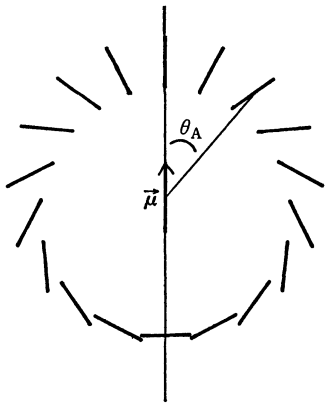

Fig. 1b. Orientation of benzene molecules in the most stable direction based on the (μ-Q) interaction.

ASIS Caused by the Dipole-induced Dipole (μ-μ') Interaction. First, the energy of the (μ-μ') interac-

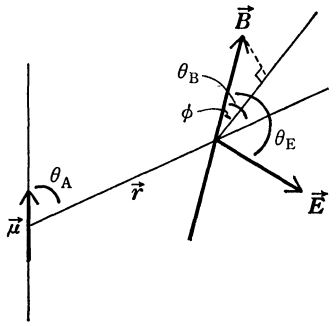

Fig. 2. A benzene molecule in a permanent dipole field of a solute molecule.

tion between one solute and one solvent is carried out. In Fig. 2 the parameters required for the calculation are defined: $\vec{\mu}$ is the permanent dipole of the solute located at the point of origin, $\vec{r}$ is the distance from the origin to the center of a solvent molecule, and θ_A is the angle between $\vec{\mu}$ and $\vec{r}$. The orientation of a benzene molecule is conveniently defined by the direction of its six-fold axis $\vec{B}$, rather than by its plane. θ_B is the angle between $\vec{B}$ and $\vec{r}$. ϕ is the dihedral angle between the plane containing $\vec{\mu}$ and $\vec{r}$ and that containing $\vec{r}$ and $\vec{B}$. $\vec{E}$ represents the electric-field vector at the benzene molecule caused by the $\vec{\mu}$ of the solute, and $|\vec{E}|$ is defined by Eq. (1):

$$E = |\vec{E}| = |\vec{\mu}|\sqrt{1+3\cos^2\theta_A}\cdot r^{-3} \tag{1}$$

θ_E is the angle between $\vec{B}$ and $\vec{E}$; it is related to θ_A, θ_B, and ϕ as is shown in Eq. (2):

$$\cos\theta_E = (\cos\theta_A\cos\theta_B - \sin\theta_A\sin\theta_B\cos\phi)/\sqrt{1+3\cos^2\theta_A} \tag{2}$$

An induced dipole, $\vec{\mu}'$, is caused in a benzene molecule when it is placed in the electric field, $\vec{E}$, as defined by Eq. (3):

$$\vec{\mu}' = \alpha\cdot\vec{E} \tag{3}$$

where α is the electric polarisability of a benzene molecule.

The energy of interaction between $\vec{\mu}$ and $\vec{\mu}'$ is given by Eq. (4):

$$U_{\mu\text{-}\mu'} = -\vec{\mu}'\cdot\vec{E} = -(1/2)\{\alpha^{\parallel}(E\cdot\cos\theta_E)^2 + \alpha^{\perp}(E\cdot\sin\theta_E)^2\} \tag{4}$$

By substituting Eqs. (1) and (2) in Eq. (4), Eq. (5) is obtained:

$$U_{\mu\text{-}\mu'} = -\mu^2\{(\alpha^{\parallel}-\alpha^{\perp})(2\cos\theta_A\cos\theta_B - \sin\theta_A\sin\theta_B\cos\phi)^2 + \alpha^{\perp}(1+3\cos^2\theta_A)\}\cdot r^{-6} \tag{5}$$

where $\alpha^{\parallel}$ and $\alpha^{\perp}$ are the parallel and perpendicular components of the electric polarisability of a benzene molecule in respect to its axis of symmetry.

As a result of this solute-solvent interaction, benzene molecules will be oriented around the solute with a decreased randomness of orientation.

As an aromatic solvent has an anisotropy of magnetic susceptibility, the shift $\delta(\mu\text{-}\mu')$ observed for a proton of the solute due to one benzene molecule at the one position is given by:

$$\delta(\mu\text{-}\mu') = \frac{\int_{\theta_B}\int_{\phi}\Delta\chi(1-3\cos^2\xi)(3R^3)^{-1}\exp(-U_{\mu\text{-}\mu'}/kT)\sin\theta_B d\theta_B d\phi}{\int_{\theta_B}\int_{\phi}\exp(-U_{\mu\text{-}\mu'}/kT)\sin\theta_B\, d\theta_B\, d\phi} \tag{6}$$

where $\Delta\chi(=\chi^{\parallel}-\chi^{\perp}=\chi^{\perp}-\chi^{\perp *})$ is the diamagnetic anisotropy of benzene, ξ is an angle between the axis $\vec{B}$ and $\vec{R}$, and $\vec{R}$ is the distance from the center of benzene to the proton in question (see Fig. 3).

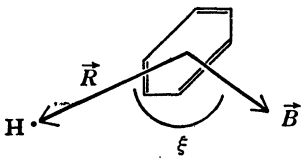

Fig. 3. Relationship between a benzene molecule and a proton in question.

By difinition, the ASIS, $\sigma(\mu\text{-}\mu')$, is the sum of the effect of all the benzene molecules around the solute; thus,

$$\sigma(\mu\text{-}\mu') = \int\rho\delta(\mu\text{-}\mu')\,d\tau \tag{7}$$

where ρ is the specific density of benzene. The integration is carried out throughout the space except for the excluded volume of the solute (as $\rho=0$). The excluded volume was defined as the region surrounding a solute molecule into which the center of a solvent molecule cannot enter.

ASIS Caused by the Dipole-Quadrupole(μ-Q) Interaction. The calculation of the ASIS caused by the interaction between the permanent electric dipole moment of a solute molecule and the permanent electric quadrupole moment of a benzene molecule was performed in the following manner. The molecular quadrupole moment along a principal axis is defined by:[13]

$$Q_{\alpha\alpha} = \frac{|e|}{2}\sum_n Z_n(3\alpha_n^2 - r_n^2) - \frac{|e|}{2}\langle 0|3\alpha_i^2 - r_i^2|0\rangle \tag{8}$$
$$\alpha = x,\ y,\ z$$

where e is the unit electric charge, Z_n is the atomic number of the n-th nucleus, α_n and α_i are the nuclear and the electric coordinates, and the summation is over the n nuclei and i electrons. $\langle 0|\ |0\rangle$ indicates the electric ground-state average value. A quadrupole tensor of a benzene molecule, calculated from the magnetic anisotropy, is given by:[13]

$$Q = \begin{vmatrix} 2.8\pm1.4 & 0 & 0 \\ 0 & 2.8\pm1.4 & 0 \\ 0 & 0 & -5.6\pm2.8 \end{vmatrix} \times 10^{-26}\ \text{esu} \tag{9}$$

The electrostatic energy of a molecular quadrupole at the position of r from the dipole is given by:

$$U_{\mu\text{-}Q} = qq'\left(\frac{2}{r_1} - \frac{1}{r_2} - \frac{1}{r_3} - \frac{2}{r_4} + \frac{1}{r_5} + \frac{1}{r_6}\right) \tag{10}$$

where q is the electric charge of the bar-dipole (solute) with the length of $2a$, where q' is the electric charge of a bar-quadrupole (solvent) with the length of $2b$, and where r_1^{-1}, r_2^{-1}, r_3^{-1}, *etc.* are given by:

$$r_1^{-1} = r^{-1}(1-2\cos\theta_A \cdot ar^{-1}+a^2r^{-2})^{-1/2}$$
$$= r^{-1}\{1+\cos\theta_A \cdot ar^{-1}+(1/2)(3\cos^2\theta_A-1)\cdot a^2r^{-2}$$
$$+ (1/2)(5\cos^3\theta_A-3\cos\theta_A)\cdot a^3r^{-3}+\cdots\cdots\} \quad (11)$$

$$r_2^{-1} = r_1^{-1}\{1+(\cos\theta_B\cos\delta-\sin\theta_B\sin\delta\cos\phi)\cdot 2br_1^{-1}+b^2r_1^{-2}\}^{-1/2}$$
$$= r_1^{-1}[1-(\cos\theta_B\cos\delta-\sin\theta_B\sin\delta\cos\phi)\cdot br_1^{-1}+$$
$$(1/2)\{3(\cos\theta_B\cos\delta-\sin\theta_B\sin\delta\cos\phi)^2-1\}\cdot b^2r_1^{-2}-$$
$$(1/2)\{5(\cos\theta_B\cos\delta-\sin\theta_B\sin\delta\cos\phi)^3-$$
$$3(\cos\theta_B\cos\delta-\sin\theta_B\sin\delta\cos\phi)\}b^3r_1^{-3}+\cdots\cdots] \quad (12)$$

$$r_3^{-1} = r_1^{-1}\{1-(\cos\theta_B\cos\delta-\sin\theta_B\sin\delta\cos\phi)\cdot 2br_1^{-1}+b^2r_1^{-2}\}^{-1/2}$$
$$= r_1^{-1}[1+(\cos\theta_B\cos\delta-\sin\theta_B\sin\delta\cos\phi)\cdot br_1^{-1}+$$
$$(1/2)\{3(\cos\theta_B\cos\delta-\sin\theta_B\sin\delta\cos\phi)^2-1\}\cdot b^2r_1^{-2}+$$
$$(1/2)\{5(\cos\theta_B\cos\delta-\sin\theta_B\sin\delta\cos\phi)^3-$$
$$3(\cos\theta_B\cos\delta-\sin\theta_B\sin\delta\cos\phi)\}\cdot b^3r_1^{-3}+\cdots\cdots] \quad (13)$$

etc., where δ is the angle between $\vec{r}$ and $\vec{r}_1$; then $\sin\delta = a\cdot\sin\theta_A/r_1$ (see Fig. 4).

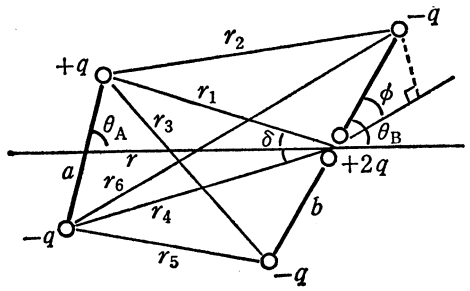

Fig. 4. Electrostatic interaction between bar-dipole and bar-quadrupole. q is the electric charge of the dipole. q' is the electric charge of the quadrupole.

The substitution of Eqs. (11), (12), (13), *etc.* into Eq. (10) and the use of the point-dipole and -quadrupole approximations, ($r \gg a$, $r \gg b$ and $\delta=0$), will give the orientation energy by means of:

$$U_{\mu\text{-Q}} = -6qq'ab^2r^{-4}\{\cos\theta_A(1-3\cos^2\theta_B)$$
$$+ 2\cos\theta_B\sin\theta_B\sin\theta_A\cos\phi\}$$
$$= -(3/2)\mu Q_{zz}r^{-4}\{\cos\theta_A(1-3\cos^2\theta_B)$$
$$+ 2\cos\theta_B\sin\theta_B\sin\theta_A\cos\phi\} \quad (14)$$

where Q_{zz} is the principal value of the quadrupole moment on the six-fold axis of a benzene molecule.

Thus, the shift, $\delta(\mu\text{-Q})$, observed for a proton of a solute molecule caused by one solvent molecule at one position is given by:

$$\delta(\mu\text{-Q}) = \frac{\int_{\theta_B}\int_{\phi} A\chi(1-3\cos^2\xi)(3R^3)^{-1}\exp(-U_{\mu\text{-Q}}/kT)\sin\theta_B d\theta_B d\phi}{\int_{\theta_B}\int_{\phi}\exp(-U_{\mu\text{-Q}}/kT)\sin\theta_B d\theta_B d\phi} \quad (15)$$

The $\sigma(\mu\text{-Q})$ ASIS can be estimated in the manner described in the previous section.

Calculation

Point-dipole (-quadrupole) approximations are employed for calculating the electrostatic interaction between the solute and the solvent. Thus, both the electric polarization of a solute molecule and the induced polarization of a benzene molecule are approximated as a point dipole, whereas the electric distribution in a benzene molecule (molecular quadrupole) was approximated as a point quadrupole at the center of the molecule. Unless the solvent molecule is in contact with the solute molecule, the dielectric constant of the medium should be considered. In our calculation, however, it was assumed to be unity for all the distances.

The energies of the dipole-induced dipole interaction and the dipole-quadrupole interaction are given by Eqs. (5) and (14) respectively. The maximum and the minimum energy of the two interactions are plotted against the distance, r, in Fig. 5. As in our calculation, the difference between the maximum and the minimum energy due to the (μ-Q) interaction at the one position at any value of r larger than 4.45 Å, the closest possible distance between the solute and benzene, was about 14 times as large as that due to the (μ-μ') interaction. This indicates that the (μ-Q) interaction is almost exclusively responsible for the orientation of the benzene molecules around the solute.

In order to obtain a general perspective as the magnitude of the ASIS caused by two interactions, a spherical-model molecule, with a diameter of 2.9 Å and a permanent dipole of 3.1 D which is located 1.5 Å

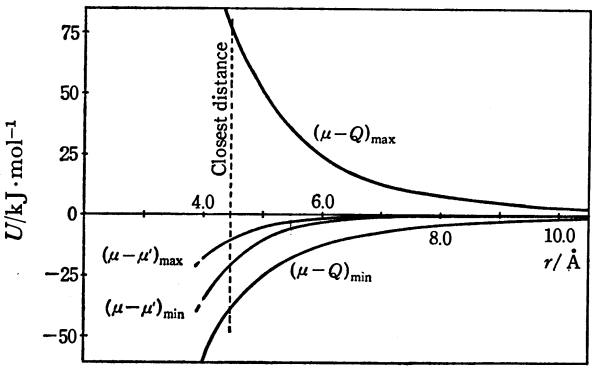

Fig. 5. The maximum energy and the minimum energy of the dipole-induced dipole interaction and the dipole-quadrupole interaction.

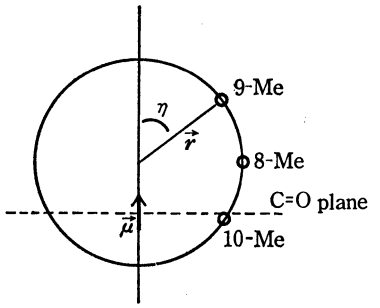

Fig. 6. A spherical "model" molecule. ↑ is the dipole, and ○ is a center of a "methyl" group on the sphere.

apart from, and pointed toward, the center of the sphere (Fig. 6), was introduced. The "average" position (proton point) of the three protons of each methyl group of camphor was on the surface of the sphere, when the dipole of camphor is superimposed on the dipole of the model. For the benzene molecule we assumed a sphere with a van der Waals radius of 1.85 Å. The values used for the calculation were as follows:

$\Delta\alpha$ (benzene): -60×10^{-25} esu

$\Delta\chi$ (benzene): -0.9×10^{-28} esu

Q_{zz} (benzene): -5.6×10^{-26} esu

ρ (benzene): 0.00679 molecule/Å^3

van der Waals radius of H: 1.2 Å.

In the computation of $\delta(\mu\text{-}\mu')$ and $\delta(\mu\text{-Q})$, the $\int_{\theta_B}\int_{\phi} f(\theta_B, \phi)d\theta_B d\phi$ integration is approximated by a double summation:

$$\sum_{\theta_B=0}^{180^\circ}\sum_{\phi=0}^{360^\circ} f(\theta_B, \phi)\Delta\theta\Delta\phi$$

with $\Delta\theta_B=10^\circ$ and $\Delta\phi=10^\circ$.**

In a similar manner, $\int\rho\delta(\mu\text{-}\mu')d\tau$ and $\int\rho\delta(\mu\text{-Q})d\tau$ are approximated by the triple summation:

$$\sum_{\theta_A=0}^{180^\circ}\sum_{\phi=0}^{360^\circ}\sum_{r=4.45\text{Å}}^{10.5\text{Å}} f(\theta_A, \phi, r)\Delta\theta_A\Delta\phi\Delta r$$

where $\Delta\theta_A$ and $\Delta\phi$ are taken as 10°† and Δr as $0.1r$. θ_A and ϕ varied from 0° to 180° and from 0° to 360° respectively, whereas r varied from 4.45 Å, which corresponds to the smallest possible distance between a benzene molecule and a solute molecule (closest distance), to 10.5 Å.††

The calculated ASIS for the model molecules based on $(\mu\text{-}\mu')$ or $(\mu\text{-Q})$ interactions are plotted against an angle in the model molecule (see Fig. 6) in Fig. 7.

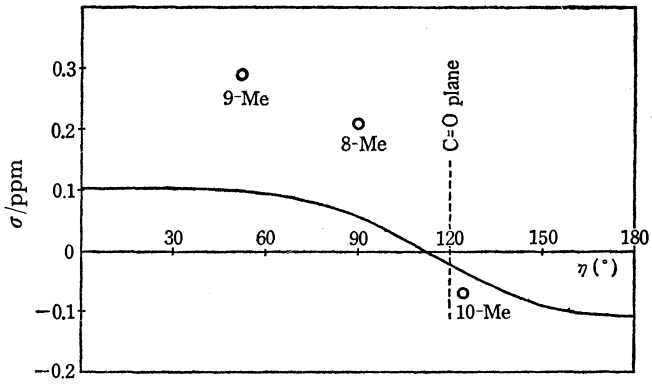

Fig. 7. The angular dependency of ASIS. η is an angle between $\vec{\mu}$ and $\vec{r}$ (a distance of a proton from the center of the sphere). A solid line represents calculated values, $\sigma(\mu\text{-}Q)$, and ○ represent observed values of ASIS of methyl groups of camphor.

Discussion

It is surprising that no quantitative calculation has ever been attempted to assess the ASIS caused by the $(\mu\text{-}\mu')$ interaction, although most, if not all, of the proposed interpretations have been based on this interaction.

Our calculations indicate that the energy of the $(\mu\text{-}\mu')$ interaction is so small that no appreciable orientation is incurred in benzene molecules. Hence, the ASIS caused by this interaction is negligibly small. On the contrary, the $(\mu\text{-Q})$ interaction seems to cause a noticeable orientation; hence, the ASIS caused is at least hundred times as large. For example, the observed ASIS for three methyl groups of camphor are plotted in Fig. 7. The locations of the proton points were estimated from the geometry of the camphor, as determined by the HGS molecular model. The agreement between the calculated and observed values proves that our assumption is qualitatively correct. In our preliminary paper,[1] we took only three possible orientations of benzene molecules into consideration, for the sake of simplicity, instead of all the possible ones as we have done in this paper. The estimated ASIS under that approximation was twice as large as the present estimation.

Far more important in predicting the ASIS is its sense (its upfield or downfield shift, as compared with the chemical shifts in a neutral solvent). This is particularly the case with carbonyl compounds where the observed ASIS is quite dependent on the relative geometry of the proton(s) in question and on the carbonyl dipole, as summarised by the so-called carbonyl plane rule.[11] According to this rule, protons lying in front of (or behind) the carbonyl plane (a plane perpendicular to $\vec{\mu}$ and through the carbonyl carbon) exhibit a positive (negative) ASIS, while protons on the plane show virtually no ASIS. This empirical rule is in good agreement with our calculated results.

Thus, for a polar solute molecule the dipole-quadrupole interaction model is a much better approximation of the ASIS than the dipole-induced dipole interaction model in estimating its magnitude and "sense." This electrostatic interaction model is now being used in our laboratories to study the solvent shifts caused by other solvents, including hexafluorobenzene and carbon disulfide.

** Much the same results were obtained with $\Delta\theta_B$ and $\Delta\phi=5^\circ$.

† Calculations were also carried out with $\Delta\theta_A$ and $\Delta\phi=5^\circ$; these results were much the same as those, given in the text.

†† At this distance, δ is almost 1/4000 of that at the closest distance.

References

1) Preliminary communication: N. Nakagawa, K. Nikki, Y. Takeuchi, and I. Kumagai; *Chem. Lett.*, **1972**, 1239.

2) J. A. Pople, W. G. Schneider, and H. J. Bernstein; "High-resolution Nuclear Magnetic Resonance, "McGraw-Hill, New York (1959), p. 427.

3) P. Laszlo; *Nucl. Magn. Resonan. Spectrosc.*, **3**, 348 (1967).

4) J. Ronayne and D. H. Williams; *Ann. Rev. Nucl. Magn. Resonance Spectrosc.*, **2**, 97 (1969).

5) E. M. Engler and P. Laszlo; *J. Amer. Chem. Soc.*, **93**, 1317 (1971).

6) A. A, Bothner-By and R. E. Glick; *J. Chem. Phys.*, **26**, 1651 (1957).
7) N. S. Bhacca and D. H. Williams; "Applications of NMR Spectroscopy in Organic Chemistry," Holden-Day, San Francisco (1966), p. 159.
8) J. Ronayne and D. H. Williams; *J. Chem. Soc., B*, **1967**, 540.
9) T. Ledaal; *Tetrahedron Lett.*, **1968**, 1683.
10) W. G. Schneider; *J. Phys. Chem.*, **66**, 2653 (1962).
11) J. D. Connoly and R. McCrindle; *Chem. Ind.* (London), **1965**, 379.
12) N. Nakagawa; "The Interpretation of NMR Spectra," Kyoritsu-Shuppan, Tokyo (1966), p. 76.
13) R. L. Shoemaker and W. H. Flygare; *J. Chem. Phys.*, **51**, 2988 (1969).
14) A. L. McClellan; "Tables of Experimental Dipole Moments," W. H. Freeman and Co., San Francisco (1963).
15) M. P. Bogaard, A. D. Buckingham, M. G. Corfield, D. A. Dunmur, and A. H. White, *Chem. Phys. Lett.*, **14**, 558 (1972).

α-Thiocarbonyl-stabilized Triphenylphosphonium Ylides: Preparation, Structure, and Alkylation Reactions

Hiroshi YOSHIDA, Hironori MATSUURA, Tsuyoshi OGATA, and Saburo INOKAWA

Department of Synthetic Chemistry, Faculty of Engineering, Shizuoka University, Johoku, Hamamatsu 430

(Received April 21, 1975)

A number of α-thiocarbonyl-stabilized ylides II were prepared in moderate yields, and their alkylation reactions were studied. II(H, MeO), II(H, EtO), II(H, i-PrO), and II(H,H) were mixtures of *cis* and *trans* isomers, and the II_{cis}/II_{trans} ratios were solvent-dependent. II(H, Ph), II(H, Me_2N), II(H, MeS), and II(H, EtS) were composed of only *cis* isomers. All these ylides II with alkyl iodide gave S-alkylation products in good yields.

The physical and chemical properties of carbonyl-stabilized phosphonium ylides (I) have been widely studied in recent years.[1] In this report we will discuss the structure and alkylation reactions of thiocarbonyl-stabilized triphenylphosphonium ylides (II).

Results and Discussion

Preparation of II(R^1,R). The reaction of triphenylphosphonium alkylide (III) with *S*-alkyl thiolcarboxylates yields phosphonium acylalkylides in good yields.[2]

The treatment of III with a two-fold excess of thionocarboxylate (IV) was performed in benzene under a nitrogen atmosphere at room temperature or under ice-water cooling. The product was then purified by crystallization. The results are collected in Table 1.

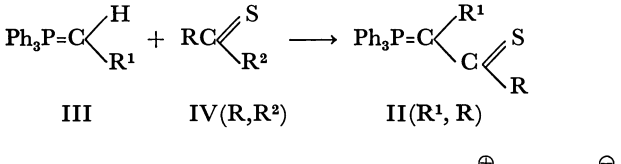

III IV(R,R^2) II(R^1, R)

Structure of II(R^1,R) and Alkylation Reaction. The NMR spectra of carbonyl-stabilized phosphonium ylides (I) have been widely studied in recent years. The NMR spectra of ester-stabilized ylides I(H, Alkyl-O) have been shown to be a mixture of *cis* and *trans* isomers;[3] however, keto-stabilized ylides I(R^1, Alkyl or Aryl) are only *cis* isomers[4] unless R is large and R^1 is strongly electron-withdrawing.[5] Keto-stabilized ylides I(Cl, Ph) and I(I, Ph) have been shown to be *cis* by X-ray studies.[6,7]

It is known that ester-stabilized ylides I(R^1, Alkyl-O) undergo alkylation with alkyl halides to give normal C-alkylation products,[8] whereas alkylation with triethyloxonium fluoroborate yields a mixture of C- and

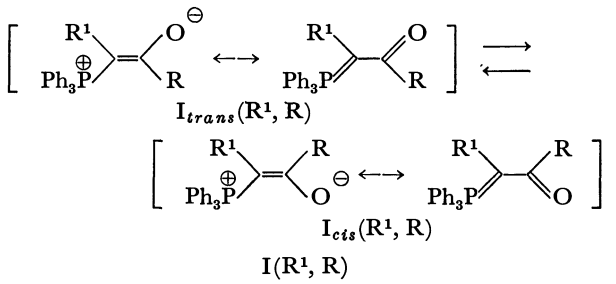

$I_{trans}(R^1, R)$ $I_{cis}(R^1, R)$ $I(R^1, R)$

Table 1. Preparation of II(R^1, R) and their physical properties

II(R^1, R)	IV	Yield (%)	Mp (°C)	II(R^1, R) in $CDCl_3$	
				Conf. (%)	NMR(δ)[a], *J* are in Hz.
II(H, MeO)	$MeOCS_2Me$	38	164—165	*cis*(45)	3.83(s, MeO), 4.32(d, *J*=26.0, methine)
				trans(55)	3.53(s, MeO), 4.64(d, *J*=26.0, methine)
II(H, EtO)	$EtOCS_2Me$	41	133—134	*cis*(40)	1.30(t, *J*=7.9, Me), 4.35(*J*=26.0, methine), 4.42(q, CH_2)
				trans(60)	0.67(t, *J*=7.9, Me), 4.23(q, CH_2), 4.68(d, *J*=25.5, methine)
II(H, *i*-PrO)	*i*-$PrOCS_2Me$	56	156—158	*cis*(21)	1.27(d, *J*=6.5, Me), 4.33(d, *J*=26.0, methine)
				trans(79)	0.72(d, *J*=6.5, Me), 4.68(d, *J*=25.9, methine), 5.52(sept, methine)
II(Me, MeO)	$MeOCS_2Me$	43	251—253	*cis*(16)	1.66(d, *J*=14.8, Me), 3.95(s, MeO)
				trans(84)	1.97(d, *J*=14.9, Me), 3.37(s, MeO)
II(H, Ph)	$PhCS_2Me$	45	179—181	*cis*(100)	5.66(d, *J*=30.0, methine)
II(H, MeS)	$MeSCS_2Me$	40	183—184	*cis*(100)	2.53(s, MeS), 5.10(d, *J*=28.1, methine)
II(H, EtS)	$EtSCS_2Et$	47	125—127	*cis*(100)	1.30(t, *J*=8.0, Me), 3.13(q, CH_2), 5.11(d, *J*=28.2, methine)
II(H, Me_2N)	Me_2NCS_2Me	28	142—144	*cis*(100)	3.28(s, Me_2N), 3.61(d, *J*=27.9, methine)
II(H, H)	HCSOMe	54	213—215	*cis*(19) *trans*(81)	see Table 4
II(Me, H)	HCSOMe	48	267—269	*trans*(100)	see Table 4

a) Phenyl protons were observed at about 7.2—7.8(m).

Table 2. Alkylation of II with alkyl iodide (R'I) in $CDCl_3$

II	R'I	V (R^1, R, R')		
		Conf.	Mp (°C)	NMR (δ in $CDCl_3$)[a], J are in Hz
II(H, MeO)	MeI	*cis*	Resinous	2.27(s, MeS), 4.33(s, MeO), 5.36(d, J=10.8, methine)
		trans		2.83(s, MeS), 3.60(s, MeO), 5.11(d, J=13.6, methine)
II(H, EtO)	MeI	*cis*	Resinous	1.51(t, J=7.9, Me), 2.29(s, MeS), 4.62(q, CH_2), 5.30 (d, J=10.9, methine)
		trans		0.73(t, J=7.8, Me), 2.83(s, MeS), 4.05(q, CH_2), 5.04 (d, J=13.9, methine)
II(H, *i*-PrO)	MeI	*cis*	Resinous	1.52(d, J=6.5, Me), 2.25(s, MeS), 5.28(d, J=10.5, methine), 5.41(sept, methine)
		trans		0.87(d, J=6.5, Me), 2.88(s, MeS), 4.78(sept, methine), 4.98(d, J=15.0, meshine)
II(H, Ph)	MeI	*cis*	198—200	1.91(s, MeS), 6.41(d, J=21.8, methine)
II(H, MeS)	MeI	*cis*	195—197	2.39(s, MeS), 2.92(s, MeS), 6.02(d, J=16.2, methine)
II(H, EtS)	MeI	*cis*	125—127	1.47(t, J=7.3, Me), 2.38(s, MeS), 3.39(q, CH_2), 5.95 (d, J=16.1, methine)
II(H, MeS)	EtI	*cis*	167—169	1.03(t, J=7.2, Me), 2.94(q, CH_2), 2.85(s, MeS), 6.04 (d, J=17.1, methine)
II(H, Me_2N)	MeI	*cis*	191—192	1.69(s, MeS), 3.39(s, Me_2N), 4.39(d, J=19.2, methine)

a) Phenyl protons were appered at about 7.2—7.8(m).

Table 3. *cis*/*trans* ratios for I[a] and II[b] in various solvents

Solvent(ε)	I(H, MeO)	II(H, MeO)	I(H, EtO)	II(H, EtO)	I(H, *i*-PrO)	II(H, *i*-PrO)
PhH(2.27)	*cis*	3.5	5.9	2.1	2.9	1.8
CD_3CN(37.5)	5	1.9	2.3	1.2	1.3	0.82
CD_3NO_2(38.6)	4.0	2.1	2.4	1.2	1.4	0.56
$CDCl_3$(4.7)	4.6	0.82	1.8	0.67	1.0	0.36

a) Taken from Ref. 3. Recorded at −10—0 °C. b) Recorded at 34.5 °C.

O-alkylation products (O-rich).[9] Keto-stabilized ylides I(R^1, Alkyl or Aryl) react with alkyl halides to give O-alkylation products.[10] Contrary to these results, the alkylation of II with alkyl iodides takes place exclusively at sulfur and easily at room temperature to give salts V in quantitative yields (Table 2).

The stereochemistry of the products was assigned on the assumptions that the protons of the R group *cis* to the phosphorus are shielded by the phenyl rings and that they appear at a higher field than the R *trans* to the phosphorus.

The variable-temperature NMR study of I(H, MeO) shows the methyl protons as a singlet above the coalescence temperature (T_c=35±3 °C for I(H, MeO)) and an unsymmetrical doublet at a lower temperature.[4] The NMR spectra of II(H, Alkyl-O) at 34.5 °C gave clean peaks of two groups corresponding to the *cis* and *trans* isomers (Table 1). These results indicate that the T_c for II (H, Alkyl-O) may be higher than the T_c for I(H, Alkyl-O). However, the rotation for II is not restricted, since II (H, Alkyl-O) reached equilibrium fairly rapidly in any solvent and the II_{cis}/II_{trans} ratio was nearly constant during the reaction with alkyl halides.

In a previous communication[11] we have reported on the effect of solvents on the II_{cis} (H, Alkyl-O)/II_{trans} (H, Alkyl-O) isomer ratios and on the effect of alkylating reagents on the V_{cis}(H, Alkyl-O, R')/V_{trans} (H, Alkyl-O, R') products ratios. Here, only representative data are collected in Table 3.

It is clear that $P^{\oplus}/O^{\ominus}$ or $P^{\oplus}/S^{\ominus}$ attraction is maximized in I_{cis} or II_{cis}. For ester-stabilized ylides I, it has been reported that a large R and an increasing solvent aggregation about the ester carbonyl favor a relatively high population of the *trans* form.[3] The regular variation in I_{cis}/I_{trans} found for ylides I is interpreted as a result of steric inhibition of solvation.[3] As is shown in Table 3, both I(H, Alkyl-O) and II(H, Alkyl-O) show similar properties. The smaller *cis*/*trans* value for II than for I seems to show a higher solvent aggregation around thiocarbonyl than that around carbonyl. This result clearly reflects the higher mesomeric character of the thiocarbonyl than the carbonyl group. This trend is especially marked in the chloroform solvent, with which negative oxygen or sulfur associates by hydrogen-bonding interaction.[3]

The ylides II(H, Ph), II(H, Me_2N), II(H, MeS), and II(H, EtS) gave only a single *cis* isomer. The structure was confirmed as follows.

The methylation of II(H, MeS) with methyl iodide gave needles whose NMR spectrum showed two *S*-methyl peaks, at δ 2.39 and 2.92 in $CDCl_3$. The ethylation of II(H, MeS) with ethyl iodide gave needles with a mp of 167—169 °C, which showed only one *S*-methyl signal, at δ 2.85. II(H, EtS) reacted with methyl iodide to give needles (mp 125—127 °C) which showed one *S*-methyl signal, at 2.38. Thus, these alkylation products were confirmed to be V_{cis}(H, MeS, Me), V_{cis}(H, MeS, Et), and V_{cis}(H, EtS, Me). These products were stable for more than 20 hr at 80—90 °C

Table 4. NMR data for II(H, H), II(Me, H) and their methylation products in $CDCl_3$.

Compound	δ_{R^1}	δ_R	J_{R^1R}	$J_{PCR'}$(Hz)	J_{PCCR}(Hz)	δ_{SMe}
II_{cis}(H, H)	5.17	9.34	8.1	30.2	45.0	
II_{trans}(H, H)	5.94	8.69	14.8	26.0	15.3	
V_{cis}(H, H, Me)	6.80	8.73	12.0	15.9	44.0	2.54
V_{trans}(H, H, Me)	a)	a)				2.81
II_{trans}(Me, H)	2.21	8.66		13.7	18.6	
V_{trans}(Me, H, Me)	2.11	7.19		13.7	21.1	2.55

a) Signals were appered in the phenyl proton region.

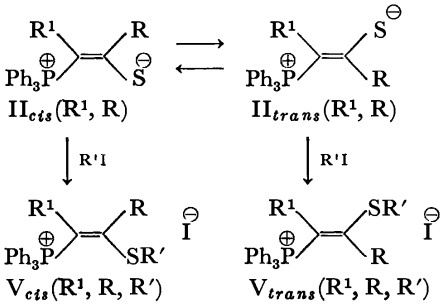

in $CDCl_3$, and they showed no isomerization. However, on irradiation with a high-pressure mercury lamp for 6 hr in $CDCl_3$, V_{cis}(H, MeS, Et) and V_{cis}(H, EtS, Me) gave the same 1 : 1 mixture of V_{cis}(H, MeS, Et) and V_{cis}(H, EtS, Me). These results indicate that the structure of the ylides II(H, MeS) and II (H, EtS) was *cis* and that alkylation products have a structure of a vinylphosphonium salt like V, not that of a carbonium ion like VI.

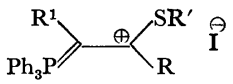

VI

The NMR spectrum of the methylation product V(H, Ph, Me) of II (H, Ph) with methyl iodide showed signals at δ 1.91 (s, MeS) and 6.41 (d, J=21.8 Hz, methine). The compound gave new peaks at 2.87 (s, MeS) and 6.38 (d, J=14.1, methine) on ultraviolet irradiation. The results show that the ylide II(H, Ph) is *cis* and that the methylation product is V_{cis}(H, Ph, Me), which gives V_{trans}(H, Ph, Me) on ultraviolet irradiation. The equilibrium ratio, V_{cis}(H, Ph, Me): V_{trans}(H, Ph, Me), was 6 : 4 after 6 hr.

The ylide II (H, Me_2N) gave an isomer on methylation, but the product showed no change on ultraviolet irradiation for 10 hr. Although we have no direct evidence, the structure of II(H, Me_2N) was assumed to be *cis* judging from the kinetic studies of methylation reaction (see the next section).

Formylmethylenetriphenylphosphorane I(H, H) exists as a mixture of *cis* and *trans* isomers, whose ratio (about 1 : 1) is constant in any solvent,[1,12,13] but I(Me, H) gives only the *trans* isomer.[1]

The NMR spectrum of II(H, H) was shown to be a mixture of *cis* and *trans* isomers, while II(Me, H) gave only *trans* (Table 4). Interestingly, II(H, H) showed a solvent dependence like that of ester-stabilized ylides I(H, Alkyl-O) and II(H, Alkyl-O); however the small solubility of II(H, H) inhibited precise studies. A sample crystallized from benzene gave a *cis*-rich product of *cis*/*trans*=7, one of *cis*/*trans*=1.1 from nitrobenzene, and one of *cis*/*trans*=0.23 from chloroform. These data were obtained by the analysis of the NMR spectra of samples in the $CDCl_3$-Et_3N (5%) solvent. A sample from benzene attained equilibrium quickly (*cis*/*trans*=0.23) without the addition of any dry sodium carbonate (in 3—5 min); with the addition of dry sodium carbonate, attaining equilibrium took rather longer (about 60 min). However, the sample attained equilibrium slowly (about 25 hr) in the $CDCl_3$–Et_2N solvent. These results indicate that the acid-catalyzed *cis-trans* isomerization is a lower energy process than the thermally induced one, as has been reported in connection with the ester-stabilized ylides I (H, Alkyl-O).[1,3]

Table 5. Second-order rate constants for the methylation of II with methyl benzenesulfonate in $CDCl_3$ at 34.5 °C

II	$k_2 \times 10^3$ l/mol·s	
	cis	*trans*
II(H MeO)	1.60	3.59
II(H, EtO)	1.77	4.13
II(H, *i*-PrO)	2.12	4.36
II(H, Ph)	11.2	
II(H, Me_2N)	24.1	
II(H, MeS)	3.45	

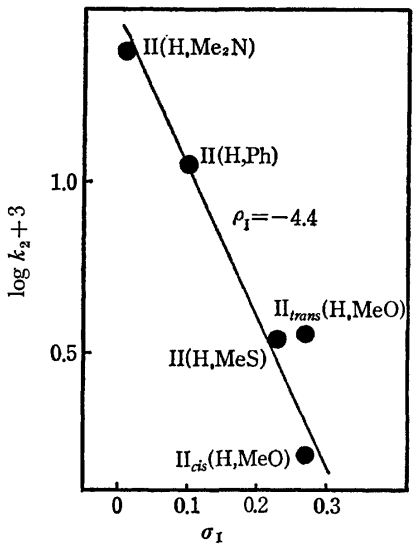

Fig. 1. The relation between σ_I and $\log k_2$.

Kenetic Studies of the Methylation of II with Methyl Benzenesulfonate. Since the reaction of II with methyl iodide was too fast to follow by means of the NMR spectra (within one min), methyl benzenesulfonate was used as the methylating reagent. The reaction gave good second-order rate constants (k_2), first-order with II and benzenesulfonate respectively. The results are shown in Table 5 and Fig. 1. The large negative ρ_I value seems to indicate that, in the transition state of the reaction, the negative charge is highly localized on the thiocarbonyl sulfur (*i.e.*, the betaine form).

As was observed on II(H, Alkyl-O), the *trans* isomer showed nearly twice as much reactivity with methyl benzenesulfonate as the *cis* isomer. The ylide II(H, Me_2N) was supposed to be *cis*, since there was a much deviation of II_{trans}(H, MeO) from the line (Fig. 1).

Experimental

Preparation of II. A suspension of triphenylmethylphosphonium bromide (5.0 g, 14 mmol) and sodium amide (1.5 g) in 50 ml of dry benzene was stirred for 12 hr in a stoppered flask at room temperature. After the separation of the precipitate, the ammonia was removed *in vacuo* to give a yellow solution of triphenylphosphonium methylide. After the solution had then been cooled in an ice-water bath, methyl methylxanthate (1.7 g, 14 mmol) in 10 ml of benzene was added in one portion, and the resulting mixture was allowed to stand for 1 hr at room temperature. The mixture was then treated with charcoal and condensed *in vacuo* to give an oil. The oil was washed several times with petroleum ether, II(H, MeO) was then obtained in a 38% yield from benzene–petroleum ether.

Similarly several other II were prepared in moderate yields; the results are collected in Table 1.

Alkylation of II. A solution of II(H,Ph) in chloroform was treated with twice as much methyl iodide at room temperature. The subsequent evaporation of the solvent *in vacuo* afforded needles (mp 198—200 °C) in a quantitative yield.

The similar treatment of II(R^1,R) with alkyl iodide (R'I) gave V(R^1,R,R') in a good yield (Table 2).

The photo-isomerization of V(H,Ph,Me), V(H,MeS,Et), and V(H,EtS,Me) in $CDCl_3$ was performed in NMR tubes (Pyrex), following at suitable time intervals by observing NMR spectral change.

Kinetic Studies. A solution of II and methyl benzenesulfonate in $CDCl_3$ was sealed in an NMR sample tube. The rate was followed at suitable time intervals by analyzing the NMR spectra of the *O*-methyl and *S*-methyl groups. The results are collected in Table 5.

References

1) C. J. Devlin and B. J. Walker, *Tetrahedron*, **28**, 3501 (1972).
2) H. J. Bestmann and B. Arnason, *Chem. Ber.*, **95**, 1513 (1962).
3) J. P. Snyder, *Tetrahedron Lett.*, **1971**, 215.
4) H. I. Zeliger, J. P. Snyder, and H. J. Bestmann, *ibid.*, **1969**, 2199.
5) I. F. Wilson and J. C. Tebby, *ibid.*, **1970**, 3769.
6) A. J. Speziale and K. W. Ratts, *J. Amer. Chem. Soc.*, **87**, 5603 (1965).
7) F. S. Stephens, *J. Chem. Soc.*, **1965**, 5640, 5658.
8) H. J. Bestmann and H. Schulz, *Tetrahedron Lett.*, **1960**, 5; *Chem. Ber.*, **95**, 2921 (1962).
9) H. J. Bestmann, R. Saalfrank, and J. P. Snyder, *Angew. Chem.*, **81**, 227 (1969); *Chem. Ber.*, **106**, 2601 (1973).
10) F. Ramirez and S. Dershowitz, *J. Org. Chem.*, **22**, 41 (1957).
11) H. Yoshida, H. Matsuura, T. Ogata, and S. Inokawa, *Chem. Lett.*, **1974**, 1065.
12) J. P. Snyder and H. J. Bestmann, *Tetrahedron Lett.*, **1970**, 3317.
13) M. L. Filleux-Blanchard and M. G. J. Martin, *C. R. Acad. Sci., Paris, C*, **270**, 1747 (1970).

Determination of Amino Acid Sequence of Peptides by the Combination of Mass Spectrometry and Edman Degradation. Alternate Use of *p*-Chloro- and *p*-Bromophenylisothiocyanate Followed by Modification of Shortened Peptide

Asao MURAI and Yoko TAKEUCHI

Central Research Laboratories, Ajinomoto Co. Inc., Suzuki-cho, Kawasaki-ku, Kawasaki 210

(Received April 30, 1975)

It was shown that the alternate use of *p*-chloro- and *p*-bromophenylisothiocyanate for Edman degradation makes it possible to determine the amino acid sequence of peptides more unambigously by mass spectrometry, *i.e.*, by the doublet molecular ions of phenylthiohydantoin derivatives of amino acids with the intensity ratio inherent to the natural abundance of each halogen atom. The amino acid sequence of the shortened peptide could also be surely determined by the deuterium labeled mixed acylation by shifting the "sequence determining peaks" to higher mass region where no interfering peaks for the interpretation of the mass spectra would appear as well as labeling them as doublets with equal intensities by the distance of 2 mass units. Two examples, a dodecapeptide H-(Pro-Pro-Gly)$_4$-OH, and an octapeptide angiotensin II, were presented.

In recent years, the combination of Edman degradation[1] with mass spectrometry is well recognized as a useful method for the determination of amino acid sequence of peptides.[2] The advantages of the method might be considered as follows; the phenylthiohydantoins produced from the sequential degradation of peptide with phenylisothiocyanate are the most desirable derivatives for the unambigous identification of amino acids by mass spectrometry, and after suitable modification the residual shortened peptide can readily be determined the amino acid sequence in one step by mass spectrometry.[3,4] Thiohydantoin derivatives of amino acids can also be identified by gas chromatography-mass spectrometry.[5,6] An automatic sequenator using Edman degradation with reaction and inlet device directly connected to mass spectrometer has already been reported.[7]

Tschesche, Wachter[8] and Weygand, Obenmeier[9] reported that the N-terminal amino acids could be more clearly identified by converting to their *p*-bromophenylthiohydantoin [PTH(Br)] derivatives by mass spectrometry because the doublet molecular and fragment ions appear on their mass spectra with approximately equal intensities by the distance of two mass units due to the isotopic bromine atoms, ^{79}Br and ^{81}Br.

It seems that the alternate use of *p*-bromo- and *p*-chlorophenylisothiocyanate [PIT(Br) and PIT(Cl), respectively] for the sequential Edman degradation followed by mass spectrometric identification of the products [amino acid-PTH(Br) or PTH(Cl)] allows more unambigous sequence determination by checking the intensity ratio of their molecular and fragment ion pairs inherent to the natural abundances of each halogen atom. This is especially advantageous for the cases where the extraction of PTH derivative is incomplete or the application to the peptides in which the same amino acid neighbours with each other.

The authors also wish to report the method for the determination of amino acid sequence of peptides shortened by the consecutive Edman degradations; mixed acylation of peptide with normal and deuterium labeled long chain acyl groups to discriminate the "sequence determining peaks" (due to the cleavages of CO-N bonds with positive charges on each carbonyl group) by marking with doublet as well as shifting them to higher mass region where no undesirable contaminant peaks would appear.

Results and Discussion

Alternate Edman Degradation with PIT(Cl) and PIT(Br). A dodecapeptide, H-(Pro-Pro-Gly)$_4$-OH, was applied to the alternate sequential Edman degradations with PIT(Cl) and PIT(Br) followed by acylation and permethylation of the shortened peptide. Series of mass spectra of the PTH(Cl or Br) derivatives obtained from first through sixth Edman degradation are illustrated in Fig. 1. The mass spectrum of the derivative of the N-terminal amino acid indicates the clear molecular ion pair at *m/e* 266 and 268 with an intensity ratio of 3 : 1 and this readily leads to identification the N-terminal amino acid as proline. The spectrum of the second Edman degradation products clearly indicates the second amino acid as proline, too, by the molecular ion pair at *m/e* 310/312 with the equal intensity ratio of proline-PTH(Br). The mass spectrum of the third Edman degradation products using PIT(Cl) exibits three doublet peaks of molecular ions. One pair of the doublet at *m/e* 226/228 with the intensity ratio of 3 : 1 must be the molecular ion of the third amino acid-PTH(Cl), glycine. Another doublets at *m/e* 266/268 (3 : 1) and *m/e* 310/312 (1 : 1) should be attributed to the first and second amino acid, proline and proline, by the incomplete extraction of the PTH derivatives in the first and second stage of the Edman degradations. A similar result can be deduced from the spectrum of the fourth Edman degradation products using PIT(Br), in which the new pair of doublet at *m/e* 310/312 (1 : 1) is indicative of the fourth amino acid, proline. The same procedures of identification of amino acid-PTH derivatives by the alternate Edman degradations resulted the determination of the sequence from first to sixth amino acid as Pro-Pro-Gly-Pro-Pro-Gly. The residual shortened peptide was then acetylated, esterified and permethylated by the method

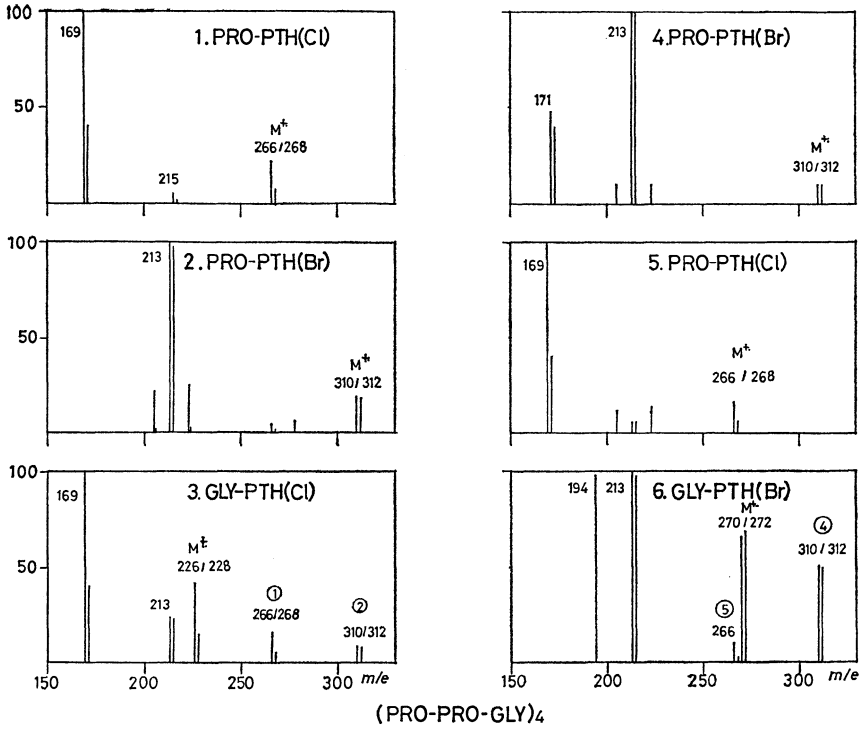

Fig. 1. Series of mass spectra of amino acid-PTH (Cl or Br) derivatives from 1st to 6th Edman degradations of (Pro–Pro–Gly)$_4$. The peaks under encircled numerals represent the molecular ions of the PTH derivatives from corresponding order of degradation.

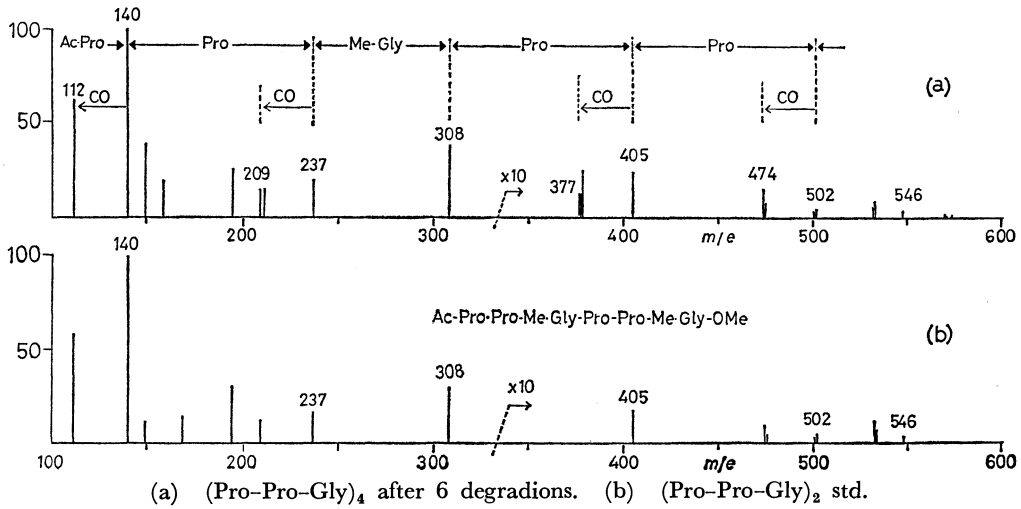

(a) (Pro–Pro–Gly)$_4$ after 6 degradions. (b) (Pro–Pro–Gly)$_2$ std.

Fig. 2. Mass spectra of the N-acetylated and permethylated peptides.
Upper: residual peptide after 6 degradations of (Pro–Pro–Gly)$_4$, lower: standard peptide (Pro–Pro–Gly)$_2$.

of Vilkas and Lederer[10] and determined the amino acid sequence by its mass spectrum as Pro–Pro–Gly–Pro-Pro–Gly. The mass spectra of the modified shortened peptide after six degradations and the standard peptide, H–(Pro–Pro–Gly)$_2$–OH, are shown in Fig. 2. The complete amino acid sequence of this dodecapeptide was then ascertained by combining with the results from alternate Edman degradation as H–(Pro–Pro–Gly)$_4$–OH

Mixed Long-chain Acylation with Unsaturation or Deuterium Labeling. Consecutive Edman degradation procedures often accumulate undesirable by-products or other artifacts by which the mass spectra are contaminated at the mass region of lower "sequence determining peaks" ($\sim m/e$ 300) of an acetylated peptide derivatives. It seems that the interpretation of mass spectra for the sequence determination must be much simplified by introducing the mixture of saturated and unsaturated acyl groups to the peptides not only because the molecular and fragment peaks would be marked by doublets by the distance of two mass units but because they would be shifted to the higher mass region where no peaks from contamination would appear. Mixed acylation

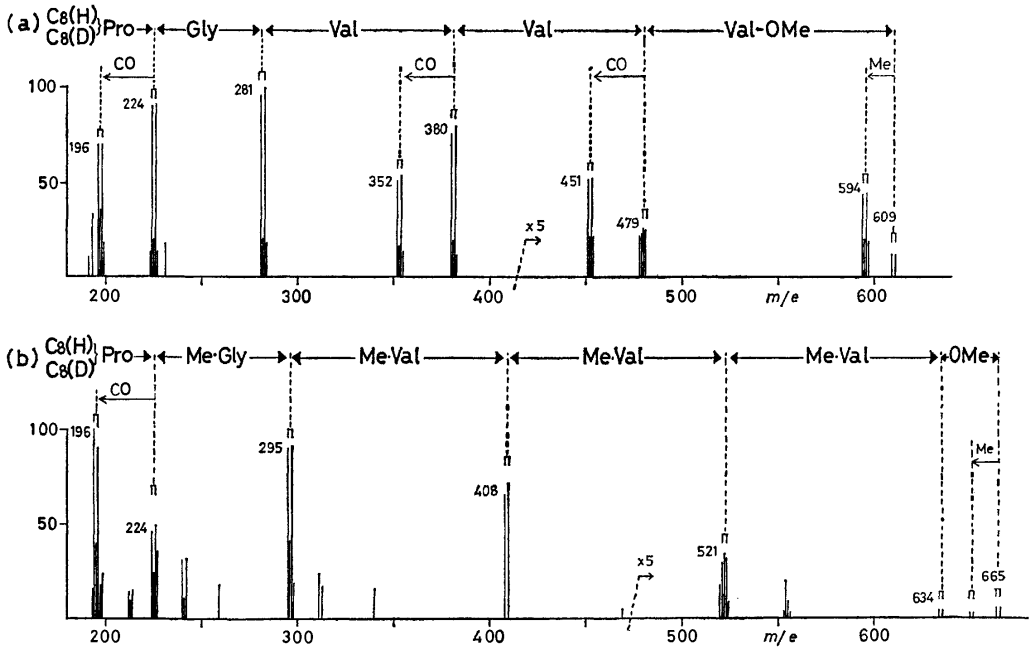

Fig. 3. Mass spectra of mixed acylated Pro-Gly-Val-Val-Val methyl ester with(b) and without(a) permethylation. $C_8(H) = C_7H_{15}CO$, $C_8(D) = C_7H_{13}D_2CO$

of peptides with C_2H_5COCl/C_2H_3COCl, $C_7H_{15}COCl/C_7H_{13}COCl$, and $C_{17}H_{35}COCl/C_{17}H_{33}COCl$ were investigated. A C_8-mixed acylation was sufficient for the "sequence determining peak" shifting. The intensity ratio of the doublets, however, differed significantly among the peaks of the molecular and fragment ions within a spectrum and moreover, the ratio varied not only with vaporization temperature but with peptide to peptide. Similar results were obtained from C_3- or C_{18}-mixed acylation.

Marking the molecular and sequence peaks by doublets was successful by the acylation of peptides with equivalent mixture of *n*-octanoyl chloride and *n*-octanoyl-3,3-d_2 chloride. Figure 3 shows the mass spectra of deuterium labeled-acylated Pro-Gly-Val-Val-Val methyl ester with (b) and without (a) permethylation. The lowest "sequence determining peaks" appear at *m/e* 224/226 (acylprolyl ion). The fragment ions appearing in higher mass region than that of the acylprolyl ion were enough simple and clear for the interpretation of sequence determination.

Permethylation of long-chain acylated peptide esters usually lowers the relative intensities of the molecular ions and does not seem to give an additional advantage on the spectra for the interpretation of sequence determination. The vaporization temperature, however, is lowered by 30—40° by permethylation.

Combination of Alternate Edman Degradation and Deuterium Labeled Long-chain Acylation of the Residual Peptide. A typical example for the sequence determination of peptides by sequential Edman degradation followed by esterification and deuterium labeled long-chain acylation of the shortened peptides is shown in Fig. 4. An octapeptide, angiotensin II, was easily proved its amino acid sequence after six alternate Edman degradations followed by deuterium labeled acylation.

There can be the case where the shortened peptide, even in the case of tripeptide such as Val-Val-Val, is extracted together with the PTH derivative by ethyl acetate by the usual separation procedures[5,6] in Edman degradation. As in these cases, the mixture of the extracted PTH derivative and the residual peptide was directly applied to esterification and *N*-acylation, then the mass spectra of the mixture were recorded at the suitable vaporization temperatures at which the PTH and peptide derivatives were separately evaporated. Alternatively, PHT derivatives can be well and selectively extracted from the residual peptides with toluene–ethyl acetate (1 : 1) instead of ethyl acetate.

Experimental

Peptides. H-(Pro-Pro-Gly)$_2$-OH, H-(Pro-Pro-Gly)$_4$-OH, and angiotensin II were purchased from Protein Research Foundation.

n-*Octanoic-3,3-d_2 Acid.* A similar method of synthesis of *n*-heptanoic-3,3-d_2 acid by Katoh *et al.*[13] was used with the starting material of *n*-hexanoic acid in place of *n*-valeric acid.

Edman Degradation. Sequential degradation of peptides with PIT (Cl or Br) was done by the method of Tschesche and Wachter.[8] PIT(Cl) and PIT(Br) were synthesized by the method described elsewhere.[11]

Peptide Modification. The shortened peptide (1—5 mg) was esterified with HCl-saturated methanol (10 ml) at room temperature for 2 hr and the excess reagents were evaporated off. To the residue, 2 ml of dried pyridine containing acid chloride 1.2—2 molar equivalent to the free amino groups was added and the solution was allowed to stand for 2 hr at room temperature. After the solvent was evaporated, the residue was dissolved in chloroform and was washed with

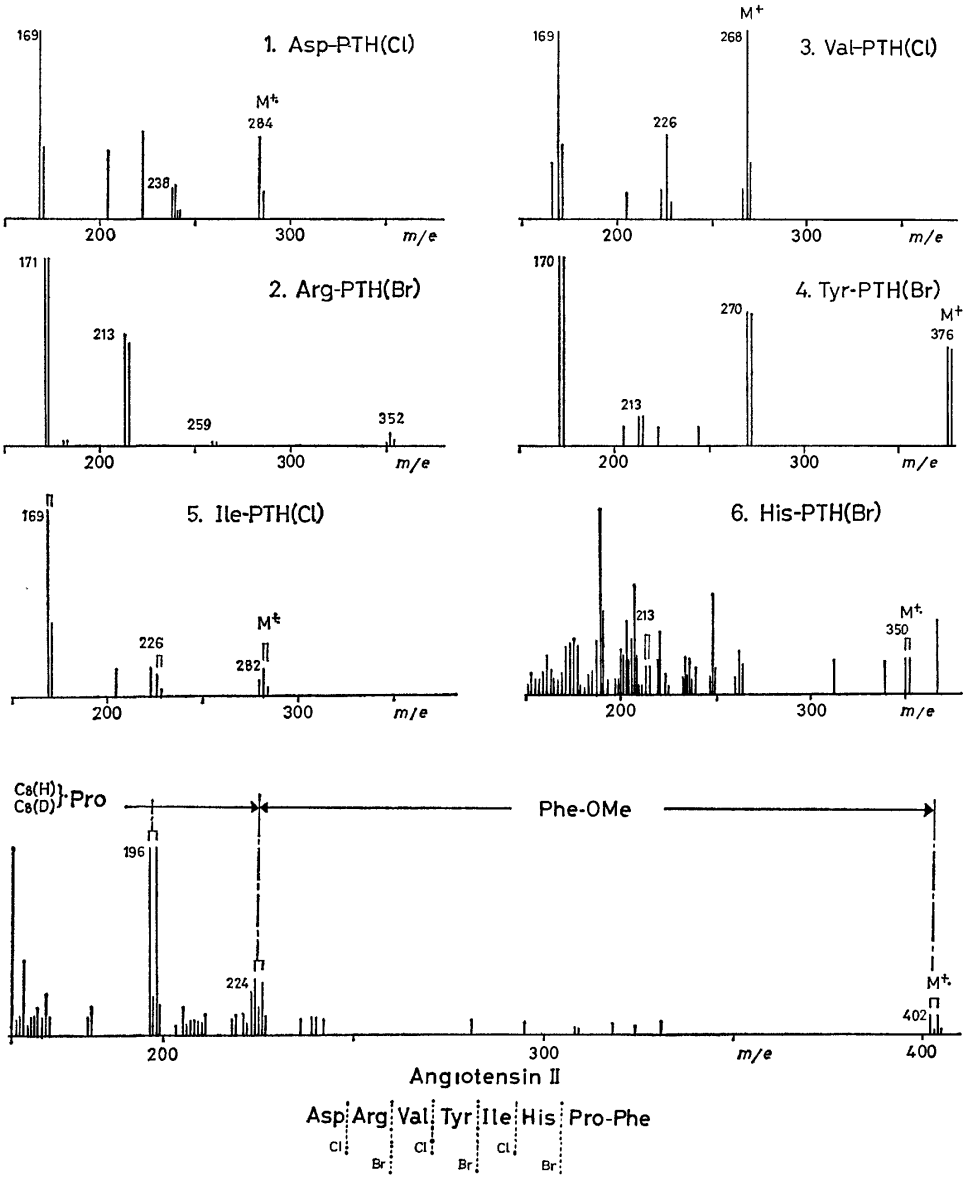

Fig. 4. Mass spectra of PTH(Cl or Br) derivatives from 1st to 6th Edman degradations of angiotensin II and residual peptide after esterification and deuterium labeled mixed acylation.

aqueous $NaHCO_3$ solution. The chloroform layer was then dried over anhydrous Na_2SO_4, and the solvent was evaporated. The oily residue was directly introduced into the ion source of mass spectrometer. Permethylation, if necessary, was carried out according to the method of Thomas[12] or Vilkas.[10]

Mass Spectrometry. A Hitachi RMU-6E Mass Spectrometer with 70 eV ionizing energy, 80 μA of emission current, and ion source temperature of 220° was used.

References

1) P. Edman, *Acta Chem. Scand.*, **4**, 283 (1950).
2) N. A. Aldanova, E. I. Vinogradova, S. A. Kazaryan, B. V. Rozynov, and M. M. Shemyakin, *Biochem. USSR.*, **35**, 742 (1970).
3) M. M. Shemyakin, *Pure Appl. Chem.*, **17**, 313 (1968).
4) E. Lederer, *ibid.*, **17**, 489 (1968).
5) H. Hagenmaier, W. Ebbighausen, G. Nicholson, and W. Votsch, *Z. Naturforsch.*, **25b**, 681 (1970).
6) R. Burgus, M. Butcher, M. Amos, N. Ling, M. Monahan, J. Rivier, R. Fellows, R. Blackwell, W. Vale, and R. Guillemin, *Proc. Nat. Acad. Sci. U.S.A.*, **69**, 278 (1972).
7) R. E. Lovins, J. Craig, T. Fairwell, and C. McKinney, *Anal. Biochem.*, **47**, 539 (1972).
8) H. Tschesche and E. Wachter, *Eur. J. Biochem.*, **16**, 187 (1970).
9) F. Weygand and R. Obermeier, *ibid.*, **20**, 72 (1971).
10) E. Vilkas and E. Lederer, *Tetrahedron*, **26**, 3089 (1968).
11) G. J. M. Van der Kerk, C. W. Pluygers, and G. de Vries, "Organic Syntheses," Vol. 45 (1965), p. 19.
12) D. W. Thomas, B. C. Das, S. D. Gero, and E. Lederer, *Biochem. Biophys. Res. Commun.*, **32**, 519 (1968).
13) M. Katoh, D. A. Jaeger, and C. Djerassi, *J. Amer. Chem. Soc.*, **94**, 3107 (1972).

The Synthesis of 1,3,4-Oxadiazolo[3,2-*b*]isoquinoline and 1,3,4-Thiadiazolo-[3,2-*b*]isoquinoline Derivatives from Homophthalic Anhydride

Masahiko TAKAHASHI, Takamitsu SHINODA, Hideshi OSADA, and Toshio NAKAJIMA

Department of Industrial Chemistry, Faculty of Engineering, Ibaraki University, Hitachi, Ibaraki 316

(Received May 2, 1975)

The synthesis of 1,3,4-oxadiazolo[3,2-*b*]isoquinoline and 1,3,4-thiadiazolo[3,2-*b*]isoquinoline derivatives is described. The reaction of homophthalic anhydride (**1**) with acylhydrazines (**2**) afforded 2-acylamino-1,2,3,4-tetrahydroisoquinoline-1,3-diones (**3**) or 1-(*o*-carboxyphenylacetyl)-2-acylhydrazines (**4**). The treatment of **3** or **4** with polyphosphoric acid gave 2-substituted 1,3,4-oxadiazolo[3,2-*b*]isoquinolin-5(5*H*)-ones (**5**) in quantitative yields. The treatment of **3** or **4** with phosphorus pentasulfide gave 2-substituted 1,3,4-thiadiazolo[3,2-*b*]-isoquinoline-5(5*H*)-thiones (**6**). 2-Phenyl-1,3,4-oxadiazolo[3,2-*b*]isoquinoline-5(5*H*)-thione (**9**) was obtained by the reaction of **5a** with phosphorus pentasulfide.

Homophthalic anhydride is a readily-available cyclic anhydride,[1] which is considered to be a useful starting material for the synthesis of various condensed isoquinoline derivatives. Homophthalic anhydride (**1**) has been condensed with *o*-phenylenediamine to give benzimidazo[1,2-*b*]isoquinoline derivatives.[2-5] On the other hand, *o*-aminobenzenethiol has been treated with 5-substituted homophthalic anhydride to form 2-substituted benzylbenzothiazoles, which were then cyclized to 9-substituted isoquinolino[3,2-*b*]benzothiazolones.[6] Thiazolo[3,2-*b*]isoquinoline derivatives[7] were similarly obtained from 2-aminoethanethiol and **1**. In the reaction of **1** with 1,2-dimethylhydrazine, 2,3-dimethyl-1,2,3,4-tetrahydro-5*H*-2,3-benzodiazepine-1,4-dione[8] has been isolated. The reaction of **1** with *S*-alkylisothiosemicarbazides has been reported to give 2-alkylthio-*s*-triazolo[1,5-*b*]isoquinolin-5-ones, and their reactions have been studied.[9] *s*-Triazolo[1,5-*b*]isoquinolin-5-ones[10,11] have also been synthesized from **1** and amidrazones.

In this paper we wish to report the synthesis of two groups of heterocycles which have new ring systems.

Results and Discussion

When **1** was treated with acyl hydrazines (**2**) in boiling acetic acid, the products isolated were 2-acylamino-1,2,3,4-tetrahydroisoquinoline-1,3-diones (**3**) or 1-(*o*-carboxyphenylacetyl)-2-acylhydrazines (**4**).

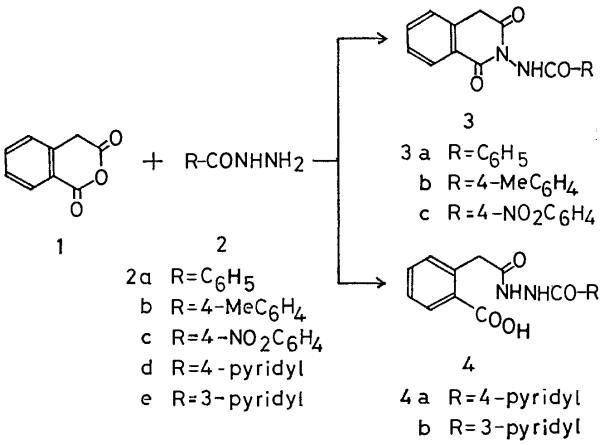

Scheme 1.

Thus, the reaction of **1** with benzohydrazide (**2a**) gave 2-benzamido-1,2,3,4-tetrahydroisoquinoline-1,3-dione (**3a**) in a 92% yield. The IR spectrum of **3a** showed an NH absorption at 3250 cm^{-1} and three carbonyl absorptions at 1735, 1695, and 1660 cm^{-1}. The reaction of **1** with (**2b**) and (**2c**) proceeded in a similar manner to give (**3b**) and (**3c**). However, the products obtained from (**2d**) and (**2e**) were 1-(*o*-carboxyphenylacetyl)-2-acylhydrazines (**4a**) and (**4b**). The physical properties and spectral data, shown in Table 1, are consistent with the structure assigned.

TABLE 1. PHYSICAL PROPERTIES AND SPECTRAL DATA OF **3** AND **4**

Compound	Reaction time (hr)	Yield (%)	Mp (°C) Solvent	Found (%) (Calcd (%)) C	H	IR (KBr, cm^{-1})	UV (λ_{max}^{MeOH} nm (log ε))
3a	4	92	190—191 MeOH	68.54 (68.56	4.48 4.32)	3250, 1735, 1695, 1660	238(4.13), 280(sh, 3.36) 290(sh, 3.23), 310(sh, 2.93)
3b	4	74	206—208 AcOH	69.19 (69.37	4.61 4.80)	3220, 1730, 1695, 1650	243(4.43), 282(sh, 3.51) 292(sh, 3.41), 310(sh, 3.30)
3c	10	76	210—211 MeOH	58.94 (59.08	3.67 3.41)	3280, 1743, 1700, 1665	251(4.33)
4a	5	66	112—115 MeOH	60.06 (60.19	4.56 4.38)	3430, 3160, 2920, 2820, 1735, 1700 1663	242(4.20), 310(sh, 3.49)
4b	16	35	166—169 EtOH	60.27 (60.19	4.66 4.38)	3540, 3160, 2980, 1730, 1670	243(4.21), 290(sh, 3.24) 310(sh, 2.86)

The dehydration of **3** with polyphosphoric acid proceeded smoothly to give the desired products (**5**) in quantitative yields. Thus, **3a** was heated with polyphosphoric acid at 125—130 °C, and the reaction mixture was treated in the usual manner to give 2-phenyl-1,3,4-oxadiazolo[3,2-*b*]isoquinolin-5(5*H*)-one (**5a**). The IR spectrum of **5a** showed no NH absorptions, only one C=O absorption at 1685 cm^{-1} and a new C=N absorption at 1652 cm^{-1}. The olefinic proton resonance of **5a** in the NMR spectrum was observed at δ 6.49 ppm. The elemental analysis and the mass-spectral molecular ion at *m/e* 262 also supported the assigned structure. A similar cyclization by polyphosphoric acid occurred in one step in the case of **4**. The **5** compounds showed characteristic IR absorptions at 1683—1685 (C=O) and 1648—1652 (C=N) cm^{-1}. The physical properties and spectral data are summarized in Table 2. The **5** compounds are heterocycles with a new ring system.

When **3** or **4** was heated with phosphorus pentasulfide in refluxing pyridine, 2-substituted 1,3,4-thiadiazolo[3,2-*b*]isoquinoline-5(5*H*)-thiones (**6**) were obtained; these heterocycles also belong to a new ring system. 2-Phenyl-1,3,4-thiadiazolo[3,2-*b*]isoquinoline-5(5*H*)-thione (**6a**) showed no NH or C=O absorptions in the IR spectrum. The NMR spectrum exhibited a signal of an olefinic proton at δ 7.31 ppm. The molecular-ion peak at *m/e* 294 and the other fragment-ion peaks in the mass spectrum were also consistent with the structure. The physical properties and spectral data of the other compounds of **6** are summarized in Table 2. These compounds show similar absorption maxima in the UV and visible spectra.

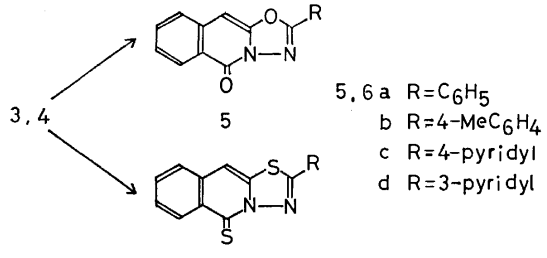

Scheme 2.

Some reactions of these new heterocycles **5** and **6** were attempted. The hydrolysis of **5a** in refluxing aqueous methanol containing sodium hydroxide afforded a crystalline product (**7**). The characteristic absorptions of the carboxyl group were observed at 2620—3340 (OH) and 1705 (C=O) cm^{-1} in the IR spectrum. The NMR spectrum of **7** indicated the presence of a methylene group at δ 4.13 ppm. From the above data, the structure of **7** was assigned to 2-(*o*-carboxybenzyl)-5-phenyl-1,3,4-oxadiazole. A similar treatment of **6a** with alkaline afforded a product (**8**). The characteristic absorption of the carboxyl group were observed at 2340—3440 and 1688 cm^{-1} in the IR spectrum. **8** was also shown to be the ring-opened product 2-(*o*-carboxybenzyl)-5-phenyl-1,3,4-thiadiazole.

When **5a** was treated with phosphorus pentasulfide

TABLE 2. PHYSICAL PROPERTIES AND SPECTRAL DATA OF 5 AND 6

Compound	Reaction time	Yield (%)	Mp (°C) Solvent	Found (%) (Calcd (%)) C	H	IR (KBr, cm^{-1})	UV (λ_{max}^{MeOH} nm (log ε))
5a	40 min	100	236—238 Pyridine	73.50 (73.27	3.78 3.84)	3040, 1685, 1652, 1610	245(sh, 4.51), 256(sh, 4.59), 263(4.61), 290(sh, 4.13), 354(sh, 3.83), 370(3.92), 385(sh, 3.79)
5b	40 min	100	290—292 Pyridine	73.72 (73.90	4.14 4.38)	3040, 1685, 1652, 1610	251(sh, 4.47), 268(4.63), 354(sh, 3.88), 368(3.95), 385(sh, 3.80)
5c	40 min	100	267—269 Pyridine	68.57 (68.43	3.46 3.45)	3045, 1685, 1650, 1620	255(4.60), 290(sh, 4.11), 380(3.73)
5d	40 min	100	249—250 MeOH	68.65 (68.43	3.66 3.45)	3060, 1683, 1648, 1620	244(sh, 4.51), 253(4.58), 261(sh, 4.55), 290(sh, 4.13), 372(3.82)
6a	4 hr	48	217—218 Pyridine	65.34 (65.30	3.65 3.43)	3040, 1600, 1530, 1472	230(4.45), 270(4.61), 294(4.51), 347(sh, 3.87) 443(4.01), 465(3.97)
6b	5 hr	49	178—180 Pyridine	66.55 (66.23	4.11 3.92)	3040, 1665, 1605, 1532	232(4.53), 274(4.57), 299(4.60), 348(sh, 3.87), 440(4.06), 463(4.03)
6c	5 hr	39	269—273 Pyridine	61.27 (61.02	3.28 3.07)	3030, 1603, 1530, 1475	225(4.42), 266(4.65), 290(4.37), 330(3.99), 350(sh, 3.93), 467(3.92)
6d	5 hr	50	251—252 Pyridine	61.12 (61.02	3.04 3.07)	3030, 1600, 1533, 1469	227(4.39), 266(4.58), 292(4.45), 326(3.94), 349(sh, 3.90), 450(3.96), 470(3.92)

in refluxing pyridine, yellow needles (**9**) were obtained in a quantitative yield. The IR spectrum of **9** showed no C=O absorption, but the C=N absorption band which was characteristic of the **5** compounds remained at 1652 cm^{-1}. The absorption maxima observed in the UV and visible spectrum were similar to those of **5a**. These spectral data and the satisfactory analytical value accorded with the structure of **9** as 2-phenyl-1,3,4-oxadiazolo[3,2-*b*]isoquinoline-5(5*H*)-thione.

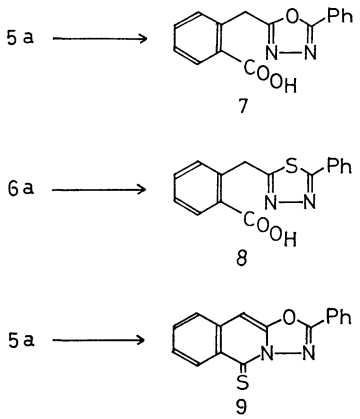

Scheme 3.

Experimental

All the melting points are uncorrected. The IR, UV, and NMR spectra were measured with a JASCO Model IRA-2, a Shimadzu Model MPS-501, and a Hitachi Model R-20 spectrometer respectively. A Shimadzu Model UM-3B apparatus was used for the elemental analysis.

*2-Benzamido-1,2,3,4-tetrahydroisoquinoline-1,3-dione (**3a**).* A mixture of **1** (724 mg, 4.5 mmol) and **2a** (618 mg, 4.5 mmol) in acetic acid (10 ml) was refluxed for 4 hr. After the concentration of the solution *in vacuo* and subsequent cooling, the crystals were filtered to give **3a** (1.15 g, 92% yield). Recrystallization from methanol afforded white crystals; mp 190—191 °C.

The other derivatives, **3b**, **3c**, **4a**, and **4b** were obtained according to methods similar to those described in the case of **3a**.

*2-Phenyl-1,3,4-oxadiazolo[3,2-b]isoquinolin-5(5H)-one (**5a**).* A mixture of **3a** (840 mg, 3.0 mmol) and polyphosphoric acid (2.7 g) was heated at 125—130 °C with gentle stirring for 40 min. After cooling, the mixture was poured into water (30 ml) and the resulting precipitates were filtered to give **5a** in a quantitative yield. Recrystallization from pyridine afforded yellow plates; mp 236—238 °C. NMR ($CDCl_3$): δ 6.49 (s, 1H, =CH–), 7.2—8.7 (m, 9H, aromatic H). Mass *m/e* (%): 262 (M^+, 100), 131 (57), 103 (57).

The other derivatives, **5b**—**5d**, were obtained from **3** or **4** according to methods similar to those described in the case of **5a**.

*2-Phenyl-1,3,4-thiadiazolo[3,2-b]isoquinoline-5(5H)-thione(**6a**).* A mixture of **3a** (560 mg, 2.0 mmol) and finely powdered phosphorus pentasulfide (450 mg. 2.0 mmol) in pyridine (3.0 ml) was refluxed for 4 hr. The insoluble materials were then filtered off from the hot solution, and the filtrate was cooled. The precipitates were filtered to give **6a** (227 mg, 48% yield). Recrystallization from pyridine afforded orange needles; mp 217—218 °C. NMR ($CDCl_3$): δ 7.31 (s, 1H, =CH–) 7.5—8.2 (m, 9H, aromatic H). Mass *m/e* (%): 294 (M^+, 100), 266 (17), 250 (44), 191 (23), 159 (40), 147 (98), 146 (65), 121 (63).

*2-(o-Carboxybenzyl)-5-phenyl-1,3,4-oxadiazole (**7**).* A solution of **5a** (262 mg, 1.0 mmol) in a mixture of aqueous sodium hydroxide (1 M, 5.0 ml) and methanol (5.0 ml) was refluxed for 5 hr. After the removal of the solvent, water (15 ml) was added to the residue, and the solution was neutralized with dilute hydrochloric acid. The resulting precipitates were filtered to give **7** (191 mg, 68% yield). Recrystallization from methanol afforded white needles; mp 174—175 °C. Found: C, 68.76; H, 4.37%. Calcd for $C_{16}H_{12}O_3N_2$: C, 68.56; H, 4.32%. IR (KBr): 3360, 3040, 2960, 2740, 2620, 1705, 1608, 1555 cm^{-1}. UV λ_{max}^{MeOH} nm (log ε): 280 (4.32). NMR (DMSO-d_6): δ 4.13 (s, 2H, $-CH_2-$), 7.4—8.3 (m, 9H, aromatic H).

*2-(o-Carboxybenzyl)-5-phenyl-1,3,4-thiadiazole (**8**).* A solution of **6a** (147 mg, 0.50 mmol) in a mixture of aqueous sodium hydroxide (1 M, 2.5 ml) and methanol (15 ml) was refluxed for 24 hr. After the subsequent evaporation of the solvent, water (15 ml) was added to the residue; the small amount of insoluble materials was then filtered off. The filtrate was neutralized with dilute hydrochloric acid, and the resulting precipitates were filtered to give **8** (111 mg, 75% yield). Recrystallization from methanol afforded white needles; mp 193—194 °C. Found: C, 64.87; H, 4.04%. Calcd for $C_{16}H_{12}O_2N_2S$: C, 64.87; H, 4.08%. IR (KBr): 3440, 2860, 2760, 2680, 2455, 2370, 1688, 1597, 1459 cm^{-1}. UV λ_{max}^{MeOH} nm (log ε): 272 (4.22).

*2-Phenyl-1,3,4-oxadiazolo[3,2-b]isoquinoline-5(5H)-thione (**9**).* A mixture of **5a** (500 mg, 2.0 mmol) and phosphorus pentasulfide (440 mg, 2.0 mmol) in pyridine (10 ml) was refluxed for 8 hr. The insoluble materials were filtered off from the hot solution, and then the filtrate was concentrated *in vacuo* to one-half volume. After cooling, the precipitates were filtered to give **9** (542 mg, 100% yield). Recrystallization from ethanol afforded yellow needles; mp 205—206 °C. Found: C, 69.44; H, 3.62%. Calcd for $C_{16}H_{10}ON_2S$: C, 69.06; H, 3.62%. IR (KBr): 3040, 1652, 1610, 1572, 1535, 1472 cm^{-1}. UV λ_{max}^{MeOH} nm (log ε): 218 (4.34), 259 (4.64), 282 (4.61), 310 (sh, 4.02), 415 (4.02), 436 (4.03).

The authors wish to express their thanks to Dr. Masatoshi Hirayama for the NMR measurements and to the Sankyo Co., Ltd., for the mass measurements.

References

1) O. Grummitt, R. Egan, and A. Buck, "Organic Syntheses," Coll. Vol., III, p. 449 (1955).
2) A. Bistrzycki and K. Fässler, *Helv. Chim. Acta*, **6**, 519 (1923).
3) M. F. Sartori, A. Oken, and H. E. Schroeder, *J. Org. Chem.*, **31**, 1498 (1966).
4) E. Schefczik, *Ann. Chem.*, **729**, 83 (1969).
5) A. Mustafa, M. I. Ali, and A. A. El-Sayed, *ibid.*, **739**, 68 (1970).
6) V. N. Bubnovskaya, G. N. Miskevich, and F. S. Babichev, *Ukr. Kim. Zh.*, **39**, 188 (1973); *Chem. Abstr.*, **78**, 147860 (1973).
7) Ger. Patent, 1960376 (1971); *Chem. Abstr.*, **75**, 63774 (1971).
8) G. Rosen and F. D. Popp, *J. Heterocycl. Chem.*, **6**, 9 (1969).
9) M. I. Ali, A. A. El-Sayed, and A. M. Abd-Elfattah, *J. Org. Chem.*, **37**, 3209 (1972).
10) A. M. Abd-Elfattah, S. M. Hussain, and M. I. Ali, *Tetrahedron*, **30**, 987 (1974).
11) M. Takahashi and N. Sugawara, *Nippon Kagaku Kaishi*, **1975**, 334.

Oxidation of Cyclopropylamines and Aziridines with Lead Tetraacetate

Tamejiro HIYAMA, Hiroshi KOIDE, and Hitosi NOZAKI

Department of Industrial Chemistry, Kyoto University, Yoshida, Kyoto 606

(Received May 6, 1975)

The title reaction of 2-phenylcyclopropylamine gives cinnamaldehyde, while that of the 1-phenyl isomer produces benzonitrile and ethylene. The similar treatment of 2-phenylaziridine provides benzaldehyde as the only isolable product. These reactions are explained by assuming the common intermediacy of nitrenium ions such as 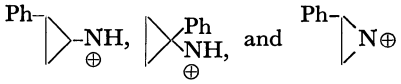 respectively. The assumption is confirmed by the oxidation of the corresponding amines with sodium hypochlorite. Entention of the reaction to 2,3-polymethyleneaziridines with R group on C-2 afforded R–CO–$(CH_2)_n$–C≡N type products (R=H, alkyl, phenyl) in preparative yields. This provides a novel method of C=C bond cleavage of cycloalkenes.

Information on reactive metastable species has been accumulating.[1] Among them much attention has been focused on the oxidation of amines with metal salts in higher valency.[2] The species involved in the oxidation are nitrenium ions, nitrogen radicals,[3] and nitrenes.[4] We wish to report that the lead tetraacetate oxidation of cyclopropylamines and aziridines proceeds *via* nitrenium ion intermediates.[5]

The *trans* isomer of 2-phenylcyclopropylamine (**1**) in dichloromethane was treated with equimolar lead tetraacetate at −78 °C to afford *trans*-cinnamaldhyde. The oxidation of the *cis* isomer of **1** gave the same product. The regioisomer, 1-phenylcyclopropylamine (**2**), reacted in a completely different way to produce benzonitrile and ethylene, the latter being ascertained by obtaining 1,2-dibromoethane.

Nitrene intermediates in these reactions are excluded on the basis of the following facts. Thermal decomposition of cyclopropyl azides results in the ring expansion to yield 1-azetines.[6] This transformation involves cyclopropylnitrene intermediates.[6c] In contrast, however, fragmentation to olefins and nitriles is observed when appropriately substituted cyclopropyl azides are decomposed.[7] The choice of either ring expansion or fragmentation seems to depend upon the substituents on the cyclopropane ring. The fragmentation is particularly favored in the one that partial positive charge being developed in the transition state resides on the remaining nitrogen upon the extrusion of nitrogen molecule.[7]

More appropriately the above oxidation can be explained by assuming the intermediacy of nitrenium ions.[8] In order to confirm this, the amines *trans*-**1** and **2** were treated successively with sodium hypochlorite and with silver perchlorate. The products obtained under such nitrenium ion producing conditions[9] were the same as in the above oxidation, *i.e.*, cinnamaldehyde from *trans*-**1** and benzonitrile from **2**.

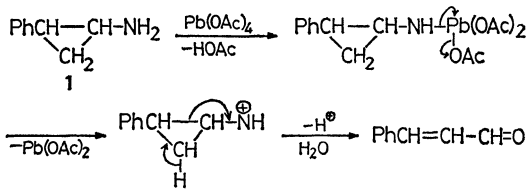

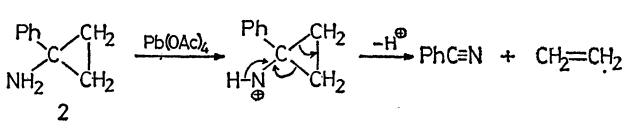

Oxidation of 2-phenylaziridine (**3**) gave benzaldehyde as a sole isolable product. Possibly the reaction involves nitrenium ion intermediate **4**[10] and the 2-azaallene cation **5**,[11] which is then oxygenated to benzaldehyde. With this observation in hand we examined lead tetraacetate oxidation of aziridines fused with medium and large rings.

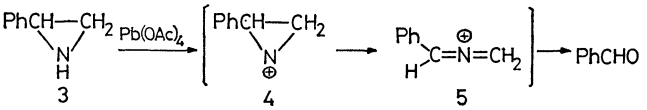

The aziridine **6a** dissolved in dichloromethane was treated with lead tetraacetate under a nitrogen atmosphere at −40 °C. Stirring for 1 hr at −40 °C, warming up to room temperature during 2 hr and work-up gave 12-cyano-2-dodecanone (**7a**). Best results were obtained upon the use of two molar equivalent of lead tetraacetate. The structure of the product was unambiguously confirmed by the alternative synthesis of **7a**. Namely, ethyl acetoacetate was alkylated with 1,9-dibromononane and the resulting product was heated in aqueous dimethyl sulfoxide containing sodium cyanide. Both decarboxylation[12] and substitution of cyano group for bromine were attained in this single operation yielding **7a**. The oxidation was extended to aziridines **6b**, **6c**, **8a**—**c**, and to the nonamethylene homologue **11a**. The yields as well as the physical properties of the products are listed in

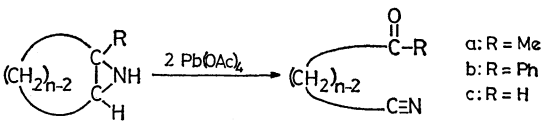

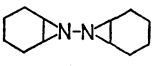

Table 2. In contrast to the above results, 7-azanorcarane (**10c**) was recovered unchanged under the typical condition, but the reaction at reflux of dichloromethane gave a product tentatively assigned as 7,7'-bi-7-azanorcarane (**13**).

The mechanism of the novel transformation can be understood by the following scheme involving two moles of lead tetraacetate. A cyclic 2-azaallene cation is readily susceptible to nucleophilic attack of acetate anion to give **14**. Addition of lead tetraacetate on the C=N bond in **14** followed by elimination yields **15**. Facile thermal rearrangement affords a *gem*-diacetate **16**, characterized by the spectrometry of the crude product (1735—1744 cm^{-1}, δ~2.0 (singlet)). Purification upon silica gel tlc induces the hydrolysis of **16** to give the corresponding ω-cyano carbonyl compound. Obviously **10c** should give a nitrenium ion which can not be isomerized to a seven-membered azaallene cation due to the strain. This accounts for the formation of **13**.

The transformation of an olefin into an ω-cyanoaldehyde has been previously achieved by the addition of nitrosyl chloride and the following Beckmann rearrangement.[13] The present method is more generally applicable, as the 2-substituted aziridines are easily obtained from cyclic ketone oximes by means of the Neber reaction[14] proceeding in the presence of Grignard reagents or organolithiums.

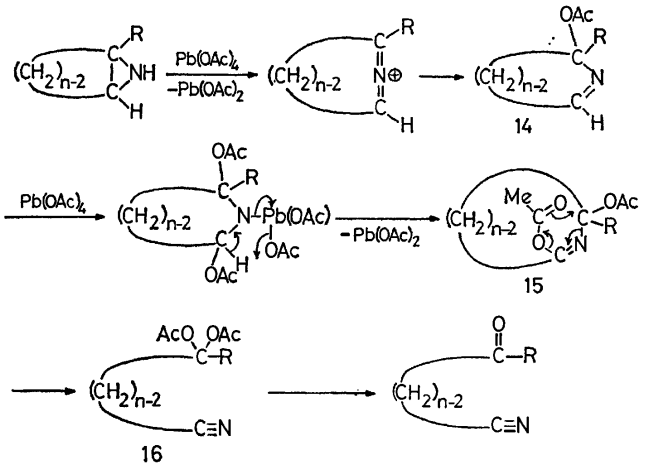

Experimental

IR spectra were recorded on a Shimadzu IR-27 G spectrometer, mass spectra on a Hitachi RMU-6L machine, and PMR spectra on a Varian EM 360 spectrometer (60 MHz) in carbon tetrachloride solution. All the temperatures recorded are uncorrected.

Oxidation of Amines ***1***, ***2***, *and* ***3*** *with Lead Tetraacetate. A General Procedure.* To a solution of lead tetraacetate (490 mg, 1.1 mmol) in dichloromethane (20 ml) an amine (1.0 mmol) dissolved in dichloromethane (5 ml) was added dropwise under a nitrogen atmosphere at −78 °C. The mixture was then gradually warmed up to room temperature in *ca.* 10 hr. Isolation of the product was accomplished by concentration of the reaction mixture, followed by preparative tlc. The product was identified by the comparison of its spectral data with those of the authentic specimen. The results are summarized in Table 1. The yields were estimated either by the isolation or glc assay as indicated.

Table 1. Oxidation of **1**, **2**, and **3**

Amine	Oxidant	Product	Yield (%)
trans-**1**	$Pb(OAc)_4$	PhCH=CHCHO	79[a]
trans-**1**	NaOCl	PhCH=CHCHO	34[a]
cis-**1**	$Pb(OAc)_4$	PhCH=CHCHO	84[a]
2	$Pb(OAc)_4$	PhC≡N[c]	69[b]
2	NaOCl	PhC≡N	21[b]
3	$Pb(OAc)_4$	PhCHO	42[b]

a) Isolation yield. b) Estimated by gas chromatographic assay. c) The accompanying ethylene was identified as 1,2-dibromoethane.

Oxidation of Amines trans-***1*** *and* ***2*** *with Sodium Hydrochlorite.* An amine (0.6 mmol) was added to ice-cooled commercially available aqueous sodium hypochlorite (5% content, 5.2 g) at 0 °C. The mixture was stirred at 0 °C for 10 min and then at room temperature for 1 hr. Extractive work-up with ether gave a crude product which was treated with silver perchlorate (166 mg) in acetone (5 ml) for a night. The results are listed in Table 1.

Oxidation of 2,3-Polymethyleneaziridines. A Typical Procedure: Aziridine **6a** (197 mg, 1.0 mmol) dissolved in dichloromethane (4 ml) was added to a solution of lead tetraacetate (1.00 g, 2.3 mmol) in dichloromethane (15 ml) under a nitrogen atmosphere at −40 °C. Precipitation of lead diacetate immediately occurred. The mixture was gradually warmed up to room temperature in 6 hr and then concentrated *in vacuo*. The product **7a** (171 mg, 82% yield) was separated from lead diacetate by preparative tlc on silica gel (*n*-hexane/ether 3 : 1, R_f 0.4). The yields and the physical properties of the products are collected in Table 2.

*1-Methyl-13-azabicyclo[10.1.0]tridecane (****6a****).* A methylmagnesium iodide solution prepared from methyl iodide (11.4 g, 80 mmol) and magnesium (2.0 g, 82 mmol) in ether (20 ml) was diluted with toluene (20 ml) and then cyclododecanone oxime (3.94 g, 20 mmol) was added. Ether was removed by heating the mixture and the remaining toluene solution was heated to reflux overnight. The mixture was poured into ice-cooled aqueous ammonium chloride and extracted with benzene. Work-up and distillation at 89—90 °C/0.1 mmHg gave the aziridine **6a** (2.19 g, 56% yield), mp 33.0—33.5 °C (*n*-hexane). IR (neat): 3250, 888 cm^{-1}, PMR: δ 0.9—2.4 (m+s (δ 1.17), methylenes, methyl and methine), mass: *m/e* 195 (M^+), 194 (M^+-1), 180 (M^+-15). Found: C, 79.8; H, 13.2; N, 7.4%. Calcd for $C_{13}H_{25}N$: C, 79.9; H, 12.9; N, 7.2%

*1-Phenyl-13-azabicyclo[10.1.0]tridecane (****6b****).* Cyclododecanone oxime (5.91 g, 30 mmol) and toluene (70 ml) were added to an ethereal solution of phenyllithium (prepared from lithium dispersion (1.75 g) in ether (50 ml) and bromobenzene (18.8 g, 120 mmol)). The resulting suspension was concentrated to remove ether and heating was continued for 24 hr (bath temperature 140 °C). Work-up and column chromatography (silica gel, *n*-hexane/ether 1 : 1) afforded **6b** (6.19 g, 80%), mp 55—56 °C (*n*-hexane). IR (Nujol): 3230, 1604, 1580, 763, 701 cm^{-1}, PMR: δ 0.5 (br s, 1H, NH), 0.8—2.2 (m, 21H, methylenes and methine), 7.10 (s, 5H, Ph). Mass: *m/e* 257 (M^+), 256 (M^+-1), 148 (100%). Found: C, 83.8; H, 10.8; N, 5.7%. Calcd for $C_{18}H_{27}N$: C, 84.0; H, 10.6; N, 5.4%.

*13-Azabicyclo[10.1.0]tridecane (****6c****).* A mixture (*ca.* 1 : 1) of *cis*- and *trans*-cyclododecene (1.66 g, 10 mmol) was treated with silver isocyanate (2.0 g, 13 mmol) and iodine (2.54 g, 10 mmol) in tetrahydrofuran (20 ml) in a similar

Table 2. Lead tetraacetate oxidation of aziridines **6**, **8**, **10** and **11**, and the physical properties of the products

Aziridine	Product	Yield(%)	Bp or Mp	IR (cm^{-1})[a]	NMR (δ)
6a	**7a**[b]	82	110 °C/0.09 mmHg (bath temp)	2260, 1713	0.9—2.0 (m, 16H, methylenes), 1.98 (s, 3H, Me), 2.1—2.5 (m, 4H, CH_2CO and CH_2CN)
6b	**7b**[c]	85	54—55OC (*n*-hexane)	2270, 1678[d] 1600, 1580	1.0—2.0 (m, 16H, methylenes), 2.27 (t, J=6 Hz, 2H, CH_2CN), 2.90 (t, J=6 Hz, 2H, CH_2CO), 7.2—7.7 (m, 3H, Ph-*m,p*), 7.8—8.1 (m, 2H, Ph-*o*)
6c	**7c**[e]	58	2,4-DNPH[f] 91—92 °C	2725, 2250 1723	1.0—2.0 (m, 16H, methylenes), 2.0—2.6 (m, 4H, CH_2CO and CH_2CN), 9.77 (t, J=1.8Hz, 1H, CHO)
8a	**9a**[g]	58	120 °C/2.5 mmHg	2260, 1711	1.0—2.0 (m, 8H, methylenes), 2.06 (s, 3H, Me), 2.2—2.6 (m, 4H, CH_2CO and CH_2CN)
8b	**9b**[h]	46	41—41.5 °C (*n*-hexane)	2255, 1677[d] 1600, 1580 742, 727, 690	0.8—2.0 (m, 8H, methylenes), 2.28 (t, J=*ca* 6 Hz, 2H, CH_2CN), 2.90 (t, J=6 Hz, 2H, CH_2CO), 7.0—7.6 (m, 3H, Ph-*m,p*), 7.8—8.1 (m, 2H, Ph-*o*)
8c	**9c**[i]	29	100 °C/0.07 mmHg 2,4-DNPH[j] 75—77 °C	2730, 2255 1722	1.0—2.0 (m, 8H, methylenes), 2.0—2.8 (m, 4H, CH_2CO and CH_2CN), 11.07 (t, J=1.4 Hz, 1H, CHO)
11a	**12a**[k]	82	140—145 °C/6mmHg (bath temp)	2260, 1716	0.6—2.0 (m, 14H, methylenes), 2.09 (s, 3H, Me), 2.1—2.6 (m, 4H, CH_2CN and CH_2CO)
10c	**13**[l]	—		955, 840, 790	0.8—2.0 (m)

a) Neat unless otherwise stated. b) Mass: *m/e* 209 (M^+). Found: C, 74.6; H, 11.1; N, 6.7%. Calcd for $C_{13}H_{23}NO$: C, 74.6; H, 11.1; N, 6.7%. c) Mass: *m/e* 291 (M^+). Found: C, 79.9; H, 9.3; N, 5.2%. Calcd for $C_{18}H_{25}NO$: C,79.7; H, 9.3; N, 5.2%. d) Nujol. e) Mass: *m/e* 195 (M^+). f) Lit., 90—92 °C (Ref. 13). g) Mass: *m/e* 153 (M^+). Found: C, 70.4; H, 10.0; N, 9.2%. Calcd for $C_9H_{15}NO$: C, 70.6; H, 9.9; N, 9.1%. h) Mass: *m/e* 215 (M^+). Found: C, 78.1; H, 8.2; N, 6.4%. Calcd for $C_{14}H_{17}NO$: C, 78.1; H, 8.0; N, 6.5%. i) Mass: *m/e* 139 (M^+). j) Lit., 76—77 °C (Ref. 13). k) Mass: *m/e* 195 (M^+). Found: C, 73.6; H, 11.1; N, 7.2%. Calcd for $C_{12}H_{21}NO$: C, 73.8; H, 10.8; N, 7.2%. l) Mass: *m/e* 192 (M^+).

manner as the reported procedure[15] to obtain methyl 2-iodocyclododecanecarbamate, mp 108—109.5 °C (*n*-hexane), IR (Nujol): 3200, 1692, 1536 cm^{-1}. Found: C, 45.9; H, 7.2; N, 3.7%. Calcd for $C_{14}H_{26}INO_2$: C, 45.8; H, 7.1; N, 3.8%.

The carbamate (1.11 g, 30 mmol) was heated in methanol (40 ml) and water (8ml) containing sodium hydroxide (2.4 g, 60 mmol) for 2 hr. Work-up followed by distillation at 120—130 °C (bath temperature)/0.2 mmHg gave the aziridine **6c** (490 mg, 90% yield), mp 46.5—47.5 °C (*n*-hexane), IR (neat): 3250, 969, 874 cm^{-1}. Found: C, 79.4; H, 12.9; N, 7.8%. Calcd for $C_{12}H_{23}N$: C, 79.5; H, 12.8; N, 7.7%.

*1-Methyl-9-azabicyclo[6.1.0]nonane (**8a**).* Cyclooctanone oxime (2.82 g, 20 mmol) was treated with methylmagnesium iodide (*ca.* 80 mmol) in toluene (10ml) and ether (25 ml) in a similar manner as **6a** to give **8a** (l. 92 g, 51% yield), bp 54 °C/4 mmHg. IR (neat): 3250, 830 cm^{-1}, PMR: δ 1.0—2.4 (m+s (δ 1.15)), mass: *m/e* 139 (M^+), 138 (M^+-1). Found: C, 77.3; H, 12.5; N, 9.8%. Calcd for $C_9H_{17}N$: C, 77.6; H, 12.3; N, 10.1%.

*1-Phenyl-9-azabicyclo[6.1.0]nonane (**8b**).* The aziridine was obtained in 62% yield, bp 103—105 °C/0.1 mmHg. IR (neat): 3230, 1601, 1496, 931, 809, 760, 742, 701 cm^{-1}, PMR: δ 0.7—2.7 (m, 14H), 7.0—7.7 (m, 5H), mass: *m/e* 201 (M^+), 200 (M^+-1). Found: C, 83.4; H, 9.7; N, 6.7%. Calcd for $C_{14}H_{19}N$: C, 83.5; H, 9.5; N, 7.0%.

*Aziridines **8c** and **10c**.* The aziridines were prepared according to the literature.[16]

*1-Methyl-12-azabicyclo[9.1.0]dodecane (**11a**).* The aziridine was obtained by the similar method from cycloundecanone oxime in 71% yield, bp 160—165 °C/22 mmHg. IR (neat): 3250, 894 cm^{-1}, PMR: δ 0.2—0.7 (br. s, 1H), 0.7—2.3 (m+s (δ 1.18), 22H), mass: *m/e* 181 (M^+). Found: C, 79.5; H, 12.8; N, 7.7%. Calcd for $C_{12}H_{23}N$: C, 79.4; H, 12.9; N, 7.6%.

*Alternative Preparation of 12-Cyano-2-dodecanone (**7a**).* Ethyl acetoacetate (1.30 g, 10 mmol) was added to sodium hydride (10 mmol) suspended in dimethoxyethane (20 ml). After the evolution of hydrogen gas ceased 1,9-dibromononane (2.86 g, 10 mmol) was added to the resulting pale yellow solution. Stirring at room temperature for two days, followed by chromatographic separation of the crude product, gave 12-bromo-3-ethoxycarbonyl-2-dodecanone (0.62 g, 54% yield based on the consumed dibromide). The alkylate was dissolved in 95% aqueous dimethyl sulfoxide (10 ml) containing sodium cyanide (9.50 g), and the solution was heated at 160—165 °C for 3 hr. Extractive work-up and the subsequent purification by preparative tlc (silica gel, ether/*n*-hexane 1 : 3, R_f 0.4—0.5) afforded **7a** (0.11 g, 28% yield). All the spectral data were identical with those of the oxidation product.

References

1) "Hannosei Chukantai (Reactive Intermediates)," ed. by K. Ichikawa, T. Saegusa, H. Tsubomura, H. Nozaki, and I. Moritani, Kagakudojin, Kyoto, 1971.

2) J. B. Aylward, *Quart. Rev.*, **25**, 407 (1971); B. Rindone, E. Santaniello, and C. Scolastico, *Tetrahedron Lett.*, **1972** 19.

3) R. S. Neale, *Synthesis*, **1971**, 1; A. Stojiljković, V. Andrejević, and M. Lj. Mihailovi, *Tetrahedron*, **23**, 721 (1967).

4) W. Lwowski, "Nitrenes," John Wiley & Sons, New York, 1970.

5) A preliminary report is found in: T. Hiyama, H. Koide, and H. Nozaki, *Tetrahedron Lett.*, **1973**, 2143.

6) a) A. B. Levy and A. Hassner, *J. Amer. Chem. Soc.*, **93**, 2052 (1971). b) D. S. Wulfman and T. R. Steinheimer, *Tetrahedron Lett.*, **1972**, 3933. c) G. Szeimies, U. Siefken, and R. Rinck, *Angew. Chem. Int. Ed. Engl.*, **12**, 161 (1973).

7) A. Hassner, A. B. Levy, E. E. McEntire, and J. E. Galle, *J. Org. Chem.*, **39**, 585 (1974).

8) Nagata *et al.* have studied the oxidation of primary amines containing olefinic moiety with lead tetraacetate to afford aziridines (W. Nagata, S. Hirai, K. Kawata, and T. Aoki, *J. Amer. Chem. Soc.*, **89**, 5045 (1967)). They suggested that the α-elimination of lead(II) and proton was assisted by the back-side attack of the π-electrons of the olefinic part (W. Nagata, S. Hirai, Y. Yoshioka, K. Tori, and T. Aoki "Abstracts of the 16th Symposium on Organic Reaction Mechanism, Japan," p. 40 (1965)). The concerted opening of the three membered ring in the oxidation of **1** cannot be excluded.

9) P. G. Gassman, *Accounts Chem. Res.*, **3**, 26 (1970).

10) Chlorination of **3** and the following solvolysis are reported to afford benzaldehyde. P. G. Gassmann and D. K. Dygos, *J. Amer. Chem. Soc.*, **91**, 1543 (1969).

11) As to the theoretical treatment on the ring opening reaction of *N*-aziridinyl cation, see R. G. Weiss, *Tetrahedron*, **27**, 271 (1971).

12) A. P. Krapcho, E. G. E. Jahngen, Jr., and A. J. Lovey, *Tetrahedron Lett.*, **1974**, 1091.

13) M. Ohno, N. Naruse, S. Torimitsu, and I. Terasawa, *J. Amer. Chem. Soc.*, **88**, 3168 (1966). M. Ohno, N. Naruse, and I. Terasawa, "Organic Syntheses," Coll. Vol. 5 (1973), p. 266.

14) R. Chaabouni and A. Laurent, *Bull. Soc. Chim. Fr.*, **1973**, 2680; R. Chaabouni, A. Laurent, and P. Mison, *Tetrahedron Lett.*, **1973** 1343; K. Kotera, K. Kitahonoki, "Organic Syntheses," Coll. Vol. 5 (1973), p. 83.

15) L. A. Paquette, D. E. Kuhla, J. H. Barret, and R. J. Haluska, *J. Org. Chem.*, **34**, 2866 (1969); S. Rosen and D. Swern, *Anal. Chem.*, **38**, 1392 (1966).

16) A. Hassner, M. E. Lorber, and C. Heathcock, *J. Org. Chem.*, **32**, 545 (1967); A. Hassner and C. Heathcock, *Tetrahedron*, **20**, 1037 (1964); S. Fujita, T. Hiyama, and H. Nozaki, *ibid.*, **26**, 4347 (1970).

Stereospecific [2π+2π+2π] Cycloaddition Reaction of Norbornadiene[1]

Iwao TABUSHI*, Kazuo YAMAMURA, Zen-ichi YOSHIDA,** and Atsushi TOGASHI**

Faculty of Pharmaceutical Sciences, Kyushu University, Fukuoka 812

***Department of Synthetic Chemistry, Kyoto University, Kyoto 606*

(Received May 27, 1975)

[2π+2π+2π] cycloaddition reaction of *cis*- or *trans*-disubstituted olefinic dienophiles (**4a–4e**) to bicyclo-[2.2.1]hepta-2,5-diene (**1**, norbornadiene) was found to be stereospecific. The cycloadducts obtained, 4,5-disubstituted tetracyclo[4.2.1.0.^{2,9}0^{3,7}]nonane (**5,6**) conserved the original stereochemistry in the dienophiles, strongly suggesting the presence of *homo*-conjugation in **1**. A striking contrast between cycloaddition reaction of quadricyclane (a valence bond isomer of **1**) and that of norbornadiene was understood by application of the principle of orbital symmetry conservation to these cycloadditions.

[2π+2π+2π] cycloaddition reaction of norbornadiene (**1**) with dienophiles are known as *homo*-Diels-Alder reaction in several cases,[2] giving tetracyclo-[4.2.1.0.^{2,9}0^{3,7}]nonanes (**2**). The unique and very interesting mode of these cycloadditions of **1** may be interpreted by means of a six-membered transition state (**3**).

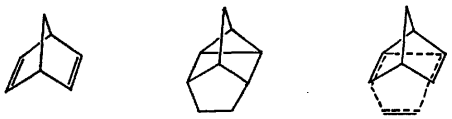

1 **2** **3**

It was suggested by Hoffmann *et al.*[3] that there exists a (through-space) conjugation between the two double bonds in the ground electronic state of **1**, and several physico-chemical investigations (photoelectron spectroscopy,[4] photoionization spectroscopy[5]) or quantum chemical studies[3,4b] afforded good evidences for the suggestion.

If the unusually effective *homo*-conjugation in **1** also strongly contributes to the assumed transition state (**3**), the cycloadducts must conserve the original stereochemistry of the starting dienophiles. No investigation appeared so far, which showed that the *homo*-Diels-Alder reactions are concerted ones, except for crotononitrile which is reported to conserve the substituents' configuration, *cis* or *trans*, in the cycloadducts.[2f] If these reactions are concerted, the difference in the symmetry of the highest occupied molecular orbital (HOMO) between norbornadiene (SA) and quadricyclane (AS) could be attributed to the striking difference in regiospecificity of the cycloaddition reactions between these two valence bond isomers.[8]

Now we wish to report stereochemistry in *homo*-Diels-Alder cycloadditions of **1** with several *cis*- and *trans*-disubstituted olefinic dienophiles (**3a**—**3e**). These cycloaddition reactions were concluded to be completely stereospecific, based on results of chemical and spectroscopic studies of the adducts, therefore, it seems to be concerted, suggesting that the *homo*-conjugation in **1** is very important to control its cycloaddition reactions.

Results and Discussion

Dimethyl fumarate (**4b**) was treated with excess amount of norbornadiene (**1**) in a sealed tube at 180 °C for 50 hr, in the presence of hydroquinone (2% to **4b**) as an inhibitor to radical polymerizations. Distillation under the reduced pressure gave an oily product (bp 120—125°/5 mmHg) in 78% yield. Determination of the product's structure was made chemically (*vide infra*) and spectroscopically. The mass spectrum of the product showed molecular peak (M^+, 236 *m/e*) and expected fragment peaks (M^+—HCO_2CH_3, 176 *m/e* and M^+—HCO_2CH_3—CO_2CH_3, 117 *m/e*). Infrared spectrum of **5b** exhibited an absorption at 800 cm^{-1}, characteristic to nortricyclane skeleton,[7] and nuclear magnetic resonance spectrum showed absorptions of two protons α to methoxycarbonyls (δ 3.42, 3.22), two protons β to methoxycarbonyls (δ 2.40, 2.32), C_7-H proton[8] (δ 2.04, 1H), and cyclopropane ring protons (δ 0.9—1.3, 3H), which also strongly supported the structure **5b**.

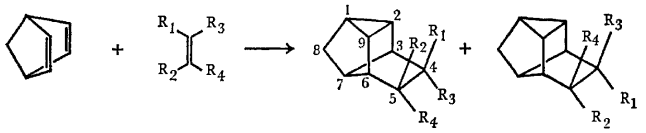

1 **4** **5** **6**

a) R_1R_2=-COOOC-; R_3=R_4=H
b) R_1=R_4=CO_2CH_3; R_2=R_3=H
c) R_1=R_2=CO_2CH_3; R_3=R_4=H
d) R_1=R_4=CN; R_2=R_3=H
e) R_1=R_2=CN; R_3=R_4=H

4,5-*trans*-Dicyanotetracyclo[4.2.1.0.^{2,9}0^{3,7}]nonane (**5d**) was obtained in 69% yield, when fumaronitrile (**4d**) was treated at 120 °C with norbornadiene in a similar manner to that described above. The structure **5d** was again supported by mass spectrum (Table 1), IR spectrum (2240 and 800 cm^{-1}), and NMR spectrum (Table 2), the latter strongly resembled to that of *trans*-dicarboxylate, **5b**, in every detail (chemical shifts and coupling patterns) except for the chemical shifts of H_{4x} and H_{5n}.

Two *homo*-Diels-Alder stereoisomers, *endo-cis*- (**5**) and *exo-cis*-4,5-disubstituted, were obtained from each of maleic anhydide (**4a**), dimethyl maleate (**4c**), and maleonitrile (**4e**) additions to **1**. The NMR spectrum of each cycloadduct (**5a**, **6a**, **5c**, **6c**) exhibited characteristic absorptions of symmetrical two α protons ($H_{4,5}$) and two β protons ($H_{3,6}$) to the substituents, CO_2X, together with absorptions of isolated bridgehead proton (H_7) and three cyclopropane ring protons, again strongly supporting the products' structure of tetracyclo-

* To whom correspondence should be addressed.

Table 1. Mass spectra of the *homo*-Diels-Alder adducts[a)]

Adduct	*m/e*
6a	p+2 192(1.8), p+1 191(14.4), p 190(100), 162(31), 118(294), 117(283), 115(47), 58(114), 51(100)
5b	p+2 238(7.3), p+1 237(15.2), p 236(100), 176(415), 145(285), 126(415), 117(769), 116 (423), 115(377), 91(392)
5c	p+2 238(5), p+1 237(26), p 236(100), 205 (69), 204(52), 177(46), 176(114), 145(106), 118(69), 117(543), 116(106), 115(91), 91(57)
6c	p+2 238(2.5), p+1 237(16), p 236(100), 205 (73), 204(44), 177(110), 145(120), 126(68), 118(41), 117(288), 116(63), 115(54)
5d	p+2 172(0.7), p+1 171(11.5), p 170(100), 169(94), 144(122), 130(89), 104(82), 92(91), 91(96)

a) Relative intensities are in parentheses.

[4.2.1.0.^{2,9}0^{3,7}]nonane skeleton. Based on all of spectral data, NMR (*vide infra*), IR, and/or mass spectra, and chemical conversion cited below, it was concluded that cycloadducts, **5a**—**5d**, **6a**—**6d** differ only in substituents or in stereochemistry at C_4 and C_5.

Product distribution in dienophiles' addition to **1** were carefully determined by means of gas liquid phase chromatography (glpc) and the results are shown in Table 3. In each case of addition of a *trans*-disubstituted olefin (**4b** and **4d**) to **1**, no or little corresponding *cis*-4,5-disubstituted isomer was produced within the precision of glpc detection (0.3%) (runs 3 and 7). It was also shown by glpc analysis of crude products that, in the cases of additions of the *cis*-disubstituted olefins (**4c** and **4f**), corresponding *trans* isomers were not detected for **4c** (run 4) or produced only in a trifling amount (5%, run 8) for **4e**. From the present results, therefore, it was concluded that the cycloadducts conserved the original stereochemistry, *cis* or *trans*, of the dienophiles.

Table 3 shows that the stereospecificity mentioned

Table 2. Chemical shifts and coupling constants of the protons of the *homo*-Diels-Alder products

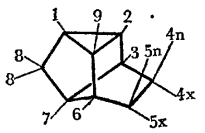

	5a[a,d] (*endo*)	**6a**[a)] (*exo*)	**5b**[a)] (*trans*)	**5c**[b)] (*endo*)	**6c**[b)] (*exo*)	**5d**[a)] (*trans*)
$H_{1,2,9}$	1.1—1.4	1.1—1.4	0.9—1.3	1.1—1.3	0.9—1.2	1.1—1.5
$H_{3,6}$	2.58	2.57	{2.40 {2.32	2.40	2.30	2.48
H_{4n}		2.58			3.15(s)	
H_{4x}	3.50(dd)		3.42(dd)	3.20(dd)		3.21(dd)
H_{5n}		3.25(s)	3.22(d)		3.15(s)	3.07(d)
H_{5x}	3.50(dd)			3.20(dd)		
H_7	2.20	1.81	2.04	2.02	1.73	2.19
H_8	1.65	1.67	1.54	1.50	1.60	1.76
CO_2CH_3			{3.72(s) {3.70(s)	3.68(s)	3.64(s)	
$J_{3,4x}$	3		4	2		4
$J_{6,5n}$		0	0		0	0
$J_{4n,5x}$			5			5

a) δ value in $CDCl_3$. b) δ value in CCl_4. c) Hertz. d) R. C. Cookson *et al.*, Ref. 2d.

Table 3. Product distribution in additions of olefinic dienophiles to **1**.

Run	Addenda	Temp. (°C)	Hydroquinone	*homo*-Diels-Alder adduct		
				cis-endo	*cis-exo*	*trans*
1	**4a**	130	2%	79	21	—
2		200	2%	66	34	—
3	**4b**	180	2%	<0.2[a)]	<0.2[a)]	>99.6
4	**4c**	150	2%	73	27	< 0.3[a)]
5		200	2%	41	24	35
6		200	4%	41	24	35
7	**4d**	120	2%	<0.3[a)]	<0.3[a)]	>99.4
8	**4e**	100[b)]	2%	*ca.* 80	*ca.* 15	5
9		120	2%	73	16	11

a) Not detected. b) The conversion was less than 2%.

above holds under the conditions of the controlled reaction temperatures for cases of *cis*-disubstituted dienophiles' additions to **1**. Thus, 35% and 11% of the *trans* isomers isomerized were produced in additions at higher temperature; from *cis* olefin **4c** at 200 °C (run 5) and **4e** at 120 °C (run 9), respectively.

Since maleonitrile (**4e**) was unstable (to isomerize to fumaronitrile, **4d**) at the higher temperatures than 130 °C, the addition reaction of **4e** with **1** was followed at 120 °C up to *ca.* 2% conversion. Glpc analysis of the crude mixture gave a product ratio : **5e** : **6e** : **5d**=73 : 16 : 11. Products **5e** and **6e** could be purified through a preparative glpc, whose IR spectra exhibited absorptions at 2230 and 800 cm^{-1}, demonstrating the presence of nortricyclane skeleton and the cyano substituents.

Chemical Conversion of the Cycloadducts. Two stereoisomers, tetracyclo[4.2.1.0.^{2,9}0^{3,7}]nonane-*endo-cis*-4,5-dicarboxylic anhydride (**5a**) and *exo-cis*-dicarboxylic anhydride (**6a**), were obtained in the ratio of 66 : 34,*** when maleic anhydride was treated with excess amount of norbornadiene at 200 °C (Table 3).

The *endo* anhydride (**5a**) was converted to the corresponding half ester on treatment with methanol, followed by estirification with diazomethane giving *endo-cis*-4,5-diester (**5c**) exclusively. Acid catalyzed esterification of the *exo* anhydride (**6a**) in HCl methanol led to the *exo-cis*-4,5-dicarboxylate (**6c**). Dicarboxylates thus obtained, **5c** and **6c**, were identical with those obtained in the reaction of dimethyl maleate (**4c**) with **1**, respectively in every detail (NMR and IR spectra, glpc retention times, see Experimental Section).

It is noteworthy that an equilibrium was attained between the three isomeric dicarboxylates (**5b** : **5c** : **6c**=95.0 : 3.7 : 1.3), when any pure sample of the three was treated with sodium methoxide in methanol at 30 °C for 10 hr.

The conversion of the *trans* dinitrile (**5d**) to the *trans* dicarboxylate (**5b**) was attempted by refluxing a solution of **5d** in HCl acidic methanol for *ca.* 8 hr. However, 4-*endo*-cyano-5-*exo*-methoxycarbonyltetracyclo[4.2.1.0.^{2,9}0^{3,7}]nonane (**8**) was isolated instead of **5b**. NMR spectroscopic evidence (next paragraph), nevertheless, strongly supported that the *trans* dinitrile (**5d**) had the same skeletal structure as the *trans* dicarboxylate (**5b**), and therefore, it was concluded that the cycloadducts (**5a**—**5d**, **6a**, and **6c**) differ only in substituents (with the same stereochemistry) or in stereochemistry (with the same substituent). Structural correlations are shown in Scheme 1.

Stereochemistry and NMR Spectra of the Cycloadducts. Careful examinations of chemical shifts data in Table 2 reveal a very characteristic trend : the δ values of the *endo* protons at C_4 (C_5) were somewhat smaller (0.05—0.25 ppm) than those of the *exo* protons at C_4 (C_5). For example, in *trans* diester **5b** (*trans* dinitrile **5d**), the chemical shift of H_{5n} was δ 3.22 (δ 3.07) and that of H_{4x} was δ 3.42 (δ 3.21). A similar trend

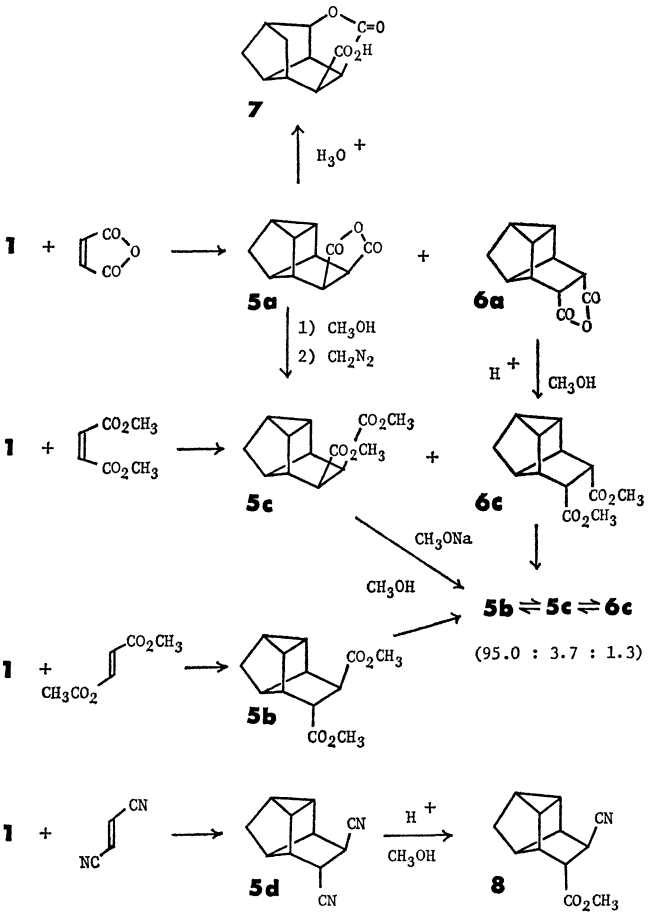

Scheme 1.

is well known in norbornanes[9] or norbornenes,[10] where the resonances of *exo* protons were observed at somewhat lower field than those of *endo* protons. These were mainly explained as the result of C–C shielding effect.[11]

The chemical shift, δ 3.50 (δ 3.20), of α protons of **5a** (**5c**) was larger than that of α protons, δ 3.25 (δ 3.15), of **6a** (**6c**). This strongly indicated that **5a** (**5c**) and **6a** (**6c**) have *exo* protons and *endo* protons, respectively, in good agreement with the structures assigned on the basis of chemical conversions.

NMR decoupling experiments of the *trans*-dicarboxylate (**5b**) (*trans*-dinitrile, **5d**) were carried out, which made it possible to calculate $J_{3,4x}$, $J_{6,5n}$, or $J_{4,5x}$ (Table 2). Apparently there observed a large coupling of the *exo* proton (H_{4x}) with the bridgehead proton ($J_{3,4x}$=4 Hz), whereas coupling between the *endo* proton (H_{5n}) and the corresponding proton (C_6-H) was not appreciable. Therefore, the appreciable coupling constants, J=3 Hz and J=2 Hz, of the resonances of α protons of **5a** and **5c**, respectively, again strongly supported that these α protons are *exo*, in good agreements with the assigned structures.

Regiospecificity and Stereospecificity of homo-*Diels-Alder Reaction.* Based on the assigned structures of the cycloadducts, it was concluded that the *homo*-Diels-Alder reaction is stereospecific as shown in Scheme 2. The regiospecificity and stereospecificity observed implies that the reaction is concerted and allowed, giving

*** Cookson *et al.*[2d] isolated only the *endo-cis* isomer (**5a**), the structure of which was determined by the fact that **5a** could be converted to lactone **7** (Scheme 1).

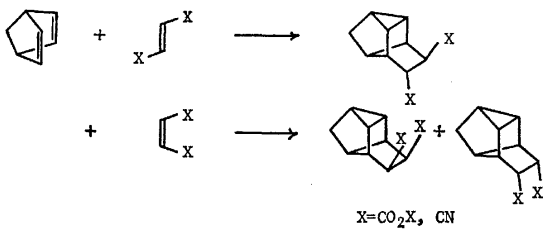

Scheme 2.

a strong evidence for the *homo*-conjugation in **1** on a reactivity ground.

The present results make a striking contrast to the [2σ+2σ+2π] cycloaddition reaction of quadricyclane reported by the authors,[6] where another type of regiospecificity (*exo*-type addition) together with stereospecificity were observed.

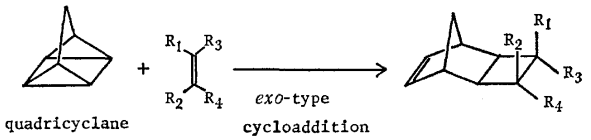

These regiospecificities and stereospecificities in Scheme 3 required a presence of an effective interaction between the two cyclopropane ring bonds in a transition state. Consideration of the usual orbital correlation diagram[12] (Fig. 1) suggests that the *homo-endo*-type cycloaddition to norbornadiene is allowed, whereas the *exo*-type addition, shown in Scheme 3, is forbidden. Thus, the present experimental results are in good agreement with the orbital symmetry consideration.

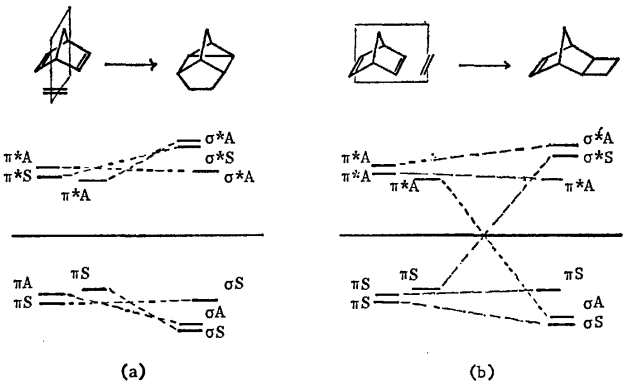

Fig. 1. Orbital correlation diagram.
(a) *homo-endo*-type cycloaddition; (b) *exo*-type cycloaddition.

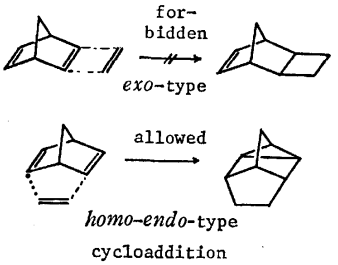

Scheme 3.

On the other hand, for quadricyclane, *exo*-type cycloaddition is allowed and *homo-endo*-type cycloaddition is forbidden. Again experimental results[6] are in good agreement with the prediction from the orbital symmetry consideration.

It is concluded, therefore, that the striking difference in regiospecificity of the cycloaddition reaction between quadricyclane and norbornadiene is attributable to the differed orbital symmetry of these two valence bond isomers.

Experimental

Measurements of nuclear magnetic resonance spectra were performed on Varian T-60, JEOL 60-H, or JEOL 100-H spectrometer. Infrared spectra were obtained with a Hitachi model 215 infrared spectrometer. Elemental analyses were performed by Microanalysis Laboratory in Faculty of Pharmaceutical Sciences, Kyushu University or by Microanalysis Center of Kyoto University. Measurements of mass spectra were performed by Analysis Laboratory of Faculty of Pharmaceutical Sciences, Kyushu University or of Department of Synthetic Chemistry, Kyoto University.

For the determination of the product distribution, glpc analyses were carried out with Shimadzu model GC 4B-IT on two different liquid phases: Silicone DC 550 and polyethylene glycol 20 M. Retention times are shown below.

*Reaction of **1** with Dimethyl Fumarate (**4b**).* A mixture of 1.00 g (6.9 mmol) of dimethyl fumarate (**4b**) and 10 ml (*ca.* 97 mmol) of norbornadiene (**1**) and 10 mg of hydroquinone was sealed in a Pyrex tube (30 ml volume). The sealed tube was heated at 180 °C in a bath for 50 hr. After the evaporation of excess of norbornadiene *in vacuo*, the residue was distilled at the reduced pressure: (**5b**); bp 120—130 °C/5 mmHg; 1.27 g (78%); IR (neat) 3080, 2950, 1735 ($\nu_{C=O}$), 1435, 1180—1200, 1038, 1015, 800, 786 cm^{-1}; Found C, 65.94; H, 6.94%. Calcd for $C_{13}H_{16}O_4$ C, 66.08; H, 6.83%.

*Reaction of **1** with Dimethyl Maleate (**4c**).* A mixture of 1.0 g (6.9 mmol) of dimethyl maleate (**4c**) and 10 ml (97 mmol) of **1** and 10 mg of hydroquinone was sealed in a Pyrex tube and heated at 200 °C for 24 hr. After the distillation off the excess of **1** *in vacuo*, the residue was distilled at the reduced pressure: bp 120—140 °C/5 mmHg; **5c** : **6c** : **5b**=41 : 24 : 35. **5c** : IR (neat) 3060, 2960, 2875, 1740 ($\nu_{C=O}$), 1438, 1200, 818, 794 cm^{-1}; glpc retention time, 18.2 min on 2 m polyethylene glycol (190 °C, H_2, 1.7 atm); Anal. Calcd for $C_{13}H_{16}O_4$ C, 66.08; H, 6.83%. Found; C, 65.45; H, 6.90%. **6c**: IR (neat) 3060, 2960, 2870, 1740 ($\nu_{C=O}$), 1438, 1120, 1195, 818, 792 cm^{-1}; glpc retention time 16.1 min on 2 m polyethylene glycol (190 °C, H_2, 1.7 atm); Found C, 65.75; H, 6.60%. Calcd for $C_{13}H_{16}O_4$: C, 66.08; H, 6.83%.

*Reaction of **1** with Maleic Anhydride (**4a**).* A mixture of 0.50 g (5.1 mmol) of maleic anhydride (**4a**) 1.0 g (*ca.* 11 mmol) of **1**, and 30 mg of hydroquinone was heated in a sealed Pyrex tube at 130 °C for 5 hr. Glpc analysis of the crude mixture on a 2.5 m column of polyethylene glycol at 230 °C (H_2, 3.0 atm) revealed that two products were formed: **5a**, 79% (retention time, 8.8 min) and **6a**, 21% (6.7 min). The product ratio at 200 °C was also shown in Table 2. Purifications of **5a** and **6a** were carried out through preparative glpc. **5a** : IR (KBr) 2980, 1860, 1780, 1220, 1080, 906, 895, 830, 800 cm^{-1}; **6a** : IR (KBr) 2960, 1860, 1780, 1212, 980, 908, 896, 830, 800 cm^{-1}. The NMR chemical shifts of the *endo* anhydride (**5a**) were identical with the values reported by Cookson *et al.*[2d]

Reaction of ***1*** *with Fumaronitrile (****4d****).* A mixture of 1.00 g (12.8 mmol) of fumaronitrile (**4d**), 10 ml of norbornadiene, and 10 mg of hydroquinone was heated in a sealed tube at 120 °C for 50 hr. After the excess of **1** was distilled off at the reduced pressure, the residue was distilled at 10 mmHg : **5d**; 1.5 g (69%); bp 165 °C/10 mmHg; mp 77—77.5 °C (from methylene chloride or methanol); IR (neat) 3070, 2950, 2240 ($\nu_{C\equiv N}$), 1305, 1210, 800 cm^{-1}; glpc retention time, 1.75 min (polyethylene glycol, 1 m, 190 °C, H_2, 1 atm); Found C, 77.83; H, 5.81%. Calcd for $C_{11}H_{10}N_2$ C, 77.62; H, 5.92%.

Reaction of ***1*** *with Maleonitrile (****4e****).* A mixture of 0.75 g (9.6 mmol) of maleonitrile (**4e**), 4 ml (43 mmol) of **1**, and 10 mg of hydroquinone was heated in a sealed tube at 100 °C for 17 hr. Glpc analysis on polyethylene glycol (1 m, 190 °C, H_2, 1 atm) showed two peaks (3.1 and 4.0 min) and a ratio of 15 : 85. IR spectrum of each product exhibited characteristic absorptions at 2240 and 800 cm^{-1}.

Chemical Conversion. ***5a*** *to* ***5c***: After 100 mg of **5a** was dissolved in 5.0 ml of methanol at 50 °C, excess methanol was distilled off *in vacuo*. Then 10 ml of ether was added and the solution was treated with etheral solution of diazomethane. After the evaporation of ether, the residue was analyzed by glpc, IR and NMR spectra.

6a *to* ***6c***: A mixture of 100 mg of **6a**, 5 ml of methanol, two drops of concentrated HCl was heated at 60 °C for 3.0 hr. The methanol solution was condensed to one third and then poured into ice cooled water, to which was added an aqueous solution of sodium bicarbonate to neutralize hydrochloric acid. The aqueous solution was extracted with 25 ml of ether twice, and the glpc analysis of the etheral solution revealed that the product was the *endo-cis*-diester (**6c**).

5d *to* ***8***: A mixture of 50 mg (0.29 mmol) of **5d**, a drop of concentrated hydrochloric acid, and 10 ml of dry methanol in a 25 ml flask was stoppered and heated at 80 °C for 8 hr. After the solution was neutralized with an aqueous solution of sodium bicarbonate, the product was extracted with chloroform. Evaporation of chloroform gave an oily product, and the product was identified as **8** by means of glpc analysis and the identical infrared spectrum with an authentic compound. **8** : retention time, 9.5 min on polyethylene glycol 20 M (2 m, 190 °C, H_2, 1 atm); IR (neat) 3070, 2948, 2240, 1740, 1438, 818, 799 cm^{-1}.

References

1) A part of this work was presented at the 24th Annual Meeting of the Chemical Society of Japan, Osaka, Preprint p. 1122 (1972). After this oral presentation, it was reported by Kobuki *et al.* that the *homo*-Diels-Alder reaction of **1** with crotonitrile took place stereospecifically (Ref. 2f).

2) (a) H. K. Hall, *J. Org. Chem.*, **25**, 42 (1960); (b) A. T. Blomquist and Y. C. Meinwald, *J. Amer. Chem. Soc.*, **81**, 667 (1959); (c) E. F. Ullman, *Chem. Ind.* (London), **1958**, 1173, (d) R. D. Cookson, J. Dance, and J. Hudec, *J. Chem. Soc.*, **1964**, 5614 (e) S. J. Cristol, E. L. Allred, and D. L. Wetzel, *J. Org. Chem.*, **27**, 4058 (1962); (f) Y. Kobuke, T. Sugimoto, J. Furukawa, and T. Fueno, *J. Amer. Chem. Soc.*, **94**, 3633 (1972).

3) R. Hoffman, E. Heibronner, and R. Gleiter, *ibid.*, **92**, 706 (1970).

4) (a) N. Bodor, M. J. S. Dewar, and S. D. Worley, *ibid.*, **92**, 19 (1970); (b) E. Heilbronner and H. -D. Martin, *Helv. Chem. Acta*, **55**, 1490 (1970); (c) D. A. Demeo and A. J. Yencha, *J. Chem. Phys.*, **53**, 4536 (1970).

5) D. A. Demeo and M. A. El-Sayed, *ibid.*, **52**, 2622 (1970).

6) I. Tabushi, K. Yamamura, and Z. Yoshida, *J. Amer. Chem. Soc.*, **94**, 787 (1972).

7) D. J. Trecker and J. P. Henry, *ibid.*, **85**, 3204 (1963); S. Winstein *ibid.*, **83**, 1516 (1961), and references cited therein.

8) S. Forsen and T. Norin, *Tetrahedron Lett.*, **1964**, 2845.

9) W. C. Wong and C. C. Lee, *Can. J. Chem.*, **42**, 1245 (1964).

10) P. Laszlo, P. v. R. Schleyer, *J. Amer. Csem. Soc.*, **89**, 2709 (1963).

11) L. M. Jackman, S. Sternhell, "Application of Nuclear Magnetic Resonance Spectroscopy in Organic Chemistry," 2nd Ed., Pergamon Press, New York, N.Y. (1969), pp. 78, 79.

12) (a) R. Hoffmann and R. B. Woodward, *J. Amer. Chem. Soc.*, **87**, 2045 (1965); (b) R. B. Woodward and R. Hoffmann, "Conservation of Orbital Symmetry," Academic Press (1970).

Stereoselective Synthesis of 1,4,4a,9a-Tetrahydro-9-fluorenone Bearing *trans* Angular Substituents

Takenori KUSUMI, Kiyoto IMAYE, and Hiroshi KAKISAWA

Department of Chemistry, Tokyo Kyoiku University, Otsuka, Bunkyo, Tokyo 112

(Received May 31, 1975)

An intramolecular Friedel-Crafts reaction of 2-methyl-1-phenyl-1,2,3,6-tetrahydrophthalic anhydride **6** followed by methylation afforded new types of fluorenones bearing *trans* angular substituents, 4a-carbomethoxy-*trans*-9a-methyl-1,4,4a,9a-tetrahydro-9-fluorenone **7** and 3-hydroxy-*trans*-9a-methyl-9-oxo-1,2,3,4,4a,9a-hexahydrofluoren-*cis*-4a-carboxylic anhydride **10**.

A number of triterpenes are found to have polycyclic systems bearing *trans* substituents at the angular positions, as exemplified by the C/D ring system of fernene **1**.[1] A few reports have appeared concerning the methods for building up such *trans* fused cyclic systems, *e.g.*, hydrocyanation,[2] olefinic cyclization,[3] and the cleavage of a cyclopropane ring.[4] In the preceding paper[5] we have reported upon the acid-catalyzed cyclization of the cyclohexenone **2**, which gives rise to the *cis*-dimethylphenanthrenone **3**.

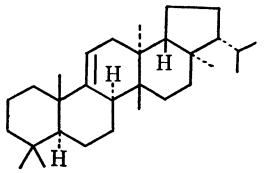

1

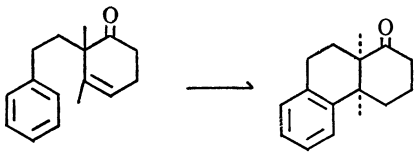

2 **3**

We report here a new method for the stereoselective synthesis of a tricyclic system carrying *trans* angular substituents using a Diels-Alder reaction and an intramolecular Friedel-Crafts reaction.

The Diels-Alder reaction of maleic anhydride and butadiene is well known to produce stereoselectively *cis*-1,2,3,6-tetrahydrophthalic anhydride. The same reaction of the anhydride **4** and butadiene affords the hydrophenanthrene derivative **5**,[5] in which the two functional groups are also oriented in a *cis* sense at the ring junctions. Thus, the cycloaddition reaction is suitable for synthesis of alicyclic compounds with two functional groups in a *cis* relation. We have devised the synthesis of polycyclic compounds having *trans* angular substituents from the *cis*-intermediate produced by a Diels-Alder reaction.

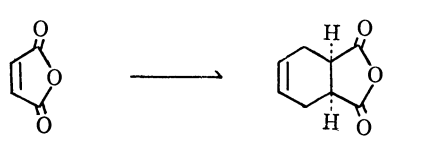

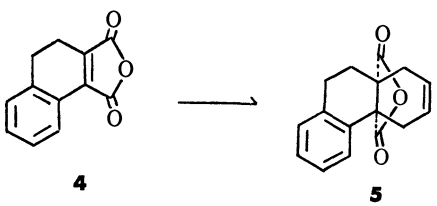

4 **5**

Results and Discussion

A Diels-Alder reaction of phenylmethylmaleic anhydride[6] and butadiene (or 3-sulfolene[7]) at 200 °C afforded the adduct **6** (mp 99.5—100 °C). Treatment of the anhydride **6** with aluminum chloride in carbon disulfide, followed by methylation with diazomethane, afforded the fluorenone **7** in 40% yield accompanied by three reaction products, the structures of which will be clarified later. The NMR spectrum of **7** shows two singlets at 1.05 (3H, angular methyl) and 3.48 (3H, $-COOCH_3$), in addition to a broad singlet at 5.8 (2H, olefinic protons) ppm. The IR (1710 and 1600 cm^{-1}) and UV (245 and 288 nm) spectra are consistent with the indanone chromophor of **7**. The structure was also verified by a further transformation; the ester **7** was reduced with lithium aluminum hydride in ether to give the diol **8**. The benzylic hydroxyl group was selectively oxidized on treatment with manganese dioxide[8] in methylene chloride to afford the crystalline hydroxy ketone **9**, which gives analytical datum and spectroscopic properties consistent with the proposed structure.

The angular substituents in these compounds (**7**–**9**) are necessarily located in the *trans* relationship because of the *cis* arrangement of the two carbonyls in the anhydride **6**.

Three other crystalline substances were also isolated from the Friedel-Crafts reaction products of the an-

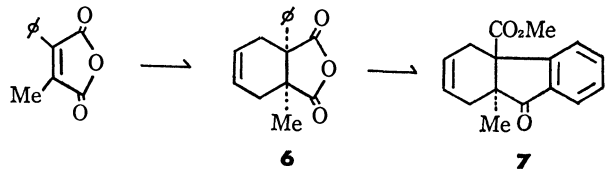

6 **7**

+ Three products

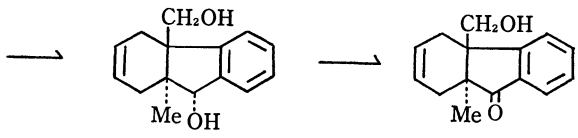

8 **9**

hydride **6**. The IR spectrum of the first crystals (40% from **6**) shows bands at 1765 and 1712 cm^{-1} and the UV spectrum exhibits absorption maxima at 247 and 290 nm, suggesting the presence of a γ-lactone and an indanone chromophor. The NMR spectrum exhibits a sharp singlet at 1.22 due to an angular methyl group and a 1H-multiplet at 4.95 ppm attributable to the proton attached to the carbinyl carbon atom of the lactone. From these properties the structure **10** was assigned for the first crystals, and this was further supported by physicochemical analyses.

The second and third crystals (7% and 2% from **6**) were found to be isomers having molecular formula $C_{16}H_{17}O_3Cl$ from the consideration of their mass spectra (*m/e* 264, M^+-CO; 266, M^++2-CO [32% height of the 264 peak]) and analytical data. The presence of chlorine atom in each compound was also detected by a Beilstein test. The IR spectra of each substance gave a pair of carbonyl bands at around 1776 (strained carbonyl) and 1720 (ester) cm^{-1}; the NMR spectra suggest the presence of a quaternary methyl (1.48/1.34 ppm, s, 3H), methoxy (3.42/3.41 ppm, s, 3H), and monosubstituted phenyl (7.29/7.28 ppm, s, 5H) groups. The signal ascribable to the proton attached to the carbon bearing chlorine atom appears around 4.5 ppm, as a multiplet. The structures **11a** and **b** can be assigned to the isomeric pair which are formed by the attack of the acyl cation to the double bond, as shown in the following scheme.

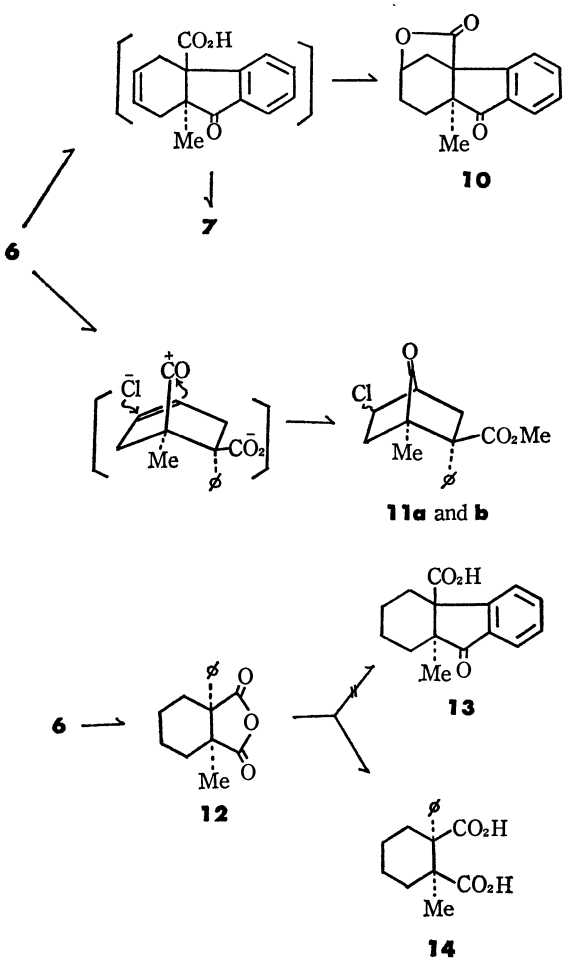

It is noteworthy that the dihydroanhydride **12**, obtainable by hydrogenation of **6** on platinum oxide, does not give rise to the hexahydrofluorenone **13** by treating with aluminum chloride, but affords the diacid **14**. The molecular models indicate that interactions between the angular substituents and hydrogens destabilize the intermediate I. On the other hand, the absence of two hydrogen atoms at C-4 and 5 makes the intermediate II more stable and easier to cyclize.

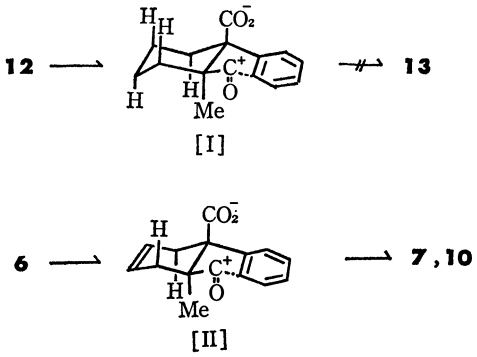

Experimental

NMR spectra were obtained with a Hitachi H-60 instrument using TMS as an internal standard. All the infrared spectra were taken on a Hitachi EPI-3T spectrophotometer. Ultraviolet spectra were taken on a Hitachi EPS-3T. Melting points and boiling points are uncorrected.

2-Methyl-1-phenyl-1,2,3,6-tetrahydrophthalic Anhydride ***6***. A solution of phenylmethylmaleic anhydride (3.76 g) and butadiene (10.8 g) in dry dioxane (12 ml) containing a small amount of hydroquinone was heated at 200 °C in a sealed tube for 65 hr. The tube was cooled in a Dry Ice–acetone bath and opened. The solvent was evaporated to afford a yellow residue, which was chromatographed on silica gel (200 g). Elution with benzene–hexane (4 : 6) gave the adduct **6** (1.24 g) followed by the recovered phenylmethylmaleic anhydride (0.87 g). The analytical sample of **6** was obtained by recrystallization from ethanol as needles, mp 99.5—100 °C; ν (KBr): 1855, 1780, 1210, 970, 760, 700 cm^{-1}; δ ($CDCl_3$): 0.98 (3H, s), 6.04 (2H, br. s), 7.28 (5H, s) ppm. Calcd for $C_{15}H_{14}O_3$: C, 74.36; H, 5.83%. Found: C, 74.16; H. 5.80%.

Intramolecular Friedel-Crafts Reaction of the Tetrahydrophthalic Anhydride ***6***. Finely powdered aluminum chloride (4.37 g) was added to a solution of the anhydride **6** (1.81 g) in dry carbon disulfide (500 ml) during 30 min with vigorous stirring under an atmosphere of nitrogen. The deep purple mixture was stirred at room temperature for 34 hr, and the solvent was removed on a rotary evaporator at 30 °C. Cold dilute hydrochloric acid (200 ml) was added to the dark red residue and the resulting light yellow oil was taken up in ether. The organic layer was separated and washed with aqueous sodium bicarbonate solution (150 ml), and dried over sodium sulfate. The ether was evaporated to give the crude γ-lactone **10** which was recrystallized from benzene (712 mg); mp 175—176 °C; ν (KBr): 1765, 1712 cm^{-1}; δ ($CDCl_3$): 1.22 (3H, s), 2.60 (2H, ABX, J_{AB}=12 Hz, J_{AX}= 5 Hz), 4.95 (1H, br. t, J=5 Hz), 7.1—7.9 (4H, m) ppm. Calcd for $C_{15}H_{14}O_3$: C, 74.36; H, 5.83%. Found: C, 74.09; H, 5.83%.

The aqueous layer was acidified with concentrated hydrochloric acid and extracted with several portions of ether.

The ethereal layer was washed with brine and dried over sodium sulfate. Removal of the ether under reduced pressure gave a brown oil; ν ($CHCl_3$): 3500—2400, 1770, 1730, 1700, 1605 cm^{-1}. The oil was dissolved in ethyl acetate–ether (1 : 2; 50 ml) and treated with excess diazomethane at 0 °C. After 3 hr the polymethylene was filtered away, and the filtrate was concentrated to afford a brown oil. Chromatography on silica gel (50 g) using benzene as eluent produced the ester **7** (700 mg) as a colorless oil; ν (film): 1730, 1710, 1600 cm^{-1}; δ ($CDCl_3$): 1.05 (3H, s), 3.48 (3H, s), 5.8 (2H, br. s), 7.0—8.0 (4H, m) ppm. Found: *m/e* 256.110. Calcd for $C_{16}H_{16}O_3$: 256.110.

Further elution with benzene gave the isomers **11a** and **b** as slightly yellow crystals; **11a** (155 mg); mp 125.5 °C; ν (KBr) 1776, 1732 cm^{-1}, δ ($CDCl_3$) 1.48 (3H, s), 3.42 (3H, s), 4.6 (1H, m), 7.29 (5H, m) ppm. Found: C, 65.59; H, 5.83%. Calcd for $C_{16}H_{17}O_3Cl$: C, 65.64; H, 5.85%. **11b** (40 mg); mp 140—141 °C; ν (KBr): 1776, 1713 cm^{-1}; δ ($CDCl_3$): 1.34 (3H, s), 3.41 (3H, s), 4.15 (1H, m), 7.28 (5H, s) ppm. Found: C, 65.59; H, 5.85%. Calcd for $C_{16}H_{17}O_3Cl$: C, 65.64; H, 5.85%.

4b-Hydroxymethyl-8a-methyl-4b,5,8,8a-tetrahydro-9-fluorenone ***9***.

Lithium aluminum hydride (4 g) was added to a solution of the ester **7** (393 mg) in dry ether (100 ml), and the reaction mixture was refluxed overnight. The excess hydride was decomposed with water followed by the addition of 10% sodium hydroxide solution. After the precipitates were removed by filtration, the filtrate was concentrated into an oil (347 mg); ν ($CHCl_3$): 3560, 3430, 1180, 1070 cm^{-1}; δ ($CDCl_3$): 0.71 (3H, s), 3.50 (2H, ABq, J_{AB}=10 Hz), 5.09 (1H, s), 5.74 (2H, br. s), 6.9—7.6 (4H, m) ppm. The crude diol (250 mg) was dissolved in methylene chloride (50 ml) and stirred with active manganese dioxide (3 g) at room temperature for 3 hr. The manganese dioxide was removed by filtration and the filtrate was concentrated. The residual oil was crystallized with benzene to give needles (200 mg); mp 122—126 °C; δ ($CHCl_3$): 1.00 (3H, s), 3.48 (2H, s), 5.76 (2H, br. s), 7.0—8.0 (4H, m) ppm. Found: C, 78.90; H, 7.12%. Calcd for $C_{15}H_{16}O_2$: C, 78.92; H, 7.06%.

1-Methyl-2-phenyl-1,2,3,4,5,6-hexahydrophthalic Anhydride ***12***. A solution of the anhydride **6** (193 mg) in ethyl acetate (15 ml) was hydrogenated in the presence of platinum oxide (18 mg). After the catalyst was filtered away, the ethyl acetate was evaporated to give a crystalline residue (190 mg); mp 110—115 °C (cubes from benzene); ν (KBr): 1870, 1855, 1780 cm^{-1}. Found: C, 73.93; H, 6.66%. Calcd for $C_{15}H_{16}O_3$: C, 73.75; H, 6.60%.

Attempted Cyclization of the Hexahydrophthalic Anhydride ***12***. A solution of the anhydride **12** (73 mg) and aluminum chloride (200 mg) in nitrobenzene (2 ml) was stirred at room temperature for 24 hr. Cold hydrochloric acid was added and the mixture was extracted with ether. Evaporation of the ether and removal of the nitrobenzene afforded the starting anhydride (20 mg). Continuous extraction of the aqueous layer with ether afforded the diacid **14** as a white powder (20 mg); ν (KBr): 3500—2400 (br.), 1710, 1695 cm^{-1}. The structure of the diacid **14** was confirmed by heating it with acetic anhydride for 4 hr. A quantitative yield of the anhydride **12** was obtained.

References

1) H. Ageta, K. Iwata, and S. Natori, *Tetrahedron Lett.*, **1964**, 3413.
2) W. Nagata, M. Yoshioka, and T. Terasawa, *J. Amer. Chem. Soc.*, **94**, 4672 (1972).
3) R. E. Ireland, C. A. Lipinsky, C. J. Kowalski, J. W. Tilley, and D. M. Walba, *ibid.*, **96**, 3335 (1974).
4) W. G. Dauben and E. J. Deviny, *J. Org. Chem.*, **31**, 3794 (1966).
5) T. Kusumi, N. Ohno, and H. Kakisawa, This Bulletin, **48**, 96 (1975).
6) J. Schreiber, *C. R Acad. Sci., Paris*, **217**, 353 (1943).
7) T. E. Sample and L. F. Hatch, *J. Chem. Educ.*, **45**, 55 (1968).
8) F. Sondheimer, C. Amendolla, and G. Rosenkranz, *J. Amer. Chem. Soc.*, **75**, 5930, 5932 (1953).

Sesquiterpenes from *Acorus calamus* L.

Masatake NIWA, Atsuko NISHIYAMA, Masanobu IGUCHI, and Shosuke YAMAMURA*

Faculty of Pharmacy, Meijo University, Showa-ku, Nagoya 468

(Received June 3, 1975)

Three new sesquiterpenes, acoragermacrone (**1**), acolamone (**2**), and isoacolamone (**3**) were isolated from *Acorus calamus* L., and their structures were elucidated. In particular, acoragermacrone, a ten-membered ring sesquiterpene, is the most important precursor of the other sesquiterpenes included in the same plant. Acoragermacrone was converted into shyobunone, epi-shyobunone, preisocalamendiol, acolamone, and isoacolamone.

Many sesquiterpenes have been isolated from the plant *Acorus calamus* L. (Japanese name "Shyobu") growing in Japan.[1] However, such a key intermediate as acoragermacrone (**1**) has not been isolated. From a biogenetic point of view, our considerable efforts have been made to search for such an important precursor as **1**, and led us to the isolation of the expected ten-membered ring sesquiterpene, named "acoragermacrone", and two selinane-type compounds, acolamone (**2**) and isoacolamone (**3**). In this paper, we wish to describe the isolation and structures of these new sesquiterpenes. Furthermore, chemical correlation among them, including thermal and acid- or base-catalyzed isomerizations of acoragermacrone **1**, is also reported.

The Structures of Acoragermacrone (1). The pluverized raw rhizomes of *Acorus calamus* L. were carefully extracted with *n*-hexane to give a brown oil, which was directly chromatographed on silica gel. Rapid elution with *n*-hexane–ether (3 : 1) afforded a mixture of two ten-membered ring sesquiterpenes after elution of shyobunone and its isomers. Further separation of this mixture was successfully carried out by repeated preparative tlc using alumina in *n*-hexane–benzene (2 : 1) to give acoragermacrone **1** and preisocalamendiol (**4**) in 6 and 18% yields, respectively.[2]

Acoragermacrone **1** is a monocyclic sesquiterpene with a molecular formula $C_{15}H_{24}O$. The presence of an α,β-unsaturated cisoid carbonyl system (Me–C(=)CH–C(=)O) can be confirmed by its IR and UV spectra (ν_{max} 1680 and 1607 cm^{-1}; λ_{max} 242 nm (ε, 6590)] coupled with NMR spectrum which has two prominent signals at δ1.97 (3H, d, J=1.0 Hz) and 5.33 ppm (1H, q, J=1.0 Hz).[3] As found in the case of preisocalamendiol **4**,[1] furthermore, this new sesquiterpene also has an isopropyl group [δ 0.94 (3H, d, J=5.7 Hz) and 1.02 ppm (3H, d, J=5.7 Hz)] as well as a methyl group attached to a trisubstituted double bond [δ 1.12 (3H, d, J=1.5 Hz) and 4.60 ppm (1H, m)[4]]. In particular, the appearance of the methyl signal in unusually higher magnetic field (δ 1.12 ppm) seems to be due to the anisotropy effect of the α,β-unsaturated carbonyl system. This fact was supported by the following chemical evidence. When treated with sodium methoxide in MeOH (room temp., 30 min), acoragermacrone **1** was readily converted into the corresponding methoxy-ketone (**5**) in 48% yield, $C_{16}H_{28}O_2$ [*m/e* 252 (M^+)], which was proved to have a partial structure [Me–C(OMe)–CH_2–C(=)O] on the basis of its spectral data [ν_{max} 1705 cm^{-1}; δ 1.41 (3H, s), 2.46 (1H, d, J=17.7 Hz), 2.93 (3H, s) and 3.03 ppm (1H, d, J=17.7 Hz)]. Furthermore, it should be noted that the methyl signal at δ 1.12 ppm in **1** is shifted to δ 1.53 ppm in **5**.

From the above spectral and chemical data it is clear that acoragermacrone must be the most important ten-membered ring sesquiterpene (**1**) that has been expected to be present in the plant. Finally, the structure of acoragermacrone including its stereostructure (**1**) was established on the basis of some chemical evidences, namely thermal and base-catalyzed isomerizations.

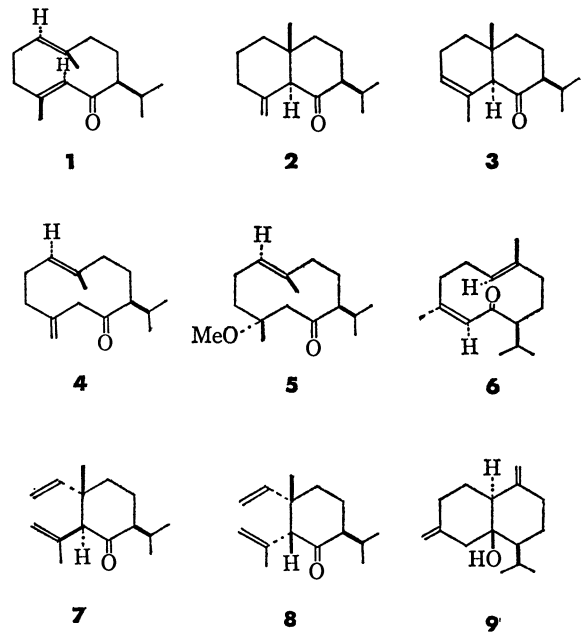

Fig. 1.

Base-catalysed Isomerization. As described earlier, action of MeONa on acoragermacrone **1** converted it into the corresponding addition product (**5**). When treated with *t*-BuOK in *t*-BuOH under N_2 (room temp., 30 min), **1** was readily converted into the known isomer (**6**)[5] in 95% yield through an enolate anion [A], as shown in Scheme 1. On the other hand, **1** reacted with 5% aq. KOH in *t*-BuOH (room temp., 24 hr) to give preisocalamendiol **4** in 84% yield, whose stereostructure had been already established in connection with shyobunone (**7**).[1] Further action of *t*-BuOK in *t*-BuOH on **4** also converted it into the most stable ten-membered ring compound, isoacoragermacrone (**6**), in almost quantitative yield.

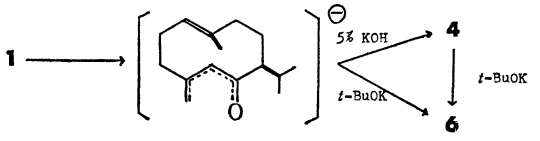

[A]

Scheme 1. Base-catalysed isomerization of acoragermacrone.

Thermal Isomerization of Acoragermacrone (1). In the cases of germacrones having an (*E,E*)-1,5-cyclodecadiene system, most of them have been known to adopt a crossed conformation.[6] In connection with the Cope rearrangement, conformations of these 1,5-cyclodecadienes have been also discussed by Takeda *et al.*[7]

The variable-temperature NMR spectrum of acoragermacrone was measured using benzene-d_6 as a solvent (24—106 °C). At 106 °C, it showed the new signal corresponding to those of shyobunone **7** in addition to the own signals, indicating that the Cope rearrangement took place to give **7**. When heated in a sealed tube at 110 °C for 30 min, acoragermacrone was completely converted into a mixture of shyobunone **7** and epi-shyobunone (**8**) (relative ratio **7**/**8**=21/4). In these experiments, shyobunone and epi-shyobunone both must be directly produced from acoragermacrone **1**, because these two elemene-type sesquiterpenes are quite stable under the same conditions. Therefore, this fact indicates that **1** has two possible conformational isomers (**1a** and **1b**) at least at higher temperature than 110 °C. Of two conformers, shyobunone **7** must be formed from the crossed conformer (**1a**) through a chair-like transition state [B], whereas epi-shyobunone **8** can be derived from the parallel one (**1b**) *via* a boat-like transition state [C]. In the above case, the chair-like one is much preferred as usual. However, it should be noted that the latter [C] leading to the formation of **8** can not be discarded, as shown in Scheme 2.[8] Under more vigorous conditions, in Scheme 2, the retro-Cope rearrangement of the elemene-type compounds takes place, leading to the formation of acoragermacrone **1** again, from which preisocalamendiol **4** and dehydroxyisocalamendiol (**9**) are readily produced.[1,5,9]

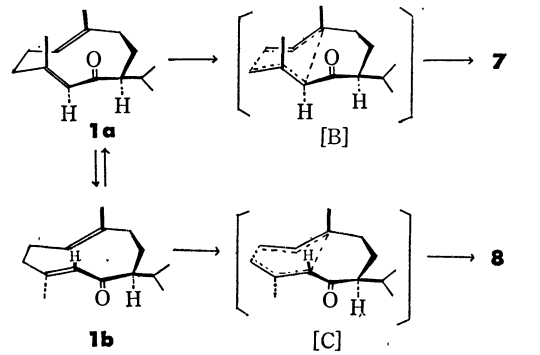

Scheme 2. Thermal isomerization of acoragermacrone (**1**).

The Structures of Acolamone (2) and Isoacolamone (3).[10] According to essentially the same procedure as that of acoragermacrone **1**, the *n*-hexane extracts were chromatographed repeatedly on different kinds of silica gel to afford acolamone **2** and isoacolamone **3** in each *ca.* 1.6% yield (from the *n*-hexane extracts) before elution of shyobunone **7** and its isomers.

Acolamone and isoacolamone both are bicyclic ketones ($C_{15}H_{24}O$; ν_{max} 1715 cm^{-1} in **2** as well as in **3**), and can be regarded as double bond isomers to each other on the basis of their NMR spectra, as shown in Table 1.

Table 1. NMR spectra of acolamone (**2**) and isoacolamone (**3**)

2	**3**
0.76(3H, s)	0.74(3H, s)
0.87(3H, d, J=6.5 Hz)	0.89(3H, d, J=6.3 Hz)
0.90(3H, d, J=6.5 Hz)	0.93(3H, d, J=6.3 Hz)
	1.76(3H, d, J=1.8 Hz)
2.90(1H, s)	3.10(1H, br. s)
5.00(1H, br. s)	
	5.42(1H, br. s)
5.95(1H, br. s)	

In the comparison of the NMR spectra between **2** and **3**, the former has two protons attached to an exocyclic double bond (δ 5.00 and 5.95 ppm), whereas **3** has one proton and the methyl group, both of which must be attached to a tri-substituted double bond (δ 5.42 and 1.76 ppm). The remaining signals are almost identical in both compounds. Furthermore, the structural relationship between acolamone and isoacolamone was established by the following thermal isomerization.

When heated in a sealed tube at 190 °C for 5 hr, acolamone **2** was converted into a mixture of two α,β-unsaturated ketones[11], whose spectral data were fairly close to each other [**10** (relative retention 2.30), ν_{max} 1690 and 1635 cm^{-1}; λ_{max} 248 nm (ε, 5600). **11** (relative retention 2.79), ν_{max} 1685 and 1638 cm^{-1}; λ_{max} 252 nm (ε, 4300)], in 60 and 27% yields, respectively. The former was completely identical with the selinane-type compound (**10**), which has been already derived from isoacoragermacrone **6** in several steps,[12] in respect of the glc and IR spectra. The compound (**10**) has also been derived from ajanol.[13] In the case of isoacolamone **3**, a mixture of **10** and **11** was also obtained in the same ratio as that of acolamone. Finally, the stereostructures of acolamone and isoacolamone were established as discussed below.

The ORD curve of acolamone showed a weak positive Cotton effect ($[\phi]^{P}_{325nm}+9°\times10^2$, $[\phi]^{T}_{280nm}-4°\times10^2$, $A=+13$), whereas that of isoacolamone has a weak negative Cotton effect ($[\phi]^{T}_{314nm}-10°\times10^2$, $[\phi]^{P}_{283nm}+7°\times10^2$, $A=-17$). In these cases, however, it is pretty dangerous to apply the octant rule to such $\beta\gamma$-unsaturated ketones as **2** and **3**. Therefore, the stereochemistry at C_5-position should be discussed in the case of the corresponding dihydro-compound (**12**, $C_{15}H_{26}O$, ν_{max} 1715 cm^{-1}),[14] which was readily

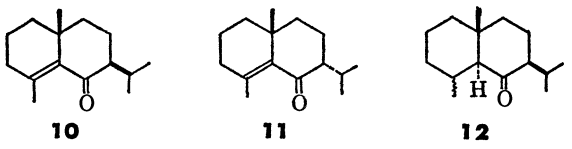

Fig. 2.

produced from acolamone as well as from isoacolamone on catalytic hydrogenation (H_2/PtO_2 in AcOEt) and has a positive Cotton effect in its ORD curve ($[\phi]^{P}_{312nm}+19°\times10^2$, $[\phi]^{T}_{274nm}-13°\times10^2$, $A=+32$), indicating that acolamone and isoacolamone should have the stereostructures (**2**) and (**3**), respectively.

From a structural view point, particularly, acolamone **2** is regarded as the higher oxidation product of junenol (**13**)[15], which must be derived from a plausible precursor (**14**). However, in consideration of the co-occurrence of acoragermacrone **1**, acolamone **2** and isoacolamone **3** both must be derived from **1** *in vivo*, as shown in Scheme 3. Thus, these two sesquiterpenes (**2** and **3**) were directly produced from acoragermacrone **1**.[16]

When treated with $AlCl_3$ in dry ether (0 °C, 1 hr), acoragermacrone afforded a pale yellow liquid, from which acolamone **2** and isoacolamone **3** were successfully separated, in each pure state, by preparative tlc in 55 and 23% yields, respectively.

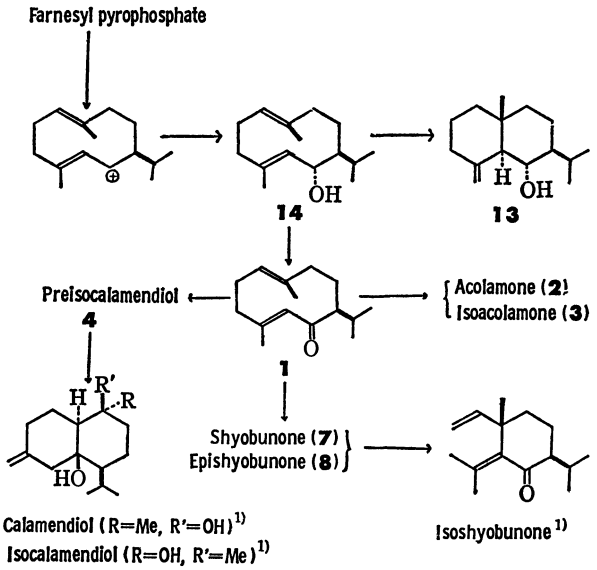

Scheme 3. Biogenesis of acoragermacrone and related sesquiterpenes.

Experimental

All mps are uncorrected. Relative retentions *vs.* calamenene as an internal standard were recorded on Shimadzu GC-1C (flame-ionizer detector) [stationary phase: 5% PEG 20M on Celite 545 (100 mesh); column [ϕ 3 mm× 1.5 m (stainless steel)] temp.: 90 °C; carrier gas: nitrogen (85 ml/min); inlet pressure: 1.2 kg/cm²], unless otherwise stated. The IR spectra were recorded on a Hitachi-215 spectrophotometer. The UV spectra were recorded on a Hitachi 124 spectrophotometer using MeOH as solvent. The NMR spectra were recorded on a Varian Associates HA-100, a Varian A-60 or a Nihondenshi JNM-C60H NMR spectrometer using $CDCl_3$ as solvent, unless otherwise stated. Chemical shifts are given in ppm relative to internal TMS, and only prominent signals are cited (d, doublet; m, multiplet; q, quartet; s, singlet; t, triplet). The mass spectra were obtained on a Hitachi RMU-6D mass spectrometer operating with an ionization energy (70 eV). The ORD curves were recorded on a JASCO ORD/UV-5 spectrophotometer using MeOH as solvent.

Isolation of Acoragermacrone (1). As expected from the previous paper,[1] such ten-membered ring compounds as preisocalamendiol **4** and isoacoragermacrone **6** seem to be more polar than those of shyobunone and its isomers. Thus, our attentions were focused on searching for the much polar fraction similar to that of preisocalamendiol **4**.

Raw sliced rhizomes of *Acorus calamus* L. (7 kg) growing in Aichi-ken, which were collected late in November, were pluverized with a mixer, and immersed in *n*-hexane (*ca.* 35 l) at room temperature for two weeks, and then filtered. The filtrates were concentrated under reduced pressure below 35 °C to leave a brown residue. The above procedure was repeated three times, and total weight of the *n*-hexane extracts so far obtained is 92 g (*ca.* 13% yield). The brown oil (20 g) was chromatographed on silica gel (Kanto Chemical Co. Ltd., 100—200 mesh) (250 g), and eluted very rapidly with *n*-hexane -Et_2O (3 : 1). The first fraction eluted with the mixed solvent (*ca.* 400 ml) afforded a mixture of shyobunone, acolamone and their isomers and undetermined hydrocarbons. Further elution with the same solvent system (*ca.* 200 ml) gave the slightly brown oil (8.4 g) corresponding to the spot of preisocalamendiol on a tlc plate. This oil (150 mg) was directly separated by repeated preparative tlc using alumina [GF_{254} (Type E), E. Merck A. G., Darmstadt] in *n*-hexane–benzene (2 : 1). From the less polar fraction, preisocalamendiol (64 mg) was obtained. From the more polar fraction, acoragermacrone (22 mg) was isolated, whose physical data were shown below.

Acoragermacrone (1). A colorless liquid; ν_{max} (film) 1680 and 1607 cm^{-1}; λ_{max} 242 nm (ε, 6590); $\delta(C_6D_6)$ 0.94 (3H, d, J=5.7 Hz), 1.02 (3H, d, J=5.7 Hz), 1.12 (3H, d, J=1.5 Hz), 1.97 (3H, d, J=1.0 Hz), 4.60 (1H, br. m) and 5.33 ppm (1H, q, J=1.0 Hz); *m/e* 220 (M^+), 215, 177 and 150 (Found: *m/e* 220.1786. Calcd for $C_{15}H_{24}O$: *m/e* 220.1825).

Reaction of Acoragermacrone with MeONa. To a solution of acoragermacrone (22 mg) in anhydrous MeOH (1 ml) was added MeONa (6 mg) with stirring. The resulting solution was further stirred at 20 °C for 30 min, and then diluted by addition of water (1 ml) and extracted with *n*-hexane. The extract was washed with water and dried over anhydrous Na_2SO_4. Evaporation of the solvent afforded a colorless liquid (21 mg), which was purified by preparative tlc [Alumina (GF_{254} (Type E), E. Merck A. G., Darmstadt); *n*-hexane–benzene (4 : 1)] to give a colorless liquid (12 mg) of the methoxy-ketone (**5**); ν_{max} (film) 1705 and 1640 cm^{-1}; δ (C_6D_6) 0.79 (6H, d, J=6.0 Hz). 1.41 (3H, s), 1.53 (3H, s), 2.46 (1H, d, J=17.7 Hz), 2.98 (3H, s), 3.03 (1H, d, J= 17.7 Hz) and 5.40 ppm (1H, br. m); *m/e* 252 and 220 (Found: *m/e* 252.2137. Calcd for $C_{16}H_{28}O_2$: *m/e* 252.2088).

Action of t-BuOK on Acoragermacrone. To a solution of acoragermacrone (22 mg) in *t*-BuOH (1.5 ml) was added *t*-BuOK (11 mg) under N_2. The resulting solution was further stirred at room temperature for 30 min, and then diluted with saturated aqueous NaCl solution (5 ml) and extracted with *n*-hexane. The extract was washed with water, and then dried over anhydrous Na_2SO_4. Removal of the solvent under reduced pressure afforded a colorless liquid (21 mg),

an analytical tlc of which showed one spot corresponding to that of isoacoragermacrone **6**[5] (tlc and IR spectrum).

Conversion of Preisocalamendiol into Isoacoragermacrone. To a solution of preisocalamendiol (47 mg) in *t*-BuOH (2 ml) was added *t*-BuOK (24 mg) under N_2 with stirring. The resulting solution was continuously stirred at room temperature for 30 min and then extracted with *n*-hexane after addition of saturated aqueous NaCl solution (10 ml). The *n*-hexane extract was washed with water, and then dried over anhydrous Na_2SO_4. Removal of the solvent gave a colorless liquid (45 mg), which was identical with the authentic sample of isoacoragermacrone **6** (tlc and IR spectrum).[5]

Conversion of Acoragermacrone into Preisocalamendiol. To a solution of acoragermacrone (25 mg) in *t*-BuOH (2.5 ml) was added 5% aqueous KOH (0.5 ml). The resulting solution was stirred at room temperature for 24 hr, and then extracted with ether after addition of water (10 ml). The ethereal extract was washed with water and dried over anhydrous Na_2SO_4, and then concentrated under reduced pressure to give a colorless liquid (25 mg), whose glc showed two peaks (relative ratio; 84 : 16). The former was completely identical with preisocalamendiol **4**, (glc, tlc and IR spectrum).

Thermal Isomerization of Acoragermacron. Acoragermacrone **1** was heated in a sealed tube under various conditions as shown in Table 2, and the thermal reaction was stopped after the starting material was completely consumed.

Table 2. The Cope rearrangement of acoragermacrone

Temp. (°C)[a]	Time (min)	Relative ratio (%)[b]	
		7	**8**
110	30	83.8	16.2
120	25	82.6	17.4
130	12	81.9	18.1
140	6	80.5	19.5
150	3	80.1	19.9
160	2	77.5	22.5

a) Under more vigorous conditions, the retro-Cope rearrangement takes place, leading to the formation of acoragermacrone **1**, from which preisocalamendiol **4** can be produced.[1,5] b) Peak area of gas-liquid chromatogram (5% PEG 20 M on Celite 545, 95 °C, N_2) was served as an approximate value of content (%).

*Isolation of Acolamone (**2**) and Isoacolamone (**3**).* The *n*-hexane extract (36 g), which was described in the case of acoragermacrone **1**, was directly chromatographed on silica gel (Katayama Chemical Co. Ltd., 100—200 mesh) (500 g), and eluted rapidly with petroleum ether–Et_2O (9 : 1). After elution of a mixture of hydrocarbons (8.0 g), further elution with the same solvent system (*ca.* 240 ml) afforded a fraction (9.0 g) containing sesquiterpenic ketones as the main component, which was rechromatographed on silica gel (Kanto Chemical Co. Ltd., 100—200 mesh) (240 g), and eluted with *n*-hexane–benzene (1 : 1). After elution of hydrocarbons (1.0 g), a mixture of two new ketones (1.2 g) was obtained from the second fraction, which was checked by analytical tlc. Further elution with the same solvent afforded shyobunone (1.6 g), epishyobunone (0.7 g) and other undetermined ketones. The mixture of the second fraction (1.2 g) was carefully chromatographed on silica gel (Mallinckrodt, 100 mesh) (50 g) and eluted with *n*-hexane–benzene (1 : 1) to give acolamone (560 mg) and isoacolamone (570 mg), in each pure state*. Their physical data are shown below.

*Acolamone (**2**).* A colorless liquid; relative retention 2.70; λ_{max} (film) 1715 and 1645 cm^{-1}; *m/e* 220 (M^+), 205, 177 and 149 (Found: *m/e* 220.1825. Calcd for $C_{15}H_{24}O$: *m/e* 220.1825).

*Isoacolamone (**3**).* A colorless liquid; relative retention 2.30; ν_{max} (film) 1715, 1660 (w) and 1640 (w) cm^{-1}; *m/e* 220 (M^+), 205, 177 and 149 (Found: *m/e* 220.1863. Calcd for $C_{15}H_{24}O$: *m/e* 220.1825).

Thermal Isomerization of Acolamone. Acolamone (30 mg) in a sealed tube was heated at 190 °C for 5 hr, and then cooled. The resulting viscous oil was separated by preparative tlc [Wakogel B-5F; *n*-hexane–benzene (1 : 1)]. From the less polar fraction, an $\alpha\beta$-unsaturated keton (**10**) (18 mg) was obtained. On the other hand, an isomer (**11**) (8 mg) was separated from the more polar fraction.

10. A colorless liquid; relative retention 2.79; ν_{max} (film) 1690 and 1635 cm^{-1}; λ_{max} 248 nm (ε, 5600); δ 0.92 (3H, d, J=6.7 Hz), 0.97 (3H, d, J=6.7 Hz), 0.98 (3H, s) and 1.74 ppm (3H, s); *m/e* 220 (M^+), 205 and 178 (Found: *m/e* 220.1821. Calcd for $C_{15}H_{24}O$: *m/e* 220.1825).

11. A colorless liquid; relative retention 2.79; ν_{max} (film) 1685 and 1638 cm^{-1}; λ_{max} 252 nm (ε, 4300); δ 0.87 (3H, d, J=5.8 Hz), 0.93 (3H, d, J=5.8 Hz), 1.00 (3H, s) and 1.75 ppm (3H, s), *m/e* 220 (M^+), 205 and 178 (Found: *m/e* 220.1823. Calcd for $C_{15}H_{24}O$: *m/e* 220.1825).

Thermal Isomerization of Isoacolamone. Under the same conditions as that of acolamone, isoacolamone (30 mg) was heated in a sealed tube, and then the resulting viscous oil was proved to be a mixture of **10** and **11** in the same ratio as that of acolamone by its glc.

Catalytic Hydrogenation of Acolamone as well as of Isoacolamone. Catalytic hydrogenation of acolamone (30 mg) in AcOEt (3 ml) was carried out over PtO_2 (4 mg) at room temperature overnight, and then filtered to remove the catalyst. The filtrate was concentrated under reduced pressure to give a colorless liquid (30 mg) of the dihydro-compound (**12**), which was also obtained, in almost quantitative yield, from isoacolamone **3** under the same conditions as that of **2**.

12. A colorless liquid; relative retention 2.32; ν_{max} (film) 1715 cm^{-1}; δ 0.86 (3H, d, J=6.8 Hz), 0.91 (3H, s), 0.92 (3H, d, J=6.8 Hz) and 1.15 ppm (3H, d, J=6.9 Hz); *m/e* 222 (M^+), 207, 138, 137 and 109 (Found: *m/e* 222.1980. Calcd for $C_{15}H_{26}O$: *m/e* 222.1982).

*Conversion of Acoragermacrone into Selinane-type Sesquiterpenes (**2** and **3**).* To a solution of acoragermacrone (50 mg) in anhydrous ether (2 ml) was added a solution of $AlCl_3$ (30 mg) in anhydrous ether (1 ml), with stirring, at 0 °C. The resulting solution was further stirred at 0 °C for 1 hr. and then diluted with ice–water and extracted with ether. The ethereal extract was washed with water, and then dried over anhydrous Na_2SO_4. Removal of the solvent afforded a pale yellow liquid (50 mg), which was separated by preparative tlc [Wakogel B-5F; *n*-hexane–benzene (1 : 1)] to give acolamone (22 mg) and isoacolamone (9 mg) in addition to the starting material (10 mg). These compounds were identified by comparing their tlc and IR spectra with those of the corresponding authentic samples.

The authors wish to thank Professor Yoshimasa Hirata (Nagoya University) for his invaluable suggestion, and Mr. Bunichi Eziri for collection of the plant.

* Analytical glc of the original *n*-hexane extract has the peaks corresponding to those of these two ketons.

Thanks are also due to Professor Akira Tatematsu (Meijo University) for measurements of high resolution mass spectra and to Dr. Yoshikazu Shizuri (Nagoya University) for measurements of NMR spectra. This research has been supported in part by grants from the Ministry of Education, to which greatful acknowledgement is made.

References

1) S. Yamamura, M. Iguchi, A. Nishiyama, M. Niwa, K. Koyama, and Y. Hirata, *Tetrahedron*, **27**, 5419 (1971) and references cited therein.

2) M. Iguchi, A. Nishiyama, S. Yamamura, and Y. Hirata, *Tetrahedron Lett.*, **1973**, 2759.

3) Irradiation at δ 1.97 ppm caused the quartet at δ 5.33 ppm to collapse to a sharp singlet. In the case of irradiation at δ 5.33 ppm, the methyl doublet at δ 1.97 ppm became a sharp singlet.

4) Irradiation at δ 4.60 ppm caused the methyl doublet at δ 1.12 ppm to collapse to sharp singlet.

5) M. Iguchi, A. Nishiyama, S. Yamamura, and Y. Hirata, *ibid.*, **1969**, 4295.

6) a) F. H. Allen and D. Rogers, *Chem. Commun.*, **1967**, 588; b) H. Yoshioka, T. J. Mabry, and H. E. Miller, *ibid.*, **1968**, 1679; c) N. S. Bhacca and N. H. Fisher, *ibid.*, **1969**, 68; d) J. McClure, G. A. Sim, P. Coggon, and A. T. McPhail, *ibid.*, **1970**, 128; e) R. K. Bently, J. G. St. C. Buchanan, T. G. Halsall, and V. Thaller, *ibid.*, **1970**, 435; f) F. Sörm, M. Suchy, M. Holub, A. Linek, I. Hodinec, and C. Nová, *Tetrahedron Lett.*, **1970**, 1893. See also Ref. 7.

7) K. Takeda, *Tetrahedron*, **30**, 1525 (1974) and references cited therein.

8) Usually, (*E,E*)-1,5-cyclodecadienes have been known to afford the corresponding Cope rearrangement products selectively *via* a chair-like transion state, but not *via* a boat-like one.[7] In the case of acoragermacrone which has an $\alpha\beta$-unsaturated carbonyl system, a boat-like transition state seems to be much stabilized by the conjugated carbonyl group, as seen from its molecular model.

9) M. Iguchi, A. Nishiyama, S. Yamamura, and Y. Hirata, *Tetrahedron Lett.*, **1970**, 855.

10) M. Niwa, A. Nishiyama, M. Iguchi, and S. Yamamura, *Chem. Lett.*, **1972**, 823.

11) D. W. Theobald, *Tetrahedron*, **20**, 2593 (1964).

12) To be published in a series of "biogenetic model reactions" (see Ref. 10).

13) V. A. Babkin, Z. V. Dubovenko, and V. A. Pentegova, *Khim. Prir. Soedin*, **1971**, 736.

14) The direct comparison of physical data between **12** and the oxidation product of dihydrojunenol has not been carried out, but these two compounds seem to be identical (see Refs. 11 and 15).

15) V. Herout, O. Motl, and F. Sörm, *Coll. Czech. Chem. Commun.*, **22**, 785 (1957); S. C. Bhattacharyya, A. S. Rao, and A. M. Shaligram, *Chem. Ind.*, **1960**, 469.

16) M. Iguchi, M. Niwa, and S. Yamamura, *Tetrahedron Lett.*, **1973**, 4367.

Ungewöhnliche Wichterle-Reaktionen. Eine Neue Synthese von Phenalenonen

Makoto KOBAYASHI und Takeshi MATSUMOTO

Chemisches Institut, Naturwissenschaftliche Fakultät der Hokkaido Universität, Sapporo 060

(Eingegangen am 9. Juni 1975)

Beim Erhitzen von 1-Methyl-1-(3-chlor-2-butenyl)-5-methoxy-2-tetralon(**10**) in HCO_2H in Gegenwart von $HClO_4$ wurde 4,7-Dimethyl-1-phenalenon(**11**) erhalten, während das Desmethoxy-Analogon, 1-Methyl-1-(3-chlor-2-butenyl)-2-tetralon(**5**) ein Phenanthren-Derivat ergibt. Es wurde gezeigt, dass die Bildung von Phenalenon über die Zwischenprodukte 2,3,9,9a-Tetrahydro-7,9-dimethyl-4-methoxy-1-phenalenon(**13**) und 2,3-Dihydro-4,7-dimethyl-1-phenalenon(**17**) verläuft. Unter den gleichen Bedingungen wurde 1-(3-Chlor-2-butenyl)-5-methoxy-2-tetralon(**21**) über 2,3-Dihydro-7-methyl-4-methoxy-1-phenalenon(**23**) in 7-Methyl-4-methoxy-1-phenalenon(**24**) umgewandelt.

In einer früheren Mitteilung haben wir über eine Modifizierung der Wichterle-Reaktion berichtet und gezeigt,[1] dass beim Erhitzen von an 2-C 3-Chlor-2-butenylierten Ketonen wie z. B. 2-Alkyl-2-(3-chlor-2-butenyl)-cyclohexanon(**1**) in HCO_2H in Gegenwart von $HClO_4$ als Katalysator Δ^2-Cyclohexenone von Typ **2** entstehen.[2] Im Gegensatz dazu lieferten die Chlor-ketone unter konventionellen Reaktionsbedingungen die verzweigten Bicyclen **3** als Hauptprodukte (Schema-1).[3] Versuche zur Übertragung der modifizierten Bedingungen auf die arylierten, 2-(3-Chlor-2-butenyl)-ketone haben einen neuen Zugang zu Phenalenonen aufgedeckt, über den wir hier berichten.[4]

Aus 1-Methyl-1-(3-chlor-2-butenyl)-2-tetralon (**5**) und 1-(3-Chlor-2-butenyl)-1-phenyl-4'-methoxy-acetophenon(**8**) wurden je die erwarteten Cyclohexenone **6** bzw. **9** erhalten(Schema-2). Im Gegensatz dazu führte die gleiche Behandlung von 1-Methyl-1-(3-chlor-2-butenyl)-5-methoxy-2-tetralon(**10**) nicht zum Hydrophnanthren-Derivat, sondern zu einem stark gelb gefärbten Produkt, $C_{15}H_{12}O$, Schmp. 118.5—119 °C. Im NMR-Spektrum dieser Substanz erscheinen zwei Singuletts für aromatisch gebundene Methylgruppen bei 2.69 und 2.78 ppm sowie drei AB-Systeme zwischen 6.6—8.5 ppm.[5] Das erste mit Dubletts bei 6.65 und 7.95 ppm ist durch eine Kopplungskonstante $J=10$ Hz charakterisiert und wird den *cis*-ständigen *vic*-Protonen eines α,β-Enon-Systems zugeordnet. Das Dublett beim tiefsten Feld(8.45 ppm)gehört zum zweiten AB-Muster mit dem breiten Dublett bei 7.48 ppm ($J=7.5$ Hz), welches durch „Long-Range" Kopplung mit einer Methylgruppe fein aufgespaltet ist. Das dritte, von aromatischen *vic*-Protonen herrührende AB-System wird durch die Dubletts bei 7.38 und 8.02 ppm ($J=8.5$ Hz) angezeigt. Die IR-Absorption der Carbonylgruppe bei 1640 cm^{-1} sowie das UV-Spektrum weisen darauf hin,[6] dass diese gelbe Verbindung ein stark konjugiertes System enthält. Auf Grund dieser spektroskopischen Befunde sowie mechanistischer Überlegungen (siehe weiter unten) folgt für das gelbe Produkt die Konstitution eines 4,7-Dimethyl-1-phenalenons(**11**).

Ein denkbarer Bildungsmechanismus für **11** ist in Schema-3 wiedergegeben. Zuerst wird das Ausgangsmaterial zum Carbonium-Ion **12** protoniert, das durch eine intramolekulare Friedel-Crafts Alkylierung zum Tetrahydro-Derivat **13** cyclisiert. Aus **13** führen die Wanderung einer Methylgruppe und die nachfolgende Wasserabspaltung zum Phenalen **15**, das über **16a** gefolgt von **16b** oder über **16b** gefolgt von **16a** in den Dihydrokörper **17** übergeht. Zuletzt muss **17** unter Dehydrierung in das Phenalenon **11** umgewandelt werden,[7] weil Phenalenone troz des 12π-konjugierten Systems aromatische Stabilität zeigen.[4] Das hier angenommene Reaktionsbild konnte in der Tat, wie folgt, bestätigt werden. Die Behandlung des Chlorketons **10** mit 90% H_2SO_4 lieferte nicht ein Hydro-

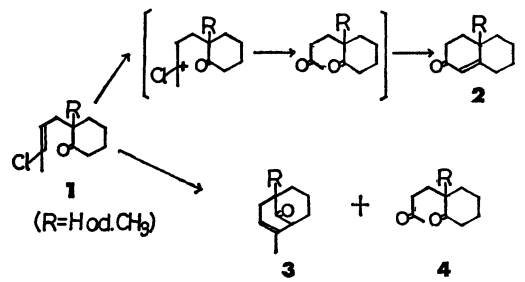

Schema 1.

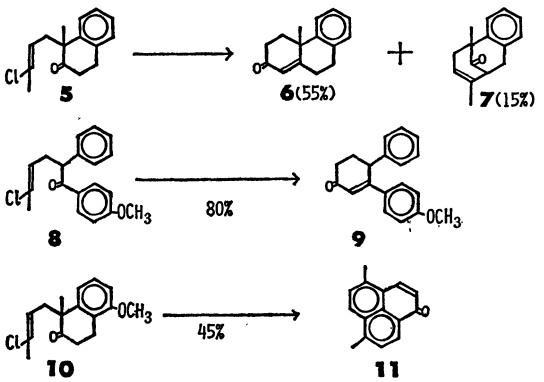

Schema 2.

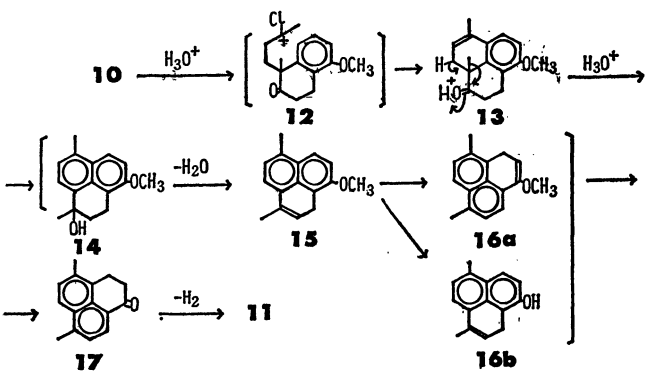

Schema 3.

phenanthren-Derivat,[8] sondern das oben als Zwischenprodukt postulierte Tetrahydro-dimethyl-methoxy-phenalenon **13**, Schmp. 78—79 °C, mit 80%-Ausbeute. Die Einwirkung von konz. H_2SO_4 (Raumtemp. 6 h.) ergab das 2,3-Dihydro-phenalenon **17**, neben dem Hauptprodukt **11**. Bei längerer Behandlung von **10** mit konz. H_2SO_4(Raumtemp. 20 h.) fand sich nur noch das Phenalenon **11** mit 30%-Ausbeute. Ausserdem wurde **13** durch Erhitzen in HCO_2H in Gegenwart von $HClO_4$ in das Phenalenon **11** und Dihydro-phenalenon **17** übergeführt. Bei kürzerer Behandlung des Chlorketons **10** mit $HClO_4$–HCO_2H wurden auch 7% der Dihydrokörper **17** neben 38% **11** erhalten. Die Konstitution der Zwichenprodukte **13** und **17** gehen aus den Analysen und spektroskopischen Daten hervor. Das NMR-Spektrum von **13** zeigt ein Singulett bei 1.15 ppm für die tertiäre Methylgruppe, ein Dublett (J=1.5 Hz)bei 1.99 ppm für die olefinische Methylgruppe, ein Singulett bei 3.78 ppm für die Methoxygruppe, ein AB-Signal bei 6.50 and 7.00 ppm (J=9 Hz) für die *o*- und *m*- Protonen des Anisolteils und ein breites Triplett bei 5.55 ppm ($J\approx$6 Hz) für das olefinische Proton, das mit der olefinisgebundenen Methylgruppe allylisch koppelt. Die Carbonylgruppe von **13** ist nicht konjugiert (1715 cm^{-1}); nach dem UV-Spektrum mit λ_{max} bei 237 nm ist die Doppelbindung zum Anisolring konjugiert.[9] Im NMR-Spektrum von **17** waren erkennbar : zwei Singuletts für aromatische Methylgruppe bei 2.49 und 2.61 ppm, ein bei 2.9 und 3.3 ppm zentriertes angenährtes A_2B_2-Muster für die Äthylengruppe, ein AB-Signal bei 7.37 und 8.11 ppm (J=7.5 Hz) für zwei aromatische *vic*-Protonen und ein zusätzliches AB-System bei 7.40 und 7.86 ppm (J= 9 Hz) für zwei weitere aromatische *vic*-Protonen. Die Carbonylgruppe ist mit dem Arylrest konjugiert (1685 cm^{-1}). In Übereinstimmung mit der Konstitution **17** und dem postulierten Reaktionsmechanismus, liess sich das Dimethyl-phenalenon **11** mit Zn-AcOH in guter Ausbeute zum Dihydro-phenalenon **17** reduzieren, das durch Erhitzen in HCO_2H mit $HClO_4$ wieder in **11** zurück verwandelt werden konnte[10] (Schema-4).

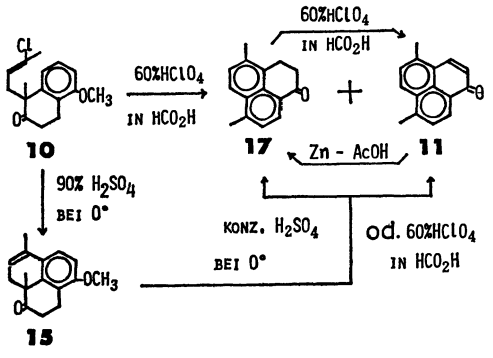

Schema 4.

Um den Anwendungsbereich und die Grenzen dieser neuen Phenalenon-Synthese zu untersuchen, wurden nachfolgende Reaktionen durchgeführt. Nicht durch Erhitzen in HCO_2H mit $HClO_4$,[11] sondern nur durch Behandlung mit konz. H_2SO_4 bei 50—60 °C oder mit FSO_3H bei Raumtemp. lieferte 1-Methyl-1-

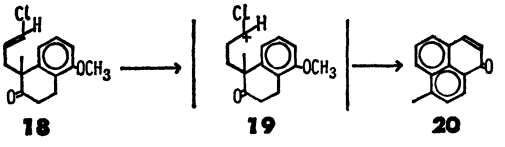

Schema 5.

(3-chlor-2-propenyl)-5-methoxy-2-tetralon(**18**) u.a. 7-Methyl-1-phenalenon(**20**), allerdings, in sehr schlechter Ausbeute (<7%).[12] Dieses Resultat zeigt, dass offensichtlich für die Phenalenon-Bildung die Stabilität der intermediären Carbonium-Ionen wie **19** sehr wichtig ist(Schema-5), und dass die Methylgruppe der Chlor-butenylgruppe in **10** für die Stabilisierung von **12** eine grosse Rolle spielt. Dadurch könnte der Anwendungsbereich auf alkylierte Phenalenone beschränkt werden.

Die Behandlung von 1-(3-Chlor-2-butenyl)-5-methoxy-2-tetralon (**21**), bei dem die anguläre Methylgruppe durch ein Wasserstoffatom ersetzt ist, liefert mit $HClO_4$–HCO_2H ein neues Phnalenon **24**, Schmp. 138—139.5 °C (zers.), in 30%-Ausbeute.[13] Das NMR-Spektrum von **24** zeigt zwei Singuletts bei 2.71 (aromatische $-CH_3$) und 4.02 (aromatische $-OCH_3$) ppm, sowie drei AB-Systeme. Das erste, zwei Dubletts bei 6.57 und 8.09 ppm, ist durch J=10 Hz charakterisiert (CH=CH–CO); das zweite bei 7.12 und 8.04 ppm (J=9.5 Hz, *o*- bzw. *m*-ständiges Proton am Anisolteil); das dritte bei 8.44 und 7.32 ppm (J=8 Hz, *o*- bzw. *m*-ständiges Proton am Toluolteil). Die Carbonylgruppe von **24** ist stark konjugiert (1633 cm^{-1}). Dem neuen Produkt kann somit die Konstitution eines 7-Methyl-4-methoxy-1-phenalenon (**24**) zugewiesen werden. Ein möglicher Mechanismus(Schema-6) für die Genese von **24** aus **21** wurde, wie folgt, bestätigt. Das NMR-Spektrum vom durch Behandlung von **21** mit Polyphosphorsäure[14] oder konz. H_2SO_4 erhaltenen Rohprodukt zeigt u.a. die folgenden Signale: ein breites Singulett bei 2.00 ppm (olefinische $-CH_3$), ein Singulett bei 3.80 ppm (aromatische $-OCH_3$), ein breites Quartett bei 5.70 ppm (Proton am cyclischen Olefin; koppelt mit der olefinischen $-CH_3$), und ein bei 6.17 und 7.09 ppm (J=8 Hz, *o*- bzw. *m*-ständiges Proton am Anisolteil) zentriertes AB-System. Das Hauptprodukt ist demgemäss 2,3,9,9a-Tetrahydro-7-methyl-4-methoxy-1-phenalenon(**22**). Bei der Säulenchromatographie des rohen **22** an SiO_2 fand aber eine Dehydrierungsreaktion statt und danach wurde nur

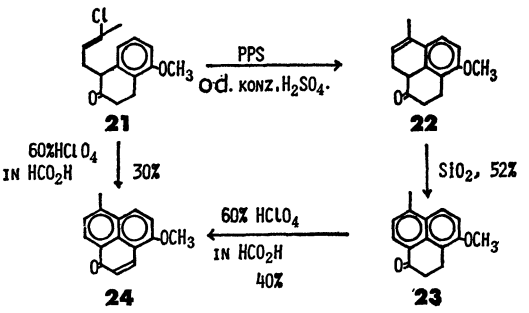

Schema 6.

2,3-Dihydro-7-methyl-4-methoxy-1-phenalenon (**23**) isoliert. Im NMR-Spektrum von **23** erkennt man ein Singulett bei 2.70 ppm(aromatische $-CH_3$), ein Singulett bei 3.98 ppm(aromatische $-OCH_3$), das 4H-Multiplett bei 2.9—3.3 ppm, bei 7.26 und 7.93 ppm (J=9.5 Hz, *o*- bzw. *m*-ständiges Proton am Anisolteil) zentriertes AB-Signal und zwei Dubletts bei 7.25 und 8.08 ppm (J=7.5 Hz, *o*- bzw. *m*-ständiges Proton am Toluolteil) eines zusätzlichen AB-Systems. Der Tetrahydrokörper **22** konnte sogar durch Dünnschichtchromatographie nicht rein erhalten werden. Schliesslich liess sich der Dihydrokörper **23** durch Behandlung in HCO_2H in Gegenwart von $HClO_4$ zu **24** mit 40%-Ausbeute überführen. Die modifizierte Wichterle-Reaktion erweist sich somit als eine neue Darstellungsmethode für 4,7-Dialkyl- sowie 7-Alkyl-4-methoxyphenalenon.

Experimenteller Teil

Die IR-Spektren wurden mit dem Jasco. IR-S und die UV-spektren in Äthanol mit dem Hitachi EPS-III gemessen. Die NMR-Spektren wurden in $CDCl_3$ oder CCl_4 mit den Geräten Hitachi R-20B oder JEOL. PS-100 aufgenommen. Die chemischen Verschiebungen sind in ppm (interner Standard; TMS=0) angegeben. Die Mass-Spektren (Abk: MS)wurden mit dem Hitachi RMU-6E oder RMS-4 erhalten. Die Schmp. wurden in einer Kapillare bestimmt und sind korrigiert. Für die Säulenchromatographie(SC) verwendete man Silikagel der Kanto Chemischen Industrie. Die Dünnschichtchromatogramme(DC) wurden auf Kieselgelplatten 60.PF_{254}, der Firma Merck ausgeführt.

Darstellung der Ausgangsverbindungen ***5***, ***8***, *und* ***10***. Ein Gemisch von aromatischem Keton(5.3 mMol) und NaH(50% ölsuspension, 6.9 mMol, verwendet ohne Waschen mit *n*-Hexan) in 10 ml Benzol wurde 1 h. unter Rückfluss, Rühren und N_2-Atomosphäre erhitzt. Nach Abkühlen auf Raumtemp. wurde 1,3-Dichlor-2-buten(*cis-trans* Gemisch, 6.9 mMol) in 10 ml Benzol zugetropft und dann die Lösung 1.5 h. gekocht. Nach der üblichen Aufarbeitung und Entfernung des Lösungsmittels chromatographierte man das Rohprodukt an der 30-fachen Menge SiO_2 mit Benzol und erhielt das ölige Chlor-keton mit 70—80%-Ausbeute.

1-Methyl-1-(3-chlor-2-butenyl)-2-tetralon (***5***): IR (Film): 1715, 1666 cm^{-1}; NMR ($CDCl_3$): 1.44 (3H, s), 1.96 ((3H, d, J=1.5 Hz), 5.70 (1H, q. t, J=1.5, 7 Hz), 7.18 (4H,m); MS : 248, 250 (M^+).

1-(3-Chlor-2-butenyl)-1-phenyl-4'-methoxy-acetophenon (***8***): IR (Film) : 1675, 1600, 1260, 1245 cm^{-1}; NMR ($CDCl_3$) 2.01 (3H, d, J=1.5 Hz), 2.75 (2H, m), 3.78 (3H, s), 4.56 (1H, t, J=7 Hz), 5.40 (1H, q. t, J=1.5, 7 Hz), 7.21 (5H, s), 6.79, 7.84 (2H, AB-q, J=8.5 Hz); MS : 314, 316 (M^+).

1-Methyl-1-(3-chlor-2-butenyl)-5-methoxy-2-tetralon (***10***); IR (Film): 1715, 1665, 1590, 1265 cm^{-1}; NMR (CCl_4) : 1.34 (3H, s), 1.94 (3H, d, J=1.5 Hz), 2.3—3.1 (6H, m), 3.78 (3H, s), 5.52 (1H, q. t, J=1.5, 7 Hz), 6.5—7.1 (3H, m); MS : 278, 280 (M^+).

Analog wurde mit 1,3-Dichlor-2-propen(*cis-trans* Gemisch) *1-Methyl-1-(3-chlor-2-propenyl)-5-methoxy-2-tetralon* (***18***) als Öl erhalten: IR(Film): 1719, 1633, 1590, 1263 cm^{-1}; NMR (CCl_4) : 1.35, 1.38 (3H, anguläre $-CH_3$), 2.1—3.3 (6H, m), 3.80 (3H, s), 5.05—5.95 (2H, olefinische Protonen), 6.5—7.3 (3H, m); MS : 264, 266 (M^+).

1-(3-Chlor-2-butenyl)-5-methoxy-2-tetralon (***21***). Eine Lösung des Pyrrolidin-enamins von 5-Methoxy-2-tetralon[15] (10 mMol) und 1,3-Dichlor-2-buten (50 mMol) in 15 ml Dioxan wurde 15 h. unter N_2-Atomosphäre gekockt. Nach Abkühlen auf Raumtemp. wurde die Lösung mit 2 ml AcOH und 8 ml H_2O versetzt und weiter 4 h. unter Rückfluss erhitzt. Die übliche Aufarbeitung und Reinigung durch SC mit Benzol als Elutionsmittel ergaben das ölige Chlorketon **21**(*ca.* 50%). Dieses Substanz ist sehr labil und zersetzt sich bei Raumtemp. innerhalb 24 h. vollständig; IR (Film): 1720, 1665, 1590, 1278 cm^{-1}; NMR ($CDCl_3$): 2.01 (3H, d, J=1.5 Hz), 3.08 (3H, s), 5.39 (1H, q. t, J=1.5, 7 Hz).

2,3,4,4a,9,10-Hexahydro-4a-methyl-phenanthren-2-on (***6***) *und 2,5-Dimethyl-6,7-benz-bicyclo*[3.3.1]*-2-nonen-9-on* (***7***). Eine Lösung von 150 mg Chlor-keton **5** in 10 ml HCO_2H wurde mit 1 ml $HClO_4$ versetzt und 1.5 h. under Rückfluss gekocht. Nach Abkühlen auf Raumtemp. wurde das Reaktionsgemisch auf 90 ml gesättigte $NaHCO_3$-Lögung gegossen und dann mit AcOEt extrahiert. Nach Entfernung des Lösungsmittels wurde der Rückstand an SiO_2 mit Benzol→Benzol/AcOEt (9 : 1) chromatographiert, und man erhielt 70 mg **6** (55%) und 20 mg **7** (15%). Die Konstitution von **6** wurde durch Vergleich mit den Daten in der Literatur bestätigt.[16]

7; Schmp. 81.5—82° (*n*-Hexan-Isopropyläther); IR(Nujol): 1715, 1670 cm^{-1}; NMR (CCl_4) 1.42 (3H, s). 1.70 (3H, d, J=2 Hz), 2.42 (2H, b), 2.8 (1H, m), 3.15 (2H, m), 5.15 (1H, m), 7.0 (4H); MS : 212 (M^+), 197 (M^+-15); Gef : C, 84.78; H, 7.61%. Ber. für $C_{15}H_{16}O$: C, 84.87; H, 7.60%.

4-Phenyl-3-(4'-methoxy-phenyl)-cyclohexenon(***9***). Zu 90 mg Chlor-keton **8** in 7 ml HCO_2H fügte man 0.7 ml $HClO_4$ und kochte 1.5 h. unter Rückfluss. Nach der Aufarbeitung wie oben wurde das Rohprodukt durch DC[Laufmittel : *n*-Hexan-Benzol (1 : 3)] gereinigt, und man erhielt 63 mg **9**(80%); Schmp. 113—114 °C (MeOH-Isopropyläther); IR (Nujol): 1660, 1575, 1253 cm^{-1}; NMR ($CDCl_3$): 2.47 (4H,m), 3.73 (3H, s), 4.29 (1H, m), 6.64 (1H, s), 7.21 (5H, s), 6.76, 7.40 (2H, AB-q, J=8.5 Hz); MS: 278 (M^+); Gef; C, 81.82; H, 6.52%. Ber. für. $C_{19}H_{18}O_2$: C, 81.98; H, 6.52%.

4,7-Dimethyl-1-phenalenon (***11***). *a) Aus* ***10***: Eine Lösung von 90 mg Chlor-keton **10** und 0.9 ml $HClO_4$ in 9 ml HCO_2H wurde 1.5 h. unter Rückfluss gekocht. Nach Abkühlen auf Raumtemp. wurde die Lösung auf gesättigte $NaHCO_3$-Lösung gegossen und mit $CHCl_3$ extrahiert. Die organischen Phasen wurden zweimal mit gesättigter $NaHCO_3$-Lösung und zweimal mit gesättigter NaCl-Lösung gewaschen. Nach Entfernung des Lösungsmittels wurde das Rohprodukt durch präparative DC gereinigt. Man erhielt 30 mg (45%) von Dimethyl-phenalenon **11** als gelbe Kristalle; Schmp. 118.5—119 °C (CH_2Cl_2-Isopropyläther); IR(Nujol) : 1640, 1618, 1589, 1559 cm^{-1}; NMR($CDCl_3$) : 2.69 (3H, s), 2.78-(3H, s), 6.65, 7.95(2H, AB-q, J=10 Hz), 7.48, 8.45(2H, AB-q, J=7.5 Hz), 7.38, 8.02(2H, AB-q, J=8.5 Hz); UV : 255(Schulter), 260.5(ε=30000), 332(ε=5300), 396(ε=11800)nm; MS : 208(M^+), 180(M^+-28), 165(M^+-43); Gef : C, 86.62; H, 5.87%. Ber. für $C_{15}H_{12}O$: C, 86.51, H, 5.87%. *b) Aus* ***17***: Zu einer Lösung von 20 mg Dihydrophenalenon **17** in 2.5 ml HCO_2H fügte man 0.2 ml $HClO_4$ und erhitzte 1 h. auf 90°. Die übliche Aufarbeitung ergab 12 mg **11** (60%).

2,3,9,9a-Tetrahydro-7,9a-dimethyl-4-methoxy-1-phenalenon (***13***). 200 mg Chlor-keton **10** wurde mit 5 ml von 90% H_2SO_4 bei 0 °C versetzt. Nach 1.5 h. wurde das Reaktionsgemisch auf Eis gegossen und mit $CHCl_3$ extrahiert. Nach der üblichen Aufarbeitung und Reinigung durch SC[Elutionsmittel: *n*-Hexan-Benzol(1 : 3)] wurde das ölige Rohprodukt aus *n*-Hexan-Isopropyläther-MeOH kristallisiert; Schmp. 78—79°; IR(Nujol): 1715, 1600, 1585, 1255 cm^{-1}; NMR-($CDCl_3$): 1.15(3H, s), 1.99(3H, d, J=1.5 Hz), 3.78(3H, s), 5.55(1H, b. t, J~6 Hz), 6.50, 7.00(2H, AB-q, J=9 Hz); UV: 273(ε=13700) nm; MS: 242(M^+); Gef: C, 79.04;

H, 7.70%. Ber. für $C_{16}H_{15}O_2$: C, 79.31; H, 7.49%.

*2,3-Dihydro-4,7-dimethyl-1-phenalenon (**17**).* *a) Reduktion von **11** mit Zn-AcOH*: Eine Lösung von 20 mg **11** in 2.5 ml AcOH wurde mit 110 mg Zn-Pulver versetzt und bei 80—95 °C unter N_2-Atmosphäre gerührt. Nach der üblichen Aufarbeitung und Reinigung durch präparative DC[Laufmittel: Benzol] erhielt man 16 mg **17**(80%). Nach Kristallisieren aus CH_2Cl_2-Isopropyläther schmolz die Substanz bei 82.5—83.5 °C; IR(Nujol): 1685, 1610, 1575 cm^{-1}; NMR($CDCl_3$): 2.49(3H, s), 2.61(3H, s), 2.9(2H, m), 3.3(2H, m), 7.37, 8.11(2H, AB-q, J=7.5 Hz), 7.40, 7.86 (2H, AB-q, J=9 Hz); UV: 221(ε=52500), 251(ε=32800), 345(ε=9450) nm; MS: 210(M^+), 195(M^+−15), 167(M^+ −43); Gef: C, 85.48; H, 6.70%. Ber. für $C_{15}H_{14}O$: C, 85.68; H, 6.71%.

*b) Aus **10***: Eine Lösung von 370 mg **10** in 17 ml HCO_2H wurde mit 3 ml $HClO_4$ versetzt und 12 h. bei Raumtemp. stehengelassen, dann langsam bis zu Siedepunkt erwärmt, und zuletzt 1 h. unter Rückfluss gekocht. Die Trennung des Rohprodukts durch SC[Elutionsmittel: $CHCl_3$] ergab 20 mg **17**(7%) und 105 mg **11**(38%).

*c) Durch Behandlung von **13** mit konz. H_2SO_4*: Eine Lösung von 100 mg **13** in 0.2 ml CH_2Cl_2 wurde bei 0 °C mit 0.3 ml konz. H_2SO_4 versetzt und 6 h. bei Raumtemp. gerührt, 8 mg **17**(9%) und 25 mg **11**(29%) wurden abgetrennt.

*d) Aus **13** mit $HClO_4$-HCO_2H*: Zu 56 mg **13** in 5 ml HCO_2H fügte man 0.5 ml $HClO_4$ und erhitzte die Lösung 1.5 h. auf 90—95°, wobei 6 mg **17**(12%) und 10 mg **11**(21%) erhalten wurden.

*7-Methyl-1-phenalenon (**20**).* Zu 90 mg Chlor-keton **18** in 0.2 ml CH_2Cl_2 fügte man 0.5 ml FSO_3H und rührte 2 h. bei Raumtemp. Nach Aufarbeitung erhielt man 45 mg als Rückstand. Die Auftrennung des Rohproduckts durch DC[Laufmittel: $CHCl_3$] lieferte 5 mg(*ca.* 7%) nicht völlig reines Monomethyl-phenalenon **20**; IR($CHCl_3$): 1643, 1623, 1585, 1565 cm^{-1} NMR($CDCl_3$): 2.82(3H, s), 6.66(1H, d, J=9.5 Hz), 7.5—7.8 (4H), 8.19(1H, m) 8.49(1H, d, J= 7.5 Hz); MS: 194(M^+), 166(M^+ − 28).

*2,3-Dihydro-7-methyl-4-methoxy-1-phenalenon (**23**).* Zu Polyphosphorsäure aus 1.7 g P_2O_5 und 1.2 ml H_3PO_4 fügte man eine Lösung von 100 mg **21** in 0.3 ml CH_2Cl_2 und rührte 1.5 h. bei Raumtemp. Danach wurde die Lösung unter Eiskühlung mit 50 ml Wasser verdünnt und wurde mit $CHCl_3$ extrahiert. Die Reinigung durch SC[Elutionsmittel: $CHCl_3$]lieferte 45 mg **23**(52%); Schmp. 87—87.5 °C (CH_2Cl_2-*n*-Hexan-Isopropyläther); IR(Film): 1680, 1614, 1583, 1270 cm^{-1}; NMR ($CDCl_3$): 2.70(3H, s), 2.9(2H), 3.3(2H), 3.98(3H, s), 7.26, 7.93(2H, AB-q, J=9.5 Hz), 7.25, 8.08(2H, AB-q, J=7.5 Hz); UV: 228(ε=52000), 253(ε=35000), 322(ε=5500), 358(ε=8700) nm; MS: 226(M^+), 211(M^+ −15), 195(M^+ −31), 183(M^+ −43); Gef: C, 79.30; H, 6.37%. Ber. für $C_{15}H_{14}O_2$: C, 79.62; H, 6.24%. Das reine Tetrahydro-Derivat **22** liess sich nicht isolieren. Die Behandlung von **21** mit konz. H_2SO_4 ergab eine niedrigere Ausbeute an **23**.

*7-Methyl-4-methoxy-1-phenalenon (**24**).* *a) Aus **21***: Eine Lösung von 155 mg **21** in 10 ml HCO_2H wurde mit 1.5 ml $HClO_4$ versetzt, allmählich erwärmt und zuletzt 1 h. unter Rückfluss gekocht. Nach der üblichen Aufarbeitung und Abtrennung erhielt man 40 mg **24**(30%), die durch Sublimation(100°/3 Torr)gereinigt wurden; Schmp. 138—139.5° (zers.); IR(Nujol): 1633, 1589, 1578, 1270 cm^{-1}; NMR ($CDCl_3$): 2.71(3H, s), 4.02(3H, s), 6.57, 8.09(2H, AB-q, J=10 Hz), 7.12, 8.04(2H, AB-q, J=9.5 Hz), 7.32, 8.44(2H, AB-q, J=8 Hz); UV: 266(ε=21000), 331.5(ε=4500), 433 (ε=11300) nm; MS: 224(M^+), 209(M^+ −15), 196(M^+ −28), 181(M^+ −43); Gef: C, 79.06; H, 5.62%. Ber. für $C_{15}H_{12}O_2$: C, 80.33: H, 5.39%.

*b) Aus **23***: Zn einer Lösung von 18 mg **23** in 1.8 ml HCO_2H fügte man 0.15 ml $HClO_4$ und erhitzte 1.5 h. unter Rückfluss. Die übliche Aufarbeitung lieferte 7 mg **24** (40%).

Wir danken Herrn Prof. Dr. H. Musso (Universität Karlsruhe) für die Durchsicht des Manuskripts.

Literaturen und Anmerkungen

1) M. Kobayashi und T. Mastumoto, *Chem. Lett.*, **1973**, 957.

2) Es wurden 99—100% HCO_2H und 60% wässrige $HClO_4$ verwendet.

3) S. Julia, *Bull. Soc. Chim. Fr.*, **21**, 780(1954); J. A. Marshall und D. J. Schaeffer, *J. Org. Chem.*, **30**, 3462(1965).

4) Übersicht über Phenalenon, D. H. Reid, *Quart. Rev.*, **19**, 274(1956).

5) Vgl. NMR-Spektrum von 4,7-Dimethoxy-1-phenalenon, M. Jarco, *J. Amer. Chem. Soc.*, **90**, 4644 (1968).

6) IR- und UV-Spektren von Phenalenonen, N. H. Cromwell und G. V. Hudson, *J. Amer. Chem. Soc.*, **75**, 872 (1953); R. D. Campell und N. H. Cromwell, *ibid.*, **79**, 3456 (1957).

7) Ähnliche Dehydrierungsreaktion, z. B., O. I. Fedrova, G. S. Grienco und V. I. Maskimov, *Zh. Org. Khim.*, **1968**, 1219; *Chem. Abstr.*, **69**, 96945 k (1968); L. J. Chinn und H. L. Dryden, Jr., *J. Org. Chem.*, **26**, 3904 (1961).

8) Die Behandlung von **5** und **8** mit konz. H_2SO_4 bei 0 °C ergab **7** (47%) bzw. 1,5-Diketon.

9) L. Dorfman, *Chem. Rev.*, **53**, 47 (1953).

10) Die Reduktion in Anwesenheit von Sauerstoff ergab schlechte Ausbeuten.

11) Das Ausgangsmaterial wurde zurückerhalten.

12) Die Konstitution wurde auf Grund spektroskopischer Daten abgeleitet.

13) Der Dihydrokörper **23** liess sich dünnschichtchromatographisch nachweisen.

14) Die Behandlung von **10** mit Polyphosphoräure ergab bei Raumtemp. **13** und bei 50—60 °C **17** als Hauptprodukt.

15) T. Matsumoto und A. Suzuki, Dieses Bulletin, **34**, 274 (1961).

16) E. Wenkert und T. E. Stevens, *J. Amer. Chem. Soc.*, **78**, 2318 (1956).

Preparation and Application of Some New Disperse Anthraquinone Dyes

Saoud A. M. METWALLY* and Karl BREDERECK**

Chemistry Department, Faculty of Science, Assiut University, Assiut, Egypt

(Received October 3, 1974)

A series of anthraquinone derivatives free from water-solubilising groups were prepared. These compounds were found to be valuable for dyeing synthetic fibers with different shades of good fastness properties.

Anthraquinone dyes remain as the most important and pre-eminent class of all dyes because of their outstanding all-round fastness. On the other hand, disperse dyes are very useful and represent the main class of dyes for coloring synthetic textile materials.

In a previous note[1] we have reported that hydroxymethylanthraquinones could be used as alkylating agents for aromatic compounds using Friedel-Crafts catalysts. This paper gives the results of some experiments in regard to the reaction course and new examples are expressed.

(Hydroxymethyl)anthraquinones (I) react with aromatic hydrocarbons in the presence of aluminium chloride or tin tetrachloride to give the corresponding (arylmethyl)anthraquinones (III).[1] An equimolecular mixture of freshly fused tin tetrachloride and 1-amino-2-(hydroxymethyl)anthraquinone gave an addition product at 60 °C and heating of the addition product at 90—95 °C yielded the corresponding chloride (II). A determination of the hydrogen chloride evolved by heating of the addition product leads to the view that the reaction proceeds in the following steps.

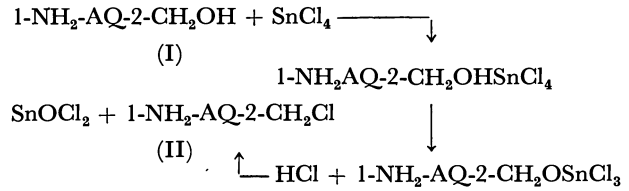

If aromatic hydrocarbon and more than equimolar amounts of tin tetrachloride are used, reaction with 1-amino-2-(chloromethyl)anthraquinone (II) yields III.

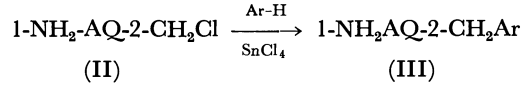

Heating of the addition product with aromatic hydrocarbon in the absence of the catalyst gave no III, indicating the necessity of two moles of tin tetrachloride to complete the reaction.

Reaction of toluene with 1,4-dihydroxy-2-(hydroxymethyl)anthraquinone gave 1,4-dihydroxy-2-(4′-methylbenzyl)anthraquinone.[1] The mass spectrum of this product is different from that of 1,4-dihydroxy-2-(2′-methylbenzyl)anthraquinone which was prepared by a modified Marschalk's method.[2] The molecular ion in the former isomer is the base peak, while that in the latter one is 57.8% as relative abundance.

Loss of water molecule from molecular ions is more intense in case of 1,4-dihydroxy-2-(2′-methylbenzyl)-anthraquinone. This may be explained by the formation of the stable six-membered ring ion resulted from the loss of hydroxyl group in the 1-position and the hydrogen atom from the *ortho* methyl group. All these steps are indicated by metastable peaks and accurate mass measurements.

1-Amino-2-(4′-hydroxybenzyl)anthraquinone has been prepared using concentrated sulfuric acid as a catalyst.[2] Our trials to obtain this product according to the patent specification gave very low yield and also different side products. The side products were identified as 1-aminoanthraquinone, 1-aminoanthraquinone-2-carbaldehyde beside a red product

TABLE 1. PRINCIPAL PEAKS IN THE MASS SPECTRUM OF 1,2-DIHYDRO-4*H*-ANTHRA[1,2-*d*][1,3]OXAZINE-7,12-DIONE

m/e	28	75	75.5	76	76.5	
Rel. int.	20.7	5.3	2.3	14.8	2.4	
m/e	77	150	151	152	153	
Rel. int.	7.1	7.0	14.1	18.2	7.1	
m/e	165	180	181	207	208	
Rel. int.	7.2	12.2	4.9	4.5	14.8	
m/e	209	220	223	234	235	
Rel. int.	5.7	6.4	6.8	4.6	7.7	
m/e	236	237	264	265 (M)	266	267
Rel. int.	40.9	12.3	100	83.0	16.2	3.8

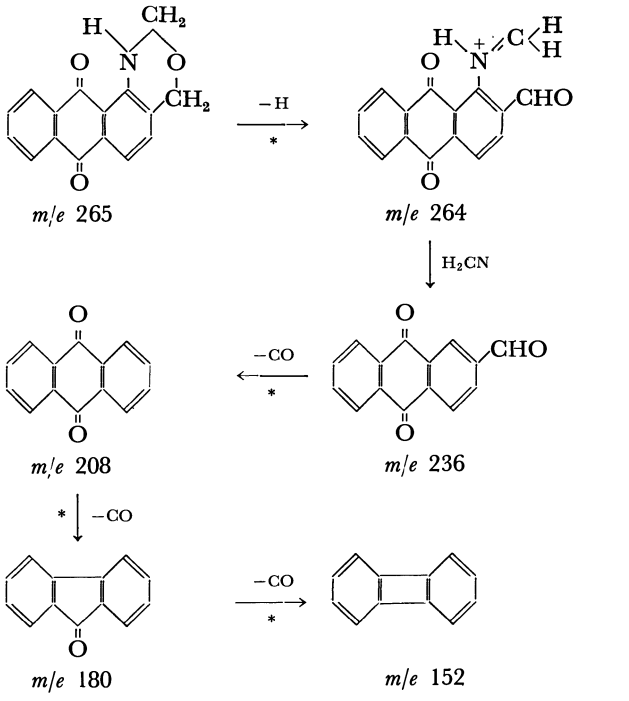

Scheme A.

* Author to whom all correspondence should be addressed.

** Present address: Institut für Textilchemie, 7-Stuttgart-80, Pfaffenwaldring 55, Deutschland.

($C_{16}H_{11}NO_3$) which indicates the presence of a secondary amino group and a bathochromic schift of 20 nm in its ultraviolet spectrum as compared with the starting 1-amino-2-(hydroxymethyl)anthraquinone. Molecular weight of the red product was 265 by the mass spectrum.

Table 1 indicates the mass spectrum of this compound (*cf.* Scheme A). The molecular ion undergoes the loss of hydrogen atom to give the base peak which can lose H_2CN *via* an α, γ-proton schift to give anthraquinonecarbaldehyde cation radical. The latter loses carbon monoxide yielding the parent anthraquinone[3]. These steps were proved by accurate mass measurements and metastable peaks determinations. According to these facts, this compound was formulated as 1,2-dihydro-4*H*-anthra[1,2-*d*][1,3]oxazine-7,12-dione (IV).

Compound IV was also prepared by the action of 70% sulfuric acid on 1-amino-2-(hydroxymethyl)-anthraquinone.

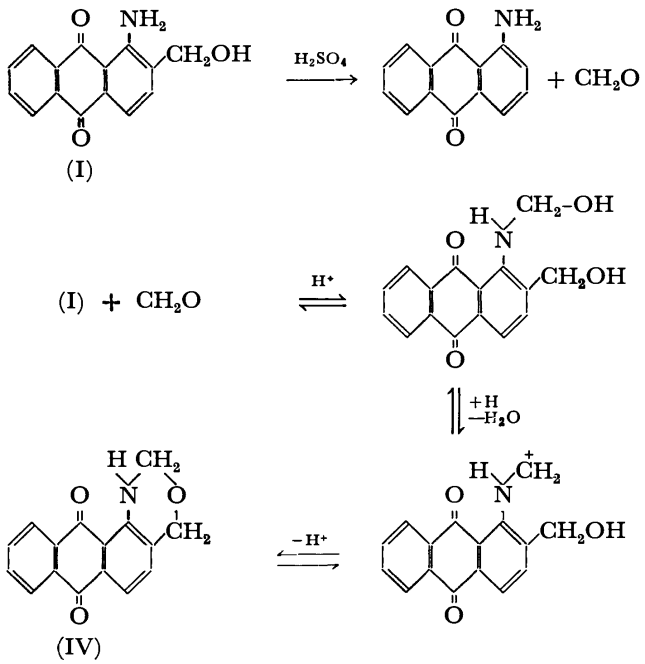

Reaction of 1-amino-2-(hydroxymethyl)anthraquinone with formaldehyde in presence of dilute hydrochloric acid gave IV quantitatively.

The formation of the 1-aminoanthraquinone-2-carbaldehyde may be due to self oxidation of the starting (hydroxymethyl)anthraquinone derivatives in acidic medium.

The (arylmethyl)anthraquinone derivatives[1] have colors ranging from yellow, orange, red, magenta and blue. The work was extended for the preparation of green disperse dyes. This was done by alkylation of a yellow anthraquinone. An example for such preparation is 1,4-diamino-2-[(4'-hydroxyanthraquinon-1-yl)methyl] anthraquinone(Vb) which was prepared by heating 1,4-diamino-2-(hydroxymethyl)-anthraquinone with 1-hydroxyanthaquinone in an inert solvent and in the presence of freshly fused tin tetrachloride.

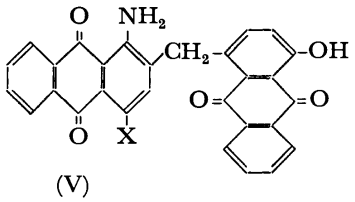

(V)

a, X=H
b, X=NH_2

The visible spectra of such green dyes are characterized by the presence of two bands, one in the yellow and the other in the blue region of the spectra.

Experimental

Melting points are uncorrected. Infrared spectra were measured on a Perkin-Elmer Model 21 spectrophotometer, ultraviolet and visible spectra were measured on a Unicum 1800 spectrophotometer. Mass spectra were obtained using an AEI MS9 mass spectrometer operating at 70 eV. Samples were introduced through a heated inlet system at *ca.* 185 °C.

Preparation of 2-(Chloromethyl)anthraquinones. (Hydroxymethyl)anthraquinone (I) (0.5 mol) was added to freshly fused tin tetrachloride (0.5 mol) in dioxane, but only a trace of hydrogen chloride evolved. On heating, the solid product began to melt at 85—90 °C and hydrogen chloride was given off freely. About 0.5 mol of hydrogen chloride was collected at 95 °C for 2 hr. The reaction mixture was added to ice-cold water and the precipitates were washed throughly with water and dried. Some examples are summarized in Table 2.

Preparation of (Arylmethyl)anthraquinones. A mixture of (hydroxymethyl)anthraquinone (1 mol), 1-hydroxyanthraquinone (1 mol) and freshly fused tin tetrachloride (2 mol) was heated in dioxane under reflux for about one hour. The reaction mixture was poured into excess 4 M sodium hydroxide solution. The precipitated product was washed with excess water, dried and recrystallized from dimethylformamide.

TABLE 2. 2-(CHLOROMETHYL)ANTHRAQUINONES

Compound	Mp °C	Yield %		Analysis (%) C	H	N	Cl	Solvent of crystallization	λ_{max}(nm) in C_6H_6	log ε
1-Amino-2-(chloromethyl)-anthraquinone	185	89	Calcd	66.31	3.71	5.16	13.10	Benzene	475	3.92
			Found	66.46	3.92	5.31	13.33			
1-Amino-2-(chloromethyl)-4-chloroanthraquinone	212	92	Calcd	58.85	2.97	4.57	23.15	Benzene	480	3.84
			Found	59.21	3.18	4.62	23.23			
1,4-Diamino-2-(chloromethyl)-anthraquinone	218	90	Calcd	62.83	3.83	9.77	12.37	Toluene	592	3.79
			Found	63.16	3.88	9.84	12.42			

Table 3. Fastness properties

Compound	WF[a]	LF[b]	Compound	WF[a]	LF[b]
1-Amino-2-benzylanthraquinone	4—5	6	1-Amino-4-bromo-2-benzylanthraquinone	4	6—7
1-Amino-2-(4′-methylbenzyl)anthraquinone	4—5	6—7	1-Amino-4-bromo-2-(4′-methylbenzyl)-anthraquinone	4—5	6
1-Amino-2-(4′-hydroxybenzyl)anthraquinone	4	6	1-Amino-4-bromo-2-(4′-hydroxybenzyl)-anthraquinone	3—4	6—7
1-Amino-2-[4′-(dimethylamino)benzyl]-anthraquinone	4—5	6—7	1-Amino-4-bromo-2-[4′-(dimethylamino)-benzyl]anthraquinone	4—5	6—7
1-Amino-2-(2′-naphthylmethyl)anthraquinone	5	6—7	1-Amino-4-bromo-2-(2′-naphthylmethyl)-anthraquinone	4—5	6
1-Amino-2-(1′-hydroxy-4′-naphthyl)-anthraquinone	3—4	5—6	1-Hydroxy-2-benzylanthraquinone	3—4	6
1,4-Diamino-2-benzylanthraquinone	4	6	1-Hydroxy-2-(4′-methylbenzyl)anthraquinone	4—5	5—6
1,4-Diamino-2-(4′-methylbenzyl)-anthraquinone	4—5	6	1-Hydroxy-2-(4′-hydroxybenzyl)anthraquinone	3	6
1,4-Diamino-2-(4′-hydroxybenzyl)-anthraquinone	4	5—6	1-Hydroxy-2-[4′-(dimethylamino)benzyl]-anthraquinone	4	6
1,4-Diamino-2-[4′-(dimethylamino)benzyl]-anthraquinone	5	4—5	1,4-Dihydroxy-2-benzylanthraquinone	3—4	5—6
1,4-Diamino-2-(2′-naphthylmethyl)-anthraquinone	4	6	1,4-Dihydroxy-2-(4′-methylbenzyl)-anthraquinone	3—4	6
1,4-Diamino-2-(1′-hydroxy-4′-naphthyl)-anthraquinone	3—4	5—6	1-Amino-2-[(4′-hydroxyanthraquinon-1-yl)-methyl]anthraquinone	3	5—6
1,8-Diamino-2-benzylanthraquinone	4—5	6	1,4-Diamino-2-[(4′-hydroxyanthraquinon-1-yl)methyl]anthraquinone	3—4	5—6
1,8-Diamino-2-(4′-methylbenzyl)anthraquinone	4	6			
1,8-Diamino-2-(4′-hydroxybenzyl)-anthraquinone	3—4	6			

a) Wash fastness. b) Light fastness.

Va; yield 81%; mp 210 °C; λ_{max}^{PhH} 450 nm (log ε 3.61) Found: C, 76.13; H, 3.92; N, 3.17%. Calcd for $C_{29}H_{17}NO_5$: C, 75.81; H, 3.70; N, 3.05%.

Vb; yield 78%; mp 235 °C; λ_{max}^{PhH} 412 nm (log ε 3.86) and 585 nm (log ε 3.25). Found: C, 73.28; H, 3.84; N, 6.12%. Calcd for $C_{29}H_{18}N_2O_5$: C, 73.41; H, 3.79; N, 5.90%

Preparation of other derivatives was reported previously.[1]

Preparation of 1,2-Dihydro-4H-anthra[1,2-d][1,3]oxazine-7, 12-dione(IV). 1-Amino-2-(hydroxymethyl)anthraquinone (0.53 g), 30% aqueous formaldehyde solution (1 ml) and concentrated hydrochloric acid (0.5 ml) were dissolved at room temperature in dioxane (100 ml). The mixture was left for 30 min and then warmed at 45 °C for 15 min. The reaction mixture was poured into ice-cold water and the precipitated red product was washed with water and dried. It was crystallized from benzene into red fine needles, mp 162 °C, yield 0.52 g.

λ_{max}^{PhH} 490 nm (log ε 3.72); IR 3252, 1592, 1660, and 1630 cm^{-1}. Found: C, 72.55; H, 4.16; N, 4.94%. Calcd for $C_{16}H_{11}NO_3$: C, 72.45; H, 4.15; N, 5.28%.

Application of Disperse Dyes to Synthetic Fibers. These disperse dyes were applied to polyamide fibres by immersing the textile materials in a dyebath containing the aqueous dispersion of these dyes and an anionic surface-active reagent. The dyeing process was done at the boil for 45 min. Table 3 indicates the fastness properties of such dyes on Nylon-66.[4]

Appreciation is expressed to the Alexander von Humboldt-Stiftung, West Germany for a grant supporting this work.

References

1) K. Bredereck and S. Metwally, *Ann. Chem.*, **1974**, 1536.
2) Imperial Chemical Industries (by C. W. Greenhalgh and W. Galin), Brit. Pat., 1927310; *Chem. Abstr.*, **74**, 127453n (1971).
3) J. H. Beynon and A. E. Williams, *Appl. Spectr.*, **14**, 156 (1960).
4) "Standard Methods for the Determination of Colour Fastness of Textiles," edited by The Society of Dyers and Colourists, Chorley and Pickargill Ltd., Leeds, England, (1960).

Electric Dipole Moment of Pyrrole and Molecular Interaction in Solution

A. N. SRIVASTAVA and V. K. JOSHI

Chemistry Department, University of Jodhpur, Jodhpur-342001, India

(Received April 26, 1975)

Literature[1] reports two values for μ_s/μ_v namely 1.06 and 0.9 for pyrrole in benzene solution. Our orientation polarisation data on pyrrole discussed in terms of Higasi's theory favours the former. Further we observe that in benzene the solute forms donor-acceptor complexes, while in carbon tetrachloride it undergoes association through hydrogen bonding.

The moment values of pyrrole both in vapour and solution state cited earlier[2] are widely divergent. A survey of literature[1,3-7] shows that though Buckingham and others have carried much work on pyrrole, yet they have shown considerable variation in apparent moment. The discrepancy may be attributed to the specific interaction in solution. Consequently the purpose of the present investigation was to re-examine the apparent moment values and then to understand the interaction operating between solute and solvent from the data so obtained, with reference to theory of Earp and Glasstone.[8]

Experimental

The practical work essentially involves the measurements of dielectric constant and density of various solutions containing different mole fractions of the solute. The method and techniques have been described elsewhere.[9]

Pyrrole[12] (Fluke A.G., Buchs S. G., Switzerland) was distilled twice in a quickfit apparatus, where there was no possibility for the liquid to be in contact with atmospheric moisture and carbon dioxide. The fraction boiling at 128 °C was used.

The solution moment value μ_s has been determined by the method of Halverstadt and Kumler.[13] The constants α, β, ε_1 and V_1 in Halverstadt and Kumler equation have been evaluated by the method of least square. Electronic polarization P_e is the same as the molecular refraction for sodium D-line and has been taken from the literature.[14] Atomic polarization P_A has not been taken into consideratoin as suggested by Debye[15] namely that the electronic polarisation calculated from the sodium D-line partly compensates the neglect of atomic polarisation for which there is still no good method of evaluation.

The excess polarisation P^E needed for the present study, has been evaluated from the expression,

P^E = (Solution polarisation) − (Total polarisation)

The solution polarisation P_{12} is given by

$$P_{12} = \frac{\varepsilon_{12}-1}{\varepsilon_{12}+1} \cdot \frac{M_1 f_1 + M_2 f_2}{d_{12}}$$

and total polarisation $= P_1 f_1 + P_2 f_2$

where P_1 and P_2 are the molar polarisation of the solvent and the solute respectively and f_1 and f_2 are their respective mole fractions.

Results and Discussion

The values available in literature for μ_s/μ_v of pyrrole in benzene are 1.06 and 0.9. However we observe that the μ_s value of pyrrole in benzene is slightly greater than that in cyclohexane. This is in agreement with the positive solvent effect (*i.e.* $\mu_s > \mu_v$) as suggested by Higasi.[16-18] Consequently our observed data in benzene favours the value 1.06 for the ratio μ_s/μ_v. The experimental data has been shown in Table 2.

The molecular interaction in solution has been discussed in terms of the theory of Earp and Glasstone.[8]

Accordingly we observe that no chemical interaction takes place in the mixture since the variation of

TABLE 1. PYRROLE

Solvent	α	β	ε_1	V_1	$P_{2\infty}$
Benzene	6.8630	−0.1848	2.2514	1.1643	121.99
Carbon tetrachloride	3.5327	+0.6154	2.2062	0.6898	103.97
Cyclohexane	5.2857	−0.2808	1.9944	1.3157	104.71

TABLE 2.

Solvent	μ_s (apparent moment values)		μ_v^2 (moment in vapour state)
	by present authors	by earlier workers[2]	
Benzene	2.26	2.2 , 1.74	1.55−1.65
Carbon tetrachloride	2.05	1.78, 1.76	1.84±0.08
Cyclohexane	2.06	1.75[3]	

TABLE 3.

			(Pyrrole+Benzene)				
$f_1 f_2$	0.0005	0.0036	0.0042	0.0064	0.0073	0.0078	0.0116
P^E	+0.041	+0.267	+0.354	+0.450	+0.502	+0.556	+0.790
			(Pyrrole+Carbon tetrachloride)				
$f_1 f_2$	0.0007	0.0012	0.0033	0.0051	0.0064	0.0066	0.0106
P^E	−0.641	−0.607	−0.511	−0.430	−0.388	−0.388	−0.170
			(Pyrrole+Cyclohexane)				
$f_1 f_2$	0.0027	0.0034	0.0062	0.007	0.0087	0.0104	0.0127
P^E	−0.177	−0.148	+0.142	+0.251	+0.304	+0.451	+0.606

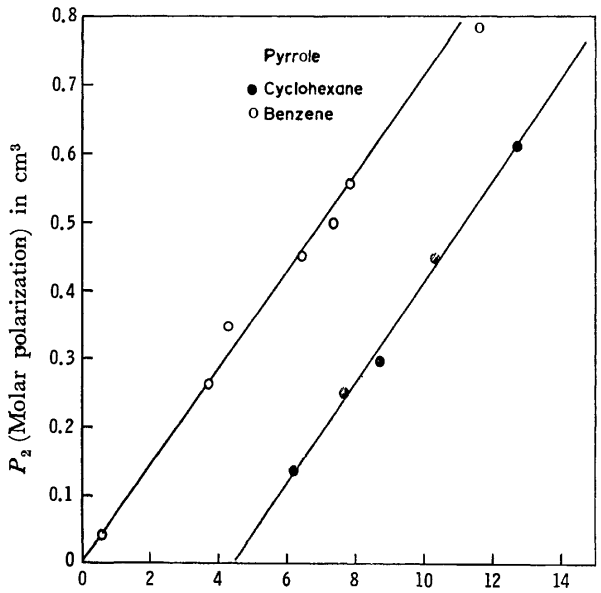

Fig. 1.

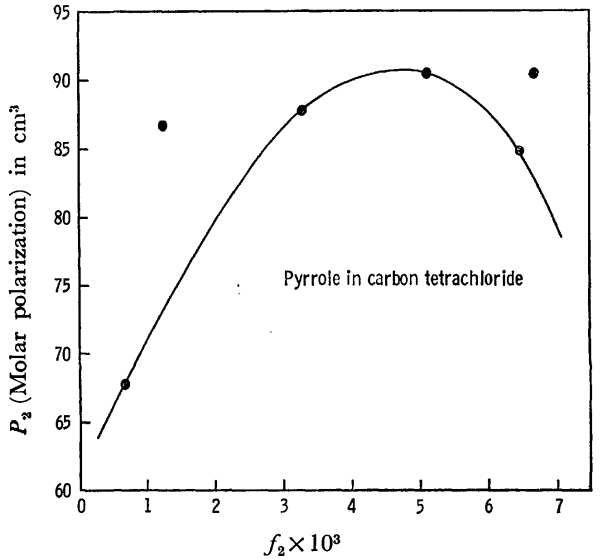

Fig. 2.

$\{(\varepsilon_{12}-1/\varepsilon_{12}+1)\}^2$ with P_{12} is linear. Further the values of P^E (the excess polarisation) in benzene and cyclohexane being positive (Table 3) eliminate the possibility of dipole association as well.

However the variation of P^E with $f_1 f_2$ (Fig. 1) for the system (pyrrole+benzene) is linear and passes through the origin. This shows the formation of charge-transfer complexes in solution. The specific interaction according to Goats and Sullivan[19] in benzene appears to be of donor-acceptor type. Literature[20] reports that pyrrole is practically non-basic and its hydrogen atom is acidic in nature. It seems probable therefore that pyrrole accepts the π electrons through its hydrogen atom from benzene. This is supported from the complex formation between benzene (donor) and carbon tetrachloride reported recently.[21] The possibility of complex formation in cyclohexane does not arise as it has no π electrons. Our experimental data fully demonstrate this fact.

The negative values of P^E in carbon tetrachloride (Table 3) suggest that pyrrole undergoes association through hydrogen bonding in this solvent. To ascertain this view, the graph between P_2 and f_2 (Fig. 2) has been plotted, which shows a maxima.[9,22] This observation is further supported from the study of infrared spectra[23,24] of pyrrole in carbon tetrachloride. A lower value of pyrrole in carbon tetrachloride suggests head to head association. There seems to be the following two possibilities during association.

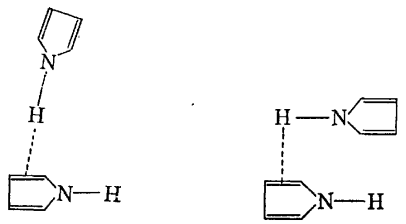

(i) (ii)

One of us (VKJ) is thankful to C.S.I.R., Govt. of India, for financing the project.

References

1) A. D. Buckingham and R. J. W. LeFevre, *J. Chem. Soc.*, **1953**, 1626.
2) A. L. McClellan, "Tables of Experimental Dipole Moment," W. H. Freeman and Co. (1963).
3) H. Lumbroso and Pappalardo, *Bull. Soc. Chim. Fr.*, **1961**, 1131.
4) V. Shomaker and L. Pauling, *J. Amer. Chem. Soc.*, **61**, 1769 (1939).
5) E. G. Cowley and J. R. Partington, *J. Chem. Soc.*, **1936**, 47.
6) C. G. LeFevre, R. J. W. LeFevre and M. R. Smith,, *ibid.*, **1959**, 1188.
7) H. Kofod, L. E. Sutton, and J. Jackson, *ibid.*, **1952**,1467.
8) D. P. Earp and S. Glasstone, *ibid.*, **1935**, 1709.
9) A. N. Srivastava, P. R. Talesara, *J. Ind. Chem. Soc.*, **48**, 359 (1971).
10) A. N. Srivastava, and P. R. Talesara, *ibid.*, **48**, 829 (1971).
11) A. N. Srivastava and P. R. Talesara, *ibid.*, **51**, 545 (1974).
12) E. G. Cowley and J. R. Partington, *J. Chem. Soc.*, **1933**, 1259.
13) I. F. Halverstadt and W. D. Kumler, *J. Amer. Chem. Soc.*, **64**, 2988 (1942).
14) J. R. Partington, "Advanced Treatise on Physical Chemistry," Vol. 4, (1953) pp. 60—61.
15) P. Debye, "Polar Molecules," Dover, New York (1929), p. 51.
16) K. Higasi, *Bull. Inst. Phys. Chem. Japan*, **14**, 146 (1935).
17) K. Higasi, *Sci. Pap. Inst. Phys. Chem. Res. Japan*, **28**, 284 (1935).
18) K. Higasi, *ibid.*, **31**, 311 (1937).
19) J. R. Goats and R. J. Sullivan, *J. Phys. Chem.* (Ithaca), **63**, 589 (1959).
20) A. R. Katritzky, "Physical Methods in Heterocyclic Compounds," Vol. 1, Academic Press (1963), p. 212.
21) G. W. Chantry, *et al.*, *Spectrochim. Acta*, **23A**, 2749 (1967).
22) B. Krishna and A. N. Srivastava, *J. Chem. Phys.*, **37**, 1574 (1962).
23) M. L. Josien, P. Pineau, and M. Paty, *ibid.*, **24**, 1261 (1956).
24) G. M. Badger, "The Chemistry of Heterocyclic Compounds," Academic Press (1961), p. 14.

NOTES

BULLETIN OF THE CHEMICAL SOCIETY OF JAPAN, VOL. 48(10), 2944 (1975)

Friedel-Crafts Benzylation of Toluene with Benzyl Chloride Catalyzed by Metal Oxides

Kazushi ARATA, Norio AZUMI, and Hiromitsu SAWAMURA
Hokkaido University of Education, Hachiman-cho, Hakodate-shi 040

(Received May 26, 1975)

Synopsis. Metal oxides were found to catalyze significantly the Friedel-Crafts type benzylation of toluene with benzyl chloride with a selectivity similar to that occurring with metal sulfates.

The benzylation of toluene with benzyl chloride, which is a typical example of Friedel-Crafts alkylations and is known to proceed over Lewis-type catalysts such as anhydrous aluminum chloride and gallium bromide,[1] has been found to be catalyzed by metal sulfates: $NiSO_4$, $MnSO_4$, etc.[2] Iron sulfates especially showed an unexpected effectiveness for this reaction.[3,4] The selectivity, however, of these studied catalysts was almost the same, indicating the analogous reaction mechanism. In order to extend the scope of this reaction, we have examined the catalytic activity as well as the selectivity of these metal oxides: ZnO, TiO_2, ZrO_2, and TiO_2-ZrO_2.

Experimental

Experiments which do not overlap with those reported in the previous paper[4] are described here.

Preparation of Catalysts. ZnO was prepared by calcining its hydroxide in air at 400 °C for 3 hr. The hydroxide was precipitated by adding 2 M aqueous ammonia to an aqueous solution of zinc chloride (1 M), followed by washing thoroughly with water until no chloride ion was detected in the filtrate and drying at 120 ° for 24 hr. TiO_2, ZrO_2, and TiO_2-ZrO_2 (molar ratio=1 : 1) were prepared by calcining H_4TiO_4, $Zr(OH)_4$, and H_4TiO_4-$Zr(OH)_4$, respectively, in air at 500 °C for 3 hr. These materials were precipitated by heating a mixed aqueous solution (5 l of 0.2 M) of titanium tetrachloride, zirconium oxychloride, or both chlorides and an excess amount of urea (300 g) on a boiling water bath for 6—9 hr, followed by thorough washing and drying at 110 °C for 30 hr.

Results and Discussion

As observed in the case of metal sulfates, the initial part of the HCl evolution was linear with time after a slight period of induction, and the over-all reaction followed first order reaction kinetics with respect to the benzyl chloride concentration.

Table 1 summarizes the initial rates and the relative rates, together with the pertinent data taken from our previous study.[2] It is shown that the present metal oxides, solid acid catalysts,[5,6] are quite active for this Friedel-Crafts reaction, especially TiO_2-ZrO_2, which is more than 400 times as active as $NiSO_4$. The products were very similar in distribution with an almost negligible amount of polymer, as shown in Table 2. This product distribution is quite similar to that by sulfates of Ni, Mn, and other metals.[2-4] This similarity of selectivity implys that the catalytic actions upon this benzylation are the same on those studied catalysts: that is, the catalytic mechanism is independent of the species of catalyst and reaction rate. Since an induction period, which is presumably the period of HCl adsorption on the catalyst surface, was observed in every reaction, it is supposed that the adsorbed HCl acts as a true catalyst. This model is attractive in explaining the similarity of the catalytic action. However, $AlCl_3$, a typical Lewis catalyst, gave a quite different selectivity (10.2% *ortho*-, 69.0% *meta*-, and 20.8% *para*-isomer) under the heterogeneous reaction condition.[2] Therefore, it is concluded that solid acids such as metal sulfates and oxides give the same selectivity arising from the same catalytic actions for the Friedel-Crafts type benzylation.

TABLE 1. CATALYTIC ACTIVITIES OF METAL OXIDES FOR BENZYLATION OF TOLUENE WITH BENZYL CHLORIDE AT 100 °C

Catalyst	Initial rate (mol/l·min·g)	Relative rate (ZnO=1)
ZnO	0.036	1.00
TiO_2	0.30	8.3
ZrO_2	0.11	3.1
TiO_2-ZrO_2	0.48[a]	13.3
$MnSO_4$[b]	0.0073	0.2
$NiSO_4$[b]	0.0012	0.03

a) The reaction was 80% completed in 5 min.
b) Ref. 2.

TABLE 2. ISOMER DISTRIBUTION OF BENZYLTOLUENE

Catalyst	Mol %		
	Ortho-	*Meta-*	*Para-*
ZnO	43.0	6.0	51.0
TiO_2	46.5	7.3	46.1
ZrO_2	44.5	7.8	47.8
TiO_2-ZrO_2	43.2	7.7	49.1

Partial support of this work by the Hokkaido Science Research Foundation is gratefully acknowledged.

References

1) G. A. Olah, "Friedel-Crafts and Related Reactions," Vol. I~IV Wiley-Interscience, New York and London, 1963~1964.
2) K. Arata, T. Takeshita, and K. Tanabe, *Shokubai*, **8**, 226 (1966).
3) K. Arata and I. Toyoshima, *Chem. Lett.*, **1974**, 929.
4) K. Arata, K. Sato, and I. Toyoshima, This Bulletin, to be published.
5) K. Tanabe, C. Ishiya, I. Matsuzaki, I. Ichikawa, and H. Hattori, This Bulletin, **45**, 47 (1972).
6) K. Shibata and T. Kiyoura, *J. Res. Inst. Catalysis, Hokkaido Univ.*, **19**, 35 (1971).

BULLETIN OF THE CHEMICAL SOCIETY OF JAPAN, VOL. 48(10), 2945—2946 (1975)

The Electronic Absorption Spectra of UV Irradiated Anilines Adsorbed on Porous Vycor Glass

Tadayoshi SAKATA, Toshihiro OKAI,* Hiroaki SUGIMOTO,** and Hiroshi TSUBOMURA
Department of Chemistry, Faculty of Engineering Science, Osaka University, Toyonaka, Osaka 560
(Received February 8, 1975)

Synopsis. Cation radicals of aniline and its derivatives were formed on porous Vycor glass plates by UV-irradiation. One of the absorption bands appearing in the visible region is assigned to the transition to the first excited state of the cation radical by comparison with the reported photoelectron spectrum. The charge resonance band of the dimer cation was also observed in the near infrared region in most cases.

The electronic absorption spectra due to the transition to the first electronic excited states of the cation radicals of anilines do not seem to have been observed, although they are expected to exist in the visible or near infrared region both from theoretical calculation[1] and photoelectron spectra (PES)[2-4] of anilines.

The porus Vycor glass (PVG) which adsorbed a large amount of anilines was exposed to ultraviolet (UV) light at 77 K by using a 250 W high pressure mercury lamp and a Toshiba glass filter UV-D25, transparent in the region from 200 to 400 nm.

The electronic absorption spectra obtained after UV-irradiation of aniline (AN), *N*-methylaniline (NMA) *N,N*-dimethylaniline (DMA), *N,N*-diethylaniline (DEA) *N,N*-dimethyl-*p*-toluidine (DMT), and *m*-phenylenediamine (MPD) are shown in Fig. 1. The peak positions of the visible strong bands obtained for the cation radicals of anilines are given in Table 1, together with those reported by others.[5] They agree fairly well with each other, though the absorption shape is rather broader in our case. The reason for this broadening might be attributed to the effect of adsorption or the high concentration of anilines. ESR (electron spin resonance) spectra were observed for the irradiated specimens containing NMA and DMA, which decayed above ~150 K. The electronic absorption spectra also changed remarkably above the same temperature. All these facts suggest that the obtained visible absorption bands are those of the cation radicals of anilines. Besides these bands there appear one or two weak bands at the longer wavelength as seen in Fig. 1.

In order to assign them, we estimated the energies of the first and second excited states of the cation radicals from the results of photoelectron spectroscopy (PES). The results are compared with ours in Table 2, showing that the peak positions of the new bands agree fairly well with those estimated from PES for AN, NMA, and MPD, each having only one new band. Therefore, the first absorption bands of these compounds seem to be attributable to the first excited state of the cation radical.[6]

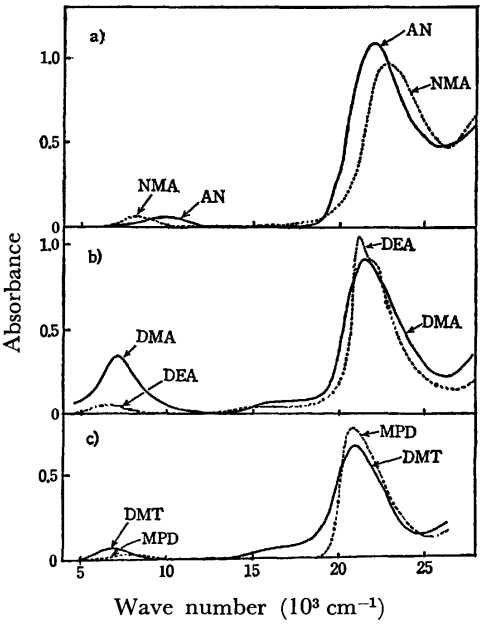

Fig. 1. The absorption spectra of the UV-irradiated anilines.
a) ——: aniline, ----: *N*-methylaniline.
b) ——: *N,N*-dimethylaniline, ----: *N,N*-diethylaniline.
c) ——: *N,N*-dimethyl-*p*-toluidine, ----: *m*-phenylenediamine.

TABLE 1. ABSORPTION MAXIMUM OF THE STRONG BAND IN THE VISIBLE REGION

Anilines	This study	Literature
AN	2.75	2.93[9]
NMA	2.85	2.91[10]
DMA	2.65	2.64[11]
DEA	2.63	2.64[12]
DMT	2.62	2.63[9]
MPD	2.61	2.56[13]

(unit: eV)

TABLE 2. THE ABSORPTION MAXIMA OF THE UV-IRRADIATED ANILINES AND THE FIRST AND SECOND EXCITED STATES OF THE CATION RADICALS ESTIMATED FROM PES

Anilines	This study	PES
AN	1.26, 2.77	1.16, 2.76[2]
NMA	1.04, 2.88	1.30, 2.51[3]
DMA	0.89, ~2.0, 2.65	1.59, 2.43[2]
DEA	0.84, ~1.9, 2.63	1.60, 2.28[3]
DMT	0.83, ~1.9, 2.62	1.59, 2.28[2]
MPD	0.87, 2.61	0.63, 2.54[4]

(unit: eV)

* Present address: Nippon Paint Co., Ltd., Osaka
** Present address: Central Research Laboratory, Sumitomo Chem. Co., Ltd., Takatsuki, Osaka

There appear two new bands in each of the case of DEA, DMA, and DMT as seen in Fig. 1. The first excited state of the cation radical estimated from PES seems to correspond well to the weak absorption band observed at 500—700 nm in these cases. Then, what is the origin of the near infrared band in these cases? To clarify this, the change of intensity with temperature from 77 K was followed for the visible band (2.65 eV), the near infrared band, and the ESR absorption of DMA cation. As shown in Fig. 2, all shows similar temperature dependency, indicating that the cation radical of DMA begins to decompose at about 150 K and almost disappears at 270 K[7]. The possibility that these bands are due to solvated electrons can be denied because they do not change by the irradiation in the visible or near infrared region.

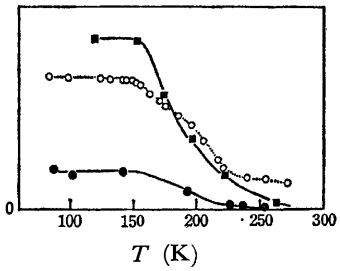

Fig. 2. The temperature dependence of the intensity on the visible band (2.67 eV) (○), the near infrared band (●), and the ESR absorption (■).
As for ESR the ordinate shows the intensity of ESR absorption multiplied by temperature, so that it represents the number of paramagnetic species.

Since in our experiments a large amount of anilines were adsorbed on PVG and only their small part is photoionized, this band can be most reasonably assigned to the charge resonance band of the dimer cation formed between the cation radical and its neutral molecule,[8] not to the charge transfer band of the cation dimers. The weakness of the charge resonance bands can be attributed to the small concentration of the dimer cations.

It is possible in the cases of AN and NMA that similar charge resonance bands exist in the energy region of the first excited band of the cation. Therefore, the observed IR bands for these cases might be a superposition of the cation band and the charge resonance band. This assumption seems fairly reasonable because the charge resonance interaction is thought to be stronger in these cases than in the other three compounds, taking account of the steric hindrance of the methyl group. If one assumes further that the IR bands consist mostly of the charge resonance bands, the excitation energies of these bands are in reasonable sequence as regarded to be the charge resonance bands for all compounds, decreasing in the order, AN, NMA, DMA, DEA, DMT, parallel to the increasing steric hindrance. From the excitation energy of these resonance bands, the intermolecular resonance integrals are estimated to be from 0.4 to 0.5 eV for these dimer cations which seem resonable. For MPD, the corresponding charge resonance band might be located in the longer wavelength region.

The authors would like to express their gratitude to Prof. T. Shida of Kyoto University for informing us his unpublished spectral data of the cation radicals of AN and DMA.

References

1) S. Katsumata and K. Kimura, This Bulletin, **46**, 775 (1973).
2) T. Kobayashi and S. Nagakura, *Chem. Lett.*, **1972**, 1013.
3) A. D. Baker, D. P. May, and D. W. Turner, *J. Chem. Soc., B*, **1968**, 22.
4) K. Tsuji, M. Saito, and T. Tani, *Denki Kagaku*, **41**, 688 (1973).
5) Prof. T. Shida of Kyoto University kindly informed us his recent spectral data of the cation radicals of aniline and *N,N*-dimethylaniline which are formed in the solid solution by γ radiolysis, according to which the first absorption band of the cation radicals of AN and DMA appears at 900 nm and 650 nm, respectively.
6) The energy and the intensity of the first excited band of AN and MPD cations were calculated by Katsumata and Kimura.[1] Our results agree well with the estimated values.
7) It is due to the unknown chemical products that the intensity of the visible band does not reach to zero.
8) B. Badger and B. Brocklehurst, *Trans. Faraday Soc.*, **65**, 2582 (1969).
9) E. J. Land and G. Porter, *ibid.*, **59**, 2027 (1963).
10) P. K. Wong and A. O. Allen, *J. Phys. Chem.*, **74**, 774 (1970).
11) S. Arimitsu, K. Kimura, and H. Tsubomura, This Bulletin, **42**, 1858 (1969).
12) T. Shida and W. H. Hamill, *J. Chem. Phys.*, **44**, 2369 (1966).
13) K. Kimura, S. Katsumata, and K. Sawada, *J. Phys. Chem.*, **76**, 639 (1972).

BULLETIN OF THE CHEMICAL SOCIETY OF JAPAN, VOL. 48(10), 2947—2948 (1975)

The Crystal and Molecular Structure of Emericellin, A Metabolite of *Aspergillus nidulans*

Keiichi FUKUYAMA, Tomitake TSUKIHARA, Shunji KISHIDA, Yukiteru KATSUBE, Masayoshi ISHIDA,* Takashi HAMASAKI,** and Yuichi HATSUDA**

Faculty of Engineering, Tottori University, Koyama, Tottori 680

(Received March 26, 1975)

Synopsis. The crystal and molecular structure of emericellin has been determined by the X-ray diffraction method. The compound crystallizes in the space group $P\bar{1}$, with $a=8.667$, $b=14.665$, $c=9.157$ Å, $\alpha=88.29$, $\beta=113.10$, and $\gamma=91.61°$. The structure was refined to an R value of 0.086 for 2151 non-zero reflections. There are two intramolecular hydrogen bonds.

Emericellin was isolated as a new metabolite of *Aspergillus nidulans* (Eidam) Winter.[1] The isolation and the chemical structure (shown below), proposed on the basis of the chemical and spectroscopic data, have been reported previously.[1] In order to confirm this, an X-ray structure analysis has been undertaken as part of the investigation of the metabolites of the genus *Aspergillus*.[2,3]

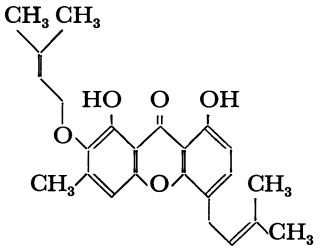

Emericellin crystallized from an ethanol solution in the form of yellow prisms. Preliminary oscillation and Weissenberg photographs showed that the crystals were triclinic and that there was no significant reflection in the region of $2\theta>110°$ (Cu $K\alpha$ radiation). Measurement was made by manually operating a Toshiba four-circle diffractometer. The cell constants were obtained by least-squares fits of the θ values for 49 reflections. Crystal data: $C_{25}H_{28}O_5$, $M=408.5$, triclinic, $P\bar{1}$, $a=8.667(5)$, $b=14.665(7)$, $c=9.157(5)$ Å, $\alpha=88.29(9)$, $\beta=113.10(9)$, $\gamma=91.61(9)°$, $V=1070$ Å^3, $Z=2$, $D_o=1.28$ g/cm^3, $D_x=1.27$ g/cm^3. The intensities of 2584 independent reflections were measured with Ni-filtered Cu $K\alpha$ radiation up to $\sin\theta/\lambda=0.531$ from a specimen with dimensions of *ca.* $0.21\times0.15\times0.06$ mm. The stationary-crystal stationary-counter method was used, with a counting time of 30 seconds. The background for each reflection was taken from plots of the background as a function of 2θ. The intensities were corrected for Lorentz and polarization factors, but not for absorption.

The structure was deduced from an interpretation of the three-dimensional Patterson map, followed by successive Fourier syntheses. The coordinates and isotropic temperature factors of all the non-hydrogen atoms were refined with the carbon scattering factor. Five oxygen atoms were assigned by an inspection of the temperature factors. When an R value reached 0.12 by further refinement with anisotropic temperature factors, the positions of all the hydrogen atoms were derived from a difference Fourier synthesis. The final refinement, made by including the hydrogen atoms, used the following weighting scheme: $w=0.0$ for $F_o=0$, $w=1.0$ for $0<F_o\leqq17$, and $w=1.0/(1.0+0.3(F_o-17))$ for $17<F_o$. The final R value is 0.086 for 2151 non-zero reflections. The final atomic parameters are given in Tables 1 and 2.

The atomic scattering factors were taken from the International Tables for X-ray Crystallography.[4] The computations were performed on a TOSBAC-3400 computer at the Tottori University Computing Center and on a NEAC 2200-N700 computer at the Computation Center of Osaka University.

The structural formula of emericellin has been confirmed by the present X-ray analysis. A stereo-

Table 1. Final atomic parameters and their estimated standard deviations ($\times10^4$) for carbon and oxygen atoms

The anisotropic temperature factors are of the form;
$\exp[-(\beta_{11}h^2+\beta_{22}k^2+\beta_{33}l^2+\beta_{12}hk+\beta_{13}hl+\beta_{23}kl)]$

	x	y	z	β_{11}	β_{22}	β_{33}	β_{12}	β_{13}	β_{23}
C(1)	259(6)	638(3)	2647(6)	209(10)	46(3)	147(8)	28(8)	159(15)	11(7)
C(2)	-919(6)	-11(3)	1838(5)	170(9)	52(3)	134(8)	32(8)	151(14)	18(7)
C(3)	-362(6)	-816(3)	1358(5)	152(9)	57(3)	135(8)	5(8)	115(13)	4(8)
C(4)	-1441(6)	-1593(4)	569(6)	168(9)	64(3)	134(8)	-8(9)	105(14)	10(8)
C(5)	-678(6)	-2347(3)	146(6)	182(10)	49(3)	139(8)	14(8)	114(14)	-5(7)
C(6)	-1601(6)	-3112(4)	-618(6)	191(10)	54(3)	176(9)	-10(9)	117(16)	-5(8)
C(7)	-830(7)	-3822(4)	-995(7)	247(12)	57(3)	184(10)	-10(10)	116(18)	-38(9)
C(8)	891(7)	-3767(4)	-606(7)	238(12)	66(3)	175(10)	31(10)	135(17)	-18(9)
C(9)	1874(6)	-3035(4)	159(6)	181(10)	60(2)	147(8)	11(9)	95(15)	4(8)
C(10)	1037(6)	-2324(3)	528(6)	189(10)	48(3)	151(8)	19(8)	126(15)	-8(8)
C(11)	1359(6)	-881(3)	1726(6)	184(10)	48(3)	147(8)	9(8)	147(15)	0(7)
C(12)	2522(6)	-219(3)	2521(6)	169(9)	55(3)	143(8)	-1(8)	122(14)	-7(8)
C(13)	1993(6)	547(3)	3019(6)	201(10)	54(3)	136(8)	-5(8)	131(15)	3(8)
C(14)	3239(7)	1272(4)	3904(7)	240(12)	60(3)	181(10)	-29(10)	124(18)	-32(9)
C(15)	-237(8)	1350(4)	4697(6)	287(13)	55(3)	172(9)	30(10)	208(18)	-7(9)
C(16)	43(7)	2260(4)	5440(6)	207(11)	61(3)	179(9)	18(9)	152(16)	-30(9)
C(17)	-1146(7)	2859(4)	5240(7)	245(12)	59(3)	197(10)	22(10)	182(18)	-13(9)
C(18)	-704(10)	3755(4)	6108(9)	402(19)	63(4)	316(15)	19(13)	395(28)	-23(12)
C(19)	-2933(9)	2717(5)	4164(11)	234(15)	98(5)	489(23)	53(14)	114(30)	-44(18)
C(20)	-2761(7)	158(4)	1424(6)	179(10)	72(3)	166(9)	37(9)	125(16)	14(9)
C(21)	3753(7)	-2982(4)	566(7)	215(11)	71(3)	190(10)	54(10)	141(17)	-9(10)
C(22)	4756(7)	-3122(4)	2324(7)	188(11)	70(3)	208(10)	31(10)	132(17)	-42(10)
C(23)	5605(7)	-3860(4)	3068(7)	195(11)	62(3)	192(10)	6(9)	134(17)	-28(9)
C(24)	5774(11)	-4666(5)	2192(8)	509(23)	73(4)	219(13)	132(16)	118(27)	-62(12)
C(25)	6550(8)	-3914(5)	4835(7)	260(14)	84(4)	210(11)	34(12)	70(20)	-15(11)
O(1)	-3465(4)	-417(3)	2292(4)	195(7)	87(3)	209(7)	25(7)	215(12)	21(7)
O(2)	-2998(4)	-1606(3)	262(5)	160(7)	74(2)	249(8)	-14(6)	156(11)	-51(7)
O(3)	-3294(5)	-3178(3)	-1012(5)	192(7)	72(2)	263(8)	-40(7)	155(12)	-68(7)
O(4)	2043(4)	-1611(2)	1294(4)	158(6)	51(2)	179(6)	10(5)	125(10)	-29(5)
O(5)	-221(5)	1433(2)	3114(4)	259(8)	52(2)	159(6)	47(6)	171(11)	10(5)

Table 2. Positional parameters ($\times10^3$) and isotropic temperature factors (Å^2) for hydrogen atoms

	x	y	z	B		x	y	z	B
H(1)	-146(7)	-442(4)	156(7)	5.2(15)	H(2)	147(7)	-432(4)	-79(7)	5.1(14)
H(3)	379(6)	-30(3)	266(6)	3.3(11)	H(4)	465(7)	118(4)	404(7)	5.6(15)
H(5)	353(8)	129(4)	512(7)	6.7(16)	H(6)	331(8)	174(4)	328(7)	6.8(16)
H(7)	63(7)	90(4)	534(7)	4.6(14)	H(8)	-139(7)	106(4)	455(7)	4.7(14)
H(9)	124(7)	246(4)	614(7)	5.1(14)	H(10)	-154(8)	375(5)	639(8)	7.0(18)
H(11)	-96(8)	430(5)	529(8)	7.0(18)	H(12)	48(9)	387(5)	684(8)	7.8(19)
H(13)	-361(10)	331(6)	335(10)	10.7(24)	H(14)	-349(10)	215(6)	468(10)	10.7(24)
H(15)	-343(10)	211(5)	332(9)	9.8(22)	H(16)	-350(6)	8(4)	18(6)	3.9(12)
H(17)	-286(7)	89(4)	177(7)	4.7(14)	H(18)	-372(8)	-106(4)	195(7)	6.2(16)
H(19)	-351(8)	-267(4)	-62(8)	6.8(17)	H(20)	408(7)	-235(4)	26(6)	4.2(13)
H(21)	404(7)	-346(4)	-8(6)	4.0(13)	H(22)	486(7)	-258(4)	309(7)	4.8(14)
H(23)	613(10)	-510(5)	272(9)	9.7(22)	H(24)	473(10)	-490(6)	134(10)	9.9(23)
H(25)	584(10)	-455(5)	112(9)	9.7(22)	H(26)	630(9)	-331(5)	503(8)	8.2(19)
H(27)	766(8)	-384(5)	506(8)	6.9(17)	H(28)	627(7)	-450(4)	529(7)	5.8(16)

* Tottori Women's College, Kurayoshi 682.

** Faculty of Agriculture, Tottori University, Koyama, Tottori 680.

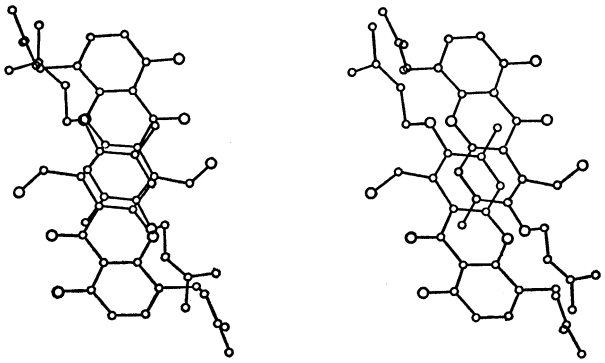

Fig. 1. Stereoscopic view of a pair of melecules.

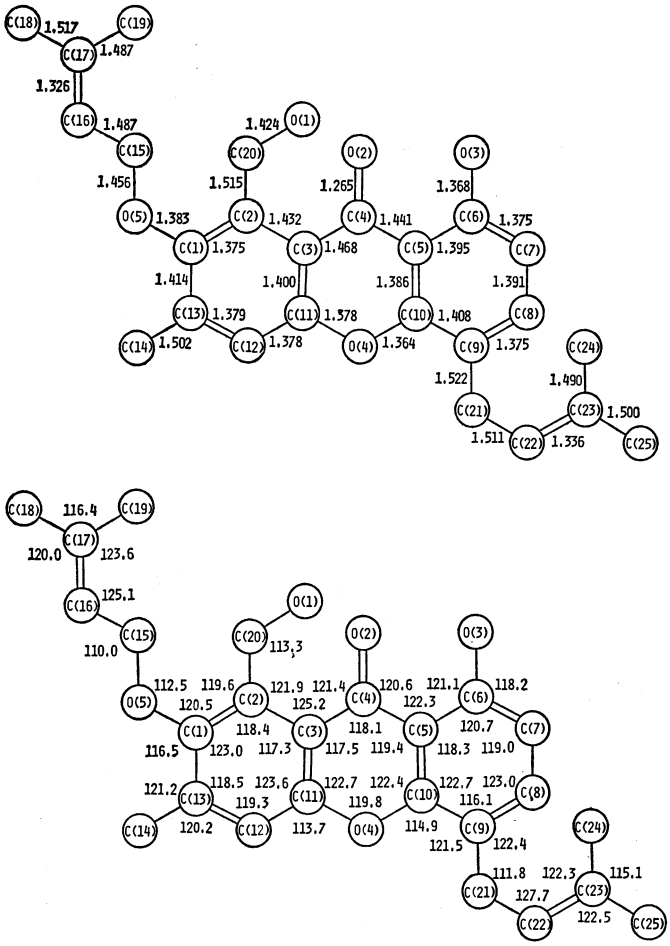

Fig. 2. Bond lengths (Å) and angles (°) for non-hydrogen atoms.
The e. s. d.'s of bond lengths and angles are about 0.008 Å and 0.5° respectively.

scopic view of the pair of molecules is shown in Fig. 1. The bond lengths and angles for non-hydrogen atoms are shown in Fig. 2. The bond lengths and angles in the xanthone skeleton are comparable with those found in sterigmatin.[2] There is a screw-like twist along the longitudinal axis of the skeleton; the twist angle between the two outer benzenoid rings is about

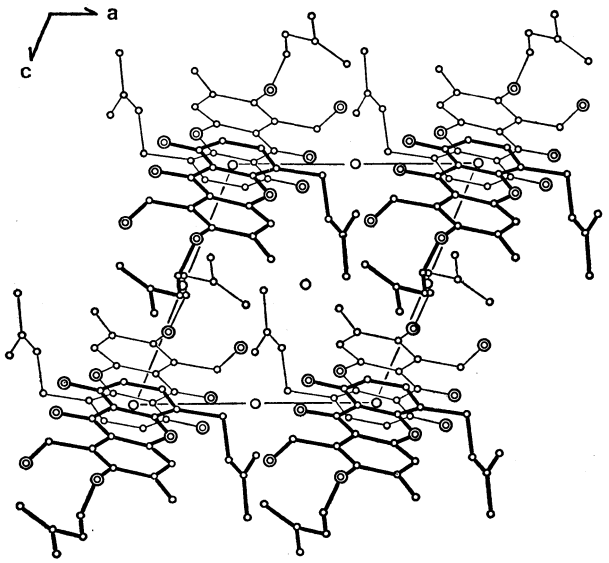

Fig. 3. The crystal structure of emericellin viewed along the b axis. The hydrogen atoms are omitted in the figure.

3°. The C(20) atom is largely displaced from the least-squares plane passing through the 14 ring atoms in the skeleton. The corresponding bond lengths and angles in the two isopentenyl groups are similar to each other. There are two intramolecular hydrogen bonds, O(1)–H(18)·····O(2) and O(3)–H(19)·····O(2). The distances of O(1)·····O(2) and O(3)·····O(2) are 2.736 and 2.575 Å respectively, while the angles of O(1)–H(18)·····O(2) and O(3)–H(19)·····O(2) are 122° and 154° respectively.

The crystal structure viewed along the b axis is shown in Fig. 3. There are only three kinds of close contacts; plane to plane contact of the xanthone skeletons around (0, 0, 0), contact between the isopentenyl group and the xanthone skeleton around (0, 0, 1/2), and head-to-tail contact between the molecules related by unit translation along the a axis. Except for these contacts, the crystal consists of a loose-packed array, and there is no intermolecular hydrogen bond. These are in accordance with the relatively low density of the crystal.

The authors wish to thank Professor Tamaichi Ashida of Nagoya University for his permission to use the block-diagonal least-squares program.

References

1) M. Ishida, T. Hamasaki, Y. Hatsuda, K. Fukuyama, T. Tsukihara, and Y. Katsube, *Agr. Biol. Chem.*, **39**(1), 291 (1975).

2) K. Fukuyama, T. Tsukihara, Y. Katsube, T. Hamasaki, Y. Hatsuda, N. Tanaka, T. Ashida, and M. Kakudo, This Bulletin, **48**, 1639 (1975).

3) Y. Katsube, T. Tsukihara, N. Tanaka, K. Ando, T. Hamasaki, and Y. Hatsuda, *ibid.*, **45**, 2091 (1972).

4) "International Tables for X-ray Crystallography", Vol. III, Kynoch Press, Birmingham (1962), p. 202.

BULLETIN OF THE CHEMICAL SOCIETY OF JAPAN, VOL. 48(10), 2949—2950 (1975)

A Structure Analysis of a Bromo Derivative of Parasiticolide A by the X-Ray Diffraction Method

Keiichi FUKUYAMA, Hiromitsu KAWAI, Tomitake TSUKIHARA, Kumiko TSUKIHARA, Yukiteru KATSUBE, Takashi HAMASAKI,* Yuichi HATSUDA,* and Harumitsu KUWANO**

Faculty of Engineering, Tottori University, Koyama, Tottori 680

(Received May 6, 1975)

Synopsis. The structure of a bromo-derivative of parasiticolide A, $C_{26}H_{29}O_8Br$, has been determined by single-crystal X-ray analysis. The compound crystallized in the space group $P2_12_12_1$, with $a=14.658$, $b=15.323$, and $c=11.181$ Å. The absolute configuration of the molecule was determined using the anomalous dispersion effect of the bromine atom for Cu$K\alpha$ radiation.

Parasiticolide A (I) was isolated as a new metabolite from a strain of *Aspergillus parasiticus* Speare IFO 4082, which produces a small amount of carcinogenic aflatoxins.[1] Although the structural formula of parasiticolide A had been determined by means of chemical and spectroscopic methods,[1] the three-dimensional structure and the absolute configuration of this compound remained unsolved. Therefore, a bromo-derivative of parasiticolide A (II) has been studied by the X-ray diffraction method in a series of works on the structures of the metabolites of the genus *Aspergillus*.[2-4]

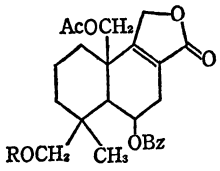

(I) R: CH_3CO-
(II) R: $BrCH_2CO$-

The bromo-derivative of parasiticolide A was prepared by the acylation of a partial hydrolysis product of parasiticolide A and bromoacetylbromide. The compound crystallized from acetone solution in the form of colorless prisms elongated along the b-axis. The cell dimensions were obtained by the least-squares fits of the Bragg angles of forty-nine reflections measured by a Toshiba four-circle diffractometer. The crystal data were as follows: $C_{26}H_{29}O_8Br$, $M=549.4$, mp 206—208 °C, orthorhombic, space group $P2_12_12_1$, $a=14.658(6)$, $b=15.323(6)$, $c=11.181(5)$ Å, $V=2511.4$ Å^3, $Z=4$, $D_o=1.45$ g/cm^3, $D_x=1.45$ g/cm^3. The intensities were measured from a specimen with dimensions of *ca.* $0.36\times0.16\times0.14$ mm on a diffractometer with a scintillation counter equipped with a pulse-height analyzer. The stationary-crystal stationary-counter method was used, with a counting time of 30 seconds. The intensities of 1782 independent reflections were measured up to $\sin\theta/\lambda=0.53$ with Ni-filtered Cu $K\alpha$ radiation. The background for each reflection was taken from plots of the background as a function of 2θ. The intensities were corrected only for the Lorentz and polarization factors.

The structure was solved by the heavy-atom method and refined by a block-diagonal least-squares method. In the early stage of the refinement, all the lighter atoms were assumed to be carbon atoms. Eight oxygen atoms were assigned on the bases of the temperature factors and of the chemical sense. The refinement with anisotropic temperature factors reduced the R value to 0.079. The absolute configuration of the molecule was determined using the anomalous dispersion effect of the bromine atom ($\Delta f'=-0.9$ and

Table 1. The comparison of calculated and observed intensities ($\times5$) of Friedel-pair reflections

h k l	$F_c(hkl)$	$F_c(\bar{h}\bar{k}\bar{l})$	$I_o(hkl)$	$I_o(\bar{h}\bar{k}\bar{l})$
1 1 1	364	341	>	
1 6 1	286	264	>	
3 1 1	509	539	<	
4 3 1	435	418	>	
2 5 2	217	203	>	
3 2 2	171	156	>	
3 6 2	267	293	<	
5 2 2	144	167	<	
1 5 3	269	255	>	
2 3 5	193	217	<	

The right-handed coordinate system is adopted.

Table 2. Final atomic parameters and their estimated standard deviations ($\times10^4$) for non-hydrogen atoms

The anisotropic temperature factors are of the form; $\exp[-(\beta_{11}h^2+\beta_{22}k^2+\beta_{33}l^2+\beta_{12}hk+\beta_{13}hl+\beta_{23}kl)]$.

	x	y	z	β_{11}	β_{22}	β_{33}	β_{12}	β_{13}	β_{23}
Br	-2633(1)	-2323(1)	-1003(1)	92(1)	49(1)	124(1)	-3(1)	-20(1)	-3(1)
C(1)	-1891(5)	3154(5)	655(7)	47(4)	51(4)	79(7)	-4(7)	5(9)	-18(9)
C(2)	-2610(5)	2463(6)	685(8)	49(4)	64(5)	102(8)	20(7)	23(9)	-14(10)
C(3)	-2877(5)	2152(6)	-563(8)	43(4)	58(4)	105(8)	-2(7)	10(9)	9(10)
C(4)	-2063(5)	1813(5)	-1287(6)	37(3)	48(4)	65(6)	0(6)	-18(7)	3(8)
C(5)	-1303(5)	2521(5)	-1275(7)	41(3)	46(4)	71(6)	3(6)	4(8)	0(8)
C(6)	-494(5)	2395(5)	-2143(7)	41(3)	40(3)	77(6)	8(6)	-7(7)	16(8)
C(7)	59(6)	3210(5)	-2346(7)	54(4)	50(4)	83(7)	-5(7)	13(9)	25(9)
C(8)	81(6)	3750(6)	-1233(8)	49(4)	50(4)	106(8)	-17(7)	-24(10)	25(10)
C(9)	-394(5)	3636(5)	-215(7)	45(4)	43(3)	85(7)	1(6)	-15(9)	23(9)
C(10)	-1010(5)	2865(5)	10(6)	41(3)	48(4)	72(6)	0(6)	-11(8)	-3(9)
C(11)	-186(7)	4357(6)	625(8)	73(5)	54(4)	106(8)	-30(9)	-8(12)	-3(10)
C(12)	625(7)	4560(6)	-1088(9)	79(6)	57(5)	122(10)	-30(9)	-32(14)	-10(12)
C(13)	-1736(5)	922(5)	-838(7)	44(4)	40(3)	96(7)	2(6)	-2(10)	-4(9)
C(14)	-2400(6)	1694(6)	-2596(8)	54(4)	56(4)	98(7)	-14(8)	-23(10)	-15(9)
C(15)	-469(5)	2202(5)	749(6)	47(4)	48(4)	72(6)	3(7)	-21(8)	10(9)
C(16)	160(6)	2115(6)	2688(7)	53(4)	63(5)	88(7)	-15(8)	-12(10)	42(10)
C(17)	298(7)	2598(8)	3838(8)	73(5)	96(7)	91(8)	14(11)	-23(11)	16(13)
C(18)	-2219(6)	-529(5)	-739(7)	59(4)	46(4)	86(7)	-7(7)	-8(10)	14(9)
C(19)	-2982(7)	-1140(6)	-1155(12)	69(5)	48(4)	194(14)	-18(8)	-63(16)	-12(14)
C(20)	612(5)	1258(5)	-2490(7)	34(3)	51(4)	98(8)	-1(6)	-2(9)	-16(9)
C(21)	1167(5)	566(5)	-1969(8)	45(4)	39(3)	102(8)	-10(6)	-7(10)	-27(9)
C(22)	1016(6)	256(6)	-811(8)	51(4)	51(4)	103(8)	-6(7)	-8(10)	8(10)
C(23)	1599(6)	-402(6)	-351(9)	63(5)	55(4)	132(10)	16(8)	-26(12)	17(12)
C(24)	2305(7)	-726(7)	-1064(11)	65(5)	54(5)	186(13)	24(8)	-40(16)	7(14)
C(25)	2436(6)	-428(6)	-2187(10)	54(4)	58(4)	150(10)	18(8)	2(13)	-31(12)
C(26)	1865(6)	234(6)	-2686(9)	56(5)	53(4)	128(9)	7(8)	32(12)	-16(11)
O(1)	-2435(3)	288(3)	-1063(5)	45(2)	45(3)	94(5)	-1(4)	1(7)	4(6)
O(2)	-1533(4)	-732(4)	-237(7)	72(4)	54(3)	188(9)	-14(6)	-88(11)	27(9)
O(3)	89(3)	1687(3)	-1681(4)	38(2)	50(2)	73(4)	21(4)	6(5)	8(6)
O(4)	599(4)	1436(4)	-3545(5)	65(3)	74(3)	71(5)	16(6)	22(7)	12(7)
O(5)	1155(6)	4895(5)	-1772(8)	111(6)	76(4)	173(9)	-77(9)	39(12)	55(11)
O(6)	449(4)	4897(4)	-6(7)	64(3)	52(3)	173(8)	-29(5)	-45(9)	0(9)
O(7)	-273(4)	2623(4)	1886(4)	56(3)	62(3)	64(4)	0(5)	-12(6)	4(6)
O(8)	377(6)	1392(5)	2491(7)	119(6)	71(4)	142(8)	40(9)	-112(12)	44(9)

* Faculty of Agriculture, Tottori University, Koyama, Tottori 680.

** Central Research Laboratories, Sankyo Co., Ltd., Tokyo.

$\Delta f''=1.5$) for Cu $K\alpha$ radiation. A comparison of the intensities between the Friedel-pair of reflections is given in Table 1. Including hydrogen atoms with fixed parameters and the anomalous dispersion effect of the bromine atom, the final refinement reduced the R value to 0.062 for 1772 reflections. The weighting scheme adopted in the final calculation was $w=0.3$ for $F_o=0$, $w=1.0$ for $0<F_o\leqq 20$, and $w=1.0/(1.0+0.5(F_o-20))$ for $20<F_o$. The final atomic parameters are given in Table 2. The absolute configuration of the molecule is correctly represented by the coordinates in Table 2 if the right-handed coordinate system is adopted. All the atomic scattering factors were taken from the International Tables for X-ray Crystallography.[5] The computations were performed on a TOSBAC-3400 computer at the Tottori University Computing Center, and on a NEAC 2200 N700 computer at the Computation Center of Osaka University.

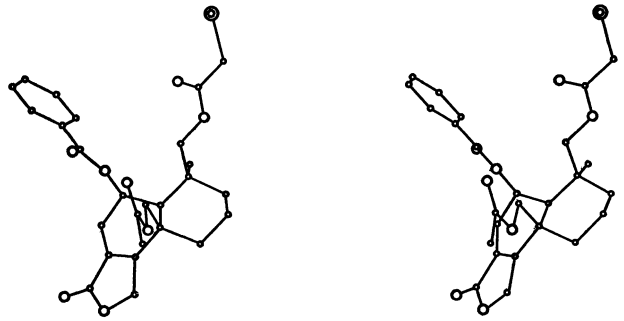

Fig. 1. Stereoscopic view of the molecule.

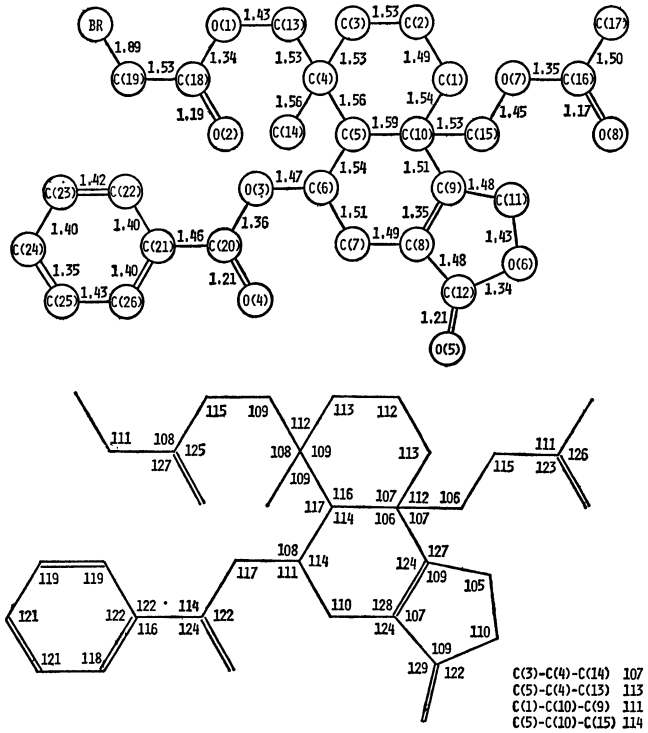

Fig. 2. Bond lengths (l/Å) and angles (φ/°) for non-hydrogen atoms. The mean estimated standard deviation of bond lengths is 0.012 Å, and that of bond angles is 0.7°.

The present analysis has established the three-dimentional structure and the absolute configuration of the bromo-derivative of parasiticolide A. A stereoscopic view of the molecule is shown in Fig. 1, which is drawn with the correct absolute configuration. The bond lengths and angles for non-hydrogen atoms are given in Fig. 2. Two six-membered rings are joined through two equatorial-type bonds. The two acetoxymethyl groups and one benzoyloxy group show a 1,3-diaxial relationship. As a consequence, the bond angles, C(4)–C(5)–C(6), C(4)–C(5)–C(10), C(6)–(5)–C(10), and C(5)–C(10)–C(15), may be widened from the regular tetrahedral angle to release these groups from crowding. The remaining bond lengths and angles seem to be normal for the respective bond types. The details of the stereochemistry of parasiticolide A itself will be published later.

The authors wish to thank Professor Tamaichi Ashida of Nagoya University for his permission to use the block-diagonal least-squares program.

References

1) T. Hamasaki, H. Kuwano, K. Isono, Y. Hatsuda, K. Fukuyama, T. Tsukihara, and Y. Katsube, *Agr. Biol. Chem.*, **39**, 749 (1975).

2) N. Tanaka, Y. Katsube, Y. Hatsuda, T. Hamasaki, and M. Ishida, This Bulletin, **43**, 3635 (1970).

3) Y. Katsube, T. Tsukihara, N. Tanaka, K. Ando, T. Hamasaki, and Y. Hatsuda, *ibid.*, **45**, 2091 (1972).

4) K. Fukuyama, T. Tsukihara, Y. Katsube, T. Hamasaki, Y. Hatsuda, N. Tanaka, T. Ashida, and M. Kakudo, *ibid.*, **48**, 1639 (1975).

5) "International Tables for X-ray Crystallography," Vol. III, Kynoch Press, Birmingham (1962), p. 202.

BULLETIN OF THE CHEMICAL SOCIETY OF JAPAN, VOL. 48(10), 2951—2952 (1975)

The Apparent Solvent Effect on the Fluorescence Efficiency of 9-Methyl-10-(chloromethyl)anthracene

Fujio TANAKA and Jiro OSUGI

Department of Chemistry, Faculty of Science, Kyoto University, Kyoto 606

(Received March 28, 1975)

Synopsis. 9-Methyl-10-(chloromethyl)anthracene (I) is immediately transformed into 9-methyl-10-(ethoxymethyl)-anthracene (II) in ethanol, and a very strong fluorescence of II is observed. While I is practically nonfluorescent, II fluoresces strongly in all solvents. These facts explain well a phenomenon misinterpreted by Melhuish as a remarkable solvent effect on the fluorescence efficiency of I.

It was reported by Melhuish that the fluorescence yield of 9-methyl-10-(chloromethyl)anthracene (I) was 0.09 in benzene and 0.73 in ethanol.[1] This remarkable difference has received some attention as a typical example of solvent effects on fluorescence yields.[2] However, the origin of this interesting phenomenon is not yet well understood. The present authors re-examined the behavior of the fluorescence of I in the course of their studies of the environment effects on the fluorescence yields of anthracene and its derivatives.

As reported by Melhuish, all alcoholic solutions of I fluoresce very strongly, while I is practically nonfluorescent in all solvents except alcohols.[3] To clarify the mechanism of the high-fluorescence efficiency in alcoholic solvents, first the spectroscopic nature of I in ethanol and benzene was investigated. The absorption spectrum of an ethanol solution of I shifts toward wavelengths shorter by *ca.* 10 nm relative to that of a benzene solution. This shift is too large compared with the corresponding values (3—4 nm) for anthracene and most derivatives. Therefore, the change in the absorption spectrum suggests the occurrence of a solvolytic reaction in ethanol. Indeed, the residue of an ethanol solution of I was identified as 9-methyl-10-(ethoxymethyl)anthracene (II) by PMR (signals of ethyl group) and mass spectrometry (M^+=250). II fluoresces strongly in both ethanol and benzene. Melhuish also reported in the same paper that the fluorescence yields of II are 0.68 in ethanol and 0.71 in benzene.[1] As a matter of course, an ethanol solution of II shows the same absorption and fluorescence spectra as an ethanol solution of I. The absorption and fluorescence spectra of I and II in ethanol and benzene are shown in Fig. 1. It is also clear from the similar changes in the absorption spectra that I is transformed into the corresponding alkoxy-compounds in other alcoholic solvents. Accordingly, the following conclusion may be drawn: the high-fluorescence efficiency in alcoholic solutions of I is not due to the solvent effect on the fluorescence efficiency of I itself, but to the transformation of I into II in alcoholic solvents.

Further, the above conclusion is confirmed by the fluorescence behavior of I in the acetonitrile-water system, where a solvolytic reaction is likewise possible. Although I is nonfluorescent in acetonitrile, a strong fluorescence appears upon the addition of some water. The residue from this solution was identified as 9-methyl-10-(hydroxymethyl)anthracene (III) by mass spectrometry (M^+=222). III also fluoresces strongly in all solvents.

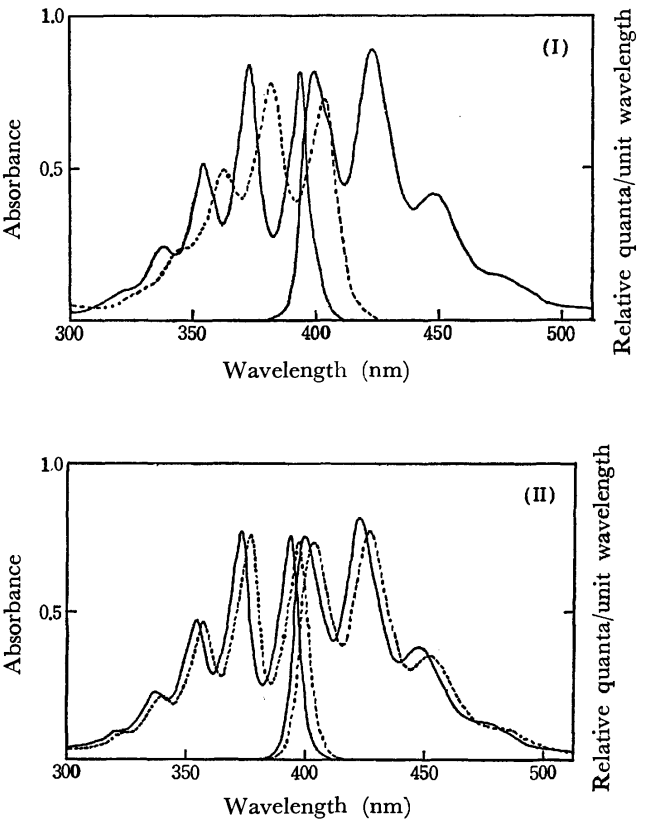

Fig. 1. Absorption and fluorescence spectra of (I) and (II) in ethanol (——) and benzene (----); 8×10^{-5} mol/l for absorption and 8×10^{-6} mol/l for fluorescence. The fluorescence spectra are normalized to the absorption spectra at the 0-0 band.

In conclusion, then, the nonfluorescent character of I is an interesting problem. A photolytic process of the C-Cl bond may be considered as the main deactivation process.

Experimental

I was prepared by the chloromethylation[4] of 9-methylanthracene[5] and was recrystallized three times from benzene. The ethanol and benzene are of a spectroscopic grade. The absorption and fluorescence spectra were measured with a Shimadzu spectrophotometer, UV 200, and a Shimadzu corrected fluorospectrophotometer, RF 502, respectively.

References

1) W. Melhuish, *New Zealand J. Sci. Tech.*, **37B**, 142 (1955).

2) R. S. Becker, "Theory and Interpretation of Fluorescence and Phosphorescence," John Wiley & Sons, New York, Chapter 11.

3) Indeed, a very weak fluorescence was observed in the benzene solution of I, but its excitation spectrum is different from the absorption spectrum of I; Rather, it resembles the absorption spectrum of III, which seems to be slightly present as impurities.

4) J. L. Adelfang and G. H. Daub, *J. Amer. Chem. Soc.*, **80**, 1405 (1958).

5) A. Sieglitz and R. Marx, *Ber.*, **56**, 1619 (1923).

BULLETIN OF THE CHEMICAL SOCIETY OF JAPAN, VOL. 48(10), 2953—2954 (1975)

The Reaction of Water Vapor and Carbon Vapor Produced by Laser Irradiation

Pil Hyon KIM, Ko TAKI,* and Susumu NAMBA

The Institute of Physical and Chemical Research, Wako-shi, Saitama 351

**Faculty of Industrial Hygiene, Kitasato University, Sagamihara-shi, Kanagawa 228*

(Received January 31, 1975)

Synopsis. The carbon vapor produced by laser irradiation was found to react with the water vapor. The main products were carbon monoxide, hydrogen, and acetylene, the last of which is not found in the water-gas. Acetylene is considered to be formed by the reaction of the C_2 species of the carbon vapor.

The present authors have previously studied the reactions of gaseous substances with the vapor of the solid target produced by laser heating.[1,2] In these cases, only a small region of the target is heated rapidly by the irradiation of the pulsed laser beam, and the gaseous substances can react with the vaporized species produced at high temperatures. Moreover, because of the localized heating and the short-pulse heating, the gaseous products are prevented from thermal decomposition.

In the reaction of hydrogen or hydrocarbons with the carbon species vaporized from the graphite carbon target,[1] acetylene was obtained as the main product; it had been assumed that the C_2 species played the main role in the product-forming step. From the above results, the carbon vapor produced by laser heating can be expected to react with the water vapor, which is most simple and easily obtainable hydrogen compound, to produce hydrocarbons as gaseous fuel.

It is well known in the fuel and coal-product industries that the reaction of heated carbon and water vapor gives a water-gas[3] which contains hydrogen and carbon monoxide as the main components, plus a small quantity of methane and carbon dioxide, but no acetylene. However, the reaction of the water vapor with the carbon vapor produced by the laser heating has never been reported.

This paper will describe the reaction of the water vapor with the carbon vapor produced from the graphite carbon target by the irradiation of the pulsed laser beam.

Experimental

The graphite carbon target and a small amount of water ($\sim 10^{-2}$ g) were placed in a 7-cm^3 Pyrex cell, as is shown in Fig. 1. The cell had been preheated to increase the vapor pressure of water ($\sim$100 Torr). Then, the target was irradiated by means of a ruby laser beam focused by a lens 35 mm in focal length. The ruby laser used was a normal laser, the output energy and pulse duration of which were about 3 J and 1 ms respectively. The temperature of the irradiated region ($\sim 10^{-3}$ cm^2) is estimated to be above 3000 K, and the carbon vapor produced is considered to be the C_1, C_2, C_3 . . . species.[4] After 5—7 pulse irradiations, the reaction products were analysed by gas chromatography using silica gel and squalane columns and by mass spectroscopy.

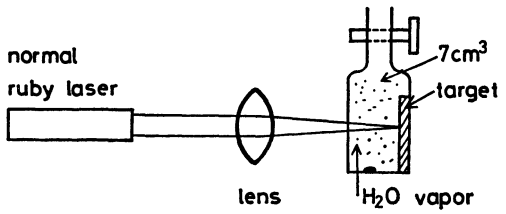

Fig. 1. Experimental block diagram.

Results and Discussion

The product yields in the reaction of water vapor with the carbon vapor produced by six pulse-laser irradiations are shown in Table 1. The yields are proportional to the number of laser irradiations. For a comparison of the product yields, the product ratios of the water-gas[3] produced by conventional heating are also shown in Table 1. In laser irradiation, the main products are carbon monoxide, hydrogen, and acetylene, the last of which is not contained in the water-gas.

TABLE 1. PRODUCT YIELD IN THE REACTION OF WATER VAPOR WITH CARBON VAPOR AFTER 6 PULSE LASER IRRADIATIONS AND RELATIVE YIELD IN WATER-GAS

Product	Yield (10^{-6} mol) in laser irrad.	Relative yield (%) in water-gas
CO	6	30—42
H_2	5	44—52
C_2H_2	2	
CO_2	$\sim 10^{-2}$	2— 8
CH_4	$\sim 10^{-2}$	0.5—1.0
C_2H_4	$\sim 10^{-2}$	
N_2		2— 6

In the case of water-gas, it has been considered that monatomic carbon reacts with water vapor to give carbon monoxide and hydrogen as the main products. In laser irradiation of the carbon target, the reaction of the C_1 species of the carbon vapor with water vapor may also give carbon monoxide and hydrogen. As has been described in a previous paper,[1] acetylene may be formed by the reaction of the C_2 species of the carbon vapor in this system. Therefore, as in the reaction of C_2 species with hydrogen or hydrocarbons, the elementary formation processes of acetylene may be considered to be as follows:

1) $C_2 + H_2O \longrightarrow \cdot C_2H + \cdot OH$

2) $\cdot C_2H + H_2O \longrightarrow C_2H_2 + \cdot OH$

By the addition of about 100 Torr NO to the reaction system, the yield of acetylene was decreased to about one-tenth, but that of carbon monoxide increased about 1.5 times. In this case, NO may scavenge the acetylene precursor, C_2, to give carbon monoxide, because it has also been reported that the C_2H radical is not affected by this scavenger.[5] Moreover, by the addition of about 100 Torr oxygen, the yield of acetylene decreased to a trace.

The reaction of the C_2 species with the hydrogen produced may also give acetylene. However, the contribution to the yield is considered to be smaller than that of the reaction with water vapor, because the partial pressure of the hydrogen produced is several Torr for about a hundred Torr of water vapor.

The two reasons for the formation of acetylene in the laser irradiation are considered to be as follows: one is that the carbon vapor produced by laser irradiation contains a considerable amount of the C_2 species, and the other is that the acetylene produced is prevented from thermal decomposition because the laser heating features rapid heating and rapid quenching.

References

1) K. Taki, P. H. Kim, and S. Namba, This Bulletin, **42**, 823 (1969); *ibid.*, **46**, 1556 (1973).

2) K. Taki, P. H. Kim, and S. Namba, *ibid.*, **45**, 2052 (1972); *Sci. Papers I.P.C.R.*, **67**, 82 (1973).

3) Chem. Soc. Jap. ed., "Kagaku-binran (in Japanese)," Maruzen (1966); F. Tamamushi *et al.* ed., "Rikagaku-jiten (in Japanese,)" Iwanami (1971).

4) H. A. Chupka and M. G. Inghram, *J. Phys. Chem.*, **59**, 100 (1955). J. Berkowitz and W. A. Chupka, *J. Chem. Phys.*, **40**, 2735 (1964). J. T. Clarke and B. R. Fox, *ibid.*, **46**, 827 (1967).

5) A. M. Tarr, O. P. Strausz, and H. E. Gunning, *Trans. Faraday Soc.*, **61**, 1946 (1965).

BULLETIN OF THE CHEMICAL SOCIETY OF JAPAN, VOL. 48(10), 2955—2956 (1975)

Micellar Effect of Alkylammonium Propionates on Reaction Rate of Keto-Enol Tautomerism in Cyclohexane

Kijiro KON-NO, Kiyoshi MIYAZAWA, and Ayao KITAHARA

Department of Industrial Chemistry, Science University of Tokyo, Kagurazaka, Shinjuku-ku, Tokyo 162

(Received May 31, 1975)

Synopsis. The rate of keto-enol transformation of acetylacetone or acetoethyl acetate was spectroscopically measured in the cyclohexane solutions in the presence of primary, secondary or tertiary alkylammonium propionate. The rate was enhanced by micelle formed. The order of effectiveness of the surfactants was that primary≫secondary> tertiary. The order coincides with the number of protons in the ammonium ion of the surfactants and the aggregation number of micelle.

Reversed micelle of oil-soluble surfactants in apolar solvents which involves polar region or ion-pairs in the interior is expected to provide active sites for reactions. Because reversed micelle is more analogous to an enzymatic model than aqueous micelle as pointed out by Fendler *et al.*,[1] micellar catalysis in apolar media seems to be more interesting than that in water media. Furthermore, reversed micellar catalysis is possible to be modified by solubilization of polar substances such as water, acids, alcohols and amines and the solubilization has been considerably studied.[2]

Enhancement of the rate constant of mutarotation of 2,3,4,6-tetramethyl-α-D-glucose and decomposition of Meisenheimer complex in benzene in the presence of alkylammonium carboxylates has been recently reported by Fendler *et al.*[3,4] They have attributed the rate enhancement to the orientation of the reactants in the micelle and the transfer of proton from the ammonium ion of the surfactant to the reactant. However, such a system has little been studied.[5] The present authors have also studied the catalytic effect of alkylammonium carboxylates on hydrolysis of *p*-nitrophenyl esters.[6]

For the further investigation on the effect of proton of surfactant molecules of ammonium type, the rate of keto-enol transformation is now studied in the presence of a surfactant of primary, secondary or tertiary ammonium type in a nonpolar solvent.

Experimental

Materials: Dodecylammonium propionate (DAP), didodecylammonium propionate (DDAP) and cetyldimethylammonium propionate (CDAP) were used as oil-soluble surfactants. The preparation and purification were described in the previous paper.[6] They were further dried under reduced pressure at 50 °C immediately before use. Cyclohexane used as the solvent was purified by the process reported[7] and dried with Molecular Sieves 4A. Acetylacetone (AA) and acetoethyl acetate (EA) used as the substrates were of the chemical grade.

Methods: The rate was measured by following UV-absorption spectra of the keto-form with the Spectrophotometer UV-200 of the Shimadzu Manufacturing Co. The absorption peaks of the keto-form used for calculation of the rate constant were 275, 285 and 304 nm for EA in the DAP solution, EA in the DDAP solution and AA in the DAP solution, respectively.

All of the rates of transformation were the pseudo-first order and the apparent rate constants (k_ψ) were obtained by the Guggenheim method.[8] In pure cyclohexane, 43% of EA or 88% of AA is present as the enol-form.[9] The initial concentration of the enol-form used throughout the present measurements was 2.5×10^{-5} M and 5.0×10^{-5} M for EA and AA, respectively. Temperature of the solutions in the cell was kept at 30 °C.

The measurement of aggregation number and critical micellar concentration (CMC) or critical aggregating concentration (CAC) were carried out with a vapor pressure osmometer, the Hitachi-Perkin-Elmer Molecular Weight Apparatus, as reported previously.[10]

Results and Discussion

The equilibrium concentration of the enol- or keto-form of EA or AA in cyclohexane is considerably different from that in water. Hence water present in the cyclohexane solution may affect the rate of the shift reaction. Hence, the reaction rate of EA was measured by varying the quantity of water in the DAP solution. The result was shown in Fig. 1. Further experiments were carried out below the 0.5 molar ratio.

Transformation reaction from enol-form to keto-form for EA and AA occurred in all of the surfactant solutions used, though the reaction did not appear in pure cyclohexane. The increasing rate constant (k_ψ) of the keto-form of EA and AA was depicted as a function of surfactant concentration in Fig. 2, with the inserted small figure enlarging lower concentration range. The aggregating number (n) and CMC or CAC obtained experimentally were listed in Table 1.

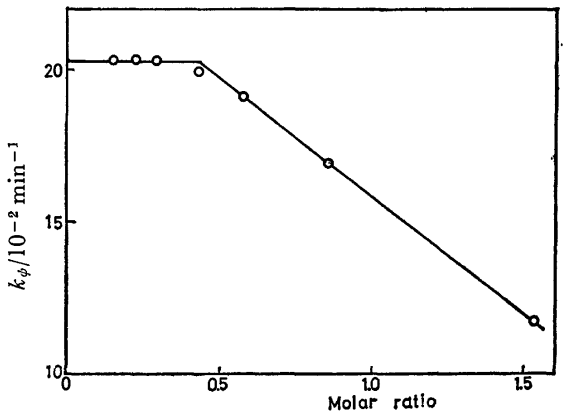

Fig. 1. Rate constant (k_ψ) of transformation to the keto-form of EA *vs.* the amount of water (molar ratio of water to the surfactant) added in the DAP solution (50 mM).

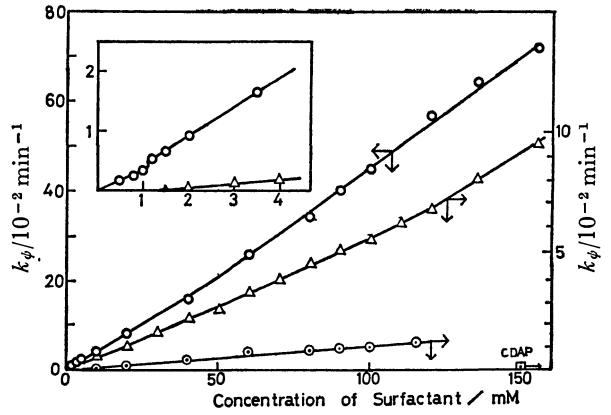

Fig. 2. Rate constant (k_ψ) of transformation to the keto-form *vs.* concentration of surfactants.
—○—: EA in the DAP solution, —△—: AA in the DAP solution, —⊙—: EA in the DDAP solution, ⊡: EA in the CDAP solution.

Table 1. The values of CMC or CAC and aggregation number (n) of surfactants (Dry systems, 30 °C)

Surfactants	CMC or CAC (mM)	n	Number of protons in ammonium ion
DAP	1.8	3.8	3
DDAP	4.4	1.2	2
CDAP	0.78	1.2	1

Combination of Fig. 2 and Table 1 elucidates the following effect of micelle on the reaction rate. Below CMC or CAC, transformation to the keto-form was too slow to calculate k_ψ for AA in the DAP solution and EA in the DDAP solutions, though k_ψ was obtained for EA in the DAP solution. That is, it can be seen that transformation to the keto-form is more enhanced by micelle than monomer, except for EA in the CDAP solution in which k_ψ was too small to be depicted in the Fig. 2 over the whole range of concentration measured. This may be due to concentration of polar groups by micelle formation which increases interaction with the substrate. It is also evident from Fig. 2 that effectiveness of the surfactant micelle on the k_ψ-values is the order of DAP≫DDAP>CDAP. The order coincides with the number of protons or hydrogen atoms in the ammonium ion and the aggregation number shown in Table 1, though the difference of n between DDAP and CDAP is ambiguous. Hence it is concluded that the surfactant having more protons and aggregation number shows the more effectiveness on the reaction rate.

It is considered from the above facts that keto-enol transformation is induced by proton transfer from the ammonium ion to the substrate. The consideration may propose a following scheme for the reaction mechanism similar to the proposition by Fendler *et al.*[3] As an example, for EA:

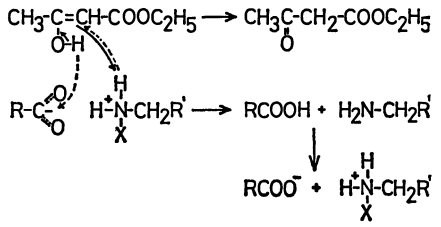

R: $CH_3(CH_2)_2$
R': $CH_3(CH_2)_{10}$
X: $CH_3(CH_2)_{11}$ or H

The inhibition effect of water shown in Fig. 1 may be due to hydration to ammonium and/or carboxylate.

References

1) E. J. Fendler, S. A. Chang, J. H. Fendler, R. T. Medary, O. A. ElSeoud, and V. A. Woods in "Reaction Kinetics in Micelles" ed. by E. H. Cordes, p. 127, Plenum Press, New York, London (1973).
2) W. D. Bascom and C. R. Singleterry, *J. Colloid Sci.*, **13**, 569 (1958); S. Kaufman, *ibid.*, **17**, 231 (1962), *J. Colloid Interface Sci.*, **25**, 401 (1967); A. Kitahara in "Cationic Surfactants," ed. by E. Jungermann, Chap 8, Marcel Dekker Inc., New York (1970).
3) E. J. Fendler, J. H. Fendler, R. T. Medary, and V. A. Woods, *J. Amer. Chem. Soc.*, **94**, 7288 (1972).
4) J. H. Fendler, E. J. Fendler, and S. A. Chang, *ibid.*, **95**, 3273 (1973).
5) S. Friberg and S. I. Ahmad, *J. Phys. Chem.*, **75**, 2001 (1971), *J. Amer. Chem. Soc.*, **94**, 5196 (1972): F. M. Menger, J. H. Donohue, and R. F. Williams, *ibid.*, **95**, 286 (1973).
6) K. Kon-no, H. Mizuno, and A. Kitahara, *Nippon Kagaku Zassi*, submitted.
7) K. Kon-no and A. Kitahara, *J. Colloid Interface Sci.*, **37**, 469 (1971).
8) E. A. Guggenheim, *Phil. Mag.*, **2** 538 (1926).
9) A. S. N. Murthy, A. Balasubramanian, C. N. R. Rao, and T. R. Kasturi, *Can. J. Chem.*, **40**, 2267 (1962).
10) K. Kon-no, T. Jin-no, and A. Kitahara, *J. Colloid Interface Sci.*, **49** 383 (1974).

BULLETIN OF THE CHEMICAL SOCIETY OF JAPAN, VOL. 48(10), 2957—2958 (1975)

The Redox Acidity Function, R_0(H) in Glycols and Their Aqueous Mixtures

V. Srinivas Rao and C. Kalidas*

Department of Chemistry, Indian Institute of Technology, Madras-600 036, *India*

(Received February 3, 1975)

Synopsis. The variation of the redox acidity function, R_0(H), based on ferrocene redox couple has been studied at 25 °C as a function of solvent composition in diethylene glycol-water and ethylene glycol-water mixtures and compared with the H_0 variation in these solvents. Further, the redox function for sulfuric acid has been reported upto 6 molal in 50 wt% diethylene glycol-water mixture as the solvent.

The indicator acidity functions have been the most extensively studied[1] among the acidity functions. However, it has been well established in recent years,[1] that these functions are not satisfactory as an index of the proton activity of the medium as they are known to vary with the nature of the indicators employed in such measurements. Strehlow and Wendt[2] proposed an alternate acidity function, the redox function, R_0(H), based on redox systems of large size of the charge type, $0/1^+$, such as ferrocene couple. Although this function has been studied in aqueous solutions,[2] practically no measurements have been reported in non-aqueous media,[3] especially in amphiprotic solvents and their aqueous mixtures. In continuation of our earlier work[4-6] on this subject in glycolic solvents, the present investigation deals with a study of the variation of R_0(H) in diethylene glycol–water and ethylene glycol–water mixtures at 0.01 mol/kg perchloric acid as also the determination of R_0(H) for sulfuric acid in 50wt% diethylene glycol as solvent.

Experimental

The purification of ethylene and diethylene glycols has been described[4,7] elsewhere. Ferrocene (E. Merck) was sublimed twice under vacuum and the resulting pure orange crystals were employed. Perchloric acid (E. Merck, Proanalysi, 70 wt %) was used in measurements in aqueous mixtures involving variation of solvent composition while methanesulphonic acid (Fluka), purified by distillation, was used in the pure organic solvents. Aqueous SCE was the reference electrode in these studies. A.R. Sulfuric acid was used in measurements in 50 wt % diethylene glycol as solvent. Mercury, mercurous sulphate electrode was employed as the reference in these measurements.

The determination of R_0(H) function is based on the evaluation of the EMF of the cell.

$$\text{Pt, } H_2(\text{g, 1 atm})\,/\,\frac{\text{acid in the given solvent}}{}\,\frac{\text{FOC, FiC}^+}{(1:1)}\,/\,\text{Pt} \qquad (1)$$

in the solvent and water and was obtained by a combination of the polarographic $E_{1/2}$ of ferrocene *vs.* SCE or mercury, mercurous sulphate electrode as reference and the EMF of the hydrogen–calomel or hydrogen–mercury, mercurou sulphate cell using the same experimental solution for both the measurements. Further details of the determination of the EMF of the cell (1) are given[8] elsewhere.

Results and Discussion

The redox function, R_0(H), is defined by

$$R_0(\text{H}) = \frac{E_s - E^\circ_w}{2.303\,RT/F} \qquad (2)$$

where E_s refers to the EMF of the cell (1) in the solvent and E°_w is the standard EMF of the cell in water which has a value of +0.400 V at 25 °C as reported[2] earlier. The EMF's of cell (1) at 0.01 mol/kg perchloric acid in various diethylene glycol–water and ethylene glycol–water mixtures and the R_0(H) data in these media at 25 °C are recorded in Table 1. The H_0 data obtained in these solvents at 0.01 mol/kg perchloric acid according to the method described[4] previously, using *p*-nitroaniline as indicator are also recorded in this table for comparison.

Table 2 presents the EMF's of cell (1) and R_0(H) data at various molalities of sulfuric acid in 50 wt% diethylene glycol as solvent.

Assuming that the neutral component of the transfer free energy of ferricinium ion is equal to that of ferrocene and neglecting the small electrostatic transfer free energy of the ferricinium ion, which is justifiable in view of the larger size of ferricinium ion (r_{fic^+} = 3.3 Å,)[9] the R_0(H) can be related to the proton activity of the medium by

$$R_0(\text{H}) = -\log\,(m_{\text{H}^+}\,{}_w\gamma_{\text{H}^+}) \qquad (3)$$

where m_{H^+} is the molality of the H^+ ion and ${}_w\gamma_{\text{H}^+}$ is the activity coefficient of the same ion on the aqueous standard state. It is seen from Table 1 that R_0(H) increases continuously with increasing additions of diethylene glycol, passes through a maximum at about 90 wt% organic solvent and then decreases. A similar result is observed in ethylene glycol–water mixtures although the maximum occurs at 95 wt% organic solvent in this case. This implies that in both organic solvent–water mixtures the proton activity of the medium initially decreases, passes through a minimum at about 90—95 wt% organic solvent and then increases. Evaluation of the proton medium effect employing the ferrocene redox couple as reference in these solvents showed[8] a variation similar to R_0(H) and thus the basicity of the medium increases with increasing addition of the organic solvent at fixed acid concentration upto 90—95 wt% organic solvent and then decreases in the pure solvent, which can be explained on the basis of the structural theory of ion solvation proposed by Feakins and Watson.[10] It is also noted from Table 1 that R_0(H) and H_0 vary similarly in these solvent mixtures with good agreement in the composition of maximum basicity region in diethylene glycol–water mixtures while it is somewhat

* For correspondence.

Table 1. R_0(H) and H_0 data in diethylene glycol-water and ethylene glycol-water mixtures at 25° C

Wt % diethylene glycol	EMF of cell(1) in V	R_0(H)	H_0	Wt % ethylene glycol	EMF of cell(1) in V	R_0(H)	H_0[a]
20.00	0.5287	2.18	2.35	30.00	0.5456	2.47	1.15
40.00	0.5635	2.77	2.42	50.00	0.5608	2.72	1.25
50.00	0.5702	2.88	—	70.00	0.5872	3.16	1.25
60.00	0.5866	3.16	2.75	90.00	0.6017	3.41	1.10
80.00	0.6469	4.18	2.80	95.00	0.6431	4.11	—
90.00	0.6607	4.41	—	100.00	0.5895	3.22	0.00
95.00	0.6548	4.31	—	—	—	—	—
100.00	0.6348	3.97	1.09	—	—	—	—

a) At 0.1 molal HCl.

Table 2. R_0(H) of sulfuric acid in 50 wt% diethylene glycol at 25 °C

Molality of H_2SO_4	EMF of cell (1) in V	R_0(H)
0.1178	0.4644	1.09
0.2335	0.4251	0.43
0.4710	0.4107	0.18
1.00	0.3945	−0.09
2.00	0.3553	−0.76
3.60	0.3171	−1.40
6.00	0.2155	−3.12

poor in ethylene glycol–water mixtures, Further, R_0(H) is generally greater than H_0 at a given solvent composition (from the data in diethylene glycol–water mixtures), the difference being given by

$$R_0(\mathrm{H}) - H_0 = \log_{w}\left(\frac{\gamma_B}{\gamma_{BH^+}}\right) \quad (4)$$

where the γ_B and γ_{BH^+} represent the activity coefficients of the indicator base and its conjugate acid on the aqueous standard state. Equation (4) was checked in diethylene glycol–water mixtures by calculation of the activity coefficient ratio from the indicator data (unpublished results) on *p*-nitroaniline in these mixtures. For this purpose, the medium effect of the indicator was obtained from solubility measurements and that of its conjugate acid was realised through the application of the ferrocene assumption to the pK data on the indicator and fair agreement was indeed observed.

It is seen from Table 2 that R_0(H) of sulfuric acid in 50 wt% diethylene glycol decreases with increasing acid concentration indicating that the proton activity of the medium is enhanced with acid concentration. The R_0(H) of an aqueous sulfuric acid solution is more negative[2] than R_0(H) in 50 wt% diethylene glycol at a given acid concentration which shows that aqueous acid solutions have higher proton activity than those in 50 wt% diethylene glycol. This indicates that this solvent is more basic than water, a result in agreement[8] with the conclusions arrived from the proton medium effect in this solvent.

One of us (V.S.R.) thanks the C.S.I.R.(India) for the award of a Senior Research Fellowship.

References

1) C. H. Rochester, "Acidity Function," Academic Press, London (1970).
2) H. Strehlow and H. Wendt, *Z. Phys. Chem. N.F.*, **30**, 141 (1961).
3) J. Vedel, *Ann. Chim.*, **2**, 335 (1967).
4) C. Kalidas and S. R. Palit, *J. Chem. Soc.*, **1961**, 3998.
5) N. Chattanathan and C. Kalidas, *Aust. J. Chem.*, **24**, 83 (1971).
6) N. Chattanathan and C. Kalidas, This Bulletin, **43**, 1004 (1971).
7) C. Kalidas and V. Srinivas Rao, *J. Chem. Engg. Data*, **19**, 201 (1974).
8) V. Srinivas Rao and C. Kalidas, *Ind. J. Chem.*, in press.
9) D. Bax, C. L. de Ligny, and A. G. Remijnse, *Rec. Trav. Chim. Pays-Bas*, **91**, 965 (1972).
10) D. Feakins and P. Watson, *J. Chem. Soc.*, **1963**, 4686.

BULLETIN OF THE CHEMICAL SOCIETY OF JAPAN, VOL. 48(10), 2959—2960 (1975)

Hydration of Perchlorate Anion in Nitrobenzene by Means of Cryoscopic Measurements

Takao TARUI

Department of Chemistry, Faculty of Science, Hiroshima University, Hiroshima 730

(Received December 21, 1974)

Synopsis. By means of cryoscopic measurements, hydration of the perchlorate anion in nitrobenzene was examined and the value of the first hydration constant was determined.

Tris(1,10-phenanthroline)iron(II) chelate cation is well extracted into nitrobenzene with certain anions.[1] As the size of anions increases, extractability increases. At the same time, a small amount of water was found to be transferred into nitrobenzene accompanied by the anions.[2,3] However, it is not as yet clear whether or not the water molecule transferred with the ion pair is associated with the ions in the organic phase. Cryoscopic measurements were carried out in order to estimate the first hydration constant of the perchlorate anion. The results were compared with those obtained by isopiestic measurements.[4]

Experimental

Preparation of the crystal of tris(1,10-phenanthroline)-iron(II) perchlorate was carried out according to the method reported previously, and its purity was checked by analysis.[4] The crystal was dehydrated by heating at 120 °C for a day just before use. Nitrobenzene was purified by washing with concentrated sulfuric acid and water successively, then dried over anhydrous calcium chloride and filtered with a filter paper. The resulting product was distilled under reduced pressure.

An appropriate amount (85—425 mg) of $Fe(phen)_3(ClO_4)_2$ was added to 20 ml of nitrobenzene solution containing various amounts of water, the freezing point depression being measured with a Beckmann thermometer. Since moisture in the air seriously affects the measurements, the amount of water was checked before and after the cryoscopic measurements and necessary correction made. Stoichiometric concentration of water was determined by means of the Karl Fischer titration.

Results and Discussion

The cryoscopic constant determined by the use of water as a solute is 6.815. The value is similar to that reported previously.[5] Some authors pointed out the occurrence of self-association of water in nitrobenzene,[6,7] but we have ignored it since the concentration of water is very low. The mixture of water and tris(1,10-phenanthroline)iron(II) perchlorate shows a smaller freezing point depression than expected from the additivity, thus indicating the occurrence of association.

From conductivity measurements, the ion pair of tris(1,10-phenanthroline)iron(II) perchlorate is considered to be completely dissociated in nitrobenzene.[8] Moreover, the amount of water co-extracted into nitrobenzene decreased with the increase[2,3] in anion size. The water co-extracted into nitrobenzene is considered to be attached to anions.

Now let us consider the degree of hydration. Since the concentration of water is very low (below 0.05 mol/l), the concentration of highly hydrated species such as di- or tri-hydrated species is assumed to be negligibly small. The mean hydration number $\bar{n}$ is described as follows:

$$\bar{n} = \frac{[ClO_4\cdot H_2O]}{[ClO_4]+[ClO_4\cdot H_2O]} = \frac{\beta_1[H_2O]_f}{1+\beta_1[H_2O]_f} = \frac{[H_2O]_{total}-[H_2O]_f}{[M]}$$

or

$$\frac{\beta_1}{1+\beta_1[H_2O]_f} = \frac{[H_2O]_{total}-[H_2O]_f}{[H_2O]_f}\cdot\frac{1}{[M]} \quad (1)$$

where $[M]=2\,[Fe(phen)_3^{2+}]=[ClO_4]$, and β_1 denotes the first hydration constant. Strictly speaking, the depression of freezing point at a certain concentration of salt might not be the linear function of the concentration of water. However, as a first approximation, the concentration of free water not associated with the perchlorate ion can be represented by the use of an apparent cryoscopic constant. The approximation is equivalent to the description that the amount of hydrated water is proportional to the stoichiometric concentration of water, and is considered to be valid from the data relating to the change of mean hydration number with free water. $[H_2O]_{total}/[H_2O]_f$ can thus be represented by K_f/K_1, where K_f is the cryoscopic constant of nitrobenzene and K_1 the apparent cryoscopic constant of nitrobenzene containing salts. Substituting the above relation into Eq. (1) we have

$$\frac{\beta_1}{1+\beta_1[H_2O]_f} = \frac{K_f-K_1}{K_1}\cdot\frac{1}{[M]}$$

If we assume that $\beta_1[H_2O]_f$ is negligibly smaller than unity, we get the following equation.

$$\frac{K_f-K_1}{K_1}\cdot\frac{1}{[M]} = \beta_1 \quad (2)$$

The results calculated by means of Eq. (2) are given in Table 1. Measurements were carried out at tem-

Table 1. Hydration constants of the perchlorate ion in nitrobenzene

M	K_1	β_1
0.00498	6.49 ±0.12	5.1±2.9
0.00999	6.270±0.094	4.5±1.4
0.0151	6.068±0.095	4.2±1.0
0.0257	5.493±0.204	4.7±1.1

peratures near 5.5 °C, the term β_2 being neglected in the treatment of data. The values of β_1 estimated at different concentration of salt are similar to each other, a mean value 4.5 being obtained within experimental errors. The constant β_1 was determined to be 1.5 ± 0.1 from the isopiestic study,[4] where the measurements were carried out at 25 °C. The results seem to be reasonable, when we take the difference of conditions of the two experiments into consideration. We can conclude that all the excess water transferred by the solvent extraction of ion pair is hydrated to the anions. This indicates that the water molecule is chemically bound to the perchlorate ion in nitrobenzene phase.

The author would like to thank Professor Yuroku Yamamoto for his helpful discussion and comments.

References

1) Y. Yamamoto, T. Tarumoto, and E. Iwamoto, *Chem. Lett.*, **1972**, 255.
2) Y. Yamamoto, T. Tarumoto, and T. Tarui, *ibid.*, **1972**, 459.
3) Y. Yamamoto, T. Tarumoto, and T. Tarui, This Bulletin, **46**, 1466 (1973).
4) T. Tarui, *J. Inorg. Nucl. Chem.*, **37**, 1213 (1975).
5) W. E. S. Turner and C. T. Pollard, *J. Chem. Soc.*, **1914**, 1751.
6) L. Ödberg and E. Hogfeldt, *Acta Chem. Scand.*, **23**, 1330 (1969).
7) J. R. Johnson, S. D. Christian, and H. E. Affsprung, *J. Chem. Soc.*, **1967**, 1924.
8) Y. Yamamoto, E. Sumimura, K. Miyoshi, and T. Tominaga, *Anal. Chim. Acta*, **64**, 225 (1973).

BULLETIN OF THE CHEMICAL SOCIETY OF JAPAN, VOL. 48(10), 2961—2962 (1975)

An Equilibrium Study of the Formation of Mixed-Ligand Nickel(II)–Aminopolycarboxylate Complexes

Mutsuo KODAMA

Department of Chemistry, College of General Education, Hirosaki University, Bunkyo, Hirosaki 036

(Received March 22, 1975)

Synopsis. The equilibria for the formation of 1 : 1 : 1 ratio mixed-ligand complexes of nickel(II)–NTA, HIDA, and -ethylenediamine-*N*,*N*′-diacetate (EDDA) complexes with the glycinate (Gly), glutamate (Glut), and aspartate (Asp) anions were studied by determining the effects of the Gly, Glut, and Asp anions on the rates of the substitution reactions of nickel(II)–NTA, -HIDA, and -EDDA complexes with EDTA-OH or DTPA.

Recently the importance of the formation of mixed-ligand complexes has been recognized, and a large number of studies have been carried out for a better understanding of the mixed-ligand complex formation.[1–3] The present author has also studied the equilibria for the formation of mixed-ligand complexes between ammonia and metal (II)-aminopolycarboxylate complexes.[4,5] In this paper, the mixed-ligand complex formation equilibria between the nickel(II)–aminopolycarboxylate complexes and the Gly, Glut, and Asp anions will be studied by investigating their effects on the rates of the substitution reactions of nickel(II)–aminopolycarboxylate complexes.

Experimental

Reagents. The EDDA, NTA, Glut, Gly, Asp, EDTA-OH, and DTPA used in this study were recrystallized as their acids from their aqueous solutions. The preparation and recrystallization of the acid form of HIDA were described previously.[6] The other chemicals used were of analytical reagent-grades and were used without further purification.

Apparatus and Experimental Procedures. The polarographs and the dropping mercury electrode (DME) used for the measurement of the DC current-voltage curves and the current-time curves were the same as those described previously.[6,7] The pH of the solution was measured with a glass electrode in combination with a pH meter (Hitachi-Horiba Model F-7). All the experimental procedures used in the kinetic study have been described previously.[8] In this study, all the measurements were conducted in solutions with an ionic strength of 0.30 ($NaClO_4$) at 25 °C. No buffer reagent was used, because the sample solutions always contained a large excess of uncomplexed aminopolycarboxyfate and had a sufficient buffer capacity in the pH range studied ($9.00<pH<10.00$). The reaction rates were determined by observing the change in the dissolution wave due to the uncomplexed DTPA or EDTA-OH under the experimental conditions where all the reactions could be treated as pseudo first-order reactions. The forward apparent rate constant, k_{ap}, was determined from the slope ol the linear relation between log (i_0/i_t) and time, t.[9]

Results and Discussion

Previously,[7] the present author reported that the rate of the reaction of EDTA with the nickel(II)–EDDA complex is reduced appreciably by the addition of Gly; he ascribed this to the formation of a mixed-ligand complex involving the Gly anion. As in the case of the EDTA reaction with the nickel(II)–EDDA complex in the presence of the Glut or Asp anion also gave a k_{ap} value which was independent of the concentrations of the uncomplexed DTPA and EDDA, but proportional to the total concentration of the nickel(II) ion$[Ni(II)]_t$. Furthermore, the Glut and Asp anions reduced the reaction rate and the plot of k_{ap}^{-1} against the uncomplexed Glut or Asp concentration, $[A^{m-}]$, invariably gave a straight line, with an intercept of a finite value (Fig. 1). In view of the conclusion obtained in the EDTA reaction with the nickel(II)–EDDA complex in the presence of the Gly anion, these findings suggest that the Glut and Asp anions also form a 1 : 1 : 1 ratio mixed-ligand complex with the nickel(II)–EDDA complex and that the rapid dissociation of the Glut or Asp anion from the mixed complex precedes the slow reaction of the DTPA anion with the 1 : 1 ratio nickel(II)–EDDA complex. Thus, the k_{ap} at a given pH should be given by the following relation:

$$k_{ap} = k\cdot[Ni(II)]_t/(1+K^{A}_{MxA}\cdot[A^{m-}]) \quad (1)$$

where K^{A}_{MxA} means the equilibrium constant for the formation of a mixed-ligand complex from the nickel-(II)–EDDA complex and the Glut or Asp anion. Therefore, the K^{A}_{MxA} value can be determined from

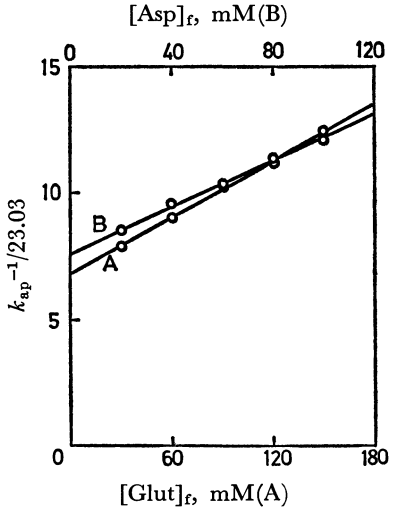

Fig. 1. The plot of the reciprocal of k_{ap} for the reaction of nickel(II)–EDMA complex with DTPA against the concentrationof uncomplexed Gly or Asp.
$\mu=0.30$, 25 °C, pH=9.35, $[DTPA]_l=1.0$ mM
$[EDDA]_f=10.0$ mM, $[Ni(II)]_t=10.0$ mM
A) $[Gly]_f$ ranged from 30 to 150 mM.
B) $[Asp]_f$ ranged from 20 to 100 mM.

the ratio of the slope to the intercept of the linear relation between k_{ap}^{-1} and $[A^{m-}]$. Although no experimental result is shown here, k in Eq. (1) could be determined to be $(k_\alpha+k_\beta\cdot[H^+])/(\alpha_H)_Y$[9] from a systematic investigation of the pH effect on the reaction rate. The K^A_{MXA} values obtained from the slope and intercept of the linear relation in Fig. 1 are listed in Table 1, together with that for the EDDA~Gly system.[7] The reactions of DTPA with the nickel(II)–NTA complex and of EDTA-OH with the HIDA complex in solutions containing the Gly, Glut, or Asp anion also showed kinetic profiles quite similar to that of the DTPA reaction with the nickel(II)-EDDA complex in the presence of Glut or Asp. In these reactions, the reaction rates of the Gly, Glut, and Asp anions were also appreciably reduced, and the plot of k_{ap}^{-1} *versus* the concentration of the Gly, Glut or Asp anion, $[A^{m-}]$ at a given pH invariably gave a straight line with an intercept of a finite value. A typical result obtained for the Asp system is reproduced in Fig. 2. In the light of the coordination natures of the nickel(II) ion and the NTA and HIDA anions, the above fact also suggests the formation of a 1 : 1 : 1 ratio mixed-ligand complex involving the Gly, Glut, or Asp anion, which is in a rapid equilibrium with the 1 : 1-ratio NTA or HIDA complex involved in the rate-determining steps. With the NTA and HIDA anions, the nickel(II) ion forms a 1 : 2 ratio complex. Therefore, the k_{ap} value for the NTA and HIDA systems should be given by $[Ni(II)]_t\cdot k/(1+K_2'\cdot[X]_f+K^A_{MXA}\cdot[A^{m-}])$ in place of Eq. (I). Here, K_2' denotes the conditional second successive formation constant of the nickel(II)–NTA or –HIDA complex, and $[X]_f$, the concentration of uncomplexed NTA or HIDA. Then, the K^A_{MXA} values for the NTA and HIDA systems were determined from the ratio of the slope to the intercept of the linear relation between k_{ap}^{-1} and $[A^{m-}]$, with the aid of the $K^A_{MXA}=(1+K_2'\cdot[X]_f)\times$slope/intercept relation. In the case of the HIDA system, no confirmative evidence which suggests the formation of a mixed-ligand complex involving the Gly anion could be obtained under the present experimental conditions. The K^A_{MXA} values obtained for the NTA and HIDA systems are also listed in Table 1. In all the systems studied in this paper, the K^A_{MXA} values determined at various solution pH's showed a satisfactory agreement with each other.

Table 1. The K^A_{MXA} values (μ=0.30, 25 °C)

System	log K^A_{MXA}	System	log K^A_{MXA}
EDDA-NH_3	1.62[11]	NTA-Gly	3.68
EDDA-Gly	1.12[8]	NTA-Glut	3.57
EDDA-Glut	1.32	NTA-Asp	3.92
EDDA-Asp	1.30	HIDA-Glut	4.84
		HIDA-Asp	4.86

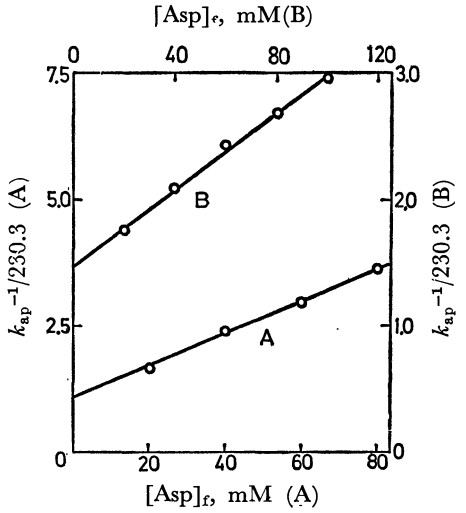

Fig. 2. The effect of aspartate on the rates of the reactions of the nickel(II)-NTA complex with DTPA and of the nickel-HIDA complex with EDTA-OH. μ=0.30, 25 °C, $[Asp]_f$ ranged from 20 to 100 mM
A) NTA system pH=9.73, $[NTA]_f$=20.0 mM $[Ni(II)]_t$=10.0 mM, $[DTPA]_l$=1.0 mM.
B) HIDA system pH=9.58, $[HIDA]_f$=28.0 mM $[Ni(II)]_t$=6.0 mM, $[EDTA\text{-}OH]_l$=0.6 mM.

Ho *et al.*[10] reported in their NMR study of mixed 1 : 1 : 1 EDDA complexes of the nickel(II) ion with the Glut and Asp anions that the mixed-ligand complex has the trans-form, and that the Glut and Asp anions in the complex are bonded to the nickel(II) ion through the glycinate chelate ring. The finding that the K^A_{MXA} value for the Gly~EDDA system is nearly identical with those for the Glut~ and Asp~ EDDA systems may support their conclusion. As is shown by the data in Table 1, the K^A_{MXA} values for the Gly, Glut, and Asp systems are slightly smaller than that for the 1 : 1 : 1 mixed complex of ammonia.[11] This is probably ascribable to the unfavourable entropy change due to the formation of the charged mixed complex from the neutral parent complex. The mixed 1 : 1 : 1-ratio NTA and HIDA complexes with the Gly, Glut, and Asp anions also have almost the same K^A_{MXA} values. This may also indicate that all three aminoacid anions in the mixed-ligand complex coordinate to the nickel(II) ion through a Gly chelate ring.

References

1) Ya. D. Fridman. Dzh. S. Sarbaev, and R. I. Sarochan, *Zh. Neorg. Khim.*, **5**, 791 (1960).
2) S. Kida, This Bulletin, **34**, 962 (1961).
3) A. E. Martell and L. G. Sillén, "Stability Constants of Metal-Ion Complexes," 2nd Ed., The Chemical Society, London (1964).
4) M. Kodama and K. Miyamoto, This Bulletin, **42**, 833 (1969).
5) M. Kodama and K. Miyamoto, *ibid.*, **42**, 1596 (1969).
6) M. Kodama, K. Namekawa, and T. Horiuchi, *ibid.*, **47**, 2011 (1974).
7) M. Kodama, *ibid.*, **47**, 1434 (1974).
8) M. Kodama, *ibid.*, **42**, 2532 (1969).
9) M. Kodama, S. Karasawa, and T. Watanabe, *ibid.*, **44**, 1815 (1971).
10) F. F. -L. Ho, L. E. Erickson, S. R. Watkins, and C. N. Reilley, *Inorg. Chem.*, **9**, 1139 (1970).
11) N. E. Jackobs and D. W. Margerum, *ibid.*, **6**, 2038 (1967).

BULLETIN OF THE CHEMICAL SOCIETY OF JAPAN, VOL. 48(10), 2963—2964 (1975)

The Solubilities and the Solubility Parameter of Heptasulfur Imide

Shuichi HAMADA, Yoshiyuki KUDO, and Masako KAWANO

Department of Chemistry, Faculty of Science, Science University of Tokyo, Kagurazaka, Shinjuku-ku, Tokyo 162

(Received March 31, 1975)

Synopsis. The solubilities of heptasulfur imide in eleven organic solvents were measured. The solubility parameter of heptasulfur imide was estimated to be 12.$_7$ at 25 °C from the solubilities and the activity deduded from the enthalpy of the fusion; we assumed the solutions to be regular.

The structure of heptasulfur imide, S_7NH, closely resembles that of cycloocta-sulfur; one of the sulfur atoms in it is, however, replaced by an NH group.[1] Only a few solubilities of heptasulfur imide have been reported—for example, those for carbon disulfide[2] and carbon tetrachloride.[3] In this work, the solubilities and the solubility parameter of this compound will be estimated.

Experimental

Materials. The heptasulfur imide was prepared by the method described by Heal;[4] the disulfur dichloride was reacted with an ammonia at −10 °C by passing the ammonia into its dimethylformamide sulution. A crude product wa; extracted with an ethyl ether, and then the heptasulfur imide was isolated chromatographically from the by-products by using a silica-gel column. The pure heptasulfur imide was obtained as pale yellow crystals by recrystallization from a benzene solution. Eleven organic solvents were used to estimate the solubilities, as Table 1 shows. All the solvents were purified in the usual ways.

Procedure. Suitable amounts of the heptasulfur imide and an organic solvent were put into a three-necked flask and were then stirred continuously for 2 hr at the temperature range from 20 to 40 °C (from 10 to 30 °C for the *n*-pentane), with a precision of ±0.03 °C. An aliquot of the solution was withdrawn through a fine Teflon tube with a glass filter by applying excessive pressure in the flask. The concentration of the solution was estimated from its optical absorbances at the range from 320 to 365 nm, after the solution has been diluted to a suitable concentration. The molalities of the solutions were estimated by using the working curves for the respective solvents previously determined by means of a double-beam spectrophotometer, model UV-200, from Shimadzu Seisakusho. The solubility was estimated repeatedly (at least three times) under the same conditions; its deviation from the average value was less than ±1.5%. The partial molar volume of the heptasulfur imide was estimated from the benzene solutions at 25 °C with a precision of ±0.01 °C by using a modified Lipkin-Davison-type pycnometer. The molar enthalpy of the fusion of the heptasulfur imide was estimated with a differential scanning calorimeter, model DSC-1B, from Perkin-Elmer. The enthalpy of the fusion was calibrated by using that of a metallic indium (0.781 kcal/mol at 156 °C).

Results and Discussion

The heptasulfur imide was isolated chromatographically three times because it could not be completely separated from the by-products by only one run. The X-ray powder diffractogram[1] and the IR spectrum[5] of the sample showed patterns attributable to heptasulfur imide only. The melting point of the sample was determined microscopically to be 113.5 °C; this value agreed with that of the purified heptasulfur imide.[6]

The solubilities, X_2 (mole fraction), at 25 °C of the heptasulfur imide in various solvents are shown in Table 1. The logarithms of the mole fractions in the saturated solutions for the respective solvents showed good linearities against the reciprocals of the absolute temperatures except for those in the acetone solution. The enthalpies of solution, ΔH^d, were estimated from the linear relationship between $\log X_2$ and $1/T$ with an accuracy of ±0.1 kcal/mol, as Table 1 shows. The solubility of the heptasulfur imide decreased abruptly with an increase in the enthalpy of solution except for that in the methanol. Though the solubilities for the acetone at 20 and 30 °C were estimated to be 1.3×10^{-2} and 1.8×10^{-2} respectively, the sulfur was detected as a decomposition product in the solution at 40 °C by means of thin-layer chromatography.

TABLE 1. SOLUBILITIES, ENTHALPIES OF SOLUTION, AND SOLUBILITY PARAMETERS OF HEPTASULFUR IMIDE AT 25 °C

Solvent	X_2 ($\times10^3$)	ΔH^d kcal/mol	δ_1[a]	δ_2
Methanol	4.1	5.7		
n-Pentane	0.45	7.7	7.1	12.$_4$
n-Hexane	0.67	7.9	7.3	12.$_4$
n-Heptane	0.81	7.8	7.5	12.$_5$
Cyclohexane	2.0	7.3	8.2	12.$_8$
Cyclooctane	4.3	7.3	8.55	12.$_7$
Benzene	14	6.4	9.15	12.$_7$
Toluene	18	5.9	8.9	12.$_3$
Chlorobenzene	14	6.3	9.5	13.$_0$
Chloroform	9.6	6.4	9.3	13.$_0$
Carbon tetrachloride	3.8	7.3	8.6	12.$_9$

a) The solubility parameters of the solvents, δ_1, were those at 25 °C.[7]

Therefore, the data are not presented in Table 1. The absorption peaks in the UV spectra of the heptasulfur imide were observed at approximately 270 and 225 nm in all the solvents except for those with strong absorption bands near 270 and 225 nm. The UV spectra of the heptasulfur imide in all the solvents did not change over a period of three days, while the color of the acetone solution at 40 °C turned light yellow.

If it is assumed that these solutions are regular solutions,[7] the following equation can be obtained:[8]

$$RT\ln a_2 = RT\ln X_2 + V_2\phi_1^2(\delta_1-\delta_2)^2 \quad (1)$$

where a_2 is the activity of the solute based on its supercooled liquid state at a given temperature; V_2, the molar volume of the solute in the liquid state; ϕ_1, the volume fraction of the solvent; δ_1 and δ_2, the solubility parameters of the solvent and the solute, and R, the gas constant. The activity of the solute can be calculated by means of the following equation:[7]

$$\ln a_2 = -\frac{\Delta H^f}{R}\left(\frac{T_f - T}{T_f T}\right) \quad (2)$$

where ΔH^f is the molar enthalpy of the fusion, and T_f, the melting point of the solute.

The molar enthalpy of the fusion of the heptasulfur imide was estimated to be 4.5 kcal/mol at its melting point by using the differential scanning calorimeter. The activity of the heptasulfur imide was calculated to be approximately 1.8×10^{-1} at 25 °C. The molar volume, V_2, of the heptasulfur imide in the supercooled liquid state was deduced from the partial molar volume (127 cm^3/mol), which was itself estimated from the benzene solutions at 25 °C.

By using the values of a_2, X_2, V_2, ϕ_1, and δ_1,[7] the solubility parameter, δ_2, of the heptasulfur imide at 25 °C was calculated from Eq. (1); the results are shown in Table 1.

The solubility parameter of the heptasulfur imide at 25 °C was estimated to be $12._7$ as an average value. This value agreed with that of cyclooctasulfur (12.7).[9]

References

1) J. Weiss, *Z. Anorg. Allgem. Chem.*, **305**, 190 (1960).
2) H. G. Heal, *Nature*, **199**, 371 (1963).
3) M. Goehring, "Ergebnisse und Probleme der Chemie der Schwefelstickstoffverbindungen," Akademie-Verlag, Berlin (1957), p. 57.
4) H. G. Heal and J. Kane, "Inorganic Syntheses," Vol. XI, ed. by W. L. Jolly *et al.*, McGraw-Hill, New York (1968), p. 184.
5) J. Nelson, *Spectrochimica*, **27A**, 1105 (1971).
6) H. Tavs, J. Schultze-Steinen, and J. E. Colchester, *J. Chem. Soc.*, **1963**, 2555.
7) J. H. Hildebrand and R. L. Scott, "The Solubility of Nonelectrolytes," Dover Publications, New York (1964), p. 66.
8) J. H. Hilderbrand and R. L. Scott, *ibid.*, p. 270.
9) J. H. Hildebrand and R. L. Scott, *ibid.*, p. 280.

BULLETIN OF THE CHEMICAL SOCIETY OF JAPAN, VOL. 48(10), 2965—2966 (1975)

Kinetic Studies of the Electron Transfer Reaction in Iron(II) and Iron(III) Systems. VII. The Electron Transfer Reaction in Solid Dimethyl Sulfoxide[1]

Goro WADA and Mikiko TABIRA

Department of Chemistry, Nara Women's University, Nara 630

(Received March 31, 1975)

Synopsis. The electron transfer reaction between Fe(II) and Fe(III) in dimethyl sulfoxide (DMSO) was investigated in the solid phase, and compared with the case in the liquid. In the temperature range between the freezing point (T_M) and the eutectic point (T_E), the reaction actually proceeds in the liquid phase where the reactants are concentrated due to the partial separation of pure DMSO solid, while below T_E the reaction occurs in the solid phase at considerable reaction rates, with a lower activation energy, 4 kcal/mol, than that in the liquid. This indicates a different probable mechanism in solid DMSO.

It has been proved that the electron transfer reaction between iron(II) and iron(III), Fe(II)+*Fe(III)=Fe(III)+*Fe(II), in aqueous media in the absence of catalytic ligand proceeds *via* a hydrogen atom transfer mechanism through a Grotthuss type conduction along the extended chains of the hydrogen bonds between the oriented solvent molecules.[2-4] As one proof of this mechanism, the occurrence of the reaction in solids of protic solvents was observed in the cases of ice[5-7] and of very concentrated perchloric acid,[8] although the reactants are frozen with no freedom of translational mass transfer in the solids of such media.

Dimethyl sulfoxide (DMSO) is typical of the aprotic solvents for which the hydrogen atom transfer mechanism is difficult. In fact, the reaction was shown to proceed not *via* the hydrogen atom transfer but rather *via* an inner-sphere mechanism in liquid DMSO.[9-11] Consequently, it seems to be of interest to test whether the reaction can proceed in solid DMSO or not.

Experimental

The procedure of determination of the rate constant was similar to that already described,[9-11] except for several points indicated below. Soon after the initiation of the reaction by mixing the two solutions of iron(II) and ^{59}Fe-labeled iron(III), equal amounts of the reaction solution were quickly delivered into eight glass tubes of the same shape and size in a thermostat at 20 °C, followed by simultaneous cooling to −78 °C. The solutions were solidified within several seconds at this temperature. Then the tubes were set in a bath at a fixed reaction temperature. The reaction temperatures adopted were −28, −48, −68, and −78 °C, which were attained by freezing mixtures of dry-ice with carbon tetrachloride, chloroform, or ethanol, according to the temperature adopted. At appropriate time intervals, one of the tubes was taken out of the bath and the quenching solution was quickly added. It took only about twenty seconds to complete dissolving the solid and quenching the reaction by using a vibrator. The concentration of perchloric acid was always 0.005 M.

For the sake of simplicity, the phase diagram of the binary system $Fe(ClO_4)_3$+DMSO was studied in the very low concentration range of $Fe(ClO_4)_3$.

Results and Discussion

As have been seen in the liquid system, McKay's plots of $\log(x_e-x)$ against time in the solid phase were also linear: here x and x_e stand for the specific radioactivities of iron(II) at reaction time t and at infinite time, respectively.[12] Thus, the rate constant k of the electron transfer reaction can be obtained from the half period of the reaction $t_{1/2}$.

$$k = \frac{0.693}{([Fe(II)]+[Fe(III)])t_{1/2}} \quad (1)$$

The Arrhenius plot of log k against reciprocal temperature is drawn in Fig. 1. The activation energy in the liquid phase is E_{liq}=9.2 kcal/mol, which is in agreement with the values in the literature.[9,11] On the other hand, the activation energy obtained from the temperature range of the solid state appears to be approximately E_{solid}=4 kcal/mol, which is much smaller than E_{liq}.

The phase diagram of the $Fe(ClO_4)_3$–DMSO binary system in the low concentration range of $Fe(ClO_4)_3$ is shown in Fig. 2. When a liquid DMSO solution of $Fe(ClO_4)_3$ at low concentration is continuously cooled, it reaches its freezing point, T_M, below which an equilibrium between pure solid DMSO and concentrated liquid solution is established. As the cooling goes on, the liquid phase becomes more concentrated with $Fe(ClO_4)_3$ due to the progressive separation of solid DMSO, until the system arrives at the eutectic temperature, T_E, approximately −45±3 °C, where the concentrated solution itself freezes as a solid solution.

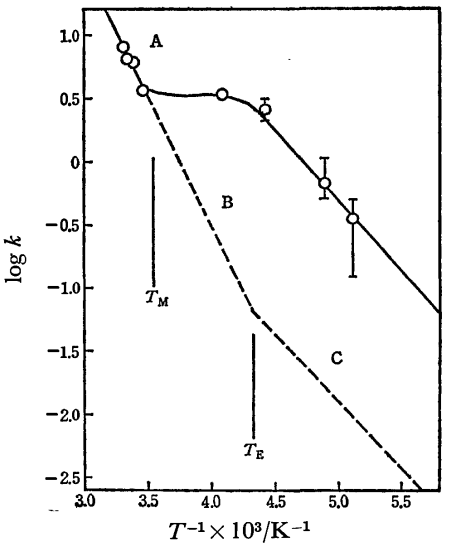

Fig. 1. Arrhenius plot for liquid and solid phase reaction,

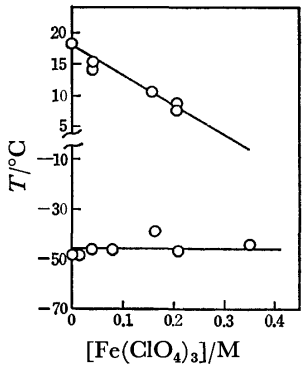

Fig. 2. Phase diagram of $Fe(ClO_4)_3$-DMSO binary system.

In the present reaction system, the phase diagram must be more complicated than this, but the fundamental tendency appearing in this simple system would be similarly valid: the concentration phenomenon of the dissolved species in the liquid phase and the eutectic freezing of the concentrated liquid would also occur.

At temperatures between T_M and T_E, the reaction system is a heterogeneous mixture of liquid solution and solid DMSO, and the reaction takes place only in the liquid phase, where the reactants are concentrated according to the reaction temperature. This results in an apparent increase in k, because the true [Fe(II)] and [Fe(III)] in the concentrated liquid phase must be larger than those used in Eq. (1). When the apparent and the true rate constants are denoted by k and k_0 respectively, k is apparently enlarged by a factor of p.

$$k = p\,k_0 \qquad (2)$$

The lower the temperature, the larger the p value. In Fig. 1, the straight line above T_M (A) is extrapolated into the T_M-T_E range, where the liquid phase reaction still continues to occur with an unchanged activation energy E_{liq}. Consequently, this extended straight line (B) gives the corrected true rate constant k_0 at the respective temperatures.

At temperatures below T_E, the reaction occurs truely in the solid phase, where p no longer varies with temperature but is a constant. Thus, another straight line (C) can be drawn in parallel with the observed one with an equal slope corresponding to E_{solid}, as is done by the broken line in Fig. 1. From the vertical shift of the straight line C from the apparent one, the p value below T_E could be roughly estimated as p=40.

Since the glass tubes containing the reaction solution were cooled far below the eutectic point as quickly as possible, the geometric sizes of the crystalline particles of both pure DMSO and solid solution might be very small, and it is likely that there remains some local heterogeneity of concentration of the reactants and that heterogeneous catalysis on the mosaic interfaces between the solid particles may affect the reaction rate. However, if the probabilities of these heterogeneous effects are small and the reaction is simply supposed to occur homogeneously in the solid phase, the averaged distance between iron(II) and iron(III) is calculated to be about 50 Å in our present case. Since in the solid phase the medium is too viscous for the reactants to diffuse so that the electron transfer reaction may proceed not through the migration of the reactants carrying electrons but through the tunnelling of electrons for long distances over several medium molecules. The extension of wave functions of the electrons is suitable for such a transfer.[13] In such a case, the low activation energy observed as E_{solid} to be 4 kcal/mol would seem to be reasonable.

In the case of aqueous media, the reaction mechanism is the same indifferent to whether in the liquid or in ice: *via* the hydrogen atom transfer along the bridges of the hydrogen bonds between water molecules. Therefore, the activation energy is also the same for both phases.[5,6] On the other hand, in the case of DMSO, the reaction mechanism must differ in going from liquid to solid, with a consequent variation in the activation energies.

According to our present study, the true rate constant of the reaction in solid DMSO at −78 °C is approximately of the order of $10^{-2}\,M^{-1}\,s^{-1}$, which roughly coincides with $7\times10^{-3}\,M^{-1}\,s^{-1}$ in a liquid mixed solvent of water : DMSO=3 : 2,[14] although the reaction mechanisms might be completely different from each other. At any rate, looking at the cases of aqueous, aqueous-DMSO, and pure DMSO media together, one problem yet remains unsolved: whether electrons can be transferred not only *via* the hydrogen atom transfer mechanism but also *via* an alternative mechanism, probably *via* electron tunneling over a considerably long distance.

References

1) Part VI of this series: G. Wada, Y. Sahira, K.Ohsaki, and F. Shinoda, This Bulletin, **47**, 851 (1974).
2) R. W. Dodson and N. Davidson, *J. Phys. Chem.*, **56**, 855 (1952).
3) W. L. Reynolds and R. W. Lumry, *J. Chem. Phys.*, **23**, 2460 (1955).
4) R. A. Horne and E. H. Axelrod, *ibid.*, **40**, 1518 (1964).
5) R. A. Horne, *J. Inorg. Nucl. Chem.*, **25**, 1139 (1963).
6) E. Nitzan and A. C. Wahl, *ibid.*, **28**, 3069 (1966).
7) M. Komor, A. Vertes, I. Deszi, and I. Ruff, *Proc. Conf. Appl. Mössbauer Eff.*, **1969**, 713; *idem.*, *Acta Chim.* (Budapest), **66**, 285 (1970); *idem.*, *Magy. Kem. Foly.*, **76**, 402 (1970).
8) D. L. Baulch, F. S. Dainton, D. A. Ledward, and H. Sugier, *Trans. Faraday Soc.*, **62**, 2200 (1966).
9) J. Menashi, W. L. Reynolds, and G. Van Auken, *Inorg. Chem.*, **4**, 299 (1965).
10) G. Wada and W. L. Reynolds, *ibid.*, **5**, 1354 (1966).
11) G. Wada, N. Yoshizawa, and Y. Sakamoto, This Bulletin, **44**, 1018 (1971).
12) H. A. C. McKay, *Nature*, **142**, 997 (1938).
13) W. F. Libby, *J. Phys. Chem.*, **56**, 863 (1952).
14) M. S. Henry and W. L. Reynolds, *Int. J. Chem. Kin.*, **4**, 37 (1972).

BULLETIN OF THE CHEMICAL SOCIETY OF JAPAN, VOL. 48(10), 2967—2968 (1975)

The Responses of the Monovalent Cation-sensitive Glass Electrode to the Cationic Activities in Different Solvents

Toshio NAKAMURA

Chemistry Department, Faculty of Science, Shinshu University, Asahi, Matsumoto 390

(Received April 9, 1975)

Synopsis. The responses of the glass electrode to the cationic activities in different solvents have been studied for several monovalent cations in several dipolar aprotic and protic solvents by comparing the potentials of the amalgam electrode with those of the glass electrode.

The Nernstian responeses of cationic glass electrodes to cations in partially aquated solvents[1,2] and in non-aqueous systems[1,3,4] have been well established. Cations are known to have quite different activities according to the solvent in which they are dissolved, and there have been some investigations in methanol[1] and hydro-organic madia[5] which confirm that the cationic glass electrodes can also respond to such a solvent effect on the cationic activities. In the present report, the potentials of the monovalent cation-sensitive glass electrode immersed in solutions of various monovalent cations were compared, in a variety of solvents, with the potentials of the corresponding amalgam or metal electrodes. To carry this out, the emf's of the following two cells were measured:

$$\text{Glass electrode} \mid \underset{(A)}{10^{-2}\,\text{M}\ \text{Et}_4\text{NClO}_4,\ x\text{M}\ \text{M}^+\text{ClO}_4^-\ (\text{D})} \parallel_{J_1} \underset{(B)}{0.1\,\text{M}\ \text{Et}_4\text{NClO}_4\ (\text{AN})} \parallel \underset{(C)}{5\times10^{-3}\,\text{M}\ \text{AgNO}_3\ (\text{AN})} \mid \text{Ag}$$

Cell I

$$\text{M(Hg)}^* \mid \underset{(A)}{10^{-2}\,\text{M}\ \text{Et}_4\text{NClO}_4,\ x\text{M}\ \text{M}^+\text{ClO}_4^-\ (\text{D})} \parallel_{J_2} \underset{(B)}{0.1\,\text{M}\ \text{Et}_4\text{NClO}_4\ (\text{AN})} \parallel \underset{(C)}{5\times10^{-3}\,\text{M}\ \text{AgNO}_3\ (\text{AN})} \mid \text{Ag}$$

Cell II

(* Ag wire for $M^+=Ag^+$)

In these cells, D shows such solvents as 1,2-dichloroethane (DCE), acetonitrile (AN), propylene carbonate (PC), methanol, water, dimethylformamide (DMF), and dimethyl sulfoxide (DMSO), and M^+, such monovalent cations as lithium, sodium, potassium, cesium, thallium, and silver ions. The concentrations of $M^+ClO^-_4$ in the compartments (A) are shown in Table 1. It should be noted that the salt bridge (B) and the reference electrode (C) in Cells I and II are always the same as each other.

TABLE 1.

	Concentration of metal in amalgam (M)	Concentration of the ion[a] in Cells I and II[b]; x values
Lithium	6.58×10^{-2}	1.00×10^{-3}
Sodium	3.02×10^{-2}	1.00×10^{-3}
Potassium	2.25×10^{-2}	5.000×10^{-4}
Cesium	1.03×10^{-2}	5.000×10^{-4}
Thallium	1.84×10^{-2}	5.00×10^{-4}
Silver	Wire	1.00×10^{-4}

a) When the solvent was DCE, saturated solution of each ion was used, and methanol solution of the cesium ion was also saturated solution. b) See text.

Experimental

Apparatus. The glass electrode was a Beckman 39047. The constructions of the cell and the amalgam electrodes have been described previously.[6,7] The reference electrode was a silver wire immersed in 5×10^{-3} M silver nitrate in AN. The salt bridge consisted of 0.1 M tetraethylammonium perchlorate in AN instead of the 0.1 M tetraethylammonium picrate in AN used in the previous report.[6,7] Except when the D solvent was water, the junction potentials of J_1 and J_2 changed by only several millivolts upon the change in the salt bridge electrolyte.[8] When the D solvent was water, the change in the junction potential was somewhat larger. The test solution in Cell II were deoxygenated by bubbling in nitrogen gas. The metal contents in the amalgams were determined titrimetrically: the amalgams were decomposed in an excess of a 0.1 M perchloric acid solution, and then the excess acid was titrated with a standard sodium carbonate solution. For the emf measurements, a Hitachi-Horiba pH meter, model F-7ss (for Cell I), and a voltmeter equipped with a voltage follower with an input impedance of $10^{11}\Omega$ (for Cell II) were used.

Reagents. The potassium perchlorate of an analytical-reagent-grade substance was recrystallized. The cesium perchlorate was prepared from cesium carbonate and perchloric acid. These perchlorates were dried at 150 °C under a vacuum. The thallium perchlorate was prepared by passing an aqueous solution of thallium formate through a column of Amberlite IRA 411 exchange resin in the OH^- form and by then neutralizing it with perchloric acid. It was dried at 70 °C under a vacuum. The silver perchlorate and silver nitrate were of an analytical-reagent-grade substance and were used after drying. The lithium perchlorate, sodium perchlorate, and tetraethylammonium perchlorate were the same as those in previous papers.[6,7] The 1,2-dichloroethane was purified by the method of Coetzee and Lok.[9] The acetonitrile, dimethylformamide, dimethyl sulfoxide, propylene carbonate, and methanol were purified by conventional methods.

Results and Discussion

The relations between the potentials of the glass electrode and those of the metal amalgam or silver wire electrodes in various solvents are shown in Fig. 1. Except for the case of the silver ion, the values of the potentials were referred to those in AN. In deaerated solutions, the potentials of the amalgam electrodes soon reached their equilibrium values and were stable

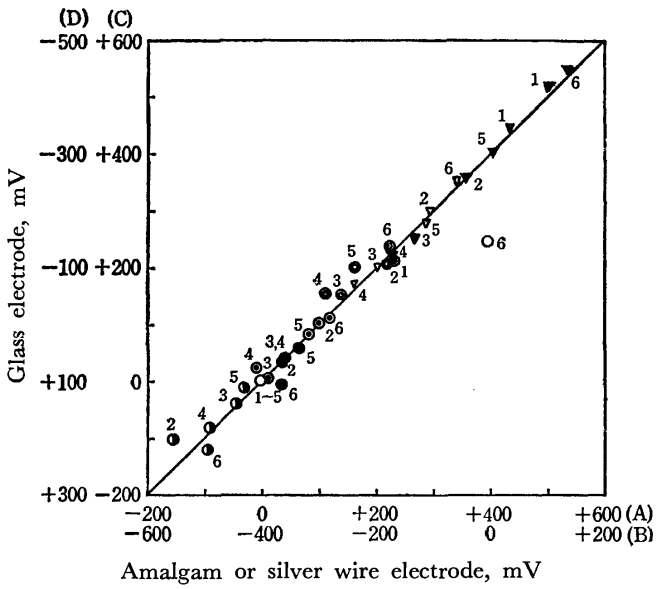

Fig. 1. The responses of the monovalent cation-sensitive glass electrode in various solvents.
(A) $E_{M(Hg)_{AN}}-E_{M(Hg)_D}$, Potentials of the amalgam electrode, (B) $E_{(Ag)_{AN}}-E_{(Ag)_D}$, Potentials of the silver wire electrode, (C) $E^{M}_{(G1)_{AN}}-E^{M}_{(G1)_D}$, Potentials of the glass electrode for M^+, (D) $E^{Ag}_{(G1)_D}$, Potentials of the glass electrode for Ag^+.
M: 1; Li, 2; Na, 3; K, 4; Cs, 5; Tl, 6; Ag
D: ◑ DCE, ○ AN, ● PC, ⊙ methanol, ◎ water, ▽ DMF, ▼ DMSO

enough during the period of the measurements. When oxygen was introduced, however, the potential changed, especially when the measurements were carried out in methanol. Generally, the response of the glass electrode was slower than that of the amalgam electrodes. To reach the equilibrium potentials, it usually took about fifteen to twenty minutes. For various cations in water and for the silver ion in AN, the stabilizations of the glass electrode potentials needed a longer time, however. In Fig. 1, the potentials of the glass electrode for the cesium, and the thallium ions in water and the sodium ion in 1,2-dichloroethane deviate somewhat from the values of the amalgam electrodes. The potential change for the silver ion in 1,2-dichloroethane, propylene carbonate, and particularly in AN also deviates from the change in the potential of the silver wire electrode. Except for these exceptional cases, though, the correspondences of the potential changes of the glass electrode with those of the amalgam or silver wire electrodes are good enough for the cations investigated in this work.

In conclusion, if we consider that the amalgam or silver wire electrodes always make Nernstian responses to the solvent effects on the activities of monovalent cations, the glass electrode can also be considered in many cases to respond in the same ways. However, it should be remembered that there exist exceptional cases in which the Nernstian response cannot be obtained.

The author wishes to express his hearty thanks to Professor Kosuke Izutsu of this department for his kind suggestions and discussions.

This work was supported in part by a Grant-in-aid for Scientific Research from the Ministry of Education.

References

1) G. Eisenman, "Advances in Analytical Chemistry and Instrumentation," Vol. 4, p. 295, C. N. Reilley, Ed., Interscience, New York, N. Y., 1965.
2) G. A. Rechnitz, *Rec. Chem. Progr.*, **26** (4), 242 (1965).
3) J. E. McClure and T. B. Reddy, *Anal. Chem.*, **40**, 2064 (1968).
4) D. Boden, presented at the Electrochemical Society Meeting, May 7—12, 1967, Dallas, Texas.
5) R. D. Lanier, *J. Phys. Chem.*, **69**, 2697 (1965).
6) K. Izutsu, T. Nomura, T. Nakamura, H. Kazama, and S. Nakajima, This Bulletin, **47**, 1657 (1974).
7) T. Nakamura, *ibid.*, **48**, 1447 (1975).
8) K. Izutsu and T. Nakamura, unpublished results.
9) J. F. Coetzee and R. M. Lok, *J. Phys. Chem.*, **69**, 2690 (1965).

BULLETIN OF THE CHEMICAL SOCIETY OF JAPAN, VOL. 48(10), 2969—2970 (1975)

A Study of Optically Active (Benzoin-α-oxime)dichlorocopper(II)

Tomikatsu KUDO, Sumio KAIZAKI, Jinsai HIDAKA,* and Yoichi SHIMURA

Department of Chemistry, Faculty of Science, Osaka University, Toyonaka, Osaka 560

(Received April 24. 1975)

Synopsis. An optically active complex, [(*S*)-benzoin-α-oxime]dichlorocopper(II), was prepared and its absorption and circular dichroism spectra were investigated in organic solvents.

(Benzoin-α-oxime)dichlorocopper(II), $[CuCl_2(cuprH_2)]$,[1] was prepared by Jennings *et al.*[2] and studied magnetochemically by Rindorf,[3] who established its monomeric nature from the effective magnetic moment of 1.91 μ_B in contrast to the polymeric subnormal 1 : 1 complex $\{Cu(cupr)\}_x$ (0.80 μ_B at 294 K). In the present paper, the dichloro complex with optically active (*S*)-benzoin-α-oxime is reported.

Experimental

Preparation. $(+)_{589}$-(S)-*Benzoin-α-oxime*: Hydrogen phthalate of benzoin was obtained from the reaction of racemic benzoin and phthalic anhydride in trimethylamine, and resolved with $(+)_{589}$-quinidine by a modified method of Kenyon *et al.*;[4] the powdered solid of phthalic anhydride was used instead of its suspension in pyridine. $(+)_{589}$-(*S*)-Benzoin was obtained by the hydrolysis of hydrogen phthalate. $[\alpha]_{589}=+119.2°$ (*c*, 0.0105, in acetone). (lit,[4] $[\alpha]_{589}=+118.4°$). $(+)_{589}$-(*S*)-Benzoin-α-oxime was prepared by the oximation of $(+)_{589}$-(*S*)-benzoin. mp 163—164 °C. $[\alpha]_{589}=+3.0°$ (*c*, 0.0472, in chloroform). Found: C, 74.02; H, 5.71; N, 6.14%. Calcd for $C_{14}H_{13}NO_2$: C, 73.99; H, 5.76; N, 6.16%.

(Benzoin-α-oxime)dichlorocopper(II): This was prepared by a new method as follows. To 30 ml of 2,2′-dimethoxypropane was added 2.7 g (0.0158 mol) of $CuCl_2\cdot 2H_2O$ with stirring. The yellow mixture obtained was kept at room temperature, stirring for 30 min. When 3.6 g (0.0159 mol) of $cuprH_2$ was added to it, the mixture turned immediately to a green solution. A pale-green fine precipitate deposited after standing at room temperature for about 10 min. The product was filtered off, washed with methanol, and then air-dried. Found: C, 45.53; H, 4.72; N, 3.60%. Calcd for $[CuCl_2(cuprH_2)]\cdot CH_3OH=C_{15}H_{17}NO_3Cl_2Cu$: C, 45.76; H, 4.35; N, 3.57%. The complex which was recrystallized from methanol, ethanol, acetone, or acetonitrile had one molecule of the solvent. The solvent of crystallization was removed by air-drying for several days. Found: C, 45.98; H, 3.71; N, 3.87%. Calcd for $[CuCl_2(cuprH_2)]=C_{14}H_{13}NO_2Cl_2Cu$: C, 46.49; H, 3.62; N, 3.87%.

[(+)$_{589}$-(S)-Benzoin-α-oxime]dichlorocopper(II): To 20 ml of 2,2′-dimethoxypropane was added 2.1 g (0.0123 mol) of $CuCl_2\cdot 2H_2O$ with stirring. After 30 min, 2.8 g (0.0123 mol) of (*S*)-$cuprH_2$ was added to this mixture; the mixture immediately turned into a green solution. In this case, however, the desired complex did not appear because of its high solubility. To the solution was added 20 ml of methanol and the resulted solution was concentrated to half of its original volume in a vacuum rotary evaporator at about 30 °C. After 80 ml of ether was added to it, the solution was kept in a refrigerator for a week. Bright emerald-green needle crystals were obtained. The complex had one molecule of methanol as solvent of crystallization, but lost it easily. Found: C, 45.46; H, 4.29; N, 3.47%. Calcd for $[CuCl_2\{(S)\text{-}cuprH_2\}]\cdot CH_3OH=C_{15}H_{17}NO_3Cl_2Cu$: C, 45.76; H, 4.35; N, 3.56%. Found: C, 46.07; H, 3.71; N, 3.79%. Calcd for $[CuCl_2\{(S)\text{-}cuprH_2\}]=C_{14}H_{13}NO_2Cl_2Cu$: C, 46.49; H, 3.62; N, 3.87%.

Tetraethylammonium trichlorocuprate(II): An aqueous solution containing $CuCl_2\cdot 2H_2O$ and $[N(C_2H_5)_4]Cl$ (1 : 1) was concentrated by evaporation to dryness. The brick red crystals obtained were recrystallized from acetone. Found: C, 31.07; H, 6.51; N, 4.41%. Calcd for $[N(C_2H_5)_4]CuCl_3=C_8H_{20}NCl_3Cu$: C, 32.01; H, 6.71; N, 4.67%.

Measurement. Visible and ultraviolet absorption spectra were measured with a Shimadzu spectrophotometer QR-50 or UV-200. Diffuse reflectance spectra were obtained by a Hitachi spectrophotometer EPU-2. CD spectra were recorded on a JASCO MOE-1 spectropolarimeter, and optical rotation were checked by a JASCO ORD/UV-5 spectropolarimeter.

Results and Discussion

The absorption and CD data of $[CuCl_2\{(S)\text{-}cuprH_2\}]$ in various organic solvents are shown in Figs. 1 and 2. The spectral behavior in the visible region depends remarkably upon the kind of solvents, which can be classified into three groups, [A], [B], and [C].

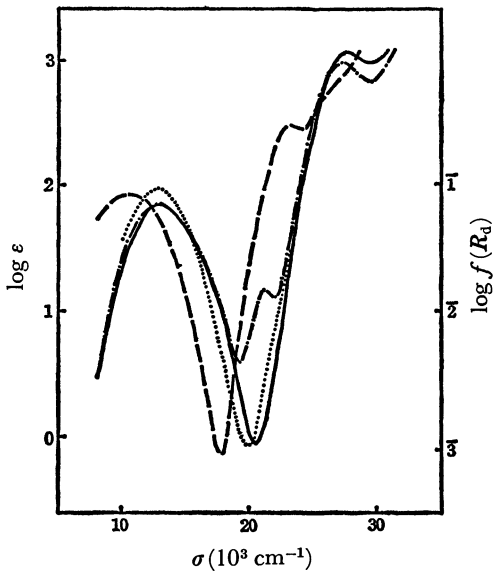

Fig. 1. Absorption curves of $[CuCl_2(cuprH_2)]$ in organic solvents (10^{-2} M): - - - Dimethylformamide ([A] group), —— Chloroform ([B] group), —·— Acetone ([C] group), and ····· Diffuse reflectance spectra (the right ordinate).

* Present address: Department of Chemistry, The University of Tsukuba, Ibaraki, 300—31.

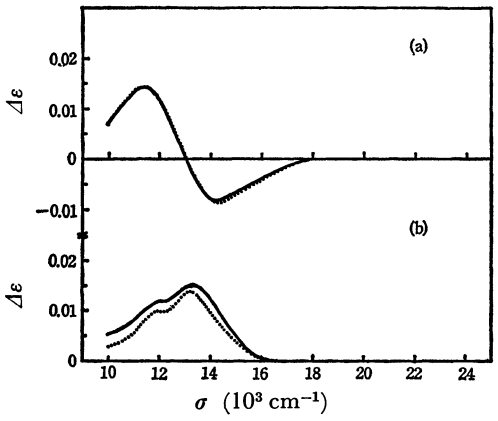

Fig. 2. CD curves of $[CuCl_2\{(S)\text{-}cuprH_2\}]$ in organic solvents; (a) Chloroform ([B] group), (b) Acetone ([C] group), (—— 10^{-2} M, ·····10^{-3} M solution).

The d-d absorption band in [A] group solvents differs markedly from those in [B] or [C] solvents (Fig. 1), and no CD band appears in the visible region. It seems that the [A] group solvents, dimethyl sulfoxide, dimethylformamide, and pyridine, coordinate strongly to copper(II) ion; accordingly, the coordinated (*S*)-$cuprH_2$ may be substituted by the solvent employed.

In the [B] group solvents, chloroform, dichloromethane, methanol, and ethanol, the complex shows a broad but relatively strong ligand field absorption band at about 13000 cm^{-1}, which obeyed Beer's law in the range 10^{-2}—10^{-4} M. The absorption spectra in [B] group solvents resemble closely the powder diffuse reflectance spectrum of the complex (Fig. 1). In the d-d absorption band region, two CD components, (+) and (−) from the lower frequency side, were observed and the net CD sign was positive.

In the [C] group solvents, acetone, acetonitrile, acetophenone, ethyl acetate, and tetrahydrofuran, a sharp absorption band appeared at about 21000 cm^{-1} in addition to the d-d band at about 13000 cm^{-1}. The intensity of the former band depends markedly upon the concentration of the solution (Fig. 3). Two positive CD bands were obtained in the d-d absorption band region, but the CD intensity also depends upon the concentration of the solution (Fig. 2). No CD band appeared in the 21000 cm^{-1} band region. The 21000 cm^{-1} absorption band was intensified by the addition of $[N(C_2H_5)_4]Cl$ to the solution. An intense d-p_π charge transfer band was observed at 21000 cm^{-1} for $[N(C_2H_5)_4]CuCl_3$ dissolved in acetone: the absorption bands appear at 8600 cm^{-1} ($\log \varepsilon_{max}=0.89$), 11000 (1.93), and 21000 (3.18). Manahan and Iwamoto[5] reported a stability constant study of the Cu^{2+}–Cl^- system in organic solvents and showed that the main species is $CuCl_3^-$. Indeed, the intensity of the 21000 cm^{-1} band of $[N(C_2H_5)_4]CuCl_3$ decreases with addition of $[N(C_2H_5)_4]Cl$ and a new band appears at 24300 cm^{-1}. The band at about 24000 cm^{-1} has been attributed to a charge transfer transition of the $CuCl_4^{2-}$ species.[6,7] In conclusion, the 21000 cm^{-1} band is ascribed to the charge transfer band of a small amount of the $CuCl_3^-$ species which is the dissociation product of $[CuCl_2(cuprH_2)]$ in the [C] group solvents.

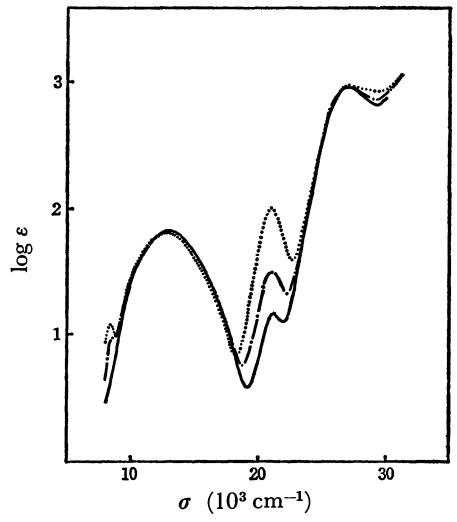

Fig. 3. Absorption curves of $[CuCl_2(cuprH_2)]$ in Acetone; —— 10^{-2} M, —·— 10^{-3} M, ····· 10^{-4} M.

The CD intensities of $[CuCl_2\{(S)\text{-}cuprH_2\}]$ in Fig. 2 are comparable to those of the (*S*)-α-amino acidato copper(II) complexes and the net CD sign is positive both in the [B] and [C] group solvents. It has been well established that the copper(II) complexes of ordinary (*S*)-α-amino acids,[8,9] their amides,[10] and simple peptides[11] have a net negative CD sign in the d-d absorption band region, and this negative Cotton effect has been explained from a true vicinal contribution[9] of the (*S*) asymmetric carbon atom, from a conformational contribution[12] of the δ chiral chelate ring, or from a regional contribution[11] of the large substituent on the (*S*) asymmetric carbon atom. A molecular model examination of the interaction between the two phenyl groups in the present ligand (*S*)-benzoin-α-oxime shows that the ligand prefers axial disposition of the phenyl group attached to the asymmetric carbon atom, producing a λ chiral chelate ring. Thus, it is concluded that the net positive CD of the present copper(II) complex is due to the regional contribution of the axial phenyl group and/or the conformational contribution of the λ chelate ring.

References

1) Benzoin-α-oxime, $C_6H_5C(NOH)CH(OH)C_6H_5$, has been called cupron, which is abbreviated as $cuprH_2$.
2) J. S. Jennings, E. Sharratt, and C. K. Wardlaw, *J. Chem. Soc.*, **1935**, 818.
3) G. Rindorf, *Acta Chem. Scand.*, **25**, 774 (1971).
4) J. Kenyon and R. L. Patel, *J. Chem. Soc.*, **1965**, 453.
5) S. E. Manahan and R. T. Iwamoto, *Inorg. Chem.*, **4**, 1409 (1970).
6) R. D. Willett and O. L. Liles, Jr., *ibid.*, **6**, 1666 (1967).
7) W. Ludwig and M. Texton, *Helv. Chim. Acta*, **54**, 1144 (1971).
8) T. Yasui, This Bulletin, **38**, 1746; T. Yasui, J. Hidaka, and Y. Shimura, *J. Amer. Chem. Soc.*, **87**, 2762 (1965).
9) C. J. Hawkins and C. L. Wong, *Aust. J. Chem.*, **23**, 2237 (1970).
10) T. Komorita, J. Hidaka, and Y. Shimura, This Bulletin, **42**, 168 (1969).
11) J. M. Tsangaris and R. B. Martin, *J. Amer. Chem. Soc.*, **92**, 4255 (1970).
12) K. M. Wellman, W. Mungall, T. G. Mecca, and C. R. Hare, *ibid.*, **89**, 3647 (1967).

BULLETIN OF THE CHEMICAL SOCIETY OF JAPAN, VOL. 48(10), 2971—2972 (1975)

Kinetics and Mechanism of the Reaction of Copper(II) with Hydroxylamine in the Presence of Bathocuproine Disulfonate

Taira IMAMURA and Masatoshi FUJIMOTO

Department of Chemistry, Faculty of Science, Hokkaido University, Sapporo 060

(Received May 6, 1975)

Synopsis. The stoichiometry and the mechanism of the electron-transfer reaction of Cu(II) with hydroxylamine are investigated by measuring a fast complex formation of Cu(II) with bathocuproine disulfonate. The data are evaluated for the rate-determining step involving a radical species.

Hydroxylamine acts as a reducing agent on various metal ions,[1] the stoichiometry of the reaction being dependent on the metal species and on the acid concentration of the medium.[2]

Bathocuproine disulfonate (4,7-diphenyl-2,9-dimethyl-1,10-phenanthroline disulfonate; abbr. BCDS) was used as a specific chelating agent for copper(I) forming a very stable complex of intense color.[3] The corresponding complex of the bivalent copper has not been reported owing to its low stability due to the steric hindrance of the ortho-methyl groups of the ligands in the square planar complex.

We report here the stoichiometry and the kinetics of the reaction between copper(II) and hydroxylamine. The copper(I) formed in the reaction was measured by stopped-flow method as a colored 1 : 2 complex of BCDS. The very fast complex formation of univalent copper ion was found to be useful as an indication of the slow redox reaction.

Experimental

Reagents. Reagent grade chemicals were used. The stock solution of copper(II) sulfate (Koso) was titrated with EDTA. Hydroxylammonium sulfate (Wako) was dissolved in distilled water free from oxygen, and stored in a refrigerator under nitrogen atmosphere. The concentration of the stock solution was determined with potassium permanganate. Disodium bathocuproine disulfonate (Dojindo) was dissolved in water to prepare a 1.00×10^{-3} M stock solution.[4] The ionic strength was adjusted at 0.15 with potassium sulfate (Koso).

Stoichiometry. The composition of the complex species was confirmed using the absorption peak of the copper(I)-BCDS complex at 483 nm ($\varepsilon_{max}=1.27\times10^4$). The stoichiometry of the reaction of copper(II) with hydroxylamine was also determined spectrophotometrically at 483 nm.

Kinetics. The reaction of copper(II) with hydroxylamine was followed spectrophotometrically at 483 nm using a Yanagimoto SPS-1 stopped-flow apparatus. Reservoirs of the reagent solutions were kept under nitrogen atmosphere to avoid air oxidation. Kinetics was studied in the acid region under the condition $[NH_2OH]_0 \gg [BCDS]_0 > [Cu(II)]_0$, $\mu=0.15$ (K_2SO_4), and at 25.0±0.2 °C.

Results and Discussion

Stoichiometry. The parent compound bathocuproine (4,7-diphenyl-2,9-dimethyl-1,10-phenanthroline) has been known to form a 1 : 2 complex with copper(I). We confirmed by the mole ratio method that the BCDS also forms a 1 : 2 complex with copper(I) as shown in Fig. 1.

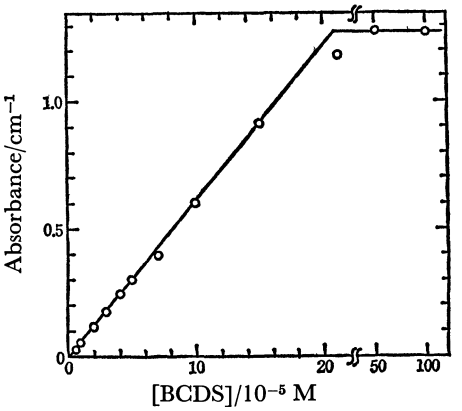

Fig. 1. Mole ratio method for the formation of Cu(I)-BCDS complex.
$[Cu(II)]_0=1.008\times10^{-4}$ M, $[NH_2OH]_0=1.23\times10^{-2}$ M, pH=4.0 (acetate buffer), $\mu=0.15$ (K_2SO_4), 25 °C.

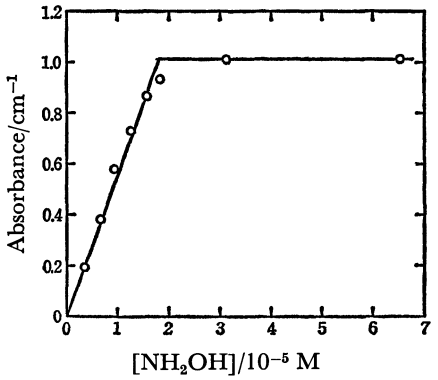

Fig. 2. Stoichiometry of the reaction of Cu(II) with hydroxylamine.
$[Cu(II)]_0=4.03\times10^{-5}$ M, $[BCDS]_0=5.08\times10^{-4}$ M, $\mu=0.15$ (K_2SO_4), pH≃5.7, 25 °C.

Figure 2 indicates that one mole of hydroxylamine reduces two moles of copper(II) to copper(I).[5]

Kinetics. Since no difference in the reaction rate was observed between two combinations of the mixing of the reactants, (A) {NH_2OH+BCDS}+{Cu(II)} and (B) {NH_2OH}+{BCDS+Cu(II)}, the combination A was mainly used to follow the kinetics. The very fast increase in the absorbance at 483 nm on mixing the solution {Cu(II)+NH_2OH} with BCDS indicates a much higher rate of the complex formation of copper(I) with BCDS than that of the redox reaction between copper(II) and hydroxylamine.

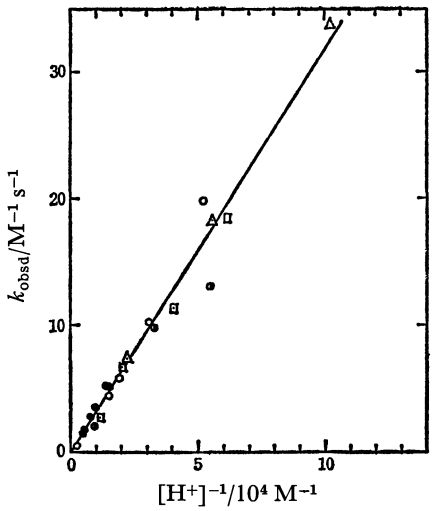

Fig. 3. Plot of the second-order rate constant k_{obsd} against $[H^+]^{-1}$ at 25 °C.
$[Cu(II)]_0$, $[BCDS]_0$, and $[NH_2OH]_0$ are, ◑: 5.04×10^{-6}, 2.03×10^{-4}, 6.10×10^{-2}; ⊡: 5.04×10^{-6}, 2.03×10^{-4}, 4.58×10^{-2}; △: 2.52×10^{-6}, 2.03×10^{-4}, 3.05×10^{-2}; ○: 5.04×10^{-6}, 2.03×10^{-4}, 1.83×10^{-2}; ●: 2.01×10^{-5}, 4.06×10^{-4}, 1.00×10^{-1} M, respectively.

Linear semi-logarithmic plot of the absorbance at 483 nm *vs.* time indicates the first-order dependence on the [Cu(II)] under the conditions $[NH_2OH]_0 \gg [BCDS]_0 > [Cu(II)]_0$. The second-order rate constant k_{obsd} thus obtained depends on the acidity, increasing with $[H^+]^{-1}$ as shown in Fig. 3.

Following rate law of the redox reaction is thus derived.

$$\frac{1}{2}\cdot\frac{d[Cu^I(BCDS)_2]}{dt} = -\frac{1}{2}\cdot\frac{d[Cu(II)]}{dt}$$
$$= k_{obsd}[NH_2OH][Cu(II)]$$
$$= \frac{k_a}{[H^+]}\cdot[NH_2OH][Cu(II)].$$

The apparent rate constant k_a is evaluated to be $3.1\times10^{-4}\ s^{-1}$ from the slope of the straight line in Fig. 3.

The acid dissociation constants for the aquo copper(II) ion and the hydroxylammonium ion are in the same order of magnitude as $K_H=[CuOH^+][H^+]/[Cu^{2+}]=10^{-6.47}$ [6] and $k_a=[NH_2OH][H^+]/[NH_3OH^+]=10^{-5.96}$ [7] at 25 °C.

Although direct evidence for the formation of the complexes of copper(II) with hydroxylamine was not obtained, it would be reasonable to assume the fast formation of copper(II) complex with hydroxylamine followed by the redox reaction, since the observed redox reaction is very slow in comparison with the complex formation of aquo copper(II) ion in general.

The formation of short-lived radical species was reported in the reaction of hydroxylamines with one-electron abstracting oxidants such as cerium(IV).[8] Though in the reaction with bivalent copper we have no direct evidence as for the radical formation, we derived the following reaction scheme involving radicals to interpret the above reaction stoichiometries.

$$\begin{array}{ccc} CuSO_4 & NH_3OH^+ & \\ \downarrow\uparrow K_1 & +H^+ \uparrow\downarrow K_2(=K_a) & \\ Cu^{2+} + NH_2OH & \overset{K}{\rightleftharpoons} & Cu^{II}\cdot NH_2OH \\ \uparrow\downarrow K_3(=K_H) & & \downarrow k_1 \\ CuOH^+ + H^+ & & \end{array}$$

$$Cu(I) + NH_2O\cdot + H^+ \quad (1)$$

$$2Cu(II) + 2NH_2O\cdot \xrightarrow{k_2}$$
$$2Cu(I) + N_2O + H_2O + 2H^+ \quad (2)$$

$$Cu(I) + 2BCDS \xrightarrow{fast} Cu^I(BCDS)_2. \quad (3)$$

The overall reaction is thus summarized as,

$$4Cu(II) + 2NH_2OH + 8BCDS \longrightarrow$$
$$4Cu^I(BCDS)_2 + N_2O + H_2O + 4H^+. \quad (4)$$

In the radical reaction (2), k_2 is postulated to be much larger than k_1K. Thus the k_{obsd} is approximated as follows:

$$k_{obsd} = \frac{k_a}{[H^+]} = \frac{k_1K}{[H^+]\{K_1[SO_4^{2-}]+1\}+K_3}.$$

Under the experimental conditions, $[H^+]\{K_1[SO_4^{2-}]+1\} \gg K_3$, and $[SO_4^{2-}]=0.1$ M.

The value of k_1K is evaluated to be $6.2\times10^{-3}\ s^{-1}$ at 25 °C. The small values of k_a and k_1K may be attributed to the small complex formation constant K.

References

1) G. Davies and K. Kustin, *Inorg. Chem.*, **8**, 484 (1968).
2) N. Hlasivcová, J. Novák, and J. Zýka, *Collect. Czech. Chem. Commun.*, **32**, 403 (1967).
3) B. Zak, J. S. Cohen, and L. A. Williams, *Microchem. J.*, **6**, 67 (1962); B. Zak, *Tech. Bull. Regist. Med. Technol.*, **28**, 98 (1958); *Am. J. Clin. Pathol.*, **29**, 590 (1958); B. Zak, G. A. Cavanaugh and L. A. Williams, *Chemist-Analyst*, **50**, 8 (1961); D. Blair and H. Diehl, *Talanta*, **7**, 163 (1961); D. C. Wharton, *J. Biol. Chem.*, **236**, 1857 (1961). *Cf.* also, G. F. Smith and D. H. Wilkins, *Anal. Chem.*, **25**, 510 (1953).
4) T. Takahashi, T. Imamura, and M. Fujimoto, *Mikrochim. Acta*, **1973**, 69.
5) It was reported[2] that dinitrogen oxide was detected by gas chromatography and infrared spectrum as an intermediate of the reaction of cerium(IV) with hydroxylamine in 0.25 M sulfuric acid. We assume the formation of dinitrogen oxide also in the reaction of copper(II) with hydroxylamine.
6) B. B. Owen and R. W. Curry, *J. Amer. Chem. Soc.*, **60**, 3074 (1938).
7) R. A. Robinson and V. E. Bower, *J. Phys. Chem.*, **65**, 1279 (1961).
8) C. J. W. Gutch and W. A. Waters, *J. Chem. Soc.*, **1965**, 751. J. W. Adams, S. W. Nicksic, and J. R. Thomas, *J. Chem. Phys.*, **45**, 654 (1966).

BULLETIN OF THE CHEMICAL SOCIETY OF JAPAN, VOL. 48(10), 2973—2974 (1975)

Organische Metallkomplexe. VIII.* Notiz über die Kupfer(II)- und Nickel(II)chelate der *N,N'*-Bis(2-phenylhydrazono-1-methyläthyliden)-α,ω-alkandiamine

Hiroshi OHTA, Yasushi KODERA, Fumie MORI, Mitsue KOYAMA, und Sumie ISHIBASHI
Chemisches Institut der Fukuoka Universität, 814 Fukuoka, Nishi-ku, Nakaduma 11

(Enigegangen am 6. Mai 1974)

Synopsis. Es wurden die Synthesen der neuen Chelatbildner, *N,N'*-Bis(2-phenylhydrazono-1-methyläthyliden)-1,2-äthandiamin und -1,3-propandiamin sowie ihrer Kupfer(II)- und Nickel(II) chelate beschrieben.

Glyoxal-, Methylglyoxal-(Pyruvinaldehyd-) und Dimethylglyoxal (Biacetyl)phenylhydrazone wurden schon früher dargestellt und charakterisiert.[1-3] Aus den Molekularmodellen erscheinen sie als N.O-Chelatbildner mit den Schwermetallionen Chelate zu bilden. In Wirklichkeit jedoch, trotz verschiedener Versuche konnten wir aus ihnen keine Metallchelate erhalten. Die schwache Acidität der am Benzolkerne haftenden NH-Gruppe im Phenylhydrazon-Reste und die stärkere Elektronegativität des Sauerstoffatoms der C=O-Gruppe erscheinen die Ursache dafür zu sein.

In Rücksicht auf die Tatsache, daß die Formazane mit den Schwermetallionen beständige Metallchelate liefern, haben wir versucht, die anderen Carbonylgruppen in die Azomethine überzüfuhren. Als Carbonylverbindungen lieferten sie alle mit den Carbonylreagenzien normale Kondensationsprodukte. So konnten wir aus ihnen die Phenylhydrazone (Phenylosazone), Oxime, Semicarbazone, und die Schiffschen Basen mit Alkanaminen und Alkandiaminen erhalten. Die Versuche, aus diesen Metallchelate darzustellen, ergaben, daß nur die Schiffschen Basen mit Alkandiaminen Metallchelate liefern, und zwar *N,N'*-Bis(2-phenylhydrazono-1-methyläthyliden)-1,2-äthan-diamin und -1,3-propandiamin beständige Kupfer(II)-und Nickel(II)chelate geben. Ferner haben wir gefunden, daß mit der Zunahme der Methylengruppe die Metallchelate schwerer zugänglich werden. Aus diesen Resultaten konnten wir einen Schluß ziehen, daß in diesen beiden Schiffschen Basen zwei NH-Gruppen und zwei C=N-Gruppen eine begünstigte Lage für die eintretenden Metallione nehmen und so daß diese Basen als 4N-Chelatbildner fungieren.

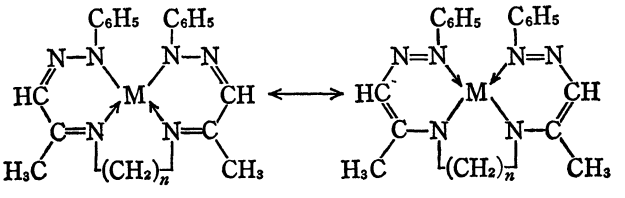

M=Cu, Ni n=2, 3

Aus den Betrachtungen der Molekularmodelle ist die tetraedrische Anordnung der Liganden um das zentrale Kupfer- bzw. Nickelatom schwierig; dagegen ist die plane Anordnung spannungsfrei. Die magnetischen Momente der Nickel(II)chelate haben darauf hingedeutet, daß in ihnen eine ebene oder fast ebene Struktur vorliegt. Man könnte daher annehmen, daß auch den Kupfer(II)chelaten die gleiche Anordnung der Liganden zukommt.

Aus dem Vergleich der Stabilität und der Absorptionsmaxima im sichtbaren Bereich der ebenen (oder fast obenen) Kupfer(II)chelate haben Nakahara *etal.*[4] festgestellt, daß innerhalb einer bestimmten Reihe von den orthokondensierten tricyclischen Kupfer(II)-chelaten, das 6-5-6-Chelatringsystem stabiler als 6-6-6-System ist, und die stabileren Chelate stets im kürzeren Wellenbereich die Absorptionsmaxima haben als die instabileren und umgekehrt. Wir haben gefunden, daß die Nakahara-sche Regel auch für unsere Kupfer(II)chelate gilt.

Beschreibung der Versuche

Die Schmelzpunkte sind nicht korrigiert. Die Absorptionsspektren im sichtbaren Bereich wurden mit dem Hitachi-Gerät, Modell 124 aufgenommen. Die magnetischen Messungen wurden mit der Gouy-schen Waage im pulverisierten Zustand bei Zimmertemperatur ausgeführt.

Darstellung der Chelatbildner.

N,N'-Bis(2-phenylhydrazono-1-methyläthyliden)-1,2-äthandiamin (PMÄ-H_2). Man fügt zur warmen Lösung von 3.2 g Methylglyoxal-al-phenylhydrazon in 10 ml Äthanol 0.9 ml 1,2-Äthandiamin zu, und erhitzt das Gemisch auf dem Wasserbade etwa 20 Min under Rückfluß. Nach dem Erkalten kristallisiert man die erhaltene kristallinische Masse aus Äthanol um. Gelbe Kristalle, Schmp. 193—94 °C. Zur Analyse und Darstellung der Metallchelate wurde eine Substanzprobe verwendet, die durch einstündiges Erhitzen unter vermindertem Druck über P_2O_5 bei 90 °C getrocknet wurde.

Gef.: C, 68.74; H, 6.91; N, 24.36%. Ber.($C_{20}H_{24}N_6$): C, 68.95; H, 6.92; N, 24.12%.

N,N'-Bis(2-phenylhydrazono-1-methyläthyliden)-1,3-propandiamin (PMP-H_2). Man stellt die Verbindung in derselben Weise wie beim PMÄ-H_2 aus 3.2 g Methylglyoxal-al-phenylhydrazon gelöst in 10 ml warmem Äthanol und 1 ml 1,3-Propandiamin dar. Gelbe Kristalle, Schmp. 145—46 °C. Zur Analyse und Darstellung der Metallchelate wurde eine Substanzprobe verwendet, die durch mehrstündiges Erhitzen unter vermindertem Druck über P_2O_5 bei 110—30 °C getrocknet wurde.

Gef.: C, 69.46; H, 7.19; N, 23.04%. Ber. ($C_{21}H_{26}N_6$): C, 69.59; H, 7.23; N, 23.18%.

Kupfer(II)chelate. *PMÄ-Cu(II)*: Man fügt zur warmen Lösung von 350 mg PMÄ-H_2 in 35 ml Äthanol eine Lösung von 220 mg Kupfer(II)acetat(Monohydrat) in 10 ml Äthanol zu. Die Farbe der Lösung schlägt sofort nach schwärzlichem Purpur um, und die glänzenden purpurroten Platte scheiden sich ab. Man kristallisiert sie aus Äthanol um.

* VII. Mitteilung: H. Ohta *et al.*, Dieses Bulletin, **42**, 3019 (1969).

Gef.: C, 58.59; H, 5.41; N, 20.52; Cu, 15.52%. Ber. ($C_{20}H_{22}N_6Cu$): C, 58.59; H, 5.41; N, 20.50; Cu, 15.50%.

PMP-Cu(II): Durch das obige Verfahren ist das Chelat aus 365 mg PMP-H_2 in 15 ml warmen Äthanol und 220 mg Kupfer(II)acetat (Monohydrat) in 10 ml Äthanol darstellbar. Aus Äthanol kristallisiert es in schwarzen Saülen.

Gef.: C, 59.35; H, 5.71; N, 19.51; Cu, 14.94%. Ber. ($C_{21}H_{24}N_6Cu$): C, 59.49; H, 5.71; N, 19.82; Cu, 14.99%.

Nickel(II)chelate. PMÄ-Ni(II): Man fügt zur Lösung von 350 mg PMÄ-H_2 in 35 ml warmem Äthanol eine Lösung von 250 mg Nickel(II)acetat (Tetrahydrat) in 10 ml Äthanol zu. Die Farbe der Lösung schlägt sofort zum Purpurrot um, und aus der Lösung beim Stehenlassen scheiden sich die glänzenden purpurroten Platte aus, die aus Äthylenglykolmonoäthyläther umkristallisiert werden können. $\mu_{eff} \approx 0$ (291 K).

Gef.: N, 20.73; Ni, 14.42%. Ber. ($C_{20}H_{22}N_6Ni$): N, 20.74; Ni, 14.49%.

PMP-Ni(II): Durch das obige Verfahren ist das Chelat aus 365 mg PMP-H_2 in 15 ml warmem Äthanol und 250 mg Nickel(II)acetat (Tetrahydrat) in 10 ml Äthanol darstellbar. Glänzende grünlich-braune Platte, die aus Äthanol umkristallisiert werden können. $\mu_{eff} \approx 0$ B. M. (291 K).

Gef.: N, 19.77; Ni, 13.91%. Ber. ($C_{21}H_{24}N_6Ni$): N, 20.05; Ni, 14.01%.

Spektroskopische Daten des PMÄ-Cu(II) und des PMP-Cu(II). (Lösungsmittel : 1,4-Dioxan)

	λ_{max}(nm)	log ε
PMÄ-Cu(II)(6-5-6-System)	414	4.61
PMP-Cu(II)(6-6-6-System)	433	4.65

Herrn Prof. Dr. Shigeo Kida der Kyushu Universität (Institut für Komplexchemie) und Herrn M. Sc. Isao Ando unseres Instituts (Anorganisch-chemisches Laboratorium) danken wir herzlichst für die magnetischen Messungen.

Literatur

1) H. O. L. Fischer und C. Taube, *Ber.*, **59**, 851 (1926).
2) G. A. Reynolds und J. A. VanAllan, "Organic Syntheses," Coll. Vol. IV, p. 633 (1963).
3) P. Petrenko-Kritschenko und E. Eltschaninoff, *Ber.*, **34**, 1699 (1901).
4) A. Nakahara, H. Yamamoto, und H. Matsumoto, Dieses Bulletin, **37**, 1137 (1964); Y. Nakao, K. Sakurai, und A. Nakahara, *ebenda*, **39**, 1471 (1966).

BULLETIN OF THE CHEMICAL SOCIETY OF JAPAN, VOL. 48(10), 2975—2976 (1975)

Nitrosylrhodium (^{14}NO and ^{15}NO) Compounds Containing Triphenylphosphine

Eiichi MIKI,* Kunihiko MIZUMACHI, and Tatsujiro ISHIMORI

Department of Chemistry, College of Science, Rikkyo University, 3-Chome, Nishi Ikebukuro, Toshima-ku, Tokyo 171

(Received May 14, 1975)

Synopsis. The oxidation states of the NO group and the geometries for the nitrosylrhodium compounds were investigated on the basis of the ^{15}N-isotopic shifts of the N–O stretching vibrations and the frequencies of the Rh–NO stretching ones. $RhCl(NO_2)(NO)(PPh_3)_2$ was found to react with NO to give $RhCl(NO_2)_2(PPh_3)_2$.

It has been reported that the oxidation states of the metal atom and the NO group in transition-metal nitrosyl complexes significantly influence the isotopic shifts of the vibrational bands due to the metal–N–O skeleton upon ^{15}NO-substitution, and control the region where these bands are observed.[1-3] Such a view may be connected with the concept of "Stereochemical Control of Valence": that the geometry of NO group is determined by the stereochemistry of the ligands attached to the metal.[4]

On the basis of these facts, the authors measured the isotopic shifts of the following nitrosylrhodium compounds: $Rh(NO)(PPh_3)_3$ (PPh_3=triphenylphosphine), $RhX_2(NO)(PPh_3)_2$, and $RhX(NO_2)(NO)(PPh_3)_2$ (X=Cl and Br), which have been the subject of great interest as homogeneous catalysts of olefin hydrogenation.[5]

Experimental

Syntheses. The examined compounds were prepared in accordance with Ref. 6—8. One of the starting materials, rhodium(III) bromide, was prepared from $RhCl_3 \cdot 3H_2O$ by heating it with concentrated hydrobromic acid on a boiling water bath to dryness. The ^{15}NO-complexes were prepared in a vacuum line by the use of *ca.* 5 mmol of ^{15}NO (^{15}N atom %=95.5—96.8) on the same scale as that used for preparing the ^{14}NO-complexes. The elementary analyses and IR spectra showed that the desired products were obtained. All of these compounds were diamagnetic.

$RhCl(NO_2)_2(PPh_3)_2$: A 6-mmol portion of NO was trapped in a reaction vessel containing 1 mmol of $RhCl(PPh_3)_3$ in 70 ml of chlorobenzene by cooling with liquid nitrogen. Then the solid solution was melted under running water and was allowed to stand for more than 2 days, changing from dark red to yellow through green. The yellow solution was condensed to less than 5 ml by the use of liquid nitrogen to give a yellow product. Yield, 150—300 mg. Found: C, 56.98; H, 3.95; N, 3.71; Cl, 4.82%. Calcd for $RhCl(NO_2)_2(PPh_3)_2$: C, 57.29; H, 3.98; N, 3.71; Cl, 4.70%. χ_g (at 291 K)$=-0.46\times10^{-6}$ (cgs).

Measurements. The magnetic susceptibility was measured by the Gouy method at room temperature. The IR spectra were measured in the region 200—4000 cm^{-1} as Nujol and hexachlorobutadiene mulls using JASCO DS-402 G and JASCO model IR-F infrared spectrophotometers. The reproducibility was about ±0.5 cm^{-1} in the region 200—2400 cm^{-1}. The Raman spectra of the powdered samples were measured in the region 100—700 cm^{-1} on a Narumi 750 Z-1200 double monochrometer equipped with a He-Ne laser.

Results and Discussion

From the comparison of the observed isotopic shifts with the calculated ones, the following rules were established:[1-3] the observed isotopic shift of the N–O stretching vibration for NO^+ complex is 36—44 cm^{-1}, while that for the NO^- one is 25—28 cm^{-1}; the metal-NO bending vibration is observed in the region 450—650 cm^{-1}, and its isotopic shift is 10—15 cm^{-1} for both NO^+ and NO^- complexes; the metal–NO stretching vibration for the NO^+ complex is observed in the region 500—650 cm^{-1}, while that for the NO^- one is seen in the region *ca.* 300 cm^{-1}, and their isotopic shifts are 2—6 cm^{-1}. The bands due to the RhNO group were assigned on this basis.

The wave numbers, isotopic shifts, and assignments of IR and Raman bands for the examined compounds are shown in Table 1.

The N–O stretching vibration of $Rh(NO)(PPh_3)_3$ was observed at 1610 cm^{-1} and shifted downwards by 49 cm^{-1} upon ^{15}NO-substitution. In the region where skeletal vibrations due to metal-NO groups have been usually observed, only a weak absorption band at 410 cm^{-1} shifted downwards by 18 cm^{-1}. This band may be assigned to the Rh–NO bending vibration. Another skeletal vibration, the Rh–NO stretching one, may be considered to overlap with the strong bands due to the coordinated PPh_3 groups. The Raman bands in the region 200—700 cm^{-1} showed no isotopic shifts. The isotopic shift of the N–O stretching vibration supports the view that the oxidation state of the NO group is I, and that of the rhodium atom, −I. The concept of "Stereochemical Control of Valence" will support the view that this compound is not a square planar one with a strongly bent RhNO group but a tetrahedral one with a linear RhNO one, if this compound is a NO^+ one,[4]

The N–O stretching vibration of $RhX_2(NO)(PPh_3)_2$ was observed in the region *ca.* 1630 cm^{-1}; the isotopic shift was 28 cm^{-1}. The band at *ca.* 590 cm^{-1} shifted downwards by *ca.* 15 cm^{-1}, and the 339 cm^{-1} band for the bromide shifted downwards by 2 cm^{-1}. The former band can be assigned to the Rh–NO bending vibration, and the latter one to the Rh–NO stretching one. The Rh–NO stretching vibration of the chloride could not be observed because of the overlapping with the strong band due to the Rh–Cl stretching one. The Rh–Cl band was observed as a single band on both IR and Raman spectra. This suggests that the two chloride ions are in a *trans* position to each other in this compound.

* Present address: Department of Chemistry, The University of Texas at Austin, Austin, Texas 78712.

Table 1. Wave numbers, observed isotopic shifts, and assignments of IR and Raman bands[a]

Assignments	$Rh(NO)(PPh_3)_3$	$RhCl_2(NO)(PPh_3)_2$	$RhBr_2(NO)(PPh_3)_2$
NO str	1610 vs (49)[b]	1632 vs (28)	1631 vs (28)
Rh-NO bend	410 w (18)	591 s (15), 598[c] (14)	586 s (15)
Rh-P str	450 s	456 s	460 s
Rh-NO str	not obsd.	not obsd.	339 m (2)
Rh-X str		341 vs, 347[c]	271 vs

Assignments	$RhCl(NO_2)(NO)(PPh_3)_2$	$RhBr(NO_2)(NO)(PPh_3)_2$
NO str	1659 vs (29), 1632 w (28)	1653 vs (28), 1625 w (29)
Rh-NO bend or NO_2 wag	577 m, br (15); 560 s (13)	573 m (17), 554 w (14)
Rh-P str	459 m	459 s
Rh-NO str	341 m (1)	320 m (2)
Rh-X str	318 vs	280 m, br

a) The bands which are characteristic of PPh_3 and the nitro group are eliminated. b) The wave numbers in parentheses indicate the observed isotopic shifts. c) Raman band.
Abbreviations: vs=very strong; s=strong; m=medium; w=weak; br=broad; str=stretching vibration; bend=bending vibration; wag=wagging vibration.

For $RhX(NO_2)(NO)(PPh_3)_2$, two N–O stretching vibrations were observed in the region 1630—1660 cm^{-1}, and these shifted downwards by 28—29 cm^{-1}. The ^{15}N-isotopic shifts of the bands which are characteristic of the nitro group were comparable to those of $[Rh(NO_2)(NH_3)_5]Cl_2$.[9] The two bands observed in the region 550—580 cm^{-1} are considered to be assigned to the wagging vibration of the NO_2 group and the Rh–NO bending vibration. These bands, however, could not be assigned distinctly because their isotopic shifts are almost equal to each other. The 320 cm^{-1} band of the bromide shifted downwards by 2 cm^{-1}, and can be assigned to the Rh–NO stretching vibration. The 341 cm^{-1} band of the chloride is considered to be the Rh–NO stretching vibration. The oxidation state of the NO group for $RhX_2(NO)(PPh_3)_2$ and $RhX(NO_2)(NO)(PPh_3)_2$ is considered to be −I, that of the rhodium atom, III. If these compounds are NO^- ones, the concept of "Stereochemical Control of Valence" will support the view that the geometries of these five-coordinate compounds are tetragonal pyramids with an apical NO^-.[4]

It is established that the metal–NO stretching vibration for the NO^- complex is in the region *ca.* 300 cm^{-1}, as observed for the nitrosylplatinum complexes such as $M_2[PtX_5(NO)]$.[2]

For $RhCl(NO_2)_2(PPh_3)_2$, no absorption bands could be observed in the region where the N-O stretching vibration has been usually observed, but the absorption bands and their ^{15}N-isotopic shifts, which are characteristic of the coordinated nitro group, could be observed in addition to the bands due to PPh_3. The IR bands and the elementary analyses show that this new compound is $RhCl(NO_2)_2(PPh_3)_2$. The reaction of NO with a square-planar d^8 complex of rhodium, such as $RhCl(PPh_3)_3$, has been reported to give a five coordinate derivative, $RhCl(NO_2)(NO)(PPh_3)_2$.[8] It was found from this study that the nitro-nitrosyl compound further reacts with NO to give the dinitro compound, $RhCl(NO_2)_2(PPh_3)_2$. The apical NO^- ion of the nitro-nitrosyl compound is considered to react with NO to give NO_2^- ion and N_2O.

$$RhCl(NO_2)(NO)(PPh_3)_2 + 2NO \longrightarrow RhCl(NO_2)_2(PPh_3)_2 + N_2O.$$

References

1) E. Miki, K. Mizumachi, T. Ishimori, and H. Okuno, This Bulletin, **46**, 3779 (1973).
2) E. Miki, K. Mizumachi, and T. Ishimori, *ibid.*, **47**, 656 (1974).
3) E. Miki, K. Mizumachi, and T. Ishimori, *ibid.*, **47**, 3068 (1974).
4) J. H. Enemark and R. D. Feltham, *Coor. Chem. Rev.*, **13**, 339 (1974).
5) J. P. Collman, N. W. Hoffman, and D. E. Morris, *J. Amer. Chem. Soc.*, **91**, 5659 (1969).
6) G. Dolcetti, N. W. Hoffman, and J. P. Collman, *Inorg. Chim. Acta*, **6**, 531 (1972).
7) M. C. Baird, *ibid.*, **5**, 46 (1971).
8) W. B. Hughes, *Chem. Commun.*, **1969**, 1126.
9) M. J. Cleare and W. P. Griffith, *J. Chem. Soc., A*, **1967**, 1144.

BULLETIN OF THE CHEMICAL SOCIETY OF JAPAN, VOL. 48(10), 2977—2978 (1975)

A Structural Investigation of the 2-Methylthiophene Trimer and Its Related Compounds†

Akira ISHIGAKI and Toshiyuki SHONO*

Nara Technical College, Yata, Yamato-Kōriyama-shi, Nara 639-11

**Department of Applied Chemistry, Faculty of Engineering, Osaka University, Yamada-kami, Suita-shi, Osaka 565*

(Received November 30, 1974)

Synopsis. A structural investigation of the 2-methylthiophene trimer and its crystalline oxidation product has been performed. These compounds have been found to be identical with 2,4-bis(5′-methyl-2′-thienyl)-2-methylthiolane and its sulfone derivative.

Thiophene and alkylthiophen react under the catalytic action of phosphoric acid to give their oligomers. The reaction was investigated by Meisel *et al.* in 1950.[1] Noting the presence of trimers in the reaction products, they proposed a reaction mechanism and elucidated the structure of the thiophene trimer, 2,4-bis-2′-thienylthiolane [**1**]. However, no structural description of the alkylthiophene trimers was undertaken.

In a previous paper,[2] the present authors investigated an oligomerization of 2-methylfuran and elucidated the structure of the 2-methylfuran tetramer. 2-Methylfuran reacts under the catalytic action of phosphoric acid to give its tetramer in a good yield. However, no trimeric compounds are found in the reaction product. Our interest in preparing the 2-methylfuran tetramer led us to reinvestigate the trimerization of thiophene and 2-methylthiophene. In this paper, the authors will try to elucidate the structure of the 2-methylthiophene trimer [**2**] and its related compounds, novel crystalline derivatives of **1** and **2**.

Experimental

*Preparation of **1** and **2**.* Reagent-grade thiophene was used after fractional distillation. The 2-methylthiophene was prepared by the ordinary method[3,4] and was used after fractional distillation; bp 112 °C (750 mmHg). The preparations of **1** and **2** were carried out by the method of Meisel *et al.*

Thiophene trimer [**1**]: bp 181—183 °C (2 mmHg); n_D^{20} 1.6455 (lit,[1] bp 167—170 °C (1 mmHg); n_D^{20} 1.6450).

2-Methylthiophene trimer [**2**]: bp 190 °C (2 mmHg); n_D^{20} 1.6103 (lit,[1] bp 190—193 °C (0.8 mmHg); n_D^{20} 1.6104).

*Preparation of the Crystalline Derivatives of **1** and **2**.* To 20 ml of glacial acetic acid we added 1.5 g (6 mmol) of **1**, followed by 20 ml of an aqueous solution of potassium permanganate (2.6 g, 8 mmol). The solution was stirred at 40—50 °C for 30 min. The resulting solution was treated with sodium hydrogen sulfite to dissolve the precipitated manganese dioxide. The solution was then extracted with two portions of ether. The combined ethereal layers were washed with a saturated sodium hydrogen carbonate solution and then successively twice with water. The ethereal extract was dried over anhydrous magnesium sulfate and concentrated. The residue was crystallized from ethanol to give 0.57 g of a crude product; mp 129.3 °C. The product was treated with active carbon in ethanol and then recrystallized to afford 0.37 g of a colorless crystalline product [**3**]; mp 133.3 °C. Found: C, 50.74; H, 4.27%, mol wt, 285.3 (measured in dioxane by means of a vapor-pressure osmometer). Calcd for $C_{12}H_{12}S_3O_2$: C, 50.67; H, 4.25%; mol wt, 284.4.

The crystalline derivative of **2** was prepared following the method of the preparation of **3**. From 1.0 g of **2**, 0.1 g of colorless fine crystals [**4**] was obtained; mp 146.5 °C. Found: C, 55.15; H, 5.68%; mol wt, 325.1. Calcd for $C_{15}H_{18}S_3O_2$: C, 55.17; H, 5.55%; mol wt, 326.5.

Results and Discussion

The NMR spectrum of **1** in CCl_4 reveals a signal at δ 6.7—7.1 (m, 6H). This signal is assigned to the protons of the two thienyl groups. This fact supports the structure of **1** proposed by Meisel *et al.*—2,4-bis-2′-thienylthiolane. Following the structure, the other signals are assigned to the six protons on the thiolane ring; the thiolane ring protons of the 2-position (δ 4.6—5.0, m, 1H), the 3-position (δ 2.0—2.5, m, 2H), the 4-position (δ 3.6—3.9, m, 1H), and the 5-position (δ 2.6—3.5, m, 2H).

The mass spectrum of **1** reveals a metastable ion at *m/e* 112. The presence of the metastable ion at *m/e* 112 (calcd: $(168)^2/252=112.0$) supports the following fragmentation process:

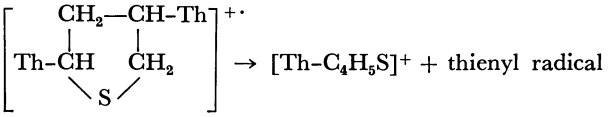

M^+ of **1**, *m/e* 252 *m/e* 168 (rel. intensity 98.8%)

Th; thienyl group

These NMR and mass spectral data are useful for investigating the unknown structure of **2**. If the trimerization of 2-methylthiophene occurs by means of the same reaction mechanism as that proposed by Meisel *et al.*, the following two kinds of structural formulas may be expected: 2,4-bis(5′-methyl-2′-thienyl)-2-methylthiolane or 2,4-bis(5′-methyl-2′-thienyl)-5-methylthiolane.

The remarkable resemblance between the NMR spectra of **1** and **2** indicates the structural resemblance between them. Thus, the signal at δ 6.3—6.8 (m,4H) is assigned to the protons of the two disubstituted thiophene nuclei, while the signal at δ 2.36 (s, 6H) is assigned to the two methyl groups substituted on the thiophene nuclei. The other signals are, then, assigned to the eight protons on the methylthiolane nucleus: the thiolane ring protons of the 3-position (δ 2.1—2.7, m, 2H; overlapped with a broad singlet at δ 2.36),

† Presented in part at the 30th Annual Meeting of the Chemical Society of Japan, Osaka, April, 1974.

the 4-position (δ 3.5—4.0 m, 1H) and the 5-position (δ 2.8—3.4, m, 2H), and the methyl protons attached to the 2-position of the thiolane ring (δ 1.8, s, 3H).

The presence of the singlet methyl signal at δ 1.8 shows that one of the two thienyl groups must be attached to the 2-position of the thiolane ring. The other thienyl group must, then, be attached to the 4-position of the thiolane ring. The structure of the two methylthienyl groups probably corresponds to that of the 5′-methyl-2′-thienyl groups, because the α and α' positions of the thiophene nucleus are actually more reactive than the β and β' positions. Therefore, the structure of **2** is identified with 2,4-bis(5′-methyl-2′-thienyl)-2-methylthiolane.

The mass spectrum of **2** reveals a metastable ion at *m/e* 131. This metastable ion supports the following fragmentation process (calcd=(196)²/294=130.6):

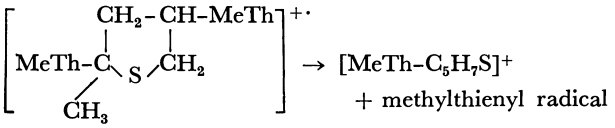

M⁺ of **2**, *m/e* 294 *m/e* 196 (rel. intensity 80.9%)
Meth; methylthienyl group

The NMR spectral pattern of **3** closely resembles that of **1**, and the two IR bands of **3** correspond to the characteristic bands due to the sulfone group: NMR ($CDCl_3$) δ 2.5—3.0 (m, 2H), 3.3—3.8 (m, 2H), 3.8—4.2 (m, 1H), 4.6—4.9 (m, 1H) and 6.9—7.4 (m, 4H); IR 1315 ($\nu_{as}SO_2$) and 1135 cm^{-1} ($\nu_{s}SO_2$). These facts support the structure of **3** as a sulfone derivative of **1**: 2,4-bis-2′-thienylthiolane 1,1-dioxide.

The structure of **4** was also identified as 2,4-bis(5′-methyl-2′-thienyl)2-methylthiolane 1,1-dioxide by the NMR and IR spectral data, and by elemental analysis: NMR ($CDCl_3$) δ 1.86 (s, 3H), 2.44 (s, 6H), 2.5—2.9 (m, 2H), 3.1—3.4 (m, 2H), 3.5—4.0 (m, 1H) and 6.5—7.0 (m, 4H); IR 1300 ($\nu_{as}SO_2$) and 1130 cm^{-1} ($\nu_{s}SO_2$).

No metastable ion peaks are found in the mass spectra of **3** and **4**. These spectral data suggest a quite different fragmentation process from those of **1** and **2**. The mass spectrum of **3** reveals the molecular ion peak at *m/e* 284 and some major peaks: *m/e* 110 (rel. intensity 100%), 220 (10%), and others. The presence of these ion peaks suggests the following possible fragmentation process for **3**:

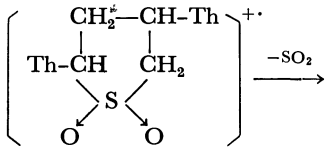

M⁺ of **3**, *m/e* 284

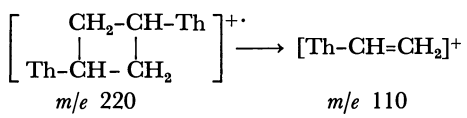

m/e 220 *m/e* 110

The mass spectrum of **4** lacks the molecular ion (*m/e* 326). However, the presence of several ion peaks at *m/e* 262 (rel. intensity 3%), 138 (100%) and 124 (21%) supports the following fragmentation process similar to that discussed in connection with the fragmentation of **3**:

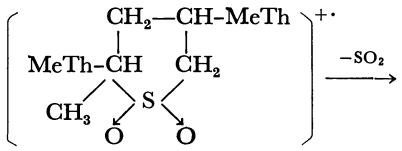

M⁺ of **4**, *m/e* 326

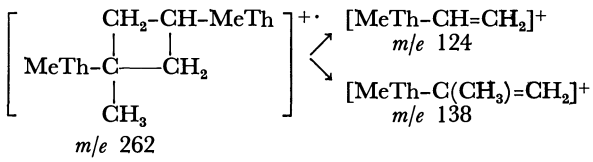

m/e 262

References

1) S. L. Meisel, G. C. Johnson, and H. D. Hartough, *J. Amer. Chem. Soc.*, **72**, 1910 (1950).
2) A. Ishigaki and T. Shono, This Bulletin, **47**, 1467 (1974).
3) A. W. Weston and R. J. Michaels, Jr., "Organic Syntheses," Vol. 31, p. 108 (1951).
4) D. Todd, "Organic Reactions," Vol. 4, p. 378 (1948).

BULLETIN OF THE CHEMICAL SOCIETY OF JAPAN, VOL. 48(10), 2979—2980 (1975)

A Theoretical Model for the Hydrogen Migration of Butyl Alcohol

Tsutomu TAKAGI and Masayoshi OIWA

Department of Applied Chemistry, Faculty of Engineering, Kansai University, Suita-shi, Osaka 564

(Received December 20, 1974)

Synopsis. The hydrogen-migration mechanism of the fragmentation of *n*-butyl alcohol in a mass spectrometer is discussed from the standpoint of the bonding interaction energy, as estimated by an all-valence electron semi-empirical SCF-MO treatment (CNDO/2-UHF), assuming the following models I and II:

$CH_2CH_2CH_2CH_2$-OH $\rightarrow$ $C_4H_8^{+}$ + H_2O (I)

H.....

$CH_3CHCH_2CH_2$-OH $\rightarrow$ $C_4H_8^{+}$ + H_2O (II)

H.....

Finally, Model I is suggested to be energetically favorable.

The elimination of H_2O from *n*-butyl alcohol[1] in the fragmentation by electron impact was suggested to be due to the intramolecular migration of a hydrogen atom from the γ- or δ-carbon to oxygen. However, the precise mechanism of the migration has not yet been elucidated, but only speculated from the mass spectra data.

The present paper is concerned with a discussion of the hydrogen migration mechanism in a mass-spectrometric fragmentation of *n*-butyl alcohol from the standpoint of the theory of the partition of the total energy.[2]

The models in the hydrogen migration are schematically represented in view of the least-motion path from the origin of migration to the terminus. It should be considered that the lengths and angles of each bond change with the migration steps of the hydrogen migration, and that the breaking of the carbon-oxygen bond requires more precise electronic structure calculations. However, in the calculations, the conformation of the molecule was already assumed to be the optimal ground state, as determined from the standard table.[3] Four steps were also chosen to form a path representing the hydrogen migration. The bond distances between the migration hydrogen (H_7 or H_9 in the two models respectively) and oxygen (O_5), and the energy profile along the migration steps, which was estimated by CNDO calculations, have also been listed in Table 1.

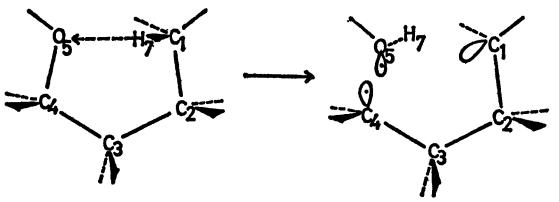

Model I

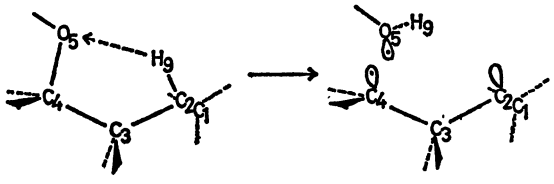

Model II

TABLE 1. COMPUTED TOTAL ENERGY AND PARTITION TERMS[a] WITH HYDROGEN MIGRATION

	Model I			
	1	2	3	4
R (H_7-O_5) (Å)	1.503	1.377	1.252	1.127
E_{total}(eV)	−1473.298	−1472.947	−1472.434	−1471.689
E^U+E^R	−2328.056	−2328.093	−2328.659	−2330.827
E^J	2954.263	2959.952	2965.194	2969.319
E^K	−75.930	−75.981	−76.068	−76.163
E^V	−6111.083	−6123.297	−6135.238	−6146.378
E^N	3243.770	3250.860	3258.260	3266.421
	Model II			
	1	2	3	4
R (H_9-O_5) (Å)	1.619	1.406	1.193	0.980
E_{total}(eV)	−1470.946	−1448.610	−1447.723	−1446.309
E^U+E^R	−2338.007	−2355.283	−2360.017	−2362.120
E^J	2755.547	2797.674	2793.019	2792.099
E^K	−75.246	−74.752	−74.962	−75.549
E^V	−5714.770	−5814.251	−5814.445	−5820.285
E^N	3043.687	3126.999	3131.315	3141.743

a) E^U is the total one electron AO energy of the electrons on atom A. E^R is the contribution of the resonance integral to the energy of the AB bond and is the main feature of the covalent bond. E^J is the repulsion of the electrons of the atoms A and B. E^K is the corresponding term of the electronic exchange interactions. E^V is the potential energy of the electrons on atom A in the field of nucleus B plus that of the electrons on atom B in the field of nucleus A. E^N represents the nuclear repulsion energy of the nuclei A and B.

Here, the driving factor for the migration was interpreted by using the partition method for the total energy. The total energies of both models increase with the hydrogen migration. The variation in the total energy in Model I is, however, smaller than that in Model II. The resonance energy term (E^U+E^R) decrease with the hydrogen migration in both models. It can be suggested that the decrease in the energy is due to the resonance effect and that the increase in the total energy results from the steric effect.

Now, the changes of the E_{AB} of each bond due to migration will be employed to estimate the bond length and the bond order.[4] The E_{AB} of the C_1–H_7

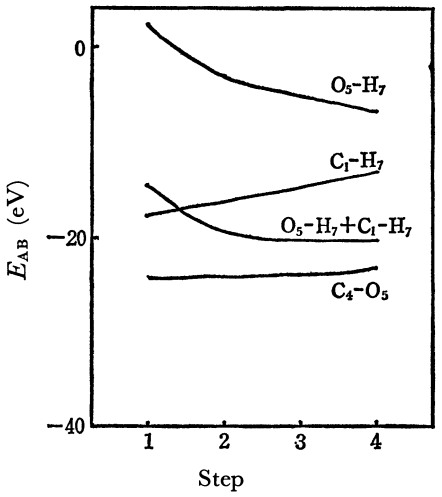

Fig. 1. Variation of E_{AB} of each bond due to migration through the least motion path in the model I.

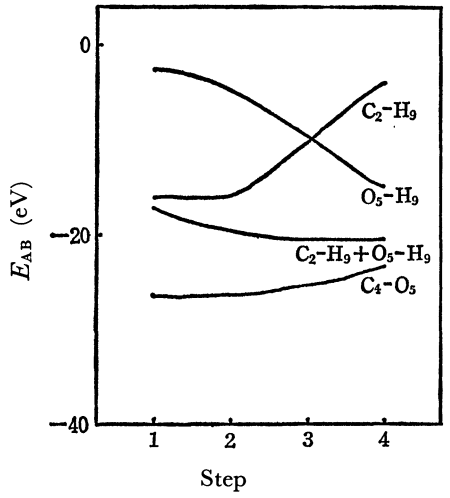

Fig. 2. Variation of E_{AB} of each bond due to migration through the least motion path in the model II.

bond becomes smaller and the E_{AB} of the O_5–H_7 bond becomes larger in Model I, as is shown in Fig. 1. Therefore, the sum of the E_{AB} values of the two bonds is significant. The sum of the E_{AB} values of the two bonds decreases along the migration steps. On the other hand, in Model II, as is shown in Fig. 2, the C_2–H_9 bond also becomes smaller, while the O_5–H_9 bond becomes larger. In the case of Model II, the sum of the E_{AB} values of the two bonds decreases with the hydrogen migration, the same tendency as in Model I. The decrease in the sum of the E_{AB} values of the two bonds implies that the bonding interaction between O_5 and the leaving hydrogen becomes strong along the coordinates representing the migration of hydrogen to O_5.

As is shown in Figs. 1 and 2, the bonding interaction energies of the C_4–O_5 bonds decrease with the approach of hydrogen to oxygen. In other words, the bonding interaction between C_4 and O_5 is weakened by the hydrogen migration. The variation in the bonding interaction of the C_4–O_5 bond in Model I was, however, smaller than that in Model II. Also, the E_{AB} values of the other carbon-carbon bonds are larger than that of the C_4–O_5 bond; the E_{AB} values of the C_4–O_5 bonds of Step 4 in Models I and II were calculated to be −23.753 eV and −23.376 eV respectively. Moreover, the E_{AB} values of the C_1–C_2, C_2–C_3, and C_3–C_4 bonds were found to be −29.124 eV, −28.497 eV, and −29.260 eV in Model I.

On the other hand, the E_{AB} values of the C_1–C_4 and C_2–C_4 non-bonds were found to change from 0.147 eV to 0.041 eV and from −0.015 eV to −0.255 eV respectively. The interaction between non-bonded carbon atoms (between C_1 and C_4 in Model I and between C_2 and C_4 in Model II) tends to change from the non-bonding to a weakly bonding state, *i.e.*, the sequence of ring formation.

Thus, these results may be related to the ease of the cleavage from the molecular ion (M ion) to the M-H_2O ion in the rearrangement reaction. Moreover, although the possibility of the hydrogen migration in Model II can not always be eliminated, the hydrogen migration *via* Model I may be estimated to be energetically favorable, judging from the variation in the total energy and the small steric effect compared with those of Model II. The simple models described in the present paper can provide sufficient information as the rearrangement reaction of *n*-butyl alcohol.

All the calculations were performed using a NEAC 2200 MODEL 700 computer at Osaka University.

References

1) H. Budzikiewcz, C. Djerassi, and D. H. Williams, "Mass Spectrometry of Organic Compounds," Helden Day, San Francisco (1967).

2) H. Fischer and H. Kollmar, *Theoret. Chim. Acta*, **16**, 163 (1970); M. S. Gordon, *J. Amer. Chem. Soc.*, **91**, 3122 (1969).

3) "Table of Interatomic Distances," Chem. Soc., Spec. Publ., No. 11 (1958); No. 18 (1965).

4) T. Yonezawa, H. Konishi, and H. Kato, This Bulletin, **42**, 933 (1969).

BULLETIN OF THE CHEMICAL SOCIETY OF JAPAN, VOL. 48(10), 2981—2982 (1975)

A Convenient Method for the Preparation of Aryl and Alkyl Isothiocyanates Using Amines, Carbon Disulfide, and a Grignard Reagent

Shizuyoshi SAKAI, Tatsuo FUJINAMI, and Toshiyuki AIZAWA

Department of Industrial Chemistry, Faculty of Engineering, Shizuoka University, Hamamatsu 432

(Received January 7, 1975)

Synopsis. The thermal decomposition of bromomagnesium *N*-aryl- or *N*-alkyl-*N*-bromomagnesio-dithiocarbamate (**3**), prepared *in situ* from amines, carbon disulfide, and a Grignard reagent, is a new and convenient method for the preparation of aryl or alkyl isothiocyanate.

The reported methods for the preparation of isothiocyanates from amines have usually involved the decomposition reactions of dithiocarbamate derivatives.[1-4] However, these methods are inconvenient, because a poisonous reagent, such as a heavy metal or a phosgene derivative, is used as the starting material. In view of this, we have already described a new method, which consists of the decomposition reaction of lithium *N*-lithio-dithiocarbamate prepared *in situ* using butyllithium. Grignard reagent appears also to have an interesting synthetic potential in isothiocyanate preparation. In this report, we will describe a more convenient and alternative approach for isothiocyanate synthesis using a Grignard reagent, and will compare this new method with that using an organolithium compound.

Aromatic amines were treated with two equivalents of ethylmagnesium bromide in tetrahydrofuran under a nitrogen atmosphere to form bis(bromomagnesio)-aniline (**2**; R=Aryl); then excess amounts to carbon disulfide were added below room temperature to give bromomagnesium *N*-aryl-*N*-bromomagnesio-dithiocarbamate (**3**; R=Aryl) *in situ*. The characteristic band of the ν_{NCS} of isothiocyanate could not be detected after the reaction mixture had been refluxed for 1 hr. After the evaporation of the mixture of tetrahydrofuran and excess carbon disulfide, the distillation residue was heated at 120—140 °C to decompose (**3**), thus affording aryl isothiocyanate (**4**; R=Aryl). The results for other amines are designated by 'Direct Method' in Table 1.

$$\underset{\mathbf{1}}{RNH_2} \xrightarrow[-2EtH]{+2EtMgBr} \underset{\mathbf{2}}{RN(MgBr)_2} \xrightarrow{+CS_2} \underset{\mathbf{3}}{RN(MgBr)CS_2MgBr} \xrightarrow[-(BrMg)_2S]{} \underset{\mathbf{4}}{RNCS} \quad (1)$$

The by-product, '$(BrMg)_2S$', could not be characterized, but it reacted violently with water to evolve hydrogen sulfide gas.

Bis(bromomagnesio)anilines are well known to be formed by the reaction of aromatic amines with a Grignard reagent.[6] However, the dimetallation reaction of primary aliphatic amines by organomagnesium is difficult to complete; therefore, the yields of alkyl isothiocyanates by the 'Direct Method' are rather low, except for cyclohexylamine (Table 1). To improve the yield of alkyl isothiocyanate, an alternative approach was tried; in it we treated alkylamine with the Grignard reagent and carbon disulfide, step-by-step, in the way described in Eq. (2) ('Step-by-step Method' in Table 1).

$$\underset{\mathbf{1}}{RNH_2} \xrightarrow[-EtH]{+EtMgBr} \underset{\mathbf{5}}{RNHMgBr} \xrightarrow{+CS_2} \underset{\mathbf{6}}{RNHCS_2MgBr} \xrightarrow[-EtH]{+EtMgBr} \mathbf{3} \xrightarrow[-(BrMg)_2S]{} \mathbf{4} \quad (2)$$

The temperature required to decompose the *N*-alkyl-*N*-bromomagnesio-dithiocarbamate (**3**; R=

Table 1. Yields of isothiocyanates in the decomposition reactions of bromomagnesium *N*-bromomagnesio-dithiocarbamates (**3**)

Amine used (RNH_2)	Direct Method (1) Yield (%)[a]	Step-by-step Method (2) Temp (°C[b])	Step-by-step Method (2) Yield (%)	Bp of RNCS (°C/mmHg)	ν_{NCS} (cm^{-1})
$EtNH_2$	—	c)	68	53—55/50	2090
n-$PrNH_2$	28	c)	93	71—72/45	2090
i-$PrNH_2$	—	c)	80	55—58/50	2090
n-$BuNH_2$	20	c)	85	83—85/50	2090
t-$BuNH_2$	21	c)	24	93—95/85	2090
Cyclo-$C_6H_{11}NH_2$	70	c)	90	104—105/10	2090
$PhNH_2$	82	~130	82	105—107/20	2070
p-$CH_3C_6H_4NH_2$	81	~130	87	106—109/10	2070
o-$CH_3C_6H_4NH_2$	71	~130	83	105—108/10	2070
α-Naphthyl-NH_2	30	—	—	125—127/0.5	2090
β-Naphthyl-NH_2	40	—	—	118—119/0.1	2110

a) Two mol of CS_2 and EtMgBr were used per one mol of amine through the reaction (1), and the reaction mixture prepared *in situ* was decomposed at 120—140 °C. b) The temperature where the carbamate (**3**) began to decompose. c) Refluxing temperature of tetrahydrofuran solution.

Alkyl) thus prepared was substantially lower than that needed for the corresponding *N*-aryl derivative (**3**; R=Aryl). The dithiocarbamate (**3**; R=Alkyl) was decomposed for 1 hr at the refluxing temperature in tetrahydrofuran, thus affording a good yield of **4**.

Contrary to the case of isothiocyanate synthesis using butyllithium, where two equivalents of carbon disulfide per mole of amine were essentially required,[5] the 'direct' and 'step-by-step' methods using the Grignard reagent needed only one equivalent of carbon disulfide. Although mechanistic comparisons of these reactions are now in progress, a four-centered scheme (**7a** or **7b** in Fig. 1) for the reaction using the Grignard reagent and a six-centered scheme (**8**) *via* a lithium intermediate can tentatively be suggested to explain the different amounts of carbon disulfide needed.

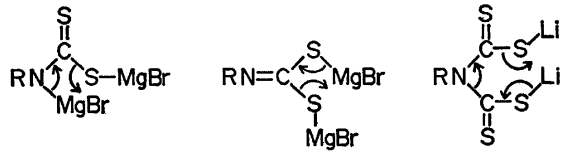

7a **7b** **8**

Fig. 1. Tentative schemes for isothiocyanate formation.

In conclusion, the Grignard reagent is superior to butyllithium both in purity and in yield of isothiocyanate obtained, except for the lower yield of isothiocyanate from sterically hindered amines such as *tert*-butylamine and α-naphthylamine.

Experimental

All the boiling points are uncorrected. The IR and NMR spectra were determined with a JASCO Model IRA-1 spectrometer and a Hitachi Perkin-Elmer Model R-24 spectrometer respectively. The tetrahydrofuran, carbon disulfide, and amines were dried using metallic sodium, diphosphorous pentoxide, and pellets of sodium hydroxide respectively, and were distilled before use. Some standard examples of the preparation of aryl and alkyl isothiocyanates are given below.

Thermal Decomposition of Bromomagnesium N-*Bromomagnesio*-N-*Phenyldithiocarbamate (**3**; R=Ph) (Direct Method).* In a flask equipped with a mechanical stirrer, a condenser, a dropping funnel, and a nitrogen inlet, ethylmagnesium bromide (110 mmol) was prepared in the usual manner from a magnesium ribbon (2.68 g; 110 mmol) and bromoethane (*ca.* 115 mmol) in dry tetrahydrofuran (80 ml) under a dry nitrogen atmosphere. To the solution we then slowly added aniline (4.66 g; 50 mmol) in dry tetrahydrofuran (5 ml), followed by 4 hrs' refluxing to form bis(bromomagnesio)aniline. The resulting suspension was treated slowly with excess amounts of carbon disulfide (7.61 g; 100 mmol) in tetrahydrofuran (5 ml) below room temperature. A violent heat evolution was observed in the reaction at room temperature; therefore, the mixture had to be cooled by mean of a water bath. The solution of the reaction mixture was heated for 1 hr and was then transferred into a distillation apparatus. After the solvent and excess carbon disulfide had then been recovered by distillation, the residue[7] was heated for 1 hr at 120—140 °C to decompose the bromomagnesium *N*-bromomagnesio-*N*-phenyldithiocarbamate (**3**; R=Ph), thus affording phenyl isothiocyanate (**4**; R=Ph). The product was redistilled *in vacuo* to separate **4** (R=Ph); yield 5.54 g (82% based on the aniline used); bp 105—107 °C/20 mmHg (Ref,[5] 96—98 °C/15 mmHg); IR(neat) ν_{NCS} 2070 cm^{-1}. The NMR and IR spectra were in good agreement with those of the authentic sample prepared by the published method.[5]

Even when an equivalent amount of carbon disulfide (3.81 g; 50 mmol) was used in the reaction with bis(bromomagnesio)aniline, phenyl isothiocyanate was obtained in a slightly lower yield (75%). However, excess amounts (two equivalents) of carbon disulfide were used in most cases; the results are summarized in Table 1.

Hydrogen sulfide was violently evolved by the addition of water to the distillation residue.

Thermal Decomposition of Bromomagnesium N-*Bromomagnesio*-N-*butyldithiocarbamate (**3**; R=Bu) (Step-by-step Method).* A solution of *n*-butylamine (3.66 g; 50 mmol) in tetrahydrofuran (5 ml) was added, drop-by-drop, to a solution of ethylmagnesium bromide (55 mmol) in tetrahydrofuran (50 ml) under dry nitrogen in the apparatus described above. After refulxing for 1 hr, the solution of **5** (R=Bu) was treated with an equivalent amount of carbon disulfide (3.81 g; 50 mmol) in tetrahydrofuran (5 ml) under cooling by water, to form the *N*-butyl-dithiocarbamate salt (**6**; R=Bu). Heat evolution was observed during this procedure at room temperature. The solution thus prepared *in situ* was treated again with ethylmagnesium bromide (55 mmol) to give bromomagnesium *N*-bromomagnesio-*N*-butyldithiocarbamate (**3**; R=Bu) and ethane. After the reaction mixture had then been heated with stirring for 1 hr under reflux, the characteristic band of isothiocyanate at 2090 cm^{-1} appeared in the IR spectrum of the product mixture. The tetrahydrofuran was recovered by distillation, and the residue was heated for 1 hr at 120—140 °C. Butyl isothiocyanate was obtained by distillation *in vacuo*; yield 4.89 g (85%); bp 64—66 °C/20 mmHg (lit,[5] 47—48 °C/10 mmHg); IR(neat) ν_{NCS} 2090 cm^{-1}.

In separate experiments, an additional amount of carbon disulfide (3.81 g; 50 mmol) was added to the solution of **3** (R=Bu), but no heat evolution was ever observed. The treatment of the reaction mixture in the same manner as has been described above afforded an 86% yield of BuNCS.

References

1) J. E. Hodgkins, W. P. Reeves, and M. G. Ettlinger, *J. Org. Chem.*, **21**, 404 (1956); **29**, 3098 (1964).

2) T. Wagner-Jauregg, H. Arnold, and H. Rausen, *Ber.*, **74**, 1372 (1941).

3) K. Itoh, I. K. Lee, I. Matsuda, S. Sakai, and Y. Ishii, *Tetrahedron Lett.*, 2667 (1967).

4) F. B. Dains, R. Q. Brewster, and C. P. Olander, "Organic Syntheses," Coll. Vol. I, p. 71 (1956).

5) S. Sakai, T. Aizawa, and T. Fujinami, *J. Org. Chem.*, **39**, 1970 (1974).

6) E. W. Abel and G. R. Willey, *J. Chem. Soc.*, **1964**, 1528.

7) Solid at room temperature but melted at the beginning of the distillation.

BULLETIN OF THE CHEMICAL SOCIETY OF JAPAN, VOL. 48(10), 2983—2984 (1975)

The Reaction of *N*-Phenylsulfonyl Thione *S*-Imide with Acyl Halides[1)]

Seizo TAMAGAKI, Keishi SAKAKI, and Shigeru OAE[2)]

Department of Applied Chemistry, Faculty of Engineering, Osaka City University, Sugimoto-cho, Sumiyoshi-ku, Osaka 558

(Received January 21, 1975)

Synopsis. Thiocarbonyl *S*-imide of 1,2-dithiole-3-thione reacted with various acyl halides producing the corresponding *N*-phenylsulfonyl-1,2-benzodithiole-3-imine and elemental sulfur. The reaction was found to proceed *via* initial acylation on the nitrogen of the imide and was essentially acyl halide-catalyzed with regard to rearrangement.

The authors have shown previously that the *N*-phenylsulfonyl thione *S*-imide(I) underwent rearrangement accompanied by desulfurization producing product(II) either by heating in neat[3)] or by treating with various nucleophiles such as amines[4)] and mercaptans.[5)]

We have now extended the investigation to the reaction of I with several electrophilic reagents and it has been found that the *S*-imide(I) produces the corresponding *N*-phenylsulfonyl imine(II) in good yield upon treatment with a variety of acyl halides. This paper describes a detailed account of the reaction.

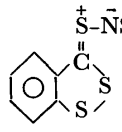
(I)

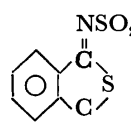
(II)

Results and Discussion

When the imide(I) was allowed to react with an equimolar amount of trichloroacetyl chloride at room temperature in CH_2Cl_2, yellowish elemental sulfur followed by a trace of hydrochloride(III) of the imide(I) precipitated from the solution within minutes, and then the imine(II) was isolated in a 75% yield along with a small amount of the reduction product, benzotrithione(IV), by preparative layer chromatography. The hydrochloride(III) seems to be produced by the reaction of imide(I) with the hydrochloric acid inevitably present or generated in normal reacting systems containing acyl halides.

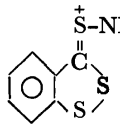
Cl⁻ (III)

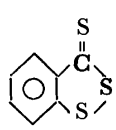
(IV)

As is seen from Table 1, only less than one-half an equimolar amount of trichloroacetyl chloride is sufficient to complete the reaction. This indicates clearly that the reaction is essentially acyl halide-catalyzed with regard to the rearrangement reaction, where the halide is utilized repeatedly during the reaction. In fact, after completion of the reaction with an equimolar amount of trichloroacetyl chloride, 75% of the halide remained unchanged.

The reactions with aroyl chlorides were likewise found to produce both the rearranged product and a trace amount of benzotrithione. The reaction times required for benzoyl chlorides bearing electron-donating substituents are longer than those with electron-capturing substituents. This implies that acylation of the nitrogen atom of the imide(I), leading to an intermediate(V), is the key step in the reaction. Meanwhile, both thionyl and sulfinyl chlorides can also react in a similar manner to produce the imine(II).

Thus, based on these results and intuitive considerations, the outline of the reaction scheme may be written as follows:

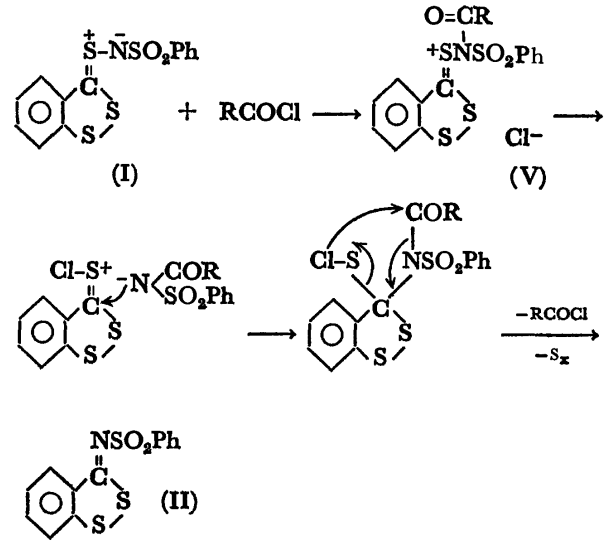

TABLE 1. ACYL HALIDE-CATALYZED REARRANGEMENT OF I IN CH_2Cl_2 AT ROOM TEMPERATURE

Halide	Mole ratio[a)]	Reaction time[b)]	Isolated yield, % II	IV
O_2N-C_6H_4-COCl	1.0	1 hr	75	trace
Cl-C_6H_4-COCl	5.0	1 hr	70	5
C_6H_5-COCl	5.0	2 hr	80	g)
MeO-C_6H_4COCl	5.0	10 hr	40	g)
CCl_3COCl[c)]	1.0	5 min	72	5
CCl_3COCl	0.5	10 min	68	8
CCl_3COCl	0.3	10 min	89	5
CCl_3COCl[d)]	1.0	10 min	43	15
CCl_3COCl[e)]	1.0	5 min	84	10
$SOCl_2$	1.2	5 min	62	10
O_2N-C_6H_4-SOCl	1.0	10 min	26[f)]	5

a) Ratio of I to acyl halide. b) Required time for the change in color of the solution from red to yellow. c) The amount of the remaining halide was determined as 75% using the IR absorption band at 1795 cm^{-1} due to the carbonyl group in trichloroacetyl chloride. d) For *p*-nitrophenylsulfonyl thione *S*-imide. e) for *p*-methylphenylsulfonyl thione *S*-imide. f) The low yield was mainly due to the formation of III. g) No yield was determined.

Experimental

A typical run is as follows. To *S*-imide(I) (339 mg, 1 mmol) in CH_2Cl_2 well-dried over $CaCl_2$ one equivalent of trichloroacetyl chloride dissolved in the same solvent was added at room temperature. After 5 min the solution turned yellow. The solvent was evaporated under reduced pressure and then the residue was separated b preparative tlc using benzene as the eluent. The yields thus obtained are listed in Table 1.

References

1) Derivatives of 1,2-Dithiole-3-thiones. Part IX.
2) Present address: Department of Chemistry, Tsukuba University, Sakura-mura, Niihari-gun, Ibaraki-ken 300-31.
3) Part II. S. Tamagaki, K. Sakaki, and S. Oae, This Bulletin, **46**, 2608 (1973).
4) Part VII. S. Tamagaki, K. Sakaki, and S. Oae, *ibid.*, **47**, 3084, (1974).
5) Part X. Submitted for publication to this Bulletin.

BULLETIN OF THE CHEMICAL SOCIETY OF JAPAN, VOL. 48(10), 2985—2986 (1975)

Kinetic Studies of the Thiol-catalyzed Rearrangement of *N*-Phenylsulfonyl Thione *S*-Imide[1)]

Seizo TAMAGAKI, Keishi SAKAKI, and Shigeru OAE[2)]

Department of Applied Chemistry, Faculty of Engineering, Osaka City University, Sugimoto-cho, Sumiyoshi-ku, Osaka 558

(Received January 27, 1975)

Synopsis. The *N*-phenylsulfonyl thione *S*-imide(I) of 1,2-dithiole-3-thione reacted catalytically with various thiols to afford the corresponding rearranged *N*-phenylsulfonyl-1,2-benzodithiole-3-imine(II) with the extrusion of the elemental sulfur together with a minor amount of reduced benzotrithione. A kinetic study of the rearrangement of I with thiobenzoic acid was performed, and a plausible mechanism is discussed.

Recently we reported the reaction of I with a variety of amines to give the corresponding rearranged(II) and amine-exchanged(III) products. A detailed kinetic study of this reaction suggested that the rate-controlling step is the attack of amine on the tetravalent sulfur atom rather than on the carbon-3 of the thione *S*-imide(I) to give the addition complex(IV), which, in the subsequent step, yields an ion-pair that eventually collapses to give the products outlined below:

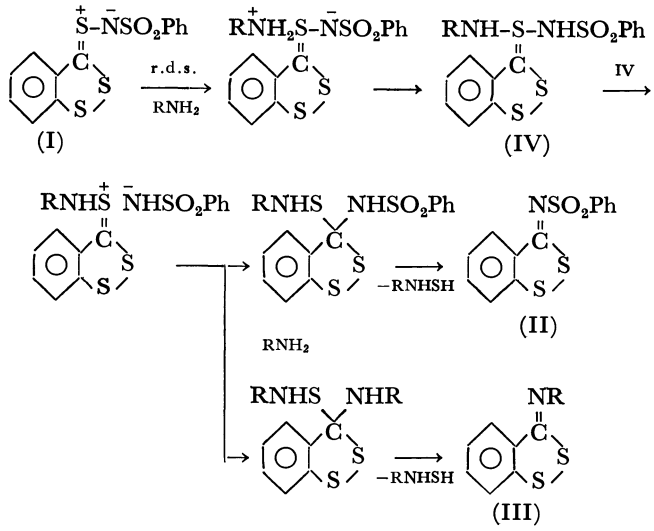

In this paper we wish to report our findings on an interesting rearrangement in which the thione *S*-imide(I) readily reacts catalytically with various thiols to afford mainly the same rearranged product(II) as in the amine-catalyzed rearrangement; however, the reaction was found to be quite different in its reaction mechanism from that with amines.

Results and Discussion

When I was treated with various inorganic sulfides, organic thiols, and thioacetic or thiobenzoic acid in CH_3CN or CH_2Cl_2 at room temperature, the precipitation of a yellowish, elemental sulfur was observed; furthermore, the rearranged product(II), benzotrithione, and the sulfonamide could be obtained.

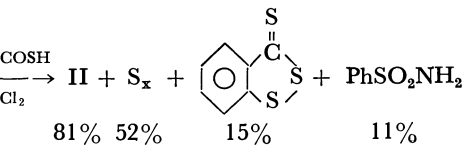

The results of the product analyses are collected in Table 1. In order to focus our attention especially on the rearrangement of this hitherto unknown type, a kinetic study of the reaction between I and thiobenzoic acid was carried out in CH_3CN at about 20 °C. At the given initial thiobenzoic acid concentrations in the range of $1—5\times10^{-5}$ mol/l, the reaction was found to follow strictly first-order kinetics with regard to the thione *S*-imide (I) up to more than half-lives.

The plot of the pseudo-first-order rate constants (k_{obsd}) thus obtained against the thiobenzoic acid concentrations showed a fairly good straight line in the $1—5\times10^{-5}$ mol/l range, as shown in Fig. 1, while in the concentrations below this range the plot was found to shift the straight line upward. It seems likely that, in the range of high concentrations of thiobenzoic acid, the over-all reaction follows second-order kinetics essentially and that the reaction rate is not much affected by the occurrence of the reduction leading to the formation of benzotrithione and the

TABLE 1. REACTION OF I WITH EQUIMOLAR AMOUNTS OF THIOLS AT ROOM TEMPERATURE

Thiol	Solvent	Product (%)			
		II	S_x	Benzotrithione	$PhSO_2NH_2$
NaSH	$CHCl_3$	24.8	a	64.5	a
H_2S	$CHCl_3$	44	a	55	46
H_2S	CH_3CN	21.2	a	76.4	39.7
EtSH	CH_2Cl_2	63	33	20	a
p-ClC_6H_4SH	CH_2Cl_2	67	65	22	21
CH_3COSH[b)]	CH_2Cl_2	49	a	30	a
CH_3COSH	CH_2Cl_2	54	a	a	a
PhCOSH	CH_2Cl_2	78	50	15	8
PhCOSH	CH_3CN	71.5	60.4	17.5	14.5
p-$MeOC_6H_4COSH$	CH_2Cl_2	69	78	17	18
p-ClC_6H_4COSH[c)]	CH_2Cl_2	72	a	23	15
p-ClC_6H_4COSH[d)]	CH_2Cl_2	81	52	15	a
$(n\text{-PrO})_2PS_2H$[e)]	CH_2Cl_2	52	a	38	a

a) Yields were not determined. b) Thirteen molar excess of thiol was used. c) One-third equiv. of thiol to I was used. d) In the presence of an equimolar amount of *p*-$MeC_6H_4SO_2NH_2$. e) Two molar excess of thiol.

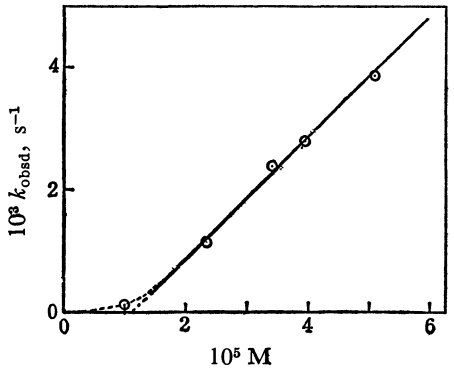

Fig. 1. Effect of acid concentration on the reaction at 1.0×10^{-4} mol/l of I in CH_3CN at 24.2 °C (X=H, Y=Cl).

Table 2. Rate constants for the reactions of *p*-substituted I[a] with *p*-substituted thiobenzoic acids[b] in CH_3CN at 24.2 °C

p-Substituent, X, in I[c]	*p*-Substituent, Y, in acid[d]	$10^3\ k_{obsd}$, s^{-1}
Br	Cl	7.59
H	Cl	3.90
Me	Cl	2.83
H	Cl	3.90[e]
H	H	2.40
H	Me	1.92
H	MeO	1.74

a) 10.0×10^{-5} mol/l. b) 5.06×10^{-5} mol/l. c) $\rho_X=+1.06$. d) $\rho_Y=+0.7$. e) $\Delta H^{\neq}=11.9\pm1.0$ kcal/mol, $\Delta S^{\neq}=-8.0\pm3.0$ eu.

sulfonamide. The fact that I was recovered in a appreciable yield when I was treated with less than a one-fifth equiv. of thiobenzoic acid implies that the added acid was completely consumed by a side-reaction before the rearrangement was completed.

In order to clarify the mechanism, especially the rate-determining step of the reaction, the effects of the substituent and temperature on the rate were examined in CH_3CN as a solvent at the thiobenzoic acid concentration of 5×10^{-5} mol/l; the results are listed in Tables 2. An inspection of the data reveals that the *rho* values (ρ_X and ρ_Y) for the para-substituents, X in I and Y in thiobenzoic acid, are both positive, *i.e.*, 1.06 and 0.7 respectively. In sharp contrast to the previously reported reaction with amines ($\rho_X=+0.13$)[3] and phosphines ($\rho_X=+0.08$),[4] where the attack of the nucleophiles on the sulfur atom is considered to be rate-determining, the rate is very sensitive to the nature of the substituent(X). Thus, the fairly large value of ρ_X is fully consistent with Pathway I, as is shown below, when the reaction proceeds *via* the initial addition of thiobenzoic acid to the S–N moiety of I prior to the rate-controlling S–NSO_2 bond cleavage, eventually leading to the products *via* an ion-pair.

Another pathway involving the rate-determining nucleophilic attack of RS^- on the sulfur atom can readily be ruled out, since the activation energy for the reaction involving the rate-determining addition

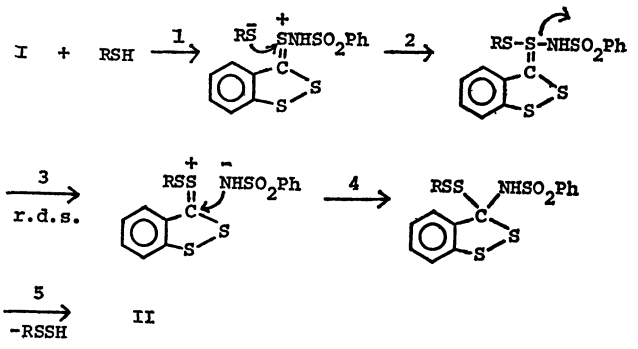

Path I.

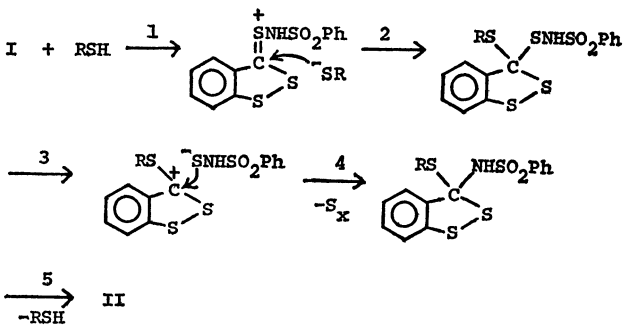

Path II.

(Step 2 in Path I) would be low; it is estimated to be around 5 kcal/mol based on the activation energeis of 4±1 and 3±2 kcal/mol for the reactions with amines and phosphines respectively.

The large ρ_X value offers strong evidence against Pathway II, which proceeds through the rate-determining carbon attack. The HASB principle also seems to support the above conclusion, since a soft nucleophile(RS^-) tends to attack a soft electrophilic sulfur center rather than a hard electrophilic carbon center.[5]

Hence, the study of the effects of substituent and temperature on the rearrangement shows that both the large ρ_X value and an energy of activation as large as 12 kcal/mol are in accordance with the mechanism involving the S–N bond breaking in the rate-determining step.

Experimental

A typical run is as follows: to the imide(I)(339 mg, 1 mmol) in CH_2Cl_2, an equivalent thiol dissolved in the same solvent was added at room temperature. After 5 min, the solution turned yellow. The solvent was evaporated under reduced pressure, and then the residue was separated by preparative tlc using benzene. The yields thus obtained are listed in Table 1. The rate constants (k_{obsd}) were determined spectrophotometrically by the usual procedure.

References

1) Derivatives of 1,2-Dithiole-3-thiones. Part X.

2) Present address: Department of Chemistry, Tsukuba University, Niiharigun, Ibaraki-ken 300-31.

3) Part VII of this series, S. Tamagaki, K. Sakaki, and S. Oae, This Bulletin, **47**, 3084 (1974).

4) S. Tamagaki, K. Sakaki, and S. Oae, *Heterocycles*, **2**, 631 (1974).

5) J. O. Edwards and R. G. Pearson, *J. Amer. Chem. Soc.*, **84**, 16 (1962); R. G. Pearson, *ibid.*, **85**, 3533 (1963).

BULLETIN OF THE CHEMICAL SOCIETY OF JAPAN, VOL. 48(10), 2987—2988 (1975)

Derivatives of 1,2-Dithiole-3-thione. XI. A Kinetic Study of the Reduction of *N*-Phenylsulfonyl Thione *S*-Imide with Halide

Seizo TAMAGAKI, Keishi SAKAKI, and Shigeru OAE*

Department of Applied Chemistry, Faculty of Engineering, Osaka City University, Sugimoto-cho, Sumiyoshi-ku, Osaka 558
**Department of Chemistry, Tsukuba University, Sakura-mura, Niihari-gun, Ibaraki-ken 300-31*

(Received March 17, 1975)

Synopsis. *N*-Phenylsulfonyl thione *S*-imide(I) was reduced with tetra-*n*-butylammonium bromide and iodide in the presence of trichloroacetic acid to yield benzotrithione and the sulfonamide in good yields. The kinetics of the reaction was performed, and the mechanism was discussed in detailed.

Earlier we reported[1] the isolation and characterization of the thione *S*-imide(I) formed in the reaction of chloramine-B with 1,2-benzodithiole-3-thione (benzotrithione).

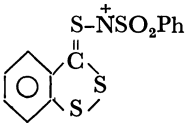

(I)

Our primary interest in this new type of the compound was to elucidate the mechanism of its formation. Previously,[2] the reaction of diphenyl sulfide with chloramine-T was found to be acid-catalyzed and to take place through an initial chlorination of the sulfur atom to give the chlorosulfonium ion, followed by nucleophilic displacement with the sulfonamide anion; the rate-limiting step is the former rather than the latter step.

Quite contrary to the rate of common sulfilimide formation, the thione *S*-imide formation did not allow us to determine its rate because the rate of the reaction was too fast for us to employ the usual techniques even at a neutral pH. The object of the present study was to examine the reduction of the thione *S*-imide with halide, since although the rate of the formation could not be followed by our usual means, as has been stated above, an examination of the reduction should clarify the mode of its reverse reaction, *i.e.* the formation, according to the microscopic reversibility principle.

Results and Discussion

When the thiocarbonyl *S*-imide(I) was treated with an equimolar amount of tetra-*n*-butylammonium bromide (Br^-) or iodide in CH_3CN containing a five-fold excess of trichloroacetic acid (H^+) at room temperature for 20 min, benzotrithione and benzenesulfonamide were both obtained in excellent yields.

The reaction was catalyzed essentially by acids with pH values of a moderate strength. In fact, a weak acid such as acetic acid with a pH of 4.76 did not catalyzed the reduction, not even in a neat acetic acid solution.

The kinetic study of the reaction of *S*-imide with bromide was carried out in some detail by adding a large excess of acid and by monitoring the increase in the absorbance due to the reduced trithione appearing at 445 nm. At high acid concentrations, as the UV spectra indicate, all the *S*-imide has been protonated on the nitrogen atom; that is, the protonated *S*-imide is the only predominant species at the initial stage of the reaction. Indeed, there is an isosbestic point at 443 nm between the benzotrithione produced and what appears to the protonated *S*-imide (Fig. 1). The data for the substituent effect on the rate are collected in Table 1, where k_0 is the observed first-order-rate constant of the reaction, which follows simple first-order kinetics.

First, we attempted to determine the kinetic order with regard to both the acid and bromide concentrations. At a large excess of acid concentrations relative to the *S*-imide, additional protic acid did not play any important role in accelerating the rate, as is shown in Fig. 2. Under these reaction conditions, kinetic experiments at different initial concentrations of bromide salt were performed and showed that the rate constants(k_0) thus determined did not follow the usual first-order kinetics with regard to the bromide concentrations, but gave a correlation represented by a down-concave curvature, as is shown in Fig. 3.

In the initial range of the plot the rate appears to obey first-order kinetics, while at the higher bromide concentrations the rate appears to be essentially independent of the bromide concentration. It thus seems clear that the reaction is indeed consistent with

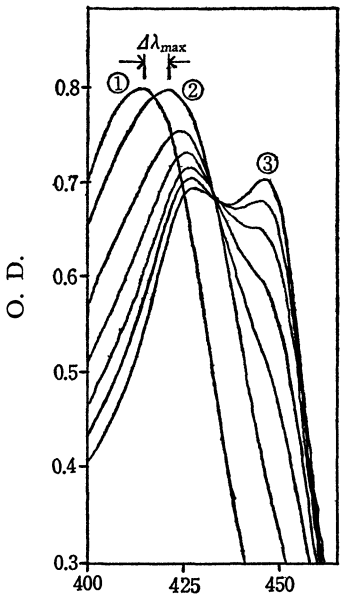

Fig. 1. Reduction of I with Br^- in the presence of Cl_3CCOOH.
①: (I) + H^+, ②: (I)+H^++Br^-, ③: benzotrithione

TABLE 1. KINETIC DATA FOR THE REDUCTION OF VARIOUS SUBSTITUTED THIOCARBONYL *S*-IMIDE WITH Br^- IN THE PRESENCE OF Cl_3CCOOH

Substituent(X)	CH_3	H	Br	*m*-NO_2
$k_0 \times 10^5$ s^{-1}	5.78	7.34	13.4	30.7

$[Br^-]=8.01\times10^{-4}$ M, $[H^+]=1.21\times10^{-1}$ M, $[I]=1.00\times10^{-4}$ M, at 25.25 °C.

step-by-step processes involving the buld-up of at least one Br^--containing intermediate, which we assumed to be an intimate ion-pair(II).

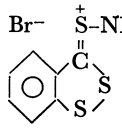

ion-pair (II)

In Fig. 3 a plot of the change of the UV maxima against varying bromide concentrations is also shown. An inspection of Fig. 3 reveals that the change in the absorption maximum by varying the bromide concentration gives a good parallelism with the change in the rates. This observation can best be accounted for by a specific solute-solute interaction between the protonated *S*-imide and Br^-; that is, the reduction takes place *via* the formation of quite a stable intimate ion-pair intermediate(II).

The Hammett plot of the data(Table 1) gives the best linear correlation with the σ_p values for the para-substituted *S*-imide. The direction of the substituent effect is shown by the large, positive value of $\rho=0.9$ indicating that, in the rate-determining step, the S-NSO_2 bond cleavage apparently takes place. The two reaction mechanisms, A and B, fit the experimental data thus obtained.

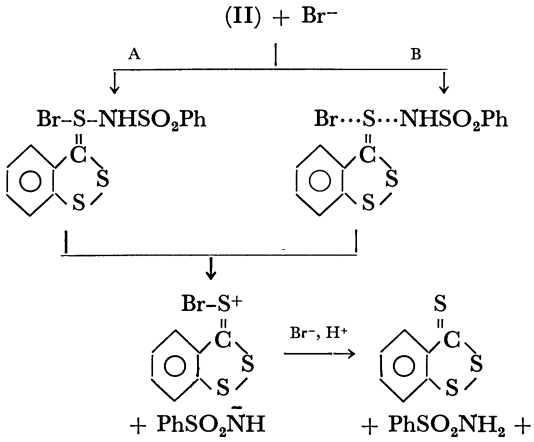

Both the activation energy and entropy, 13 kcal/mol and −25 eu respectively, at $[Br^-]=8.01\times10^{-4}$ M and $[H^+]=1.21\times10^{-1}$ M are well consistent with these mechanisms. The first one (A) involves the addition-elimination of the nucleophilic Br^- ion on the sulfur atom, followed by the rate-determining N-S bond cleavage, leading to a bromonium salt and eventually giving the reduced trithione. Meanwhile, the (B) mechanism resembles that outlined for a usual S_N2 reaction on a carbon atom; this process requires a one-step displacement of the leaving sulfonamide anion by the bromide anion.

Based on only the limited data available it is difficult to decide whether or not this reduction involves an discrete addition intermediate. However, a more plausible mechanism would be the process like A which includes the intervention of an addition complex in which the entering and leaving groups are bonded to the central sulfur atom. Such a hypervalent intermediate has been documented in other substitution reactions[3] and, in some cases, isolated.[4] In fact, quite a structurally similar planar compound has recently been synthesized.[5]

Finally, it should be emphasized that the Br^--reduction itself is the reverse of the formation of the

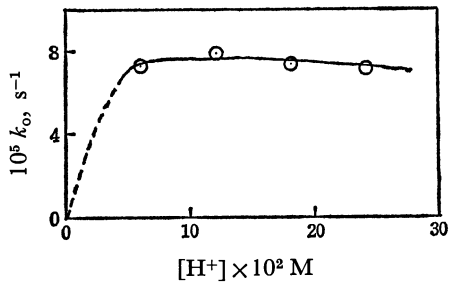

Fig. 2. Plot of the rate constant against acid concentration at 25 °C in CH_3CN. $[Br^-]=8.01\times10^{-4}$ M, $[I]=1.00\times10^{-4}$ M.

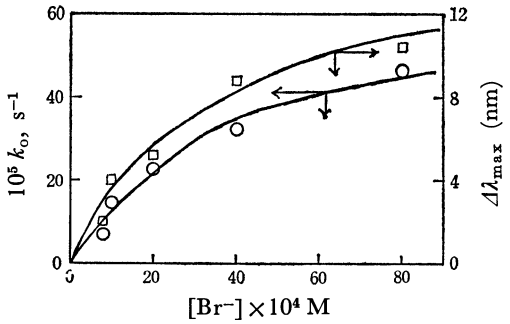

Fig. 3. Plots of the rate constant and $\Delta\lambda_{max}$ against Br^- concentration in the presence of a large excess of acid at 25 °C in CH_3CN. $[CCl_3COOH]=1.21\times10^{-1}$ M, $[I]=1.00\times10^{-1}$ M.

S-imide from the trithione and chloramine-B. From a consideration of the microscopic reversibility, it can be said that the *S*-imide is probably produced not by the mechanism involving the initial halogenation as the rate-controlling step, but rather, by the rate-determining attack of the sulfonamide anion on the halogenated trithione in sharp contrast to the mechanism of the formation of the sulfilimide where the halogenation is the rate-determing step.[2]

Experimental

Kinetics. The rates were determined spectrophotometrically by employing the usual techniques.

Products. The *S*-imide (339 mg) was treated with an equimolar amount of tetra-*n*-butylammonium bromide and a five-fold excess of Cl_3CCOOH in CH_3CN at room temperature. After 20 min, the solvent was evaporated *in vacuo* and the residue was treated with a dilute $Na_2S_2O_3$ solution. Extraction with ether, the evaporation of the ether, and the chromatographic separation of the extract on silica plates, using benzene as the eluent, gave benzotrithione (85.9%) as well as benzenesulfonamide (91.1%)

References

1) Part I of this series, S. Tamagaki and S. Oae, *Tetrahedron Lett.*, **1972**, 1159; Part VII of this series, S. Tamagaki, K. Sakaki, and S. Oae, This Bulletin, **47**, 3084 (1974).

2) K. Tsujihara, N. Furukawa, K. Oae, and S. Oae, This Bulletin, **43**, 263 (1969).

3) E. Ciuffarin and G. Cuaraldi, *J. Amer. Chem. Soc.*, **91**, 1745 (1969); F. A. Davis, S. Divald, and A. H. Confer, *Chem. Commun.*, **1971**, 194.

4) J. C. Martin and R. J. Arhart, *J. Amer. Chem. Soc.*, **93**, 2339 (1971); J. M. Shreeve, *Accounts Chem. Res.*, **6**, 387 (1973); E. F. Perozzi, J. C. Martin, and I. C. Paul, *J. Amer. Chem. Soc.*, **96**, 578 (1974).

5) I. Pomerantz, L. Miller, E. Lustig, D. Mastbrook, E. Hausen, R. Barron, N. Oates, and J. Y. Chen, *Tetrahedron Lett.*, **1969**, 5307; R. D. Gilardi and I. L. Karle, *Acta Crystallogr., Sect. B.*, **27**, 1073 (1971).

BULLETIN OF THE CHEMICAL SOCIETY OF JAPAN, VOL. 48(10), 2989—2990 (1975)

The Conversion of Penicillin *S*-Oxides into Cephalosporin *S*-Oxides

Toshiyasu ISHIMARU and Tsuneo IMAMOTO

The Institute of Scientific and Industrial Research, Osaka University, Yamadakami, Suita, Osaka, 565

(Received April 3, 1975)

Synopsis. The reaction of penicillin *S*-oxides (**1a,b**) with *N*-bromosuccinimide afforded sulfinyl bromides (**2a,b**) in high yields. The bromides were converted into cephalosporin *S*-oxides (**4a**, **4b**, **6a**, and **7a**) in fairly good yields.

It is well known that sulfenic acid is generated by a thermal sigmatropic rearrangement of penicillin *S*-oxide. The highly reactive sulfenic acid has been trapped by several methods.[1,2] We have also investigated a method for trapping sulfenic acid with the objective of the preparation of a useful intermediate for the synthesis of cephalosporin analogues. In this paper the reaction of penicillin *S*-oxides with *N*-bromosuccinimide (NBS) is described and a few examples of the conversion of the produced sulfinyl bromides into cephalosporin *S*-oxides are noted.

The reaction of methyl 6-phthalimidopenicillinate 1-oxide (**1a**) with 1 equivalent of NBS in boiling CCl_4 afforded sulfinyl bromide (**2a**) in high yield. The NMR spectrum of **2a** resembles closely that of the corresponding sulfinyl chloride, prepared by the reaction of **1a** with sulfuryl chloride according to the method of Kukolja *et al.*[3] The structural assignment of **2a** is also supported by the reaction of **2** with aniline; readily reacted with 2 equivalents of aniline to give sulfinamide (**3a**).

A noteworthy fact is that **2a** was successfully converted into cephem *S*-oxide by the action of 1 equivalent of tertiary amine. When **2a** was treated with triethylamine in CCl_4, the ring-closed product **4a** was obtained in 47% yield. In a similar manner, trichloroethyl ester *S*-oxide (**1b**) was transformed into the corresponding cephem *S*-oxide (**4b**).

In connection with the above results, we examined the preparation of 3-bromomethyl cephem *S*-oxide (**6a**) and 3-acetoxymethyl cephem *S*-oxide (**7a**). The reaction of **2a** with NBS in the presence of benzoyl peroxide (BPO) in boiling CCl_4 provided **5a** (not isolated), which, on subsequent treatment with triethylamine, gave **6a** in 33% yield. The direct bromination of **4a** with excess NBS in the presence of BPO in boiling benzene also afforded **6a**. The bromide **6a** was then acetoxylated by the action of AgOAc in AcOH to give **7a** in 45% yield.

Experimental

Preparation of Methyl 3-Methyl-2-(2-bromosulfinyl-4-oxo-3-phthalimido-1-azetidinyl)-3-butenoate (2a). A mixture of methyl 6-phthalimidopenicillinate 1-oxide (**1a**) (376 mg, 1 mmol) and NBS (178 mg, 1 mmol) in 15 ml of CCl_4 was refluxed for 1.5 hr under N_2. The precipitated succinimide was removed by filtration and the filtrate was evaporated to afford a yellow amorphous solid. This product was found from its NMR spectrum to be a 2 : 1 mixture of the two diastereomers of the compound **2a** which were epimeric at sulfur.[4] Yield, 442 mg (97%). NMR ($CDCl_3$): major component, δ 1.96 (3H, br. s), 3.84 (3H, s), 5.03 (2H, br. s), 5.20 (1H, br. s), 5.85 (1H, d, J=5 Hz), 6.08 (1H, d, J=5 Hz), 7.83 (4H, m); minor component, δ 2.00 (3H, br. s), 3.84 (3H, s), 4.90 (2H, br. s), 5.12 (1H, br. s), 5.82 (1H, d, J=5 Hz), 6.08 (1H, d, J=5 Hz), 7.83 (4H, m).

Reaction of 2a with Anilline. Into the solution of **2a** in CCl_4, prepared from 1 mmol of **1a** by the above procedure, anilline (232 mg, 2.5 mmol) was added with stirring at 0 °C. The mixture was then diluted with CH_2Cl_2, washed with water, and dried ($MgSO_4$). The evaporated residue was purified by silica gel chromatography using C_6H_6-AcOEt (2 : 1) as the eluent to give the pale yellow amorphous solid of methyl 3-methyl-2-(2-anilinosulfinyl-4-oxo-3-phthalimido-1-azetidinyl)-3-butenoate (**3a**) (389 mg, 83% yield). Softening point 100—120 °C. UV (EtOH): λ_{max} 207 nm (ε 40700), 221 (50400), and 290 (2400). IR (KBr): 1790 (β-lactam) and 1065 cm^{-1} (S=O). NMR ($CDCl_3$): δ 1.92 (3H, br. s),

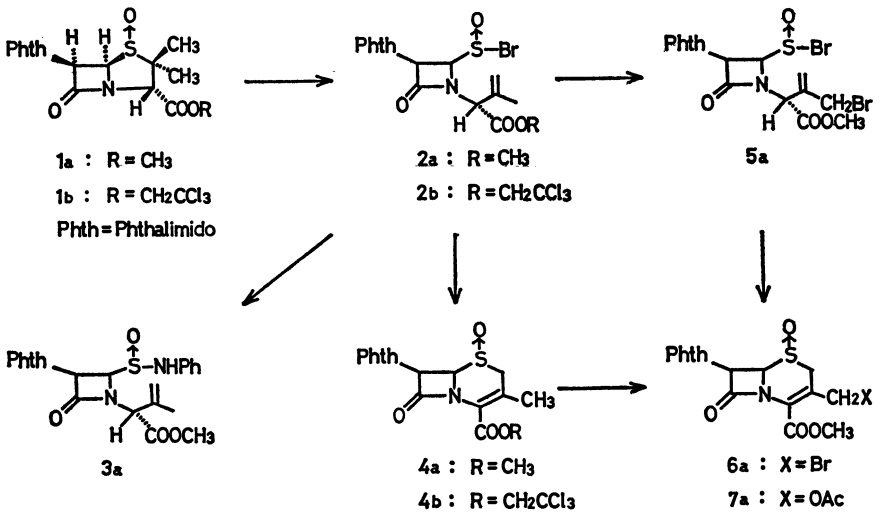

3.59 (3H, s), 4.73 (1H, br. s), 4.82 (1H, br. s), 5.02 (1H, br. s), 5.86 (1H, d, J=5 Hz), 6.29 (1H, d, J=5 Hz), 6.80 (5H, m), 7.63 (1H, s), 7.81 (4H, m). Found: C, 59.21; H, 4.67; N, 8.52%. Calcd for $C_{23}H_{21}N_3O_6S$: C, 59.09; H, 4.53; N, 8.99%.

Reaction of ***2a*** *with Triethylamine.* Into the solution of **2a** in CCl_4, prepared from 1 mmol of **1a** by the above procedure, triethylamine (120 mg, 1.2 mmol) was added at 0 °C. After stirring for 20 min, the mixture was diluted with CH_2Cl_2, washed with water, and dried ($MgSO_4$). The evaporated residue was chromatographed on silica gel using AcOEt as the eluent to afford methyl 3-methyl-7-phthalimido-3-cephem-4-carboxylate 1-oxide (**4a**) (175 mg, 47% yield); mp 212—214 °C (dec) (from MeOH) (lit,[3] 215 °C (dec)). UV (EtOH): λ_{max} 221 nm (ε 40700) and 264 (4900). IR (KBr): 1795 (β-lactam) and 1055 cm^{-1} (S=O). NMR ($CDCl_3$): δ 2.35 (3H, s), 3.49 (1H, d, J=16 Hz), 3.84 (3H, s), 4.13 (1H, d, J=16 Hz), 4.65 (1H, d, J=5 Hz), 6.03 (1H, d, J=5 Hz), 7.79 (4H, m). Found: C, 54.34; H, 3.75; N, 7.37%. Calcd for $C_{17}H_{14}N_2SO_6$: C, 54.54; H, 3.77; N, 7.48%.

*Preparation of Trichloroethyl 3-Methyl-7-phthalimido-3-cephem-4-carboxylate 1-Oxide (****4b****).* In a procedure similar to that described above, **4b** was obtained in 54% yield. Mp 200—202 °C (dec) (from MeOH). UV (EtOH): λ_{max} 221 nm (ε 50900) and 271 (5700). IR (KBr): 1800 (β-lactam) and 1055 cm^{-1} (S=O). NMR ($CDCl_3$): δ 2.44 (3H, s), 3.67 (1H, d, J=16 Hz), 4.19 (1H, d, J=16 Hz), 4.68 (1H, d, J=5 Hz), 4.90 (2H, s) 6.07 (1H, d, J=5 Hz), 7.81 (4H, m). Found: C, 44.20; H, 2.72; N, 5.97%. Calcd for $C_{18}H_{13}N_2O_6SCl_3$: C, 43.96; H, 2.66; N, 5.70%.

*Preparation of Methyl 3-Bromomethyl-7-phthalimido-3-cephem-4-carboxylate 1-Oxide (****6a****).* *Method A*: A mixture of **1a** (3.76 g, 10 mmol) and NBS (1.78 g, 10 mmol) in 150 ml of CCl_4 was heated at refluxing temperature for 1.5 hr under N_2. After cooling to room temperature, NBS (2.67 g, 15 mmol) and BPO (300 mg) were added and the mixture was refluxed for 3 hr under N_2. The reaction mixture was then chilled in an ice bath, and triethylamine (1.50 g, 15 mmol) was added. After stirring for 20 min, the mixture was diluted with CH_2Cl_2, washed with water, and dried ($MgSO_4$). The evaporated residue was purified repeatedly by chromotography on silica gel using C_6H_6-AcOEt (2 : 1) as the eluent to give the amorphous solid of **6a** (1.40 g, 33% yield). Softening point 130—140 °C. UV (EtOH): λ_{max} 221 nm (ε 43200) and 278 (8500). IR (KBr): 1800 (β-lactam) and 1045 cm^{-1} (S=O). NMR ($CDCl_3$): δ 3.68 (1H, d, J=16 Hz), 3.92 (3H, s), 4.23 (1H, d, J=16 Hz), 4.55 (2H, s), 4.73 (1H, d, J=5 Hz), 6.08 (1H, d, J=5 Hz), 7.85 (4H, m). Found: C, 45.29; H, 2.94; N, 6.26%. Calcd for $C_{17}H_{13}N_2O_6SBr$: C, 45.05; H, 2.89; N, 6.18%.

Method B: A solution of **4a** (374 mg, 1 mmol), NBS (445 mg, 2.5 mmol), and BPO (50 mg) in 20 ml of benzene was refluxed for 3 hr. The reaction mixture was worked up in a similar procedure to that described above to give **6a** (80 mg, 18% yield).

*Preparation of Methyl 3-Acetoxymethyl-7-phthalimido-3-cephem-4-carboxylate 1-Oxide (****7a****).* To a solution of **6a** (453 mg, 1 mmol) in 4 ml of AcOH, a suspension of AgOAc (200 mg, 1.2 mmol) in 4 ml of AcOH was added with stirring; the stirring was continued for 1 hr. The reaction mixture was filtered to remove the silver salts, and the filtrate was diluted with AcOEt. The solution was then washed successively with water, 3% $NaHCO_3$, and water. After drying over $MgSO_4$, the solvent was evaporated and the residue was purified by chromatography on silica gel using C_6H_6-AcOEt (1 : 1) as the eluent to give the colorless amorphous solid of **8a** (178 mg, 45% yield). Softening point 105—125 °C. UV (EtOH): λ_{max} 221 nm (ε 45100) and 267 (5600). IR (KBr): 1800 (β-lactam) and 1045 cm^{-1} (S=O). NMR ($CDCl_3$): δ 2.10 (3H, s), 3.58 (1H, d, J=16 Hz), 3.89 (3H, s), 4.14 (1H, d, J=16 Hz), 4.68 (1H, d, J=5 Hz), 4.91 (1H, d, J=14 Hz), 5.79 (1H, d, J=14 Hz), 6.06 (1H, d, J=5 Hz), 7.82 (4H, m). Found: C, 52.92; H, 3.77; N, 6.46%. Calcd for $C_{19}H_{16}N_2O_8S$: C, 52.77; H, 3.73; N, 6.48%.

The authors wish to express their sincere appreciation to Mr. Osamu Sakanaka for his assistance.

References

1) R. D. G. Cooper and D. O. Spry in "Cephalosporins and Penicillins," E. H. Flynn, Ed., Academic Press, New York, N. Y., 1972, Chapter 5; R. D. G. Cooper, L. D.Hatfield, and D. O. Spry, *Accounts Chem. Res.*, **6**, 32 (1973); T. Kamiya, *Yuki Gosei Kagaku Kyokai Shi*, **33**, 24 (1975).

2) D. H. R. Barton, I. H. Coats, D. G. Sammes, and C. M. Copper, *Chem. Comm.*, **1973**, 303; T. Kamiya, T. Teraji, Y. Saito, M. Hashimoto, O. Nakanishi, and T. Oku, *Tetrahedron Lett.*, 3001 (1973); T. S. Chou, J. R. Burgtorf, A. L. Ellis, S. R. Lammert, and S. P. Kukolja, *J. Amer. Chem. Soc.*, **96**, 1609 (1974); I. H. Coats and P. G. Sammes, *ibid.*, **96**, 1459 (1974); T. S. Chou, *Tetrahedron Lett.*, 725 (1974).

3) S. Kukolja and S. R. Lammert, *Angew. Chem.*, **85**, 40 (1973); *Angew Chem. Int. Ed., Engl.* **12**, 67 (1973).

4) The reaction of **1a** with 1 equivalent of *N*-chlorosuccinimide in boiling CCl_4 for 1.5 hr afforded the corresponding sulfinyl chloride in quantitative yield. The NMR spectrum of this product was completely superimposable on that of the chloride prepared from **1a** and SO_2Cl_2 according to the method described in Ref. 3). This result indicates that two diastereomers were produced in the same ratio (2 : 1) in both reactions.

BULLETIN OF THE CHEMICAL SOCIETY OF JAPAN, VOL. 48(10), 2991—2992 (1975)

Cryptate Chemistry. I. The Reaction of Potassium Alkanoates with Alkyl Halides in the Presence of 4,7,13,16,21,24-Hexaoxa-1,10-diazabicyclo[8.8.8]hexacosane

Sadatoshi AKABORI and Michiko OHTOMI

Department of Chemistry, Faculty of Science, Tōho University, Funabashi, Chiba 275

(Receieved April 19, 1975)

Synopsis. Potassium alkanoates reactes with organic halides in the presence of bicyclopolyether (III) in benzene to give esters in high yields.

In recent years, many papers[1-3] have been published reporting that such crown ethers as I and II increase the solubility of salts and the reactivity of anions in aprotic solvents. For example, Sam and Simmons[4] have reported that the complexes of potassium halide and potassium hydroxide with dicyclohexyl-18-crown-6 (II) show strong nucleophilic and basic properties.

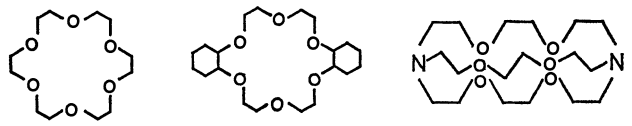

(I) (II) (III)

Liotta *et al.*[5] have observed that potassium fluoride and the potassium acetate complex of 18-crown-6 (I), which he termed the "naked anion" in non-polar aprotic solvents, have shown unusual properties and reactivities. Dietlich *et al.*[6-7] have reported the preparation and properties of a number of macrobicyclic polyethers with bridgehead nitrogens, such as 4,7,13,16,21,24-hexaoxa-1,10-diazabicyclo[8.8.8]-hexacosane (III). It was shown that these compounds form stable complexes, cryptate, with alkali, alkaline earth, and other cations, and that the complexing ability of the cryptates could be correlated with the number of ligand sites, the approximate cavity size of the bicyclopolyether, and the relative cation radius in question. Our interest in the reactivities of these cryptates in aprotic solvents led us to examine the reactivities of the potassium salts of acids with some halides in the presence of III in benzene.

Nucleophilic substitution was carried out by the following method. The carboxylate complex of III was prepared by dissolving a catalytic amount of III in 7 ml of dry benzene and by then adding an appropriate amount of dry potassium salts of acids. After the heterogenious system had then been stirred for 30 min, the alkyl halide was added all at once and the mixture was stirred for a further 3 hr at 15 or 83 °C. Table 1 summarizes the results.

The data in the table clearly show that the cryptates prepared by mixing III with potassium alkanoates in benzene are sufficiently reactive to form organic esters from organic halides at an appropriate temperature. Indeed, in the absence of III, no reaction takes place under the same conditions. Benzyl bromide gives less than 2% benzyl acetate after 10 hr at room temperature when it is treated with potassium acetate in the absence of III, whereas benzyl acetate is formed quantitatively within 3 hr when III is present. The reaction of the cryptate complex from potassium propionate with 1,2-dibromoethane afforded a mixture of ethylene dipropionate and 2-bromoethyl propionate. The ratio of the two substances is dependent upon which reagent is present in excess. Another

TABLE 1. REACTIONS OF THE CRYPTATE WITH ORGANIC HALIDES

Organic bromide ($\times 10^{-3}$ mol)	Potassium carboxylate ($\times 10^{-3}$ mol)	III ($\times 10^{-3}$ mol)	Reaction temp. (°C)	Yield[a] (%)	Products
$PhCH_2Br$ (0.812)	CH_3COOK (2.40)	(0.160)	15	99	$PhCH_2OCOCH_3$
$PhCH_2Br$ (0.810)	CH_3CH_2COOK (2.50)	(0.151)	15	85	$PhCH_2OCOCH_2CH_3$
$PhCH_2Br$ (0.304)	$(CH_3)_2CHCOOK$ (0.873)	(0.093)	15	95	$PhCH_2OCOCH(CH_3)_2$
$CH_3(CH_2)_6CH_2Br$ (0.500)	CH_3COOK (1.60)	(0.106)	83	85	$CH_3(CH_2)_6CH_2OCOCH_3$
$CH_3(CH_2)_6CH_2Br$ (0.301)	CH_3CH_2COOK (0.574)	(0.154)	83	90	$CH_3(CH_2)_6CH_2OCOCH_2CH_3$
$CH_3(CH_2)_6CH_2Br$ (0.404)	$(CH_3)_2CHCOOK$ (1.00)	(0.106)	83	99	$CH_3(CH_2)_6CH_2OCOCH(CH_3)_2$
$BrCH_2CH_2Br$ (0.500)	CH_3CH_2COOK (2.00)	(0.133)	83	89 11	$CH_3CH_2COOCH_2CH_2OCOCH_2CH_3$ $BrCH_2CH_2OCOCH_2CH_3$

a) The values are those obtained by glc. b) All products show the same retention time with authentic sample and mass spectra were consistent with the proposed structure. Reaction of *n*-octyl bromide with potassium alkanoates afforded octene in less than 0.3% yield.

feature of the reaction with the aid of the cryptate is the low degree of the formation of the olefin. *n*-Octyl bromide afforded less than 0.3% of 1-octene.

The main conclusions to be drawn from these results are as follows: 1) cryptate carboxylate can be used as an extremely valuable reagent in the preparation of alkyl esters in non-polar aprotic solvents such as benzene, and 2) cryptate carboxylate is a powerful nucleophile but a weak base.

Experimental

The gas chromatograms were obtained on a Hitachi K 23 apparatus using the following column; 10% FFAP on Chromosorb W AW/DMCS 1 m×3 mm. The mass spectra were recorded on a gas-chromatography mass spectrometer, Shimadzu LKB 9000, at an ionizing voltage of 70 eV.

Materials. Compound (III) was prepared according to the procedures described in the literature.[6] Potassium alkanoates of the Tokyo Kasei Kogyo Co., Ltd., were used without further purification. *n*-Octyl bromide and benzyl bromide of the Tokyo Kasei Kogyo Co., Ltd., were purified by distillation prior to use.

Solvent. The solvent used was purified by distillation.

General Procedure. To a solution of III in 7 ml of benzene, we added potassium alkanoate, after with the mixture was stirred for 30 min at room temperature. To the mixture we then added organic halide and continued stirring for a further 3 hr at 15 °C or 83 °C. At the end of the reaction, the organic layer was analyzed by gas chromatography and gas-chromatography mass spectrometer.

The authors wish to express their gratitude to Professor Michinori Ōki, the University of Tokyo, for his valuable discussions and suggestions.

References

1) C. J. Pedersen, *J. Amer. Chem. Soc.*, **92**, 391 (1970); **89** 7017 (1967); **92** 386 (1970).
2) G. W. Gokel and D. J. Cram, *Chem. Commun.*, **1973**, 481.
3) R. N. Greene, *Tetrahedron Lett.*, **1972**, 1793.
4) D. J. Sam and H. E. Simmons, *J. Amer. Chem. Soc.*, **96**, 2252 (1974). D. J. Sam and H. E. Simmons, Org. Crg. Conference, Cape Cod, Oct, 1973, Abstr. No. 11.
5) C. L. Liotta and H. P. Harris, *J. Amer. Chem. Soc.*, **96**, 2250 (1974); C. L. Liotta, H. P. Harris, M. McDermont, Tom, Gonzalez and K. Smith, *Tetrahedron Lett.*, **1974**, 2417.
6) B. Dietlich, J. M. Lehn and J. P. Sauvage, *Tetrahedron Lett.*, **1969** 2885.
7) B. Dietlich, J. M. Lehn, and J. P. Sauvage, *Chem. Commun.*, **1970**, 1055, B. Dietlich, J. M. Lehn, J. P. Sauvage and J. Blanzat, *Tetrahedron*, **29**, 1629 (1973); J. M. Lehn, J. P. Sauvage and B. Dietlich, *J. Amer. Chem. Soc.*, **92**, 2916 (1970); J. M. Lehn and J. P. Sauvage, *Chem. Commun.*, **1973**, 15; B. Dietlich, J. M. Lehn, and J. P. Sauvage, *Tetrahedron*, **29**, 1647 (1973); B. Dietlich and J. M. Lehn, *Tetrahedron Lett*, **1973**, 1225.

BULLETIN OF THE CHEMICAL SOCIETY OF JAPAN, VOL. 48(10), 2993—2994 (1975)

Synthesis and NMR Spectra of *para*-Substituted Benzyl Hydrodisulfides and Related Compounds

Shunichi KAWAMURA, Toyokazu HORII, Takeshige NAKABAYASHI, and Masayuki HAMADA

Radiation Center of Osaka Prefecture, Shinke-cho, Sakai, Osaka 593

(Received May 29, 1975)

Synopsis. The titled compounds were synthesized and their NMR spectra were measured. The chemical shifts of benzyl hydrodisulfides were not related to σ or σ_R, while those of the corresponding thiols were related to σ.

In an NMR study of *para*-substituted phenyl hydrodisulfides, we have found a novel correlation for the chemical shifts of the mercapto protons.[1] The correlation, $\tau_{SSH}=0.263\sigma_R+6.653$ ($r=0.993$),[2] includes the chemical shift which is only related to the resonance term, and includes also a large positive ρ value. It has thus been postulated that the substituent effect in the *para*-substituted phenyl hydrodisulfides is conducted to the terminal protons anisotropically.

In the present work, the synthesis of *para*-substituted benzyl hydrodisulfides through a slightly modified route has been attempted, and the NMR spectra of the compounds have also been measured. The chemical shifts of mercapto and methylene protons of the compounds are interesting, because different correlations for the two kinds of protons are anticipated; the chemical shifts of mercapto protons should be related to σ_R, and those of methylene, to σ.

α-Toluenethiols having methoxy, methyl, or chlorine at the *para*-position (**1a, 1b**, and **1d**) were allowed to react with *N*-chlorosuccinimide, giving *N*-(*p*-substituted benzylthio)succinimides in 22—35% yields (**2a, 2b**, and **2d**).[3] By the condensation of the *N*-aralkylthiosuccinimides with thioacetic acid, acetyl *p*-substituted benzyl disulfides (**3a, 3b**, and **3d**) were obtained in moderate yields. This reaction is an application of the synthesis of thiolsulfonates from *N*-(arylthio)-succinimides and arenesulfinic acids.[4] Acetyl disulfides **3e** and **3f** were prepared by the reactions of **1e** and **1f** with acetylsulfenyl chloride, respectively.[5] Compound **3c** could be obtained by both methods mentioned above. The acetyl *p*-substituted benzyl disulfides obtained were ethanolyzed in the presence of hydrogen chloride. Of the resulting hydrodisulfides, **4b, 4d**, and **4e** were distilled under high vacuum to give products in 18—54% yields. However, **4a** and **4f** were unstable on distillation; in the case of **4a**, only 2.5% of the product was isolated and no product was obtained for **4f** (see experimental). The hydrodisulfides **4a—f** were stable in solvents such as carbon tetrachloride and chloroform.

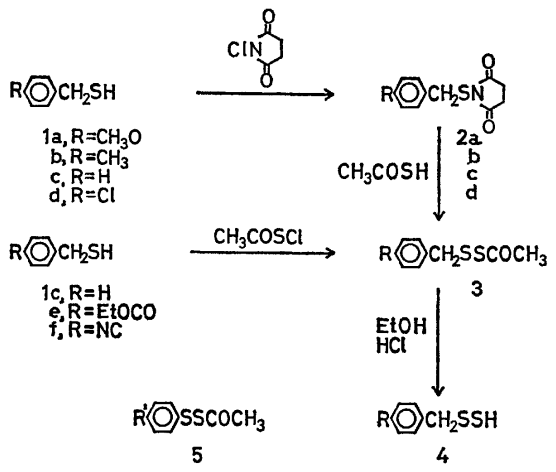

The chemical shifts of the benzyl hydrodisulfides and related compounds are shown in Table 1. The chemical shifts of mercapto protons of *p*-substituted α-toluenethiols fit the thermodynamic relationship, $\tau_{SH}=-0.149\,\sigma+8.496$ ($r=0.978$). The ρ value (−0.149) is about a half of that for benzenethiols,[6] which is reasonable because it has been demonstrated that the insertion of methylene carbon atom into a side chain (in the present case, R-C_6H_4-CH_2-SH) diminishes ρ to 1/2—1/3 of its original value.[7] For the methylene protons of the α-toluenethiols, $\tau_{CH_2}=-0.103\,\sigma+6.330$ ($r=0.929$) was obtained. The correlation coefficient is not sufficiently large, and ρ is too small for protons of R-C_6H_4-CH(SH)-**H**. These facts imply that some other effects, *e.g.*, a stereochemical effect as well as an electronic effect, reflect the chemical shift of the protons.

The chemical shifts of protons (both SSH and CH_2) of *p*-substituted benzyl hydrodisulfides **4** were related

Table 1. NMR chemical shift data (in CCl_4, τ, ppm)

R	1		4		3[a]		5[b]
	-CH_2-	-SH	-CH_2-	-SSH	-CH_2-	-CH_3	-CH_3
MeO	6.359	8.532	6.199	7.300	6.102	7.646	7.628
Me	6.352	8.528	6.196	7.303	6.096	7.655	7.603
H	6.309	8.4875	6.156	7.289	6.066	7.662	7.578
Cl	6.332	8.463	6.193	7.277	6.114	7.635	
EtOCO	6.268	8.437	6.128	7.2815	6.0445	7.648	
NC	6.262	8.382	6.142	7.250	6.063	7.628	

a) In $CDCl_3$. b) Some other acetyl phenyl disulfides were measured: for EtO, 7.628; *t*-Bu, 7.592; Me_3Si, 7.576; F, 7.600; Br, 7.587.

Table 2. Acetyl *p*-substituted benzyl disulfides, $RC_6H_4CH_2SSCOCH_3$

	R	Mp, °C	Yield, %	Found (Calcd) % C	H	N	S+Cl
3a	CH_3O	22	77	52.60 (52.55)	5.30 (5.37)		28.08 (27.96)
3b	CH_3	36.5—37.5	55	56.57 (56.60)	5.70 (5.77)		30.20 (29.66)
3d	Cl	31—31.9	53	46.44 (46.16)	3.90 (3.85)		42.78 (42.04)
3e	EtOCO	54.5—57.7	81	53.31 (53.16)	5.22 (5.25)		23.72 (23.55)
3f	NC	86.5—88	45	53.79 (53.64)	4.06 (3.92)	6.27 (5.91)	28.71 (29.92)

neither to σ nor to σ_R, the correlation coefficients did not exceed 0.90. It should be noted that even the chemical shifts of the methylene protons of the hydrodisulfides were not represented by the Hammett equation. These complicated results remind us of the restricted rotation of the sulfur-sulfur bond.[8] If it is true that the sulfur-sulfur group in the phenyl hydrodisulfide was almost fixed in the same plane as the benzene ring, the CH_2-S-S-H group would be relaxed in motion owing to its methylene carbon, and this relaxation would bring about a deviation from a correlation with the chemical shift.

The chemical shifts of acetyl disulfides **3** and **5** were also measured in connection with the above compounds. The shifts of methyl protons of **5** showed no relation for σ or σ_R. A similar relaxation of the restricted rotation of S-S bond can be also seen in this case. The differences among the chemical shifts of the methyl protons of **3a**—**f** are small; these protons seem too distant from the substituents for any substituent effect to be detected. Also, the methylene protons of these compounds were not connected to the character of the substituents.

Experimental

Melting points are corrected. NMR spectra were recorded on a JEOL MH-100 Spectrometer using carbon tetrachloride or deuteriochloroform as solvent and TMS as internal lock. Chemical shifts were determined by use of a frequency counter. The chemical shifts reported in Table 1 were values at infinite dilution, which were obtained by extrapolation of four concentrations (2.5, 5, 7.5, and 10 w/v%).

Benzyl hydrodisulfide[5] and acetyl *p*-substituted phenyl disulfides[1] were obtained by the procedures described previously.

*N-(p-Substituted benzylthio)succinimides (**2a**, **2b**, and **2d**)* were prepared by the reaction[3] of *N*-chlorosuccinimides with *p*-substituted α-toluenethiols.[9] Two recrystallizations from ethanol (70 °C) gave **2a**, mp 139.2—140.2 °C (22%); **2b**, mp 180.7—181.3 °C (26%); **2d**, mp 188.2—189.5 °C (35%).

Found for **2a**: C, 57.18; H, 5.21; N, 5.27; S, 12.11%. Calcd for $C_{12}H_{13}O_3NS$; C, 57.35: H, 5.21; N, 5.57; S, 12.76%.

Found for **2b**: C, 61.37; H, 5.56; N, 5.73; S, 13.19%. Calcd for $C_{12}H_{13}O_2NS$: C, 61.25; H, 5.57; N, 5.95; S, 13.62%.

Found for **2d**: C, 51.75; H, 3.89; N, 5.30; S+Cl, 25.57%. Calcd for $C_{11}H_{10}O_2ClNS$: C, 51.67; H, 3.94; N, 5.48; S+Cl, 26.40%.

Acetyl p-Substituted Benzyl Disulfides. *A. Procedure for **3a**—**d***: These compounds were obtained by a method similar to that of thiolsulfonate synthesis from *N*-(*p*-tolylthio)-succinimide and *p*-toluenesulfinic acid.[4] A mixture of **2a** (7 mmol), thioacetic acid (7.35 mmol, 5% excess), and benzene (30 ml) was stirred for 2 hr at room temperature. The mixture was allowed to stand overnight. The white precipitate of succinimide formed was filtered off. The filtrate was evaporated under reduced pressure. Crude **3a** was crystallized out from the solution of the residue in petroleum ether by cooling (−18 °C, then 2 °C). Immediate pumping out of the solvent after recrystallization from petroleum ether (2 °C) produced 77% yield of **3a** with mp 22 °C. Disulfides **3b** and **3d** were prepared similarly. Disulfide **3c** obtained by Procedure A showed mp 54.5—56 °C (*cf.* by Procedure B, mp 54—55 °C). The analytical data is summarized in Table 2.

*B. Procedure for **3e** and **3f***: To a solution of *p*-ethoxycarbonyl-α-toluenethiol (10 mmol) in ether (20 ml) was added a solution of acetylsulfenyl chloride (10 mmol) in carbon tetrachloride with stirring and cooling (−2 °C to −5 °C) for 10 min. After 1 hr, the solution was evaporated *in vacuo*. To the residue 3 ml of petroleum ether was added, and then the treatment described in A was followed. Disulfide **3e** was obtained in a good yield. Disulfide **3f** was prepared similarly; its analytical data as well as those for **3e** are listed in Table 2.

p-Substituted Benzyl Hydrodisulfides. A mixture of acetyl *p*-substituted benzyl disulfide (**3a**, **3b**, **3d**, **3e**, or **3f**, 0.5 g) and 0.83 M ethanolic hydrogen chloride (6 ml) was stirred at 26—28 °C under a nitrogen atmosphere. After several hours (4 hr for **3a**, **3b**, and **3d**, 5 hr for **3e**, and 7 hr for **3f**), the resulting solution was evaporated under reduced pressure. The oil obtained was distilled under vacuum. On distillation, *p*-methoxybenzyl hydrodisulfide **4a** was unstable and its major portion decomposed. *p*-Cyanobenzyl hydrodisulfide **4f** was quite unstable and decomposed immediately after its formation, unless it was dissolved in solvents such as carbon tetrachloride and chloroform.

Such being the case, the NMR spectrum of **4f** was measured using a carbon tetrachloride solution of a neat sample without distillation. It was confirmed with all the other hydrodisulfides mentioned here that the differences between the chemical shifts of a sample obtained from distilled hydrodisulfide and those without distillation were within 0.5 Hz (av. 0.2 Hz).

The yields and boiling points of the hydrodisulfides were as follows: **4a** 2.5%, *ca.* 90 °C, decomp/0.01 mmHg; **4b**, 38%, 91—96 °C/0.02 mmHg; **4d**, 54%, 90—95 °C/0.01 mmHg; **4e**, 18%, 117—120 °C/0.01 mmHg.

References

1) S. Kawamura, T. Horii, and J. Tsurugi, *J. Org. Chem.*, **36**, 3677 (1971).

2) In the previous paper, chemical shifts were shown by frequencies form TMS at 60 MHz. They were re-calculated to τ, for comparison with the present data at 100 MHz.

3) Y. Abe, T. Nakabayashi, and J. Tsurugi, This Bulletin, **46**, 1898 (1973).

4) Y. Abe and J. Tsurugi, *Chem. Lett.*, **1972**, 441

5) J. Tsurugi and T. Nakabayashi, *J. Org. Chem.*, **24**, 807 (1959).

6) S. H. Marcus and S. I. Miller, *J. Phys. Chem.*, **68**, 331 (1964). The correlation, $\tau_{SH}=-0.283\sigma+6.760$ ($r=0.993$), has been reported.

7) S. H. Marcus, W. F. Reynolds, and S. I. Miller, *J. Org. Chem.*, **31**, 1872 (1966).

8) W. A. Pryor, "Mechanisms of Sulfur Reactions," McGraw-Hill Book Co., Inc., New York (1962), p. 19.

9) a) E. E. Reid, "Organic Chemistry of Bivalent Sulfur," Vol. I, Chemical Publishing Co., Inc., New York, N. Y. (1958), p. 32. b) "Beilstein," EII, Vol. 10, p. 142.

BULLETIN OF THE CHEMICAL SOCIETY OF JAPAN, VOL. 48(10), 2995—2996 (1975)

Diels-Alder Reaction of 2-Methyl-2-cyclohexenone and Substituted Butadienes[1)]

Isao NAGAKURA, Haremi OGATA, Masako UENO, and Yoshio KITAHARA*

Department of Chemistry, Faculty of Science, Tohoku University, Aramaki, Aoba, Sendai 980

(Received June 16, 1975)

Synopsis. Diels-Alder adducts of 2-methyl-2-cyclohexenone and substituted butadienes were obtained in a high yield in the presence of catalytic aluminum chloride.

Eremophilane type sesquiterpenoids possess the basic skeleton (I) and syntheses of these compounds have been reported.[2-5)] One of the important problems for elaboration of eremophilane type skeleton is a construction of *cis* fused six-membered rings. Diels-Alder reaction is expected to be a useful method for synthesis of these *cis* fused rings. Although Diels-Alder reactions of 2-methyl-2-cyclohexenone with substituted butadienes have been reported,[6-8)] the addition products were generally formed in a low yield. It has been known that some of the Diels-Alder reactions are catalyzed by Lewis acids,[9)] but dienes are unstable under these acidic conditions. Now we found that in the presence of catalytic aluminum chloride, Diels-Alder reaction afforded the adducts in a satisfactory yield (Table 1).

The reaction between 2-methyl-2-cyclohexenone and butadiene proceeded smoothly at room temperature in the presence of one tenth mole of aluminum chloride to dienophile in methylene chloride and adduct (II) was obtained in a good yield (95%). A small amount of hydroquinone was added to prevent polymerization of diene. Under the same reaction condition, however, both reactions of 3-methyl-2-cyclohexenone and 2,3-dimethyl-2-cyclohexenone with butadiene did not give any addition products. On the other hand, the reaction of 2-methyl-2-cyclohexenone with isoprene or piperylene in methylene chloride gave the adducts (III or IV) in a poor yield and a resinous material was obtained. The reason may be due to that the rate of the polymerization of diene is faster than that of the addition of diene to dienophile. In benzene, the adduct, III or IV, was obtained, but the reaction was very slow. When this reaction was carried out in the presence of one forth mole of aluminum chloride to dienophile in benzene, the reaction took place smoothly, and the adducts III and IV were obtained in a high yield. Structures of the adducts described above were determined by NMR.

These results seem to be of considerable utility for building up *cis* fused rings of eremophilane type sesquiterpenoids and several examples of the successful total syntheses have been reported.[9)]

TABLE 1. DIELS-ALDER ADDITIONS OF 2-METHYL-2-CYCLOHEXENONE AND SUBSTITUTED BUTADIENE IN THE PRESENCE OF $AlCl_3$

Diene	Enone-$AlCl_3$ mol ratio	Solvent	Yield (%)[a)]	Product (ratio)
Butadiene	10 : 1	CH_2Cl_2	93	II
	1 : 1	CH_2Cl_2	47	II
			30[b)]	II
Isoprene	10 : 1	CH_2Cl_2	20	IIIa
	4 : 1	Benzene	88	IIIa
			64[c)]	IIIa(9), IIIb(1)[c)f)]
Piperylene	10 : 1	CH_2Cl_2	26	IVa(2.2), IVb(7.8)[e)]
	4 : 1	Benzene	76	IVa(2.2), IVb(7.8)
		Toluene	17[d)]	IVa(2.7), IVb(7.3)

a) Based on enone. b) Based on diene, quoted from Ref. 5b. c) Based on diene, quoted from Ref. 7. d) Quoted from Ref. 8. e) Ratio was evaluated from integration of tertiary methyl group in NMR data (Varian 60 MHz). f) See Ref. 10.

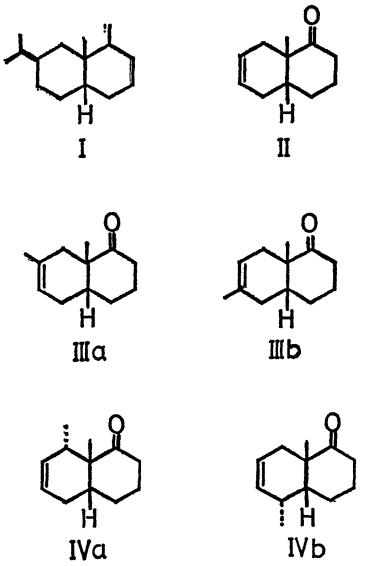

Experimental

General Procedure. To an ice cooling suspension of $AlCl_3$ in solvent was added dropwise dienophile. $AlCl_3$ was dissolved to give a colored solution, to which hydroquinone was added. The reaction flask was provided with a dry ice condenser, and then butadiene was absorbed in the reaction mixture. After the reaction flask was closed with stoppers, the mixture was stirred at room temperature for several days. The reaction process was traced by gas chromatography. After excess butadiene was recovered, the mixture was extracted with CCl_4. The organic layer was washed with water, dried and concentrated. The residue was distilled to give the adduct.

Reaction of 2-Methyl-2-cyclohexenone and Butadiene. To

* To whom all correspondences should be addressed.

a suspension of 6.5 g (0.048 mol) of powdered anhydrous $AlCl_3$ in 650 ml of CH_2Cl_2 was added 55 g (0.5 mol) of 2-methyl-2-cyclohexenone and then 100 g of butadiene. The mixture was stirred for 4 days. Work-up as described gave 75.5 g (93%) of adduct (II), bp 80—90 °C/5 mmHg (lit,[7b] bp 58—65 °C/0.4 mmHg). IR(neat): 3020, 1725, 1655, 925 cm^{-1}. NMR(CCl_4): 1.08 (s, 3H), 5.58—5.62 ppm (m, 2H).

Reaction of 2-Methyl-2-cyclohexenone and Isoprene. 2-Methyl-2-cyclohexenone (11 g, 0.1 mol) was added to a suspension of 3.3 g (0.025 mol) of $AlCl_3$ in 120 ml of dry benzene. $AlCl_3$ was gradually dissolved to form a paste, to which was added dropwise with ice cooling 20 ml of isoprene. After the mixture was stirred for 2 days, 20 ml of isoprene was added again. Up to the end of the reaction after additional 3 days, a heterogeneous mixture became homogeneous reddish brown. Work-up as described gave 15.6 g (88%) of the adduct (IIIa). IR(neat): 3010, 1705, 995, 920 cm^{-1}, NMR ($CDCl_3$): 1.13 (s, 3H), 1.70 (s, 3H), 5.36 ppm (m, 1H).

Reaction of 2-Methyl-2-cyclohexenone and Piperylene. The adduct (IV) was prepared from 2.2 g (20 mmol) of 2-methyl-2-cyclohexenone, 0.66 g (5 mmol) of $AlCl_3$ and 5 ml of piperylene in 24 ml of benzene. The reaction mixture was stirred for 2 days. After work-up in usual way, the residue was chromatographed on silica gel with CH_2Cl_2 and gave 2.7 g (76%) of IV. The IR and NMR spectra of the mixture of (IVa) and (IVb) matched the published data of that mixture.

References

1) Published in part in *Yuki Gosei Kagaku Kyokai Shi*, **31**, 251 (1973).
2) E. Piers and D. Smillie, *J. Org. Chem.*, **35**, 3997 (1970).
3) J. A. Marshall and G. M. Cohen, *Tetrahedron Lett.*, **1970**, 3865; *J. Org. Chem.*, **36**, 877 (1971).
4) A. K. Torrence and A. R. Pinder, *Tetrahedron Lett.*, **1971**, 745; *J. Chem. Soc., C*, **1971**, 3410.
5) E. Piers, M. B. Geraghty, and D. Smillie, *Chem. Commun.*, **1971**, 614; *Can. J. Chem.*, **51**, 2166 (1973).
6) a) W. G. Dauben, J. B. Rogan and E. J. Blanz, Jr., *J. Amer. Chem. Soc.*, **76**, 6384 (1954) b) A. M. Gaddis and L. W. Butz, *ibid.*, **69**, 117 (1947).
7) I. N. Nagarow and G. P. Kugatona, *Chem. Abstr.*, **50**, 6405 (1956).
8) P. Beslin, R. Bloch, G. Moinet, and J. M. Conia, *Bull. Soc. Chim. Fr.*, **1969**, 509.
9) Presented in part at the 15th Symposium on the Chemistry of Natural Product, Nagoya, Oct. 1971 Abstracts, p. 239.
10) A. S. Onishchenko, "Diene Synthesis": Israel Program for Scientific Translations, Jerusalem, **1964**, 144.
11) a) P. Yates and P. Eaton, *J. Amer. Chem. Soc.*, **82**, 4436 (1960) b) G. J. Fray and R. Robinson, *ibid.*, **83**, 249 (1961) c) T. Inukai and T. Kojima, *J. Org. Chem.*, **32**, 872 (1967) and references cited therein.

BULLETIN OF THE CHEMICAL SOCIETY OF JAPAN, VOL. 48(10), 2997—2998 (1975)

Metal Derivatives of Amidoximes. VII. Synthesis of Bis(1,3,5,2-Oxadiazaborol-2-yloxy)tetrabutyldistannoxanes

A. B. GOEL and V. D. GUPTA
Chemistry Department, Rajasthan University, Jaipur-302004, India

(Received March 24, 1975)

Synopsis. Bis(1,3,5,2-oxadiazaborol-2-yloxy)tetrabutyldistannoxanes have been synthesized by the reaction of amidoxime, boric acid and dibutyltin oxide. A probable structure for the dimeric species has been proposed on the basis of molecular weight and IR spectral data.

Industrial importance of polymers like silicones[1] has given impetus to the study of metalloboroxanes containing B-O-M linkage.[2] In continuation to our earlier report[3] we briefly communicate here the synthesis and characterization of the dibutylstannoxy boron derivatives containing amidoxime ring.

Bis(1,3,5,2-oxadiazaborol-2-yloxy)tetrabutyldistannoxanes (I) have been synthesized from the mixture of dibutyltin oxide, boric acid and amidoxime by removing water azeotropically with benzene.

$$2Bu_2SnO + 2H_3BO_3 + 2R\underset{NH_2}{\overset{NOH}{C}} \xrightarrow{C_6H_6}$$

$$\left[\begin{array}{l} N\!-\!O \\ \| \quad\quad B\text{-}O\text{-}SnBu_2\text{-} \\ R\text{-}C \quad\quad\quad\quad -O \\ \quad\; N \\ \quad\; H \end{array}\right]_2 + 5H_2O$$

(I)

(R=Me, Et, Pr or Ph)

The reactivity of dibutyltin oxide with amidoxime[4] and boric acid[5] in refluxing benzene indicates that probably amidoxime reacts preferentially with boric acid with the formation of $[R(HN)C{=}N\text{-}OB\text{-}]_2\text{-}O$ (II) which with dibutyltin oxide gives the final product (I). This has been substantiated by the interchange reaction of II[6] with dibutyltin oxide which furnishes I.

These products are white crystalline solids re-crystallizable from hot benzene and are dimeric in refluxing benzene as revealed by molecular weight data.

Infrared spectrum of I shows the characteristic bands[7] due to νNH in the region 3250—3350 cm^{-1}, νC=N at 1646±5 cm^{-1} and νN–O at 920±10 cm^{-1}. Bands at 1275±5 and 1240±10 cm^{-1} due to νB–O (–Sn) and at 595 and 565±5 cm^{-1} due to ν(Sn–O–Sn) indicate the possibility of ladder type structure[8] for these products (I).

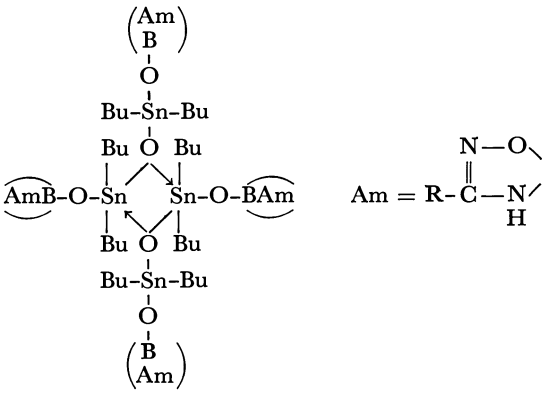

The more detailed structural work is in progress.

Experimental

Dibutyltin oxide (Nitto Kasei) and boric acid were used as supplied. Amidoximes were prepared by standard methods.[9] Boron, tin and nitrogen were estimated by the methods reported earlier.[3] Infrared spectra were recorded on Nujol on Perkin-Elmer 337 spectrophotometer in the range 4000—400 cm^{-1} using KBr optics. Molecular weights were determined on an ebulliometer (Gallenkamp).

TABLE 1. PREPARATION OF $[R(NH)C{=}N\text{-}O\text{-}B\text{-}O\text{-}SnBu_2\text{-}]_2\text{-}O$ (I)

Reactants (mmol)			Refluxed for (hr)	Yield (%)	Product (I) (mp °C)	Analysis(%) Found(Calcd)			Mol. wt. Found (Calcd)
$R(NH_2)C{=}NOH$ R=	Boric acid	Bu_2SnO			R=	B	Sn	N	
Me									
12.5	12.3	12.4	16	88	Me(155—158)	3.10 (3.18)	34.7 (34.9)	8.13 (8.24)	1405 (679.6)
Et									
9.5	9.5	9.4	13	90	Et(150—157[a])	3.0 (3.06)	33.4 (33.50)	7.84 (7.93)	1438 (707.6)
Pr									
9.3	9.4	9.4	12	85	Pr(110—115[a])	2.88 (2.94)	32.0 (32.3)	7.60 (7.62)	1506 (735.6)
Ph									
12.7	12.7	12.8	10	92	Ph(90—92)	2.63 (2.69)	29.6 (29.5)	7.40 (7.47)	1587 (803.8)

a) With decomposition.

Reaction between Dibutyltin Oxide, Boric Acid and Amidoxime. Removal of water azeotropically with benzene (~60 ml) from an equimolar mixture of dibutyltin oxide, boric acid and amidoxime left a clear solution. After removing the solvent *in vacuo*, the product (I) is obtained as white solid recrystallizable from benzene. The details are given in Table 1.

Reaction between II(R=Ph) and Dibutyltin Oxide. A mixture of II,[6] R=Ph (0.98, 3.23 mmol) and dibutyltin oxide (1.61 g, 6.47 mmol) was refluxed in benzene (~40 ml) for about 9 hr leaving a clear solution. On removing excess benzene a white product (2.36 g, 90% yield, mp 90—92 °C) crystallized out. Found: B, 2.62; Sn, 29.5; N, 7.30%. Calcd for I (R=Ph), B, 2.69; Sn, 29.5; N, 7.47%.

One of the authors (A.B.C.) is grateful to UGC New Delhi for a Junior Research Fellowship.

References

1) M. F. Lappert and G. J. Leigh, "Developments in Inorganic Polymer Chemistry," Elsevier, New York (1962).
2) S. K. Mehrotra, G. Srivastava, and R. C. Mehrotra, *J. Organometal. Chem.*, **74**, 277 (1974).
3) A. B. Goel and V. D. Gupta, *ibid.*, **77**, 183 (1974).
4) A. B. Goel and V. D. Gupta, to be published.
5) S. K. Mehrotra, G. Srivastava, and R. C. Mehrotra, *J. Organometal. Chem.*, **65**, 367 (1974).
6) A. B. Goel and V. D. Gupta, *J. Heterocycl. Chem.*, in press.
7) A. B. Goel and V. D. Gupta, *Aust. J. Chem.*, **27**, 2319 (1974).
8) T. Tanaka, *Organometal. Chem. Rev.*, **5**, 1 (1970).
9) F. Eloy and R. Lenaers, *Chem. Rev.*, **62**, 155 (1962).

BULLETIN OF THE CHEMICAL SOCIETY OF JAPAN, VOL. 48(10), 2999—3000 (1975)

The Volatilization of Cadmium from Polyvinyl Chloride–Cadmium Mixtures on Heating

Ryoichi TSUNODA

Industrial Research Institute of Kanagawa Prefecture, Showa-machi, Kanazawa-ku, Yokohama-shi 236

(Received February 17, 1975)

Synopsis. The volatilization of cadmium from a PVC–cadmium stearate mixture on heating was studied by the X-ray diffraction analysis of the products volatilized, which were identified as $CdCl_2$ in air metal Cd and $CdCl_2$ in N_2.

In papers dealing with the decomposition of PVC, there have been much discussion of the effects of metal soaps, but no attention has been paid to the volatilization of metal elements from metal soaps in PVC compositions.[1–6]

About 1.2 mg of cadmium stearate was weighed, sandwich-like, into a platinum sample dish (5 mm $\phi \times$ 5 mm) containing about 40 mg of PVC, mixed well by tapping the bottom and side of the dish lightly, and heated at a heating rate of 5 °C/min in a small electric furnace. The electric furnace, shown in Fig. 1, was a Rigaku Denki Thermoflex, the heating unit of which was employed as the heating apparatus.

The products volatilized after the decomposition of the PVC-cadmium stearate were trapped on the wall of a quartz tube placed in the furnace and were examined by X-ray diffraction analysis by means of an X-ray diffractometer, Rigaku Denki Geigerflex, using Ni filter-CuKα radiation. The residues, heated in platinum sample dishes, were oxidized with sulfuric and nitric acids, and the Cd was determined by atomic absorption spectrometry by means of an atomic absorption spectrometer, Perkin Elmer 403, at a wavelength of 2288 Å.

The percentage of cadmium retained and the X-ray diffraction diagrams of the products volatilized from PVC–cadmium stearate on heating are shown in Figs. 2 and 3 respectively, from which the difference in the volatilization processes of cadmium between that in air and that in nitrogen was observed.

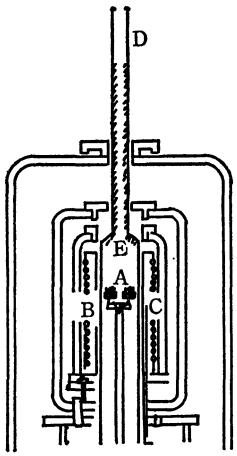

Fig. 1. Electric furnace.
A: Platinum sample dishes, B: heater, C: CA thermocouple, D: Quartz tube, E: Position where volatilized products were trapped.

By the way, the generation of metal chloride by the interaction of metal carboxyrate with pyrolytically eliminated hydrogen chloride was previously reported,[1] but not that of metal. In order to ascertain the formation and volatilization of metal Cd, the cadmium

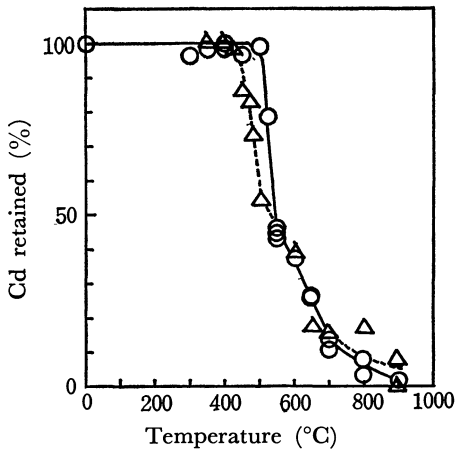

Fig. 2. Percentage of Cd retained in PVC–cadmium stearate on heating.
△: in N_2, ○: in air.

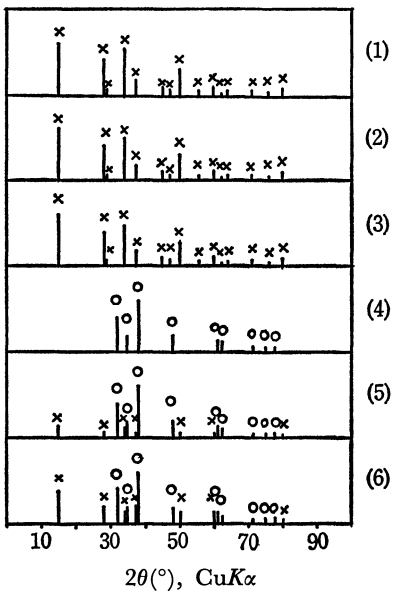

Fig. 3. X-Ray diffraction diagrams of products volatilized from PVC–cadmium stearate on heating up to:
(1) 550 °C, (2) 700 °C, (3) 900 °C in air
(4) 500 °C, (5) 550 °C, (6) 900 °C in N_2
×: $CdCl_2$, ○: Cd.

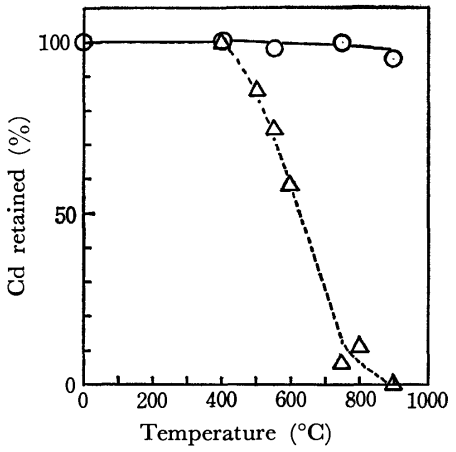

Fig. 4. Percentage of Cd retained on heating of cadmium stearate.
△: in N_2, ○: in air.

stearate was heated in N_2 or in air and subsequently examined in the same way. This showed the volatilization and existence of metal Cd in the residues heated in N_2. The percentage of Cd retained is shown in Fig. 4.

These results show that, in air, the cadmium in PVC–cadmium stearate was volatilized as $CdCl_2$[7] above *ca.* 500 °C, while in nitrogen the cadmium was volatilized as metal Cd[8] above *ca.* 400 °C, and as a mixture of metal Cd and $CdCl_2$ above *ca.* 500 °C.

References

1) A. H. Frye and R. W. Horst, *J. Polym. Sci.*, **40**, 419 (1959); **45**, 1 (1960).
2) A. H. Frye, R. W. Horst, and M. A. Paliobagis, *J. Polym. Sci., Part A*-2, **2**, 1765 (1964); **2**, 1785 (1964); **2**, 1801 (1964).
3) W. C. Geddes, *Rubber Chem. Technol.*, **40**, 177 (1967).
4) E. N. Zilberman, A. E. Kulilova, S. B. Meiman, N. A. Okladnov, and V. P. Lebedev, *J. Polym. Sci., Part A-1*, **8**, 2631 (1970).
5) M. M. O'Mara, *J. Polym. Sci., Part A*-1, **8**, 1887 (1970).
6) G. A. Rasuvaev, L. S. Troitskaya, and B. B. Troitskii, *J. Polym. Sci., Part A*-1, **9**, 2673 (1971).
7) ASTM 9—401.
8) ASTM 5—674.

COMMENTS

BULLETIN OF THE CHEMICAL SOCIETY OF JAPAN, VOL. 48(10), 3001 (1975)

Comment on "Some Considerations on the Electronic Spectra of Cyclic Polyenes"[1]

E. HEILBRONNER

Physikalisch-chemisches Institut der Universität Basel, Klingelbergstrasse 80, CH-4056 Basel, Switzerland

(Received April 25, 1975)

Whatever the merit of the combined application of a FE-treatment and the hole/particle formalism, proposed by Basu[1] for the calculation of the electronic spectra of all-*cis* cyclic polyenes containing n π-electrons in a perimeter system of at least D_{nh} symmetry, the experimental results known to date do *not* constitute proof that the predicted convergence limit for the $^1L_b \leftarrow {}^1A$ transition does exist. In fact they agree much better with the assumption that for $n\rightarrow\infty$ the difference $\Delta E = E(^1L_b) - E(^1A)$ does not differ much from zero. The limit of ΔE for $n\rightarrow\infty$ is definitely much smaller than suggested by Fig. 1 of Ref. 1, which is based on wrong or inadequate data.[2]

Many-electron SCF treatments including configuration interaction[2,3] indicate that ΔE for the longwave $^1L_b \leftarrow {}^1A$ transition of all-*cis* cyclopolyenes satisfying Hückel's rule should depend on n according to $\Delta E \propto \sin(\pi/n)$. Using the data given in Ref. 2 for cyclic π-systems with n=6, 10, 14, 18 we find

$$\Delta E = [(-1.47\pm1.93) + (85.99\pm6.57)\sin(\pi/n)]\times 10^3\ \mathrm{cm}^{-1}$$

a regression line which does not miss the origin $\sin(\pi/\infty)=0$ significantly. (Predicted 90% security confidence limits for n=22 : 8.8 to $12.8\times10^3\ \mathrm{cm}^{-1}$; n=26 : 6.7 to $11.1\times10^3\ \mathrm{cm}^{-1}$; n=30 : 5.1 to $9.9\times10^3\ \mathrm{cm}^{-1}$). Of course linear extrapolation beyond $n\approx30$ is dangerous, because of higher order terms which are not accounted for, if one uses the transformation of the independent variable n into the new variable $\sin(\pi/n)$. However, the analysis clearly indicates that the value of the upper limit of ΔE for $n\rightarrow\infty$ must be at best of the order of $5\times10^3\ \mathrm{cm}^{-1}$, especially if the lack of planarity of some of the reference systems is taken into account. This value is close to the highest frequency vibrational modes and thus "zero" for all practical purposes.

References

1) S. Basu, This Bulletin, **48**, 368 (1975).

2) H. R. Blattmann, E. Heilbronner, and G. Wagnière, *J. Amer. Chem. Soc.*, **90**, 4786 (1968); and references given therein.

3) W. Moffit, *J. Chem. Phys.*, **22**, 320 (1954); H. C. Longuet-Higgins, and L. Salem, *Proc. Roy. Soc.*, **A251**, 172 (1959), **A255**, 435 (1960); **A257**, 445 (1960); E. Heilbronner and J. N. Murrell, *Mol. Phys.*, **6**, 1 (1963).

Trans-Gauche Equilibrium of 1,2-Dibromoethane and Dipole-interactions in Solutions

Masao KAKIMOTO and Tsunetake FUJIYAMA*

Department of Chemistry, Faculty of Science, The University of Tokyo, Hongo, Bunkyo-ku, Tokyo 113
**Department of Chemistry, Faculty of Science, Tokyo Metropolitan University, Fukazawa, Setagaya-ku, Tokyo 158*

(Received December 2, 1974)

The relative absorption intensities of the scissoring vibration bands of *trans*- and *gauche*-1,2-dibromoethanes were measured in pure liquid and in solutions of *cis*-1,2-dichloroethylene or tetrachloroethylene at various concentrations. The relative populations of the rotational isomers were determined from the intensity data. An attempt was made to describe quantitatively the observed concentration-dependence of the relative population on the basis of a semi-molecular theory of dipole-interaction. An equation is proposed for the averaged interaction energy of a molecule with its surrounding molecules, which is expressed in terms of the dipole moments and the polarizabilities of the solute and the solvent molecules.

The problem of rotational isomerism has been one of the major subjects in the field of physical chemistry.[1-3] Many investigations have been concerned with the determination of the energy difference, ΔE, between rotational isomers. In doing so, one uses the van't Hoff's relation and plots the logarithms of the relative intensities (either absorption or scattering) of two isomers against $1/T$, where T is the absolute temperature, and obtains ΔE from the slope of the plot. There remain two problems, however. One is that a straight-line relation is assumed in the plot. This means that ΔE is assumed to be independent of the temperature or, more generally, of intermolecular interactions. Although the assumption holds effectively in many cases, the present authors[4] recently showed that ΔE depends on the temperature in the case of liquid 1,2-dibromoethane. The other problem is that, in general, only the relative intensities, and not the relative populations, can be known from spectroscopic measurements. If one wants to discuss the equilibrium properties of rotational isomers, however, the relative populations must be known experimentally. Fortunately, the present authors[4] succeeded in obtaining the relative populations at several temperatures from the relative intensities of Raman lines in the case of liquid 1,2-dibromoethane. This permits one to discuss the equilibrium property of liquid 1,2-dibromoethane in some detail.

The present investigation concerns the quantitative description of the concentration-dependence of the relative populations of *trans*- and *gauche*-1,2-dibromoethanes. The solvents used were *cis*-1,2-dichloroethylene and tetrachloroethylene: they were chosen because the former is strongly polar, while the latter is nonpolar. *gauche*-1,2-Dibromoethanes and *trans*-1,2-dibromoethanes are also characterized by their dipole moments; the former is strongly polar, while the latter is nonpolar. The effects of intermolecular dipole-interactions on ΔE are estimated in this paper; a good agreement is obtained between the calculated and observed concentration-dependencies of the relative populations of *trans*- and *gauche*-1,2-dibromoethanes.

Experimental

All the chemicals used in the present study were commercial products. Purchased samples showed no trace of impurity in the infrared spectra covering the range of 400—4000 cm^{-1} and were used without further purification. Solutions of 1,2-dibromoethane in *cis*-1,2-dichloroethylene or in tetrachloroethylene were prepared just before the observations so as to obtain the appropriate concentrations by measuring the weight of each component. On determining the mole percents and the molar concentrations, the density data from a standard table[5] were used. The additivity of the volumes of the components was assumed in this process.

The infrared absorption spectra were measured for the scissoring vibration of 1,2-dibromoethane (ν_{15} of the *trans* form, and ν_3 and ν_{13} of the *gauche* form) in pure liquid and in solutions by the use of a Perkin-Elmer 112G single-beam infrared spectrometer. The spectrometer was operated under a resolution of about 1 cm^{-1} and at room temperature (25 °C). The effects of a finite slit-width on the observed band shapes and on the intensities were ascertained to be very small. The observed spectra were reduced to the absorption-index curves, $k(\nu)$'s.[6] It is known that the effects of the refractive index often spoil the observed relative intensity data when the absorption bands are strong.[7] In the present case, however, all the absorption bands observed was very weak, so no special correction for the observed intensity data was made.

The observed spectra, as is shown in Figs. 1 through 3, contain two absorption bands arising from the *trans* and the *gauche* isomers of 1,2-dibromoethane. We separated the two slightly overlapping bands by the method of least-squares,

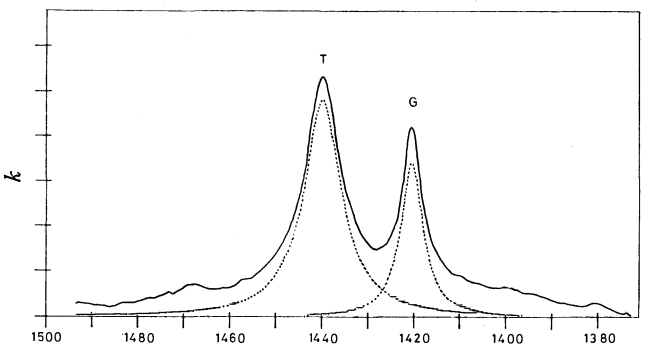

Fig. 1. Absorption index curve for the scissoring vibration bands of liquid 1,2-dibromoethane. Solid line; observed curve, broken line; calculated Lorentzian curve.

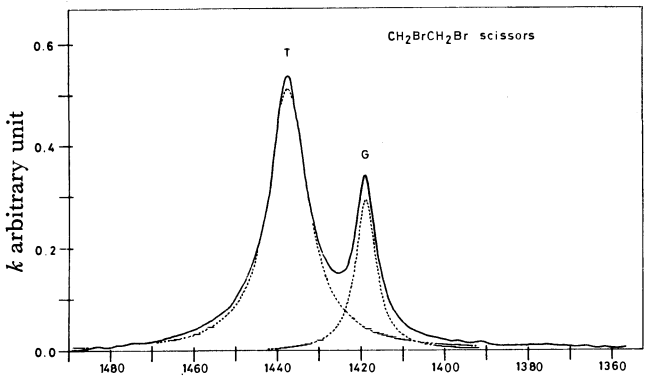

Fig. 2. Absorption index curve for the scissoring vibration bands of 20 mol% solution of 1,2-dibromoethane in *cis*-1,2-dichloroethylene. The unit of the ordinate is arbitrary. Meanings of the lines are the same as in Fig. 1.

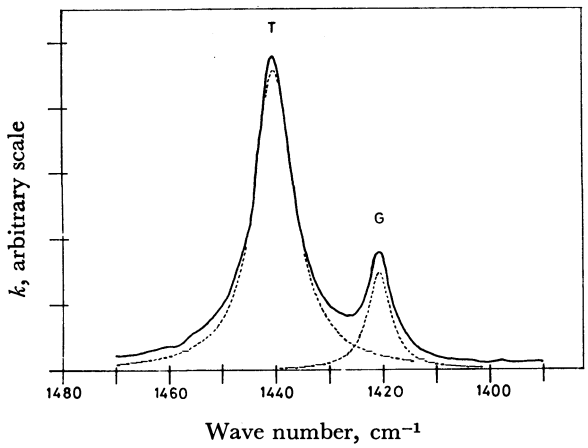

Fig. 3. Absorption index curve for the scissoring vibration bands of 20 mol% solution of 1,2-dibromoethane in tetrachloroethylene. The unit of the ordinate is arbitrary. Meanings of the lines are the same as in Fig. 1.

TABLE 1. CONCENTRATION-DEPENDENCE OF THE RELATIVE POPULATION OF *trans*- AND *gauche*-1,2-DIBROMOETHANES IN SOLUTIONS

mol %	I_t/I_g	$\ln\left(\frac{I_t}{I_g}\right)$	$\ln\left(\frac{n_t}{n_g}\right)$	$-H/kT$	$\frac{A+}{(\Delta E^\circ/kT)}$
— Solutions in *cis*-1,2-dichloroethylene —					
100.00	3.37(0.13)	1.215	0.300[a)]	0.508	0.808
79.76	3.16(0.16)	1.151	0.236	0.605	0.841
59.89	2.82(0.14)	1.037	0.122	0.705	0.827
39.59	2.55(0.14)	0.936	0.021	0.800	0.821
20.22	2.35(0.23)	0.854	−0.061	0.884	0.823
— Solutions in tetrachloroethylene —					
79.84	3.64(0.18)	1.292	0.377	0.395	0.772
59.98	4.12(0.22)	1.416	0.501	0.291	0.792
40.21	4.47(0.20)	1.497	0.582	0.209	0.791
21.75	5.17(0.32)	1.643	0.728	0.136	0.864

I_t/I_g is the relative intensity of the scissoring vibration bands. Numbers in parentheses indicate the standard deviations. n_t/n_g is the relative population obtained from $\ln(I_t/I_g)$ (see the text). H is calculated through Eq. (15). The sixth column is the sum of the fourth and the fifth columns. a) See Ref. 4.

assuming a Lorentzian band shape, and estimated the relative values of the integrated intensities. The separated bands are illustrated by the broken lines in Figs. 1 through 3. Table 1 contains the relative intensity at each concentration thus obtained. The standard deviations attached to the relative intensities in Table 1 were estimated from the deviation between the observed and the calculated absorption curves.

The logarithmic relative population, $\ln(n_t/n_g)$, differs from the corresponding logarithmic relative intensity, $\ln(I_t/I_g)$, only by a constant which is independent of the concentration, if the absolute intensities of the *trans* and the *gauche* isomers do not change in the concentration-variation.[8] The constant was determined so as to make $\ln(n_t/n_g)$ in pure liquid equal to

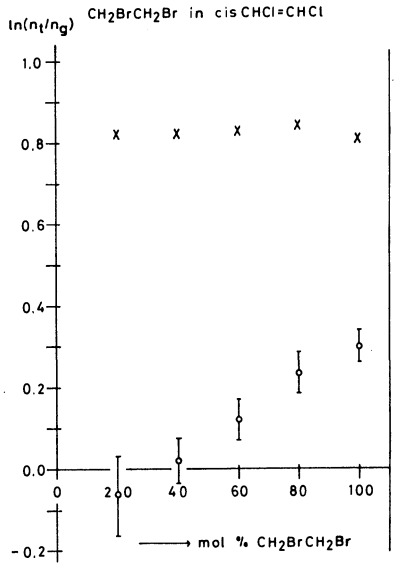

Fig. 4. Concentration-dependence of the relative population of *trans*- and *gauche*-1,2-dibromoethanes in *cis*-1,2-dichloroethylene solution. Open circles; experimental values of the relative population. Crosses; values of the relative population corrected for the effect of dipole interaction (see the text). Vertical lines show the standard deviations.

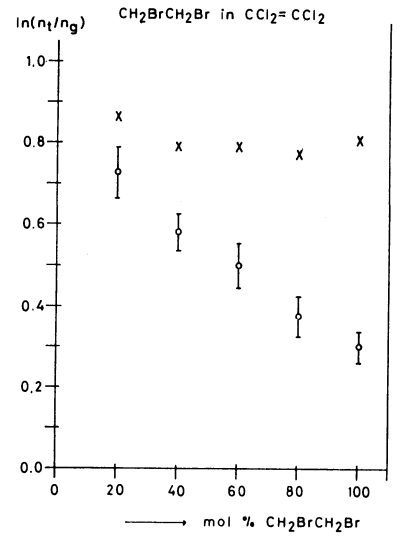

Fig. 5. Concentration-dependence of the relative population of *trans*- and *gauche*-1,2-dibromoethanes in tetrachloroethylene solution. Meanings of the symbols are the same as in Fig. 4.

0.300, the value of which had previously been determined by the present authors.[4] The value of $\ln(n_t/n_g)$ was determined at each concentration from the corresponding $\ln(I_t/I_g)$ by substracting the constant. The results are shown in Table 1 and Figs. 4 and 5.

Theory

Usually the enrgy difference, ΔE, and the relative population, n_t/n_g, are related by the van't Hoff equation:

$$\ln(n_t/n_g) = A + (\Delta E/kT) \tag{1}$$

where A is a constant, k is the Boltmann's constant, and T is the absolute temperature. Let us consider the effect of intermolecular interaction on the magnitude of ΔE. The effect is, in principle, a function of the temperature, the concentration, and other parameters characterizing the system. We may write:

$$\Delta E = \Delta E^\circ + H \tag{2}$$

and

$$\ln(n_t/n_g) = A + (\Delta E^\circ/kT) + (H/kT) \tag{3}$$

where ΔE^0 means the intrinsic energy difference or the energy difference of the rotational isomers when they are well isolated from other molecules, and where H is the effect of intermolecular interactions.

From the microscopic point of view, the *gauche* and the *trans* isomers are considered to differ only in that the former possesses a dipole moment, while the latter does not. The other physical properties may be regarded as almost identical for the two isomers. H, then, arises from the dipole-interaction of a *gauche* isomer with other molecules. In the following, we will focus our attention on a special *gauche* isomer, which will be designated as "central", and try to find the energy of its dipole interaction with the surrounding molecules. It may be expedient to distinguish here the following four types of dipoles which interact with the central *gauche*-dipole; (1) the dipole moments of other *gauche* molecules, (2) the dipole moments of solvent molecules (if any), (3) the dipole moments of other molecules of 1,2-dibromoethane (*gauche*+*trans*) induced by the central *gauche*-dipole, and (4) the dipole moments of solvent molecules induced by the central *gauche*-dipole. The reason why we do not distinguish the *trans* and the *gauche* isomer in (3) is that the refractive index, and hence the polarizability, is known only for the equilibrium mixture of the *trans* and the *gauche* isomers.

Let the polar coordinates of the central *gauche*-dipole, $\boldsymbol{\mu}_g$, of another dipole, $\boldsymbol{\mu}$, and of the radius vector, $\boldsymbol{r}$, pointing from $\boldsymbol{\mu}_g$ to $\boldsymbol{\mu}'$, be (θ_g, φ_g), (θ', φ'), and (θ_r, φ_r) respectively. $\boldsymbol{\mu}'$ can be any one of the aforementioned four types of interacting dipoles. The dipole, $\boldsymbol{\mu}'$, induces an electric field at the point of $\boldsymbol{\mu}_g$. The component of the field along the direction of $\boldsymbol{\mu}_g$ is written as:[11]

$$F = -\frac{\mu'}{r^3}(A+B+C+D+E+F) = -\frac{\mu'}{r^3}\Omega \tag{4}$$

where A, B, C, D, E, and F are expressed in terms of the spherical harmonic with respect to polar coordinates, (θ_g, φ_g), (θ', φ'), and (θ_r, φ_r),[11] and where Ω means the sum of these six terms. Similarly, $\boldsymbol{\mu}_g$ induces an electric field in the surroundings and produces an induced moment, $\boldsymbol{\mu}_i$:

$$\mu_i = -\frac{\alpha\mu_g}{r'^3}\Omega' \tag{5}$$

where α is the polarizability of the molecule in the surroundings. The primes on r and Ω in Eq. (5) show that r Ω of Eq. (5) are not necessarily the same as those in Eq. (4). The induced moment, $\boldsymbol{\mu}_i$, in turn induces and electric field on the position of $\boldsymbol{\mu}_g$. The component of the field along the direction of $\boldsymbol{\mu}_g$ is, according to Eq. (4):

$$F = \frac{\alpha\mu_g}{r'^6}\Omega'^2 \tag{6}$$

Now we can write the induced field at the position and along the direction of the central $\boldsymbol{\mu}_g$:

$$F_1 = -\frac{\mu_g}{r_g^3}\Omega_g \tag{7a}$$

$$F_2 = -\frac{\mu_s}{r_s^3}\Omega_s \tag{7b}$$

$$F_3 = \frac{\alpha_m\mu_g}{r_m^6}\Omega_m^2 \tag{7c}$$

$$F_4 = \frac{\alpha_s\mu_g}{r_s^6}\Omega_s^2 \tag{7d}$$

where all the quantities suffixed with g, s, or m, except for the μ_g in Eq. (7c) or (7d), which stands for the dipole moment of the central *gauche* isomer, are related with the surrounding *gauche* isomers. the solvent molecules, or the mixture of the *trans* and the *gauche* isomers, respectively. The total interaction energy, $\mathcal{H}$, of the central *gauche* isomer is, then:

$$\mathcal{H} = \mu_g(F_1+F_2+F_3+F_4) \tag{8}$$

To obtain H of Eq. (2) or (3), one must average Eq. (8) over all the possible orientations and distances of the interacting pair. In doing so, it must be considered that the relative orientation of two dipole moments is distributed according to their interaction energy; that is, energetically more stable configurations are distributed more than the less stable configurations. This concept is considered in the averaging process by introducing the Boltzmann distribution function:

$$W = w\exp(-\mathcal{H}/kT) \tag{9}$$

where w is a constant which is to be determined by the normalization condition:[12]

$$w\int_v d\tau = n \tag{10}$$

where v indicates a sphere of the unit volume, at the center of which the central *gauche*-dipole is situated, where $d\tau$ is the volume element:

$$d\tau = r^2\sin\theta d\theta d\varphi dr \tag{11}$$

and where n is the number of molecules in v. Now, the average way be expressed in terms of an integral:

$$H = \sum_i w_i\int\mu_g F_i\exp(-\mu_g F_i/kT)d\tau \tag{12}$$

where the suffix i corresponds to the four terms of Eq. (7). In Eq. (12), it is assumed that the averages of the four terms of Eq. (8) can be taken independently. In other words, the orientational correlation between neighbour dipoles is assumed to have no effect on the interaction of the dipoles with the central *gauche*-dipole.

To calculate the integral in Eq. (12), we expand the exponential and neglect the higher terms than the second:[13]

$$H = \sum_i w_i \int \mu_g F_i [1 - (\mu_g F_i / kT)] \mathrm{d}\tau \qquad (13)$$

Integration over orientations is performed by the use of the orthonormality of the spherical harmonics, which results in:[13]

$$\int \Omega \mathrm{d}\tau' = \int \Omega^3 \mathrm{d}\tau' = 0$$

and

$$\int \Omega^2 \mathrm{d}\tau' = \frac{128}{3}\pi^3 \qquad (14)$$

where $\mathrm{d}\tau'$ is the angular part of the volume element. A lower limit, a_0, must exist for the integration over the distance; the meaning of this is that two molecules can not come closer than a_0. We estimated the a_0 from the density and the molecular weight, assuming a rigid sphere for each molecule.[14] The result is:

$$H = -\frac{4\pi^2}{27}\frac{\mu_g^4}{kT}\frac{\rho}{W_m}c_m\frac{N_a^2}{1+(n_t/n_g)} - \frac{4\pi^2}{27}\alpha_m\mu_g^2\frac{\rho}{W_m}c_m N_a^2 - \frac{32\pi^2}{27}\left(\frac{\mu_g^2\mu_s^2}{kT}+\alpha_s\mu_g^2\right)\frac{c_{ms}N_a^2}{\left[\left(\frac{W_m}{\rho}\right)^{1/3}+\left(\frac{W_{ms}}{\rho_s}\right)^{1/3}\right]^3} \qquad (15)$$

where N_a is Avogardo's number, where W_m, ρ, and c_m are the molecular weight, the density, and the molar concentration (mol/cm^3) respectively of the solute, and where the same symbols suffixed with s refer to those of the solvent molecule.

Results and Discussion

Figures 4 and 5 show the experimental values of the relative populations of *trans*- and *gauche*-1,2-dibromoethanes in solutions. It may be seen from the figures that the population varies on going from pure liquid to dilute solutions: it increases in a tetrachloroethylene solution. In other words, the numbers of the *gauche* isomer increase as the polarity of the environment increases.

To see whether or not the model of dipole interaction, developed in the last section, is appropriate, we calculate H/kT from Eq. (15) at each concentration and subtract it from the observed value of $\ln(n_t/n_g)$. The resultant value should be $A+(\Delta E^0/kT)$, as may be seen from Eq. (2), and should remain constant over all concentrations. In the calculation, α_m and α_s were estimated from the values of the refractive indices[5] using the Lorentz-Lorenz formula, the densities were taken from a standard table,[5] and μ_g and μ_s (of *cis*-1,2-dichloroethylene) were taken to be 2.20 D[15] and 1.89 D[16] respectively. The results of the subtraction are shown in Table 1 and in Figs. 4 and 5. It may be seen from the table and the figures that the resultant value remains almost constant for all the concentrations; this indicates the validity of the model used in the calculation. Thus, it may be concluded that the equilibrium properties of the *trans*- and *gauche*-1,2-dibromoethanes in solutions are fully described by the model of dipole-interaction, Eq. (15).

Incidentally, Eq. (15) tells us that the energy difference, ΔE, should change in value according to the change in temperature as well as that in concentration. The temperature-effect data of the reference[4] can also be explained by the use of Eq. (15).

It should be noted that, in the present calculation, we are considering the environments to be built up of gas-like molecules dispersed in a vacuum to give the actual density, instead of looking them as continuous dielectrics. The latter model yields the famous reaction field of Onsager.[17] The present approach has a close resemblance to the latter in concept, but it has resulted in a quite different equation which is expressed in terms of the dipole moment and the polarizability instead of the dielectric constant, a very macroscopic quantity. The present theory is not, however, a fully molecular theory in the sense that the polarizability is calculated from such macroscopic quantities as the refractive index and the density through the Lorentz-Lorenz formula, and in that the molecular radius is estimated in the same way as in Onsager.[14,17] A comparison of the numerical results of the present equation with those based on the reaction field shows that the two approaches do not give the same results for the averaged electric field acting on a molecule.[4] It can be said at the same time that the present model can well describe the magnitude of the change in the averaged electric field in the concentration- or temperature-variation. To clarify the difference existing between the two approaches is interesting and may be a problem for the future.

The authors are indebted to all the members of the Shimanouchi laboratory for their helpful correspondence about this work. They are particularly grateful to Professor Takehiko Shimanouchi of the University of Tokyo for giving them the opportunity of publishing this work.

References

1) S. Mizushima, "Structure of Molecules and Internal Rotation," Academic Press, New York (1954).

2) Y. Morino, S. Mizushima, K. Kuratani, and M. Katayama, *J. Chem. Phys.*, **18**, 754 (1950).

3) I. Watanabe, S. Mizushima, and Y. Masiko, *Sci. Pap. Inst. Phys. Chem. Research* (Tokyo), **40**, 425 (1943).

4) T. Fujiyama and M. Kakimoto, to be published.

5) "International Critical Tables," National Research Council, McGraw-Hill, New York (1928).

6) M. Kakimoto and T. Fujiyama, This Bulletin, **45**, 3021 (1972).

7) T. Fujiyama and B. Crawford, Jr., *J. Phys. Chem.*, **72**, 2174 (1968).

8) In the discussions of the text, it is assumed that the absolute intensity of a *gauche* or a *trans* isomer does not change in dilution. This assumption, however, is not strictly true. The authors are going to show, in a subsequent paper,[9] tha the absolute intensities of the infrared absorption bands may change, in some cases about a factor of two, on going from a pure liquid to a dilute solution. An equation is to be presented to describe the intensity change: the basic concept is that the transition moment, m_1, differs in liquid media from that of an isolated molecule, μ_1:

$$m_1 = \mu_1 + \alpha_1 \langle \mathscr{F} \rangle_{av}$$

where α_1 is the transition polarizability and where $\langle \mathscr{F} \rangle_{av}$ is the averaged field acting on the absorbing molecule. The most contributing term in $\langle \mathscr{F} \rangle_{av}$ is, in the case of liquid 1,2-dibromoethane;

$$\frac{4\pi^2}{27} N_a \frac{\mu_g^2}{kT} \left(\frac{\rho}{W_m} \right)^2 \frac{1}{1+(n_t/n_g)}$$

where the notations are the same as in the text. We must remember that, among the two scissoring vibrations of *trans*-1,2-dibromoethane, one (b_u) is Raman-inactive ($\alpha_1=0$) and the other (a_g) is infrared-inactive ($\mu_1=0$). Therefore, one might expect that the absolute intensity of the scissoring vibration of the *trans* isomer does not change. On the other hand, the two scissoring vibrations (*a* and *b*) of the *gauche* isomer are active in both the infrared and Raman spectra, so one must consider the intensity-change in this case. The results of the present measurement, combined with the value of the relative population in Table 1, yield 504 cm^2/mol for the absolute intensity of the scissoring vibration band (*a* and *b* combined) of the *gauche* isomer, after the Polo-Wilson correction.[10] This corresponds to m_1 of 0.0449 D. If α_1 is assumed to be 0.1 $Å^3$, which might be unrealistically large for this vibration, then μ_1 becomes 0.0441 D and the corresponding intensity is 487 cm^2/mol. Therefore, the change in the absolute intensity is only about 3.5% even for the large value of α_1, on going from a pure liquid to a very dilute solution in nonpolar solvents. Thus, the intensity-change does not exceed the experimental errors in the present work.

9) M. Kakimoto and T. Fujiyama, This Bulletin, **48**, 2258 (1975).

10) S. R. Polo and M. K. Wilson, *J. Chem. Phys.*, **23**, 2376 (1955).

11) See, for example, M. Bersohn and J. C. Baird, "An Introduction to Electron Paramagnetic Resonance," (W. A. Benjamin, New York, 1966), Appendix B–1, or A. Abragam, "The Principles of Nuclear Magnetism," (Oxford, Clarendon Press, 1961), Chapter IV.

12) More precisely, Eq. (10) should be written as:

$$w \int_v \exp(-\mathscr{H}/kT) d\tau = n.$$

However, the higher-order terms than the first, in the expansion of the exponential, yield only very small contributions to the result, and so Eq. (10) is justified.

13) The next nonvanishing term in the expansion of H can be calculated by the use of this relation:

$$\int \Omega^4 d\tau' = \frac{1536}{25} \pi^3.$$

Calculation showed that the contribution from the next nonvanishing term is, at most, about 1% of Eq. (15) in the case of 1,2-dibromoethane in solutions.

14) In principle, one must use a radial distribution function in the integration of the radial part in Eq. (13). The radial distribution function can not, however, be used for large molecules. The present assumption is identical with putting the radial distribution function equal to unity for $r \geqq a_0$ and to 0 for $r < a_0$.

15) I. Watanabe, I. Miyagawa, and Y. Morino, *Repts. Radiation Chem. Res. Inst.* (Tokyo Univ.), **3**, 25 (1947).

16) A. A. Maryott, M. E. Hobbs, and P. M. Gross, *J. Amer. Chem. Soc.*, **63**, 659 (1941).

17) L. Onsager, *ibid.*, **58**, 1486 (1936).

Coagulation-dispersion and Precipitation-flotation Behavior of Bentonite and Cadmium-ion Flotation

Toyono INAKAZU,* Koichi KOBAYASHI,** and Tsunetaka SASAKI***

Department of Chemistry, Faculty of Science, Tokyo Metropolitan University, Setagaya, Tokyo 158

(Received December 9, 1974)

The states of dispersion and the precipitation-flotation behavior of bentonite particles in an aqueous solution of hexadecyltrimethylammonium chloride (HTAC) were studied, and the effect of the HTAC on the coagulation and dispersion was discussed in connection with its adsorption on bentonite. The coagulation precipitation of bentonite began to occur at the ratio of the adsorbed amount to an exchange capacity, A/T, of about 0.05. It changed to coagulation flotation in the vicinity of $A/T=1.2$. The change was very sharp. The results suggest that the change from precipitation to flotation is produced by the adsorption of HTAC a little in excess of the first-layer formation, where a slight hydrophilization begins. It seems likely that, in the above state, the bubbles are easily accessible to bentonite particles because the agglomerates assume an open structure. The redispersion occurred near the point of sufficient hydrophilization of bentonite particles because of the adsorption of the second layer of cationic surfactant molecules.

There have been a number of studies of the coagulation and redispersion of suspension by the addition of inorganic electrolytes, macromolecular substances, and surfactants.[1-4] Thus, the sensitizing and stabilizing action of gelation on hydrophobic sol; the addition to the colloidal suspension of an electrolyte with a polyvalent ion with the charge opposite to that of the colloidal, particle, known as the irregular series, is a popular instance.[5] The effect of the addition of ionic[4,6] and nonionic surfactants[7] on the flocculation-deflocculation behavior of sulfathiazole and other suspensions, in particular the bentonite suspension, has also been reported. In such cases, the suspension often foams and the suspended particles coagulate and float. However, such phenomena have not received much attention,[2,8] though they are properly suitable to the removal of many different ions from solutions.

In the present paper, the coagulation and redispersion, accompanied by the precipitation and flotation upon the addition of a cationic surfactant, will be described for the bentonite suspension. The adsorption of the surfactant on bentonite was also studied, and the mechanisms of the coagulation, flotation, and redispersion of bentonite will be discussed in connection with its adsorption on bentonite. Further, the ion flotation of Cd^{2+} ions will be studied in parallel with the bentonite flotation.

Experimental

Materials. The bentonite used was of a commercial grade (origin; Gunma, Japan, montmorillonite type) and was supplied by the Wako Pure Chemical Co., Ltd; the fraction passing through a 350-mesh sieve was collected. A stock suspension of bentonite was prepared first by dispersing the bentonite in distilled water; then it was allowed to stand for 24 hr after shaking. Then, the supernatant solution was taken in the visking dialysis tube and dialyzed while the suspension was being stirred by passing nitrogen gas through it. The dialysis was continued for 5 days, frequently exchanging the outer water with fresh ion-exchange water. The dialysis of the bentonite suspension was continued until a constant specific conductivity of about 10^{-5} Ω/cm was reached. The stock suspension of about 10000—20000 ppm bentonite thus obtained was well shaken before use. A preliminary experiment showed that the bentonite suspension thus prepared scarecely sedimentated at all within a week, but no solution aged longer than a week was used. Pure-grade hexadecyltrimethylammonium chloride (HTAC), supplied by the Kao Soap Co., Ltd., was dried under reduced pressure and kept in a desiccator containing silica gel. The sodium octadecylsulfate (SOS) used for titrating HTAC was obtained from the Kao Soap Co., Ltd., and was used without further treatment.

A stock solution of Cd^{2+} ions of a 1.78×10^{-4} mol/l concentration was prepared by dissolving in nitric acid pure metals (purity>99.99%) kindly supplied from the Laboratory of General Chemistry of our department.

Water was refluxed overnight with a mixture of sulfuric acid and potassium permanganate and then triply distilled using a borosilicate glass apparatus.

All the experiments were carried out at room temperatures from 25 to 27 °C.

Measurement of the Coagulation and Redispersion of Bentonite. Varying amounts of the bentonite suspension and of the HTAC solution were placed in a test tube with a ground-glass stopper, 1.5 cm in inner diameter and 13 cm in length, and the total volume of the solution was made up to 10 ml with water. The pH values of suspension thus prepared ranged from 5.7 to 6.4. The test tube was turned upside down 3 times, then shaken by hand for 10 s again turned upside down 3 times, and finally allowed to stand for 30 min. The appearances of the dispersion, coagulation precipitation, coagulation flotation, and redispersion of the suspension were judged by the naked eye, and the regions of the compositions of systems showing these phenomena were plotted as a diagram.

Measurement of the Adsorption of HTAC on Bentonite. In the ground test tube, a fixed amount of the dialyzed bentonite suspension and varying amounts of the HTAC solution were placed. The volume of the solution was made up to 10 ml with water. After shaking the test tube for 10 s or by turning the test tube upside down 20 times with a 2-min period, bentonite particles were removed from the solution by (a) centrifugation, (b) ultrafiltration, or (c) electrodialysis

* Present address: Century Research Center, 2-3, Nihonbashi-Honcho, Chuo-ku, Tokyo 103.

** Address all correspondence to present address: Laboratory of Chemistry, Musashi Institute of Technology, 1-28-1, Tamatsutsumi, Setagaya, Tokyo 158.

*** Present address: Department of Chemistry, Faculty of Science, Tokai University, Hiratsuka, Kanagawa 259-12.

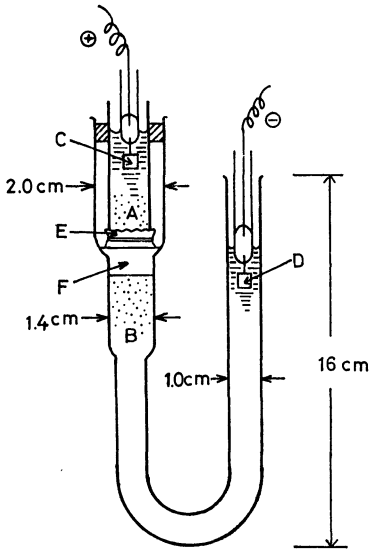

Fig. 1. Apparatus used for electrodialysis. A: glass tube with visking membrane E, B: glass U-tube, C, D: platinum electrodes, F: clear solution for analysis.

as the case required. The concentration of HTAC remaining in the solution was titrated with a SOS solution of a known concentration, with the addition of dilute hydrochloric acid and of bromophenol blue as an indicator.[9]

The amount of HTAC adsorbed on the bentonite was calculated from the difference between the HTAC concentration before and after adsorption. (a) Centrifugation. A suspension containing bentonite particles was centrifuged for 10 min at about 2500 rpm. The aqueous supernatant thus obtained was used for the determination of the HTAC concentration. (b) Ultrafiltration. The aqueous suspension was filtered using a visking membrane supported by a glass filter with a porosity of No. 4 under reduced pressure. The filtrate was then used for the determination of the HTAC concentration. (b) Electrodialysis. Electrodialysis was carried out for a stable suspension containing concentrated HTAC; neither method, (a) or (b), could be applied. The apparatus used for the electrodialysis is shown in Fig. 1.[10] In this figure, a glass tube, A, with a semipermeable visking membrane, E, closing its bottom and a glass U-tube, B, were filled with the solution of a stable bentonite suspension to be dialysed. The tube, A, was adjusted so that the membrane just touched the surface of the solution in the tube, B. The solution in A was renewed after being allowed to stand for 30 min. The electrodialysis was then carried out for 2 to 3 hrs applying a 200-V DC between two platinum electrodes inserted in the solution, as is shown in Fig. 1. The electrodes were 27 cm apart from each other along the axis of the tubes. After the electrodialysis, a transparent layer of the solution was obtained in the tube, B, just below the membrane, which was then carefully taken out for the determination of the HTAC concentration.

Measurement of the Total Base Exchange Capacity of Bentonite.[11] A suspension containing about 4 g of bentonite in 100 ml of a 0.1 M aqueous $BaCl_2$ solution was prepared, and the mixture was stirred for 4 hrs. The precipitates of Ba-bentonite, thus obtained were removed by centrifuging (2500 rpm for 20 min), and the precipitates separated were dispersed in triply distilled water. The free $BaCl_2$ remaining was then removed by dialysis, and the precipitates of Ba-bentonite were again dispersed in a 2: 1 (vol) water–ethanol mixture. The suspension thus obtained was conductometrically titrated with a 0.2 M $MgSO_4$ solution, and the total base exchange capacity of the bentonite was determined from the amount of Mg^{2+} ions added until a sudden increase in the conductance appeared.

Measurement of the Flotation of Cd^{2+} Ions by HTAC. The apparatus and procedure used in the present experiment were the same as have been described in a previous paper.[12] Nitrogen gas humidified with water vapor and controlled to a constant rate of gas flowing was bubbled through a glass filter (No. 4) into a flotation cell containing 10 ml of the sample solution. The concentrations of Cd^{2+} ions before and after flotation were determined by using an atomic absorption spectrometer (Techtron Pty., Ltd., Model-AA-100).

The flotation rate (F) of Cd^{2+} ions is conventionally given by:

$$F = (1 - C_f/C_i) \times 100\%$$

where C_i and C_f denote the concentrations of the Cd^{2+} ions before and after flotation respectively.

Results and Discussion

Coagulation-dispersion Behavior of Bentonite upon the Addition of HTAC. The change in the dispersion state of the bentonite suspension upon the addition of the cationic surfactant HTAC is shown in Fig. 2. As may be seen in the figure, each region—dispersion, coagulation precipitation, coagulation flotation, and redispersion— is distinct.

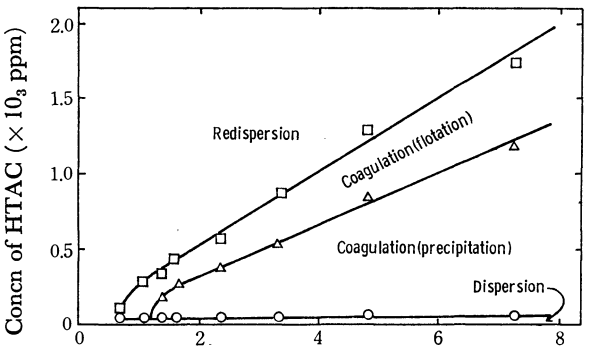

Fig. 2. Effect of HTAC on bentonite suspension.

Dispersion Region. Immediately after the preparation of the solution, the aggregates form slightly, but after shaking they disappear and the suspension is stable even after 30 min. The amount of HTAC is thus insufficient to produce coagulation in this region.

Coagulation Precipitation Region. On an increase in the amount of HTAC, with the amount of bentonite kept constant, fluffy aggregates begin to precipitate. The sedimentation volume increases with a further increase in the amount of HTAC, and a turbid supernatant gradually changes to a clear one.

Coagulation Flotation Region. On a further increase in the amount of HTAC, a sharp point is arrived at which aggregates change suddenly the state of precipitation to that of flotation, while the bentonite particles are still in an aggregated state. In this region, the suspension is readily coagulated by shaking and the coagulates quickly rise to the aqueous surface, leaving a transparent solution below.

Redispersion Region. On continuing the addition of HTAC, the state is arrived at in which the aqueous phase begins to become turbid; this turbidity increases with an increase in the amount of HTAC, while the amount of bentonite floated decreases until the coagulates completely disappear. The foam formation is observed for a sufficiently concentrated solution of HTAC.

The above observation of the change in the dispersion state with an increase on the amount of HTAC leads to the consideration that the coagulation-redispersion and precipitation-flotation phenomena are closely related to the nature of the outermost surface of the bentonite particles modified by the increasing adsorption of HTAC with the concentration. The increase in the amount of adsorption is considered to change the surface properties gradually from those favorable for coagulation precipitation through coagulation flotation to redispersion. To confirm such a reasoning, the following measurements were carried out.

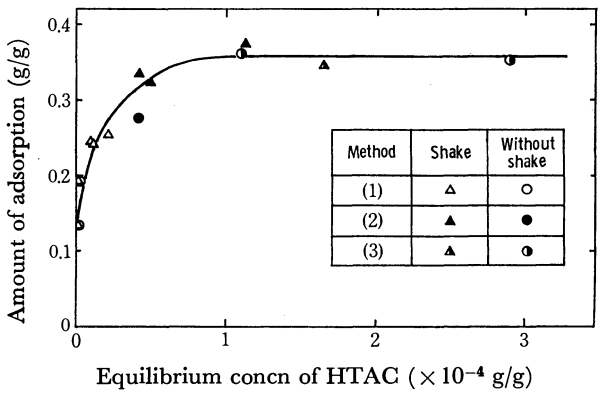

Fig. 3. Adsorption isotherm of HTAC on bentonite.
(1) centrifuge, (2) dialysis, (3) ultrafiltration

Amount of the Adsorption of HTAC. The amount of HTAC adsorption of bentonite is plotted against the equilibrium concentration in Fig. 3. The values obtained by the various methods mentioned above may be seen to agree with each other. A sharp initial increase in the amount of adsorption and the saturated adsorption at a low HTAC concentration show the almost complete adsorption of added HTAC on the bentonite up to saturation. Such behavior is indicative of the exchange adsorption being rapid and quantitative. The saturated adsorption is obtained in the region of equilibrium HTAC concentrations larger than 1×10^{-4} g/g water. The fact that the amount adsorption is independent of the shaking also shows that the adsorption of HTAC on air bubbles is negligible.

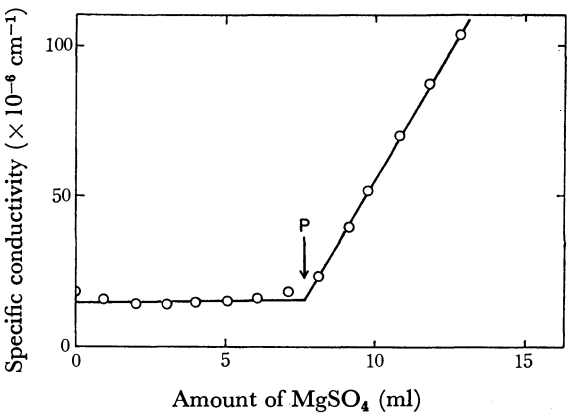

Fig. 4. Conductometric titration of Ba-bentonite. P: total exchange capacity of bentonite.

Total Base Exchange Capacity of Bentonite. In order to measure the exchange capacity of bentonite, the conductance of the Ba-bentonite suspension is plotted against the volume of $MgSO_4$ added in Fig. 4. The exchange capacity, as calculated from the break point corrected for the moisture content of the bentonite, is 42.5 m. e./100 g dry bentonite. The value obtained is somewhat smaller than the value from 60 to 100 m. e./100 g previously reported for bentonite.[13]

Effect of the HTAC Adsorption on Coagulation and Redispersion. In order to study the relation between the adsorption of HTAC and the coagulation-redispersion behavior of bentonite shown in Fig. 2, the amount of adsorption of HTAC on the bentonite was calculated for the system corresponding to the points on the line of Fig. 2. The amount of adsorption, Γ, can be calculated as the intersection of the isotherm, Γ *vs.* C, shown in Fig. 3 and the straight line where M and m denote the

$$M = m\Gamma - CV$$

total amount of HTAC and the amount of bentonite taken up respectively, and V, the volume of the solution, all of which are known constants corresponding to a given point in Fig. 2. The amount of adsorption thus calculated is shown in Table 1, together with the ratio of the adsorbed amount (A) to the exchange capacity (T).

Table 1. Effects of HTAC adsorption on coagulation—dispersion and precipitation—flotation

Concn of bentonite (ppm)	Coagulation precipitation		Coagulation flotation		Redispersion	
	A[a]	A/T[b]	A[a]	A/T[b]	A[a]	A/T[b]
3000	0.016	0.12	0.154	0.13	0.236	1.75
4000	0.009	0.07	0.162	1.19	0.243	1.79
6000	0.007	0.05	0.165	1.21	0.245	1.80

a) Minimum amount of adsorption. b) Ratio of minimum amount of adsorption (A) to exchange capacity (T).

It may be seen that coagulation begins at a very low A/T ratio of about 0.05 and that the coagulation precipitation changes to the coagulation flotation at about $A/T=1.2$, *i.e.*, at an amount of adsorption slightly above the exchange capacity, and that the redispersion begins at an A/T ratio larger than about 1.8. On the basis of these experimental results, the state of the adsorption of the cationic surfactant on the bentonite to produce coagulation and redispersion is illustrated in Fig. 5.

In this figure, (a) and (b) show the HTAC adsorption on the single bentonite particle and the state of aggregation of such particles respectively in each concentration range of Fig. 2. At a very concentration of HTAC, the bentonite is dispersed despite the adsorption of the

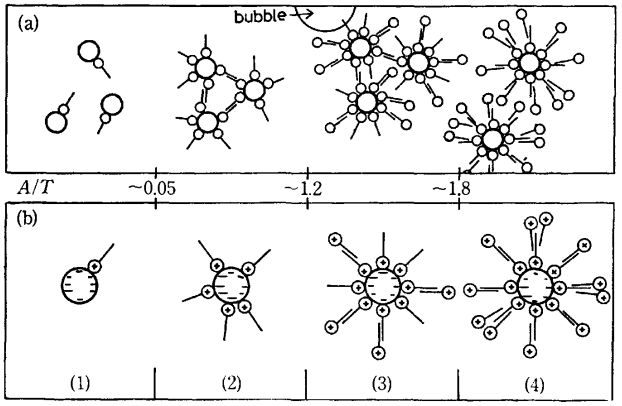

Fig. 5. Adsorption of HTAC and state of dispersion of bentonite (a) and adsorption of HTAC on a bentonite particle (b). (1) dispersion, (2) coagulation precipitation, (3) coagulation flotation, (4) redispersion.

cationic surfactant. With an increase in the concentration of the cationic surfactant, the surface of the particles is rendered hydrophobic by the increasing amount of the adsorption of HTAC, with its hydrophobic tail directed outward, and the coagulation of particles is promoted by the hydrophobic binding of these adsorbed molecules. Since there are no sufficient molecules available for adhering to bubbles, coagulated particles precipitate. As the amount of adsorption increases and comes slightly to exceed the exchange capacity, namely, $A/T>1.2$, double-layer adsorption takes place, as is shown in Fig. 5, and the coagulates assume an open structure favorable for bubble attachment, resulting in coagulation flotation. At A/T ratios larger than 1.8, the double-layer adsorption is nearly completed and the bentonite particles are rendered hydrophilic, resulting in a redispersion of the particles. In this state, the bentonite particles have sufficient positive charges as a result of the adsorption of the cationic surfactant.[14] This reversl. of the charge was also confirmed by electrodialysis measurements.

Flotation of Cd^{2+} Ions by HTAC and Bentonite. There are various possible types of methods of ion flotation.[15] The combined use of bentonite and a cationic surfactant is especially effective for the removal of both anion and cations in the solution.[16] From this fact, together with the phenomena of coagulation flotation and precipitation mentioned above, the bentonite-cationic surfactant system is considered to be suitable for the flotation of ions in an aqueous solution. Here, cadmium ions are selected as the ions to be floated. The flotation was carried out for a solution containing 1.78×10^{-5} mol/l Cd^{2+}, 1000 ppm bentonite, and varying concentrations of HTAC under a gas-flow rate and a time of 10 ml/min and 7 min respectively and at pH 11.2. The results are shown in Fig. 6.

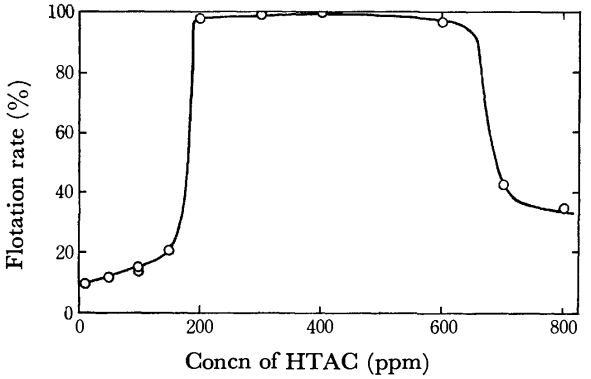

Fig. 6. Rate of Cd^{2+} ion flotation *vs.* concn of HTAC. Cd^{2+}: 1.78×10^{-5} mol/l, bentonite: 1000 ppm, pH: 11.2, gas-flow time: 7 min, gas-flow rate: 10 ml/min, pH adjusted by NaOH.

As may be seen, the flotation rate, F, increases rapidly at an HTAC concentration of about 150 ppm, shows a flat maximum of about 98% in the region of HTAC concentrations from 200 ppm to 600 ppm, and decreases at concentrations of HTAC larger than about 600 ppm. In the region of HTAC concentrations from 200 ppm to 600 ppm, the solutions after flotation look quite transparent, while in the other region of HTAC concentrations they look opaque. These facts indicate that the region of coagulation flotation shown in Fig. 2 corresponds to the optimum region of ion flotation, although the former does not coincide with the latter, perhaps because of difference in the pH at which the flotation measurements were carried out. A rapid decrease in the flotation rate above 600 ppm HTAC may be explained by a redispersion of the bentonite in addition to the replacement of the Cd^{2+} ions on the bentonite by HTAC. It was further confirmed that a stable foam layer was produced for the bentonite concentrations larger than about 400 ppm.

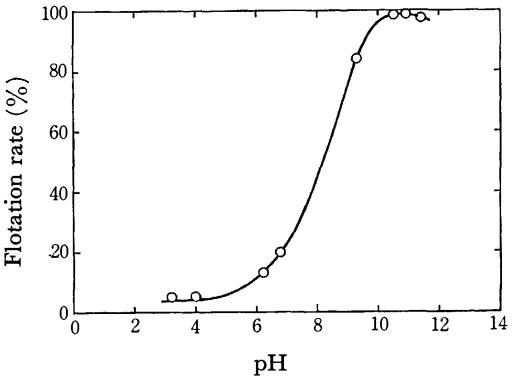

Fig. 7. Rate of Cd^{2+} ion flotation *vs.* pH. Cd^{2+}: 1.78×10^{-5} mol/l, bentonite: 600 ppm, HTAC: 200 ppm, gas-flow time: 7 min, gas-flow rate: 10 ml/min, pH adjusted by NaOH.

Figure 7 shows the flotation rate *vs.* pH curve under the optimum conditions specified in the figure. As may be seen, the flotation rate begins to increase from almost zero at around pH; the maximum flotation rate of 99% was observed at about pH 11. From these experiments, it may be concluded that the optimum conditions for the bubble flotation of Cd^{2+} ions exist in the region of coagulation flotation and that the region is relatively wide with respect to the amount of HTAC, while it is rather narrow for hydrogen-ion-concentration change, as expressed by the pH. Since the bentonite and the HTAC are confirmed to be removed together with the Cd^{2+}, the above conditions are also the optimum ones for these additives.

References

1) A. S. Michael, *Ind. Eng. Chem.*, **46**, 1485 (1954); M. Noda, *Kogyo Yosui*, No. 25, 60 (1960); *ibid.*, No. 26, 26 (1960); *ibid.*, No. 27, 34 (1960); Y. Toyoshima, *ibid.*, No. 30, 34 (1961); *ibid.*, No. 31, 50 (1961); K. Meguro, *Kogyo Kagaku Zasshi*, **58**, 905 (1955); *Nippon Kagaku Zasshi*, **77**, 72 (1956); **77**, 77 (1956); K. Meguro and T. Kondo, *Nippon Kagaku Zasshi*, **76**, 642 (1955); This Bulletin, **32**, 267 (1959); H. Arai, F. Shigehiro and I. Maruta, *Kogyo Kagaku Zasshi*, **68**, 1090 (1965).

2) V. H. Lange, *Kolloid-Z*, **211**, 106 (1966).

3) R. E. Grim, W. H. Allaway, and F. L. Cuthbert, *J. Amer. Ceram. Soc.*, **30**, 137 (1947); *ibid.*, **30**, 142 (1947).

4) J. P. Law, Jr., and G. W. Kunze, *Soil Sci. Soc. Amer. Proc.*, **30**, 321 (1966); *ibid.*, **30**, 327 (1966).

5) H. R. Kruyt, "Colloid Science," Vol. II, Elsevier Pub. Co. Inc., New York (1949), p. 207.

6) Y. Nakamura, A. Otsuka, and M. Nakagaki, *Yakugaku Zasshi*, **94**, 833 (1974).

7) M. Nakagaki, and N. Kawamura, *ibid.*, **90**, 699 (1970); A. Otsuka, H. Sunada, and Y. Yonezawa, *J. Pharm. Sci.*, **62**, 751 (1973).

8) T. Sasaki, In "Bunri to Seisei," Jikken Kagaku Koza, Ser. 2, Vol. 2, Sec. 15, pp. 565—603; T. Sasaki, *Nippon Kogyo Kaishi*, **85**, 610 (1969).

9) G. S. Hartley and D. F. Runnicler, *Proc. Roy. Soc., Ser. A*, **168**, 420 (1938).

10) S. Okazaki and T. Sasaki, *Kolloid-Z*, **178**, 97 (1961).

11) M. M. Martley and J. L. Mellor, *Soil Sci. Soc. Amer. Proc.*, **18**, 363 (1954).

12) K. Kobayashi, This Bulletin, **48**, 1180 (1975).

13) T. Sudo, "Clay Mineral," Iwanami Zensho, (1969), p. 197.

14) L. Ter. Minassian-Saraga, *J. Chim. Phys.*, **63**, 1278 (1966).

15) R. Lemlich, "Adsorptive Bubble Separation Techniques," Academic Press, New York and London (1972).

16) E. Fukada, K. Kobayashi, and T. Sasaki, This Bulletin, to be published.

Surface Dilational Properties of Adsorbed Monolayers of Aqueous Sodium Dodecyl Sulfate Solutions

Masao NAKAMURA*

Department of Chemistry, Faculty of Science, Tokyo Metropolitan University, Setagaya, Tokyo 156

(Received January 6, 1975)

The surface pressure relaxation of a freshly formed surface and the surface area creep at a constant surface pressure have been studied for aqueous surface of sodium dodecyl sulfate solutions. It was found that the area stress after the formation of a fresh surface undergoes relaxation according to the generalized Maxwell model, and that the surface area viscosity is not constant during the process but increases with the surface area. The concept of two-dimensional open system rheology was introduced and the observed phenomena were discussed. A surface equation of state applicable under such dynamic conditions has been derived.

Numerous studies[1-3] have been carried out on the adsorption kinetics of surface-active solute from aqueous solutions onto their surfaces in connection with the variation of surface tension with time. For such studies, it is necessary to change the measured surface tension (pressure) data into the amount of solute absorbed at each moment. However, there is no non-equilibrium surface equation of state that can be applied during the course of adsorption.

The rheological properties of the surface containing adsorbed surfactants have often been the cause of the stability of dispersion.[4] Four independent surface rheological paramenters are taken into consideration, surface shear viscosity and elasticity, and surface dilational (or area) viscosity and elasticity. The surface area modulus, the reciprocal of surface compressibility, is zero at equilibrium for the adsorbed surface, when the equilibrium surface tension of surfactant solution is constant, independent of the area at a constant temperature. The surface viscosity and elasticity contribute to foam drainge *via* surface transport phenomena.[5] The surface area viscosity seems to influence the damping of ripples a great deal.[6] As regards the measurement of the surface area viscosity, only a few reports have appeared for surfactant solutions.[7]

The expansion or contraction of the surface in equilibrium produces an area strain, and the corresponding stress changes the surface pressure (or tension) from the equilibrium value. Under the action of surface area viscosity, the surface pressure usually returns to its equilibrium value. This seems to be due to the relaxation of area stress. The change of surface tension after the formation of a fresh surface is a special case.

The process of the change of surface area under a constant surface pressure differing from the equilibrium value corresponds to the creep of the area strain under a constant stress, and under the action of the surface area viscosity. In the present paper, the relaxation and creep processes for the aqueous surface containing adsorbed film in contact with bulk of the solution were studied. Aqueous sodium dodecyl sulfate solutions were chosen for this purpose.

Experimental

Sodium dodecyl sulfate (SDS) was prepared by the reaction of pure dodecanol with chlorosulfonic acid in ether followed by neutralization with sodium hydroxide. The product was purified twice by addition of active charcoal to its hot saturated ethanol solution followed by recrystallization from the cold solution.[8] The product was sufficiently pure, showing no minima in the surface tension *vs.* concentration curve.

The surface pressure against pure water was measured within an error of ± 0.02 dyn/cm by the Wilhelmy method using a vertical glass plate, peripheral length 4.790 cm.[9] The glass plate was cleaned by immersing it in concentrated aqueous alkaline–alcohol solution overnight, dipping in a hot chromic acid mixture for *ca.* 1 hr, and rinsing with water.

The stock solution of SDS was prepared and subjected to aging for *ca.* 17 hr before each measurement, since the variation of surface tension with time is considered to depend upon age. The water used for dissolving SDS was freshly distilled and boiled for *ca.* 1 hr to remove dissolved gas, which otherwise formed bubbles on the paraffin-coated walls during the course of measurement.

A Langmuir type trough of $60 \times 15 \times 1$ cm size coated with paraffin was used. Water from a thermostat was circulated beneath the trough, and the solution was maintained at 30 ± 0.3 °C. The trough and the tensiometer, contained in a closed chamber of air thermostat at 30 ± 1 °C, were protected from atmospheric contaminations. For measurements under a constant area, glass barriers coated with paraffin were used to clean and to provide a specified surface area. For measurements under a constant surface pressure, one of the barriers was driven by a motor to change the surface area continuously.

Reproducible surface pressure could be obtained after allowing the solution to stand in the trough for 1 hr and then sweeping its surface at least 10 times with three barriers. The error of the surface pressure measurement due to the fall of water level produced by the surface evaporation during the course of measurement was confirmed to be negligible as compared with the overall error.

Results and Discussion

Relaxation Process under a Constant Area Strain. Figure 1 shows the variation of surface pressure π with time t after the formation of fresh surface for aqueous SDS solutions of varying concentrations under a constant area *ca.* 400 cm^2, and pH *ca.* 6. Since the surface pressure did not attain a constant value except for a very dilute solution (1×10^{-4} mol/l), the equilibrium surface pressure π_e was obtained by extrapolating plot π *vs.* $1/t$ to $1/t = 0$.[10]

From a rheological point of view, the process shown in

* Present address: Department of Chemistry, Faculty of Science, Tokai University, Hiratsuka, Kanagawa 259-12.

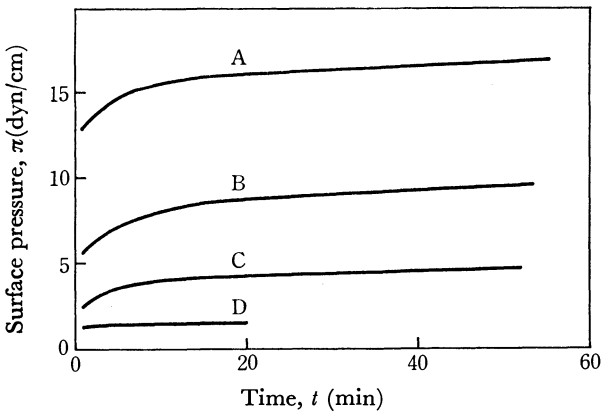

Fig. 1. Surface pressure *vs.* time plot for aqueous SDS solutions at 30 °C. Surface area: 400 cm².
Concn of SDS: A,2.02; B, 1.05; C, 0.52; D, 0.10×10^{-3} mol/l.

Fig. 1 is regarded as one in which the stress

$$\Delta\pi = \pi_e - \pi \tag{1}$$

produced by a constant area strain undergoes relaxation according to the generalized Maxwell model as given by

$$\Delta\pi = \sum_i^n K_i e^{-t/\tau_i}, \tag{2}$$

where K_i and τ_i are constants. At $t=0$, Eqs. (1) and (2) give

$$\sum_i^n K_i = \pi_e \tag{3}$$

since $\pi=0$ at $t=0$.

As regards the τ_i and K_i values, the largest value, τ_1, with the corresponding K_1 value can be determined from the linear part of the plot log $\delta\pi$ *vs.* t for sufficiently large value of t, and the next largest value, τ_2, with the corresponding K_2 value can be obtained from the linear part of the plot log $(\delta\pi - K_1e^{-t/\tau_1})$ *vs.* t. Figure 2 shows such a plot. The values obtained (Table 1) express the curves in Fig. 1 within ±0.05 dyn/cm. It is the shorter relaxation time τ_2 which should be compared with thin

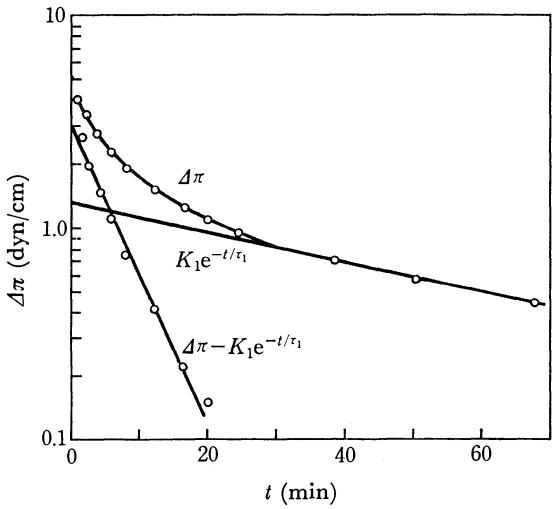

Fig. 2. $\Delta\pi$, K_1e^{-t/τ_1}, and $\Delta\pi - K_1e^{-t/\tau_1}$ *vs.* t plot.
Concn of SDS: 2.02×10^{-3} mol/l.
Surface area: 400 cm².

Table 1. Relaxation times (τ_1, τ_2) and initial stresses (K_1, K_2) for the freshly formed surfaces of aqueous SDS solutions and their equilibrium surface pressures (π_e) at 30 °C

	Concn (mol/l) $\times10^{-3}$	π_e (dyn/cm)	τ_1 (min)	τ_2 (min)	K_1 (dyn/cm)	K_2 (dyn/cm)
A	2.02	17.20	63	6.1	1.31	3.10
B	1.05	10.40	39	4.5	2.31	2.65
C	0.52	5.45	82	3.4	1.67	1.78

film relaxation times of the order of minutes, measured by Razouk and Mysels[11] for the aqueous SDS solutions.

In all the cases, K_1+K_2 is not equal to the equilibrium surface pressure π_e. This means that the value of surface pressure (Fig. 1) extrapolated to $t=0$ is not zero and suggests the existence of at least one more relaxation element something like "semi-dynamic surface tension" postulated by Bouteric and Berthier[12] and Ross.[13] The presence of two relaxation elements has been reported,[14] when the relaxation was measured after expanding the lamellae of bovine hemoglobin solution.

Equations (1) and (2) give

$$\pi = \sum_i^n K_i(1-e^{-t/\tau_i}). \tag{4}$$

The two longest relaxation times of τ_i were thus determined. The remaining shorter relaxation times can not be measured by the vertical plate technique. They might be detected by a more rapid measurement, such as the jet method.

Creep Process under a Constant Stress. The change of surface area A under a constant surface pressure was determined with time t for solutions whose area stress relaxation had been measured. The results are shown in Fig. 3. Measurements were made first by sweeping the surface with a paraffin-coated glass barrier to form a fresh surface and then with a motor-driven barrier to expand the surface in order to keep the surface pressure within 0.5 dyn/cm of the predetermined value of π_s. Surface area A thus obtained was plotted against time t.

Since the rate of area strain is expressed by $(1/A)(dA/dt)$ and the stress by $\delta\pi=(\pi_e-\pi_s)$, the area viscosity η_A is defined by

$$\Delta\pi = \eta_A \frac{1}{A}\cdot\frac{dA}{dt}, \tag{5}$$

according to Boussinesq.[15] By integration under the assumption that $\delta\pi$ and η_A are constant, we have

$$\ln A - \ln A_i = \frac{\Delta\pi}{\eta_A}\cdot t, \tag{6}$$

where A_i is the value of A at $t=0$. Thus, log A should change linearly with t. However, this was not the case actually, the dependence of η_A on A or t being shown. Equation (5) combined with the $A(dt/dA)$ *vs.* A relation gives

$$\frac{\eta_A}{\Delta\pi} = \frac{rA}{1+qA} + s, \tag{7}$$

where q, r, and s are constants.

The fact that η_A increases with area is in line with the result of van Voorst Vader's experiments in which $(1/A)$

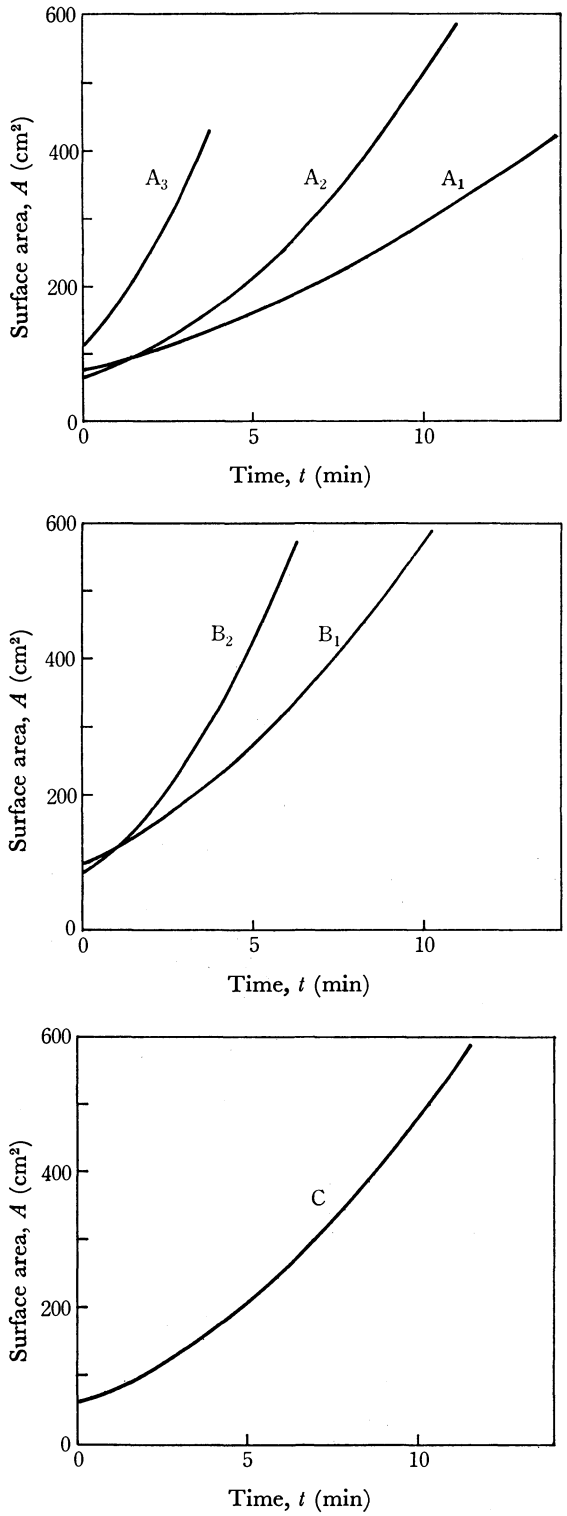

Fig. 3. Surface area *vs.* time plot under constant area stress.

	A_1	A_2	A_3	B_1	B_2	C
Concn of SDS ($\times 10^{-3}$ mol/l)	2.02	2.02	2.02	1.05	1.05	0.52
Area stress, $\Delta\pi$ (dyn/cm)	2.02	2.68	3.34	3.14	3.80	1.13

(dA/dt) is kept constant.[7] We see that the relation of $\delta\pi$ *vs.* $(1/A)(dA/dt)$ at a given A of the same solution (A_1, A_2, and A_3, or B_1 and B_2 in Fig. 6) gives a relation similar to the curve in the steady state obtained by van Voorst Vader *et al.*[7] The area viscosity obtained can be separated into two parts, if two Maxwell elements are considered. It would be reasonable to divide η_A into two portions in a ratio of τ_1K_1 and τ_2K_2, since

$$\eta_{Ai} = \tau_i\varepsilon_{Ai}, \tag{8}$$

in which ε_{Ai} is the area elastic modulus of the i'th element, to which K_i is proportional. Since K_1 and K_2 are of the same order of magnitude (Table 1), η_{A1} and η_{A2} would be roughly proportional to τ_1 and τ_2. If there are more relaxation elements as given by Eq. (2), area viscosity should be separated into more than two elements.

Rheology of Two-dimensional Open System. The system treated here differs essentially from the ordinary rheological system in that the number of molecules involved in the system changes in the former (open system), and remains constant in the latter (closed system). In the rheology of a two-dimensional system, the open system treatment is required when the area of liquid surface with its soluble adsorbed film changes. The above four rheological parameters are similarly defined for both open and closed systems, but the molecular behavior brought about by an area strain is quite different for the two systems. Thus, in the closed system, the stress relaxation after area strain is due to the change in the rearrangement, orientation, conformation and/or other chemical change of the molecules in the system, while in the open system the relaxation involves the transfer of the molecules into or out of the system, *i.e.*, the adsorption from or desorption into bulk of the solution, in addition to the above changes of the closed system. As a result, the area viscosity is much more significant in the mechanical behavior of the two-dimensional open system than the volume viscosity of the three-dimensional closed system.

The surface film flows and the adsorbed molecules in the surface generally rearrange themselves by the pressure gradient due to the compression or expansion of the surface. Since the surface shear viscosity is sufficiently below the order of magnitude of 10^{-4} surface poise for an adsorbed film of pure SDS,[16] the surface flow would rapidly follow the surface expansion in the creep experiment and the surface might be regarded to be uniform as a whole. The rate of orientation of adsorbed molecules on the water surface is also considered to be fairly rapid in a dilute solution of SDS, similar to that of water molecules on the surface, though the exact rate is not known.[17] The measured rheological properties might be governed mainly by the transfer of molecules from bulk of the solution to the surface.

In such a case, when the rate of adsorption is constant and the rate of desorption simply depends upon the surface pressure, the relaxation due to the process would be rather simple. On the other hand, when an unstirred diffusion layer of certain thickness exists just below the surface, several exponential terms should be taken into account in order to elucidate the relaxation mechanism, regardless of the presence of energy barrier at the surface, as Sutherland suggested.[18] The relation between relaxation and creep observed might be discussed as rheology of an open system.

Since the adsorption of surfactant molecules is the

principal cause common to both the relaxation of area stress and the creep of area strain observed as an open system, a certain relation might be expected to exist between these phenomena. Because of the lack of exact equation of state available for the adsorbed film under such dynamic conditions, surface pressure is first assumed to be proportional to the surface density of adsorbed SDS molecules, namely, an ideal gas type equation is assumed to hold:

$$\pi A = nkT, \tag{9}$$

where n is the total amount of adsorbed SDS, k the Boltzmann constant, and T absolute temperature. Thus at a given moment of surface area expansion, the relation between creep and relaxation is given by

$$A\left(\frac{\partial\pi}{\partial t}\right)_A = \pi\left(\frac{\partial A}{\partial t}\right)_\pi. \tag{10}$$

This is derived by differentiation of Eq. (9) with respect to time t keeping π or A constant. In order to examine the validity of Eq. (10), $(\partial A/\partial t)\pi$ and $(\partial\pi/\partial t)_A$ obtained by drawing tangents to the curves shown in Figs. 3 and 4, respectively, are used. However, both sides of Eq.

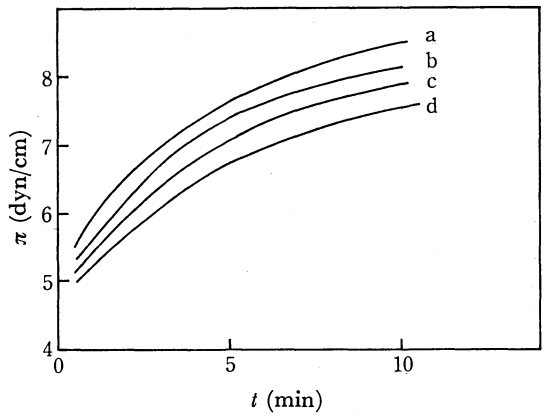

Fig. 4. Area effect on π *vs.* t curve for aqueous SDS solution.
Concn of SDS: 1.0×10^{-3} mol/l.
Surface area: a, 55; b, 100; c, 175; d, 250–400 cm².

(10) calculated differed from each other by about one order of magnitude. It was also found that Amagat's type of equation of state does not hold in the present case. We assume a surface equation of expanded film type

$$(\pi+\pi_0)(A-A_0) = nkT, \tag{11}$$

where π_0 and A_0 are constants. A similar calculation gives the following equation:

$$(A-A_0)\left(\frac{\partial\pi}{\partial t}\right)_A = (\pi+\pi_0)\left(\frac{\partial A}{\partial t}\right)_\pi. \tag{12}$$

Neither Eq. (12) nor Eq. (11) holds, since π_0 found was not constant but increased in proportion to π. However, we found at least experimentally that the relation

$$A - A_0 = p\pi_s\left(\frac{\partial A}{\partial t}\right)_{\pi_s}\left(\frac{\partial t}{\partial\pi}\right)_A \tag{13}$$

holds as a whole with constants A_0=25 cm² and p=0.13 (Fig. 5) for the systems of B_1 and B_2 under a constant π_s. The original state of equation corresponding to Eq. (13)

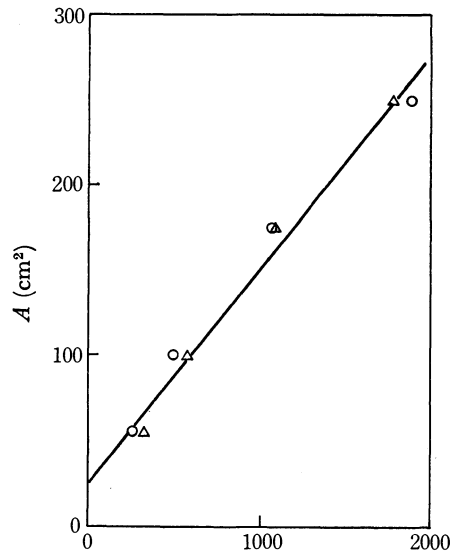

Fig. 5. A *vs.* $\pi_s\left(\frac{\partial A}{\partial t}\right)_{\pi_s}\left(\frac{\partial t}{\partial\pi}\right)_A$ plot.
○: B_1, △: B_2.

would then take the form

$$\pi(A-A_0)^p = \alpha n, \tag{14}$$

where α is a constant. We see that π decreases rapidly with increasing A in the region of small A with an asymptote at $A=A_0$ while the decrease is small in the region of large A as compared with π *vs.* A relation for ideal gas film. This suggests that the curve π *vs.* A shifts towards the region of larger area than that of ideal gas film, and that a large apparent repulsive force prevails. The ionic nature and steric factor are also considered to have certain relations.

The values $(\partial\pi/\partial t)_A$ at sufficiently large A were calculated by means of Eq. (14) and compared with the observed values. According to Eq. (13), we have

$$\left(\frac{\partial\pi}{\partial t}\right)_A = p\pi_s\left(\frac{\partial A}{\partial t}\right)_{\pi_s}\Big/(A-A_0). \tag{15}$$

In order to obtain an empirical formula for $(\partial A/\partial t)\pi_s$, a trial and error method was attempted and the following relation was found to hold (Fig. 6):

$$A\left(\frac{\partial t}{\partial A}\right)_{\pi_s} = \frac{rA}{1+0.002A} + s. \tag{16}$$

The values of r and s are given in Table 2. Substituting $(\partial A/\partial t)\pi_s$ of Eq. (16) into Eq. (15), the value $(\partial\pi/\partial t)_A$ at infinite A is obtained as

$$\left(\frac{\partial\pi}{\partial t}\right)_{A_\infty} = p\pi_s q/r, \tag{17}$$

where q=0.002 cm^{-2}. The values $(\partial\pi/\partial t)_{A\infty}$ calculated by means of Eq. (17) are given in Table 2 together with the observed values obtained at π_s from Fig. 1.

The values agree as a whole, although the disagreement is not small in some cases. The discrepancy might come from the nature of Eq. (14) for the open system under dynamic conditions, together with the fact that the states of the film in an immediate vicinity of the

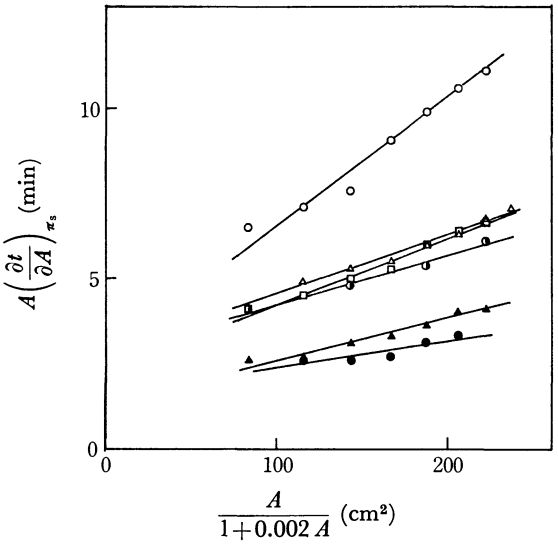

Fig. 6. $A\left(\frac{\partial t}{\partial A}\right)_{\pi_s}$ *vs.* $\frac{A}{1+0.002A}$ plot.
○: A_1, ◑: A_2, ●: A_3, △: B_1, ▲: B_2, □: C (see Fig. 3).

Table 2. Observed and calculated values of $(\partial\pi/\partial t)_{A\infty}$, and r and s in Eq. (16)

	Concn (mol/l) $\times 10^{-3}$	π_S (dyn/cm)	$\left(\frac{\partial\pi}{\partial t}\right)_{A\infty}$ (dyn/cm·min) obsd	calcd	r (min/cm²)	s (min)
A_1	2.02	15.18	0.17	0.11	0.038	2.8
A_2	2.02	14.56	0.28	0.24	0.016	2.6
A_3	2.02	14.06	0.36	0.35	0.011	1.1
B_1	1.05	7.26	0.17	0.094	0.020	2.4
B_2	1.05	6.60	0.28	0.13	0.014	1.2
C	0.52	4.32	0.013	0.048	0.023	1.8

barrier and rim of the trough differ from those in the main part of the film. It may be further inferred that A_0 in Eq. (14) when expressed per molecule seems to correspond to the co-area of Amagat's equation, but it may involve contribution of some other factors, which reduce the area effective for adsorption.

The author wishes to express his hearty thanks to Professer Tsunetaka Sasaki for his encouragement and guidance.

References

1) J. L. Moilliet and B. Collie, "Surface Activity," D. van Nostrand, New York (1951), p. 84.
R. Defay and J. R. Hommelen, *J. Colloid Sci.*, **13**, 533 (1958); **14**, 411 (1959).
2) H. Lange, *ibid.*, **20**, 50 (1965).
3) K. L. Sutherland, *Aust. J. Chem.*, **12**, 1 (1959).
4) J. A. Kitchener, "Recent Progress in Surface Science," Vol. 1, ed. by J. F. Danielli, K. G. A. Pankhurst, and A. C. Riddirord, Academic Press, New York (1964), p. 51.
M. van den Tempel, "Surface Chemistry," ed. by P. Ekwall, K. Groth, and V. Runnstrom-Reio, Munksgaad, Copenhagen (1965), p. 306.
B. Stuke, *Chem. Ing. Techn.*, **33**, 173 (1961).
5) W. E. Evers and K. L. Sutherland, *Aust. J. Sci. Res.*, **A5**, 697 (1952).
6) M. van den Tempel and R. P. van de Riet, *J. Chem. Phys.*, **42**, 2769 (1965).
7) F. van Voorst Vader, Th. F. Erkens, and M. van den Tempel, *Trans. Faraday Soc.*, **60**, 1170 (1964).
8) E. F. Williams, N. T. Woodberry, and J. K. Dixon, *J. Colloid Sci.*, **12**, 452 (1957).
9) M. Nakamura and T. Sasaki, *J. Sci. Instrum.*, **44**, 855 (1967).
10) M. Nakamura and T. Sasaki, This Bulletin, **43**, 3667 (1970).
11) R. I. Razouk and K. J. Mysels, *J. Amer. Oil Chem. Soc.*, **45**, 481 (1968).
12) A. Bouteric and P. Berthier, *J. Chim. Phys.*, **36**, 1 (1939).
13) S. Ross, *J. Phys. Chem.*, **49**, 377 (1945).
14) L. K. James, Jr., *J. Sci. Instrum.*, **42**, 762 (1965).
15) M. J. Boussinesq, *Ann. Chim. Phys.*, **29**, 349 (1913).
16) W. E. Ewers and R. A. Sack, *Aust. J. Chem.*, **7**, 40 (1953).
17) A. E. Vandegrift, *J. Colloid Interface Sci.*, **23**, 43 (1967).
18) K. L. Sutherland, *Aust. J. Sci. Res.*, **A5**, 683 (1952).

Heat Capacity Changes of Alkyl-substituted Ammonium Chlorides in Aqueous Solutions

Kunio TAMAKI, Satoru YOSHIKAWA, and Mitsuyoshi KUSHIDA
Department of Chemistry, Yokohama City University, Kanazawa-ku, Yokohama 236
(Received January 21, 1975)

The changes in the heat capacity for the dissolution in water, ΔC_p°, of *n*-alkylammonium chlorides (methyl to hexyl), di-*n*-alkylammonium chlorides (methyl to butyl), and tri-*n*-alkylammonium chlorides (methyl to propyl) at the room temperature were determined from measurements of the relation between the heats of solution of these salts in water and the temperature, and the results were compared with the ΔC_p° values for tetraalkylammonium salts in the literature. It was found that the effect of the coordination of the charge-bearing nitrogen atom by alkyl groups was definitely reflected in the ΔC_p° values. In the cases of $MeNH_3Cl$, $EtNH_3Cl$, Me_2NH_2Cl, and Me_3NHCl, the ΔC_p° values are negative, while in the cases of other higher homologues, the ΔC_p° values are positive; the increments in the ΔC_p° values per methylene group are discussed in terms of the hydrophobic hydration and the steric effect of alkyl chains.

Recently, studies of the behavior of electrolytes with attached nonpolar groups, particularly of tetraalkylammonium salts, R_4NX, have been extensively carried out by various experimental methods.[1-5] Measurements of the heat capacities of aqueous electrolytes solutions produce useful information about the influences of ions on the structure of solvent water.[6] The changes in the heat capacities for the dissolution in water of simple salts indicate negative values, whereas the changes in the heat capacities for the dissolution in water of nonpolar solutes indicate positive values. This characteristic relation has been applied to the study of R_4NX salts in water, and the behavior of R_4NX salts has been discussed in terms of the modification of the water structure around the nonpolar parts.[6-12] To elucidate the role of the alkyl groups on the coordination of the charge-bearing nitrogen atom, it seems of great interest to study the behavior of incompletely alkylated ammonium salts in water.

In this paper, we will report our experimental results on the changes in the heat capacity for the dissolution in water of *n*-alkylammonium chlorides RNH_3Cl (methyl to hexyl), di-*n*-alkylammonium chlorides R_2NH_2Cl (methyl to butyl), and tri-*n*-alkylammonium chlorides R_3NHCl (methyl to propyl); we will discuss the results in terms of the balance of two types of hydration-namely, electrostrictive hydration due to the ionic part and hydrophobic hydration due to the nonpolar part.

The change in the heat capacity for the dissolution at infinite dilution, ΔC_p°, may be obtained from the relation between the heat of solution at infinite dilution, ΔH_s°, and the temperature, T:[13]

$$d\Delta H_s^\circ/dT = \Delta C_p^\circ = \bar{C}_p^\circ - C_p \quad (1)$$

where $\bar{C}_p^\circ$ is the partial molal heat capacity of the solute at infinite dilution, and C_p the heat capacity of the pure salt.

Experimental

NH_4Cl was a commercial sample of a G. R. grade. The other organic chemicals were obtained from Tokyo Kasei Kogyo Co. RNH_3Cl salts were the same samples as have been described elsewhere.[14] Pr_2NH_2Cl, Bu_2NH_2Cl, and Pr_3NHCl were prepared by the neutralization of the respective amines with gaseous hydrogen chloride in benzene. All the organic salts were recrystallized from suitable solvents: ethanol for Me_2NH_2Cl, Et_2NH_2Cl, Pr_2NH_2Cl, and Me_3NHCl; ethyl acetate for Pr_3NHCl; and ethanol–ethyl acetate mixtures for Bu_2NH_2Cl and Et_3NHCl. Water was redistilled from an alkaline permanganate solution.

The heats of solution were measured by means of a twin conduction microcalorimeter (Model CM-204D1 of Ōyodenki Kenkyujo) described in a previous paper.[15] The uncertainties of the heat-of-solution data obtained in this work were estimated to be within 0.03 kcal/mol at 10—25 °C and 0.05 kcal/mol at 30—45 °C. The concentration of the measured solution was 0.01 M, and the heat of dilution from a solution at 0.01 M to one at a large dilution is about $-0.03 \sim -0.04$ kcal/mol for NH_4Cl, $MeNH_3Cl$, Me_2NH_2Cl, and Me_3NHCl.[16] In view of this situation, the mean values of the heats of solution repeatedly measured at 0.01 M are presented in this paper. The ΔC_p° values are obtained by assuming that the change in the heat capacity at 0.01 M is equal to that at infinite dilution.[15]

Results

The heats of solution obtained for three homologous series of RNH_3Cl, R_2NH_2Cl, and R_3NHCl are listed in Table 1. The ΔH_s° values at 25 °C reported by Krishnan and Friedman[17] for RNH_3Cl salts, Me_2NH_2Cl, Bu_2NH_2Cl, and Me_3NHCl are also included in Table 1. Except for Bu_2NH_2Cl, the heats of solution obtained in this work at 25 °C are in fairly good agreement with those reported by Krishnan and Friendman.[17] Taking account of the experimental uncertainties described above, the heats of solution can be regarded as approximately a linear function of the temperature over the range studied. The approximate linear relation between the heat of solution and the temperature in the range of room temperature has sometimes been reported.[10] The mean ΔC_p° values in the range of measurements are obtained from the average slope of the linear plots of the heats of solution against the temperature: the results are listed in Table 2. For comparison, the ΔC_p° values at room temperature reported for R_4NBr salts in the literature[7,10] are also included in Table 2. As will be explained below, the difference in ΔC_p° values due to the variation in halide ions for the same cation is very small. Therefore, the ΔC_p° values of R_4NBr salts may well be

Table 1. Heat of solution

R	10 °C kcal/mol	25 °C kcal/mol	40 °C kcal/mol	45 °C kcal/mol
		RNH_3Cl		
H	4.01	3.54	—	2.90
Me	1.80	1.42	—	0.97
		1.42[a]		
Et	2.15	2.05	2.00	1.94
		2.08[a]		
Pr	0.24	0.38	0.56	0.60
		0.33[a]		
Bu	−0.96	−0.64	−0.31	—
		−0.64[a]		
Pen	−0.76	−0.20	0.34	—
		−0.23[a]		
Hex	−0.50	0.31	1.16	—
		0.28[a]		

R	10 °C kcal/mol	15 °C kcal/mol	25 °C kcal/mol	35 °C kcal/mol
		R_2NH_2Cl		
Me	0.69	—	0.48	0.34
			0.47[a]	
Et	—	0.17	0.38	0.57
Pr	−2.55	—	−1.80	−1.28
Bu	−2.61	—	−1.43	−0.65
			−1.61[a]	

R	10 °C kcal/mol	25 °C kcal/mol	30 °C kcal/mol	35 °C kcal/mol
		R_3NHCl		
Me	1.01	0.85	0.80	—
		0.83[a]		
Et	0.68	1.04	—	1.29
Pr	−2.66	−1.51	—	−0.76

a) Ref. 17

Table 2. Change in heart capacity for dissolution (ΔC_p°) and increase in ΔC_p° per methylene group ($\Delta C_p^\circ/-CH_2-$)

R	ΔC_p° cal/K mol		$\Delta C_p^\circ/-CH_2-$ cal/K mol	
		RNH_3Cl		
H	−32			
			8	
Me	−24			
			18	
Et	−6			
			16	
Pr	10			
			12	
Bu	22			
			15	
Pen	37			
			18	
Hex	55			
		R_2NH_2Cl		
Me	−14			
			17	
Et	20			
			15.5	
Pr	51			
			13.5	
Bu	78			
		R_3NHCl		
Me	−11			
			12	
Et	24			
			17	
Pr	76			
		R_4NBr		
Me	−11.3[a]	−10.1[b]	10.3[a]	10.8[b]
Et	30[a]	33[b]	19[a]	20[b]
Pr	106[a]	112.5[b]	15[a]	17[b]
Bu	176[a]	179[b]		

a) Ref. 10, b) Ref. 7.

used in place of R_4NCl salts for the purpose of considering the effect of alkyl chains on the behavior of alkyl-substituted ammonium salts in water.

Discussion

The $\Delta\bar{C}_p^\circ$ Value as the Ion-solvent Interaction Parameter. The $\bar{C}_p^\circ$ value is of thermodynamical importance for the study of electrolyte solutions.[18] The $\bar{C}_p^\circ$ value can be obtained by the measurement of the heat capacities of solutions at dilute concentrations.[18] There have been reports about the $\bar{C}_p^\circ$ values for methyl- and ethylammonium chlorides by Rüterjans, Schreiner, Sage, and Ackermann,[19] for a series of *n*-alkylammonium bromide by Leduc, Fortier, and Desnoyers.[20] and for some di-*n*-alkylammonium chlorides by Cobani, Conti, Martinelli, and Matteoli.[21] Alternatively, if the C_p value is known, the $\bar{C}_p^\circ$ value can be obtained by adding the C_p and ΔC_p° values by means of Eq. (1). Furthermore, it is assumed that the $\bar{C}_p^\circ$ value consists of two contributions; the first is the intrinsic heat capacity of the ions in the absence of ion-solvent interactions, while the second is the contribution arising from the influence which the ions exert on the solvent structure:[11]

$$\bar{C}_p^\circ = \bar{C}_p^\circ(\text{int}) + \bar{C}_p^\circ(\text{solv}) \quad (2)$$

Thus, in order to discuss the interaction of ion with solvent using the data of the $\bar{C}_p^\circ$ value, we must obtain the $\bar{C}_p^\circ$ (solv) value by substracting the appropriate value of the $\bar{C}_p^\circ$(int) value from the $\bar{C}_p^\circ$ value. For the $\bar{C}_p^\circ$(int) value, Visser and Somsen[11,12] adopted the hypothetical liquid state of the salt. On the other hand, Leduc, Fortier, and Desnoyers[20] assumed two limiting cases for the $\bar{C}_p^\circ$(int) value; one is as the liquid state, and the other is as the solid crystalline.

If we regard $\bar{C}_p^\circ$(int) as the capacity of the solid crystalline, ΔC_p° in Eq. (1) corresponds to $\bar{C}_p^\circ$(solv) in Eq. (2). In other words, the ΔC_p° value is a measure of ion-solvent interactions if the standard state of the salt is taken as the solid state.

A variety of simple salts show negative $\bar{C}_p^\circ$ values in water, which may be interpreted in terms of electrostrictive hydration.[22] For example, the $\bar{C}_p^\circ$ values for NaCl, NaBr, and NaI are −22.1, −23.3, and −23.4 cal/K mol at 25 °C respectively.[23] If we use 11.9, 12.5, and 13.0 cal/K mol for the corresponding C_p values at 25 °C in the literature,[24] the ΔC_p° values become −34.0, −35.8, and −36.4 cal/K mol respectively. Likewise we can conclude that the ΔC_p° values for other alkali halides do not vary greatly with the different halide ions, such as Cl^-, Br^-, and I^- ions. On the other hand, the ΔC_p° values for organic solutes with nonpolar groups, such as alkyl alcohol,[25] alkane carboxylic acids,[26] and alkylamines,[26] are all positive, which may be interpreted in terms of the promotion of the water structure around the nonpolar groups in water (hydrophobic hydration).

RNH_3Cl Salts. NH_4Cl is a typical simple salt, the ΔC_p° value being as low as -32 cal/K mol, as may be seen in Table 2. In a previous study of viscosity B coefficients,[14] we proposed that the $-NH_3^+$ ionic part is an electrostrictive structure-breaker. Table 2 indicates the negative ΔC_p° values for $MeNH_3Cl$ and $EtNH_3Cl$. Leduc, Fortier, and Desnoyers[20] showed that the $\bar{C}_p^\circ$—$\bar{C}_p^\circ$(int) values for $MeNH_3Br$ and $EtNH_3Br$ are negative, whether the $\bar{C}_p^\circ$(int) value is taken as a liquid or a solid state. Therefore, it may be concluded that the electrostrictive hydration due to the charge-bearing nitrogen atom may interfere with the interaction of hydrophobic methyl or ethyl groups with water in RNH_3Cl salts. In the cases of $PrNH_3Cl$ and higher homologues, the ΔC_p° values become positive, and they increase with an increase in the chain length. They are classifiable as hydrophobic structure-making solutes. The average increment in the ΔC_p° values per methylene group from $MeNH_3Cl$ to higher homologues is about 16 cal/K mol; this value corresponds approximately to the value in the series of nonelectrolytes such as alcohol.[25]

Previous studies of the viscosity B coefficient[14] and the surface activity[27] seem to indicate that $EtNH_3Cl$ may be classified as a weak hydrophobic structure-making solute. Although it is difficult to draw any definite conclusions, the ambiguity in the behavior of this salt in water is probably attributable to the fact that $EtNH_3Cl$ is a borderline solute.

R_2NH_2Cl Salts. As may be seen in Table 2, the ΔC_p° value for Me_2NH_2Cl is negative, but the value is less negative than that of $MeNH_3Cl$, showing the cooperative hydrophobic effect of the two methyl groups. In the cases of Et_2NH_2Cl, Pr_2NH_2Cl, and Bu_2NH_2Cl, the ΔC_p° values become positive, and they are hydrophobic structure-makers. The increments in the ΔC_p° values per methylene group from Me_2NH_2Cl to Bu_2NH_2Cl are about 15 cal/K mol, suggesting that the two alkyl chains can interact independently with water in R_2NH_2Cl series.

R_3NHCl and R_4NBr Salts. The ΔC_p° values for Me_3NHCl and Me_4NBr are about -11 cal/K mol, only slightly less negative than that of Me_2NH_2Cl. Although the ΔC_p° values for ethyl salts and higher homologues are positive in R_3NHCl and R_4NBr salts, the increments in the ΔC_p° values per methylene group from methyl salt to ethyl salt are 10—12 cal/K mol; the values are smaller than the average value of 16 cal/K mol in a series of straight-chain solutes. These facts suggest that methyl and ethyl groups cannot freely interact with water due to the steric configuration in both series. However, judging from the increments in the ΔC_p° values per methylene group from Et_3NHCl to Pr_3NHCl salts and from Et_4NBr to Bu_4NBr salts, the methylene groups of the C-3 position and the longer parts of the alkyl chains attached to the charge-bearing nitrogen atom are free from the steric effect on the interaction with water in both series.

In conclusion, all the methyl salts of the four types of alkyl-substituted ammonium salts in water are predominantly governed by electrostrictive hydration. $EtNH_3Cl$ is probably a borderline solute. The other salts studied are hydrophobic structure-makers, but the effect of alkyl groups on the hydrophobic hydration is slightly weakenened as a result of the steric configuration in R_3NHCl and R_4NX series.

References

1) S. Saito, *Hyomen*, **4**, 584 (1968).
2) M. J. Blandamer, *Quart. Rev.*, **24**, 169 (1970).
3) W-Y. Wen, "Water and Aqueous Solutions, Structure, Thermodynamics, and Transport Processes," ed. by R. A. Horne, Wiley-Interscience, New York, N. Y. (1972), p. 613.
4) W-Y. Wen, *J. Solution Chem.*, **2**, 253 (1973).
5) T. S. Sarma and J. C. Ahluwalia, *Chem. Soc. Rev.*, **2**, 203 (1973).
6) H. S. Frank and W-Y. Wen, *Discuss. Faraday Soc.*, **24**, 133 (1957).
7) T. S. Sarma, R. K. Mohanty, and J. C. Ahluwalia, *Trans. Faraday Soc.*, **65**, 2333 (1969).
8) T. S. Sarma and J. C. Ahluwalia, *ibid.*, **67**, 2528 (1971).
9) R. K. Mohanty and J. C. Ahluwalia, *J. Chem. Thermodyn.*, **4**, 53 (1972).
10) E. M. Arnett and J. J. Campion, *J. Amer. Chem. Soc.*, **92**, 7097 (1970).
11) C. de Visser and G. Somsen, *J. Chem. Thermodyn.*, **5**, 147 (1973).
12) C. de Visser and G. Somsen, *J. Chem. Soc. Faraday* 1, **69**, 1440 (1973).
13) C. M. Criss and J. W. Cobble, *J. Amer. Chem. Soc.*, **83**, 3223 (1961).
14) K. Tamaki, Y. Ōhara, H. Kurachi, M. Akiyama, and H. Odaki, This Bulletin, **47**, 384 (1974).
15) K. Tamaki, Y. Isomura, and Y. Ōhara, *ibid.*, **45**, 2939 (1972).
16) H. Streeck, *Z. Phsik. Chem.*, **A 169**, 103 (1934).
17) C. V. Krishnan and H. L. Friedman, *J. Phys. Chem.*, **74**, 3900 (1970).
18) K. S. Pitzer and L. Brewer, "Thermodynamics," McGraw-Hill, New York, N. Y. (1961), p. 373.
19) H. Rüterjans, F. Schreiner, U. Sage, and Th. Ackermann, *J. Phys. Chem.*, **73**, 986 (1969).
20) P-A. Leduc, J-L. Fortier, and J. E. Desnoyers, *ibid.*, **78**, 1217 (1974).
21) S. Cabani, G. Conti, A. Martinelli, and E. Matteoli, *J. Chem. Soc., Faraday 1*, **69**, 2112 (1973).
22) J. T. Edsall and J. Wyman, "Biophysical Chemistry," Vol. 1, Academic Press, New York, N. Y. (1958), p. 173.
23) Ref. (18), p. 652.
24) Landolt-Börnstein, "Zahlenwerte und Funktionen," 2 Band, 4 Teil, Springer-Verlag (1961), p. 201.
25) E. M. Arnett, W. B. Kover, and J. V. Carter, *J. Amer. Chem. Soc.*, **91**, 4028 (1969).
26) J. Konicek and I. Wadsö, *Acta Chem. Scand.*, **25**, 1541 (1971).
27) K. Tamaki, *Colloid Polymer Sci.*, **252**, 547 (1974).

The Determination of the Activity Coefficients of Pb(II), Cd(II), and Zn(II) Chlorides in *N,N'*-Dimethylformamide by Means of Electromotive-force Measurements of the M(Hg)/MCl_2(DMF)/AgCl; Cells*

Makoto SAITO and Akemi KANAMORI**

Department of Chemistry, College of Liberal Arts, Toyama University, 3190 Gofuku, Toyama 930

(Received January 21, 1975)

Electromotive-forces have been measured for the cells of the M(Hg)/MCl_2(DMF)/AgCl;Ag type at 25.00± 0.01 °C, where M are Pb, Cd, and Zn metals and were M(Hg) are amalgams saturated with these metals. The standard potentials of the corresponding metals relative to the silver-silver chloride have been determined, and the mean activity coefficients and the standard free-energies of formation have been calculated for the solvated salts of $PbCl_2$, $CdCl_2$, and $ZnCl_2$ from the electromotive-foce data. Experimental works were carried out by using an H-shaped Pyrex glass cell which was coated externally with silicon grease to eliminate electrical leakage from the water bath. The electromotive-force measurements were made with a digital voltmeter, the voltage sensitivity and the input impedance of which were 10 μV and 100 megohms respectively. The standard potentials for the cells of the M/MCl_2(DMF)/AgCl;Ag type were 0.327_1 V for $PbCl_2$, 0.576_2 V for $CdCl_2$, and 0.898_6 V for $ZnCl_2$.

In the early measurements of electromotive-force, Ulisch and Spiegel[1] discussed the reproducibilities of silver silver chloride and calomel electrodes in acetonitril as a solvent containing chloride ions. Pavlopoulos and Strehlow[2] measured the standard electrode potentials for various first kind electrodes in formamide. Luksha and Criss[3] determined the standard electromotive-forces for cells of the M(Hg)/MX(NMF)/AgX; Ag type, where M is Li, Na, K, or Cs and where X is either Cl^- or Br^-, and determined the activity coefficients of alkali metal ions in anhydrous *N*-methylformamide (NMF). Marple[4] studied the nonpolarizability of Cd(Hg)/$CdCl_2$ as reference electrode for polarographic studies in anhydrous *N,N'*-dimethylformamide (DMF). Studies of various reversible chloride electrodes which are used in dimethylsulfoxide, DMF, and propylene carbonate were carried out by Synott and Butler.[5] According to their paper, thallium, lead, and cadmium chloride electrodes were all stable in DMF, but the $CdCl_2$ was apparently the most stable in potential. The initial potential, 1.653 V, varied by less than 1 mV over the next 12 hr. In the present study, the electromotive-forces have been measured for cells of the M(Hg)/MCl_2/AgCl; Ag type, where M are Pb, Cd, and Zn metals and where M(Hg) are amalgams saturated with these metals. The standard potentials of the corresponding metals relative to the silver-silver chloride electrode were determined, and the mean activity coefficients and standard free-energies of formation were obtained for the solvated salts of $PbCl_2$, $CdCl_2$, and $ZnCl_2$.

Experimental

Solvent. DMF purified by the method described in a previous paper[6] was used. The specific conductivity of the DMF used was $7.0\sim7.5\times10^{-8}$ ohm^{-1} cm^{-1} at 25 °C. Karl-Fisher titrations indicated the water content in the distilled DMF to be less than 0.03%.

Anhydrous Metal Chlorides. Anhydrous metal chloride was prepared from hydrated metal chloride by treating it with thionyl chloride according to Tyree's method.[7]

Amalgams. Lead, cadmium, and zinc amalgams were prepared by the method of Kolthoff.[8] A quantity of metal was gently heated together with mercury and a small amount of diluted sulfuric acid, and then the amalgam thus prepared was carefully washed with diluted sulfuric acid and stocked under diluted sulfuric acid. The amalgam used as a heterogeneous (saturated) one.

All the other reagents used were of an analytical grade.

Electrodes. The Ag-AgCl electrode was prepared from Pt wire plated with silver by means of the electrolytic method.[9-10] The electrode was made up from 0.50 cm-diameter Pt wire sealed in Pyrex glass. Lengths of wire up to 15 cm were left exposed and spiralled, and then it was plated with silver by means of electrolysis from a mixed solution of silver nitrate and potassium cyanide. Eight electrodes were prepared at a time, and those with a bias potential greater than 0.3 mV were discarded. All the electrodes were stored in double-distilled water before use. The dropping analgam electrode used had a flow rate of 1~ 2 s/drop. No effect of the flow rate on the electromotive force (EMF) of the cells could be observed as had been reported by Walfenden *et al.*[11] and Scatchard and Tefft.[12]

Apparatus. The H-cell was made of Pyrex glass, and the two electrodes inserted into the cell were fixed with a silicon rubber stopper. The cell, coated externally with silicon grease to eliminate an electrical leakage from the water bath, was thermostatted on the water bath at 25.00±0.01 °C.

All the electromotive-force measurements were made with a Kuwano Electric Instruments, model DM-750, digital voltmeter. The voltage sensitivity and the input impedance of this voltmeter were 10 μV and 100 megohms respectively.

Experimental Procedures. About a 0.1 molal metal chloride DMF stock solution was prepared by dissolving a quantity of anhydrous metal chlorides in DMF in an ice bath. The concentration of metal chloride in the stock solution was determined by chelatometric titration[13] with EDTA before the solution was used in each experiment.

The electromotive-foce measurements were carried out in

* Presented at the 22nd Annual Meeting of the Japan Society for Analytical Chemistry, Fukuoka, November 23—26, 1973.

** Present address.: Scientific Investigation Research Laboratory, Toyama Prefectural Police Headquarters, 1-7 Shinsogawa, Toyama 930.

the manner described by Luksha and Criss.[3] Readings were taken approximately every 2 min, for a period of 45 min in general, but in a few cases for as long as 90 min.

Results and Discussion

The electromotive-force of a cell containing 2—1 electrolytes and with its electrodes in their standard states is given by:

$$E = E^\circ - \frac{3RT}{nF} \ln m\gamma_\pm, \quad (1)$$

where the symbols have their usual meanings. The expanded Debye Hückel equation gives the mean activity coefficient for the 2—1 electrolyte as:

$$\log \gamma_\pm = -\delta_\gamma \sqrt{m} + \beta m,$$

where: $$\delta_\gamma = 6.3213 \times 10^6 \frac{\rho_0^{1/2}}{(\varepsilon T)^{3/2}}, \quad (2)$$

β is a constant, m is the molality, and ρ_0 and ε are the density and the dielectric constant of the solvent respectively. For DMF at 25 °C, ε is 36.7 and ρ_0 is 0.944 g/cm^3, giving a value of 0.1148 kg/mol for δ_γ. The substitution of Eq. (2) into Eq. (1) and the rearrangement of the terms give:

$$E + \frac{3RT}{nF} \ln m - \frac{(2.303)3RT\delta_\gamma \sqrt{m}}{nF} = E^\circ - \frac{(2.303)3RT\beta m}{nF}, \quad (3)$$

The substitution of the appropriate constants into Eq. (3) leads to

$$E + 0.0887 \log m - 0.455\sqrt{m} = E^\circ - 0.0887\beta m, \quad (4)$$

The cell employed in this experiment is written as:

$$M(Hg)/MCl_2(DMF)/AgCl;\ Ag. \quad (a)$$

The measured potential of the (a) cell is not the electromotive force represented by E in Eq. (4), but, rather, a potential, E', related to E by:

$$E' = E - E'', \quad (5)$$

where E'' is the potential of a cell of this type:

$$M/MCl_2(soln)/M(Hg). \quad (b)$$

To correct the observed potential to that which one would obtain for a pure metallic electrode, the E'' value must be added to the observed potential. Making this substitution and setting the left-hand side of Eq. (4) equal to E''' gives:

$$E''' = E^\circ - 0.0887\beta m. \quad (6)$$

The resultant potentials then refer to a cell employing a pure metallic electrode and may be written as the (c) cell:

$$M/MCl_2(DMF)/AgCl;\ Ag \quad (c)$$

The relationships between the electromotive-force and the time of measurements at various concentrations are shown in Fig. 1 for the zinc chloride cell. As may be seen from Fig. 1, the potentials reached an equilibrium within 10 min from the begining of the measurements. The data obtained are summarized in Table 1. The first two columns give the molality of the cell solution and the measured potential respectively. The third column gives the potential required to correct the observed potential to that for a pure metallic electrode that is, the potential corresponding to the electromotive-force for cells of the (b) type cell. The values of the potential are listed from the literature.[13,14] The fourth column gives the values of E''' in Eq. (6), and the fifth column gives the potentials for cells of (c) type cell. The E''' values are plotted against the molality and extrapolated to an infinite dilution by the method of least-squares to obtain E°. Some typical results obtained are shown in

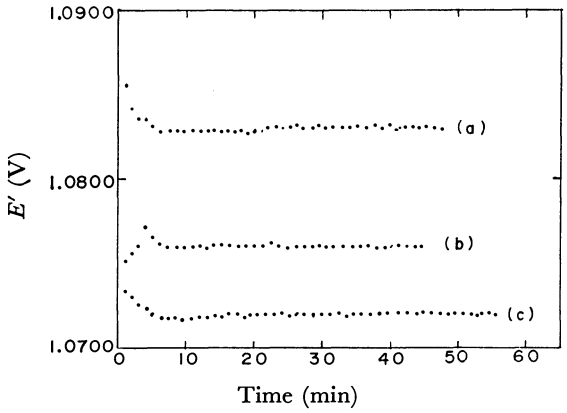

Fig. 1. Stability of electromotive-force for cell of type(a). (a): 0.1117 m $ZnCl_2$, (b): 0.1861 m $ZnCl_2$, (c): 0.2606 m $ZnCl_2$.

Table 1. Electromotive-force data for electrolytes in DMF at 25 °C

Molality	E'	E''	E'''	E
		$PbCl_2$		
0.0053	0.5587	0.0058	0.3311	0.5645
0.0106	0.5397	0.0058	0.3235	0.5455
0.0212	0.5208	0.0058	0.3118	0.5266
0.3018	0.5141	0.0058	0.3055	0.5199
0.0424	0.5086	0.0058	0.2989	0.5144
0.0529	0.5041	0.0058	0.2889	0.5099
0.0635	0.5000	0.0058	0.2848	0.5058
0.0741	0.4973	0.0058	0.2795	0.5037
		$CdCl_2$		
0.0065	0.7473	0.0505	0.5719	0.7978
0.0131	0.7394	0.0505	0.5707	0.7899
0.0196	0.7328	0.0505	0.5681	0.7833
0.0261	0.7291	0.0505	0.5656	0.7796
0.0327	0.7262	0.0505	0.5628	0.7769
0.0457	0.7239	0.0505	0.5583	0.7744
0.0537	0.7221	0.0505	0.5510	0.7708
0.0588	0.7211	0.0505	0.5502	0.7697
0.0653	0.7111	0.0505	0.5500	0.7616
		$ZnCl_2$		
0.0185	1.1060	0.0000	0.8882	1.1060
0.0372	1.0961	0.0000	0.8815	1.0961
0.0745	1.0878	0.0000	0.8635	1.0878
0.1117	1.0828	0.0000	0.8461	1.0828
0.1489	1.0790	0.0000	0.8299	1.0790
0.1861	1.0760	0.0000	0.8163	1.0760
0.2234	1.0736	0.0000	0.8006	1.0736
0.2606	1.0718	0.0000	0.7875	1.0718
0.2987	1.0703	0.0000	0.7751	1.0703

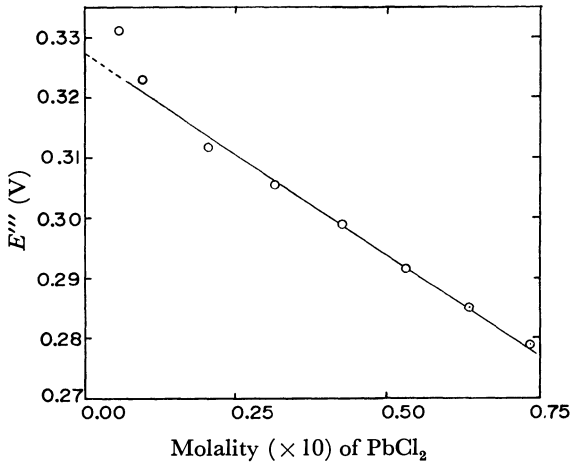

Fig. 2. Relationship between E''' and molality for $PbCl_2$ cell.

Fig. 2. Although the plots in the case of a concentration higher than 0.1 mol of a cell solution are not shown in Fig. 2, the relationship between the electromotive-force and the concentration of metal chloride makes a curve with a gentle slope. It may be considered that the dissociation of metal chloride in DMF becomes difficult in proportion to the increasing concentration of the salt. The standard potentials for the cells of the (c) type as evaluated by the least-squares treatment, are given in

Table 2. Standard potentials for cell of type (C)

Cell	$E°$ (V)
Pb|$PbCl_2$ (DMF)|AgCl; Ag	0.327_1
Cd|$CdCl_2$ (DMF)|AgCl; Ag	0.576_2
Zn|$ZnCl_2$ (DMF)|AgCl; Ag	0.988_6

Table 2. From the data of the electromotive-force measurements of the (c) type cells and the standard potential, the activity coefficients of the corresponding salts in DMF are obtained. The rearrangement of Eq. (1) gives:

$$\log \gamma_{\pm} = \frac{E°-E}{0.0887} - \log m \qquad (7)$$

from which $\gamma\pm$ values for various electrolytes have been evaluated. The smoothed values of E and the activity

Table 3. Smoothed values of E and activity coefficients for round concentrations for cell (C)

Molality	$PbCl_2$		$CdCl_2$		$ZnCl_2$	
	E	$\gamma_{\pm}$	E	$\gamma_{\pm}$	E	$\gamma_{\pm}$
0.01	0.5450	0.349	0.7936	0.354	1.116	0.354
0.02	0.5275	0.275	0.7837	0.229	1.105	0.236
0.03	0.5205	0.220	0.7765	0.184	1.099	0.184
0.04	0.5150	0.190	0.7730	0.151	1.095	0.153
0.05	0.5150	0.171	0.7708	0.128	1.092	0.133
0.06	0.5070	0.156	0.7690	0.112	1.090	0.114
0.07	0.5040	0.145	0.7677	0.104	1.089	0.102
0.08	0.5015	0.135	0.7667	0.103	1.0885	0.091
0.09	0.5010	0.124	0.7660	0.102	1.0882	0.081
0.10	0.500	0.110	0.7655	0.101	1.0880	0.073

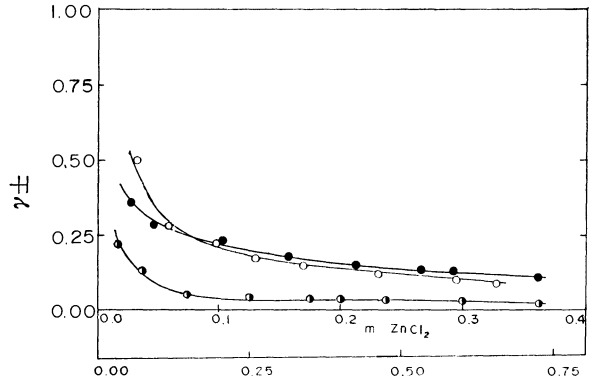

Fig. 3. Relationships between activity coefficients and molalities of metal chlorides in DMF.
—○—: $PbCl_2$, —●—: $CdCl_2$, —◑—: $ZnCl_2$.

coefficients for a round concentration of metal chloride in cells of the (c) type listed in Table 3. The plots of the activity coefficients against the concentrations of metal chlorides related to this work are shown in Fig. 3.

Standard Free-energies of the Solvated Electrolytes. The general reaction for the (c) cell is:

$$M(s) + 2AgCl(s) = 2Ag(s) + MCl_2(soln),$$

and the corresponding standard free-energy change for this reaction is:

$$\Delta G° = G°_{f_{MCl_2(soln)}} + 2G°_{f_{Ag(s)}} - G°_{f_{M(s)}} - 2G°_{f_{AgCl(s)}} = -nFE° \qquad (8)$$

where $G°_{f_{MCl_2(soln)}}$ is the standard free-energy of the formation of a solvated MCl_2. The standard free-energy of the formation of a solvated salt, MCl_2, is then given by:

$$G°_{f_{MCl_2(soln)}} = 2G°_{f_{AgCl(s)}} - nFE° \qquad (9)$$

The values for the standard free-energies of formation have also been calculated for the corresponding solvated salts; they are listed in Table 4.

Table 4. Standard free-energies of formation of solvated metal chlorides in DMF

Salt	$-G_f°$ (kcal/mol)	
	DMF	H_2O
$PbCl_2$	67.54	68.51
$CdCl_2$	79.03	81.28
$ZnCl_2$	93.90	97.88

The standard free-energy of the formation for silver chloride was obtained from Lange:[16] $G°_{f_{AgCl(s)}} = -26.22$ kcal/mol. The standard free-energies of the formation of solvated lead, cadmium, and zinc chlorides in aqueous solutions are also listed in Table 4, thus facilitating a comparison of these data. As may be seen from Table 4, the free-energy values in DMF were larger than in the aqueous solution. It may, therefore, be considered that these metal chlorides in DMF have larger solvation energies than in aqueous solutions, for the free-energy of the formation of MCl_2 (s) is always the same in these solvents.

References

1) H. Ulisch and G. Spiegel, *Phys. Chem.*, **177**, 103 (1936).
2) T. Pavlopoulos and H. Strehlow, *Z. Phys. Chem.* (Frankfurt), **2**, 89 (1954).
3) E. Luksha and C. M. Criss, *J. Phys. Chem.*. **70**, 1949 (1966).
4) L. S. Marple, *Anal. Chem.*, **39**, 844 (1967).
5) J. C. Synnott and J. N. Butler, *ibid.*, **41**, 1890 (1969).
6) M. Saito, *ibid.*, **47**, 1784 (1975).
7) S. Y. Tyree, Jr., "Inorganic Syntheses," Vol. 4, McGraw-Hill Inc., N.Y. (1953), p. 104.
8) I. M. Kolthoff, "Volumetric Analysis," Vol. III, Interscience Pub. Inc., N. Y. (1957), p. 19.
9) W. H. Harnibrook, G. J. Janz, and A. B. Gordon, *J. Amer. Chem. Soc.*, **64**, 513 (1942).
10) H. S. Harned, R. W. Ehlers, *ibid.*, **55**, 2179 (1933).
11) J. H. Wolfenden, C. P. Wright, N. L. Ross Kane, and R. I. Buckley, *Trans. Faraday Soc.*, **23**, 491 (1927).
12) G. Scatchard and R. F. Refft, *J. Amer. Chem. Soc.*, **52**, 2265 (1930).
13) W. Biedermann and G. Schwarenbach, *Chimia* (Switz), **2**, 56 (1948); H. Flaschka, *Mikrochim. Acta*, **39**, 38 (1952).
14) W. R. Crmody, *J. Amer. Chem. Soc.*, **51**, 2095 (1929).
15) W. J. Clayton and W. C. Vosburg, *ibid.*, **58**, 2093 (1936).
16) N. D. Lange, "Handbook of Chemistry," 10th Ed., McGraw-Hill, Inc., N. Y. (1961), p. 1576.

The *cis-trans* Isomerization of 2-Butenes Photosensitized by Adsorbed Acetone

Kiyoshi OTSUKA and Akira MORIKAWA

Department of Chemical Engineering, Tokyo Institute of Technology, Ookayama Meguro-ku, Tokyo 152

(Received January 23, 1975)

The anomalous acceleration of the rate of the *cis-trans* isomerization of 2-butenes is observed in the photosensitization of acetone adsorbed on porous Vycor glass. The anomaly is explained by means of a chain mechanism which is compatible with the triplet-triplet energy transfer mechanism. The chain carrier may be radicals formed by the dissociation of the lowest triplet acetone, resulting from the less efficient quenching of the triplet acetone by butenes at lower butene pressures. The preferential quenching of the acetone by the *cis* isomer to by the *trans* isomer of 2-butenes suggests that the geometrical factor plays a significant role in the reaction in the adsorption phase.

It was shown in a previous report[1] that the photosensitized isomerization of 2-butenes by ketones adsorbed on porous Vycor glass proceeds by means of the mechanism of the triplet-triplet energy transfer from ketones to 2-butenes. At a low pressure of 2-butenes, anomalously high rates of isomerization have been observed when acetone is used as a sensitizer. This anomaly cannot be explained in terms of the reaction scheme proposed previously.[1] We intend to report here the details of the isomerization of 2-butenes photosensitized by the adsorbed acetone on the porous Vycor glass and to suggest a mechanism for interpreting the anomaly mentioned above.

Experimental

The properties and the pretreatment of the porous Vycor glass, and the apparatus and the method used in the photosensitized isomerization, were identical with those described in the previous report.[1] The light from a Toshiba H-400-P medium-pressure mercury lamp was filtered by passing it through 1-cm path of water and a Toshiba UV-29 glass filter (transparent >270 nm), so that the adsorbed acetone was excited to its lowest singlet state. The adsorption of acetone and the sensitized reaction were carried out at room temperature. The amount of acetone remaining in the gas phase was negligibly small during the course of the reaction.

The *cis*-2-butene was a high-purity product of the Phillips Petroleum Co. The *trans*-2-butene and 1-butene were purchased from Takachiho Kagaku Kogyo Co. The butenes were further purified by trap-to-trap distillation in a high-vacuum apparatus. A spectro-pure-grade acetone obtained from Wako Pure Chemical Industries, Ltd., was purified in a similar manner. The nitric oxide was an extra-pure-grade product of the Takachiho Kagaku Kogyo Co. and was used without further purification.

Results and Discussion

The illumination of the porous Vycor glass plate on which acetone has been preadsorbed induces the *cis-trans* isomerization of 2-butenes without any double-bond migration reaction. Using 100% of *cis*-2-butene as the starting material, the initial rates of *trans*-2-butene formation, $R^0_{c\text{-}t}$, were obtained at the various amounts of the adsorbed acetone. Figure 1 shows the relation between $R^0_{c\text{-}t}$ and I, the relative light intensities absorbed by acetone at different coverages (θ=0.13~0.49).

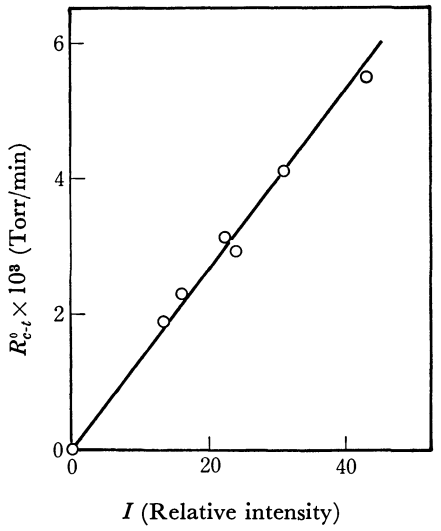

Fig. 1. The relation between $R^0_{c\text{-}t}$ and I.
The initial pressure of *cis*-2-butene, $P^0_{c\text{-}B}$ is 120 Torr.

The proportionality between them guarantees that the *cis-trans* isomerization will be sensitized by adsorbed acetone.

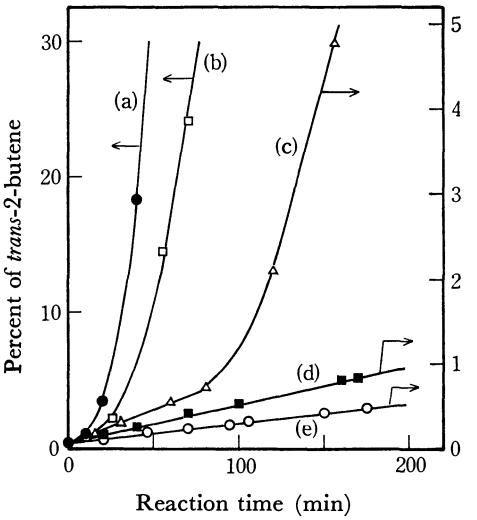

Fig. 2. The time-courses of the photosensitized isomerization at various $P^0_{c\text{-}B}$.
The coverage of the adsorbed acetone, θ_A, is 0.24.
(a); 14 Torr, (b); 18 Torr, (c); 41 Torr, (d); 80 Torr, (e); 125 Torr.

The time-course of the formation of *trans*-2-butene at different initial pressures of *cis*-2-butene are indicated in Fig. 2. At high pressures, *trans*-2-butene is formed at a constant rate, while at pressures less than ~40 Torr the rate of the *trans* isomer formation is accelerated. Although the scattering of the incident light by the porous adsorbent results in an inaccurate estimate of the absolute quantum yield, the roughly calculated values for the *trans*-2-butene formation after the acceleration, for instance, for the curves of (a) or (b) in Fig. 2, exceed 10 at a reaction time longer than 40 min. However, those for the data at high butene pressures never exceed unity.

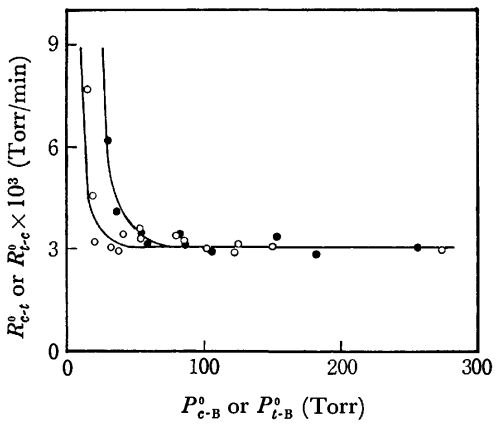

Fig. 3. The effect of butene pressure on the initial rate of the photoisomerization.
$\theta_A=0.24$, —○—; $R^0_{c\text{-}t}$, —●—; $R^0_{t\text{-}c}$.

The pressure effect on $R^0_{c\text{-}t}$ and $R^0_{t\text{-}c}$, the initial rate of *cis*-2-butene formation from 100% *trans*-2-butene, is indicated in Fig. 3. The rates observed at low pressures show a very steep increase with a decrease in the pressure, and $R^0_{t\text{-}c}$ is always greater than $R^0_{c\text{-}t}$, while at high pressures of butenes neither rate depends on the pressure and both give the same value.

The most general mechanism for the photosensitized *cis-trans* isomerization by acetone on the solid surface is given by the following processes:[1]

$$^0A(a) \xrightarrow{h\nu} {}^1A(a) \longrightarrow {}^3A(a) \quad (1)$$

$$^3A(a) \longrightarrow {}^0A(a)\ (+\text{heat or } h\nu) \quad (2)$$

$$^3A(a) + {}^0A(a) \longrightarrow 2{}^0A(a) \quad (3)$$

$$^3A(a) + t\text{-}{}^0B(a) \longrightarrow {}^0A(a) + {}^3B(a) \quad (4)$$

$$^3A(a) + c\text{-}{}^0B(a) \longrightarrow {}^0A(a) + {}^3B(a) \quad (5)$$

$$^3B(a) \longrightarrow \alpha\cdot t\text{-}{}^0B(a) + (1-\alpha)\cdot c\text{-}{}^0B(a) \quad (6)$$

where ^0A and ^3B represent the ground-state acetone and the triplet 2-butene respectively, when the other symbols have their usual meanings,[1] and where the suffix (a) indicates the adsorbed state of the individual species.

Steady-state approximations for $^3A(a)$ and $^3B(a)$ give the following equations:

$$R^0_{t\text{-}c} = (1-\alpha)I_0\phi_{isc}k_4[t\text{-}{}^0B]/(k_2+k_3[{}^0A]+k_4[t\text{-}{}^0B]) \quad (7)$$

$$R^0_{c\text{-}t} = \alpha I_0\phi_{isc}k_5[c\text{-}{}^0B]/(k_2+k_3[{}^0A]+k_5[c\text{-}{}^0B]) \quad (8)$$

Here, the quantum yield of $^3A(a)$ or ϕ_{isc} must be close to unity, as has been verified in the liquid phase.[2] The independence of both rates from the change in the butene pressure at $P^0_{t\text{-}B}>\sim 60$ Torr and $P^0_{c\text{-}B}>\sim 40$ Torr, as is shown in Fig. 3, may reasonably be ascribed to the triplet-energy transfer by means of Eq. (4) or (5) being faster than that by the deactivation (Eqs. (2) and (3)).[1] The proportionality between $R^0_{c\text{-}t}$ and I also suggests that Process (3) is slow compared to Process (5) or (4).

The rapid increase in the rates and the anomalously high quantum yield in the low-pressure range can not be explained only by Processes (1)~(6). The difference between the photostationary state ratio, $([t\text{-}{}^0B]/[c\text{-}{}^0B])_{pss}$, at a high pressure of butene, 2.8~3.0, and that at a low pressure, 2.2~2.4, suggests that the dominant mechanisms for the two pressure ranges are different. The following mechanism conceivably predominates in the low-pressure range:

$$^3A(a) \longrightarrow R\cdot(a) \quad (9)$$

$$R\cdot(a) + c\text{-}{}^0B(a) \longrightarrow R\text{–}B\cdot(a) \quad (10)$$

$$R\cdot(a) + t\text{-}{}^0B(a) \longrightarrow R\text{–}B\cdot(a) \quad (11)$$

$$R\text{–}B\cdot(a) \longrightarrow R\cdot(a) + \beta\cdot t\text{-}{}^0B(a) + (1-\beta)\cdot c\text{-}{}^0B(a) \quad (12)$$

$$R\cdot(a) + R\cdot(a) \longrightarrow P(a) \quad (13)$$

where R· is presumably the methyl or acetyl or a reactive product produced from these radicals; R–B·, a complex between 2-butene and R· in which the π-bond opening of butene may be established, and P, the termination product of R·. The *cis-trans* conversion occurs in Process (12), accompanying a regeneration of the chain carrier, R·. It is conceivable that, at low butene pressures, the formation of the chain carrier, R·, from the triplet acetone (Process (9)) becomes remarkable, since the efficiency of the triplet quenching by butenes (Process (4) or (5)) is low. The assumptions that the chain carrier, R·, and, accordingly, R–B·, accumulate with the time give an explanation for the accelerating rate and the high quantum yield mentioned above. The acceleration appears in the earlier stage of the reaction for lower pressures of butenes because of the fast accumulation of radicals. The abnormally high rates in the low-pressure range (Fig. 3) must be attributed to the difficulty of obtaining the initial rate, excluding the contribution of the chain mechanism, because of a rapid acceleration.

In the course of the reaction at the butene pressure of 86 Torr, the butene in the gas phase was condensed by means of a liquid-nitrogen trap at Point (A) in Fig. 4, followed by a sudden vaporization after 15 min at (B). The very rapid formation of *trans*-2-butene is seen in the first analysis of the butenes after Point (B). Then, the reaction proceeded steadily, with a velocity identical with that observed before the condensation. The rapid formation of *trans*-2-butene in Fig. 4 may also be caused by the accumulation of R· during the condensation of butene in the gas phase. The addition of 0.7 Torr of nitric oxide to 17.3 Torr of *cis*-2-butene prevented the acceleration of the rate, and the *trans*-2-butene production proceeded proportionally with the time under the low conversion, as had been seen at high pressures of butene.[3] This suggests that the R· must be captured by Process (14) resulting in no accumulation of the radicals:

$$R\cdot + NO \longrightarrow RNO \longrightarrow \text{stabilized} \quad (14)$$

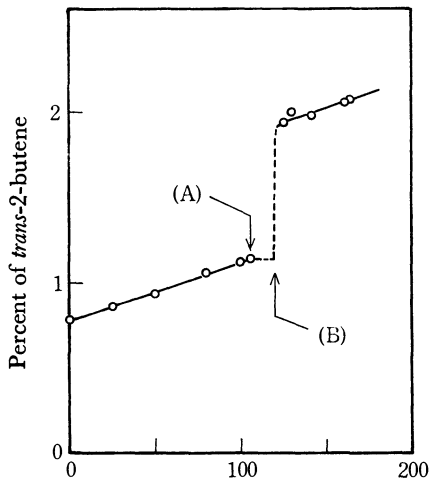

Fig. 4. The effect of condensation of butenes during the photoisomerization.
$P^0_{c\text{-}t}$=86 Torr, θ_A=0.24
At point (A); condensation, (B); vaporization.

At pressures of butene higher than 60 Torr, the ratio of $R^0_{c\text{-}t}$ to $R^0_{t\text{-}c}$ is unity (Fig. 3). Then, the blanching ratio, α, is obtained as 0.5 from Eq. (15):

$$R^0_{c\text{-}t}/R^0_{t\text{-}c} = \alpha/(1-\alpha) = 1.0 \quad (15)$$

k_5/k_4 was estimated to be 2.8~3.0 from Eq. (16):

$$([t\text{-}^0\mathrm{B}]/[c\text{-}^0\mathrm{B}])_{pss} = (k_5/k_4)(\alpha/(1-\alpha)) = 2.8\sim3.0 \quad (16)$$

In the liquid phase, the ratios of the quenching rate constant for the *cis* and *trans* isomers of 2-pentene sensitized by acetone were estimated to be 1.0 and 1.30 by Borkman and Kearns[2b] and Saltiel *et al.*[5] respectively. In contrast to these results, we have concluded that the preferential quenching by the *cis* isomer occurs in the adsorbed layer. This is consistent with the result that the contribution of the chain mechanism is remarkably more pronounced in $R^0_{t\text{-}c}$ than in $R^0_{c\text{-}t}$ under the same pressure (See the low-pressure range in Fig. 3). Although the features of the complex formation in the quenching of acetone by 2-butenes are not clear at present, the difference in the geometrical structures of 2-butene isomers may play an important role in establishing the ease of such complex formation so far as the reaction in the adsorbed layer is concerned.

References

1) K. Otsuka and A. Morikawa, This Bulletin, **47**, 2335 (1974).

2) R. F. Borkman and D. R. Kearns, a) *J. Chem. Phys.*, **44**, 945 (1966); b) *J. Amer. Chem. Soc.*, **88**, 3467 (1966).

3) The appreciably lower rate than the constant value at high butene pressure was observed by addition of nitric oxide, since nitric oxide is an effective quencher for the triplet ketones.[4]

4) Y. Kubokawa and M. Anpo, *J. Phys. Chem.*, **78**, 2442 (1974).

5) J. Saltiel, K. R. Neuberger, and M. Wrighton, *J. Amer. Chem. Soc.*, **91**, 3658 (1969).

Uranyl Ion-Sensitized Isomerization of the Stilbenes in Solution

Ryoka MATSUSHIMA,* Tsuneo KISHIMOTO, and Morio SUZUKI

Department of Industrial Chemistry, Faculty of Engineering, Shizuoka University, Hamamatsu 432

(Received March 20, 1975)

By selective excitation of the uranyl ion with light of $\lambda \geqq 365$ nm, a deoxygenated acetone solution containing *cis*- or *trans*-stilbene and the uranyl ion finally reaches a photostationary state, whose isomer ratio, $(t/c)_{pss}$, varies from 1 to 3 depending on the concentrations of the uranyl ion and the stilbenes. A close correlation is found between the features in the sensitized isomerization and the phosphorescence quenching of the sensitizer. Comparison with the results of halogen radical induced isomerization suggests that catalytic isomerization by free radicals is not an important process. A triplet-triplet energy transfer mechanism is proposed, which is supported by the oxygen effect and considerations on the lowest excited state of the uranyl ion, *i.e.*, its long lifetime and triplet energy level higher than that of the stilbenes.

The uranyl ion in solution at room temperature is both phosphorescent and reactive towards many organic compounds.[1,2] This allows a possible elucidation of the reaction mechanism as regards both primary and secondary processes.[3,4] Kemp and his co-workers have studied the excited state and radical intermediates in the photoredox reactions of the uranyl ion with organic compounds by laser flash absorption spectroscopy[5] and ESR detection.[6]

Uranyl ion as a photosensitizer does not seem to have been studied.[2] We reported on the aquation of the hexacyanocobaltate (III) ion[7] and *cis-trans* isomerization of the stilbenes[8] sensitized by the uranyl ion in solution, triplet-triplet energy transfer process being suggested in both cases. In the uranyl ion-sensitized isomerization of the stilbenes an abnormal value of the photostationary state isomer ratio was observed,[8] which suggests some special effects of organic-inorganic interactions in the excited states. The present work was undertaken to investigate the features and the mechanism of the uranyl ion-sensitized *cis-trans* isomerization of the stilbenes in solution.

Experimental

All the reagents and solvents were of guaranteed grade. Acetone solutions of the uranyl ion were dried over anhydrous sodium sulfate, after uranyl nitrate hexahydrate had been dissolved in acetone. Acetone solutions containing stilbene and uranyl ion were put into 7 mdm^3 ampoules and were deoxygenated by bubbling purified nitrogen current followed by sealing. The sealed ampoules were irradiated with light of $\lambda \geqq 365$ nm from a 100 W high-pressure mercury lamp with glass filters, in order to avoid direct excitation of the stilbenes. Temperature was maintained near 10 °C during the course of photolyses. After irradiation acetone was evaporated under reduced pressure at 40 °C, 50 Torr a small amount of alcohol being added in order to eliminate the acetone completely. The residue was shaken with aliquots of chloroform and 0.1 mol·dm^{-3} aqueous perchloric acid. The chloroform layer, which was washed with water followed by drying through anhydrous sodium sulfate, was adequately diluted with ethanol for measurement of the absorbance. The relative concentrations of the stilbenes were calculated from absorbances at 320 nm and a calibration graph.

Photoreaction quantum yields were measured by the optical train system with two cells (each having two plane parallel windows) arranged in series and a monochromatic parallel light beam from a 500 W high-pressure mercury lamp with a suitable arrangement for obtaining a monochromatic and parallel light. Ferric oxalate solution was used as an actinometer.

Quenching constants were obtained from the Stern-Volmer plot for the emission intensity at the 510 nm peak with excitation at 436 nm. Measurements were carried out without deoxygenation since no significant effect of dissolved oxygen was observed. Absorption and emission measurements were carried out with a Hitachi 124-type spectrophotometer and a Hitachi 204-type fluorescence spectrophotometer, respectively.

Results and Discussion

Photostationary States. The changes in the absorption spectra of the stilbenes (in ethanol after elimination of acetone and the uranyl ion from the reaction mixture) due to the uranyl ion-sensitized *cis*→*trans* and *trans*→*cis* isomerizations in deoxygenated acetone solution with $\lambda \geqq 365$ nm are shown in Fig. 1. An isosbestic point appears near 260 nm. After a long period of irradiation both the sensitized *cis*→*trans* and *trans*→*cis* isomerizations give the same isomer ratio (*c*-4, *t*-5).

Under similar conditions, but in the absence of the uranyl ion, no significant (direct) photoisomerization took place. No thermal isomerization was found for the uranyl–stilbene mixture in deoxygenated acetone solution after being left to stand at 40—45 °C in the dark for 5 hr.

Figure 2 shows the change in the *trans*/*cis* mole fraction against the time of irradiation under experimental conditions identical with those in Fig. 1. The existence and constancy of the photostationary state can be confirmed. The isomer ratios at the photostationary state, $(t/c)_{pss}$, obtained in a similar manner to that shown in Fig. 1, for various concentrations of the stilbenes and the uranyl ion, are summarized in Table 1. The concentration dependence of $(t/c)_{pss}$ can be noted. The $(t/c)_{pss}$ values in Table 1 are in the range 1—3, whereas those for the triplet-sensitized isomerization of the stilbenes with organic sensitizers whose triplet energies are 230—250 kJ/mol are in the range 0.31—0.43.[10]

Figure 3 shows the plot of the reciprocal of the quantum yield of the sensitized *cis*→*trans* isomerization, $1/\phi$, *vs.* the reciprocal of the initial concentration of *cis*-stilbene, $1/[cis]$, giving a straight line with an intercept of 16.5 and a slope of 6.5×10^{-3} mol/dm^3. The Stern-Volmer quenching of the uranyl phosphorescence by *cis*

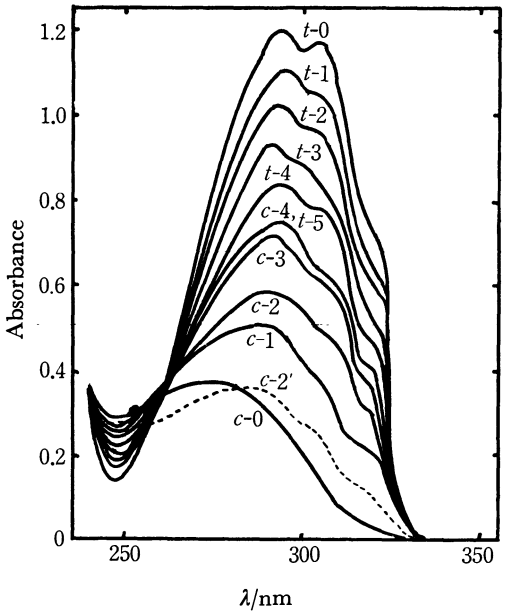

Fig. 1. The changes in the absorption spectra of the stilbenes (in ethanol after elimination of the uranyl ion and acetone from the reaction mixtures) due to the uranyl ion-sensitized *cis*→*trans* and *trans*→*cis* isomerization with light of $\lambda \geq 365$ nm. Both concentrations of the uranyl ion and the stilbenes were 2×10^{-3} mol/dm^3. The irradiation periods for the sensitized *cis*→*trans* isomerization were, *c*–0: 0 min, *c*–1: 30 min, *c*–2: 90 min, *c*–2′: 90 min irradiated without deoxygenation, *c*–3: 120 min, *c*–4: 360 min, and for the sensitized *trans*→*cis* isomerization, *t*–0: 0 min, *t*–1: 30 min, *t*–2: 60 min, *t*–3: 90 min, *t*–4: 180 min, *t*–5: 360 min.

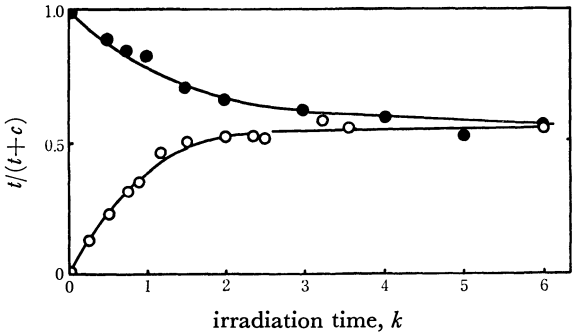

Fig. 2. Photostationary state reached after a long period irradiation of the mixture of the uranyl ion and the stilbenes. Conditions were the same as those shown in Fig. 1.

Table 1. The $(t/c)_{pss}$ values at various concentrations of the uranyl ion (U) and the stilbenes (S)

[S]$\times 10^3$ mol/dm^3	[U]$\times 10^2$ mol/dm^3	$(t/c)_{pss}$
2.0	0.02	0.96
2.0	0.20	1.25
2.0	2.0	1.63
2.0	10	1.77
20	0.20	3

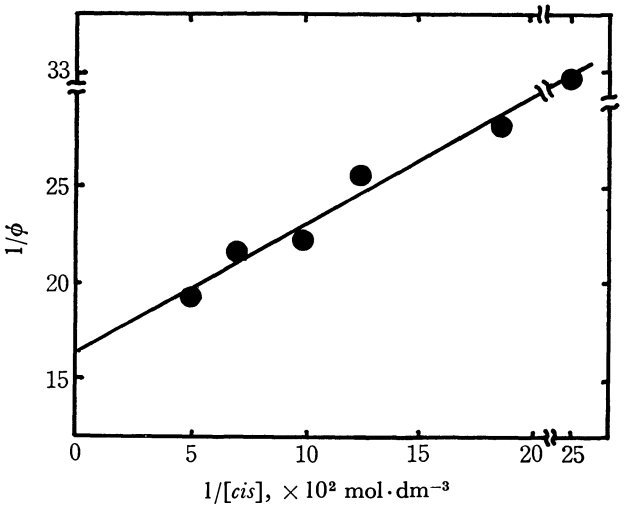

Fig. 3. Plot of $1/\phi$ *vs.* $1/[cis]$. The concentration of the uranyl ion was 2×10^{-3} mol/dm^3.

stilbene was $(4 \pm 2) \times 10^3$ dm^3/mol under similar conditions though no precise value was available because of the weak phosphorescence intensity of a 0.002 mol/dm^3 uranyl ion in acetone as compared to the solvent (impurity) emission. The ratio of the intercept to the slope in Fig. 3, 2.5×10^3 dm^3/mol, is compatible with the quenching constant.

Effects of Dissolved Oxygen. No significant oxygen effect on the phosphorescence intensities of the uranyl ion was observed either in the presence or absence of quenchers (stilbenes).

The lack of oxygen quenching on the phosphorescent emission in solutions has been reported for some rare earth metal ions,[11] which is assumed to be due to the well-shielded inner shells. In contrast, a significant interference effect of the dissolved oxygen was found on the sensitized isomerization, (curve *c*-2′, Fig. 1 irradiated without deoxygenation) as compared to the curve *c*-2. The curve *c*-2′ indicates a decrease in the total concentration of the stilbenes, or oxidation. These effects of oxygen might suggest the intermediacy of either an exciplex or the triplet stilbenes. The latter possibility can be excluded since the lifetime of the stilbene triplet is too short (10^{-8} s) to be effectively intercepted by the dissolved oxygen;[9] the effect of oxygen might reflect the interception of uranyl-stilbene triplet exciplex.

Rate Parameters. Since the uranyl ion is excited to its lowest triplet state[12] (E_T=245 kJ,[3] $\tau_p = 10^{-4} - 10^{-6}$ s[1,5]) whose level is higher than the lowest triplet states of the stilbenes (200 and 230 kJ[10]), triplet energy transfer from the excited uranyl ion to the stilbenes is feasible. Thus the correlation between the features in the phosphorescence quenching and the sensitization processes suggests triplet energy transfer mechanism as the major process for the sensitized isomerization. On the other hand, studies on the quenching of the uranyl phosphorescence by a series of aromatic hydrocarbons indicate that the primary interaction involves the formation of exciplexes between the excited uranyl ion and the aromatic hydrocarbons.[3]

Thus the following scheme can be postulated for the sensitized *cis*→*trans* isomerization, where S, S′, U, ^{3}U*,

and $^3U^*\cdots S$ represent *cis*-and *trans*-stilbenes, the ground state and the excited state uranyl ions, and the exciplex, respectively.

$$U + h\nu \longrightarrow {}^3U^* \xrightarrow{k_p} U + h\nu_p \quad (1)$$

$$^3U^* \xrightarrow{k_d} U \quad (2)$$

$$^3U^* + S \underset{k_b}{\overset{k_q}{\rightleftharpoons}} {}^3U^*\cdots S \xrightarrow{k_t} U + S' \quad (3)$$

$$^3U^*\cdots S \xrightarrow{k_c} U + S \quad (4)$$

Since the reverse dissociation of the exciplex is an endothermic process, the rate constant k_b is assumed to be negligible as compared to k_t and k_c which are assumed to be of rapid exothermic processes. Thus, the steady state assumption for $^3U^*\cdots S$ might lead to

$$\frac{I_p^\circ}{I_p} = 1 + \left(\frac{k_q}{k_p+k_d}\right)[S] \quad (5)$$

$$\frac{1}{\phi} = \frac{k_c+k_t}{k_t}\left(1+\frac{k_p+k_d}{k_q[S]}\right) \quad (6)$$

The plot of $1/\phi$ *vs.* $1/[S]$ should give a straight line, and the ratio of the intercept to the slope should be equal to the Stern-Volmer quenching constant. These requirements are satisfied. From Eq. (6) and the intercept in Fig. 3, the decay ratio k_t/k_c is estimated to be 15.5 which differs a great deal from the corresponding value, 1.6, expected from pure triplet energy transfer processes with sensitizers whose triplet energies are 230—240 kJ.[10]

An alternative mechanism to the triplet energy transfer would include catalytic isomerization of the stilbenes by paramagnetic species or free radical intermediates of the photoredox reaction between the uranyl ion and the solvent molecules, since free rsdicals and certain paramagnetic substances have been found to be very effective catalysts for *cis*→*trans* isomerizations of olefins.[13] Some free radicals have also been detected in the photoreactions of alcohols, aldehydes, ketones, and carboxylic acids, with uranyl ion.[6] If the catalytic process by free radicals or paramagnetic species is the major one for the present reaction, it should lead exclusively to the *trans* isomer which is thermodynamically more stable. It is unlikely that such a catalytic process is the major process in the present photoreaction, since the mole fraction of the *cis* isomer at the photostationary state is 0.45 or more. Partial involvement of such a catalytic process, however, might be possible, which would lead to larger $(t/c)_{pss}$ values than those expected from pure triplet energy transfer processes.

Exclusion of Free Radical Induced Isomerization. In order to test the possible contamination of free radical processes in the uranyl ion-sensitized isomerization of the stilbenes, free radical induced isomerization of the stilbenes has been investigated under comparable conditions. Addition of 0.02 mol/dm^3 *n*-propanol did not alter the $(t/c)_{pss}$ value in the uranyl ion-sinsitized *cis-trans* isomerization of the stilbenes in acetone (uranyl ion 0.02 mol/dm^3, stilbene 0.002 mol/dm^3), indicating that *cis-trans* isomerization by the free radical $R_2\dot{C}OH$[3,6] produced in the photoredox reaction is of no significance. The inefficiency can be ascribed to the very short lifetime of the aliphatic radicals. Table 2 shows that the catalyzed *cis-trans* isomerization of stilbenes by bromine or iodine atom does not occur in acetone, whereas iodine atom-induced isomerization occurrs in hexane to give exclusively the *trans* isomer in accord with thermodynamic considerations. These results suggest no significant contamination of free radical processes in the uranyl ion-sensitized isomerization of the stilbenes in acetone.

TABLE 2. FREE RADICAL INDUCED ISOMERIZATION OF THE STILBENES BY IRRADIATION WITH LIGHT OF $\lambda \geqq 400$ nm.

Solvent	Initial isomer[a]	I_2 10^2 mol/dm^3	Br_2 10^2 mol/dm^3	Irradiation time, hr	$\left(\frac{t}{c+t}\right)_{final}$
n-Hexane	*cis*	2.0		5	1.0
	trans	2.0		4	1.0
Acetone	*cis*	2.0		6	0.0
	cis		2.0	7	0.0
	trans	2.0		10	1.0
	trans		2.0	6	1.0

a) Initial stilbene concentration was 0.02 mol/dm^3 in each run.

Another mechanism in which stilbene cation radical ion intermediate is involved can be considered, since the excited state uranyl ion is a powerful oxidizing agent towards various organic compounds. However the degree of the charge transfer (δ) in the exciplexes of a series of aromatic hydrocarbons with the uranyl ion has been estimated to be small, $\delta \leqq 0.2$, in an acetone–water solution.[3] The small δ value implies that the formation of aromatic radical cation intermediates (which corresponds to complete charge transfer, $\delta = 1$) is unlikely.

The large difference in k_c/k_t and $(t/c)_{pss}$ as compared to those for organic triplet sensitized isomerization might at least partly be related to internal paramagnetic and/or heavy atom effects on the decay ratio k_c/k_t of the uranyl-stilbene exciplex. More probably, the π-electron density of the ethylenic bond in the stilbene moiety (in the uranyl-stilbene exciplex) would decrease due to the electron donation from the stilbene to the uranyl moiety, *i.e.*, $(U^{*\delta-}\cdots S^{\delta+})$, so that the formation of thermodynamically more stable *trans* isomer would be favorable.

The change in $(t/c)_{pss}$ with that in the concentration of of the uranyl ion or the stilbenes may suggest that, in addition to the unimolecular decay of the exciplex ((3) and (4)), bimolecular deactivation of the exciplex by the ground state uranyl ion or the stilbenes with a deactivation ratio k_c'/k_t' different from k_c/k_t for the unimolecular decay process becomes significant. No satisfactory explanation for the concentration dependence of $(t/c)_{pss}$ is available as yet.

References

1) E. Rabinowitch and R. L. Belford, "Spectroscopy and Photochemistry of Uranyl Compounds," Pergamon Press, Oxford, 1964.

2) H. D. Burrows and T. J. Kemp, *Chem. Soc. Rev.*, **3**, 139 (1974).

3) R. Matsushima, *J. Amer. Chem. Soc.*, **94**, 6010 (1972).

4) S. Sakuraba and R. Matsushima, This Bulletin, **44**,

2915 (1971).
5) D. M. Allen, H. D. Burrows, A. Cox, R. J. Hill, T. J. Kemp, and T. J. Stone, *Chem. Commun.*, 1973, 59; *J. Chem. Soc. Faraday 1*, **70**, 847 (1974).
6) D. Greatorex, R. J. Hill, T. J. Kemp, and T. J. Stone, *ibid.*, **68**, 2059 (1972); **70**, 216 (1974).
7) R. Matsushima and S. Sakuraba, *Chem. Lett.*, **1973**, 115.
8) R. Matsushima and S. Sakuraba, *ibid.*, **1973**, 1077.
9) J. Saltiel, J. T. D'Agostino, W. G. Herkstroeter, G. Saint-Ruf, and N. P. Buu-Hoi, *J. Amer. Chem. Soc.*, **95**, 2543 (1973).
10) J. Saltiel and G. S. Hammond, *ibid.*, **85**, 2515 (1963); G. S. Hammond, J. Saltiel, A. A. Lamola, N. J. Turro, J. S. Bradshaw, D. O. Cowan, R. C. Counsell, V. Vogt, and C. Dalton, *ibid.*, **86**, 3197 (1964).
11) I. A. Taha and H. Morawetz, *ibid.*, **93**, 829 (1971); V. Balzani, R. Ballardini, M. T. Gandolfi, and L. Moggi, *ibid.*, **93**, 339 (1971); D. J. Binet, E. L. Goldberg, and L. S. Forster, *J. Phys. Chem.*, **72**, 3017 (1968).
12) S. P. McGlynn and J. K. Smith, *J. Mol. Spectrosc.*, **6**, 164 (1961); J. T. Bell and R. E. Biggers, *ibid.*, **18**, 247 (1965); **25**, 312 (1968).
13) K. J. Laidler and L. F. Loucks, in "Comprehensive Chemical Kinetics," ed. by C.H. Bamford and C.F.H. Tipper, Elsevier, London, Vol. 5, (1972), p. 34.

The Effect of the Pressure on the Electrical Conductivity of Zinc Sulfate in Water

Yoshihiro TANIGUCHI, Takashi WATANABE, and Keizo SUZUKI

Department of Chemistry, Faculty of Science and Engineering, Ritsumeikan University, Kita-ku, Kyoto 603

(Received March 22, 1975)

The electrical conductivity of $ZnSO_4$ in water was measured at high pressures up to 3000 kg/cm² and at 25 °C. The dissociation constant of the ion pair (K_m) increased with an increase in the pressure. The volume change ($\Delta V°$) accompanying the dissociation was -8.0 ± 0.5 ml/mol at 25 °C. The distance of the closest approach (å) of the ion pair, calculated using the observed K_m value and the theoretical equation of Bjerrum, increased with an increase in the pressure. In view of these $\Delta V°$ and å values, the ion pair of $ZnSO_4$ was assumed to be of the solvent-separated type. It was also concluded that the number of water molecules separating the ions constituting an ion pair increases with an increase in the pressure.

The structure of the ion pairs of metal sulfates in water has been studied from electrochemical and thermodynamical measurements,[1-3] ultrasonic absorption measurements,[4-6] and spectroscopic measurements.[6-8] As a result, it has been found that there exist two types of ion pairs. One is the contact type, and the other is the separated one with one or more solvent molecules between sandwiched. From the heat of dilution data, Larson[3] has concluded that ion pairs of $MgSO_4$, $NiSO_4$, and $ZnSO_4$ are separated by more water molecules than those of $CaSO_4$, $CuSO_4$, and $CdSO_4$. Their tendency to form a contact ion pair is in the same order as their ionic radii, which is in good agreement with the results from IR reported by Larsson[7] and those from the visible absorption spectrum reported by Smithson and Williams.[8]

The information as to the volume change accompanying the dissociation of the ion pair, $\Delta V°$, obtained from dilatometry[9] and the pressure effect on the dissociation constants of ion pairs[10-15] may be a useful indication of whether a particular ion pair is of the "solvent-separated" or "contact" type. It is well known that the volume change accomapanying the dissociation of electrolytes shows a negative sign upon electrostriction, a negative sign caused by the electrostatic interaction between ions and their surrounding solvent molecules.[16] Therefore, the magnitude of the volume decrease accompanying the dissociation of ion pairs may be expected to be smaller for the solvent-separated type, in which the ions are hydrated in the ion-pair state, than for the contact type.

In the present experiment, we attempted to measure the electrical conductivity of $ZnSO_4$ in water up to 3000 kg/cm² at 25 °C and to clarify the structure of the ion pair by considering the $\Delta V°$ value together with the value of the ionic distance of the closest approach of the ion pair at high pressures.

Experimental

Materials. Zinc sulfate of a special grade was used without further purification. The conductivity water was prepared by repeatedly distilling the water from a mixed-bed deionizing column. The specific conductivity of this water was 1.320×10^{-6} mho/cm at 25 °C. The solutions of zinc sulfate were prepared in the approximate concentration range from 5.0×10^{-4} to 1.0×10^{-3} M at 25 °C.

Method. The apparatus and the procedure used to obtain the electrical conductivity under high pressures have been described in detail elsewhere.[17]

Results and Discussion

The measured equivalent conductances (Λ) are listed in Table 1, together with the limiting equivalent conductances ($\Lambda°$), which were determined by the extrapolation of the Kohlrausch plots,[18] Λ *vs.* $\sqrt{c}$, to an infinite dilution. From these data, the dissociation constants of the ion pair were calculated by the method by Hamann, Pearce, and Strauss.[12] The dissociation degree (α) of the ion pair was determined by inserting the experimental conductances (Λ) and the theoretical values (Λ^i), calculated from Eq. (2) and given by Davies, Otter, and Prue,[19] into Eq. (1):

Table 1. Equivalent conductances (Λ) and limiting equivalent conductances ($\Lambda°$) of $ZnSO_4$ at 25 °C and at various pressures.

Pressure kg/cm²	Concentration at 1 atm, equiv./l (10^{-4})					
	$\Lambda°$	Λ				
	0.0	5.0	6.0	7.5	9.0	10.0
1 (atms)	132.8	116.0	114.4	112.1	110.1	108.8
500	135.4	119.8	118.1	116.2	114.2	113.2
1000	135.5	120.0	119.4	117.4	115.8	114.7
1500	134.4	121.0	119.8	118.0	116.4	115.4
2000	132.8	120.4	119.2	117.4	116.0	115.2
2500	131.0	119.3	118.3	116.9	115.4	114.6
3000	129.0	118.2	117.0	115.8	114.5	113.8

$$\alpha = \frac{\Lambda}{\Lambda^i} \tag{1}$$

$$\Lambda^i = \Lambda° - \left[\frac{R\Lambda°}{1+B\text{å}\sqrt{2\alpha c}} + E\right]\frac{2\sqrt{\alpha c}}{1+2B\text{å}\sqrt{\alpha c}} \tag{2}$$

where:

$$R = \frac{32.816\times10^7}{(\varepsilon T)^{3/2}} \tag{3}$$

$$B = \frac{5.029\times10^9}{(\varepsilon T)^{1/2}} \tag{4}$$

$$E = \frac{165.00}{\eta(\varepsilon T)^{1/2}} \tag{5}$$

$$\mathring{a} = \frac{2e^2}{\varepsilon k T} \tag{6}$$

Here, ε and η are the dielectric constant and the viscosity of water respectively, k is the Boltzmann constant, T is the absolute temperature, e is the protonic charge, and c is the molarity. The activity coefficient ($f_\pm$) was predicted by the Debye-Hückel limiting law at the c concentration as follows:

$$-\log f_\pm = \frac{2A\sqrt{\alpha c}}{(1+2B\mathring{a}\sqrt{\alpha c})} \tag{7}$$

where A is $7.2984\times 10^6/(\varepsilon T)^{3/2}$. In applying the above equation to the conditions under a high pressure, the ε values calculated by the Owen-Brinkley equation[20] and the η data observed by Cappi[21] were used.

The dissociation constant (K_m) is given by:

$$K_m = \frac{m\alpha^2 f_\pm^2}{1-\alpha} \tag{8}$$

where m[22] donates the molality of $ZnSO_4$ and where the activity coefficient of ion pairs is assumed to be unity. The K_m values obtained are listed in Table 2. The pres-

Table 2. Dissociation constants (K_m) and average dissociation constants $(K_m)_{av}$ of $ZnSO_4$ at 25 °C and at various pressures.

Pressure kg/cm²	$(K_m)_{av}$	K_m, equiv./l (10^{-3}) Concentration at 1 atm, equiv./l (10^{-4})				
		5.0	6.0	7.5	9.0	10.0
1(atm)	4.554±0.046	4.454	4.541	4.555	4.581	4.640
500	5.461±0.096	5.386	5.295	5.546	5.478	5.599
1000	6.252±0.146	5.916	6.221	6.279	6.447	6.398
1500	7.677±0.096	7.437	7.701	7.726	7.755	7.763
2000	8.865±0.076	8.787	8.888	8.774	8.844	9.030
2500	10.17±0.207	9.722	10.11	10.49	10.20	10.35
3000	11.72±0.266	11.66	11.12	11.98	11.83	12.02

ent value at atmospheric pressure, 4.55×10^{-3} equiv./l, may be compared with that of 4.90×10^{-3} equiv./l observed by Owen and Gury[24] and by Patterson and Freitag,[25] that of 4.4×10^{-3} equiv./l observed by Denney and Monk[26] from their electrical conductivity measurements, and that of 4.17×10^{-3} mol/l observed by Nair and Nancollas[1] from the electromotive force. These results, ranging from 4.17×10^{-3} to the 4.90×10^{-3} mol/l presented above, rather deviate from the value of 3.24×10^{-3} mol/l reported by Izatt *et al.*[27] on the basis of their calorimetrical determinations and from that of 5.4×10^{-3} equiv./l reported by Davies[28] on the basis of the electrical conductivity. Table 2 shows that K_m increases with an increase in the pressure. Therefore, the formation of the ion pair is depressed by an increase in the pressure.

The $\Delta V°$ value at 1 atm accompanying the dissociation of the $ZnSO_4$ ion pair was obtained graphically by the following equation:

$$\Delta V° = -RT(\partial \ln K_m/\partial P)_T \tag{9}$$

where R is the gas constant. The obtained $\Delta V°$ value of -8.0 ± 0.5 ml/mol agrees with that of -8.2 ml/mol for $ZnSO_4$[29] and is close to those of -8.5 ml/mol[10] and -7.7 ml/mol[14] for $MgSO_4$ and that of -7.4 ml/mol[11] for $MnSO_4$, but it is larger than that of -10.2 ml/mol[14] for $CaSO_4$. The absolute $\Delta V°$ values of the above divalent metal sulfate ion pairs are much smaller than those of -20.4 ± 0.5 ml/mol[30] and -28.9 ml/mol[31] accompanying the dissociation of H_2O and NH_4OH respectively. The smallness of the absolute values of $\Delta V°$ in comparison with the values for the ionization of weak acid and bases shows that the ions are extensively hydrated in the ion-pair state. The order of the $\Delta V°$ values for divalent metal sulfates is independent of their ionic radii. The tendency to form a solvent-separated ion pair shown by the data of the volume change is not in good agreement with the results obtained from the heat of dilution.[3]

Information about the distance of the closest approach of ion pairs derived from both the observed dissociation constant and the theory of the ion association by Bjerrum will contribute to clarifying the structure of ion pairs. The K_m is related theoretically to $\mathring{a}$ by:

$$K_m = \frac{1000}{4\pi N Q(b)\rho}\left(\frac{\varepsilon k T}{4e^2}\right)^3 \tag{10}$$

where:

$$Q(b) = \int_2^b x^{-4}e^x dx \tag{11}$$

$$b = \frac{4e^2}{\mathring{a}\varepsilon k T} \tag{12}$$

ρ is the density of water at a given temperature and pressure,[23] and the relation between log $Q(b)$ and b obtained by Harned and Owen[32] was used. Table 3 shows the $\mathring{a}$ values obtained at each pressure up to 3000 kg/cm². The value at 1 atm, 4.3 Å is larger than that of 3.47 Å for the interionic distance of the $ZnSO_4$ crystal.[33] Therefore, the solvent-separated type is assumed for the ion pair. This is the same as the conclusion obtained from the volume change.

Table 3. Distance of the closest approach ($\mathring{a}$) of $ZnSO_4$ ion pair at 25 °C under various pressures.

Pressure, kg/cm²	$\mathring{a}$, Å
1 (atm)	4.3
500	4.4
1000	4.5
1500	4.8
2000	5.0
2500	5.3
3000	5.5

The present results, to be found in Table 3, show an increase in the $\mathring{a}$ value with an increase in the pressure; this is in disagreement with the results derived by Nakahara *et al.*,[13] Inada *et al.*,[14] and Ueno *et al.*[15] However, from the study of the pressure effect on the equilibrium of tight ion pairs⇄loose ion pairs for sodium and lithium fluorenyl in tetrahydrofuran, Claesson *et al.*[34] found that the pressure shifted the equilibrium towards the loose ion pairs. The fact that the structure of the solvated ion pairs strongly depends on the dielectric constant of the solvent has been clarified in a nonaqueous system by Griffiths and Symons.[35] They showed

that the tendency to form the solvent-separated ion pair increased with the increase in the dielectric constant of the solvent. The application of pressure causes an increase in the dielectric constant of the solvent. Therefore, the increase in the δ value with an increase in the pressure suggests that the ion pair may be expected to become more hydrated as the pressure increases, in spite of the contraction of the water in the hydration sheath of the ion pair by the compression. This consideration was already predicted about small free ions, *i.e.*, sodium and potassium ions, by Kay and Evans[36] from the point of view of the structural change of bulky water as a result of the pressure effect on the Walden product. On the contrary, Horne[37] has suggested that the pressure breaks up the structure of the hydration of small ions. Nakahara *et al.*,[38] have reported that no pressure effect can be found in the hydration number of potassium chloride up to 5000 kg/cm^2, assuming that the average volume of water molecules in the hydration sheath is equal to that of bulky water under pressure. The conclusions about the structure of the solvated ions derived from the pressure effect on the electrical conductivity have thus been conflicting. In order to solve this problem, information about the density of the water in the hydration sheath under pressure will be necessary, along with that about the structure of the bulky water under pressure.

References

1) V. S. K. Nair and G. H. Nancollas, *J. Chem. Soc.*, **1959**, 3934.
2) W. L. Masterton and T. Bierly, *J. Phys. Chem.*, **74**, 139 (1970).
3) J. W. Larson, *ibid.*, **74**, 3392 (1970).
4) M. Eigen and K. Tamm, *Z. Electrochem.*, **66**, 93 (1962).
5) D. P. Fay and N. Purdie, *J. Phys. Chem.*, **74**, 1160 (1970).
6) P. Hemmes and S. Petrucci, *ibid.*, **72**, 3986 (1968).
7) R. Larsson, *Acta Chem. Scand.*, **18**, 1923 (1964).
8) J. M. Smithson and R. J. P. Williams, *J. Chem. Soc.*, **1958**, 457.
9) J. G. Spiro, A. Revesz, and J. Lee, *J. Amer. Chem. Soc.*, **90**, 4000 (1968).
10) F. H. Fisher, *J. Phys. Chem.*, **66**, 1607 (1962).
11) F. H. Fisher and D. F. Davies, *ibid.*, **69**, 2595 (1965).
12) S. D. Hamann, P. J. Pearce, and W. Strauss, *ibid.*, **68**, 375 (1964).
13) M. Nakahara, K. Shimizu, and J. Osugi, *Rev. Phys. Chem. Japan*, **40**, 12 (1970).
14) E. Inada, K. Shimizu, and J. Osugi, *Nippon Kagaku Zasshi*, **92**, 1096 (1971).
15) M. Ueno, K. Shimizu, and J. Osugi, *Rev. Phys. Chem., Japan*, **43**, 33 (1973).
16) S. D. Hamann, "Modern Aspects of Electro-Chemistry," Vol. 9, ed. by B. E. Conway and J. O. M. Bockris, Plenum, New York-London (1974), p. 47.
17) K. Suzuki, Y. Taniguchi, and T. Watanabe, *J. Phys. Chem.*, **77**, 1918 (1973).
18) Osugi *et al.*[13-15] already reported that Kohlrausch plots were satisfied in the concentration range 5×10^{-4} M to 1×10^{-3} M under pressure.
19) W. G. Davies, R. J. Otter, and J. E. Prue, *Discuss. Faraday Soc.*, **24**, 103 (1957).
20) B. B. Owen and S. R. Brinkley, *Phys. Rev.*, **64**, 32 (1943).
21) J. B. Cappi, Ph. D. Thesis, London University, 1964; K. E. Bett and J. B. Cappi, *Nature*, **207**, 620 (1965).
22) The values of m is given approximately in dilute solution by dividing c at 1 atm by the density ρ[23] of water at the given temperature and pressure.
23) P. W. Bridgman, *Proc. Amer. Acad. Arts Sci.*, **47**, 441 (1912).
24) B. B. Owen and R. W. Gurry, *J. Amer. Chem. Soc.*, **60**, 3074 (1938).
25) A. Patterson jun and H. Freitag, *J. Electrochem. Soc.*, **108**, 529 (1961).
26) T. O. Denney and C. B. Monk, *Trans. Faraday Soc.*, **47**, 992 (1951).
27) R. M. Izatt, D. Eatough, J. J. Christensen, and C. H. Bartholomew, *J. Chem. Soc., A*, **1969**, 48.
28) C. W. Davies, *ibid.*, 2093 (1938).
29) G. Tammann and A. Rohmann, *Z. Anorg. Allg. Chem.*, **183**, 1 (1929).
30) S. D. Hamann, *J. Phys. Chem.*, **67**, 2233 (1963).
31) J. Buchanan and S. D. Hamann, *Trans. Faraday Soc.*, **49**, 1425 (1953).
32) H. S. Harned and B. B. Owen, "The Physical Chemistry of Electrolyte Solutions," Reinhold, New York, N. Y. (1957), p. 170.
33) L. Pauling, "The Nature of the Chemical Bond," Cornell Univ. Press (1960).
34) S. Claesson, B. Lundgren, and M. Szware, *Trans. Faraday Soc.*, **66**, 3053 (1970).
35) T. R. Griffiths and M. C. R. Symons, *Mol. Phys.*, **3**, 90 (1960).
36) R. L. Kay and D. F. Evans, *J. Phys. Chem.*, **70**, 2325 (1966).
37) R. A. Hone, *Nature*, **200**, 418 (1963); "Advances in High Pressure Research," Vol. 2, ed. by R. S. Bradley, Academic Press, New York, N. Y. (1969), p. 169.
38) M. Nakahara, K. Shimizu, and J. Osugi, *Rev. Phys. Chem. Japan*, **42**, 12 (1972).

CNDO/2 Difference Electron Density Contours in Saturated Three-membered Rings

Tetsuzo Ito

The Institute of Physical and Chemical Research, Wako-shi, Saitama 351

(Received April 19, 1975)

Theoretical difference electron density contours in the NCC, CCC, and OCC ring planes of ethyleneimine quinone, *cis*-1,2,3-tricyanocyclopropane and tetracyanoethylene oxide molecules, respectively, were calculated by the CNDO/2 molecular orbital method. They are qualitatively in good agreement with the experimental contours, and have reproduced the most characteristic features of the observed electron distributions in the bent bonds in the three-membered rings. The theoretical difference contours in the three-membered ring planes of aziridine, cyclopropane and oxirane molecules have shown essentially the same bonding electron distributions as the corresponding contours in the more complex molecules mentioned above.

The saturated CCC, NCC, and OCC three-membered rings are typical examples of highly strained structures. Coulson and Moffitt[1] have shown the bent bond nature in cyclopropane by a valence bond treatment of the molecule. Several diffraction studies of electron distributions have also revealed the bent bonds in these three-membered rings: the CCC rings in 2,5-dimethyl-7,7-dicyanonorcaradiene[2] and in *cis*-1,2,3-tricyanocyclopropane,[3] the OCC ring in tetracyanoethylene oxide,[4] and the NCC ring in ethyleneimine quinone.[5]

Although various kinds of molecular orbital calculations have recently been reported on these three-membered ring systems,[6] the results are not given in a form suitable for comparison with diffraction observations. In the present work, therefore, appropriate difference electron density contours were calculated by the semi-empirical CNDO/2 molecular orbital method,[7] and compared with the experimental contours.[3-5]

Theoretical Model

Let us first summarize the definition of the X-ray difference electron density. It is usually defined as:

$$\overline{\Delta\rho}_o(\boldsymbol{r}) = \bar{\rho}_{cryst}(\boldsymbol{r}) - \sum_j^{atoms} \bar{\rho}_j(\boldsymbol{r}), \quad (1)$$

where $\bar{\rho}_{cryst}$ is the observed electron density in the crystal; the second term is the calculated electron density of the "free atoms model", in which the atoms (or the ions) in the unit cell of the crystal are assumed to be free atoms (or free ions) with spherical electron distributions ρ_j, and be placed at the same positions as they occupy in the crystal. The bars on the ρ's indicate the time-average over thermal vibration.

In practice, however, $\overline{\Delta\rho}_o$ is obtained by Fourier summation of the differences between the observed and calculated structure factors, F_o—F_c, over lattice planes:

$$\overline{\Delta\rho}_o(\boldsymbol{r}) = (1/V)\sum_h\sum_k\sum_l [F_o(hkl) - F_c(hkl)] \times \exp[-2\pi i \boldsymbol{S}_{hkl}\cdot\boldsymbol{r}], \quad (2)$$

where V is the unit cell volume of the crystal, and $\boldsymbol{S}_{hkl}$ is the scattering vector of a plane, *hkl*. F_c is the Fourier transform of the second term in Eq. (1); it can be calculated by:

$$F_c(hkl) = \sum_j^{atoms} f_j T_j \exp 2\pi i \boldsymbol{S}_{hkl}\cdot\boldsymbol{r}_j, \quad (3)$$

where f_j is the theoretical free atom scattering factor of the j-th atom in the unit cell, whereas the nuclear position $\boldsymbol{r}_j$ and the thermal vibration factor T_j can be obtained from crystal structure analysis. The X-ray difference density defined by Eqs. (1)—(3) is called the difference Fourier synthesis or the D-synthesis.

A theoretical difference electron density can be defined in analogy with Eq. (1) as follows:

$$\Delta\rho_c(\boldsymbol{r}) = \rho_{mol}(\boldsymbol{r}) - \sum_j^{atoms} \rho_j(\boldsymbol{r}), \quad (4)$$

where ρ_{mol} is the theoretical electron density of a free molecule; the second term represents again the "free atoms model", the summation extending over the atoms which constitute the molecule. The theoretical difference density of Eq. (4) was originally introduced by Roux and coworkers.[8] For a molecule in a closed shell electron configuration, the molecular electron density can be expressed as:

$$\rho_{mol}(\boldsymbol{r}) = 2\sum_i^{occ} \psi_i^2(\boldsymbol{r}), \quad (5)$$

where ψ_i is the i-th molecular orbital, and the summation is taken over the molecular orbitals occupied with pairs of electrons.

In the CNDO/2 approximation,[7] molecular orbitals are obtained as linear combinations, with coefficients $\boldsymbol{C}_o$, of the orthogonalized atomic orbitals of the valence shells. Therefore, deformation of the 1s core electrons by molecule formation is ignored in the present model. Eq. (5) can be evaluated in a straightforward way by transforming the coefficients $\boldsymbol{C}_o$ to the coefficients $\boldsymbol{C}_s$ for the Slater type atomic orbitals by the Löwdin transformation $\boldsymbol{C}_s = \boldsymbol{S}^{-1/2}\ \boldsymbol{C}_o$.[9] The electron density of a spherical free atom, ρ_j in Eq. (4), can be represented by a single valence s atomic orbital $\chi_{s,j}$:

$$\rho_j(\boldsymbol{r}) = N_j \chi_{s,j}^2(\boldsymbol{r}), \quad (6)$$

where N_j is the number of the valence electrons of the j-th neutral free atom; N_j is 1, 4, 5, and 6 for H, C, N, and O atoms, respectively. Eq. (6) is consistent with the CNDO/2 scheme in which the 2s and 2p atomic orbitals of an atom are given the same Slater exponent; in this case, spherically averaged density distribution of a 2p electron is identical with the density distribution of a 2s electron. The theoretical difference density defined by Eqs. (4)—(6) may be called the "molecule—free atoms" density.

It is evident from the definitions that both the experi-

mental and theoretical difference densities represent the deviations of the densities in a crystal or in a molecule from those of the "free atoms model". Although both densities represent approximately the same physical quantity, the following two factors distinguish between the two. (a) The effect of thermal vibration (the thermal smearing of the electron density) is not taken into account in $\Delta\rho_c$, whereas $\overline{\Delta\rho}_o$ is inevitably influenced by thermal vibration. The effect will be examined in future studies. (b) The effect of the crystal field (the intermolecular interaction) is ignored in the calculation of ρ_{mol}. The effect is considered to be generally small compared with that of chemical bonding, but strong interactions such as hydrogen bonding may not be ignored.

Results and Discussion

The theoretical difference electron density contours in the NCC, CCC, and OCC ring planes of ethyleneimine quinone, *cis*-1,2,3-tricyanocyclopropane and tetracyanoethylene oxide molecules, respectively, were calculated by Eqs. (4)—(6), and compared with the experimental contours.[3-5] The molecular geometries found in the crystal[3-5] were used for the CNDO/2 calculations.

Ethyleneimine Quinone. The electron density in ethyleneimine quinone, 2,5-di(1-aziridinyl)-*p*-benzoquinone, $C_6H_2O_2(NC_2H_4)_2$, was studied by X-ray at 110 K.[5] The two aziridinyl groups are equivalent in the crystal because the molecule lies on an inversion center.

The CNDO/2 calculations[7] were performed for the whole molecule with 72 valence electrons. The "molecule–free atoms" map in the NCC ring plane (Fig. 1) may be compared with the X-ray contours (Fig. 2).

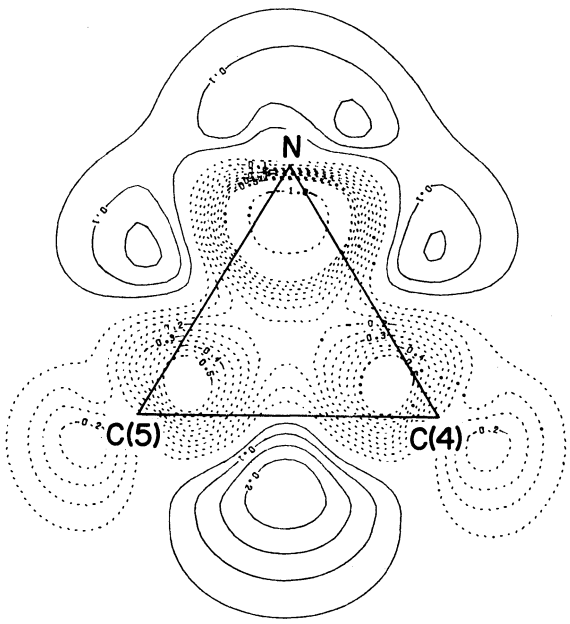

Fig. 1. Theoretical difference electron density contours, the "molecule—free atoms" map, in the NCC ring plane of ethyleneimine quinone.
Negative contours are dotted and zero contours are omitted. The contours are at intervals of 0.05 above −0.5, and 0.5 below −0.5 e.Å^{-3}.

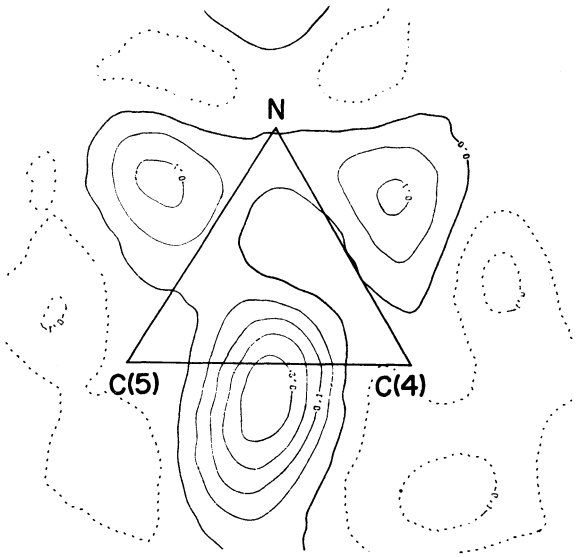

Fig. 2. X-Ray difference Fourier map in the NCC ring plane of ethyleneimine quinone.[5]
Negative contours are dotted. The contours are at intervals of 0.05 e.Å^{-3}.

The two maps are qualitatively in good agreement in the internuclear regions where both the theoretical and experimental densities are less influenced by systematic errors (see below). Both maps clearly illustrate characteristic features of the bent bond; bonding electron peaks of about 0.1 and 0.2 e.Å^{-3} are observed in the N–C and C–C bonds respectively, but displaced outside of the NCC triangle. The broad peak at the back of the nitrogen atom in the theoretical map is a tail-off of the nitrogen lone pair electrons.

The sharp depressions near the nuclear positions in the theoretical map are absent in the X-ray map. The following systematic errors in $\overline{\Delta\rho}_o$ and $\Delta\rho_c$ may account for the discrepancies: (a) The atomic parameters (the nuclear positions $\boldsymbol{r}_j$ and the thermal parameters T_j) determined by the X-ray structure analysis may be systematically in error. In fact, they were so determined as to give the best fit between the observed and calculated structure factors, that is, to minimize $\overline{\Delta\rho}_o$ in Eq. (2). Therefore, any aspherical features of electron distributions around the nuclear positions which could be fitted by the expression Eq. (3) were absorbed into apparent changes of atomic parameters, especially into those of anisotropic thermal parameters. In this respect, determination of the atomic parameters by neutron diffraction is preferable.[10] (b) Thermal vibration which will considerably smear out the sharp depressions is not taken into account in the present theoretical model. (c) The CNDO/2 electron density near the nuclear position may be a poor approximation to the true density.

cis-1,2,3-Tricyanocyclopropane. The electron density in *cis*-1,2,3-tricyanocyclopropane, $(CHCN)_3$, was studied by Hartman and Hirshfeld[3] by X-ray at room temperature. The molecule lies on a three-fold symmetry axis through the center of the ring in the crystal. Bonding electron peaks of 0.05 e.Å^{-3} have been observed in the C–C bonds, 0.32 Å outside of the CCC triangle.[3]

The molecule has 42 valence electrons. The "mole-

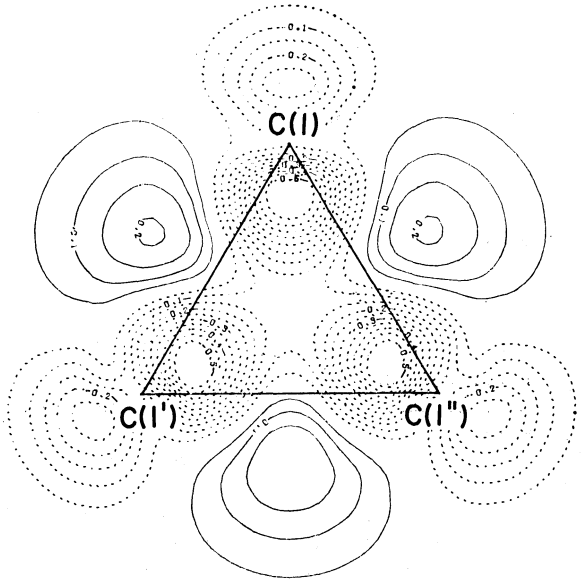

Fig. 3. The "molecule—free atoms" map in the CCC ring plane of *cis*-1,2,3-tricyanocyclopropane. The scale is the same as in Fig. 1.

cule—free atoms" map in the ring plane is shown in Fig. 3. The distribution of the bonding electrons is in qualitative agreement with the X-ray observations.[3] However, the theoretical peak heights of 0.15 e.Å^{-3} are three times higher than the experimental ones.

Tetracyanoethylene Oxide. The electron density in tetracyanoethylene oxide, $OC_2(CN)_4$, was studied by Matthews and Stucky[4] by a combined use of X-ray and neutron diffraction at room temperature. In this case, the electron density of the "free atoms model" in Eqs. (1)—(3) was calculated with the atomic parameters determined by neutron diffraction; a difference electron density map obtained with X-ray F_o and neutron F_c is called an X—N map.[10] The X—N map in the OCC ring plane of the molecule has revealed a bonding peak

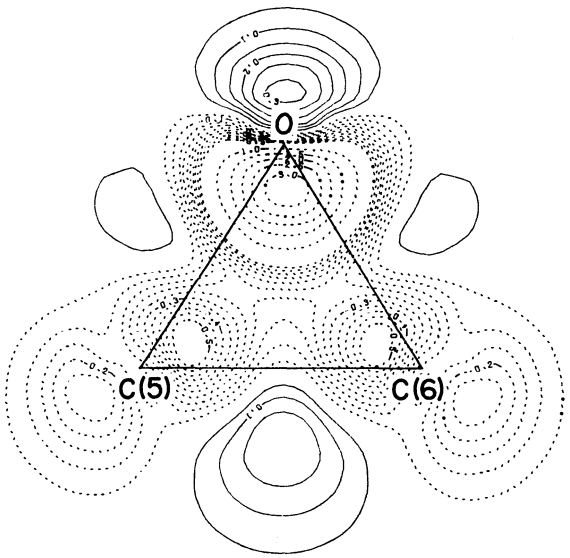

Fig. 4. The "molecule—free atoms" map in the OCC ring plane of tetracyanoethylene oxide. The scale is the same as in Fig. 1.

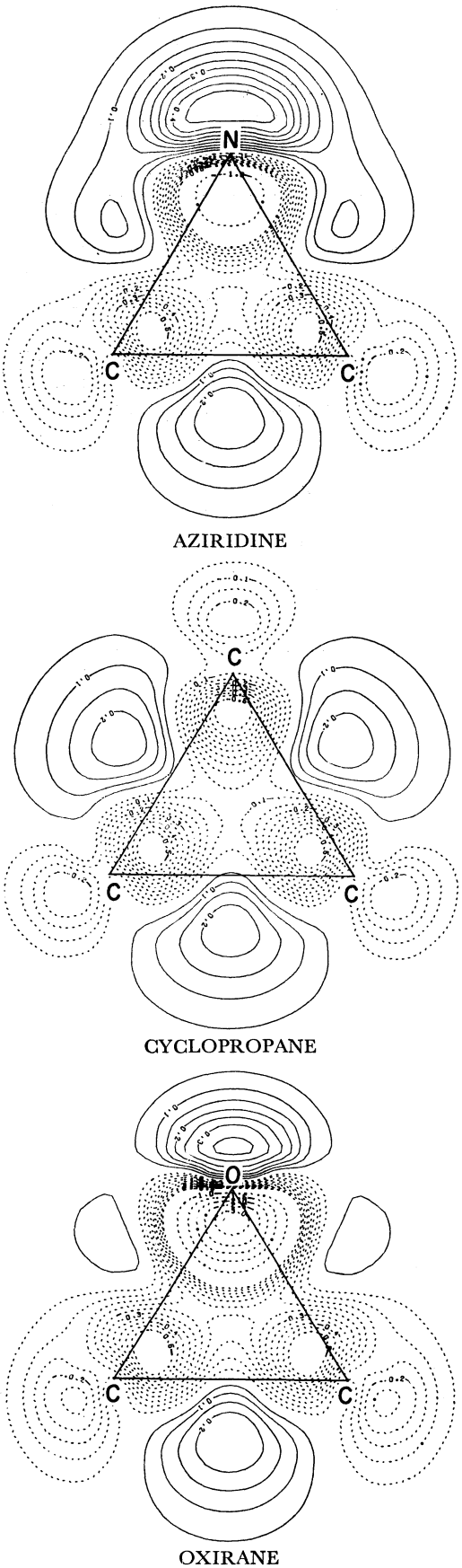

Fig. 5. The "molecule—free atoms" maps in the three-membered ring planes of aziridine, cyclopropane and oxirane. The scale is the same as in Fig. 1.

of 0.45 e.Å^{-3} in the C–C bent bond region, but the bend in the C–O bonds has been obscured by the tail-off of the broad peak of 0.35 e.Å^{-3} at the center of the ring.[4]

The molecule has 50 valence electrons. The "molecule—free atoms" map in the ring plane is shown in Fig. 4. The positive peak in the C–C bent bond is much higher than those in the C–O bonds, qualitatively in agreement with the experimental observations. Quantitatively, however, the theoretical peak heights are about three times lower than the experimental ones. The experimentally observed electron build-up at the center of the ring is not reproduced in the theoretical map.

It should be noted that in this case of tetracyanoethylene oxide, in which the experimental difference density was obtained with the neutron atomic parameters, the sharp depressions near the nuclear positions in the theoretical map are in qualitative agreement with the experimental observations.[4]

Related Molecules. The "molecule—free atoms" maps in the ring planes of aziridine, $NH(CH_2)_2$, cyclopropane, $(CH_2)_3$ and oxirane, $O(CH_2)_2$ molecules were also calculated (Fig. 5). The molecular geometries used were taken from the literature.[11] The electron distributions in the bent bond regions are essentially the same as those obtained for ethyleneimine quinone, *cis*-1,2,3-tricyanocyclopropane and tetracyanoethylene oxide, respectively.

The numerical calculations were performed on the FACOM 230—75 computer of this Institute. The author wishes to thank Dr. Tsunetoshi Kobayashi of the University of Tokyo for his valuable advice in performing the CNDO/2 calculations.

References

1) C. A. Coulson and W. E. Moffitt, *Phil. Mag.*, **40**, 1 (1949).
2) C. J. Fritchie, *Acta Crystallogr.*, **20**, 27 (1966).
3) A. Hartman and F. L. Hirshfeld, *ibid.*, **20**, 80 (1966).
4) D. A. Matthews and G. D. Stucky, *J. Amer. Chem. Soc.*, **93**, 5954 (1971).
5) T. Ito and T. Sakurai, *Acta Crystallogr.*, **B29**, 1594 (1973).
6) For example, C. Ghio and J. Tomasi, *Theoret. Chim. Acta*, **30**, 151 (1973), and the references 4–27 cited therein.
7) J. A. Pople and D. L. Beveridge, "Approximate Molecular Orbital Theory," McGraw-Hill, New York (1970).
8) M. Roux, S. Besnainou and R. Daudel, *J. Chim. Phys.*, **53**, 218 (1956).
9) P. O. Löwdin, *J. Chem. Phys.*, **18**, 365 (1950).
10) P. Coppens, *Acta Crystallogr.*, **B30**, 255 (1974).
11) "Interatomic Distances," ed. by L. E. Sutton, The Chemical Society, London (1958, 1965).

Electron Scavenging by Bromobenzene in the Radiolysis of Heptane, 1-Hexene and Their Mixtures

Masatoshi BABA and Kenji FUEKI

Department of Synthetic Chemistry, Nagoya University, Chikusa-ku, Nagoya 464

(Received April 28, 1975)

A quantitative study has been made of electron scavenging by bromobenzene in the radiolysis of heptane, 1-hexene and their mixtures. Experimental data were analyzed using Schuler's scavenging function. It has been found that the total ion yields are 4—5 G units in these liquids and the value of the reactivity parameter decreases with increasing fraction of 1-hexene. Further analysis of the data was made in terms of the exponential spatial distribution function for the electrons. A discussion is given to physical parameters derived from such analysis.

In recent years considerable efforts have been focussed on reactions of electrons in irradiated liquid hydrocarbons. Chemical and physical methods have both been applied to elucidation of quantitative aspects of electron reactions in liquid hydrocarbons. Most previous studies of electron reactions were concerned with electrons in alkanes.

In the present work we have made a quantitative study of electron scavenging by bromobenzene in the radiolysis of heptane, 1-hexene and their mixtures. We have determined the total ion yields and values of the reactivity parameter from the Schuler plot of experimental data. We have further analyzed the experimental data in terms of the exponential spatial distribution function for the electrons and derived from such analysis some physical parameters that are related to the behavior of electrons in these liquid hydrocarbons. We also include in this paper a comparative study of electron distributions in irradiated cyclohexane and 2,2,4-trimethylpentane.

Experimental

Bromobenzene (Nakarai Kagaku research grade) was distilled and passed through a column of activated alumina. Heptane (Merck spectrograde) was passed through a column of activated silica gel. The purity of heptane was 99.9% and a major impurity was hexane. 1-Hexene (Tokyo Kagaku Seiki standard material, >99% stated purity) was used as received. Impurities in 1-hexene were not identified.

Samples containing the desired amount of bromobenzene were degassed by freeze-pump-thaw cycles and sealed off the vacuum line. The samples were irradiated at 23 °C with ^{60}Co γ-rays for one hour at a dose rate of 3.19×10^{19} eV g^{-1}.hr^{-1}. The dose absorbed in the samples was determined by correction for the appropriate electron density differences. The benzene produced from bromobenzene was measured by a Hitachi K53 gas chromatograph with a flame ionization detector. The column used in the gas chromatograph was 30% hexatriacontane on Celite 545.

Results and Discussion

Yield of Electrons Scavenged by Bromobenzene in Heptane–1-Hexene Solutions. Figure 1 shows plots of the yield of benzene produced *vs.* the concentration of 1-hexene for heptane–1-hexene solutions. In Fig. 1, curves a and b show such plots for the solutions containing 0.238 and 0.0143 M bromobenzene, respectively. It is seen in

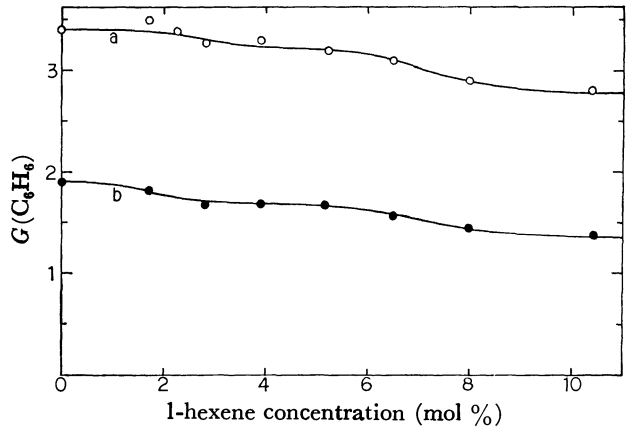

Fig. 1. The yield of benzene *vs.* concentration of 1-hexene in heptane–1-hexene solutions containing (a) 0.238 M and (b) 0.0143 M bromobenzene.

Fig. 1 that the yield of benzene decreases gradually with increasing 1-hexene concentration. It appears that significant decreases in benzene yield are observed around 2 and 7 mol% 1-hexene. The decrease of the benzene yield at 10.5 mol% 1-hexene amounts to 0.6 and 0.5 G units for the solutions containing 0.238 and 0.0143 M bromobenzene, respectively. Further, we have measured the yield of benzene as a function of the bromobenzene concentration for (a) heptane solutions, (b) heptane–1-hexene solutions (5.54 mol% 1-hexene), (c) heptane–1-hexene solutions (10.5 mol% 1-hexene) and (d) 1-hexene solutions. The concentration of bromobenzene was varied from 1.4×10^{-2} to 3.2×10^{-1} M. The data have been treated by assuming the reaction mechanism presented in the previous paper[1] and applying the scavenging function (Eq. (1)) developed by Schuler and his coworkers.[2]

$$\frac{1}{G(C_6H_6)-G_{fi}}=\frac{1}{G_{gi}}+\frac{1}{G_{gi}\alpha^{1/2}S^{1/2}} \qquad (1)$$

where G_{fi} and G_{gi} represent the yields of free and geminate ions, respectively, S is the concentration of bromobenzene, and α is a parameter which represents the reactivity of the electron toward the solute relative to the recombination processes. Figure 2 shows plots of Eq. (1) for four sets of experimental data. These results indicate that the data correspond to the predicted concentration dependence. Since it was difficult to measure the free ion yield by our analytical technique, values of G_{fi} for pure heptane and 1-hexene were taken from Ref.

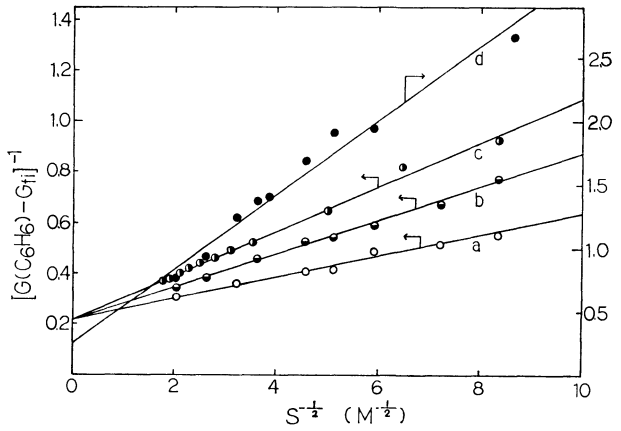

Fig. 2. Plots of $[G(C_6H_6)-G_{fi}]^{-1}$ *vs.* [bromobenzene]$^{-1/2}$ for heptane–1-hexene solutions. a: heptane, b: heptane–5.54 mol% 1-hexene, c: heptane–10.5 mol% 1-hexene, d: 1-hexene.

3, and those for the heptane–1-hexene mixtures were estimated in a manner that will be described later. The geminate ion yield and the total ion yield, G_t, determined from Eq. (1) are given in Table 1 together with the free ion yield used. The values of G_t thus obtained are 4.7—4.8 for pure heptane and heptane–1-hexene mixtures, and 4.0 for pure 1-hexene. The G_t values of 4.7—4.8 are somewhat higher than those obtained for alkanes in the previous work.[1] The G_t value of 4.0 for 1-hexene is based on the data points more scattered than those for the other solvents, and this value of G_t is perhaps a lower limit for the total ion yield in 1-hexene. Values of the reactivity parameter α are also given in Table 1. It is seen in Table 1 that the value of α decreases with increasing fraction of 1-hexene and the α value in 1-hexene is about 1/36 of that in heptane. The significance of this trend in α will be discussed later.

Prior to a further analysis of the present experimental data, we will make a comparative study of spatial distribution functions and scavenging functions for electrons in cyclohexane and 2,2,4-trimethylpentane because such a study should provide a basis for further analyzing our data on the heptane–1-hexene systems.

Table 1. Values of the parameters derived from Schuler's scavenging function

Fraction of 1-hexene (mol %)	G_{fi}	G_{gi}	G_t	α (M^{-1})
0	0.13[a]	4.5_5	4.7	27
5.54	0.12[b]	4.7	4.8	10
10.5	0.12[b]	4.6	4.7	6.3
100	0.062[a]	3.9_5	4.0	0.75

a) Ref. 3. b) See text.

Spatial Distribution and Scavenging Functions for Electrons in Cyclohexane and 2,2,4-Trimethylpentane. Spatial Distributions: First, we attempt to compare the exponential spatial distribution function (Eq. (2))[4] for electrons in cyclohexane and 2,2,4-trimethylpentane with the corresponding spatial distribution function (Eq. (4))[5,6] derived from Schuler's lifetime distribution function[7] by assuming the time-distance relation given by Eq. (3).[8]

$$\left.\begin{aligned}\phi(r) &= 0 && \text{for } r \leq r_0\\ \phi(r) &= (4\pi br^2)^{-1}\exp[(r_0-r)/b] && \text{for } r \geq r_0\end{aligned}\right\} \quad (2)$$

where b is the electron range parameter, r_0 is the reaction radius and r is the ion-electron separation distance.

$$t = r^3/(3Dr_c) \quad (3)$$

Here D is the sum of the diffusion constants of the ion and electron, and r_c is the Onsager distance $r_c=e^2/\varepsilon kT$, where e is the electronic charge, ε is the dielectric constant of a liquid, k is Boltzmann's constant and T is the absolute temperature.

$$\phi_g(r) = \frac{\lambda}{4\pi Dr_c}\left[\left(\frac{3Dr_c}{\pi\lambda r^3}\right)^{1/2} - \exp\left(\frac{\lambda r^3}{3Dr_c}\right)\operatorname{erfc}\left(\frac{\lambda r^3}{3Dr_c}\right)^{1/2}\right] \quad (4)$$

where $\lambda=k/\alpha$ and k is the rate constant for reaction of the electron with a scavenger. Since Eq. (4) is applicable to geminate electrons, it is required for a quantitative comparison between the two distribution functions that the exponential distribution function also be normalized with respect to the geminate electron distribution. Therefore, we have actually used Eq. (5) for comparison instead of Eq. (2).

$$\phi_g(r) = (G_t/G_{gi})[1-\exp(-r_c/r)]\phi(r) \quad (5)$$

The probability of finding the geminate electrons between r and $r+dr$ is given by Eq. (6).

$$\Phi(r)dr = 4\pi r^2\phi_g(r)dr \quad (6)$$

Values of physical parameters used in the calculations are listed in Table 2. Since the diffusion constant of the electron is usually much greater than that of the ion, the diffusion constant D may be approximated by the diffusion constant of the electron, D_e, which is related to the electron mobility μ_e by $D_e=kT\mu_e/e$.

Figures 3 and 4 show the spatial distribution $\Phi(r)$ for the geminate electrons in cyclohexane and 2,2,4-trimethylpentane, respectively. In these figures, curve a represents the exponential distribution function and curve b shows Schuler's distribution function. It is seen in Figs. 3 and 4 that curve a is very close to curve b down to the ion-electron separation distance $r\sim35$ Å for cyclo-

Table 2. Physical parameters used in the calculation of spatial distributions of electrons in cyclohexane and 2,2,4-trimethylpentane

Solvent	r_c (Å)	b (Å)	μ_e ($cm^2\ V^{-1}\ s^{-1}$)	Solute	α (M^{-1})	k ($M^{-1}\ s^{-1}$)
Cyclohexane	279[a]	57.5[b]	0.24[c]	CCl_4	12[e]	2.7×10^{12} [g]
2,2,4-Trimethylpentane	291[a]	96.1[b]	7[d]	C_2H_5Br	5[f]	6.3×10^{12} [c]

a) Ref. 3. b) Ref. 1. c) Ref. 14. d) Ref. 16. e) Ref. 17. f) Ref. 18. g) Ref. 19.

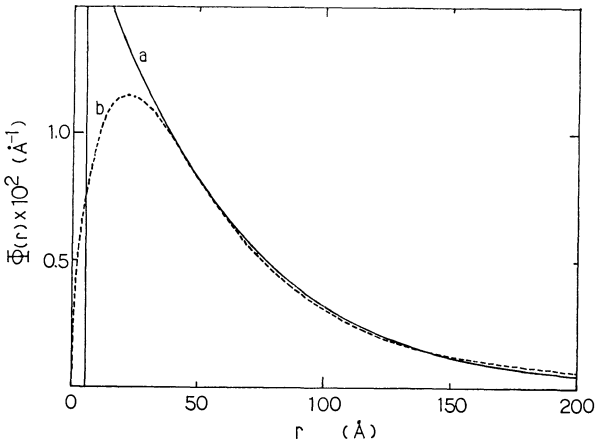

Fig. 3. Spatial distributions of electrons in cyclohexane. a: exponential function (r_0=5 Å), b: Schuler's function. See Table 2 for parameters used in the calculations.

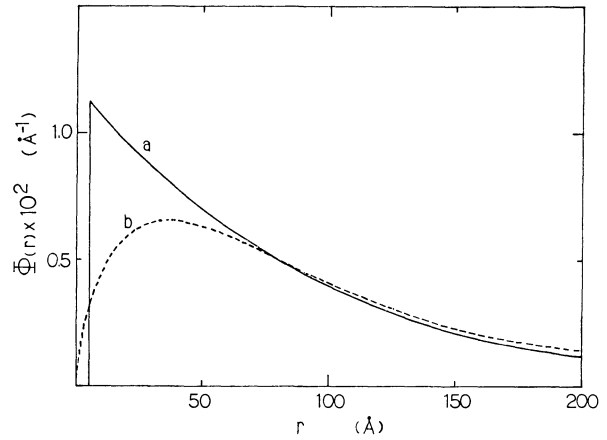

Fig. 4. Spatial distributions of electrons in 2,2,4-trimethylpentane. a: exponential function (r_0=5 Å), b: Schuler's function. See Table 2 for parameters used in the calculations.

hexane and $r\sim60$ Å for 2,2,4-trimethylpentane. Experimentally, quantitative kinetic studies of electron scavenging in liquid hydrocarbons are usually made at solute concentrations less than 0.5 M. It can be shown that most of the electrons scavengeable in scavenging experiments are distant from their parent ions farther than the distances mentioned above.[9] Thus, it is expected that the exponential distribution function would be able to account for experimental results on electron scavenging in liquid hydrocarbons. This also implies that the choice of the reaction radius is practically a trivial problem. It should be stressed that the exponential distribution function has the advantage that the range parameter b can be readily determined from the free ion yield by Eq. (7).

$$\int_0^\infty \phi(r) \exp(-r_c/r) 4\pi r^2 dr = G_{fi}/G_t \tag{7}$$

A calculation is described below on the concentration dependence of electron scavenging in cyclohexane and 2,2,4-trimethylpentane.

Scavenging Functions: It has been shown by Hummel[10] that the recombination probability $P_{q,r}$ of an ion-electron pair separated by r in the presence of scavenger is given by Eq. (8).

$$P_{q,r} = \frac{2\exp(-qr)[1-\exp(-r_c/r)]}{1+\exp(-2qr)+2qr^2r_c^{-1}[1-\exp(-r_c/r)]} \tag{8}$$

where $q=(kS/D)^{1/2}$ and S is the concentration of scavenger. The yield of electrons scavenged, $G(e_{sc}^-)$, in the presence of scavenger is given by Eq. (9).

$$G(e_{sc}^-) = G_t\int_0^\infty \phi(r)(1-P_{q,r})4\pi r^2 dr \tag{9}$$

Empirically, the concentration dependence of the yield of electrons scavenged by a scavenger in liquid hydrocarbons can be well described by Schuler's scavenging function (Eq. (10)).[2]

$$G(e_{sc}^-) = G_{fi} + G_{gi}\{(\alpha S)^{1/2}/[1+(\alpha S)^{1/2}]\} \tag{10}$$

Figures 5 and 6 show the concentration dependence of the yields of electrons scavenged by carbon tetrachloride in cyclohexane and by ethyl bromide in 2,2,4-trimethyl-

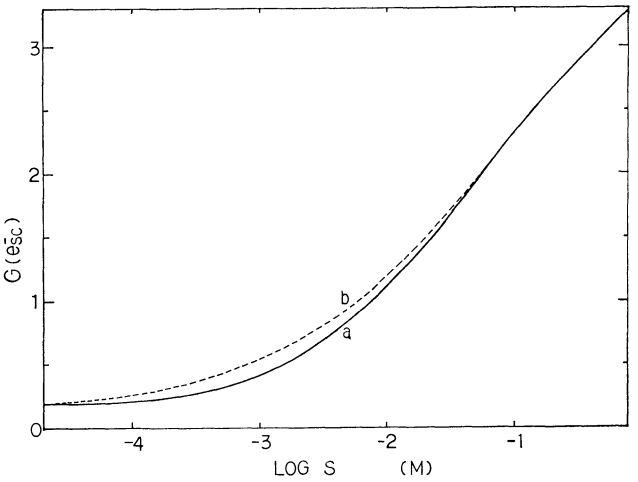

Fig. 5. The calculated concentration dependence of the yield of electrons scavenged by carbon tetrachloride in cyclohexane. a: calculated from Eq. (9) using the exponential distribution function, b: calculated from Schuler's scavenging function (Eq. (10)).

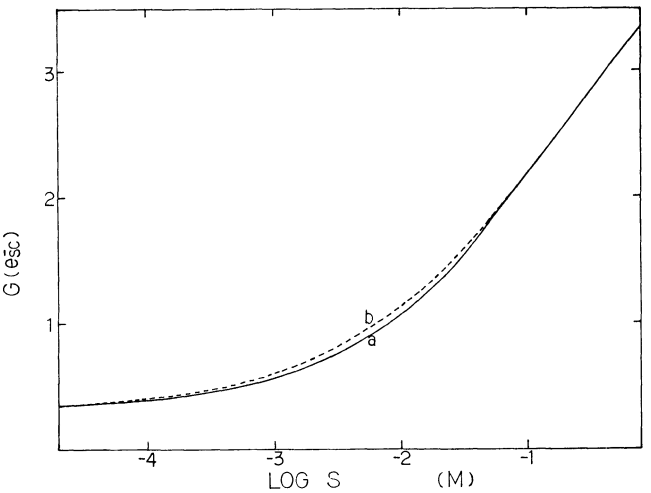

Fig. 6. The calculated concentration dependence of the yield of electrons scavenged by ethyl bromide in 2,2,4-trimethylpentane. a: calculated from Eq. (9) using the exponential distribution function, b: calculated from Schuler's scavenging function (Eq. (10)).

pentane, respectively. In these figures, curve a was calculated from Eq. (9) using the exponential distribution function for $\phi(r)$ and curve b was obtained from Eq. (10). It is seen in Figs. 5 and 6 that the shape of curve a is similar to that of curve b over the entire range of the scavenger concentration studied. Although there is some discrepancy between curves a and b around $S\sim10^{-3}$M for cyclohexane, the experimental data points lie between the two curves in this concentration region.[7] Thus, we have been able to demonstrate that the exponential distribution function can well account for the concentration dependence of electron scavenging in liquid hydrocarbons and that this is due to the fact that the exponential distribution function is similar in its significant portion to Schuler's distribution function.

Analysis of Experimental Data on Electron Scavenging by Bromobenzene in Heptane, 1-Hexene and Their Mixtures. In this section, we will describe the procedure to evaluate physical parameters of the hydrocarbon mixtures, analyze using the exponential distribution function the concentration dependence of the yield of electrons scavenged by bromobenzene in heptane, 1-hexene and their mixtures, and discuss the significance of physical parameters derived from such analysis.

Physical Parameters of Heptane-1-Hexene Mixtures: The electron range b of a mixture is given by Eq. (11).[11]

$$(bd)^{-2} = x_1(b_1d_1)^{-2} + x_2(b_2d_2)^{-2} \qquad (11)$$

Here the density d of the mixture is obtained as $d=x_1d_1+x_2d_2$, where d_1 and d_2 are the densities of the mixture components, and x_1 and x_2 are their mole fractions. The free ion yield in a mixture can be determined from Eq. (7) using b in Eq. (11). The free ion yields thus obtained are given for the heptane–1-hexene mixtures in Table 1. The dielectric constant ε of a mixture can be calculated from the Clausius-Mosotti equation (Eq. (12)).

$$\varepsilon = [1+(8\pi\bar{\alpha}n/3)]/[1-(4\pi\bar{\alpha}n/3)] \qquad (12)$$

Here the isotropic polarizability $\bar{\alpha}$ of the mixture is given by $\bar{\alpha}=x_1\bar{\alpha}_1+x_2\bar{\alpha}_2$, where $\bar{\alpha}_1$ and $\bar{\alpha}_2$ are the isotropic polarizabilities of the mixture components, and the number density n of molecules in the mixture is given by $n^{-1}=x_1n_1^{-1}+x_2n_2^{-1}$.[12]

Comparison between the Calculated and Observed Yields of Electrons Scavenged: Using Eqs. (7), (8), and (9) we have calculated the yields of electrons scavenged by bromobenzene in heptane, 1-hexene and their mixtures. Figure 7 shows the calculated and observed yields of electrons scavenged plotted against the concentration of bromobenzene. It is seen in Fig. 7 that the calculated curves agree well with the experimental data within experimental error. The parameters used in the calculations are b, k, and D. The electron range b was obtained from the free ion yield as already mentioned. The rate constant k for reaction of the electron with a scavenger and the diffusion constant D appear only as the ratio of k/D in Eq. (8). Accordingly, k/D is the only adjustable parameter in the calculations. The curves shown in Fig. 7 were calculated with the properly chosen values of k/D by best fitting them to the experimental data. The values of k/D thus obtained are given in Table 3. Knowing the value of D or the electron mobility, we can get the value of k. Unfortunately, values of D are not known for electrons in our systems, so we are unable to determine values of k. The relative values of k/D are also given in Table 3 as $(k/D)_N/(k/D)_1$, where $(k/D)_1$ stands for heptane. It is seen in Table 3 that the relative value of k/D decreases with increasing fraction of 1-hexene. If the reaction of the electron with bromobenzene in these liquid hydrocarbons is diffusion-controlled, *i.e.*, k is directly proportional to D, the relative value of k/D should be unity for all the hydrocarbons studied. It is not the case for our systems. This result indicates that electron scavenging by bromobenzene in these hydrocarbons is not a diffusion-controlled reaction. For comparison we have also calculated the relative value of k/D using the time-distance relationship derived from the Nernst-Einstein relation. In this approximation, Eq. (13) holds.[13]

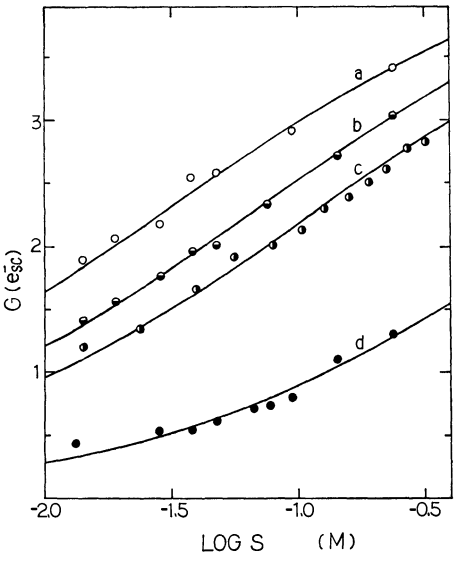

Fig. 7. The calculated and observed yields of electrons scavenged *vs.* concentration of bromobenzene in heptane–1-hexene solutions. a: heptane, b: heptane–5.54 mol% 1-hexene, c: heptane–10.5 mol% 1-hexene, d: 1-hexene. Curves show the calculated yields.

$$k/D = 3\alpha r_c/b^3 \qquad (13)$$

From Eq. (13) we can calculate k/D with known values of α, r_c and b. The relative values of k/D thus obtained are given in the last column of Table 3. It can be seen from Table 3 that these relative values of k/D are in good agreement with those derived from the theoretical scavenging function. Such an agreement implies that the effect of Brownian motion on the behavior of electrons in the Coulomb field is rather small for the electrons scavengeable at the scavenger concentrations studied.

It has recently been shown[14] that the rate constant k for reaction of the electron with a scavenger in different hydrocarbon solvents is, in some cases, proportional to the square root of the electron mobility μ_e in the corresponding solvents. If we assume that this relation between k and μ_e holds for our systems, we can calculate the relative value of μ_e from that of k/D. The relative values of μ_e thus calculated are given in Table 3 as μ_N/μ_1, where μ_1 stands for heptane. It is seen in Table 3 that

Table 3. Some physical parameters derived for electrons in heptane, 1-hexene and their mixtures

Fraction of 1-hexene (mol %)	k/D[a] ($10^{14}M^{-1}$ cm^{-2})	N	$\frac{(k/D)_N}{(k/D)_1}$[a]	μ_N/μ_1[b]	$\frac{(k/D)_N}{(k/D)_1}$[c]
0	2.3	1	1	1	1
5.54	1.1	2	0.47	4.5	0.41
10.5	0.67	3	0.29	12	0.27
100	0.20	4	0.087	130	0.082

a) Determined from the best fit of the calculated scavenging curve to the experimental data. b) Based on the assumption that k is proportional to $\mu_e^{1/2}$. c) Calculated using the Nernst-Einstein relation.

the value of μ_N/μ_1 increases with increasing fraction of 1-hexene, and the electron mobility in 1-hexene is two orders of magnitude greater than that in heptane. If we assume that the electron mobility in heptane is 0.06 $cm^2\ V^{-1}\ s^{-1}$ based on the electron mobility in hexane (0.09,[16] 0.07,[20] 0.08[14] $cm^2\ V^{-1}\ s^{-1}$), we obtain $\mu_e=$ 7.8 $cm^2\ V^{-1}\ s^{-1}$ for electrons in 1-hexene, which is of the same order of magnitude as the electron mobilities in 2-methylpropene (1.44 $cm^2\ V^{-1}\ s^{-1}$),[21] *cis*-2-butene (2.2 $cm^2\ V^{-1}\ s^{-1}$),[21] 2-methyl-2-butene (3.6 $cm^2\ V^{-1}\ s^{-1}$)[20] and 2,3-dimethyl-2-butene (5.8 $cm^2\ V^{-1}\ s^{-1}$).[21] It is possible, however, that the value of μ_e thus derived for electrons in 1-hexene is somewhat overestimated, since the reactivity parameter α is rather sensitive to the experimental data on electron scavenging.

References

1) M. Tanaka and K. Fueki, *J. Phys. Chem.*, **77**, 2524 (1973).
2) J. M. Warman, K.-D. Asmus, and R. H. Schuler, *ibid.*, **73**, 931 (1969).
3) W. F. Schmidt and A. O. Allen, *ibid.*, **72**, 3730 (1968).
4) G. C. Abell and K. Funabashi, *J. Chem. Phys.*, **58**, 1079 (1973).
5) S. Sato and T. Oka, This Bulletin, **44**, 856 (1971).
6) M. Tachiya, *J. Chem. Phys.*, **56**, 4377 (1972).
7) R. H. Schuler and P. P. Infelta, *J. Phys. Chem.*, **76**, 3812 (1972).
8) F. Williams, *J. Amer. Chem. Soc.*, **86**, 3954 (1964).
9) M. Baba and K. Fueki, unpublished results.
10) A. Hummel, *J. Chem. Phys.*, **48**, 3268 (1968).
11) W. F. Schmidt and A. O. Allen, *ibid.*, **52**, 2345 (1970).
12) R. G. Brown and H. T. Davis, *Chem. Phys. Lett.*, **27**, 78 (1974).
13) J. M. Warman and S. J. Rzad, *J. Chem. Phys.*, **52**, 485 (1970).
14) A. O. Allen and R. A. Holroyd, *J. Phys. Chem.*, **78**, 796 (1974).
15) R. M. Minday, L. D. Schmidt, and H. T. Davis, *ibid.*, **76**, 442 (1972).
16) W. F. Schmidt and A. O. Allen, *J. Chem. Phys.*, **52**, 4788 (1970).
17) G. W. Klein and R. H. Schuler, *J. Phys. Chem.*, **77**, 978 (1973).
18) S. J. Rzad and K. M. Bansal, *ibid.*, **76**, 2374 (1972).
19) A. O. Allen, T. E. Gangwer, and R. A. Holroyd, *ibid.*, **79**, 25 (1975).
20) R. M. Minday, L. D. Schmidt, and H. T. Davis, *J. Chem. Phys.*, **54**, 3112 (1971).
21) J.-P. Dodelet, K. Shinsaka, and G. R. Freeman, *ibid.*, **59**, 1293 (1973).

Kinetic Analysis of the Transitory Overshooting of the H^+ Concentration in the Cation-exchange Membrane System

Noriaki TAKEGUCHI, Isamu HORIKOSHI, and Shigeo TANAKA
Faculty of Pharmaceutical Sciences, University of Toyama, Gofuku, Toyama 930
(Received May 6, 1975)

Overshooting with respect to the H^+ concentration was studied quantitatively. Systems of two species of cation and one species of anion were studied for example, the 0.2 M-NaCl (initial, s-side): Collodion-Polystyrene sulfonic acid membrane: 0.02 M-NaCl+0.002 M-HCl (l-side, constant). The volume of the l-side solution was greatly larger than that of the s-side solution. The composition of the former was not altered measurably by the transport of ions across the membrane. Because the cation-exchange membrane used was not highly selective, both cation and anion were permeable. The final composition of the s-side solution became equal to the composition of the l-side solution. In the course of changes toward the final equilibrium, the H^+ or HCl concentration temporarily reached far above the final value. An analytical interpretation with two parameters was given, in which the concentration of the most slowly movable ion in the membrane, Cl^-, was assumed to decrease monotonously. Moreover, the concentration of next slowly movable ion, Na^+, was assumed to change as a result of the force which tends to bring the system toward the imaginary Donnan equilibrium. The Na^+ concentration at the imaginary Donnan equilibrium toward which the s-side solution is approaching at any given instant was obtained as follows. The (H^+ concentration)/(Na^+ concentration) ratio at the equilibrium is the same as the corresponding ratio in the l-side. Moreover, the total concentration of H^+ and Na^+ at the imaginary Donnan equilibrium is equal to the existing Cl^- concentration in the s-side solution.

Teorell[1] investigated the transport of ions against their concentration difference between two solutions across a cation-exchange membrane separating these solutions under the simultaneous influence of a concentration gradient and a potential gradient within the membrane. The ions are transported against their concentration difference between outside solutions, but they move in the direction of their electrochemical potential difference. Woermann[2] reinvestigated the Teorell model quantitatively at a steady state.

Neihof and Sollner[3] and Sollner[4] presented electrochemical models which might have potential biological significance in explaining the abilities of living cells. These abilities are: (1) to accumulate electrolytes in their sap up to concentrations far in excess of the surrounding milieu and (2) to take up different species of the same charge in ratios which are vastly different from the ratio in which these ions are present in the surrounding milieu. The Sollner models are based on the transitory effects called the "overshooting" and "depletion" effects. The transitory effects arise in the course of the spontaneous drift toward the Donnan membrane equilibrium of systems in which two or more species of ions of the same charge, coexisting in one solution, exchange at greatly different rates across a membrane of a high anionic or high cationic selectivity against some other species of ions in the other solution. They assumed the existence of a partial membrane equilibrium in which the permeability of the most slowly movable ion was taken to be negligibly small until the system had attained the maximum drift. From the partial membrane equilibrium, they estimated the maximum drift of the effect. Their experimental values of the maximum drifts from the final equilibria were about 90% of the estimated values. In the Sollner model, the membrane of a high anionic or high cationic selectivity was used. That is, only cationic or anionic species of ions are permeable across the cationic or anionic membrane respectively.

It seemed that it would be interesting to extend the Sollner model to a more general membrane model in which a membrane is not perfectly ionic-selective, that is, in which it is permeable to both cation and anion. This makes it possible to apply the overshooting effect to such leaky (low-electrical-resistance) membranes as gastric mucosa and the collecting tubule in the kidney. In this paper we will report on the overshooting with respect to the H^+ concentration in systems which have two species of cation and one species of anion, using membranes which do not have perfect cationic selectivity.

Another point we wish to report on here is a quantitative analysis of the overshooting effect. As has been described above, Neihof and Sollner[3] estimated only the value of the maximum drift. We will formulate the full-time course of the H^+ overshooting effect, using a kinetic theory together with the imaginary Donnan equilibrium, to which the system tends to approach.

Description of Systems

The isothermal systems studied in this paper are composed of three compartments; one is the membrane phase that separates the other two compartments of ionic solutions. We shall call these two solutions the s-side and the l-side solutions hereafter. We assumed that the changes in the concentrations of the ionic species in the l-side solution were negligibly small during the experiment. This assumption was made possible by taking the volume of the l-side solution as extremely large compared with that of the s-side solution. For the H^+ overshooting effect, the following system was studied. The s-side solution included only NaCl at the initial state (its initial concentration, c_i). The l-side solution included NaCl (c_1) and HCl (c_2), where $c_i > (c_1+c_2)$. In the system, the H^+ concentration is equal to the HCl concentration because the system has only one species of anion, Cl^-. The ionic selectivity of the

cation-exchange membrane used here was not too high, so the anionic species of ion could also permeate slowly across the membrane. The permeation velocity of Cl^- was very slow compared with the fast permeations of the cations, however. When the test-tube-shaped membrane, which has the s-side solution inside, was immersed in the l-side solution, the H^+ concentration in the s-side solution began to increase rapidly as a result of interdiffusions. In due time, the H^+ concentration reached a maximum that far exceeded the final equilibrium value. Next, it gradually decreased. Finally, it settled to the final equilibrium value, *i.e.*, the H^+ concentration in the l-side solution. It should be noted that, if the system did not have the overshooting effect ($c_i < (c_1 + c_2)$), the H^+ concentration reached its final value without exceeding the final equilibrium value.

Materials and Methods

The test-tube-shaped membranes, 8 cm in length and 2 cm in diameter, were made of sulfonated polystyrene and collodion. The polystyrene sulfonic acid was synthesized following the method by Kato, Nakagawa, and Akamatsu;[5] its % of sulfonation was about 75%. Polystyrene sulfonic acids (1.59 g for Membranes 1 and 2 and 2.17 g for Membrane 3) were mixed with 300 ml of a 5% w/w collodion solution. Table 1 summarizes

Table 1. Characteristics and properties for membranes

	Membrane number		
	1	2	3
Membrane thickness (mm)	0.22	0.10	0.024
Water content	0.715	0.359	0.093
θ(M)	-8.3×10^{-3}	-1.07×10^{-2}	-7.14×10^{-2}
Electric resistance (Ω cm^2)	250	240	260
k_1 (min^{-1})	0.043	0.015	0.0028
k_2 (min^{-1})	0.556	0.193	0.0997

the characteristic data of these membranes—that is, the average membrane thickness, the water content of the membrane, the effective charge density of the membrane in the KCl solution, and the electric resistance of the membrane. The water content of the membrane is defined as the net weight of water absorbed in the membrane phase divided by the total weight of the wet membrane. The effective charge density of the membrane, θ(M), was measured following the method described in a paper by Kobatake, Takeguchi, Toyoshima, and Fujita.[6] The electrical resistance of the membrane (Ω cm^2) was measured on a membrane which had been soaked in a 0.1 M-NaCl solution at 30 °C prior to the measurement.

The s-side solution (20 ml) was placed in the test-tube-shaped membrane. A combination electrode (Beckmann, Type 39030, Calif., U.S.A.) was immersed in the s-side solution in order to measure the continuous change in the H^+ concentration. The volume of the l-side solution was about 20 l. Both solutions were stirred by bubbling air, and their temperatures were kept at 35 $\pm$0.1 °C

Results

In Fig. 1, the solid lines show the changes in the H^+ concentration in the s-side solution as a function of the time for Membranes 1, 2, and 3. The initial concentrations of NaCl in the s-side solution were 0.2042 M for Membranes 1 and 3 and 0.1950 M for Membrane 2. Moreover, the l-side solution contained 0.0247 M-NaCl and 0.0022 M-HCl for Membranes 1 and 3 and 0.0220 M-NaCl and 0.0024 M-HCl for Membrane 2.

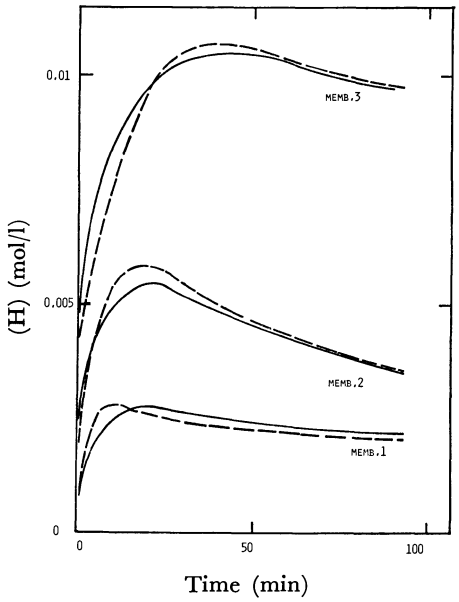

Fig. 1. Time dependencies of the H^+ concentration in the s-side solution. Solid lines show experimental curves for Membranes 1, 2, and 3. Broken lines show calculated curves from Eq. (8) with k_1 and k_2.

The H^+ concentrations of the s-side started from zero and thereafter increased rapidly beyond the final equilibrium values in a few minutes. They went up to the maximum values of 0.0028 M, 0.0054 M, and 0.010 M for Membranes 1, 2, and 3 respectively. Their maximum values were 1.32 times (Membrane 1), 2.25 times (Membrane 2), and 4.37 times (Membrane 3) as large as their final values. After reaching their maximum values, the H^+ concentrations descreased gradually. It took a long time to attain the final equilibrium values (3—24 hr after the start of the experiments).

Discussion

First, we will check the applicability of the concept of the partial membrane equilibrium to our present system. Following the idea by Neihof and Sollner,[3] the maximum values of the H^+ concentration can be calculated on the basis of the partial membrane equilibrium. The maximum values of the H^+ concentration were calculated as 0.0165 M for Membranes 1 and 3 and 0.0192 for Membrane 2. However, the experimental values were about 1/6, 1/4, and 2/3 times as

large as the calculated maximum values for Membranes 1, 2, and 3 respectively. These large discrepancies between the maximum experimental values and the maximum calculated values mean that the permeation of the most slowly movable ion, Cl^-, cannot be neglected even in the initial process. Therefore, we cannot apply the explanation based on the partial membrane equilibrium to a membrane which has a relatively low ionic selectivity, such as the membrane used here.

We shall now propose a kinetic analysis which can formulate the whole time dependence of the transitory effect. The water permeability of the membrane was assumed to be negligibly small. In the system there exist three kinds of ionic species which are movable across the membrane. As for the permeability velocities of these ions through the cation-exchange membrane, the fastest one is H^+, because of its large ionic mobility, the second is Na^+, and the slowest is Cl^-, because of its repulsive interaction with fixed negative membrane charges. Below, the ionic concentration (in M) will be placed within parentheses.

Because its movement in the membrane is the slowest, the transport of Cl^- through the membrane might be rate-determining for this kind of interdiffusion. Hence, its time-dependent change in the concentration is expected to be relatively monotonous in the system. It was assumed that an equation for the first-order reaction could express the decrease in the Cl^- concentration in the s-side solution, (Cl). That is,

$$(Cl) = [(Cl)_i - (Cl)_f] \exp(-k_1 t) + (Cl)_f \quad (1)$$

where $(Cl)_i$ and $(Cl)_f$ are the initial and final concentrations of Cl^- in the s-side solution respectively ($(Cl)_i = c_i$ and $(Cl)_f = (c_1 + c_2)$) and where k_1 is the velocity rate parameter for Cl^-.

The system, in the course of changing toward the final equilibrium, is not in a steady state, but in a transient state. Therefore, we cannot expect the Donnan equilibrium to be materialized during the experiment except at the end. However, there still exists a driving force which tends to bring the system to the imaginary Donnan equilibrium. The imaginary Donnan equilibrium can be calculated as follows. We made two additional assumptions in the calculation of the imaginary Donnan equilibrium. One is that the permeability of Cl^- is negligibly small in this calculation only. The other is that the activity coefficients of all ions in solutions are unity. The ratio of the imaginary concentrations of two permeable ions in the s-side solution, *i.e.*, $(H)_{imaginary}/(Na)_{imaginary}$, should be identical with the ratio of their corresponding concentrations in the l-side solution from the Donnan equilibrium. That is,

$$c_2/c_1 = (H)_{imaginary}/(Na)_{imaginary}. \quad (2)$$

From the electric neutrality condition, the total imaginary cation concentration in the s-side solution may be said to be equal to the existing Cl^- concentration in the s-side solution, *i.e.*:

$$(H)_{imaginary} + (Na)_{imaginary} = (Cl). \quad (3)$$

From Eqs. (2) and (3), we obtain:

$$(Na)_{imaginary} = [c_1/(c_1+c_2)](Cl) \equiv \gamma(Cl) \quad (4)$$

where $\gamma(=c_1/(c_1+c_2))$ is considered to be constant during the experiment.

An important assumption was made regarding the transport of Na^+. The Na^+ concentration in the s-side solution was forced to change by the driving force, which would tend to bring the Na^+ concentration, (Na), toward the calculated Na^+ concentration of the imaginary Donnan equilibrium, (Na)imaginary. This follows:

$$d(Na)/dt = -k_2[(Na) - (Na)_{imaginary}] \quad (5)$$

where k_2 is another velocity rate parameter for Na^+. Here, $k_2 > k_1$ because the permeability of Na^+ is much greater than that of Cl^-. By combining Eqs. (1), (4), and (5) and by integrating, we get:

$$(Na) = [k_2\gamma/(k_2-k_1)][(Cl)_i - (Cl)_f] \exp(-k_1 t) + \gamma(Cl)_f + I_0 \exp(-k_2 t) \quad (6)$$

where I_0 is the integral constant. The I_0 is determined from the initial condition; *i.e.*, at $t=0$, $(Na)=(Cl)=(Cl)_i$. That is,

$$I_0 = (Cl)_i - [k_2\gamma/(k_2-k_1)][(Cl)_i - (Cl)_f] - \gamma(Cl)_f. \quad (7)$$

The H^+ concentration in the s-side solution, (H), is given as follows from the electric neutrality condition:

$$(H) = (Cl) - (Na) = (1-\gamma)(Cl)_f + [1 - k_2\gamma/(k_2-k_1)] \times [(Cl)_i - (Cl)_f][\exp(-k_1 t) - \exp(-k_2 t)] - [(Cl)_f - \gamma(Cl)_f] \exp(-k_2 t). \quad (8)$$

In order to determine the two parameters, k_1 and k_2, from the experiment, we got a limiting equation from Eq. (8). Considering γ as near unity ($c_1 \gg c_2$) and neglecting the term of $\exp(-k_2 t)$ in the third brackets on the right-hand side of Eq. (8) compared with the term of $\exp(-k_1 t)$ in the range of large t values because $k_2 > k_1$, we obtain:

$$\log[(H) - (1-\gamma)(Cl)_f] = -k_1 t/2.303 + \log\{[1 - k_2\gamma/(k_2-k_1)][(Cl)_i - (Cl)_f]\}. \quad (9)$$

In Fig. 2, the left-hand side of Eq. (9) is plotted against t for Membranes 1, 2, and 3. From their gradients and the intercepts of straight broken lines in the range of large t values, k_1 and k_2 were obtained. In Table 1,

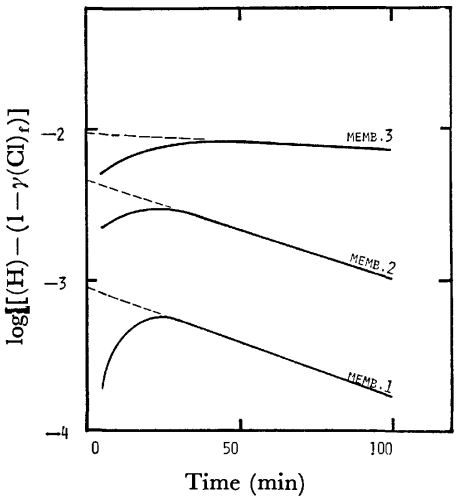

Fig. 2. Plots of $\log[(H)-(1-\gamma)(Cl)_f]$ *vs.* time t.
From gradients and intercepts of straight broken lines, k_1 and k_2 were obtained. Solid lines show experimental data.

k_1 and k_2 are shown along with other membrane characteristics.

The time dependencies of the H^+ concentration for Membranes 1, 2, and 3 calculated from Eq. (8) with k_1 and k_2 in Table 1 are represented in broken lines in Fig. 1. The coincidence between experimental curves and calculated curves was found to be generally good. Although it is felt that the analysis is rather too simple, this good coincidence could mean that the most significant aspects of the phenomena are included in the above analysis. It may be noted that the overshooting effect becomes larger as k_1 and k_2 become smaller and as the effective charge density of the membrane, θ, becomes larger.

A partial derivative of Eq. (8) with time becomes zero at the time when the overshooting effect reaches its maximum. Thus, the time t at the maximum effect, t_{max}, is given as:

$$(k_2-k_1)t_{max} = \ln(k_2/k_1) + \ln I_0 - \ln[1-k_2\gamma/(k_2-k_1)] - \ln[(Cl)_i-(Cl)_f]. \quad (10)$$

The t_{max} values were calculated from Eq. (10) to be 8, 17, and 39 min for Membranes 1, 2, and 3 respectively. The calculated t_{max} values are in good agreement with the experimental values. When $(Cl)_i<(Cl)_f$, Eq. (10) has no solution. In fact, experiments under the condition of constant 1-side composition (0.0247 M-NaCl+0.0022 M-HCl) showed that the overshooting effects were not found at 0.01 M and 0.02 M-NaCl initial concentrations in the s-side solution, although the effects *were* observed at an initial concentration higher than 0.05 M-NaCl in the s-side solution.

References

1) T. Teorell, *Progr. Biophys. Biophys. Chem.*, **3**, 305 (1953).
2) D. Woermann, *J. Amer. Chem. Soc.*, **90**, 3020 (1968).
3) R. Neihof and K. Sollner, *J. Phys. Chem.*, **61**, 159 (1957).
4) K. Sollner, *J. Macromol. Sci.- Chem.*, **A3**, 1 (1969).
5) M. Kato, T. Nakagawa, and H. Akamatsu, This Bulletin, **33**, 322 (1960).
6) Y. Kobatake, N. Takeguchi, Y. Toyoshima, and H. Fujita, *J. Phys. Chem.*, **69**, 3981 (1965).

Chemical Reaction of Electron Donor-Acceptor System: A New Mechanism for the Tricyanovinylation Reaction of Some Aromatic Amines with Tetracyanoethylene

Takashi NOGAMI, Yoshiki HASEGAWA, Yasuhiko SHIROTA, and Hiroshi MIKAWA

Department of Applied Chemistry, Faculty of Engineering, Osaka University, Yamadakami, Suita, Osaka 565

(Received May 13, 1975)

The tricyanovinylation reactions of several aromatic amines with tetracyanoethylene (TCNE) were investigated kinetically by observing the change of the absorbance of the charge-transfer (CT) band in 1,2-dichloroethane. The pseudo first order rate coefficient of the decay of the CT-complex (k_{obsd}) was found to obey the relation, $k_{obsd}=kKD^n/(1+KD)$ (K: association constant of CT-complex; D: initial concentration of donor molecule), where $n=1$ in *N,N*-diethylaniline (DEA)–TCNE and *N,N*-di-*n*-butylaniline (DBA)–TCNE systems and $n=2$ in *N*-methyl-*N*-ethylaniline (MEA)–TCNE system. Since the currently accepted mechanism for the tricyanovinylation reaction cannot explain the case of $n=1$, we have proposed a new reaction mechanism which can explain all the kinetic data reported hitherto. Two characteristic points are involved in the new mechanism, *i.e.*, one is the unimolecular reaction of the CT-complex or the bimolecular reaction between reactants to form the σ-complex, and the other the decomposition of the σ-complex back to the component molecules. The reactions of MEA, DEA, and DBA with TCNE were discussed based on the new mechanism.

There have been extensive studies on the role of charge-transfer (CT) interaction in chemical reactions.[1] The tricyanovinylation (TCV) reactions of several aromatic amines with tetracyanoethylene (TCNE)[2-11] are the most typical reaction systems involving the formation of CT-complex. The clarification of the TCV reaction mechanism is very important, since it gives us fundamental information as to the role of the CT-complex to the reaction which has been left ambiguously yet.

Z. Rappoport studied systematically the TCV reactions of *N,N*-dimethylaniline (DMA) and *N*-methylaniline (MA) with TCNE for the first time,[2,3] and found that the 1 : 1 CT-complex (DA) formed between reactants gradually disappears to form the intermediate zwitterionic σ-complex (σ) or neutral adduct tetracyanoethane derivative (NA), and thereafter the final tricyanovinyl compound (TCVP) is slowly produced. The reaction scheme proposed by him is shown as Scheme 1. These two steps of reactions could be followed independently by an electronic absorption measurement because of the large difference in the reaction rates. In the first step, the decay of the CT-complex followed the rate equation (I-1),

$$-\frac{d[DA]}{dt}=k_{obsd}[DA]=\frac{kKD^2}{1+KD}[DA] \qquad (I\text{-}1)$$

where [DA], D, K, k_{obsd}, and k denote the CT-complex, initial concentration of a donor molecule (D), association constant of the CT-complex, pseudo first order rate coefficient of the CT-complex and the coefficient for the process between the CT-complex and the σ-complex, respectively. This kinetic equation has to date been understood by the mechanism as described in Scheme 1. Namely, Z. Rappoport has postulated in this mechanism a bimolecular reaction between DA and D, which is considered to be inevitable in order to introduce D^2 term in the numerator of k_{obsd}, and he considered an exchange reaction of a complexed D and a free D in this process. The reactions of D with σ and NA have been considered as the proton abstraction reactions from σ and NA with D.

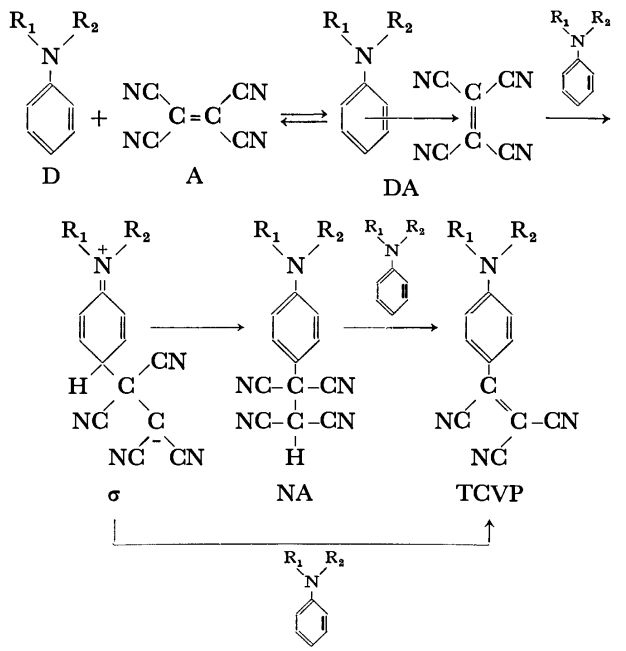

$R_1=H$, $R_2=CH_3$: MA
$R_1=R_2=CH_3$: DMA
$R_1=CH_3$, $R_2=C_2H_5$: MEA
$R_1=R_2=C_2H_5$: DEA
$R_1=R_2=n\text{-}C_4H_9$: DBA

Scheme 1.

The kinetic studies on the cycloaddition reactions of electron-donating olefins with TCNE[12,13] and on the ionization reaction in *N,N*-diethyl-*p*-toluidine–TCNE system[14] have revealed that the reaction should be interpreted as either a unimolecular transformation of the CT-complex or a bimolecular reaction of D with A. Namely, the bimolecular reaction between CT-complex and D has not been involved in these reaction kinetics. We have had questions for a long time why a bimolecular reaction of CT-complex with free D must be involved only in the TCV reaction, and this question prompted us to study the TCV reactions of higher *N*-alkylanilines, *N*-methyl-*N*-ethylaniline (MEA),

N,N-diethylaniline (DEA) and *N,N*-di-*n*-butylaniline (DBA), with TCNE in order to make clear the role of the CT-complex in the reaction. As the results, unimolecular reaction of the CT-complex or the bimolecular reaction between reactants were observed in DEA–TCNE and DBA–TCNE systems as shown later in this paper, being inconsistent with the currently accepted Rappoport mechanism. Therefore, we wish now to propose another mechanism for TCV reaction which can explain all the kinetic data reported hitherto and is considered to be more reasonable than the currently accepted one.

Experimental

Materials. DMA, DEA, and DBA were purchased from Tokyo Kasei Kogyo Co., Ltd. MEA was synthesized according to the literature.[15] All these amines were refluxed with sodium and thereafter distilled *in vacuo*. Special attention was made in the distillation of DBA to exclude *N*-monobutylaniline contained. The purity of the amines was confirmed by a gas chromatography. TCNE was purified by repeated sublimations. Commercially available 1,2-dichloroethane was shaken with KOH, washed with water, followed by extraction dried with $CaCl_2$ one day, refluxed with CaH_2, and finally distilled.

Measurements. The electronic absorption spectra and kinetic studies were made by a Hitachi 124 spectrophotometer. Thermostated water was circulated around the quartz observation-cell compartment (optical path length is 10 mm), and the donor and acceptor reservoirs. Donor and acceptor solutions were mixed directly in the observation cell. Initial absorption measurements could be made within 15 s after mixing.

Results and Discussion

Spectroscopic Course of the Reaction. The reactions in MEA–TCNE, DEA–TCNE, and DBA–TCNE systems were followed spectroscopically at a room temperature, using 1,2-dichloroethane as a solvent. Figure 1 shows the spectral change in MEA–TCNE system as a typical example. As the decrease of the CT-band at the long wavelength region, two new absorption bands, one locating at 440 nm with the vibrational structure and the other at 530 nm, increase gradually. The former band is assigned as a well-known TCNE anion radical[16] and the latter as tricyanovinylated product, *p*-tricyanovinyl-*N*-methyl-*N*-ethylaniline. The $TCNE^-$ band was observed for about one hour, and disappeared completely after all. The fate of $TCNE^-$ is unknown yet, but one possibility is that $TCNE^-$ is an intermediate for the formation of TCVP. Although we cannot answer to this possibility at present, independent study showed that TCVP is produced mostly through NA as shown below. The mixture of the equimolar ratio of MEA and TCNE showed the absorption band at 288 nm, and this band decreased gradually to produce TCVP. Although we could not isolate the species peaking at 288 nm because of its conversion into TCVP, it is safely assigned as NA in view of its quite similar absorption spectrum to that of the authentic NA in DMA–TCNE system.[5]

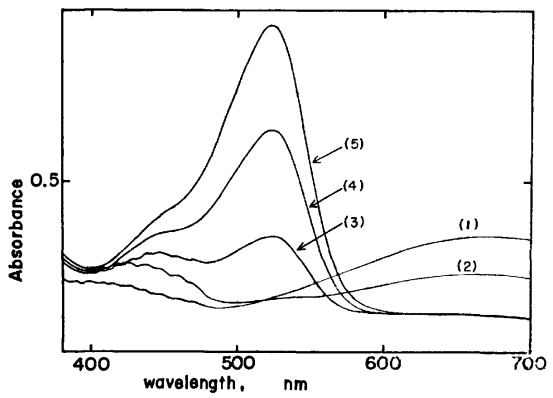

Fig. 1. Spectroscopic course of the reaction in MEA–TCNE system in 1,2-dichloroethane measured at a room temperature. $[MEA]=3.0\times10^{-2}$ M, $[TCNE]=3.0\times10^{-4}$ M. (1) 20 s, (2) 8 min, (3) 45 min, (4) 87 min, (5) 122 min after mixing.

Almost similar spectroscopic change was observed also in DEA–TCNE and DBA–TCNE systems, and TCVP was found to be produced mostly from NA. However, these systems produced also pentacyanopropenide anion (PCP)[17] (λ_{max}=410, 430 nm) as another reaction product. PCP is probably produced by the reaction of $TCNE^-$ with TCNE as evidenced previously.[17]

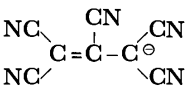

PCP

Yields of Reaction Products. The yields of TCVP and PCP under the kinetic work condition were estimated by measureing the electronic absorption spectra of the mixtures of the donor and acceptor solutions after keeping them for a few days at room temperature (Table 1). In these cases, the authentic extinction coefficients of PCP[17] and TCVP[18] were used. Each TCVP tends to increase slowly even several days after mixing the donor and acceptor solutions. Therefore, the yields of TCVP become higher than those in Table 1 day by day. This fact is due to the slow reaction rate from NA to TCVP. In other words, these reaction systems produce NA relatively fast, and it converts into TCVP very slowly. Therefore, the decrease in the CT-absorption does not correspond to the increase of TCVP. Furthermore, the correspondence between the decrease of the CT-complex and the increase of NA

Table 1. Yields of TCVP and PCP

	Yield of TCVP (%)	Yield of PCP (%)
$[MEA]=0.4$ M, $[TCNE]=1.0\times10^{-3}$ M	90[a]	—
$[DEA]=0.4$ M, $[TCNE]=1.0\times10^{-3}$ M	24[a]	23[a]
$[DBA]=0.8$ M, $[TCNE]=8.3\times10^{-4}$ M	49[b]	9[b]

a) Measured two days after mixing. b) Measured six days after mixing.

could not be measured because of the overlap of the absorption band of NA with those of the component molecules. No noticeable reaction product other than TCVP and PCP was observed in these systems. Table 1 shows that the formation of TCVP is the main reaction at least in MEA–TCNE and DBA–TCNE systems.

Thermodynamic Parameters of the CT-complex. The association constant of the CT-complex was obtained from the extrapolation of the decay of the CT-complex to zero time to make Benesi-Hildebrand (B-H) plot by the least-squares method. Figures 2, 3, and 4 show the B-H plots of MEA–TCNE, DEA–TCNE, and DBA–TCNE systems, respectively, in 1,2-dichloroethane at several temperatures. Clearly 1:1 CT-complexes are formed in these systems. The Arrhenius plots of the association constants of the CT-complexes (K) in these systems give straight lines to obtain the standard enthalpy ($\Delta H°$) and the entropy ($\Delta S°$) changes. The values of K, $\Delta H°$, and $\Delta S°$ in these systems together with those

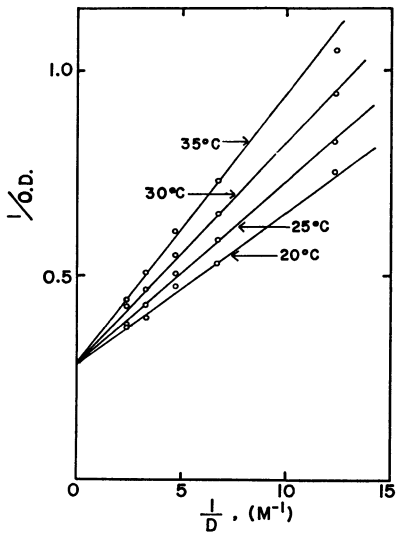

Fig. 2. Benesi-Hildebrand plot in MEA–TCNE system in 1,2-dichloroethane measured at the temperatures indicated. [TCNE]$=1.059\times10^{-3}$ M.

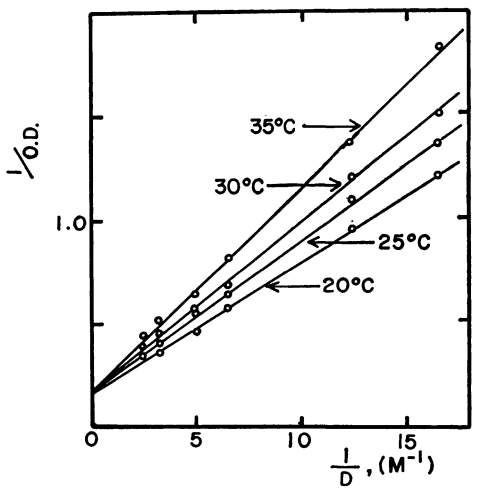

Fig. 3. Benesi-Hildebrand plot in DEA–TCNE system in 1,2-dichloroethane measured at the temperatures indicated. [TCNE]$=1.008\times10^{-3}$ M.

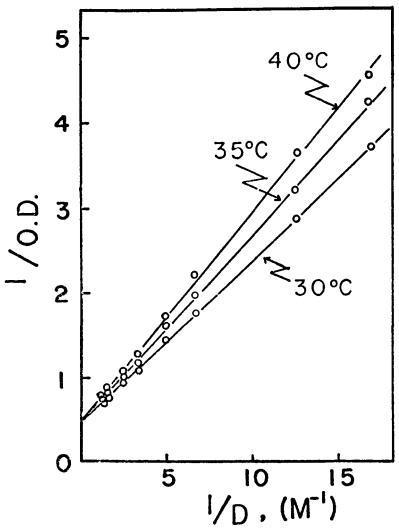

Fig. 4. Benesi-Hildebrand plot in DBA–TCNE system in 1,2-dichloroethane measured at the temperatures indicated. [TCNE]$=4.98\times10^{-4}$ M.

Table 2 Thermodynamic parameters of CT-complex in 1,2-dichloroethane

	Temp. (°C)	K (M^{-1})	$\Delta H°$ (kcal/mol)	$\Delta S°$ (e.u.)
DMA–TCNE	30	5.04	−4.92	−12.5
	35	4.39		
	40	3.89		
MEA–TCNE	20	7.34	−5.72	−15.3
	25	6.24		
	30	5.42		
	35	4.55		
DEA–TCNE	20	2.64	−4.21	−14.3
	25	2.34		
	30	2.12		
	35	1.74		
DBA–TCNE	30	2.25	−4.75	−14.3
	35	1.98		
	40	1.75		

in DMA–TCNE systems measured in 1,2-dichloroethane are summarized in Table 2. The value of K at each temperature is used in the analysis of the following decay kinetics of the CT-band.

The Decay Kinetics of the CT-band. The decay of the CT-band was followed at the appropriate band positions (DMA–TCNE, 675 nm; MEA–TCNE, 750 nm; DEA–TCNE, 800 nm; DBA–TCNE, 800 nm) with the donors in large excess over TCNE. Varying the concentration of the donor keeping that of TCNE constant, plots of log I_{CT} (I_{CT}: the absorbance of the CT-complex at the wavelength measured) against time (t) give straight lines at several temperatures in all systems studied as shown for DBA–TCNE system as a typical example in Fig. 5, which shows that the decay rate of the CT-complex is of the first order with respect to the CT-complex. It was also found that the decay rate of the CT-complex is independent of the initial concentration of TCNE. Table 2 shows the values of the pseudo first order rate coefficients of the CT-complex

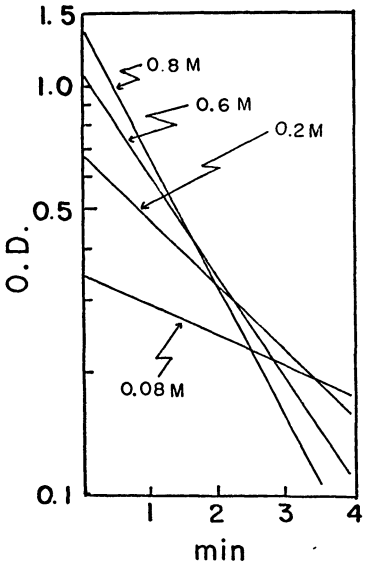

Fig. 5. The decay of the CT-band with time measured at 30 °C. [TCNE]=4.98×10^{-4} M. The concentration of DBA is indicated in the figure.

(k_{obsd}) in these systems, those of $k_{obsd}(1+KD)$ and of $k_{obsd}(1+KD)/D$ at various initial donor concentrations (D). The values of $k_{obsd}(1+KD)/D$ are almost constant irrespective of the initial donor concentrations within the experimental error in DMA–TCNE and MEA–TCNE systems but vary with the change of the donor concentrations in DEA–TCNE and DBA–TCNE systems. Fig. 6 shows the plot of $k_{obsd}(1+KD)/D$ against KD in MEA–TCNE system, and Figs. 7 and 8 those of $k_{obsd}(1+KD)$ against KD in DEA–TCNE and DBA–TCNE systems, these plots being obtained by the least squares method. The former and the latter plots are designated hereafter as "second order plot" and "first order plot," respectively, since $k_{obsd}(1+KD)$ is quadratic with D in the former plot and linear with D in the latter. One can see from Figs. 6, 7, and 8 that MEA–TCNE system gives straight lines in the second order plot and DEA–TCNE and DBA–TCNE systems in the first order plot at several temperatures measured. The kinetic studies on the TCV reactions of DMA–TCNE and *N*-methylaniline (MA)–TCNE systems have shown that the second order plots are linear in these systems,[2,3] and this is also confirmed in the former system in this study. On the other hand, the values of $k_{obsd}(1+KD)$ was found to be proportional to D^3 in the *N*-tricyanovinylation reactions of aniline (A)–TCNE system[10] (such a D^3 dependence is designated as "third order plot"). Therefore, the following results are derived from the kinetic studies on the TCV reactions carried out hitherto.

First order plot (DEA–TCNE,[19] DBA–TCNE[19])

$$k_{obsd}=\frac{kKD}{1+KD}$$

Second order plot (MA–TCNE,[3] DMA–TCNE,[2] MEA–TCNE[19])

$$k_{obsd}=\frac{kKD^2}{1+KD}$$

Third order plot (A–TCNE[10])

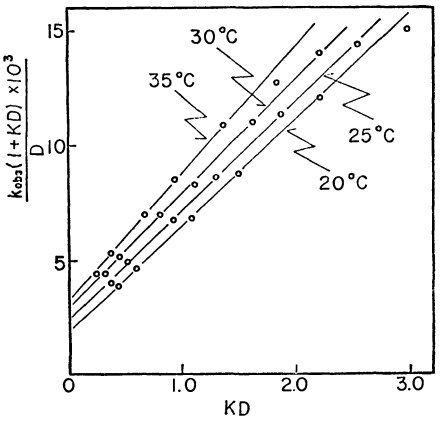

Fig. 6. Plots of $k_{obsd}(1+KD)/D$ against KD in MEA–TCNE system in 1,2-dichloroethane measured at the temperatures indicated. [TCNE]=1.059×10^{-3} M.

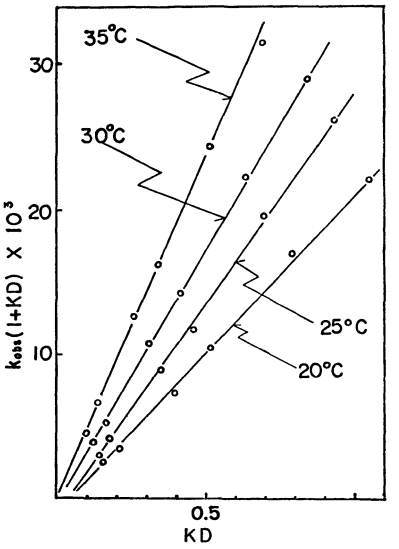

Fig. 7. Plots of $k_{obsd}(1+KD)$ against KD in DEA–TCNE system in 1,2-dichloroethane measured at the temperatures indicated. [TCNE]=1.008×10^{-3} M.

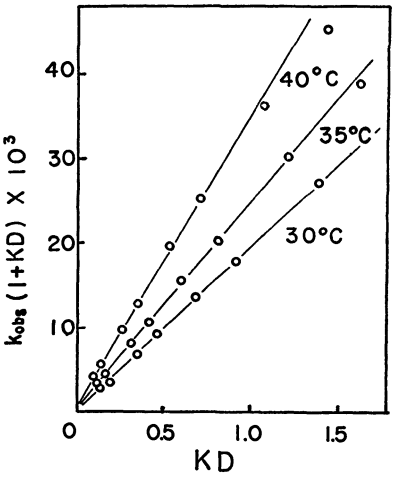

Fig. 8. Plots of $k_{obsd}(1+KD)$ against KD in DBA–TCNE system in 1,2-dichloroethane measured at the temperatures indicated. [TCNE]=4.98×10^{-4} M.

Table 3. Values of pseudo first-order rate coefficients (k_{obsd}), $k_{obsd}(1+KD)$, and $k_{obsd}(1+KD)/D$ in 1,2-dichloroethane

	Temp (°C)	[D], (M)	[A]×10, (M)	$k_{obsd}\times 10^2$, (s^{-1})	$k_{obsd}\times$ $(1+KD)$	$k_{obsd}\times$ $(1+KD)/D$
DMA–TCNE	30	0.059	0.975	0.089	0.00115	0.0195
		0.148		0.338	0.00591	0.0399
		0.295		0.769	0.01913	0.0648
	40	0.059	0.975	0.089	0.00109	0.0185
		0.148		0.350	0.00551	0.0372
		0.295		0.833	0.01789	0.0606
MEA–TCNE	20	0.060	1.059	0.164	0.00237	0.0394
		0.205		0.721	0.01806	0.0881
		0.405		1.535	0.06098	0.1506
	35	0.060	1.059	0.209	0.00266	0.0444
		0.205		0.911	0.01761	0.0859
		0.405		1.808	0.05319	0.1269
DEA–TCNE	20	0.197	1.008	0.685	0.01041	0.0529
		0.301		0.945	0.01696	0.0563
		0.400		1.068	0.02196	0.0549
	35	0.197	1.008	1.205	0.01331	0.0821
		0.301		1.587	0.02418	0.0803
		0.400		1.855	0.03146	0.0787
DBA–TCNE	30	0.149	0.498	0.494	0.00660	0.0443
		0.298		0.809	0.01351	0.0454
		0.599		1.128	0.02648	0.0442
	40	0.149	0.498	0.761	0.00959	0.0644
		0.298		1.273	0.01937	0.0650
		0.599		1.743	0.03570	0.0596

$$k_{obsd} = \frac{kKD^3}{1+KD}$$

The first order plot obtained in this study is the first example for the TCV reaction, although the first order plot is rather general in many reaction systems involving CT-complex such as 2+2 and 4+2 cycloaddition reactions[12,13] and ionization reactions.[14] As stated previously, Z. Rappoport and P. G. Farrell explained the second order plot in the TCV reaction as resulting from the bimolecular exchange reaction between a complexed donor and a free donor, and this assumption has been accepted to be general for the TCV reaction (Scheme 1). By this currently accepted mechanism, however, the first order plots observed in DEA–TCNE and DBA–TCNE systems are difficult to understand. We considered, therefore, that a more general reaction scheme must exist for the TCV reaction, and the decay kinetics of the CT-complex obeys first order plot or second order plot, and sometimes third order plot, by applying the special conditions to the new reaction scheme.

New Mechanism for the TCV Reaction. We wish now to propose another mechanism which can also satisfy all the kinetic data reported hitherto as described in Scheme 2.

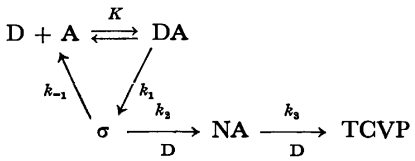

Scheme 2.

Two characteristic points are involved in the new mechanism, *i.e.*, (1) unimolecular reaction from CT-complex to zwitterionic σ-complex, and (2) dissociation reaction of zwitterionic σ-complex back to the component molecules. The other reaction steps (the reactions from σ to NA and from NA to TCVP) are the same as the currently accepted mechanism, and the introductions of D in these steps are due to the proton abstraction reactions from σ and NA with basic D molecule (see Scheme 4).

Applying the steady state approximations to the unstable σ-complex,[20] the decay of the CT-complex is derived as follows.

$$\frac{d[DA]}{dt} = k_{obsd}[DA] = \frac{k_1k_2KD^2}{(1+KD)(k_{-1}+k_2D)}[DA] \quad \text{(II-1)}$$

$$\approx \frac{(k_1k_2/k_{-1})KD^2}{1+KD}[DA] \quad (k_{-1} \gg k_2D) \quad \text{(II-2)}$$

$$\approx \frac{k_1KD}{1+KD}[DA] \quad (k_{-1} \ll k_2D) \quad \text{(II-3)}$$

The equation (II-1) reduces to (II-2) to give the second order plot if $k_{-1} \gg k_2D$ holds, and (II-2) is essentially identical with (I-1), *i.e.*, k in (I-1) is reinterpreted in the new mechanism as (k_1k_2/k_{-1}). That is to say, in the currently accepted mechanism the presence of DA+D reaction has been assumed in order to make the D term in the numerator of k_{obsd} quadratic, and in our new mechanism this is effected by introducing a back reaction from the σ-complex to the reactants. On the contrary, if $k_{-1} \ll k_2D$ holds, the equation (II-1) reduces

to (II-3) to give the first order plot. In other words, in our new mechanism if the rate of the decomposition of the σ-complex to the component molecules (k_{-1}) is much faster than that of the conversion of the σ-complex to neutral adduct (k_2D), the second order plot is obtained and if in the reverse case, the first order plot is obtained.

We insist here that the former condition may hold in MA–TCNE and DMA–TCNE systems. Concerning the MEA–TCNE system, we observed the TCV reaction as well as the ionization reaction of the component molecules. The existence of the ionization process in this system is the characteristic point as compared with MA–TCNE and DMA–TCNE systems. The second order plot observed in MEA–TCNE system is considered to result from the fact that the TCV reaction occurs with the former condition ($k_{-1} \gg k_2D$), and that the TCV reaction dominates over the ionization reaction.[21] It cannot be necessarily said, however, that the latter condition ($k_{-1} \ll k_2D$) holds in DEA– and DBA–TCNE systems. The discussions on these two systems are shown later in this paper.

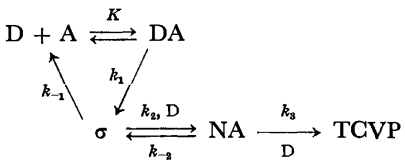

Scheme 3.

The cubic dependence of D in the numerator of k_{obsd} (third order plot) observed in aniline–TCNE system[10] is interpreted in our new mechanism in terms of the reversibility of both processes of the σ-complex and the neutral adduct formations probably due to the instability of the neutral adduct in this system. This is consistent with the fact that the absorption band of neutral adduct could not be detected by an electronic absorption spectra in this system. The reaction scheme for this system is given as Scheme 3. Applying the steady state approximations to the σ-complex and neutral adduct, the following kinetic equations are derived, where k_{-2} denote the reaction rate coefficient from neutral adduct to σ-complex.

$$-\frac{d[DA]}{dt} = k_{obsd}[DA]$$

$$= \frac{k_1k_2k_3KD^3}{(1+KD)(k_{-1}k_2+k_{-1}k_3D+k_2k_3D^2)}[DA] \quad \text{(III-2)}$$

$$\approx \frac{(k_1k_2k_3/k_{-1}k_{-2})KD^3}{1+KD}[DA] \quad \text{(III-2)}$$

$$(k_{-1} \gg k_2D, \text{ and } k_{-2} \gg k_3D)$$

The rate equation (III-1) reduces to (III-2), the third order plot, if $k_{-1} \gg k_2D$ and $k_{-2} \gg k_3D$ hold simultaneously.

Discussions on the New Mechanism. At present, we have no direct evidence for the new mechanism, but we beleive that the new mechanism is more reasonable from the following reasons.

(1) The reaction of a complexed TCNE with a free donor, the currently accepted mechanism, is difficult to understand in such an electrophilic substitution reaction as TCV reaction, because the electron accepting property of the complexed TCNE may be sufficiently weakened. Furthermore, no experimental evidence has been found which shows the existence of the exchange reaction between a complexed donor and a free donor.

(2) The kinetic deuterium isotope effect was found to exist for the decay of the CT-complex between DMA–TCNE and 4-deuterio-*N*,*N*-dimethylaniline–TCNE systems.[7] The currently accepted mechanism cannot explain this result, since hydrogen abstraction reaction is not involved in the reaction of DA with D. On the other hand, the new mechanism can explain the isotope effect in view of the fact that the rate of hydrogen abstraction reaction from σ-complex (k_2) is involved in k_{obsd}, *viz.*,

$$k_{obsd} \approx \frac{(k_1k_2/k_{-1})KD^2}{1+KD}.$$

(3) The kinetic studies for the 2+2 and 4+2 cycloaddition reactions of electron donating olefins with TCNE[12,13] and ionization reaction in *N*,*N*-diethyl-*p*-toluidine–TCNE system[14,21] have revealed that the reaction should be understood as either unimolecular transformation of the CT-complex or bimolecular reaction between a free donor and an acceptor molecules. These results suggest that the unimolecular transformation of the CT-complex is favored over the bimolecular reaction between the CT-complex and a free donor. Thus, the primary process of the chemical reaction involving the formation of the CT-complex is systematically understood by the same mechanism.

(4) The assumption of back process of the zwitterionic σ-complex to the component molecules is reasonable, which has recently been evidenced in the 2+2 cycloaddition reaction of isomeric enol ethers with TCNE.[22]

(5) The new mechanism which involves σ-complex as an unstable intermediate and neutral adduct tetracyanoethane derivative as an accumulating intermediate is in accord with the fact that the latter has actually been isolated,[7,8] while the former cannot be detected even by the spectroscopic technique. The explanation in the literature[7] that the isolable neutral adduct may arise by rapid rearrangement of the σ-complex and may not be on the reaction path of the overall TCV reaction under the kinetic work conditions seems to be unattractive.

Discussions on the TCV Reaction in DEA–TCNE and DBA–TCNE Systems. As stated above, the decay of the CT-complex obeyed the first order plot in DEA–TCNE and DBA–TCNE systems. These results are now discussed based on the new mechanism. The following three cases can be considered as the reason of the first order plots in these systems.

(1) As stated in the description of the new mechanism, these systems are in the condition that the decomposition rate of σ-complex is much slower than the reaction rate from σ-complex to neutral adduct, *i.e.*, $k_{-1} \ll k_2D$. This may be rationalized by the stability of the σ-complexes in these systems because of the increasing donor properties of DEA and DBA as compared

with MA, DMA, and MEA, and the decomposition rate of the σ-complex back to the component molecules may be considerably reduced.

(2) The steric effect of the bulky alkyl groups attached to the amino nitrogens of DEA and DBA hinder the proton abstraction reaction of these amines from the σ-complex, and the conversion of the σ-complex into the neutral adduct is a unimolecular reaction.[23] Thus, in this case k_2D in equation (II-1) must be replaced by k_2 to give

$$k_{obsd} = \frac{(k_1k_2/(k_{-1}+k_2))KD}{1+KD}.$$

(3) The ionization reaction dominates over TCV reaction.[21] Which of these three cases actually holds is now under investigation.

Concerning the ionization reaction, three mechanisms are conceivable, *i.e.*, ionization from (1) component molecules, (2) CT-complex, and (3) σ-complex. In order to know the ionization mechanism, the ESR studies are now under investigation.[14]

Comments. The followings are the additional comments to be noted. (1) We have discussed the mechanism based on the unimolecular transformation of CT-complex to the σ-complex (Scheme 2). However, another mechanism is also possible in which σ-complex is produced from the component free molecules and the CT-complex exists in a side reaction as shown in Scheme 2'. The reaction scheme and rate equation are as follows.

$$D + A \overset{K}{\rightleftharpoons} DA$$

$$\sigma \xrightarrow[D]{k_2} NA \xrightarrow[D]{k_3} TCVP$$

$$-\frac{d[DA]}{dt} = \frac{k_1'k_2D^2}{(1+KD)(k_{-1}+k_2D)}[DA] \qquad (II'-1)$$

Scheme 2'.

Where, k_1' is the rate coefficient from the component molecules to the σ-complex. The two mechanisms,

TCV reaction

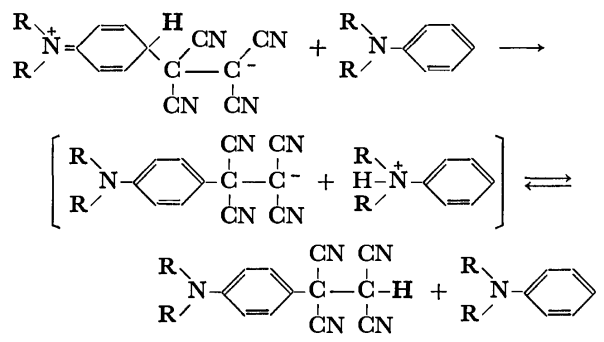

Cycloaddition reaction

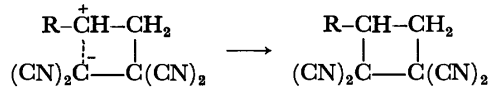

Scheme 4.

Schemes 2 and 2', are indistinguishable kinetically. The detailed discussions will be reported in the near future.

(2) It has been reported that the decay of the CT-complex obeys the first order plot in many cycloaddition reactions of electron rich olefins with TCNE.[12,13] The apparent difference in the rate equations for the decay of the CT-complex between the TCV reaction and the cycloaddition reaction is understandable as resulting from the fact that in the TCV reaction one more donor molecule participates in abstracting a proton from the σ-complex in the neutral adduct formation process, while in the cycloaddition reaction such a process is not involved (Scheme 4).[24]

(3) It has been to date insisted that the CT-complex is the essential intermediate in the TCV reaction based on the mechanism of the bimolecular reaction of the complexed donor and a free donor. In the new mechanism, however, the kinetic data alone cannot tell whether or not the CT-complex is the true intermediate in the TCV reaction.[24]

References

1) E. M. Kosower, "Progress in Physical Organic Chemistry," ed. by S. G. Cohen, A. Streitwieser, Jr., and R. W. Taft, Interscience Publishers, N. Y. (1965), p. 81.
2) Z. Rappoport, *J. Chem. Soc.*, **1963**, 4498.
3) Z. Rappoport and A. Horowitz, *ibid.*, **1964**, 2348.
4) R. Foster and P. Hanson, *Tetrahedron*, **21**, 255 (1965).
5) Z. Rappoport and E. Shohamy, *J. Chem. Soc., B*, **1969**, 77.
6) P. G. Farrell and R. K. Wojtowski, *ibid.*, **1970**, 1390.
7) P. G. Farrell and J. Newton, *ibid.*, **1970**, 1630.
8) Y. Shirota, S. Ezaki, S. Kusabayashi, and H. Mikawa, This Bulletin, **45**, 836 (1972).
9) S. Garbutt and D. L Gerrand, *J. Chem. Soc., Perkin II*, **1972**, 782.
10) P. G. Farrell and P. N. Ngo, *ibid.*, **1973**, 974.
11) Y. Shirota, T. Nogami, Y. Hasegawa, and H. Mikawa, *Chem. Lett.*, **1974**, 1009.
12) J. Nagata, K. Furushita, T. Nogami, Y. Shirota, and H. Mikawa, 5th Symposium on the Charge-transfer Cymplex, Osaka, Dec., 1973, preprint p. 25.
13) T. Arimoto and J. Osugi, *Chem. Lett.*, **1974**, 271.
14) To be published in the forthcoming paper.
15) J. M. Fayadh and G. A. Swan, *J. Chem. Soc., C*, **1969**, 1781.
16) O. W. Webster, W. Mahler, and R. E. Benson, *J. Amer. Chem. Soc.*, **84**, 3678 (1962).
17) W. J. Middleton, E. J. Little, D. D. Coffman, and V. A, Engerhardt, *ibid.*, **80**, 2795 (1958). PCP may be in the form of salt as shown below (see, P. G. Farrell and R. K. Wijtowski, *J. Chem. Soc., C*, **1970**, 1394.)

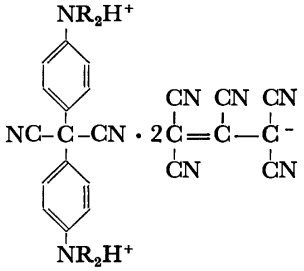

18) B. C. McKusick, R. E. Heckert, T. L. Cairs, D. D. Coffman, and H. F. Mower, *J. Amer. Chem. Soc.*, **80**, 2806 (1958).
19) Present study.
20) The change of the [σ] with time is assumed to be negligibly small as compared with those of the other reaction species.
21) Concerning the ionization reaction involving the CT-complex, we have carried out kinetic studies on *N,N*-diethyl-*p*-toluidine–TCNE system in which no TCV reaction is expected to occur, and found that the decay of the CT-complex obeys the first order plot.[14] We think that the ionization reactions involving the CT-complex may be generalized as the first order plot.
22) R. Huisgen and G. Steiner, *J. Amer. Chem. Soc.*, **95**, 5055 (1973).
23) The steric hindrance of proton abstraction of *N*-alkylanilines were discussed by H. T. Taylor. The basicities of *N*-alkylaniline increase passing from DMA to DEA, but decrease for the larger *N*-alkylanilines by the steric effect. H. T. Taylor, *Nature*, **181**, 265 (1958).
24) The isolable neutral adduct tetracyanoethane derivative might exist as a carbanion species (see Scheme 4).

The Application of Molecular-flame-absorption Spectroscopy to the Elucidation of Chemical Interferences in Indium Atomic Absorption Spectrometry

Hiroki HARAGUCHI and Keiichiro FUWA*

Department of Chemistry and Physics, The National Institute for Environmental Studies, Yatabe-machi, Tsukuba-gun, Ibaraki 300-21

**Department of Agricultural Chemistry, Faculty of Agriculture, The University of Tokyo, Yayoi, Bunkyo-ku, Tokyo 113*

(Received May 17, 1975)

The atomic absorption spectrometry of indium was investigated in air-acetylene and nitrous oxide-acetylene flames. The atomic absorptions of indium were significantly interfered by HCl, $HClO_4$, and HBr in both the flames. The chemical interferences can be explained by the formation of diatomic molecules, such as InCl and InBr, the molecular absorption spectra of which were really observed in flames.

The atomic absorption spectrometry of indium has been studied by several workers.[1-4] It has been established by the studies that indium is interfered with by several cations[2] and anions[4] in the air-acetylene flame and even in the nitrous oxide-acetylene flame. Popham and Schrenk reported analytical interferences by HCl, HBr, H_2SO_4, and H_3PO_4 in the concentration range of less than 1M and suggested an interfering mechanism resulting from the formation of diatomic molecules in the flames.[4]

Recently, the molecular absorption spectra of various species in flames have been investigated, and such molecular species as SO_2, PO, InF, InCl, InBr, InO, AlF, AlCl, and AlO have been found.[5-11] Furthermore, it has been shown that these molecular absorption spectra in the flames can be used not only for the determination of non-metallic elements,[5-7] but also for the elucidation of the chemical interferences.[8,9] Hence, in this paper, the chemical interferences due to various hydrogen acids in indium atomic absorption spectrometry have been investigated by means of molecular absorption spectroscopy.

Experimental

Samples. The indium oxide (In_2O_3; 99.9%) was purchased from Mitsuwa Chemical Ind. Co. The acids used were of a guaranteed ragent grade. The sample solutions were prepared by dissolving properly weighed amounts of indium oxide in acidic aqueous solutions.

Instruments. A Hitachi 207 Atomic Absorption Spectrophotometer was used for the measurements of the atomic and molecular absorptions. The hollow cathode-discharge tube of indium was obtained from Hitachi Manufacturing Ltd., and that of the deuterium lamp, from the Hamamatsu TV Co. A Hitachi 207-0100 High-voltage Power Source was used as the power supply for the deuterium lamp.

Procedures. The experimental conditions for the measurements of the atomic and molecular absorptions in the air-acetylene and nitrous oxide-acetylene flames are summarized in Table 1. In the case of the atomic absorption spectrometry, the "sample flow rates," which are referred to the volumes of the sample solutions aspirated into the burner for a minute, are affected to some extent by the viscosities of the solutions and change the atomic absorptions of indium. Therefore, the dependences of the atomic absorptions on the sample-flow rates have been investigated. The results are shown in Fig. 1, where the sample flow rates were changed by using several kinds of capillary tubes with different diameters and lengths. The sample flow rates were measured with a graduated cylinder.

Table 1. Experimental conditions in atomic and molecular absorption spectrometry

I) Atomic absorption	
Analytical lines	303.9 nm, 325.6 nm, 412.5 nm, 451.1 nm
Lamp	hollow cathode lamp of indium
Lamp current	15 mA
Flame height	10—20 mm
Air-acetylene flame;	
air flow rate	13 l/min
acetylene flow rate	3 l/min
Nitrous oxide-acetylene flame[a];	
nitrous oxide flow rate	6 l/min
acetylene flow rate	4 l/min
Spectral band width	0.34 nm
II) Molecular absorption[b]	
Analytical lines	(303.9 nm for In)
	273.0 nm for InO
	267.2 nm for InCl
	284.6 nm for InBr
Lamp	hollow cathode lamp of deuterium
Lamp current	25—35 mA

a) A water-cooled burner for nitrous oxide-acetylene flame was used. b) Other conditions were the same with those in atomic absorption spectrometry.

The molecular flame absorption spectrum shown in Fig. 5 was obtained by measureing the absorbances at wavelengths separated by intervals of 1Å, as has been reported previously,[11] the deutrium lamp was used as a continuous light source. The dependences of the atomic and molecular absorptions of In, InO, and InCl on the HCl concentration, which are shown in Fig. 4, were also measured using the deuterium lamp.

Results and Discussion

The calibration curve for the atomic absorption of indium was linear in the concentration range from 0 to 10 μg/ml when 0.1—1 M HNO_3 aqueous solutions of indium with various concentrations were used as the sample solutions. The sensitivity (1% absorption) for

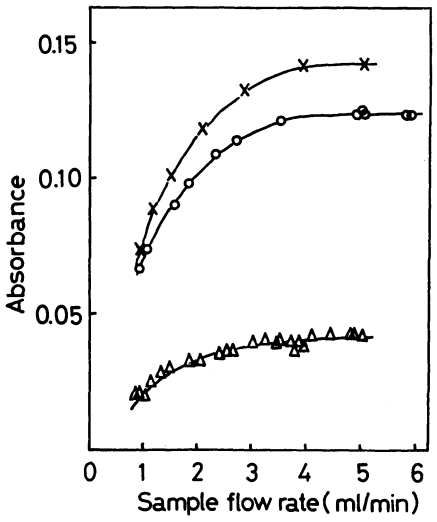

Fig. 1. Sample flow rate *vs.* atomic absorptions of indium at several analytical lines in the air–acetylene flame.
The concentration of indium is 20 μg/ml.
—×—: 303.9 nm, —○—: 325.6 nm
—△—: 412.5 nm, 451.1 nm.

the analytical lines of 303.9, 324.6, 410.5, and 451.1 nm were 0.5, 0.6, 1.7, and 1.7 μg/ml respectively.

Dependences of the Atomic Absorptions on the Sample-flow Rate. The atomic absorptions of indium are much affected by the sample-flow rates. The experimental curves for the relation between the absorbances of atomic indium in the air-acetylene flame and the sample-flow rates are shown in Fig. 1; these curves correspond to the results with respect to some analytical lines. In all the cases, the absorbances of indium significantly decrease when the sample-flow rates become smaller than 3.5 ml/min, while they are almost constant over 3.5 ml/min. Similar results have been obtained by Fuwa *et al.* in flame-emission spectrometry[12] and by Takada and Nakano in atomic absorption spectrometry.[13] In the emission spectrometry, the intensity is very dependent on the sample-flow rate, and the maximum intensity was observed clearly at a definite sample-flow rate.[12] These results have been explained in terms of the cooling effect of the aspirated water on the flame temperature. This is because the population of atoms in the exited states, which determines the sensitivity of emission, depends much on the flame temperature. In atomic absorption spectrometry, on the other hand, the population of atoms in the ground state determines the sensitivity; it dose not depend greatly on the change in the flame temperature.[13] Therefore, the results in Fig. 1 indicate that the changes in the sample-flow rates are not so meaningful in atomic absorption spectrometry as in emission spectrometry.

Interferences of Hydrogen Acids. The dependences of atomic absorptions in the air–acetylene flame on the concentration of hydrogen acids are shown in Fig. 2. When the concentrations of acids become larger, the viscosities of the sample solutions increase and the sample-flow rates decrease significantly, below 3.5 ml/min in some cases. Such effects of acids were particularly remarkable in the cases of H_2SO_4 and $HClO_4$.

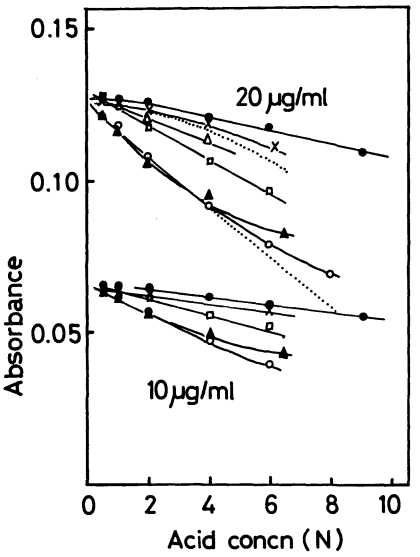

Fig. 2. Chemical interfering effects of hydrogen acids on atomic absorptions of indium at 303.9 nm in the air–acetylene flame.
The concentration of indium is 10 and 20 μg/ml. The dotted lines show the obserbed values in the cases of H_2SO_4 and $HClO_4$, and the continuous lines do the corrected values with respect to the viscosities of the sample solutions in the respective case.
—●—: HNO_3, —×—: H_2SO_4, —△—: HI,
—□—: HBr, —▲—: HCl, —○—: $HClO_4$.

These circumstances are shown in Fig. 2, where the observed values have been corrected using the results shown in Fig. 1. In the cases of other acids, the effects of the viscosities of the solutions were smaller or negligible. From Fig. 3, it can be seen that the stomic absorptions of indium are considerably interfered with by various hydrogen acids as the acid concentrations increase. The interferences become larger in the following order; $HNO_3 < H_2SO_4 < HI < HBr < HClO_4 \cong HCl$. These interferences can not be excluded even in the nitrous oxide–acetylene flame, as is shown in Fig. 3. It should be noted here that indium in $HClO_4$ is interfered with to almost the same extent as that in HCl.

Sastri *et al.* investigated the atomic absorptions of Ti, Zr, Ta, Hf, and so on in cyclopentadiene and acetylacetonate complexes, and suggested that the dissociations of metal complexes into atoms in the flame are controlled by the atoms directly coordinated with the central metal ion in ligands.[15,16] According to their investigation of the distributions of cobalt atoms in the flame, Fujiwara *et al.* also suggested the formation of intermediate molecules between the central metal ion and the coordinating atom in the case of cobalt(III) complexes.[17] Moreover, Popham and Schrenk explained the interferences of hydrogen acids less than 1 M with the atomic absorptions of indium by suggesting the formation in the flame of such intermediate compounds as InO and InCl.[4] Actually, Marks and Welcher observed the flame emissions of such diatomic molecules as AlO and TiO and interpreted the metallic inter-element interferences in aluminum atomic absorption spectrometry as occurring because of the reaction between the diatomic molecules.[18] The studies cited

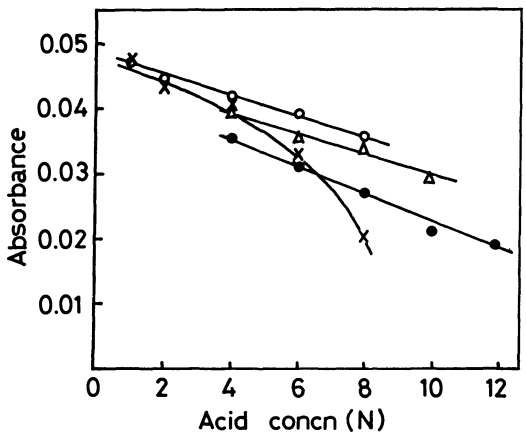

Fig. 3. Chemical interfering effects of hydrogen acids on atomic absorptions of indium at 303.9 nm in the nitrous oxide–acetylene flame.
The concentration of indium is 10 μg/ml.
—○—: HNO_3, —△—: HBr, —●—: HCl
—×—: $HClO_4$.

above suggest the important roles of the intermediate molecules, such as the diatomic molecules, in the chemical-interfering phenomena. With respect to the HCl and HBr solutions of indium, the molecular absorptions of InCl and InBr have been observed in the air–acetylene flame, when the solutions are aspirated into the flame.[8-11]

TABLE 2. DISSOCIATION ENERGIES OF DIATOMIC MOLECULES OF INDIUM[21]

Molecule	Dissociation energy (eV)
InO	3.3 ±0.5
InI	3.35±0.15
InBr	4.0 ±0.15
InCl	4.5 ±0.15
InF	5.35±0.15
InH	2.5[a]

a) Cited from "Flame Spectroscopy" by R. Mavrodineanu and H. Boiteux, John Wiley & Sons, New York (1965).

It has been established by the ^{115}In-NMR study that indium ions in various hydrogen acids exist as such complexes as $In(H_2O)_6^{3+}$ in HNO_3 and $HClO_4$, $In(SO_4)_2^-$ in H_2SO_4, and $In(H_2O)_{6-n}X_n^{3-n}$ in HCl, HBr, and HI, where X is Cl, Br, and I and where n is 0—4.[19,20] If we take into consideration the suggestions with respect to the decompositions of various complexes in the flames, as proposed by Sastri *et al.*[15,16] and Fujiwara *et al.*,[17] it is possible that indium in various acidic solutions produces, in the flame, such diatomic molecules as InO, InS, InCl, InBr, and InI as intermediate compounds. If so, the interferences due to hydrogen acids may have some correlation with the dissociation energies of the suggested diatomic molecules. The dissociation energies of the diatomic molecules are listed in Table 2.[21] The order of magnitudes of the dissociation energies is really consistent with that of the interferences due to hydrogen acids except for the case of $HClO_4$. This may support the idea of the formation of diatomic molecules in the flame. Indium in the $HClO_4$ solution behaves similarly to that in HCl in both the air–acetylene and nitrous oxide–acetylene flames. This may be ascribed to the formation of InCl by a secondary reaction in the flame in the case of $HClO_4$. This interfering mechanism will be elucidated in the next section.

The reason why the interferences of acids cannot be overcome even in the nitrous oxide–acetylene flame may be ascribed to the fact that the dissociation energies of the diatomic molecules shown in Table 2 are large enough so that the diatomic molecules are dissociated into atoms only with difficulty, even in the nitrous oxide–acetylene flame.

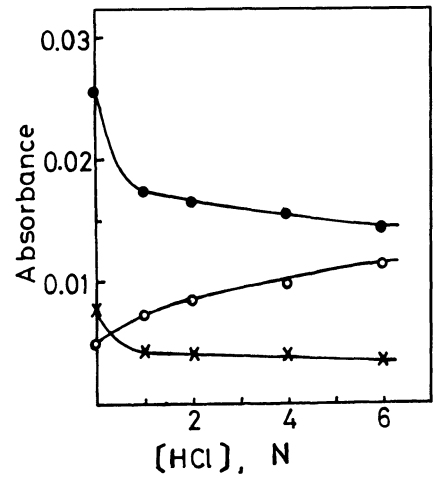

Fig. 4. Concentration of HCl *vs.* atomic and molecular absorptions of indium in the air–acetylene flame.
The concentration of indium is 0.05 M, and a deuterium lamp was used.
—●—: In at 303.9 nm, —×—: InO at 273.0 nm,
—○—: InCl at 267.2 nm.

Interfering Mechanisms. In order to elucidate the interfering mechanisms suggested above, the atomic and molecular absorptions for the indium atoms, InO and InCl, in the air–acetylene flame were measured in terms of the HCl solution of indium, using a deuterium lamp. The results are shown in Fig. 4, where the concentration of indium was 0.05 M and where the analytical lines for In, InO, and InCl were 303.9 nm, 273.0 nm, and 267.2 nm[11] respectively. As the concentration of HCl increase, the absorbances of InCl increase, while those of In and InO decrease. This fact indicates that the interfering effect of HCl is apparently due to the formation of InCl in the flame. The increase of the interference at the high concentrations of HCl may also be affected by that of the complex formation of indium with chlorine in solution.[20] In the case of HBr, result similar to that in Fig. 4 was obtained, and it was ascertained that the formation of InBr is essential to the interfering effect of HBr.

In Fig. 5 the absorption spectrum is shown; it was measured by aspirating the $HClO_4$ solution of indium into the air–acetylene flame. It should be noted here that the broad bands observed in the range from 265 to

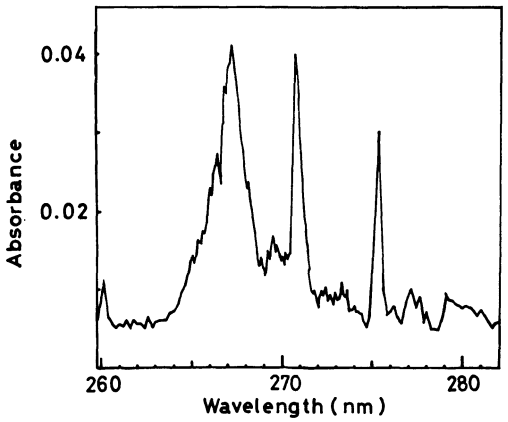

Fig. 5. Absorption spectrum in the airacetylene flame, which are measured with aspirating an 2 N $HClO_4$ solution of 0.05 M indium into the flame.

270 nm correspond to those of InCl.[11] This result indicates that the following reactions for the formation of InCl occur in the flame and that InCl is produced:

$$In(ClO_4)_3 \xrightarrow{\Delta} In^* + 3Cl^{**} + 6O_2$$
$$HClO_4 \xrightarrow{\Delta} Cl^{**} + OH + 3/2O_2$$
$$In^* + Cl^{**} \longrightarrow InCl$$

where Δ indicates a pyrolysis reaction. The formation of InCl in the case of the $HClO_4$ solution of indium explains well the results of atomic absorption spectrometry shown in Figs. 2 and 3.

References

1) J. E. Allen, *Spectrochim. Acta*, **18**, 259 (1962).
2) C. E. Mulford, *Atomic Absorption Newsletter*, **5**, 28 (1966).
3) C. E. Mulford, *ibid.*, **5**, 88 (1966).
4) P. E. Popham and W. G. Schrenk, *Spectrochim. Acta, Part B*, **24**, 223 (1969).
5) K. Fuwa and B. L. Vallee, *Anal. Chem.*, **41**, 188 (1969).
6) K. Fuwa, H. Haraguchi, and S. Toda, International Congress on Analytical Chemistry, Kyoto, Japan, 1972.
7) K. Fuwa, H. Haraguchi, K. Okamoto, and T. Nagata, *Bunseki Kagaku*, **27**, 945 (1972).
8) H. Haraguchi and K. Fuwa, *Chem. Lett.*, **1972**, 913.
9) H. Haraguchi, M. Shiraishi, and K. Fuwa, *ibid.*, **1973**, 251.
10) K. Fuwa, IV-th International Conference on Atomic Spectroscopy, Toronto, 1973.
11) H. Haraguchi and K. Fuwa, *Spectrochim. Acta, Part B*, in press.
12) K. Fuwa, R. E. Thiers, B. L. Vallee, and M. R. Baker, *Anal. Chem.*, **31**, 2039 (1959).
13) T. Takada and K. Nakano, *Nippon Kagaku Zasshi*, **90**, 279 (1969).
14) A. Walsh, *Spectrochim. Acta*, **7**, 108 (1955).
15) V. S. Sastri, C. L. Chakrabalti, and D. E. Willis, *Talanta*, **16**, 1093 (1969).
16) V. S. Sastri, C. L. Chakrabalti, and D. E. Willis, *Can. J. Chem.*, **47**, 583 (1969).
17) K. Fujiwara, H. Haraguchi, and K. Fuwa, *Anal. Chem.*, **44**, 1895 (1972).
18) J. Y. Marks and G. G. Welcher, *ibid.*, **42**, 1033 (1970).
19) T. H. Cannon and R. E. Richards, *Trans. Faraday Soc.*, **62**, 1378 (1966).
20) H. Haraguchi, K. Fuwa, and S. Fujiwara, *J. Phys. Chem.*, **77**, 1497 (1973).
21) A. G. Gaydon, "Dissociation Energies and Spectra of Diatomic Molecules," 3rd Ed., Chapman and Hall London (1968).

An Adiabatic Calorimeter for High-resolution Heat Capacity Measurements in the Temperature Range from 12 to 300 K

Masami TATSUMI, Takasuke MATSUO, Hiroshi SUGA, and Syûzô SEKI
Department of Chemistry, Faculty of Science, Osaka University, Toyonaka, Osaka 560
(Received May 23, 1975)

Construction of a high resolution calorimeter of an adiabatic type for single crystals is described. It uses a bank of thermistors for high resolution measurements in addition to a miniature platinum resistance thermometer. The results of heat-capacity measurements on benzoic acid as a standard material showed the inaccuracy of $\pm 0.1\%$ and the imprecision was confirmed to be less than $\pm 0.05\%$ between 50 and 275 K.

Singularities observed in thermodynamic properties of a substance at the critical point are characterized by the quantities known as the critical exponents. These quantities are of paramount importance in the study of critical phenomena and their determination as well as verification of various relation expected to hold among them are central problems of experimental and theoretical investigations in this field.[1,2] Elucidation of the nature of a phase transition by determining reliable values of the critical exponents requires measurement of the thermodynamic quantities with high resolution both in the independent variable (particularly, the temperature) and in the quantity measured. Although the heat capacity exponents have been evaluated for a number of substances, lack of sufficient resolution in the measurement diminishes their reliability in a large number of cases. Among the notable exception in this respect is the excellent high resolution heat capacity measurement performed by Buckingham, Fairbank and Keller[3] on the λ-transition in liquid ^{4}He. Other critical phase transitions which have been studied include those in magnetic and dielectric substances and binary liquid mixtures.[4-10] As to the dielectric transitions, with which we are concerned mainly, reliable high resolution heat capacity data are deplorably limited in number and in the substance dealt with.

There are two types of calorimeter used for high-resolution measurement which operate on different principles. One is the discontinuous heating method (the DC method) and the other the stationary state method (the AC method).[11] We adopted the DC method, in view of the problem of the present interest. Although the AC method has desirable features that the measurements can be made with smaller amount of the sample and easily operated automatically, it has the demerits: the specimens to be studied are limited to non-volatile substances and the absolute values of the heat capacities are very difficult to determine. On the other hand, the DC method has no restrictions on specimens and yields the absolute value of heat capacities and is able to detect a minute 1-st order component which sometimes accompany the critical point. This last possibility is also important for characterization of the phase transition phenomenon.

This paper describes an adiabatic-type high-resolution calorimeter which works in the temperature range between 12 and 300 K. The accuracy of this apparatus was determined by the measurement of heat capacities of benzoic acid. The results[12] of the high resolution measurement on the single crystal of $SnCl_2 \cdot 2H_2O$ revealed the reliability of this apparatus.

Experimental

Construction of Apparatus. The calorimeter consists of four major parts, *viz.*, the cryostat, the adiabatic-control circuit, the temperature-measuring circuits and the energy supply and its measuring circuit (Fig. 1). A special feature of the apparatus is that it is equipped with two thermometers, a platinum resistance thermometer and a thermistor thermometer. The former provides an accurate temperature scale based on the International Practical Temperature Scale 1968, while the latter enables precise measurement of small temperature increment of the calorimeter. The platinum resistance thermometer is also used for calibrating the thermistor. This feature endows the apparatus with a unique capability of measuring the heat capacity with high accuracy and precision. Details of the calorimeter design and construction are described in the following.

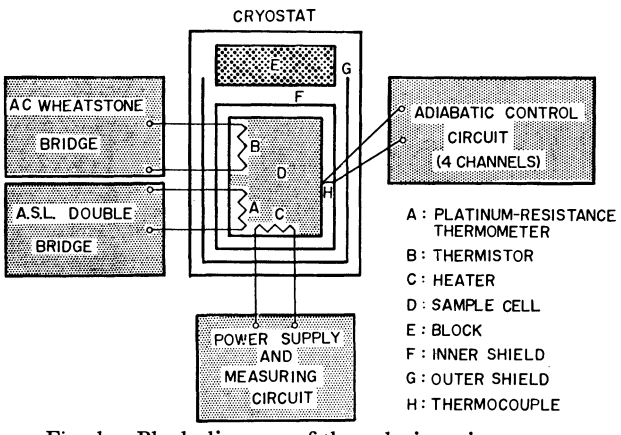

Fig. 1. Block diagram of the calorimetric system.

1) Cryostat. Figure 2 shows a schematic drawing of the cryostat. The calorimeter cell (A), whose detailed construction is given below, is suspended in the inner adiabatic jacket (B) with a 0.5 mm thick nylon cord at the top. Its horizontal position relative to the jacket is adjusted to the center of the jacket with three thinner nylon cords attached at the bottom of the cell. The inner jacket of a thin copper shell of 0.5 mm thickness consists of three parts, *i.e.*, a cylinder, upper cone (these two weighing 114 g) and a bottom cone (22 g). The bottom cone is firmly attached to the cylinder with three pairs of screw. The temperature of the inner

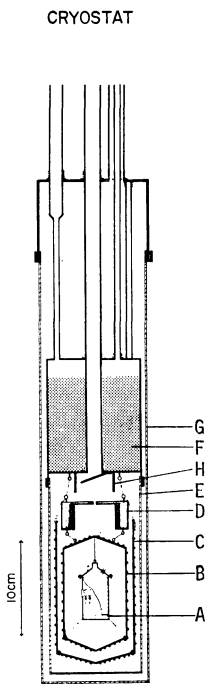

Fig. 2. Sectional view of the crystat
A, Sample cell; B, Inner jacket; C, Outer jacket; D, Block; E, Inner vacuum can; F, Coolant container; G, Outer vacuum can; H, Sleeve

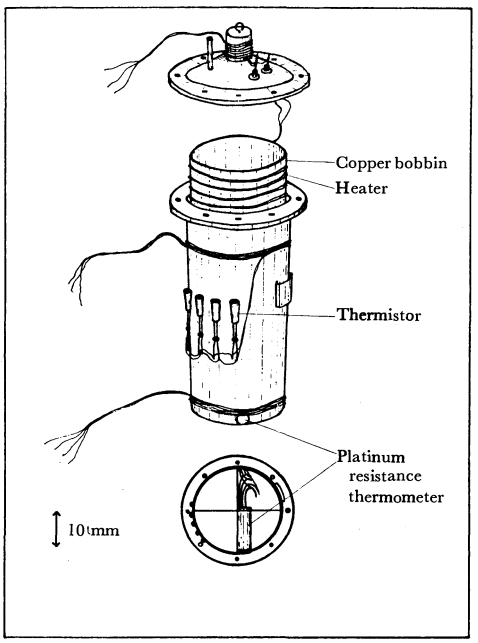

Fig. 3. Sketch of the calorimeter cell for single crystals. The bobbin is slightly lifted for better illustration.

jacket is controlled relative to that of the cell. The outer jacket (C) is also a temperature-regulated copper cylinder (275 g) whose function is to prompt establishment of the adiabatic condition of the cell by keeping a stabilized temperature difference between the inner jacket and itself. The copper block (D) is a temperature-controlled heat reservoir, which helps the inner jacket to work correctly by tempering the thermal agitation coming down through the leads. The block has a large mass for this purpose and a copper bobbin for winding the heater wires. These three temperature-controlled components are suspended in the inner vacuum can (E) from the bottom of the coolant container (F). The latter is surrounded by the outer vacuum can (G) which is normally immersed in an appropriate coolant, usually liquid nitrogen or methanol-dry ice mixture according to the temperature region being studied.

The leads for the thermometers, heaters, and thermocouples are tightly wound around the inner jacket and the block, and then around the sleeve (H) attached to the bottoms of the inner coolant container in turn and finally led out through a Dekhochinsky seal and a glass-hermetic seal. The lead wires to the calorimeter cell are connected with terminals insulated by teflon attached to the inner jacket. The spaces in the inner can and between the inner and the outer can are evacuated independently to *ca.* 0.2 mPa by an oil vacuum pump.

2) Calorimeter Cell. The calorimeter cell for the samples of single crystals is shown schematically in Fig. 3. This is a chromium-plated copper cylinder, about 30 mm in diameter and 60 mm long with the wall 0.3 mm thick.

A dismountable lid on the top end of the cell allowed loading it with a large snugly-fitting single crystal. The vacuum-tight closure was achieved by applying a thin layer of Apiezon N grease between the lapped faces of the flanges of the cylinder and the lid and fixing them tightly together with eight pairs of screw. An indium O-ring with 0.5 mm diameter can also be used. This closure could hold cell at 0.1 mPa. The two types of thermometers are attached to the outside of the cell. One is a miniature platinum-resistance thermometer (Model S 1059, the Minco Products, USA). It is 13 mm long and 3 mm in diameter and has a nominal resistance 100 Ω at 0 °C. It is placed in a closely fitting copper tube soldered on the bottom face of the cell. The other is a bank of five glass-bead thermistors (Shibaura Denshi, model NSB) for the high resolution measurements. The glass beads were wrapped in a small piece of thin copper sheet, and soldered on the side of the cell side by side. Nominal resistance of each of the thermistor is 4 kΩ at 0 °C and 0.13 kΩ at 100 °C. The connection of the five thermistors was changed so as to obtain the resultant resistance of 10—20 kΩ in the temperature interval of interest. This cell had a copper bobbin, 0.2 mm thick and of a slightly smaller diameter than the inner diameter of the cell itself. On this bobbin the calorimeter heater was wound bifilarly and cemented in place with GE adhesive. The heater wire was double silk wrapped constantan (Driver & Harris AWG No. 36) with total resistence of 100 Ω. The primary role of the bobbin is to promote temperature homogeneity in the cell during the heat-on period. Helium gas for improving thermal conduction within the sample space could be admitted before seal-off.

3) Adiabatic Control. The heat-transfers between calorimeter cell and its environment may be caused by three factors, that is, the convective heat leak which was eliminated by maintaining vacuum in the calorimeter system, the radiative heat transfer and the heat transfer by conduction along the leads bundle. As regards the radiative heat transfer it was reduced by gold-plating the inner surface of the radiation jacket and chromium-plating the outer surface of the calorimeter cell to obtain high reflectivity. To minimize the heat transfer by conduction, the leads to the calorimeter cell must be as thin as possible, but it is in conflict with the requirement of high electric conductivity of leads. To minimize heat exchange by the second- and third-mentioned mechanisms, the temperature of the inner jacket, about which leads were wound tightly, must be equalized to that of the

outer surface of the calorimeter cell, and especially to minimize the temperature gradient along both surfaces is required in order to reduce the radiation heat transfer. Temperatures of the bottom cone and other part of the inner jacket are controlled separately. The resistances of the heater wires were adjusted so as to make the power dissipation in the side and cone proportional to their respective mass (cylinder, uppercone 100 Ω and bottom cone 50 Ω). Thermocouples (Chromel P-constantan) were attached at five locations on the inside and outside of the cylinder and at three locations on the bottom cone. The two thermocouples insulated by cellophane adhesive tape were covered with small thin phosphor bronze plates which were attached to the inner bottom cone with two screws. These thermocouples detects temperature difference between the cell and the side and between the cell and the bottom of the adiabatic jacket. During a test run of the apparatus, it was found that the thermal conductivity between the inner and outer jackets was so small that the inner jacket, especially its bottom was liable to over-heat. It was remedied by linking thermally the bottoms of the two jackets with copper wire of appropriate length and diameter. The thermocouples (Chromel P-constantan) sense the temperature differences between the block and the inner jacket and between the outer jacket and the inner jacket, and the currents flow through the heater of the block (200 Ω) and the outer jacket (197 Ω). The temperatures of the block and the outer jacket were usually maintained lower than that of the inner jacket by several kelvin. On-off type of the regulator action, even if it is satisfactory in regard to the stability of the regulation, would caused strong noise in the thermometer circuits to the point of saturating the detectors. This difficulty was overcome by proportional mode of action which regulates the input power to the jacket heater smoothly in proportional to the temperature imbalance. The control system only with the proportional function could not automatically follow the temperature variation of the calorimeter cell at the early stage of and immediately after the heating period. Therefore, the off-set voltages, which were determined at an equilibration and a heating periods respectively, had to be readjusted quickly. To reduce the labor of paying attention to the off-set signal indicators, an integral action was added to the proportional action. In this improved regulator system (Fig. 4) the thermocouple voltage was measured and amplified with DC microvoltmeter (Keithley model 149), the output of which was fed into the proportional-integrating circuit as an error signal, and drove the jacket heater. The heater current was normally less than 50 mA. By using this circuit the temperature difference between the inner jacket and the calorimeter cell was less than 0.5 mK during both equilibration and heating periods.

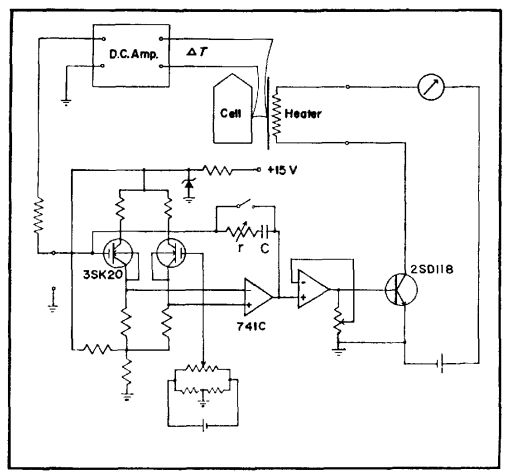

Fig. 4. Electric proportioning-integrating circuit.

4) Measurements of the Temperature. a) Circuit System for the Platinum Resistance Thermometer: The miniature platinum resistance thermometet was used as a temperature sensor which determined the absolute temperature scale. The precision AC double bridge (Automatic System Laboratory Inc. Model H8) with inductively coupled ratio arms was used to measure the thermometer resistance. This bridge has the merit that it requires only one balancing operation, since use of alternating current eleminates the effect of thermal emf's. However, some care had to be paid to the characteristics of the apparatus on using it in low temperature calorimeter, as will be described below. The basic circuit of this bridge is shown in Fig. 5 which, for the sake of clarity, does not contain

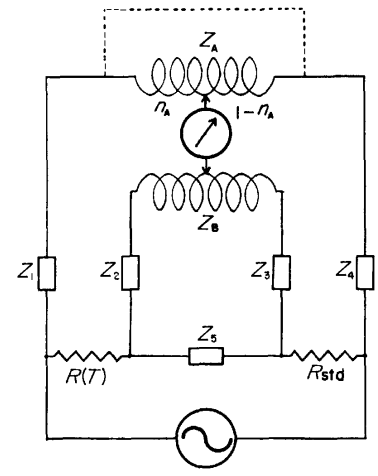

Fig. 5. Basic circuit of the ASL AC double bridge.

any phase balancing component. $R(T)$ is a resistance of the thermometer, R_{std} is a resistance of the standard resistor and Z_1, Z_2, Z_3, Z_4, and Z_5 represent lead impedances. Z_A and Z_B are impedance of the inductive ratio arms which have 4×10^5 Ω at 390 Hz and n_A and n_B the ratios of the arms. The equation of the balance which is that of the Kelvin double bridge is given precisely by

$$R(T) = R_{std}\left[\frac{n_AZ_A+Z_1}{(1-n_A)Z_A+Z_4}+Z_5\frac{(1-n_B)Z_B+Z_3}{Z_B+Z_2+Z_3+Z_5}\times\frac{n_AZ_A+Z_1}{(1-n_A)Z_A+Z_4}-\frac{n_BZ_B+Z_2}{(1-n_B)Z_B+Z_3}\right]. \quad (1)$$

In this bridge $Z_A=Z_B$, $Z_1=Z_2$, $Z_3=Z_4$ and Z_A and Z_B are much larger than Z_1, Z_2, Z_3, Z_4, and Z_5, so if n_A and n_B are not close to unity or zero, this equation is simplified as given below,

$$R(T) = R_{std}\frac{n_A}{1-n_A}\left[1+\frac{Z_1}{n_AZ_A}-\frac{Z_4}{(1-n_A)Z_A}\right]. \quad (2)$$

If ultimately high-precision measurement of the resistance is required, the ratio n_A must lie between 0.2 and 0.8, so the value of the standard resistor has to be varied in accordance with the resistance of the thermometer. For this purpose, three standard resistors (100 Ω, 6.238453 Ω, 0.390430 Ω) were prepared and kept in the box thermostated within ±0.03 K.

Three corrections had to be made in the measurements by using this AC double bridge. The first was correction for eliminating the effects of the impedance of the leads. If Z_1 and Z_4 were much smaller than Z_A, the last two terms in Eq. (2) were neglected, so Eq. (2) becomes to be $R(T)=R_{std}n_A/(1-$

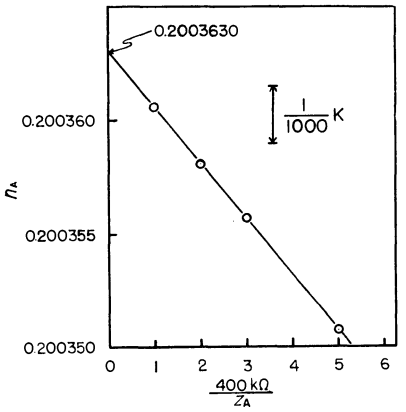

Fig. 6. Correction for the impedance of the leads to the platinum resistance thermometer.

n_A). But the condition $Z_A \gg Z_1$, Z_4 is not always satisfied because the thermometer-lead impedance could not be reduced below a few ohms. The correction for this effect was achieved by connecting resistors in parallel with Z_A in turn, which is indicated by the dashed lines in Fig. 5. The "n_A" are plotted against the 400/(resultant resistance) in Fig. 6. Extrapolation of this straight line to the infinite resultant resistance gives the corrected n_A. This means that, since no current flows in this circuit because of its infinite resistance, the voltage drop due to Z_1 does not occur, so the extrapolated n_A corresponds to that which would be obtained if Z_1 is zero. The slope of this straight line increases with increasing $R(T)$ and R_{std}. The magnitude of this correction was less than 3/1000 K at any temperature range studied. The second correction is concerned with the self-heating of the thermometer. Since the Minco thermometer has the higher resistance and smaller volume than the platinum resistor of normal type, the effect of self-heating due to the current flow for measurements could not be neglected. This effect could be eliminated, however, in the following manner. A set of measurements with various bridge carrier voltages was plotted against the power dissipated in the thermometer and the n_A at the zero power dissipation was determined by extrapolation. This n_A value corresponds to that measured at condition where no current flowed in the thermometer. In actual heat capacity measurements, the power dissipation in the thermometer was typically 5 μW. The third correction, *i.e.*, the effect of the inductance of the thermometer element is not quite clear. The inductance of the Minco thermometer (~30 μH) is considerably larger than that of the typical L & N Pt-thermometer (~1.5 μH). Therefore, the DC resistance and the apparent AC resistance of the Minco thermometer can possibly be appreciably different from each other. This possible effect was taken into account by making the calibration of the Minco thermometer at a fixed frequency (390 Hz), while the standard thermometer (L & N Pt-resistor) was measured with DC current. The calibration table is given in the apparent resistance of the Minco thermometer against temperature. In principle, the calibration may have been performed at several frequencies to determine the DC resistance by extrapolation, but it was impracticable because of the instrumental limitation. This caused no inconvenience because the Minco thermometer was always used in conjunction with the ASL AC double bridge at the fixed carrier frequency.

b) Calibration of the Platinum Resistance Thermometer: The Minco platinum resistance thermometer was calibrated against the standard capsule type Leeds & Northrup Pt-thermometer which was recalibrated according to the IPTS-68. Two thermometers were mounted side by side in the well drilled in a copper block and set in the cryostat. The resistance of the standard thermometer was measured with the DC Müller bridge (Leeds & Northrup 8071-B Type G-3), while that of the Minco thermometer by the AC bridge mentioned above. The calibration was carried out at the eight temperatures from 13.81 to 373.15 K. Three measurements were made at each of the internationally defined fix points: *i.e.*, the triple and boiling points of equilibrium H_2, O_2, H_2O, equilibrium H_2 at 25/76 atm and the boiling point of Ne. The accurate values of resistance for the Minco thermometer at these fixed points were determined by interpolation. The temperature determined from the calibration table of the standard thermometer and the resistances of the Minco thermometer were corrected according to the procedure described above.

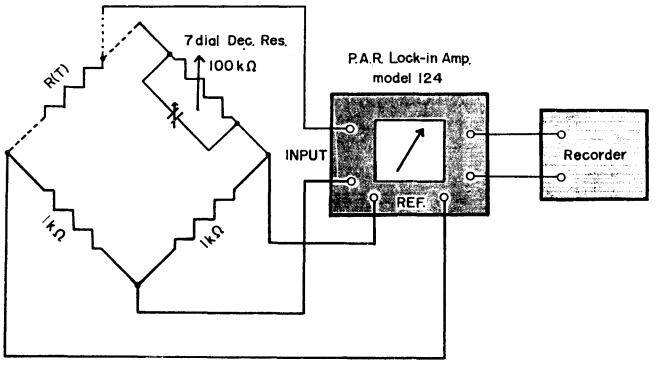

Fig. 7. AC Wheatstone bridge for the thermistor thermometer.

c) Circuit System for the Thermistor Resistance Measurement: Figure 7 shows the AC Wheatstone bridge for the thermistors which was used in the high resolution measurements. A lock-in amplifier (Princeton Applied Research Corp. Model 124) was employed as a high sensitivity detector. The balance of the resistive and the reactive components could be performed easily. The variable air-capacitor connected in parallel with decade resistor was used in balancing a reactive component. The fixed-arm resistors and the seven dial decade resistor box were kept in an air thermostat. Each dial of the decade resistor was calibrated against the 10 kΩ standard resistor by the decade-for-decade method. The leads of the thermistor represented by the dashed lines in Fig. 7 have the same length so as to compensate their impedance effects. Induction noises to the thermometer leads were reduced by twisting the lead wires with each other. All the other lead wires (for the thermocouples and heaters, which were potential noise sources) were also twisted in go-and-return pairs with different pitches.

d) Calibration of the Thermistor: The thermistor was calibrated against the Minco platinum thermometer (IPTS-68) at each measurement. On determining the relation between the temperature scale and the resistance of the thermistor, the equation $T=\sum_{i=1}^{n} A^i(\ln R)^i$ (n=2,3 or 4) was assumed and the expansion coefficients were determined by the least square fit. The deviations of the observed values from this equation were found to be less than 1×10^{-3} K, which was precise enough to determine absolute temperatures by means of this method (Fig. 8).

5) Circuit System for Energy Supply. The power supply and measureing circuit is shown in Fig. 9. A constant voltage circuit was used for the power supply and a digital voltmeter (Takeda Riken Model TR-6515D) for the measurements of

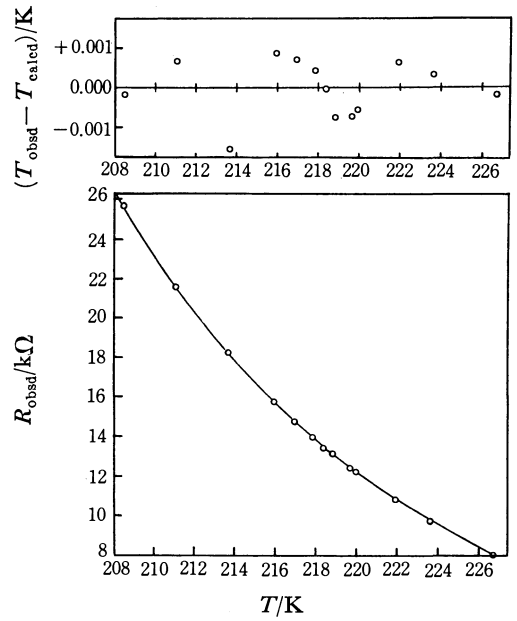

Fig. 8. Relation between the temperature and the net resistance of the five thermistors connected in parallel (lower), and the deviation of the calibration points from this curve (upper).

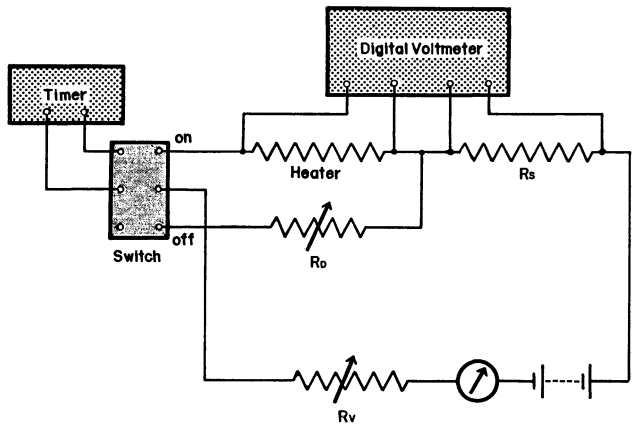

Fig. 9. Power supply and measuring circuit.

the current and voltage. The duration of the heat-on period was measured with a digital multifunction counter (Takeda Riken Model TR-5104). When the switch was put in position "on," the current start to flow through the calorimeter heater and counting of the timer begins. The current through the heater was determined by measuring the potential difference across the standard resistance R_s(100 Ω). A dummy resistor provided a by-pass circuit for the heater current. This device stabilized the out-put of the power supply when the calorimeter heater was switched off.

Results and Discussion

Determination of Heat Capacity of Benzoic Acid. The measurements and calculations of the gross heat capacity were carried out as follows. After the initial temperature T_i; *i.e.* the steady state temperature before heating, was measured, the electrical energy Q was introduced into the calorimeter. When the equilibrium state was confirmed after switching the heater current off, the final temperature T_f was determined. The steady state temperatures T_i and T_f were determined by following the temperature drifts as a function of time. If the natural drifts due to the imperfection of the adiabatic regulation were present, an additional corrections would be required. The electrical energy Q was determined as the product of the average calorimeter heater voltage $\bar{e}$, the current $\bar{i}$, and the time interval t, of the applied power input: *i.e.* $Q=\bar{e}\bar{i}t$. From the knowledge of these quantities, the gross heat capacity was determined by the equation: $Q/(T_f-T_i)$ at the mean temperature $(T_i+T_f)/2$. In the case of the high resolution measurements, the adiabatic regulation was strictly adjusted in order to eliminate the temperature drift for a long time. The precise determination of the heat capacity employing the small temperature increment is more liable to be affected by the heat leak. The thermistor was calibrated over the range of about 30 K including the temperature interval of the high-resolution measurement. The heat capacity is given by the equation, $C=Q/(\mathrm{d}T/\mathrm{d}R)_{T=T_{av}}\Delta R$, where $T_{av}=\{T(R_f)+T(R_i)\}/2$ and $\Delta R=|R_f-R_i|$. This calculation was performed on NEAC 2200 Model 700. In order to ascertain the over-all accuracy of the whole apparatus, the heat capacity measurement was performed on the benzoic acid as standard material which was prepared by the US National Bureau of Standards. The weight of the sample was 12.6106 g. The experimental values of the molar heat capacity are given in Table 1. Fig. 10 shows the deviation plots of our individual data points from the smoothed heat capacity of benzoic acid recommended by the US Calorimetry Conference.[13] The data by Furukawa *et al.*[14] and Cole *et al.*[15] are also plotted. These data were originally based on the IPTS-48, while our measurements were performed on the basis of the new temperature scale (IPTS-68). In order to compare these data with ours, they were converted into IPTS-68.[16]

Deviation of our heat capacity data from the smoothed curve is about 1% of the total heat capacity at 20 K, 0.5% between 25 and 50 K ($\Delta T\approx 1.5$ K) and 0.1%

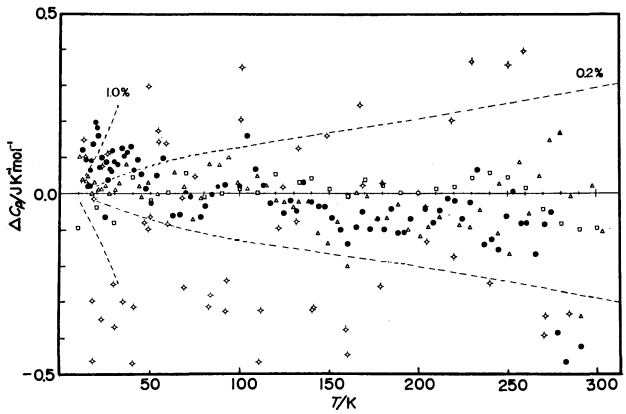

Fig. 10. Deviation plot of the measured values for the heat capacity of benzoic acid. ● the present data; □ Furukawa *et al.*; △ Cole *et al.*; ☼ Gorbunov *et al.* The abscissa is a statistical-smoothed-value of the data of several authors which include the results of Furukawa *et al.* and Cole *et al.*

Table 1. Heat capacity of benzoic acid

T/K	C_p/$JK^{-1}mol^{-1}$	T/K	C_p/$JK^{-1}mol^{-1}$	T/K	C_p/$JK^{-1}mol^{-1}$	T/K	C_p/$JK^{-1}mol^{-1}$
12.51	3.95	35.54	27.65	113.15	68.98	212.85	108.27
14.17	5.29	37.32	29.34	117.14	70.42	217.04	110.11
15.54	6.47	39.16	31.02	124.85	73.27	221.17	111.90
16.63	7.58	41.12	32.67	128.59	74.70	225.27	113.64
17.56	8.55	43.19	34.43	132.28	76.04	229.31	115.46
18.38	9.44	45.34	36.12	135.99	77.52	233.34	117.33
19.14	10.27	47.82	38.00	140.02	78.98	237.31	118.89
19.82	11.04	50.61	39.96	143.91	80.44	241.39	120.73
20.47	11.73	53.56	42.03	147.73	81.89	245.57	122.58
21.12	12.42	56.72	44.07	151.81	83.42	249.73	124.55
21.87	13.22	60.18	46.17	156.14	85.06	253.86	126.50
22.64	14.01	63.66	47.89	160.41	86.68	257.93	128.27
23.36	14.83	66.93	49.62	164.62	88.37	261.97	130.13
24.16	15.76	70.03	51.23	168.78	90.06	265.98	131.89
25.05	16.55	72.99	52.65	172.89	91.65	270.10	133.89
25.89	17.65	75.82	54.00	176.94	93.30	274.17	135.80
26.70	18.48	78.56	55.14	180.96	94.90	278.22	137.34
27.50	19.38	81.20	56.32	184.91	96.57	282.56	139.26
28.24	20.18	84.19	57.62	188.83	98.11	287.00	141.23
28.96	21.01	87.89	59.14	192.71	99.71	291.24	143.35
29.90	21.97	91.87	60.77	196.56	101.35	295.44	145.22
31.18	23.23	100.55	64.19	200.36	102.84	299.62	147.07
32.54	24.68	104.86	65.98	204.39	104.67	303.75	148.97
33.95	26.13	109.09	67.49	208.65	106.44		

between 50 and 275 K ($\Delta T \approx 4$ K). It should be noted that the weight of the samples employed by the different authors are considerably different, *i.e.*, 12.6106 g (ours), 100.99 g (Cole *et al.*) and 6.16 g ((Gorbunov *et al.*).[17] Taking into account of the dependence of the precision of the measurement on the amount of the samples, our data are quite satisfying.

Sources of Inaccuracy in the Measurement. Next, we consider two aspects of the errors, namely, the systematic error (contributing to inaccuracy) and the random error (contributing to imprecision). A measure of the former is the deviation of the smoothed curve from the (unknown) "true" heat capacity, while the latter appears as the scattering of the data points about the smoothed curve. Several factors contribute to these errors; *i.e.*, errors in determination of the input energy and temperature and those due to the heat leak. The calorimeter heater voltage and current were determined to within 10 parts per million and the time interval within 1 ppm. Thus the errors due to the energy measurement are not a decisive factors in both the inaccuracy and the imprecision. The deviation of the thermometer calibration from the IPTS-68 was typically 4 mK and varied smoothly with temperature. The inaccuracy of the heat capacity due to the error in the temperature scale was estimated to be 0.3% at the lowest temperature and less than 0.02% at 200 K. The resistance resolution by the ASL bridge was better than 1×10^{-5} Ω which corresponds to 2.3×10^{-4} K at 15 K. At the higher temperatures, the temperature resolution is better than 1×10^{-4} K. Thus, the temperature measurement is not the largest source of the imprecision of the observed heat capacity, provided that the temperature step for one measurement is not too small (1~3 K). The main factor contributing to the imprecision appears to be the heat leak to or from the sample cell. It is caused by transient deviation from the ideal adiabatic condition as well as by any stray emf in the difference-thermocouple circuits. The adiabatic condition in the equilibration period is achieved by eliminating the temperature change of the sample cell. This was done by adjusting the zero shifting emf at the input circuit of the DC microvoltmeter so as to cancel the stray emf in the thermocouple leads, the resultant zero drift rate being taken as the indication of the optimum condition. Once adjusted suitably, the constant zero shifting emf served over a reasonably long series of measurements. If undisturbed, the adiabatic control system can keep the temperature of the sample cell constant within 0.3 mK for 24 hr at the desired temperature. The apparent temperature difference between the cell and the inner jacket was regulated to less than 0.5 mK during heating period. But this temperature difference does not take into account the possible temperature gradient along the surface of the cell and the inner jacket. Error due to this effect is difficult to estimate. But one of the method for its estimation would be to compare the heat capacity data obtained by different heating rates. This has not been done yet with the present calorimeter. At present, the temperature gradient effect and the stray emf, especially its variation with time, seems to be the most important factors limiting the precision of the measurement. In the high resolution measurement, the principle and procedure of the operation are essentially the same as in the ordinary measurement discussed

above, but more ingenuity and experience are required for successful operation because of the small temperature steps (two orders of magnitude smaller than in the ordinary measurements). The temperature was measured by the AC Wheatstone bridge with the imprecision less than 5×10^{-6} K. The heat leak during the equilibration period was minimized by optimizing the zero shifting emf in the difference-thermocouple circuits of the adiabatic jacket as mentioned above. This was done at the beginning of a series of measurements to within a drift rate ±2 μK for at least 30 min. This procedure was facilitated by displaying the out-put signal of the null detector (P.A.R. model 124 lock-in-amplifier) of the bridge. Heat leak during the heating is again difficult to estimate, but it is believed to be less significant than in the ordinary measurement because the lower heater power disturbs the thermal uniformity of the jacket to the lesser extent. The relatively short heating period (60~100 s) is also an advantageous factor in this respect. Figure 11 shows an example of the recorder trace of the

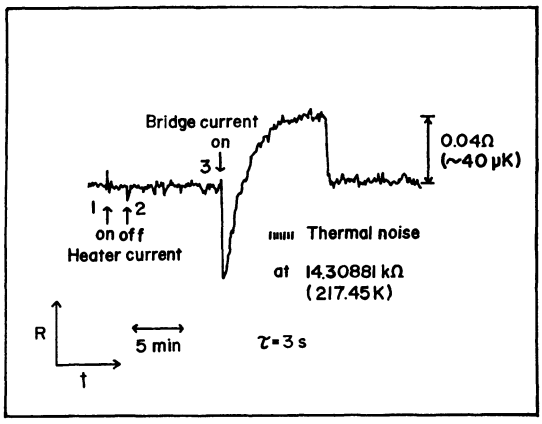

Fig. 11. An example of the high resolution measurement at 217.45 K.
R: the resistance of the thermistors.
t: the time.
τ: the time constant of the lock-in amplifier.

output signal (at 217.45 K) of the bridge null detector. The temperature remains constant within 5 μK after settling in the equilibrium value. It should be noted that the thermal noise from the the thermistor calculated by the Nyquist formula corresponds to about 5 μK. The power dissipated in the thermometer was 0.5 μW.

By use of this calorimeter, we have perfomed high resolution heat capacity measurements in the vicinity of phase transition of $SnCl_2\cdot2H_2O$,[12] $SnCl_2\cdot2D_2O$[18] and Rochelle salt.[19] The imprecision in these measurements was about 0.05%. The accuracy was also found to be satisfactorily high since it was found that the high resolution data agreed closely with those obtained by the ordinary measurement where the latter is available.

References

1) L. P. Kadanoff, W. Götze, D. Hamblen, R. Hecht, E.A.S. Lewis, V. V. Palciauskas, M. Rayl, J. Swift, D. Aspnes, and J. Kane, *Rev. Mod. Phys.*, **39**, 395 (1967).
2) H. E. Stanley, "Introduction to Phase Transitions and Critical Phenomena," Oxford Univetsity Press, London (1971).
3) M. J. Buckingham and W. M. Fairbank, "Progress in Low Temperature Physics," Vol. 13, ed. by C. J. Gorter, North Holland, Amsterdam (1961), p. 80.
4) A. V. Voronel, S. R. Garber, and V. M. Mamnitskii, *Zh. Eksp. Teor. Fiz.*, **55**, 2017 (1968).
5) F. J. Cook, *J. Phys. Chem. Ref. Data*, **2**, 11 (1973).
6) W. Reese and L. F. May, *Phys. Rev.*, **162**, 510 (1967); *ibid.*, **167**, 504 (1968); *ibid.*, **181**, 905 (1969).
7) P. Schwartz, *Phys. Rev.*, **B4**, 920 (1971).
8) E. N. Kostina and G. A. Mil'ner, *Sov. Phys. Solid State*, **14**, 2923 (1973).
9) I. Hatta and A. Ikushima, *J. Phys. Chem. Solids*, **34**, 57 (1973).
10) K. Govindarajan, B. Viswanathan, and E. S. R. Gopal, *J. Chem. Thermodynamics*, **5**, 73 (1973).
11) Ya. A. Kraftmakher, *Zh. Prikl. Mekhan. i Tekhn. Fiz.*, **5**, 176 (1962).
12) T. Matsuo, M. Tatsumi, H. Suga, and S. Seki, *Solid State Commun.*, **13**, 1829 (1973).
13) R. A. Robie and B. S. Hemingway, *Geological Survey Professional Paper* **755**, United States Government Printing Office, Washington (1972).
14) G. T. Furukawa, R. E. McCosky, and G. J. King, *J. Res. Nat. Bur. Stand.*, **47**, 256 (1951).
15) A. G. Cole, J. O. Hutchens, R. A. Robie, and J. W. Stout, *J. Amer. Chem. Soc.*, **82**, 4807 (1960).
16) The International Practical Temperature Scale of 1968, *Metrologia*, **5**, 35 (1969).
17) V. E. Gorbunov and V. A. Palkin, *Zh. Fiz. Khim.*, **46**, 1625 (1972).
18) Read before the 9-th Japanese Calorimetry Conference, Osaka (1973).
19) M. Tatsumi, T. Matsuo, H. Suga, and S. Seki, *Proc. Japan Acad.*, **50**, 476 (1974).

Pulse Radiolysis of $Hg(CN)_2$ in Aqueous Solutions

Shin-ichi FUJITA, Hideo HORII, Toshiaki MORI, and Setzuo TANIGUCHI
Radiation Center of Osaka Prefecture, Shinke-cho, Sakai, Osaka 593

(Received June 2, 1975)

The reduction of $Hg(CN)_2$ in deaerated aqueous solutions was studied by the pulse radiolysis technique. $Hg(CN)_2$ reacts with the e_{aq} with $k(e_{aq}+Hg(CN)_2)=(1.3\pm0.1)\times10^{10}$ M^{-1} s^{-1} to yield a transient species of HgCN having an absorption maximum at 285 nm. $Hg(CN)_2$ is also reduced by CO_2^- with $k(CO_2^-+Hg(CN)_2)=(3.4\pm0.2)\times10^9$ M^{-1} s^{-1}. The extinction coefficient of HgCN at 285 nm was determined as $(3.8\pm0.1)\times10^3$ M^{-1} cm^{-1}. HgCN recombines with $2k=(3.4\pm0.5)\times10^9$ M^{-1} s^{-1} to produce another absorption species, assigned as $(HgCN)_2$, in an unstable state. The decay rate of the dimer was accelerated by some additives, such as alcohols and sodium formate. Making use of a proposed mechanism, $(HgCN)_2\rightarrow Hg(aq)+Hg(CN)_2$, the absorption coefficient of atomic mercury in water was evaluated as $(2.8\pm0.1)\times10^3$ M^{-1} cm^{-1}.

The radiolysis of aqueous solutions of some metal ions gives various species in unstable valence states by the action of the reactive primary products coming from water, such as OH radicals, H radicals, and hydrated electrons. The technique of pulse radiolysis, as is well known, is useful in investigating the reaction processes of such short-lived species.[1]

By means of this method the radiolytic reduction of mercuric ions has, recently, been carried out in aqueous solutions.[2-4] The unstable monovalent mercurous ion formed initially behaves differently depending on pH of solutions. In an acidic solution at about pH 4,[3] the stable mercurous ion, Hg_2^{2+}, is formed *via* an additional step after disproportionation of the initial species:

$$Hg^+ + Hg^+ \longrightarrow Hg(0) + Hg(II)$$
$$Hg(0) + Hg(II) \longrightarrow Hg_2^{2+}$$

While in the neutral solution,[4] where the transient mercurous ion exists in the form of HgOH, the dimerization occurs in one step:

$$Hg^+ \longleftrightarrow HgOH$$
$$2HgOH \longrightarrow (HgOH)_2$$

The direct recombination is similar to the case of HgCl formed in the reduction of $HgCl_2$.[5]

Another interesting point on radiolytic reduction of mercuric ion in the neutral solution was the finding of Hg_2O,[4] which had not been proved to exist before.

In comparison with these results, the pulse technique has been applied to aqueous $Hg(CN)_2$ solutions. Another transient mercurous species, HgCN, and its unstable dimer were found optically. The reaction mechanisms are discussed based on some kinetic data.

Experimental

The experimental details of pulse radiolysis measurement have been described previously.[3,4]

Reagent grade $Hg(CN)_2$, HCO_2Na, methanol, ethanol, isopropyl alcohol and *tert*-butyl alcohol (all are supplied from Wako Pure Chemical Industries) were used without further purification.

Triply distilled water was used at natural pH for all the experiments. All the solutions were deaerated by bubbling with argon. When necessary, solutions were saturated with N_2O (special pure grade, $O_2<0.1\%$, Suzuki Shokan Co.)

Product analysis in aqueous $Hg(CN_2)$ solutions containing isopropyl or *tert*-butyl alcohol was carried out on irradiation of 7.9 kCi ^{60}Co source at a dose rate of 1.29×10^5 r/hr. Acetone, being one of the products, was determined on a gas-chromatograph (Hitachi 063) using a column of 1 m Carbowax 20 M at 50 °C.

Results and Discussion

Figure 1 shows typical oscillograms of the changes in optical absorptions at 290 and 210 nm after pulse irradiation in a deaerated aqueous solution of 200 μM $Hg(CN)_2$. The absorption at 285 nm decays approximately according to a second order kinetics. The half life was about 30 μs for a dose of about 2.5 krads per pulse. While, the absorption at 210 nm decays only partly and thereafter remains constant within about 1 ms.

Figure 2 shows the spectra of the absorption immediately and 1 ms after the pulse. The initial spectrum has a peak at 285 nm and rises at wavelengths shorter

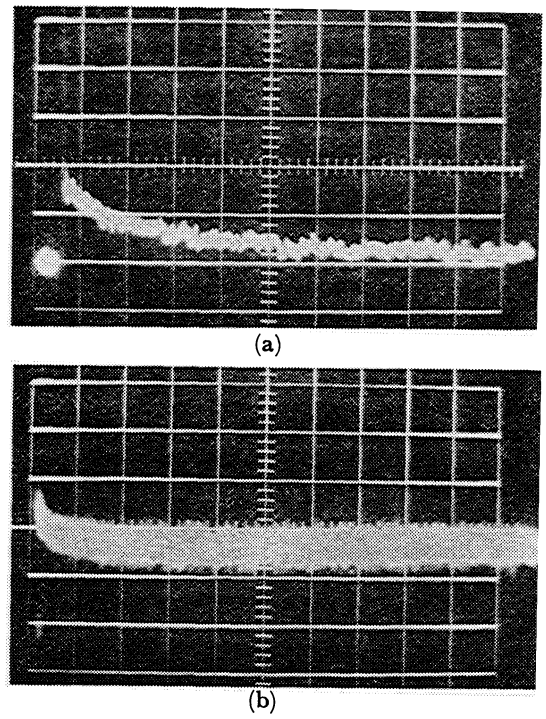

Fig. 1. Oscilloscope traces obtained in a deaerated aqueous solution of 2×10^{-4} M $Hg(CN)_2$: pulse dose, 2.5 krads; ordinates, 4.5 %/large division; (a): at 285 nm, time scale, 20 μs/large division; (b): at 210 nm, time scale, 0.5 ms/large division.

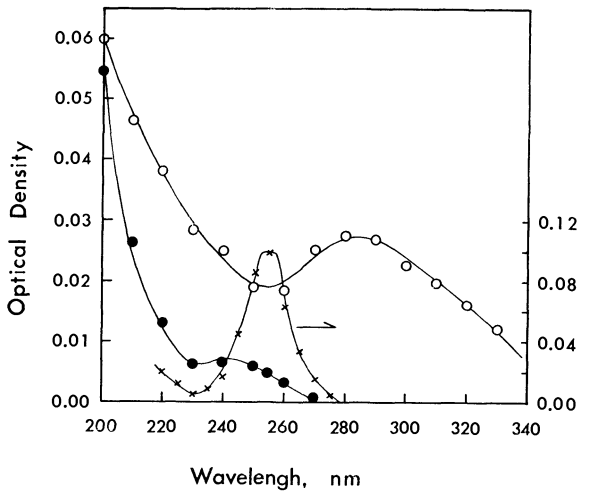

Fig. 2. Absorption spectra in a deaerated aqueous solution of 2×10^{-4} M $Hg(CN)_2$: average dose, 2.0 krads; immediately (○), 2 ms (●) after the pulse; (×), the spectrum about a few minutes after ten repeated pulses.

than 260 nm. The spectrum of the remaining absorption is different from that of the initial one. These absorption did not appear in solutions saturated with N_2O, but were hardly affected by the presence of 10 mM *tert*-butyl alcohol.

Absorption of the electron energy in water liberates the free radicals and molecular products represented by

$$H_2O \longrightarrow e_{aq}^-,\ H,\ OH,\ H_2,\ H_2O_2,\ etc. \qquad (1)$$

It has been well known that N_2O and *tert*-butyl alcohol react rapidly with the e_{aq}^- and the OH radical, respectively:

$$e_{aq}^- + N_2O \longrightarrow N_2 + OH + OH^- \qquad (2)$$

$$OH + t\text{-BuOH} \longrightarrow H_2O + \dot{t}\text{-BuOH} \qquad (3)$$

where $k_2=5\times10^9\ M^{-1}\,s^{-1}$ [6] and $k_3=2.5\times10^8\ M^{-1}\,s^{-1}$.[7] Therefore, the scavenging effects suggest that the optical absorption appearing initially in aqueous solutions of $Hg(CN)_2$ could be due to the mercurous species, the reduced product of $Hg(CN)_2$ by the hydrated electron.

$$e_{aq}^- + Hg(CN)_2 \longrightarrow Hg(I) \qquad (4)$$

The H radical would also function as a reducing agent for $Hg(CN)_2$, by analogy with the cases of other mercuric ions,[3,5,8,9]

$$H + Hg(CN)_2 \longrightarrow Hg(I) \qquad (5)$$

though the contribution to the transient is small due to the low yield ($G_H/G_{aq}^-=0.2$).[10]

Reaction Kinetics of the e_{aq}^- and the CO_2^- Ion with $Hg(CN)_2$. In order to determine the rate constant of Reaction 4, the decay of the hydrated electron after the pulse of about 0.5 μs duration was monitored at 500 nm in the absence and presence of $Hg(CN)_2$. This monitoring wavelength is considerably longer than the absorption band of the transient product of Reaction 4. Under our experimental conditions, where 10 mM *tert*-butyl alcohol was present as a scavenger for the OH radical, the first half-life of the e_{aq}^- was roughly 15 μs. With increasing $Hg(CN)_2$ concentrations from

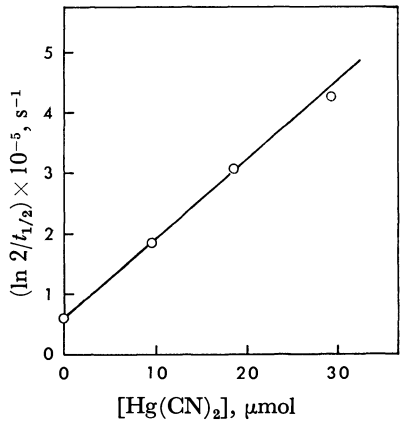

Fig. 3. Dependence of the pseudo-first-order decay rate of the e_{aq}^- on $Hg(CN)_2$ concentration, monitored at 500 nm.

10^{-5} to 3×10^{-5} M the decay of the hydrated electron became first order and the half-life progressively diminished. As seen in Fig. 3, pseudo-first-order rate constants, calculated from these half-lives, were proportional to added substrate concentration over the range investigated. The second-order rate constant, obtained from data in Fig. 3, is $(1.3\pm0.1)\times10^{10}\ M^{-1}\,s^{-1}$. This is about half of the similar reaction to HgO[4] and about one third to $HgCl_2$.[5]

On pulse radiolysis of a 200 μM $Hg(CN)_2$ solution containing 10 mM HCO_2Na and saturated with nitrous oxide, an analogous absorption species was also obtained by about 2 times in the absorption intensity, though the formation rate was slower. As a matter of fact, the spectrum immediately after the pulse was somewhat different from the spectrum in Fig. 2. In a short period of time after the pulse, however, the absorption built-up is observed in the wavelength region longer than 275 nm and shorter than 225 nm, while the absorption around 250 nm starts decaying at the end of the pulse. Within about ten μs the resultant spectrum of the absorption became analogous to the initial one in Fig. 2.

The HCO_2^- ion reacts with the OH or H radical to form a strong reducing species, CO_2^-, that has an optical absorption maximum at 250 nm:[12]

$$OH \text{ or } H + HCO_2^- \longrightarrow CO_2^- + H_2O \text{ or } H_2 \qquad (6)$$

Thus it may be concluded that, similarly to the case of reduction by hydrated electron, the transient mercurous species results also from the reaction of $Hg(CN)_2$ with the CO_2^- radical ion:

$$CO_2^- + Hg(CN)_2 \longrightarrow CO_2 + Hg(I) \qquad (7)$$

On analysis of the formation of the absorption at 285 nm, the plots of $\ln(D_\infty - D_t)$ *vs.* time, where D is the optical density, became linear and the slope was proportional to $Hg(CN)_2$ concentration. An example of the oscilloscope trace and kinetic plots are given in Fig. 4. In solutions of 50 and 100 μM $Hg(CN)_2$ a mean bimolecular rate constant for Reaction 7 was obtained as $(3.4\pm0.2)\times10^9\ M^{-1}\,s^{-1}$ at an average dose of 1.2 krads.

The experiments in the presence of some sorts of alcohols demonstrated that the transient mercurous species was not formed by the action of the radicals,

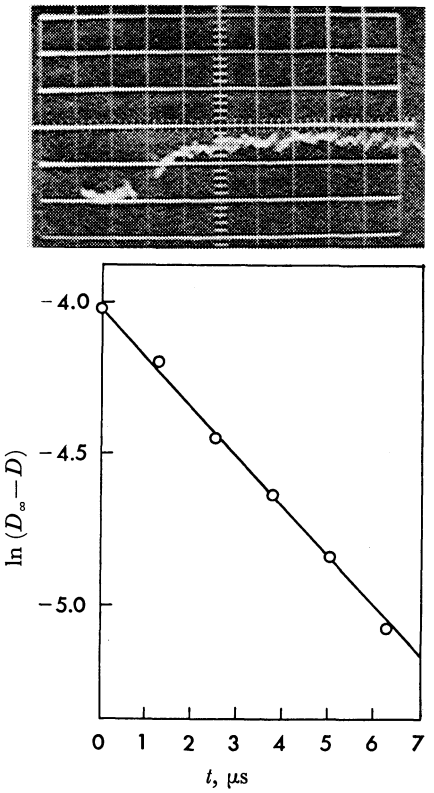

Fig. 4. An oscilloscope trace and first-order plots for the built-in of absorption at 285 nm in a N_2O saturated solution of 50 μM $Hg(CN)_2$ containing 10 mM HCO_2Na; dose, 1.2 krads; ordinates 4.5%/large division; time scale, 5 μs/large division.

such as $\dot{C}H_2OH$, $CH_3\dot{C}HOH$, $(CH_3)_2\dot{C}OH$, and $(CH_3)_2C(OH)\dot{C}H_2$. These radicals were produced by the reactions of the corresponding alcohols with the OH radicals and have been known as reducing agents[13] except the last radical. Such results are different from the case where $HgCl_2$ is the reactant toward the alcoholic radicals. Nazhat and Asmus[5] have reported that $HgCl_2$ is reduced by the isopropyl alcohol radical to form a transient mercurous chloride, HgCl.

Characteristics of the Initial Transient Species. The optical density of the absorption immediately after the pulse at 285 nm was linear against dose up to about 3 krads/pulse in deaerated aqueous solutions of more than a few mM $Hg(CN)_2$ and HCO_2Na. The molar extinction coefficient of the species, ε^{285}, is $(3.8\pm0.1)\times10^3$ M^{-1} cm^{-1}, assuming $G_{Hg(I)}=G_{e^-_{aq}}+G_H+G_{OH}=6.1$[10] in a 10 mM $Hg(CN)_2$ solution containing 5 mM HCO_2Na.

A possibility that might be argued on the assumption concerning the G value of the transient is the addition of H atoms or OH radicals to the -C≡N bond and subsequent oxidation of the ligand. Such reactions possibly take place with rapid rates when H atoms or OH radicals react with HCN or free CN^-.[14] To confirm this possibility, pulse radiolysis of N_2O saturated aqueous solutions containing a concentration of benzene (200 μM) and several concentrations of $Hg(CN)_2$ was carried out. In such solutions most of initial reactive species are OH radicals that react with benzene to produce the hydroxycyclohexadienyl radical with an absorption maximum at 313 nm ($\varepsilon^{313}=4.7\times10^3$ M^{-1} cm^{-1}).[15] No decrease in the absorption due to the radicals was observed with addition of $Hg(CN)_2$ up to 1 mM. Considering the competitive kinetics, the result demonstrates that the OH radical does not react with $Hg(CN)_2$ to a significant extent in these solutions. The nonreactivity of the -C≡N bond seems to be similar to the case for the reaction of the H radical with the $Fe(CN)_6^{4-}$ ion,[16] though there is no data concerning the reactivity against the OH radical in Ref. 16.

Figure 5a shows the test of a second order rate law for the decay of the transient at 285 nm, for different doses, in a 1 mM $Hg(CN)_2$ and 5 mM HCO_2Na solution. In both cases in which the dose per pulse was 2.1 and 4.0 krads, respectively, the plots of $1/D$ *vs.* time are linear. Thus, the kinetics indicate the following reaction:

$$2Hg(I) \longrightarrow \text{product} \qquad (8)$$

and then the slope corresponds to $2k_8/\varepsilon l$, where ε is the extinction coefficient of the absorption and l the optical path length (1.5 cm here). All the slopes obtained for various combinations of $Hg(CN)_2$ concentration (0.2—10 mM) and HCO_2Na (1—100 mM) were in good agreement with a value of $2k_8/\varepsilon^{285}l=(5.9\pm0.4)\times10^5$ s^{-1}. The value was also not affected by the existence of $NaClO_4$ up to 100 mM in a solution containing the substrates in low concentration, as seen in Fig. 5a. Substituting the values of ε^{285} and l, $2k_8$ can be calculated as $(3.4\pm0.5)\times10^9$ M^{-1} s^{-1}.

According to the Debye-Hückel theory of reaction rates in solution, the lack of the effect of ionic strength on the rate suggests that the transient does not carry any charge on it and be assigned most likely to HgCN. It is concluded in addition that the species is not subject to

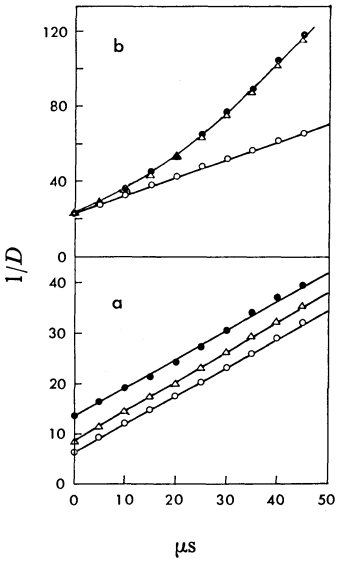

Fig. 5. Second-order plots for the decay of transient absorption at 285 nm, (a): $[Hg(CN)_2]=1.0$ mM, $[HCO_2Na]=5$ mM; ○: dose, 4.0 krads; ●: dose, 2.1 krads; △: 0.1 M $NaClO_4$ further contained, dose, 3.0 krads; (b): $[Hg(CN)_2]=1.0$ mM, dose, 2.6 krads; ○: without additives; ●: 1 mM MeOH; △: 100 mM MeOH.

additional complexing with the HCO_2^- ion, since all the spectral observations and kinetic results were not influenced by addition of the ion. Figure 5b shows similar plots of the transient obtained in a solution containing methanol to scavenge the OH radical. In this case, the decay is no longer of simple second order. The shapes of the decay curves were not influenced at all by methanol concentration in the range from 1 to 100 mM. It might be concluded, therefore, that 1 mM of methanol is enough to scavenge all OH radical to form CH_2OH and that the increase in decay rate with the addition of methanol is due to the onset of the reaction:

$$\dot{C}H_2OH + HgCN \longrightarrow \text{products} \quad (9)$$

If the assumption is right, the rate of decay of HgCN will be given by

$$-d[HgCN]/dt = k_9[\dot{C}H_2OH][HgCN] + 2k_8[HgCN]^2$$

An approximate estimate of k_9 can be obtained from a comparison of the initial decay rate with that in the presence of 5 mM HCO_2Na.[17] Let the initial decay rates of HgCN in the presence of the alcohol and HCO_2-Na be R_1 and R_2, respectively. Then from the data we find $R_1=2.01\ R_2$ and

$$R_1 - R_2 = k_9[\dot{C}H_2OH]_0[HgCN]_0$$

$$1.01 = k_9[\dot{C}H_2OH]_0/2k_8[HgCN]_0.$$

Since the H radical reacts slowly with methanol,[18] it should contribute to the formation of HgCN and the initial yield of $\dot{C}H_2OH$ should be equal to G_{OH}. Then using $[\dot{C}H_2OH]_0/[HgCN]_0=G_{OH}/G_{e^-_{aq}+H}=0.85$, k_9 can be calculated as $4.0\times10^9\ M^{-1}\ s^{-1}$. Similar treatments were also made for solutions of 1 mM $Hg(CN)_2$ containing 5 mM ethanol, isopropyl alcohol, and *tert*-butyl alcohol, wherein respective alcohol radicals must be taken into account. Here, the H radical may also be regarded to contribute to the formation of HgCN.[19] All the results are listed in Table 1, together with k(OH +HgCN) obtained in a solution without any OH scavenger. In Fig. 5b is also shown a result obtained in a 1 mM $Hg(CN)_2$ solution. The plots are found to be rather close to a linear one. It may be explained by the fact that the OH radical is consumed more rapidly by the combination reaction (k(OH+OH)$=8\times10^9$ $M^{-1}s^{-1}$,)[20] than the similar reaction of the alcohol radicals.[21]

Table 1. Reaction rate constants of HgCN with the OH and some alcohol radicals, $[Hg(CN)_2]=1$ mM, $[ROH]=5$ mM

Additive	R_1/R_2	$k(\dot{R}OH+HgCN)$, $M^{-1}s^{-1}$
MeOH	2.01	4.0×10^9
EtOH	1.98	3.9×10^9
2-PrOH	1.59	2.4×10^9
t-BuOH	1.41	1.6×10^9
Nothing	1.77	3.1×10^9 [a]

a) The value will represent the reaction rate constant of the OH radical with HgCN.

It is of interest whether Reaction 9′ gives a stable organomercury compound,

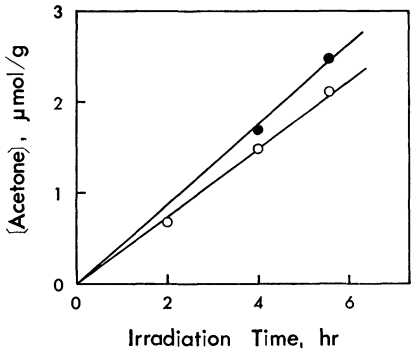

Fig. 6. Dependence of acetone yield on irradiation time in aqueous solutions of 10 mM isopropyl alcohol; ●: with saturated N_2O, ○: with 10 mM $Hg(CN)_2$; the radiation source: 7.9 kCi ^{60}Co, dose rate$=1.3\times10^5$ r/hr.

$$\dot{R}OH + HgCN \longrightarrow \text{products} \quad (9')$$

where $\dot{R}OH$ means an alcohol radical. In order to obtain a few information about it, some experiments were performed in ^{60}CO γ-ray irradiation. Figure 6 shows the dependence of the amount of acetone produced on doses in an aqueous 25 mM isopropyl alcohol solution with 25 mM $Hg(CN)_2$ or with saturated N_2O. In each case the amount increases linearly with doses. From this data the G values of acetone were calculated as 3.0 ± 0.3 and 2.6 ± 0.3 in the solutions with $Hg(CN)_2$ and with N_2O, respectively.

In a N_2O saturated solution, all of the primary reactive species produced by irradiation of water are expected to contribute to hydrogen abstraction from isopropyl alcohol in the form of OH and H radicals,[18] since the e^-_{aq} is converted to the OH radical according to Reaction 2. The resultant radical, $(CH_3)_2\dot{C}OH$, would disproportionate to produce acetone with the G value of $1/2(G_{e^-_{aq}}+G_{OH}+G_H)=3.1$. The experimental result is in good agreement with this expectation. While, in the solution with $Hg(CN_2)$ the e^-_{aq} and the H radical contribute to the formation of HgCN. If Rection 9′ gives rise to a product, such as an organomercury compound that liberates no acetone molecule, the yield of acetone should be smaller than $1/2\cdot G_{OH}=1.4$. From this consideration our result of G(acetone)$=2.6$ in this system demonstrates that most of the isopropyl radical reacts with HgCN to produce Hg(0) and acetone. The small decrease in the yield here may be explained by the contribution of Reaction 8. This conclusion is reasonable in view of the fact that the radical is a strong reducing agent.[13]

On the contrary the opposite conclusion seemed to be reached in the case of the *t*-BuOH radical that has not any reducing properties. Kelm *et al.* have proposed[22] that the radical is rapidly reduced to isobutene by the unstable Ni^+ ion on the radiolysis of an aqueous solution of $NiSO_4$ containing *t*-BuOH. However, no sign of isobutene formation was obtained gas-chromatographically on ^{60}CO γ-ray irradiation of an aqueous solution of $Hg(CN)_2$ with *t*-BuOH. Thus, the experimental result might present indirect evidence for the formation of an organomercury compound, such as $(CH_3)_2$-$C(OH)CH_2HgCN$.

Long-lived Species. In general, attempts to produce $Hg_2(CN)_2$ lead only to $Hg(CN)_2$ and mercury, although it has been suggested that it might be formed in non-aqueous solvents at low temperatures.[23] The unstability of $Hg_2(CN)_2$ has been explained by the reason that the CN^- ion forms a stable complex, $Hg(CN)_2$, with Hg^{2+} through the equilibrium, $Hg_2^{2+} \longleftrightarrow Hg + Hg^{2+}$ ($K = 1.15 \times 10^{-2}$). As seen in the case of Hg_2O,[4] however, a dimer complex of mercurous cyanide is also expected to be found in an unstable state. Thus, the residual absorption species in Fig. 2 may be assigned to a dimerized product, maybe as $(HgCN)_2$. As has been mentioned earlier, the second order reaction kinetics also supports this assignment, thus:

$$2HgCN \longrightarrow (HgCN)_2 \qquad (8')$$

A similar spectrum was obtained also with the doubled yield of absorption in solutions containing the HCO_2^- ion up to 100 mM. The dimerization of the initial species is expected to be fully attained in this solution, where there should be no reactant consuming the initial transient. Considering the stoichiometry in Reaction 8', the absorption coefficient of the dimer was evaluated as $(5.2 \pm 0.2) \times 10^3$ M^{-1} cm^{-1} at 220 nm and $(1.1 \pm 0.05) \times 10^4$ M^{-1} cm^{-1} at 210 nm, from the slope of the yields against pulse doses in a solution of 3 mM $Hg(CN)_2$ and 5 mM HCO_2Na.

In solutions with alcohols, however, the absorption was somewhat larger at shorter wavelengths, which may indicate the contribution from the products arising from Reaction 9 or 9'.

As expected, the long-lived absorption observed at 210 nm was found to decay slowly in the solution without any additives. The decay kinetics did not follow either a first or a second order rate law. The initial half-life is (4 ± 1) s independently of $Hg(CN)_2$ concentration in the range from 0.1 to 10 mM. Since the lifetime was not affected by the presence of 100 mM H_2O_2 added before irradiation, the decay was not due to the reaction with H_2O_2 produced by pulse electron irradiation. In solutions with additives, however, the decay rates become faster. The rates seemed to become constant at more than 5 mM of respective additives, although they were considerably scattered in every solutions. The most plausible half-lives obtained in each solution are listed in Table 2.

Table 2. Most plausible half-lives of $(HgCN)_2$ in 1 mM $Hg(CN)_2$ solutions with some additives

Additive	mM	$[Hg(CN)_2]$ mM	λ_{obsd} nm	$t_{1/2}$ s
no		0.2—1.0	210	4 ± 1
			220	5 ± 1
MeOH	5—100	1.0	220	7×10^{-1}
EtOH	10	1.0	220	1×10^{-1}
2-PrOH	10	1.0	220	8×10^{-2}
t-BuOH	5	1.0	210	2.5×10^{-1}
HCO_2Na	5—10	1.0	220	10×10^{-3}

Figure 2 also shows an absorption spectrum about one minute after ten repeated pulses. The spectrum is very similar to that of atomic mercury dissolved in water.[24] Considering the low solubility of mercury[25] and the short optical path length of the analytical light, however, the absorption in its stable state is expected to be far lower. Thus, it is concluded that mercury dissolved temporarily in excess is produced following the decomposition of $(HgCN)_2$.

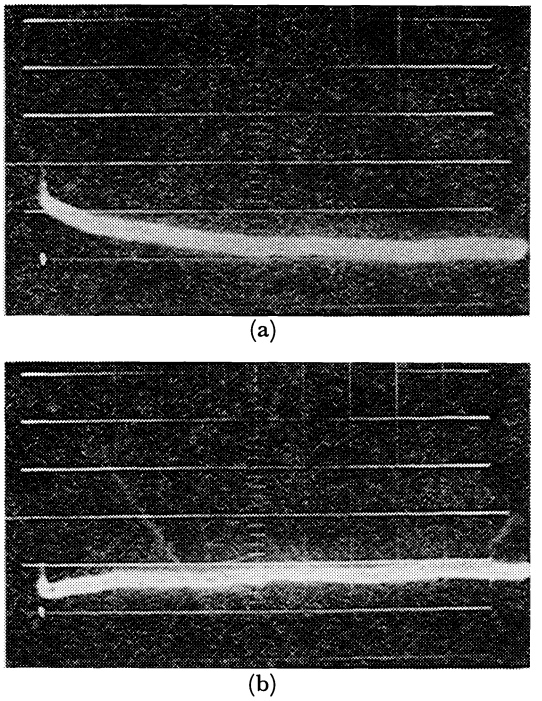

Fig. 7. Decay of the long-lived species at 220 nm (2.6 krads): (a); and increase of absorption at 254 nm (3.2 krads): (b); observed in a 1 mM $Hg(CN)_2$ solution containing 5 mM HCO_2Na; ordinates: 11%/large division, time scale: 5 ms/large division.

$$(HgCN)_2 \longrightarrow Hg(0) + Hg(CN)_2 \qquad (10)$$

A similar behavior has been found in the decomposition of Hg_2O produced by pulse electron irradiation in the neutral solution of mercuric oxide.[4] This conclution is further confirmed by the comparison of absorption changes with time between 254 and 220 nm. Figure 7 shows an example of a couple of oscilloscopic traces at the respective wavelengths obtained in a solution of 1 mM $Hg(CN)_2$ and 5 mM HCO_2Na. Simultaneous changes in absorption are found between the decay of the long-lived species at 220 nm and the formation of the additional absorption at 254 nm. The presence of alcohols as additives also gave similar results. These observations reasonably indicate that the species, the absorption of which increases slowly at 254 nm, has a dimerized mercurous cyanide molecule as its precursor. In solution without any additives, however, such increase in absorption at 254 nm was uncertain, maybe, due to a slow precipitation process of the dissolved mercury.

$$Hg(aq) \longrightarrow Hg(liquid) \qquad (11)$$

Since the decay of the dimer is more rapid in a solution containing HCO_2Na, Process 11 would be negligible at the time when the absorption just become constant in Fig. 7. Thus, if it is assumed that all the absorption

at 254 nm, 50 ms after the pulse, is due to the dissolved mercury arising from Reaction 10, the extinction coefficient can be evaluated. Considering that the concentration of Hg(aq) is equal to that of its precursor, $(HgCN)_2$, ε^{254} of Hg(aq) is calculated as $(2.8\pm0.1)\times 10^3$ M^{-1} cm^{-1} from Fig. 7.

The kinetic behavior of the dimerized species in the presence of these additives seems to be similar to that in a neutral solution of unstable mercurous oxide, $(HgOH)_2$.[4] It is, however, still in question how the decay process is controlled.

References

1) G. E. Adams, J. H. Baxendale, and J. W. Boag, *Proc. Chem. Soc.*, **1963**, 241; D. Meyerstein and W. A. Mulac, *J. Phys. Chem.*, **72**, 784 (1968); A. S. Ghosh-Mazumdar and E. J. Hart, *Adv. Chem. Ser.*, **81**, 193 (1968); *etc.*

2) M. Faraggi and A. Amozig, *Int. J. Radiat. Phys. Chem.*, **4**, 353 (1972).

3) S. Fujita, H. Horii, and S. Taniguchi, *J. Phys. Chem.*, **77**, 2868 (1973).

3) S. Fujita, H. Horii, T. Mori, and S. Taniguchi, *ibid.*, **79**, 960 (1975).

5) N. B. Nazhat and K.-D. Asmus, *ibid.*, **77**, 614 (1973).

6) J. H. Baxendale *et al.*, *Nature* (London), **201**, 468 (1964).

7) M. Anbar and P. Neta, *Int. J. Appl. Radiat. Isotop.*, **18**, 493 (1967).

8) M. Faraggi and J. Désalos, *Int. J. Radiat. Phys. Chem.*, **1**, 335 (1969).

9) E. Hayon and M. M. Moreau, *J. Chim. Phys.*, **62**, 391 (1965).

10) *G* represents the number of species per 100 eV absorbed energy. Primary reactive species in Reaction 1 are produced with $G(e^-_{aq})=2.7$, $G(OH)=2.8$, and $G(H)=0.6$, respectively.[11]

11) M. S. Matheson and L. M. Dorfman, "Pulsed Radiolysis," The M. I. T. Press, Cambridge, Mass. (1969).

12) J. P. Keene, Y. Raef, and A. J. Swallow, "Pulse Radiolysis," ed. by M. Ebert, J. P. Keene, A. J. Swallow, and J. H. Baxendale, Academic Press, London (1965), p. 99.

13) J. Lilie, G. Beck, and A. Henglein, *Ber. Bunsenges. Phys. Chem.*, **75**, 458 (1971); J. Lilie, *J. Phys. Chem.*, **76**, 1487 (1972).

14) M. Anbar and P. Neta, *Int. J. Appl. Radiat. Isotop.*, **18**, 493 (1967); D. Behar, *J. Phys. Chem.*, **78**, 2660 (1974).

15) A. Mantaka, D. G. Marketos, and G. Stein, *ibid.*, **75**, 3886 (1971).

16) D. Zehavi and J. Rabani, *ibid.*, **78**, 1368 (1974).

17) G. E. Adams, J. W. Boag, J. Currant, and B. D. Michael, "Pulse Radiolysis," ed. by M. Ebert, J. P. Keene, A. J. Swallow, and J. H. Baxendale, Academic Press, London (1965), p. 117.

18) J. Rabani, *J. Phys. Chem.*, **66**, 361 (1962).

19) (a) A. Appleby, G. Scholes, and M. Simic, *J. Amer. Chem. Soc.*, **85**, 3891 (1963); (b) J. Rabani, *J. Phys. Chem.*, **66**, 361 (1962); *J. Chem. Phys.*, **37**, 1865 (1962).

20) M. S. Matheson, *Radiat. Res. Suppl.*, **4**, 1 (1964).

21) M. Simic, P. Neta, and E. Hayon, *J. Phys. Chem.*, **73**, 3794 (1969).

22) M. Kelm, J. Lilie, A. Henglein, and E. Janata, *ibid.*, **78**, 882 (1974).

23) B. J. Aylet, "Comprehensive Inorganic Chemistry," Vol. 3, ed. by J. C. Bailar, H. J. Emeleus, R. Nyholm, and A. F. Trotman-Dickenson, Perganon Press, Oxford (1973), p. 291

24) H. Reichardt and K. F. Bonhoeffer, *Z. Elektrochem.*, **36**, 753 (1930); *Z. Phys.*, **67**, 780 (1931).

25) S. S. Choi and D. G. Tuchk, *J. Chem. Soc.*, **1962**, 4080, A. Stock, *Z. Anorg. Allg. Chem.*, **217**, 241 (1934).

Electron Scavenging by Benzene Derivatives in Alcohol Glasses

Akira NAMIKI, Masato NODA, and Takenobu HIGASHIMURA
Research Reactor Institute, Kyoto University, Kumatori-cho, Sennan-gun, Osaka 590-04
(Received June 6, 1975)

Electron scavenging efficiencies by benzene derivatives in alcohol glasses were studied by employing gamma radiolysis at 77 K. Scavenging efficiencies, $1/[S]_{1/2}$, were quasi-linear with the adiabatic electron affinities (*EA*) of the acceptors and they increased as the solvation time of the trapped electron became long. Electron scavenging was explained as a tunneleing of the unsolvated electron; the pre-exponential factor in the tunneling rate was calculated by employing the Morse function developed by Wentworth *et al.* in the gas phase, which gave an *EA* dependence in accordance with the experimental results.

A variety of molecules can capture a low energy electron in the gas phase to form molecular anions or dissociate into fragment radicals and anions. In the condensed matrices, also. the electron capture process has been studied extensively by using polar and non-polar solvents. But few reports have been published which discuss the relation between mechanisms of electron scavenging in the gas and the condensed matrices. This paper is a first step to explain the mechanism of electron scavenging in the glass in terms of reactions in the gas phase.

It has been widely admitted that, in the glass, the trapped or solvated electrons (e_t^- or e_s^-) react withsolutes and their parent positive ions through tunneling. The simple expressions of the tunneling theory were given by Miller[1] and he succeeded in estimating the tunneling distances between e_s^- and solute molecules and also the decay of e_s^- over a very wide range of time.[1,2] However, there are some discrepancies between the estimated values and the experimental results, especially in polar matrices. For example, the experimental tunneling distance of e_s^- in a benzene solution of ethanol was much smaller ($\leq$17 Å) than the estimated value.[1] The observed decay of e_s^- was much slower than the calculated curve for the case of NO_3^- in the alkaline water glass.[2] These discrepancies may result from an oversimplification in his theory, in which the nature of the acceptor molecule is not taken into consideration and in which the tunneling occurs only from the solvated state. The electronic level of the anion of the acceptor molecule must resonate with that of the trapped electron. The transition from the neutral state to the anionic state occurs without changing the nuclear configurations before and after accepting the electron (Franck-Condon principle). In this paper, the Franck-Condon restriction is taken into consideration in the pre-exponential factor of the tunneling rate along with the treatment developed in the gas phase studies.[3,4]

In polar matrices, the electron is stabilized in pre-existing shallow traps.[5] The depth of these potential wells changes with time upon solvation. Miller suggested that the extremely restricted tunneling to benzene in ethanol occurs within 1 μ sec when the traps are shallow.[1] Steen also suggested the importance of tunneling of the pre-solvated electrons.[6] The reactivity of e_t^- in shallow traps in ethanol at 4K was noticably larger than that of e_s^- at 77K, which can be attributed to a more efficient tunneling from shallow traps than from the solvated state.[7]

Halogenated benzene derivatives have been studied as regards the attachment of a low energy electron in the gas phase by both the electron beam experiments[8,9] and the thermal electron attachment experiments.[3,4] Wentworth *et al.*, obtained the formulation for the electron attachment rate using the simple Morse function and succeeded in explaining qualitatively both experimental results.[4] They estimated the adiabatic electron affinities for some halogenated benzenes, which play the most important role in the electron capture process.[4] In this report, Steelhammer and Wentworth's method is extended to the electron attachment through tunneling in condensed media.

Experimental

Reagent grade methanol, ethanol, *n*- and *iso*-propanol were used as solvents without further purification. Reagent grade of benzene derivatives were added aerobically without purification.

The solutions were quenched to glasses by the usual rapid cooling technique in suprasil cells of 0.2 cm thickness. The glasses were irradiated at 77 K by ^{60}Co gamma ray with a dose rate of 1.88×10^{20} eV/g·hr for 3 min in the case of MeOH (5 mol% H_2O) and EtOH glasses and for 5 min in the cases of *n*-PrOH and *iso*-PrOH glasses. The optical density (O.D.) at the peak in the absorption spectrum of e_s^- was measured at 77 K within 1 min after the irradiation.

Dissociative electron attachments to chloro-, bromo-, and iodobenzene do not produce any free radicals, except the solvent radical in the alcohol at 77 K. The anions of benzene, alkylated benzene, and fluorobenzene are protonated, and converted to the hexadienyl type radicals which show an absorption spectrum in the near UV region.[10] Therefore, the O.D. at the peak of e_s^- in the visible region could be obtained accurately for all benzene derivatives.

Results and Discussion

Experimental Results. Figure 1 shows the plots of log O.D. *vs.* the concentrations of the added scavengers in ethanol at 77K. Good linearlity was also obtained for other solvents and solutes. The concentrations, $[S]_{1/2}$, which reduce the e_s^- yield to a half of those in pure solvents, were determined from these semilogarithmic plots and are shown in Table 1.

Experimental tunneling distances, *a*, as defined by Miller,[1] were obtained by the formula:

$$a = \left(\frac{10^3}{8.0\pi}\frac{\ln 2}{[S]_{1/2}}\frac{M}{d}\right)^{1/3} \text{(Å)} \qquad (1)$$

Table 1. $[S]_{1/2}$ in mol %; experimental tunneling distance a and simulated tunneling distance a' in Å

Formula	MeOH			EtOH			*n*-PrOH			*iso*-PrOH		
	$[S]_{1/2}$	a	a'[a]	$[S]_{1/2}$	a	a'	$[S]_{1/2}$	a	a'	$[S]_{1/2}$	a	a'
1,3,5-$C_6H_3(CH_3)_3$				0.77	12.7							
p-$C_6H_4(CH_3)_2$				0.64	13.5							
$C_6H_5CH_3$	0.85	11.0		0.67	13.4		0.265	19.9		0.25	20.4	
C_6H_6	0.88	10.9		0.68	13.3		0.24	20.5		0.24	20.7	
C_6H_5F	0.75	11.4		0.40	15.9		0.17	23.0		0.145	24.4	
o-$C_6H_4CH_3Cl$	0.64	12.1	6.4[b]	0.35	16.6	10.2	0.165	23.3	12.7	0.10	27.7	14.0
C_6H_5Cl	0.62	12.2	12.4	0.265	18.2	20.3	0.14	24.6	22.7	0.095	28.2	24.1
o-$C_6H_4CH_3Br$	0.52	12.9	10.7	0.25	18.5	18.5	0.145	24.3	21.0	0.09	28.6	22.3
C_6H_5Br	0.49	13.2	13.1	0.23	19.1	21.0	0.125	25.5	23.4	0.08	29.8	24.8
C_6H_5I	0.49	13.2	14.9	0.20	20.0	22.8	0.12	25.9	25.3	0.07	31.2	26.6
o-$C_6H_4Cl_2$	0.465	13.4	15.5	0.18	20.7	23.4	0.11	26.6	25.9	0.065	31.9	27.2
p-$C_6H_4Cl_2$				0.15	22.0							
1,3,5-$C_6H_3Cl_3$				0.11	24.3							

a) τ was assumed to be 10 ns. The same values as in other solvents were inserted for the other parameters.
b) Only this value was estimated from Eq. (7').

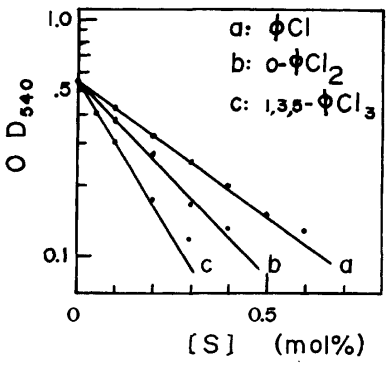

Fig. 1. Semilogarithmic plots of the yields of e_s^- (O.D. at 540 nm) *vs.* scavenger concentrations in ethanol at 77 K.

where M and d are the molecular weight and the density of the solvent and $[S]_{1/2}$ is in mol %. The values of a are tabulated for each solvent in the second column of Table 1.

In Fig. 2 the scavenging efficiencies, the reciprocals of $[S]_{1/2}$, were plotted against the *adiabatic electron affinity*, *EA*,[4] for *o*-$C_6H_4CH_3Cl$, C_6H_5Cl, *o*-$C_6H_4CH_3Br$, C_6H_5-Br, and *o*-$C_6H_4Cl_2$. The scavenging efficiency is nearly linear with the electron affinities of the solutes in all the different alcohols. The deviation from linearity is especially small in ethanol. Because the *EA*'s of C_6H_6, C_6H_5F, and C_6H_5I are unknown, these *EA*'s are estimated by putting their scavenging efficiencies on the best fit line in ethanol. They are −0.75, −0.52, and 0.0 eV, respectively. For these three additional points (a, b, and c in Fig. 2), the linearity is still as good as for other three solvents.

From Fig. 2 and Table 1 we can find two main results.

(1) For various benzene derivatives in each solvent, the scavenging efficiency, $1/[S]_{1/2}$, and the experimental tunneling distance, a, become large as *EA* increases. $1/[S]_{1/2}$ *vs.* *EA* is roughly linear.

(2) $1/[S]_1/_2$ and a are strongly dependent upon the nature of the matrix. The order of increase is MeOH, EtOH, *n*-PrOH, and *iso*-PrOH.

Simple Model for Acceptor. The exponential dependence of the yield of e_s^- on the scavenger concentration in Fig. 1 shows that the scavenging is due to the epithermal electron capture or to the tunneling of the trapped electron. If we take the former process, it is difficult to explain the strong dependence of scavenging efficiency on the matrix because the degradation spectrum of the epithermal electron must not differ so much among these alcohol solvents.

Result (1) of the preceeding section implies clearly that the contribution from *EA* of the acceptor should not be ignored in the tunneling model. Result (2) suggests that tunneling occurs mainly when the potential well of the trapped electron is shallow. The times for the trapped electron to reach the stable spectra at 77K are <3, ~7, ~40, and ~100 μs for MeOH, EtOH, *n*-PrOH,

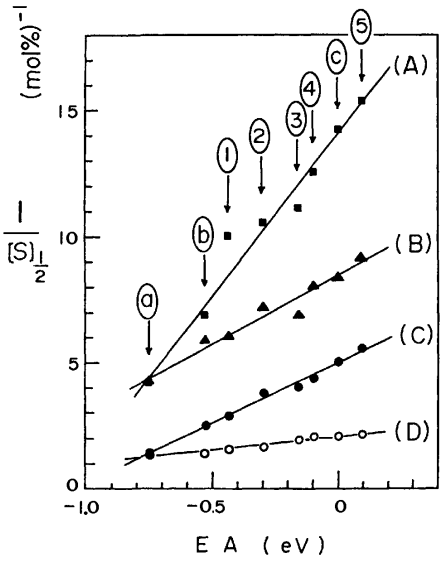

Fig. 2. Plots of $[S]_{1/2}^{-1}$ *vs.* *EA*. The solvents are *iso*-PrOH (A) ■, *n*-PrOH (B) ▲, EtOH (C) ● and MeOH (D) ○.
EA of *o*-$C_6H_4CH_3Cl$ ①, C_6H_5Cl ②, *o*-$C_6H_4CH_3Br$ ③, C_6H_5Br ④, and *o*-$C_6H_4Cl_2$ ⑤ are from Ref. 4, while *EA* of C_6H_6 ⓐ, C_6H_5F ⓑ and C_6H_5I ⓒ were determined from the line (C).

and *iso*-PrOH, respectively.[11] This order is the same as that in result (2).

In order to simplify the ploblem, we make the following assumptions. The secondary electron is stabilized in the pre-solvated state, and it tunnels to the acceptor molecules or it becomes solvated after surviving for a life time of τ. There is only one kind of shallow trap with a depth of V. Once the electron is solvated, it cannot tunnel to the acceptor.

The usual tunneling procedure refers to the final state of the electron in the free continuum. In our case, however, the final state is the electron in a molecular orbital of the anion. Therefore, the expression of the tunneling rate, k_{tun},[12] must be modified by introducing F into the pre-exponential factor as

$$k_{tun} = \nu F \exp\left\{-\frac{2a}{\hbar}\sqrt{2m(V-E)}\right\}, \quad (2)$$

where ν is the impinging frequency of e_t^- in the potential well, a is the tunneling distance or the barrier width, $\hbar$ is Planck's constant divided by 2π, m is the electron mass, V is the depth of the well measured from the bottom of the conduction band, and E is the energy of e_t^- measured from the bottom of the well. F has a meaning close to the Franck-Condon factor and it must be written as a function of the EA of the acceptor. The resonance electron transfer from e_t^- to the acceptor is so fast that the nuclear configuration of the acceptor cannot change during the electron tunneling. Therefore, it can be written as the vertical transition between the two adiabatic potential energy curves of the neutral state and the negative-ion state. For the calculation of F we follow Steelhammer and Wentworth's treatment, which explained successfully the vertical electron attachment process in the gas.[3,4]

When the incident electron has the energy E_v, the vertical transition requires the following energy relation:

$$E_v = -2kD_{AB}^{\circ}e^{-\beta(r-r_o)} + D_{AB}^{\circ}e^{-2\beta(r-r_o)} - EA_{A\text{ or }B} + D_{AB} \quad (3)$$

where the parameters are the same as those in Ref. 4: namely, k is the parameter to determine the potential energy curve of the acceptor anion, D_{AB}° is the bond dissociation energy referenced to the minimum of the function, r_o is the equilibrium internuclear separation for the C–X bond (X=halogen), $\beta=\nu_0(2\pi^2\mu/D_{AB}^{\circ})^{1/2}$, ν_0 is the fundamental vibrational frequency for the C–X stretching mode, μ is the reduced mass, EA_A is the electron affinity of the aromatic radical in the case of the formation of the molecular negative ion and EA_B is that of the halogen atom in the case of a dissociative negative-ion, and D_{AB} is the bond dissociation energy measured from the zero-point energy level.

In condensed media, the energy of e_t^- is $(V-E)$ under the quasi-free electron level. Because the latter is V_o above the vacuum level, the trapped electron state is expressed as $V_o-(V-E)$ referenced to the vacuum level. When the electron is captured by the neutral molecule, the molecular negative ion is stabilized by the medium electronic polarization energy of P_-. Therefore, the electron energy to be given to the acceptor has the following equation:

$$E_v = V_o-(V-E)-P_-. \quad (4)$$

Upon tunneling, the internuclear separation of the neutral molecule, r, must satisfy Eqs. (3) and (4). The probability density, $p(E_v)$, of finding the nuclear configulation at r in the zero vibrational state of the neutral molecule is[4]

$$p(E_v)dE_v = \frac{\sqrt{\alpha/\pi}e^{-\alpha(r-r_o)^2}}{2\beta D_{AB}^{\circ}(e^{-2\beta(r-r_o)}-ke^{-\beta(r-r_o)})}dE_v, \quad (5)$$

where $\alpha=\sqrt{\mu f/\hbar^2}$ and f is the force constant for the C–X bond.

If we assume that the density of the resonance state of the trapped electron is unity within the small range of ΔE_v around E_v and vanishes in the other region, F is expressed as

$$F = p(E_v)\Delta E_v. \quad (6)$$

Under the condition of $\nu F\tau \geqq 10$,[13] the tunneling distance a' is

$$a' \cong 5.0 + \frac{1}{\sqrt{V-E}}\ln(\nu p(E_v)\Delta E_v\tau)\ (\text{Å}), \quad (7)$$

where 5.0 is added as the correction term from the radii of both the trapped electron cavity and the acceptor, and $(V-E)$ is in eV. When $\nu F\tau < 10$,[13] a' is

$$a' \cong 5.0 + \frac{1}{\sqrt{V-E}}(6\nu p(E_v)\Delta E_v\tau)^{1/3}\ (\text{Å}). \quad (7')$$

Miller estimated 10^{15}/s for ν as the case of the one dimensional problem.[1] But if we take into consideration the attenuation from the fractional solid angle into which the electron enters,[14] ν must be reduced by a factor of about 10^2 for the tunneling distances in our results. ΔE_v is the width of the resonant vibrational levels. Though we have no exact knowledge about this width, ΔE_v is assumed to be the order of several spans of the lattice vibration of the matrix around the trapped electrons and less than the vibrational spacings of the acceptor molecule. Tentatively we take $\Delta E_v=10^{-2}$ eV for all solutes and solvents. The absorption band of the pre-solvated electron in ethanol at 4 K shows a threshold at about 0.5 eV. Since the absorption of the pre-solvated electron is a bound-free transition,[15] we take $(V-E)=0.5$ eV. In the case of the other solvents, photo-ionization thresholds of the pre-solvated electron have not been determined, and therefore we assume the same value for the other solvents. There is no direct information for V_o and P_- given by experiment. Fueki *et al.*[16] calculated successfully the energy of the trapped electron in ethanol for the case of $V_o \geq 0$. Allen *et al.*[17] claimed the polarization energy of SF_6^- in the non-polar liquid as about -0.65 eV. Therefore, we have assumed that (V_o-P_-) is roughly 1.0 eV, leading to $E_v=0.5$ eV.

$p(E_v)$'s of different halobenzene molecules were calculated to explain the line shapes of the electron attachment cross-sections but were given in arbitrary units.[4] In this paper, we recalculated $p(E_v)$ absolutely for various E_v using the same values of parameters in Morse functions as in Ref. 4. Molecular negative-ion potential energy curves were taken for *o*-$C_6H_4CH_3Cl$, C_6H_5Cl, *o*-$C_6H_4CH_3Br$, C_6H_5Br, and *o*-$C_6H_4Cl_2$ and the dissociative negative-ion potential energy curve for C_6H_5I as in the case of Steelhammer and Wentworth.[4] These

Table 2. $p(E_v)$ in $(eV)^{-1}$

	o-$C_6H_4CH_3Cl$	C_6H_5Cl	o-$C_6H_4CH_3Br$	C_6H_5Br	C_6H_5I	o-$C_6H_4Cl_2$
$p(E_v)$	0.157×10^{-3}	0.174	0.524×10^{-1}	0.282	1.04	1.57

imply that the trapped electron tunnels to the π^* orbital for the five Cl or Br substituted benzenes and to the σ^* orbital of the C–X bond for C_6H_5I. The values of $p(E_v)$ at $E_v=0.5$ eV are listed in Table 2.

The halflife of the pre-solvated electron, τ, in ethanol at 77K was measured to be about 2.5 μs at 1260 nm.[18] The τ's in *n*- and *iso*-PrOH at 77K were not obtained, but the absorption spectra of the trapped electron in these matrices and in the EtOH matrix became stable at 40 and 100 μs and at 7 μs after the pulse respectively.[11] The half-lives in *n*- or *iso*-PrOH were then assumed as $2.5/7\times40$ or $2.5/7\times100$ μs respectively by normalizing the above times, which were required for reaching the stable spectra in EtOH. The tunneling distances, a', obtained from Eq. (7) are shown in Table 1. Similar calculations were carried out on MeOH, assuming that τ in this matrix is 10 ns.

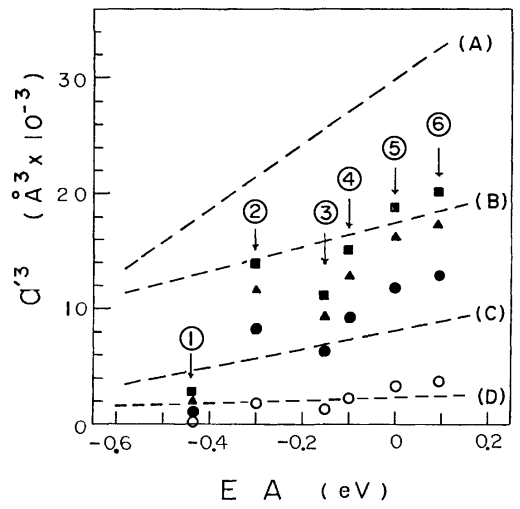

Fig. 3. Plots of a'^3 *vs.* *EA*. The dotted lines are experimental one; (A) *iso*-PrOH, (B) *n*-PrOH, (C) EtOH, and (D) MeOH. Other notations are same as those in Fig. 2 with exceptions of C_6H_5I ⑤ and o-$C_6H_4Cl_2$ ⑥.

Discussion of the Model Calculation. The simulated values of a'^3 are compared to the experimental values of a^3 in Fig. 3. $EA=0.0$ eV for C_6H_5I was tentatively assumed from Fig. 2 for convenience in comparison, though the present model states that the electron tunneling occurs directly to the dissociative state of the orbital for a C–I bond. The simulated values in EtOH and *n*-PrOH are consistent with the experimental ones, not only in the tendency with *EA* but also in their absolute values. In *iso*-PrOH the deviation is serious. This deviation comes partly from the uncertainty of the numerical values in each parameter. Especially τ in *iso*-PrOH may be underestimated, since the absorption spectrum observed by a pulse experiment extended far into the infrared region even at 100 μs after a pulse.[11]

In MeOH, the trapped electron prior to solvation was observed neither by the pulse radiolysis at 77 K[11] nor by the gamma ray radiolysis at 4 K.[5] The spectra obtained in those experiments show that the electron has already been solvated. Therefore, it is reasonable to consider that the solvation time in MeOH is very short. In this paper, a solvation time of 10 ns gives the best fitting in the scavenging curves, as is shown in Fig. 3.

The linear relationship between a'^3 and *EA* can not be proved directly from Eq. (8) *via* Eq. (5). In Eq. (5), k in the case of the molecular negative ion state contains *EA* of the acceptor as

$$k^2=\frac{EA+(D^\circ_{AB}-EA_A)-\frac{1}{2}h\nu_{0AB}+\frac{1}{2}h\nu_{0AB^-}}{D^\circ_{AB}}, \quad (8)$$

where $h\nu_{0AB}$ and $h\nu_{0AB^-}$ are the vibrational energies of the C–X streching mode in the neutral and ionic states.[4] In Fig. 3, o-$C_6H_4CH_3Cl$ and o-$C_6H_4CH_3Br$ deviate seriously. These deviations are partly removed if we take E_v larger than 0.5 eV, though $p(E_v)$ of o-$C_6H_4Cl_2$ decreases in this energy region since the peak in $p(E_v)$ exists at an energy lower than 0.5 eV. But the present simple model cannot explain the linearity of a^3 *vs.* *EA* obtained experimentally.

We checked the possibility of the electron tunneling to the molecular negative-ion state for the case of C_6H_5I. The tentatively assumed value the $EA=0.0$ eV from Fig. 2 is inserted into Eq. (8), neglecting the zero vibrational energy, and gives $k=0.321$. Using this value, we can get $p(E_v)=0.332\times10^{-2}$/eV at $E_v=0.5$ eV. But this value gives a very small tunneling distance for C_6H_5I. This fact suggests that tunneling to the π^* orbital is not involved for C_6H_5I as much as the electron attachment in the gas phase.[3,4] Bond dissociation occurs rather dominantly at C–I rather than C–Br in p-C_6H_4BrI, while both bond dissociations occured at C–Br and C–Cl in p-C_6H_4ClBr.[10] These facts support the contention that the dissociative electron tunneling goes through via a molecular negative-ion state for Cl or Br substituted benzenes, but proceeds by a direct dissociation process for I substituted benzenes.

For an appropriately improved model to explain especially the linear relationship between a'^3 and *EA*, the following features should be taken into consideration. (1) The dynamical process of the solvation by the trapped electrons is more complicated. Though how exactly make the solvation proceed is unclear, it is more realistic to deepen the well continuously rather than discretely. Then, k_{tun} must be a function of time through $(V-E)$. (2) The pre-solvated electrons exist in traps with different potential depths.[15] There may exist more shallowly trapped electrons than 0.5 eV in quicker periods. The distribution of the potential depths must be taken into consideration for k_{tun} in the improved model. This effect may be important especially for small *EA* acceptors.

The condition that $E_v>-EA$, is necessary for the

tunneling of the trapped electron. Since EA is -0.75 or -0.52 eV for C_6H_6 or C_6H_5F as estimated above, this condition is violated for these solutes if E_v is 0.5 eV. But tunneling can occur to C_6H_5F or C_6H_6 experimentally. This difficulty may be partly removed by considering the above situations.

Electron Affinity. There remain remarkable discrepancies among the reported EA values of C_6H_6 and C_6H_5F.[19] EA's in the abscissa in Fig. 2 for the five Cl or Br substituted benzenes were determined through Eq. (8) and, following Eq. (9),[4]

$$k = 1 - \frac{E_v^p + EA_A + \frac{1}{2}h\nu_0}{2D_{AB}^\circ}. \quad (9)$$

This may be also applicable to C_6H_6 or C_6H_5F if we take D_{AB}° of the C–H bond in C_6H_6 and of the C–F bond for C_6H_5F. We tried to test the validity of EA of C_6H_6 or C_6H_5F estimated from Fig. 2 using these relations. The D_{AB}° of the C–H or C–F bond in benzene is 102 or 115 kcal/mol. Neglecting the zero vibrational energy, we obtained $E_v^p=1.5$ eV for C_6H_6 or $E_v^p=1.1$ eV for C_6H_5F by using our estimated values of $EA=-0.75$ or -0.52 eV, respectively. These E_v^p values should be compared to the peak energies in the energy loss resonance, which were interpreted to be a temporary negative ion resonance.[9,20] Compton *et al.*[20] reported that these peak energies were 1.55 eV for C_6H_6 and 1.35 eV for C_6H_5F; here agreement between the estimated E_v^p values and the measured values is good, suggesting that the estimation of the adiabatic electron affinities of benzene derivatives can be determined reasonably well by using the lines in Fig. 2.

Table 3. EA in eV

Formula	EA (eV)
1,3,5-$C_6H_3(CH_3)_3$	-0.78 ± 0.10
1,4-$C_6H_4(CH_3)_2$	-0.72 ± 0.10
$C_6H_5CH_3$	-0.73 ± 0.10
C_6H_6	-0.75 ± 0.10
C_6H_5F	-0.52 ± 0.10
p-$C_6H_4Cl_2$	0.35 ± 0.15
1,3,5-$C_6H_3Cl_3$	0.85 ± 0.20

In Table 3 we tabulated the EA values so determined from the line of EtOH for methylated benzenes and chlorinated or fluorinated benzenes. Large changes in EA are recognized by halogen atom substitution. Addition of one Cl atom to the ring increases EA by about 0.4—0.5 eV, suggesting that additivity in EA is also valid for Cl as well as for F.[21] On the other hand, no large change in EA is seen in C_6H_6 or other methylated benzenes, implying that the effect of the CH_3 group on EA is small compared to the case of a halogen.

The anion of C_6H_6 is known to exist stably in the condensed media,[22] though the EA of C_6H_6 is negative. The condition that the anion can be stable in the condensed medium is

$$V_0 - P_- + EA > 0. \quad (10)$$

Due to the factor of V_0-P_-, stable existence of the benzene anion does not imply necessarily that $EA>0$. In this sense, the recent conclusion that $EA>0$[19a] for C_6H_6 is questionable.

References

1) J. R. Miller, *J. Chem. Phys.*, **56**, 5173 (1972).
2) J. R. Miller, *Chem. Phys. Lett.*, **23**, 180 (1973).
3) W. E. Wentworth, R. George, and H. Keith, *J. Chem. Phys.*, **51**, 1791 (1969).
4) J. C. Steelhammer and W. E. Wentworth, *ibid.*, **51**, 1802 (1969).
5) H. Hase, T. Warashina, M. Noda, A. Namiki, and T. Higashimura, *ibid.*, **57**, 1039 (1972).
6) H. B. Steen, *ibid.*, **61**, 3387 (1974).
7) (a) T. Higashimura, A. Namiki, M. Noda, and H. Hase, *J. Phys. Chem.*, **76**, 3744 (1972); (b) T. Higashimura, *Int. J. Radiat. Phys. Chem.*, **6**, 397 (1974).
8) L. G. Christophorou, R. N. Compton, G. S. Hurst, and P. W. Reinhardt, *J. Chem. Phys.*, **45**, 536 (1966).
9) R. N. Compton, L. G. Christophorou, and R. H. Huebner, *Phys. Lett.*, **23**, 656 (1966).
10) A. Namiki, *J. Chem. Phys.*, **62**, 990 (1975).
11) L. Kevan, *ibid.*, **56**, 838 (1972).
12) K. I. Zamaraev and R. F. Khairutdinov, *Chem. Phys.*, **4**, 181 (1974).
13) M. Tachiya and A. Mozumder, *Chem. Phys. Lett.*, **28**. 87 (1974).
14) B. Brocklehurst, *Chem. Phys.*, **2**, 6 (1973).
15) A. Namiki, M. Noda, and T. Higashimura, *Chem. Phys. Lett.*, **23**, 402 (1973).
16) K. Fueki, D. F. Feng, and L. Kevan, *J. Chem. Phys.*, **56**, 5351 (1972).
17) A. O. Allen, T. E. Gangwer, and R. A. Holroyd, *J. Phys. Chem.*, **79**, 25 (1975).
18) J. T. Richards and J. K. Thomas, *Chem. Phys. Lett.*, **8**, 13 (1971).
19) Recent publications about EA of C_6H_6 include (a) L. G. Christophorou and R. E. Goans, *J. Chem. Phys.*, **60**, 4244 (1974); (b) I. Nenner and G. J. Schulz, *ibid.*, **62**, 1747 (1975).
20) R. N. Compton, R. H. Huebner, P. W. Reinhardt, and L. G. Christophorou, *J. Chem. Phys.*, **48**, 901 (1968).
21) W. T. Naff, C. D. Cooper, and R. N. Compton, *J, Chem. Phys.*, **49**, 2784 (1968).
22) C. Chachaty, *J. Chim. Phys.*, **64**, 614 (1966).

Topochemical Studies. VII. The Crystal and Molecular Structures of Tetrachlorophthalic Acid Hemihydrate and Tetrabromophthalic Anhydride

Kuniaki Ito, Keigo Moriya,* Setsuo Kashino, and Masao Haisa
Department of Chemistry, Faculty of Science, Okayama University, Tsushima, Okayama 700
(Received June 14, 1975)

The crystal structures of tetrachlorophthalic acid hemihydrate (TCPH) and tetrabromophthalic anhydride (TBPA) have been determined from visually estimated Cu$K\alpha$ data. The crystals of TCPH are monoclinic, space group A2/a, $a=19.81(1)$, $b=7.091(5)$, $c=16.22(1)$ Å, $\beta=101.2(2)°$ and $Z=8$. Those of TBPA are monoclinic, space group $P2_1/n$, $a=13.39(3)$, $b=6.19(2)$, $c=12.66(3)$ Å, $\beta=91.1(3)°$ and $Z=4$. The structures of TCPH and TBPA were solved from the sharpened Patterson maps, and refined by the block-diagonal least-squares method to R values of 0.112 and 0.112 for 1287 and 1278 non-zero reflections, respectively. The molecules of TCPH related by a twofold screw axis are linked together by hydrogen bonds between the carboxylic groups to form a chain along the b axis and the chains are held together by hydrogen bonds through water molecules to form a sheet parallel to the (100) plane. The sheets are stacked by van der Waals forces. The dihedral angles of the carboxylic groups with the benzene ring are 68.2 and 48.9°. The crystals of TBPA are isomorphous to those of tetrachlorophthalic anhydride. The benzene ring of TBPA are distorted by the attachment of five membered ring. There is considerable molecular overlap in TCPH, while in TBPA there is no overlap.

The conformation of the benzene ring overcrowded with halogen atoms is of considerable interest. Coulson and Stocker[1] have discussed the planarity of *o*-dihalogenobenzenes on calculations of potentials between halogen atoms, but the problem for more overcrowded benzenes has not always been settled. Strand[2] has shown that the planar molecule of *o*-dibromobenzene belongs to C_{2v} symmetry but the angle between the C–Br bonds is enlarged. Gafner and Herbstein[3] have noted that the intramolecular Br···Br distance of 1,2,4,5-tetrabromobenzene is significantly shorter than the usual van der Waals separation in different molecules. Rudman[4] has determined the structure of tetrachlorophthalic anhydride (TCPA) and pointed out that an anisotropic van der Waals radius plays an important role in the contacts of the halogen atoms. It is of additional interest that some multi-halogenated benzoic acids bear a distinct parallelism between the superdelocalizability for nucleophilic reaction and auxin activity or carcinogenic activity,[5] but the parallelism involves some conflicts to be solved in view of the detailed molecular structures.

Previous work on the topochemical studies has been carried out with 2,5-pyridinedicarboxylic acid–*N*,*N*-dimethylformamide complex monohydrate[6] in order to study the role of π-electron interaction and hydrogen bonding in molecular stacking and overlap on crystal structure formation. The present investigation was undertaken in order to compare the overlappings of the title overcrowded molecules and to study the effects of

Table 1. Crystallographic data and experimental details

	Tetrachlorophthalic acid hemihydrate	Tetrabromophthalic anhydride
Chemical formula	$C_8H_2O_4Cl_4\cdot 1/2H_2O$	$C_8O_3Br_4$
F.W.	312.9	463.7
mp (°C)	*ca.* 98 (anhydrated)	280
Crystal system	monoclinic	monoclinic
Space group	A2/a-C_{2h}^6, No. 15	$P2_1/n$-C_{2h}^5, No. 14
Systematic absences	hkl $h+l$ odd	$h0l$ $h+l$ odd
	$h0l$ h odd	$0k0$ k odd
a(Å)	19.81(1)	13.39(3)
b(Å)	7.091(5)	6.19(2)
c(Å)	16.22(1)	12.66(3)
β(°)	101.2(2)	91.1(3)
Z	8	4
D_x (g/cm^3)	1.859	2.935
D_m (g/cm^3)	1.88	2.90
Flotation mixture	$ZnBr_2$ aq. soln.	HCOOTl aq. soln.
μ (cm^{-1}) for Cu $K\alpha$	97.8	209
F(000)	1240	828
Dimensions of crystal used (mm)	$0.1\times0.3\times0.2$	$0.08\times1.1\times0.05$
Layers photographed	$h0l$ to $h5l$	$h0l$ to $h4l$
No. of observed reflections	1287	1278
Percent to Cu$K\alpha$ sphere	50	52
B (Å^2) from Wilson's plot	4.04	3.27

* Present address: Central Research Laboratory, Kanto Denka Co., Shibukawa, Gunma 377.

overcrowding on the conformation of the benzene rings.

Experimental

Tetrachlorophthalic acid hemihydrate (TCPH) was recrystallized from a hot aqueous solution by cooling as thin plates elongated along the b axis. Crystals of tetrabromophthalic anhydride (TBPA) were obtained from a hot acetone solution by evaporation as prisms elongated along the b axis. Crystallographic data and experimental details are listed in Table 1. The intensity data were collected by the equi-inclination Weissenberg method using Cu$K\alpha$ radiation (λ= 1.5418 Å). Intensities were estimated visually and corrected for Lorentz and polarization factors and for spot shape, but not for absorption. The structure of TCPH was assumed to be centric from the distribution of normalized structure factors and the space group A2/a was confirmed by the analysis.

Structure Determination and Refinement

The structures were solved from three-dimensional sharpened Patterson maps. The hydrogen atoms of TCPH were located by a difference Fourier synthesis. Parameters of all the atoms were refined by the block-diagonal least-squares method. The weighting scheme used was:

$$w = 1.0 \quad \text{for} \quad 0 < |F_o| \leq F_{max}$$

$$\text{and} \quad w = (F_{max}/|F_o|)^2 \quad \text{for} \quad |F_o| > F_{max},$$

where F_{max}=16.0 and 30.0 for TCPH and TBPA, respectively. The final R value of TCPH was 0.112 for 1287 non-zero reflections and that of TBPA 0.112 for 1278. The observed and calculated structure factors are listed in Table 2,** and the final atomic parameters in Table 3.

The atomic scattering factors were taken from International Tables for X-ray Crystallography.[7] The computations were carried out on an NEAC 2200-500 computer at the Okayama University Computer Center. The programs used were HBLS-5 and DAPH.[8]

Table 3. Final atomic parameters and estimated standard deviations ($\times 10^4$)
The anisotropic thermal parameters are defined as: $\exp(-\beta_{11}h^2-\beta_{22}k^2-\beta_{33}l^2-\beta_{12}hk-\beta_{13}hl-\beta_{23}kl)$.

	x	y	z	β_{11}	β_{22}	β_{33}	β_{12}	β_{13}	β_{23}
Tetrachlorophthalic acid hemihydrate (TCPH)									
Cl(1)	834(1)	1619(4)	435(1)	39(1)	297(8)	33(1)	60(4)	7(1)	−9(4)
Cl(2)	187(1)	5045(4)	1158(2)	31(1)	221(8)	51(1)	52(3)	−1(1)	21(4)
Cl(3)	422(1)	5641(4)	3083(2)	34(1)	172(8)	56(1)	32(3)	28(2)	−39(4)
Cl(4)	1368(1)	2905(4)	4288(1)	37(1)	232(8)	36(1)	−10(3)	19(1)	−38(3)
O(1)	1671(3)	−1277(10)	3943(4)	30(2)	267(20)	39(3)	−19(9)	17(4)	44(11)
O(2)	2621(3)	−288(9)	3515(4)	24(2)	210(18)	47(3)	2(8)	11(3)	19(10)
O(3)	1695(3)	−2475(9)	2070(4)	35(2)	138(16)	52(3)	0(9)	37(4)	17(11)
O(4)	2101(4)	−714(10)	1148(4)	45(3)	236(20)	51(3)	54(11)	53(5)	81(12)
C(1)	1536(4)	1033(12)	2896(5)	25(2)	103(22)	34(3)	−14(10)	12(4)	10(11)
C(2)	1434(4)	755(12)	2034(5)	24(2)	130(24)	37(3)	5(10)	16(4)	−6(12)
C(3)	1010(4)	2010(13)	1494(5)	20(2)	194(28)	35(3)	4(10)	7(4)	9(12)
C(4)	708(4)	3524(13)	1830(5)	21(2)	181(25)	35(3)	13(9)	6(4)	−7(12)
C(5)	803(4)	3774(13)	2681(6)	20(2)	121(24)	52(4)	7(9)	16(5)	−22(14)
C(6)	1219(4)	2545(13)	3216(6)	21(2)	173(26)	48(4)	−3(10)	18(4)	−7(15)
C(7)	2001(5)	−256(12)	3484(5)	28(2)	151(24)	29(3)	1(11)	8(4)	−4(11)
C(8)	1765(5)	−890(13)	1695(5)	27(3)	212(26)	31(3)	25(12)	15(4)	−5(13)
O(5)	2500(0)	−3414(13)	5000(0)	32(3)	177(24)	35(3)	0(0)	19(5)	0(0)
H(1)	2063(64)	−2271(178)	4383(86)	B=5.8(3.3) Å^2					
H(2)	1981(73)	−3619(207)	1802(91)	7.8(4.1)					
H(3)	2736(83)	−4135(220)	4503(100)	8.5(4.3)					
Tetrabromophthalic anhydride (TBPA)									
Br(1)	1174(2)	805(4)	5670(2)	50(1)	191(10)	51(1)	−54(5)	−6(2)	17(5)
Br(2)	3279(2)	1940(4)	6960(2)	60(1)	176(9)	40(1)	−9(5)	−30(2)	49(5)
Br(3)	4564(2)	6208(4)	6335(2)	48(1)	231(10)	46(1)	−58(5)	−38(2)	12(5)
Br(4)	3882(2)	9139(5)	4247(2)	61(1)	201(11)	53(1)	−74(5)	−11(2)	52(5)
O(1)	832(11)	6281(28)	3106(11)	44(8)	246(61)	45(9)	10(34)	−33(14)	−9(37)
O(2)	−7(13)	3391(35)	3837(15)	56(10)	384(81)	68(13)	−114(45)	−21(19)	31(50)
O(3)	1931(16)	8945(36)	2755(14)	103(16)	302(85)	57(12)	−7(52)	−8(23)	169(46)
C(1)	1644(13)	4579(33)	4489(13)	39(10)	40(74)	26(9)	13(36)	−7(15)	−52(35)
C(2)	1925(14)	3187(34)	5304(12)	39(10)	107(77)	19(9)	−23(38)	−23(14)	−3(35)
C(3)	8243(12)	3715(37)	5822(13)	25(9)	213(84)	26(9)	−56(38)	−27(14)	−2(39)
C(4)	3406(14)	5440(37)	5528(15)	36(10)	141(86)	39(11)	23(40)	−34(17)	−82(43)
C(5)	3126(13)	6807(36)	4697(13)	33(10)	141(81)	25(9)	−27(38)	−6(15)	−16(38)
C(6)	2223(14)	6247(41)	4185(13)	42(11)	318(95)	13(8)	−70(47)	−34(16)	39(41)
C(7)	1751(20)	7331(44)	3300(15)	95(19)	164(95)	23(10)	−1(61)	−20(22)	1(44)
C(8)	774(12)	4583(38)	3837(13)	20(8)	256(86)	26(9)	−49(39)	−9(14)	30(42)

** Table 2 is kept as Document No. 7524 at the Chemical Society of Japan.

Results and Discussion

Figure 1 shows the crystal structures of TCPH (a) and TBPA (b) viewed along b axes. The molecular overlappings are shown in Fig. 2. Bond lengths and angles are shown in Fig. 3 for TCPH (a) and TBPA (b) together with intramolecular distances. The least-squares planes and deviations of the atoms from the re-

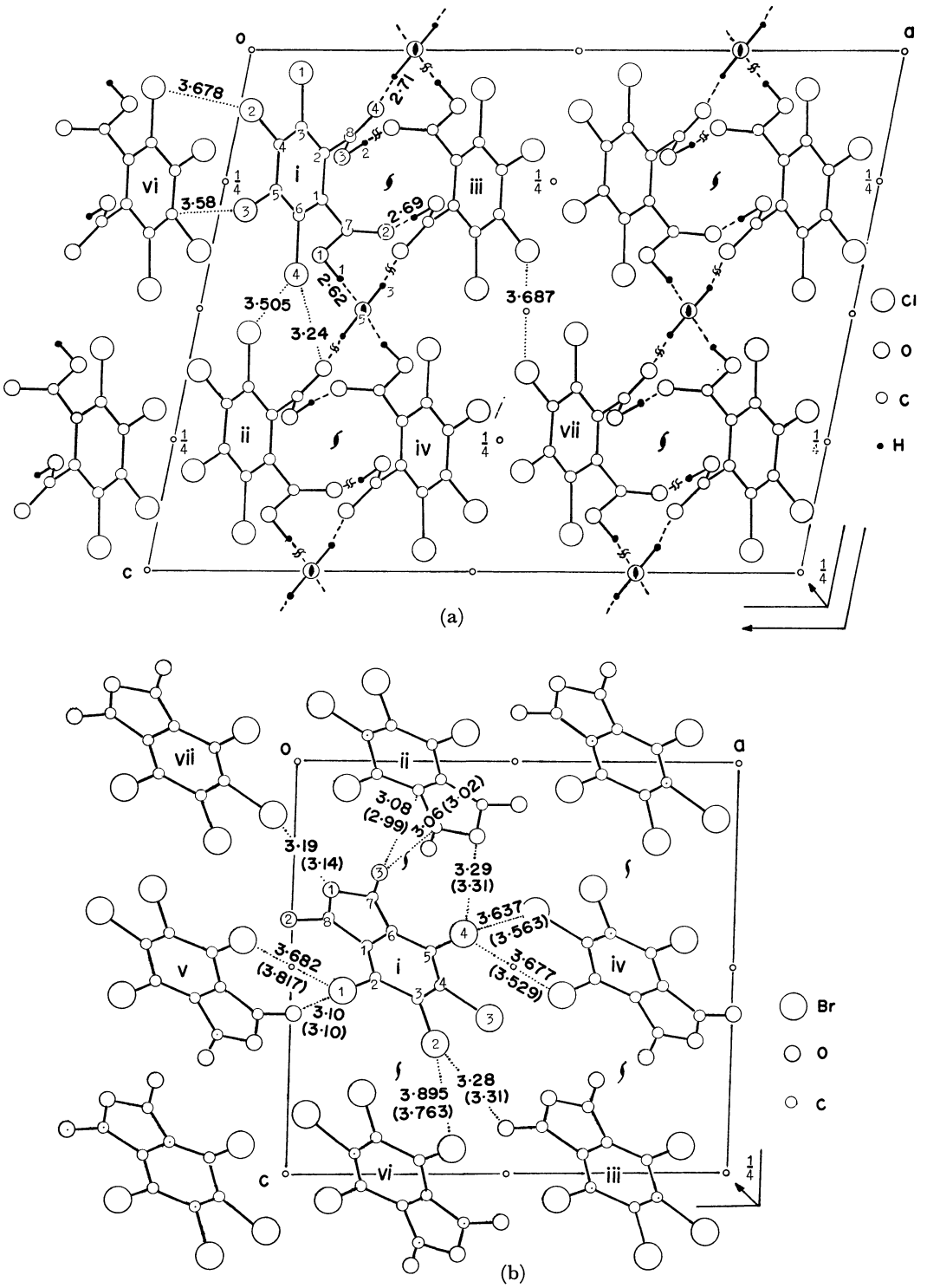

Fig. 1. Projections of the crystal structures of (a) TCPH and (b) TBPA along b axes, together with intermolecular contacts. Figures for TCPA are shown in parentheses for comparison.

Symmetry code: For TCPH, i x, y, z; ii x, $1/2+y$, $1/2+z$; iii $1/2-x$, $1/2+y$, $1/2-z$; iv $1/2-x, y, 1-z$; v x, $-1/2+y$, $1/2+z$; vi $-x$, $1/2-y$, $1/2-z$; vii $1/2+x$, $3/2-y$, $1/2+z$; viii $1/2-x$, $-1/2+y$, $1/2-z$.

For TBPA, i x, y, z; ii $1/2-x$, $1/2+y$, $1/2-z$; iii $1/2+x$, $1/2-y$, $1/2+z$; iv $1-x$, $2-y$, $1-z$; v $-x$, $-y$, $1-z$; vi $1/2-x$, $1/2+y$, $3/2-z$; vii $-1/2+x$, $3/2-y$, $-1/2+z$; viii $1-x$, $1-y$, $1-z$; ix $-x$, $1-y$, $1-z$; x x, $1+y$, z.

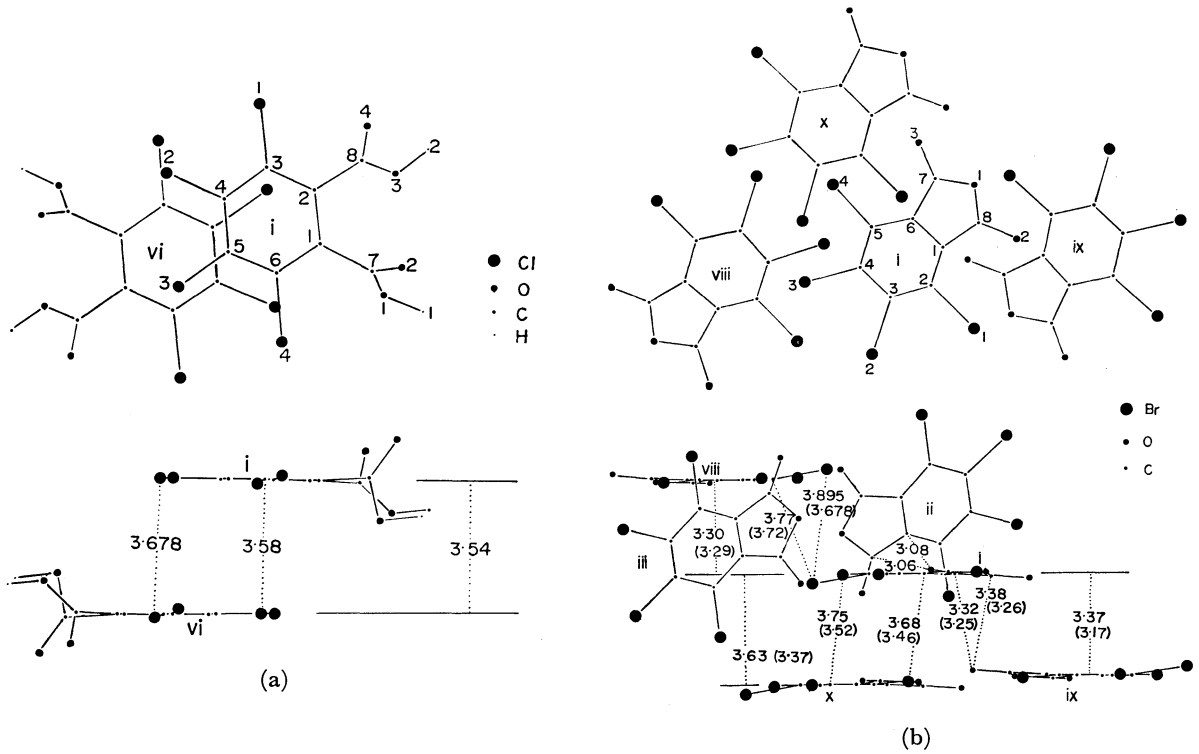

Fig. 2. The molecular overlappings for (a) TCPH and (b) TBPA. Figures are intermolecular distanes (Å). Values for TCPA are shown in parentheses for comparison. Symmetry code is given in the legend of Fig. 1.

spective planes are listed in Table 4.

Crystal Structures. *(a) TCPH*: The molecules related by the twofold screw axis at $x=1/4$ and $z=1/4$ are linked by the hydrogen bonds between the carboxylic groups to form a chain along the b axis. The chains are held together by the hydrogen bonds through the water molecules on the twofold axis at $x=1/4$ and $z=1/2$ to form a sheet parallel to the (100) plane, which is in accordance with the observed cleavage. The sheets are stacked along the a axis by van der Waals forces.

Geometry of the hydrogen bonds are listed in Table 5. It can be seen that the O–H·····O bonds are nearly linear and the O·····O·····O angles are close to the tetrahedral angle.

As seen from Fig. 2 (a), the perpendicular spacing between the adjacent benzene-ring planes is close to that found in hexachlorobenzene (3.52 Å)[9] and in 1,2,3-trichlorobenzene (3.53 Å).[10]

Table 4. The least-squares planes and deviations from the planes $X=ax+cz\cos\beta$, $Y=by$, $Z=cz\sin\beta$ (Å).

(a) TCPH

I. Benzene ring

$0.8193X+0.5720Y-0.0395Z=1.9827$

Atom	Shift (Å)	Atom	Shift (Å)	Atom	Shift (Å)
Cl(1)	0.112	O(3)	0.898	C(5)*	0.006
Cl(2)	0.004	O(4)	−0.771	C(6)*	0.001
Cl(3)	−0.003	C(1)*	−0.004	C(7)	−0.047
Cl(4)	−0.044	C(2)*	0.000	C(8)	0.021
O(1)	1.050	C(3)*	0.007	H(1)	0.96
O(2)	−1.030	C(4)*	−0.010	H(2)	0.81

II. 1-Carboxyl group

$-0.0113X+0.7132Y+0.7009Z=3.7275$

O(1)*	−0.001	C(1)*	−0.001	H(1)	0.02
O(2)*	−0.001	C(7)*	0.003		

III. 2-Carboxyl group

$0.7127X+0.1743Y+0.6795Z=3.8561$

O(3)*	−0.007	C(2)*	−0.006	H(2)	−0.04
O(4)*	−0.008	C(8)*	0.020		

Dihedral angle I and II 68.2°, I and III 48.9°

(b) TBPA

I. Benzene ring

$-0.4979X+0.5857Y+0.6396Z=4.2372$

Br(1)	0.07	O(2)	−0.15	C(4)*	−0.00
Br(2)	0.00	O(3)	0.02	C(5)*	−0.01
Br(3)	−0.18	C(1)*	−0.02	C(6)*	0.02
Br(4)	0.02	C(2)*	0.01	C(7)	0.04
O(1)	−0.04	C(3)*	0.00	C(8)	−0.06

II. Five-membered ring

$-0.4661X+0.6108Y+0.6400Z=4.4007$

Br(1)	0.17	O(2)	−0.04	C(4)	−0.07
Br(2)	−0.00	O(3)	−0.04	C(5)	−0.08
Br(3)	−0.30	C(1)*	0.01	C(6)*	−0.01
Br(4)	−0.12	C(2)	0.04	C(7)*	0.01
O(1)*	−0.01	C(3)	−0.01	C(8)*	−0.00

Dihedral angle I and II 2.3°

* Atoms with asterisks were used for calculations of the planes.

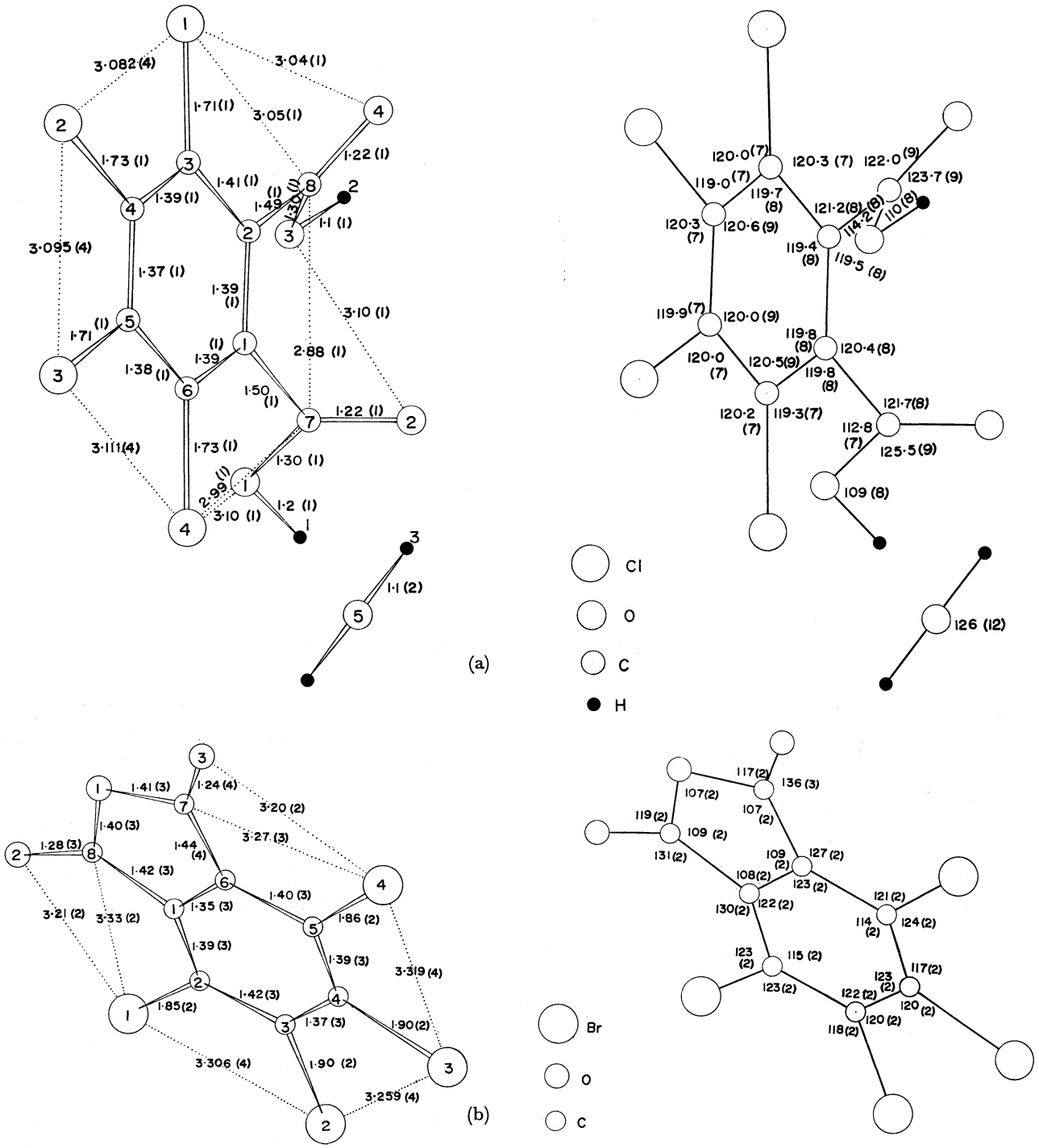

Fig. 3. Bond lengths (Å) and angles (°) of (a) TCPH and (b) TBPA, together with some intramolecular distances (Å). The estimated standard deviations are shown in parentheses.

(b) TBPA: The crystals of TBPA are isostructural with those of TCPA.[4] The molecules related by a center of symmetry, a b translation, and a twofold screw axis pack together by van der Waals forces along the a, b, and c axes, respectively.

The distances Br(1)···Br(1^{v}) and Br(1)···O(2^{v}) are shorter than those expected from the van der Waals radii, and are unexpectedly not longer than the corresponding distances in TCPA, respectively.

As seen from Fig. 2 (b), the perpendicular distance between the planes of the benzene rings of the molecules i and x is close to the distances 3.61 and 3.63 Å found in the 1 : 1 complex of hexabromobenzene with 1,2,4,5-tetrabromobenzene.[11] This distance is determined by the carbon-bromine contacts. On the other hand, the distance between the molecules i and viii is determined by the contacts of the O(3) atom with C(6^{ii}) and C(7^{ii}) atoms. The carbon-oxygen contacts are also found between the molecules i and ix.

Molecular Structures. (a) TCPH: The benzene ring keeps a planar form of regular hexagon within experimental error, but the Cl(1) and Cl(4) atoms are

Table 5. Hydrogen-bond distances (Å) and angles (°) in TCPH

D–H···A	Symmetry	D···A	H···A	Angle
O(1)–H(1)···O(5)	(i, i, i)	2.616(11)	1.44(14)	173(12)
O(3)–H(2)···O(2)	(iii, iii, i)	2.686(9)	1.56(15)	176(13)
O(5)–H(3)···O(4)	(i, i, viii)	2.706(12)	1.62(16)	161(14)

O···O···O	Symmetry	Angle
O(1)···O(5)···O(1)	(i, i, iv)	109.2(4)
O(1)···O(5)···O(4)	(i, i, viii)	97.3(4)
O(1)···O(5)···O(4)	(i, i, v)	124.3(4)
O(4)···O(5)···O(4)	(viii, i, v)	105.9(4)

Symmetry code is given in the legend of Fig. 1.

displaced to both sides of the benzene-ring plane because of the short contacts between the Cl(1) and O(4) atoms, and the Cl(4) and O(1) atoms, respectively. The average C–Cl bond length 1.716 (10) Å is near to the normal value.[4] The distances between the adjacent chlorine atoms are not far from the average value of 3.096 Å. The dihedral angles of both carboxylic groups with respect to the benzene ring are rather large because of cooperative effect of formation of the hydrogen bonds and a repulsive interaction between the O(2) and O(3) atoms.

(b) TBPA: The benzene ring is somewhat distorted from the regular hexagon, the angles C(1)–C(2)–C(3) and C(4)–C(5)–C(6) being significantly smaller than the sp^2 angle. The average C–Br bond length 1.88 (2) Å is close to the normal value.[12] The distance between the Br(2) and Br(3) atoms is shorter than that between the Br(1) and Br(2) atoms, or the Br(3) and Br(4) atoms, as found in TCPA. As seen from Table 4, the molecule is nearly planar but the Br(3) and O(2) atoms deviate from the benzene-ring plane in the same sense as in TCPA.

Comparison of the Mode of Molecular Overlapping. Different modes of overlapping are found for the overcrowded molecules; these is considerable molecular overlap in TCPH, while in TBPA these is no overlap. As noted above, this reflects in the spacings of stacking in both compounds: the spacing in TCPH is rather large and determined by the carbon-chlorine contacts, while in TBPA there are two short spacings determined by the carbon-oxygen contacts in addition to one spacing determined by the carbon-bromine contacts.

Effects of Overcrowding on the Conformation of the Benzene Rings. The observed distances between halogen atoms attached to adjacent carbon atoms on a benzene ring are much less than the sum of the van der Waals radii of the halogen atoms in both TBPA and TCPH. However, the benzene ring in TCPH is not distored. As an explanation for this fact an anisotropic van der Waals radius can be considered as follows. Let the z axis be perpendicular to the benzene ring plane, and the x axis be along the carbon-chlorine bond, then the direction of the $3p_y$ orbital, which is assumed to participate in the van der Waals interaction, deviates outward by 30° from the line between the chlorine atoms. On this model for usual geometry the possible extent of the $3p_y$ orbital is estimated to be 1.80 Å, which is equal to the Pauling's van der Waals radius.

The decrease in the C(1)–C(2)–C(3) and C(4)–C(5)–C(6) bond angles as found in TBPA is commonly observed in the benzene rings attached by five-membered ring as listed in Table 6. Therefore, the decrease is not attributed to the overcrowding of the halogen atoms, but to the attachment of five-membered ring as pointed out recently by Bechtel, *et al.*[16]

Table 6. Decrease in the bond angles of C(1)–C(2)–C(3) and C(4)–C(5)–C(6) in the benzene ring with five-membered ring fused at the C(1) and C(6) atoms

Compound	Angles (°)	
TBPA[a]	114	115
TCPA[4]	113.4	115.8
Xanthotoxin[13]	115.5	117.6
Dibenzofuran[14]	116.7	117.9
Alkaloid lycorine[15]	116.7	117.3
2-(*p*-Bromophenyl)indane-1,3-dione[16]	115.0	117.1
	117.5	117.7
Phthalimide[17]	116.6	116.8
5-Methoxytryptamine[18]	117.7	117.8
N-Acetyl-L-tryptophane[19]	117.9	118.7
Melatonin[20]	117.1	118.4
2-Thio-1-(β-D-ribofuranosyl)-3*H*-benzimidazole[21]	115.7	116.8
5-Methylbenzofurazan-1-oxide[22]	115.7	117.8
Benzotriazole[23]	114.7	115.6
	115.6	115.6
	115.0	117.0
	115.8	116.6

a) This work.

References

1) C. A. Coulson and D. Stocker, *Mol. Phys.*, **2**, 397 (1959).
2) T. G. Strand, *J. Chem. Phys.*, **44**, 1611 (1966).
3) G. Gafner and F. H. Herbstein, *Acta Crystallogr.*, **13**, 706 (1960).
4) R. Rudman, *ibid.*, **B27**, 262 (1971).
5) K. Fukui, C. Nagata, and T. Yonezawa, *J. Amer. Chem. Soc.*, **80**, 2267 (1958).
6) K. Ito, S. Kashino, and M. Haisa, *Acta Crystallogr.*, **B31**, in the press. "Topochemical Studies. VI. The Crystal and Molecular Structure of 2,5-Pyridinedicarboxylic Acid-*N*,*N*-Dimethylformamide Complex Monohydrate." Received May 6, 1975 and accepted June 26, 1975.
7) "International Tables for X-ray Crystallography," Vol. III, Kynoch Press, Birmingham (1962), p. 202.
8) "The Universal Crystallographic Computing System-Osaka," The Computation Center, Osaka University. (1973).
9) G. M. Brown and O. A. W. Strydom, *Acta Crystallogr.*, **B30**, 801 (1974).
10) R. G. Hazell, M. S. Lehmann, and G. S. Pawley, *ibid.*, **B28**, 1388 (1972).
11) G. Gafner and F. H. Herbstein, *J. Chem. Soc.*, **1964**, 5290.
12) M. N. G. James and G. J. B. Williams, *Acta Crystallogr.*, **B29**, 1172 (1973).
13) N. R. Stemple and W. H. Watson, *ibid.*, **B28**, 2485 (1972).
14) O. Dideberg, L. Dupont, and J. M. André, *ibid.*, **B28**, 1002 (1972).
15) R. Roques and J. Piquion, *ibid.*, **B30**, 296 (1974).

16) F. Bechtel, G. Bravic, J. Gaultier, and C. Hauw, *Acta Crystallogr.*, **B30**, 1499 (1974).
17) E. Matzat, *ibid.*, **B28**, 415 (1972).
18) W. G. Quarles, D. H. Templeton, and A. Zalkin, *ibid.*, **B30**, 95 (1974).
19) M. Cotrait and Y. Barans, *ibid.*, **B30**, 510 (1974).
20) W. G. Quarles, D. H. Templeton, and A. Zalkin, *ibid.*, **B30**, 99 (1974).
21) P. Prusiner and M. Sundaralingam, *ibid.*, **B29**, 2328 (1973).
22) D. Britton and W. E. Noland, *ibid.*, **B28**, 1116 (1972).
23) A. Escande, J. L. Galigné, and J. Lapasset, *ibid.*, **B30**, 1490 (1974).

Photochemistry in the Adsorbed Layer. VI. The Type I Selectivity in the Photolysis of Adsorbed 2-Pentanone

Masakazu ANPO and Yutaka KUBOKAWA

Department of Applied Chemistry, College of Engineering, University of Osaka Prefecture, Mozu-Umemachi, Sakai, Osaka 591

(Received June 18, 1975)

A marked high selectivity of the type I reaction in the photolysis of adsorbed 2-pentanone decreases with increasing amount of 2-pentanone adsorbed, approaching the selectivity in the water solution photolysis. In the solution photolysis the type I selectivity decreases in the order water>methanol>*n*-heptane. From these results together with comparison of the blue shifts of the (n,π^*) bands in solution and in the adsorbed layer it has been concluded that such an enhancement of the type I reaction in the adsorbed layer is attributed to a heterogeneity of the surface, *i.e.*, the presence of special active sites, as well as to the surface polarity.

The Norrish type II reactions of alkyl ketones having γ-hydrogen atoms have been investigated by a number of workers.[1-3] On the other hand, there have been few or no studies for the type I reactions of these compounds. We have found that in the adsorbed layer the type I selectivity in the 2-pentanone photolysis is enhanced compared to that in the gas phase.[4] In order to obtain information on the nature of such enhancement, it seems necessary to investigate its photolysis in solution and to compare these results with those in the adsorbed layer. In the present work therefore it has been undertaken to study the solvent effect upon the type I selectivity in the 2-pentanone photolysis and to examine how the type I selectivity in the adsorbed layer photolysis varies with the amount adsorbed in connection with this problem.

Experimental

Materials. All the compounds used in this work were available commercially (Tokyo Kasei Kogyo Co. Ltd., Grade SG) and purified by fractional distillation. Deionized double-distilled water was degassed by alternate freezing and thawing *in vacuo*. Particular care was taken to remove water completely from the solvents and reactants. Porous Vycor glass (Corning, No. 7930) was used as adsorbent.

Apparatus and Procedure. Details of the apparatus and procedure used in the photolysis in the adsorbed layer were described in the previous paper.[4] A conventional vacuum system was used in conjunction with a special quartz cell capable of studying the spectra and photolysis in the adsorbed layer. The specimen of porous Vycor glass which had been heated in oxygen to remove carbonaceous impurities was introduced to the cell and degassed at temperatures ranging from 100 to 800 °C for 7 hr. After a certain amount of 2-pentanone had been adsorbed on the specimen, photolysis was carried out using an ultra high pressure mercury lamp without filter.

Liquid phase photolyses were carried out in a rectangular quartz cell (4.0×1.0 cm) of path length 0.5 cm, having two outlets. One was sealed off after admission and degassing of the sample solution. Another had a breakable seal which made it possible to attach the cell to a conventional analytical system after irradiation. The cell was immersed in a thermostat having a quartz window. The irradiation was carried out using an ultra high pressure mercury lamp without filter. The analytical system consisted of three traps and a modified Ward still. The gaseous products were separated by fractional distillation and analyzed by gas chromatography using a flame-ionization detector.

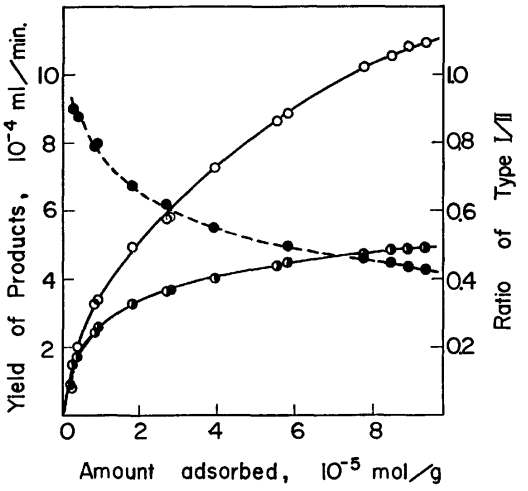

Fig. 1. Effect of amount adsorbed upon the photolysis of 2-pentanone at 25 °C. Irradiation time, 20 minutes. ○, Ethylene; ◑, Propane; ●, Ratio of Type I/II.

Results

In Fig. 1 the rates of propane and ethylene formation are plotted against the amount of 2-pentanone adsorbed. It is seen that the rates of formation increase with increasing amount adsorbed. In the range of the small amounts adsorbed the extent of the increase is large, but decreases with increasing amount adsorbed. Such a trend is more significant for the propane than for the ethylene formation. Accordingly, the ratio of propane (Norrish type I reaction) to ethylene (Norrish type II reaction) decreases with increasing amount adsorbed, finally approaching 0.40.

Results of 2-pentanone photolysis in various solvents are shown in Table 1. The major gaseous products

Table 1. The rates of 2-pentanone photolysis in various solvents[a] (10^{-4} ml/hr)

	Heptane	Methanol	Water
Ethylene	618.0	674.0	755.0
Propane	67.0	167.0	303.0
Ratio of type I/II	0.11	0.25	0.40

a) These values were the corrected rates of formation divided by the relative ε_{max} values (Table 2). The concentration of 2-pentanone was 2.0×10^{-4} mol (0.1 mol%). Photolysis was carried out at 30 °C.

formed are propane and ethylene. The amounts of minor products such as methane, ethane, propylene, and butane did not exceed 10% of the amount of propane, indicating that the rate of the type I reaction is approximately equal to the rate of propane formation. It is seen that the rate of formation increases slightly for ethylene while significantly for propane in the order heptane<methanol<water, *i.e.*, with increasing polarity of the solvents.[5-7] It should be noted that with increasing polarity of the solvent the ratio of propane to ethylene formation increases. The ratio obtained with water solution is essentially the same as the smallest corresponding value in the adsorbed layer photolysis.

TABLE 2. THE (n, π^*) TRANSITION OF 2-PENTANONE IN SOLUTION AND IN ADSORBED LAYER AT 25 °C

	Gas phase	Heptane[a]	Methanol[a]	Water[a]	Vycor glass[b]
Absorption max. (nm)	279	280	275	273	273
Relative ε_{max}	—	1.0	1.1	1.3	—

a) The concentration of 2-pentanone was 2×10^{-4} mol (0.1 mol%). b) Porous Vycor glass was pretreated at 500 °C for 7 hr in vacuum. The amount of 2-pentanone adsorbed was 9×10^{-5} mol/g. The magnitude of the blue shift of the (n, π^*) transition scarcely changed with increasing amount of 2-pentanone adsorbed.

As seen in Table 2, the blue shift of the (n, π^*) transition of 2-pentanone increases in the order *n*-heptane< methanol<water. Similar magnitudes of the blue shift have been obtained by Rao *et al.*[8] As described in the previous paper,[4] we have shown that the blue shift observed for the alkyl ketones adsorbed on porous Vycor glass is attributable to hydrogen bonding between the surface OH groups and C=O groups of the alkyl ketones and can be used as a measure of the polarity of the surface OH groups. This suggests that the surface polarity of Vycor glass may be similar to that for water solution.

Discussion

Wagner *et al.*[2,3] have carried out extensive studies of the solvent effect upon the type II reaction, which show that the rate of the type II reaction increases with increasing polarity of the solvent owing to stabilization of the 1,4-biradical intermediate, *i.e.*, a decreased probability for return of the γ-hydrogen in the biradical (formed by the intramolecular hydrogen abstraction in the excited states) due to hydrogen bonding between the polar solvent and the hydroxyl group of the biradical. The effects of the surface pretreatments upon the yields of the type II reaction of adsorbed 2-pentanone have been interpreted on a similar basis.[9] On the other hand, there have been no studies of the solvent effect upon the type I reaction. The increase in the rate of the type I reaction may be interpreted as follows: As the polarity of the solvent increases, the interaction of the radicals formed in the primary process with the solvent will increase. Such an increase in the interaction would result in the increase in stabilization of the radicals, leading to suppression of the recombination of the alkyl-acyl radical pairs formed in the primary process as well as increased probability of α-cleavage in the excited triplet states, *i.e.*, formation of these radical pairs. Both effects may contribute to enhancement of the yield of the type I reaction.

In the range of the amount adsorbed about 9.00×10^{-5} mol/g the magnitude of the blue shift of the (n, π^*) transition as well as the ratio of the yield for the type I to that for the type II reaction is essentially the same as that observed for water solution. This suggests that at least in this range of the amount adsorbed enhancement of the type I reaction in the adsorbed layer may arise from the surface polarity which is reflected by the magnitude of the blue shift. Such a significant role of the surface polarity in determining the ratio of the yield for the type I to that for the type II reaction is apparent from the effect of surface pretreatments upon the photolysis of adsorbed 2-pentanone described previously.[9] As seen in Fig. 2 this ratio decreases with increasing degassing temperature, *i.e.*, with decreasing surface polarity owing to the decrease in the concentration of surface OH groups.

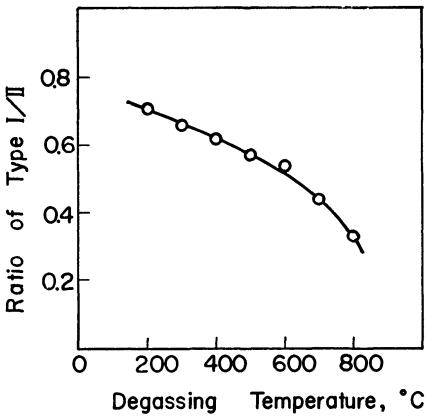

Fig. 2. Effect of degassing temperature upon the photolysis of adsorbed 2-pentanone at 25 °C. Amount of 2-pentanone adsorbed was 2.2×10^{-5} mol/g.

In the range of the amount adsorbed below 4.00×10^{-5} mol/g a marked increase in the type I selectivity as well as the overall yield of the photolysis occurs. Although the true nature of such a marked increase in the type I selectivity is not yet clear, such behavior may be explained by assuming a heterogeneity of the surface, *i.e.*, the presence of special active sites, since the amount adsorbed of 4.5×10^{-5} mol/g corresponds to $\theta=0.05$ using 25 A^2 per one molecule.

It has been reported by Turkevich and Fujita,[10] and by Gesser and his co-workers[11,12] that the radicals produced by the photolysis of methyl iodide adsorbed on porous Vycor glass are trapped much more strongly on a limited number of active sites than other sites. Thus, a significant increase in the radical stabilization would be expected on such special active sites, where suppression of the recombination of the radical pair as well as an increase in the probability of α-cleavage described above would be much more significant than that for other ordinary sites. In addition, it seems necessary to

take into account the following possibility: The type I reaction will be enhanced because of the contribution of hydrogen abstraction from the surface OH groups, which takes place more efficiently in the small amounts adsorbed as described in the previous paper.[13] Furthermore, the presence of special active sites capable of abstracting hydrogen efficiently from 2-pentanone molecules may retard the intramolecular γ-hydrogen abstraction leading to the type II reaction. The presence of such kind of active sites has already been suggested by Low *et al.*[14] for the Vycor glass-acetone system.

We would like to express our thanks to Mr. T. Shimatani for carrying out some parts of the experiments.

References

1) N. C. Yang and S. P. Elliot, *J. Amer. Chem. Soc.*, **91** 7550 (1969).
2) P. J. Wagner and G. S. Hammond, *ibid.*, **88**, 1245 (1966). P. J. Wagner, *Tetrahedron Lett.*, **1968**, 5385; **1967**, 1753; *Accounts Chem. Res.*, **4**, 168 (1971).
3) J. A. Barltrop and J. D. Coyle, *Tetrahedron Lett.*, **1968**, 3235.
4) Y. Kubokawa and M. Anpo, *J. Phys. Chem.*, **78**, 2442 (1974).
5) H. H. Jaffé and M. Orchin, "Theory and Applications of Ultraviolet Spectroscopy," Wiely, New York (1962), p. 186.
6) C. Reichardt, *Angew. Chem.*, **77**, 30 (1965).
7) E. S. Stern and C. J. Timmons, "Electronic Absorption Spectroscopy in Organic Chemistry," Edward Arnold, London (1970), p. 28.
8) A. Balasubramanian and C. N. R. Rao, *Spectrochimica Acta*, **18**, 1337 (1962). C. N. R. Rao, G. K. Goldman, and A. Balasubramanian, *Can. J. Chem.*, **38**, 2508 (1960).
9) M. Anpo, T. Wada, and Y. Kubokawa, This Bulletin, **48**, 2663 (1975).
10) J. Turkevich and Y. Fujita, *Science*, **152**, 1619 (1966).
11) M. Fujimoto, H. D. Gesser, B. Garbutt, and A. Cohan, *ibid.*, **154**, 381 (1966). M. Fujimoto, H. D. Gesser, B. Garbutt, and M. Shimizu, *ibid.*, **156**, 1105 (1967).
12) M. Shimizu and H. D. Gesser, *Can. J. Chem.*, **46**, 3517 (1968); **47**, 1375 (1969). B. Garbutt and H. D. Gesser, *ibid.*, **48**, 2685 (1970).
13) M. Anpo, S. Hirohashi, and Y. Kubokawa, This Bulletin, **48**, 985 (1975).
14) J. C. McManus, Y. Harano, and M. J. D. Low, *Can. J. Chem.*, **47**, 2545 (1969).

The Catalytic Action of TiO_2 for the Isomerization of Butenes

Kunimitsu MORISHIGE, Hideshi HATTORI, and Kozo TANABE
Department of Chemistry, Faculty of Science, Hokkaido University, Sapporo 060
(Received June 27, 1975)

The isomerization of 1-butene or *cis*-2-butene and the co-isomerization of *cis*-2-C_4H_8 and *cis*-2-C_4D_8 were carried out at 120 °C over TiO_2 calcined *in air*. It has been found that induction period appeared and the ratio of *cis*-2-butene to *trans*-2-butene in the isomerization of 1-butene was unusually high (5—20). The double bond migration and *cis-trans* isomerization occurred by an intramolecular hydrogen transfer reaction and the kinetic isotope effect (k_H/k_D) was 4—5. The activity was completely or almost lost by poisoning with pyridine or nitric oxide. The isomerization was concluded to proceed by a π-allyl anion mechanism, where the *cis-trans* interconversion is highly restricted and the C–H bond cleavage is involved in the rate-determining step of the double bond migration. Main active sites were suggested to consist of both Lewis acid sites and basic sites (surface oxygen ion, O^{2-}).

TiO_2 has been generally classified as a solid acid on the basis of the experiment on the chemical adsorption of basic Hammett indicators and pyridine.[1] Recently, however, Shannon *et al.* reported that TiO_2 calcined in air showed the similar selectivity as basic catalysts for the isomerization of *n*-butene.[2] From the experiment on co-isomerization of the mixture of C_4H_8 and C_4D_8, they concluded that both the double bond migration and *cis-trans* isomerization were mainly intermolecular and each isomerization proceeded *via* separate mechanisms. However, it seems to be difficult to determine whether the isomerizations are inter- or intra-molecular, since their results showed that considerable isotopic scrambling occurred independently of the isomerizations.

In our previous work, the nature of active sites on TiO_2 was found to depend strongly on the method of preparation and pretreatment of the catalyst.[3] Over TiO_2 prepared by calcining titanic acid *in vacuo* at low temperatures, the ratio of *cis*-2-butene/*trans*-2-butene (abbreviated as *cis*-/*trans*-) from 1-butene was nearly 1, indicating Brönsted acid as active sites. When TiO_2 was prepared by calcining titanic acid *in vacuo* at high temperatures, it gave the high *cis*-/*trans*- ratio. Since the activity of the latter catalyst was decreased by oxygen treatment, the active sites were concluded to be mainly Ti^{3+} ions formed by the reduction of Ti^{4+}. On the other hand, it was reported that the activity of TiO_2 calcined *in air* was not affected by oxygen treatment,[2] though no study was made on the nature of active sites.

The purpose of the present work is to elucidate the reaction mechanism as well as the nature of active sites for the isomerization of *n*-butene over TiO_2 prepared by calcining titanic acid *in air* and to learn about the relation of the acid sites on the catalyst with the basic character giving the high *cis*-/*trans*- ratio.

Experimental

Catalyst and Reagents. TiO_2 was prepared by hydrolyzing $TiCl_4$ with NH_4OH in the solution of $(NH_4)_2SO_4$ and calcining the precipitate in air at 500 °C for 3 hr. X-Ray diffraction of the sample showed a structure of an anatase type. Butenes (Takachiho pure grade) were purified by distilling through a molecular sieves 4A maintained at the temperature of dry ice–ethanol. Perdeuterio-*n*-butenes were prepared by exchange of 1-butene with D_2 over MgO at room temperature, the isomers being separated on a preparative scale chromatographic column.[4] Pyridine (GR of Kanto Chem. Co.) was purified by repeating three times the procedure of a freeze-thaw outgassing cycle after passing over zeolite 13X. NO of more than 95.0% purity supplied by the Gaschro Industry Co. was purified by a vacuum distillation.

Reaction Procedure. The isomerization of *n*-butenes was carried out in a circulating system of *ca.* 330 ml at 120 °C. A small amount (*ca.* 1%) of the reaction products was withdrawn out of the system by expansion at appropriate time intervals and analyzed by gas chromatography using a 7 m column (Cu tubing of 4 mm in diameter) containing 30% propylene carbonate on 30—60 mesh Uniport C. The column was operated at 0 °C. Before use, a catalyst (0.2 g) was treated in a vacuum of 10^{-4} mmHg at 450 °C for 2 hr. Between runs, the catalyst was degassed at 400 °C for 30 min. The same activity and selectivity as those of the first run were maintained by this simple treatment through all the kinetic runs. The surface area of the catalyst was 72 m^2/g.

For co-isomerization experiments, a mixture containing about equal amounts of light *cis*-2-butene (*cis*-C_4H_8) and heavy *cis*-2-butene (*cis*-C_4D_8) was co-isomerized on TiO_2 (18.9 mg) in a static system of 26 ml at 5 cmHg. The isomerized products were condensed into a liquid nitrogen trap, separated by preparative scale gas chromatography and analyzed for the isotopic composition by mass spectrometry. Four runs were carried out and each run was stopped at different conversions. The mixtures of heavy 1-butene (12%) and light *cis*-2-butene (88%) were also co-isomerized at 3.5 cmHg in order to determine the main path in the interconversion from *cis*- to *trans*-2-butene.

Poisoning, IR and ESR Measurements. For poisoning experiment, the prepared catalyst was evacuated at 450 °C, equilibrated with a vapor of pyridine (0.5 cmHg) at room temperature for 30 min, evacuated again overnight at the same temperature and then heated *in vacuo* for 1—2 hr at different temperatures. The activities for the isomerization of 1-butene were examined after the above treatment. The isomerization was also carried out on the catalyst in the presence of NO (2.45 cmHg).

IR spectrum of the catalyst which was evacuated at 200 °C after exposed to pyridine vapor in *in situ* cell was measured at room temperature. ESR spectra of the catalyst with or without pyridine poisoning were measured at −195 °C before and after the introduction of 1-butene (5 cmHg) at 120 °C.

Results

Kinetics of the Isomerizations of n-*Butenes.* The time courses of the isomerizations of 1-butene and *cis*-2-butene are shown in Fig. 1. 1-Butene isomerized pre-

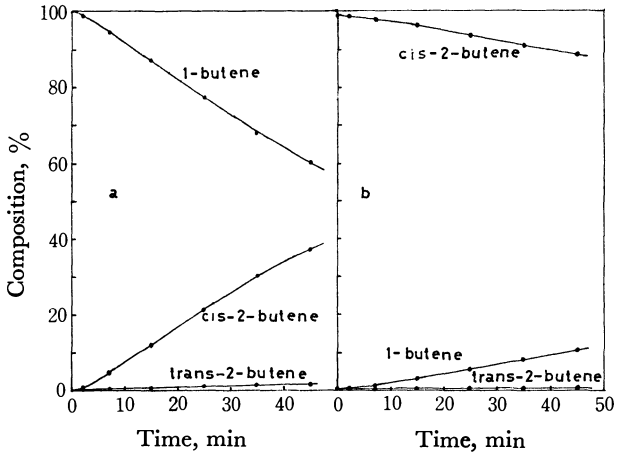

Fig. 1. Isomerization of 1-butene (a) and *cis*-2-butene (b) over TiO_2. Pressure of butenes: 11 cmHg.

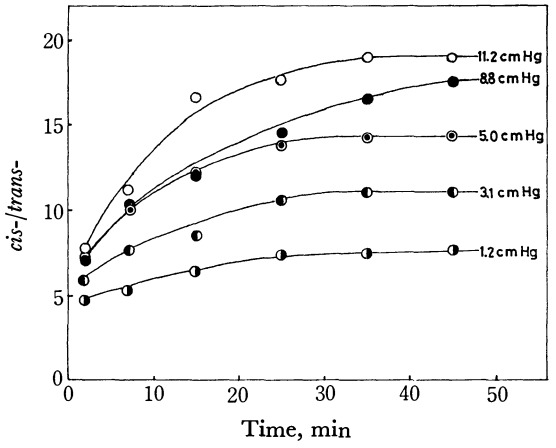

Fig. 2. Ratio of *cis*-2-butene/*trans*-2-butene in isomerization of 1-butene *vs.* reaction time at different pressures.

ferentially to *cis*-2-butene and *cis*-2-butene preferentially to 1-butene, in accord with the results observed by Shannon *et al.*[2] It is interesting that induction periods were observed in our case. Figure 2 shows the time course of the *cis*-/*trans*- ratio when 1-butene was isomerized over the catalyst at different pressures. The figure indicates the two remarkable features which have not been reported before for the isomerization of *n*-butene. The first one is that the *cis*-/*trans*- ratio becomes increasingly far from the equilibrium value as the isomerization progresses. The second one is that the higher the initial pressure, the larger the *cis*-/*trans*- ratio. Similarly, the increase in 1-/*trans*- ratio with reaction time and increasing initial pressure was observed for the isomerization of *cis*-2-butene.

The time courses of the *n*-butene isomerizations obeyed the reversible first order kinetics except the induction period. The initial rate, R_0, was calculated from the first order plots. Assuming that reactant butene is in adsorption equilibrium of Langmuir type and that the surface reaction of the adsorbed molecule is rate-determining, R_0, is given by the equation.

$$R_0 = kKP_0/(1+KP_0), \qquad (1)$$

where P_0 is the initial pressure of the reactant, K the

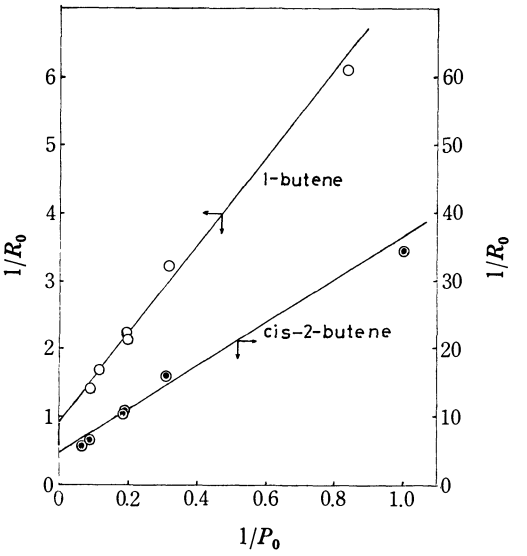

Fig. 3. Plots of reciprocals of initial rates against reciprocals of pressures for isomerizations of 1-butene and *cis*-2-butene.

adsorption constant of the reactant and k the rate constant of the surface reaction. In accord with the above equation, plots of the reciprocals of the initial rates against the reciprocals of reactant pressures were linear as shown in Fig. 3. The intercepts and slopes provided the adsorption constants (K_1 and K_c) of 1-butene and *cis*-2-butene. The adsorption constant of *trans*-2-butene could not be determined by the same way, because the reactivity of *trans* isomer was very low. In order to obtain the adsorption constant, the isomerization of 1-butene was carried out in the presence of different partial pressures of *trans* isomer, where the initial pressure of 1-butene was maintained at 5 cmHg. The initial rate, R_1, was calculated from the first order plots of the disappearance of 1-butene, where the amount of the products from the isomerization of *trans*-2-butene was neglected. The rate data were represented by the competitive reaction equation of Langmuir type.

$$R_{0(1)}/R_1 = K_tP_t/(1+K_1P_1) + 1, \qquad (2)$$

where P_1, P_t, K_1, and K_t are the initial pressures and the adsorption constants of 1-butene and *trans*-2-butene,

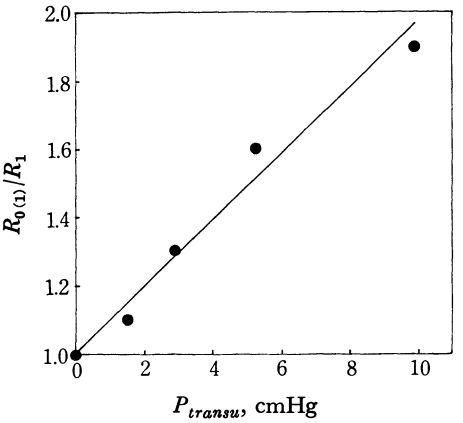

Fig. 4. Effect of partial pressure of *trans*-2-butene on initial rate of isomerization of 1-butene.

respectively. The plots of the Eq. (2) gave a straight line as shown in Fig. 4. K_t was calculated from the slope and K_1. Thus, K_1, K_c, and K_t were obtained to be 0.15 0.17, and 0.18 $cmHg^{-1}$, respectively.

Co-isomerization. From the results of the co-isomerization of a mixture of *cis*-2-C_4H_8 and *cis*-2-C_4D_8, isotope effects and intermolecular hydrogen exchange were determined. The data were analyzed by the method devised by Hightower and Hall.[5] For each isomer, the light fraction is given by the formula.

$$\frac{1}{2}N_4+\sum_{i=0}^{3}N_i \quad (3)$$

where N_i is the mole fraction of each isotopic species containing i deuterium atoms. The heavy fraction is then given by the formula.

$$\frac{1}{2}N_4+\sum_{i=5}^{8}N_i \quad (4)$$

The isotope effects were calculated from the relative activities of the two species; namely, the ratios of light materials to heavy materials in the products divided by the ratio in the starting materials.

Table 1. Product distribution from co-isomerization of *cis*-2-C_4H_8 and *cis*-2-C_4D_8 over TiO_2 at 120 °C

	Composition of products	Isotopic composition, %								
		Light fraction					Heavy fraction			
		d_0	d_1	d_2	d_3	d_4	d_5	d_6	d_7	d_8
1-C_4'	19.2	44.0	3.0	0	0	0	0	0.7	4.2	48.2
trans	8.9	65.5	3.0	0	0	0	0	0	3.6	27.9
cis	71.8	45.8	1.8	0	0	0	0	0	3.7	48.6

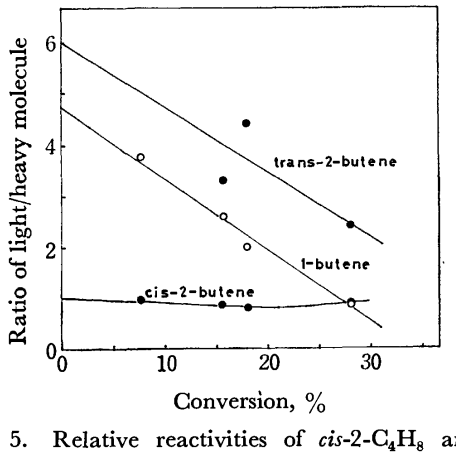

Fig. 5. Relative reactivities of *cis*-2-C_4H_8 and *cis*-2-C_4D_8 over TiO_2 at 120 °C.

Table 1 shows the isotopic distribution and Fig. 5 the ratio of light to heavy material for each isomer at various conversions. The data of Table 1 indicate that double bond migration and *cis-trans* isomerization are much faster than intermolecular H–D exchange. Evidently, both reactions do not involve the intermolecular exchange reaction, *i.e.*, the hydrogen transfers are intramolecular. Since the ratio of light molecule to heavy molecule in products represents kinetic isotope effect, Fig. 5 shows the existence of the large isotope effects, 4—5, in both isomerizations.

Table 2. Poisoning with pyridine and NO

	No poison	pyridine[a]	pyridine[b]	pyridine[c]	NO	NO[e]
Activity	0.451	0	0.049	0.294	0.05[d]	0.294
$(cis/trans)_s$	15		13	16	4	9

Activity: cmHg min^{-1} g^{-1}, $(cis/trans)_s$: selectivity in a stationary state calculated from the plots analogous to Fig. 7.
a) Degassed at 200 °C for 2 hr. b) Degassed at 300 °C for 1 hr. c) Degassed at 400 °C for 1 hr. d) Poisoning occurred increasingly in progress of isomerizartion. e) After adsorption of NO (1.78 cmHg), the catalyst was degassed for 1 hr at 120 °C.

In the co-isomerization of a mixture of 1-C_4D_8 (12%) and *cis*-2-C_4H_8 (88%), the ratio of heavy molecule to light molecule in *trans*-2-butene was 0.093 at the stage of 2% formation of *trans*-2-butene, while the value in *cis*-2-butene was 0.019.

The Results of Poisoning and IR and ESR Spectra. The effects of poisoning with pyridine and NO on the isomerization of 1-butene are shown in Table 2, where the activities are the initial rates evaluated from the reversible first order plots. The catalyst on which pyridine was adsorbed showed no activity even after evacuation at 200 °C. By the poisoning with NO, the activity was decreased to less than one tenth. The selectivities were affected by poisoning with NO, but not with pyridine.

IR spectra of the catalyst poisoned with pyridine exhibited only the pyridine molecules coordinately bonded to the Lewis acid sites, in accord with the literatures.[6-8] ESR spectra of the above sample did not show the existence of dipyridil anion radical which was observed in the cases of the alkaline earth oxides.[9] The intensities of ESR signals[3] indicating Ti^{3+} for both catalysts with and without pyridine poisoning increased about four times on the introduction of 1-butene.

Discussion

Reaction Mechanism. The isomerization of 1-butene or *cis*-2-butene is known to give high ratio of *cis*-2-butene to *trans*-2-butene or 1-butene to *trans*-2-butene over basic catalysts such as MgO, CaO, Na–Al_2O_3 *etc.*[10-13] Since the adsorption constants of each butene isomer were almost the same in the present work, the basic feature of the selectivities, *i.e.*, the very high ratios of *cis*-/*trans*- and 1-/*trans*-, observed for TiO_2 seems not to result from a selective adsorption of *cis*-2-butene or 1-butene in the *cis* configuration on active sites, whose model was once presented for 1-butene isomerization over γ-Al_2O_3 by Gerberich and Hall.[14] In other words, the configurational differences among three isomers do not exert any influence on the adsorption of each isomer. The basic feature of the observed selectivity would result from the difference in the rate of interconversion among each isomer adsorbed on TiO_2.

The data on co-isomerization shown in Table 1 reveal that the hydrogen transfers involved in double bond migration and *cis-trans* isomerization are intramolecular. The large isotope effect observed for *cis-trans* isomeriza-

tion does not reflect the effect for the direct interconversion step, because, in the co-isomerization of 1-C_4D_8 (12%) and *cis*-2-C_4H_8 (88%), the ratio of heavy to light molecule in *trans*-2-butene was larger than that in *cis*-2-butene. Actually, at a reaction temperature (200 °C) at which direct *cis-trans* interconversion becomes predominant, the isotope effect was not observed.[2] Therefore, it is very likely that C–H bond cleavage is involved in the rate-determining step of the double bond migration. These features together with the high *cis/trans* ratio and slow direct *cis-trans* isomerization can be well explained only by a π-allyl anion mechanism,[13] in which the *cis* allyl anion is thermodynamically more stable than the *trans* form and the *cis-trans* conversion is highly restricted.

Active Sites. The activity for the isomerization was completely lost by the adsorption of pyridine. Since pyridine was adsorbed on Lewis acid site to form its coordinately bonded molecule according to IR spectra and not on basic site (surface oxygen ion, O^{2-}) to form the dipyridyl anion[9] according to ESR spectra, Lewis acid sites are considered to participate in active sites for the isomerization. On the other hand, the activity was considerably decreased by poisoning with NO, which is known to react with basic site (O^{2-}) to form nitrato-compound.[15] These facts strongly suggest that the active sites consist of Lewis acid site-basic site pair. The concept that acid-base pair sites are active sites for the isomerization is also proposed for η-Al_2O_3 on the basis of the experiments on the reactivity of substituted olefins.[16]

The active sites on TiO_2 prepared by calcining titanic acid *in vacuo* were previously reported to be Ti^{3+} formed by the reduction of Ti^{4+} on the surface.[3] Since the activity of the present catalyst prepared by calcining titanic acid *in air* and then evacuated was decreased to two thirds of the activity by treating with dry air at 450 °C for 1 hr, the possibility that Ti^{3+} is a part of active sites can not be excluded. However, main active sites on the present catalyst are considered to be Lewis acid (Ti^{4+}) and oxygen ion (O^{2-}) pair. It should be emphasized that the main active sites on TiO_2 for the isomerization are varied by changing preparation condition of the catalyst.

Induction Period and Pressure Dependence of Selectivity.

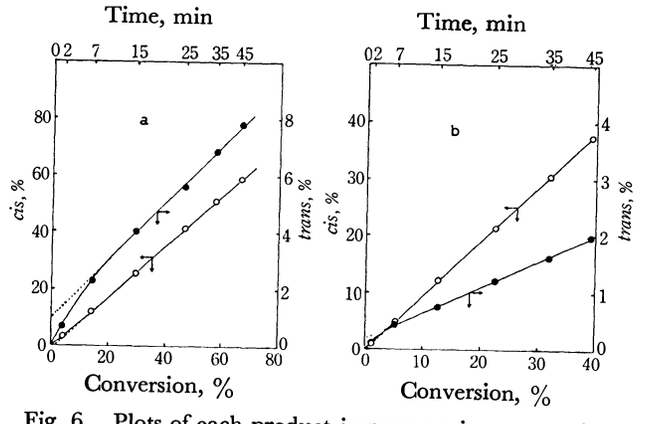

Fig. 6. Plots of each product isomers against conversion % for isomerization of 1-butene. Pressure of 1-butene: a) 1.2 cmHg, b) 11.2 cmHg.

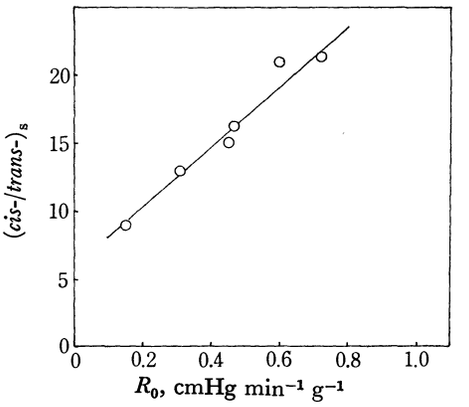

Fig. 7. Correlation between initial rates and selectivities of isomerization of 1-butene in a stationary state.

The remarkable results concerning selectivity and induction period found in the present work were not observed by Shannon *et al.*[2] The difference is presumably due to the difference in the reaction conditions. They carried out the isomerization in a static system at a lower pressure (*ca.* 1.6 cmHg) and at higher temperatures (130—168 °C) than in our case. Only two examples of induction period have been reported for *n*-butene isomerization over solid catalysts. One is for Cu 13X zeolite[17] and another for metal ion exchanged resin.[18] In those cases, the induction period is considered to be caused by the reduction process of Cu^{2+} to Cu^{+} or the complex formation of butene with metal ion, respectively. In our case, a part of Ti^{4+} was reduced to form Ti^{3+} by introducing 1-butene on both catalysts with and without pyridine poisoning. However, the catalyst poisoned with pyridine was completely inactive, though the catalyst without poisoning was active. Hence, the formation process of Ti^{3+} does not seem to cause the induction period.

The plots of % of *cis*- and *trans*-2-butene produced from 1-butene against the % conversion are shown in Fig. 6. The figure clearly indicates that a stationary state in selectivity is reached within 15 min, in accord with time-course curve in Fig. 1. The selectivities in a stationary state are obtained from the ratio of the slope for *cis*-isomer to that for *trans*-isomer in the linear parts. As shown in Fig. 7, the *cis-/trans-* ratio in a stationary state linearly increases with the rate in stationary state. As the initial rate obeyed the rate expression of Langmuir type, it is proportional to the adsorbed amount. Eventually, the larger the adsorbed amount of butenes is, the more the formation of *cis*-2-butene becomes predominant.

References

1) K. Tanabe, "Solid Acids and Bases," Kodansha, Tokyo, Academic Press, New York, London (1970).

2) I. R. Shannon, I. J. S. Lake, and C. Kemball, *Trans. Faraday Soc.*, **67**, 2760 (1971).

3) H. Hattori, M. Itoh, and K. Tanabe, *J. Catal.*, in press.

4) T. Sumiyoshi, K. Tanabe, and H. Hattori, *Bull. Japan Petroleum Inst.*, **17**, 65 (1975).

5) J. W. Hightower and W. K. Hall, *J. Amer. Chem. Soc.*, **89**, 778 (1967).

6) N. D. Parkyns, Conference on Chemisorption and Catalysis, Hydrocarbon Research Group, London, 150 (1970).
7) G. D. Parfitt, J. Ramsbotham, and C. H. Rochester, *Trans. Faraday Soc.*, **67**, 1500 (1971).
8) M. Primet, P. Pichat, and M. V. Mathieu, *J. Phys. Chem.*, **75**, 1221 (1971).
9) T. Iizuka and K. Tanabe, This Bulletin, **48**, 2527 (1975).
10) N. F. Foster and R. J. Cvetanović, *J. Amer. Chem. Soc.*, **82**, 4274 (1960).
11) W. O. Haag and H. Pines, *ibid.*, **82**, 387 (1960).
12) K. Tanabe, Y. Yoshii, and H. Hattori, *Chem. Commun.*, **1971**, 464; H. Hattori, N. Yoshii, and K. Tanabe, *Proc. 5th Intern. Congr. Catalysis*, Miami Beach, **10**-233(1973).
13) S. Bank, A. Schriesheim, and C. A. Rowe, Jr., *J. Amer. Chem. Soc.*, **87**, 3244 (1965).
14) H. R. Gerberich and W. K. Hall, J. Catal., **5**, 99 (1966).
15) M. Primet, M. Che, C. Naccache, M. V. Mathieu, and B. Imelik, *J. Chim. Phys.*, **67**, 1629 (1970).
16) Gy. Gati and H. Knözinger, *Proc. 5th Intern. Congr. Catalysis*, Miami Beach, **56**-819(1973).
17) C. Dimitrov and H. F. Leach, *J. Catal.*, **14**, 336 (1969).
18) T. Uematsu, K. Tsukada, M. Fujishima, and H. Hashimoto, *ibid.*, **32**, 369 (1974).

Effects of Foreign Gases on Dual Fluorescences of Pyrene Vapor

Kohji CHIHARA and Hiroaki BABA

Division of Chemistry, Research Institute of Applied Electricity, Hokkaido University, Sapporo 060

(Received July 29, 1975)

The characteristics of the dual fluorescences of pyrene vapor at 170 °C and 0.2—0.3 Torr have been investigated in the presence of cyclohexane or oxygen. With increasing cyclohexane pressure, the S_1-fluorescence shows a blue shift and an increase in quantum yield and in lifetime, while the S_2-fluorescence shows only a slight blue shift and a marked decrease in yield and in lifetime. Oxygen efficiently quenches the S_1- and S_2-fluorescence according to the Stern-Volmer relation. The experimental results are well explained by kinetic analyses based on the following assumptions: (1) The internal conversion is reversible and is much faster than other radiative and radiationless processes; (2) cyclohexane causes only vibrational relaxation which can be described in terms of a simple stepladder model; (3) oxygen acts as a quencher on both S_1- and S_2-fluorescence emissions. It is found that one collision with cyclohexane removes on the average a vibrational energy of the order of 1000 cm^{-1} or less from S_1 or S_2 of pyrene, and that one collision with oxygen quenches S_1 or S_2 with a probability close to unity. It is concluded that the S_2-fluorescence consists mainly of a slow component originating from S_2 which is in equilibrium with S_1.

In relation to the theories of radiationless transitions in isolated molecules,[1,2] a number of experimental studies[3,4] have recently been made of the emission properties of organic compounds in the vapor phase at low pressure, where molecules are free from collision during their emission lifetimes. Under such conditions the fluorescence of organic molecules presents peculiar features that cannot be seen in a condensed phase or in a vapor at a high pressure. Thus, in the low-pressure vapor, pyrene and related compounds are known to exhibit distinct fluorescence emission from the second excited singlet state (S_2) in addition to the ordinary fluorescence from the first excited singlet (S_1).[5-9]

In previous papers,[5,6] hereafter referred to as Papers I and II respectively, the following observations were reported on the dual fluorescences of pyrene and its simple derivatives in the vapor phase. (1) As the excitation energy increases, the S_2-fluorescence shifts to the red in much the same way as the S_1-fluorescence, and both S_1- and S_2-fluorescence bands become broad. (2) The quantum yield of the S_2-fluorescence (Φ_{2F}) increases rapidly with excitation into successively higher singlet states, whereas the yield of the S_1-fluorescence (Φ_{1F}) decreases only slowly with increasing excitation energy. The ratio Φ_{2F}/Φ_{1F} is roughly related to ρ_2/ρ_1, where ρ_1 and ρ_2 are the densities of vibrational states in S_1 and S_2 at the energy of excitation. (3) Addition of cyclohexane as an inert foreign gas to the pyrene vapor results in a marked decrease in Φ_{2F}/Φ_{1F}. (4) Most of the S_2-fluorescence emission seems to occur through the mechanism involving reverse internal conversion.

In the presence of cyclohexane, pyrene must undergo vibrational relaxation in its excited state. On the other hand, the excited singlet state of many aromatic compounds including pyrene is known to be quenched by oxygen very efficiently.[10,11] It is to be expected that the changes in emission characteristics caused by addition of such foreign gases are different between the S_1- and S_2-states of pyrene vapor.

The purpose of the present study is to gain a deeper insight into the nature of the dual fluorescences through a detailed examination of the effects of foreign gases, cyclohexane and oxygen, on the S_1- and S_2-emissions of the pyrene molecule in the vapor phase.

Experimental

Pyrene and cyclohexane were purified in the same way as in Paper I. Oxygen obtained from Takachiho Kagaku Kogyo Co. (purity, 99.8%) was used as received. The methods for preparation of the sample vapor, measurement and correction of fluorescence spectra, and for determination of fluorescence quantum yields were the same as described in Paper I, unless otherwise stated. All the experiments were conducted at 170 °C and at pyrene pressures in the range 0.2—0.3 Torr.

Measurements of fluorescence emission of low intensity were made on a high-sensitivity emission spectrophotometer constructed recently in our laboratory. In this spectrophotometer, light from a 150-W xenon lamp was dispersed by a Czerny-Turner double monochromator with an f number of 4.5, consisting of a quartz prism and a grating (1200 lines/mm), to give monochromatic excitation beam. The fluorescence emitted from the sample at right angles to the excitation beam was dispersed by another Czerny-Turner monochromator with an f number of 4.5, consisting of a 1200 lines/mm grating alone. The resulting monochromatic fluorescence emission was detected by the photon counting method, using a Hamamatsu R585 photomultiplier which showed at room temperature a very low dark current corresponding to $\sim$1 count/s. Both excitation and emission wavelengths were scanned discontinuously with the aid of a pulse motor. Fluorescence with a quantum yield as low as 10^{-7} can be measured with this spectrophotometer, provided that an optimum concentration of sample material is used. For fluorescence of higher intensity another emission spectrophotometer was used which was constructed by attaching a photon counting system, similar to the one mentioned above, to the optical system of a Hitachi MPE-2A fluorescence spectrophotometer.

The fluorescence decay was observed using a breakdown spark generated in 2-atm oxygen gas as the exciting light source. The breakdown was induced by a Japan Electron Optics Laboratory JLS-R3A giant pulse ruby laser with a peak output of 150 MW. The oxygen breakdown spark has a high intensity and a duration of about 70 ns, and covers the necessary wavelength range of 210—330 nm. The light beam from the breakdown spark was passed through the following filter systems (a) and (b) for exciting the pyrene molecule into its S_3- and S_4-states, respectively; (a) consists of an interference filter with a transmittance maximum of 17.5% at 264.5 nm and a half bandwidth of 14 nm and a solution filter obtained by dissolving 1.1 mg of 2,7-dimethyl-

3,6-diazacyclohepta-1,6-diene perchlorate in 25 ml water, and (b) is an interference filter with a transmittance maximum of 19% at 234 nm and a half bandwidth of 23 nm. Note that the solution filter in (a) cuts off the stray light falling into the wavelength region of S_2-fluorescence. A monochromator was used for selecting the emission wavelength. For the measurement of S_1-fluorescence decay in the absence of a foreign gas, excitation was made at each of the vibrational peaks belonging to individual electronic absorption bands. In this case, a monochromator was used for selecting the wavelength of the exciting light of the breakdown spark, with the bandwidth being set to 8 nm, and the emission beam was passed through filters of UV-D2 and UV-35 from Toshiba Electric Co., which excluded the scattered exciting light and the S_2-fluorescence emission. All the fluorescence lifetimes were determined by the deconvolution method.[12]

Results

The excited singlet states associated with the four electronic absorption transitions of pyrene appearing in the near ultraviolet region (Paper I) are denoted by S_1,⋯, S_4 in order of increasing energy, and the ground singlet state by S_0. The zero vibrational level of each of the electronic states will be represented by a superscript 0, *e.g.*, S_2^0. The $S_0 \rightarrow S_2$,$\rightarrow S_3$, and $\rightarrow S_4$ transitions show a prominent progression in a totally symmetric carbon stretching vibration of 1400 cm^{-1} frequency (*cf.* Papers I and II). The vibrational levels related to this progression will be expressed as S_2^v *etc.*, where v refers to the quantum number of the vibration concerned (v=0, 1, 2, ⋯).

The effects of cyclohexane added as an inert foreign gas on the S_1- and S_2-fluorescence were examined by exciting the pyrene molecule into various vibronic levels. As an example, changes in fluorescence spectrum caused by addition of different pressures of cyclohexane are shown in Fig. 1 for excitation into S_4^0. Similar spectral

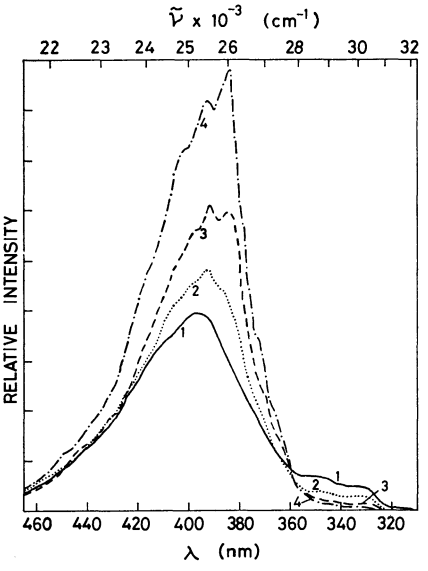

Fig. 1. Fluorescence spectra of pyrene vapor excited at 234 nm (S_4^0) in the presence of cyclohexane of different pressures: (1) 0; (2) 6.3; (3) 23.4; (4) 47.5 Torr. The relative intensity means relative quanta per unit wave-number interval.

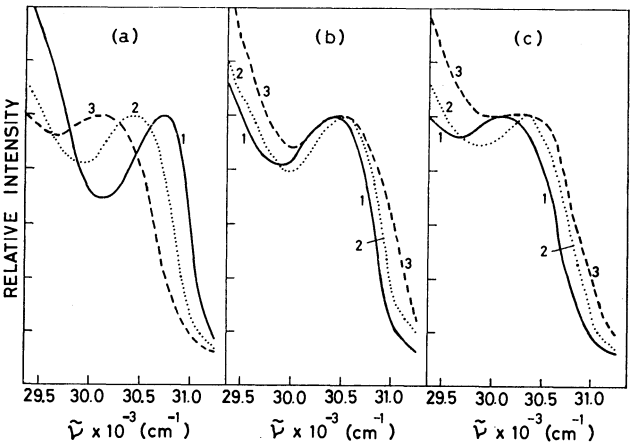

Fig. 2. S_2-fluorescence spectra (normalized) of pyrene vapor. (a) Excited in the absence of cyclohexane at different wavelengths: (1) 298 nm (S_2^2); (2) 266 nm (S_3^0); (3) 234 nm (S_4^0). (b) Excited at 266 nm (S_3^0) in the presence of cyclohexane of different pressures: (1) 0; (2) 12.5; (3) 164 Torr. (c) Excited at 234 nm (S_4^0) in the presence of cyclohexane of different pressures: (1) 0; (2) 23.4; (3) 164 Torr. The relative intensity as in Fig. 1.

changes were observed for excitation into other vibronic levels. As is seen from Fig. 1, cyclohexane has considerable effects on the fluorescence spectra both in position and in intensity. With increasing cyclohexane pressure, the S_1-fluorescence shows a blue shift and an increase in intensity, while the S_2-fluorescence shows only a slight blue shift and a marked decrease in intensity.

The blue shift of the S_1-fluorescence spectrum is clearly seen in Fig. 1. The spectral shifts of the S_2-fluorescence due to the added cyclohexane are illustrated in Fig. 2 for excitation into S_3^0 and S_4^0, together with the frequency shift that occurs on changing the excitation energy in the absence of cyclohexane, *i.e.*, in the pure pyrene vapor. The quantum yields of S_1- and S_2-fluorescence are plotted against the cyclohexane

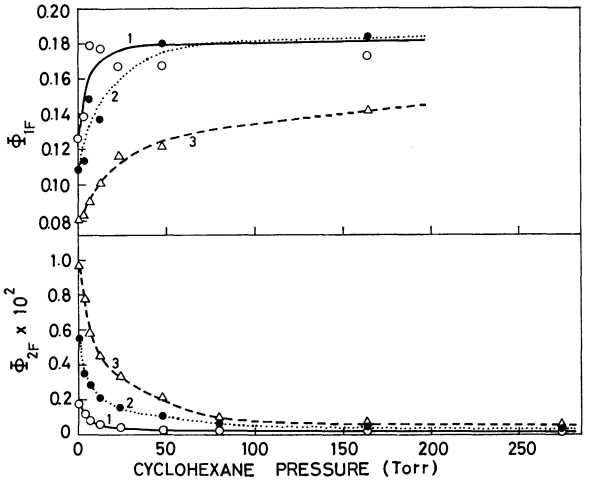

Fig. 3. Plots of Φ_{1F} and Φ_{2F} for pyrene vapor *vs.* the pressure of cyclohexane. Exciting wavelengths: (1) 298 nm (S_2^2); (2) 266 nm (S_3^0); (3) 234 nm (S_4^0).

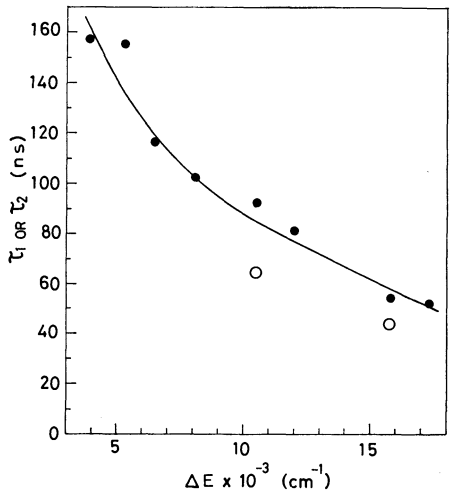

Fig. 4. Plots of τ_1 (●) and τ_2 (○) for pyrene vapor *vs.* ΔE.

pressure in Fig. 3 for excitation into different vibronic levels.

The lifetimes of the S_1- and S_2-fluorescence in the absence of cyclohexane, τ_1 and τ_2, are plotted in Fig. 4 against ΔE, which represents the excitation energy in excess of the $S_0^0 \rightarrow S_1^0$ transition energy. Both τ_1 and τ_2 are found to decrease with increasing ΔE. In the presence of cyclohexane, vibrational relaxation must occur in each of the excited electronic states, so that the molecules are distributed among various vibrational levels. The apparent lifetimes obtained in such a condition will be denoted by $\bar{\tau}_1$ and $\bar{\tau}_2$ (instead of τ_1 and τ_2) for S_1- and S_2-fluorescence, respectively. Figure 5 shows $\bar{\tau}_1$ and $\bar{\tau}_2$ as a function of the cyclohexane pressure. It is seen that the lifetime $\bar{\tau}_1$ increases but $\bar{\tau}_2$ decreases with the inert gas pressure, irrespective of excitation energy.

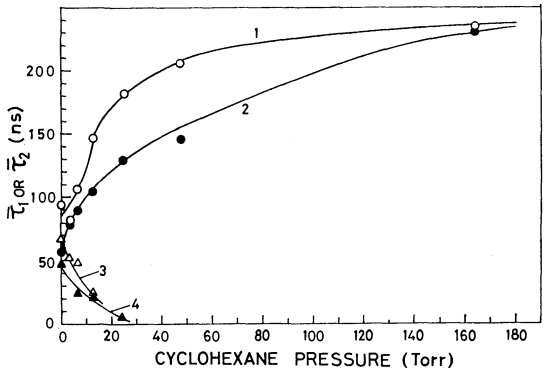

Fig. 5. Plots of $\bar{\tau}_1$ (1, 2) and $\bar{\tau}_2$ (3, 4) for pyrene vapor *vs.* the pressure of cyclohexane. Exciting and monitoring wavelengths: (1) 264.5 nm ($\sim S_3^0$), 400 nm (S_1); (2) 234 nm (S_4^0), 400 nm (S_1); (3) 264.5 nm ($\sim S_3^0$), 330 nm (S_2); (4) 234 nm (S_4^0), 330 nm (S_2).

The effects of added oxygen on the fluorescence properties of pyrene vapor are quite different from the effects of cyclohexane. The spectral changes accompanying the addition of various pressures of oxygen are shown in Figs. 6 and 7, respectively, for S_2^2 and S_4^0 excitation. It is seen that in contrast to the case of cyclohexane oxygen acts as a quencher on both S_1- and

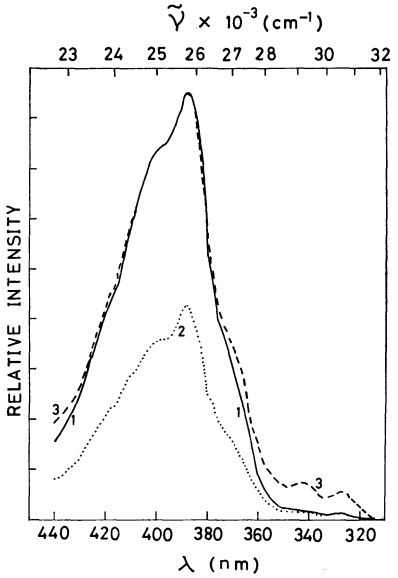

Fig. 6. Fluorescence spectra of pyrene vapor excited at 298 nm (S_2^2) in the presence of oxygen of different pressures: (1) 0; (2) 10.2; (3) 350 Torr. The relative intensity as in Fig. 1. The maximum intensities of spectra 1 and 3 are normalized to a common value (I_{max}); the maximum intensity of spectrum 2 is normalized to $I_{max}/2$.

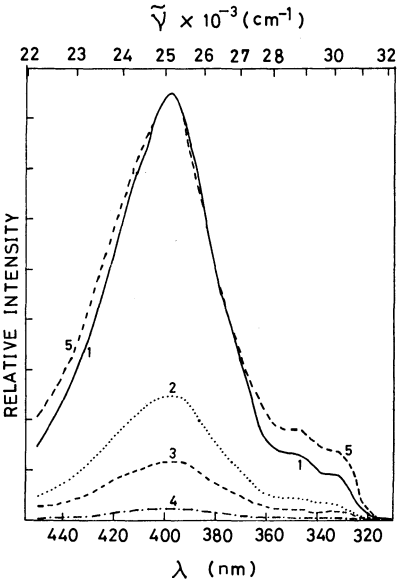

Fig. 7. Fluorescence spectra of pyrene vapor excited at 234 nm (S_4^0) in the presence of oxygen of different pressures: (1) 0; (2) 6; (3) 15; (4) 102; (5) 350 Torr. The relative intensity as in Fig. 1. The intensities of spectra 1—4 are given according to the respective observed emission signals; the maximum intensity of spectrum 5 is normalized to that of spectrum 1.

S_2-fluorescences, and that the quantum yield ratio Φ_{2F}/Φ_{1F} increases, though slightly, with increasing oxygen pressure.

In Fig. 8 Φ_{1F}^0/Φ_{1F} and Φ_{2F}^0/Φ_{2F} are plotted against the oxygen pressure for S_2^2, S_3^0, and S_4^0 excitation; here, the fluorescence quantum yields in the absence and presence of oxygen are denoted by Φ_{1F}^0 (or Φ_{2F}^0) and Φ_{1F} (or Φ_{2F}),

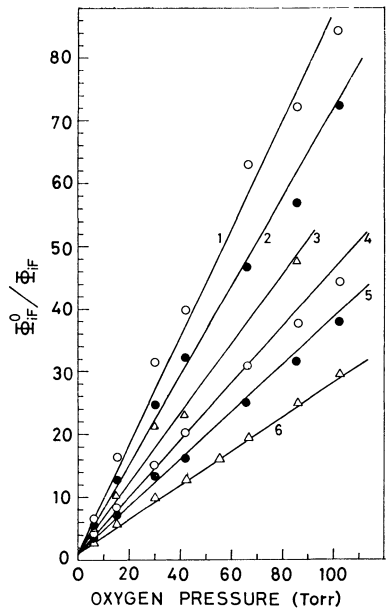

Fig. 8. Stern-Volmer plots for quenching of S_1-fluorescence (1, 2, 5) and S_2-fluorescence (3, 4, 6) of pyrene vapor by oxygen. Exciting wavelengths: (1) 298 nm (S_2^2); (2) 266 nm (S_3^0); (3) 298 nm (S_2^2); (4) 266 nm (S_3^0); (5) 234 nm (S_4^0); (6) 234 nm (S_4^0). For Φ_{iF}^0/Φ_{iF}, $i=1$ or 2.

respectively. The plots are found to be linear over a wide range of the quantum yield ratio, Φ_{1F}^0/Φ_{1F} or Φ_{2F}^0/Φ_{2F}, indicating that the Stern-Volmer equation holds in every case.

Discussion

As has been mentioned, the present experiments were made with the pyrene vapor at 0.2—0.3 Torr and 170 °C. Under these conditions, the mean time between collisions of pyrene molecules (*cf.* Paper I) is somewhat longer than the observed fluorescence lifetimes τ_1 and τ_2 (Fig. 4). It is assumed here, to the first approximation, that the pyrene molecule in the absence of a foreign gas is free from collisions in its excited state S_1 or S_2.

Intramolecular radiative and radiationless processes in polyatomic molecules can be treated both quantum-mechanically and kinetically.[2] In the following, the effects of foreign gases on the dual fluorescences of pyrene vapor will be discussed on the basis of a kinetic scheme involving reverse internal conversion, as in the case of Paper I.

For the pure pyrene vapor, the above scheme predicts that most of the S_2-fluorescence emission should occur through the reverse internal conversion, with its lifetime (τ_2) equal to that of the S_1-fluorescence (τ_1). The S_2-emission of this sort may be called slow S_2-fluorescence, because the lifetime τ_2 is very long compared not only with the lifetime of the direct or prompt S_2-fluorescence but also with the radiative lifetime of S_2 which is to be determined from the integrated absorption intensity. The experiments on the fluorescence quenching by oxygen clearly indicate that the S_2-emission is ascribable almost exclusively to the slow S_2-fluorescence. Also, the lifetime measurements show that τ_2 is comparable, though not strictly equal, to τ_1 in length.

In the absence of a foreign gas, the kinetic analysis given in Paper I is applicable. It is thus assumed that an isolated pyrene molecule is excited directly or indirectly to S_2*, *i.e.* a vibrationally excited level of S_2, and then passes to S_1* whose energy $E(S_1^*)$ is equal to the energy of S_2*, $E(S_2^*)$. It is further assumed that the molecule may return to S_2* from S_1*.

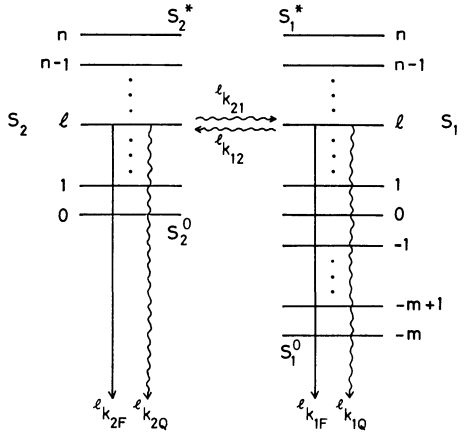

Fig. 9. A schematic diagram showing a stepladder model for vibrational relaxation in S_1- and S_2-states together with various electronic processes involved. Straight-line arrows denote radiative processes, and wiggly-line arrows radiationless processes.

Effects of Cyclohexane. In order to have an understanding of the effects of an inert foreign gas X, *i.e.* cyclohexane in this study, on the emission properties of pyrene vapor, we consider a simple stepladder relaxation model[13] illustrated in Fig. 9. We assume that only a finite series of vibrational levels, represented by $l=n, n-1, \cdots, 0$ for S_2 and by $l=n, \cdots, 0, \cdots, -m$ for S_1, participates in the collision-induced vibrational relaxation, with n, 0, and $-m$ corresponding to S_2* (or S_1*), S_2^0, and S_1^0, respectively. For $n \geqq l \geqq 0$, the vibrational levels $l(S_2)$ and $l(S_1)$ in the stepladder model are isoenergetic with each other, and reversible internal conversion is supposed to occur between them. The difference in energy between any two adjacent levels with $l \geqq 0$ or $l \leqq 0$ is equated to the amount of energy $\triangle\varepsilon$ or $\triangle\varepsilon'$ removed on the average by one collision between a pyrene and an X molecule. Thus we have simple relations $[E(S_2^*)-E(S_2^0)]/\triangle\varepsilon=n$ and $[E(S_2^0)-E(S_1^0)]/\triangle\varepsilon'=m$, where $\triangle\varepsilon'$ may or may not be equal to $\triangle\varepsilon$. Various rate constants for radiative and radiationless processes are defined in Fig. 9.

If the concentration of pyrene in a vibrational level $l(S_i)$ ($i=1$ or 2) in the stepladder model is expressed as $[l]_i$, the following general rate equations are obtained by reference to Fig. 9:

$$\frac{d[l]_2}{dt} = k_C[X][l+1]_2 + {}^{l}k_{12}[l]_1 - {}^{l}\lambda_2[l]_2 \quad (1)$$

$$\frac{d[l]_1}{dt} = k_C[X][l+1]_1 + {}^{l}k_{21}[l]_2 - {}^{l}\lambda_2[l]_1 \quad (2)$$

where

$${}^{l}\lambda_2 = {}^{l}k_{2F} + {}^{l}k_{2Q} + {}^{l}k_{21} + k_C[X] \quad (3)$$

$$ {}^{l}\lambda_1 = {}^{l}k_{1F} + {}^{l}k_{1Q} + {}^{l}k_{12} + k_C[X] \quad (4) $$

k_C is the bimolecular rate constant for the vibrational relaxation by collision and [X] is the concentration of the inert gas X; namely, $k_C[X]$ is the frequency of collision of a pyrene molecule with X molecules. Equations (1) and (3) apply to $n \geqq l \geqq 0$, and (2) and (4) to $n \geqq l \geqq -m$. However, for $l=n$, $[l+1]_i$ in Eqs. (1) and (2) is taken as equal to zero; for $l=0$ and $-m$, the term $k_C[X]$ is removed from Eqs. (3) and (4), respectively; and for $-1 \geqq l \geqq -m$, ${}^{l}k_{21}[l]_2$ in Eq. (2) and ${}^{l}k_{12}$ in Eq. (4) are eliminated. Further, in the case of steady photo-excitation, the rate of excitation (I_0) should be added to the right-hand side of Eq. (1) for $l=n$.

As will be shown later, the following relations exist among the rate constants for the pyrene molecule:

$$ {}^{l}k_{21} \gg {}^{l}k_{2F} + {}^{l}k_{2Q} \quad (5) $$

$$ {}^{l}k_{12} \gg {}^{l}k_{1F} + {}^{l}k_{1Q} \quad (6) $$

$$ {}^{l}k_{21} \gg {}^{l}k_{12} \quad (7) $$

Although the term $k_C[X]$ increases with the inert gas pressure, we have

$$ {}^{l}k_{21} \gg k_C[X] \quad (8) $$

$$ {}^{l}k_{12} \gg k_C[X] \text{ or } {}^{l}k_{12} \gtrsim k_C[X] \quad (9) $$

under the present experimental conditions.

Let us first consider the case of steady excitation. Under photostationary conditions $d[l]_i/dt=0$ in Eqs. (1) and (2). When $l=n$, it follows from Eq. (2) and inequality (6) that

$$ [n]_1/[n]_2 = {}^{n}k_{21}/({}^{n}k_{12}+k_C[X]) \quad (10) $$

Using inequalities (5)—(9), we can verify from Eqs. (1) and (2) that

$$ [l]_1/[l]_2 = {}^{l}k_{21}/{}^{l}k_{12} \quad (n-1 \geqq l \geqq 0) \quad (11) $$

It is useful to define a sort of equilibrium constant ${}^{l}K$ and an effective rate constant ${}^{l}k_{\text{eff}}$ for $n \geqq l \geqq 0$ by

$$ {}^{l}K = {}^{l}k_{21}/{}^{l}k_{12} \quad (12) $$

$$ {}^{l}k_{\text{eff}} = ({}^{l}k_2 + {}^{l}K\,{}^{l}k_1)/(1+{}^{l}K) \quad (13) $$

where

$$ {}^{l}k_i = {}^{l}k_{iF} + {}^{l}k_{iQ} \quad (i=1 \text{ or } 2) \quad (14) $$

Also, for $n \geqq l \geqq 0$, we put

$$ [l]_1 + [l]_2 \equiv [l] \quad (15) $$

We can then derive the following equations:

$$ [n] = I_0/({}^{n}k_{\text{eff}} + k_C[X]) \quad (16) $$

$$ [l-1] = [l]\frac{k_C[X]}{{}^{l-1}k_{\text{eff}} + k_C[X]} \quad (n \geqq l \geqq 1) \quad (17) $$

$$ [l-1]_1 = [l]_1\frac{k_C[X]}{{}^{l-1}k_1 + k_C[X]} \quad (0 \geqq l \geqq -m+2) \quad (18) $$

$$ [-m]_1 = [-m+1]_1 k_C[X]/{}^{-m}k_1 \quad (19) $$

Combining inequalities (7) and (8) with Eqs. (10)—(12), we obtain the relations $[l]_2 \ll [l]_1$ and ${}^{l}K \gg 1$ for $n \geqq l \geqq 0$. Hence

$$ [l]_1 \simeq [l] \quad (n \geqq l \geqq 0) \quad (20) $$

$$ [n]_2 \simeq [n]\frac{1 + k_C[X]/{}^{n}k_{12}}{{}^{n}K} \quad (21) $$

$$ [l]_2 \simeq [l]/{}^{l}K \quad (n-1 \geqq l \geqq 0) \quad (22) $$

If $k_C[X]$ is so large that ${}^{l}k_{\text{eff}} \ll k_C[X]$ for $n \geqq l \geqq 0$ and ${}^{l}k_1 \ll k_C[X]$ for $-1 \geqq l \geqq -m$, it follows from Eqs. (16)—(20) that

$$ I_0/(k_C[X]) \simeq [n] \simeq [n-1] \simeq \cdots \simeq [0] \simeq [-1]_1 \simeq \cdots \simeq [-m+1]_1 \ll [-m]_1 = I_0/{}^{-m}k_1 \quad (23) $$

We are now in a position to discuss fluorescence quantum yields. To the approximation adopted in the present study, it follows from the kinetic analyses given in Paper I that the S_1- and S_2-fluorescence quantum yields obtained on exciting the molecule to the lth level in the absence of the inert gas are

$$ {}^{l}\Phi^0_{1F} = \begin{cases} {}^{l}k_{1F}/{}^{l}k_{\text{eff}} & (n \geqq l \geqq 0) \\ {}^{l}k_{1F}/{}^{l}k_1 & (-1 \geqq l \geqq -m) \end{cases} \quad (24) $$

$$ {}^{l}\Phi^0_{2F} = {}^{l}k_{2F}/({}^{l}K\,{}^{l}k_{\text{eff}}) \quad (n \geqq l \geqq 0) \quad (25) $$

When the molecule is excited to the nth level in the presence of the inert gas, the S_1- and S_2-fluorescence quantum yields, denoted by Φ_{1F} and Φ_{2F} respectively, are given by

$$ \Phi_{1F} = \sum_{l=-m}^{n} {}^{l}k_{1F}[l]_1/I_0 \quad (26) $$

$$ \Phi_{2F} = \sum_{l=0}^{n} \frac{{}^{l}k_{2F}[l]}{{}^{l}K I_0} \quad (27) $$

Here we assume for the sake of simplicity that $k_C[X]$ is negligible in Eq. (10) or (21) compared with ${}^{n}k_{12}$. Strictly speaking, this assumption is not always valid (*cf.* (9)). We can show, however, that even if the above assumption is omitted, the results remain essentially unchanged. Under photostationary conditions the rate of excitation must be equal to the rate of deactivation, so that

$$ I_0 = \sum_{l=0}^{n} {}^{l}k_2[l]_2 + \sum_{l=-m}^{n} {}^{l}k_1[l]_1 $$

Neglecting $k_C[X]$ compared with ${}^{n}k_{12}$ as before, we can rewrite this equation as

$$ I_0 = \sum_{l=0}^{n} {}^{l}k_{\text{eff}}[l] + \sum_{l=-m}^{-1} {}^{l}k_1[l]_1 \quad (28) $$

From Eqs. (24)—(28) and Eq. (20), we obtain

$$ \Phi_{1F} = \frac{\sum_{l=0}^{n} {}^{l}\Phi^0_{1F}\,{}^{l}k_{\text{eff}}[l] + \sum_{l=-m}^{-1} {}^{l}\Phi^0_{1F}\,{}^{l}k_1[l]_1}{\sum_{l=0}^{n} {}^{l}k_{\text{eff}}[l] + \sum_{l=-m}^{-1} {}^{l}k_1[l]_1} \quad (29) $$

$$ \Phi_{2F} = \frac{\sum_{l=0}^{n} {}^{l}\Phi^0_{2F}\,{}^{l}k_{\text{eff}}[l]}{\sum_{l=0}^{n} {}^{l}k_{\text{eff}}[l] + \sum_{l=-m}^{-1} {}^{l}k_1[l]_1} \quad (30) $$

If $k_C[X]$ is large enough for the relation (23) to hold good,[14] we have

$$ \Phi_{1F} \simeq {}^{-m}\Phi^0_{1F} \quad (31) $$

$$ \Phi_{2F} \simeq \sum_{l=0}^{n} {}^{l}\Phi^0_{2F}({}^{l}k_{\text{eff}}/k_C[X]) \quad (32) $$

On the basis of the foregoing kinetic considerations, we examine the spectral data on S_1- and S_2-fluorescence. Referring to Eqs. (29) and (30), we see that Φ_{1F} and Φ_{2F} are closely related to the concentration $[l]$ of the pyrene molecules belonging to the individual levels l. According to Eqs. (16)—(19), as [X] increases, (i) $[l]/[n]$ $(n-1 \geqq l \geqq 0)$ and $[l]_1/[n]$ $(-1 \geqq l \geqq -m)$ increase though $[n]$ itself decreases; and (ii) $[l-1]/[l]$ $(n \geqq l \geqq 1)$,

$[-1]_1/[0]$, and $[l-1]_1/[l]_1$ $(-1 \geqq l \geqq -m+1)$ increase with increasing [X]. The experimental results reported in Paper I indicate that[15]

$$ {}^{n}\Phi_{1F}^{0} < {}^{n-1}\Phi_{1F}^{0} < \cdots < {}^{-m}\Phi_{1F}^{0} \qquad (33a) $$

By combining (ii) with (33a), it can be strictly verified that Φ_{1F} given by Eq. (29) possesses its lowest value ${}^{n}\Phi_{1F}^{0}$ at [X]=0, increases with increasing [X], and finally reaches its highest value ${}^{-m}\Phi_{1F}^{0}$ (see Eq. (31)).

On the other hand, the data in Paper I show that

$$ {}^{n}\Phi_{2F}^{0} > {}^{n-1}\Phi_{2F}^{0} > \cdots > {}^{0}\Phi_{2F}^{0} \qquad (33b) $$

It follows from (ii) and (33b) that, in contrast to Φ_{1F}, the quantum yield Φ_{2F} given by Eq. (30) decreases with increase in [X]. We note that ${}^{l}\Phi_{2F}^{0}$ falls off markedly with a decrease in the number l (Paper I). On increasing [X] from zero, therefore, Φ_{2F} decreases rapidly from its highest value ${}^{n}\Phi_{2F}^{0}$. At sufficiently large [X], Φ_{2F} is expressed in the form of Eq. (32), and hence it is finally reduced to zero.

These considerations are in good agreement, at least qualitatively, with the results of experiments on the intensities (Fig. 1) and quantum yields (Fig. 3) of the S_1- and S_2-fluorescence.

In order to obtain more quantitative information about the dependence of Φ_{2F} on cyclohexane pressure, we made a calculation on the basis of the stepladder model. We treated a case where the initially excited level n corresponds to $S_4{}^0$. The difference between $E(S_4{}^0)=E(S_2{}^*)$ and $E(S_2{}^0)$ is known to be about 12000 cm^{-1} (Paper I). Referring to the literature,[13] we tentatively adopted two values (500 and 1000 cm^{-1}) as $\Delta\varepsilon$. It then follows that $n=24$ and 12, respectively, for $\Delta\varepsilon=$ 500 and 1000 cm^{-1}. According to Eqs. (16), (25), and (27), Φ_{2F} can be expressed in the form

$$ \Phi_{2F} = \sum_{l=0}^{n} {}^{l}\Phi_{2F}^{0} \frac{{}^{l}k_{eff}}{{}^{n}k_{eff}+k_C[X]} \frac{[l]}{[n]} \qquad (34) $$

In Eq. (34), the observed S_2-fluorescence quantum yield as a function of excitation energy (Paper I) was used for ${}^{l}\Phi_{2F}^{0}$. The effective rate constant ${}^{l}k_{eff}$ was assumed to be equal to the reciprocal of the S_1-fluorescence lifetime τ_1 (*vide infra*), which has been measured in the present study as a function of excitation energy (Fig. 4). The rate constant k_C was determined from the standard gas kinetic theory, molecular diameters of 8 and 4 Å being assigned to pyrene and cyclohexane, respectively; the result is $k_C=9.8\times10^6$ $Torr^{-1}$ s^{-1} at 170 °C. The ratio of concentrations, $[l]/[n]$, can be calculated by using Eq. (17) repeatedly. The curves thus obtained theoretically for Φ_{2F} as a function of cyclohexane pressure reproduce fairly well the experimental data, *i.e.*, the lower curve 3 in Fig. 3. The experimental curve lies between the two theoretical ones corresponding to $\Delta\varepsilon=500$ and 1000 cm^{-1}; the latter $\Delta\varepsilon$ value leads to a more favorable result.

The changes in position and shape of the fluorescence spectra on increasing the inert gas pressure must be caused by changes of the extents to which different levels l contribute to the fluorescence transitions concerned.

From Eqs. (16)—(20), (23), and (26) or (29) we may predict that the S_1-fluorescence band will shift toward the position of the emission originating from lower levels, *i.e.* toward the blue, upon increasing the inert gas pressure; and finally, as is seen from Eq. (31), the S_1-fluorescence will originate from the lowest vibrational level of S_1 which gives emission at the shortest wavelengths. The above prediction is in agreement with the behavior of S_1-fluorescence shown in Fig. 1.

The numbers l of the levels responsible for the S_2-fluorescence are such that $n \geqq l \geqq 0$. According to the relations (17) and (23), $[n]>[n-1]>\cdots>[0]$ for any value of [X], and $[n]\simeq[n-1]\simeq\cdots\simeq[0]$ for large [X]. Moreover, as has been mentioned, ${}^{l}\Phi_{2F}^{0}$ decreases rapidly with decreasing l. It then follows from Eq. (27) or (30) that the emissions from the levels with higher l numbers make relatively large contributions to the S_2-fluorescence, irrespective of inert gas pressure. This accounts for the finding that the S_2-fluorescence band shows only small blue shifts even at high inert gas pressures, in contrast to the case where the excitation energy is decreased (Paper II and Fig. 2).

We next proceed to the case of transient processes following the pulse excitation by the breakdown spark. We substitute n for l in both Eqs. (1) and (2), and remove the first terms of the right-hand sides of these equations. In the absence of the inert gas, the fourth terms on the right-hand sides of Eqs. (3) and (4) also are removed. The solution of Eqs. (1) and (2) thus modified is well known.[12] When the relations (5) and (6) hold, $[n]_2$ and $[n]_1$ are expressed in the forms

$$ [n]_2 = [n]_2^0 \left\{ \frac{{}^{n}K}{1+{}^{n}K} \exp(-{}^{n}\tilde{\lambda}_2 t) + \frac{1}{1+{}^{n}K} \exp(-{}^{n}\tilde{\lambda}_1 t) \right\} \qquad (35) $$

$$ [n]_1 = [n]_2^0 \frac{{}^{n}K}{1+{}^{n}K} \{ -\exp(-{}^{n}\tilde{\lambda}_2 t) + \exp(-{}^{n}\tilde{\lambda}_1 t) \} \qquad (36) $$

where

$$ {}^{n}\tilde{\lambda}_2 = {}^{n}k_{21} + {}^{n}k_{12} \qquad (37) $$

$$ {}^{n}\tilde{\lambda}_1 = {}^{n}k_{eff} \equiv 1/{}^{n}\tau_{eff} \qquad (38) $$

$[n]_2$ at $t=0$ is written as $[n]_2^0$, while $[n]_1$ is assumed to be zero at $t=0$.

Since ${}^{n}\tilde{\lambda}_2 \gg {}^{n}\tilde{\lambda}_1$, after a very short time, δt, of the order of $1/({}^{n}k_{21}+{}^{n}k_{12})$, $[n]_2$ and $[n]_1$ will decay with a common rate constant, ${}^{n}k_{eff}$. In the range of time longer than δt, it follows from Eqs. (35) and (36) that $[n]_1/[n]_2={}^{n}K$, that is, a sort of dynamic equilibrium is attained.[12] Note that this equation is obtained also by putting [X] $=0$ in Eq. (10).

Because of the duration (~70 ns) of the flash employed, the present experiments on the time behavior of the dual fluorescences must be concerned with the range of time ($>\delta t$) mentioned above. It is thus expected that the observed lifetimes τ_1 and τ_2 are identical and both are equal to ${}^{n}\tau_{eff}$ defined by Eq. (38). Since ${}^{n}K \gg 1$ in Eq. (13). ${}^{n}\tau_{eff}$ is nearly equal to $1/{}^{n}k_1$, which is estimated to be about 10^2 ns and is much longer than the radiative lifetime ($1/{}^{n}k_{2F}$) of S_2, 6 ns from the integrated absorption intensity (Paper I). The lifetime data given in Fig. 4 indicate that τ_2 is, indeed, considerably longer than the radiative lifetime of S_2. In contrast to the results of kinetic considerations, however, τ_2 is slightly shorter than τ_1. This discrepancy in value between the two lifetimes has been interpreted by Deinum *et al.* as due in part to sequence congestion effects.[8]

Suppose now that the pyrene molecule is excited into the level with $l=n$ by a light pulse in the presence of cyclohexane. As the time proceeds, the lower levels $l=n-1$, $n-2$, $\cdots$ are populated owing to the vibrational relaxation caused by the collision, and the fluorescence is emitted also from these levels. On account of the relations (5)—(9), a dynamic equilibrium will be reached in each of the emitting levels. It is then expected from the relations (33a) and (33b) that an increase in cyclohexane pressure will result in a decrease and an increase in decay rate of the S_1- and S_2-fluorescence, respectively. In other words, the apparent lifetime $\bar{\tau}_1$ will be lengthened but $\bar{\tau}_2$ will be shortened, in agreement with the observations illustrated in Fig. 5.

Effects of Oxygen. When oxygen is added to the pyrene vapor, the S_1- and S_2-fluorescence emissions are quenched, but their spectral shapes and positions are little changed (see Figs. 6 and 7), suggesting that the vibrational relaxation is not induced by collision with oxygen. We are therefore concerned here solely with the vibronic level S_2*, which is initially excited (directly or indirectly), and its isoenergetic partner S_1*. The rate equations and related quantities that have hitherto been used for the vibrational level, $l=n$, can be applied to the case of oxygen quenching by making pertinent modifications. The superscript n will hereafter be eliminated.

The oxygen-quenching rate of the vibronic state S_i* may be expressed in the form $wk_C[Y][S_i^*]$, where [Y] is the concentration of the quencher Y, *i.e.* oxygen, and w is a factor representing the probability that one collision quenches S_i*. In the present study the following relations hold: $k_{21} \gg wk_C[Y]$ and $k_{12} \gg wk_C[Y]$ or $k_{12} \gtrsim wk_C[Y]$ (*cf.* relations (8) and (9)). Thus, under photostationary conditions, it follows from Eqs. (16), (20), and (21) that

$$\Phi_{1F} = k_{1F}/(k_{eff}+wk_C[Y]) \tag{39}$$

$$\Phi_{2F} = \frac{k_{2F}}{k_{eff}+wk_C[Y]} \frac{1+wk_C[Y]/k_{12}}{K} \tag{40}$$

where K and k_{eff} are defined by Eqs. (12) and (13). The quantum yields in the absence and the presence of Y will be denoted, respectively, by Φ_{iF}^0 and Φ_{iF}. Then Eqs. (39) and (40) lead to the following equations of the Stern-Volmer type:

$$\Phi_{1F}^0/\Phi_{1F} = 1 + wk_C\tau_{eff}[Y] \tag{41}$$

$$\frac{\Phi_{2F}^0}{\Phi_{2F}} = \frac{1+wk_C\tau_{eff}[Y]}{1+wk_C[Y]/k_{12}} \tag{42}$$

with $\tau_{eff}=1/k_{eff}$. Unless $wk_C[Y]$ is of comparable magnitude to k_{12}, the denominator on the right-hand side of Eq. (42) may be equated to unity.

The Stern-Volmer plots shown in Fig. 8 are in general agreement with the prediction from Eqs. (41) and (42), except that two straight lines resulting from the plots of the quantum yield ratios Φ_{1F}^0/Φ_{1F} and Φ_{2F}^0/Φ_{2F} which were measured with the same excitation energy have somewhat different slopes. Such a difference between the slopes may be attributed to the fact that the observed lifetimes τ_1 and τ_2, which are both identified as τ_{eff}, are not strictly equal to each other, as has already been mentioned.

Table 1. Kinetic data on quenching of S_1- and S_2-fluorescence by oxygen

Fluorescing state	Exciting wavelength (nm)	Slope of Stern-Volmer plot ($Torr^{-1}$)	Lifetime τ_1 or τ_2 (ns)	$wk_C \times 10^{-11}$ (1 mol^{-1}. s^{-1})	w
S_1	324 (S_2^0)	1.14	157	2.00	0.77
	298 (S_2^2)	0.93	116	2.20	0.85
	266 (S_3^0)	0.71	92	2.14	0.82
	257 (S_3^1)	0.66	81	2.26	0.87
	234 (S_4^0)	0.39	54	1.98	0.75
	226 (S_4^1)	0.36	52	1.93	0.74
S_2	298 (S_2^2)	0.54	—	—	—
	266 (S_3^0)	0.43	65	1.83	0.71
	257 (S_3^1)	0.40	—	—	—
	234 (S_4^0)	0.30	45	1.84	0.71
	226 (S_4^1)	0.24	—	—	—

The values for the quenching rate constant wk_C, obtained at various exciting wavelengths, are listed in Table 1, together with the slopes and lifetimes from which the wk_C values were derived. In contrast to the considerable variation of the lifetimes with exciting wavelength, both S_1- and S_2-fluorescence emissions show comparatively constant wk_C values, ranging from 1.8×10^{11} to 2.3×10^{11} l mol^{-1} s^{-1}, regardless of the excitation energy. Assuming molecular diameters to be 8 and 2 Å for pyrene and oxygen, respectively, we obtain $k_C=2.6\times 10^{11}$ l mol^{-1} s^{-1} (or 9.4×10^6 $Torr^{-1}$ s^{-1}) at 170 °C from the gas kinetic theory. Dividing the experimental wk_C value by the theoretical k_C, we get the probability factor w. The w values thus determined are found to be rather close to unity (Table 1). Although some assumptions are involved in the evaluation of w, it may be concluded that the quenching of the dual fluorescences of pyrene vapor by oxygen is very efficient.

Inspection of the data in Table 1 at exciting wavelengths of 234 and 266 nm reveals that the difference in question between the slopes of the Stern-Volmer plots is due mainly to the difference between τ_1 and τ_2. For a given exciting wavelength, the S_2-fluorescence has a small slope compared with the S_1-fluorescence, so that the intensity of the S_2-fluorescence spectrum relative to that of the S_1-fluorescence increases with the oxygen pressure. As a result, the S_2-fluorescence spectrum becomes more distinct at higher oxygen pressures (see Figs. 6 and 7). In the case of spectral curve 3 in Fig. 6 (S_2^2 excitation at 350-Torr oxygen pressure), the S_2-fluorescence can be observed very clearly, and its intensity relative to the intensity of the S_1-fluorescence is somewhat higher than expected from extrapolation of the linear plots shown in Fig. 8. A conceivable reason for the occurrence of this phenomenon is that in the case concerned the denominator on the right-hand side of Eq. (42) is appreciably larger than unity.

Relations between Rate Constants. In Paper I we attempted to determine the values of the rate constants k_{21} and k_{12}. For that purpose the S_2-fluorescence quantum yield Φ_{2F} was divided into two parts, that is, $\Phi_{2F}=\phi_{2F}+\phi_{12F}$, where ϕ_{2F} and ϕ_{12F} correspond to the quantum yields of the prompt and slow fluorescence

emissions, respectively. The ratio of ϕ_{12F} to ϕ_{2F} was then expressed as

$$\phi_{12F}/\phi_{2F} = \Phi_{1F}(k_{12}/k_{1F}) \quad (43)$$

On the assumption that the residue of S_2-fluorescence at a high pressure of cyclohexane (~70 Torr) ocrresponds to ϕ_{2F}, the ratio ϕ_{12F}/ϕ_{2F} was estimated to be 25 for S_4^0 excitation. As is seen in Fig. 3, Φ_{2F} is still decreasing at a cyclohexane pressure of 70 Torr. Furthermore, the contribution of thermal repopulation to Φ_{2F} (Paper I) cannot be ignored at high cyclohexane pressures. The figure 25 for ϕ_{12F}/ϕ_{2F}, therefore, should be regarded as a tentative one.

As has been mentioned, oxygen quenches the S_1 and S_2 states of pyrene very efficiently, so that practically no vibrational relaxation takes place even at oxygen pressures higher than 100 Torr. Hence, it is not necessary to take account of the thermal repopulation effect when oxygen is used as a foreign gas. So far as the Stern-Volmer plot based on Eq. (42) is linear, the prompt fluorescence yield, ϕ_{2F}, should be negligible compared with ϕ_{12F}. On the basis of these considerations, we inferred from such experimental data as shown in Figs. 6—8 that $\phi_{12F}/\phi_{2F} \gtrsim 10^2$ irrespective of excitation wavelength. It then follows from Eq. (43) that $k_{12} \gtrsim 10^9$ s^{-1}, since k_{1F} is 10^6 s^{-1} (Paper I). On the other hand, according to Paper I,

$$k_{21} \simeq k_{12}\frac{\Phi_{1F}}{\Phi_{2F}}\frac{k_{2F}}{k_{1F}} \quad (44)$$

Φ_{1F}/Φ_{2F} is ~10 for S_4^0 excitation and increases with decreasing excitation energy, and k_{2F} is known to be 1.7×10^8 s^{-1} (Paper I); hence $k_{21} > 10^{12}$ s^{-1}. Thus, it may safely be said that the relations (5)—(7) hold at excitation wavelengths adopted in the present study.

Concluding Remarks. In this paper we hold the view that electronic processes in an isolated pyrene molecule may be treated kinetically on the basis of a scheme in which internal conversion is reversible between S_1* and S_2*, and thereby we can explain, to a good extent, the effects of cyclohexane and oxygen on the dual fluorescences of pyrene vapor. Along this line, it is concluded from the results of the present study that the S_2-fluorescence consists mainly of a slow component originating from S_2* which is in equilibrium with S_1*.

Quantum-mechanically, an intermediate strong coupling[8,16] is expected to occur between S_2* and S_1* because of a small electronic energy gap (3900 cm^{-1}) between the S_2 and S_1 states of the pyrene molecule. The coupling of an S_2* vibronic state with S_1* states that are quasidegenerate with S_2* yields compound states, and results in an anomalously long lifetime of the S_2-fluorescence. Thus, a good correspondence between the kinetic and quantum-mechanical schemes is obtained, as has recently been pointed out by Lahmani *et al.*[2]

Although it is predicted from each of the two schemes that the lifetimes τ_1 and τ_2 for the S_1- and S_2-fluorescence emissions should be equal, there is a slight but systematic difference between the actually obtained values of τ_1 and τ_2. Owing to sequence congestion, the thermal distribution of vibrational energy in the electronic ground state is transferred to the excited state even if a molecular system is excited with light of a given energy. According to Deinum *et al.*[8] the sequence congestion, along with the rapid increase of Φ_{2F}/Φ_{1F} with the excess vibrational energy, may account for about half of the lifetime difference. Further studies must be made to settle this problem.

We wish to express our thanks to Mr. Yoshio Shindo, Mr. Masahisa Fujita, and Mr. Masakatsu Aoi for their help in carrying out the experiments.

References

1) B. R. Henry and W. Siebrand, "Organic Molecular Photophysics," Vol. 1, ed. by J. B. Birks, John Wiley & Sons, London (1973), Chap. 4.
2) F. Lahmani, A. Tramer, and C. Tric, *J. Chem. Phys.*, **60**, 4431 (1974).
3) A. Frad, F. Lahmani, A. Tramer, and C. Tric, *ibid.*, **60**, 4419 (1974).
4) Papers cited in Refs. 2) and 3).
5) H. Baba, A. Nakajima, M. Aoi, and K. Chihara, *J. Chem. Phys.*, **55**, 2433 (1971).
6) H. Baba and M. Aoi, *J. Mol. Spectrosc.*, **46**, 214 (1973).
7) P. A. Geldof, R. P. H. Rettschnick, and G. J. Hoytink, *Chem. Phys. Lett.*, **4**, 59 (1969).
8) T. Deinum, C. J. Werkhoven, J. Langelaar, R. P. H. Rettschnick, and J. D. W. van Voorst, *ibid.*, **27**, 206, 552 (1974).
9) P. Wannier, P. M. Rentzepis, and J. Jortner, *ibid.*, **10**, 102 (1971).
10) T. Brewer, *J. Amer. Chem. Soc.*, **93**, 775 (1971).
11) J. E. Haebig, *J. Phys. Chem.*, **71**, 4203 (1967).
12) J. B. Birks, "Photophysics of Aromatic Molecules," Wiley-Interscience, London (1970).
13) a) M. Boudart and J. T. Dubois, *J. Chem. Phys.*, **23**, 223 (1955); b) A. M. Halpern and W. R. Ware, *ibid.*, **53**, 1969 (1970); c) B. S. Rabinovitch, H. F. Carroll, J. D. Rynbrandt, J. H. Georgakakos, B. A. Thrush, and R. Atkinson, *J. Phys. Chem.*, **75**, 3376 (1971).
14) In this case, it follows from the simplest stepladder model being adopted here that vibrational levels other than S_1^0 are little populated. In reality the lower vibrational levels are to be populated according to Boltzmann's distribution.
15) See also C. J. Werkhoven, T. Deinum, J. Langelaar, R. P. H. Rettschnick, and J. D. W. van Voorst, *Chem. Phys. Lett.*, **32**, 328 (1975).
16) A. Nitzan, J. Jortner, and P. M. Rentzepis, *Proc. Roy. Soc. Ser. A*, **327**, 367 (1972).

Vapor-Phase Photolysis of *cis*- and *trans*-4,5-Dimethylcyclohexenes

Yoshihisa INOUE,* Setsuo TAKAMUKU, and Hiroshi SAKURAI

The Institute of Scientific and Industrial Research, Osaka University, Yamadakami, Suita, Osaka 565

(Received April 12, 1975)

Direct and sensitized photolyses of 4,5-dimethylcyclohexene vapor were investigated using a stereochemical approach at room temperature over the pressure range from 1 to 9 Torr. In the direct photolysis, decomposition of the retro-Diels-Alder type was the main course of the reaction, leading to the formation of 2-butene and 1,3-butadiene with the retention of the original configuration; 3,4-dimethyl-1-methylenecyclopentane was also formed as a minor product from a pressure-independent process. Mercury sensitization, on the other hand, produced *cis*- and *trans*-2-butenes, butadiene, 2,3-dimethyl-1-vinylcyclobutane, and *cis-trans* isomers of the substrate together with radical-induced products, *i.e.*, hydrogen, 1,2-dimethylcyclohexane, and dimeric products. The intermediacy of a "*hot*," "*triplet*" *biradical* was suggested from the pressure-dependence of the *trans*- to *cis*-2-butene ratio in the mercury sensitization. The differences in the results between the direct and sensitized photolyses are interpreted in terms of spin correlation effects.

Few studies have been reported on the direct photolysis of cycloalkenes, although there is some literature on the mercury-sensitized photolysis of this species.[1] Regarding the cyclohexene derivatives dealt with in the present report, Gunning *et al.* have investigated in detail the kinetics of the mercury-sensitized photolysis of cyclohexene itself.[1a] They proposed a biradical

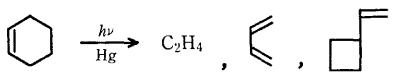

mechanism for the formation of ethylene, butadiene and vinylcyclobutane, which involves an alkyl-allyl biradical produced by the familiar allylic C–C bond cleavage, and the kinetics seem to support this mechanism. De Maré has reported on the mercury-sensitized photolysis of 3-methylcyclohexene vapor *via* a similar reaction mechanism.[2] However, little evidence has been obtained regarding the nature of the intermediate species and the mechanism involved. We have elucidated the reaction mechanism of the vapor-phase photolysis of cycloalkene using a stereochemical approach.

Recently it has been shown that the spin multiplicity of the intermediate 1,4-biradical drastically affects the stereochemistry of the reaction in Norrish type-II photocleavage,[3] as well as in other systems.[4] A study of the direct and sensitized photolyses of *cis*- and *trans*-4,5-dimethylcyclohexenes (**1c** and **1t**) is of interest since the results are expected to provide insight into both the reaction mechanism and the spin correlation effects.

Experimental

Materials. *cis*- and *trans*-4,5-Dimethylcyclohexenes were prepared according to procedures similar to those described by Peter *et al.*[5] *cis*-4,5-Dihydroxymethylcyclohexene, prepared by the reduction of *cis*-cyclohexene-4,5-dicarboxylic anhydride with $LiAlH_4$ in ether, was converted into ditosylate by a reaction with *p*-toluenesulfonyl chloride in dry pyridine. The *cis*-ditosylate was reduced in turn to *cis*-4,5-dimethylcyclohexene by $LiAlH_4$ in ether. The dimethyl ester of *trans*-cyclohexene-4,5-dicarboxylic acid, prepared by a Diels-Alder reaction of dimethyl fumarate with 1,3-butadiene at 200 °C for 3 hr in an autoclave,[6] was reduced to *trans*-4,5-dimethylcyclohexene by similar successive treatments with $LiAlH_4$, *p*-toluenesulfonyl chloride, and again $LiAlH_4$. All the compounds prepared were identifield by means of infrated and NMR spectrometry. *cis*- and *trans*-Dimethylcyclohexenes thus obtained were purified by preparative gas chromatography (gc) on a 6 m polyethylene glycol-6000 column. Quantitative analysis by gc indicated that the purities of **1c** and **1t** are at least 99.9 and 98.0%, respectively. Samples of **1t** contained a small amount (1%) of **1c** as an impurity. A correction was applied to all of the data for the presence of the impurity. The samples of **1c** and **1t** were admitted to a vacuum line, dried over evaporated sodium, and degassed at liquid nitrogen temperature before use.

The NMR spectra of **1c** and **1t** were in good agreement with those reported by Peter *et al.*[5] Their steric configurations were confirmed by the gc comparison of commercially available *cis*- and *trans*-1,2-dimethylcyclohexanes with the saturated compounds obtained from the hydrogenation of **1c** and **1t** on 5% Pd–charcoal.

Apparatus and Procedure. All the experiments were carried out at room temperature and under static conditions. A cylindrical cell, 5 cm long and 5 cm in diameter, made of Suprasil and a mercury-free vacuum system were available for the vapor-phase direct photolysis. The direct irradiation was run using a 30 W low-pressure mercury lamp fitted with a Suprasil envelope, the light path being flushed with nitrogen gas. The mercury-sensitized photolysis was carried out using a quartz cell of similar size, a conventional vacuum system, and the same mercury lamp fitted with a Toshiba UV-25 filter which removes the 1849-Å resonance line of mercury. The lamp was allowed to warm up for at least 30 min before each run in order to reach stable operating conditions. The quantum yields in mercury-sensitization were determined by ethylene (100 Torr) actinometry.[7] The absorption of the incident radiation was incomplete in the cell and appropriate corrections were made in the determination of the quantum yields.

After each run, materials were trapped in a capillary at liquid nitrogen temperature. The noncondensable products were analyzed and measured by a combination of Toepler pump, gas burette, and Pd-chamber. The condensable material was analyzed by gc on a 6 m column of 20% β,β'-oxydipropionitril (ODPN) on 60/80 Celite 545 at 50—70 °C. The stereoisomers of 2-butene were clearly separated from one another under these conditions, while a trace amount of the stereoisomers of **1** could not be separated from one another enough for quantitative analysis, especially in the higher pressure (>3 Torr) experiments. The analyses of the dimeric products from the mercury-sensitization were conducted by gc on a 3 m column of polyethylene glycol-6000 on Celite at 150 °C and a 1.5 m column of FFAP on Celite at 150 °C. The molecular weights of the dimers were confirmed

using a Hitachi RMS-4 gc-mass spectrometer.

Identification of 2,3-Dimethyl-1-vinylcyclobutane (3). Mercury sensitization of **1c** was carried out on a prepatative scale using the mercury lamp and an apparatus composed of a 5 l Pyrex vessel, two 100 ml quartz cells for irradiation, and a thermosiphon for circulation of the gas. The irradiation of **1c** with 10% nitric oxide in the presence of mercury was run at 1 Torr for 15 hr. The photolyzed sample was trapped at liquid nitrogen temperature and then subjected to preparative gc in order to isolate **3**. The NMR spectrum of **3** was obtained with TMS as an internal standard in CCl_4 and showed three vinyl protons at δ 5.5—6.0(m), 4.9(d), and 4.95(d), six methyl protons at 1.0(d), and five cyclobutyl protons at 1.2—2.2(m). The mass spectrum indicated the following relative intensities: *m/e*, 110(2.1), 95(28.3), 81(40.5), 69(45.5), 68(67.8), 67(70.7), 56(35.1), 55(100), and 54(6.4). These spectral data indicate a 2,3-dimethylvinylcyclobutane structure of **3**, but its steric configuration is not known. The mercury sensitization of **1t** also produced a compound which has the same retention time on the gc and an identical mass spectrum with that of **3**. Consequently, it is considered that the mercury sensitization of both **1c** and **1t** produced dimethylvinylcyclobutane **3** with an identical steric configuration.

Identification of 3,4-Dimethyl-1-methylenecyclopentane (2). Eighty mg of **1c** in a sealed Suprasil tube, 2 mm in diameter, was photolyzed in the liquid phase without a solvent using a 30 W low-pressure mercury lamp. The irradiation was continued for 350 hr resulting in a conversion of *ca.* 10% and the photolyzed sample was subjected to preparative gc to isolate **2c**. The NMR spectrum of **2c** was obtained with TMS in CCl_4, and showed two olefinic protons at δ 3.5(s), six methyl protons at 0.86(d), and six other protons at 1.8—2.4(m). The mass spectrum of **2c** indicated the following relative intensities: *m/e*, 110(26.9), 95(100), 81(32.6), 69(20.0), 68(32.3), 67(60.0), 55(47.7), and 54(26.2). The gc analysis on an ODPN column indicated that the isolated C_8H_{14} isomer has a shorter retention time relative to those of the authentic samples of *cis*-3,4-*trans*-4,5-, *cis*-4,5-, 2,3-, 1,2-dimethylcyclohexenes and 2-methyl-1-methylenecyclohexane, and that the retention time of the saturated compound, prepared by hydrogenation of **2c** on Pd–charcoal, is different from that of *trans*- or *cis*-1,2-dimethylcyclohexane. All the data described above suggest a 3,4-dimethyl-1-methylenecyclopentane structure for **2c**, the steric configuration of which is deduced to be *cis* from that of the starting material(**1c**).

Vapor-phase direct photolysis of **1c** produced the same C_8H_{14} compound (**2c**), the mass spectrometric, gas chromatographic, and chemical (hydrogenation) features of which were identical with those of the **2c** obtained in the liquid-phase photolysis of **1c**. Vapor-phase photolysis of **1t** afforded another C_8H_{14} isomer (**2t**), which has a shorter retention time on ODPN relative to that of **2c**. The mass spectrum of **2t** indicated: *m/e*, 110(33.0), 95(100), 81(41.7), 69(33.0), 68 (46.1), 67(60.0), and 55(54.8). The structure of **2t** was identified to be *trans*-3,4-dimethyl-1-methylenecyclopentane on the basis of resemblance of the mass spectra.

Results

Direct Photolysis. As major decomposition products, 2-butene and 1,3-butadiene were obtained together with a minor isomeric product, 3,4-dimethyl-1-methylenecyclopentane (**2**), in the direct photolysis of **1c** and **1t** at a substrate pressure of 5 Torr, as shown in Table 1. Dimeric products and a vinylcycloalkane derivative, which are usually produced in the mercury-sensitized photolysis of cycloalkenes,[1] were not detected in significant yields. The total yield of 2-butenes was equal to that of butadiene. The photolysis of **1c** and **1t** at 5 Torr gave almost selectively *cis*- and *trans*-2-butenes at *cis-trans* ratios of 16: 1 and 1: 20, respectively. Irradiation of **1** through a UV-25 filter did not result in any products under comparable conditions.

TABLE 1. PRODUCTS OF DIRECT PHOTOLYSIS OF **1**

Compd	Press, Torr	Exposure time, min	Products, μmol $\times 10^3$				
1c	5.0	1.0	53.8	3.4	61.7	5.1	a)
1t	5.0	1.0	2.8	57.0	61.7	a)	6.1

a) Not detected.

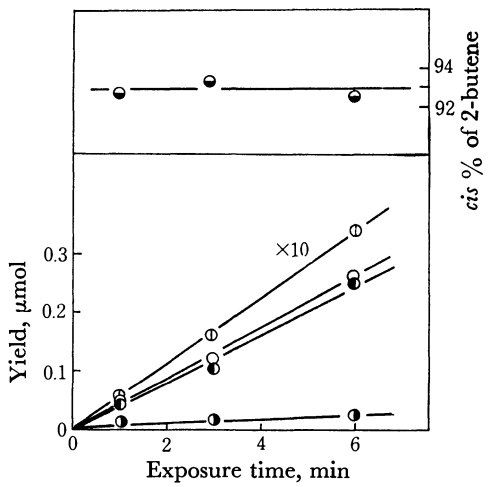

Fig. 1. Product yields as a function of exposure time in direct photolysis of **1c** (8 Torr). ◐, *cis*-2-butene; ◑, *trans*-2-butene; ○, 1,3-butadiene; ⊕, *cis*-3,4-dimethyl-1-methylenecyclopentane (×10); ◒, *cis* % of 2-butene.

The effects of exposure time on the product yields were examined in the photolysis of **1c** at a pressure of 8 Torr, since the further irradiation of initially formed 2-butene could produce isomeric 2-butene.[8] According to the data appearing in Fig. 1, all the yields increase linearly with exposure time, which indicates that these are the products from the primary process. The percentage of *cis*-2-butene, on the other hand was constant over the range of 1—6 min, and therefore, the isomeric 2-butene cannot result from the further photoisomerization. Direct photolysis of **1c** was performed over the pressure range of 1—8 Torr. The results are shown in Fig. 2. Although the pressure range was limited by the low vapor pressure of the substrate, the suppressing effect of pressure on the formation of butene and butadiene is evident from the data. The percentage of *cis*-2-butene was independent of the pressure, in spite of the decrease in the yields with increasing pressure. The yield of **2c** remained constant over the entire pressure range.

Mercury-sensitized Photolysis. The products of the mercury sensitization were hydrogen, 2-butene,

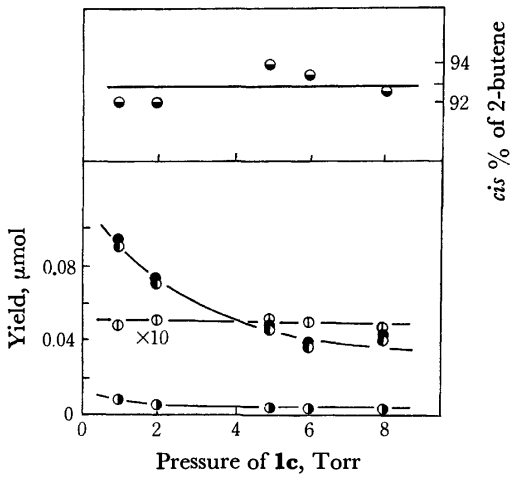

Fig. 2. Product yields as a function of initial substrate pressure in direct photolysis of **1c**. Exposure time is 1 min. ◐, *cis*-2-butene; ◑, *trans*-2-butene; ●, 1,3-butadiene; ⦶, *cis*-3,4-dimethyl-1-methylenecyclopentane (×10); ◒, *cis* % of 2-butene.

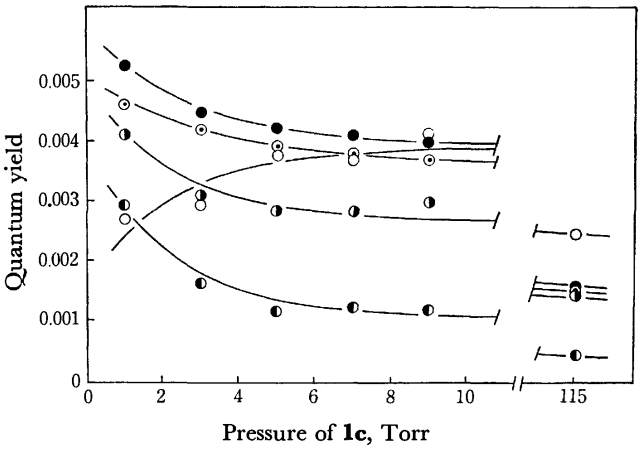

Fig. 3. Product yields as a function of pressure in mercury-sensitized photolysis of **1c**. Exposure time is 3 min. Plots at a pressure of 115 Torr were obtained by adding xenon (112 Torr) to **1c** (3 Torr). ◐, *cis*-2-butene; ◑, *trans*-2-butene; ●, 1,3-butadiene; ⊙, 2,3-dimethyl-1-vinylcyclobutane; ○, *cis*-1,2-dimethyl cyclohexane.

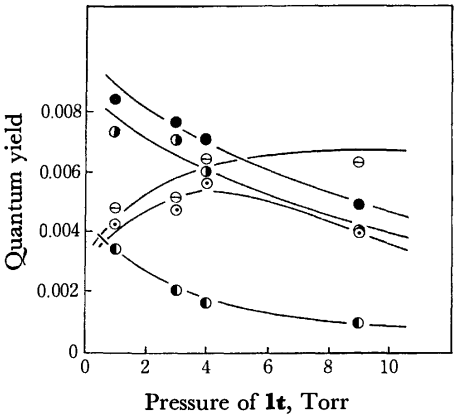

Fig. 4. Product yields as a function of substrate pressure in mercury-sensitized photolysis of **1t**. Exposure time is 3 min. ◐, *cis*-2-butene; ◑, *trans*-2-butene; ●, 1,3-butadiene; ⊙, 2,3-dimethyl-1-vinylcyclobutane; ⊖, *trans*-1,2-dimethylcyclohexane.

1,3-butadiene, 2,3-dimethylvinylcyclobutane (**3**), 1,2-dimethylcyclohexanes, and some dimeric products. The gas chromatographic and mass spectrometric analyses of the dimeric products showed that the dimeric fraction is composed of at least five compounds, the molecular weights of which are in the range of 218—222. The mass spectra of the dimers appears to suggest the absence of cyclodimers of **1**. On the basis of these results and observations in other systems,[1] the dimeric products were assumed to have a bicyclohexyl, cyclohexylcyclohexene, or bicyclohexenyl skeleton. The quantum yields of all products except the dimers are shown in Table 2. The distribution of the products from shorter exposure time (1 min) experiments is in good agreement with this result. The total yield of the 2-butenes equals that of butadiene. The 2-butene resulting from the mercury sensitization was predominantly *trans* even when **1c** was used. In addition, the photolysis of both **1c** and **1t** produced dimethylvinylcyclobutane having the same steric configuration as the major product.

A pressure-dependent study was also carried out for the mercury sensitization of **1c** and **1t**. In order to further examine the pressure effects, a higher pressure experiment was also performed above vapor pressure limit of the substrate using **1c** (3 Torr) with xenon added (112 Torr). The results are plotted in Figs. 3 and 4. While the suppressing effect of the pressure on the yields of 2-butene, butadiene, and **3** is evident, the 1,2-dimethylcyclohexane yields show no pressure dependence above *ca.* 5 Torr in the photolysis of both **1c** and **1t**.

An inhibiting experiment was performed with a small amount of nitric oxide added since radical-initiated reactions caused by excited mercury atoms are well-known in the mercury sensitization of hydrocarbons.[9] As can be seen from Table 3, the formation of 1,2-dimethylcyclohexane and the dimeric products were completely suppressed by the addition of nitric oxide which acts as a radical scavenger, while the yields of the other products merely decreased to a small extent.

Table 2. Products of mercury-sensitized photolysis of **1**

Compd	Press, Torr	Exposure time, min	Products, $\Phi \times 10^3$						
									H_2
1c	9.0	3.0	1.2	3.0	4.0	3.7	3.7	a)	27.2
1t	9.0	3.0	0.6	3.0	3.7	3.0	a)	4.8	b)

a) Not detected. b) Not determined.

TABLE 3. EFFECTS OF NITRIC OXIDE ON MERCURY-SENSITIZED PHOTOLYSIS OF **1**

Press, Torr		Exposure time, min	Products, μmol × 10^3					
1c	NO							Dimers
5.0	0	3.0	4.0	9.7	14.4	13.4	12.9	138
5.0	0.5	3.0	5.5	7.5	9.0	10.0	a)	a)

a) Not detected.

In other experiments, it was observed qualitatively that (i) the sensitized decomposition of **1c** (5 Torr) at 2537 Å in the vapor phase with benzene vapor (5 Torr) as a sensitizer did not produce detectable amounts of any products and (ii) irradiation at 1849 Å of **1c** in the liquid phase with no solvent produced no detectable yields of 2-butene, butadiene, or **3**. The only detectable products were saturated *cis*-1,2-dimethylcyclohexane and isomerized *cis*-3,4-dimethyl-1-methylenecyclopentane (**2c**).

Over the temperature range of 400—700 °C, pyrolyses of **1c** and **1t** were conducted using a Shimadzu PYR-2A pyrolyzer-gas chromatograph. The products of the pyrolysis were merely decomposition products of lower molecular weight, and no 2-butene, butadiene or isomeric product was detected in significant amounts.

Discussion

Decomposition of the retro-Diels-Alder type appears to be the main course of the direct photolysis of **1** in the vapor phase, which results in the stereospecific formation of 2-butene together with an equimolar amount of butadiene. No detectable amounts of 2-butene and butadiene were formed in the direct photolysis of **1** in the liquid phase. Irradiation through a UV-25 filter produced no products in the direct photolysis of **1** in the vapor phase. From these results and the stereospecificity of the reaction, it is inferred that **1** is promoted to an electronically excited singlet state principally by the 1849 Å resonance line of mercury and then decomposes directly or *via* a short-lived biradical produced by an allylic C–C bond cleavage into 2-butene and butadiene with the retention of its original configuration. It is, however, difficult to determine if these are direct products from the electronically-excited states or if significant amounts are formed as a result of decomposition after internal conversion to a vibrationally-excited ground state.

The most significant observation in the direct photolysis of **1c** is the effect of pressure, resulting in a decrease in the yields of the decomposition products with increasing pressure, whereas the yield of *cis*-3,4-dimethyl-1-methylenecyclopentane (**2c**) remains constant. The **2c** observed is, therefore, considered to be formed in a pressure-independent process,* probably from an electronically-excited singlet state which has a lifetime short compared to the effective time between deactivating collisions even at higher pressures. On the other hand, the high pressure dependence of the yields of the other decomposition products suggests that these are the products from a vibrationally-excited ground state, since with molecules of this size, the lifetimes should be long enough to permit collisional deactivation of any energetic ground-state species which might be formed *via* an internal conversion process. This elucidation is also supported by the observation that only **2c** is formed in the liquid-phase photolysis of **1c**, in which vibrational energy is quickly removed. Although 2-butene and butadiene were not detected in the attempted pyrolysis of **1** at 400—700 °C, the vibrationally-excited ground state species as the intermediate in direct photolysis cannot be eliminated from this result since raising the temperature from room temperature to 700 °C is considered to involve very little energy difference relative to the large energy input of the direct photolysis.

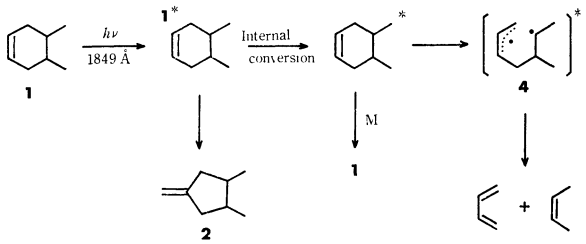

Scheme 1.

The detailed mechanism of the photodecomposition of **1** to 2-butene and butadiene is of interest in this work. The fact that several % *trans*-2-butene is formed from **1c** and also *cis*-2-butene from **1t** seems to suggest the biradical mechanism as opposed to the concerted path. However, there may be another possibility that the electronically-excited singlet state of **1** undergoes inter-

* The formation mechanism of **2** is of interest. Fields and Kropp have reported that only tetrasubstituted alkenes undergo photorearrangement of the alkyl group *via* π,R(3*s*) Rydberg excited states on direct irradiation in a pentane solution; T. R. Fields and P. J. Kropp, *J. Amer. Chem. Soc.*, **96**, 7759 (1974).

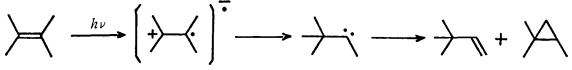

In the present system, although the nature of the electronically-excited state involved is uncertain, the disubstituted alkene **1** seems to undergo a similar photorearrangement producing **2** upon direct irradiation in both the liquid and vapor phases. We have also observed photoisomerization of cycloheptene to carbene-derived products, *i.e.*, methylenecyclohexane and norcarane, on direct photolysis in the liquid phase. The detailed mechanism and the nature of the intermediate of these rearrangements are under investigation and will be the subject of a separate report.

system crossing in part to a triplet species, which would give nonstereospecific 2-butene in a manner similar to the sensitized photolysis described below. Although such a process is important in the photolysis of aromatic and carbonyl compounds,[10] it is believed that the large difference in energy causes singlet-triplet intersystem crossing to be very slow in such a monoolefin. The absence of the vinylcyclobutane **3** in the direct photolysis of **1** also indicates the low efficiency of the intersystem crossing since photoisomerization to **3** is characteristic of triplet species as shown in the mercury sensitization of **1**. It is therefore concluded that the photodecomposition of **1** proceeds *via* the short-lived singlet biradical **4**.

In mercury sensitization, 2,3-dimethyl-1-vinylcyclobutane **3**, the *cis-trans* isomers of **1**, and the radical-induced products were obtained in addition to the decomposition products, as shown in Table 2. Since the formation of 1,2-dimethylcyclohexane and the dimeric products was completely suppressed by the radical scavenger NO, these products, and probably hydrogen, are considered to be formed from the well-known hydrogen abstraction reaction initiated by the excited mercury atom.[1a,9] The mechanism for the formation of hydrogen, 1,2-dimethylcyclohexane and the dimers is deduced to be as follows:

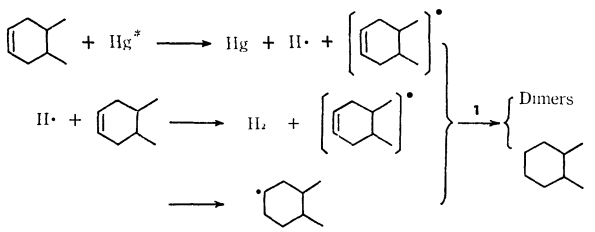

Scheme 2.

In contrast to direct photolysis, the 2-butene resulting from the mercury sensitization of **1** is predominantly *trans* even when **1c** was used. Furthermore, the mercury sensitizations of both **1c** and **1t** produced 2,3-dimethylvinylcyclobutane having the same steric configuration as a major product, and in addition the isomerization of **1c** to **1t** was confirmed at low pressure. On the basis of these results and the generally accepted view of mercury photosensitization of olefins,[1,9,11] it is suggested that the vibrationally-excited triplet state of **1**, produced by energy transfer from the excited mercury atom, undergoes the usual allylic C–C bond fission resulting in an allylic triplet biradical **4**, where rotation about the C–C bond adjacent to the alkyl radical site is possible. Then the biradical ^{3}**4** decomposes into *cis*- and *trans*-2-butenes with an equimolar amount of butadiene, and/or combines to **1** or **3**.

Spin inversion is required in order for the triplet biradical ^{3}**4** to undergo decomposition and/or ring closure. Although the present intermediate is an alkyl-allyl biradical, ring closure of the photolytically derived singlet 1,4-biradical has been shown to be fast relative to the time required for free rotation about the C–C bonds.[12] If the same is true in this system, equilibrium will be established among triplet, not singlet, biradical rotamers. The rate-determining step

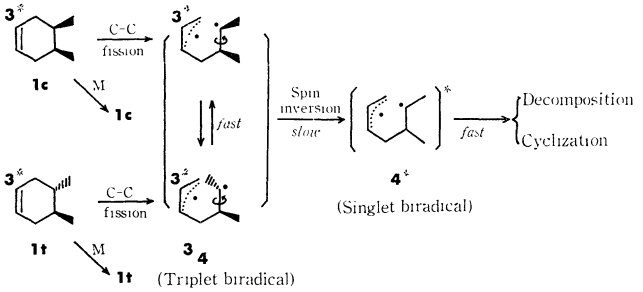

Scheme 3.

in the sensitized photolysis may, therefore, be the spin inversion of the triplet biradical.

As for benzene photosensitization in the vapor phase, it has been shown by Schmidt and Lee[13] that energy transfer from the benzene triplet to olefins is fast enough to produce olefin triplets in most cases. It is therefore noted that the triplet state of **1** produced in benzene sensitization resulted in no photoproducts. The difference between the benzene- and mercury-sensitizations can be attributed to the triplet energy of the sensitizers, 84 and 113 kcal/mol, respectively. The triplet state of **1** produced by mercury sensitization is considered to have a larger vibrational energy by *ca.* 30 kcal/mol than that produced by benzene sensitization. Consequently, the excess vibrational energy is suggested to play a singificant role in the triplet reaction.

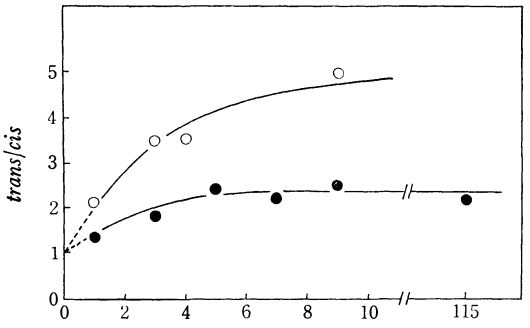

Fig. 5. Pressure dependence of *trans-cis* ratio of 2-butene in mercury-sensitized photolysis of **1c** (●) and **1t** (○). Plot at a pressure of 115 Torr was obtained by adding xenon (112 Torr) to **1c** (3 Torr).

The *trans-cis* ratio of 2-butene in the mercury sensitization of **1** was found to depend on the substrate pressure as shown in Fig. 5. Regardless of which isomer is used, the value of the *trans-cis* ratio seems to approach unity at 0 Torr, while it increases with increasing pressure. The higher pressure experiment with xenon added showed that, although the *trans-cis* ratio decreases considerably at lower pressure (<3 Torr), the ratio is constant from 5 to 115 Torr in the mercury sensitization of **1c**. An explanation of the results may be found in the vibrational energy of the triplet biradical **4**, this alkyl-allyl biradical being a novel instance of a "hot," "triplet" biradical produced in the vapor phase, although a hot, triplet biradical of the alkyl-thiyl type has recently been reported by Dice and Steer.[14] The biradical **4** formed from **1t** is considered to have a

lower vibrational energy than that formed from **1c** by an amount equal to the difference in the stabilities ($\triangle H_f$) of the two isomers, **1t** and **1c**. In the absence of deactivating collisions, the hot, triplet biradical **4** has a large amount of excess vibrational energy, which renders insignificant the slight differences in stabilities, and therefore, the *trans-cis* ratio approaches unity in the sensitized photolysis of both **1c** and **1t**. At higher pressures, the difference between the energies of **4** resulting from **1c** and **1t** has a considerable influence on the value of the *trans-cis* ratio. Because of the lower vibrational energy, the biradical formed from **1t** produces much more *trans*-2-butene than that from **1c** at a comparable pressure. These estimations appear to explain the present results reasonably well, and also suggest that the lifetime of the biradical **4** is not long enough to be deactivated by collisions because the *trans-cis* ratio from **4** is different at higher pressures.

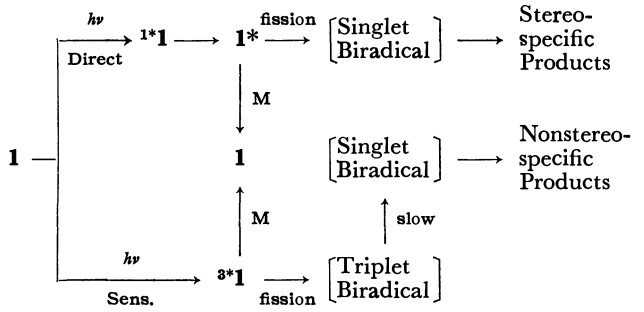

Scheme 4.

The excess energy in the direct photolysis is larger by *ca.* 40 kcal/mol than that in the mercury sensitization, which in itself may account for the different reactivities between the direct and sensitized photolyses, since with increasing excess energy the lifetime of the intermediates should decrease favoring decomposition over rearrangement. If this is the case, it is expected that the stereospecificity of butene-formation in direct photolysis must decrease with increasing pressure, since collisional deactivations diminish the excess energy of the intermediates to give nonstereospecific 2-butene. However, the *trans-cis* ratio of 2-butene in the direct photolysis is not affected by increasing the pressure in spite of the considerable decreases in yield (see Fig. 2). The rate-determining step of the direct photolysis may be the allylic C–C bond cleavage. The different results for the direct and sensitized photolyses are, therefore, attributed to the difference in the spin states of the intermediates.

References

1) a) G. R. De Maré, O. P. Strausz, and H. E. Gunning, *Can. J. Chem.*, **43**, 1329 (1965); b) W. A. Gibbons, W. F. Allen, and H. E. Gunning, *ibid.*, **40**, 568 (1962); c) S. Takamuku, K. Moritsugu, and H. Sakurai, This Bulletin, **44**, 2562 (1971); d) Y. Inoue, M. Kadohira, S. Takamuku, and H. Sakurai, *Tetrahedron Lett.*, **1974**, 459.

2) G. R. De Maré, *Bull. Soc. Chim. Belges*, **81**, 459 (1972).

3) N. C. Yang and S. P. Elliot, *J. Amer. Chem. Soc.*, **91**, 7550 (1969); L. M. Stephenson, P. R. Cavigli, and J. L. Partlett, *ibid.*, **93**, 1984 (1971).

4) P. D. Bartlett and N. A. Porter, *ibid.*, **90**, 5317 (1968).

5) H. Peter, R. A. Archer, and H. S. Mosher, *J. Org. Chem.*, **32**, 1382 (1967).

6) I. N. Nazarov and V. F. Kucherov, *Izvest. Akad. Nauk S.S.S.R., Otdel. Khim. Nauk*, **1954**, 329; *Chem. Abstr.*, **49**, 5328e (1955).

7) K. Yang, *J. Amer. Chem. Soc.*, **86**, 3941 (1964).

8) J. P. Chesick, *J. Chem. Phys.*, **45**, 3934 (1966); P. Borrel and F. C. James, *Trans. Faraday Soc.*, **62**, 2452 (1966).

9) J. G. Calvert and J. N. Pitts, Jr., "Photochemistry," Wiley, New York, N.Y. (1966), Chapter 2.

10) J. G. Calvert and J. N. Pitts, Jr., *ibid.*, Chapter 4.

11) R. J. Cvetanović and L. C. Doyle, *J. Chem. Phys.*, **37**, 543 (1962).

12) C. P. Casey and R. A. Boggs, *J. Amer. Chem. Soc.*, **94**, 6457 (1972); H. A. J. Carless, J. Metcalfe, and E. K. C. Lee, *ibid.*, **94**, 7221 (1972).

13) M. W. Schmidt and E. K. C. Lee, *ibid.*, **92**, 3579 (1970).

14) D. R. Dice and R. P. Steer, *ibid.*, **96**, 7361 (1974).

The Additions of Acetic Acid to Limonene Catalyzed by Sulfuric Acid

Tohr YAMANAKA

Central Research Laboratory of Takasago Perfumery Co., Ltd., Kamata, Ohta-ku, Tokyo 144

(Received May 13, 1975)

The additions of acetic acid (AcOH) to limonene (IV) catalyzed by H_2SO_4 ($(0.367—8.39)\times10^{-2}$ mol/l), without a solvent, were studied. The mole ratio of IV to AcOH was less than 1: 19, and the reaction temperature was 28.5—92.5 °C. The products were α- and β-terpinyl acetates (I and II), and a mixture of *p*-menthadienes (III) as isomers of IV. The selectivity for I and II against III was not affected by the amount of H_2SO_4. The rate constants for I, II, and III were proportional to the amount of H_2SO_4. The apparent activation energy was 10.9 kcal/mol for I and II, and 13.7 kcal/mol for III. Both the proton concentration and the acidity function (h_0) in the reaction medium were regarded as proportional to the H_2SO_4 concentration. It was concluded that the formations of I and II were related to the A-2-type solvolytic mechanism, while that of III was related to the A-1-type specific hydrogen-ion mechanism.

An acid-catalyzed addition of AcOH to an olefin is a convenient method for introducing a hydroxy group into the olefin. However, there have been only a few papers about this reaction.[1] In order to form α-terpinyl acetate (I), some investigators have studied the additions of AcOH or chlorinated acetic acids to limonene (IV) or pinene in the liquid phase, with homogeneous and heterogeneous proton-acid catalysts.[2] Their efforts were concentrated mainly on identifying the products and on improving the yield of I, because the olefinic terpenes are liable to shift double bonds and to resinify in the presence of a strong acid catalyst. So far as the AcOH addition to a terpene is concerned, though, there has been no systematic study of the reaction kinetics and the catalytic mechanism.

We obtained some kinetic data on the additions of AcOH to IV, and the simultaneous isomerizations of IV, under various concentrations of H_2SO_4. The effects of the acid property in the system on catalytic activities and selectivities were discussed. The kinetic study was simplified by using a large excess of AcOH over the stoichiometric requirement, without a solvent; these species are miscible homogeneously within the limited concentration used in this study.

Experimental

Materials. Limonene (IV), a fraction of orange terpenes, was purified by fractional distillation. The fraction used as the starting material consists of IV of 96.7 wt% and two unknown impurities (one: 2.5 wt% and the other: 0.5 wt%), as determined by gas chromatographic (glc) analysis. The AcOH and 98 wt% H_2SO_4 were of a guaranteed reagent grade and were used without further purification.

Procedure. 24.3 g of AcOH and the desired amount of H_2SO_4 were weighed into a 100-ml Erlenmeyer flask equipped with a condenser. An appropriate amount of naphthalene (of a guaranteed reagent grade) was added as an internal standard substance for the glc analysis prior to each reaction run. Then IV was weighed into the flask, and the mixture was promptly stirred with a magnetic stirrer in a water bath with a thermostat. At any reaction time, 2—3 ml of the reaction mixture was sampled, diluted with 70 ml of water saturated with NaCl to stop the reaction, and extracted with hexane. The extract was washed with NaCl-saturated water and, after concentration, used for the glc analysis. Sampling was repeated at arbitrary time intervals. 0.069—0.944 mol/l of IV, 3.67×10^{-3}—8.39×10^{-2} mol/l of H_2SO_4, and 17.5 mol/l (an amount corresponding to a large excess over the stoichiometric requirement) of AcOH were used. The reference volume of the reaction mixture used to express concentrations of species in it was taken at 28 °C.

Analysis of the Products. Quantitative analysis was done by means of an internal-standard method, using a Shimadzu GC-3AH apparatus on a 3 m×3 mmϕ column packed with 10 wt% of polyethylene glycol on Diasolin. At a column temperature of 172 °C, the IV, I, and II peaks all appeared in the chromatogram. Under those column conditions, the mixture of all the *p*-menthadienes except IV showed one peak. The difference between the initial content of IV and the sum of the contents of I, II, III, and IV in the reaction mixture was regarded as the resin content.

Identification of the Products. Gas chromatography-mass spectroscopy (Hitachi RMU-6MG) was used for the identifications. The addition products of AcOH to IV were identified as I and II. III was estimated to be a mixture of 1,3-*p*-menthadiene, 1,4-*p*-menthadiene, and 2,8-*p*-menthadiene.

Results

Conversion-Time Curves. Figure 1 shows that the conversions of I and II decrease after each maximum. On the contrary, the formation of isomers (III) shows no maximum in the curve. This suggests that the acetates (I and II) are formed reversibly or as intermediates to cause the irreversible formation of III by the elimination of AcOH. Consequently, the following scheme can be postulated.

In the reaction with 3.68×10^{-3} mol/l of H_2SO_4, 0.54 mol/l of IV, and 15.0 mol/l of AcOH, the maximum con-

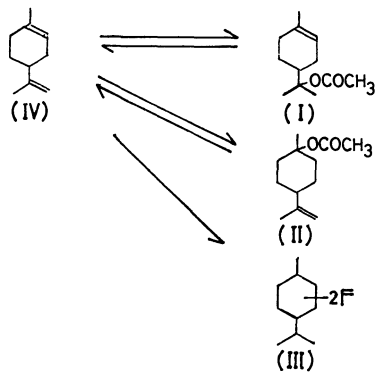

Scheme 1.

versions were from 0.198 to 0.08 for I and from 0.05 to 0.02 for II at 35—92 °C.

Order of Reaction. The formation rates of I, II, and III were defined as $dC_i/d\theta$, where θ denotes the reaction time (hr) and where C denotes the concentration of a product, i; i=1, 2, and 3 indicates I, II, and III. Each rate at $\theta=0$ was plotted against the initial concentration of IV (C_0) in Fig. 2. The initial rate for each product is proportional to C_0 when C_0 is less than 0.66 mol/l. Consequently, the rates will be first-order with respect to the concentration of IV; $dC_i/d\theta=k_iC$. C denotes the concentration of IV, and k_i denotes a rate constant. The effect of the concentration of AcOH on the rates was regarded as constant, because the initial mole ratio of AcOH to IV was 28: 1 to 19: 1. The conversion-time curve for each product could be approximated to a straight line when the total conversion of IV was less than 10 mol%.

Effect of H_2SO_4. In Fig. 3, the log k_i values are plotted against log C', where C' is defined by the amount of H_2SO_4 used as a catalyst and not by the amount of the "H_2SO_4 molecule" in the reaction medium. From the linear correlation with a slope of 1.0 in Fig. 3, every k_i is proportional to C'.

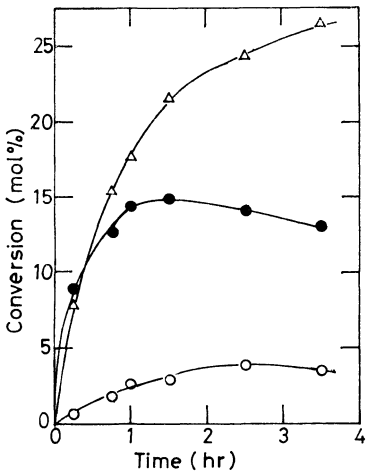

Fig. 1. Conversion-time curves of IV for I (●), II (○), and III (△) with H_2SO_4 3.68×10^{-3} mol/l and limonene 0.540 mol/l at 55 °C.

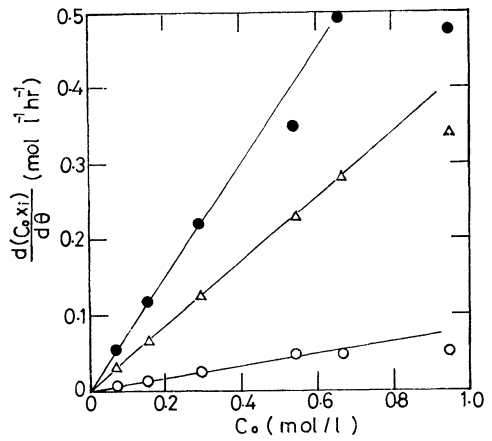

Fig. 2. Correlation between initial rate and initial concentration of limonene with H_2SO_4 2.27×10^{-2} mol/l and AcOH 15.0 mol/l at 35 °C. ●, I; ○, II; △, III.

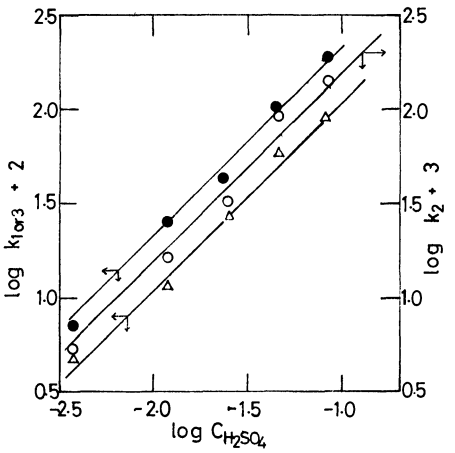

Fig. 3. Correlation between log $C_{H_2SO_4}$ and log k_i with limonene 0.606 mol/l and AcOH 15.0 mol/l at 28 °C. ●, I; ○, II; △, III.

TABLE 1. KINETIC DATA

Products	E_i (kcal/mol)	A_i[a] (hr^{-1})
α-terpinyl acetate	10.9	8.90×10^6
β-terpinyl acetate	10.9	6.91×10^5
isomers of limonene	13.7	5.24×10^8

a) The values are at $C'=3.68\times10^{-3}$ mol/l and AcOH: 15.01 mol/l.

Apparent Activation Energies and Pre-exponential Factors. The apparent activation energies (E_i) and the pre-exponential factors (A_i) shown in Table 1 were determined from the Arrhenius plots in Fig. 4. Here, the E_i values for I and II are the same, while the E_3 value for the III isomers is higher than they. This suggests that the mechanism of the formation of III may be different from that of the acetates (I and II), which have the same mechanism and rate-determining step.

The selectivity to form I against II depends entirely on the A_i's; $A_1/A_2\approx13$ from Table 1. This may be interpreted by considering the relative reactivity of the double bonds in the isopropenyl group and in the hexene

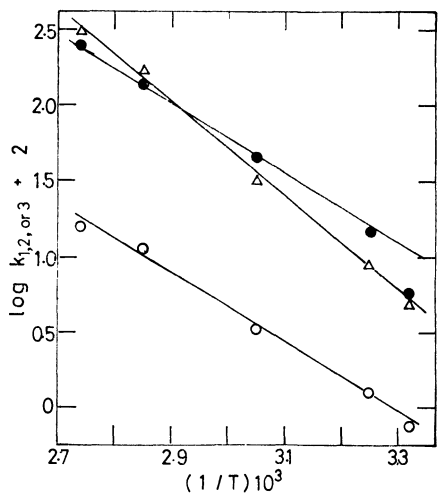

Fig. 4. Arrhenius plots for I (●), II (○), and III (△) with H_2SO_4 3.68×10^{-3} mol/l, limonene 0.540 mol/l and AcOH 15.0 mol/l.

ring of IV. On the other hand, the $A_3/(A_1+A_2)\approx 55$ ratio may be interpreted in terms of the difference between the mechanisms.

Discussion

Isomerization of IV. Bates *et al.* and many other investigators have interpreted the acid-catalyzed isomerizations of *p*-menthadienes in terms of a carbonium-ion mechanism.[4] The isomerization of IV to form III, namely, 1,3-*p*-menthadiene, 2,8-*p*-menthadiene, and 1,4-*p*-menthadiene, will be interpreted to proceed *via* carbonium ions in a similar scheme.

Carbonium ions are also formed by the elimination of the AcO^- anion from the acetates (I and II), as well as by the protonation of IV, which sometimes become isomerized products (III) or resin. The elimination of the AcO^- anion is supported by the decrease in the concentration of I and II after the maxima are reached.

In the isomerization of IV, the rate-determining step is the step of forming carbonium ions from a protonated double bond:[4,5]

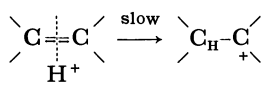

where H_2SO_4 acts as a specific hydrogen-ion catalyst. Therefore, the isomerization rate (also k_3) is proportional[5] to the acidity function, h_0[9], of the medium rather than to $C_{AcOH_2^+}$.

The acidity function, h_0, of H_2SO_4 in a water–AcOH solution has been related to C' by George *et al.*[6] The following relation was obtained from their data, where C' is less than 2.52 mol/l and where the water content is less than 0.99 wt%:[6] $h_0=(C')^{1.1}$. Here, h_0 indicates the ability of proton donation of an acid medium to weak, uncharged, indicator bases. This relation is applicable to estimating the h_0 in the present medium by assuming that h_0, the ability of proton donation to IV, is equal to, or at least proportional to, the h_0 to the indicator bases. Moreover, (1) the effect of IV and naphthalene on h_0 can be neglected, because their concentrations were less than 1 mol/l; (2) the trace of water contained with H_2SO_4 (98 wt%) and the other substances will make an amount not more than 1 wt% in the medium, and (3) C' is $(3.67—8.4)\times 10^{-2}$ mol/l. Consequently, the present h_0 value is nearly proportional to C', and the proportionality of k_3 to C' is observed.

Mechanism of the Acetates Formation. The addition of AcOH will proceed *via* $AcOH_2^+$ in the presence of a strong acid.[8] According to the facts that the formation rates of I and II are proportional to C' and have the same E_i, we propose the following mechanism, like the A-2-type solvolytic reaction defined by Hammett *et al*;[7]

$$HA + AcOH \rightleftharpoons (AcOH_2^+\ A^-) \rightleftharpoons AcOH_2^+ + A^-$$

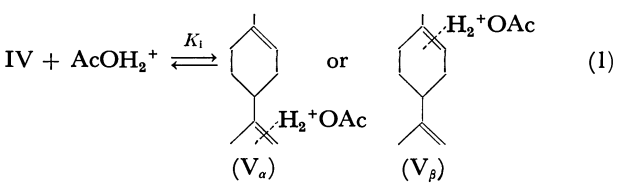

(1)

$$\left.\begin{aligned} V_\alpha &\rightleftharpoons X_\alpha^* \longrightarrow I \\ V_\beta &\rightleftharpoons X_\beta^* \longrightarrow II \end{aligned}\right\} \text{rate-determining step} \qquad (2)$$

where HA denotes H_2SO_4. This mechanism corresponds to one of the hypothetical mechanisms derived by Corriu *et al.* for the addition of AcOH to cyclohexene.[1] They also supposed the slow formation of a carbonium ion by the elimination of AcOH from a coordination product like V_α and V_β, and the subsequent, rapid addition of AcOH to the carbonium ion; the rate-determining step is the same as the isomerization. The present case cannot be explained by this mechanism, which suggests that $E_1=E_2=E_3$.

The observed activation energies, E_1 and E_2, correspond, respectively, to the sum of the heat of the reaction in Step (1) and the activation energy in the rate-determining step (2). Because E_1 and E_2 are the same in value, the structural changes to the activated complexes, X_α^* and X_β^*, from IV and $AcOH_2^+$ are considered to affect the change of the potential energies in almost the same way. The difference between A_1 and A_2 depends entirely on the difference between the overall changes in entropy from IV and $AcOH_2^+$ to the activated complexes.

In the above scheme, the formation rates of I and II are proportional to the concentration of the solvated proton ($AcOH_2^+$). In such a solvolytic acid-catalyzed reaction of the A-2 types, $C_{AcOH_2^+}$ can be a better measure of the acidity than the acidity function.[9] In fact, the effect of C' on rates other than *via* $C_{AcOH_2^+}$ is not significant considering the small dielectric constant and ionic strength in the AcOH medium,[8] and assuming an analogy between the activated complex (X^*) and $AcOH_2^+$ with respect to the charged part.[7] Consequently, it can be deduced that $C_{AcOH_2^+}$ is proportional to C' in the present medium.

Aspects of the Selectivity of the Acetates. From the above discussion, it must be noted that the similar proportionality shown in Fig. 3 for the AcOH addition and the isomerization is effected *via* two different mechanisms: k_1 and $k_2\propto C_{AcOH_2^+}\approx\gamma C'$, and $k_3\propto h_0\approx\delta C'$. ($\gamma$ and δ are defined as constants in the present medium.) This conclusion suggests that it is impossible to improve the selectivity of the acetates (I and II) against the isomers (III) by changing C', for an increase in C' beyond the present concentration will cause a remarkable increase in δ, while γ probably decreases or, at most, remains constant with an increase in C', as a result of the low dielectric constant of AcOH.[7,8] In fact, we obtained plenty of resin from IV by using the higher C' value than in the present study.

We wish to thank the Takasago Perfumery Co., Ltd., for its permission to publish this article.

References

1) R. Corriu, J. Guenzet, M. Camps, et C. Reye, *Bull. Soc. Chim. Fr.*, **1970**, 3679.

2) Y. Matsubara, K. Tanaka, M. Urata, and M. Kuwata, *Proc. of 17th Congr. on Perfumery, Terpene, and Essential Oil Chemistry*, Okayama, 1973, 2T 710.

3) Y. Matsubara, T. Fujiwara, and K. Tanaka, *Yuki Gosei Kagaku Kyokai Shi*, **31**, 924 (1973).

4) P. B. Bates, E. S. Caldwell, and H. P. Klein, *J. Org. Chem.*, **34**, 2615 (1969).
5) R. W. Taft, Jr., *J. Amer. Chem. Soc.*, **74**, 5372 (1952).
6) S. T. Valenta and J. George, Thesis ("Acidity Function Values of the Four Acids—Perchloric, Surfuric, *p*-Toluenesulfonic and Camphorsulfonic—in Acetic Acid Solutions"), St. Louis Univ., 1962.
7) a) F. A. Long and M. A. Paul, *Chem. Rev.*, **57**, 935 (1957). b) L. Zucker and L. P. Hammett, *J. Amer. Chem. Soc.*, **61**, 2791 (1939).
8) I. M. Kolthoff and S. Bruckenstein, *ibid.*, **78**, 1 (1956).
9) L. P. Hammett and A. J. Deyrup, *ibid.*, **54**, 2721 (1932).

The Radiation Synthesis of Hydrogen Cyanide from the Nitrogen-ethylene System. The Effect of Fission-fragment Irradiation

Yasumasa IKEZOE and Shoichi SATO

Japan Atomic Energy Research Institute, Tokai-mura, Ibaraki-ken, 319-11

(Received May 30, 1975)

Upon irradiation by (FF+n+γ), the G(HCN) value from the nitrogen–ethylene system increased with the rise in the pressure, while upon γ and (n+γ) radiations it decreased. This pressure effect was explained in terms of the high concentration of the active species in the FF tracks. At a high pressure, Reaction (5) is considered to take place in the tracks;

$$N_2^+ + e^- \longrightarrow 2N \quad (5)$$

At low pressures, Reaction (6) predominates, as in the γ-ray radiolysis, over Reaction (5) even in the FF tracks,

$$N_2^+ + C_2H_4 \longrightarrow N_2 + C_2H_4^+ \quad (6)$$

and nitrogen molecule cations do not contribute to the formation of hydrogen cyanide.

Hydrogen cyanide is formed from the nitrogen–ethylene system by ionizing irradiation.[1-3] In a previous paper,[2] it was shown that both nitrogen atoms and excited nitrogen molecules were the precursors of hydrogen cyanide in the γ radiolysis.

In the present investigation, the hydrogen-cyanide formation was studied by means of ^{60}Co γ-rays and mixed reactor radiations (n+γ) and by fission-fragment (FF) radiation. The pressure dependence of the G(HCN) value by the FF irradiation differed significantly from that of the G(HCN) value by γ and (n+γ) irradiation. A new mechanism is proposed for the hydrogen-cyanide formation upon the FF irradiation, which is closely related to the structure of the FF tracks.

Experimental

Premixed gas (C_2H_4; 5.25% in N_2, pure gas mixed by Takachiho Chemical) and ethylene (Takachiho research grade, 99.9%) were used as reactant gases without further purification. A stainless steel capsule (inner vol., 43 ml) with a rupture plate at one end was used as the irradiation vessel. The capsule was washed successively with trichloroethylene, ethanol, and hot distilled water, and then vacuum dried. After evacuating the capsule to a vacuum of 5×10^{-3} Torr and purging three times with the reactant gas, a known amount of the gas was charged in the capsule, the pressure being measured by means of a stainless steel Bourdon gauge.

Irradiations were carried out by γ-rays from a 45 kCi ^{60}Co source or by means of reactor mixed radiations with or without an FF source in the Low Temperature Fissiochemical Loop (LTFL).[4] Without the FF source, neutrons and γ-rays, (n+γ), were absorbed by the reactant. With a piece of thin U-Pd alloy foil[5] set at the center of the capsule, the reactant was irradiated by fission fragments, neutrons, and γ-rays, (FF+n+γ). The absorbed dose was determined both by means of a gaseous chemical dosimeter[6] and by calculation using the data of the neutron flux and the average range of an FF in the gas.[7] The resultant dose rates were 0.9 Mrad/h (γ-rays), 5 Mrad/h (n+γ),[8] and 12—40 Mrad/h (FF+n+γ),[9] depending on the amount of the U-Pd alloy foil. The hydrogen cyanide formed was measured by the titration method using a 10^{-4} M mercuric nitrate solution, using copper diethyldithiocarbamate as an indicator.[2] The yields were measured at doses from 5 to 8 Mrad. The G(HCN) value was determined on the basis of the energy absorbed by nitrogen.

Results and Discussion

The Pressure Dependence of G(HCN). In the previous paper,[2] the G(HCN) value upon γ-ray irradiation was found to decrease with the rise in the total pressure from 0.05 to 1.5 atm. In this study, the pressure dependence of the G(HCN) value was examined on three radiations, γ, (n+γ), and (FF+n+γ). The results are shown in Fig. 1.

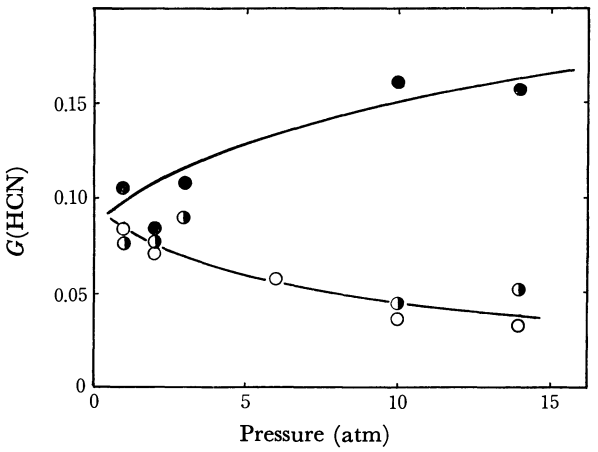

Fig. 1. Pressure effect on $G_{FFn\gamma}$, $G_{n\gamma}$, and G_γ.
N_2; 94.75%, C_2H_4; 5.25%, 43 ml stainless steel capsule, 5—8 Mrad. ●; $G_{FFn\gamma}$, 12—40 Mrad/h. ◑; $G_{n\gamma}$, 5 Mrad/h. ○; G_γ, 0.9 Mrad/h.

The G(HCN) values obtained by γ and by (n+γ) (G_γ and $G_{n\gamma}$, hereafter) decreased from 0.08 to 0.04 with the rise in the total pressure from 1 to 14 atm. This pressure dependence can be explained by the mechanism which was proposed previously[2] for the hydrogen cyanide formation in the γ-ray radiolysis:

$$N_2 \rightsquigarrow N, N_2^+, N_2^*, e^- \quad (1)$$

$$N_2^* \longrightarrow 2N \quad (2)$$

$$N_2^* + M \longrightarrow N_2 + M \quad (3)$$

$$N + C_2H_4 \longrightarrow HCN + CH_3 \quad (4)$$

The formation of nitrogen atoms by Reaction (2) is suppressed by the competitive Reaction (3) with a rise in the total pressure, resulting in a lowering of the

G(HCN) value.

The pressure dependence of the G(HCN) value upon (FF+n+γ) irradiation, $G_{FFn\gamma}$, differed distinctly from those of G_γ and $G_{n\gamma}$. The experimental $G_{FFn\gamma}$ value increased from 0.10 to 0.15 in the same pressure range. However, the ratio of the FF energy to the total energy was not exactly constant.[9] Therefore, for further discussion, the G(HCN) value obtained solely with FF, G_{FF}, was obtained by Eqs. (1) and (2), assuming that the experimental $G_{FFn\gamma}$ value is the mean value of the G_{FF} and $G_{n\gamma}$, weighted with the absorbed energies of the FF and (n+γ):

$$G_{FFn\gamma} = G_{FF}\varepsilon_{FF} + G_{n\gamma}\varepsilon_{n\gamma} \quad (1)$$

$$\varepsilon_{FF} + \varepsilon_{n\gamma} = 1 \quad (2)$$

where ε_{FF} or $\varepsilon_{n\gamma}$ is the ratio of the absorbed dose of FF or (n+γ) to the total dose. The $G_{n\gamma}$ value observed and the G_{FF} value thus calculated are shown in Table 1.

Table 1. Effect of pressure on G_{FF} and $G_{n\gamma}$[a]

Pressure (atm)	1	3	10	14
$G_{n\gamma}$ (observed)	0.08	0.09	0.05	0.05
G_{FF} (calculated)[b]	0.11	0.12	0.22	0.23

a) Absorbed dose; 5—8 Mrad, N_2; 94.75%, C_2H_4; 5.25%, 43 ml stainless steel capsule. b) Calculated by Eq. (1) in the text.

At 1 atm, the G_{FF} value, 0.11, is nearly equal to the $G_{n\gamma}$ value, 0.08, while at 14 atm the G_{FF} value is four times as large as the $G_{n\gamma}$ value. This pressure dependence of the G_{FF} value indicates that a quite different mechanism of the hydrogen-cyanide formation must be considered under the FF irradiation.

FF Tracks. According to Mozumder's model,[10] it is possible to detetmine the core radius and the temperature of the FF tracks in a condensed medium; the core radius is given by the impulse principle of Bohr or by the range of 100 eV electrons. In the gas phase, however, the latter is always longer than the former. By use of the model, the core radius of this system may be regarded as equal to a range of 100 eV electrons.

The concentration of the active species and the temperature in the tracks can be estimated if the core radius is determined. These values at 1 and 10 atm are shown in Table 2.

Table 2. FF tracks[a]

Pressure p (atm)	Core radius r (Å)	Temperature elevation ΔT (°C)	Concentration of active species: $C_{N_2^+=C_e^-}$ (cm^{-3})	$C_{N_2^*}$ (cm^{-3})	C_N (cm^{-3})
1	1.2×10^4	0.2	2.6×10^{13}	4.4×10^{13}	4.4×10^{12}
10	1.2×10^3	15.1	2.6×10^{16}	4.4×10^{16}	4.4×10^{15}

a) Calculated in Appendix.

Chemical Reaction in the Core. The concentrations of active species in the core are several orders of magnitude higher than those of the γ-ray radiolysis (see Appendix). Because of this local high concentration of active species, the recombination of a nitrogen molecule cation[11-13] with an electron may be assumed in the FF track core:

$$N_2^+ + e^- \longrightarrow 2N \quad (5)$$

By Reaction (5), two kinds of nitrogen atoms, N(^{4}S) and N(^{2}D), are formed mainly,[14] and each state of the nitrogen atom is known to react with ethylene to form hydrogen cyanide[15,16], according to Reaction (4).

In the γ-ray radiolysis, the charge on a nitrogen cation is transferred to an ethylene molecule, and no contribution is expected to the hydrogen cyanide formation:

$$N_2^+ + C_2H_4 \longrightarrow N_2 + C_2H_4^+ \quad (6)$$

In the FF radiolysis, Reactions (5) and (6) can compete with each other. The rates of the two reactions in the track core were calculated at 1 and 10 atm, as is shown in Table 3. At 1 atm, Reaction (5) is much slower than Reaction (6) even in the track core, and Reaction (5) can be neglected, as in the γ-ray radiolysis. At 10 atm, however, Reaction (5) predominates over Reaction (6), resulting in the formation of excess nitrogen atoms. The higher the total pressure, the more excess nitrogen atoms are formed in the core by this mechanism. This is in qualitative agreement with the experimental results (Table 1).

Table 3. Reaction rate in the track core

Pressure (atm)	rate of reaction (5);[a] $N_2^+ + e^- \rightarrow 2N$ (cm$^{-3}\cdot$s^{-1})	rate of reaction (6);[b] $N_2^+ + C_2H_4 \rightarrow N_2 + C_2H_4^+$ (cm$^{-3}\cdot$s^{-1})
1	2.0×10^{20}	1.0×10^{22}
10	2.0×10^{26}	1.0×10^{26}

The concentrations of N_2^+ and e^- are given in Table 2. The ethylene concentration is 1.2×10^{18} and 1.2×10^{19} cm^{-3} at 1 and 10 atm (5% C_2H_4 in N_2).
a) Rate constant of reaction (5); $k_5=3\times10^{-7}$ cm$^3\cdot$s^{-1}.[16] b) Rate constant of reaction (6); $k_6=3\times10^{-10}$ cm$^3\cdot$s^{-1}, is estimated from similar reactions.[19]

The Role of Ethylene Molecules. The effect of the ethylene concentration on the $G_{FFn\gamma}$ value was studied in order to clarify the role of ethylene molecules in the formation of hydrogen cyanide upon the FF irradiation. If the mechanism of hydrogen-cyanide formation

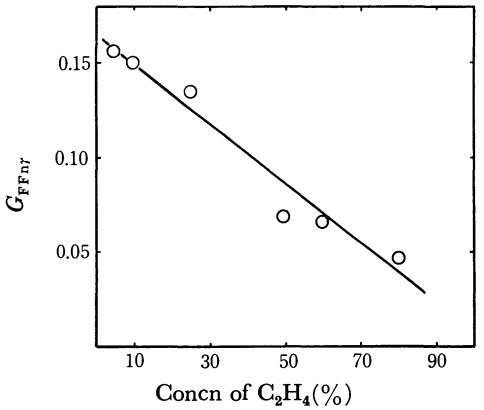

Fig. 2. Effect of ethylene concentration on $G_{FFn\gamma}$.[a] (FF+n+γ); 12 Mrad/h, 6.8 Mrad, ε_{FF}; 0.66, N_2+C_2H_4; 14 atm in 43 ml stainless steel capsule.
a) The G(HCN) value was calculated on the basis of the energy absorbed by nitrogen.

proposed above holds, the G(HCN) value should decrease with the rise in the ethylene concentration because of Reaction (6).

As is shown in Fig. 2, the G(HCN) value actually decreased with the ethylene concentration. Thus, this mechanism is again in agreement with the experimental results.

Local Temperature Effect. Since a small increase in the G_r value has been observed upon reaction-temperature elevation at a low total pressure,[2] the effect of the local temperature rise within the FF track core might be expected on the G_{FF} value also at the high total pressure studied. The measured G_r value was indeed found to increase as the temperature was raised, as is shown in Fig. 3. However, the increase was not large enough to explain the high G_{FF} value obtained. The G_r values were 0.04 and 0.07 at 40 and 400 °C respectively.

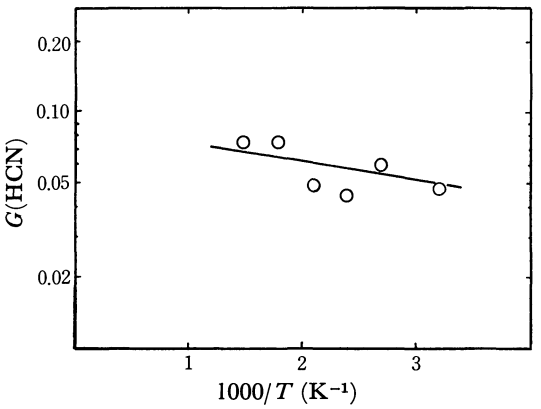

Fig. 3. Arrhenius' plot of G_r.
γ-rays; 0.9 Mrad/h, 4.3 Mrad. N_2; 15.1 g/l, C_2H_4; 5.25% in N_2.

The temperature effect in this system can be neglected because of the small increase in the G_r value with the reaction temperature elevation and because of the low temperature rise in the track cores (Table 2).

Appendix

Radius and Temperature of the Track Cores.[10] The radius of the FF track cores in this system is given by this equation: $r=r_0\rho_0/\rho$, where r_0 is the range of 100 eV electrons in water (15 Å), ρ_0 and ρ, the desities of water and the reactant gas. The temperature rise in the cores is given by this equation: $\Delta T=S/\pi C_v r^2$, where S is the energy loss per unit length (0.4 eV/Å$=0.64\times10^{-11}$ J/cm at 1 atm,[17] and 4 eV/Å$=6.4\times10^{-11}$ J/cm at 10 atm), and C_v, the specific heat at a constant volume (0.75 J/deg·g). Thus, $\Delta T=0.2$ and 15.1 °C at 1 and 10 atm.

Concentrations of Active Species in the Cores. The concentration of an active species, C_A, is given by this equation: $C_A=Sg_A/100\pi r^2$, where g_A is the initial G(A) value. Using appropriate g_A value ($g_{N_2^+}=g_{e^-}=3$, $g_{N_2^*}=5$, and $g_N=0.5$[8]), the concentrations of these active species are found to be as is shown in Table 2. The ratio is $(N)/(N_2)=1.8\times10^{-7}$ at 1 atm. This value is several orders of magnitude greater than the corresponding one in the γ-ray radiolysis (0.9×10^{-13}).[2]

The authors wish to acknowledge the technical assistance in the sample preparation and irradiation provided by Messrs. T. Kobayashi, S. Shimizu, and H. Nakajima of the authors' Institute, and the valuable guidance afforded by Professors K. Oshima and Y. Tabata of the University of Tokyo and Professor A. Danno of Kagoshima University. Discussions with Professor S. Sato of the Tokyo Institute of Technology are also gratefully acknowledged.

References

1) T. Oka, R. Kato, S. Sato, and S. Shida, This Bulletin, **41**, 2192 (1968); T. Oka, Y. Suda, and S. Sato, *ibid.*, **42**, 3083 (1969).
2) Y. Ikezoe, S. Sato, and A. Danno, *ibid.*, **46**, 1154 (1973).
3) A. T. Podkhalyuzin, A. E. Trishkin, and I. V. Vereshchinskii, *Int. J. Radiat. Phys. Chem.*, **5**, 3 (1973).
4) S. Sato, N. Moriyama, Y. Ikezoe, T. Ishii, M. Hirata, Y. Yamazaki, A. Danno, and K. Oshima, *J. Nucl. Sci. Technol.*, **10**, 379 (1973).
5) The uranium–palladium alloy foil used in this work was given to our group by the courtesy of Messrs. B. Manowitz and M. Steinberg of the Brookhaven National Laboratory. The foil contained 0.503 mg $^{235}U/cm^2$ foil, and the 2.1 μm-thick alloy layer was covered on both sides with 0.2 μm-thick platinum layers.
6) Y. Ikezoe, S. Sato, and A. Danno, *J. Nucl. Sci. Technol.*, **8**, 394 (1971); S. Sato, N. Moriyama, Y. Ikezoe, and A. Danno, *ibid.*, **11**, 141 (1974).
7) S. Sato, N. Moriyama, Y. Ikezoe, S. Shimizu, T. Kobayashi, Y. Yamazaki, and A. Danno, JAERI-M 4717 (1972).
8) The (n+γ) rays (total, 5.0 Mrad/h) were constituted of γ-rays (4.1 Mrad/h), fast neutrons (*ca.* 0.01 Mrad/h), and protons arising from the nuclear reaction of thermal neutons, $^{14}N(n,p)^{14}C$ (0.9 Mrad/h).
9) In the case of (FF+n+γ) irradiation, the area of the foil was determined so that the ratio of the absorbed dose by FF to the total dose, ε_{FF}, fell in a relatively narrow range, 0.60—0.87.
10) A. Mozumder, "Advances in Radiation Chemistry," Vol. 1, ed. by M. Burton and J. Magee, Wiley-Interscience, New York (1969), p. 1; A. Mozumder, A. Chatterjee, and J. L. Magee, "Radiation Chemistry," Vol. 1, Advances in Chemistry Series, No. 81, American Chemical Society, Washington (1968), p. 27.
11) Because of the fast clustering reaction: $N_2^+ + 2N_2 \rightarrow N_4^+ + N_2$ ($k=6\times10^{-29}$ cm^{-6} s^{-1}), the recombination of both N_2^+ and N_4^+ with electrons may be considered. Also, the formation of N atoms by the recombination of N_4^+ with an electron is energetically possible because of the low binding energy of N_2^+ with N_2 (0.5 eV).[12] However, the equilibrium concentration of N_4^+ is presumably lower than that of N_2^+, as was estimated in the case of O_2^+—O_4^+.[13]
12) R. N. Varney, *J. Chem. Phys.*, **31**, 1314 (1959).
13) K. Fueki and J. L. Magee, *Discuss. Faraday Soc.*, **36**, 21 (1963).
14) C. S. Warke, *Phys. Rev.*, **144**, 120 (1966).
15) J. Dubrin, C. MacKay, and R. Wolfgang, *J. Chem. Phys.*, **44**, 2208 (1966).
16) A. N. Wright and C. A. Winkler, "Active Nitrogen," Academic Press, New York (1968), p. 68 and 121.
17) R. D. Evans, "The Atomic Nucleus," McGraw-Hill Book Co., New York (1967), p. 668.
18) S. Dondes, P. Harteck, and C. Kunz, *Z. Naturforsh.* **19a**, 6 (1964).
19) E. W. McDaniel, V. Čermák, A. Dalgarno, E. E. Ferguson, and L. Friedman, "Ion-Molecule Reactions," Wiley-Interscience, New York (1970), p. 325.

The Synthesis and Ion-exchange Properties of $TiH_2(PO_4)_2 \cdot 1/2H_2O$

Etsuro KOBAYASHI

National Chemical Laboratory for Industry, Hon-machi, Shibuya-ku, Tokyo 151

(Received November 28, 1974)

In order to develop an ion-exchanger for industrial use, a new compound, titanium dihydrogen bis (phosphate) hemihydrate, was prepared by means of a reflux between titanium phosphate and concentrated phosphoric acid; then the conditions of synthesis and the ion-exchange properties of the products were investigated. The amorphous titanium phosphate used as the starting material was formed by the reaction of titanium tetrachloride with phosphoric acid in diluted hydrochloric acid. The phase equilibrium of the TiO_2–P_2O_5–H_2O system has been studied at the refluxing temperatures of the mother liquors. The solid phase in equilibrium with the mother liquor containing 13—64% P_2O_5 had the components of TiO_2 (29—32%), P_2O_5 (53—54%), and H_2O (15—16%); its composition was $TiH_2(PO_4)_2 \cdot H_2O$, which had already been known, but the solid phase in equilibrium with the mother liquor containing more than 64% P_2O_5 had as components TiO_2 (31—32%), P_2O_5 (57—58%), and H_2O (10—11%); therefore, its composition corresponded to $TiH_2(PO_4)_2 \cdot 1/2H_2O$. The X-ray diffraction pattern of this compound was entirely different from that of monohydrate, and some large *d*-values were recognized. From the DTA and TGA, the processes of the dehydration of monohydrate and hemihydrate were also different from each other; however, both compounds were converted to titanium pyrophosphate (TiP_2O_7) at 800 °C. $TiH_2(PO_4)_2 \cdot H_2O$ can adsorb sodium ions, but the ions of a large radius, such as potassium and cecium, are not adsorbed. In contrast to this, $TiH_2(PO_4)_2 \cdot 1/2H_2O$ had an excellent ion-exchange property; its ion-exchange capacities were 4.0 meq/g to K^+ and 2.0 meq/g to Cs^+ at pH 4. These capacities were about eight times those of monohydrate. The solubilities of the phosphate used as an ion-exchanger were remarkably low. Therefore, the titanium dihydrogen bis (phosphate) hemihydrate thus obtained may be utilized as a useful inorganic ion-exchanger for potassium and cesium ions.

The phosphates of poly-valence metals such as chromium,[2] zirconium,[3] and tin,[4] have hitherto been known as inorganic ion-exchangers. In order to develop an inorganic ion-exchanger capable of recovering potassium from sea water, we have previously investigated the ion-exchange characters of magnesium, calcium, aluminium, and iron phosphate,[5] further synthesized iron trihydrogen bis (phosphate), which was fairly stable to phosphoric acid as a regenerant of the exchanger, and examined its ion-exchange character.[6] The phosphates of bivalent and trivalent metals, however, generally do not have enough stability to be good inorganic ion-exchangers.

In the present work, titanium phosphate, which is an economical raw material, has been examined. Titanium phosphates with the composition of $3TiO_2 \cdot P_2O_5 \cdot xH_2O$ ($x=1, 3, 6$) are already known.[7] Also, crystalline titanium hydrogen phosphate with the composition of $TiH_2(PO_4)_2 \cdot H_2O$ was prepared by the reflux of amorphous titanium phosphate with phosphoric acid at the boiling point, and its ion-exchange property was examined.[8] This compound showed a higher resistance to hydrolysis than the amorphous titanium phosphate; it adsorbed Li^+ and Na^+, but not the ions of a large radius, such as K^+ and Cs^+. Therefore, this crystalline titanium hydrogen phosphate is not suitable as an industrial ion-exchanger. Recently, titanium phosphate with the composition of $(TiO)_{0.535}(HPO_4)_{0.639}(OH)_{0.17} \cdot aq.$ was synthesized, and it could recover cesium in radioactive waste materials.[9] The molar ratio of Ti to P in this non-stoichiometric compound is larger than that in the above crystalline titanium phosphate, so it may be supposed that this compound is lacking in chemical resistance to an acidic eluent. Titanium phosphate-silicate for the separation of radioactive materials was also synthesized.[10] In the study of the TiO_2–P_2O_5–H_2O system at 20 °C, $Ti(OH)PO_4 \cdot 2H_2O$ and $TiH_2(PO_4)_2$ existed as solids in the system.[11] However, in the general method of preparing inorganic ion-exchanger by the reflux of amorphous phosphate with phosphoric acid, the data of the above equilibrium system cannot be applied to the preparation because of the difference between the refluxing temperature and room temperature.

When the phase equilibrium of the Fe_2O_3–P_2O_5–H_2O system was examined,[6] the existence of several kinds of iron hydrogen phosphate was known. In the present work, it is supposed that titanium hydrogen phosphate, as the solid phase of the equilibrium to concentrated phosphoric acid, also exists in the TiO_2–P_2O_5–H_2O system. From the results of the phase equilibrium on the reflux of amorphous titanium phosphate with phosphoric acids of various concentrations, it is known that $TiH_2(PO_4)_2 \cdot 1/2H_2O$, which differs in its molar ratio of the water of crystallization, is present. The X-ray diffraction pattern of this compound was entirely different from that of $TiH_2(PO_4)_2 \cdot H_2O$, and large *d*-values were noticed in it. The investigation of its ion-exchange properties showed this salt to have an adsorption capacity to ions of a larger ionic radius, such as K^+ and Cs^+. In this paper, an experimental study of the preparation of titanium dihydrogen bis (phosphate) hemihydrate and its ion-exchange properties will be described.

Experimental

Synthesis. Amorphous titanium phosphate, used as the raw material, was initially prepared in the following way: 800 ml of 2 M HCl placed in a beaker and mixed with 50 g of $TiCl_4$ solution. To this was slowly added 800 ml of 1.45 mol/l H_3PO_4, while simultaneously the mixture in the beaker was vigorously stirred at room temperature. Thus, amorphous titanium phosphate was precipitated. This was allowed to

stand overnight and then separated from the mother liquor by the use of a centrifugal separator. The product was washed with distilled water, centrifugally separated from the wash liquid, and finally vacuum-dried over phosphorus pentoxide for 24 h.

Crystalline titanium phosphate was prepared in the following way: 10 g of amorphous titanium phosphate, prepared previously, was placed in a Kjeldahl flask and mixed with 150—180 ml of phosphoric acid of an appropriate concentration. The mixture was kept at a proper temperature by the evaporation of a little water, and then heated at its boiling point for 12—36 h after the reflux condenser had been connected to the flask. Immediately the resulting precipitate was separated centrifugally from the mother liquor. To the precipitate alcohol or acetone was added, and the mixture was vigorously shaken up; then the precipitate was separated from the wash liquid by using the centrifugal separator. The product thus obtained as the precipitate was washed enough by repeating this procedure several times, and finally it was vacuum-dried over phosphorus pentoxide for 24 h.

Analysis. P_2O_5: A 0.5 g portion of the product was weighed exactly and then refluxed with 50 ml of 1 M NaOH in a stainless steel flask for 60 min. The amorphous precipitate obtained by this treatment was separated from the mother liquor by filtration and washed sufficiently with hot water. The mother liquor and wash liquid were put together, and the volume of the solution was adjusted to 250 ml. The phosphorus content was determined gravimetrically as magnesium pyrophosphate.

TiO_2: A 0.1 g portion of the product was weighed exactly and then refluxed with 10 ml of 18 M H_2SO_4 and 5 g of $(NH_4)_2SO_4$ in a Kjeldahl flask until it had dissolved completely. The volume of the sample solution was then adjusted to 250 ml with distilled water. 10 ml of 9 M H_2SO_4 and 10 ml of 3% H_2O_2 were added to a 25 ml portion of the diluted solution; the meta-titanic acid peroxide thus turned yellow. The titanium content was determined colorimetrically at 420 nm. The content of TiO_2 in titanium phosphate was also derived as follows:

$$100\% - (P_2O_2)\% - (H_2O)\% = (TiO_2)\%$$

H_2O: A 0.2 g portion of the product was weighed exactly and then heated in an electric furnace regulated to 800 °C for about 2 h until it had reached a constant weight. In this case, the weight loss corresponds to the water content of the product. The water content was also given by thermal gravimetric analysis.

The Components in the Liquid Phases: Exactly a 10 ml portion of the mother liquor was taken, and the specific gravity was measured. The volume of the sample solution was adjusted to 250 ml. A 100 ml portion of the diluted solution was neutralized with a sodium hydroxide solution. The white precipitate thus obtained was separated from the mother liquor and washed with hot water. The TiO_2 content was determined gravimetrically by the calcination of the precipitate. On the other hand, the mother liquor and wash liquid were put together, and the volume of the solution was adjusted to 250 ml. The P_2O_5 content was determined gravimetrically as magnesium pyrophosphate by using a portion of the solution.

X-Ray Diffraction Pattern: The X-ray diffraction pattern was obtained by using a Rigaku-Denki model 2001 diffractometer with Ni-filtered Cu$K\alpha$ radiation, with 20 KVP and 15 mA.

DTA and TGA: The differential thermal analysis (DTA) and thermogravimetric measurements (TGA) were performed simultaneously at a heating rate of 5 °C/min with a Rigaku-Denki model DC-C1-S thermal analyzer.

Ion-exchange Titration Curve: A 0.200 g portion of a product was placed in a 50 ml stoppered Erlemeyer flask, and 25 ml of the solution, mixed in the proper ratio of 0.1 M MCl to 0.1 M MOH (M=Na, K, Cs), was added to it. The contents in the flask were shaken up at times, and the pH of the solution was measured after 24 h. Then, the ion-exchange titration curve was drawn from the relations between the pH and the ion-exchange capacity, which was estimated from the mixed ratio of 0.1 M HCl to 0.1 M MOH.

Results and Discussion

Preparation of $TiH_2(PO_4)_2 \cdot H_2O$ and $TiH_2(PO_4)_2 \cdot 1/2H_2O$. The conditions of synthesizing crystalline titanium hydrogen phosphates and the results of the analysis of the products are summarized in Table 1.

Composition by Chemical Analysis: Amorphous titanium phosphate, with the composition of $1.9TiO_2$, P_2O_5, $3.7H_2O$, was used as the raw material. The reaction product No. 1, which was obtained by refluxing amorphous titanium phosphate with a suitable amount of 10%

Table 1. Synthesis and analysis of hydrogen titanium phosphates

No.	Reaction condition[a]					Reaction product				
	Temp. (°C)	Time (h)	Mother liquor (s.g)	P_2O_5%	TiO_2%	Washing liquid	TiO_2 (%)	P_2O_5 (%)	H_2O (%)	$TiO_2:P_2O_5:H_2O$ (Mole ratio)	Estimated formura
1	104	36	1.043	6.9	0.0	Acetone	35.9	41.2	22.9	1.55:1.00:4.39	(Non-crystal)
2	107	24	1.141	13.2	0.1	Acetone	32.3	55.2	14.9	1.04:1.00:2.13	$TiH_2(PO_4)_2 \cdot H_2O$
3	110	12	1.244	30.3	0.2	Acetone	28.8	54.6	16.6	0.94:1.00:2.38	$TiH_2(PO_4)_2 \cdot H_2O$
4	120	12	1.429	45.7	0.3	Ethanol	31.1	53.7	15.2	1.03:1.00:2.23	$TiH_2(PO_4)_2 \cdot H_2O$
5	144	12	1.652	56.1	0.4	Acetone	31.7	55.0	14.9	1.02:1.00:2.14	$TiH_2(PO_4)_2 \cdot H_2O$
6	160	12	1.648	58.8	0.4	Acetone	29.9	54.5	15.6	0.97:1.00:2.26	$TiH_2(PO_4)_2 \cdot H_2O$
7	165	12	1.670	62.0	0.3	Ethanol	31.9	52.6	15.5	1.08:1.00:2.34	$TiH_2(PO_4)_2 \cdot H_2O$
8	176	24	1.687	65.5	0.4	Ethanol	32.2	57.8	10.0	0.99:1.00:1.36	$TiH_2(PO_4)_2 \cdot 1/2H_2O$
9	176	36	1.712	66.1	0.3	Acetone	32.2	57.3	10.5	1.00:1.00:1.44	$TiH_2(PO_4)_2 \cdot 1/2H_2O$
10	170	30	1.687	64.5	0.4	Ethanol	30.9	58.0	11.1	0.95:1.00:1.51	$TiH_2(PO_4)_2 \cdot 1/2H_2O$
Raw material						Water–ethanol	42.9	40.2	18.9	1.90:1.00:3.71	

a) The mixture of amorphous titanium phosphate (raw material, 10) and phosphoric acid (150—160 ml) was refluxed under a certain condition.

phosphoric acid (P_2O_5, 7.3%) for 36 h, was still the non-crystalline powder. It could be expected that when phosphoric acid of a comparatively lower concentration was used, the reaction could not reach the equilibrium state even by means of a reaction at a refluxing temperature for a fairly long time. In the No. 2—7 products, which were equilibrium-solid phases with a 13—62% P_2O_5 content in the mother liquor, their compositions were found to be 29—32% TiO_2, 53—54% P_2O_5, and 15—16% H_2O, and its components corresponded to those of $TiH_2(PO_4)_2 \cdot H_2O$ known already. In the No. 8—10 products, which were equilibrium-solid phases with a P_2O_5 content of more than 64% in the mother liquor and at a refluxing temperature 170—180 °C, the compositions were found to be 31—32% TiO_2, 57—58% P_2O_5, and 15—16% H_2O. From these results, the expected composition was given as $TiH_2(PO_4)_2 \cdot 1/2H_2O$.

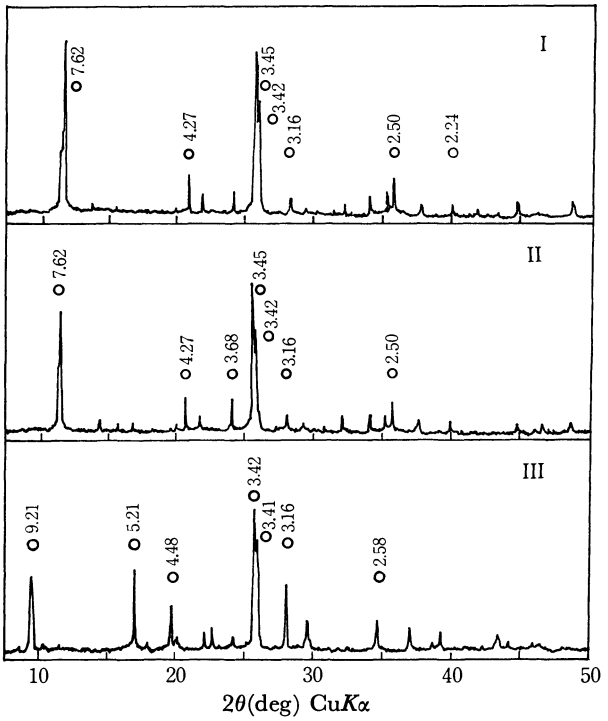

Fig. 1. X-Ray diffraction patterns of titanium hydrogen phosphates.
I: Product obtained by reflux in phosphoric acid of P_2O_5 13.2% at 107 °C for 24 h (No. 2). II: Product obtained by reflux in phosphoric acid of P_2O_5 58.8% at 160 °C for 12 h (No. 6). III: Product obtained by reflux in phosphoric acid of P_2O_5 66.1% at 176 °C for 36 h (No. 9).
Numerals near peaks indicate distance (Å) between planes in crystals.

X-Ray Diffraction Patterns: The X-ray diffraction patterns of the products, which are prepared in different concentrations of phosphoric acid in the mother liquor, are shown in Fig. 1. I and II are the X-ray diffraction patterns for monohydrate, known already. These diffraction data agreed almost entirely with those of the ASTM X-ray data cards and also with those of $TiH_2(PO_4)_2 \cdot H_2O$, prepared by Alberti *et al.*[8] III is the pattern for hemihydrate obtained by the reflux of amorphous titanium phosphate with concentrated phosphoric acid. In this diagram, diffraction lines newly appeared at the positions of 9.21, 5.21, 4.38 Å, *etc.* The X-ray diffraction values of hemihydrate were clearly different from those of monohydrate, as is shown in Table 2. For the formation of two crystalline titanium phosphates having a Ti/P atomic ratio of exactly 1.0, a fairly long time was needed, even at the reflux temperature. The course of the formation of hemihydrate by the reaction between amorphous titanium phosphate and concentrated phosphoric acid is shown in Fig. 2 by the X-ray diffraction patterns changing successively.

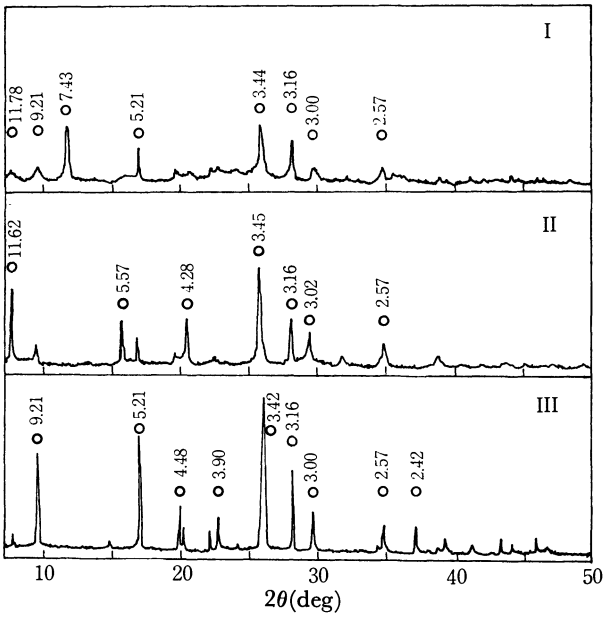

Fig. 2. X-Ray diffraction patterns on course of formation of modification titanium hydrogen phosphate.
I: Product obtained by reflux in phosphoric acid of 63.5% P_2O_5 at 176 °C for 5 h. II: Product obtained by reflux in phosphoric acid of 63.5% P_2O_5 at 176 °C for 12 h. III: Product obtained by reflux in phosphoric acid of 63.5% P_2O_5 at 176 °C for 24 h (No. 8).
Numerals near peaks indicate distance (Å) between planes in crystals.

When the concentration of phosphoric acid in the mother liquor was low, as has been mentioned above, the reaction product did not crystallize easily, so a slight crystallization of the product occurred upon refluxing for several hours, as is shown in I. It was observed from the X-ray patterns that a metastable crystalline product was produced by refluxing for 12 h at 176 °C and also by refluxing for a fairly long time at 170 °C. The X-ray diffraction pattern for this product is shown in II; in the diagram peculier diffraction lines appeared at 11.6 and 5.57 Å. The object, hemihydrate as a stable form, was obtained by refluxing for more than about 20 h at above 170 °C. The X-ray diffraction pattern of hemihydrate is shown in III.

Effect on the Concentration of Phosphoric Acid in the Mother Liquor: From the TiO_2–P_2O_5–H_2O system at the refluxing temperatures of the mother liquors, we ascertained the existences of $TiH_2(PO_4)_2 \cdot H_2O$ and $TiH_2(PO_4)_2 \cdot 1/2H_2O$ as the solid phase in the equilibrium

state to the mother liquor. If pyrophosphoric acid is contained in the liquid phase, it may be supposed, as a matter of course, that another solid phase appears. However, the pure phosphoric acid of P_2O_5 66% theoretically does not contain pyrophosphoric acid.[12] In fact, the existence of condensed phosphoric acids in this liquid phase was not observed by paper or ion-exchange chromatography. The amount of TiO_2 dissolved in the liquid phase was nearly zero when the concentration of phosphoric acid was low; it slightly increased with the increase in the concentration of phosphoric acid.

Change in Titanium Hydrogen Phosphate upon Heating. The DTA and TGA curves for two crystalline titanium phosphates are shown in Fig. 3. The X-ray diffraction values for some titanium phosphates previously registered on ASTM X-ray data cards, the products obtained in this work, and their heated products are summarized in Table 2. In the DTA curve for monohydrate (I), the broad endothermic peak at 70—100 °C seemed to be due to the elimination of water adhering to the crystal powder. It was confirmed from the X-ray diffraction, which characterized pyrophosphate in the heated product at 185 °C, that the endothermic peak at 210 °C was a result of the dehydration of the water of crystallization and the condensation. The endothermic peaks at 260 and 510 °C were also due to the condensation. However, the reason why these condensations take place progressively upon heating is not yet known. The behavior of the DTA and TGA curves for hemihydrate (II) differed from those of I, a dehydration gradually occurred from 100 °C to about 300 °C, and a weight loss corresponding to the weight of the water of crystallization of this salt was observed in this temperature range. Then a large endothermic peak, which was due to the condensation, appeared at 415 °C.

Table 2. X-ray diffraction data for titanium hydrogen phosphate, reaction product and its heating product

$TiH_2P_2O_8 \cdot H_2O$[a]	$H_2(Ti(PO_4))\cdot H_2O$[b]	Product No. 4	Product No. 8	Heating product of No. 4 or No. 8 (800 °C)	TiP_2O_7[c]
			11.47W		
			9.21M		
7.62 S	7.55 S	7.62 S			
			5.21 S		
4.62W			4.48M	4.57W	
4.27M	4.23W	4.27W	4.39W		4.20M
	4.02W	4.02W			
3.80M			3.90W	3.95 S	3.82 S
			3.71W		
		3.68W	3.66W		
3.44 S	3.44 S	3.45 S		3.53 S	3.45 S
	3.41M	3.42 S	3.42 S		
3.51W	3.15W	3.13W	3.16M	3.22M	3.15 S
	3.03W	3.05W	3.00W		
2.77M		2.76W		2.79W	
	2.61W	2.61W			
	2.53W	2.53W	2.57W		
2.59 S	2.49W	2.49W			
			2.42W		
2.38W	2.38W	2.38W		2.38W	
			2.29W		2.34M
2.24M	2.24M	2.24W			
2.16W	2.16W			2.18W	2.15W
			2.08W		
2.02W	2.02W	2.02W	2.04W		
1.96M	1.96W	1.96W	1.97W		
	1.94W	1.94W			
				1.91W	1.89M
1.87M	1.86W	1.87W		1.76W	1.74M
				1.61W	1.60M
				1.52W	1.50 S
				1.39W	1.38M

a) According to data on Deutsche Akad. der Wissensch., Berlin, Inst. f. Anorg. Chem. (1968). b) According to Michel and Weiss (1967). c) According to Levi and Peyronel (1935). These data were registered in ASTM X-ray data cards.

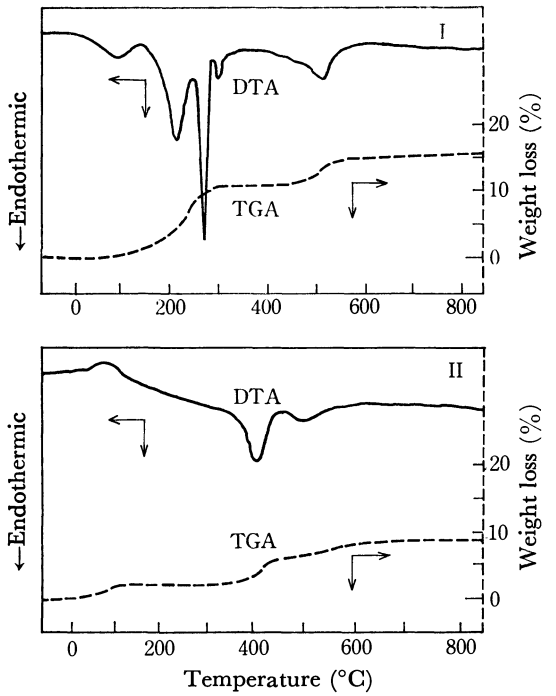

Fig. 3. DTA and TGA curves for titanium hydrogen phosphates.
I: Titanium hydrogen phosphate (No. 3). II: Modification titanium hydrogen phosphate (No. 8).
Sample: 200 mg, heating rate: 5 °C/min.

Hemihydrate and the product obtained by heating it at 185 °C for 2 h gave almost the same X-ray diffraction pattern. Therefore, at this heating temperature, pyrophosphate was not yet formed. However, the X-ray diffraction values of the heated products of monohydrate and hemihydrate at 800 °C were all the same, and these values agreed with the diffraction data of TiP_2O_7 registered on an ASTM X-ray data. It was also confirmed by means of chemical analysis that the two heated products both had the composition of $TiO_2 \cdot P_2O_5$.

Ion-exchange Properties of Titanium Hydrogen Phosphates. It has already been reported that the ion-exchange capacity of $TiH_2(PO_4)_2 \cdot H_2O$ showed values as high as

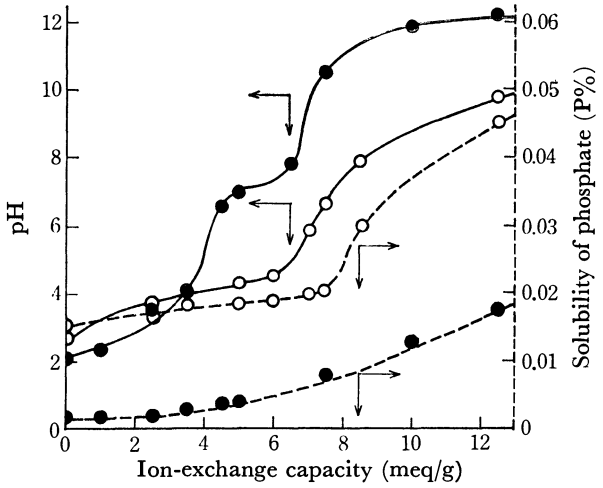

Fig. 4. Na ion-exchange titration curve and solubility of titanium hydrogen phosphates.
○: Titanium hydrogen phosphate, $TiH_2(PO_4)_2 \cdot H_2O$ (No. 3). ●: Modification titanium hydrogen phosphate, $TiH_2(PO_4)_2 \cdot 1/2H_2O$ (No. 8).
Ion-exchanger: 0.200 g, mixed solution of 0.1 mol/l NaOH and 0.1 mol/l NaCl: 25.0 ml.

~7 meq/g for Li^+ and Na^+, but ions with a large radius, such as K^+ and Cs^+, were scarcely adsorbed.[8] The $TiH_2(PO_4)_2 \cdot 1/2H_2O$ prepared in this work gave large *d*-values in the X-ray diffraction data. Therefore, it was supposed that there was a layer structure in the crystal and that, among the layers, various cations could be adsorbed.

Ion-exchange Capacities of Phosphates to Na^+: The sodium ion-exchange titration curves of monohydrate and hemihydrate and their solubilities are shown in Fig. 4. The ion-exchange capacities of monohydrate at pH 4 and 7 were 3.6 and 7.5 meq/g respectively; these capacities were the same as those previously reported.[8] On the other hand, the ion-exchange capacities of hemihydrate at pH 4 and 7 were 3.3 and 5.1 meq/g respectively. In an acid solution the solubility of the ion-exchanger was reduced by about one seventh as compared with that of monohydrate.

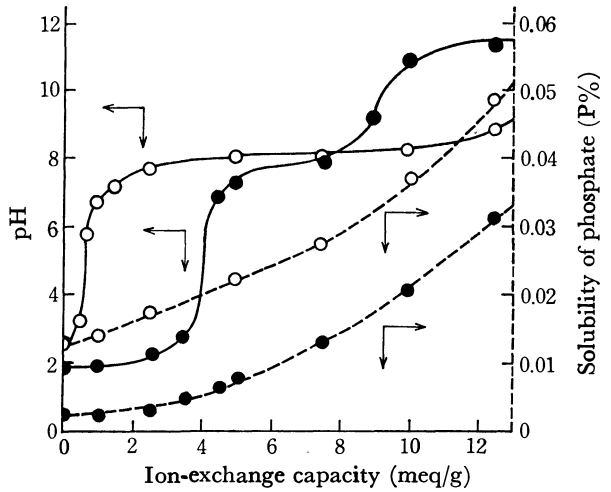

Fig. 5. K ion-exchange titration curve and solubility of titanium hydrogen phosphates.
○: Titanium hydrogen phosphate, $TiH_2(PO_4)_2 \cdot H_2O$ (No. 3). ●: Modification titanium hydrogen phosphate, $TiH_2(PO_4)_2 \cdot 1/2H_2O$ (No. 8).
Ion-exchanger: 0.200 g, mixed solution of 0.1 mol/l KOH and 0.1 mol/l KCl: 25.0 ml.

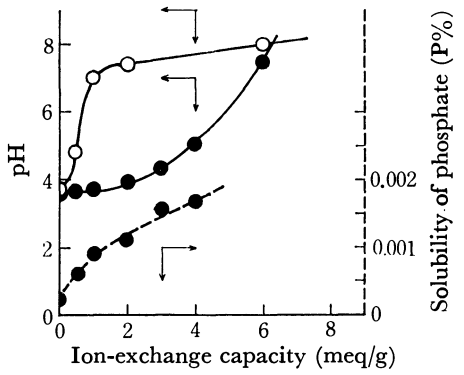

Fig. 6. Cs ion-exchange titration curve and solubility of titanium hydrogen phosphates.
○: Titanium hydrogen phosphate, $TiH_2(PO_4)_2 \cdot H_2O$ (No. 3). ●: Modification titanium hydrogen phosphate, $TiH_2(PO_4)_2 \cdot 1/2H_2O$ (No. 8).
Ion-exchanger: 0.200 g, mixed solution of 0.1 mol/l CsOH and 0.1 mol/l CsCl: 25.0 ml.

Ion-exchange Capacities of Phosphates to K^+: The potassium ion-exchange titration curves of monohydrate and hemihydrate and their solubilities are shown in Fig. 5. The ion-exchange capacities of monohydrate at pH 4 and 7 were 0.5 and 7.5 meq/g respectively. On the other hand, the ion-exchange capacities of hemihydrate at pH 4 and 7 were 4.0 and 4.7 meq/g respectively, and in an acid solution with the same conditions as above the adsorption of the potassium ion was about 8 times that of monohydrate. Besides, the solubility of the ion-exchanger was consideably less than that of monohydrate.

Ion-exchange Capacities of Phosphates to Cs^+: The cesium ion-exchange titration curves of monohydrate and hemihydrate and the solubilities of the latter are shown in Fig. 6. It has previously been reported that the Cs^+ with a large ionic radius was scarcely adsorbed in monohydrate.[8] In the present study, however, a little adsorption was observed, as is shown in the diagram. The ion-exchange capacities of hemihydrate at pH 4 and 7 were 2.0 and 5.5 meq/g respectively, and the solubility of the ion-exchanger was extremely small. The solubility of the monohydrate used as an ion-exchanger could not be estimated, because a colloidal solution was formed by the dissolution of the salt as the pH rose.

As has been mentioned above, the crystalline titanium hydrogen bis(phosphate) hemihydrate could also adsorb such large ions as K^+ and Cs^+; therefore, it may be expected to be an inorganic ion-exchanger.

References

1) The article was presented at the 32th Annual Meeting of the Chemical Society of Japan, Tokyo, April, 1975.
2) D. Betteridge and G. N. Stradling, *J. Inorg. Nucl. Chem.*, **29**, 2652 (1967).

3) C. B. Amphlett, L. A. McDonald, J. S. Burgess, and J. C. Maynard, *J. Inorg. Nucl. Chem.*, **10**, 69 (1959).
4) M. G. Fuller, *ibid.*, **33**, 559 (1971).
5) E. Kobayashi and T. Goto, *Kogyo Kagaku Zasshi*, **73**, 692 (1970); Reports of Government Chemical Industrial Research Institute, Tokyo, **66**, 313 (1971).
6) E. Kobayashi, *Kogyo Kagaku Zasshi*, **73**, 1797 (1970); Reports of Government Chemical Industrial Research Institute Tokyo, **66**, 326 (1971).
7) "Gmelins Handbuch der anorganischen Chemie," System-Number **41**, Titan, Ti, 380 (1951), GmbH., Weinheim/Bergs.
8) G. Alberti, P. Cardini-Gallt, U. Costantino, and E. Torracca, *J. Inorg. Nucl. Chem.*, **29**, 571 (1967).
9) J. Gremer, *Nucl. Appl.*, **1968**, 5(2), 64.
10) S. J. Nagvi, D. Huys, and L. H. Baetsle, *J. Inorg. Nucl. Chem.*, **33**, 4317 (1971).
11) A. P. Shtin, A. M. Gorelov, and S. V. Zolotavina, Tr. Inst. Khim., Akad. Nauk SSSR, Ural. Filial, 1970, No. 20, 111.
12) J. R. Van Wazer, "Phosphorus and its Compounds I," Interscience New York (1958), p. 748.

Preparation and Stereochemistry of the Cobalt(III) Complexes with *N,N'*-Polymethylenedi(salicylideneamine) and Its Related Compounds

Fujio EBINA, Eishin KYUNO, Akira UEHARA, and Ryokichi TSUCHIYA
Department of Chemistry, Faculty of Science, Kanazawa University, Kanazawa 920
(Received February 5, 1975)

Preparation of two series of the cobalt(III) complexes, Na[Co(CN)$_2$(SB)] and [Co(acac)(SB)], was carried out. CN, acac and SB respectively refer to cyanide anion, acetylacetonate anion and the quadridentate Schiff base anion, *N,N'*-polymethylenedi(salicylideneamine), *N,N'*-polymethylenedi(α-methylsalicylideneamine) or *N,N'*-polymethylenedi(2-hydroxy-1-naphthylmethyleneamine). Efforts to obtain Na[Co(CN)$_2$(SB)] only containing the last Schiff base were unsuccessful. It was concluded from their PMR spectra that, for the dicyano complexes, the structure changes from a *trans*-form to a *cis*-one *via* a distorted *trans*-form, whereas for the acetylacetonato complexes, it changes from a distorted *cis*-β-form to an undistorted one with an increase in the length of carbon chain in the bridged polymethylene group of the Schiff bases.

The preparation of the first transition, bivalent metal complexes with salrn as the Schiff base is well-known. Salrn is the abbreviated form of *N,N'*-polymethylenedi(salicylideneamine), $HOC_6H_4CH{=}N(CH_2)_nN{=}CHC_6H_4OH$, which is indicated by salen, saltn and salbn when $n=2$, 3, and 4, respectively. Their structures change from the planar coordination of Schiff base to nonplanar tetrahedral coordination with an increase in the length of carbon chain in the bridged polymethylene group of the Schiff bases from $n=2$ through $n=4$ in Co(II), Ni(II), Cu(II), and Zn(II) complexes.[1-13]

In the tervalent metal complexes, only the cobalt(III) complex containing the above Schiff base as a ligand, where $n=2$, is known.[1,14,15] No other complexes containing bases where n is greater than 3 have been prepared.

Since tervalent metal complexes generally prefer a hexacoordinated octahedral structure, the coordination feature of the Schiff base seems to depend on both the potential denticity of the ligand simultaneously coordinated and the length of carbon chain of the polymethylene bridge.

In the series Na[Co(CN)$_2$(salrn)], when $n=2$, the complex is known to take a *trans*-form structure.[16,17] However, the greater the carbon chain lengthens, the greater the steric strain on the *trans*-form structure.

On the other hand, in the series [Co(acac)(salrn)], when $n=2$, the complex is assumed to take a remarkably distorted *cis*-β-form structure, due to the occupancy of adjacent sites by bidentate acetylacetonate.[18-20] However, as the length of the carbon chain of the polymethylene bridge increases, the above distortion is expected to disappear in contrast to the complexes Na[Co(CN)$_2$(salrn)].

In the present work, the change in the expected steric effect was studied by measuring the PMR spectra of the two series.

In order to confirm the results of PMR spectra of the complexes containing salrn, similar studies were carried out for Na[Co(CN)$_2$(Me-salrn)] and [Co(acac)(Me-salrn)] (Me-salrn is the abbreviated form of *N,N'*-polymethylenedi(α-methylsalicylideneamine) anion, $HOC_6H_4C(CH_3){=}N(CH_2)_nN{=}C(CH_3)C_6H_4OH$, which is indicated by Me-salen, Me-saltn, and Me-salbn when $n=2$, 3, and 4, respectively). Preparation was also made of the cobalt(III) complexes [Co(acac)(Np-salrn)], and their PMR spectra were measured for the sake of stereochemical comparison with the corresponding three types of Schiff base complexes (Np-salrn is the abbreviated form of *N,N'*-polymethylenedi(2-hydroxy-1-naphthylmethyleneamine) anion, $HOC_{10}H_6CH{=}N(CH_2)_nN{=}CHC_{10}H_6OH$, which is indicated by Np-saltn and Np-salbn when $n=3$ and 4, respectively).

Experimental

Preparation. Co(II) Complexes: The Schiff bases and the cobalt(II) complexes containing them were prepared by the procedure given by Hariharan and Urbach[4] and identified by elemental analysis.

Co(III) Complexes. 1) trans-*Sodium Dicyano*-N,N'-*ethylenedi(salicylideneaminato)cobaltate(III)*, trans-*Na[Co(CN)$_2$(salen)] (I)*: Ten milliliters of aqueous solution containing 0.022 mol of sodium cyanide was added to 100 ml of ethanolic solution containing 0.01 mol of Co(II)-Schiff base complex, [Co(salen)] in suspension, and the resulting solution was stirred for 10 min. On being oxidized by blow of air for 2—10 h, yellowish orange powder was precipitated. Needle crystals were separated out by recrystallization from aqueous solution containing a small amount of sodium cyanide. Yield, about 50%. Found: N, 13.90; C, 53.98; H, 3.85%. Calcd for Na[Co(CN)$_2$(salen)]: N, 14.00; C, 54.01; H, 3.53%.

2) trans-*Sodium Dicyano*-N,N'-*trimethylenedi(salicylideneaminato)cobaltate(III) Monohydrate*, trans-*Na[Co(CN)$_2$(saltn)]·H$_2$O (II)*: The procedure of preparation was similar to that for Complex I, [Co(saltn)] being used as Co(II) Schiff base complex of the starting materials, in place of [Co(salen)]. When the resulting solution was oxidized, concentrated to 15 ml at 20 °C, and then allowed to stand overnight in a refrigerator, brown needle crystals were separated out. Recrystallization was achieved by the same procedure as that used for Complex I. Yield, about 40%. Found: N, 12.88; C, 54.81; H, 4.20%. Calcd for Na[Co(CN)$_2$(saltn)]·H$_2$O: N, 12.96; C, 52.78; H, 4.21%.

3) cis-β-*Sodium Dicyano*-N,N'-*tetramethylenedi(salicylideneaminato)cobaltate(III) Trihydrate*, cis-β-*Na[Co(CN)$_2$(salbn)]·3H$_2$O (III)*: This complex was prepared by a procedure similar to that employed for Complex II, [Co(salbn)] being used in place of [Co(saltn)]. Brown cubic crystals were obtained. Recrystallization was carried out from ethanol–ether mixture. Yield, about 30%. Found: N, 11.72; C, 50.92; H, 5.34%. Calcd for Na[Co(CN)$_2$(salbn)]·3H$_2$O: N, 11.62; C, 49.83; H, 5.02%.

4) trans-*Sodium Dicyano*-N,N'-*ethylenedi(α-methylsalicylideneaminato)cobaltate(III) Monohydrate*, trans-*Na[Co(CN)$_2$(Me-salen)]·H$_2$O (IV)*: This complex was prepared and recrystallized by a procedure similar to that employed for Complex I, Me-salen being used in place of salen as a Schiff base. Orange crystals were obtained. Yield, 50%. Found: N, 12.40; C, 54.18; H, 4.44%. Calcd for Na[Co(CN)$_2$(Me-salen)]·H$_2$O: N, 12.56; C, 53.83; H, 4.53%.

5) trans-*Sodium Dicyano*-N,N'-*trimethylenedi(α-methylsalicylideneaminato)cobaltate(III) Dihydrate*, trans-*Na[(CN)$_2$(Me-saltn)]·2H$_2$O (V)*: This complex was also prepared and recrystallized by a procedure similar to that employed for Complex II, Me-saltn being used in place of saltn as a Schiff base. Brown needle crystals were obtained. Yield, about 40%. Found: N, 11.48; C, 54.54; H, 5.38%. Calcd for Na[Co(CN)$_2$(Me-saltn)]·2H$_2$O: N, 11.71; C, 52.72; H, 5.07%.

6) cis-α-*Sodium Dicyano*-N,N'-*tetramethylenedi(α-methylsalicylideneaminato)cobaltate(III) Dihydrate*, cis-α-*Na[Co(CN)$_2$(Me-salbn)]·2H$_2$O (VI)*: This complex was also prepared and recrystallized by a procedure similar to that employed for Complex III, Me-salbn being used in place of salbn as a Schiff base. Yellowish green needle crystals were obtained. Yield, about 20%. Found: N, 11.32; C, 54.97; H, 5.44%. Calcd for Na[Co(CN)$_2$(Me-salbn)]·2H$_2$O: N, 11.38; C, 53.66; H, 5.33%.

Coordination of the cyano group for Complexes I—VI was confirmed from the IR spectra. The charge of these complexes was confirmed by the behavior to an anion exchanger.

7) cis-β-*Acetylacetonato*-N,N'-*ethylenedi(salicylideneaminato)cobalt(III) Quarterhydrate*, cis-β-*[Co(acac)(salen)]·0.25H$_2$O (VII)* This complex was prepared by a modification of the procedure of Fujii *et al.*[17] Ten milliliters of aqueous solution containing 0.006 mol of potassium acetylacetonate was added to 100 ml of methanolic solution suspending 0.005 mol of Co(II)-Schiff base complex, [Co(salen)], and the solution was oxidized by hydrogen peroxide. The resulting solution was refluxed for 1 h and concentrated to *ca.* 20 ml. When the solution was let to stand overnight in a refrigerator, dark green crystals were separated out. They were recrystallized from methanol. Yield, about 70%. Found: N, 6.49; C, 58.60; H, 5.01%. Calcd for [Co(acac)(salen)]·0.25H$_2$O: N, 6.53; C, 58.80; H, 5.06%.

8) cis-β-*Acetylacetonato*-N,N'-*trimethylenedi(salicylideneaminato)cobalt(III) Quarterhydrate*, cis-β-*[Co(acac)(saltn)]·0.25H$_2$O (VIII)*: This complex was prepared and recrystallized by a procedure similar to that employed for Complex VII, saltn being used in place of salen. Dark green crystals were obtained. Yield, about 70%. Found: N, 6.20; C, 59.92; H, 5.44%. Calcd for [Co(acac)(saltn)]·0.25H$_2$O: N, 6.33; C, 59.65; H, 5.36%.

9) cis-β-*Acetylacetonato*-N,N'-*tetramethylenedi(salicylideneaminato)cobalt(III) Hemihydrate*, cis-β-*[Co(acac)(salbn)]·0.5H$_2$O (IX)*: This complex was also prepared and recrystallized by a procedure similar to that employed for Complex VII, salbn being used in place of salen. Bluish green crystals were obtained. Yield, about 60%. Found: N, 5.93; C, 59.75; H, 6.04%. Calcd for [Co(acac)(salbn)]·0.5H$_2$O: N, 6.07; C, 59.86; H, 6.04%.

10) cis-β-*Acetylacetonato*-N,N'-*ethylenedi(α-methylsalicylideneaminato)cobalt(III)*, cis-β-*[Co(acac)(Me-salen)] (X)*: This complex was also prepared and recrystallized by a procedure similar to that employed for Complex VII, Me-salen being used in place of salen. Dark green crystals were obtained. Yield, about 70%. Found: N, 6.18; C, 61.03; H, 15.66%. Calcd for [Co(acac)(Me-salen)]: N, 6.18; C, 61.05; H, 15.58%.

11) cis-β-*Acetylacetonato*-N,N'-*trimethylenedi(α-methylsalicylideneaminato)cobalt(III) Monohydrate*, cis-β-*[Co(acac)(Me-saltn)]·H$_2$O (XI)*: This complex was also prepared and recrystallized by a procedure similar to that employed for Complex VII, Me-saltn being used in place of salen. Dark green crystals were separated out. Yield, about 70%. Found: N, 5.78; C, 59.55; H, 5.96%. Calcd for [Co(acac)(Me-saltn)]·H$_2$O: N, 5.78; C, 59.49; H, 6.05%.

12) cis-β-*Acetylacetonato*-N,N'-*tetramethylenedi(α-methylsalicylideneaminato)cobalt(III)*, cis-β-*[Co(acac)(Me-salbn)] (XII)*: This complex was also prepared and recrystallized by a procedure similar to that employed for Complex VII, Me-salbn being used in place of salen. Bluish green crystals were obtained. Yield, about 60%. Found: N, 5.57; C, 62.26; H, 6.17%. Calcd for [Co(acac)(Me-salbn)]: N, 5.83; C, 62.49; H, 6.10%.

13) cis-β-*Acetylacetonato*-N,N'-*trimethylenedi(2-hydroxy-1-naphthylmethyleneaminato)cobalt(III) Hemihydrate*, cis-β-*[Co(acac)-(Np-saltn)]·0.5H$_2$O (XIII)*: To 0.01 mol of bis-(acetylacetonato)cobalt(II) dihydrate in 150 ml of chloroform was added 0.01 mol of the Schiff base, Np-saltnH$_2$, in 20 ml of chloroform. When the solution was refluxed for 1 hr, the color of the solution turned from pink to dark green. The resulting solution was concentrated to *ca.* 20 ml and let to stand overnight in a refrigerator. Dark green columnar crystals were separated out. They were recrystallized from methanol–chloroform mixture. Yield, about 70%. Found: N, 5.12; C, 65.16; H, 5.36%. Calcd for [Co(acac)(Np-saltn)]·0.5H$_2$O; N, 5.12; C, 65.80; H, 5.17%.

14) cis-β-*Acetylacetonato*-N,N'-*tetramethylenedi(2-hydroxy-1-naphthylmethyleneaminato)cobalt(III) Monohydrate*, cis-β-*[Co(acac)-(Np-salbn)]·H$_2$O (XIV)*: This complex was prepared and recrystallized by a procedure similar to that employed for Complex XIII, Np-salbn being used in place of Np-saltn. Bluish green columnar crystals were obtained. Yield, about 60%. Found: N, 5.23; C, 64.72; H, 5.47%. Calcd for [Co(acac)(Np-salbn)]·H$_2$O: N, 4.91; C, 65.25; H, 5.49%.

Coordination of the acetylacetonate group for Complexes VII—XIV was confirmed from the IR spectra; the characteristic absorption band of coordinated acetylacetonate was observed in the vicinity of 1515 cm^{-1}. Preparation of the cobalt(III) complexes with Np-salen was unsuccessful.

Measurement. The PMR spectra of the complexes were measured with a JEOL JNM-MH-60 spectrometer (60 MHz) at 25 °C using D$_2$O, CD$_3$OD or CDCl$_3$ as a solvent. TMS or NaTMS was used as an internal reference in all the PMR measurements.

The visible and UV absorption spectra were measured with a 323 Hitachi recording spectrophotometer at room temperature using H$_2$O or CHCl$_3$ as a solvent.

Results and Discussion

1) *Dicyano Complexes, Na[Co(CN)$_2$(SB)].* Three geometrical isomers, *trans*, *cis*-α and *cis*-β-form, are possible for a mixed cobalt(III) complex with a quadridentate ligand and two unidentate ligands. Yamada *et al.*[16] reported that [Co(CN)$_2$(salen)]$^-$ ion has a *trans*-form structure. On the other hand, from a consideration of the molecular model it is presumed that it becomes difficult for [Co(CN)$_2$(salrn)]$^-$ ion to have a *trans*-form with an increase in the length of the bridged polymethylene group owing to increasing distortion. The coordination structure of Na[Co(CN)$_2$(salrn)] and Na[Co(CN)$_2$(Me-salrn)] is thus expected to change from *trans*- to *cis*-form depending on the increase in the

Table 1. PMR spectral data of the dicyano complexes

Complex	Solvent	Peaks of Schiff base (ppm)			
		CH=N or CH_3–C=N	Aromatic ring	=N–CH_2–	–CH_2–
Complex I	D_2O	7.73	6.30—7.30[a]	3.68	
II	D_2O	7.40	6.20—7.20	3.70—3.90[a]	1.87—2.20[a]
III	D_2O	7.67, 8.23	6.50—7.50	3.40—3.77	1.67—2.20
IV	D_2O	2.63	6.50—7.83	3.83	
V	CD_3OD	2.71	6.50—7.50	3.70—3.93	1.85—2.15
VI	CD_3OD	2.51	6.40—7.60	3.80—4.10	1.63—2.00

a) Multiplet peaks.

length of the bridged polymethylene group.[21]

The PMR spectral data of the dicyano complexes, I through VI, are summarized in Table I. The assignment of each signal in their spectra was given on the basis of the corresponding assignment in the complexes[17] which have similar structures to those of dicyano complexes. In Complexes I and IV, one signal of azomethine proton and one signal of azomethyl proton were observed, respectively. In Complexes II and V, patterns similar to those of Complexes I and IV, respectively, were observed. By referring the patterns to those determined to be *trans*-form,[17] the structures of Complexes I, II, IV, and V can all be assigned to a *trans*-form.

However, the azomethine signal of Complex II is found to shift to higher magnetic field as compared with that of Complex I. From a consideration of the molecular model, such a shift seems to be attributed to the fact that the distortion owing to the steric strain of trimethylene group results in a decreased donation power of the ligand to cobalt(III) ion and, consequently, in an increased electron density of ligand in itself and in an increased shielding effect against the methine proton.

On the other hand, in Complex III, since two signals of azomethine proton were observed, the structure can be assigned to a *cis*-β-form.[17]

Similar features found in Complexes I and II could not be distinctly observed in IV and V. The PMR spectrum of Complex IV was measured in D_2O owing to the small solubility in CD_3OD and, inversely, that of Complex V was measured in CD_3OD owing to the small solubility in D_2O. However, in Complex VI, one signal of azomethyl proton was observed in a higher magnetic field region than in Complex V. The structure of Complex VI seems to be forced into a *cis*-form by the steric strain of the bridged tetramethylene group. From the observation of only one signal concerning azomethyl proton, its structure could be assigned to a *cis*-α-form.

2) *Acetylacetonato Complexes, [Co(acac)(SB)].* For these complexes two geometrical isomers, *cis*-α and *cis*-β-form, are possible since acetylacetonate anion acts as a bidentate ligand. Calligaris *et al.*[18] found by X-ray analysis that the structure of Complex VII takes a distorted *cis*-β-form. This structure is in approximate agreement with that expected by Fujii *et al.*[17] The distortion seems to be due to the shorter length of the bridged ethylene group on salen. It is expected that the greater the length of the bridged group (from salen to salbn), the more weakened the distortion in *cis*-β-form.

The PMR spectral data of the acetylacetonato complexes in chloroform are summarized in Table 2. The assignment of each signal in their spectra was made by referring to that of Complex VII.[17,22] In Complexes VII, VIII, and IX, both the signals of azomethine proton of the coordinated Schiff base and methyl proton of coordinated acetylacetonate were split into two peaks, their four signals being in a relative intensity of 1 : 1 : 3 : 3. In Complexes X, XI, and XII, and Complexes XIII and XIV, similar splittings were observed in relative intensities of 3 : 3 : 3 : 3 and 1 : 1 : 3 : 3, respectively. These patterns correspond to those of *cis*-β-form and, therefore, the structures of all the acetylacetonato complexes can be assigned to a *cis*-β-form.

Some characteristics were found in the spectra: in each of the salrn complexes VII, VIII, and IX, and Mesalrn complexes X, XI, and XII, the apparent separation of two split methyl signals of coordinated acetyl-

Table 2. PMR spectral data of the acetylacetonato complexes in $CDCl_3$

Complex	Peaks of Schiff base (ppm)				Peaks of acac (ppm)	
	CH=N or CH_3–C=N	Aromatic ring	=N–CH_2–	–CH_2–	CH=C	CH_3–
Complex VII	7.60, 7.83	6.40—7.45[a]	3.87—4.13[a]		5.43	1.81, 2.00
VIII	7.43, 7.60	6.30—7.35	3.22—3.70	2.10—2.50[a]	5.45	1.92, 2.12
IX	7.44, 7.63	6.35—7.30	3.00—4.00	1.85—2.50	5.35	1.64, 2.05
X	2.61, 2.76	6.45—7.75	3.90—4.30		5.39	1.82, 1.84
XI	2.62, 2.69	6.40—7.45	3.45—4.04	1.95—2.30	5.26	1.40, 1.78
XII	2.64, 2.71	6.20—7.45	3.50—4.00	1.80—2.20	5.21	1.25, 1.67
XIII	7.89, 8.25	7.06—7.80	3.50—4.00	2.00—2.50	5.40	1.83, 1.92
XIV	8.10, 8.22	7.00—7.80	3.30—3.80	1.80—2.50	5.26	1.53, 1.95

a) Multiplet peaks.

acetonate increases with the increase in the length of the bridged group, where one signal is apparently fixed and the other is shifted to a higher magnetic field. Two methine signals of the coordinated Schiff base for Np-salrn complexes XIII and XIV are shifted to a lower magnetic field than that of salrn complexes VIII and IX. The apparent separation of the corresponding split signals also has a tendency to increase in VIII and IX, and also XIII and XIV, with an increase in the length of the bridged group.

The first tendency may be related to the degree of distortion of the coordination structure in these complexes, but the origin is still obscure. The anisotropic effects of phenyl and naphthyl skeleton of the coordinated Schiff bases seem to play a less important role because of the large distance between methyl groups of acetylacetonate and these skeletons.[23] Other effects, such as solvent effect *etc*, might play an effective role. The origin of the second tendency may be related to the greater deshielding effect of the naphthyl skeleton in Complexes XIII and XIV than that of the phenyl skeleton in Complexes VIII and IV.

The authors wish to express their hearty thanks to Dr. Y. Fujii, Ibaraki University, for his valuable suggestions.

References

1) R. H. Holm, G. W. Everett, Jr., and A. Chakravorty, *Progr. Inorg. Chem.*, **7**, 83 (1966).
2) W. P. Schafer and R. E. Marsh, *Acta Crystallogr.*, **B 25**, 1675 (1970).
3) H. Weigold and B. O. West, *J. Chem. Soc., A*, **1967**, 1310.
4) M. Hariharan and F. L. Urbach, *Inorg. Chem.*, **8**, 556 (1969).
5) J. Manassen, *ibid.*, **9**, 966 (1970).
6) H. Montgomery and B. Morosin, *Acta Crystallogr.*, **12**, 551 (1961).
7) L. M. Shkol'nikova, E. A. Shugam, and L. G. Makarevich, *Zh. Strukt. Khim.*, **4**, 927 (1963).
8) R. H. Holm, *J. Amer. Chem. Soc.*, **82**, 5632 (1960).
9) W. C. Hoyt and G. W. Everett, Jr., *Inorg. Chem.*, **8**, 2013 (1969).
10) D. Hall and T.N. Waters, *J. Chem. Soc., A*, **1960**, 2644.
11) E. Sinn and C. M. Harris, *Coord. Chem. Rev.*, **4**, 391 (1969); S. J. Gruber, C. M. Harris, and E. Sinn, *Inorg. Nucl. Chem. Lett.*, **4**, 107 (1968); *J. Inorg. Nucl. Chem.*, **30**, 1805 (1968).
12) T. P. Cheeseman, D. Hall, and T. N. Waters, *Proc. Chem. Soc.* (London), **1963**, 379.
13) G. E. Batley and D. P. Graddon, *Aust. J. Chem.*, **20**, 885 (1967).
14) M. Calligaris, G. Nardin, and L. Randaccio, *Coord. Chem. Rev.*, **7**, 385 (1972).
15) M. D. Hobday and T. D. Smith, *ibid.*, **9**, 311 (1972).
16) S. Yamada, H. Nishikawa, and E. Yoshida, *Proc. Japan Acad.*, **40** 211 (1964).
17) Y. Fujii, A. Osawa, Y. Furukawa, F. Ebina, and S. Takahashi, This Bulletin, **45**, 2459 (1972).
18) M. Calligaris, G. Manzini, G. Nardin, and L. Randaccio, *J. Chem. Soc., Dalton*, **1972**, 543.
19) N. A. Bailey, B. M. Higson, and E. D. McKenzie, *ibid.*, **1972**, 503.
20) D. Cummins, B. M. Higson, and E. D. McKenzie, *ibid.*, **1973**, 1359.
21) G. T. Morgen and J. D. Smith, *J. Chem. Soc.*, **127**, 2030 (1925).
22) R. J. Cozens and K. S. Murray, *Aust. J. Chem.*, **25**, 911 (1972).
23) H. M. McConnell, *J. Chem. Phys.*, **29**, 1012 (1958).

The Thermal Changes in Gels of the SiO_2–Al_2O_3–Sc_2O_3–H_2O System

Mitsuhiro KASAI and Shuichi HAMADA

Department of Chemistry, Faculty of Science, Science University of Tokyo, Kagurazaka, Shinjuku-ku, Tokyo 162

(Received February 7, 1975)

The DTA patterns of synthesized coprecipitated gels, the SiO_2–Al_2O_3–Sc_2O_3–H_2O system, resembled that of allophane as well as those of coprecipitated gels, the SiO_2–Al_2O_3–M_2O_3–H_2O system (M: Fe, Ga, or In). The exothermic reaction around 980 °C in the DTA was confirmed to arise from the formation of mullite. The scandium-rich coprecipitated gels showed a new small exothermic peak at about 1000 °C, based on the formation of thortveitite in the DTA. The apparent activation energy for the mullite formation on the coprecipitated gels decreased with an increase in the scandium content. A large portion of the scandium in the coprecipitated gels was deposited as the thortveitite by heating, while that in the mixed gels was deposited as the scandium oxide. The behavior of such trivalent cations as gallium, iron(III), indium, and scandium in the silicoalumina gels was discussed.

In previous papers,[1–3] the properties of amorphous coprecipitated gels in the systems of SiO_2–Al_2O_3–M_2O_3–H_2O (M: Fe, Ga, and In) were found to resemble those of allophane. Scandium ions are considered to replace aluminum ions in the allophane structure, judging from the similarity in their chemical properties. The thermal properties of the gels, the system of SiO_2–Al_2O_3–Sc_2O_3–H_2O, have not been studied, while Toropov *et al.*[4] reported the phase diagram of the Sc_2O_3–Al_2O_3 system. In this paper, the thermal changes in the scandium-bearing coprecipitated gels were studied.

Experimental

Materials. The coprecipitated samples were prepared in the following manner;[1–3] the coprecipitated gels were obtained by boiling mixed solutions of sodium silicate, aluminum sulfate, and scandium sulfate at pH 5.0—5.7, a pH value obtained by adding hexamethylenetetramine; then they were washed by decantation and air-dried for three weeks. The concentration of the scandium ion in the mixed solutions was varied at the constant ratio of 2.0 as $SiO_2/(Al_2O_3+Sc_2O_3)$. All the coprecipitated samples were identified as amorphous from the X-ray powder diffractograms. The scandium-mixed samples were prepared by mixing a synthesized allophane, free from scandium, and an amorphous hydrated scandium oxide in order to compare the properties of the coprecipitated samples. The amorphous hydrate scandium oxide was prepared at pH 5.5 by using hexamethylenetetramine, because the precipitates obtained with ammonia water were identified as crystalline phases of γ-ScOOH[5] or $Sc(OH)_3$.[6]

Procedure. The amounts of SiO_2, Al_2O_3, and $H_2O(\pm)$[7] in the samples were estimated gravimetrically, while that of Sc_2O_3 was estimated by the chelatometry after it has been separated with a cation-exchange resin (Dowex 50W-X8, H-type).[8]

The differential thermal analysis of the samples was carried out in the temperature range from room temperature to 1100 °C at the heating rate of 10 °C/min with a Rigaku Denki Thermoflex, model 8002, differential thermal analyzer.

The X-ray powder diffraction patterns of the samples were taken with an X-ray diffractometer, model JDX-5P, from the Japan Electron Optics Laboratory Co. The samples were heated at 800, 900, 1000, 1100, and 1200 °C for 5 h in order to examine their thermal changes. The relative amounts of the firing-products were identified and estimated by using the diffraction peaks at (120) and (210) of the mullite, those at (110) and (021) of the thortveitite, and that at (222) of the scandium oxide. The unit-cell dimensions of the mullite, one of the firing-products at 1200 °C, were calculated by using the diffraction peaks at (041), (331), and (002) of the mullite. The diffraction angles were calibrated by using those of silicon.

Results

The chemical compositions of the samples are shown in Table 1.

The Differential Thermal Analysis of the Samples. The results of the differential thermal analysis are shown in Fig. 1. Both the coprecipitated and the mixed samples showed a broad endothermic peak and a sharp exothermic peak in the DTA curves at about 100 and 980 °C respectively. The profile of the DTA curves in these samples was similar to that observed in the allophane. The exothermic-peak temperature in the DTA on the coprecipitated gels was scarcely changed in spite of the variation in the scandium content, unlike as in the case of gallium-coprecipitated samples.[2] A new small exothermic peak was observed at about 1000 °C in the coprecipitated samples with more than 7.23 wt% of Sc_2O_3 (the Sc-7C, -8C, and -9C samples).

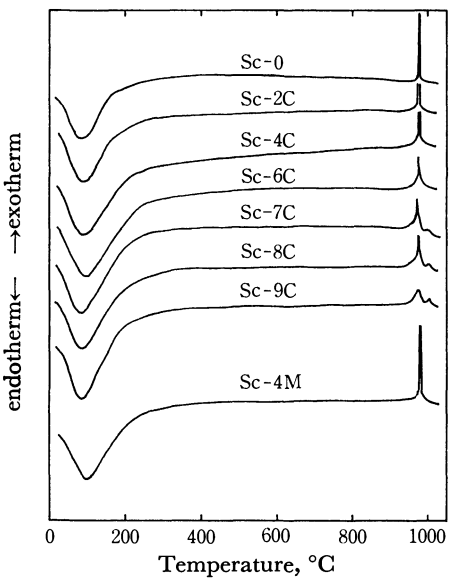

Fig. 1. DTA curves of scandium-bearing samples.

Table 1. Chemical compositions of scandium-bearing samples

Sample	Chemical composition, wt%					Molar ratio	
	SiO_2	Al_2O_3	Sc_2O_3	H_2O (±)	Total	$\frac{SiO_2}{R_2O_3}$[a]	$\frac{H_2O\ (\pm)}{R_2O_3}$
Sc-0[b]	28.01	30.59	—	41.35	99.95	1.55	7.66
Sc-1C[c]	24.87	32.71	0.40	41.90	99.88	1.28	7.19
Sc-2C	24.15	31.45	1.15	42.49	99.24	1.27	7.45
Sc-3C	22.72	32.75	2.22	42.58	100.27	1.12	7.02
Sc-4C	23.25	30.69	2.77	42.61	99.32	1.21	7.37
Sc-5C	23.43	31.06	3.78	41.86	100.13	1.17	7.00
Sc-6C	25.72	28.39	6.00	40.07	100.18	1.33	6.92
Sc-7C	28.57	25.85	7.23	38.16	99.81	1.55	6.93
Sc-8C	28.04	25.54	8.40	38.43	100.41	1.50	6.86
Sc-9C	26.53	23.87	11.33	38.67	100.40	1.40	6.79
Sc-10M[c]	27.84	30.41	0.37	41.38	100.0[d]	1.54	7.64
Sc-11M	27.69	30.24	0.69	41.38	100.0[d]	1.53	7.62
Sc-12M	27.12	29.61	1.88	41.39	100.0[d]	1.49	7.57
Sc-13M	26.57	29.02	3.01	41.40	100.0[d]	1.44	7.51

a) R_2O_3: $Al_2O_3+Sc_2O_3$ b) The sample is the allophane free from scandium. c) The postscript "C" and "M" denote the scandium-coprecipitated and -mixed samples respectively. d) Calculated.

The causes of the exothermic peaks in the DTA were examined as follows: the samples were preheated in the DTA equipment up to temperatures just below and just above their peak temperatures. The phases of the preheated samples were found by X-ray powder diffractometry to be as shown in Table 2. The exothermic reaction at about 980 °C in the coprecipitated samples was found to arise from the formation of mullite, and that at about 1000 °C, from the formation of thortveitite.

The apparent activation energy for the formation of mullite was estimated by means of the method described by Kissinger.[9] The results for the coprecipitated samples are shown in Table 3.

Table 2. Phases of preheated samples

Sample	Peak temp. of original state (°C)	Phase after heat treatment	
		below peak temp. (°C)	above peak temp. (°C)
Sc-0	980	A (975)	M (998)
Sc-2C	982	A (970)	M (987)
Sc-4C	983	A (946)	M (982)
Sc-6C	979	A (967)	M (989)
Sc-8C	981	A (970)	M (993)
	1000		M, T (1010)
Sc-9C	984	A (968)	M (982)
	1000		M, T (1014)
Sc-13M	985	A (962)	M (995)

A; Amorphous, M; Mullite, T; Thortveitite, S; Scandium oxide

Table 3. Apparent activation energies for exothermic change around 980 °C

Sample	E_a, kcal/mol
Sc-0	247
Sc-1C	227
Sc-3C	222
Sc-5C	187
Sc-7C	171
Sc-8C	145
Sc-9C	148

The Variation in the Firing-products in the Samples during Heat Treatment. The crystalline phases formed in the heat-treated samples at 800, 900, 1000, 1100, and 1200 °C for 5 h were identified as the mullite, the thortveitite,[10] and the scandium oxide[11] by means of X-ray powder diffractometry. The firing-products at each temperatures are shown in Table 4. All the samples formed the mullite above 900 °C, while they were amorphous at 800 °C except for the Sc-12M and -13M samples. The scandium component deposited as the thortveitite in the coprecipitated gels with more than 2.22 wt% of Sc_2O_3, but deposited as the scandium oxide only above 800 °C in the mixed samples. The formation temperature of the thortveitite decreased with an increase in the scandium content. The coprecipitated gel of the SiO_2–Sc_2O_3–H_2O system, with the

Table 4. Firing-products in the samples

Sample	Temperature, °C				
	800	900	1000	1100	1200
Sc-0	A	M	M	M	M
Sc-1C	A	M	M	M	M
Sc-2C	A	M	M	M	M
Sc-3C	A	M	M	M	M,T
Sc-4C	A	M	M	M,T	M,T
Sc-5C	A	M	M	M,T	M,T
Sc-6C	A	M	M	M,T	M,T
Sc-7C	A	M	M,T	M,T	M,T
Sc-8C	A	M	M,T	M,T	M,T
Sc-9C	A	M,T	M,T	M,T	M,T
Sc-10M	A	M	M	M	M
Sc-11M	A	M	M,S	M,S	M,S
Sc-12M	S	M,S	M,S	M,S	M,S
Sc-13M	S	M,S	M,S	M,S	M,S

A; Amorphous, M; Mullite, T; Thortveitite, S; Scandium oxide

SiO_2/Sc_2O_3 molar ratio of 1.79 and free from aluminum, formed the scandium oxide and the thortveitite, while the mixed gels with the same composition formed only the scandium oxide at 1000 °C.

The Unit-cell Dimensions of the Mullite formed in the Heat-treated Samples. The relationships between the unit-cell lengths, a_0, b_0, and c_0, of the mullite formed at 1200 °C for 5 h in the coprecipitated samples and the scadium content in the original samples are shown in Fig. 2. While all the unit-cell lengths increased with an increase in the scandium content up to approximately 4—5 wt%, the increasing tendency in the c_0 was less than those in the a_0 and the b_0. The spacings of the thortveitite formed at 1200 °C were scarcely changed in spite of the variation in the scandium content, while they were slightly smaller than those of a native thortveitite.[10]

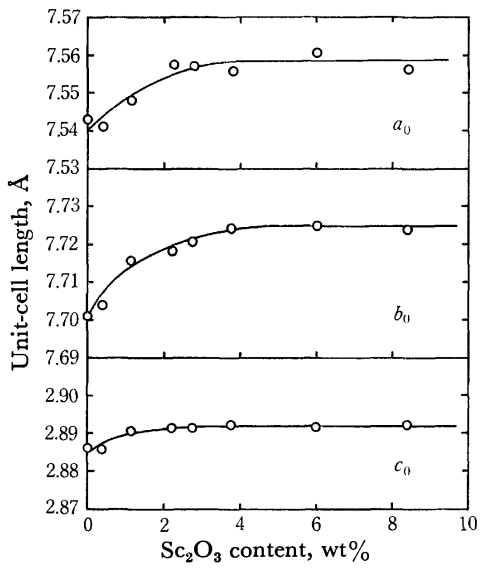

Fig. 2. Relationships between unit-cell length, a_0, b_0, and c_0, of scandium-bearing mullite formed at 1200 °C and Sc_2O_3 content of original gel.

Ďurovič[12] confirmed that the mullite lattice consisted of a AlO_6 octahedron and AlO_4 and (Si, Al)O_4 tetrahedra, that the AlO_6 octahedra were composed of chains, parallel to the [001] direction, by sharing their edges, and that the chains were linked by the AlO_4 and the (Si, Al)O_4 tetrahedra. Judging from the ratio of the ionic radii of Sc^{3+} and O^{2-} (0.73 and 1.32 Å),[13] the scandium ions replace the aluminum ions only in the octahedra of the mullite lattice. Variations in the unit-cell lengths, a_0, b_0, and c_0, of the mullite were found to be nonidentical, as is shown in Fig. 2. Because two octahedra slanting to the [100] and the [010] directions are situated in the <110> directions for each unit-cell of the mullite, though only one octahedron slants in the [001] direction, the replacement of the scandium ions would bring about larger enlargements of the a_0 and the b_0 than that of the c_0. Furthermore, the distortion of the octahedra based on the repulsion between the aluminum ions was considered to decrease slightly by the replacement of the scandium ions, as had also been observed in the octahedra in the α-AlOOH[14] and the α-ScOOH.[15] Therefore, the a_0 and b_0 would be further expanded by this effect.

Discussion

A clear difference between the kinds of firing products obtained from the coprecipitated and the mixed gels has been observed in the SiO_2–Al_2O_3–M_2O_3–H_2O systems (M: Fe, Ga, In, and Sc) in this series of works.[1-3] Judging from these facts, such trivalent cations as iron (III), gallium, indium, and scandium ions were obvious substitutes for the aluminum ions in the allophane structure of the coprecipitated gels. Such trivalent cations were included in the mullite by heating, and they enlarged the lattice; the degree of enlargement is governed by several factors—for example, the amount of the substituting cation, its ionic radius, and the crystallographic geometry, all related to each other.

The order of the amount of trivalent cations includible in the mullite as a solid solution was found to be Ga≫Fe>Sc>In. This result was considered to be reasonable, judging from the ionic radii of the trivalent cations in these systems (Al^{3+}: 0.51, Ga^{3+}: 0.62, Fe^{3+}: 0.64, Sc^{3+}: 0.73, and In^{3+}: 0.81 Å respectively).[13]

Léonard *et al.*[16] have investigated the coordination states of aluminum ions and the structure change in the amorphous hydrated silicoalumina gels by means of X-ray fluorescence spectroscopy and IR spectroscopy. They stated that the aluminum ions were stabilized by forming octahedra sharing corners of the tetrahedra of the SiO_4 and hydroxy-groups in the hydrated silicoalumina gel structure, and that then the sixfold-coordinated aluminum ions were altered to the fourfold-coordinated state as dehydration proceeded upon heating.

The aluminum ion is well known to take both the sixfold- and the fourfold-coordinated states; the gallium ion also can take both the states—for example, in the structure of the β-gallia,[17] though less frequently than the aluminum ion. The iron (III), however, was not found to form the tetrahedra. The clear difference between the gallium and the iron (III) ions in the degree of substitution was considered to be caused by a variability in the coordination state of the gallium ion in spite of the similarity in their ionic radii.

Though the scandium and the indium ions, having large ionic radii, would replace the aluminum ions to some extent by forming the octahedra in the hydrated silicoalumina gels, the stability of the gels would decrease as a result of the great distortion as dehydration proceeded. The apparent activation energies for the formation of mullite or silicoalumina spinel,[1,2] a precursor of the mullite, at the coprecipitated gels decreased with an increase in the content of the substituted cations; this decreasing tendency in the scandium- and the indium-coprecipitated samples was larger than that in the gallium-coprecipitated gels. These facts support the above consideration. Though the scandium ions replaced the aluminum ions in the original allophane structure, a large portion of the scandium is probably excluded by heating from the mullite lattice, because the scandium ion took the sixfold-coordinated state only. The deposition of scandium as disilicate in the

coprecipitated gels would be caused by its lithophilic nature, and the thortveitite, which has only the sixfold-coordinated sites for metal[18] in it, is likely to be stable both thermodynamically and crystallographically.

References

1) J. Ossaka, S. Iwai, M. Kasai, T. Shirai, and S. Hamada, This Bulletin, **44**, 716 (1971).
2) M. Kasai, Y. Kudo, and S. Hamada, *ibid.*, **46**, 3091 (1973).
3) M. Kasai, Y. Kudo, and S. Hamada, *ibid.*, **48**, 1608 (1975).
4) N. A. Toropov and V. A. Vail'eva, *Proc. Acad. Sci. USSR*, **152**, 856 (1963).
5) W. O. Milligan and J. L. McAtee, *J. Phys. Chem.*, **60**, 273 (1956).
6) K. Schubert and A. Seitz, *Z. Anorg. Allgem. Chem.*, **256**, 226 (1948).
7) The values were estimated from the ignition loss.
8) H. Hamaguchi, R. Kuroda, K. Aoki, R. Sugishita, and N. Onuma, *Talanta*, **10**, 153 (1963).
9) E. H. Kissinger, *Anal. Chem.*, **29**, 1702 (1957).
10) K. Sakurai, K. Nagashima, and A. Kato, This Bulletin, **35**, 1776 (1962).
11) H. E. Swanson and R. K. Fuyat, NBS Circular 539, Vol. 4, p. 25 (1955).
12) S. Ďurovič, *Chem. Zvesti*, **23**, 113 (1969).
13) "Handbook of Chemistry and Physics," ed. by R. C. Weast, CRC Press, Cleveland (1974), p. F-194.
14) W. R. Busing and H. A. Levy, *Acta Crystallogr.*, **11**, 798 (1958).
15) A. N. Christensen and S. J. Jensen, *Acta Chem. Scand.*, **21**, 121 (1967).
16) A. Léonard, S. Suzuki, J. J. Fripat, and C. De Kimpe, *J. Phys. Chem.*, **68**, 2608 (1964).
17) S. Geller, *J. Chem. Phys.*, **33**, 676 (1960).
18) "Comprehensive Inorganic Chemistry," Vol. 3, ed. by J. C. Bailar *et al.*, Pergamon Press, Oxford (1973), p. 332.

The Preparation and Absorption Spectra of the Cyanocarbonatotriammine- and Cyanooxalatotriammine-type Complexes of Cobalt(III)

Shoji NAKASHIMA and Muraji SHIBATA

Department of Chemistry, Faculty of Science, Kanazawa University, Kanazawa 920

(Received March 18, 1975)

The complexes of the $[CoCN(O\text{–}O)(N)_3]$ type (O–O represents CO_3^{2-} or $C_2O_4^{2-}$, and $(N)_3$ represents three NH_3, one NH_3 plus one en, or one dien) have been prepared starting from the $[Co(CO_3)_3]^{3-}$ complex, and their characterization has been achieved on the basis of the absorption and PMR spectra. Among these, each of the *fac*(N) isomers of the carbonato complexes shows a shoulder in the second absorption band and no shoulder in the first absorption band. In contrast, each of the corresponding *fac*(N) isomers of the oxalato complexes shows no such shoulder in the second absorption band, but does show a shoulder in the first absorption band. The same phenomena have been found in the spectra of the *trans*(N)-$[Co(O\text{–}O)(mda)(NH_3)]^-$ complexes (mda stands for the methyliminodiacetate ion).

In our previous studies concerning the preparation of mixed-ligand cobalt(III) complexes containing the cyanide ion as a ligand, we succeeded in obtaining such complexes as $[CoCN(NH_3)_5]^{2+}$,[1] *mer*-$[Co(CN)_3(NH_3)_3]$,[1] *cis*-$[Co(CN)_2(CO_3)_2]^{3-}$,[2] and *cis-cis*-$[Co(CN)_2(CO_3)(NH_3)_2]^-$.[3] The present work was undertaken in connection with those studies and in order to prepare the cyanocarbonatotriammine-type and the cyanooxalatotriammine-type complexes, which are represented by the formula $[CoCN(O\text{–}O)(N)_3]$ ($(N)_3$ represents three NH_3, one NH_3 plus one en, or one dien). These complexes are of interest not only in such preparative work, but also in electronic spectroscopy: Since the three kinds of donor atoms differ greatly in their ligand-field strengths, marked splittings of both the first and second absorption bands were expected for some of these complexes. In practice, the carbonato complexes with a geometrical form with respect to donor atoms showed shoulders in their second absorption bands, whereas the corresponding oxalato complexes showed shoulders in their first absorption bands.

Experimental

Preparation. *1) Cyanocarbonatotriamminecobalt(III), $[CoCN(CO_3)(NH_3)_3]$*: To a cold, green solution of tricarbonatocobaltate(III) (0.1 mol scale)[4] we added potassium cyanide (13 g, 0.2 mol) in portions; the mixture was then stirred vigorously at room temperature for 20 min, whereby a deep red solution was obtained. To this solution we added conc. aqueous ammonia (40 ml, 0.56 mol), after which the mixture was stirred at 50 °C for 40 min. The resulting dark red solution was carefully neutralized with aqueous perchloric acid under an iced condition and then filtered to remove any precipitated material. The filtrate was charged on a column of Dowex 50 WX-8 resin (100—200 mesh, Na-form, 50×400 mm). With careful washing with water, two bands colored yellow-brown and red, descended after the minor band of negatively charged species had been effused. These two bands were collected in fractions labeled A-1 and A-2. Each fraction was concentrated to a small volume, and a small amount of ethanol was added to the concentrate. When the mixture was kept in a refrigerator, fine crystals were deposited. The complexes thus obtained were also named A-1 and A-2. The formation ratio of A-1/A-2 was found to be about 1/5.

2) Cyanocarbonatoammineethylenediaminecobalt(III), $[CoCN(CO_3)(NH_3)(en)]\cdot H_2O$: Concentrated aqueous ammonia (20 ml, 0.28 mol) was added to a deep red solution prepared in the same way (0.1 mol scale) as in 1), and the mixture was stirred at 40 °C for 30 min. The resulting solution was neutralized with aqueous perchloric acid and filtered. To the filtrate ethylenediamine (0.1 mol) was added, after which the mixture was stirred at 40 °C for an hour. The resulting dark red solution was neutralized again with aqueous perchloric acid under an iced condition and filtered to remove any precipitates. The filtrate was chromatographed in the same manner as in 1); two bands, colored yellow-brown and red, were collected in fractions labeled B-1 and B-2. When each concentrate from the fractions was kept in a refrigerator, crystals of the desired complex were deposited. The formation ratio of B-1/B-2 was about 1/10.

3) Cyanocarbonatodiethylenetriaminecobalt(III), $[CoCN(CO_3)(dien)]$: The procedure was the same as that in 1), except for the use of diethylenetriamine (10.3 g, 0.1 mol) instead of conc. ammonia. The chromatographic separation gave three bands, colored yellow-brown, red, and red. These were collected in fractions labeled C-1, C-2, and C-3. Very fine crystals were obtained from C-1 and C-3, whereas no complex was isolated from C-2 because the species was too unstable to be isolated. The formation ratio of C-1/C-3 was found to be about 1/5.

4) Cyanooxalatotriammine-type Complexes, $[CoCN(ox)(N)_3]$: A cyanocarbonato complex, A-1 (10 g, 0.05 mol), which had been obtained in *1)*, was treated with 60% perchloric acid (0.1 mol), and then potassium oxalate (18.4 g, 0.1 mol) was added to the acid-hydrolyzed solution. The resulting solution was stirred at 40 °C for 2 h and then neutralized with an aqueous solution of potassium hydroxide. After the precipitated material had been removed by filtration, the filtrate was chromatographed in the same manner as that in *1)*; two yellow-brown bands, labeled A′-1 and A′-2, were thus obtained. The amount of the second band (A′-2) formed was less than that of the first one (A′-1). One yellow-brown band was obtained when the A-2 complex was used as the starting material, and the complex obtained from this band was the same as A′-2. The other oxalato complexes, labeled B′-1 and B′-2 for the $[CoCN(ox)(NH_3)(en)]$ complex, and C′-1 and C′-3 for the $[CoCN(ox)(dien)]$ complex, were obtained in the same manner as above. The oxalato complexes thus obtained were less soluble in water than the corresponding carbonato complexes. Therefore, the recrystallization of the oxalato complexes was achieved by dissolving them in an aqueous solution of sulfuric acid and by then adding ethanol.

5) Potassium Carbonatomethyliminodiacetatomonoamminecobaltate (III), $K[Co(CO_3)(mda)(NH_3)]\cdot 2.5H_2O$: The ligand, methyliminodiacetic acid (H_2mda), was prepared from methylamine and sodium monochloroacetate according to the method

in the literature.[5] To a solution of $K[Co(CO_5)_2(NH_3)_2]\cdot H_2O$[6] (13.5 g, 0.05 mol) in water, we added an aqueous solution of the ligand (K_2mda, 0.05 mol); the mixture was then stirred for 4 h at 45 °C, whereby a red-blue solution was obtained. It was carefully neutralized with aqueous perchloric acid under an iced condition and then filtered. The filtrate was charged on a column of an anion-exchange resin (Dowex 1X-8, 100—200 mesh, Cl-form, 50×400 mm). When the adsorbed band was eluted with a 0.07 M aqueous KCl solution, one red-violet band was obtained. This fraction was concentrated to a small volume at *ca.* 40 °C. A small amount of methanol was added to remove the KCl used for the elution. When the solution was then kept in a refrigerator, the desired complex was deposited. The recrystallization was performed from water.

6) Potassium Oxalatomethyliminodiacetatomonoamminecobaltate (III), K[Co(ox)(mda)(NH_3)]: This complex was easily obtained by treating an aqueous solution of the carbonato complex obtained in *5)* with a little excess of oxalic acid.

Measurements. The absorption spectra were measured with a Hitachi Model 323 spectrophotometer. The proton magnetic resonance spectra were recorded on a JEOL JNM-PS-100 NMR spectrometer at *ca.* 22 °C, with 20% D_2SO_4 in D_2O as the solvent. The values of the chemical shifts were referred to internal sodium 2,2-dimethyl-2-silapentane-5-sulfonate (DSS) or sodium D_4-trimethylsilylpropionate (TMSP).

Results and Discussion

The possible geometrical isomers of the [CoCN(O–O)$(N)_3$] type complexes are illustrated in Fig. 1, where *mer* and *fac* represent *trans-cis* and *cis-cis* arrangements of the three N atoms, and where the *s-* and *u-* symbols are used to distinguish between the isomer with a plane of symmetry and the one without such a plane.

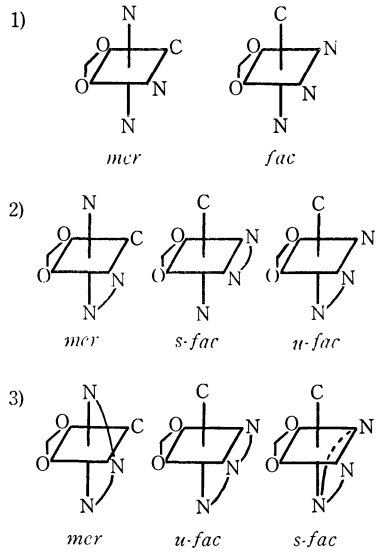

Fig. 1. Possible geometrical isomers of the [CoCN(O–O)$(N)_3$]-type complexes; 1) triammine complex, 2) ammine-ethylenediamine complex, and 3) diethylenetriamine complex.

The results of elemental analysis are given in Table 1 (no elemental analysis of the B′-1 complex was carried out because of the poor yield); these figures are in close agreement with the calculated values. The absorption spectral data are also summarized in Table 1, but that of the A′-1 complex was not measured because of its low solubility. Figure 2 shows the absorption spectra of the cyanocarbonato complexes, A-2, B-2, and C-3. Each spectrum shows a shoulder and a maximum in the second absorption band region. A similar feature of the

Table 1. Elemental analyses and absorption spectral data

Label	Complex	Elemental analyses, %[a] C	H	N	I band $\tilde{\nu}/10^3$ cm^{-1}	log ε	II band $\tilde{\nu}/10^3$ cm^{-1}	log ε
A-1	*mer*(N)-[CoCN$(CO_3)(NH_3)_3]\cdot H_2O$	11.76 (11.22)	4.98 (5.18)	26.03 (26.17)	20.6	2.05	28.8	2.05
A-2	*fac*(N)-[CoCN$(CO_3)(NH_3)_3$]	12.42 (12.25)	4.85 (4.63)	28.83 (28.58)	20.2	2.03	29.0 sh26.5	2.20
A′-2	*fac*-(N)-[CoCN(ox)$(NH_3)_3]\cdot 0.5H_2O$	16.10 (15.46)	4.27 (4.32)	24.26 (24.04)	21.2 sh18.0	1.95	29.4	2.15
B-1	*mer*(N)-[CoCN$(CO_3)(NH_3)$(en)]$\cdot H_2O$	20.26 (20.01)	5.40 (5.46)	23.64 (23.33)	20.6	2.06	28.8	2.08
B-2	*u-fac*-(N)-[CoCN$(CO_3)(NH_3)$(en)]$\cdot H_2O$	19.95 (20.01)	5.91 (5.46)	23.18 (23.33)	20.6	2.07	29.0 sh26.5	2.16
B′-2	*u-fac*-(N)-[CoCN(ox)(NH_3)(en)]$\cdot 0.5H_2O$	23.42 (23.18)	4.64 (4.67)	21.64 (21.62)	21.4 sh18.0	2.07	29.4	2.26
C-1	*mer*(N)-[CoCN(CO_3)(dien)]	29.02 (29.04)	5.49 (5.28)	22.00 (22.58)	20.4	2.18	28.6	2.20
C-3	*s-fac*(N)-[CoCN(CO_3)(dien)]	29.04 (29.04)	5.45 (5.28)	22.79 (22.58)	20.8	2.21	29.0 sh26.5	2.26
C′-1	*mer*(N)-[CoCN(ox)(dien)]$\cdot H_2O$	28.32 (28.58)	5.46 (5.14)	19.32 (19.05)	20.6	2.13	29.0	2.26
C′-3	*s-fac*-(N)[CoCN(ox)(dien)]$\cdot H_2O$	28.68 (28.58)	5.22 (5.14)	18.52 (19.05)	21.4 sh18.3	1.82	29.4	1.99
	trans(N)-K[Co(CO_3)(mda)$(NH_3)]\cdot 2.5H_2O$	20.32 (20.23)	4.34 (4.24)	7.95 (7.86)	18.4	2.06	26.4 sh23.9	1.99
	trans(N)-K[Coox(mda)(NH_3)]	24.28 (24.15)	3.11 (2.89)	7.98 (8.05)	18.2 sh16.5	2.08	25.6	2.32

a) ( ): calcd. sh: shoulder.

spectrum has been reported for the *mer*(*trans*)-[$Co(CO_3)$-(α-am)$(NH_3)_2$] complexes (*trans* refers to the NH_3 groups, and α-am represents the glycinate, alaninate, or valinate ion),[7,8] and also with the *mer*(N)-[$Co(CO_3)$-(*i*-dtma)] complexes (*i*-dtma stands for *N*,*N*-bis(2-aminoethyl)glycinate ion).[9] The spectrum of the *i*-dtma complex is included in Fig. 2 as an example. Moreover, it has been reported[10] that the absorption spectrum of the *trans*-$[Co(CO_3)_2(py)_2]^-$ complex shows an explicit shoulder in the second absorption band region and that the shoulder is assignable to a split component of the second band on the basis of Yamatera's predictions.[11] Therefore, the band positions for the present $[CoCN(CO_3)(NH_3)_3]$ complex were calculated by means of Yamatera's predictions; the parameters concerning the first and second bands, δ^{I} and δ^{II}, were treated as $\delta^{I}=\delta^{I}_{\sigma}+\delta^{I}_{\pi}$ and $\delta^{II}\approx\delta^{II}_{\sigma}$. The numerical values were estimated from the absorption maxima of the $[Co(NH_3)_6]^{3+}$, $[Co(CO_3)_3]^{3-}$,[4] and *fac*-$[Co(CN)_3(NH_3)_3]$[12] complexes ($\delta^{I}(NH_3-CO_3)=4466$, $\delta^{II}(NH_3-CO_3)=6700$ cm^{-1}; $\delta^{I}(CN-NH_3)=10770$, $\delta^{II}(CN-NH_3)=10130$ cm^{-1}). The predicted positions are given in Table 2.

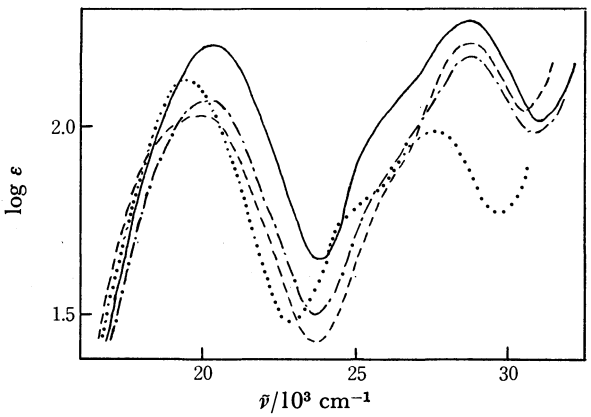

Fig. 2. Absorption spectra of $[CoCN(CO_3)(N)_3]$-type complexes, A-2 (------), B-2 (-·-·-) and C-3 (——), and of *mer*(N)-$[Co(CO_3)$(*i*-dtma)] (·····).

TABLE 2. PREDICTED BAND POSITIONS FOR $[CoCN(CO_3)(NH_3)_3]$

Geometry	I band (in cm^{-1})	II band (in cm^{-1})
fac(N)	18700, 22500, 22500	27500, 27500, 31700
mer(N)	19900, 21400, 22500	27500, 29200, 30000

From the table it may be seen that the separations between the lowest-energy and highest-energy components in both the first and the second band for the *fac*(N) geometry are considerably greater than those for the *mer*(N) geometry. This fact suggests that a splitting of the second absorption band is to be expected for the *fac*(N) complex (namely, A-2). Thus, the remaining complexes, B-2 and C-3, may also be regarded as *fac*(N) isomers from the similarity in the spectrum. It is, however, not possible to differentiate between the *s*- and *u*-configurations for the B-2 and C-3 complexes.

Figure 3 shows the absorption spectra measured with solutions of the *fac*(N)-$[CoCN(CO_3)(N)_3]$ complexes (A-2, B-2, and C-3) acidified with aqueous perchloric

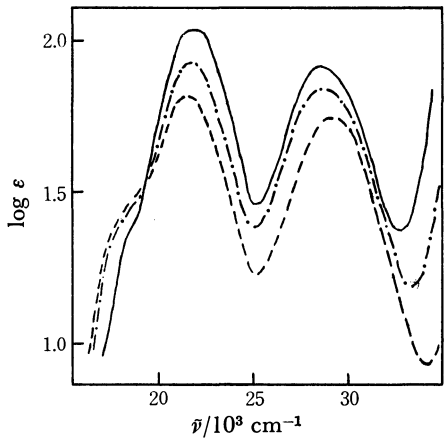

Fig. 3. Absorption spectra of $[CoCN(H_2O)_2(N)_3]$-type complexes derived from A-2 (------), B-2 (-·-·-), and C-3 (——).

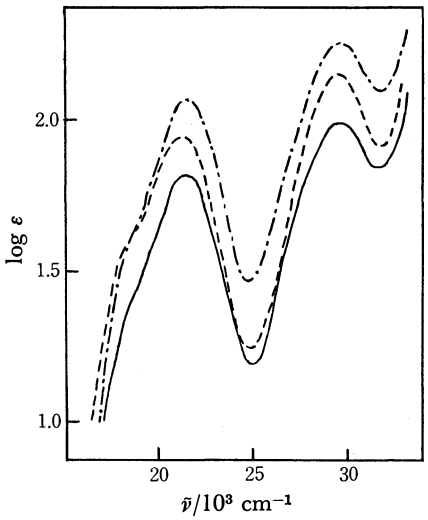

Fig. 4. Absorption spectra of $[CoCN(ox)(N)_3]$-type complexes, A′-2 (------), B′-2 (-·-·-), and C′-3 (——), in *ca.* 20% H_2SO_4.

acid to give acid-hydrolyzed species. Figure 4 shows the spectra of the $[CoCN(ox)(N)_3]$ complexes, A′-2, B′-2, and C′-3. In both figures, each spectrum reveals a shoulder in the first absorption band and no shoulder in the second absorption band. Similar splitting of the first absorption bands have been observed in the spectra of the *mer*(*trans*)-[Co(α-am)$(H_2O)_2(NH_3)_2]^{2+}$ and of the *mer*(*trans*)-[Coox(α-am)$(NH_3)_2$] complexes.[8] On this basis, the A′-2, B′-2, and C′-3 complexes can be identified as the *fac*(N) isomers which correspond, in geometrical configuration, to the above-mentioned *mer*-(*trans*) isomers.

Figure 5 shows the spectrum of the $[CoCN(CO_3)$-(dien)] complex, C-1, and that of the corresponding oxalato complex, C′-1. There are no shoulders in either the first or second absorption band. Similarly shaped spectra have been reported with the *fac*(N)-$[Co(CO_3)$(α-am)$(NH_3)_2]$[8] and also with the *fac*(N)-$[Co(CO_3)$(*i*-dtma)].[9] As for *cis*-$[Co(CO_3)_2(py)_2]^-$, no shoulders have been reported in the first and second absorption bands.[10] Thus, the C-1 and C′-1 complexes can be identified as the *mer*(N) isomers. The same

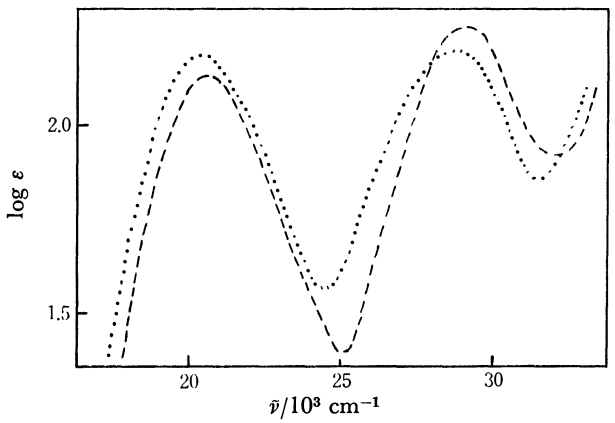

Fig. 5. Absorption spectra of [CoCN(CO_3)(dien)] complex, C-1 (·····) and [CoCN(ox)(dien)] complex, C′-1 (------).

assignment can be made for the remaining complexes (A-1, B-1, A′-1, and B′-1). In addition the elution orders in the chromatographic separations support the foregoing assignments; the earlier eluted species in each run of the chromatographic separations is the *mer*(N) isomer.[7-9]

The PMR spectrum of the *mer*(N)-[CoCN(ox)(dien)] complex, whose structural assignment could be made on the basis of the absorption spectrum, is presented in Fig. 6-a, the spectrum of the corresponding *fac*(N) complex being presented in Fig. 6-b. By a comparison of the two spectra, each peak resonating in a down field (5.7 ppm for the *mer* and 6.9 ppm for the *fac*) is attributed to the NH proton, the two peaks resonating in a middle field (4.8 and 4.4 ppm for the *mer* and 4.3 and 4.1 ppm for the *fac*) being attributed to the NH_2 protons. The integrated ratio of these three peaks is estimated to be 1: 2: 2.

A molecular model for the *mer*(N) isomer indicates that the two protons of each of the two NH_2 groups of the chelated dien are not equivalent with respect to the complexed CN^- ion; one of the protons is located in a position near to the CN^- ion, while the other is far from the CN^- ion. Thus, the observed two peaks for the *mer*(N) complex can be interpreted in terms of such environmentally different situations of the NH_2 protons by assuming the effect of the CN^- ion on the NH_2 resonances. Provided the *fac*(N) complex has the *s-fac*(N) structure, the two peaks due to the NH_2 protons can be interpreted in the same way. If the *u-fac*(N) structure is assumed, its spectrum would have three peaks due to the NH_2 resonances with the integrated ratio of 1: 1: 2. The fact that the CN^- ion affects the NH_2 resonances is clearly recognized in the PMR spectrum of the *cis-cis*-$[Co(CN)_2(H_2O)_2(en)]^+$ complex[13] (Fig. 6-c); there are four peaks corresponding to the four protons of the two NH_2 groups of the chelated en. This fact supports the *s-fac*(N) structure of the C′-3 complex. As to the corresponding carbonato complex, the PMR spectrum was measured in 20% D_2SO_4 (under this condition the complex was converted into [CoCN-$(H_2O)_2$(dien)]$^{2+}$ species). The spectrum exhibited two broad peaks due to the NH_2 resonances, although one peak at a lower field contained a weak peak due to the NH resonance. On the basis of this obervation, the structure of the carbonato complex (C-3) is regarded as of the *s-fac*(N) form.

In establishing the structures of the isomers of the *fac*(N)-[CoCN(ox)(NH_3)(en)] complex, the PMR spectral approach did not play a part because similar spectra were expected for both the *s*- and *u*-geometries; the spectrum measured showed two peaks due to the NH_2 groups and one peak due to the NH_3 molecule. Taking into consideration the fact that the *u-fac*(N) isomer of the [CoCN(ox)(dien)] could not be isolated, the present NH_3-en complex may be regarded as a *u-fac*(N) isomer which corresponds to the *s-fac*(N) isomer of the dien complex. From the same point of view, the [CoCN-$(CO_3)(NH_3)$(en)] complex (B-2) may be regarded as a *u-fac*(N) isomer.

When the absorption spectra of the [CoCN$(CO_3)(N)_3$] type complexes are again examined in relation to their established structures, it is found that every complex exhibiting a shoulder in the second absorption band has such a configuration that no chelate ring is formed in a co-plane with the carbonate chelate ring and that the axial positions are occupied by the donor atoms exerting stronger ligand fields than the other donor atoms on the planar positions.

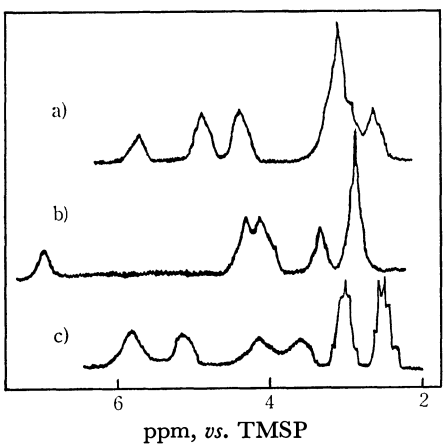

Fig. 6. PMR spectra of;
a) *mer*(N)-[CoCN(ox)(dien)], (b) *s-fac*(N)-[CoCN(ox)-(dien)], c) *cis-cis*-$[Co(CN)_2(H_2O)_2(en)]^+$.

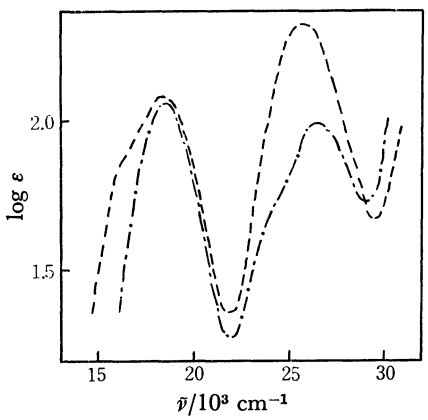

Fig. 7. Absorption spectra of mda complexes of; *trans*(N)-[Co(CO_3)(mda)$(NH_3)]^-$ (-·-·-) and *trans*(N)-[Coox(mda)$(NH_3)]^-$ (------).

In order to confirm such restrictions in configuration, an additional experiment was designed to prepare the $[Co(CO_3)(mda)(NH_3)]^-$ complex; three geometrical isomers, two *cis*(N) and one *trans*(N), can possibly exist, but only one isomer was isolated, as has been mentioned in the Experimental section. The absorption spectrum of the complex is shown in Fig. 7, together with the spectrum of the corresponding oxalato complex. The splitting of the second absorption band is observed for the carbonato complex, whereas that of the first absorption band is observed for the oxalato complex. These facts correspond to those observed for the cyanotriammine complexes and indicate that both the mda complexes are to be their *trans*(N) isomers. This assignment is supported by the PMR spectrum of the oxalato complex (where there is observed an AB pattern due to the two CH_2 groups of the chelated mda).

References

1) M. Shibata, M. Mori, and E. Kyuno, *Inorg. Chem.*, **3**, 1573 (1964).
2) S. Fujinami and M. Shibata, This Bulletin, **46**, 3443 (1973).
3) Y. Enomoto, T. Ito, and M. Shibata, *Chem. Lett.*, **1974**, 423.
4) M. Shibata, *Proc. Japan. Acad.*, **50**, 779 (1974).
5) A. Uehara, E. Kyuno, and R. Tsuchiya, This Bulletin, **43**, 1394 (1970).
6) M. Shibata, *Nippon Kagaku Zasshi*, **87**, 771 (1966).
7) S. Kanazawa and M. Shibata, This Bulletin, **44**, 2424 (1971).
8) K. Nakai, S. Kanazawa, and M. Shibata, *ibid.*, **45**, 3544 (1972).
9) S. Nakashima and M. Shibata, *ibid.*, **47**, 2069 (1974).
10) Y. Ida, K. Kobayashi, and M. Shibata, *Chem. Lett.*, **1974**, 1299.
11) H. Yamatera, This Bulletin, **31**, 95 (1958).
12) H. Siebert, C. Siebert, and K. Wieghardt, *Z. Anorg. Allg. Chem.*, **380**, 30 (1971).
13) T. Ito, and M. Shibata, unpublished.

The Polarography of *trans*-Cobalt(III) Complexes of Tetradentate Schiff Bases and α-Methylbenzylamine in *N,N*-Dimethylformamide and Methanol Solutions

Mutsuo KODAMA

Department of Chemistry, College of General Education, Hirosaki University, Bunkyo, Hirosaki 036

(Received April 21, 1975)

The polarographic behavior of mixed-ligand cobalt(III) complexes of tetradentate Schiff bases and α-methylbenzylamine (pheNH$_2$) of the general formula of [CoZ(pheNH$_2$)$_2$]$^+$ in methanol and *N,N*-dimethylformamide solutions was studied. At the dropping mercury electrode, these metal complexes give well-defined, two-step waves corresponding to the reduction of cobalt(III) to cobalt(II) and that of cobalt(II) to cobalt(I). A careful and systematic study of their polarographic behavior revealed that the reaction mechanism in the presence of uncomplexed pheNH$_2$ can be formulated as:

$$[CoZ(pheNH_2)_2]^+ + e^- \rightleftarrows [CoZ(pheNH_2)_2]^0$$
$$[CoZ(pheNH_2)_2]^0 + e^- \rightleftarrows [CoZ(pheNH_2)_2]^-$$

while, in the absence of pheNH$_2$, the reaction mechanism for the second step of the *N,N'*-ethylenebis(acetylacetoneiminato) and *N,N'*-ethylenebis(benzoylacetoiminate) systems is given by:

$$[CoZ(pheNH_2)_2]^0 + e^- \rightleftarrows [CoZ(pheNH_2)]^- + pheNH_2$$

This can be ascribed to the labile nature of the axial ligand, pheNH$_2$, in these two complexes. The introduction of halogen atoms on the methyl or methylene carbon of *N,N'*-ethylenebis(acetylacetoneiminato) and that of the benzene ring on the framework of the equatorial ligand remarkably shifted the half-wave potential towards more positive potentials. This fact suggests the electron withdrawal from the cobalt atom by these groups. Furthermore, by examining the nature of the half-wave potentials the redox orbitals of *N,N'*-ethylenebis(salicylideneaminato) and *o*-phenylenebis(salicylideneaminato) systems were concluded to be essentially different from those of other Schiff-base systems.

Previously,[1] the present author studied the polarographic behavior of a series of mixed *β-cis* and *trans*-cobalt(III) complexes of tetradentate Schiff-base dianions, baen and salen,[2] in an *N,N*-dimethylformamide (DMF) solution. All these complexes gave two well-defined polarographic steps corresponding to the reduction of cobalt(III) to cobalt(II) and that of cobalt(II) to cobalt(I). A thorough investigation of these led to the conclusion that the planar nature of baen and salen plays an important role in trapping the metal ion in an uncommon oxidation state. In order to get a deeper insight into the nature of the Schiff-base as a equatorial ligand, it seemed that it would be worthwhile to investigate the influence of tetradentate Schiff bases on the polarographic behavior of cobalt(III) complexes. In this paper, the present author will describe a polarographic study of *trans* mixed-ligand cobalt(III) complexes of tetradentate Schiff-base dianions (Z^{2-}) and methylbenzylamine (pheNH$_2$) with the general formula of [CoZ(pheNH$_2$)$_2$]$^+$ [2] in DMF and methanol solutions.

Experimental

Reagents. All the cobalt(III) complexes, [CoZ(pheNH$_2$)$_2$]ClO$_4$, used in this study were obtained from Dr. Y. Fujii (Department of Chemistry, Ibaraki Uiversity, Bunkyo, Mito, Ibaraki). The purification of DMF was described previously.[3] The tetraethylammonium perchlorate (TEAP) was prepared by the method given by Fujinaga *et al.*[4] The methanol used in this study was purified by employing the method given in a previous paper.[5] All the other chemicals used in this study were of a reagent grade and were used without further purification.

Apparatus and Experimental Procedures. The DC polarographic waves were measured by using a manual polarograph similar to Kolthoff and Lingane's or a Yanagimoto pen-recording polarograph, P-8. All the AC polarograms were recorded automatically by employing the above pen-recording polarograph. The DC polarographic data given in this paper were corrected for the residual current and the ohmic drop of the cell circuit (4.2 kΩ). The characteristics of the dropping mercury electrode (DME) used have been given previously.[6] As reference electrodes, a saturated calomel electrode (SCE) and a silver-silver chloride electrode (Ag/AgCl) were used in the DMF and methanol solutions respectively. The Ag/AgCl electrode was prepared by employing the method of Mizuguchi and Ueno.[7] TEAP for the DMF system and LiCl for the methanol system were used as supporting electrolytes. All the other experimental procedures employed were described in a previous paper.[1]

Results and Discussion

As is illustrated by the DC polarogram of [Co(benacen)(pheNH$_2$)$_2$]$^+$ complex in Fig. 1, all the cobalt(III) complexes in DMF and methanol containing an excess of uncomplexed pheNH$_2$ gave two cathodic waves, the limiting currents of which were exactly proportional to their bulk concentration and to the square-root of the effective pressure on the DME. Furthermore, their diffusion-current constants were nearly identical to that of the reduction wave of the tris(acetylacetonate) cobalt(III) complex in the DMF solution, suggesting a one-electron reduction[1] for both steps. The plot of log $(I/(I_d-I))$ against the DC potential, E, invariably gave a straight line with a reciprocal slope falling in the range from −57 mV to −70 mV (20 °C). This indicates that the electrode reactions at both steps proceed reversibly in the polarographic sense. This explanation could be also confirmed AC-polarographically. An AC polarogram with two sharp maximal

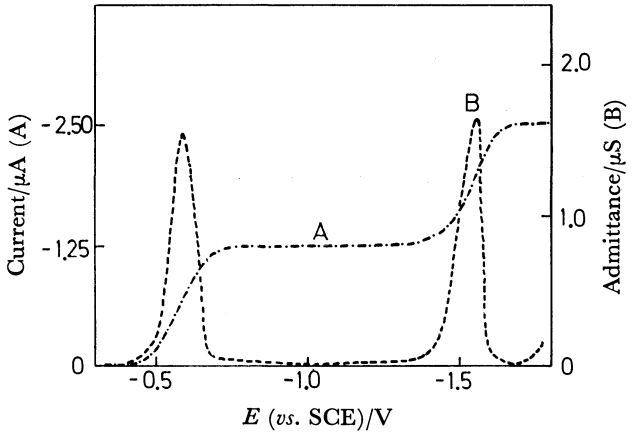

Fig. 1. DC (A) and AC (B) polarograms of 1.20 mM $[Co(benacen)(pheNH_2)_2]^+$ in DMF solution containing an excess of $pheNH_2$.
[TEAP]=0.20 M, $[pheNH_2]$=0.32 M.

currents corresponding to the DC reduction steps was obtained (Fig. 1). The concentration of the excess $pheNH_2$, when higher than 10 mM*, had no effect on the half-wave potential and the wave-height. These findings clearly suggest that the electron-transfer step is not accompanied by the dissociation of $pheNH_2$ from the complex; hence, the reaction mechanisms for the first and second steps can be expressed by Eqs. (1) and (2) respectively:

$$[CoZ(pheNH_2)_2]^+ + e^- \rightleftarrows [CoZ(pheNH_2)_2]^0 \quad (1)$$

$$[CoZ(pheNH_2)_2]^0 + e^- \rightleftarrows [CoZ(pheNH_2)_2]^- \quad (2)$$

The electrode reaction at the second step in the absence of $pheNH_2$ also proceeded reversibly in the polarographic sense. However, the first step became extended, showing an irreversible nature. The plot of $\log(I/(I_d-I))$ against E gave a straight line with a reciprocal slope falling in the range from −75 mV to −85 mV. Furthermore, a prestep appeared at a less negative potential, and its wave-height increased with the time at the expense of the first wave-height (Fig. 2). This prestep can probably be ascribed to the reduction of the $[CoZ(pheNH_2)]^+$ or CoZ^+ formed upon the dissociation of the axial ligand, $pheNH_2$, because the transformation of $[CoZ(pheNH_2)_2]^+$ into $[CoZ(pheNH_2)]^+$ or CoZ^+ lowers the energy level of the redox orbital,[8] which will then accept the electron in the course of the reduction process. The wave-height of the prestep at a given time was almost parallel with the following order of the rate constants for the dissociation of the axial ligand, $pheNH_2$, from the $[CoZ(pheNH_2)_2]^+$, lending strong support to the above explanation:

$$baen > benacen > salen > saloph > tfbaen^{9)}$$

In the light of the above findings, the irreversible nature of the first step in the absence of $pheNH_2$ can probably be ascribed to the slow partial dissociation of the axial ligand in the course of the electron-transfer step. The finding that the second step of the tfbaen complex gave a straight line with a reciprocal slope of −65 mV between $\log(I/(I_d-I))$ and E, while that of the substitution-labile benacen complex gave a linear relationship between $\log(I^2/(I_d-I))$ and E, also supports the above explanation (Fig. 3). The linear relation between $\log(I^2/(I_d-I))$ and E clearly suggests the following reaction mechanism for the second step of the benacen complex:

$$[CoZ(pheNH_2)_2]^0 + e^- \rightleftarrows [CoZ(pheNH_2)]^- + pheNH_2 \quad (3)$$

In the methanol solution, the second step of the baen system merged into the base current. Therefore, no accurate log-plot examination could be achieved under the present experimental conditions. However, in the DMF solution, quite a similar result was obtained by conducting the above log-plot examination. This indicates that the electrode reaction in the second step of the baen system in the absence of $pheNH_2$ can also be given by Eq. (3).

The equatorial ligand will have a profound effect on the physicochemical properties and the reactivity of the ligand at the axial position. With a given axial ligand, the coordination of the equatorial tetradentate ligand,

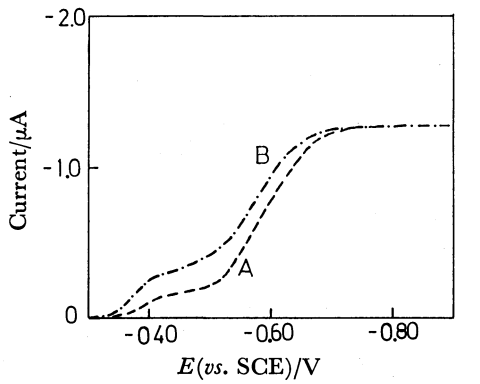

Fig. 2. DC polarogram of 1.20 mM $[Co(baen)(pheNH_2)_2]^+$ in DMF solution not containing $pheNH_2$.
[TEAP]=0.20 M
A) Time, t=10 min. B) t=30 min.

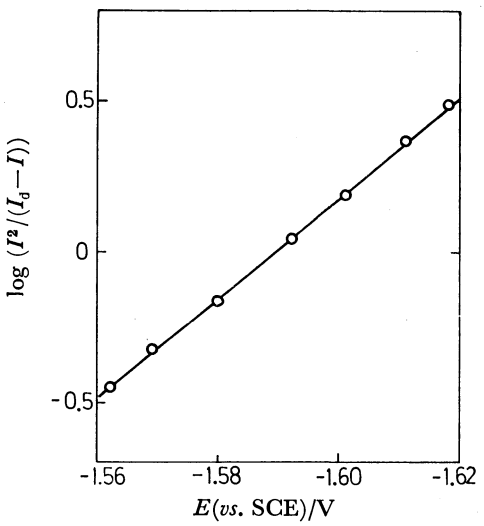

Fig. 3. The linear relation between the $\log(I^2/(I_d-I))$ and E for the 2nd step of 1.0 mM $[Co(benacen)(pheNH_2)_2]^+$.
[TEAP]=0.20 M

* M is mol dm^{-3}.

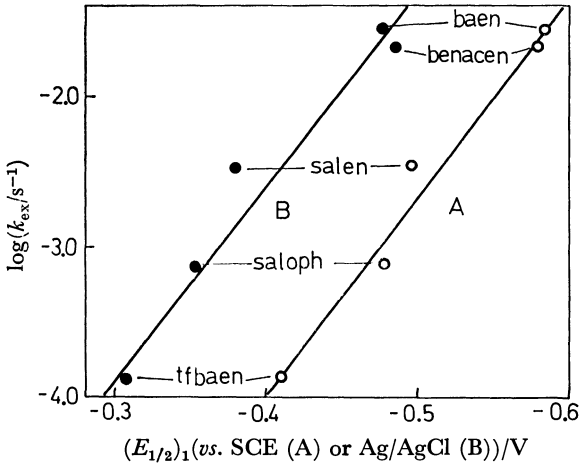

Fig. 4. The relation between the half-wave potential for the 1st step and log (k_{ex}/s^{-1}).
[pheNH$_2$]=0.32 M
A) DMF solution; [TEAP]=0.20 M
B) Methanol solution; [LiCl]=0.30 M

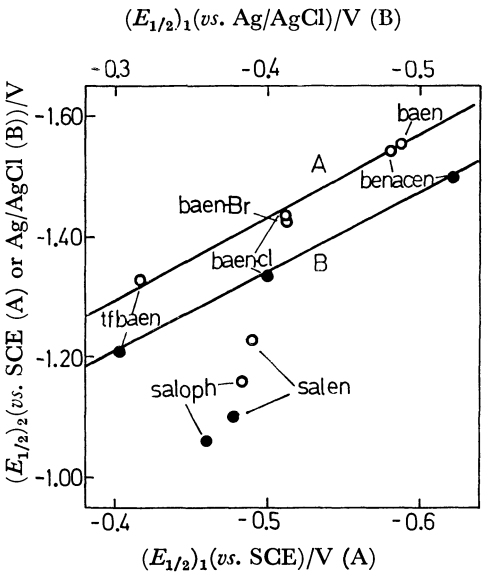

Fig. 5. The relation between the half-wave potentials for the 1st, ($E_{1/2}$)$_1$ and 2nd steps, ($E_{1/2}$)$_2$.
[pheNH$_2$]=0.32 M
A) DMF solution; [TEAP]=0.20 M
B) Methanol solution; [LiCl]=0.30 M

which gives the increase in the effective charge on the cobalt atom, will weaken the coordination bond in the axial positions and will shift the half-wave potential towards more negative potentials. Therefore, a close relationship between the half-wave potential and the magnitude of the exchange-rate constant of the axial ligand, pheNH$_2$, can be expected. As is illustrated in Fig. 4, a linear relation was found between the half-wave potential for the first step and the logarithm of the exchange-rate constant, log (k_{ex}/s^{-1}),[9] measured in the methanol solution by employing an NMR method. The half-wave potential determined in the presence of an excess of pheNH$_2$ was compared with log (k_{ex}/s^{-1}), because, only when the electrode process is rigorously reversible and the chemical reactions, including the dissociation of axial ligands which follows the electron transfer can be kept slow enough to be studied separately, the polarographic half-wave potential can give quantitative information concerning the thermodynamic aspects of the interaction of the axial ligand with the rest of the molecule.[10] As is shown by the results in Fig. 4, the replacement of the methyl group of the baen by the phenyl group (benacen) has no appreciable effect on the half-wave potential or the exchange rate of the axial ligand, pheNH$_2$. However, the replacement of the methyl hydrogen atoms of baen by fluorine (tfbaen) and the introduction of the benzene ring onto the framework of the equatorial ligand (salen and saloph) remarkably shifted the half-wave potential towards more positive potentials and reduced the rate of the exchange reaction of pheNH$_2$. The introduction of a chlorine (baen-Cl) or bromine (baen-Br) atom on the 3-position of baen also gave a positive shift of the half-wave potential (Fig. 5). As has been stated above, the half-wave potential gives a relative measure of the electron density on the cobalt atom.[11,12] Therefore, the above findings suggest that the benzene group on the framework of the equatorial tetradentate ligand and the halogen atom on the methyl or methylene carbon of baen can effectively decrease the electron density on the cobalt atom, hence enhancing the strength of the cobalt-pheNH$_2$ bond.

Finally, the present author wants to mention the following fact. As is shown by the results in Fig. 5, a linear relation holds in the DMF solution between the half-wave potentials of the first and second waves for all the tetradentate Schiff-base systems other than the salen and saloph systems. In the methanol solution, a similar linear relation also roughly holds. This probably indicates that the redox orbitals of the salen and saloph systems are essentially different from those of the other Schiff-base systems investigated. In order to describe precisely the nature of the redox orbital, though, further systematic investigation is required.

The author wishes to express his heartfelt thanks to Dr. Yuki Fujii of the Department of Chemistry, Faculty of Sciences, Ibaraki University, for his kind gift of the pure cobalt(III) complexes used in this study.

References

1) M. Kodama, Y. Fujii, and M. Sakurai, This Bulletin, **45**, 1729 (1972).
2) The following abbreviations are used throughout: baen *N,N'*-ethylenebis(acetylacetoneiminato) dianion; baen-X, *N,N'*-ethylenebis(3-halogenoacetylacetoiminato) dianion; tfbaen, *N,N'*-ethylenebis(trifluoroacetylacetoniminato) dianion; benacen, *N,N'*-ethylenebis(benzoylacetoiminato) dianion; salen, *N,N'*-ethylenebis(salicylideneaminato) dianion; saloph, *o*-phenylenebis(salicylideneaminato) dianion.
3) T. Fujinaga, K. Izutsu, K. Umemoto, T. Arai, and K. Takaoka, *Nippon Kagaku Zasshi*, **89**, 105 (1968).
4) T. Fujinaga, K. Izutsu, and K. Takaoka, *J. Electroanal. Chem.*, **12**, 203 (1966).
5) C. K. Mann, in "Electroanalytical Chemistry," Vol. 3, ed. by A. J. Bard, Marcel Dekker, New York (1969), p. 57.
6) M. Kodama, This Bulletin, **47**, 1434 (1974).

7) J. Mizuguchi and K. Ueno, *Rev. Polarog.* (Kyoto), **18**, 52 (1972).
8) F. Basolo and R. G. Pearson, "Mechanisms of Inorganic Reactions," 2nd Ed., J. Wiley, New York (1967).
9) Y. Fujii, private communication.
10) G. Costa, *Coord. Chem. Rev.*, **8**, 63 (1972).
11) G. Costa, G. Mestroni, A. Ruxeddu, and E. Reisenhofer, *J. Chem. Soc., A*, **1970**, 2870.
12) M. J. Carter, D. P. Rillema, and F. Basolo, *J. Amer. Chem. Soc.*, **96**, 392 (1974).

Electronic Spectra of Tetraphenylporphinatoiron(III) Methoxide

Hiroshi KOBAYASHI, Tadatoshi HIGUCHI, Youkoh KAIZU,
Hisajiro OSADA, and Masaru AOKI

Department of Chemistry, Tokyo Institute of Technology, Ookayama, Meguro-ku, Tokyo 152

(Received April 26, 1975)

Tetraphenylporphinatoiron(III) methoxide in the high-spin state $S=5/2$ gives rise to an absorption spectrum which has been assigned to that of low-spin iron(III) porphyrins. The excited states characteristic of the spectrum of high-spin iron(III) porphyrins are the configuration-interaction admixtures of the lowest triplet and singlet porphyrin (π,π^*) excited states and the low-lying "porphyrin to iron(III)" charge-transfer excited states. The charge-transfer excited states in tetraphenylporphinatoiron(III) methoxide, however, are so high that the charge-transfer excited states are not sufficiently mixed with the lowest triplet (π,π^*) excited states. Thus the high-spin methoxo complex does not exhibit a spectrum characteristic of high-spin iron(III) porphyrins.

Possible spin states of the iron(III) ion embedded in porphyrin ligand are the high-spin state $S=5/2$ and the low-spin state $S=1/2$ depending upon its axial ligand field. The intermediate spin state $S=3/2$ is not obtained for a typical ligand field of porphyrin.[1-3] George, Beetlestone and Griffith separated the high- and low-spin spectral types for the ferrihemoproteins by combining spectroscopic and magnetic data.[4] They could get limiting spectra from the mixture spectra of the two spin states $S=5/2$ and $S=1/2$ in equilibrium. On the other hand, Caughey found that a high-spin iron(III) porphyrin, methoxo iron(III) deuteroporphyrin-IX dimethyl ester, shows an absorption spectrum characteristic of low-spin iron(III) porphyrins.[5,6]

In this paper, an interpretation of the low-spin type of spectrum observed for high-spin porphyrinatoiron(III) methoxides is presented on the basis of experimental observations for tetraphenylporphinatoiron(III) methoxide.

Experimental

Synthesis of the Metal-free Base of Tetraphenylporphin (H_2TPP). H_2TPP was synthesized by the method of Adler *et al.*[7] Chromatographic purification was repeated on activated alumina columns using chloroform as a solvent and also as an eluent. The elute was concentrated, and then excess methanol was added. Purple needle crystals thus obtained were identified by elemental analysis.

Found: C, 86.18; H, 4.61; N, 8.96%. Calcd for $C_{44}H_{30}N_4$: C, 85.97; H, 4.92; N, 9.11%.

Synthesis of Tetraphenylporphinatoiron(III) Chloride (TPPFe(III)Cl). TPPFe(III)Cl was prepared in dimethylformamide (DMF). H_2TPP (0.3 g) and $FeCl_2\cdot 4H_2O$ (1.5 g) were dissolved in DMF (200 ml) and refluxed for 3 h. When the solution was cooled, dilute hydrochloric acid were added in small portions. The dark purple crystals thus precipitated were collected by filtration. The complex was recrystallized twice from a mixture of 1,2-dichloroethane and *n*-hexane.

Found: C, 74.94; H, 3.85; N, 7.92; Fe, 7.97; Cl, 5.10%. Calcd for $C_{44}H_{28}N_4FeCl$: C, 75.07; H, 4.01; N, 7.96; Fe, 7.93; Cl, 5.04%.

Synthesis of Tetraphenylporphinatoiron(III) Methoxide (TPPFe(III)OCH_3). A methanol solution of sodium methoxide prepared by dissolving metal sodium (1 g) in dry methanol (100 ml) was added to a solution of TPPFe(III)Cl (0.7 g) in dry benzene (350 ml). The mixture was refluxed for 3 h and then filtered. The filtrate was concentrated under reduced pressure until crystals appeared and then a small amount of dry methanol was added. The blue crystals thus obtained were collected by filtration, washed with dry methanol, and dried *in vacuo* over silica gel.

Found: C, 77.72; H, 4.64; N, 7.87; Fe, 7.91%. Calcd for $C_{45}H_{31}N_4OFe$: C, 77.26; H, 4.47; N, 8.01; Fe, 7.98%.

Synthesis of Bisimidazoletetraphenylporphinatoiron(III) Perchlorate ([TPPFe(III)$(Im)_2$]ClO_4). TPPFe(III)Cl (35 mg) was dissolved in benzene (5 ml). Silver perchlorate (10 mg) was added to the solution. After being refluxed for 4 h, silver chloride was filtered off and then imidazole (6 mg) was added. Reddish purple crystals precipitated upon the addition of imidazole. When the precipitation was completed, unreacted silver perchlorate and imidazole were dissolved by addition of ethyl ether (5 ml). The precipitate thus obtained was dissolved in 1,2-dichloroethane and then filtered for separation of the contaminating silver chloride. The filtrate was condensed under reduced pressure. Benzene was then added for precipitation. Pure crystals were obtained by recrystallization from a mixture of 1,2-dichloroethane and benzene.

Found: C, 66.18; H, 3.67; N, 12.50; Fe, 6.08%. Calcd for $C_{50}H_{36}N_8FeClO_4$: C, 66.42; H, 4.01; N, 12.39; Fe, 6.18%.

Synthesis of μ-Oxo-bis(tetraphenylporphinatoiron(III)) ([TPPFe(III)]$_2O$). The complex was obtained by shaking a benzene solution of TPPFe(III)Cl with aqueous KOH.[8] The resulting benzene solution was evaporated to dryness. The residue was dissolved in chloroform and then methanol was added. The purple crystals thus precipitated were collected and washed with methanol. The complex was purified by chromatography in a column packed with Sephadex LH-20 using tetrahydrofuran as a solvent and an eluent. The first fraction of the elute was evaporated to dryness. The residue was recrystallized from a mixture of 1,2-dichloroethane and *n*-hexane.

Found: C, 77.74; H, 4.07; N, 8.08%. Calcd for $C_{88}H_{56}N_8OFe_2$: C, 78.11; H, 4.17; N, 8.28%.

Measurements of Absorption and Magnetic Circular Dichroism Spectra. The electronic absorption spectra were recorded on a Shimadzu recording spectrophotometer Model MPS-50. Solvents were benzene, and 1,2-dichloroethane purified by fractional distillation using a 1.5 m Dixson-ring packed column and dried by the usual procedure.[9]

The absorption spectra of the powder samples were measured by the opal glass method.[10] Instead of an opal glass plate, a sheet of tracing paper smeared with the solid sample was placed in front of the window of a head-on type photomultiplier in the Shimadzu spectrophotometer.

The circular dichroism under an external magnetic field (MCD) was measured on a JASCO automatic recording spectropolarimeter Model ORD/UV-5 with its CD attachment and electro-magnet. The magnetic field was set at

10000 Gauss.

Magnetic Susceptibility. The magnetic susceptibilities of the complexes were measured at room temperature by means of the Gouy method. After a calibration of the diamagnetic term by the conventional method, the magnetic moments of the complexes were evaluated.[11]

Infrared Spectra. The infrared spectra of the complexes in KBr disk were taken on a Hitachi infrared spectrometer Model EPI-G3.

ESR Spectra. The ESR spectra were obtained with a Japan Electron Optics Laboratory spectrometer Model JES-ME3X. The static magnetic field was calibrated by means of a proton-resonance gaussmeter.

Results and Discussion

The electronic absorption spectrum of TPPFe(III)Cl is typical of high-spin iron(III) porphyrins. Three other iron(III) porphyins, TPPFe(III)OCH_3, [TPPFe(III)$(Im)_2$]ClO_4 and [TPPFe(III)]$_2O$, exhibit spectra resembling each other, but differing in profile from the spectrum characteristic of high-spin iron(III) porphyrins The absorption and MCD spectra are presented in Figs. 1 and 2.

The absorption spectrum of [TPPFe(III)$(Im)_2$]ClO_4 in 1,2-dichloroethane (Fig. 1) is a typical low-spin spectrum. The low-spin spectrum was also obtained for [TPPFe(III)$(Im)_2$]Cl and [TPPFe(III)$(Im)_2$]ClO_4 in chloroform which consists of ten times or more excess imidazole. La Mar and Walker also observed in their NMR studies that the proton signals of the low-spin species were detected only in the presence of eight times excess imidazole in deuterochloroform.[12] In chloroform, however, a drift of the absorption spectrum was observed for a few hours even in the presence of excess imidazole. This indicates the dissociation of coordinated imidazole in solution. In 1,2-dichloroethane, the absorption spectrum does not change for a few days after the sample is dissolved in the absence of excess imidazole.

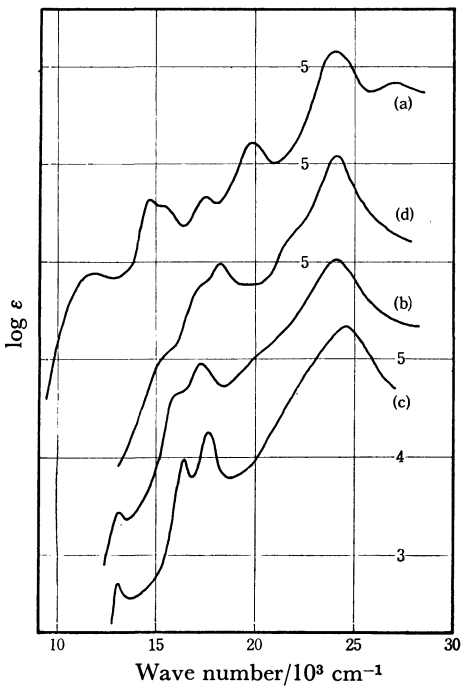

Fig. 1. Absorption spectra of TPPFe(III)Cl(a), TPPFe(III)OCH_3(b) and [TPPFe(III)]$_2O$(c) in benzene, and [TPPFe(III)$(Im)_2$]ClO_4(d) in 1,2-dichloroethane.

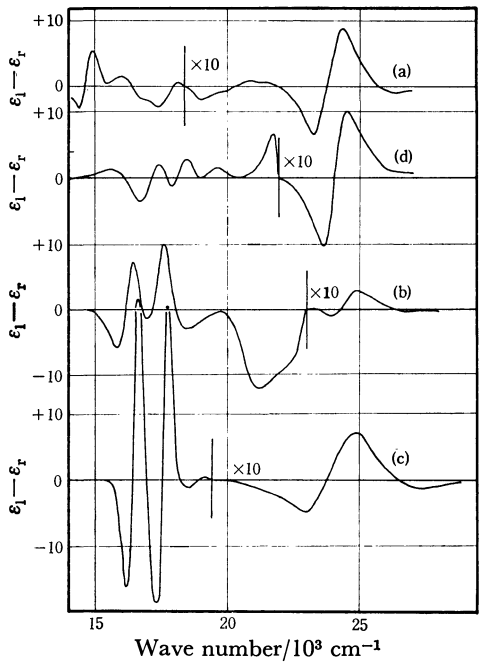

Fig. 2. MCD spectra of TPPFe(III)Cl(a), TPPFe(III)-OCH_3(b) and [TPPFe(III)]$_2O$(c) in benzene, and [TPPFe(III)$(Im)_2$]ClO_4(d) in 1,2-dichloroethane.

The absorption spectrum of TPPFe(III)OCH_3 dissolved in dry benzene (Fig. 1) is very similar to that of [TPPFe(III)$(Im)_2$]ClO_4. Unless the solvent and the

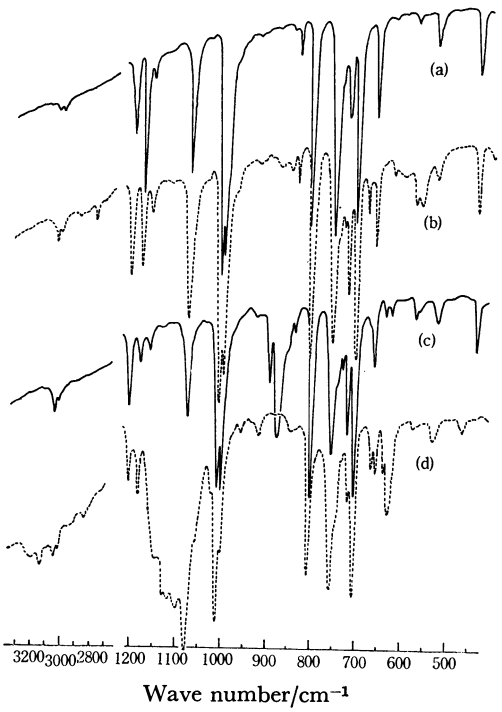

Fig. 3. IR spectra of TPPFe(III)Cl(a), TPPFe(III)-OCH_3(b), [TPPFe(III)]$_2O$(c), and [TPPFe(III)-$(Im)_2$]ClO_4(d) in KBr disk.

apparatus are sufficiently dried, the absorption spectrum gradually changes to that of $[TPPFe(III)]_2O$. The moisture in solution reacts with $TPPFe(III)OCH_3$ forming $[TPPFe(III)]_2O$, a dimer with Fe–O–Fe bridge.[13] $[TPPFe(III)]_2O$ exhibits two strong IR peaks of antisymmetric vibrations of Fe–O–Fe at 875 cm^{-1} and 895 cm^{-1}.[8,13] $TPPFe(III)OCH_3$ lacks such IR peaks in the region but shows a C–H stretching peak of coordinated OCH_3 group at 2800 cm^{-1}. The IR spectra are shown in Fig. 3.

Table 1. Magnetic moments of TPPFe(III)Cl, $TPPFe(III)OCH_3$ and $[TPPFe(III)(Im)_2]ClO_4$

Complex	χ (10^{-6} cgs/mol)	Temperature (K)	μ_{eff} (B.M.)	Spin state
$[TPPFe(III)(Im)_2]ClO_4$	2493	291.7	2.41	$S=1/2$
TPPFe(III)Cl	14733	292.8	5.87	$S=5/2$
$TPPFe(III)OCH_3$	14489	293.3	5.83	$S=5/2$

The magnetic moments which were measured by the Gouy method are given in Table 1. The measurement reveals that the solid sample of $TPPFe(III)OCH_3$ is in the high spin state $S=5/2$, although the absorption spectrum in benzene is of low-spin type. The ESR spectrum of solid $TPPFe(III)OCH_3$ measured at 77 K ($g_\perp=5.30$, $g_{//}=2.00$) is also a spectrum characteristic of high-spin species such as TPPFe(III)Cl ($g_\perp=6.00$, $g_{//}=2.00$).[14] The ESR spectra are shown in Fig. 4. Since an interconversion of the spin state was possible upon dissolution of the sample into a solvent, the absorption spectra of the solid samples were examined by the opal glass method. They were found, however, to coincide qualitatively with the solution spectra (Fig. 5). A spectral change to be attributed to a spin interconversion does not occur on dissolution. The solution spectrum is less dependent upon solvents unless the solvent molecules replace the axial ligands.

The lowest excited states, which are responsible for the absorption spectra of high-spin iron(III) porphyrins and of high-spin manganese(III) porphyrins, are well described as a configuration-interaction admixture of the lowest triplet and singlet (π, π^*) excited states of porphyrin and the "porphyrin to metal" charge-transfer (CT) excited states.[15] Since the ground state of the high-spin iron(III) porphyrin is $^6A_1$ the allowed photo-excited states should be spin-sextet. The energies of the (π, π^*) excited states $^6E_T(\pm 9a)$, $^6E_T(\pm 1a)$, $^6E_Q(\pm 9b)$

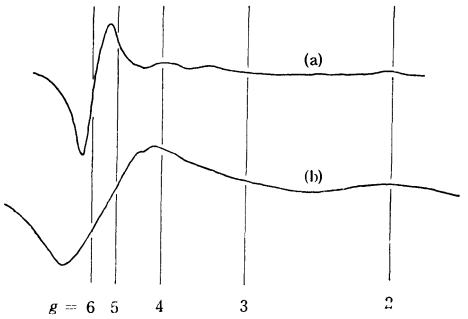

Fig. 4. ESR spectra of TPPFe(III)Cl(a) and TPPFe-(III)OCH_3(b) in the solid state at 77 K.

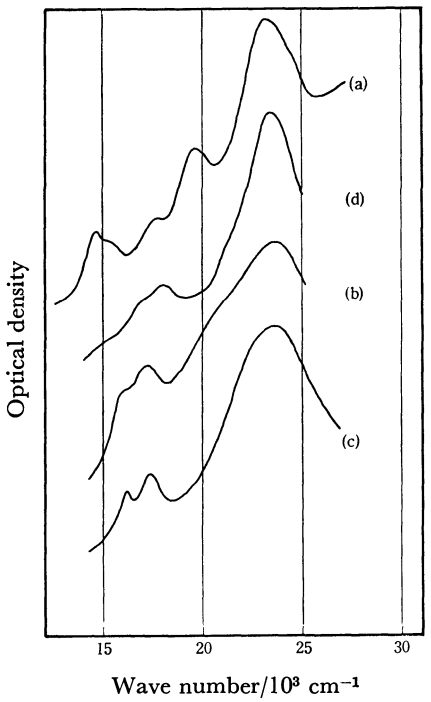

Fig. 5. Absorption spectra of TPPFe(III)Cl(a), TPPFe-(III)OCH_3(b), $[TPPFe(III)]_2O$(c) and $[TPPFe(III)(Im)_2]ClO_4$(d) in the solid state.

and $^6E_B(\pm 1b)$ and the CT excited states $^6E_{CT}(\pm 5)$ and $^6E_{CT}(\mp 3)$ are given in terms of energy parameters E, K_9, K_1, and E_{CT}.[15] The mixing terms of the excited sextets are given in terms of the delocalization parameter β and the off-diagonal corrections ε, ε', and ε'' for the assumption of an accidental degeneracy in the highest filled porphyrin orbitals. The molecular param-

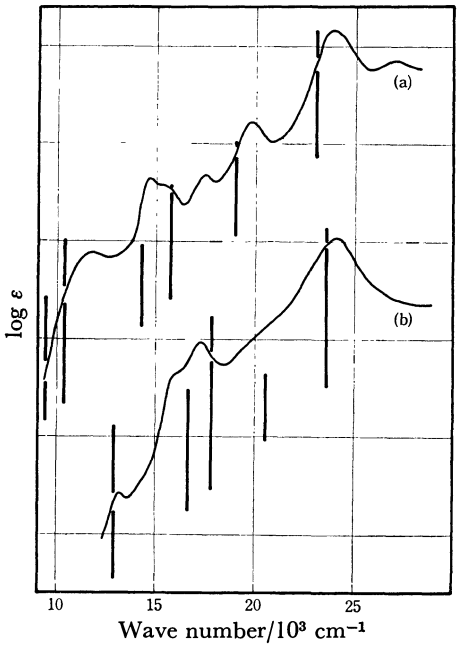

Fig. 6. The calculated lowest excitations of TPPFe(III)-Cl(a)($E_{CT}=12500\,cm^{-1}$) and $TPPFe(III)OCH_3$(b)($E_{CT}=17500\,cm^{-1}$). The assumed parameter values are $E=13070\,cm^{-1}$, $K_1=4600\,cm^{-1}$, $K_9=2730\,cm^{-1}$, $\beta=-3000\,cm^{-1}$, $\varepsilon=1340\,cm^{-1}$, $\varepsilon'=-1340\,cm^{-1}$, and $\varepsilon''=0\,cm^{-1}$.

TABLE 2. CALCULATED COMPOSITIONS OF THE EXCITED SEXTET STATES OF THE HIGH-SPIN IRON(III) PORPHYRIN ($E_{CT}=17500$ cm^{-1})

	a^{6}E	b^{6}E	c^{6}E	d^{6}E	e^{6}E	f^{6}E
Excitation energy (cm^{-1})	10700	12800	16700	17800	20400	23500
log ε	2.08	3.02	3.49	4.28	3.67	5.12
$^6E_{CT}$ ($\Lambda_z=\pm5$)	0.2652	−0.3794	0.5246	0.2326	0.6673	−0.1056
$^6E_{CT}$ ($\Lambda_z=\mp3$)	0.2541	0.3675	0.0206	0.7899	−0.2382	−0.3453
^6E_T ($\Lambda_z=\pm9$)	0.6593	−0.5700	−0.4210	−0.0051	−0.2510	0.0150
^6E_T ($\Lambda_z=\pm1$)	0.6517	0.5980	0.1413	−0.4178	0.1271	0.0810
^6E_Q ($\Lambda_z=\pm9$)	0.0654	−0.1654	0.7077	−0.0268	−0.6223	0.2823
^6E_B ($\Lambda_z=\pm1$)	0.0391	0.1058	−0.1610	0.3829	0.1778	0.8850
Λ_z ($\hbar$)	±4.53	±3.85	±7.52	∓1.27	±6.16	±1.21
Number of the transferred charge	0.135	0.279	0.276	0.678	0.502	0.130

The assumed parameter values are $E=13070$ cm^{-1}, $K_1=4600$ cm^{-1}, $K_9=2730$ cm^{-1}, $\beta=-3000$ cm^{-1}, $\varepsilon=1340$ cm^{-1}, $\varepsilon'=-1340$ cm^{-1}, and $\varepsilon''=0$ cm^{-1}.

eters except E_{CT} were estimated to reproduce the transition energies and the intensity ratio of the Q and B bands of TPPCo(III)Cl in pyridine. The transition energies and intensities for the lowest excited sextets of high-spin iron(III) porphyrins were calculated for a variety of E_{CT}. The calculated lowest excited sextets can well reproduce the observed lowest excited states of TPPFe(III)Cl for $E_{CT}=12500$ cm^{-1}. The electronic absorption spectrum of TPPFe(III)OCH_3 is also reproduced for the same molecular parameters of TPPFe(III)-Cl except a high E_{CT} value of 15000 cm^{-1} or 17500 cm^{-1}. The calculated lowest excited states of TPPFe(III)X are shown with the observed spectra in Fig. 6. In the case of a high-spin iron(III) porphyrin with $E_{CT}=12500$ cm^{-1}, the "porphyrin to iron(III)" charge-transfer excited states crucially mix with the lowest triplet (π, π^*) excited states and give rise to a blue shift of the excited state which is essentially assigned to the Q (π, π^*) state. This results in a typical spectrum of high-spin iron(III) porphyrins. In the case of a high-spin iron(III)porphyrin with $E_{CT}=17500$ cm^{-1}, on the other hand, the charge-transfer excited states do not mix sufficiently with the triplet (π, π^*) excited states, the high-spin iron(III) porphyrin thus exhibiting a spectrum differing from the typical spectrum of high-spin iron(III) porphyrins. Contributions of the composite excited states to each of the lowest excited states are presented in Table 2, together with the calculated values of orbital angular momentum and transferred charge from "porphyrin to iron(III)" in the excited states.

An increase in the charge-transfer energy in high-spin porphyrinatoiron(III) methoxides is attributed to a reduction in the dπ electron affinity of the central iron-(III) ion for a greater charge donation by the coordinated OCH_3. The magnitude of the zero-field splitting of the $^6A_1$ components of ferric ion ($\Delta E_1 \equiv E(^6A_1 \mp 3/2) - E(^6A_1 \pm 1/2)$) has been directly measured by far-infrared spectroscopy on the methoxide and chloride of ferric deuteroporphyrin-IX dimethyl ester (ΔE_1-(OCH_3)$=9.3$ cm^{-1}; ΔE_1(Cl)$=17.9$ cm^{-1}).[16,17] Here, ΔE_1 is given by $2D$ in terms of $D=\zeta^2/5(E_4-E_6)$, where ζ is the spin-orbit coupling constant and E_4-E_6 is the first-order energy difference between $^4A_2(\theta\xi^2+1-1)$ and $^6A_1(\varepsilon\theta\zeta+1-1)$ states.[18] For a strong axial field, an energy difference between ε and θ is reduced and then $^4A_2$ lies higher. This implies that an increase in the axial ligand field results in a reduction in ΔE_1. Thus the observed zero-field splitting supports a greater charge donation by the coordinated OCH_3^-.

The authors wish to express their sincere thanks to Professor W. S. Caughey who brought the low-spin type of spectrum in a high-spin porphyrinatoiron(III) methoxide to their attention during the course of collaboration by one of the authors (H. K.) in Johns Hopkins Medical School. The authors are indebted to Professor J. Higuchi and Dr. T. Ito for the measurements of ESR spectrum.

References

1) J. S. Griffith, *Proc. Roy. Soc., Ser. A*, **235**, 23 (1956).
2) J. S. Griffith, *Discuss. Faraday Soc.*, **26**, 81 (1956).
3) J. S. Griffith, "The Theory of Transition-Metal Ions," Cambridge University Press (1961), p. 366.
4) P. George, J. Beetlestone, and J. S. Griffith, "Haematin Enzymes," ed. by J. E. Falk, R. Lemberg, and R. K. Morton, Pergamon Press, Oxford (1961), p. 105.
5) W. S. Caughey, J. L. York, and P. K. Iber, "Magnetic Resonance in Biological Systems," ed. by A. Ehrenberg, B. G. Malmström and T. Vänngard, Pergamon Press, Oxford (1967), p. 25.
6) W. S. Caughey, "Inorganic Biochemistry," Vol. 2, ed. by G. L. Eichhorn, Elsevier, Amsterdam (1973), p. 829; See also the spectrum of methoxo iron(III) deuteroporphyrin-IX dimethyl ester reported by J. O. Alben, W. H. Fuchsman, C. A. Beaudreau, and W. S. Caughey, *Biochemistry*, **7**, 624 (1968).
7) A. D. Adler, F. R. Longo, J. D. Finavells, J. Goldmacher, J. Assour, and L. Korsakoff, *J. Org. Chem.*, **32**, 476 (1967).
8) E. B. Fleischer and T. S. Srivastava, *J. Amer. Chem. Soc.*, **91**, 2403 (1969).
9) D. D. Perrin, W. L. F. Armarego, and D. R. Perrin, "Purification of Laboratory Chemicals," Pergamon Press, Oxford (1966).
10) K. Shibata, "Methods of Biochemical Analysis," Vol. 7, ed. by C. Glick, Interscience Publishers, New York (1959), p. 77.

11) B. N. Figgis and J. Lewis, "Modern Coordination Chemistry," ed. by J. Lewis and R. G. Wilkins, Interscience Publishers, New York (1960), p. 415.
12) G. N. La Mar and F. A. Walker, *J. Amer. Chem. Soc.*, **94**, 8607 (1972).
13) I. A. Cohen, *ibid.*, **91**, 1980 (1969).
14) J. S. Griffith, "The Theory of Transition-Metal Ions," Cambridge University Press (1961), p. 352.
15) H. Kobayashi, Y. Yanagawa, H. Osada, S. Minami, and M. Shimizu, This Bulletin, **46**, 1471 (1973).
16) P. L. Richards, W. S. Caughey, H. Eberspaecher, G. Feher, and M. Malley, *J. Chem. Phys.*, **47**, 1187 (1967).
17) G. C. Brackett, P. L. Richards, and W. S. Caughey, *ibid.*, **54**, 4383 (1971).
18) J. S. Griffith, "The Theory of Transition-Metal Ions," Cambridge University Press (1961), p. 369.

Complex Formation of Indium(III) with Murexide and the Decomposition of Murexide in the Presence of Indium(III) in Acid Perchlorate Media

Yoichi KAWAI,* Taira IMAMURA, and Masatoshi FUJIMOTO
Department of Chemistry, Faculty of Science, Hokkaido University, Sapporo 060
(Received April 28, 1975)

Kinetic and equilibrium data on the complex formation between In(III) and murexide are derived using stopped-flow method and also from the rate of decomposition of the ligand in acid perchlorate media. The rate of complex formation is independent of the acid concentration over the wide range of [H] between 0.001 and 0.5 M. The discrepancies of the stability constants obtained from the direct and the indirect methods are discussed.

Murexide, ammonium purpurate, has long been used as a very useful metallochromic indicator[1] except for acid region, where it decomposes to uramil and alloxan.[2,3] The rate of the decomposition depends on the acid concentration.[2] We are interested in the reaction mechanism of the complex formation between indium(III) and murexide in connection with the possibility of catalytic action of indium(III) on the decomposition of murexide.

The rates of metal complex formations in general are affected by the acid concentration due to the contribution of hydrolyzed forms of the metal ion.[4] The kinetic data on the metal complex formations with murexide in the neutral region were reported in detail by Geier.[5] In the case of indium(III) and murexide, however, we observed no dependence on the hydrogen-ion concentration of the rate of complex formation. In the present report the complex formation between indium(III) and murexide and the decomposition of murexide in the presence of indium(III) ion are studied over a wide range of the hydrogen-ion concentrations 0.001—0.5 M.

Experimental

Materials. Deionized water was distilled. Reagent grade materials were used unless otherwise specified. Indium(III) perchlorate solution was prepared by dissolving indium(III) oxide in a small excess of concentrated perchloric acid. The concentration was titrimetrically determined with EDTA using Xylenol Orange as indicator. Weighed amount of commercial or prepared murexide[6] was dissolved in water immediately before use.

Acidity and ionic strength of the solutions were adjusted with perchloric acid and sodium perchlorate. The stock solution of perchloric acid was standardized by titration with sodium hydroxide. The stock solution of sodium perchlorate was kept for a couple of weeks to precipitate trace amount of metal impurities together with silicates and filtered through a glass filter. An aliquot of the solution was passed through a column of cation-exchange resin (Dowex 50W-X8) in the H-form and titrated with sodium hydroxide.

Measurements. The rates of decomposition and the spectra were measured with a Hitachi EPS-3T spectrophotometer equipped with a recorder. The thermostated reactant solutions were pipetted and mixed with shaking in a thermostated optical cell.

A Yanagimoto SPS-1 stopped-flow apparatus was used to measure the rate of complex formation. The optical cell and the reservoirs were thermostated by circulating the water from a thermostat.

Results

Stability Constant of the Complex Measured by Stopped-flow Method at [H]=0.5 M. Equilibrium data of the complex in the acid range were directly derived from the change in absorbance as measured by stopped-flow technique.

Formation of 1 : 1 complex between indium(III) and murexide (MX) was confirmed by the mole ratio method. The absorption maximum of the complex (InMX) lies at 470 nm with the molar extinction coefficient $\varepsilon_{InMX}=8.82\times10^3$ at [H]=0.5 M and ionic strength 2.0 M ($NaClO_4$). The value ε_{MX} at 470 nm was evaluated to be 4.51×10^3.

Under high acid concentration the rapid complex formation is followed by the slow decomposition of murexide. Stability constant of the complex K_{1a} at 25 °C and [H]=0.5 M was calculated from the change in absorbance at 470 nm memorized on the screen of oscilloscope.

Stability constant K_{1a} is written as follows.

$$K_{1a}=\frac{[InMX]}{\{[In]_0-[InMX]\}\{[MX]_0-[InMX]\}},$$

$$A=\varepsilon_{MX}[MX]_0+(\varepsilon_{InMX}-\varepsilon_{MX})[InMX], \text{ and}$$

$$[InMX]=\frac{A-\varepsilon_{MX}[MX]_0}{\varepsilon_{InMX}-\varepsilon_{MX}},$$

where $[In]_0$ and $[MX]_0$ are the initial concentrations of indium(III) and murexide respectively, and A, ε_{InMX}, and ε_{MX} denote the observed absorbance, the molar extinction coefficients of the complex and the ligand at 470 nm respectively.

The plot of $\{[In]_0-[InMX]\}\{[MX]_0-[InMX]\}$ *versus* [InMX] gave a straight line as shown in Fig. 1 and value of K_{1a} was evaluated from the slope to be 7.2×10^3 M^{-1} at [H]=0.5 M, μ=2.0 M ($NaClO_4$) and at 25 °C.

Rate of Complex Formation and Stability Constants. The rate of complex formation between indium(III) and murexide was measured by following the increase in the absorbance of the complex with time. The rate

* Present address: Sumitomo Chemical Industries, Ltd., Niihama, Ehime.

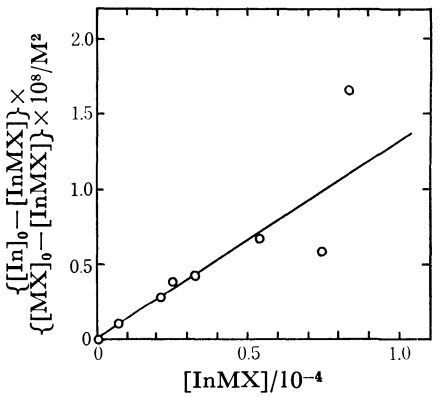

Fig. 1. Plot of $\{[In]_0-[InMX]\}\{[MX]_0-[InMX]\}$ *vs.* [InMX] at 25 °C, μ=2.0 ($NaClO_4$), and [H]=0.5 M.

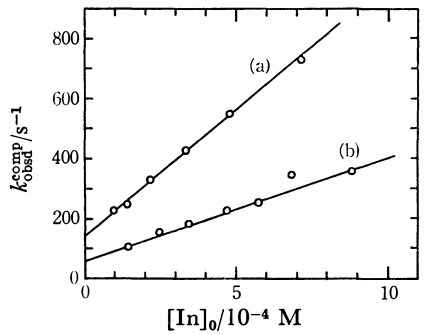

Fig. 2. Plot of k_{obsd}^{comp} *vs.* total concentration of In(III) at [H]=0.5 M and μ=2.0 ($NaClO_4$).
(a) $[MX]_0=4.08\times10^{-5}$ M and at 25 °C; (b) $[MX]_0=1.08\times10^{-5}$ M and at 10 °C.

of complex formation is increased with increasing concentration of indium(III). Figure 2 shows the dependence of the pseudo-first-order rate constant on indium(III) concentration under the conditions of $[In]_0 \gg [MX]_0$, [H]=0.5 M, μ=2.0 M ($NaClO_4$) and at 10 or 25 °C.

The values of $\vec{k}$, $\overleftarrow{k}$ and K_{1b} for the reaction

$$In + MX \underset{\overleftarrow{k}}{\overset{\vec{k}}{\rightleftharpoons}} InMX$$

are evaluated as shown in Table 1.

Table 1. Kinetic and equilibrium data of the indium(III)-murexide complex, measured at [H]=0.5 M and μ=2.0 ($NaClO_4$).

T (°C)	$\vec{k}$ ($M^{-1}\cdot s^{-}$)	$\overleftarrow{k}$ (s^{-1})	$K_{1b}=\vec{k}/\overleftarrow{k}$ (M^{-1})
10	$3.5_4\times10^5$	$57._6$	$6.1_4\times10^3$
25	$8.5_2\times10^5$	130	$6.5_5\times10^3$

Table 2 shows the rate constants k_{obsd}^{comp}, $\vec{k}$ and $\overleftarrow{k}$ for the wide range of acid concentrations at ionic strength 2.0 M ($NaClO_4$) and 10 °C. Since the pseudo-first-order rate constant k_{obsd}^{comp} does not depend on the acid concentration, it would be reasonable to conclude that the both rate constants $\vec{k}$ and $\overleftarrow{k}$ do not depend on the acid concentration.

Effect of $[MX]_0$ *and* $[H]$ *on the Rate of Decomposition of Murexide.* The absorption maximum of murexide

Table 2. [H]-Dependence of the rate of complex formation between indium(III) and murexide at 10 °C and μ =2.0 ($NaClO_4$). ($[In]_0$= 4.77×10^{-4} M, $[MX]_0=5.10\times10^{-5}$ M).

[H] (M)	k_{obsd}^{comp} (s^{-1})	$\vec{k}=(k_{obsd}^{comp}-\overleftarrow{k})/[In]_0$ ($M^{-1}\cdot s^{-1}$)
0.5	230	3.61×10^5
0.4	(162)[b]	$(4.42)^{b}\times10^5$
0.3	(156)[b]	$(4.17)^{b}\times10^5$
0.2	190	2.78×10^5
0.1	230	3.61×10^5
0.05	250	4.03×10^5
0.01	210	3.20×10^5
0.005	220	3.40×10^5
0.001	230	3.61×10^5

a) The value of $\overleftarrow{k}$ was evaluated to be 57.6 s^{-1} (see Table 1). b) The values in parentheses are those from other series of data with $[In]_0=2.36\times10^{-4}$ M and $[MX]_0=2.65\times10^{-5}$ M. Experimental errors for the values of k_{obsd}^{comp} are *ca.* ±8%.

Table 3. $[MX]_0$-Dependence of the rate of the decomposition of murexide at 25 °C, μ=2.0 ($NaClO_4$) and [H]=0.5 M.

$[MX]_0$ (M)	k_{obsd}^{dec} (s^{-1})
2.5×10^{-6}	0.11
5.0×10^{-6}	0.11
2.5×10^{-5}	0.10
1.0×10^{-4}	0.093
1.5×10^{-4}	0.085

lies at 530 nm at [H]=0.5 M and μ=2.0 M ($NaClO_4$) in the concentration range between $[MX]_0=1.0\times10^{-4}$ and 2.5×10^{-6} M. The effect of initial concentration of murexide on the rate of decomposition is shown in Table 3. Though the rate shows some dependence on the concentration of murexide, the observed tendency of decrease was quite small despite of the large concentration change of murexide more than two orders of magnitude. The similar tendency is also reported in Ref. 2.

The decomposition of murexide is accelerated by acid. Figure 3 shows that the reciprocal of the pseudo-first-order rate constant for the decomposition of murexide has a linear relation to $[H]^{-1}$. The proposed reaction scheme is thus as follows.

$$MX + H \underset{}{\overset{K_{2a}}{\rightleftharpoons}} MXH$$

$$MXH \xrightarrow{k_{2a}} Uramil + Alloxan,$$

where MX and MXH denote purpurate anion and purpuric acid respectively.

The rate of decomposition is written as

$$k_{obsd}^{dec\,-1} = \frac{1}{k_{2a}} + \frac{1}{k_{2a}K_{2a}}\cdot\frac{1}{[H]}.$$

According to the above equation the values $k_{2a}K_{2a}$ and k_{2a} are evaluated to be $k_{2a}K_{2a}=0.16$ M^{-1} s^{-1} and $k_{2a}=$ 1.2 s^{-1} from the slope and the intercept respectively. The constant K_{2a} is therefore calculated to be about 0.13 M^{-1}. However, as the intercept passes through

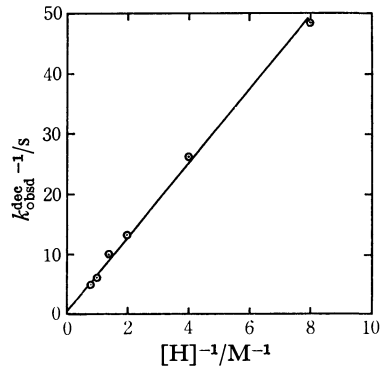

Fig. 3. Plot of $k_{obsd}^{dec\ -1}$ *vs.* inverse of hydrogen-ion concentration.
at 530 nm, 25 °C, μ=2.0 ($NaClO_4$), and $[MX]_0$= 1.02×10^{-4} M.

very near the origin, each value of k_{2a} and K_{2a} has eventually a great inaccuracy of 50%. More accurate value of K_{2a} is given by K_{2b} in the next section from the effect of indium(III) on the decomposition of murexide.

Rate of Decomposition of Murexide in the Presence of Indium(III). The rate of decomposition of murexide was also studied by following the change in absorbance at the absorption peak of the complex at constant acid concentration [H]=0.5 M. The apparent rate of decomposition was decreased with increasing concentration of indium(III). This result is ascribed to the inertness of the indium(III) complex against the decomposition of the ligand murexide.

Now let us write the reaction scheme as follows.

$$In + MX \overset{K_{1c}}{\rightleftarrows} InMX$$

$$MX + H \overset{K_{2b}}{\rightleftarrows} MXH$$

$$MXH \xrightarrow[+H_2O]{k_{2b}} Uramil + Alloxan.$$

The rate of decomposition is written as

$$k_{obsd}^{dec\ -1} = \frac{[H]K_{2b}+1}{[H]k_{2b}K_{2b}} + \frac{K_{1c}}{[H]k_{2b}K_{2b}}\cdot[In]_0.$$

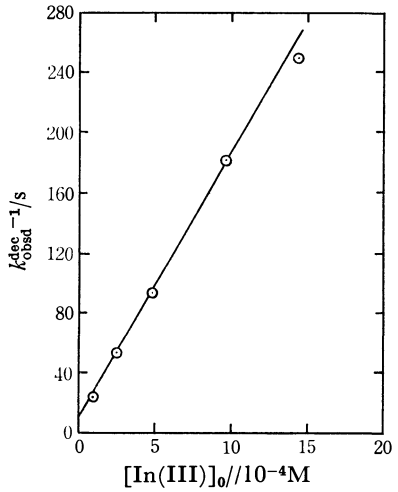

Fig. 4. Plot of $k_{obsd}^{dec\ -1}$ *vs.* total concentration of In(III).
At 470 nm, 25 °C, [H]=0.5, μ=2.0 ($NaClO_4$), and $[MX]_0=1.02\times10^{-4}$ M.

Table 4. Equilibrium data measured at 25 °C, μ=2.0 ($NaClO_4$) and [H]=0.5 M.

$K_{1a}=7.2\times10^3$ M^{-1}	
$K_{1b}=6.5_5\times10^3$ M^{-1}	$K_{2a}=0.13$ M^{-1}
$K_{1c}=14\times10^3$ M^{-1}	$K_{2b}=0.13$ M^{-1}

From the intercept and the slope of the straight line as shown in Fig. 4, the values of K_{2b} and K_{1c} are determined to be 0.13 and 1.4×10^4 M^{-1} at 25 °C, respectively. The data are summarized in Table 4.

Discussion

Stability constant K_{1c} evaluated from the rate of decomposition is about twice as large as the constants K_{1a} and K_{1b} given by the stopped-flow measurements. These results show that the complex formation between indium(III) and murexide plays a role of negative catalysis on the decomposition of murexide under the experimental conditions.

The complex formed between metal ions and the ligand murexide does not show a large molar extinction coefficient until the "nitrogen" atom at the center of the ligand molecule *does* coordinate to the metal ion to form a terdentate structure.[7] The complex followed at 470 nm is thus assigned to the one involving murexide as a terdentate ligand. The terdentate structure of the complex usually stabilizes the ligand molecule against decomposition.[8,9] Therefore the observed larger value of K_{1c} suggests the existence of other type of complexes or some ion pairs that are stable and less active to the acid decomposition of murexide, though not experimentally ascertained.

The result that the rate of the complex formation between indium(III) and murexide does not depend on the acid concentration is very interesting from a point of view that the rate of complex formation of hydroxo metal ion is generally by about 100 times higher than that of the corresponding aquo metal ion.[10-12] The larger value of K_{1c} from the decomposition rate of the ligand as compared with the values of K_{1a} and K_{1b}, and the lack of effect of the hydrogen-ion concentration on the rate of complex formation suggest the contribution of a sort of complex different from the one followed at 470 nm to the reaction system. Then K_{1c} may include the stability constants of the other complexes. Further details of the problem will be discussed elsewhere.

Furthermore it is of practical interest to note that the kinetic results of the acid decomposition suggest the possibility of determining the acid dissociation constant of the organic compounds which are too unstable to determine the constant by static method.

The present work was supported by a grant-in-aid for Scientific Research from the Ministry of Education.

References

1) G. Schwarzenbach and H. Gysling, *Helv. Chim. Acta*, **32**, 1108, 1314 (1949). J. H. Moser and M. B. Williams, *Anal. Chem.*, **25**, 1414 (1953). G. Brunisholz, *Helv. Chim. Acta*, **37**, 1546 (1954).

2) N. A. Ramaiah, S. L. Gupta, and J. Vishnu, *Z. Naturforsch.*, **12b**, 189 (1957).
3) R. K. Chaturvedi, *Z. Phys. Chem.* (Leipzig), **221**, 127 (1962).
4) M. Eigen, "Advances in the Chemistry of the Coordination Compounds," ed. by S. Kirschner MacMillan, New York, N.Y. (1961), p. 371.
5) G. Geier, *Ber. Bunsenges. Phys. Chem.*, **69**, 617 (1965); *Helv. Chim. Acta*, **51**, 94 (1968).
6) D. Davidson, *J. Amer. Chem. Soc.*, **58**, 1821 (1936).
7) H. Gysling and G. Schwarzenbach, *Helv. Chim. Acta*, **52**, 1484 (1949).
8) G. L. Eichorn and N. D. Marchand, *J. Amer. Chem. Soc.*, **78**, 2688 (1956).
9) A. Nakahara, This Bulletin, **32**, 308 (1959).
10) J. Miceli and J. Stuehr, *J. Amer. Chem. Soc.*, **90**, 6967 (1968).
11) N. D. Lukomskaya, T. V. Malikova, and K. B. Yatsimirskii, *Zh. Neorg. Khim.*, **12**, 2462 (1967).
12) Y. Kawai, T. Takahashi, K. Hayashi, T. Imamura, H. Nakayama, and M. Fujimoto, This Bulletin, **45**, 1417 (1972).

The Crystal Structure of β-$K_4SiW_{12}O_{40}\cdot 9H_2O$, Containing an Isomer of the Keggin Ion

Kazuko Y. MATSUMOTO,* Akiko KOBAYASHI, and Yukiyoshi SASAKI

Department of Chemistry, Faculty of Science, The University of Tokyo, Hongo, Bunkyo-ku, Tokyo 113

(Received April 30, 1975)

β-$K_4SiW_{12}O_{40}\cdot 9H_2O$ is orthorhombic, with the space group Pnma and $a=20.62(1)$, $b=15.57(1)$, $c=12.95(1)$ Å, $D_m=4.88$ g cm^{-3} and $D_x=5.04$ g cm^{-3} for $Z=4$. The crystal contains a discrete β-$SiW_{12}O_{40}^{4-}$ polyanion, a geometrical isomer of the α-$SiW_{12}O_{40}^{4-}$ with the well known Keggin structure. The idealized Keggin ion has a T_d symmetry, but the β-isomer has only a C_s symmetry. Mutual transformation between the α- and β-structures is possible through a 60° rotation of one of the four W_3O_{13} units, which make a cage around a SiO_4 tetrahedron in both structures. The other possible geometrical isomers of the Keggin structure are discussed.

The 12-tungstosilicic acid and its salts were first synthesized in 1863 by Marignac. Later he reported the existence of two isomers, "*silicotungstic acid*" and "*tungstosilicic acid*" or "*iso-silicotungstic acid*," and found that all the salts also always have two forms, the crystal habit and solubility different from one to another.[1] Similar isomers have also been found in 12-tungstoboric acid, $H_5BW_{12}O_{40}$, and its salts.[2] Though at the begining of this century, Copaux claimed to have confirmed these results,[3,4] the existence of such isomerism was still often regarded as doubtful because of the close resemblance in the chemical properties of each pair of isomers.

Some early workers naturally contrived structural models of the two isomers. Pfeiffer proposed two isomeric structures based upon a Werner-type isomerism of an octahedral coordination around the silicon atom.[5] Pauling thought that one was a dimer of the other.[6] However, no one went beyond speculations. Though, in 1934, Keggin[7] first solved, by the powder X-ray diffraction technique, the structure of $PW_{12}O_{40}^{3-}$, which is isomorphous with $BW_{12}O_{40}^{5-}$ and $SiW_{12}O_{40}^{4-}$, successive similar X-ray investigations of the 12-tungstoborates[8,9] denied the existence of any isomerism in the $BW_{12}O_{40}^{5-}$ polyanion.

Recently, however, these isomers were confirmed by Souchay with the aid of modern physicochemical techniques, together with synthetic works; they were named the α- and β-forms.[10-17] In addition to the 12-tungstosilicate[10] and 12-tungstoborate[11] mentioned above, 12-tungstogermanate,[10] 12-molybdosilicate,[12,13] 12-molybdogermanate,[14] 12-molybdophosphate,[15,16] and 12-molybdoarsenate[15,17] have also been reported to have similar kinds of isomers.

The β-isomers are generally unstable compared to the corresponding α-isomers.[10-17] In 1909 Copaux examined the crystals prepared by Marignac 40 years before and found that the β-tungstosilicic acid samples had been transformed into the α-form in an appreciable amount. When the β-crystals are placed in contact with a saturated aqueous solution in a sealed tube, the transition is completed within one hour at 150 °C.[3] In an aqueous solution, the rate of the transformation depends on the kind of the hetero atom; the stability lies in this order; Si>Ge>P>As.

The 12-heterotungstates are generally more stable than the corresponding 12-heteromolybdates. The transformation from β to α is considerably retarded by the addition of an organic solvent, such as alcohol or dioxane. The present authors have found that the addition of a small amount of a base to an aqueous solution of the β-form accelerates its transformation. The polarographic studies of the α and β isomers show that the β-isomer is more easily reduced than the corresponding α-isomer.[10,11,13,16,17] The features of their polarographic curve are independent of the kind of hetero atom except in the case of β-12-tungstoborate. The polarogram and also the UV absorption spectra suggest that the β-12-tungstoborate anion differs from other β-isomers in its structure.

The crystal-structure determination of β-12-heteropoly acids or their salts has been considered to be indispensable to the elucidation of the structural relation between α and β isomers. With this in mind, β-$K_4SiW_{12}O_{40}\cdot 9H_2O$ has been subjected to X-ray crystal structure analysis, since it appeared suitable for a structural study because of its stability in air and because of the relatively low amount of water of crystallization.

Experimental

Originally β-$K_4SiW_{12}O_{40}\cdot 9H_2O$ was prepared in a very low yield, together with the main product, α-$K_4SiW_{12}O_{40}\cdot 17H_2O$.[1] Recently Souchay, Tézé, and Hervé reported a new synthetic method which gives almost pure β-$SiW_{12}O_{40}^{4-}$.[10] The β-$SiW_{12}O_{40}^{4-}$ was prepared by the acidification of sodium tungstate, followed by the addition of acidified water glass, while the acidification of the mixed solution of sodium tungstate and water glass solutions gave α-$SiW_{12}O_{40}^{4-}$. For purification, β-$SiW_{12}O_{40}^{4-}$ was extracted with hydrochloric acid and ether; then the ether was removed from the extract according to the procedure applied to the α-isomer (see Ref. 18 for the details). The addition of a saturated solution of potassium chloride precipitates β-$K_4SiW_{12}O_{40}\cdot 9H_2O$. The precipitate was recrystallized from water in order to remove a small amount of the α-isomer. The β-isomer is slightly more soluble in water than the α-form.

The crystals of β-$K_4SiW_{12}O_{40}\cdot 9H_2O$ thus prepared are faint yellow, rhombic, and stable in air, while the α-isomer is colorless.

Preliminary oscillation and Weissenberg photographs showed that the crystal is orthorhombic, with the space group Pnma. The crystals quite often gave smeared reflection spots. A specimen was chosen which gave well-shaped reflection spots, its size being $0.1\times 0.12\times 0.07$ mm. The intensities of the reflections were measured on a Rigaku four-circle

* Formerly Kazuko Yamamura in Ref. 21.

diffractometer with Mo$K\alpha$ radiation ($\lambda=0.71069$ Å). The ω-2θ scan technique was employed; 2007 independent reflections, for which $|F_o|\geqq 110$ (F_o: absolute scale) up to $2\theta=60°$, were obtained. The data were corrected for Lorentz and polarization factors. Though the crystals have a large μ value, no absorption correction could be made bacause of the irregular shape of the sample and because of its brittleness, which made polishing of the specimen practically impossible. The unit-cell dimensions and their standard deviations are $a=20.62(1)$, $b=15.57(1)$, $c=12.95(1)$ A; $V=4157$ Å^3 at 23 °C, $D_m=4.88$, $D_x=5.04$ g cm^{-3} for $Z=4$, F.W. 3157.3, μ(Mo$K\alpha$)$=376.2$ cm^{-1}.

Solution and Refinement of the Structure

The structure was solved by the heavy atom method. All the coordinates of the atoms of the polyanion were obtained by several Fourier syntheses. Refinements were carried out with anisotropic temperature factors for the tungsten and potassium atoms and with isotropic ones for all the oxygen and silicon atoms to the final R value of 0.138. A weighting scheme, $w=0.2$ if $|F_o|<150$ and $w=1$ otherwise, was employed. The atomic scattering factors were taken from Ref. 19, and corrections for anomalous dispersion were made for the tungsten, potassium, and silicon atoms.[20] The atomic parameters and their estimated standard deviations are listed in Table 1. The F_c—F_o table is kept at the office of this Bulletin as Document No. 7523. A preliminary report of this work has already been published elsewhere.[21] All the calculations were performed on a HITAC 8700/8800 Computer at the Computer Centre of the University of Tokyo, using a local version of UNICS.[22]

Description of the Structure and Discussion

A recent investigation of α-$Ba_2SiW_{12}O_{40}\cdot 16H_2O$[23] and α-$K_4SiW_{12}O_{40}\cdot 17H_2O$[24] proved that the α-$SiW_{12}O_{40}^{4-}$ anion has the well-known Keggin structure[7]

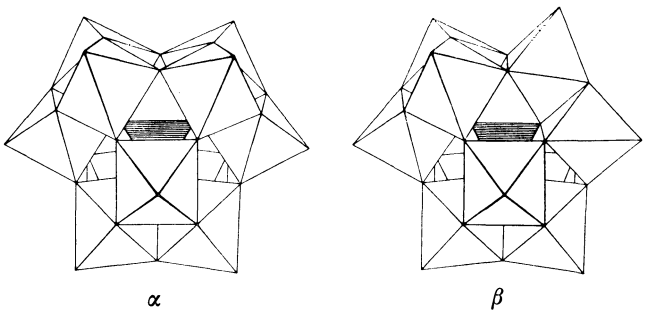

α β

Fig. 1. Polyhedral models of α- and β-$SiW_{12}O_{40}^{4-}$ polyanions. The central SiO_4 tetrahedra are shaded. The model α represents the Keggin structure found in α-$Ba_2SiW_{12}O_{40}\cdot 16H_2O$.[23]

Table 1. Atomic parameters

(a) Positional and thermal parameters for tungsten and potassium atoms ($\times 10^4$), with their estimated standard deviations in parentheses. The B_{ij}'s are defined by: $\exp[-(h^2B_{11}+k^2B_{22}+l^2B_{33}+2hkB_{12}+2hlB_{13}+2klB_{23})]$.

	x	y	z	B_{11}	B_{22}	B_{33}	B_{12}	B_{13}	B_{23}
W(1)	2764 (2)	5224 (3)	6114 (4)	4 (1)	24 (2)	17 (2)	1 (1)	0 (1)	−5 (2)
W(2)	1610 (2)	6300 (3)	7331 (3)	3 (1)	21 (2)	23 (2)	−1 (1)	1 (1)	−1 (2)
W(3)	3121 (2)	6310 (3)	8283 (3)	3 (1)	19 (2)	17 (2)	1 (1)	−1 (1)	1 (2)
W(4)	4416 (3)	7500 (0)	6895 (5)	2 (1)	20 (3)	17 (4)	0 (0)	−2 (2)	0 (0)
W(5)	4066 (2)	6428 (4)	4712 (4)	4 (1)	24 (2)	21 (2)	1 (1)	3 (1)	−3 (2)
W(6)	2783 (3)	7500 (0)	3248 (5)	7 (1)	36 (4)	13 (4)	0 (0)	−2 (2)	0 (0)
W(7)	1622 (2)	6428 (4)	4515 (3)	5 (1)	23 (2)	20 (2)	−3 (1)	−4 (1)	0 (2)
K(1)	21(20)	2500 (0)	7037(41)	16(10)	19(17)	81(41)	0 (0)	−12(17)	0 (0)
K(2)	7023(24)	7500 (0)	4908(49)	18(13)	52(31)	96(50)	0 (0)	−12(19)	0 (0)
K(3)	301(14)	4896(25)	2482(30)	9 (5)	65(20)	75(26)	3(10)	26(10)	−27(22)

(b) Positional and isotropic thermal parameters for the silicon and oxygen atoms ($\times 10^4$).

	x	y	z	B/Å^2		x	y	z	B/Å^2
Si	2756(25)	7500 (0)	5922(43)	2.3 (9)	O(13)	3278 (37)	6649(56)	3721 (65)	2.2(16)
O (1)	909(41)	5902(56)	7982(64)	2.3(15)	O(14)	4297(140)	7500 (0)	4263(242)	11.9(88)
O (2)	1362(51)	6642(76)	5983(90)	4.5(24)	O(15)	4454 (53)	5714(81)	3887 (93)	4.7(25)
O (3)	2709(37)	6606(55)	6586(64)	2.2(15)	O(16)	4630 (32)	6717(51)	6019 (59)	1.5(13)
O (4)	2214(29)	6224(42)	8435(48)	0.7(10)	O(17)	3631 (41)	7500 (0)	5681 (70)	0.5(15)
O (5)	1573(55)	7500 (0)	7714(89)	1.8(20)	O(18)	3518 (28)	5710(44)	5425 (51)	0.6(11)
O (6)	1892(35)	5321(51)	6838(61)	1.6(13)	O(19)	5152 (40)	7500 (0)	7689 (72)	0.4(14)
O (7)	1034(29)	5787(46)	3924(53)	0.8(11)	O(20)	3952 (37)	6536(55)	7505 (68)	2.3(16)
O (8)	1199(45)	7500 (0)	4109(83)	1.0(17)	O(21)	3410 (55)	5910(78)	9393 (87)	4.7(24)
O (9)	2075(32)	6633(49)	3244(58)	1.4(13)	O(22)	2986 (47)	7500 (0)	8642 (85)	1.3(19)
O(10)	2218(39)	5673(54)	5044(62)	2.0(14)	O(23)	3163 (32)	5234(46)	7530 (46)	1.2(12)
O(11)	2358(76)	7500 (0)	5074(126)	4.3(35)	O(24)	2882 (33)	4251(48)	5794 (57)	1.4(13)
O(12)	3026(95)	7500 (0)	1918(158)	6.5(48)					

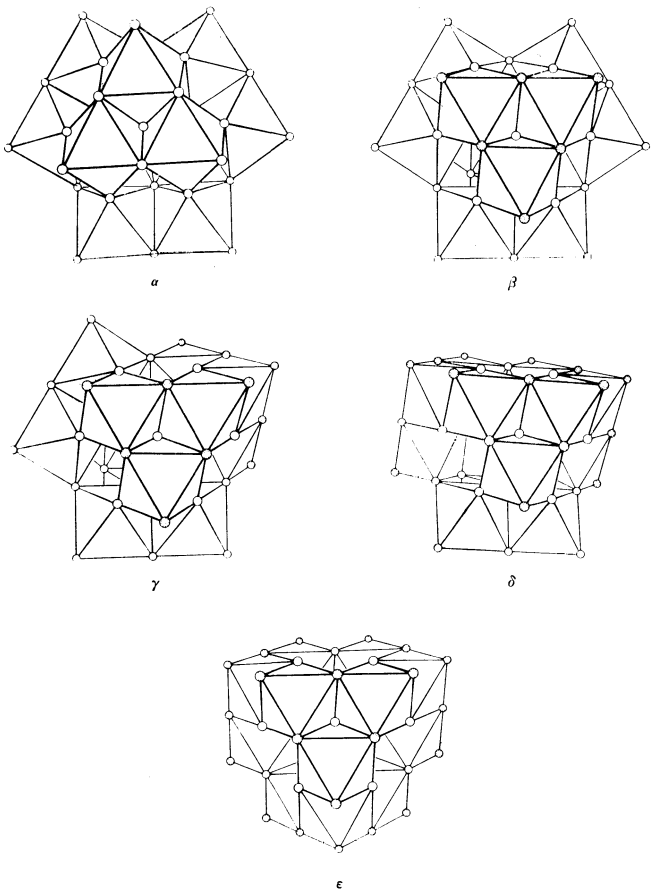

Fig. 2. Five possible isomeric structures of the Keggin structure. The models $A^tB_{12}O_{40}$ are constructed by idealized regular tetrahedra A^tO_4 and BO_6 octahedra. White and dotted balls represent oxygen atoms. The β, γ, δ, and ε (Jahr structure) models are made by rotating one, two, three, and all the four W_3O_{13} moieties of the α (Keggin structure) by 60°. The W_3O_{13} units with dotted balls are rotated parts.

(*cf.* Fig. 1α and 2α). The present work has revealed that the β-$SiW_{12}O_{40}^{4-}$ anion has the structure shown in Figs. 1β and 2β. Note that the β-isomer results from a 60° rotation about the threefold axis of one of the trigonal edge-sharing W_3O_{13} units of the α-isomer and from reattachment again *via* corner sharing. The possibility of such geometrical isomers has been predicted by Baker and Figgis[24] on the basis of stoichiometric and structural speculations.

Table 2 lists the interatomic distances within the anion, along with their standard deviations.

The central SiO_4 tetrahedron is largely distorted, the Si–O distances ranging from 1.37 to 1.83 Å. Each WO_6 octahedron is also greatly distorted. The oxygen atoms are classified into four groups, which will be called O_a, O_b, O_c, and O_d. The positions of these types of oxygen atoms are indicated in Fig. 3, which represents one of the W_3O_{13} units and the central SiO_4 tetrahedron. The O_a oxygen atoms are shared between three WO_6 octahedra and one SiO_4 tetrahedron. The O_b oxygen atoms are shared between adjacent W_3O_{13} units. The O_c oxygen atoms are shared between $2WO_6$ octahedra in a W_3O_{13} unit. The O_d oxygen atoms are unshared with other

Table 2. Interatomic distances within the anion with their estimated standard deviations

W(1)–O(18)	b	1.94 (6) Å	W(5)–O(14)	c	1.83(12) Å
O (6)	c	2.03 (7)	O(17)	a	2.27 (6)
O(23)	c	2.01 (7)	O(15)	d	1.73(12)
O(10)	b	1.92 (8)	O(18)	b	1.84 (6)
O (3)	b	2.24 (8)	O(13)	b	2.10 (8)
O(24)	d	1.58 (7)	O(16)	c	2.10 (7)
W(2)–O (2)	b	1.90(11)	W(6)–O (9)	c	1.99 (7)
O (5)	b	1.93 (3)	O(12)	d	1.79(20)
O (6)	c	1.75 (7)	O(11)	a	2.53(16)
O (1)	d	1.78 (8)	O(13)	b	1.78 (8)
O (4)	c	1.90 (6)	W(7)–O (2)	b	2.00(11)
O (3)	b	2.50 (7)	O (7)	d	1.75 (6)
W(3)–O (3)	b	2.40 (8)	O(10)	b	1.83 (8)
O(21)	d	1.68(11)	O (8)	c	1.95 (5)
O (4)	c	1.88 (5)	O(11)	a	2.36(11)
O(22)	b	1.93 (3)	O (9)	b	1.92 (7)
O(20)	b	2.02 (8)	Si–O(11)	a	1.37(17)
O(23)	c	1.94 (7)	O(17)	a	1.83 (9)
W(4)–O(16)	c	1.72 (7)	O (3)	b	1.64 (8)
O(19)	d	1.83(68)			
O(17)	a	2.25 (8)			
O(20)	b	1.94 (8)			

O (1)–O (2)	2.99(14)	O (9)–O (9)′	2.70(15)
O (4)	2.79(10)	O(10)	2.79(11)
O (5)	2.86(10)	O(11)	2.79(16)
O (6)	2.67(11)	O(12)	2.93(19)
O (2)–O (3)	2.88(13)	O(13)	2.55(10)
O (5)	2.65(15)	O(10)–O(11)	2.85 (8)
O (6)	2.57(14)	O(18)	2.72 (9)
O (7)	3.07(13)	O(24)	2.77(11)
O (8)	2.79(15)	O(11)–O(13)	2.90(16)
O(10)	2.62(13)	O(17)	2.73(17)
O(11)	2.71(17)	O(12)–O(13)	2.74(19)
O (3)–O (3)′	2.78(17)	O(13)–O(13)′	2.64(17)
O (4)	2.67(10)	O(14)	2.58(26)
O (5)	3.09(12)	O(15)	2.83(13)
O (6)	2.63(11)	O(17)	2.96(11)
O(10)	2.67(11)	O(18)	2.70(10)
O(11)	2.51(15)	O(14)–O(15)	2.84(14)
O(17)	2.63(10)	O(16)	2.67(28)
O(18)	2.65(10)	O(17)	2.29(31)
O(20)	2.82(11)	O(15)–O(16)	3.20(14)
O(22)	3.06(12)	O(18)	2.77(13)
O(23)	2.63(11)	O(16)–O(16)′	2.43(16)
O (4)–O (5)	2.56 (9)	O(17)	2.43(10)
O (6)	2.59(10)	O(18)	2.89 (9)
O(21)	2.80(12)	O(19)	2.71(34)
O(22)	2.55 (8)	O(20)	2.40(11)
O(23)	2.75 (9)	O(17)–O(18)	2.82 (6)
O (6)–O(10)	2.48(11)	O(20)	2.88(11)
O(23)	2.77(10)	O(18)–O(23)	2.92 (9)
O(24)	2.96(10)	O(24)	2.65 (9)
O (7)–O (8)	2.70 (7)	O(19)–O(20)	2.90(70)
O (9)	2.66 (9)	O(20)–O(20)′	3.00(17)
O(10)	2.85(10)	O(21)	2.86(14)
O (8)–O (9)	2.51(10)	O(22)	2.89(12)
O(11)	2.69(18)	O(23)	2.59(10)
		O(21)–O(22)	2.80(12)
		O(23)	2.68(13)
		O(23)–O(24)	2.78(10)

Prime refers to the transformation x, 0.5 $-y$, z.

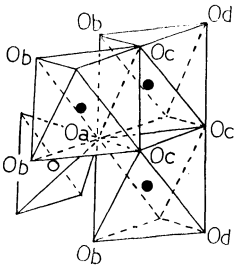

Fig. 3. One of the W_3O_{13} units in β-$SiW_{12}O_{40}^{4-}$ with the central SiO_4 tetrahedron (see text).

polyhedra. The O_a–O_c edges are shared between two WO_6 octahedra. The W–O distances are W–O_a 2.24—2.53, W–O_b 1.74—2.10, W–O_c 1.75—2.10, and W–O_d 1.59—1.80 Å. These values show that the tungsten atoms are off-centered in the respective WO_6 octahedron and that all the tungsten atoms are displaced toward the outside of the anion. Similar displacements have been observed for the tungsten atoms in $PW_{12}O_{40}^{3-}$,[7] $CoW_{12}O_{40}^{5-}$,[26] and α-$SiW_{12}O_{40}^{4-}$,[23,24] and also for the molybdenum atoms in $TeMo_6O_{24}^{6-}$,[26] $As_4Mo_{12}O_{50}^{8-}$,[28] and $CeMo_{12}O_{42}^{8-}$,[29] such displacement is considered to be a characteristic feature of not only Keggin-type structures but also of other types of heteropolymolybdates and heteropolytungstates.

The crystal structure projected along the b and c axes are presented in Figs. 4 and 5 respectively. Two anions lie on the crystallographic mirror plane at $y=1/4$, and other two, on the mirror plane at $y=3/4$. The rotated W_3O_{13} unit is dipicted as W6–W7–W7^{I}. An attempt to locate the water molecules was not successful, since many

Table 3. Interanionic and inter cation-anion distances (less than 3.5 Å)

O (1)^{III}	–O(19)^{I}	3.06(42) Å
	O(16)^{I}	3.20(11)
O (2)^{III}	–O(19)^{I}	3.31(63)
O (4)^{IV}	–O(24)^{I}	3.16 (9)
O (5)^{III}	–O(19)^{I}	2.97(81)
O (7)	–O(21)^{III}	2.94(13)
O (9)	–O(23)^{III}	3.09(10)
	O(24)^{III}	3.47(10)
O(10)	–O(21)^{III}	2.90(14)
O(21)^{III}	–O(24)^{III}	3.23(13)
K (1)^{III}	–O(14)	3.22(31)
K (2)	–O (4)^{IV}	2.96 (7)
	O(22)^{IV}	2.74(11)
	O(24)^{I}	2.88 (7)
K (3)^{II}	–O (1)^{III}	2.85 (9)
	O(15)	2.80(12)

Roman numeral superscripts refer to the following transformations of the coordinates:

I	$1-x$,	$1-y$,	$1-z$
II	$0.5+x$,	y,	$0.5-z$
III	$0.5-x$,	$1-y$,	$-0.5+z$
IV	$0.5+x$,	y,	$1.5-z$
V	$1-x$,	$-0.5+y$,	$1-z$
VI	$0.5+x$,	$0.5-y$,	$1.4-z$

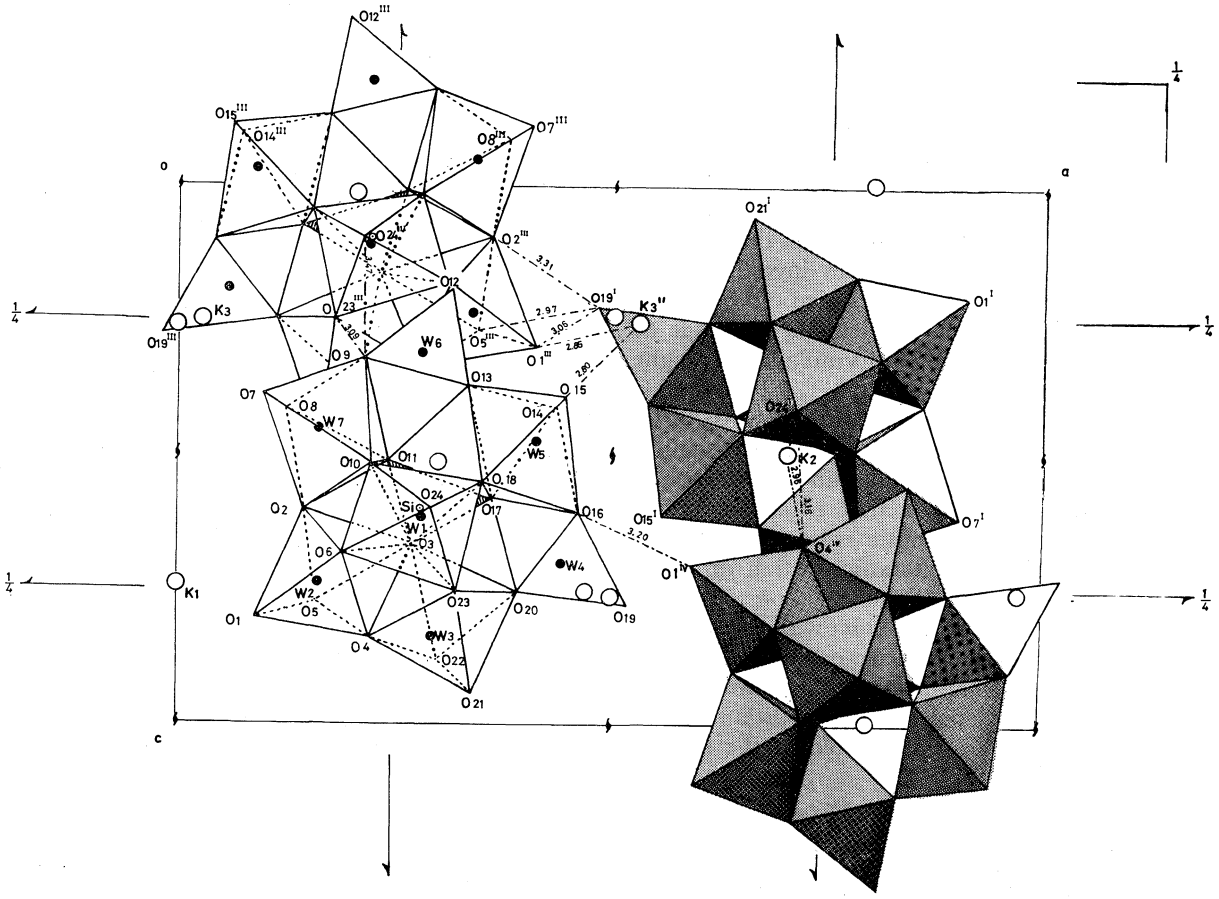

Fig. 4. The crystal structure of β-$K_4SiW_{12}O_{40}\cdot 9H_2O$ projected along the b axis.

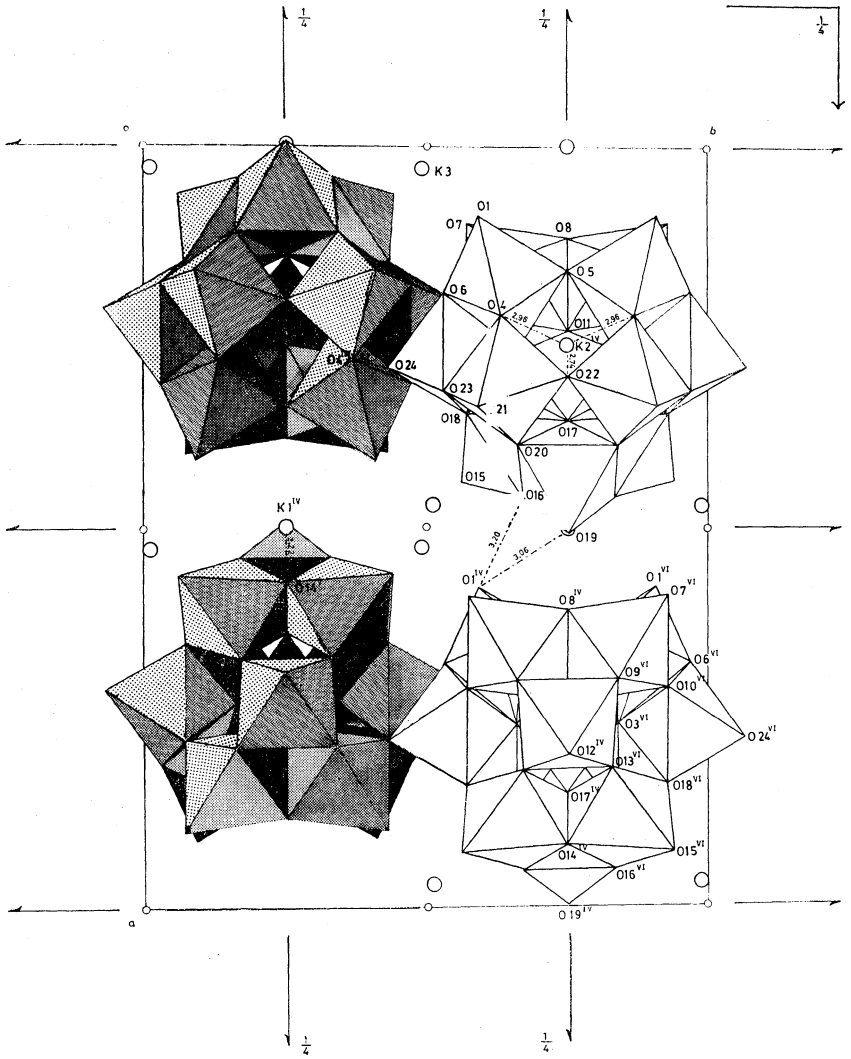

Fig. 5. The crystal structure of β-$K_4SiW_{12}O_{40}\cdot 9H_2O$ projected along the c axis.

electron density peaks, which were lower than those of the anion oxygens, were smeared out in the cavities between the polyanions. In order to investigate the crystal water, thermal analysis was carried out on β-$K_4SiW_{12}O_{40}\cdot 9H_2O$. The results confirm the presence of a total of nine water molecules per formula unit (weight loss at 230 °C: calcd 5.1%, obsd 4.9%). The crystals begin to lose the water at a temperature as low as 70 °C, which, together with the X-ray diffraction study, suggest that the present crystals possibly contain mobile zeolitic water. It has been established that heteropoly compounds very often contain zeolitic water in the crystals.[11,29] Interanionic and interanion-cation distances less than 3.5 Å are listed in Table 3. Some parts of adjacent anions seem to come in contact with one another directly. All the potassium ions are partly coordinated by anion oxygens, the remaining coordination numbers being presumably completed by the addition of the water oxygens, which were not located in the present work.

The structural relationship between the α- and β-isomers has been clarified for the first time by this investigation, though with large standard deviations of the positions of the light elements, as is shown in Tables 1 and 2.

On the Other Possible Geometrical Isomer of the Keggin Structure

Figure 2 shows all five possible isomers of $SiW_{12}O_{40}^{4-}$ or the Keggin ion in general. The models are constructed of idealized octahedra (WO_6) and tetrahedra (SiO_4). In the β-model, one W_3O_{13} of the Keggin ion (α) is rotated by 60°; such a reorientation of two, three, and all four W_3O_{13} moieties leads to γ, δ, and ε isomers successively. The ε model was once proposed for 12-heteropolyanions by Jahr[31] and later found by Johansson in the $Al^tO_4Al_{12}(OH)_{24}(H_2O)_{12}^{7+}$ ion,[32,33] where Al^tO_4 denotes AlO_4 tetrahedron and where the other 12 aluminum atoms are surrounded by an octahedral array of 6 oxygen atoms.

None of the five isomers can be optically active, and a close-packing of the oxygen atoms is realized only in δ and ε. If we use A, B, and C to label the layers of oxygen atoms, as is common in discussions of the close-packing (ABAB for a hexagonal close-packing and ABCABC for a cubic one), the arrangements of the oxygen atom layers in δ and ε are ABCB and ABCA. In both anions, the A and B layers both contain 12 atoms and C, 10, while the last B layer in δ and the last A in ε contain 6 oxygen atoms each. One isomer of $BW_{12}O_{40}^{4-}$, which gives

unique polarographic waves among all the 12-heteropoly acids, might have a γ, δ, or ε structure; an X-ray diffraction study of the crystals containing this anion is highly desirable.

The present work was partly supported by a Grant in aid for Cooperated Research of the Ministry of Education. The authors are also indebted to the late Professor P. Souchay, Dr. A. Tézé, and Dr. G. Hervé of the University of Paris for their advice about the procedure of preparing the β-isomers. Thanks are also due to Dr. H. Iwasaki of the Institute of Physical and Chemical Research for reading through the manuscript and for his advice.

References

1) C. Marignac, *Ann. Chim. Phys.*, [4], **3**, 5 (1864).
2) D. Klein, *ibid.*, [5], **28**, 350 (1883).
3) M. H. Copaux, *Bull. Soc. Chim. Fr.*, [4], III, 101 (1908).
4) M. H. Copaux, *Ann. Chim. Phys.*, **17**, 217 (1909).
5) P. Pfeiffer, *Z. Anorg. Allg. Chem.*, **105**, 26 (1918).
6) L. Pauling, *J. Amer. Chem. Soc.*, **51**, 2868 (1929).
7) J. F. Keggin, *Proc. Roy. Soc., Ser. A*, **114**, 75 (1934).
8) R. Signer and H. Gross, *Helv. Chim. Acta*, **17**, 1076 (1934).
9) O. Kraus and F. Mussgnug, *Naturwissenschaften.*, **28**, 238 (1940).
10) P. Souchay, A. Tézé, and G. Hervé, *C. R. Acad. Sci. Paris, Ser. C.*, **275**, 1013 (1972).
11) P. Souchay, *Bull. Soc. Chim. Fr.* [5], **18**, 365 (1951).
12) J. D. H. Strickland, *J. Amer. Chem. Soc.*, **74**, 862 (1953).
13) R. Massart, *Ann. Chim.*, [14], **3**, 507 (1968).
14) P. Souchay, A. Tézé, and G. Hervé, Proceedings of XV I. C. C. C., Moscow, **1972**, p. 481.
15) P. Souchay, R. Content, and M. Fruchart, *C. R. Acad. Sci. Paris, Ser. C.*, **264**, 976 (1967).
16) J. M. Fruchart and P. Souchay, *ibid.*, **266**, 1571 (1968).
17) P. Souchay and R. Content, *ibid.*, **265**, 723 (1967).
18) "Inorganic Synthesis," McGraw-Hill Book Co., 1939, Vol. I, p. 129.
19) "International Tables for X-Ray Crystallography," Vol. III, Kynoch Press, Birmingham (1962), p. 210.
20) D. T. Cromer, *Acta Crystallogr.*, **18**, 17 (1965).
21) K. Yamamura and Y. Sasaki, *Chem. Commun.*, **1973**, 648.
22) "The Universal Crystallographic Computation Program System," Crystallographic Society of Japan (1967).
23) A. Kobayashi and Y. Sasaki, This Bulletin, **48**, 885 (1975).
24) P. M. Smith, *Dissertation Abstr.*, **32**, 5136-B (1972).
25) L. C. W. Baker and J. S. Figgis, *J. Amer. Chem. Soc.*, **92**, 3794 (1970).
26) N. F. Yannoni, Dissertation, Boston University (1961).
27) H. T. Evans, Jr., *J. Amer. Chem. Soc.*, **90**, 3275 (1968).
28) T. Nishikawa and Y. Sasaki, *Chem. Lett.*, **1975**, 1185.
29) D. D. Dexter and J. V. Silverton, *J. Amer. Chem. Soc.*, **90**, 3589 (1968).
30) S. F. West and F. Audrieth, *J. Phys. Chem.*, **59**, 1069 (1955).
31) K. F. Jahr, *Naturwissenschaften*, **29**, 505 (1941).
32) G. Johansson, *Acta Chem. Scand.*, **14**, 771 (1960).
33) G. Johansson, *Arkiv Kemi*, **20**, 321 (1963).

The Structure of Polyvanadotungstates. II. The Crystal Structure of $K_7V_5W_8O_{40}\cdot 12H_2O$

Keiko NISHIKAWA,* Akiko KOBAYASHI, and Yukiyoshi SASAKI

Department of Chemistry, Faculty of Science, The University of Tokyo, Hongo, Bunkyo-ku, Tokyo 113

(Received May 7, 1975)

Crystals of $K_7V_5W_8O_{40}\cdot 12H_2O$ are cubic, with the space group of $P\bar{4}3m$ and with the cell dimension of $a=10.62(1)$ Å. The structure was determined by the single-crystal X-ray diffraction technique. All the non-hydrogen atoms were located, and the final R value was 0.057. The $V_5W_8O_{40}^{7-}$ anion has the Keggin structure, with a central VO_4 tetrahedron. The twelve outer metal positions are randomly occupied by four vanadium and eight tungsten atoms. A detailed discussion of the configuration isomers is impossible because of the orientational disorder. The present work, and the former X-ray structure determination of $V_2W_4O_{19}^{4-}$ show that polyvanadotungstates can be regarded as substituted homologues of isopolytungstates: $V_nW_{6-n}O_{19}^{(n+2)-}$ ($n=1, 2$) has a hexaniobate-type structure, and $V^tV_nW_{n-12}O_{40}^{(n+3)-}$ ($n=2, 3, 4$), the Keggin structure, where V^t represents the central vanadium atom.

When a solution of orthotungstate (WO_4^{2-}) and metavanadate (VO_3^-) salts is acidified, polyvanadotungstate crystals are precipitated.[1] Several species of polyvanadotungstates have been reported as salts, their composition varies with the pH, the constitution, and the concentration.[1-4] Recently, Pope and Flynn proposed, in their preparative studies,[5-7] that these polyvanadotungstate anions can be divided into two groups: $V_nW_{6-n}O_{19}^{(n+2)-}$($n=1,2$) and $V^tV_nW_{12-n}O_{40}^{(n+3)-}$(where V^t is the vanadium in the center of the tetrahedron, $n=2,3,4$). For the former series, we have determined the crystal structure of α-$(CN_3H_6)_4V_2W_4O_{19}$ and showed[8] that, as Pope proposed, it has the "*hexaniobate structure*"[9] shown in Fig. 1. This paper will report the structure of $K_7V_5W_8O_{40}\cdot 12H_2O$, which belongs to the latter series.

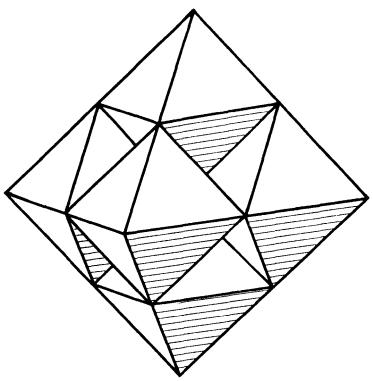

Fig. 1. The coordination polyhedra model of $V_2W_4O_{19}^{4-}$ anion. All the octahedra are idealized.

Experimental

Crystals of $K_7V_5W_8O_{40}\cdot 12H_2O$ were prepared by Pope's method.[7] Potassium tungstate, K_2WO_4 was added to an aqueous solution of potassium metavanadate, KVO_3; the mixture was acidified with formic acid to pH=3 and then heated until just before boiling. From the red-brown crystals obtained after cooling, a single crystal $0.2\times0.2\times0.15$ mm in size was chosen for the X-ray diffraction experiments. The reflection data were collected on a Rigaku four-circle diffractometer with Mo$K\alpha$ radiation monochromatized by a graphite crystal ($\lambda=0.7107$ Å). The $\omega-2\theta$ scan technique was employed, and 256 independent reflections with intensities larger than 3σ were obtained to $2\theta=60°$. The intensities were corrected for the Lorentz and polarization factors, but not for absorption. The crystal data are as follows:

$K_7V_5W_8O_{40}\cdot 12H_2O$

cubic

$a = 10.62(1)$ Å

$V = 1199$ Å^3

space group $P\bar{4}3m$

$Z = 1$ ($D_m=4.0$ g cm^{-3}, $D_x=3.97$ g cm^{-3})

(Mo$K\alpha$) = 233.3 cm^{-1}

The conventional heavy atom method was used to solve the structure.** The positional parameters and anisotoropic thermal parameters for all the non-hydrogen atoms were refined by the block-diagonal, least-squares method to $R=0.057$. No significant peak was found on the residual electron density map. The F_o—F_c table is kept by the Chemical Society of Japan as Document No. 7525. A weighting scheme of $w=0.5$ for $|F_o|<104.4$ and $w=1$ otherwise was employed. The atomic scattering factors were taken from the "International Tables for X-Ray Crystallography," but those for W and V were corrected for the anomalous dispersion.[10] The calculations were performed on a HITAC 8700/8800 computer at the Computer Centre of the University of Tokyo using a local version of UNICS.[11]

Results and Discussion

The Structure of the Polyanion. As is shown in Fig. 2, one unit cell contains one Keggin-type polyanion, $V^tM_{12}O_{40}^{7-}$, where V^t represents the central vanadium atom of the VO_4 tetrahedron and where M_{12} means 4V

* Present address: Department of Chemistry, Faculty of Science, Gakushuin University, Mejiro, Toshima-ku, Tokyo 171.

** The possible space groups observed in connection with the systematic extinctions are $P\bar{4}3m$, $Pm3m$, and $P432$. Considering the composition of the polyanion, the Patterson map was solved only by assuming the positional disorder of metal atoms. A trial structure obtained on the assumption of the $P\bar{4}3m$ space group gave an R value of 0.27; however, $Pm3m$ and $P432$ gave 0.8—0.9.

TABLE 1. FINAL POSITIONAL COORDINATES ($\times 10^4$) AND ANISOTROPIC TEMPERATURE FACTORS ($\times 10^4$)[a]
(The temperature factor is of the form: $\exp[-h^2\beta_{11}+k^2\beta_{22}+l^2\beta_{33}+2hk\beta_{12}+2hl\beta_{13}+2kl\beta_{23})]$)

	x	y	z	β_{11}	β_{22}	β_{33}	β_{12}	β_{13}	β_{23}
M[b]	2351 (2)	2351 (2)	−30 (2)	18 (2)	18 (2)	36 (2)	−5 (1)	3 (7)	3 (7)
V[b]	0	0	0	28 (5)	28 (5)	28 (5)	0	0	0
Oa[c]	948(110)	948(110)	−948(110)	58(47)	58(47)	58(47)	24(58)	24(58)	24(58)
Ob	1101 (35)	2806 (50)	2806 (50)	40(28)	38(28)	38(45)	35(32)	35(32)	21(32)
Oc	1428 (40)	1428 (40)	−3211 (49)	53(35)	53(35)	34(49)	23(46)	0(32)	0(32)
Od	3476 (30)	3476 (30)	182 (44)	39(24)	39(24)	30(65)	9(31)	11(22)	11(22)
K(1)	5000	0	0	24(19)	33(13)	33(13)	0	0	0
K(2)	5000	5000	1423 (37)	58(17)	58(17)	124(40)	0	0	0
H_2O	3113 (47)	3113 (47)	5234(100)	161(51)	161(51)	86(53)	30(65)	80(74)	80(74)

a) The estimated standard deviations in parantheses here and elsewhere are in units of the last significant digit.
b) $M=\frac{4V+8W}{12}$, see text. c) The Evans classification of oxygen atoms in the Keggin structure (see text).[12]

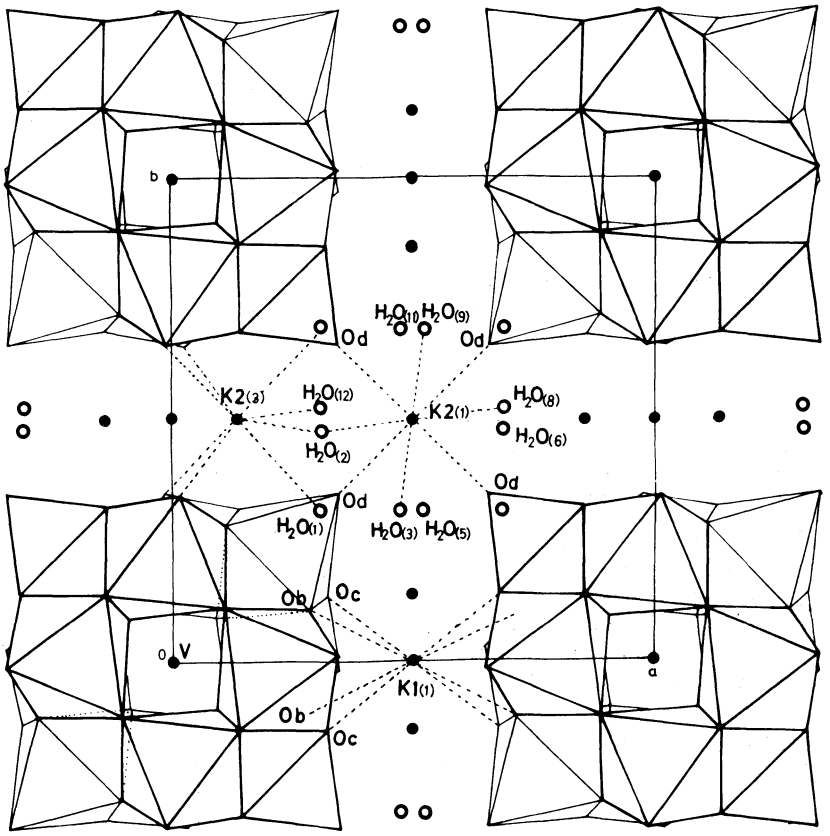

Fig. 2. A view of the structure as projected down the c axis. The $V_5W_8O_{40}^{7-}$ anion has three two fold axes parallel to the crystal axes. The coordination bonds around K^+ are designated by dotted lines.

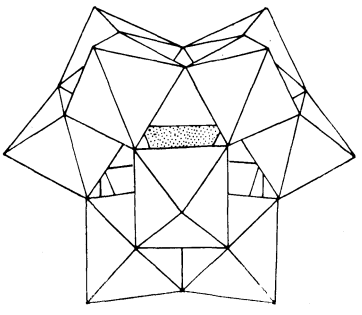

Fig. 3. The coordination polyhedral model of Keggin structure.

and 8W atoms randomly mixed. In Fig. 3 the polyanion is shown as a coordination polyhedral model. Three MO_6 octahedra link together by sharing edges to form a M_3O_{13} unit with a trigonal symmetry (Fig. 4). Four such M_3O_{13} units link in a T_d symmetry with a central hetero-atom by sharing corners to build the structure known as the Keggin ion.[13]

The twelve metal positions are occupied by four vanadium and eight tungsten atoms with a 4: 8 probability. The space-group symmetry requires that twelve metal positions are crystallographically equivalent; it is impossible to discriminate the 38 possible isomers with a different distribution of four vanadium and eight tung-

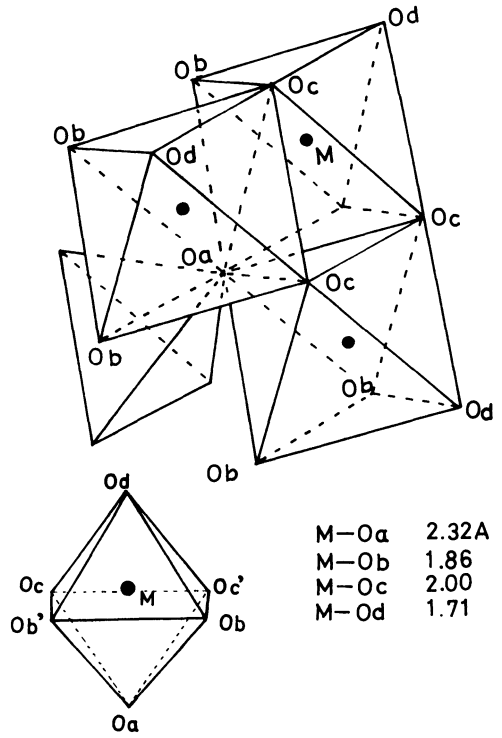

Fig. 4. The coordination polyhedral model of M_3O_{13} unit and central VO_4 tetrahedron and MO_6 octahedron. The classification of the oxygen atoms conform to those given by Evans.[12]

sten atoms on the twelve metal positions in a $V^tM_{12}O_{40}^{7-}$ anion. The assumption that the sample is a mixed crystal of many configurational isomers cannot be definitely ruled out on the basis of the present diffraction data. There is no evidence for the tungsten atoms being randomly mixed in the central vanadium position.

Oxygen atoms in the polyanion are classified into four groups—Oa, Ob, Oc, and Od, as is shown in Fig. 4. Oa is the oxygen atom bound to one central vanadium atom and to three metal atoms, while Ob is shared by two metal atoms of different M_3O_{13} units. Oc is bound to two metal atoms in the same M_3O_{13} unit. Od is the terminal oxygen atom combined with only one metal.

TABLE 2. INTERATOMIC DISTANCES (d/Å) AND ESTIMATED STANDARD DEVIATIONS WITHIN THE ANION $V_5W_8O_{40}^{7-}$

(1) The metal–metal interatomic distances	
M–M (in M_3O_{10} unit)	3.486 (9)
M–M (nearest M–M in different M_3O_{13} units)	3.578(11)
M–V^t	3.532 (9)
(2) The distances between metal and oxygen atoms	
M–Oa	2.32(12)
M–Ob	1.86 (5)
M–Oc	2.00 (5)
M–Od	1.71 (4)
V^t–Oa	1.75(12)
(3) The distances between oxygen atoms	
Oa–Ob	2.94(13)
Oa–Oc	2.51(13)
Ob–Oc	2.74 (8)
Oc–Od	2.78 (8)

The M–O distances in Table 2 (2) are the weighted average of the W–O and V–O distances, since the M in each position is occupied by randomly distributed V and W atoms. All the MO_6 octahedra are deformed. The M atom is not at the center of the octahedra, but near Od; it is displaced 0.35 Å outside the plane made by two Ob and two Oc atoms. Three Oc atoms form a triangle 0.43 Å inside the plane which three Od atoms make. On the other hand, one Oa and six Ob atoms form an almost perfect plane.

The $V^tV_4W_{12}O_{40}^{7-}$ is the sole example of the Keggin structure containing a vanadium (V) atom in the center as V^t. From the standpoint of vanadium structure chemistry, it is interesting to see whether or not the V^t-$(Oa)_4$ tetrahedron is deformed, because, in general, VO_4 has a remarkable tendency to deviate from the tetrahedral symmetry. For instance, Evans reported that, in VO_4 (tetrahedron),[14] VO_5 (trigonal bipyramid), or VO_6 (octahedron),[15] two V–O bonds are always shorter, suggesting the existence of bent O–V–O bondings stronger than other V–O bonds. Banks, Greenblatt, and Post, in their structure study of K_3VO_4, found that the deformation of VO_4^{3-} is more remarkable than that of AsO_4^{3-}.[16] In the present case, however, the polyanion apparently has the T_d symmetry. As a result, such a deformation of the $V(Oa)_4$ tetrahedron, if it occurred at all, must have been smeared out by the orientational disorder. Though the large observed standard deviations in the positional and thermal parameters of the Oa atoms, and consequently the large errors in the V–Oa distances, are consistent with this model of the random orientation of the deformed polyanion, there is no difinite proof of it.

TABLE 3. BOND ANGLES (φ/°) AND ESTIMATED STANDARD DEVIATIONS WITHIN A MO_6 UNIT

Oa–M–Ob	88.8 (35)
Oa–M–Oc	70.6 (34)
Oa–M–Od	162.8 (34)
Ob–M–Ob′	87.2 (24)
Ob–M–Oc	159.3 (22)
Ob–M–Oc′	90.7 (22)
Ob–M–Od	103.6 (23)
Oc–M–Oc′	84.1 (20)
Oc–M–Od	97.0 (20)

Potassium Ions and Water of Crystallization. One unit cell contains seven potassium ions, of which three, K(1), the 3d sites, are at (1/2, 0, 0; 0, 1/2, 0; 0, 0, 1/2). Other four ions, K(2), are distributed among the sixfold positions, 6g ($\pm x$, 1/2, 1/2; 1/2, $\pm x$, 1/2; 1/2, 1/2, $\pm x$) with equal probability. This assumption explains the peak heights on Fourier maps [K(1): K(2): O (oxygen atom of H_2O)=4: 2: 1] and gives reasonable temperature factors and the lowest R value. Both K(1) and K(2) are coordinated by eight oxygen atoms, as is shown in Fig. 2. The K(1) is surrounded by four Oc and four Ob atoms, and K(2), by four water molecules and four terminal Od atoms of the polyanions. Table 4 shows the K–O distances. The coordination numbers of potassium ions by oxygen atoms are known to be 6, 7, 8, 9, 10, and 12,[17] and for the 8 coordination, the K–O

Table 4. Interatomic distances (d/Å) shorter than 3.5 Å outside the polyanion

K(1)-Ob	2.86 (4)
K(1)-Oc	2.87 (5)
K(2)-Od	2.64 (6)
K(2)-H_2O	2.70 (8)
H_2O-H_2O	3.13(10)
Oc-H_2O	3.38 (8)

distance has been reported to be in the range from 2.66 to 3.10 Å.[17] The present data of bond lengths seem to be typical.

Water of Crystallization. Water molecules are used only as ligands to potassium cations. There is no hydrogen bonding between the oxygen of the polyanion and water molecules (the shortest distance, H_2O–Oc, is 3.38 Å).

Comparison with Isopolyvanadates and Isopolytungstate. Isopolytungstates in the solid phase have always been found in the solid phase as discrete polyanions, such as $W_6O_{19}^{2-}$,[18] $W_{10}O_{32}^{4-}$,[19] $H_2W_{12}O_{42}^{10-}$ (paratungstate),[20] and $H_2W_{12}O_{40}^{4-}$ (metatungstate)[21]. No infinite polymer has been reported; these polyanions seem all to exist in aqueous solutions. On the other hand, all the isopolyvanadate crystals so far studied, with the sole exception of $K_2Zn_2V_{10}O_{28}\cdot 16H_2O$ crystals containing discrete $V_{10}O_{28}^{6-}$ [15] anions, have infinite polymeric structures.

The CsV_3O_8 crystals contain a plane sheet consisting of VO_6 octahedra-sharing edges,[22] $K_3V_5O_{14}$ consists of VO_5 square pyramids, and VO_4 of tetrahedra bound by sharing corners.[23] The equilibria of isopolyvanadates in an aqueous solution are fairly complicated. The following species have been reported:[24] VO_2^+, $H_2V_{10}O_{28}^{4-}$, $HV_{10}O_{28}^{5-}$, $HV_6O_{17}^{3-}$, $HV_2O_7^{3-}$, $V_2O_7^{4-}$, HVO_3, VO_3^-, H_3VO_4, $H_2VO_4^-$, HVO_4^{2-}, and VO_4^{3-}. However, the existence of any infinite polymer in the aqueous phase has never been proved.

We have already determined the structures of the five polyvanadotungstates, $(CN_3H_6)_4V_2W_4O_{19}$,[8] $K_7V_5W_8O_4\cdot 12H_2O$, $Ag_4V_2W_4O_{19}$,[25] and $(CN_3H_6)_5HV_2^{IV}W_4O_{19}$,[26] but no isopolyvanadate-like infinite polymer has been found; the structures are always similar to those of the isopolytungstates.

These results support Pope's proposal[5–7] that all the polyvanadotungstates form two homologous series, $V_nW_{6-n}O_{19}^{(n+2)-}$ (n=1,2) and $V^tV_nW_{12-n}O_{40}^{(n+3)-}$ (n=2,3,4). According to him, the two series are derived from the hexatungstate $W_6O_{19}^{2-}$ with the hexaniobate structure and from the hypothetical heteropolytungstate, $V^tW_{12}O_{40}^{3-}$, which is a Keggin ion as a result of the partial replacement of W(VI) by V(V). The Keggin ions are stable in acidic solutions, and the niobate-type anion, $V_2W_4O_{19}^{4-}$, is reversibly converted to a Keggin ion, $V_4W_9O_{40}^{6-}$, on acidification.

In the both series, a lower pH stabilizes polyanions containing fewer vanadium atoms. This may be correlated with the facts that the basicity of V(V) is stronger than that of W(VI) and that the VO_2^+ cation is stable in acidic media.

References

1) A. Rosenheim und M. Pieck, *Z. Anorg. Chem.*, **98**, 223 (1916).
2) F. Chauveau, *Bull. Soc. Chim. Fr.*, **5**, 834 (1960).
3) F. Chauveau et P. Souchay, *ibid.*, **8**, 561 (1963).
4) A. B. Bekturov, D. U. Begalieva, and A. K. I'lyasova, *Russian J. Inorg. Chem.*, **15**, 1932, (1970).
5) M. Flynn and M. T. Pope, *Inorg. Chem.*, **10**, 2524 (1971).
6) M. Flynn and M. T. Pope, *ibid.*, **10**, 2745 (1971).
7) M. Flynn and M. T. Pope, *ibid.*, **11**, 1950 (1972).
8) K. Nishikawa, A. Kobayashi, and Y. Sasaki, This Bulletin, **48**, 889 (1975).
9) I. Lindqvist, *Arkiv Kemi*, **5**, 247 (1953).
10) "International Tables for X-ray Crystallography," Vol. III, Kynoch Press, Birmingham (1962), p. 201.
11) "The Universal Crystallographic Computation Program System," Crystallographic Society of Japan (1967).
12) H. T. Evans, Jr., *Perspectives Struct. Chem.*, **4**, 1 (1971).
13) J. F. Keggin, *Proc. Roy. Soc., Ser A*, **144**, 75 (1934).
14) H. T. Evans, Jr., *Z, Kristallogr.*, **114**, 257 (1960).
15) H. T. Evans, Jr., *Inorg. Chem.*, **5**, 967 (1966).
16) E. Banks, M. Greenblatt, and B. Post, *Inorg. Chem.*, **9**, 2259 (1970).
17) Ref. 10, p. 258.
18) G. Henning and A. Hüllen, *Z. Kristallogr.*, **130**, 162 (1969).
19) K. J. Fuchs, H. Hartl, and W. Schiller, *Angew. Chem., Int. Edit. Engl.*, **12**, 409 (1973).
20) R. Allmann, *Acta Crystallogr.*, **B27**, 1393 (1971).
21) A. Kobayashi and Y. Sasaki, to be published.
22) H. T. Evans, Jr., and S. Block, *Inorg. Chem.*, **5**, 1808 (1966).
23) A. M. Byström and H. T. Evans, Jr., *Acta Chem. Scand.*, **13**, 377 (1959).
24) M. Pope and B. W. Dale, *Quart. Rev.*, **22**, 527 (1968).
25) K. Nishikawa, A. Kobayashi, and Y. Sasaki, to be published.
26) K. Nishikawa, to be published.

Chemical Vapor Growth of Titanium Diboride Whisker

Seiji MOTOJIMA, Fumio SUGIMORI, Yasutaka TAKAHASHI, and Kohzo SUGIYAMA
Department of Synthetic Chemistry, Faculty of Engineering, Gifu University, Gifu 504
(Received May 14, 1975)

Titanium diboride whisker was grown by chemical vapor deposition from a gaseous mixture of $TiCl_4$, BCl_3, H_2, and Ar. The relations between the growth conditions and the crystal morphologies were investigated. The predominant factors for whisker growth were found to be the substrate temperature and the kind of impurities painted on the substrate. The optimum temperature was determined as 1050—1070 °C where whiskers grew up to 250 μm in length and 0.1 to 1 μm in diameter for 30 min. Au, Pt, and Pd were found to be promissing impurities for whisker growth. From an observation of the droplet on whisker tip, the growth mechanism for the whiskers was supposed to be VLS mechanism. The form of whisker grown was tetragonal and hexagonal pillar, and the growth direction was determined as [100]direction.

A few investigations have been reported on the single crystal growth of titanium diboride by Verneuil's process,[1,2] and from fused metal solutions.[3,4] However, few papers have been published on the single crystal growth by chemical vapor deposition (CVD) except for polycrystalline coatings.[5-7] In this paper, chemical vapor growth conditions of titanium diboride whisker were studied in relation to the effects of impurities to the whisker morphology and growth mehcanism.

Experimental

Figure 1 shows the apparatus for whisker growth. A gaseous mixture of hydrogen and argon passed through a $TiCl_4$ saturator which consisted of an evaporator and a condenser, the top temperature of which was regarded as saturating temperature. Another gas stream of chlorine was flowed into a boron trichloride generator filled with boron carbide regulated at 800 °C. Two gas streams were mixed to flow into reaction tube of quartz glass (27 mm i.d.). Substrate and atmosphere were heated doubly by four rods of outer and a rod of inner carborundum resistants. A quartz glass tube (8 mm i.d.) was used as substrate for whisker growth, and the inner carborundum rod was inserted to the substrate tube. Surface temperature of the substrate was measured by an optical pyrometer and was corrected by a calibration curve. As an impurity, various salts of metals were painted on the substrate scratched by abrasives in the form of the aqueous solutions, and decomposed or reduced to the respective metal, in hydrogen atmosphere at 1000 °C.

The term of whisker length in this paper means the average length of ten samples selected in the order from the longest in the field of microscope magnified by 150.

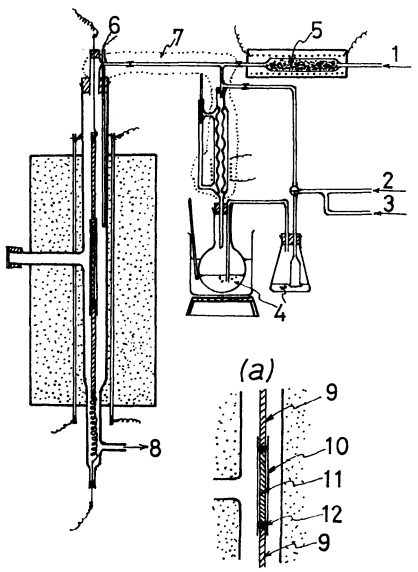

Fig. 1. Schematic diagram of the experimental apparatus. (1) Cl_2, (2) H_2, (3) Ar, (4) $TiCl_4$, (5) B_4C, (6) Pt-PtRh thermocouple, (7) thermal insulator, (8) outlet, (9) electrode, (10) quartz substrate, (11) SiC heater, (12) carbon powder.

Results and Discussion

The Effects of Impurities. In preliminary experiments, the optimum conditions were roughly determined as follows; substrate temperature of 1070 °C, gas phase temperature of 870 °C, total gas flow rate of 2.3 cc/s (NTP), and the concentration of boron trichloride, titanium tetrachloride, hydrogen, and argon of 9, 17, 44, and 30 vol%, respectively. Under these conditions, the impurities of In, Cr, Cu, Co, Ni, Fe, Mn, and V

Table 1. Impurity effects on whisker growth and eutectic temperature of binary alloys

	Impurity effects[a]		Eutectic temperature (°C)[b]	
	TiB_2	Boron[8]	Ti-impurity	Boron-impurity
Co	—	++	1135 (22.4)	1095 (18.5)
Ni	—	++	955 (75.5)	1080 (18.4)
Mn	—		1175 (60.8)	
Fe	—	+	1080 (71)	1149 (17)
In	—			
V	—			
Cr	—	+		*ca.* 1570 (*ca.* 13)
Cu	—	++	880 (27)	1060 (10.7)
Ag	+			
Pd	+	++	1080 (71.5)	845 (27)
Rh	+	++		
Pt	+	++	1310 (84.4)	830 (40)
Au	++	++	peritectic	

Reaction temperature: 1070 °C; $BCl_3/TiCl_4/H_2/Ar$= 8.8/17.5/43.4/30.2 (vol%). a) (—): Non or negative effect; (+): Weak positive effect (up to 200—300 μm); (++): Positive effect (longer than 300 μm). b) Atomic percent of titanium and boron metal in corresponding binally alloy systems, are shown in the parenthesis, respectively.

compounds resulted in no or even negative effects for whisker growth. In these cases, titanium diboride deposition took place in a form of homogeneous coatings or fine crystallites, and the thickness of the coatings or deposits on impurity painted zone was the same as or rather thinner than those on upainted zone. On the contrary, the compounds of Au, Ag, Pt, Pd, and Rh resulted in positive effects to titanium diboride deposition. Whisker grew on the half part of substrate near to outlet, while coatings or fine crystallites on the other half part near to inlet. Of the positive effect elements, Au was the most effective one, and Pt and Pd were found to be considerably effective. Rh exhibited weak effect and Ag also gave an effect only at somewhat lower temperature range than that of Au. These impurity effects for titanium diboride whisker growth are summarized in Table 1 together with those for the boron whisker growth[8] and the eutectic temperature of relevant binary systems. It is interesting that the excellent impurities for boron whisker growth such as Co, Ni, Cu metals are in effective in titanium diboride whisker growth.

Figure 2 shows the appearance of whiskers commonly grown with Au impurity at 1050 °C (a) and hexagonal pillar crystals grown with Pd impurity at 1120 °C (b and c). Hereafter the results were taken under painting of 2% chloroauric acid unless otherwise described.

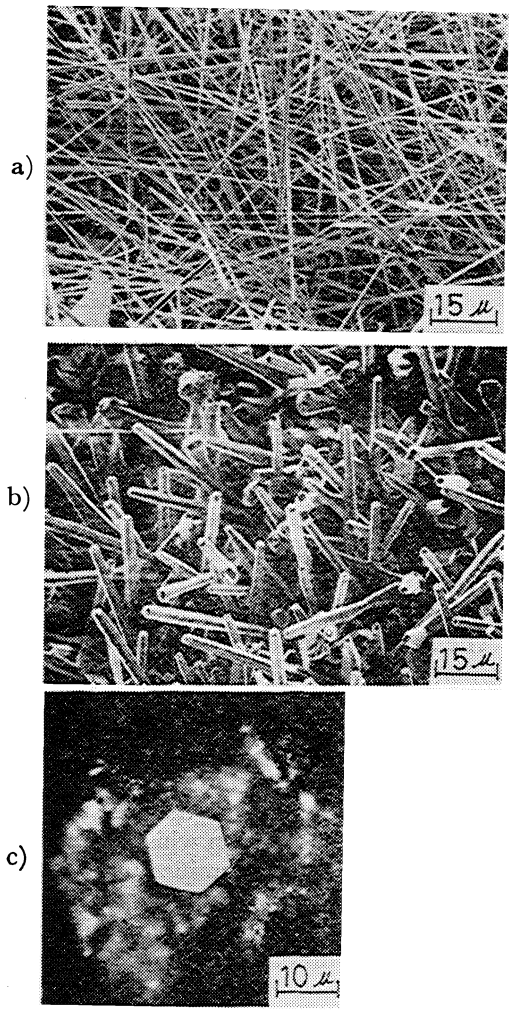

Fig. 2. Appearances of TiB_2 whiskers and pillar crystals. (a) Whiskers, impurity: Au; substrate tempeature: 1050 °C. (b) Pillar crystals, impurity: Pd; substrate temperature: 1120 °C. (c) Cross section of pillar crystal.

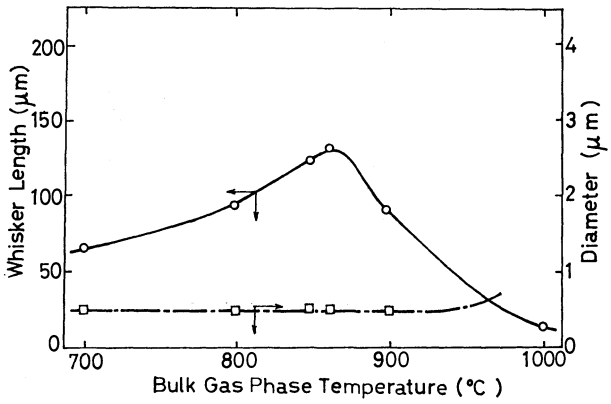

Fig. 3. Effect of temperature of bulk gas phase. Substrate temperature: 1100 °C; reaction time: 30 min.

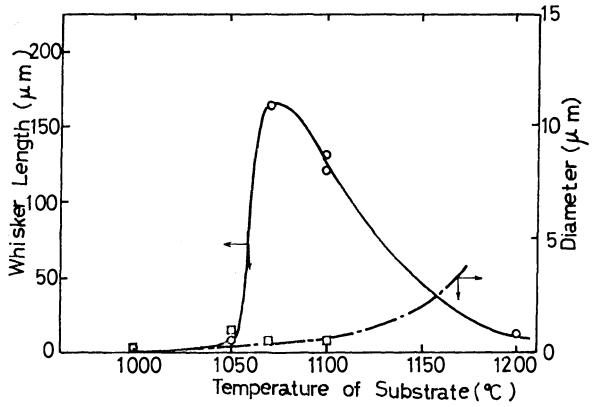

Fig. 4. Effect of substrate temperature. Bulk gas phase temperature: 870 °C; reaction time: 30 min; total flow rate: 2.3 cc/s; $TiCl_4/BCl_3/H_2/Ar$= 8.8/17.5/43.5/30.2 (vol %).

The Effect of Temperature. When the substrate temperature was kept at 1100 °C, whisker length and its diameter after 30 min are moderately varied with the gas phase temperature as shown in Fig. 3. The whisker length became the shorter above 870 °C. Therefore, the gas phase temperature of 870 °C was selected hereafter. On the other hand, the substrate temperature exhibited a sharp effect for whisker growth (Fig. 4). The longest whisker grew at 1060—1080 °C, above which decrease of length and increase of diameter took place gradually, and at the temperature higher than 1100 °C, pillar crystals and thick polycrystalline coatings deposited (Fig. 5). On the contrary, at the substrate temperature lower than 1050 °C whiskers did not grow to observable length.

Time Dependence of Whisker Growth. Average whisker length increased with time up to 30 min, then decreased apparently as shown in Fig. 6. This results may be explained by rapid linear growth, followed by gradual thickning to touch each other especially at the foot part of the whiskers.

In Fig. 7, whisker length and diameter are plotted

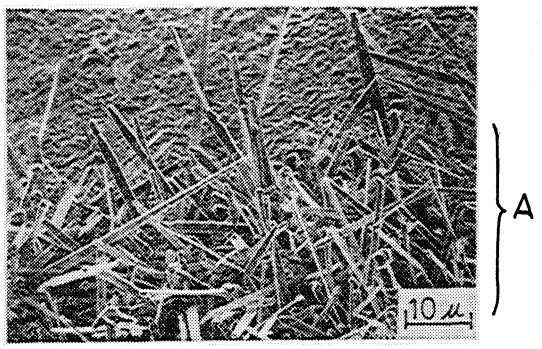

Fig. 5. Appearances of pillar crystals.
Substrate temperature: 1100 °C.

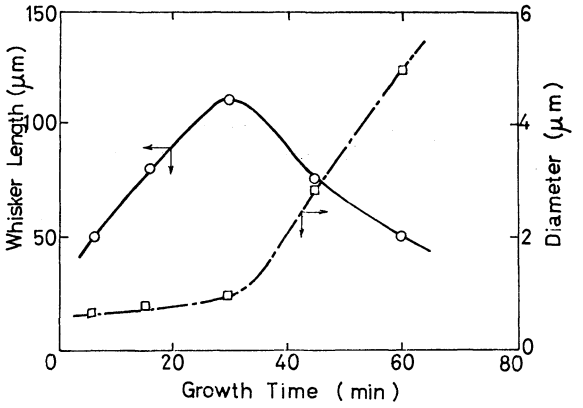

Fig. 6. Effect of reaction time.
Bulk gas phase temperature: 870 °C; substrate temperature: 1070 °C; total flow rate: 2.3 cc/s; $TiCl_4/BCl_3/H_2/Ar=13.1/13.1/45.6/28.2$ (vol %).

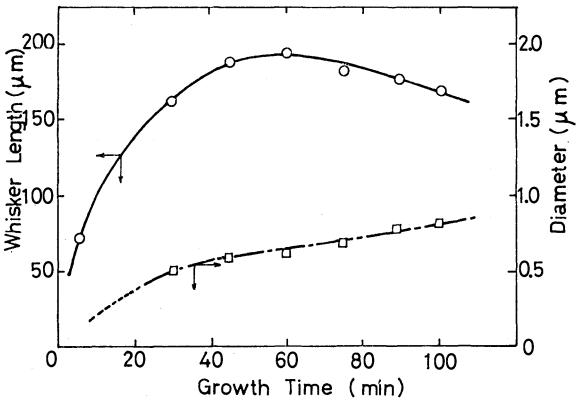

Fig. 7. Effect of growth time with repeptive painting of gold.

against the reaction time during which repetitive gold paintings of about 0.05 mg/cm² of substrate area were carried out. It is found that the repetitive paintings resulted in only a slight effect and the average whisker length increased to 200 μm (maximum length of 350 μm) up to 60 min of growth time, and average diameters also increased up to 0.9 μm for 100 min.

Effect of the Gas Flow Rate and its Composition. In Fig. 8, total flow rate for obtaining the longest whisker is found at 2.0—3.0 ml/s. The average whisker diameters retain 0.9—1.0 μm above the flow rate of 2.5 ml/s. In Fig. 9, the concentration of titanium tetrachloride is

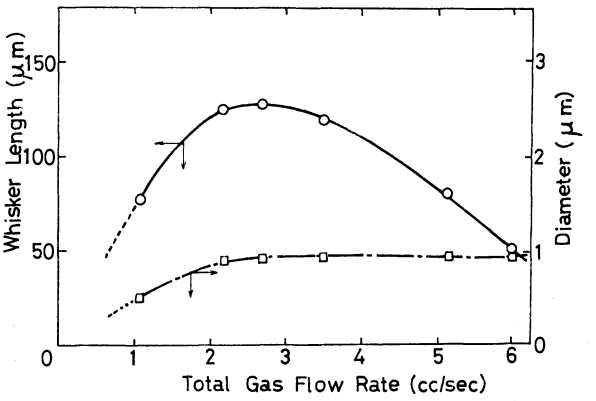

Fig. 8. Effect of total gas flow rate.
Bulk gas phase temperature: 870 °C; substrate temperature: 1070 °C; reaction time: 30 min; $TiCl_4/BCl_3/H_2/Ar=10/20/50/20$ (vol %).

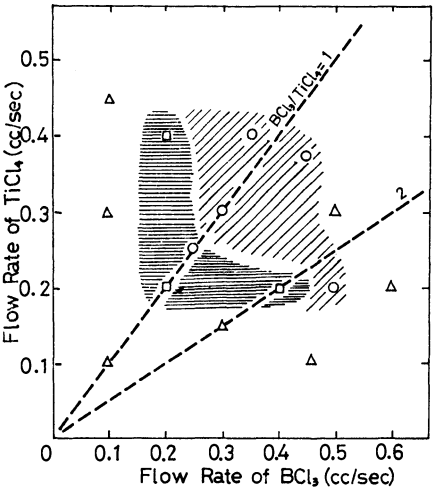

Fig. 9. Effects of the gas flow rate and its composition
Bulk gas phase temperature: 870 °C; substrate temperature: 1070 °C; reaction time: 30 min; total flow rate: 2.3 cc/s, (△): below 100 μm; (○): 100—150 μm; (□): above 150 μm.

plotted against that of boron trichloride in relation to whisker length under a total flow rate of 2.3 ml/s, and the optimum growth conditions are in the hatched range. The longest whiskers were not obtained at the concentration ratio of $BCl_3/TiCl_4=2$, which corresponds to the stoichiometric ratio of the reaction of

$$2BCl_3 + TiCl_4 + 5H_2 = 10HCl + TiB_2,$$

but at a ratio of $BCl_3/TiCl_4 \approx 1$. At the concentration range of boron trichloride higher than the range shown in Fig. 9 the formation of boron whisker was detected, however, which could not be identified by X-ray diffraction for its low diffraction ability, but was discriminated against the titanium diboride whisker by thin curled appearance and by easy dissolution in nitric acid.

Morphologies and Growth Mechanism of TiB_2 Crystals. Some interesting morphologies are shown in Fig. 10. The whisker growth along the hexagonal edges (10a), and from a center of a hexagonal to the six corners of it (10b) are seen when Ag was painted as impurity. When substrate was scratched by pure gold plate, the gold are

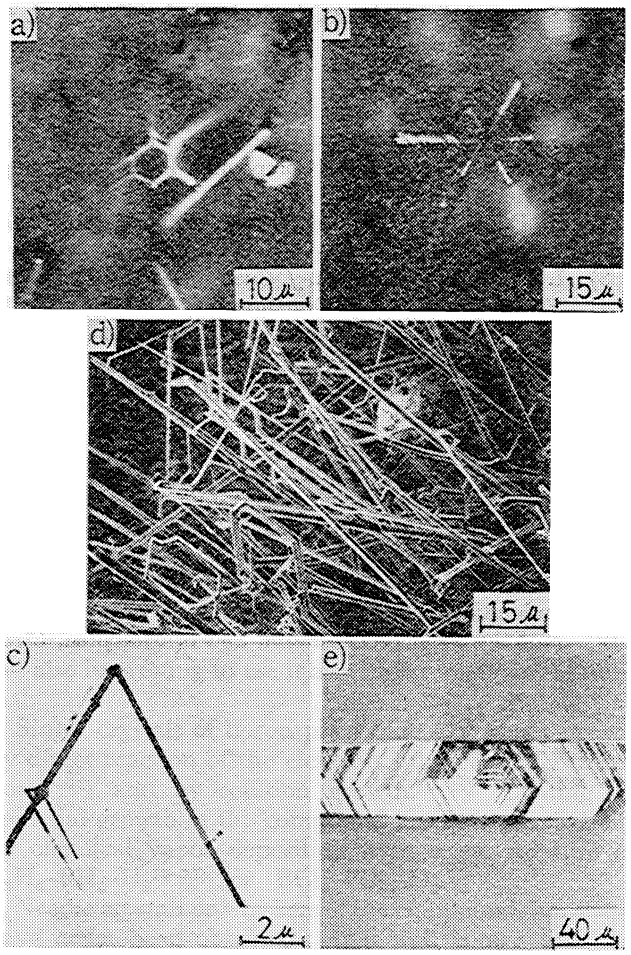

Fig. 10. Some interesting morphologies of TiB_2 whiskers.
a) Whisker grown along a hexagonal edges, b) whiskers grown from the center of hexagonal, c) and d) kinked whiskers, e) growth steps on the side of pillar crystal.

regarded as one of the heaviest dopings. On the zone scratched by gold, whiskers are apt to grow with two kinds of kink angles of 60° (Fig. 10c) and 120° (Figs. 10c and 10d). On the sides of tetragonal pillar crystals (Fig. 10e), multiple growth steps of hexagonal patterns are found, and six fold symmetry axis perpendicular to the side plane was confirmed by Laue photograph. Also additional information for growth direction was obtained from X-ray diffraction diagrams as shown in Fig. 11. The whiskers as grown gave a diagram (Fig. 11b) having peak intensities like those of powder diffraction (Fig. 11a). On the contrary, when about one milligram of whiskers was thoroughly disintegrated in a few drops of water, poured on a holder glass, and dried, the X-ray diffraction diagram is deficient of (10$\bar{1}$1) peak (Fig. 11d) which is the strongest one in powder diffraction peaks (Fig. 11a). From above results, the whisker shape is considered to be tetragonal pile, and the growth direction to be ⟨100⟩axis. Then the kink angles of 60° and 120° are reasonable for equivalent ⟨100⟩directions.

It may be seen in Fig. 5 that pillar whiskers grow only on the part of Au impurity painted zone (A-part), furthermore, on the tip of whisker a droplet can be seen as in Fig. 12a. The existence of a cap on the whisker tip leads to the VLS mechanism for whisker growth. There

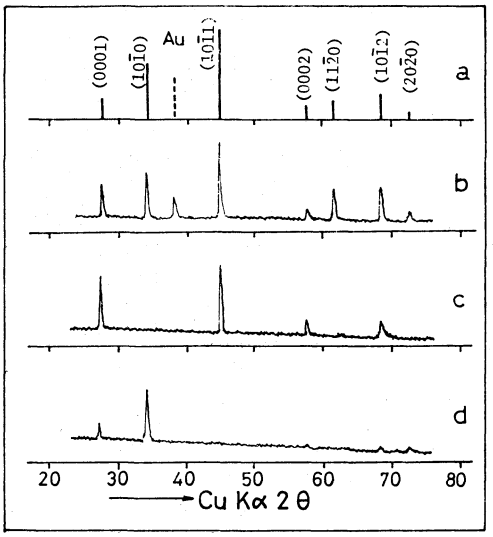

Fig. 11. X-ray diffraction profiles.
a) ASTM data for pulverized TiB_2, b) whiskers as grown, c) hexagonal piles as grown, d) whiskers dispersed on glass.

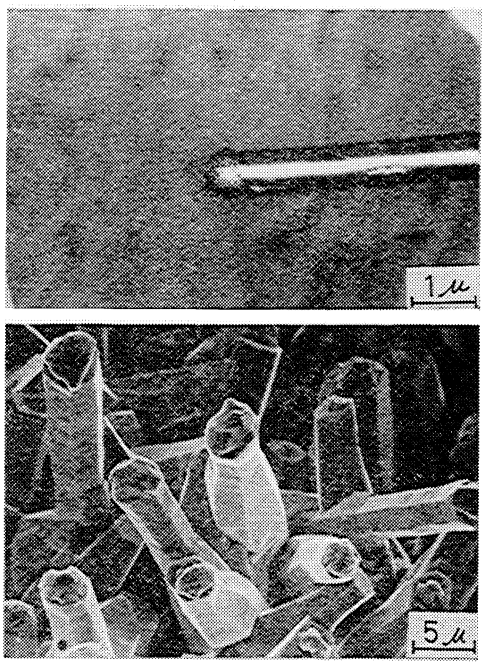

Fig. 12. The tips of the whiskers and pillar crystals.
a) Impurity: Au, substrate temperature: 1050 °C.
b) Impurity: Pd, substrate temperature: 1120 °C.

is, however, a problem to support the mechanism, that is, no liquid phase is found in the binary systems Ti–Au,[9] Ti–B,[9] and Au–B, below 1063 °C which is the melting point of Au. Whiskers grew above 1050 °C. Then the liquid phase may be formed by contamination with silicon from the substrate as reported on the titanium nitride whisker growth[10] or by lowering of liquidus in ternary system Ti–Au–B compared with any of relevant binary systems.

On the other hand, the growth process of hexagonal piles are supposed from their appearance (Figs. 2b and 2c) that the piles grew to [001] direction under the influence of impurity at first, followed by the growth to the direction perpendicular to c-axis.

In Fig. 12b, which is the sample grown on the Pd painted zone near inlet, droplets are also found on the tips, but have different figure from that of Fig. 12a. These hexagonal piles are grown from a BCl_3 rich atmosphere relative to that for the whisker which was grown on the half part substrate near outlet. By the deposition of polycrystalline TiB_2 on the half part of substrate near inlet, the ratio of $BCl_3/TiCl_4$ in gas stream may steeply decrease from unity at inlet to nearly zero outlet. Then, hexagonal piles grown on the zone painted of Pd near inlet are considered to grow under a condition of VS (Vapor-Solid) growth, that is, high concentrations of reactants and high temperature (1120 °C). It is supposed that VS growth rate to [001] direction is low as seen from the hexagonal steps in Fig. 10e. The stacking of the atomic planes to the direction of [001] of titanium diboride consisted of alternative planes of boron and titanium, whereas the stacking to the direction of [100] is that of self-consistent plane of titanium diboride. If one of the reasons for the low growth rate to [001] direction is assumed to be the nucleation of boron, the role of palladium impurity is recognized by easier nucleation of boron plane from a liquid phase of Pd–B alloy, and VS growth from the nuclear along the (0001) plane develops the figure shown in Fig. 12b.

References

1) S. A. Mersol, C. T. Lynch, and F. W. Vahldick, Anisotropy Single Cryst. Refract. Compounds Proc. Int. Symp. Dayton, Ohio, **2**, 41 (1967).
2) A. D. Kiffer, U. S. Dept. Com., Office Tech. Serv., PB Report 161792, 24 (1960).
3) I. Higashi and T. Atoda, *J. Cryst. Growth*, **1**, 251 (1970).
4) V. N. Gurin, A. P. Obukhov, T. I. Mazina, Z. P. Terenteva, I. R. Kozlova, and M. M. Korsukova, *Izv. Akad. Nauk. SSSR, Neorg. Mater.*, **5**, 11 (1969).
5) P. Peshev, *Izv. Inst. Obshta. Neorg. Khim., Bulg. Akad. Nauk.*, **4**, 53 (1966).
6) R. L. Hough, *AIAA J.*, **4**, 107 (1966).
7) T. Takahashi, K. Sugiyama, and Y. Suzuki, *J. Cryst. Growth*, **10**, 139 (1971).
8) S. Motojima, Y. Miura, Y. Takahashi, and K. Sugiyama, Unpublished data.
9) M. Hansen, "Constitution of Binary Alloys," McGraw-Hill, London (1958), pp. 237, 260.
10) K. Sugiyama, Y. Takahashi, and S. Motojima, *Chem. Lett.*, **1975**, 363.

Metallic Impurity-Activated Crystal Growth of Boron Phosphide by Chemical Vapor Deposition and Its Physical Properties

Seiji MOTOJIMA, Yasuo MIURA, Kohzo SUGIYAMA, and Yasutaka TAKAHASHI
Department of Synthetic Chemistry, Faculty of Engineering, Gifu University, Gifu 504
(Received May 26, 1975)

Needle single crystals of boron monophosphide as large as 5—100 μm in diameter and 4 mm in length were obtained by chemical vapor deposition on an impurity painted zone of quartz substrate at 1060—1120 °C. The impurities such as Mn, Ni, Pt, Ag or Au were painted on the substrate in a form of aqueous solution of their salts and decomposed or reduced to the respective metal in hydrogen atmosphere at 1000 °C. Needle crystals with the homo p-n junction were also prepared using Ni impurity. The colors of grown crystals varied with the change of gas composition. Differences of electrical resistivity and thermoelectric power were found between the crystals of different colors.

Cubic boron monophosphide (BP, boron phosphide hereafter) has been extensively investigated during the past decade for its eminent properties as semiconductor.[1-3] Other properties of the compound, such as high melting point (about 3000 °C), high hardness (4000 kg/mm^2),[4] high oxidation resistance in air,[5] and high corrosion resistance in various chemicals,[6-8] moreover, are also interesting to use it as a high temperature material.

Single crystals of boron phosphide have been grown by direct reaction of the elements,[9] by chemical transport[10-12] and by solution growth.[13-14] Coating or epitaxial growth of the compound has been carried out by chemical vapor deposition from a gas mixture of B_2H_6–PH_3–H_2[15-17] or BCl_3–PCl_3–H_2.[18]

Needle crystals or whiskers of the compound, however, have never been obtained. It is well known that the existence of some kind of impurities accelerates the growth of whisker or needle crystals. In the present work, the growth conditions of the single crystal of boron phosphide in use of metal impurities by chemical vapor deposition from a gas mixture of boron trichloride, phosphorus trichloride, hydrogen and argon were investigated together with some physical properties of the grown crystals.

Experimental

Materials. Commercial G. R. grade phosphorus trichloride, boron carbide, and liquefied chlorine were used without further purification. Boron trichloride was prepared from boron carbide *in situ* (*vide infra*).

Preparation of Boron Phosphide. Apparatus is shown in Fig. 1. A quartz tube (7 mm o.d. and 50 mm in length), in which SiC heater was inserted, was placed at a center of reaction tube (quartz of 23 mm i.d.) as a substrate for the crystal growth. The substrate was heated at 900—1200 °C dually from outside and inside. A chlorine stream was flowed into a boron carbide bed kept at 800 °C to form boron trichloride, and the other stream of argon was bubbled through a phosphorus trichloride saturator maintained at 0 °C. The two streams were mixed at the growth zone. The surface temperature of the substrate was measured by an optical pyrometer through a window (corrected with emmision factor) and the bulk gas phase temperature by a C–A thermocouple.

Aqueous solutions of eleven compounds such as nickel acetate, hexachloroplatinic acid, tetrachloroauric acid, silver nitrate, *etc.* were painted as impurities on the substrate scratched by abrasives and decomposed or reduced to fine particles or islands of the respective metals in hydrogen atmosphere at 1000 °C.

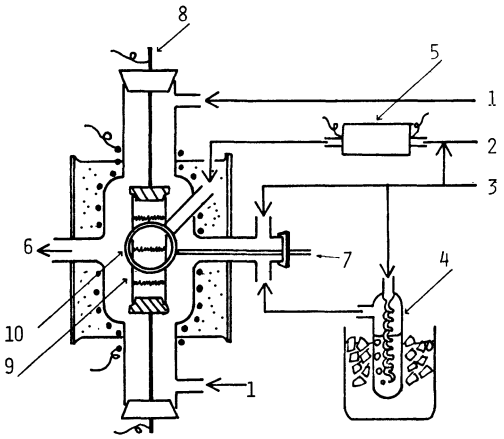

Fig. 1. The apparatus for BP growth.
(1) H_2, (2) Cl_2, (3) Ar, (4) PCl_3 saturator, (5) B_4C, (6) outlet, (7) C–A thermocouple, (8) electrode, (9) quartz substrate, (10) window.

In this paper, length of needle crystals is shown by the average length of about twenty samples selected in the order from the longest in the field of microscopy magnified by 150. Reaction time was fixed at 30 min, unless otherwise described.

Electrical Resistivity Resistivity measurements of needle crystals were performed under argon atmosphere at the temperature range of 20—120 °C using a DC wheatstone bridge (Ando Elec. Co., Model LCR-4) by conventional two probe method using a silver paste (Fujikura Chemicals, Dotite D-550) to contact the leads.

Thermoelectric Power. Crystal was bridged and attached between two copper plates (3×5 mm) separated 1 mm each other, one of which was heated by nichrome heater, where temperature difference of two edges of the crystals was measured by an iron-constantan thermocouple, and controlled in the range of 1—1.5 °C. Thermoelectric power was measured by a potentiometer.

I—V Measurements. The relationship between the current and the applied voltage (DC) was taken by a current interruptor (Hokuto Denki Co., CL-2515).

Results and Discussion

Identification of Products and Impurity Effect. In the preliminary experiment, it was found that the forms of

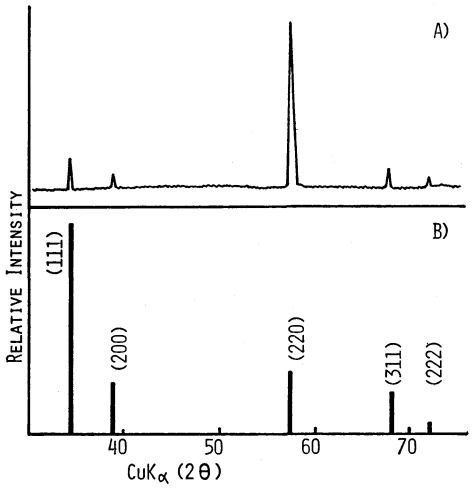

Fig. 2. X-Ray diffraction profiles.
A) BP pillar crystals set aside along the growth axis, B) BP-ASTM (No. 11—119).

deposits varied from polycrystalline coatings in the absence of nickel impurity to pillar crystals in the presence of it at 1070 °C. Although X-ray diffraction peaks of pillar crystals set aside along the growth direction shown in Fig. 2A are in good accordance with those of powder

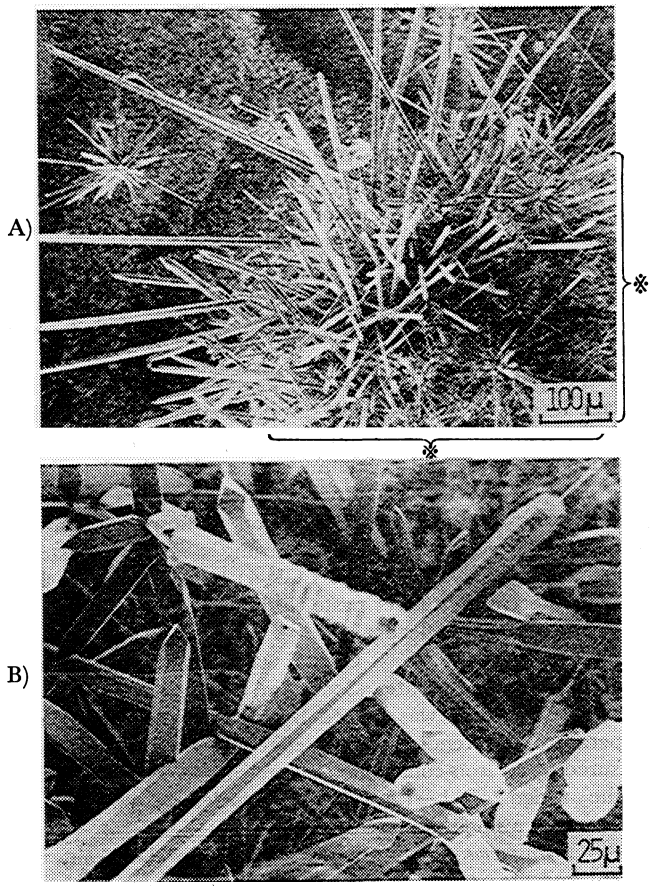

Fig. 3. Appearance of pillar crystals.
A) Pillar orange crystals, temperature: 1090 °C; reaction time; 30 min; $BCl_3/PCl_3/H_2/Ar=0.15/0.03/1.0/1.4$ (cc/s); impurity: Ni, ※ Impurity pained zone. B) Pillar black crystals, temperature: 1090 °C; reaction time: 30 min; $BCl_3/PCl_3/H_2/Ar=0.7/0.02/1.0/1.2$ (cc/s); impurity: Ni.

Table 1. Impurity effects

	Impurity (mp)	Impurity (painted forms)	Eutectic temp of binary alloy (°C) Boron-impurity	Eutectic temp of binary alloy (°C) Phosphorus-impurity	Impurity effects (crystal colors)
Fe	1535	$FeCl_3$	1149	1050	—
Co	1495	Co-$(CH_3COO)_2$	1095	1023	—
Ni	1445	Ni-$(CH_3COO)_2$	1080	880	++ (red and black)
Rh	1966	$RhCl_3$	1131	1300	+ (black)
Pd	1549	$PdCl_2$	845	788	—
Pt	1774	H_2PtCl_6	830	588	++ (black), + (red)
Cu	1083	$CuCl_2$	1060	714	—
Ag	960.5	$AgNO_3$		878	++ (red and black)
Au	1063	$HAuCl_4$		935	++ (red and black)
Zn	419.5	$ZnCl_2$			—
Sb	630.5	$SbCl_3$		612	—
Nd	840	$NdNO_3$			—
Cr	1890	$CrCl_3$	1550±50	1370	—
Mn	1260	$MnSO_4$		960	+ (red and black)

Reactions: conditions: Temperature; 1090 °C; reaction time, 30 min; $BCl_3/PCl_3/H_2/Ar=0.12/0.03/0.8/1.5$ (cc/s). a) (−): no or negative effects, (+): weak positive effects (below 1 mm long), (++): strong positive effects (longer than 1 mm).

data of the boron phosphide[19] (Fig. 2B), from the anomalous intensity of (110) in Fig. 2A and from the hexagonal shape (Fig. 12), it is supposed that the growth direction is ⟨111⟩, thus the side planes (110). The different growth conditions and impurities resulted in the needle or pillar crystals of different colors such as black, dark-red, and orange or yellow, while the structures and the growth directions were determined as the same as the pillar crystals grown at 1070 °C with nickel impurity described above.

When nickel impurity is painted on the substrate, pillar crystals grow only on the impurity painted zone as shown in Fig. 3A, indicating the impurity indispensable for pillar crystal growth. In Table 1, impurity effects of various metals on the pillar crystal growth at 1090 °C are summarized together with the eutectic temperatures of the relevant binary alloys.[20-22] Of the examined impurities, chromium, cobalt, iron, palladium, and copper resulted in no or negative effect on pillar crystal growth at 1090 °C, where deposition took place in a form of coatings or polygonals. On the contrary, manganese, nickel, platinum, silver, and gold indicated a positive effect at the same temperature as above, affording a straight and well-formed pillar crystal as large as 2 mm for 30 min and up to 4 mm for 90 min.

Of cource, the impurity effect varies with growth temperature. In Fig. 4, the temperature ranges of substrate for respective impurities where pillar crystal growth is possible are shown by vertical lines at the eutectic temperatures of the systems, boron–impurities. It is found that cobalt, rhodium, and iron indicate the positive effect at the higher temperature. It may be seen that

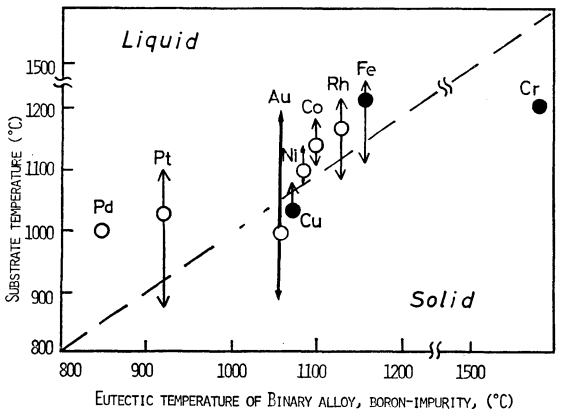

Fig. 4. Relationship between the substrate temperature and the eutectic temperature of binary alloys, boron and impurities, in BP pillar crystal growth.
(○): up to 1 mm long, (●): below 1 mm, In the case of Au impurity, the mp of Au metal it self are shown because boron is not dissolved in it.

the higher the eutectic temperature of the system of boron-impurity, the higher temperature is required for pillar crystal growth.

Hereafter nickel or platinum was used as an impurity, unless otherwise noted. The surface concentration of the impurity was fixed at *ca.* 50 μg/substrate area (cm^2) without reasons.

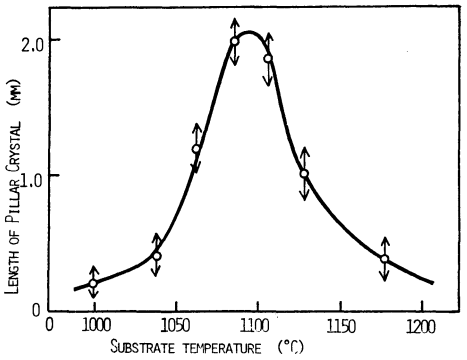

Fig. 5. Effect of substrate temperature on the length of pillar crystal.
Impurity: Pt; reaction time: 30 min; $BCl_3/PCl_3/H_2/Ar=0.05/0.023/1.3/1.25$ (cc/s).

The Effect of Substrate Temperature. The predominant factor to control the maximum length of pillar crystal is the substrate temperature. One of the results is shown in Fig. 5, where platinum was used as the impurity. An average length of 1.8—2.0 mm and the thickness of 10—50 μm was attained at 1070—1100 °C, above or below which the maximum length steeply decreased below 500 μm.

Effects of Gas Composition and Flow Rate on Pillar Crystal Growth. In the Case of Platinum Impurity: The effect of the concentration of BCl_3 and PCl_3 on the pillar crystal length is shown in Fig. 6, where total flow rate was fixed at 2.6 cc/s. According to the reaction:

$$BCl_3 + PCl_3 + 3H_2 = BP + 6HCl$$

stoichiometric ratio of $BCl_3/(BCl_3+PCl_3)$ equals to 0.5. However, the longest pillar crystal of black and hexa-

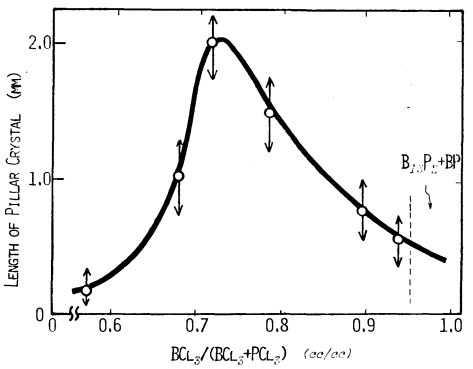

Fig. 6. Effect of the flow ratio $BCl_3/(BCl_3+PCl_3)$ on pillar crystals growth.
Impurity: Pt; reaction temperature: 1080 °C; reaction time: 30 min; H_2: 1.3 cc/s, total flow rate: 2.6 cc/s.

gonal or trigonal shape was obtained between the ratios of 0.7—0.8. Woolly and faint yellow whiskers were grown at the ratio of higher than 0.95, and were determined as the mixture of boron phosphide and tridecaboron diphosphide.

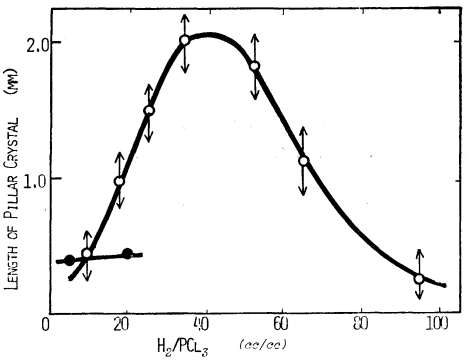

Fig. 7. Effect of the flow ratio H_2/PCl_3 on pillar crystal growth.
Impurity: Pt; reaction temperature: 1090 °C; reaction time: 30 min; $BCl_3/PCl_3=4$ (cc/cc); total flow rate: 2.4 cc/s. (○): black crystal, (●): red-orange crystal.

Phosphorus trichloride is readily reduced by hydrogen to phosphorus element. Thus the ratio of H_2/PCl_3 is expected to affect the boron phosphide crystal growth. In Fig. 7, the relationship between the length of pillar crystal and the ratio of H_2/PCl_3 in the feed stream is shown where the ratio of $BCl_3/(BCl_3+PCl_3)$ was fixed at 0.8. In spite of the dilution of phosphorus trichloride and boron trichloride by hydrogen, the length of the pillar crystal increases with the ratio up to 40, which corresponds to the phosphorus trichloride concentration of 2.5% and to the total chloride concentration of 10%. At the dilution (H_2/PCl_3) lower than twenty the color of grown crystals varied to red-orange. When the concentrations of boron trichloride, phosphorus trichloride, hydrogen, and argon calculated from the feed rates are kept at 2.0, 1.0, 50, and 47 vol %, respectively, the total flow rate to grow the longest whisker was between 2.3—3.0 cc/s which corresponds to the linear velocity of about 3 cm/s at the growth temperature of 1090 °C.

In the Case of Nickel Impurity. It was found that

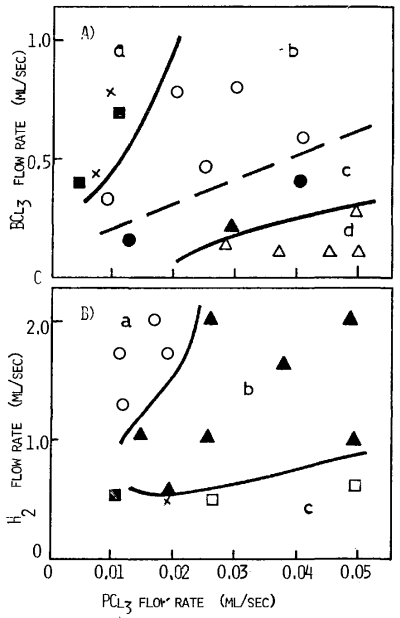

Fig. 8. Effect of relevant gas flow rates on the crystal colors and the compositions.
Impurity: Ni; (○): black pillar crystal; (●): black and orange pillar crystal; (△): orange or yellow pillar crystal; (▲): red-orange and black pillar crystal; (×): black coatings of boron and boron phosphide; (□): black coatings or brown woolly crystals of BP and $B_{13}P_2$; (■): blown and white woolly crystals of boron and boron phosphide.
A) H_2 flow rate: 1.0 cc/s, B) $BCl_3/PCl_3=0.7$ (cc/cc).

the kind of impurity affects not only morphologies of grown crystal, but also the colors of it. In Fig. 8, the distributions of the colors and the compounds of grown crystals are shown in relation with the flow rates of boron trichloride, hydrogen, and phosphorus trichloride using nickel impurity. It is found that the colors of the pillar crystals of boron phosphide vary from black of b-region to orange or faint yellow of d-region in Fig. 8A, and also from black of a-region to orange of b-region in Fig. 8B. The preferable concentration ratio of BCl_3/PCl_3 to grow the black pillar crystal of boron phosphide is about twenty, which is far rich in boron trichloride compared with the result in the case of platinum impurity, where the ratio was about three as seen from Fig. 6.

Preparation of the Crystal with Homo p-n Junction.
During the CVD experiment of boron phosphide, it was found that the pillar crystal with the homo junction between the p-type black and n-type orange boron phosphide grew spontaneously by a local fluctuation of gas composition. The growth condition of the experiment was substrate temperature of 1090 °C, the gas concentration of $BCl_3/PCl_3/H_2/Ar$ of (3.7—7.4)/(1.1—1.5)/(37—38)/(55—58) vol%, and total flow rate of 2.6—2.8 cc/s in use of nickel as an impurity. The black and the orange pillar crystals are apt to grow in mixture at the part near inlets of boron trichloride and phosphorus trichloride only when nickel was used as an impurity. It was supposed that the variation of colors of pillar crystals arised from unexpected change of the ratio BCl_3/PCl_3. Thus, during the growth the inlets of boron trichloride and phosphorus trichloride was exchanged

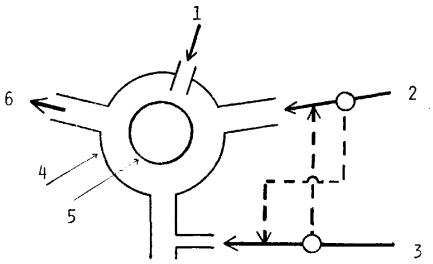

Fig. 9. Apparatus (cross section) for obtaining the pillar crystal with homo p–n junction.
1) H_2, 2) PCl_3, 3) BCl_3, 4) reaction tube, 5) quartz substrate, 6) outlet.

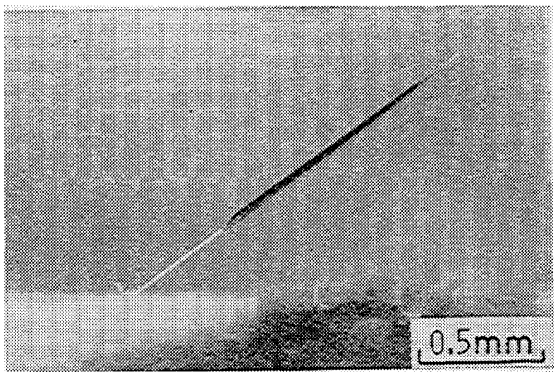

Fig. 10. Pillar crystal with homo p–n junction.
Impurity: Ni; reaction temperature: 1090 °C; reaction time; 60 min; $BCl_3/PCl_3/H_2/Ar=0.2/0.03/1.0/1.4$ (cc/s).

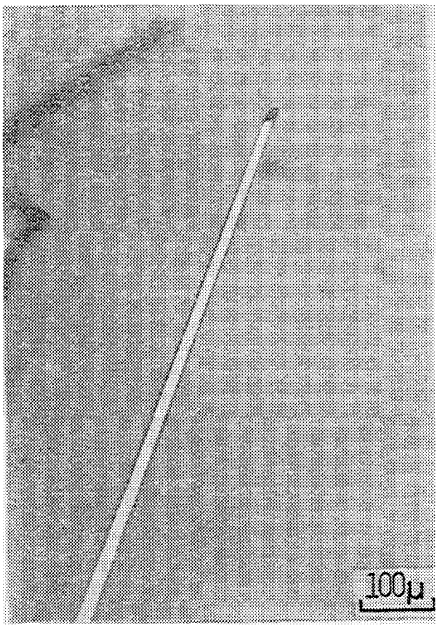

Fig. 11. Typical orange pillar crystal.
Impurity: Ni; reaction temperature: 1090 °C; reaction time: 30 min; $BCl_3/PCl_3/H_2/Ar=0.2/0.04/1.0/1.6$ (cc/s).

each other after the growth time of 30 min from the heavy lines in Fig. 9 to the dashed line, and the growth was continued for 15—30 min. The color of the pillar crystal changed from orange at the first step to black partly near tip at the second step. In Fig. 10, one of the grown crystals is shown. The black part consists of the

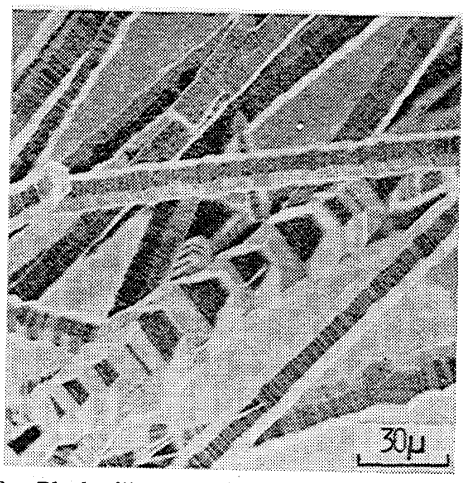

Fig. 12. Black pillar crystals with multiple growth steps on the side.
Impurity: Pt; reaction temperature: 1090 °C; reaction time: 30 min; $BCl_3/PCl_3/H_2/Ar=0.1/0.025/1.5/1.3$ (cc/s).

outer black layer and the orange core. The I–V property of the crystal will be shown later.

Crystal Morphologies and Growth Mechanism of Pillar Crystals. In contrast with the well formed red-orange crystals grown in use of nickel impurity (Fig. 11), multiple growth steps were seen frequently on the side of black pillar crystals in use of platinum impurity as shown in Fig. 12. The cross section of these crystals was commonly hexagonal- or trigonal-shaped irrespective of their colors.

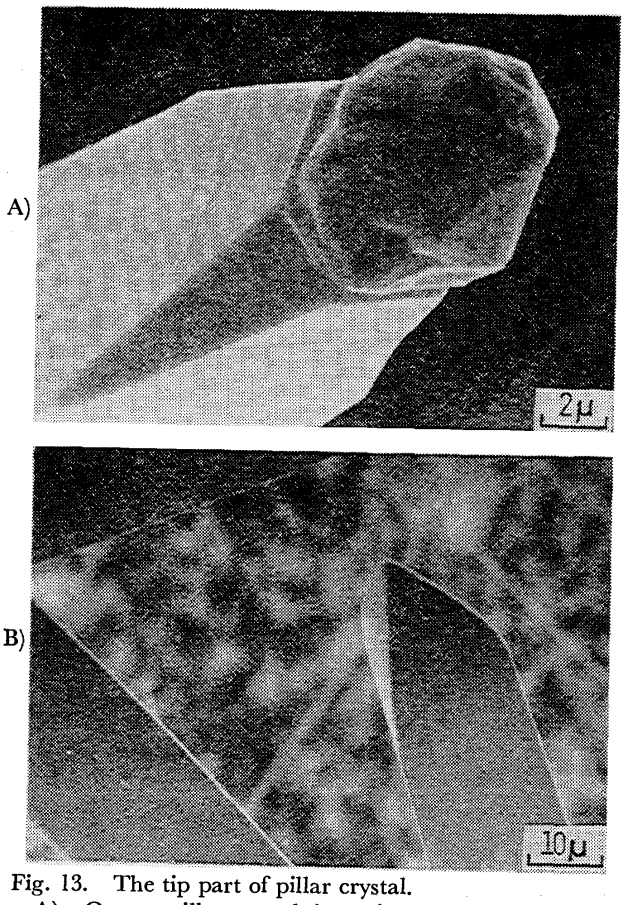

Fig. 13. The tip part of pillar crystal.
A) Orange pillar crystal, impurity: Ni.
B) Black pillar crystal, impurity: Pt.

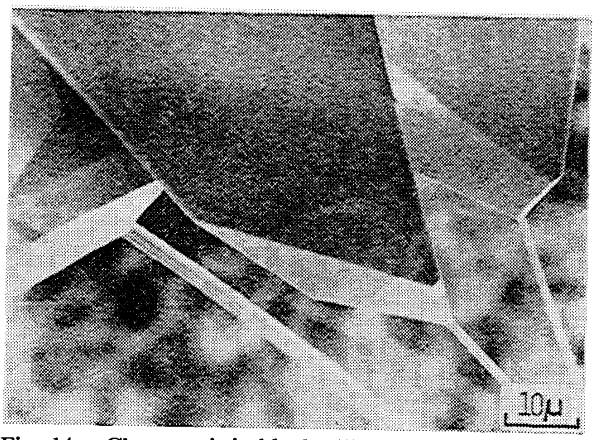

Fig. 14. Characteristic black pillar crystal grown on an orange whisker.
Impurity: Ni; reaction temperature: 1090 °C; reaction time: 30 min; $BCl_3/PCl_3/H_2/Ar=0.7/0.02/1.0/1.2$ (cc/s).

The impurities, intended to be a liquid forming agent, are indispensable for the growth of pillar crystals as described above. When nickel was used as an impurity, on the tip of the orange pillar crystal there can be seen commonly globules which may be considered to be impurity drops (Fig. 13A). On the contrary, no globules were seen on the tip of black pillar crystals irrespective of the kind of impurities (Fig. 13B). In Fig. 14, the foot part of black crystals is shown. The whole of them has yellow thin leg, from which the growth mechanism is supposed to be fast linear growth of yellow crystal by "VLS" mechanism followed by growth of black crystal by slow "VS" mechanism to the direction perpendicular to the growth axis. Unfortunately, such a double structure can be seen only when nickel was used. Thus the

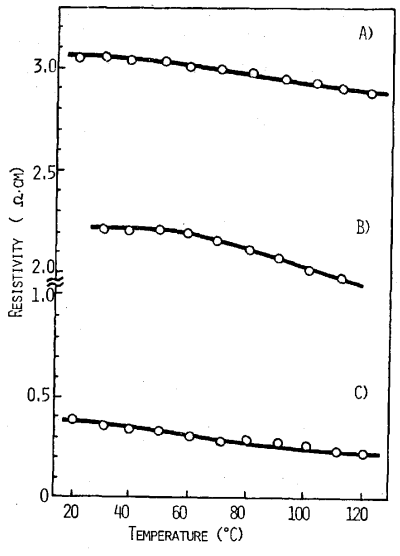

Fig. 15. Temperature dependence of electrical resistivity.
A) Impurity: Pt; $BCl_3/PCl_3/H_2/Ar=0.05/0.025/1.3/1.25$ (cc/s); black crystal.
B) Impurity: Ni; $BCl_3/PCl_3/H_2/Ar=0.3/0.035/1.0/1.45$ (cc/s); dark-red crystal.
C) Impurity: Ni; $BCl_3/PCl_3/H_2/Ar=0.12/0.03/0.8/1.5$ (cc/s); orange crystal.

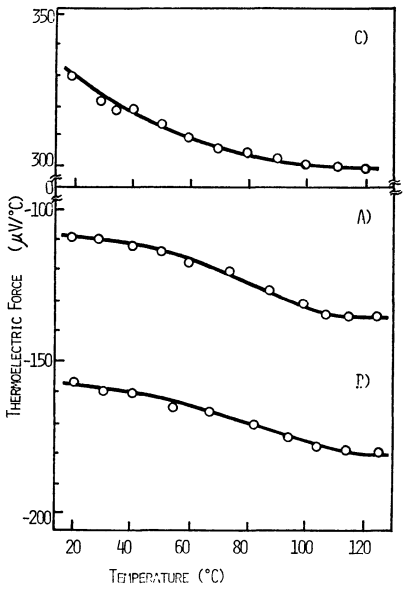

Fig. 16. Temperature dependence of thermoelectric force.

growth mechanism for other impurities than nickel remains open to further investigations.

Properties of Boron Phosphide Crystals. Electrical Resistivity: The resistivities of well-formed black, dark-red and orange or yellow crystals of hexagonal or trigonal pillars are shown in Fig. 15. These crystals were obtained in use of Pt, Ni, and Ni metal as an impurity, respectively. Although the measurements were carried out on three crystals of respective colors, the results were characteristic of respective colors within the experimental errors. Figure 15 shows that the resistivity decreases with increasing temperature, showing a characteristic semiconductor behavior. Crystal of black, dark-red, and orange have the resistivities of 3.1, 2.2, and 0.4 Ω·cm at room temperature, respectively. Chu *et al.*[12] and Nishinaga *et al.*[15] reported that the resistivities of boron phosphide were 0.5 Ω·cm (for single crystal of p-type) and 5×10^{-3} Ω·cm (for undoped layers of n-type), respectively. The resistivity of orange crystals is in good accordance with that of the former.

Thermoelectric Power. Thermoelectric powers of boron phosphide crystals of three colors, black, dark-red, and orange, are shown in Fig. 16, indicating the thermoelectric powers of −110, −160, +330 μV/°C at room temperature, respectively, and decrease with temperature. These values obtained roughly agree with the value of 240 μV/°C reported by Grinberg *et al.*[23]

Conduction types were determined as p, p, and n for crystal of black, dark-red, and orange, respectively.

Schono *et al.*[17] reported that boron phosphide of p-type and n-type was grown epitaxially on a silicon substrate at low and high flow rates of phosphine, in the reaction of phosphine, boran, and hydrogen at 950—1100 °C, respectively. Takenaka *et al.*[24] obtained a thin red-brown layer of n-type boron phosphide. From the results obtained by Schono *et al.*[17] and in present work, it is supposed that the conduction types of boron phosphide are determined by excess boron or phosphorus as p or n, respectively. Thus the transition of the growth mechanism from "VLS" (orange whisker) to "VS" (black pillar) may be resulted from the solubility change of boron in impurity liquid with the whisker length because of the temperature decrease from hot surface of substrate to warm wall of reaction tube.

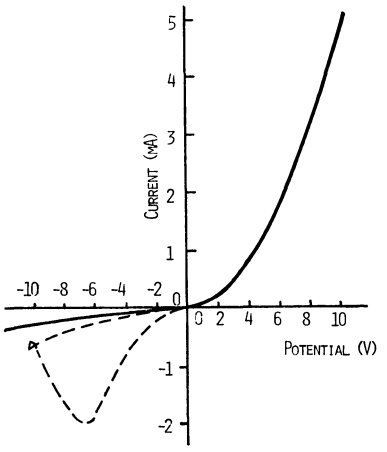

Fig. 17. I—V curve of the pillar crystal with homo p–n junction.

I—V Curve. The relationship of the applied voltage and the current of the crystal with homo p–n junction indicates a considerable rectification (Fig. 17).

References

1) C. C. Wang, M. Cardona, and A. G. Fischer, *RCA Rev.*, **25**, 159 (1964).
2) R. J. Archer, R. Y. Koyama, E. E. Loebner, and R. C. Lucas, *Phys. Rev. Lett.*, **12**, 538 (1964).
3) B. Stone and D. Hill, *Phys. Rev. Lett.*, **6**, 282 (1960).
4) V. I. Matkovich, *J. Amer. Chem. Soc.*, **83**, 1804 (1961).
5) R. C. Vickery, *Nature*, **184**, Suppl. No. 5, 268 (1959). (*Chem. Abstr.*, **54**, 7392 (1960)).
6) F. V. Williams and R. A. Rueherwein, *J. Amer. Chem. Soc.*, **82**, 1330 (1960).
7) J. Cueilleron and F. Thevenot, *Bull. Soc. Chem. Fr.*, **1965**, 402. (*Chem. Abstr.*, **62**, 14164 (1965)).
8) I. Yu. Andreeva and G. V. Efremov, *Vestn. Leningr. Univ. Ser. Fiz. i Khim.*, **19**, No. 2, 130 (1964).
9) K. P. Ananthanarayanan, C. Mothanty, and P. J. Gielisse, *J. Cryst. Growth*, **20**, 63 (1973).
10) Z. S. Medvedeva, J. H. Greenberg, E. G. Zukov, and N. P. Lužnaja, *Kristall Technick*, **2**, 523 (1967).
11) Z. S. Medvedeva, J. H. Greenberg, and E. G. Zukov, *ibid.*, **4**, 487 (1969).
12) T. L. Chu, J. M. Jackson, and R. K. Smeltzer, *J. Cryst. Growth*, **15**, 254 (1972).
13) B. V. Baranov, Ya. A. Oksman, V. D. Prochukhan, and V. N. Smirnov, *Opt. Spectrosk.*, **19**, 987 (1965).
14) T. L. Chu, J. M. Jackson, and R. K. Smeltzer, *J. Electrochem. Soc.*, **120**, 802 (1973).
15) T. Nishinaga, H. Ogawa, H. Watanabe, and T. Arizumi, *J. Cryst. Growth*, **13/14**, 346 (1972).
16) T. L. Chu, J. M. Jackson, A. F. Hyslop, and S. C. Chu, *J. Appl. Phys.*, **42**, 420 (1971).
17) K. Schono, M. Takigawa, and T. Nakada, *J. Cryst. Growth*, **24/25**, 193 (1974).
18) J. Lindström, K. Fundell, and A. Lind, "Proceedings of the 4th International Conference on CVD (1973)," Electrochem. Soc. (1973), p. 546.
19) J. A. Perri, S. Laplaca, and B. Post, *Acta Crystallogr.*, **11**, 310 (1958).

20) M. Hansen and K. Anderco, "Constitution of Binary Alloys," McGraw-Hill, New York, Toronto, London (1958).
21) R. P. Elliot, *ibid.*, First Supplement (1964).
22) F. A. Schunk, *ibid.*, Second Supplement (1969).
23) Ya. Kh. Grinberg, Z. S. Medvedva, A. A. Elisseve, and E. G. Zhukov, *Doklady*, **160**, 337 (1965).
24) T. Takenaka, M. Takigawa, and K. Schono, *Japan J. Appl. Phys.*, **14**, 579 (1975).

An NMR and Mössbauer Spectroscopic Study of Mixed-valence Iron Fluoride Heptahydrate and Related Compounds

Takuhiko SAKAI and Takeshi TOMINAGA*

Department of Chemistry, Faculty of Science, The University of Tokyo, Bunkyo-ku, Tokyo 113

(Received May 17, 1975)

The powder X-ray patterns of $Fe^{III}Fe^{II}F_5 \cdot 7H_2O$, $AlFe^{II}F_5 \cdot 7H_2O$, $Fe^{III}ZnF_5 \cdot 7H_2O$ and $AlZnF_5 \cdot 7H_2O$ indicate that they are all isomorphous. When the Mössbauer spectra of the fluorides containing iron were measured, Fe^{II} and/or Fe^{III} oxidation states were recognized distinctly. The ^{19}F NMR spectra reveal that all the fluorine atoms are bonded to the trivalent metal ion (Al or Fe^{III}) in these compounds. On the basis of these results, a possible structure is proposed for $Fe^{III}Fe^{II}F_5 \cdot 7H_2O$.

Although a few works have been reported on the Mössbauer spectrum[1,2] and the X-ray powder pattern[3] of the mixed-valence iron fluoride heptahydrate, $Fe^{III}Fe^{II}F_5 \cdot 7H_2O$, no previous study has elucidated the bonding of ligands to iron in this compound. While Mössbauer spectroscopy can be used to recognize different oxidation states of central iron atoms in such mixed-valence systems, the ^{19}F and proton NMR spectra may provide us with important information concerning the bonding of ligands to central atoms. Hence, we have recently investigated $Fe^{III}Fe^{II}F_5 \cdot 7H_2O$ and several related compounds, such as $Fe^{III}ZnF_5 \cdot 7H_2O$, $AlFe^{II}F_5 \cdot 7H_2O$ and $AlZnF_5 \cdot 7H_2O$ (containing paramagnetic and/or non-magnetic metal ions), by means of Mössbauer and/or NMR spectroscopy, and have concluded that all the fluoride ions are bonded to the ferric iron.[4] The object of this article is to report the results of our recent work in further detail.

Experimental

Materials. *$Fe^{III}Fe^{II}F_5 \cdot 7H_2O$*: This compound was prepared as has been reported previously.[2] Found: Fe(III), 16.8; Fe(II), 16.8; F, 28.3%. Calcd for $Fe^{III}Fe^{II}F_5 \cdot 7H_2O$: Fe(III), 16.8; Fe(II), 16.8; F, 28.6%.

$AlFe^{II}F_5 \cdot 7H_2O$: A hot 20% HF solution containing iron powder was heated for several hours on a water bath under a reducing atmosphere. The resulting Fe^{2+}–HF solution was filtered, and more iron powder was added to the filtrate so as to ensure the complete reduction of Fe^{3+} to Fe^{2+} in the solution. The solution was then filtered and poured over iron wire, immediately mixed with an equivalent amount of $Al(OH)_3$, and heated for one hour on a water bath. After the solution had stood for several hours, pale green crystals of $AlFe^{II}F_5 \cdot 7H_2O$ were filtered, washed with water and dried in air. Found: Al, 9.1; Fe(II), 18.3; F, 31.7%. Calcd for $AlFe^{II}F_5 \cdot 7H_2O$: Al, 8.9; Fe(II), 18.4; F, 31.3%.

$Fe^{III}ZnF_5 \cdot 7H_2O$: This was prepared by modifying Weinland's method[5] as follows: $Fe(OH)_3$ was dissolved in a hot 20% HF solution, to which an equivalent amount of $ZnCO_3$ was then added. After the solution had been condensed by heating on a water bath, it was kept standing overnight at room temperature. Then, white crystals of $Fe^{III}ZnF_5 \cdot 7H_2O$ were filtered out, washed with water and dried in air. Found: Fe(III), 16.3; Zn, 19.1; F, 28.2%. Calcd for $Fe^{III}ZnF_5 \cdot 7H_2O$: Fe(III), 16.3; Zn, 19.1; F, 27.8%.

$AlZnF_5 \cdot 7H_2O$: The procedure of preparation was similar to that used for $Fe^{III}ZnF_5 \cdot 7H_2O$, except that $Al(OH)_3$ was used as the starting material instead of $Fe(OH)_3$. Found: F, 30.6%. Calcd for $AlZnF_5 \cdot 7H_2O$: F, 30.3%. The determination of the metal contents was interfered with by the presence of fluoride ions.

$Fe^{III}CoF_5 \cdot 7H_2O$ and $Fe^{III}NiF_5 \cdot 7H_2O$: They were prepared by procedures similar to that used for $Fe^{III}ZnF_5 \cdot 7H_2O$, except that basic cobalt carbonate or basic nickel carbonate was used instead of $ZnCO_3$.

Measurements. The powder X-ray patterns of $Fe^{III}Fe^{II}F_5 \cdot 7H_2O$, $Fe^{III}ZnF_5 \cdot 7H_2O$, $AlFe^{II}F_5 \cdot 7H_2O$ and $AlZnF_5 \cdot 7H_2O$ were obtained at room temperature by using Cu$K\alpha$ radiation. The observed data were calibrated by referring to the spectrum of the quartz added as an internal standard.

The Mössbauer spectra of $Fe^{III}Fe^{II}F_5 \cdot 7H_2O$, $Fe^{III}ZnF_5 \cdot 7H_2O$, and $AlFe^{II}F_5 \cdot 7H_2O$ at 80, 195, and 293 K, as well as those of $Fe^{III}CoF_5 \cdot 7H_2O$ and $Fe^{III}NiF_5 \cdot 7H_2O$ at 80 and 293 K, were measured by means of a Shimadzu MEG-2 Mössbauer Spectrometer with a ^{57}Co source diffused into copper foil.

The NMR measurements of the powder samples of these compounds were made at 298 and 113 K by a Varian VF-16 broad-line NMR Spectrometer operating at 7.994 MHz or at about 16 MHz.

Results and Discussion

Powder X-Ray Patterns. The powder X-ray patterns of the four fluorides shown in Fig. 1 appear to be generally alike except for an unimportant difference observed in the vicinity of the diffraction angle, $2\theta \sim 20°$. The lattice constants of these compounds were calculated for the tetragonal symmetry from the data calibrated by referring to the spectrum of the quartz used as the internal standard. The lattice constants obtained in the

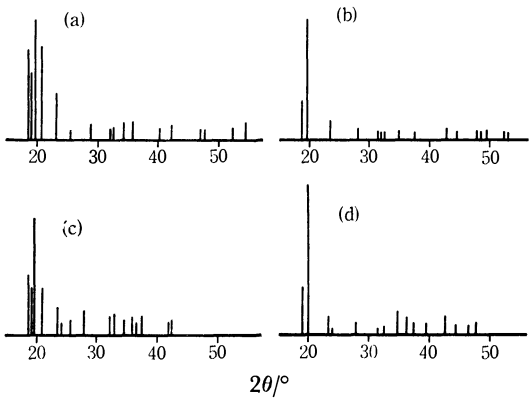

Fig. 1. Powder X-ray patterns of (a) $Fe^{III}Fe^{II}F_5 \cdot 7H_2O$, (b) $AlFe^{II}F_5 \cdot 7H_2O$, (c) $Fe^{III}ZnF_5 \cdot 7H_2O$, and (d) $AlZnF_5 \cdot 7H_2O$.

* To whom all correspondence should be addressed.

present work (±0.03 Å) are: $a=12.64$ and $b=7.05$ Å for $Fe^{III}Fe^{II}F_5\cdot 7H_2O$; $a=12.89$ and $b=6.94$ Å for $Fe^{III}ZnF_5\cdot 7H_2O$; $a=12.71$ and $b=6.99$ Å for $AlFe^{II}F_5\cdot 7H_2O$, and $a=12.75$ and $b=7.01$ Å for $AlZnF_5\cdot 7H_2O$. The results indicate that these four compounds ($M^{III}M'^{II}F_5\cdot 7H_2O$) are all isomorphous.

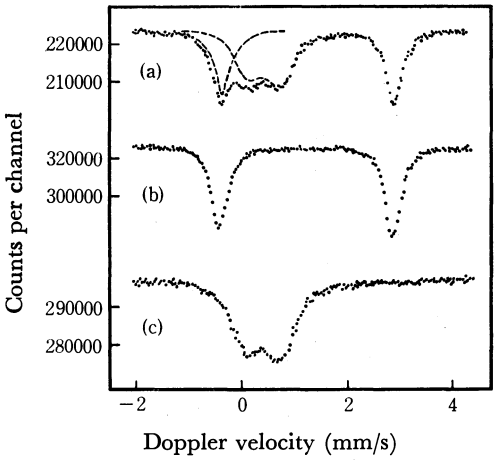

Fig. 2. Mössbauer spectra at 293 K of (a) $Fe^{III}Fe^{II}F_5\cdot 7H_2O$, (b) $AlFe^{II}F_5\cdot 7H_2O$, and (c) $Fe^{III}ZnF_5\cdot 7H_2O$.

Table 1. Mössbauer parameters of $M^{III}M'^{II}F_5\cdot 7H_2O$

Compound	Isomer shift[a] (mm/s)			Quadrupole splitting (mm/s)		
	293 K	195 K	80 K	293 K	195 K	80 K
	(±0.02)			(±0.02)		
$Fe^{III}Fe^{II}F_5\cdot 7H_2O$ Fe^{II}	1.26	1.34	1.39	3.28	3.52	3.55
Fe^{III}	0.45	0.52	0.54	0.51	0.52	0.59
$AlFe^{II}Fe_5\cdot 7H_2O$	1.24	1.30	1.38	3.27	3.51	3.63
$Fe^{III}ZnF_5\cdot 7H_2O$	0.41	0.48	0.53	0.47	0.47	0.52
$Fe^{III}CoF_5\cdot 7H_2O$	0.44		0.53	0.44		0.58
$Fe^{III}NiF_5\cdot 7H_2O$	0.42		0.53	0.52		0.53

a) With respect to the centroid of the spectrum of iron foil at 293 K.

Mössbauer Spectra. Some typical Mössbauer spectra of $Fe^{III}Fe^{II}F_5\cdot 7H_2O$, $AlFe^{II}F_5\cdot 7H_2O$, and $Fe^{III}ZnF_5\cdot 7H_2O$ obtained at 293 K are shown in Fig. 2. In Table 1 are summarized the Mössbauer parameters of these compounds at 80, 195, and 293 K, together with those of $Fe^{III}CoF_5\cdot 7H_2O$ and $Fe^{III}NiF_5\cdot 7H_2O$ at 80 and 293 K. The Mössbauer spectrum of $Fe^{III}Fe^{II}F_5\cdot 7H_2O$ appears to consist of two sets of doublets of nearly equal intensities. The outer doublet corresponds to Fe(II), while the inner doublet is ascribed to Fe(III). At 80, 195, and 293 K, the Mössbauer parameters of the Fe(II) doublet in $Fe^{III}Fe^{II}F_5\cdot 7H_2O$ are in good agreement with those of the doublet in $AlFe^{II}F_5\cdot 7H_2O$. The spectrum of $Fe^{III}Fe^{II}F_5\cdot 7H_2O$ can be resolved to reveal the Fe(III) peaks distinctly by subtracting the superposed Fe(II) doublet (the broken lines in Fig. 2a). The shape of the Fe(III) peaks thus obtained is similar to the spectra of $Fe^{III}ZnF_5\cdot 7H_2O$, $Fe^{III}CoF_5\cdot 7H_2O$, and $Fe^{III}NiF_5\cdot 7H_2O$. Accordingly, the Mössbauer results are compatible with the conclusion based on the X-ray data, indicating that these compounds are all isomorphous. Furthermore, it is worth mentioning that the shape of the Fe(III) peaks in either $Fe^{III}Fe^{II}F_5\cdot 7H_2O$ or $Fe^{III}ZnF_5\cdot 7H_2O$ (Fig. 2) appears to be a composite of at least two sets of unresolved doublets. Accordingly, the spectra of $Fe^{III}Fe^{II}F_5\cdot 7H_2O$ and $Fe^{III}ZnF_5\cdot 7H_2O$ were analyzed by means of a computer fitting based on the assumption that the Fe(III) peaks were composed of two sets of doublets. The best-fit curves obtained imply the presence of at least two different Fe(III) sites (Fig. 3).

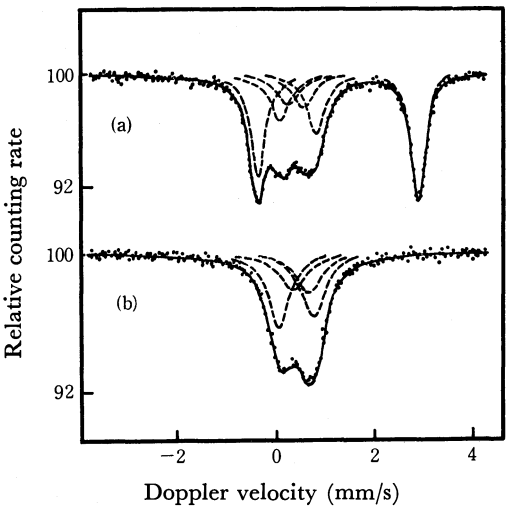

Fig. 3. Computer-fitting analysis of Mössbauer spectra (293 K) of (a) $Fe^{III}Fe^{II}F_5\cdot 7H_2O$, and (b) $Fe^{III}ZnF_5\cdot 7H_2O$.

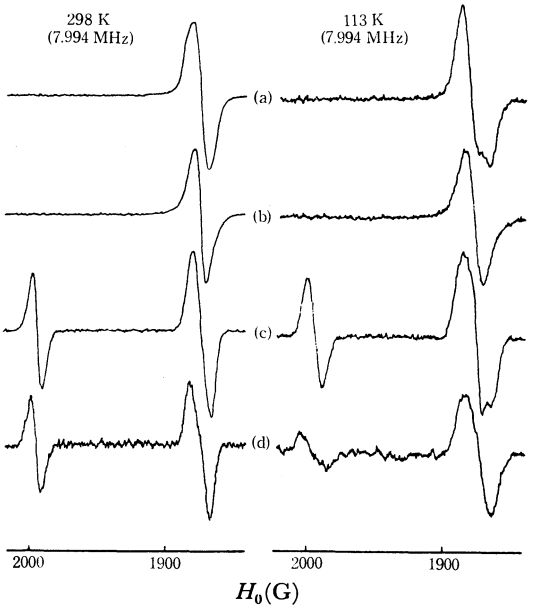

Fig. 4. NMR spectra at 298 K (left) and 113 K (right) of (a) $Fe^{III}Fe^{II}F_5\cdot 7H_2O$, (b) $Fe^{III}ZnF_5\cdot 7H_2O$, (c) $AlFe^{II}F_5\cdot 7H_2O$, and (d) $AlZnF_5\cdot 7H_2O$.

^{19}F NMR Spectra. Figure 4 represents the nuclear magnetic resonances of ^{19}F and protons in these fluorides observed at 113 and 298 K. The signals at about 2000 G and 1880 G indicate the NMR lines of ^{19}F and the protons respectively. As is shown in Fig. 4, the ^{19}F nuclear magnetic resonances are observed only in $AlFe^{II}F_5\cdot 7H_2O$ and $AlZnF_5\cdot 7H_2O$, not in $Fe^{III}ZnF_5\cdot 7H_2O$ and $Fe^{III}Fe^{II}F_5\cdot 7H_2O$. Since the comparison of

the area under the ^{19}F and proton signals in the NMR spectra of $AlFe^{II}F_5 \cdot 7H_2O$ and $AlZnF_5 \cdot 7H_2O$ indicates the $^{19}F/^{1}H$ ratio of 5/14, it may be presumed that all the ^{19}F and ^{1}H nuclear spins are detected in these compounds.

While the ^{19}F resonance signals in paramagnetic compounds would, in general, be unobservable because of the large internal dipole or hyperfine field arising from the electronic spins,[6] the resonance signals of the ^{19}F atoms bonded to such diamagnetic ions as Al^{3+} and Zn^{2+} should be observable because of the weak influence on ^{19}F of the magnetic field due to the diamagnetic ions. The absence of the ^{19}F resonance signals in $Fe^{III}ZnF_5 \cdot 7H_2O$ reveals that all the ^{19}F atoms are bonded to Fe^{3+}, but not to Zn^{2+}, and that these ^{19}F atoms are possibly influenced by the very strong internal magnetic field due to the paramagnetic spins of the Fe^{3+} ions. The ^{19}F NMR spectra thus indicate that all the fluorine atoms are bonded to M^{III} (Al^{3+} or Fe^{3+}) in these fluorides. Since the X-ray and Mössbauer data have shown that they all isomorphous, the structures of the four fluorides, $M^{III}M'^{II}F_5 \cdot 7H_2O$ ($M^{III}=Fe^{III}$ or Al, and $M'^{II}=Fe^{II}$ or Zn), may be generally represented as $[M^{III}F_5OH_2] \cdot [M'^{II}(OH_2)_6]$, and we may presume the structure of $Fe^{III}Fe^{II}F_5 \cdot 7H_2O$ to be $[Fe^{III}F_5OH_2] \cdot [Fe^{II}(OH_2)_6]$.

Proton NMR Spectra. In the proton NMR spectra at 7.994 MHz, the proton signals of $Fe^{III}Fe^{II}F_5 \cdot 7H_2O$ and $AlFe^{II}F_5 \cdot 7H_2O$ at 113 K appear to be asymmetric (Fig. 4). In order to make a more detailed analysis convenient, the proton NMR spectra of these fluorides, together with those of $Fe^{III}CoF_5 \cdot 7H_2O$ and $Fe^{III}NiF_5 \cdot 7H_2O$ were also measured during operation at 16 MHz; asymmetric signals were obtained at 113 K in all the compounds except $Fe^{III}ZnF_5 \cdot 7H_2O$ (Fig. 5). In accordance with the proposed structures, these results may be generally explained as follows. The asymmetric proton NMR signals reflect the influence of the magnetic anisotropy of the paramagnetic ion with a short spin-relaxation time (*i.e.*, Fe(II), Co(II), or Ni (II)), to which the water molecules are bonded. If a water molecule is bonded to a ferric ion with a long spin-relaxation time, however, the local magnetic field changes slowly and the proton experiences various magnetic fields. Hence, the proton NMR line-width is so broadened that the resonance can hardly be detected. Since all proton signals can be observed in $AlFe^{II}F_5 \cdot 7H_2O$, its spectrum is composed of asymmetric signals reflecting the magnetic anisotropy of Fe(II) and the superimposed, unperturbed signals from protons of the water bonded to Al. In $Fe^{III}ZnF_5 \cdot 7H_2O$ we observed only the symmetrical signals of protons of water bonded to Zn(II), which are not perturbed magnetically.

The proton NMR spectra of these compounds observed at 298 K are all symmetrical (Figs. 4 and 5). This may be attributable to the disappearance of the magnetic anisotropy because of the accelerated motion of protons around the oxygen atom at elevated temperatures.

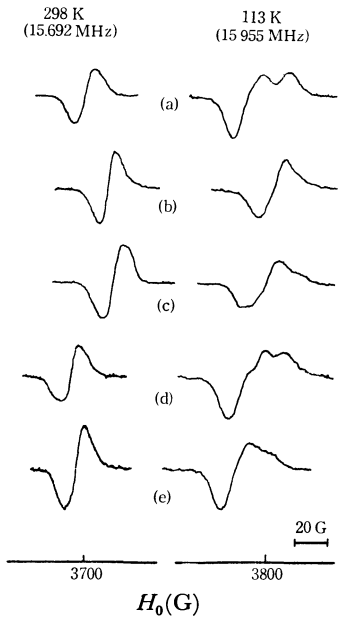

Fig. 5. Proton NMR spectra at 298 K (left) and 113 K (right) of (a) $Fe^{III}Fe^{II}F_5 \cdot 7H_2O$, (b) $Fe^{III}ZnF_5 \cdot 7H_2O$, (c) $AlFe^{II}F_5 \cdot 7H_2O$, (d) $Fe^{III}CoF_5 \cdot 7H_2O$, and (e) $Fe^{III}NiF_5 \cdot 7H_2O$.

The authors wish to thank Professor Nobufusa Saito for his encouragement and support and to Drs. Yoji Arata and Akira Yamasaki for many helpful discussions. They are also greatly indebted to Dr. Keikichi Nakamura of the National Research Institute of Metals for the NMR measurements. Their thanks are also due to Dr. Takamitsu Yamanaka of the Department of Mineralogy, the University of Tokyo, where the X-ray powder patterns were made and the computer analysis done, and to Dr. Fumitoshi Ambe of the Institute of Physical and Chemical Research, where the computer analysis of the Mössbauer data was done.

References

1) P. Imbert, Y. Macheteau, and F. Varret, *J. Phys.* (Paris), **34**, 49 (1973).
2) T. Sakai and T. Tominaga, *Radioisotopes*, **23**, 347 (1974).
3) G. Brauer and M. Eichner, *Z. Anorg. Allg. Chem.*, **296**, 13 (1958).
4) T. Sakai and T. Tominaga, *Radiochem. Radioanal. Lett.*, **22**, 11 (1975).
5) R. Weinland and O. Köppen, *Z. Anorg. Allg. Chem.*, **22**, 266 (1899).
6) R. G. Shulman and V. Jaccarino, *Phys. Rev.*, **108**, 1219 (1957).

Metal Complexes of Amino Acids. VIII.[1] Carbon-13 Nuclear Magnetic Resonances of Cobalt(III) Complexes Containing L-Aspartic and L-glutamic Acids

Takaji YASUI and Tomoharu AMA

Faculty of Arts and Sciences, Kochi University, Asakura, Kochi 780

(Received June 5, 1975)

The ^{13}C NMR spectra of cobalt(III) complexes containing L-aspartic acid or L-glutamic acid as unidentate, bidentate, or bridged ligand were measured, and the relationship between the coordination types and the changes in chemical shift of carboxyl carbons in these amino acid complexes was discussed. Two structural isomers were newly separated for the *trans*(O)-[Co en_2(L-aspH_2 or L-gluH_2)$_2$]X_3 complex by a column chromatographic method. The structures of the earlier eluted isomers for the *trans*(O)-[Co en_2(L-aspH_2)$_2$]X_3 and -[Co en_2(L-gluH_2)$_2$]X_3 complexes were assigned to *trans*(O_0, O_γ) and *trans*(O_0, O_δ) (O_0, O_γ and O_δ indicate the coordinated oxygen atoms of C_0OO, $C_\gamma OO$, and $C_\delta OO$), respectively, and the structures of the later eluted isomers for the both complexes to *trans*(O_0, O_0), on the basis of the shift patterns of carboxyl carbons.

It is well known that the ^{13}C NMR technique gives many useful informations about structural analyses of organic compounds.[2,3] Recently this technique has been applied to the metal complexes.[4–7] In the previous paper[8] we studied the ^{13}C NMR of cobalt(III) complexes containing various amino acids.

In the present paper, the relationship between the coordination types and the changes in chemical shift of carboxylate groups in amino acid-cobalt(III) complexes containing L-aspartic and L-glutamic acids as unidentate, bidentate and bridged ligands will be discussed on the basis of their ^{13}C NMR spectra. Furthermore the structural assignments for the newly obtained structural isomers of the *trans*(O)-[Co en_2(L-aspH_2)$_2$]X_3 and [Co en_2(L-gluH_2)$_2$]X_3 complexes will be made.

Experimental

Preparation of Complexes. Trans(O_0,O_γ)- and trans(O_0, O_0)-[Co en_2(L-aspH_2)$_2$]$Br_3\cdot H_2O$: To an aqueous solution containing 5.2 g (0.01 mol) of [Co$(OH_2)_2en_2$]$(ClO_4)_3$ in 50 ml of water was added 3.2 g (0.024 mol) of L-aspartic acid, and the mixture was gradually evaporated to dryness on a steam-bath. The residue was dissolved in 20 ml of water, and the solution was evaporated again. This procedure was repeated three or four times more. The final residue was dissolved in about 300 ml of water, and the solution was poured into a SP-Sephadex cation-exchange column (C-25, K-form, $\phi 4.5\times 50$ cm). After two days two purplish-red bands were separated from the upper adsorbed band by sweeping with 0.03 M aqueous solution of KBr which was slightly acidified with hydrobromic acid. Each split band was taken out and transfered into a short column. The purplish-red solution obtained from each column by elution with concentrated KBr solution was concentrated by using a vacuum evaporator at 30—35 °C. The deposited KBr was removed by filtration and the filtrate was evaporated almost to dryness. The purplish-red complex was extracted from the residue with methanol and the solution was filtered. The crude complex was obtained by evaporation of the methanolic solution. Purification of the complex was carried out by adding acetone to a concentrated aqueous solution. The purplish-red powder (*trans*(O_0,O_γ) isomer) and crystals (*trans*(O_0,O_0) isomer) were obtained from the earlier and later eluted fractions, respectively, and yields were 0.20 g and 0.75 g.

Found: C, 20.85; H, 4.79; N, 11.88% for *trans*(O_0,O_γ) isomer and C, 20.76; H, 4.83; N, 12.02% for *trans*(O_0,O_0) isomer. Calcd for $C_{12}H_{32}N_6O_9Br_3Co$: C, 20.50; H, 4.60; N, 11.95%.

Trans(O_0,O_δ)- and trans(O_0,O_0)-[Co en_2(L-gluH_2)$_2$]Br_3. These isomers were obtained by a similar procedure to that for the L-aspartic acid complex except for use of 3.5 g of L-glutamic acid. In the case of L-glutamic acid, however, at the first stage three purplish-red bands were separated from the adsorbed band. All of the complexes eluted from these bands showed the absorption spectra pattern corresponding to the type *trans*(O)-[CoN_4O_2] complex,[9] but unfortunately no analytically pure complex was isolated from the first eluting band. The purplish-red powder (*trans*(O_0,O_δ) isomer) and crystals (*trans*(O_0,O_0) isomer) were obtained from the second and third eluted fractions by the same way as used for the L-aspartic complex, respectively, and yields were 0.15 g and 0.50 g.

Found: C, 23.82; H, 4.80; N, 12.10% for *trans*(O_0,O_δ) isomer, and C, 23.36; H, 4.59; N, 11.50% for *trans*(O_0,O_0) isomer. Calcd for $C_{14}H_{34}N_6O_8Br_3Co$: C, 23.57; H, 4.81; N, 11.79%.

[Co(NH_3)$_5$(L-glnH)]$Br_3\cdot H_2O$. This complex was prepared by modification of the method described in previous paper.[9,10] To an aqueous solution containing 4.8 g (0.01 mol) of [Co$(NH_3)_5(OH_2)$]$(ClO_4)_3\cdot H_2O$ in 50 ml of water was added 2.0 g (excess) of L-glutamine, and the mixture was gradually evaporated to 10 ml on a water-bath at 55—60 °C. The resulting solution was filtered and the filtrate was diluted to 100 ml with water and poured into a short column ($\phi 7\times 5$ cm) containing SP-Sephadex cation-exchanger (C-25, Na-form). The orange eluting solution obtained by elution with 0.03—1.0 M aqueous solution of KBr was evaporated by using a vacuum evaporator. The deposited KBr was removed by filtration and the filtrate was evaporated again. The crude complex obtained was recrystallized from an aqueous solution by adding methanol. The orange complex deposited as plate crystals was filtered and washed with 90% methanol, 99% methanol and then ether, and dried in air.

Found: C, 10.86; H, 5.17; N, 18.22%. Calcd for $C_5H_{27}N_7O_4Br_3Co$: C, 10.95; H, 4.98; N, 17.89%.

[Co(NH_3)$_5$(L-asnH)](ClO$_4$)$_3$.[11] This complex was obtained as orange needle crystals by the same method as for the L-glutamine complex.

(+)$_D$-[Co(L-asp)en_2]$ClO_4\cdot 2H_2O$, (+)$_D$-[en_2Co(L-asp)Co(NH_3)$_5$](ClO$_4$)$_4\cdot H_2O$, (+)$_D$-[en_2Co{(L-asp)Co en_2}$_2$](ClO$_4$)$_5\cdot 5H_2O$, (+)$_D$-[Co(L-glu)en_2]ClO_4, (+)$_D$-[en_2Co(L-glu)Co(OH_2)en_2](ClO$_4$)$_4\cdot 2H_2O$, and (+)$_D$-[en_2Co{(L-glu)Co en_2}$_2$](ClO$_4$)$_5\cdot 4H_2O$. Preparations of these complexes are described in

the previous study.[12]

Measurements. The absorption spectra were obtained by using a Hitachi Model EPS-3T spectrophotometer. The ^{13}C NMR spectra were recorded on a JEOL-MFT-100 spectrometer with JEC-6 spectrum computer in pulse Fourier transform/proton noise decoupled mode at 25.15 MHz and at room temperature. An internal D_2O rocking form was used for the measurements. Peak positions were measured relative to external benzene, and D_2O is used as solvent of the samples. Chemical shifts are reported relative to TMS using the relation $\delta_{TMS}=\delta_{benzene}-128.5$ ppm.[3] Experimental errors were ± 0.1 ppm. Some samples were converted to the chloride to obtain higher solubility in D_2O.

Results and Discussion

Structural Isomers of trans*(O)-[Co en$_2$(L-aspH$_2$ or L-gluH$_2$)$_2$]X$_3$ Complex.* L-Aspartic and L-glutamic acids have three functional groups, two carboxylates and one amino. Therefore, these amino acids will provide the complexes of three coordination types containing them as unidentate, bidentate,[13–17] and terdentate[18,19] ligands It is well known that a large number of amino acids form easily unidentate complexes in which the amino acids coordinate to cobalt(III) with only carboxylates.[9–11] However, the unidentate complexes containing L-aspartic and L-glutamic acids have not been isolated so far. In this study we attempted to prepare the type *trans*(O)-[Co en$_2$(L-aaH$_2$)$_2$]X$_3$ complex containing L-aspartic acid or L-glutamic acid as unidentate ligand. There are three structural isomers possible in this type complex, that is, *trans*(O$_\gamma$,O$_\gamma$), *trans*(O$_0$,O$_\gamma$) and *trans*-(O$_0$,O$_0$) isomers for L-aspartic acid complex, and *trans*-(O$_\delta$,O$_\delta$), *trans*(O$_0$,O$_\delta$) and *trans*(O$_0$,O$_0$) isomers for L-glutamic acid complex, as shown in Fig. 1. Indeed the existence of three structural isomers for the L-glutamic acid complex was confirmed on a column chromatogram. These isomers showed the absorption spectra corresponding to the typical *trans*(O)-[Co N_4O_2] complex[9] as shown in Fig. 2, but unfortunately it was unsuccessful to isolate the analytically pure complex from the earliest eluted fraction (perhaps *trans*(O$_\delta$,O$_\delta$) isomer) of three split bands because of its unstability in aqueous solution. On the other hand in the L-aspartic acid complex the bands corresponding to two structural isomers, *trans*(O$_0$,O$_\gamma$) and *trans*(O$_0$, O$_0$), were confirmed on a column chromatogram, but another one (*trans*(O$_\gamma$, O$_\gamma$) was not detected on it.

The structural assignment of each isomer will be mentioned in section of ^{13}C NMR spectra. The notations of all carbon atoms in L-aspartic and L-glutamic acids are shown below.

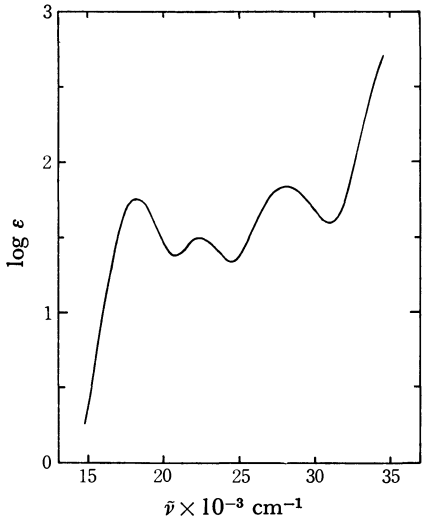

Fig. 2. Absorption spectra of *trans*(O)-[Co en$_2$(L-aspH$_2$ or L-gluH$_2$)$_2$]$^{3+}$ ion.

NH_3^+
$^-OOC_0-C_\alpha H-C_\beta H_2-C_\gamma OOH$
L-Aspartic Acid (L-aspH$_2$)

NH_3^+
$^-OOC_0-C_\alpha H-C_\beta H_2-C_\gamma H_2-C_\delta OOH$
L-Glutamic Acid (L-gluH$_2$)

^{13}C NMR Spectra. The observed ^{13}C NMR shifts of L-aspartic and L-glutamic acids and of their cobalt(III) complexes are listed in Table 1, and their shift patterns are shown in Figs. 3 and 4. The resonance of carboxyl carbons, α-carbons and methylene carbons (C_β and C_γ) of the free and coordinated L-aspartic and L-glutamic acids, and ethylene carbons of ethylenediamine were observed in the ranges of 171.9—187.4, 49.8—58.1, 24.5—39.7, and 42.8—45.9 ppm, respectively.

As described in the previous paper[8] the carboxyl carbon resonances of various α-amino acids show upfield shifts in the range of 2.5—3.0 ppm in acidic solution, compared with those in neutral solution. Quite similar behaviors in ^{13}C chemical shift are also observed for two carboxyl carbons in L-aspartic and L-glutamic acids of the present study, as shown in Figs. 3 and 4. The changes in chemical shifts of these carboxyl groups can be related to the changes of their chemical environments. Horsley[20] and Quirt[21] have demonstrated from the pH titration studies for various amino acids that the carboxyl carbon resonance exhibits large shift with pH

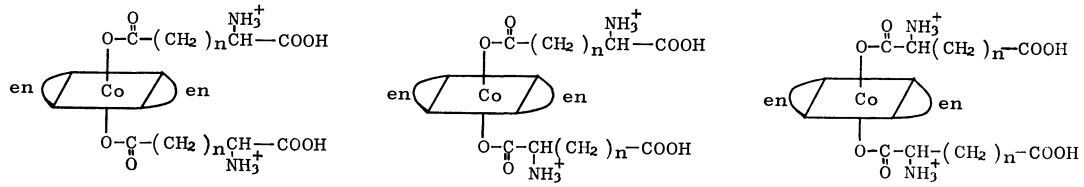

Fig. 1. The structures of three possible isomers in *trans*(O)-[Co en$_2$(L-aspH$_2$ or L-gluH$_2$)$_2$]X$_3$ complex.

TABLE 1. OBSERVED ^{13}C NMR SHIFTS (IN ppm FROM TMS) OF L-ASPARTIC AND L-GLUTAMIC ACID COMPLEXES

Label	Compound	C_0OO	$C_\gamma OO$	$C_\delta OO$	C_α	C_β	C_γ	C_{en}			
I	L-asp$H_3^{+a)}$	171.9	174.9		49.8	33.5					
II	L-aspH^-	176.0	179.3		52.5	36.8					
III	L-asp^{2-}	184.4	182.3		54.1	43.3					
IV	$(+)_D$-[Co(L-asp)en_2]$^+$	187.4	179.2		55.1	39.1		45.6	44.8	42.8	
V	$(+)_D$-[Co(L-aspH)en_2]$^{2+}$	186.9	176.6		54.4	36.5		45.9	45.1	43.6	
VI	$(+)_D$-[en_2 Co(L-asp)Co$(NH_3)_5$]$^{4+}$	187.0	183.8		54.9	39.7		45.8	44.9	43.3	
VII	$(+)_D$-[en_2 Co{(L-asp)Co en_2}$_2$]$^{5+}$	186.7	184.4		54.5	39.0		45.9	45.5	44.5	43.0
VIII	[Co$(NH_3)_5$ (L-asnH)]$^{3+}$	179.1	175.6		51.0	34.5					
IX	*trans*(O_0,O_γ)-[Co en_2(L-aspH_2)$_2$]$^{3+}$	178.7	182.4		50.4	36.5		45.1			
		172.8	175.1		50.1	34.1					
X	*trans*(O_0,O_0)-[Co en_2(L-aspH_2)$_2$]$^{3+}$	178.7	175.1		50.0	34.0		45.0			
XI	L-glu$H_3^{+a)}$	172.5		178.4	52.8	24.5	29.2				
XII	L-gluH^-	176.2		183.0	54.8	26.8	33.4				
XIII	L-glu^{2-}	185.0		184.7	56.3	32.0	34.5				
XIV	$(+)_D$-[Co(L-glu)en_2]$^+$	186.5		183.5	58.1	28.5	34.0	45.5	45.0	44.7	43.6
XV	$(+)_D$-[Co(L-gluH)en_2]$^{2+}$	186.5		178.7	57.4	27.3	30.1	45.6	45.0	44.7	43.5
XVI	$(+)_D$-[en_2 Co(L-glu)Co$(OH_2)en_2$]$^{4+}$	185.8		185.8	57.9	28.4	34.1	45.3	44.8	44.4	43.6
								43.2			
XVII	$(+)_D$-[en_2 Co{(L-glu)Co en_2}$_2$]$^{5+}$	186.1		187.4	57.4	28.2	33.7	45.5	44.8	43.4	
XVIII	[Co$(NH_3)_5$(L-glnH)]$^{3+}$	179.5		179.0	54.4	25.9	31.2				
XIX	*trans*(O_0,O_δ)-[Co en_2(L-gluH$_2$)$_2$]$^{3+}$	179.5		186.4	53.5	25.5	32.9	45.0			
		172.9		177.9	52.4	25.0	29.9				
XX	*trans*(O_0,O_0)-[Co en_2(L-gluH$_2$)$_2$]$^{3+}$	179.7		178.0	53.6	25.1	30.1	45.4			

a) Dissolved in 30% D_2SO_4 solution. b) Dissolved in 10% NaOD Solution.

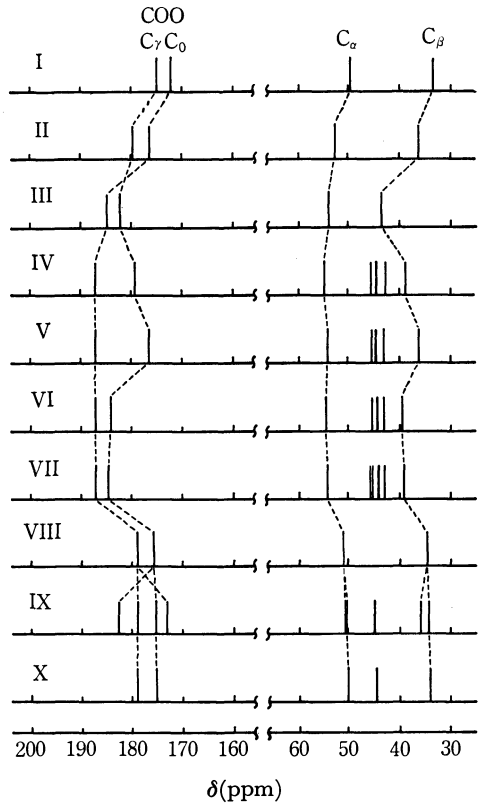

Fig. 3. ^{13}C NMR patterns of L-aspartic acid and its complexes.

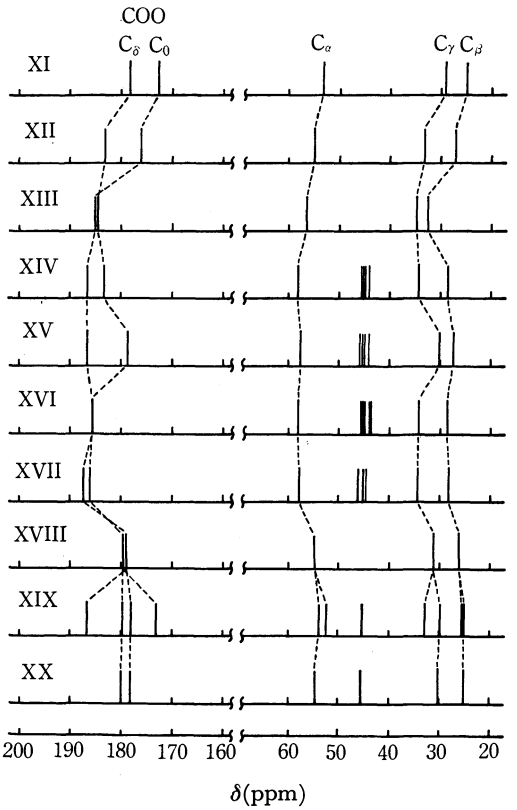

Fig. 4. ^{13}C NMR patterns of L-glutamic acid and its complexes.

change. Generally the protonation (acidic solution) and deprotonation (alkaline solution) of the amino acid provide upfield and downfield shift changes for the carboxyl carbon resonance, respectively. Such upfield shift changes also appear on protonations of uncoordinated carboxyl groups ($C_\gamma OO$ and $C_\delta OO$) in IV and XIV complexes. On the other hand the α-carboxyl carbons in chelated complexes (IV, V, XIV, and XV)

show downfield shifts, relative to those in unidentate complexes and free amino acids,[8] and their chemical shifts are almost constant within the range of 186.3—187.4 ppm. This constant shift can be applied to assignments of the chelated α-carboxyl carbons in the μ-L-aspartato (VI and VII) and μ-L-glutamato (XVI and XVII) complexes.

The structural assignments of two newly obtained isomers for the type *trans*(O)-[Co en_2(L-aaH_2)$_2$]X_3 complex can be easily made from the shift patterns of the carboxyl carbons. These isomers show considerably different shifts patterns from each other, that is, the earlier eluted isomers (IX and XIX) exhibit double peaks for each of two carboxyl carbons (C_0 and C_γ for L-aspartic acid complex, and C_0 and C_δ for L-glutamic acid complex), α-methine, β- and γ-methylene carbons, while the later eluted isomers (X and XX) do single peak. On the other hand for four carbons of two chelated ethylenediamines in these isomers only one resonance peak was observed. This means that four carbons are equivalent in chemical environment, and suggests that two isomers are structural ones taking *trans*(O) structure.

The peaks at 178.7 ppm of IX and X correspond well to the peak at 179.1 ppm of the coordinated carboxyl C_0 in VIII where L-asparagine coordinates with α-carboxyl group as a unidentate ligand, while the peaks at 175.1 ppm of IX and X do to the peak at 174.9 ppm of carboxyl C_γ in the protonated L-aspartic acid (I). Therefore the former peak of 178.7 ppm can be assigned to the coordinated carboxyl carbon (C_0) and the latter one (175.1 ppm) to the uncoordinated and protonated carbon (C_γ). The peaks at 172.8 and 182.4 ppm of IX correspond to the peaks of the protonated α-carboxyl C_0 in I (171.9 ppm) and of the coordinated carboxyl C_γ in VI and VII (183.8 and 184.4 ppm), respectively. From these results it is concluded that one of two L-aspartic acids contained in IX coordinates to cobalt(III) with C_0OO group and the other with $C_\gamma OO$ group as a unidentate ligand, while those in X coordinate with C_0OO groups only.

The same discussion can be made about two structural isomers (XIX and XX) of the L-glutamic acid complex. The peak at 179.5 ppm of XIX and that at 179.7 ppm of XX may correspond to that at 179.5 ppm of the coordinated α-carboxyl C_0 in XVIII where L-glutamine coordinates to cobalt(III) as a unidentate ligand. The peak at 177.9 ppm of XIX and that at 178.0 ppm of XX correspond to the peak at 178.4 ppm of the protonated carboxyl C_δ in XI, and the peaks at 172.9 and 186.4 ppm of XIX to that at 172.5 ppm of the protonated α-carboxyl C_0 in XI and to those at 185.8 and 187.4 ppm of the coordinated carboxyl C_δ in XVI and XVII, respectively. Therefore, for two structural isomers (XIX and XX) of L-glutamic acid complex the structures of (B) and (C) shown in Fig. 1 can be assigned.

References

1) Part VII of this series: T. Yasui, This Bulletin, **48**, 454 (1975).
2) J. B. Stothers, "Carbon-13 NMR Spectroscopy," Academic Press, New York (1972).
3) G. C. Levy and G. L. Nelson, "Carbon-13 Nuclear Magnetic Resonance for Organic Chemists," John Wiley & Sons, Inc., New York (1972).
4) M. Hirota, Y. Koike, H. Ishizuka, A. Yamasaki, and S. Fujiwara, *Chem. Lett.*, **1973**, 853.
5) R. Hagen, J. P. Warren, D. H. Hunter, and J. D. Roberts, *J. Amer. Chem. Soc.*, **95**, 5712 (1973).
6) B. J. Fuhr and D. L. Rabenstein, *ibid.*, **95**, 6944 (1973).
7) O. W. Howarth, P. Moore, and N. Winterton, *J. Chem. Soc., Dalton*, **1974**, 2271; *ibid.*, **1975**, 360.
8) T. Ama and T. Yasui, *Chem. Lett.*, **1974**, 1295.
9) T. Yasui, J. Hidaka, and Y. Shimura, This Bulletin, **39**, 2417 (1966).
10) J. Fujita, T. Tasui, and Y. Shimura, *ibid.*, **38**, 654 (1965).
11) C. J. Hawkins and P. J. Lawson, *Inorg. Chem.*, **9**, 6 (1970).
12) T. Yasui, H. Kawaguchi, Z. Kanda, and T. Ama, This Bulletin, **47**, 2393 (1974).
13) M. Shibata, H. Nishikawa, and K. Hosaka, *ibid.*, **40**, 236 (1967).
14) J. H. Dunlop, R. D. Gillard, and N. C. Payne, *J. Chem. Soc., A*, **1967**, 1469.
15) R. D. Gillard, R. Maskill, and A. Pasini, *ibid.*, **1971**, 2268.
16) J. I. Legg and J. Steele, *Inorg. Chem.*, **10**, 2177 (1971).
17) Y. Kojima and M. Shibata, *ibid.*, **12**, 1009 (1973).
18) J. I. Legg and D. W. Cooke, *J. Amer. Chem. Soc.*, **89**, 6854 (1967).
19) S. Yamada, J. Hidaka, and B. E. Douglas, *Inorg. Chem.*, **10**, 2187 (1971).
20) W. J. Horsley and H. Sternlicht, *J. Amer. Chem. Soc.*, **90**, 3738 (1968).
21) A. R. Quirt, J. R. Lyerla, Jr., I. R. Peat, J. S. Cohen, W. F. Reynolds, and M. H. Freeman, *ibid.*, **96**, 570 (1974).

Preparation of the Co(III) Complexes with a Tridentate Hexaniobato and a Bi- or Tri-dentate Amino Carboxylato Ligand

Yutaka HOSOKAWA, Jinsai HIDAKA,* and Yoichi SHIMURA

Department of Chemistry, Faculty of Science, Osaka University, Toyonaka, Osaka 560

(Received June 7, 1975)

Twelve new Co(III) complexes containing a hexaniobate ion $Nb_6O_{19}^{8-}$ as a tridentate ligand were synthesized. The hexaniobato ligand coordinates facially, and the remaining three coordination sites are occupied by a tridentate amino carboxylato ligand or by a bidentate amino carboxylato ligand and NH_3 or H_2O. Two glycinato complexes, $[Co(Nb_6O_{19})(gly)(X)]^{6-}$ ($X=NH_3$ or H_2O), were optically resolved, and a L-valinato complex $[Co(Nb_6O_{19})(L\text{-val})(NH_3)]^{6-}$ was separated into two diastereomers. The structures of these complexes were determined from their visible and ultraviolet absorption, circular dichroism, and proton magnetic resonance spectra.

Several papers have appeared for the heteropoly-condenced compounds containing Co(III) ion, but only a few concerned to a hybrid type between ordinary metal complex and heteropoly oxoanion, such as $K_5[SiCoW_{11}O_{39}(NH_3)]\cdot 14H_2O$,[1] $(+)_{589}$-$Na_4[Co_4I_3O_{18}(OH_2)_4(L\text{-ala})]\cdot 8H_2O$,[2] and $Na_5[CoNb_6O_{19}(OH_2)(en)]\cdot 17H_2O$.[3] The last named compound was prepared by Flynn and Stucky in a reaction of *trans*-$[CoCl_2(en)_2]Cl$ with $Na_7HNb_6O_{19}\cdot 15H_2O$. They assumed that the hexaniobate ion $Nb_6O_{19}^{8-}$ coordinates to the central Co(III) ion through three niobium-bridging oxygen atoms and the remaining three coordination sites of Co(III) octahedron are occupied by ethylenediamine (en) and H_2O. This means that the hexaniobate ion is functioning as a bulky tridentate ligand. This kind of coordination was confirmed from an X-ray study on the crystal of $Na_{12}[Mn(Nb_6O_{19})_2]\cdot 15H_2O$.[4] The free ligand $Nb_6O_{19}^{8-}$ consists of six NbO_6 octahedra condenced by edge-sharing and has a m3m(O_h) point group symmetry as in Fig. 1.[5] The

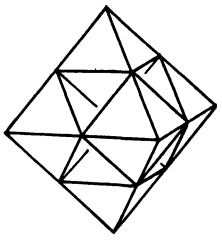

Fig. 1, Structure of $Nb_6O_{19}^{8-}$

present study is concerned with the preparation of new hexaniobato Co(III) complexes with some kinds of tridentate or bidentate ligands and with subsequent electronic absorption and circular dichroism (CD) investigations of the complexes. The tridentate ligands used are iminodiacetate(ida), L-aspartate(L-asp), L-methioninate(L-methio), and diethylenetriamine(dien), and the bidentate ligands glycinate (gly), L-valinate (L-val), and L-alaninate(L-ala).

Experimental

Preparation. *(1)* *$Na_5[Co(Nb_6O_{19})(dien)]$*: This complex was prepared by the similar method to that of $Na_5[Co(Nb_6O_{19})(OH_2)(en)]\cdot 17H_2O$.[3] Sodium hydrogenhexaniobate $Na_7HNb_6O_{19}\cdot 15H_2O$ (1.3 g; 1 mmol) and *mer*-$[CoCl_3(dien)]$ (0.27 g; 1 mmol) were dissolved in 40 cm³ of boiling water. After a 10 cm³ portion of 1 M NaOH had been added to the resulting violet-red solution, it was concentrated to about two-thirds of its original volume on a water bath. The concentrated solution was boiled for 1 hr. The solution was cooled to room temperature, filtered, and an appropriate amount of methanol was gradually added to the filtrate. After the filtrate had been kept in a refrigerator overnight, the purple product deposited was separated by a centrifuge, recrystallized from water by adding methanol and dried in a desiccator over $CaCl_2$. Found: C, 4.22; H, 1.90; N, 3.63%. Calcd for $Na_5[Co(Nb_6O_{19})(dien)]$: C, 4.22; H, 1.26; N, 3.69%.

(2) *$Li_7[Co(Nb_6O_{19})(L\text{-}asp)]\cdot 13H_2O$*, *$Li_7[Co(Nb_6O_{19})(L\text{-}asp)(OH_2)]\cdot 16H_2O$*, *$Li_7[Co(Nb_6O_{19})(L\text{-}asp)(NH_3)]\cdot 13H_2O$*: A solution of 2.7 g (10 mmol) of $K[Co(CO_3)_2(NH_3)_2]$ in 80 cm³ of water was added to a solution of 13.7 g (10 mmol) of $K_7HNb_6O_{19}\cdot 13H_2O$ in 200 cm³ of water, and to this mixture was added 0.6 g (10 mmol) of KOH. The color of solution changed from violet to blue green and then dark green. The pH was about 10.6. The solution was evaporated to about 50 cm³ and a small amount of light green precipitate resulted, which seemed to be a salt of unreacted $Nb_6O_{19}^{8-}$, was filtered off. After a little amount of methanol had been added to the filtrate, it was kept in a refrigerator overnight. The viscous dark green product deposited was dried on a vacuum desiccator, after the supernatant had been decanted. The crude product was crystallized from water by addition of ethanol. This complex, which seems to be $K_7[Co(Nb_6O_{19})(CO_3)(NH_3)]$, is very useful as a starting material for the syntheses of amino carboxylato complexes (2)—(5).

To a solution of 1.2 g of $K_7[Co(Nb_6O_{19})(CO_3)(NH_3)]$ in 80 cm³ of water was added a mixed solution of 0.12g (0.9 mmol) of L-aspartic acid and 0.1 g of KOH in 40 cm³ of water. The mixture was gradually evaporated almost to dryness on a water bath at about 70 °C. The resulting material was dissolved in a little amount of water and the solution was poured into a column (3 cm×60 cm) of strong base anion-exchanger (QAE Sephadex A-25, chloride form). The adsorbed band was eluted with 0.35 M LiCl solution at a rate of about 0.5 cm³/min. Three colored bands, blue one, blue green one and green one, were eluted in this order. The three eluates were separately concentrated to about 20 cm³ at 30 °C in a rotatory evaporator, and a large volume of ethanol was added to each of the concentrated solutions. After the solution had been kept in a refrigerator overnight, the product deposited was collected by a centrifuge and washed several times with ethanol and then acetone–water mixture. Each of the complexes was recrystallized from water by adding

* Present address: Department of Chemistry, The University of Tsukuba, Ibaraki 300-31

ethanol and washed repeatedly with ethanol and ether. Found for the blue complex: C, 3.69; H, 2.13; N, 2.21%. Calcd for $Li_7[Co(Nb_6O_{19})(L\text{-asp})(NH_3)]\cdot 13H_2O$: C, 3.76; H, 2.13; N, 2.19%. Found for the blue green complex: C, 3.53; H, 2.46; N, 1.19%. Calcd for $Li_7[Co(Nb_6O_{19})(L\text{-asp})]\cdot 13H_2O$: C, 3.60; H, 2.35; N, 1.05%. Found for the green complex: C, 3.35; H, 2.73; N, 1.07%. Calcd for $Li_7[Co(Nb_6O_{19})(L\text{-asp})(OH_2)]\cdot 16H_2O$: C, 3.41; H, 2.80; N, 0.99%.

(3) $Li_7[Co(Nb_6O_{19})(ida)]\cdot 14H_2O$: The same procedure to that of the L-aspartato complex (2) was adopted using iminodiacetic acid instead of L-aspartic acid. In this case, however, the reaction was carried out at 65 °C. The column chromatography showed only one green band. Found: C, 4.28; H, 2.39; N, 0.99%. Calcd for $Li_7[Co(Nb_6O_{19})(ida)]\cdot 14H_2O\cdot 1/2C_2H_5OH$: C, 4.29; H, 2.60; N, 0.99%.

(4) $Li_6[Co(Nb_6O_{19})(S.C\text{-}methio)]\cdot 8H_2O$: This complex was prepared by a similar method to (2). The column chromatography showed only a bluish-green band. Found: C, 4.75; H, 2.80; N, 1.20%. Calcd for $Li_6[Co(Nb_6O_{19})(L\text{-methio})]\text{-}8H_2O$: C, 4.72; H, 2.16; N, 1.10%.

(5) $Li_6[Co(Nb_6O_{19})(am)(OH_2)]\cdot nH_2O$ *and* $Li_6[Co(Nb_6O_{19})(am)(NH_3)]\cdot nH_2O$ *(am=amino carboxylate)*: The complex with glycinate, L-valinate or L-alaninate was prepared by the same method as that of L-aspartato complex described in (2). The reaction temperature was 65 °C. Each of the products separated on the column gradually into two colored bands, blue one and green one, when eluted with 0.30 M LiCl solution. In the case of L-valinato complex, however, the blue band further separated gradually into two bands F_1 and F_2 (denoted by the elution order), with the formation ratio $F_1/F_2=2$. Each of the complexes isolated was purified by the same method as that of the L-aspartato complex. Found for the blue glycinato complex: C, 2.13; H, 2.87; N, 2.18%. Calcd for $Li_6[Co(Nb_6O_{19})(gly)(NH_3)]\cdot 12H_2O\cdot 1/8C_2H_5OH$: C, 2.12; H, 2.53; N, 2.19%. Found for the green glycinato complex: C, 1.95; H, 2.18; N, 1.29%. Calcd for $Li_6[Co(Nb_6O_{19})(gly)(OH_2)]\cdot 10H_2O$: C, 1.95; H, 2.18; N, 1.13%. Found for the blue L-valinato complex (F_1): C, 4.69; H, 3.15; N, 2.05%. Calcd for $Li_6[Co(Nb_6O_{19})(L\text{-val})(NH_3)]\cdot 13H_2O$: C, 4.58; H, 2.98; N, 2.11%. Found: for the blue L-valinato complex (F_2): C, 7.31; H, 3.67; N, 1.82%. Calcd for $Li_6[Co(Nb_6O_{19})(L\text{-val})(NH_3)]\cdot 19H_2O\cdot 9/4C_2H_5OH$: C, 7.42; H, 3.84; N, 1.82%. Found for the green L-valinato complex: C, 4.51; H, 2.93; N, 1.09%. Calcd for $Li_6[Co(Nb_6O_{19})(L\text{-val})(OH_2)]\cdot 13H_2O$: C, 4.51; H, 2.89; N, 1.09%. Found for the blue L-alaninato complex: C, 2.74; H, 2.53; N, 2.24%. Calcd for $Li_6[Co(Nb_6O_{19})(L\text{-ala})(NH_3)]\cdot 11H_2O$: C, 2.84; H, 2.21; N, 2.47%. Found for the green L-alaninato complex: C, 2.83; H, 2.58; N, 1.16%. Calcd for $Li_6[Co(Nb_6O_{19})(L\text{-ala})(OH_2)]\cdot 10H_2O$: C, 2.88; H, 2.27; N, 1.16%.

(6) Resolution of $[Co(Nb_6O_{19})(gly)(X)]^{6-}$ *(X=*NH_3 *or* H_2O*)*: A solution of 0.12 g of $(+)_{589}$-$[Co(en)_3]Br_3$ in 500 cm^3 of water was gradually added with mechanical stirring to a solution of 0.35 g of $Li_6[Co(Nb_6O_{19})(gly)(NH_3)]\cdot 12H_2O$ in 1 dm^3 of water. The mixed solution was evaporated to about 300 cm^3 in air stream. The dark yellow-green diastereomer deposited was isolated by filtration and washed with water and then methanol several times. This sparingly soluble diastereomer was stirred mechanically in an aqueous solution containing cation-exchange resin (Dowex 50 W×8, Na^+ form). When the color of solution changed to blue, the solution was filtered to remove the resin, and the filtrate was concentrated to obtain the blue sodium salt, $\Delta\varepsilon_{546}=+0.61$, $\Delta\varepsilon_{589}=-0.028$.

The resolution of $[Co(Nb_6O_{19})(gly)(OH_2)]^{6-}$ was made by the same method; $(+)^{CD}_{546}$-$[Co(Nb_6O_{19})(gly)(OH_2)]^{6-}$ which was derived from the less soluble diastereomer has $\Delta\varepsilon_{546}=+0.061$ and $\Delta\varepsilon_{589}=-0.012$.

Measurements. Electronic absorption spectra of the complexes in the visible and near ultraviolet regions were measured by a Shimadzu UV-200 spectrophotometer in aqueous solutions. Circular dichroism spectra were recorded on a Jasco Model J-20 spectropolarimeter with a CD attachment. A Yanagimoto spectropolarimeter was used to check the optical rotations. The proton magnetic resonance spectra were measured in deuterium oxide with a Varian XL-100-15 NMR spectrophotometer, using *tert*-butyl alcohol (TBA) as an internal reference. The infrared spectra were obtained with a Hitachi EPI-001 infrared photometer with NaCl prisms using KBr disks. All measurements were made at room temperature.

Results and Discussion

The hexaniobato Co(III) complexes obtained are summarized in Table 1 with their d–d absorption data and the representative absorption curves are shown in Figs. 3 and 4. It is expected stereochemically that only one complex is possible for each of $[Co(Nb_6O_{19})(dien)]^{5-}$, $[Co(Nb_6O_{19})(ida)]^{7-}$, $[Co(Nb_6O_{19})(L\text{-asp})]^{7-}$, and $[Co(Nb_6O_{19})(L\text{-methio})]^{6-}$, and this was chromatographically confirmed. Two diastereomers (Fig. 2) are

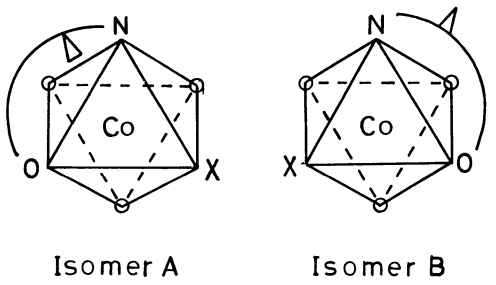

Fig. 2. Diastereomers of $[Co(Nb_6O_{19})(L\text{-am})X]^{6-}$: X= OH_2 or NH_3; N–O=L-ala or L-val. The circled three apices are occupied by $Nb_6O_{19}^{8-}$.

possible for $[Co(Nb_6O_{19})(L\text{-val})(NH_3)]^{6-}$ and this was also confirmed by the chromatographic separation of F_1(earlier eluted) and F_2 (later eluted) isomers. In addition, the corresponding glycinato complexes, $[Co(Nb_6O_{19})(gly)(NH_3)]^{6-}$ and $[Co(Nb_6O_{19})(gly)(OH_2)]^{6-}$, were resolved into their optical isomers. These facts support the Flynn and Stucky's inference for the structure of ethylenediamine complex $[Co(Nb_6O_{19})(OH_2)(en)]^{5-}$. Diastereomers are also expected for the other complexes with L-aminocarboxylate as a bidentate ligand, but the present chromatographic separation procedure was uneffective for the separation of the isomers. As is seen in Fig. 3 and Table 1, the first and second absorption bands of the complexes shift to shorter wave lengths reasonably in the order of complex type CoO_5N→*cis*-CoO_4N_2→*fac*-CoO_3N_3. The first absorption band of CoO_5N type complex shows a vague shoulder at lower energy of the absorption maximum and that of *cis*-CoO_4N_2 type at higher energy. These are in accordance with the facts that $(+)^{CD}_{546}$-$[Co(Nb_6O_{19})(gly)(OH_2)]^{6-}$ shows three CD components in the first absorption band region, and $(+)^{CD}_{546}$-$[Co(Nb_6O_{19})(gly)(NH_3)]^{6-}$ two CD components (Table 2 and Fig. 5). The *fac*-CoO_3N_3 type complex shows a sharp first

Table 1. Absorption data of the complexes

Type	Complex	σ_{max}[a] (log ε) I band	II band
CoO_5N	$[Co(Nb_6O_{19})(gly)(OH_2)]^{6-}$	16.5 (1.87)	23.8 (1.95)
	$[Co(Nb_6O_{19})(L\text{-val})(OH_2)]^{6-}$	16.6 (1.89)	23.9 (1.95)
	$[Co(Nb_6O_{19})(L\text{-ala})(OH_2)]^{6-}$	16.7 (1.86)	23.7 (1.87)
	$[Co(Nb_6O_{19})(L\text{-asp})(OH_2)]^{7-}$	16.7 (1.92)	23.6 (1.88)
	$[Co(Nb_6O_{19})(L\text{-asp})]^{7-}$	16.9 (1.95)	23.9 (1.94)
	$[Co(Nb_6O_{19})(ida)]^{7-}$	16.9 (1.98)	23.9 (2.11)
cis-CoO_4N_2	$[Co(Nb_6O_{19})(en)(OH_2)]^{5-}$	16.8 (1.84)	24.7 (1.73)
	$[Co(Nb_6O_{19})(gly)(NH_3)]^{6-}$	17.0 (1.89)	24.8 (1.95)
	$[Co(Nb_6O_{19})(L\text{-val})(NH_3)]^{6-}$	17.0 (1.90)	24.4 (1.95)
	$[Co(Nb_6O_{19})(L\text{-ala})(NH_3)]^{6-}$	17.0 (1.87)	24.5 (1.86)
	$[Co(Nb_6O_{19})(L\text{-asp})(NH_3)]^{7-}$	17.1 (1.89)	24.7 (1.94)
fac-CoO_3N_3	$[Co(Nb_6O_{19})(dien)]^{5-}$	18.2 (1.80)	25.6 (1.80)
CoO_4NS	$[Co(Nb_6O_{19})(L\text{-methio})]^{6-}$	17.1 (2.06)	*ca.* 24 (shoulder)

a) In the unit of 10^3 cm^{-1}.

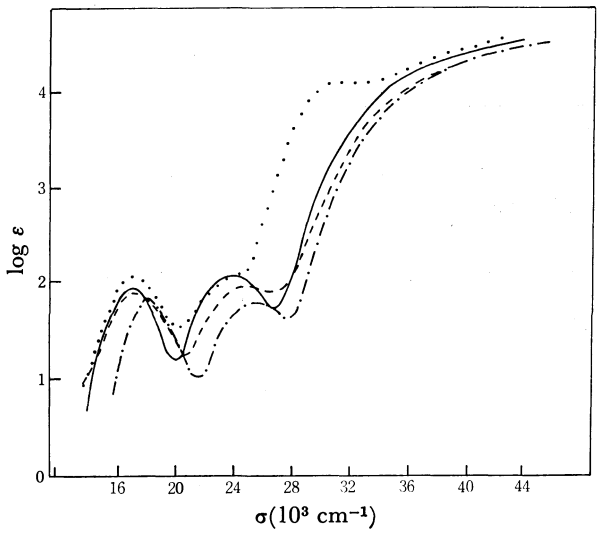

Fig. 3. Absorption spectra of $[Co(Nb_6O_{19})(ida)]^{7-}$ (——), $[Co(Nb_6O_{19})(gly)(NH_3)]^{6-}$ (----), $[Co(Nb_6O_{19})(dien)]^{5-}$ (-·-·-) and $[Co(Nb_6O_{19})(L\text{-methio})]^{6-}$ (·····).

absorption band. These spectral behaviors agree well with those which can be expected from the semi-empirical rule for d–d absorption bands.[6] The second absorption band of $[Co(Nb_6O_{19})(L\text{-methio})]^{6-}$ appears as a shoulder because of overlapping by the thioether charge transfer band,[7] which is located at 31300 cm^{-1} with log ε=4.07. For all the complexes studied, a strong absorption band due to the coordinated hexaniobate appears in a region of 38000—40000 cm^{-1}, and its position and intensity are independent of the pH change from 6.5 to 14, though a 41300 cm^{-1} band of the free $Nb_6O_{19}^{8-}$ ion depends strongly upon the pH. The two resembling complexes, $[Co(Nb_6O_{19})(L\text{-asp})]^{7-}$ and $[Co(Nb_6O_{19})(L\text{-asp})(OH_2)]^{7-}$, were distinguished from each other by the pmr spectra. The former complex shows an ABX pattern due to $-CHCH_2-$ protons of the tridentate L-aspartato ligand,[8] whereas the latter shows a more complicated pattern, which suggests the mixing of two ABX patterns resulted from the coexistene of two diastereomers.

The CD data of the present complexes are summarized in Table 2. The CD curve of $(+)^{CD}_{546}$-$[Co(Nb_6O_{19})(gly)(NH_3)]^{6-}$ obtained from the less soluble diastereomer with $(+)_{589}$-$[Co(en)_3]Br_3$ is shown in Fig. 5. As is seen in Fig. 4, the CD curves of two L-valinato isomers differ remarkably from that of $(+)^{CD}_{546}$-$[Co(Nb_6O_{19})(gly)(NH_3)]^{6-}$, and the difference may be attributed to the vicinal contribution due to the L-valinato ligand. When the additivity rule for the configurational and vicinal CD contributions is applied for the CD curves of L-valinato diastereomers,[9,10] the calculated configurational CD curve does not agree well with the observed CD curve of $(+)^{CD}_{546}$-$[Co(Nb_6O_{19})(gly)(NH_3)]^{6-}$ (Fig. 5). But the sign pattern suggests that the configuration of $(+)^{CD}_{546}$-$[Co(Nb_6O_{19})(gly)(NH_3)]^{6-}$ corresponds to

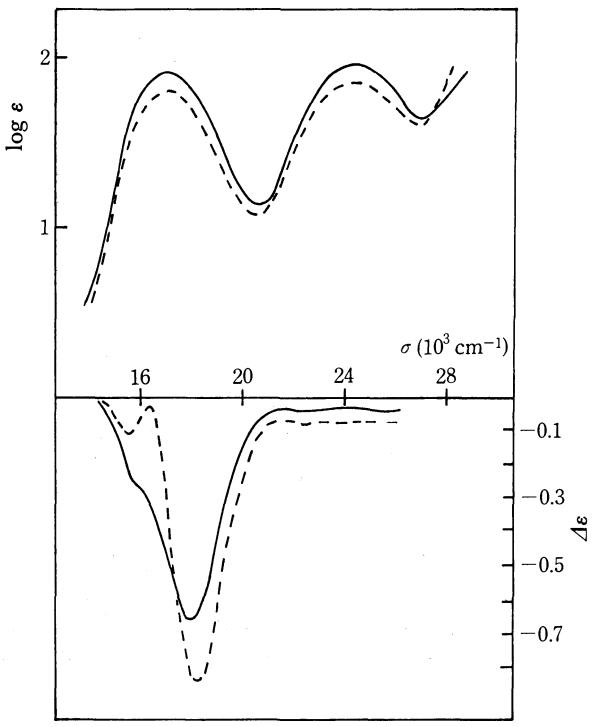

Fig. 4. Absorption and CD spectra of $[Co(Nb_6O_{19})(L\text{-val})(NH_3)]^{6-}$, F_1 (——) and F_2 (----).

Table 2. CD data of the complexes

Complex	σ_{ext} [a] ($\Delta\varepsilon$) I band	II band
$[Co(Nb_6O_{19})(L\text{-methio})]^{6-}$	17.2 (+1.23)	25.0 (−0.22)
$[Co(Nb_6O_{19})(L\text{-asp})]^{7-}$	14.8 (−0.1)	*ca.* 24 (+0.06)
	16.4 (+0.14)	
	18.5 (−0.11)	
$(+)^{CD}_{546}$-$[Co(Nb_6O_{19})(gly)(OH_2)]^{6-}$	14.6 (+0.20)	23.5 (−0.06)
	16.0 (−0.26)	27.4 (+0.05)
	17.9 (+0.08)	
$[Co(Nb_6O_{19})(L\text{-val})(OH_2)]^{6-}$ [b]	15.8 (−0.29)	24.0 (−0.03)
$[Co(Nb_6O_{19})(L\text{-ala})(OH_2)]^{6-}$ [b]	16.8 (−0.31)	22.5 (+0.01)
$[Co(Nb_6O_{19})(L\text{-asp})(OH_2)]^{7-}$ [b]	15.6 (−0.21)	*ca.* 23 (+0.02)
$(+)^{CD}_{546}$-$[Co(Nb_6O_{19})(gly)(NH_3)]^{6-}$	16.4 (−0.21)	22.7 (+0.04)
	18.3 (+0.61)	24.6 (−0.06)
$[Co(Nb_6O_{19})(L\text{-val})(NH_3)]^{6-}$: F_1	*ca.* 16 (−0.25)	
	18.1 (−0.66)	
F_2	15.6 (−0.11)	
	18.4 (−0.84)	
$[Co(Nb_6O_{19})(L\text{-ala})(NH_3)]^{6-}$ [b]	17.9 (−0.26)	*ca.* 22 (−0.03)
$[Co(Nb_6O_{19})(L\text{-asp})(NH_3)]^{7-}$ [b]	16.2 (+0.10)	22.5 (−0.02)
	18.3 (−0.40)	*ca.* 25 (+0.01)

a) In the unit of 10^3 cm^{-1}. b) Unresolved complex.

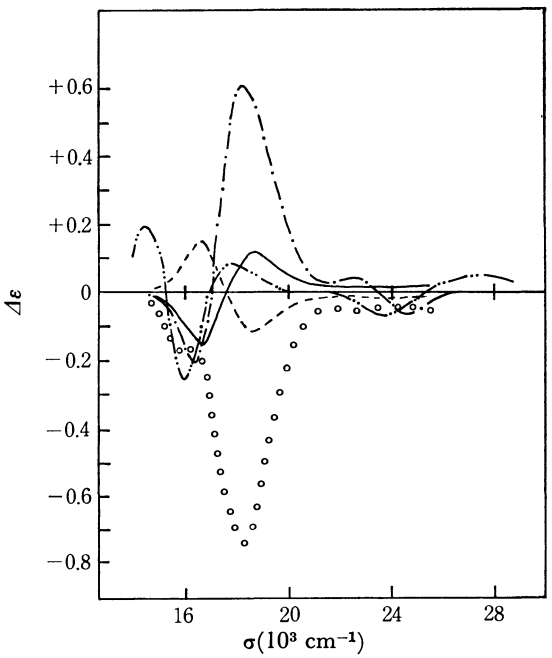

Fig. 5. Calculated configurational (F_1' ——, F_2' ----) and vicinal (oooo) CD curves of $[Co(Nb_6O_{19})(L\text{-val})(NH_3)]^{6-}$. Observed CD spectra of $(+)^{CD}_{546}$-$[Co(Nb_6O_{19})(gly)(NH_3)]^{6-}$ (-·-·-) and $(+)^{CD}_{546}$-$[Co(Nb_6O_{19})(gly)(OH_2)]^{6-}$ (-···-).

the L-valinato F_1 isomer. The formation ratio of F_1 to F_2 is about 2 as described in Experimental section. This fact suggests that the F_1 diastereomer is (A) in Fig. 2, since a less interaction is expected between the $-CH(CH_3)_2$ substituent and the coordinated hexaniobato ligand in the isomer (A) than in (B).

The configurational chirality in the present complexes is the same type as in the $[Co(am)NH_3(tame)]^{2+}$ complexes recently studied in this laboratory,[11] where the ligand tame is 1,1,1-tris(aminomethyl)ethane. In this $CoON_5$ type complexes the additivity of the configurational and vicinal CD contributions was reasonably well in contrast to the present hexaniobato complexes. The reason for such difference between the $CoON_5$ and the present CoO_4N_2 types still remaines unknown.

References

1) L. C. W. Baker and J. S. Figgis, *J. Amer. Chem. Soc.*, **92**, 3794 (1970).
2) T. Ama, J. Hidaka, and Y. Shimura, This Bulletin, **46**, 2145 (1973).
3) C. M. Flynn, Jr., and G. D. Stucky, *Inorg. Chem.*, **8**, 178 (1969).
4) C. M. Flynn, Jr., and G. D. Stucky, *ibid.*, **8**, 335 (1969).
5) I. Lindqvist, *Arkiv Kemi*, **5**, 247 (1953).
6) H. Yamatera, This Bulletin, **31**, 95 (1958).
7) J. Hidaka, S. Yamada, and Y. Shimura, *Chem. Lett.*, **1974**, 1487.
8) L. R. Froebe, S. Yamada, J. Hidaka, and B. E. Douglas, *J. Coord. Chem.*, **1**, 183 (1971).
9) N. Matsuoka, J. Hidaka, and Y. Shimura, This Bulletin, **9**, 719 (1970).
10) K. Okamoto, J. Hidaka, and Y. Shimura, *ibid.*, **44**, 1601 (1971).
11) K. Yamanari, J. Hidaka, and Y. Shimura, *ibid.*, **48**, 1653 (1975).

Studies of the Ruthenium Complexes. XI.[1] The Reaction Mechanism of the Base Hydrolysis of Halogenopentaammineruthenium(III) Complexes[2]

Akira OHYOSHI, Hiroyuki SAKAMOTO, Haruo MAKINO, and Keijiro HAMADA

Department of Industrial Chemistry, Faculty of Engineering, Kumamoto University, Kumamoto 860

(Received June 9, 1975)

The base hydrolysis of halogenopentaammineruthenium(III) complexes, $[RuX(NH_3)_5]X$, (X=Cl, Br, and I), has been studied in a solution with a 0.03—0.2 M hydroxide ion concentration in order to clarify the reaction mechanism. Some deviations from the first-order rate plots were observed early in the reaction. By the analysis of these results, it was proved that the concentration change with time for each species participating in the reaction was expressed by a linear combination of two exponential functions. The reaction can be well accounted for by a mechanism involving S_N2 CB and S_N2 processes:

$$[RuX(NH_3)_5]^{2+} + OH^- \underset{k_{-1}}{\overset{k_1}{\rightleftharpoons}} [RuX(NH_3)_4(NH_2)]^+ + H_2O$$

$$[RuX(NH_3)_4(NH_2)]^+ + OH^- \xrightarrow[H_2O]{k_2} [Ru(OH)(NH_3)_5]^{2+} + X^- + OH^-$$

$$[RuX(NH_3)_5]^{2+} + OH^- \xrightarrow{k_3} [Ru(OH)(NH_3)_5]^{2+} + X^-$$

The rate constants, k_1, k_{-1}, k_2, and k_3, at 15 °C were determined to be 9.29×10^{-2} M^{-1} s^{-1}, 2.65×10^{-2} s^{-1}, 6.78×10^{-1} M^{-1} s^{-1}, and 1.13×10^{-1} M^{-1} s^{-1} respectively for the chloropentaammine complex.

Among the several investigations[3-10] of the base hydrolysis of the metal-ammine complexes, Broomhead and his co-workers[9,10] have reported that the reaction of the halogenopentaammineruthenium(III) complex proceeds *via* the S_N1 conjugated-base (S_N1 CB) mechanism in a solution with a 3.78×10^{-4}—2.65×10^{-3} M hydroxide ion concentration. Certainly, this interpretation is reasonable. However, other mechanisms are possible considering the strong affinity of the ruthenium(III) ion for the oxygen atom. Thus, the base hydrolysis of halogenopentaammineruthenium(III) complexes, $[RuX(NH_3)_5]^{2+}$, X=Cl, Br, and I, has been studied at high concentrations of hydroxide ions (from 0.03 M to 0.2 M). On the basis of the experimental results, we assumed three types of elementary reactions for the mechanism and examined their validities by means of computer-simulation analysis.

Experimental

Preparation of Complexes. The complexes, $[RuX(NH_3)_5](ClO_4)_2$, were prepared by the method of the literature.[9] The complexes were confirmed by elemental analysis and by the visible and UV spectra. Found: H, 3.47; N, 16.32%. Calcd for $[RuCl(NH_3)_5](ClO_4)_2$: H, 3.60; N, 16.65%. Found: H, 3.40; N, 14.49%. Calcd for $[RuBr(NH_3)_5](ClO_4)_2$: H, 3.25; N, 15.06%. Found: H, 2.87; N, 13.58%. Calcd for $[RuI(NH_3)_5](ClO_4)_2$: H, 2.95; N, 13.68%.

Kinetic Run. The reaction solutions were adjusted to the ionic strength of 1.0 M and the hydroxide-ion concentration of 0.03—0.2 M with sodium hydroxide and sodium perchlorate. The reaction temperature was kept constant within ±0.1 °C by circulating water from a thermostated bath. A change in the concentration of $[RuX(NH_3)_5]^{2+}$ (or $[Ru(OH)(NH_3)_5]^{2+}$) as a function of time was followed by measuring the absorbance at λ_{max} of the spectra of the respective complexes, using a Hitachi 124 recording spectrophotometer.

Results and Discussion

The changes in the spectra during the base hydrolysis of bromopentaammine are shown in Fig. 1. The absorption band (398 nm) of the original complex rapidly decreases, with a slight shift to the low-wavelength region, and a new peak appears at about 300 nm. This peak grows with the shift to a constant wavelength (298 nm), a tendency which is in agreement with that of the hydroxo-complex.[9] Similar results were observed in the base hydrolysis of the other two complexes.

As is shown in Fig. 2, some deviations from the straight lines of the first-order plots are observed in the initial period of the reaction. This fact can be interpreted by assuming that the measured absorbance involves that of a short-lived intermediate in addition to that of the reactant. If the intermediate is an amido-

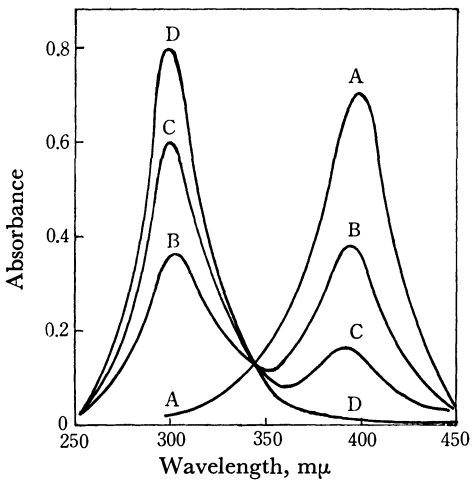

Fig. 1. Spectral changes during the base hydrolysis of $[RuBr(NH_3)_5]^{2+}$.
$[OH^-]$: 0.03 M, μ=1.0, Temp.=10.0 °C.
A; initial B; 30 s C; 60 s D; final (250 s)

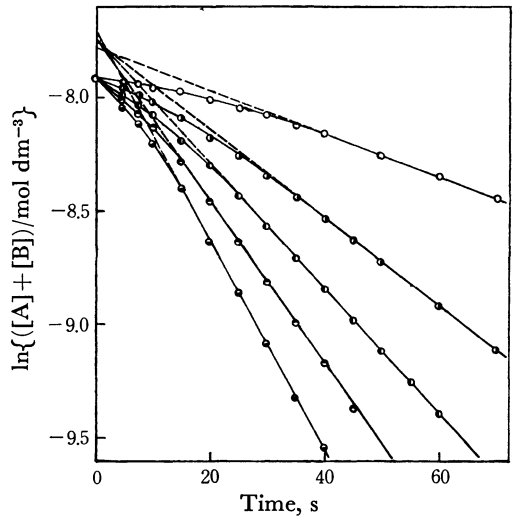

Fig. 2. Plots of ln ([A]+[B]) *vs.* reaction time.
A: $[RuBr(NH_3)_5]^{2+}$, B: $[RuBr(NH_3)_4(NH_2)]^{+}$.

complex, which is a conjugated base of the reactant, it may be acceptable that the values of λ_{max} and the extinction coefficient of the intermediate are nearly equal to those of the reactant.

Thus, we assumed the following three types of elementary reactions:

Mechanism I (S_N1 CB):

$$[RuX(NH_3)_5]^{2+} + OH^- \underset{k_{-1}}{\overset{k_1}{\rightleftharpoons}} [RuX(NH_3)_4(NH_2)]^{+} + H_2O \quad (1)$$

$$[RuX(NH_3)_4(NH_2)]^{+} \xrightarrow{k_2} [Ru(NH_3)_4(NH_2)]^{2+} + X^- \quad (2)$$

$$[Ru(NH_3)_4(NH_2)]^{2+} + H_2O \xrightarrow{\text{fast}} [Ru(OH)(NH_3)_5]^{2+} \quad (3)$$

$$[A] = \{(\lambda_1-k_{-1}'-k_2)e^{-\lambda_1 t}-(\lambda_2-k_{-1}'-k_2)e^{-\lambda_2 t}\}[A]_0/(\lambda_1-\lambda_2) \quad (4)$$

$$[B] = (-e^{-\lambda_1 t}+e^{-\lambda_2 t})k_1'[A]_0/(\lambda_1-\lambda_2) \quad (5)$$

$$[A] + [B] = \{(\lambda_1-p)e^{-\lambda_1 t}-(\lambda_2-p)e^{-\lambda_2 t}\}[A]_0/(\lambda_1-\lambda_2) \quad (6)$$

where $[A] = [RuX(NH_3)_5]^{2+}$, $[B] = [RuX(NH_3)_4(NH_2)]^{+}$, $\lambda_1=(p+\sqrt{p^2-4q})/2$, $\lambda_2=(p-\sqrt{p^2-4q})/2$, $p=k_1'+k_{-1}'+k_2$, $q=k_1'k_2$, $k_1'=k_1[OH^-]$, and $k_{-1}'=k_{-1}[H_2O]$. The zero subscript indicates the initial concentration.

Mechanism II (CB and S_N2):

$$[RuX(NH_3)_5]^{2+} + OH^- \underset{k_{-1}}{\overset{k_1}{\rightleftharpoons}} [RuX(NH_3)_4(NH_2)]^{+} + H_2O \quad (7)$$

$$[RuX(NH_3)_5]^{2+} + OH^- \xrightarrow{k_2} [Ru(OH)(NH_3)_5]^{2+} + X^- \quad (8)$$

$$[A] = \{(\lambda_1-k_{-1}')e^{-\lambda_1 t}-(\lambda_2-k_{-1}')e^{-\lambda_2 t}\}[A]_0/(\lambda_1-\lambda_2) \quad (9)$$

$$[B] = (-e^{-\lambda_1 t}+e^{-\lambda_2 t})k_1'[A]_0/(\lambda_1-\lambda_2) \quad (10)$$

$$[A] + [B] = \{(\lambda_1-k_1'-k_{-1}')e^{-\lambda_1 t} - (\lambda_2-k_1'-k_{-1}')e^{-\lambda_2 t}\}[A]_0/(\lambda_1-\lambda_2) \quad (11)$$

where $p=k_1'+k_{-1}'+k_2'$, $q=k_{-1}'k_2'$, and $k_2'=k_2[OH^-]$. The other notations are the same as those for Mechanism I.

Mechanism III (S_N2 CB and S_N2):

$$[RuX(NH_3)_5]^{2+} + OH^- \underset{k_{-1}}{\overset{k_1}{\rightleftharpoons}} [RuX(NH_3)_4(NH_2)]^{+} + H_2O \quad (12)$$

$$[RuX(NH_3)_4(NH_2)]^{+} + OH^- \xrightarrow[H_2O]{k_2} [Ru(OH)(NH_3)_5]^{2+} + X^- + OH^- \quad (13)$$

$$[RuX(NH_3)_5]^{2+} + OH^- \xrightarrow{k_3} [Ru(OH)(NH_3)_5]^{2+} + X^- \quad (14)$$

$$[A] = \{(k_1'+k_3'-\lambda_2)e^{-\lambda_1 t}-(k_1'+k_3'-\lambda_1)e^{-\lambda_2 t}\}[A]_0/(\lambda-\lambda_2) \quad (15)$$

$$[B] = (-e^{-\lambda_1 t}+e^{-\lambda_2 t})k_1'[A]_0/(\lambda_1-\lambda_2) \quad (16)$$

$$[A] + [B] = \{(k_3'-\lambda_2)e^{-\lambda_1 t}-(k_3'-\lambda_1)e^{-\lambda_2 t}\}[A]_0/(\lambda_1-\lambda_2) \quad (17)$$

where $p=k_1'+k_{-1}'+k_2'+k_3'$, $q=k_1'k_2'+k_{-1}'k_3'+k_2'k_3'$, $k_2'=k_2[OH^-]$, and $k_3'=k_3[OH^-]$.

For all the mechanisms, [A]+[B] is expressed by Eq. 18:

$$[A] + [B] = C_1e^{-\lambda_1 t} + C_2e^{-\lambda_2 t} \quad (18)$$

Where C_1 and C_2 are the constants.

In the stationary-state period, the first term on the right-hand of Eq. 18 is nearly equal to zero. Therefore we can obtain the λ_2 value from the plots of ln{([A]+[B])} *vs.* the time. The values of λ_2 and λ_1 correspond to the respective slopes of the straight lines in Figs. 2 and 3. As $-\lambda_1$ and $-\lambda_2$ are roots of the quadratic equation, $\lambda_1+\lambda_2$ and $\lambda_1\cdot\lambda_2$ are equal to p and q respectively. Plots of $(\lambda_1+\lambda_2)$ (=p) and $\lambda_1\cdot\lambda_2$ (=q) *vs.* the concentration of hydroxide ions are shown in Fig. 4.

Let us examine the validity of the reaction mechanisms. For Mechanism I, k_1' has a linear dependence on the concentration of hydroxide ions, and the plot of p *vs.* the hydroxide-ion concentration should be a straight line, with an intercept corresponding to $(k_{-1}+$

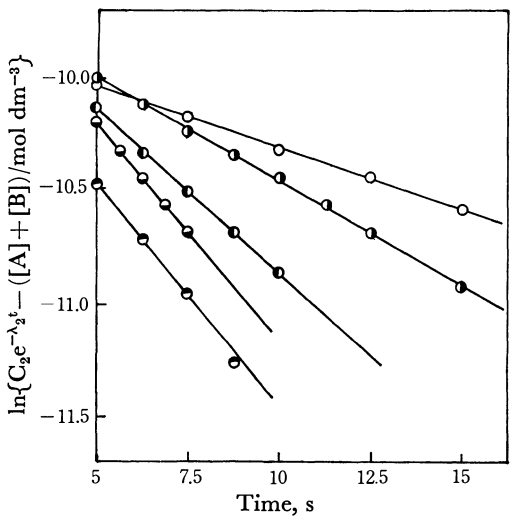

Fig. 3. Plots of $\ln\{C_2e^{-\lambda_2 t}-([A]+[B])\}$ *vs.* reaction time.
A: $[RuBr(NH_3)_5]^{2+}$, B: $[RuBr(NH_3)_4(NH_2)]^{+}$.
$[OH^-]$; -○- 0.03 M, -◑- 0.07 M, -◐- 0.11 M, -◒- 0.16 M, -◓- 0.20 M.

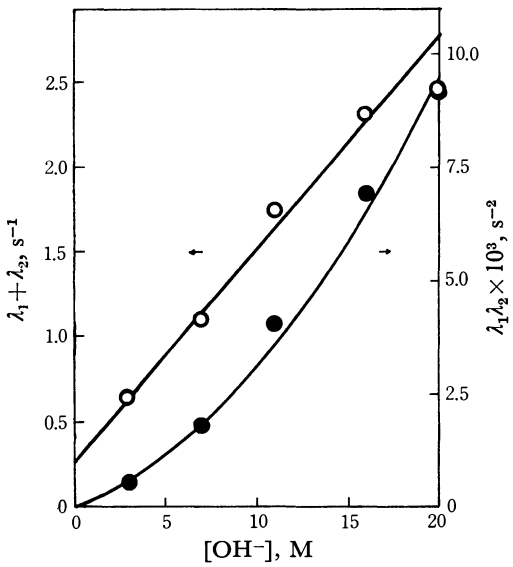

Fig. 4. Plots of $\lambda_1+\lambda_2$ and $\lambda_1\cdot\lambda_2$ *vs.* [OH$^-$].

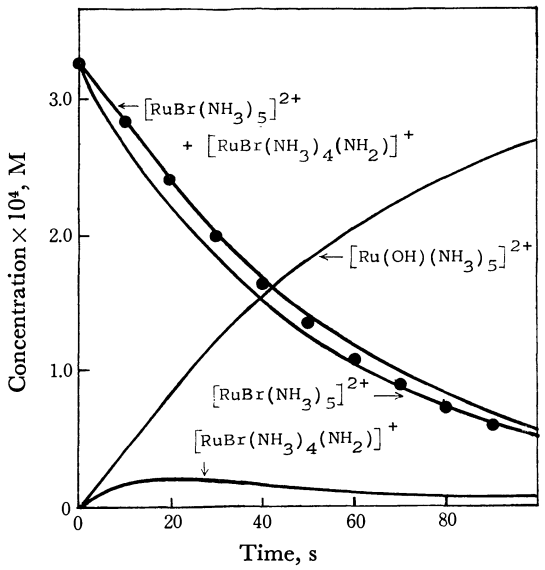

Fig. 5. Concentration variation of chemical species participating in the base hydrolysis of chloropentaammineruthenium(III).
$[RuCl(NH_3)_5]_0^{2+}=3.267\times10^{-4}$ M, $[OH^-]=0.11$ M, Temp.$=15.0$ °C, $\mu=1.0$ mol·kg^{-1}, k_1, k_2, k_3, and k'_{-1} are 9.29×10^{-2} M^{-1} s^{-1}, 6.78×10^{-1} M^{-1} s^{-1}, 1.13×10^{-1} M^{-1} s^{-1}, and 2.65×10^{-2} s^{-1} respectively.
●, Experimental; ——, Simulation.

k_2). Just as in the case of Mechanism I, a linear relationship can be expected to hold for Mechanisms II and III. Plots of q *vs.* the concentration of hydroxide ions should be straight lines for Mechanisms I and II, while a quadratic curve can be expected for Mechanism III; that is, the types of curves for Mechanisms II and III should be different. The former has the same double real roots, but the latter, two different real roots.

Judging from Fig. 4, the relation is not linear but quadratic, and the curve favors Mechanism III. Especially, if the reaction proceeds by means of Mechanism I, no irregularities should be allowed in the initial stage of the reaction.

Table 1. Rate constants and kinetic parameters of the base hydrolysis for chloropentaammineruthenium(III) complex

	Rate constants (Temp., °C)	Frequency factor, A, s^{-1}	E_a (kcal/mol)	ΔS^* (e.u.)	ΔH^* (kcal/mol)
k_1, $10^{-2}\cdot M^{-1}\cdot s^{-1}$	2.4 ±0.2 (3.0) 3.4 ±0.3 (6.0) 5 ±1 (10.0) 9 ±2 (15.0) 14 ±5 (19.0)	3.1×10^{12}	18	−3.3	17
k_{-1}, $10^{-2}\cdot s^{-1}$	2.01±0.08(3.0) 2.2 ±0.1 (6.0) 2.4 ±0.6 (10.0) 2.7 ±0.3 (15.0) 2.9 ±0.5 (19.0)	1.5×10^{10}	3.6	−55	3.1
k_2, $10^{-2}\cdot M^{-1}\cdot s^{-1}$	8.5 ±0.4 (3.0) 14.5 ±0.5 (6.0) 29 ±1 (10.0) 68 ±5 (15.0) 131 ±9 (19.0)	4.3×10^{20}	27	34	27
k_3, $10^{-2}\cdot M^{-1}\cdot s^{-1}$	2.1 ±0.8 (3.0) 3.2 ±0.2 (6.0) 5.9 ±0.4 (10.0) 11 ±2 (15.0) 19 ±3 (19.0)	6.9×10^{15}	22	12	22
k_{obsd}, $10^{-2}\cdot M^{-1}\cdot s^{-1}$	2.7 ±0.1 (3.0) 4.9 ±0.1 (6.0) 9.4 ±0.5 (10.0) 26 ±2 (15.0) 52 ±4 (19.0)	1.1×10^{22}	30	40	29

Table 2. Rate constants and kinetic parameters of the base hydrolysis for bromopentaammineruthenium(III) complex

	Rate constants (Temp., °C)	Frequency factor, A, s^{-1}	E_a (kcal/mol)	$\Delta S^{\ddagger}$ (e.u.)	$\Delta H^{\ddagger}$ (kcal/mol)
k_1, $10^{-2}\cdot M^{-1}\cdot s^{-1}$	1.18±0.08 (3.0) 2.5 ±0.2 (6.0) 7 ±1 (10.0) 23 ±6 (15.0) 57 ±9 (19.0)	6.6×10^{28}	39	11	38
k_{-1}, $10^{-2}\cdot s^{-1}$	1.48±0.06 (3.0) 1.9 ±0.1 (6.0) 2.7 ±0.1 (10.0) 4.0 ±0.6 (15.0) 5.4 ±0.7 (19.0)	2.6×10^{8}	13	−22	12
k_2, $10^{-2}\cdot M^{-1}\cdot s^{-1}$	21.6 ±0.6 (3.0) 29.6 ±0.8 (6.0) 44 ±2 (10.0) 73 ±7 (15.0) 107 ±9 (19.0)	1.1×10^{12}	16	−5.3	16
k_3, $10^{-2}\cdot M^{-1}\cdot s^{-1}$	2.0 ±0.3 (3.0) 3.0 ±0.3 (6.0) 6.7 ±0.4 (10.0) 15 ±2 (15.0) 28 ±4 (19.0)	2.6×10^{19}	27	29	26
k_{obsd}, $10^{-2}\cdot M^{-1}\cdot s^{-1}$	3.0 ±0.2 (3.0) 5.8 ±0.5 (6.0) 12.0 ±0.9 (10.0) 22 ±4 (15.0) 44 ±3 (19.0)	1.4×10^{19}	26	27	26

Table 3. Rate constants and kinetic parameters of the base hydrolysis for iodopentaammineruthenium(III) complex

	Rate constants (Temp., °C)	Frequency factor, A, s^{-1}	E_a (kcal/mol)	$\Delta S^{\ddagger}$ (e.u.)	$\Delta H^{\ddagger}$ (kcal/mol)
k_1, $10^{-2}\cdot M^{-1}\cdot s^{-1}$	0.33±0.04 (3.0) 0.70±0.06 (6.0) 3.3 ±0.7 (10.0) 16 ±3 (15.0) 53 ±4 (19.0)	6.1×10^{37}	51	113	50
k_{-1}, $10^{-2}\cdot s^{-1}$	1.18±0.09 (3.0) 1.5 ±0.1 (6.0) 2.2 ±0.2 (10.0) 2.7 ±0.2 (15.0) 4.4 ±0.4 (19.0)	9.5×10^{7}	13	−24	12
k_2, $10^{-2}\cdot M^{-1}\cdot s^{-1}$	32 ±1 (3.0) 35 ±2 (6.0) 38 ±2 (10.0) 42 ±3 (15.0) 45 ±4 (19.0)	1.3×10^{2}	3.3	−51	2.7
k_3, $10^{-2}\cdot M^{-1}\cdot s^{-1}$	1.2 ±0.1 (3.0) 1.9 ±0.2 (6.0) 4.1 ±0.4 (10.0) 9.3 ±0.3 (15.0) 15 ±1 (19.0)	2.9×10^{18}	26	24	25
k_{obsd}, $10^{-2}\cdot M^{-1}\cdot s^{-1}$	2.7 ±0.03 (3.0) 3.05±0.06 (6.0) 7.0 ±0.2 (10.0) 19.5 ±0.3 (15.0) 38 ±3 (19.0)	5.8×10^{18}	26	25	25

Now, let us estimate the rate constants based on Mechanism III. In Fig. 4, the slope and intercept of the straight line indicate $(k_1+k_2+k_3)$ and k_{-1} respectively. Since the variation in the concentration (=$\{[A]+[B]\}$) is almost linear in the initial stage of the reaction, as is shown in Fig. 5, the k_3 value can be obtained from the slope of the initial line. The values of k_1 and k_2 are calculated by the relation of p and q. Thus, all the rate constants were determined; they are given in Tables 1—3. It seems that the dissociation of hydrogen is very difficult in comparison with the hydrogen-exchange reaction of the hexaammineruthenium(III) complex.[10]

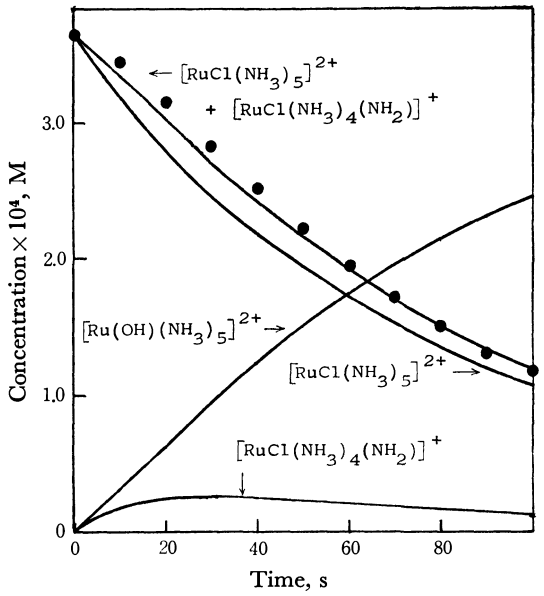

Fig. 6. Concentration variation of chemical species participating in the base hydrolysis of bromopentaammineruthenium(III).
$[RuBr(NH_3)_5]_0^{2+}=3.654\times10^{-4}$ M, $[OH^-]=0.11$ M, Temp.=10.0 °C, $\mu=1.0$ mol kg^{-1}, k_1, k_2, k_3, and k'_{-1} are 6.79×10^{-2} M^{-1} s^{-1}, 4.46×10^{-1} M^{-1} s^{-1}, 6.74×10^{-2} M^{-1} s^{-1} and 2.65×10^{-2} s^{-1} respectively.
● Experimental; —— Simulation.

Finally, we carried out a simulation analysis based on Eqs. 15—17 in order to check the validity of the estimated rate constants. The calculated results are shown in Figs. 5 and 6. The concentration of $[Ru(OH)(NH_3)_5]^{2+}$ was calculated by means of $([A]_0-[A]-[B])$. The curves showing the concentration change with the reaction time for the original and intermediate complexes obtained from the simulative calculation are in agreement with the experimental results.

As has already been pointed out[11] in connection with the influence of hydrogen peroxide on the reaction rate of the base hydrolysis of metal ammine complexes, the rate constant decreases upon the addition of hydrogen peroxide for the base hydrolysis with the S_N1 CB mechanism, while it increases for the reaction process of the S_N2 mechanism.

In the present experiment on the base hydrolysis, the rate constant in the solution of each 0.11 M hydroxide ion and hydrogen peroxide is about three times larger than that in the 0.11 M hydroxide ion solution. This fact indicates that the S_N2 mechanism favors the base hydrolysis reaction of halogenopentaammineruthenium(III).

The calculations were performed on a FACOM 230-25 computer at the Engineering Research Center of Kumamoto University.

The authors wish to thank the Ministry of Education for the financial support (No. 847009) granted to this research.

References

1) Part X. of this series; K. Ohkubo, F. Kitagawa, H. Sakamoto, and A. Ohyoshi, This Bulletin, **48**, 774 (1975).
2) A part of this paper was briefly reported, H. Sakamoto, H. Makino, K. Hamada, and A. Ohyoshi, *Chem. Lett.*, **1975**, 631.
3) G. C. Lalor and J. Long, *J. Chem. Soc.*, **1963**, 5620.
4) S. C. Chan, K. Y. Hui, J. Miller, and W. S. Tsang, *ibid.*, **1965**, 3207.
5) W. A. Levine, T. P. Jones, W. E. Harris, and W. J. Wallace, *J. Amer. Chem. Soc.*, **83**, 2453 (1961).
6) A. E. Ogard and H. Taube, *ibid.*, **80**, 1084 (1958).
7) G. W. Bushnell, G. C. Lalor, and E. A. Moelwyn-Hughes, *J. Chem. Soc., A*, **1966**, 719.
8) S. A. Johnson, F. Basolo, and R. G. Pearson, *J. Amer. Chem. Soc.*, **85**, 1741 (1963).
9) J. A. Broomhead, F. Basolo, and R. G. Pearson, *Inorg. Chem.*, **3**, 826 (1964).
10) J. A. Broomhead and L. Kane-Maguire, *ibid.*, **8**, 2124 (1969).
11) A. D. Allen and C. V. Senoff, *Can. J. Chem.*, **45**, 1337 (1967).
12) J. W. Palmer and F. Basolo, *J. Inorg. Nucl. Chem.*, **15**, 279 (1960).
13) F. Basolo and R. G. Pearson, "Mechanisms of Inorganic Reactions," 2nd Ed.. John Wiley & Sons, Inc., New York (1967), p. 192.

Thermal Dehydration Reactions of Bivalent Transition Metal Malonate Dihydrates in Solid State

Kenzo NAGASE, Kazuo MURAISHI,* Kozo SONE,** and Nobuyuki TANAKA***

College of General Education, Tohoku University, Kawauchi, Sendai 980

**Department of Chemistry, Faculty of Science, Yamagata University, Koshirakawa, Yamagata 990*

***Department of Chemistry, Faculty of Science, Ochanomizu University, Otsuka, Bunkyo-ku, Tokyo 112*

****Department of Chemistry, Faculty of Science, Tohoku University, Aoba, Aramaki, Sendai 980*

(Received July 21, 1975)

The kinetics of the thermal dehydration reactions of $MC_3H_2O_4 \cdot 2H_2O$(M=Mn(II), Fe(II), Co(II), Ni(II), and Zn(II)) were studied by the Freeman-Carroll and Coats-Redfern methods on the basis of the TG and DTG in nitrogen. The most reasonable reaction order for all the salts was found to be 2/3, indicating that the rate is controlled by the chemical process at a phase-boundary. This was also confirmed by the microscopic observations. The values of activation energy and frequency factor were 70—90 kJ mol^{-1} and 10^7—10^{10} s^{-1}, respectively. The enthalpy changes for all the salts were determined to be 60—80 kJ mol^{-1} by the DSC measurements. The X-ray powder diffractograms, infrared absorption and diffuse reflectance spectra of the hydrates and anhydrous salts were also examined to obtain informations on their crystal and bonding structures.

The thermal elimination reactions of the salts containing volatile ligands such as water, ammonia and pyridine have been extensively investigated both kinetically and calorimetrically in connection with the strengths of metal-volatile ligand bonds and with the structural changes caused by the eliminations.

Most metal dicarboxylates crystallize as hydrates. Oxalates of bivalent transition metals, in many cases, contain two water molecules, which were found by the X-ray analyses to be coordinated to the metals.[1] One of water molecules in copper succinate dihydrate was found by the X-ray analysis[2] to be coordinated to the metal and it was predicted that the water molecules in the succinates of other metals are also coordinated to the metals.[3] As for the malonates investigated in this study, each of them contains two water molecules, and some preliminary experiments indicate that both of them are coordinated to the metals, so that it may be possible to characterize their dehydration reactions by appropriate kinetic and calorimetric parameters related to the strength of metal–OH_2 bonds.

Several studies dealing with the thermal dehydration reactions of metal malonates have been reported in recent years: Yttrium and scandium malonate hydrates[4] lose all of their water almost continuously, while lanthanum,[4] europium[5] and uranyl[6] malonate hydrates lose water molecules into two steps. Sodium,[7] iron,[8] nickel,[9] cobalt[10] and barium[7] malonate hydrates lose their 1, 2, 2, 2, and 0.8 moles of water in one step, while potassium malonate hydrate[7] loses one mole of water at 323—363 K and another one mole at 423—463 K. Although thermal dehydration of copper malonate trihydrate or tetrahydrate has been investigated by several workers,[11] the results are divergent, since the dehydration is followed immediately by the decomposition of its anhydrous salt.

Experimental

Materials. To prepare each of the malonates investigated, the corresponding metal carbonate was dissolved into an aqueous solution of malonic acid (10% excess) at 343 K. Precipitation of the malonate crystals occurred immediately; after the solution was allowed to stand overnight at room temperature, the crystals were filtered, washed with water, ethanol and ether, dried in air, and sieved (Tyler mesh size: 170—200) before use. The results of the elemental analyses for C, H, and metal are given in Table 1.

Table 1. Analytical data for metal malonate dihydrates

M	C(%)		H(%)		Metal(%)	
	Found	Calcd[a]	Found	Calcd[a]	Found	Calcd[a]
Mn	18.65	18.67	3.12	3.13	28.42	28.46
Fe	18.81	18.58	3.19	3.12	28.70	28.46
Co	18.23	18.29	3.01	3.07	29.76	29.91
Ni	18.29	18.31	3.07	3.07	29.81	29.83
Zn	17.83	17.71	2.98	2.97	32.03	32.13

a) Calculated for $MC_3H_2O_4 \cdot 2H_2O$ (M=metal).

Measurements. The Mössbauer spectrum of the iron salt was measured with a constant acceleration spectrometer equipped with a 400 channel pulse-height analyzer (Elron, Oxford). The lines of the sample appeared at about 0.5 and 2.3 mm s^{-1}, offering the evidence for bivalent iron.

The crystal and bonding structures of the hydrates and anhydrous salts were examined by X-ray diffraction analysis and infrared and reflectance spectroscopy. The X-ray diffractograms were obtained with a Rigaku Denki diffractometer DS, using Cu$K\alpha$ or Fe$K\alpha$ radiations. The infrared measurements were made in a frequency region of 4000—250 cm^{-1} with a Hitachi 215 spectrophotometer by the KBr disk method. The diffuse reflectance spectra in the visible region were measured with a Hitachi EPS-3T spectrophotometer equipped with a standard integrating sphere attachment.

Non-isothermal kinetic measurements were made using a Shinku Riko TGD-3000 differential thermal microbalance. Samples of about 15 mg were heated at a scanning rate of 0.083 K s^{-1} (5 K min^{-1}) under nitrogen stream with a flow rate of 1 ml s^{-1}.

A Rigaku Denki DSC-8002 differential scanning calorimeter, calibrated by the heat of transition of KNO_3 (ΔH= 51.3 kJ mol^{-1} at 401 K), was used for the heat measurements. The details of experimental conditions were described previously.[12]

Kinetic Procedures. The values of reaction order (n) and activation energy (E_a) were found graphically using the Freeman-Carroll method[13]

$$\frac{-E_a \Delta\left(\frac{1}{T}\right)}{2.3R\,\Delta \log (W-W_c)} = -n + \frac{\Delta \log \frac{dW}{dt}}{\Delta \log (W-W_c)}$$

where W=sample weight at temperature T; W_c=sample weight at the completion of reaction; dW/dt=the rate of change in sample weight at temperature T. The values of $(W-W_c)$ and dW/dt were determined directly from TG and DTG curves, respectively, in terms of 15—20 divisions.

The frequency factor (A) was calculated using the basic relation:

$$\frac{d\alpha}{dt} = Ae^{-E_a/RT}(1-\alpha)^n$$

where α means the degree of reaction, $(W_0-W)/(W_0-W_c)$ (W_0=initial sample weight).

The values of E_a and n obtained using the Freeman-Carroll method were checked by the Coats-Redfern method[14] which allows a good linearization if the correct n value is assumed:

$$\log\left[\frac{1-(1-\alpha)^{1-n}}{T^2(1-n)}\right] = \log\frac{AR}{\phi E_a}\left[1-\frac{2RT}{E_a}\right] - \frac{E_a}{2.3RT}$$

where ϕ means heating rate.

Results and Discussion

Dihydrates. Recently, the diffraction and crystallographic data of several malonates have been reported;[8,10,15] according to them, the crystals of manganese and iron malonate dihydrates belong to the orthorhombic system, and those of cobalt, nickel and zinc to the monoclinic system. The authors have also obtained the X-ray diffractograms of all these salts, together with their infrared absorption spectra given in Fig. 1. The salts of the same crystal system give similar spectra, whereas there are apparant differences between the spectral pattern of the salts of the orthorhombic system and that of the salts of the monoclinic system. Most of absorptions can be assigned easily by applying the bands assignments made successfully with sodium malonate,[16] but two absorptions in the region of 900—850 cm^{-1}, observed only with the salts of Co, Ni and Zn (monoclinic system), could not be assigned. Sodium malonate, malonic acid and di- or tri-malonato complexes do not show any absorption in this region.[16] Some particular bonding manner may exist in these salts.

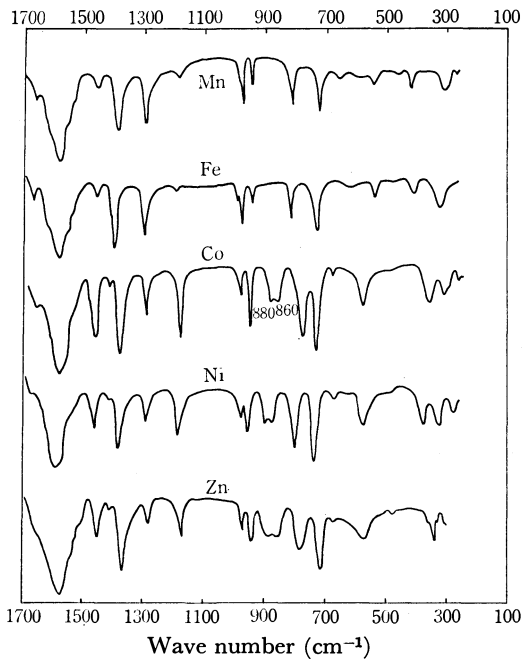

Fig. 1. Infrared absorption spectra of metal malonate dihydrates.

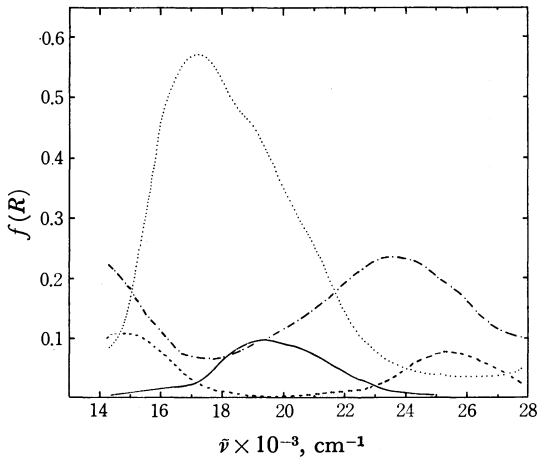

Fig. 2. Reflectance spectra of malonate dihydrates and anhydrous malonates. ——: $CoC_3H_2O_4\cdot 2H_2O$, ……: $CoC_3H_2O_4$, ----: $NiC_3H_2O_4\cdot 2H_2O$, -·-·-: $NiC_3H_2O_4$.

The diffuse reflectance spectra of the cobalt and nickel salts in Fig. 2 indicate that each metal is surrounded octahedrally by six oxygen atoms.[17] Since a malonate ion has four oxygen atoms, two water molecules of $MC_3H_2O_4\cdot 2H_2O$ (M=Co and Ni) seem to be coordinated to the metals.

Dehydration Reactions. The TG, DTA, DTG, and DSC curves were obtained in a nitrogen atmosphere for all the salts investigated. All the curves corresponding to the dehydration were smooth so that the dehydration reactions seems to take place in one step. The initial weight-loss temperatures (T_i), weight-loss values (W_0-W_c) and peak temperatures of DTG (T_m) are given in Table 2. The weight-loss data confirm the formura $MC_3H_2O_4\cdot 2H_2O$. Both T_i and T_m vary considerably with the metals and the variations are similar to those of metal oxalate dihydrates in which two water molecules are coordinated to the metals. Moreover, T_i, and T_m of the malonates are relatively higher than the ordinary values for the elimination of crystalline water. These facts support the view that

Table 2. Initial weight-loss temperatures (T_i), DTG peak temperatures (T_m) and weight-loss values (W_0-W_c) for the reaction

$MC_3H_2O_4\cdot 2H_2O(s) \rightarrow MC_3H_2O_4(s)+2H_2O(g)$

M	T_i/K	T_m/K	$(W_0-W_c)_{obsd}$ (%)	$(W_0-W_c)_{calcd}$ (%)
Mn	393	453	18.4	18.7
Fe	392	456	17.4	18.6
Co	396	456	17.1	18.3
Ni	430	501	19.7	18.3
Zn	342	395	16.8	17.7

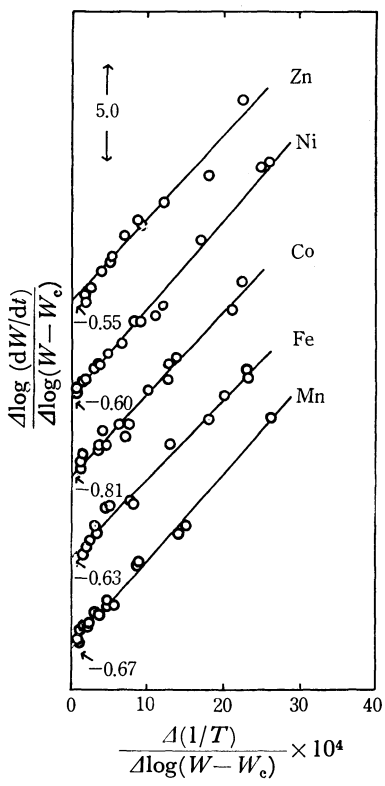

Fig. 3. Plots by the Freeman-Carroll method.

TABLE 3. REACTION ORDERS (n), ACTIVATION ENERGIES (E_a), FREQUENCY FACTORS (A) AND ENTHALPY CHANGES (ΔH) FOR THE REACTION

$MC_3H_2O_4 \cdot 2H_2O(s) \rightarrow MC_3H_2O_4(s) + 2H_2O(g)$

M	n	E_a/KJ·mol^{-1}		A/s^{-1}	ΔH/ KJ·mol^{-1}
		F-C[a]	C-R[b]		
Mn	0.67±0.23	88.6±4.2	86.9	5.2×10^9	73.6
Fe	0.63±0.19	80.7±2.9	76.9	2.3×10^7	65.6
Co	0.81±0.21	83.6±3.8	76.5	3.6×10^8	77.3
Ni	0.60±0.13	92.0±2.5	80.7	4.2×10^7	77.7
Zn	0.55±0.14	80.7±4.2	76.5	4.3×10^9	69.4

a) Freeman-Carroll method. b) Coats-Redfern method.

the water molecules in all the malonates are also coordinated.

The kinetic analyses of the traces of the TG and DTG curves lead to the plots shown in Fig. 3, yielding the values of activation energy and reaction order given in Table 3 (Freeman-Carroll method). For all the salts, a reaction order of 2/3 was found to fit best the experimental results, indicating that the dehydration begins on the surface of the crystals and propagates uniformly to their centers. Consequently it is probable that the overall reaction rate is controlled by the chemical process at the phase-boundary formed by the reactant and the product.

Figure 4 shows the microscopic photographs of partially dehydrated manganese malonate heated up to 434 K in nitrogen, indicating that the reaction proceeds from the outer surface of each particle inwards. The crystalline hydrate became finally amorphous on dehydration. As shown in Fig. 5, the change of the X-ray powder diffraction patterns for the manganese salt correspond well to the microscopic observations. Other anhydrous salts were also found to be amorphous to X-rays, supporting the former reports on iron[8] and cobalt[9] salts.

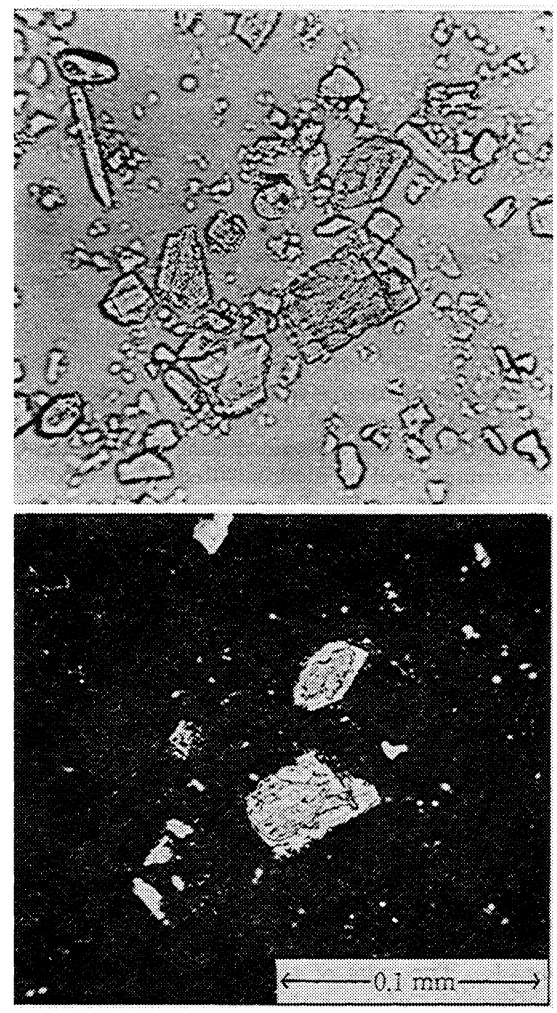

Fig. 4. Microscopic photographs of partially dehydrated manganese malonate; the lower one was taken between crossed polarizers.

When n is assumed to be 2/3, the plots by the Coats-Redfern method give good straight lines to yield E_a given in Table 3. The values agreed with those obtained by the Freeman-Carroll method, although the former values are somewhat lower. The bond strength of M–OH_2 is expected to be a function of the size of the metal ion if electrostatic attraction between it and the oxygen lone-pair is assumed, or to follow the well-known Irving-Williams order if ligand field effect is taken into consideration; but the variation of E_a in Table 3 with the metals are not as expected and the value for the manganese salt is apparently quite high. The bond strengths of M–OH_2 thus seem to be better reflected on T_i (or T_m) rather than on E_a.

The heat changes caused by the dehydration are given in Table 3. These values correspond to the average enthalpy changes per one mole of H_2O. Since the enthalpy changes obtained involve the amount corresponding to the change in the physical state of

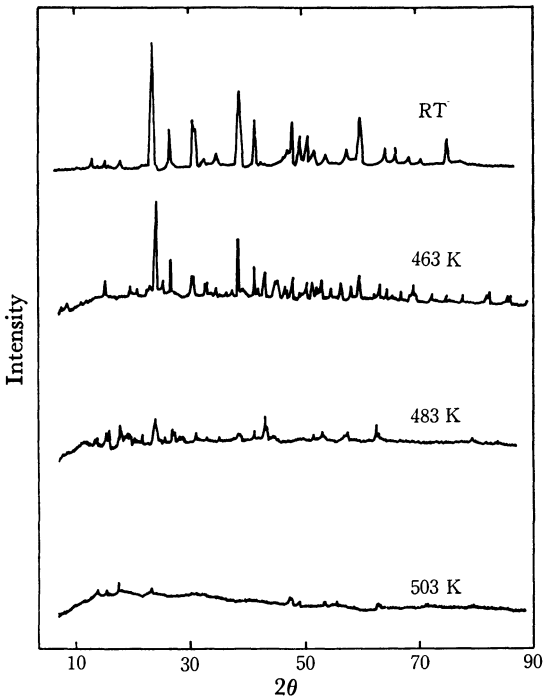

Fig. 5. X-Ray diffraction patterns of manganese malonate dihydrate and its dehydration products heated at various temperatures.

H_2O (ΔH_w), the net increases of enthalpy caused by dehydration may be 10—30 KJ mol^{-1} if ΔH_w is assumed to be in the vicinity of the heat of sublimation of ice (52 KJ mol^{-1}).

With a few exceptions, the ΔH of the malonates tends to increase with the increase of E_a, as shown in many elimination reactions. There are also remarkable differences in ΔH between the malonates and the oxalates.[18] The value for a malonate is always 10—20 KJ mol^{-1} larger than that for the corresponding oxalate. Since the values of T_i, which is seemingly a measure of the bond strengths of M–OH_2, are not so much different between the malonates and the oxalates, the differences in ΔH may be due to other factors. Other differences between these two carboxylates observed during dehydration are as follows: (1) all of the anhydrous malonates give broad infrared absorption bands, whereas anhydrous oxalates (as well as all the hydrates) give narrow bands; (2) the anhydrous malonates are poorer than the anhydrous oxalates in their crystallinity; (3) in the case of colored salts, the dehydration of the malonates are accompanied with more drastic color changes than that of the oxalates (*cf.* Table 4). These observations suggest that, compared with the anhydrous oxalates, the anhydrous malonates are composed of networks of more loosely linked polymers with higher potential energy.

Table 4. Color and spectral changes accompanying dehydration of malonate and oxalate dihydrates

Compound	Color	$\tilde{\nu}_{max}/cm^{-1}$
$Co(mal)\cdot 2H_2O$	pink→bluish violet	19400→17100
$Ni(mal)\cdot 2H_2O$	greenish blue→yellow	25400→23500
$Co(ox)\cdot 2H_2O$	pink→reddish violet	19200—20400→19900
$Ni(ox)\cdot 2H_2O$	blue→yellowish green	27100→25700

References

1) J. P. Lagier, H. Pezernat, and J. Dubernat, *Rev. Chim. Miner.*, **6**, 1081 (1968).
2) B. H. O'Conner and E. N. Maslen, *Acta Crystallogr.*, **20**, 824 (1966).
3) a) P. Sharrock and T. Theophanides, *Can. J. Chem.*, **53**, 98 (1975). b) K. Nagase, H. Yokobayashi, K. Muraishi, and K. Sone, This Bulletin, **48**, 1612 (1975); the structural remarks in this paper must be taken with reserve, because they are based chiefly on the earier view of Kuroda and Kubo (*J. Phys. Chem.*, **64**, 759 (1960)) on the structure of copper succinate, overlooking the X-ray work[2] of O'Conner and Maslen. The experimental findings described in this paper will, however, retain their own interest. The data on Co(II) salt coincide, in the main, with those of Sharrock and Theophanides[3a] published very shortly before it, although their structural view is somewhat different.
4) B. S. Azikov and V. V. Serebrennikov, *Zhur. Neorg. Khim.*, **12**, 445 (1967).
5) B. S. Azikov and V. V. Serebrennikov, *Tr. Tomsk. Gos. Univ. Ser. Khim.*, **185**, 118 (1965), *Chem. Abstr.*, **66**: 43327s (1965).
6) J. A. Herrero, J. Bermudez, and R. E. Gutierrez, *Quim. Ind.*, **18**, 15 (1972); *Chem. Abstr.*, **78**: 37301k (1972).
7) S. Shishido and K. Ogasawara, *Sci. Rep. Niigata Univ. Ser. C*, (3) 23 (1971).
8) A. Kwiatkowsky, J. Prezedmojsky, and B. Pura, *Mat. Res. Bull.*, **4**, 765 (1969).
9) K. A. Jones, R. J. Acheson, B. R. Wheeler, and A. K. Galway, *Trans. Faraday Soc.*, **64**, 1887 (1968). L. V. My, G. Perinet, F. Boubli, and R. Lafont, *C. R. Acad. Sci. Paris. Ser. C*, **271**, 69 (1970).
10) A. K. Galway, D. M. Jamieson, M. L. Van, and C. Berro, *Thermochim. Acta*, **10**, 161 (1974).
11) J. Ploquin, *Bull. Soc. Chim. Fr.*, **1951**, 757. F. Charbonnier, *Thermochim. Acta*, **10**, 269 (1974).
12) K. Nagase and H. Yokobayashi, This Bulletin, **47**, 2036 (1974).
13) E. S. Freeman and B. Carroll, *J. Phys. Chem.*, **62**, 394 (1958).
14) A. W. Coats and J. P. Redfern, *Nature*, **201**, 68 (1964).
15) M. L. Walter-Levy, J. Perrotey, and J. W. Visser, *Bull. Soc. Chim. Fr.*, **1973**, 2596.
16) M. J. Schmelz, I. Nakagawa, S. Mizushima, and J. W. Quaglino, *J. Amer. Chem. Soc.*, **81**, 287 (1959).
17) The fact that the Co^{2+} ion in anhydrous $CoC_3H_2O_4$ is 6-coordinated is, however, not quite certain, because bis(dipivaloylmethanato)cobalt(II), which is a tetrahedral CoO_4 type chelate, is known to show visible and near infrared spectra which are quite similar to those of the common octahedral chelates, although the band intensities in the former are considerably higher (F. A. Cotton, R. H. Soderberg, *Inorg. Chem.*, **3**, 1 (1964)). The same remarlk may be applicable to the spectrum of $K_2[Co(C_2O_4)_2]$ (K. Nagase, K. Sato, N. Tanaka, This Bulletin, **48**, 868 (1975)).
18) K. Nagase, K. Sato, and N. Tanaka, This Bulletin, **48**, 439 (1975).

Adducts of Bis(hexafluoroacetylacetonato)metal(II) with Uni- and Bidentate Nitrogenous Bases

Fujio IZUMI,* Ryoko KUROSAWA, Hiroshi KAWAMOTO, and Hideo AKAIWA

**National Institute for Researches in Inorganic Materials, Sakura-mura, Niihari-gun, Ibaraki-ken 300-31*
Department of Chemistry, Faculty of Technology, Gunma University, Tenjin-cho, Kiryu-shi, Gunma-ken 376

(Received July 31, 1975)

Base adducts of the types: $M(hfa)_2(py)_2$, $M(hfa)_2phen$, and $M(hfa)_2bpy$ [M=Co(II), Ni(II), Cu(II), and Zn(II); Hhfa=hexafluoroacetylacetone; py=pyridine; phen=1,10-phenanthroline; bpy=2,2'-bipyridine] were prepared, and their infrared spectra were examined in detail. These adducts have a *cis*-octahedral configuration except for $Ni(hfa)_2(py)_2$. The metal-oxygen stretching frequencies of the adducts in the 405—370 cm^{-1} region decrease along the series: nickel(II)>cobalt(II)>copper(II)>zinc(II). Adduct formation leads to the marked weakening of Cu–O bonds in the copper(II) adducts, which is ascribable to the equatorial ligation of the neutral bases. The mass spectral studies of $M(hfa)_2phen$ and $M(hfa)_2bpy$ revealed that the addition of a neutral ligand affects the fragmentation of the complex remarkably. The exceptional behavior of $Cu(hfa)_2phen$ under electron impact is explained in terms of the tendency of copper(II) ion to undergo valency change.

Bis(β-diketonato)metal(II) complexes behave as Lewis acids and form five- or six-coordinate adducts with neutral donor molecules.[1] The stability of an adduct depends both on the basicity of a β-diketonate and on that of a neutral ligand. Introduction of an electron-withdrawing group such as CF_3- into β-diketone increases the affinity of a central metal ion for ligation.[2-6] For example, bis(trifluoroacetylacetonato)copper (II) and bis(hexafluoroacetylacetonato)copper(II) form isolable 1:2 adducts with pyridine,[2,5,7] whereas bis(acetylacetonato)copper(II) forms only an unstable 1:1 adduct that loses pyridine on exposure to air.[8] It is also known that the more basic a neutral ligand is, the more stable the resulting adduct tends to be.[9]

Most of the studies on base adducts have been concerned with the coordinatively saturated 1:2 ones containing unidentate ligands such as pyridine and its derivatives,[1] pyridine *N*-oxide,[10] aniline and its derivatives.[11] Single crystal X-ray studies revealed that these adducts are of *cis*- or *trans*-octahedral configuration. Bidentate neutral ligands also add to metal(II) β-diketonates to form *cis*-octahedral 1:1 adducts more stable than those of unidentate donors owing to the chelate effect.[12-14] Even bis(acetylacetonato)copper(II) was found to form a six-coordinate adduct with ethylenediamine, which is stable under dry conditions.[14] However, only copper(II) complexes have been referred to in these reports, and the structures as well as the properties of the adducts of other metal(II) β-diketonates should be investigated in some detail.

The present paper describes the mixed ligand complexes of the types: $M(hfa)_2(py)_2$, $M(hfa)_2phen$,[15] and $M(hfa)_2bpy$, where M=Co(II), Ni(II), Cu(II), and Zn(II); Hhfa=hexafluoroacetylacetone; py=pyridine; phen=1,10-phenanthroline; bpy=2,2'-bipyridine. The phen and bpy adducts are expected to be most stable because of both the presence of CF_3- groups and the chelate effect by the bidentate neutral ligands. Infrared spectroscopy was mainly used for estimation of the structures and the strength of metal-ligand bonds. Thus far few reports have been published on the infrared spectra of base adducts, while those of metal β-diketonate complexes have been studied extensively. The mass spectra of the phen and bpy adducts were also investigated in order to obtain information on the stabilities of the adducts against electron impact.

Experimental

Preparation of Complexes. $M(hfa)_2$[16]: A KOH solution was neutralized with Hhfa. This solution was mixed with a metal(II) acetate solution in a 2:1 molar ratio. The precipitate immediately formed was filtered, dried over P_2O_5, and recrystallized from methanol. $M(hfa)_2(py)_2$: $M(hfa)_2$ was dissolved in hot neat pyridine, and crystals formed on slow cooling were filtered and dried carefully. $M(hfa)_2phen$ and $M(hfa)_2bpy$: Methanol solutions of $M(hfa)_2$ and each nitrogenous base were mixed in a 1:1 molar ratio. After standing overnight, crystallized adduct was filtered and dried over P_2O_5. The analytical data for isolated complexes are given in Table 1.

Table 1. Analytical data for the isolated adducts

Compound	C(%)		H(%)		N(%)	
	Calcd	Found	Calcd	Found	Calcd	Found
$Co(hfa)_2(py)_2$	38.06	38.46	1.92	2.11	4.44	5.00
$Ni(hfa)_2(py)_2$	38.06	39.47	1.92	1.87	4.44	4.14
$Cu(hfa)_2(py)_2$	37.78	37.72	1.90	1.88	4.41	4.40
$Zn(hfa)_2(py)_2$	37.67	38.52	1.90	2.16	4.39	4.98
$Co(hfa)_2phen$	40.46	41.00	1.54	1.60	4.29	4.49
$Ni(hfa)_2phen$	40.46	41.56	1.54	1.66	4.29	4.63
$Cu(hfa)_2phen$	40.17	40.21	1.53	1.56	4.26	4.42
$Zn(hfa)_2phen$	40.06	41.37	1.53	1.64	4.25	4.65
$Co(hfa)_2bpy$	38.18	38.62	1.61	1.68	4.45	4.57
$Ni(hfa)_2bpy$	38.19	38.46	1.61	1.64	4.45	4.65
$Cu(hfa)_2bpy$	37.90	37.78	1.59	1.60	4.42	4.45
$Zn(hfa)_2bpy$	37.73	37.55	1.59	1.58	4.40	4.42

Apparatus and Measurements. Infrared spectra were measured using a Hitachi EPI-G3 (4000—700 cm^{-1}) and a Nippon Bunko IR-F (700—200 cm^{-1}) infrared spectrophotometer. Samples were in the form of Nujol mulls between sodium chloride (4000—700 cm^{-1}) or KRS-5 (700—200 cm^{-1}) plates. X-Ray powder diffraction patterns were obtained using a Rigaku Denki 4051-5055 X-ray diffractometer with Cu$K\alpha$ radiation. Mass spectra were obtained on a Nihon Denshi JMS-07 mass spectrometer under the following conditions: ion source temperature 300 °C, ionization voltage 30 V, ion accelerating voltage 3 kV, ionization current 300 μA.

Results and Discussion

The infrared spectra of the adducts exhibited no band due to free carbonyl group or free nitrogenous base, which shows these complexes to be six-coordinate. Of course, the only reasonable structure for the phen or bpy adduct is *cis*-octahedral one, whereas either *cis* or *trans* isomer may be present in the case of the pyridine adduct.

Strong absorption bands due to the C–O stretching modes[1] were observedaround 1650 cm^{-1}. Published works have often referred to C–O stretching vibrations for the purpose of obtaining indirect information on the metal–oxygen bonds. However, it seems to us that no clear correlation exists between the perturbed C–O stretching vibration and the strength of M–O bond.[18,19]

Table 2. Metal-sensitive bands of $M(hfa)_2(py)_2$, $M(hfa)_2$phen, and $M(hfa)_2$bpy (cm^{-1})

$Co(hfa)_2(py)_2$	$Ni(hfa)_2(py)_2$	$Cu(hfa)_2(py)_2$	$Zn(hfa)_2(py)_2$	Assignment
667 s	673 s	667 s	665 s	$\nu(M-O)_1$
635m	636m	648 sh	637m	py (6a)
585 s	588 s	583 s,br	584 s	$\nu(M-O)_2$
428m, 422 sh	436m	443m, 434m	426m, 419.5 sh	py (16b)
384w	404w	376m	372.5m	$\nu(M-O)_3$
341w	345w	333w	340w	$\nu(M-O)_4$
315m	326m	314.5m	311m	$\nu(M-O)_5$
255 sh	250 m,br	264m	255w	
236.5m		240 sh	211m	
$Co(hfa)_2$ phen	$Ni(hfa)_2$ phen	$Cu(hfa)_2$ phen	$Zn(hfa)_2$ phen	Assignment
667.5 s	670 s	665 s	663 s	$\nu(M-O)_1$
646w	648 sh	652 sh	647 sh	phen
585 s	586 s,br	585 s, 578 sh	583 s,br	$\nu(M-O)_2$
427m	429m	433.5m	427m	phen
387w	393m	379w	374w	$\nu(M-O)_3$
343w	346.5w	337w	342.5w	$\nu(M-O)_4$
314w	317m	a	308w	$\nu(M-O)_5$
291m	298m	308m	290m	phen
252m	258 m,br	265 m,br	252w	
240 sh	244 sh,br	235w	240w	
$Co(hfa)_2$ bpy	$Ni(hfa)_2$ bpy	$Cu(hfa)_2$ bpy	$Zn(hfa)_2$ bpy	Assignment
665 s	669.5 s	665 s	664 s	$\nu(M-O)_1$
637w	640w	643w	636w	bpy
585 s	587 s	587 s, 579 sh	584.5 s	$\nu(M-O)_2$
413m	415m	416m	412m	bpy
385w	392.5w	380w	372.5w	$\nu(M-O)_3$
343w	347w	337w	343w	$\nu(M-O)_4$
316.5w	319.5w	312w	313w	$\nu(M-O)_5$
278m	289m	294.5m		
250w	259m	261w	250m	

a) Overlapped by the neighboring band.

Table 2 summarizes the metal-sensitive bands of the adducts in the far-infrared region. Above 700 cm^{-1}, almost all the bands observed are associated with vibrational modes of the ligands. The spectra in this region are very similar, and each band exhibited almost no sensitivity to a metal. Therefore, no further effort was devoted to examining the spectra above 700 cm^{-1}.

The pyridine ring vibrations located at 405 cm^{-1} (vibration 16b, out-of-plane ring deformation) and at 604 cm^{-1} (vibration 6a, in-plane ring deformation) in free pyridine are known to suffer marked shifts toward higher frequencies upon coordination to a metal.[20] In the pyridine adducts, the frequencies of the above bands showed the following order: cobalt(II)<nickel(II)<copper(II)>zinc(II). This is the same order as that reported in the literatures,[21,22] in which it is suggested that in a series of isostructural complexes, the frequencies of these two bands increase with a decrease in ionic radius of a metal. This conclusion is doubtful because the effective ionic radii of six-coordinate cobalt(II), nickel(II), copper(II), and zinc(II) ions are reported to be 0.73, 0.77, 0.81, and 0.83 Å, respectively.[23] Doublings of the 405 cm^{-1} band took place except for the case of the nickel(II) adduct, which is ascribed to the result of some interaction between different pyridine molecules.[22]

The assignments of phen and bpy vibrations in Table 2 are based on the work of Huchinson *et al.*[24] It is worth noting that the observed frequencies of the bidentate ligands vibrations showed the same order with the case of the pyridine ones. The frequencies of these vibrations may be reflection of some factors such as metal–nitrogen bond length, the strength of back-bonding, the polarizing power of metal ion.[21]

Metal-oxygen (M–O) stretching bands were assigned on the basis of the metal ion substitution technique applied extensively by Thornton *et al.*[25–27] It is generally recognized that in a series of isostructural complexes, substitution of a metal ion by another leads to a remarkable shift in a metal-ligand stretching frequency. The infrared spectra of the adducts showed five metal-sensitive bands in common in the 700—300 cm^{-1} region. These bands are considered to contain M–O stretching character to a varying degree bacause of the strong coupling between various vibrational modes. The bands observed at 405—370 cm^{-1} can be assigned to the least-coupled M–O stretching modes because they exhibit the maximum sensitivity to the metal ions. Since the transition metal(II) ions in the present study have similar masses, the variation in M–O stretching frequency may be considered to reflect the variation in the force constant of the M–O bond to a first approximation.

The M–O stretching frequencies of the adducts were found to decrease as follows: nickel(II)>cobalt(II)>copper(II)>zinc(II), which is inconsistent with the so-called Irving-Williams stability order: cobalt(II)<nickel(II)<copper(II)>zinc(II). The M–O stretching frequencies of metal(II) β-diketonates have been shown to follow this natural rule.[25,28] Hancock and Thornton[17] assigned the band at 427 cm^{-1} of $Cu(hfa)_2 \cdot H_2O$ to the copper-oxygen (Cu–O) stretching vibration, and the present study shows that M–O stretching frequencies of $Ni(hfa)_2$ and $Zn(hfa)_2$ are 404 and 385 cm^{-1}, respectively.

The above results revealed that adduct formation

causes a low-frequency shift of the M–O stretching band except for the case of $Ni(hfa)_2(py)_2$. The magnitudes of shifts were 11—13 cm^{-1} for nickel(II), zinc(II) complexes and about 50 cm^{-1} for copper(II), respectively. The shifts in the cobalt(II) complexes would be as large as those in the nickel(II) and zinc(II) complexes.[29]

These shifts can generally be explained in terms of the electrostatic repulsion between a neutral base and hfa. Anhydrous $M(hfa)_2$ are estimated to have a polynuclear octahedral geometry [M=Co(II), Ni(II), and Zn(II)] like acetylacetonate analogues of these metals.[1] A considerable "crowding" of donor ligands exists in the six-coordinate complex of a first-row transition metal(II). Thus, the coordination of more basic nitrogenous base in place of bridging oxygen atoms leads to the increased repulsion toward hfa, with the result that M–O distances are slightly lengthened. This interaction may be assumed to be caused by induced charges through the d orbital of the metal(II) ion.[7] Similar low-frequency shifts have been reported for bis-(nitrogenous base) adducts of nickel(II) acetylacetonate[11] and metal(II) thenoyltrifluoroacetonates.[29] The Lewis acidity of a metal(II) β-diketonate is enhanced by the introduction of an electron-withdrawing substituent to the β-diketone ligand. This fact may be ascribable to the reduction in the repulsion described above owing to a decrease in the electron density around the central metal(II) ion.

In the case of the copper(II) complexes, exceptionally large shifts of about 50 cm^{-1} were observed, which cannot be ascribed only to the repulsion effect. There are two possible interpretations for these results. One is that the coordination number of copper(II) changes from five in $Cu(hfa)_2 \cdot H_2O$ to six in the adducts. Increased coordination number generally causes a considerable low-frequency shift of metal-ligand stretching bands.[26] However, the shift as much as 50 cm^{-1} seems to be too large even if the change in coordination number is taken into consideration.

A more plausible explanation can be offered by considering a structure that has Jahn-Teller distortion arising from the d^9 electron configuration of copper(II) ion.[29] The *cis*-equatorial structure of $Cu(hfa)_2(py)_2$ and $Cu(hfa)_2$bpy has been established by single crystal X-ray studies.[7,12] In view of the fact that the Cu–O stretching bands of the three copper(II) adducts appeared at approximately the same frequency, $Cu(hfa)_2$-phen is thought to have a *cis*-equatorial structure as well (Fig. 1). The coordinating ability of phen is evidently higher than that of hfa which is the least basic in a series of β-diketonate ions.[30] The significant back-donation as well as the chelate effect will stabilize the bonds between copper(II) and phen. It is, therefore, reasonable to conclude that phen occupies the equatorial sites, forming a most stable chelate ring with copper(II) ion.

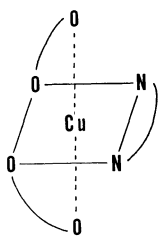

Fig. 1. The estimated structure of $Cu(hfa)_2$phen.

In each copper(II) adduct, one oxygen atom in hfa occupies the equatorial position. On the other hand, the other oxygen coordinates along the axial direction, which results in a longer and weaker Cu–O bond than the former. The observed Cu–O stretching bands of the adducts are considered to exhibit a character intermediate between the long and the short Cu–O bonds because of the vibrational coupling.[31] Consequently, the Cu–O stretching band of the copper(II) adduct appears at much lower frequency than that of $Cu(hfa)_2 \cdot H_2O$ in which the four equatorial sites are estimated to be occupied by hfa.

It should be noted that the nickel-oxygen (Ni–O) stretching band of $Ni(hfa)_2(py)_2$ showed a negligible low-frequency shift on adduct formation. This fact seems to exclude the possibility of $Ni(hfa)_2(py)_2$ having the *cis* arrangement of pyridine molecules because the Ni–O steretching bands of $Ni(hfa)_2$phen and $Ni(hfa)_2$-bpy, for which only a *cis*-octahedral structure is assumed. shifted toward the lower frequencies to the same extent as the other phen and bpy adducts. Single crystal X-ray studies[7] revealed that bis pyridine adducts of $Cu(hfa)_2$ and $Zn(hfa)_2$ are of *cis*-octahedral geometry, $Cu(hfa)_2(py)_2$: monoclinic, $P2_1/c$; $Zn(hfa)_2(py)_2$: monoclinic, C2/c. Figure 2 gives the X-ray powder patterns of the pyridine adducts. Since $Co(hfa)_2(py)_2$ was isomorphous with $Zn(hfa)_2(py)_2$, a *cis* structure is also implied. On the other hand, $Ni(hfa)_2(py)_2$ did not show any feature of isomorphism with the *cis* $Cu(hfa)_2$-$(py)_2$ and $Zn(hfa)_2(py)_2$ species. As Horrocks *et al.* suggested,[32] there is little energy difference between *cis* and *trans* forms of such adducts, and a *trans* isomer may well be present in the crystalline state. However,

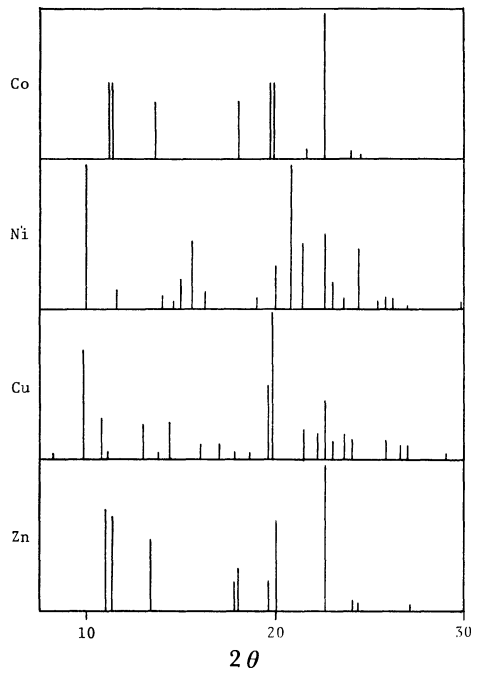

Fig. 2. X-ray powder patterns of $M(hfa)_2(py)_2$.

it is impossible at present to make a conclusive decision regarding a *trans* arrangement in $Ni(hfa)_2(py)_2$.

It has been established that the increased donor capacity of a nitrogenous base for a metal ion leads to a reduction in M–O stretching frequency.[11,29] However, the pyridine, phen, and bpy complexes showed no marked difference in M–O stretching frequencies. Incorporation of strongly electron-withdrawing CF_3-groups into β-diketone must result in weaker and longer M–O bonds. Thus, the interaction between hfa and a neutral ligand may be relatively weak, and the strength of M–O bonds is hardly affected by slight differences in the basicities of the three nitrogenous bases[33] (pK_a: py 5.22, phen 4.86, bpy 4.35).

The metal–nitrogen (M–N) stretching vibrations are expected to lie below 300 cm^{-1}. However, the assignment of metal pyridine stretching band has been subject to some confusion. In the infrared spectrum of $Ni(acac)_2(py)_2$ (Hacac=acetylacetone), the 249 cm^{-1} band was assigned to the nickel-nitrogen (Ni–N) stretching mode by Nakamoto *et al.*,[34] whereas Haigh *et al.*[11] indicated the absence of any band due to Ni–N stretching mode in the region above 200 cm^{-1}. To our knowledge, no reports have been published on the assignment of the M–N stretching vibration of six-coordinate mono phen or bpy complex. Therefore, we did not make any effort to assign the M–N stretching bands of the adducts although a few netal-sensitive bands were observed between 300 and 200 cm^{-1}.

The mass spectrometry of $M(hfa)_2$phen and $M(hfa)_2$bpy was investigated in order to examine the fragmentation of the adducts under electron impact. Though the mass spectra of metal β-diketonates have been studied extensively,[35–37] those of base adducts are still unknown. Table 3 lists the relative intensities of the main fragment peaks. The spectra in the *m/e* region greater than 500 where parent peaks might appear could not be measured because of the limitation of the apparatus used.

Table 3. Relative intensities of metal-containing ions in the mass spectra of $M(hfa)_2$phen and $M(hfa)_2$bpy L: hfa, B: phen or bpy

Ion	$M(hfa)_2$phen				$M(hfa)_2$bpy		
	Co	^{58}Ni	^{63}Cu	^{64}Zn	Co	^{58}Ni	^{64}Zn
LMB^+	100	100	100	100	100	100	74
$(L_2M-CF_3)^+$			37	45	8		100
$(L_2M-2CF_3)^+$			15				
$F\text{-}MB^+$	34	50		45	38	21	22
MB^+			78				
$(LM-CF_3)^+$			77				

The previous study[38] on the thermal stability of the synergistic adducts of copper(II) β-diketonates has demonstrated that a unidentate pyridine base is readily released during thermal decomposition process. The thermal stability of phen or bpy adduct is expected to be enhanced far more exceedingly than that of pyridine adduct because of the chelate effect. In fact, no thermal decomposition of the adducts was observed during the mass spectral measurement except for the case of $Cu(hfa)_2$bpy.

It became evident that $Cu(hfa)_2$bpy decomposed into $Cu(hfa)_2$ and bpy prior to electron impact since the mass spectrum of $Cu(hfa)_2$bpy corresponded to just a superposition of that of $Cu(hfa)_2$ and bpy. The observed difference in the thermal stability between $Cu(hfa)_2$phen and $Cu(hfa)_2$bpy is mainly ascribable to the decreased rigidity of bpy molecule in comparison with that of phen. As the result of the above reaction, bpy molecule comes to rotate freely around the C–C bond between the two aromatic rings, which contributes positively to the entropy term of the free energy change in the decomposition reaction. A more reduced d_π–p_π interaction in the adduct of bpy having a shorter conjugated system may also play an important part.

(a) $M(hfa)_2$phen (M=Co and Ni) and $Ni(hfa)_2$bpy

$$L_2MB^+ \xrightarrow{-L} LMB^+ \xrightarrow{-188} F\text{-}MB^+$$

(b) $Cu(hfa)_2$phen

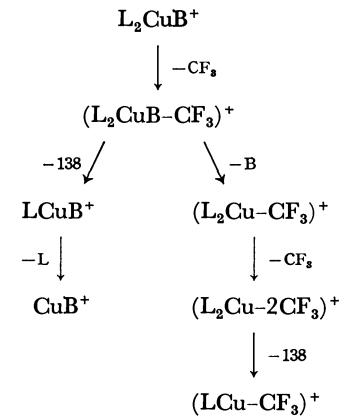

(c) $Zn(hfa)_2$phen and $M(hfa)_2$bpy (M=Co and Zn)

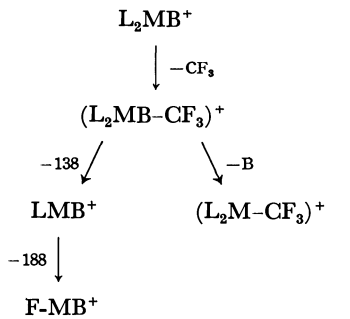

Chart 1. Mass fragmentations of $M(hfa)_2$phen and $M(hfa)_2$bpy.
L: hfa, B: phen or bpy

The fragmentation sequences assumed with regard to metalcontaining ions are shown in Chart 1. The fragmentation of L_2MB^+ to LMB^+ may occur *via* initial loss of CF_3 and subsequent loss of $CF_3COCHCO$ (mass 138). The nitrogenous beses in the group (a) adducts are bound more firmly to metal ions than those belonging to groups (b) and (c). In the latter complexes, the fragment ions containing no nitrogenous base, $(L_2M-CF_3)^+$ were detected. It is reported that

elimination of CF_2 occurs with migration of a fluorine atom to the metal in $Zn(hfa)_2$ and $Al(hfa)_3$.[36] The whole residual ligand $CF_3COCHCOCF_2$ (mass 188) was lost in the corresponding process of the phen and bpy adducts.

After loss of one hfa radical, $Cu(hfa)phen^+$ undergoes quite a unique fragmentation, *i.e.*, $Cu(hfa)phen^+ \longrightarrow Cu\text{-}phen^+ + \cdot hfa$. It is interesting to note that $Cu\text{-}phen^+$ formally involves Cu(I). Of the present four metals, only copper is relatively stable in the univalent state. A decrease in valency of a metal generally leads to increased covalent character of the metal-ligand bonds.[36] Thus, the copper-nitrogen bonds in $Cu\text{-}phen^+$ are fairly stabilized through the strong copper(I)-to-ligand back-donation.

References

1) D. P. Graddon, *Coord. Chem. Rev.*, **4**, 1 (1969).
2) R. D. Gillard and G. Wilkinson, *J. Chem. Soc.*, **1963**, 5885.
3) W. R. Walker and N. C. Li, *J. Inorg. Nucl. Chem.*, **27**, 2255 (1965).
4) N. C. Li, S. M. Wang, and W. R. Walker, *ibid.*, **27**, 2263 (1965).
5) L. L. Funck and T. R. Ortolano, *Inorg. Chem.*, **7**, 567 (1968).
6) W. Partenheimer and R. S. Drago, *ibid.*, **9**, 47 (1970).
7) J. Pradilla-Sorzano and J. P. Fackler, Jr., *ibid.*, **12**, 1174 (1973).
8) D. P. Graddon and E. C. Watton, *J. Inorg. Nucl. Chem.*, **21**, 49 (1961).
9) Y. Marcus and A. S. Kertes, "Ion Exchange and Solvent Extraction of Metal Complexes," Wiley-Interscience, New York, N. Y. (1969), p. 815.
10) W. D. Horrocks, Jr., D. H. Templeton, and A. Zalkin, *Inorg. Chem.*, **7**, 1552 (1968).
11) J. M. Haigh, N. P. Slabbert, and D. A. Thornton, *J. Mol. Struct.*, **7**, 199 (1971).
12) M. V. Veidis, G. H. Schreiber, T. E. Gough, and G. J. Palenik, *J. Amer. Chem. Soc.*, **91**, 1859 (1969).
13) D. E. Fenton, R. S. Nyholm, and M. R. Truter, *J. Chem. Soc., A*, **1971**, 1577.
14) T. Kurauchi, M. Matsui, Y. Nakamura, S. Ooi, S. Kawaguchi, and H. Kuroya, This Bulletin, **47**, 3049 (1974).
15) Preliminary communication was presented in F. Izumi, R. Kurosawa, H. Kawamoto, and H. Akaiwa, *Chem. Lett.*, **1975**, 379.
16) M. L. Morris, R. W. Moshier, and R. E. Sievers, *Inorg. Chem.*, **2**, 411 (1963).
17) R. D. Hancock and D. A. Thornton, *J. Mol. Struct.*, **4**, 377 (1969).
18) L. J. Bellamy and R. F. Branch, *J. Chem. Soc.*, **1954**, 4491.
19) B. Rao and H. B. Mathur, *J. Inorg. Nucl. Chem.*, **33**, 2919 (1971).
20) K. Nakamoto, "Infrared Spectra of Inorganic and Coordination Compounds," Wiley-Interscience, New York, N. Y. (1970), p. 212.
21) N. S. Gill, R. H. Nuttal, D. E. Scaife, and P. W. A. Sharp, *J. Inorg. Nucl. Chem.*, **18**, 79 (1961).
22) R. J. H. Clark and C. S. Williams, *Inorg. Chem.*, **4**, 350 (1969).
23) E. J. W. Whittaker and R. Muntus, *Geochim. Cosmochim. Acta*, **34**, 945 (1970).
24) B. Hutchinson, J. Takemoto, and K. Nakamoto, *J. Amer. Chem. Soc.*, **92**, 3335 (1970).
25) G. S. Shephard and D. A. Thornton, *Helv. Chim. Acta*, **54**, 2212 (1971).
26) G. C. Percy and D. A. Thornton, *J. Inorg. Nucl. Chem.*, **35**, 2719 (1973).
27) C. A. Fleming and D. A. Thornton, *J. Mol. Struct.*, **17**, **79**. (1973).
28) R. D. Hancock and D. A. Thornton, *J. South African Chem. Inst.*, **23**, 71 (1970).
29) H. Akaiwa, H. Kawamoto, and F. Izumi, *J. Inorg. Nucl. Chem.*, **37**, 65 (1975).
30) L. G. Van Uitert, W. C. Fernelius, and B. E. Douglas, *J. Amer. Chem. Soc.*, **75**, 457 (1953).
31) M. Mikami, I. Nakagawa, and T. Shimanouchi, *Spectrochim. Acta*, **23A**, 1037 (1967).
32) W. D. Horrocks, Jr., D. H. Templeton, and A. Zalkin, *Inorg. Chem.*, **7**, 1552 (1968).
33) A. A. Schilt, "Analytical Applications of 1,10-Phenanthroline and Related Compounds," Pergamon Press, London (1969), pp. 4, 6.
34) K. Nakamoto, C. Udovich, and J. Takemoto, *J. Amer. Chem. Soc.*, **92**, 3973 (1970).
35) S. Sasaki, Y. Itagaki, T. Kurokawa, and K. Nakanishi, This Bulletin, **40**, 76 (1967).
36) C. Reichert, J. B. Westmore, and H. D. Gesser, *Chem. Commun.*, **1967**, 782.
37) C. Reichert and J. B. Westmore, *Can. J. Chem.*, **48**, 3213 (1970).
38) H. Akaiwa, H. Kawamoto, and M. Abe, *J. Inorg. Nucl. Chem.*, **34**, 1763 (1972).
39) R. G. Pearson, *J. Chem. Educ.*, **45**, 581, 643 (1968).

An X-Ray Diffraction Study of the Structures of the Hexachloro- and Hexabromoplatinate(IV) Ions in Aqueous Solution

Masunobu MAEDA, Takeshi AKAISHI, and Hitoshi OHTAKI

Laboratory of Solution Chemistry, Tokyo Institute of Technology, O-okayama, Meguro, Tokyo 152

(Received August 6, 1975)

The structures of the $PtCl_6^{2-}$ and $PtBr_6^{2-}$ complexes in aqueous solution were determined by means of X-ray diffraction measurements of concentrated solutions of hexachloro- and hexabromoplatinic acids. Analysis of X-ray scattering data showed that the $PtCl_6^{2-}$ and $PtBr_6^{2-}$ complexes have a regular octahedral symmetry. The interatomic distances within the complexes are: Pt–Cl, 2.33 Å; *cis*-Cl–Cl, 3.30 Å; *trans*-Cl–Cl, 4.66 Å; Pt–Br, 2.47 Å; *cis*-Br–Br, 3.50 Å; *trans*-Br–Br, 4.94 Å. These distances are in good agreement with those reported in crystals of hexahalogenoplatinate(IV) compounds.

It is well known that platinum(IV) has a coordination number of six and forms stable hexahalogeno complexes with halide ions, which have an octahedral symmetry in the solid state.[1-3] Results from infrared and Raman spectroscopic measurements suggested that hexahalogenoplatinate(IV) complexes have a regular octahedral configuration in aqueous solutions.[4]

Vaughan *et al.*[5] carried out X-ray scattering measurements of solutions of hexachloro- and hexabromoplatinic acids, and they concluded that the observed data are in accord with the octahedral model of these complexes and that the platinum–halogen distances within the complexes are 2.39 Å for Pt–Cl and 2.43 Å for Pt–Br. The former is *ca.* 0.06 Å longer than that in crystals and the latter is shorter by 0.03 Å. Moreover, the peaks which corresponded to the *trans*–halogen–halogen distances were not seen in their radial distribution curves.

In a previous work,[6] we found that the $AuCl_4^-$ and $AuBr_4^-$ complexes have a square planar symmetry and the gold–halogen distances within the complexes are 2.29 Å for Au–Cl and 2.43 Å for Au–Br, which are very similar to those in crystals.

This paper describes X-ray scattering measurements on concentrated solutions of hexachloro- and hexabromoplatinic acids and compares the values of interatomic interactions within these complexes with the results reported by Vaughan *et al.* in aqueous solutions[5] and those in crystals.[1-3]

Experimental

Preparation and Analysis of Sample Solutions. Sample solutions of hexachloro- and hexabromoplatinic acids were prepared by dissolving metallic platinum of 99.99% purity in solutions of hydrochloric and hydrobromic acids, respectively, containing nitric acid and by removing the nitric acid by repeated evaporation with the corresponding hydrohalogenic acids.

The content of platinum in the sample solutions was determined gravimetrically both by reduction of platinum(IV) to metal with formic acid and by ignition of precipitates of ammonium hexahalogenoplatinate(IV) to platinum metal.[7] The results of analysis obtained by the two procedures agreed each other within the error of 0.2%. The chloride- and bromide-ion concentrations were determined gravimetrically as AgCl and AgBr, respectively, after reduction of the platinum(IV) with formic acid. The hydrogen-ion concentrations were calculated from the relation $[H^+]=[X^-]-4[Pt^{4+}]$.

The density of the solutions was determined with a pycnometer.

Table 1. Compositions of the solutions (in g-atom/l)

	Hexachloroplatinic acid solution	Hexabromoplatinic acid solution
Pt	2.882	2.739
Br	—	17.11
Cl	18.57	—
O	36.89	34.75
H	80.81	75.64

The compositions of the sample solutions are given in Table 1.

Measurements and Treatment of X-Ray Diffraction Intensities. X-Ray scattering measurements were carried out with an X-ray diffractometer (JEOL Co., Tokyo) in a room thermostated at 25±1 °C according to procedures described in previous papers.[8,9] Mo$K\alpha$ radiation ($\lambda=0.7107$ Å) was used for the irradiation of the sample solutions. The slit-openings were 1/12°, 1/4°, and 1° over the scattering angle ranges of 2° to 12°, 6° to 30°, and 12° to 140°, respectively. The scattered intensities were measured at discrete points between the scattering angle $2\theta=2°$ and 140°. The whole angle range was scanned twice in order to examine the reproducibility of the measured intensities. The intensities measured at the same angle usually agreed within 2%. The measured intensities $I(s)$, which were normalized to a common slit width, and then corrected for polarization in the solution and in the monochromator and scaled to electron units by means of the usual ways,[6,8,9] were used to calculate the reduced intensities $i(s)$ according to the following equation.

$$i(s) = I(s) - \sum_i n_i[(f_i(s)+\Delta f_i')^2 + (\Delta f_i'')^2 + \Phi(s)\cdot I_i^{\mathrm{inco}}(s)] \quad (1)$$

Here $s=4\pi\sin\theta/\lambda$, n_i represents the number of atom i, $f_i(s)$ the scattering factor of atom i at angle s, $\Delta f_i'$ and $\Delta f_i''$ the real and imaginary parts of the anomalous dispersion, respectively, $\Phi(s)$ the fraction of the incoherent radiation $I_i^{\mathrm{inco}}(s)$ reaching the counter.

All the calculations were referred to a stoichiometric volume of a solution containing one Pt atom.

The reduced intensities thus evaluated are shown in Fig. 1 in the form of $s\cdot i(s)$ *vs.* s.

The coherent and incoherent scattering factors for Pt were taken from Cromer and Waber[10] and from Cromer,[11] respectively. The values for anomalous dispersion of Pt were those given by Cromer and Lieberman,[12] which were corrected for the Breit-Dirac factors. The values for coherent, incoherent, and anomalous scatterings of other atoms were the same as those used in a previous paper.[6]

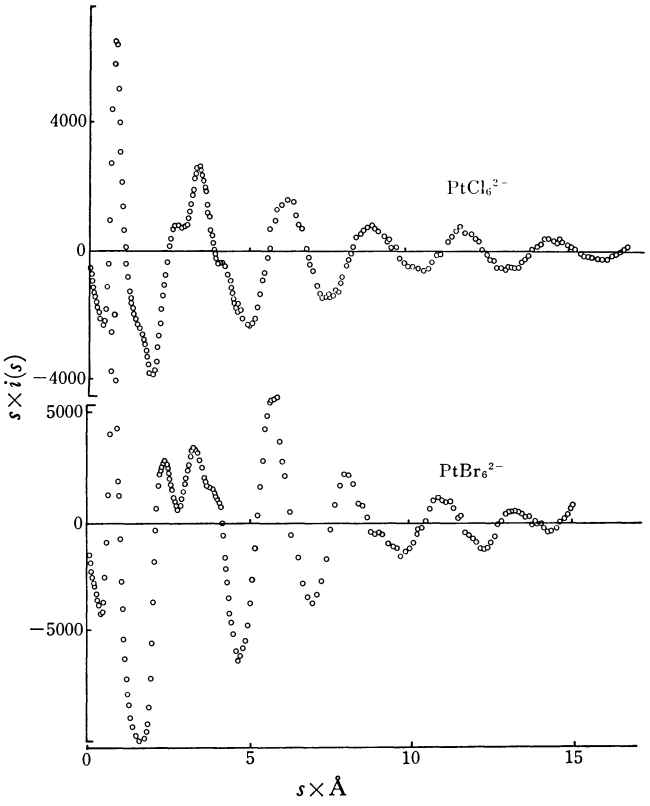

Fig. 1. Values $s\cdot i(s)$ for the chloride and bromide solutions as a function of s.

Results and Discussion

The radial distribution functions $D(r)$ were calculated from the reduced intensities $i(s)$ according to Eq. (2). The calculations were carried out with the aid of the computer program KURVLR.[13]

$$D(r) = 4\pi r^2\rho_0 + 2r\pi^{-1}\int_0^{s_{max}} s\cdot i(s)\cdot M(s)\cdot\sin(sr)ds \qquad (2)$$

Here ρ_0 denotes the average scattering density of the solution in electron units. The modification function $M(s)$ was chosen to be $(f_{Pt}^2(0)/f_{Pt}^2(s))\exp(-0.01\,s^2)$.

Spurious peaks below 1 Å in the distribution curves, which could not correspond to any interatomic distances, were used to correct the reduced intensities for low-frequency additions.

The radial distribution curves $D(r)$ for the two solutions thus calculated are shown in Fig. 2. Each distribution curve shows three peaks. The first dominant peak appeared at around 2.3 Å for the chloride solution and 2.5 Å for the bromide solution. These peaks can be identified as being due to Pt–Cl and Pt–Br distances within the complexes. The number of halide ions coordinated to a Pt(IV) ion was estimated to be about six both for the chloride and bromide solutions from the peak areas under the first peaks according to graphical procedures.[9] The second and third peaks appeared at around 3.3 Å ($\simeq$2.3 Å$\times\sqrt{2}$) and 4.6 Å ($\simeq$2.3 Å$\times$2) for the chloride solution, and at around 3.5 Å ($\simeq$2.5 Å$\times\sqrt{2}$) and 5 Å ($\simeq$2.5 Å$\times$2) for the bromide solution. These second and third peaks may be due to Cl–Cl and Br–Br contacts. The relation among the distances of

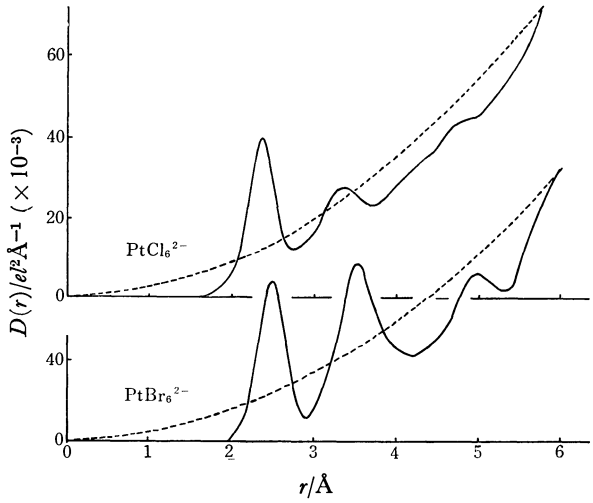

Fig. 2. Radial distribution curves for the chloride and bromide solutions. The brocken curves denote $4\pi r^2\rho_0$.

the three peaks in each $D(r)$ curve is that expected from a regular octahedral structure.

In order to refine the values for the structures of the complexes, analysis of the reduced intensity curve was carried out by means of a least squares method, in which a minimum was sought for the function $\sum s^2(i(s)-i_{calc}\cdot(s))^2$. Here, $i_{calc}(s)$ is the theoretical intensity due to interatomic interactions calculated from Eq. (3).

$$i_{calc}(s) = \sum_i\sum_j f_i(s)f_j(s)\frac{\sin(r_{ij}s)}{r_{ij}s}\exp(-b_{ij}s^2) \qquad (3)$$

where r_{ij} denotes the distance between two atoms i and j, $f_i(s)$ and $f_j(s)$ the scattering factor, and b_{ij} the temperature factor corresponding to the interaction between i and j atoms. For each interatomic interaction within the complexes the values of three parameters were refined: the distance r_{ij}, the temperature factor b_{ij}, and the frequency factor n_{ij}. For the refinement various subsets of the intensity data from different s ranges larger than 4 were used in order to detect errors in the refined parameters caused by a contribution to the intensity from the intermolecular interactions and experimental errors in the data. Two types of refinement (A and B) were carried out. In A type of refinement only the platinum–halogen bonds were included for $i_{calc}(s)$. The distance, the temperature factor, and the frequency factor were refined. In B type contacts for the platinum–halogen and the halogen–halogen at the *cis*-position were taken into account, and six parameters in all were changed simultaneously. The *trans*-halogen–halogen interactions were not included because of their small contributions to the intensities in the s ranges used for the calculations, as is seen from the theoretical intensities of interactions within the complexes in Fig. 3; the curves being calculated with the final parameter values in Table 3. Table 2 summarizes the results of the two types of refinement. As shown in Table 2 the number of the Pt–Cl and Pt–Br bonds per Pt atom does not differ from the value of 6 expected for the PtX_6^{2-} complex. The number of *cis*- Cl–Cl and Br–Br interactions (in B) was not definitely determined, but it is not so different from the expected value of 12 if the standard deviations are

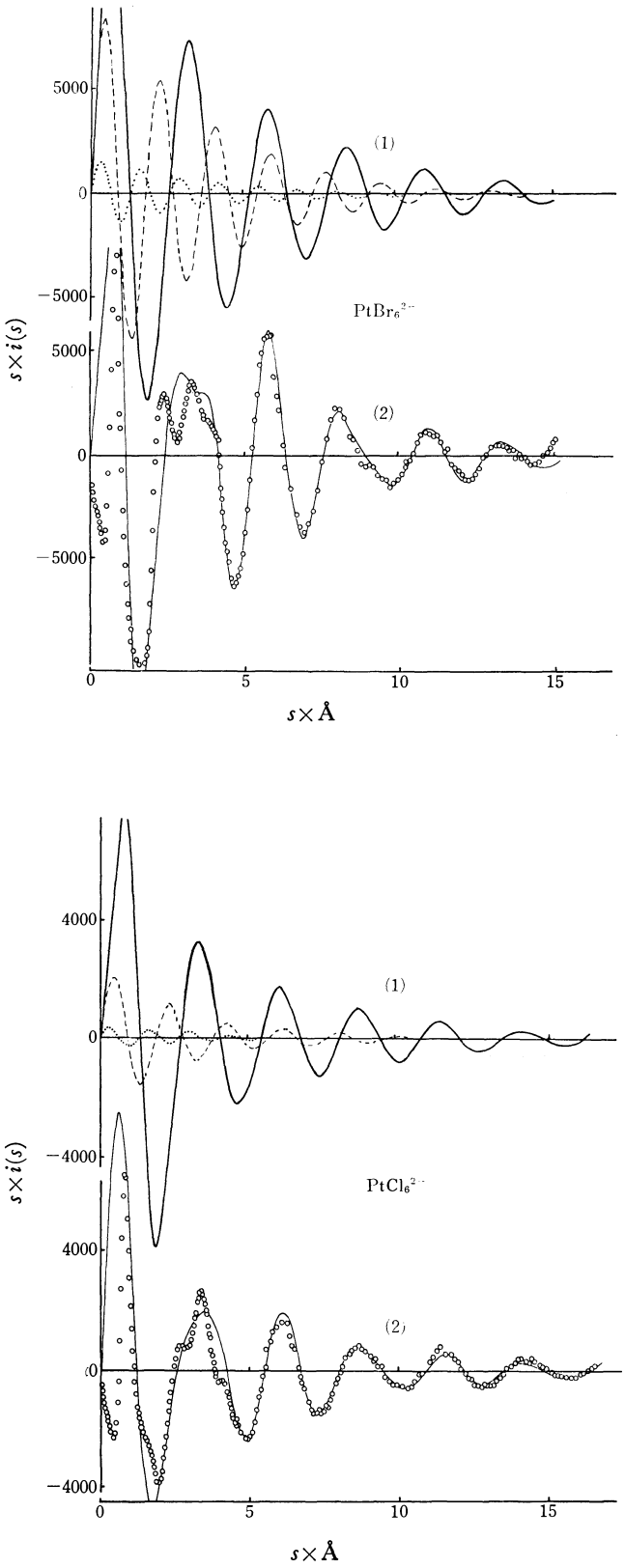

Fig. 3. Observed and calculated $s \cdot i(s)$ values for the chloride and bromide solutions.
(1) Calculated $s \cdot i(s)$ values for the interactions within the PtX_6^{2-} ions; Pt–X full drawn line, *cis*-X–X dashed line and *trans*-X–X dotted line.
(2) Comparison between observed $s \cdot i(s)$ values (circles) and calculated $s \cdot i(s)$ values (full line).

Table 2. Summary of the results of the least-squares refinements

	$PtCl_6^{2-}$	$PtBr_6^{2-}$
A	$r_{Pt-Cl}=2.332\,(5)$ Å	$r_{Pt-Br}=2.480\,(10)$ Å
	$b_{Pt-Cl}=0.0022\,(4)$ Å^2	$b_{Pt-Br}=0.0038\,(7)$ Å^2
	$n_{Pt-Cl}=6.0\,(4)$	$n_{Pt-Br}=6.1\,(4)$
B	$r_{Pt-Cl}=2.328\,(6)$ Å	$r_{Pt-Br}=2.474\,(7)$ Å
	$b_{Pt-Cl}=0.0015\,(4)$ Å^2	$b_{Pt-Br}=0.0033\,(5)$ Å^2
	$n_{Pt-Cl}=5.6\,(2)$	$n_{Pt-Br}=6.2\,(3)$
	$r_{cis\text{-}Cl\text{-}Cl}=3.30\,(4)$ Å	$r_{cis\text{-}Br\text{-}Br}=3.52\,(3)$ Å
	$b_{cis\text{-}Cl\text{-}Cl}=0.010\,(4)$ Å^2	$b_{cis\text{-}Br\text{-}Br}=0.0064\,(9)$ Å^2
	$n_{cis\text{-}Cl\text{-}Cl}=17\,(7)$	$n_{cis\text{-}Br\text{-}Br}=13\,(5)$

Numbers in the parentheses are least-squares standard deviations.

Table 3. Final parameter values for the hexachloro- and hexabromoplatinate (IV) ions

$PtCl_6^{2-}$	$PtBr_6^{2-}$
$r_{Pt-Cl}=2.33$ Å	$r_{Pt-Br}=2.47$ Å
$b_{Pt-Cl}=0.002$ Å^2	$b_{Ft-Br}=0.003$ Å^2
$n_{Pt-Cl}=6$	$n_{Pt-Br}=6$
$r_{cis\text{-}Cl\text{-}Cl}=3.30$ Å	$r_{cis\text{-}Br\text{-}Br}=3.49$ Å
$b_{cis\text{-}Cl\text{-}Cl}=0.010$ Å^2	$b_{cis\text{-}Br\text{-}Br}=0.006$ Å^2
$n_{cis\text{-}Cl\text{-}Cl}=12$	$n_{cis\text{-}Br\text{-}Br}=12$
$r_{trans\text{-}Cl\text{-}Cl}=4.66$ Å	$r_{trans\text{-}Br\text{-}Br}=4.94$ Å
$b_{trans\text{-}Cl\text{-}Cl}=0.015$ Å^2	$b_{trans\text{-}Br\text{-}Br}=0.015$ Å^2
$n_{trans\text{-}Cl\text{-}Cl}=3$	$n_{trans\text{-}Br\text{-}Br}=3$

taken into account. The ratio between the halogen–halogen and the platinum–halogen distances, which were refined independently in B, is about 1.42, which is close to the expected value of $\sqrt{2}$ for the regular octahedral configuration.

The final parameter values for the regular octahedral hexachloro- and hexabromoplatinate(IV) complexes are given in Table 3, in which the temperature factors for the halogen-halogen interactions at the *trans* position were roughly estimated from the corresponding peak shapes.

The intensities calculated by the use of the parameter values in Table 3 are compared with the observed ones in Fig. 3. It is seen that the agreement is satisfactory except at the low-angle part of the curves where the long range intermolecular interactions contribute significantly to the $s \cdot i(s)$ curves.

The theoretical peak shapes for intramolecular interactions were calculated by the use of the values in Table 3, and the peaks are compared with those of the radial distribution curves in Fig. 4. The residual curves obtained by subtraction of the calculated peaks from the radial distribution curves show two broad peaks at around 3.2 Å and 4.9 Å for the chloride solution and two distinct peaks at around 3.4 Å and 5 Å for the bromide solution. These peaks may be ascribed to the contacts between water molecules and halide ions unbonded and bonded to the platinum(IV) ions. In fact, the peak positions of 3.2 Å and 3.4 Å, respectively, are compatible with the distances of Cl–OH_2 and Br–OH_2 in the first hydration sphere so far reported.[14-15] The second peaks at 4.9 Å and 5 Å are in agreement with those found by

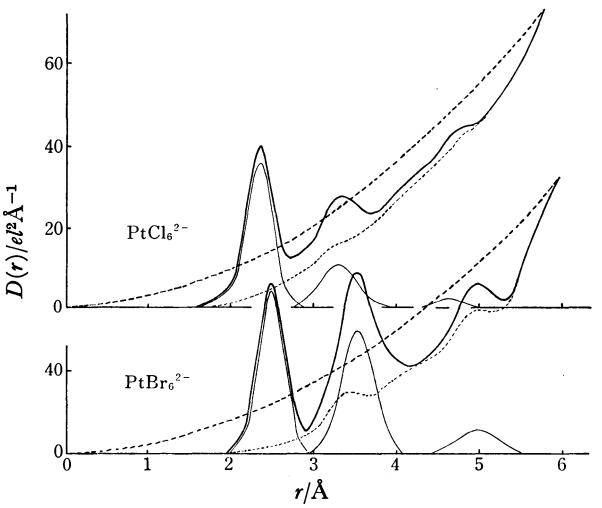

Fig. 4. Comparison between radial distribution curves and peak shapes calculated for the interactions within the PtX_6^{2-} ions using the parameter values given in Table 3. The difference between the distribution curve and the calculated peaks is shown by the dashed line.

Lawrence and Kruh in aqueous metal halide solutions.[14] They ascribed these peaks to the interactions of Cl–OH_2 and Br–OH_2 in the second hydration sphere. That the peaks for the chloride solutions are smaller than the corresponding ones for the bromide solutions is associated with the smaller scattering power of Cl than Br. No other marked peaks, which can be related to intramolecular interactions, are seen in the residual curves.

The Pt–Cl distance of 2.33 Å found in this work is shorter by 0.06 Å than that reported by Vaughan *et al.*[5] and is in good agreement with the average distance of 2.33 Å found in crystals of hexachloroplatinate (IV) compounds.[1,2] On the other hand, our Pt–Br distance of 2.47 Å is somewhat longer than that (2.43 Å) found by Vaughan *et al.* and our value agrees with the distance of 2.46 Å obtained in K_2PtBr_6 crystal.[3]

The work was supported by the Asahi Glass Foundation for the Contribution to Industrial Technology.

References

1) F. J. Ewing and L. Pauling, *Z. Krist.*, **72**, 482 (1930).
2) G. Engel, *ibid.*, **90**, 341 (1935).
3) H. D. Grundy and I. D. Brown, *Can. J. Chem.*, **48**, 1151 (1970).
4) Y. M. Bosworth and R. J. H. Clark, *J. Chem. Soc., Dalton*, **1974**, 1749, and references cited therein.
5) P. A. Vaughan, J. H. Sturdivant, and L. Pauling, *J. Amer. Chem. Soc.*, **72**, 5477 (1950).
6) M. Maeda, H. Ohtaki, and G. Johansson, This Bulletin, **47**, 2229 (1974).
7) W. W. Scott, "Standard Methods of Chemical Analysis," 5th Ed., Van Nostrand, New York (1939).
8) H. Ohtaki and M. Maeda, This Bulletin, **47**, 2197 (1974).
9) H. Ohtaki, M. Maeda, and S. Ito, *ibid.*, **47**, 2217 (1974).
10) D. T. Cromer and J. T. Waber, *Acta Crystallogr.*, **18**, 104 (1965).
11) D. T. Cromer, *J. Chem. Phys.*, **50**, 4875 (1969).
12) D. T. Cromer and D. Lieberman, *J. Chem. Phys.*, **53**, 1891 (1970).
13) G. Johansson and M. Sandström, *Chem. Scripta*, **4**, 195 (1973).
14) R. M. Lawrence and R. F. Kruh, *J. Chem. Phys.*, **47**, 4758 (1967).
15) A. H. Narten, F. Vaslow, and H. A. Levy, *ibid.*, **58**, 5017 (1973).

Photolysis of Methyl Benzenesulfonate in Methanol

Yasuji IZAWA and Naoki KUROMIYA

Department of Industrial Chemistry, Faculty of Engineering, Mie University, Tsu, Mie 514

(Received November 18, 1974)

The irradiation of methyl benzenesulfonate (**1**) in methanol undergoes a photolysis ($\Phi_{disapp}=0.07\pm0.005$) leading to benzene (5—34%), biphenyl (9—15%), and anisole (trace), in place of a photo-addition of methanol to give bicyclohexene derivatives. The rate of desulfonation of **1** is only slightly affected by triethylamine. Stern-Volmer quenching by piperylene occurs and the results suggest a significant singlet participation in this photolysis.

It has been reported that irradiation of benzene and alkylbenzenes in alcohols gives alkoxybicyclo[3.1.0]-hexenes by 1,3-addition of alcohols.[1-5] During the course of studies of the photochemical behavior of various monosubstituted benzenes, *e.g.*, anisole, *N,N*-dimethylaniline, benzoates, and phenylacetates, in protic solvents, it was discovered that, upon irradiation in methanol, methyl benzenesulfonate readily undergoes a photolysis to give benzene, biphenyl, and anisole, in place of a photo-addition of methanol; the results will be reported in this paper.

$$\underset{\mathbf{1}}{PhSO_3Me} \xrightarrow[MeOH]{h\nu} \begin{cases} -//\rightarrow \text{bicyclohexene derivatives} \\ \longrightarrow \underset{\mathbf{2}}{PhH} + \underset{\mathbf{3}}{Ph\text{-}Ph} + \underset{\mathbf{4}}{Ph\text{-}OMe} + \underset{\mathbf{5}}{\text{others}} \end{cases}$$

Although photochemical reactions beginning with an initial Ph-S bond cleavage have been reported for diaryl sulfone, sulfoxide, and sulfide in benzene,[6] little information is available on the photochemical reactions of benzenesulfonates.

Results and Discussion

A solution of **1** (1.7 g, 0.04 M) in methanol was irradiated with an unfiltered 300 W high pressure Hg lamp for 17 hr at about 10 °C, with N_2 gas being bubbled into the mixture during irradiation. After irradiation the photoproducts were separated by column chromatography on silica gel, giving colorless crystals (0.2 g), mp 69—70 °C, and other products (**5**) (44 mg) containing solid and polymeric materials. On the basis of mp and spectroscopic properties, the crystal was identified to be biphenyl (**3**). No bicyclohexene derivatives were detected in the other photoproducts. On the other hand, the formation of benzene and anisole was evident from glc on Carbowax 20 M of the reaction mixture. Thus, it has been shown that the benzene sulfonate (**1**) is photochemically desulfonated to give benzene, biphenyl, and anisole in methanol. Table 1 shows the relation between the yields of photoproducts and the initial concentration of **1**. As shown in Table 1, the relative yields of biphenyl to benzene decrease as the concentration of **1** is lowered. Furthermore, when a methanol solution of 0.7 mM of **1** was irradiated in a sealed quartz cell, after 30 min irradiation the spectrum of the solution became identical with that of benzene. That is, no biphenyl was detected in a dilute solution of **1**. These results suggest undoubtedly that benzene and biphenyl are derived from phenyl radicals produced by Ph-S bond cleavage. The quantum yield for disappearance of **1** was estimated to be 0.07 ± 0.005 at 254 nm at room temperature, using a ferrioxalate actinometer.

Table 1. PHOTOLYSIS OF METHYL BENZENESULFONATE (**1**) IN METHANOL USING 300W HIGH PRESSURE Hg LAMP

[**1**] M	Conv. (%)	Yield (%)[a]			Product ratio [**3**]/[**2**]
		2	**3**	**4**	
0.5	14	5.1	9.9	trace	1.9
0.1[b]	38	8.0	9.1	trace	1.1
0.2	30	21.9	15.3	trace	0.7
0.1	46	34.4	10.1	trace	0.3
0.05	43	24.0	12.0	trace	0.5

a) Determined by glpc after 20 hr, based on **1** consumed. b) 30W Low pressure Hg lamp.

Quenching by 1,3-pentadienes was carried out in order to obtain information about an excited state of **1**. The photolysis of **1** is quenched by 1,3-pentadienes to give a linear Stern-Volmer plot, whose slope ($k_q\tau$) is 18.6 M^{-1}. Assuming that the quenching is diffusion-controlled, the value of τ, the mean life time of an excited state of **1**, may be estimated. Hence, assuming again the bimolecular diffusion-controlled rate constant for neat methanol at 20 °C to be 1.06×10^{10} M^{-1} s^{-1} on the basis of the Debye expression, the value of τ is calculated to be 1.8×10^{-9} s. On the other hand, the fluorescence of **1** in methanol is quenched by 1,3-pentadienes[7] to give a linear Stern-Volmer plot, whose slope ($k_q\tau_f$, fluorescence quenching constant) is 14.0 M^{-1} at 30 °C. From the slope τ_f is estimated to be 1.1×10^{-9} s, which is in agreement with the value of τ. Thus, it seems that the photolysis proceeds *via* a singlet state rather than a triplet state of **1**.

In order to examine whether the present desulfonation is induced by a photochemical electron transfer (ETR)[8] from methanol to **1**, the photolysis was carried out in the presence of triethylamine, which is an efficient electron domor.[9] If ETR takes place, the relative rates of disappearance of **1** would increase with addition of triethylamine. As shown in Table 2, however, the relative rates are about unity. These facts suggest that an electron transfer from amine to **1** to give a radical anion (**6**) does not occur and/or that the sulfonate group is less able to

Table 2. EFFECT OF NEt_3 ON THE PHOTO-DESULFONATION OF **1**

$[NEt_3]/[1]$ (Molar ratio)	0	0.5	1.0	2.0
Relative rate[a] (k/k_0)	1.00	1.00	0.98	1.07

a) Relative rates (k/k_0) of disappearance of **1** were determined by comparison with the rate (k_0) without triethylamine.

leave as an anion from **6**. This result implies that a similar ETR does not occur for methanol, since the I_p (10.85 eV[10]) of methanol is higher than that (7.50 eV[10a]) of the amine.

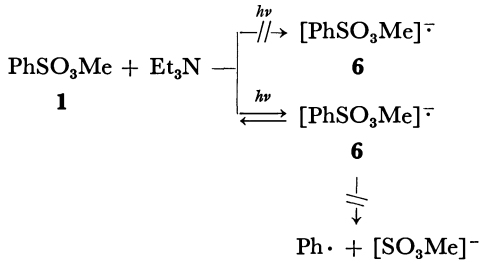

On the basis of these facts, the possible reaction pathways of photo-desulfonation of **1** to give benzene, biphenyl, and anisole can be postulated as follows:

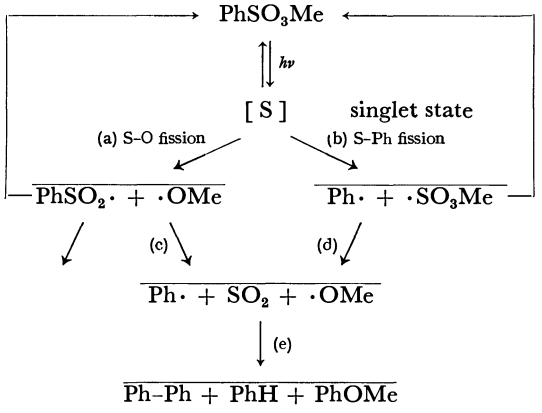

Scheme 1.

Step (c), however, may be less probable, since a desulfonation of $PhSO_2\cdot$ radical to give Ph· radical may be significantly endothermic,[11] and it is known that two arylsulfonyl radicals react with each other to produce a sulfonic anhydride and thiosulfonate *via* a mixed sulfonic sulfinic anhydride.[12] Accordingly, the reaction pathway (b→d→e) beginning with the homolysis of Ph-S bond appears to play an important role in the photolysis of **1** leading to benzene, biphenyl, and anisole.

Experimental

The glpc analysis was carried out on a Yanagimoto GC-1800 apparatus equipped with hydrogen-flame detectors. The IR spectra were measured with a JASCO IR-G grating instrument and the UV spectra were recorded with a Shimadzu UV-200 spectrophotometer. The NMR data were obtained with a JEOL JNM MH-100 spectrometer. Monochromatic irradiation (254 nm) was performed with a monochrometer of the Hitachi MPF-2A type fluorescence spectrophotometer (150 W Xe lamp).

Materials. Methyl benzenesulfonate (**1**) was prepared from benzenesulfonyl chloride and methanol according to the known procedure,[13] bp 110—114 °C/1.5—3 mmHg, λ_{max}^{MeOH} (ε): 252.5 (390), 257.5 (680), 264.8 (980), and 272 (85) nm; δ (CCl_4): 3.70 (s, $-CH_3$) and 7.42—8.00 (m, -Ph); 1365 and 1189 cm^{-1} (liq. film, $-SO_2-$). Methanol was dried over Mg metal and distilled. Triethylamine was dried over Na metal and distilled. Silica gel Woelm containing an inorganic fluorescent indicator was used for column chromatography and silica gel PF_{254} containing $CaSO_4$ (Merk) was used for tlc. Piperylene (a mixture of isomers) of a g.r. grade supplied by the Nakarai Chemicals, Ltd. was distilled ,bp 41.8—42.0 °C. Other reagents were of the first grade commercial materials.

Preparative Scale Irradiation. The irradiation was carried out using an immersion type Halos 300W high pressure Hg lamp without filter. A solution of **1** (1.7 g) in methanol (250 ml) was placed in a reaction vessel, which was immersed in a water-bath, equipped with a N_2 gas inlet, thermometer, and a condensor. The solution was irradiated under N_2 at about 10 °C for 17 hr. After irradiation, the reaction mixture was carefully neutralized with aqueous sodium hydroxide solution and then evaporated under reduced pressure below 30 °C. Separation of photo-products was carried out by liquid chromatography with silica gel column (Nylon column, diameter: 3 cm, height: 35 cm), using a mixed solution of hexane and acetone (50: 1) as a eluent, to give **3** (0.2 g), brownish viscous liquid **5** (44 mg), and **1**. Furthermore, in order to detect the presence or absence of bicyclohexene derivatives, the viscous liquid (**5**) was then subjected to silica gel tlc using 50: 1 hexane-acetone solution as a developer. Three products were isolated and subjected to IR and NMR analyses. However, the existence of bicyclohexene derivatives could not be demonstrated.

Irradiation for Analtyical Purposes. The solutions (5 ml) of 0.05—0.5 M **1** in methanol were placed in 12-mm o.d. quartz tubes, and these were capped with polyethylene-stopples after flushing with N_2 gas at 0 °C for 5 min. A Halos 300 W high pressure Hg lamp with a water cooling quartz jacket was used without filter. The tubes and lamp were placed in a water-bath and irradiation was carried out at about 10 °C for 20 hr. After irradiation, the analysis of the reaction mixtures was done by means of glpc. The agreement of the retention times of the peaks with those of authentic samples established their identity. The conditions for glpc were as follows: 2 m×3 mm column of 13% Apiezon L on 60—80 mesh Diasolid L at 50 °C for benzene (**2**) and at 100 °C for anisole (**4**); 1 m×3 mm column of 5% PEG 20 M on 60—80 mesh Diasolid L at 130 °C for methyl benzenesulfonate (**1**) and biphenyl (**3**). The yields were estimated by glpc on the basis of **1** consumed.

Quantum Yield. These experiments were performed with 254 nm radiation from the monochrometer at room temperature and the quantum yields were determined by means of a liquid phase actinometer using potassium ferrioxalate. Cylindrical (ϕ=2 cm) fused-quartz cells with optically flat windows were used for the photolysis (path length 2 cm, 5 ml) and actinometer (path length 5 cm, 15 ml) cells. A solution of 0.4 mM **1** in methanol was placed in the photolysis cell; irradiation was started by opening a shutter and continued for 1 hr. The actinometer was photolyzed simultaneously. Photolysis was carried to 5% or less conversion and the number of molecules of consumed **1** in the cell was determined spectrophotometrically. The quantum yield was the average of the two analyses.

Effect of Added Triethylamine on the Photolysis. The solutions of 0.7 mM **1** and 0—1.4 mM triethylamine in methanol were flushed with N_2 gas at 0 °C for 5 min and sealed in 12 mm o.d. quartz tubes. The tubes were then irradiated on a merry-go-round apparatus using 30 W Halos low pressure Hg lamp without filter at room temperature for 10 min. The amount of consumed **1** in the tubes was determined spectrophotometrically. The relative rates (k/k_0) of disappearance of **1** were determined by comparison with the rate (k_0) without amine.

Quenching of Photolysis. The solutions of 7.1 mM **1** in

methanol with or without piperylenes were placed in closed 12 mm o.d. quartz tubes. The tubes were then irradiated on a merry-go-round apparatus using 300 W high pressure Hg lamp without filter at about 20 °C for 5 hr. Five concentrations (0.7—5.6 mM) of piperylenes, in addition to blanks containing no piperylenes, were used for the Stern-Volmer plot. The amount of consumed **1** in the tubes was determined spectrophotometrically.

Fluorescence Quenching of 1. A methanol solution of **1** showed a structureless fluorescence spectrum with a maximum at 289 nm. A stock solution of **1** in methanol (35.8 mM) was prepared and varying amounts of 1,3-pentadienes were added to aliquots of the stock; [dienes]=6.9—34.5 mM. Six solutions were used for the quenching experiment. The fluorescence spectra were recorded at room temperature (about 30 °C) and the relative intensities at 289 nm in the absence and presence of the dienes (I_0/I) were plotted with concentration of the dienes. A linear Stern-Volmer plot was obtained.

References

1) E. Farenhorst and A. F. Bickel, *Tetrahedron Lett.*, **1966**, 5911.

2) L. Kaplan, J. S. Ritscher, and K. E. Wilzbach, *J. Amer. Chem. Soc.*, **88**, 2881 (1966).

3) H. Newman, *Tetrahedron Lett.*, **1968**, 2417, 2421.

4) J. A. Berson and N. M. Hasty, Jr., *J. Amer. Chem. Soc.*, **93**, 1549 (1971).

5) L. Kaplan, D. J. Rausch, and K. E. Wilzbach, *ibid.*, **94**, 8638 (1972).

6) a) N. Kharasch and A. I. A. Khodair, *Chem. Commun.*, **1967**, 98; b) M. Nakai, N. Furukawa, and S. Oae, This Bulletin, **45**, 1117 (1972).

7) Singlet quenching of various alkylbenzenes by diene (see P. M. Froehlich and H. A. Morrison, *J. Amer. Chem. Soc.*, **96**, 332 (1974)) has been reported.

8) N. Mataga, T. Okada, and N. Yamamoto, *Chem. Phys. Lett.*, **1**, 119 (1967); A. Weller, *Pure Appl. Chem.*, **16**, 115 (1968); H. Yamashita and M. Koizumi, This Bulletin, **41**, 2313 (1968); S. G. Cohen and N. M. Chao, *J. Amer. Chem. Soc.*, **90**, 165 (1968); C. Pac and H. Sakurai, *Chem. Commun.*, **1969**, 20; idem, *Kogyo Kagaku Zasshi*, **72**, 230 (1969); M. T. McCall, G. S. Hammond, O. Yonemitsu, and B. Witkop, *J. Amer. Chem. Soc.*, **92**, 6991 (1970); C. Pac, H. Sakurai, and T. Tosa, *Chem. Commun.*, **1970**, 1311; S. G. Cohen and N. M. Stein, *J. Amer. Chem. Soc.*, **93**, 6542 (1971); S. G. Cohen, G. A. Davis, and W. D. K. Clark, *ibid.*, **94**, 869 (1972); Y. Saburi, T. Yoshimoto, and K. Minami, *Nippon Kagaku Kaishi*, **1974**, 905; C. Pac, T. Tosa, and H. Sakurai, This Bulletin, **45**, 1169 (1972).

9) For example, photo-induced dechlorination of 4-chlorobiphenyl by aliphatic amines (see M. Ohashi, K. Tsujimoto, and K. Seki, *Chem. Commun.*, **1973**, 384.) has been reported.

10) K. Watanabe, *J. Chem. Phys.*, **26**, 542 (1957).

10a) K. Watanabe and J. R. Mottl, *ibid.*, **26**, 1773 (1957).

11) J. L. Kice, "Free Radicals," Vol. 2, ed. by J. K. Kochi, John Wiley & Sons, New York (1973), p. 736.

12) C. M. M. da Silva and W. A. Waters, *J. Chem. Soc., C*, **1968**, 1874.

13) M. S. Morgan and L. H. Cretcher, *J. Amer. Chem. Soc.*, **70**, 375 (1948).

Reactions of Vinyloxyboranes with Carbonyl Compounds, Nitriles, and Formates[1]

Masayoshi MURAKI,* Katsuhiko INOMATA, and Teruaki MUKAIYAMA
Laboratory of Organic Chemistry, Tokyo Institute of Technology, Ookayama, Meguro-ku, Tokyo 152
(Received February 25, 1975)

A new vinyloxyborane derivative, Id, was found to be formed in reaction of phenyl di-*n*-butylthioboronite (II) with methyl vinyl ketone. In order to explore its utilization in organic synthesis, the reactivity of Id and other known vinyloxyboranes was variously examined. Id and Ie gave β-hydroxyketones (IVa—c, Va—d) in fairly good yields when they were allowed to react with carbonyl compounds. The reaction of Ia′ and Ib with nitriles, followed by hydrolysis, afforded β-iminothioates (VIa—c) and β-ketoesters (VIIa—d) respectively. It was also found that the borane (Ib) reacted with formates or formamides at room temperature to give ethyl α-formylhexanoate.

In a previous paper,[2] it was reported that β-hydroxythioates are produced in high yields by the reaction[3] of thioboronites, ketene, and carbonyl compounds *via* the key intermediates, vinyloxyboranes (Ia). Similarly,

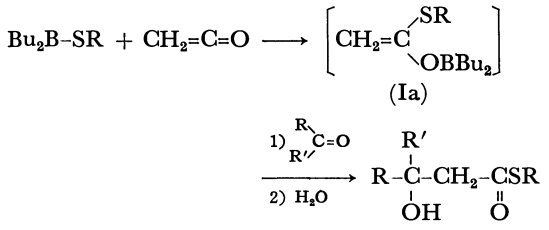

vinyloxyboranes[4] (Ib, Ic) prepared from tri-*n*-butylborane and ethyl diazoacetate or diazoacetophenone reacted with carbonyl compounds to afford β-hydroxyesters and β-hydroxyketones respectively.[1,3]

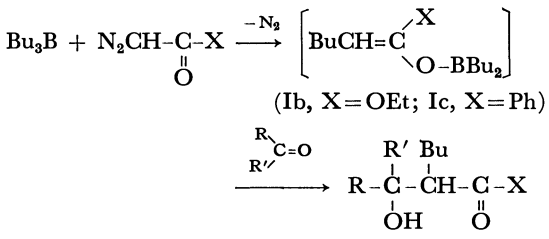

We have subsequently been studying the formation and reactivity of vinyloxyborane derivatives and now wish to report the formation of a new vinyloxyborane (Id), which was obtained from methyl vinyl ketone and thioboronite (II), and the reactivity of Id and Ie, which were prepared from tri-*n*-butylborane and methyl vinyl ketone,[5] with various carbonyl compounds. This paper will also describe the reactions of Ia′ and Ib with such electophiles as nitriles, acyl halides, and formates.

A new vinyloxyborane (Id) was formed by the reaction of methyl vinyl ketone with thioboronite according to the following procedure: an equimolar amount of *S*-phenyl di-*n*-butylthioboronite (II) was added to a solution of methyl vinyl ketone in CCl_4, and then the mixture was kept standing at room temperature for 30 min. The product was not isolated, but its structure was confirmed to be (1-methyl-3-phenylthio-1-propenyloxy)di-*n*-butylborane (Id) by PMR analysis. This assignment was also supported by the observation that the hydrolysis of Id in aqueous methanol afforded 4-phenylthiobuta-2-one (III) in an 86% yield. The reactivity of this intermediate (Id) to carbonyl compounds was then examined.

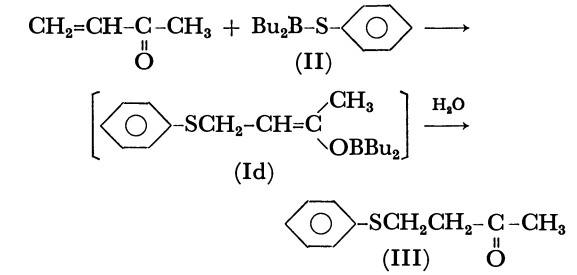

When Id was allowed to react with various carbonyl compounds in dry ether at room temperature, the corresponding β-hydroxy-α-(phenylthiomethyl)-ketones (IVa—c) were obtained in fairly good yields. The results are summarized in Table 1. This reaction proceeds in a mode similar to that with other vinyloxyboranes (Ia—c) described in a previous paper.[2]

Similarly, the vinyloxyborane (Ie), prepared from methyl vinyl ketone and tri-*n*-butylborane according to the method of Suzuki *et al.*,[5] was caused to react with carbonyl compounds to give β-hydroxy-α-*n*-pentyl ketones (Va—d) (Table 1). The reaction of Id, Id′, or Ie with aldehydes gave favorable results, whereas the yields of the products (IVc, Vc, d) were comparatively low when these boranes were treated with ketones.

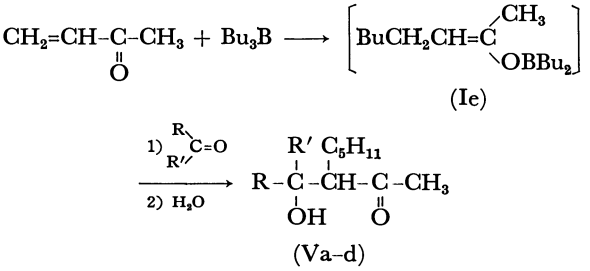

(Va–d)

The addition of a solution of *S*-benzyl diazothioacetate in ether to tri-*n*-butylborane led to the liberation of the nitrogen. On the treatment of the resulting solution with a solution of benzaldehyde or propiophenone in ether, the corresponding α-butyl-β-hydroxyalkanethioates were obtained in 51% and 81% yields respectively. The structure of the intermediate was identified as If, in analogy with Ib:

* Present address: Organic Chemistry Research Laboratory, Tanabe Seiyaku Co., Ltd., 2-2-50, Kawagishi, Toda, Saitama 335.

Table 1. Yields of β-hydroxyketone[a]

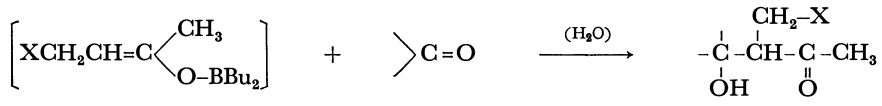

(Id, d′, e) (IVa—d, Va—d)

Vinyloxyboranes	Carbonyl compounds	Reaction time	Products	Isolated yield(%)
Id (X=–S–)	–CHO	1.5 hr	IVa	93
	n-C_3H_7CHO	1 day	IVb	83
	CH_3COCH_3	3 day	IVc	20[b]
Id′ (X=–S–CH_2)	–CHO	13 hr	IVd	72
Ie (X=n-Bu)	–CHO	0.5 hr	Va	91
	n-C_3H_7CHO	1 day	Vb	71
	CH_3COCH_3	1 day	Vc	15
	=O	1 day	Vd	38

a) In THF at room temperature. b) Isolated III in 42% yield.

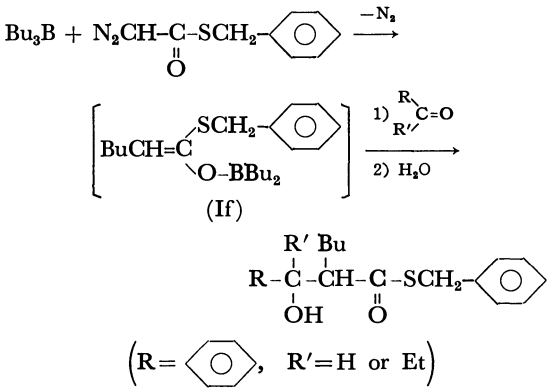

(If)

The reaction of ethyl diazoacetate, 9-borabicyclo-[3.3.1]nonane (9-BBN), and benzaldehyde were tried in order to know the migrating tendency of the substituents on the boron atom in 9-BBN.[6,7] Ethyl β-hydroxyhydrocinnamate was consequently obtained in a 43% yield by the same procedure as in the case of tri-n-butylborane. It was found that the preferential cleavage of the B–H bond in 9-BBN occurred to form the vinyloxyborane (Ig) as follows:

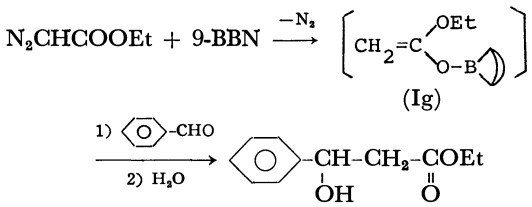

(Ig)

The experimental results in both the previous and

Table 2. Reactions of various vinyloxyboranes with benzaldehyde

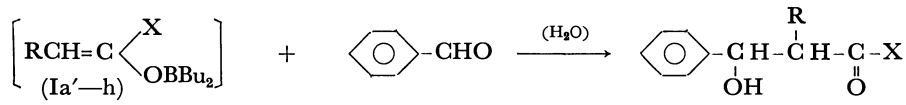

(Ia′—h)

Starting materials			Vinyloxyboranes (R)		(X)	Isolated yield (%)
CH_2=CHCCH$_3$ (O)	+	Bu_2BS	Id	–CH_2S	CH_3	93[3]
CH_2=CHCCH$_3$ (O)	+	Bu_3B	Ie	$-C_5H_{11}$	CH_3	91
$N_2CHCOOEt$	+	Bu_3B	Ib	Bu	OEt	81[2]
$N_2CHCOSCH_2$	+	Bu_3B	If	Bu	–SCH_2	51
N_2CHC– (O)	+	Bu_3B	Ic	Bu	–	98[2]
$N_2CHCOOEt$	+	9-BBN	Ig[a]	H	OEt	43
CH_2=C=O	+	Bu_2BS	Ia′	H	–S	96[2]
CH_3CH(Br)–COBr	+ Zn +	Bu_2BS	Ih	Me	–S	85[3]

a) The substituent group of the boron is not n-butyl but 1,5-cyclooctylene.

Table 3. Yields of β-iminothioates[a]

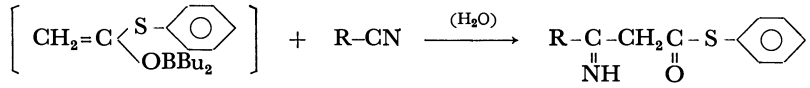

(Ia′) (VIa—c)

Nitriles	Products	Isolated yield (%)
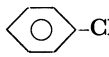	VIa	37
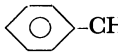	VIb	39
CH_3CN	VIc	35

a) 1 day in ether at room temperature.

present papers show that vinyloxyboranes (Ia—h: R=H, alkyl, cyclohexyl, or thiomethyl; X=OR, SR, alkyl, or aryl) easily react with carbonyl compounds to afford the corresponding β-hydroxy- esters, thioates, or ketones in good yields. As an example, the reactions of these vinyloxyborane derivatives with benzaldehyde are listed in Table 2.

Next, the reaction of vinyloxyboranes with nitriles was attempted. When vinyloxyborane (Ia′; Ia, R=Ph), prepared from S-phenyl di-*n*-butylthioboronite (II) and ketene, was allowed to react with nitriles at room temperature for 1 day under argon, β-iminothioates (VIa—c) were obtained after hydrolysis (Table 3).

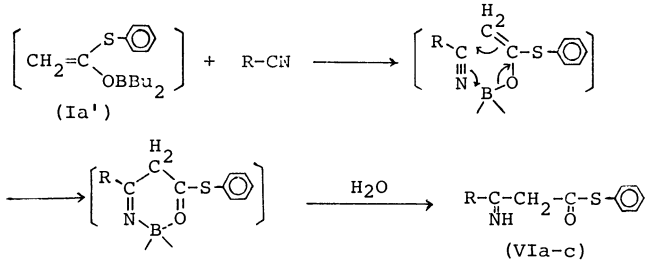

(Ia′) (VIa-c)

Similarly, Ib reacted with some nitriles to afford α-butyl-β-ketoesters in about 55—70% yields after hydrolysis, as is shown in Table 4.

Furthermore, the reactions of Ib with various carboxylic acid derivatives, such as acyl halides, esters, and amides, were examined. Benzoyl bromide and phenylacetyl chloride gave the corresponding β-ketoesters in 31% and 9% yields respectively when they were submitted to a reaction with Ib at room temperature under argon, followed by hydrolyses.

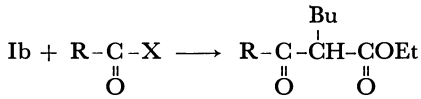

It was found that Ib hardly reacts at all with any esters or amides except for formic and oxalic acid derivatives. The borane (Ib) reacted with formic acid derivatives, such as ethyl or *p*-nitrophenyl formate and *N*,*N*-dimethylformamide, to afford ethyl α-formyl-*n*-hexanoate (Table 5). In general, such formyl compounds are prepared by the mixed Claisen condensation of esters and formate in the presence of strong bases. According to the present reaction, however, the formyl compounds are produced under almost neutral conditions.

Diethyl oxalate, which is often used in the mixed Claisen condensation, also reacted with Ib at room temperature to give ethyl α-ethoxalylhexanoate in a 46% yield.

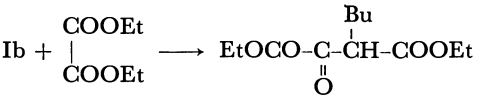

There are two possible pathways for the reaction of vinyloxyborane with carboxylic acid derivatives: Path (a), similar to that of vinyloxyboranes with carbonyl compounds, and Path (b), accompanied by the initial fission of the C–OR′ or C–NR'_2 bond of formate or formamide, as is sketched below:

Table 4. Yields of α-butyl-β-keto esters[a]

(Ib) (VIIa–d)

Nitriles	Reaction time	Products	Isolated yield (%)
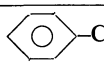	16 hr	VIIa	71
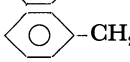	10 hr	VIIb	61
MeCN	1 day	VIIc	57
n-C_3H_7CN	5 hr	VIId	54

a) In THF at room temperature.

Table 5. Yields of ethyl α-formylhexanoate[a)]

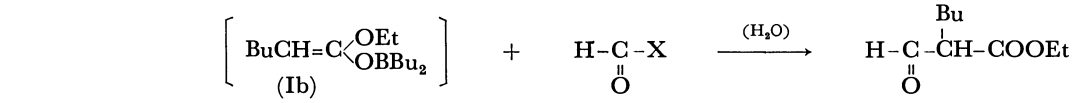

Formyl derivatives (X)	Reaction time	Isolated yield (%)
-OMe	16 hr	65
-OEt	13 hr	60
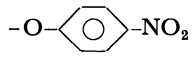	16 hr	44
$-NMe_2$	1 day	40
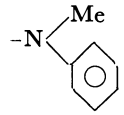	12 hr	8

a) In ether at room temperature.

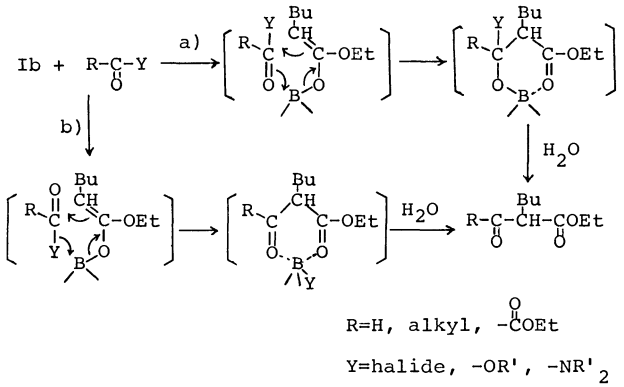

It should be noted that vinyloxyboranes, which react, under mild conditions, with carbonyl compounds, nitriles, or formates, may be useful as intermediates for the synthesis of a variety of β-hydroxy, β-keto- or α-formyl- ester, thioate, and ketone derivatives.

Experimental[9)]

Materials. Tri-*n*-butylborane was prepared from boron trifluoride diethyl etherate and *n*-butylmagnesium bromide in dry ether under argon. *S*-Phenyl di-*n*-butylthioboronite was prepared from tri-*n*-butylborane and thiophenol at 180 °C.[3)]

Reaction of S-*Phenyl Di*-n-*butylthioboronite and Methyl Vinyl Ketone.* To a solution of *S*-phenyl di-*n*-butylthioboronite (235 mg, 1.0 mmol) in CCl_4, we added methyl vinyl ketone (80 mg, 1.1 mmol) at room temperature under argon. After 30 min, the PMR spectrum of the solution was measured to show the formation of a vinyloxyborane (Id). PMR (CCl_4) δ 1.78 (s, 3H), 3.36 (d, J=8 Hz, 2H), 4.77 (t, J=8 Hz, 1H). The solution was then hydrolyzed with aqueous methanol and extracted with ether. The ethereal extracts were washed with water, dried over Na_2SO_4, and concentrated *in vacuo*. The residue was separated by preparative tlc to give 4-phenylthiobutan-2-one (III) in an 86% yield; bp 135—136 °C/8 mmHg. IR 1715, 1580, 1475, 740, 690 cm^{-1}. PMR ($CDCl_3$) δ 2.09 (s, 3H), 2.6—3.3 (m, 4H), 7.32 (s, 5H).

Reaction of Vinyloxyborane (Id) with n-*Butyraldehyde.* To a solution of (1-methyl-3-phenylthio-1-propenyloxy)di-*n*-butylborane (Id) prepared from *S*-phenyl di-*n*-butylthioboronite (319 mg, 1.4 mmol) and methyl vinyl ketone (100 mg, 1.4 mmol) in ether, we added a solution of butyraldehyde (94 mg, 1.3 mmol) in abs. ether (1 ml). The mixture was allowed to stand overnight and concentrated, and the residue was treated with water and bubbled air for 1 hr and then further extracted with ether. The ethereal layers were washed successively with 5% $NaHCO_3$ and H_2O, dried over Na_2SO_4, and evaporated. The residual oil was purified by preparative tlc (silica gel/$CHCl_3$) to give the pure oil of 4-hydroxy-3-phenylthiomethylheptan-2-one (IVb); 274 mg (83%); IR 3440, 1695 cm^{-1}. PMR ($CDCl_3$) δ 0.8—1.5 (m, 7H), 2.22 (s, 3H), 2.5 (broad s, 1H), 2.8—3.0 (m, 1H), 3.2 (d, 2H), 3.9 (d, 1H), 7.32 (m, 5H). Found: C, 66.48; H, 8.11; S, 12.79%. Calcd for $C_{14}H_{20}O_2S$: C, 66.62; H, 7.99; S, 12.71%.

The IR and PMR spectra and analysis of the other β-hydroxy-α-thiomethyl ketones (IVa, c, d) are consistent with the assigned structure. IVa; IR 3440, 1700 cm^{-1}. PMR ($CDCl_3$) δ 1.97 (s, 3H), 2.9—3.4 (m, 4H), 4.8—5.0 (m, 1H), 7.17 (s, 5H), 7.30 (s, 5H). Found: C, 70.85; H, 6.53; S, 11.28%. Calcd for $C_{17}H_{18}O_2S$: C, 71.28; H, 6.33; S, 11.19%. IVc; IR 3420, 1695 cm^{-1}. PMR ($CDCl_3$) δ 1.22 (s, 6H), 2.28 (s, 3H), 2.1—2.4 (broad s, 1H), 2.8—3.35 (m, 3H), 7.29 (s, 5H). Found: C, 65.28; H, 7.48; S, 13.32%. Calcd for $C_{13}H_{18}O_2S$: C, 65.51; H, 7.61; S, 13.45%. IVd; IR 3410, 1695 cm^{-1}. PMR ($CDCl_3$) δ 1.88 (s, 3H), 2.6—3.4 (m, 4H), 3.70 (s, 2H), 4.65—4.8 (m, 1H), 7.15 (s, 5H), 7.20 (s, 5H). Found: C, 71.70; H, 6.97; S, 10.88%. Calcd for $C_{18}H_{20}O_2S$: C, 71.97; H, 6.71; S, 10.68%.

Reaction of Vinyloxyborane (Ie) with Benzaldehyde. A solution of methyl vinyl ketone (150 mg, 2.1 mmol) and tri-*n*-butylborane (450 mg, 2.4 mmol) in abs. THF was stirred at room temperature under nitrogen containing a little oxygen overnight to give (1-methyl-1-heptenyloxy)di-*n*-butylborane (Ie). To the solution we then added a solution of benzaldehyde (160 mg, 1.5 mmol) in abs. THF. After 30 min, the solvent was removed. The residue was treated with a mixture of MeOH (20 ml) and 30% H_2O_2 (1 ml) for 1 hr, and further water was added. The mixture was concentrated *in vacuo* to remove the MeOH and extracted with ether. The extracts were washed with 5% $NaHCO_3$ and water, dried over Na_2SO_4, and evaporated. The oil was separated by preparative tlc to give 3-(α-hydroxybenzyl)octan-2-one (Va), both *threo* type (240 mg, 68%) and *erythro*-type (79 mg, 23%). Va of the *threo* type: IR 3420, 1700 cm^{-1}; PMR (CCl_4) δ 0.6—1.8 (m, 11H), 2.06 (s, 3H), 2.73 (m, 1H), 3.32 (s, 1H), 4.56 (d, 1H), 7.23 (s, 5H). Va of the *erythro* type: IR 3420, 1695 cm^{-1}: PMR (CCl_4) δ 0.6—1.8 (m, 11H), 1.83 (s, 3H), 2.70 (m, 1H), 3.15 (s, 1H), 4.70 (d, 1H), 7.23 (s, 5H).

The IR and PMR spectra of the other β-hydroxy-γ-pentylketones (Vb—d) are consistent with the assigned structure.

Vb; IR 3410, 1690 cm^{-1}: PMR (CCl_4) δ 0.7—1.9 (m, 18H), 2.13 (s, 3H), 2.3—2.7 (m, 1H), 3.17 (s, 1H), 3.5—3.9 (m, 1H). Vc; IR 3440, 1690 cm^{-1}: PMR (CCl_4) δ 0.6—1.8 (m, 11H), 1.10 (s, 3H), 1.15 (s, 3H), 2.13 (s, 3H), 2.3—2.9 (m, 2H). Vd; IR 3470, 1685 cm^{-1}: PMR (CCl_4) δ 0.6—2.0 (m, 21H), 2.15 (s, 3H), 2.53 (t, 1H), 2.65 (broad s, 1H).

Reaction of Vinyloxyborane (Ia') and Benzyl Cyanide. To a solution of *S*-phenyl di-*n*-butylthioboronite (419 mg, 1.8 mmol) in asb. ether (10 ml), we added 45 ml of gaseous ketene (prepared by the thermal cracking of acetone) at −78° under argon. After 10 min, we added benzyl cyanide (174 mg, 1.5 mmol) to the solution of vinyloxyborane (Ia') at room temperature. The reaction mixture was then allowed to stand for 21 hr and concentrated. MeOH was added to the residue and then, after 12 hr, removed *in vacuo*. The residual oil was separated by preparative tlc to give *S*-phenyl β-imino-γ-phenylbutyrothioate (VIb) 155 mg (39%). Recrystallization from cyclohexane: mp 74.0 °C. IR 3455, 3305, 1615, 1520 cm^{-1}. Found: C, 71.27; H, 5.75; N, 5.02; S, 11.88%. Calcd for $C_{16}H_{15}NOS$: C, 71.36; H, 5.61; N, 5.20; S, 12.14%.

The IR and analyses of the other β-iminothioates (VIa, c) are consistent with the assigned structure. VIa (mp 111—112 °C); IR 3380, 3290, 3200, 1610, 1520 cm^{-1}. Found: C, 70.70; H, 5.10; N, 5.68; S, 12.53%. Calcd for $C_{15}H_{13}NOS$: C, 70.58; H, 5.13; N, 5.49; S, 12.53%. VIc (oil); IR 3410, 3305, 3200, 1607, 1520 cm^{-1}. Found: C, 61.95; H, 6.04; N, 6.96; S, 16.56%. Mol wt, 193 (mass spectrometry). Calcd for $C_{10}H_{11}NOS$: C, 62.16; H, 5.74; N, 7.25; S, 16.51%. Mol wt, 193.2.

Reaction of Vinyloxyborane (Ib) with Benzonitrile. A solution of ethyl diazoacetate (242 mg, 2.1 mmol, dried over P_2O_5) in THF (1 ml) was stirred into a solution of tri-*n*-butylborane (398 mg, 2.1 mmol) in THF (3 ml) at room temperature under argon. N_2 was immediately evolved, and the yellow coloration characteristic of ethyl diazoacetate disappeared. After 5 min, a solution of benzonitrile (108 mg, 1.1 mmol) in THF was added to the solution. The reaction mixture was then allowed to stand at room temperature for 16 hr, after which the solution was treated with a mixture of 5% HCl (2 ml), MeOH (3 ml), and 30% H_2O_2 (1.5 ml) for 4 hr. Water was added to the solution, and the mixture was concentrated *in vacuo* to remove most of the THF and MeOH and extracted with ether. The ether layer was washed with 5% $NaHCO_3$ and satd. NaCl and dried over Na_2SO_4, and the solvent was removed. The crude oil was purified by preparative tlc (silica gel, benzene) to give the pure oil of ethyl α-benzoylhexanoate (VIIa); 184 mg, 71%. IR 1740, 1695 cm^{-1}. PMR (CCl_4) δ 0.65—2.4 (m, 13H), 4.10 (q, J=7 Hz, 2H), 7.4—7.6 (m, 3H), 7.8—8.05 (m, 2H). Found: C, 72.42; H, 8.18%. Calcd for $C_{15}H_{20}O_3$: C, 72.55; H, 8.12%.

The IR and PMR spectra of the other β-ketoesters (VIIb—d) are consistent with the assigned structure. VIIb; IR 1740, 1715 cm^{-1}; PMR (CCl_4) δ 0.7—2.0 (m, 12H), 3.47 (t, J=6 Hz, 1H), 3.73 (s, 2H), 4.10 (q, J=7 Hz, 2H), 7.17 (s, 5H). VIIc; IR 1740, 1720 cm^{-1}: PMR (CCl_4) δ 0.7—2.4 (m, 13H), 2.17 (s, 3H), 4.10 (q, J=7 Hz, 2H), VIId: IR 1745, 1715 cm^{-1}. PMR (CCl_4) δ 0.6—2.6 (m, 18H), *ca.* 3.2 (m, 2H), 4.08 (q, J=7 Hz, 2H).

Reaction of Vinyloxyborane (Ib) with Ethyl Formate. A solution of ethyl diazoacetate (2.74 g, 24 mmol) in asb. ether (5 ml) was stirred into a solution of tri-*n*-butylborane (3.65 g, 20 mmol) and ethyl formate (1.85 g, 25 mmol) in ether (20 ml) at room temperature under argon. The solution was then allowed to stand at room temperature for 16 hr, and ether was added. The solution was washed with a 5% solution of $NaHCO_3$ and water and then dried over anhydrous Na_2SO_4, after which the solvent was evaporated to give a crude oil. The oil was purified by silica-gel-column chromatography to give the pure oil of ethyl α-formylhexanoate (1.95 g, 60%); bp 88—91 °C/9 mmHg. (lit,[10] bp 94—96 °C/10 mmHg). IR 1740 (shoulder), 1720, 1660 cm^{-1}. Found: C, 62.57; H, 9.45%. Mol wt, 172 (mass spectrometry). Calcd for $C_9H_{16}O_3$: C, 62.76; H, 9.36%; Mol wt, 172.2.

References

1) Preliminary Communication: T. Mukaiyama, K. Inomata, and M. Muraki, *J. Amer. Chem. Soc.*, **95**, 967 (1973).
2) K. Inomata, M. Muraki, and T. Mukaiyama, This Bulletin, **46**, 1807 (1973).
3) T. Mukaiyama and K. Inomata, *ibid.*, **44**, 3215 (1971).
4) The reaction of trialkylborane with diazo esters or ketone was developed by Hooz and his coworker [J. Hooz and S. Linke, *J. Amer. Chem. Soc.*, **90**, 5936, 6891 (1970)] and the structure of the intermediate, vinyloxyborane, was confirmed by Pasto and Wojtkowski [D. J. Pasto and P. W. Wojtkowski, *Tetrahedron Lett.*, **1970**, 215.].
5) A. Suzuki, A. Arase, H. Matsumoto, M. Itoh, H. C. Brown, M. M. Rogić, and M. W. Rathke, *J. Amer. Chem. Soc.*, **89**, 5708 (1967).
6) H. C. Brown and M. M. Rogić, *ibid.*, **91**, 2146 (1969).
7) J. Hooz and D. M. Gunn, *Tetrahedron Lett.*, **1969**, 3455.
8) K. Inomata, T. Kawahara, and T. Mukaiyama, *Chem. Lett.*, **1974**, 245.
9) All melting and boiling points are not corrected.
10) M. Regitz and F. Menz. *Chem. Ber.*, **101**, 2622 (1968).

The Reaction of Alkyl Halides with Mercuric Thiocyanate in Tetrahydrofuran. The Solvent Incorporation and the Intermediacy of *O*-Alkyltetrahydrofuranium Ions.

Nanao WATANABE,* Sakae UEMURA, and Masaya OKANO**
Institute for Chemical Research, Kyoto University, Uji, Kyoto 611
(Received March 12, 1975)

The reaction of alkyl halides with mercuric thiocyanate in tetrahydrofuran (THF) affords mainly the THF-incorporated products, $R[O(CH_2)_4]_nNCS$ and $R[O(CH_2)_4]_nSCN$ (mostly $n=1$ and 2), where the isomer ratios (N/S ratios) are nearly 1. The reaction of $EtO(CH_2)_mBr$ ($m=2$—5) with mercuric thiocyanate in THF or *n*-Bu_2O proceeds rapidly only in the case of $m=4$ to give $EtO(CH_2)_4NCS$ and $EtO(CH_2)_4SCN$, the N/S ratio being also nearly 1, and gives EtNCS and EtSCN when $m=5$, while the reaction with potassium thiocyanate in DMF affords a good yield of $EtO(CH_2)_mSCN$ ($m=2$—5) as nearly the only product. It is suggested that the titled reaction involves the initial formation of a five-membered oxonium ion, *O*-alkyltetrahydrofuranium ion, and a subsequent attack by $XHg(SCN)_2^-$.

Previously, we reported that alkyl halides react with $Hg(SCN)_2$ in less polar solvents such as di-*n*-butyl ether and *n*-hexane to afford predominantly alkyl isothiocyanates (RNCS), in contrast to the reaction with the potassium salt in DMF, where alkyl thiocyanates (RSCN) are the main products.[1] When the former reaction was carried out in tetrahydrofuran (THF) as a solvent, it was found that the THF-incorporated products, $R[O(CH_2)_4]_nNCS(-SCN)$ ($n=1$ and 2), were mainly obtained instead of the expected substitution products, RNCS(–SCN). Here, the ratios of isothiocyanates to thiocyanates (hereinafter abbreviated as the N/S ratio) in the THF-incorporated products were nearly 1, regardless of the structure of the alkyl halides. In the present paper we wish to describe the results of the reaction and discuss its reaction mechanism.

Results and Discussion

When the reaction of various alkyl halides with $Hg(SCN)_2$ was carried out in THF at 65—70 °C (in the case of MeI, at 35—40 °C) for several hours, the THF-incorporated products (**1** and **2**) were mainly obtained, together with small amounts of the expected products (**3** and **4**), as shown in scheme 1. Typical results are summarized in Table 1. Besides the products listed in Table 1, small amounts of high-boiling substances which seemed to be **1** and **2** ($n=3$) were always detected in glc analysis. As can be seen from Table 1, the N/S ratios in **3** plus **4** increased upon changing from primary halides to secondary ones; this is in good agreement with the reported result of the reaction in *n*-Bu_2O.[1] On the other hand, the N/S ratios in **1** plus **2** were generally *ca.* 1, regardless of the structure of alkyl halides used. The reactions using $Cu(NCS)_2$ and AgSCN instead of Hg salt gave mainly 4-alkoxybutyl halide and a mixture of **3** and **4**, respectively, whereas the yields of **1** and **2** were very low even for a longer reaction time (see Experimental). Here the N/S ratio in **1** plus **2** was *ca.* 0.1, in sharp contrast to that in the Hg case. Therefore, the formation of nearly equal amounts of **1** and **2** as main products is a characteristic of the reaction with $Hg(SCN)_2$. Similar phenomena were also observed in reactions of EtI with metal bromides in THF, where the bromide analogue of **1** and **2** ($n=1$ and 2) was obtained in good yields by using $HgBr_2$, while the reaction occurred only slightly by using Cu(II) and Ag(I) bromides.[2]

$$RX + Hg(SCN)_2 + THF \longrightarrow \underset{\mathbf{1}}{R[O(CH_2)_4]_nNCS} + \underset{\mathbf{2}}{R[O(CH_2)_4]_nSCN} + \underset{\mathbf{3}}{RNCS} + \underset{\mathbf{4}}{RSCN} \quad (1)$$

Table 1. REACTION OF RX WITH $Hg(SCN)_2$ IN THF[a]

RX (40 mmol) R	RX (40 mmol) X	React. temp (°C)	React. time (hr)	Products Yields (%),[b] (N/S ratios)[c] **1**+**2** ($n=1$)	**1**+**2** ($n=2$)	**3**+**4**
Me	I	35—40	28	15 (47/53)	10 (48/52)	1 (8/92)
Et	I	65—70	3	32 (49/51)	13 (52/48)	2 (30/70)
n-Pr	I	65—70	3	36 (49/51)	12 (53/47)	6 (34/66)
n-Bu	I	65—70	3	32 (51/49)	—[d]	4 (33/67)
i-Pr	I	65—70	2	30 (50/50)	17 (50/50)	5 (77/23)
c-C_6H_{11}	I[e]	65—70	5	1 (53/47)	—[d]	1 (75/25)
n-Bu	Br	65—70	4	3 (47/53)	2 (45/55)	1 (38/62)
i-Pr	Br	65—70	6.5	34 (49/51)	15 (50/50)	2 (70/30)

a) $Hg(SCN)_2$, 40 mmol. THF, 30 ml. b) Isolated yield. c) Determined by glc. d) Not determined. e) Other product: cyclohexene, 64%.

* Koei Chemical Co. Ltd., Joto-ku, Osaka 536

** To whom correspondence should be addressed.

Considering the well-clarified mechanism of the polymerization of THF under the influence of trialkyloxonium salts,[3] together with the finding that no reaction proceeded between THF and a mixture of ethyl thiocyanate and isothiocyanate by heating at 65—70 °C for 3 hr in the presence of $Hg(SCN)_2$, we propose a pathway for the formation of **1** and **2** such as that shown in scheme 2, where the *O*-alkyltetrahydofuranium ion is formed as an initial intermediate from RX and THF.

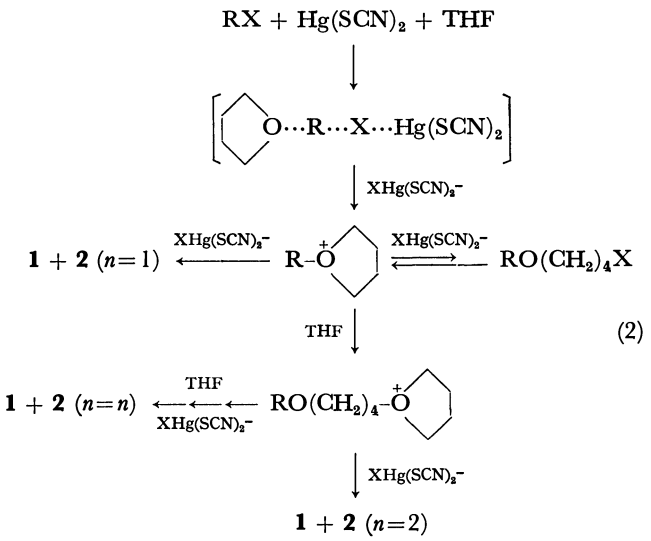

Since the yields of **1** plus **2** from primary alkyl iodides were generally comparable to that from *i*-PrI (see Table 1), it seems unlikely that free R^+ plays a part in the oxonium ion formation. When more polar 1,2-dichloroethane ($\varepsilon=10.36$) was used as a solvent instead of THF ($\varepsilon=7.58$) (a favorable condition for the S_N1 process), the conversion in the reaction of *i*-PrBr with $Hg(SCN)_2$ was only 0.5% at 65 °C for 7 hr. On the contrary, the reaction in THF showed a high conversion (see Table 1), suggesting a nucleophilic participation of the solvent. Therefore it seems to be reasonable to assume that both the push by THF and the pull by the Hg salt are involved in the formation of *O*-alkyltetrahydrofuranium ion. The resulting cation reacts with $XHg(SCN)_2^-$[1] to afford a mixture of **1** and **2** ($n=1$) and 4-alkoxybutyl halide, or with another THF molecule with ring opening to give a new tetrahydrofuranium ion, which in turn can react with $XHg(SCN)_2^-$ to afford **1** and **2** ($n=2$) or can add to another THF molecule. Although the formation of 4-alkoxybutyl halide was only slightly observed in this reaction, the halide became the main product in the reaction of EtI and $Hg(CN)_2$, instead of $Hg(SCN)_2$, in THF (see Experimental). Furthermore, we found that 4-butoxybutyl bromide reacted very rapidly with $Hg(SCN)_2$ in THF to afford **1** and **2** (*i.e.*, almost all of the bromide disappeared after 20 min at 65—70 °C), the N/S ratio in **1** plus **2** being *ca.* 1. Therefore it seems very likely that even if 4-alkoxybutyl halide is formed, the equilibrium is quite unfavorable to this halide in the presence of $Hg(SCN)_2$.

In the solvolysis of ω-methoxy-*n*-alkyl brosylates, $CH_3O(CH_2)_mOBs$, a considerable rate enhancement has been observed in the cases of $m=4$ and 5, as compared to those of $m=2$ and 3, and this has been attributed to the formation of a cyclic oxonium ion intermediate.[4] Furthermore, a favorable nucleophilic attack occurs at the O-methylene C atoms of the ring for a five-membered oxonium ion ($m=4$), while it occurs at the methyl C atom of the side chain for a six-membered one ($m=5$).[5] In order to obtain further evidence for scheme 2, namely the participation of *O*-alkyltetrahydrofuranium ion as an intermediate, we carried out the reaction of $EtO(CH_2)_m$-Br with $Hg(SCN)_2$ in THF and *n*-Bu_2O and obtained results similar to those described above. Thus the reaction proceeded rapidly when $m=4$, while ethyl thiocyanate and isothiocyanate were obtained only in the case of $m=5$ (Scheme 3, Table 2). The extent of rate

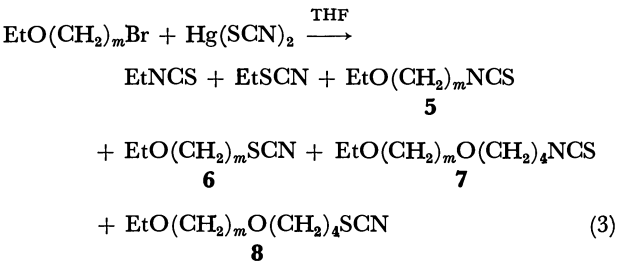

enhancement by the introduction of an alkoxy group at 4-position in *n*-BuBr is such that the reaction of 4-ethoxy-*n*-butyl bromide with $Hg(SCN)_2$ in *n*-Bu_2O gave a 77% yield of a mixture of **5** and **6** ($m=4$) at 65—70 °C for 1 hr (see Table 2), while only a 23% yield of *n*-BuN-

Table 2. Reaction of $EtO(CH_2)_mBr$ with $Hg(SCN)_2$ in THF and *n*-Bu_2O[a]

$EtO(CH_2)_mBr$ (20 mmol) *m*	Solvent (15 ml)	React. time (hr)	Products Yields (%),[b] (N/S ratios)[b] EtNCS+EtSCN	5 + 6	7 + 8
2	THF	4	0	0.2 (15/85)	1[c] (51/49)
2	*n*-Bu_2O	20	0	0	0
3	THF	4	0	1 (23/77)	2[c] (47/53)
3	*n*-Bu_2O	20	0	0	0
4	THF	1.5	0	42[d] (48/52)	17[d] (50/50)
4	*n*-Bu_2O	1	0	77[d] (64/36)	0
5	THF	4	12 (53/47)	4[e] (43/57)	—[f]
5	*n*-Bu_2O	24	12 (55/45)	7 (48/52)	0

a) $Hg(SCN)_2$, 20 mmol. React. Temp., 65—70 °C. b) Determined by glc. c) Not characterized. d) Isolated yield. Here **5**+**6** and **7**+**8** correspond to **1**+**2** (R=Et, $n=1$) and **1**+**2** (R=Et, $n=2$), respectively. e) Other products: $EtO(CH_2)_4NCS(-SCN)$ 5.7%, N/S ratio=44/56. f) Not determined.

CS(–SCN) was obtained from the reaction with *n*-BuBr, even at 80—90 °C for 50 hr.[1] Considering these findings it is obvious that the reaction proceeds through a cyclic oxonium ion intermediate when $m=4$ and 5 (Scheme 4). It should be noted here that the N/S ratio

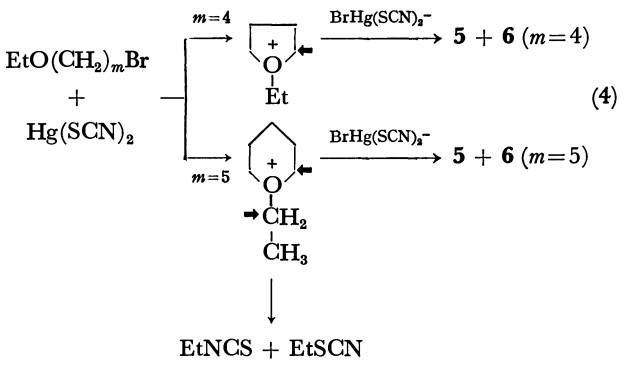

in **5** plus **6** ($m=4$) was nearly 1 in THF solvent, which is in good agreement with that in **1** plus **2** shown in Table 1. This fact clearly supports scheme 2, where the reaction of RX with $Hg(SCN)_2$ in THF is supposed to involve an *O*-alkyltetrahydrofuranium ion as an intermediate.

In separate experiments we confirmed that almost no isomerization occurs between the produced alkyl isothiocyanate and thiocyanate under the conditions shown in Tables 1 and 2. Therefore, it can be concluded that the N/S ratios in both Tables are kinetically controlled.

In contrast to the reaction of $RO(CH_2)_mBr$ with $Hg(SCN)_2$ described above, the reaction with KSCN in DMF proceeded smoothly with all kinds of $RO(CH_2)_mBr$; alkoxyalkyl thiocyanate was nearly the only product (Table 3). Here, the presence of alkoxy groups showed almost no significant effects on either the reaction rate or the yield of the products. In the reaction using THF as a solvent, where the rate was slow compared to that in DMF, none of the THF-incorporated products was formed and alkoxyalkyl thiocyanate was also nearly the only product. These results clearly indicate that the

Table 3. Reaction of $RO(CH_2)_mBr$ with KSCN in DMF and THF[a]

$RO(CH_2)_mBr$ (20 mmol) R	m	Solvent (15 ml)	React. temp. (°C)	React. time (hr)	Yield of product (%)[b] $RO(CH_2)_mSCN$
Et	2	DMF	65—70	1	78
Et	3	DMF	65—70	1	86
Et	4	DMF	65—70	1	89
n-Bu	4	DMF	65—70	1	93
n-Bu	4	THF	65—70	24	38
Et	5	DMF	65—70	1	92

a) KSCN, 40 mmol. b) Isolated yield. Each product contained 0.6—0.8% of $RO(CH_2)_mNCS$ (by glc).

reaction of alkoxyalkyl bromide with KSCN is S_N2 type in either solvent, as expected.[1]

In a previous paper[1] we reported that the N/S ratios of the products in the reaction of alkyl halides with $Hg(SCN)_2$ are 21/79—34/66 for primary alkyl halides (S_N2 type) and 85/15—99/1 for secondary and tertiary ones (S_N1 type). A high selectivity for N attack was ascribed to the structure of $Hg(SCN)_2$, where Hg is S-bonded. As described above, the N/S ratio in **1** plus **2** was nearly 50/50 (more precisely 47/53—53/47) regardless of the structure of alkyl halides used; this ratio was thought to be determined by the step of the attack on the intermediate oxonium ion. In order to confirm this point we prepared $Et_3O^+BF_4^-$ separately and carried out the reaction of this oxonium ion with a mixture of KBr and $Hg(SCN)_2$ in 1,2-dichloroethane. As a result, although the yield was low, a mixture of EtNCS and EtSCN was obtained, with a N/S ratio of 66/34 (see Experimental). Here, neither THF nor n-Bu_2O could be used as a solvent because of the polymerization of the solvent or an alkyl exchange reaction. For comparison, when the reaction of $EtO(CH_2)_5Br$ with $Hg(SCN)_2$ was carried out in 1,2-dichloroethane at 65—70 °C for 4 hr, a mixture of EtNCS and EtSCN was obtained in 38% yield, with a N/S ratio of 61/39, together with **5** and **6** ($m=5$)

Table 4. Boiling points and analytical data of new compounds

Compounds[a]	Bp(°C/mmHg)	Found (Calcd) C (%)	H (%)	N (%)
1 + **2** (R=Me, $n=1$)	70—75 /5	49.19 (49.63)	8.07 (7.64)	9.34 (9.65)
1 + **2** (R=Et, $n=1$)	77—85 /5	52.44 (52.80)	8.64 (8.23)	8.55 (8.80)
1 + **2** (R=*n*-Pr, $n=1$)	81—88 /2	54.88 (55.45)	8.98 (8.73)	7.89 (8.08)
1 + **2** (R=*i*-Pr, $n=1$)	91—102/6	55.16 (55.45)	9.05 (8.73)	7.96 (8.08)
1 + **2** (R=*n*-Bu, $n=1$)	93—104/3	57.68 (57.71)	9.38 (9.15)	7.58 (7.48)
1 + **2** (R=Me, $n=2$)	119—126/2	55.53 (55.27)	9.32 (8.81)	6.29 (6.45)
1 + **2** (R=Et, $n=2$)	145—157/4	56.70 (57.11)	9.51 (9.15)	5.78 (6.05)
1 + **2** (R=*n*-Pr, $n=2$)	131—137/2	58.22 (58.74)	9.72 (9.45)	5.68 (5.71)
1 + **2** (R=*i*-Pr, $n=2$)	127—132/2	58.44 (58.74)	9.97 (9.45)	5.66 (5.71)
$EtO(CH_2)_2SCN$	99—101/22	45.27 (45.78)	7.12 (6.92)	10.56 (10.68)
$EtO(CH_2)_3SCN$	75—76 /6.5	49.01 (49.63)	7.95 (7.64)	9.47 (9.65)
$EtO(CH_2)_4SCN$[b]	95—96 /6			
$EtO(CH_2)_5SCN$	109—111/5.5	55.22 (55.45)	9.01 (8.73)	8.04 (8.08)
n-$BuO(CH_2)_4SCN$[c]	120—121/6.5			

a) The N/S ratios in **1** plus **2** are shown in Table 1. $RO(CH_2)_mSCN$ contains 0.6—0.8% of $RO(CH_2)_mNCS$. b) Corresponds to **2** (R=Et, $n=1$). c) Corresponds to **2** (R=*n*-Bu, $n=1$).

(16% yield, N/S=55/45). The fact that the N/S ratios of the products, EtNCS and EtSCN, are nearly the same in both reactions shows that the latter reaction proceeds through an ethyloxonium ion, and also supports the reaction mechanism shown in schemes 2 and 4. The reason why the attack by N is more preferred in the reaction with the oxonium ion (N/S=47/53—53/47) than in that with primary halides (N/S=21/79—34/66) seems to be explained by the symbiotic effect in the HSAB principle proposed by Pearson,[6] since both reactions are supposed to be of the S_N2 type. This effect states that in an S_N2 reaction a grouping of either several hard ligands or several soft ligands on the central carbon atom should stabilize the transition state and cause an increased rate of reaction. Namely, the carbon bearing a harder ligand as the leaving group is apt to be attacked more preferably by a harder atom in an ambident ion. In our case, R_2O in R_3O^+ is harder than X^- in RX as the leaving group, and the N atom in the attacking species, $XHg(SCN)_2^-$, is harder than the S atom.[7]

Experimental

The N/S ratios in mixtures of alkyl thiocyanates and isothiocyanates were determined by gas chromatography (glc). Glc analyses were carried out on a Shimadzu 5APTF apparatus using EGSS-X (1 m), Apz-L (1 m), and PEG-6000 (3 m) columns (carrier gas, N_2). The retention time of RSCN was longer than that of RNCS in EGSS-X and PEG-6000 columns, while the reverse was observed by using Apz-L column. The NMR spectra were recorded with a Varian A-60 spectrometer in CCl_4, using TMS as an internal standard. The IR spectra were taken with a Hitachi EPI-S2 spectrometer.

Materials. All the organic substances, including the solvents, were used after distillation, while commercial inorganic salts were used without further purification. $Cu(NCS)_2$ was prepared from $CuSO_4 \cdot 5H_2O$ and KSCN by the reported method.[8] Alkoxyalkyl bromides, $RO(CH_2)_mBr$, were prepared by PBr_3 bromination of the corresponding alcohols which were synthesized from RBr and $NaO(CH_2)_mOH$:[9] R=Et and m=2, bp 126—127 °C (lit,[10] bp 126—127 °C); R=Et and m=3, bp 147—148 °C (lit,[9] bp 147—150 °C); R=Et and m=4, bp 78—80 °C/30 mmHg (lit,[11] bp 69 °C/15 mmHg); R=Et and m=5, bp 91—92 °C/20 mmHg (lit,[11] bp 185—192 °C/741 mmHg); R=*n*-Bu and m=4, bp 105—108 °C/25 mmHg (lit,[12] bp 57 °C/1.5 mmHg).

Reaction of Alkyl Halides with Mercuric Thiocyanate in THF. The following example shows a typical procedure. To a suspension of $Hg(SCN)_2$ (12.7 g, 40 mmol) in THF (30 ml) was added *i*-PrI (6.8 g, 40 mmol) drop by drop at 65—70 °C; the resulting yellowish-green homogeneous solution was kept for 2 hr under stirring while orange precipitates gradually came out. After being cooled down to room temperature, Et_2O (200 ml) was added and the precipitated inorganic salt was filtered off. The filtrate was washed several times with aqueous KI in order to remove a small amount of dissolved mercuric salt and then dried over $MgSO_4$. Distillation afforded the following products: **3**+**4** (R=*i*-Pr), bp 45—50 °C/40 mmHg, 0.2 g (5% yield); **1**+**2** (n=1, R=*i*-Pr), bp 91—102 °C/6 mmHg, 2.1 g (30% yield); **1**+**2** (n=2, R=*i*-Pr), bp 127—132 °C/2 mmHg, 1.7 g (17% yield).

Reaction of $RO(CH_2)_mBr$ with KSCN in DMF. The following example shows a typical procedure. To a homogeneous solution of KSCN (7.8 g, 80 mmol) in DMF (30 ml) was added $EtO(CH_2)_2Br$ (6.1 g, 40 mmol) at 65—70 °C. After being kept for 1 hr under stirring, the mixture was cooled down to room temperature, poured into water, and then extracted with Et_2O (200 ml). Distillation of the ether extract gave 4.1 g (78% yield) of $EtO(CH_2)_2SCN$, which contains a small amount of isothiocyanate (N/S=0.7/99.3); bp 99—101 °C/22 mmHg. IR 2150 (ν_{SCN}), 1120 (ν_{C-O}) cm^{-1}. NMR δ 1.21 (t. 3H, J=7 Hz, methyl), 3.1 (t. 2H, J=5.5 Hz, $-OCH_2-C\underline{H}_2S-$), 3.53 (q. 2H, J=7 Hz, $CH_3C\underline{H}_2O-$), 3.7 (t. 2H, J=5.5 Hz, $-OC\underline{H}_2CH_2S-$).

The boiling points and analytical data of all new compounds in Tables 1—3 are summarized in Table 4. All IR and NMR spectra were reasonably explained.

Reaction of Isopropyl Iodide with $Cu(NCS)_2$ or AgSCN in THF. When the heterogeneous mixture of $Cu(NCS)_2$ (7.2 g, 40 mmol) and *i*-PrI (6.8 g, 40 mmol) in THF (30 ml) was heated at 65—70 °C for 10 hr, the following compounds were obtained: *i*-PrNCS(-SCN) 0.24 g (6% yield, N/S=6/94), **1**+**2** (R=*i*-Pr, n=1) 0.52 g (7.5% yield, N/S=11/89), *i*-PrO-$(CH_2)_4I$ 1.65 g (17% yield), a small amount of unidentified product, and a residue (1.1 g). *i*-$PrO(CH_2)_4I$: bp 96—97 °C/20 mmHg, IR 1130 (ν_{C-O}) cm^{-1}. NMR δ 1.08 (d. 6H), 1.4—2.2 (m. 4H), 3.0—3.7 (m. 5H). Found: C, 34.93; H, 6.57%. Calcd for $C_7H_{15}OI$: C, 34.73; H, 6.25%.

A similar reaction using AgSCN at 65—70 °C for 24 hr afforded 0.6 g (14% yield) of *i*-PrNCS(-SCN) (N/S=24/76) and 0.35 g (5% yield) of **1**+**2** (N/S=14/86). Almost no reaction occurred at 65—70 °C for 1 hr in either case.

Reaction of Ethyl Iodide with $Hg(CN)_2$ in THF. A homogeneous solution of EtI (6.3 g, 40 mmol) and $Hg(CN)_2$ (10 g, 40 mmol) in THF (20 ml) was heated at 70 °C for 24 hr. The products were 4-ethoxybutyl iodide (1.1 g, 12% yield) and 0.86 g of an unidentified compound, probably $EtO-(CH_2)_4O(CH_2)_4I$. Almost no reaction occurred by heating for 1.5 hr. 4-Ethoxybutyl iodide: bp 87—89 °C/23 mmHg. IR 1130 (ν_{C-O}) cm^{-1}. NMR δ 1.15 (t. 3H), 1.4—2.25 (m. 4H), 3.1—3.6 (m. 6H).

Reaction of $Et_3O^+BF_4^-$ with $Hg(SCN)_2$ and KBr in 1,2-Dichloroethane. To 1,2-dichloroethane (5 ml) solution of $AgBF_4$ (1.0 g, 5 mmol) was added Et_2O (1 ml) and then EtBr (1 ml) at 15—20 °C under N_2 atmosphere.[13] After stirring for 1 hr the resulting AgBr was filtered off and washed with 1,2-dichloroethane (5 ml). A solid mixture of KBr (1.1 g, 5 mmol) and $Hg(SCN)_2$ (1.6 g, 5 mmol) was added to the combined 1,2-dichloroethane solution and the resulted heterogeneous mixture was stirred at 40 °C for 4 hr under N_2. Glc analysis of the mixture using *n*-BuNCS as an internal standard showed the presence of 5 mg (0.06 mmol, 1.2% yield based on $AgBF_4$) of a mixture of EtNCS and EtSCN (N/S=66/34). The reaction with KSCN was similarly carried out to give 11.6% yield of a mixture of EtNCS and EtSCN (N/S=2/98). Although it was conceivable that excess EtBr instead of $Et_3O^+BF_4^-$ reacted to give the product, we confirmed that EtBr did not react at all with $Hg(SCN)_2$ or KSCN under similar conditions.

References

1) N. Watanabe, M. Okano, and S. Uemura, This Bulletin, **47**, 2745 (1974).

2) N. Watanabe, S. Uemura, and M. Okano, unpublished data.

3) H. Perst, "Oxonium Ions in Organic Chemistry," Verlag Chemie, Weinheim (1971), p. 78 and 141.

4) S. Winstein, E. Allred, R. Heck, and R. Glick, *Tetrahedron*, **3**, 1 (1958).

5) E. L. Allred and S. Winstein, *J. Amer. Chem. Soc.*, **89**, 3991, 4012 (1967).

6) R. G. Pearson and J. Songstad, *ibid.*, **89**, 1827 (1967).
7) R. G. Pearson, *Chem. Brit.*, **3**, 103 (1967).
8) C. L. Jenkins and J. K. Kochi, *J. Org. Chem.*, **36**, 3095 (1971).
9) L. I. Smith and J. A. Sprung, *J. Amer. Chem. Soc.*, **65**, 1276 (1943).
10) E. Schmidt, *Ann. Chem.*, **337**, 60 (1904).
11) S. Oae, *J. Amer. Chem. Soc.*, **78**, 4030 (1956).
12) R. E. Gilbert and N. B. Lorette, U. S. 3303221; *Chem. Abstr.*, **67**, 21628j (1967).
13) H. Meerwein, "Methoden der Organischen Chemie (Houben-Weyl)," ed. by E. Müller, 4th Ed., Vol. VI/3, Georg Thieme Verlag, Stuttgart (1965), p. 338.

Synthesis of D-Ribofuranosylpyrazolecarboxamides

Osamu MAKABE, Masakazu NAKAMURA, and Sumio UMEZAWA

Department of Applied Chemistry, Faculty of Engineering, Keio University, Hiyoshi, Kohoku-ku, Yokohama, Kanagawa 223

(Received March 13, 1975)

Several carbamoylpyrazole-nucleosides were synthesized by fusion of 1-*O*-acetyl derivatives of ribofuranoses with pyrazole derivatives in the presence of bis(*p*-nitrophenyl) hydrogen phosphate as an acidic catalyst. NMR and UV spectral studies revealed the orientation in *N*-glycosylation of the substituted pyrazoles.

The pyrazole-nucleoside antibiotic pyrazomycin[1] (3-(β-D-ribofuranosyl)-4-hydroxypyrazole-5-carboxamide) has been found to be an inhibitor of virus multiplication. On the other hand, 1-β-D-ribofuranosyl-1,2,3-triazole-4-carboxamide, previously synthesized in our laboratory,[2] was found to possess activity against vaccinia viruses, and, 1-β-D-ribofuranosyl-1,2,4-triazole-3-carboxamide (virazole), synthesized by Witkowski *et al.*,[3] was reported to possess activity against DNA and RNA viruses. These facts prompted us to investigate the structure-activity relationship of pyrazolecarboxamide nucleosides. This paper describes the synthesis of several carbamoylpyrazoles and related nucleosides.

In the present synthesis, blocked derivatives of pyrazoles were coupled with 1-*O*-acetyl derivatives of blocked ribofuranoses by the fusion procedure in the presence of bis(*p*-nitrophenyl)hydrogen phosphate (BNPP)[4] to give blocked nucleosides. Another purpose of the present investigation was to study the orientation in the *N*-glycosylation of pyrazole derivatives.

Fusion of ethyl pyrazole-3-carboxylate[5] (**1**) with 1-*O*-acetyl-2,3,5-tri-*O*-benzoyl-β-D-ribofuranose[6] (**4**) in the presence of BNPP gave a mixture of two major nucleosides, namely ethyl 1-(2,3,5-tri-*O*-benzoyl-β-D-ribofuranosyl)pyrazole-3-carboxylate (**6**) and -5-carboxylate (**7**), which were separated by chromatography to give **6** and **7** in a ratio of approximatly 8: 1. Treatment of **6** and **7** with methanolic ammonia gave 1-β-D-ribofuranosylpyrazole-3-carboxamide (**18β**) and 5-carboxamide (**19β**), respectively.

In an attempt to prepare the corresponding α-nucleosides, 1-*O*-acetyl-2,3,5-tri-*O*-benzyl-D-ribofuranose

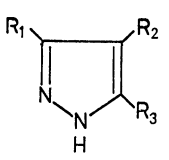

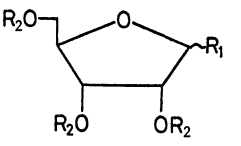

1, R_1=CO_2Et, R_2=R_3=H
2, R_1=R_3=CO_2Et, R_2=H
3, R_1=R_3=CO_2Et, R_2=NO_2

4, R_1=β-OAc, R_2=Bz
5, R_1=OAc, R_2=Bn

Chart 1.

(**5**), which has a benzyl group at *C*-2 as a non-participating group, was prepared and condensed with **1** by the fusion procedure to give ethyl 1-(2,3,5-tri-*O*-benzyl-α-D-ribofuranosyl)pyrazole-3-carboxylate (**10α**), its β-anomer (**10β**), and β-5-carboxylate (**11β**) in a ratio of approximately 2.6: 1.6: 1. Upon treatment with methanolic ammonia, these gave the carboxamide derivatives, (**14α**), (**14β**), and (**15β**), respectively. Catalytic hydrogenolysis of these products afforded 1-α-D-ribofuranosylpyrazole-3-carboxamide (**18α**), its β-isomer (**18β**), and β-5-carboxamide (**19β**), respectively.

Next, several pyrazole-3,5-dicarboxamide nucleosides, namely, 1-β-D-ribofuranosylpyrazole-3,5-dicarboxamide (**20β**), 4-nitro-1-(β-D-ribofuranosyl)pyrazole-3,5-dicarboxamide (**21β**), 4-amino-1-(β-D-ribofuranosyl)pyrazole-3,5-dicarboxamide (**22β**), and its α-anomer (**22α**) were synthesized. The fusion of ethyl pyrazole-3,5-dicarboxylate (**2**) with **4** gave ethyl 1-(2,3,5-tri-*O*-benzoyl-β-D-ribofuranosyl)pyrazole-3,5-dicarboxylate (**8**), which led to **20β** by the treatment with methanolic ammonia. Similar condensation of **2** with the benzyl sugar **5** also afforded a

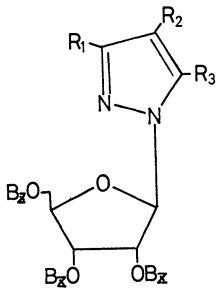

6, R_1=CO_2Et, R_2=R_3=H
7, R_3=CO_2Et, R_1=R_2=H
8, R_1=R_3=CO_2Et, R_2=H
9, R_1=R_3=CO_2Et, R_2=NO_2

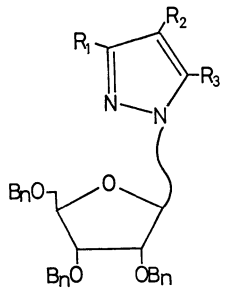

10β, R_1=CO_2Et, R_2=R_3=H
10α, R_1=CO_2Et, R_2=R_3=H
11β, R_3=CO_2Et, R_1=R_2=H
12β, R_1=R_3=CO_2Et, R_2=H
13β, R_1=R_3=CO_2Et, R_2=NO_2
13α, R_1=R_3=CO_2Et, R_2=NO_2

14β, R_1=$CONH_2$, R_2=R_3=H
14α, R_1=$CONH_2$, R_2=R_3=H
15β, R_3=$CONH_2$, R_1=R_2=H
16β, R_1=R_3=$CONH_2$, R_2=H
17β, R_1=R_3=$CONH_2$, R_2=NO_2
17α, R_1=R_3=$CONH_2$, R_2=NO_2

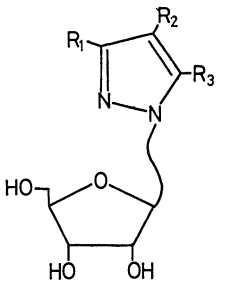

18β, R_1=$CONH_2$, R_2=R_3=H
18α, R_1=$CONH_2$, R_2=R_3=H
19β, R_3=$CONH_2$, R_1=R_2=H
20β, R_1=R_3=$CONH_2$, R_2=H
21β, R_1=R_3=$CONH_2$, R_2=NO_2
22β, R_1=R_3=$CONH_2$, R_2=NH_2
22α, R_1=R_3=$CONH_2$, R_2=NH_2

Chart 2

β-nucleoside (**12β**) which led to **20β** through **16β**. In an attempt to prepare 4-amino nucleosides, ethyl 4-nitropyrazole-3,5-dicarboxylate (**3**) was prepared and coupled with **4** to give ethyl 1-(2,3,5-tri-*O*-benzoyl-β-D-ribofuranosyl)-4-nitropyrazole-3,5-dicarboxylate (**9**); subsequent amidation yielded the 4-nitro-3,5-dicarbamoyl derivative (**21β**), and catalytic reduction afforded the 4-amino derivative (**22β**). Similar fusion of **3** with the benzyl sugar **5** gave a mixture (approximately 1:1) of (**13α**) and (**13β**), which were separated by chromatography; subsequent amidation gave (**17α**) and (**17β**), respectively, and catalytic reduction yielded the 4-amino nucleosides (**22α**) and **22β**.

The structures of the above mentioned pyrazole-nucleosides were assigned on the basis of their NMR spectral data. An apparent difference in the chemical shift for the anomeric proton signals in the 3-carboxamides (**18α**, **18β**) and 5-carboxamide (**19β**) is consistently observed. The large downfield shift of the latter is attributable to the close location of the anisotropic carbamoyl group. The same effect has been observed in other nucleosides.[7-9] The proton of 3,5-dicarboxamide (**20β**) also showed a similar downfield shift. The ultraviolet spectra of the 3-carboxamides (**18α**, **18β**) and 5-carboxamide (**19β**) also showed a characteristic difference, as shown in Table 1.

Table 1. Ultraviolet absorption data for pyrazole-3- and 5-carboxamide derivatives

Compound No.	Solvents λ_{max} nm and ε					
	pH 7 H_2O		pH 1 HCl		pH 13 NaOH	
	λ_{max}	ε	λ_{max}	ε	λ_{max}	ε
18α	214	11500	215	12700	227	11000
18β	212	11100	213	11200	227	12200
19β	220	12500	221	12200	227	8400

Assignment of the anomeric configuration is also supported by the NMR spectral data. The *H*-1′ signal for 1′,2′-*trans*-nucleosides has been shown[10] to appear at higher field than the *H*-1′ signal of the corresponding 1′,2′-*cis*-nucleosides. No formation of α-anomers corresponding to **11β** and **12β** was detected in this procedure; however, their β-configurations were characterized by the small $J_{1'2'}$ values (2.0 Hz).

The data of the NMR spectra also shows that *N*-glycosylation causes a chemical shift: the proton at *C*-5 adjacent to glycosylated nitrogen is at a lower field than that of the proton at *C*-3 adjacemt to nitrogen which is not glycosylated. A similar trend has been observed in the case of the proton at *C*-5 of 1,2,3-triazoles glycosylated at *N*-1.[11]

Among the pyrazole-nucleosides prepared in this paper, the 3-carboxamide (**18β**), which is a carbon bioisostere of virazole, and 3,5-dicarbamoyl-4-nitro derivative (**21β**) were found to have antileuchemic and antitumor activities.[12]

Experimental

Melting points were determined on a micro hot stage and were uncorrected. Thin layer chromatography (tlc) was conducted by the use of a Wakogel B-5. Silica gel column chromatography was carried out by using a Wakogel G-200. UV-Spectra were taken with a Hitachi Perkin-Elmer UV-VIS spectrometer 139. The NMR spectra were measured with a Varian A-60D spectrometer (TMS as an internal standard).

Ethyl Pyrazole-3-carboxylate (1). Prepared by the method of K. V. Auewrs[5]; NMR ($CDCl_3$): δ 7.95 (d, 1H, H-5), 7.01 (d, 1H, H-4), 4.55 (q, 2H, CH_2-ester), 1.47 (t, 3H, CH_3-ester).

Ethyl Pyrazole-3,5-dicarboxylate (2). Pyrazole-3,5-dicarboxylic acid[13] (10.0 g, 64 mmol) was dissolved in a 70% hydrogen chloride ethanol solution (100 ml) and refluxed for 4 hr. After removal of the solvent, the residue was dissolved in ethyl acetate and chromatographed on a silica gel column (200 g) using benzene–ethyl acetate (3:1) as a solvent. The main fraction was evaporated to give colorless crystals of **2**, 9.8 g (72%); mp 49—51 °C. NMR ($CDCl_3$): δ 7.50 (s, 1H, H-4), 4.52 (q, 4H, CH_2-ester), 1.41 (q, 6H, CH_3-ester). Found: C, 50.80; H, 5.72; N, 13.14%. Calcd for $C_9H_{12}O_4N_2$: C, 50.94; H, 5.70; N, 13.20%.

Ethyl 4-Nitropyrazole-3,5-dicarboxylate (3). 3-Methyl-4-nitropyrazole-5-carboxylic acid[14] (10.0 g, 58.5 mmol) was dissolved in water (100 ml), to which powdered potassium permanganate (0.13 mol) was gradually added for 30 min under stirring. The solution was heated at 100 °C for 8 hr under stirring. After filtration, the solution was evaporated to dryness. 3 M Sulfulic acid (30 ml) was added and the precipitate was filtered. The dried crude precipitate was suspended in a 70% ethanolic hydrogen chloride solution (65 ml) and the solution was refluxed for 4 hr. After evaporation of the solvent, the residual syrup was dissolved in acetone (10 ml) and silica gel (6.5 g) was added; the mixture was evaporated and the crude product was purified by chromatography on a column (2.5×90 cm) of silica gel (130 g) using benzene–ethyl acetate (4:1) as a solvent, to give pale yellow crystals of **3**, 6.3 g (42%); mp 82—84 °C. Found: C, 41.96; H, 4.11; N, 16.18%. Calcd for $C_9H_{11}O_6N_3$: C, 42.03; H, 4.31; N, 16.34%.

1-O-Acetyl-2,3,5-tri-O-benzyl-D-ribofuranose (5). 2,3,5-Tri-*O*-benzyl-D-ribose[15] (10.0 g, 23.8 mmol) was dissolved in anhydrous pyridine (50 ml) and acetic anhydride (5 ml) was added. The mixture was stirred at room temperature for 12 hr. After evaporation of the solvent, the crude syrup was dissolved in ethyl acetate and chromatographed on a column of silica gel (400 g, 5×100 cm, packed with benzene) and eluted with benzene–ethyl acetate (20:1). The main fraction was evaporated to give a syrup of **5** (9.55 g, 87%); NMR ($CDCl_3$): δ 7.40 (s, 15H, Ar), 6.38 (s, 1H, H-1′), 4.8—3.9 (m, 9H, CH_2-Ar, H-2′, H-3′, H-4′), 3.71 (m, 2H, H-5′, 5″), 1.90 (s, 2.9H, CH_3), 1.87 (s, 0.1H, CH_3), α: β=1:29 (from acetyl peak). Found: C, 72.65; H, 6.50%. Calcd for $C_{28}H_{30}O_6$: C, 72.71; H, 6.54%.

Ethyl 1-(2,3,5-Tri-O-benzoyl-β-D-ribofuranosyl)pyrazole-3-carboxylate (6) and Ethyl 1-(2,3,5-Tri-O-benzoyl-β-D-ribofuranosyl)pyrazole-5-carboxylate (7). A mixture of ethyl pyrazole-3-carboxylate[5] (**1**) (0.62 g, 4.43 mmol) and 1-*O*-acetyl-2,3,5-tri-*O*-benzoyl-β-D-ribofuranose[6] (**4**) (2.0 g, 3.97 mmol) was heated to 140 °C. To the melt was added BNPP (4 mg) and the mixture was heated at 140 °C under reduced pressure about 20 min until the evolution of acetic acid ceased. The resulting mixture was dissolved in ethyl acetate and was placed on a column of silica gel (130 g, 2.5×90 cm, packed with benzene) and eluted succesively with benzene (150 ml) and benzene–ethyl acetate (20:1). The effluent was fractionized into 12 mls.

Fraction Nos 11—21 gave **7**, colorless syrup, 255 mg (11%); $[\alpha]_D^{25}$ −6.7° (*c* 1.73, chloroform). NMR ($CDCl_3$): δ 8.15

(m, 6H, Ar), 7.73 (d, 1H, H-3), 7.51 (m, 10H, Ar, H-1'), 7.02 (d, 1H, H-4), 6.50 (m, 2H, H-2', H-3'), 4.80 (m, 3H, H-4', H-5', 5''), 4.40 (q, 2H, CH_2-ester), 1.40 (t, 3H, CH_3-ester). Found: C, 65.49; H, 5.01; N, 4.58%. Calcd for $C_{32}H_{28}O_9N_2$: C, 65.75; H, 4.83; N, 4.79%.

Fraction Nos 31—49 gave **6**, colorless syrup, 1.92 g (83.5%); $[\alpha]_D^{25}$ −40.0° (*c* 3.2, chloroform). NMR ($CDCl_3$): δ 8.15 (m, 6H, Ar), 7.85 (d, 1H, H-5), 7.55 (m, 10H, Ar, H-1'), 6.95 (d, 1H, H-4), 6.30 (m, 2H, H-2', H-3'), 4.85 (m, 3H, H-4', H-5', 5''), 4.46 (q, 2H, CH_2-ester), 1.40 (t, 3H, CH_3-ester). Found: C, 65.49; H, 5.01; N, 4.58%. Calcd for $C_{32}H_{28}O_9N_2$: C, 65.75; H, 4.85; N, 4.79%.

Ethyl 1-(2,3,5-Tri-O-benzoyl-β-D-ribofuranosyl)pyrazole-3,5-dicarboxylate (8). A mixture of ethyl pyrazole-3,5-dicarboxylate (**2**) (630 mg, 2.97 mmol) and 1-*O*-acetyl-2,3,5-tri-*O*-benzoyl-β-D-ribofuranose (1.50 g, 2.97 mmol) was fused in the presence of BNPP (2 mg) in the same manner as described for the preparation of **7**. The resulting mixture was dissolved in hot acetone (50 ml) and 1.5 g charcoal was added. After heating the mixture on boiling water, the charcoal was filtered off and the filtrate was evaporated under reduced pressure. The syrup was crystallized from isopropylalcohol to give **8**, 1.66 g (85.1%); mp 106—107 °C. $[\alpha]_D^{25}$ −25.6° (*c* 0.96, chloroform). NMR ($CDCl_3$): δ 8.15 (m, 6H, Ar). 7.50 (m, 11H, Ar, H-4, H-1'), 6.45 (m, 2H, H-2', H-3'), 4.81 (m, 3H, H-4', H-5', 5''), 4.48 (q, 4H, CH_2-ester), 1.40 (t, 6H, CH_3-ester). Found: C, 64.24; H, 5.09; N, 4.06%. Calcd for $C_{35}H_{32}O_{11}N_2$: C, 64.02; H, 4.91; N, 4.27%.

Ethyl 1-(2,3,5-Tri-O-benzoyl-β-D-ribofuranosyl)-4-nitropyrazole-3,5-dicarboxylate (9). A mixture of ethyl 4-nitropyrazole-3,5-dicarboxylate (**3**) (765 mg, 2.98 mmol) and 1-*O*-acetyl-2,3,5-tri-*O*-benzoyl-β-D-ribofuranose (**4**) (1.5 g, 2.98 mmol) was fused at 138 °C in the presence of BNPP in the same manner as described for the preparation of **7**. The resulting mixture was dissolved in hot acetone (40 ml) and treated with charcoal. After removal of the charcoal, the acetone solution was evaporated under reduced pressure. The resulting syrup was crystallized from isopropylalcohol to give **9**, 1.38 g (66%); mp 92—93 °C. $[\alpha]_D^{25}$ −51.2° (*c* 1.0, chloroform). NMR ($CDCl_3$): δ 8.15 (m, 6H, Ar), 7.60 (m, 9H, Ar), 7.12 (d, 1H, $J_{1',2'}$=2.0 Hz, H-1'), 6.5—6.2 (m, 2H, H-2', H-3'), 4.80 (m, 3H, H-4', H-5', 5''), 4.49 (dq, 4H, CH_2-ester), 1.39 (t, 6H, CH_3-ester). Found: C, 60.01; H, 4.53; N, 5.83%. Calcd for $C_{35}H_{31}O_{13}N_3$: C, 59.91; H, 4.45; N, 5.99%.

Ethyl 1-(2, 3, 5-Tri-O-benzyl-β-D-ribofuranosyl)pyrazole-3-carboxylate (10β), Its α-anomer (10α) and Ethyl 1-(2,3,5-Tri-O-benzyl-β-D-ribofuranosyl)pyrazole-5-carboxylate (11β). A mixture of **1** (525 mg, 3.04 mmol) and **5** (1.40 g, 3.03 mmol) and a catalytic amount of BNPP were fused for 10 min in the same manner as described for the preparation of **7**. The resulting residue was dissolved in chloroform (5 ml) and silica gel (2 g) was added. The mixture was evaporated and then chromatographed on a column of silica gel (120 g) using *n*-hexane–isopropylether (2: 1) as a solvent. The effluent was fractionized into 13 mls.

Fraction Nos 31—43 gave **11β**, a colorless syrup, 282 mg (17.2%); $[\alpha]_D^{25}$ −1.4° (*c* 5.0, chloroform). NMR ($CDCl_3$): δ 7.65 (d, 1H, H-3), 7.41 (s, 15H, Ar), 7.15 (d, 1H, $J_{1',2'}$= 2.0 Hz, H-1'), 6.99 (d, 1H, H-4), 4.78—4.25 (m, 9H, CH_2-Ar, H-2', H-3', H-4'), 4.45 (q, 2H, CH_2-ester), 3.72 (m, 2H, H-5', 5''), 1.38 (t, 3H, CH_3-ester). Found: C, 70.53; H, 6.02; N, 4.64%. Calcd for $C_{32}H_{34}O_6N_2$: C, 70.83; H, 6.32; N, 5.16%.

Fraction Nos 49—53 gave **10β**, a colorless syrup, 455 mg (27.2%); $[\alpha]_D^{25}$ −30.1° (*c* 1.0, chloroform). NMR ($CDCl_3$): δ 7.88 (d, 1H, H-5), 7.40 (s, 15H, Ar), 6.83 (d, 1H, H-4), 6.17 (d, 1H, $J_{1',2'}$=2.4 Hz, H-1'), 4.80—4.20 (m, 11H, CH_2-Ar, H-2', H-3', H-4', CH_2-ester), 3.77 (t, 2H, H-5', 5''), 1.40 (t, 3H, CH_3-ester). Found: C, 70.51; H, 6.26; N, 4.97%. Calcd for $C_{32}H_{34}O_6N_2$: C, 70.83; H, 6.32; N, 5.16%.

Fraction Nos 56—67 gave **10α**, a colorless syrup, 727 mg (44.4%); $[\alpha]_D^{25}$ +35.8° (*c* 0.98, chloroform). NMR ($CDCl_3$): δ 8.17 (d, 1H, H-5), 7.40 (s, 15H, Ar), 6.95 (d, 1H, H-4), 6.44 (d, 1H, $J_{1',2'}$=4.9 Hz, H-1'), 4.70—4.15 (m, 11H, CH_2-ester, CH_2-Ar, H-2', H-3', H-4'), 3.62 (t, 2H, H-5', 5''), 1.38 (t, 3H, CH_3-ester). Found: C, 70.63; H, 6.37; N, 5.08%. Calcd for $C_{32}H_{34}O_6N_2$: C, 70.83; H, 6.32; N, 5.16%.

Ethyl 1-(2,3,5-Tri-O-benzyl-β-D-ribofuranosyl)pyrazole-3,5-dicarboxylate (12β). A mixture of ethyl pyrazole-3,5-dicarboxylate (**2**) (286 mg, 1.35 mmol) and 1-*O*-acetyl-2,3,5-tri-*O*-benzyl-D-ribofuranose (**5**) (622 mg, 1.35 mmol) was fused in the presence of BNPP (2 mg) in the same manner as described for the preparation of **7**. The resulting mixture was dissolved in ethyl aeetate and chromatographed on a column of silica gel (40 g, 2.5×30 cm) using *n*-hexane–isopropyl-ether (2: 1) as a solvent. The effluent was fractionized into 8 mls. Fractjon lNos 38—64 gave **12β**, a colorless syrup, 530 mg (63%); $[\alpha]_D^{25}$ −28.3° (*c* 1.0, chloroform). NMR ($CDCl_3$): δ 7.42 (t, 16H, H-4, Ar), 7.10 (d, 1H, $J_{1',2'}$=2.0 Hz, H-1'), 4.77—4.25 (m, 13H, CH_2-ester, CH_2-Ar, H-2', H-3', H-4'), 3.73 (m, 2H, H-5', 5''), 1.40 (t, 6H, CH_3-ester). Found: C, 68.08; H, 6.11; N, 4.36%. Calcd for $C_{35}H_{38}O_8N_2$: C, 68.39; H, 6.23; N, 4.57%.

Ethyl 1-(2,3,5-Tri-O-benzyl-β-D-ribofuranosyl)-4-nitropyrazole-3,5-dicarboxylate (13β) and Its α-Anomer (13α). A mixture of ethyl 4-nitropyrazole-3,5-dicarboxylate (**3**) (599 mg, 2.32 mmol) and the sugar component **5** (1.07 g, 2.32 mmol) was fused in the presence of BNPP (2 mg) and worked up in a similar manner to the above, using a silica gel column (80 g, 2.8×35 cm). The effluent was fractionized into 11 mls.

Fraction Nos 38—46 gave **13β**, a colorless syrup, 550 mg (36%); $[\alpha]_D^{25}$ −55.8° (*c* 2.0, chloroform), NMR ($CDCl_3$): δ 7.40 (t, 15H, Ar), 6.52 (d, 1H, $J_{1',2'}$=2.0 Hz, H-1'), 4.8—4.5 (m, 9H, H-2', H-3', H-4', CH_2-Ar), 4.42 (q, 4H, CH_2-ester), 3.52 (d, 2H, H-5', 5''), 1.35 (t, 6H, CH_3-ester). Found: C, 64.03; H, 5.56; N, 6.10%, Calcd for $C_{35}H_{37}O_{10}N_3$: C, 63.72; H, 5.65; N, 6.37%.

Fraction Nos 49—61 gave **13α**, a colorless syrup, 580 mg (38%); $[\alpha]_D^{25}$ −9.3° (*c* 3.0, chloroform). NMR ($CDCl_3$): δ 7.42 (t, 15H, Ar), 6.77 (d, 1H, $J_{1',2'}$=3.3 Hz, H-1'), 4.75—4.50 (m, 9H, H-2', H-3', H-4', CH_2-Ar), 4.42 (q, 4H, CH_2-ester), 3.65 (d, 2H, H-5', 5''), 1.35 (t, 6H, CH_3-ester). Found: C, 63.98; H, 5.46; N, 6.13%. Calcd for $C_{35}H_{37}O_{10}N_3$: C, 63.72; H, 5.65; N, 6.37%.

1-(2,3,5-Tri-O-benzyl-β-D-ribofuranosyl)pyrazole-3-carboxamide (14β). A sample of **10β** (400 mg, 0.785 mmol) in absolute methanol (40 ml) saturated with ammonia at 0°C was kept at room temperaturefor 12 hr, and evaporated under reduced pressure at 40 °C. The residual syrup was washed with *n*-hexane and dried at 80 °C for 10 hr to give a colorless oil of **14β**, 318 mg (84%); $[\alpha]_D^{25}$ −22.5° (*c* 1.0, chloroform). NMR ($CDCl_3$): δ 7.75 (d, 1H, H-5), 7.38 (d, 15H, Ar), 6.87 (d, 1H, H-4), 6.60 (br s, 2H, $CONH_2$), 6.03 (d, 1H, $J_{1',2'}$=3.2 Hz, H-1'), 4.70—4.20 (m, 9H, CH_2-Ar, H-2', H-3', H-4'), 3.70 (t, 2H, H-5', 5''). Found: C, 70.14; H, 6.14; N, 8.22%. Calcd for $C_{30}H_{31}O_5N_3$: C, 70.16; H, 6.08; N, 8.18%.

1-(2,3,5-Tri-O-benzyl-α-D-ribofuranosyl)pyrazole-3-carboxamide (14α). The same procedure as described above was applied to **10α** (700 mg, 1.29 mmo.) in absolute methanol saturated with ammonia (70 ml) to give a colorless oil of **14α**, 546 mg (82%); $[\alpha]_D^{25}$ +45.2° (*c* 0.92, chloroform). NMR

($CDCl_3$): δ 8.25 (d, 1H, H-5), 7.40 (m, 15H, Ar), 7.00 (d, 1H, H-4), 6.45 (br s, 2H, $CONH_2$), 6.31 (d, 1H, $J_{1'2'}$=5.2 Hz, H-1'), 4.80—4.13 (m, 9H, CH_2-Ar, H-2', H-3', H-4'), 3.67 (d, 2H, H-5', 5''). Found: C, 70.15; H, 6.12; N, 8.24%. Calcd for $C_{30}H_{31}O_5N_3$: C, 70.16; H, 6.08; N, 8.18%.

1-(2,3,5-Tri-O-benzyl-β-D-ribofuranosyl)pyrazole-5-carboxamide (15β). The same procedure as described above was applied to **11β** (260 mg, 0.48 mmol) in absolute methanol saturated with ammonia (26 m.) to give a colorless oil of **15β**, 196 mg (80%); $[\alpha]_D^{25}$ −2.5° (*c* 3.0, chloroform), NMR ($CDCl_3$): δ 7.60 (d, 1H, H-3), 7.40 (d, 15H, Ar), 7.18 (d, 1H, H-4), 6.60 (br d, 3H, $CONH_2$, $J_{1'2'}$=1.8 Hz, H-1'), 4.95—4.30 (m, 9H, CH_2-Ar, H-2', H-3', H-4'), 3.74 (m, 2H, H-5', 5''). Found: C, 70.47; H, 6.24; N, 8.27%, Calcd for $C_{30}H_{31}O_5N_3$: C, 70.16; H, 6.08; N, 8.18%.

1-(2,3,5-Tri-O-benzyl-β-D-ribofuranosyl)pyrazole-3,5-dicarboxamide (16β). The same procedure as described above was applied to **12β** (420 mg, 0.685 mmol) in absolute methanol (42 ml) saturated with ammonia. The residual syrup was chromatographed on a column of silica gel (30 g) using benzene–ethyl acetate (3: 1) as a solvent, to give a colorless glass of **16β**, 351 mg (92%); $[\alpha]_D^{25}$ −23.3° (*c* 1.0, dioxane). NMR (CD_3OD): δ 7.40 (t, 16H, Ar, H-4), 7.20 (d, 1H, $J_{1'2'}$=1.8 Hz, H-1'), 4.8—4.3 (m, 9H, CH_2-Ar, H-2', H-3', H-4'), 3.30 (d, 2H, H-5', 5''). Found: C, 66.66; H, 5.79; N, 9.96%. Calcd for $C_{31}H_{32}O_6N_4$: C, 66.89; H, 5.80; N, 10.07%.

4-Nitro-1-(2,3,5-tri-O-benzyl-β-D-ribofuranosyl)pyrazole-3,5-dicarboxamide (17β). A sample of **13β** (400 mg, 0.606 mmol) was led to its amide in a similar manner to that described above. The residual oil was washed with *n*-hexane and crystallized from benzene to give **17β**, 314 mg (81%); mp 82—83° C. $[\alpha]_D^{25}$ −27.5° (*c* 1.0, chloroform). NMR (CD_3OD): δ 7.42 (s, 15H, Ar), 6.27 (d, 1H, $J_{1'2'}$=3.1 Hz, H-1'), 4.8—4.4 (m, 9H, H-2', H-3', H-4', CH_2-Ar), 3.70 (m, 2H, H-5', 5''). Found: C, 61.78; H, 5.23; N, 11.58%. Calcd for $C_{31}H_{31}O_8N_5$: C, 61.89; H, 5.19; N, 11.64%.

4-Nitro-1-(2,3,5-tri-O-benzyl-α-D-ribofuranosyl)pyrazole-3,5-dicarboxamide (17α). By the same procedure as described above, **15α** gave **17α**, 296 mg (81%), crystallized from benzene–isopropylether; mp 161—162 °C. $[\alpha]_D^{25}$ −14.5° (*c* 1.0, chloroform). NMR (CD_3OD): δ 7.40 (d, 15H, Ar), 6.52 (d, 1H, $J_{1'2'}$=4.9 Hz, H-1'), 4.70—4.10 (m, 9H, H-2', H-3', H-4', CH_2-Ar), 3.68 (m, 2H, H-5', 5''). Found: C, 62.01; H, 5.22; N, 11.47%. Calcd for $C_{31}H_{31}O_8N_5$: C, 61.89; H, 5.19; N, 11.64%.

1-α-D-Ribofuranosylpyrazole-3-carboxamide (18α). A sample of **14α** (500 mg, 0.975 mmol) in 10 ml methanol was hydrogenated over a palladium black catalyst at 50 lb/sq inch for 24 hr. After removal of the catalyst, the methanol layer was evaporated and recrystallized from ethanol and benzene to give **18α**, 187 mg (79%); mp 175.5 °C. $[\alpha]_D^{25}$ +33.4° (*c* 1.0, water). NMR (DMSO-d_6): δ 8.15 (d, 1H, H-5), 7.44 (br d, 2H, $CONH_2$), 6.78 (d, 1H, H-4), 6.14 (d, 1H, $J_{1'2'}$=5.3 Hz, H-1'), 5.32 (t, 2H, OH), 4.47 (t, 1H, OH), 4.57—4.13 (m, 3H, H-2', H-3', H-4'), 3.60 (m, 2H, H-5', 5''). Found: C, 44.61; H, 5.41; N, 17.48%. Calcd for $C_9H_{13}O_5N_3$: C, 44.44; H, 5.39; N, 17.28%.

1-β-D-Ribofuranosylpyrazole-3-carboxamide (18β).

A. From 14β: A sample of **14β** (300 mg, 0.585 mmol) was hydrogenated and worked up in a similar manner to that described above. It was recrystallized from methanol to give **18β**, 111 mg (78%); mp 137 °C. $[\alpha]_D^{25}$ −41.6° (*c* 0.5, water). NMR (DMSO-d_6): δ 8.20 (d, 1H, H-5), 7.47 (br d, 2H, $CONH_2$), 6.83 (d, 1H, H-4), 5.85 (d, 1H, $J_{1'2'}$=4.0 Hz, H-1'), 5.50 (d, 1H, OH), 5.18 (d, 1H, OH), 4.95 (t, 1H, OH), 4.55—3.90 (m, 3H, H-2', H-3', H-4'), 3.71 (m, 2H, H-5', 5''). Found: C, 44.14; H, 5.37; N, 17.09%. Calcd for $C_9H_{13}O_5N_3$: C, 44.44; H, 5.39; N, 17.28%.

B. From 6: A sample of **6** (1.2 g, 2.06 mmol) in absolute methanol (120 ml) saturated with ammonia at 0 °C was kept at room temperature for 3 days and then evaporated under reduced pressure at 40 °C. The residual syrup was dissolved in water (30 ml) and washed with ether (5 ml × 10). The aqueous layer was evaporated to dryness to give 18β, 370 mg (72%).

1-β-D-Ribofuranosylpyrazole-5-carboxamide (19β).

A. From 15β: A sample of **15β** (180 mg, 0.351 mmol) was debenzylated by catalytic hydrogenation in a similar manner to that described above, in (A) of **18β**. After removal of methanol, the residual syrup was dissolved in aqueous ammonia and chromatographed on a column of silica gel (8 g, 1 × 10 cm) using butanol–ethanol–chloroform–17% aqueous ammonia (4: 4: 2: 3) as a solvent, to give **19β**, colorless crystals, 61.5 mg (72%); mp 150—151 °C. $[\alpha]_D^{25}$ −64.5° (*c* 1.91, water). NMR (DMSO-d_6): δ 7.85 (br d, 2H, $CONH_2$), 7.72 (d, 1H, H-3), 7.00 (d, 1H, H-4), 6.86 (d, 1H, $J_{1'2'}$=3.0 Hz, H-1'), 5.28 (d, 1H, OH), 5.02 (d, 1H, OH), 4.83—3.80 (m, 4H, OH, H-2', H-3', H-4'), 3.58 (m, 2H, H-5', 5''). Found: C, 44.73; H, 5.52; N, 17.43%. Calcd for $C_9H_{13}O_5N_3$: C, 44.44; H, 5.39; N, 17.28%.

B. From 7: A sample of **7** (230 mg, 0.394 mmol) in absolute methanol (50 m.) saturated with ammonia at 0 °C was kept at room temperature for 3 days. After removal of the methanol, water (10 ml) was added and the aqueous solution was extracted with ether (5 ml × 10). The aqueous layer was evaporated and the residual syrup was chromatographed in a similar manner as described above to give **19β**, 74 mg (75%).

1-β-D-Ribofuranosylpyrazole-3,5-dicarboxamide (20β).

A. From 8: A sample of **8** (600 mg, 0.91 mmol) was subjected to ammonolysis in a similar manner to that described for the preparation (*B*) of **19β**. The residual syrup was chromatographed on a column of silica gel (30 g), using butanol–ethanol–chloroform–17% aqueous ammonia (4: 4: 2: 3) as a solvent. The main fraction was evaporated to give a colorless glass of **20β**, 188 mg (72%); $[\alpha]_D^{25}$ −31.3° (*c* 1.0, water); NMR (DMSO-d_6): δ 7.80 (br d, 2H, $CONH_2$), 7.40 (s, 1H, H-4), 6.89 (d, 1H, $J_{1'2'}$=3.0 Hz, H-1'), 5.40 (d, 1H, OH), 5.00 (d, 1H, OH), 4.60 (m, 3H, OH, H-2', H-3'), 3.90 (m, 1H, H-4'), 3.60 (m, 2H, H-5', 5''). UV: λ_{max}^{water} 205 nm (ε 19700), λ_{max}^{pH1} 207 nm (ε 20600), λ_{max}^{pH13} 219 nm (ε 12500). Found C, 42.06; O, 5.00; N, 19.35%. Calcd for $C_{10}H_{14}O_6N_4$: C, 41.96; H, 4.93; N, 19.58%.

B. From 16β: A sample of **16β** (300 mg, 0.54 mmol) in 8 ml methanol was hydrogenated over a palladium black catalyst at 50 lb/sq inch for 70 hr. After filtration of the catalyst, the filtrate was evaporated and chromatographed on a column of silica gel with butanol–ethanol–chloroform–17% aqueous ammonia (4: 4: 2: 3) to give **20β**, 94.3 mg (61%).

4-Nitro-1-(β-D-ribofuranosyl)pyrazole-3,5-dicarboxamide (21β). A sample of 9 (800 mg, 1.14 mmol) was subjected to ammonolysis and worked up in a similar manner to that described for the preparation (*A*) of **20β** to give a colorless glass of **21β**, 272 mg (72%); $[\alpha]_D^{25}$ −23.5° (*c* 1.0, water); NMR (DMSO-d_6): δ 8.04 (br d, 4H, $CONH_2$), 5.82 (d, 1H, $J_{1'2'}$=3.7 Hz, H-1'), 5.55 (d, 1H, OH), 5.52 (d, 1H, OH), 4.80—3.90 (m, 4H, OH, H-2', H-3', H-4'), 3.60 (d, 2H, H-5', 5''). UV: λ_{max}^{water} 201 nm (ε 24500), 270 nm (ε 11200), λ_{max}^{pH1} 207 nm (ε 21200), 268 nm (ε 10600), λ_{max}^{pH13} 219 nm (ε 17300), 276 nm (ε 11100). Found: C, 35.98; H, 4.21; N, 20.90%. Calcd for $C_{10}H_{13}O_8N_5$: C, 36.26; H, 3.96; N, 21.14%.

4-Amino-1-(β-D-ribofuranosyl)pyrazole-3,5-dicarboxamide (22β).

A. From 17β: A sample of **17β** (200 mg, 0.332 mmol) in 6 ml methanol was hydrogenated over a palladium black

catalyst at 50 lb/sq inch for 24 hr. The catalyst was filtered off and the filtrate was evaporated. Recrystallization from water gave **22β**, 74 mg (74%); mp 227—229 °C. $[\alpha]_D^{25}$ −68.2° (*c* 1.0, water). NMR (DMSO-d_6): δ 7.50 (br s, 4H, $CONH_2$), 6.45 (d, 1H, $J_{1'2'}$=3.6 Hz, H-1′), 5.40 (br d, 3H, OH, NH_2), 5.00 (d, 1H, OH), 4.70 (m, 2H, H-2′, OH), 4.45—3.80 (m, 2H, H-3′, H-4′), 3.50 (m, 2H, H-5′, 5″). UV: λ_{max}^{water} 210 nm (ε 26000), 301 nm (ε 6330), $\lambda_{max}^{pH\ 1}$ 208 nm (ε 21200), 304 nm (ε 2470), $\lambda_{max}^{pH\ 13}$ 219 nm (ε 19300), 303 nm (ε 6620). Found: C, 39.50; H, 4.98; N, 23.10%. Calcd for $C_{10}H_{15}O_6N_5$: C, 39.37; H, 5.02; N, 23.25%.

B. From ***21β***: A sample of **21β** (200 mg, 0.604 mmol) was hydrogenated in the same way as above to give **22β**, 82 mg (82%).

*4-Amino-1-(α-*D*-ribofuranosyl)pyrazole-3,5-dicarboxamide (**22α**).* A sample of **17α** (250 mg, 0.415 mmol) was hydrogenated in the same manner as above. Recrystallization from methanol and benzene gave **22α**, 100 mg (80%); mp 206—207 °C. $[\alpha]_D^{25}$ +35.0° (*c* 0.5, water). NMR (DMSO-d_6): δ 7.55 (br d, 4H, $CONH_2$), 6.80 d, 1H, $J_{1'2'}$=5.7 Hz, H-1′), 5.25 (br s, 2H, NH_2), 5.2—4.8 (m, 3H, OH), 4.5—4.0 (m, 3H, H-2′, H-3′, H-4′), 3.60 (d, 2H, H-5′, 5″). UV: λ_{max}^{water} 211 nm (ε 27700), 300 nm (ε 6900), $\lambda_{max}^{pH\ 1}$ 208 nm (ε 22500), 300 nm (ε 28600), $\lambda_{max}^{pH\ 13}$ 219 nm (ε 20100), 302 nm (ε 6800). Found: C, 39.64; H, 5.03; N, 23.01%. Calcd for $C_{10}H_{15}O_6N_5$: C, 39.37; H, 5.02; N, 23.25%.

The authors wish to thank Mr. Saburo Nakada of our laboratory for the microanalysis and Mr. Takehiro Ogasa for his technical assistance. We are also thankful for a cancer research grant from the Ministry of Education.

References

1) K. Gerzon, R. H. Williams, M. Hoehn, M. Gorman, and D. C. DeLong, 2nd Intern. Cong. Heterocyclic Chemistry, Montpellier, France, July 10, 1969, Abstr. C-30.
2) O. Makabe, S. Fukatsu, and S. Umezawa, This Bulletin, **45**, 2577 (1972).
3) J. T. Witkowski, R. K. Robins, R. W. Sidwell, and L. N. Simon, *J. Med. Chem.*, **15**, 1150 (1972).
4) T. Hashizume and H. Iwamura, *Tetrahedron Lett.*, **1965**, 3095; *idem*, *J. Org. Chem.*, **33**, 1796 (1968).
5) K. V. Auwers and F. Cauer, *Ann.*, **470**, 287 (1929).
6) E. F. Recondo and H. Rinderknecht, *Helv. Chim. Acta*, **42**, 1171 (1959).
7) G. R. Revankar and L. B. Townsend, *J. Heterocycl. Chem.*, **7**, 1329 (1970).
8) G. P. Kreishman, J. T. Witkowski, R. K. Robins, and M. P. Schweizer, *J. Amer. Chem. Soc.*, **94**, 5894 (1972).
9) S. R. Naik, J. T. Witkowski, and R. K. Robins, *J. Heterocycl. Chem.*, **11**, 57 (1974).
10) C. A. Dekker and L. Goodman in "The Carbohydrates" Vol. IIA, W. Pigman and D. Horton, Eds., Academic Press, New York, N. Y., 1970, Chapter 29, p. 53.
11) F. A. Lehmkuhl, J. T. Witkowski, and R. K. Robins, *J. Heterocycl. Chem.*, **9**, 1195 (1972).
12) The details of the biological activities will be reported and discussed elsewhere.
13) R. V. Rosenburg, *Ber.*, **27**, 1098 (1894).
14) C. Musante, *Gazz. Chim. Ital.*, **75**, 121 (1945).
15) R. Baker and H. G. Fletcher, Jr., *J. Org. Chem.*, **26**, 4605 (1961).

Photochemistry in Micellar System. II. Photochemical Reduction of β-Arylquinonesulfonates in the Presence of Cationic Surfactants.[1]

Koji KANO, Yuzo TAKADA, and Taku MATSUO*

Department of Organic Synthesis, Faculty of Engineering, Kyushu University, Hakozaki, Higashi-ku, Fukuoka 812

(Received March 14, 1975)

The photochemical reduction of sodium 9,10-phenanthraquinone-3-sulfonate (PQ) and sodium 1,2-naphthoquinone-4-sulfonate (NQ) to the corresponding diols has been studied in water containing cationic surfactants. Photoreduction of PQ was markedly accelerated in the presence of cationic surfactants whereas that of NQ was highly retarded. Both the acceleration and retardation of the photoreaction of these quinonesulfonates in the presence of cationic surfactants are explained as due to the formation of association complexes betwen the quinones and the surfactants.

The chemistry in heterogeneous systems is important in relation to that of biological systems. The rates of many bimolecular reactions have been found to be considerably affected in the presence of surfactant micelles which provide a convenient heterogeneous model system.[2-4] These micellar effects are generally explained in terms of the solubilization of substrate into the micellar interior, where the electrostatic or hydrophobic interaction between substrate, reactant and micelles is so large that the rate of reaction is modified. In the case of photochemical reaction, the nature of photoexcited state of the substrate would also be modified when it is solubilized into apolar micellar interior. The micellar catalysis in photochemical reactions is expected to be large than that in thermal reactions. Hautala and Letsinger have found that the nucleophilic substitution of 4-methoxy-1-nitronaphthalene with cyanide ion is enhanced by a factor of about 6800 by the addition of cetyltrimethylammonium chloride (CTACl);[5] the enhancement factor is unexpectedly large in comparison with that of the micellar effects in thermal reactions.[2-4]

We reported that the photochemically generated radical anions of 9,10-anthraquinonesulfonates are remarkably stabilized in the presence of either anionic or non-ionic surfactant.[6] We have investigated the photochemistry of β-arylquinonesulfonates in water containing various surfactants and the results are given in this paper. In the case of sodium 9,10-phenanthraquinone-3-sulfonate (PQ), the photoreduction was enhanced by the cationic surfactants, neither anionic nor non-ionic ones having any effect at all. The photoreduction of sodium 1,2-naphthoquinone-4-sulfonate (NQ), on the other hand, was highly retarded by cationic surfactants in comparison with that in pure water.[7] These effects of surfactants were recognized even at a concentration far below the critical micelle concentrations (CMC) of the surfactants. The formation of association complexes between the β-arylquinonesulfonates and the cationic surfactants was suggested to account for the experimental observation.

Experimental

Spectroscopic measurements were made with a Shimadzu UV-200 recording spectrometer, a Bruker WH-90 FT NMR spectrometer (90 MHz) and a JEOL JES-ME-3X ESR spectrometer (X-band).

Materials. PQ was prepared according to the procedure given by Werner.[8] Reagent grade NQ (Tokyo Kasei Kogyo Co. Ltd.) was further purified by recrystallization from aqueous methanol. Cetyltrimethylammonium bromide (CTABr) and chloride (CTACl) were recrystallized from water and methanol, respectively. Water was distilled and deionized with a column of ion-exchange resin.

Irradiation. The solution in a pyrex tube (φ 15 mm) was irradiated with a Riko 100W high-pressure mercury lamp combined with a Riko rotary photolysis apparatus RH400-10W at room temperature. The photolysis was undertaken under the aerobic conditions unless otherwise stated.

Quantum Yield. Monochromatic light was isolated from a Ushio 500W super high-pressure mercury arc USH-500D either with a combination filter of a Toshiba UV-D25, an aqueous nickel sulfate solution, and a glass plate (313 nm) or with a combination filter of a Toshiba UV-D1C and a UV-35 (365 nm). The light intensity was determined with a potassium ferrioxalate actinometer.

Results

Photolysis of PQ and NQ. NQ in water is photoreduced to sodium 1,2-dihydroxynaphthalene-4-sulfonate (NQH_2).[7] The quantum yield for the disappearance of NQ was determined to be 0.118 ± 0.007 (pH 6.80). On the other hand, PQ in an aerobic phosphate buffer (pH 6.80) is considerably stable against irradiation. The quantum yield for the disappearance of PQ ($[PQ]_0 = 1.0 \times 10^{-3}$ M) at 313 nm is $(5.5 \pm 1.5) \times 10^{-4}$. Under the unaerobic conditions, the photolysis of PQ is accelerated about two-fold, no photoproducts being identified by UV spectra. The photolysis of PQ (5.0×10^{-4} M) is markedly accelerated, however, in the presence of CTABr (4.0×10^{-3} M). Upon irradiation, new absorption bands appear at 232, 254, 258, 275, and 318 nm, the intensities of the absorption due to PQ at 260, 264, 324, and 416 nm decreasing. The spectrum of the photoproduct is in complete agreement with that of the authentic sample of sodium 9,10-dihydroxyphenanthrene-3-sulfonate (PQH_2) prepared by the zinc dust-hydrochloric acid reduction. The isosbestic points are observed at 262, 283, and 327 nm up to the 70% conversion. The quantum yield for the disappearance of PQ ($[PQ]_0 = 1.0 \times 10^{-3}$ M) in the presence of CTABr (4.0×10^{-3} M) is $(1.3 \pm 0.1) \times 10^{-2}$. CTACl ($4.0 \times 10^{-3}$ M) catalyzes the photoreduction more effectively than CTABr ($\phi_{CTACl}/\phi_{CTABr} = 2.3$).

* To whom inquiries should be addressed.

Unlike the case of PQ, the photoreduction of NQ (5.0×10^{-4} M) in water is highly retarded in the presence of CTACl (5.0×10^{-3} M) ($\phi_{CTACl}/\phi_0=0.076$). Since the photoreduction of NQ in water is not affected by the addition of Cl^- (2.0×10^{-3} M) ($\phi_{NaCl}/\phi_0=0.99$) in contrast to the case of Br^- ($\phi_{KBr}/\phi_0=0.45$), the retarding effect of CTACl should be ascribed to the binding of NQ with the surfactant.

Photoreaction of either PQ or NQ is not affected by the addition of anionic (sodium lauryl sulfate) or nonionic (polysorbate 80) surfactant above the CMC.

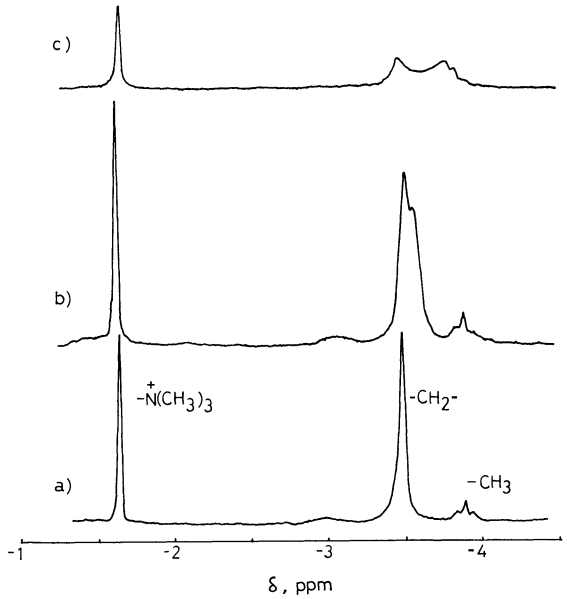

Fig. 1. NMR spectra of 2.0×10^{-2} M CTACl in D_2O: a) in the absence of PQ; b) with 4.0×10^{-3} M PQ; c) with 8.0×10^{-3} M PQ. The spectra were obtained by accumulation of 100-scans and the chemical shifts are expressed as measured downfield from HDO signal.

NMR of Quinone-CTACl System. The NMR spectra were examined in order to study the binding effect of the quinones with the CTACl-micelles. The variation of proton signals of CTACl in deuterium oxide with the concentration of PQ is shown in Fig. 1. The signals of $(CH_3)_3N^+$ and terminal $-CH_3$ protons are scarcely affected by the addition of PQ. As to the methylene protons, a part of the signal is shifted so that partially resolved two peaks are observed on the addition of PQ. At higher concentration of PQ, about a half of the methylene proton signals are shifted upfield, all the spectra showing considerable broadening due to the increased viscosity of the CTACl solution. Bunton studied the effects of added sodium alkylbenzenesulfonates on the proton signals of CTABr above the CMC and found appreciable broadening and upfield shift of the $(CH_3)_3N^+$ proton signals;[9] the methylene proton signals are separated into two groups, one shifted upfield and the other downfield. Bunton thus suggested that the phenyl group is inserted into the micelles so that the sulfonate group is in the aqueous environment (Fig. 2a). In the present experiment, the NMR spectra of the PQ-CTACl indicates that the $(CH_3)_3N^+$ protons are not affected by the magnetic anisotropy of the aromatic ring.

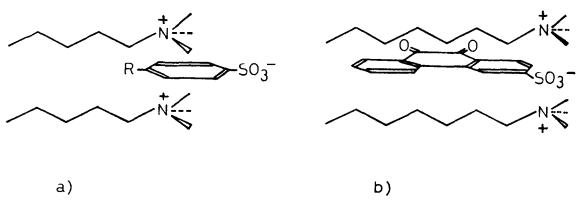

Fig. 2. Models of the binding of anionic substrates with cationic micelles: a) alkylbenzenesulfonate-CTABr; b) PQ-CTACl.

The SO_3^- group of PQ is considered to be associated with the $(CH_3)_3N^+$ of the surfactant so that the aromatic ring is incorporated into the hydrophobic micelle core (Fig. 2b).

Essentially the same results were obtained with the NQ–CTACl system.

Effect of Surfactant Concentration. If the effects of cationic surfactants on the photoreductions are due to the ordinary micellar effects, both the acceleration (PQ) and retardation (NQ) should become appreciable as the concentrations of the surfactants exceed the CMC. The effect of CTABr concentration on the photoreduction rate of PQ is shown in Fig. 3. Since the CMC generally

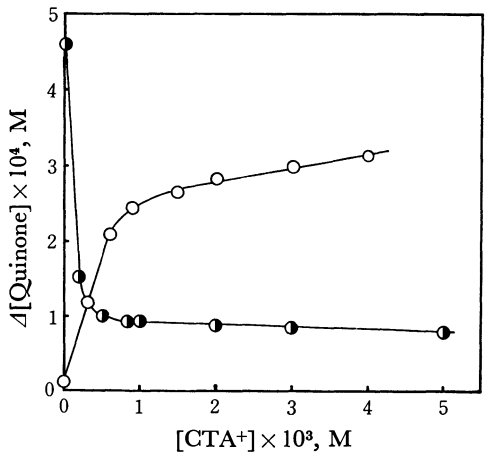

Fig. 3. The effect of cationic surfactant concentration on the β-arylquinones photochemistry. The aerobic aqueous solutions of PQ (—○—) and NQ (—◑—) (5.0×10^{-4} M) were irradiated for 15 and 2 min, respectively, at room temperature.

decreases on the addition of inorganic salts,[2-4] the experiments were carried out in non-buffered system (pH *ca.* 5.8). As shown in Fig. 3, the rate of photoreduction is significantly enhanced at the concentration of CTABr far below the CMC ($\sim10^{-3}$ M).[2] The onset of sharp decrease in the reaction rate of NQ was also located at CTACl concentration below the CMC (Fig. 3).[10] Further addition of surfactants above the CMC gave no effect on the photoreduction of either PQ or NQ. The results suggest that the effects of the cationic surfactants on the photoreactions of these β-arylquinonesulfonates are not attributed to the ordinary micellar effects. A similar effect of CTABr was observed in the fluorescent probe experiments with 8-toluidinyl-1-naphthalenesulfonate where the fluorescent yield is enhanced in the presence of CTABr below the CMC.[11]

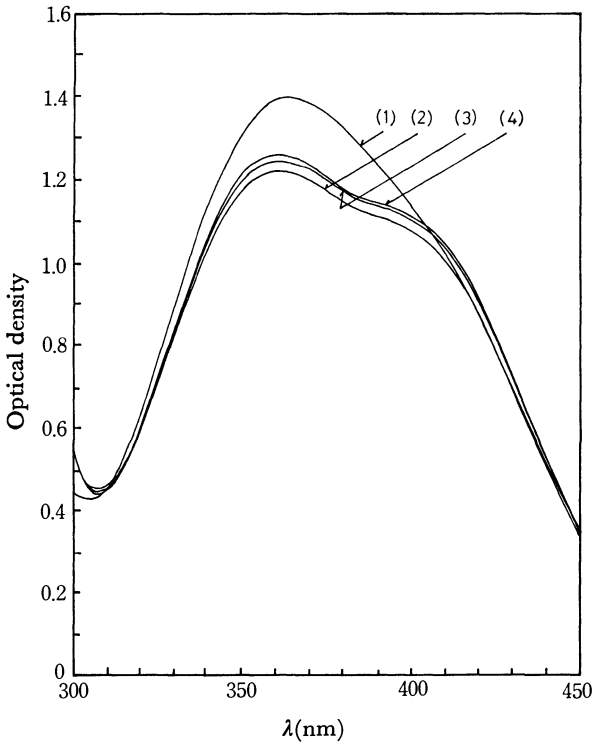

Fig. 4. Electronic absorption spectra of NQ in the presence of CTACl at various concentrations: none (1), 2.0×10^{-4} (2), 5.0×10^{-4} (3), $0.08-1.0\times10^{-2}$ M CTACl (4).

Association Complex of Quinonesulfonate and Cationic Surfactant. The NMR spectra indicate that the quinones with negatively charged group (SO_3^-) are associated with the positively charged nitrogen of the cationic surfactant. In fact, the association complex of PQ and CTABr gradually separated out of the freshly prepared equimolar solution of PQ and CTABr: mp 147—151 °C. IR (KBr disk) ν_{SO_2}, 1050, 1186; $\nu_{C=O}$, 1684; ν_{CH_2}, 2850, 2925; and δ_{CH_2}, 1465 cm^{-1}. The formation of the association complex was also verified by means of electronic absorption spectroscopy. The absorption spectra of NQ in the presence of various amounts of CTACl are shown in Fig. 4. When a small amount of CTACl is added to the aqueous NQ solution, the absorption band of NQ at 364 nm (ε_{max} 2.80×10^3) in water is split into two bands with λ_{max} at 361 (ε_{max} 2.50×10^3) and ~400 nm (ε_{max} $\sim2.0\times10^3$), respectively. The spectra of NQ in the presence of CTACl were in good agreement with those in organic solvents such as acetonitrile and alcohols. It is noteworthy that the absorption spectrum changes appreciably at the CTACl concentration far below the CMC. It may be suggested that the main body of NQ is in the hydrophobic environment which is provided by the long alkyl chain of the associated CTACl. The suggestion is supported by an examination of the absorption spectra of the equimolar solutions (5.0×10^{-4} M) of NQ and CTACl in water containing various amounts of acetonitrile. The π,π^* absorption band at 361 nm in water is shifted to 364 nm, and the one near 400 nm becomes obscure in 20—30% (v/v) acetonitrile–water solutions. The absorption spectrum observed in the 20—30% (v/v) acetonitrile–water agrees with that of NQ itself in water. At higher concentrations of acetonitrile (>40% (v/v)), the two absorption maxima at 361 and ~400 nm were restored. A possible explanation for the spectrophotometric behavior of the association complex in 20—30% (v/v) acetonitrile–water might be that the alkyl chain of the complex is elongated by the organic additive so that the water in the bulk phase become accessible to the main body of NQ.

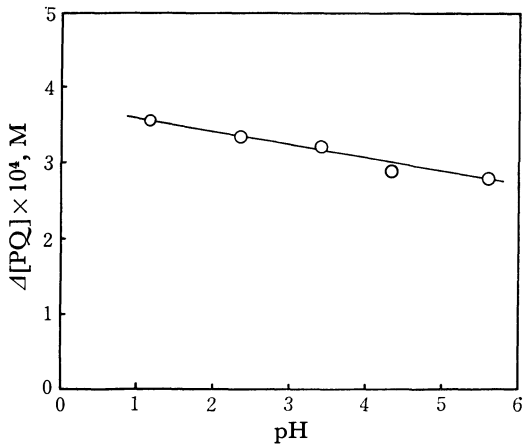

Fig. 5. Effect of pH on the disappearance of PQ in the presence of CTABr: $[PQ]_0=5.0\times10^{-4}$ M, $[SO_4^{2-}]=5.5\times10^{-2}$ M. The solutions were irradiated for 5 min at room temperature.

pH Effect. The pH effect on the photodecomposition of PQ in the presence of CTABr above the CMC is shown in Fig. 5. The pH (1.18—5.61) and the concentration of the sulfate ion ($[SO_4^{2-}]=0.055$ M) were adjusted with sulfuric acid and sodium sulfate, respectively. Disappearance of PQ is slightly depressed at higher pH. It appears that the photolysis of PQ is hardly affected by the hydroxide ions which are locally concentrated at the Stern layer of the cationic surfactant.

Deuterium Oxide Isotope Effect. The rate of formation of NQH_2 from NQ under irradiation in 99.8% D_2O is reduced in comparison with that in H_2O ($k_{H_2O}/k_{D_2O}=1.8$).[7] In the case of PQ (5.0×10^{-4} M), however, neither the disappearance of PQ nor the formation of

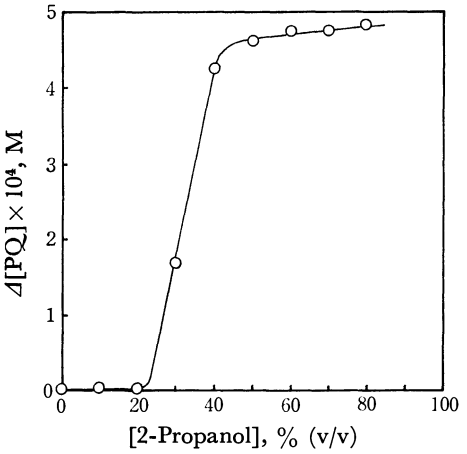

Fig. 6. Effect of 2-propanol concentration on the photoreduction of PQ in water. The solution of PQ (5.0×10^{-4} M) were irradiated for 2 min.

PQH_2 was affected by the use of deuterium oxide ($k_{H_2O}/k_{D_2O}=1.1$) in the presence of CTABr (4.0×10^{-3} M).

Photoreduction of PQ in 2-Propanol–water. In order to clarify the nature of the lowest photoexcited state of PQ in water, we examined the photochemical reduction of PQ in aqueous 2-propanol solutions. Figure 6 shows the effects of the concentration of 2-propanol on the photoreduction of PQ. Rapid photoreduction proceeds when the concentration of 2-propanol exceeds 20% (v/v), whereas PQ is scarcely photolyzed at low 2-propanol concentration. A linear relationship between the reciprocal of the quantum yields of the photoreduction and the reciprocal of the concentrations of 2-propanol is expected if the same chemical species is responsible for the reaction throughout the concentration range of 2-propanol investigated.[12] Contrary to expectation, a typical sigmoid profile was obtained (Fig. 6). The result suggests that the lowest excited state of PQ in water is an inactive π,π^* triplet, while that in 2-propanol is a n,π^* triplet. The critical concentration of 2-propanol for this disposition of the photoexcited species seems to be approximately 20% (v/v). The lowest photoexcited states of NQ are similarly suggested to be a π,π^* triplet in water and n,π^* triplet in organic media.[7]

Discussion

In the photoreduction of NQ in water to NQH_2,[7] it was found that:

1) The yield of NQH_2 is *ca.* 50%.

2) The quantum yield for the disappearance of NQ under irradiation at 365 nm is 0.118 ± 0.007 (pH5.00—6.80).

3) The radical anion of NQ ($NQ^{\cdot-}$) is detected by the ESR spectra when NQ is irradiated at pH 6.80, while no signal is observed at pH *ca.* 5.8.

4) The reactive species in this photoreduction is the π,π^* triplet of NQ.

5) The deuterium oxide isotope effect for the formation of NQH_2 (k_{H_2O}/k_{D_2O}) is 1.8.

Table 1. Effect of substrate concentration on quantum yields for the disappearance of NQ in water at 365 nm

$[NQ]\times10^3$, M	Quantum Yield
1.97	0.122
3.99	0.076
5.98	0.064
8.00	0.049
10.00	0.045

We have found in the present work that the quantum yields for the disappearance of NQ decrease with increase of the initial concentrations of NQ (Table 1). Therefore the D/D* scheme postulated in the photoreaction of 9,10-anthraquinone-2-sulfonate[13,14] should be excluded from the possible mechanisms.

$$NQ^* + NQ \longrightarrow NQ^{\cdot-} + NQ^{\cdot+} \quad (1)$$

We suggest the following sequence of reactions which lead to the photoreduction of NQ in water:[7]

$$NQ^* + OH^- \longrightarrow NQ^{\cdot-} + \cdot OH \quad (2)$$

$$NQ^{\cdot-} + H^+ \longrightarrow NQH\cdot \quad (3)$$

$$2NQH\cdot \longrightarrow NQH_2 + NQ \quad (4)$$

$$NQ + \cdot OH \longrightarrow NQ(OH)\cdot \quad (5)$$

The mechanism has not been confirmed, but it should be emphasized that water must be the reducing agent in the photoreduction of NQ.

The NMR spectra of the CTACl–micellar system containing NQ show that the SO_3^- group of NQ is associated with the positively charged nitrogen of CTACl so that the aromatic ring is incorporated into the hydrophobic micelle core. The electronic absorption spectra of NQ indicate that NQ is associated with CTACl so that the long alkyl chain surrounds the main body of NQ. Thus water can be excluded from the reaction site even at the concentrations of CTACl below the CMC. The photoreaction of NQ will be thus retarded in the presence of CTACl both above and below the CMC.

The photoreduction of PQ to PQH_2 was accelerated by the addition of the cationic surfactants (CTABr and CTACl). Neither ESR signal nor deuterium oxide isotope effect was observed in this case. Thus the mechanism of the photoreduction of PQ should differ from that of NQ in water. The surfactant concentration profile (Fig. 3) clearly indicates that the acceleration of the photolysis of PQ by cationic surfactants is not due to the ordinary micellar effects. As in the case of NQ–CTACl system, PQ and CTABr seem to form an association complex so that the main body of PQ would be surrounded by the long alkyl chain. The model might also be used to explain the fact that PQH_2 is completely stabilized toward oxidation with air in the presence of CTABr, whereas PQH_2 in pure water is rapidly oxidized to the original quinone. Under these circumstances, the photoexcited PQ would easily abstract hydrogen atom from the alkyl chain of the associated CTABr. If the hydrogen atom is abstracted from a free CTABr molecule, it is hardly expected for the reaction yield to reach an asymptotic value at such low CTABr concentration as in Fig. 3. The small deuterium oxide isotope effects is also explained by the same model. The photoreduction of PQ is influenced neither by the addition of sodium lauryl sulfate nor by polysorbate 80, inspite of the fact that they are expected to be better hydrogen donor than CTABr and CTACl due to the presence of $-OCH_2-$ group. All the data could be explained if the nature of the photoexcited state and its chemical reactivity vary with the change in environment surrounding PQ as summarised below.

1) The photoexcited PQ in water is considered to be the π,π^* triplet state. Since hydrogen abstraction is hardly induced by this particular species, no photoreduction takes place even in the presence of good hydrogen donors.

2) The lowest excited state of the association complex between PQ and CTABr is considered to be a n,π^* triplet so that hydrogen abstraction is easily induced in this case.

3) The hydrogen abstraction in the associated complex may be facilitated by the proximity effects of the alkyl chain (hydrogen donor) around the photoexcited PQ.

Table 2. The effects of solvents and organic additives on the photolysis of association complex between PQ and CTABr[a)]

Solvent	Additive	Irradiation time, min	$\Delta[PQ]\times10^4$, M
H_2O[b)]	—	15	2.09
CH_3CN	—	20	0.84
CH_3CN	CTABr(5.0×10^{-3}M)	20	0.15
CH_3CN	2-propanol (1 vol%)	1.25	4.30

a) $[\text{Association complex}]_0=5.0\times10^{-4}$ M. b) $[PQ]_0=5.0\times10^{-4}$ M, $[CTABr]=6.0\times10^{-4}$ M.

The effects of solvents and organic additives were examined in order to study the photochemical behavior of the association complex between PQ and CTABr (Table 2). The rate of reduction in acetonitrile was considerably less than that in water. The alkyl chain of CTABr surrounding the main body of associated PQ in water would be elongated in organic solvents. The rate of the hydrogen abstraction from the alkyl chain can be consequently reduced in acetonitrile. Addition of excessive CTABr quenches the photoreaction of the association complex in acetonitrile as expected from the heavy atom effects. It should be recalled, however, that the presence of CTABr in excess amounts did not quench the photolysis of PQ in water (Fig. 3). The difference in the effect of CTABr between these two solvents can be attributed to whether the reaction center of PQ is surrounded by the alkyl chain or not.

The same type of intramolecular hydrogen abstraction may also be expected to take place in the NQ-CTACl system as in the case of PQ-CTABr association complex. However, the photodecomposition of NQ in water was simply retarded on the addition of CTACl. It is suggested that the quantum efficiency for the hydrogen abstraction in the association complex between NQ and CTACl is much lower than that for the electron abstraction of NQ from the hydroxide ion.

References

1) Contribution No. 364 from the Department of Organic Synthesis, Faculty of Engineering, Kyushu University.
2) E. J. Fendler and J. H. Fendler, "Advances in Physical Organic Chemistry," Vol. 8, ed. by V. Gold, Academic Press, New York, N. Y., (1970), p. 271.
3) E. H. Cordes and C. Gitler, "Progress in Bioorganic Chemistry," Vol. 2, ed. by E. T. Kaiser and F. J. Kézdy, John Wiley and Sons, New York, N. Y., (1973), p. 1.
4) Ed. by E. H. Cordes, "Reaction Kinetics in Micelles," Plenum Publishing Co., New York, N. Y., (1973).
5) R. R. Hautala and R. L. Letsinger, *J. Org. Chem.*, **36**, 3762 (1971).
6) K. Kano and T. Matsuo, This Bulletin, **47**, 2836 (1974).
7) K. Kano and T. Matsuo, *Tetrahedron Lett.*, **1974**, 4323.
8) A. Werner, *Ann. Chem.*, **321**, 341 (1902).
9) C. A. Bunton, "Reaction Kinetics in Micelles," ed. by E. H. Cordes, Plenum Publishing Co., New York, N. Y., (1973), p. 73.
10) Although the CMC of CTACl has not been exactly determined, we roughly estimate the CMC to be 10^{-3} M from the photoinduced hydrolysis of *m*-nitrophenyl phosphate in the presence of CTACl.
11) R. R. Hautala, N. E. Schore, and N. J. Turro, *J. Amer. Chem. Soc.*, **95**, 5508 (1973).
12) N. J. Turro, "Molecular Photochemistry," W. A. Benjamin, Inc., New York, N. Y., (1965).
13) G. O. Phillips, N. W. Worthington, J. F. McKellar, and R. R. Sharpe, *J. Chem. Soc. A*, **1969**, 767.
14) K. P. Clark and H. I. Stonehill, *J. Chem. Soc. Faraday I*, **68**, 577, 1676 (1972).

The Photosensitized Oxygenation of Furanoeremophilanes. I. The Isomeric Hydroperoxides from Petasalbin and Their Transformations to Lactones

Keizo NAYA, Reizo KANAZAWA, and Michikazu SAWADA

Department of Chemistry, Faculty of Science, Kwansei Gakuin University, Uegahara, Nishinomiya, Hyogo 662

(Received April 3, 1975)

The photosensitized oxygenation of petasalbin I gave almost quantitatively a crystalline mixture of two isomeric hydroperoxides, V-a and V-b, both of which were then transformed to the corresponding lactones, VI-a and VI-b, respectively, in good yields. The stereochemistry of these hydroperoxides and lactones has been established by spectral and chemical methods. Furthermore, two natural lactones, III and IV, were prepared by the reduction of the hydroperoxides.

Petasalbin I has been isolated from *Petasites*[1] and *Ligularia*[2,3] species, and its absolute configuration has already been established. Then, from *Petasites officinalis* an interesting compound, II, was isolated by Šorm *et al.*, and for its formation it was postulated that the peroxides of methanol must play a role in a plant.[4,5] On the other hand, the dye-sensitized photooxygenation of furans has been extensively studied[6,7] and the oxygenation mode in methanol has been demonstrated, in that the reaction proceeds to give a cyclic peroxide by the 1,4-addition of oxygen to a furan ring, an addition which is often followed spontaneously by the addition of methanol, thus affording a 2-methoxy-2,5-dihydrofuran derivative.[6]

We have oureselves previously investigated the photosesnsitized oxygenation[8] of petasalbin I isolated from *Petasites japonicus* Maxim. as a biogenetic-type oxidation to the lactone homologues, such as the known 6β-hydroxyeremophilenolide, III,[2] and the newly isolated 6β,8β-dihydroxyeremophilenolide, IV, included in the same plant.

The present paper will report on the physical and chemical properties of the hydroperoxides, VI-a and VI-b, prepared from petasalbin I, and also on the stereochemistry of the hydroperoxides, VI-a,b, and their derivatives. Furthermore, the reduction products of VI-a,b were examined and found to include the same products as the natural lactones, III and IV.

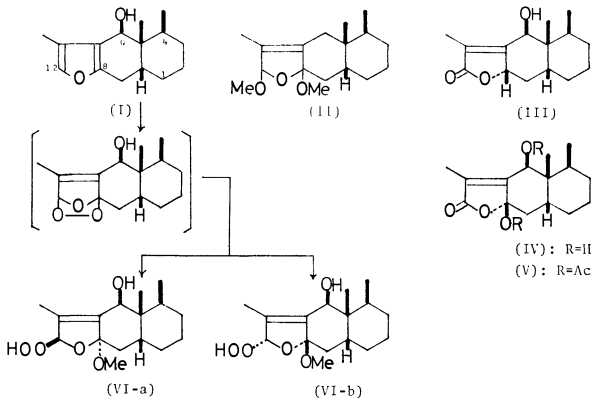

Scheme 1

Petasalbin I in methanol was photooxygenated, in the presence of Rose Bengal as a sensitizer, by irradiation with a circular fluorescent lamp (30 watt) under a bubbling of air. The reaction mixture was found on tlc to contain two compounds, which were separated by careful fractional crystallization to afford two hydroperoxides, (VI-a) (mp 119.3—119.5 °C (dec)) and (VI-b) (mp 116.0—116.5 °C (dec)). Both compounds have the same molecular formula, $C_{16}H_{26}O_5$, and both are positive to a peroxide test (KI–AcOH). Thus, there was no symptom of the exsistence of a cyclic ozonide-like intermediate, as in Scheme 1, and we could initially obtain the methanol adducts, VI-a,b, whose IR, UV, and NMR spectra were very similar to each other, suggesting that both are stereoisomers caused by a newly introduced 2-methoxy-5-hydroperoxy-2,5-dihydrofuran grouping. They showed these UV spectra: end absorption in both; IR bands at 3480 and 3350 (H-bonded OH), 1700 and 1630 cm^{-1} (C=C double bond) in VI-a, and at 3400 and 3330 (H-bonded OH), 1700 and 1630 cm^{-1} (C=C double bond) in VI-b; NMR signals (acetone-d_6): δ 11.13 (s, OO–H), 5.58 (s, OOCH), 3.08 (s, OCH_3) in VI-a, and 11.25 (s, OO–H), 5.70 (s, OOCH), 3.15 (s, OCH_3) in VI-b, besides the common signals with the original petasalbin I. The above results, therefore, led to the VI-a and VI-b structures for the hydroperoxides except for the configuration of the 8-methoxy and 12-hydroperoxy groups. These hydroperoxides, VI-a,b, were relatively stable in the crystalline state, but decomposed considerably in solution or upon chromatography on silica gel (Merck, grade II). Furethermore, the reduction of the hydroperoxides, VI-a,b, with sodium sulfite, sodium borohydride, and a platinum catalyst gave no principal or selective reduction product and rather complicated results, accompanied by decomposition, as will be described in detail later.

Finally, the hydroperoxides, VI-a,b, were quantita-

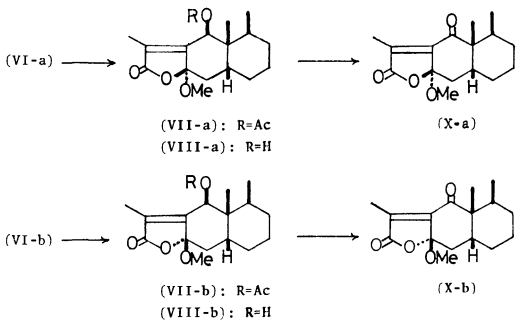

Scheme 2

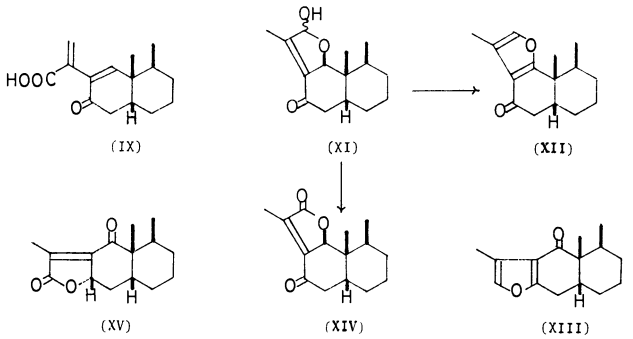

Scheme 3

tively converted to two substances, epimeric 6β-acetoxy-8α-methoxylactone (VII-a) (mp 106.5—108.0 °C) and the corresponding 8β-methoxylactone (VII-b) (mp 174.5—175.5 °C) by acetylation with acetic anhydride–pyridine.

For the determination of the configuration, therefore, each hydroperoxide was transformed into a 6-oxo derivative, X-a,b, according to Scheme 1—that is, by acetylation followed by the partial hydrolysis of the 6β-acetoxy group and subsequently by oxidation with Jones' reagent. Both the first products, VII-a and VII-b, showed similar IR bands at 1760 (α,β-unsaturated lactone C=O), and 1740 cm^{-1} (C=C double bond) and similar NMR spectra (cf. Table 1 and Experimental section). By subsequent partial hydrolysis, compounds VII-a and VII-b gave 6β-hydroxy derivatives, (VIII-a) (mp 167.5—168.0 °C) and (VIII-b) (mp 129.5—130.2 °C), respectively, both of which showed NMR spectra closely similar to that of 6β-hydroxyeremophilenolide III except for the signals due to the 8-methoxy groups instead of the 8β-proton in III. On the other hand, a mixture of the 6β-acetoxy-8(α and β)-methoxylactones, VII-a,b, was treated with an excess of alkaline to afford quantitatively an acid (IX) as the sole product. The IX acid, $C_{15}H_{20}O_3$ (mp 96.0—97.0 °C), exhibited IR bands at 3400—2400 (OH in carboxyl group), 1695 (C=O in carboxyl group), 1680 (α,β-unsaturated ketone), 1615 (C=C double bond), 950 cm^{-1} (end-methylene in a conjugated diene system); NMR signals at δ 6.70 (s, 1H, 6-H), 6.28 and 5.69 (each d, J=1.5 Hz, 13-CH_2=), and its UV maximum at 239 nm. The above results led to the IX structure for the acid; hence, the 6β-acetoxy compounds, VII-a and VII-b, obviously became epimers with regard to the configuration of the 8-methoxy groups.

The configurational assignments of the 8-methoxy groups in the corresponding epimers (VI—VIII, and IX) were achieved by a comparison of the NMR spectra, ORD–CD curves, specific rotations, and adsorption properties (Table 1, Fig. 1, and Fig. 2).

The conformation of α,β-unsaturated keto-group in a pair of 6-oxolactones, (X-a) (mp 99.0—100.0 °C) and (X-b) (mp 160.5—161.5 °C), was defined by the ORD–CD curves. Similar effects[9] observed in the cisoid α,β-unsaturated ketones are to be expected for the 6-oxo compounds, X-a,b. The X-a,b epimers have opposite signs; those enantiomeric chiralities seemed to be dominated by the helicity of the α,β-unsaturated ketone moiety. Thus, on the basis of a consideration with the Dreiding model, a pair of 6-oxolactones, X-a,b, with intense negative and positive Cotton effects in the 250—

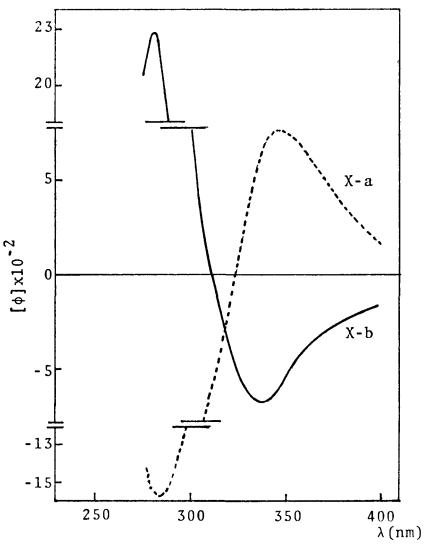

Fig. 1. Optical rotatory dispersion curves of 6-oxo-8-methoxylactones X-a and X-b.

Table 1. Comparison of chemical shifts (δ-values), specific rotations, and R_f values of the corresponding isomers

Compound	Solvent	15-Me	14-Me	13-Me	6-H	$[\alpha]_D^\circ$ ($CHCl_3$)	R_f (C_6H_6:AcOEt)
VI-a	CD_3COCD_3	0.78s	0.94d J=7.2	1.73d J=1.0	4.72b*	+2.5[a]	0.50 (3: 1)
VI-b	CD_3COCD_3	1.00s	0.72d J=5.5	1.73s	4.36s	+46.1[a]	0.40 (3: 1)
VII-a	$CDCl_3$	0.85s	0.97d J=7.6	1.85d J=1.4	5.92d J=1.4	−190.4	0.75 (10: 1)
VII-b	$CDCl_3$	0.98s	0.77d J=5.5	1.94s	5.62s	+185.5	0.66 (10: 1)
VIII-a	$CDCl_3$	0.78s	0.98d J=7.0	2.02d J=1.5	4.95d J=1.5	−187.0	0.73 (3: 1)
VIII-b	$CDCl_3$	1.08s	0.75d J=5.0	1.87s	4.49s	+205.1	0.66 (3: 1)
X-a	$CDCl_3$	1.04s	0.90d J=7.7	1.98s		−13.6	0.60 (30: 1)
X-b	$CDCl_3$	1.15s	0.66d J=6.0	1.96s		−16.6	0.60 (30: 1)

b*: broad singlet. a): measured with a methanol solution.

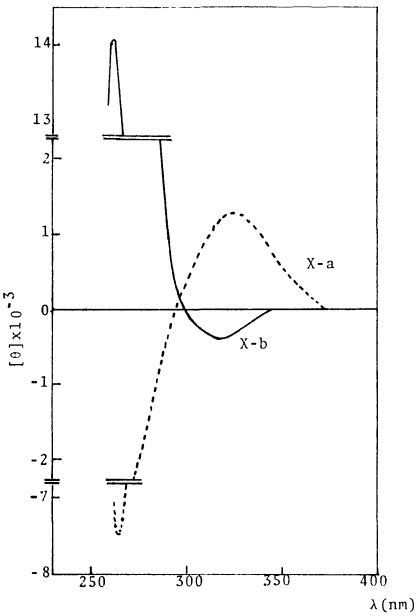

Fig. 2. Circular dichroism curves of 6-oxo-8-methoxylactone X-a and X-b.

400 nm region have been alloted the X-a and X-b formulas, those which have left- and right-handed helicities respectively.

In the NMR spectra, only the 8α-methoxy derivatives showed homoallylic couplings[10] (1.0—1.5 Hz) between 6–H and 13–CH_3. Upon the Dreiding model, the angles between the two bonds lie around 90° and 20° in the 8α- and 8β-methoxy derivatives respectively. The observed coupling, therefore, is consistent with the above assignment.

A further comparison between the corresponding 8-methoxy epimers also revealed the characteristics of this configurational correlation. The NMR spectra of the 8α-methoxy compounds exhibited chemical shifts due to 14-methyls at a lower field than those due to 15-methyls, and the chemical shifts were reversed in the 8β-epimers. The 8β-methoxy compounds have stronger positive rotations than the 8α-series except for the 6-oxo derivatives. The 8β-methoxy derivatives showed stronger adsorptive properties than the 8α-epimers, suggesting that the 8β- and 8α-series have *cis*- and *trans*-like geometries respectively, in agreement with the above configurational assignment.

Now the configuration of the hydroperoxides, VI-a and VI-b, can be explained in terms of the approved mechanism that the *cis*-1,4-addition of an oxygen molecule should occur from one side to the furan ring surface, followed by the attack of methoxide from another side to give hydroperoxides as in the stereoformulas, VI-a and VI-b.

Next we examined several reduction methods for the stabilization of the labile hydroperoxy group.

a) By Sodium Sulfite. After the photooxygenation of petasalbin I in methanol, the solution was immediately subjected to reduction with sodium sulfite without any isolation of hydroperoxides. The products were separated by repeated column chromatography on silica gel to afford 6β-hydroxyeremophilenolide (III, 7%) (mp 204.0—205.0 °C), 6β-hydroxy-8α-methoxyepieremophilenolide VIII-a (5%), and two other unknown products, (IV, 1.8%) and (XI, 36%).

The IV product, $C_{15}H_{22}O_4$ (mp 209.0—211.5 °C, $[\alpha]_D$ +172°), showed the presence of hydroxyl groups at 3500 and 3250 cm^{-1}, α,β-unsaturated γ-lactone groups at 1730 and 1695 cm^{-1}, and its UV maximum at 218 nm. The MS spectrum indicated the presence of two hydroxyl groups, *i. e.*, *m/e* 266 (M^+), *m/e* 248 (M−18), and *m/e* 230 (M−36). The structure was proved by a comparison of the NMR spectrum with those of 6β-hydroxyeremophilenolide III and the epimeric 6β-hydroxy-8-methoxylactones, VIII-a,b. The configuration of the 8-hydroxyl group was identified as β-substituent from the chemical shifts of the 14- and 15-methyls, and also from the absence of homoallylic coupling between 6–H and 13–CH_3, according to the generality mentioned above.

On the other hand, the crude extract from the rhizomes of *Petasites japonicus* Maxim. was reinvestigated in order to examine the lactone components by chromatography on silica gel; the natural 6β,8β-dihydroxyeremophilenolide (IV) (mp 211.0—212.0 °C, $[\alpha]_D$ +169°) was isolated from the polar part.

The XI product was a colorless oil and was positive to an Ehrlich test. XI showed IR bands at 3400 (OH), 1685, and 1650 cm^{-1} and its UV maximum at 250 nm (α,β-unsaturated ketone). The appearance of the above keto-group can be derived from the fission of the dihydrofuran ring, followed by the isomerization of the double bond and recyclization with the 6β-hydroxyl group. As the above color-test suggested that XI is closely connected with a furan derivative, XI was heated in acetic anhydride at 90 °C for 1 hr to afford quantitatively isoligularone (XII)[11] (mp 147.0—148.0 °C, $[\alpha]_D$ +39.0°), which was an isomer of ligularone (XIII)[1-b,c] (mp 66.0—67.5 °C), prepared from petasalbin I with chromium trioxide-pyridine. Jones' oxidation of XI gave 8-oxoisoeremophilenolide (XIV) (mp 76.5—77.5 °C, $[\alpha]_D$ +31.5°), which showed IR bands at 1760 (lactone C=O), 1695, and 1660 cm^{-1} and its UV maximum at 245 nm (α,β-unsaturated ketone). Its NMR spectrum showed signals at 5.42 (q, J=2.5 Hz, 6–H) and 1.92 (d, J=2.5 Hz, 13–CH_3) with homoallylic coupling. The XIV lactone distinctly differs from the isomeric ketolactone (XV)[1-a] (mp 124.0—126.0 °C, $[\alpha]_D$ −27.1°), prepared from 6β-hydroxyeremophilenolide III by Jones' oxidation. The configuration, therefore, can be assigned the XIV formula.

The former alcohol, XI, was indicated to be an epimeric mixture attributable to the orientation of the 12-hydroxyl group in its NMR spectrum—namely, pairs of signals centered at 5.32 and 5.12 (1H), 5.69 and 5.55 (1H), and 0.78 and 0.70 due to the 6–H, 12–H, and 15–CH_3 groups respectively. However, attempts to separate the mixture were unsuccessful.

b) By Sodium Borohydride. A crystalline mixture of hydroperoxides, VI-a,b, was treated with a methanol solution of sodium borohydride at room temperature, and the product was chromatographed on deactivated alumina (Merck, grade IV) to afford petasalbin I (30.2 %) and 6β-hydroxyeremophilenolide III (20%).

c) By a Platinum Catalyst. On hydrogenation with a platinum catalyst in acetic acid, the hydroperoxides,

VI-a,b, gave III (3.7%), 6β-hydroxy-8α-methoxyepieremophilenolide VIII-a (18.4%), and 6β,8β-dihydroxyeremophilenolide IV (24.5%).

When a mixture of the VI-a,b hydroperoxides was chromatographed on silica gel (Merck, grade II) in order to separate them, the eluate included recovered hydroperoxides (52%), IV (21%), and a mixture of lactones VIII-a,b (9%).

These reductions and silica gel chromatography invariably showed poor reproducibilities in the yield ratios of their products.

Experimental

The IR, UV, ORD-CD, and mass spectra were taken with Hitachi EPI-G3, Cary 14, JASCO ORD-5, and Hitachi RMU-6 spectrophotometers respectively. The NMR spectra were recorded with a Hitachi R-20B (60 MHz) spectrometer, and the chemical shifts are reported in δ-values (with TMS as the internal reference). The optical rotations were measured with a Perkin-Elmer 141 polarimeter. The tlc were run on Kieselgel G (Merck).

Isolation of Petasalbin (I), 6β-Hydroxyeremophilenolide (III), and 6β,8β-Dihydroxyeremophilenolide (IV). The dried rhizomes of *Petasites japonicus* Maxim. were extracted with ether at room temperature. The neutral oil (24 g) was chromatographed on neutral alumina (400 g, grade III). Elution with benzene and then benzene–ethyl acetate (20: 1) gave two fractions, including mainly petasalbin I and 6β-hydroxyeremophilenolide III respectively. Each fraction was purified by repeated chromatography on alumina or silica gel and by subsequent recrystallization to afford petasalbin I (2 g, tlc: R_f, 0.30, benzene) and 6β-hydroxyeremophilenolide III (1.9 g, tlc: R_f, 0.50, benzene–ethyl acetate, 5: 1).

The collected polar fraction (40 g), eluted with benzene–ethyl acetate (20: 1), was chromatographed on silica gel (400 g) with the same solvent to give crude III (1.4 g) and 6β,8β-dihydroxyeremophilenolide IV (2.2 g, R_f, 0.53, benzene–ethyl acetate, 2: 1).

Petasalbin (I):[1c] mp 79.0—81.0 °C, colorless needles (from ether or light petroleum), $[\alpha]_D^{22}$ −13.0° (*c*, 1.0, $CHCl_3$). (Found: C, 76.64; H, 9.40%).

6β-Hydroxyeremophilenolide (III):[2] mp 204.5—205.5 °C, colorless prisms (from ethyl acetate), $[\alpha]_D^{23}$ +203° (*c*, 1.01, $CHCl_3$). (Found: C, 72.05; H, 8.80%). The spectral data of the above compounds, I and III, are consistent with those reported in the lit. for 1-c and 2).

6β,8β-Dihydroxyeremophilenolide (IV): mp 211.0—212.0 °C, prisms (from methanol or ethyl acetate); $[\alpha]_D^{16}$ +169° (*c*, 0.985, $CHCl_3$); IR ($CHCl_3$): 3525, 3250, 1760, 1005, 990 cm^{-1}; NMR ($CDCl_3$): 4.60 (s, 6-H), 2.70 (br s, 2×OH), 2.07 (s, 9-CH_2), 1.87 (s, 13-CH_3), 1.11 (s, 15-CH_3), 0.78 (non-resolvable methyl signal, 14-CH_3).

Found: C, 67.46; H, 8.42%. Calcd for $C_{15}H_{22}O_4$: C, 67.64; H, 8.33%.

6β,8β-Diacetoxyeremophilenolide (V). 6β,8β-Dihydroxyeremophilenolide IV (241 mg) was dissolved in acetic anhydride (2.5 ml) and pyridine (1 ml), and the mixture was left at room temperature for 3 days. Subsequent working up in the usual manner gave quantitatively a crude diacetate, which was crystallized from isopropyl ether as prisms; mp 119.5—120.5 °C; $[\alpha]_D^{23}$ +64.7° (*c*, 1.00, $CHCl_3$); IR(KBr): 1780, 1760, 1740, 1250, 1170, 993 cm^{-1}, ($CHCl_3$): 1765, 1740sh, 1240, 993 cm^{-1}; NMR (CCl_4): 5.78 (s, 6-H), 1.95 (s, 13-CH_3), 1.90 (s, 2×OAc), 0.95 (s, 15-CH_3), 0.83 (non-resolvable methyl signal, 14-CH_3).

Found: C, 64.89; H, 7.36%. Calcd for $C_{19}H_{26}O_6$: C, 65.12; H, 7.48%.

The Photosensitized Oxygenation of Petasalbin (I) and Isolation of Hydroperoxides, (VI-a) and (VI-b). A stirred solution of petasalbin I (1.19 g) and Rose Bengal (47.5 mg) in methanol (60 ml) was irradiated with a circular fluorescent lamp (30 watt) for 3 hr under the bubbling of air. After the subsequent evaporation of the methanol *in vacuo*, the residue was extracted with benzene. The benzene extract was washed with water, and passed through a column filled with anhydrous sodium sulfate for drying and taking out the dye-stuff. On tlc, the benzene solution showed the existence of two products. The removal of the solvent *in vacuo* gave a colorless, crystalline mixture (1.4 g) of hydroperoxides, VI-a (R_f, 0.50, benzene–ethyl acetate, 3: 1) and VI-b (R_f, 0.40). The mixture was separated by fractional recrystallization from benzene. Thus, the evaporation of the solvent to some extent deposited a less-soluble compounds, VI-a; subsequently the mother liquor was fractionated by crystallization to collect VI-a and then VI-b.

Hydroperoxide (VI-a): mp 119.3—119.5 °C, colorless needles (from benzene), $[\alpha]_D^{24}$ +2.5° (*c*, 1.02, MeOH); positive to a peroxide test (KI–AcOH); IR(KBr): 3480, 3350, 1700, 1630, 1140, 1060, 930 cm^{-1}; MS: *m/e* 280 (M^+-18), *m/e* 109 (base peak); NMR (acetone-d_6): 11.13 (s, OO-H), 5.58 (s, OO-CH), 4.72 (split br s, 6-H), 4.13 (s, 6-OH), 3.08 (s, OCH_3), 1.99 (s, 9-CH_2), 1.73 (d, J=1.0 Hz, 13-CH_3), 0.94 (d, J=7.2 Hz, 14-CH_3), 0.78 (s, 15-CH_3).

Found: C, 64.37; H, 8.74%. Calcd for $C_{16}H_{26}O_5$: C, 64.40; H, 8.78%.

Hydroperoxide (VI-b): mp 116.0—116.5 °C, $[\alpha]_D^{24}$ +46.1° (*c*, 1.01, MeOH); positive to a peroxide test; IR(KBr): 3400, 3330, 1700, 1630, 1135, 1075, 980 cm^{-1}; MS: *m/e* 262 (M^+-36), *m/e* 78 (base peak); NMR (acetone-d_6): 11.25 (s, OO-H), 5.70 (s, OO-CH), 4.36 (s, 6-H), 4.22 (s, 6-OH), 3.15 (s, OCH_3), 1.73 (s, 13-CH_3), 1.00 (s, 15-CH_3), 0.72 (d, J=5.5 Hz, 14-CH_3).

Found: C, 64.75; H, 9.02%. Calcd for $C_{16}H_{26}O_5$: C, 64.40; H, 8.78%.

6β-Acetoxy-8α-methoxyepieremophilenolide (VII-a). Hydroperoxide VI-a (171.4 mg) was dissolved in pyridine (0.5 ml) and acetic anhydride (1 ml), and the mixture was left overnight at room temperature. Subsequent working up in the usual manner gave quantitatively the VII-a acetate, which was then crystallized from isopropyl ether as prisms: mp 106.5—108.0 °C, $[\alpha]_D^{24}$ −190.4° (*c*, 1.01, $CHCl_3$); UV: λ_{max}^{MeOH} 217 nm (ε, 10500); IR(KBr): 1760, 1740, 1700, 1230, 1060, 960 cm^{-1}; NMR ($CDCl_3$): 5.92 (d, J=1.4 Hz, 6-H), 3.20 (s, 8-OCH_3), 2.16 (s, 6-OAc), 1.85 (d, J=1.4 Hz, 13-CH_3), 0.97 (d, J=7.6 Hz, 14-CH_3), 0.85 (s, 15-CH_3).

Found: C, 67.10; H, 8.15%. Calcd for $C_{18}H_{26}O_5$: C, 67.06; H, 8.13%.

6β-Acetoxy-8β-methoxyeremophilenolide (VII-b). Hydroperoxide VI-b (125.5 mg) was acetylated in a similar manner to afford the acetate (VII-b, 118.2 mg), which was then crystallized from isopropyl ether as prisms: mp 174.5—175.5 °C, $[\alpha]_D^{23}$ +185.5° (*c*, 1.03, $CHCl_3$); IR(KBr): 1760, 1740, 1700, 1250, 1180, 1080, 925 cm^{-1}; NMR ($CDCl_3$): 5.62 (s, 6-H), 3.00 (s, 8-OCH_3), 2.05 (s, 6-OAc), 1.94 (s, 13-CH_3), 0.98 (s, 15-CH_3), 0.77 (d, J=5.5 Hz, 14-CH_3).

Found: C, 67.25; H, 8.13%. Calcd for $C_{18}H_{26}O_5$: C, 67.06; H, 8.13%.

Alkaline Hydrolysis of Acetates, (VII-a) and (VII-b). *a) 6β-Hydroxy-8α-methoxyepieremophilenolide (VIII-a).* The acetate VII-a (65.7 mg) was dissolved in an equimolecular potassium hydroxide–methanol solution (0.93 ml, 0.22 N), after which the mixture was left at room temperature for 1 hr. After the removal of the solvent and acidification with 1% sulfuric

acid, the reaction mixture was extracted with ether. The extract was washed with a saturated sodium hydrogen carbonate solution and water. The subsequent evaporation of the solvent gave 6β-hydroxy-8α-methoxyepieremophilenolide VIII-a (50 mg), which was then crystallized from light petroleum as needles: mp 167.5—168.0 °C, $[\alpha]_D^{23}$ −187.0° (*c*, 0.96, $CHCl_3$); IR(KBr): 3460, 1740, 1680, 1165, 1080, 1070, 940 cm^{-1}; UV: λ_{max}^{MeOH} 225 nm (ε, 7500); MS: *m/e* 280 (M^+), *m/e* 109 (base peak); NMR ($CDCl_3$): 4.95 (d, J=1.5 Hz, 6-H), 3.14 (s, 8-OCH_3), 2.62 (s, OH), 2.02 (d, J=1.5 Hz, 13-CH_3), 0.98 (d, J=7.0 Hz, 14-CH_3), 0.78 (s, 15-CH_3).

Found: C, 68.60; H, 8.68%. Calcd for $C_{16}H_{24}O_4$: C, 68.54; H, 8.63%.

b) 6β-Hydroxy-8β-methoxyeremophilenolide (VIII-b). The hydrolysis of the acetate VII-b (222 mg) was performed in a similar manner. The product was obtained quantitatively and was crystallized from ethyl acetate–light petroleum as prisms: mp 129.5—130.2 °C, $[\alpha]_D^{23}$ +205.1° (*c*, 1.01, $CHCl_3$); IR(KBr): 3450, 1730, 1690, 1210, 1190, 1130, 1090, 920 cm^{-1}, ($CHCl_3$): 3500, 1755, 1010, 1002, 992, 970, 930 cm^{-1}; NMR ($CDCl_3$): 4.49 (s, 6-H), 3.27 (s, 8-OCH_3), 2.71 (s, 6-OH), 2.00 (s, 9-CH_2), 1.87 (s, 13-CH_3), 1.08 (s, 15-CH_3), 0.75 (d, J=5.0 Hz, 14-CH_3).

Found: C, 68.87; H, 8.71%. Calcd for $C_{16}H_{24}O_4$: C, 68.54; H, 8.63%.

Alkaline Hydrolysis of the Mixture of 6β-Acetoxy-8(α and β)-Methoxylactones, (VII-a) and (VII-b). A mixture of 6β-acetoxy-8(α and β)-methoxylactones, VII-a, b was prepared from petasalbin I by photooxidation as has been described above, followed by acetylation. The crystalline mixture (6.138 g) was dissolved in a 1.84 N potassium hydroxide–methanol solution (80 ml) and then left at room temperature for 36 hr. After acidification with 2 N sulfuric acid, the mixture was extracted with ether. Subsequent working up in the usual manner gave a viscous oil (5.41 g), which crystallized on standing. The crystalline mass was recrystallized from isopropyl ether-light petroleum to afford the pure unsaturated acid IX (4.07 g) as needles: mp 96.0—97.0 °C, $[\alpha]_D^{22}$ +20.5° (*c*, 1.09, $CHCl_3$); IR (CCl_4): 3400—2300, 1695, 1680, 1615, 950, 928 cm^{-1}; UV: λ_{max}^{MeOH} 239 nm (ε, 5580); MS: *m/e* 248 (M^+), 133 (base peak); NMR (CCl_4): 10.5 (br s, COOH), 6.70 (s, 6-H), 6.28 and 5.69 (each d, J=1.5 Hz, 13-CH_2=), 1.13 (s, 15-CH_3), 0.92 (d, J=6.7 Hz, 14-CH_3).

Found: C, 72.24; H, 7.88%. Calcd for $C_{15}H_{20}O_3$: C, 72.55; H, 8.12%.

Jones' Oxidation. a) 6-Oxo-8α-methoxyepieremophilenolide (X-a). Jones' reagent (0.18 ml) was added to a stirred solution of 6β-hydroxy-8α-methoxylactone VIII-a (97.8 mg) in acetone (4 ml) over a period of 0.5 hr under cooling with ice-water. After stirring for a further 2.5 hr and after the decomposition of the excess reagent with methanol, the mixture was extracted with ether. Subsequent working up as usual gave, quantitatively, 6-oxo-8α-methoxyepieremophilenolide, X-a (mp 99.0—100.0 °C), as needles (from isopropyl ether), $[\alpha]_D^{23}$ −13.6° (*c*, 1.04, $CHCl_3$); IR (KBr): 1760, 1698, 1660, 1160, 1070, 915 cm^{-1}; UV: λ_{max}^{MeOH} 230 nm (ε, 8300); NMR ($CDCl_3$): 3.16 (s, 8-OCH_3), 2.35 (m, 3H), 1.98 (s, 13-CH_3), 1.04 (s, 15-CH_3), 0.90 (d, J=7.7 Hz, 14-CH_3); ORD (*c*, 0.116, MeOH): *cf.* Fig. 1; CD (*c*, 0.108, MeOH): Fig. 2.

Found: C, 69.04; H, 8.14%. Calcd for $C_{16}H_{22}O_4$: C, 69.04; H, 7.97%.

b) 6-Oxo-8β-methoxyeremophilenolide (X-b). Compound VIII-b (103.7 mg) was oxidized by a method similar to that described above to yield 6-oxo-8β-methoxyeremophilenolide, X-b (94.3 mg) (mp 160.5—161.5 °C), as prisms (from isopropyl ether); $[\alpha]_D^{23}$ −16.6° (*c*, 1.04, $CHCl_3$); negative to a Zimmermann test;[12] UV: λ_{max}^{MeOH} 230 nm (ε, 7630); IR (KBr): 1775, 1695, 1175, 995, 925 cm^{-1}, ($CHCl_3$): 1763, 1690, 1178, 998, 927 cm^{-1}; NMR ($CDCl_3$): 3.14 (s, 8-OCH_3), 2.26 (s, 3H), 1.96 (s, 13-CH_3), 1.15 (s, 15-CH_3), 0.66 (d, J=6.0 Hz, 14-CH_3); ORD (*c*, 0.118, MeOH): *cf.* Fig. 1; CD (*c*, 0.099, MeOH): Fig. 2.

Found: C, 69.02; H, 8.08%. Calcd for $C_{16}H_{22}O_4$: C, 69.04; H, 7.97%.

Chromatography of Hydroperoxides on Silica Gel. A crystalline mixture of hydroperoxides, VI-a, b (1.109 g), was chromatographed on silica gel (26.5 g, grade II). Elution with benzene–ethyl acetate (50: 1 and 20: 1) gave a mixture of 6β-hydroxy-8(α and β)-methoxylactones VII-a, b (94 mg), the recovered starting hydroperoxides, VI-a, b (576 mg), and 6β,8β-dihydroxyeremophilenolide IV (209 mg). The compounds, VII-a, b and VI-a, b, were identified by tlc analysis.

Compound IV was crystallized from ethyl acetate as prisms; mp 209.0—211.5 °C, $[\alpha]_D^{24}$ +172° (*c*, 0.97, $CHCl_3$).

Found: C, 67.52; H, 8.32%. Calcd for $C_{15}H_{22}O_4$: C, 67.64; H, 8.33%.

The acetate was prepared in a similar manner and crystallized from isopropyl ether as prisms; mp 119.5—120.5 °C.

Found: C, 65.31; H, 7.58%. Calcd for $C_{19}H_{26}O_6$: C, 65.12; H, 7.48%. Compound IV and its acetate were identified with the natural samples by a mixed-melting-point determination and by a comparison of their IR, UV, and NMR spectra.

Reduction of Hydroperoxides (VI-a, b). a) By Sodium Sulfite. A mixture of petasalbin I (500 mg) and Rose Bengal (30 mg) in methanol (50 ml) was photooxygenated as has been described above. A solution of sodium sulfite (700 mg) in water (10 ml) was added to the stirred mixture, and stirring was continued for 15 hr. After the removal of the methanol and the addition of water, the mixture was extracted with ether. The extract was worked up in the usual manner to give a crude product (427 mg), which was then chromatographed on silica gel (15 g, grade II). Elution with benzene–ethyl acetate (30: 1) gave 6β-hydroxy-8α-methoxyepieremophilenolide VIII-a (30 mg), hemiacetal XI (193 mg), 6β-hydroxyeremophilenolide III (38 mg), and 6β,8β-dihydroxyeremophilenolide IV (10.5 mg).

The above compounds, III (mp 204.0—205.0 °C: prisms from ethyl acetate; $[\alpha]_D^{23}$ +212° (*c*, 1.02, $CHCl_3$), was found to be identical with the natural specimen by a mixed-melting-point determination and by a comparison of their IR and NMR spectra.

Hemiacetal (XI): a colorless oil, positive to an Ehrlich test; IR (film): 3400, 1685, 1650, 1245, 1110, 995 cm^{-1}; UV: λ_{max}^{MeOH} 250 nm (ε, 4500); NMR (CCl_4): 5.7—5.5 (two signals centered at 5.69 and 5.55, 1H), 5.4—5.1 (two signals centered at 5.32 and 5.12, 1H), 4.18 (OH), 1.88 (s, 13-CH_3), 0.93 (d, J=7.0 Hz, 14-CH_3), 0.78 and 0.70 (each s, 15-CH_3). This compound was found to afford isoligularone (XII) on glc (SF-96, 2.6 m; column temperature, 200 °C; H_2-flow rate, 60 ml/min).

b) By Sodium Borohydride. A crystalline mixture of hydroperoxides, VI-a, b (224.8 mg), was treated with sodium borohydride (73.4 mg) in methanol (14 ml) at room temperature for 19 hr. Subsequent working up as usual gave a crude product (230 mg), which was chromatographed on alumina (6 g, grade IV). Elution with benzene and benzene–ethyl acetate (30: 1) afforded petasalbin I (68 mg) and 6β-hydroxyeremophilenolide III (48 mg). The products, I and III, were identified by a comparison of the tlc and the IR spectra and by a mixed-melting-point determination with natural samples.

c) By a Platinum Catalyst. Hydroperoxide VI-a (202 mg) in acetic acid (4 ml) was hydrogenated over platinum oxide (52.6 mg) at room temperature until the hydrogen-uptake

had ceased (0.91 mol). After working up as usual, the chromatography of the crude product (175 mg) on silica gel (4 g) with benzene–ethyl acetate (50: 1 and 20: 1) gave 6β-hydroxy-8α-methoxyepieremophilenolide, VIII-a (34.4 mg); 6β-hydroxyeremophilenolide, III (6.1 mg), and 6β,8β-dihydroxyeremophilenolide, IV (43.7 mg). All the products were found to be identical with the authentic samples by a comparison of the tlc and the IR spectra and by a mixed-melting-point determination.

Isoligularone (XII)[11] *from Hemiacetal (XI).* A solution of hemiacetal XI (70 mg) in acetic anhydride (1.5 ml) was warmed at 90 °C for 1 hr. The reaction mixture was then diluted with water (3 ml) and extracted with ether. The ethereal extract was washed with a saturated sodium hydrogen carbonate solution and then water, and dried. The removal of the solvent gave a crystalline product, isoligularone XII (68 mg), which was crystallized from methanol as needles: mp 147.0—148.0 °C, $[\alpha]_D^{23}$ +39.0° (*c*, 0.98, $CHCl_3$); positive to a Zimmermann test; IR (KBr): 3125, 3060, 1660, 1547, 1280 cm^{-1}; UV: λ_{max}^{MeOH} 269 nm (ε, 5100); MS: *m/e* 232 (M^+), 175 (base peak); NMR ($CDCl_3$): 7.02 (q, *J*=1.5 Hz, 6-H), 2.86 (dd, *J*=18, 13 Hz, 9α-H), 2.16 (d, *J*=1.5 Hz, 13-CH_3), 1.28 (s, 15-CH_3), 0.91 (d, *J*=7.5 Hz, 14-CH_3); tlc: R_f, 0.50 (benzene–ethyl acetate, 15: 1).

Found: C, 77.50; H, 8.73%. Calcd for $C_{15}H_{20}O_2$: C, 77.55; H, 8.68%.

Oxidation of Hemiacetal (XI). Jones' reagent (0.15 ml)[13] was added to a solution of hemiacetal XI (80 mg) in acetone (3 ml) over a period of 15 min under ice-cooling. After stirring for a further 45 min, the excess reagent was decomposed with methanol (5 drops), diluted with water, and extracted with ether. The extract was then worked up in the usual manner to give a crude oil (66 mg), which was subsequently chromatographed on silica gel (2 g). Elution with light petroleum–benzene (1: 1) gave 8-oxoisoeremophilenolide XIV (47 mg), which was crystallized from isopropyl ether as colorless needles; mp 76.5—77.5 °C, $[\alpha]_D^{23}$ +31.5° (*c*, 0.73, $CHCl_3$); positive to a Zimmermann test; IR(KBr): 1760, 1695, 1195 cm^{-1}; UV: λ_{max}^{MeOH} 245 nm (ε, 7700); NMR (CCl_4): 5.42 (q, *J*=2.5 Hz, W1/2=5 Hz, 6-H), 3.63 (dd, *J*=16.5, 6.5 Hz, 9α-H), 1.92 (d, *J*=2.5 Hz, 13-CH_3), 1.05 (d, *J*=7.5 Hz, 14-CH_3), 0.79 (s, 15-CH_3); tlc: R_f, 0.66 (benzene–ethyl acetate, 10: 1).

Found: C, 72.39; H, 8.13%. Calcd for $C_{15}H_{20}O_3$: C, 72.55; H, 8.12%.

Ligularone (XIII).[1b,c] Compound XIII was prepared from petasalbin I (100 mg) by chromium trioxide (80mg) in pyridine (6.8 ml). The crude product was chromatographed on alumina (800 mg) and then crystallized from light petroleum to afford ligularone XIII as prisms: mp 66.0—67.5 °C, $[\alpha]_D^{25}$ −50.0° (*c*, 1.03, $CHCl_3$); tlc: R_f, 0.90 (benzene); (Found: C, 77.48; H, 8.87%). This compound was found to be identical with natural specimen by a comparison of the IR and NMR spectra and by a mixed-melting-point determination.

6-Oxoeremophilenolide (XV).[1-a] Jones' reagent (0.26 ml) was stirred over a period of 30 min under ice-cooling into a solution of 6β-hydroxyeremophilenolide III (148 mg) in acetone (5 ml). After stirring for a further 2 hr, the reaction mixture was worked up as has been described above to afford 6-oxoeremophilenolide XV (136 mg), which was subsequently crystallized from isopropyl ether as prisms: mp 124.0—126.0 °C, $[\alpha]_D^{24}$ −27.1° (*c*, 1.07, $CHCl_3$); IR(KBr): 1740, 1690, 1190, 1150, 1090, 1050, 930 cm^{-1}; UV: λ_{max}^{MeOH} 240 nm (ε, 11100); NMR (CCl_4): 4.88 (m, W1/2=21 Hz, 8-H), 1.85 (d, *J*=2.2 Hz, 13-CH_3), 1.11 (s, 15-CH_3), 0.63 (d, *J*=6.0 Hz, 14-CH_3); tlc: R_f, 0.75 (benzene–ethyl acetate, 10: 1).

Found: C, 72.51; H, 8.21%. Calcd for $C_{15}H_{20}O_3$: C, 72.55; H, 8.12%.

The authors wish to thank the staff of the Shionogi Research Laboratory, Shionogi and Co., Ltd., for the microanalysis, and the Institute of Food Chemistry for the measurement of the MS and NMR spectra.

References

1) a) L. Novotný, V. Herout, and F. Sorm, *Coll. Czech. Chem. Commun.*, **29**, 2189 (1964). b) H. Ishii, T. Tozyo, and H. Minato, *Tetrahedron*, **21**, 2605 (1965). c) K. Naya, M. Nakagawa, M. Hayashi, K. Tsuji, and M. Naito, *Tetrahedron Lett.*, **1971**, 2961.

2) H. Ishii, T. Tozyo, and H. Minato, *J. Chem. Soc.*, **1966**, 1545.

3) H. Nagano, Y. Tanahashi, Y. Moriyama, and T. Takahashi, This Bulletin, **46**, 2840 (1973).

4) L. Novotný, Z. Samek, and F. Sorm, *Coll. Czech. Chem. Commun.*, **31**, 371 (1966).

5) F. Sorm, *Pure Appl. Chem.*, **21**, 281 (1970).

6) C. S. Foote, M. T. Wuesthoff, S. Wexler, I. G. Burstain, R. Denny, G. O. Schenck, and K. H. Schulte-Elte, *Tetrahedron*, **23**, 2583 (1967).

7) G. O. Schenck, *Angew. Chem.*, **57**, 101 (1944), **69**, 579 (1957); E. Koch and G. O. Schenck, *Chem. Ber.*, **99**, 1984 (1966).

8) K. Naya, H. Takashina, M. Sawada, and R. Kanazawa, 15th Symposium on the Chemistry of Terpenes, Essential Oils, and Aromatics, Symposium Papers (1971), p. 87.

9) C. Djerassi, R. Records, E. Bunnenberg, K. Mislow, and A. Moscowwitz, *J. Amer. Chem. Soc.*, **84**, 870 (1962).

10) N. S. Bhacca and D. H. Williams, "Application of NMR Spectroscopy in Organic Chemistry," Holden-Day, San Francisco (1964), p. 110.

11) M. Tada and T. Takahashi, *Tetrahedron Lett.*, **1973**, 3999.

12) T. J. King and C. E. Newall, *J. Chem. Soc.*, **1962**, 367.

13) J. Mainwald, J. Crandall, and W. E. Hymans, "Organic Syntheses," Coll. Vol. V, p. 866 (1973).

Autoxidation of Atactic Polypropylene and Related Alkanes. Rates and Reactivities toward Peroxy Radicals

Etsuo NIKI and Yoshio KAMIYA

Department of Reaction Chemistry, Faculty of Engineering, University of Tokyo, Hongo, Tokyo 113

(Received April 12, 1975)

Rates of autoxidations of atactic polypropylene, polystyrene, and several alkanes in solution initiated by azobiscyclohexanecarbonitrile were measured at 90 °C in the absence and presence of added hydroperoxide and the reactivities toward *tert*-butylperoxyl and tetralylperoxyl radicals were measured. Atactic polypropylene was found to be oxidized faster than expected from the related alkanes. On the other hand, polystyrene was quite resistant to autoxidation. The relative reactivities of secondary and tertiary hydrogens toward *t*-butylperoxyl radical were obtained as 1: 9.7 and that for primary hydrogen was estimated to be quite small. The observed reactivity of 2,2,4-trimethylpentane was much smaller than the calculated reactivity from the results of simple alkanes, whereas the observed reactivity of atactic polypropylene was higher than the calculated one. The high reactivity of atactic polypropylene for oxidation and toward peroxyl radicals was interpreted as being due to a fast intramolecular propagation. Tetralylperoxyl radical was 3.6 times as reactive as *t*-butylperoxyl radical toward both atactic polypropylene and 2,6,10,14-tetramethylpentadecane.

The oxidation of polymers by molecular oxygen is probably the most important reaction in the ageing, deterioration, and degradation of plastics, fiber, rubber, and food. This autoxidation proceeds by a radical chain mechanism, in which the chain carrying species are the peroxyl and alkoxyl radicals.[1] We have previously reported that the reactivities of atactic polypropylene and polystyrene toward *t*-butoxyl radical are considerably smaller than those of the corresponding simple model compounds.[2] The peroxyl radicals may be a more important chain carrier in the oxidation of polyolefins especially at ambient temperature. However, the relative reactivities of polyolefins and alkanes toward a specific peroxyl radical have not yet been reported. The objective of the present paper is to determine the relative reactivities of atactic polypropylene, polystyrene, and several simple low molecular weight model compounds toward *t*-butylperoxyl and 1-tetralylperoxyl radicals generated from corresponding hydroperoxide.

Experimental

Materials. Atactic polypropylene supplied by Mitsui Petrochemical Industries was first soaked in benzene at room temperature for several days and the insoluble fraction was separated by filtration. Then a soluble fraction was purified by the conventional method, using benzene and methanol as solvent and precipitant respectively. Finally it was dried to a constant weight under vacuum at room temperature. The glc analysis showed that the dried polypropylene contained little benzene or methanol. The average molecular weight of the purified polypropylene was obtained as 8400 from its intrinsic viscosity. The infrared spectrum of the purified polypropylene showed strong absorption at 975 cm^{-1}, but little absorption at 997 cm^{-1}, indicating that little isotactic polypropylene was present.[3] Polystyrene supplied by Asahi Dow Industries was purified as described previously.[2] The purified polystyrene had an intrinsic viscosity of 0.825 at 45 °C in benzene, and the number average molecular weight was 2×10^5. A monodisperse polystyrene was also used to examine the effect of the molecular weight. This polystyrene standard was obtained from Pressure Chemical Co. and was used without further purification. Decane, tridecane, 2,6,-10, 14-tetramethylpentadecane, and chlorobenzene were washed successively with acid, water, alkali and water, dried, and distilled. 2,4-Dimethylpentane, 2,2,4-trimethylpentane, and 3-methyloctane were percolated through an activated alumina column prior to use.

Commercial *t*-butyl hydroperoxide was purified by fractional distillation, 44 °C/27 mmHg, and stored over sodium carbonate. The purity determined by iodometric titration was always higher than 98%. Tetralyl hydroperoxide was prepared by air oxidation of tetralin at 50 °C and by repeated recrystallization from hexane. Azobiscyclohexanecarbonitrile (ACN) and 2,6-di-*t*-butyl-4-methylphenol (BMP) were recrystallized from methanol. Commercial oxygen and nitrogen were used as received.

Procedures. The polymer solutions were prepared by dissolving a weighed amount of polypropylene or polystyrene into chlorobenzene in a volumetric tube. All polymers dissolved completely both at room temperature and at 90 °C and the solutions were always homogeneous.

The oxidation was carried out in an ampoule immersed in a silicone oil bath carefully maintained at constant temperature (±0.02 °C). The rate of oxidation was measured either by following the pressure change using a pressure transducer or by measureing the initial and final amounts of oxygen in the reaction vessel by a Toepler pump and subsequent gas analysis by gas chromatography or Cu–CuO furnace.[4] Plots of pressure change as a function of time gave excellent straight lines without any noticeable autocatalytic or autoretarding effect at the initial stage of the oxidation. The rate of decomposition of ACN was measured from the rate of nitrogen evolution and the rate of initiation was determined from the induction period in the presence of inhibitor.[5] BMP was used as the inhibitor.

Results and Discussion

Rates of Oxidation of Atactic Polypropylene, Polystyrene, and Alkanes at 90 °C. The rates of oxidation of atactic polypropylene, polystyrene, and several alkanes initiated with ACN at 90 °C are summarized in Table 1. To obtain the rate of oxidation in the propagation step, the observed rate of oxidation was corrected for nitrogen evolution from ACN and oxygen absorption and evolution associated with initiation and termination by

$$R_{prop} = R_{obsd} + \frac{R_i}{2e} - \frac{7}{4}R_i \qquad (1)$$

where R_i is the rate of initiation and e is the efficiency of

Table 1. Oxidation of atactic polypropylene, polystyrene, and several alkanes in chlorobenzene at 90 °C

Substrate, M	[ACN]$\times 10^2$, M	$R_{prop}\times 10^6$, M/s	$k_p/(2k_t)^{1/2}\times 10^3$, $(Ms)^{-1/2}$
Decane, 2.57	0.996	0.55	0.32
Tridecane, 2.05	1.02	0.56	0.40
3-Methyloctane, 2.79	1.01	0.73	0.57
2,6,10,14-Tetramethylpentadecane, 1.46	1.00	1.76	1.79
2,2,4-Trimethylpentane, 3.03	1.01	0.18	0.041
Polypropylene, 0.999	2.00	1.41	1.48
Polystyrene,[a] 1.00	1.00	—0	
Polystyrene 20400,[b] 0.975	1.00	—0	

a) Polystyrene with $M_n=2\times 10^5$. b) Monodisperse polystyrene, $mw=20400$ and $M_w/M_n<1.10$.

initiation by ACN.[4] The ratio of the rate constants, $k_p/(2k_t)^{1/2}$, was calculated from the rate of oxidation by

$$k_p/(2k_t)^{1/2} = R_{prop}/[RH]R_i^{1/2} \quad (2)$$

where k_p and k_t are the rate constants for the propagation and termination reactions respectively.

Table 1 shows that $k_p/(2k_t)^{1/2}$ for tridecane is 1.25 times as large as that for decane, which corresponds well with the ratio of the number of secondary hydrogens in tridecane to that in decane, 22/16=1.38. This probably indicates that the rate constants for propagation (per active hydrogen) and termination reactions are similar for decane and tridecane. The high $k_p/(2k_t)^{1/2}$ for 2,6,10,14-tetramethylpentadecane must be ascribed to a relatively high k_p and low k_t due to the four tertiary hydrogen atoms. However, 2,2,4-trimethylpentane has an extraordinarily low $k_p/(2k_t)^{1/2}$, apparently due to the low reactivity of its tertiary hydrogen atom (see later text and Ref. 2). On the other hand, atactic polypropylene has a rather high $k_p/(2k_t)^{1/2}$. It is interesting that atactic polypropylene is as oxidizable as 2,6,10,14-tetramethylpentadecane. This may be because of a low k_t due to the tertiary alkylperoxyl radicals, but more probably because of a high k_p due to the fast intramolecular propagation. The rates of oxidation of polystyrenes were too small to permit the calculation of reliable $k_p/(2k_t)^{1/2}$. Considering that polystyrene has tertiary benzylic hydrogen, this extraordinarily low oxidizability is surprising. It may occur because of a very low reactivity of polystyrene toward oxy radicals[2] and high termination rate constants.

Oxidation with Added Hydroperoxide. Hydroperoxide is quite reactive toward peroxyl radical and therefore it is quite an efficient chain transfer agent in the autoxidation.[6] Accordingly, the addition of hydroperoxide changes the chain carrying peroxyl radical from substrate peroxyl radical to the peroxyl radical derived from the added hydroperoxide. When the added hydroperoxide (BOOH) gives a tertiary peroxyl radical ($BO_2\cdot$), the termination reactions proceed as follows:[7]

$$BO_2\cdot + BO_2\cdot \xrightarrow{\alpha} BOOB + O_2 \quad (3)$$

$$\xrightarrow{1-\alpha} 2\,BO\cdot + O_2 \quad (4)$$

$$BO\cdot + BOOH \longrightarrow BOH + BO_2\cdot \quad (5)$$

The alkoxyl radical generated from the non-terminating interactions of tertiary peroxyl radicals exclusively abstracts hydrogen from the hydroperoxide before it reacts with the substrate or cleaves. The rate of oxygen evolution in the termination step (R_{term}) is then given by[7]

$$R_{term} = R_i/2\alpha \quad (6)$$

where α is the fraction of the interactions of tertiary peroxyl radicals that are terminating.

The results of the oxidations of atactic polypropylene, polystyrene, and several alkanes at 90 °C in the presence of initially added *t*-butyl and 1-tetralyl hydroperoxides

Table 2. Oxidation of atactic polypropylene, polystyrene, and alkanes in chlorobenzene in the presence of hydroperoxide at 90 °C

Substrate, M	[ACN] $\times 10^2$, M	Hydroperoxide M	R_{prop} $\times 10^6$, M/s	k_{BR}[c] $(Ms)^{-1}$	k_{TR} $(Ms)^{-1}$
Decane, 2.05	1.01	*t*-Butyl, 1.60	7.72	0.612 (0.619)	
Tridecane, 1.64	1.02	*t*-Butyl, 1.60	8.79	0.863 (0.851)	
3-Methyloctane, 2.23	1.02	*t*-Butyl, 0.80	9.12	0.658	
3-Methyloctane, 2.23	1.02	*t*-Butyl, 1.60	10.20	0.736 (0.763)	
2,6,10,14-Tetramethylpentadecane, 1.17	1.02	*t*-Butyl, 1.60	16.80	2.31 (2.02)	
2,6,10,14-Tetramethylpentadecane, 1.46	0.992	Tetralyl, 0.102	1.73		8.36
2,2,4-Trimethylpentane, 3.03	0.992	*t*-Butyl, 1.60	3.15	0.170 (0.453)	
Polypropylene, 0.717	1.00	*t*-Butyl, 1.60	4.31	0.977 (0.453)	
Polypropylene, 2.0	2.00	Tetralyl, 0.0513	1.28		3.14
Polypropylene, 2.0	2.00	Tetralyl, 0.100	1.34		3.29
Polystyrene,[a] 0.795	1.02	*t*-Butyl, 1.60	0	0 (0.453)[d]	
Polystyrene 20400,[b] 0.780	1.02	*t*-Butyl, 1.60	0	0 (0.453)[d]	

a) b) See footnote of Table 1. c) Numbers in the parentheses are k_{BR} calculated with $k_{prim}=0$, $k_{sec}=0.0387$, and $k_{tert}=0.376\ M^{-1}\,s^{-1}$ (see text). d) The contribution of benzyl resonance is neglected (see Ref. 2).

are summarized in Table 2. In the presence of *t*-butyl hydroperoxide, the rate of oxidation in the propagation step was obtained by correcting the observed rate of gas absorption for nitrogen evolution from ACN and oxygen absorption and evolution associated with the initiation and termination steps by

$$R_{prop} = R_{obsd} + \frac{R_i}{2e} - R_i + \frac{R_i}{2\alpha} \quad (7)$$

The value of α for *t*-butylperoxyl radicals was determined from the rate of oxygen evolution in the induced decomposition of *t*-butyl hydroperoxide by ACN in chlorobenzene at 90 °C: the value of 0.059 was obtained. This shows that only 5.9% of the bimolecular interactions of *t*-butylperoxyl radicals are terminating and about 94% are non-terminating to give *t*-butoxyl radicals. It was assumed that the increase in the macroscopic viscosity due to atactic polypropylene and polystyrene had no effect on α.[8] For the oxidation with added tetralyl hydroperoxide, which gives a secondary peroxyl radical, the observed rate of gas absorption was corrected by Eq. (8) with the assumption that all the bimolecular interactions of tetralylperoxyl radicals are terminating.[9]

$$R_{prop} = R_{obsd} + \frac{R_i}{2e} - \frac{R_i}{2} \quad (8)$$

Tables 1 and 2 show that the addition of *t*-butyl hydroperoxide increased the rate of oxidation for every substrate except polystyrene. This is apparently due to a low termination rate constant for *t*-butylperoxyl radicals.[10]

The rate constant k_{BR} for the hydrogen atom abstraction from the substrate by *t*-butylperoxyl radical was calculated from Eq. (9)[6]

$$k_{BR} = R_{prop}/[RH](R_i/2k_{tBB})^{1/2} \quad (9)$$

where k_{tBB} is the rate constant for direct termination by *t*-butylperoxyl radical.[10] The absolute termination rate constant was calculated as $2k_{tBB}=1.2\times10^4$ M^{-1} s^{-1} at 90 °C from the literature value,[11]

$$\log(2k_{tBB}) = 9.2-8.5/2.303RT \quad (10)$$

This k_{BR} shows the reactivities of the substrate toward a *t*-butylperoxyl radical. The rate constants for hydrogen atom abstraction from primary, secondary, and tertiary carbon-hydrogen bonds by *t*-butylperoxyl radical were calculated from k_{BR} for decane, tridecane, 3-methyloctane, and 2,6,10,14-tetramethylpentadecane. The best results are $k_{prim}=0$, $k_{sec}=0.0387$, and $k_{tert}=0.376$ M^{-1} s^{-1} (per hydrogen). The rate constant for primary hydrogen was obtained as a negative value and so is estimated as zero, since this is obtained as a small difference between large quantities and a small experimental error would produce a large error in k_{prim}. The calculated k_{BR} from the above k_{prim}, k_{sec}, and k_{tert} is also shown in Table 2. The agreement between the observed and calculated k_{BR} values is satisfactory for decane, tridecane, 3-methyloctane, and 2,6,10,14-tetramethylpentadecane. However, the observed k_{BR} for 2,2,4-trimethylpentane is much lower than the calculated k_{BR}. This lower reactivity of 2,2,4-trimethylpentane toward *t*-butylperoxyl radical must be due to its preferred conformation as observed toward *t*-butoxyl radical.[2] The observed reactivity of atactic polypropylene was larger than the calculated one by a factor of more than 2. Since atactic polypropylene also has an alternate methyl group along the main chain, the tertiary hydrogens must be sterically protected from the attack of *t*-butylperoxyl radical. The high k_{BR} for atactic polypropylene must imply the contribution of intramolecular propagation even in the presence of a high concentration of *t*-butyl hydroperoxide. On the other hand, polystyrene was found to be quite stable toward a *t*-butylperoxyl radical. This may be ascribed to a profound steric protection by phenyl groups on the alternating carbon atoms.

The oxidation of alkanes has been studied by several investigators. Allara *et al.*[12] estimated the relative reactivities of primary, secondary, and tertiary hydrogens toward peroxyl radicals as 1: 10: 80 at 100 °C. In the oxidation of isobutane, primary hydrogen was found to be stable and only tertiary hydrogen was oxidized selectively.[13] Mill *et al.*[14] obtained the relative reactivities of primary and secondary hydrogens as 1: 45 in the oxidation of butane at 100 °C. On the other hand, Van Sickle *et al.*[15] reported that the ratio of attack by peroxyl radicals at primary and secondary hydrogens was 1: 38.5 in the oxidation of pentane at 100 °C. Bennett, Brown, and Mile[16] measured the relative reactivities of primary, secondary, and tertiary hydrogens by product analyses in the oxidation of 2-methylpentane and obtained the ratio of 1: 18: 133 at 20 °C. Some of these relative reactivities are not toward a specific peroxyl radical but toward composite peroxyl radicals and, in some cases, the contribution of an alkoxyl radical is also possible.

From Table 2, the relative reactivities of secondary and tertiary hydrogens toward *t*-butylperoxyl radical is obtained as $k_{sec}: k_{tert}=1: 9.7$. This is in satisfactory agreement with the literature value shown above. Since the relative reactivities of primary, secondary, and tertiary hydrogens toward *t*-butoxyl radical was 0.14: 1: 2.9 at 45 °C,[2] *t*-butylperoxyl radical is more selective than *t*-butoxyl radical, as was expected.

Bennett, Eyre, and Summers[17] measured the absolute termination rate constant in the oxidation of 2,6,10,14-tetramethylpentadecane and obtained $2k_t=3.0\times10^6$ M^{-1} s^{-1} at 88 °C. With this $2k_t$ and $k_p/(2k_t)^{1/2}$ in Table 1, we obtain $k_p=3.1$ M^{-1} s^{-1}, which is in fair agreement with k_{BR} in Table 2. The fact that k_p is about 30% higher than k_{BR} may be partly because of the contribution of the secondary peroxyl radicals, which are more reactive than the *t*-butylperoxyl radical.

In Table 2 is shown the effect of addition of 1-tetralyl hydroperoxide. The rate constants k_{TR} for the reactions of 1-tetralylperoxyl radical and 2,6,10,14-tetramethylpentadecane and atactic polypropylene were calculated from

$$k_{TR} = R_{prop}/[RH](R_i/2k_{tTT})^{1/2} \quad (11)$$

where k_{tTT} is the constant for the termination reaction of 1-tetralylperoxyl radicals, which was calculated from the literature value:[18]

$$k_{tTT} = 4.3\times10^9 \exp(-4300/RT) \quad (12)$$

The calculated k_{TR} are shown in Table 2. The reactivities of both atactic polypropylene and 2,6,10,14-tetramethylpentadecane toward 1-tetralylperoxyl radical are

higher than those toward *t*-butylperoxyl radical. 1-Tetralylperoxyl radical is more reactive than *t*-butylperoxyl radical by a factor of 3.6. Table 2 shows, however, that the rate of oxidation in the presence of 1-tetralyl hydroperoxide is considerably lower than that in the presence of *t*-butyl hydroperoxide. This is due to a higher termination rate constant for 1-tetralylperoxyl radical (1.1×10^7 M^{-1} s^{-1} at 90 °C) than that for *t*-butylperoxyl radical (6.0×10^3).

When the rate constans k_{BR} and k_{TR} are calculated from the rate of oxidation in the presence of initially added hydroperoxide as described above (Eqs. (9) and (11)), it is required that all the chain carriers are changed from the substrate peroxyl radical to the peroxyl radical derived from hydroperoxide.[19,20] In other words, if the contribution of the substrate peroxyl radical in either the propagation or the termination step is not negligiblly small, Eqs. (9) and (11) do not hold. This complication is especially important for reactive substrates at higher temperature. However, the substrates studied in this work are much less reactive than the hydroperoxide. Moreover, the contribution of the substrate peroxyl radical in the propagation or termination step should give less error, if any, in the relative k_{BR} and k_{TR} and therefore in the relative reactivities of primary, secondary, and tertiary hydrogens.

Another complication that must be considered is the reaction of *t*-butoxyl radical in the oxidation with added *t*-butyl hydroperoxide. For Eq. (7) to hold, a *t*-butoxyl radical generated from the non-terminating interactions of *t*-butylperoxyl radicals should exclusively abstract hydrogen from *t*-butyl hydroperoxide before it reacts with the substrate or cleaves to acetone and methyl radical. It may well be concluded that this condition is satisfied in this study from the experimental data that the observed α was independent of the concentration of *t*-butyl hydroperoxide when it was higher than 0.80 M.

References

1) E. Niki, C. Decker, and F. R. Mayo, *J. Polym. Sci., Polym. Chem. Ed.*, **11**, 2813 (1973).
2) E. Niki and Y. Kamiya, *J. Org. Chem.*, **38**, 1403 (1973); *J. Chem. Soc., Perkin II*, in press.
3) J. P. Luongo, *J. Appl. Polym. Sci.*, **3**, 302 (1960).
4) E. Niki, Y. Takaishi, and Y. Kamiya, *Nippon Kagaku Kaishi*, **1975**, 1559.
5) C. E. Boozer, G. S. Hammond, C. E. Hamilton, and J. N. Sen, *J. Amer. Chem. Soc.*, **77**, 3233 (1955).
6) J. A. Howard, W. J. Schwalm, and K. U. Ingold, *Adv. Chem. Ser.*, Vol. 75, *Amer. Chem. Soc.*, (1968), p. 6.
7) J. R. Thomas, *J. Amer. Chem. Soc.*, **87**, 3835 (1965).
8) E. Niki and Y. Kamiya, *ibid.*, **96**, 2129 (1974).
9) G. A. Russell, *ibid.*, **79**, 3871 (1957).
10) J. A. Howard, *Adv. Free Radical Chem.*, **4**, 49 (1971).
11) S. Korcek, J. H. B. Chenier, J. A. Howard, and K. U. Ingold, *Can. J. Chem.*, **50**, 2285 (1972).
12) D. L. Allara, D. Edelson, and K. C. Irwin, *Int. J. Chem. Kinet.*, **4**, 345 (1972).
13) D. L. Allara, T. Mill, D. G. Hendry, and F. R. Mayo, *Adv. Chem. Ser.*, Vol. 76, *Amer. Chem. Soc.*, (1968), p. 40.
14) T. Mill, F. R. Mayo, H. Richardson, K. C. Irwin, and D. C. Allara, *J. Amer. Chem. Soc.*, **94**, 6802 (1972).
15) D. E. Van Sickle, T. Mill, F. R. Mayo, H. Richardson, and C. W. Gould, *J. Org. Chem.*, **38**, 4435 (1973).
16) J. E. Bennett, D. M. Brown, and B. Mile, *Trans. Faraday Soc.*, **66**, 386 (1970).
17) J. E. Bennett, J. A. Eyre, and R. Summers, *J. Chem. Soc., Perkin II*, **1974**, 977.
18) J. A. Howard and K. U. Ingold, *Can. J. Chem.*, **44**, 1119 (1966).
19) E. Niki, K. Okayasu, and Y. Kamiya, *Int. J. Chem. Kinet.*, **6**, 279 (1974).
20) J. A. Howard and J. B. Chenier, *ibid.*, **6**, 527 (1974).

Kinetics of the Thermal Decompositions of Diaryl and Dialkyl Disulfides

Tokuji MIYASHITA, Minoru MATSUDA,* and Masashi IINO
Chemical Research Institute of Non-aqueous Solutions, Tohoku University, Sendai 980
(Received April 25, 1975)

A kinetic study of the thermal decomposition of diphenyl disulfide, its *p*-methoxy, *p*-methyl, and *p*-chloro derivatives, and di-*n*-butyl and di-*t*-butyl disulfides in tetralin was made. The rate of decomposition was followed by the decrease of disulfide and the spontaneous first-order rate constants for these disulfides at 196, 207, and 217 °C and the activation parameters were obtained. It was observed that the rates of the decompositions for diaryl disulfides are increased by *p*-substituents ($CH_3O > Cl \simeq CH_3 > H$) and that that of di-*t*-butyl disulfide is comparable to diaryl disulfides, whereas, di-*n*-butyl disulfide shows no decomposition under these conditions. A reaction scheme of the decomposition including induced decomposition is proposed from the kinetic results and product analysis. Moreover, the properties of a thiyl radical in relation to the above results are discussed from the electronic and ESR spectra of the aryl thiyl radicals generated from the photolysis of corresponding thiols in a glass of 2-methyltetrahydrofuran at −196 °C.

Although it is well known that the S—S bonds in organic disulfides are cleaved homolytically by heat or light yielding thiyl radicals,[1] there are few kinetic studies of the thermal decomposition of organic disulfides. The dissociation of tetramethylthiuram (TMTD) and 2,2'-dibenzothiazolyl (DBTD) disulfides into their thiyl radicals has been demonstrated from magnetic measurements[2] and these radicals initiate the radical polymerization of styrene and methyl methacrylate (MMA)[3,4] at temperatures above 60 °C. The first-order rate constants for the decomposition of TMTD at two temperatures (60 °C and 80 °C) have been estimated by Ferington and Tobolsky[3] from kinetic studies of styrene and MMA polymerizations initiated by the disulfide, and Davis and Perrin[5] have also determined the rate constants for both TMTD and DBTD at 56 °C and 100 °C using diphenylpicrylhydrazyl (DPPH) as a scavenger for radicals formed thermally. However, for both diaryl and dialkyl disulfides the first-order rate constants have so far not been reported, though the formation of thiyl radicals from the homolytic scission of disulfides has already been indicated from the fact that the reaction of diphenyl disulfide with benzyl alcohol gives both aldehyde and thiophenol[6] and that such a disulfide dehydrogenates from hydrocarbons.[7,8] Leandri and Tundo[9] have investigated the effects of substituents on the extent of the decomposition of diaryl disulfides at 170 °C from molecular weight measurements, but they have not determined the rate constants.

The purpose of this paper is to determine the first-order rate constants for the thermal decompositions of some symmetric diaryl and dialkyl disulfides in tetralin, and to obtain a relationship between the structure and the susceptibility to decomposition, as well as other information about the properties of thiyl radicals.

Experimental

Materials. Commercially available, diphenyl, di-*t*-butyl, and di-*n*-butyl disulfides were recrystallized three times from ethanol. Di-*p*-chlorophenyl and di-*p*-methylphenyl disulfides were prepared from the oxidations of the corresponding thiols and recrystallized from ethanol. Di-*p*-methoxyphenyl disulfide was prepared by the method of Tarbell and Fukushima[10] and recrystallized three times from ethanol. Tetralin was washed successively with concentrated sulfuric acid, water, 10% aqueous sodium carbonate, water, and then dried over anhydrous sodium sulfate and distilled from sodium metals. The distillate was refluxed over DPPH and redistilled before use.

Kinetics. A weighed sample of disulfide was dissolved in a known volume of tetralin. The solution was placed in a Pyrex glass-reaction tube, degassed many times (usually 6—9 times) by the freeze-thaw method, and finally the reaction tube was filled with nitrogen, sealed off and immersed in an oil bath which was maintained at the desired temperature to within ±0.1 °C. An aliquot of the solution was withdrawn after a definite time interval into a sample tube attached to the reaction tube, and evacuated by a high-vacuum pump through a stopcock. Then, the quantity of residual disulfide in the aliquot was determined by the following method:[11] the disulfide in the aliquot was reduced to the corresponding thiol with sodium borohydride and aluminum chloride and the quantity of the resulting thiol was determined by titration with silver nitrate using dithizone as an indicator.[12] Since the reaction mixture contained the thiol formed from the hydrogen abstraction of the thiyl radical, the disulfide content was determined by subtracting the amount of thiol in an unreduced aliquot from that obtained after reduction. It has been reported that the thiol and sulfide formed during the decomposition of disulfides (see the following section) are unchanged by the reduction and the presence of these compounds does not interfere with the reduction and titration.[11] The preliminary experiments show that the accuracy of the titration for diphenyl, di-*p*-methoxyphenyl, di-*p*-methylphenyl, di-*p*-chlorophenyl, and di-*n*-butyl disulfides is 99.0—99.5, 99.2—99.7, 93.0—93.5, and 98.5—99.0%, respectively.

The rate of decomposition is known to be represented generally by the following equations,[15]

$$-\mathrm{d[P]}/\mathrm{d}t = k_1[\mathrm{P}] + k_i[\mathrm{P}]^n = k_{obsd}[\mathrm{P}] \quad (1)$$

$$k_{obsd} = k_1 + k_i[\mathrm{P}]^{n-1} \quad (2)$$

where [P] is the concentration of the decomposed substance (disulfide, in this case) and k_1 and k_i are the first-order (spontaneous) rate constant and a constant including the rate constant for induced decomposition, respectively. The apparent first-order rate constants for various initial concentrations of disulfide were obtained from the slopes in the first-order plots (line (a) in Fig. 1) in a region of low conversion ($[\mathrm{P}] \simeq [\mathrm{P}]_0$), and then, these were treated according to Eq. (2) in order to obtain k_1 and n, as will be described in the section on the Results. In our experiments, first-order plots gave straight lines to at least a 20% conversion.

Analysis of Products for a Large Scale Experiment. A solution of 4.36 g (0.02 mol) of diphenyl disulfide in 70 ml of tetralin was deaerated with nitrogen gas and allowed to react at a reflux temperature (270.2 °C) for 90 hr. Most of the tetralin and thiophenol were distilled from the reaction mixture and then 1.32 g (0.012 mol) of thiophenol was isolated as a yellow crystal of lead salt (I) by the reaction of thiophenol with lead acetate.[13] This yield of thiophenol was almost equal to that obtained by titration with silver nitrate.

Found: C, 34.07; H, 2.16%. Calcd for $C_{12}H_{10}PbS_2$ (I): C, 33.86; H, 2.35%.

The residual mixture was analyzed by chromatography on a silica gel column in the usual way. Elution with petroleum ether gave tetralin, and then using a 90: 10 petroleum ether–benzene mixture, unreacted diphenyl disulfide (0.006 mol, 1.3 g). The oily product was eluted with a 80: 20 petroleum ether–benzene mixture and identified as 1,2,3,4-tetrahydro-1-phenylthionaphthalene (II) (0.006 mol, 1.4 g): NMR (δ, CCl_4): 4.45 (1H, t, CH), 1.6—2.0 (4H, m, CH_2), 2.4—2.8 (2H, m, $-CH_2-C_6H_4-$), 6.9—7.4 ppm (9H, m, arom).

Found: C, 80.76; H, 7.11; S, 14.00%. Calcd for $C_{16}H_{16}S$ (II): C, 79.95; H, 6.71; S, 13.34%. The yellow oily fraction (about 0.3 g) containing both sulfur (14.2%) and tetralin fragments was eluted with a 50: 50 petroleum ether–benzene mixture. Elution with diethyl ether produced a brown oily fraction (about 0.4 g) containing sulfur (6.9%) and tetralin fragments. The formation of a small amount of naphthalene was observed using glc.

Spectra of Thiyl Radicals. The electronic spectra of aryl thiyl radicals generated by the photolysis of the corresponding thiols in a rigid glass of 2-methyltetrahydrofuran (2-MTHF) at liquid nitrogen temperature have been obtained (matrix isolation technique[14]). The concentration of each thiol was 0.01 mol/l and a super-high-pressure mercury lamp was used for the photolysis.

Results

Kinetics. The thermal decompositions of various disulfides were studied in tetralin which is a good hydrogen-donating compound. In Fig. 2 (n=2 in Eqs. 1 and 2), the apparent first-order rate constants (k_{obsd}) for various initial concentrations are plotted against the initial concentrations of the disulfides. Nozaki and Bartlett[15] have indicated in their studies on the decomposition of the substituted benzoyl peroxides that the order n of the induced decomposition in Eq. (1) (and Eq. 2) can vary between 0.5 and 2.0, depending on which radicals attack the parent molecules and on the type of radicals participating in the termination step. In our experiments the

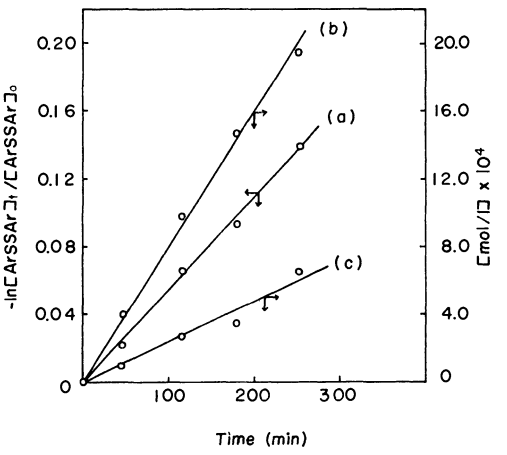

Fig. 1. (a) Plot of the first-order kinetics for the decomposition of di-*p*-methoxyphenyl disulfide (0.010 M) at 207 °C. (b) Rate of thiol formation determined by the titration with silver nitrate. (c) Rate of "other product" formation estimated from the subtraction of the rate of thiol formation from that of di-*p*-methoxyphenyl disulfide decomposition.

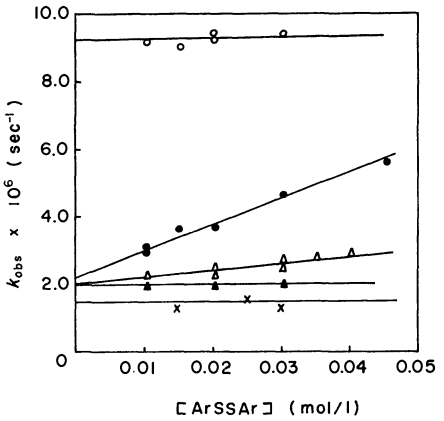

Fig. 2. Plots of k_{obs} *vs.* the concentration of disulfide at 207 °C: (×) diphenyl disulfide; (●) di-*p*-chlorophenyl disulfide; (○) di-*p*-methoxyphenyl disulfide; (△) di-*p*-methylphenyl disulfide; (▲) di-*tert*-butyl disulfide.

Table 1. First-order rate constants and activation parameters for the thermal decomposition of diaryl and dialkyl disulfides in tetralin.

Disulfide	Temp. °C	$k_1 \times 10^6$ s^{-1}	ΔS cal mol^{-1}	E_a kcal mol^{-1}
Diphenyl disulfide	196	0.47		
	207	1.1	1.5	43.0
	217	3.3		
Di-*p*-chlorophenyl disulfide	196	0.80		
	207	2.2	−4.0	40.0
	217	5.0		
Di-*p*-methoxyphenyl disulfide	196	3.3		
	207	9.0	0.5	40.6
Di-*p*-methylphenyl disulfide	207	2.0	−5.4	39.4
	217	4.6		
Di-*t*-butyl disulfide	207	1.9[a]		
Di-*n*-butyl disulfide	207	No decomposition[b]		

a) Value estimated from the amount of thiol formed. b) No decomposition occurs at 207°C for 20 hr.

trial and error method for determining n in Eq. (2) gives straight lines with different slopes for di-*p*-chlorophenyl and di-*p*-methylphenyl disulfides when n is equal to 2. Thus, it is suggested that a considerable amount of induced decomposition occurs in the decomposition of di-*p*-chlorophenyl disulfide and probably a small amount in that of di-*p*-methylphenyl disulfide, whereas, for the other disulfides no appreciable concentration effect was observed. The values of k_1 for both di-*p*-chlorophenyl and di-*p*-methylphenyl disulfides were estimated from an extrapolation of the straight lines to zero concentration; these values of k_1 were found to be 0.8×10^{-6}, 2.2×10^{-6}, and 5.0×10^{-6} s^{-1} at 196, 207, and 217 °C, respectively. The k_1 values for other disulfides at 196, 207, and 217 °C and the activation parameters are shown in Table 1. Since di-*t*-butyl disulfide was not reduced quantitatively with sodium borohydride, the k_1 value was estimated from the amount of the thiol formed and so this value may be considered to be the lower limit of the true value.

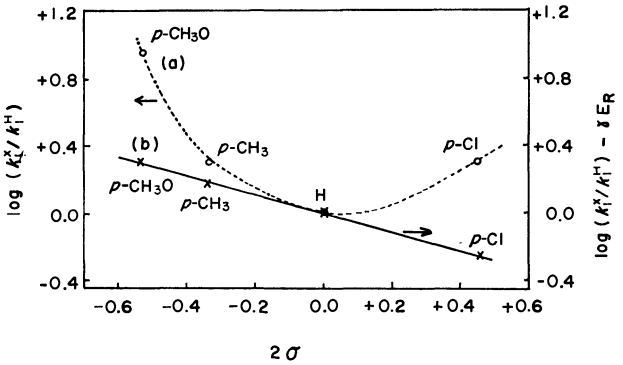

Fig. 3. Hammett plots of the first-order rate constants for the decompositions of di-*p*-substituted phenyl disulfides: (a) Log (k_1^X/k_1^H) *vs.* Hammett's σ values. (b) Log $(k_1^X/k_1^H)-\gamma E_R$ (Yamamoto-Otsu's equation) *vs.* Hammett's σ value ($\rho=-0.55$, $\gamma=3.0$).

The Effects of p-*Substituents on the Values of* k_1. Fig. 3(a) shows a plot of $\log k_1^X/k_1^H$ *vs.* 2σ, where k_1^H and k_1^X are the first-order rate constants for diphenyl and di-*p*-substituted phenyl disulfides, respectively, and σ is the usual Hammett substituents sigma-value. This plot does not give a straight line, but rather a curve which has a minimum value for diphenyl disulfide. The Yamamoto-Otsu equation,[16]

$$\log k_1^X/k_1^H = 2(\rho\sigma+\gamma E_R) \quad (3)$$

which is a modified Hammett equation including the resonance term, was applied to the present data of k_1 (Fig. 3(b)) in which σ and E_R are the polar and resonance substituent constants and ρ and γ are the reaction constants giving the susceptibilities for the polar and resonance effects of the substituents respectively. A constant 2 is used here, since symmetrically-substituted phenyl disulfide has two substituents. As shown in Fig. 3(b), the values of -0.55 and 3.0 for ρ and γ, respectively, are found to give a straight line.

Products Analyses. The rate of formation of the thiol obtained by titration with silver nitrate and that of "products" other than thiol are indicated by (b) and (c), respectively, in Fig. 1. This latter rate was obtained by the subtraction of the rate of the formation of thiol from that of the decomposition of the disulfide, and since these products are not reduced by sodium borohydride and aluminum chloride, they are, therefore, probably aryl sulfide (see Experimental). Fig. 1 indicates that the thermal decomposition of 1 mol of disulfide yielded about 1.5 mol of thiol and 0.5 mol of "other products". The analysis of products obtained from a large scale experiment for diphenyl disulfide at a reflux temperature of tetralin indicates the formation of thiophenol (0.90 mol), 1,2,3,4-tetrahydro-1-phenylthionaphthalene (0.41 mol) per 1 mol of diphenyl disulfide consumed, and unidentified oily products containing sulfur and tetralin fragments. Nakasaki[7] has reported that thiophenol and naphthalene were formed from the decomposition of diphenyl disulfide in tetralin at 260 °C. Ritter and Sharpe[8] have also found a similar dehydrogenation of tetralin by *iso*-amyl disulfide. Both authors have used disulfides as dehydrogenation reagents and thus the concentrations of disulfides in their experiments (11—18 mol/l) are much higher than that in those reported here (0.29 mol/l).

Discussion

Mechanism. The following reactions can be considered as the elementary steps in the thermal decomposition of disulfides in tetralin,

$$\mathrm{ArSSAr} \xrightarrow{k_1} 2\mathrm{ArS}\cdot \quad (4)$$

$$\mathrm{ArS}\cdot + \mathrm{RH} \xrightarrow{k_2} \mathrm{ArSH} + \mathrm{R}\cdot \quad (5)$$

$$\mathrm{ArS}\cdot + \mathrm{R}\cdot \xrightarrow{k_3} \mathrm{ArSR} \quad (6)$$

$$\mathrm{R}\cdot + \mathrm{R}\cdot \xrightarrow{k_4} \text{product} \quad (7)$$

$$\mathrm{ArS}\cdot + \mathrm{ArSSAr} \xrightarrow{k_5} \mathrm{ArS}\cdot + \text{product} \quad (8)$$

$$\mathrm{R}\cdot + \mathrm{ArSSAr} \xrightarrow{k_6} \mathrm{ArS}\cdot + \text{product} \quad (9)$$

where RH and R· are tetralin and its derived radical, respectively. A thiyl radical (ArS·) formed from step 4 abstracts α-hydrogen from tetralin (step 5) and the tetralinyl radical thus formed terminates with a thiyl radical or other tetralinyl radical. The step involving the addition of a thiyl radical to a phenyl ring is ignored since no such product was obtained.

Pryor, Gojon, and Stanley[17] have reported that the self-termination of the thinyl radicals is the only significant termination reaction in the reaction of the cyclohexyl thiyl radical with cumene at 80 °C. However, the reverse reaction of step 4 (self-termination) outside of the solvent-cage was ignored because of the situation described below. Probably due to the greater stability of the phenyl thiyl radical compared to that of the cyclohexyl thiyl radical, our preliminary experiment on the flash photolysis of *p*-chlorothiophenol in tetralin at room temperature[18] shows that the decay of the *p*-chlorophenyl thiyl radical obeyed first-order kinetics, that is, the thiyl radical reacts with tetralin and not with each other (the rate constant for this hydrogen abstraction reaction by the thiyl radical being found to be 1.5×10^2 $M^{-1}s^{-1}$), whereas, in a cyclohexane solution the thiyl radical decayed with second-order kinetics, indicating the self-termination of the thiyl radicals (the rate constant for the self-termination reaction was $2k_t=1.2\times10^9$

M^{-1} s^{-1}, this value being consistent with that of Thyrion[19]). Since the activation energy for hydrogen abstraction may be greater than that for a coupling reaction, these results can be used to consider our reaction scheme (our decomposition experiments were conducted at much higher temperatures than those on flash photolysis), and the rate constants obtained here are the values extrapolated to zero concentration of the disulfides, *i.e.*, they were obtained in extremely unfavorable conditions for the self-termination of thiyl radicals.

The k_{obsd} obtained in the decomposition of diphenyl and di-*p*-methoxyphenyl disulfides hardly varied with the initial concentrations of the disulfides, and these results are expected for the two following cases: (1) for $k_{obsd}=k_1$, and (2) for $k_{obsd}=k_1+k_i$, which is derived from $n=1.0$ in Eq. (1) (that is, in this case the decomposition proceeds by steps 4, 5, 6, and 9). The contribution of induced decomposition to k_{obsd}, such as in the second case, can be excluded experimentally by the presence of radical scavengers (a stable radical is used in these experiments), but this common method of using a stable free radical could not be applied at these high temperatures. For the following reasons, however, the process consisting of steps 4, 5, 6, and 9 leading to $n=1.0$ in Eq. (1) (and Eq. 2) can be neglected. First, as shown in Fig. 1, about 1.5 mol of the thiol (hydrogen abstraction product from tetralin by the thiyl radical) were obtained per mol of disulfide consumed. If a considerable amount of induced decomposition for $n=1$ occurs, the thiol yield should be less than 1 mol from steps 6 and 9. The yield (1.5 mol) greater than 1 mol indicates that all or a large portion of the thiyl radical was formed by step 4 (the maximum value being 2 mol when the termination occurs only due to step 7 which may not be the case from the fact that ArSR (product from step 6) was formed with a considerable yield). Second, step 9 is the attack of the disulfide by the tetralinyl radical. Tsuda and Otsu[20] have reported that a kinetic study of the induced decomposition of di-*p*-substituted phenyl disulfides with the polystyryl radical (the same benzyl-type radical as the tetralinyl radical) resulted in +0.23 for ρ in the Yamamoto-Otsu equation. Thus, if step 9 occurs at a high rate, the present ρ value should be a positive value, however, it is found to be −0.55. Moreover, the results reported by Nakasaki[7] and Ritter and Sharpe[8] suggest that the tetralinyl radical does not attack the disulfide, unlike the case of the reactive phenyl radical.[21] Therefore, the thermal decompositions of diphenyl and di-*p*-methoxyphenyl disulfides, for which the induced decomposition is found to be negligibly small, as shown in Fig. 2, seem to proceed *via* a process consisting of steps 4, 5, 6, and 7.

Steps 8 and 9 are considered to be induced decompositions by thiyl and tetralinyl radicals, respectively, which may occur in the thermal decomposition of both di-*p*-chlorophenyl and di-*p*-methylphenyl disulfides. The kinetic equation of the decomposition, assuming step 9 to be an induced decomposition, is not consistent with the present data, because the order *n* in Eq. (1) is not 2.0. However, if step 8 is assumed, the order *n* is 2.0, regardless of the type of termination step (step 6 or 7), in agreement with the present experimental results. From steps 4, 5, 6, and 8, the following equation can be derived:

$$-\frac{d[ArSSAr]}{dt} = k_1[ArSSAr] + \frac{k_1k_5[ArSSAr]^2}{k_2[RH]} \quad (10)$$

It appears reasonable that the thiyl radical induces the decomposition, while the tetralinyl radical does not, and thus, the latter radical may be more stable and less reactive than the thiyl radical. If induced decomposition by the tetralinyl radical under the present experimental conditions (high temperature and low disulfide concentration) occurs in a manner similar to that in the case of the polystyryl radical for the disulfide as previously described, di-*p*-methoxyphenyl disulfide should also be susceptible to induced decomposition. Benati and his coworkers[22] have reported interesting reactions of the thiyl radical with halogenobenzene; the phenyl thiyl radical formed from the homolytic scission of diphenyl disulfide in halogenobenzene attacks the carbon being substituting for the halogen atom and produces phenyl sulfide. From this result, reaction (11) is speculated to be the reaction of the thiyl radical with di-*p*-chlorophenyl disulfide.

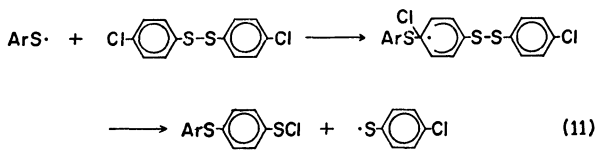

(11)

Rate Constants and Activation Parameters. Table 1 shows that the homolytic scission of S—S bonds in disulfides is more difficult than of O–O bonds in peroxides for which the bond dissociation energy is 34—37 kcal/mol for diaryl peroxides and nearly 30 kcal/mol for dibenzoyl peroxide.[23] Although, from thermochemical studies, the bond energies of S–S bonds in dialkyl and diphenyl disulfides (in gas phase) are calculated to be 67—68[24] and 64 kcal/mol,[25] respectively, the bond dissociation energies of S–S bonds obtained experimentally for polysulfides (*e.g.*, dimethyltetrasulfide and S_8 ring), TMTD, DBTD, and benzhydrylhydro disulfide in solution are 36,[26] 31.6,[3] 26,[5] and 20 kcal/mol,[27] respectively, which are comparable to those of the O–O bonds in peroxides. Thus, the activation energies obtained (39.4—43.0 kcal/mol) for the decomposition of diaryl disulfides are reasonable values.

The Effects of Structure on the Decomposition. The following results suggest that the stability of thiyl radicals formed from decomposition is an important factor in the decomposition of the disulfide; the homolytic scission of S–S bonds in diaryl disulfides is easier than that of S–S bonds in dialkyl disulfides (for example, compare with di-*n*-butyl disulfide in Table 1). This can be explained from the greater stability (resonance stabilization) of aryl thiyl radicals in comparison with that of alkyl thiyl radicals.[28] The rates of the decompositions of the di-*p*-substituted phenyl disulfides are increased by a *p*-substituent, and the order of decreasing rates is $CH_3O > Cl \simeq CH_3 > H$. This order might be expected from the stability of thiyl radicals, which is increased by the resonance interaction of the *p*-substituent with the aromatic ring.[29] Similar curves for the Hammett plots have also been obtained for the decompositions of substituted benzoyl peroxides in acetophenone,[30] the dissociation of

hexaaryl ethane into triaryl methyl radicals,[31] and some substituent effects on the free-radical properties such as the λ_{max} shift in the electronic spectra of some nitrogen-centered radicals.[32]

It has been reported that, in the thermal decomposition of di-*p*-substituted benzoyl peroxides and of peresters, electron-donating substituents increase the rate of decomposition, since these substituents increase the difference in the electronegativity between the peroxide oxygens and the aromatic ring, and the repulsion between the negative charges located on the peroxide oxygen destabilizes the parent molecule in the ground state of the decomposition. Thus, the ρ value is negative in the Hammett equation, whereas, peroxides having electron-attracting substituents are subject to induced decomposition, with the ρ value being positive.[33] In the present study the ρ value (−0.55) in the Yamamoto-Otsu equation is also negative (the value of γ is 3.0), that is, electron-donating substituents destabilize the disulfide and increase the rate of thermal decomposition, probably for the same reason as that in the case of peroxides. It is interesting that the rate of decomposition of di-*t*-butyl disulfide is high and comparable to that of diaryl disulfides, whereas, di-*n*-butyl disulfide did not decompose under the same conditions. In the decomposition of dialkyl peroxides, however, it has been reported[34] that di-*t*-butyl and diethyl peroxides have the same dissociation energy. Therefore, the high reactivity of di-*t*-butyl disulfide, which is less strained than di-*t*-butyl peroxide, cannot be explained in terms of strain.

It may be concluded from the present study that *p*-substituents in di-*p*-substituted phenyl disulfides influence both the destabilization of the disulfide and the stabilization of the thiyl radical formed from thermal decomposition, and these two factors accelerate the rate of thermal decomposition of the disulfides.

Table 2. λ_{max} in the electronic spectra of aryl thiyl radicals in 2-MTHF at −196 °C and of benzyl-type radicals

Radical	λ_{max} (nm)		
p-Methoxyphenyl thiyl[a]		410 (418)[b]	530
p-Methylphenyl thiyl	312	397 (396)[b]	513
p-Chlorophenyl thiyl	318	386 (381)[b]	516
Phenyl thiyl	308	390 (387)[b]	
Benzyl[c]	318	452	
Phenoxy[d]	300	403	
Anilino[e]	307	400	

a) Value obtained from the photolysis of di-*p*-methoxyphenyl disulfide. b) Ref. 14(b). c) Ref. 35(a). d) Ref. 35(b). e) Ref. 35(c).

Electronic Spectra of Aryl Thiyl Radicals. Electronic spectra of *p*-substituted phenyl thiyl radicals were observed by the photolysis of the thiols in a 77 K-matrix of 2-MTHF in order to obtain some information about the electronic states of aryl thiyl radicals and the interaction between the *p*-substituent and the odd electron of the radical. The absorption maxima of aryl thiyl radicals are summarized in Table 2 together with other benzyl-type radicals such as benzyl, phenoxy, and anilino radicals. Table 2 shows that the absorption maxima of phenyl thiyl radical at 310 and 390 nm are shifted by the *p*-substituents (the ESR spectrum of the phenyl thiyl radical being characterized by a large anisotropic *g* value ($g_{//}$=2.020 and $g_{\perp}$=2.019) under the same conditions). Similar absorption maxima around 300 and 400 nm being assigned to the π-electronic spectra of benzyl, phenoxy, and anilino radicals, the shift of the absorption maxima due to substituents have been observed by Porter and his co-workers,[35] and the molecular orbitals of the radicals have been calculated theoretically.[36] A comparison with the position of the absorption maxima of benzyl-type radicals and the considerable change in position due to *p*-substituents suggest that the thiyl radicals should be π-type radicals, which is supported by some theoretical and ESR studies,[37] and the present kinetic results, suggesting the importance of the conjugation among the sulfur atom, the phenyl ring, and the *p*-substituent.

Finally, it is found from a comparison of the first-order rate constants at 207 °C calculated from activation parameters taken from the literature[38] (Table 3), that the homolytic scission of S–S bonds in disulfides is most improbable in comparison with such related compounds as $ArS(=O)_2-SAr$, $ArS-S(=O)_2Ar$, $ArS(=O)-SAr$, $ArS(=O)_2-S(=O)_2Ar$, and $ArS(=O)-S(=O)Ar$, which differ in the oxidation state of the sulfur atom in the S–S bonds. Kice[39] has explained the change in the rate of the homolytic scission of these compounds by the difference in the stability of the radicals, stating that ArSO· is more stable than either ArS· or $ArSO_2$·.

We would like to thank Dr. K. Kikuchi and Dr. O. Ito for helpful discussions concerning the spectroscopic studies.

References

1) For example, W. A. Pryor, "Mechanism of Sulfur Reactions," McGraw-Hill Book Co., New York, N. Y., 1962, pp. 42—57.
2) H. G. Cutforth and P. D. Selwood, *J. Amer. Chem. Soc.*, **70**, 278 (1948).
3) T. E. Ferington and A. V. Tobolsky, *ibid.*, **77**, 4510

Table 3. Ease of homolytic dissociation for various S–S bonds at 207 °C

Compd.	$Ar-S(=O)_2-S-Ar$[a]	$Ar-S(=O)-S(=O)_2-Ar$[b]	$Ar-S(=O)-S-Ar$[c]	$Ar-S(=O)_2-S(=O)_2-Ar$[e]	$Ar-S(=O)-S-Ar$	$Ar-S-S-Ar$[e]
k_1 s^{-1}	Very large	7.6×10^{2}	3.4	1×10^{-2}	—	$(1—9)\times10^{-6}$

a) Ref. 38(c). b) Ref. 38(a). c) Ref. 38(b). d) Ref. 38(c). e) This work.

(1955); **80**, 3215 (1958).
4) T. Otsu, *J. Polym. Sci.*, **21**, 559 (1956).
5) R. E. Davis and C. Perrin, *J. Amer. Chem. Soc.*, **82**, 1590 (1960).
6) A. Schönberg and Mustafa, *J. Chem. Soc.*, **1949**, 889; *J. Amer. Chem. Soc.*, **73**, 2401 (1951).
7) M. Nakasaki, *Nippon Kagaku Zasshi*, **74**, 403 (1953).
8) J. J. Ritter and E. D. Sharpe, *J. Amer. Chem. Soc.*, **59**, 2351 (1937).
9) G. Leandri and A. Tundo, *Ann. Chim.* (Rome), **44**, 63 (1954); *Chem. Abstr.*, **49**, 4563d (1955).
10) D. S. Tarbell and D. K. Fukushima, "Organic Syntheses," Vol. 27, p. 81 (1947).
11) C. R. Stahl and S. Siggia, *Anal. Chem.*, **29**, 154 (1957).
12) R. K. Kunkel, *ibid.*, **31**, 1098 (1959).
13) P. Borgstrom, L. M. Ellis, and E. E. Reid, *J. Amer. Chem. Soc.*, **51**, 3649 (1929).
14) a) I. Norman and G. Porter, *Proc. Roy. Soc., Ser. A*, **230**, 399 (1955); b) F. Feher, T. Gladden, and D. Kurz, *Z. Natureforsch*, **25b**, 1215 (1970).
15) K. Nozaki and P. D. Bartlett, *J. Amer. Chem. Soc.*, **68**, 1686 (1946).
16) T. Yamamoto and T. Otsu, *Chem. and Ind.*, **1967**, 787.
17) W. A. Pryor, G. Gojon, and J. P. Stanley, *J. Amer. Chem. Soc.*, **95**, 945 (1973).
18) Unpublished data. The rate of decay of the thiyl radical is determined by the 500 nm absorption band of the thiyl radical. In both cumene and *p*-cymene, the thiyl radical also decay with first-order kinetics. Photolysis lamp: a xenon filled flash lamp, discharge energy: 128 J, peak duration: 10 μsec.
19) F. C. Thyrion, *J. Phys. Chem.*, **77**, 1478 (1973).
20) K. Tsuda and T. Otsu, This Bulletin, **39**, 2206 (1966).
21) W. A. Pryor and P. K. Platt, *J. Amer. Chem. Soc.*, **85**, 1496 (1963). W. A. Pryor and H. Guard, *ibid.*, **86**, 1150 (1964). W. A. Pryor and K. Smith, *ibid.*, **92**, 2731 (1970).
22) L. Benati, C. M. Camaggi, and G. Zanardi, *J. Chem. Soc., Perkin I*, **1972**, 2817.
23) W. A. Pryor, "Free Radicals," McGraw-Hill Book Co., New York, N. Y., 1966, pp. 84—91.
24) H. Mackle, *Tetrahedron*, **19**, 1159 (1963).
25) H. Mackle and R. G. Mayrick, *Trans. Faraday Soc.*, **58**, 238 (1962).
26) I. Kende, T. L. Pickering, and A. V. Tobolsky, *J. Amer. Chem. Soc.*, **87**, 5582 (1965).
27) T. Nakabayashi and J. Tsurugi, *J. Org. Chem.*, **28**, 813 (1963).
28) Ref. 1, p. 19.
29) U. Schmidt, *Angew. Chem.*, **76**, 629 (1964).
30) A. T. Blomquist and A. J. Busell, *J. Amer. Chem. Soc.*, **73**, 3883 (1951).
31) Summerized in M. J. Dewar, "Electronic Theory of Organic Chemistry," The Claredon Press, Oxford (1949), p. 245.
32) R. I. Walter, *J. Amer. Chem. Soc.*, **88**, 1923, 1930 (1966).
33) Ref. 15, A. T. Blomquist and I. A. Berstein, *J. Amer. Chem. Soc.*, **73**, 5546 (1951); C. Walling, "Free Radicals in Solution," John Wiley & Sons, Inc., New York (1957).
34) W.A. Pryor, D.M. Huston, T.R. Fiske, T.L. Pickering, and E. Ciuffarin, *J. Amer. Chem. Soc.*, **86**, 4237 (1964).
35) a) G. Porter and E. Strachan, *Trans. Faraday Soc.*, **54**, 1595 (1958); b) E. J. Land, G. Porter, and E. Strachan, *ibid.*, **57**, 1885 (1961); c) E. J. Land and G. Porter, *ibid.*, **59**, 2027 (1963).
36) a) A. Hinchiffe, R. E. Stainbank, and M. A. Ali, *Theort. Chim. Acta* (Berl.), **5**, 95 (1966); b) H. C. Longuet-Higgins and J. A. Pople, *Proc. Phys. Soc.* (London), **A68**, 591 (1955).
37) a) Y. Kurita and W. Gordey, *J. Chem. Phys.*, **34**, 282 (1961); b) W. Rundel, *Chem. Ber.*, **102**, 359 (1969).
38) a) J. L. Kice and N. E. Pawloski, *J. Amer. Chem. Soc.*, **86**, 4898 (1964); b) P. Koch and A. Fava, *ibid.*, **90**, 3868 (1968); c) J. L. Kice and N. Faustritsky, *J. Org. Chem.*, **35**, 114 (1970).
39) Ref. 38 (c); J. L. Kice "Sulfur in Organic and Inorganic Chemistry," Vol. 1, A. Senning, Ed., Marcel Dekker, Inc., New York, N. Y., 1971, p. 153.

The Asymmetric (Enantioface Differentiating) Hydrogenation of the C=O Double Bond with Modified Raney Nickel. XXIX.

Tadao HARADA

Division of Organic Chemistry, Institute for Protein Research, Osaka University, Yamadakami, Suita, Osaka 565

(Received April 28, 1975)

In the asymmetric (enantioface differentiating) hydrogenation of methyl acetoacetate with modified Raney nickel catalysts, the effects of the modifying pH on the amounts of the modifying reagents adsorbed and the enantioface differentiating abilities of the catalysts were studied using glycolic acid, mandelic acid, and 2-hydroxy-3-phenylpropionic acid as the modifying reagents. The results indicate that the modifying pH governs the adsorption mode of the modifying reagent. Thus, the change in the adsorption mode of the modifying reagent with the change in the modifying pH results in changes in the amount of the modifying reagent adsorbed and in the enantioface differentiating ability of the catalyst.

The asymmetric hydrogenation of methyl acetoacetate to methyl 3-hydroxybutyrate has been previously studied by our research group[1,2] in the presence of Raney nickel catalysts modified with optically active 2-amino or 2-hydroxy acid (modifying reagent). This reaction can be classified as an enantioface differentiating reaction,[2,3] because in this reaction process the catalyst differentiates between the two sides of the enantiotopic plane (the enantiofaces) of methyl acetoacetate. The enantioface differentiating hydrogenation of methyl acetoacetate is shown in Fig. 1. In the course of our studies, it was found that the enantioface differentiating ability of the catalyst[4] and the amount of the modifying reagent adsorbed on the catalyst were both strongly affected by the pH of the aqueous solution of the modifying reagent (the modifying pH.)[5,6] In order to understand the change in the enantioface differentiating ability of the catalyst with the change in the modifying pH, it is essential to clarify the relationship between the enantioface differentiating ability of the catalyst and the amounts of the modifying reagent adsorbed at various modifying pH values.

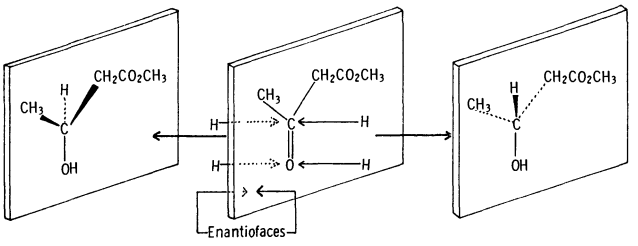

(*S*)-Isomer Methyl acetoacetate (*R*)-Isomer

Fig. 1. Enantioface differentiating hydrogenation of methyl acetoacetate.

In the present work, the effects of the modifying pH on the amount of the modifying reagent adsorbed and on the enantioface differentiating ability of the catalyst were investigated by means of catalysts modified with 2-monohydroxy monocarboxylic acids, such as glycolic acid, mandelic acid, and 2-hydroxy-3-phenylpropionic acid.

Results and Discussion

The modified Raney nickel catalysts were prepared with glycolic acid, DL-mandelic acid, and L-2-hydroxy-3-phenylpropionic acid at various modifying pH values.

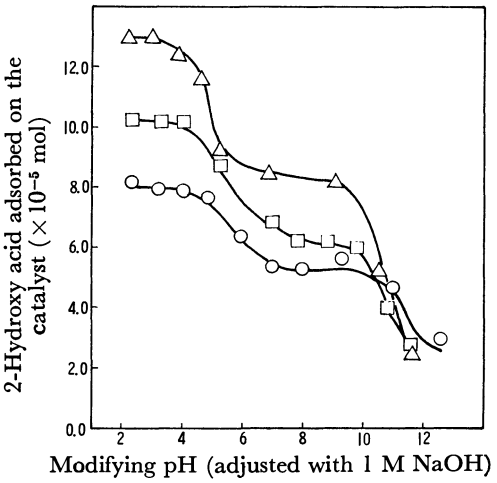

Fig. 2. Effects of the modifying pH on the amounts of the modifying reagents adsorbed.
△: glycolic acid
○: DL-mandelic acid
□: L-2-hydroxy-3-phenylpropionic acid
An amount of 1.5 g of Raney alloy (Ni: Al=42: 58) was used for each preparation of the catalyst.
Modifying solution: 100 ml of a 1% aqueous solution of the modifying reagent.

Plots of the amounts of the modifying reagent adsorbed against the modifying pH are shown in Fig. 2.

The amount of the modifying reagent (RCH(OH)-COOH) adsorbed at each modifying pH depends on the nature of the R group. However, on modification with these compounds, the changes in the amounts show a similar figure with the change in the midifying pH, regardless of the drastic changes in the R groups (*i.e.* H to phenyl). That is, the amounts of these compounds adsorbed are constant below pH 4 and at pH 6(7)—9, while they vary steeply at pH 4—6(7) and above pH 9. These observations indicate that the curve can be divided into four segments; that is, below pH 4(A), pH 4—6(7)(B), pH 6(7)—9(C), and above pH 9(D).

The enantioface differentiating abilities of the catslysts modified with L-2-hydroxy-3-phenylpropionic acid and L-mandelic acid were studied at various modifying pH values; the results are shown in Fig. 3. The enantioface differentiating abilities of the catalysts and the amounts of the modifying reagents adsorbed change in a fashion similar to each other with the change in the modifying

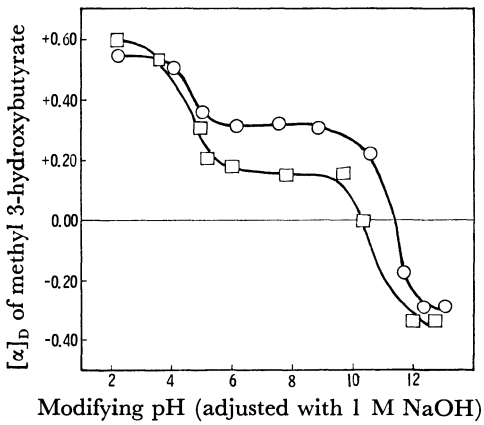

Fig. 3. Effects of the modifying pH on the enantioface differentiating abilities of the catalysts.
○: L-mandelic acid[a)]
□: L-2-hydroxy-3-phenylpropionic acid[b)]
a) The hydrogenation of 3.5 ml of methyl acetoacetate was carried out with the catalyst prepared from 0.3 g of Raney alloy (Ni: Al=42: 58).
b) The hydrogenation of 17.5 ml of methyl acetoacetate was carried out with the catalyst prepared from 1.5 g of the alloy.

pH. That is, the ability of the catalyst does not change in A and C, but does change drastically in B and D. However, the ratio of the enentioface differentiating ability in A to that in C is dependent on the nature of the R group, while the ratio of the amount of the modifying reagent adsorbed in A to that in C is independent of the nature of the R group, as is shown in Tables 1 and 2. From the data in Tables 1 and 2, it is clear that the ratio of the enantioface differentiating ability of the catalyst in A to that in C cannot be interpreted simply on the basis of the amount of the modifying reagent adsorbed. However, the similarity between the modifying pH dependence of the amount of the modifying reagent adsorbed and that of the enantioface differentiating ability of the catalyst suggests that there are some common factors which control both of them. The present author introduces the term of the adsorption mode to account for these common factors. Thus, the modifying pH governs the adsorption mode of the modifying reagent; the change in the adsorption mode results in the change in the amount of the modifying reagent adsorbed and that in the enentioface differentiating ability of the catalyst. The adsorption mode is determined by the adsorption species and the conditions of the catalyst surface.

Furthermore, on modifications with L-2-hydroxy-3-phenylpropionic acid and L-mandelic acid the direction of the optical rotation ($[\alpha]_D$) of the hydrogenation product is (−) above pH 12, while it is (+) below pH 10. These findings also support the dependence of the adsorption mode on the modifying pH.

The modifying pH dependence of the enentioface differentiating abilities observed with the catalysts modified with other 2-monohydroxy monocarboxylic acids can be explained in the same way, since our research group has obtained similar results with L-3,3-dimethyl-2-hydroxybutyric acid[7)] and L-2-hydroxy-3-methylbutyric acid.

Studies of the absorption modes of the modifying reagent in A, B, C, and D are in progress and will be reported soon.

Experimental

The preparation of the modified Raney nickel catalyst, the hydrogenation of methyl acetoacetate, and the measurement of the enantioface differentiating ability of the catalyst were carried out by the procedures described in the previous paper.[8)]

The modification of the catalyst was carried out at 0 °C for 90 min. During the modification, the mixture of the modifying solution and the catalyst was shaken every 15 min. After the midification, the catalyst was washed once with 10 ml of deionized water and then with three 50 ml portions of methanol.

Elution of the Modifying Reagent from the Catalyst Surface. A mixture of the modified Raney nickel and 10 ml of M sodium hydroxide was allowed to stand for 2 hr at 100 °C in a 50 ml, round-bottomed flask fitted with a condenser. The catalyst was removed by filtration and washed with deionized water. The filtrate and the washings were then combined and diluted accurately to 50 ml with deionized water. This solution was used for the determination of the modifying reagent adsorbed on the catalyst.

The Determination of L-2-Hydroxy-3-phenylpropionic Acid and

Table 1. The amounts of the modifying reagents adsorbed on the catalysts in A and C[a)]

Modifying Reagent	A_a[b)] (midifying pH)	C_a[b)] (modifying pH)	C_a/A_a
Glycolic acid	14×10^{-5} (2.2)	8.6×10^{-5} (6.9)	0.61
DL-Mandelic acid	8.2×10^{-5} (2.3)	5.3×10^{-5} (7.0)	0.64
L-2-Hydroxy-3-phenylpropionic acid	10×10^{-5} (2.3)	6.0×10^{-5} (7.8)	0.60

a) The catalyst was prepared from 1.5 g of Raney nickel alloy (Ni: Al=42: 58). Modifying solution: 100 ml of a 1% aqueous solution of the modifying reagent. b) A_a (C_a): the amount (expressed in mole) of the modifying reagent adsorbed on the catalyst in A(C).

Table 2. The enantioface differentiating abilities of the catalysts modified in A and C

Modifying reagent	A_e[a)] (modifying pH)	C_e[a)] (modifying pH)	C_e/A_e
L-Mandelic acid	+0.55[b)] (2.4)	+0.32[b)] (7.5)	0.58
L-2-Hydroxy-3-phenylpropionic acid	+0.60[c)] (2.3)	+0.15[c)] (7.8)	0.25

a) $A_e(C_e)$: The enantioface differentiating ability of the catalyst modified in $A(C)$. b) The hydrogenation of 3.5 ml of methyl acetoacetate was carried out with the catalyst prepared from 0.3 g of Raney nickel alloy (Ni: Al=42: 58). c) The hydrogenation of 17.5 ml of methyl acetoacetate was carried out with the catalyst prepared from 1.5 g of the alloy.

DL-*Mandelic Acid.* These compounds were determined by the measurement of the absorbance at 258 nm, using a reagent blank as the reference.

The Determination of Glycolic Acid. The glycolic acid was determined by the procedure of Sasakawa *et al.*, using 2,7-dihydroxynaphthalene.[9]

The author wishes to express his thanks to Professor Yoshiharu Izumi and Assistant Professor Akira Tai for their valuable discussions and encouragement throughout this work.

References

1) Part XXVII: T. Tanabe, This Bulletin, **46**, 1482 (1973).
2) Part XXVIII: H. Ozaki, A. Tai, and Y. Izumi, *Chem. Lett.*, **1974**, 935.
3) The definition of the enantioface differentiating reaction was proposed in *Kagakusosetsu*, **4**, 85 (1974).
4) The ability is represented by the optical rotatory power ($[\alpha]_D$) of the hydrogenation product, methyl 3-hydroxybutyrate.
5) Y. Izumi, M. Imaida, H. Fukawa, and S. Akabori, This Bulletin, **36**, 21 (1963).
6) S. Tatsumi, *ibid.*, **41**, 408 (1968).
7) Y. Izumi, T. Tanabe, S. Yajima, and M. Imaida, *ibid.*, **41**, 941 (1968).
8) Y. Izumi, T. Harada, T. Tanabe, and K. Okuda, *ibid.*, **44**, 1418 (1971).
9) T. Sasakawa and T. Kimura, *Seikagaku*, **28**, 816 (1956).

An Evaluation of the Effects of the Phosphorus Ligands on the Stereoselectivity of a Nickel-catalyzed Reaction. The Reaction of Norbornadiene with Acrylonitrile

Susumu YOSHIKAWA,* Kunihiro AOKI, Jitsuo KIJI, and Junji FURUKAWA
Department of Synthetic Chemistry, Kyoto University, Kyoto 606

(Received May 2, 1975)

The effects of nineteen phosphorus ligands on the nickel-catalyzed 4+2 cycloaddition reaction of norbornadiene to acrylonitrile have been studied. The cone angle and the ν_{CO} stretching frequency of $Ni(CO)_3L$ (where L is the phosphorus ligand) are used as measures of their steric and electronic parameters respectively. The steric factor of the phosphorus ligands is correlated with the ratio of the *exo*- and *endo*-isomers of the product. Consequently, this effect is important in determining the steric course of the reaction. The electronic property and the solvent effect are less influential.

Many stereoselective reactions are catalyzed by transition metal complexes. In these catalytic reactions, the reaction participants are both electronically and sterically influenced by the effects of the ligands. Therefore, the transition metal-catalyzed homogeneous reactions have many advantages, *e.g.*, the available coordination sites for the reactions can be modified by adding some appropriate ligands, thus controlling a desired reaction. Such a modification has widely been used in synthetic and mechanistic studies of such transition metal-catalyzed reactions as the polymerization and oligomerization of olefins, hydrogenation, hydroformylation, and so on.[1] The electronic properties of phosphorus ligands have been evaluated from the infrared stretching frequencies of the ν_{CO} of $Ni(CO)_3L$ (where L is the phosphoru sligand).[2] On the other hand, the steric parameters of phosphorus ligands are somewhat complicated. Tolman has proposed the concept of a "cone angle", which encloses the van der Waals radii of the outermost atoms of the phosphorus ligand.[3-5] Until now, though, no satisfactory study of the electronic and steric effects of the phosphorus ligand on the transition metal-catalyzed homogeneous reaction has been made, because the reaction consists of many complicated steps. It seems that only a simple reaction can be discussed.

The reaction of norbornadiene with acrylonitrile is known to occur catalytically by means of nickel complexes.[6] This 4+2 cycloaddition is one of the most satisfactory model reactions for the evaluation of the stereochemical course of a transition metal-catalyzed reaction, because the *endo-exo* isomerization of the products is negligibly slow under the reaction conditions and the reaction can probably be explained by a simple intermediate which involves the coordination of two reactants and the phosphorus ligand.[7,8] In the past several years, the reactions of diolefins catalyzed by nickel complexes have been developed in our laboratory, and mechanistic studies have also been carried out.[9] The present study forms a part of this systematic investigation. This paper will deal with an evaluation of the effects of both the electronic and the steric factors of the phosphorus ligands on the reaction of norbornadiene with acrylonitrile as a model reaction.

* Present address: Government Industrial Research Institute, Osaka, Midorigaoka, Ikeda, Osaka 563.

Results and Discussion

The reaction of norbornadiene with acrylonitrile gives two products, I and II (Eq. 1). Around 100 °C no appreciable 2+2 reaction (Eq. 2) occurs. Some nickel catalysts are effective for the reaction (Eq. 1) at lower temperatures. Schrauzer and Eicheler have reported the bis(acrylonitrile)nickel-catalyzed reaction in the presence of a phosphorus ligand, but they did not discuss the stereoisomers in detail.[6] It has been found that the catalytic reaction, unlike the thermal reaction, affords the *exo* isomer predominantly, and that this stereoselectivity is influenced delicately by an added phosphorus ligand.[10] To gain insight into the effects of the ligands on the stereoselectivity of the reaction, various phosphorus compounds and triphenylarsine were prepared and used with bis(acrylonitrile)nickel, $Ni(AN)_2$. Bis(acrylonitrile)nickel itself, without a phosphorus ligand, had no catalytic activity under these conditions. Metal acetylacetonates, such as $Cr(C_5H_7O_2)_2$, $Mn(C_5H_7O_2)_3$, $Fe(C_5H_7O_2)_3$, $Co(C_5H_7O_2)_3$, $Ni(C_5H_7O_2)_2$, $Cu(C_5H_7O_2)_2$, and $V(C_5H_7O_2)_3$, combined with sodium borohydride were used in the presence of triphenylphosphine. None of these complexes except $Ni(C_5H_7O_2)_2$ catalyzed the reaction.

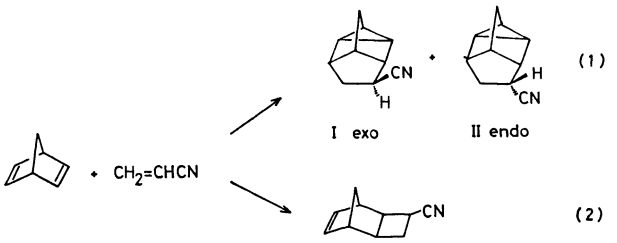

Before the systematic investigation, the optimum ratio of triphenylphosphine to the nickel complex was studied. The yields were increased with the amount of added triphenylphosphine, while the ratio of the *exo* to *endo* isomers was not influenced by its amounts (Fig. 1). Bis(acrylonitrile)nickel is slightly soluble under the present reaction conditions. The addition of triphenylphosphine seems to increase the solubility of $Ni(AN)_2$, thus increasing the yield. This observation reveals that the active species is specified only by the kind of the phosphorus ligand, not by its amount.

All the reactions were carried out between 70 and 130

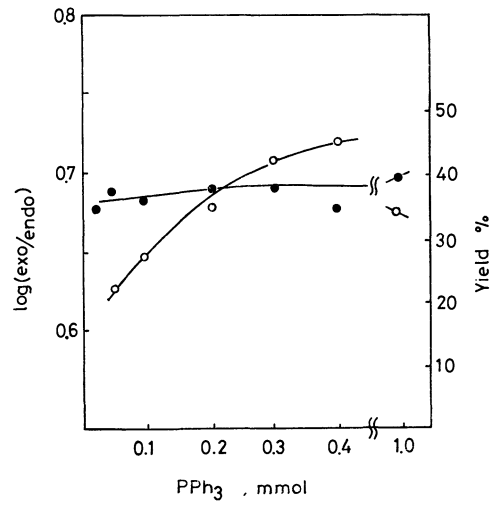

Fig. 1. Effect of added $(C_6H_5)_3P$ on the reaction at 80 °C. Conditions: $Ni(AN)_2$. 0.05 mmol; C_3H_3N, 6 mmol; C_7H_8, 6 mmol; reaction time, 10 hr.
(○): Yield (●): Isomer ratio

°C. Under these conditions, neither *retro*-reaction nor isomerization occurred. That is, the product (I or II) was separated by gas chromatography and heated in the presence of $Ni(AN)_2$–$(C_6H_5)_3P$ at 100 °C. After 20 hr, no isomerization occurred and I or II was recovered unchanged. Consequently, the isomeric ratio reflects the ratio of the rates of their formation; thus the reaction is kinetically controlled.

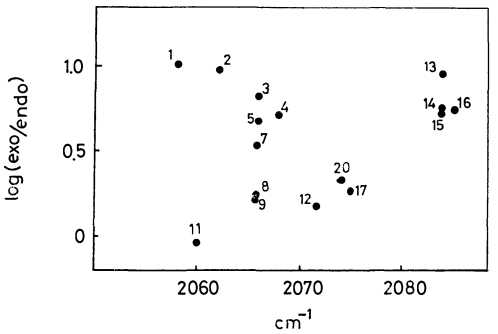

Fig. 2. Plot of *exo/endo* ratio at 80 °C against $\nu_{CO}(A_1)$ of $Ni(CO)_3L$ of phosphorus ligand (L) used with $Ni(AN)_2$. Ligand number refers to experimental section.

In general, ligand effects may be separated into electronic and steric factors. The electronic properties of the phosphorus ligands have been estimated by means of the ν_{CO} stretching frequency of $Ni(CO)_3L$ complex (where L is the phosphorus compound).[2] This spectrochemical estimation is applicable to some discussion of the catalytic process. Wilkinson and his co-workers[11] have employed this estimation for the explanation of the catalysis of tris(triarylphosphine)rhodium chloride. As is shown in Fig. 2, however, there is no correlation between the *exo/endo* ratio at 80 °C or 130 °C and the electronic properties of the added ligands. For example, there is a marked difference in the electronic properties between $(o\text{-}CH_3OC_6H_4)_3P$ and $(o\text{-}CH_3C_6H_4O)_3P$ (**1** and **13** in Fig. 2). The ratio of the isomers is nearly equal. All the phosphite ligands $P(OR)_3$ except $(o\text{-}CH_3C_6H_4O)_3P$ gave products in similar yields (see Experimental section). The electronic character of the phosphorus ligand has no appreiable influence on the reaction rate. This is a marked contrast to the dimerization of olefins or acetylenes. For example, the ratio of the stereoisomers (*exo-trans-exo* and *endo-trans-exo*) of the 2+2 cyclodimer of norbornadiene is strongly influenced by the electronic factor.[12]

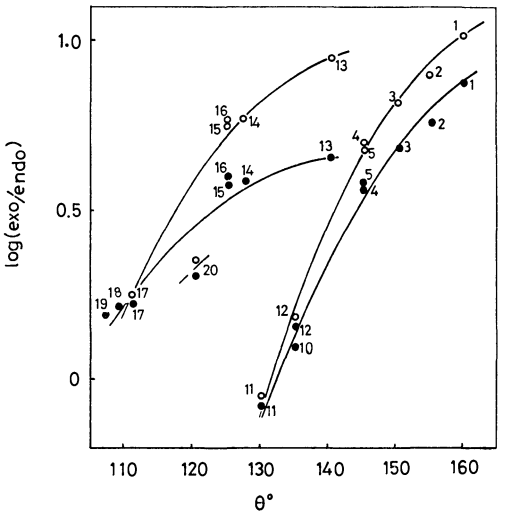

Fig. 3. Plot of *exo/endo* ratio against cone angle (θ) of the phosphorus ligands.
(○): 80 °C (●): 130 °C

Contrary to the electronic factor, an estimation of the steric factor of the phosphorus ligand is rather complicated. One measure of its bulkiness is the cone angle, θ, which is the maximum clearance angle for the rotation of the phosphorus ligand around its three-fold axis.[3] When this value is used as a measure of the steric parameter, it is shown in Fig. 3 that the steric factor is much more important than the electronic factor in determining the steric course of the reaction. The cone angles of the phosphorus ligand used and the ratio of *exo/endo* are correlated with each other. In Fig. 3 the phosphorus ligands are divided mainly into two groups; the first is a phosphite group, and the other, phosphine. The effect of $(C_6H_5)(C_2H_5O)_2P$ (**20**) is intermediate between those of the phosphites and phosphines. Within the phosphorus homologs, excellent correlations of log *exo/endo* with the cone angles are observed. The steric effect is more predominant at 80 °C than at 130 °C. These facts can reasonably be explained in terms of steric interaction between the coordinated acrylonitrile and the phosphorus ligand in the coordination sphere of the reaction intermediate.

Here it may be postulated that, among the four available coordination sites of the zero-valent nickel, two are occupied by diene and one by acrylonitrile,[8] and that their coordination takes place in the less-hindered tetrahedral configuration between the CN group and the phosphorus ligand (Fig. 4). Therefore, when a bulky phosphorus ligand is used, the less hindered coordination (Fig. 4 right) is favorable; thus the *exo* isomer is formed.

The steric effect of the phosphorus ligand on the reaction is further illustrated by the following facts. When

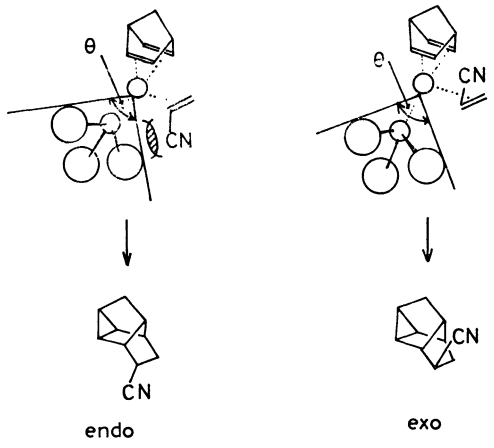

Fig. 4. Proposed structure of the intermediates.

the more bulky (o-$CH_3C_6H_4)_3P$ was used as the ligand, no appreciable reaction occurred between 80 and 130 °C. In the case of $(CH_3OC_6H_4)_3P$, the *ortho* isomer gave a lower yield than the other isomers. The fact that phosphites have a different steric effect on the reaction from that of the phosphine analogue cannot be explained by the present study. The effect of diphosphines (**7**—**9**) is too complicated to discuss, since diphosphines coordinate to the nickel competitively with norbornadiene and retard the reaction.

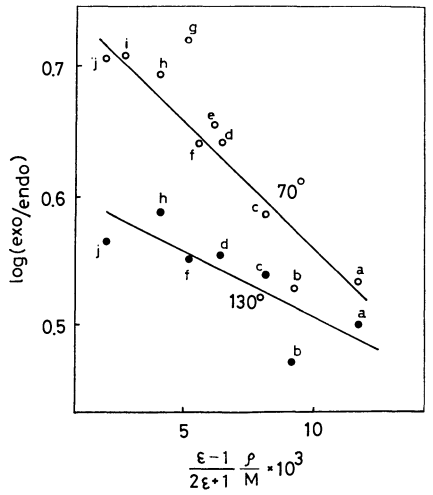

Fig. 5. Plot of *exo*/*endo* ratio against molar polarization of the solvent used.
(○): 70 °C (●): 130 °C
a, methanol; b, acetonitrile; c, ethanol; d, acetone; e, 2-propanol; f, pyridine; g, tetrahydrofuran; h, ethyl acetate; i, benzene; j, triethylamine.

The solvent effect was also investigated by using aprotic and protonic solvents, using triphenylphosphine as the auxiliary ligand. A linear free-energy relationship was observed for all the solvent. The polar solvent preferred the *endo* isomer. This can be explained by the dipolar interaction between the intermediate (Fig. 4) and the solvent. Thus, the intermediate (Fig. 4), which gives the *endo* isomer, is considered to have a larger total dipole moment than the other intermediate giving the the *exo* isomer and is stabilized by the polar solvent.[13] However, this effect on the reaction is smaller than that of the ligands.

Experimental

Commercially available phosphorus compounds were used without further purification. The other phosphorus compounds were prepared by the known methods. The products of the reaction of norbornadiene with acrylonitrile were identified by comparing their infrared and NMR spectra with those of the reported ones. Quantitative analyses were performed by gas chromatography on a column, Silicon DC 550 on Celite, 3 m at 150 °C, using tetralin as the internal standard. The *exo* isomer was eluted faster than the *endo* isomer. The cone angles and the stretching frequencies of $\nu_{CC}(A_1)$ were estimated by the reported methods. The Stewart molecular model was used for the estimation of the cone angle (θ). The values estimated in the present study are as follows:
$P(C_6H_5)(o\text{-}C_6H_4OCH_3)_2$ (**2**), 155; $P(C_6H_5)_2(o\text{-}C_6H_4OCH_3)$ (**3**), 150; $P(p\text{-}C_6H_4CH_3)_3$ (**5**), 145; $P(C_6H_5)(C_2H_5)_2$ (**10**), 135; $As(C_6H_5)_3$ (**12**), 135; $P(O\text{-}o\text{-}C_6H_4CH_3)_3$ (**13**), 140; $P(O\text{-}m\text{-}C_6H_4CH_3)_3$ (**14**), 127; $P(O\text{-}p\text{-}C_6H_4CH_3)_3$ (**15**), 125; $P(O\text{-}n\text{-}C_4H_9)_3$ (**17**), 111; $P(C_6H_5)(OC_2H_5)_2$ (**20**), 121.

Reaction. All the reactions were carried out in a glass tube (8 mm in diameter), as in the case of the dimerization of butadiene reported earlier.[14] In the glass tube, $Ni(AN)_2$ (0.05 mmol), the solvent (1 ml), norbornadiene (6 mmol), acrylonitrile (6 mmol), the phosphorus ligand (0.2 mmol), and tetralin (130 mg, as the internal standard for the gas chromatographic analysis) were placed under an atmosphere of argon. The tube was sealed with a flame and then heated without agitation. The total yields (*exo* and *endo* isomers) of the reactions in the presence of the various ligands shown in Figs. 2 and 3 are as follows (% at 80, 130 °C for 10 hr):
$P(o\text{-}C_6H_4OCH_3)_3$ (**1**) (26.9, 12.4), **2** (27.9, 11.2), **3** (27.4, 17.7), $P(C_6H_5)_3$ (**4**) (48.9, 28.1), **5** (42.5, 30.9), $NiBr_2[P(C_6H_5)_3]_2$ (**6**) (18.6, 15.7), $(C_6H_5)_2P(CH_2)_3P(C_6H_5)_2$ (**7**) (59.7, 28.4), $(C_6H_5)_2P(CH_2)_2P(C_6H_5)_2$ (**8**) (47.9, 25.0), $(C_6H_5)_2PCH_2P(C_6H_5)_2$ (**9**) (17.6, 19.1), $P(C_6H_5)(C_2H_5)_2$ (**10**) (42.1, 27.0), $P(n\text{-}C_4H_9)_3$ (**11**) (16.6, 8.4), **12** (17.6. 5.9), **13** (24.8, 12.9), **14** (49.9, 26.7), **15** (50.4, 29.5), $P(OC_6H_5)_3$ (**16**) (47.9, 26.7), **17** (58.7, 28.1), $P(OC_2H_5)_3$ (**18**) (58.2, 26.1), $P(OCH_3)_3$ (**19**) (57.2, 25.0), **20** (57.2, 27.5).

The authors are grateful to Drs. Yoshiaki Kobuke and Takuji Sugimoto for their helpful discussion.

References

1) G. N. Schrauzer (Ed.), "Transition Metals in Homogeneous Catalysis," Marcel Dekker, New York, N. Y. (1971).
2) C. A. Tolman, *J. Amer. Chem. Soc.*, **92**, 2953 (1970).
3) C. A. Tolman, *ibid.*, **92**, 2956 (1970).
4) C. A. Tolman, W. C. Seidel, and L. W. Gosser, *ibid.*, **96**, 53 (1974).
5) W. C. Trogler and L. G. Marzilli, *ibid.*, **96**, 7589 (1974).
6) G. N. Schrauzer and S. Eicheler, *Chem. Ber.*, **95**, 2764 (1962).
7) G. N. Schrauzer, "Advances in Organometallic Chemistry," Vol. 2, ed. by F. G. A. Stone and R. West, Academic Press (1964), p. 1.
8) R. Noyori, I. Umeda, H. Kawauchi, and H. Takata, *J. Amer. Chem. Soc.*, **97**, 812 (1975).
9) J. Furukawa and J. Kiji, "Organotransition-Metal

Chemistry," ed. by Y. Ishii and M. Tsutsui, Plenum Publisher, (1975) p. 119 and references cited therein.

10) The thermal reaction at 150 °C gives the *endo* isomer (II) predominantly. Y. Kobuke, T. Sugimoto, J. Furukawa, and T. Fueno, *J. Amer. Chem. Soc.*, **94**, 3633 (1972).

11) S. Montetatici, A. van der Ent, J. A. Osborn, and G. Wilkinson, *J. Chem. Soc. A*, **1968**, 1054.

12) S. Yoshikawa, J. Kiji, and J. Furukawa, presented at the 31st Annual Meeting of the Chemical Society of Japan, Sendai, 1974.

13) There are few data for calculating the dipole moment of the intermediates. When 3.4D for Ni–PPh_3 [J. Chatt and F. A. Hart, *J. Chem. Soc.*, **1960**, 1378] and 3.6D for Ni–C_7H_8 (estimated from 4.07D for tetramethyl-1,4-benzoquinone-Ni–C_7H_8 [P. W. Jolly and G. Wilke, "The Organic Chemistry of Nickel," Vol. 1, Academic Press, New York (1974), p. 294] by assuming that the dipole moment of the 1,4-benzoquinone–Ni is comparable with that of OC–Ni) are used, the intermediate giving the *endo* isomer is considered to have larger dipole moment than the other.

14) J. Kiji, K. Masui, and J. Furukawa, This Bulletin, **44**, 1956 (1971).

Novel Synthesis of Anhydronucleosides *via* the 2′,3′-*O*-Sulfinate of Purine Nucleosides as Intermediates

Tsuneo Sowa and Kozo Tsunoda

Research Section, Foodstuff Plants, Asahi Chemical Ind. Co., Ltd., Nobeoka, Miyazaki 882

(Received May 6, 1975)

The synthesis of 8,2′-*O*-anhydro(9-β-D-arabinofuranosyl)-8-hydroxyadenine (**3c**) and 8,2′-*S*-anhydro(9-β-D-arabinofuranosyl)-8-mercaptoadenine (**3a**) is described. The active intermediates, 2′,3′-*O*-sulfinyl 8-bromoadenosine (**2a**), 2′,3′-*O*-sulfinyl-8-hydroxyadenosine (**2c**), and 2′,3′-*O*-sulfinyl-8-bromoguanosine (**2d**), were prepared from the corresponding nucleosides (**1a**, **1c** or **1d**) by successive treatment with thionyl chloride in the presence of pyridine in acetonitrile and with water. The anhydronucleosides, **3a** and **3c**, were formed in good yields by heating the intermediates (**2a** or **2c**) in *n*-butanol in the presence of thiourea or in *N*,*N*-dimethylformamide in the presence of sodium acetate. All attempts at the cyclization of Compound **2d** failed. The reaction product of 8-mercaptoadenosine (**1b**) with thionyl chloride was identified as the bis(2′,3′-*O*-sulfinyl adenosin-8-yl) disulfide (**2b**), which could not be transformed to Compound **3a**.

Anhydronucleosides are important analogues of natural nucleosides. 8,2′-Anhydronucleosides are key intermediates in the synthesis of many biologically active compounds and have provided new routes for the nucleotides.[1,2] Anhydronucleosides have been synthesized, by several procedures, from natural or unnatural nucleosides *via* the corresponding activated intermediates, such as tosyl,[3] triisopropylbenzene sulfonyl[4] or carbonyl derivatives,[5] but most of these methods are tedious.

The present authors[6] have previously reported that anhydropyrimidinenucleosides can be conveniently prepared in high yields *via* the corresponding 2′,3′-*O*-sulfinates as intermediates. In the present paper we wish to describe a simple and efficient method for the anhydropurine nucleosides.

Results and Discussion

Ogilvie[5] prepared 8,2′-thioanhydro(9-β-D-arabinofuranosyl)-8-mercaptoadenine by heating 2′,3′-*O*-carbonyl-8-bromoadenosine in the presence of thiourea in *n*-butanol. The essential step in the preparation of anhydronucleosides is the introduction of a good leaving group to the 2′ and 3′-positions in the ribose moiety of nucleosides, as is outlined in Scheme 1. In order to establish a convenient method applicable for large-scale preparation, a cyclic sulfinyl group[6] was used as the leaving froup; it was considered to be more active than the cyclic carbonyl group.

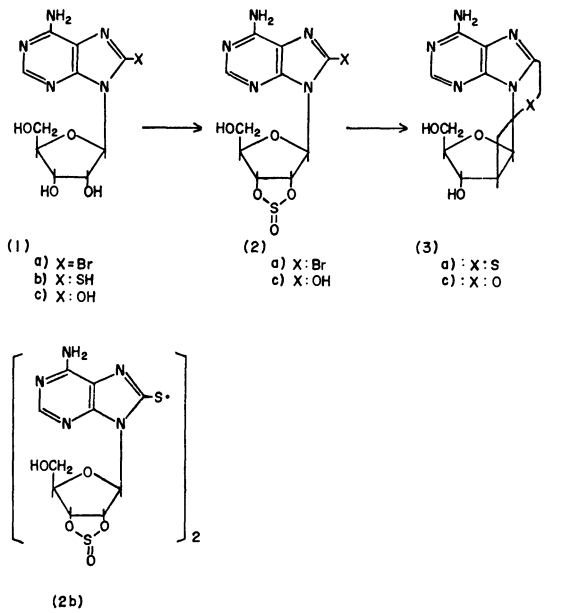

Scheme 1.

Thionyl chloride was allowed to react with 8-bromoadenosine (**1a**) in the presence of pyridine in acetonitrile at the temperature of 5 °C for 3 hr. Paper chromatography showed the presence of a single spot with an R_f-value of 0.91 other than that of the **1a** meterial (0.71). The reaction product was isolated in a 64% yield by pouring the reaction mixture into ice water and by then adjusting the pH of the resulting solution to pH 2.5 with sodium bicarbonate. The structure of the acylation product was identified as 2′,3′-*O*-sulfinyl-8-bromoadenosine (**2a**), which was negative to a periodate-benzidine test[7] and which gave ultraviolet spectra similar to those of **1a**. The alkaline hydrolysis of **2a** eliminated the cyclic sulfinyl group to give the **1a** material. The **2a** product had a broad band due to S=O stretching and three sharp bands associated with the five-membered cyclic sulfinyl group at 1201, 1205, and 1210 cm^{-1} in the infrared spectrum.[8] The elemental analysis of **2a** agreed with the proposed structure.

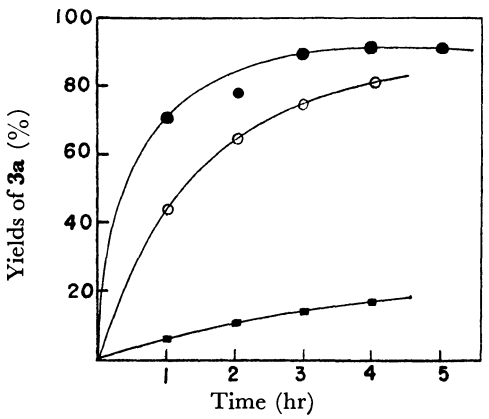

Fig. 1. Effect of reaction temperature of the preparation of **3a**.
Experimental conditions: 2′,3′-*O*-sulfinyl-8-bromoadenosine 1 mmol, thiourea 4 mmol, *n*-butanol 100 ml at 119 °C (●), 100 °C (○), 70 °C (■).

Table 1. Properties of nucleoside derivatives

Compound	Mp °C (d)[a]	R_f, PPC		UV-Spectrum λ_{max}, nm
		Solv. A	Solv. B	
1a	196	0.08	0.67	263
2a	146—148	—	0.90	260
3a	212—214	0.12	0.61	276
4a	184—188	0.38	0.49	257
1b	171—173	0.14	0.68	221, 243, 308
2b	142	—	0.91	281
1c	237—238	0.25	0.31	264, 284
2c	85— 92	—	0.82	264, 284
3c	202—202.5	0.45	0.25	260
4c	190—191	0.53	0.18	223, 248, 308
5c	252	0.19	0.45	257
1d	180	0.39	0.29	260
2d	175—177	—	0.85	258

a) d: decompose.

In *n*-butanol, **2a** was stable at the temperature of 80 °C in the presence of thiourea but was transformed to **3a** at an elevated temperature (Fig. 1). When **2a** was refluxed in *n*-butanol in the presence of thiourea, the reaction went essentially to completion after 4 hr to form a 8,2′-thioanhydro-linkage. The reaction product was isolated in a 70% yield and was identified as 8,2′-*S*-anhydro(9-β-D-arabinofuranosyl)-8-mercaptoadenine (**3a**) by a comparison of the physical properties with those of an authentic sample.[5] Compound **3a** was easily converted to 2′-deoxyadenosine (**4a**) by reducing it with Raney-Ni.

The treatment of 8-mercaptoadenosine (**1b**) with thionyl chloride under the same conditions as **1a** gave a single product, with an R_f-value of 0.9, by paper chromatography. Compound **2b** had a λ-maximum at 281 nm in the aqueous solution at pH 2.0, and its ultraviolet spectrum differed from that of the **1b** material (307 nm). Though the **2b** product had a broad band due to S=O stretching at 1000—1050 cm^{-1} and three fairly sharp bands associated with a five-membered cyclic sulfinyl group at 1200, 1205, and 1210 cm^{-1}, the specific absorption peak due to the SH group could not be found at 2550 cm^{-1} in the infrared spectrum. These facts show that the structure of the **2b** product is the bis(2′,3′-*O*-sulfinyladenosin-8-yl) disulfide. The elemental analysis of **2b** agreed with the proposed structure. All attempts at the cyclization of **2b** failed.

8-hydroxyadenosine (**1c**) was allowed to react with thionyl chloride under the same conditions as **1a** to give 2′,3′-*O*-sulfinyl-8-hydroxyadenosine (**2c**) as the single product, as shown by paper chromatography. By heating **2c** in *N*,*N*-dimethylformamide at 115 °C for 1 hr in the presence of sodium acetate, 8,2′-*O*-anhydro(9-β-D-arabinofuranosyl)-8-hydroxyadenosine (**3c**) was obtained in a 44.3% yield. The physicochemical properties of **3c** were in good agreement with those of an authentic sample.[9] By treatment with hydrogen sulfide in pyridine, **3c** was easily converted to 9-β-D-arabinofuranosyl-8-mercaptoadenine (**4c**), which was then transformed to 9-β-D-arabinofuranosyladenine (**5c**) by treating it with Raney-Ni. The physical properties of **4c** and **5c** are listed in Table 1; they are identical with those of authentic samples. Though the 2′,3′-*O*-sulfinyl-8-bromoguanosine (**2d**), much like **2a**, was formed quantitatively by treating 8-bromoguanosine (**1d**) with thionyl chloride, Compound **2d** could not be transformed to the corresponding anhydronucleoside, presumably because Compound **2d** is conformationally the "Syn" form.

The above method of synthesizing the anhydropurine nucleosides is superior to those of Ikehara[9] and Ogilvie[5] with respect to the yield and the simplicity of the procedure.

Experimental

The ultraviolet spectra were recorded on a Hitachi EPS-3T spectrophotometer, and the infrared spectra, on a Hitachi EPI-G2. The paper chromatography of the reaction products was carried out by the ascending technique on Toyo-Roshi No. 51 paper (40 cm × 40 cm) using the following solvent system: Solv. A; *n*-butanol–acetic acid–water (4: 1: 5); Solv. B; 2-propanol–saturated ammonium sulfate–1 M-sodium acetate (2: 79: 19). The UV and chromatographic properties are shown in Table 1.

2′,3′-O-Sulfinyl-8-bromoadenosine (2a). Freshly distilled thionyl chloride (21.6 ml, 300 mmol) and pyridine (24 ml, 300 mmol) were placed in 100 ml of acetonitrile, after which the mixture was set aside at the temperature of 5 °C. To the solution we then added 8-bromoadenosine (34.7 g, 100 mmol), and the mixture was stirred at 5 °C for 3 hr. Then, 300 ml of water was mixed with the reaction mixture to destroy the reactant under vigorous stirring. Paper chromatography showed the presence of a single spot with an R_f value of 0.9 (solvent B); an aqueous extract of it showed an absorption maximum at 260 nm (pH 1.0). The resulting reaction mixture was adjusted to pH 2.5 with sodium bicarbonate and was then kept in the refrigerator overnight. The white precipitates thus obtained were collected by filtration, washed with water, and dried to yield 24.4 g (64%) of 2′,3′-*O*-sulfinyl-8-bromoadenosine; mp 146—148 °C (dec.).

Found: C, 31.6; H, 2.5; N, 18.0, Br, 19.5; S, 8.1%. Calcd for $C_{10}H_{10}N_5O_5S \cdot Br$: C, 30.6; N, 2.5, H, 17.8; Br, 20.4; S, 8.2%.

2′,3′-O-Sulfinyl-8-bromoguanosine (2d). Into a mixed solution of thionyl chloride (21.6 ml), pyridine (24 ml), and acetonitrile (100 ml), we vigorously stirred 8-bromoguanosine (100 mmol); the reaction solution was then maintained for

3 hr at 5 °C. A 300 ml portion of water was then added to the reaction mixture, and the pH of the resulting solution was adjusted to 2.5 with sodium bicarbonate. The white precipitates thus obtained were collected, washed with water, and then dried to yield 25.4 g (64.3%) of 2′,3′-*O*-sulfinyl-8-bromoguanosine. Mp 175—177 °C (dec.); R_f 0.85 (solv. B), λ_{max} 258 nm (pH 2.0).

Found: C, 30.8; N, 17.1; S, 7.89%. Calcd for $C_{10}H_{10}N_5O_6Br$: C, 29.4; N, 17.1; S, 7.8%.

*2′,3′-O-Sulfinyl-8-hydroxyadenosine (**2c**).* Into a mixed solution of thionyl chloride (3.6 ml, 50 mmol), pyridine (2.4 ml, 30 mmol), and acetonitrile (30 ml), we vigorously stirred 8-hydroxyadenosine (2.8 g, 10 mmol), after which the reaction solution was maintained for 2 hr at 0 °C. A 250 ml portion of acetonitrile was added to the resulting mixture, and the solid thus precipitated was collected by filtration, washed with acetonitrile and twice with ether, and then dried to yield 2.84 g (85.7%) of 2′,3′-*O*-sulfinyl-8-hydroxyadenosine hydrochloride. Mp 85—92 °C (dec.); R_f 0.82 (solv. B).

Found: C, 32.5; H, 3.2; N, 17.3; S, 7.87; Cl, 10.14%. Calcd for $C_{10}H_{11}O_6N_5S\cdot HCl$: C, 32.8; H, 3.3; N, 19.2; S, 8.74; Cl, 9.71%.

*Bis(2′,3′-O-sulfinyladenosin-8-yl) Disulfide (**2b**).* Into a mixed solution of thionyl chloride (10.8 ml, 150 mmol), pyridine (12 ml, 150 mmol), and acetonitrile (50 ml), we vigorously stirred 8-mercaptoadenosine (15 g, 50 mmol), after which the reaction solution was maintained for 3 hr at 0 °C. A 300 ml portion of water was added to the reaction mixture under vigorous stirring to destroy the reactant. The resulting aqueous solution was adjusted to pH 2.5 with sodium bicarbonate and was then kept in the refrigerator overnight. The precipitates were collected by the filtration and then washed with water and dried to yield 12.6 g of bis(2,3′-*O*-sulfinyladenosin-8-yl) disulfide. Mp 142 °C (dec.); R_f 0.9 (solv. B), λ_{max} 281 nm (pH 2.0).

*8,2′-S-Anhydro(9-β-D-arabinofuranosyl)-8-mercaptoadenine (**3a**).* 2′,3′-*O*-Sulfinyl-8-bromoadenosine (21 g, 50 mmol) and thiourea (14 g, 200 mmol) were dissolved in 5 l of *n*-butanol, and the solution was refluxed for 4 hr. After drying the reaction mixture *in vacuo*, the residual product was dissolved in hot water and then cooled. The solid thus precipitated was collected by filtration and then washed with cold water and dried to give 10.2 g (70%) of 8,2′-*S*-anhydro(9-β-D-arabinofuranosyl)-8-mercaptoadenine. Mp 212—214 °C (dec.); $[\alpha]_D^{20}$ −178.1° (*c*, 0.5, H_2O) λ_{max} 276 nm (pH 2.0), R_f 0.12 (solv. A), 0.61 (solv. B). Found: C, 41.0; H, 4.2; N, 23.2; S, 9.67%. Calcd for $C_{10}H_{11}N_5O_3S\cdot 1/2H_2O$: C, 41.4; H, 4.1; N, 24.1; S, 11.0%.

*8,2′-O-Anhydro(9-β-D-arabinofuranosyl)-8-hydroxyadenine (**3c**).* 2′,3′-*O*-sulfinyl-8-hydroxyadenosine hydrochloride (5.5 g, 15 mmol) and sodium acetate (2.8 g, 45 mmol) were heated in *N,N*-dimethylformamide (1500 ml) for 45 min at 115 °C. After the reaction mixture had been dried *in vacuo*, the residual product was dissolved in 1 l of water; then the aqueous solution was submitted to electrodialysis with an ion-exchange membrane. The resulting solution was evaporated *in vacuo*, and white precipitates were collected, washed with water, and dried to yield 1.32 g (44.3%) of 8,2′-*O*-anhydro(9-β-D-arabinofuranosyl)-8-hydroxyadenine monohydrate. Mp 202—202.5 °C (dec.); λ_{max} 260 nm (pH 2.0).

Found: C, 42.90; H, 4.38; N, 24.7%. Calcd for $C_{10}H_{11}O_4N_5\cdot H_2O$: C, 42.40; H, 4.59; N, 24.73%.

*2′-Deoxyadenosine (**4a**).* 8,2′-*S*-Anhydro(9-β-D-arabinofuranosyl)-8-mercaptoadenine (4.6 g, 16.9 mmol) and Raney-Ni (30 g, Ni-content 50%) were mixed with 400 ml of water. The mixture was then refluxed for 2 hr. The nickel was removed by filtration, and the filtrate and washings (hot water) were combined and evaporated *in vacuo* to about 40 ml. A 100 ml portion of methanol was added to the concentrated solution, and the solid thus precipitated was collected by filtration, washed with water, and dried to give 2.88 g (67%) of 2′-deoxyadenosine. Mp 184—188 °C (dec.); R_f 0.49 (solv. B), λ_{max} 257 nm (pH 2), λ_{min} 232 nm (pH 2).

Found: C, 47.83; H, 5.11; N, 26.73%. Calcd for $C_{10}H_{13}N_5O_3$: C, 47.81; H, 5.18; N, 26.89%.

*8-Mercapto-9-β-D-arabinofuranosyl Adenine (**4c**).* 8-Mercapto-9-β-D-arabinofuranosyl adenine was prepared by Ikehara's method.[9] 8,2′-*O*-Anhydro(9-β-D-arabinofuranosyl)-8-hydroxyadenine monohydrate (1.1 g, 4 mmol) was dissolved in pyridine (40 ml) and liquid H_2S (obtained by cooling with dry-ice–acetone, 40 g). The mixture was sealed in a steel tube and heated at 100 °C for 16 hr. The tube was then cooled with dry-ice and N_2 gas was bubbled through to remove the H_2S completely. The pyridine was removed by the distillation *in vacuo*, and the residual product was crystallized from water to yield 1.0 g (78.4%) of 8-mercapto-9-β-D-arabinofuranosyl adenine monohydrate. Mp 190—191 °C (dec.); λ_{max} 223, 248, 208 nm (pH 2).

Found: C, 37.81; H, 4.75; N, 21.98; S, 9.95%. Calcd for $C_{10}H_{13}N_5O_4S\cdot H_2O$: C, 37.85; H, 4.73; N, 22.08; S, 10.09%.

9-β-D-Arabinofuranosyl Adenine[9] *(**5c**).* 8-Mercapto-9-β-D-arabinofuranosyl adenine monohydrate (4.5 g, 15 mmol) dissolved in 750 ml of water, and Raney-Ni (7.5 g) was added. The mixture was refluxed for 3 hr. The nickel was removed by filtration, and the filtrate and washings (hot water) were combined and concentrated *in vacuo*. The solid thus precipitated was collected by filtration, washed with water, and dried to yield 4.05 g (90%) of 9-β-D-arabinofuranosyl adenine monohydrate. Mp 252 °C (dec.); λ_{max} 257 nm (pH 2.0), R_f 0.19 (solv. A), 0.45 (solv. B).

Found: C, 42.15; H, 5.33; N, 24.28%. Calcd for $C_{10}H_{13}N_5O_4\cdot H_2O$: C, 42.10; H, 5.23; N, 24.56%.

References

1) M. Ikehara, *Accounts Chem. Res.*, **2**, 47 (1969).
2) M. Ikehara, S. Uesugi, and M. Yasumoto, *J. Amer. Chem. Soc.*, **92**, 4735 (1970).
3) M. Ikehara and H. Tada, *Chem. Pharm. Bull.*, **15**, 94 (1967).
4) M. Ikehara and M. Kaneko, *ibid.*, **18**, 2401 (1970).
5) K. K. Ogilvie and L. Slotin, *Chem. Commun.*, **1971**, 890; K. K. Ogilvie, L. Slotin, J. B. Westmore, and D. Lin, *Can. J. Chem.*, **50**, 2250 (1970).
6) T. Sowa and K. Tsunoda, This Bulletin, **48**, 505 (1975).
7) M. Viscontini *et al.*, *Helv. Chim. Acta*, **38**, 642 (1955).
8) L. J. Bellamy, "The Infrared-Spectra of Complex Molecules," ed. by L. J. Bellamy, Richard Clay and Company, Great Britain (1960), p. 360.
9) M. Ikehara, *Tetrahedron*, **24**, 3489 (1968); *ibid.*, **28**, 3695 (1972); *J. Amer. Chem. Soc.*, **88**, 3165 (1966).

Ethanol and Lactic Acid Sensors Using Electrodes Coated with Dehydrogenase-Collagen Membranes

Shuichi SUZUKI, Fujio TAKAHASHI, Ikuo SATOH, and Nobuyuki SONOBE

Research Laboratory of Resources Utilization, Tokyo Institute of Technology, Ookayama, Meguro-ku, Tokyo 152

(Received May 7, 1975)

Electrochemical and enzymatic reactions were studied for the purpose of making sensors of ethanol and lactic acid. The dehydrogenase-collagen membrane coated onto a platinum plate was prepared by the electroshaping method. The substrates were dehydrogenated and nicotinamide adenine dinucleotide (NAD) was reduced to form the reduced NAD (NADH) by an enzymatic reaction on the collagen membrane. Flavin mononucleotide (FMN) was chosen as an electroactive substance which could oxidize NADH to return NAD. The reduced FMN ($FMNH_2$) was easily oxidized at the anode and a current was obtained. From the above reactions, the concentrations of ethanol and lactic acid in solutions were found to be determined by a current-substrate concentration relation. The accuracy was estimated to be within 10% error. The activity and stability of enzymes immobilized in the collagen membrane were investigated.

Since 1962, the characteristics of biochemical reaction cells have been studied in this laboratory.[1] These cells have been found not to generate a large quantity of power. However, these cells have a specificity that only one substrate in the mixture selectively reacts in the enzymatic reaction to form an electroactive substance which in turn reacts at the electrode to generate electricity. One of the present authors has already reported on the application of several sensors for the detection and analysis of hydrogen peroxide and uric acid using biochemical reaction cells.[2] It has been found that NAD can be utilized as one of electroactive substances in the biochemical reaction cells.[3] It has been found that NAD is involved in more than 200 kinds of enzymatic reactions as a coenzyme.[4] Therefore, it is expected that many kinds of substrates might be detected or determined by the measurement of the anodic reaction of NADH produced by the enzymatic reaction with each substrate.

The purpose of this study is to produce a sensor which combines the electrochemical reaction and the enzymatic reaction with NAD. The necessary conditions for the sensor are (1) to obtain the relative value of the potential or current corresponding to the substrate concentration, (2) to allow the electrochemical reaction to occur with a constant concentration of NAD, and (3) to be capable of using the enzyme repeatedly. It is already known that NADH is hardly oxidized at the anode electrochemically.[3] Therefore, it was proposed that another redox system, as an electroactive substance which can easily react with NADH, be introduced in the biochemical reaction cell as follows:

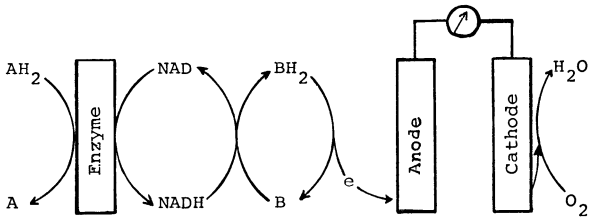

AH_2: Substrate, A: product, B,BH_2: electroactive substance

This paper reports on the studies of electrochemical and enzymatic reactions for making ethanol and lactic acid sensors.

Experimental

Materials and Preparation of Collagen Membrane. Alcohol dehydrogenase (ADH) and lactate dehydrogenase (LDH) were supplied by Oriental Yeast Co. All the other chemicals were of reagent grade or the best commercially available. ADH-collagen membranes were prepared, according to the method of Karube, as shown in Fig. 1, by an electrochemical method using collagen fibril suspensoid which was obtained from hide.[5]

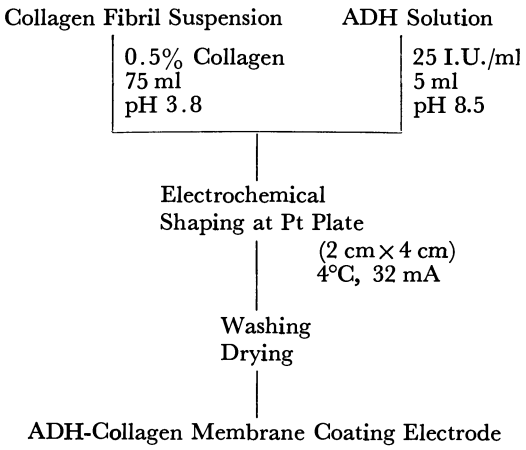

Fig. 1. Preparation of ADH-collagen membrane.

In the case of LDH-collagen membrane, the collagen fibril in the suspensoid was treated with pepsin to digest and to produce an almost transparent solution before adding LDH. The LDH-collagen membrane-coated anode was dipped in a glutaraldehyde solution and then washed with distilled water. NAD, NADH, and FMN were determined by UV spectrophotometry. The ADH was analyzed by measuring the zinc content in the enzyme by atomic absorption spectrophotometry. The ADH and LDH activities were determined by measuring NADH which was formed as a product of the enzymatic reaction.

Instruments. Absorption spectra and atomic absorption spectra were obtained using a Shimadzu spectrophotometer UV-200 and a Varian atomic absorption spectrophotometer A-A1000, respectively. A Toa Electric recorder EPR-2T and a Kikusui 114 Millivolt-ammeter were used for measuring the current. The potentials were determined with reference to a saturated calomel electrode.

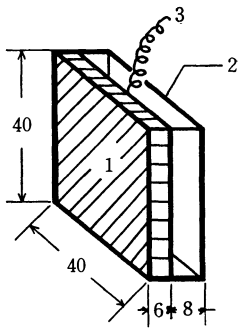

Fig. 2. The cathode.
1. Carbon, 2. plastic plate, 3. lead wire. unit: mm

Procedure and Measurement of Electrochemical Reaction. The electrochemical reaction was carried out with the following mounting: Anode: an intact or enzyme-collagen membrane-coated platinum plate (2 cm×4 cm). Cathode: a box-shaped cathode, as shown in Fig. 2. One surface of the carbon plate (4 cm×4 cm×0.6 cm) was soaked in the catholyte and the other side was exposed to air. The anolyte was 0.1 mol/l of a phosphate buffer solution (pH 7.7) containing substrates (ethanol or lactic acid), NAD and an electroactive substance. The enzyme was added to the anolyte when an intact platinum plate was used as the anode. The catholyte was 0.1 mol/l of a phosphate buffer solution (pH 7.7). The anolyte and catholyte in each beaker were connected *via* an agar bridge. When the circuit of the biochemical reaction cell was open, the anode potential went to less noble because of the enzymatic reaction in the anolyte, as shown in Fig. 3. Nearly 30 min after the enzymatic reaction were required to reach equilibrium in the anolyte. Then the discharge was started and the current was measured. During this procedure, nitrogen gas was bubbled into the anolyte.

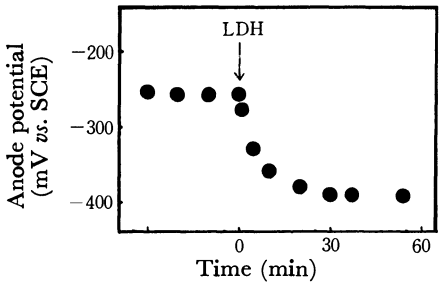

Fig. 3. Anode potential-time curve.

Results

The Electroactive Substances. FMN, thioglycolate, methyl viologen and phenazine methosulfate (PMS) were used as electroactive substances which reacted with NADH. In this biochemical reaction cell, 40 ml of an anolyte containing 1.5 mmol/l of the electroactive substance and 1 mmol/l of NADH, and an intact platinum anode were used. The values of current obtained from short-circuit discharging after the redox reaction between the NADH and the electroactive substance are summarized in Table 1. In the case when the anolyte contained only NADH, the current decreased to zero within 5 min after discharging. PMS oxidized NADH so rapidly that a high current was observed. But the PMS was unstable. It appears that the electrochemical reactions of thioglycolate and methylviologen are remarkably slow. It was found that an almost constant current was maintained after 1 minute in the case of FMN. From these results FMN was chosen as the electroactive substance for subsequent experiments.

Influence of Substrate, NAD, and FMN to the Current. The anode reaction process in process (1) includes 3 steps. For the purpose of the assignment of the rate-determining step in process (1), the current was measured in the ethanol-ADH system and in the lactic acid-LDH system in the anolyte containing various concentrations of the substrate, NAD and FMN. An intact platinum plate was used as the anode in the anolyte. The results are shown in Figs. 4, 5 and 6. The values of the current are thoughtsto be reliable to within 10%. The substrate concentration–current relation did not fall on a straight line.

Electrochemical Reaction Using an Enzyme-Collagen Mem-

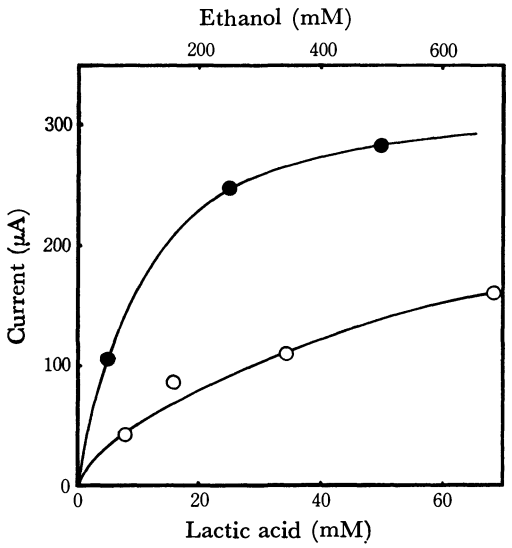

Fig. 4. Substrate–current relation.
—○—: Ethanol, —●—: lactic acid

Table 1. Electroactive substances

Compound (1.5 mmol/l)	NADH (mmol/l)	Anode potential (mV *vs.* SCE)	Current (μA) 1 min after closing the circuit
None	1	−262	10
Thioglycolic acid	1	−132	0
Methylviologen	1	−134	0
Phenazine methosulfate[a)]	1	−155	150
FMN	1	−440	207
FMN	0	−180	0

0.1 mol/l of a phosphate buffer (pH 7.7), 25 °C. a) 2 mmol/l.

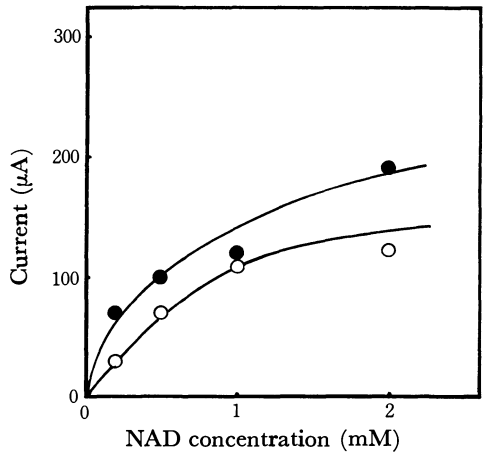

Fig. 5. NAD-current relation.
—○—: Ethanol, —●—: lactic acid.

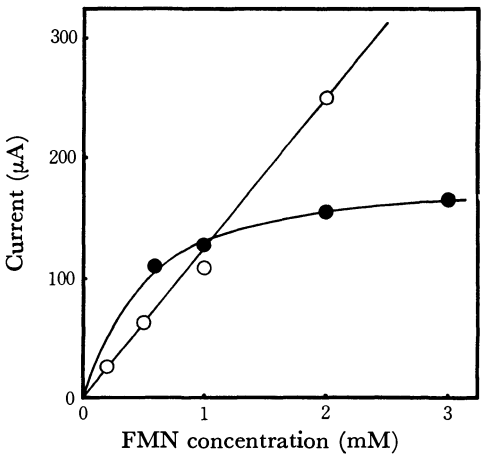

Fig. 6. FMN-current relation.
—○—: Ethanol, —●— lactic acid.

brane-Coated Anode. The enzyme was immobilized in the collagen membrane, so that the enzyme might be used repeatedly. The anode reaction was studied using an anode coated with an enzyme-collagen membrane, which was prepared by means of the electrochemical process shown in Fig. 1. The enzyme content, activities and other properties of the enzyme-collagen membrane were determined (Table 2). The substrate-current relation was measured in the same way as in Fig. 4. The results (Fig. 7) showed a tendency similar to that in Fig. 4, but the current was lower. The same anode coated with an enzyme-collagen membrane was used repeatedly and its activity was determined with the hope of maintaining the same activity for each measurement. The anolyte contained 0.34 mol/l of ethanol, 1 mmol/l of NAD and 2 mmol/l of FMN.

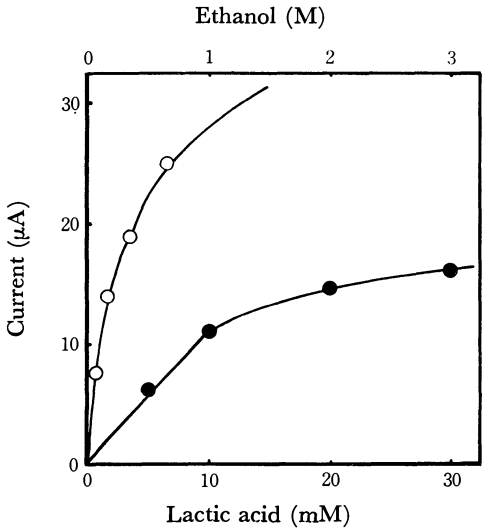

Fig. 7. Substrate-current relation (Enzyme-collagen membrane coating electrode).
—○—: Ethanol, —●— : lactic acid.

After each measurement of the current, the anolyte used was replaced by a new one and the same process was repeated. The enzyme activity was not found to decrease. The average value of current over 5 measurements was 33 ± 4 μA.

In the case of the LDH-collagen membrane, the enzyme activities were determined in a solution containing 12.5 mmol/l of lactic acid and 1 mmol/l of NAD and it was found that the activity remained constant over 8 measurements.

Discussion

It is clear that the reactions in process (1) can be utilized as a sensor. It was concluded, using the anode coated with ADH and LDH-collagen membranes, that (1) the value of the current increased non-linearly with the substrate concentration, (2) ethanol and lactic acid can be determined to within an accuracy of 10% error, (3) the enzyme activity remained constant over more than 5 measurements and (4) the necessary conditions for temperature, pH and concentrations of ethanol and lactic acid were lower than 30 °C, 6~8, 1 mol/l and 25 mmol/l, respectively.

Process (1) can be rearranged into 3 reactions as follows:

$$AH_2 + NAD^+ \longrightarrow A + NADH + H^+ \quad (2)$$

$$NADH + FMN + H^+ \longrightarrow NAD^+ + FMNH_2 \quad (3)$$

$$FMNH_2 \longrightarrow FMN + 2H^+ + 2e \quad (4)$$

If reaction (2) is the rate-determining step, the current

TABLE 2. PROPERTIES OF ENZYMES IN COLLAGEN MEMBRANE

Properties	Alcohol dehydrogenase	Lactate dehydrogenase
Enzyme content or activity	2% (from Zn content)	0.4 unit[a)]
pH Stability	5—10	5—10
Thermal stability	less than 35 °C	less than 35 °C
Reusability	5 times	8 times

a) In collagen membrane on platinum anode (2 cm×4 cm).

should be proportional to the substrate or total NAD concentration for a constant concentration of the NAD or substrate, respectively. However, Figs. 4 and 5 indicate that there is no linearity. If reaction (3) is the rate-determining step, the NADH concentration has to be constant during the reaction, and the concentration of $FMNH_2$ formed in the reaction could be negligible because of the rapid oxidation at the anode. The reaction velocity should be proportional to the product of the NADH concentration and the total FMN concentration. In turn, this velocity would be proportional to the current. If reaction (4) is the rate-determining step, the $FMNH_2$ concentration has to be constant in a steady state. Accordingly, the current remains constant during the electrochemical reaction, thus,

$$i \propto [FMNH_2] \quad (5)$$

From the result in Fig. 6, it can be said that reaction (4) should be the rate-determining step in lactic acid case, although it cannot be determined which step is the rate-determining one, reaction (3) or (4), in the ethanol case.

References

1) J. Mizuguchi, S. Suzuki, F. Takahashi, and K. Kashiwaya, *Kogyo Kagaku Zasshi*, **65**, 1606 (1962); J. Mizuguchi S. Suzuki, K. Kashiwaya, and M. Tokura, *ibid.*, **67**, 410 (1964).

2) M. Aizawa, I. Karube, and S. Suzuki, *Anal. Chim. Acta*, **69**, 431 (1974). S. Suzuki, N. Sonobe, I. Karube, and M. Aizawa, *Chem. Lett.*, **1974**, 9.

3) F. Takahashi, M. Aizawa, J. Mizuguchi, and S. Suzuki, *Kogyo Kagaku Zasshi*, **73**, 908, 912 (1970).

4) T. E. Barman; "Handbook of Enzymes," Vol. 1, Springer-Verlag, New York (1969), p. 23.

5) I. Karube, S. Suzuki, S. Kinoshita, and J. Mizuguchi, *Ind. Eng. Chem. Prod. Res. Develop.*, **10**, 2 (1971).

Favorable Conformations of 2-Amino-2-deoxy-D-hexopyranose Derivatives

Tooru TAGA and Kenji OSAKI

Faculty of Pharmaceutical Sciences, Kyoto University, Sakyo-ku, Kyoto 606

(Received May 12, 1975)

The conformational free energies of 2-amino-2-deoxy (hydrochloride) and 2-acetamido-D-deoxy derivatives of D-glucose, D-galactose, and D-mannose were calculated by using the empirical potential functions. The most stable conformations of these amino sugars were obtained for α- and β-anomers in the Cl and 1C chair forms through the procedure of searching for the energy minimum. The results of the energy calculations indicate that the increased anomeric effect in the protonated and *N*-acetylated amino derivatives in an aqueous solution is mainly due to the electrostatic interaction between the positive-charged amino group on C(2) and the hydroxyl group on the anomeric carbon atom, C(1).

This paper will present a theoretical calculation of the conformational free energies of the protonated, non-protonated, and *N*-acetylated amino derivatives of 2-amino-2-deoxy-D-glucose, -D-galactose, and -D-mannose. The anomeric equilibria of these amino sugars in an aqueous solution have been studied by many workers using the NMR[1] or optical rotatory methods.[2-9] The present work was undertaken in order to determine the most favored conformation of each of these amino sugars and to explain the increased proportion of the α-anomer in the protonated and *N*-acetylated amino derivatives of D-glucose and D-galactose, as pointed out by Neuberger and Fletcher.[8]

The theoretical prediction of the favored conformation of simple reducing sugars has been attempted by many workers by considering various factors, including the Hassel-Ottar effect,[9] the $\triangle_2$ effect[10,11] and the anomeric effect.[12-16] Angyal[14] has assigned the interaction energies for aldopyranoses by using the empirical rule. Rao *et al.*[17-19] have shown that the energy calculations taking the nonbonded and electrostatic interactions into account are consistent with the experimental data for aldopyranoses. In the present work, the potential energies for α- and β-anomers of each amino sugar in the Cl and 1C conformations have been calculated from the empirical potential functions, using a modification of the method of Rao *et al.*[18] The conformational entropies have also been estimated and added to the corresponding potential energies to obtain the total free energies.

Calculation of Free Energy

Potential Energy. The potential energy of a molecule can be expressed in terms of the nonbonded interaction, the electrostatic interaction, and the steric effect associated with the bond distortion.

The nonbonded interaction energy was evaluated by the use of the Lennard-Jones '6—12'-type potential function:

$$V_n = \frac{A}{R_{ij}^{12}} - \frac{B}{R_{ij}^{6}} \quad (1)$$

where R_{ij} is the distance between the interacting atoms, i and j. The A and B coefficients determined by Scott and Sheraga[20] were used in the present calculation.

The electrostatic interaction energy was calculated by using the following function:

$$V_e = \frac{Q_i \cdot Q_j}{\varepsilon \cdot R_{ij}} + \frac{Q_i \cdot \mu \cdot \cos\phi_i}{\varepsilon \cdot R_i^2} \quad (2)$$

where Q_i and Q_j are the charges of a pair of interacting atoms, i and j, where R_{ij} is the distance between them, ε is the effective dielectric constant of the medium, μ is the dipole moment of the lone pairs on the ring-oxygen atom, R_i is the distance between the i atom and the ring-oxygen atom, and Φ_i is the angle between the dipole vector on the ring-oxygen atom and the vector directed from the ring-oxygen atom to the i atom. The first term in Expression (2) is the Coulombic interaction between the partial charges localized at each atom. The values of Q used in the calculation are given in Table 3. They were obtained from the results of the molecular orbital calculations for aldopyranose and amino acid molecules by several workers.[19,21,23] The second term in Expression (2) is the charge-dipole interaction. The value of the dipole moment of the unshared electron pairs on the ring-oxygen atom is 0.37D, a value derived from the results of the theoretical calculation for 2-methoxytetrahydropyran by Zhadanov *et al.*[24] The effective dielectric constant, ε, is usually much smaller than the actual dielectric constant.[20] In the present calculation, the value of 4.5 was assigned, since the use of this value gave a good agreement between the calculated and observed free energies for aldopyranoses in an aqueous solution.

The energy caused by the steric effect of the covalent bonds was evaluated with the deviation of a single-bond angle, θ, from the normal tetrahedral angle, θ_t (109.5°), by using the following function:

$$V_b = \kappa \cdot (\cos\theta - \cos\theta_t)^2 \quad (3)$$

where κ is a constant dependent on the bonded atoms involved. The values of κ were assigned as 65 kcal/mol for C–C–C and C–C–O, 55 kcal/mol for O–C–O, and 45 kcal/mol for C–C–H and O–C–H.[25]

The energies associated with the internal rotation and the intramolecular hydrogen bond were neglected.

Entropy. The conformational entropy can be calculated by using the formula:

$$S = R \ln N \quad (4)$$

were R is the gas constant and where N is the total number of possible conformations of the molecule.[18]

Generally, the OH bond in the equatorial hydroxyl group has three favored orientations of the staggered form, while the OH bond in the axial hydroxyl group

has two favored orientations. Since, in an aqueous solution, the sugar molecules are extensively hydrated through hydrogen-bonding with the surrounding water molecules, the OH bond might be directed to the oxygen atom of the neighboring water molecule to form a strong hydrogen bond. Therefore, the orientations of the OH bonds are greatly restricted, not only by the intramolecular interactions, but also by the intermolecular hydrogen bonds. As a result, the possible orientations of the OH bond are dependent on the position of the hydroxyl group linked to the ring. For instance, the OH bond of the equatorial hydroxyl group linked to C(1) has only two favorable orientations. By taking account of all the possible orientations of OH bonds, together with the orientations of the CH_2OH and amino groups, the total number of possible conformations was calculated for each derivative.

Procedure of Calculation. The ring atoms and atoms linked directly to the ring were fixed in the Cl and 1C chair forms by using average values derived from 25 crystal structure analyses of pyranoses.[26-33] The CH_2OH side group was fixed in the *gauche-trans* conformation, which is one of the preferable orientations often found in the crystals.[34] The hydrogen atoms in the hydroxyl groups were fixed in one of the favorable staggered forms. The atoms in amino groups were fixed by using the bond lengths and angles given in Table 2. The NH_2 and *N*-acetyl groups were assumed to be planar. The positional parameters given for β-D-glucose are listed in Table 1. The bond lengths and angles calculated from these parameters are in good agreement with the values given by Arnott *et al.*[27]

The most stable conformation of each derivative was determined from the initial structure by the following procedure. As has been mentioned before, the OH bond in the equatorial hydroxyl group has three favored orientations, and the most favorable orientation of the three might be determined by taking the relative positions of the neighboring OH bonds into account. Thus, in the first step, the most preferable conformation was selected from the 81 possibilities which arose from the different orientations of OH bonds in the staggered form. The interaction energies were calculated for each conformation by using the (1) and (2) potential functions, and their values were compared. In the next step, the OH, CH_2OH, and amino groups were independently rotated around their free rotational bonds, and the minimum energy position of each substituent group was sought by the reiterative process. For example, the O(1)–H(O1) bond was rotated around the C(1)–O(1) bond at suitable angular intervals, and at each position the interaction energy between H(O1) and each fixed atom was calculated by using the (1) and (2) functions.

Table 1. Positional parameters (Å) of β-D-glucopyranose

Atom	*X*	*Y*	*Z*
C(1)	1.406	0.090	−0.231
C(2)	0.761	−1.212	0.209
C(3)	−0.692	−1.272	−0.231
C(4)	−1.437	−0.024	0.222
C(5)	−0.692	1.227	−0.231
C(6)	−1.314	2.504	0.281
O(1)	2.676	0.177	0.313
O(2)	1.481	−2.323	−0.296
O(3)	−1.304	−2.435	0.317
O(4)	−2.741	0.005	−0.346
O(5)	0.655	1.191	0.262
O(6)	−0.572	3.601	0.048
H(1)	1.441	0.178	−1.229
H(2)	0.800	−1.266	1.219
H(3)	−0.710	−1.314	−1.252
H(4)	−1.523	−0.021	1.224
H(5)	−0.673	1.278	−1.245
H(61)	−1.322	2.482	1.512
H(62)	−2.262	2.559	0.179
H(O1)	2.608	0.125	1.542
H(O2)	1.483	−2.304	−1.064
H(O3)	−1.266	−2.412	1.546
H(O4)	−2.678	−0.004	−1.113
H(O6)	−0.983	4.446	0.387

Table 2. Bond lengths and angles in amino groups

Nonprotonated amino group			
C(2)–N(2)	1.48 Å	C(2)–N(2)–H(N)	120°
N(2)–H(N)	1.0 Å	H(N)–N(2)–H′(N)	120°
Protonated amino group			
C(2)–N(2)	1.50 Å	C(2)–N(2)–H(N)	109.5°
N(2)–H(N)	1.0 Å	H(N)–N(2)–H′(N)	109.5°
N-Acetylated amino group			
C(2)–N(2)	1.47 Å	C(2)–N(2)–C(7)	123°
N(2)–C(7)	1.33 Å	C(2)–N(2)–H(N)	115°
C(7)–C(8)	1.47 Å	C(7)–N(2)–H(N)	122°
C(7)–O(7)	1.24 Å	N(2)–C(7)–C(8)	118°
N(2)–H(N)	1.0 Å	N(2)–C(7)–O(7)	123°
C(8)–H(8)	1.0 Å	C(8)–C(7)–O(7)	119°
		C(7)–C(8)–H(8)	109.5°
		H(8)–C(8)–H′(8)	109.5°

Table 3. Partial charges on the atoms for the amino sugars in fractions of an electronic charge

Atom name	Fractional charge
C(1)	0.19
C(2), C(5), C(6)	0.06
C(3), C(4)	0.12
O(1)	−0.445
O(3), O(4), O(6)	−0.455
O(5)	−0.25
All hydrogen atoms linked to the carbon atoms	0.05
All hydrogen atoms in the hydroxyl group	0.30
N(2) in NH_2 group	−0.53
H(N) in NH_2 group	0.22
N(2) in NH_3 group	0.13
H(N) in NH_3 group	0.25
N(2) in *N*-acetyl group	−0.305
C(7) in *N*-acetyl group	0.45
C(8) in *N*-acetyl group	−0.12
O(7) in *N*-acetyl group	−0.12
H(N) in *N*-acetyl group	0.27

The minimum energy position for H(O1) was sought. After fixing the H(O1) atom in its minimum-energy position, the H(O2) atom was fixed in the same manner and the process was continued until all atoms were located. A similar reiterative procedure was applied to determine the distortion of the bond angles about the ring carbon atoms. In this process, each of the OH, CH_2OH, and amino groups and each of the hydrogen atoms linked to the ring were sequentially tilted by varying the bond angles about the ring atoms. For each bond angle, the steric energy was calculated using the (3) function, and the interaction energy, using the (1) and (2) functions, thus, the minimum-energy position was determined for each substituent group. The rotation and tilting procedures were repeated alternatively until, after four cycles, a convergence was observed. The potential energy of the molecule was found by the summation of the nonbonded and electrostatic interactions and the steric energies calculated in the last cycle.

The entropy of each derivative was calculated by using Formula (4), and the contribution of the entropy term, $-ST$, was added to the corresponding potential energy to obtain the total free energy at 300 K. The values of the entropies assigned for the amino derivatives are given in Table 4.

Table 4. Conformational entropies of various amino hexose derivatives

Amino hexose derivative	Calculated conformational entropy(S) in cal·mol^{-1}·deg^{-1}			
	α-anomer		β-anomer	
	Cl	1C	Cl	1C
2-Amino-2-deoxy-D-glucose	8.98	6.31	11.30	8.49
2-Amino-2-deoxy-D-galactose	8.85	6.31	11.10	8.49
2-Amino-2-deoxy-D-mannose	10.18	7.69	10.18	8.38
2-Amino-2-deoxy-D-glucose HCl	8.80	7.12	10.18	9.47
2-Amino-2-deoxy-D-galactose HCl	8.32	7.12	9.70	9.47
2-Amino-2-deoxy-D-mannose HCl	10.18	7.12	8.80	6.31
2-Acetamido-2-deoxy-D-glucose	12.17	8.49	12.74	9.51
2-Acetamido-2-deoxy-D-galactose	11.53	8.49	12.10	9.51
2-Acetamido-2-deoxy-D-mannose	11.37	8.49	11.37	9.51

Table 5. Free energy (kcal/mol) for some aldopyranoses

Sugar	Calculated value		Angyal's value	
	Cl	1C	Cl	1C
α-D-glucose	0.45	4.45	0.35	4.5
β-D-glucose	0.0	6.01	0.0	5.95
α-D-galactose	0.84	2.97	0.80	4.25
β-D-galactose	0.57	5.78	0.45	5.7
α-D-mannose	0.43	3.68	0.45	3.5
β-D-mannose	1.05	5.65	0.90	5.6

Results and Discussion

The conformational free energies calculated for D-glucose, D-galactose, and D-mannose in the Cl and 1C conformations are given in Columns 2 and 3 of Table 5. These values are in good agreement with Angyal's values,[14] given in Columns 4 and 5 of the same table. The results of the energy calculations for the amino derivatives are given in Table 6. The free energies given in Columns 2—5 of Table 6 show that the Cl conformation is more stable than the 1C conformation for all the derivatives and that the α-anomers in the Cl form are more stable than the β-anomers except in the cases of 2-amino-2-deoxy-D-glucose and -galactose and 2-amino-2-deoxy-D-mannose hydrochloride. The percentages, p, of the proportions of the α- and β-anomers in the Cl and 1C conformations in an equilibrium mixture of each derivative were calculated using the following formula:

$$p_i = \frac{\exp(-F_i/RT)}{\sum_i \exp(-F_i/RT)} \qquad (5)$$

where the summation includes all four conformations and where F_i is the free energy of the i component. Calculations by means of Expression (5) incorporating the free energy values given in Table 6 show that the proportions of both anomers existing in the 1C conformation in an equilibrium mixture are negligible for all amino derivatives except for α-D-glucosamine hydrochloride. The calculated anomeric ratios (α/β) in an equilibrium mixture of each derivative are given in Column 2 of Table 7, while the corresponding NMR and optical rotatory data observed from aqueous solutions are given in Columns 3 and 4 of the same table. The α/β ratios calculated here include both Cl and 1C conformations, whereas the NMR ratios are derived from the Cl peaks only. However, it is possible that the Cl peaks may include contributions from the 1C conformation, and, as the energy calculation indicates that the Cl conformation is much more stable than the 1C, a valid comparison can be made. In the case of D-glucosamine hydrochloride, the α/β ratio calculated from the Cl conformation is 52:48; this value is slightly different from the observed value.

As is well known, the anomeric effect makes an equatorial group on the anomeric carbon of D-glucose less stable than it would be in other positions on the ring. This effect has been explained in terms of the unfavorable parallel interaction between the anomeric carbon-oxygen dipole and the dipole formed by the unshared electron pairs on the ring-oxygen atom.[12,13] In the present case, such an anomeric effect seems likely to be increased further. However, we have no evidence that such dipole-dipole interaction would be enhanced by the amino group on C(2). Table 6 shows that the electrostatic interaction terms given in Columns 6—9 tend to reduce the free energy of the α-anomer significantly in the case of the protonated and *N*-acetylated amino derivatives. It may be, therefore, that the main factor responsible for the increased anomeric effect in these amino sugars is the charge-charge interaction between the positively charged amino group and the hydroxyl group on the anomeric carbon atom. The presence of an oxygen atom in the pyranose ring produces a significant deformation as compared with the cyclohexane ring, with the result

Table 6. Free energies and electrostatic interaction energies for 2-amino-2-deoxy-hexose derivatives

Name of amino sugar	Free energy (kcal/mol)				Electrostatic interaction energy (kcal/mol)			
	α-anomer		β-anomer		α-anomer		β-anomer	
	Cl	1C	Cl	1C	Cl	1C	Cl	1C
2-Amino-2-deoxy-D-glucose	4.47	7.48	4.13	8.99	3.14	3.51	3.65	2.89
2-Amino-2-deoxy-D-galactose	4.66	6.48	4.50	8.51	3.32	2.75	3.83	2.81
2-Amino-2-deoxy-D-mannose	3.45	6.49	4.21	9.20	2.70	3.06	3.45	3.00
2-Amino-2-deoxy-D-glucose HCl	41.37	42.22	41.43	46.18	9.47	7.93	9.92	9.87
2-Amino-2-deoxy-D-galactose HCl	41.75	44.17	42.02	48.35	9.62	10.30	10.25	12.55
2-Amino-2-deoxy-D-mannose HCl	41.65	43.46	40.88	46.45	10.38	9.38	9.16	9.29
2-Acetamido-2-deoxy-D-glucose	70.80	72.82	71.05	75.54	8.89	8.60	9.62	8.92
2-Acetamido-2-deoxy-D-galactose	70.93	73.24	71.23	76.90	9.05	8.88	9.82	10.09
2-Acetamido-2-deoxy-D-mannose	70.56	73.98	70.67	76.68	9.03	9.50	9.26	9.49

Table 7. Anomer ratio (α/β) in equilibrium mixtures of amino sugar derivatives

Amino sugar derivative	Calcd	From NMR[a]	From optical rotation	Ref.
2-Amino-2-deoxy-D-glucose	36:64	—	39:61	2
2-Amino-2-deoxy-D-galactose	39:61	—	—	—
2-Amino-2-deoxy-D-mannose	78:22	—	—	—
2-Amino-2-deoxy-D-glucose HCl	61:39	63:37	63.3:36.7	3
2-Amino-2-deoxy-D-galactose HCl	62:38	47:53	56.3:43.7	4
2-Amino-2-deoxy-D-mannose HCl	22:78	43:57	—	—
2-Acetamido-2-deoxy-D-glucose	61:39	68:32	65.8:34.2	5
2-Acetamido-2-deoxy-D-galactose	63:37	65:35	64:36	6
2-Acetamido-2-deoxy-D-mannose	55:45	57:43	55:45	7

a) The NMR data was taken from Ref. 1.

that the amino group on C(2) is closer to the hydroxyl group on C(1) in the α-anomer than that in the β-anomer. This unequal distance in the two anomers might cause the increased anomeric effect.

The most stable conformations derived from several amino sugars by means of the potential energy calculations indicate the following structural features of the amino sugars. The hydroxyl group in an axial position has a tendency to be tilted toward the equatorial orientation as a result of the repulsive interaction between the axial substituents. The C–C–O angles outside of the ring for the axial hydroxyl group are larger than those for the equatorial group by 1° on the average. The CH_2OH side group in an axial position also has a similar tendency. It is more tilted when the hydroxyl groups occupy the axial positions of the C(1) and C(3) ring atoms. For example, the C(4)–C(5)–C(6) angles are calculated as 115° for α-D-glucose in the 1C form and as 117° for β-D-glucose in the 1C form, while the mean value of the corresponding angles in the equatorial epimers is 113°. However, the amino groups do not show such a tendency. In this case, the C–C–N angle is close to the tetrahedral angle in both the axial and the equatorial groups. This may be accounted for by the electrostatic attractive force due to the positive charge on the amino group. The stable conformation of the NH_3 group with respect to the pyranose ring is the staggered form, as observed in the β-D-galactosamine hydrochloride crystal.[28] The planar NH_2 and *N*-acetyl groups have two possible conformations when they link to the equatorial position of C(2) in a Cl-chair form. Each conformfftion is close to a *trans* form about C(2)–N, whith the N–H bond *trans*-antiparallel with respect to the hydrogen atom on C(2). The present calculations give the minimum energies at 90° and 145° for the C(1)–C(2)–N(2)–C(7) torsional angle. These calculated angles may be compared with the corresponding angles of 137°, 83°, 72°, and 113° observed in the crystal structures of the *N*-acetylated derivatives of α-D-glucose,[30] α-D-galactose,[31] α-D-muramic acid,[32] and 4-*N*-(α-D-glucopyranosyl)-L-asparagine[33] respectively.

The authors wish to thank Mr. Masanori Senma for his data collection of the crystal structures used in this work. All the computations were performed by using the FACOM 230-60 in the Data Processing Center, Kyoto University.

References

1) D. Horton, J. S. Jewel, and K. D. Philips, *J. Org. Chem.*, **31**, 4022 (1966).
2) A. Neuberger and A. P. Fletcher, *J. Chem. Soc., B*, **1969**, 178.
3) J. C. Irvine and J. C. Earl, *J. Chem. Soc.*, **121**, 2370 (1922).
4) I. Werner, *Mikrochem.*, **39**, 133 (1952).
5) R. Kuhn and F. Haber, *Chem. Ber.*, **86**, 722 (1953).
6) M. Stacey, *J. Chem. Soc.*, **1940**, 272.
7) C. T. Spivak and S. Roseman, *J. Amer. Chem. Soc.*, **81**, 2403 (1959).
8) A. Neuberger and A. P. Fletcher, *Carbohyd. Res.*, **17**, 79 (1971).
9) O. Hassel and B. Ottar, *Acta Chem. Scand.*, **1**, 929 (1947).
10) R. E. Reeves, *Advan. Carbohyd. Chem.*, **6**, 107 (1951).
11) R. B. Kelly, *Can. J. Chem.*, **35**, 149 (1957).
12) J. T. Edward, *Chem. Ind.* (London), **1955**, 1102.
13) R. U. Lemieux and H. J. Chu, *Abstr. Pap. Amer. Chem. Soc. Meeting*, **133**, 31 (1958).

14) S. J. Angyal, *Aust. J. Chem.*, **21**, 2737 (1968).
15) S. Wolf, A. Rauk, L. M. Tel, and I. G. Csizmadia, *J. Chem. Soc., B*, **1971**, 126.
16) P. L. Durette and D. Horton, *Advan. Carbohyd. Chem.*, **26**, 49 (1971).
17) V. S. R. Rao, K. S. Vijayalakshmi, and P. R. Sundararajan, *Carbohyd. Res.*, **17**, 341 (1971).
18) K. S. Vijayalaksnmi and V. S. R. Rao, *ibid.*, **22**, 413 (1972).
19) P. R. Sundararajan and V. S. R. Rao, *Tetrahedron*, **24**, 289 (1968).
20) R. A. Scott and H. A. Scheraga, *J. Chem. Phys.*, **42**, 2209 (1965).
21) A. Salinas and J. F. Sproviero, *Carbohyd. Res.*, **16**, 243 (1971).
22) Y. A. Zhadanov, V. I. Minkin, Y. A. Ostroumov, and G. N. Dorofeenko, *ibid.*, **7**, 156 (1968).
23) G. Del Re, B. Pullman, and T. Yonezawa, *Biochem. Biophys. Acta*, **75**, 153 (1963).
24) Y. A. Zhadanov, R. M. Minyaev, and V. I. Minkin, *J. Mol. Struct.*, **16**, 357 (1973).
25) E. L. Eliel, N. L. Allinger, S. J. Angyal, and G. A. Morrison, "Conformational Analysis," John Wiley, New York (1965), Chapter 7.
26) G. A. Jeffrey and R. D. Rosenstein, *Advan. Carbohyd. Chem.*, **19**, 7 (1964).
27) S. Arnott and W. E. Scott, *J. Chem. Soc., Perkin II*, **1972**, 324.
28) S. S. C. Chu and G. A. Jeffrey, *Proc. Roy. Soc., Ser.A*, **285**, 470 (1964).
29) M. Takai, S. Watanabe, T. Ashida, and M. Kakudo, *Acta Crystallogr.*, **B28**, 2370 (1972).
30) L. N. Johnson, *Acta Crystallogr.*, **21**, 885 (1966).
31) R. D. Gilardi and J. L. Flippen, *ibid.*, **B30**, 2931 (1974).
32) J. R. Knox and N. S. Murthy, *ibid.*, **B30**, 365 (1974).
33) L. T. J. Delbaere, *Biochem. J.*, **143**, 197 (1974).
34) M. Sundaralingam, *J. Amer. Chem. Soc.*, **87**, 599 (1965).

Azafulvenes. 2.[1] Formation of Iminium Salt from Pyrrole- and Indolecarbaldehyde and Its Reaction with Bases

Takashi KOBAYASHI, Shoji KAJIGAESHI, and Shuji KANEMASA

Department of Industrial Chemistry, Faculty of Engineering, Yamaguchi University, Tokiwadai, Ube 755

(Received May 12, 1975)

Pyrrole- and indolecarbaldehyde reacted with secondary ammonium perchlorate to produce the corresponding iminium perchlorate, which did not afford azafulvene, but instead its dimer, in good yield by deprotonation. These results indicate that the iminium perchlorate from pyrrole- and indolecarbaldehyde appears to be a convenient precursor of azafulvene.

In a preceding communication, the authors have reported that attempts to isolate 6-amino-1-azafulvene (**1**) from the reactions of pyrrole-2-carbaldehyde with secondary amines were unsuccessful because of a tendency to dimerize thermally. It has also been described that the thermal decomposition of dimer **2** regenerated **1** which was trapped as the corresponding [6+2] cycloadducts with isocyanates and isothiocyanate.[1]

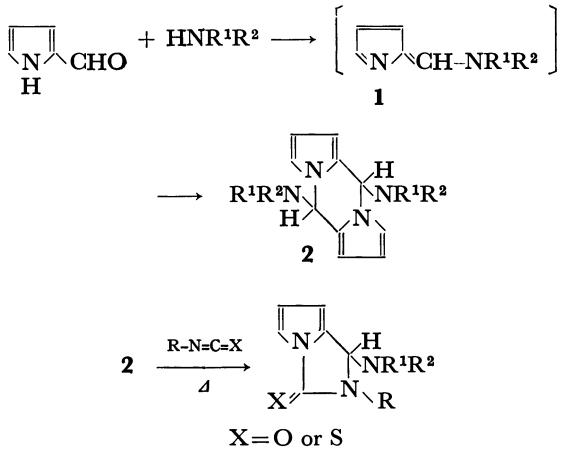

X=O or S

It is well known that an enamine can be protonated to yield a stable iminium salt[2] which is also directly obtainable by the reaction of a carbonyl compound with the secondary ammonium salt.[3] Protonation of **1** containing an enamine system in its molecular structure would probably make itself stable enough to be isolated. Although two structures, iminium salt **A** and azafulvenium salt **B**, are possible as protonated products of **1**, both of them are possible as convenient precursors of 6-amino-1-azafulvene **1**.

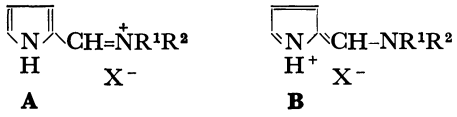

We have investigated which type of salt, iminium or azafulvenium salt, is formed from the reaction of pyrrole-2-, indole-2- and indole-3-carbaldehyde with secondary ammonium perchlorates and also examined whether these salts liberate the corresponding azafulvenes by deprotonation.

Results and Discussion

Preparation of Iminium Perchlorate. The reactions of pyrrole-2-carbaldehyde (**3**) with morpholinium (**4a**) and pyrrolodinium perchlorate (**4b**) in ethanol under refluxing conditions produced colorless prisms, **5a** and **5b**, in 57 and 40% yields, respectively. The molecular formulae of these products agree with those of the compounds derived from the 1:1 adduct with the elimination of water. The IR spectrum of **5a** showed the characteristic band of perchlorate salt at 1100 cm^{-1} and the band assignable to >NH and $-CH=\overset{+}{N}<$ absorption at 3220 and 1640 cm^{-1}, respectively. The compound **5a** exhibited an absorption maximum at 331 nm in its UV spectrum in ethanol and no absorption in the visible region, while it has been reported by Hafner and Pfeiffer[4] that 6,6-diphenyl-1-azafulvenium fluoroborate was of a deep yellow color (λ_{max} in CH_2Cl_2: 413, 363 and 267 nm). The corroborating evidence for the structure of **5a** was afforded by its NMR spectrum in trifluoroacetic acid, which revealed signals at τ 1.59 (1H, s, $-C\underline{H}=\overset{+}{N}<$), 2.38, 2.55 and 3.28 (each 1H, m, pyrrole ring protons) and 5.72 (8H, m, morpholino methylenes). The down field shift of the α-methylene protons of morpholino moiety are based on the electron affinity of the adjacent ammonium nitrogen atom.

From the above UV and NMR data, **5a** was deduced to be, not 6-morpholino-1-azafulvenium perchlorate **B** (X=ClO_4), but 2-pyrrolylmethylenemorpholinium perchlorate **A** (X=ClO_4). The compound **5b** has already been prepared by Sonnet[5] and identified to be *N*-(2-pyrrolylmethylene)pyrrolidinium perchlorate. No formation of azafulvenium salt **B** should occur due to

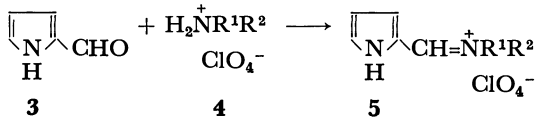

a: R^1R^2= **b**: R^1R^2=

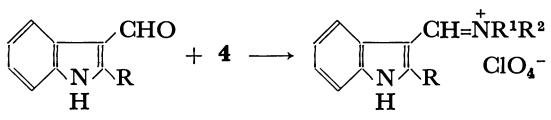

6: R=H
8: R=CH_3

7a: R=H, R^1R^2=
7b: R=H, R^1R^2=
7c: R=H, R^1=R^2=CH_3
9a: R=CH_3, R^1R^2=
9b: R=CH_3, R^1R^2=

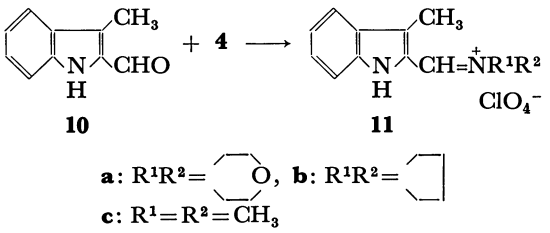

a lack of the stabilizing energy of the pyrrole ring, whereas iminium salt formation does not require any loss of energy.

The reactions of indole-3-carbaldehyde (**6**) with **4a**, **4b** and dimethylammonium perchlorate (**4c**) afforded the respective colorless crystals, **7a**, **7b** and **7c**, in excellent yield which were clearly identified to be 3-indolylmethyleneammonium perchlorates on the basis of their IR, NMR and UV spectra as well as elemental analyses.

Similarly, the corresponding 3-(2-methylindolyl)-methyleneammonium perchlorates, **9a** and **9b**, were obtained on heating 2-methylindole-3-carbaldehyde (**8**) with **4a** and **4b** in ethanol.

Although no reactions of 3-methylindole-2-carbaldehyde (**10**) with **4** took place during ethanol refluxing, **10** reacted with **4** to produce 2-(3-methylindolyl)-methyleneammonium perchlorate (**11**) when heated under reflux with continuous removal of the water formed in the reaction. The structures of **9** and **11** were also established by their spectroscopic results and elemental analyses.

Deprotonation of Iminium Perchlorate. For the purpose of the liberation of aminoazafulvenes, the deprotonation reactions of the iminium perchlorates, **5**, **7**, **9** and **11**, were investigated using bases such as triethylamine, tetramethylguanidine and potassium *tert*-butoxide.

The treatment of **5a** with tetramethylguanidine in ethanol gave pyrrole-2-carbaldehyde **3** which can be derived from the hydrolysis of the starting iminium perchlorate **5a** or 6-morpholino-1-azafulvene **1a** (NR^1R^2=N⟨O⟩). The fact that the iminium perchlorate **5a** considerably resists hydrolysis in ethanol indicates azafulvene **1a** is formed at first in this reaction, followed by hydrolysis into **3**. Therefore, the reaction under anhydrous conditions was carried out and afforded another product **2a** which was identical to the dimer of **1a**, 5,10-dimorpholinodipyrrolo[1,2-*a*: 1′,2′-*d*]pyrazine, obtained by heating **3** with morpholine in benzene.[1]

The new compound **13a**, mp 242—243 °C (decomp.), was yielded quantitatively by the reaction of **11a** with triethylamine in benzene. The molecular formula of **13a** corresponds to the dimer of azafulvene **12a**. The NMR spectrum of **13a** in deuteriochloroform showed two methyls- and two methines-protons at τ 7.64 (6H) and 4.10 (2H) as singlets, respectively. On the basis of the spectral data, **13a** was identified to be 6,13-dihydro-5,12-

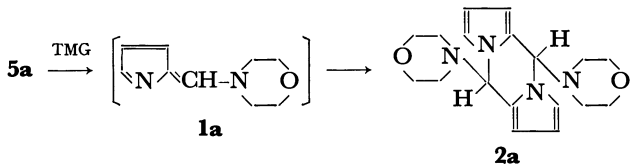

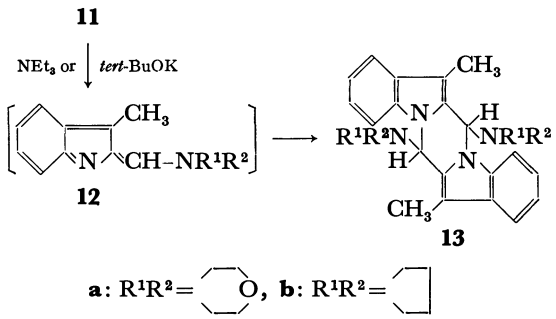

dimethyl-6,13-dimorpholinodiindolo[1,2-*a*: 1′,2′-*d*]-pyrazine.

Two isomers with the methine protons at the 6- and 13-positions of the pyrazine ring are possible for **13a**. Actually, both the *cis* and *trans* isomers have been isolated[1] in the case of the dimer of 6-(*N*-pyrrolidinyl)-1-azafulvene (**1b**), which is analogous to **13a**. The compound **13a** was determined to be the *trans* isomer because of the equivalence of the two methyls-protons and of the two methines-protons in the NMR spectrum.[1] Similarly, *trans*-6,13-dihydro-5,12-dimethyl-6,13-di(*N*-pyrrolidinyl)diindolo[1,2-*a*: 1′,2′-*d*]pyrazine (**13b**) was also obtained in excellent yield by treating **11b** with potassium *tert*-butoxide in benzene, while **11b** could not be deprotonated with triethylamine.

The above results show that 1-azafulvene is formed as an unstable intermediate[6] upon deprotonation of the corresponding iminium perchlorate and dimerized by [6+6] cycloaddition. This cyclodimerization reaction is considered to be reversible.[7] Therefore, the ease of the dimerization is attributable to the large difference between the stabilizing energies of 1-azafulvene and its dimer *via* a resonance. In particular, benzo[*b*]-1-azafulvene **12** has a tendency to change into the dimer **13** owing to the additional *o*-quinoid cyclic system in **12**.

On the other hand, benzo[*c*]-2-azafulvene, which is possible to be derived from the iminium salt **7** or **9**, is expected to be more thermally stable than benzo[*b*]-1-azafulvene. The reaction of **9a** with aqueous sodium hydroxide at −5 °C or with potassium *tert*-butoxide in benzene at room temperature gave a colorless product which was contaminated with 2-methylindole-3-carbaldehyde **8**. This moisture-sensitive product was not isolated in pure form and did not give reliable spectral data. Moreover, reduction with lithium aluminum hydride resulted in hydrolysis into **8**. The quantitative conversion of this product to **8** by the moisture in an atmosphere is explained by the guess that this water-

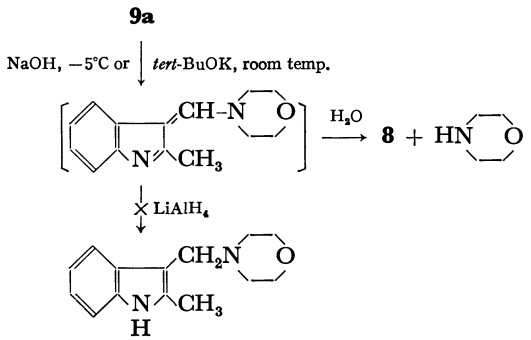

sensitive product is benzo[*c*]-2-azafulvene, which is thermally stable but subject to hydrolysis due to the nature of enamines.

Although similar deprotonation reactions of **7** gave products which did not include any halogen ions, the structures of these products have not yet been clarified.

Experimental

All melting points were determined using a Mitamura Riken micro melting point apparatus and are uncorrected. The IR spectra were taken in KBr disks with a Nihon Bunko IRA-1 spectrometer. The NMR spectra were obtained at 100 MHz using a Nihon Denshi JNM-MH-100 spectrometer with TMS as an internal reference. The mass spectra were determined with a Nihon Denshi JMS-06 mass spectrometer equipped with a direct inlet and at an ionization energy of 75 eV.

Materials. Pyrrole-2-(**3**); mp 44—47 °C, bp 128 °C/20 Torr (lit,[8] bp 78 °C/2 Torr), indole-3-(**6**); mp 193—195 °C (lit,[9] mp 194 °C) and 2-methylindole-3-carbaldehyde (**8**); mp 201—202 °C (lit,[10] mp 202—203 °C) were prepared by the Vilsmeier reaction of the corresponding pyrroles and indoles. 3-Methylindole-2-carbaldehyde (**10**) was obtained by oxidation of 2-(3-methylindolyl)methanol with activated manganese dioxide in a 58% yield; mp 139—141 °C (lit,[11] mp 138—140 °C).

N-*(2-Pyrrolylmethylene)morpholinium Perchlorate (**5a**).* The mixture of 0.95 g (0.01 mol) of **3** and 1.88 g (0.01 mol) of **4a** was heated under reflux in 20 ml of ethanol for 1 hr. On cooling, the precipitated product was filtered and washed with a benzene–ethanol (1:1 vol/vol) mixture giving 1.50 g (57%) of **7a**. Recrystallization from ethanol produced colorless prisms; mp 142—143 °C (decomp.). IR (KBr) cm^{-1}: 3220 (>NH), 1640 (–CH=$\overset{+}{N}$<) and 1100 (ClO_4). NMR (CF_3COOH) τ: 1.59 (1H, s, –C<u>H</u>=$\overset{+}{N}$<), 2.30, 2.47, 3.40 (each 1H, m, pyrrole ring protons) and 5.72 (8H, m, morpholino methylenes). UV (EtOH): 331 nm. Found: C, 40.75; H, 4.74; N, 10.43%. Calcd for $C_9H_{13}N_2O_5Cl$: C, 40.84; H, 4.95; N, 10.58%.

N-*(2-Pyrrolylmethylene)pyrrolidinium Perchlorate (**5b**).* Prepared in the same way as **5a**, starting with 0.95 g of **3** and 1.72 g of **4b** in 20 ml of ethanol. Colorless prisms from ethanol; mp 103—104 °C (decomp.). IR (KBr) cm^{-1}: 3220 (>NH), 1640 (–CH=$\overset{+}{N}$<) and 1100 (ClO_4). NMR (CF_3COOH) τ: 1.65 (1H, s, –C<u>H</u>=$\overset{+}{N}$<), 2.58, 2.82, 3.46 (each 1H, m, pyrrole ring protons), 6.01 and 7.77 (each 4H, m, pyrrolidinyl methylenes). UV (EtOH): 329 nm. Found: C, 43.40; H, 5.14; N, 11.19%. Calcd for $C_9H_{13}N_2O_4Cl$: C, 43.47; H, 5.27; N, 11.27%.

N-*(3-Indolylmethylene)morpholinium Perchlorate (**7a**).* A 1.45 g (0.01 mol) of **6** and 1.88 g (0.01 mol) of **4a** were refluxed in 20 ml of ethanol for 2 hr. After cooling, 2.80 g (89%) of **7a** were precipitated. Recrystallization from ethanol yielded colorless prisms; mp 242—244 °C (decomp.). IR (KBr) cm^{-1}: 3240 (>NH), 1640 (–CH=$\overset{+}{N}$<) and 1100 (ClO_4). NMR (CF_3COOH) τ: 1.31 (1H, s, –C<u>H</u>=$\overset{+}{N}$<), 1.64 (1H, d, 2-H of indole ring), 2.13—2.60 (4H, m, aromatic protons) and 5.66 (8H, m, morpholino methylenes). UV (EtOH): 288 nm. Found: C, 49.55; H, 4.79; N, 8.95%. Calcd for $C_{13}H_{15}N_2O_5Cl$: C, 49.61; H, 4.80; N, 8.90%.

N-*(3-Indolylmethylene)pyrrolidinium Perchlorate (**7b**).* The method used here is virtually identical with that used for **7a**: 1.45 g of **6** and 1.72 g of **4b** were refluxed for 2 hr. Colorless prisms from ethanol; mp 249—250 °C (decomp.). Yield: 2.43 g (81%). IR (KBr) cm^{-1}: 3280 (>NH), 1640 (–CH=$\overset{+}{N}$<) and 1100 (ClO_4). NMR (CF_3COOH) τ: 1.26 (1H, s, –C<u>H</u>=$\overset{+}{N}$<), 1.89 (1H, d, 2-H of indole ring), 2.08—2.68 (4H, m, aromatic protons), 5.95 and 7.64 (each 4H, m, pyrrolidinyl methylenes). UV (EtOH): 352 nm. Found: C, 52.07; H, 4.91; N, 9.40%. Calcd for $C_{13}H_{15}N_2O_4Cl$: C, 52.27; H, 5.06; N, 9.38%.

N-*(3-Indolylmethylene)*-N,N-*dimethylammonium Perchlorate (**7c**)* The same procedure as that for **7a** using 2.9 g of **6** and 2.92 g of **4c** in 40 ml of ethanol afforded 4.44 g (78%) of **7c**; colorless prisms from ethanol; mp 217—220 °C (decomp.). IR (KBr) cm^{-1}: 3260 (>NH), 1640 (–CH=$\overset{+}{N}$<) and 1100 (ClO_4). NMR (CF_3COOH) τ: 1.60 (1H, s, –C<u>H</u>=$\overset{+}{N}$<), 1.96 (1H, d, 2-H of indole ring), 2.24—2.73 (4H, m, aromatic protons), 6.28 and 6.50 (each 3H, s, =$\overset{+}{N}$(C<u>H</u>$_3$)$_2$). Found: C, 48.82; H, 4.82; N, 10.07%. Calcd for $C_{11}H_{13}N_2O_4Cl$: C, 48.63; H, 4.82; N, 10.31%.

N-*(2-Methyl-3-indolylmethylene)morpholinium Perchlorate (**9a**).* To the stirred suspension of **8** (3.2 g, 0.02 mol) in 40 ml of ethanol was added 3.76 g (0.02 mol) of **4a** and which were refluxed for 2 hr. On cooling, **9a** (6.34 g, 98%) was filtered and recrystallized from ethanol to give colorless prisms, mp 248—249 °C (decomp.). IR (KBr) cm^{-1}: 3280 (>NH), 1640 (–CH=$\overset{+}{N}$<) and 1100 (ClO_4). NMR (CF_3COOH) τ 1.48 (1H, s, –C<u>H</u>=$\overset{+}{N}$<), 2.36—2.67 (4H, m, aromatic protons), 5.65 (8H, m, morpholino methylenes) and 7.23 (3H, s, –C<u>H</u>$_3$). UV (EtOH): 289 nm. Found: C, 51.65; H, 5.05; N, 8.54%. Calcd for $C_{14}H_{17}N_2O_5Cl$: C, 51.15; H, 5.21; N, 8.52%.

N-*(2-Methyl-3-indolylmethylene)pyrrolidinium Perchlorate (**9b**).* The same method as that for **9a** starting from **8** (1.59 g) and **4b** (1.72 g) gave 2.31 g (74%) of **9b**; colorless prisms from ethanol; mp 238—239 °C (decomp.). IR (KBr) cm^{-1}: 3250 (>NH), 1640 (–CH=$\overset{+}{N}$<) and 1100 (ClO_4). NMR (CF_3COOH) τ: 1.67 (1H, s, –C<u>H</u>=$\overset{+}{N}$<), 2.21—2.78 (4H, m, aromatic protons), 5.84, 7.74 (each 4H, m, pyrrolidinyl methylenes) and 7.32 (3H, s, –C<u>H</u>$_3$). UV (EtOH): 344 nm. Found: C, 54.09; H, 5.46; N, 9.04%. Calcd for $C_{14}H_{17}N_2O_4Cl$: C, 53.77; H, 5.48; N, 8.96%.

N-*(3-Methyl-2-indolylmethylene)morpholinium Perchlorate (**11a**).* A heterogeneous mixture of **10** (1.1 g, 0.069 mol), **4a** (1.3 g, 0.069 mol) and 3 drops of morpholine in 100 ml of benzene was heated under reflux for 5 hr with stirring, while water was continuously removed by means of Dean-Stark trap. The separated solid was collected by filtration, washed with a small amount of ethanol. Colorless prisms from ethanol; mp 240—242 °C (decomp.). Yield: 1.82 g (80%). IR(KBr) cm^{-1}: 3320 (>NH), 1630 (–CH=$\overset{+}{N}$<) and 1100 (ClO_4). NMR (CF_3COOH) τ: 1.57 (1H, s, –C<u>H</u>=$\overset{+}{N}$<), 2.26—2.90 (4H, m, aromatic protons), 5.64 (8H, m, morpholino methylenes) and 7.36 (3H, s, –C<u>H</u>$_3$). Found: C, 51.20; H, 5.63; N, 8.74%. Calcd for $C_{14}H_{17}N_2O_5Cl$: C, 51.15; H, 5.21; N, 8.52%.

N-*(3-Methyl-2-indolylmethylene)pyrrolidinium Perchlorate (**11b**).* The similar procedure to that of **11a** using 1.2 g of **10**, 1.29 g of **4b** and 3 drops of pyrrolidine, but being refluxed for 10 hr, gave 2.13 g (91%) of **11b**. Recrystallization from ethanol afforded colorless prisms; mp 265—266 °C (decomp.). IR (KBr) cm^{-1}: 3320 (>NH), 1630 (–CH=$\overset{+}{N}$<) and 1100 (ClO_4). NMR (CF_3COOH) τ:1.43 (1H, s, –C<u>H</u>=$\overset{+}{N}$<), 2.18—2.81

(4H, m, aromatic protons), 5.72, 7.68 (each 4H, m, pyrrolidinyl methylenes) and 7.33 (3H, s, $-C\underline{H}_3$). Found: C, 53.51; H, 5.84; N, 8.87%. Calcd for $C_{14}H_{17}N_2O_4Cl$: C, 53.77; H, 5.48; N, 8.96%.

*N-(3-Methyl-2-indolylmethylene)-N,N-dimethylammonium Perchlorate (**11c**).* A mixture of **10** (0.31 g), **4c** (0.28 g) and a few drops of dimethylamine was refluxed in 70 ml of benzene for 17 hr to give 0.34 g (60%) of **11c**. Colorless prisms from ethanol; mp 257 °C (decomp.). IR (KBr) cm^{-1}: 3325 (>NH), 1640 ($-CH=\overset{+}{N}<$) and 1100 (ClO_4). NMR (CF_3COOH) τ: 1.55 (1H, s, $-C\underline{H}=\overset{+}{N}<$), 2.12—2.78 (4H, m, aromatic protons), 6.06, 6.14 (each 3H, s, $=\overset{+}{N}(C\underline{H}_3)_2$) and 7.28 (3H, s, $-C\underline{H}_3$).

*The Reaction of **5a** with Tetramethylguanidine.* To the suspension of **5a** (0.27 g) in 5 ml of dry tetrahydrofuran was added 0.12 g of tetramethylguanidine which was stirred at room temperature for 10 min. The resulting solution was dried *in vacuo*, and the residue was washed with water and then dried. Recrystallization from methanol gave 0.16 g (95%) of 5,10-dihydro-5,10-dimorpholinodipyrrolo[1,2-*a*: 1′,2′-*d*]-pyrazine (**2a**), mp 190—193 °C (decomp.) (lit,[1] mp 190—193 °C (decomp.)).

*The Reaction of **11a** with Triethylamine.* 1.0 g of **11a** was suspended in 6 ml of dry benzene added to an excess of triethylamine. After refluxing for 3 hr, benzene was evaporated to give a colorless powder which was washed with water. Recrystallization from ether gave colorless needles of 6,13-dihydro-5,12-dimethyl-6,13-dimorpholinodiindolo-[1,2-*a*: 1′,2′-*d*]pyrazine (**13a**), mp 242—243 °C (decomp.). Yield 0.7 g (100%). NMR ($CDCl_3$) τ: 2.44—2.96 (8H, m, aromatic protons), 4.10 (2H, s, $>C\underline{H}$–N<), 6.38, 7.16 (each 8H, m, morpholino methylenes) and 7.64 (6H, s, $-C\underline{H}_3$). Mass (*m/e*): 456 (M^+), 370 $\left(M^+-\text{N}\langle\rangle\text{O}\right)$, 284 $\left(370^+-\text{N}\langle\rangle\text{O}\right)$ and 228 (M^{2+}). Found: C, 74.23; H, 6.96; N, 11.99%. Calcd for $C_{24}H_{32}N_4O_2$: C, 73.66; H, 7.06; N, 12.27%.

*The Reaction of **11b** with Potassium* tert*-Butoxide.* The mixture of 0.9 g of **11b**, 0.35 g of potassium *tert*-butoxide in 30 ml of dry benzene was refluxed for 5 hr. The residue obtained by evaporation was washed with water to yield 0.43 g (70%) of 6,13-dihydro-5,12-dimethyl-6,13-(*N*-pyrrolidinyl)diindolo[1,2-*a*: 1′,2′-*d*]pyrazine (**13b**), mp 204—205 °C (decomp.). Colorless prisms from ether. NMR ($CDCl_3$) τ: 2.40—3.00 (8H, m, aromatic protons), 3.76 (2H, s, $>C\underline{H}$–N<), 7.13, 8.32 (each 8H, m, pyrrolidinyl methylenes) and 7.62 (6H, s, $-C\underline{H}_3$). Mass (*m/e*): 424 (M^+), 354 $\left(M^+-\text{N}\langle\rangle\right)$, 284 $\left(354^+-\text{N}\langle\rangle\right)$ and 212 (M^{2+}). Found: C, 79.81; H, 8.16; N, 12.97%. Calcd for $C_{24}H_{32}N_4$: C, 79.20; H, 7.60; N, 13.20%.

*The Reaction of **9a** with Aqueous Sodium Hydroxide.* The suspension of 0.62 g of **9a** in 10 ml of methylene dichloride was cooled to −5 °C with ice-salt and then 10 ml of a 10% sodium hydroxide solution was added dropwise under vigorous stirring. As soon as the addition was completed, the organic layer was separated and dried with anhydrous magnesium sulfate. Evaporation of the solvent below 20 °C gave 0.40 g of colorless crystals, which were tentatively assigned to be 3-morpholinomethylene-2-methyl-3*H*-indole.

References

1) Part 1 of this series: M. Watanabe, T. Kobayashi, S. Kajigaeshi, and S. Kanemasa, *Chem. Lett.*, **1975**, 607.
2) J. V. Pauksteilis, "Enamines," ed. by A. G. Cook, Marcel Dekker, New York and London (1969), p. 169.
3) N. J. Leonard and J. V. Pauksteilis, *J. Org. Chem.*, **28**, 3021 (1963).
4) K. Hafner and K. Pfeiffer, *Tetrahedron Lett.*, **1968**, 4311.
5) P. E. Sonnet, *J. Org. Chem.*, **37**, 925 (1972).
6) Unpublished results: 1-azafulvene generated by deprotonation of the iminium perchlorates were trapped as corresponding [6+2] cycloadducts with isocyanate, ketene and sulfene.
7) The dimer of 6-amino-1-azafulvene regenerates its original azafulvene on pyrolysis: see Ref. 1.
8) R. M. Silverstein, E. E. Ryskiewicz, C. Willard, and R. Koehler, *J. Org. Chem.*, **20**, 668 (1955).
9) G. F. Smith, *J. Chem. Soc.*, **1954**, 3842.
10) G. Barger and A. J. Evins, *Biochem. J.*, **11**, 59 (1917).
11) A. Chatterjee and K. M. Biswas, *J. Org. Chem.*, **38**, 4002 (1973).

Cycloaddition Reactions of *N*-Sulfinylsulfonamides with Ketenimines

Toru MINAMI, Futoshi TAKIMOTO, and Toshio AGAWA

Department of Petroleum Chemistry, Faculty of Engineering, Osaka University, Yamadakami, Suita, Osaka 565

(Received May 16, 1975)

N-Sulfinylsulfonamides, **1a, b**, reacted with ketenimines, **2**, in ether to give the unstable [2+2] cycloadducts, 3-ylidene-1,2,4-thiadiazetidin-1-oxides, **3**, which were then readily hydrolyzed to the *N,N'*-disubstituted amidine derivative, **4**, in good yields. The reaction of *N*-sulfinylmethanesulfonamide (**1b**) with diphenylketen-*N*-*p*-tolylimine (**2d**) at 130 °C gave the exchange product, *N*-sulfinyl-*p*-toluidine (**5**) in a 70% yield *via* the intermediate cycloadduct. In contrast to **2d**, the reaction of *N*-sulfinyl-*p*-toluenesulfonamide (**1a**) and phenylethylketen-*N*-phenylimine (**2f**), under the same conditions, led to the formation of a mixture of *N*-phenyl-*N'*-*p*-toluenesulfonyl-2-phenyl-*trans*- (**6a**) and *cis*-2-butenoamidine (**6b**) in an 81% yield.

We previously demonstrated that *N*-sulfinylamines react with heterocumulenes, such as isocyanate and isothiocyanate, to give exchange products *via* the intermediate [2+2] cycloadducts.[1,2]

However, recently we reported that, in contrast to the above heterocumulenes, carbodiimides afford the unstable [2+2] cycloadducts in reactions with *N*-sulfinylsulfonamides.[3] In the course of such studies of the chemical reactivities of *N*-sulfinylamines, we have observed that the reactions with ketenimines similarly yield the corresponding unstable cycloadducts. We wish to report here on the structures of the cycloadducts and their reactivities.

Results and Discussion

N-Sulfinyl-*p*-toluenesulfonamide (**1a**) was allowed to react with dimethylketen-*N*-phenylimine (**2a**) at the ambient temperature in ether to give, smoothly, a 1:1 cycloadduct, **3a**, which was precipitated on standing in a 79% yield. The infrared spectrum exhibits the characteristic absorption bands for the C=C group and the S=O group at 1580 and 1090 cm^{-1} respectively. The mass spectrum shows the molecular ion at *m/e* 362 and the fragment ions at 223 and 139 due to ($Me_2C{=}C{=}NTs^+$) and ($PhNSO^+$). The NMR spectrum ($CDCl_3$) indicates two singlet isopropylidene methyl (6H), *p*-methyl (3H), and phenyl protons (9H) at 1.94 and 2.00, 2.40, and 7.20—7.96 ppm respectively. Thus, the structure of **3a** was identified as 2-*p*-toluenesulfonyl-3-isopropylidene-4-phenyl-1,2,4-thiadiazetidin 1-oxide. Furthermore, this structure was confirmed by the hydrolysis of **3a** to *N*-phenyl-*N'*-*p*-toluenesulfonyl-isobutyramidine (**4a**) in a good yield.

The reaction of *N*-sulfinylmethanesulfonamide (**1b**) with **2a** similarly afforded the [2+2] cycloadduct **3b** in an 85% yield.

However, in the reactions of **1a** (or **1b**) with other ketenimines, **2b**—**e**, the expected cycloadducts, **3**, could not be isolated in pure forms since they are unstable and are readily hydrolyzed to the corresponding amidines, **4b**—**e**. The physical and analytical data and the yields of the cycloadducts and the amidines obtained above are shown in Table 1.

No 1:2-cycloadduct was obtained in any of the above reactions nor in the reactions between *N*-sulfinylsulfonamides and carbodiimides,[3] although the 1:2-cycloadducts are well known to be formed in the reactions of

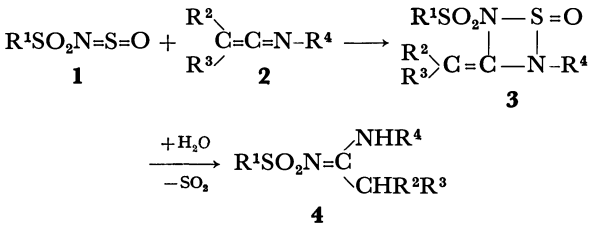

1a, R^1=*p*-MeC_6H_4
1b, R^1=Me
2a, R^2=R^3=Me, R^4=Ph
2b, R^2=R^3=Me, R^4=*p*-MeC_6H_4
2c, R^2=R^3=Me, R^4=C_6H_{11}
2d, R^2=R^3=Ph, R^4=*p*-MeC_6H_4
2e, R^2=H, R^3=Ph, R^4=C_6H_{11}

3a, R^1=*p*-MeC_6H_4, R^2=R^3=Me, R^4=Ph
3b, R^1=R^2=R^3=Me, R^4=Ph
4a, R^1=*p*-MeC_6H_4, R^2=R^3=Me, R^4=Ph
4b, R^1=*p*-MeC_6H_4, R^2=R^3=Me, R^4=*p*-MeC_6H_4
4c, R^1=*p*-MeC_6H_4, R^2=R^3=Me, R^4=C_6H_{11}
4d, R^1=R^4=*p*-MeC_6H_4, R^2=R^3=Ph
4e, R^1=Me, R^2=H, R^3=Ph, R^4=C_6H_{11}

Scheme 1.

TABLE 1. 3-YLIDENE-1,2,4-THIADIAZETIDIN 1-OXIDES **3** AND AMIDINES **4** FROM *N*-SULFINYLSULFONAMIDES **1** AND KETENIMINES **2**

3 or 4	Substituents				Yield %	Mp °C	Formula	Calcd %			Found %		
	R^1	R^2	R^3	R^4				C	H	N	C	H	N
3a	*p*-MeC_6H_4	Me	Me	Ph	79	117	$C_{17}H_{18}N_2O_3S_2$	56.35	5.01	7.73	56.07	5.23	7.88
3b	Me	Me	Me	Ph	85	125	$C_{11}H_{14}N_2O_3S_2$	46.15	4.93	9.79	46.31	4.84	9.86
4a	*p*-MeC_6H_4	Me	Me	Ph	78	84	$C_{17}H_{20}N_2O_2S$	64.54	6.37	8.86	64.21	6.47	8.72
4b	*p*-MeC_6H_4	Me	Me	*p*-MeC_6H_4	78	128	$C_{18}H_{22}N_2O_2S$	65.44	6.71	8.48	65.52	6.77	8.40
4c	*p*-MeC_6H_4	Me	Me	C_6H_{11}	58	127	$C_{17}H_{26}N_2O_2S$	63.33	8.13	8.69	63.23	8.24	8.56
4d	*p*-MeC_6H_4	Ph	Ph	*p*-MeC_6H_4	85	168	$C_{28}H_{26}N_2O_2S$	73.99	5.77	6.16	74.01	5.73	6.19
4e	Me	H	Ph	C_6H_{11}	77	187	$C_{15}H_{22}N_2O_2S$	61.20	7.53	9.52	61.13	7.61	9.66

carbodiimides with isocyanates.[4] Therefore, in contrast to the reactions between carbodiimides and isocyanates, the cycloaddition reactions of *N*-sulfinylsulfonamides with heterocumulenes can be said probably to proceed *via* a concerted mechanism rather than *via* a step-by-step mechanism, although further kinetic evidence is necessary for the establishment of the mechanism.

A reaction using *N*-sulfinylarylamines or *N*-sulfinylalkylamines in place of reactive *N*-sulfinylsulfonamides afforded no cycloadduct.

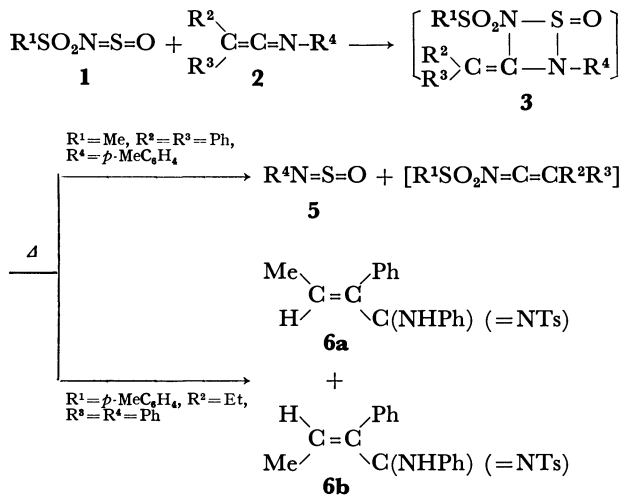

Scheme 2.

On the other hand, the reaction of **1b** with diphenylketen-*N*-*p*-tolylimine (**2d**) at 130 °C for 1 hr under reduced pressure gave *N*-sulfinyl-*p*-toluidine (**5**) as a volatile liquid, which is an exchange product *via* the intermediate cycloadduct, in a 70% yield along with the residual polymeric product. However, the similar treatment of a mixture of **1a** and phenylethylketen-*N*-phenylimine (**2f**) containing hydrogen on the α carbon resulted in the formation of a mixture of *N*-phenyl-*N'*-*p*-toluenesulfonyl-2-phenyl-*trans*- (**6a**) and *cis*-2-butenoamidine (**6b**), the ratio of which was found by NMR to be approximately 5: 3, in an 81% yield. Their formations could be explained in terms of the elimination of sulfur monoxide from the [2+2] cycloadduct, **3**, which would be initially yielded from **1a** and **2f**, followed by a proton shift on the delocalized anionic nitrogen moiety. Such thermal decomposition is of interest since similar results have not been observed in the reactions of *N*-sulfinylamines with other heterocumulenes.

Experimental

All the melting points were determined with a Yanagimoto micro melting apparatus and are uncorrected. The NMR spectra were obtained on a JEOL LMM 3H-60 spectrometer, with tetramethylsilane as the internal standard. The IR spectra were recorded with a Jasco IR-E spectrometer. The mass spectra were taken with a Hitachi RMU-6E spectrometer.

Materials. The *N*-sulfinyl-*p*-toluenesulfonamide,[5] *N*-sulfinylmethanesulfonamide,[5] dimethylketen-*N*-phenyl-,[6] -*N*-*p*-tolyl-,[6] and -*N*-cyclohexyl-,[6] phenyl-*N*-cyclohexyl-,[6] and diphenyl-*N*-*p*-tolylketenimines[7] were prepared according to the established procedures.

2-p-Toluenesulfonyl-3-isopropylidene-4-phenyl-1,2,4-thiadiazetidin 1-Oxide (3a). Dimethylketen-*N*-phenylimine (**2a**, 1.02 g, 7 mmol) in 20 ml of dry ether was added, drop by drop, into a solution of 1.52 g (7 mmol) of *N*-sulfinyl-*p*-toluenesulfonamide (**1a**) in 30 ml of dry ether. After being stirred at the ambient temperature for 1 hr, the solution was allowed to stand overnight to give 2.0 g (79%) of a white solid, **3a**. Recrystallization from hexane–benzene afforded the analytical sample; mp 117—119 °C; IR (Nujol) ν 1600, 1580 (C=C), 1300 (SO_2), 1155 (SO_2), and 1090 cm^{-1} (SO); NMR ($CDCl_3$) δ 1.94 (s, 3H, $\underline{Me}>C=C<$), 2.00 (s, 3H, $\underline{Me}>C=C<$), 2.40 (s, 3H, $\underline{Me}Ar$), and 7.20—7.96 (m, 9H, phenyl protons); mass spectrum (70 eV) *m/e* 362 (M^+), 314 (M^+-SO), 223 (Me_2CCNTs^+), 145 (Me_2CCNPh^+), and 139 ($PhNSO^+$).

2-Methanesulfonyl-3-isopropylidene-4-phenyl-1, 2, 4-thiadiazetidin 1-Oxide (3b). This substance was prepared in the same way as **3a** by the reaction of **2a** (1.45 g, 0.01 mol) with *N*-sulfinylmethanesulfonamide (**1b**, 1.41 g, 0.01 mol). After the removal of the solvent, the resulting residue was recrystallized from hexane–benzene to give 2.45 g, (85%) of pure **3b**; mp 125—126 °C; IR (Nujol) ν 1600 (C=C), 1290 (SO_2), 1160 (SO_2), and 1130 cm^{-1} (SO); NMR ($CDCl_3$) δ 1.90 (s, 3H, $\underline{Me}>C=C<$), 1.95 (s, 3H, $\underline{Me}>C=C<$), 3.10 (s, 3H, $\underline{Me}SO_2$), and 7.25—7.75 (m, 5H, phenyl protons); mass spectrum (70 eV) *m/e* 286 (M^+), 238 (M^+-SO), 159 (M^+-MeSO_2), and 147 ($Me_2CCNSO_2Me^+$).

Base Catalyzed Hydrolysis of 3a. A solution of **3a** (1.09 g, 3 mmol) in 95% ethanol (20 ml) containing sodium hydroxide (0.12 g, 3 mmol) was refluxed for 1 hr. After the removal of the solvent, the residue was washed with water and then dried. The white solid thus obtained was recrystallized from ethanol to give pure *N*-phenyl-*N'*-*p*-toluenesulfonylisobutyramidine (**4a**, 0.74 g, 78%); mp 84—86 °C; IR (Nujol) ν 3240 (NH), 1560 (C=N), 1525 (NH), 1250 (SO_2), and 1135 cm^{-1} (SO_2); NMR ($CDCl_3$) δ 0.85—1.35 (m, 6H, methyl protons), 2.40 (s, 3H, $\underline{Me}Ar$), 3.60 (q, J=7 Hz, 1H, methine proton), 6.95—7.95 (m, 9H, phenyl protons), and 9.50—10.10 (broad, 1H, NH); mass spectrum (70 eV) *m/e* 316 (M^+), 247 ($TsNHPh^+$), and 224 (M^+-PhNH).

Reactions of N-Sulfinylsulfonamides, 1a—b, with Ketenimines, 2b—e. These reactions were carried out in a similar manner. After similar treatments, the cycloadducts corresponding to **3a** (or **3b**) could not be isolated in pure forms because of their easy hydrolysis. Therefore, the reaction products were chromatographed on alumina to give the amidine derivatives, **4b—e**, which are hydrolysis products, in good yields, as is shown in Table 1. The amidines, **4b—e**, had the following physical properties:

N-p-*Tolyl*-N'-p-*toluenesulfonyl-isobutyramidine (4b)*: IR (Nujol) ν 3280 (NH), 1560 (C=N), 1525 (NH), 1250 (SO_2), and 1135 cm^{-1} (SO_2); NMR ($CDCl_3$) δ 0.85—1.35 (broad d, 6H, methyl protons), 2.34 (s, 3H, $\underline{Me}Ar$), 2.40—2.90 (m, 4H, $\underline{Me}Ar$ and methine proton), 6.90—7.95 (m, 8H, phenyl protons), and 9.10—9.40 (broad, 1H, NH); mass spectrum (70 eV) *m/e* 330 (M^+), and 261 ($TsNHC_6H_4Me^+$).

N-*Cyclohexyl*-N'-p-*toluenesulfonyl-isobutyramidine (4c)*: IR (Nujol) ν 3290 (NH), 1570 (C=N), 1530 (NH), 1260 (SO_2), and 1130 cm^{-1} (SO_2); NMR ($CDCl_3$) δ 1.0—2.05 (m, 16H, two methyl and cyclohexyl protons), 2.40 (s, 3H, $\underline{Me}Ar$), 2.50—2.90 (m, 1H, methine proton), 3.50—3.90 (m, 1H, methine proton), 5.50—5.90 (broad, 1H, NH), and 7.05—7.85 (dd, 4H, phenyl protons); mass spectrum (70 eV) *m/e* 322 (M^+) and 241 ($TsNHC_6H_9^+$).

N-p-*Tolyl*-N'-p-*toluenesulfonyldiphenylacetamidine (4d)*: IR

(Nujol) ν 3200 (NH), 1570 (C=N), 1510 (NH), 1270 (SO_2), and 1130 cm^{-1} (SO_2); NMR ($CDCl_3$) δ 2.35 (s, 6H, methyl protons), 5.03 (s, 1H, methine proton), 6.80—7.70 (m, 18H, phenyl protons), and 9.55—9.85 (broad, 1H, NH); mass spectrum (70 eV) *m/e* 454 (M^+).

N-*Cyclohexyl*-N'-*methanesulfonyl-phenylacetamidine (4e)*: IR (Nujol) ν 3220 (NH), 1555 (C=N), 1540 (NH), 1270 (SO_2), and 1140 cm^{-1} (SO_2); NMR (DMSO-d_6) δ 1.0—2.15 (m, 12H), 2.80 (s, 3H, methyl protons), 3.25—3.40 (broad, 1H, methine proton), 3.65—4.10 (broad, 1H, NH), and 7.40—8.05 (m, 5H, phenyl protons); mass spectrum (70 eV) *m/e* 294 (M^+).

Exchange Reaction between ***1b*** *and Diphenylketen*-N-p-*tolylimine (2d)*. To 0.71 g (5 mmol) of **1b** in 20 ml of ether, we added, drop by drop, 1.42 g (5 mmol) of **2d** in 10 ml of ether. After the subsequent evaporation of the solvent under reduced pressure, the vacuum distillation of the residue at 130 °C for 1 hr under reduced pressure (15 mmHg) yielded 0.54 g (70%) of *N*-sulfinyl-*p*-tolylamine (**5**), whose structure was determined by a comparison of its IR spectrum and glpc behavior with those of an authentic sample.[8] No identification of the residue was attempted.

N-*Phenyl*-N'-p-*toluenesulfonyl-2-phenyl-2-butenoamidine (6)*.

The reaction mixture of **1a** (2.17 g, 0.01 mol) with phenylethylketen-*N*-phenylimine (**2f**, 2.21 g, 0.01 mol) was similarly thermolyzed. The crude product was recrystallized from ethanol to give a mixture (3.13 g, 81%) of *N*-phenyl-*N'*-*p*-toluenesulfonyl-2-phenyl-*trans*- (**6a**) and *cis*-2-butenoamidine (**6b**), whose ratio was determined by means of its NMR spectrum. The attempted isolation of pure samples of individual **6a** and **6b** was unsuccessful. The analytical and physical data of the product are as follows.

Mp 185—187 °C; IR (Nujol) ν 3260 (NH), 1565, 1510, 1275 (SO_2), and 1180 cm^{-1} (SO_2); NMR ($CDCl_3$) δ 1.70 (d, J=6 Hz, 3H, $\underline{Me}\rangle C{=}C\langle^{Ph}$), 1.82 (d, J=6 Hz, 3H, $\underline{Me}\rangle C{=}C\langle^{Ph}$), 2.32 (s, 3H, $\underline{Me}$Ar), 2.44 (s, 3H, $\underline{Me}$Ar), 5.80—6.25 (m, J=6 Hz, 1H, $^{\underline{H}}_{Me}\rangle C{=}C\langle_{Ph}$ and $^{Me}_{\underline{H}}\rangle C{=}C\langle_{Ph}$), 6.75—8.0 (m, 14H, phenyl protons), and 10.0—10.25 (broad, 1H, NH); mass spectrum (70 eV) *m/e* 390 (M^+), 247 ($PhNHTs^+$) and 235 (M^+-Ts).

Financial support from the Takeda Science Foundation is gratefully acknowledged.

References

1) T. Minami, H. Miki, and T. Agawa, *Kogyo Kagaku Zasshi*, **70**, 1831 (1967).

2) T. Minami and T. Agawa, *Tetrahedron Lett.*, **1968**, 2651.

3) T. Minami, M. Fukuda, M. Abe, and T. Agawa, This Bulletin, **46**, 2156 (1973).

4) H. Ulrich, B. Tucker, F. A. Stuber, and A. A. R. Sayigh, *J. Org. Chem.*, **43**, 2250 (1969).

5) G. Kresze and W. Wucherphennig, *Angew. Chem.*, **79**, 109 (1967).

6) C. L. Stevens and J. C. French, *J. Amer. Chem. Soc.*, **76**, 4398 (1954).

7) C. L. Stevens and G. H. Singhal, *J. Org. Chem.*, **29**, 34 (1964).

8) D. Klamann, C. Sass, and M. Zelenka, *Chem. Ber.*, **92**, 1910 (1959).

Chemistry of Nitrosoimines. X.[1] Reactions of 3-Substituted 2-Nitrosoimino-2,3,-dihydrobenzothiazoles with Aryl and *t*-Butyl Grignard Reagents

Kin-ya AKIBA, Takayuki KAWAMURA, Motoyuki HISAOKA, and Naoki INAMOTO

Department of Chemistry, Faculty of Science, The University of Tokyo, Hongo, Tokyo 113

(Received May 20, 1975)

3-Substituted 2-nitrosoimino-2,3-dihydrobenzothiazoles (**1**) react with arylmagnesium bromide to give 3-substituted 2,2-diaryl-2,3-dihydrobenzothiazoles as the major product and 2-*N'*-arylhydrazono-2,3-dihydrobenzothiazoles as a minor product. **1** reacts also with *t*-butylmagnesium chloride to give 3-substituted 2-*t*-butyl- and 2-*N'*-*t*-butylhydrazono-2,3-dihydrobenzothiazoles and 2,3-dihydrobenzothiazol-2-one. Reaction of **1** with mesitylmagnesium bromide gave a similar result to that with *t*-butylmagnesium chloride.

Simple nitrosoimines are thermally unstable and apt to decompose unimolecularly to the corresponding carbonyl compounds and nitrogen. Sterically hindered nitrosoimines have been prepared as rather unstable compounds, some of their reactions being reported.[2] Resonance-stabilized nitrosoimines were found to be considerably unstable. 2-Nitroso-1,1,3,3-tetraphenyl guanidine is the only one compound which gave correct elemental analysis.[3]

On the other hand, nitrosoimines are known to be stable when the nitrosoimino group is contained in heterocycles such as benzothiazole, 1,2,4-thiadiazole,[4] and 1,3,4-thiadiazole.[5]

We have chosen 3-substituted 2-nitrosoimino-2,3-dihydrobenzothiazole (**1**) as a model and investigated reactions of **1** with nucleophiles such as Grignard reagents,[6] lithium aluminum hydride,[1,7] organolithiums,[8] and Grignard type and lithium reagents of 3-substituted 2-imino-2,3-dihydrobenzothiazoles.[9] Preliminary results have been interpreted to be due to large contribution of an ambident character to **1**.

We recently obtained direct evidence for the contribution of ambident structures (**1'**, **1''** and **1'''**) to the ground state of **1** by UV[3] and ESCA study.[10a]

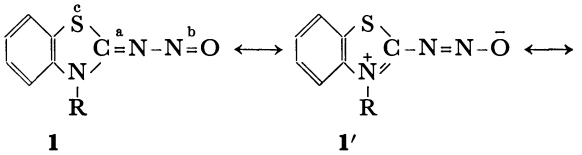

1 **1'**

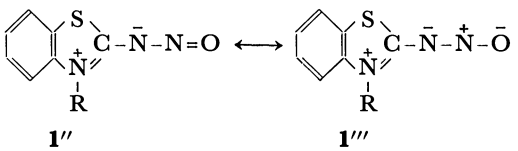

1'' **1'''**

a, R=Me, **b**, R=Ph, **c**, R=Et

The result suggests that **1** has three possible reactive centers for nucleophiles, *i.e.*, the C-2 position of the ring (a), the nitrogen atom of the nitroso group (b), and the sulfur atom of the ring (c). We investigated the reactions of **1** with Grignard reagents and organolithiums.

From an investigation on the chemistry of nitrosoimines to prepare and investigate the nature of the nitrosoimino group, a new functionality, studies were turned to reactions of nucleophiles toward ambident cation (**1**). In this connection, it is necessary to mention the extensive studies on cyclic azosulfones by Hünig.[10b] He mainly studied the oxidative coupling of azosulfones with active methylenes and phenols, paying attention to the ambident nature of quaternary salts of azosulfones. A couple of reactions of 2-azido-3-ethylbenzothiazolium ions with nucleophiles have recently been interpreted by means of HSAB principle as the nucleophilic addition of bases to ambident aromatic cations.[10c] This paper describes the reactions of **1** with arylmagnesium and *t*-butylmagnesium halides.

Excess phenylmagnesium bromide reacted with 2-nitrosoimino-3-phenyl-2,3-dihydrobenzothiazole (**1b**) in ether at 0 °C under nitrogen to give 2,2,3-triphenyl-2,3-dihydrobenzothiazole (**2b**, 48%), a small amount of bis(*o*-anilinophenyl) disulfide (**3b**) and 3-phenyl-2-*N'*-phenylhydrazono-2,3-dihydrobenzothiazole (**4b**, 17%).

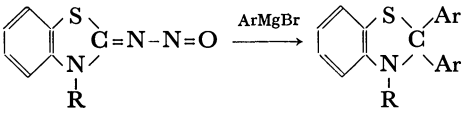

1 **2** Ar=Ph; **6** Ar=*p*-MeC$_6$H$_4$

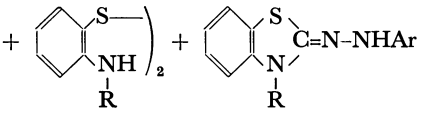

a, R=Me; **b**, R=Ph — **3** — **4** Ar=Ph; **7** Ar=*p*-MeC$_6$H$_4$

The structures of **2b** and **4b** were confirmed by elemental analyses, NMR, IR and MS. The structure of **3b** was confirmed by comparing the spectral data with those of an authentic sample[11] prepared from 3-phenyl-2,3-dihydrobenzothiazol-2-one (**5b**) and potassium hydroxide.

A similar reaction with 3-methyl derivative (**1a**) gave the corresponding **2a** (22%), **3a** (5%), and **4a** (*ca.* 15%), but **4a** could not be sufficiently purified for elemental analysis.

p-Tolylmagnesium bromide reacted with **1a** to afford 3-methyl-2,2-bis(*p*-tolyl)-2,3-dihydrobenzothiazole (**6a**, 66%) and 3-methyl-2-*N'*-*p*-tolylhydrazono-2,3-dihydrobenzothiazole (**7a**, 12%), and with **1b** to give the corresponding **6b** (50%) and **7b** (8%).

Reactions of **1a** were also carried out, but separation of the reaction products was unsuccessful. In particular,

fractions containing mainly *N'*-arylhydrazono type compounds were unstable in the atmosphere, gradually producing a purple red tar.

Mesitylmagnesium bromide reacted with **1a** in a similar manner to give 2-mesityl- (**8**, 46%) and 2-*N'*-mesitylhydrazono-3-methyl-2,3-dihydrobenzothiazoles (**9**, 18%), and 3-methyl-2,3-dihydrobenzothiazol-2-one (**5a**, 10%).

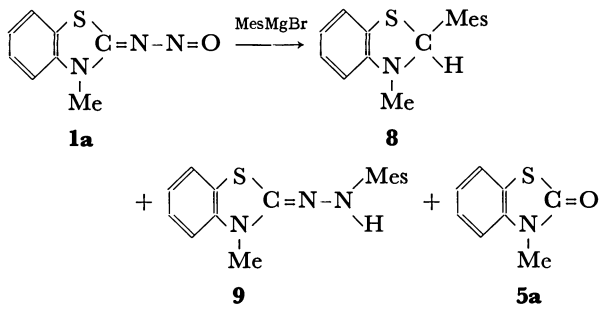

1a **8** **9** **5a**

The formation of 2-monosubstituted compound (**8**) is in contrast to that of 2,2-disubstituted compounds (**2** and **6**) in the case of phenyl and *p*-tolyl Grignard reagents. The difference is attributable to the difference of the bulkiness of Grignard reagents. It was found that the reaction of **1** with *t*-butylmagnesium chloride gives the corresponding 3-substituted 2-*t*-butyl- (**10**), 2-*N'*-*t*-butylhydrazono-2,3-dihydrobenzothiazoles (**11**) and 3-substituted 2,3-dihydrobenzothiazol-2-one (**5**). The result is given below.

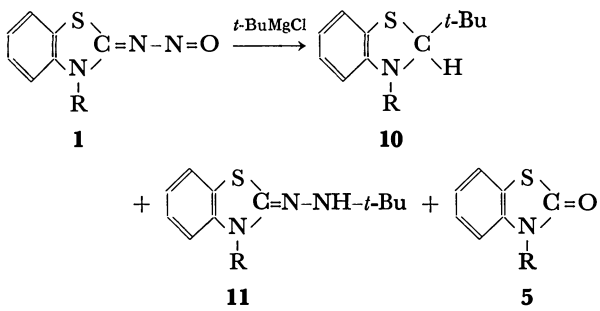

1 **10** **11** **5**

	10 (%)	**11** (%)	**5** (%)
1a	39	8	13
1b	50	15	22

2,2-Diaryl (**2** and **6**), 2-mesityl (**8**) and 2-*t*-butyl (**10**) derivatives are considered to be formed *via* the common 1,4-addition intermediate between **1** and Grignard reagent, a diazonium salt (**A**), which reacts with Grignard reagent to give 2,2-disubstituted derivatives (*path a-i*) or loses nitrogen to give magnesium bromide 2-mesitly (or *t*-butyl)-2,3-dihydrobenzothiazol-2-yl oxide (**B**). The formation of **8** and **10** is explained below (*path a-ii*, *a-iii*).

The fate of **A** seems to depend on the bulkiness of Grignard reagents. Bulky Grignard reagents such as mesityl and *t*-butyl prefer the latter path (*path a-ii*).

The *path a-ii* was supported by the fact that the evolved gas was only nitrogen in the reaction of **1b** with *t*-butylmagnesium chloride, the amount (76%) being nearly equal to the sum (72%) of the amounts of **10** and **5b**.

N'-Substituted hydrazono derivatives (**4**, **7**, **9**, and **11**) are considered to be produced as follows.

1 first reacts with Grignard reagent to give 1,2-addition intermediate (**C**), **C** then reacting with excess Grignard reagents to give **D**.

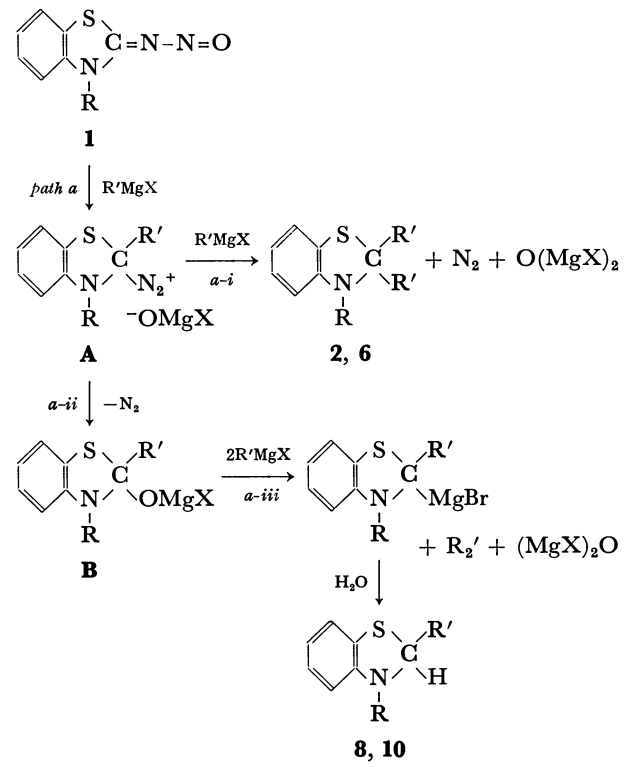

1 **A** **2, 6** **B** **8, 10**

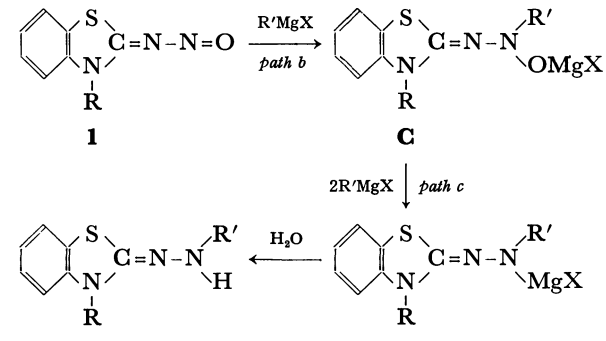

1 **C** **4, 7, 9, 11** **D**

p-Cresol (4 mmol) was actually obtained in the reaction of **1b** (24 mmol) with *p*-tolylmagnesium bromide (100 ml). This seems to support OMgX-MgX exchange for *path c* producing R'OMgX as Wieland and Roseeu reported for the reaction of nitrosobenzene with phenylmagnesium bromide.[12]

However, their postulate was not substantiated by Gilman, who found that the following should be the case,[13] this being now accepted.

$$Ph_2NOMgBr + 2\,PhMgBr \longrightarrow Ph_2NMgBr + Ph_2 + (MgBr)_2O$$

This type of reaction is sensitive to the structure of both reagents. However, no systematic investigation has been carried out. We prefer Gilman's postulate. This can also be the case for *path a-iii*, although exact mechanism may be more complex.

The mechanism of formation of **3** will be discussed in a succeeding paper.[14]

Thiazolones (**5**) are formal products in the thermal decomposition of **1**, but **1** is completely stable under

the reaction conditions. The reason why **5** is produced in considerable amount in the reaction with bulky Grignard reagents is obscure.

We see that aryl and *t*-butyl Grignard reagents react at positions a (major) producing diazonium salt (**A**) as an intermediate and at b (minor) producing hydroxylamine type intermediate (**C**).

Experimental

All the melting and boiling points are uncorrected. NMR spectra were recorded with Hitachi R-20B and R-24 spectrometers (60 MHz) using TMS as an internal standard. IR spectra were taken with a Hitachi EPI-G2 spectrometer. MS were measured with a Hitachi RMU-6L mass spectrometer at 70 eV.

Materials. 3-Methyl- (**1a**, mp 143 °C (dec.))[15] and 3-phenyl-2-nitrosoimino-2,3-dihydrobenzothiazoles (**1b**, mp 140 °C (dec.))[16] were prepared by reported methods. Mesityl bromide was prepared by the bromination of mesitylene,[17] bp 80—85 °C/6 mmHg.

All the reactions were carried out under nitrogen except the one for the determination of evolved gas (argon).

*Reaction of 2-Nitrosoimino-3-phenyl-2,3-dihydrobenzothiazole (**1b**) with Phenylmagnesium Bromide.* To a stirred solution of Grignard reagent prepared from magnesium turnings (3.60 g, 0.15 mol) and bromobenzene (23.55 g, 0.15 mol) in anhydrous ether (150 ml), was added **1b** (7.61 g, 30 mmol) portionwise over a period of 1 hr at 0 °C. The reaction took place immediately with vigorous evolution of gas, stirring being continued for 3 hr. The reaction mixture was treated with saturated aqueous ammonium chloride and the resulting precipitates were filtered off. The precipitates were extracted with ether (100 ml×2) and benzene (100 ml). The extracts and ether layer of the filtrate were combined and dried over anhydrous magnesium sulfate. The solvent was evaporated in a vacuum and the residue was chromatographed on silica gel. 2,2,3-Triphenyl-2,3-dihydrobenzothiazole (**2b**, 5.25 g, 48%) was eluted with benzene and recrystallized from benzene–ethanol (1: 1) as yellowish crystals, mp 191.5—192.5 °C; MS: *m/e* 365 (M^+, 23%) and 288 (M^+—Ph, 100%).

Found: C, 82.35; H, 5.36; N, 3.79; S, 8.64%. Calcd for $C_{25}H_{19}NS$: C, 82.17; H, 5.24; N, 3.84; S, 8.76%.

A small amount of bis(*o*-anilinophenyl) disulfide (**3b**) was eluted with benzene as a yellow oil. The structure was confirmed by comparison with the spectral data of an authentic sample[11] prepared from 3-phenyl-2,3-dihydrobenzothiazol-2-one (**5b**) and potassium hydroxide in ethanol. 3-Phenyl-2-*N'*-phenylhydrazono-2,3-dihydrobenzothiazole (**4b**, 1.57 g, 17%) was eluted with dichloromethane–chloroform (1: 1) and recrystallized from benzene–ethanol (1: 1), mp 157—158 °C; IR (KBr): 3230 (NH), 1595, and 1585 cm^{-1}; NMR ($CDCl_3$): δ 3.45 (broad s, 1H, N–H) and 6.70—7.65 (m, 15H, Ar-H); MS: *m/e* 317 (M^+, 100%) and 225 (M^+—PhNH, 41%).

Found: C, 71.92; H, 4.77; N, 13.31; S, 9.80%. Calcd for $C_{19}H_{15}N_3S$: C, 71.91; H, 4.76; N, 13.24; S, 10.08%.

*Reaction of 3-Methyl-2-nitrosoimino-2,3-dihydrobenzothiazole (**1a**) with Phenylmagnesium Bromide.* To a stirred Grignard solution prepared from magnesium (3.63 g, 149 mmol) and bromobenzene (23.26 g, 148 mmol) in ether (100 ml) was added **1a** (4.80 g, 24.3 mmol) portionwise over a period of 2.5 hr at 0 °C and the mixture was stirred for 13.5 hr. After a similar work-up, 3-methyl-2,2-diphenyl-2,3-dihydrobenzothiazole (**2a**, 1.63 g, 22%) was eluted with *n*-hexane, mp 142—143 °C (from $CHCl_3$); NMR ($CDCl_3$): δ 2.59 (s, 3H, N-Me) and 6.12—7.63 (m, 14H, Ar-H); MS: *m/e* 303 (M^+, 16%) and 226 (M^+—Ph, 100%).

Found: C, 79.37; H, 5.37; N, 4.64; S, 10.43%. Calcd for $C_{20}H_{17}NS$: C, 79.17; H, 5.65; N, 4.62; S, 10.57%.

Bis(*o*-methylaminophenyl) disulfide (**3a**, 0.657 g, 5%) was eluted with *n*-hexane–benzene (1: 1) as yellow crystals, mp 66.5—67.0 °C (from chloroform–ethanol) (lit,[18] 64—68 °C).

A fraction corresponding to 3-methyl-2-*N'*-phenylhydrazono-2,3-dihydrobenzothiazole (**4a**, 1.0 g, 15%) was obtained, **4a** decomposing slowly during the course of isolation.

*Reaction of **1a** with* p-*Tolylmagnesium Bromide.* To a stirred Grignard solution prepared from magnesium (4.80 g, 0.20 mol) and *p*-bromotoluene (34.20 g, 0.20 mol) in ether (150 ml) was added **1a** (7.72 g, 40 mmol) portionwise at 0 °C and the mixture was stirred for 1 hr. After a similar work-up 3-methyl-2,2-bis(*p*-tolyl)-2,3-dihydrobenzothiazole (**6a**, 8.8 g, 66%) was eluted with benzene as yellowish crystals, mp 141.0—141.5 °C (from benzene–methanol (1: 1)); NMR ($CDCl_3$): δ 2.35 (s, 6H, 2 Me), 2.65 (s, 3H, Me), and 6.7—7.5 (m, 12H, Ar–H).

Found: C, 79.72; H, 6.16; N, 3.92; S, 9.59%. Calcd for $C_{22}H_{21}NS$: C, 79.73; H, 6.39; N, 4.23; S, 9.66%.

Red brown tarry material (2.45 g) was eluted with chloroform–ether (7: 1) and crystallized partly on standing, mp 155.0—156.5 °C. The compound was assigned as 2-*N'*-*p*-tolylhydrazono-3-methyl-2,3-dihydrobenzothiazole (**7a**) by comparison of its IR data with those of **4b** and **7b**. IR (KBr): 3350 (NH), 1610 (C=N), 1595, and 1590 cm^{-1}.

*Reaction of **1b** with* p-*Tolylmagnesium Bromide.* To a stirred Grignard solution prepared from magnesium (2.51 g, 0.10 mol) and *p*-bromotoluene (17.13 g, 0.10 mol) in ether (100 ml) was added **1b** (6.14 g, 24 mmol) portionwise at room temperature and the mixture was stirred for 2 hr. After a similar work-up, extraction with 20% aqueous sodium hydroxide gave *p*-cresol (0.43 g, 4 mmol), whose spectral data were in agreement with those of an authentic sample. The residue was chromatographed on silica gel. Elution with *n*-hexane–benzene (1: 1) gave a mixture of bi-*p*-tolyl and 3-phenyl-2,2-bis(*p*-tolyl)-2,3-dihydrobenzothiazole (**6b**), but separation of the mixture was very difficult. The yield of **6b** was estimated to be 4.7 g (50%) by its NMR spectrum, and the structure was determined by the following data; NMR ($CDCl_3$): δ 2.56 (s, 6H, 2 Me) and 6.15—7.20 (m, 19H, Ar-H).

Elution with benzene–dichloromethane (1: 1) gave a reddish purple tarry material (1.48 g), which was treated with dry column chromatography (silica gel) to give 3-phenyl-2-*N'*-*p*-tolylhydrazono-2,3-dihydrobenzothiazole (**7b**, 0.672 g, 8%), mp 186.5—187.5 °C (from chloroform–ethanol); IR (KBr): 3270 (NH), 1610, 1590, and 1580 cm^{-1}; NMR ($CDCl_3$): δ 2.23 (s, 3H, Me) and 6.30—7.53 (m, 13H, Ar-H) (N–H signal was obscure); MS: *m/e* 331 (M^+, 100%). Compound **7b** was unstable in solvents.

Found: C, 72.35; H, 5.18; N, 12.72%. Calcd for $C_{20}H_{17}N_3S$: C, 72.48; H, 5.14; N, 12.68%.

*Reaction of **1a** with Mesitylmagnesium Bromide.* To a stirred Grignard solution prepared from magnesium (4.8 g, 0.20 mol) and mesityl bromide (39.8 g, 0.20 mol) in ether (150 ml) was added **1a** (7.72 g, 40 mmol) portionwise and the mixture was treated and chromatographed in the usual way. Elution with benzene with 2-mesityl-3-methyl-2,3-dihydrobenzothiazole (**8**, 4.9 g, 46%) as yellowish crystals, mp 222.0—223.5 °C (from ethanol); NMR ($CDCl_3$): δ 2.1 (s, 3H, Me), 2.3 (s, 6H, 2 Me), 3.2 (s, 3H, Me), 5.0 (s, 1H, CH), and 6.7—7.4 (m, 6H, Ar-H).

Found: C, 75.62; H, 6.90; N, 5.18; S, 12.01%. Calcd for $C_{17}H_{19}NS$: C, 75.81; H, 7.11; N, 5.20; S, 11.88%.

Elution with dichloromethane gave 3-methyl-2,3-dihydrobenzothiazol-2-one (**5a**, 0.64 g, 10%), mp 74—75 °C (75—

76 °C,[11] 76 °C[15]). Elution with dichloromethane–chloroform (1: 1) gave 2-*N'*-mesitylhydrazono-3-methyl-2,3-dihydrobenzothiazole (**9**, 2.1 g, 18%), mp 152.0—154.5 °C; IR (KBr): 3310 (NH), 1610, and 1590 cm^{-1}. IR supports structure **9**.

Reaction of ***1b*** *with* t-*Butylmagnesium Chloride.* To a stirred solution of Grignard reagent prepared from magnesium (3.60 g, 0.15 mol) and *t*-butyl chloride (13.50 g, 0.146 mol) in ether (150 ml), was added **1b** (7.71 g, 30 mmol) portionwise over a period of 1 hr at 0 °C. Stirring was continued for 3 hr. 2-*t*-Butyl-3-phenyl-2,3-dihydrobenzothiazole (**10b**, 3.70 g, 50%) was eluted with benzene, mp 61—62 °C (from ethanol); NMR ($CDCl_3$): δ 1.00 (s, 9H, Me_3C), 5.10 (s, 1H, >C–H), and 6.85—7.25 (m, 9H, Ar-H); MS: *m/e* 279 (M^+, 8.9%) and 212 ($M^+ - t$-Bu, 100%).

Found: C, 75.81; H, 7.11; N, 5.20; S, 11.88%. Calcd for $C_{17}H_{19}NS$: C, 76.02; H, 7.15; N, 5.20; S, 11.60%.

3-Phenyl-2,3-dihydrobenzothiazol-2-one (**5b**, 1.48 g, 22%) was eluted with benzene–dichloromethane (1: 3), mp 78—79 °C (from *n*-hexane) (lit,[16] 75—76 °C). 2-*N'*-*t*-Butylhydrazono-3-phenyl-2,3-dihydrobenzothiazole (**11b**, 1.33 g, 15%) was eluted with dichloromethane, mp 161—162 °C (from ethanol); IR (KBr): 3230 (NH), 1615, 1590, and 1580 cm^{-1}; NMR ($CDCl_3$): δ 1.10 (s, 9H, Me_3C), 3.05 (broad s, 1H, N–H), and 6.7—7.6 (m, 9H, Ar-H); MS: *m/e* 297 (M^+, 88%) and 282 ($M^+ - Me$, 100%).

Found: C, 68.38; H, 6.22; N, 14.06; S, 10.99%. Calcd for $C_{17}H_{19}N_3S$: C, 68.66; H, 6.44; N, 14.13; S, 10.76%.

Reaction of ***1a*** *with* t-*Butylmagnesium Chloride (Reverse Addition Method).* *t*-Butylmagnesium chloride free of excess magnesium, prepared from magnesium (2.59 g, 0.106 mol) and *t*-butyl chloride (8.06 g, 87.1 mmol) in ether (100 ml), was added dropwise over a period of 1 hr at 0 °C with stirring to a suspension of **1a** (3.00 g, 15.5 mmol) in ether (50 ml). Stirring was continued for 1 hr. The reaction mixture was chromatographed on silica gel after the usual work-up. 2-*t*-Butyl-3-methyl-2,3-dihydrobenzothiazole (**10a**, 1.05 g, 39%) was eluted with *n*-hexane–benzene (1: 1) as an oil. The structure was confirmed by the following NMR data: NMR ($CDCl_3$): δ 0.93 (s, 9H, Me_3C), 2.99 (s, 3H, N–Me), 4.62 (s, 1H, >C–H), and 6.35—7.46 (m, 4H, Ar-H).

3-Methyl-2,3-dihydrobenzothiazol-2-one (**5a**, 0.346 g, 13%) was eluted with benzene, mp 76.0—76.5 °C (lit,[15] 76 °C). 2-*N'*-*t*-Butylhydrazono-3-methyl-2,3-dihydrobenzothiazole (**11a**, 0.307 g, 8%) was eluted with benzene–dichloromethane (1: 1) and chloroform as an oil. The structure was confirmed by the following spectral data: IR (KBr): 3220 (NH), 1630 and 1580 cm^{-1}: NMR ($CDCl_3$): δ 1.19 (s, 9H, Me_3C), 2.76 (broad s, 1H, N–H), 3.44 (s, 3H, N–Me), and 6.7—7.9 (m, 4H, Ar–H). By addition of D_2O, a broad singlet at δ 2.76 disappeared.

Determination of the Evolved Gas. *t*-Butylmagnesium chloride was prepared from magnesium (0.43 g, 18 mmol) and *t*-butyl chloride (1.67 g, 18 mmol) in ether (50 ml) under argon. In a closed system, **1b** (0.92 g, 3.6 mmol) was added to the above solution at 0 °C under stirring. The amount of evolved gas was 61.5 ml (76%). The gas was found to be pure nitrogen by MS. No dinitrogen oxide (*m/e* 44) was detected.

References

1) For Part IX see: K. Akiba, M. Hisaoka, N. Inamoto, T. Ohta, and H. Kuroda, *Chem. Lett.*, **1975**, 347.

2) C. J. Thoman, S. J., and I. M. Hunsberger, *J. Org. Chem.*, **33**, 2852 (1968).

3) K. Akiba, S. Matsunami, C. Eguchi, and N. Inamoto, This Bulletin, **47**, 935 (1974).

4) a) J. Goerdeler, A. Huppertz, and K. Wember, *Chem. Ber.*, **87**, 69 (1954). b) D. S. Hector, *Ber.*, **22**, 1176 (1889); **23**, 357 (1980); **25**, 799 (1892).

5) A. S. Shawai and A. O. Abdelhamid, *Tetrahedron Lett.*, **1975**, 163.

6) K. Akiba, T. Kawamura, M. Hisaoka, and N. Inamoto, *Chem. Lett.*, **1973**, 201.

7) K. Akiba, T. Kawamura, M. Ochiumi, and N. Inamoto, *Heterocycles*, **1**, 35 (1973).

8) K. Akiba, M. Hisaoka, and N. Inamoto, *Chem. Lett.*, **1974**, 1267.

9) K. Akiba, K. Ishikawa, and N. Inamoto, *Heterocycles*, **2**, 555 (1974).

10) a) K. Akiba, M. Hisaoka, N. Inamoto, T. Ohta, and H. Kuroda, *Chem. Lett.*, **1975**, 347. b) S. Hünig, *Angew. Chem.*, **80**, 343 (1968). c) H. Balli, *Helv. Chim. Acta*, **57**, 1912 (1974).

11) A. I. Kiprianov and Z. N. Pazenko, *J. Gen. Chem.*, **19**, 1523 (1949); *Chem. Abstr.*, **44**, 3487g (1950).

12) H. Wieland and A. Roseeu, *Ber.*, **45**, 494 (1912); **48**, 1117 (1915).

13) H. Gilman and R. McCracken, *J. Amer. Chem. Soc.*, **49**, 1052 (1927).

14) K. Akiba, M. Hisaoka, T. Kawamura, N. Inamoto, This Bulletin, **48**, 3270 (1975).

15) E. Besthorn, *Ber.*, **43**, 1519 (1910).

16) H. Passing, *J. Prakt. Chem.*, **153**, 1 (1939).

17) L. I. Smith, "Organic Syntheses," Coll. Vol. II, p. 95 (1943).

18) C. D. Harries and E. Loewenstein, *Ber.*, **27**, 861 (1894).

Chemistry of Nitrosoimines. XI.[1] Reactions of 3-Substituted 2-Nitrosoimino-2,3-dihydrobenzothiazoles with Benzyl and Allylic Grignard Reagents

Motoyuki HISAOKA, Kin-ya AKIBA, and Naoki INAMOTO

Department of Chemistry, Faculty of Science, The University of Tokyo, Hongo, Tokyo 113

(Received May 20, 1975)

3-Substituted 2-nitrosoimino-2,3-dihydrobenzothiazoles (**1**) react with benzylmagnesium chloride to give 3-substituted 2,2-dibenzyl- (**2**), 2-*N'*-benzylidenehydrazono- (**3**) and 2-*N'*,*N'*-dibenzylhydrazono-2,3-dihydrobenzothiazoles (**4**). The main reaction (formation of **3** and **4**) occurrs on the nitroso group of **1**, which proceeds *via* 1,2-addition intermediate (**B**). Allylmagnesium bromide and cinnamylmagnesium chloride also react with 3-methyl derivative (**1a**) to afford 2-*N'*,*N'*-diallyl- and 2-*N'*-(1-phenyl-2-propenyl)hydrazono-3-methyl-2,3-dihydrobenzothiazoles, respectively.

In a previous paper,[1] it was shown that the major reaction of 3-substituted 2-nitrosoimino-2,3-dihydrobenzothiazoles (**1**) with aryl and *t*-butyl Grignard reagents occurs on the C-2 of the benzothiazoline ring (*path a*) and the minor one on the nitrogen of the nitroso group (*path b*). In order to clarify a correlation between structure of Grignard reagents and reaction center in **1** which has an ambident character,[2] reactions of **1** were carried out with benzyl, allyl and cinnamyl Grignard reagents, which are resonance-stabilized carbanions. Reactions of **1** with benzylmagnesium chloride, in particular, were investigated in detail.

Table 1. Reaction products of **1** with excess (4 eqv.) benzylmagnesium chloride

Run	Reaction condition	Yield (%) 2	3	4
1[a]	**1a**, Et_2O, r.t. (4 hr)	8	44	19
2	**1a**, Et_2O, r.t. (4 hr) and then reflux (3 hr)	8	14	31
3	**1b**, Et_2O, r.t. (2.5 hr) and then reflux (1 hr)	4	9	25
4	**1c**, THF, r.t. (2.5 hr)	2	30	11
5[b]	**1a**, THF, r.t. (2.5 hr)	7	43	3

a) Neither $PhCH_2OH$ nor $PhCH_2Cl$ was detected by glc.
b) Reverse addition of Grignard reagent to a suspension of **1a** and $MgCl_2$. 2-*N'*-Benzylhydrazono-3-methyl-2,3-dihydrobenzothiazole (**5a**) was also isolated in 2% yield.

To an excess benzylmagnesium chloride in ether or tetrahydrofuran (THF) was added **1** under nitrogen. The reaction products were 2,2-dibenzyl- (**2**), 2-*N'*-benzylidenehydrazono- (**3**) and 2-*N'*,*N'*-dibenzylhydrazono-2,3-dihydrobenzothiazoles (**4**). The results are shown in Table 1.

From a comparison of the result of run 2 with that of run 1 (Table 1), it is seen that the yield of **2a** remains unchanged by reflux of the solvent, but that of **3a** decreases, accompanied by the increase of **4a**, the total

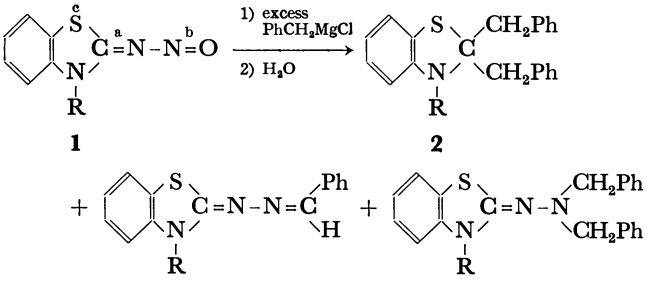

1 **2** **3** **4**

a; R=Me, **b**; R=Ph, **c**; R=Et

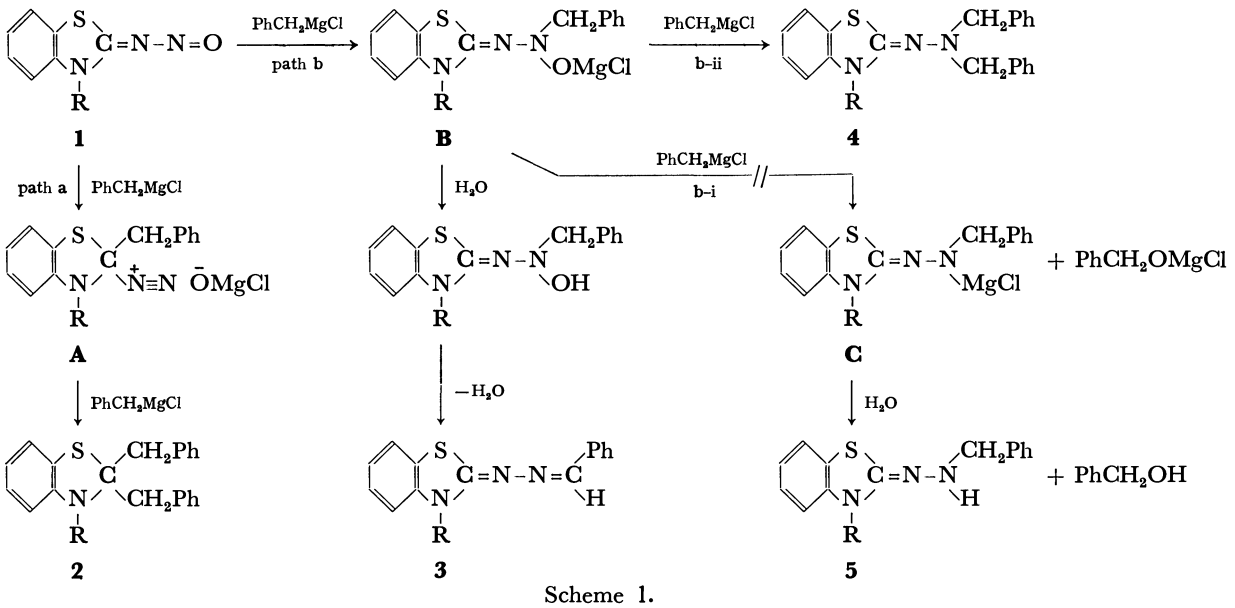

1 **B** **4** **A** **C** **2** **3** **5**

Scheme 1.

yield of **3a** and **4a** being almost the same as that of run 1. This suggests that **3a** and **4a** are produced through a common intermediate (**B**).

Similarly, 3-phenyl (**1b**, run 3) and 3-ethyl (**1c**, run 4) derivatives were allowed to react with excess benzylmagnesium chloride at room temperature. After 2.5 hr (run 3), the reaction mixture was refluxed to give a similar result to that of run 2. The result of run 4 was very similar to that of run 1.

From the results obtained in runs 1—4, paths of formation of **2**, **3** and **4** are proposed as shown in Scheme 1.

Nitrosoimines (**1**) react with benzylmagnesium chloride to produce initially 1,2- (**B**) and 1,4-addition intermediates (**A**).[1] Unsymmetric azines (**3**) and hydrazones (**4**) are formed *via* the common intermediates (**B**). Azines (**3**) are produced by the hydrolysis and dehydration of the intermediate (**B**). Two paths can be considered for the formation of **4** from **B**. One is the apparent exchange of the OMgCl group to give magnesium salt of hydrazones (**C**), which can proceed by Gilman's mechanism producing bibenzyl, Wieland's mechanism producing benzyl alcohol not being excluded *a priori*.[1] The other is the path along which a second Grignard reagent attacks directly on the nitrogen atom of the nitroso group to give **4** (*b-ii*). Two possibilities for the former path were ruled out since no benzyl alcohol could be detected in the reaction mixture by gas chromatography (glc) and no residual benzyl chloride was detected in the Grignard solution before use. The formation of **4** is accelerated by heating.

In the case of slow reverse addition of Grignard reagent to a suspension of **1a** and magnesium(II) chloride in THF (run 5), 2-*N'*-benzylhydrazono-3-methyl-2,3-dihydrobenzothiazole (**5a**) was also isolated in 2% yield together with **2a**, **3a** and **4a**. Thus, the path of formation of **5a** is explained as follows: the OMgCl-MgCl exchange between the 1,2-addition intermediate (**Ba**) and magnesium (II) chloride probably produces magnesium salt (**Ca**), which is hydrolyzed to produce **5a** (Scheme 2).

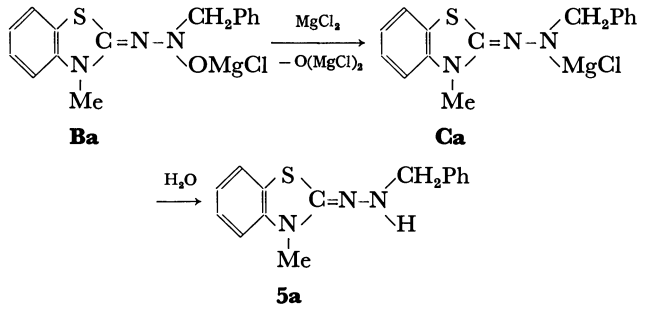

Scheme 2.

It is noteworthy that the benzyl protons of **2a** and **2c** appear as quartet whereas those of **2b** appear as singlet. The difference can be attributed to the presence of phenyl group in **2b**, although the exact reason is not clear.

Excess allylmagnesium bromide reacts with **1a** in ether at room temperature to give 2-*N'*,*N'*-diallylhydrazono-3-methyl-2,3-dihydrobenzothiazole (**6**) in 30% yield, together with an oily product, which is tentatively assigned as 2-allyl-2-(α-hydroxyallyl)-3-methyl-2,3-dihydrobenzothiazole (**7**, 27%) from spectral data. However, the mechanism of formation is obscure.

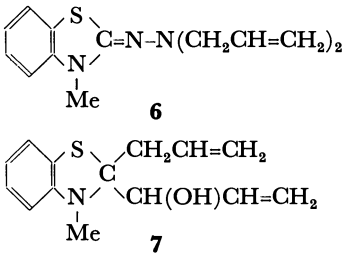

Excess cinnamylmagnesium chloride, which reacts easily with cinnamyl chloride to give a mixture of coupling products even without heating,[3] was allowed to react with **1a**, as soon as possible after the preparation. The isolated and identified products were found to be a mixture of 1,4-diphenyl- (main) and 1,6-diphenyl-1,5-hexadienes (minor) as coupling products and 3-methyl-2-*N'*-(1-phenyl-2-propenyl) hydrazono-2,3-dihydrobenzothiazole (**8**) in 8% yield. This result can be explained in terms of the equilibrium in the Grignard reagent and the apparent exchange between the OMgCl group of the addition product (**B**) and the MgCl group of Grignard reagent as shown in Scheme 3.

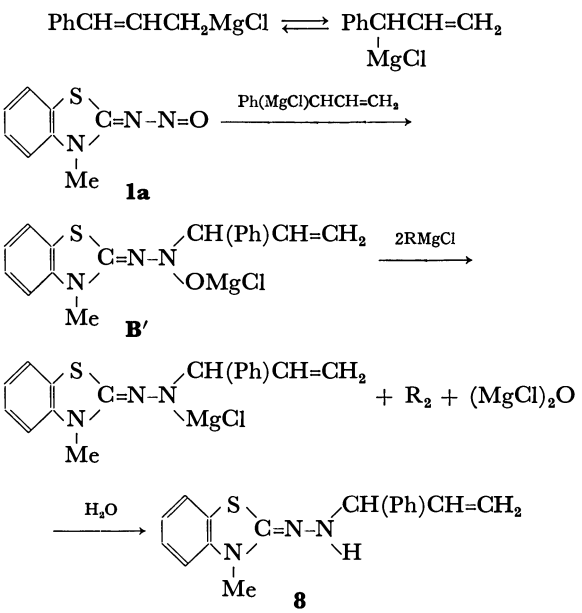

Scheme 3.

The main reaction of resonance-stabilized Grignard reagents such as benzyl, allyl, and cinnamylmagnesium halides with **1** occurs on the nitroso group (*path b*), accompanied by a minor reaction on the C-2 of the ring (*path a*). The results are in contrast with those reported for aryl- and *t*-butylmagnesium halides.[1] This can be explained as follows: resonance-stabilized Grignard reagents are not reactive enough to add on the C-2 and to cut off the entire conjugation between the benzothiazoline ring and the nitrosoimino group, whereas the latter type Grignard reagents are reactive enough. We should keep in mind the fact that C–C bond

formation is, in general, highly (or exclusively) favorable to C–N bond formation by Grignard reagents.[4]

Experimental

Materials. 3-Methyl (**1a**), 3-phenyl (**1b**) and 3-ethyl derivatives (**1c**) of 2-nitrosoimino-2,3-dihydrobenzothiazole were prepared by the reported methods: **1a**,[5] mp 143 °C (dec.); **1b**,[6] mp 140 °C (dec.); **1c**,[7] mp 143—144 °C (dec.). Cinnamyl chloride was prepared according to the method of Koch.[3]

In all cases, the reactions were carried out under nitrogen. MS spectra were measured at 70 eV.

Reaction of 3-Methyl-2-nitrosoimino-2,3-dihydrobenzothiazole (1a) with Benzylmagnesium Chloride in Ether at Room Temperature. To a stirred Grignard reagent prepared from magnesium (4.94 g, 0.20 mol) and benzyl chloride (12.99 g, 0.10 mol) in ether (100 ml) was added **1a** (4.83 g, 25.0 mmol) portionwise over a period of 1 hr at room temperature. Stirring was continued for 3 hr. The reaction mixture was treated with 20% aqueous solution of ammonium chloride, the resulting precipitates being filtered off and extracted with ether, benzene, and dichloromethane. The extracts and the ether layer of the filtrate were combined and washed with water and dried over anhydrous magnesium sulfate. After the solvents had been evaporated, the residue was chromatographed on silica gel. 2,2-Dibenzyl-3-methyl-2,3-dihydrobenzothiazole (**2a**, 0.63 g, 8%) was eluted with *n*-hexane–benzene (3: 2), mp 86.5—87.5 °C (from chloroform–ethanol). NMR ($CDCl_3$, 60 MHz): δ 2.90 (s, 3H, N–CH_3), 3.18 (AB q, J_{AB}=13 Hz, $\Delta\delta_{AB}$=20 Hz, 4H, 2PhCH_2), and 6.00—7.22 (m, 14H, Ar-H); MS: *m/e* (M^+, trace) and 240 (M^+-PhCH_2, 100%).

Found: C, 79.75; H, 6.44; N, 3.96%. Calcd for $C_{22}H_{21}NS$: C, 79.72; H, 6.39; N, 4.23%.

2-*N'*-Benzylidenehydrazono-3-methyl-2,3-dihydrobenzothiozole (**3a**, 3.06 g, 44%) was eluted with benzene and benzene–dichloromethane (1: 1) as pale yellow crystals, mp 162—163 °C (from benzene–ethanol).[5]

2-*N'*,*N'*-Dibenzylhydrazono-3-methyl-2,3-dihydrobenzothiazole (**4a**, 1.67 g, 19%) was eluted with benzene–dichloromethane (1: 1), mp 116.5—117.5 °C (from benzene–ethanol). IR (KBr): 1600 and 1580 cm^{-1}; NMR ($CDCl_3$): δ 3.31 (s, 3H, N–CH_3), 3.85 (s, 4H, 2PhCH_2), and 6.25—7.50 (m, 14H, Ar-H); MS: *m/e* 359 (M^+, 13%), 240 ($M^+-PhCH_2-N_2$, 50%), and 91 ($PhCH_2^+$, 100%).

Found: C, 73.61; H, 5.70; N, 11.95; S, 8.70%. Calcd for $C_{22}H_{21}N_3S$: C, 73.50; H, 5.88; N, 11.69; S, 8.92%.

Reaction of 1a with Benzylmagnesium Chloride in Ether at Room Temperature and Then with Reflux. To a stirred solution of Grignard reagent, prepared from magnesium (3.21 g, 0.13 mol) and benzyl chloride (8.60 g, 0.068 mol) in ether (80 ml), was added **1a** (3.24 g, 16.8 mmol) portionwise over a period of 1 hr at room temperature, stirring being continued for 3 hr. The reaction mixture was then refluxed for additional 3 hr. Compounds **2a**, **3a**, and **4a** were isolated in the amounts of 0.46 g (8%), 0.59 g (14%), and 1.90 g (31%), respectively.

Reaction of 2-Nitrosoimino-3-phenyl-2,3-dihydrobenzothiazole (1b) with Benzylmagnesium Chloride in Ether at Room Temperature and Then with Reflux. To a stirred Grignard solution prepared from magnesium (4.86 g, 0.20 mol) and benzyl chloride (12.71 g, 0.10 mol) in ether (100 ml) was added **1b** (5.20 g, 20.8 mmol) portionwise over a period of 0.5 hr at room temperature and stirring was continued for additional 2 hr. The reaction mixture was then refluxed for 1 hr. 2,2-Dibenzyl- (**2b**), 2-*N'*-benzylidenehydrazono- (**3b**), and 2-*N'*,*N'*-dibenzylhydrazono-3-phenyl-2,3-dihydrobenzothiazoles (**4b**) were eluted with *n*-hexane and *n*-hexane–benzene (1: 1), benzene–dichloromethane (1: 1), and benzene–dichloromethane (1: 1), respectively. All the products were recrystallized from chloroform–ethanol.

2b (0.33 g, 4%); mp 145.0—145.5 °C; NMR ($CDCl_3$): δ 3.20 (s, 4H, 2PhCH_2) and 6.25—7.50 (m, 19H, Ar-H); MS: *m/e* 393 (M^+, trace) and 302 (M^+-PhCH_2, 100%).

Found: C, 82.55; H, 5.77; N, 3.40; S, 8.18%. Calcd for $C_{27}H_{23}NS$: C, 82.40; H, 5.89; N, 3.56; S, 8.15%.

3b (0.64 g, 9%), pale yellow crystals; mp 124.5—125.0 °C; IR (KBr): 1605, 1575, and 1525 cm^{-1}; NMR ($CDCl_3$): δ 6.6—7.9 (m, 14H, Ar-H) and 8.25 (s, 1H, –N=CH–); MS: *m/e* 329 (M^+, 100%).

Found: C, 72.95; H, 4.58; N, 12.74; S, 9.73%. Calcd for $C_{20}H_{15}N_3S$: C, 72.92; H, 4.59; N, 12.76; S, 9.73%.

4b (2.18 g, 25%); mp 85.0—85.5 °C; IR (KBr): 1605, 1590, and 1575 cm^{-1}; NMR ($CDCl_3$): δ 3.81 (s, 4H, 2PhCH_2) and 6.32—7.60 (m, 19H, Ar-H); MS: *m/e* 421 (M^+, 13%), 302 (M^+-PhCH_2, 43%), and 91 ($PhCH_2^+$, 100%).

Found: C, 77.23; H, 5.78; N, 10.06; S, 7.71%. Calcd for $C_{27}H_{23}N_3S$: C, 76.93; H, 5.50; N, 9.97; S, 7.61%.

Reaction of 3-Ethyl-2-nitrosoimino-2,3-dihydrobenzothiazole (1c) with benzylmagnesium Chloride in Tetrahydrofuran (THF) at Room Temperature. To a stirred Grignard solution prepared from magnesium (4.84 g, 0.16 mol) and benzyl chloride (12.90 g, 0.10 mol) in THF (100 ml) was added **1c** (5.64 g, 27.2 mmol) portionwise over a period of 1 hr at room temperature, stirring being continued for 1.5 hr. 2,2-Dibenzyl-3-ethyl-2,3-dihydrobenzothiazole (**2c**, 0.37 g, 2%) was eluted with *n*-hexane–benzene (1: 1), mp 132—133 °C (from benzene–ethanol). NMR ($CDCl_3$): δ 1.20 (t, J=7 Hz, 3H, $C\underline{H}_3CH_2$), 3.24 (AB q, J_{AB}=14 Hz, $\Delta\delta_{AB}$=21 Hz, 4H, 2PhCH_2), 3.39 (q, J=7 Hz, 2H, $CH_3C\underline{H}_2$–N), and 5.95—7.45 (m, 14H, Ar-H); MS: *m/e* 345 (M^+, trace) and 254 (M^+-PhCH_2, 100%).

Found: C, 80.16; H, 6.69; N, 3.84; S, 9.21%. Calcd for $C_{23}H_{23}NS$: C, 79.96; H, 6.71; N, 4.05; S, 9.28%.

2-*N'*-Benzylidenehydrazono-3-ethyl-2,3-dihydrobenzothiazole (**3c**) was eluted with *n*-hexane–benzene (1: 1) and benzene as a yellow oil. The oil was rechromatographed on silica gel and eluted with *n*-hexane–benzene (2: 1 and 1: 1) and benzene to give an oil, 2.28 g (30%). The oil solidified to give yellow crystals (mp 51.0—52.2 °C (from *n*-hexane–benzene)) after being left to stand for several months. IR (KBr): 1610, 1570, and 1530 cm^{-1}; NMR ($CDCl_3$): δ 1.25 (t, J=7.5 Hz, 3H, $C\underline{H}_3CH_2$), 4.02 (q, J=7.5 Hz, 2H, $CH_3C\underline{H}_2$–N), 6.6—8.0 (m, 9H, Ar-H), and 8.39 (s, 1H, –N=CH–); MS: *m/e* 281 (M^+, 100%).

Found: C, 68.27; H, 5.09; N, 15.02%. Calcd for $C_{16}H_{15}N_3S$: C, 68.30; H, 5.37; N, 14.93%.

2-*N'*,*N'*-Dibenzylhydrazono-3-ethyl-2,3-dihydrobenzothiazole (**4c**) was eluted with benzene–dichloromethane (1: 1) as an oil. The oil was rechromatographed on silica gel and eluted with benzene and benzene–dichloromethane (1: 1) to give 1.19 g (11%) of **4c**, mp 108.5—109.0 °C (from chloroform–ethanol). IR (KBr): 1600 and 1580 cm^{-1}; NMR ($CDCl_3$): δ 1.10 (t, J=7 Hz, 3H, $C\underline{H}_3CH_2$), 3.86 (s, 4H, 2PhCH_2), 3.87 (q, J=7 Hz, 2H, $CH_3C\underline{H}_2$), and 6.57—7.58 (m, 14H, Ar-H); MS: *m/e* 373 (M^+, 12%), 254 ($M^+-PhCH_2-N_2$), and 91 ($PhCH_2^+$, 100%).

Found: C, 74.18; H, 6.18; N, 11.40; S, 8.60%. Calcd for $C_{23}H_{23}N_3S$: C, 73.96; H, 6.21; N, 11.25; S, 8.58%.

Reaction of 1a with Benzylmagnesium Chloride in THF at room Temperature in the Presence of Magnesium (II) Chloride (Reverse Addition of Grignard Reagent). A Grignard solution was prepared from magnesium (4.56 g, 0.19 mol) and benzyl chloride (11.93 g, 0.09 mol) in THF (100 ml) and transferred

to a dropping funnel through a Teflon tube fitted with glass wool in order to filter the unchanged magnesium under nitrogen. Seven-tenths of this solution, containing 66 mmol of benzylmagnesium chloride, was added dropwise to a suspension of **1a** (4.27 g, 22.1 mmol) and magnesium (II) chloride (0.25 g, 26 mmol) in THF (50 ml) over a period of 0.5 hr at room temperature with stirring, stirring being continued for 2 hr. Compounds **2a** (0.54 g, 7%), **3a** (2.53 g, 43%), and **4a** (0.22 g, 3%) were eluted with *n*-hexane–benzene (1: 1), benzene, and benzene–dichloromethane (1: 1), respectively. 2-*N'*-Benzylhydrazono-3-methyl-2,3-dihydrobenzothiazole (**5a**, 0.12 g, 2%) was also eluted with benzene–dichloromethane (1: 1), mp 143.5—144.5 °C (from chloroform–ethanol). IR (KBr): 3230 (NH), 1615 and 1580 cm^{-1}; NMR ($CDCl_3$): δ 3.07 (dd, $J_{vic}=7$ Hz, $J_{gem}=2.4$ Hz, 2H, $PhCH_2$), 3.30 (s, 3H, CH_3–N), 4.42 (t, $J_{vic}=7$ Hz, 1H, N–H), and 6.6—7.5 (m, 9H, Ar-H); MS: *m/e* 269 (M^+, 100%).

Reaction of ***1a*** *with Allylmagnesium Bromide.* To a stirred Grignard solution prepared from magnesium (11.00 g, 0.45 mol) and allyl bromide (18.43 g, 0.15 mol) in ether (150 ml) was added **1a** (4.38 g, 22.7 mmol) portionwise over a period of 1.5 hr at room temperature. Stirring was continued for 2.5 hr. 2-*N'*,*N'*-Diallylhydrazono-3-methyl-2,3-dihydrobenzothiazole (**6**) was eluted with benzene and recrystallized from *n*-hexane to give pure **6** (1.75 g, 30%), mp 50.5—51.5 °C. IR (KBr): 1610 and 1585 cm^{-1}; NMR ($CDCl_3$): δ 3.34 (d, $J_{CX}=6$ Hz, 4H, allylic-H_X), 3.38 (s, 3H, N–CH_3), 5.03 (dd, $J_{AC}=10$ Hz, $J_{AB}=2$ Hz, 2H, vinylic-H_A), 5.13 (dd, $J_{BC}=18$ Hz, $J_{AB}=2$ Hz, 2H, vinylic-H_B), 5.95 (dt, $J_{BC}=18$ Hz, $J_{AC}=10$ Hz, $J_{CX}=6$ Hz, 2H, vinylic-H_C), and 6.63—7.38 (m, 4H, Ar-H); MS: *m/e* 259 (M^+, 19%), 190 (M^+-CH_2CH-CH_2-N_2, 30%), and 41 ($CH_2=CHCH_2^+$, 100%).

Found: C, 64.79; H, 6.82; N, 16.16; S, 12.30%. Calcd for $C_{14}H_{17}N_3S$: C, 64.83; H, 6.61; N, 16.21; S, 12.36%.

Elution with dichloromethane gave crude 2-allyl-2-(α-hydroxyallyl)-3-methyl-2,3-dihydrobenzothiazole (**7**, 1.51 g, 27%) as an oil. Purification was difficult and no analytically pure sample was obtained. IR (neat): 3225 (OH), 1610, 1580, and 1470 cm^{-1}; NMR ($CDCl_3$): 2.33 (t, $J=6$ Hz, 2H, CH_2), 3.33 (s, 3H, N–Me), 3.62 (q, $J=6$ Hz, 1H, CH), 4.06 (s, 1H, OH), 4.86—5.37 (m, 4H, $2CH_2$–CH), 5.50—6.22 (m, 2H, $2CH_2=CH$), and 6.60—7.40 (m, 4H, Ar-H); MS: *m/e* 247 (M^+, 8.4%) and 218 ($M^+-HC=O$, 100%).

Reaction of ***1a*** *with Cinnamylmagnesium Chloride.* Cinnamylmagnesium chloride, prepared *in situ*, was allowed to react with **1a**. After a small amount of ethereal solution (100 ml) of cinnamyl chloride (15.10 g, 99 mmol) had been added to magnesium (7.67 g, 0.32 mol) covered with ether (15 ml) to start the reaction, **1a** (4.34 g, 22.4 mmol) was added with stirring. To this suspension, cooled with ice, was added the residual solution dropwise over a period of 8 hr. Stirring was continued for 0.5 hr after the addition. The reaction mixture was chromatographed on silica gel after usual work-up. A mixture (4.09 g, 21 mmol) of 1,4-diphenyl- (main) and 1,6-diphenyl-1,5-hexadienes (minor) was eluted with *n*-hexane and distilled to give an analytically pure sample, bp 160—162 °C/4 mmHg (lit,[3] 115 °C/0.005 mmHg).

Found: C, 92.46; H, 7.92%. Calcd for $C_{18}H_{18}$: C, 92.46; H, 7.84%.

3-Methyl-2-*N'*-(1-phenyl-2-propenyl) hydrazono-2,3-dihydrobenzothiazole (**8**), the only one identified product in this reaction, was eluted with dichloromethane–ether (1: 1) and ether, contaminated with a deep red oil, and recrystallized from ethanol to give 0.51 g (8%) of a pure sample, mp 103.5 °C. IR (KBr): 3225 (NH), 1620 and 1580 cm^{-1}: NMR ($CDCl_3$): δ 3.34 (s, 3H, CH_3–N), 4.2 (broad s, 1H, N–H), 4.9 (d, $J_{CX}=7$ Hz, 1H, allylic-H_X), 5.17 (dd, $J_{AC}=10$ Hz, $J_{AB}=2$ Hz, 1H, vinylic-H_A), 5.25 (dd, $J_{BC}=17$ Hz, $J_{AB}=2$ Hz, 1H, vinylic-H_B), 6.12 (sep, $J_{BC}=17$ Hz, $J_{AC}=10$ Hz, $J_{CX}=7$ Hz, 1H, vinylic-H_C), and 6.69—7.62 (m, 9H, Ar-H); MS: *m/e* 295 (M^+, 10%) and 178 ($M^+-CH_2CHCHPh$, 100%).

Found: C, 69.27; H, 5.67; N, 13.98; S, 10.87%. Calcd for $C_{17}H_{11}N_3S$: C, 69.12; H, 5.80; N, 14.22; S, 10.85%.

References

1) For Part X see K. Akiba, T. Kawamura, M. Hisaoka, and N. Inamoto, This Bulletin, **48**, 3262 (1975).
2) K. Akiba, M. Hisaoka, M. Inamoto, T. Ohta, and H. Kuroda, *Chem. Lett.*, **1975**, 347.
3) H. P. Koch, *J. Chem. Soc.*, **1948**, 1111.
4) R. B. Moffett and W. M. Hoehn, *J. Amer. Chem. Soc.*, **69**, 1792 (1974); H. Gilman and R. H. Kirby, *ibid.*, **55**, 1265 (1933).
5) E. Besthorn, *Ber.*, **43**, 1519 (1910).
6) H. Passing, *J. Prakt. Chem.*, **153**, 1 (1939).
7) R. F. Hunter, *J. Chem. Soc.*, **1930**, 125.

Chemistry of Nitrosoimines. XII.[1] Reactions of 3-Substituted 2-Nitrosoimino-2,3-dihydrobenzothiazoles with Alkyl Grignard Reagents

Kin-ya AKIBA, Motoyuki HISAOKA, Takayuki KAWAMURA, and Naoki INAMOTO
Department of Chemistry, Faculty of Science, The University of Tokyo, Hongo, Tokyo 113

(Received May 20, 1975)

3-Substituted 2-nitrosoimino-2,3-dihydrobenzothiazole (**1**) reacts with primary or secondary alkyl Grignard reagents to afford bis[*o*-(*N*-substituted amino)phenyl] disulfide, 3-substituted 2-*N'*-alkyl- and 2-*N'*,*N'*-dialkylhydrazono-2,3-dihydrobenzothiazoles as major products. In the reactions with secondary alkyl Grignard reagents, 3-substituted 2-*N'*-alkylidenehydrazono-2,3-dihydrobenzothiazole was also produced. The general feature of the reaction of **1** with Grignard reagents has been summarized and is discussed.

In a previous paper,[2] it was reported that reactions of 3-substituted 2-nitrosoimino-2,3-dihydrobenzothiazole (**1**) with arylmagnesium or *t*-butylmagnesium halides give the corresponding 2,2-di- or 2-monosubstituted benzothiazolines in good yields (*path a*). Such Grignard reagents attack the nitrogen atom of the nitroso group of **1** to give 2-(*N'*-substituted hydrazono) derivatives (*path b*).

The reaction of **1** with benzylmagnesium chloride afforded 2,2-dibenzylbenzothiazolines as minor products (*path a*) and azines and 2-(*N'*,*N'*-dibenzylhydrazono) derivatives (*path b*) as major products.[1]

This paper describes the reactions of **1** with alkyl Grignard reagents in detail[3] and gives a summary of the general aspect of the reaction of **1** with Grignard reagents.

2-Nitrosoimino-3-phenyl-2,3-dihydrobenzothiazole (**1b**) reacts with excess *n*-butylmagnesium bromide in ether at 0 °C under nitrogen to afford 2,2-di-*n*-butyl- (**2b**, 6%), 2-*N'*,*N'*-di-*n*-butylhydrazono-3-phenyl-2,3-dihydrobenzothiazoles (**3b**, 26%), and bis(*o*-anilinophenyl) disulfide (**4b**, 23%).

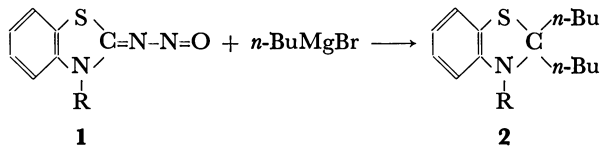

1 **2**

a, R=Me
b, R=Ph

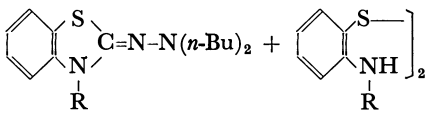

3 **4**

A similar reaction of **1a** with *n*-butylmagnesium bromide was found to give 2-*N'*-*n*-butylhydrazono-3-methyl-2,3-dihydrobenzothiazole (**5c**, 20%) and bis[*o*-(*N*-methyl-*N*-valeroylamino)phenyl] disulfide (**6**, 11%) together with **2a** (7%), **3a** (15%), and **4a** (12%).

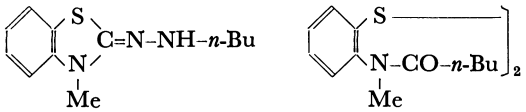

5c **6**

Reaction of **1a** with *sec*-butylmagnesium bromide gives **4a** (13%), 2-*N'*-*sec*-butylhydrazono- (**5a**, 18%), and 2-*N'*-*sec*-butylidenehydrazono-3-methyl-2,3-dihydrobenzothiazoles (**7a**, 22%).

Reaction of **1a** with cyclohexylmagnesium chloride gives **4a** (8%), **5b** (20%), **7b** (14%), and 2-*N'*,*N'*-dicyclohexylhydrazono-2,3-dihydrobenzothiazole (**8b**, 6%). The reaction scheme is shown below.

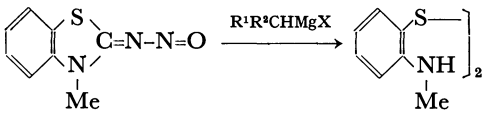

1a **a**, R^1=Me, R^2=Et **4a**
b, R^1R^2=$-(CH_2)_5-$

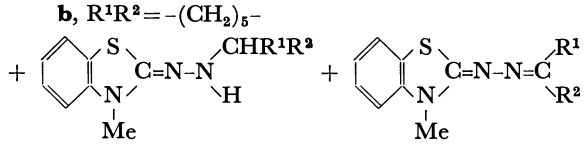

5 **7**

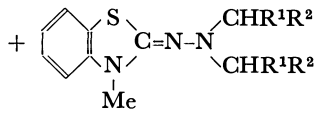

8

Reaction of **1a** with *t*-butylmagnesium chloride affords 2-*t*-butyl (**9**, 39%), 2-*N'*-*t*-butylhydrazono-3-methyl-2,3-dihydrobenzothiazoles (**10**, 8%), and 3-methyl-2,3-dihydrobenzothiazol-2-one (**11**, 13%).

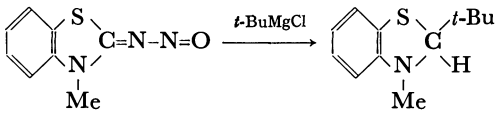

1a **9**

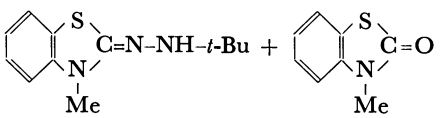

10 **11**

2,2-Disubstituted and 2-(*N'*-substituted hydrazono) derivatives are formed *via* the corresponding 1,4- (**A**) and 1,2-addition intermediates (**B**), respectively.[2]

2-*N'*-Alkylidenehydrazono derivatives in the case of secondary alkylmagnesium halides are produced by dehydration through the intermediate (**B**) because of the thermodynamic stability of the product. 2-*N'*,*N'*-Dialkylhydrazono derivatives can be formed through the intermediate (**B**) by direct attack with the second Grignard reagent (*path b-ii*) as was evidenced in the reactions with benzylmagnesium chloride in refluxing ether.[1]

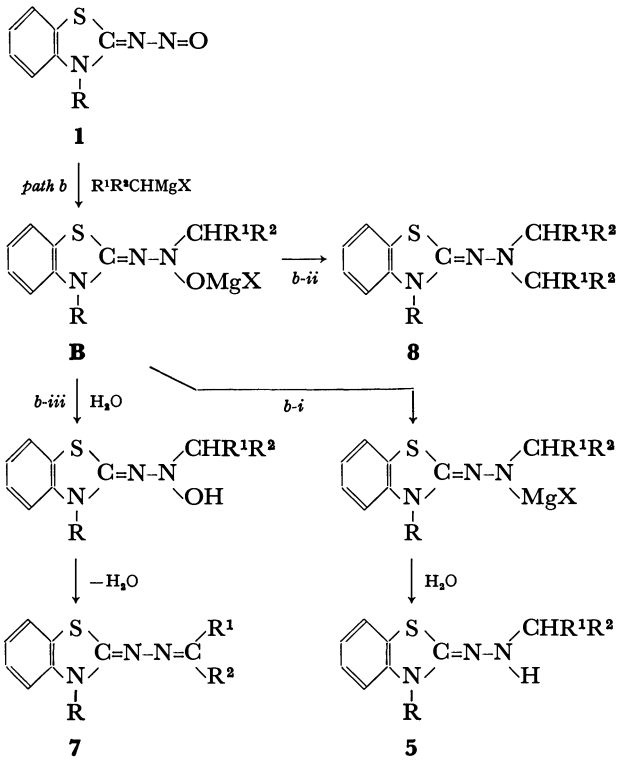

Scheme 1.

The formation of disulfide (**4**) can be explained as follows. The direct attack of a Grignard reagent on the C-2 position of **1** gives the diazonium intermediate (**A**) (*path a-i*) and the corresponding ring-opened nitrosoimine (**C**) followed by loss of nitrogen to give the corresponding amide (**D**) (*path a-ii*). The magnesium salt (**D**) then reacts with the Grignard reagent to afford the corresponding *S,N*-dimagnesium salt, which, by hydrolysis followed by oxidation, gives disulfide (**4**).

The presence of the amide (**D**) was confirmed by the isolation of **6** in the case of the reaction of **1a** with *n*-butylmagnesium bromide. Nitrogen loss from the ring-opened nitrosoimine (**C**) should proceed rapidly, as seen from the decomposition of *N*-nitrosoketimines[4] and 1,1,3,3-tetrasubstituted 2-nitrosoguanidines.[5]

The yields of reaction products of **1a** with Grignard reagents are summarized in Table 1. The yields were estimated from the amount of isolated products by column chromatography followed by recrystallization, and not optimized. The apparent yield should thus be lower than that in the reaction mixture, cases where products did not crystallize easily being affected. This was especially the case for e) in Table 1. However, it sufficiently shows the general nature of the reaction.

Table 1. Yields[a] of reaction products of **1a** with RMgX

R	Reaction path[b]				Reaction path[c]			
	X	*a-i*	*a-ii*	*a*	*b-i*	*b-ii*	*b-iii*	*b*
a) $PhCH_2$	Cl	8	—	8	—	19	44	63
b) $Me(CH_2)_3$	Br	7	23	30	20	15	—	35
c) MeEtCH	Br	—	13	13	18	—	22	40
d) *cyclo*-C_6H_{11}	Cl	—	8	8	20	6	14	40
e) Me_3C	Cl	39	—	39	8	—	—	8
f) *p*-MeC_6H_4	Br	66	—	66	17	—	—	17
g) 2,4,6-$Me_3C_6H_2$	Br	46	—	46	18	—	—	18

a) Numerical values show the yield (mol %) of products based on **1a**. b) *a*, *a-i*, and *a-ii* correspond to the reaction paths shown in Scheme 2. c) *b*, *b-i*, *b-ii*, and *b-iii* correspond to the reaction paths shown in Scheme 1.

It is apparent from Table 1 that Grignard reagents can be classified into two groups:

group α (more reactive), consisting of aryl and *t*-butyl groups (e—g).

group β (less reactive), consisting of primary and secondary alkyl groups (a—d).

General features of the reaction are summarized and rationalized as follows:

1) The main path of group α is *path a* and that of group β *path b* (see Schemes 1 and 2). This is consistent with the nature of the ground state of **1**[6] and the

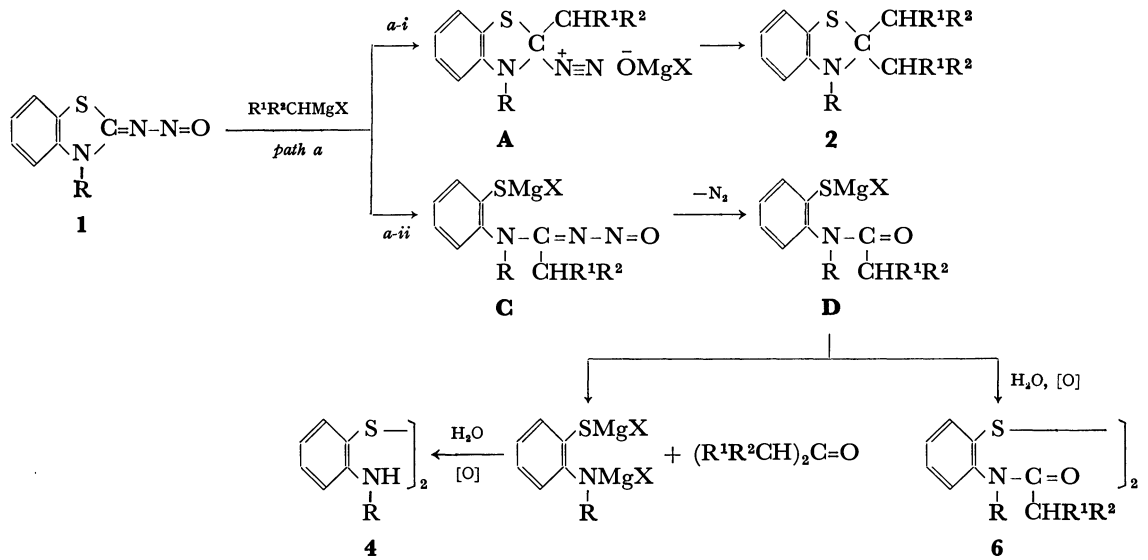

Scheme 2.

expected relative reactivity of Grignard reagents, since *path a* should be of a higher energy process than *path b*, the entire conjugation between the benzothiazoline ring and the nitrosoimino group being cut off in the former but conjugation between the ring and the imino group is retained in the latter. Here we must keep in mind that Grignard reagents add almost exclusively on the carbon of Schiff's base but not on the nitrogen.[7]

2) For *path a*, group α reacts exclusively through *path a-i*, whereas *path a-ii* is preferred by group β except benzylmagnesium chloride. This can be realized mainly by the electronic effect of the substituent (R), where R can stabilize positive charge on the C-2 more effectively, *path a-i* becomes predominant. It is noteworthy to mention that *path a-i* was not observed with secondary Grignard reagents, probably because of the balance between electronic and steric effects.

3) For *path b*, group α reacts exclusively through *path b-i*, whereas *paths b-i*, *b-ii*, and *b-iii* are competitive for group β. When the intermediate **B** is stabilized thermodynamically by dehydration, *path b-iii* is preferred as a typical one for benzylmagnesium chloride. *Path b-ii*, alkylation of Grignard type reagent of hydroxylamine by Grignard reagent, has not been observed so far. However, this was substantiated with benzylmagnesium chloride by refluxing the solvent.[1] The reason is not clear why group α does not follow *path b-ii* at all. However, it is understandable if we consider the nature of R-N-OMgX bond in the intermediate **B** (Ar-N-OMgX and *t*-Bu-N-OMgX compared with Alkyl-N-OMgX).

Experimental

Materials. 3-Methyl- (**1a**, mp 143 °C (dec.))[8] and 3-phenyl-2-nitrosoimino-2,3-dihydrobenzothiazoles (**1b**, mp 140 °C (dec.))[9] were prepared by the reported methods. All the reactions were carried out under nitrogen.

Reaction of 3-Methyl-2-nitrosoimino-2,3-dihydrobenzothiazole (1a) with n-*Butylmagnesium Bromide.* **1a** (4.78 g, 24.7 mmol) was added portionwise over a period of 0.5 hr at room temperature to a stirred Grignard solution prepared from magnesium turnings (2.76 g, 0.11 mol) and *n*-butyl bromide (13.82 g, 0.10 mol) in ether (100 ml). Stirring was continued for 3 hr. The reaction mixture was treated with saturated aqueous ammonium chloride and the resulting precipitates were filtered off. The precipitates were extracted with ether (100 ml×2) and benzene (100 ml). The extracts and ether layer of the filtrate were combined and dried over anhydrous magnesium sulfate. The solvent was evaporated *in vacuo* and the residue was chromatographed on silica gel. 2,2-Di-*n*-butyl-3-methyl-2,3-dihydrobenzothiazole (**2a**, 0.49 g, 7%) was eluted with *n*-hexane as an oil. The structure of **2a** was confirmed by the following spectral data: NMR ($CDCl_3$): δ 0.53—2.13 (m, 18H, $2CH_3CH_2CH_2CH_2$), 2.67 (s, 3H, N–CH_3), and 5.95—7.16 (m, 4H, Ar-H); Mass: *m/e* 263 (M^+, 7%) and 206 (M^+-n-Bu, 100%).

Bis(*o*-methylaminophenyl) disulfide (**4a**, 0.39 g, 12%) was eluted with *n*-hexane–benzene (1: 1) and recrystallized from chloroform–ethanol, mp 66.5—67.0 °C (lit,[10] 64—68 °C. Disulfide **4a** (0.13 g) was refluxed in acetic anhydride (8 ml) for 1 hr to give diacetylated compound (0.15 g, 87%), mp 173.0—173.8 °C (from chloroform–ethanol). IR (KBr): 1670 cm^{-1} (CO); NMR ($CDCl_3$): δ 1.85 (s, 6H, $2CH_3CO$), 3.26 (s, 6H, 2N–CH_3), and 7.05—7.72 (m, 8H, 2Ar–H); Mass: *m/e* 360 (M^+, 1.8%), 180 ($M^+/2$, 28%), and 148 ($M^+/2-S$, 100%).

Found: C, 59.76; H, 5.69; N, 7.60; S, 17.77%. Calcd for $C_{16}H_{20}N_2O_2S_2$: C, 59.97; H, 5.59; N, 7.77; S, 17.79%.

2-*N'*,*N'*-Di-*n*-butylhydrazono-3-methyl-2,3-dihydrobenzothiazole (**3a**, 1.44 g, 20%) was eluted as an oil and the structure was confirmed by the following results: IR (KBr): 1620 and 1580 cm^{-1}; NMR ($CDCl_3$): δ 0.66—1.92 (m, 14H, $2CH_3CH_2CH_2$), 2.15—2.80 (m, 4H, 2N–CH_2–*n*-Pr), 3.48 (s, 3H, N–CH_3), and 6.75—7.47 (m, 4H, Ar–H). 2-*N'*-*n*-Butylhydrazono-3-methyl-2,3-dihydrobenzothiazole (**5c**, 0.88 g, 15%) was eluted with dichloromethane, mp 66.0—66.5 °C (from chloroform–methanol). IR (KBr): 3200 (NH), 1620, and 1580 cm^{-1}; NMR ($CDCl_3$): δ 0.71—1.75 (m, 7H, $CH_3CH_2CH_2$), 3.03 (t, J=7.0 Hz, 2H, *n*-$PrCH_2$–N), 3.41 (s, 3H, N–CH_3), 4.02 (broad s, 1H, N–H, disappeared by addition of D_2O), and 6.73—7.45 (m, 4H, Ar–H); Mass: *m/e* 235 (M^+, 100%).

Found: C, 61.43; H, 7.44; N, 18.04%. Calcd for $C_{12}H_{17}N_3S$: C, 61.24; H, 7.28; N, 17.85%.

Bis[*o*-(*N*-methyl-*N*-valeroylamino)phenyl] disulfide (**6**, 0.65 g, 11%) was eluted with dichloromethane, mp 87.5—88.5 °C. The structure was confirmed by the following spectral data; IR (KBr): 1665 cm^{-1} (CO); NMR ($CDCl_3$); δ 0.58—2.20 (m, 18H, $2CH_3CH_2CH_2CH_2$), 3.23 (s, 6H, 2N–CH_3), and 7.0—7.7 (m, 8H, Ar-H); Mass: *m/e* 444 (M^+, trace) and 139 ($M^+/2$+H–*n*-PrCHCO, 100%).

Reaction of 2-Nitrosoimino-3-phenyl-2,3-dihydrobenzothiazole (1b) with n-*Butylmagnesium Bromide.* To a stirred Grignard solution prepared from magnesium (3.60 g, 0.15 mol) and *n*-butyl bromide (20.55 g, 0.15 mol) in ether (100 ml) was added **1b** (7.61 g, 29.8 mmol) portionwise at 0 °C, and the mixture was stirred for 1 hr. After the usual work-up, the reaction mixture was chromatographed on silica gel. Elution with benzene gave crude 2,2-di-*n*-butyl-3-phenyl-2,3-dihydrobenzothiazole (**2b**), which was purified by preparative thin layer chromatography with benzene–*n*-hexane (1: 3) to give pure **2b** (0.60 g, 6%) as colorless oil; NMR ($CDCl_3$): δ 0.90 (t, 6H, 2Me), 1.30—1.85 (m, 12H, $2(CH_2)_3$), and 6.75—7.40 (m, 9H, Ar–H). Elution with benzene gave tarry material (1.39 g, 23%). The IR spectrum was in agreement with that of bis(*o*-anilinophenyl) disulfide (**4b**).[11] Elution with dichloromethane–chloroform (2: 1—1: 5) and chloroform afforded red brown tarry material (3.34 g). The compound was purified twice by preparative thin layer chromatography with dichloromethane to give colorless viscous material (**3b**), which partly solidified on being left to stand for 2 weeks. **3b** (2.75 g, 26%); mp 40.0—41.5 °C; IR (KBr): 1610 (C=N) and 1580 cm^{-1}; NMR ($CDCl_3$): δ 0.85 (t, 6H, 2Me), 1.35 (m, 8H, $2(CH_2)_2$), 2.55 (t, 4H, $2CH_2$–N), and 6.7—7.4 (m, 9H, Ar–H); Mass: *m/e* 353 (M^+, 40%) and 310 ($M^+-C_3H_7$, 100%).

Reaction of 1a with sec-*Butylmagnesium Bromide.* **1a** (4.60 g, 23.8 mmol) was added portionwise over a period of 0.5 hr at room temperature to a stirred solution of Grignard reagent prepared from magnesium (2.77 g, 0.11 mol) and *sec*-butyl bromide (13.78 g, 0.10 mol) in ether (100 ml). Stirring was continued for 2 hr. The resulting reaction mixture was chromatographed on silica gel after the usual work-up. Bis(*o*-methylaminophenyl) disulfide (**4a**, 0.42 g, 13%) was eluted with *n*-hexane–benzene (1: 1) and the structure was confirmed by comparing its physical properties with those of an authentic sample.[2] 2-*N'*-*sec*-Butylidenehydrazono-3-methyl-2,3-dihydrobenzothiazole (**7a**, 1.47 g, 22%) was eluted with benzene, benzene–dichloromethane (3: 1 and 1: 1) and dichloromethane, mp 81.5—82.5 °C (from chloroform–ethanol). IR (KBr): 1635 and 1580 cm^{-1}; NMR ($CDCl_3$): δ 1.15 (t, J=7 Hz, 3H, =Ċ–$CH_2C\underline{H}_3$), 2.04 (s, 3H, =Ċ–CH_3), 2.34 (q, J=7 Hz, 2H, =Ċ–$C\underline{H}_2CH_3$), 3.44 (s, 3H, N–CH_3), and 6.65—7.39 (m, 4H, Ar-H); Mass: *m/e* 233 (M^+, 100%).

Found: C, 62.01; H, 6.53; N, 17.77; S, 13.72%. Calcd for $C_{12}H_{15}N_3S$: C, 61.77; H, 6.48; N, 18.01; S, 13.74%.

2-*N'*-*sec*-Butylhydrazono-3-methyl-2,3-dihydrobenzothiazole (**5a**, 1.05 g, 18%) was eluted with dichloromethane as an oil. The structure was confirmed by the following spectral data: IR (neat): 3200 cm^{-1} (NH); NMR ($CDCl_3$): δ 1.05 (t, J=7 Hz, 3H, $C\underline{H}_3$-CH_2), 1.10 (d, J=7 Hz, 3H, $C\underline{H}_3$-CHEt), 3.45 (s, 3H, N-CH_3), 3.82 (broad s, 1H, N-H), and 6.78—7.60 (m, 4H, Ar-H). Two multiplets, assignable to a methine proton and two methylene protons, overlapped each other.

Reaction of ***1a*** *with Cyclohexylmagnesium Chloride.* **1a** (4.47 g, 23.1 mmol) was added portionwise over a period of 0.5 hr at room temperature to a stirred solution of Grignard reagent prepared from magnesium (2.75 g, 0.11 mol) and cyclohexyl chloride (11.78 g, 99 mmol) in ether (100 ml). Stirring was continued for 4 hr. The reaction mixture was chromatographed after the usual work-up. 2-*N'*,*N'*-Dicyclohexylhydrazono-3-methyl-2,3-dihydrobenzothiazole (**8b**, 0.49 g, 6%) was eluted with *n*-hexane–benzene (1: 1), mp 121—122 °C (from ethanol). IR (KBr): 1615 and 1590 cm^{-1}; NMR ($CDCl_3$): δ 0.87—2.15 (m, 20H, $10CH_2$), 2.85 (broad s, 2H, 2CH), 3.47 (s, 3H, N-CH_3), and 6.67—7.36 (m, 4H, Ar-H); Mass: *m/e* 343 (M^+, 42%) and 150 ($M^+ - C_6H_{11}$-$C_6H_{10}N_2$, 100%).

Found: C, 70.11; H, 8.73; N, 12.24; S, 9.42%. Calcd for $C_{20}H_{29}N_3S$: C, 69.93; H, 8.51; N, 12.23; S, 9.33%.

Bis(*o*-methylaminophenyl) disulfide (**4a**, 0.27 g, 8%) was eluted with *n*-hexane–benzene (1: 1), mp 66.5—67.0 °C (from chloroform–ethanol) (lit,[10] 64—68 °C). 2-*N'*-Cyclohexylidenehydrazono-3-methyl-2,3-dihydrobenzothiazole (**7b**, 0.89 g, 14%) was eluted with benzene–dichloromethane (1: 3) as yellow crystals, mp 114.5 °C (from benzene–chloroform). IR (KBr): 1620, 1580, and 1575 cm^{-1}; NMR ($CDCl_3$): δ 1.4—2.9 (m, 10H, $5CH_2$), 3.50 (s, 3H, N-CH_3), and 6.74—7.46 (m, 4H, Ar-H); Mass: *m/e* 259 (M^+, 59%) and 121 ($C_7H_9N^+$, 100%).

Found: C, 65.02; H, 6.86; N, 16.32; S, 12.50%. Calcd for $C_{14}H_{17}N_3S$: C, 64.83; H, 6.61; N, 16.20; S, 12.36%.

2-*N'*-Cyclohexylhydrazono-3-methyl-2,3-dihydrobenzothiazole (**5b**, 1.21 g, 20%) was eluted with benzene–dichloromethane (1: 1) as pale yellow crystals, mp 112.5—114.0 °C (from chloroform–ethanol). IR (KBr): 3175 (NH), 1618, 1600, and 1580 cm^{-1}; NMR ($CDCl_3$): δ 0.85—2.18 (m, 10H, $5CH_2$), 2.95 (broad s, 1H, >CH), 3.41 (s, 3H, N-CH_3), 3.50 (broad s, 1H, N-H), and 6.65—7.44 (m, 4H, Ar-H). The singlet at δ 3.50 disappeared by addition of D_2O, a new singlet due to HDO appearing at δ 4.61. Mass: *m/e* 261 (M^+, 100%).

Found: C, 64.29; H, 7.23; N, 16.29; S, 12.37%. Calcd for $C_{14}H_{19}N_3S$: C, 64.33; H, 7.33; N, 16.08; S, 12.27%.

References

1) For Part XI see: M. Hisaoka, K. Akiba, and N. Inamoto, This Bulletin, **48**, 3266 (1975).
2) K. Akiba, T. Kawamura, M. Hisaoka, and N. Inamoto, This Bulletin **48**, 3262 (1975).
3) Preliminary report: K. Akiba, T. Kawamura, M. Hisaoka, and N. Inamoto, *Chem. Lett.*, **1973**, 201.
4) C. J. Thoman, S. J. and I. M. Hunsberger, *J. Org. Chem.*, **33**, 2852 (1968).
5) K. Akiba, S. Matsunami, C. Eguchi, and N. Inamoto, This Bulletin, **47**, 953 (1974).
6) K. Akiba, M. Hisaoka, N. Inamoto, T. Ohta, and H. Kuroda, *Chem. Lett.*, **1975**, 347.
7) R. B. Moffett and W. M. Hoehn, *J. Amer. Chem. Soc.*, **69**, 1792 (1947).
8) E. Besthorn, *Ber.*, **43**. 1519 (1910).
9) H. Passing, *J. prakt. Chem.*, **153**, 1 (1939).
10) C. D. Harries and E. Loewenstein, *Ber.*, **27**, 861 (1894). A. I. Kiprianov and Z. N. Pazenko, *J. Gen. Chem.*, **19**, 1523 (1949); *Chem. Abstr.*, **44**, 3487 (1950).
11) A. I. Kiprianov and I. K. Ushenko, *J. Gen. Chem.*, **17**, 2201 (1947); *Chem. Abstr.*, **42**, 5016 (1948).

Chemistry of Nitrosoimines. XIII.[1] Reactions of 3-Substituted 2-Nitrosoimino-2,3-dihydrobenzothiazoles with Organolithiums

Motoyuki HISAOKA, Kin-ya AKIBA, and Naoki INAMOTO
Department of Chemistry, Faculty of Science, The University of Tokyo, Hongo, Tokyo 113
(Received May 20, 1975)

Reactions of 3-substituted 2-nitrosoimino-2,3-dihydrobenzothiazoles (**1**) with phenyl- and *n*-butyllithiums give the corresponding (*N*-substituted *o*-amino)phenyl sulfides as the major product due to direct attack on the sulfur atom of the benzothiazoline ring, while that with benzyllithium gives 2,2-dibenzyl derivatives and bis[*o*-(*N*-substituted amino)phenyl] disulfides. The difference between the reactions of **1** with Grignard reagents and those with organolithiums has been explained by the difference of the coordination site, thiophilicity and the ionic character of the reagents.

The reactions of 3-substituted 2-nitrosoimino-2,3-dihydrobenzothiazoles (**1**) with Grignard reagents give different types of main products depending on the structure of Grignard reagents.[1-3]

In this paper, the reaction of **1** with organolithiums,[4] which differ from those with Grignard reagents in their main reaction paths, are described in detail. The reason for the apparent difference in reactivity is also discussed.

3-Substituted 2-nitrosoimino-2,3-dihydrobenzothiazoles (**1**) were allowed to react with excess phenyllithium (about five molar equivalents) in ether for 1 hr at 0 °C under nitrogen. 3-Substituted 2,2-diphenyl-2,3-dihydrobenzothiazole (**2**), the main product in the corresponding Grignard reaction,[2] was obtained only in a very low yield. The major product was phenyl *N*-substituted *o*-aminophenyl sulfide (**3**) and benzophenone. Refluxing of **3** in acetic anhydride gave the corresponding acetylated derivative (**4**) in a high yield.

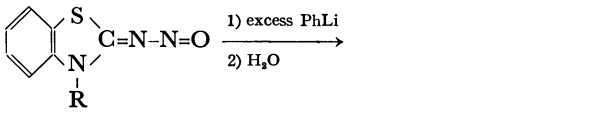

1 **2** **3**

	R	2	3	Ph_2CO
a)	Me	trace	36%	52%
b)	Ph	trace	38%	58%

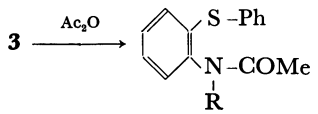

4

When excess *n*-butyllithium was added to a suspension of **1b** in ether under nitrogen at 0 °C, 2,2-di-*n*-butyl-3-phenyl-2,3-dihydrobenzothiazole (**5**, 10%), bis(*o*-anilinophenyl) disulfide (**6b**, 3%), *o*-anilinophenyl *n*-butyl sulfide (**7**, 43%), and 2-*N'*-*n*-butylidenehydrazono-3-phenyl-2,3-dihydrobenzothiazole (**8**, 10%) were obtained.

Attack on the C-2 position of the benzothiazoline ring became the main path, when **1a** and benzyllithium were allowed to react in tetrahydrofuran (THF) under almost the same conditions, giving **9** and **6a** in 16 and 38% yields, respectively.

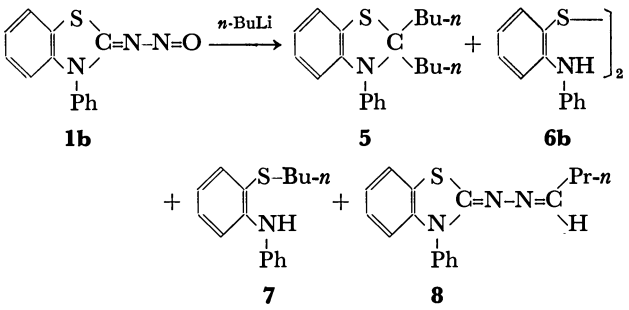

1b **5** **6b**

7 **8**

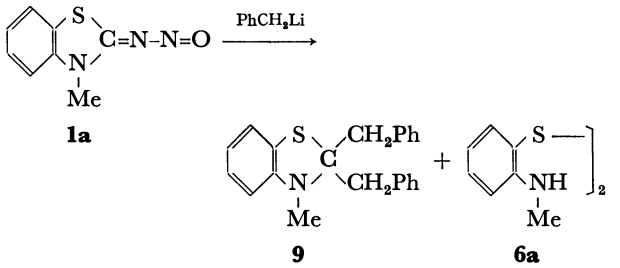

1a **9** **6a**

Mechanism of Formation. The formation of products other than **3** and **7** can be explained by a mechanism analogous to that for the reactions with Grignard reagents.[1-3] The path of formation of **3** and **7** is explained as shown in Scheme 1.

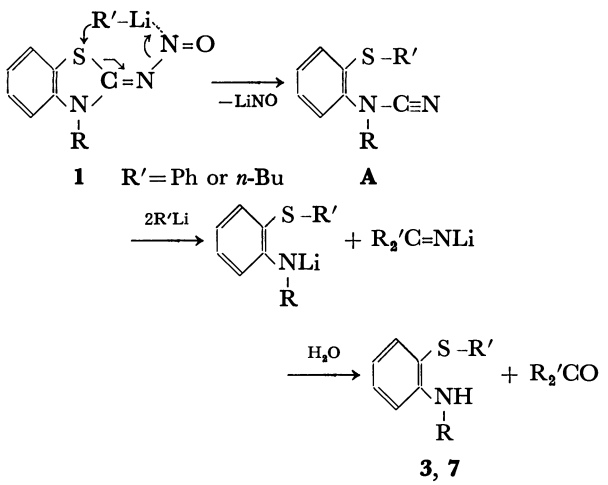

1 R'=Ph or *n*-Bu **A**

3, 7

Scheme 1.

Phenyl- and *n*-butyllithium directly attack the sulfur atom of the benzothiazoline ring *via* lithium–nitrogen coordination and cleavage of the carbon–sulfur linkage followed by loss of NO^- anion to give the corresponding phenyl and *n*-butyl *N*-substituted *o*-cyanaminophenyl sulfides (**A**) as a primary product. **A** reacts further with excess organolithium to produce **3** or **7** and benzophenone after hydrolysis.

The cyano group in **A** behaves as a pseudo-halogen, undergoing nucleophilic displacement or metal-cyanide exchange. In fact, the cyano group is transferred from *N,N*-diphenylcyanamide to phenylmagnesium bromide[5] and from *N*-methyl-*N*-phenylcyanamide to phenyllithium.[6] These results support the second step of Scheme 1.

The formation of **6** is ascribable to the intermediacy of ring-opened nitrosoimine (**C**) (Scheme 2), which is similar to that of Grignard reagent.[1]

Path a-iii is assumed to be another route for **6**, due to the large ionic character of the –O–Li bond in contrast to the –O–MgX bond. The same kind of difference was observed in the reaction of **1** with lithium and Grignard reagents of the corresponding 2-iminobenzothiazolines.[7]

Direct attack on the sulfur atom of the benzothiazoline ring, which was the main path in the case of phenyl- and *n*-butyl–lithium, was observed neither in the case of benzyllithium nor in the reactions with Grignard reagents.

Discussion on the Difference between the Reactions with Grignard Reagents and Those with Organolithiums. Based on the results of the spectral study on **1**,[8] the reactions of **1** with nucleophiles are expected to take place on three possible reaction centers, *i.e.*, the C-2 position of the benzothiazoline ring (*a*), the nitrogen atom of the nitroso group (*b*) and the sulfur atom of the ring (*c*).

The difference between the reactions of **1** with Grignard reagents and those with organolithiums can primarily be attributed to the difference in the coordination position of organomagnesium and organolithium compounds to the nitrosoimino group of **1**.

This postulate is supported by the reactions of nitrosobenzene with Grignard reagents[9–12] and phenyllithium.[13] The reaction with an equimolar amount of phenylmagnesium bromide has been shown to give the corresponding hydroxylamine,[9,11,12] which reacts successively with excess Grignard reagent to give diphenylamine and biphenyl.[11] On the other hand, nitrosobenzene reacts with excess phenyllithium to give diphenylamine and phenol, but the reaction of *N,N*-diphenylhydroxylamine with excess phenyllithium does not produce diphenylamine and phenol, recovering the hydroxylamine.[13]

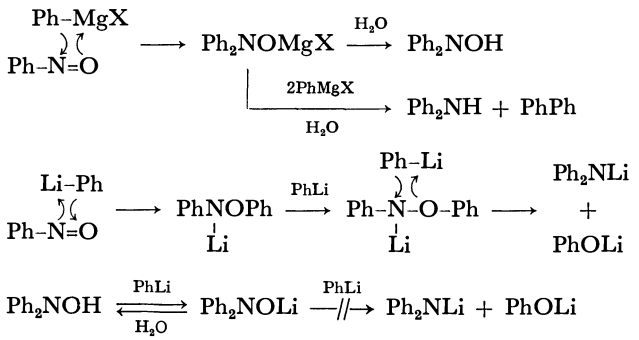

It was proposed from the results that the reaction of nitrosobenzene with phenyllithium initially gives not *O*-lithio compound but *N*-lithio compound, which is then attacked by another phenyllithium to give diphenylamine and phenol.[13]

Let us propose that organolithiums are coordinated by the nitrogen atom of the nitroso group and attack the sulfur atom of the benzothiazoline ring (*path c*) and competitively the C-2 position of the ring (*path a*). *Path c* may be a process of higher energy than *path a*, since benzyllithium follows *path a* exclusively.

On the other hand, we propose that Grignard reagents are coordinated by the oxygen atom of the nitroso group and attack the position *a* to give the corresponding diazonium salt (*path a-i*) and/or the ring-opened nitrosoimine (*path a-ii*) and competitively the position *b* to

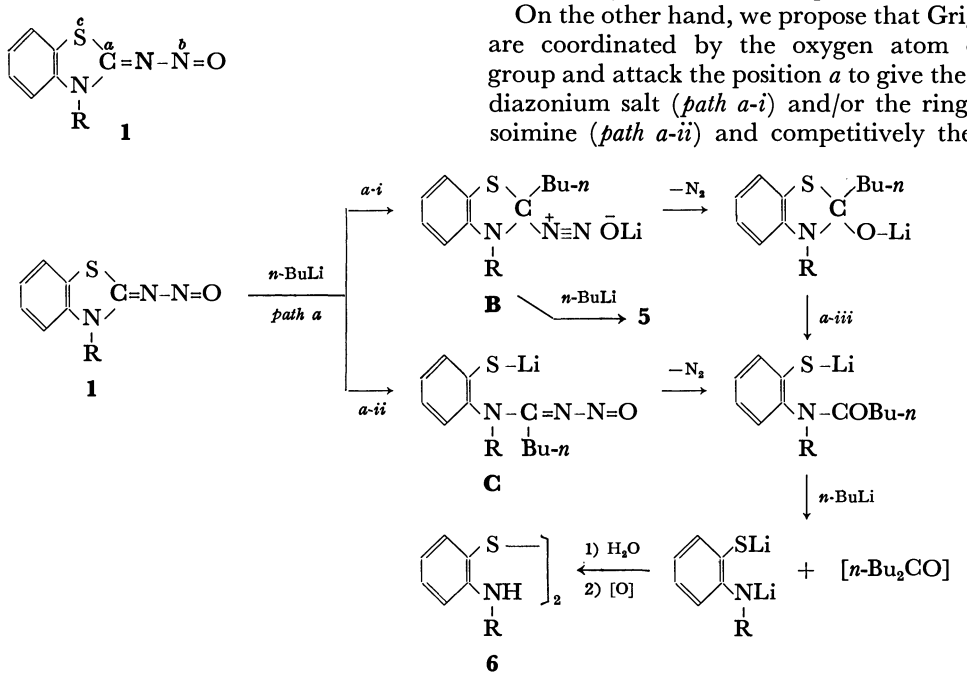

Scheme 2.

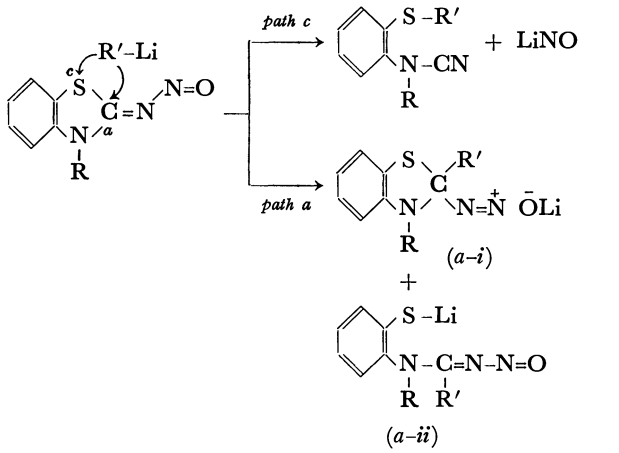

produce the magnesium salt of the corresponding hydrazono derivative (*path b*). Contribution of these paths to the reaction depends on the nature of Grignard reagents.[1]

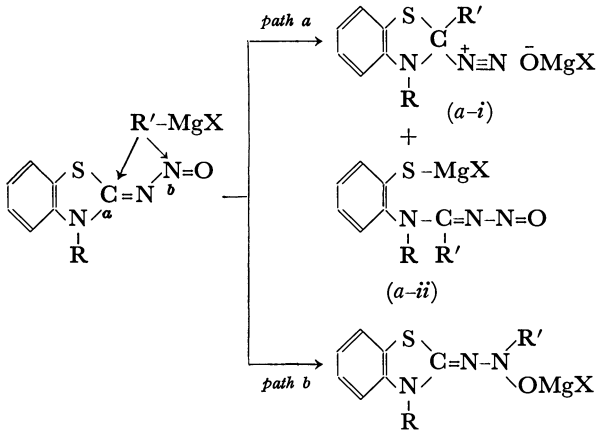

It should be kept in mind that addition of Grignard reagents and organolithiums occurs exclusively on the carbon atom of Schiff's base[14] and that organolithiums are usually more reactive than Grignard reagents as shown by the addition of methyllithium to *N*-benzylidene-*t*-butylamine which is inert to methylmagnesium bromide.[15]

There may be another factor contributing to the difference in reactivity of Grignard reagents and organolithiums, *viz.*, thiophilicity.

Organometallics have been shown to attack the sulfur of thioketones[16] and thioketenes,[17] generating the corresponding carbanions. There is no definite comparison of thiophilicity of organolithiums and Grignard reagents. However, the fact that the yield of benzhydryl phenyl sulfide was 70% (isolated yield) and 37% (glc yield), respectively, when thiobenzophenone reacted with phenyllithium and phenylmagnesium bromide[17] shows greater thiophilicity of phenyllithium than that of phenylmagnesium bromide.

Thus, the difference in reactivity between organolithiums and Grignard reagents can be ascribed to three factors, *i.e.*, i) coordination site, ii) thiophilicity, and iii) ionic character of both reagents.[18]

Experimental

Materials. Benzyl methyl ether was prepared from benzyl chloride, methanol, and sodium hydroxide,[19] bp 48—49 °C/10 mmHg (lit,[19] 170.5 °C). Commercial *n*-butyllithium in *n*-hexane was used. Phenyllithium was prepared from lithium and bromobenzene in ether under nitrogen by the method of Jones and Gilman.[20] Excess lithium was filtered off before use. Benzyllithium was prepared from benzyl methyl ether and lithium in THF at −27——5 °C according to the method of Gilman and McNinch.[21] Excess lithium was filtered off before use. 3-Methyl- (**1a**, mp 143 °C (dec.))[22] and 3-phenyl-2-nitrosoimino-2,3-dihydrobenzothiazoles (**1b**, mp 140 °C (dec.))[23] were prepared by the reported methods.

All the reactions were carried out under nitrogen.

Reaction of 2-Nitrosoimino-3-phenyl-2,3-dihydrobenzothiazole (1b) with Phenyllithium. **1b** (4.91 g, 19.2 mmol) was added portionwise over a period of 0.5 hr at 0 °C to a stirred solution of phenyllithium prepared from lithium (1.71 g, 0.25 mol) and bromobenzene (15.87 g, 0.10 mol) in ether (100 ml). Stirring was continued for further 0.5 hr after the addition. The reaction mixture was treated with 100 ml of 17% aqueous ammonium chloride, and extracted with ether. The extracts were washed with water and dried over anhydrous magnesium sulfate. After evaporation of ether, the residue was chromatographed on silica gel. A trace amount of 2,2,3-triphenyl-2,3-dihydrobenzothiazole (**2b**) was eluted with *n*-hexane, mp 191.5—192.5 °C (from benzene–ethanol) (lit,[2] 191.5—192.5 °C). *o*-Anilinophenyl phenyl sulfide (**3b**) was eluted with *n*-hexane–benzene (1 : 1) and recrystallized from benzene–ethanol as pale yellow crystals, yield 1.83 g, (38%), mp 93.0—94.5 °C. IR (KBr): 3350 (NH) and 1585 cm^{-1}; NMR ($CDCl_3$): δ 6.35—7.65 (m, ArH). A signal due to N–H proton was obscure. Mass: *m/e* 277 (M^+, 100).

Found: C, 78.15; H, 5.22; N, 5.12; S, 11.53%. Calcd for $C_{18}H_{15}NS$: C, 77.94; H, 5.45; N, 5.05; S, 11.56%.

Compound **3b** (0.19 g, 0.7 mmol) was refluxed in acetic anhydride (5 ml) for 1.5 hr to give *N*-acetylated derivative (**4b**, 0.18 g, 80%), mp 107.0—107.5 °C (from ethanol). IR (KBr): 1670 cm^{-1} (CO); NMR ($CDCl_3$): δ 2.08 (s, 3H, CH_3) and 7.0—7.5 (m, 14H, ArH); Mass: *m/e* 319 (M^+, 8.9%), 277 (M^+–$H_2C{=}C{=}O$, 65), and 210 (M^+–PhS, 100).

Found: C, 75.37; H, 5.12; N, 4.30; S; 9.80%. Calcd for $C_{20}H_{17}NOS$: C, 75.21; H, 5.36; N, 4.39; S, 10.04%.

Benzophenone (1.81 g, 58%) was also eluted with *n*-hexane–benzene (1:1), benzene and benzene–dichloromethane (1:1), bp 123 °C/4 mmHg (lit,[24] 187—190 °C/15 mmHg). The spectral data (NMR and IR) were in agreement with those of an authentic sample.

Reaction of 3-Methyl-2-nitrosoimino-2,3-dihydrobenzothiazole (1a) with Phenyllithium. In a manner similar to run a), **1a** (4.91 g, 17.2 mmol) was allowed to react with phenyllithium (0.10 mol) in ether (100 ml). The reaction mixture was chromatographed on silica gel after the usual work-up. A trace amount of 2,2-diphenyl-3-methyl-2,3-dihydrobenzothiazole (**2a**, 0.11 g, 0.35 mmol) was eluted with *n*-hexane, mp 142—143 °C (from chloroform) (lit,[2] 142—143 °C). *o*-Methylaminophenyl phenyl sulfide (**3a**, 1.97 g, 36%) was eluted with *n*-hexane–benzene (1: 1) as an oil. The structure of **3a** was confirmed by the following spectral data: IR (neat): 3400 cm^{-1} (NH); NMR ($CDCl_3$): δ 2.75 (s, 3H, CH_3–N), 4.82 (broad s, 1H, N–H), and 6.5—7.6 (m, 9H, ArH); Mass: *m/e* 215 (M^+, 100%). Compound **3a** (0.57 g, 2.66 mmol) was refluxed in acetic anhydride (6 ml) for 1.5 hr to afford the *N*-acetyl derivative (**4a**, 0.47 g, 68%) as an oil, which was chromatographed on silica gel (dry column method) to give an analytically pure sample of **4a**. IR (neat): 1670 cm^{-1} (CO); NMR ($CDCl_3$): δ 1.85 (s, 3H, $COCH_3$), 3.23 (s, 3H CH_3–N), and 7.03—7.69 (m, 9H, ArH); Mass: *m/e* 257 (M^+, 4.1%), 215 (M^+–$CH_2{=}C{=}O$, 11), and 148 (M^+–PhS,

100).

Found: C, 69.72; H, 6.14; N, 5.24%. Calcd for $C_{15}H_{15}NOS$: C, 70.01; H, 5.87; N, 5.44%.

Benzophenone (1.624 g, 52%) was eluted with *n*-hexane–benzene (1: 1).

Reaction of ***1b*** *with* n-*Butyllithium.* *n*-Butyllithium (68 mmol) in *n*-hexane was added dropwise to a suspension of **1b** (4.90 g, 19.2 mmol) in ether (70 ml) over a period of 1 hr with stirring at 0 °C. Stirring was continued for 3 hr after the addition. After the usual work-up, the reaction mixture was chromatographed on silica gel. 2,3-Di-*n*-butyl-3-phenyl-2,3-dihydrobenzothiazole (**5**, 0.65 g, 10%) was eluted with *n*-hexane as an oil and the structure of **5** was confirmed by the following spectral data: NMR ($CDCl_3$): δ 0.5—2.2 (m, 18H, $2CH_3CH_2CH_2CH_2$) and 6.0—7.5 (m, 9H, ArH); Mass: *m/e* 325 (M^+, 12%) and 268 (M^+–*n*-Bu, 100). Bis(*o*-anilinophenyl) disulfide (**6b**, 0.13 g, 3%) was eluted with *n*-hexane–benzene (1: 1) as an oil. IR (neat): 3350 cm^{-1} (NH); MS: *m/e* 400 (M^+). The structure of **6b** was confirmed by comparing its spectral data (IR and NMR) with those of an authentic sample prepared from 3-phenyl-2,3-dihydrobenzothiazol-2-one and potassium hydroxide in ethanol.[25] *o*-Anilinophenyl *n*-butyl sulfide (**7**, 2.12 g, 43%) was eluted with *n*-hexane–benzene (1: 1) as an oil. The structure of **7** was confirmed by the following spectral data: IR (neat): 3350 cm^{-1} (NH); NMR ($CDCl_3$): δ 0.6—1.8 (m, 7H, $CH_3CH_2CH_2$), 2.7 (t, 2H, $-CH_2-S$), and 6.4—7.7 (m, 9H, ArH); Mass: *m/e* 257 (M^+, 97) and 201 ($M^+-CH_2=CHCH_2CH_3$, 100). 2-*N'*-*n*-Butylidenehydrazono-3-phenyl-2,3-dihydrobenzothiazole (**8**, 0.59 g, 10%) was eluted with benzene–dichloromethane (1: 1) as pale yellow crystals, mp 112—113 °C. The structure of **8** was confirmed by the following spectral data: IR (KBr): 1615, 1580, 1560, and 1550 cm^{-1}; Mass: *m/e* 295 (M^+, 55%) and 225 (M^+–*n*-PrCH=N, 100).

Reaction of ***1a*** *with Benzyllithium.* **1a** (3.44 g, 17.8 mmol) was added portionwise over a period of 0.5 hr at room temperature to a stirred solution of benzyllithium prepared from lithium (3.27 g, 0.47 mol) and benzyl methyl ether (14.07 g, 0.12 mol) in THF (320 ml). Stirring was continued for an additional 3 hr. After the usual work-up, the reaction mixture was chromatographed on silica gel. 2,2-Dibenzyl-3-methyl-2,3-dihydrobenzothiazole (**9**, 0.96 g, 16%) was eluted with *n*-hexane–benzene (1: 1), mp 86.5—87.5 °C (from chloroform–ethanol) (lit,[3] 86.5—87.5 °C). Bis(*o*-methylaminophenyl) disulfide (**6a**, 0.95 g, 38%) was eluted with *n*-hexane–benzene (1: 1) and benzene, mp 66.5—67.0 °C (from chloroform–ethanol) (lit,[2] 66.5—67.0 °C).

References

1) For Part XII see: K. Akiba, M. Hisaoka, T. Kawamura, and N. Inamoto, This Bulletin, **48**, 3270 (1975).

2) K. Akiba, T. Kawamura, M. Hisaoka, and N. Inamoto, This Bulletin, **48**, 3262 (1975).

3) M. Hisaoka, K. Akiba, and N. Inamoto, This Bulletin, **48**, 3266 (1975).

4) Preliminary paper: K. Akiba, M. Hisaoka, and N. Inamoto, *Chem. Lett.*, **1974**, 1267.

5) Dr. C. Eguchi of our laboratory found that the reaction of diphenylcyanamide (0.20 mol) in THF (40 ml) with phenylmagnesium bromide prepared from bromobenzene (0.26 mol) and magnesium (0.266 mol) in THF (36 ml) afforded diphenylamine (0.15 mol, 77%) and benzonitrile (0.17 mol, 83%) at room temperature, giving an example of the cyano group transformation.

6) R. J. Ambrose and M. L. Hergenrother, *Macromolecules*, **5**, 275 (1972).

7) K. Akiba, K. Ishikawa, and N. Inamoto, *Heterocycles*, **2**, 555 (1974).

8) K. Akiba, M. Hisaoka, N. Inamoto, T. Ohta, and H. Kuroda, *Chem. Lett.*, **1975**, 347.

9) H. Wieland and A. Roseeu, *Ber.*, **45**, 494 (1912).

10) H. Wieland and A. Roseeu, *ibid.*, **48**, 1117 (1915).

11) H. Gilman and R. McCracken, *J. Amer. Chem. Soc.*, **49**, 1052 (1927).

12) K. Maruyama, This Bulletin, **37**, 1013 (1964).

13) P. Buck and G. Köbrich, *Tetrahedron Lett.*, **1967**, 1563.

14) R. B. Moffett and W. M. Hoehn, *J. Amer. Chem. Soc.*, **69**, 1792 (1947); H. Gilman and R. H. Kirby, *ibid.*, **55**, 1265 (1933).

15) B. L. Embing, R. J. Horvath, A. J. Saraceno, E. F. Ellermeyer, L. Hail, and L. D. Hudac, *J. Org. Chem.*, **24**, 657 (1959).

16) P. Beak and J. W. Worley, *J. Amer. Chem. Soc.*, **94**, 597 (1972).

17) E. Schaumann and W. Walter, *Chem. Ber.*, **107**, 3562 (1974).

18) L. Pauling, "The Nature of the Chemical Bond," Chap. 3, Cornell University Press (1960).

19) W. T. Olson, H. F. Hipsher, C. M. Buess, I.A. Goodman, I. Hart, J. H. Lamneck, Jr., and L. C. Gibbons, *J. Amer. Chem. Soc.*, **69**, 2451 (1947).

20) R. G. Jones and H. Gilman, *Org. Reactions*, **4**, 339 (1951).

21) H. Gilman and H. A. McNinch, *J. Org. Chem.*, **26**, 3723 (1961).

22) E. Besthorn, *Ber.*, **43**, 1519 (1910).

23) H. Passing, *J. Prakt. Chem.*, **153**, 1 (1939).

24) C. S. Marvel and W. M. Sperry, "Organic Syntheses," Coll. Vol. **1**, 95 (1967).

25) A. I. Kiprianov and Z. N. Pazinko, *J. Gen. Chem.*, **19**, 1523 (1949); *Chem. Abstr.*, **44**, 3487 g (1950).

Syntheses of Tetracyclo[7.3.0.0^{3,7}.0^{4,10}]dodecane-2,8-dione ("[8]Diisotwistane-2,8-dione"[1]) and 8,9-Benzotricyclo[4.3.1.0^{3,7}]decane ("Benzoisotwistane")

Masao NAKAZAKI, Koichiro NAEMURA, and Hiroyuki YOSHIHARA

Department of Chemistry, Faculty of Engineering Science, Osaka University, Toyonaka, Osaka 560

(Received May 21, 1975)

Tetracyclo[7.3.0.0^{3,7}.0^{4,10}]dodecane-2,8-dione ("[8]diisotwistane-2,8-dione") was synthesized from *trans-anti*-2,5-dioxo-7,8-diethoxycarbonylbicyclo[2.2.2]octane which was prepared by the Diels-Alder reaction of hydroquinone with diethyl fumarate. 8,9-Benzotricyclo[4.3.1.0^{3,7}]decane ("benzoisotwistane") was also synthesized from 2-oxo-5-*endo*-ethoxycarbonyl-7,8-benzotricyclo[2.2.2]octane which was obtained by the Diels-Alder reaction of β-naphthol with ethyl acrylate.

We have been interested in the preparation of "gyrochiral"[2] cage-shaped compounds such as twistane (D_2 point group) (**1**)[3] and twist-brendane (C_2 point group) (**2**)[4] as well as in the study of their chiroptical properties.

1 **2**

Although twistane (**1**) can be regarded as being constructed by the double 1–4 and 2–5 ethano-bridging over and below twist-cyclohexane (D_2 symmetry), one can also visualized it as being formed by the single diagonal ethano-bridging between 2 and 5 positions of bicyclo[2.2.2]octane (**3**). On continuance of this type of diagonal ethanol-bridging on twistane, there arise successively ditwistane (C_2 point group) (**4**)[5] and tritwistane (D_3 point group) (**5**). There remains another possible ethano-bridging, *i.e.* the collateral bridging between 3 and 5 positions this time, and this type of bridging on parent bicyclo[2.2.2]octane gives isotwistane (C_s point group) (**6**), "[8]diisotwistane"(C_2 point group) (**7**),[6] and the pentacyclic hydrocarbon (C_2 point group) (**8**)[8] successively.

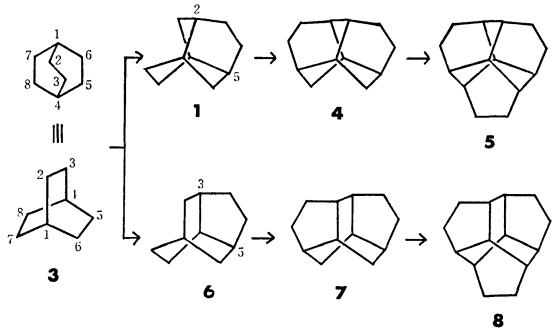

We have been making efforts to synthesize these "gyrochiral" tetra and pentacyclic compounds, and this paper reports the preparation of [8]diisotwistane-2,8-dione (**9**) as the first member of the tetracyclic compound with this unique structure. Although 8,9-benzotricyclo-[4.3.1.0^{3,7}]decane ("benzoisotwistane") (**10**) is achiral, since its preparation incidentlly follows an analogous scheme to the compound (**9**) in securing the starting material as well as in its final synthetic step, the synthesis of this compound will also be reported in the latter part of this paper.

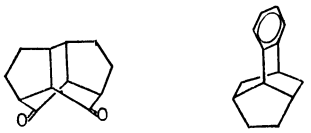

9 **10**

[8]Diisotwistane-2,8-dione

Heating a mixture of hydroquinone and diethyl fumarate under a nitrogen atmosphere for 63 hr at 200—220 °C and chromatographic separation of the adduct gave two ketonic substances in a 3: 1 ratio; the major product melting at 88—89 °C and the minor product melting at 104.5—105.5 °C. The stereoisomeric nature of these compounds were demonstrated by their conversion to the same *trans*-2,3-dicarboxybicyclo[2.2.2]-octane (**11**) on Wolff-Kishner reduction. We resorted to the NMR spectra (Table 1) of their ketal derivatives (**14**) and (**15**) to securing the informations about their stereochemistry. A W-letter long-range coupling between proton H_a and proton H_d in ketalester (**14**) from the minor product which is clearly revealed on a spin decoupling experiment afforded the evidence to

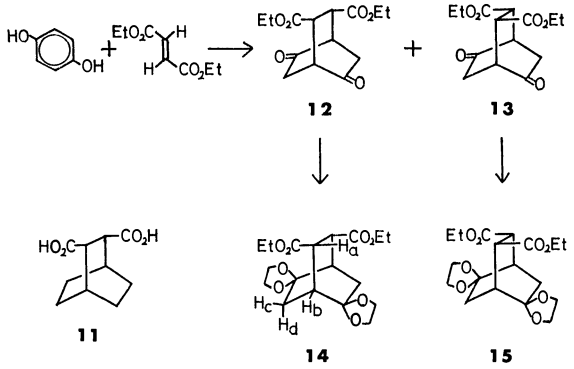

12 **13** **11** **14** **15**

TABLE 1. NMR SPECTRA (IN $CDCl_3$) OF **14** AND **15**

	14	**15**
Carboethoxy	δ 1.22 (t, 6H)	δ 1.21 (t, 6H)
	4.18 (q, 4H)	4.10 (q, 4H)
H_c	1.77 (q, 2H)	1.78 (q, 2H)
H_d	2.18 (q, 2H)	2.12 (q, 2H)
H_b	2.28 (m, 2H)	2.51 (m, 2H)
H_a	3.42 (d, 2H)	3.05 (d, 2H)
Ethylenedioxy	3.85—4.00 (m, 8H)	3.62—3.90 (m, 8H)

assign the *anti*-structure[9] (**12**) to the minor adduct whereas the *syn*-structure[9] (**13**) to the major adduct.

This assignment was further supported by their chemical behaviors as follows. Lithium aluminum hydride reduction converted these two ketals into two alcohols (**16**) and (**17**). Whereas treatment of *anti*-ketalalcohol (**16**) with 5% sulfuric acid led to the corresponding ketoalcohol (**18**), the same procedure led the *syn*-ketalalcohol (**17**) to the hemi-ketal (**19**) whose structure was confirmed by the IR spectrum.

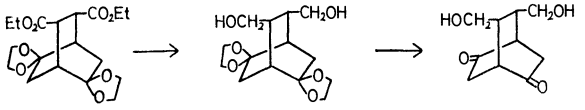

14 **16** **18**

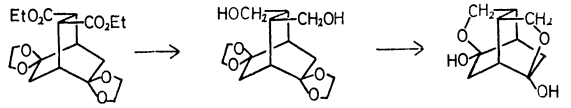

15 **17** **19**

Thus being convinced of the stereochemistry, we could carry on our syntheses. Tosylation of the *anti*-alcohol (**16**) provided the ketaltosylate (**20**) which was treated with sodium cyanide in DMF to give the *anti*-nitrile (**21**). Alkaline hydrolysis of the *anti*-nitrile (**21**) afforded the *anti*-carboxylic acid (**22**), which was reduced with lithium aluminum hydride to yield the *anti*-alcohol (**23**). After mesylation of the *anti*-alcohol (**23**), ketal functions were removed by treatment with 10% sulfuric acid. The resultant *anti*-ketomesylate (**25**) was treated with sodium hydride in DMF. Chromatography on silica gel followed by sublimation of the reaction product yielded a dione mp 88—89 °C, to which the structure (**26**) was assigned on the basis of the following spectral data. The NMR spectrum exhibited two multiplet signals centered at δ 2.53 due to protons H_b and at 2.83 due to protons H_c. The IR spectrum showed a carbonyl absorption at 1710 cm^{-1}. The UV spectrum showed absorption maxima at 258 (ε=40) and 289 (42) nm.

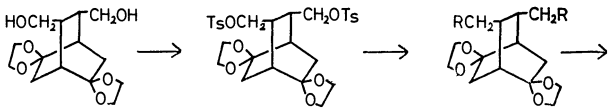

16 **20** **21** R=CN
22 R=CO_2H

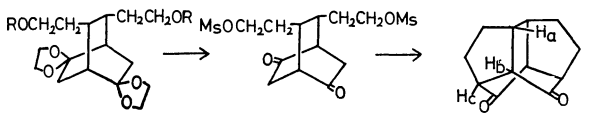

23 R=H
24 R=Ms
25 **26**

It seems in order here to divert attention from [8]diisotwistane series of compound to our sterile efforts to [8]ditwistane series of compound. The same procedure described for *anti*-form converted the *syn*-ketalalcohol (**17**) into *syn*-nitrile (**28**), *syn*-carboxylic acid (**29**), and *syn*-ketalalcohol (**30**) successively. On treatment with methanesulfonyl chloride and pyridine the *syn*-ketalalcohol (**30**) gave a corresponding ketal-mesylate (**31**) whose structure was confirmed on the basis of its NMR and IR spectra. But various fruitless attempts to remove the ketal functions at this stage forced us to abandon the hope to proceed further.

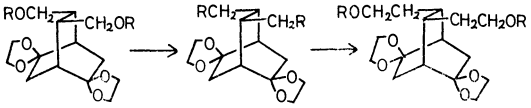

17 R=II
27 R=Ts
28 R=CN
29 R=CO_2H
30 R=H
31 R=Ms

Benzoisotwistane

Diels-Alder reaction which was proved convenient to secure starting materials with functional groups suitable for the synthesis of the cage-shaped compound as described above, encouraged us to apply this reaction to β-naphthol and ethyl acrylate. Although formation of the four isomers (**32**)—(**35**) was theoretically expected, analysis of the adduct, bp 137—140 °C at 0.1 mmHg, by glc revealed a formation of only two components in a ratio of 2: 3. Reflection on steric and electric effects involved in the Diels-Alder reaction led to the conclusion that 2-oxo-5-ethoxycarbonyl-7,8-benzobicyclo[2.2.2]-octanes (**32**) and (**33**) should be formed preferentially over 2-oxo-6-ethoxycarbonyl-7,8-benzobicyclo[2.2.2]-octanes (**34**) and (**35**). Further structural information was accessible from the NMR spectrum which showed two three-protons triplets centered at 1.11 and 1.26 (relative ratio 4: 6 respectively). These signals were due to methyl protons of carboethoxy groups. The high field signal was assigned for *exo*-isomer (**33**)[10] and the low field one was due to *endo*-isomer (**32**).[10]

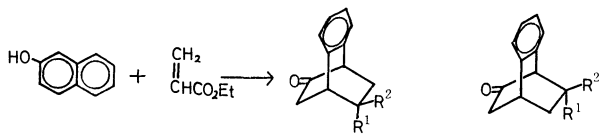

32 R^1=CO_2Et, R^2=H
33 R^1=H, R^2=CO_2Et
34 R^1=CO_2Et, R^2=H
35 R^1=H, R^2=CO_2Et

No attempt was made at this stage to separate these isomers because of difficulty encountered to accomplish the separation, and the product after ketalization with ethylene glycol was treated with lithium aluminum hydride to give a mixture of the ketalalcohols (**38**) and (**39**). Upon treatment with *p*-toluenesulfonyl chloride and pyridine the mixture of the ketalalcohols (**38**) and (**39**) was converted into the mixture of the tosylates (**40**) and (**41**). At this stage one isomer of the tosylates was separated as crystals and the other was liquid. The fact that this crystalline isomer was eventually led to benzoisotwistane implies the isomer has *endo*-structure (**40**) whereas the liquid one has *exo*-structure (**41**).

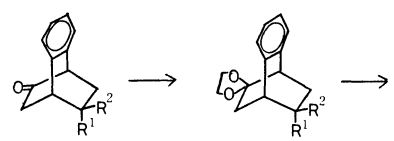

32 R^1=CO_2Et, R^2=H
33 R^1=H, R^2=CO_2Et
36 R^1=CO_2Et, R^2=H
37 R^1=H, R^2=CO_2Et

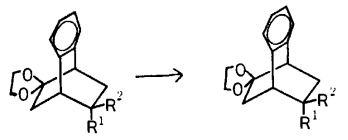

38 $R^1=CH_2OH$, $R^2=H$ **40** $R^1=CH_2OTs$, $R^2=H$
39 $R^1=H$, $R^2=CH_2OH$ **41** $R^1=H$, $R^2=CH_2OTs$

Upon treatment with sodium cyanide in DMF, the *endo*-tosylate (**40**) gave the *endo*-nitrile (**42**). Alkaline hydrolysis of the substance afforded the *endo*-carboxylic acid (**43**), which was reduced with lithium aluminum hydride to yield the *endo*-alcohol (**44**). After hydrolysis of the ketal function, the resultant ketoalcohol (**45**) was converted into the *endo*-ketomesylate (**46**), which was treated with sodium hydride in DMF. Sublimation of a solid product gave a tricyclic ketone mp 85—86 °C. We assigned benzoisotwistan-2-one (**47**) to the product on the basis of the NMR spectrum exhibiting double doublet signal centered at 3.38 for a proton H_a and this pattern ruled out twistane structure (**48**). The Wolff-Kishner reduction of the ketone (**47**) yielded benzoisotwistane (**10**) mp 56—57 °C.

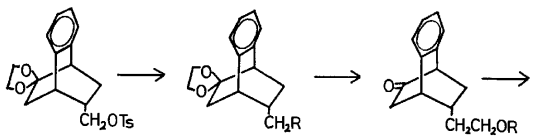

40 **42** R=CN **45** R=H
43 R=CO_2H **46** R=Ms
44 R=CH_2OH

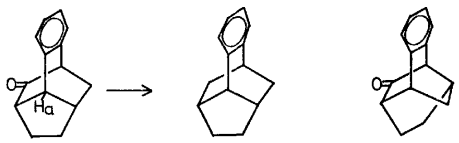

47 **10** **48**

Turning to the oily *exo*-tosylate (**41**), the substance gave also a crystalline *exo*-nitrile (**49**), which was converted into the *exo*-carboxylic acid (**50**), ketalalcohol (**51**), ketoalcohol (**52**), and Ketomesylate (**53**) by the same procedure described for *endo*-isomer. The *exo*-mesylate (**53**) was treated with sodium hydride in DMF, but a cyclized product was not obtained.

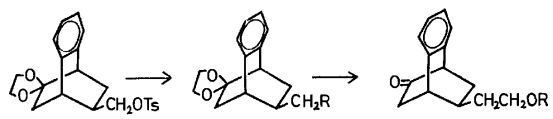

41 **49** R=CN **52** R=H
50 R=CO_2H **53** R=Ms
51 R=CH_2OH

Finally we made an effort to prepare the lower homolog of benzoisotwistane; 7,8-benzotricyclo[3.3.1.$0^{3,6}$]nonan-2-one (**56**). Upon treatment with acetone and *p*-toluenesulfonic acid, the *endo*-ketaltosylate (**40**) gave the *endo*-ketotosylate (**54**), which was heated with sodium hydride in DMF. Chromatographic separation of a product yielded a cyclized compound. It was not an expected ketone but an alcoholic compound. On oxidation with 8N Jones' reagent the substance gave a ketonic compound mp 90 °C, whose UV spectrum (Table 2) was very similar with that of benzoisotwistan-2-one (**47**). From the fact we assigned the structure (**56**) to the compound and its NMR and IR spectra were also consistent with the structure (**56**).

TABLE 2. UV SPECTRA (IN ISOOCTANE SOLUTION) OF **47** AND **56**

47		**56**	
nm	ε	nm	ε
259.5 (sh)	330	260 (sh)	320
265	409	265.5	368
271.5	361	272	327
291 (sh)	213	289 (sh)	268
299.5	261	296.5	309
309	254	305.5	297
319 (sh)	147	316 (sh)	177

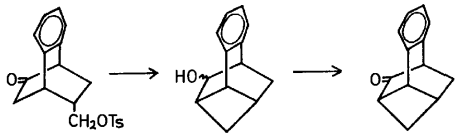

54 **55** **56**

Experimental

All the melting points and the boiling points are not corrected. The IR spectra were measured with Hitachi EPI-S2 spectrophotometer. The NMR spectra were obtained on LNM-C-60HL and JNM-MH-100 spectrometer. The UV spectra were measured with Beckman DB spectrometer.

Diels-Alder Reaction of Hydroquinone with Diethyl Fumarate. A mixture of 160 g of hydroquinone and 320 g of diethyl fumarate was heated for 36 hr at 200—220 °C under a nitrogen atmosphere. After cooling, 105 g of hydroquinone was recovered by filtration and a liquid reaction mixture was distilled to recover 220 g of diethyl fumarate. A residue was chromatographed on neutral alumina (Woelm, activity III) and ealier fractions eluted with benzene gave an oily product, which was distilled to yield 14.6 g of **13**, bp 170—180 °C at 1.5 mmHg. This adduct was crystallized in a reciever, mp 88—89 °C. Followed fractions eluted with benzene gave a solid, which was recrystallized from benzene to yield 5.5 g of **12**, mp 104.5—105.5 °C.

13: IR (KBr): 1720 (s), 1260 (m), 1240 (m), 1190 (s), 1112 (m), and 1022 (m) cm^{-1}.

NMR ($CDCl_3$): δ 1.30 (t, 6H, J=7 Hz), 2.52—2.67 (m, 4H), 3.02—3.25 (m, 2H), 3.55 (s, 2H), and 4.20 (q, 4H, J= 7 Hz).

Found: C, 59.15; H, 6.54%. Calcd for $C_{14}H_{18}O_6$: C, 59.56; H, 6.43%.

12: IR (KBr): 1720 (s), 1253 (m), 1239 (m), 1190 (s), 1175 (m), and 1030 (m), cm^{-1}.

NMR ($CDCl_3$): δ 1.25 (t, 6H, J=7 Hz), 2.42—2.55 (m, 4H), 3.04—3.18 (m, 2H), 3.15 (s, 2H), and 4.18 (q, 4H, J= 7 Hz).

Found: C, 59.48; H, 6.42%. Calcd for $C_{14}H_{18}O_6$: C, 59.56; H, 6.43%.

trans-2,3-Dicarboxybicyclo[2.2.2]octane (11). *From* ***12***: A mixture of 1.37 ml of 80% hydrazine hydrate, 1.34 g of potassium hydroxide, 14 ml of triethylene glycol and 1.33 g of **12** was heated for 3 hr at 130—140 °C and then water was removed from the reaction mixture. A residual solution was heated for further 6 hr at 200 °C and then diluted with water.

After washing with ether, a water layer was acidified with hydrochloric acid and extracted with ether. The extract was washed with water and dried over magnesium sulfate. Removal of the solvent gave a solid which was recrystallized from ethanol to yield 692 mg of **11**, mp 232 °C (lit,[11] mp 234 °C).

Found: C, 60.74; H, 7.19%. Calcd for $C_{10}H_{14}O_4$: C, 60.59; H, 7.12%.

From ***13***: *trans*-2,3-Dicarboxybicyclo[2.2.2]octane (550 mg) was obtained from 1.25 g of **13** by the same method described above.

trans-anti-*2,5-Bisethylenedioxy-7,8-diethoxycarbonylbicyclo[2.2.2]octane (**14**).* A solution of 3.34 g of **12**, 24 mg of *p*-toluenesulfonic acid, and 40 ml of ethylene glycol in 176 ml of benzene was boiled for 25 hr during which time water generated was removed from the reaction mixture as the azeotrope with benzene. After cooling to room temperature, benzene layer was separated and washed with satd. aqueous sodium bicarbonate and water. Removal of the solvent gave a solid which was recrystallized from hexane to yield 4.22 g of **14**, mp 80—81 °C.

IR (KBr): 1728 (s), 1288 (m), 1220 (m), 1185 (s), 1110 (s), 1032 (s), and 1025 (s) cm^{-1}.

Found: C, 58.20; H, 7.27%. Calcd for $C_{18}H_{26}O_8$: C, 58.37; H, 7.08%.

trans-syn-*2,5-Bisethylenedioxy-7,8-diethoxycarbonylbicyclo[2.2.2]octane (**15**).* *syn*-Ketoester (**13**) (8.54 g) was converted into **15** (7.34 g), mp 98—98.5 °C, by the same method described above.

IR (KBr): 1740 (s), 1730 (s), 1312 (m), 1235 (m), 1185 (s), 1150 (m), 1105 (s), and 1020 (s) cm^{-1}.

Found: C, 58.38; H, 7.17%. Calcd for $C_{18}H_{26}O_8$: C, 58.37; H, 7.08%.

trans-anti-*2,5-Bisethylenedioxy-7,8-bis(hydroxymethyl)bicyclo[2.2.2]octane (**16**).* To a suspension of 1.15 g of lithium aluminum hydride in 50 ml of dry ether was added a solution of 6.30 g of **14** in 150 ml of dry ether at room temperature and then the mixture was refluxed for 2 hr. After cooling with ice, to the chilled reaction mixture was carefully added satd. aqueous ammonium chloride solution and then a solid was filtered off. A filtrate was washed with water and dried over magnesium sulfate. Removal of the solvent gave a solid which was recrystallized from acetone to yield 5.27 g of **16** mp 163—165 °C.

IR (KBr): 3350 (s), 1130 (m), 1098 (m), 1062 (s), 1038 (m), and 990 (m) cm^{-1}.

Found: C, 58.70; H, 7.80%. Calcd for $C_{14}H_{22}O_6$: C, 58.73; H, 7.75%.

trans-syn-*2,5-Bisethylenedioxy-7,8-bis(hydroxymethyl)bicyclo[2.2.2]octane (**17**).* Reduction of 14.0 g of **15** with 3.4 g of lithium aluminum hydride in dry ether afforded 9.65 g of **17**, mp 132 °C, by the same procedure described above.

IR (KBr): 3300 (s), 1155 (m), 1090 (s), 1045 (s), and 995 (s) cm^{-1}.

Found: C, 58.55; H, 7.81%. Calcd for $C_{14}H_{22}O_6$: C, 58.73; H, 7.75%.

trans-anti-*2,5-Dioxo-7,8-bis(hydroxymethyl)bicyclo[2.2.2]octane (**18**).* A solution of 500 mg of **16** in 10 ml of 5% sulfuric acid was kept for 3 days at room temperature. The reaction mixture was neutralized with solid sodium bicarbonate and concentrated under reduced pressure. Acetone was added to a residue and an insoluble solid was filtered off. A filtrate was concentrated to give a solid which was recrystallized from acetone to yield 210 mg of **18**, mp 126—127 °C.

IR (KBr): 3400 (s), 1725 (s), 1705 (s), 1080 (m), 1070 (m), and 1020 (s) cm^{-1}.

Found: C, 60.36; H, 7.17%. Calcd for $C_{10}H_{14}O_4$: C, 60.59; H, 7.12%.

Hydrolysis of trans-syn-*2,5-Bisethylenedioxy-7,8-bis(hydroxymethyl)bicyclo[2.2.2]octane (**17**).* A mixture of 10.3 g of **17** and 5% sulfuric acid was kept for 3 days at room temperature. After working up as the same manner described above, a solid product was recrystallized from acetone to give 3.83 g of **19**, mp 125 °C.

IR (KBr): 3300 (s), 1160 (m), 1090 (m), 1070 (m), and 980 (s) cm^{-1}.

Found: C, 60.46; H, 7.27%. Calcd for $C_{10}H_{14}O_4$: C, 60.59; H, 7.12%.

trans-anti-*2,5-Bisethylenedioxy-7,8-bis(cyanomethyl)bicyclo[2.2.2]octane (**21**).* To a solution of 5.05 g of **16** in 25 ml of dry pyridine was added 15.0 g of *p*-toluenesulfonyl chloride with ice cooling and then the mixture was stirred for 2 hr at this temperature. After standing overnight at room temperature, the mixture was poured onto ice water and acidified with hydrochloric acid. A solid was collected and washed with dilute hydrochloric acid, satd. aqueous sodium bicarbonate, and water. After drying over calcium chloride, 9.05 g of tosylate (**20**) was obtained, mp 156—157 °C. A mixture of 9.00 g of **20**, 4.7 g of sodium cyanide and 45 ml of *N,N*-dimethylformamide (DMF) was heated for 4 hr at 120—130 °C and then for further 8 hr at 140—150 °C. After cooling to room temperature, a solid was filtered off and a filtrate was concentrated under reduced pressure. A residue was poured into water and a solid was collected, which was washed with water. Recrystallization from benzene gave 4.10 g of **21**, mp 162—164 °C.

IR (KBr): 2260 (w), 1135 (s), 1110 (m), 1053 (s), 1025 (s), 983 (s), and 950 (m) cm^{-1}.

Found: C, 63.31; H, 6.69; N, 9.20%. Calcd for $C_{16}H_{20}O_4N_2$: C, 63.14; H, 6.62; N, 9.21%.

trans-syn-*2,5-Bisethylenedioxy-7,8-bis(cyanomethyl)bicyclo[2.2.2]octane (**28**).* Tosylation of 7.90 g of **17** with 15.7 g of *p*-toluenesulfonyl chloride and 42 ml of pyridine was carried out by the same procedure described above and 11.3 g of **27** was obtained. A mixture of 11.0 g of **27**, 5.8 g of sodium cyanide, and 55 ml of DMF was heated for 4 hr at 120—130 °C and then for further 10 hr at 140—150 °C. After working up as described above, a solid was collected and recrystallized from benzene to yield 2.09 g of **28**, mp 217—219 °C.

IR (KBr): 2260 (w), 1140 (s), 1100 (s), 1075 (s), 980 (m), and 960 (m) cm^{-1}.

Found: C, 63.25; H, 6.69; N, 9.06%. Calcd for $C_{16}H_{20}O_4N_2$: C, 63.14; H, 6.62; N, 9.21%.

trans-anti-*2,5-Bisethylenedioxy-7,8-bis(carboxymethyl)bicyclo[2.2.2]octane (**22**).* A mixture of 3.82 g of **21**, 4.23 g of potassium hydroxide and 35 ml of ethylene glycol was heated for 6 hr at 150—160 °C. After cooling to room temperature, the reaction mixture was diluted with water and acidified with hydrochloric acid. A solid was collected, washed with water, and dried over calcium chloride to yield 1.92 g of **22**, mp 208 °C dec.

IR (KBr): 2900 (broad), 1705 (s), 1295 (m), 1140 (m), 1120 (m), 1020 (m), and 998 (m) cm^{-1}.

Found: C, 55.65; H, 6.51%. Calcd for $C_{16}H_{22}O_8$: C, 56.13; H, 6.48%.

trans-syn-*2,5-Bisethylenedioxy-7,8-bis(carboxymethyl)bicyclo[2.2.2]octane (**29**).* Hydrolysis of 9.22 g of **28** with potassium hydroxide in ethylene glycol gave 3.95 g of **29**, mp 238 °C dec., by the same procedure described above.

IR (KBr): 2900 (broad), 1720 (s), 1205 (m), 1130 (m), 1090 (s), and 960 (m) cm^{-1}.

Found: C, 55.97; H, 6.44%. Calcd for $C_{16}H_{22}O_8$: C, 56.13; H, 6.48%.

trans-anti-*2,5-Bisethylenedioxy-7,8-bis(2-hydroxyethyl)bicyclo-*

[2.2.2]octane (23). To a suspension of 0.48 g of lithium aluminum hydride in 20 ml of dry tetrahydrofuran (THF) was added a solution of 1.82 g of **22** in 20 ml of dry THF at room temperature and then a mixture was heated under reflux for 2 hr. After cooling with ice, satd. aqueous ammonium chloride solution was carefully added to the chilled reaction mixture and a solid was filtered off. A filtrate was dried over magnesium sulfate and removal of the solvent gave a solid which was recrystallized from acetone to yield 1.39 g of **23**, mp 138—139 °C.

IR (KBr): 3300 (s), 1140 (m), 1118 (s), 1060 (m), 1012 (s), 995 (m), and 948 (m) cm^{-1}.

Found: C, 61.09; H, 8.52%. Calcd for $C_{16}H_{26}O_6$: C, 61.13; H, 8.34%.

trans-syn-*2,5-Bisethylenedioxy-7,8-bis(2-hydroxyethyl) bicyclo-[2.2.2]octane (30).* Reduction of **29** (3.95 g) with lithium aluminum hydride was carried out by the same procedure described above and recrystallization of a product gave 2.10 g of **30**, mp 183 °C.

IR (KBr): 3450 (m), 1110 (s), 1060 (m), 1045 (m), and 970 (m) cm^{-1}.

Found: C, 61.26; H, 8.28%. Calcd for $C_{16}H_{26}O_6$: C, 61.13; H, 8.34%.

[8]Diisotwistane-2,8-dione (26). To a solution of 1.6 g of **23** in 20 ml of dry pyridine was added 2.28 g of methanesulfonyl chloride at 0—5 °C and then a reaction mixture was stirred for 2 hr at this temperature. After standing for further 20 hr at room temperature, it was poured onto ice and extracted with ether. The extract was washed with dilute hydrochloric acid, satd. aqueous sodium bicarbonate, water, and dried over magnesium sulfate. Removal of the solvent gave 1.11 g of **24**, to which was added 30 ml of 10% sulfuric acid. After standing for 3 days at room temperature, it was extracted with ether. The extract was washed with satd. aqueous sodium bicarbonate, water, and dried over magnesium sulfate. Removal of the solvent afforded 0.78 g of **25** as an oily product.

IR (neat film): 1725 (s), 1350 (m), 1175 (m), and 945 (m) cm^{-1}.

The mesylate (**25**), without purification, was dissolved in 25 ml of dry DMF and a solution was added to a suspension of 1.0 g of sodium hydride in 10 ml of dry DMF. A reaction mixture was heated for 48 hr at 60—70 °C under a nitrogen atmosphere. After cooling to room temperature, a few drops of methanol was added to the mixture and then it was diluted with water and extracted with ether. The extract was washed with dilute hydrochloric acid, satd. aqueous sodium bicarbonate, water, and dried over magnesium sulfate. After evaporation of the solvent, a residue was chromatographed on neutral alumina (Woelm, activity III) and fractions eluted with ether–pentane (1:1 volume) gave a wax. The wax was sublimed to yield 85 mg of [8]diisotwistane-2,8-dione (**26**), mp 88—89 °C (in a sealed tube). A sample for elemental analysis was further purified by tlc (Kieselgel 60 PF_{254}, Merck) and sublimation.

IR (KBr): 1710 (s), 1222 (m), 1160 (m), and 1030 (m) cm^{-1}.

NMR ($CDCl_3$): δ 1.6—2.2 (m, 10H), 2.45—2.60 (m, 2H), and 2.68—2.88 (m, 2H).

UV: $\lambda_{max}^{ethanol}$ 258 nm (ε=40), 289 nm (42).

Found: C, 75.68; H, 7.49%. Calcd for $C_{12}H_{14}O_2$: C, 75.76; H, 7.42%.

Mesylation of 30. To a solution of 1.90 g of **30** in 20 ml of dry pyridine was added 2.70 g of methanesulfonyl chloride with ice cooling. After stirring for 5 hr at 0—5 °C, a mixture was stand overnight at room temperature and then poured onto ice. A solid was collected and washed with water to give 2.08 g of **31**, mp 169 °C dec.

IR (KBr): 1335 (s), 1170 (s), 985 (m), and 840 (m), cm^{-1}.

NMR ($CDCl_3$): δ 1.6—2.1 (m, 6H), 2.4—2.5 (m, 2H). 3.09 (s, 6H), 3.60—3.70 (m, 12H), and 4.22—4.31 (m, 4H),

Found: C, 45.78; H, 6.44; S, 13.56%. Calcd for $C_{18}H_{30}O_{12}S_2$: C, 45.95; H, 6.43; S, 13.60%.

Attempts to Hydrolyze Ethylenedioxy Group of 31. Mesylate (**31**) was quantitatively recovered unchanged from 10% sulfuric acid (for 2 days at room temperature), *p*-toluenesulfonic acid in acetone (for 4 days at room temperature), 1 N hydrochloric acid in THF (for 5 hr at room temperature), and 50% aqueous acetic acid (for 1 hr at 70 °C).

Diels-Alder Reaction of β-Naphthol with Ethyl Acrylate. A mixture of 90 g of β-naphthol and 120 g of ethyl acrylate was heated for 70 hr at 170—180 °C under a nitrogen atmosphere. From the reaction mixture, 75 g of ethyl acrylate was recovered by distillation. A residue was chromatographed on alumina (Sumitomo). Fractions eluted with benzene were distilled to give 22.1 g of a mixture of adducts, bp 137—140 °C at 0.1 mmHg. Analysis by glc on a 10% SE-30 column at 190 °C revealed the presence of two components having relative retention times 1.00: 1.24 (relative yield 39: 61 respectively). The structure (**33**) was assigned to a minor adduct and **32** to a major adduct.

IR (neat film): 1720 (s), 1625 (w), 1600 (w), 1170 (m), and 755 (m) cm^{-1}.

NMR ($CDCl_3$): δ 1.11 (t, J=7 Hz, 1.0*), 1.26 (t, J=7 Hz, 1.5), 1.8—3.0 (m, 4.5), 3.4—4.3 (m, 3.5), 7.13 (s, 1.5), and 7.16 (s, 2.0).

Found: C, 73.49; H, 6.63%. Calcd for $C_{15}H_{16}O_3$: C, 73.75; H, 6.60%.

*Ketalization of a mixture of 2-Oxo-5-*endo*-ethoxycarbonyl-7,8-benzobicyclo[2.2.2]octane (32) and 2-Oxo-5-*exo*-ethoxycarbonyl-7,8-benzobicyclo[2.2.2]octane (33).* A solution of 22.0 g of a mixture of **32** and **33**, 300 ml of ethylene glycol, 1.40 g of *p*-toluenesulfonic acid in 1400 ml of benzene was boiled for 30 hr. During this period, the water generated was separated as benzene azeotrope from the reaction mixture. After cooling to room temperature, a benzene layer was separated and washed with satd. aqueous sodium bicarbonate, water and dried over magnesium sulfate. After evaporation of the solvent, a residue was distilled to give 23.8 g of a mixture of **36** and **37**, bp 153—155 °C at 0.1 mmHg.

IR (neat film): 1725 (s), 1625 (w), 1600 (w), 1185 (m), 1120 (m), 1095 (m), 1030 (m), 1010 (m), and 755 (m) cm^{-1}.

Found: C, 69.51; H, 8.33%. Calcd for $C_{17}H_{24}O_4$: C, 69.83; H, 8.27%.

*A Mixture of 2-Ethylenedioxy-5-*endo*-hydroxymethyl-7,8-benzobicyclo[2.2.2]octane (38) and 2-Ethylenedioxy-5-*exo*-hydroxymethyl-7,8-bicyclo[2.2.2]octane (39).* A solution of 23.7 g of a mixture of **36** and **37** in 200 ml of dry ether was added to a suspension of 5.00 g of lithium aluminum hydride in 150 ml of dry ether at room temperature. It was refluxed for 2 hr and then cooled with ice. A chilled reaction mixture was added with satd. aqueous ammonium chloride solution and a solid was filtered off. A filtrate was washed with water and dried over magnesium sulfate. After evaporation of the solvent, a residue was distilled to yield 16.6 g of a mixture of **38** and **39**, bp 172—173 °C at 0.1 mmHg.

IR (neat film): 3400 (s), 1625 (w), 1600 (w), 1120 (m), 1080 (m), 1030 (m), and 750 (s) cm^{-1}.

Found: C, 72.98; H, 7.38%. Calcd for $C_{15}H_{18}O_3$: C, 73.14; H, 7.37%.

Tosylation of a Mixture of 38 and 39. To a solution of 16.5 g of a mixture of **38** and **39** in 40 ml of dry pyridine was

* Relative ratio of peak areas.

added 16.0 g of *p*-toluenesulfonyl chloride at 0—5 °C. The mixture was agitated at this temperature for 2 hr and then kept for further 24 hr at room temperature. After pouring onto ice, it was acidified with hydrochloric acid and extracted with benzene. The extract was washed with satd. aqueous sodium bicarbonate, water, and dried over magnesium sulfate. After evaporation of the solvent, a residue was added with ether and a solid precipitated was collected. The solid was recrystallized from benzene to yield 9.10 g of **40**, mp 139—140 °C.

IR (KBr): 1360 (s), 1175 (s), and 750 (m) cm^{-1}.

Found: C, 66.09; H, 6.11; S, 7.69%. Calcd for $C_{22}H_{24}O_5S$: C, 65.99; H, 6.04; S, 7.99%.

The solvent was removed from a filtrate to give 15.4 g of an oily substance (**41**), which was, without further purification, used for a subsequent reaction.

IR (neat film): 1360 (s), 1175 (s), and 755 (m) cm^{-1}.

*2-Ethylenedioxy-5-*endo*-cyanomethyl-7,8-benzobicyclo[2.2.2]octane (42).* A mixture of 11.5 g of **40**, 6.30 g of sodium cyanide, and 75 ml of DMF was heated for 1 hr at 120 °C and then for further 8 hr at 150—160 °C. After cooling to room temperature, a solid was filtered off and a filtrate was concentrated under reduced pressure. A residue was diluted with water and extracted with ether. The extract was washed with dilute hydrochloric acid, satd. aqueous sodium bicarbonate, water, and dried over magnesium sulfate. Removal of the solvent gave a solid, which was recrystallized from benzene–hexane to yield 6.10 g of **42**, mp 120—120.5 °C.

IR (KBr): 2250 (w), 1125 (m), 1090 (m), 1035 (m), 1010 (m), and 750 (m) cm^{-1}.

Found: C, 75.58; H, 6.78; N, 5.58%. Calcd for $C_{16}H_{17}O_2N$: C, 75.27; H, 6.71; N, 5.49%.

*2-Ethylenedioxy-5-*exo*-cyanomethyl-7,8-benzobicyclo[2.2.2]octane (49)* Treatment of 15.3 g of **41** with 8.20 g of sodium cyanide by the same manner described above yielded a solid which was recrystallized from benzene–hexane to give 5.20 g of **49**, mp 116.5—118 °C.

IR (KBr): 2250 (w), 1095 (s), 1075 (s), 1030 (m), 1015 (m), and 755 (m), cm^{-1}.

Found: C, 75.51; H, 6.78; N, 5.55%. Calcd for $C_{16}H_{17}O_2N$: C, 75.27; H, 6.71; N, 5.49%.

*2-Oxo-5-*endo*-(2-hydroxyethyl)-7,8-benzobicyclo[2.2.2]octane (45).* A mixture of 5.80 g of **42**, 10.0 g of potassium hydroxide, and 85 ml of ethylene glycol was heated for 2 hr at 120 °C and then for further 8 hr at 150—160 °C. After cooling to room temperature, a reaction mixture was diluted with water and acidified with hydrochloric acid. It was extracted with ether. The extract was washed with water and dried over magnesium sulfate. Removal of the solvent gave 6.53 g of an oily product (**43**), which was dissolved in 200 ml of dry ether. A solution was slowly added to a suspension of 2.00 g of lithium aluminum hydride in 50 ml of dry ether and a mixture was refluxed for 3 hr. After cooling with ice, to the chilled mixture was carefully added satd. aqueous ammonium chloride solution. A solid was filtered off and a filtrate was concentrated to give 5.92 g of a viscous oily product (**44**).

IR (neat film): 3450 (s), 1050 (m), 1110 (m), 1080 (m), 1030 (m), 1010 (m), and 755 (m) cm^{-1}.

To a solution of this substance in 400 ml of acetone was added 1.00 g of *p*-toluenesulfonic acid and the mixture was allowed to stand overnight at room temperature. After removal of acetone under reduced pressure, a residue was diluted with water and extracted with ether. The extract was washed with satd. aqueous sodium bicarbonate, water, and dried over magnesium sulfate. After evaporation of the solvent, a residue was distilled to yield 3.64 g of **45**, bp 180 °C at 0.5 mmHg.

IR (neat film): 3450 (s), 1725 (s), 1625 (w), 1600 (w), 1050 (m), and 755 (m) cm^{-1}.

Found: C, 76.99; H, 7.33%. Calcd for $C_{14}H_{16}O_2$: C, 77.75; H, 7.46%.

The substance was very hygroscopic.

*2-Ethylenedioxy-5-*exo*-carboxymethyl-7,8-benzobicyclo[2.2.2]octane (50).* Hydrolysis of 4.17 g of **49** with 8.00 g of potassium hydroxide in 70 ml of ethylene glycol was carried out by the same manner described above. A solid was obtained and recrystallized from benzene–hexane to yield 4.06 g of **50**, mp 119.5—120 °C.

IR (KBr): 3000 (broad), 1710 (s), and 755 (m) cm^{-1}.

Found: C, 70.27; H, 6.65%. Calcd for $C_{16}H_{18}O_4$: C, 70.05; H, 6.61%.

*2-Oxo-5-*exo*-(2-hydroxyethyl)-7,8-benzobicyclo[2.2.2]octane (52).* Reduction of 4.20 g of **50** with 2.10 g of lithium aluminum hydride in dry ether gave 3.66 g of an oily product (**51**).

IR (neat film): 3450 (s), 1050 (m), 1110 (m), 1080 (m), 1030 (m), 1010 (m), and 755 (m) cm^{-1}.

The substance was dissolved in 280 ml of acetone and to the solution was added 0.72 g of *p*-toluenesulfonic acid. The solution was stirred for 8 hr at room temperature and then worked up as described above to yield 2.30 g of **52**, bp 167—168 °C at 0.2 mmHg.

IR (neat film): 3450 (s), 1720 (s), 1050 (m), and 755 (m) cm^{-1}.

Found: C, 77.66; H, 7.50%. Calcd for $C_{14}H_{16}O_2$: C, 77.75; H, 7.46%.

8,9-Benzotricyclo[4.3.1.0^{3,7}]decan-2-one (47). To a solution of 3.32 g of **45** in 10 ml of dry pyridine was added 3.42 g of methanesulfonyl chloride with ice cooling and then a mixture was kept for 20 hr at room temperature. It was poured onto ice and acidified with hydrochloric acid. It was extracted with ether. The extract was washed with satd. aqueous sodium bicarbonate, water, and dried over magnesium sulfate. Removal of the solvent gave 4.40 g of **46**.

IR (neat film): 1720 (s), 1350 (s), 1170 (s), and 755 (m) cm^{-1}.

The methanesulfonate (**46**) was, without purification, dissolved in 45 ml of dry DMF and the solution was added to a suspension of 8.00 g of sodium hydride in 100 ml of dry DMF. It was stirred for 22 hr at 60 °C under a nitrogen atmosphere. After cooling with ice, to a chilled reaction mixture was added 3 ml of methanol and then poured onto ice. It was extracted with ether. The extract was washed with dilute hydrochloric acid, satd. aqueous sodium bicarbonate, water, and dried over magnesium sulfate. After evaporation of the solvent, to a residue was added pentane to give a solid which was collected and sublimed to yield 2.62 g of **47**, mp 85—86 °C (in a sealed tube).

IR (KBr): 1725 (s), 1630 (w), 1475 (m), 1455 (m), and 755 (s) cm^{-1}.

NMR (CCl_4): δ 1.4—1.6 (m, 2H), 1.6—2.3 (m, 4H), 3.17 (t, 2H), 3.38 (d,d, J=3.3 Hz, J=1.4 Hz, 2H), and 7.12 (s, 4H).

Mass spectrum: *m/e* 198 (parent peak).

Found: C, 84.60; H, 7.15%. Calcd for $C_{14}H_{14}O$: C, 84.81; H, 7.12%.

Tosylhydrazone; mp 182 °C dec.

Found: C, 69.11; H, 6.38; N, 7.32; S, 8.56%. Calcd for $C_{21}H_{22}O_2N_2S$: C, 68.83; H, 6.05; N, 7.65; S, 8.74%.

8,9-Benzotricyclo[4.3.1.0^{3,7}]decane (10). A mixture of 300 mg of **47**, 0.13 g of potassium hydroxide, 0.22 ml of 80% hydrazine hydrate, and 2 ml of triethylene glycol was heated for 90 min at 160 °C and then water was removed from the

reaction mixture. A residual solution was heated for further 3 hr at 200 °C and then diluted with water. It was extracted with pentane. The extract was washed with water and dried over magnesium sulfate. Removal of the solvent gave a solid which was sublimed to yield 131 mg of **10**, mp 56—57 °C (in a sealed tube).

IR (KBr): 2920 (m), 2870 (m), 1480 (m), 1450 (m), and 755 (s) cm^{-1}.

NMR (CCl_4): δ 1.3—2.1 (m, 10H), 2.81 (m, 2H), and 7.03 (s, 4H).

Mass spectrum: *m/e* 184 (parent peak).

Found: C, 90.98; H, 8.85%. Calcd for $C_{14}H_{16}$: C, 91.25; H, 8.75%.

Attempt to Cyclize exo-*Methanesulfonate (53).* Treatment of 2.30 g of **52** with 2.50 g of methanesulfonyl chloride and 7 ml of dry pyridine by the same manner described for *endo*-isomer gave 2.28 g of **53**, which was dissolved in 30 ml of dry DMF. This solution was added to a suspension of 4.80 g of sodium hydride in 60 ml of dry DMF. The mixture was agitated for 25 hr at 60 °C under a nitrogen atmosphere and 2 ml of methanol was added to the reaction mixture with ice cooling. It was then poured onto ice and extracted with ether. The extract was washed with dilute hydrochloric acid, satd. aqueous sodium bicarbonate, water, and dried over magnesium sulfate. Removal of the solvent gave an oily product which was chromatographed on neutral alumina (Woelm, activity III). But 8,9-benzotricyclo[4.3.1.$0^{3,7}$]-decan-2-one (**47**) was not obtained.

Hydrolysis of Ethylenedioxy Group of 40. A mixture of 8.21 g of **40**, 1.50 g of *p*-toluenesulfonic acid and 600 ml of acetone was stirred for 2 days at room temperature. The mixture was concentrated under reduced pressure and a residue was diluted with water. It was extracted with ether. The extract was washed with satd. aqueous sodium bicarbonate, water, and dried over magnesium sulfate. After evaporation of the solvent, a residue was added with benzene–hexane to yield 6.31 g of **54**, mp 121.5—123 °C.

IR (KBr): 1730 (s), 1595 (m), 1355 (s), 1175 (s), 970 (s), 845 (s), and 755 (m) cm^{-1}.

Found: C, 68.04; H, 6.01; S, 8.78%. Calcd for $C_{20}H_{20}O_4S$: C, 67.40; H, 5.66: S, 8.98%.

7,8-Benzotricyclo[*3.3.1.*$0^{3,6}$]*nonan-2-ol (55).* A solution of 4.50 g of **54** in 50 ml of dry DMF was added to a suspension of 8.00 g of sodium hydride in 100 ml of dry DMF and a mixture was agitated for 72 hr at 70 °C. After cooling to room temperature, the reaction mixture was diluted with water and extracted with ether. The extract was washed with dilute hydrochloric acid, satd. aqueous sodium bicarbonate, water, and dried over magnesium sulfate. After evaporation of the solvent, a residue was chromatographed on silica gel (Mallinckrodt) and fractions eluted with ether–pentane (1: 1 volume) gave 0.23 g of **55**, mp 95—98 °C.

IR (KBr): 3250 (s), 1030 (s), and 745 (s) cm^{-1}.

Mass spectrum: *m/e* 186 (parent peak).

Found: C, 83.78; H, 7.68%. Calcd for $C_{13}H_{14}O$: C, 83.83; H, 7.58%.

7,8-Benzotricyclo[*3.3.1.*$0^{3,6}$]*nonan-2-one (56).* To a solution of 150 mg of **55** was added 0.5 ml of 8N-Jones' reagent at 0—5 °C and a mixture was stirred for 30 min at the same temperature. After dilution with ether, it was washed with satd. aqueous sodium bicarbonate, water, and dried over magnesium sulfate. Removal of the solvent gave a solid which was sublimed to yield 61 mg of **56**, mp 90 °C (in a sealed tube).

IR (KBr): 1720 (s) and 750 (s) cm^{-1}.

NMR ($CDCl_3$): δ 1.4—1.7 (m, 2H), 2.30 (m, 1H), 2.70 (m, 3H), 3.82 (m, 2H), and 7.12 (s, 4H).

Mass spectrum: *m/e* 184 (parent peak).

Found: C, 84.80; H, 6.54%. Calcd for $C_{13}H_{12}O$: C, 84.75; H, 6.57%.

References

1) Presented at the 30th Annual Meeting of the Chemical Society of Japan, Osaka, April, 1974, preprint Vol. III p. 1798.

2) This name has been given to describe symmetry of a shape which is chiral but not asymmetric. Collectively we call a shape "gyrochiral" when it belongs to anyone of C_n ($n \neq 1$), D_n, T, O, and I point groups.

3) H. W. Whitlock, Jr., *J. Amer. Chem. Soc.*, **84**, 3412 (1962). J. Gauthier and P. Deslongchamps, *Can. J. Chem.*, **45**, 297 (1967). K. Adachi, K. Naemura, and M. Nakazaki, *Tetrahedron Lett.*, **1968**, 5467. M. Tichy and J. Sicher, *Collect. Czech. Chem. Commun*, **37**, 3106 (1972).

4) B. R. Vogt, *Tetrahedron Lett.*, **1968**, 1579. R. R. Sauers and J. A. Whittle, *J. Org. Chem.*, **34**, 3579 (1969). K. Naemura and M. Nakazaki, This Bulletin, **46**, 888 (1973).

5) K. Hirao, T. Iwakura, M. Taniguchi, E. Abe, O. Yonemitsu, T. Date, and K. Kotera, *Chem. Commun.*, **1974**, 691.

6) According to the proposed nomenclature[5,7], we name tetracyclo[7.3.$0^{3,7}$.$0^{4,10}$]dodecane (**7**) [8]diisotwistane.

7) W. D. Graham, P. v. R. Schleyer, E. W. Hagaman, and E. Wenkert, *J. Amer. Chem. Soc.*, **95**, 5785 (1973).

8) The symmetry of the parent compound (**3**) forces the last ethano-bridging to become diagonal.

9) As a matter of convenience, an isomer with 7 and 8-carboxyl groups near to 2 and 5-keto groups respectively is termed *syn*-form and the other is named *anti*-form.

10) We call an isomer with 5-carboxy group near to benzene ring *exo*-form and the other isomer *endo*-form.

11) O. Diels and K. Alder, *Ann.*, **478**, 152 (1930).

Peptides Containing Aminophosphonic Acids. III. The Synthesis of Tripeptide Analogs Containing Aminomethylphosphonic Acid

Kiyoshi YAMAUCHI, Yasuhiro MITSUDA, and Masayoshi KINOSHITA
Department of Applied Chemistry, Osaka City University, Sumiyoshi-ku, Osaka 558
(Received May 22, 1975)

A synthetic method for tripeptide analogs containing aminomethylphosphonic acid has been described.

Since β-aminoethylphosphonic acid was discovered from marine organisms,[1] human beings, *etc.*,[2] its potential biological roles have been investigated actively; the results have suggested the occurence of the compound in lipid[3] as well as in peptide.[4] These aspects of an aminophosphonic acid have stimulated the study of the synthesis of peptides containing aminophosphonic acid;[5] we ourselves reported previously the first attempt at the preparation of a tripeptide containing aminomethylphosphonic acid in the center.[6]

In the present paper, we wish to describe the synthesis of tripeptide analogs containing more than one aminomethylphosphonic acid unit. Unlike an amino acid, a phosphonic acid group of aminophosphonic acid must be converted to the phosphonochloridate group in order to couple with an amino group of amino acid or aminophosphonic acid.

Thus, diethyl phthalimidomethylphosphonate (I), which could be easily prepared by the reaction of *N*-bromomethylphthalimide with triethyl phosphite, was chlorinated with a slight excess of phosphorus pentachloride to the corresponding phosphomonochloridate (II). On the other hand, Compound (I) was treated with one equivalent of hydrazine in ethanol at room temperature to generate diethyl aminomethylphosphonate (III) in a 70% yield. The chloride (II) was then allowed to react with the amine (III), affording a phosphorus analog of the dipeptide (IV) in a fairly good yield. The further extension of IV by aminomethylphosphonic acid was performed by the dephthalylation of IV with hydrazine to the corresponding amine

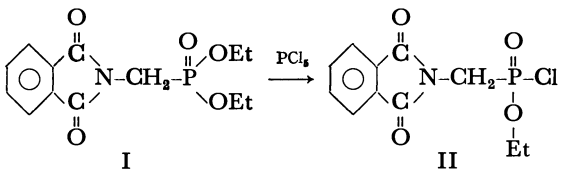

I II

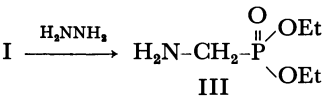

III

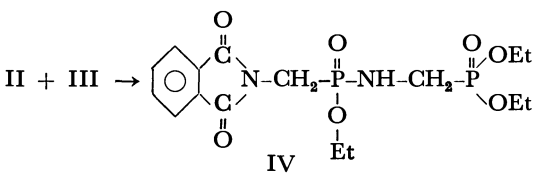

IV

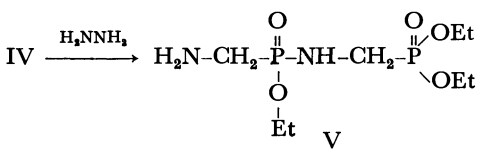

V

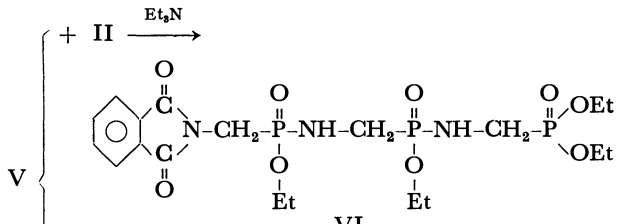

VI

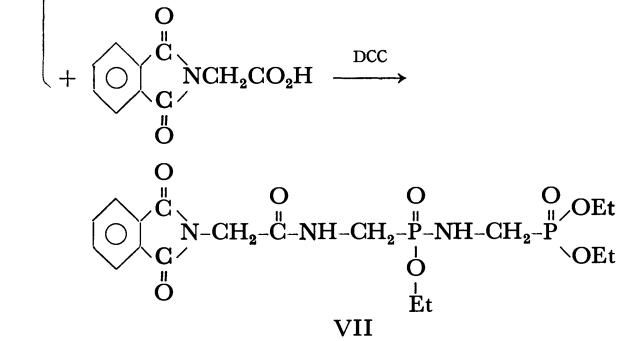

VII

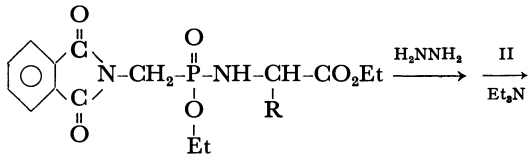

VIII: R=H
IX: R=CH_3

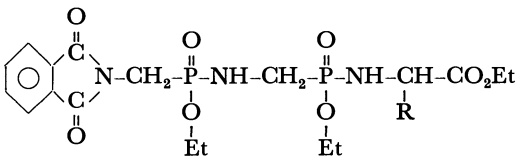

X: R=H
XI: R=CH_3

(V), followed by a reaction with II to provide a tripeptide analog (VI). Compound (V) was coupled also with phthalylglycine by means of dicyclohexylcarbodiimide to form VII. Similarly, dipeptides (VIII and IX) could each be elongated by one aminomethylphosphonic acid unit to tripeptide analogs (X and XI).

The above successive processes enable us to synthesize the higher analogs of peptides containing aminophosphonic acid; our studies in this direction are continuing.

Experimental

The infrared spectra (IR) were measured on a Jasco Model IR-G spectrometer. The nuclear magnetic resonance spectra (NMR) were recorded with a Hitachi-Perkin Elmer R-20 spectrometer, with a dilute solution in deuteriochloroform and tetramethylsilane as the internal standard.

Preparation of O-Ethyl Phthalimidomethylphosphonochloridate (II). Compound (I, 4.34 g, 0.0146 mol) was refluxed with phosphorus pentachloride (3.06 g, 0.0147 mol) in benzene (50 ml) for 15 hr. The light-boiling substances were distilled out from the reaction mixture under reduced pressure to give a slightly yellow liquid, which, upon standing at room temperature, solidified as crystals; 3.58 g (85%) (tetrahydrofuran-ether); mp 92—94 °C; IR ($CHCl_3$); 1780 (w), 1725 (s), 1600 (w), 1385 (s), 1300 (m), 1250 (m), and 720 (m) cm^{-1}; NMR: τ 1.8 (m, 4, phthalyl), 5.40 (d, 2, $C\underline{H}_2P$), 5.50 (m, 2, $POC\underline{H}_2$), and 8.55 (qua, 3, $C\underline{H}_3$).

Found: C, 46.21; H, 4.03; N, 5.10; Cl, 12.76%. Calcd for $C_{11}H_{11}ClNO_4P$: C, 45.93; H, 3.85; N, 4.87; Cl, 12.33%.

Preparation of Diethyl Aminomethylphosphonate (III). A mixture of diethyl phthalylimidomethylphosphonate (I, 4.34 g, 0.0146 mol)[6] in ethanol (30 ml) and hydrazine hydrate (100%, 1.2 ml) was kept at room temperature overnight and then refluxed for 2 hr. The resulting phthalyl hydrazide was removed by filtration, and the filtrate was concentrated to give diethyl aminomethylphosphonate as a light-yellow liquid; 1.7 g (70%); IR (neat): 3300 (s), 2820 (w), 1600 (s), 1505 (m), 1195 (s), and 1005 (s) cm^{-1}; NMR: τ 5.87 (qua, 4, $2OC\underline{H}_2$), 6.75 (s, 2, $N\underline{H}_2$), 7.02 (d, 2, $C\underline{H}_2P$) and 8.70 (t, 6, $2C\underline{H}_3$). A subsequent purification by distillation under reduced pressure resulted only in decomposition. Therefore, III was utilized for the next reaction without further purification.

Preparation of Peptide Analogs (IV.) A THF solution of II (50 ml) was added, drop by drop, to an ice-cooled chloroform solution (50 ml) of a mixture of the amine (III) and triethylamine (4 ml) over a 15-min period; the solution was then stirred at room temperature for 10 hr. After the subsequent removal of the triethylammonium chloride, the solution was concentrated. The residue was dissolved in chloroform (100 ml), and the solution was washed with saturated sodium hydrogen carbonate, and water and then dried with Drierite. The evaporation of the solvent and the recrystallization of the residue from THF-diethyl ether afforded white crystals of IV; 3.44 g (56%); 108—109 °C; IR (KBr): 3350 (w), 3100 (w), 1770 (w), 1720 (s), 1410 (m), 1200 (s), 1020 (s), 960 (m), and 720 (m) cm^{-1}; NMR: τ 2.15 (m, 4, phthalyl), 5.60—6.10 (m, 6, 3 $OC\underline{H}_2$), 5.90 (d, 2, PHT-$C\underline{H}_2$), 6.60 (s, 2, NH-$C\underline{H}_2$-P), 7i70 (t, 6, $2C\underline{H}_3$), and 8.72 (t, 3, $C\underline{H}_3$).

Found: C, 45.49; H, 5.58; N, 6.62%. Calcd for $C_{16}H_{24}N_2O_7P_2$: C, 45.93; H, 5.79; N, 6.70%.

VI. Dipeptide (IV, 1.25 g, 0.0030 mol) in ethanol (15 ml) was first treated with hydrazine hydrate (0.3 ml) to give its free amine (V) as a yellow viscous liquid; IR (neat): 3170 (m), 2930 (m), 1745 (s), 1655 (m), 1480 (w), 1200 (s), 1035 (s) and 680 (w); NMR: τ 5.90 (qua, 2, $COC\underline{H}_2$), 5.94 (qua, 2, $POC\underline{H}_2$), 6.5 (b, 2, $N\underline{H}_2$), 8.68 (t, 3, CH_3), 8.65 (t, 3, $C\underline{H}_3$). The amine (V) was subsequently allowed to react with II (0.89 g, 0.0031 mol) in the presence of triethylamine (1.5 ml) in a manner similar to that mentioned above, thus giving 0.53 g (32%) of VI; mp 136—138 °C (THF-diethyl ether); IR (KBr): 3350 (w), 3150 (w), 1770 (w), 1710 (s), 1410 (m), 1305 (w), 1220 (s), 1030 (s), 960 (s), 830 (m), and 720 (m) cm^{-1}; NMR: τ 2.18 (m, 4, phthalyl), 5.60—6.10 (m, 8, $4OC\underline{H}_2$), 5.90 (d, 2, PHT-$C\underline{H}_2$), 6.30—6.80 (m, 6, $2NC\underline{H}_2P$, and 2N$\underline{H}$), 8.70 (t, 6, $2C\underline{H}_3$), and 8.72 (t, 6, $2C\underline{H}_3$).

Found: C, 40.90; H, 5.69; N, 7.79%. Calcd for $C_{19}H_{32}N_3O_9P_3$: C, 41.44; H, 5.60; N, 7.71%.

VII. The amine (V), which was obtained *via* the dephthalylation of IV (1.34 g, 0.0032 mol), was stirred with phthalylglycine (0.65 g, 0.0032 mol) and DCC (0.68 g, 0.0033 mol) in THF (20 ml) at room temperature overnight. Aqueous acetic acid (40%, 1.5 ml) was then added to the reaction mixture, and the solution was kept at room temperature for 2 hr. The resulting dicyclohexylurea was filtered off, and the filtrate was concentrated. The residue was dissolved in chloroform, and the solution was washed with aqueous sodium hydrogen carbonate and water and dried with Drierite. The subsequent evaporation of the solvent afforded crystals of VII; 0.68 g (45 %); mp 149—150 °C (THF); IR (KBr): 3300 (w), 1770 (w), 1730 (s), 1660 (m), 1420 (s), 1200 (s), 1040 (s), 960 (s), and 710 (w) cm^{-1}; NMR: τ 1.65 (broad s, 1, CON$\underline{H}$), 2.15 (m, 4, phthalyl), 5.53 (s, 2, PHT-$C\underline{H}_2$), 5.5—6.10 (m, 8, $4OC\underline{H}_2$), 6.20—6.80 (m, 5, $2NC\underline{H}_2P$, and PN$\underline{H}$), 8.66 (t, 6, $2C\underline{H}_3$) and 8.69 (t, 3, $C\underline{H}_3$).

Found: C, 45.66; H, 5.73; N, 8.99%. Calcd for $C_{18}H_{27}N_3O_8P_2$: C, 45.48; H, 5.73; N, 8.84%.

X. A solution of the dipeptide (VIII, 1.95 g, 0.0055 mol) in ethanol (30 ml) was dephthalylated with hydrazine hydrate (0.4 ml) at room temperature overnight to give the corresponding amine through a procedure similar to that described in the preparation of III. The amine in THF (50 ml) was then added, drop by drop, to the chloride (II, 1.58 g, 0.0055 mol) in chloroform (50 ml), which had been precooled in an ice-water bath. After the mixture has been stirred further at room temperature overnight, it was processed in a manner essentially similar to that used in the preparation of IV, thus producing X; 0.56 g (22%); mp 159—160 °C (THF); IR (KBr): 3400 (w), 3150 (m), 2950 (w), 2900 (w), 1705 (s), 1410 (m), 1300 (m), 1060 (s), 960 (m), 900 (m), 830 (m), and 720 (m) cm^{-1}; NMR: τ 2.22 (m, 4, phthalyl), 5.60—6.10 (m, 9, $OC\underline{H}_2$, $2POC\underline{H}_2$, and PN$\underline{H}$,-$C\underline{H}_2$C) 5.90 (d, 2, PHT-$C\underline{H}_2$), 6.4—6.9 (m, 3, PN$\underline{H}C\underline{H}_2$P), 8.61 (t, 6, $2OC\underline{H}_3$), and 8.66 (t, 3, $C\underline{H}_3$).

Found: C, 45.55; H, 5.59; N, 8.96%. Calcd for $C_{18}H_{27}N_3O_8P_2$: C, 45.48; H, 5.73; N, 8.84%.

XI. The tripeptide analog (XI) was similarly synthesized from IX (1.19 g, 0.0032 mol) and II (0.92 g, 0.0032 mol), using triethylamine (0.7 ml); 0.185 g (12%); mp 140 °C; IR (KBr): 3300 (w), 1770 (w), 1740 (w), 1720 (s), 1405 (m), 1205 (s), 1160 (m), 1040 (s), 955 (m), 900 (w), and 720 (m) cm^{-1}; NMR: τ 2.20 (m, 4, phthalyl), 5.6—6.4 (m, 8, $3C\underline{H}_2$, and N$\underline{H}C\underline{H}C\underline{H}_3$), 6.4—6.7 (m, 3, N$\underline{H}C\underline{H}_2$P), 5.90 (d, 2, PHT-$C\underline{H}_2$), 8.56 (d, 3, $CHC\underline{H}_3$), 8.70 (t, 6, $2OC\underline{H}_3$), and 8.73 (t, 3, $OC\underline{H}_3$).

Found: C, 45.21; H, 5.93; N, 8.62%. Calcd for $C_{19}H_{29}N_3O_8P_2$: C, 45.63; H, 5.97; N, 8.59%.

References

1) M. Horiguchi and M. Kandatsu, *Nature*, 184, **901** (1959); J. S. Kittredge, E. Roberts, and D. G. Simonsen, *Biochemistry*, **1**, 624 (1962); L. D. Quinn, *ibid.*, **4**, 324 (1965); H Hori, O. Itasaka, H. Inoue, and K. Yamada, *J. Biochem.* (Tokyo), **56**, 447 (1964).

2) J. A. Alhadeff and G. D. Davies, Jr., *Biochemistry*, **9**, 4866 (1970); *Biochim. Biophys. Acta*, **244**, 211 (1971).

3) E. Baer and N. Z. Stanacev, *J. Biol. Chem.*, **239**, 3209 (1964).

4) L. D. Quin, *Science*, **144**, 1133 (1964).

5) W. F. Gilmore, and H. A. McBride, *J. Pharm. Sci*, **63**, 965 and 1087 (1974); M. Hariharan, R. J. Motekaitis, and A. E. Martell, *J. Org. Chem.*, **40**, 470 (1975).

6) K. Yamauchi, M. Kinoshita, and M. Imoto, This Bulletin, **45**, 2528, 2531 (1972).

Reactions between Nucleophiles and Sulfonium Ions Containing Electron-withdrawing Substituents

Haruo MATSUYAMA, Hiroshi MINATO, and Michio KOBAYASHI

Department of Chemistry, Faculty of Science, Tokyo Metropolitan University, Fukazawa, Setagaya, Tokyo 158

(Received May 27, 1975)

Sulfonium ions containing electron-withdrawing substituents are formed by the reactions between sulfonium ylides and suitable electrophiles. Reactivities of these sulfonium ions ($MeR\overset{+}{S}-CX(CO_2Me)_2$) with nucleophiles ($Y^-$) are investigated. The products found are those of 1) C-attack ($MeSR+YCX(CO_2Me)_2$), 2) Me-attack ($MeY+RSCX(CO_2Me)_2$) and 3) R-attack ($RY+MeSCX(CO_2Me)_2$). When R is (+)-2-octyl and Y^- is bromide ion, the RY found is (−)-2-octyl bromide with 59% optical purity. The mechanism of these reactions are discussed.

It has been shown that the reactions between trialkylsulfonium ions and nucleophiles yielding sulfides and alkylated nucleophiles have features different from ordinary S_N1, S_N2 or competitive S_N1-S_N2 reactions on carbon atoms.

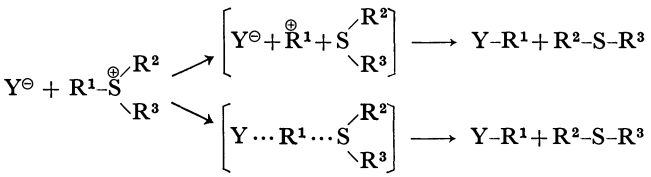

In ordinary S_N2 reactions on carbon atoms (for instance, the leaving groups are halides), the relative reactivities of benzyl and methyl compounds are not much different from unity,[1] whereas benzylation predominates in the reaction of dimethyl-1-phenylethylsulfonium ion with nucleophiles.[2] When di-*t*-butylmethylsulfonium ion reacts with methyl sulfide, exclusive *t*-butylation takes place with no methylation accompanied.[3] Thus when sulfides are leaving groups, the behavior of the substitution are occasionally quite different from that with halides or ammonium ions as leaving groups. No comprehensive explanations have been proposed yet.

In an attempt to understand the reactions between sulfonium ions and nucleophiles, the reactivities of the sulfonium ions containing electron-withdrawing substituents have been investigated, and the results are described in this paper.

Results and Discussion

Sulfonium ions containing electron-withdrawing substituents were prepared by the reaction between sulfonium ylides and suitable electrophiles.

When sulfonium bis(methoxycarbonyl)methylide (**1**) was mixed in chloroform with Br–Br, Cl–Cl, PhS–Cl, PhS–Br, MeS–Br or H–Br, they reacted instantaneously at room temperature. Usually it was not possible to

Table 1. Reactions of sulfonium ions with nucleophiles

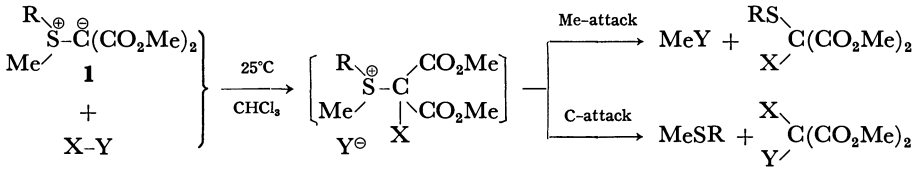

1	R	X	Y	Products (mol%) Me-attack MeY	Me-attack $(RS)XC(CO_2Me)_2$	C-attack MeSR	C-attack $XYC(CO_2Me)_2$
1a	Me	Br	Br	94	99	0	0
		Cl	Cl	95	84	0	0
		H	Br	100	100	0	0
		PhS	Cl	84	85	0	0
		PhS	Br[a]	92	64	0	0
		MeS	Br[b]	(25)	0	75	84
1b	Ph	Br	Br	100	86	0	0
		Cl	Cl	100	88	0	0
		H	Br	34	34	66	66
		PhS	Cl	0	0	84	88
		PhS	Br[c]	(36)	0	65	97
		MeS	Br[d]	(20)	0	80	83

a) Since PhSBr contains about 36% of free bromine, 36% of $Br(MeS)C(CO_2Me)_2$ was produced from the reaction of free bromine. b) From the reaction of free bromine, methyl bromide (25%) was produced. c) From the reaction of free bromine, methyl bromine (36%) was produced. d) From the reaction of free bromine, methyl bromide (20%) was produced.

Table 2. Reaction of dialkylsulfonium ions with nucleophiles

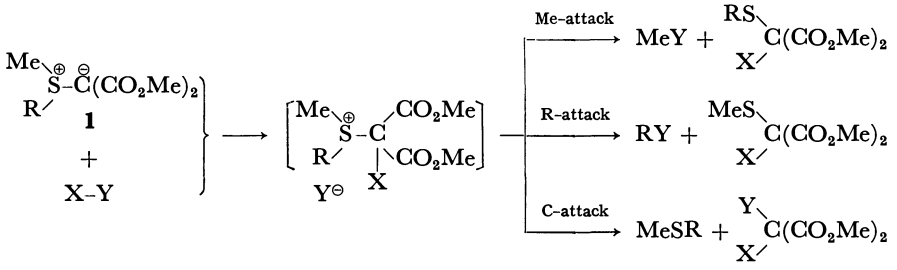

1	R	X	Y	Products (mol%)					
				Me-attack		R-attack		C-attack	
				MeY[a]	(RS)XCQ$_2$[b,c]	RY[d]	(MeS)XCQ$_2$[c,d]	MeSR[a]	XYCQ$_2$[b,c]
1c	Et	Br	Br	56	66	(34)	34	0	0
1d	*n*-Bu			81	81	(19)	19	0	0
1e	*i*-Pr			19	28	(72)	72	0	0
1f	*sec*-C_8H_{17}			21	21	(79)	79	0	0
1g	$PhCH_2$			0	0	100	97	0	0
1h	$MeSCH_2$			0	0	100	95	0	0
1c	Et	Cl	Cl	57	63	(37)	37	0	0
1e	*i*-Pr			23	33	(67)	67	0	0
1g	$PhCH_2$			0	0	97	95	0	0
1h	$MeSCH_2$			0	0	100	100	0	0
1c	Et	PhS	Cl	52	56	(44)	44	0	0
1e	*i*-Pr			18	25	(75)	75	0	0
1g	$PhCH_2$			0	0	90	90	0	0
1h	$MeSCH_2$			0	0	100	100	0	0
1c	Et	H	Br	73	73	(11)	11	16	(16)
1d	*n*-Bu			68	68	(12)	12	20	(20)
1e	*i*-Pr			61	62	(13)	13	25	(25)
1g	$PhCH_2$			0	0	100	100	0	0
1h	$MeSCH_2$			0	0	100	100	0	0

a) Determined from its methyl singlet absorption. b) The CO_2Me (δ 3.77—3.86, broad singlet) absorptions of (RS)XCQ$_2$, (MeS)XCQ$_2$ and XYCQ$_2$ usually could not be resolved. The amount of (MeS)XCQ$_2$ was determined from its MeS singlet, and that of XYCQ$_2$ was estimated by assuming the equimolar formation of MeSR and XYCQ$_2$. Then the amount of (RS)XCQ$_2$ could be calculated. c) Q=CO_2Me. d) The amounts of $PhCH_2Y$ (or $MeSCH_2Y$) were determined from its singlet near 4.50 ppm. The amounts of other RY's were estimated from the assumption of equimolar formation of RY and (MeS)XCQ$_2$ (determined from its MeS singlet).

isolate the sulfonium salts. It was possible to isolate a white solid sulfonium salt from the reaction between **1a** (R=Me) and HBr; they decomposed when they were dissolved in chloroform and allowed to stand at room temperature for 5 hrs. The products of the reaction of **1a** (R=Me) and **1b** (R=Ph) with several electrophiles are listed in Table 1.

When R in **1** is an alkyl group, competitive S_N2 attacks on the methyl and alkyl groups are expected. Ylide **1** with various alkyl groups was allowed to react with X—Y, and the products are shown in Table 2.

The results shown in Tables 1 and 2 can be summarized as follows. The ylides and electrophiles react and form sulfonium ions and anions $Y^{\ominus}$, which further react in three different ways (namely, Me-attack, R-attack and C-attack).

The course of the reaction depends upon the structure of the sulfonium ion (R and X) and the nucleophile $Y^{\ominus}$.

1) When R is Me, methyl attack of $Y^{\ominus}$ predominates

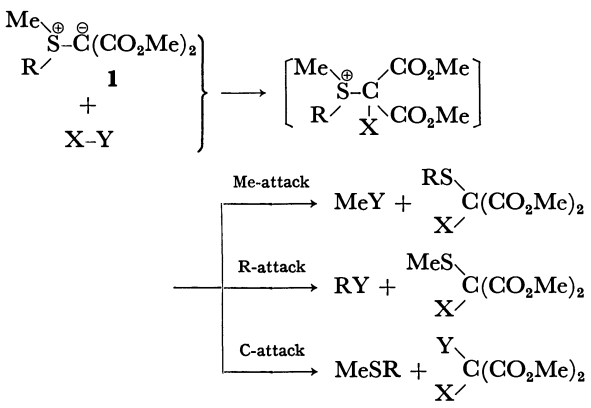

except one case, in which X is MeS.

When X is MeS, Me_2S group easily leaves from $Me_2\overset{\oplus}{S}-C(SMe)(CO_2Me)_2$; it is known that R—S groups can stabilize the adjacent carbonium ion by resonance effect as shown below.[4]

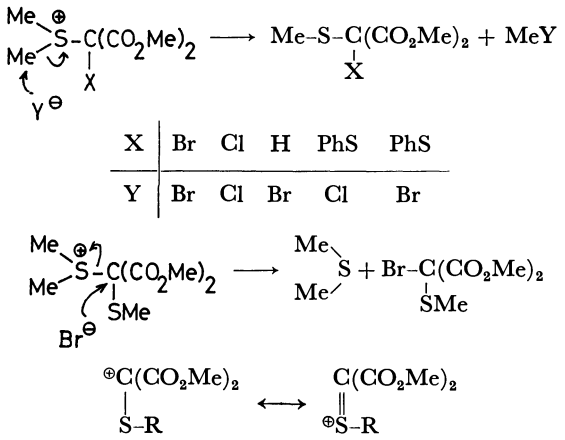

X	Br	Cl	H	PhS	PhS
Y	Br	Cl	Br	Cl	Br

When X is PhS, such resonance effect is not great enough to help the elimination of Me_2S.

2) When R is Ph, and X is MeS or PhS, the elimination of PhSMe and the apparent C-attack of $Y^{\ominus}$ predominate.

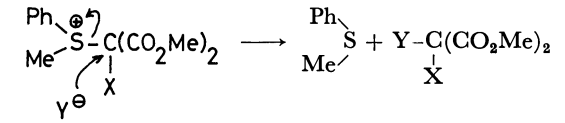

X	PhS	PhS	MeS
Y	Cl	Br	Br

Apparently PhSMe is a better leaving group than Me_2S,[5] and even when X is PhS (a poorer resonance-stabilizing group), the elimination of PhSMe takes place readily.

3) When X is Br or Cl, the main reaction is methyl attack of $Y^{\ominus}$ and RSMe elimination is not observed.

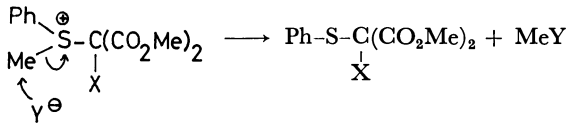

It is reasonable that the carbon atom containing three electron-withdrawing groups (two CO_2Me's and one halogen) does not allow the RSMe elimination resulting in the formation of a carbonium ion.

4) When R=Ph and X=H, both the RSMe elimination and the methyl attack of $Y^{\ominus}$ take place.

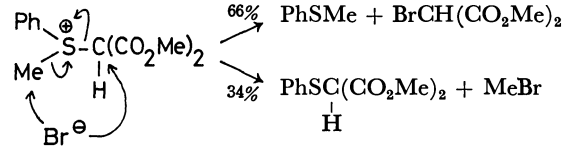

It is interesting to note that when one of the substituents is benzyl or methylthiomethyl group, the reaction is exclusive benzylation or methylthiomethylation of the nucleophile with no accompanying methylation. The ratio between the yields of methylated and alkylated products are calculated and summarized in Table 3. They are quite different from what are expected for ordinary S_N2 reactions on carbon. For instance, the relative reactivities of alkyl bromides with bromide anion in acetone at 25 °C are Me 1.0, Et 0.013, *i*-Pr 0.0086, and $PhCH_2$ 1.0.[6] The remarkable feature in the results shown in Table 3 is that the reactivity of methyl group is comparable to that of ethyl group, smaller than that of isopropyl group, and far smaller than that of benzyl group.

The relative reactivities of phenylmethylalkylsulfonium perchlorates with iodide anion in acetone at 50 °C are Me 1.0, Et 0.20, *n*-Pr 0.16, and *i*-Pr 0.05, and apparently these reactions involve S_N2 attack on the sulfonium alkyl groups.[7]

Table 3 shows that benzyl and methylthiomethyl are far more reactive than methyl group. These results suggest that these reactions may involve an S_N1-like process. In the reactions of **1** with hydrogen bromide, however, the reactivity of isopropyl group is smaller than that of methyl group. Thus, *sec*-alkyl groups are more reactive than methyl group only when the α atom in X is a hetero atom such as Br, Cl or S.

Reversible bond-formation between sulfonium sulfur atom and an anion is a possible process, since evidence for the formation of a tetracovalent sulfur intermediate from a sulfonium ion and chloride ion has been presented,[8] and many examples of tetracovalent sulfur intermediates were described in a recent review.[9] In an attempt to elucidate the mechanism of these reactions, a sulfonium ylide with optically active (+)-2-C_8H_{17}

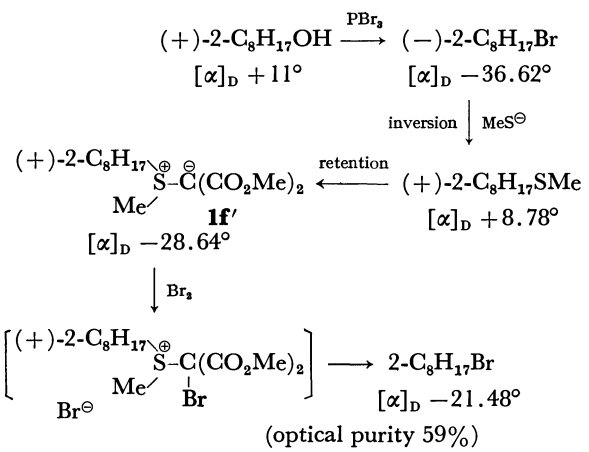

Scheme.

Table 3. Relative reactivities of alkyl groups of sulfonium ions with nucleophiles[a]

Sulfonium ion	Nucleophile	Relative reactivity, k_R/k_{Me}						
		Me	Et	*n*-Bu	*i*-Pr	*sec*-C_8H_{17}	$PhCH_2$	$MeSCH_2$
$MeRS^{\oplus}$-$BrC(CO_2Me)_2$	$Br^{\ominus}$	(1.0)	0.61	0.23	3.79	3.76	∞	∞
$MeRS^{\oplus}$-$ClC(CO_2Me)_2$	$Cl^{\ominus}$	(1.0)	0.65	—	2.91	—	∞	∞
$MeRS^{\oplus}$-$(PhS)C(CO_2Me)_2$	$Cl^{\ominus}$	(1.0)	0.85	—	4.17	—	∞	∞
$MeRS^{\oplus}$-$HC(CO_2Me)_2$	$Br^{\ominus}$	(1.0)	0.15	0.18	0.21	—	∞	∞

a) Relative reactivities are the ratio RY/MeY, calculated from Table 2.

group (**1f'**) was prepared and its reaction with bromine was examined according to the Scheme shown.

The reactivity of 2-C_8H_{17} group is about 4 times that of methyl group. The results of optical measurements show that the main course of the reaction is the inversion at the asymmetric carbon accompanied by some racemization.

If a sulfurane intermediate is produced by the bond-formation between the sulfonium sulfur atom and bromide ion, the collapse of the sulfurane should yield (+)-2-C_8H_{17}–Br with retention of configuration. The optical data show that such sulfurane intermediates are probably not formed in the reaction between **1f'** and bromine.

It is of interest that $k_{i\text{-Pr}}$ is smaller than k_{Me} in the reactions between MeRS⊕—Ph $ClO_4^\ominus$ and $I^\ominus$,[7] and $k_{i\text{-Pr}}$ is greater than k_{Me} in the reactions between MeRS⊕—CX-$(CO_2Me)_2$ and $Y^\ominus$ only when the α atom in X is a hetero atom. One possible explanation is the formation of the following intramolecular sulfurane.

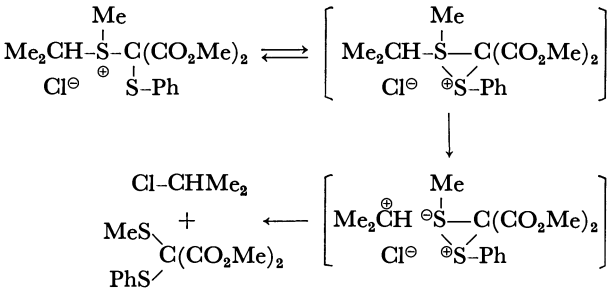

A similar intramolecular sulfurane has been proposed between a sulfonium ion and the neighboring nitro group.[10]

If the PhS group interacts with the solfonium sulfur atom, some positive charge is expected on the PhS sulfur atom. In order to check the possibility, sulfonium ion **2a** was prepared, and allowed to react with pyridine.

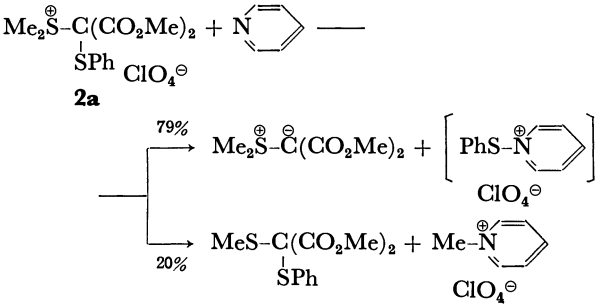

The product of the nucleophilic attack of pyridine on the PhS sulfur atom was found in 79% yield. These results suggest that the PhS sulfur atom has a partial positive charge in agreement with the above hypothesis.

Reactions of **2a** with $Cl^\ominus$ or Me_2S gave the results consistent with those shown in Table 1.

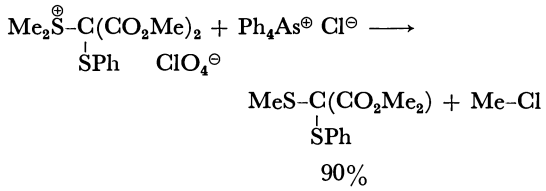

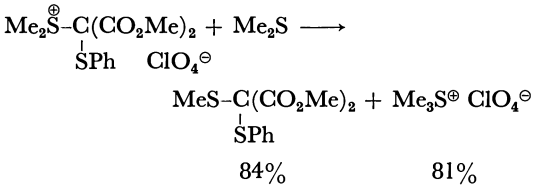

The results of the reaction between optically-active **1f'** and Br_2 may be rationallized by assuming some elongation of the R-S⊕ bond, development of positive charge on R, and the attack of $Br^\ominus$ taking place mainly from the backside.

Ōki and Kobayashi studied the reaction between (+)-α-phenylpropyl methyl sulfide and methanesulfenyl chloride, and found that $Cl^\ominus$ attacked the intermediate sulfonium ion, PhEtC*H—S⊕Me(SMe), forming (−)-PhEtCH—Cl with 70% inversion and 30% racemization.[11]

Experimental

Materials. Sulfonium bis(methoxycarbonyl)methylides **1a—h** were prepared by copper salts-catalyzed decomposition of dimethyl diazomalonate in large excess sulfides[12] and by transylidation.[13] Benzenesulfenyl chloride (bp 50 °C/2 mmHg) was synthesized by the methods described in the literature.[14] Benzenesulfenyl bromide (or methanesulfenyl bromide) was prepared by mixing equimolar amounts of phenyl disulfide (or methyl disulfide) and bromine in carbon tetrachloride. Sulfonium salt **2a** was prepared by dropwise addition of a CCl_4 solution of benzenesulfenyl chloride (1.45 g, 10 mmol) to a nitromethane solution of **1a** (1.94 g, 10 mmol) and silver perchlorate (2.07 g, 10 mmol) at 0 °C. Yield, 3.6 g (90%); recrystallized from ethanol; mp 105—106 °C; IR (KBr), 1740 cm^{-1} (ν_{CO}); NMR (DMSO-d_6), δ 7.60 (5H, s, PhS), 3.93 (6H, s, CO_2Me) and 3.20 (6H, s, $Me_2\overset{\oplus}{S}$–). Found: C, 38.26; H, 4.25%. Calcd for $C_{13}H_{17}O_8ClS_2$: C, 38.96; H, 4.27%. This salt partially decomposed when it was allowed to stand at room temperature for several days.

Reactions of Ylides 1a or 1b with Bromine. (a) When Br_2 (1.65 g, 10.3 mmol) was added to a chloroform (18 g) solution of **1a** (1.97 g, 10.0 mmol), they reacted instantaneously, and the solution turned from red to colorless. The ylide carbonyl absorptions (1630 and 1670 cm^{-1}) were replaced by the ester absorption (1730 cm^{-1}). The amounts of the products were determined by NMR spectroscopy with nitromethane as an internal standard. The low-boiling fractions from the mixture were trapped in liquid nitrogen, and the presence of MeBr was shown by NMR (δ 2.62, s). The high-boiling fractions were chromatographed (Florisil), and the oils obtained from the benzene eluate were found to be Br(MeS)$C(CO_2Me)_2$ (2.54 g, 9.9 mmol, 99%; IR (neat), 1740 cm^{-1} (ν_{CO}); NMR (CCl_4), δ 3.86 (6H, s, CO_2Me) and 2.22 (3H, s, MeS). Found: C, 27.76; H, 3.68%. Calcd for $C_6H_9O_4BrS$: C, 27.29; H, 3.44%). (b) A mixture of a $CHCl_3$ (10 g) solution of **1b** (1.25 g, 5.0 mmol) and Br_2 (0.80 g, 5.0 mmol) gave MeBr (δ 2.62, s) and Br(PhS)$C(CO_2Me)_2$ (liquid, 1.37 g, 0.43 mmol, 86%; IR (neat), 1740 cm^{-1} (ν_{CO}); NMR (CCl_4), δ 7.30—7.60 (5H, m, PhS) and 3.76 (6H, s, CO_2Me). Found: C, 41.26; H, 3.56%. Calcd for $C_{11}H_{11}O_4BrS$: C, 41.40; H, 3.47%).

Reactions of Ylides 1a or 1b with Chlorine. (a) The reaction between a $CHCl_3$ (10 g) solution of **1a** (1.0 g, 5.14 mmol) and a CCl_4 solution of Cl_2 (0.42 g, 6.0 mmol) was exothermic and instantaneous, and gave MeCl (δ 3.0, s) and Cl(MeS)C-$(CO_2Me)_2$ (liquid, 0.92 g, 4.34 mmol, 84%; IR (neat), 1740

cm^{-1} (ν_{CO}); NMR ($CDCl_3$), δ3.88 (6H, s, CO_2Me) and 2.25 (3H, s, MeS). Found: C, 32.75; H, 3.82%. Calcd for $C_6H_5O_4ClS$: C, 32.82; H, 4.13%).

(b) In a similar manner, a mixture of a $CHCl_3$ (19 g) solution of **1b** (2.61 g, 10.3 mmol) and a CCl_4 solution of Cl_2 (0.78 g, 11.0 mmol) gave MeCl (δ 2.97, s) and $Cl(PhS)C(CO_2Me)_2$ (liquid, 2.49 g, 9.09 mmol, 88%; IR (neat), 1740 cm^{-1} (ν_{CO}); NMR (CCl_4), δ 7.30—7.60 (5H, m, PhS) and 3.68 (6H, s, CO_2Me). Found: C, 48.17; H, 3.92%. Calcd for $C_{11}H_{11}O_4ClS$: C, 48.10; H, 4.04%). Methyl phenyl sulfide (PhSMe, δ 2.49, s) was not found.

Reactions of Ylides ***1a*** *or* ***1b*** *with Benzenesulfenyl Chloride.*

(a) When PhSCl (1.60 g, 11.1 mmol) was added to a chloroform (15 g) solution of **1a** (1.98 g, 10.3 mmol), they reacted instantaneously, and the solution turned from red to colorless. The amounts of the products were determined by NMR spectroscopy with nitromethane as an internal standard. From the low-boiling fraction trapped in liquid nitrogen, methyl chloride was identified by NMR (δ 2.97, s). The high-boiling fraction solidified at room temperature, and recrystallization from benzene yielded white crystals of $MeS(PhS)C(CO_2Me)_2$. 2.51 g (8.77 mmol, 85%): mp 71—72 °C; IR (KBr), 1730 cm^{-1} (ν_{CO}); NMR (CCl_4), δ 7.30 (5H, s, PhS), 3.64 (6H, s, CO_2Me) and 2.15 (3H, s, MeS). Found: C, 50.52; H, 4.93%. Calcd for $C_{12}H_{14}O_4S_2$: C, 50.33; H, 4.93%.

(b) In a similar manner, a mixture of a $CHCl_3$ (9 g) solution of **1b** (1.75 g, 6.87 mmol) and PhSCl (1.01 g, 7.0 mmol) gave PhSMe (from hexane eluates; 0.71 g, 5.75 mmol, 84%), $Cl(PhS)C(CO_2Me)_2$ (oil from benzene eluates; 1.66 g, 6.05 mmol, 88%).

Reactions of Ylides ***1a*** *or* ***1b*** *with Benzenesulfenyl Bromide.*

(a) A mixture of a $CHCl_3$ (14 g) solution of **1a** (1.95 g, 10.0 mmol) and a CCl_4 (6 g) solution of PhSSPh (1.1 g, 5.0 mmol) and bromine (0.8 g, 5.0 mmol) reacted instantaneously, and gave MeBr (δ 2.64, s) and MeS (PhS) C $(CO_2Me)_2$ (1.83 g, 6.4 mmol, 64%; mp 71—72 °C).

(b) A mixture of a $CHCl_3$ (10 g) solution of **1b** (2.54 g, 10.0 mmol) and a CCl_4 (10 g) solution of PhSSPh (1.1 g, 5.0 mmol) and bromine (0.8 g, 5.0 mmol) gave PhSMe (δ 2.49, from hexane eluates; 0.81 g, 6.50 mmol, 65%) and $Br(PhS)C(CO_2Me)_2$ (oil from benzene eluates; 3.09 g, 7.70 mmol, 97%).

Reactions of Ylides ***1a*** *or* ***1b*** *with Methanesulfenyl Bromide.*

(a) In a similar manner, a mixture of a $CHCl_3$ (10 g) solution of **1a** (1.92 g, 10 mmol) and a CCl_4 (9 g) solution of MeSSMe (0.42 g, 5.0 mmol) and bromine (0.8 g, 5.0 mmol) reacted instantaneously, and gave Me_2S (δ 2.10, s, 75%), MeBr (δ 2.64, s, 25%; produced from the reaction of free bromine) and $Br(MeS)C(CO_2Me)_2$ (oil from benzene eluates; 2.24 g, 8.40 mmol, 84%).

(b) A mixture of a $CHCl_3$ (10 g) solution of **1b** (1.90 g, 10 mmol) and a CCl_4 (8 g) solution of MeSSMe (0.42 g, 0.5 mmol) and bromine (0.8 g, 5.0 mmol) gave PhSMe (δ 2.49, s; from hexane eluates; 1.0 g, 8.0 mmol, 80%), MeBr (δ 2.64, s, 20%; produced from the reaction of free bromine) and $Br(MeS)C(CO_2Me)_2$ (oil from benzene eluates; 2.21 g, 8.30 mmol, 83%).

Reactions of Ylides ***1a*** *or* ***1b*** *with Hydrogene Bromide.* (a) When hydrogene bromide gas was bubbled through a $CHCl_3$ solution of **1a**, its NMR spectrum showed the formation of a sulfonium salt ($Me_2\overset{\oplus}{S}-$, δ 3.42, s). Evaporation of the solvent yielded white solids (NMR ($CHCl_3$), δ 4.01 (6H, s, CO_2Me) and 3.42 (6H, s, $Me_2\overset{\oplus}{S}-$)). When they were dissolved in $CHCl_3$ and allowed to stand for 5 hr at room temperature, the NMR spectrum showed the quantitative formation of MeBr (δ 2.63, s) and $MeSCH(CO_2Me)_2$ (δ 2.25, s).

(b) When a CCl_4 solution of hydrogen bromide was added to a $CHCl_3$ solution of **1b**, they reacted instantaneously, and it was not possible to isolate the sulfonium salt. The amounts of MeBr (δ 2.62, s, 34%) and PhSMe (δ 2.46, s, 66%) were determined by use of nitromethane as an internal standard.

Reactions of Ylides ***1c—h*** *with Halogens, PhSCl or HBr.*

The $CDCl_3$ solutions of Ylides **1c—h** (0.7—1.0 mmol) and X—Y (0.8—1.1 mmol) containing nitromethane (internal standard, 50 μl, 0.79 mmol) were let to react in NMR tubes at 25 °C, and the amounts of the reaction products were determined from their singlet methyl absorption by NMR spectroscopy (see Table 2); Me–Br (δ 2.62—2.64), Me–Cl (2.90—2.98), MeSEt (2.05—2.12), MeSBu-*n* (2.07), MeSPr-*i* (2.10), $MeSC_8H_{17}$-*sec* (1.99), $MeSCH_2Ph$ (1.92), $MeSCH_2$-SMe (2.10), $Br(MeS)C(CO_2Me)_2$ (2.23), $Cl(MeS)C(CO_2Me)_2$ (2.23), $MeS(PhS)C(CO_2Me)_2$ (2.19—2.20) and $MeSCH(CO_2Me)_2$ (2.25).

*Synthesis of (+)-2-Octylmethylsulfonium Bis(methoxycarbonyl)-methylide (***1f′***).* (−)-2-Octyl bromide was prepared from the reaction between (+)-2-octanol (purchased from Fluka, $[\alpha]_D$ +11°) (15 g) and PBr_3 (34.8 g) below +5 °C; yield, 13.8 g (62.6%); bp 55 °C/3 mmHg (lit,[15] 61 °C/3 mmHg); $[\alpha]_D^{26.6}$ −36.62° (*c* 8.36, 95% ethanol) (lit,[15] $[\alpha]_D^{25}$ −34.25°).

(+)-2-Octyl methyl sulfide was prepared from the reaction between (−)-2-octyl bromide (11.1 g) and sodium methylmercaptide (20% aq solution, 42 g) in ethanol; yield, 75.0%; bp 84—85.5 °C/10 mmHg; $[\alpha]_D^{26.5}$ +8.78° (*c* 11.8, $CHCl_3$).

Ylide **1f′** was not obtained by copper-catalyzed decomposition of methyl diazomalonate in the sulfide.[12] Therefore, it was prepared by transylidation.[13] A chloroform (11.5 g) solution of **1b** (3.04 g), (+)-2-octyl methyl sulfide (6.0 g) and dimethoxy disulfide (1.3 g; a catalyst) was kept at 40 °C. After 4 days, its NMR spectrum showed the complete disappearance of **1b**. Sulfides and the catalyst were distilled off under reduced pressure at 55 °C/3 mmHg, and the NMR spectrum of the residual oil showed that it is ylide **1f′**; yield, 2.5 g (72%); IR (neat), 1620 and 1670 cm^{-1} (ν_{CO}); NMR ($CDCl_3$), δ 3.74 (6H, s, CO_2Me), 2.88 (3H, s, $Me\overset{\oplus}{S}-$) and 0.88—1.44 (16H, m, 2-octyl group); $[\alpha]_D^{28.2}$ −28.64° (*c* 10.5, $CHCl_3$).

Reactions of Ylide ***1f′*** *with Bromine.* A CCl_4 (13.8 g) solution of Br_2 (1.38 g, 8.62 mmol) was added drop by drop to a $CHCl_3$ (21 g) solution of **1f′** (2.5 g, 8.62 mmol). The completion of the reaction was ascertained by the IR spectrum (ν_{CO}, 1730 cm^{-1}). The NMR spectrum showed the formation of 2-octyl bromide (79.3%) and methyl bromide (20.7%). After the reaction mixture was concentrated under reduced pressure, the residue was subjected to column chromatography (Florisil), and the *n*-hexane eluates yielded 2-octyl bromide. Its purity was checked by gas chromatography. $[\alpha]_D^{25.2}$ −21.48° (*c* 5.96, 95% ethanol).

Reactions of Sulfonium Ion ***2a*** *with Nucleophiles.* (a) A nitromethane solution of **2a** (1.0 mmol) and tetraphenylarsonium chloride (2.0 mmol) was heated at 50 °C for 5 min. After evaporation, the NMR spectrum of the residue (soluble in CCl_4) showed the presence of $MeS(PhS)C(CO_2Me)_2$ (δ 2.20, s, MeS; 90%).

(b) A DMSO-d_6 solution of **2a** (1.0 mmol) and methyl sulfide (1.5 mmol) was placed in an NMR tube at 25 °C. After 4 days, the amounts of trimethylsulfonium salt (δ 2.89, s, $Me_3\overset{\oplus}{S}$; 81%) and $MeS(PhS)C(CO_2Me)_2$ (δ 2.17, s, MeS; 84%) were determined by NMR spectroscopy.

(c) A DMSO-d_6 solution of **2a** (1.0 mmol) and pyridine (2.0 mmol) was placed in an NMR tube at 25 °C. After 2 hr, the amounts of **1a** (δ 2.88, s, $Me_2\overset{\oplus}{S}-$; 79%) and $MeS(PhS)C(CO_2Me)_2$ (δ 2.17, s, MeS; 20%) were determined by NMR spectroscopy.

Reaction of Ylide **1e** *with Methanesulfenyl Chloride.* In an NMR tube a $CDCl_3$ solusion of **1e** (1.0 mmol) and a CCl_4 solution of MeSCl were mixed. Rapid reaction took place, yielding MeSPr-*i* and $Cl(MeS)C(CO_2Me)_2$ quantitatively. The NMR spectrum showed the absence of isopropyl chloride.

References

1) A. Streitwieser, *Chem. Rev.*, **56**, 571 (1956).
2) H. M. R. Hoffmann, *J. Chem. Soc.*, **1965**, 823; H. M. R. Hoffmann and E. D. Hughes, *ibid.*, **1964**, 1259; S. H. Harvey, P. A. T. Hoye, E. D. Hughes, and C. K. Ingold, *ibid.*, **1960**, 800.
3) H. Minato, T. Miura, F. Takagi, and M. Kobayashi, *Chem. Lett.*, **1975**, 211.
4) T. Nakai, Y. Ueno, and M. Okawara, *Tetrahedron Lett.*, **1967**, 3831; T. Nakai and M. Okawara, *ibid.*, **1967**, 3835; T. Nakai, Y. Ueno, and M. Okawara, This Bulletin, **43**, 156 (1970); T. Nakai and M. Okawara, *ibid.*, **43**, 1864 (1970); C. P. Lillya, E. F. Miller, P. Miller, and R. A. Sahatjian, *Int. J. Sulfur Chem.*, **1**, 79 (1971).
5) T. Cohen, G. Herman, T. M. Chapman, and D. Kuhn, *J. Amer. Chem. Soc.*, **96**, 5627 (1974).
6) P. B. D. de la Mare, *J. Chem. Soc.*, **1955**, 3180; P. B. D. de la Mare and E. D. Hughes, *ibid.*, **1956**, 845.
7) H. Matsuyama, W. Ando, and T. Migita, unpublished results.
8) D. C. Owsley, G. K. Helmkamp, and S. N. Spurlock, *J. Amer. Chem. Soc.*, **91**, 3606 (1969); D. C. Owsley, G. K. Helmkamp, and M. F. Rettig, *ibid.*, **91**, 5239 (1969).
9) N. E. Hester, *Int. J. Sulfur Chem.*, **8**, 124 (1973).
10) E. N. Givens and H. Kwart, *J. Amer. Chem. Soc.*, **90**, 378, 386 (1968).
11) M. Ōki and K. Kobayashi, This Bulletin, **43**, 1223 (1970).
12) W. Ando, T. Yagihara, S. Tozune, S. Nakaido, and T. Migita, *Tetrahedron Lett.*, **1969**, 1979.
13) H. Matsuyama, H. Minato, and M. Kobayashi, This Bulletin, **46**, 2845 (1973).
14) "Organic Syntheses," Coll. Vol. 4, p. 934.
15) C-M. Hsueh and C. S. Marvel, *J. Amer. Chem. Soc.*, **50**, 856 (1928).

Influence of Anhydrous Hydrogen Fluoride on Hen Egg-White Lysozyme. I. Effects on Native Hen Egg-White Lysozyme

Saburo AIMOTO and Yasutsugu SHIMONISHI

Institute for Protein Research, Osaka University, Yamada-kami, Suita, Osaka 565

(Received May 31, 1975)

The influences of anhydrous hydrogen fluoride on the native form of hen egg-white lysozyme under standard conditions of peptide synthesis were investigated by measuring the enzymatic activities of materials recovered from mixtures of anhydrous hydrogen fluoride and hen egg-white lysozyme. The enzymatic activity of hen egg-white lysozyme gradually decreased on incubation with anhydrous hydrogen fluoride at a given temperature. After incubation of the mixture at 0 °C for 60 min, at least three fractions could be separated by gel-filtration on Sephadex G-50. One of these was eluted in the same position as native lysozyme and was fully active enzymatically. Its ultra-violet, and circular dichroism absorptions were identical with those of native lysozyme, and the tetragonal crystals obtained from this fraction could not be distinguished from those of native lysozyme.

The authors are now studying the chemical synthesis of the native form of the well-characterized protein molecule, hen egg-white lysozyme (HEL). At present they are interested in establishing how much of the intact structure of this enzyme is retained after exposure to anhydrous liquid hydrogen fluoride (HF) under usual conditions for peptide synthesis and how much of the original enzyme can be recovered in an intact form after this treatment.

HF was first used in peptide synthesis by Sakakibara *et al.*[1,2] and since then it has been widely used for releasing free peptide, because it does not show any troublesome side reactions with simple protected peptides. However, in the synthesis of complicated polypeptides, it is uncertain whether it can be used to release free polypeptides from protected derivatives without causing side reactions. HF was originally used in studies on the chemistry of peptides and proteins by Katz[3] and Katz *et al.*[3,4] examined its effects on some natural polyepptide hormones, such as insulin and corticotropin, and also on enzymes such as ribonuclease and lysozyme. They reported that the biological activities of these compounds were not irreversibly affected by HF, provided that the temperature of exposure was low (−78 °C) and the exposure time was short (<2 hr). This suggests that a considerable amount of starting material might remain in an intact form during treatment with HF under these conditions. On the other hand, they found that considerable inactivation occurred on exposure to HF at a higher temperature (0—25 °C) and for a longer time (≥2 hr), particularly in the cases of ribonuclease and lysozyme. These findings indicate that highly oriented macromolecules may be considerably affected by prolonged exposure to HF at high temperature. However, unfortunately protecting groups can only be removed from protected complicated polypeptides under these conditions. Since the syntheses of complicated polypeptide hormones and enzymes have recently become of major interest, it will be very valuable to examine the influence of HF on complicated polypeptides or enzymes under conditions generally used for peptide synthesis.

In the present study, the influences of HF on the native form of HEL were investigated in the preliminary studies of the chemical synthesis of HEL. First, the effect of the conditions of HF-treatment on the enzymatic activity of HEL was examined. Second, the attempts were made to isolate intact HEL after treatments of native HEL with HF. The results show the possibility to recover intact HEL from native HEL treated with HF under the conditions generally used for peptide synthesis.

Materials and Methods

Substrates and Reagents. Spray-dried cells of *Micrococcus lysodeikticus* (Lot. No. 21—88—778) were purchased from Seikagaku Fine Biochemicals. Sephadex was purchased from Pharmacia Co. (Uppsala) and hydrogen fluoride was a product of Daikin Ind. Co. (Osaka). Urea of reagent grade was recrystallized from ethanol before use. All other chemicals used were of analytical grade.

Hen Egg-White Lysozyme (HEL). Hen egg-white lysozyme (6 x crystallized Lot. No. 7103) from Seikagaku Fine Biochemicals was used without further purification. It was dissolved in dilute acetic acid, lyophilized and then dried over P_2O_5 *in vacuo*. The freeze-dried powder was used in all experiments.

Treatments of Native HEL with HF. The freeze-dried powder (*ca.* 30 mg) of native HEL was weighed in a Daiflon cylinder of the HF-reaction apparatus.[2] HF (5 ml) was distilled into a cylinder containing HEL previously cooled to −78 °C in a dry-ice/methanol bath. The resulting solution was stirred at 0 °C or 25 °C for the required period. Under these conditions, the start of the reaction period was taken as 30 min after transferring the sample from the bath at −78 °C to that at 0 °C or 25 °C. After a given period, HF was completely removed from the reaction mixture by evaporation *in vacuo*, and the residue of the HF-solution of native HEL was dissolved in M/15 sodium phosphate buffer solution at pH 6.2 (30 ml), and stirred at room temperature for 20—24 hr. Then, its enzymatic activity was assayed.

Enzyme Assays. The specific activity of HEL after treatment with HF was determined by measuring the initial rate of lysis of *Micrococcus lysodeikticus* cells suspended in M/15 sodium phosphate buffer solution at pH 6.2 containing 0.1% sodium chloride at 37 °C using the method of Jolles,[5] with six times recrystallized native HEL as a standard. The extent of lysis was measured spectrophotometrically at 540 nm.

Desalting of Protein. Protein solutions containing various salts were charged on a column of Sephadex G-10 (3×60 cm), and eluted with 0.1M acetic acid. The fractions of eluate with absorption at 280 nm were collected and lyophilized.

Gel-filtration. The lyophilized powder of the material recovered after treatment of native HEL with HF was dis-

solved in a buffer containing 1M acetic acid and 5M urea and charged on a column of Sephadex G-50 (fine, 2.2×95 cm), equilibrated with the same buffer. The column was eluted with the same buffer and the absorption of each fraction at 280 nm was determined.

Ion-Exchange Chromatography. The lyophilized powder obtained after treatment of native HEL with HF was dissolved in a small volume of 0.2M sodium phosphate buffer solution at pH 7.15 and charged on a column of Bio-rex 70 (1.9×54 cm), equilibrated with the same buffer. The absorptions at 280 nm of the fractions eluted with the same buffer were measured and fractions in each peak were combined and lyophilized.

Ultra-violet and Circular Dichroism Absorption Spectra. Ultra-violet absorption spectra were measured using a Hitachi UV-spectrophotometer type-124, equipped with a recording attachment. Circular dichroism spectra were measured in a Jasco automatic spectropolarimeter J-20, equipped with a CD-attachment. $[\theta]_R$ represents the molecular ellipticity based on the mean residue weight. Protein concentration was calculated using the value, $E^{1\%}_{1cm}=23.7$ at 280 nm. The cell length was 1 mm for the range of wavelengths of 220 to 250 nm and 1 cm for those of 290 to 300 nm. The solvent was 0.1M sodium chloride, adjusted to pH 3.0 with hydrochloric acid. Spectra were measured at 25 °C.

Crystallization of HF-Treated HEL. Crystallization was carried out by the method of Berthou and Jolles[6] with some modifications. The lyophilized protein (35 mg) was dissolved in distilled water (0.50 ml), and then first 0.2M acetate buffer solution at pH 4.7 (0.063 ml) and distilled water (0.187 ml) and then 10% sodium chloride solution (0.75 ml) were added. The protein concentration was adjusted to 2.33% and the solution was allowed to stand in a refrigerator at 5 °C for 3 days. Crystals were deposited from solutions of biologically fully active materials.

Results

Treatment of Native HEL with HF. The freeze-dried native HEL was first treated with HF at 0 °C or 25 °C. After a given period of 60 to 240 min, the reaction was stopped by complete evaporation of the HF from the HF-solution of the freeze-dried native HEL. The residue was dissolved in M/15 sodium phosphate buffer solution at pH 6.2 containing 0.1% sodium chloride and after 20—24 hr its lytic activity on *Micrococcus lysodeikticus* was compared with that of standard HEL.

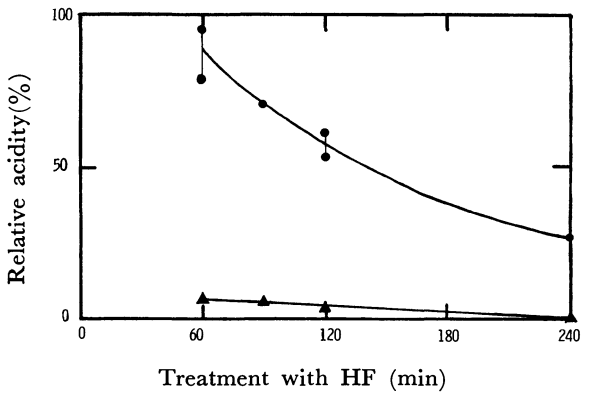

Fig. 1. Relative activity of HF-treated native HEL. The procedure used for treatment of HEL with HF and the method used of enzymatic assay of HF-treated HEL are given in the text.
—●—: treated at 0 °C, —▲—: treated at 25 °C.

The enzymatic activity of the solution of the freeze-dried native HEL treated with HF at 0 °C for 60 min was about 80% of that of standard HEL and decreased gradually on longer treatment. On the other hand, after treatment at 25 °C for 60 min its activity was only 10% of that of standard HEL and after 240 min-treatment it was almost inactive. These results are summarized in Fig. 1.

Gel-Filtration of HF-Treated Native HEL on Sephadex G-50. The material recovered from an HF-solution of the freeze-dried native HEL was desalted on Sephadex G-10 and subjected to chromatography on Sephadex G-50 using buffer solution containing 1M acetic acid and 5M urea. The chromatogram of the material recovered after treatment of the freeze-dried native HEL with HF at 0 °C for 60 min is shown in Fig. 2. These fractions (I, II and III) were separated. The first fraction (I) was eluted in the void voulme, and the

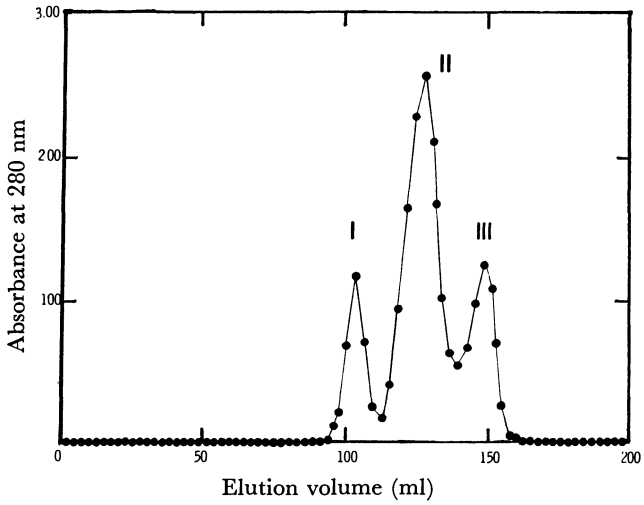

Fig. 2. Gel-filtration of native HEL treated with HF at 0 °C for 60 min on Sephadex G-50 (2.2×95 cm) using buffer containing 1 M acetic acid and 5 M urea. The flow rate was 10 ml per hr.

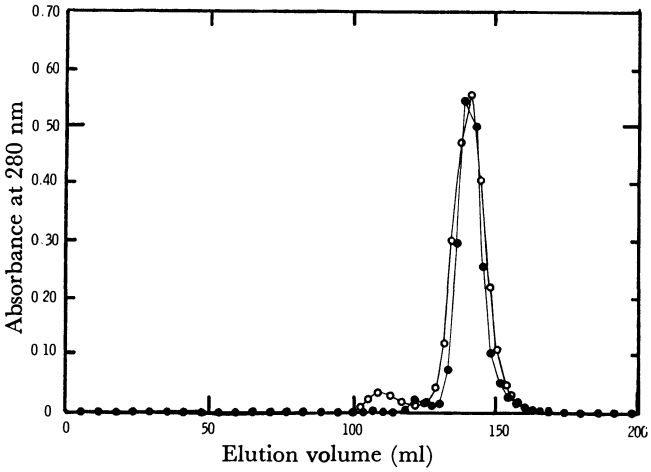

Fig. 3. Rechromatogram of fraction III of Fig. 2 on Sephadex G-50 (2.2×95 cm) using buffer containing 1 M acetic acid and 5 M urea. The flow rate was 10 ml per hr. —●—: fraction III of Fig. 2, —○—: native HEL.

third fraction (III) in the same position as standard native HEL under the same chromatographic conditions. Fraction III was rechromatographed on Sephadex G-50 using buffer containing 1M acetic and 5M urea as shown in Fig. 3. When the freeze-dried native HEL which had been treated with HF under various conditions was subjected to gel-filtration on Sephadex G-50 using buffer containing 1M acetic acid and 5M urea, different chromatograms were obtained depending on the conditions of HF-treatment. On prolongation of the reaction period at a given temperature the amount of fraction II increased and the amount of fraction III decreased. Furthermore, it was found that with a constant reaction period the amount of fraction III decreased on increasing the reaction temperature. Typical chromatograms are shown in Figs. 4 and 5.

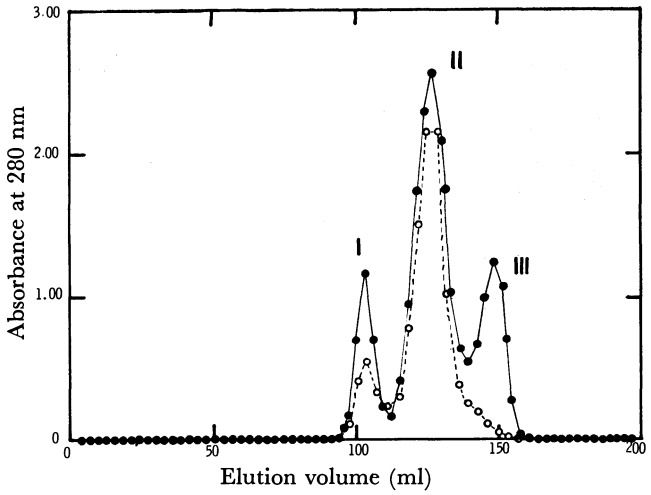

Fig. 4. Gel-filtration of native HEL treated with HF at 0 °C for 60 min (—●—) or 240 min (—○—) on Sephadex G-50 (2.2×95 cm) using buffer containing 1 M acetic acid and 5 M urea. The flow rate was 10 ml per hr.

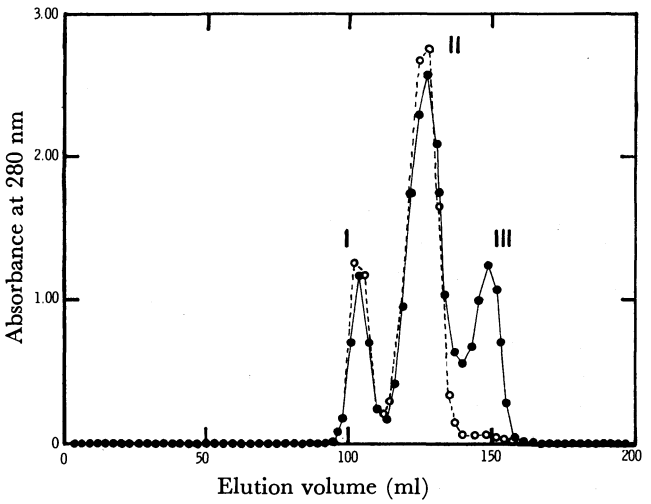

Fig. 5. Gel-filtration of native HFL treated with HF for 60 min at 0 °C (—●—) or 25 °C (—○—) on Sephadex G-50 (2.2×95 cm) using buffer containing 1 M acetic acid and 5 M urea. The flow rate was 10 ml per hr.

Effects of Various Buffers on the Recovery of Fraction III. The freeze-dried native HEL was treated with HF at 0 °C for 60 min and then stood in various buffers at room temperature for 20 hr. Then the solution was desalted and lyophilized and the residues were subjected to gel-filtration on Sephadex G-50. The recovery of fraction III corresponding to native HEL was calculated from its absorbance, as shown in Table 1.

Table 1. Effects of various buffers on the recovery of fraction III from HF-treated native HEL

Sodium phosphate buffer		Average recovery of fraction III
mol concn (M)	pH	(%)
0.067	3.5	46
0.067	6.2	47
0.067	8.0	54
0.1	6.2	49
0.1	8.0	55
0.2	6.2	40

Ion-Exchange Chromatography. The freeze-dried native HEL was treated with HF at 0 °C for 60 min and then chromatographed on Sephadex G-50. The fraction III obtained was subjected to chromatography on Biorex 70 using 0.2M sodium phosphate buffer solution at pH 7.15. This procedure is generally used for purification of crude HEL isolated from natural sources. It was found that fraction III was eluted in the same position as native HEL, as shown in Fig. 6.

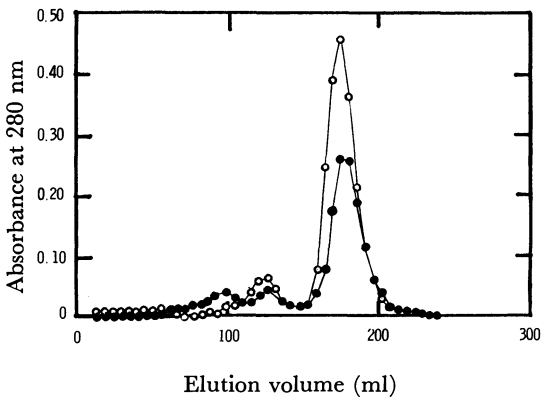

Fig. 6. Ion-exchange chromatogram of HEL on Biorex 70 (1.9×54 cm) using 0.2 M sodium phosphate buffer solution (pH 7.15). The flow rate was 16 ml per hr. —●—: fraction III of Fig. 2, —○—: native HEL.

Enzymatic Activity of the Fractions of HF-Treated Freeze-dried Native HEL. The lytic activities of various fractions of HF-treated freeze-dried native HEL, separated by gel- and ionexchange-chromatographes, were determined relative to that of standard HEL on *Micrococcus lysodeikticus* cell walls. Table 2 shows the

Table 2. Relative activities of fractions I, II, and III

HF-treatment	Fraction I	Fraction II	Fraction III
0 °C, 60 min	0%	45—66%	97—106%
25 °C, 60 min	0	10—15	—

specific activities of fractions I, II and III, separated by gel-filtration on Sephadex G-50. Fraction III consistently showed full specific activity after treatment with HF at 0 °C for 60, 90, 120 or 240 min. The main fraction separated by chromatography of fraction III on Bio-rex 70 (Fig. 6) was also fully active. However, the fraction II's, separated after treatment of the freeze-dried native HEL with HF under different conditions, showed different specific activities.

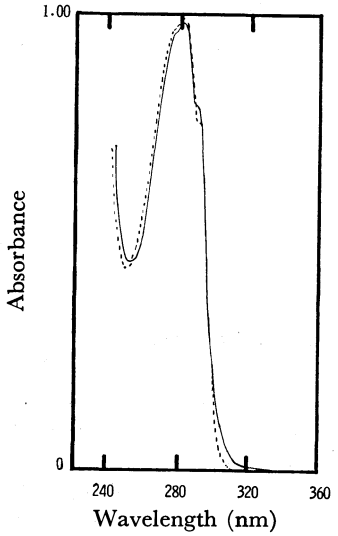

Fig. 7. Ultra-violet absorption spectra of fraction II of Fig. 2 (——) and native HEL (----). Solvent: Buffer containing 1 M acetic acid and 5 M urea.

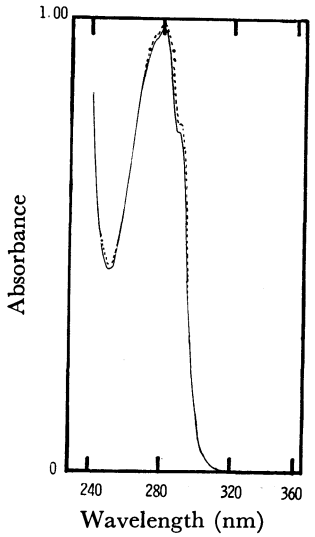

Fig. 8. Ultra-violet absorption spectra of fraction III of Fig. 2 (——) and native HEL (----). Solvent: Buffer containing 1 M acetic acid and 5 M urea.

Absorption Spectra. Figures 7 and 8 show the ultraviolet absorption spectra of fractions II and III, respectively in Fig. 2. The spectrum of fraction II was slightly different from that of the native HEL, while that of fraction III was the same as that of native HEL. In Fig. 9 the circular dichroism of fraction III of Fig. 2 is compared with that of native HEL. The two spectra are identical in the range of wavelengths measured.

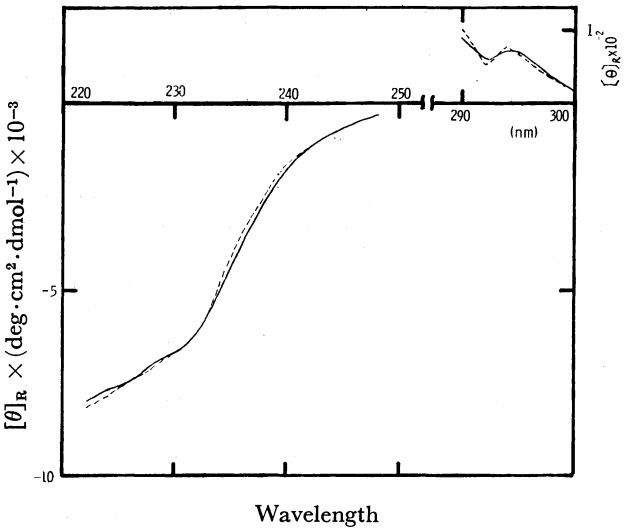

Fig. 9. Circular dichroism spectra of fraction III of Fig. 2 (——) and native HEL (----). Solvent: 0.1 M sodium chloride buffer solution adjusted to pH 3.0 with hydrochloric acid.

Crystallization of Fraction III. The material, recovered from fraction III in Fig. 2 was stood under conditions inducing crystallization. The tetragonal crystals obtained were like those of native HEL, as shown in Fig. 10.

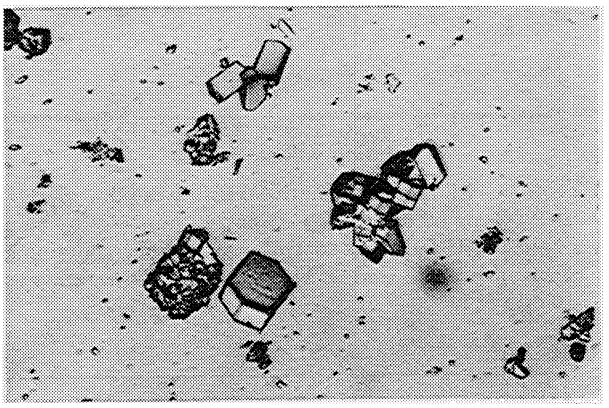

Fig. 10. Microphotograph of crystals of the material from fraction III obtained by the method of Berthou and Jolles.[7]

Discussion

The enzymatic activities of native HEL decreased during treatment with HF. This suggests that HF may affect structures which are essential for enzymatic activity. After treatment of native HEL with HF three fractions could be separated by gel-filtration in 1M acetic acid and 5M urea buffer. The first fraction eluted, fraction I, was inactive, the second, fraction II, was not fully active and the last, fraction III, was fully active. This suggests that molecules of native HEL were not affected uniformly by treatment with HF, some being only slightly affected and others greatly affected. This is supported by the finding that on prolongation of the period of treatment of native HEL with HF, the amount of fraction II increased while that of fraction III decreased.

The properties of fractions I, II and III were compared with those of native HEL. Fraction I seemed to contain polymeric material formed during treatment of native HEL with HF, because it was eluted in the void volume on gel-filtration, and because it was poorly soluble in a buffer and was enzymatically inactive. On gel-filtration fraction II was eluted before native HEL. The fraction II, separated after treatment of native HEL with HF at 0 °C for 60 min, had 45—66% of the activity of native HEL. However, preparations obtained after different conditions of treatment had different activities. Fraction II could be further separated into two fractions, IIa and IIb by gel-filtration in 5% NaCl and 5M urea buffer solution.[7] After treatment of native HEL with HF at 0 °C for 60 min, fraction II had 45—66% of the activity of native HEL, while fraction IIa had 2.5% and fraction IIb had about 85% of the activity of native HEL. Chromatograms of fractions IIa and IIb on Bio-rex 70 showed different patterns from that of native HEL.[7] Furthermore, when the material in fraction II was reduced and refolded under the method of Saxena and Wetlaufer,[8] the resultant material did not move in the position of fraction III on gel-filtration in 1M acetic acid and 5M urea buffer. Thus fraction II was a mixture of at least two components formed by modification of the structure of HEL during treatment with HF.

On gel-filtration fraction III was eluted in the same position as native HEL, and it also gave the same pattern on Bio-rex 70 as native HEL. These results suggest that fraction III has the similar properties to native HEL. In addition, the yield of fraction III was about 50% of the initial amount of native HEL. Accordingly, the properties of fraction III were further investigated. The ultra-violet and circular dichroism absorption spectra of fraction III were the same as those of native HEL over the range of wavelengths examined. Moreover, the crystals obtained from fraction III under the same conditions used to crystallize native HEL could not be distinguished from the latter.

The results described above indicate clearly that material which was indistinguishable in various properties from native HEL could be recovered in a crystalline state after treatment of native HEL with HF under usual conditions of peptide synthesis. The authors are now attempting to recover intact HEL from the reduced HEL treated with HF and refolded.[9] These studies should demonstrate the usefulness of HF in chemical synthesis of HEL.

References

1) S. Sakakibara and Y. Shimonishi, This Bulletin, **38**, 1412 (1965).
2) S. Sakakibara, Y. Shimonishi, Y. Kishida, M. Okada, and H. Sugihara, *ibid.*, **40**, 2164 (1967).
3) J. J. Katz, *Arch. Biochem. Biophys.*, **51**, 293 (1954).
4) A. L. Koch, W. A. Lamont, and J. J. Katz, *ibid.*, **63**, 106 (1956).
5) P. Jolles, "Methods in Enzymology," ed by S. P. Colowick and N. O. Kaplan, Vol. 5, Academic Press, New York (1962), p. 137.
6) J. Berthou and P. Jolles, *FEBS Lett.*, **31**, 189 (1973).
7) S. Aimoto and Y. Shimonishi, unpublished data.
8) V. P. Saxena and D. B. Wetlaufer, *Biochemistry*, **9**, 5015 (1970).
9) S. Aimoto and Y. Shimonishi, unpublished data.

Nucleophilic Displacement Catalyzed by Transition Metal. I. General Consideration of the Cyanation of Aryl Halides Catalyzed by Palladium(II)

Kentaro TAKAGI, Tadashi OKAMOTO,* Yasumasa SAKAKIBARA,** Atsuyoshi OHNO,* Shinzaburo OKA,* and Naomi HAYAMA

College of Liberal Arts and Science, Okayama University, Tsushima, Okayama 700

(Received June 6, 1975)

The displacement reaction of various non-activated aryl halides with cyanide ions was investigated in the presence of palladium salts. Various aryl iodides and bromides were converted into the corresponding aryl cyanides in good yields under mild conditions. The addition of certain substances, such as potassium hydroxide and potassium carbonate, enhanced the catalytic activity. Hexamethylphosphoric triamide, in which potassium cyanide was scarcely soluble, was an outstanding solvent for the reaction. The reduced palladium species was supposed to be the active catalyst.

The inertness of aryl halides in the nucleophilic substitution reaction is generally recognized. The reaction with ordinary nucleophiles does not proceed unless the substrates are activated by electron-withdrawing groups.[1] Recently the great affinity of low-valent transition metal complexes for various halides has been reported.[2] Aryl halides, for example, exhibit a remarkable reactivity in oxidative addition to the complexes and sometimes produce isolable adducts in the presence of certain ligands, such as phosphines or isonitriles.[3] This fact suggests that the reversible oxidative addition of an aryl halide to a transition metal, when carried out in the presence of another nucleophile, may produce a product of a displacement reaction.

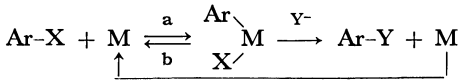

a: oxidative addition, b: reductive elimination, M: transition-metal catalyst, Ar-X: aryl halide, Y^-: nucleophile

Thus, a net nucleophilic aromatic substitution may take place with the aid of a transition-metal catalyst with otherwise inert substrates. From this point of view, the present authors intended to replace a halogen atom in aryl halide with a cyanide ion and found that palladium (II) salts in *N,N*-dimethylformamide (DMF) did indeed give satisfactory results. When the facile catalytic reaction at a moderate temperature was preliminarily communicated,[4] it was emphasized that the method is more useful for the syntheses of aryl cyanides than the conventional Rosenmund-von Braun reaction.[5] At almost the same time, a catalytic cyanation by a nickel catalyst was also reported.[6] In this paper the results of detailed studies of the reaction conditions will be presented.

Results and Discussion

Outline of the Reaction. Palladium salt, potassium cyanide, and iodobenzene were mixed in an appropriate solvent, and the reaction was carried out under nitrogen, Because of the poor solubility of potassium cyanide, the reaction mixture consisted of a heterogeneous system. The reaction mixture was colorless or pale yellow at the beginning and again at the end of the reaction, whereas it was deep yellow or reddish-brown during the reaction. Sometimes black precipitates appeared, presumably colloidal palladium metal. Benzonitrile, was almost the sole organic product.

$$C_6H_5I + KCN \xrightarrow[Pd(II)]{} C_6H_5CN + KI$$

Occasionally, small amounts of benzene and biphenyl were detected. Small amounts of water and air stopped the reaction before it reached completion. Under certain conditions, the presence of a co-catalyst such as potassium hydroxide was required to initiate the reaction (*vide infra*).

TABLE 1. Pd(II) CATALYZED CYANATION OF ARYL HALIDES

Run No.	Ar-X	Reaction temp. (°C)	Reaction time (hr)	Ar-X/Pd mole ratio	Other reaction conditions	Yield %
1	C_6H_5-I	100	4.5	100	a)	97.5
2	C_6H_5-I	140	0.2	50	b)	84
3	C_6H_5-I	60	9.0	65	c)	99
4	*p*-CH_3-C_6H_4-I	100	2.0	100	a)	93
5	*o*-CH_3-C_6H_4-I	100	2.0	100	a)	96
6	*m*-Cl-C_6H_4-I	100	5.5	100	a)	70 (*m*-Cl) 21 (*m*-CN)
7	*p*-NH_2-C_6H_4-I	100	10.0	50	a)	0
8	*p*-NO_2-C_6H_4-I	100	10.0	100	a)	70
9	C_6H_5-Br	153	11.5	50	b)	80[f]
10	C_6H_5-Br	100	0.3	6.5	d)	93
11	C_6H_5-Br	90	2.3	65	c)	94
12	C_6H_5-Cl	90	1.5	65	c)	2
13	C_6H_5-I	140	1.0	50	e)	0

a) $Pd(OAc)_2$ 0.005 mmol, KCN 0.7 mmol, HMPA-(NaOEt incld) 3 ml. b) $Pd(OAc)_2$ 0.04 mmol, KCN(without recrystallization) 4 mmol, DMF 2 ml. c) $Pd(OAc)_2$ 0.015 mmol, KCN 2 mmol, KOH 0.0005 mmol, KI 0.09 mmol, HMPA 1.5 ml. d) $Pd(OAc)_2$ 0.033 mmol, KCN 0.33 mmol, PPh_3 0.066 mmol, $Ca(OH)_2$ 0.03 mmol, DMF 1 ml. e) H_2O 5 μl; other conditions are the same as b. f) Conversion 91%; yield based on consumed bromobenzene.

* Institute for Chemical Research, Kyoto University, Uji, Kyoto 611.

** Chemical Laboratory of Textile Fibers, Kyoto University of Industrial Arts and Textile Fibers, Kyoto 606.

The Catalytic Cyanation of Various Aryl Halides. The results from catalytic cyanation with various aryl halides are listed in Table 1.

Aryl iodides, except for amino derivatives (Run 7), produce the corresponding aryl cyanides, in which a cyano group replaces the iodo atom. An *ortho* substituent in aryl iodide does not affect the reaction (Run 5), however, as may be seen in Table 1.

Catalytic cyanation with aryl bromides required more severe conditions than with aryl iodides. That is, a higher temperature (Run 9) or a larger amount of the catalyst and the addition of triphenylphosphine (Run 10) were necessary to complete the reaction. However, the presence of a small amount of potassium iodide promotes the reaction efficiently (Run 11).[7,8]

Chlorobenzene was the least reactive, and even the addition of potassium iodide was scarcelly effective in this case (Run 12). The marked difference in the reactivities of iodo and chloro atoms can also be observed from the experiment cited as Run 6 in Table 1.

The above difference in the reactivities of a series of aryl halides, I>Br>Cl, suggests that the bond dissociation is a crucial step in the catalytic reaction and that the formation of an activated aromatic system, *e.g.*, the π-complex, is not crucial. If such an intermediate should play an important role, the reactivity of aryl halides would decrease in the Cl>Br>I order as in the classical S_NAr reaction with activated aryl halides.[9,10]

The Catalyst System. The catalytic abilities of various palladium (II) salts for the reaction of iodobenzene in hexamethylphosphoric triamide (HMPA) were examined at various temperatures; the results are shown in Table 2. All the palladium salts, except for potassium tetracyanopalladate (II), are effective without the co-operation of any additives. In the presence of a small amount of potassium hydroxide, the reactivity of the catalyst system was greatly enhanced (Table 2). Other active co-catalysts are sodium ethoxide, potassium carbonate, and sodium phenoxide. The palladium complex in the zero oxidation state is also effective as a co-catalyst. The results are shown in Table 3.

Table 2. Activity of various catalyst system (correlation of catalytic activity and reaction temperature)

Catalyst system	Reaction temperature			
	120 °C	100 °C	80 °C	60 °C
$K_2Pd(CN)_4$	C	C	C	C
$Pd(CN)_2$	A	C	C	C
$PdCl_2$	A	B	C	C
$Pd(acac)_2$	A	B	C	C
PdI_2	A	A	B	B
$Pd(OAc)_2$	A	A	B	B
$Pd(OAc)_2$+KOH	A	A	A	A
PdI_2+KOH	A	A	A	A
$Pd(acac)_2$+KOH	A	A	C	C
$Pd(CN)_2$+KOH	A	C	C	C
$K_2Pd(CN)_4$+KOH	C	C	C	C

Reaction condition: C_6H_5I 2 mmol, KCN 4 mmol, HMPA 3 ml, PdX_2 0.03 mmol, KOH (when used) 0.001 mmol.
A represents that the reaction proceeds to completion. B represents that the slower and unpractical reaction takes place or the reaction stops in the middles. C represents that the reaction dose not take place.

Since these co-catalysts have been widely used to reduce transition-metal ions of a higher valence to their corresponding lower-valent ones,[11] the above results seem to suggest the importance of zero-valent palladium. The inertness of cyanide salts ($Pd(CN)_2$, $K_2Pd(CN)_4$) and the solvent effect (*vide infra*) support this idea: since cyanide ion possesses a positive value as the oxidation potential of the next reaction, palladium cyanides may be hard to reduce, and the reduction of palladium cyanides can be achieved only at higher temperatures.[12]

$$Pd + 4X^- = PdX_4^{2-} + 2e^-$$
$$E^0(V) = -0.18\,(X=I),\ +0.4\,(X=CN)^{13}$$

Table 3. Effect of various co-catalysts

Run No.	$Pd(OAc)_2$ mmol	Co-catalyst (mmol)	Reaction temp. °C	Reaction time hr	Aryl halide (mmol)	KCN mmol	HMPA ml	Conversion %
14	0.015	—	70	1	C_6H_5I (1)	2	1.5	>1
15	0.015	KOH (0.15)	70	4.5	C_6H_5I (1)	2	1.5	100
16	0.015	K_2CO_3 (0.09)	70	7.5	C_6H_5I (1)	2	1.5	100
17	0.015	NaOPh (0.015)	70	4	C_6H_5I (1)	2	1.5	100
18	0.0065	NaOEt (0.0013)	100	0.5	C_6H_5I (0.33)	1	7.5	100
19	0.015	NaOAc (0.15)	60	2	C_6H_5I (1)	2	1.5	0
20	0.015	Na_2HPO_4 (0.15)	70	1.5	C_6H_5I (1)	2	1.5	0
21	0.015	KOH (0.0005)	60	12	C_6H_5I (1)	2	1.5	100
22	0.015	KOH (0.0005)	90	13	C_6H_5Br (1)	2	1.5	25
11	0.015	KOH (0.0005) KI (0.09)	90	2.3	C_6H_5Br (1)	2	1.5	100
23	0.01	$Pd(PPh_3)_4$ (0.001)	60	0.5	C_6H_5I (0.5)	1.3	1	18.5
24	0.01	PPh_3 (0.006)	60	0.5	C_6H_5I (0.5)	1.3	1	2.9
25[a]	—	$Pd(PPh_3)_4$ (0.01)	70	0.8	C_6H_5I (0.5)	0.7	1	<1

a) Recently $Pd(PPh_3)_4$ catalysed cyanation of aryl iodides in tetrahydrofuran was reported: A. Sekiya and N. Ishikawa, *Chem. Lett.*, **1975**, 278.

In fact, palladium acetate is spontaneously reduced to palladium metal on standing in HMPA at room temperature under nitrogen, whereas palladium cyanide resists the reduction.[14]

Solvent Effect. The catalytic cyanation of iodobenzene was examined in various solvents. The results are shown in Table 4. It is apparent that the solvent affects the catalytic reaction in a striking manner.

Table 4. Solvent effect

Run No.	Solvent	Reaction temp. °C	Other condition	Conversion %
	DMSO, sulfolane, acetic acid,[a] 1-butanol,[a] diethylene glycol diethyl ether, acetonitrile,[a,b] propionitrile[a,b]	140	A	0
	DMF, PC, DMAc, NMP, TMU, HMPA	140	A	100
	DMF, PC, DMAc, NMP	90	A	0
26	HMPA	90	A	100
27	TMU	90	A	50
28	DMF	120	A	98
29	DMF	100	B	>1
30	DMF	100	C	80
31	DMF	100	D	100

a) reflux, b) convesion<5%
Reaction condition A: $Pd(OAc)_2$ 0.015 mmol, KCN 2 mmol, KOH 0.0005 mmol, C_6H_5I 1 mmol, Solvent 1 ml. Reaction condition B: $Pd(OAc)_2$ 0.033 mmol, KCN 0.5 mmol, C_6H_5I 0.2 mmol, DMF 1 ml. Reaction condition C: $Pd(OAc)_2$ 0.033 mmol, KCN 0.33 mmol, C_6H_5I 0.2 mmol, DMF 1 ml. Reaction condition D: $Pd(OAc)_2$ 0.033 mmol, KCN 0.33 mmol, $Ca(OH)_2$ 0.1 mmol, C_6H_5I 0.2 mmol, DMF 1 ml.

In such protic solvents as acetic acid and 1-butanol, the reaction did not occur under the conditions examined. Some dipolar aprotic solvents, such as acetonitrile, propionitrile, sulfolane, dimethyl sulfoxide (DMSO), and diethylene glycol dimethyl ether, also gave unfavorable results, while DMF, *N,N*-dimethylacetamide (DMAc), HMPA, tetramethylurea (TMU), propylene carbonate (PC), and *N*-methylpyrrolidone (NMP) gave satisfactory results. The favorable dipolar aprotic solvents may be further classified into two groups. The more favorable ones include HMPA and TMU, while the others consist of DMF, DMAc, PC, and NMP. That is, the catalytic reaction takes place at lower temperatures in solvents of the former group than in those of the latter (Runs 26, 27).

The advantage of dipolar aprotic solvents in organic reactions has generally been attributed to the stabilization of transition states by its high polarizability and to the formation of so-called naked anions by strong solvation to counter cations.[15] However, the solvent effect here observed could not be interpreted by the general concept alone. The difference in the concentrations of potassium cyanide in these solvents must be taken into account, because the present reaction system is heterogeneous. The solubilities of potassium cyanide in DMSO, DMF, or HMPA, as representatives of the three distinct groups mentioned above, were determined. The results suggest that the most favorable solvent is the one which dissolves potassium cyanide with most difficulty. This conclusion is supported by the fact that sodium cyanide could not be used in place of potassium cyanide as a source of cyanide ions, not even in HMPA: the former is more soluble in HMPA than the latter, which may mean that the cyanide anion itself inhibits the reaction, probably by forming an inert palladium-cyanide bond (*cf.* the discussion of the catalyst system above).[16]

Thus, the ratio of the concentrations of palladium to that of cyanide ions must be kept large for facile catalytic reactions. For example, the catalytic reaction took place at 60 °C in HMPA, whereas it did not occur below 120 °C in DMF (Runs 21, 28), into which potassium cyanide dissolves relatively well, with the same concentration of the catalyst. However, when the amount of the catalyst was increased greatly, the reaction in DMF took place at 100 °C (Runs 29—31).

Experimental

Materials. The palladium acetate,[17] potassium tetracyanopalladate,[18] palladium acetylacetonate,[19] tetrakis(triphenylphosphine)palladium,[20] and substituted iodobenzene[21] were prepared following the literature. The other materials were commercial products.

General Procedure and Analysis. All the reactions were performed in a test tube equipped with a magnetic stirrer and a three-way trap under a nitrogen stream following the procedures described in the previous section. Analytical glc were performed on a Hitachi Perkin-Elmer F 6D gas chromatograph: 35% silicon DC 200 on celite 545, 2 m for the analysis of iodobenzene, *p*-iodotoluene, *o*-iodotoluene, *m*-chloroiodobenzene, bromobenzene, and chlorobenzene at 140 °C (0.8 kg/cm² of a nitrogen carrier) and 20% silicon DC 200 on celite 545, 1 m for the analysis of *p*-iodoaniline and *p*-nitroiodobenzene at 160 °C (0.7 kg/cm² of a nitrogen carrier). The yields were determined by using internal standards.

A Typical Example of the Catalytic Reactions. Reaction of *p*-iodotoluene: To a mixture of 45.5 mg (0.7 mmol) of KCN (recrystallized from water), 109 mg (0.5 mmol) of *p*-iodotoluene, and 1.1 mg (0.005 mmol) of $Pd(OAc)_2$, a 3 ml portion of HMPA (NaOEt was dissolved) was added. The reaction system was then flushed with nitrogen under stirring and kept at 100 °C. After stirring for 2 hr, aqueous sodium chloride (5 ml) and benzonitrile (50 mg, internal standard) were added to the reaction mixture. The organic products were extracted with ether (5 ml), washed with aqueous sodium chloride (5 ml), and dried over sodium sulfate. The glc analysis showed the formation of 54 mg (0.47 mmol) of *p*-tolunitrile (yield, 93%).

Reaction of Bromobenzene with Potassium Iodide. A suspension of 200 mg (1.2 mmol) of KI, 78 mg (0.5 mmol) of bromobenzene, 3.4 mg (0.015 mmol) of $Pd(OAc)_2$, 6.7 mg (0.1 mmol) of NaOEt, and 1.5 ml of HMPA was heated at 100 °C for 4 hr under a nitrogen. Analysis showed the complete absence of iodobenzene in the solution.

Solubilities of Potassium Cyanide in HMPA, DMF, and DMSO. After a suspension of potassium cyanide in a solvent had been stirred overnight at room temperature under a nitrogen, the potassium metal in the solution was determined with an atomic

absorption spectrophotometer (Nippon Jarrell Ash, Type AA-I). One liter of HMPA, DMF, or DMSO dissolved about 0.1, 10, or 200 mmol of KCN respectively. (The solvents used contained, respectively, 10^{-4}, 10^{-5}, and 10^{-4} g of water per 1 ml of the solvent.)

References

1) J. Miller, "Aromatic Nucleophilic Substitution," Elsevier, Amsterdam (1968), p. 66.

2) J. P. Collman, *Accounts Chem. Res.*, **11**, 136 (1968); M. F. Semmelhack, *Org. React.*, **19**, 115 (1972).

3) P. Fitton and E. A. Rick, *J. Organometal. Chem.*, **28**, 287 (1971); M. Hidai, T. Kashiwagi, T. Ikechi, and Y. Uchida, *J. Organometal. Chem.*, **30**, 279 (1971); S. Otsuka, A. Nakamura, Y. Yoshida, M. Naruto, and K. Ataka, *J. Amer. Chem. Soc.*, **95**, 3180 (1973); G. W. Parshall, *ibid.*, **96**, 2360 (1974).

4) K. Takagi, T. Okamoto, Y. Sakakibara, and S. Oka, *Chem. Lett.*, **1973**, 471.

5) C. A. Ruehler and D. E. Pearson, "Survey of Organic Syntheses," Wiley, New York (1970), p. 939.

6) L. Cassar, *J. Organometal. Chem.*, **54**, C57 (1973).

7) The intermediacy of iodobenzene in this reaction was discarded on the basis of the fact that even a trace amount of iodobenzene was not formed by a bromobenzene–potassium iodide–palladium(II) salt system (see Experimental) and that cyanide ion is much better nucleophile than iodide ion.

8) Recently the catalytic effect of iodide ion in the oxidative addition of alkyl halides to Rh(I) was reported; D. Forster, *J. Amer. Chem. Soc.*, **97**, 951 (1975).

9) J. F. Bunnett, *Quart. Rev.*, **12**, 1 (1958).

10) M. F. Semmelhack and H. T. Hall, *J. Amer. Chem. Soc.*, **96**, 7091 (1974) and references cited therein. They observed that the order of reactivity for the series of π-(halobenzene)-chromium tricarbonyl complexes with carbanion is F>Cl>I.

11) see for example: J. Chatt and B. L. Shaw, *J. Chem. Soc.*, **1962**, 5075; L. Malatesta, *ibid.*, **1955**, 3942.

12) A. McKillop and E. C. Taylor, "Advances in Organometallic Chemistry," Vol. 11, ed. by F. G. A. Stone and R. West, Academic Press, New York (1973), p. 172.

13) P. M. Maitlis, "Organic Chemistry of Palladium," Vol. 1, Academic Press, New York (1971), p. 32.

14) K. Takagi, Unpublished data.

15) A. J. Parker, *Chem. Rev.*, **69**, 1 (1969).

16) 18.76 g of NaCN is soluble in 100 g of DMF: R. C. Paul and B. R. Sreenathan, *Indian J. Chem.*, **4**, 382 (1966).

17) T. A. Stephenson, S. M. Morehouse, A. R. Powell, J. P. Heffer, and G. Wilkinson, *J. Chem. Soc. (A)*, **1965**, 3632.

18) J. H. Bigelow, *Inorg. Synth.*, **2**, 245 (1946).

19) R. West and R. Riley, *J. Inorg. Nucl. Chem.*, **5**, 295 (1958).

20) S. Takahashi, K. Sonogashira, and N. Hagihara, *Nippon Kagaku Zasshi*, **87**, 610 (1966).

21) F. G. Mann and E. J. Chaplin, *J. Chem. Soc.*, **1937**, 527.

Racemization of Amino Acid Residues Fused in Thiazoline, Oxazoline, and Imidazoline Rings

Ken YONETANI, Yoshihiro HIROTSU, and Tetsuo SHIBA

Department of Chemistry, Faculty of Science, Osaka University, Toyonaka, Osaka 560

(Received June 9, 1975)

For the purpose of study on racemization of *exo* methine carbon atom of thiazoline, oxazoline or imidazoline ring, the following four compounds were synthesized from amino acid imino ether: 2-(1-benzyloxycarbonylaminoethyl)-2-thiazoline (I), methyl 2-(1-benzyloxycarbonylaminoethyl)-2-thiazoline-4-carboxylate (II), methyl 2-(1-benzyloxycarbonylaminoethyl)-2-oxazoline-4-carboxylate (III), and 2-(1-benzyloxycarbonylaminoethyl)-2-imidazoline (IV). A racemization rate of the alanine residue was measured from an optical rotation of 2,4-dinitrophenyl derivative obtained from the acid hydrolyzate and from hydrogen-deuterium exchange reaction at α-carbon atom. All these compounds were found to be racemized very easily particularly in the presence of proton source. From the experimental results, a plausible mechanism for racemization peculiar to such heterocyclic compounds through protonation-deprotonation process was presented.

Bacitracin A is a peptide antibiotic which involves a unique structure of the thiazoline ring in its molecule. Among peculiar chemical characters of this antibiotic, the racemization at the *N*-terminal isoleucine residue seems to be significantly important, since it is directly related to decrease of the biological activity against microorganisms. Thus, Konigsberg *et al.*[1,2] recognized that a "high potency" form of bacitracin A was converted to a "low potency" form on standing under weak acidic condition and both forms became nearly equal in amounts after two days. This interconversion between the two forms took place even under nearly neutral condition. Meanwhile, it was observed that L-isoleucine of *N*-terminal residue linked to the thiazoline ring in the "high potency" form was isomerized to D-alloisoleucine in the "low potency" one without any change in the rest of the molecule. This epimerization proceeded according to the first-order kinetics in weak acidic media. As pointed out in our previous paper,[3] we postulated that the ease of the isomerization in this case could be attributed to the particular position of the asymmetric center at C-2 *exo* methine of the thiazoline ring.

In the present paper, optical properties of the amino acid components of the peptides containing imidazoline or oxazoline ring as well as the thiazoline ring were investigated in order to clarify the reaction mechanism in more detail. Four model peptides *i.e.*, 2-(1-benzyloxycarbonylaminoethyl)-2-thiazoline (I), methyl 2-(1-benzyloxycarbonylaminoethyl)-2-thiazoline-4-carboxylate (II), methyl 2-(1-benzyloxycarbonylaminoethyl)-2-oxazoline-4-carboxylate (III), and 2-(1-benzyloxycarbonylaminoethyl)-2-imidazoline (IV) were synthesized by iminoether method[4] according to the scheme as outlined in Fig. 1.

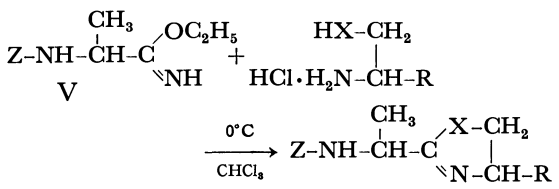

I X=S R=H
II X=S R=COOCH$_3$
III X=O R=COOCH$_3$
IV X=NH R=H

Fig. 1.

The thiazoline derivatives (I and II) were prepared by coupling of iminoether (V) derived from L-alanine with 2-aminoethanethiol hydrochloride and methyl L-cysteinate hydrochloride respectively in chloroform at 0 °C. Similarly, the oxazoline derivative (III) was synthesized by coupling of V with methyl L-serinate hydrochloride. The imidazoline derivative (IV) was also obtained by coupling of V with ethylenediamine in the same solvent at 0 °C.

An optical purity of the alanine residue in each compound was determined by means of the following two methods. First method was based on a measurement of an optical rotation of 2,4-dinitrophenyl (DNP)-alanine. Thus, acid hydrolyzate of the sample given was dinitrophenylated and DNP-alanine was isolated by preparative thin-layer chromatography (tlc). The optical rotation of DNP-alanine thus obtained was measured at 550 nm in aqueous sodium hydrogencarbonate solution and the concentration of the material in the same solution was calculated from UV absorbance at 360 nm compared with those of authentic DNP-L-alanine.[5]

The observed value of the optical purity of the alanine residue in thiazoline derivative (I) was found to be 48% by the DNP-method, whereas the same residue was completely racemized after standing of I at room temperature for a longer period than four weeks or even in the course of its purification procedure either by recrystallization or by silica gel column chromatography. When the oily thiazoline derivative (II) was purified by passing through silica gel column, the alanine residue in this compound was also perfectly racemized. In the case of oxazoline derivative (III), warming at 40 °C for 16 h caused complete racemization at the alanine residue, though the optical purity of this amino acid was maintained as L-form of 98% in the original compound III. When the oily oxazoline (III) was kept at around 20 °C for a couple of weeks, hydrolysis of III occurred by participation of moisture in air and crystals of optically pure benzyloxycarbonylalanylserine methyl ester corresponding to the open chain form of III was deposited. This finding may also mean that the racemization proceeded only in the

heterocyclic form. Although imidazoline derivative (IV) was obtained as crystals keeping an optical purity of 78% at the alanine residue, it was most easily racemized even during recrystallization. The racemization degrees in the above discussion were all obtained by the DNP method. However in the case of the compound I or IV where only one asymmetric center was involved, a racemization of the alanine residue can be determined simply by measurement of an optical rotation of the heterocyclic compound itself. Both methods can be applied to follow the progress of the racemization in the time course.

On the other hand, observation of NMR spectra of those compounds (I, II, III, and IV) in 0.5M CD_3OD solution indicated that the intensity of signal for methine proton on the alanine residue gradually decreased, and at the same time, the signal of methyl proton on the same residue changed to singlet from doublet. Hence, a rate of hydrogen-deuterium exchange on the α-carbon atom of the alanine residue could be calculated by comparison of integrated intensities of singlet and doublet signals due to methyl proton.

Discussion

The reaction times ($t_{1/2}$) of racemization and deuterium exchange reaction on the α-carbon atom of the *N*-terminal alanine residue of model peptides (I)—(IV) are summarized in Table 1. The reaction rates for those compounds at 30 °C are shown in Fig. 2.

Table 1. Reaction time ($t_{1/2}$, h) of racemization and deuterium exchange reaction

Compound	10 °C	30 °C	50 °C
I	1000[b]	140[a]	5[b]
		80[b]	
		22[c]	
II	550[b]	62[b]	8[b]
III	1300[b]	176	43
IV	3.2	0.5[a]	

a) Racemization (0.5 M CH_3OH solution). b) D-Exchange (0.5 M CD_3OD solution). c) D-Exchange (0.5 M solution in CD_3OD containing *ca.* 5% D_2O). The values with no mark represent the cases where both times for racemization and D-exchange reaction coincided each other.

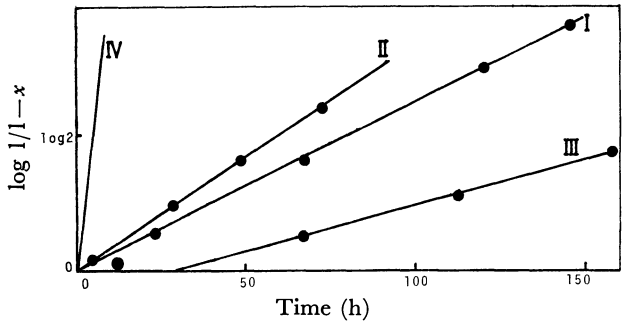

Fig. 2. The rates of racemization or D-exchange reaction at 30 °C.
For the Compound I, only the racemization rate is depicted.

Since an abscissa represents the time on a semilog scale, the straight lines in Fig. 2 indicate first-order kinetics either for racemization or deuterium exchang reaction. From the result in Table 1, it was shown that a higher temperature accelerates the reaction rate on each compound. The rates of racemization on oxazoline (III) and imidazoline (IV) are in agreement with those of deuterium exchange reaction with exception of the case of thiazoline derivative (I). The reaction rates on the compound I were further investigated as shown in Fig. 3. The reaction at 30 °C in CD_3OD

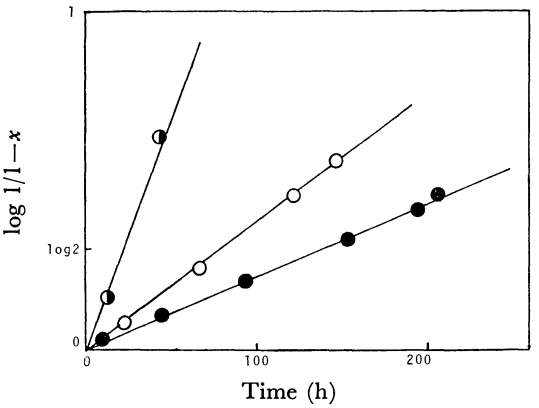

Fig. 3. The rate of racemization or D-exchange reaction in thiazoline compound (I) at 30 °C.
●: Racemization (0.5 M CH_3OH solution).
○: D-Exchange reaction (0.5 M CD_3OD solution).
◑: D-Exchange reaction (0.5 M solution in CD_3OD containing *ca.* 5% D_2O).

was shown to become faster in the presence of D_2O. This indicates that the reaction rate of thiazoline (I) is greately influenced by the presence of a trace amount of water or D_2O in the solvent. This effect may be a reason for discrepancy of reaction rates depending on the measurement condition in the case of the compound (I). Concerning a solvent effect for the racemization, the alanine residue of oxazoline (III) was partly racemized even at the stage of the coupling in methanol. On the other hand, no racemization occurred in chloroform in a preparation of III. This experimental fact suggests that the racemization depends on protic character of the solvent significantly. In this connection, an effect of the solvent was thoroughly investigated on imidazoline (IV) which was racemized most rapidly

Table 2. Racemization time ($t_{1/2}$) of imidazoline (IV) in 0.5 M solution at 30 °C

Solvent	$t_{1/2}$ min
CH_3OH	26
CH_3OH–$CHCl_3$ 1:1	68
$CHCl_3$	*ca.* 1000
$CHCl_3$+0.5 eq. AcOH	26
$CHCl_3$+2.5 eq. AcOH	137
$CHCl_3$+5 eq. AcOH	*ca.* 600
CH_3OH+0.5 eq. AcOH	28
CH_3OH–12 M HCl 1:1	∞
CH_3OH+1 eq. NEt_3	27
$CHCl_3$+1 eq. NEt_3	*ca.* 3000

among four model peptides. The racemization time ($t_{1/2}$) obtained in various media is shown in Table 2. The reaction rate was much faster in methanol as protic solvent than in chloroform as aprotic one. In chloroform containing a little amount of acetic acid, the reaction rate was as fast as in methanol. However, the rate decreased as the acid concentration increased, and racemization did not proceed eventually in strong acid media. From these results, it was proved that a deprotonation at the α-carbon atom of alanine residue is inhibited in acidic solvent, though the racemization requires the presence of proton. Furthermore, it seems unlikely that the racemization proceeds through proton abstraction directly at the α-carbon atom since the reaction was not catalyzed on addition of triethylamine as base. Consequently, the most plausible mechanism through protonated intermediate can be now presented for this racemization as depicted in Fig. 4. It should be

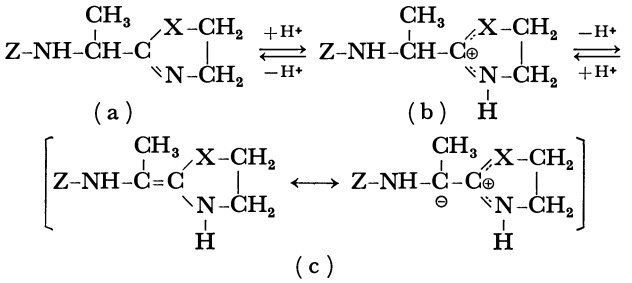

Fig. 4.

emphasized again that racemization and deuterium exchange reaction proceed in almost the same rates. From this fact it is assumed that protonation process from (c) to (b) is very rapid and the rate-determining step is deprotonation step from (b) to (c).[6,7] No effect of the base on racemization can be explained by assumption that either deprotonation from (b) to (a) proceeds predominantly or the protonation process from (a) to (b) might be inhibited. According to this mechanism, the reaction rate must be followed to first-order kinetics for the concentration of cation (b). This assumption is compatible with the results in model peptides I, II, and IV. Only exception is found in the rate of oxazoline (III) which showed the time lag for the reaction initiation. Although this phenomenon can not be elucidated unambiguously yet, an autocatalysis participated by some species formed in the process of deprotonation from (b) to (c) may be considered as one possibility since any protonation step should be rapid and seems to be improbable for explanation of such time lag.

Iminoether (V) used as starting material for the preparation of these model peptides was never racemized when it was treated under any coupling condition nor exchanged with deuterium at all even at 50 °C after 200 h. These results indicate that the racemization reaction is characteristic of heterocyclic structures such as thiazoline, oxazoline, and imidazoline rings. The cation protonated at N-3 of these heterocyclic compounds is stable owing to delocalization of the ring electron. The following deprotonation occurs concertedly with the shift of the inner double bond in the heterorings to the exocyclic position. Consequently, the racemization can take place in cases that the carbon atoms adjacent to C-2 of the heterorings are asymmetric. Therefore, it is useful to employ deuterium exchange as a detection method of racemization in these cases. It should be taken into consideration that racemization may occur always in the synthesis of such a heterocyclic compound, even when it is involved as an intermediate. At the same time, the possibility of electrophilic substitution on the carbanion adjacent to C-2 can be now suggested. For this purpose, the heterocyclic compound derived from glycine may be employed as substrate, and aldehyde or halide as electrophile. One can expect that the coupling product after hydrolysis is β-hydroxy-α-amino acid derivative or α-amino acid derivative respectively. A study along this line is in progress.

In conclusion, we not only clarified the racemization mechanism of heterocyclic compounds derived from amino acids but also pointed out the possibility for a new synthetic method of amino acid.

Experimental

All melting points are uncorrected. Nuclear magnetic resonances spectra were measured on a Varian T-60 spectrometer with tetramethylsilane as an internal standard. Optical rotations were observed with a JASCO ORD/UV-5 spectrophotometer. Ultraviolet spectra were obtained on a Hitachi 124 spectrophotometer. IR spectra were obtained on a JASCO IR-5 spectrophotometer.

Determination of Optical Purity of Alanine Residue. The sample (*ca.* 100 mg) was heated in 6M hydrochloric acid under reflux for 3 h. After evaporation *in vacuo*, the residue was dissolved in water (10 ml). Evaporation of the solvent was repeated. The hydrolyzate thus obtained was dissolved in 5% aqueous sodium hydrogencarbonate (12 ml). To the solution was added 1-fluoro-2,4-dinitrobenzene (*ca.* 200 mg) in 95% ethanol (24 ml). The reaction mixture was stirred at room temperature for 3 h and then concentrated *in vacuo*. The residue was dissolved in water (200 ml) and washed with ether. The aqueous layer was acidified with 6M hydrochloric acid to Congo red and extracted with ether. The ethereal extract was washed with water, dried over sodium sulfate and evaporated *in vacuo*. The residue was applied to preparative tlc on silica gel H to obtain DNP-alanine which was then dissolved in 1% aqueous sodium hydrogencarbonate (10 ml). The specific optical rotation of the solution was observed at 550 nm and the concentration of the same solution was calculated from the extinction coefficient at 360 nm: authentic DNP-L-alanine: $[\alpha]_{550}^{19}$ +197° (*c* 0.34, 1% $NaHCO_3$); $\lambda_{max}^{1\%\ NaHCO_3}$ 360 nm (ε 1.72×10^4).

2-(1-Benzyloxycarbonylaminoethyl)-2-thiazoline (I). To a solution of L-2-benzyloxycarbonylaminopropioimino ethyl ether[4] (3.00 g, 12 mmol) in chloroform (80 ml) was added 2-aminoethanethiol hydrochloride (1.8 g, 16 mmol) in anhydrous methanol (10 ml) with stirring at 0 °C under nitrogen atmosphere over a period of 2 h. The reaction mixture was stirred for additional 18 h and then concentrated *in vacuo* below 25 °C. The oily residue was dissolved in chloroform, washed with water and dried over magnesium sulfate. Evaporation of the solvent gave an oily material which was crystallized on addition of anhydrous *n*-hexane; yield, 2.06 g (64%); mp 51—53 °C; $[\alpha]_D^{28}$ −6.9° (*c* 1.5, CH_3OH); IR (Nujol): 1630 cm^{-1} (C=N), 1720, 1680 cm^{-1} (C=O); NMR (in $CDCl_3$): δ 7.4 (s, 5H), 5.8 (bd, 1H), 5.1 (s, 2H), 4.6 (q, 1H: J=7 Hz), 4.2 (t, 2H: J=8 Hz), 3.2 (t, 2H, J=8 Hz),

and 1.4 (d, 3H: J=7 Hz). The optical purity of the alanine residue in this material was found to be 84% by DNP method. When this sample was recrystallized from ethyl acetate–*n*-hexane, the obtained crystals were completely racemized: mp 93—95 °C; IR (Nujol): 1630 cm^{-1} (C=N), 1720 cm^{-1} (C=O); λ_{max}^{EtOH} 252 nm (ε 2.9×10³), $\lambda_{max}^{EtOH-12\ M\ HCl}$ 268 nm (ε 6.9×10³). Found: C, 59.08; H, 6.05; N, 10.43; S, 12.15%. Calcd for $C_{13}H_{16}O_2N_2S$: C, 59.06; H, 6.10; N, 10.60; S, 12.13%.

*Methyl 2-(1-Benzyloxycarbonylaminoethyl)-(*R*)-2-thiazoline-4-carboxylate (II).* To a solution of L-2-benzyloxycarbonylaminopropioimino ethyl ether (0.90 g, 3.6 mmol) in chloroform (40 ml) was added methyl L-cysteinate hydrochloride (0.70 g, 4.1 mmol) with stirring at 0 °C under nitrogen atmosphere. After the reaction mixture was stirred for 24 h, it was treated in a similar manner to that in preparation of I. The crude oily product (1.0 g) obtained was dissolved in anhydrous ether (10 ml) and subjected to silica gel (Merck silica gel 0.05—0.2 nm, 30 g) column. The column was eluted with anhydrous *n*-hexane–ether–acetone to give oily but pure II: yield, 0.80 g (69%); $[\alpha]_D^{23}$ +40.8° (*c* 2.7, CH_3OH); IR (Nujol): 1620 cm^{-1} (C=N); NMR (in $CDCl_3$): δ 7.4 (s, 5H), 5.6 (bd, 1H), 5.2 (s, 2H), 5.1 (t, 1H: J=9 Hz), 4.7 (q, 1H: J=7 Hz), 3.8 (s, 3H), 3.6 (d, 2H: J=9 Hz), and 1.5 (d, 3H: J=7 Hz). Found: C, 55.51; H, 5.51; N, 8.62; S, 9.78%. Calcd for $C_{15}H_{18}O_4N_2S$: C, 55.85; H, 5.63; N, 8.69; S, 9.95%. The alanine residue in II was found to be DL-form by DNP method.

*Methyl 2-(1-Benzyloxycarbonylaminoethyl)-(*S*)-2-oxazoline-4-carboxylate (III).* A solution of iminoether (V) (4.80 g, 19 mmol) and methyl L-serinate hydrochloride (3.80 g, 25 mmol) in chloroform (50 ml) was stirred at room temperature for 16 h. The reaction mixture was concentrated *in vacuo*. Purification by silica gel column chromatography, gave an oily product III: yield, 4.15 g (72%); $[\alpha]_D^{13}$ +30.0° (*c* 3.3, CH_3OH); IR (Nujol): 1670 cm^{-1} (C=N); NMR (in $CDCl_3$): δ 7.3 (s, 5H), 5.8 (bd, 1H), 5.1 (s, 2H), 4.1—4.9 (m, 4H), 3.7 (s, 3H), and 1.4 (d, 3H: J=7 Hz). Found: C, 58.79; H, 6.07; N, 9.08%. Calcd for $C_{15}H_{18}O_5N_2$: C, 58.81; H, 5.92; N, 9.15%.

An optical purity of the alanine residue in III was shown to be 98% by DNP method. When the oily product III (1.5 g) itself was allowed to stand at room temperature for a couple of weeks in an open vessel, crystals of benzyloxycarbonyl-L-alanyl-L-serine methyl ester were formed. This open chain peptide was recrystallized from ethyl acetate–*n*-hexane: yield, 1.2 g (76%); mp 133—134 °C; $[\alpha]_D^{28}$ −18.9° (*c* 1.1, CH_3OH). (lit,[8]: L-L form: mp 134.5—135.5 °C; $[\alpha]_D^{28}$ −17.7° (*c* 3.43, CH_3OH)). IR (Nujol): 3500 cm^{-1} (OH); NMR (in $CDCl_3$): δ 7.4 (s, 5H), 7.3 (b, 1H), 5.8 (bd, 1H), 5.1 (s, 2H), 4.2—4.8 (m, 2H), 3.9 (d, 2H, J=4 Hz), 3.8 (s, 3H), 3.3 (s, 1H), and 1.4 (d, 3H: J=6 Hz). Found: C, 55.49; H, 6.24; N, 8.59%. Calcd for $C_{15}H_{20}O_6N_2$: C, 55.55; H, 6.22; N, 8.64%.

When the oxazoline (III) was prepared in methanol, an optical purity of the alanine residue was found to be 70—90% by DNP method.

2-(1-Benzyloxycarbonylaminoethyl)-2-imidazoline (IV). To a solution of iminoether (V) (3.60 g, 14.4 mmol) in chloroform (30 ml) was added ethylenediamine (1.10 g, 20 mmol). The reaction mixture was stirred at 0 °C for 158 h and then evaporated *in vacuo* below 25 °C. The residue was readily crystallized on addition of anhydrous ether. The crystals were collected and washed with anhydrous ether: yield, 1.44 g (41%); mp 100—103 °C; $[\alpha]_D^{23}$ −24.9° (*c* 2.1, CH_3OH); IR (Nujol): 1620 cm^{-1} (C=N); NMR (in $CDCl_3$): δ 7.4 (s, 5H), 6.1 (bd, 1H), 5.1 (s, 2H), 4.4 (q, 1H: J=7 Hz), 3.6 (s, 4H), and 1.4 (d, 3H: J=7 Hz).

An optical purity of the alanine residue in VI was found to be 78% by DNP method. On recrystallization from acetone–ether, IV was changed to completely racemized form: mp 111—113 °C. Found: C, 63.11; H, 7.09; N, 16.68%. Calcd for $C_{13}H_{17}O_2N_3$: C, 63.14; H, 6.93; N, 16.99%.

References

1) W. Konigsberg, R. H. Hill, and L. C. Craig., *J. Org. Chem.*, **26**, 3867 (1961).
2) W. Konigsberg and L. C. Craig, *J. Amer. Chem. Soc.*, **81**, 3452 (1959).
3) Y. Hirotsu, T. Shiba, and T. Kaneko, This Bulletin, **43**, 1870 (1970).
4) Y. Hirotsu, T. Shiba, and T. Kaneko, *ibid.*, **40**, 2945 (1967); **43**, 1564 (1970).
5) General and conventional application of combination of the measurements of optical rotation and UV absorbance of DNP amino acid to an evaluation of the optical purity of amino acid in minute amount will be reported soon elsewhere.
6) C. Hsu, C. Ingold, and C. Wilson, *J. Chem. Soc.*, **1938**, 78.
7) D. Cram, B. Bickborn, C. Kingsbury, and P. Haberfield, *J. Amer. Chem. Soc.*, **83**, 3678 (1961).
8) T. Kaneko, I. Takeuchi, and T. Inui, This Bulletin, **41**, 974 (1968).

Ethylation and Transethylation of Naphthalene[1]

Keizo SHIMADA and Shizuo NAGAHAMA

Central Research Institute, Teijin Limited, Asahigaoka, Hino, Tokyo 191

(Received June 9, 1975)

Transethylation of naphthalene by ethylxylenes and ethylbenzene in the presence of $AlCl_3$ as a catalyst was studied and compared with ethylation by ethyl bromide. When ethylxylenes were used, it was observed that the β-isomer of ethylnaphthalene initially formed (96.8%) was isomerized to the α-isomer. This was attributed to steric hindrance of the α-position in the transition state of reactions proceeding by the hydride abstraction mechanism. However, the formation of considerable proportion of the α-isomer (25%) was observed in the case of transethylation by ethylbenzene, as well as of ethylation with ethyl bromide (60% α-isomer). Thus, the S_N2 mechanism should be operative, at least partly, in the transethylation by ethylbenzene. The rates of transethylation by ethylxylenes were found to be in the order: 1,2-diMe-4-Et-≒1,3-diMe-4-Et-＞1,4-diMe-2-Et-≫1,3-diMe-5-5-Et-benzene. The equilibrium composition of ethylnaphthalene was found to contain 8.7—8.8% α-isomer.

Ethylation of naphthalene has been investigated a long time ago.[2] However, the nature of the isomer distribution of the ethylnaphthalene produced was obscure. Nickels and Kutz[3] described a product of 80% β- and 20% α-isomers by ethylation with ethylene using a silica-alumina catalyst.

Lien and McCaulay[4] reported that the β-isomer was formed exclusively by the transethylation of naphthalene with ethylbenzene in the presence of $HF-BF_3$. Karakureva *et al.*[5] also reported that the transethylation of naphthalene with ethylbenzene, diethylbenzene, and ethylxylene, prepared *in situ* from xylene and ethylene, in the presence of $AlCl_3$, all produced the β-isomer.

Here, the nature of the isomer distribution of the product obtained by ethylation and transethylation of naphthalene catalyzed by aluminium chloride is reported.

Experimental

1,3-Dimethyl-5-ethylbenzene. To a mixture of 244 g of *m*-xylene (95% pure) and 70 g of $AlCl_3$, 72.3 g of ethyl bromide was added with stirring. The reaction mixture was stirred for 24 h at 30 °C. The lower complex layer was separated and poured onto crushed ice, and the organic layer which appeared was washed with aqueous sodium hydroxide and water, and dried over potassium carbonate. *m*-Xylene was recovered and the residue was fractionated by a spinning band column. A fraction (bp 184 °C) of 97.3% purity was obtained.

1,3-Dimethyl-4-ethylbenzene. To a mixture of 650 g of *m*-xylene and 20 g of $AlCl_3$, 146 g of ethyl bromide was added and the reaction mixture was stirred for 2 h. The upper layer was separated by decantation and treated as above. A fraction (bp 188 °C) 85.7% pure and containing 14.2% 1,3-dimethyl-2-ethylbenzene and 0.1% 1,3-dimethyl-5-ethylbenzene was obtained.

1,4-Dimethyl-2-ethylbenzene was synthesized from *p*-xylene and ethyl bromide with $AlCl_3$ and was distilled. Bp 187 °C, purity 97.5%.

1,2-Dimethyl-4-ethylbenzene was synthesized from *o*-xylene and ethyl bromide as above and distilled by a spinning band column. Bp 190 °C, purity 97.5%.

Naphthalene was purified by sublimation, purity 99.7%.

Reactions. Ethylation was carried out using naphthalene (0.1 mol), ethyl bromide (0.025 mol) and $AlCl_3$ (0.01 mol) in 50 g of *n*-heptane at 30 °C. Transethylation by ethylxylenes was carried out using a mixture containing 0.1 mol each of naphthalene and ethylxylene, 0.02 mol of $AlCl_3$ in 30 g of *n*-heptane at 30 °C. In the case of transethylation by ethylbenzene, 0.2 mol of ethylbenzene was used without *n*-heptane at 20 °C.

Aliquots of the samples were taken at appropriate times, poured into ice water and ether to decompose the catalyst, washed and dried. The samples were analyzed by gas chromatography, using an MB MA Golay column (45 m) at 160 °C.

Results

Ethylation with Ethyl Bromide. The isomer distribution and the reaction time are shown in Table 1. The data clearly show the initial attack favorable to the α-position, followed by rapid isomerization to the β-position. By extrapolating to zero time, an initial isomer distribution of about 60% α-isomer was obtained.

Table 1. Isomer distribution in the ethylation of naphthalene with ethyl bromide

Time (min)	Ethylnaphthalenes (%) α	Ethylnaphthalenes (%) β	Conversion[a] (%)
5	45	55	1.1
10	30	70	2.2
15	16	84	3.5
30	14	86	6.8
90	12	88	9.7
210	10	90	12
24 (h)	8.8	91.2	

a) Calculated from the peak area of the gas chromatogram, (ethylnaphthalene+diethylnaphthalene)/(naphthalene+ethylnaphthalene+diethylnaphthalene).

Transalkylation with Ethylbenzene. The isomer distribution and the reaction time are shown in Table 2. The initial β-attack increased as compared with ethyl bromide ethylation. By extrapolation to zero time, an initial isomer distribution of about 25% α-isomer was obtained.

If transethylation proceeded by the hydride abstraction mechanism, the initial attack would be more probable at the β-position, and thus, isomerization from the β- to the α-isomer may be expected. However, isomerization from the α- to the β-isomer was none the less ob-

Table 2. Isomer distribution in the transethylation of naphthalene with ethylbenzene

Time (min)	Ethylnaphthalenes (%) α	Ethylnaphthalenes (%) β	Conversion (%)
2	20	80	1.5
5	15	85	5.5
15	9.7	90.3	14.5
30	8.9	91.1	19.5
60	8.8	91.2	28

served.

Transethylation with Ethylxylenes. The isomer distributions and the reaction times obtained from the reaction of individual ethylxylene isomers with naphthalene are shown in Tables 3—6.

It is observed, in all cases, that the initial products are rich in the β-isomer compared to the equilibrium composition. Thus, isomerization of the β-isomer to the α-isomer was observed.

Table 3. Isomer distribution in the transethylation of naphthalene with 1,4-dimethyl-2-ethylbenzene

Time (h)	Ethylpaththalenes (%) α	Ethylpaththalenes (%) β	Conversion (%)
1/4	4.2	95.8	3.5
1/2	5.3	94.7	8.7
1	5.3	94.7	17
2	5.7	94.3	32
3	6.0	94.0	40
5	6.2	93.8	46
7	6.4	93.6	48
24	7.8	92.2	57

Table 4. Isomer distribution in the transethylation of naphthalene with 1,3-dimethyl-5-ethylbenzene

Time (h)	Ethylnaphthalenes (%) α	Ethylnaphthalenes (%) β	Conversion (%)
3	3.2	96.8	1.5
5	3.2	96.8	3.4
7	3.9	96.1	10
15	5.1	94.9	38
24	5.9	94.1	54
26	6.3	93.7	57
32	7.3	92.7	62

Table 5. Isomer distribution in the transethylation of naphthalene with 1,3-dimethyl-4-ethylbenzene

Time (h)	Ethylnaphthalenes (%) α	Ethylnaphthalenes (%) β	Conversion (%)
1/12	3.5	96.5	9
1/4	3.5	96.5	23
1/2	3.8	96.2	36
1	4.2	95.8	47
2	5.0	95.0	57
3	5.8	94.2	60
24	8.7	91.3	61

Table 6. Isomer distribution in the ethylation of naphthalene with 1,2-dimethyl-4-ethylbenzene

Time (h)	Ethylbenzenes (%) α	Ethylbenzenes (%) β	Conversion (%)
1/2	3.2	96.8	8
1/4	3.3	96.7	34
1/2	3.3	96.7	50
1	4.3	95.7	59
2	6.7	93.3	59
3	7.0	93.0	60
24	8.7	91.3	61

As a result, the rates of transethylation with ethylxylene isomers decrease in the order 1,2-diMe-4-Et-≧1,3-diMe-4-Et>1,4-diMe-2-Et≫1,3-diMe-5-Et.

The equilibrium composition of ethylnaphthalene was found to contain 8.7—8.8% α-isomer.

Discussion

The mechanism of transethylation has received the attention of many researchers. McCaulay and Lien,[6] and later, Brown and Smoot[7] proposed an S_N2 mechanism without the formation of a free primary carbonium ion. On the other hand, Streitwieser and Reif[8] proposed a hydride abstraction mechanism, in which the formation of a secondary benzyl cation was characteristic, based on an experiment using $GaBr_3$ as the catalyst.

One of the present authors[9] (K.S.) reported on the transethylation of toluene to show that both mechanisms operate with an aluminum chloride catalyst and that the hydride abstraction mechanism is favored when an ethylalkylbenzene of stronger basicity is used. More precisely, ethyl-*m*-xylene produced *p*-ethyltoluene in greater prevalence over its *ortho*-isomer than did ethyl-*o*- and *p*-xylenes.

In the present work, it was found that there is virtually no difference in the initial isomer distribution among the ethylxylene isomers. Namely, 3.2—3.5% α- and 96.8—96.5% β-isomer was obtained. This may be due to the basicity of the reactants which is in the order, naphthalene>ethylxylenes>toluene.

However, the fact that the initial isomer distribution was richer in the β-isomer than at equilibrium, shows the strong steric hindrance of the α-position in the transition state. This means that the hydride abstraction mechanism was operated preferentially as discussed previously.[9]

On the other hand, the formation of considerable proportions of α-ethylnaphthalene was observed in the case of transethylation by ethylbenzene. Therefore, the transethylation of naphthalene with ethylbenzene should, at least partly, proceed by a mechanism, which shows lesser steric hindrance at the α-position as in the ethylation by ethyl bromide, namely, the S_N2-type mechanism.

The authors are indebted to Dr. Shoichi Sakajiri,

Director of the Central Research Institute, Teijin Limited, for his permission to publish this article.

References

1) The Alkylation and Transalkylation Reaction of Aromatic Hydrocarbons V. Part IV: *Sekiyu Gakkaishi*, **18**, 34 (1974).

2) For References on previous researches, see S. H, Patinkin and B. S. Friedman in "Friedel-Crafts and Realted Reactions," edited by G. A. Olah, Vol. 2, Interscience Publishers, New York, N. Y. (1964), pp. 68—71.

3) J. E. Nickels and W. M. Kutz, U. S. 2570263 (1951).

4) A. P. Lien and D. A. McCaulay, U. S. 2837583 (1958).

5) G. I. Karakuleva, A. V. Bondarenko, M. I. Farberov, and Z. V. Smirnova, *Neftekhimiya*, **5**, (6) 856 (1965).

6) D. A. McCaulay and A. P. Lien, *J. Amer. Chem. Soc.*, **75**, 2407, 2411 (1953).

7) H. C. Brown and C. R. Smoot, *ibid.*, **78**, 2185 (1956).

8) A. Streitwieser, Jr. and L. Reif, *ibid.*, **82**, 5003 (1960); **86**, 1988 (1964).

9) K. Shimada, *Nippon Kagaku Zassi*, **90**, 1041 (1969).

Photochemical Reactions of Azido-1,3,5-triazines with Hydrocarbons and Ketones

Ryuichi KAYAMA, Haruo SHIZUKA, Shizen SEKIGUCHI, and Kohji MATSUI

Department of Synthetic Chemistry, Faculty of Engineering, Gunma University, Kiryu, Gunma 376

(Received June 12, 1975)

2-Azido-4,6-dimethoxy-1,3,5-triazine (**1**) produced 2-cyclohexylamino-4,6-dimethoxy-1,3,5-triazine as the sole major product upon irradiation at 254 nm in cyclohexane by the intermolecular insertion of the triazinyl nitrene into cyclohexane, while in the reaction with cyclohexene a derivative of the aziridine type was produced by the addition of triazinyl nitrene to the double bond of cyclohexene. In the photochemical reaction of **1** with ketones, 3,3-dialkyl derivatives of 5,7-dimethoxy-3*H*-[1,2,4]oxadiazolo[4.3-*a*]-*s*-triazine were obtained. The reaction is assumed to proceed *via* the electrophilic attack of the singlet nitrene on the carbonyl oxygen of the ketones followed by cyclization to give the final products. However, in the thermal reaction of **1** with ketones only 2-amino-4,6-dimethoxy-1,3,5-triazine was obtained.

In a previous paper,[1] the authors reported that the thermal reactions of azido-1,3,5-triazines with non-olefinic hydrocarbons proceed *via* a nitrene intermediate producing insertion and hydrogen abstraction products and that the reactions with olefinic hydrocarbons take place *via* a bimolecular mechanism involving the formation of an intermediate of the triazoline type to give alkenylamino- and amino-1,3,5-triazines as the final products.

Photolyses of a number of organic azides involving the formation of nitrene intermediates have been extensively investigated.[2] Although little is known about the photochemical reactions of azido nitrogenheteroaromatics, the reactions are considered to proceed *via* a nitrene intermediate producing amines,[3] azo-compounds,[3,4] insertion,[5] and ring contraction products,[6] *etc.* Recently, the formation of a nitrene intermediate was observed in the photolysis of azido-1,3,5-triazine;[7] amino-1,3,5-triazines were obtained upon irradiation of azido-1,3,5-triazines in methanol.[8] However, the details of the photochemical reactions of azido-1,3,5-triazines have not yet been determined. On the other hand, the photolysis of azido-1,3,5-triazines is of interest from the view point of the effect of the presence of three ring nitrogen atoms—the effect of an electron-attracting aryl nucleus on the photochemical reaction of arylazide. In addition, the photolysis of azido-1,3,5-triazines may provide useful and convenient methods for the preparation of a number of 1,3,5-triazine derivatives which would otherwise be difficult to prepare. This paper reports the photochemical reactions of azide-1,3,5-triazines with some hydrocarbons and ketones.

Results and Discussion

Photochemical Reactions of Azido-1,3,5-triazines with Hydrocarbons. When azido-1,3,5-triazines were irradiated in cyclohexane at 254 nm, a regular spectral change with isosbestic points was observed in every case, regardless of constituents of the 1,3,5-triazine nucleus, as is shown in Fig. 1.

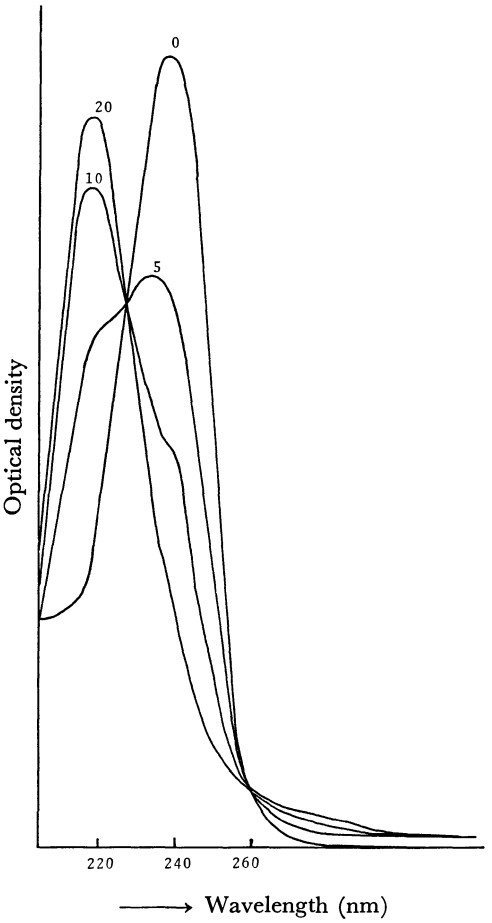

Fig. 1. Spectral change of cyclohexane solution of 2-azido-4,6-dimethoxy-1,3,5-triazine with lapse of time at 254 nm. Numbers refer to time at measurement in min.

In the photochemical reaction of 2-azido-4,6-dimethoxy-1,3,5-triazine (**1**) in cyclohexane, 2-cyclohexylamino-4,6-dimethoxy-1,3,5-triazine (**2**) was obtained as the sole major photoproduct; in the reaction mixture, no amount of the corresponding amino-1,3,5-triazine (**3**) was observed.

On the other hand, when azido-1,3,5-triazines were irradiated at 254 nm in EPA at 77 K, a new spectrum involving vibrational structure assignable to the corresponding triplet nitrene appeared in the long-wavelength region[9] in all cases. These triplet nitrenes should result from an intersystem crossing of the singlet nitrenes produced by the photodecomposition of the azido-1,3,5-triazines. Ordinary monoazido-1,3,5-triazines are

thermally very stable,[1] thus without irradiation they did not react with cyclohexane at room temperature. The photochemical reaction of azido-1,3,5-triazine with cyclohexane can be said to proceed *via* a singlet nitrene intermediate, judging from the formation of cyclohexylamino-1,3,5-triazine and the absence of the hydrogen abstraction product (amino-1,3,5-triazine) in the reaction mixture.

It has been pointed out that in the photochemical reactions of ordinary arylazides with hydrocarbons,[10,11] intermolecular nitrene insertion products are not obtained as the major product. However, in the case of azido-1,3,5-triazine, the reaction proceeded in a similar manner to those of acyl and sulfonyl azides to give the intermolecular insertion products. Thus, even though the 1,3,5-triazine nucleus is an aromatic group, the 1,3,5-triazinyl nitrene behaves as if it were acyl or sulfonyl nitrene rather than ordinary aryl nitrene; the peculiar situation of 1,3,5-triazinyl nitrenes correlates with the strong electron-withdrawing power of this heteroaromatic nucleus.

On the other hand, the photochemical reaction of compound **1** in cyclohexene yielded many kinds of by-products along with one major product. Since isolation and purification of the major product were found to be difficult, the reaction mixture was treated with dimethylamine and hydrochloric acid. The former treatment gave 2-(2-dimethylaminocyclohexylamino)-4,6-dimethoxy-1,3,5-triazine (**4**) while the latter gave 2-(2-chlorocyclohexylamino)-4,6-dimethoxy-1,3,5-triazine (**5**), suggesting that the major photoproduct of **1** with cyclohexene is a derivative of the aziridine type (**6**) resulting from the addition of 1,3,5-triazinyl nitrene to the double bond of cyclohexene. If 2-(cyclohexenylamino)-4,6-dimethoxy-1,3,5-triazine were produced during the photolysis as in the thermal reaction,[1] the final products **4** and **5** would not be produced by these treatments.

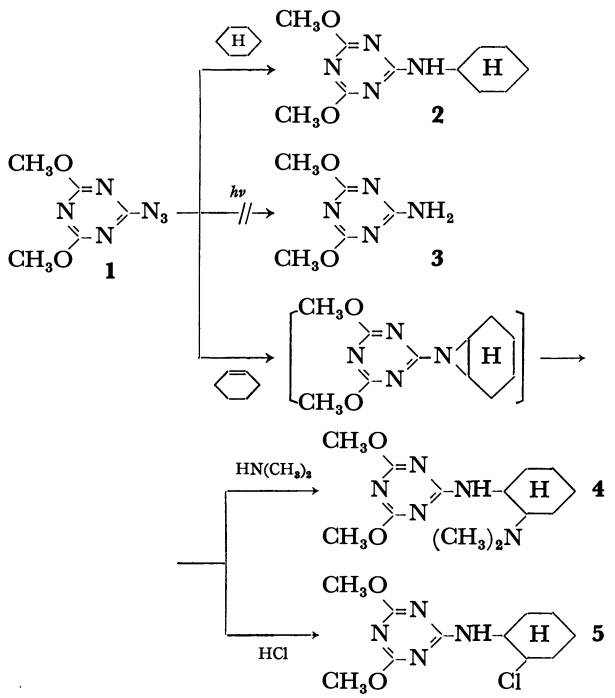

Photochemical Reactions of Azido-1,3,5-triazines with Ketones. Although there are many studies on the photochemical reactions of organic azides, little is known about the photochemical reactions of azides with ketones; only recently, it was reported that ethyl azidoformate reacts with acetone photochemically to give 2-ethoxy carbonyl-3,3-dimethoxyloxazirane, acetonyl carbamate, *etc.*[12] On the other hand, the present authors have recently reported that azido-1,3,5-triazine reacts photochemically with some nitriles to give the derivatives of *s*-triazolo[4.2-*a*]-1,3,5-triazine by the cycloaddition of triazinyl nitrene to nitriles.[9] When 2-azido-4,6-dimethoxy-1,3,5-triazine was irradiated at 254 nm

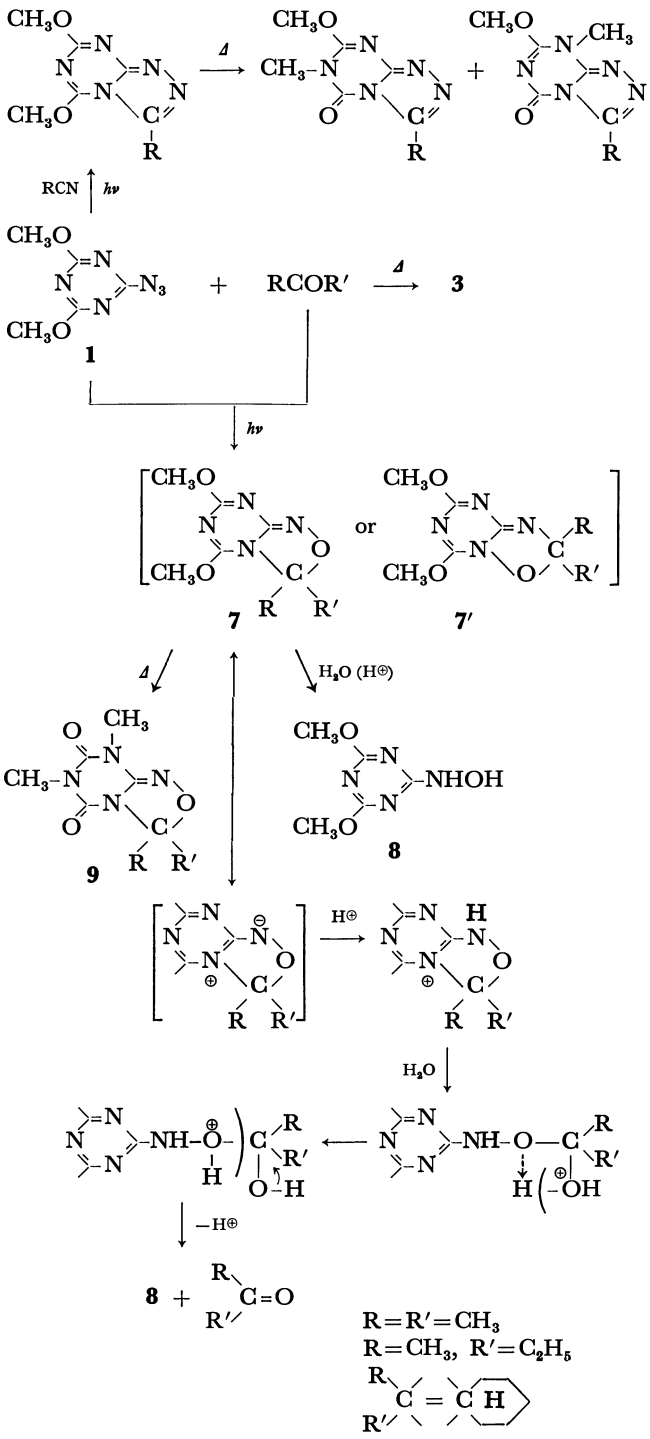

in acetone, an adduct consisting of the corresponding nitrene and acetone in a molar ratio of 1: 1 was obtained. The compound has two kinds of methoxyl groups and the lack of the characteristic IR band of the saturated aliphatic carbonyl group indicates that the compound has a bicyclic structure resulting from the cycloaddition of the nitrene to acetone, as is shown by **7** or **7'**. Similar photoproducts were obtained when **1** was irradiated at 254 nm in methylethyl ketone and cyclohexanone. On the other hand, it is known that the attempted intermolecular reaction of sulfonyl nitrene with cyclohexanone failed to give any products arising from the nitrene addition.[13] Therefore, even though 1,3,5-triazinyl nitrene behaves similarly to acyl and sulfonyl nitrenes, 1,3,5-triazinyl nitrene is not a mere adherent of acyl or sulfonyl nitrene. From the spectral data, it is difficult to distinguish between the two possible isomers **7** and **7'**. However, these photoproducts were readily hydrolyzed by dilute acid to give hydroxyamino-1,3,5-triazine (**8**) in a good yield indicating that **8** was derived from 7 (3,3-dialkyl derivatives of 5,7-dimethoxy-3*H*-[1,2,4]oxadiazolo[4.3-*a*]-*s*-triazine), because hydroxyamino-1,3,5-triazines do not result from **7'** by hydrolysis in the presence of an acid. The acidic hydrolysis of the photoproducts to give hydroxyamino-1,3,5-triazine (**8**) can be accounted for by the preceding scheme.

From these results, the photoproducts of **1** with ketones and nitriles are found to be very closely related to each other in chemical composition. In the photochemical reaction of **1** with nitriles, the cycloaddition of 1,3,5-triazinyl nitrene is known to proceed *via* a singlet nitrene. On the other hand, the photocycloadditions of carbethoxynitrene to acetone and nitriles[14,15] yielding 2-ethoxycarbonyl-3,3-dimethyloxazirane[12] and 2-alkyl-5-ethoxy-1,3,4-oxadiazoles also are known to proceed *via* a singlet nitrene.

In this case also, the photocycloaddition of triazinyl nitrene to ketones is assumed to proceed *via* a singlet nitrene; the singlet mechanism may be supported by the following data. The starting material (**1**) in aliphatic ketones absorbs more than 95% of the 254 nm incident light, although the solvent has a weak absorption band ($n\rightarrow\pi^*$) at 254 nm ($\varepsilon<4$),[16] and the singlet nitrene should be formed by the decomposition of the excited singlet azido-1,3,5-triazine, whose quantum yield is close to unity.[9] The solvents of ketones, themselves, are triplet quenchers of the starting material, and no effect of the quenchers or dissolved oxygen on the photocycloaddition would oppose the triplet pathway. It is known that the singlet nitrenes are electrophilic. Therefore, it seems likely that the initial step in the present reaction is

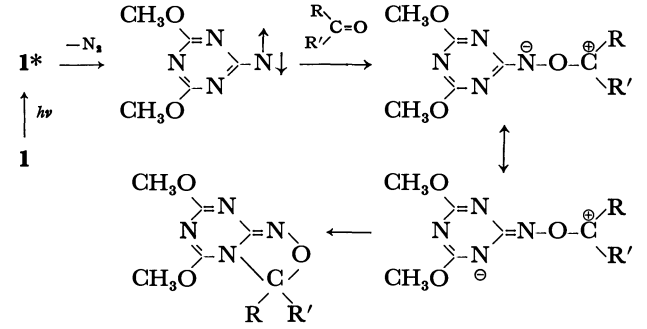

the electrophilic attack of the singlet nitrene on the carbonyl oxygen in the ketones followed by cyclization producing the final products, where **1*** is an excited singlet state of **1**. On the other hand, in the thermal reactions of azido-1,3,5-triazines with ketones no product arising from the nitrene addition was produced, for example, when **1** was heated at 180 °C in acetone, 2-amino-4,6-dimethoxy-1,3,5-triazine (**3**) was obtained as the sole major product in a 67% yield. The formation of **3** in this case can be understood in terms of the hydrogen abstraction reaction of the triplet 1,3,5-triazinyl nitrene. In the thermal reaction, there is another possibility that compound **7**, even if produced, decomposes owing to its thermal instability to give compound **3**. However, when compound **7** was heated at 180—190 °C in acetone, the main product obtained was found to be compound **9** resulting from the O→N migration of the methyl groups with a small amount (7%) of compound **3**. Thus, the formation of **7** as an intermediate in the thermal reaction can be neglected; it is apparent that the photochemical and thermal reactions of azido-1,3,5-triazine with ketones proceeded *via* different routes.

Experimental

All the melting points are uncorrected.

2-Azido-4,6-dimethoxy-1,3,5-triazone (**1**) was prepared by the condensation of 2-chloro-4,6-dimethoxy-1,3,5-triazine with sodium azide.[1] Irradiated solutions were concentrated and crystallized products were separated and purified by column chromatography and recrystallization. The assignments of the photoproducts were performed by means of NMR, IR, UV, and mass spectra, elemental analyses and by a mixed-melting-point test with an authentic sample. A low pressure mercury lamp was used as the 254 nm radiation source with a Vycor glass filter.

Photochemical Reaction of Compound 1 with Cyclohexane. A solution of 2.0 g of compound **1** in 300 ml of cyclohexane was irradiated for 10 days. From the irradiated solution 850 mg of the starting material was recovered. Crude 2-cyclohexylamino-4,6-dimethoxy-1,3,5-triazine obtained by purification using column chromatography (silica gel; benzene–acetone= 10: 1 by volume) was recrystallized from methanol to give 720 mg (yield 48%) of the pure product. Mp 125—127 °C (lit,[1] 127—128 °C).

Photochemical Reaction of Compound 1 with Cyclohexene. In this case the primary photoproduct formed in the beginning was found to decompose gradually upon further irradiation. Therefore, the irradiation was stopped at the point of 25% conversion of the starting material. After the solvent hat been evaporated *in vacuo*, the residue was dissolved in 30 ml of acetone and the solution was treated with 10 g of a 40% dimethylamine solution. After standing for 2 hr at room temperature, the solution was treated with an excess of a 2M hydrochloric acid solution to make the mixture acidic, and then, the solution was extreacted with benzene. The aqueous layer was neutralized with sodium carbonate and was extracted with ether to give 800 mg of a pasty substance from which 200 mg (yield 13%) of 2-(2-dimethylaminocyclohexylamino)-4,6-dimethoxy-1,3,5-triazine was obtained by recrystallization from methanol–water. Mp 119.5—120.5 °C. (Found: C, 55.25; H, 8.03; N, 25.11%. Calcd for $C_{13}H_{23}N_5O_2$: C, 55.48; H, 8.24; N, 25.28%) NMR ($CDCl_3$), δ 1.50 (m, 8H), 2.21 (s, 6H), 2.44 (m, 1H), 3.60 (m, 1H), 4.00 (s, 6H), 6.17 (broad, 1H). The benzene layer was evaporated and the residue was dissolved in

a small amount of ethanol. From the ethanolic solution the crystalline precipitate of 2-(2-chlorocyclohexylamino-4,6-dimethoxy-1,3,5-triazine was obtained by the addition of a small amount of water. Mp 170—171 °C (benzene–ligroin). Yield: 580 mg (39%). (Found: C, 48.71; H, 6.43; N, 20.78%. Calcd for $C_{11}H_{17}ClN_4O_2$: C, 48.44; H, 6.28; N, 20.54%) Mass: m/e=272. NMR ($CDCl_3$), δ 1.60 (m, 9H), 4.00 (s, 7H), 6.20 (broad, 1H). Thus, in the photochemical reaction of compound **1** with cyclohexene, the yield of the derivative of the aziridine type should exceed 50% of the decomposed azide.

Photochemical Reaction of Compound 1 with Ketones. A typical run is the case of the reaction of compound **1** with acetone. A solution of 1.0 g of compound **1** in 20 ml of acetone was irradiated for 24 hr. The solvent was evaporated *in vacuo* and the residue was purified by column chromatography (alumina: benzene–acetone= 10: 5 by volume) to give 300 mg of the starting material and 3,3-dimethyl-5,7-dimethoxy-3*H*-[1,2,4]oxadiazolo[4.3-*a*]-*s*-triazine in a 30% yield. Mp 144—145 °C (benzene–ligroin). (Found: C, 45.05; H, 5.43; N, 26.22%. Calcd for $C_8H_{12}N_4O_3$: C, 45.28; H, 5.70; N, 26.40%) Mass: m/e=212. NMR ($CDCl_3$), δ 1.70 (s, 6H), 3.92 (s, 3H), 4.07 (s, 3H). IR (KBr, cm^{-1}) (C=N), 1665.

Hydrolysis of Compound 7 in the Presence of Hydrochloric Acid. A mixture of 800 mg of compound **7** and 7 ml of a dilute hydrochloric acid solution (the pH of the solution was about 3.0) was warmed in a water bath for 3 min. After cooling, the solution was neutralized with sodium carbonate to give 550 mg (yield 85%) of hydroxyamino-4,6-dimethoxy-1,3,5-triazine as a crystalline precipitate. Mp 174—175 °C (under decomposition) (Methanol). (Found: C, 35.10; H, 4.82; N, 32.35 %. Calcd for $C_5H_8N_4O_3$: C, 34.88; H, 4.68; N, 32.55%). The compound was identified by a mixed-melting-point test with an authentic sample prepared by the condensation of 2-chloro-4,6-dimethoxy-1,3,5-triazine with hydroxylamine in the presence of sodium carbonate.

Similarly, in the reaction of compoun **1** with methyl ethyl ketone, compound **7** (R=CH_3, R′=C_2H_5) was obtained in a 52% yield. Mp 110—111 °C (benzene–ligroin). (Found: C, 47.83; H, 6.42; N, 24.92%. Calcd for $C_9H_{14}N_4O_3$: C, 47.78; H, 6.23; N, 24.76%). NMR ($CDCl_3$), δ 0.98 (t, 3H), 1.67 (s, 3H), 2.00 (m, 2H), 3.94 (s, 3H), 4.10 (s, 3H).

In the reaction of compound **1** with cyclohexanone, compound **7** was obtained in a 46% yield. Mp 137—138 °C (benzene–ligroin). (Found: C, 52.51; H, 6.44; N, 21.98%. Calcd for $C_{11}H_{16}N_4O_3$: C, 52.37; H, 6.39; N, 22.21%) NMR ($CDCl_3$), δ 1.80 (m, 10H), 3.94 (s, 3H), 4.08 (s, 3H).

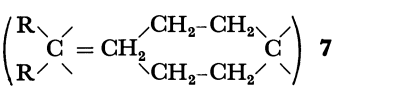

7

Rearrangement of Compound 7 in Acetone. When a solution of 600 mg of compound **7** (R=R′=CH_3) in 50 ml of acetone was heated at 180—190 °C in an autoclave, 30 mg (7% yield) of crude 2-amino-4,6-dimethoxy-1,3,5-triazine [mp 210—214 °C (dioxane) (lit.,[17] 219 °C)] and 150 mg (yield 25%) of a product of mp 87—88 °C (methanol) were obtained. The latter compound was assigned to compound **9**, on the basis of the follwoing data. (Found: C, 45.45; H, 5.85; N, 26.31%. Calcd for $C_8H_{12}N_4O_3$: C, 45.28; H, 5.70; N, 26.40%). Mass: m/e=212. IR (KBr, cm^{-1}) (C=O), 1700, 1750: (C=N), 1650. NMR (CCl_4), δ 1.70 (s, 6H), 3.19 (s, 3H), 3.23 (s, 3H).

Thermal Reaction of Compound 1 with Acetone. When a solution of 3.0 g of compound **1** in 50 ml of acetone was heated at 180 °C for 12 hr in an autoclave, 2-amino-4,6-dimethoxy-1,3,5-triazine [mp 211—214 °C (dioxane)] was obtained in a 67% yield.

References

1) R. Kayama, S. Hasunuma, S. Sekiguchi, and K. Matsui, This Bulletin, **47**, 2825 (1974).

2) For example: a) A. Reiser and H. M. Wagner, The Chemistry of the Azido Group," ed by S. Patai, Interscience Publishers (1971), p. 441; b) "Nitrenes," ed by W. Lwowsky, Interscience Publishers (1970); c) H. Kashiwagi, S. Iwata, T. Yamaoka, and S. Nagakura, This Bulletin, **46**, 417 (1973); d) R. Breslow, A. Feiring, and F. Herman, *J. Amer. Chem. Soc.*, **96**, 5937 (1974).

3) B. Stanovnik, *Tetrahedron Lett.*, **1971**, 3211.

4) A. C. Mair, M. F. G. Stevens, *J. Chem. Soc., Perkin I*, **1972**, 161.

5) J. A. Hyatt, J. S. Swenton, *J. Heterocycl. Chem.*, **9**, 409 (1972); J. V. VanAllan, G. A. Renolds, and D. P. Maier, *J. Org. Chem.*, **34**, 1691 (1969).

6) C. Wentrup, *Helv. Chim. Acta*, **55**, 565 (1972); T. Sasaki, K. Kamematsu, and M. Murata, *Tetrahedron*, **29**, 529 (1973).

7) R. M. Moriarty, M. Rahman, and G. J. King, *J. Amer. Chem. Soc.*, **88**, 842 (1966).

8) B. E. Pape and M. J. Zabik, *J. Agr. Food Chem.*, **20**, 316 (1972).

9) H. Yamada, H. Shizuka, and K. Matsui, *J. Org. Chem.*, **40**, 1351 (1975).

10) W. E. Doering and R. A. Odum, *Tetrahedron*, **22**, 81 (1966).

11) L. Horner, O. Christmann, and A. Gross, *Chem. Ber.*, **96**, 399 (1963).

12) T. Hiyama, H. Taguchi, S. Fujita, and H. Nozaki, This Bulletin, **45**, 1863 (1972).

13) G. P. Balabanov, Y. I. Dergunov, and V. A. Gal'perin, *J. Org. Chem. USSR*, **2**, 1797 (1966).

14) W. Lwowskii, A. Hartenstein, C. deVita, and R. L. Smick, *Tetrahedron Lett.*, **1964**, 2497.

15) Ref. 2-b, p. 214.

16) J. G. Calvert and J. N. Pitts, Jr., "Photochemistry," John Wiley & Sons, Inc., New York (1967), pp. 368—369.

17) J. Thurston, J. Dudley, D. Kaiser, I. Hechenbleickner, F. Schaefer, and D. Holm-Hansen, *J. Amer. Chem. Soc.*, **73**, 2981 (1951).

Low-temperature NMR Studies of the Conformations of 3-Aryl-1,2,3-oxathiazolidine 2-Oxides

Fukiko YAMADA, Tomihiro NISHIYAMA, and Hiroshi SAMUKAWA

Department of Applied Chemistry, Faculty of Engineering, Kansai University, Senriyama, Suita, Osaka 564

(Received June 12, 1975)

A complete iterative NMR spectral analysis has been carried out for twelve 3-aryl-1,2,3-oxathiazolidine 2-oxides at several low temperatures over a range of 111 °C. The magnitudes of the two vicinal coupling constants either increased or decreased markedly with a decrease in the temperature. On the basis of the resulting vicinal coupling constants, the correlations between the ratios of the vicinal coupling constants and the corresponding torsion angles were obtained and made it possible to assign their twist-envelope conformations. From the experimental data, the parameters of the Karplus equation could be given:

$$J\,\mathrm{vic} = 5.3 - \cos(135\pm\theta) + 4.3\cos 2(135\pm\theta)$$
$$+45^\circ \geq \theta \geq -45^\circ$$

In a previous paper of this series, the twist-envelope conformations have been assigned to the oxathiazolidine ring of 3-aryl-1,2,3-oxathiazolidine 2-oxides (**1**) on the basis of the vicinal coupling constants at room temperature.[1] These assignments are consistent with the results of the solvent-shift determinations.

The present study was initiated in order to examine the NMR spectral data at several low temperatures for the following compounds:

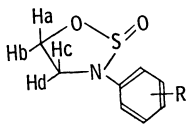

1

I, R=H	IIIc, R=*p*-OCH_3
IIa, R=*o*-CH_3	IV, R=*p*-Br
IIb, R=*m*-CH_3	Va, R=*o*-Cl
IIc, R=*p*-CH_3	Vb, R=*m*-Cl
IIIa, R=*o*-OCH_3	Vc, R=*p*-Cl
IIIb, R=*m*-OCH_3	VI, R=2,4,6-tri-Cl

Experimental

Compounds. A series of **1** compounds was prepared and was then purified by a previously reported method.[2,3] The reaction conditions and the physical properties of **1** were reported in our previous paper.[1]

NMR Spectral Determination. All the NMR spectra were recorded at 100 MHz on a Japan Electron Optics Model JNM-PS-100 spectrometer equipped with a Japan Electron Optics Model JNM-VT-3C variable-temperature controller, using acetone-d_6 as the solvent (0.5 mmol/ml). The probe temperature was measured both with a thermocouple and by the peak separation of a calibrated methyl alcohol sample; it is considered accurate to ±2 °C. The chemical shifts were reported in ppm downfield from the internal TMS. The details of the analyses and the stereochemical assignments were also provided in the previous paper.[1]

Results and Discussion

Spectra at Low Temperatures in an Acetone-d_6 Solution. Table 1 shows the NMR spectral data for the methylene protons of the **1** compounds at room temperature. Insignificant variations are observed in the NMR parameters in acetone-d_6 solutions relative to those in CCl_4 or $CDCl_3$–CCl_4 solutions at room temperature.[1] In this study, the shapes of all the NMR signals at several low temperatures over a range of 111 °C are quite similar. That is, cooling a sealed NMR tube containing one of the **1** compounds in acetone-d_6 at temperatures down to −85 °C (with the exception of the VI compound) produced no major change in the signals.

TABLE 1. CHEMICAL SHIFTS AND COUPLING CONSTANTS OF THE METHYLENE PROTONS OF THE **1** COMPOUNDS, IN ACETONE-d_6 AT 26 °C

Compd.	Chemical shifts, δ ppm				Geminal, Hz		Vicinal, Hz				r	θ
	H_a	H_b	H_c	H_d	J_{ab}	J_{cd}	J_{ac}	J_{bd}	J_{ad}	J_{bc}	J_{ad}/J_{bc}	(degree)
I	4.995	4.784	3.949	3.755	8.4	8.9	6.4	6.7	8.4	4.5	1.87	12.0
IIa	4.915	4.560	4.108	3.702	8.0	9.3	6.9	6.6	4.4	7.9	1.80[a]	−11.3
IIb	4.968	4.732	3.919	3.722	8.5	8.9	6.4	6.8	8.3	4.4	1.89	12.2
IIc	4.958	4.713	3.916	3.722	8.3	8.9	6.5	6.9	7.8	4.9	1.59	9.0
IIIa	4.864	4.508	3.936	3.713	8.3	9.1	6.9	7.1	5.1	7.0	1.37[a]	−6.2
IIIb	4.975	4.747	3.927	3.733	8.6	9.0	6.4	6.7	8.5	4.3	1.98	13.1
IIIc	4.935	4.660	3.934	3.731	8.3	9.0	6.4	6.6	7.0	5.7	1.23	4.0
IV	5.005	4.790	3.937	3.737	8.4	8.9	6.3	6.8	8.6	4.2	2.05	13.8
Va	4.930	4.563	4.123	3.785	7.9	9.3	6.9	6.7	4.2	8.3	1.98[a]	−13.1
Vb	5.031	4.824	3.975	3.772	8.5	8.8	6.3	6.8	8.8	4.0	2.20	15.2
Vc	5.016	4.800	3.955	3.758	8.4	8.8	6.3	6.8	8.5	4.3	2.00	13.5
VI	5.013	4.829	4.092	3.621	8.6	8.6	5.8	6.9	10.3	2.3	4.48	28.6

a) Values for J_{bc}/J_{ad}

Chemical Shifts. The chemical shifts for the methylene protons, H_a, H_b, H_c, and H_d, at several low temperatures are shown in Figs. 1-a and 1-b. From these observations, it is clear that the chemical shifts of the methylene protons of the **1** compounds are dependent on the temperatures, moving either to a lower or a higher field with a decrease in the temperature.

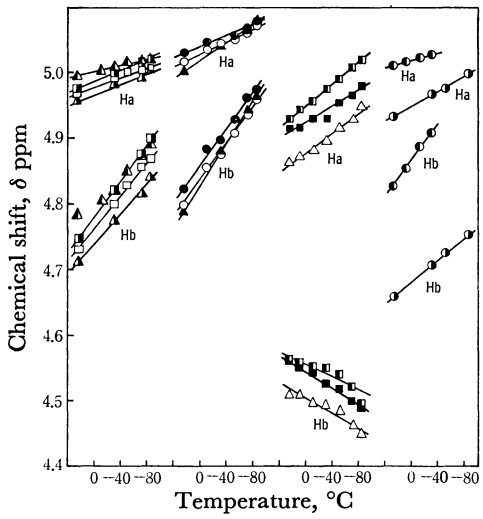

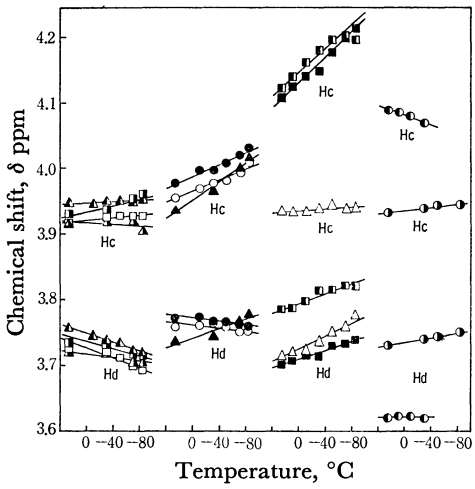

Figs. 1-a and 1-b. Temperature-dependence of the chemical shifts of the methylene protons of the **1** compounds.
Group 1a ▲, I; □, IIb; ◭, IIc; ◨, IIIb
Group 1b ▲, IV; ●, Vb; ○, Vc
Group 2 ■, IIa; △, IIIa; ◧, Va
Group 3, 4 ◑, IIIc; ◐, VI

In the previous paper,[1] we proposed that the conformations of the **1** compounds could be divided roughly into several groups on the basis of their well-defined patterns of the appearance of the methylene-proton signals, the ratios (r values) of the vicinal coupling constants (that is, J_{ad}/J_{bc} or J_{bc}/J_{ad}), their torsion angles, and the data of the solvent-shift studies in benzene (Table 2). In this present study, the characteristic properties of these groups are reflected in the temperature-dependence of their methylene-proton chemical shifts. In particular, with a decrease in the temperature the H_b proton shifts of the IIa, IIIa, and Va compounds in Group 2 move markedly toward a higher field in comparison with those of other H_b protons. This interesting feature may be caused by the presence of an *o*-substituent.

Table 2. Classification of the conformations of the **1** compounds

Group	R	r value	θ°
1a	H, *m*-CH_3, *p*-CH_3, *m*-OCH_3	1.59—1.89[a] (1.8—2.2)[b]	9.0—13.1 (11—15)
1b	*p*-Br, *m*-Cl, *p*-Cl	2.00—2.20 (1.9—2.2)	13.5—15.2 (12—15)
2	*o*-CH_3, *o*-OCH_3, *o*-Cl	1.37—1.98 (1.3—1.8)	−6.2—−13.1 (−5—−11)
3	*o*-OCH_3, *p*-OCH_3	1.23—1.37 (1.2—1.3)	−6.2—+4.0 (−5—+4)
4	tri-Cl	4.48 (4.7)	28.6 (≥30)

a) The values in upper line are obtained in this study.
b) The values obtained in the previous paper[1] are shown in parentheses.

Geminal Coupling. Two geminal coupling constants of the **1** compounds have been determined in this study; they were found not to vary significantly in the temperature range of 111 °C. This phenomenon means that the angle of neither H_a–C_5–H_b nor H_c–C_4–H_d changes, not even at low temperatures.

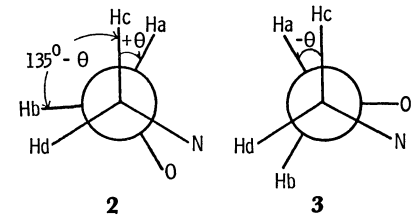

2 **3**

Fig. 2. Diagrams of **2** and **3** forms of the parts of methylene protons of **1**.
Dihedral angle (ϕ) = 135 °±Torsion angle (θ).

Vicinal Coupling. As has been discussed in our previous study,[1] the vicinal coupling data for the four methylene protons of the **1** compounds corroborate the explanations that the distortions of the compounds with an *m*- or *p*-substituent are in the direction of the **2** projection (in Fig. 2), while those with an *o*-substituent cause distortion toward the **3** projection. Furthermore, the r values, J_{ad}/J_{bc} for the **2** projection and J_{bc}/J_{ad} for the **3** projection, have been found to be nearly independent of the electronegativity of the substituent and of other factors, and to be dependent only on each dihedral angle. It was, therefore, possible to determine the conformational effects by means of the r value.

Figures 3-a and 3-b show the vicinal coupling constants, J_{ad}, J_{bd}, J_{ac}, and J_{bc}, of the **1** compounds at various low temperatures. The value of J_{ad} or J_{bc} increased with a decrease in the temperature, whereas J_{bc} or J_{ad} decreased with a decrease in the temperature. These figures clearly show that the values of J_{ad} and J_{bc} of the **1** compounds change almost linearly with the temperatures in the range from 26 to −85 °C. When the two straight lines for J_{ad} and J_{bc} are extended, the

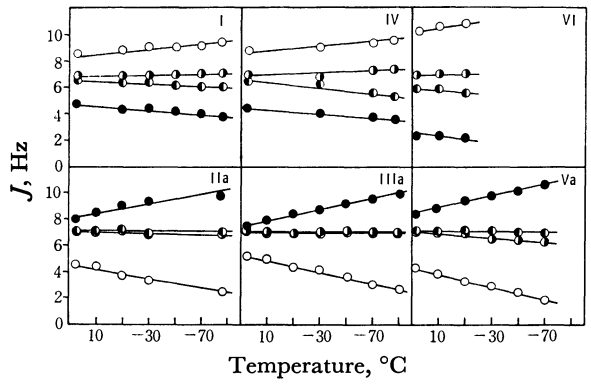

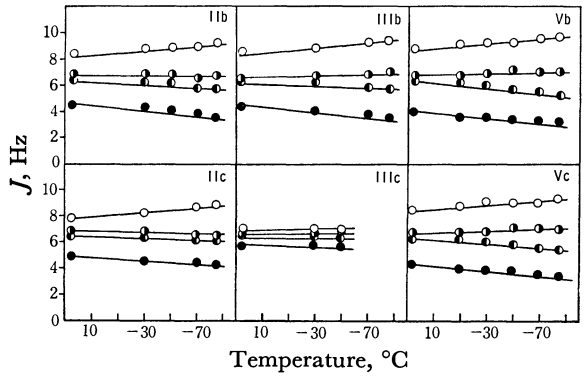

Figs. 3-a and 3-b. Vicinal coupling constants of the **1** compounds at various temperatures.
○, J_{ad}; ◑, J_{bd}; ◐, J_{ac}; ●, J_{bc}

two lines intersect around 6.3, are symmetrical with respect to the line which is parallel with the x-axis, and pass through the point of 6.3 on the y-axis. That is, the average value of J_{ad} and J_{bc} obtained from the experimental data (118 pieces) of all the **1** compounds is 6.331. The results indicate that, at each intersection point, the values of both J_{ad} and J_{bc} are the same and are very close to 6.3 Hz; therefore, their r value becomes 1.000.

In the case of the well-known Karplus equation ($90 \leq \theta \leq 180°$), the curve passes through the inflection point at 135°.[4] From our results presented above that the increasing and decreasing straight lines are symmetrical and show the same gradient, it is possible to get a rough idea of the value of the projection angle of a CH_2 group—that is, the angles of H_a–C_5–H_b and H_c–C_4–H_d. (Fig. 2). We therefore suggest that, in the case of the oxathiazolidine ring, the projection angle is no longer 120°, but is close to the value of 135°, corresponding to the above inflection point.

On the other hand, the projection angle of a CH_2 group in the five-membered rings, must be larger than the 120° in the six-membered rings. At present, it is not possible to obtain an accurate value of the projection angle in the five-membered rings. However, it was necessary to estimate the size of this angle. Usually the value of 120° in the six-membered rings has been used for the calculation of Karplus-type equations of the five-membered rings.[1,5-7]

On the basis of the above observations and the results of the previous investigation,[1] we may set the following parameters of the Karplus equation by means of a "trial

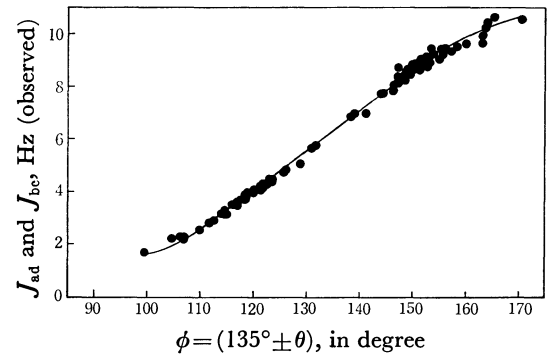

Fig. 4. Plots of the observed vicinal coupling constants, J_{ad} and J_{bc}, of all the **1** compounds at various temperatures *vs.* the dihedral angles.
——, Calculated curves by Karplus eq.
●, J_{ad} or J_{bc}; number of dots in this figure is 118 pieces.

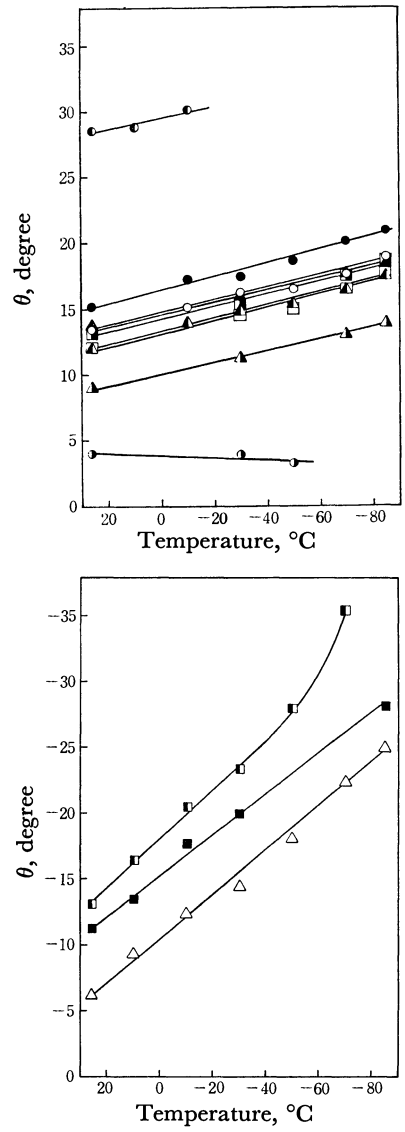

Figs. 5-a and 5-b. Temperature dependence of the torsion angles of the **1** compounds.
Group 1a: ◭, I; □, IIb; ▲, IIc; ◨, IIIb
Group 1b: ▲, IV; ●, Vb; ○, Vc
Group 2: ■, IIa; △, IIIa; ▮, Va
Group 3: ◑, IIIc
Group 4: ◐, VI

and error" procedure;

$$r = (J_{ad}/J_{bc}) \text{ or } (J_{bc}/J_{ad})$$
$$= \frac{5.3-\cos(135+\theta)+4.3\cos 2(135+\theta)}{5.3-\cos(135-\theta)+4.3\cos 2(135-\theta)}$$
$$+45° \geq \theta \geq -45°$$

After setting the above parameters, we evaluated the correlation among the θ, J, and r values. Then, the torsion angles can be obtained from the observed values of J_{ad} and J_{bc} by using this relation. Figure 4 shows the plots of the observed vicinal coupling constants, J_{ad} and J_{bc}, of all the **1** compounds at various low temperatures *vs.* the dihedral angles obtained by means of the above procedure. The experimental data clearly fall on the calculated Karplus curve for the above parameters.

Torsion Angles at Low Temperatures. The torsion angles of the **1** compounds at 26 °C are shown in Table 1. Figures 5-a and 5-b show the data at various low temperatures. The values of θ increased with the decrease in the temperature, except in the IIIc compound. As can be seen in these figures, the compounds belonging each group show a similar tendency toward increasing the torsion angle. These findings indicate that each group shows a sterically different feature.

References

1) F. Yamada, T. Nishiyama, and H. Samukawa, This Bulletin, **48**, 1878 (1975).
2) T. Nishiyama and F. Yamada, *ibid.*, **44**, 3037 (1971).
3) F. Yamada, T. Nishiyama, M. Kinugasa, and M. Nakatani, *ibid.*, **43**, 3611 (1970).
4) L. M. Jackman and S. Sternhell, "Applications of Nuclear Magnetic Resonance Spectroscopy in Organic Chemistry," Vol. 5, ed. by D. H. R. Barton and W. Doering, Pergamon Press, London (1969), p. 281.
5) J. B. Lambert, J. J. Papay, E. S. Magyar, and M. K, Neuberg, *J. Amer. Chem. Soc.*, **95**, 4458 (1973).
6) P. Haake, J. P. McNeal, and E. J. Goldsmith, *ibid.*, **90**. 715 (1968).
7) J. B. Lambert, *Accounts Chem. Res.*, **4**, 87 (1971).

Cyclic Dimerization of Ethyl 1-Arylethylidenecyanoacetates with Grignard Reagents

Shoji HAYASHI, Takami ANII, and Taizo TAMANO

Department of Chemistry, Faculty of Science, Kwansei Gakuin University, Uegahara, Nishinomiya, Hyogo 662

(Received June 24, 1975)

The treatment of ethyl 1-arylethylidenecyanoacetates (I) with Grignard reagents, especially mesitylmagnesium bromide, gave ethyl 2,4-diaryl-5-cyano-5-ethoxycarbonyl-6-imino-4-methyl-1-cyclohexenecarboxylates (II), a dimer of I.

The preparation of ethyl *t*-alkylcyanoacetate by the conjugate addition of Grignard reagents to ethyl 1-alkylethylidenecyanoacetate has been reported.[1] The treatment of ethyl 1-arylethylidenecyanoacetate (I)[2] with isopropylmagnesium bromide yielded ethyl 3-aryl-2-cyano-3-isopropylbutanoate and an unknown yellow compound II, which is a dimeric product. It was found that ester I reacted with mesitylmagnesium bromide (MesMgBr) to give only the same unknown dimeric product. Other Grignard reagents also yielded the dimeric product, as shown in Table 1. The structure of the dimeric product was assumed to be ethyl 2,4-diaryl-5-cyano-5-ethoxycarbonyl-6-imino-4-methyl-1-cyclohexenecarboxylate (II) on the basis of the mechanism of base-catalyzed dimerization shown in Chart 1.

TABLE 1. YIELD (%) OF DIMER II

I	RX for RMgX				
	MeI	EtBr	*i*-PrBr	*t*-BuCl	MesBr
Ia	6.1	5.8	21.3	1.9	30.2
Ib	1.8	6.1	42.7	3.5	52.4

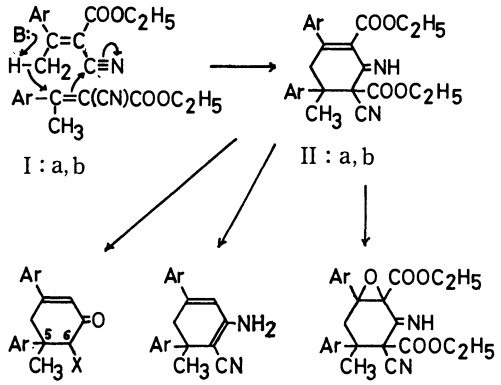

a: Ar=C_6H_5 b: Ar=*p*-$CH_3C_6H_4$

Chart 1

The IR spectrum of compound IIa showed the presence of two ester groups (an α,β-unsaturated and a saturated ester), a cyano and an imino group (see Experimental). The NMR spectrum showed signals assigned to a tertiary methyl, a methylene group, and two ethoxy groups (see Experimental).

Compound IIa was stable for refluxing in conc. hydrochloric acid; however, the treatment of IIa with an acetic acid-concd hydrochloric acid solution under reflux gave white crystals (IIIa). The IR spectrum showed no absorption band due to the ester, cyano, and imino groups, but carbonyl bands due to α,β-unsaturated ketone and an amide group were observed. The UV spectrum showed an absorption maximum at 293 nm characteristic of 3-phenyl-2-cyclohexenone systems.[3] The above results, therefore, indicate that the imino group of compound IIa was hydrolyzed with the simultaneous hydrolytic decarboxylation of two ethoxycarbonyl groups.

The NMR spectrum of IIIa showed the presence of a vinyl, a tertiary methyl, a methylene (ABX-type), a methine (singlet), and an amide proton (see Experimental). The methine singlet due to H-6 indicates the presence of two groups (phenyl and methyl) on C-5. Therefore, the amide group is located on C-6.

From these data, compound IIIa was assigned to 6-carbamoyl-5-methyl-3,5-diphenyl-2-cyclohexenone.

The alkaline hydrolysis of IIa with potassium hydroxide in boiling ethylene glycol afforded pale yellow crystals (IVa). The IR spectrum showed the presence of an amino and a cyano group, and the NMR spectrum revealed signals due to the ABX system, in which the AB pattern of methylene appeared at δ 2.94 and the X part (a vinylic proton) at 6.02. From the results, IVa was assigned to 2-amino-6-methyl-4,6-diphenyl-1,3-cyclohexadienecarbonitrile.

The oxidation of IIa with alkaline hydrogen peroxide in acetone gave epoxide (Va). The epoxidation of the double bond caused the shift of the UV absorption band of a conjugated system to that of a simple aromatic system (see Experimental).

IIb was assigned to ethyl 5-cyano-5-ethoxycarbonyl-6-imino-4-methyl-2,4-di(*p*-tolyl)-1-cyclohexenecarboxylate from spectral analysis (see Experimental).

In contrast with the acid hydrolysis of IIa, IIb gave a product (IIIb) with the simultaneous loss of carbonyl groups. The analogy in the ring system was supported by the UV spectrum (λ_{max} 296 nm).[4]

IIb gave 2-amino-6-methyl-4,6-di(*p*-tolyl)-1,3-cyclohexadienecarbonitrile (IVb) by alkaline hydrolysis.

The epoxidation of IIb gave no crystalline products.

Experimental

All melting points are uncorrected. Unless otherwise noted, UV, IR, and NMR spectra were measured in 95% ethanol, chloroform, and deuteriochloroform (with TMS as an internal standard), and presented in λ_{max} nm (log ε), ν_{max} cm^{-1}, and δ ppm, respectively. The instruments used for the measurements are a Cary 14 recording spectrophotometer, a JASCO model DS-402G infrared spectrophotometer, and a JEOLCO model

C-60 spectrometer.

Materials. Ethyl 1-phenylethylidenecyanoacetate (Ia) was prepared according to the method of McElvain and Clemens,[5] bp 149.5—153 °C/3 Torr (lit,[5] 135—160 °C/0.35 Torr); Ethyl 1-(*p*-tolyl)ethylidenecyanoacetate (Ib) was prepared accoding to the methob of Cope,[6] bp 122—123 °C/ 3.5×10^{-3} Torr (lit,[6c] 160—170 °C/10 Torr).

Reaction of Ethyl 1-Arylethylidenecyanoacetate (I) with Grignard Reagent. To a Grignard solution, prepared from 2.92 g (0.12 mol) of magnesium, 0.12 mol of alkyl halide, and 22 ml of absolute ether, was added 0.1 mol of I in 30 ml of refluxing absolute ether over a period of 20 min. The mixture was refluxed under stirring for 1 hr and then left to stand overnight. An excess of the Grignard reagent was decomposed by the addition of aqueous ammonium chloride. The reaction mixture was extracted with ether and the ethereal extract was dried. After removal of the solvent, the residue dissolved in ethanol was treated with active carbon, and cooled with ice. The resulting yellow crystals were washed with cold ethanol, and recrystallized from ethanol to give II. The filtrate was concentrated *in vacuo* and analyzed by chromatography on silica gel. Elution with benzene-ethyl acetate (10: 1, v/v) gave yellow crystals (II). Combined II was recrystallized from 50% ethanol (the yield is indicated in the yield table). A pure sample was obtained after several recrystallizations.

a) IIa: Mp 134.5—135.0 °C. IR: 3400 (=NH), 2221 (C≡N), 1746, 1706 (C=O), and 1626 (C=C). UV: 240 (4.05) and 324 (3.97). NMR: 0.75 (t, 3H, J=7 Hz), 1.31 (t, 3H, J=7 Hz), 1.70 (s, 3H), 3.08 (ABq, 2H, J=18 Hz, $\nu_0\delta$=8.7 Hz), 3.88 (q, 2H, J=7 Hz), 4.27 (q, 2H, J=7 Hz), and 6.95—7.61 (m, 11H, 2 Ph and =NH). Found: C, 72.70; H, 6.01; N, 6.37%. Calcd for $(C_{13}H_{13}O_2N)_2$: C, 72.54; H, 6.09; N, 6.51%.

b) IIb: Mp 149.0—150.0 °C. IR: 3405 (=NH), 2219 (C≡N), 1741, 1702 (C=O), and 1617 (C=C). UV: 246 (4.07) and 336 (4.03). NMR: 0.80 (t, 3H, J=7 Hz), 1.29 (t, 3H, J=7 Hz), 1.65 (s, 3H), 2.30 (s, 6H), 3.01 (ABq, 2H, J=17 Hz, $\nu_0\delta$=10.5 Hz), 3.87 (q, 2H, J=7 Hz), 4.21 (q, 2H, J=7 Hz), and 6.80—7.37 (m, 9H). Found: C, 73.33; H, 6.57; N, 5.94%. Calcd for $(C_{14}H_{15}O_2N)_2$: C, 73.34; H, 6.59; N, 6.11 %.

Acid Hydrolysis of II. A mixture of 1 g of II, 10 ml of acetic acid and 5 ml of conc. hydrochloric acid was boiled under reflux for 13 hr. Carbon dioxide was evolved during the reaction. The reaction mixture was concentrated under reduced pressure. The residue dissolved in ether was washed with saturated aqueous sodium bicarbonate and the solvent was distilled off. The residue dissolved in benzene was analyzed by chromatography on silica gel and eluted with benzene. Elution with benzene gave white crystals, which, after recrystallization from ethanol, gave a pure sample (III).

a) IIIa: Yield 80 mg, mp 181.0—181.5 °C. IR (KBr disk): 3382, 3164 (NH_2), 1686 (amide I), 1632 (C=O), and 1600 (C=C). UV: 293 (4.22) and 255^{sh} (4.01). NMR (DMSO-d_6, JEOLCO PS-100 spectrometer): 1.51 (s, 3H), 3.38 (ABX, 2H, J_{AB}=18.5 Hz, J_{BX}=2 Hz, $\Delta\nu_{AB}$=12 Hz), 3.91 (s, 1H), 6.30 (d, 1H, J=2 Hz), 7.32 (s, 2H), 7.54 (m, 5H), and 7.77 (m, 5H). Found: C, 78.47; H, 6.28; N, 4.39%. Calcd for $C_{20}H_{19}O_2N$: C, 78.66; H, 6.27; N, 4.59%.

b) IIIb: Yield 450 mg, mp 105.0—106.5 °C. IR: 1655 (C=O) and 1607 (C=C). UV: 296 (4.29), 217^{sh} (4.22), and 231^{sh} (4.00). NMR (CCl_4): 1.41 (s, 3H), 2.28 (s, 3H), 2.36 (s, 3H), 2.59 (d, 2H, J=9 Hz), 2.89 (d, 2H, J=6 Hz), 6.21 (s, 1H), 7.06 (m, 4H), and 7.24 (m, 4H). Found: C, 87.12; H, 7.81%. Calcd for $C_{21}H_{22}O$: C, 86.85; H, 7.64%.

Alkaline Hydrolysis of II. A mixture of 1 g of II, 4.3 g (76.6 mmol) of potassium hydroxide and 280 ml of ethylene glycol was refluxed for 3 hr. The reaction mixture was poured into cold water, and extracted with ether. The ethereal extract was washed with saturated aqueous sodium chloride, drted and evaporated producing pale yellow crystals.

a) IVa: Yield 230 mg, mp 158.0—159.0 °C. Several recrystallizations from ethanol gave a pure sample, mp 158.5—159.0 °C. IR: 3399, 3490 (NH_2), 2193 (C≡N), 1645, and 1621 (C=C). UV: 271 (4.20) and 358 (4.06). NMR: 1.61 (s, 3H), 2.94 (ABX, 2H, J_{AB}=17 Hz, J_{AX}=1.8 Hz, $\Delta\nu_{AB}$= 14.4 Hz), 4.51 (s, 2H), 6.02 (d, 1H, J_{AX}=1.8 Hz), and 7.30 (m, 10H). Found: C, 83.95; H, 6.53; N, 9.95%. Calcd for $C_{20}H_{18}N_2$: C, 83.88; H, 6.34; N, 9.78%.

b) IVb: Yield 800 mg, mp 171.5—174.5 °C. Several recrystallizations from ethanol gave a pure sample, mp 174.0—175.0 °C. IR: 3490, 3399 (NH_2), 2190 (C≡N), 1642, and 1620 (C=C). UV: 275 (4.20) and 358 (4.05). NMR: 1.62 (s, 3H), 2.25 (s, 3H), 2.32 (s, 3H), 2.92 (ABX, 2H, J_{AB}=17 Hz, J_{AX}=1.8 Hz, $\Delta\nu_{AB}$=14.4 Hz), 4.44 (s, 2H), 6.02 (d, 1H, J_{AX}=1.8 Hz), and 7.00—7.40 (m, 8H). Found: C, 84.20; H, 7.24; N, 8.95%. Calcd for $C_{22}H_{22}N_2$: C, 84.04; H, 7.05; N, 8.91%.

Hydrogen Peroxide Oxidation of IIa. To a mixture of 1 g (2.33 mmol) of IIa, 25 ml of 30% hydrogen peroxide and 35 ml of acetone was added 3 ml of 10% aqueous sodium carbonate at room temperature over a period of 20 min. The mixture was heated in a water bath for 3 min and then left to stand for two days. The excess of hydrogen peroxide was decomposed by the addition of aqueous sodium thiosulfate. The reaction mixture was evaporated under reduced pressure, and then cooled with ice-water. The resulting white crystals were recrystallized several times from 50% aqueous ethanol to give a pure sample, mp 157.5—158.0 °C, yield 300 mg. IR: 3425 (=NH), 2227 (C≡N), 1751, and 1718 (C=O). UV: 266 (4.13). NMR: 0.72 (t, 3H, J=7 Hz), 1.31 (t, 3H, J=7 Hz), 1.70 (s, 3H), 2.59 (ABq, 2H, J=15 Hz, $\nu_0\delta$=21.3 Hz), 3.75 (q, 2H, J=7 Hz), 4.22 (q, 2H, J=7 Hz), 6.47 (m, 1H), and 7.07—7.44 (m, 10H). Found: C, 70.07; H, 5.89; N, 6.37%. Calcd for $C_{26}H_{26}O_5N_2$: C, 69.94; H, 5.87; N, 6.27%.

The authors are indebted to Professors Takeo Sakan and Toshio Miwa of Osaka City University, for fruitful discussions.

References

1) E. R. Alexander, J. D. McCollum, and D. E. Paul, *J. Amer. Chem. Soc.*, **72**, 4791 (1950).

2) Ester I used here is a mixture of *Z*- and *E*-isomers; T. Hayashi, *J. Org. Chem.*, **31**, 3253 (1966).

3) The absorption maxima of 3-phenyl-2-cyclohexenone are 222 (log ε=4.21) and 283 nm (log ε=4.28); H. O. House and R. L. Wasson, *J. Amer. Chem. Soc.*, **79**, 1488 (1957).

4) The absorption maximum of 4-(*p*-tolyl)-3-buten-2-one is 296 nm (log ε=4.40); P. Grammaticakis and J. Chauvelier, *C. R. Acad. Sci., Paris*, **242**, 1189 (1956).

5) S. M. McElvain and D. H. Clemens, "Organic Syntheses," Coll. Vol. IV, p. 463 (1963).

6) (a) A. C. Cope, C. M. Hofman, C. Wyckoff, and E. Hardenburgh, *J. Amer. Chem. Soc.*, **63**, 3452 (1941). (b) E. J. Cragoe, C. M. Robb, and J. M. Sprague, *J. Org. Chem.*, **15**, 381 (1950). (c) R. P. Gandhi, O. P. Vig, and S. M. Mukherji, *Tetrahedron*, **7**, 236 (1959).

Anomeric Effect Involving Carboxyl and Ethynyl Group in Sulfur-Containing Heterocycles

Kazutaka ARAI, Hiizu IWAMURA, and Michinori ŌKI

Department of Chemistry, Faculty of Science, The University of Tokyo, Tokyo 113

(Received June 24, 1975)

Normal anomeric effect is found in 1,3-dithiane-2-carboxylic acid, 1,3,5-trithiane-2-carboxylic acid, and their esters, in contrast to a report that oxane-2-carboxylic acid derivatives exhibit reverse anomeric effect. The results are interpreted from the difference in bond lengths between oxanes and polythianes which affects the extent of 1,3-diaxial interaction. The anomeric effect is found to be larger in 1,3-dithianes than in 1,3,5-trithianes. The differences is discussed on the ground of the energy levels of available electrons. Phenylethynyl derivatives also show small but definite anomeric effect.

During the course of other study, we needed a pair of 2,4,5-trimethyl-1,3,5-trithiane-2-carboxylic acids. Since the electrophilic reaction of 1,3,5-trithianide or 1,3-dithianide anion is known to proceed from the equatorial side,[1,2] it is no wonder to obtain 2,*c*-4,*c*-6-trimethyl-1,3,5-trithiane-*r*-2-carboxylic acid (**1e**) on treatment of 1,3,5-trithianide anion with carbon dioxide. We then tried to equilibrate **1e** with 2,*t*-4,*t*-6-trimethyl-1,3,5-trithiane-*r*-2-carboxylic acid (**1a**) with the aid of an acidic catalyst. The result was, however, almost a complete conversion to **1a**.

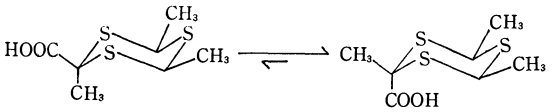

1e **1a**

The result indicates that the carboxyl-axial form is more stable than the carboxyl-equatorial form by *ca.* 2 kcal/mol or more and aroused our interest for the following reasons. The equilibration results may be explained by the stabilization of isomers governed by the anomeric effect,[3] since the carboxyl group is electronegative and provides a low-lying lowest unoccupied molecular orbital (LUMO). The anomeric effect in trithiane is known to be strong.[4] Contrary to these considerations, however, methyl oxanecarboxylate derivatives were found to be more stable in the methoxycarbonyl-equatorial conformation[5] and the phenomenon is referred to as reverse anomeric effect.

This sharp contrast of the trithiane case to the case of oxanes stimulated the further study on the reverse and/or normal anomeric effect and a series of studies of the polythiane cases have been undertaken. This paper is to describe the results of such studies, which conclude the presence of anomeric effect in the carboxypolythianes.

Syntheses and Structural Assignment

The monocarboxylic acids were prepared by carbonation of the corresponding lithio derivatives. Esters of the acids were prepared by the action of diazomethane on the free acids. Action of thionyl chloride to form acid chloride gave satisfactory results with the stable carboxylic acids but caused isomerization when applied to the less stable ones.

Phenylethynyl derivatives were prepared from chloropolythianes and phenylethynylmagnesium bromide.

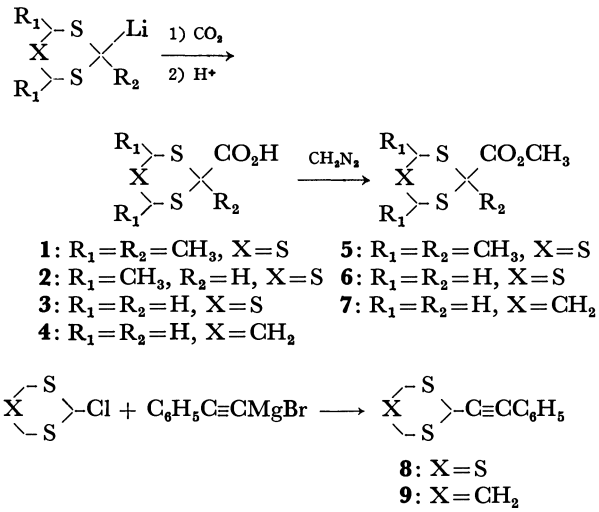

1: $R_1=R_2=CH_3$, X=S **5**: $R_1=R_2=CH_3$, X=S
2: $R_1=CH_3$, $R_2=H$, X=S **6**: $R_1=R_2=H$, X=S
3: $R_1=R_2=H$, X=S **7**: $R_1=R_2=H$, X=CH_2
4: $R_1=R_2=H$, X=CH_2

8: X=S
9: X=CH_2

When a compound in question carries an α-proton to the carboxyl or methoxycarbonyl group, the structural assignment is straightforward. The proton gives a singlet signal and the paramagnetic shift is observed for the axial proton owing to the anisotropy of the C–S bonds.[6] Therefore the carboxyl-axial form gives a singlet signal at a higher field than the counterpart. In addition, the axial isomer gives a broad signal for the equatorial proton due to the presence of W-type long range coupling.[7] The difference in chemical shifts of methylene protons is also a clue for diagnosis of the conformation of 2-substituted 1,3,5-trithianes. The substituent-axial conformation gives larger difference in chemical shifts than the counterpart because of the anisotropy effect of the substituent.[4]

Those which possess a methyl group in α-position may be assigned in a similar manner. However, ambiguity may arise because of the long averaged distance of the methyl protons from the C–S bonds. Firm evidence for the configurations of **5a** and **5e** was obtained by measurement of the nuclear Overhauser effect. On irradiation of the methyl protons in position 2 of compound **5e**, the absorption intensity of the methine protons in positions 4 and 6 increased by 16%. In contrast, the same operation for the isomer **5a** caused no measurable enhancement. The results unambiguously show that 4- and 6-H's and 2-methyl are located closely in compound **5e** and consequently compound **5e** has the structure as shown.

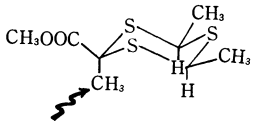

5e

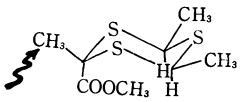

5a

Results and Discussion

Equilibration of Polymethyltrithianecarboxylic Acids. Equilibration was carried out by using boron trifluoride etherate as a catalyst in various solvents and the results are summarized in Table 1.

Table 1. Conformational equilibrium data of polymethylpolythianecarboxylic acids and their derivatives at 23 °C

System	Solvent	ε	K	$\Delta G°$ (kcal/mol)
1a⇄**1e**	CCl_4	2.2	<0.02	>2.3
	CH_3CN	37.5	<0.02	>2.3
5a⇄**5e**	CCl_4	2.2	<0.005	>3.2
	$ClCH_2CH_2Cl$	10.7	<0.005	>3.2
	CH_3CN	37.5	~0.01	~2.7
2a⇄**2e**	CH_3CN	37.5	0.4	0.24

The results indicate that the axial form **1a** is one-sidedly more stable than the equatorial isomer **1e** in various solvents. The solvent effect on population is hardly seen because of the strong stabilization of the axial isomer: it is only acetonitrile that enabled us to measure the population of the less stable form of the ester and to calculate the difference in free energies at 23 °C which was obtained as 2.7 kcal/mol. In a series of cyclohexane derivatives, A values for methyl and methoxycarbonyl groups are known to be 1.7 and 1.2 kcal/mol, respectively.[8,9] Therefore the difference in conformational energies between cyclohexane analogs of **1a** and **1e** may amount to 0.5 kcal/mol: if we assume the same steric conditions in polythianes, the methyl-equatorial form is favored over the methyl-axial form and the ratio may be 1/3—1/2 with the former predominating. Since the ratio in reality is large in favor of the methyl-equatorial form, there must be reasons which stabilize that form and/or destabilize the other form. Anomeric effect can be present in these compounds because the carboxyl group has a low-lying LUMO. If the above-cited solvent effect is taken to be significant, it also supports the presence of anomeric effect because the magnitude of stabilization by the anomeric effect is suppressed in polar solvents.[3]

The equilibration of 4,6-dimethyl-1,3,5-trithiane-2-carboxylic acid (**2**) should provide data which are only affected by the conformational energy of the carboxyl group. As is seen in Table 1, $\Delta G°$ value becomes smaller because of the erasure of the effect of the methyl group, but the axial form (**2a**) is still favored in acetonitrile. Unfortunately, equilibration in other solvents failed because of extensive deterioration of the substrate.

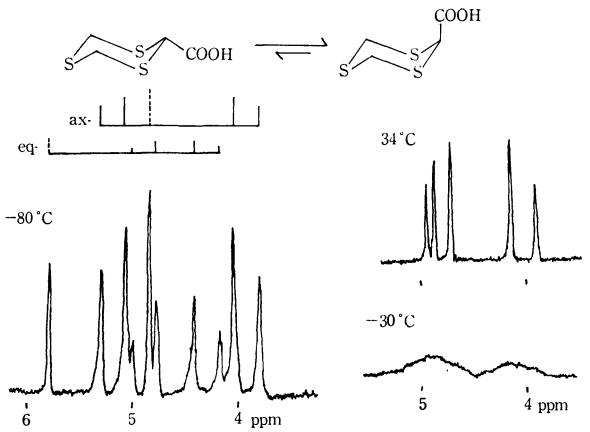

Fig. 1. ^1H NMR spectra of **3** in acetone-d_6 at three temperatures.

Low Temperature NMR Study of Polythianecarboxylic Acids. The difficulty seen in equilibration allured us to investigate the flexible polythianecarboxylic acids at low temperature. 1,3,5-Trithiane-2-carboxylic acid (**3**) and its methyl ester (**6**) showed only averaged signals at room temperature. The signal, however, broadened considerably at −40——50 °C,[10] and split into two sets of 2-H and 4,6-H's at −80 °C (Fig. 1). The results are shown in Table 2. It is interesting to note that the

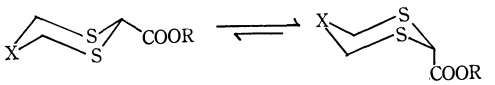

3e **3a** R=H, X=S
4e **4a** R=H, X=CH_2
6e **6a** R=CH_3, X=S
7e **7a** R=CH_3, X=CH_2

Table 2. Data concerned with conformational equilibria of polythianecarboxylic acids and their derivatives at −80 °C

Compound	Solvent	Chemical shift of 2-H (δ) e-Form	Chemical shift of 2-H (δ) a-Form	a-Form/e-Form	$\Delta G°$ (kcal/mol)	A-Value
3	CD_3COCD_3	5.75	4.82	1.5	0.15	1.43
	CD_3COCD_3–$CDCl_3$ (3:1)	5.71	4.69	2.35	0.31	
4	CD_3COCD_3	5.42	4.48	5.5	0.66	
6	CD_3COCD_3	5.75	4.88	3.0	0.43	1.22
	CD_3COCD_3–$CDCl_3$ (3:1)	5.70	4.87	5.0	0.54	
7	CD_3COCD_3	5.44	4.53	8.5	0.83	
	CD_3COCD_3–$CDCl_3$ (3:1)	5.20	4.34	9.5	0.87	
	CS_2–$CDCl_3$ (1:1)	5.02	4.10	20	1.15	

difference in chemical shifts of the axial and equatorial protons in 2-position is almost constant at 0.9 ppm in these compounds.

One can clearly see, from the data in Table 2, that the axial form is preferred in every case. The results are contrary to the case of 2,4,6-trimethyl-1,3,5-trithianes[11] in which the *cis* form is more stable because it has no axial methyl group. Anomeric effect is a probable cause again for the presence of the axial form. Solvent effects on the populations of the axial and the equatorial forms are in agreement with the anomeric effect: the less polar is the solvent, the more is the axial form preferred. We may now conclude that the anomeric effect is seen in polythianecarboxylic acids.

The magnitude of anomeric effect may be expressed by the following equation.[3]

$$\Delta\Delta G^\circ = (\Delta G^\circ_{\text{substituent}})_{\text{hetero ring}} - (\Delta G^\circ_{\text{substituent}})_{\text{cyclohexane}}$$

Comparison of the results reveals that the magnitude of the anomeric effect is larger in 1,3-dithiane than in 1,3,5-trithiane.

The results seem to be explained by the delocalization of electrons. The UV spectra of 1,3-dithiane and 1,3,5-trithiane[12] indicate that the lone pair electrons in the latter are more delocalized than those in the former. Sweigart and Turner reported the results of photoelectron spectroscopy which reveal that the ionization potential of lone pair electrons in 1,3,5-trithiane is higher than those in 1,3-dithiane.[13] Thus transfer of lone pair electrons on sulfur to the antibonding orbital involving the axial substituent, as discussed by Hoffmann *et al.*,[14] must be smaller in its extent in trithianes (**10**) than in dithianes (**11**). By taking advantage of the above discussion, we may understand the weaker anomeric effect and consequently less population of the substituent-axial isomer of 1,3,5-trithiane derivatives than those of the 1,3-dithianes.

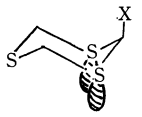

10

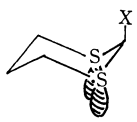

11

The anomeric effect is larger with the free carboxylic acids than the corresponding esters, both in trithiane series and in dithiane series. It is also known that the methoxycarbonyl group gives less preference in free energy than the carboxyl group in cyclohexane series, although the equatorial form is favored in this case.[9] The differences are almost constant at 0.2 kcal/mol. These results suggest that the difference is not of the electronic or electric origin but of the steric origin. Since the carboxyl group shows less preference of the axial form than the corresponding esters in polythianes, the latter may be taken as giving less steric effect. This is reasonable because the acid dimerizes under the conditions of the NMR measurement. Negligence of the electronic-electic effect will not give an important defect, since Hammett σ_m values of the carboxyl and methoxycarbonyl groups are 0.36 and 0.32, respectively.[15]

Comparison of the above results with those of oxane series is worthy of note. Methyl 5-*t*-butyloxane-2-carboxylate (**12**) was equilibrated with a base catalyst to show that the methoxycarbonyl-equatorial form (**12e**) is predominant in the equilibrium mixture. The phenomenon has been referred to as reverse anomeric effect.

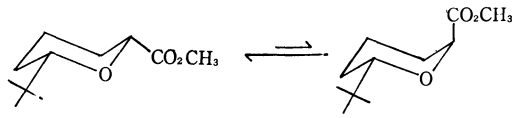

12e **12a**

However, owing to the short distance of the C–O bond in oxanes, the 1,3-*syn*-diaxial interaction must be more severe in oxane series.[5] This disfavors the axial conformation. In trithianes and dithianes, the C–S bond is much longer than the C–O and the 1,3-diaxial interaction is surpressed to a great extent. Normal anomeric effect thus becomes detectable as conformational equilibrium constants.

Eliel *et al.* prepared ethyl 2,4-dimethyl-1,3-dioxane-2-carboxylate (**13**) under the conditions of thermodynamic control and found that the ethoxycarbonyl-axial conformation (**13a**) is disfavored in less polar solvents. The results are in line with the reverse anomeric effect,

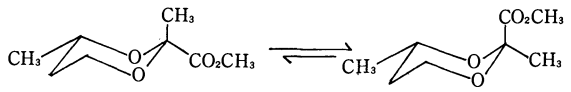

13e **13a**

but the system may be too complicated to interprete in a straightforward manner, as suggested by the authors.[16]

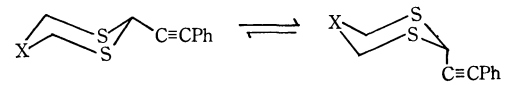

8e **8a** X=S
9e **9a** X=CH_2

Finding the presence of anomeric effect in polythianecarboxylic acids, we were allured to investigate the case of phenylethynylpolythianes. The results are shown in Table 3.

Table 3. Data concerned with conformational equilibria of 2-phenylethynylpolythianes at −80 °C

Compd.	Solvent	Chemical Shift of 2-H (δ) e-Form	Chemical Shift of 2-H (δ) a-Form	a-Form / e-Form	ΔG° (kcal/mol)
8	CD_3COCD_3	6.00	5.68	1.18	0.07
	CS_2–$CDCl_3$ (1:1)	5.21	4.96	3.3	0.46
9	CD_3COCD_3	5.62	5.21	1.57	0.18
	CS_2–$CDCl_3$ (1:1)	5.16	4.73	3.1	0.44

The data suggest the presence of small but distinct anomeric effect in the phenylethynyl compounds: the axial forms (**8a** and **9a**) are preferred over the equatorial forms (**8e** and **9e**) in the solvents examined and the preference becomes less in more polar solvents. The 2-phenylethynyl group, providing a low-lying LUMO,

seems to be effective in accepting the electrons from the sulfur atoms in 1 and 3 positions.

Experimental

^1H NMR Measurement. The ^1H NMR spectra were recorded on a Hitachi R 20B spectrometer (60 MHz) equipped with a temperature variation accessory. Temperature was read by the difference in chemical shifts between protons of methanol.

Preparation of Carboxylic Acids and Their Esters. A general procedure of preparation of carboxylic acids will be described by taking the case of 1,3-dithiane-2-carboxylic acid (**4**) as an example. To a solution of 2.0 g (16.7 mmol) of 1,3-dithiane in 100 ml of tetrahydrofuran was added 18.5 mmol of butyllithium in 30 ml of ether at −20 °C and the mixture was stirred for 1 h at that temperature under a nitrogen atmosphere. Dried carbon dioxide was introduced into the solution for 3 h, during which time the temperature was allowed to rise to 0 °C, and the mixture was left to stand overnight. The solvent was evaporated and the residue was shaken with a mixture of dilute aqueous sodium hydroxide and ether. The aqueous layer was separated, acidified with hydrochloric acid, and extracted with ether. The ethereal solution was dried over magnesium sulfate and evaporated. 1,3-Dithiane-2-carboxylic acid (**4**), mp 112—113.5 °C, was obtained in 1.8 g (66%) yield. Found: C, 36.48; H, 4.69; S, 39.11%. Calcd for $C_5H_8O_2S_2$: C, 36.57; H, 4.91; S, 39.04%. IR: 1685—1690 cm^{-1} ($\nu_{C=O}$). ^1H NMR: (δ, $CDCl_3$): 2.1 (m, 2H), 2.4—3.7 (m, 4H), 4.17 (s, 1H), *ca.* 9 (s, 1H).

The methyl ester (**7**) was prepared almost quantitatively by treatment of the acid with diazomethane in ether. It was purified by chromatography on silica gel with benzene, oil (mp between 20 and 30 °C). Found: C, 40.53; H, 5.59; S, 35.81%. Calcd for $C_6H_{10}O_2S_2$: C, 40.43; H, 5.65; S, 35.97%. IR: 1730 cm^{-1} ($\nu_{C=O}$). ^1H NMR (δ, $CDCl_3$): 3.77 (s, 3H), 2.10 (m, 2H), 2.4—2.8 (m, 2H), 3.2—3.65 (m, 2H), 4.20 (s, 1H).

It could also be prepared by treating the corresponding acid with thionyl chloride in carbon tetrachloride–chloroform (9: 1) at reflux temperature for 5 to 7 h followed by treatment with methanol.

*1,3,5-Trithiane-2-carboxylic acid (**3**)*, mp 273 °C (decomp.), was prepared similarly from 1,3,5-trithiane. Found: C, 26.65; H, 3.35; S, 52.57%. Calcd for $C_4H_6O_2S_3$: C, 26.37; H, 3.32; S, 52.77%. IR: 1690 cm^{-1} ($\nu_{C=O}$). ^1H NMR (δ, acetone-d_6): 4.02 and 4.77 (q, J=14.5 Hz, 4H), 4.83 (s, 1H).

The methyl ester (**6**) melted at 96—97 °C. Found: C, 30.83; H, 4.34; S, 49.22%. Calcd for $C_5H_8O_2S_3$: C, 30.59; H, 4.11; S, 49.00%. IR: 1715 cm^{-1} ($\nu_{C=O}$). ^1H NMR (δ, CCl_4): 3.78 (s, 3H), 3.46 and 5.06 (q, J=15 Hz, 4H), 4.22 (s, 1H).

Treatment of *cis*-2,4,6-trimethyl-1,3,5-trithiane with butyllithium followed by carbonation gave 2,*c*-4,*c*-5-trimethyl-1,3,5-trithiane-*r*-2-carboxylic acid (**1e**), mp 137—138.5 °C, as a sole product. Found: C, 37.72; H, 5.14; S, 42.77%. Calcd for $C_7H_{12}O_2S_3$: C, 37.48; H, 5.39; S, 42.87%. IR: 1703 cm^{-1} ($\nu_{C=O}$). ^1H NMR (δ, $CDCl_3$): 1.59 (d, 6H), 2.07 (s, 3H), 4.39 (q, 2H), *ca.* 9 (s, 1H).

The methyl ester (**5e**) melted at 53—54 °C. Found: C, 40.25; H, 5.72; S, 40.35%. Calcd for $C_8H_{14}O_2S_3$: C, 40.31; H, 5.92; S, 40.35%. IR: 1737 cm^{-1} ($\nu_{C=O}$). ^1H NMR (δ, CCl_4): 1.54 (d, 6H), 1.95 (s, 3H), 3.82 (s, 3H), 4.29 (q, 2H).

Treatment of *cis*-2,4-dimethyl-1,3,5-trithiane with butyllithium followed by carbonation afforded *c*-4, *c*-6-dimethyl-1,3,5-trithiane-*r*-2-carboxylic acid (**2e**), mp 165—166 °C (decomp.), as a sole product. Found: C, 34.35; H, 5.03; S, 45.51%. Calcd for $C_6H_{10}O_2S_3$: C, 34.26; H, 4.79; S, 45.73%. IR: 1695 cm^{-1} ($\nu_{C=O}$). ^1H NMR (δ, acetone-d_6): 1.53 (d, 6H), 5.26 (s, 1H). The carboxyl proton was obscured because of the presence of water in the solvent.

*t-4,t-6-Dimethyl-1,3,5-trithiane-r-2-carboxylic Acid (**2a**).* *c*-4,*c*-6-Dimethyl-1,3,5-trithiane-*r*-2-carboxylic acid (**2e**) (0.2 g) was dissolved in 5 ml of dry acetonitrile and heated at 80 °C with 0.1 ml of boron trifluoride etherate for 3 h. The solvent was evaporated and the residue was shaken with a mixture of 20 ml of ether and 10 ml of 1 M hydrochloric acid. Evaporation of the ether layer afforded a mixture of *ca.* 3: 2 **2a** and **2e** which was extracted with carbon tetrachloride. Concentration of the carbon tetrachloride solution followed by standing afforded *ca.* 0.05 g (25%) of **2a**, mp 114—115 °C. Found: C, 33.99; H, 4.76%. Calcd for $C_6H_{10}O_2S_3$: C, 34.26; H, 4.79%. IR: 1685 cm^{-1} ($\nu_{C=O}$). ^1H NMR (δ, CCl_4): 1.50 (d, 6H), 4.76 (q, 2H), 4.58 (s, 1H), *ca.* 11.5 (s, 1H).

*2,c-4,c-6-Trimethyl-1,3,5-trithiane-r-2-carboxylic Acid (**1a**)*, mp 135.0—135.5 °C, was similarly prepared by heating 2.0 g of **1e** with 10 ml of boron trifluoride etherate at 60 °C in 75% yield. Found: C, 37.32; H, 5.12; S, 42.44%. Calcd for $C_7H_{12}O_2S_3$: C, 37.48; H, 5.39; S, 42.87%. IR: 1690 cm^{-1} ($\nu_{C=O}$). ^1H NMR (δ, $CDCl_3$): 1.55 (d, 6H), 1.78 (s, 3H), 4.69 (q, 2H), *ca.* 10 (s, 1H).

The methyl ester (**5a**) melted at 33.5—34.5 °C. Found: C, 40.52; H, 5.84; S, 40.41%. Calcd for $C_8H_{14}O_2S_3$: C, 40.31; H, 5.92; S, 40.35%. IR: 1728 cm^{-1} ($\nu_{C=O}$). ^1H NMR (δ, CCl_4): 1.51 (d, 6H), 1.70 (s, 3H), 3.70 (s, 3H), 4.66 (q, 2H).

Equilibration. Either of the equatorial or the axial form of the substrate (0.2 g) was dissolved in 2 ml of an appropriate solvent, mixed with 0.031 ml (*ca.* 1/3 equivalent) of boron trifluoride etherate, and allowed to stand at 23±2 °C. The progress of equilibration was followed by ^1H NMR spectra. It took *ca.* 60 days for equilibration of **1** in acetonitrile which required the longest time among the solvents used.

The analyses of the products were performed with integration of the ^1H NMR signals and the error is estimated to be ±2%. The esters were analyzed with vapor phase chromatography and the results are believed to be accurate within the error of ±0.5%.

*2-Phenylethynyl-1,3-dithiane (**9**).* To a solution of 2.2 g (18.5 mmol) of 1,3-dithiane in 20 ml of sodium-dried benzene was added 2.7 g (20.3 mmol) of *N*-chlorosuccinimide during a 15 min period at 20 °C under a nitrogen atmosphere. The mixture was stirred for 15 min under the same conditions and filtered. To this solution was added phenylethynylmagnesium bromide in ether which was prepared from 2.55 g (25 mmol) of phenylacetylene and isopropylmagnesium bromide (from 3.25 g of isopropyl bromide, 0.7 g of magnesium and 50 ml of ether) at 35 °C. The mixture was stirred for 2 h at room temperature and treated with dilute hydrochloric acid. Extraction of the mixture with chloroform afforded 2.6 g of crude 2-phenylethynyl-1,3-dithiane, which was purified by chromatography on silica gel. Elution with benzene–hexane (8: 2) gave a pure compound, mp 54—55.5 °C in 35% yield. Found: C, 65.40; H, 5.54%. Calcd for $C_{12}H_{12}S_2$: C, 65.41; H, 5.49%. IR: 2220 cm^{-1} ($\nu_{C\equiv C}$). ^1H NMR (δ, CCl_4): 1.8—2.3 (m, 2H), 2.5—3.5 (m, 4H), 4.63 (s, 1H), 7.3 (m, 5H).

*2-Phenylethynyl-1,3,5-trithiane (**8**)*, mp 66—67 °C, was similarly prepared from 1,3,5-trithiane. Found: C, 55.17; H, 4.03; S, 40.19%. Calcd for $C_{11}H_{10}S_3$: C, 55.42; H, 4.23; S, 40.35%. IR: 2205 cm^{-1} ($\nu_{C\equiv C}$). ^1H NMR (δ, $CDCl_3$): 3.91 and 4.83 (q, J=14.5Hz, 4H), 5.04 (s, 1H), 7.39 (m, 5H).

References

1) M. Fukunaga, K. Arai, H. Iwamura, and M. Ōki, This Bulletin, **45**, 302 (1972).
2) A. A. Hartmann and E. L. Eliel, *J. Amer. Chem. Soc.*, **93**, 2572 (1971).
3) E. L. Eliel and C. A. Giza, *J. Org. Chem.*, **33**, 3745 (1968) and references therein.
4) M. Ōki, T. Sugawara, and H. Iwamura, This Bulletin, **47**, 2457 (1974).
5) C. B. Anderson and D. T. Sepp, *J. Org. Chem.*, **33**, 3272 (1968).
6) E. Campaign, N. F. Chamberlain, and B. E. Edwards, *ibid.*, **27**, 135 (1962).
7) J. M. Jackmann and S. Sternhell, "Applications of Nuclear Magnetic Resonance Spectroscopy in Organic Chemistry," 2nd Ed., Pergamon Press, London (1969), p. 334.
8) E. L. Eliel, N. Allinger, S. J. Angyal, and G. A. Morrison, "Conformational Analysis," Interscience Publishers, New York (1965), pp. 439—441.
9) E. L. Eliel and M. C. Reese, *J. Amer. Chem. Soc.*, **90**, 1560 (1968).
10) This means that the inversion-barriers of these 1,3,5-trithianes are about 11 kcal/mol, which is the standard value for the exchange between two chair forms.
11) M. Fukunaga, Ph. D. thesis, The University of Tokyo (1971).
12) J. Barrett and M. J. Hitch, *Spectrochim. Acta*, **25A**, 407 (1969); L. K. Dyall and S. Winstein, *ibid.*, **27A**, 1619 (1971).
13) A. Sweigart and D. W. Turner, *J. Amer. Chem. Soc.*, **94**, 5599 (1972).
14) S. David, O. Eisenstein, W. H. Hehre, L. Salem, and R. Hoffmann, *ibid.*, **95**, 3806 (1973).
15) H. H. Jaffé, *Chem. Revs.*, **53**, 191 (1953).
16) W. F. Bailey and E. L. Eliel, *J. Amer. Chem. Soc.*, **96**, 1798 (1974).

The Substituent Effect. VI. Inductive and π-Electronic Effects in the Phenol Hydroxyl Chemical Shifts in DMSO

Yuho Tsuno,[1] Mizue Fujio, and Yasuhide Yukawa*

Department of Chemistry, Faculty of Science, Kyushu University, Hakozaki, Fukuoka 812
**Institute of Scientific and Industrial Research, Osaka University, Yamada-kami, Osaka 565*

(Received December 10, 1974)

Substituent effects on the NMR chemical shifts of the hydroxyl proton of *m*- and *p*-substituted phenols in DMSO have been studied by means of the LSFE equation. The effect of substituents was found to be considerably modified in the DMSO solution as compared with that in aqueous solution through strong substituent-solvent interactions. The LSFE equation was applied to the apparent substituent effects of such solvent-modified systems, and the practical set of parameters for the inductive and the π-electronic effects of the DMSO-modified substituents were estimated. The treatment was successful for $+R$ substituents but not for $-R$ substituents. This may be attributed to the much stronger solvent-substituent interactions. Characteristic features of LSFE treatment were discussed in comparison with Taft and Swain-Lupton treatments. It is suggested that the dual resonance reaction constants for $+R$ and $-R$ *para* substituents are required for Taft-type correlations.

Substituent effects on chemical and physical properties in a number of benzene derivatives have been treated by the following *Linear Aromatic Substituent Reactivity* (LArSR) *Relationship*:[2]

$$\log (k/k_0) \text{ or } P-P_0 = \rho\bar{\sigma} = \rho(\sigma^0+r^+\Delta\bar{\sigma}_R^+ + r^-\Delta\bar{\sigma}_R^-) \quad (1)$$

where $\Delta\bar{\sigma}_R^+$ and $\Delta\bar{\sigma}_R^-$ are the resonance substituent constants describing the capability of π-electron delocalization of conjugatively electron releasing ($-R$) and electron attracting ($+R$) *para* substituents, respectively. r^+ or r^- is the resonance reaction constant characteristic of given reaction giving a measure of the resonance exaltation. This equation gives a purely empirical description of the substituent effect on reactivities of substituted benzene derivatives in terms of the unexalted polar effect of substituted phenyl groups and aryl resonance exaltation effect. From the success of the treatment and particularly from the generality of the resonance parameters $\Delta\bar{\sigma}_R^+$ and $\Delta\bar{\sigma}_R^-$ for various types of reactions, we have extended Eq. (1) to an alternative theoretically simple expression, the *Linear Substituent Free Energy* (LSFE) *Relationship*:

$$\log (k/k_0)_p = \rho\bar{\sigma}_p = \rho(\sigma_i + q_r^+\sigma_\pi^+ + q_r^-\sigma_\pi^-) \quad (2)$$

$$\log (k/k_0)_m = \rho\bar{\sigma}_m = \rho(1.17\sigma_i + 0.50\sigma_\pi^\pm) \quad (2')$$

where the substituent effect is given as a first approximation by the combination of inductive and resonance effects of given substituents.[3] σ_i is the inductive substituent constant, which remains constant for a given substituent independent of its variable resonance contribution. σ_π^+ and σ_π^- are the parameters for the capabilities of $-R$ and $+R$ classes of substituents respectively to donate or withdraw electron through π-electronic delocalization, being constants characteristic only of substituents and not dependent upon the nature of reactivities, systems, and perhaps, detection variables. q_r^+ and q_r^- are the characteristic variables of a given reaction or system, indicating the degree of π-electronic interaction of $+R$ and $-R$ groups with detection center. Both q_r^+ and q_r^- are standardized by definition to be unity in the σ_p^0 scale; *i.e.*, $\sigma_p^0 = 1.00\,\sigma_i + 1.00\,\sigma_\pi^\pm$. σ_π^+ corresponds numerically to 0.42 $\Delta\bar{\sigma}_R^+$ and σ_π^- to 0.73 $\Delta\bar{\sigma}_R^-$.[4] The σ_i values are proportional to the relative inductive strength of substituents in the saturated system, and correspond to 0.74 σ'.

The applicability of Eqs. (1) and (2) to conjugatively electron attracting ($+R$) substituents in the nucleophilic exalted-resonance reactions has not yet been examined sufficiently, due to the lack of data on $+R$ substituents. In this series of studies, we have thus dealt with the effect of conjugatively electron attracting substituents, especially in various types of nucleophilic reactions, in order to ascertain the applicability and limitation of our treatment of the substituent effects in the benzene system.[4,5]

We reported a complete set of NMR chemical shift data of the hydrogen-bonding hydroxyl proton of *m*- and *p*-substituted phenols in DMSO,[5] and demonstrated a satisfactory fit of the substituent chemical shifts to Eq. (1), giving a ρ value of 1.53 and r^- 0.67. The apparent substituent constant for particular substituents differs significantly from the standard one. However, the effects remained essentially the same in the related series of the hydroxyl chemical shifts of 4-substituted 2- and 3-cresols and 2,6-xylenols in DMSO, as evidenced by excellent linear $\Delta\delta$—$\Delta\delta$ plots.

We have treated these series of chemical shift data in terms of Eq. (2), and attempted to estimate a practically useful set of the π-electronic and inductive substituent parameters, $(\sigma_\pi)_{DMSO}$ and $(\sigma_i)_{DMSO}$, for the DMSO-modified substituent groups. The present paper includes a comparison of the results with those of similar treatments based on Taft[6] and Swain-Lupton Equations.[7]

Results and Discussion

Table 1 gives the apparent substituent constants derived from the NMR chemical shifts of the hydroxyl proton of phenols in DMSO.[5] The constants obtained from 4-substituted phenols were identical with those derived from the corresponding 2- and 3-cresols[8] and 2,6-xylenols using appropriate ρ values.

According to Eq. (1), enhancement of the apparent $\bar{\sigma}_p$ values from corresponding σ^0 values are proportional to the resonance parameters, $\Delta\bar{\sigma}_R^-$ or $\Delta\bar{\sigma}_R^+$. Figure 1 gives a plot of apparent enhancement $\bar{\sigma}_p - \sigma_p^0$ for conjugatively electron attracting ($+R$) substituents in *p*-substituted phenols against standard $\Delta\bar{\sigma}_R^-$. Most substi-

Table 1. Apparent substituent constants in DMSO

No.	Subst.	$\bar{\sigma}_p$	$\bar{\sigma}_m$
1	NO_2	1.121	0.722
2	CN	0.844	0.583
3	CHO	0.840	0.411
4	SO_2CH_3	0.825	0.596
5	$SOCH_3$	0.498	0.422
6	SO_2NH_2	0.613	
7	SCN	0.583	
8	$SMe_2{}^+I^-$	0.926	0.721
9	$NMe_3{}^+I^-$	0.547	0.601
10	COC_6H_5	0.735	0.356
11	$COCH_3$	0.655	0.297
12	$COOCH_3$	0.658	0.337
13	COOEt	0.647	0.318
14	$CONH_2$	0.410	0.184
15	CF_3	0.635	0.508
16	$CH{=}CHNO_2$	0.713	0.305
17	CH=CHCOOEt	0.449	0.201
18	$CH{=}NC_6H_5$	0.536	
19	$N{=}CHC_6H_5$	0.122	
20	$N{=}NC_6H_5$	0.652	
21	C_6H_5	0.151	
22	H	0.002	
23	I	0.238	0.288
24	Br	0.244	0.369
25	Cl	0.229	0.367
26	F	0.025	0.359
27	SCH_3	0.079	0.115
28	OC_6H_5	0.011	0.181
29	NHAc	−0.112	0.008
30	NHC_6H_5	−0.198	−0.085
31	*t*-Bu	−0.138	−0.088
32	Et	−0.149	
33	CH_3	−0.162	−0.071
34	OCH_3	−0.276	0.030
35	OH	−0.467	−0.113
36	NMe_2	−0.467	−0.210
37	NH_2	−0.643	−0.323
38	$(CH_3)_2$		−0.151
39	Cl_2		0.725

tuents fall near the correlation line, but certain carbonyl and sulfonyl derivatives deviate from it. The deviation is large for the $CONH_2$ and SO_2NH_2 groups; that of the latter in particular suggests an unlikely electron releasing resonance contribution of this group. The scattered pattern is similar to that observed in DMF solution.[4] These deviations may arise from solvent-modification of the electronic nature of substituents in the DMSO solution. Since the standard $\sigma_p{}^0$ is the parameter referable to the substituents modified with water, the quantities $\bar{\sigma}_p-\sigma_p{}^0$ should include certain extraneous effects due to the change of solvents from H_2O to DMSO. The deviations in the above correlation are not merely due to the solvent-modification of π-electronic interaction of substituents but include changes in the inductive nature of substituents caused by solvation. It appears necessary to deal with the solvent-modified substituent effects in terms of both inductive and π-electronic effects.

From Eqs. (2) and (2′), we can eliminate the inductive contribution by using the unique *para*/*meta* inductive

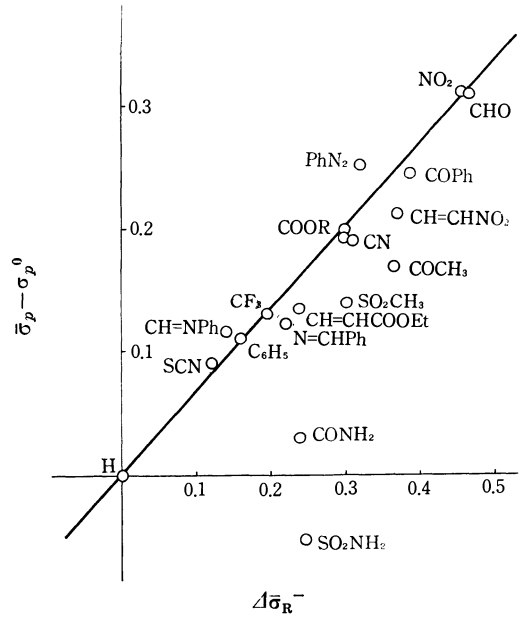

Fig. 1. Plot of the apparent resonance enhancements $\bar{\sigma}_p-\sigma_p{}^0$ against standard $\Delta\bar{\sigma}_R{}^-$ values for $+R$ substituents.

contribution ratio of 0.85 (=1/1.17) and obtain the following equation as the simplest linear resonance free energy relationship.

$$\log (k/k_0)_p - 0.85 \log (k/k_0)_m = \rho(\bar{\sigma}_p-0.85\bar{\sigma}_m) = \rho(q_r{}^{\pm}-0.425)\sigma_\pi{}^{\pm} \quad (3)$$

This relationship should also be valid for the solvent-modified substituent. $q_r{}^+$ is not generally identical with $q_r{}^-$ in nucleophilic or electrophilic resonance-exalted reactions. Accordingly, both $+R$ and $-R$ substituents can not be treated with a single q_r parameter. This paper deals with the effect of conjugatively electron attracting ($+R$ class) substituents, for which the results are successfully correlated.

The π-electronic effect of DMSO-modified +R substituents of interest can thus be given for the present system by the following equation since $\sigma_\pi{}^-=0.73\,\Delta\bar{\sigma}_R{}^-$ by definition.

$$(\Delta\delta_p-0.85\Delta\delta_m)/1.529 = C^-_{DMSO}(\sigma_\pi{}^-)_{DMSO} = 0.73C^-_{DMSO}(\Delta\bar{\sigma}_R{}^-)_{DMSO} \quad (4)$$

where C^-_{DMSO} is a coefficient giving the degree of effective resonance contributions from $+R$ substituents in the given system in DMSO and corresponds to $q_r{}^--0.425$ for the system. $(\sigma_\pi{}^-)_{DMSO}$ or $(\Delta\bar{\sigma}_R{}^-)_{DMSO}$ denotes the π-electronic (resonance) substituent parameters for the DMSO-modified $+R$ substituent. The correlation of the same type can be derived for $-R$ substituents, while the coefficient C^+_{DMSO} is not necessarily the same as the C^-_{DMSO} even in the same system.

The C^-_{DMSO} can be determined experimentally from the slope of the plots of $(\bar{\sigma}_p-0.85\bar{\sigma}_m)_{DMSO}$ against $(\Delta\bar{\sigma}_R{}^-)_{DMSO}$ or $(\bar{\sigma}_\pi{}^-)_{DMSO}$. We may utilize standard $\Delta\bar{\sigma}_R{}^-$ values for $(\Delta\bar{\sigma}_R{}^-)_{DMSO}$ since the effect of solvent modification is relatively small for most substituents. This process in turn can be used to determine a set of $(\Delta\bar{\sigma}_R{}^-)_{DMSO}$ and $(\sigma_\pi{}^-)_{DMSO}$. Figure 2 shows the plot for $+R$ substituents of the present phenol system against standard $\Delta\bar{\sigma}_R{}^-$,

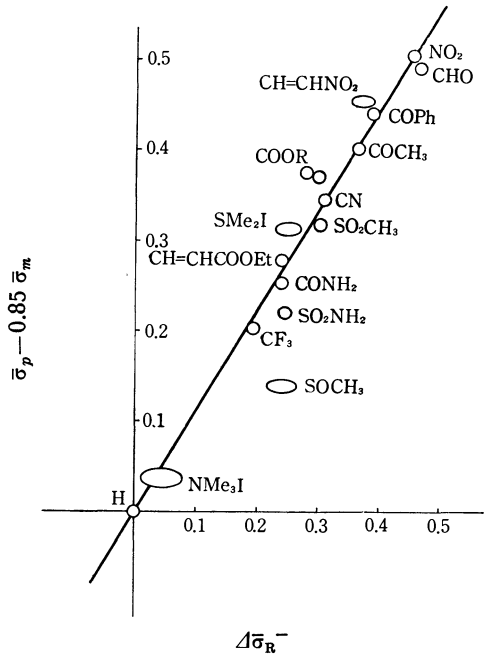

Fig. 2. Plot of the quantities $\bar{\sigma}_p-0.85\,\bar{\sigma}_m$ against standard $\Delta\bar{\sigma}_R^-$ values, for $+R$ substituents.

giving the slope of 1.12 with satisfactory linearity; correlation coefficient 0.987 and standard deviation ±0.028. A similar correlation has been obtained for the corresponding resonance quantities of the same series in DMF solution.[4] The modification of substituents with DMSO and DMF solvents is related more closely to each other than to those in aqueous solution, because of similarity in their aprotic and basic character. $(\Delta\bar{\sigma}_R^-)_{DMF}$ in fact give a much better correlation ($s=\pm0.010$ and $R=0.998$) than standard $\Delta\bar{\sigma}_R^-$. From the slope 1.12, $(\Delta\bar{\sigma}_R^-)_{DMSO}$ is obtained, and converted into $(\sigma_\pi^-)_{DMSO}$; *i.e.*, $(\sigma_\pi^-)_{DMSO}=0.818$ $(\bar{\sigma}_p-0.85\bar{\sigma}_m)$. The inductive substituent constants are given by

$$(\sigma_i)_{DMSO}=\bar{\sigma}_p-1.43(\Delta\bar{\sigma}_R^-)_{DMSO}.$$

$(\sigma_p^0)_{DMSO}$ can also be derived by combining $(\sigma_\pi^-)_{DMSO}$ and $(\sigma_i)_{DMSO}$. These sets of substituent constants are compared with corresponding standard parameters (Table 2).

Comparison of the DMSO-modified substituent parameters with standard σ^0 and σ^- parameters suggests that NO_2, CHO, CN, CF_3, COC_6H_5, and COOMe can be classified as well-behaving substituents even in the aprotic solvent since for these groups the effect of solvent-modification is negligible. Discrepancies are significant in $COCH_3$, $SOCH_3$, $CONH_2$, SO_2NH_2, Me_3N^+, and Me_2S^+ groups. In the first two loss of the hydrogen-bonding at the oxygen with aqueous solvents appears to be an important factor to lower the electron attracting power of these groups in aprotic DMSO.[4,5] For the amides the negative charge arising from the donating hydrogen-bonding to DMSO makes these groups less electron-attracting. The charged substituents are known to be highly sensitive to changes of solvents and reaction conditions, so that even the standard parameter values have not been definitely evaluated.[9] However, it is of interest to note that the Me_3N^+ group in the present system is effectively more electron attracting from *meta* than *para* position (Table 1). The trend $\bar{\sigma}_p<\bar{\sigma}_m$ is generally observed for this group as in the pK_a of benzoic acids and of phenols in various solvents.[10] According to Taft's assumption $\sigma_I^m=\sigma_I^p$, this group should be conjugatively electron releasing since $\bar{\sigma}_p-\bar{\sigma}_m<0$. In our treatment this group appears to be a weak $+R$ class or almost exclusively inductive class,[11] as indicated by the small positive value of $\bar{\sigma}_p-0.85\,\bar{\sigma}_m$. On the other hand, Me_2S^+ group is suggested from either treatment to be considerably strong $+R$ class substituent, not depending on solvent.

We see that the resonance parameters $(\Delta\bar{\sigma}_R^-)_{DMSO}$ as well as $(\sigma_\pi^-)_{DMSO}$ are generally in agreement with the standard values within uncertainty of average ±0.01 or so in σ unit except for $SOCH_3$ group (Table 2). The $(\sigma_i)_{DMSO}$ values are consistently less positive than the standard values for all substituents. The difference between the two values is significant for about a half of the entries, and particularly remarkable for SO_2NH_2 and $CONH_2$ and charged substituents Me_3N^+ and Me_2S^+. The substantial changes can be explained at least quali-

Table 2. DMSO-Modified substituent parameters for $+R$ groups

Subst.	$\Delta\bar{\sigma}_R^-$	$(\Delta\bar{\sigma}_R^-)_{DMSO}$	σ_π^-	$(\sigma_\pi^-)_{DMSO}$	σ_i	$(\sigma_i)_{DMSO}$	σ_p^0	$(\sigma_p^0)_{DMSO}$	σ_p^-	$(\sigma_p^-)_{DMSO}$
NO_2	0.455	0.454	0.332	0.331	0.46	0.473	0.800	0.804	1.255	1.26
CHO	0.47	0.440	0.34	0.321	0.22	0.212	*ca.*0.53	0.533	1.030	0.97
CN	0.309	0.311	0.226	0.227	0.42	0.400	0.653	0.627	0.96	0.94
CF_3	0.196	0.182	0.143	0.133	0.34	0.375	0.50	0.508	0.686	0.69
$COCH_3$	0.365	0.361	0.266	0.264	0.214	0.140	0.491	0.404	0.850	0.77
COC_6H_5	0.387	0.387	0.28	0.283	0.20	0.183	0.49	0.466	0.877	0.85
$COOCH_3$	0.30	0.333	0.22	0.243	0.23	0.183	0.46	0.426	0.76	0.76
COOEt	0.28	0.337	0.20	0.246	0.24	0.166	0.45	0.412	0.73	0.75
SO_2CH_3	0.302	0.285	0.22	0.208	0.46	0.418	0.69	0.626	0.99	0.91
$CH=CHNO_2$	*ca.*0.37	0.406	0.27	0.296	*ca.*0.23	0.134	*ca.*0.50	0.430	0.88	0.84
CH=CHCOOEt		0.249		0.182		0.144		0.326		0.58
$CONH_2$	0.24	0.227	0.175	0.166	*ca.*0.20	0.086	*ca.*0.38	0.252	0.62	0.48
SO_2NH_2	0.25	0.197	0.18	0.144	*ca.*0.46	0.332	*ca.*0.65	0.476	0.90	0.67
$SOCH_3$	0.24	0.124	0.175	0.091	0.31	0.321	0.49	0.412	0.73	0.54
$SMe_2^+I^-$	*ca.*0.25	0.280	0.18	0.204	*ca.*0.82	0.526	1.0	0.730	*ca.*1.25	1.01
$NMe_3^+I^-$	*ca.*0.05	0.032		0.023	0.7	0.501	0.8	0.524	0.80	0.56

tatively in terms of the specific substituent-solvent interactions with DMSO, as discussed before.[4,5] The discrepancies of these DMSO values from ordinary σ_p^0 and σ_p^- appear to be caused largely by the modification of the inductive nature of substituents in DMSO, as far as $+R$ class substituents are concerned. Only the $SOCH_3$ group, with an exceptional behavior, shows a remarkable decrease in the π-electronic contribution without noticeable decrease in the inductive contribution in DMSO solution. This suggests that in hydroxylic solvents the contribution of the cannonical structure, O^-–S^+–CH_3, is particularly enhanced through hydrogen bonding, but in aprotic DMSO the decreased polarization due to loss of hydrogen-bonding makes the (p—d)π interaction far less effective giving no noticeable change in the inductive polarity.

It is possible that the specific magnetic term which does not correlate with any ordinary substituent parameters might fortuitously be cancelled out by process (4) to result in a set of parameters proportional to the resonance substituent constants. Such a non-electronic effect may be accommodated in the residual parameters, so that the resulting $(\sigma_i)_{DMSO}$ parameters are no longer proportional to the ordinary σ_i values. However, this does not seem reasonable from the fact that the deviation of $(\sigma_i)_{DMSO}$ from the standard σ_i value is remarkable in only carbamido and sulfonamide groups while negligible in other carbonyl and sulfonyl groups. Accordingly, any specific magnetic effect, if operative at all, is not so important that it does not overcome the solvent-modification of substituent inductive effects. This conclusion is further supported by the fact that the $(\sigma_i)_{DMSO}$ values essentially parallel the changes of ^{19}F NMR chemical shift of *m*-substituted fluorobenzenes in the same solvent.[6b]

When we consider the process of the derivation, $(\sigma_i)_{DMSO}$ and even $(\sigma^0)_{DMSO}$ and $(\sigma^-)_{DMSO}$ might be less reliable than $(\Delta\bar{\sigma}_R^-)_{DMSO}$ or $(\sigma_\pi^-)_{DMSO}$ parameters. However, the parameters, especially the resonance parameters, should serve as a useful measure to estimate the substituent effects in the aprotic DMSO. For the substituents whose standard parameter values are not yet known precisely, the present set of parameters should have practical value for estimation of the conjugative powers of the substituents. As an example, $CH{=}CHNO_2$ and $CH{=}CHCOOC_2H_5$ would have relatively strong electron-attracting resonance-ability. The set of DMSO-parameters can be applied to reactions in most anhydrous aprotic solvents, and to even those in aqueous organic solvent, more satisfactorily than the standard set of parameters.

For conjugatively electron releasing ($-R$) substituents, quantities $(\bar{\sigma}_p - 0.85\,\bar{\sigma}_m)$ give poor linear correlation with standard $\Delta\bar{\sigma}_R^+$ values. This is perhaps due to the deviation from the basic requirement that the solvent-modification of the nature of substituents should be of minor significance as compared with the electronic change of the detection site by substituents. The deviations of OH and NH_2 substituents are the most remarkable. The nature of the substituents is modified by DMSO to the same extent as the changes of the detection function OH or NH_2 caused by the hydrogen-bonding with DMSO. The interaction of such a substituent with DMSO should considerably differ at *meta* and *para* positions, to the same extent as the detection site being affected by a substituent from both positions. Thus the solvent-modification of a substituent could not be assumed to be the same for *meta* and *para* positions, which is especially important for a substituent capable of strong substituent-DMSO interaction. In view of the fit of the $+R$ substituents in the above treatment (4), however, it is reasonable that the quantities $(\bar{\sigma}_p - 0.85\,\bar{\sigma}_m)$ for most $-R$ groups in DMSO solution would be also, as a first approximation, proportional to the plausible $(\Delta\bar{\sigma}_R^+)_{DMSO}$ values. If the present set of apparent $\bar{\sigma}_p$ for $-R$ groups are assumed to be of the σ_p^0 class,[4] the C^+_{DMSO} value of 0.575 can be given for the $-R$ substituents, from the *meta*/*para* π-contribution ratio of 0.50 which is characteristic of the σ^0 scale. The resonance contribution scale of these substituents can be roughly approximated on this basis:

$$(\bar{\sigma}_p - 0.85\bar{\sigma}_m) = 0.242(\Delta\bar{\sigma}_R^+)_{DMSO} \qquad (5)$$

This leads also to a crude estimation of $(\sigma_i)_{DMSO}$ values for $-R$ substituents. The results are very close to those obtained in the treatment of the chemical shift in DMF solution. The uncertainty in the contribution scale of resonance for $-R$ substituents does not permit further discussion of these parameter values especially of $(\sigma_i)_{DMSO}$ values. It might be said that their general application can not yet be warranted for this class of substituents. However, we might conclude that the contribution scale of the $-R$ resonance in this system does not differ much from the scale in standard σ^0 constant; at most, less than that of the σ_p scale.[12]

Comparison with Related Treatment. From the above results, the hydroxyl chemical shifts of *para*-substituted derivatives in DMSO can be given by

$$\Delta\delta_p = 1.529[(\sigma_i)_{DMSO} + (\sigma_\pi^+)_{DMSO} + 1.96(\sigma_\pi^-)_{DMSO}] \qquad (6)$$

The second term applies to the $-R$ class and the third to $+R$ class substituents.[13] The use of the standard substituent constants in place of the DMSO values does not appear to affect the characteristics of the correlation at least for the $+R$ groups even though the precision of fit would be a little lowered. The higher q_r^- value evidently indicates the important contribution from only $+R$ class *para* substituents in this system, while the $q_r^- = 1.96$ is less than the q_r^- value $= 2.37$ for the pK_a of phenols in water, suggesting that the resonance contribution of *para* $+R$ substituents to the hydroxyl hydrogen-bonding is less important than that to the dissociation of the hydroxyl proton.

Fischer *et al.*[14] have applied the Taft equation

$$\log(k/k_0) = \rho_I\sigma_I + \rho_R\sigma_R^0 \qquad (7)$$

for sixteen *para* substituents in Traynham's data[15] to give the correlation

$$\Delta\delta_p = 1.53(\sigma_I + 1.54\sigma_R^0).$$

Although no detail of the treatment was given, it appears that the exaltation of resonance for $+R$ groups suggested by the $\rho_R/\rho_I = 1.54$ is significantly less than that expected from $q_r^- = 1.96$, since σ_R^0 values for the $+R$ groups are numerically of the order of 1/2 or less of the corresponding σ_π^- values.[16] It should be noted that this treatment

appears similar to but stands on a considerably different basis from ours. As the wide applicability of Eq. (1) indicates,[2] the general σ^+ class electrophilic reactivity is such that only the resonance effect of $-R$ but not of $+R$ class substituents is significantly exalted, and the reverse is held in the general σ^- class nucleophilic resonance reactivities. Such characteristics of exalted resonance for both classes are still retained in Eq. (2) with the introduction of dual parameters q_r^- and q_r^+ each for $+R$ and $-R$ class substituents. With this flexibility of π-electronic contributions, a full range of various types of reactivities from an extreme σ^+ class to the other extreme σ^- class can generally be treated by a single equation (2).[4,6a]

Apart from the question of fit, treatment with a single resonance reaction constant inevitably gives an indiscriminate change (parallel increase or decrease) in the resonance contributions from both $+R$ and $-R$ class *para* substituents in a given reaction. In the Taft treatment using a single ρ_R coefficient for both $-R$ and $+R$ groups, no combinations of σ_I and σ_R^0 can reproduce even Brown's σ^+ constants or σ^- constants where either the $-R$ or the $+R$ class substituents exerts the exalted resonance contribution. The results of Fischer *et al.*[14] do not offer any indication whether the system is of the σ^- or σ^+ type. The same criticism applies also to the Swain and Lupton equation,[7] $\log k/k_0=fF+rR$, which in principle does not differ from Eq. (7). From a slightly different view, Wiley and Miller[17] have questioned the significance of the Swain and Lupton f, r or % R values.

Although many correlations using Eq. (7) as well as the related equations with the single resonance coefficient have been reported for σ^+ or σ^- type reactivities, in most cases, the numbers of $-R$ and $+R$ substituents examined were not well balanced, so that the correlations obtained should be judged as those weighted more or less heavily on the effect of either $+R$ or $-R$ substituents. The correlations can be generally improved by excluding either $+R$ or $-R$ class substituents from the data set. Swain and Lupton gave[7] a satisfactory correlation for σ_p^- values with reasonable precision in terms of the F-R combination or the equation, $\log k/k_0=a\sigma_m+b\sigma_p$, while a few effective $-R$ groups were included in their calculation. For the same set of data, an excellent correlation can be obtained when the treatment is made only for $+R$ substituent groups; the latter treatment of the σ_p^- values for only $+R$ substituents gives a correlation, $\sigma_p^-=-0.13\sigma_m+3.44\sigma_p-0.011$, with remarkably improved precision of a correlation coefficient 0.996 and a standard deviation ±0.027.[18] The same is true for the correlation of σ_p^+ values for only the $-R$ substituents.[19] The results cast doubts upon the applicability of the single resonance coefficient treatments. It appears that the different ρ_R coefficients which are characteristic of reactions should be required for the effects of each $+R$ and $-R$ class substituents in exalted resonance type reactions as long as the resonance parameters σ_R^0 derived from the σ^0-reactivity are used. For such restrictions, Taft has noted[6c] that Eq. (7) with a single ρ_R (in terms of σ_I and σ_R^0) should be applied as a useful approximation to a limited class of substituted phenyl reactivities effectively insulated from the resonance interaction with the reaction site, and that apparent resonance parameters $\bar{\sigma}_R$ given by the difference between apparent $\bar{\sigma}_p$ and corresponding σ_I is applicable for most of substituents in only closely related types of reactions.[6] It is necessary for this treatment to utilize a most suitable set of apparent $\bar{\sigma}_R$ values for a given reaction, since any set of $\bar{\sigma}_R$ values does not cover evenly over a series of $+R$ and $-R$ substituents.[3,6,18] Consequently, the increase in the number of required sets of σ_R parameters is inevitable when a single ρ_R is employed.[20] Taft has demonstrated[6a] that at least four distinctive sets of $\bar{\sigma}_R$ parameters are required in practice for his treatment, depending on the σ^0, σ, σ^+, and $\bar{\sigma}^-$ type of reactivity. This is clearly not in line with Taft's original aim to accomplish an unified treatment of the aromatic substituent effect, retaining the simplicity of the linear free energy relationship. This very important deficiency is believed to arise primarily from an improper definition of the effective scale of the substituent inductive effect in the substituted benzene system. As relationship (2) shows, only with the assumption of the inductive scale for the *p*-substituted benzene system being $0.74\,\sigma_I$ instead of $1.00\,\sigma_I$, a universal set of π-electronic effect parameters can be obtained by $\bar{\sigma}-0.74\sigma_I$ from any class of reactivity.[3,4] Disagreement between both treatments appears to depend simply upon whether or not one might accept the continuum of the π-electronic contribution of respective substituents over a wide spectra of the reactivity changes from an extreme σ^+ to the other extreme σ^- classes, as well as the existence of a set of π-electronic parameters of substituents independent of reactivity classes.

Nevertheless, a separate determination of both q_r^+ and q_r^- parameters is not convenient, and the single q_r treatment has a practical advantage over the dual q_r treatment, especially when the number of substituents in a given data set is limited. From a practical point of view, the employment of a Taft-type equation only with a proper set of resonance parameters might be acceptable as a useful approximation. According to Eq. (2), any particular scale of the π-electronic effects over a range from extremely electron-releasing to -attracting substituents can reasonably be given for any class of $\bar{\sigma}_p$'s, by setting a proper ratio of q_r^- to q_r^+ values. Thus, the LSFE equation with dual q_r values can be easily reduced to the equation with a single q_r coefficient,[21] although the range of validity of such treatment with a fixed q_r^+/q_r^- ratio may be limited to a similar extent as that of the Taft equation.

References

1) To whom inquiries should be addressed.

2) Y. Yukawa and Y. Tsuno, This Bulletin, **32**, 960, 965, 971 (1959); Y. Yukawa, Y. Tsuno, and M. Sawada, *ibid.*, **39**, 2274 (1966); Y. Yukawa, Y. Tsuno, and M. Sawada, *ibid.*, **45**, 1198 (1972).

3) Y. Yukawa and Y. Tsuno, *Nippon Kagaku Zasshi*, **86**, 873 (1965); Y. Yukawa and Y. Tsuno, *Memoir, ISIR, Osaka Univ.*, **23**, 71 (1966).

4) Y. Tsuno, M. Fujio, Y. Takai, and Y. Yukawa, This Buletin, **45**, 1519 (1972).

5) M. Fujio, M. Mishima, Y. Tsuno, Y. Yukawa, and

Y. Takai, *ibid.*, **48**, 2127 (1975).

6) a) S. Ehrenson, R. T. C. Brownlee, and R. W. Taft, "Progress in Physical Organic Chemistry," Vol. 10 (1973), p. 1. The authors are indebted to Prof. R. W. Taft for making these data available prior to publication. b) R. W. Taft, E. Price, I. R. Fox, I. C. Lewis, K. K. Andersen, and G. T. Davis, *J. Amer. Chem. Soc.*, **85**, 709 (1963); J. Hirst and S. J. Una, *J. Chem. Soc., B*, **1969**, 646. c) P. R. Wells, S. Ehrenson, and R. W. Taft, "Progress in Physical Organic Chemistry," Vol. 6 (1968), p. 147.

7) C. G. Swain and E. C. Lupton, Jr., *J. Amer. Chem. Soc.*, **90**, 4328 (1968).

8) In the case of 4-substituted 3-cresols, dimethylamino, acetamino, nitro, acetyl, and carbethoxy derivatives were deviated from the correlation. This may reasonably be attributed to the steric inhibition of resonance of the 4-substituents by 3-methyl group.

9) C. D. Ritchie and E. S. Lewis, *J. Amer. Chem. Soc.*, **84**, 591 (1962); M. Hojo, M. Utaka, and Z. Yoshida, *Tetrahedron*, **27**, 4031 (1971).

10) J. D. Roberts, R. A. Clement, and J. J. Drysdale, *J. Amer. Chem. Soc.*, **73**, 2181 (1951); F. G. Bordwell and P. J. Boutan, *ibid.*, **78**, 87 (1956).

11) However, see, A. R. Katritzky and R. D. Topsom, *Angew. Chem. (Intern. Ed.)*, **9**, 87 (1970); P. J. Q. English, A. R. Katritzky, T. T. Tidwell, and R. D. Topsom, *J. Amer. Chem. Soc.*, **90**, 1767 (1968).

12) M. Fujio, Y. Tsuno, Y. Yukawa, and Y. Takai, This Bulletin, **48**, 3330 (1975).

13) Equation (6) is not result of overall least squares calculation. The coefficient 1.0 for $-R$ substituents (2nd term) is less reliable.

14) A. Fischer, M. C. A. Opie, J. Vaughan, and G. J. Wright, *J. Chem. Soc., B*, **1972**, 319.

15) J. G. Traynham and G. A. Knesel, *J. Org. Chem.*, **31**, 3350 (1966); M. T. Tribble and J. G. Traynham, *J. Amer. Chem. Soc.*, **91**, 379 (1969).

16) The σ_R^0 for $+R$ substituents are too small and less reliable as the relative measure of the resonance capabilities of these substituents.

17) G. R. Wiley and S. I. Miller, *J. Org. Chem.*, **37**, 767 (1972).

18) M. Fujio, Ph D thesis, March, 1972, Osaka University.

19) The correlation $\sigma_p^+ = 2.37\sigma_p - 1.17\sigma_m + 0.017$ was obtained for 14 representative $-R$ substituents, with $R = 0.997$ and $s = \pm 0.040$.

20) However, see ref. 6c), p. 155.

21) The π-electronic effects involved in the representative substituent constants, σ_p^0, σ_p, σ_p^+, and σ_p^-, can be given for first three sets by $q_r^- = 1.00$ but $q_r^+ = 1.00$, 1.65, and 3.38, respectively, and for σ_p^-, $q_r^- = 2.37$ and $q_r^+ = 1.00$. The corresponding sets of π-electronic substituent parameters $\bar{\sigma}_\pi$ to the above sets of substituent constants can thus be obtained from these q_r values.

The Substituent Effect. VII. Substituent Chemical Shifts of NH Proton of Acetanilides[1a)]

Mizue FUJIO, Yuho TSUNO,[1b)] Yasuhide YUKAWA,* and Yoshio TAKAI*

Department of Chemistry, Faculty of Science, Kyushu University, Hakozaki, Fukuoka 812

**Institute of Scientific and Industrial Research, Osaka University, Yamada-kami, Suita, Osaka 565*

(Received December 10, 1974)

NMR chemical shifts of the NH proton of fifty-three *m*- and *p*-substituted acetanilides were determined in dilute DMSO solutions. The substituent chemical shifts were correlated with σ^0 constants with considerable scatter. Deviations were particularly significant for $-R$ groups having α-hydrogen. Improved correlation was found for $-R$ substituents with $(\sigma^0)_{DMSO}$ values which had been derived from the phenol hydroxyl chemical shifts in DMSO. Application of the LArSR equation using the DMSO-modified substituent parameters gave a good linear correlation for all substituents; $\Delta\delta^{NHAc}=0.686\ [(\sigma^0)_{DMSO}+0.277\ (\Delta\bar{\sigma}_R^-)_{DMSO}]$. These results indicate that the deviations are caused primarily by solvent-modification of substituents, the modification being essentially the same for both the acetanilide and the phenol systems in DMSO. The lower r^- value 0.277 in the chemical shifts for the acetanilides than for the phenols suggests that the π-electronic contribution of $+R$ *para* substituents is less important in the acetanilide system than in the phenol one. The resonance substituent parameter for these solvent-modified substituents was found to be proportional to both $(\bar{\sigma}_p^{OH}-\bar{\sigma}_p^{NH})$, the difference between the apparent $\bar{\sigma}_p$ constants of the two systems, and to $\bar{\sigma}_p-0.85\,\bar{\sigma}_m$ of each series. Estimation of a practical set of inductive and resonance substituent parameters for DMSO-modified substituents is attempted.

Foregoing investigations[2-4)] have indicated the following: The hydroxyl chemical shift of *m*- and *p*-substituted phenols in DMF or DMSO is closely related to the chemical reactivities; the substituent effect can be described successfully in terms of the LArSR and LSFE relationships;[5)] the solvent-modification of substituents is of considerable importance in these aprotic solvents. The effect of solvent on the substituent effect in chemical reactivities and physical properties has received considerable attention.[6)] However, hardly any studies have been carried out to elucidate quantitatively such solvent effect on the basis of the linear free energy relationship. The solvent-modification of the nature of substituents can be measured by the deviations in the LArSR or LSFE correlation by means of the sets of substituent parameters which were determined from the reactivity data in aqueous media.

From our interest in the substituent effect in aromatic derivatives, we attempted to estimate the practical measure of inductive and π-electronic effects of "the solvent-modified substituents" in DMF and DMSO solutions.[2,3)] Evaluation of the resonance parameters $(\sigma_\pi)_M$ for the solvent-modified substituents in medium M was carried out by means of the following relation derived from the LSFE equation.[5)]

$$(\sigma_\pi)_M = (\bar{\sigma}_p-0.85\bar{\sigma}_m)_M/C_M \qquad (1)$$

where $\bar{\sigma}_p$ and $\bar{\sigma}_m$ are the apparent substituent constants obtained from the above system in medium M. The characteristic coefficient 0.85 corresponds to the ratio of inductive contributions of the substituent from *para* and *meta* positions in the LSFE relationship. C_M was determined by employing the standard σ_π in place of $(\sigma_\pi)_M$ parameters. The σ_i and σ_p^0 parmeters for solvent-modified substituents in DMF and DMSO were also derived.

This approach stands essentially upon the generality of the unique ratio 0.85 of *para*/*meta* inductive effects. It will be possible to establish significance of the inductive ratio by confirming its validity in chemical and physical properties whose requirements of resonance widely differ. For one of such systems, the substituent chemical shifts of the NH proton of *m*- and *p*- substituted acetanilides in DMSO have been chosen. The NH chemical shift in this system was found to follow the σ^0 parameters. The resonance exaltation for $+R$ class substituents does not appear to be so important as in the case of phenol hydroxyl chemical shift. Accordingly the comparison of the apparent $\bar{\sigma}_p$ values for both systems should provide interesting information on the resonance (π-electronic) and the inductive effects of the DMSO-modified substituent groups. Such a study would confirm generality of the LArSR and LSFE relationships.

Results and Discussion

The NH proton signal of acetanilides in DMSO is considerably more broadened than the hydroxyl proton signal of phenols in DMSO. However, the DMSO solution seems to give the sharpest and most stable signals of the NH proton, no significant dilution shift being observed. The experimental uncertainty appears to be slightly larger in the NH chemical shifts than the phenol OH chemical shift values. It is estimated that in most cases the error involved in the infinite dilution values does not exceed ±0.5 Hz, although in a few cases the uncertainty may be as high as ±1 Hz. The chemical shifts of NH proton of acetanilides are given in Table 1. Bennett *et al.*[7a)] and Rae *et al.*[7b)] have reported the chemical shift data of several acetanilides in the same solvent, their data being only of *p*-substituted derivatives. The chemical shift values reported were in good agreement with the present results.

Niwa reported the chemical shifts of NH protons of *meta* and *para* substituted formanilides in DMSO.[8)] His data can be compared with the present data to give a good linear relation; correlation coefficient 0.996 and standard deviation ±0.025.

$$\Delta\delta^{NHAc} = 1.003\Delta\delta^{NHCHO}$$

This suggests that there is no significant difference in the substituent effects on the shifts in both systems.

Asabe and Tsuzuki reported on α-NH protons of sub-

Table 1. Chemical shifts of NH protons of *m*- and *p*-substituted acetanilides in DMSO

No.	Subst.	$\Delta\delta_p^{TMS}$	$\Delta\delta_m^{TMS}$
1	NO_2	10.485	10.357
2	CN	10.302	10.218
3	CHO	10.308	
4	SO_2CH_3	10.335	10.288
5	SO_2NH_2	10.215	10.185
6	SCN	10.178	
7	COC_6H_5	10.282	10.138
8	$COCH_3$	10.217	10.082
9	$COOCH_3$	10.222	10.110
10	COOEt	10.218	10.110
11	$CONH_2$	10.090	10.005
12	CF_3	10.245	10.222
13	$N{=}NC_6H_5$	10.260	
14	C_6H_5	9.987	
15	H	9.872	
16	I	9.975	9.970
17	Br	10.018	10.047
18	Cl	10.003	10.058
19	F	9.927	10.090
20	SCH_3	9.887	
21	OC_6H_5	9.920	9.968
22	NHAc	9.790	9.863
23	NHC_6H_5	9.725	
24	*t*-Bu	9.795	
25	CH_3	9.775	9.788
26	OCH_3	9.728	9.850
27	OH	9.597	9.732
28	NMe_2	9.562	
29	NH_2	9.435	9.552
30	OAc	9.948	10.032
31	Me_2		9.702
32	Cl_2		10.200

stituted phenylureas in DMSO.[9] Although no *meta* substituents were included, *para* substituents can be correlated linearly with our data by

$$\Delta\delta^{urea} = 1.282\Delta\delta^{NHAc}$$

with excellent precision, $R=0.998$ and $s=\pm0.023$, suggesting that essentially the same interaction mechanism is operating for both systems. The analysis we have made in the present study will be applied in the same way for these systems. The α-NH chemical shift in urea is significantly more susceptible to substituent changes than those in the other NH chemical shifts.

Relative NH chemical shifts of the substituted acetanilides (Table 1) are plotted against the standard σ^0 constants in Fig. 1. The general trends that electron attracting groups tend to shift the NH-resonance position toward low field and the chemical shifts appear to reflect the charge density at the NH-site are borne out, while substantial scatter does not permit us to draw any quantitative conclusion. However, following facts are obvious. No significant exaltation in the resonance contributions of conjugatively electron attracting ($+R$) substituents relative to σ_p^0 scale is observed, employment of σ^- values not improving the fit. This indicates that the present data belong to the so called σ^0 class reactivity. Deviations of higher halogens are attributed to the sub-

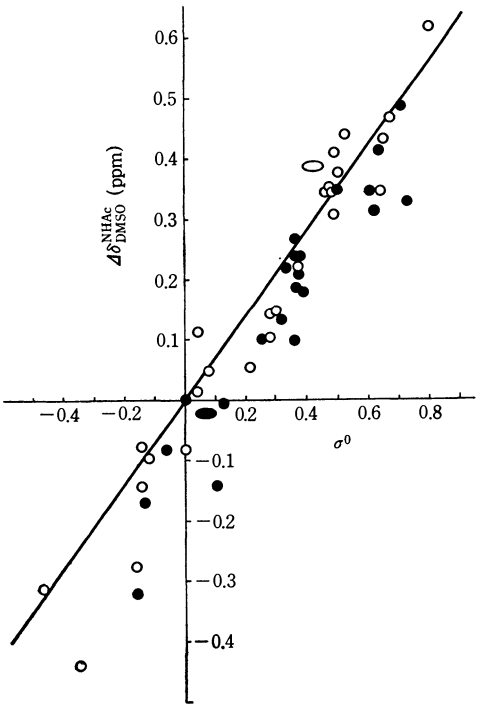

Fig. 1. The plot of $\Delta\delta^{NHAc}_{DMSO}$ against standard σ^0: open circles *p*-substitute l and closed circles *m*-substituted acetanilides.

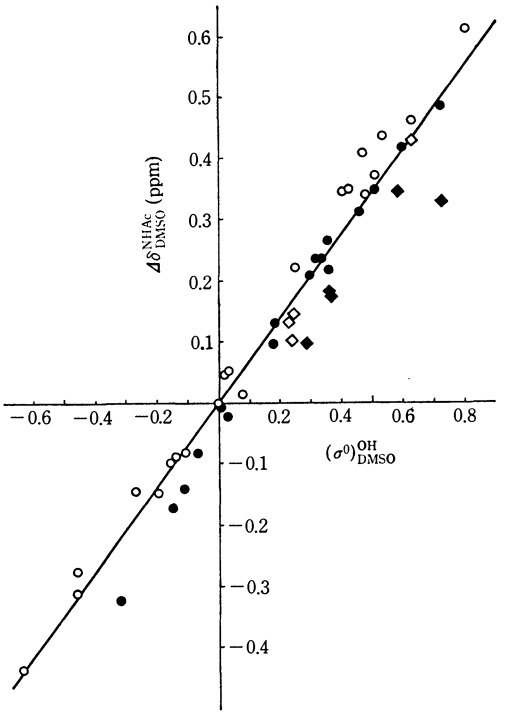

Fig. 2. The plot of $\Delta\delta^{NHAc}_{DMSO}$ against $(\sigma^0)^{OH}_{DMSO}$: open circles *para*, closed circles *meta*, and squares anisotropic substituents.

stituent anisotropy effect. Deviations of the $-R$ substituents with acidic α-hydrogens are all large but similar to the behavior observed in the phenol chemical shift in DMSO. It is most plausible to ascribe these deviations mainly to the substantial substituent-solvent interactions.

The substituent effect is appreciably modified by DMSO.[3] The solvent-modified substituents in DMSO may be assumed to be essentially the same in the acetanilide as in the phenol system. We could thus expect a good correlation between the present data and the $(\sigma^0)_{DMSO}$ derived from the phenol hydroxyl chemical shifts in DMSO.[3] The good correlation obtained is shown in Fig. 2. $-R$ *para* substituents fall on a straight line determined by *meta* substituents, whereas all the $+R$ *para* substituents deviate slightly but systematically to the direction of enhancing resonance. No improved correlation was observed for the anisotropic halogen groups.

Although the exaltation of resonance contribution of $+R$ class *para* substituents does not appear very significant, the effect may be described by

$$\Delta\delta = \rho(\sigma^0 + r^-\Delta\bar{\sigma}_R^-) \quad (2)$$

The following equation should be employed in place of Eq. (2) utilizing the modified substituent constants $(\sigma^0)_{DMSO}$ and $(\Delta\bar{\sigma}_R^-)_{DMSO}$.[5]

$$\Delta\delta^X = \rho[(\sigma^0)_{DMSO} + r^-(\Delta\bar{\sigma}_R^-)_{DMSO}] \quad (3)$$

The equation agreed excellently with the chemical shift data excluding halogen groups, giving ρ value of 0.686 and r^- of 0.277 with a correlation coefficient 0.994 and a standard deviation $\pm$0.030.[10] The ρ value obtained is, within experimental uncertainty, identical with the value derived from the correlation (Fig. 2). Using this ρ value, the apparent substituent constants $\bar{\sigma}^{NH}$ can be determined (Table 2). The small r^- value indicates that the through-conjugation interaction between conjugatively electron attracting ($+R$) *para* substituents and the NHAc site is not important in the present system in contrast to the phenol system. This can be explained by the deviation from coplanarity of the NHAc site with the benzene ring. Since an insignificant degree of through-conjugation operates for $+R$ *para* substituents, no significant exaltation of resonance with the $-R$ detection site would be expected for $-R$ *para* substituents. The substituent effect observed in the present system can be regarded as the effect of nearly unexalted σ^0 class. Hence, the excellent fit of $-R$ class substituents to the above correlation, to the first approximation, indicates the validity of $(\sigma_p^0)_{DMSO}$ values of $-R$ groups derived from the hydroxyl chemical shift of phenols.

On the basis of this correlation, we can determine a set of $(\sigma^0)_{DMSO}$. Because of the small r^- value of 0.277, possible errors involved in the $(\Delta\bar{\sigma}_R^-)_{DMSO}$ values do not significantly affect the resulting set of $(\sigma^0)_{DMSO}$ values. This suggests that the new set of $(\sigma^0)_{DMSO}$ values might be more reliable than the previous one at least for the $+R$ groups (*cf.* Table 3). The solvent-modified parameters $(\sigma^0)_{DMSO}$ as well as apparent substituent constants $\bar{\sigma}^{NH}$ are composed of the inductive and the π-electronic effects of the solvent-modified substituents in DMSO.

Table 2. Apparent substituent constants in DMSO

No.	Subst.	$\bar{\sigma}_p$	$\bar{\sigma}_m$
1	NO_2	0.903	0.717
2	CN	0.637	0.516
3	CHO	0.647	
4	SO_2CH_3	0.685	0.618
5	SO_2NH_2	0.510	0.466
6	SCN	0.457	
7	COC_6H_5	0.607	0.399
8	$COCH_3$	0.513	0.316
9	$COOCH_3$	0.520	0.357
10	COOEt	0.516	0.357
11	$CONH_2$	0.328	0.204
12	CF_3	0.554	0.520
13	$N{=}NC_6H_5$	0.575	
14	C_6H_5	0.178	
15	H	0.010	
16	I	0.160	0.153
17	Br	0.224	0.265
18	Cl	0.202	0.283
19	F	0.090	0.328
20	SCH_3	0.032	
21	OC_6H_5	0.080	0.151
22	NHAc	−0.109	−0.001
23	NHC_6H_5	−0.204	
24	*t*-Bu	−0.102	
25	CH_3	−0.131	−0.111
26	OCH_3	−0.198	−0.022
27	OH	−0.390	−0.194
28	NMe_2	−0.441	
29	NH_2	−0.626	−0.456
30	OAc	0.122	0.243
31	Me_2		−0.237
32	Cl_2		0.468

Solvent-Modified Substituent Parameters

The substituent effects in benzene systems are generally described by the LSFE relationship, to the first approximation, in terms of the combination of mutually independent inductive and π-electronic contributions:[5]

$$\log (k/k_0)_p = \rho(\sigma_i + q_r^+ \sigma_\pi^+ + q_r^- \sigma_\pi^-)$$
$$\log (k/k_0)_m = \rho(1.17\sigma_i + 0.50\sigma_\pi^\pm) \quad (4)$$

where σ_i is the inductive substituent constant, which is independent of q_r's, a measure of reaction-dependent contributions of its resonance effect. σ_π^+ and σ_π^- are the substituent constants measuring the capability of $-R$ and $+R$ class substituents respectively to donate and withdraw electron through π-electronic delocalization. σ_π^+ corresponds numerically to 0.42 $\Delta\bar{\sigma}_R^+$ and σ_π^- to 0.73 $\Delta\bar{\sigma}_R^-$. By the aid of the characteristic ratio 0.85 or 1/1.17 of the inductive contributions from *para* and *meta* substituents in Eq. (4), a linear π-electronic free energy relationship can be derived which should be free from any inductive contributions:

$$\log (k/k_0)_p - 0.85 \log (k/k_0)_m = \rho C^- \sigma_\pi^- \text{ or } = \rho C^+ \sigma_\pi^+ \quad (5)$$

where C^- and C^+ are parameters measuring the susceptibility to the π-electronic effects of $+R$ and $-R$ substituents respectively in a given reaction. A convenient modification to accommodate effects of the $+R$ groups in the present system gives Eq. (1).

We have demonstrated the utility of the quantities $\bar{\sigma}_p - 0.85\ \bar{\sigma}_m$ or $\Delta\delta_p - 0.85\ \Delta\delta_m$ for the hydroxyl chemical shifts of phenols in DMSO, as a measure of relative

resonance capabilities of the solvent-modified substituents.[2,4] The resonance substituent constants of the DMSO-modified substituents denoted by $(\sigma_\pi^{\pm})_{DMSO}$ or by $(\Delta\sigma_R^{\pm})_{DMSO}$ were determined by Eq. (1) providing 0.73 $C^-=1.12$ and $0.42C^+=0.24$.[4] The inductive and normal substituent constants denoted by $(\sigma_i)_{DMSO}$ and $(\sigma^0)_{DMSO}$ for the DMSO-modified substituents were subsequently determined from $(\sigma_\pi)_{DMSO}$. The same sort of treatment is expected to be applicable also to the present system. The most important feature of the LSFE treatment, Eq. (4), is the introduction of dual reaction constants for the π-electronic effect, q_r^+ and q_r^-, each for $-R$ and $+R$ substituents. The subsequent treatment has therefore to be applied separately for $+R$ and $-R$ substituent effects. Since our purpose has been to establish the general applicability of our treatment for conjugatively electron attracting ($+R$) groups, we have chosen the present acetanilide system where the effects of $+R$ *para* substituents significantly differ from those in the phenol chemical shifts.[3,4] Thus, Eq. (5) will be applied first to the analysis of $+R$ substituent effects.

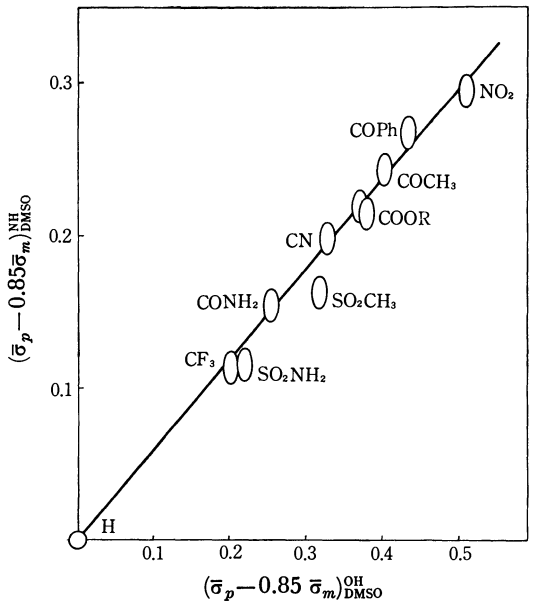

Fig. 3. The plot of $(\bar{\sigma}_p-0\bar{\sigma}.85_m)^{NH}_{DMSO}$ against $(\bar{\sigma}_p-0.85\,\bar{\sigma}_m)^{OH}_{DMSO}$ for $+R$ substituents.

Treatment of $+R$ Substituents. If the assumption of the solvent-modified substituent holds generally, Eq. (1) could be applied to the acetanilide system as well as to the phenol system in the same solvent. Equation (6) would hold provided that $(\Delta\bar{\sigma}_R^-)_{DMSO}$ for a series of $+R$ substituents are essentially independent of systems.

$$(\bar{\sigma}_p-0.85\bar{\sigma}_m)^{NH}=\alpha(\bar{\sigma}_p-0.85\bar{\sigma}_m)^{OH} \quad (6)$$

It follows that a plot of the quantities $(\bar{\sigma}_p-0.85\,\bar{\sigma}_m)^{NH}_{DMSO}$ against $(\bar{\sigma}_p-0.85\,\bar{\sigma}_m)^{OH}_{DMSO}$ for various $+R$ substituents should be a straight line of slope α. Figure 3 shows such a straight line with a correlation coefficient 0.997 and a standard deviation ±0.010. Using $\alpha=0.603$ in Eq.(6), $(\Delta\bar{\sigma}_R^-)_{DMSO}$ for $+R$ substituents can be derived from the apparent $\bar{\sigma}$ values from the acetanilides, and $(\sigma_\pi^-)_{DMSO}$ by $(\sigma_\pi^-)_{DMSO}=0.73\ (\Delta\bar{\sigma}_R^-)_{DMSO}$. The values are in precise agreement with those obtained from the phenol system, no serious corrections being required for the parameter values previously obtained. In this treatment, we have assumed that the *para/meta* inductive contribution ratio is a constant, 0.85, for all substituents irrespective of reactions. The good agreement thus may offer confirmation of the generality of 0.85 for the inductive contribution ratio.

We can apply the LArSR equation[5b] which is modified to (3) to accommodate the effect of DMSO-modified substituents on the chemical shift. If Eq. (3) is applicable to both the phenol and acetanilide systems, it follows that

$$(\Delta\bar{\sigma}_R^-)_{DMSO}=(\bar{\sigma}_p^{OH}-\bar{\sigma}_p^{NH})_{DMSO}/(r^{OH}-r^{NH})$$
$$=(1/\Delta r)(\bar{\sigma}_p^{OH}-\bar{\sigma}_p^{NH})_{DMSO} \quad (7)$$

The coefficient Δr can be determined from the slope of the correlation of $(\bar{\sigma}_p^{OH}-\bar{\sigma}_p^{NH})_{DMSO}$ against $(\Delta\bar{\sigma}_R^-)_{DMSO}$. Equation (7) is just the same expression as the basic one of the LArSR theory, indicating that the set of the differences between two sets of apparent $\bar{\sigma}_p$ in any two independent systems with different r's should be equivalent to the relative measure of resonance capabilities of the substituent.[5b] If Eqs. (3) and (4) are valid, the set of resonance quantities in Eq. (6) is proportional to another set of relative resonance capacities of substituents, namely,

$$(\bar{\sigma}_p-0.85\bar{\sigma}_m)^{OH}_{DMSO}=\beta(\bar{\sigma}_p^{OH}-\bar{\sigma}_p^{NH})_{DMSO} \quad (8)$$

A reasonably good linear correlation (Fig. 4) verifies the equivalency of these two sets of resonance measures.[11] An exceptionally large deviation indicated by the CN group is attributable to the anisotropy effect which appears to be considerably effective only in the acetanilide but not in the phenol chemical shifts.

The correlation could be applied for estimating the $(\Delta\bar{\sigma}_R^-)_{DMSO}$ parameter. However, because of the smallness of $(\bar{\sigma}_p^{OH}-\bar{\sigma}_p^{NH})$ quantities, the uncertainty would be larger for the parameter values derived from this set of quantities than those from the $(\bar{\sigma}_p^{NH}-0.85\,\bar{\sigma}_m^{NH})$ quantities. The former evaluation depends on the uncertainty of two independent ρ values, whereas in the latter based upon Eq. (6) any error involved in ρ values is practically unimportant for the evaluation of $(\Delta\bar{\sigma}_R^-)_{DMSO}$ parameters, since we can utilize directly two sets of experimental quantities $(\Delta\delta_p-0.85\,\Delta\delta_m)_{DMSO}$ instead of $(\bar{\sigma}_p-0.85\,\bar{\sigma}_m)_{DMSO}$. It is therefore more reasonable to evaluate a set of $(\Delta\bar{\sigma}_R^-)_{DMSO}$ parameters by Eq. (6), in comparison with the previous values derived from the phenol hydroxyl chemical shift (Table 3). $(\sigma_i)_{DMSO}$ and then $(\sigma^0)_{DMSO}$ parameters can be determined from $(\Delta\sigma_R^-)_{DMSO}$ or $(\sigma_\pi^-)_{DMSO}$ (Table 3). As anticipated, these sets of parameters derived from NH chemical shifts are identical within experimental uncertainty with the corresponding parameters derived from the phenol hydroxyl chemical shift. The identity between the corresponding sets from two independent sources with reasonable precision is a strong evidence for the generality of the LArSR and LSFE relationships. This proves also the validity of the assumption that the substituent effect in a given solvent can be treated as the effect of the solvent-modified substituents, independent of reactions or systems, at least for conjugatively electron

Table 3. Modified substituent parameters in DMSO for $+R$ groups

No.	Subst.	Acetanilides			Phenols		
		$(\sigma_\pi^-)_{DMSO}$	$(\sigma_t)_{DMSO}$	$(\sigma_p^O)_{DMSO}$	$(\sigma_\pi^-)^{OH}_{DMSO}$	$(\sigma_t)^{OH}_{DMSO}$	$(\sigma_p^0)^{OH}_{DMSO}$
1	NO_2	0.326	0.470	0.796	0.331	0.473	0.804
2	CN	0.220	(0.345)	(0.565)	0.227	0.400	0.627
3	CF_3	0.124	0.389	0.513	0.133	0.375	0.508
4	$COCH_3$	0.271	0.154	0.425	0.264	0.140	0.404
5	COC_6H_5	0.297	0.213	0.510	0.283	0.183	0.466
6	$COOCH_3$	0.240	0.201	0.441	0.243	0.183	0.426
7	COOEt	0.237	0.202	0.439	0.246	0.166	0.412
8	SO_2CH_3	0.177	0.450	0.627	0.208	0.418	0.626
9	$CONH_2$	0.172	0.099	0.271	0.166	0.086	0.252
10	SO_2NH_2	0.126	0.342	0.468	0.144	0.332	0.476

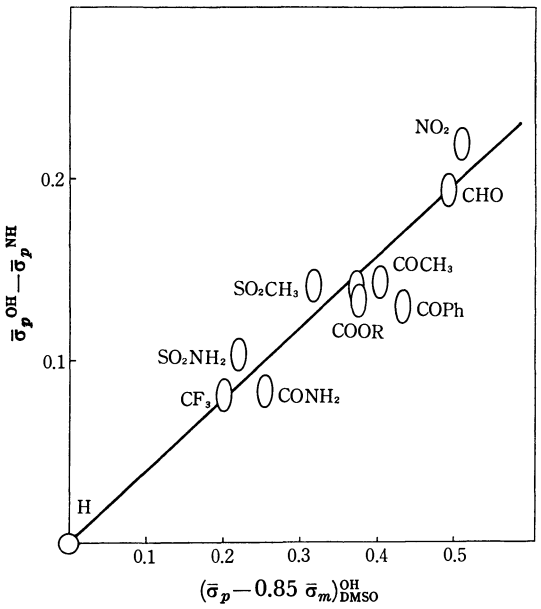

Fig. 4. The plot of $\bar{\sigma}_p^{OH}-\bar{\sigma}_p^{NH}$ against $(\bar{\sigma}_p-0.85\,\bar{\sigma}_m)^{OH}_{DMSO}$.

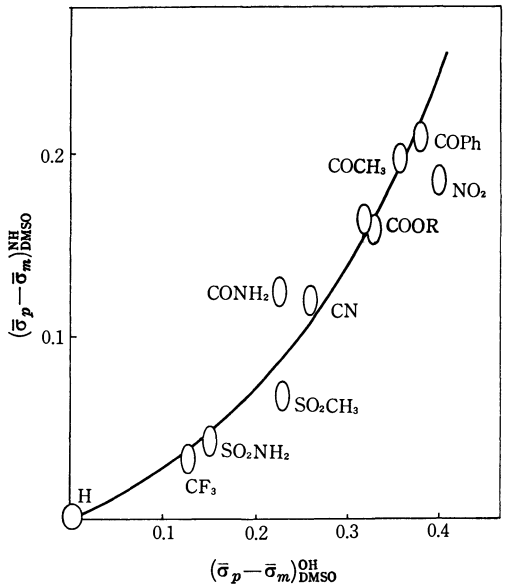

Fig. 5. The relation between Taft's apparent resonance quantities, $(\bar{\sigma}_p-\bar{\sigma}_m)^{NH}_{DMSO}$ and $(\bar{\sigma}_p-\bar{\sigma}_m)^{OH}_{DMSO}$.

attracting substituents.

In order to rationalize the results, it is necessary to compare them with the results of the corresponding analysis of the present shift data according to Taft's equation.[12] Taft's treatment is based on the assumption of i) the equal inductive contributions from a given substituent at *meta* and *para* positions, and ii) the view that the σ_I parameters of any substituent essentially are invariant irrespective of the nature of reaction. Of course, the solvent-variation of these parameters may be imposed. From his theory, the apparent resonance parameters $\bar{\sigma}_R$ of the solvent-modified substituents in DMSO can be given by

$$(\bar{\sigma}_R)_{DMSO} = (\bar{\sigma}_p)_{DMSO} - (\bar{\sigma}_I)_{DMSO}$$

The equal inductive contribution from *meta* and *para* positions implies that the π-electronic effect (or resonance) parameters should be proportional to the difference between *meta* and *para* apparent substituent constants, $\bar{\sigma}_p-\bar{\sigma}_m$, in a given system, namely,

$$(\bar{\sigma}_R)_{DMSO} = \alpha'(\bar{\sigma}_p-\bar{\sigma}_m)_{DMSO} \quad (9)$$

where α' is a proportionality constant. If Eq. (9) were valid for various systems, $(\bar{\sigma}_p-\bar{\sigma}_m)_{DMSO}$ quantities for two systems may be expected to be linearly related. Figure 5 shows the correlation of the two sets of Taft's resonance quantities derived from phenol and acetanilide systems in DMSO solution. The correlation is less satisfactorily linear ($R=0.961$ and $s=\pm0.021$) than that given by Eq. (6). The plot appears to be better described by a smooth curve; otherwise, the deviation of the unsubstituted derivative is significant. Such non-linearity between any two sets of Taft's resonance parameters $\bar{\sigma}_R$ derived from various classes of $\bar{\sigma}$ values is generally observed even in chemical reactivities. For instance, similar resonance quantities $\bar{\sigma}_p-\bar{\sigma}_m$ for $+R$ substituents from the standard σ^- constants are not reasonably linear against the corresponding quantities from the other references σ^0 or σ parameters.[13] This is in contrast to the present results based on our LArSR and LSFE treatment. Taft has concluded that there are no general or universal parameters of resonance effects of substituents.[12] Generalized treatment of the same kind as we have employed could not be possible with Taft's equation based on the equal *meta* and *para* inductive contribution model.

Treatment of $-$R *Substituents.* In contrast to the remarkable success in correlating effects of conjugatively electron attracting substituents, the analysis of con-

jugatively electron releasing substituent effects does not appear to be so simple. The same sort of difficulty was observed in the analysis of phenol chemical shifts.[2,4] Neither σ_π nor σ_i parameters obtained were linear against the ordinary sets of corresponding parameters. Thus we can not attain ultimate accuracy in the evaluation of parameters of the solvent-modified substituents from the present data. Nevertheless, it appears of value to estimate somewhat rough but still useful measures of the apparent inductive and π-electronic effects of the so-called solvent-modified substituents.

Since the *para/meta* inductive contribution ratio of 0.85 is believed to be valid for $-R$ as well as $+R$ substituents, the quantities $(\bar{\sigma}_p - 0.85\,\bar{\sigma}_m)_{\mathrm{DMSO}}$ for $-R$ groups in either the phenol or the acetanilide system should give a relative measure of the resonance capability of DMSO-modified substituents. Thus, even though they might not be proportional to the standard σ_π^+ or $\Delta\bar{\sigma}_R^+$ parameters, it is anticipated that both sets of quantities are correlated linearly with each other; that is, Eq. (6) holds for $-R$ substituents. Since the apparent substituent constants $\bar{\sigma}_p$ for $-R$ *para* substituents in both systems are identical within their uncertainty and appear both to be of the σ^0 class, the slope α of the correlation should be close to unity. However, the result is not in line with anticipation. The fit does not appear to be satisfactory and the slope α corresponds to roughly 2/3. This implies that the C_M scale in Eq. (1) is not the same for the two apparent stes of $(\sigma_\pi)_{\mathrm{DMSO}}$. A similar treatment based upon Taft's assumption, Eq. (9) for $-R$ substituents, gives no reasonable correlation.

Assuming the effect of $-R$ groups to be of the σ^0 class, the conversion coefficient for $-R$ class substituents can be given as follows, provided that the ordinary resonance contribution scale $q_r^+ = 1.0$ for *para* $-R$ substituents and $q_r^m = 0.50$ for *meta* substituents by means of Eq. (4);

$$(\bar{\sigma}_p - 0.85\bar{\sigma}_m) = 0.575(\sigma_\pi^+)_{\mathrm{DMSO}} \qquad (10)$$

An apparent set of inductive parameters $(\sigma_i)_{\mathrm{DMSO}}$ can thus be given by

$$(\sigma_i)_{\mathrm{DMSO}} = \bar{\sigma}_p - (\sigma_\pi^+)_{\mathrm{DMSO}} = 1.48\bar{\sigma}_m - 0.74\bar{\sigma}_p \qquad (11)$$

The inadequacy of the scale of $(\sigma_\pi^+)_{\mathrm{DMSO}}$ parameters should reflect the consistency of the resulting set of $(\sigma_i)_{\mathrm{DMSO}}$ values. The reliability of the former parameters can be judged in turn from the consistency of the $(\sigma_i)_{\mathrm{DMSO}}$ values. The best practical way of critical examination of both parameters is to compare the $(\sigma_i)_{\mathrm{DMSO}}$ values with a certain reliable measure of the inductive effects of substituents obtained from a completely independent source in the same solvent. As such a reference measure, we have chosen the relative ^{19}F NMR chemical shifts of *m*-substituted fluorobenzenes, correlating with the inductive substituent constants alone.[14] We assume, to a first approximation, that the solvent-modified substituents remain essentially the same in the same solvent regardless of change of the system from acetanilides to *m*-substituted fluorobenzenes. In Fig. 6 the inductive quantities, $(\sigma_i)_{\mathrm{DMSO}}$ for $+R$ groups (Table 3) and those derived from Eq. (11) for $-R$ groups, are plotted against $\Delta\delta^{\mathrm{F}}_{m-\mathrm{X}}$ in DMSO. The $+R$ groups satisfy a linear correlation, while almost

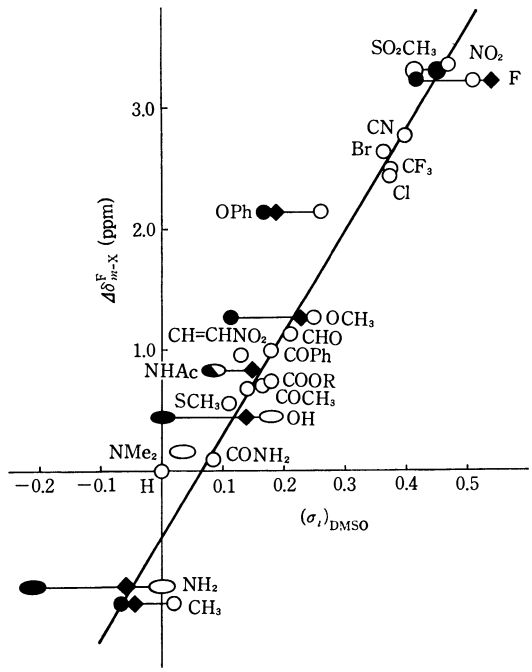

Fig. 6. The plot of ^{19}F substituent chemical shifts of *m*-substituted fluorobenzenes against DMSO-modified inductive substituent parameters, σ_i: open circles $(\sigma_i)^{\mathrm{OH}}_{\mathrm{DMSO}}$, closed circles $(\sigma_i)^{\mathrm{NH}}_{\mathrm{DMSO}}$, and squares $(\sigma_i)^{\mathrm{Corr}}_{\mathrm{DMSO}}$.

all $-R$ substituents deviate considerably from the correlation line. The fit of $+R$ substituents is excellent (correlation coefficient 0.986 and standard deviation ± 0.024) so that the correlation can give rise to a set of the inductive measure $(\sigma_i)^{\mathrm{F}}$, by

$$(\sigma_i)^{\mathrm{F}} = 0.118\Delta\delta^{\mathrm{F}}_{m\text{-}\mathrm{X}} + 0.066$$

As 0.85 for the *para/meta* inductive ratio is presumed to be valid for $-R$ groups in this system, the relative π-electronic contribution should be proportional to the quantities $(\bar{\sigma}_p - 0.85\,\bar{\sigma}_m)$. This gives the following equation concerning the π-electronic effect of $-R$ class substituent.

$$\bar{\sigma}_p{}^{\mathrm{NH}} - (\sigma_i)^{\mathrm{F}} = \gamma(\bar{\sigma}_p - 0.85\bar{\sigma}_m)^{\mathrm{NH}} \qquad (12)$$

The best-fit gave γ value of 2.36 for $-R$ groups in the acetanilide system. The $(\sigma_\pi^+)^{\mathrm{Corr}}_{\mathrm{DMSO}}$ values derived on this basis and $(\sigma_i)^{\mathrm{Corr}}_{\mathrm{DMSO}}$ values given by $\sigma_p - (\sigma_\pi^+)^{\mathrm{Corr}}_{\mathrm{DMSO}}$ are given in Table 4 in comparison with those from the phenol chemical shifts. $(\sigma_i)^{\mathrm{Corr}}_{\mathrm{DMSO}}$ for $-R$ substituents satisfy the correlation determined by $+R$ groups with an excellent precision (Fig. 6); especially, the sub-

Table 4. Modified substituent parameters in DMSO for $-R$ groups

No.	Subst.	Acetanilides		Phenols	
		$(\sigma_\pi^+)^{\mathrm{Corr}}_{\mathrm{DMSO}}$	$(\sigma_i)^{\mathrm{Corr}}_{\mathrm{DMSO}}$	$(\sigma_\pi^+)^{\mathrm{OH}}_{\mathrm{DMSO}}$	$(\sigma_i)^{\mathrm{OH}}_{\mathrm{DMSO}}$
1	F	−0.45	0.54	−0.49	0.51
2	OC_6H_5	−0.11	0.19	−0.25	0.26
3	NHAc	−0.26	0.15	−0.21	0.10
4	CH_3	−0.09	−0.04	−0.18	0.02
5	OCH_3	−0.42	0.23	−0.52	0.25
6	OH	−0.53	0.14	−0.64	0.18
7	NH_2	−0.56	−0.06	−0.64	0.00

stituents carrying acidic hydrogen at the α-position are brought closer to the line. The excellent fit of $-R$ substituents suggests that the quantity $(\bar{\sigma}_p - 0.85\,\bar{\sigma}_m)$ measures the relative capabilities of the π-electronic contributions of solvent-modified substituents, even though the γ value is not 1/0.575 expected for the system of the σ^0 class. On the other hand, the phenol system gives a correlation for $-R$ groups using $(\sigma_i)^F$ values;

$$\bar{\sigma}_p{}^{OH} - (\sigma_i)^F = (1.00+0.08)(\sigma_\pi{}^+)_{DMSO}.$$

The unit slope indicates that the scale of the π-electronic effect parameters estimated from the phenol system is reasonable, while deviations of $-R$ groups are considerably large.

The best correspondence to $\Delta\delta^F_{m-X}$ is observed with $(\sigma_i)^{Corr}_{DMSO}$ parameters (Fig. 6). Accordingly, $(\sigma_\pi{}^+)^{Corr}_{DMSO}$ derived from acetanilides seems to give a better measure of the π-electronic effect of solvent-modified substituents in DMSO than the other, while it is necessary to justify the higher γ value for the acetanilides before one may draw any conclusion. The identity of the apparent $\bar{\sigma}_p$ values of $-R$ groups in acetanilides and phenols indicates that the resonance contribution scale of $-R$ *para* groups, $q_r{}^+$ or r^+, should be essentially the same in both systems. The ambiguity of the contribution scale of π-electronic effect of *p*-substituents in either system, even if they differ from the σ^0-scale, does not theoretically cause any serious deviation in the γ-value. The contradiction has to be ascribed only an inadequate estimation of the contribution scale of resonance from *meta* substituents. The high γ-value requires the enhanced resonance contribution from *meta* substituents. The $-R$ *meta* groups exert more enhanced electron release in the NHAc than in the phenol chemical shifts. The apparent *meta* substituent constants $\bar{\sigma}_m^{NH}$ can be correlated with $\bar{\sigma}_m^{OH}$, taking into account the resonance exaltation in terms of modified LArSR equation:

$$\bar{\sigma}_m{}^{NH} = 1.03\bar{\sigma}_m{}^{OH} + 0.14(\sigma_\pi{}^+)$$

This means that the relative resonance effect of $-R$ *meta* substituents in the acetanilides is some 20% more effective than that in the phenol system. The resonance exaltation of *meta* substituents is unusual in general chemical reactivities in which the *meta* resonance remains constant $0.50\,\sigma_\pi{}^\pm$ regardless of the nature of substituents and independent of the type of reactions,[5] as evidenced by general reaction-independency of σ_m constants.

On the other hand, it has been pointed out that NMR chemical shifts of the proton attached to the *meta*-position relative to substituents do not precisely correlate with σ_m but rather with $\sigma_p{}^0$ values.[15] A plausible explanation for this behavior, based on the ring-current model, was proposed by Yukawa and co-workers:[16] The benzene ring current should be disrupted by the disturbance of π-electron distribution with the exo-delocalization with conjugative (either $-R$ or $+R$) substituents. Such an effect may be parallel to the capability of substituents to alter the π-electronic distribution; that is, parallel to $\sigma_\pi{}^\pm$ values. It would follow from this concept that the $-R$ substituents give the apparent resonance exaltation in the *meta* proton chemical shifts. The enhanced π-electronic contribution from *meta*-substituents in the present system can be explained if such an effect is effective in the chemical shifts of hydrogen-bonded NH proton of the acetanilides.

Experimental

Almost all *m*- and *p*-substituted acetanilides were prepared by the acetylation of substituted anilines with acetic anhydride sometimes with addition of pyridine. Anilines made available from other studies of substituent effects were used. The melting points and other physical constants agreed with established values.

References

1) a) Presented in summary at the first IUPAC Symposium on Physical Organic Chemistry at Cran sur Sierre, Switzerland, September, 1972. b) To whom inquiries should be addressed.

2) Y. Tsuno, M. Fujio, Y. Takai, and Y. Yukawa, This Bulletin, **45**, 1519 (1972).

3) M. Fujio, M. Mishima, Y. Tsuno, Y. Yukawa, and Y. Takai, *ibid.*, **48**, 2127 (1975).

4) Y. Tsuno, M. Fujio, and Y. Yukawa, *ibid.*, **48**, 3324 (1975).

5) a) Y. Yukawa and Y. Tsuno, *Nippon Kagaku Zasshi*, **86**, 873 (1965); Y. Yukawa and Y. Tsuno, *Memoir, ISIR* Osaka *Univ.*, **23**, 71 (1966). b) Y. Yukawa and Y. Tsuno, This Bulletin, **32**, 960, 965, 971 (1959); Y. Yukawa, Y. Tsuno, and M. Sawada, *ibid.*, **39**, 2274 (1966); Y. Yukawa, Y. Tsuno, and M. Sawada, *ibid.*, **45**, 1198 (1972).

6) M. Hojo, M. Utaka, and Z. Yoshida, *Tetrahedron Lett.*, **1966**, 19, 25; *Tetrahedron*, **27**, 2713, 4013, 4255 (1971); C. D. Ritchie and G. H. Megerle, *J. Amer. Chem. Soc.*, **89**, 1447 (1967); C. D. Ritchie and R. E. Uschold, *ibid.*, **90**, 3415 (1968); C. D. Ritchie and E. S. Lewis, *ibid.*, **84**, 591 (1962); A. Fischer, G. J. Leary, R. D. Topsom, and J. Vaughan, *J. Chem. Soc. B*, **1967**, 846; C. D. Ritchie and R. E. Uschold, *J. Amer. Chem. Soc.*, **90**, 2821 (1968); T. Matsui and N. Tokura, This Bulletin, **44**, 756 (1971).

7) a) J. Bennett, M. Delmas, and J. C. Maire, *Org. Magnetic Resonance*, **1**, 319 (1969); b) I. D. Rae, *Can. J. Chem.*, **46**, 2589 (1968); J. M. Appleton, B. D. Andrews, I. D. Rae, and B. E. Reicher, *Aust. J. Chem.*, **23**, 1667 (1970).

8) J. Niwa, This Bulletin, **42**, 1926 (1969).

9) Y. Asaba and Y. Tsuzuki, *ibid.*, **44**, 3482 (1971).

10) 38 data points were included into calculation; *m*- and *p*-halogens, cyano, acetoxy groups and *p*-phenylazo, *p*-phenyl and thiocyano groups were excluded.

11) M. T. Tribble and J. G. Traynham, "Advances in Linear Free Energy Relationships," N. B. Chapman and J. Shorter, Ed., Chapt. 4, Plenum (1972), p. 143.

12) a) P. R. Wells, S. Ehrenson, and R. W. Taft, "Progress in Physical Organic Chemistry," Vol. 6 (1968), p. 147. b) S. Ehrenson, R. T. C. Brownlee, and R. W. Taft, *ibid.*, Vol. 10 (1973), p. 1. The authors are indebted to Prof. R. W. Taft for making these data available prior to publication.

13) M. Fujio, PhD thesis, March, 1972, Osaka University.

14) R. W. Taft, E. Price, I. R. Fox, I. C. Lewis, K. K. Andersen, and G. T. Davis, *J. Amer. Chem. Soc.*, **85**, 709 (1963); J. Hirst and S. J. Una, *J. Chem. Soc., B.* **1969**, 646.

15) Y. Yukawa, Y. Tsuno, and N. Shimizu, This Bulletin, **44** 2843 (1971).

16) H. Yamada, Y. Tsuno, and Y. Yukawa, *ibid.*, **43**, 1459 (1970).

The Substituent Effect. VIII. Solvolysis of *m*- and *p*-Substituted α-Methylbenzyl Chlorides

Yuho Tsuno,* Yoshiaki Kusuyama, Masami Sawada, Takahiro Fujii, and Yasuhide Yukawa

The Institute of Scientific and Industrial Research, Osaka University, Suita, Osaka 565

(Received December 10, 1974)

The rates of solvolysis of twenty-two *m*- and *p*-substituted α-methylbenzyl chlorides were determined in 80% aqueous acetone. The relative rates at 45 °C are not correlated linearly with σ^0 or σ. The use of Brown's σ^+ improves the fit but the resulting correlation is still concave. An excellent correlation, $\log k/k_0 = -4.950$ ($\sigma^0 + 1.147\,\Delta\bar{\sigma}_R^+$), was obtained by applying the LArSR equation. The r value 1.15 suggests that the π-electronic contribution relative to the inductive contribution of $-R$ *para* substituents at the transition states differs with reaction, and is more important in the present α-methylbenzyl than Brown's *t*-cumyl solvolysis ($r = 1.00$ by definition). A set of $\Delta\bar{\sigma}^+$ and σ^+ corresponding to the substituent constants for unit r were calculated. The calculated σ^+ values are in precise agreement with Brown's primary σ^+ values. The generality of the LArSR equation and some new substituent constants are illustrated.

Although Brown's $\rho\sigma^+$ treatment is successful for describing substituent effects in the solvolysis and aromatic substitutions,[1] there is substantial evidence that the actual blend of inductive and resonance effects varies with reaction.[2,3] Taking this into account, we proposed the equation,

$$\log (k/k_0) = \rho(\sigma^0 + r\Delta\bar{\sigma}_R^+) \quad (1)$$

and illustrated its applicability to various electrophilic reactions.[4-6] σ^0 is the normal substituent constant which does not involve any additional π-electronic interaction between substituents and the reaction center. $\Delta\bar{\sigma}_R^+$ is the resonance substituent constant measuring the capability for π-electron delocalization of conjugatively electron releasing ($-R$) substituents and is defined by $\sigma_p^+ - \sigma_p^0$. The r parameter is the resonance reaction constant describing the required resonance stabilization of the transition state of given reaction; $r = 1.00$ is referred to Brown's σ_p^+ scale and $r = 0.00$ to the unexalted σ_p^0 scale. Equation (1) has been employed for various reactivity data.[7,8] In order to confirm the applicability and the possible limitation of our treatment, it is necessary to reconfirm the validity of the required substituent parameters. Since the resonance substituent constant $\Delta\bar{\sigma}_R^+$ is based on two reference sets of substituent constants σ^0 and σ^+, our studies have been carried out along two principal lines of reconfirmation of both reference sets of the substituent parameters.[9] For the reexamination of σ^+ as well as $\Delta\bar{\sigma}_R^+$, we need data of the effects of a variety of substituents on the solvolytic system similar to Brown's reference reaction. Only a few data were available to test the applicability of Eq. (1). The system to be studied should be a simple reaction having a similar transition state to Brown's system. The solvolysis of *m*- and *p*-substituted α-methylbenzyl chlorides was chosen for study. The kinetic data of this series appear to be important in connection with the comparison of substituent effects in secondary and tertiary carbonium ion reactions. Results of several less extensive studies on this system are available,[10-12] but none are satisfactory.

We carried out kinetic studies of the solvolysis of various series of substituted arylmethylcarbinyl chlorides in various solvents. Parts of the results have been reported.[6,13,14] Several sets of interesting data of similar kinetic studies have also been reported.[14-16] A complete set of our data is presented with a discussion in comparison with the relevant data. Our studies include the solvolysis of substituted phenyl-, α-naphthyl,[17] 3′- and 4′-substituted biphenyl-,[18a] and 7-substituted 2-fluorenyl-[18b] derivatives.

The present paper is concerned with the substituent effects on the solvolysis of *m*- and *p*-substituted α-methylbenzyl chlorides in 80% aqueous acetone.

Results and Discussion

The rates of solvolysis of *m*- and *p*-substituted α-methylbenzyl chlorides were determined in 80% aqueous acetone at convenient temperatures to give moderate rates for respective derivatives. All the runs followed accurately the first order kinetic law, the rate constants being obtained with accuracy of 1%, except for *p*-methoxy derivative. Rate constants (Table 1) are in good agreement within the usual accuracy with the values in literature. Extrapolation of these data was made solely by means of the Arrhenius equation at 45 °C. The relative rate varies remarkably with substituent changes over a range of six powers of ten, and the reactivities for both the highest and lowest ends are not presumed to be less reliable. Especially for *p*-methoxy derivative a rather large uncertainty will be expected because of experimental difficulties in measuring the rapid reaction at extremely low temperatures and uncertainty in the extrapolation to 45 °C. *m*-Halogen derivatives may also involve somewhat large uncertainty because of extrapolation from measurements at temperatures higher than the boiling point of the solvent. From remarkable divergence of the reactivities, however, minor errors involved are not expected to affect the following discussion of the substituent effect. Logarithms of relative rates at 45 °C are linearly correlated in excellent precision ($s = \pm 0.030$, $R = 0.9999$) with those at 25 °C giving a slope of 0.9615. The same

* To whom inquiries should be addressed. Department of Chemistry, Faculty of Science, Kyushu University, Hakozaki, Fukuoka 812.

Table 1. Solvolysis rates of *m*- and *p*-substituted α-methylbenzyl chlorides in 80% aqueous acetone

Subst.	Temp. °C	10^5k s^{-1}	$(k/k_0)_{45°C}$	E_a kcal mol^{-1}	log A
H	45.00	0.729; 0.733[c]	1.00	22.2	10.14
	55.00	2.13			
	65.00	5.84			
p-CH_3O	−30.0	7.89; 8.03[c]	5.8×10^4	17.6	11.69
	−21.0	28.0			
	−15.0	65.6[c]			
	−13.9	77.8			
	45.0	42000[a]			
p-CH_3S	−15.0	2.64	3.33×10^3	18.7	11.20
	−10.0	4.77			
	−5.00	9.90			
	0.00	18.8			
	3.00	28.1			
	5.00	34.0			
	10.00	63.1			
	45.00	2430[a]			
p-C_6H_5O	3.00	8.67	1.23×10^3	19.3	11.19
	10.00	21.1			
	20.00	66.9			
	45.00	894[a]			
2-Fluorenyl	0.00	1.940	554	20.4	11.63
	3.00	3.08			
	12.00	9.69			
	15.00	13.15			
	18.00	19.5			
	25.00	46.5; 47.9[c]			
	45.00	404[a]			
p-CH_3	45.00	31.0; 31.8[c]	42.5		
p-C_2H_5	45.00	24.9	34.2		
p-*i*-Pr	45.00	19.8	27.2		
p-*t*-Bu	45.00	14.4	19.8		
p-C_6H_5	39.65	4.16	10.4	21.5	10.65
	45.00	7.98; 8.57[c]			
	49.75	12.97			
	55.00	20.72			
2-Napht	45.00	5.18; 5.03[c]	7.11		
m-CH_3	45.00	1.46	2.00		
p-F	45.00	2.11	2.89		
m-CH_3O	55.00	1.26	0.584	22.6	10.16
	70.00	5.87			
	80.00	14.6			
	45.00	0.426[a]			
m-C_6H_5	70.00	2.96	0.288	23.0	10.14
	80.00	8.72			
	90.00	19.0			
	45.00	0.210[a]			
m-CH_3S	70.00	1.81	0.176	23.0	9.91
	80.10	4.76			
	90.00	11.6			
	45.00	0.128[a]			
p-Cl	55.00	0.711	0.331	22.2	9.61
	60.00	1.18			
	70.00	3.14			
	80.00	7.94			
	45.00	0.246[a]			
p-Br	54.90	0.419[c]	0.207	22.9	9.85
	60.00	0.802			
	70.00	2.07			
	80.00	5.06			

Table 1 (continued)

Subst.	Temp. °C	$10^5 k\ s^{-1}$	$(k/k_0)_{45°C}$	E_a kcal mol^{-1}	log A
	45.00	0.151[a]			
p-I	70.00	2.38	0.248	22.5	9.68
	80.00	6.29			
	90.00	14.6			
	45.00	0.181[a]			
m-F	80.00	0.626	0.0213		
	45.00	0.0155[b]			
m-Cl	70.00	0.146	0.0133	23.6	9.19
	80.00	0.393			
	90.00	1.53			
	45.00	0.00969[a]			
m-Br	70.00	0.134	0.0113	24.2	9.53
	80.00	0.366			
	90.00	1.49			
	45.00	0.00826[a]			

a) Extrapolated from the rate constant at other temperatures by the Arrhenius equation. b) Estimated from the rate constant at 80°C on the basis of linear log k–log k relation between the rates at 80°C and those at 45°C. c) Average values of repeated determinations.

is true in the log-log plot of relative rates at 45 °C *vs.* those at 80 °C. Thus, an arbitrary choice of the reference temperature 45 °C also does not affect the present discussion, except for the minor temperature effect on the ρ-value.

As anticipated for the typical benzylic S_N1-solvolysis reactions, σ^0 or σ is unable to correlate linearly the present reactivity data as shown by the σ-plot in Fig. 1, in which *meta* substituents fall on a straight line to give a ρ_m value of -4.964 ± 0.025, but all $-R$ *para* substituents deviate upwards from the *meta* line. Brown's σ^+ provides a much better correlation (Fig. 2) with a ρ^+ value of

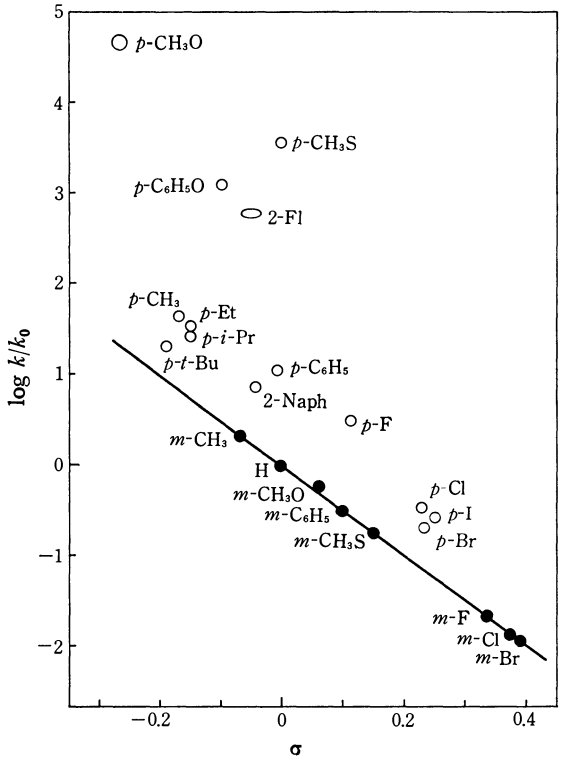

Fig. 1. Hammett plot of the solvolysis of α-methylbenzyl chlorides in 80% aq. acetone at 45 °C.

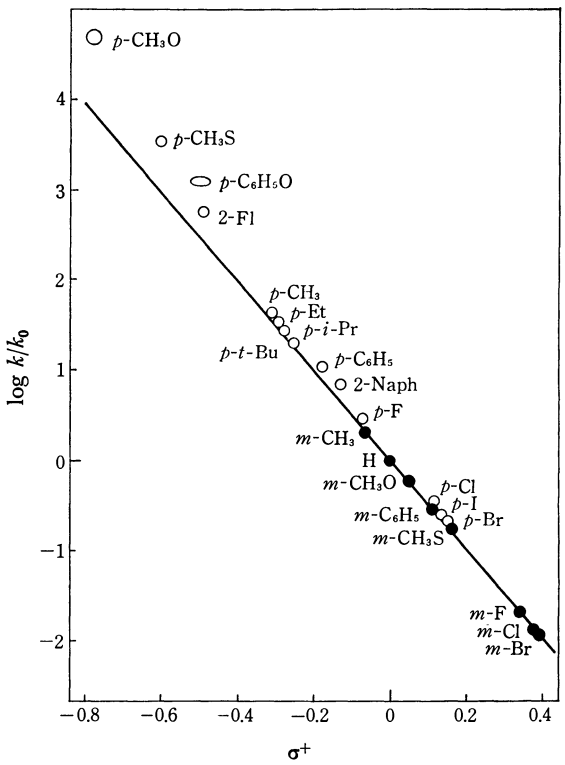

Fig. 2. Hammett-type plot against Brown's σ^+.

-5.51 (standard deviation ±0.17 and correlation coefficient 0.995). The line is not for the best fit correlation but is drawn through the points for *m*-substituents. The best-fit ρ^+ value is considerably higher (more negative) than the ρ_m value based on *meta* substituents. Points for weakly conjugative *para* groups appear to fall near the the ρ_m-line, whereas strongly electron-releasing ($-R$) groups, such as *p*-methoxy, *p*-phenoxy, 2-fluorenyl and *p*-methylthio groups, deviate significantly to the direction of enhanced reactivity from the ρ_m-line. Excluding four such faster reacting groups, an improved partial σ^+ correlation within a range of substituents from *p*-methyl

to *m*-bromo groups can be obtained with correlation coefficient 0.999 and standard deviation ±0.057, to give $\rho^+ = -4.980 \pm 0.060$, which is close to the ρ_m value. This indicates that Brown's $\rho\sigma^+$ treatment can practically be applied to the present reactivity set only within a limited range of weakly conjugative substituent groups. Even though the deviation of *p*-methoxy group might be ascribed to the error in its relative rate at 45 °C due to experimental difficulties, such serious errors are not expected for the rates of *p*-phenoxy and *p*-methylthio-derivatives. Deviation of these substituents should be due to difference in stabilization of the transition states between the present and cumyl system. The overall $\rho\sigma^+$ correlation is represented by a smooth upward curvature.[19] Brown's treatment can not describe adequately the effect of strongly electron-donating *para* substituents in the present reaction.

From the above ρ_m value, we can derive a set of apparent substituent constants ($\bar{\sigma}$) of the σ^+-type from the relative rates of the present solvolysis by

$$\bar{\sigma} = (\log k/k_0)/(-4.964)$$

As an operational definition, this set of apparent substituent constants are completely independent of and should be equivalent in nature to Brown's σ^+ parameters determined by the same procedure from the *t*-cumyl solvolysis rates. The apparent σ values for *m*-substituents, $\bar{\sigma}_m$, agree precisely with Brown's $\bar{\sigma}_m{}^+$, even better than with the standard σ_m values, while the σ values for all *—R para* substituents (Table 2) are consistently more negative than the corresponding Brown's σ^+ values. This suggests that the additional resonance contribution from *—R para* substituents is more important in the transition state of the secondary benzylic carbonium ion structure than in the latter tertiary carbonium ion transition state, and that there is no unique set of σ^+ constants applicable to electrophilic exalted resonance type reactivities. The blend of resonance and inductive effects represented by Brown's σ^+ constants appears to be only a sufficiently good average to fit most cases. The varied contribution of the resonance effect can be taken into account, as a precise approximation, by application of Eq. (1) from which it immediately follows that

$$(\log k/k_0)/\rho = \sigma^0 + r\Delta\bar{\sigma}_R{}^+ \qquad (2)$$

This indicates that the exaltation of apparent $\bar{\sigma}_p$ from σ^0,

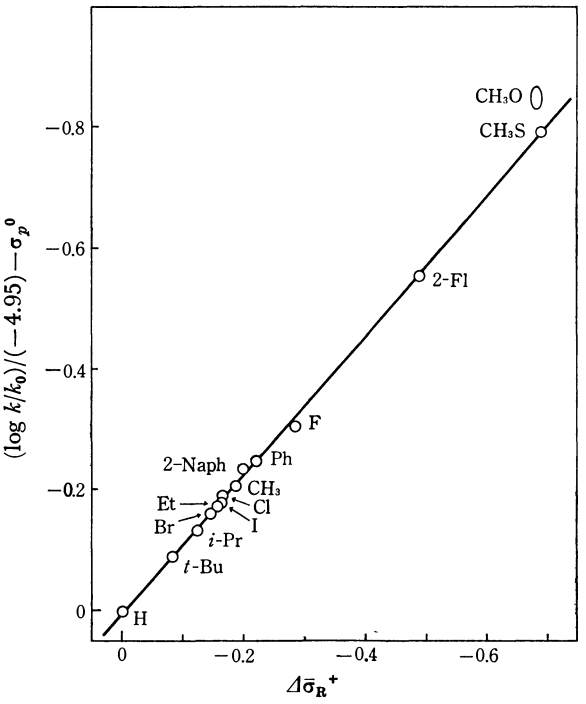

Fig. 3. Plot of the apparent resonance exaltation, (log *k*/*k*$_0$)/(−4.95) $-\sigma_p{}^0$, in the solvolysis against $\Delta\bar{\sigma}_R{}^+$

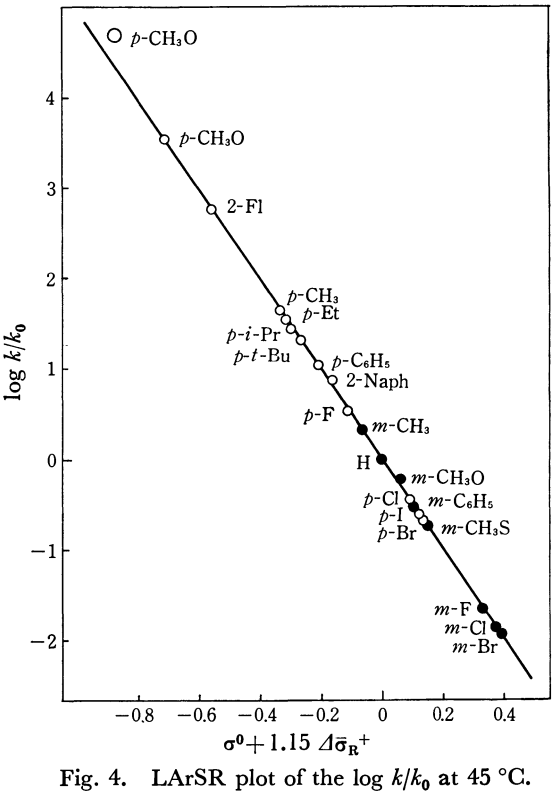

Fig. 4. LArSR plot of the log k/k_0 at 45 °C.

Table 2. Calculated values of substituent parameters

Subst.	$\bar{\sigma}$[a]	$(\Delta\bar{\sigma}_R{}^+)_{calcd}$[b]	σ^+_{calcd}	σ^+[d]
p-CH_3O	−0.959	−0.755	−0.855	−0.778
p-CH_3S	−0.709	−0.697	−0.614	−0.604
p-C_6H_5O	−0.622	−0.602	−0.539	(−0.5)
2-Fluorenyl	−0.553	−0.487	−0.486	−0.490
p-CH_3	−0.328	−0.182	−0.306	−0.311
p-C_2H_5	−0.309	−0.160	−0.291	−0.295
p-*i*-Pr	−0.289	−0.120	−0.276	−0.280
p-*t*-Bu	−0.261	−0.080	−0.254	−0.256
p-C_6H_5	−0.205	−0.219	−0.180	−0.179
2-Napht	−0.172	−0.207	−0.145	−0.135
p-F	−0.093	−0.270	−0.058	−0.073
p-Cl	0.093	−0.167	0.114	0.115
p-Br	0.138	−0.141	0.155	0.150
p-I	0.122	−0.157	0.141	0.135
H	0.000	0.000	0.000	0.000

a) Apparent $\bar{\sigma}$ values given by $\bar{\sigma} = \log k/k_0/(-4.964)$; use of $\rho = -4.950$ instead of $\rho_m = -4.964$ does not affect the results. b) Giving by $[\log k/k_0/(-4.950) - \sigma_p{}^0]/1.15$. c) $\sigma^+ = (\Delta\bar{\sigma}^+{}_R)_{calcd} + \sigma_p{}^0$. d) Brown's primary σ^+ values taken from Ref. 1.

the quantities $(\log k/k_0)/\rho-\sigma^0$, should be proportional to the resonance parameter $\Delta\bar{\sigma}_R^+$. Figure 3 illustrates such a plot. The slope should correspond to the r value. It is obvious that there is no trend of curvature in the plot but only the *p*-methoxy group clearly deviating from the line. The deviation can be attributed to the error in the relative rate of this group. The linear plot offers confirmation of the validity of our LArSR relationship. The ordinary LArSR plot for the present reaction is shown in Fig. 4. No trend of curvature except for the *p*-methoxy group is indicated. Least squares calculation gives a ρ-value −4.953 and r 1.147 excluding *p*-methoxy group (standard deviation ±0.040 and correlation coefficient 0.9997). Substituent constants utilized are given in

Table 3. Substituent parameters

Subst.	σ_m^0	σ_p^0	$\Delta\bar{\sigma}_R^+$
CH_3O	0.060	−0.100	−0.678
CH_3S	0.15	0.083	−0.687
C_6H_5O		0.063	
2-Fluorenyl		0.001	−0.491
CH_3	0.069	−0.124	−0.187
C_2H_5		−0.131	−0.164
i-Pr		−0.156	−0.124
t-Bu		−0.174	−0.082
C_6H_5	0.10	0.039	−0.218
2-Napht		0.062	−0.197
F	0.337	0.212	−0.285
Cl	0.373	0.281	−0.167
Br	0.391	0.296	−0.146
I		0.298	−0.163

Table 3. The ρ-value is identical within experimental uncertainty to the ρ_m value based on *m*-substituents alone and appreciably less than that given by the σ^+-resorting. The high r-value is consistent with the view that the resonance contribution from $-R$ *para* substituents to the stabilization of the transition state is more important in the present series than in Brown's cumyl system. Putting $r=1.15$ and $\rho=-4.950$ in Eq. (1), we can obtain a calculated set of $\Delta\bar{\sigma}_R^+$ values and a secondary set of σ^+ values in Brown's scale ($r=1.00$). They are compared with Brown's primary values (Table 2). Both sets of σ^+ are in precise agreement within ±0.007 in σ unit for all *para* substituents except the *p*-methoxy group. The rates of solvolysis of several polynuclear arylmethylcarbinyl chlorides under the same conditions[12] have been treated on the basis of the above correlation in order to derive the σ^+ and $\Delta\bar{\sigma}_R^+$ constants for these aryl moieties as derivatives of the parent phenyl compound. The applicability of these parameters for other reactions was shown in a previous paper.[13] Kusuyama and Ikeda[14a] recently determined the rates of hydrolysis of *p*-cyclopropyl- and *p*-(β,β-dichloro-cyclopropyl)-α-methylbenzyl chlorides and obtained, on the basis of the above correlation, the σ^+ and $\Delta\bar{\sigma}_R^+$ constants for cyclopropyl and β,β-dichlorocyclopropyl groups.[14a] The results are given in Table 4. The σ_p^+ for *p*-cyclopropyl group is consistent with the estimation from the *t*-cumyl reactivity.[14] The particularly large $\Delta\bar{\sigma}_R^+$ value of −0.36 as compared with ordinary alkyl groups is striking, and suggests that the donating resonance power of this group is roughly close to that of

Table 4. Estimation of substituent parameters

Substrate	$\bar{\sigma}$ [a]	σ^0 [b]	$(\Delta\sigma_R^+)_{calcd}$ [c]	σ^+_{calcd} [d]
Phenyl	0.000	0.000	0.000	0.000
4-Biphenylyl	−0.212	0.039	−0.219	−0.180
	−0.209[e]			
2-Naphthyl	−0.176	0.062	−0.207	−0.145
	−0.174[e]			
2-Phenanthryl	−0.144[e]	0.131	−0.240	−0.109
3-Phenanthryl	−0.230[e]	0.109	−0.296	−0.187
2-Fluorenyl	−0.558	0.001	−0.487	−0.486
9-Phenanthryl	−0.197[e]	0.113	(−0.270)[g]	(−0.157)[g]
1-Naphthyl	−0.251[f]	0.048	(−0.239)[g]	(−0.191)[g]
p-c-C_3H_5-phenyl	−0.515[h]	−0.10[h]	−0.362	−0.462[i]
p-c-$C_3H_3Cl_2$-phenyl	−0.019[h]	0.05[h]	−0.06	−0.01

a) Apparent substituent constant given by $\bar{\sigma}=(\log k/k_0)/(-4.950)$. b) Taken from Ref. 13. c) Calculated by $(\bar{\sigma}-\sigma^0)/1.147$. d) $\sigma^+_{calcd}=\sigma^0+(\Delta\bar{\sigma}_R^+)_{calc}$. e) Ref. 12. f) Ref. 17. g) The parameter value does not appear to be practically applicable because of the reaction-dependent *peri*-effect. h) Ref. 14a. i) Shechter reported the same value of the primary σ^+ (Ref. 14b).

2-fluorenyl and much stronger than that of *p*-phenyl or ordinary alkyl groups.

The σ^+ values for *p*-methylthio, *p*-phenoxy, and 2-fluorenyl have seldom been applied to typical electrophilic reactions and have not yet been examined in detail. For the *p*-phenoxy group even the primary σ^+ value has not been determined. The present results will thus give some support for validity of σ^+ values for these groups. Clementi *et al.* studied the effect of *p*-CH_3S group on electrophilic aromatic substitutions in order to confirm the reliability of the σ^+ value and also illustrated far better results with LArSR treatment of the reactions whose r values differ from unity.[20a]

Equation (2) implies that, as a good approximation, the variation of apparent substituent constants of a given *para* substituent should be a linear function of r for varying reaction. The slope of the relation should correspond to the $\Delta\bar{\sigma}_R^+$ and the intercept to the σ^0 of the substituent.

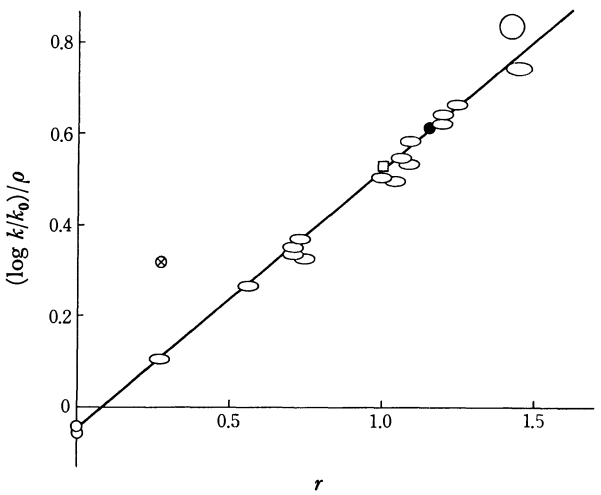

Fig. 5. Plot of the apparent substituent constants, $\bar{\sigma}=(\log k/k_0)/\rho$, for *p*-phenoxy group against r.
●: present study, □: σ^+_{calc}, ⊗: pK_a of benzoic acids.

Ordinary substituents satisfy this relation.[5] Figure 5[20c] shows the plot for *p*-phenoxy group. Both $\Delta\bar{\sigma}_R^+$ and σ^0 for this group estimated from this correlation are in good agreement with the above values, suggesting its applicability to various reactions. Similarly good correlations are obtained for *p*-phenyl and 2-fluorenyl derivatives.[5,13]

The *p*-methoxy group is in most cases the only substituent which has a particularly large $\Delta\bar{\sigma}_R^+$ value as compared with other ordinary substituents, such as alkyls and halogens. The best fit correlation should thus be determined most effectively by the *p*-methoxy group and might be constrained by the error involved in its reactivity. Since the above three groups, *p*-CH_3S, *p*-C_6H_5O, and 2-fluorenyl, are sufficiently stable under ordinary solvolytic conditions, use of these groups may be recommended as a good alternative of *p*-methoxy group for the correlational analysis of substituent effects and as auxiliary substituents for estimation of $-R$ resonance requirement of given reactions.

The point for the pK_a of benzoic acids in Fig. 5 deviates seriously from the correlation line, while the points for the saponification of benzoic esters and other σ-type reactivities having the comparable *r*-value (round 0.28) fall on the line. This suggests a limited applicability of the σ-value-0.32, recommended by Brown and McDaniel.[21] The σ value of -0.10 derived from the hydrolysis of substituted ethyl benzoates in aq. ethanol[22] is in accord with the calculated value from the above correlation (Fig. 5).

Another fact of interest is observed in the behavior of *p*-phenyl substituent. The lower $\Delta\bar{\sigma}_R^+$ value of *p*-phenyl group, or the smaller slope in the apparent $\bar{\sigma}$ *vs.* *r* plot, than that of 2-fluorenyl indicates a considerable decrease in the transition state resonance due to the deviation from the coplanarity of both benzene rings in the former. Stock and Brown suggested,[23] on the basis of their observation of a non-linear selectivity relation for *p*-phenyl but for fluorenyl derivatives in electrophilic aromatic substitutions, that the substituent phenyl-ring in the former should be forced to lie in a nearer coplanarity to get a maximum possible overlap of both π-systems as the demand of donative resonance of the reaction site becomes larger. On the other hand, Neuman pointed out that the log p_f for 2-fluorenyl was at least as good a linear function of log p_f for *p*-phenyl as that for *p*-methyl, and that the fluorenyl did not fit the selectivity relation much better than *p*-phenyl group.[24] Deviations in these relations were quite large in both plots and the failure of Brown's selectivity treatment is partly associated with variations of *r*-value. It may be expected that the twisting causes certain failure in the $(\log k/k_0)/\rho$ *vs.* *r* correlation for phenyl group. Since *r* can be regarded as a measure of the demand of resonance of the reaction site, the coplanarity of both phenyl rings may increase as the *r* increases, and cause a parallel increase in the resonance power ($\Delta\bar{\sigma}_R^+$) of phenyl group to approach the $\Delta\bar{\sigma}_R^+$ for 2-fluorenyl. No such effect is detectable in the present treatment, the plot for phenyl being as precisely linear against *r* as that for fluorenyl derivative. *p*-Phenyl group appears thus to be a well-behaving $-R$ substituent in the usual electrophilic reactions. As far as the ordinary solvolysis and aromatic electrophilic substitution reactions are concerned, the changes in the electron deficiency of reactions cause no significant changes in the twisting angle of the biphenyl at the transition states of varied reactions.

We see that the LArSR equation can describe the present reaction far more precisely than Brown's $\rho\sigma^+$ treatment. However, a sophisticated treatment with an additional term should give more satisfactory results than the simpler treatment. From a practical point of view the simpler $\rho\sigma^+$ treatment can provide satisfactory correlation for the present system within the limit of usual accuracy of linear free energy relationships. This is not inconsistent with the significance of the additional resonance parameter, because we have chosen the present reaction as the reference reaction mechanistically close to Brown's reference reaction. Essentially a small difference in the *r*-value between the present and Brown's reference reactions may not result in significant improvement of the correlation with the LArSR treatment.

Brown estimated the secondary σ^+ values for polynuclear aryl moieties from the solvolysis of α-arylethyl chlorides,[12] on the basis of a linear log *k*–log *k* relation of 4 common derivatives.[25] The σ^+ values compared in Table 4 are in good agreement with ours. The σ^+ treatment seems to be practically applicable to the solvolysis of α-arylethyl chlorides including these polynuclear aryl derivatives, even if the applicability might be limited in the choice of substituents as well as in accuracy. Streitwieser *et al.*[16] demonstrated the applicability of a set of σ^+ for these moieties to several benzylic carbonium ion reactions. The σ^+ was applied to the desilylation of aryltrimethylsilanes[26] and also to the pK_{BH}^+ of aryl methyl ketones.[13] The results support Brown's single σ^+ treatment, as a practical approximation of the simple linear free energy relationship, in a broad range

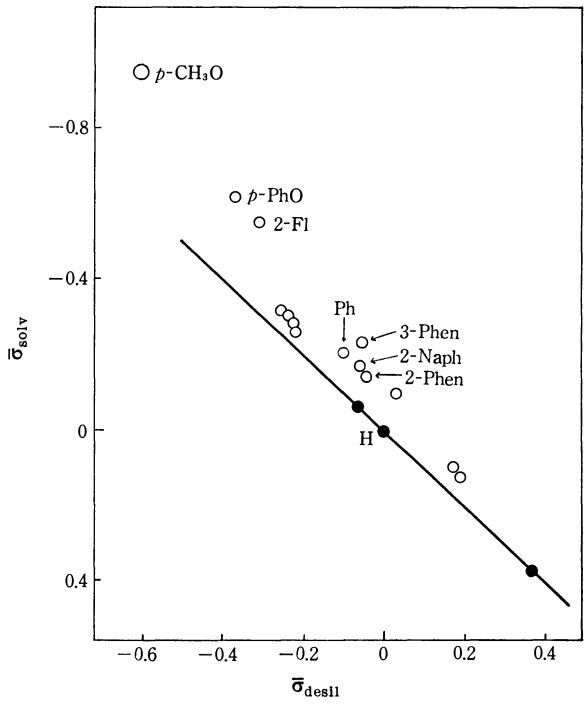

Fig. 6. Correlation of the apparent substituent constants between the present solvolysis and protodesilylation.

of electrophilic type conjugation reactions. We are not concerned here with the difference in the precision of fit with Eq. (1) and Brown's basis treatment, since introduction of more parameter should inevitably improve the precision of fit. Nevertheless, it must be pointed out that even through the σ^+ treatment is valid as a practical approximation both for the present solvolysis and the desilylation, the $\bar{\sigma}$ values from both reactions can not correlate linearly with each other (Fig. 6), giving a quite similar pattern to that in Fig. 1. —*R para* substituents as well as polynuclear aryls in Fig. 6 deviate more or less seriously from the *meta*-correlation line, apparently depending upon their resonance capabilities. The partial correlation with respect to polynuclear aryls is of poor quality. This arises from the significant difference in the r values of both reactions 0.7 and 1.15. The correlation between pK_{BH^+} of aryl methyl ketones and the present solvolysis is much the same as above.

σ^+ appears to be the best average to fit most cases and practically applicable within satisfactory precision to the electrophilic reactions having r value in the range 0.8—1.2, while a definite set of σ^+ can not describe the substituent effect in the reaction having the r value outside of this range. Examples are the acetolysis of neophyl brosylates[27] and β,β-diarylethyl tosylates[28] and the like which require r of about 0.5. The r-parameter has been verified to be a useful measure of the degree of resonance contribution from substituents in the rate determining transition state and is applicable to the estimation of the electronic structure of transition states. In a comparison of the solvolysis of benzyl, α-methylbenzyl, and *t*-cumyl chlorides, the r parameter appears to decrease in the order, 1.5 (approximate value), 1.15, and 1.00 as the number of α-methyl substitution increases.[6] The increased stabilization of the charged reaction center at the transition state by the α-methyl group should cause decreased demand of the electron releasing resonance contribution from *para* substituents. This predicts the above decreasing order of r-values. The distinctly low r-value for acetolysis of neophyl brosylates and the related derivatives might indicate the different mechanism of stabilization of the rate determining transition state from that of ordinary benzyl-type carbonium ion reactions.

As a possible factor affording a higher r value in the present reaction, we can not rule out the gradual change in the mechanism within respective series due to incursion of the S_N2-type solvent participation. This effect is observed in the case of substituted benzyl tosylates, for which our treatment fails.[5,6] The solvolysis of α-methylbenzyl chlorides is also a borderline case. The nucleophilic solvent participation might play an important role in the reaction of derivatives carrying stronger electron attracting substituents. The monotonic change in mechanism from limiting S_N1 to non-limiting solvolysis can be expected as the substituent becomes more electron attracting. If this is the case, the σ^+ plot might be monotonically concave upwards and subsequently a lower ρ value given by slow solvolyzing substituents may afford a higher r-value. For such a case, the LArSR equation provides a less precise correlation or none at all as an extreme case.[5,6] Evidently this is not the present case.

From the α-deuterium kinetic isotope effect on the solvolysis of substituted α-methylbenzyl chlorides, Shiner *et al.* suggested that derivatives faster solvolyzing than the unsubstituted were solvolyzed by the limiting mechanism but the reaction of *m*-bromo derivative which had a lower isotope effect should involve the S_N2 character to a certain extent.[15] In contrast, there is no consistent trend in LArSR correlation which might point to mechanistic change related to the substituent change. An excellent quality of the correlation leads to the conclusion that no serious change in mechanism is involved in the present solvolysis in this medium, at least down to *m*-halogen substituted derivatives. The constant isotope effect for faster reacting derivatives suggests that the deviation of *p*-methoxy derivative observed in Fig. 4 is not due to change in mechanism. The lower isotope effect value for *m*-bromo derivative of course does not indicate complete loss of the S_N1 character. Even though the incursion of S_N2 mechanism may be the case, we believe that the influence of concurrent S_N2 to the solvolysis rate is negligible in this group and throughout a series of substituents we examined. Determination of the reactivity should be extended further to the derivatives substituted by more strongly electron attracting groups than *m*-halogen.

Since the S_N2 process or the nucleophilic solvent participation depends on both the nucleophilicity and the ionizing power of the solvent, the effect of solvent changes on the correlation should provide important evidence for the above consideration. However, no noticeable effect was observed by changing solvents from 90% to 50% aqueous acetone, in the correlation of the substituent effects within the same range of substituents.[29] The data of Mechelynch-David and Fierens in less nucleophilic aqueous dioxane–formic acid[10] give a linear free energy correlation with the present data. The acetolysis rates also can be correlated by Eq. (1), giving an r higher than unity.[30] Thus, the high r value is characteristic of the transition state of this reaction. This is further supported by the fact that pyrolysis rates of α-methylbenzyl chlorides are correlated linearly to the present data. No irregularity was observed even in the behavior of strongly electron-attracting *p*-cyano derivative.[31] A strictly linear correlation by Eq. (1) may be taken as a criterion for the operation of a unique mechanism throughout the series of substituted members included.

Experimental

Acetophenones were obtained by the usual Friedel-Crafts acetylation of appropriate substituted benzenes. *m*-Bromoacetophenone was obtained by the bromination of acetophenone in the presence of anhydrous aluminum chloride. *m*-Methoxyacetophenone (bp 135—137 °C/20 mmHg) was obtained by treating *m*-hydroxyacetophenone with dimethyl sulfate in an alkaline solution. *m*-Methylthioacetophenone (bp 127—128 °C/2 mmHg) was prepared by converting *m*-aminoacetophenone with potassium ethylxanthate into the thiophenol, and treating with dimethyl sulfate.

α-Methylbenzyl Alcohols. Acetophenones were reduced with lithium aluminum hydride to the corresponding α-

Table 5. Melting and boiling points of substituted α-methylbenzyl alcohols and the chlorides

Subst.	α-Methylbenzyl alcohol		α-Methylbenzyl chloride	
	observed[a]	lit. value	observed[a]	lit. value
p-OCH_3	81°/0.7mm	109—110°/2.5mm[32]	b)	
p-SCH_3	105°/0.55mm (47—48°)	(38—40°)[33]	(59—59.5°)	
p-OC_6H_5	145—147°/2mm	138—140°/0.7mm[15] 160—162°/2mm[34]	b)	
2-Fluorenyl	(138—138.5°)	(139—140°)[35]	(92—93°)	(90.5—92.0°)[39]
p-CH_3	103°/15mm	102—103°/11mm[36]	64°/3mm	92°/12mm[36]
p-C_2H_5	131—132°/25mm	120°/14mm[37]	70°/4mm	152°/80mm[46]
p-*i*-C_3H_7	95°/3.5mm	127—129°/15mm[38]	81°/4mm	180°/176mm[46]
p-*t*-C_4H_9	104°/4mm	149—153°/30mm[27]	88°/4.5mm	179°/130mm[46]
p-C_6H_5	(97°)	(96.4—97.5°)[39]	(52.0—52.5°)	(52.6—53.7°)[39]
2-Napht	(74°)	(71.3—72.1°)[39]	(68°)	(66.4—67.3°)[39]
p-F	90°/10mm	91°/10mm[40]	47—48°/4.2mm	75°/10mm[36]
H	70°/5mm	93°/16mm[41] 106°/20mm[36]	51—52°/6mm	75°/15mm[36]
m-CH_3	76°/3.5mm	103—105°/6mm[42]	61°/3.8mm	69—73°/2.5mm[36]
m-OCH_3	103—103.5°/1mm	115—120°/5.5mm[43]	73°/1mm	
p-Cl	93.5°/4.5mm	99°/5mm[42]	64°/1.5mm	105°/10mm[36]
m-C_6H_5	163—165°/3mm	146—149°/1mm[44]	147—148°/2mm	
p-I	(50.5—51.5°)	(40°)[45]	92°/0.4mm	
p-Br	114—115°/5 mm	128°/10mm[36]	89.5—90.0°/3mm	72°/1mm[36]
m-SCH_3	125—126°/1.5mm		100°/0.25mm	
m-F	121—122°/4.5mm		64.5—66.5°/6—6.5mm	
m-Cl	95°/4mm	99—104°/4mm[42]	72—73°/5mm	
m-Br	91—92°/2.5mm	108—110°/2mm[42]	66—67°/1.5mm	

a) Boiling point °C (uncorrected) under a given pressure, mmHg. Mp's are given in brackets. b) Used without purification.

arylethyl alcohols in 80—90% yields by the usual procedure. *m*-Methyl, *m*-phenyl, *m*-fluoro, and *m*-chloro-α-methylbenzyl alcohols were prepared by the Grignard reaction of the corresponding bromobenzenes with acetaldehyde in about 60% yields. They were purified before being converted into chlorides by distillation under reduced pressure or recrystallization from petroleum benzine. The physical constants of alcohols are summarized in Table 5.

α-Methylbenzyl Chlorides. Most *m*- and *p*-substituted α-methylbenzyl chlorides, α-(2-fluorenyl)ethyl chloride and α-(2-naphthyl)ethyl chloride were prepared by the following method. The alcohol in ether containing anhydrous calcium chloride was treated under cooling in an ice-bath with a stream of dry hydrogen chloride, through a concd. sulfuric acid trap, and the resulting solution was decanted and treated with hydrogen chloride in the presence of fresh anhydrous calcium chloride for *ca.* 3 h. The ether was removed under reduced pressure and the residue was purified by fractionation through a column or recrystallized from appropriate solvents. *p*-Methoxy and *p*-phenoxy-α-methylbenzyl chlorides were used without further purification for kinetic measurements immediately after evaporation of ether as completely as possible, since they were quite unstable. Unsubstituted and *m*- and *p*-halo-substituted and *m*-methoxy, *m*-phenyl and *m*-methylthio-α-methylbenzyl chlorides were obtained by the following procedure. Benzene solution of α-methylbenzyl alcohol (1 equivalent) was dropwise added with stirring into a benzene solution of thionyl chloride (2 equivalent). The mixture was kept overnight, and evaporated under reduced pressure. The residue was purified by distillation under nitrogen *in vacuo* (yield, 70—80%). Physical constants of the chlorides are summarized in Table 5. Chlorides were prepared in small portions each time before use. Some stable chlorides were stored in a refrigerator in sealed ampoules and were repurified before use.

Solvent. 80% aqueous acetone was prepared by mixing 8 volumes of purified acetone and 2 volumes of distilled water. Different batches of solvent were standardized each time by adding a small amount of water or acetone to give an identical solvolysis rate for the reference sample.

Kinetic Measurement. The procedure of the rate determination is essentially the same as that described by Brown and Okamoto.[1] The reaction temperature was controlled within ±0.01 °C in the range 15—18 °C, and ±0.02 °C or less at temperature outside of this range; very low temperature was estimated to be less accurate than ±0.1 °C. The rate studies were carried out by using freshly prepared or repurified samples before each run. Measurements at temperatures 10—30 °C were carried out in a long-necked flask with a ground joint stopper. A weighed amount of chloride was quickly dissolved in a small amount of the solvent and made up to the volume corresponding to 0.02 M with the solvent preheated to the reaction temperature in a volumetric flask, shaken vigorously and transferred to a reaction flask immersed in a thermostated bath. At appropriate time intervals, 10 ml aliquots were quenched by pouring into ice-cold acetone (50 ml) and the hydrochloric acid liberated was titrated with aqueous sodium hydroxide solution (*ca.* 0.03 M). Bromocresol purple was used as an indicator. The initial concentration was obtained from the infinity reading determined after 10 half-lives of the reaction. Measurements above 30 °C for slow reacting chlorides were carried out in sealed ampoules. Ten ml aliquot was used for each determination. Two of the sealed ampoules were allowed to

react for at least 10 half-lives, or for the corresponding period at higher temperature, in order to get the infinity reading. Reactions were followed to 75% completion or more, during which period generally more than ten determinations were made. The reaction followed first order kinetics in all cases for two half-lives and in optimum case for up to three half-lives, except the reaction of *p*-methyl derivative, in which a certain drop took place in the first order reaction rate with time. Lewis *et al.* reported a similar phenomenon but gave no clear reason.[11] The experimental errors in respective runs were generally less than 1.0% and correlation coefficients were better than 0.999. Rate constants from repeated runs were reproducible within an accuracy 1.5%. During the course of studies for several years, determinations were made repeatedly by different workers using different samples of the halide in different batches of the solvent. Nevertheless, the repeated runs gave mostly identical rate constants within the limit of our estimated accuracy. The rate constant 3.10×10^{-4} for *p*-methyl (obtained by Y. K. who carried out most measurements) was in agreement with average 3.18×10^{-4} of nine repeated runs by the others.

For the measurements below 10 °C for faster reacting chlorides aliquots were quenched with a large amount of dry ice cold acetone and titrated with aqueous ethanolic sodium hydroxide solution (*ca.* 0.03 M). Titration in a very cold (*ca.* −50 °C) less aqueous solution suffered from the slow response of indicator and the end point could hardly be determined. Rapid titration at an allowable high temperature and the use of a mixed indicator, bromocresol green—methyl red (3: 2), were more favorable. The rate constants for the most reactive *p*-methoxy derivative at low temperatures were less accurate. Respective runs gave good first order rate plots of the order of correlation coefficient not less than 0.99. The rate constants from 7 repeated runs at −30 °C agreed within a range of ±4%. The rate constant extrapolated to 45 °C is estimated for this derivative to be of ±10% uncertainty.

References

1) H. C. Brown and Y. Okamoto, *J. Amer. Chem. Soc.*, **79**, 1974 (1957); *ibid.*, **80**, 4979 (1958); H. C. Brown, "Advances in Physical Organic Chemistry," Vol. 1, Academic Press, New York (1963), Chap. 2.

2) Y. Tsuno, T. Ibata, and Y. Yukawa, This Bulletin, **32**, 960 (1959); Y. Yukawa and Y. Tsuno, *ibid.*, **32**, 965 (1959).

3) P. R. Wells, *Chem. Rev.*, **63**, 171 (1963); R. W. Taft, Jr., *J. Phys. Chem.*, **64**, 1805 (1960); R. W. Taft, Jr., and I. C, Lewis, *J. Amer. Chem. Soc.*, **80**, 2436 (1959); R. W. Taft, Jr., S. Ehrenson, I. C. Lewis, and R. E. Glick, *ibid.*, **81**, 5354, (1959); H. van Bekkum, P. E. Verkade, and B. M. Wepster. *Rec. Trav. Chem. Pays-Bas*, **78**, 815 (1959); S. Ehrenson, "Progress in Physical Organic Chemistry," Vol. 2, John Wiley and Sons (1964), p. 195; C. D. Ritchie and W. F. Sager, *ibid.*, Vol. 2, p. 323; S. Ehrenson, R. T. C. Brownlee, and R. W. Taft, *ibid.*, Vol. 10 (1973), p. 1; C. G. Swain and E. C. Lupton, *J. Amer. Chem. Soc.*, **90**, 4328 (1968); M. J. S. Dewar and P. J. Grisdale, *ibid.*, **84**, 3539, 3546, 3548 (1962).

4) Y. Yukawa and Y. Tsuno, This Bulletin, **32**, 971 (1959); Y. Tsuno, *Memoir. ISIR, Osaka Univ.*, **16**, 197 (1959).

5) Y. Yukawa, Y. Tsuno, and M. Sawada, This Bulletin, **39**, 2274 (1966); Y. Yukawa and Y. Tsuno, *Memoir, ISIR, Osaka Univ.*, **23**, 71 (1966).

6) Y. Yukawa and Y. Tsuno, *Nippon Kagaku Zasshi*, **86**, 873 (1965).

7) H. Yamada, Y. Tsuno, and Y. Yukawa, This Bulletin, **43**, 1459 (1970); Y. Yukawa, Y. Tsuno, and H. Yamada, *Memoir, ISIR, Osaka Univ.*, **23**, 79 (1966); T. Imamoto, Y. Tsuno, and Y. Yukawa, This Bulletin, **44**, 1632, 1639, 1644, 2776 (1971).

8) C. Eaborn and K. C. Pande, *J. Chem. Soc.*, **1961**, 297; C. Eaborn and J. A. Waters, *ibid.*, **1961**, 542; R. Bader, R. W. Bott, C. Eaborn, and P. P. M. Greasley, *ibid.*, **1964**, 627; R. W. Bott, C. Eaborn, and D. R. M. Walton, *ibid.*, **1965**, 384; R. Taylor, G. G. Smith, and W. H. Wetzel, *J. Amer. Chem. Soc.*, **84**, 4817 (1962); R. Taylor and G. G. Smith, *Tetrahedron*, **19**, 937 (1963); L. A. Singer and D. J. Cram, *J. Amer. Chem. Soc.*, **85**, 1080 (1963); M. Sheehan and D. J. Cram, *ibid.*, **91**, 3553 (1969); T. Inukai, This Bulletin, **35**, 400 (1962); K. Miyazaki, *Tetrahedron Lett.*, **1968**, 2793; R. O. C. Norman and G. K. Radda, *ibid.*, **1962**, 125; R. W. Bott and C. Eaborn, *J. Chem. Soc.*, **1963**, 2139; J. E. Dubois and A. F. Hegarty, *ibid.*, **1969**, 638; J. E. Dubois and W. V. Wright, *Tetrahedron Lett.*, **1967**, 3101; J. E. Dubois, A. F. Hegarty, and E. D. Bergmann, *J. Org. Chem.*, **37**, 2218, 2222 (1972); E. P. Shepel, V. V. Sinev, and O. F. Ginsburg, *J. Org. Chem. USSR*, **6**, 163 (1970); D. S. Noyce and R. L. Casternson, *J. Amer. Chem. Soc.*, **95**, 1247 (1973); J. Mindl and M. Vecera, *Collection Czechoslov. Chem. Commun.*, **35**, 950 (1970); G. A. Olah and H. C. Lin, *J. Amer. Chem. Soc.*, **96**, 2892 (1974); G. M. Loudon and C. Berke, *ibid.*, **96**, 4508 (1974).

9) Y. Yukawa, Y. Tsuno, and M. Sawada, This Bulletin, **45**, 1198 (1972).

10) C. Mechelynch-David and P. J. C. Fierens, *Tetrahedron*, **6**, 232 (1957); R. Anantara and M. R. Nair, *Can. J. Chem.*, **44**, 2415 (1966).

11) E. S. Lewis, R. R. Johnson, and G. M. Coppinger, *J. Amer. Chem. Soc.*, **81**, 3140 (1959); T. G. Traylor and J. C. Ware, *ibid.*, **89**, 2304 (1967).

12) E. Berliner and N. Shieh, *ibid.*, **79**, 3849 (1957).

13) Y. Yukawa, Y. Tsuno, and M. Sawada, This Bulletin, **45**, 1210 (1972).

14) a) Y. Kusuyama and Y. Ikeda, *ibid.*, **46**, 204 (1973). b) L. B. Jones and V. K. Jones, *Tetrahedron Lett.*, **1966**, 1493; H. C. Brown and J. D. Cleveland, *J. Amer. Chem. Soc.*, **88**, 2015 (1966); R. C. Hahn, T. F. Corbin, and H. Shechter, *ibid.*, **90**, 3403 (1968).

15) V. J. Shiner, Jr., W. E. Buddenbaum, B. L. Murr, and G. Lamaty, *J. Amer. Chem. Soc.*, **90**, 418 (1968).

16) A. Streitwieser, Jr., H. A. Hammond, R. H. Jagow, R. M. Williams, R. G. Jesaitis, C. J. Chang, and R. Wiolf, *ibid.*, **92**, 5141 (1970).

17) Y. Tsuno, M. Sawada, T. Fujii, and Y. Yukawa, This Bulletin, **48**, 3347 (1975); Y. Tsuno, M. Sawada, T. Fujii, Y. Tairaka, and Y. Yukawa, *ibid.*, **48**, 3356 (1975).

18) a) Y. Tsuno, Wei-Yuen Chong, Y. Tairaka, M. Sawada, and Y. Yukawa, unpublished. b) Y. Tsuno, M. Sawada, Y. Tairaka, and Y. Yukawa, unpublished.

19) The least squares calculation gave Brown's σ^+ correlation, log $k/k_0=(-5.995\pm0.170)\sigma^+ -0.104$, for 12 derivatives reacting faster than the unsubstituted one (excluding *p*-phenoxy group) with a standard deviation ±0.130 and a correlation coefficient 0.996.

20) a) S. Clementi and P. Linda, *Tetrahedron*, **26**, 2869 (1970). b) S. Clementi and P. Linda, *J. Chem. Soc., Perkin II*, **1973**, 1887; R. Taylor, *ibid. B*, **1971**, 1450. c) Data are taken mostly from our previous compilation (Ref. 5), and the other three points correspond to demercuration (O. A. Reutov, *et al.*, *J. Org. Chem. USSR*, **4**, 344, 532, 1077 (1968)).

21) D. H. McDaniel and H. C. Brown, *J. Org. Chem.*, **23**, 420 (1958).

22) Y. Yukawa, Y. Tsuno, and Sawada, unpublished.

23) L. M. Stock and H. C. Brown, *J. Amer. Chem. Soc.*, **84**, 1242 (1962); *ibid.*, **84**, 3298 (1962); "Advances in Physical Organic Chemistry," Vol. 1 (1963), Chap. 2; H. C. Brown,

et al., *J. Amer. Chem. Soc.*, **84**, 1229, 1233, 1236, 1238 (1962).
24) R. C. Neuman, Jr., *J. Amer. Chem. Soc.*, **84**, 3025 (1962).
25) H. C. Brown and T. Inukai, *ibid.*, **83**, 4825 (1961).
26) C. Eaborn, Z. Lasocki, and D. E. Webster, *J. Chem. Soc.*, **1959**, 3034; R. C. O. Norman and R. Taylor, "Electrophilic Substitution in Benzenoid Compounds," Elsevier (1965), pp. 234—241.
27) R. Heck and S. Winstein, *J. Amer. Chem. Soc.*, **79**, 3432 (1957); H. Tanida, T. Tsuji, H. Ishitobi, and T. Irie, *J. Org. Chem.*, **34**, 1086 (1969); Y. Tsuno, M. Mishima, and K. Shibata, unpublished data.
28) Y. Tsuno, M. Fujio, S. G. Kim, and Y. Maeda, unpublished.
29) Y. Tsuno, M. Sawada, T. Fujii, M. Mishima, and Y. Yukawa, unpublished.
30) Y. Tsuno, Y. Kusuyama, N. Shimizu, and Y. Yukawa, unpublished.
31) M. R. Bridge, D. H. Davies, A. Maccoll, R. A. Ross, B. Stephenson, and O. Banjoko, *J. Chem. Soc., B*, **1968**, 805.
32) R. Fuchs and C. A. VanderWerf, *J. Amer. Chem. Soc.*, **76**, 1631 (1954).
33) G. B. Bachman and C. L. Carlson, *ibid.*, **73**, 2857 (1951).
34) A. McCoubrey and D.M. Zausmer, *Brit. J. Pharmacol.*, **9**, 289 (1954).
35) E. D. Hughes, C. K. Ingold, and N. A. Taher, *J. Chem. Soc.*, **1940**, 949.
36) M. Protiva, L. Navak, and Z. Sedivy, *Collection Czechoslov. Chem. Commun.*, **27**, 2102 (1962).
37) M. Sulzbacher and E. Bergman, *J. Org. Chem.*, **13**, 303 (1948).
38) J. M. Vander Zauden and A. P. Ter Borg, *Rec. Trav. Chim.*, **75**, 1115 (1956).
39) R. Adams and C. R. Noller, "Organic Syntheses," Coll. Vol. 1 (1967), p. 109.
40) M. W. Renoll, *J. Amer. Chem. Soc.*, **68**, 1159 (1946).
41) E. L. Eliel, *ibid.*, **71**, 3970 (1949).
42) C. G. Overberger, J. H. Saunder, R. E. Allen, and R. Gander, "Organic Syntheses," Coll. Vol. 3, p. 200.
43) K. Kaji and H. Nagashima, *J. Pharm. Soc. Japan*, **76**, 1371 (1956).
44) W. F. Hyber, Reonoll, A. G. Rossow, and D. T. Mowry, *J. Amer. Chem. Soc.*, **68**, 1109 (1946).
45) R. W. Straussburg, R. A. Gregg, and C. Walling, *ibid.*, **69**, 2141 (1947).
46) R. Arantraman and M. R. Nair, *Can. J. Chem.*, **44**, 2415 (1966).
47) G. Baddenly, J. Chadwick, and H. T. Taylor, *J. Chem. Soc.*, **1954**, 2405; E. S. Lewis, R. R. Johnson, and G. M. Coppinger, *J. Amer. Chem. Soc.*, **81**, 3140 (1959); J. Steigman and L. P. Hammett, *ibid.*, **59**, 2536 (1937).

The Substituent Effect. X. Solvolysis of 3- and 4-Substituted 1-(1-Naphthylethyl) Chlorides

Yuho Tsuno,* Masami Sawada, Takahiro Fujii, and Yasuhide Yukawa
The Institute of Scientific and Industrial Research, Osaka University, Suita, Osaka 565
(Received December 18, 1974)

The rates of the solvolysis of eleven 3- and 4-substituted 1-(1-naphthylethyl) chlorides were determined in 80% (v/v) aqueous acetone solution at 45 °C. The effect of substituents in 3- and 4-positions of the naphthalene can be correlated with the LArSR relationship ($\log k/k_0)_{3\alpha,4\alpha} = -5.12\,(\sigma^0 + 1.04\,\Delta\bar{\sigma}_R^+) - 0.12$ (correlation coefficient, 0.999; standard deviation, ± 0.12). The ρ value in the naphthalene is slightly larger and the r value is slightly smaller than values in the corresponding benzene system under the same condition ($\rho = -4.95$, $r = 1.15$). The difference is reasonably interpreted in terms of the steric effect for the *peri*-hydrogen relative to the reaction center at the α-position of the naphthalene. The effect of substituents can be correlated with the LSFE relationship for conjugatively electron releasing groups with high precision ($R > 0.999$) in the series, 3α and 4α; ($\log k/k_0 = \rho_i\sigma_i + \rho_\pi{}^+\sigma_\pi{}^+$). In this solvolysis, the $3\alpha/4\alpha$ inductive ratio, $\rho_{i,3\alpha}/\rho_{i,4\alpha}$, was 1.37, only slightly larger than the *meta*/*para* inductive ratio of 1.17 for the corresponding reaction in the benzene series. The applicability of these equations to 3- and 4-substituted α-naphthyl system is also shown for some other reactivities.

In our studies of the substituent effect on chemical reactivities, we established that the following Linear Aromatic Substituent Reactivity (LArSR) relationship[1-3] is, in general, applicable to electrophilic and nucleophilic reactions of *meta*- and *para*-substituted benzene derivatives:

$$\log k/k_0 = \rho(\sigma^0 + r^+\Delta\bar{\sigma}_R{}^+ + r^-\Delta\bar{\sigma}_R{}^-) \quad (1)$$

This holds on the assumption of additive description of the substituent effect in terms of the unexalted polar effect of substituted phenyl groups and the aryl resonance exaltation effect.

It has been generally assumed that the electronic effect of substituents consists, to a first approximation, of inductive and π-electronic effects.[4-7] We have shown that the substituent effect on benzene reactivities can be successfully correlated with the Linear Substituent Free Energy (LSFE) relationship[3a-3d,8] based on the σ_i—$\sigma_\pi^\pm$ combination in place of the σ^0—$\Delta\bar{\sigma}_R^\pm$ combination in Eq. (1):

$$\log k/k_0 = \rho(C_i\sigma_i + q_r{}^+\sigma_\pi{}^+ + q_r{}^-\sigma_\pi{}^-) \quad (2)$$

The first term, $C_i\sigma_i$, represents the contribution of inductive effect and the last two, $q_r{}^+\sigma_\pi{}^+$ and $q_r{}^-\sigma_\pi{}^-$, the contributions of π-electronic effects for conjugatively electron releasing ($-R$) and attracting ($+R$) substituents, respectively. σ_i is the inductive substituent constant characteristic of given substituents and independent of the resonance requirement of their reactions. $\sigma_\pi{}^+$ or $\sigma_\pi{}^-$ is the π-electronic substituent constant characteristic of a given substituent describing the capability to donate or attract electron through π-electron delocalization. Both C_i and $q_r{}^+$ ($q_r{}^-$) are characteristic variables giving a measure of the inductive and π-electronic interactions with the reaction center, respectively.

From a statistical analysis of substituted benzene reactivities by means of Eq. (2), we arrived at two significant conclusions.[3a-3d,8] (i) The transmission coefficient of the inductive effect, C_i, depends only on the position of substituents and remains constant independent of reactions in the benzene system, that is, C_i is 1.00 for the *para* and 1.17 for the *meta* position. (ii) The contribution of the π-electronic effect, $q_r{}^+$ or $q_r{}^-$, effectively varies only for substituents that may conjugate with the reaction center and is a function of given reactions. Both $q_r{}^+$ and $q_r{}^-$ are standardized to be unity in $\sigma_p{}^0$ scale and $q_r{}^\pm$ is 0.50 in *meta* position. These are summarized in the following generalized forms.

$$\log (k/k_0)_p = \rho(1.00\sigma_i + q_r{}^+\sigma_\pi{}^+ + q_r{}^-\sigma_\pi{}^-)$$
$$\log (k/k_0)_m = \rho(1.17\sigma_i + 0.50\sigma_\pi{}^\pm) \quad (3)$$

In naphthalene derivatives, there are ten positional combinations between substituents and reaction centers, excluding *ortho* and *peri* combinations. It is expected that contributions of both the inductive and the π-electronic effects may differ from each other, depending upon the relative position of substituents in any single reaction. Since the substituent constants, σ_i and $\sigma_\pi{}^\pm$, are believed to be characteristic of substituents independent of the parent hydrocarbon, the application of Eq. (2) to the substituent effect on the naphthalene system offers important information on the positional transmittance of the inductive and π-electronic effects in naphthalene reactivities.

Very few substituent effect data have been reported on naphthalene, as compared with those on benzene reactivities. Three electrophilic reactions have been reported in which the effects of a wide range of substituents at almost all of the positions in the naphthalene system are systematically investigated: (1) dissociation of naphthoic acids in 50% aq. EtOH,[6,9] (2) alkaline hydrolysis of naphthoic acid esters in aq. organic solvents,[10,11] (3) detritiation of tritionaphthalenes in CF_3COOH.[12,13] The first two reactions are representative σ-type reactivities in the benzene system, having no large contribution of the π-electronic effect. Since an acidic solvent was utilized in the last reaction, there were some problems, *e.g.*, the methoxy substituent was evidently modified by direct solvent-substituent interaction; only methyl and halogens could be treated as ordinary substituents. In order to get more information on the substituent effect for naphthalene reactivities in which electron requirement of the reaction center a great

* To whom inquiries should be addressed. Present address; Department of Chemistry, Faculty of Science, Kyushu University, Hakozaki, Fukuoka 812

deal differs from the first two, we choose the solvolysis of substituted 1-(1-naphthylethyl) chlorides in an ordinary aqueous organic solvent. This reaction is representative of carbonium-ion type reactions and gives comparatively large π-electronic effects of $-R$ substituents at the conjugative positions in the naphthalene.

The present paper is mainly concerned with the treatment based on Eqs. (1) and (2) on the substituent effect of the solvolysis of 3- and 4-substituted 1-(1-naphthylethyl) chlorides in 80% aqueous acetone at 45 °C. These effects can be directly compared with those of *meta*- and *para*-substituted 1-phenylethyl chlorides which have been studied extensively under the same conditions.[3e]

Experimental

Materials. *3- and 4-Substituted 1-Acetylnaphthalenes*: Commercial 1-acetylnaphthalene was purified by recrystallization of the picrate (mp 119—120 °C),[14] followed by fractional distillation of the regenerated ketone. No impurities were detected by vpc. 4-Methyl-, 4-chloro-, 4-bromo-, and 4-methoxy-1-acetylnaphthalenes were prepared by the Friedel-Crafts acetylation of the corresponding 1-substituted naphthalenes and fractionated or recrystallized.[15-17] 1-Acetyl-4-cyanonaphthalene was synthesized from 1-acetyl-4-bromonaphthalene by the method of Friedmann and Shechter[18] (45% yield), using CuCN in DMF.

1-Acetyl-4-ethylnaphthalene: 1-Ethylnaphthalene was obtained by the Wolff-Kishner reduction[19] of 1-acetylnaphthalene in 84% yield. Friedel-Crafts acetylation of 1-ethylnaphthalene (32 g) with AcCl (19 g) and $AlCl_3$ (33 g) in CS_2 gave 1-acetyl-4-ethylnaphthalene in 63% yield; bp 159—159.5 °C/2.5 mmHg.[20]

1-Acetyl-3-chloronaphthalene: 1-Bromo-3-chloronaphthalene was prepared according to the prescription of Fischer *et al.*[21] Chlorination of *N*-acetyl-4-bromo-1-naphthylamine (mp 195—196 °C from MeOH or 95% aq. EtOH)[21,22] gave *N*-acetyl-4-bromo-2-chloro-1-naphthylamine; mp 233—233.5 °C from MeOH or 95% EtOH.[21] 1-Bromo-3-chloronaphthalene distilled at 141—145 °C/5 mmHg,[21,23] solidified on being left to stand (mp 45—50 °C), was obtained by deamination of crude 4-bromo-2-chloro-1-naphthylamine (mp 108—110 °C)[21] prepared by hydrolysis of the above naphthalide in EtOH–aq. H_2SO_4 solution.

A mixture of the bromochloronaphthalene and CuCN in DMF solution was refluxed for 4 hr.[18] The crude 3-chloro-1-naphthonitrile obtained (mp 88—94 °C) was hydrolyzed in AcOH–aq. H_2SO_4 solution. The resulting 3-chloro-1-naphthoic acid was purified by recrystallization from aq. EtOH and aq. AcOH; mp 229—232 °C.[21]

The acid was successfully converted into the 1-acetyl-3-chloronaphthalene by application of Browman's procedure[24] in 75% yield; *via* 3-chloro-1-naphthoyl chloride (mp 77—83 °C from hexane). The fractionated product was recrystallized from hexane.

1-Acetyl-3-bromonaphthalene: 3-Bromo-1-naphthoic acid (mp 234—237 °C from EtOH)[25] was prepared by a similar synthetic route by Dewar and Grisdale;[25] mercuration[26,27] of 3-bromonaphthalic acid anhydride (mp 243.5—244.5 °C)[25,28] and subsequent decomposition of the mercurated product.[26] The acid was converted into 3-bromo-1-naphthoyl chloride and subsequently to 1-acetyl-3-bromonaphthalene by the method described for the 3-chloro derivative.

1-Acetyl-3-cyanonaphthalene: This ketone (7 g) was obtained from 1-acetyl-3-bromonaphthalene (10 g) and purified by recrystallization from benzene–hexane.

1-Acetyl-3-methoxynaphthalene: 4-Bromo-2-naphthylamine (mp 71 °C)[29,30] was obtained, according to the prescription of Bergman,[29] from 1-bromo-3-nitronaphthalene (mp 128—130 °C)[29] derived from the deamination of the diazonium solution of 4-bromo-2-nitro-1-naphthylamine (mp 198—201 °C).[29] The 4-bromo-2-naphthylamine obtained was converted into 4-bromo-2-naphthol (bp 130—132 °C/1.5 mmHg, mp 117—120 °C)[31] by the usual diazonium method; the diazonium sulfate was decomposed by the dropwise addition to *ca.* 40% aq. H_2SO_4 solution at about 80 °C. Methylation of the 2-naphthol with Me_2SO_4 in an alkaline solution gave 1-bromo-3-methoxynaphthalene (mp 112—114 °C).

Reaction of the bromide and CuCN in DMF and working up by Friedmann's procedure[18] gave crude 3-methoxy-1-naphthonitrile (mp 102—104 °C). Direct hydrolysis of the

Table 1. Physical constants and analytical data of 3- and 4-substituted (X) 1-acetylnaphthalenes

X	Bp or Mp*	Carbon		Hydrogen		Other	
		Found	Calcd	Found	Calcd	Found	Calcd
4-MeO-α	147°C/1.5mmHg, 71—72°C[a]	77.74	77.98	5.94	6.04		
4-Me-α	136°C/1.5mmHg[b]	84.57	84.75	5.82	6.57		
4-Et-α	159—159.5°C/2.5mmHg[c]	84.87	84.82	7.06	7.11		
H-α	133—135.5°C/4mmHg[d]	84.92	84.64	5.76	5.92		
4-Cl-α	142°C/1mmHg[e]	70.31	70.43	3.80	4.43	17.60	17.32(Cl)
4-Br-α	141—143°C/0.7mmHg[f]	58.26	57.86	3.00	3.64	31.87	32.08(Br)
4-CN-α	134—135°C	79.54	79.98	4.36	4.65	7.19	7.17(N)
3-MeO-α	140—143°C/1mmHg	78.10	77.98	5.96	6.04		
3-Cl-α	169—171°C/8mmHg,37—37.5°C	70.50	70.43	4.26	4.43	17.06	17.32(Cl)
3-Br-α	137—138°C/1mmHg	57.85	57.86	3.63	3.64	32.04	32.08(Br)
3-CN-α	154—156°C	80.31	79.98	4.38	4.65	7.32	7.17(N)

a) Lit, bp 224—225 °C/15 mmHg,[17] mp 72—74 °C; G. G. Joshi and N. M. Shah, *J. Indian Chem.* **29**, 225 (1952): *Chem Abstr.*, **47**, 5924 (1953), mp 69—71 °C; N. J. Leonard and A. M. Hyson, *J. Amer. Chem. Soc.*, **71**, 1392 (1949). b) Lit, bp 172—174 °C/12 mm Hg, mp 38 °C,[15] bp 174—175 °C/15 mmHg; R. D. Haworth and C. R. Mavin, *J. Chem. Soc.*, **1932**, 2720. c) Lit, bp 182 °C/10 mmHg.[20] d) Lit, bp 127 °C/1 mmHg.[1] e) Lit, bp 140—142 °C/1.5 mmHg,[16] mp 35—37 °C; F. H. Bassilios, Y. A. Salem, M. Shawky, and M. Zaki, *Ann. Chim.* (Rome), **1968**, 1139: *Chem. Abstr.* **70**, 67979q (1969).f) Lit, 165—175 °C/2—4 mmHg,[16] bp 141—143 °C/0.6 mmHg, mp 45—46 °C; S. Berkovic, *Israel J. Chem.*, **1**, 1 (1963): *Chem. Abstr.*, **60**. 1667a (1964). *) All boiling and melting points were uncorrected.

Table 2. Physical constants and analytical data of 3- and 4-substituted (X) 1-(1-naphthylethanols)

X	Mp or Bp*	Carbon		Hydrogen		Other	
		Found	Calcd	Found	Calcd	Found	Calcd
4-Me-α	79—80.5°C	83.73	83.83	7.48	7.58		
4-Et-α	162—168°C/4—5mmHg	83.72	83.96	8.04	8.05		
H-α	65.5—66.5°C[a]	84.00	83.69	6.90	7.02		
4-Cl-α	78—78.5°C[b]	70.07	69.74	5.22	5.37	17.19	17.15(Cl)
4-Br-α	70—72°C[c]	57.92	57.39	4.02	4.42	31.68	31.84(Br)
4-CN-α	79°C	78.94	79.17	5.33	5.62	6.99	7.10(N)
3-Cl-α	102—103°C	69.66	69.74	5.22	5.37	16.87	17.15(Cl)
3-Br-α	71—72°C	57.54	57.39	4.22	4.42		
3-CN-α	82—84°C	79.34	79.17	5.59	5.62	7.41	7.10(N)

a) Lit, mp 62.5—63.5 °C,[34] mp 62—64 °C; Y. Okamoto and H. C. Brown, *J. Amer. Chem. Soc.*, **79**, 1903 (1957). b) Lit, mp 75.5—76 °C; C. C. Price and Sing-Tuh Voong, *J. Org. Chem.*, **14**, 111 (1949). c) Lit, mp 72—73 °C; S. Berkovic, *Israel J. Chem.*, **1**, 1 (1963); *Chem. Abstr.*, **60**, 1667a (1964). *) All melting and boiling points were uncorrected.

nitrile in AcOH–aq. H_2SO_4 gave 3-methoxy-1-naphthoic acid. This material was purified by recrystallization from MeOH; mp 220—223 °C. 1-Acetyl-3-methoxynaphthalene was prepared by the same method as described before.

3- and 4-Substituted 1-(1-Naphthylethanols). Alcohols were prepared by the $LiAlH_4$ reduction of the corresponding ketones in the ethereal solution,[3e,32] unless otherwise stated. The mixture was gently refluxed for about 1 hr and allowed to stand overnight at room temperature, and treated in the usual manner. The crude alcohols were purified by fractionation or recrystallization from appropriate solvents.

$NaBH_4$ in MeOH[33] was utilized for the reduction of bromo-, chloro-, and cyano-ketones. Gentle refluxing of the reaction mixture was continued until the ketone was consumed, which was confirmed by the disappearance of the 2,4-dinitrophenylhydrazone of the corresponding ketone. The methanol solution was decomposed by dil. HCl, neutralized, concentrated, and extracted with benzene.

The physical properties and the elemental analytical data for ketones and alcohols are listed in Tables 1 and 2, respectively.

3- and 4-Substituted 1-(1-Naphthylethyl) Chlorides. All the chlorides except for 3-chloro, and 3- and 4-cyano derivatives were obtained by passing a stream of dry HCl gas into the ethereal solution of purified alcohols at room temperature in the presence of $CaCl_2$.[3-,34] After prompt filtration, the ether was evaporated under reduced pressure. The crude product, dissolved in petroleum ether, was treated with excess K_2CO_3, filtered and evaporated. The same treatment was repeated twice. After final evaporation, the chloride was purified by fractionation or recrystallization from appropriate solvents (*e.g.*, petroleum ether). In the case of methoxy derivatives, the chlorinated products were directly employed for the rate measurements without further purification.

For 3- and 4-cyano- and 3-chloro-1-(1-naphthylethanols), chlorination with excess $SOCl_2$ in benzene was utilized. The solution was gently refluxed until the peaks of O–H vibration in IR spectra disappeared, and refluxing was further continued for 1 hr. Excess $SOCl_2$ was removed by azeotropic distillation, dry benzene being added twice. The chlorides obtained were purified by recrystallization from benzene–hexane or fractionation (Table 3).

Solvent. Acetone which had been refluxed with $KMnO_4$ for over 6 hr was distilled, dried over K_2CO_3 for several days. and fractionated. The stock solutions of 80% and 95% aqueous acetone were prepared by mixing the nominal volumes of acetone and freshly-boiled deionized water, both components being measured at 25 °C.

Kinetic Measurements. The rates of the solvolysis of 3- and 4-substituted chlorides were determined in 80% (v/v) or 95% (v/v) aqueous acetone solutions at appropriate temperatures by means of the usual titration method. The procedure employed for these measurements was essentially the same as that given in the literature.[3e,34] The bath temperature was controlled to ±0.02 °C. For reactions studied at below 0 °C, the runs were carried out in a thermo-

Table 3. Physical constant and analytical data of 3- and 4-substituted (X) 1-(1-naphthylethyl) chlorides

X[a]	Bp or Mp*	Carbon		Hydrogen		Chlorine	
		Found	Calcd	Found	Calcd	Found	Calcd
4-Me-α	103—104°C/1mmHg,41—41.5°C	76.19	76.28	6.22	6.40	17.50	17.32
4-Et-α	31.5—32°C	76.75	76.88	6.79	6.91	16.23	16.21
H-α	116—118°C/2mmHg[b]	75.85	75.79	5.77	5.82	18.87	18.59
4-Cl-α	59—60°C	64.08	64.03	4.22	4.48	31.73	31.50
4-CN-α	76—78°C	72.94	72.39	4.57	4.67	16.21	16.44
3-Cl-α	116.5—118°C/1mmHg	63.89	64.03	4.38	4.48	31.68	31.50
3-Br-α	137—138°C/1mmHg	53.56	53.47	3.63	3.74	13.02	13.15
3-CN-α	78—79.5°C	72.30	72.39	4.58	4.67	16.28	16.44

a) 4-Br-α derivative, bp 137—139 °C/1 mmHg; mp 58—60 °C. b) Lit, bp 128—129 °C/4 mmHg,[34] bp 125—126 °C/2 mmHg; Y. Okamoto and H. C. Brown, *J. Amer. Chem. Soc.*, **76**, 1903 (1957). *) All boiling and melting points were uncorrected.

stated bath maintained at ±0.05 °C or better with cooling by an external bath containing a dry ice–acetone solution.

All the runs at 45 °C and above were carried out at the initial concentration of the chloride, *ca.* 0.02 mol/l in aqueous acetone, in sealed tubes. After the ampoules (more than 10) had been brought to bath temperature, each ampoule was withdrawn at appropriate intervals and quickly immersed into an ice–water bath with vigorous shaking to stop the reaction. A 10 ml aliquot was pipetted, poured into *ca.* 50 ml ice-cooled distilled acetone, and titrated with standardized NaOH aqueous solution. Bromocresol purple or bromothymol blue was employed as an indicator. The two ampoules were allowed to react for at least 10 half-lives in a water bath at *ca.* 90 °C in order to get the infinity reading.

Kinetic runs below 45 °C were conducted in a stoppered Erlenmeyer flask. Ten ml sample solutions were pipetted out, at appropriate intervals, quenched with ice-cooled acetone (*ca.* 50 ml) except for 4-MeO-α derivative, and titrated immediately. For the 4-MeO-α one, about 100 ml acetone which had been cooled about −60 °C with dry ice–acetone was used to stop the reaction.

All the runs involving more than 10 measurements were covered up to 70—85% reaction. In the case of 4-CN-α derivative, calculated values of infinity titers were employed and runs were covered up to *ca.* 50% reaction. Rate constants were determined from the integrated form of the first-order rate equation by means of least squares calculation. The experimental uncertainty of a run was estimated to be less than ±1% and the rate constants from duplicated runs agreed within ±2%.

Table 4. Rate constants of 3- and 4-X-1-(1-naphthylethyl) chlorides in 80 and 95% aq. acetone

X	Solvent %(V/V)	Temp (°C)	$k_1 \times 10^5$ (s^{-1})
H-α	80	45	12.7[a]
4-Me-α	80	25	44.1
		15	13.5
4-Et-α	80	25	33.6
		15	9.83
4-Cl-α	80	45	2.79
4-Br-α	80	45	2.09
4-CN-α	80	95	0.64
		75	0.099
3-MeO-α	80	45	3.42
3-Cl-α	80	85	5.79
		75	2.14
3-Br-α	80	85	5.54
		65	0.746
3-CN-α	80	93	2.61
		85	1.19
		75	0.475
4-MeO-α	95	−10	25.6
		−20	9.71
		−30	2.97
4-Me-α	95	45	2.36
5-MeO-α[b]	95	85	8.98
		75	3.55
6-MeO-β[b]	95	45	6.85
6-MeS-β[b]	95	45	1.36

a) Lit,[34] 12.3×10^{-5}. b) Data taken from Part XI; Y. Tsuno *et al.*, This Bulletin, **48**, 3356 (1975).

Results and Discussion

The rate constants of the solvolysis of 3- and 4-substituted 1-(1-naphthylethyl) chlorides (denoted by 3α and 4α, respectively) in 80% (v/v) aq. acetone at various temperatures are listed in Table 4. The solvolysis of 4-MeO-α derivative was too fast to follow by our method in 80% aq. acetone even at −35 °C, and an extrapolation from the rates in 95% (v/v) aq. acetone solution was employed. The reaction was retarded about 100-fold in the latter solvent, and could then be followed by titration in the temperature range from −10 °C to −30 °C. The rates of four derivatives, 4-Me-α, 5-MeO-α, 6-MeO-β, and 6-MeS-β derivatives in both 80% and 95% aq. acetone (Table 5) are correlated by

$$\log k_{80\%} = 0.847 \log k_{95\%} + 1.462 \quad (4)$$

with a correlation coefficient of 0.9991 and a standard deviation of ±0.031 (Fig. 1). From Eq. (4), the rate constant of the 4-MeO-α derivative in 80% aq. acetone can be estimated to be 1.22 s^{-1} at 45 °C. The extrapolation is supported by the substituent effect for substituted 1-phenylethyl chlorides;[3f] the solvent change from 80% to 90% aq. acetone mainly brings about a change in the ρ value but not in the *r* value of the LArSR Eq. (1). The relative rates in 80% aq. acetone at 45 °C, together with the activation parameters, are summarized in Table 5.

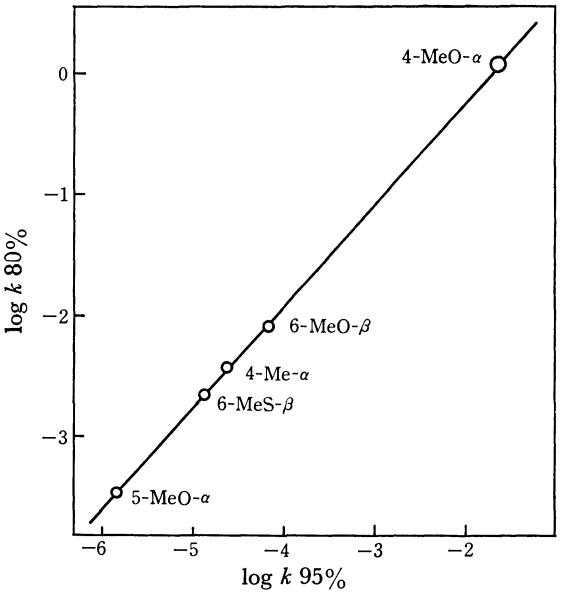

Fig. 1. Logarithmic plot of the present solvolysis rates between 80% and 95% aq. acetone at 45°C.

Comparison between Naphthalene and Benzene Systems. In 3- and 4-substituted 1-(1-naphthylethyl) chlorides, the reaction center and substituent groups are in the same relative positions as in *m*- and *p*- substituted 1-phenylethyl chlorides, respectively. Figure 2 shows the logarithmic plot of relative rates between the naphthalene and the benzene systems under the same conditions; in 80% aq. acetone at 45 °C. The correlation line suggests that the degree of the π-electronic effect of substituents is slightly less effective in the naphthalene system than in the corresponding benzene one.

Table 5. RATE CONSTANTS AND log k/k_0 VALUES IN 80% (v/v) AQ. ACETONE AT 45 °C

X	$k_1\times10^5$ [c] s^{-1}	$\log(k/k_0)_{naph}$ [a]	E_a kcal/mol	log A	$\log(k/k_0)_{benz}$ [b]
H-α	12.7	0.000			0.000
4-MeO-α	1.22×10^5** (2.38×10^3*)	3.98**			4.76
4-Me-α	379* (2.36)	1.475	20.3	11.5	1.628
4-Et-α	313*	1.391	21.0	11.9	1.534
4-Cl-α	2.79	−0.658			−0.480
4-Br-α	2.09	−0.784			−0.684
4-CN-α	0.0039*	−3.51*	23.8	8.9	
3-MeO-α	3.42	−0.570			−0.234
3-Cl-α	0.0730*	−2.241*	24.8	10.9	−1.876
3-Br-α	0.0778*	−2.213*	24.2	10.5	−1.947
3-CN-α	0.0179	−2.852*	24.0	9.7	
5-MeO-α	33.0[d] (0.150*)				
6-MeO-β	813*[d] (6.85)				
6-MeS-β	223*[d] (1.36)				

a) Values of the present solvolysis of substituted 1-(1-naphthylethyl) chlorides. b) Values of the solvolysis of the corresponding *meta*- and *para*- substituted 1-phenylethyl chlorides in 80% (v/v) aq. acetone at 45 °C; data taken from Ref. 3e. c) Rate constants in 95% (v/v) aq. acetone at 45 °C are listed in parenthesis. d) Ref. 38. * Values were obtained by extrapolation from rates at other temperatures. ** See text.

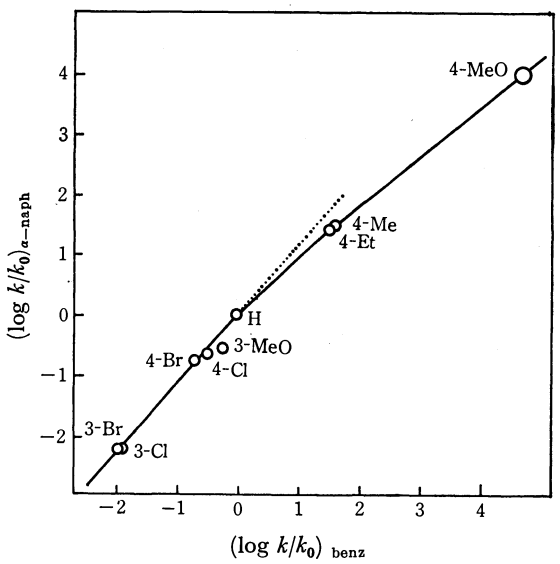

Fig. 2. Log-log plot of the solvolysis rates between α-naphthyl and benzene systems in 80% aq. acetone at 45 °C.

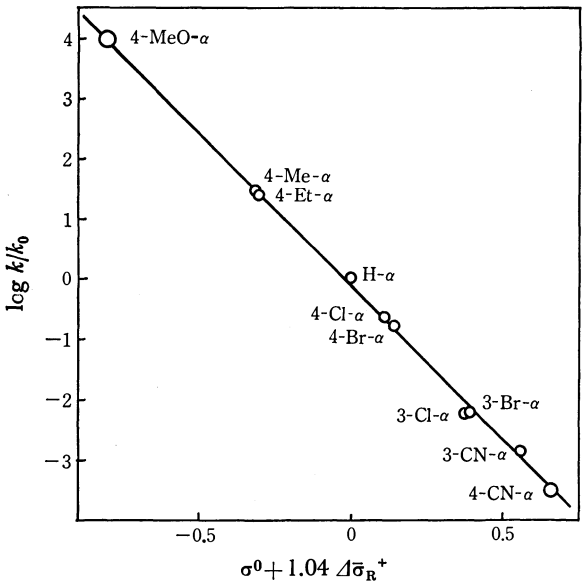

Fig. 3. LArSR plot for the solvolysis of 3- and 4-X-α-naphthylmethylcarbinyl chlorides in 80% aq. acetone at 45 °C.

Equation (1) is applied to the solvolysis rates in the naphthalene derivatives using the σ^0 parameters derived from benzene reactivities to give a correlation

$$\log(k/k_0)_{3\alpha,4\alpha} = -5.12(\sigma^0+1.04\Delta\bar{\sigma}_R^+)-0.12$$

with a correlation coefficient of 0.9990 and a standard deviation of ±0.116 (n=10) (Fig. 3). The corresponding solvolysis rates in the benzene system under the same conditions satisfy Eq. (1) with high precision (R=0.9997).[3e,35]

$$\log(k/k_0)_{m,p} = -4.95(\sigma^0+1.15\Delta\bar{\sigma}_R^+)-0.023$$

The ρ value in the present naphthalene system is slightly larger but the r value is slightly smaller than that in the benzene system. The difference in the r value of the two systems results in the curvature in Fig. 2.

Even if the inductive effect of the substituents may be transmitted through space or carbon-carbon bond or both, it is reasonably assumed from the geometrical similarity that the contributions of the inductive effect from 3α and 4α positions are approximately equal to those from *meta* and *para* positions, respectively. If there are any differences, they would be the slight differences in bond length and/or bond order between the parent naphthalene and the benzene.

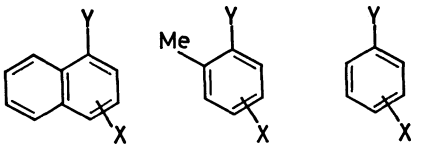

(I) (II) (III)

Chart 1

One model in which the steric requirement at the reaction center is analogous to the α-naphthyl derivative (I) is the benzene derivative with a methyl group *ortho* to the reaction site (II). In the dissociation of benzoic acids in 50% aq. EtOH, the ρ value is 1.77 with (II),[36a] and 1.51 without an *ortho* methyl group (III).[36b] In the substituent chemical shifts of the hydroxyl proton of substituted phenols in DMSO, ρ is 1.60 in (II)[3b] and 1.53 in (III),[3a] both values having high precision. The results indicate that, when a group is introduced into the proximity of the reaction site, the ρ value is not necessarily identical with that in the simple benzene system, possibly because of the difference in the solvation around the reaction center. In the analysis of the substituent effect on naphthalene reactivities, it was assumed that the ρ value in the α-naphthyl system (I) is identical with that in the benzene system (III).[6,9,10b] However, we consider that the assumption may not always be the case.

The *r* value for naphthalene solvolysis, 1.04, is smaller than 1.15 for the corresponding benzene solvolysis. In α-naphthyl derivatives, the *peri*-hydrogen prevents maximum overlap of the vacant orbital of the reaction site developed in the transition state with the ring π-orbitals. The *peri*-hydrogen steric effect causes a decrease in the bond order between the reacting carbon and the ring α-carbon. In the absence of the steric effect, it is suggested by the MO reactivity indices that the π-electronic effect in the conjugated 4α position in the naphthalene is more effective than in the *para* position in the benzene system.[6,12,13,37] Thus we may reasonably conclude that the increased contribution of the π-electronic effect in the 4α position is over-compensated by the decreased bond order due to the effective *peri*-hydrogen steric effect, resulting in a smaller *r* value in the present solvolysis.

The same type of approach is applicable to the data of alkaline hydrolysis of ethyl 3- and 4-substituted 1-naphthoates in 85% aq. EtOH at 50 °C.[10] Figure 4 shows the log-log plot of the relative rates between the naphthalene and the corresponding benzene systems. An excellent linear free energy correlation is obtained for all the substituents except 4-NO_2 and 4-NMe_2. The deviations are reasonably interpreted in terms of the non-coplanarity of these substituents with the ring due to the *peri*-hydrogen steric effect.[3b] The application of Eq. (1) to the hydrolysis of ethyl 1-naphthoates, except for the above two substituents, leads to an excellent linear correlation. The standard deviation from the regression line is ±0.03 and the correlation coefficient, 0.999(n= 10).

$$\log (k/k_0)_{3\alpha,4\alpha} = 2.19(\sigma^0+0.27\Delta\bar{\sigma}_R^+) + 0.02$$

On the other hand, the hydrolysis of ethyl benzoates (85% aq. EtOH, 25 °C)[38,39] is correlated by

$$\log (k/k_0)_{m,p} = 2.54(\sigma^0+0.27\Delta\bar{\sigma}_R^+) + 0.04$$
$$(R=0.997,\ s=\pm 0.08)$$

Nearly the same *r* value for both the naphthalene and benzene systems is evident.

In this hydrolysis, the increased contribution of the π-electronic effect in the 4α in the naphthalene is perhaps compensated by the decreased bond order between the ring α-carbon and the ethoxycarbonyl carbon, and consequently the overall contribution of the π-electronic effect becomes close to that in the *para* in the benzene system.

The present solvolysis is a typical carbonium-ion reaction and is known to show an exalted contribution of resonance (π-electronic) effect from the substituents at the conjugated position, whereas the ester hydrolysis is a typical σ-fit reaction having a small contribution of π-electronic effect. Thus it appears from the results in both reactions that the substituent effect on 3- and 4-substituted naphthalene α-reactivities can be treated successfully by means of Eq. (1) in the same way as on *m*-

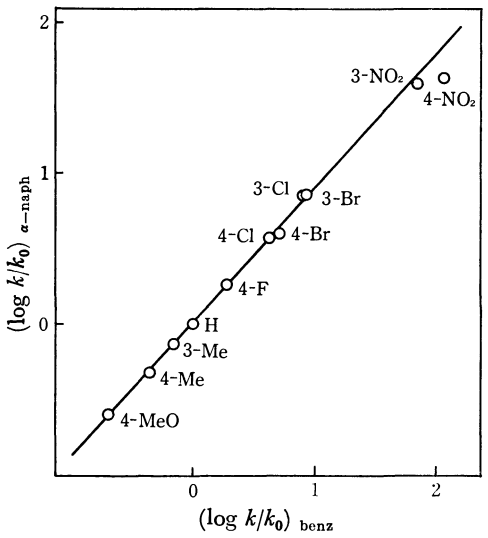

Fig. 4. Log-log plot of the alkaline hydrolysis rates between ethyl α-naphthoates (50 °C) and ethyl benzoates (25 °C).

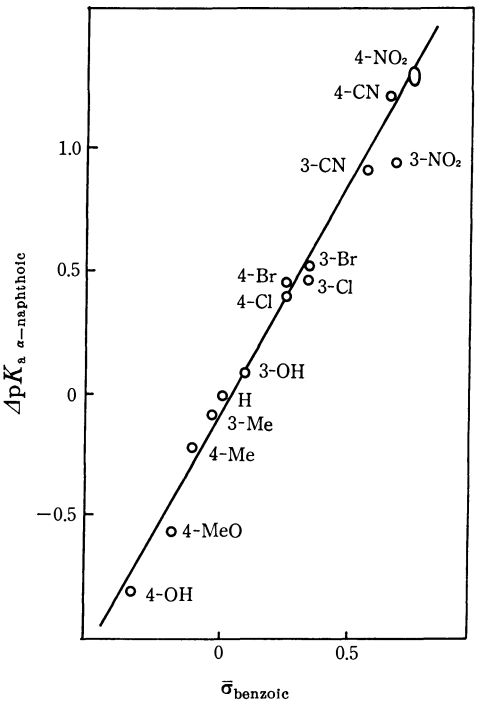

Fig. 5. The plot of ΔpK_a of α-naphthoic acids *vs.* the apparent $\bar{\sigma}$ values from ΔpK_a of benzoic acids in 50% aq. EtOH.

and *p*-substituted benzene reactivities, at least as far as electrophilic reactions are concerned.[40] Figure 5 shows the plot of ΔpK_a values of substituted 1-naphthoic acids in 50% aq. EtOH[6,9] against the apparent $\bar{\sigma}$ values calculated from the dissociation of benzoic acids in the same solvent.[36] In this case, however, considerable scattering is observed in the correlation.

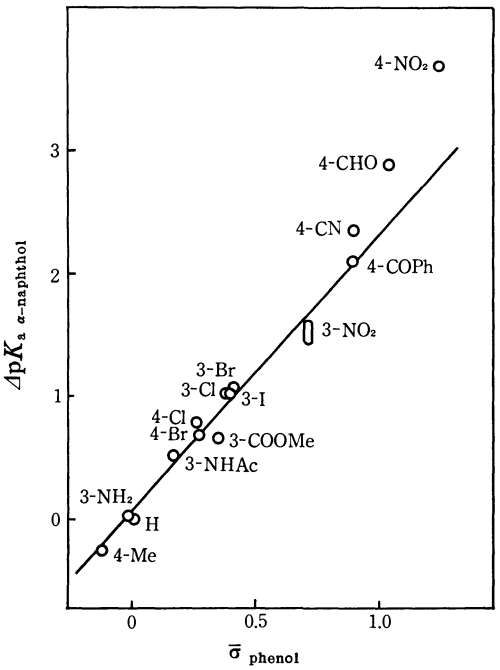

Fig. 6. Relation between ΔpK_a in α-naphthols and the apparent $\bar{\sigma}$ derived from ΔpK_a in phenols in H_2O.

The above argument may be consistent with the results of the application of Eq. (1) to nucleophilic reactivities of α-naphthyl system. An example is found in the substituent effect for dissociation of 3- and 4-substituted 1-naphthols in water at 25 °C.[41] Figure 6 shows the correlation of ΔpK_a in the 1-naphthols with the apparent $\bar{\sigma}$ derived from ΔpK_a in *m*- and *p*-substituted phenols in water. NO_2, CHO, and COC_6H_5 substituents in the 4-position may be forced out of coplanarity with the parent naphthalene ring by *peri*-hydrogen steric effect. Nevertheless the correlation line appears to be curved upward. The vertical deviations for these $+R$ substituents in 4-position from the line determined by 3α substituents and $-R$ 4α ones suggest a larger contribution of electron attracting π-electronic effect in the naphthols than that in the phenols. These findings of the direction of the change of *r* in both the naphthalene and the benzene systems are the same as the prediction based on the simple MO theory, presumably because of the less effective *peri*-hydrogen steric effect around the reaction site in this dissociation.

Application of LSFE Eq. (2) to α-Naphthyl Reactivities. According to Eq. (3), the contribution of inductive effect from substituents in *meta* position is transmitted 1.17 times more effectively to a reaction center than in *para* position. In the case of naphthalenes, the extent of the inductive contribution is also expected reasonably to depend upon the relative position of substituents to a reaction center, such as 4α, 5α, 6α, and so on. When substituents are attached to another ring of the naphthalene, *i.e.*, 5, 6, and 7-positions, the actual substituent effects may, in general, not be described successfully by any single set of substituent constants derived from the benzene system. The π-electronic contributions relative to inductive contributions from substituents at any positions of naphthalene system may differ from the relative π-electronic contributions in the benzene system.

In the pioneering studies of the substituent effect for dissociation of 1-naphthoic acids, Dewar and Grisdale proposed the *FM* equation[6]

$$\sigma_{ij} = 1/r_{ij}F + q_{ij}M$$

They considered simply that the field effect which corresponds to inductive effect in our sense was assumed to be transmitted with reciprocal of the simple distance between the ring carbons at which both substituents and COOH group were attached. Later, similar or revised treatments were employed by several authors in order to interpret other electrophilic reactivities in the naphthalene system.[42–46] However, these treatments are heavily based on the assumption of the transmission coefficients ($1/r_{ij}$ and q_{ij}) in the parent naphthalene ring.

On the other hand, Taft *et al.* adopted an alternative approach,[47] not based on any presumption of the transmission coefficients. They utilized the substituent parameters, σ_I and σ_R^0, derived from the benzene system, and analysed the substituent effect in the naphthalene system empirically; the transmission coefficients were determined by

$$\log k/k_0 = \rho_I\sigma_I + \rho_R\sigma_R^0 \qquad (5)$$

By means of statistical analysis, they examined the relative abilities of transmissions of both the inductive effect (ratio of ρ_I) and π-electronic effect (ratio of ρ_R) for a series of relative substituent positions. However, this treatment based on the substituent constant pair, σ_I and σ_R^0, must not be applied to general electrophilic reactivities such as the present solvolysis.

We have attempted a similar statistical approach by means of Eq. (2), where unique substituent constants, σ_i and $\sigma_\pi^\pm$, were employed instead of σ_I and σ_R^0. It would be expected that the relative transmission coefficients of inductive effect, C_i, can be derived from a given reaction. The expectation had been justified by the statistical analysis for both electrophilic and nucleophilic reactivities in the benzene system; C_i for *meta* relative to C_i for *para* is 1.17.

Conjugatively electron releasing ($-R$) substituents and conjugatively electron attracting ($+R$) substituents should be treated independently by Eq. (2)[1–3,8]; q_r^+ and q_r^- are substantially independent in any single reaction except for a σ^0-type reaction. Then, the present solvolysis rates for only $-R$ substituents were analysed by the least squares application of the equation

$$\log k/k_0 = \rho_i\sigma_i + \rho_\pi{}^+\sigma_\pi{}^+ \qquad (6)$$

The obtained statistical values are listed in Table 6, together with the results for other electrophilic reactivities available in 3α and 4α series. The substituent parameters utilized in this analysis are listed in Table 7.

It is evident from the results that all of the four reactivities are successfully described by Eq. (6) with high

Table 6. Statistical analysis of α-naphthyl reactivities for $-R$ substituents

$$\log k/k_0 = \rho_i\sigma_i + \rho_\pi{}^+\sigma_\pi{}^+ + \delta$$

Reaction	Series	ρ_i	$\rho_\pi{}^+$	δ	R[a]	$\pm s$[b]	n[c]
Solvolysis[d]	3α	−6.96	−2.56	−0.00	0.999	0.01	4(MeO, Cl, Br, H)
	4α	−5.09	−17.6	−0.06	0.999	0.07	5(MeO, Et, Me, Cl, Br, H)
Detritiation[e]	3α	−7.81	−1.13				3(Me, Cl, H)
	4α	−5.87	−23.4	−0.09	0.996	0.14	5(Me, F, Cl, Br, H)
Ester Hydrolysis[f]	3α	2.52	0.27	0.00	0.999	0.02	4(Me, Cl, Br, H)
	4α	2.13	3.71	0.04	0.993	0.08	6(MeO, Me, F, Cl, Br, H)
Acid Dissociation[g]	3α	1.48	0.61	0.02	0.995	0.04	5(OH, Me, Cl, Br, H)
		1.90[h]	0.88[h]	0.04[h]	0.997	0.04[h]	5(OH, Me, Cl,[h] Br,[h] H)
	4α	1.38	3.08	0.06	0.991	0.09	8(NH_2,OH, MeO, Me, F, Cl, Br, H)

a) Correlation coefficient. b) Standard deviation. c) Number of substituents. d) Present study. e) Data taken from Ref. 13. f) Data taken from Ref. 10. g) Data taken from Refs. 6 and 9. h) Corrected ΔpK_a for Br and Cl were employed; Ref. 38.

Table 7. Substituent parameters, σ_i and $\sigma_\pi{}^+$[a]

Substituent	σ_i	$\sigma_\pi{}^+$
NH_2	0.06	−0.42
OH	0.19	−0.34
CH_3O	0.185	−0.281
CH_3	−0.045	−0.078
C_2H_5	−0.045	−0.069
H	0.000	0.000
F	0.363	−0.118
Cl	0.348	−0.070
Br	0.337	−0.054

a) Parameters taken from Ref. 8.

precision (R>0.99). The reliability of both ρ_i and $\rho_\pi{}^+$ values obtained in this approach is strongly dependent upon both the number of the substituents involved in the calculation and a wide variety of the electronic nature of the substituents. Although the numbers of substituents involved here are not sufficient in respective series of reactivities given in Table 6, typical $-R$ substituents such as alkoxy, alkyl, halogen, and hydrogen, are involved in the present solvolysis and in almost all of the remainder.

Since rate data for 3α series are limited in number by comparison with the *meta* series of the benzene system, the precision with which the parameters ρ_i and $\rho_\pi{}^+$ are determined is inevitably restricted, nevertheless the inductive contribution ratio, $\rho_{i,3\alpha}/\rho_{i,4\alpha}$, 1.37, appears to be slightly large as compared with 1.17 for the corresponding series in benzene systems. Similar ratios, 1.33, 1.19, and 1.38[48] are found in the detritiation, the ester hydrolysis, and the acid dissociation, respectively. The significance of these results might not be clear, but it is suggested that the transmission coefficient for 3α series relative to 4α in the naphthalene ring may differ slightly from that in the benzene ring. This might indicate that $\sigma_p{}^0$ and $\sigma_m{}^0$ are not exactly applicable to 4α and 3α series in the naphthalene reactivity. The LArSR treatment might be restricted for the application especially to the effects of substituents in another ring positions in the naphthalene. The LSFE treatment should be promising for these cases.

References

1) Y. Yukawa, Y. Tsuno, and M. Sawada, This Bulletin, **39**, 2274 (1966); *ibid.*, **45**, 1198 (1972); *ibid.*, 1206 (1972); *ibid.*, 1210 (1972).

2) Y. Yukawa and Y. Tsuno, *ibid.*, **32**, 971 (1959); Y. Tsuno, *Memoir, ISIR, Osaka Univ.*, **16**, 197 (1959).

3) a) Y. Tsuno, M. Fujio, Y. Takai, and Y. Yukawa, This Bulletin, **45**, 1519 (1972); b) M. Fujio, M. Mishima, Y. Tsuno, Y. Yukawa, and Y. Takai, *ibid.*, **48**, 2127 (1975); c) Y. Tsuno, M. Fujio, and Y. Yukawa, *ibid.*, **48**, 3324 (1975). d) M. Fujio, Y. Tsuno, Y. Yukawa, and Y. Takai, *ibid.*, **48**, 3330 (1975). e) Y. Tsuno, Y. Kusuyama, M. Sawada, T. Fujii, and Y. Yukawa, *ibid.*, in press. f) Y. Tsuno *et al.*, unpublished.

4) R. W. Taft and I. C. Lewis, *J. Amer. Chem. Soc.*, **80**, 2436 (1958); *ibid.*, **81**, 5343 (1959); R. W. Taft, S. Ehrenson, I. C. Lewis, and R. E. Glick, *ibid.*, **81**, 5354 (1959).

5) S. Ehrenson, "Progress in Physical Organic Chemistry," Vol. 2, John Wiley and Sons (1964), p. 195; C. D. Ritchie and W. F. Sager, *ibid.*, Vol. 2, p. 323; P. R. Wells, S. Ehrenson, and R. W. Taft, *ibid.*, Vol. 6, p. 147 (1968); S. Ehrenson, R. T. C. Brownlee, and R. W. Taft, *ibid.*, Vol. 10 (1973), p. 1.

6) M. J. S. Dewar and P. J. Grisdale, *J. Amer. Chem. Soc.*, **84**, 3539, 3546, 3548 (1962). ΔpK_a values of 3-Me-α, 4-Cl-α 4-F-α, 3-NO_2-α, and 4-NO_2-α were taken from Ref. 9.

7) C. G. Swain and E. C. Lupton, *ibid.*, **90**, 4328 (1968).

8) Y. Yukawa and Y. Tsuno, *Nippon Kagaku Zasshi*, **86**, 863 (1965); Y. Yukawa and Y. Tsuno, *Memoir, ISIR, Osaka Univ.*, **23**, 71 (1966).

9) P. R. Wells and W. Adcock, *Aust. J. Chem.*, **18**, 1365 (1965).

10) A. Fischer, J. D. Murdoch, J. Packer, R. D. Topsom, and J. Vaughan, *J. Chem. Soc.*, **1957**, 4358; A. Fischer, H. H. Fountain, and J. Vaughan, *ibid.*, **1959**, 1310; see also Ref. 21.

11) P. R. Wells and W. Adcock, *Aust. J. Chem.*, **19**, 221 (1966).

12) C. Eaborn, P. Golborn, R. E. Spillett, and R. Taylor, *J. Chem. Soc.*, **1968**, 1112; R. W. Bott, R. E. Spillett, and C. Eaborn, *Chem. Commun.*, **1965**, 147.

13) C. Eaborn and A. Fischer, *J. Chem. Soc., B*, **1969**, 152.

14) C. W. Hurd, *J. Amer. Chem. Soc.*, **47**, 2777 (1925); *J. Org. Chem.*, **13**, 164 (1948).

15) J. Sauer, R. Huisgen, and A. Hauser, *Chem. Ber.*, **91**, 1461 (1958).

16) T. Jacobs, S. Winstein, J. W. Ralls, and J. Robson, *J. Org. Chem.*, **11**, 27 (1946).

17) W. Schneider and F. Kunau, *Ber.*, **54**, 2304 (1921); S. Ruhemann and S. Levy, *ibid.*, **53**, 270 (1920).

18) L. Friedmann and H. Shechter, *J. Org. Chem.*, **26**, 2522 (1961).
19) Huang-Minlon, *J. Amer. Chem. Soc.*, **68**, 2487 (1946); D. Todd, "Organic Reactions," Vol. 4, Chap. 8, John Wiley and Sons (1949).
20) G. Lock, *Monatsh.*, **83**, 865 (1952).
21) A. Fischer, W. J. Mitchell, G. S. Ogilvie, J. Packer, J. E. Packer, and J. Vaughan, *J. Chem. Soc.*, **1958**, 1462.
22) H. H. Hodgson and S. Birtwell, *ibid.*, **1943**, 321.
23) H. H. Hodgson and D. E. Hathway, *ibid.*, **1944**, 538.
24) R. E. Bowman, *ibid.*, **1950**, 322.
25) M. J. S. Dewar and P. J. Grisdale, *J. Amer. Chem. Soc.*, **84**, 3541 (1962).
26) F. C. Whitmore and A. L. Fox, *ibid.*, **51**, 3363 (1923).
27) G. J. Leuck and R. P. Perkins, *ibid.*, **51**, 1831 (1929).
28) H. G. Rule and S. B. Thompson, *J. Chem. Soc.*, **1937**, 1764.
29) E. D. Bergmann and J. Blum, *J. Org. Chem.*, **26**, 3214 (1961).
30) A. Bryson, *J. Amer. Chem. Soc.*, **82**, 4862 (1960).
31) H. H. Hodgson and S. Birtwell, *J. Chem. Soc.*, **1943**, 468; *ibid.*, **1944**, 539; A. Bryson and R. W. Mattews, *Aust. J. Chem.*, **16**, 401 (1963).
32) W. G. Brown, "Organic Reactions," Vol. 6, John Wiley and Sons (1942), Chap. 10.
33) S. W. Chaikin and W. G. Brown, *J. Amer. Chem. Soc.*, **71**, 122 (1949); D. S. Noyce and G. V. Kaiser, *J. Org. Chem.*, **34**, 1008 (1969).
34) E. Berliner and N. Shieh, *J. Amer. Chem. Soc.*, **79**, 3849 (1957).
35) n=15; *p*-MeS, *p*-Ph, 2-Naph, *p*-Me, *p*-Et, *p*-*i*-Pr, *p*-*t*-Bu, *p*-F, *p*-Cl, *p*-Br, *m*-Me, *m*-F, *m*-Cl, *m*-Br, and H derivatives were employed for the calculation.
36) a) Data taken from J. D. Roberts and J. A. Yancey, *J. Amer. Chem. Soc.*, **73**, 1011 (1951); b) Data taken from D. H. McDaniel and H. C. Brown, *J. Org. Chem.*, **23**, 420 (1958).
37) A. Streitwieser, "Molecular Orbital Theory for Organic Chemists," John Wiley and Sons (1964).
38) Y. Yukawa, Y. Tsuno, and M. Sawada, unpublished.
39) n=19; *p*-Me, *m*-Me, *p*-Et, *p*-F, *m*-F, *p*-Cl, *m*-Cl, *p*-Br, *m*-Br, *p*-MeO, *p*-MeS, *p*-NH_2, *p*-NO_2, *m*-NO_2, *m*-I, H, *m*,*m*-Me_2, 2-Naph, and *p*-Ph.
40) In the case of the detritiation for 3α and 4α series,[12,13] ρ is calculated to be −6.43 and *r*, 1.13 (R=0.997, s=±0.14, n=7; 3-Me-α, 3-Cl-α, H-α, 4-Me-α, 4-F-α, 4-Cl-α, and 4-Br-α). The precise *r* value in the corresponding benzene system can not be determined because of insufficient data.
41) L. K. Creamer, A. Fischer, B. R. Mann, J. Packer, R. B. Richards, and J. Vaughan, *J. Org. Chem.*, **26**, 3148 (1961); A. Bryson and R. W. Matthews, *Aust. J. Chem.*, **16**, 401 (1963).
42) K. C. C. Bancroft and G. R. Howe, *Tetrahedron Lett.*, **1967**, 4207.
43) W. Adcock and M. J. S. Dewar, *J. Amer. Chem. Soc.*, **89**, 379 (1967).
44) M. J. S. Dewar, R. Golden, and J. M. Harris, *ibid.*, **93**, 4187 (1971).
45) D. S. Noyce and R. W. Nichols, *Tetrahedron Lett.*, **1972**, 3889.
46) D. A. Forsyth, *J. Amer. Chem. Soc.*, **95**, 3594 (1973).
47) P. R. Wells, S. Ehrenson, and R. W. Taft, "Progress in Physical Organic Chemistry," Vol. 6, Interscience (1968), p. 147.
48) $\rho_{t,3\alpha}=1.90$ was employed (see Table 6).

The Substituent Effect. XI. Solvolysis of 5-, 6-, and 7-Substituted 1-(1-Naphthylethyl) Chlorides

Yuho Tsuno,* Masami Sawada, Takahiro Fujii, Yoshihiko Tairaka, and Yasuhide Yukawa

The Institute of Scientific and Industrial Research, Osaka University, Suita, Osaka 565

(Received December 18, 1974)

Fourteen 5-, 6-, and 7-substituted 1-(1-naphthylethyl) chlorides were prepared and the solvolysis rates were determined in 80% (v/v) aqueous acetone at 45 °C. The effects of $-R$ substituents at respective positions were treated on the basis of the equation, $\log k/k_0=\rho_i\sigma_i+\rho_\pi{}^+\sigma_\pi{}^+=\rho(C_{1j}\sigma_i+q_{r\,1j}^+\sigma_\pi{}^+)$. The position dependency of the inductive effect was given by $C_{1j}(=\rho_i/\rho_{i,4\alpha})$; $C_{3\alpha}=1.37$, $C_{4\alpha}=1.00$, $C_{5\alpha}=0.75$, $C_{6\alpha}=0.57$, and $C_{7\alpha}=0.72$. The C_{1j} values appear to be correlated with Dewar's simplified field function $1/r_{1j}$. The position dependency of *Pi*-electronic effect given by the ratio $\rho_\pi{}^+/\rho_{i,4\alpha}=q_{r\,1j}^+$ was consistent with the prediction from the MO indices, such as Forsyth's $\Delta q_{1j}(\mathrm{ArCH_2}^+)$ parameters. The same treatment was applied also to three other naphthalene reactivities, detritiation, pK_a of α-naphthoic acids and pK_a of naphthylammonium ions. The linear $\rho_i-\rho_i$ relation holds among these reactions, suggesting a reaction-independent scheme of the inductive transmission. The $q_{r\,1j}^+$ values vary at conjugate positions with reaction but not at non-conjugate positions irrespective of reactions. The results are discussed in comparison with those of relevant treatments.

We have found that the effects of substituents at the A ring positions of the α-naphthyl derivatives were successfully correlated with the following LArSR Eq. giving $\rho=-5.12$, $r=1.04$.[1]

$$\log k/k_0 = \rho(\sigma^0+r\Delta\bar{\sigma}_R{}^+) \quad (1)$$

This indicates that the substituent parameters, σ^0 and $\Delta\bar{\sigma}_R{}^+$, which were derived from the benzene system, are valid also for both 3α and 4α series in the naphthalene system. A more fundamental separation of the substituent effects into inductive and π-electronic effects was also examined by means of the equation

$$\log k/k_0 = \rho_i\sigma_i + \rho_\pi{}^+\sigma_\pi{}^+ \quad (2)$$

using inductive and π-electronic substituent parameters, σ_i and $\sigma_\pi{}^+$. Application to the 3α and 4α series gave excellent correlations, indicating that the parameters derived from the benzene system are valid again for the α-naphthyl A ring system. It seems that the substituent effects are given by a certain blend of unique substituent parameters, σ_i and σ_π, characteristic of only substituents and independent of parent hydrocarbons. The blend depends remarkably upon reactions and characteristically upon substituent positions as well as parent hydrocarbons. In this study a 3α/4α inductive ratio of 1.37 was observed, which is slightly larger than the 1.17 *meta*/*para* inductive ratio. The difference might not be unreasonable since the parent hydrocarbons differ.

Our interest in the analysis of substituent effects led us to carry out further studies on the naphthalene B ring positions. LSFE treatment of aromatic reactivities beyond the original benzene system enables us to accomplish the following objectives. The generality of the σ_i and especially $\sigma_\pi{}^+$ parameters can be tested most critically. If they are physically meaningful quantities characteristic of the substituent, they should be applied to any aromatic systems (naphthalene in the present case) as well as the benzene system, independent of different resonance requirement of the reactions. The study provides evidence to clarify the ambiguity in the scale of inductive parameters and subsequently in the definition of π-electronic parameters. The parametric analysis of the apparent substituent effect into the two basic components from different aromatic positions may shed light on the mode of operation of substituent effects.

The present paper is concerned with the treatment based on Eq. (2) of the substituent effects in the solvolysis of substituted 1-(1-naphthylethyl) chlorides in 80% aq. acetone, and also in other types of reactions of α-naphthyl derivatives; detritiation of α-tritionaphthalenes in CF_3COOH studied by Eaborn's group,[2-4] dissociation of α-naphthoic acids in 50% aq. EtOH,[5] and of α-naphthylammonium ions in H_2O.[6]

Experimental

Materials. Preparation of 5-, 6-, and 7-substituted 1-naphthoic acids was carried out by the standard method with slight modifications. The positions of substituents at substituted 1-acetylnaphthalenes were confirmed by the NMR splitting pattern of the *peri*-hydrogen relative to that of the acetyl group.

1-Acetyl-5-bromonaphthalene: 1-Naphthoic acid was prepared by the acid hydrolysis (H_2SO_4: AcOH: H_2O=1: 1: 1)[7] of 1-naphthonitrile (bp 123—126 °C/4 mmHg) obtained from 1-bromonaphthalene with CuCN in DMF.[8] The crude acid (mp 156—159 °C; lit, mp 160 °C[9]) was brominated according to the direction of Short.[9] Recrystallization from AcOH gave (average yields 60%) 5-bromo-1-naphthoic acid, mp 263—264 °C; lit, mp 262 °C,[10] 256—256.5 °C,[9,11] 258—259 °C.[12] Purification was carried out by further recrystallization from MeOH–AcOH, mp 264—265 °C.[13]

5-Bromo-1-naphthoic acid was converted into the corresponding methyl ketone by the application of Bowman's method.[14] 5-Bromo-1-naphthoic acid was chlorinated with $SOCl_2$ to give 5-bromo-1-naphthoyl chloride; mp 85—86 °C from hexane–benzene; lit,[11] mp 84—84.5 °C. A dry benzene solution (*ca.* 300 ml) of the above chloride (70 g) was added to an excess of diethylethoxymagnesio-malonate (0.6 mol) in benzene with cooling. The mixture was refluxed for 4 h, decomposed with dil. H_2SO_4, and extracted with benzene. The crude acylmalonate was refluxed for 2 h with propionic acid (180 g) and H_2SO_4 (50 drops). Dil. H_2SO_4 was then

* To whom inquiries should be addressed. Present address; Department of Chemistry, Faculty of Science, Kyushu University, Hakozaki, Fukuoka 812

added slowly, refluxing being continued for 22 hr. After addition of AcONa, 1-acetyl-5-bromonaphthalene was distilled to give pale yellow liquid, bp 179—182 °C/7 mmHg, which solidified soon on being left to stand (average yield, 73%); mp 55.5—56.5 °C from ligroin.

1-Acetyl-5-methoxynaphthalene: 5-Bromo-1-nitronaphthalene was prepared following the method of Newman,[15] by the bromination of 1-nitronaphthalene; mp 119—122 °C from EtOH–$CHCl_3$, (63% yield); lit, mp 118—122 °C,[15] 121 °C,[16] 122 °C.[10,17] 5-Bromo-1-nitronaphthalene was reduced with iron powder in aq. EtOH–HCl, 4 hr, giving 5-bromo-1-naphthylamine on distillation at 180—185 °C/7 mmHg (lit,[18] bp 156—158 °C/1.5 mmHg) which solidified on being left to stand, mp 69—71 °C (92% yield); lit, mp 69.5—71 °C[18] 69 °C,[10,17] 64—69 °C.[15] 5-Bromo-1-naphthylamine hydrochloride was diazotized in aq. AcOH solution of HCl, decomposed by dropwise addition to a boiling 40% aq. H_2SO_4, and extracted with benzene. The alkaline extract on acidification gave 5-bromo-1-naphthol in 40% yield, mp 142 °C from hexane–benzene, lit,[10,19] mp 137 °C. Alternate process, the conversion of 5-bromo-1-naphthylamine through 5-cyano-1-naphthylamine into 5-cyano-1-naphthol, appears to be more successful. 5-Bromo-1-naphthylamine (130 g) was converted with CuCN (53 g) and DMF (150 ml) into 5-cyano-1-naphthylamine in 70% yield; bp 205—210 °C/6 mmHg, mp 141.5—142 °C (from aq. EtOH); lit,[20] mp 140 °C. 5-Cyano-1-naphthol was prepared quantitatively by the diazonium method.[20] The diazotized mixture of 5-cyano-1-naphthylamine (39 g) in AcOH (300 ml) and 40% aq. H_2SO_4 (400 ml) with aq. $NaNO_2$ (16 g) solution was filtered and decomposed by dropwise addition to a boiling 40% aq. H_2SO_4 solution during a period of 1 h. After being boiled for further 1.5 hr, the solid product was collected, washed, and dried (38 g). Alkaline extract from the benzene solution gave on acidification practically pure 5-cyano-1-naphthol, mp 207—210 °C. Further recrystallization from MeOH gave mp 214—215 °C; lit,[20] mp 209.5 °C.

The 5-cyano-1-naphthol was hydrolyzed in aq. KOH solution. On acidification, 5-hydroxy-1-naphthoic acid was obtained. The aq. alkaline solution of the crude acid was methylated with Me_2SO_4 to give 5-methoxy-1-naphthoic acid (35 g); mp 234—235.5 °C from EtOH; lit, mp 232.5 °C,[20] 230—232 °C.[12] 5-Methoxy-1-naphthoic acid (28 g) was converted into 5-methoxy-1-naphthoyl chloride (24 g, mp 78—81 °C from ligroin; lit,[21] mp 80—81 °C) and then to 1-acetylmethoxynaphthalene (bp 160—175 °C/7 mmHg), in the same way as the preparation of 5-bromo-1-naphthyl derivative. The yellow distillate (15 g) solidified on standing; mp 88—89 °C from ligroin.

1-Acetyl-5-ethylnaphthalene: 1-Bromo-5-ethylnaphthalene (22 g) was prepared by the Wolff-Kishner reduction[22] of 1-acetyl-5-bromonaphthalene (35 g) by a method similar to that for 1-ethylnaphthalene;[1] bp 130—150 °C/5 mmHg; main fraction 144—145 °C/5 mmHg. The distillate was converted without purification into 1-cyano-5-ethylnaphthalene with CuCN in DMF and then into 5-ethyl-1-naphthoic acid, using alkaline and acid hydrolysis; recrystallized. from 70% aq. EtOH, mp 150—153 °C. 1-Acetyl-5-ethylnaphthalene was synthesized from the acid by the method described for 5-bromo-1-derivative in 75% yield from the corresponding naphthoyl chloride; bp 157—160 °C/5 mmHg, mp 35.5—36 °C from hexane.

1-Acetyl-5-chloronaphthalene: 1-Chloro-5-cyanonaphthalene was synthesized from the diazonium solution of 5-cyano-1-naphthylamine. The diazotized solution of 5-cyano-1-naphthylamine (40 g) in AcOH (400 ml) and aq. HCl (concd. HCl, 100 ml) was poured into the freshly-prepared CuCl[23] in concd. HCl (130 ml) with cooling, and allowed to stand two days at room temperature. The precipitates were dissolved in benzene, treated with alkaline solution and the solvent was evaporated. The crude 1-chloro-5-cyanonaphthalene (33 g) obtained was hydrolyzed by refluxing with AcOH (200 ml), H_2SO_4 (100 ml), and H_2O (100 ml) for 18 h. The acid obtained was purified by distillation of the methyl ester (27 g); bp 171—172 °C/10 mmHg (mp 63—64 °C); lit,[24] bp 130 °C/2 mmHg (mp 42 °C), mp 65—66 °C; and followed by recrystallization of the regenerated 5-chloro-1-naphthoic acid (from EtOH), mp 254—255 °C; lit, mp 246—247 °C,[11,12] 245 °C.[24] The acid (15 g) was similarly converted into the corresponding methyl ketone *via* the naphthoyl chloride; lit,[11] mp 68—69 °C. Recrystallization from hexane gave 1-acetyl-5-chloronaphthalene (9 g), mp 69.5—70 °C.

1-Acetyl-6-methoxynaphthalene: 6-Methoxy-1-naphthoic acid was prepared by the reaction of furoic acid and anisole with $AlCl_3$.[25] The acid obtained was purified by distillation of the methyl ester; methyl 6-methoxy-1-naphthoate (25 g), bp 180—186 °C/7—8 mmHg. After alkaline hydrolysis, 6-methoxy-1-naphthoic acid was recrystallized from benzene, mp 191.5—192 °C; lit, mp 180—180.5 °C,[25] 179—180 °C.[12] The acid (19 g) was converted into the corresponding methyl ketone (10 g), distilled at 156—159 °C/4 mmHg. Recrystallization from ligroin yielded 1-acetyl-6-methoxynaphthalene, mp 66—66.5 °C; lit,[26] mp 64—65 °C.

1-Acetyl-6-chloronaphthalene: 6-Chloro-1-naphthoic acid was prepared by the condensation of furoic acid and chlorobenzene with $AlCl_3$.[25] The product contaminated with 7-chloro-1-isomer[24] was recrystallized from benzene (67 g), mp 193—194 °C (lit,[25] mp 188—189 °C), and esterified with MeOH and concd. H_2SO_4. Vacuum distillation at 167—170 °C/4 mmHg (65 g) and repeated recrystallization from MeOH gave methyl 6-chloro-1-naphthoate (30 g) melting at 66.5—67 °C; lit, mp 66—66.5 °C,[24] 68—69 °C.[25] Alkaline hydrolysis yielded pure 6-chloro-1-naphthoic acid (28 g), mp 221—222 °C, lit,[12] mp 216—216.5 °C. The acid (20 g) was converted in the usual way into 1-acetyl-6-chloronaphthalene, being distilled at 155—156 °C/3 mmHg (14 g).

1-Acetyl-6-methylnaphthalene: 6-Methyl-1-naphthoic acid was derived by Price's method;[25] mp 182.5—183 °C from benzene; lit, mp 178—179 °C,[12] 176.5—177 °C.[25] 1-Acetyl-6-methylnaphthalene was derived from the corresponding acid and purified by repeated fractional distillation, bp 143—146 °C/4 mmHg.

1-Acetyl-7-methoxynaphthalene: 2-Acetylaminonaphthalene (mp 134.5—135 °C from benzene; lit,[27,28] mp 131—132 °C) was acetylated by the application of Brown's procedure,[28] with Ac_2O in CS_2 in the presence of $AlCl_3$, and the products were recrystallized twice from 50% aq. EtOH in average yield of 47%, mp 147.5—148 °C; lit, mp 149—150 °C,[27] 151 °C.[28] 1-Acetyl-7-acetylaminonaphthalene (40 g) was hydrolyzed in aq. EtOH in the presence of H_2SO_4 in average yield of 90%, and recrystallized from aq. MeOH, mp 111—112 °C; lit, mp 110—111 °C,[28] 108.5—110 °C.[27,29]

1-Acetyl-7-aminonaphthalene (25 g) was diazotized in the usual manner in a solution of H_2SO_4 (45 ml)–H_2O (200 ml) in AcOH (100 ml), and decomposed with aq. H_2SO_4. The product was dissolved into benzene, filtered, and evaporated to give practically pure 1-acetyl-7-hydroxynaphthalene (23 g), mp 150—152 °C. Recrystallization from benzene–ligroin raised the mp to 152.5—153.5 °C; lit,[27,30] mp 149—150 °C. The usual methylation with Me_2SO_4 gave 1-acetyl-7-methoxynaphthalene, bp 160—162 °C/5 mmHg, as a colorless liquid in 80% yield; mp 63.5—64 °C from hexane–benzene; lit,[27] mp 63 °C.

1-Acetyl-7-chloronaphthalene: Diazotization of 1-acetyl-7-

aminonaphthalene (22 g) in aq. HCl was carried out in the usual manner. The filtered diazonium chloride solution was poured into the ice-cooled freshly-prepared CuCl[23] in HCl (100 ml). Benzene was added to the mixture with vigorous stirring and left to stand at room temperature for 2 days. The benzene layer was separated, filtered, and washed with aq. alkali and water, and crude 1-acetyl-7-chloronaphthalene was distilled at 160—172 °C/5 mmHg, which was solidified soon (12 g) and recrystallized, mp 65—65.5 °C from hexane; lit,[28] mp 64—65 °C (bp 158—160 °C/4 mmHg).

1-Acetyl-7-cyanonaphthalene: The diazonium chloride solution of 1-acetyl-7-aminonaphthalene (50 g) was poured into an aq. solution of CuCN (40 g), NaCN (20 g), and KCN (50 g) with cooling and stirring. After being left to stand overnight, brown precipitates were collected, washed with aq. alkali and water, and dried. Yellow 1-acetyl-7-cyanonaphthalene was distilled at 197—205 °C/5—6 mmHg (23 g); mp 124—125 °C from 95% EtOH.

The cyanide (10 g) was hydrolyzed with the solution of AcOH (100 ml), H_2SO_4 (50 ml), and water (50 ml) for 27 hr to give 8-acetyl-2-naphthoic acid (10 g); mp 235.5—236 °C from 80% aq. EtOH. Found: C, 72.62; H, 4.58%. Calcd for $C_{13}H_{10}O_3$: C, 72.89; H, 4.71%.

1-Acetyl-7-methylthionaphthalene: The diazonium chloride solution of 1-acetyl-7-aminonaphthalene (16 g) was poured into the cooled solution of potassium ethoxyxanthate (30 g) in water (200 ml). After being left to stand overnight, solution was added to aq. KOH (30 g) solution. The mixture was hydrolyzed, made alkaline with 30 g KOH, and methylated with Me_2SO_4. Extraction with benzene, washing with aq. alkali and water, and evaporation of benzene gave crude 1-acetyl-7-methylthionaphthalene which was distilled at 180—205 °C/8 mmHg as yellow viscous liquid (9 g); the product solidified was recrystallized from 80% aq. EtOH, mp 63.5—64.5 °C.

1-Acetyl-7-bromonaphthalene: 2-Bromonaphthalene, bp 130—132 °C/8 mmHg, mp 56—57 °C (lit, bp 122—127 °C/4.5 mmHg, mp 54—56 °C,[31] 56—56.5 °C[28]) prepared from a commercial 2-naphthylamine-1-sulfonic acid,[31] was acetylated according to the method of Girdler *et al.*,[32] using AcCl and $AlCl_3$ in nitrobenzene. The acetylated product distilled at bp 183 °C/9 mmHg was extracted with hot petroleum ether to give a product of mp 62 °C(A). The remaining oily product was purified by column chromatography on Al_2O_3 using hexane–benzene as an eluent. The first and the second fractions gave impure product (mp 70—90 °C from ligroin or hexane), which was repeatedly recrystallized from hexane to give 2-acetyl-6-bromonaphthalene, mp 104.5—105 °C; lit, mp 104—105 °C,[20] 100.5 °C[32] The mother-liquor gave a substance melting at *ca.* 50 °C, which combined with the product (A) was purified by repeated recrystallization from ligroin to give 1-acetyl-7-bromonaphthalene, mp 60—63 °C; lit, mp 63—64 °C,[28] 62—63 °C.[32]

Alcohols and chlorides were prepared according to the reported method.[1] The physical properties and the elemental analytical data of the ketones, alcohols, and chlorides are

Table 1. Physical constants and analytical data of 5-, 6-, and 7-substituted 1-acetylnaphthalenes

Subst.	Mp or (bp)	Carbon		Hydrogen		Other	
		Found	Calcd	Found	Calcd	Found	Calcd
5-MeO-α	88—89°C	78.43	77.98	6.01	6.04		
5-Et-α	35.5—36°C	84.90	84.81	6.90	7.12		
5-Cl-α	69.5—70°C	70.39	70.43	4.72	4.43	17.20	17.32(Cl)
5-Br-α	55.5—56.5°C	58.00	57.86	3.52	3.64	32.40	32.08(Br)
5-CN-α	90—91°C	79.60	79.98	4.38	4.65	6.98	7.17(N)
6-MeO-α	66—66.5°C	77.78	77.98	6.03	6.04		
6-Me-α	(143—146°C/4mmHg)	84.63	84.75	6.50	6.57		
6-Cl-α	(155—156°C/3mmHg)	70.17	70.43	4.22	4.43	17.65	17.32(Cl)
7-MeO-α	63.5—64°C[a]	77.79	77.98	6.07	6.04		
7-MeS-α	63.5—64.5°C	71.99	72.19	5.68	5.59	14.87	14.82(S)
7-Cl-α	65—65.5°C[a]	70.34	70.43	4.43	4.43	17.20	17.32(Cl)
7-Br-α	60—63°C[a]	57.86	57.86	3.62	3.64	31.82	32.08(Br)
7-CN-α	124—125°C	79.95	79.98	4.71	4.65	7.29	7.17(N)

a) For mp in the literature, see Experimental.

Table 2. Physical constants and analytical data of 5-, 6-, and 7-substituted 1-(1-naphthylethanols)[a]

Subst.	Mp	Carbon		Hydrogen		Other	
		Found	Calcd	Found	Calcd	Found	Calcd
5-Et-α	86—87°C	84.01	83.96	8.00	8.05		
5-Cl-α	63—63.5°C	69.92	69.74	5.48	5.37		
5-Br-α	89°C	57.58	57.39	4.29	4.42	31.60	31.82(Br)
6-MeO-α	67—67.5°C	77.09	77.20	6.81	6.98		
6-Me-α	60.5°C	83.69	83.83	7.34	7.58		
6-Cl-α	82—82.5°C	69.82	69.74	5.16	5.36	17.42	17.15(Cl)
7-MeO-α	37—38°C	76.97	77.20	7.08	6.98		
7-MeS-α	37—38°C	71.80	71.52	6.19	6.46		
7-Cl-α	72—73°C	69.65	69.74	5.14	5.37	16.96	17.15(Cl)

a) 5-MeO-α, liq.; it was chlorinated without further purification. 5-CN-α, mp 88.5—90 °C. H-α, mp 65.5—66 °C, bp 133—136 °C/3 mmHg.

Table 3. Physical properties and analytical data of 5-, 6-, and 7-substituted 1-(1-naphthylethyl) chlorides[a)]

Subst.	Mp or (bp)	Carbon		Hydrogen		Chlorine	
		Found	Calcd	Found	Calcd	Found	Calcd
5-MeO-α	39.5—40.5°C	70.35	70.75	5.87	5.94	16.17	16.06
5-Cl-α	62—64°C	64.12	64.03	4.39	4.48	31.39	31.50
5-Br-α	70—71°C	53.42	53.47	3.51	3.74		
6-MeO-α	47—48°C	70.75	70.75	5.80	5.94	16.27	16.06
6-Me-α	34.5—35°C	75.47	76.28	6.15	6.40	17.59	17.32
6-Cl-α	37—37.5°C	63.96	64.03	4.32	4.48	31.92	31.50
7-MeS-α	37—38°C	66.21	65.95	5.48	5.53	14.74	14.97
7-Cl-α	(154—157°C/1mmHg)	64.30	64.03	4.52	4.48	31.42	31.50
7-CN-α	80—82°C	72.44	72.39	4.70	4.67	16.18	16.44

a) 5-CN-α, mp 83—84 °C. 7-MeO-α, liq.; a slightly colored sample was employed for kinetic runs without purification. 7-Br-α, bp 145—147 °C/0.7 mmHg. H-α, bp 131—131.5 °C/5 mmHg.

Table 4. Rate constants of substituted 1-(1-naphthylethyl) chlorides in 80% (v/v) aq. acetone

Series	Subst.	Temp. (°C)	$k_1\times10^5$ (s^{-1})	Series	Subst.	Temp. (°C)	$k_1\times10^5$ (s^{-1})
5α[a)]	MeO	45	33.0	7α[c)]	MeO[d)]	25	43.2
		25	3.13			15	14.4
	Et	45	17.7			0	2.23
		25	1.67		MeS	35	27.5
	Cl	45	0.820			25	8.90
	Br	65	6.30			15	2.59
		45	0.692		Cl	65	17.9
	CN	85	8.38			45	2.12
		75	3.54		Br	65	12.9
		65	1.28			45	1.56
6α[b)]	MeO	45	16.0		CN	85	10.3
	Me	45	20.7			75	3.99
	Cl	45	1.54				

For respective series, a slightly different rate constant for the parent 1-(1-naphthylethyl) chloride was obtained; a) $k_1=12.7\times10^{-5}$, b) $k_1=12.1\times10^{-5}$, c) $k_1=11.1\times10^{-5}$. Relative rates (Table 5) were calculated by use of the corresponding k_1 value. d) slightly colored sample solutions were employed.

given in Tables 1, 2, and 3, respectively.

Solvent and Kinetics. The solvent 80% (v/v) aqueous acetone was prepared by mixing one volume of water with 4 of acetone. Different batches of aqueous acetone which gave only slightly differing rate constants (Table 4) were used without calibration for each series of rate measurements. Solvolysis was carried out at a concentration of *ca.* 0.02 mol/l.[1)] All the runs followed first order kinetics covering over 60—90% reaction within experimental error of *ca.* ±1%, and the rate constants from duplicated runs agreed within ±2% or better. The rate constants obtained at various temperatures are listed in Table 4. Almost all the rate data were based on least squares calculation with at least 10 points covering 2 half lives; those for 7-CN-α were based on initial 5 points (*ca.* 50% reaction) since the rate drifted down slightly with time.

Results and Discussion

The values of log k/k_0 for the solvolysis of substituted chlorides studied in 80% (v/v) aq. acetone at 45 °C are given in Table 5, which also includes the data for 3α and 4α derivatives.[1)] Log k/k_0 varies widely with respect to not only substituent changes but also changes of substituent position. The reactivities of MeO group at the conjugate positions are evidently higher than those at non-conjugate one, and those in the B ring positions are fairly lower than those in the A ring, the lowest being at 5α position; 4α>7α>5α>6α>3α. Schreiber and Byers found a similar sequence in the solvolysis of the methoxy-substituted 1-naphthylmethyl bromides in 80% aq. acetone and in acetic acid.[33)] The effects of Cl substituent at all positions are consistently negative and follow the sequence, 4α>7α>6α>5α>3α, which differs slightly from that of the MeO substituent. The different sequence between both substituents reflects delicately the different blends of the contribution of their *I* and *Pi* effects from respective positions.

The logarithmic relative rates for the present solvolysis at 45 °C are plotted in Fig. 1 against those for the detritiation of substituted 1-tritionaphthalenes in CF_3COOH at 70 °C.[2)] The linear relation suggests that the contributions of the *Pi* effect relative to the *I* effect from corresponding substituents at respective positions are very close to each other in both reactions. The deviations of MeO derivative from the correlation might result from the decreased rate of the detritiation due to the special interaction of the substituent with the acidic solvent.[34)] From the slope of the plot (0.80), the ρ value for the detritiation can be estimated to be −6.3 (least squares calculation, $R=0.998$, $n=11$). This value is consistent with the ρ value (−6.4) obtained from 3α and

Table 5. Log k/k_0 values of substituted 1-(1-naphthylethyl) chlorides in 80% (V/V) aq. acetone at 45 °C

Series	Subst.	log k/k_0	E_a (kcal/mol)	log A
3α[a)]	MeO	−0.570		
	Cl	−2.241*	24.8	10.9
	Br	−2.213*	24.2	10.5
	CN	−2.852*	24.0	9.7
4α[a)]	MeO	3.98*		
	Me	1.475*	20.3	11.5
	Et	1.391*	21.0	11.9
	Cl	−0.658		
	Br	−0.784		
	CN	−3.51*	23.8	8.9
5α	MeO	0.415	22.2	11.8
	Et	0.144	22.2	11.5
	Cl	−1.190		
	Br	−1.264	23.6	11.0
	CN	−1.91*	22.6	9.7
6α	MeO	0.121		
	Me	0.233		
	Cl	−0.895		
7α	MeO	1.48*	19.2	10.7
	MeS	0.862*	20.9	11.2
	Cl	−0.719	22.8	11.0
	Br	−0.852	22.6	10.7
	CN	−1.84*	23.6	10.4

*) Values were obtained by extrapolation from other temperatures. a) Ref. 1.

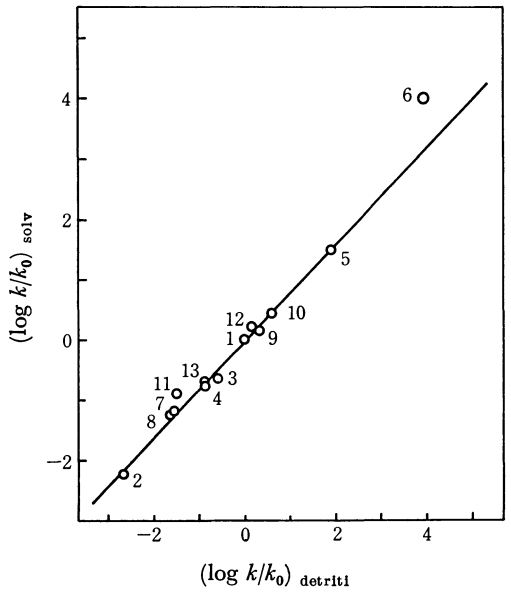

Fig. 1. LFER between the solvolysis and the detritiation rates (slope, 0.80). The points are identified as follows: (1) H-α, (2) 3-Cl-α, (3) 4-Cl-α, (4) 4-Br-α, (5) 4-Me-α, (6) 4-MeO-α, (7) 5-Cl-α, (8) 5-Br-α, (9) 5-Me-α, (10) 5-MeO-α, (11) 6-Cl-α, (12) 6-Me-α, (13) 7-Cl-α.

4α derivatives by the application of Eq. (1) (r=1.13, R=0.997, s=±0.14, n=7). Logarithms of relative rates of the present solvolysis are plotted in Fig. 2 against ΔpK_a of the corresponding substituted 1-naphthoic acids in 50% aq. EtOH.[5,35] In contrast with the plot

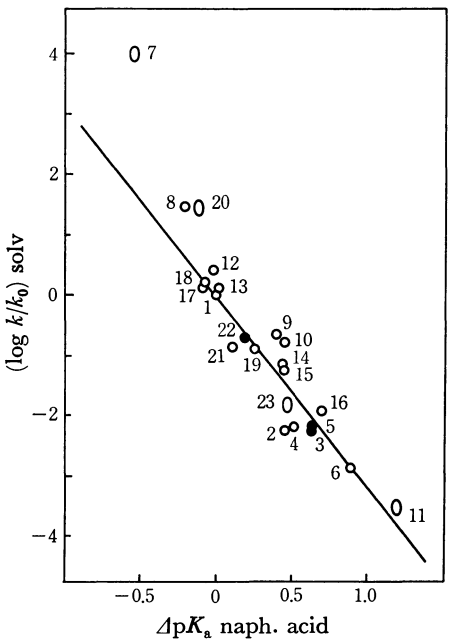

Fig. 2. Total plot of the solvolysis log k/k_0 against ΔpK_a for naphthoic acids (● corrected value for ΔpK_a was employed).
The points are identified as follows: (1) H-α, (2) 3-Cl-α, (3) corrected 3-Cl-α, (4) 3-Br-α (5) corrected 3-Br-α, (6) 3-CN-α, (7) 4-MeO-α, (8) 4-Me-α, (9) 4-Cl-α, (10) 4-Br-α, (11) 4-CN-α, (12) 5-MeO-α, (13) 5-Et-α, (14) 5-Cl-α, (15) 5-Br-α, (16) 5-CN-α, (17) 6-MeO-α, (18) 6-Me-α, (19) 6-Cl-α, (20) 7-MeO-α, (21) 7-Br-α, (22) corrected 7-Cl-α, (23) 7-CN-α.

in Fig. 1, the correlation is not linear, but appears to be quite analogous to that observed in the case of benzene derivatives against the σ-constants. This is reasonable since the pK_a's of naphthoic acids could be regarded as the essentially unexalted σ-type reactivity.

According to the LArSR assumption,[1] such a plot for an electrophilic resonance reaction against σ may be expected only for conjugatively electron releasing (−R) substituents at the conjugate position to give the substantial upward deviations, the extents of which depend upon their resonance contribution, as observed in the benzene reactivities. The correlation line may be drawn through the origin and the points for CN derivatives for which no exaltation of resonance might be expected. The weakly conjugating groups at the less effective conjugate position lie more closely to the correlation line. With respect to the σ^+ type reactivities, on the other hand, the theory predicts for any kinds of substituents to give no downward deviations from the correlation line. The figure seems to be satisfactory for most substituents except 3α- and 7α-halogen substituents. Unfavorable dispositions of 3α- and 7α-halogens may probably be due to the improper pK_a values for the corresponding naphthoic acids. This is suggested by the following facts. Such deviations of 3α- and 7α-halogen groups were not observed in similar logarithmic plots of the present data against pK_a's of naphthylamines[6] and also those against log k/k_0 of the hydrolysis of naphthoic esters.[36,37] The calibrated points on this basis (closed circles, Fig. 2) fall in fact near the correlation line determined by non- or

less conjugative derivatives. It is apparent that all the substituents at the non-conjugate 3 and 6 positions as well as the $+R$ substituents at any position fall on the correlation line for the unexalted substituent effect. The exalted contribution of substituents at any conjugate positions follows the usual order of $\Delta\bar{\sigma}_R^+$ values, MeO>Me> Cl, Br, as seen in the benzene reactivities, and that the enhancement of a $-R$ substituent, for example, the most effective MeO group, becomes less extensive by the positional change in the order, $4\alpha>7\alpha>5\alpha>3\alpha$, 6α. This is essentially valid also for the other $-R$ substituents. The exaltation of the substituent effects in the present electrophilic reactivities is observed only for the $-R$ class substituents at the conjugate position, but not for $+R$ class substituents even at the conjugate position.

The results are in line with the general features of the substituent effects observed in the Hammett-type treatment of the benzene reactivities, especially with those characteristic of the electrophilic σ^+-type reactivities in the benzene system.[38]

From a survey of the naphthalene reactivity data in the literature, including copious ones, the reaction dependence of the substituent effect can not be overlooked.

The Hammett-type description of the naphthalene reactivities requires several sets of substituents constants such as σ_{ij}, σ_{ij}^+, and σ_{ij}^-. As seen in the benzene case, however, each set of substituent constants should be applied within the limit of closely related classes of reactivities. This is clearly illustrated by a comparison of the plots in Figs. 1 and 2. The results suggest that the exalted-resonance type electrophilic naphthalene reactivities can be treated in the same way as that for benzene by means of the equation

$$\log k_{ij}/k_0 = \rho(\sigma_{ij}+r_{ij}^+\Delta\sigma_{R,ij}^+) \qquad (1')$$

where the subscripts i and j represent the respective naphthalene positions to which are attached substituents (i) and the reacting side-chain (j=α in the present case). The exalted resonance contribution of substituents at effectively conjugative positions (4α,5α,7α) can be given by the second term in Eq. (1'). For all $+R$ substituents and $-R$ ones at weak conjugate positions (3α, 6α), the second term should be zero. The values of $\Delta\sigma_{R,ij}^+$ may be defined by the differences of the apparent substituent constants between any two reference reactions in the same way as in the definition of $\Delta\bar{\sigma}_R^+$ in the benzene system. The treatment is applicable not only to the effect of substituents in the A ring,[1] but also might be applicable to that of substituents at all positions in the B ring, if the standard set of naphthalene σ values for respective substituents at respective positions, σ_{ij}, or more preferably the naphthalene σ_{ij}^0 parameters are determined. In this treatment, both σ_{ij} and $\Delta\sigma_{R,ij}^+$ are assumed to be the parameters characteristic of a substituent as well as constants of respective naphthalene positions. The r_{ij} should then be given as a constant of a given reaction and independent of substituent positions. This treatment will be most convenient for practical use. However, a fundamental set is not immediately available nor sufficient data to verify its general applicability.

For the present purpose, to determine the position dependency of inductive and π-electronic components of substituent effects, the LSFE treatment (2) using σ_i and σ_π^+ constants appears to be more reasonable. Accordingly, we employed Eq. (2) statistically for each naphthalene position with respect to only conjugatively electron releasing ($-R$) substituents. The correlational parameters obtained by the method of least squares are given in Table 6 and substituent constants, σ_i and σ_π^+, in Table 8. The reliability of statistical ρ_i and ρ_π^+ parameters is strongly dependent upon the number of substituents involved as well as the variation of electronic nature of substituents. Although the limited rate data in our study restrict the precision of fit with which the parameters ρ_i and ρ_π^+ are determined, respective series involves at least one of each representative type of $-R$ substituents, alkoxy, halogen, and hydrogen, and covers an extensive change of reactivity.

It is seen from Table 6 that most correlations are excellent (R>0.999) and the substituent effects of $-R$ substituents at each position in the present naphthalene system can be correlated quite successfully by means of Eq. (2). The same treatment can be applied also to the effects of $-R$ substituents in other naphthalene reactivities; detritiation of substituted α-tritionaphthalenes[2] and dissociation of substituted α-naphthylammonium ions[6] and of substituted α-naphthoic acids.[5,35] The results for these reactivities are given in Table 7. In the case of detritiation, the methoxy group was not included in the calculation because of the special interaction with the acidic solvent, CF_3COOH; only methyl and halogens can be treated as ordinary substituents. Eaborn stated that the kinetic data of halogen substituents at 70 °C are of probable 15% errors due to experimental difficulties.[3] One unpreferable feature resulting from the statistical application to less sufficient data appears as the positive ρ_π^+ value for 6α series, to which we can not give any physical significance; probably the ρ_i and ρ_π^+ values for 6α series in this reaction is not reliable (see Table 7). The correlations for the amine series (R> 0.997) appear to be more reliable than those for the acid series.

Table 6. Correlational parameters for the present solvolysis data with respect to $-R$ substituents

$$\log k/k_0 = \rho_i\sigma_i + \rho_\pi^+\sigma_\pi^+ + \delta$$

Series	ρ_i	ρ_π^+	δ	R[a]	$\pm$s[b]	n[c]
3α[d]	−6.96	−2.56	0.00	0.999	0.01	4(MeO, Cl, Br, H)
4α[d]	−5.09	−17.6	−0.06	0.999	0.07	6(MeO, Me, Et, Cl, Br, H)
5α	−3.82	−4.40	−0.17	0.988	0.17	5(MeO, Et, Cl, Br, H)
6α	−2.90	−2.43	−0.04	0.997	0.07	4(MeO, Me, Cl, H)
7α	−3.66	−7.74	−0.01	0.999	0.03	5(MeO, MeS, Cl, Br, H)

a) Correlation coefficient. b) Standard deviation. c) Number of substituents involved in the calculation. d) Previous results; Ref. 1.

Table 7. Correlational parameters for the data of α-naphthyl reactivities[a)]

Reaction	Series	ρ_i	ρ_π^+	δ	R	±s	n
Detriti.[2)]	3α	−7.81	−1.31				3(Me, Cl, H)
	4α	−5.87	−23.4	−0.09	0.996	0.14	5(Me, F, Cl, Br, H)
	5α	−4.83	−3.12	−0.07	0.997	0.10	5(Me, F, Cl, Br, H)
	6α	(−4.11)[b)]	(+0.83)[b)]				3(Me, Cl, H)
	7α	−3.28	−4.01				3(Me, Cl, H)
Amine[6)]	3α	3.48	0.24	0.07	0.997	0.06	6(OH, MeO, Me, Cl, Br, H)
	4α	(2.50)[c)]	(2.41)[d)]				2(Br, H)
	5α	1.81	1.03	0.01	0.997	0.05	4(NH_2, OH, Cl, H)
	6α	1.45	0.93	0.00	0.999	0.02	4(OH, MeO, Cl, H)
	7α	1.60	1.67	0.02	0.999	0.03	4(OH, MeO, Cl, H)
Acid[5,35)]	3α	1.48	0.61	0.02	0.995	0.04	5(OH, Me, Cl, Br, H)
		1.90[e)]	0.88[e)]	0.04[e)]	0.997[e)]	0.04[e)]	5(OH, Me, Cl,[e)] Br,[e)] H)
	4α	1.38	3.08	0.06	0.991	0.09	8(NH_2, OH, MeO, Me, F, Cl, Br, H)
	5α	1.16	0.98	0.08	0.971	0.08	7(NH_2, OH, MeO, Me, Cl, Br, H)
	6α	0.87	0.92	0.02	0.996	0.02	6(OH, MeO, Me, Cl, Br, H)
	7α	0.50	0.69	−0.02	0.993	0.02	5(OH, MeO, Me, Br, H)
		0.74[f)]	0.86[f)]	−0.01[f)]	0.998	0.01[f)]	5(OH, MeO, Me, Cl,[f)] H)

a) Symbols are the same as those in Table 6. b) Less reliable value because of positive ρ_π^+ value. c) Estimated value from the interpolation of the $\rho_i-\rho_i$ plot. See text. d) Estimated value. See Table 11, footnote. e) Corrected ΔpK_a values were employed; Cl(0.64) and Br(0.64). f) Corrected ΔpK_a value was employed; Cl (0.19).

Table 8. Substituent parameters[a)]

Subst.	σ_i	σ_π^+
NH_2	0.06	−0.42
OH	0.19	−0.34
MeO	0.185	−0.281
MeS	0.368	−0.285
Me	−0.045	−0.078
Et	−0.045	−0.069
H	0.000	0.000
F	0.363	−0.118
Cl	0.348	−0.070
Br	0.337	−0.054

a) Values taken from Ref. 38.

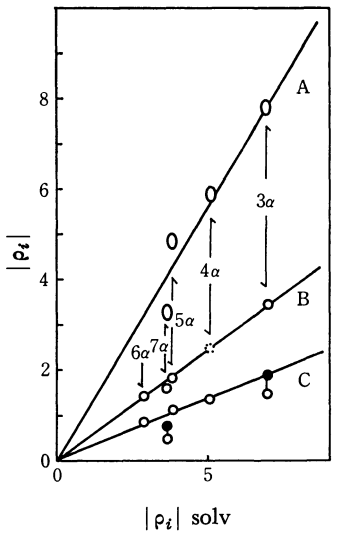

Fig. 3. $\rho_i-\rho_i$ plots.
A: the detritiation, B: the dissociation of naphthylammonium ions ($\rho_{i,4\alpha}$ can be interpolated from B line), C: the dissociation of naphthoic acids (● corrected value was employed).

Figure 3 shows the linear relations of the sets of ρ_i's for the detritiation (A), the dissociations of amines (B), and acids (C) with the corresponding ρ_i values obtained from the present solvolysis. The linear ρ_i—ρ_i relationship holds. The deviations of 6α and 7α in the plot A may arise from the inaccuracy of ρ_i values due to insufficient number of data in the detritiation. Deviations of 3α and 7α in C might be attributed to the unreasonable pK_a values.

The dissociation of naphthoic acids can reasonably be expected to be a representative σ class reactivity. The pK_a of substituted α-naphthylammonium ions should be a typical nucleophilic reactivity, that is, the resonance exaltation of $+R$ substituents at conjugate positions are significant, while the effect of the $-R$ substituents in this set could be regarded as the unexalted class even for those at conjugate positions. Both the present solvolysis and the detritiation should belong to the electrophilic reactivity. Evidently the linear ρ_i—ρ_i relationship is generally valid in various types of reactions (Fig. 3); between reactions not only of similar contributions but also of distinctly different contributions of the π-electronic effects.

In view of the positional consistency of the inductive components, it appears to be convenient to express Eq. (2) as follows.

$$\log k/k_0 = \rho(C_{ij}\sigma_i + q^+_{r,ij}\sigma_\pi^+) \qquad (3)$$

where i and j represent the naphthalene ring positions bearing a substituent and a reaction site, respectively. C_{ij} is the positional constant concerning the transmission of the inductive effects. The $q^+_{r,ij}$ is the characteristic variable of reactions as well as of substituted positions, giving a measure of the π-electronic interaction of substituents at respective positions with a reaction site. The

ρ value in Eq. (3) should be identical to $\rho_{i,4\alpha}$ (-5.09 for the solvolysis) by definition.

The reference set of C_{ij} can be determined from the ratios of the ρ_i values for the present solvolysis data, since they provide the relatively precise correlations and cover a more sufficient range of reactivity changes. The $\rho_{i,4\alpha}$ value is taken as a standard, as referred to the definition of σ_i scale for benzene derivatives. The values of C_{ij} obtained are as follows. $C_{3\alpha}=1.37$, $C_{4\alpha}\equiv 1.00$, $C_{5\alpha}=0.75$, $C_{6\alpha}=0.57$, and $C_{7\alpha}=0.72$.

In order to interpret the total substituent effects in the naphthalene reactivities, various correlational equations have been developed by various workers. Dewar and Grisdale have treated the dissociation of α-naphthoic acids in terms of the equation[5]

$$\sigma_{1j} = 1/r_{1j}F + q_{1j}M \quad (4)$$

The field effect is simply assumed to be proportionally transmitted with the reciprocal of the simplified distance between ring carbons, which is taken into account in the first term. The second term represents the mesomeric effect, whose position dependency is assumed to be proportional to the NBMO charge of each naphthalene position.

The same type of approach was developed to interpret the substituent effects on the detritiation of α- and β-tritionaphthalenes:[2,3,39]

$$\sigma_{1j}^{W} = 1/r_{1j}F + q_{1j}^{W}M^{+} \quad (5)$$

The main improvement lies in the employment of the other set of M^+ constants instead of M in Eq. (4). In these approaches, the transmission schemes of both *I* and *Pi* effects are restricted by *a priori* assumptions based upon simplified consideration. The transmission schemes were assumed to be reaction-independent. However, all these treatments were applied only to a single set of reactivities, and no definite evidence of the generality has yet been offered. Though a precise comparison may not be possible, it appears that these correlations are of considerably poorer quality than the present results. The present study does not lie on the same line of approach but aims at a purely empirical determination of the transmission schemes of *I* and *Pi* effects by means of Eq. (2). Taft and his co-workers developed the latter line of approach, not based on an *a priori* transmission scheme.[40] Their treatment is based on the assumption that the effects of substituents at respective positions can be given by the statistical blends of the terms proportional to their σ_I and σ_R^0 parameters, as represented by

$$\log k/k_0 = \rho_{I,ij}\sigma_I + \rho_{R,ij}\sigma_R^0 \quad (6)$$

The transmission schemes of the inductive and resonance effects were thus determined as the relative $\rho_{I,ij}$ and $\rho_{R,ij}$ values, by means of the statistical application of Eq. (6) for all the substituents, both $+R$ and $-R$ classes, at respective naphthalene positions. However, it should be noted that Eq. (6) can only be applied within the limited range of the unexalted σ^0- or at most σ-type reactivities, as noted by Taft. Otherwise the correlation of the reactivities at the conjugate position would not be so reliable. A similar treatment was also employed for the dissociation of naphthoic acids by Swain and Lupton, in terms of their F and R parameters.[41] The same limitation discussed above applies to this treatment.

Dewar's treatment and its modifications assume that the so-called inductive polar effect of dipolar substituents is mainly controlled by the field effect. Such a field effect is ordinarily taken into account as a first approximation by certain functions of the distances, r_{ij}; $1/r_{ij}$ or $\cos\theta/r_{ij}^2$ for a special case.[5,35] It is of interest to compare the empirical C_{ij} values with familiar functions of distance accounting for the transmission of electrostatic interaction across space. The relevant parameter values are listed in Table 9. Most of the theoretical parameters

Table 9. Comparison between C_{1j} values and varisou functions of distance

Series	C_{1j}	Ratio of $1/r$[a]	Ratio of $1/R'$[b]	Ratio of $(\cos\theta/R^2)$[c]
3α	1.37	1.15	1.15	1.11
4α	1.00	1.00	1.00	1.00
5α	0.75	0.75	0.87	0.71
6α	0.57	0.67	0.85	0.72
7α	0.72	0.75	1.00	0.58

a) r is distance between ring carbons; Refs. 5 and 35. b) R' is distance between ring carbon and reaction center; Ref. 40 ($1/r_{rX}$ for $\gamma=1$). c) R is distance between center of substituent dipole and reaction center; Ref. 35.

indicate roughly the same trend and do not differ significantly from the characteristic order of the C_{ij} values, $C_{3\alpha}>C_{4\alpha}>C_{5\alpha},C_{7\alpha}>C_{6\alpha}$, in which the most striking feature is $C_{5\alpha}\simeq C_{7\alpha}$. As far as the α-naphthyl system is concerned, however, the simplest Dewar function, the dependence on $1/r_{ij}$, appears to be the best in various field-functions, explaining completely the characteristic order as well as the magnitude of C_{ij}'s. The more sophisticated one does not appear to provide any improvement in the parallelism with the empirical C_{ij}. It is apparent that any orientational factor (function of θ or angular dependence of the field effect of dipolar substituents) is of little practical consequence. The effect, if operative at all, is relatively unimportant at least in the α-naphthyl reactivities.

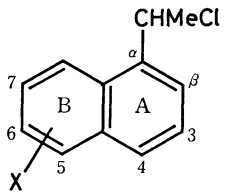

It might be concluded as follows. (1) The positional dependence of the inductive contribution can be given by the ratio of ρ_i parameters, *i.e.*, by $C_{ij}=\rho_i/\rho_{i,4\alpha}$, and remains generally a constant in the naphthalene system, independent of reactions, or more precisely, of the varied contributions of the *Pi* effects in any types of reactions. (2) Dewar's simplest field function $1/r_{ij}$ may be applicable, to a practically useful approximation, generally as the transmission factor of the *I* effects in the naphthalene reactivities. The results provide in part an evidence justifying the validity of the description of the substituent effects in the naphthalene system by means of Eq. (2).

Table 10. Comparison between the solvolysis ρ_π^+ and various theoretical values

Series	ρ_π^+	$q_r^{+a)}$	$q_{1j}^{b)}$	$\pi_{1j}^{c)}$	$\pi'_{rX}{}^{d)}$	$q_{1j}^{W\ e)}$	$\Delta q_{1j}(ArH^+)^{f)}$	$\Delta q_{1j}(ArCH_2^+)^{g)}$
3α	−2.56	0.5	0.000	0.018	0.000	0.000	0.006	(0.010)
4α	−17.6	3.5	0.200	−0.139	0.180	0.364	0.228	(0.207)
5α	−4.40	0.9	0.050	−0.023	0.045	0.091	0.082	(0.078)
6α	−2.43	0.5	0.000	0.007	0.000	0.000	0.046	(0.046)
7α	−7.74	1.5	0.059	−0.033	0.062	0.091	0.112	(0.104)

a) Value in Eq. (3), $\rho_\pi^+/\rho_{i,4\alpha}$. b) Dewar's formal charge; Refs. 5and 43. c) Atom-atom polarizability; Refs. 5 and 35. d) Bond-atom polarizability, $\pi_{Rr,i}$ in Ref. 40. e) Eaborn's parameter; Ref. 3. f) Forsyth's regional charge difference; Ref. 44. g) Approximate value; Ref. 45.

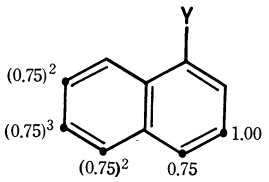

Chart 1. C_{ij} values are approximately represented as power dependence; bond fall off model.

Another instructive feature illustrated in Chart 1, where C_{ij} values are given as a power dependence upon numbers of intervening bonds to a good approximation, is of interest. It suggests that successive polarization of intervening bonds also plays an important role in the contribution of the σ-inductive effect, C_{ij}. A transmission factor per one carbon–carbon bond appears to be 0.75, when C_{ij} values are compared with each other in the naphthalene A or B ring. However, although the number of intervening C–C bond between the carbons i and j is equal for 4α, 5α, and 7α derivatives (through the most effective route), C_{ij} for 5α or 7α is 0.75 times smaller than that for 4α. This gap between rings A and B might reflect the effect of the branched ring-carbon at 9 or 10 position, at which the transmission route is separated into two ways. An explanation in terms of such branched carbons can also be applied to the fact that the ratio $C_{3\alpha}/C_{4\alpha}$ is slightly larger than C_{meta}/C_{para}, since two similar transmission routes are possible from *para* position to a reaction site in the benzene system.

Success in the separation of the contribution of the position-dependent *I* effects from the total electronic effects may provide sufficient reliability for a discussion on the remaining *Pi* effects, if the assumption of the additivity of the two effects is valid. The set of ρ_π^+ for the solvolysis (Table 6) shows that the contributions of the electron donative *Pi* effect of substituents at any conjugate position are evidently more effective than those from substituents at non-conjugate positions, just as the HMO theory predicts. The magnitude of ρ_π^+'s for the conjugate ones is appreciably different; the resulting order of the effectiveness is $3\alpha \simeq 6\alpha < 5\alpha < 7\alpha < 4\alpha$. Since the identical sequence is also found for other electrophilic reactivities such as the sets of ρ_π^+'s for the detritiation and the dissociation of amines (Table 7), it can be concluded that the sequence generally holds for $-R$ substituents in electrophilic reactivities and is inherent to the parent naphthalene π-electron system. This has been recently confirmed for $+R$ substituents in nucleophilic reactivities such as the substituent chemical shifts of OH protons of naphthols in a DMSO solution.[42]

The set of ρ_π^+'s empirically derived from the solvolysis could reasonably be compared with various sets of theoretical indices for the parent naphthalene or related hydrocarbons. The MO parameters of interest in connection with the transmission coefficient are listed in Table 10. As far as conjugate positions are concerned, the correspondence of ρ_π^+ with any HMO indices appears to be good to a rough approximation, but not necessarily complete, since small but definite electron donative *Pi* contributions are observed in the empirical set for non-conjugate 3 and 6 positions. Forsyth proposed a new set of theoretical index based on CNDO/2 approximations, $\Delta q_{ij}(ArH^+)$ or $\Delta q_{ij}(ArCH_2^+)$, in which the numerical values are derived from the difference of the regional charges at i'th carbon between a transition state and an initial state model.[44] The plot of the solvolysis ρ_π^+ *vs* $\Delta q_{ij}(ArCH_2^+)$[45] seems to be satisfactorily linear for all positions well within the limit of approximation (Fig. 4).

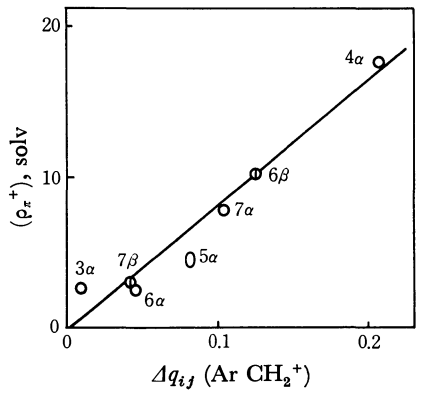

Fig. 4. The plot of solvolysis ρ_π^+ *vs.* $\Delta q_{1j}(ArCH_2^+)$.[45] (Data for 6β and 7β will be seen in a next paper).

This index can take account for not only the presence of electron donative contributions at non-conjugate positions, but also the relative magnitudes of ρ_π^+'s at conjugate ones. The good coincidence between the empirical and theoretical coefficients gives another evidence verifying the description of the substituent effects in the naphthalene system in terms of the *I* and *Pi* effects by means of Eq. (3).

The results of all four different reactions indicate that the π-electronic components are dependent not only upon the substituent positions but also upon reactions even at a given conjugate position. The most intuitive parameter illustrating such a reaction dependency of the *Pi* effects is the $q_{r,1j}^+$ value in Eq. (3), which is equivalent to the *r* value for the *para* position of benzene system in Eq. (1). The values are calculated as $\rho_\pi^+/\rho_{i,4\alpha}$ and summarized in Table 11.

Table 11. Comparison of $q_{r,ij}$ values for some electrophilic α-naphthyl reactivities

Series	Reaction[a]			
	Solv.	Detriti.	Acid	Amine
3α	0.5	0.2	0.4* (0.6)[b]	0.1[c]
4α	3.5	4.0	2.2	1.0[c,d]
5α	0.9	0.6	0.7	0.4[c]
6α	0.5		0.7	0.4[c]
7α	1.5	0.7*	0.5*(0.6*)[b]	0.7[c]

*) Value is less reliable since certain discrepancies are observed in the ρ_i—ρ_i plot in Fig. 3. a) See Table 7. b) Corrected ΔpK_a value was employed. c) Secondary value based on the estimated $\rho_{i,4\alpha}$ of 2.50. d) From ΔpK_a of 4-Br-α, $\rho_{\pi,4\alpha}^{+}$ was estimated as 2.41, using the parameter of Br in Table 8.

Although the crudeness of data does not permit a precise discussion, the results appear to suggest the following. The characteristic order of the $q_{r,ij}^{+}$ for the conjugate positions, 4α>7α>5α, obtained in the present solvolysis can be observed also in other reactivity sets. The $q_{r,ij}^{+}$ for any B ring position is much smaller and at most half as large as that for the 4α position. These are in qualitative agreement with the scheme of π-electronic transmission expected from MO indices mentioned above. However, the $q_{r,ij}^{+}$ is evidently reaction-dependent, in contrast to the reaction-independent C_{ij} value for the inductive contribution, and that for the conjugate position varies from reaction to reaction depending upon the reactivity classes or the amount of charge at the site delocalized through π-electronic interaction. It should be noted that the value for a given conjugate position, especially that for 4α position, shows practically the same dependency upon reactions as the q_r^{+} (and in the analogous way to the r value) for the same reactions of *para* substituted benzene derivatives. In the reaction of smaller electron demand such as the dissociation of naphthoic acids and naphthylamines, the $q_{r,ij}^{+}$ only for 4α is significant but those for 7 and 5 positions diminish to a value comparable to that for non-conjugate positions. Concerning the $q_{r,ij}^{+}$'s for non-conjugate positions (Table 11), although the number of substituents and of reactions examined are limited, it would be reasonable to consider that the $q_{r,ij}^{+}$ for the non-conjugate position remains practically constant in spite of the variation of reaction (*e.g.*, $q_{r,3\alpha}^{+}=0.4\pm0.3$ and $q_{r,6\alpha}^{+}=0.5\pm0.2$). This is in contrast to the behavior of the $q_{r,ij}^{+}$ for conjugate positions but in line with the general reaction-independency of σ_m values observed in benzene reactivities.[38]

Finally, the $q_{r,ij}^{+}$ values for the σ^0-class reactivity (*i.e.*, $q_{r,ij}^{0}$) may reasonably be expected to be close to the least exalted $q_{r,ij}^{+}$ values obtained for the pK_a of naphthylammonium ions and probably very close to 0.5 for all positions except 1.0 for 4α position, as far as the $-R$ substituents are concerned. A typical $+R$ cyano substituent at any position in Fig. 2 essentially satisfies the correlation determined by 3α and 6α substituents. This suggests that the exaltation of π-electronic effect of the $+R$ group even at strongly conjugative positions does not occur in the σ^+-type electrophilic reactivity of the naphthalene in the same way as in the benzene system.[38]

In fact, the apparent σ_{ij} values of the CN group in the present solvolysis can be calculated as a good approximation with the above $q_{r,ij}^{0}$ for σ^0-class reactivity (combined with C_{ij} values) but not with the set of $q_{r,ij}^{+}$ values for the solvolysis. It is apparent that the dual q_r values, $q_{r,ij}^{+}$ and $q_{r,ij}^{-}$, should generally be required each for $-R$ and $+R$ class substituents. The σ^0 class reactivity may thus be defined as the reactivity which shows minimal exaltation of both $-R$ and $+R$ resonance; *i.e.*,

$$q_{r,ij}^{+} = q_{r,ij}^{-} = q_{r,ij}^{0}.$$

From the results, we can figure out the general pattern of the transmission of the substituent effect in the naphthalene system. The substituent effect in the naphthalene system can be separable as a useful approximation into the reaction-independent inductive contribution and the reaction-dependent *pi*-electronic contributions from $+R$ and $-R$ substituents by means of the equation

$$\bar{\sigma}_{ij} = (\log k/k_0)/\rho = C_{ij}\sigma_i + q_{r,ij}^{+}\sigma_\pi^{+} + q_{r,ij}^{-}\sigma_\pi^{-} \qquad (3')$$

The last term applies to the effect of $-R$ substituents. The C_{ij} is generally independent of reactions. The $q_{r,ij}$ for non-conjugate positions also remains to be $q_{r,ij}^{0}$ regardless of reaction. The reaction dependency of the apparent substituent constants $\bar{\sigma}_{ij}$ is attributable to the changes of the $q_{r,ij}^{+}$ and/or $q_{r,ij}^{-}$ for the conjugate positions with reactions. The characteristic ratio $q_{r,ij}^{+}/q_{r,ij}^{-}$ reflects the nature of the reaction center at the transition state.[46]

Dewar's *FM* assumption is in line with the present statistical results at least with respect to the inductive transmission scheme. However, with respect to the *pi*-electronic transmission scheme it appears to be inconsistent with our conclusion, in two points. According to the present analysis there is no reaction-independent general-scheme of the *pi*-effect transmission, as Dewar assumed to be given by a fixed set of NBMO q_{ij} coefficients.[5] Even if it is valid as a first approximation, the application will be limited to some very narrow range of reactivity class. Use of Eaborn's q_{ij}^{w} scheme as in Eq. (5) for the electrophilic σ^+-type reaction gave better results.[2] The different reaction-dependency of the *pi*-effect transmission scheme for the $+R$ and $-R$ substituents was not taken into account in the *FM* treatment. The better fit for the σ^+-type reactivities by the use of q_{ij}^{w} in place of q_{ij} is consistent with our observation, since the values of q_{ij}^{w} are approximately 2-fold of q_{ij}, respectively for conjugate positions. However, in such highly electrophilic reactivities, the unexalted *pi*-effect transmission scheme (the $q_{r,ij}^{0}$ set) was evidently retained for the $+R$ substituents even at a strongly conjugative position. Incorporated application of the M^+ parameters which were derived from σ^+ constant in Eq. (5), instead of M from σ, is reasonably expected to improve the situation,[39] since the higher ratio of q_{ij}^{+}/q_{ij}^{-} required for electrophilic reactivities may partly be adjusted by the exalted $-R/+R$ resonance contribution ratio of the σ^+ constants.[47] The authors however do not agree to the use of multiple sets of resonance parameters.[46]

Taft suggested that there is no universal set of resonance parameters (providing the parameter $\bar{\sigma}_R$ is defined by $\bar{\sigma}_p-\sigma_I$) and that at least four fundamental sets of the resonance parameters, σ_R,[0] σ_R, σ_R^{+}, and σ_R^{-}, should be

required for different reactivity classes.[48] Consequently in the case of $-R$ exalted-resonance reactivities, such as the present solvolysis in the naphthalene system, the σ_R^+ should be employed instead of σ_R^0 in Eq. (6) as the most suitable set for the substituents at strongly conjugative position. However, σ_R^0 should be still utilized for the substituents at non-conjugative 3α and 6α positions. There appears however to be no definite rule for the choice of the most proper set of the parameters for the substituents at intermediate or moderately strong conjugate 5α and 7α positions. The best parameter could only be chosen as to give a best fit correlation. Presumably such $\bar{\rho}_I$ and $\bar{\rho}_R$ values could not be compared with each other within the same series or between different sets of reactivities.

The success in describing the substituent effects in the naphthalene beyond the benzene derivatives provides strong support for the possibility that a unique set of σ_i and σ_π^+ substituent constants can be utilized practically as universal substituent constants.

References

1) Part X: Y. Tsuno, M. Sawada, T. Fujii, and Y. Yukawa, This Bulletin, **48**, 3347 (1975).
2) C. Eaborn and A. Fischer, *J. Chem. Soc., B*, **1969**, 152.
3) C. Eaborn, P. Golborn, R. E. Spillett, and R. Taylor, *ibid.*, **1968**, 1112.
4) R. W. Bott, R. W. Spillett, and C. Eaborn, *Chem. Commun.*, **1965**, 147.
5) M. J. S. Dewar and P. J. Grisdale, *J. Amer. Chem. Soc.*, **84**, 3546, 3548 (1962); also see Ref. 43.
6) A. Bryson, *ibid.*, **82**, 4862 (1960).
7) F. C. Whitmore and A. L. Fox, *ibid.*, **51**, 3363 (1929).
8) L. Friedmann and H. Shechter. *J. Org. Chem.*, **26**, 2522 (1961).
9) W. F. Short and H. Wang, *J. Chem. Soc.*, **1950**, 991.
10) J. B. Shoesmith and H. Rubli, *ibid.*, **1927**, 3098.
11) I. G. Bystritskii and L. S. Solodar, *Zh. Prikl. Khim.*, **1968**, 2332; *Chem. Abstr.*, **70**, 67980h (1969).
12) M. J. S. Dewar and P. J. Grisdale, *J. Amer. Chem. Soc.*, **84**, 3541 (1962).
13) Methyl 5-bromo-1-naphthoate, recrystd. from MeOH, mp 65—65.5 °C; lit, mp 66—67 °C,[9] 64.5—65 °C.[11]
14) R. E. Bowman, *J. Chem. Soc.*, **1950**, 322.
15) M. S. Newman, D. MacDowell, and S. Swainathan, *J. Org. Chem.*, **24**, 509 (1959).
16) G. Lock, *Monatsh*, **81**, 850 (1950): *Chem. Abstr.*, **45**, 4229d (1951).
17) J. B. Shoesmith and H. Rubli, *J. Chem. Soc.*, **1927**, 3098.
18) L. H. Klemm, J. W. Sprague, and E. T. K. Mak, *J. Org. Chem.*, **22**, 161 (1957).
19) R. L. Dannley and M. Gippin, *J. Amer. Chem. Soc.*, **74**, 332 (1952).
20) G. W. Gray and B. Jones, *J. Chem. Soc.*, **1954**, 678.
21) J. B. Shoesmith and H. Rubli, *ibid.*, **1926**, 3241.
22) Huang-Minlon, *J. Amer. Chem. Soc.*, **68**, 2487 (1946); D. Todd, "Organic Reactions," Vol. 4, Chap. 8, John Wiley and Sons (1949).
23) "Organic Syntheses," Coll. Vol. 1, p. 170.
24) T. L. Jacobs, S. Winstein, R. B. Henderson, J. B. Jack, W. Ralls, D. Seymour, and W. H. Florsheim, *J. Org. Chem.*, **11**, 229 (1946).
25) C. C. Price, E C. Chapin, A. Goldman, F. Krebs, and H. M. Shafer, *J. Amer. Chem. Soc.*, **63**, 1857 (1941).
26) I. N. Nazarov, G. P. Verkholetova, S. N. Ananchenko, I. V. Targov, and G. V. Aleksandrova, *Zhur. Obshchei Khim.*, **26**, 1482 (1956); *Chem. Abstr.*, **50**, 14683h (1956).
27) N. J. Leonard and A. M. Hyson, *J. Org. Chem.*, **13**, 164 (1948).
28) R. F. Brown, T. L. Jacobs, S. Winstein, E. F. Levy, H. R. Moss, and M. L. Ott, *ibid.*, **11**, 163 (1946).
29) N. J. Leonard and A. M. Hyson, *J. Amer. Chem. Soc.*, **71**, 1392 (1949).
30) G. G. Joshi and N. M. Shah, *J. Indian Chem. Soc.*, **31**, 325 (1954): *C. A.*, **49**, 12407i (1955).
31) F. A. Vingiello, T. J. Delia, P. Poiss, and D. Farrier, *J. Chem. Educ.*, **40**, 544 (1963): *C. A.*, **59**, 15223h (1963).
32) R. B. Girdler, P. H. Gore, and J. A. Hoskins, *J. Chem. Soc. C*, **1966**, 518.
33) K. C. Schreiber and R. G. Byers, *J. Amer. Chem. Soc.*, **84**, 859 (1962).
34) R. W. Taft, E. Price, I. R. Fox, I. C. Lewis, K. K. Anderson, and G. T. Davis, *ibid.*, **85**, 709 (1963).
35) P. R. Wells and W. Adcock, *Aust. J. Chem.*, **18**, 1365 (1965).
36) A. Fischer, W. J. Mitchell, G. S. Ogilve, J. Packer, J. E. Packer, and J. Vaughan, *J. Chem. Soc.*, **1958**, 1426; A. Fischer, H. M. Fountain, and J. Vaughan, *ibid.*, **1959**, 1310.
37) C. C. Price, E. C. Mertz, and J. Wilson, *J. Amer. Chem. Soc.*, **76**, 5131 (1954).
38) Y. Yukawa and Y. Tsuno, *Nippon Kagaku Zasshi*, **86**, 863 (1965).
39) K. C. C. Bancroft and G. R. Howe. *Tetrahedron Lett.*, **1967**, 4207.
40) P. R. Wells, S. Ehrenson, and R. W. Taft, "Progress in Physical Organic Chemistry," Vol. 6, Interscience Publishers (1968), p. 147.
41) C. G. Swain and E. C. Lupton, *J. Amer. Chem. Soc.*, **90**, 4328 (1968).
42) Y. Tsuno, M. Fujio *et al.*, unpublished.
43) M. J. S. Dewar, R. Golden, and J. M. Harris, *J. Amer. Chem. Soc.*, **93**, 4187 (1971).
44) D. A. Forsyth, *ibid.*, **95**, 3594 (1973).
45) $\Delta q_{1j}(ArCH_2^+)$ which would be more suitable for the present case than $\Delta q_{1j}(ArH^+)$ were not given for all naphthalene positions. However, since the former is proportional to the latter, use of the latter does not affect the discussion. A linear relation between both parameters for 6 aromatics (Ref. 44) gives approximate $\Delta q_{1j}(ArCH_2^+)$ parameters for naphthalene positions (Table 10).
46) Y. Tsuno, M. Fujio, and Y. Yukawa, This Bulletin, **48**, 3324 (1975); M. Fujio, Y. Tsuno, Y. Yukawa, and Y. Takai, *ibid.*, **48**, 3330 (1975).
47) The q_r^+/q_r^- ratio involved in the σ_p^+ constant is estimated to be 3.38 (Ref. 46).
48) S. Ehrenson, R. T. C. Brownlee, and R. W. Taft, "Progress in Physical Organic Chemistry," Vol. 10, p. 1 (1973). The authors are indebted to Professor R. W. Taft for making his recent data available to them prior to publication.

The Effects of the Properties of Trunk Polymers on the Flocculating Action of Graft Copolymers

Namiko MIYATA, Isao SAKATA* and Ryoichi SENJU*

Nakamura Gakuen College, Befu, Nishi-ku, Fukuoka 814

**Department of Forest Products, Faculty of Agriculture, Kyushu University, Hakozaki, Higashi-ku, Fukuoka 812*

(Received January 27, 1975)

Acryl amide (AM) was graft copolymerized onto hydroxy ethyl cellulose(HEC), polyvinyl alcohol (PVA), amylose (AL), and amylopectin (AP), whose molecular extensions in an aqueous solution are different. The graft copolymers were then purified by means of fractional precipitation. The effects of the properties of the trunk polymers of the graft copolymers on their flocculating action for kaolin suspensions were examined. It was found that: 1) when the molecular weights ($\overline{M}_n$) of the copolymers were equal, their flocculating action was much influenced by the kind of trunk polymer (HEC, AL, PVA, and AP) and decreased in that order; 2) the differences in their flocculating action are due to the differences in their molecular extensions in an aqueous solution; and 3) the flocculating action of the copolymers increased with an increase in the $\overline{M}_w$ of the branched poly AM (PAM), but was, however, scarcely affected by a small number of grafted PAM per trunk polymer molecule.

High-molecular polyacrylamide (PAM) is now used in large amounts as a flocculant for the treatment of waste water; however, it has some disadvantages, *e.g.*, the abscission of its molecular chains easily occures in a dissolution process because of its high molecular weight. Consequently, the development of flocculants whose molecular weight is relatively low and whose flocculating action is superior to that of high-molecular PAM has been attempted.

It seemed, therefore, that it would be interesting to study the graft copolymers of cellulose, starch, *etc.*, as flocculants. Up to now, in some studies[1] of water-soluble graft copolymers as flocculants, the flocculating action of a reaction mixture composed of graft copolymers, homopolymers, and unreacted trunk polymers has been examined, but that of pure graft copolymers has not yet been investigated. Previously, the present authors[2] proved that the flocculating action of the fractionated water-soluble hydroxyethyl cellulose (HEC)-AM graft copolymers was superior to that of PAM because of the rigid molecular chains and the large molecular extension of HEC.

In this paper, in order to make the relation clearer between the flocculating action of the copolymers and their molecular extensions in an aqueous solution, the flocculating action of the fractionated graft copolymers of the trunk polymers, polyvinyl alcohol (PVA, flexible), amylose (AL), amylopectin (AP, branched) and HEC (rigid), which have different molecular chains, was studied. Moreover, the effects of the molecular weight and the number of the grafted PAM on the flocculating action of the copolymers were examined. Graft copolymerization was carried out by means of the Ce (IV) salt method.[3]

Experimental

Materials. PVA, AL, AP, and HEC: Commercial PVA, AL, AP, and high-molecular HEC (*h*-HEC) were used without further purification. Their molecular weights ($\overline{M}_n$) were 8×10^4, 7×10^4, 1.9×10^5, and 1.8×10^5 respectively. The degree of the hydroxyethylation of HEC was 1.2 as the molar substitution (MS).[4] Low-molecular HEC ($\overline{M}_n$ of *l*-HEC: 7×10^4) was synthesized as has been described in a previous paper.[2] Ammonium cerium(IV) nitrate, AM, CCl_4, and kaolin: they were described in a previous paper.[2]

Graft Copolymerization and Fractionation of Graft Copolymers. Graft Copolymerization: Graft copolymerization was carried out by the Ce(IV) salt method[3] under a stream of N_2 at 40 °C for 30—220 min. In a polymerization apparatus, 0.4 g of the trunk polymers, 2.0—2.5 g of AM, the fixed Ce salt, and HNO_3, and 40 ml of water were added. The concentrations of Ce salt for grafting onto PVA, HEC, AL, and AP were 1.3×10^{-4}—4.0×10^{-4} mol/l, 8.0×10^{-4}—2.2×10^{-2} mol/l 1.8×10^{-3}—2.2×10^{-2} mol/l, and 3.7×10^{-3}—2.2×10^{-2} mol/l respectively, while those of HNO_3 were 0.05—0.07 mol/l (PVA) and 0.014—0.28 mol/l (others). For the preparation of the graft copolymers with low-molecular grafted PAM, a 2—4 ml portion of CCl_4 was added to serve as a regulator.

Fractionation of Graft Copolymers: In order to obtain the fractionated graft copolymers, the precipitation properties of the trunk polymers and PAM in an aqueous acetone sytem were examined, as is shown in Fig. 1. It can be seen from

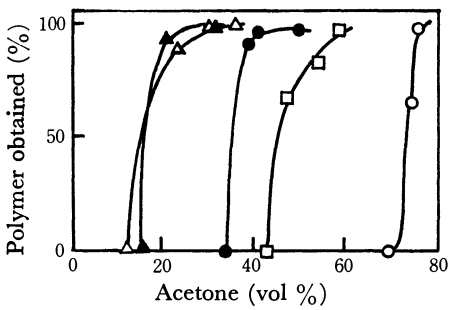

Fig. 1. The precipitation properties of the trunk polymers and PAM in an aqueous acetone system.
●: PAM, ○: HEC, □: PVA, △: Amylopectin, ▲: Amylose. 0.5% aqueous polymer solution at 30 °C.

Fig. 1 that the respective graft copolymers of HEC, PVA, AP, and AL are precipitated when the concentrations of acetone in a solution are 40—70%, 40—48%, 28—36%, and 23—36% respectively. The graft copolymers were precipitated fractionally at the above concentrations of acetone. These fractionated products were confirmed respectively by IR, turbidimetric titration in an aqueous acetone system, and the determination of the nitrogen by means of the Kjeldahl method.

Determination of the Molecular Weight and Intrinsic Viscosity ([η]). The molecular weight ($\overline{M}_n$) of the graft copolymers was measured with a 502-type high-speed membrane

Table 1. Characterization of graft copolymers

Sample		$\bar{M}_n$ of copolymer		M.W. of branch of copolymer		Number[a] of branches per one trunk polymer	Chemical composition ratio[b] (wt.) Branch/Trunk polymer
		Obsd ($\times 10^{-5}$)	Calcd[c] ($\times 10^{-5}$)	$\bar{M}_n$ ($\times 10^{-5}$)	$\bar{M}_w$ ($\times 10^{-5}$)		
h-HEC	1	2.3	3.4	2.5	6.1	0.64	0.89
	2	3.4	4.0	3.2	9.0	0.69	1.23
	3	4.2	5.5	3.7	12.8	1.0	2.05
	4	—	16.2	4.5	11.5	3.2	8.00
	5	6.0	6.8	5.6	13.8	0.90	2.80
	6	6.7	7.6	7.2	17.7	0.80	3.22
	7	7.9	9.4	12.6	31.6	0.60	4.18
	8	—	16.7	18.0	45.0	0.83	8.30
l-HEC	1	1.8	2.5	2.2	5.4	0.82	2.58
	2	2.3	3.0	3.0	7.6	0.75	3.21
	3	2.9	3.6	3.4	8.5	0.84	4.08
	4	3.7	4.3	5.0	12.3	0.72	5.14
	5	5.1	5.9	8.1	19.5	0.64	7.41
	6	7.9	8.6	9.8	25.0	0.81	11.3
	7	8.9	9.5	11.0	28.0	0.80	12.6
	8	—	11.4	14.7	36.0	0.73	15.3
	9	—	14.8	18.6	46.0	0.76	20.2
PVA	1	1.3	1.7	1.0	2.9	0.88	1.10
	2	2.7	3.4	3.8	9.5	0.67	3.18
	3	5.9	6.8	8.4	20.5	0.72	7.56
	4	8.5	9.4	9.5	24.0	0.85	10.1
	5	9.2	10.7	11.0	26.9	0.89	12.4
	6	—	15.2	12.0	33.1	1.2	18.0
	7	—	18.9	9.5	24.0	1.9	22.6
	8	—	20.0	19.2	47.4	1.0	24.0
AP	1	3.7	4.5	3.3	8.4	0.79	1.37
	2	5.0	5.4	3.6	9.2	0.97	1.84
	3	5.6	6.0	3.7	9.8	1.1	2.13
	4	—	10.0	3.0	7.8	2.7	4.26
	5	—	7.5	3.5	8.5	1.6	2.96
	6	9.1	10.1	6.8	16.3	1.2	4.29
	7	7.5	8.3	7.5	18.9	0.85	3.36
	8	—	12.9	11.0	27.9	1.0	5.79
AL	1	1.3	1.7	0.9	2.2	1.1	1.41
	2	—	2.7	1.1	2.6	1.9	2.85
	3	3.6	4.2	3.5	8.7	1.0	4.96
	4	5.7	6.4	5.2	12.6	1.1	8.14
	5	7.3	7.9	8.4	20.0	0.86	10.3
	6	1.6	1.8	1.0	2.4	1.1	1.57
	7	—	1.2	0.7	1.5	0.75	0.75

a) ($\bar{M}_n$ of trunk polymer) × (chemical composition ratio)/$\bar{M}_n$ of branch. b) Obtained by Kjeldahl method.
c) $\bar{M}_n$ of trunk polymer + ($\bar{M}_n$ of branch) × (number of branches).

osmometer manufactured by Hewlett Packard Co., while the molecular weights ($\bar{M}_w$ and $\bar{M}_n$) of the grafted PAM were determined from the following viscosity equations as has been described in a previous paper;[2] $[\eta]^{30°C}_{N\text{-}NaNO_3}=3.73\times10^{-4}\ \bar{M}_w^{0.66}$ and $[\eta]^{30°C}_{H_2O}=6.8\times10^{-4}\ \bar{M}_n^{0.66}$ [5]

Characterization of Graft Copolymers. This is shown in Table 1.

Flocculation Test. The flocculating action of the flocculants was measured by means of the sedimentation rate,[9] with a 25 ml graduated cylinder, and the transmittance of a supernatant solution, with a Shimadzu Bausch and Lomb Spectronic 20 colorimeter, which has been described in a previous paper.[2]

Results and Discussion

Effect of Difference in Kind of Trunk Polymers. Figures 2 and 3 show the effects of the difference in the kind of trunk polymers on the sedimentation rate and the transmittance respectively. Even though the $\bar{M}_n$ of the respective graft copolymers of *h*-HEC, *l*-HEC, AL, PVA, and AP are equal, the sedimentation rate and the transmittance decreased in that order, as is shown in Figs. 2 and 3.

It has been proposed[6,7] that the flocculation of kaolin suspensions with nonionic polymer flocculants is caused by a bridging of kaolin particles with the adsorbed poly-

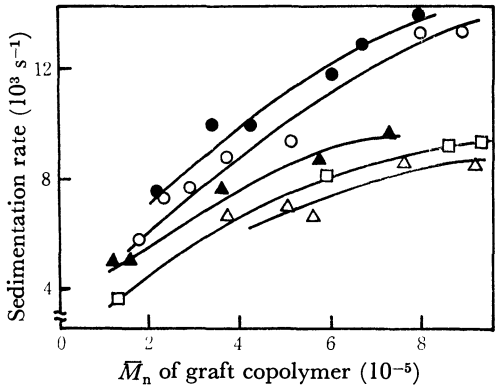

Fig. 2. Effect of the kind of the trunk polymers on the sedimentation rate.
○: *l*-HEC graft copolymer, ●: *h*-HEC graft copolymer, □: PVA graft copolymer, △: AP graft copolymer, ▲: AL graft copolymer.
Dosage of flocculant: 1 mg/l suspension.

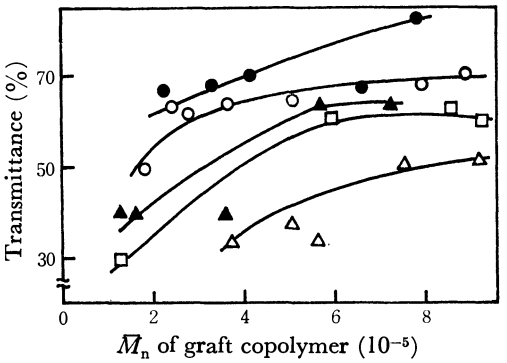

Fig. 3. Effect of the kind of the trunk polymers on the transmittance in 0.8% kaolin suspensions.
Symbols are the same as those in Fig. 2.
Dosage of flocculant: 1 mg/l suspension.

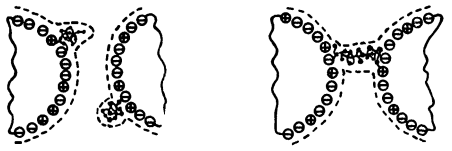

Fig. 4. Schematic representation of flocculation by a bridging of kaolin particles with polymers.
○: Kaolin particle, •: Polymer.

mers. Consequently, their flocculating action must be determined by two factors. One is the molecular extension, which the molecular chains of the adsorbed polymers can bridge between particles; if the molecular extension of polymers in a solution is small, an interparticle bridging will be unfavorable. This is shown schematically in Fig. 4. The other is the adsorption properties of the flocculants on suspended particles. The adsorption properties of these graft copolymers on the kaolin particles used in this study were not determined. It seems, however, that the adsorption properties are almost identical because of the hydrophilic trunk polymers, which have only hydroxl groups. The difference in the flocculating action of these graft copolymers seems to arise from the difference in their molecular extensions caused by the properties of the trunk polymers. That is, the extension of the HEC graft copolymers seems to be the largest, because of the rigid molecular chains and the large extension of the trunk-polymer HEC. That of the AL graft copolymers appears to be the next largest, because AL has indeed bulky anhydrous glucose groups, just as HEC does, but it is not rigid. That of the PVA graft copolymers seems to be the third largest, because of the flexible and randomly coiled chains of PVA. The smallest one appears to be that of the AP graft copolymers, because of the small extension of AP on the ground of its branching chain structure.

Difference in Molecular Extension in an Aqueous Solution. The difference in the flocculating action of the graft copolymers seems to be due to the difference in their molecular extensions in an aqueous solution caused by the properties of the trunk polymers. In order to make sure of this, the molecular extensions of the graft copolymers were examined. No definitive theoretical equation of the molecular extensions of graft and block copolymers in an aqueous solution has yet been elucidated. It seemed that it would be interesting, however, to compare the extensions of the molecular chains by means of the dimensions (R_e: the radius) of Flory's non-draining equivalent sphere model.[8] The relation between R_e, the molecular weight ($\bar{M}$), and ($[\eta]$) is as follows: $[\eta]=KR_e^3/\bar{M}$[8] (K: constant). Consequently, $[\eta]\ \bar{M}_n$ was represented as the evaluation of the molecular extensions of the graft copolymers. When the $\bar{M}_n$ values of the copolymers are equal to each other, the molecular extensions ($\bar{M}_n[\eta]$) of the respective graft copolymers of HEC, AL, AP, and PVA decreased in that order, as is shown in Fig. 5. The order of the flocculating action of

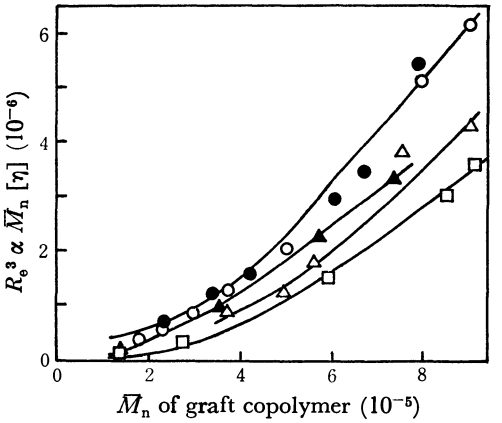

Fig. 5. Relation between the molecular extensions ($\bar{M}_n[\eta]$) and the $\bar{M}_n$ of the graft copolymers.
Symbols are the same as those in Fig. 2.

the graft copolymers was well in accord with that of their molecular extensions ($\bar{M}_n[\eta]$), except that the graft copolymers of PVA and AP were reversed. The plots of the extensions of the graft copolymers *vs.* the transmittance and the sedimentation rate gave an approximately linear relation regardless of the kind of the flocculants used in this study, as is shown in Fig. 6.

In conclusion, the difference in the flocculating action of the graft copolymers must be due to the difference in their molecular extensions in an aqueous solution, determined on the basis of the properties of the trunk poly-

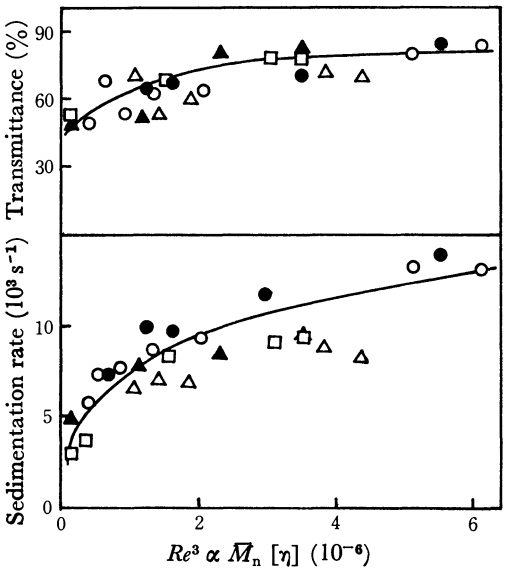

Fig. 6. Relation between the molecular extensions ($\bar{M}_n[\eta]$) and the sedimentation rate and the transmittance of 3% kaolin suspensions.
Symbols are the same as those in Fig. 2.
Dosage of flocculant: 1 mg/l suspension.

mers.

Effects of the Molecular Weight and Number of the Branched PAM of Graft Copolymers. Figures 7 and 8 show the effects of the molecular weight ($\bar{M}_w$) of the branched PAM of the graft copolymers on the sedimentation rate and the transmittance of a supernatant solution respectively. As is shown in Fig. 7, the sedimentation rate increased with an increase in the $\bar{M}_w$ of the branched PAM in all the different trunk polymers. This result suggests that kaolin particles are sedimented by means of the bridging mechanism.[6] That is, the higher the $\bar{M}_w$ is, the more effective the bridging flocculation may be. The transmittance also increased with the increase in the $\bar{M}_w$ as well as the sedimentation rate, up to 3.5×10^6 of the $\bar{M}_w$ of the branched PAM. However, at the $\bar{M}_w$ values above that value, there was little effect of the $\bar{M}_w$ on the

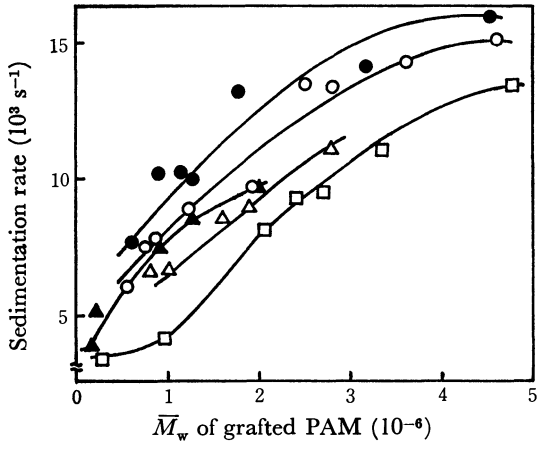

Fig. 7. Effect of the $\bar{M}_w$ of the grafted PAM of the graft copolymers on the sedimentation rate.
Symbols are the same as those in Fig. 2.
Dosage of flocculant: 1 mg/l suspension.

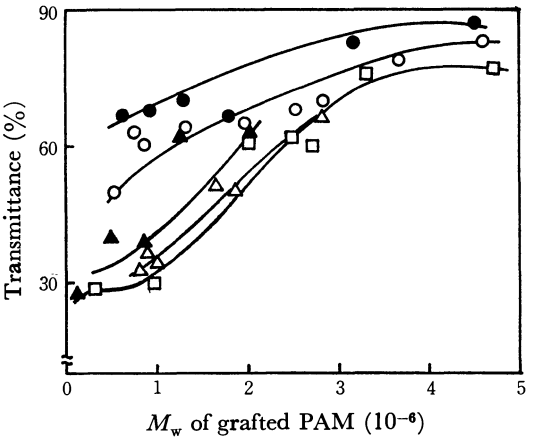

Fig. 8. Effect of the $\bar{M}_w$ of the grafted PAM of the graft copolymers on the transmittance of 0.8% kaolin suspensions.
Symbols are the same as those in Fig. 2.
Dosage of flicculant: 1 mg/l suspension.

clarification. This may be because the clarification results from the reduction of the electrostatic repulsion between the colloidal fine particles, which could not be sedimented thoroughly by the bridging alone.

When the $\bar{M}_w$ values of the branched PAM were equal to each other, the flocculating action of the respective graft copolymers of HEC, AL, AP, and PVA decreased in that order. The difference in their flocculating action seems to be due to the difference in the molecular extensions caused by the properties of the trunk polymers. This was discussed before. The flocculating action of the *h*-HEC graft copolymers was superior to that of the *l*-HEC graft copolymers even if the $\bar{M}_w$ values of their branched PAM were equal. This must be due to the easier bridging with the former compared with the latter, because the molecular weight ($\bar{M}_n$) of the former was, as a whole, higher than that of the latter.

Figure 9 shows the effect of the number (1—3) of the

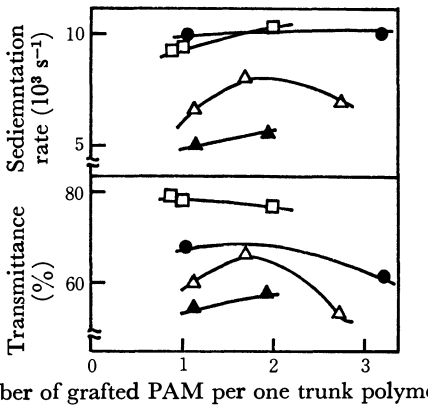

Fig. 9. Effect of the number of the grafted PAM per one trunk polymer molecule on the sedimentation rate and the transmittance of 3% kaolin suspensions.
$\bar{M}_n$ of grafted PAM:
●: *h*-HEC graft copolymer (4.0×10^5)
□: PVA graft copolymer (9.5×10^5)
△: AP graft copolymer (3.5×10^5)
▲: AL graft copolymer (1.0×10^5)
Dosage of flocculant: 1 mg/l suspension.

branched PAM on the sedimentation rate and the transmittance. The flocculating action of the graft copolymers which had two branched PAM was a little superior to that of others. However, on the whole, the flocculating action was scarcely affected by the number of the branched PAM, even if the kind of the trunk polymer was different.

References

1) M. Inano, *Kogyo Kagaku Zasshi*, **72**, 2298 (1969); T. Hirano and T. Hasegawa, *ibid.*, **74**, 91, 456 (1971).

2) N. Miyata, I. Sakata, and R. Senju, *Nippon Kagaku Kaishi*, **1974**, 1782.

3) G. Mino and S. Kaizerman, *J. Polym. Sci.*, **31**, 242 (1958); H. Narita and S. Machida, *Seni Gakkaishi*, **27**, 162 (1971).

4) P. W. Morgan, *Ind. Eng. Chem. Anal. Ed.*, **18**, 500 (1946).

5) "New Product Bulletin," No. 34, 2, American Cyanamide Co., New York (1955).

6) A. S. Michaels, *Ind. Eng. Chem.*, **46**, 1485 (1954).

7) A. S. Michaels and O. Morelos, *ibid.*, **47**, 1801 (1955).

8) P. J. Flory, *J. Chem. Phys.*, **17**, 303 (1949).

9) This was represented by the reciprocal of the time required for the solid-liquid boundary to sediment by 10 ml in a 25 ml graduated cylinder. The sedimentation with uniform rate was observed when the height of the solid-liquid boundary fall between 2 ml and 12 ml.

NOTES

BULLETIN OF THE CHEMICAL SOCIETY OF JAPAN, VOL. 48 (11), 3372 (1975)

Aromatic Substitution of Olefins. XXII. Unusual Reaction of *p*-Bromostyrene with Benzene in the Presence of Palladium(II) Acetate[1]

Hidetsugu TANAKA, Yuzo FUJIWARA, Ichiro MORITANI, and Shiichiro TERANISHI

Department of Chemistry, Faculty of Engineering Science, Osaka University, Machikaneyama, Toyonaka, Osaka 560

(Received June 19, 1975)

Synopsis. The reaction of *p*-bromostyrene with benzene in the presence of palladium(II) acetate gave unexpected bibenzyl (**2**) and *trans*-stilbene (**3**) in 12% and 5% yields respectively, in addition to the usual substitution product (**1**, 47%). This result shows that dehalogenation and subsequent hydrogenation accompany the aromatic substitution of olefins when both iodides and bromides are used.

We have reported a novel reaction of olefins with aromatic compounds to produce aromatic-substituted olefins *via* direct substitution in the presence of palladium (II) salts.[2]

In the course of our study on the aromatic substitution of olefins, we have performed the reaction of *p*-bromostyrene with benzene in the presence of $Pd(OAc)_2$ in the hope of obtaining *p*-bromo-*trans*-stilbene as the sole product. However, from this reaction, we obtained bibenzyl (**2**) and *trans*-stilbene (**3**) in yields of 12% and 5% respectively with a 47% yield of the usual substitution product, *p*-bromo-*trans*-stilbene (**1**).[3] This suggested that the bromine atom of bromostyrene was replaced with hydrogen by the action of $Pd(OAc)_2$. To chek this point, the dehalogenation and hydrogenation of halobenzenes with $Pd(OAc)_2$ were examined. Refluxing of bromobenzene with $Pd(OAc)_2$ gave the hydrogenolysis product (benzene) in 16% yield and, from iodobenzene, a 55% yield of benzene was obtained.[4]

These results show that $Pd(OAc)_2$ causes the dehalogenation-hydrogenation reaction and that the reactivity of halobenzenes is I>Br≫Cl. Thus it would be possible to describe two paths (a and b) for formation of **3**: one is the route *via* styrene which is derived from a debromination-hydrogenation of *p*-bromostyrene, and the other is the route involving a debromination-hydrogenation of **1**, which is the usual aromatic substitution product.[5] Compound **2** is formed *via* hydrogenation of **3**.[5] The reaction paths are shown in the following Scheme:

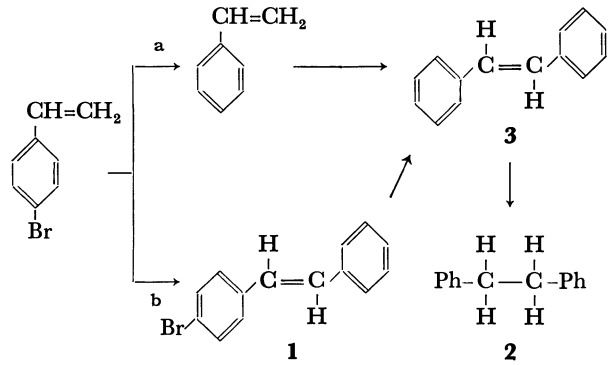

It has been reported that low-valent palladium reacts with halides (RX) to form organopalladium σ-complexes (R–Pd–X) *in situ*.[6] In the present case, an aryl-palladium σ-complex such as (H_2C=CH- 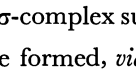 -PdBr) would also be formed, *via* the oxidative addition of Pd, but it would be decomposed by hydrogen to give hydrogenolysis products[5] without any further reaction with the olefins.

The results described here call for attention when halides, especially iodides and bromides, are employed in the aromatic substitution of olefins by palladium (II) salts.

Experimental

p-Bromostyrene was prepared from dehydration of 1-(*p*-bromophenyl)ethanol, bp_{16} 88—89 °C.

Reaction of p-*Bromostyrene with Benzene.* A solution of $Pd(OAc)_2$ (4.6 mmol), and *p*-bromostyrene (4.6 mmol) in a mixture of benzene (50 ml) and acetic acid (10 ml) was heated at 80 °C with stirring for 8 hr. The resulting mixture was worked up as described already.[7] The products were separated by preparative glc to give **1**, **2**, and **3**, which were all assigned by a comparison with authentic samples, mp of **1**, 138—139 °C (EtOH) (lit,[8] mp 139 °C).

Dehalogenation-hydrogenation of Aryl Halides. A solution of $Pd(OAc)_2$ (4.6 mmol) and bromobenzene (50 ml) was refluxed for 8 hr using octane as an internal standard. After work-up, glc analysis showed a 16% yield of benzene. Similarly, iodobenzene was refluxed using nonane as an internal standard to give a 55% yield of benzene. Under similar reaction conditions, chlorobenzene did not result in any formation of benzene.

References

1) Taken in part from the M. S. Thesis of H. Tanaka, Osaka University, 1971; Part XXI: M. Watanabe, M. Yamamura, I. Moritani, Y. Fujiwara, and S. Teranishi, This Bulletin, **47**, 1035 (1974).

2) For a review see I. Moritani and Y. Fujiwara, *Synthesis*, **1973**, 524.

3) Yields are all based on palladium acetate used.

4) Hydrogen would be derived mainly from the saturated hydrocarbons used as internal standards.

5) Hydrogen evolved from the usual aromatic substitution reaction would be used for the debromination-hydrogenation.

6) For example see P. Fitton and E. A. Rick, *J. Organometal. Chem.*, **28**, 287 (1971); K. Mori, T. Mizoroki, and A. Ozaki, This Bulletin, **46**, 1505 (1973); A. Schoenberg, I. Bartoletti, and R. F. Heck, *J. Org. Chem.*, **39**, 3318 (1974).

7) Y. Fujiwara, I. Moritani, R. Asano, and S. Teranishi, *J. Amer. Chem. Soc.*, **91**, 7166 (1969).

8) F. Bergman, J. Weizman, and D. Schapiro, *J. Org. Chem.*, **9**, 408 (1944).

BULLETIN OF THE CHEMICAL SOCIETY OF JAPAN, VOL. 48 (11), 3373—3374 (1975)

Nuclear Magnetic Resonance Studies of Bicyclic Thiophene Derivatives. III. Through Space H-F Coupling over Seven Bonds

Toshiyuki HIROHASHI, Shigeho INABA, and Hisao YAMAMOTO

Institute for Biological Science, Sumitomo Chemical Co., Takatsukasa, Takarazuka, Hyogo 665

(Received October 18, 1974)

Synopsis. Bicyclic thiophene derivatives, 1,5-dimethyl-(**1**) and 3,5-dimethyl-4-(*o*-fluorophenyl)-1,2-dihydrothieno[2,3-*d*]-pyrimidin-2-ones (**3**), 2-acetylamino-3-(*o*-fluorobenzoyl)-4-methylthiophene (**5**), and some derivatives (**2**, **4**, **6**, **7**), have been prepared. ^{1}H, ^{19}F Spin couplings over seven bonds, $^7J_{HF}$, attributable to a through-space mechanism have been observed in the ^{1}H NMR spectra of these compounds.

In a previous paper,[1] we reported that long-range spin couplings over six bonds were observed between the fluorine and H_β of the thiophene rings in 4-(*o*-fluorophenyl)thienopyrimidines, 2-acetylamino-3-(*o*-fluorobenzoyl)thiophenes, 5-(*o*-fluorophenyl)-1,4-thienodiazepines, and 5-(*o*-fluorophenyl)-1,4-thienodiazepine-4-oxides, the synthesis of all of which are of interest biologically. The coupling was considered to arise from a through-space mechanism.[2] Thus, we have examined the ^{1}H NMR spectra of other kinds of bicyclic thiophene derivatives, **1**—**7**, and discovered that there are long-range spin couplings between methyl or dichloromethyl protons of the thiophene ring and the fluorine of the benzene ring over seven bonds, $^7J_{HF}$, which were also considered to be through-space couplings, as has hitherto been reported in a few papers.[3-6] In this paper, we will present our experimental results on the $^7J_{HF}$ found in these new compounds.

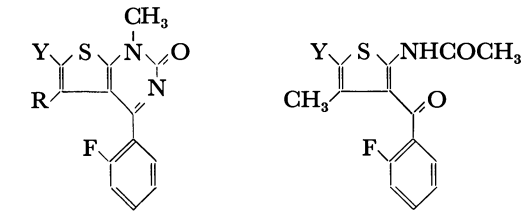

(**1**: Y=H_α, R=CH_3)
(**2**: Y=Cl, R=CH_3)
(**7**: Y=Cl, R=$CHCl_2$)

(**5**: Y=H_α)
(**6**: Y=Cl)

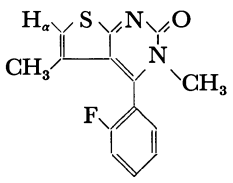

(**3**)

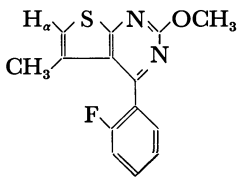

(**4**)

TABLE 1. NMR DATA ON BICYCLIC THIOPHENE DERIVATIVES

Compound	$^7J_{HF}$ (Hz)	δ (β-CH_3)	δ(H_α)	δ (NH)
1	1.0	1.85[a]	6.55	—
2	1.1	1.81	—	—
3	b)	1.50[c]	6.55	—
4	1.0	1.94[d]	6.86	—
5	0.5	1.73[e]	6.33	11.92
6	0.5	1.69	—	11.90
7	0.7	6.09[f]	—	—

a) $^4J(H_\alpha,5\text{-}CH_3)=1.1$ Hz. b) Not detectable. c) $^4J(H_\alpha,5\text{-}CH_3)=1.4$ Hz. d) $^4J(H_\alpha,5\text{-}CH_3)=1.1$ Hz. e) $^4J(H_\alpha,4\text{-}CH_3)=1.0$ Hz. f) Chemical shift of the dichloromethyl proton.

As is shown in Table 1, the β-methyl signals of the thiophene ring in **3** exhibited no detectable coupling with the fluorine. However, in **1** and **4**, which are isomers of **3**, $^7J_{HF}$ was observed (both 1.0 Hz). On the chlorination of the α-position of the thiophene ring, $^7J_{HF}$ was not practically influenced (in **2**, 1.1 Hz). The difference between the J_{HF} in **3** and those in **1**, **2**, and **4** should be due to the difference in steric hindrance; the torsional angle between the thiophene and the benzene planes should be greater for **3** than for **1**, **2**, and **4** as a result of the steric hindrance between the benzene and the *N*-methyl group in **3**. Accordingly, the internuclear distance between the fluorine and the methyl protons in **3** is so long that the through space coupling can not be detected. The dichloromethyl proton signal in **7** appears as a doublet (J=0.7 Hz), whose spacing is smaller than that of **2** (J=1.1 Hz). The difference might arise from the fact that, since the dichloromethyl group is bulkier than the methyl group, the torsional angle between the thiophene and the benzene planes should be greater for **7** than for **2**. Furthermore, $^7J_{HF}$ was also observed between the methyl protons of the thiophene ring and the fluorine in **5** and **6** (J=0.5 Hz). The difference between the $^7J_{HF}$ in **5** and **6** and those in **1** and **2** is probably due to the difference in the torsional angle between the thiophene and the benzene planes; the angle should be greater for **5** and **6** than for **1** and **2**, as has been reported in the case of $^6J_{HF}$ in the previous paper.[1]

Experimental

Measurements. The ^{1}H NMR spectra (δ, ppm) were recorded on a Hitachi R-20-B spectrometer at 60 MHz and at a probe temperature of 35 °C, using $CDCl_3$ solutions (about 10% w/v), with TMS as the internal reference. The chemical shifts are expressed in δ with a precision of $\pm$0.01. The coupling constants were measured by several sweepings at an expanded sweep width (60 or 120 Hz) with an accuracy of $\pm$0.1 Hz. The IR spectra (wave number, cm^{-1}) were recorded as Nujol mulls on a Hitachi EPI-G-3 spectrophotometer. The UV spectra (wavelength, nm) were determined in 95% ethanol with a Hitachi-323 spectrophotometer. The melting points were measured on a Thomas-Hoover melting-point apparatus and are uncorrected.

Materials. The Synthetic Procedures for 4-(o-Fluorophenyl)-1,5-dimethyl-1,2-dihydrothieno[2,3-d]-pyrimidin-2-one (1), 4-(o-

Fluorophenyl)-3, 5-dimethyl-2, 3-dihydrothieno[*2, 3*-d]-*pyrimidin-2-one (3), and 4-(*o-*Fluorophenyl)-2-methoxy-5-methylthieno*[*2,3*-d]-*pyrimidine (4)*: 2-Amino-3-(*o*-fluorobenzoyl)-4-methylthiophene was prepared from *ω*-cyano-*o*-fluoroacetophenone and mercaptoacetone as reported in a previous paper.[7] It was then heated with ethyl cabamate to give 4-(*o*-fluorophenyl)-5-methyl-1,2-dihydrothieno[2,3-*d*]-pyrimidin-2-one, which was methylated with methyl iodide to afford Compounds **1**, **3**, and **4**.

*2-Amino-3-(*o-*fluorobenzoyl)-4-methylthiophene.* Yield, 35.5%, mp 163—164 °C (from ethanol). IR: 3320, 3200, 3100, 1590, and 1560.

*4-(*o-*Fluorophenyl)-5-methyl-1,2-dihydrothieno*[*2,3*-d]-*pyrimidin-2-one.* Yield, 76.1%, it was used the next step without any further purification.

Compound 1. Yield, 18.0%, mp 275—277 °C (from $CHCl_3$–ethanol). IR: 3050, 1658, 1643, and 1608. NMR: 1.85 (3H, d-d, 5-CH_3), 3.75 (3H, s, *N*-CH_3) and 6.55 (1H, q, H_α). UV: 251 (26100) and 346 (5100). Found: C, 61.30; H, 4.17; N, 10.24%. Calcd for $C_{14}H_{11}N_2OSF$: C, 61.30; H, 4.04; N, 10.21%.

Compound 3. Yield, 10.0%, mp 178—181 °C (from $CHCl_3$–ethanol) IR: 3050 and 1655. NMR: 3.41 (3H, d, *N*-CH_3). UV: 220 (19700), 255 (23700), 295 (3000) and 373 (3900). Found: C, 61.33; H, 4.09; N, 10.10%. Calcd for $C_{14}H_{11}N_2OSF$: C, 61.30; H, 4.04; N, 10.21%.

Compound 4. Yield, 4.4%, mp 177—179 °C (from $CHCl_3$–ethanol). IR: 3065 and 1615. NMR: 1.94 (3H, d-d, 5-CH_3), 4.11 (3H, s, OCH_3) and 6.86 (1H, q, H_α). UV: 244 (34600) and 316 (3500). Found: C, 61.30; H, 4.17; N, 10.24%. Calcd for $C_{14}H_{11}N_2OSF$: C, 61.30; H, 4.04; N, 10.21%.

The other compounds were prepared according to the methods described previously.[7]

*2-Acetylamino-3-(*o-*fluorobenzoyl)-4-methylthiophene (5).* Yield, 74.0%, mp 96—96.5 °C (from ether). IR: 3200, 3080, 1690, and 1600. UV: 244.5 (10300), 282.5 (10700), and 351 (6400). Found: C, 60.84; H, 4.32; N, 5.14%. Calcd for $C_{14}H_{12}NO_2SF$: C, 60.64; H, 4.36; N, 5.05%.

*2-Acetylamino-5-chloro-3-(*o-*fluorobenzoyl)-4-methylthiophene (6).* Yield, 82.4%, mp 140—140.5 °C (from ether). IR: 3180, 1695 and 1605. UV: 250 (14400) and 358 (6700). Found: C, 53.86; H, 3.43; N, 4.29%. Calcd for $C_{14}H_{11}NO_2SClF$: C, 53.94%; H, 3.56; N, 4.49%.

*6-Chloro-1, 5-dimethyl-4-(*o-*fluorophenyl)-1, 2-dihydrothieno*[*2, 3*-d]-*pyrimidin-2-one (2).* Yield, 34.5%, mp 175—176 °C (from ethanol–ether). IR: 1660 and 1610. UV: 255 (26000) and 353 (5500). Found: C, 54.71; H, 3.44; N, 8.97%. Calcd for $C_{14}H_{10}N_2OSClF$: C, 54.46; H, 3.26; N, 9.07%.

*6-Chloro-5-dichloromethyl-4-(*o-*fluorophenyl)-1-methyl-1, 2-dihydrothieno*[*2,3*-d]-*pyrimidin-2-one (7).* This was prepared from **1** with an excess of sulfurylchloride. Yield, 28.2%, mp 215—216 °C. IR: 1675 and 1610. UV: 219 (19300), 251 (16900), 282 (8000), and 347 (6000). Found: C, 44.46; H, 2.19; N, 7.55%. Calcd for $C_{14}H_8N_2OSCl_3F$: C, 44.52; H, 2.13; N, 7.42%.

The authors wish to thank Professor Masamichi Tsuboi, The University of Tokyo, and Dr. Makoto Sunagawa of this Institute for valuable suggestions, and Mr. Hiromi Sato for his cooperation in the synthetic experiments.

References

1) Part II: T. Hirohashi, S. Inaba, and H. Yamamoto, This Bulletin, **48**, 947 (1975).
2) See ref. 1 and references therein.
3) M. S. Newman, R. G. Mentzer, and G. Slomp, *J. Amer. Chem. Soc.*, **85**, 4018 (1963).
4) R. Filler and E. W. Choe, *ibid.*, **91**, 1862 (1969).
5) I. Agranat, M. Pabivovitz, I. Gosnay, and A. Weitzen-Dagan, *ibid.*, **94**, 2889 (1972).
6) R. J. Abraham, D. F. Wileman, G. R. Bedford, and D. Greatbanks, *Org. Magne. Resonance*, **4**, 343 (1972).
7) T. Hirohashi, S. Inaba, and H. Yamamoto, This Bulletin, **48**, 147 (1975).

BULLETIN OF THE CHEMICAL SOCIETY OF JAPAN, VOL. 48 (11), 3375—3376 (1975)

ESR Studies of the Triplet-state Dimers of Michler's Ketone Metal Ketyls in Glassy Solutions

Hideo FUJITA, Saburo KAKO, Hiroaki OHYA-NISHIGUCHI,* and Yasuo DEGUCHI

Department of Chemistry, College of Liberal Arts and Sciences, Kyoto University, Kyoto 606

**Department of Chemistry, Faculty of Science, Kyoto University, Kyoto 606*

(Received February 15, 1975)

Synopsis. The ESR spectra (the $\Delta M_s = \pm 1$ and $\Delta M_s = \pm 2$ transitions) of the triplet-states of Michler's ketone metal ketyl dimers are observed in glassy solutions at 77 K. For these metal ketyl dimers, the correlation of the mean separation between spins to the radius of the counter cation was experimentally examined.

Several ESR studies have shown that the ESR spectra due to the magnetic dipole-dipole interactions of spins in glassy solutions can offer important information on the electronic and geometrical structures of the biradical-like dimeric species.[1-5]

In a previous paper,[6] it has been shown that, in the 4,4'-tetramethyldiaminobenzophenone (Michler's ketone) anion radical, the unpaired electron is mainly localized in the vicinity of its carbonyl group.[7]

In the present paper the authors will report their observations of the ESR spectra of the triplet-state in the system of Micher's ketone metal ketyls as produced by several alkali metals in ethereal solvents.

Experimental

A commercially obtained Michler's ketone was purified by recrystallization from ethyl alcohol (mp 179 °C). Its metal ketyls were prepared by the standard alkali metal reduction method, while both ketyls with lithium and calcium were prepared by the use of amalgams of both metals. The solvents used in the present study were 2-methyltetrahydrofuran (MeTHF), tetrahydrofuran (THF), 1,2-dimethoxyethane (DME), diethylene glycol dimethyl ether (diglyme), and triethylene glycol dimethyl ether (triglyme), each of which was treated by the standard purification method.

The ESR spectra were observed at 77 K by means of an X-band ESR spectrometer (JEOL ME-3) with 100 kHz field modulation. The zero-field splitting (ZFS) parameter, D, was determined by measuring the peak-to-peak separation of the $2F$ splitting, because no ZFS parameter, E, could be observed (see Fig. 1). The intensity of the weak signal for the half-field ($\Delta M_s = \pm 2$) transition was enhanced by the signal accumulation method of 32 or 64 scans by using a JEOL EC-6-type spectral computer. Thus, the ESR signals for the $\Delta M_s = \pm 2$ transitions could be observed in every case listed in Table 1. The magnetic field was calibrated by the hyperfine splittings of Mn^{2+} doped in MgO and of ^{14}N of the peroxylamine-disulfonate ion. The spectral simulations were carried out at the Computer Center of Kyoto University.

Results and Discussion

In Fig. 1 the observed and simulated ESR spectra of the triplet-state of Michler's ketone lithium ketyl dimer in MeTHF are shown as examples. In Fig. 1 (a), which depicts the spectrum for the full-field ($\Delta M_s =$

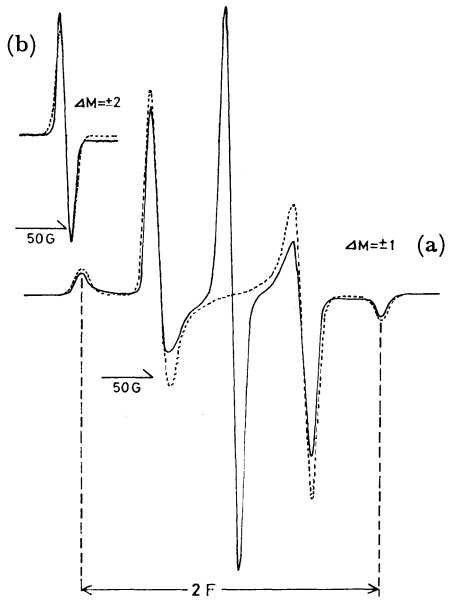

Fig. 1. The full line is the observed ESR spectrum of the triplet-state of Michler's ketone lithium metal ketyl dimer in MeTHF at 77 K, and the dotted line is its simulated one.

In the spectrum for the $\Delta M_s = \pm 1$ transition (a), the ZFS parameter D is 140.5 G. The spectrum for the $\Delta M_s = \pm 2$ transition (b) was enhanced by accumulation of 32 scans of the signal with the computer.

TABLE 1. THE ZERO-FIELD SPLITTING PARAMETERS FOR MICHLER'S KETONE METAL KETYL AT 77 K

Solvent and cation		$\lvert D \rvert$ (G)	$\lvert D \rvert / hc$ (cm^{-1})	$\bar{r}_{1,2}$ (Å)
MeTHF	Li^+	140.5	0.01312	5.83
	Na^+	113.8	0.01063	6.26
	K^+	97.6	0.00911	6.59
	Rb^+	84.4	0.00788	6.92
	Cs^+	75.2	0.00702	7.19
	Ca^{2+}	118.2	0.01104	6.19
THF	Li^+	119.4	0.01115	6.16
	Na^+	112.3	0.01049	6.29
	K^+	94.6	0.00883	6.66
	Rb^+	93.5	0.00873	6.68
	Cs^+	86.4	0.00807	6.86
	Ca^{2+}	102.9	0.00961	6.47
Diglyme	Li^+	121.8	0.01137	6.12
	Na^+	105.3	0.00983	6.42
	K^+	96.9	0.00905	6.61
	Rb^+	89.3	0.00834	6.79
	Cs^+	69.9	0.00653	7.37
	Ca^{2+}	101.9	0.00952	6.49

± 1) transitions, the sharp central absorption can be assigned to the paramagnetic monomer, its integrated intensity being about 10 per cent of the total absorption. Then, the residual part of the absorption (about 90 per cent) is attributable to the paramagnetic dimer.

In Fig. 1(a) the measured value of the ZFS parameter, D, is 140.5 G ($2F$=281.0 G), where the microwave frequency used is 9198.0 MHz and the g-value is 2.0036. The values of the ZFS parameter, D, as measured in different combinations of cations and solvents are summarized in Table 1.

The spectral simulations carried out under the assumption of the ZFS parameter, E, being zero are exhibited as dotted lines in Figs. 1(a) and (b). These simulated spectra fit well with those observed. From these results, we may safely conclude that $E=0$ in the ground-triplet-state spin Hamiltonian. Then, using the theoretical ZFS parameter, D ($D=-2/3g^2\beta^2\langle 1/r_{1-2}^3\rangle$),[1,2] the average distances ($\bar{r}_{1,2}$) between two unpaired electrons in every dimer for these metal ketyls are calculated and tabulated in Table 1, where the values of $\bar{r}_{1,2}$ measured in DME and triglyme are omitted since they are nearly equal to the corresponding values of diglyme.

In Fig. 2 the values of $\bar{r}_{1,2}$ for the system of MeTHF in

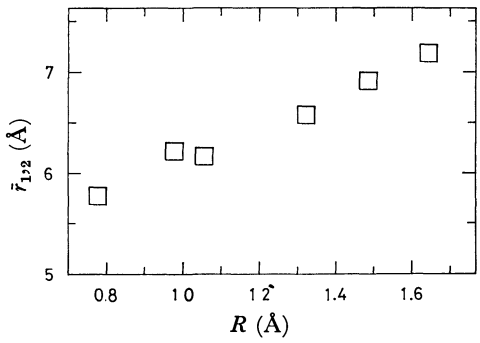

Fig. 2. The values of $\bar{r}_{1,2}$ in MeTHF are plotted against the values of R.

Table 1 are plotted against the radius (R) of the counter cations, for each of which the values of Goldschmidt's ionic radii (Li^+, 0.78; Na^+, 0.98; K^+, 1.33; Rb^+, 1.49; Cs^+, 1.65; and Ca^{2+}, 1.06 Å) were adopted.[8] The fact that $\bar{r}_{1,2}$ increases linearly with an increase in R may be understood if one considers each model as having either a triple-ion structure $(Me_2N\phi)_2CO^-M^+{}^-OC(\phi NMe_2)_2$ or an ion-quadruplet structure $(Me_2N\phi)_2CO^-{}^{M^+}_{M^+}{}^-OC(\phi NMe_2)_2$ with respect to two ketyls.[3,5,9] However, theoretical or quantitative explanation for this result is not yet available.

The authors are sincerely grateful to Professor Kohichi Itoh of Osaka University for offering the simulation program of the triplet-state ESR spectrum and also for his useful suggestions during the course of this work. They are also indebted to Dr. Jun Yamauchi and his collaborators for their helpful discussions.

References

1) N. Hirota, "Radical Ions," ed. by E. T. Kaiser and L. Kevan, Interscience, New York, N. Y. (1968), p. 68.
2) J. H. Sharp and M. C. R. Symons, "Ions and Ion Pairs in Organic Reactions," ed. by M. Szwarc, John Wiley & Sons, New York & London (1972), p. 177.
3) C. A. McDowell and F. Nakano, *J. Phys. Chem.*, **75**, 1205 (1971).
4) H. Fujita, S. Kako, H. Ohya-Nishiguchi, and Y. Deguchi, *Chem. Lett.*, **1974**, 131.
5) S. W. Mao, K. Nakamura, and N. Hirota, *J. Amer. Chem. Soc.*, **96**, 5341 (1974).
6) H. Fujita, S. Kako, J. Yamauchi, H. Ohya-Nishiguchi, and Y. Deguchi, This Bulletin, **47**, 1541 (1974).
7) P. H. Riger and G. H. Fraenkel, *J. Chem. Phys.*, **37**, 2811 (1962).
8) V. M. Goldschmidt, *Trans. Faraday Soc.*, **25**, 253 (1929).
9) N. Hirota and S. I. Weissman, *J. Amer. Chem. Soc.*, **86**, 2538 (1964). I. M. Brown, S. I. Weissman, and L. C. Snyder, *J. Chem. Phys.*, **42**, 1105 (1965); M. C. R. Symons, *J. Phys. Chem.*, **71**, 172 (1967).

BULLETIN OF THE CHEMICAL SOCIETY OF JAPAN, VOL. 48 (11), 3377—3378 (1975)

The Dehydration and Dehydrogenation of Ethanol Catalyzed by TiO_2–ZrO_2

Kazushi ARATA and Hiromitsu SAWAMURA
Hokkaido University of Education, Hachiman-cho, Hakodate 040

(Received February 17, 1975)

Synopsis. Ethanol was converted into ether, ethylene, and butadiene over TiO_2–ZrO_2 with various contents of ZrO_2 in a flow system. Maximum acidity and activity were obtained at 50% ZrO_2. The butadiene formation was explained by both dehydration and dehydrogenation reactions on acidic and basic sites, implying that TiO_2–ZrO_2 is an acid-base bifunctional catalyst.

Binary metal oxides such as SiO_2–ZrO_2,[1] TiO_2–ZnO,[2] and SiO_2–TiO_2[3] have been found to show remarkable acidic properties and catalytic activity. Shibata and Kiyoura have recently found a new mixed oxide, TiO_2–ZrO_2, which exhibits a quite significant acidic property,[4] and Watanabe *et al.* have showed that its catalytic activity for the amination reaction of phenol to aniline was higher than that of SiO_2–Al_2O_3.[5]

The present study was undertaken to examine the correlation between the acidic property of TiO_2–ZrO_2 and its catalytic activity, as well as the selectivity for the reaction of ethanol.

Experimental

Catalyst. TiO_2–ZrO_2 of various compositions was prepared by two different methods reported by Shibata *et al.*[4] (1): a 1850 ml of 2.16 M ammonia water was added at the rate of 10 ml/min to a mixed aqueous solution (11 of 1 M) of titanium tetrachloride and zirconium oxychloride with stirring. (2): a mixed aqueous solution (5 l of 0.2 M) of titanium tetrachloride, zirconium oxychloride, and an excess amount of urea (300 g=5 M) was heated on a boiling water bath for 6—9 h.

The precipitates prepared by both methods were washed thoroughly with distilled water until no chloride ions were detected in the filtrate. They were dryed in air at 110 °C for 30 hr and finally calcined in air at 500 °C for 3 h.

Properties of Catalyst. The acidic properties of the catalysts were determined by the titration method with *n*-butylamine using a series of Hammett indicators. The differential thermal analyses were obtained in the range from room temperature to 720 °C.

Reaction Procedure and Analyses. The reaction was carried out by a conventional flow method using nitrogen as carrier gas at 300—360 °C. Ethanol, purified by distillation over anhydrous calcium oxide, and nitrogen were passed through the catalyst bed (2 g) at the flow rates of 7.5 ml/h and 1.0 l/h, respectively. The reaction products were analyzed by a gas chromatograph with FID using a column of PEG 1000 on Flusin T. The catalytic activity and selectivity were obtained from the product yields, given by the gas chromatograph peak areas (uncorrected), at 25 min after the reaction was initiated.

Results and Discussion

The catalytic activity of TiO_2–ZrO_2 (1: 1) precipitated by ammonia was 20% higher than that by urea.

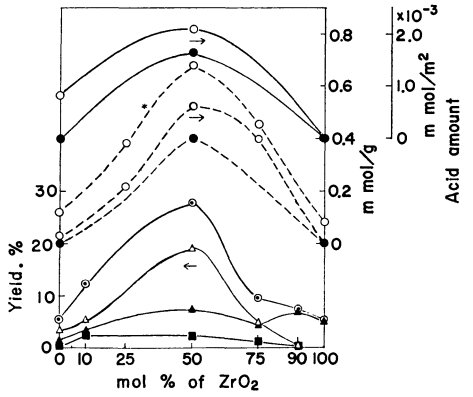

Fig. 1. Catalytic activity and acidity ($pK_a=-3.0$) of TiO_2–ZrO_2.
Reaction temperature: 300 °C, total conversion (—⊙—), yield of ether (—△—), ethylene (—▲—), butadiene (—■—).
Acidity: (○) and (●), for the samples precipitated by urea and ammonia, respectively; solid line, mmol/m²; broken line, mmol/g.
*$pK_a=6.8$.

Therefore, the TiO_2–ZrO_2 catalysts with various compositions prepared by the former method were mainly studied. The amount of acetaldehyde formed by the dehydrogenation of ethanol was almost negligible over all of the catalysts.

The catalytic activity, that is, the total conversion of ethanol, fairly well correlated with the acitidy*, as is shown in Fig. 1. TiO_2–ZrO_2 (1: 1) was most active, and the amount of ether formed was larger than that of ethylene. It is of interest that the total acidity of the sample prepared by urea was higher than that by ammonia, and the shapes of the curves were similar.

The catalytic conversion of ethanol to butadiene has been reported to proceed over solid acids such as Al_2O_3–ZnO,[6,7] though those to ethyl ether and ethylene are usually observed when catalyzed by ordinary solid acids. Therefore, this reaction was tested over the ZnO catalyst, which was prepared by the same procedure as TiO_2–ZrO_2, *i.e.*, the ammonia precipitation of $ZnCl_2$

* The acid amounts of TiO_2–ZrO_2 (1: 1) at various acid strengths were determined. The sample precipitated by ammonia showed 0.563 ($pK_a=6.8$), 0.440 (3.3), 0.363 (1.5), 0.400 (−3.0), 0.140 (−5.6), and 0.073 (−8.2), while the sample precipitated by urea exhibited 0.684 ($pK_a=6.8$), 0.460 (2.0), 0.520 (−3.0), 0.414 (−5.6), and 0.250 (−8.2). The acid amount of the sample prepared by urea was higher at each acid strength, in contrast to the observations with TiO_2–ZnO.[2] The amount at $pK_a=1.5$ or 2.0 was lower than that at $pK_a=-3.0$ in both samples, although the former value should be higher than the latter one. These unusual but interesting results seem to suggest an unusual surface property of TiO_2–ZrO_2.

aqueous solution. The products at 340 °C were 9.6% ethyl ether and 3.8% ethylene (13.4% in the total conversion). The butadiene yield increased at the higher reaction temperature, 330 °C, to 0.7, 2.3, 4.8, 12.4, 7.3, and 2.1% for ZrO_2, TiO_2–ZrO_2 (1: 9, 1: 3, 1: 1, 9: 1), and TiO_2, respectively. TiO_2–ZrO_2 (1: 1) also showed the highest activity for the formation of butadiene as well as that of ethylene and ethyl ether. Niiyama and coworkers have studied the butadiene formation from ethanol over SiO_2–MgO, which is an acid-base bifunctional catalyst, and concluded that the rate-controlling step is the acetaldehyde formation catalyzed by the basic sites.[8] Thus, it seems likely that the TiO_2–ZrO_2 catalyst also has basic sites which are effective for producing butadiene, and that the basicity increases by mixing TiO_2 and ZrO_2. In fact, TiO_2–ZrO_2 (1: 1) changed 2,4,6-trinitroaniline ($pK_a=12.2$) to its basic color, though B.T.B. ($pK_a=7.2$) did not change visibly to the basic color over TiO_2 and ZrO_2.

Table 1. Catalytic activity and selectivity of ZrO_2 for dehydration of ethanol at 360 °C

Temperature of calcination (°C)	Acidity[a] ($pK_a=6.8$) (mmol/g)	Conversion (%)	Products (%)	
			Ethylene	Butadiene
400	0.142	80.6	72.2	8.4
500	0.077	30.8	29.1	1.7
600	0.047	30.0	29.0	1.0

a) 0.230, 0.237 mmol/g at 200, 300 °C, respectively.

ZrO_2 produced no ether, resulting in a high selectivity for ethylene. A similar selectivity by ZrO_2 was also observed in the dehydration of *sec*-butanol, where 1-butene was formed in more than 90% selectivity.[9] The catalytic activity and selectivity of ZrO_2 at 360 °C are shown in Table 1. High selectivity for ethylene and also for butadiene implies that basic sites exist on this catalyst. Yamaguchi *et al.* also pointed out the basic character of ZrO_2 from its catalytic action in the isomerization of 1-butene.[9]

The strong exothermic peak at around 410 °C observed in DTA with ZrO_2, which is assigned to the crystallization of the amorphous state, moved to 510 to 640 °C as the ratio of TiO_2 mixed increased from 1: 9 to 1: 3. However, no peak was detected up to 720 °C with TiO_2–ZrO_2 (1: 1), probably being observed at above 720 °C. These discrepancies of peak might be related to acidity and catalytic activity.

We wish to express our thanks to Professor Kozo Tanabe (Faculty of Science, Hokkaido University) for his suggestions and interest in this work. Partial support of this work by Hokkaido Science Research Foundation is also gratefully acknowledged.

References

1) K. Tanabe, "Solid Acids and Bases," Kodansha, Tokyo, Academic Press, New York, London (1971).
2) K. Tanabe, C. Ishiya, I. Ichikawa, and H. Hattori, This Bulletin, **45**, 47 (1972).
3) K. Tanabe, M. Ito, and M. Sato, *Chem. Commun.*, **1973**, 723.
4) K. Shibata and T. Kiyoura, *J. Res. Inst. Catal., Hokkaido Univ.*, **19**, 35 (1971).
5) Y. Watanabe and N. Nojiri, *Nippon Kagaku Kaishi*, **1974**, 540.
6) S. K. Bhattacharyya and S. K. Sanyal, *J. Catal.*, **7**, 152 (1967).
7) S. K. Bhattacharyya and B. N. Avasthi, *Ind. Eng. Chem.*, **2**, 45 (1963).
8) H. Niiyama, S. Morii, and E. Echigoya, This Bulletin, **45**, 655 (1972).
9) T. Yamaguchi, H. Sasaki, and K. Tanabe, *Chem. Lett.*, **1973**, 1017.

BULLETIN OF THE CHEMICAL SOCIETY OF JAPAN, VOL. 48 (11), 3379—3380 (1975)

X-Ray Photoelectron Spectroscopy of 1,10-Phenanthroline Metal Chelates

Tooru YOSHIDA and Shigemasa SAWADA

Osaka Prefectural Industrial Research Institute, Enokojima, Nishi-ku, Osaka 550

(Received March 20, 1975)

Synopsis. Photoelectron spectra of several phenanthroline metal chelates were measured and the shifts of the N(1s) binding energy were plotted against the electronegativities of the metals. The plotted points appeared to fall into two groups, one for transition-metal chelates and the other for the other metal chelates.

The use of X-ray photoelectron spectrometry (XPS) to determine the effect of co-ordination on the electron density of a ligand is based on the fact that changes in the electron density about an atom are reflected in changes of the binding energies of the core electrons. The authors have previously reported results on the XPS of several metal chelate compounds.[1-3] It is well known that 1,10-phenanthroline (phen) and 2,2′-bipyridine (bipy), both having electron-donating and accepting capabilities, form very stable complexes with various cations, especially the Fe(II) ion.[4]

In this note, the results for several phen and bipy metal chelates using an XPS method will be presented.

Binding energies were measured employing an AEI ES200 photoelectron spectrometer under the control of a DS100/32 computer data-processing system using AlK_α radiation (E=1486.6 eV) as the photon source. All the metal complexes given in Table 1 were prepared according to the procedures of Schilt and Taylor.[5] The samples were ground to powder, dusted onto double-backed adhesive tape, and set inside the measuring chamber. The measurements were run at room temperature under a vacuum of about 10^{-7} Torr. However, a freezing technique was used for a few volatile samples.

The binding energy of the O(1s) peak was used as the energy standard throughout the present experiments; it was taken to be 532.0 eV, the O(1s) binding energies for all the samples being assumed to be constant. The C(1s) peak was, however, used for compounds having no perchlorate group as a constituent.

TABLE 1. N(1s) ELECTRON BINDING ENERGY VALUES

Samples	B.E. of N(1s)[a] (eV)	ΔE[b] (eV)	χ[c]	r[d] (Å)	pK[e]
phen	398.9				
phen(H_2O)	398.9				
phen($HClO_4$)	401.2; 398.9				
Mn(II)(phen)$_3$(ClO_4)$_2$	399.6	0.7	1.5	0.80	10.1
Fe(II)(phen)$_3$(ClO_4)$_2$	399.9	1.0	1.8	0.74	21.3
Co(II)(phen)$_3$(ClO_4)$_2$	399.7	0.8	1.8	0.72	19.9
Ni(II)(phen)$_3$(ClO_4)$_2$	399.7	0.8	1.8	0.69	24.8
Cu(II)(phen)$_2$(ClO_4)$_2$	399.9	1.0	1.9	0.72	11.0
Zn(II)(phen)$_3$(ClO_4)$_2$	399.7	0.8	1.6	0.71	17.5
Cd(II)(phen)$_3$(ClO_4)$_2$	399.5	0.6	1.7	0.97	14.3
Hg(II)(phen)$_3$(ClO_4)$_2$	399.0	0.1	1.9	1.10	23.3
Cu(I)(phen)$_2$(ClO_4)	399.4	0.5	1.7[f]	0.96	—
Ag(I)(phen)$_2$(ClO_4)	399.1	0.2	1.8[f]	1.31	12.0
bipy($HClO_4$)	401.2; 398.9				
Fe(II)(bipy)$_3$(ClO_4)$_2$	399.9	1.0			
Ni(II)(bipy)$_3$(ClO_4)$_2$	399.6	0.7			

a) Uncertainties are less than or equal to ±0.2 eV. b) Chemical shift of the N(1s) electron binding energy. c) Pauling electronegativity of the metal. d) Ionic radius of the metal. e) The logarithms of the overall stability constants of the chelates.[10] f) The value corrected according to Pauling.[12]

The measured values for the N(1s) electron binding energies are listed in Table 1 with other constants reported in the literature. Figure 1 shows the N(1s) electron spectra of phen($HClO_4$) and Fe(II)(phen)$_3$(ClO_4)$_2$. As can be seen from the figure, there are two kinds of nitrogen atoms in phen($HClO_4$), in addition to those observed in bipy($HClO_4$). The N(1s) spectrum of phen is a single peak with a full width at half height (FWHH) of 1.4 eV, and its binding energy value, 398.9 eV, agrees well with that of the peak with the lower binding energy of the two in phen($HClO_4$). Therefore, it can be concluded that the higher binding energy peak of the two in phen($HClO_4$) can be assigned to the protonated nitrogen atom and the lower to the unprotonated nitrogen atom.

The N(1s) binding energy value of phen(H_2O) is the same as that of phen, so the effect of the presence of a hydrogen bond in the molecule cannot be detected by XPS. The N(1s) spectrum of Fe(II)(phen)$_3$(ClO_4)$_2$ is a single peak with a FWHH of 1.4—1.5 eV, as are those of all other metal chelates. It can be concluded that all nitrogen atoms in the chelate molecule have equivalent charge densities.

The O(1s) electron spectra of all the compounds containing a perchlorate group are single peaks with a FWHH of 1.7—1.9 eV.

The chemical shifts ΔE are the differences between the N(1s) electron binding energies for the free phen and that for the chelates. Figures 2 and 3 show the chemical shifts which are plotted against the Pauling electronegativity of the metal and the ionic radius, respectively. In Fig. 2, the points appear to fall into two groups. The points for the transition-metal chelates (d^5, d^6, d^7, d^8, and d^9 complexes) Mn(II), Fe(II), Co(II), Ni(II), and Cu(II) fall near one straight line. On the other hand, the points for the Zn(II), Cd(II), Cu(I), Hg(II), and Ag(I) chelates (d^{10} complexes) fall near another straight line having a negative slope, the chemical shift in this case decreasing with increasing electronegativity of the metal. In Fig. 3, the points for all the chelates fall near one straight line, the chemical shift decreasing with increasing ionic radius.

In the charge-potential model,[6] the chemical shift can be expressed in terms of the charge on the atom and the Coulomb potential energy of an electron due to the other atoms in the molecule. In general, the neglect of the Coulomb potential energy may cause serious errors for ionic compounds, but for the covalent compounds as studied here, the chemical shift should be dominated by the charge on the atom concerned.

The difference just noted in Fig. 2 suggests that a fundamental difference of some sort may exist between the structures of the two groups of chelates. The most obvious difference between the transition-metal cations

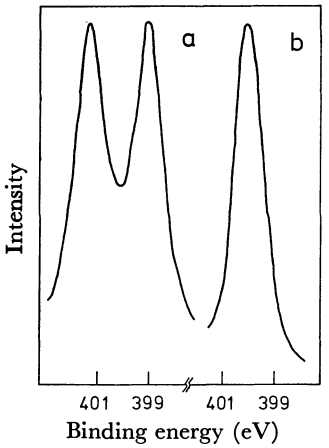

Fig. 1. N(1s) electron spectra of (a) phen($HClO_4$), and (b) Fe(II)$(phen)_3(ClO_4)_2$.

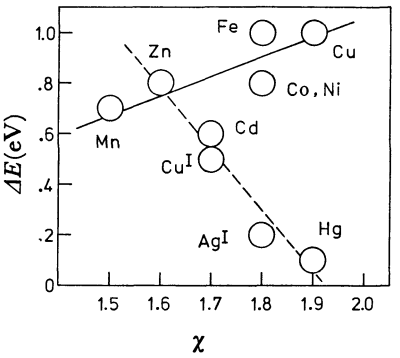

Fig. 2. Relation between electronegativity and chemical shift.

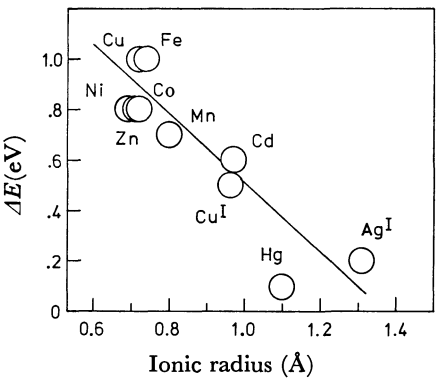

Fig. 3. Relation between ionic radius and chemical shift.

and the other metal cations mentioned is the presence of available 3d orbitals in the former. A possible explanation, then, for the difference noted is the participation of 3d orbitals in the metal–ligand bonding. However, Craig *et al.*[7] have reported on the basis of magnetic susceptibility measurements of $Ni(bipy)_3^{2+}$ that 3d-orbitals may not be involved in metal–ligand bonding for this chelate, and even if involved, not to the extent of forming a $3d^24s4p^3$ hybridized bond.

In general, the bond between a ligand and a metal for coordinate compounds is explained by a σ-bonding (the coordination of a lone pair electrons of a ligand to a metal) and a π-bonding (back-domation from filled metal ion orbitals to empty ligand orbitals) in many cases. These two effects work in opposite directions as for the electron density on the donor atom of the ligand.

If the σ-bonding is more important in the complex formation than the π-bonding, it can be said that the covalent character of the bonds between the metal ions and the ligand increases with the metal ion electronegativity, and that the degree of complex stability is affected by this character.[8] Furthermore, more covalent coordinate bonding is considered to decrease the electron density on the donor atoms, which appears in the increase of the electron binding energies.

When the π-bonding is important, there is no longer correlation between the metal ion electronegativity and the electron density of the donor atoms, as was stated above.

For EDTA, anthranilic acid and oxine chelates in which the double bond with the metal atom is not present or is weak, the plots of the N(1s) chemical shift as a function of the electronegativity of the metal actually showed that all the points for the transition and the other metal chelates appeared to fall near one straight line.[1,2,9]

It has been reported by Busch *et al.*[10] that the chemical behavior and properties of phen and bipy complexes are best described in terms of σ-bonds formed between the metal and the methine nitrogens, and of π-bonds resulting from interaction of the unhybridized d-electron pairs of the metal atom with the π-system of the ligand.

In this study, the fact that the N(1s) chemical shifts of the Hg(II) and the Ag(I) chelates are small compared to those of the Ni(II) and the Cu(II) chelates, as is seen in Fig. 2, which have stabilities similar to the former two chelates (the logarithms of the stability constants of the Hg(II) and the Ag(I) chelates are 23.3 and 12.0, respectively, while those of the Ni(II) and the Cu(II) chelates are 24.8 and 11.0, respectively)[11] may be attributed in part to the greater contribution of the dative π-bond in the metal-ligand bond of the Hg(II) and the Ag(I) chelates.

In the phen metal chelates, the ionic radii of metal ions may be one of the important factors that affect the electron density of the donor atom in view of the relation in Fig. 3. This may be correlated with the geometrical structure characteristic of the phen molecule that the distance between the two donor nitrogen atoms is invariable.

The authors wish to thank Mr. Taichiro Hirohara for the elemental analysis of all the samples.

References

1) T. Yoshida and S. Sawada, This Bulletin, **47**, 1024 (1974).
2) T. Yoshida and S. Sawada, *ibid.*, **48**, 333 (1975).
3) T. Yoshida and S. Sawada, *ibid.*, **48**, 345 (1975).
4) W. W. Brandt, F. P. Dwyer, and E. C. Gyarfas, *Chem. Rev.*, **54**, 959 (1954).
5) A. A. Schilt and R. C. Taylor, *J. Inorg. Nucl. Chem.*, **9**, 211 (1959).
6) K. Siegbahn, C. Nordling, G. Johansson, J. Hedman, P. F. Heden, K. Hamrin, U. Gelius, T. Bergmark, L. O. Werme, R. Manne, and Y. Baer, "ESCA Applied to Free Molecules," North-Holland, Amsterdam (1969).
7) D. P. Craig, A. Maccoll, R. S. Nyholm, L. E. Orgel, and L. E. Sutton, *J. Chem. Soc.*, **1954**, 332.
8) L. G. Van Uitert, W. C. Fernelius, and B. E. Douglas, *J. Amer. Chem. Soc.*, **75**, 2736 (1953).
9) T. Yoshida and S. Sawada, to be published.
10) D. H. Busch and J. C. Bailar, *J. Amer. Chem. Soc.*, **78**, 1137 (1956).
11) K. Ueno and T. Sakaguchi, "Kinzoku Kireito," Vol. 3, Nankodo Co., Tokyo (1967), p. 65.
12) L. Pauling, "The Nature of the Chemical Bond," 2nd ed., Cornel University Press, New York (1945), pp. 65—72.

BULLETIN OF THE CHEMICAL SOCIETY OF JAPAN, VOL. 48 (11), 3381—3382 (1975)

Studies of the $\pi \rightarrow \pi^*$ Absorption Bands of α-Santonin

Akira KUBOYAMA, Yoshikuni SATO,* and Fumio KOBAYASHI
National Chemical Laboratory for Industry, Shibuya-ku, Tokyo 151

(Received March 29, 1975)

Synopsis. The $\pi \rightarrow \pi^*$ S–S absorption spectra of α-santonin in solutions up to the vacuum UV region were obtained. Based on the results of the MO calculations, the observed four $\pi \rightarrow \pi^*$ bands of α-santonin could be favorably assigned.

Heretofore, the electronic spectrum of α-santonin in the wavelength region shorter than 220 nm has never been reported.[1] We have measured the spectra of α-santonin in solutions up to the vacuum UV region. We have also carried out MO calculations on the π-electronic system of α-santonin, which is similar to that of 1,4-cyclohexadiene-3-one, in order to assign the observed $\pi \rightarrow \pi^*$ bands.

The electronic spectra were measured in the same manner as in the previous works.[2] The solvents—*n*-heptane, 1,1,1,3,3,3-hexafluoroisopropanol (HFIP), and ethanol—were the same as those used in the previous works. α-Santonin of the Japan pharmacopaeia was used without further purification (mp 171.5—172.5 °C).

In the P-P-P method calculations, the electronic integral values which were used in the calculations on *p*-benzoquinone, *etc.* in one[2a] of the previous works were used. All the singly-excited configurations were included. In this work, according to the results of the X-ray analysis of 2-bromo-α-santonin,[3] the π-electronic system of α-santonin was assumed to be planar and to be of the C_{2v} symmetry. The atomic distances of the conventional C=O, C–C, and C=C bonds were assumed to be 1.22, 1.47, and 1.35 Å respectively.[3,4] In the calculations, the intramolecular environmental effect on the π-electronic system of α-santonin was ignored.

The longest-wavelength singlet absorption band of α-santonin is the $n \rightarrow \pi^*$ band near 340 nm.[5] In Fig. 1, four $\pi \rightarrow \pi^*$ bands can be observed in an *n*-heptane solution near 255, 230, 200, and 180 nm. These $\pi \rightarrow \pi^*$ bands are denoted as Bands A, B, C, and D (Table 1).

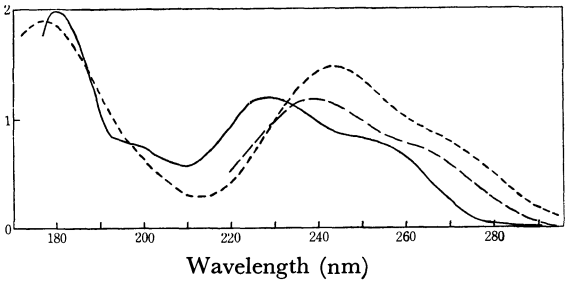

Fig. 1. Absorption spectra of α-santonin in various solvents. ——: *n*-heptane, — —: ethanol, ----: 1,1,1,3,3,3-hexafluoroisopropanol.
(In an *n*-heptane solution the scale of the ordinate is arbitrary.)

* Permanent address: The Tokyo Metropolitan Industrial Technology Center, Kita-ku, Tokyo.

TABLE 1. WAVELENGTHS AND MOLAR ABSORPTION COEFFICIENTS OF THE ABSORPTION MAXIMA (the values in parentheses are the latter)

n-Heptane (nm)	Ethanol	HFIP	Band name
~255	~265 (7060)	~270 (7950)	A
229.5	238.5 (11900)	243.5 (14700)	B
~200			C
180		177 (19000)	D

TABLE 2. CALCULATED EXCITATION ENERGIES, OSCILLATOR STRENGTHS, AND SYMMETRY SPECIES OF THE SINGLET π,π^* EXCITED STATES AND THE CORRESPONDING $\pi \rightarrow \pi^*$ BANDS IN AN *n*-HEPTANE SOLUTION

	Calcd			Obsd	
No.	Symmetry	E(eV)	f	Band name	E(eV)
1	B_2	5.139	0.042	A	~4.9
2	A_1	5.343	0.577	B	5.4
3	B_2	6.058	0.041	C	~6.2
4	A_1	7.156	0.033		
5	A_1	7.367	1.036	D	6.9

Bands A and C can be observed as shoulders. As for the solvent effects on the $\pi \rightarrow \pi^*$ bands in Fig. 1, Band D in a HFIP solution is far broader than that in an *n*-heptane solution. Furthermore, in a HFIP solution, Bands A and B shifts greatly toward longer wavelengths, while Band D shifts a little toward shorter wavelengths, in comparison with those in an *n*-heptane solution. In a HFIP solution, Band C can hardly be observed because of its blue-shift in comparison with that in an *n*-heptane solution. These solvent effects may be due to the strong hydrogen-bond formation between α-santonin and HFIP.[2b] Based on the calculated results, these four $\pi \rightarrow \pi^*$ bands can be reasonably assigned, as is shown in Table 2. The first column of this table denotes the numbering of the magnitude of the calculated excitation energies. In this table, the data on the higher excited states with small f-values have been omitted. Since the energy difference between the Nos. 4 and 5 states is small, the $\pi \rightarrow \pi^*$ band corresponding to the No. 4 state may be hidden by Band D. Based on the calculated results, it may be concluded that Bands B and D and Bands A and C are polarized parallel to, and perpendicular to, the C–O bond axis respectively. It is interesting that, according to the calculated results, the excited state of Band D is largely localized in two vinyl groups (*ca.* 66%). The above-mentioned fact that the excitation energies of Band D in an *n*-heptane and a HFIP solutions are relatively close to each other can be reasonably ex-

plained by this calculated result regarding Band D. The broadness of Band D in a HFIP solution may be due to an intensification of the $\pi \rightarrow \pi^*$ band corresponding to the No. 4 state, in addition to the above-mentioned blue-shift of Band C, comparison with those in an *n*-heptane solution.

The quinols have a π-electronic system similar to that of α-santonin. In the $\pi \rightarrow \pi^*$ absorption spectrum of 6-acetoxy-3-oxo-bicyclo-0,3,4-nonadiene-(1,4), which is classified as one of the quinols, in an ethanol solution, as reported by Wessely *et al.*,[6] two $\pi \rightarrow \pi^*$ bands, corresponding to Bands A and B, can be observed. On the other hand, in the absorption spectrum of spiro-5,5-undeca-1,4-dien-3-one, which also has a π-electronic system similar to that of α-santonin, in an *n*-hexane solution, up to the vaccum UV region, as reported by Boschi *et al.*,[7] $\pi \rightarrow \pi^*$ bands corresponding to Bands A and C can hardly be observed. The assignment of its two $\pi \rightarrow \pi^*$ bands, corresponding to Bands B and D, by Boschi *et al.*,[7] based on the P-P-P method calculation, agrees with that in Table 2.

We have also carried out similar MO calculations on other various planar conjugated dienones. According to the calculated results, in all the cross-conjugated dienones, among the singlet excited states and the lowest state does not have the largest *f*-value, unlike as in the cases of the linearly-conjugated dienones.

References

1) a) L. Ruzicka, C. L. Cohen, M. Furter, and Fch. van der Sluys-Veer, *Helv. Chim. Acta*, **21**, 1737 (1938); b) F. D. Gunstone and R. M. Heggie, *J. Chem. Soc.*, **1952**, 1437; c) D. Arigoni, H. Bosshard, H. Bruderer, G. Büchi, O. Jeger, and L. J. Krebaum, *Helv. Chim. Acta*, **40**, 1732 (1957).

2) a) A. Kuboyama, S. Matsuzaki, M. Takagi, and H. Arano, This Bulletin, **47**, 1604 (1974); b) A. Kuboyama, F. Kobayashi, and S. Morokuma, *ibid.*, to be published.

3) J. D. M. Asher and G. A. Sim, *J. Chem. Soc.*, **1965**, 6041.

4) a) E. A. Cherniak and C. C. Costain, *J. Chem. Phys.*, **45**, 104 (1966); b) J. Trotter, *Acta Crystallogr.*, **13**, 86 (1960).

5) G. Marsh, D. R. Kearns, and M. Fisch, *J. Amer. Chem. Soc.*, **92**, 2252 (1970).

6) F. Wessely, J. Kotlan, and W. Metlesics, *Monatsch. Chem.*, **85**, 72 (1954).

7) R. Boschi, A. S. Dreiding, and E. Heilbronner, *J. Amer. Chem. Soc.*, **92**, 123 (1970).

BULLETIN OF THE CHEMICAL SOCIETY OF JAPAN, VOL. 48 (11), 3383—3384 (1975)

Structural Changes of Iron Oxides by Ball-Milling in Different Media

Yasuhiko UEHARA

Electron Tube Division, Hitachi Ltd., Hayano, Mobara, Chiba 297

(Received April 18, 1975)

Synopsis. γ-Fe_2O_3, Fe_3O_4, and α-Fe_2O_3 subjected to steel ball-milling in water changed into a spinel-type solid solution, while in polar organic media no remarkable changes occurred. In non-polar media, the γ-Fe_2O_3 and a part of the Fe_3O_4 were transformed into α-Fe_2O_3, although α-Fe_2O_3 remained unchanged. The diffraction lines of the resulting α-Fe_2O_3 broadened markedly.

γ-Fe_2O_3 is known to be transformed irreversibly into α-Fe_2O_3 by such treatments as applying high pressure and grinding mechanically.[1,2] The transformation proceeds *via* the reconstruction of close-packed oxygen ion layers together with the displacement of ferric ions located at the interstices between the oxygen ions.[3,4] The present paper describes the structural changes of γ-Fe_2O_3, Fe_3O_4, and α-Fe_2O_3 caused by the ball-milling in different liquid media in order to clarify the effect of the medium.

The structure of γ-Fe_2O_3 is an inverse spinel with a lattice parameter of 8.350 Å accompanied by a superstructure which has an ordered arrangement of cation vacancies and ferric ions in a ratio of 1 : 3 at the octahedral sites. Fe_3O_4 is crystallographically isomorphous with γ-Fe_2O_3, having a lattice parameter (8.396 Å) slightly larger than that of γ-Fe_2O_3 (8.350 Å). Fe_3O_4 and γ-Fe_2O_3 form a γ-Fe_2O_3–Fe_3O_4 solid solution; this can be expressed by $\square_{x/3}Fe_{3-x/3}O_4$, where $\square$ is the cation vacancy and x is the degree of oxidation. α-Fe_2O_3 has a corundum-type rhombohedral structure, its unit cell having the lattice parameters $a=5.427$ Å and $\alpha=55°17'$.

The γ-Fe_2O_3 used in this experiment showed a characteristic lattice parameter of 8.350 Å. The Fe_3O_4 used has the lattice parameter of 8.386 Å, indicating a slight oxidation of the stoichiometric Fe_3O_4. The particle shape of γ-Fe_2O_3 is rod-like approximately 0.8 μ in length and 0.2 μ in diameter. Both α-Fe_2O_3 and Fe_3O_4 are spherical particles about 0.3 μ in diameter. γ-Fe_2O_3, Fe_3O_4, and α-Fe_2O_3 powders were wet-milled in a steel ball mill having a capacity of 1.32 l. For each run, 30 g of the sample and 90 ml of the medium of extrapure grade were loaded into the ball mill. After milling at 90 rpm for 80 h, the resultant product was dried under reduced pressure and then examined by X-ray diffraction, using Mn-filtered FeK_α radiation. In order to compare the effect of different milling procedures, wet-milling in a porcelain ball mill and dry-grinding in an agate mortar were also carried out.

Table 1 shows the crystal structure, lattice parameter, and half-value width of each characteristic X-ray pattern of the products from γ-Fe_2O_3, Fe_3O_4, and α-Fe_2O_3 after 80 h of milling in the steel ball mill in the presence of different media. The structural changes occurred may be classified as follows:

1) In water, the spinel phase was stable and no significant line broadening of the X-ray diffraction lines was observed.

2) In polar organic media, neither structural changes nor line broadening was observed.

3) In a non-polar organic medium, the α-Fe_2O_3 phase was stable and nearly half of Fe_3O_4 was transformed into α-Fe_2O_3. However, a remarkable broadening of the diffraction patterns of both oxides was observed.

When γ-Fe_2O_3 was milled in the steel ball mill in the

TABLE 1. CHANGES IN CRYSTAL STRUCTURE, LATTICE PARAMETER, AND HALF-VALUE WIDTH OF EACH CHARACTERISTIC X-RAY PATTERN OF THE PRODUCTS FROM γ-Fe_2O_3, Fe_3O_4, AND α-Fe_2O_3 AFTER 80 hr OF MILLING IN THE STEEL BALL MILL IN DIFFERENT MEDIA

Medium		Dipole moment (D)	Starting material	Resultant product	Lattice parameter[b] (Å)	Half-value width[c] (degree)
Water		1.84	γ-Fe_2O_3	Spinel[a]	8.371	0.30
			Fe_3O_4	Spinel[a]	8.393	0.25
			α-Fe_2O_3	Spinel[a]	8.371	0.30
Polar organic medium	Methyl alcohol	1.69	γ-Fe_2O_3	γ-Fe_2O_3	8.350	0.31
			Fe_3O_4	Fe_3O_4	8.386	0.26
			α-Fe_2O_3	α-Fe_2O_3	5.427	0.25
	Isopropyl alcohol	1.66	γ-Fe_2O_3	γ-Fe_2O_3	8.350	0.30
			Fe_3O_4	Fe_3O_4	8.386	0.24
			α-Fe_2O_3	α-Fe_2O_3	5.427	0.25
	Acetone	2.69	γ-Fe_2O_3	γ-Fe_2O_3	8.350	0.31
Non-polar organic medium	Cyclohexane	0	γ-Fe_2O_3	α-Fe_2O_3	5.43	1.2
			Fe_3O_4	α-Fe_2O_3+Fe_3O_4	5.43	1.0
			α-Fe_2O_3	α-Fe_2O_3	5.43	1.0

a) Spinel: γ-Fe_2O_3–Fe_3O_4 solid solution. b) Lattice parameters of starting materials. γ-Fe_2O_3: 8.350 Å, Fe_3O_4: 8.386 Å, α-Fe_2O_3: 5.427 Å. c) Half-value widths for starting materials. γ-Fe_2O_3 (311): 0.27°, Fe_3O_4 (311): 0.20°, α-Fe_2O_3 (422): 0.22°.

presence of water, the lattice parameter changed from 8.350 Å to 8.371 Å, the superstructure lines such as (210), (211), and (300) disappeared completely and the color changed from brown to black. These facts indicate that γ-Fe_2O_3 was reduced during the milling to give a γ-Fe_2O_3–Fe_3O_4 solid solution. Fe_3O_4 was also reduced to some extent to give Fe_3O_4 containing less oxygen than the original Fe_3O_4, accompanied with a change in the lattice parameter from 8.386 Å to 8.393 Å. α-Fe_2O_3 showed a complete transformation from the rhombohedral into the spinel structure with a lattice parameter of 8.371 Å which coincides with that of the milled γ-Fe_2O_3. Meanwhile, the color of α-Fe_2O_3 changed from red to black. However, when γ-Fe_2O_3, Fe_3O_4, and α-Fe_2O_3 were milled in a porcelain ball mill, no changes in the structure, lattice parameter, and color occurred. Therefore, it is likely that a mechano-chemical reaction is characteristic of the milling in the steel ball mill.

When γ-Fe_2O_3, Fe_3O_4, and α-Fe_2O_3 were milled in such polar organic media as methyl alcohol, isopropyl alcohol, and acetone, their structures, lattice parameters, and colors remained unchanged. The diffraction lines were as sharp as they were in the case of milling in water.

When milled in non-polar cyclohexane, γ-Fe_2O_3 was completely transformed into α-Fe_2O_3. In the case of Fe_3O_4, nearly half of the sample was transformed into α-Fe_2O_3; the diffraction lines of the resultant α-Fe_2O_3 were found to be remarkably broadened. Nearly identical results were obtained from an experiment by dry-grinding in an agate mortar.

During the milling, a microstrain concentrates in the lattice increasing the lattice distortion and the strain energy.[5] The increase in the lattice distortion results in the X-ray line broadening.[6] At the same time, the fresh surface produced by the milling is reactive with respect to the adsorption of polar molecules decreasing the surface energy and the fracture stress.[7] The fact that the X-ray diffraction lines remained as sharp as before can be explained, if one accepts that the adsorption of polar molecules decreases the fracture stress avoiding a remarkable increase in the microstrain concentration in the lattice. In the case of milling in non-polar media, on the other hand, the microstrain concentration increases gradually in the lattice and the X-ray diffraction lines become broader. In the case of milling in water, the sample is reduced to give a spinel phase containing less oxygen. In this reduction reaction during the milling, the mechano-chemical reaction between the sample, the water, and the fresh iron surfaces should be taken into consideration.

References

1) Y. Goto, *Japan J. Appl. Phys.*, **3**, 739 (1964).
2) M. Senna, S. Tojo, and H. Kubo, *Nippon Kagaku Zasshi*, **92**, 780 (1971).
3) S. Kachi, K. Momiyama and S. Shimizu, *J. Phys. Soc. Japan*, **18**, 106 (1963).
4) J. Hornstra, *J. Phys. Chem. Solids*, **15**, 311 (1960).
5) D. Lewis, D. O. Northwood, and R. C. Reeve, *J. Appl. Cryst.*, **2**, 156 (1969).
6) *e.g.*, A. R. Stokes and A. J. C. Wilson, *Proc. Phys. Soc.*, **56**, 174 (1944).
7) P. Rehbinder, *Z. Phys.*, **72**, 191 (1931).

BULLETIN OF THE CHEMICAL SOCIETY OF JAPAN, VOL. 48 (11), 3385—3386 (1975)

Weak Fluorescence from [2.2]Metacyclophane

Haruo SHIZUKA, Toshio OGIWARA, and Toshifumi MORITA

Department of Chemistry, Faculty of Technology, Gunma University, Kiryu, Gunma 376

(Received April, 8, 1975)

Synopsis. Weak fluorescences from [2.2]metacyclophane (MCP) were observed: the normal and intramolecular excimer fluorescences were at 305 and 361 nm respectively. It has been shown that a rapid radiationless deactivation due to the interaction between the two benzene rings in MCP occurs preferentially and the excimer formation responsible for the photocyclization takes place to a small extent.

Recently, the transannular π-electronic interaction in [2.2]metacyclophane (MCP) has come to be of interest.[1-3] In contrast to that in [2.2]paracyclophane,[4] the assumption of the interaction in MCP was denied in both the ground[1] and the excited states.[2]

However, the transannular interaction between the two benzene rings in the excited state of MCP has been recently suggested from the abnormal photochemical behaviors: the small reaction quantum yields (less than 0.01), the large quantum yield for the radiationless deactivation process (0.99), and the lack of emission.[3]

The reason why the two central hydrogen atoms in the intermediate M resulting in the photocyclization should be *cis*-form[3] has not been given. In order to elucidate further the photochemical and photophysical behaviors in MCP, we have made measurements on the emission from MCP, using a highly sensitive single photon counter.

Experimental

The chemical reagents and procedures were essentially as previously described.[3] Samples were degassed by a freeze-pump-thaw method.

The fluorescence from MCP was measured by a single photon counter similar to that reported by Hikida *et al.*[5] It was possible to measure the fluorescence quantum yields up to $\sim 10^{-6}$. The yields for normal and excimer fluorescences of MCP at 270 nm were measured by comparison with quinine bisulfate 0.1 N H_2SO_4 at 366 nm. The absolute yield at 366 nm was determined to be 0.54 by Melhuish.[6] The light intensities at 270 and 366 nm were also measured using a quantum counter (an 8 g/l solution of rhodamine B).[7]

Results and Discussion

Figure 1 shows the fluorescence from MCP in degassed cyclohexane at room temperature. The fluorescence spectrum comprises two bands at 305 and 361 nm. From the mirror image in Fig. 1, the band at 305 nm was assigned to the normal fluorescence from MCP. The band at 361 nm was assigned to the intramolecular excimer fluorescence[8] judging from the broad and structureless fluorescence band which was shifted by 5100 cm^{-1} to lower frequencies relative to the normal fluorescence. The quantum yields for the normal and the excimer fluorescences in degassed cyclohexane at 270 nm

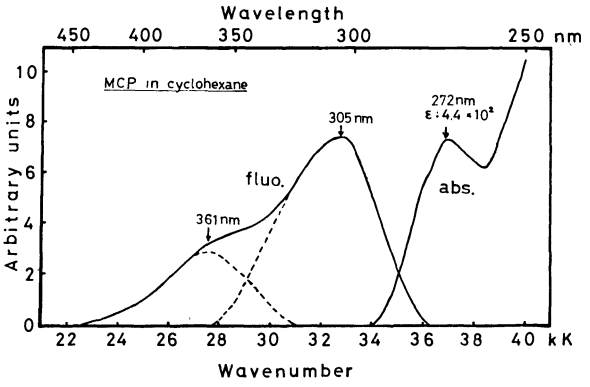

Fig. 1. Absorption and fluorescence spectra of 1.6×10^{-3} M cyclohexane solution of MCP.

and 15° were 2 $(\pm 0.1) \times 10^{-5}$ and $5._6(\pm 0.5) \times 10^{-6}$, respectively. The lifetime τ_{s1} of the lowest excited singlet state S_1, which corresponds to the $^1B_2$ state of the locally excited state of benzene, was estimated to be *ca.* 10 ps, from the values of the fluorescence quantum yield (2×10^{-5}) and the rate constant of k_f ($\sim 2.5 \times 10^6\ s^{-1}$) for the radiative transition from S_1 to S_0. No phosphorescence from MCP could be observed in MP at 77 K.

From these results, a rapid radiationless deactivation process k_d (see Fig. 2) should be involved in the S_1 state of MCP. A possible explanation for the large k_d is that rotational motions of the two benzene rings in S_1 may facilitate the internal conversion. It is well known that the deactivation process in the excited state of some dyes, such as auramine O and crystal violet, is enhanced by the rotational motion.[9-11]

Although the interacting chromophores in MCP are not separated by three carbon atoms ($n=3$ rule),[12] the sandwich configuration of MCP can be attained by rotating the benzene rings around the central carbon atoms. It is known that in the ground state this rotation with a large activation energy (>27 kcal/mol) is very difficult to take place.[13-15] This may be due to the fact that the transannular interaction[16] in the excited state gives an attractive force between them, resulting in the formation of MCP excimer. The excimer formation

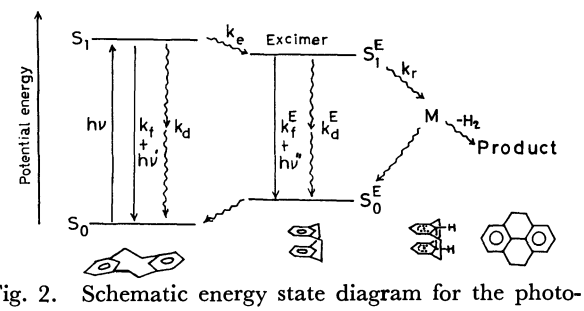

Fig. 2. Schematic energy state diagram for the photochemical processes in MCP.

of MCP has a very close relation with the intermediate M in the photochemical cyclization of MCP.[3] The "sandwich" excimer structure is responsible for the M formation, followed by the thermal reaction to give the products (4,5,9,10-tetrahydropyrene plus a hydrogen molecule) or the starting material.[3] The behavior in the excited state of MCP can be accounted for by the scheme shown in Fig. 2. Thus, the reason why the central hydrogen atoms in M should be in a *cis*-configuration can be well understood. The efficiency for the intramolecular excimer formation becomes small because of the rapid deactivation competing with the excimer formation.

In conclusion, it is obvious that the transannular interaction due to the proximity of two benzene rings exists in the excited MCP.

The authors wish to thank Dr. Takeo Sato, Tokyo Metropolitan University, for the supply of [2.2]metacyclophane.

References

1) E. Lange and H. Lehner, *Tetrahedron*, **29**, 375 (1973).
2) E. Lange and H. Lehner, *Monatsh. Chem.*, **104**, 644 (1973).
3) K. Sorimachi, T. Morita, and H. Shizuka, This Bulletin, **47**, 987 (1974).
4) D. J. Cram, N. L. Allinger, and H. Steinberg, *J. Amer. Chem. Soc.*, **76**, 6132 (1954).
5) T. Hikida, T. Ichimura, and Y. Mori, *Chem. Phys. Lett.*, **27**, 548 (1974). The blank test gave no emission from the solvent (s.g.-cyclohexane). Unfortunately, another solvents (MP and EPA) at the 270 nm excitation gave emissions from their impurities in the fluorescence spectral range.
6) M. H. Melhuish, *J. Phys. Chem.*, **65**, 299 (1961).
7) J. Yguerabide, *Rev. Sci. Inst.*, **39**, 1048 (1968).
8) For intramolecular excimer fluorescences, see W. Klöpffer, "Organic Molecular Photophysics," Vol. 1, ed. by J. B. Birks, Wiley-Interscience, London, 1973, and the many references cited therein.
9) G. Oster and Y. Nishijima, *J. Amer. Chem. Soc.*, **78**, 1581 (1956).
10) Th. Förster and G. Hoffmann, *Z. Phys. Chem. N.F.*, **75**, 63 (1971).
11) D. Magde and M. W. Windsor, *Chem. Phys. Lett.*, **24**, 144 (1974).
12) F. Hirayama, *J. Chem. Phys.*, **42**, 3163 (1965).
13) R. W. Griffin, Jr., and R. A. Coburn, *Tetrahedron Lett.*, **1964**, 2571; *J. Amer. Chem. Soc.*, **89**, 4638 (1967).
14) I. Gault, B. J. Price, and I. O. Sutherland, *Chem. Communn.*, **1967**, 540.
15) T. Sato, S. Akabori, M. Kainosho, and K. Hata, This Bulletin, **39**, 856 (1966); *ibid.*, **41**, 218 (1968).
16) J. B. Birks, "Photophysics of Aromatic Molecules," Chapter 7, Wiley-Interscience, London, 1970, and references therein. The transannular interaction in the excited state comprises charge resonance, excitation resonance, and dipole-dipole interactions between two chromophores. The dipole-dipole interaction in the excited MCP may be the smallest among them, because the excited state has a $^1B_2$ character as described in the text.

BULLETIN OF THE CHEMICAL SOCIETY OF JAPAN, VOL. 48 (11), 3387—3388 (1975)

Proton Transfer Reactions in Oxygen-Containing Molecules and Ammonia Mixtures

Akira MATSUMOTO, Satoshi OKADA,* Setsuo TANIGUCHI,* and Teruo HAYAKAWA

Department of Chemistry, Faculty of Liberal Arts and Sciences, University of Osaka Prefecture, Sakai, Osaka 593

**Radiation Center of Osaka Prefecture, Sakai, Osaka 593*

(Received April 19, 1975)

Synopsis. Ion-molecule reactions leading to the formation of NH_4^+ in a number of mixtures of oxygen-containing molecules and ammonia have been studied using pulsed-source mass spectrometry. Some unique features in the reactivities of $C_2H_4O^+$ and CHO^+ ions from ethylene oxide have been found.

The gas-phase ion chemistry of oxygen-containing molecules has been investigated by several investigators.[1-4] Blair and Harrison[1] have recently reported that the $C_2H_4O^+$ ion initially formed by electron impact of ethylene oxide is unreactive but undergoes a collisional modification to a more reactive species which shows a different reactivity from that of the $C_2H_4O^+$ ion from acetaldehyde. They have pointed out two possibilities: the difference arises from structural effects or from energy effects.

In this paper we report the rate constants of proton transfer reactions from the prominent ions in the mass spectra of oxygen-containing molecules including acetaldehyde and ethylene oxide to ammonia as a common neutral molecule. The results offer additional evidence for the unique features of ionic species from ethylene oxide. The rate constants of the hydrogen atom transfer reactions from oxygen-containing molecules to ammonia ion were also determined.

Experimental

The experiments were performed on a Hitachi-RMU5 mass spectrometer fitted with a pulsed ion source as described previously.[4]

Acetaldehyde prepared from paraldehyde, commercial dimethyl ether, and methanol were purified by vacuum distillation. The purities of these samples were more than 99%. Ethylene oxide and ammonia purchased from Takachiho Kagaku Co., Ltd., in research grade purity of 99.9% were used without further purification. The rate constants of the ion-molecule reactions studied were calibrated with reference to the reported rate constant, $k=1.22\times10^{-9}$ cm^3mol^{-1} s^{-1}, for the reaction $CH_4^+ + CH_4 \rightarrow CH_5^+ + CH_3$.[5]

Results and Discussion

As a preliminary to the study of the proton transfer reactions in mixtures containing ammonia, the reactions forming NH_4^+ ion in pure ammonia were investigated at 12—25 eV electron energies. NH_3^+, NH_2^+, and NH^+ were observed as the primary ions. However, as has been suggested by Derwish and co-workers,[6] NH^+ was not a reactant ion for forming NH_4^+ with ammonia. The rate constants of proton transfer reactions of NH_3^+ and NH_2^+ ions were determined from the analysis of $I_{NH_2^+}/I_{NH_3^+}$ *vs* delay time plots. The results obtained are given in Table 1 and are in agreement with those reported by Harrison and co-workers,[5] except for Reaction 2. It should be pointed out here that impact electron energies higher than 12 eV were employed for all the experiments, since k_1 varies with the energy of the impact electron below 12 eV.[7]

In the mixtures of an oxygen-containing molecule and ammonia, the significant primary ions, omitting the ions from ammonia, are as follows: $CH_3OCH_3^+$, $CH_3OCH_2^+$, $C_2H_3O^+$, and CHO^+ for dimethyl ether, $C_2H_4O^+$, $C_2H_3O^+$, and CHO^+ for acetaldehyde and ethylene oxide, and CH_4O^+, CH_3O^+, and CHO^+ for methanol. Table 1 shows the possible reactions leading to the formation of an NH_4^+ ion in each system.

The secondary ion current of NH_4^+ ($m/e=18$) can be generally described for the dimethyl ether–ammonia system by

$$I_{18} = \left\{k_1I_{17}+k_2I_{16}+k_3I_{46}+k_4I_{45}+k_5I_{43}+k_6I_{29} + k_7I_{17}\frac{[CH_3OCH_3]}{[NH_3]}\right\}[NH_3]t + C_1$$

Table 1. Rate constants of ion-molecule reactions in pure ammonia and oxygen-containing molecule-ammonia mixtures

	Reaction	Rate constant, $k\times10^{10}$ (cm^3 mol^{-1} s^{-1})
	NH_3	
1	$NH_3^+ + NH_3 \longrightarrow NH_4^+ + NH_2$	10.7(10.0[a])
2	$NH_2^+ + NH_3 \longrightarrow NH_4^+ + NH$	7.99(6.5[a])
	$CH_3OCH_3-NH_3$ mixture	
3	$C_2H_6O^+ + NH_3 \longrightarrow NH_4^+ + C_2H_5O$	8.43
4	$C_2H_5O^+ + NH_3 \longrightarrow NH_4^+ + C_2H_4O$	4.73
5	$C_2H_3O^+ + NH_3 \longrightarrow NH_4^+ + C_2H_2O$	<0.5
6	$CHO^+ + NH_3 \longrightarrow NH_4^+ + CO$	11.2
7	$NH_3^+ + C_2H_6O \longrightarrow NH_4^+ + C_2H_5O$	9.37
	$CH_3CHO-NH_3$ mixture	
8	$C_2H_4O^+ + NH_3 \longrightarrow NH_4^+ + C_2H_3O$	12.0
9	$C_2H_3O^+ + NH_3 \longrightarrow NH_4^+ + C_2H_2O$	<0.5
10	$CHO^+ + NH_3 \longrightarrow NH_4^+ + CO$	11.1
11	$NH_3^+ + C_2H_4O \longrightarrow NH_4^+ + C_2H_3O$	4.37
	$C_2H_4O-NH_3$ mixture	
12	$C_2H_4O^+ + NH_3 \longrightarrow NH_4^+ + C_2H_3O$	<0.1
13	$C_2H_3O^+ + NH_3 \longrightarrow NH_4^+ + C_2H_2O$	<0.1
14	$CHO^+ + NH_3 \longrightarrow NH_4^+ + CO$	1.8
15	$NH_3^+ + C_2H_4O \longrightarrow NH_4^+ + C_2H_3O$	5.46
	CH_3OH-NH_3 mixture	
16	$CH_4O^+ + NH_3 \longrightarrow NH_4^+ + CH_3O$	34.0
17	$CH_3O^+ + NH_3 \longrightarrow NH_4^+ + CH_2O$	8.57
18	$CHO^+ + NH_3 \longrightarrow NH_4^+ + CO$	10.4
19	$NH_3^+ + CH_4O \longrightarrow NH_4^+ + CH_3O$	9.00

a) From Ref. 5).

where k_i is the rate constant for reaction (i), I_M the intensity of ion (m/e=M), [NH_3] and [CH_3OCH_3] are the concentrations of the reactant molecules, t is the delay time, and C_1 is a constant. Similar relations consisting of several reactions shown in Table 1 can be applied to the other systems investigated. By analysis of the results obtained under various impact electron energies and mixing ratios of reactant molecules, the rate constants of the reactions leading to the formation of NH_4^+ were determined and are shown in Table 1.

The rate constants for a proton transfer reaction from the parent ions to ammonia are strongly dependent on ion species: highest for methanol, lowest ($<1\times10^{-11}$ $cm^3mol^{-1}s^{-1}$) for ethylene oxide. Taking into account our experimental conditions, in which the reaction time did not exceed 2 μs, the very low reactivity of the $C_2H_4O^+$ ion from ethylene oxide is in agreement with the result observed for initially formed $C_2H_4O^+$[1] prior to the collisional modification. Another interesting result is that the CHO^+ ions derived from dimethyl ether, acetaldehyde, and methanol show a high reactivity of about 11×10^{-10} $cm^3mol^{-1}s^{-1}$, while the CHO^+ ion from ethylene oxide is less reactive. Since the proton transfer processes of CHO^+ and $C_2H_4O^+$ ions from ethylene oxide and acetaldehyde to ammonia are all quite exothermic, a simple thermochemical consideration cannot explain the low reactivities of CHO^+ and $C_2H_4O^+$ ions derived from ethylene oxide.

The fragment ions $CH_3OCH_2^+$ and CH_3O^+ react with significant rates to give NH_4^+ ion, while the $C_2H_3O^+$ ions are unreactive.

The rate constants for the hydrogen atom transfer reaction from oxygen-containing molecules to ammonia ion are less specific compared with those of the proton transfer reactions.

References

1) A. S. Blair and A. G. Harrison, *Can. J. Chem.*, **51**, 703 (1973).
2) J. L. Beauchamp and R. C. Dunbar, *J. Amer. Chem. Soc.*, **92**, 1477 (1970).
3) M. T. Bowers and P. R. Kemper, *ibid.*, **93**, 5352 (1971).
4) S. Okada, A. Matsumoto, T. Dohmaru, S. Taniguchi, and T. Hayakawa, *Mass Spectroscopy* (Japan), **20**, 311 (1972).
5) S. K. Gupta, E. G. Jones, A. G. Harrison, and J. J. Myher, *Can. J. Chem.*, **45**, 3107 (1967).
6) G. A. Derwish, A. Galli, A. Giardini-Guidoni, and G. G. Volpi, *J. Chem. Phys.*, **39**, 1599 (1963).
7) W. T. Huntress, Jr., and R. F. Pinizzotto, Jr., *ibid.*, **59**, 4742 (1973).

BULLETIN OF THE CHEMICAL SOCIETY OF JAPAN, VOL. 48 (11), 3389—3390 (1975)

Electronic Absorption Spectra of the Disulfone Radical Anion. Conjugative Effect of the Sulfone Group

Osamu Ito and Minoru Matsuda

Chemical Research Institute of Non-aqueous Solutions, Tohoku University, Katahira-2, Sendai 980

(Received April 24, 1975)

Synopsis. Disulfone radical anions produced by γ-irradiation show a characteristic absorption band at a longer wavelength region (655—695 nm) than that of the mono-sulfone radical anion (*ca.* 400 nm). The former band is attributed to the charge-resonance originated from the delocalization of an unpaired electron between the linked two sulfone moieties.

The radical anions containing the sulfone group show a pronounced conjugative effect through the sulfone group.[1] The effect was studied by means of the electron spin resonance. We showed that the measurement of the absorption spectrum is useful for elucidating the effect from the absorption band appearing in a longer wavelength region.[2] In this note, we report on our findings that the radical anions of disulfones ($R–SO_2–SO_2–R$) show an absorption band in a longer wavelength region (655—695 nm) than that of the mono-sulfone radical anions such as phenyl methyl sulfone (*ca.* 400 nm). It is expected that the band appearing in a longer wavelength region is related to the effective conjugation of the disulfone moieties.

Experimental

Di-*n*-hexyl disulfone[3] and diaryl disulfones[4] were synthesized by the reported methods. Radical anions containing sulfone moieties were produced by the γ-irradiation (^{60}Co: *ca.* 1 Mrad) of degassed methyltetrahydrofuran (MTHF) glassy solution at 77 K, since the disulfone radical anions formed by the alkali metal reduction were not stable.

Results and Discussion

It is expected that the disulfone radical anion can be produced by γ-irradiation according to the electron (e^-)-capture as follows:

$$MTHF \overset{\gamma}{\rightsquigarrow} MTHF^+ + e^- \quad (1)$$

$$e^- + R–SO_2–SO_2–R \longrightarrow (R–SO_2–SO_2–R)^- \quad (2)$$

A glassy blue solution, obtained by γ-irradiation of diphenyl disulfone, exhibited a strong absorption band at 695 nm and a weak band at 368 nm (Fig. 1a). As a possible species in the blue solution other than the disulfone radical anion, the benzene sulfonyl radical ($Ph–\dot{S}O_2$) might be produced by the direct scission of $–SO_2–SO_2–$ bond or by the dissociative electron attachment process:

$$e^- + R–SO_2–SO_2–R \longrightarrow R–\dot{S}O_2 + R–SO_2^- \quad (3)$$

However, the benzene sulfonyl radical, which can be produced by the UV-irradiation of diphenyl disulfone or benzene sulfonyl halides at 77 K, shows an absorption band at 382 nm. Thus, the absorption spectrum of the blue species (Fig. 1a) can be assigned to the diphenyl disulfone radical anion.

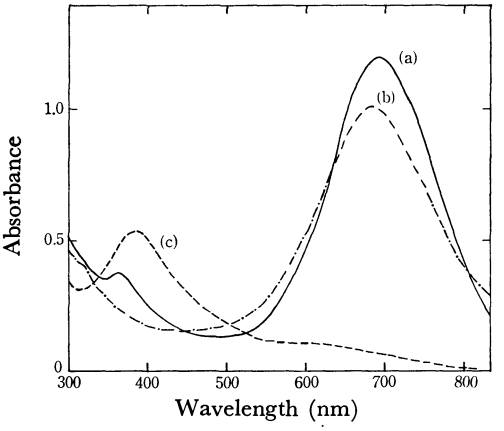

Fig. 1. Absorption spectra of the disulfone radical anions in MTHF at 77 K (5×10^{-3} mol/l in 2 mm cell); (a) diphenyl disulfone, (b) di-*n*-hexyl disulfone, and (c) phenyl methyl sulfone.

The radical anion of di-*n*-hexyl disulfone, an alkyl derivative of disulfone, was also produced by γ-irradiation. It shows a similar spectrum (Fig. 1b) to that of the diphenyl disulfone radical anion. This indicates that the electronic transitions of the disulfone radical anion appearing at *ca.* 690 nm are characteristic of two sulfone moieties and that the π-systems on the phenyl rings do not play an appreciable role in the transition. Moreover, the phenyl methyl sulfone ($Ph–SO_2–CH_3$) radical anion, a mono-sulfone, shows only one absorption band at 398 nm (Fig. 1c). An added electron to this mono-sulfone locates mainly on the sulfone moiety.[2] We see that, in the disulfone radical anion, the absorption band at *ca.* 690 nm results from the linked two sulfone moieties.

It is to be noted that the absorption spectra of the disulfone radical anions resemble those of the [2.2]paracyclophane radical anion (a strong band at 760 nm and a weak band at 360 nm) and biphenyl radical anion (two bands at 625 and 400 nm) as reported by Ishitani and Nagakura.[5] Their theoretical study of the [2,2]-paracyclophane and biphenyl radical anions indicates that the absorption bands appearing in a longer wavelength region than the benzene radical anion are assigned to the charge-resonance band originating from the delocalization of an unpaired electron between two phenyl rings. Thus, in the case of the disulfone radical anion, it can be suggested that the band appearing at *ca.* 690 nm has a charge-resonance character and that an added electron to disulfone is delocalized between the linked two sulfone moieties.

The absorption spectra of the disulfide radical anions

were reported by Shida.[6] Since the absorption band of the diphenyl disulfide radical anion appeared in the same region as that of the dialkyl disulfide radical anion (420—435 nm), he indicated that an unpaired electron added to disulfide is localized on the sulfur atoms. Although the diphenyl sulfide radical anion shows an absorption band in the same region as the diphenyl disulfide radical anion, the intensity of the band is reported to be very weak as compared with that of the disulfide.[7] Thus, there is a pronounced difference between the disulfide and disulfone radical anions; in the former the intensity of the band differs from that of mono-sulfide, and in the latter the position of the band differs from that of mono-sulfone. Since it is well established that the σ^*-orbital of the disulfide accepts an added electron, the different behavior in the spectra of the disulfone radical anion would be caused by the large π-character of O=S=O bond and/or large d-orbital participation on O=S=O bond.

Table 1. Absorption maxima of the diphenyl disulfone (X-C$_6$H$_4$-SO$_2$-SO$_2$-C$_6$H$_4$-X) radical anions

X	λ_1 (nm)	λ_2 (nm)
H–	695	368
CH_3–	665	366
CH_3O–	655	360

An abnormal shift by the substituents on the phenyl rings was observed in the absorption band appearing in a longer wavelength region (Table 1). When electron-donating substituents such as CH_3– and CH_3O– are introduced to *para*-positions, the absorption peaks shift towards shorter wavelength. In the case of the *para*-substituted diphenyl disulfide radical anions, however, an opposite tendency was observed by Miyashita, Iino and Matsuda (CH_3O–: 440 nm, CH_3–: 425 nm, and H–: 420 nm).[8] The red shift by the electron-donating substituents observed in the disulfide radical anions agrees with the well-known red shift of the substituted benzene molecules.[9] This is understandable if we assume that the transition energy of the charge-resonance band is approximately proportional to the electron density on each sulfone moiety, which might increase by the electron-donating substituents. Precise molecular orbital calculations might be necessary to elucidate the opposite substituent effect of the disulfone radical anions.

The authors are indebted to Mr. N. Tsuchihashi and Mr. K. Furukawa for their help in the γ-irradiation experiments.

References

1) M. M. Urberg and E. T. Kaiser, "Radical Ions," ed. E. T. Kaiser and L. Kevan, John Wiley & Sons, N. Y. (1968), p. 301.
2) O. Ito and M. Matsuda, *Chem. Lett.*, **1974**, 909.
3) P. Allen, Jr., L. S. Karger, J. D. Hygood, Jr., and J. Shrensel, *J. Org. Chem.*, **16**, 767 (1951).
4) T. P. Hilditch, *J. Chem. Soc.*, **93**, 1526 (1908).
5) A. Ishitani and S. Nagakura, *Mol. Phys.*, **12**, 1 (1967).
6) T. Shida, *J. Phys. Chem.*, **72**, 2597 (1968).
7) J. Wendenburg and H. Möckel, *Z. Naturforsch.*, **23b** 1171 (1968).
8) T. Miyashita, M. Iino, and M. Matsuda, unpublished data.
9) H. H. Jaffé and M. Orchin, "Theory and Applications of Ultraviolet Spectroscopy," John Wiley & Sons, N. Y. (1962), p. 242.

BULLETIN OF THE CHEMICAL SOCIETY OF JAPAN, VOL. 48 (11), 3391—3392 (1975)

Solvent Effect on the Dimerization of Tetracyanoquinodimethane Anion Radical

Tadayoshi SAKATA, Akihiro NAKANE,* and Hiroshi TSUBOMURA

Department of Chemistry, Faculty of Engineering Science, Osaka University, Toyonaka, Osaka 560

(Received May 12, 1975)

Synopsis. The thermodynamic quantities of the dimerization of tetracyanoquinodimethane (TCNQ) anion radical in water–ethanol mixtures were determined. The free energy of dimerization $-\Delta G$ showed a monotone decrease with an increase in ethanol content, whereas the enthalpy and the entropy of dimerization, $-\Delta H$ and $-\Delta S$, showed a maximum. This unusual behavior is explained by proposing a solvation model in which the water molecules are attracted more strongly around the $TCNQ^-$ dimer than are the ethanol molecules. The entropy was found to play an important role in the dimerization.

Dimerizations of organic ion radicals in solutions have been extensively studied.[1-7] The dimerization is strikingly influenced by the solvents. For example, the anion radical of tetracyanoquinodimethane ($TCNQ^-$) dimerizes strongly in water at room temperature, whereas it does not in ethanol even at 77K. In order to clarify this remarkable solvent effect we determined the thermodynamic quantities of dimerization of $TCNQ^-$ in the water–ethanol system.

Li^+TCNQ^-, Na^+TCNQ^-, and K^+TCNQ^- used in this experiment were prepared by the method described in the literature.[8] Deionized water and distilled ethanol were used. Since $TCNQ^-$ is easily oxidized by oxygen, all solutions were prepared and transferred to an absorption cell by using the vacuum line technique.

The equilibrium constant K for the dimerization was determined spectroscopically using the molar extinction coefficients of the monomer and dimer anions obtained by Boyd and Phillips.[2] The changes of the extinction coefficients in the mixed solvents were neglected, since the anions were found to exhibit the same spectral features up to 50 volume % of ethanol. The concentrations at various temperatures were corrected by use of the expansion coefficients for water and ethanol, assuming that the volume of the mixture is equal to the sum of the components.[9] The plots of log K *vs.* T^{-1} gave good straight lines, from which the change in enthalpy ΔH and that in entropy ΔS of the dimerization ($2A^- \rightleftarrows (A^-)_2$) were obtained.

Figure 1 shows the dependency of the thermodynamic quantities on the volume ratio of ethanol to water. The change in free energy $-\Delta G$ at 25 °C decreases with an increase in ethanol content throughout the range studied, whereas both $-\Delta H$ and $-\Delta S$ increase at first, reach a maximum at 30~40% ethanol, and then decrease. In the region where the ethanol content exceeds 50%, the dimer formation was found to be so scanty even at low temperatures (−50 °C~−60 °C) that the thermodynamic constants could not be determined. In the region of small ethanol content (<20%), the change

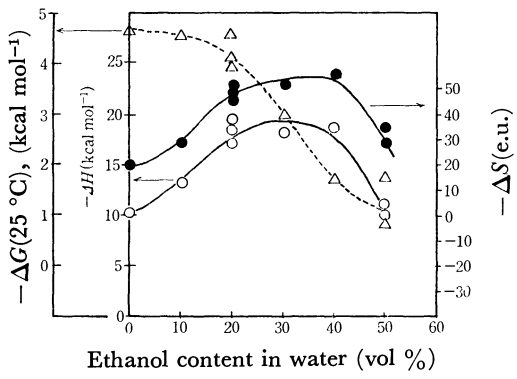

Fig. 1. Observed thermodynamic quantities for the dimerization of $TCNQ^-$ in the water–ethanol mixture.
△: $-\Delta G$(25 °C), ●: $-\Delta S$, ○: $-\Delta H$

in the enthalpy $-\Delta H$ with the ethanol concentration is opposite to that in the free energy $-\Delta G$. This behavior shows the important role of the entropy factor $T\Delta S$ in the free energy change $-\Delta G$ for the dimerization of $TCNQ^-$.

The presence of a maximum for $-\Delta H$ and $-\Delta S$ as seen in Fig. 1 is quite unusual,[10] and hard to explain by the usual understanding of the solvent polarization energy. By using Born's equation and dielectric constants for water and ethanol, the contributions of solvation in the $-\Delta H$ and $-\Delta S$ values can be calculated; the result shows a simple increase with an increase in ethanol content, and amounts to only 0.5 kcal mol^{-1} and 2.6 eu, respectively at 50% in ethanol content. Therefore, a model of a continuous and uniform medium cannot explain the experiment.

In order to understand this unusual behavior, we propose a simple model for the microscopic structure of the solvation sphere. The electrostatic field due to the dimer is considered to be must stronger than that of the monomer, because the charge of the dimer is twice as large as that of the monomer, and the effective radius is less than twice that of the monomer. Therefore, it attracts water molecules rather than ethanol ones into the solvation sphere more strongly than the monomer, since water is more polar than ethanol. Consequently, at small ethanol content, the ratio of the number of molecules in ethanol to that in water inside the solvation sphere may be lower than that in the bulk of the solution. The situation is illustrated schematically in Fig. 2. This will bring about more stabilization for the dimer anion than for the monomer anion, leading to larger $|\Delta H|$ values for the dimer formation. As the ethanol concentration becomes higher, this effect on ΔH and ΔS will diminish. Thus, the changes in enthalpies with the

* Present Address: Toray Co. Ltd., Minato-ku, Nagoya.

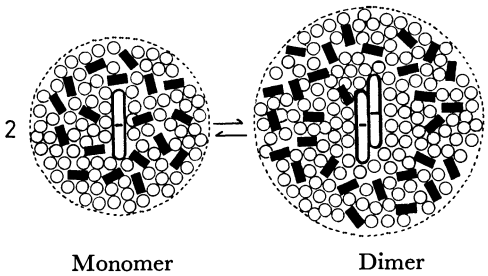

Fig. 2. Schematic illustration representing the enhanced participation of water molecules in the solvation sphere around the dimer compared to the monomer in the water–ethanol mixture.
○: water, ■: ethanol, (⊟): $TCNQ^-$.

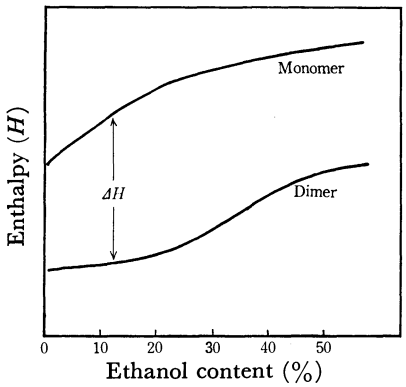

Fig. 3. Qualitative curves explain the behaviors of the enthalpies of the monomer and dimer in the water–ethanol mixture.

ethanol content for the dimer and monomer will be such as given qualitatively in Fig. 3, from which the appearance of a maximum for $-\Delta H$ in the monomer⇄dimer reaction can be understood. The appearance of a maxima in entropy $-\Delta S$ can be understood similarly.

The influence of counter cations on the thermodynamic quantities in the monomer⇄dimer reaction in water was also investigated. The result is that there is no essential difference in the thermodynamic quantities by changing the counter ions from Li^+ to Na^+ and K^+. No substantial change was detected for a solution containing LiCl 100 times more than the concentration of $TCNQ^-$. These results suggest that the counter ions exhibit a very small influence on the dimer-monomer equilibrium, and presumably they do not exist in a region very close to the anions in water.

References

1) K. H. Hausser and J. N. Murrell, *J. Chem. Phys.*, **27**, 500 (1975).
2) R. H. Boyd and W. D. Phillips, *ibid.*, **43**, 2927 (1965).
3) K. Uemura, S. Nakayama, Y. Seo, K. Suzuki, and Y. Ooshika, This Bulletin, **39**, 1348 (1966).
4) K. Kimura, H. Yamada, and H. Tsubomura, *J. Chem. Phys.*, **48**, 440 (1968).
5) K. Kimura, T. Yamazaki, and S. Katsumata, *J. Phys. Chem.*, **75**, 1768 (1971).
6) M. Itoh, This Bulletin, **45**, 1947 (1972).
7) S. Nakayama and K. Suzuki, *ibid.*, **46**, 3694 (1973).
8) L. R. Melbey, R. J. Harder, W. R. Hertler, W. Mahler, R. E. Benson, and W. E. Mochel, *J. Amer. Chem. Soc.*, **84**, 3374 (1962).
9) The errors arising from this approximation were estimated from the experimentally obtainable densities of water–ethanol mixtures, and are found to be within the experimental errors.
10) The same behaviors of the thermodynamic quantities were observed in the water–methanol system.

BULLETIN OF THE CHEMICAL SOCIETY OF JAPAN, VOL. 48 (11), 3393—3394 (1975)

Dipole Moments of the Iodine Compounds Complexed with Some Aliphatic Amines

Koichi TOYODA and Motoo IMAI*

Department of Chemistry, Faculty of Sciences, Kumamoto University, Kurokami-machi, Kumamoto 860

(Received May 13, 1975)

Synopsis. The dipole moments of some iodine compounds complexed with some aliphatic amines in benzene solution were obtained: 6.81D for EtH_2N–I_2; 6.78D for Et_2HN–I_2; 6.72D for Me_3N–ICl; 7.22D for Me_3N–IBr; 6.46D for Me_3N–ICN.

One of the present authors has recently reported the dipole moments of the electron-donor-acceptor (EDA) complexes between iodine and two aliphatic amines as follows: 12.4D in dioxane,[1] 6.78D in benzene,[2] 5.49D in cyclohexane,[2] for the triethylamine–iodine (Et_3N–I_2) complex, and 10.0D in dioxane,[1] 6.32D in benzene,[3] 5.25D in cyclohexane,[3] for the trimethylamine–iodine (Me_3N–I_2) complex. It was found that the experimental values of the dipole moments for these two complexes were strongly dependent on the solvents. The dipole moment of the Et_3N–I_2 complex was found to be time-dependent after mixing the two components. From the dipole moment of the Me_3N–I_2 complex in cyclohexane and the X-ray analysis data by Stroemme,[4] the contribution of the charge transfer (CT) structure in the ground state (b^2+abS) was evaluated to be about 0.30. Recently ESCA[5] and NQR[6] of pyridine–ICl (Py–ICl), for the gas phase and the solid state respectively, were measured. The charge distribution densities on each N, I, and Cl atoms has been directly evaluated from these data under certain assumptions. The dipole momemt measurement in solution at room temperature, however, is one of the most useful methods by which a direct measure for (b^2+abS) could be supplied. (b^2+abS) is one of the most basic constants of EDA complexes. The importance of the complex as a typical example is so great that extra efforts to obtain accurate data are justified.

Experimental

Cyclohexane, benzene, iodine, and Me_3N were purified by the method reported previously.[2,3] Ethylamine(EtH_2N) and diethylamine (Et_2HN) were purified by Nagakura's method.[7] ICl and IBr were prepared by the methods reported by Cornog and Karges,[8] and Popov and Skelly,[9] respectively. ICN, which was prepared by the method of Bak and Hillebert,[10] was colorless and melted at 145 °C in a sealed capillary. The apparatus for the measurements of dielectric constants, the picnometer for the measurements of densities, and the procedure of handling have been reported previously.[2] The temperature was kept constant at 25.00±0.05 °C or 20.00±0.05 °C throughout the series of measurements. The dipole moment of nitrobenzene obtained by means of this apparatus was 4.03D in a benzene solution at 25 °C. In each series of measurements, benzene solutions containing a fixed concentration of the amines and various concentrations of iodine, ICl, IBr, and ICN were used. The concentrations of the iodine compounds ranged from 0 to 1.8×10^{-3} mol/l in the benzene solution and did not exceed a tenth of that of amine in the solution. The dipole moments of the complexes were obtained by use of the Kobinata-Nagakura method.[11]

Results and Discussion

The experimentally observed dielectric constants (ε_{123}) and the densities (d_{123}) of the solutions were found to be linearly dependent upon the weight fractions (w_3) of the molecular complexes, as previously described.[2,3] The dipole moments of the complexes were evaluated from the slopes of these lines using only the first term of the Kobinata-Nagakura equation.[11] In spite of the low concentrations of the complexes, which were $(1.5-6)\times10^{-3}$ for EtH_2N–I_2 and $(1.8-7)\times10^{-3}$ for Et_2HN–I_2 in weight fraction and corresponded to about a tenth of the values in Nagakura's experiments,[11] the same results were obtained. As seen in Table 1, the dipole moments of the complexes increased with an increase in the amine concentration in a mixed solvent containing benzene and amine.

For the complexes between Me_3N and ICl, IBr, or ICN the dipole moments in benzene solution are presented in Table 1. The measurements in cyclohexane and hexane solution gave dispersed plots because the solubility in these solvents was a tenth of that in benzene. The geometries of the Et_2HN–I_2 and EtH_2N–I_2 complexes were assumed to be the same as that of Me_3N–I_2 by Nagakura *et al.*[11] Thus μ_1 was estimated to be 17.7D in the equation, $\mu_N=\mu_1(b^2+abS)$.[12] The X-ray diffraction study of Me_3N–ICl has been already reported

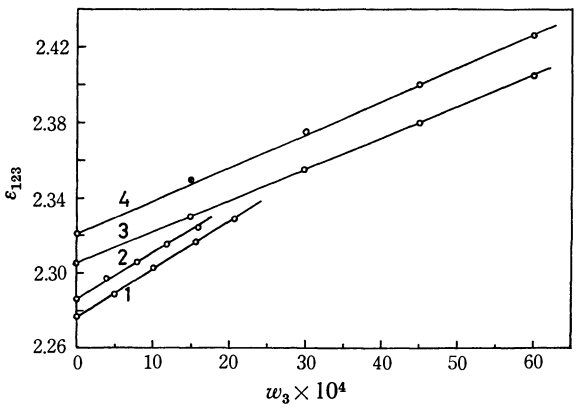

Fig. 1. The relation between the dielectric constant of benzene solutions (ε_{123}) and the weight fraction of complexes (w_3); (1) Me_3N–ICl; (2) Me_3N–ICN; (3) Et_2HN–I_2; (4) EtH_2N–I_2.

* Present address: Idemitzu Kosan Central Research Institute, Analytical Laboratory, Sodegaura-cho, Chiba-ken 299-02.

Table 1. Dipole moments (μ_N in debye units) and dielectric constants of mixed solvents (ε_{12})

Complex	Solvent	t°C	μ_N	ε_{12}	b^2+abS I[a]	b^2+abS II[b]
EtH_2N-I_2	benzene	20	6.67	2.3235	0.38	
			6.72	2.3590	0.38	
			6.76	2.3309	0.38	
			7.10	2.4350	0.40	
Et_2HN-I_2	benzene	20	6.60	2.3100	0.37	
			6.86	2.3050	0.39	
			6.89	2.3383	0.39	
Me_3N-ICl	benzene	25	6.42	2.2798	0.38	0.28
			6.82	2.2804	0.40	0.30
			6.92	2.2812	0.41	0.30
Me_3N-IBr	benzene	20	7.21	2.2869	0.42	0.31
			7.23	2.2885	0.42	0.31
Me_3N-ICN	benzene	20	6.43	2.2880		
			6.46	2.2890		
			6.50	2.2886		
$Py-I_2$[c]	cyclohexane		4.50		0.25	

a) Assuming that a negative charge is located on the center of the I–X molecule. b) Assuming that a negative charge is located on the X-atom of the I–X molecule. c) C. Reid and R. S. Mulliken, *J. Amer. Chem. Soc.*, **76**, 3869 (1954).

by Hassel *et al*,[13] in which the bond lengths of I–Cl and N–I were 2.52Å and 2.30Å, respectively. Then the estimated values of (b^2+abS) are shown in Table 1. The assumption was made that μ_1 of Me_3N-IBr was equal to μ_1 of Me_3N-ICl. According to the NQR study on solid Py–ICl by Hanna *et al*,[6] negative charge concentrates upon the Cl atom. Assuming that the positive charge concentrates upon the N atom, the (b^2+abS) values are obtained; these are shown in II of Table 1.

Several authors[14,16] have recently pointed out the importance of the induced polarization in the observed dipole moments of the molecular complexes. The (b^2+abS) values in Table 1, however, are estimated by the conventional procedure without giving any allowance for the polarization effects. The amounts of charge transfer Δq at the Py–ICl complex were estimated to be 0.1 for the gas phase by the ESCA[5] and 0.16 for the solid state by the NQR.[6] The (b^2+abS) in the solid state, in general, gives larger values than in the gas phase.[15] Δq obtained by the ESCA and NQR for the Py–ICl complex are the same order to the ionic character, which was estimated by considering the dipole moments of the two components in the $Py-I_2$ complex. These experimental Δq's were quite large as compared with those calculated (Δq, 0.018) for the NH_3-I_2 complex[16] by the MINDO/2.

References

1) K. Toyoda and W. B. Person, *J. Amer. Chem. Soc.*, **88**, 1629 (1966).
2) A. Funatsu and K. Toyoda, This Bulletin, **43**, 279 (1970).
3) H. Mihono and K. Toyoda, *ibid.*, **44**, 272 (1971).
4) K. O. Stroemme, *Acta Chem. Scand.*, **13**, 268 (1959).
5) A. Mostad, S. Svensson, R. Nilsson, E. Basilier, U. Gelius, C. Nordling, and K. Siegbahn, *Chem. Phys. Lett.*, **23**, 157 (1973).
6) H. C. Fleming and M. W. Hanna, *J. Amer. Chem. Soc.*, **93**, 5030 (1971).
7) H. Yada, J. Tanaka, and S. Nagakura, This Bulletin, **33**, 1660 (1960).
8) J. Cornog and R. A. Karges, "Inorganic Syntheses," Vol. 1, McGraw-Hill Book Co., Inc., New York, N. Y. (1939), p. 165.
9) A. I. Popov and N. E. Skelly, *J. Amer. Chem. Soc.*, **77**, 3722 (1955).
10) B. Bak and A. Hillebert, "Organic Syntheses," Vol. 32, (1952), p. 29.
11) S. Kobinata and S. Nagakura, *J. Amer. Chem. Soc.*, **88**, 3905 (1966).
12) R. S. Mulliken, *ibid.*, **74**, 811 (1952).
13) O. Hassel and H. Hope, *Acta Chem. Scand.*, **14**, 391 (1966).
14) M. W. Hanna, *J. Amer. Chem. Soc.*, **90**, 285 (1968). M. Manitone, *Theoret. Chim. Acta*, **11**, 119 (1968).
15) J. Yarwood and W. B. Person, *J. Amer. Chem. Soc.*, **90**, 594, 3930 (1968).
16) T. Ohta, T. Fujikawa, and H. Kuroda, This Bulletin, **47**, 2115 (1974).

BULLETIN OF THE CHEMICAL SOCIETY OF JAPAN, VOL. 48 (11), 3395—3396 (1975)

Mechanism of the Acceleration Effect of 1,10-Phenanthroline on the Rate of Color Change of Xylenol Orange in the Chelatometric Titration of Nickel(II)

Teisuke MURAYAMA and Michio TAKEMURA

Department of Industrial Chemistry, Faculty of Engineering, Shizuoka University, Johoku, Hamamatsu 432

(Received April 4, 1975)

Synopsis. The effect in the title was studied kinetically. Experimental results indicate that the color change reaction in the presence of 1,10-phenanthroline proceeds according to a mechanism proposed by Nakagawa and Wada.

It is essential for a metallochromic indicator to be released rapidly from the metal-indicator complex at the equivalence point in the chelatometric titration of the metal. The lack of this property causes a sluggish color change at the equivalence point, and introduces a titration error.

Because Xylenol Orange (XO) forms an inert complex with copper(II) or nickel(II), its color change is slow in direct titrations of these metals with EDTA. Pribil observed that the rate of the XO color change was markedly improved by addition of a small amount of 1,10-phenanthroline (phen) in the titration of copper.[1] He explained this effect by supposing a reaction scheme comprised of two rapid substitution reactions:

$$MI + X = MX + I \quad (1)$$

$$MX + Y = MY + X \quad (2)$$

where M is the metal ion, I the indicator, X an auxiliary complex-forming agent (namely, phen in this case), and Y a chelatometric titrant (namely, EDTA in this case).

Recently Nakagawa and Wada published results of an extensive study on effects of auxiliary complex-forming agents on the rate of color change of metallochromic indicators, and criticized Pribil's explanation on the ground of the smallness of the stability constant difference between copper-XO and copper-phen complexes.[2] They proposed another reaction scheme involving a mixed ligand complex.

$$MI + X = MIX \quad (3)$$

$$MIX + Y = MY + I + X \quad (4)$$

They, however, did not supply any kinetic data supporting this scheme.

The purpose of the present study is to examine the two schemes kinetically in the case of the titration of nickel(II).

Experimental

All chemicals used were of reagent grade, and all solutions were prepared with redistilled water. A standard solution of disodium salt of EDTA and stock solutions of XO and phen were prepared by dissolving weighed amounts. The concentration of nickel sulfate solution was determined by titration with the standard solution of EDTA, where murexide was used as indicator.[3] Acetate buffers of pH 4.54 to 5.33 were used for the control of hydrogen ion concentration of the reaction mixtures.

A solution of 50 ml was prepared by mixing nickel sulfate, XO, phen, an acetate buffer, and EDTA of insufficient amount to be equivalent to the amount of nickel sulfate, and by filling to the mark with water. The concentration of nickel sulfate was prepared to be 5.00_0 mM, and the ionic strength of the solution was controlled to 0.2. The solution, in a measuring flask, was placed in a thermostat kept at 25 °C. After equilibration a meaured volume (0.17 to 0.46 ml) of the EDTA solution was added to the solution to make the concentration of EDTA to be 1% excess of nickel sulfate. This was rapidly followed by thorough mixing and transfer of the solution into a quartz cell with light path of 10 mm. The change of transmittance of the solution with time was followed by a Hitachi Model 101 spectrophotometer, its cell compartment being kept at 25.0 °C. The transimittance was measured at 582 nm, where the nickel-XO complex showed an absorption peak and the free XO did not absorb to any appreciable degree.

Results and Discussion

The rate of the substitution reaction of the nickel-XO complex with EDTA follows the second-order rate law both in the presence and in the absence of phen, as shown in Fig. 1, where a and b are the initial concentrations of the nickel-XO complex and EDTA, respectively, and $(a-x)$ and $(b-x)$ are the concentrations of the respective species at time t.* Although the rate constant in the presence of phen, k_1, and that in the absence of phen, k_2, were both susceptible to the influence of con-

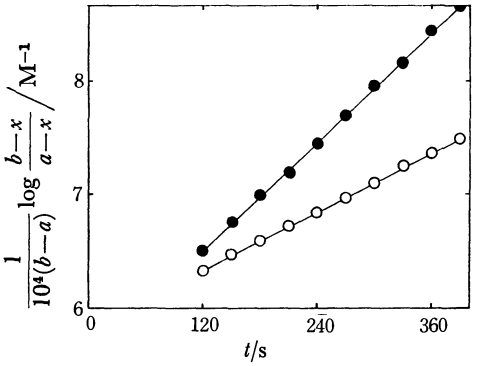

Fig. 1. Second-order rate plots of the substitution reaction of the nickel-XO complex with EDTA. pH of reaction mixtures, 4.92. Concentration of XO, 5.0 μM. Concentration of EDTA added just at the start, $20._0$ μM. Concentration of phen: ○, 0 μM; ●, 1.0 μM.

* XO, EDTA, and phen in solutions can exist in forms with different numbers of protons. Concentrations of these species were calculated, however, irrespective of the number of protons because the concentration of hydrogen ions had no influence on (k_1-k_2), about which we are concerned.

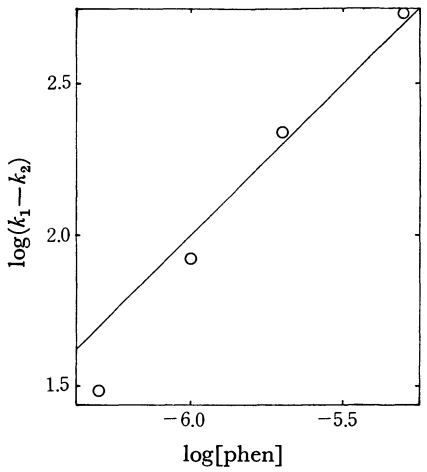

Fig. 2. Dependence of log (k_1-k_2) on log[phen]. The solid line is a straight line with a slope of 1. Units of [phen] and (k_1-k_2) are M and M^{-1} s^{-1}, respectively. pH of reaction mixtures, 4.92. Concentration of XO, 5.0 μM. Concentration of EDTA added just at the start, $30._0$ μM.

centrations of hydrogen ions and XO, the difference (k_1—k_2) was not. This difference, representing the acceleration effect of phen, varies with the first power of the concentration of phen, as shown in Fig. 2.

In Pribil's scheme the rate-determining step may be either Reaction (1) or (2). Neither case leads to the second-order rate law described above. Nakagawa-Wada's scheme, on the other hand, can satisfy this rate law if Reaction (6) is the rate-determing step as given by

$$MI + X \overset{K}{\rightleftharpoons} MIX \quad (5)$$

$$MIX + Y \overset{k}{\longrightarrow} MY + I + X \quad (6)$$

and if the equilibrium constant K is so small as to fulfill the relation $[X] \gg [MIX]$. Under these conditions the rate is written as

$$\text{rate} = kK[X][MI][Y] \quad (7)$$

which agrees with experimental observations. Hence Nakagawa-Wada's mechanism works in the case of titration of nickel(II).

References

1) R. Pribil, *Talanta*, **3**, 91 (1959).
2) G. Nakagawa and H. Wada, *ibid.*, **20**, 829 (1973).
3) G. Schwarzenbach, "Complexometric Titrations," Methuen, London (1957), p. 80.

BULLETIN OF THE CHEMICAL SOCIETY OF JAPAN, VOL. 48 (11), 3397—3398 (1975)

The Phase Transition of Bismuth(III) Oxide Prepared by the Thermal Decomposition of Bismuth Sulfate

Ryoko MATSUZAKI, Hagio MASUMIZU, and Yuzo SAEKI

Research Laboratory of Resources Utilization, Tokyo Institute of Technology, Ookayama, Meguro-ku, Tokyo 152

(Received April 16, 1975)

Synopsis. The phase transitions of α-Bi_2O_3 prepared by the thermal decomposition of $Bi_2(SO_4)_3$ on heating and cooling are revealed. The phase transition on cooling is remarkably affected by the existence of a small amount of SO_4, such as 0.05%, in the Bi_2O_3.

The phase transition of α-Bi_2O_3 (monoclinic[1]), prepared by the thermal decomposition of $Bi_2(SO_4)_3$, has been examined with special attention paid to the effect of a small amount of SO_4 in the Bi_2O_3 on its phase transition.

The $Bi_2(SO_4)_3$ used as the starting material was prepared by dissolving high-purity commercial bismuth (Bi: 99.9999%) in HNO_3, followed by treatment with an excess of H_2SO_4.[2] Two samples of α-Bi_2O_3 were obtained as follows.

Sample A: According to a previous report of the present authors,[2] α-Bi_2O_3 was prepared by heating 15 g of $Bi_2(SO_4)_3$ placed in a platinum boat at 950 °C for about 130 hr in an argon stream. The SO_4 in the product was not detected by the indirect determination of a small amount of SO_4^{2-} using solid barium chromate.[3]

Sample B: Bi_2O_3 was prepared by heating $Bi_2(SO_4)_3$ at 950 °C for about 110 hr. The SO_4 content in the product was 0.05%. X-Ray analysis showed it to be α-Bi_2O_3.

The phase transitions of Bi_2O_3 on heating and cooling were examined by DTA. The heating and cooling rates of 5 °C/min were employed. Sample holders made of platinum were used, and α-Al_2O_3 was used as a reference. The accuracy of the temperature measurements was ±4 °C. The experimental results of DTA were followed by high-temperature X-ray diffractometry in order to examine the phase transition of Bi_2O_3. Ni-filtered Cu radiation was used, and the scanning speed of 2°/min was employed. The details of the techniques of DTA and high-temperature X-ray diffractometry were described in a preceding paper.[4]

The phase transitions of Samples A and B on heating were examined. The experimental results showed that both samples transformed to δ-Bi_2O_3 (cubic[5]) at 730 °C, which then melted at 827 °C. The phase transitions of Samples A and B on heating were the same as those of the α-Bi_2O_3 prepared by the thermal decompositions of $Bi(NO_3)_3 \cdot 5H_2O$, $(BiO)_2CO_3$, and bismuth nitrate oxide.[4]

The phase transitions of Samples A and B on cooling from temperatures of 740—890 °C were examined. The results for Sample A are shown in Table 1. The peak temperature of the DTA curve is shown as the transition temperature. When the DTA curve showed a supercooling effect and the peak temperature became higher than the temperature at which the exotherm started, the latter is shown as the transition temperature and is marked with an asterisk.

Table 1. Phase transition of sample A on cooling (Cooling rate: 5 °C/min)

Temperature before cooling (°C)	Phase transition
740	$\delta \xrightarrow{702°C} \alpha$
750	$\delta \xrightarrow{695°C} \alpha$
760	$\delta \xrightarrow{648°C*} \alpha$
770	$\delta \xrightarrow{650°C} \beta \xrightarrow{545°C*} \alpha$
800	$\delta \xrightarrow{648°C} \beta \xrightarrow{545°C*} \alpha$
810	$\delta \xrightarrow{650°C} \beta \xrightarrow{547°C*} \alpha$
840	melt $\longrightarrow \delta \xrightarrow{637°C} \beta \xrightarrow{503°C*} \alpha$
860	melt $\longrightarrow \delta \xrightarrow{635°C} \beta \xrightarrow{500°C*} \alpha$
880	melt $\longrightarrow \delta \xrightarrow{635°C} \beta \xrightarrow{500°C*} \alpha$
890	melt $\longrightarrow \delta \xrightarrow{625°C*} \alpha$

Note: Temperature accuracy, ±4 °C

The experimental results given in Table 1 show that the variation in the phase transition of Sample A with the temperature before cooling was similar to those of Bi_2O_3 prepared from $Bi(NO_3)_3 \cdot 5H_2O$, $(BiO)_2CO_3$, and bismuth nitrate oxide.[4,7]

The results for Sample B, which are shown in Table 2, were compared with those for Sample A shown in Table 1. The phase transitions of Sample B on cooling from

Table 2. Phase transition of sample B on cooling (Cooling rate: 5 °C/min)

Temperature before cooling (°C)	Phase transition
740	$\delta \xrightarrow{698°C} \alpha$
760	$\delta \xrightarrow{650°C*} \alpha$
770	$\delta \xrightarrow{640°C} \beta \xrightarrow{525°C*} \alpha$
780	$\delta \xrightarrow{640°C} \beta \xrightarrow{525°C*} \alpha$
800	$\delta \xrightarrow{642°C} \beta \xrightarrow{523°C*} \alpha$
810	$\delta \xrightarrow{645°C} \alpha$
840	melt $\longrightarrow \delta \xrightarrow{630°C} \alpha$
860	melt $\longrightarrow \delta \xrightarrow{632°C} \alpha$
890	melt $\longrightarrow \delta \xrightarrow{630°C} \alpha$

Note: Temperature accuracy, ±4°C

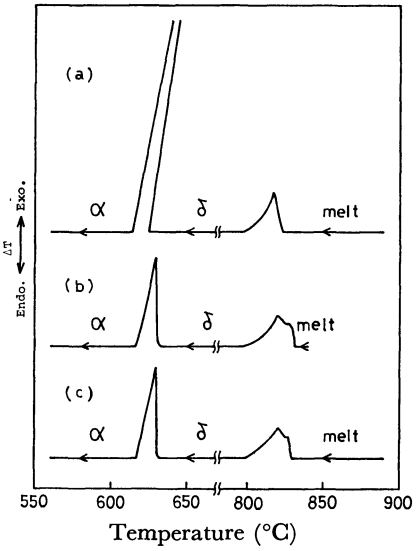

Fig. 1. DTA curves for the melt→δ→α transitions of Samples A and B
(a): Sample A on cooling from 890 °C
(b): Sample B on cooling from 840 °C
(c): Sample B on cooling from 890 °C

temperatures below 800 °C were the same as those of Sample A. However, the transition temperatures of δ→β and β→α for Sample B were lower than those for Sample A. When Sample B was allowed to cool from temperatures above 810 °C, δ-Bi_2O_3 transformed directly to α-Bi_2O_3 without passing through β-Bi_2O_3, regardless of the temperature before cooling. On the other hand, the phase transition of Sample A was dependent on the temperature before cooling, and the melt→δ→α transition occurred when Sample A was allowed to cool from 890 °C. This is the most remarkable difference between the phase transitions of Samples A and B.

The DTA curves observed when the melt→δ→α transitions occurred in Samples A and B are shown in Fig. 1.

By comparing the observations of Sample A (Fig. 1 (a)) with those of Sample B(Fig. 1(b), (c)), it was found that the DTA curve for the δ→α transition of Sample A showed a marked supercooling effect, which caused the sample temperature to increase remarkably. On the other hand, no such supercooling effect was observed in the DTA curve for the δ→α transition of Sample B. It was roughly estimated that the area of the exothermic peak due to the δ→α transition of Sample B was about one-fourth of that of Sample A. Also, the exothermic peak representing the solidification of Sample B had a shoulder. These differences may be due to the existence of SO_4 in Sample B.

The above-mentioned experimental results revealed that the phase transition of Bi_2O_3 on cooling was remarkably affected by the existence of a small amount of SO_4, such as 0.05%, in the Bi_2O_3.

References

1) ASTM card, 14-699.
2) R. Matsuzaki, A. Sofue, H. Masumizu, and Y. Saeki, *Chem. Lett.*, **1974**, 737.
3) I. Iwasaki, S. Utsumi, K. Hagino, T. Tarutani, and T. Ozawa, *Nippon Kagaku Zasshi*, **79**, 32 (1958).
4) R. Matsuzaki, A. Sofue, and Y. Saeki, *Nippon Kagaku Kaishi*, **1973**, 491.
5) ASTM card, 16-654.
6) ASTM card, 18-244.
7) R. Matsuzaki, H. Masumizu, and Y. Saeki, *Denki Kagaku*, **42**, 578 (1974).

BULLETIN OF THE CHEMICAL SOCIETY OF JAPAN, VOL. 48 (11), 3399—3400 (1975)

A Kinetic Study on the Complex Formation of Iron(III) with *o*-Cresolsulfonphthalein: A Quinoidal Complex*

Hiroaki NAKAYAMA** and Masatoshi FUJIMOTO
Department of Chemistry, Faculty of Science, Hokkaido University, Sapporo 060
(Received May 22, 1975)

Synopsis. The kinetics of the 1: 1 complex formation of Fe(III) with *o*-Cresol Red is studied. The reaction scheme is quite different from that for the monophenolato complexes of Fe(III), and interpreted by the formation of a quinoidal complex.

A pH indicator *o*-Cresolsulfonphthalein, *o*-Cresol Red (abbr. CR), is a phenolic and quinoidal ligand with conjugated π-systems and hardly behaves as a chelating agent. It is interesting to note whether the given ligand forms a phenolato complex or a quinoidal complex with tervalent iron, and in what mechanism it reacts with the metal ion in comparison with monophenols.[1]

Experimental

Reagent grade *o*-Cresol Red (Wako), which gave only one spot on paper chromatogram,[2] was used. Other reagents and apparatus were described in detail in a previous report.[1]

Kinetic measurements were performed in aqueous perchlorate media of $\mu=0.1$ and at 25.0 ± 0.2 °C. Analytical concentration of the ligand, C_{CR}, was kept at 1.00×10^{-4} M. C_{Fe} was changed from 3.62 to 51.2×10^{-3} M. Hydrogen-ion concentration [H] was calculated from the observed pH value without correction of the activity coefficients. Absorbance change was followed at 580 nm, where the absorption of the ligand was weak.

Results and Discussion

Owing to the strong absorption band of the ligand chromophore in the visible region[3] it was rather difficult to obtain the absorption spectra of the unstable complex of Fe(III) with Cresol Red except for the distinct increase in absorbance at 550—600 nm in the tail region of the absorption band of the ligand. Observed difference spectra are shown in Fig. 1.

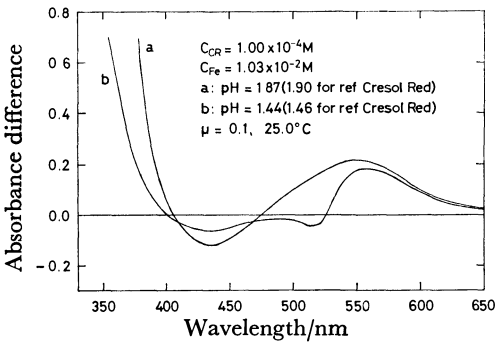

Fig. 1. Difference spectra between Fe(III)-Cresol Red and Cresol Red.

Formation constant of the complex could not be determined by the usual spectrophotometric method, since some slow side-reactions[5] involving the decomposition of the ligand ensued. At 580 nm, however, pseudo-first-order relaxation curves were obtained for the fast reaction process under the conditions of a large excess of Fe(III). Following discussions are concerned with this fast process regarded as the complex formation.

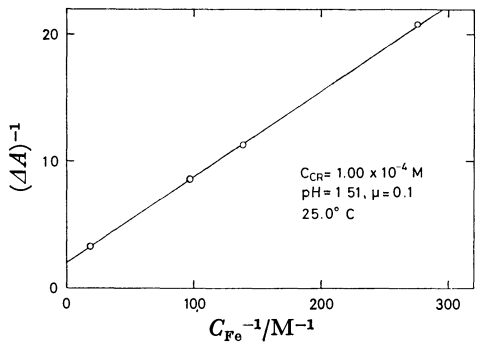

Fig. 2. Plot of $1/\Delta A$ at 580 nm *vs.* $1/C_{Fe}$.

Apparent rate constant k_{obsd} decreased with increasing [H]. It showed no significant change through more than ten-fold change in C_{Fe}. Absorbance changes, ΔA, on the complex formation were obtained from the difference in absorbance in the stopped-flow signals.[6] The values of ΔA showed no significant dependence on [H], but depends on C_{Fe} (see Fig. 2). Scheme 1 is proposed to account for these results. It clearly contrasts with the Scheme 2 for the complex formation between Fe(III) and monophenols (HA).[1]

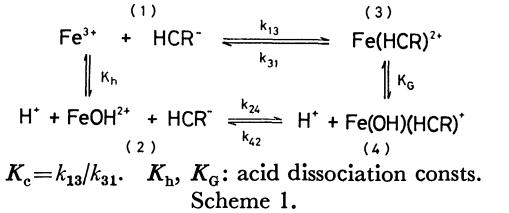

$K_c=k_{13}/k_{31}$. K_h, K_G: acid dissociation consts.

Scheme 1.

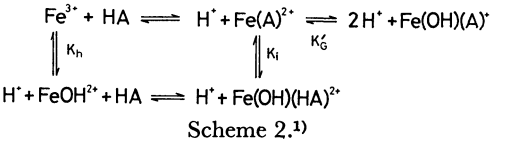

Scheme 2.[1]

The predominant species after the fast complex formation reached equilibrium may be Fe^{3+}, HCR^-, and $Fe(HCR)^{2+}$. The following approximate equation is derived:

$$1/\Delta A = (1+1/C_{Fe}\cdot K_c)/\Delta\varepsilon\cdot C_{CR},$$

$$\Delta\varepsilon = \varepsilon_{FeHCR} - \varepsilon_{HCR},$$

where ε_{FeHCR} and ε_{HCR} denote the apparent molar ex-

* Presented in part at the 1971 Winter Meeting in Hokkaido of the Chemical Society of Japan and the Japan Society for Analytical Chemistry, Sapporo, February, 1971.

** Present address: Kagawa Nutrition College, Sakado-machi, Saitama.

tinction coefficient at 580 nm, and $K_C=[Fe(HCR)^{2+}]/[Fe^{3+}][HCR^-]$. Thus ΔA becomes independent of [H]. The linear plot of $(\Delta A)^{-1}$ *versus* C_{Fe}^{-1} as shown in Fig. 2 confirms that only 1 : 1 complex formation is concerned. From the slope and the intercept,[7] $\Delta\varepsilon=5.05\times10^3$ $M^{-1}cm^{-1}$ and $K_C=29.3$ M^{-1}.

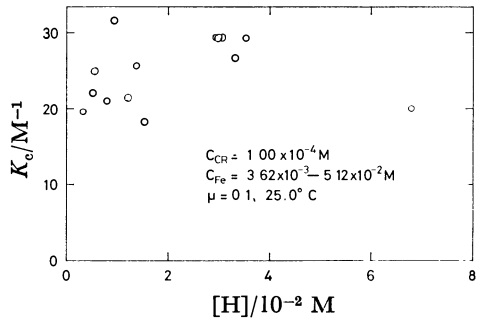

Fig. 3. Apparent stability constants K_c calculated from the absorbance change in the stopped-flow signals.

Spectrophotometric measurement gave $\varepsilon_{HCR}\leqq170$ so that ε_{FeHCR} is 5.2×10^3 $M^{-1}cm^{-1}$. Assuming the one-step mechanism[8] and the equilibrium for very fast proton transfer during the relaxation process, we obtained

$$k_{obsd}\simeq k_fC_{Fe}+k_r,$$

$$k_f=([H]k_{13}+K_hk_{24})/([H]+K_h)$$

and

$$k_r=([H]k_{31}+K_Gk_{42})/([H]+K_G).$$

Here, k_{obsd} was independent of C_{Fe}, so that $k_{obsd}=k_r$. Considering the Coulombic factor in the dissociative process, we assumed that $[H]k_{31}\ll K_Gk_{42}$, giving the approximation

$$k_{obsd}^{-1}\simeq[H]/K_G\cdot k_{42}+1/k_{42}.$$

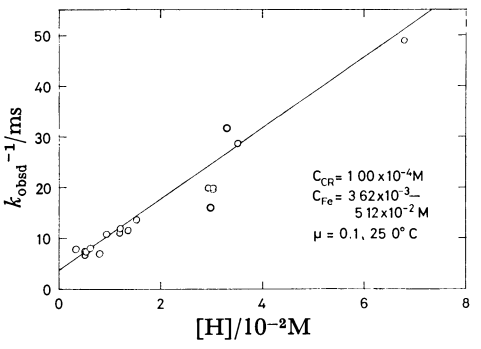

Fig. 4. Plot of $1/k_{obsd}$ *vs.* hydrogen-ion concentration.

A plot of k_{obsd}^{-1} *versus* [H] gave a straight line (Fig. 4). From the slope and the intercept, $k_{42}=270$ s^{-1} and $K_G=5.6\times10^{-3}$ M. An anionic ligand HCR^- thus may be a comparably weak donor as H_2O, for the K_G is in the same order of magnitude as K_h (4.1×10^{-3} M).[9] The rate constant k_{24} was calculated from the given data to be $k_{24}=(K_GK_C/K_h)\cdot k_{42}=1.1\times10^4$ $M^{-1}s^{-1}$. This value is similar to the complex formation rate for Br^- and $Fe(OH)^{2+}$,[10] and significantly larger than that for monophenols and $Fe(OH)^{2+}$ (1×10^3 $M^{-1}s^{-1}$).[1,11] Thus, the experimental results are consistently interpreted on the basis of the Scheme 1, regarding k_{obsd} as k_r.

Though the following Path I is postulated in the Scheme 1, another intermediate $Fe(CR)^+$, which is isoprotonic to $Fe(OH)(HCR)^+$, can also be taken into

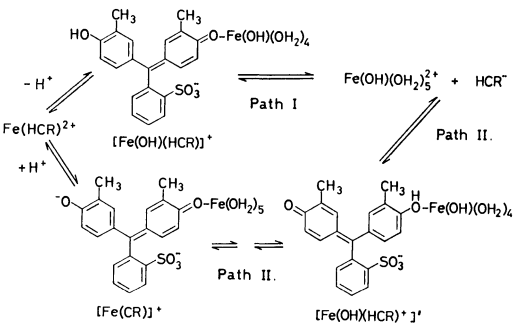

consideration (Path II). Going along the dissociative process, electronic configuration change of $Fe(CR)^+$ followed by intramolecular proton transfer results another isoprotonic intermediate $[Fe(OH)(HCR)^+]'$, which readily releases HCR^-. The observed K_G value is, however, only slightly larger than K_h and much larger than the acid dissociation constant of HCR^-. It is thus approved that the observed K_G concerns rather with the coordinated water than the phenolic hydroxyl group, though the coordination of quinoidal oxygen to Fe(III) may increase the dissociation of phenolic proton. Moreover, Path I is more favorable than Path II for the complex formation process when the charge densities on the two oxygen atoms of the ligand are considered.[12]

Temperature dependence of k_{obsd} was investigated at pH 1.81 and $C_{Fe}=1.65\times10^{-2}$ M. Apparent activation energy was found to be 68.81 $kJ\cdot mol^{-1}$.

References

1) K. Nakamura, T. Tsuchida, A. Yamagishi, and M. Fujimoto, This Bulletin, **46**, 456 (1973).

2) Y. Kawai, T. Takahashi, K. Hayashi, T. Imamura, H. Nakayama, and M. Fujimoto, *ibid.*, **45**, 1417 (1972).

3) Molar extinction coefficient of HCR^- at 435 nm (ε_{max}) was reported to be 1.80×10^4 M^{-1} cm^{-1}.[4]

4) M. Murakami, T. Yoshino, and S. Harasawa, *Talanta*, **14**, 1293 (1967).

5) At 435 nm the difference of the absorbance decreased monotonously, at 550 nm once increased and then decreased, and at 500 nm showed complicated feature.

6) Dead time of the stopped-flow apparatus was 1.7 ± 0.2 ms. In the present experiment absorbance may be estimated too small in the case of lower [H], with $k_{obsd}^{-1}=7$ ms.

7) Using the intercept value 1.98, each set of C_{Fe} and ΔA derives the value of K_c, which is plotted against [H] (Fig. 3).

8) Two-step mechanism involving a very stable intermediate gives k_{obsd} which is independent of C_{metal} and is concerned with the formation process. See Eq. (2) in Ref. 2.

9) R. M. Milburn and W. C. Vosburgh, *J. Amer. Chem. Soc.*, **77**, 1352 (1955).

10) P. Matthies and H. Wendt, *Z. Physik. Chem., N. F.*, **30**, 137 (1961).

11) According to the authors' mind the pre-equilibrium constants[2] for the ion-pair formation, which depend mainly on the charges and the radii of the solvated species involved, may characterize the complex formation rate constants of $Fe(OH)^{2+}$ with various ligands.

12) The possibility of the direct protolytic transformation between species $[Fe(OH)(HCR)]^+$ (A) and $[Fe(OH)(HCR)^+]'$ (B) is assumed to be quite small, since the contribution of the intervening resonance forms involving an intermediate protonated quinoid cation to the proton transfer between A and B is lowered because of the propeller-like distortion of the π-systems in the benzene and the quinoidal ring.

BULLETIN OF THE CHEMICAL SOCIETY OF JAPAN, VOL. 48 (11), 3401—3402 (1975)

A Stoichiometric Investigation of the Reaction of Nitrosylpentaamminechromium(2+) with Ethylenediaminetetraacetatoaquachromate(II)

Hiroshi OGINO, Keiichi TSUKAHARA, and Nobuyuki TANAKA

Department of Chemistry, Faculty of Science, Tohoku University, Aoba, Aramaki, Sendai 980

(Received June 9, 1975)

Synopsis. The reaction of $Cr(NH_3)_5NO^{2+}$ with $Cr^{II}(edta)(H_2O)^{2-}$ gives four chromium products: $Cr^{III}(edta)(H_2O)^-$, $Cr(NH_3)_6^{3+}$, a reddish-violet species which is considered to be a chromium dimer with a +2 charge, and a trace amount of $Cr(H_2O)(NH_3)_5^{3+}$.

Recently, Armor *et al.* studied the reaction of $Cr(NH_3)_5NO^{2+}$ with $Cr(H_2O)_6^{2+}$ (Cr^{2+}) and observed at least five different chromium(III) products.[1] In this work, the products of the reaction of $Cr(NH_3)_5NO^{2+}$ with ethylenediaminetetraacetatoaquachromate(II) ($Cr^{II}(edta)(H_2O)^{2-}$) are examined, and the results compared with those obtained by Armor *et al.*

Experimental

Materials. The $[Cr(NH_3)_5NO](ClO_4)_2$ complex was prepared by the method of Mori *et al.*[2] The solutions of Cr^{2+} and $Cr^{II}(edta)(H_2O)^{2-}$ were prepared as has been reported previously.[3]

Identification and Analyses of Products. The reaction of $Cr(NH_3)_5NO^{2+}$ with $Cr^{II}(edta)(H_2O)^{2-}$ was carried out in an acetate-buffer solution under a nitrogen atmosphere. The reaction was completed within 5 s under the present experimental conditions. The complex ions, $Cr(NH_3)_5NO^{2+}$, were always treated with more than four equivalents of $Cr^{II}(edta)(H_2O)^{2-}$. After the solution of the reaction mixture had been exposed to air, it was diluted with five times as much water and then poured into an SP-Sephadex C-25 column. The species which passed through the column without any affinity to the resin was identified as $Cr^{III}(edta)(H_2O)^-$ from the measurement of the visible and ultraviolet absorption spectra. After the column had then been washed with water, the adsorbed species on the column were eluted with an 0.2 M $NaClO_4$–0.1 M $HClO_4$ solution. Three distinct bands were observed—reddish-violet, reddish-orange (trace amount), and yellow from the bottom to the top of the column. The eluate from the lowest band was concentrated with a rotary evaporator below 40 °C. Reddish-violet crystals were thus deposited. However, the attempted isolation of crystals sufficiently pure to be subjected to elemental analyses has not yet been successful because of the highly hygroscopic nature of this compound. From the flow rate on the Sephadex column, this species was estimated to have a +2 charge. The visible absorption spectrum shows two maxima, at 566 nm ($\varepsilon=17$) and 406 nm ($\varepsilon=19$).[4] The reddish-orange and yellow bands were eluted out with an 0.5 M $NaClO_4$–0.1 M $HClO_4$ solution. The reddish-orange species was characterized as $Cr(H_2O)(NH_3)_5^{3+}$ from the measurement of the visible absorption spectra. When the yellow eluate was concentrated with a rotary evaporator, yellow crystals were deposited. They were identified as $[Cr(NH_3)_6](ClO_4)_3$ from the measurement of the infrared, visible, and ultraviolet absorption spectra. The chromium content of each fraction was determined spectrophotometrically as CrO_4^{2-} after oxidation with an alkaline hydrogen-peroxide solution. The visible and ultraviolet absorption spectra were recorded with a Hitachi EPS-3 spectrophotometer.

Results and Discussion

The quantitative product distribution was determined at 25 °C with a solution (total volume, 4.00 ml) with an ionic strength of 0.3 ($NaClO_4$) and a pH of 4.3 which had initially contained 3.68×10^{-3} M $Cr(NH_3)_5NO^{2+}$, 1.83×10^{-2} M $Cr^{II}(edta)(H_2O)^{2-}$, 6.7×10^{-3} M EDTA, and an acetate buffer with 0.125 M acetate. For the separation of the chromium products, a Sephadex column 1.4 cm in diameter and 5 cm in height was used; into it the reaction mixture was poured. From the chromium content of each product separated, the concentrations of $Cr(NH_3)_6^{3+}$, the reddish-violet species, and $Cr^{III}(edta)(H_2O)^-$ were determined to be 2.59×10^{-3} M, 2.21×10^{-3} M, and 1.64×10^{-2} M respectively. The following stoichiometry can be assigned to the formation of $Cr(NH_3)_6^{3+}$:

$$Cr(NH_3)_5NO^{2+} + 4Cr^{II}(edta)(H_2O)^{2-} + 5H^+ \longrightarrow Cr(NH_3)_6^{3+} + 4Cr^{III}(edta)(H_2O)^- + H_2O \quad (1)$$

The concentration of chromium in the reddish-violet species is equal to $2\times([Cr(NH_3)_5NO^{2+}]-[Cr(NH_3)_6^{3+}])$. Therefore, the reddish-violet species is considered to be a chromium dimer having a +2 charge:

$$Cr(NH_3)_5NO^{2+} + Cr^{II}(edta)(H_2O)^{2-} \longrightarrow \text{reddish-violet species}^{2+} \quad (2)$$

The product distribution revealed that 70% of the $Cr(NH_3)_5NO^{2+}$ was converted to $Cr(NH_3)_6^{3+}$ and the rest, to the reddish-violet species. The formation of $Cr(NH_3)_6^{3+}$ from $Cr(NH_3)_5NO^{2+}$ is chemical evidence that the nitrosyl group in $Cr(NH_3)_5NO^{2+}$ is a nitrogen-bonded ligand.

The chromium products of the reaction of $Cr(NH_3)_5NO^{2+}$ with Cr^{2+} were found to be $Cr(H_2O)_6^{3+}$, $Cr(H_2O)(NH_3)_5^{3+}$, $(H_2O)_4Cr(OH)_2Cr(H_2O)_4^{4+}$, and two polymeric products which may be represented by the formula $(NH_3)_5Cr\text{–}X\text{–}Cr(H_2O)_4Y^{n+}$, X=$OH^-$ or NH_2OH, Y=H_2O or NH_2OH.[1] These products are quite different from the products observed in the present reaction. According to the results obtained by Armor *et al.*[1], 1 mol of $Cr(NH_3)_5NO^{2+}$ reacts with 2 mol of Cr^{2+} to give 1 mol of NH_2OH. On the other hand, at least 70% of the nitrosyl group in $Cr(NH_3)_5NO^{2+}$ is reduced to NH_3 by $Cr^{II}(edta)(H_2O)^{2-}$ reduction. Therefore, the kind of ligand coordinated to the chromium(II)ions dramatically changes the products of the reactions of $Cr(NH_3)_5NO^{2+}$ with chromium(II). A similar observation was

also made of the reduction of NO_3^-. The reaction of NO_3^- with Cr^{2+} gives $Cr(H_2O)_5NO^{2+}$ [5], and the further reaction with Cr^{2+} yields NH_2OH.[6] The reaction of NO_3^- with $Cr^{II}(edta)(H_2O)^{2-}$ gives NH_4^+.[7,8] The difference between the reaction with Cr^{2+} and that with $Cr^{II}(edta)(H_2O)^{2-}$ may primarily come from the difference in their reduction potentials.[9] It is also apparent that the nature of the central metal ion inherently coordinated to the nitrosyl group controls the extent of the reduction of the nitrosyl group, because it is known that $Ru(NH_3)_5NO^{3+}$ reacts with Cr^{2+} to give $Ru(NH_3)_6^{2+}$.[10]

The absorption spectra of $Cr(NH_3)_5NO^{2+}$ change slowly in $NaClO_4$–$HClO_4$ media. It seems worthwhile to present some observations on these spectral changes (at 25 °C and at an ionic strength of 1.0 ($NaClO_4$–$HClO_4$)). When the hydrogen-ion concentration is higher than 0.2 M, absorbances over the whole range of the visible region decrease with the time. The rate of this change increases with an increase in the concentrations of hydrogen ions. For example, the rate constants of this process, as estimated by the Guggenheim method,[11] are 6.5×10^{-4} s^{-1} at $[H^+]=0.313$ M and 8.4×10^{-4} s^{-1} at $[H^+]=0.783$ M. When the hydrogen-ion concentration falls below 0.1 M, the reaction mentioned above can be neglected and another reaction occurs. The initial stage of the spectral changes shows isosbestic points at 351 nm and 430 nm. The rate constant of this process was determined to be 7.1×10^{-5} s^{-1} at $[H^+]=0.0940$ M. Then, the isosbestic points collapse and the spectra change in a complicated manner, suggesting the occurrence of some consecutive reactions. The spectrum which was obtained after heating the solution on a boiling water bath shows absorption bands at 390 nm (shoulder, $\varepsilon=94$), 447 nm ($\varepsilon=116$), and 566 nm ($\varepsilon=31$). This spectrum coincides satisfactorily with that of $Cr(H_2O)_5NO^{2+}$ reported by Griffith.[12] Therefore, the spectral changes at $[H^+]<0.1$ M may correspond to the following reaction:

$$Cr(NH_3)_5NO^{2+} + nH_3O^+ \longrightarrow Cr(H_2O)_n(NH_3)_{5-n}NO^{2+} + nNH_4^+ \quad (3)$$

where $1\leq n\leq 5$.

The authors wish to thank the Ministry of Education for Scientific Research Grant-in-aid No. 954144.

References

1) J. N. Armor, M. Buchbinder, and R. Cheney, *Inorg. Chem.*, **13**, 2990 (1974).
2) M. Mori, S. Ueshiba, and S. Kawaguchi, This Bulletin, **36**, 796 (1963).
3) H. Ogino and N. Tanaka, *ibid.*, **41**, 1622 (1968).
4) The intensities, ε, are given per one chromium ion.
5) H. Ogino, K. Tsukahara, and N. Tanaka, This Bulletin, **47**, 308 (1974).
6) J. N. Armor and M. Buchbinder, *Inorg. Chem.*, **12**, 1086 (1973).
7) N. Tanaka and T. Ito, This Bulletin, **39**, 1043 (1966).
8) N. Tanaka, T. Kano, H. Ogino, and A. Yamada, *ibid.*, **47**, 3064 (1974).
9) R. L. Pecsok, L. D. Shields, and W. P. Schaefer, *Inorg. Chem.*, **3**, 114 (1964).
10) J. N. Armor, *ibid.*, **12**, 1959 (1973).
11) E. A. Guggenheim, *Phil. Mag.*, [7] **2**, 538 (1926).
12) W. P. Griffith, *J. Chem. Soc.*, **1963**, 3286.

BULLETIN OF THE CHEMICAL SOCIETY OF JAPAN, VOL. 48 (11), 3403—3404 (1975)

Solubility of Transition Metal Complexes in Aqueous Salt Solutions. II. Tris(1,10-phenanthroline)iron(II) Perchlorate in Hydrophobic Salt Solutions

Katsuhiko MIYOSHI, Chiyori SHIMADA, and Hayami YONEDA

Department of Chemistry, Faculty of Science, Hiroshima University, Higashisenda-machi, Hiroshima 730

(Received June 9, 1975)

Synopsis. Solubility of tris(1,10-phenanthroline)-iron(II) perchlorate in water was found to be much increased by the addition of hydrophobic ions. This was interpreted in terms of hydrophobic interaction of the complex cation with hydrophobic ions added.

It is generally accepted that ions in aqueous solutions are classified into three groups according to the nature of their interaction with water; structure-maker, structure-breaker, and hydrophobic structure-maker.[1-3] In our preceding paper of this series,[4] we proposed that $[Fe(phen)_3]^{2+}$ (phen=1,10-phenanthroline) belongs to the last group despite its relatively high charge. In order to ascertain our proposal, solubility of $[Fe(phen)_3](ClO_4)_2$ was measured at 25 °C in aqueous solutions of various hydrophobic salts as a function of total ionic strength.

$[Fe(phen)_3](ClO_4)_2 \cdot H_2O$ was prepared in the same manner as before.[4] Sodium alkane carboxylates (formate to octanoate) were prepared and purified in a similar manner to that described by Sakurai[5] and Tamaki *et al.*[6] Tetraalkylammonium bromides (methyl to *n*-butyl) were dried at 100 °C. Solubility measurements were carried out at 25±0.1 °C in the same manner as before.[4] Usually it took 7 to 8 h to attain solution equilibrium.

In Fig. 1 is plotted the solubility ratio S/S_0, *i.e.*, the ratio of solubility (mol/l) of the complex in aqueous salt solutions to that in pure water, against square root of total ionic strength I for sodium alkane carboxylate solutions. Also drawn are theoretical curves estimated by the Debye-Hückel approximation with $a=8$ and 9 Å.[4,7] It is seen that S/S_0 is more and more increased as the number of methylene groups in alkane carboxylates is increased,[8] *i.e.*, as the added anions bear more hydrophobic character,[9] and that higher carboxylates[10] (hexanoate to octanoate) show an increasingly positive curvature contrary to the prediction from the Debye-Hückel theory.

S_0 is so low (8.99×10^{-4} mol/l) as compared with the concentration of added salts that the co-sphere[2] of $[Fe(phen)_3]^{2+}$ overlaps predominantly with that of added anions rather than that of ClO_4^-. As a result, it follows that the increment in S/S_0 depends on whether the complex cation is cooperative or antagonistic with added

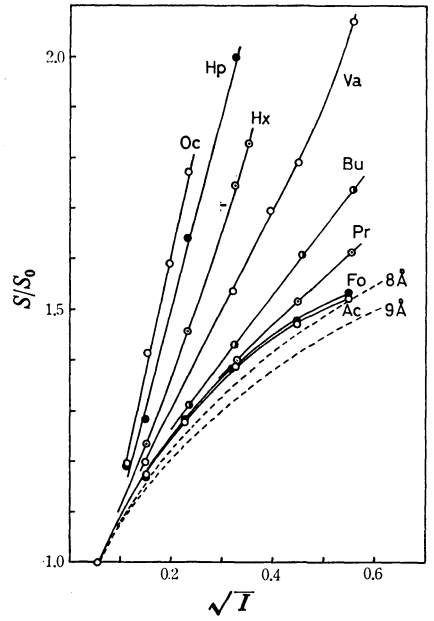

Fig. 1. Dependence of the solubility ratio S/S_0 on square root of ionic strength I for sodium alkane carboxylate solutions. Fo, Ac, Pr, Bu, Va, Hx, Hp, and Oc refer to sodium formate, acetate, propionate, butyrate, valerate, hexanoate, heptanoate, and octanoate solutions, respectively. Dotted lines represent theoretical values estimated by the Debye-Hückel approximation

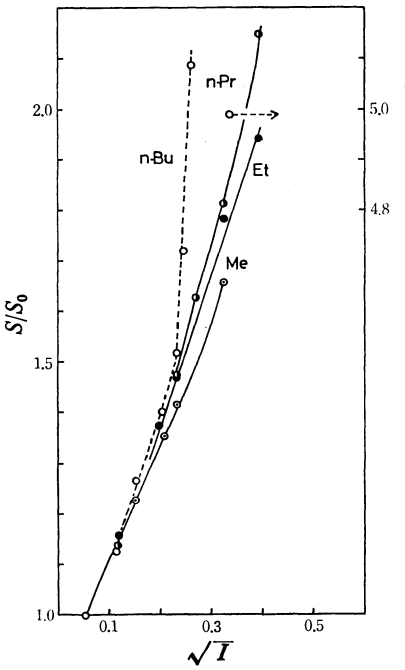

Fig. 2. Dependence of the solubility ratio S/S_0 on square root of ionic strength I for tetraalkylammonium bromide R_4NBr solutions. Me, Et, *n*-Pr, and *n*-Bu refer to Me_4NBr, Et_4NBr, *n*-Pr_4NBr, and *n*-Bu_4NBr solutions, respectively. Only one point in the most concentrated solution of *n*-Bu_4NBr corresponds to the right-hand scale.

anions with respect to their influence on the water structure, as pointed out by Steigman and Dobrow,[11] and Desnoyers *et al.*,[12] if ion association is negligible. Since added anions are all singly charged, their electrostatic association with the complex cation is not so extensive, at least at low salt concentrations.[4] Thus, it is confirmed from Fig. 1 that $[Fe(phen)_3]^{2+}$ is cooperative with hydrophobic anions.

Figure 2 shows similar plots for tetraalkylammonium bromide solutions and indicates that S/S_0 does not differ appreciably from salt to salt added when the salt concentration is relatively low. This is to be expected since the co-sphere of the complex cation firstly interacts with that of Br^- ion, which is common to all salt solutions. However, as the salt concentration is increased, S/S_0 begins to diverge; the more hydrophobic the added cation is,[13] the more S/S_0 increases (structural salting-in[3] or cation-cation interaction). In particular for tetra-*n*-butylammonium bromide (*n*-Bu_4NBr) solutions, S/S_0 suddenly increases greatly at *ca.* 0.05 mol/l. The critical micelle concentration (cmc) of *n*-Bu_4NBr is reported to be *ca.* 0.04 mol/l at 25 °C by Lindenbaum and Boyd.[14] Thus, this abnormal increase in S/S_0 is attributed to so-called solubilization of the complex cation into micelles composed of *n*-Bu_4N^+, though the electrostatic repulsion is expected between the complex and the micelles. Therefore, the complex cation is cooperative with hydrophobic cations, too.

In conclusion, $[Fe(phen)_3]^{2+}$ belongs to the hydrophobic structure-maker group and is stabilized by the hydrophobic interaction[15] with added hydrophobic ions in aqueous solutions.

References

1) H. S. Frank and W.-Y. Wen, *Discuss. Faraday Soc.*, **24**, 133 (1957); H. S. Frank, *Z. Phys. Chem. (Leipzig)*, **228**, 365 (1965).

2) W. R. Guney, "Ionic Processes in Solution," McGraw-Hill Book Co., New York, N. Y. (1953).

3) J. E. Desnoyers and C. Jolicoeur, "Modern Aspects of Electrochemistry," Vol. 5, ed. by J. O.'M. Bockris, and B. E. Conway, Plenum Publishing Corp., New York, N. Y. (1969), p. 1.

4) K. Miyoshi, T. Taura, C. Shimada, and H. Yoneda, This Bulletin, **48**, 1783 (1975).

5) M. Sakurai, *ibid.*, **46**, 1596 (1973).

6) K. Tamaki, Y. Ohara, H. Kurachi, M. Akiyama, and H. Odaki, *ibid.*, **47**, 384 (1974).

7) R. A. Robinson, and R. H. Stokes, "Electrolyte Solutions," Butterwoth, London (1959), p. 223.

8) If Gurney's suggestion that formate ion is a weaker structure-maker than acetate ion, is really correct (Ref. 2, p. 201), it is reasonable that S/S_0 for formate solutions is larger than that for acetate solutions, since structure-makers are antagonistic with hydrophobic structure-makers.[4]

9) Hydrophobic nature of some alkane carboxylate ions has been recently examined and discussed by some workers, H. Snell and J. Greyson, *J. Phys. Chem.*, **74**, 2148 (1970); Refs. 5 and 6.

10) The cmc of potassium octanoate is reported to be *ca.* 0.4 mol/l at 25 °C. Thus, all alkane carboxylates examined here do not form micelles under our experimental conditions. See the following references, K. Shinoda, "Colloidal Surfactants," Academic Press Inc., New York, N. Y. (1963); R. M. Diamond, *J. Phys. Chem.*, **67**, 2413 (1963).

11) J. E. Steigman and J. Dobrow, *ibid.*, **72**, 3424 (1968).

12) J. E. Desnoyers, M. Arel, G. Perron, and C. Jolicoeur, *ibid.*, **73**, 3346 (1969).

13) Hydrophobic nature of R_4N^+ ion has been reviewed by W.-Y. Wen, "Water and Aqueous Solutions," ed. by R. A. Horne, John Wiley & Sons, Inc., New Yoerk, N. Y. (1972), p. 613; *J. Solution Chem.*, **2**, 253 (1973). In particular, it is noteworthy that Desnoyers *et al.* (*Can. J. Chem.*, **43**, 3232 (1965)), Wirth and LoSurdo (*J. Phys. Chem.*, **72**, 751 (1968)), and Arnett *et al.* (*J. Amer. Chem. Soc.*, **92**, 7039 (1970)) have found the solubility of benzene in water to be much increased by the addition of tetraalkylammonium bromides.

14) S. Lindenbaum and G. E. Boyd, *J. Phys. Chem.*, **68**, 911 (1964).

15) G. Nemethy, *Angew. Chem. Int. Ed. Engl.*, **6**, 195 (1967).

BULLETIN OF THE CHEMICAL SOCIETY OF JAPAN, VOL. 48 (11), 3405—3406 (1975)

The Preparation of 1- and 2-Aminophenazine Derivatives

Masao TADA

The Research Institute for Tuberculosis, Leprosy and Cancer, Tohoku University, Hirosemachi, Sendai 980

(Received February 3, 1975)

Synopsis. The reactions of chlorophenazines and their *N*-oxides with sodium azide in dimethyl sulfoxide or dimethylformamide yielded the corresponding aminophenazine derivatives.

In previous papers,[1,2] the reactions of halogenophenazines with piperidine, morpholine, sodium carboxymethyl mercaptide, and sodium methyl mercaptide were reported. During the study on the potential biological activities of phenazine derivatives, the preparation of aminophenazine derivatives was required. Pachter *et al.*[3] have reported that 2-aminophenazine (I) was prepared from 2-chlorophenazine (II) with aqueous ammonia by heating in an autoclave. This note describes the application of the transformation of a halogeno group into an amino group by the use of sodium azide.[4]

The reaction of 1-chlorophenazine (III) with sodium azide in dimethyl sulfoxide (DMSO) at 130 °C for 48 h gave 1-aminophenazine (IV).[5] The treatment of 1-chlorophenazine 5-oxide (V) with sodium azide in DMSO at 130 °C for 24 h gave 1-aminophenazine-5-oxide (VI), which was converted into IV by the reduction with zinc dust in acetic acid.

The reaction of II with sodium azide in DMSO or dimethylformamide (DMF) afforded a 2-amino compound (I). The reactions of 2-chloro- (VII) and 3-chlorophenazine 5-oxides (VIII) with sodium azide in DMSO gave the corresponding aminophenazine 5-oxides (IX and X). Both compounds IX and X were converted into I by reduction.

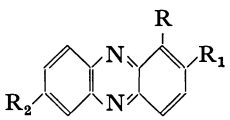

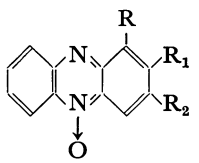

I: $R=R_2=H$; $R_1=NH_2$ V: $R=Cl$; $R_1=R_2=H$
II: $R=R_2=H$; $R_1=Cl$ VI: $R=NH_2$; $R_1=R_2=H$
III: $R=Cl$; $R_1=R_2=H$ VII: $R=R_2=H$; $R_1=Cl$
IV: $R=NH_2$; $R_1=R_2=H$ VIII: $R=R_1=H$; $R_2=Cl$
XI: $R=H$; $R_1=R_2=Cl$ IX: $R=R_2=H$; $R_1=NH_2$
XII: $R=H$; $R_1=NH_2$; $R_2=Cl$ X: $R=R_1=H$; $R_2=NH_2$

The heating of a mixture of VIII and sodium azide in DMF for 1 h under reflux afforded I, II, and X in yields of 3, 28, and 45%, respectively. Prolonged reflux (3 h), however, lead to the formation of I, II, and X in yields of 21, 19, and 20%, respectively. The results suggest that *N*-oxides are partially converted into the parent bases during the course of the displacement of a chlorine atom. This has been well confirmed by heating a solution of VIII in DMF, as shown in Table 1. Such a simple deoxygenation of *N*-oxide by DMF is hitherto unknown.[6]

A similar phenomenon was also observed in the heating of V and VII in DMF.

Table 1. Deoxygenation of 3-chlorophenazine 5-oxide (VIII)

Reflux time in DMF (h)	Deoxygenation product, II (%)	Recovery (%)
10	13	80
20	35	56
40	93	0

The amination of 2,7-dichlorophenazine (XI) gave 2-amino-7-chlorophenazine (XII) which also had been derived from VIII *via* nitration and reduction.[7]

Experimental

All the melting points are uncorrected. Absorption spectra were recorded with a Hitachi Model EPI-S_2 infrared spectrophotometer and a Hitachi Model 124 spectrophotometer.

1-Aminophenazine (IV). From 1-Chlorophenazine (III): To a hot solution of III (2.0 g) in DMSO (20 ml), sodium azide (1.0 g) was added. The mixture was then heated at 130 °C for 48 h, cooled, and poured into water. The crystals thereby separated were analyzed by chromatography on alumina, using benzene as the solvent, and then recrystallized from aqueous methanol to yield IV (520 mg, 29%), mp 176 °C, which showed no decrease in melting point on admixture with an authentic specimen.[5] Unchanged III (800 mg, 40%) was recovered.

From 1-Aminophenazine 5-Oxide (VI): Into a solution of VI (210 mg) in acetic acid (5 ml), zinc dust (1.5 g) was added. The mixture was then warmed in a water bath for 10 min, and filtered while hot. After usual treatment, recrystallization of the product from aqueous methanol afforded IV (150 mg, 77%), mp 176 °C.

1-Aminophenazine 5-Oxide (VI). A mixture of V (1.15 g) and sodium azide (450 mg) in DMSO (12 ml) was heated at 130 °C for 24 h, and treated as described above to afford crystals. Recrystallization from a mixture of chloroform and methanol (1: 1) gave VI (mp 226—227 °C (dec.), 400 mg) as reddish-violet micro-prisms in a 38% yield. Found: C, 67.98; H, 4.29; N, 19.98%. Calcd for $C_{12}H_9N_3O$: C, 68.23; H, 4.30; N, 19.90%. IR (KBr): 3440 and 3330 cm^{-1}. UV: λ_{max}^{MeOH} 252 (log ε=4.49), 289 (4.61), 367 (3.75), 384 (3.72), and 515 (3.60) nm.

2-Aminophenazine (I). In DMSO: A mixture of II (2.6 g) and sodium azide (1.1 g) in DMSO (30 ml) was heated at 130 °C for 10 h, and then diluted with water. The precipitate was dissolved in ethyl acetate. The solution was then passed through a column of alumina and eluted with ethyl acetate. From the effluent, reddish-orange crystals were obtained. Recrystallization from chloroform gave fine red crystals (900 mg, 38%), mp 267—268 °C (dec), which were identified with I[3] by a comparison of their infrared spectra.

In DMF: A suspension of II (1.2 g) and sodium azide (450 mg) in DMF (20 ml) was gently refluxed for 5 h, and then treated in a similar way to yield I (550 mg, 56%), mp 267—268 °C (dec).

2-Aminophenazine 5-Oxide (IX). A suspension of VII

(1.2 g) and sodium azide (450 mg) in DMSO (12 ml) was heated at 130 °C for 4 h, and then treated as in the procedure used in the preparation of I to give crystals, which were recrystallized from ethanol to afford IX (mp 260—261 °C (dec), 500 mg) as deep-violet micro-crystals in a 47% yield. Found: C, 68.34; H, 4.19; N, 19.72%. Calcd for $C_{12}H_9N_3O$: C, 68.23; H, 4.30; N, 19.90%. IR (KBr): 3400 and 3320 cm^{-1}. UV: λ_{max}^{MeOH} 279 (log ε=4.81), 333 (3.75), 350 (3.84), 371 (3.98), 391 (4.22), and 500 (3.82) nm.

IX (210 mg) was treated with zinc dust (0.5 g) in acetic acid (5 ml) to yield I (120 mg, 62%), mp 267—268 °C (dec).

3-Aminophenazine 5-Oxide (X). *In DMSO*: A mixture of VIII (1.16 g) and sodium azide (0.3 g) in DMSO (20 ml) was heated at 130 °C for 3 h, and then treated as in the above experiment to afford crystals. Recrystallization of the product from ethanol gave X (mp 253—254 °C (dec), 700 mg) as red micro-prisms in a 66% yield. Found: C, 68.45; H, 4.29; N, 20.10%. Calcd for $C_{12}H_9N_3O$: C, 68.23; H, 4.30; N, 19.90%. IR (KBr): 3400 and 3320 cm^{-1}. UV: λ_{max}^{MeOH} 241 (log ε= 4.22), 285 (4.75), 366 (3.79), 384 (4.08), and 500 (4.00) nm.

In DMF: A suspension of VIII (2.31 g) and sodium azide (0.6 g) in DMF (25 ml) was refluxed for 1 h to give I (50 mg, 3%), II (600 mg, 28%), and X (950 mg, 45%).

X (210 mg) was treated with zinc dust (0.5 g) in acetic acid (5 ml) to yield I (110 mg, 56%).

Deoxygenation of Chlorophenazine 5-Oxides. A solution of chlorophenazine 5-oxide (1.16 g) in DMF (20 ml) was refluxed, and then diluted with water. The crystals thereby separated were dissolved in benzene. The benzene solution was passed through a column of alumina, and eluted with benzene. From the first effluent, a deoxygenation product was obtained, and 5-oxide was recovered from the second effluent.

2-Amino-7-chlorophenazine (XII). A suspension of XI (1.25 g) and sodium azide (390 mg) in DMSO (30 ml) was heated at 130 °C for 4 h, and then treated as in the case of I to give red needles (450 mg, 39%), mp 252 °C, which showed no decrease in melting point on admixture with an authentic specimen.[7]

The author is grateful to Professor Yusaku Ikegami of Tohoku University for his encouragement, and to Miss Mieko Sasaki for her experimental cooperation.

References

1) H. Endo, M. Tada, and K. Katagiri, This Bulletin, **42**, 502 (1969); **42**, 506 (1969); **42**, 566 (1969).

2) M. Tada, *ibid.*, **47**, 1803 (1974).

3) I. J. Pachter and M. C. Kloetzel, *J. Amer. Chem. Soc.*, **74**, 971 (1952).

4) For examples, M. Tada, This Bulletin, **39**, 1954 (1966); C. Temple, L. L. Kussner, and J. A. Montgomery, *J. Org. Chem.*, **34**, 2102 (1969).

5) A. Albert and H. Duewell, *J. Soc. Chem. Ind.*, **66**, 11 (1947).

6) A. R. Katritzky and J. M. Lagowski, "Chemistry of the Heterocyclic *N*-Oxides," Academic Press, London (1971), p. 209 and 229.

7) H. Otomasu, *Chem. Pharm. Bull.*, **4**, 117 (1956).

BULLETIN OF THE CHEMICAL SOCIETY OF JAPAN, VOL. 48 (11), 3407—3408 (1975)

Mechanism of the Formation of Phenyltolylmethane by the Reaction of Toluene with Phosphorus Trichloride and Oxygen

Yoshiki OKAMOTO and Hiroshi SAKURAI

The Institute of Scientific and Industrial Research, Osaka University, Yamada-kami, Suita, Osaka 565

(Received February 7, 1975)

Synopsis. The formation of phenyltolylmethane by the reaction of toluene with PCl_3 and oxygen was shown to proceed by electrophilic attack on toluene by the benzyl cation, resulting from the decomposition of the trichlorobenzyloxyphosphoranyl peroxy radical ($PhCH_2OPCl_3OO\cdot$).

The formation of phenyltolylmethane (I) by the reaction of toluene with PCl_3 and oxygen was reported in a previous paper,[1] in which the mechanism of the formation was explained by the electrophilic attack on toluene by benzyl cation, resulting from the electron transfer from the benzyl radical to PCl_3 with the participation of oxygen as shown in Scheme 1.

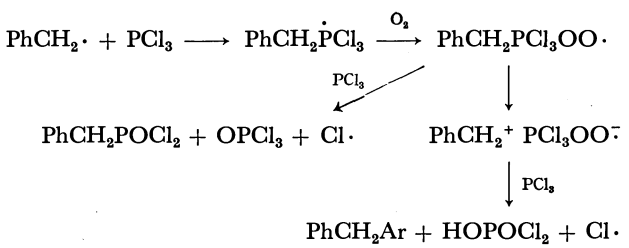

Scheme 1.

However, it has been found that when the initial ratio of PCl_3 to toluene was reduced under a constant flow rate of oxygen, or when the oxygen gas pressure was diminished by dilution with nitrogen with a constant initial ratio of PCl_3 to toluene, the ratio of I to benzylphosphonic dichloride (II) in the product decreased (Table 1).

TABLE 1. THE PRODUCT RATIO (I/II) OBTAINED BY CHLOROPHOSPHONATION OF TOLUENE, CARRIED OUT UNDER SEVERAL CONDITIONS

Reactant ratio (Toluene/PCl_3)	Oxygen (%)	Time (h)	Yield (g)	Product ratio (I/II)
0.02	100	3	3.0	7
0.1	100	3	4.9	29
0.2	100	3	4.8	50
5	100	3	1.6	230
0.2	50	6	7.0	41
0.2	10	30	5.3	21

These results cannot be explained by Scheme 1, in which the benzyl radical reacts with PCl_3 exclusively to give a trichlorobenzylphosphranyl radical as an intermediate. It is well known that tervalent phosphorus compounds have high reactivities with free radicals, such as RO·, RS·, and methyl.[2] However, recently Dulog, Nielich, and Verhelst reported that resonance-stabilized radicals, such as $Ph_3C\cdot$, fail to react with PCl_3.[3] The reactivities of the free radical with PCl_3 decrease in the following order: $C_6H_5\cdot > t\text{-}C_5H_9\cdot > (CH_3)_2\dot{C}CN > (C_6H_5)_3C\cdot$. Bentrude also suggested that methyl and ethyl radicals react with $(C_6H_5)_2POR$, but that the more stable radicals, such as benzyl, do not appreciably react with $(C_6H_5)_2POR$,[4] because the ΔH_{PZ_4} for the reaction of $(C_6H_5)_2POR$ and benzyl radical (the enthalpy change of the formation of the phosphoranyl radical intermediate) is too small to form a phosphoranyl radical.[2,4] The ΔH_{PZ_4} is analyzed into three contributing terms: (1) the phosphorus orbital reorganization energy (ORE), (2) the strength of the bond to phosphorus being formed (ΔH_{PZ}), and (3) any resonance stability imparted to the phosphoranyl radical by the substituents on phosphorus (RE). Differences in the enthalpies of formation for strengths of the new bonds being formed and the resonance-stability difference (if ORE is assumed constant). The bond strength of benzyl is not known but is assumed to be considerably smaller than that for other free radicals, such as RO·, RS·, and methyl.[2] It is also supposed that PCl_3 may be less reactive than $(C_6H_5)_2POR$ because, in the former case, the effect of no resonance stability imparted to the phosphoranyl radical can be expected.

On the other hand, it is well known that the addition of oxygen to the radical is extremely fast and is probably diffusion controlled in many instances.[5] An extremely resonance-stabilized radical, such as $Ph_3C\cdot$, is very reactive with oxygen even though it is relatively inert with other species.[6]

Therefore, the benzyl radical may react preferentially with oxygen to form a benzyl peroxy radical (reaction 1) rather than with PCl_3 to form a trichlorobenzylphosphoranyl radical,

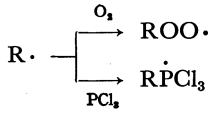

(1)

(2)

The benzyl peroxy radical is deoxygenated with PCl_3 to yield the benzyloxy radical (reaction 3),[3] which is trapped again with PCl_3 to form a trichlorobenzyloxyphosphoranyl radical (III),

$$ROO\cdot + PCl_3 \longrightarrow RO\cdot + POCl_3 \quad (3)$$

$$RO\cdot + PCl_3 \longrightarrow R\dot{O}PCl_3 \text{ (III)} \quad (4)$$

Radical III reacts with oxygen to give a trichlorobenzyloxyphosphoranyl peroxy radical (IV), thus

$$R\dot{O}PCl_3 + O_2 \longrightarrow ROPCl_3OO\cdot \text{ (IV)} \quad (5)$$

In the case of R≒benzyl, radical IV reacts with PCl_3 to give alkyl phosphorochloridate, $POCl_3$ and Cl.[7,8] However, when R has a lower ionization potential, such as for the benzyl radical (7.76 eV), the electron transfer from a benzyl group to an $OPCl_3OO$ group may occur to give an ionic structure such as IV′:

$$ROPCl_3OO\cdot \longrightarrow R^+(OPCl_3OO\cdot)^- \text{ (IV')} \quad (6)$$

The electrophilic attack of benzyl cation (IV') on toluene gives phenyltolylmethane (I) as a final product, thus

$$IV' + C_6H_5CH_3 \xrightarrow{PCl_3} I + HOPOCl_2 + POCl_3 + Cl\cdot \quad (7)$$

The formation of α-methylstyrene and its dimers by the chlorophosphonation of isopropylbenzene[1] can be explained in a similar manner.

But in this case, IV″ leads to α-methylstyrene by intramolecular proton-migration, thus

$$C_6H_5\overset{\overset{CH_3}{|}}{\underset{\underset{CH_3}{|}}{C^+}}\ OPCl_3OO^- \xrightarrow{PCl_3} \text{(IV'')}$$

$$C_6H_5\overset{\overset{CH_3}{|}}{C}=CH_2 + HOPOCl_2 + POCl_3 + Cl\cdot \quad (8)$$

The possibility of the direct formation of a benzyl cation from radical III (reaction 9) can be eliminated by the results that no α-methylstyrene and its dimers could be detected in the thermally-decomposed products of bis(α,α-dimethylbenzyl) peroxide in PCl_3 in a nitrogen atomsphere:

$$\dot{R}OPCl_3 \text{ (III)} \longrightarrow R^+ \dot{O}PCl_3^- \quad (9)$$

The remarkable formation of alkylphosphorodichloridate was observed in the chlorophosphonation of alkyl halide,[8] thus

$$ROPCl_3OO\cdot + PCl_3 \longrightarrow ROPOCl_2 + POCl_3 + Cl\cdot \quad (10)$$

Therefore, there is another possilibity of the formation of a benzyl cation: the reaction *via* the heterolytic dissociation of the C–O bond of benzylphosphorodichloridate (V), thus

$$ROPOCl_2 \text{ (V)} \longrightarrow R^+ OPOCl_2^- \quad (11)$$

However, the possibility of this reaction can also be eliminated, because a mixture of dibenzylphosphorochloridate, toluene, PCl_3 and $POCl_3$ did not gave I in the presence of a trace of HCl at 0—5 °C.

Experimental

The general and detailed procedure was described in a previous paper.[1]

Chlorophosphonation. A mixture (130 ml) of the prescribed ratio of toluene/PCl_3 was placed in a reaction vessel. Oxygen or a mixture of oxygen and nitrogen gas was bubbled into the reaction mixture at a flow rate of 300 ml/min at a temperature of −15—0 °C. After the removal of a large portion of the unreacted materials and $POCl_3$, the residue was distilled *in vacuo*.[9] The I/II ratios were determined by glc analysis after treating the distillate with ethanol–triethylamine.

Thermal Decomposition of Bis(α,α-dimethylbenzyl) Peroxide in PCl_3. Bis(α,α-dimethylbenzyl) peroxide (0.1 mol) in PCl_3 (50 ml) was heated (70—80 °C) in a nitrogen atmosphere for a period of approximatately 6 h. The reaction mixture was poured into ice water and an oily layer was extracted with ether. No α-methylstyrene or its dimers were detected but a small amount of phenol was found by glc.

Reaction of Toluene with Dibenzylphosphorochloridate in the Presence of PCl_3, $POCl_3$, and HCl. The mixture of toluene (9.2 g, 0.1 mol), dibenzylphosphorochloridate (29 g, 0.1 mol), PCl_3 (24 g, 0.2 mol), $POCl_3$ (15 g, 0.1 mol) and a trace of HCl was stirred for a period of approximately 12 h at 0—5 °C. The mixture was poured into ice water. And oily layer was analyzed by glc. No. I was detected.

References

1) T. Okada, Y. Okamoto, and H. Sakurai, This Bulletin, **47**, 2251 (1974).
2) W. G. Bentrude, "Free Radical," Vol. 2, ed. by J. K. Kochi, John Wiley & Sons, Inc., New York (1973), p. 595.
3) L. Dulog, F. Nielich, and A. Verhelst, *Chem. Ber.*, **105**, 874 (1972).
4) W. G. Bentrude, J-J. L. Fu, and P. E. Rogers, *J. Amer. Chem. Soc.*, **95**, 3625 (1973).
5) K. U. Ingold, "Free Radical," Vol. 1, ed. by J. K. Kochi, John Wiley & Sons, Inc., New York (1973), p. 37.
6) J-J. L. Fu and W. G. Bentrude, *J. Amer. Chem. Soc.*, **94**, 7710 (1972); L. P. Lorand and P. D. Bartlett, *ibid.*, **88**, 3294 (1966).
7) C. B. C. Boyce, S. B. Webb, and L. Phillips, *J. Chem. Soc., Perkin I*, **1974**, 1960.
8) Y. Okamoto, T. Okada, and H. Sakurai, This Bulletin, **48**, 484 (1975).
9) A substantial amount of I was also detected by direct glc analysis on the undistilled and cooled (0 °C) reaction mixture, and on the oily product obtained after hydrolysis of the mixture with ice water.

BULLETIN OF THE CHEMICAL SOCIETY OF JAPAN, VOL. 48 (11), 3409—3410 (1975)

Reactions of Diazomethyl-1,3,5-triazines with Cyclohexane

Akio KUMAGAI, Shizen SEKIGUCHI, and Kohji MATSUI
Department of Chemistry, Gunma University, Kiryu, Gunma 376

(Received March 28, 1975)

Synopsis. Diazomethyl-1,3,5-triazines reacted with cyclohexane thermally and photochemically to give cyclohexylmethyl-1,3,5-triazines as the major product. The reactions took place *via* a carbene intermediate; however, the hydrogen abstraction products (methyl-triazines) were not obtained in these cases.

There have been a number of studies of the reactions of aliphatic diazo compounds.[1] In recent years the reactions of diazoalkyl derivatives of heteroaromatics, such as triazole,[2] furan,[3-5] thiophene,[5,6] and pyridine,[6-8] have been investigated.

Diazomethyl-1,3,5-triazines have been known for a long time;[9-11] however, the thermal and photochemical reactions of diazomethyl-1,3,5-triazines have not yet been investigated.

On the other hand, the thermolysis and photolysis of diazomethyl-1,3,5-triazines may provide useful and convenient routes for the preparation of 1,3,5-triazine derivatives, which would otherwise be difficult to prepare.

This paper will report on the thermal and photochemical reactions of diazomethyl-triazines with cyclohexane.

Structure of Diazomethyl-1,3,5-triazines. 4,6-Dichloro-(1),[9,10] 4,6-dimethoxy- (2),[9] and 4,6-bis(dimethylamino)-2-diazomethyl-1,3,5-triazine (3)[10] are thermally stable; they can be purified by sublimation under reduced pressure. Generally, 2-diazomethyl nitrogen heteroaromatics are considered to exist in a diazomethyl-azomethine-triazole equilibrium. In the diazomethyl derivatives of pyridine, the equilibrium lies strongly on the side of triazole,[6-8,12] while in the derivatives of 1,3,5-triazine the triazole form is considered to be excluded on the basis of the mode of their reactions and the presence of the characteristic IR band of aliphatic diazo compound.[9]

The IR spectra of Compounds 1, 2, and 3 in KBr discs have a strong and sharp characteristic band near 2120 cm^{-1} assignable to the diazomethyl group, indicating that these compounds exist in the diazomethyl form in a solid state. In addition, the PMR spectra of Compounds 2 and 3 in CCl_4, $CDCl_3$, and DMSO-d_6 at 20 and 60 °C showed a signal assignable to $-OCH_3$ or $-N(CH_3)_2$ as a singlet in every case, in spite of the wide diversity in the nature of the solvent (see Table 1); this shows the absence of tautomeric triazole, which should possess two kinds of methoxyl or dimethylamino groups. Contrary to expectations, ordinary diazomethyl-1,3,5-triazines exist only in the diazomethyl form, not only in the solid state, but also in a solution, regardless of the solvent employed.

Table 1. PMR data of diazomethyl-triazines

Solvent	Chemical Shift (δ)[a]			
	Compound 2		Compound 3	
	$-CHN_2$	$-OCH_3$	$-CHN_2$	$-N(CH_3)_2$
DMSO-d_6	5.9	3.9	5.4	3.0
CCl_4	5.2	4.0	4.0	3.1
$CDCl_3$	5.1	3.9	4.7	3.1

a) Measured at 20 °C using TMS as the internal standard.

In diazomethyl-1,3,5-triazines, electrons poured into the aromatic nucleus from the side chain should spread over the 3-ring nitrogen atoms; therefore, interaction between one of these nitrogen atoms and the terminal nitrogen atom of the side chain would be weaker than in the cases of diazines and pyridine. Thus, it may generally be said that an increase in the number of ring nitrogen atom prevents the formation of a stable bicyclic tautomer in azido, diazoalkyl, and related derivatives of nitrogen heteroaromatic compounds.

Reactions of Diazomethyl-1,3,5-triazines with Cyclohexane. When compound 2 was heated in cyclohexane at 180 °C, 2-cyclohexylmethyl-4,6-dimethoxy-1,3,5-triazine (yield, 12%) was obtained as the sole isolable product;[13] however, the corresponding methyl-triazine was not detected in the reaction mixture by tlc.

On the other hand, when a cyclohexane solution of Compound 2 was irradiated at 254 nm, several photoproducts were produced, along with one major product. The major product was 2-cyclohexylmethyl-4,6-dimethoxy-1,3,5-triazine (yield, 14%); in this case also, the corresponding methyl-triazine was not obtained. The monodiazomethyl-triazines are thermally stable (the decomposition point of Compound 2 is 190 °C, and that of Compound 3 is 195 °C); therefore, without irradiation they did not react with cyclohexane at room temperature. Since most of the 254 nm incident light is absorbed by diazomethyl-triazine, the photochemical reaction with cyclohexane should take place *via* a carbene intermediate formed by the decomposition of the excited diazomethyl-triazine, even though the presence of the corresponding carbene could not be confirmed when diazomethyl-triazines were irradiated at 254 nm in EPA at 77 K.[14] The formation of cyclohexylmethyl-triazine in the photochemical and thermal reactions can be understood in terms of the intermolecular insertion of the singlet triazinyl carbene.

Similarly, 2-diazomethyl-4,6-bis(dimethylamino)-1,-3,5-triazine (3) reacted thermally and photochemically with cyclohexane to yield the corresponding cyclohexylmethyl-triazine as the sole isolable product (the yields were 10% and 16% respectively). The assumption that the thermal reaction of diazomethyl-triazines proceeds *via* a carbene intermediate may be supported by kinetic measurements of the reactions.

When diazomethyl-triazines were heated in hydrocarbons, an evolution of nitrogen was observed. There-

fore, for the kinetic measurements, an increase in the volume of nitrogen evolved in various substrates was followed after a lapse of time; however, in the reaction with cyclohexane the kinetic runs were carried out by measureing the decrease in the intensity of the $-CHN_2$ IR band after heating in small, sealed glass tubes.[16] The first-order rate constants for the decomposition of Compound 2 are listed in Table 2.

Table 2. Rate constants for the decomposition of 2-diazomethyl-4,6-dimethoxy-1,3,5-triazine in various substrates

Substrate	$k_1 \times 10^4$ (s^{-1})		
	180 °C	170 °C	160 °C
Cyclohexane	5.55	2.26	0.98
Decalin	3.25	1.43	0.41
Tetralin	2.57	—	—
Diphenyl ether	2.44	—	—

From Table 2 it is obvious that, in these reactions, there is little variation in the rate in spite of the wide diversity in the nature of the substrates, suggesting that the rate-determining step of these reactions is the loss of nitrogen to give a carbene species.

For a detailed discussion, the temperature dependence of the reaction constant was measured in decalin and cyclohexane; the activation parameters for the reactions are listed in Table 3.

Table 3. Activation parameters for the decomposition of 2-diazomethyl-4,6-dimethoxy-1,3,5-triazine

Substrate	$\Delta H^{\ddagger}$ (kcal·mol^{-1})	$\Delta S^{\ddagger}$(170 °C) (cal·deg^{-1}·mol^{-1})
Cyclohexane	33.5	−0.4
Decalin	39.7	+12.7

The entropies of the activation of −0.4 and +12.7, which were comparable in magnitude to those of the reactions of other diazomethyl derivatives with similar substrates,[15] support the idea that the reaction is of the first order, involving the carbene intermediate.

Experimental

All the melting points are uncorrected. The assignments of the reaction products were performed by means of NMR, IR spectra, and elemental analyses. A low-pressure mercury lamp with a Vycor glass filter was used as the 254 nm radiation source.

Materials. The diazomethyl-triazines were prepared by the condensation of cyanuric chloride with diazomethane,[9,10] followed by treatment with sodium methoxide[9] or dimethylamine,[10] (Compound 1, mp 112—113 °C) (lit,[9,10] 111.5—112.5 °C) (Compound 2, mp 103—104 °C) (lit,[9] 105—106 °C) (Compound 3, mp 93—94 °C) (lit,[10] 94 °C). The reaction mixtures were concentrated, purified by column chromatography (silica-gel; benzene: acetone = 10: 1 by volume), and dried *in vacuo*. 2-Cyclohexylmethyl-4,6-dimethoxy-1,3,5-triazine. Viscous oil. Found: C, 60.85; H, 8.10; N, 17.92%. Calcd for $C_{12}H_{19}N_3O_2$: C, 60.73; H, 8.07; N, 17.71%. NMR (CCl_4), δ 1.0 (m, 11H), 2.55 (d, 2H), 4.0 (s, 6H). 2-Cyclohexylmethyl-4,6-bis(dimethylamino)-1,3,5-triazine, mp 58—58.5 °C (Ligroin). Found: C, 64.20; H, 9.52; N, 26.73%. Calcd for $C_{14}H_{25}N_5$: C, 63.84; H, 9.57; N, 26.59%. NMR (CCl_4), δ 1.6 (m, 11), 2.3 (d, 2H), 3.1 (s, 12). The procedures of the kinetic measurements were almost the same as those previously described.[16]

References

1) B. Eistert, M. Regitz, G. Heak, and H. Schwall, "Methoden zur Herstellung und Umwandlung von Aliphtischen Diazoverbindungen," in Houben-Weyl "Methoden der Organischen Chemie," 4th Ed. ed by E. Mueller, Band **10/4** (1968), p. 482.

2) P. A. S. Smith and J. G. Wirth, *J. Org. Chem.*, **33**, 1145 (1968).

3) T. Sasaki, S. Eguchi, and A. Kojima, This Bulletin, **41**, 1658 (1968).

4) T. Sasaki, S. Eguchi, and A. Kojima, *J. Heterocycl. Chem.*, **5**, 243 (1968).

5) J. B. F. N. Engberts, G. van Brugger, J. Strating, and H. Wynberg, *Rec. Trav. Chim. Pays-Bas*, **84**, 1610 (1965).

6) H. Reimlinger, *Chem. Ber.*, **97**, 3493 (1964).

7) W. D. Crow and C. Wentrup, *Tetrahedron Lett.*, **1968**, 6149.

8) W. D. Crow, M. N. Paddon-row, and D. S. Sutherland, *ibid.*, **1972**, 2239.

9) C. Grundmann and E. Kober, *J. Amer. Chem. Soc.*, **79**, 944 (1957).

10) J. A. Hendry, F. L. Rose, and A. L. Walpole, *J. Chem. Soc.*, **1958**, 1134.

11) J. S. Gillespie, Jr., S. P. Acharya, and R. E. Davis, *J. Heterocycl. Chem.*, **8**, 723 (1971).

12) J. H. Boyer and N. Golbel, *J. Org. Chem.*, **25**, 304 (1950).

13) In the thermal and photochemical reactions of diazomethyl-triazines with cyclohexane, cyclohexylmethyl-triazine can be said to be the major product in every case without taking a formation of a large amount of tarry matter into account. And all our trials have failed to obtain pure minor by-products by tlc, column or gas chromatography.

14) When azido-triazines were irradiated at 254 nm in EPA at 77 K, a new spectrum involving a vibrational structure assignable to the corresponding triplet nitrene appeared in the long wavelength region in every case. H. Yamada, H. Shizuka, and K. Katsui. *J. Org. Chem.*, **40**, 1351 (1975).

15) For example: D. Betholl, D. Whittacker, and J. D. Calliscer, *J. Chem. Soc.*, **1965**, 2466.

16) R. Kayama, S. Hasunuma, S. Sekiguchi, and K. Matsui, This Bulletin, **47**, 2825 (1974).

BULLETIN OF THE CHEMICAL SOCIETY OF JAPAN, VOL. 48 (11), 3411—3412 (1975)

On the Trimorphism of 7-Hydroxy-3-(*p*-methoxyphenyl)-4,6-dimethyl-1-indanone

Masayuki TAKATORI and Kazuko KANOMATA*

Department of Chemistry, Faculty of Education, Fukushima University, Hamadacho, Fukushima 960

(Received April 5, 1975)

Synopsis. The reaction of 2′-hydroxy-4-methoxy-3′,5′-dimethylchalcone with anhydrous $AlCl_3$ in benzene gave three kinds of crystals having different melting points. It is concluded that the crystals are three modifications of 7-hydroxy-3-(*p*-methoxyphenyl)-4,6-dimethyl-1-indanone on the basis of their mutal transformations, IR spectra and X-ray analysis.

Although the transformation of chalcone into indanone using $AlCl_3$ has already been reported,[1] the indanone obtained by the present authors showed an interesting behavior-polymorphism. Thus, a brief report on the study is presented here.

The attempt to obtain 4,2′-dihydroxy-3′,5′-dimethylchalcone (**1**)[2] from the corresponding 4-methoxychalcone (**2**)[2] by demethylation with the aid of anhydrous $AlCl_3$ in benzene gave colorless needles (**3a**), mp 81—82 °C, colorless plates (**3b**), mp 87—88 °C, and colorless needles (**4**), mp 211—212 °C, besides a small amount of expected **1**.

Compound **3b** ($C_{18}H_{18}O_3$; M^+=282) produced the following UV spectrum (in methanol): 222 (log ε, 4.47), 261.5 (4.03), 286.5 (3.63) and 334 nm (3.26), suggesting the presence of substituted aromatic carbonyl. The NMR spectrum (in CCl_4) of **3b** showed signals due to two methyls (δ=1.77s and 2.13s), one methoxyl (δ=3.66s), five aromatic hydrogens (δ=6.64d, 6.83d each J=9 Hz and δ=6.97 s) and one hydroxyl (δ=9.09 s). The signals (δ=2.36 dd, J=2 and 18 Hz, δ=3.04 dd, J=8 and 18 Hz, and δ=4.29 dd, J=2 and 8 Hz) could be assigned to the $-COCH_2CH=$ group. The IR spectral data are shown in Table 1. All of these results indicate that **3b** is 7-hydroxy-3-(*p*-methoxyphenyl)-4,6-dimethyl-1-indanone with an intramolecular hydrogen bonding between the hydroxyl and the carbonyl groups (Fig. 1).[3] Since dimethyl ether of **4** was identical with methyl ether of **3b**, **4** proved to be 7-hydroxy-3-(*p*-hydroxyphenyl)-4,6-dimethyl-1-indanone. This conclusion was also supported by the spectral data.

Both **3a** and **3b** transformed into colorless crystals (**3c**), mp 95—96 °C, upon heating near to their melting points followed by solidification. It was proved that the structures of **3a** ($C_{18}H_{18}O_3$) and **3c** ($C_{18}H_{18}O_3$) are

TABLE 1. IR SPECTRA OF **3**

Phase	**3a**		**3b**		**3c**	
	ν(OH) cm^{-1}	ν(CO) cm^{-1}	ν(OH) cm^{-1}	ν(CO) cm^{-1}	ν(OH) cm^{-1}	ν(CO) cm^{-1}
KBr	3350	1668	3310	1668	3360	1672
Nujol	3350	1671	3320	1677	3360	1678
In CCl_4 and CS_2	ν(OH) 3310, ν(CO) 1678 cm^{-1}					

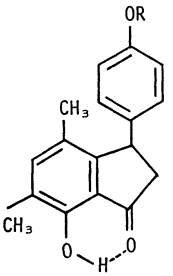

(**3**) R=CH_3
(**4**) R=H

Fig. 1.

identical with that of **3b** by the comparison of their spectra. After crystallizing **3b** as well as **3c** from a small excess of methanol or 75% acetone, metastable **3a** was first separated out and then transformed into **3b**. The modifications **3b** and **3c** remained unchanged on standing at room temperature for five years, but **3a** transformed very slowly into **3b**.

The X-ray diffraction patterns of powdered samples of **3a**, **3b**, and **3c** were entirely different, as shown in Fig. 2. Analysis of the Weissenberg photographs indicated that crystals of both **3a** and **3b** belong to a monoclinic system, and that their lattice constants are a=11.2, b=

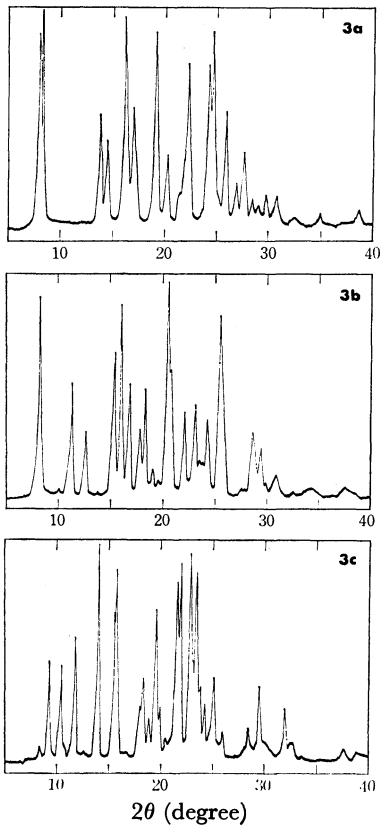

Fig. 2. X-Ray diffraction patterns of **3a**, **3b**, and **3c** by means of Ni filtered Cu$K\alpha$ radiation.

* Present address: Fukushimaken Education Center, Fukushima.

Table 2. Derivatives of indanones (**3** and **4**)

Compound	Color and crystals	Molecular formula	Mp (°C)	Elementary analysis Found (%)	Elementary analysis Calcd (%)	Yield (%)
Methyl ether of **3** (Dimethyl ether of **4**)	Colorless plates	$C_{19}H_{20}O_3$	75— 76	C 76.91 H 6.80	C 77.00 H 6.80	76[a] (79)
Benzoate of **3**	Colorless plates	$C_{25}H_{22}O_4$	183—184	C 77.77 H 5.88	C 77.70 H 5.74	73[a]
Oxime of **3**	Colorless needles	$C_{18}H_{19}NO_3$	151—152 (decomp)	N 4.75	N 4.71	80[a]
2,4-DNPH of **3**	Red needles	$C_{24}H_{22}N_4O_6$	282—284 (decomp)	N 11.83	N 12.12	83[a]
2,4-DNPH of **4**	Reddish orange needles	$C_{23}H_{20}N_4O_6$	285—287 (decomp)	N 12.61	N 12.50	85

a) These values show yields of the derivatives of **3b**. The yields of the derivatives of **3a** and **3c** are nearly the same as those of **3b**.

6.2, $c=10.2$ and $\beta=114°$ for **3a** and $a=10.7$, $b=15.6$, $c=9.3$ and $\beta=100°$ for **3b**. There is a small difference in the IR spectra of these three modifications in KBr and Nujol mull phases. The wave numbers of the absorption bands, ν(OH) and ν(CO), are shown in Table 1.

As mentioned above, it was found that the properties of **3a**, **3b**, and **3c** are different from each other in the solid state. However, the behavior of these modifications is identical in solution. They produced the same oxime, 2,4-DNPH, methyl ether and a benzoyl derivative; in two different solvent systems, their respective R_f values of tlc were the same and they produced identical UV and IR spectra (in CCl_4 and CS_2, Table 1).

Thus, it is concluded that **3a**, **3b**, and **3c** are three modifications of 7-hydroxy-3-(*p*-methoxyphenyl)-4,6-dimethyl-1-indanone.[4-6] The formation of these modifications might be due to differences in the packing mode of the molecule connected with hydrogen bonding in crystals.

Experimental

All melting points are uncorrected. The UV, IR and mass spectra were measured using Hitachi EPS-3T, JASCO IR-G (or DS-701G) and Hitachi RM-50GC spectrometers, respectively. The NMR spectra were recorded on a JEOL MH-100 spectrometer using TMS as an internal standard, and the X-ray analysis was carried out using a Rigakudenki Geigerflex D-2.

Indanone (3 and 4) and Chalcone (1). To a benzene solution of 5.0 g of **2**, 10 g of anhydrous $AlCl_3$ was added, and this suspension was kept at 50 °C for 2 h with stirring. The reaction mixture was hydrolyzed and then steam distilled. The black nonvolatile residue was dissolved in benzene, and to this solution, a 20% aqueous sodium hydroxide was added giving a yellow precipitate. a) From the precipitate; the precipitate was washed with benzene, then acetone and recrystallized from acetone with a small amount of methanol to give lemon yellow needles (**5**), mp about 240 °C (decomp). Compound **5** appeared to be a sodium salt of **3**, but was not further purified. A suspension of **5** in water was acidified, the precipitated white substance was collected and recrystallized from 75% acetone to give 0.61 g (12%) of **3b**. Modifications **3a** and **3c** were also obtained in the above manner. **3a**; Found: C, 76.53; H, 6.54%; mol wt (Rast), 282. **3b**; Found: C, 76.39; H, 6.24%; $M^+=282$. **3c**; Found: C, 76.63; H, 6.28%; $M^+=282$. Calcd for $C_{18}H_{18}O_3$ of **3a**, **3b**, and **3c**: C, 76.58; H, 6.43%; mol wt, 282.3. The R_f values of tlc on polyamide (Merck) were the same, 0.53 (Me_2CO: H_2O 3: 1) and 0.86 (*n*-BuOH: AcOH: H_2O 4: 1: 2) for **3a**, **3b** and **3c**. b) From the filtrate obtained by filtering off **5**; water was added to this filtrate, a benzene layer was taken off, and the precipitate which was produced by passing CO_2 into this sodium hydroxide solution was treated with acetic acid. The insoluble substance was recrystallized from ethanol to give 0.090 g (1.8%) of **4**. Found: C, 76.11; H, 6.08%; $M^+=268$. Calcd for $C_{17}H_{16}O_3$: C, 76.10; H, 6.01%; mol wt, 268.3. NMR (in $CDCl_3$): $\delta=1.87$s and 2.14s (2 CH_3), $\delta=2.55$dd, $J=3$ and 20 Hz, $\delta=3.29$dd, $J=8$ and 20 Hz, $\delta=4.47$dd, $J=3$ and 8 Hz ($-COCH_2CH=$), $\delta=4.87$s and 9.30s (2 OH), $\delta=6.77$d and 6.97d, each $J=8$ Hz and $\delta=7.19$s (aromatic 5H). IR: ν (KBr), 3460, 3330 (2OH) and 1667 cm^{-1} (CO). Compound **4** was also obtained in a 16% yield by refluxing **2** with anhydrous $AlCl_3$ in benzene for 2 hr. The acetic acid solution from which **4** was filtered off was diluted with water. A yellow precipitate was produced and recrystallized from a mixture of benzene and ethanol to give 0.10 g (2.2%) of **1** in the form of orange prisms, mp 190—191 °C. This compound had no mixed melting point decrease with authentic chalcone.[2]

Derivatives from 3a, 3b, and 3c (melthyl ethers, benzoates, oximes and 2,4-DNPH) and from 4 (dimethyl ether and 2,4-DNPH). They were prepared by the usual methods. No pairs of methyl ethers and dimethyl ether, of benzoates and of oximes produced mixed melting point depressions, and the IR spectra and melting points of each derivative from **3a**, **3b**, and **3c** were identical to each other. The NMR spectrum of the methyl ether of **3** showed the presence of two methoxyls ($\delta=3.73$s and 3.93s), and its MW was found to be 296 (Rast). Other properties of these derivatives are shown in Table 2.

The authors wish to thank Professor S. Sasaki of the Miyagi University of Education for reading the manuscript and Assistant Professor T. Ito of Hokkaido University for the lattice constant determinations.

References

1) A. Sammour and M. Elkasaby, *U. A. R. J. Chem.*, **13**, 409 (1970).
2) M. Takatori, *Ann. Rep. Gakugei Faculty Iwate Univ.*, **18**, 31 (1961).
3) V. C. Farmer, N. F. Hayes, and R. H. Thomson, *J. Chem. Soc.*, **1956**, 3600.
4) M. Hirota, *Yuki Gosei Kagaku Kyokai Shi*, **23**, 99 (1965).
5) G. D. Buckley, *J. Chem. Soc.*, **1953**, 1325.
6) G. Sprengling, S. Beatly, and K. B. Adams, *J. Amer. Chem. Soc.*, **72**, 4313 (1950).

BULLETIN OF THE CHEMICAL SOCIETY OF JAPAN, VOL. 48 (11), 3413—3414 (1975)

Studies on Nitro Sugars. VI.[1] Synthesis of Methyl 2-Deoxy-2-nitro-α-D-glucopyranoside Derivatives

Tetsuyoshi TAKAMOTO and Rokuro SUDOH

Department of Chemistry, Tokyo Institute of Technology, Ookayama, Meguro-ku, Tokyo 152

(Received April 28, 1975)

Synopsis. Oxidation of methyl 3-*O*-benzyl-4,6-*O*-benzylidene-2-oximino-α-D-*arabino*-hexopyranoside (**5**) with trifluoroperoxyacetic acid afforded in 76% yield the corresponding 2-nitro-glucopyranoside (**6**) which has a twist-boat conformation in chloroform.

During the course of our synthetic studies[2,3] on nitro sugars by oxidation[4] of sugar oximes with trifluoroperoxyacetic acid, we have presented[5] the synthesis of benzyl 2-deoxy-3,4-*O*-isopropylidene-2-nitro-β-D-arabino- and ribopyranoside from the corresponding 2-oximino derivative. On their PMR spectroscopic conformational discussion, a slightly twisted 1*C* and a twist-boat conformation were elucidated, respectively.

In continuation of this study on 2-deoxy-2-nitropyranosides, we now describe the synthesis and the conformational discussion of methyl 2-deoxy-2-nitro-α-D-glucopyranoside derivatives.

On preparation of 2-nitro sugars in this manner, starting materials should have a free hydroxyl group at the C-2 position. 3-*O*-Benzyl-5,6-di-*O*-acetyl-1,2-*O*-isopropylidene-α-D-glucofuranose[6] (**1**) was heated under reflux in methanol containing 3% hydrogen chloride[7] to afford syrupy methyl 3-*O*-benzyl-α-D-glucopyranoside (**2**) which was easily converted to methyl 3-*O*-benzyl-4,6-*O*-benzylidene-α-D-glucopyranoside (**3**) in 71% overall yield from **1** in the usual manner.

Assignment of α-D-glucopyranoside structure to **3** was based upon a specific rotation of +69.5° (acetone) and coupling constants, $J_{1,2}=3$ and $J_{2,3}=8$ Hz, on the PMR spectrum.

DMSO oxidation of **3** afforded in 54% yield amorphous powder of the corresponding 2-ulose (**4**), 1745 cm^{-1} ($\nu_{C=O}$), which was led to 2-oximino derivative (**5**) in 67% yield. Oxime **5** proved to be either single *syn*- or *anti*-form on the PMR spectrum (Table 1), although oxime is generally obtained as a mixture of them in such a reaction.

Oxidation of **5** with trifluoroperoxyacetic acid[8] at 42—43 °C gave selectively methyl 3-*O*-benzyl-4,6-*O*-benzylidene-2-deoxy-2-nitro-α-D-glucopyranoside (**6**), 1560 cm^{-1} (ν_{asNO_2}), in 76% yield.

On the structural discussion of **6**, the configuration at the C-2 only might be determined because it is unchangeable at the anomeric and the C-3 position in such a oxidation. As shown in Table 1, coupling constants, $J_{2,3}=0$, $J_{3,4}=9$, and $J_{4,5}=8$ Hz which were obtained by the use of decoupling technics for deutrated **6**,[9] indicate that dihedral angles, ϕ_{23}, ϕ_{34}, and ϕ_{45}, are ~100, ~160, and ~170 °, respectively.

All the data, consequently, are consistent with D-gluco form which has a twist-boat conformation. Moreover, for completion of the configurational assignment, **6** was treated with acetic anhydride in the presence of concentrated sulfuric acid to give methyl 3-*O*-benzyl-2-deoxy-4,6-di-*O*-acetyl-2-nitro-α-D-glucopyranoside (**7**). The coupling constants, $J_{2,3}=9$, $J_{3,4}=10$, and $J_{4,5}=11$ Hz, indicate that H^2, H^3, H^4, and H^5 have diaxial relationship each other. Therefore diacetate **7** has obviously a *C*1 conformation, being different from the case of **6**.

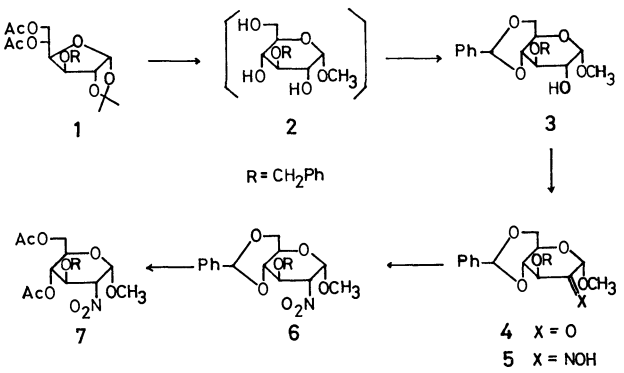

Experimental

General. Melting points were determined in capillaries and are uncorrected. Specific rotations were measured with a Carl Zeiss photoelectric polarimeter. PMR spectra were recorded at 100 MHz with a JEOL spectrometer (Type JNM-4H-100) and tetramethylsilane as an internal standard. IR spectra were obtained with a Hitachi EPI-S2 instrument.

TABLE 1. PMR DATA FOR RING PROTONS (H^1–H^4) AND OTHER SUBSTITUENTS OF METHYL 3-*O*-BENZYL-α-D-GLUCOPYRANOSIDE DERIVATIVES (in $CDCl_3$)

Compound	Chemical shift (ppm)				Coupling constant (Hz)				Chemical shift (ppm)			
	H^1	H^2	H^3	H^4	J_{12}	J_{23}	J_{34}	J_{45}	$PhCH_2$	OCH_3	PhCH	OAc
3	4.72	4.25	?	?	3	8	?	?	4.83	3.57	5.50	—
5	5.82	—	4.54	?	—	—	10	?	4.80	3.39	5.53	—
6	5.22	4.61	4.63	?	3	0	9	8	4.86	3.36	5.59	—
7	5.17	5.05	4.60	4.53	3	9	10	11	4.70	3.34	—	2.04 1.96

Methyl 3-O-benzyl-4,6-O-benzylidene-α-D-glucopyranoside (3). To a suspension of 3-*O*-benzyl-5,6-di-*O*-acetyl-1,2-*O*-isopropylidene-α-D-glucofuranose[6] (**1**) (20 g) and anhydrous methanol (125 ml), was added acetyl chloride (6 ml)[7] slowly. After refluxed for 6 h, the reaction mixture was cooled to room temperature and poured into saturated sodium bicarbonate solution with stirring. Removal of inorganic substances by using ethanol and evaporation of the solvent gave syrup (16.7 g, negative Fehling test) which was stirred vigorously with benzaldehyde (50 ml) in the presence of zinc chloride (10 g) for 14 h. Work up in the usual manner gave crude solid which was recrystallized from ethanol to give fine crystals (13.4 g, 71%): mp 180—180.5 °C, $[\alpha]_D^{20}$ +69.5° (*c* 1, acetone). Found: C, 67.90; H, 6.60%. Calcd for $C_{21}H_{24}O_6$: C, 67.73; H, 6.50%.

Methyl 3-O-benzyl-4,6-O-benzylidene-α-D-arabino-hexopyranosid-2-ulose (4). After a mixture of **3** (0.74 g), distilled dimethyl sulfoxide (6 ml), and distilled acetic anhydride (4 ml) was stirred for 24 h at room temperature, the mixture was evaporated *in vacuo* below 60 °C. The solution of the residue in ethyl acetate (30 ml) was washed with water and evaporated to give yellowish solid which was reprecipitated from ethanol: amorphous powder 0.4 g (54%), 1745 cm^{-1} ($\nu_{C=O}$). Found: C, 67.79; H, 5.99%. Calcd for $C_{21}H_{22}O_6$: C, 68.07; H, 5.99 %.

Methyl 3-O-benzyl-4,6-3-O-benzylidene-2-oximino-α-D-arabino-hexopyranoside (5). A solution of **4** (1.3 g) in a mixture of pyridine (7 ml) and ethanol (7 ml) was heated under reflux in the presence of hydroxylamine hydrochloride (1 g) for 2 h. The mixture was evaporated *in vacuo* to give syrupy residue which was washed with water several times and put on a column (7.0×3.5 cm) of silica gel. After elution of benzene (100 ml), oxime **5** was eluted with a solvent system 19 : 1 benzene–methanol. Removal of the solvent gave amorphous solid which was reprecipitated from ethanol to give **5** (0.9 g, 67%): mp 182—183 °C, $[\alpha]_D^{20}$ −54.3° (*c* 0.8, acetone), 3280 cm^{-1} (ν_{OH}). Found: C, 65.21; H, 6.02; N, 3.90%. Calcd for $C_{21}H_{23}O_6N$: C, 65.44; H, 6.02; N, 3.63%.

Methyl 3-O-benzyl-4,6-O-benzylidene-2-deoxy-2-nitro-α-D-glucopyranoside (6). To oxidizing reagent[8] prepared by mixing successively 90% hydrogen peroxide (0.25 ml), trifluoroacetic anhydride (1.5 ml), acetonitrile (5 ml), dibasic sodium phosphate (5.75 g), and urea (45 mg), was added a solution of **5** (1 g) in acetonitrile (40 ml) dropwisely with manual stirring. After the mixture was kept at 42—43 °C for 1 h, the solvent was removed *in vacuo* to give solid which was dissolved in chloroform and washed with water three times. Evaporation *in vacuo* gave crude product which chromatographed on a column of silica gel with benzene. The eluate that showed a single spot at R_f 0.71 on tlc in a solvent system 30 : 1 benzene–acetone, was evaporated *in vacuo* to give the product (0.9 g, 86%). Recrystallization from ethanol–petroleum ether gave **6** (0.79g, 76%): mp 121—122 °C, $[\alpha]_D^{20}$ +75.4° (*c* 1, acetone), 1560 cm^{-1} (ν_{asNO_2}). Found: C, 62.67; H, 6.04; N, 3.56%. Calcd for $C_{21}H_{23}O_7N$: C, 62.83; H, 5.78; N, 3.49%.

Methyl 3-O-benzyl-2-deoxy-4,6-di-O-acetyl-2-nitro-α-D-glucopyranoside (7). **6** (207 mg) was treated with acetic anhydride (500 mg) in the presence of concentrated sulfuric acid (6 mg) at room temperature. After 30 min, the red mixture was poured into sodium bicarbonate solution and extracted with dichloromethane. The extracts were washed with water and dried over sodium sulfate, and then was evaporated to give the product which was recrystallized from ethanol–petroleum ether: white needles (60 mg, 30%), mp 148—149 °C, $[\alpha]_D^{20}$ +96° (*c* 1, chloroform), 1555 cm^{-1} (ν_{asNO_2}). Found: C, 54.19; H, 5.65; N, 3.59%. Calcd for $C_{18}H_{23}O_9N$: C, 54.40; H, 5.83; N, 3.53%.

The authors are indebted to Mitsubishi Gas Chemical Co., Inc., for the gift of 90% hydrogen peroxide and to Mr. H. Matsumoto for recording the PMR spectra.

References

1) Part V, T. Takamoto, H. Tanaka, and R. Sudoh, *Chem. Lett.*, **1972**, 1125.

2) T. Takamoto, R. Sudoh, and T. Nakagawa, *Carbohyd. Res.*, **27**, 135 (1973).

3) T. Takamoto, Y. Yokota, R. Sudoh, and T. Nakagawa, This Bulletin, **46**, 1532 (1973).

4) Baer and Chiu reported that the oxidation of 3-amino-glycopyranoside derivatives with *m*-chloroperbenzoic acid to give the corresponding 3-nitro and 3-nitroso sugars; H. H. Baer and S. L. Chiu, *Can. J. Chem.*, **51**, 1812 (1973).

5) T. Takamoto, M. Ohki, R. Sudoh, and T. Nakagawa, This Bulletin, **46**, 670 (1973).

6) K. Freudenberg, W. Dürr, and J. Von Hochstetter, *Ber.*, **61**, 1735 (1928).

7) 3% Solution of hydrogen chloride in methanol was prepared from acetyl chloride and methanol; L. F. Fieser and M. Fieser, "Reagents for Organic Synthesis", Vol. 1, John Wiley & Son, Inc., New York (1967), p. 11,.

8) W. D. Emmons and A. S. Pagano, *J. Amer. Chem. Soc.*, **77**, 4557 (1955).

9) Deutration at the C-2 position was performed by treatment with 1% NaOD in acetonitrile.

BULLETIN OF THE CHEMICAL SOCIETY OF JAPAN, VOL. 48 (11), 3415—3416 (1975)

Oxidation of Isocyanides by Hg(II), Tl(III), and Pb(IV) Acetates

Sakuya TANAKA, Hiroshi KIDO, Sakae UEMURA, and Masaya OKANO*

Institute for Chemical Research, Kyoto University, Uji, Kyoto 611

(Received May 2, 1975)

Synopsis. Isocyanides were oxidized to isocyanates in acetic acid in the presence of Hg(II), Tl(III), or Pb(IV) acetate through acetoxymetallation. The reaction of an isocyanide with Tl(III) acetate in various alcohols gave the corresponding carbamates in good yields.

Oxymetallations of isocyanides (α-addition) have recently been proposed in the carbamate formation from isocyanides by use of Tl(III) nitrate[1] and Hg(II) salts.[2] We now report the oxidation of isocyanides to the corresponding isocyanates by Hg(II), Tl(III), or Pb(IV) acetate in acetic acid which seems to proceed through acetoxymetallation. Various other reagents for such oxidation are cited in a review by Saegusa and Ito.[3]

Results and Discussion

When cyclohexyl isocyanide was treated with Hg(II), Tl(III), or Pb(IV) acetate in a mixture of benzene and acetic acid (9: 1 by volume) at 5—10 °C, cyclohexyl isocyanate was obtained as the product. The reaction also proceeded in acetic acid at 20 °C, but the yield of isocyanate was slightly lower. The metal acetates were reduced to Hg metal and Tl(I) and Pb(II) acetates, respectively. Some typical results are listed in Table 1. In the absence of metal acetates, no isocyanate was formed under any conditions shown in Table 1. An

Table 1. Isocyanates from isocyanides[a]

R–NC (10 mmol) R	Metal acetate (10 mmol)	React. temp. (°C)	React. time (h)	Yield of R–NCO (%)[b]
c-C_6H_{11}	$Hg(OAc)_2$	5—10	2.5	69
c-C_6H_{11}	$Hg(OAc)_2$	20	3	64[c]
c-C_6H_{11}	$Tl(OAc)_3$	5	3	54
c-C_6H_{11}	$Pb(OAc)_4$	5	3	54
c-C_6H_{11}	$Pb(OAc)_4$	80	0.2	19
C_6H_5	$Pb(OAc)_4$	5	3	41

a) Solvent: Benzene+AcOH (9: 1 by volume) 20 ml. b) Determined by glc. c) Solvent: AcOH 20 ml.

elongation of the reaction time or an elevation of the temperature resulted in a decrease of the yield of isocyanate because of the formation of formamide from isocyanide and acetic acid and also of the secondary reaction of isocyanate with acetic acid. The reaction with Mn(III) and Co(III) acetates[4] instead of the above metal acetates gave only a trace amount of the isocyanate and almost all of the starting isocyanide was recovered. Moreover, although the oxidations of alkylbenzenes and olefins with Pb(IV), Mn(III), and Co(III) acetates are known to involve radical pathways,[5] no products which seemed to result from a radical reaction could be detected even at higher reaction temperatures.

Considering the well-known nature of Hg(II), Tl(III), and Pb(IV) acetates to afford oxymetallates of olefins and acetylenes and a proposal of oxymetallation of isocyanides,[1,2] it seems to be reasonable to assume that the reaction proceeded through acetoxymetallation as shown in Scheme 1. All attempts to isolate the intermediate acetoxymetallate of cyclohexyl and phenyl isocyanides were unsuccessful.

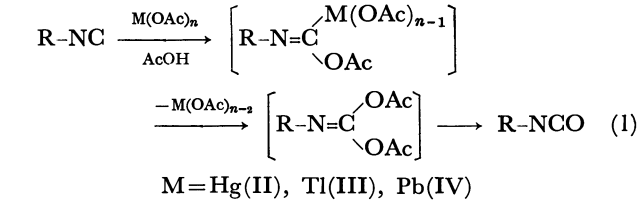

M=Hg(II), Tl(III), Pb(IV)

Table 2. Carbamates from cyclohexyl isocyanide[a]

Alcohol (20 ml) R′ in R′OH	React. temp. (°C)	React. time (h)	Yield of *c*-$C_6H_{11}NHCO_2R'$[b] (%)
Me	65	1	62
Et	65—70	1	68
n-Pr	65—70	1	72
i-Pr	65—70	1	75
t-Bu	65—70	2	49
CH_2CH_2OH	65—70	1	36[c]

a) *c*-$C_6H_{11}NC$ 10 mmol, $Tl(OAc)_3$ 10 mmol. b) Determined by glc. A small amount (<10%) of *c*-$C_6H_{11}NHCOCH_3$ was always formed. c) *c*-$C_6H_{11}NHCO_2CH_2CH_2OAc$.

It has been reported that Tl(III) nitrate is a good reagent for synthesis of carbamates from isocyanides, but unfortunately only in methanol.[1] As we found that Tl(III) acetate could be used successfully in various alcohols for this purpose, we would like to add here the results obtained by using cyclohexyl isocyanide (Table 2). Carbamates may be formed mainly *via* alkoxythallation of the isocyanide, followed by redox decomposition to iminocarbonates which react with acetic acid (Scheme 2).

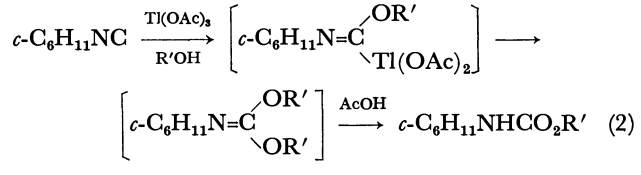

The protolysis of iminocarbonates to give carbamates has already been reported.[6] When ethylene glycol was used as an alcohol component, the expected carbamate, *c*-$C_6H_{11}NHCO_2CH_2CH_2OAc$, which may be derived from ethylene *N*-cyclohexyl iminocarbonate, was obtained as the only product.

* To whom correspondence should be addressed.

Experimental

The IR spectra were taken with a Hitachi EPI-S2 spectrometer. Glc analyses were carried out with a Shimadzu 5APTF apparatus, using Apiezon L(30%)-Celite (1m) and EGSS-X(30%)-Chromosorb W (1m) columns (N_2 as the carrier gas).

Materials. Isocyanides (R–NC) were prepared by the method of Ugi *et al*:[7] R=*c*-C_6H_{11}, bp 65—69 °C/20 mmHg (lit,[7] bp 56—58 °C/11 mmHg); R=C_6H_5, bp 57.5 °C/19.5 mmHg (lit,[7] bp 50—51 °C/11 mmHg). Other organic materials including the solvents were purified before use by distillation. Commercial inorganic materials were used without further purification. $Tl(OAc)_3$ was prepared from Tl_2O_3 and acetic acid. Mn(III) and Co(III) acetates were prepared by the reported method.[4]

Reaction of Isocyanides with Metal Acetates in Acetic Acid. A typical experimental procedure is given below. To a stirred suspension of $Tl(OAc)_3$ (3.82 g, 10 mmol) in a mixture of benzene (18 ml)–AcOH (2 ml) was added slowly cyclohexyl isocyanide (1.09 g, 10 mmol) under cooling with an ice-bath and the resulting mixture was stirred for 3 h at 5 °C. After the precipitated TlOAc was filtered off from the reaction mixture, the filtrate was combined with benzene (50 ml) and washed with 50 ml of cold water and with aq. $NaHCO_3$ (50 ml). After being dried over Na_2SO_4, the benzene was evaporated to leave *ca.* 5 ml of a residue. Glc analysis of the residue by using iodobenzene as an internal standard revealed the presence of 5.4 mmol (54% yield based on $Tl(OAc)_3$ charged) of cyclohexyl isocyanate. Distillation gave 0.25 g of a pure compound: bp 52 °C/24 mmHg; IR, 2250 ($\nu_{N=C=O}$) cm^{-1}.

Reaction of Cyclohexyl Isocyanide with Tl(OAc)$_3$ in Alcohols. As an example, the reaction in ethanol is given below. To an orange suspension of $Tl(OAc)_3$ (3.82 g, 10 mmol) in ethanol (20 ml) was added cyclohexyl isocyanide (1.09 g, 10 mmol) at room temperature and the resulting mixture was heated for 1 h at 65—70 °C. After being cooled down to room temperature, the precipitated TlOAc (1.4 g, 5.3 mmol) was filtered off. The filtrate was treated as described above. Glc analysis of the residue by using ethyl benzoate as an internal standard showed the presence of 6.8 mmol (68% yield) of ethyl *N*-cyclohexyl carbamate. Distillation gave 0.5 g of crude product, which was recrystallized from *n*-hexane: mp 53.5—55 °C (lit,[8] mp 55—56 °C).

In a similar way, the following carbamates (*c*-$C_6H_{11}NHCO_2R'$) were obtained: R'=Me, mp 72—73.5 °C (lit,[8] mp 75 °C); R'=*n*-Pr, mp 40—41 °C from *n*-hexane; R'=*i*-Pr, mp 65—66.5 °C (lit,[9] mp 66.5—67 °C); R'=*t*-Bu, mp 65—68 °C (lit,[10] mp 68—69 °C); R'=CH_2CH_2OAc, mp 77—79 °C (lit,[11] mp 83.5 °C). The last compound was identified by comparison of IR and NMR spectra with an authentic sample prepared from the reaction of ethylene *N*-cyclohexyl iminocarbonate with acetic acid in ethylene glycol or benzene.[6]

References

1) F. Kienzle, *Tetrahedron Lett.*, **1972**, 1771.
2) H. Sawai and T. Takizawa, *ibid.*, **1972**, 4263.
3) T. Saegusa and Y. Ito, "Isonitrile Chemistry," ed. by I. Ugi, Academic Press, New York, N. Y. (1971), p. 79.
4) S. Uemura, A. Spencer, and G. Wilkinson, *J. Chem. Soc. Dalton*, **1973**, 2565.
5) E. I. Heiba, R. M. Dessau, and W. J. Koehl, Jr., *J. Amer. Chem. Soc.*, **91**, 6830 (1969), and references cited therein.
6) T. Mukaiyama, T. Fujisawa, and T. Hyugaji, This Bulletin, **35**, 687 (1961).
7) I. Ugi and R. Meyr, *Chem. Ber.*, **93**, 239 (1960).
8) M. Barker, L. Hunter, and N. G. Reynolds, *J. Chem. Soc.*, **1948**, 874.
9) Z. G. Hajos, D. R. Parrish, and M. W. Goldberg, *J. Org. Chem.*, **30**, 2849 (1965).
10) M. Okano, Y. Ito, T. Shono, and R. Oda, This Bulletin, **36**, 1314 (1963).
11) R. Delaby, A. Sekera, P. Chabrier, and P. Piganiol, *Bull. Soc. Chim. Fr.*, **1951**, 392.

BULLETIN OF THE CHEMICAL SOCIETY OF JAPAN, VOL. 48 (11), 3417—3418 (1975)

Iron Carbonyl-catalyzed Reactions of Allyl Ethers and Amines Involving Claisen-type Rearrangement

Jitsuo KIJI, Satoshi NISHIMURA, Kazuyoshi YAMAMOTO, and Junji FURUKAWA
Department of Synthetic Chemistry, Kyoto University, Sakyo-ku, Kyoto 606

(Received May 2, 1975)

Synopsis. The iron carbonyl-catalyzed reaction of diallyl ether with morpholine gives 1,4-dienylamine. Diallylamine isomerizes to 4-aza-6-methyl-1,4-nonadiene.

Allylic compounds such as allyl alcohol or diallyl ether undergo a variety of reactions under the influence of transition metal complexes. Palladium-,[1] nickel-,[2] rhodium-,[3] and ion carbonyl-[4] catalyzed reactions have already been reported. These reactions attracted our attention from a view-point of synthetic application. Iron carbonyl reacts with cyclic compounds, which have a nitrogen or oxygen atom at the allylic position, resulting in interesting intermediates.[5,6] These reports prompted us to investigated the iron carbonyl-catalyzed reactions of some allylic compounds.

Results and Discussion

In the presence of $Fe_2(CO)_9$ diallyl ether (I) reacted with morpholine to give 1,4-dienylamine (II) in moderate yield, while nickel[2] and palladium[7]-catalyzed reactions give allyl amine (II'). A considerable amount of diallyl ether was recovered unchanged in each case.

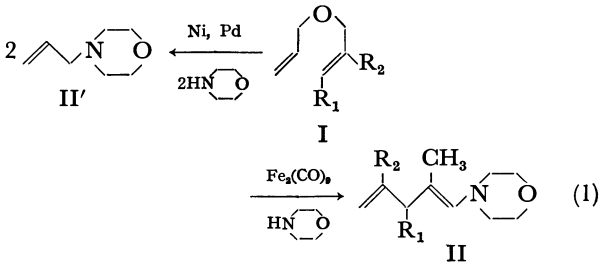

II′ I II (1)

a: $R_1=R_2=H$, 40%.
b: $R_1=CH_3$, $R_2=H$, 27%.
c: $R_1=H$, $R_2=CH_3$, 17%.

The structure of II is indicated by spectroscopic data. This reaction can be explained reasonably by the isomerization of the double bond, followed by Claisen rearrangement and condensation of the substituted 4-pentanal (III) with morpholine. In fact, the diallyl ether isomerized to III in a very low yield without morpholine. Morpholine was superior to piperidine and benzylamine with regard to the yield of II.

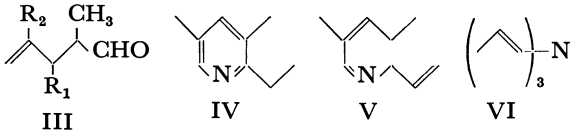

III IV V VI

These facts show that the $Fe_2(CO)_9$–morpholine system plays a significant role in the isomerization of the double bond. Under these conditions, however, no reaction was observed with dimethallyl ether and allyl phenyl ether.

The reaction of the allylamines is interesting to note. The reaction of diallylamine catalyzed by $Fe(CO)_5$ or $Fe_2(CO)_9$ in a sealed tube at 160 °C gave 2,3,5-trisubstituted pyridine (IV). However, at *ca.* 112 °C (reflux) linear amine (V) was formed in moderate yield (see Table 1). Falbe *et al.*[8] have reported that the reaction of allylamine $C_3H_5NH_2$ catalyzed by $Fe(CO)_5$ at 250 °C at a high pressure of carbon monoxide forms IV through the formation of V in a 30% yield. The reaction of diallylamine takes place under more mild conditions than those of the latter. Therefore, it seems probable that the first step of the Falbe reaction is the formation of diallylamine, since the primary amine is converted to the secondary or tertiary amine under the influence of transition metal catalysts.[9]

This reaction is also explainable in terms of Claisen-"type" rearrangement. Triallylamine seems to be a key intermediate of this reaction. To gain insight into the reaction, triallylamine was allowed to react in the presence of $Fe_2(CO)_9$. In this case, however, rapid isomerization of the double bond occurred and VI was formed in high yield (>80%), *i.e.*, this isomerization is so fast that Claisen-"type" rearrangement does not take

Table 1. Reaction of allylamines

Run No.	Allylamine (mmol)	Catalyst (mmol)	Reaction Temp. (C)	Reaction Time (h)	Product yield % (mmol)
1	$(C_3H_5)_2NH$, 8.1	$Fe(CO)_5$, 0.5	160	20	V, 42 (1.7)
2	$(C_3H_5)_2NH$, 16.2	$Fe_2(CO)_9$, 0.1	112	10	V, 52 (4.2)
3	$(C_3H_5)_3N$, 6	$Fe_2(CO)_9$, 0.03	120	7	VI>80
4	$(C_3H_5)_3N$, 6	$Pd(NO_3)_2$, 0.15; n-Bu_3P 0.4	110	20	VI, 14
5	$(C_3H_5)_3N$, 6; Morpholine, 1 ml	$Fe_2(CO)_9$, 0.1	120	20	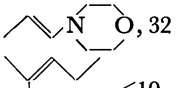 , 32
6	$(C_3H_5)_2N$-Bu^n, 6	$Fe_2(CO)_9$, 0.1	160	20	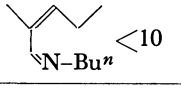 <10

place. The use of morpholine as the solvent in this reaction resulted in the formation of *N*-(1-propenyl)morpholine (II'). The isomerization of the double bonds of triallylamine by $Fe_2(CO)_9$ proceeded more smoothly than the *t*-BuOK-catalyzed isomerization. Gas chromatographic analysis of the products of the latter reaction showed the presence of many isomers and the yields were in general low.

Experimental

Reactions. All the reactions were carried out in a sealed glass tube (8 mm in diameter).

Diallyl Ether with Morpholine: Iron enneacarbonyl (0.06 mmol) was placed in the tube. The tube was fitted with a three-way stopcock, through which the reagents were introduced by a syringe. Diallyl ether (0.5 ml, *ca.* 4 mmol) and morpholine (1 ml) were added in an atmosphere of argon. The tube was sealed with a flame and heated at 120 °C for 20 h.

Allylamines: All the reactions except run 2 (Table 1) were carried out in a manner similar to that described above. The reaction conditions are summarized in Table 1.

Analysis and Identification. Gas chromatographic analysis was performed on a column of Silicon DC 550 on Celite, 3 m in height, at 100—200 °C, using tetralin or *p*-xylene as an internal standard. The products were identified by analyzing the mass, IR and NMR spectra of the samples collected by gas chromatography.

References

1) W. Hafner, H. Prigge, and J. Smidt, *Liebig Ann. Chem.*, **693**, 109 (1966).
2) J. Furukawa, J. Kiji, K. Yamamoto, and T. Tojo, *Tetrahedron*, **29**, 3149 (1973).
3) A. Bright, J. F. Malone, J. K. Nicholson, J. Powell, and B. L. Shaw, *Chem. Commun.*, **1971**, 712.
4) F. G. Cowherd and J. L. von Rosenberg, *J. Amer. Chem., Soc.*, **91**, 2157 (1969).
5) R. Auman, K. Fröhlich, and H. Ring, *Angew. Chem.*, **86**, 309 (1974).
6) Y. Becker, A. Eisenstadt, and Y. Shvo, *Tetrahedron*, **30**, 839 (1974).
7) K. Takahashi, A. Miyake, and G. Hata, This Bulletin, **45**, 230 (1970).
8) J. Falbe, M. Weitkamp, and F. Korte, *Tetrahedron Lett.*, **1965**, 2677.
9) G. Brieger and T. J. Nestrick, *Chem. Rev.*, **74**, 567 (1974).

BULLETIN OF THE CHEMICAL SOCIETY OF JAPAN, VOL. 48 (11), 3419—3420 (1975)

Phenolysis of 1,1- and 3,3-Dimethylallyl Chlorides. Rates and Product Distributions

Ken'ichi TAKEUCHI, Yoshinobu FUJII, and Kunio OKAMOTO

Department of Hydrocarbon Chemistry, Faculty of Engineering, Kyoto University, Kyoto 606

(Received May 29, 1975)

Synopsis. The phenolyses of 1,1- and 3,3-dimethylallyl chlorides were shown by kinetic studies to undergo S_N1 solvolysis. The distributions of the products, dimethylallyl phenyl ethers and (dimethylallyl)phenols, supported the mechanism that involves both localized ion-pairs and mesomeric ion-pairs.

Since the finding of the significance of ion-pair intermediates by Young, Winstein and Goering[1] for the solvolysis of 1,1-dimethylallyl chloride, various efforts have been made to characterize the intermediates involved in the solvolysis of allylic compounds.[2,3] Recent works by Sneen and his coworkers[4] and by Wiberg and Nakahira[5] on the solvolyses of allylic compounds appear to have provided clear-cut evidence for the presence of discrete unsymmetrical ion-pairs preceding the formation of a symmetrical mesomeric ion-pair.

In the course of our study of solvolytic reactions in phenol,[6] the present authors have shown that phenol is characterized as a typical solvolytic solvent[7a] and that the phenolysis products provide useful information concerning the characteristics of the intermediates due to the ambident nature of the phenol molecule as a nucleophile.[7b] Consequently, the present study of the rates and products of the solvolysis of 1,1- and 3,3-dimethylallyl chlorides in binary mixtures of phenol with benzene was undertaken in the hope of distinguishing the intermediates I, II, and III which have occasionally been postulated in the solvolysis of the two isomeric chlorides.[1-4]

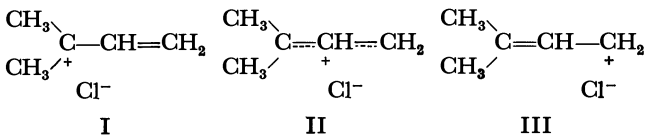

I II III

The rates of solvolysis were determined titrimetrically in phenol-benzene (1:9—3:7 by wt.) buffered with triethylamine. As expected from previous work,[1] the first-order plots for the solvolysis of 1,1-dimethylallyl chloride (1,1-DMAC) exhibited a downward drift as the reaction proceeded, showing concurrent rearrangement to 3,3-dimethylallyl chloride (3,3-DMAC). The

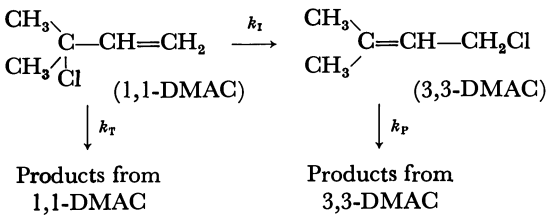

first-order rate constants (k_T, k_P, and k_I) were determined following the method of Young, Winstein and Goering[1] and are summarized in Table 1. The plots of the rate constants as a function of the Y-values[7a] provided

Table 1. Titrimetric phenolysis rates of 1,1- and 3,3-dimethylallyl chlorides in phenol–benzene at 25 °C[a]

Solvent[b]	Chloride M	Et_3N M	k_T	k_P $\times 10^5$ s^{-1}	k_I
1,1-Dimethylallyl chloride					
10% PhOH	0.0440	0.0571	12.2	—	17.3
20% PhOH	0.0462	0.0555	110	—	180
30% PhOH	0.0486	0.0554	408	—	450
3,3-Dimethylallyl chloride					
10% PhOH	0.0458	0.0553	—	3.89	—
20% PhOH	0.0392	0.0554	—	33.9	—
30% PhOH	0.0482	0.0644	—	120	—

a) The temperature controlled at ±0.05°C. b) Percent by weight of phenol in phenol–benzene.

Grunwald-Winstein m-values[8] of 0.95, 0.96, and 0.91 for k_T, k_P, and k_I, respectively. The magnitude of the present m-values of approximately 1.0 provides an evidence for the S_N1 character of the phenolysis of 1,1- and 3,3-dimethylallyl chlorides.

The products, 1,1- and 3,3-dimethylallyl phenyl ethers and *o*- and *p*-(dimethylallyl)phenols, were isolated by tlc. Control experiments revealed that the phenyl ethers neither interchanged with each other, nor isomerized to alkenylphenols during the reaction and work-up. The isolated yields of the products were divided by the recovery percents which were determined from the control experiments. The corrected yields thus calculated are shown in the first column under the respective starting chlorides in Table 2. As pointed out above, 1,1-DMAC isomerizes to 3,3-DMAC during phenolysis. Therefore, the product in the solvolysis of 1,1-DMAC is actually a

Table 2. Product distribution in the phenolysis of 1,1- and 3,3-dimethylallyl chlorides in phenol–benzene (1:4 by wt) at 25 °C

Product[a]	1,1-DMAC		3,3-DMAC		1,1-DMAC (Estimated)	
	Yield %	Ratio[b]	Yield %	Ratio[b]	Yield %	Ratio[b]
R_POPh	17.0	1.0	21.2	1.0	10.1	1.0
R_TOPh	38.6	2.3	31.0	1.5	51.0	5.0
o-R_PPhOH	12.8	1.0	20.0	1.0	10.1	1.0
p-R_PPhOH	13.6	1.1	12.9	0.65	14.7	1.5
o-R_TPhOH	≦0.25	~0	≦0.25	~0	≦0.25	~0
p-R_TPhOH	0.0	0.0	0.0	0.0	0.0	0.0
Total[c]	82.2		85.3		86.1	

a) R_P=3,3-dimethylallyl, R_T=1,1-dimethylallyl b) Ratios based on R_POPh for the ethers and on *o*-R_PPhOH for the phenols. c) The rest is presumed to have been lost as hydrocarbon products.

blend of those from 1,1- and 3,3-DMAC. Thus the product distribution from 1,1-DMAC itself was estimated by utilizing the rate constants k_T, k_P, and k_I and the yields of the products from 3,3-DMAC alone. The results are shown in the fifth and sixth columns of Table 2. The ratio of the amount of tertiary alkenyl phenyl ether to that of the primary ether is 5.0 in the phenolysis of 1,1-DMAC, while it is 1.5 for 3,3-DMAC. Since kinetic studies showed that the phenolyses of the both chlorides are classified as S_N1-type solvolysis, the product spread[2a] in the ether formation will be explained most reasonably by postulating that the localized ion-pairs I and III are first formed from the corresponding chlorides.

The finding that 1,1-DMAC gives a larger *para*: *ortho* product ratio in (3,3-dimethylallyl)phenol than 3,3-DMAC appears to require the presence of another intermediate which attacks the phenol nucleus with higher *para* selectivity than the intermediate III. The postulation of a mesomeric intermediate II, which is present in equilibrium with III, gives a plausible explanation, since it is presumed that the intermediate II exhibits a larger steric requirement than the localized ion-pair III in *ortho* substitution, which leads to higher *para* selectivity.

It should be pointed out that no *p*-(1,1-dimethylallyl)-phenol could be detected in the product to within experimental error, with the corresponding *ortho*-isomer produced being less than 0.25%, if at all present. The absence of (1,1-dimethylallyl)phenol in the products is in accord with the absence of the same product in the reaction of isoprene with phenol catalyzed by phosphoric acid.[9] Presumably, the tertiary carbonium ion center is more sterically hindered to nucleophilic approach of the phenol nucleus than the primary carbonium ion center. A similar phenomenon has been observed in the trapping of intermediates with borohydride and in the *t*-butanolysis of 1,1- and 3,3-DMAC.[10]

The present results support the presence of two localized ion-pairs (I and III) and one mesomeric ion-pair (II).

Experimental

Materials. The isomeric chlorides were prepared by the method reported by Sneen and Kay[4b] and stored at −78 °C in the presence of small amounts of anhydrous potassium carbonate. The purity of each chloride was checked by glpc[10] just prior to use; 1,1-DMAC, bp 33.9—34.2 °C/150 Torr, n_D^{20} 1.4190; 3,3-DMAC, bp 59—66 °C/160 Torr, n_D^{20} 1.4489. Other organic reagents employed were of analytical grade and were fractionated before use.

Kinetic Measurement. The pipetting technique[7a] was employed and the first-order rate constants determined in the manner described in the literature.[1]

Isolation of the Phenolysis Product. To 1,1-DMAC (525.7 mg, 5.02 mmol) was added 100 ml of phenol–benzene (1:4 by wt.) containing 0.055 M of triethylamine which had been previously equilibrated at 25 °C. After 4 h at this temperature, the solution poured into 200 ml of chilled ether. The ether solution was washed with chilled water and then with a chilled 10% sodium hydroxide solution, and dried over magnesium sulfate. After evaporation of the ether, the products were separated by tlc (silica gel) into three fractions, alkenyl phenyl ethers, *o*- and *p*-alkenylphenols. The isomer distribution in each fraction was determined by NMR. The phenolysis of 3,3-DMAC was carried out in the same manner except that the reaction was conducted for 16 h.

References

1) W. G. Young, S. Winstein, and H. L. Goering, *J. Amer. Chem. Soc.*, **73**, 1958 (1951).

2) For reviews see a) R. H. DeWolfe and W. G. Young, *Chem. Rev.*, **56**, 794 (1956). b) P. B. D. de la Mare, "Molecular Rearrangements," Vol. 1, ed. by P. de Mayo, Interscience Publishers, New York, N. Y. (1963), Chapter 2.

3) P. B. D. de la Mare and C. A. Vernon, *J. Chem. Soc.*, **1954**, 2504.

4) a) R. A. Sneen and W. A. Bradley, *J. Amer. Chem. Soc.*, **94**, 6975 (1972). b) R. A. Sneen and P. S. Kay, *ibid.*, **94**, 6983 (1972). c) R. A. Sneen and J. V. Carter, *ibid.*, **94**, 6990 (1972).

5) K. B. Wiberg and T. Nakahira, *Tetrahedron Lett.*, **1974**, 1769, 1773.

6) K. Okamoto, T. Kinoshita, Y. Takemura, and H. Yoneda, *J. Chem. Soc. Perkin II*, **1975**, in press, and previous work cited therein.

7) a) K. Okamoto, K. Matsubara, and T. Kinoshita, This Bulletin, **45**, 1191 (1972). b) K. Okamoto and T. Kinoshita, *Chem. Lett.*, **1974**, 1037.

8) E. Grunwald and S. Winstein, *J. Amer. Chem. Soc.*, **70**, 846 (1948).

9) A. R. Bader and W. C. Bean, *ibid.*, **80**, 3073 (1958).

10) M. Eckert-Maksić, Z. Majerski, S. Borčić, and D. E. Sunko, *Tetrahedron*, **27**, 2119 (1971).

BULLETIN OF THE CHEMICAL SOCIETY OF JAPAN, VOL. 48 (11), 3421—3422 (1975)

The Synthesis of the Benzofuro[2,3-*b*]benzofuran Derivative

Mutsumu NANBU, Kaishû MOMONOI, Susumu OGURO, and Yoshiyuki KAWASE

Department of Chemistry, Faculty of Literature and Science, Toyama University, Gofuku, Toyama 930

(Received May 15, 1975)

Synopsis. The synthesis of 2,9-dimethoxybenzofuro-[2,3-*b*]benzofuran from its 5a,10b-dihydro-compound was carried out by bromination with *N*-bromosuccinimide, followed by dehydrobromination. The attempted preparation of 2,9-dimethyl-, 2,9-dichloro-, and 2,4,7,9-tetrachloro-derivatives was unsuccessful.

The synthesis of the halo-derivatives of benzofuro-[2,3-*b*]benzofuran (**3**) has been carried out by Riemschneider and his co-workers[1-3] through the condensation of halo-phenols or their methyl ethers with chloral, followed by the cyclization of the products. On the other hand, the halo-[2,3] and methyl-derivatives[5] of 5a,10b-dihydrobenzofuro[2,3-*b*]benzofuran (**1**) have been prepared by the condensation of substituted-phenols or -anisoles with dichloroacetal, followed by the cyclization of the products. Also, the **1** compounds have been prepared in one step by the condensation of substituted-phenols with glyoxal.[4,5]

Now, in the present experiments, we have attempted the preparation of several derivatives of **3** from the corresponding dihydro-compounds (**1**) in order to investigate the electrophilic substitution of **3**.

The starting compounds (**1a**—**d**), among which the 2,9-dimethoxy-derivative (**1a**) was newly synthesized, were brominated with *N*-bromosuccinimide in carbon tetrachloride in the presence of benzoyl peroxide. The dehydrobromination of the brominated compounds was attempted by heating them with potassium acetate in ethanol to give the **3** compounds. The attempts succeeded only in the case of **1a**, and the structure of the product was determined to be **3a** from its elemental analysis and spectral data; the shape of the UV absorption curve was different from that of **1a** and was analogous to that of **3d**.[1] Moreover, the peaks due to 5a- and 10b-hydrogen of **1a** disappeared in the NMR spectrum in the case of **3a**. The intermediate brominated compound seems to be the 10b-bromo-compound (**2a**) by analogy to the case of **1c**. In the case of the 2,9-dimethyl-derivative (**1b**), the product was proved to be the 2-ethoxymethyl-9-methyl-derivative of **1** by its elemental analysis and by NMR spectroscopy; the formation of the compound seems to be due to bromination at the methyl group, followed by a reaction with ethanol. In the case of the 2,9-dichloro-derivative (**1c**), the brominated compound was obtained in a pure state and was considered to be the 10b-bromo-derivative (**2c**) from the absence of the doublet peaks due to the 10b-hydrogen in the NMR spectrum. However, the dehydrobromination of **2c** with potassium acetate was difficult. The brominated compound (**2d**) was also obtained from the 2,4,7,8-tetrachloro-derivative (**1d**), but the dehydrobromination was unsuccessful. Some attempts at the direct dehydrogenation as well as the hydroxylation of **2** were fruitless.

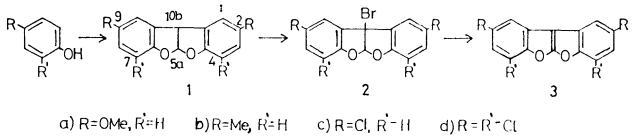

Experimental

The melting points are uncorrected. IR spectra; Hitachi Model EPI-S, UV spectra; Hitachi Model 124, NMR spectra; JEOL Model JNM-C-60H (60 MHz), Mass spectra; JEOL Model JMS-OIS.

*The Preparation of the 5a,10b-Dihydrobenzofuro[2,3-*b*]benzofurans (1).* 2,9-Dimethyl-[4,5] (**1b**), 2,9-dichloro-[3,5] (**1c**), and the 2,4,7,9-tetrachloro-derivative[2,3] (**1d**) of **1** were prepared by the reported methods. The 2,9-dimethoxy-derivative (**1a**) was prepared by an analogous method, which will be described below.

*2,9-Dimethoxy-5a,10b-dihydrobenzofuro[2,3-*b*]benzofuran (1a).* (a) Concentrated sulfuric acid (40 ml) was stirred, over a 1.5 h period and at 20—25 °C, into a mixture of *p*-methoxyphenol (24.8 g, 0.2 ml), a 40% aqueous glyoxal solution (28 g, 0.15 mol), and acetic acid (100 ml). After stirring for 40 min at that temperature, the mixture was poured into ice water; the precipitate thus formed was collected, washed with a dilute aqueous sodium hydroxide solution, and dried. Extraction by cyclohexane using a percolater and the recrystallization of the extract from ethanol gave 3 g (11% yield) of **1a**; mp 177—177.5 °C. UV: λ_{max}^{EtOH} nm (log ε) 210 (4.18), 220sh (4.12), 303 (3.93). NMR: $\delta(CDCl_3)$ 3.77 (6H, s, $-OCH_3$), 4.92 (1H, d, J=6 Hz, 10b-H), 6.75—6.95 (7H, m, arom-H and 5a-H). Mass: M^+ (*m/e*) 270. Anal. Found: C, 71.13; H, 5.26%. Calcd for $C_{16}H_{14}O_4$: C, 71.10; H, 5.22%. (b) Concentrated sulfuric acid (25 ml) was added, at 5—10 °C over a 2 h period, to a solution of *p*-methoxyphenol (12.4 g, 0.1 mol) and dichloroacetal (9 g, 0.05 mol) in acetic acid (25 ml); the mixture was stirred at room temperature for 20 h, and then concentrated sulfuric acid (25 ml) was added once more in a similar manner. The mixture was poured into ice water, extracted with ethyl acetate, and the crude 2,2-dichloro-1,1-bis(5-methoxy-2-hydroxyphenyl)-ethane obtained from the extract was refluxed for 2 h with methanol (100 ml) saturated with ammonia. The solvent was then distilled off, and the residue was crystallized from ethanol to give 0.4 g (6.5% yield) of **1a** (mp 177—177.5 °C, identical with that of the other sample).

*The Bromination of 1 and the Dehydrobromination of the Product to Give Benzofuro[2,3-*b*]benzofuran (3). In the Case of 1a*: A solution of **1a** (1.4 g ,0.005 mol) and *N*-bromosuccinimide (NBS) (1.8 g, 0.01 mol) in carbon tetrachloride (350 ml) was refluxed for 30 h with the addition of benzoyl peroxide (0.05 g). Most of the solvent was then distilled off, the residue was dissolved in chloroform, and the solution was washed with an aqueous sodium bicarbonate solution. The crude product obtained from the chloroform solution was dissolved in ethanol, and the solution was refluxed for 5 h with the addition of potassium acetate (2 g, 0.02 mol). The reaction mixture was then poured into ice water, extracted

with ether, and the ethereal solution was washed with the aqueous sodium bicarbonate solution. The residual product obtained from the ethereal solution was distilled (bp 150—250 °C/2 mmHg (bath-temperature)) and then crystallized from ethanol to give 0.7 g (50% yield) of 2,9-dimethoxybenzofuro[2,3-*b*]benzofuran (**3a**); mp 124.5—125 °C. UV: λ_{max}^{EtOH} nm (log ε) 204sh (4.37), 226 (4.57), 276 (4.28), 283 (4.27), 290 (4.26), 298 (4.14). NMR: δ (CCl_4) 3.84 (6H, s, $-OCH_3$), 6.70 (2H, dd, J=3 and 9 Hz, 3,8-H), 7.07 (2H, d, J=3 Hz, 1,10-H), 7.32 (2H, d, J=9 Hz, 4,7-H). Mass: M^+ (*m/e*) 268.

In the Case of ***1b***: The crude product obtained from **1b** (2.4 g, 0.01 mol) by a procedure similar to that described above was purified by chromatography, with alumina and benzene as the solvents. A fairly large amount of the **1b** was obtained at first, and then a small amount (*ca.* 50 mg) of 2-ethoxymethyl-9-methyl-5a,10b-dihydrobenzofuro[2,3-*b*]benzofuran (mp 95—96 °C (from ethanol)) was obtained. NMR: δ ($CDCl_3$) 1.24 (3H, t, J=7 Hz, $-CH_2-C\underline{H}_3$), 2.30 (3H, s, $-CH_3$), 3.53 (2H, q, J=7 Hz, $-C\underline{H}_2-CH_3$), 4.45 (2H, s, $-O-CH_2-$arom.), 4.96 (1H, d, J=6 Hz, 10b-H), 6.70—7.45 (7H, m, arom.-H and 5a-H). Found: C, 76.40; H, 6.29%. Calcd for $C_{18}H_{18}O_3$: C, 76.57; H, 6.43%.

In the Case of ***1c***: The bromination of **1c** (1.4 g, 0.005 mol) by the procedure described above gave a crude brominated compound which was easily purified by crystallization from acetic acid and then from ethanol to give 10b-bromo-2,9-dichloro-5a,10b-dihydrobenzofuro[2,3-*b*]benzofuran (**2c**); mp 188—188.5 °C; 0.8 g (45% yield). NMR: δ (CCl_4) 6.81 (2H, d, J=9 Hz, 4,7-H), 6.90 (1H, s, 5a-H), 7.15 (2H, dd, J=2 and 9 Hz, 3,8-H), 7.46 (2H, d, J=2 Hz, 1,10-H). Found: C, 46.82; H, 1.80%. Calcd for $C_{14}H_7BrCl_2O_2$: C, 46.94; H, 1.97%. The dehydrobromination of **2c** by the method described before was unsuccessful.

In the Case of ***1d***: A brominated compound, 10b-bromo-2,4,7,9-tetrachloro-5a,10b-dihydrobenzofuro[2,3-*b*]benzofuran (**2d**), was obtained by the crystallization of the crude brominated compound from **1d** (2.1 g, 0.006 mol); mp 195—195.5 °C (from acetone); 1.3 g (51% yield). The structure was determined on the basis of the results of the elemental analysis and by analogy to the case of **2c** (the NMR spectrum could not be measured, as it was insoluble in the apropriate solvent). Found: C, 39.22; H, 1.06%. Calcd for $C_{14}H_5BrCl_4O_2$: C, 39.38; H, 1.18%. The dehydrobromination of **2d** was also unsuccessful.

References

1) R. Riemschneider and W. Cohnen, *Chem. Ber.*, **90**, 2720 (1957).

2) R. Riemschneider and W. Cohnen, *ibid.*, **91**, 2600 (1958).

3) R. Riemschneider, I. Ahrlé, W. Cohnen, and E. Heilmann, *ibid.*, **92**, 900 (1959).

4) B. S. Thyagarajan, K. K. Balsubramanian, and R. B. Rao, *Can. J. Chem.*, **44**, 733 (1966).

5) E. C. M. Coxworth, *ibid.*, **45**, 1777 (1967).

BULLETIN OF THE CHEMICAL SOCIETY OF JAPAN, VOL. 48 (11), 3423—3424 (1975)

The Fries Rearrangement of Acetoxybenzofuran Derivatives and the Synthesis of Furochromenonecarboxylic Acids

Mutsumu NANBU, Seiji YAMAGUCHI, Yasuo SUGIMASA, Tatsuya MIYAURA, and Yoshiyuki KAWASE

Department of Chemistry, Faculty of Literature and Science, Toyama University, Gofuku, Toyama 930

(Received June 4, 1975)

Synopsis. The Fries rearrangement of 4-, 5-, 6-, and 7-acetoxy-2,3-dimethylbenzofurans was studied and the *o*-hydroxy-ketones obtained were converted to dimethylfuro derivatives of 4*H*-chromen-4-one-2-carboxylic acid.

It has been reported that the Fries rearrangement of 6-acetoxy-3-methylbenzofuran gave a 2-acetyl compound[1] and that of 6-acetoxy-3-methylbenzofuran-2-carboxylic acid gave a 7-acetyl compound.[2] In the present experiments, the Fries rearrangement of *bz*-acetoxy-2,3-dimethylbenzofurans was studied, and the *o*-hydroxy-ketones obtained were converted to the corresponding furochromenonecarboxylic acid derivatives to test the pharmacological activity.

Four isomeric 4-, 5-, 6-, and 7-acetoxy-2,3-dimethylbenzofurans (**1**, **5**, **8**, and **11**) were heated with anhydrous aluminum chloride at 120 °C for 15 min and the reaction mixture was treated as usual to give the products, the structures of which were determined by comparing their melting points and IR spectra with those of authentic samples.[3,4] The products obtained from **5**, **8**, and **11** were the *o*-hydroxy-ketones **6**, **9**, and **12**, respectively, and a small amount of *p*-hydroxy-ketone (**13**) was also obtained in the case of **11**. But, in the case of **1**, the main product was *p*-hydroxy-ketone (**3**), as well as a small amount of the *o*-hydroxy-ketone (**2**). The same reaction in carbon disulfide at room temperature for 24 h gave some amounts of the *p*-hydroxy-ketone **3** or **13**, respectively, from **1** or **11**, while no reaction occured in the case of **5** and **8**. The *o*-hydroxy-ketones **2**, **6**, **9**, and **12** thus obtained were converted to furochromenonecarboxylic acid derivatives **4**, **7**, **10**, and **14**, respectively, by condensation with ethyl oxalate followed by hydrolysis and cyclization.[5,6]

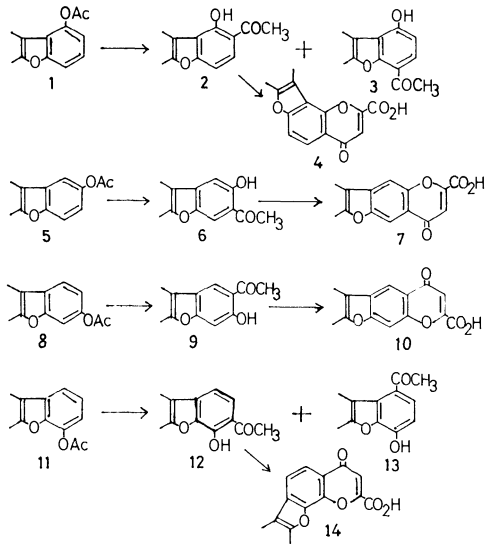

Experimental

All the melting points and boiling points are uncorrected. IR spectra: Hitachi Model EPI-S. UV spectra: Hitachi Model 124. NMR spectra: JEOL Model JNM-MH-60 (60 MHz).

The Preparation of 4-, 5-, 6-, and 7-Acetoxy-2,3-dimethylbenzofurans (1, 5, 8, and 11). These compounds were prepared by heating the corresponding hydroxy-compounds[7] with acetic anhydride and sodium acetate. Compound **1**; bp 163—167 °C/22 Torr, ν_{CO} 1765 cm^{-1}. Found: C, 70.34; H, 6.05%. Calcd for $C_{12}H_{12}O_3$: C, 70.57; H, 5.92%. Compound **5**; mp 60 °C (from *n*-hexane), ν_{CO}^{KBr} 1760 cm^{-1}. Found: C, 70.79; H, 5.84%. Calcd for $C_{12}H_{12}O_3$: C, 70.57; H, 5.92%. Compound **8**; mp 54—55 °C (from *n*-hexane), ν_{CO}^{KBr} 1760 cm^{-1}. Found: C, 70.79; H, 5.84%. Calcd for $C_{12}H_{12}O_3$: C, 70.57; H, 5.92%. Compound **11**; bp 165—167 °C/20 Torr, ν_{CO} 1770 cm^{-1}. Found: C, 70.69; H, 6.13%. Calcd for $C_{12}H_{12}O_3$: C, 70.57; H, 5.92%.

The Fries Rearrangement of the Acetoxybenzofurans. *Method A*: A mixture of the acetoxybenzofuran (4.1 g) and powdered anhydrous aluminum chloride (3.2 g) was heated with stirring at 120 °C for 15 min. The cooled mixture was treated with diluted hydrochloric acid, extracted with ether, and the ethereal layer was extracted with dilute aqueous sodium hydroxide solution. The product obtained from the ethereal solution was *o*-hydroxy-ketone, and the precipitate obtained by the acidification of the alkaline extract was *p*-hydroxy-ketone. In the case of **1**, 0.04 g (1% yield) of 5-acetyl-2,3-dimethyl-4-hydroxybenzofuran (**2**), mp 47—50 °C (lit,[4] mp 58.5—60 °C), and 1.6 g (40% yield) of 7-acetyl isomer (**3**), mp 204—206 °C (lit,[4] mp 206—208 °C), were obtained. In the case of **5**, 1.8 g (45% yield) of 6-acetyl-2,3-dimethyl-5-hydroxybenzofuran (**6**), mp 139—142 °C (lit,[3] mp 141 °C) was obtained. In the case of **8**, 1 g (24% yield) of 5-acetyl-2,3-dimethyl-6-hydroxybenzofuran (**9**), mp 119—121 °C (lit,[3] mp 122 °C) was obtained. In the case of **11**, 2 g (49% yield) of 6-acetyl-2,3-dimethyl-7-hydroxybenzofuran (**12**), mp 129—130 °C (lit,[3] mp 130 °C) and 0.01 g (0.3% yield) of 4-acetyl-2,3-dimethyl-7-hydroxybenzofuran (**13**), mp 164—165 °C (lit,[3] mp 169 °C) were obtained.

Method B: A mixture of the acetoxybenzofuran (4.1 g), anhydrous aluminum chloride (3.2 g) and carbon disulfide (20 g) was stirred at room temperature for 24 h. The reaction mixture was treated similarly to the method described for method A. In the case of **1**, 0.6 g (15% yield) of **3** was obtained, and in the case of **11**, 0.4 g (10% yield) of **13** was obtained. In the cases of **5** and **8**, almost all of the starting compounds were recovered.

The Preparation of Furochromenonecarboxylic Acids. The *o*-hydroxy-ketone (1 g) and ethyl oxalate (2 g) were added to a suspension of powdered sodium metal (0.5 g) in xylene (75 ml) and the mixture was refluxed for 1 h. The cooled mixture was treated with ethanol to destroy the excessive

sodium metal and then with water. The alkaline aqueous layer was separated and acidified with dilute hydrochloric acid. The precipitate formed was crystallized from acetic acid to give the following furochromenone-carboxylic acids: 1,2-Dimethyl-6*H*-furo[2,3-*h*]chromen-6-one-8-carboxylic acid (**4**) was obtained from **2** in a 29% yield; mp 300—302 °C; ν_{CO}^{KBr} cm^{-1}: 1730 (COOH) and 1640 (γ-pyrone); λ_{max}^{EtOH} nm (log ε): 220 (4.54), 252 (4.41), and 322 (3.65); δ (DMSO-d_6): 2.18 (3H, s, 1-CH_3), 2.31 (3H, s, 2-CH_3), 6.70 (1H, s, 7-H), 7.27 (1H, d, J=9 Hz, 4-H), and 7.57 (1H, d, J=9 Hz, 5-H). Found: C, 65.30; H, 4.18%. Calcd for $C_{14}H_{10}O_5$: C, 65.12; H, 3.90%. 2,3-Dimethyl-8*H*-furo[2,3-*g*]chromen-8-one-6-carboxylic acid (**7**) was obtained from **6** in a 47% yield; mp 293—295 °C; ν_{CO}^{KBr} cm^{-1}: 1740 (COOH) and 1630 (γ-pyrone); λ_{max}^{EtOH} nm (log ε): 220 (4.39), 242 (4.22), and 325 (4.20); δ (DMSO-d_6): 2.15 (3H, s, 3-CH_3), 2.41 (3H, s, 2-CH_3), 6.83 (1H, s, 7-H), 7.65 (1H, s, 4-H), and 7.88 (1H, s, 9-H). Found: C, 64.84; H, 3.79%. Calcd for $C_{14}H_{10}O_5$: C, 65.12; H, 3.90%. 2,3-Dimethyl-5*H*-furo[3,2-*g*]chromen-5-one-7-carboxylic acid (**10**) was obtained from **9** in a 42% yield; mp 310—312 °C, ν_{CO}^{KBr} cm^{-1}: 1730 (COOH) and 1640 (γ-pyrone); λ_{max}^{EtOH} nm (log ε): 211 (4.57), 251 (4.54), and 343 (3.82); δ (DMSO-d_6): 2.15 (3H, s, 3-CH_3), 2.40 (3H, s, 2-CH_3), 6.80 (1H, s, 6-H), 7.70 (1H, s, 9-H), and 7.96 (1H, s, 4-H). Found: C, 64.88; H, 3.86%. Calcd for $C_{14}H_{10}O_5$: C, 65.12; H, 3.90%. 2,3-Dimethyl-6*H*-furo[3,2-*h*]chromen-6-one-8-carboxylic acid (**14**) was obtained from **12** in a 31% yield; mp 275—277 °C; ν_{CO}^{KBr} cm^{-1}: 1730 (COOH) and 1640 (γ-pyrone); λ_{max}^{EtOH} nm (log ε): 214 (4.30), 261 (4.36), and 327 (3.90); δ (DMSO-d_6): 2.21 (3H, s, 3-CH_3), 2.57 (3H, s, 2-CH_3), 6.97 (1H, s, 7-H), 7.57 (1H, d, J=8 Hz, 4-H), and 7.90 (1H, d, J=8 Hz, 5-H). Found: C, 64.35; H, 4.04%. Calcd for $C_{14}H_{10}O_5$: C, 65.12; H, 3.90%.

References

1) N. M. Shah and P. M. Shah, *Chem. Ber.*, **92**, 2927 (1957).
2) N. M. Shah and P. M. Shah, *ibid.*, **92**, 2933 (1959).
3) R. Royer, E. Bisagni, A.-M. Laval-Jeantet, and J.-P. Marquet, *Bull. Soc. Chim. Fr.*, **1965**, 2607.
4) Y. Kawase, M. Nanbu, and F. Miyoshi, This Bulletin, **41**, 2676 (1968).
5) A. Schönberg and A. Sina, *J. Amer. Chem. Soc.*, **72**, 1611 (1950).
6) A. Mustafa, N. A. Starkowsky, and T. I. Salama, *J. Org. Chem.*, **26**, 886 (1961).
7) R. Royer, E. Bisagni, C. Hudry, A. Cheutin, and M.-L. Desvoye, *Bull. Soc. Chim. Fr.*, **1963**, 1003.

BULLETIN OF THE CHEMICAL SOCIETY OF JAPAN, VOL. 48 (11), 3425—3426 (1975)

A Conversion of 4α-Bromoshionan-3-one into D: B-Friedobacchara-1,5(10)-dien-3-one and A Preparation of D: B-Friedo-bacchar-5(10)-en-3-one

Kazuo TACHIBANA, Sachiko YAMADA, Shūzō YAMADA, Takahiko TSUYUKI, and Takeyoshi TAKAHASHI

Department of Chemistry, Faculty of Science, The University of Tokyo, Bunkyo-ku, Tokyo 113

(Received June 5, 1975)

Synopsis. A mixture of D: B-friedo-bacchar-5(10)-en-3-one (**2**) and D: B-friedo-bacchar-5-en-3-one (**4**), prepared from 4α-bromoshionan-3-one (**3**) by the known procedures, was converted into a mixture of 2ξ-bromo-D: B-friedobacchar-5(10)-en-3-one (**6**) and 2ξ-bromo-D: B-friedo-bacchar-5-en-3-one (**7**) by bromination with pyridinium tribromide. The mixture (**6** and **7**) was subjected to dehydrobromination to give D: B-friedo-bacchara-1,5(10)-dien-3-one (**5**). Hydrogenation of the dienone (**5**) gave D: B-friedo-bacchar-5(10)-en-3-one (**2**).

In connection with studies on a backbone rearrangement of 3α,4α-epoxyshionane (**1**),[1] a pure sample of D: B-friedo-bacchar-5(10)-en-3-one (**2**) was required for identification of rearrangement products. It has been reported that 4α-bromoshionan-3-one (**3**) was treated with silver acetate to give a mixture[2] of D: B-friedo-bacchar-5(10)-en-3-one (**2**) and D: B-friedo-bacchar-5-en-3-one (**4**) and that a treatment of the mixture (**2** and **4**) in acetic acid with hydrochloric acid at 100 °C resulted in an isomerization of a double bond in **4** to give mainly **2** (mp 78—80 °C).[2] However, the 5(10)-en-3-one (**2**) thus prepared was found to be always contaminated with some amounts of **4**. An attempt to separate the the mixture (**2** and **4**) by chromatography under various conditions was hardly successful.

We now wish to report a synthesis of D: B-friedo-bacchara-1,5(10)-dien-3-one (**5**) and a preparation of pure D: B-friedo-bacchar-5(10)-en-3-one (**2**) from **5**.

Treatment of 4α-bromoshionan-3-one (**3**)[2] with silver acetate gave a mixture (mp 81—82 °C) of **2** and **4** in a ratio of about 1: 1. Signals due to an olefinic proton of **4** appeared at δ 5.70 as a broad multiplet with an integrated intensity due to about a half proton. Then the mixture (**2** and **4**) was brominated with pyridinium tribromide in acetic acid[3,4] to yield a mixture of 2ξ-bromo-D: B-friedo-bacchar-5(10)-en-3-one (**6**) and 2ξ-bromo-D: B-friedo-bacchar-5-en-3-one (**7**) as white crystals, mp 136—137 °C, which showed PMR signals at δ 4.57—5.00 (1H, m; $C_{(2)}$–H) and 5.75 (*ca.* 0.5H, br; $C_{(6)}$–H of **7**). In the mass spectrum the molecular ion peaks appeared at *m/e* 506 and *m/e* 504. The mixture (**6** and **7**) was dehydrobrominated with hexamethylphosphoric triamide[5] to give D: B-friedo-bacchara-1,5-(10)-dien-3-one (**5**). The conjugated dienone (**5**) was a yellow oil and showed a characteristic ultra violet absorption maximum at 324 nm (ε 5300) and PMR signals due to olefinic protons at δ 5.98 (1H, d, J=10 Hz) and 7.12 (1H, d, J=10 Hz).

Finally, the dienone (**5**) was hydrogenated in the presence of palladium-charcoal to afford pure D: B-friedo-bacchar-5(10)-en-3-one (**2**), mp 84—84.5 °C. No other enone such as the 5-en-3-one (**4**) was formed. D: B-Friedo-bacchar-5(10)-en-3β-ol (**8**)[2] free from its 5-en-3β-ol isomer was also prepared by reduction of pure **2** with lithium aluminium hydride.

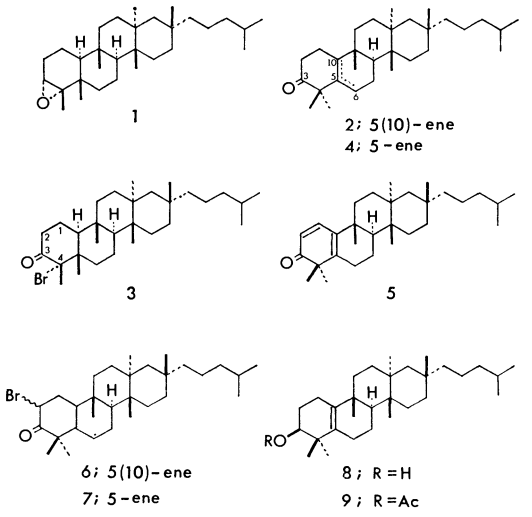

Experimental

IR spectra were measured on a Hitachi EPI-G2 spectrometer. UV spectra were measured using a Hitachi EPS-2 spectrometer. Mass spectra were taken on a Hitachi RMU-6-Tokugata mass spectrometer operating at 70 eV with a direct inlet system. PMR spectra were measured using a JEOL JNM PS-100 (100 MHz), a Hitachi R-20 (60 MHz) or a Hitachi R-24 (60 MHz) spectrometer. Chemical shifts were expressed in ppm downfield from TMS as an internal standard (δ value) and coupling constants in Hz. Thin layer chromatography (tlc) was carried out on Kieselgel G or PF_{254} (E. Merck) in 0.25 mm thickness. Wakogel C-200 (Wako Pure Chemical Ind.) was used for column chromatography. All melting points were determined on a hot block and reported uncorrected.

Treatment of 4α-Bromoshionan-3-one (3) with Silver Acetate. 4α-Bromoshionan-3-one[2] (**3**; mp 122—123 °C; 2.62 g) in ether (600 ml) was added to a solution of silver acetate (2.63 g) in acetic acid (1 l) and water (60 ml). The mixture was heated, concentrated until the vapor temperature reached to 110 °C and then refluxed for 2 h. The reaction mixture, after removal of precipitates, was evaporated under reduced pressure and the residue was extracted with ether. The ethereal layer was washed with water, 10% aqueous sodium carbonate solution and then with brine, and dried over sodium sulfate. On evaporation, an oily residue (2.31 g) was obtained, which was subjected to separation by silica gel (150 g) column chromatography using benzene as an eluent to give an oil (1.23 g). This was crystallized from dichloro-

methane–methanol to afford a mixture (672 mg) of D: B-friedo-bacchar-5(10)-en-3-one (**2**) and D: B-friedo-bacchar-5-en-3-one (**4**), mp 81—82 °C (lit,[2] 81—81.5 °C); IR (KBr) 1710 and 825 cm^{-1}; PMR (60 MHz, $CDCl_3$) δ 5.70 (*ca.* 0.5H, br).

Bromination of the Mixture of D: B-Friedo-bacchar-5(10)-en-3-one (2) and D: B-Friedo-bacchar-5-en-3-one (4). A mixture (3.62 g) of the enones (**2** and **4**) in acetic acid (100 ml) was treated at 60 °C with pyridinium tribromide (4.53 g) for 15 min. The brownish solution, after removal of the solvent under reduced pressure, was extracted with ether. The ethereal extract was washed with water, 10% aqueous sodium carbonate solution, and with brine, and then dried over sodium sulfate. The solvent was removed and the residue was dissolved in petroleum ether. The solution was passed through a column of silica gel (450 g). Elution with a mixture of petroleum ether–benzene (2: 1 and then 1: 1) gave a mixture (1.75 g) of 2ξ-bromo-D: B-friedo-bacchar-5(10)-en-3-one (**6**) and 2ξ-bromo-D: B-friedo-bacchar-5-en-3-one (**7**) as an oil, which was crystallized from dichloromethane–methanol to give white crystals (1.22 g), mp 136—137 °C; IR (KBr) 1720, 760, 655, and 630 cm^{-1}; PMR (60 MHz, $CDCl_3$) δ 4.57—5.00 (1H, m) and 5.75 (*ca.* 0.5H, br); mass spectrum *m/e* 506, 504 (M^+; $C_{30}H_{49}OBr$), and 261 (base peak).

Dehydrobromination of the Mixture of 2ξ-Bromo-D: B-friedo-bacchar-5(10)-en-3-one (6) and 2ξ-Bromo-D: B-friedo-bacchar-5-en-3-one (7). A mixture (64 mg) of the bromo-derivatives (**6** and **7**) was dissolved in freshly distilled hexamethylphosphoric triamide (5 ml) and the solution was heated at 130—140 °C for 10 h under a nitrogen atmosphere. The reaction mixture, after cooling, was poured into ice water, extracted with petroleum ether. The organic layer was washed with water, 2M hydrochloric acid, 20% aqueous sodium carbonate solution, and with brine and then dried over sodium sulfate. The residue, after removal of the solvent, was dissolved in a mixture of chloroform and benzene (1: 1), passed through a column of silica gel (100 g) and eluted with the same solvent mixture to give D: B-friedo-bacchara-1,5(10)-dien-3-one (**5**; 11 mg), a yellow oil, IR (liquid) 1655 and 1620 cm^{-1}; UV λ_{max}^{EtOH} 324 nm (ε 5300); PMR (100 MHz, $CDCl_3$) δ 5.98 (1H, d, J=10 Hz) and 7.12 (1H, d, J=10 Hz); molecular weight (by high resolution mass spectrometry) Found: 424.3642. Calcd for $C_{30}H_{48}O$: 424.3705; mass spectrum *m/e* 424 (M^+) and 203 (base peak).

Hydrogenation of D: B-Friedo-bacchara-1,5(10)-dien-3-one (5). The dienone (**5**; 11 mg) in ethanol (5 ml) was hydrogenated in the presence of palladium–charcoal (10%, 2 mg) for 3 h. A yellow color of the solution faded and finally a colorless solution was obtained, which on filtration followed by evaporation, gave a colorless oil. The oil was subjected to separation by preparative tlc (SiO_2, 0.25 mm in thickness, developed with benzene) to give a colorless oil (5 mg), which was crystallized from methanol to give D: B-friedo-bacchar-5(10)-en-3-one (**2**) as fine needles, mp 84—84.5 °C (lit,[2] mp 78—80 °C); IR (KBr) 1715 cm^{-1}; PMR (60 MHz, $CDCl_3$) δ 2.40 (2H, m), no signal due to olefinic proton; mass spectrum *m/e* 426 (M^+; $C_{30}H_{50}O$) and 109 (base peak).

Reduction of D: B-Friedo-bacchar-5(10)-en-3-one (2) with Lithium Aluminium Hydride. To a solution of D: B-friedo-bacchar-5(10)-en-3-one (**2**; 37 mg), obtained by the above procedure, in ether (5 ml) was added lithium aluminium hydride (in excess), and the reaction mixture was allowed to stand overnight. After dilution with additional ether, the solution was washed with 1M hydrochloric acid, 5% aqueous sodium hydrogen carbonate solution and with brine, and then dried over sodium sulfate. On removal of the solvent, an oily residue was obtained, which gave a major spot with a smaller R_f value accompanied by a minor spot due to 3α-isomer on tlc developed with chloroform.

The major product was separated by preparative tlc developed with chloroform to afford D: B-friedo-bacchar-5(10)-en-3β-ol (**8**), mp 141.5—142 °C (lit,[2] mp 140.5—141 °C); IR (Nujol) 3350, 1065, 1040, 1025, and 975 cm^{-1}; PMR (60 MHz, $CDCl_3$) δ 3.42 (1H, dd, J=5 and 10 Hz), no signal due to olefinic proton; mass spectrum *m/e* 428 (M^+; $C_{30}H_{52}O$) and 135 (base peak).

Acetylation of D: B-Friedo-bacchar-5(10)-en-3β-ol (8). D: B-Friedo-bacchar-5(10)-en-3β-ol (**8**; 23 mg) in pyridine (0.2 ml) was treated with acetic anhydride (0.1 ml), and was kept at room temperature overnight. Usual work-up and crystallization from chloroform–methanol gave D: B-friedo-bacchar-5(10)-en-3β-yl acetate (**9**; 18 mg), mp 146.5—149 °C (lit,[2] mp 148.5—149.5 °C); IR (KBr) 1730, 1250, 1110, and 975 cm^{-1}; PMR (60 MHz, $CDCl_3$) δ 2.03 (3H, $-COCH_3$), 4.64 (1H, dd, J=5 and 10 Hz), no signal due to olefinic proton.

References

1) S. Yamada, S. Yamada, Y. Moriyama, Y. Tanahashi, and T. Takahashi, *Tetrahedron Lett.*, **1972**, 5043.

2) Y. Tanahashi, Y. Moriyama, T. Takahashi, F. Patil, J. F. Biellmann, and G. Ourisson, *Bull. Soc. Chim. Fr.*, **1966**, 1670.

3) J. M. Beaton, F. S. Spring, R. Stevenson, and J. L. Stewart, *Tetrahedron*, **2**, 246 (1958).

4) J. W. ApSimon, R. R. King, and J. J. Rosenfeld, *Can. J. Chem.*, **47**, 1989 (1969).

5) R. Hanna, *Tetrahedron Lett.*, **1968**, 2105.

BULLETIN OF THE CHEMICAL SOCIETY OF JAPAN, VOL. 48 (11), 3427—3428 (1975)

Antineoplastic Agents. The Preparation of 5-Fluorouracil-1-acetic Acid Derivatives

Masao TADA

The Research Institute for Tuberculosis, Leprosy and Cancer, Tohoku University, Hirosemachi, Sendai 980

(Received June 23, 1975)

Synopsis. The condensations of 5-fluorouracil with α-halogenoacetic acid derivatives in the presence of alkali gave the 5-fluorouracil-1-acetic acid derivatives.

5-Fluorouracil (I)[1] and 1-(2-tetrahydrofuryl)-5-fluorouracil (II)[2] as antineoplastic agents have received much attention because of their antitumor activities. In a previous paper,[3] the preparations of various 1-acyl, 1-alkanesulfonyl-, and 1-arenesulfonyl-5-fluorouracils from I were reported. In an attempt to improve the antitumor activities, the introduction of the acetic acid group into the 1-position of I has been attempted. The preparations of 5-fluorouracil-1-acetic acid derivatives will be reported here.

The condensation of I with α-chloroacetic acid in the presence of potassium hydroxide in water afforded 5-fluorouracil-1-acetic acid (III) in a 66% yield; this acid formed ammonium salt (IV) upon subsequent treatment with ammonium hydroxide. The reaction of I with ethyl α-bromoacetate in the presence of anhydrous potassium carbonate in dimethylformamide gave both ethyl 5-fluorouracil-1-acetate (V) in a 57% yield and diethyl 5-fluorouracil-1,3-diacetate (VI) in a 22% yield.

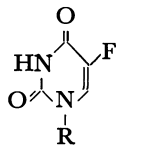

I: R=H

II: R=

III: R=CH_2CO_2H

IV: R=$CH_2CO_2NH_4$

V: R=$CH_2CO_2C_2H_5$

VII: R=$CH_2CO_2CH_3$

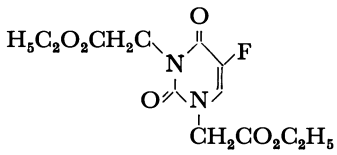

VI

The acid hydrolysis of V gave the corresponding carboxylic acid, III, in a quantitative yield; this acid was subsequently converted into V by esterification with ethanol in the presence of such catalysts as sulfuric acid and *p*-toluenesulfonic acid. Compound III was treated with methanol to afford the methyl ester (VII) in a good yield; this ester was then hydrolyzed with hydrochloric acid to give III. Compound VII was also obtained from I by the reaction of I with methyl α-bromoacetate.

TABLE 1. ULTRAVIOLET SPECTRAL DATA

Comp.	Solvent	λ nm max (log ε)	λ nm min (log ε)
III	0.1M HCl	269 (3.98)	234 (3.35)
	0.1M NaOH	271 (3.84)	247 (3.58)
V	0.1M HCl	268 (4.00)	233 (3.35)
	0.1M NaOH	272 (3.75)	248 (3.50)
VI	0.1M HCl	269 (3.96)	235 (3.30)
	0.1M NaOH	272 (3.92)	236 (3.43)
VII	0.1M HCl	268 (3.98)	233 (3.30)
	0.1M NaOH	272 (3.87)	247 (3.62)

1-Substitution on I has been established by a comparison of the absorption spectra (Table 1) of the products with those of authentic 5-fluorouracil derivatives.[4-6] The structures of the products have been further supported by their NMR spectra.

The above products are now being used for animal testing; the results will be reported elsewhere.

Experimental

All the melting points are uncorrected. The ultraviolet spectra were taken with a Hitachi Model 124 spectrophotometer. The NMR spectra were recorded in DMSO-d_6 (internal TMS standard) with a Varian Model 60T spectrophotometer.

5-Fluorouracil-1-acetic Acid (III). *From I*: Into a solution of I (1.3 g, 10 mmol) and potassium hydroxide (1.12 g, 20 mmol) in water (7.5 ml), a solution of α-chloroacetic acid (950 mg, 10 mmol) in water (4 ml) was stirred at room temperature. The pH of the reaction mixture was adjusted to, and kept at, 10 by the drop-by-drop addition of a potassium hydroxide aqueous solution. The mixture was then refluxed for 2 h, cooled, and acidified to pH 2 by the addition of concentrated hydrochloric acid. The crystals which separated were collected and washed with a little cold water to give III (1.24 g) in a 66% yield. The products were dissolved in saturated aqueous potassium bicarbonate and reprecipitated with concentrated hydrochloric acid to give colorless needles; mp 276—277 °C.

Found: C, 38.38; H, 2.72; N, 14.64%. Calcd for $C_6H_5FN_2O_4$: C, 38.31; H, 2.68; N, 14.89%.

NMR (DMSO-d_6): δ 4.40 (2H singlet, 1-CH_2-), 8.09 (1H doublet, J=7 Hz, H_6), 11.18 (1H broad singlet, 3-NH).

From V: A solution of V (430 mg, 2 mmol) in 12N hydrochloric acid (6 ml) was gently refluxed for 2.5 h and then diluted with water (6 ml). The crystals thereby separated were collected and washed with cold water to give III (240 mg). After the removal of the solvent, an additional 120 mg portion of III was obtained from the mother liquor. The total yield of III was 96%.

From VII: Compound VII was treated as in the case described above to give III (95%).

Ammonium 5-Fluorouracil-1-acetate (IV). To a suspension of III (940 mg, 5 mmol) in water (5 ml), concentrated ammonia water (0.6 ml) was added. The mixture was warmed on a water bath for 5 min. After the removal of the solvent under reduced pressure, the residue was recrystallized from diluted ethanol to give IV (0.5 g, 49%); mp 225—227 °C.

Found: C, 35.28; H, 4.12; N, 20.17%. Calcd for $C_6H_8FN_3O_4$: C, 35.13; H, 3.93; N, 20.48%.

The Reaction of 5-Fluorouracil (I) with Ethyl α-Bromoacetate. Into a suspension of powdered I (5.2 g, 40 mmol) and

anhydrous potassium carbonate (3.04 g, 44 mmol) in dimethylformamide (60 ml), ethyl α-bromoacetate (7.34 g, 44 mmol) was added. The reaction mixture was vigorously stirred at 100 °C for 10 h, cooled to room temperature, and then filtered off. The filtrate was evaporated to dryness under reduced pressure, and the residue was then extracted with absolute ethanol. The extract was concentrated by evaporation. After dilution with water, the crystals which separated were collected. Recrystallization from ethanol afforded needles (4.9 g) of ethyl 5-fluorouracil-1-acetate (V) in a 57% yield; mp 164—165 °C.

Found: C, 44.37; H, 4.39; N, 12.70%. Calcd for $C_8H_9FN_2O_4$: C, 44.45; H, 4.20; N, 12.96%.

From the mother liquor, the crystals were obtained after evaporation under reduced pressure. Recrystallization from diluted ethanol formed diethyl 5-fluorouracil-1,3-diacetate (VI), (2.60 g) as needles in a 22% yield; mp 84—85 °C.

Found: C, 47.66; H, 4.98; N, 9.58%. Calcd for $C_{12}H_{15}FN_2O_6$: C, 47.68; H, 5.00; N, 9.27%.

NMR (DMSO-d_6): δ 1.22 (6H triplet, J=7 Hz, $-OCH_2CH_3$), 4.18 (4H, quartet, J=7 Hz, $-OCH_2CH_3$), 4.60 (4H singlet, $1\text{-}CH_2-$), 8.30 (1H, doublet, J=7 Hz, H_6).

Ethyl 5-Fluorouracil-1-acetate (V). A solution of III (940 mg, 5 mmol) in absolute ethanol (30 ml) and concentrated sulfuric acid (0.2 ml) was refluxed for 8 h and then concentrated to one-third its original volume. After the addition of ice water, sodium bicarbonate was added to the reaction mixture. The crystals thereby separated were collected and washed with cold water to give V (750 mg, 69%). The mother liquor was then extracted with chloroform. The chloroform extract was washed with water and dried over anhydrous magnesium sulfate; an additional 50 mg portion of V was thus obtained; mp 164—165 °C. The total yield of V was 74%.

A solution of III (940 mg) and *p*-toluenesulfonic acid (0.5 g) in absolute ethanol (30 ml) was treated as in the above experiment to give V (425 mg, 40%).

Diethyl 5-Fluorouracil-1,3-diacetate (VI). Into a suspension of powdered I (2.6 g, 20 mmol) and anhydrous potassium carbonate (1.52 g, 11 mmol) in absolute ethanol (60 ml), ethyl α-bromoacetate (3.67 g, 22 mmol) was added. The mixture was refluxed with stirring for 10 h and then filtered off. The filtrate was concentrated under reduced pressure to give both I (350 mg, 14%) and V (300 mg, 7%). From the mother liquor, crystals (1.72 g, 29%, mp 84—85 °C) of VI were obtained after further concentration under reduced pressure.

Methyl 5-Fluorouracil-1-acetate (VII). *From I*: Into a suspension of powdered I (1.3 g, 10 mmol) and anhydrous potassium carbonate (1.52 g, 11 mmol) in dimethylformamide (30 ml), a solution of methyl α-bromoacetate (1.68 g, 11 mmol) in dimethylformamide (5 ml) was stirred. The reaction mixture was then further stirred at 100 °C for 10 h and treated as in the above experiment to give VII (960 mg, 48%). Recrystallization from methanol afforded needle; mp 185—186 °C.

Found: C, 41.63; H, 3.53; N, 13.65%. Calcd for $C_7H_7FN_2O_4$: C, 41.59; H, 3.49; N, 13.86%.

From III: A solution of III (1.88 g, 10 mmol) in absolute methanol (60 ml) and concentrated sulfuric acid (0.6 ml) was refluxed for 8 h, after which the reaction mixture was treated as in the procedure used in the preparation of the ethyl ester, V, to give VII (1.05 g, 52%).

The author is grateful to Professor Yusaku Ikegami and Dr. Masafumi Yasunami, Tohoku University, for their encouragement, and to Mitsui Pharmaceuticals, Inc., for supplying the 5-fluorouracil.

References

1) R. Duschinsky, E. Pleven, and C. Heidelberger, *J. Amer. Chem. Soc.*, **79**, 4559 (1957); C. Heidelberger, *Cancer Res.*, **30**, 1549 (1970).

2) S. A. Giller, R. A. Zhnk, M. J. Lidak, and A. A. Zidermane, British Pat. 1168391 (1969); Japan Pat. 10510 (1974).

3) M. Tada, *Chem. Lett.*, **1975**, 129.

4) M. J. Robins and S. R. Naik, *J. Amer. Chem. Soc.*, **93**, 5277 (1971).

5) I. Wempen and J. J. Fox, *ibid.*, **86**, 2474 (1964).

6) B. R. Baker and G. D. F. Jackson, *J. Pharm. Sci.*, **54**, 1758 (1965).

BULLETIN OF THE CHEMICAL SOCIETY OF JAPAN, VOL. 48 (11), 3429—3430 (1975)

α-(3-Phenoxymethyl-7-oxo-4-thia-2,6-diazabicyclo[3.2.0]hept-2-ene-6-yl)-α-isopropenylacetates, Useful Intermediate from Penicillin to Cephalosporin

Hiroshi TANIDA, Ryonosuke MUNEYUKI, and Tadahiko TSUSHIMA
Shionogi Research Laboratory, Shionogi and Co., Ltd., Fukushima-ku, Osaka 553

(Received July 24, 1975)

Synopsis. Reaction of α-[2-(Benzothiazol-2-yl)-dithio-3-phenoxyacetamido-4-oxoazetidin-1-yl]-α-isopropenylacetates with phosphorus pentasulfide afforded the title compound. The first step in this reaction is suggested as an intramolecular nucleophilic attack of the thioamide function, initially resulted from the 3-acetamido groups, towards the disulfide-sulfur at the 2 position.

Warming of a penicillanic acid sulfoxide ester (**1**) with 2-mercaptobenzothiazol gave in an excellent yield the disulfide (**3**).[1,2] It has been evidenced that the formation of **3** is a result of intermolecular thiol trapping of the sulfenic acid intermediate (**2**) existing in a thermal equilibrium with **1**.[3,4] Since cleavage of the disulfide linkage and recyclization into new series of penicillin and cephalosporin is possible under mild conditions, the disulfide derived from 2-mercaptobenzothiazol may be a useful intermediate more than those from other thiols.[2] We have suggested that the side chain at C-6 might participate in reactions with the sulfenic acid (Formula **5**→**6**). Based on this hypothesis, we undertook an experiment to transform **3** into the thioamide **7**, because the thioamide function is known as a good nucleophile,[6] perhaps, better than the acetamide.

The reaction of **3** (R=$PhOCH_2$), derived from Penicillin V, with diphosphorus pentasulfide was tried. When a benzene solution of **3** containing 1.1 mol equivalents of phosphorus pentasulfide was refluxed for 30 min, there was found to form mainly the thiazoline-azetidinone **8** (the title compound) by liberating 2-mercaptobenzothiazol. The structure of **8** was established by comparing with an authentic sample prepared by the reported method.[7]

Reaction of **1** with trimethyl phosphite in refluxing benzene is known to give **8**.[7] This reaction has been considered as an initial formation of the sulfenic acid followed by reduction by the trivalent phosphorus reagent into a thiol which attacks at the amide-carbon as a nucleophile to give the cyclized **8**. Reduction of the disulfide **3** into a thiol by the pentavalent phosphorus reagent, diphosphorus pentasulfide, is improvable. Alternatively, it seems us doubtless that the thioamide-sulfur in **7**, initially formed by an action of diphosphorus pentasulfide on **3**, reacts as a nucleophile toward the sulfide-sulfur to give **6** (X=S) which does not unfortunately survive under the reaction conditions but, as a result of several steps of thermal rearrangements as shown in the last formulas, affords the stable **8** by eliminating sulfur.

Finally, it should be pointed out that the present reaction is a simple procedure to obtain **8**, which is known as an important intermediate for the conversion of penicillin derivatives into cephalosporin derivatives.[2,4]

Experimental

Reaction of 3 (R=$PhOCH_2$-) with P_2S_5. a) With the Methyl Ester (R'=CH_3): A solution of 329 mg (0.62 mmol) of **3** in 5 ml of benzene suspended with 35 mg (0.16 mmol) of P_2S_5 was refluxed for 30 min. The reaction mixture was filtered, evaporated under a reduced pressure and extracted with carbon tetrachloride.

After evaporation of the solvent, the residue (377 mg) was separated by thin-layer chromatography (benzene–ethyl acetate=4:1). The main fraction was the thiazolin derivative **8** (the title methyl ester) in 37.5% yield: IR ($CHCl_3$) 1780 and 1745 cm^{-1} (C=O), NMR ($CDCl_3$) δ 1.76 (s, 3, allylic CH_3), 3.77 (s, 3, $COOCH_3$), 4.93 (s, 2, $PhOCH_2$), 4.83 (s, 1, $-CHCOOCH_3$), 5.10 (broad, m, 1, vinyl H), 4.50 (d, 1, vinyl H, J=9.0 Hz), and 5.97 (m, 2, azetidinone H); CD (c=0.1467, in dioxane) 270 mμ ([θ]-1040), 245 (+13300), and 209.5 (−29300).

b) With the 2,2,2-Trichloroethyl Ester (R'=$-CH_2CCl_3$): The corresponding **8** (R'=$-CH_2CCl_3$), mp 139—141 °C, was similarly obtained by the above procedure.

References

1) T. Kamiya, T. Teraji, Y. Saito, M. Hashimoto, O, Nakaguchi, and T. Oku, *Tetrahedron Lett.*, **1973**, 3001.
2) T. Kamiya, *Yuki Gosei Kagaku Kyokai Shi*, **33**, 24 (1975).

3) a) D. H. R. Barton and P. G. Sammes, *Proc. Roy. Soc., Ser. B*, **179**, 345 (1971); b) D. H. R. Baton, *Pure Appl. Chem.*, **33**, 1 (1973).

4) R. D. G. Cooper and D. O. Spry, "Cephalosporins and Penicillins Chemistry and Biology," ed. by E. H. Flynn, Academic Press, New York, N. Y., and London (1972), Chapter V.

5) H. Tanida, R. Muneyuki, and T. Tsushima, *Tetrahedron Lett.*, **1975**, 3063.

6) S. Winstein and R. Boschan, *J. Amer. Chem. Soc.*, **72**. 4669 (1950).

7) R. D. G. Cooper and F. L. José, *ibid.*, **92**, 2575 (1970).

The Calculations of Dipole Polarizabilities and Anisotropies by the CNDO Method: The Effect of an Extended-basis Set

Hiroyuki SHINODA and Tatsuo AKUTAGAWA

Department of Applied Chemistry, Faculty of Science and Engineering, Waseda University, Nishi-Ohkubo, Shinjuku-ku, Tokyo 160

(Received January 10, 1975)

The dipole polarizabilities and the anisotropies of several small molecules have been calculated according to a formula derived from the time-dependent perturbation theory. The wave functions and the energies were calculated by means of the CNDO-CI version, with an extended-basis set. The effects on the calculated results of the introduction of the atomic vacant orbitals into the basis set have been discussed.

Theoretical calculations of polarizabilities within the framework of the CNDO version have been performed by several investigators.[1-4] Miyazaki and one of the present authors[1] reported their theoretical calculations of polarizabilities according to the formula derived from the time-dependent perturbation theory. They calculated the polarizabilities by the use of the wave functions and the energies, which were evaluated by the CNDO-CI method using the valence-orbital-basis set. They discussed the effects of the parameters in the CNDO method on the calculated polarizabilities and concluded that the calculated polarizabilities were generally smaller than the experimental results and that the calculated anisotropies were larger than the observed results. Hush and Williams[2] used the finite perturbation theory with the valence-orbital-basis set in order to investigate the polarizabilities and the anisotropies of axial symmetric molecules. Their calculated values of polarizability-anisotropy, $\alpha_{\parallel}$-$\alpha_{\perp}$, were in good agreement with the experimental ones. However, the calculated values of the polarizabilities were small in comparison with the experimental ones, and the calculated vaules of the anisotropies were larger than the observed ones. They improved the calculated results by adding the correction terms to the diagonal elements of the molecular polarizability tensors.[3] Davies[4] calculated the polarizabilities of several small molecules by the use of the self-consistent perturbation method. From a comparison between the results of calculations in which the 2p-orbitals of the hydrogen atoms are considered and those in which they are not, he concluded that the valence-orbital-basis set is inadequate for the representation of the perturbed wave functions. At any rate, the polarizabilities calculated within the framework of the CNDO version with the valence-orbital-basis set were not in agreement with the experimental ones.

The purpose of this work is to investigate the effect on the calculated polarizabilities of the introduction of the atomic vacant orbitals into the basis set. The RCNDO method proposed by Salahub and Sandorfy[5] is a modified CNDO method with the extended-basis set. This method is, however, not always appropriate for the calculation of the polarizability, as will be shown later. Then the trial method, which differs from the RCNDO method, has been used to obtain the wave functions and the energies. Discussions have been based on a comparison of the results calculated by several approaches.

Methods of Calculations

Polarizability and Anisotropy: The polarizability, α, of a system in the electromagnetic field as a perturbation can be derived from the time-dependent perturbation theory.[1] By averaging the vector quantities over all the orientations of the system with respect to the field, α can be given as:

$$\alpha = \frac{2}{3h}\sum_b \frac{\nu_{ba}|\langle\Psi_a^\circ|e\sum_i \boldsymbol{r}_i|\Psi_b^\circ\rangle|^2}{\nu_{ba}^2-\nu^2}, \quad (1)$$

where $\boldsymbol{r}_i$ is the position vector of the i-th electron; ν is the frequency of the incident light, and $h\nu_{ba}=E_b-E_a$; here E_a is the energy of the unperturbed ground state described by the wave function, Ψ_a°, and E_b is the energy of the unperturbed excited state with the wave function of Ψ_b°. The anisotropy, k, is expressed by the components of the polarizability tensor as follows:

$$k^2 = \{(\alpha-\alpha_1)^2+(\alpha-\alpha_2)^2+(\alpha-\alpha_3)^2\}/6\alpha^2, \quad (2)$$

where α_1, α_2, and α_3 are the principal polarizabilities of the system.

Molecular Orbital Calculations: The molecular wave function, Ψ_a°, of an unperturbed ground state is described as the single Slater-determinant with a closed-shell structure, while those of unperturbed excited states, Ψ_b°'s, are described as linear combinations of all the singly-excited configurations obtained by the configuration-interaction (CI) treatment.

The atomic vacant orbitals considered in this work, in addition to the valence orbitals, have been restricted to those with a principal quantum number (p.q.n.) greater by 1 than that of the valence orbitals, and the effective nuclear charges for the atomic vacant orbitals are taken to be equal to those for the valence orbitals as determined by Slater's rule. Within the framework of the CNDO version, the diagonal element of the SCF energy matrix in the Roothaan LCAO-SCF equation[6] can be written as follows:[7]

$$F_{\mu\mu} = -I_\mu - (Z_A-1)\gamma_{AA}^{n\bar{m}} - \sum_{B\neq A} Z_B\gamma_{AB}^{n\bar{m}} + \left(P_{AA}^{nn}-\frac{1}{2}P_{\mu\mu}\right)\gamma_{AA}^{nn} + \sum_{m\neq n}^{A} P_{AA}^{mm}\gamma_{AA}^{nm} + \sum_{B\neq A}\sum_{m}^{B} P_{BB}^{mm}\gamma_{AB}^{nm}, \quad (3)$$

where n is the p.q.n. of the atomic orbital, φ_μ, which belongs to the A atom; I_μ, the average ionization potential of φ_μ; Z_A and Z_B, the core charges of the A and B atoms respectively; $P_{\mu\mu}$, the charge density of φ_μ; and P_{AA}^{mm}, the sum of the charge densities of

TABLE 1. AVERAGE IONIZATION POTENTIALS, I_μ, FOR ATOMIC VACANT ORBITALS (eV)

Atom	Orbital	I_μ
H	2s	3.399
	2p	3.399
C	3s	3.735
	3p	2.509
	3d	1.551
N	3s	4.329
	3p	3.144
	3d	2.456
O	3s	4.378
	3p	3.053
	3d	2.657

the atomic orbitals with the p.q.n. -m on the A atom; γ_{AB}^{nm} represents the repulsion between electrons in φ_μ and in the atomic orbital with the p.q.n. -m on the B atom, and $\bar{m}$ in $\gamma_{AB}^{n\bar{m}}$ is the p.q.n. of the valence orbital on the B atom. The electronic repulsion integral, γ_{AB}^{nm}, is calculated as a Coulomb integral including the ns and ms Slater orbitals. The values of the average ionization potentials for valence orbitals followed those of the CNDO/1 method,[7] while those of the vacant orbitals were evaluated from the table in Ref. 8 and are shown in Table 1. The off-diagonal element of the SCF energy matrix is described as follows:

$$F_{\mu\nu} = \beta_{AB}^{nm} S_{\mu\nu} - \frac{1}{2} P_{\mu\nu} \gamma_{AB}^{nm}, \tag{4}$$

where n is the p.q.n. of φ_μ on the A atom; m, the p.q.n. of φ_ν on the B atom; $S_{\mu\nu}$, the overlap integral between φ_μ and φ_ν, and $P_{\mu\nu}$, the bond order between φ_μ and φ_ν. The bonding parameter, β_{AB}^{nm}, is approximated by:

$$\beta_{AB}^{nm} = \frac{1}{2} \kappa (\beta_A^\circ + \beta_B^\circ), \tag{5}$$

where the values of the β_A° and β_B° are the same as those used in the CNDO/1 method[7] and where the κ parameter is determined as will be described below. The value of κ for the interaction between valence orbitals is taken to be unity, as in the CNDO/1 method. The average ionization potentials of the 2p-orbitals for the first-row elements are nearly equal to a half of the values of the β_A° and are roughly five times the average ionization potentials of 3p-orbitals. Therefore, the value of κ for the interaction between vacant orbitals is taken to be 0.2. The value of κ for the valence orbital-vacant orbital interaction is taken to be 0.6, the mean of 1.0 and 0.2. The geometries of the molecules followed the data listed in Ref. 9.

Results and Discussion

By the use of the molecular wave functions obtained from the CNDO/2-CI treatment including all the singly- and the doubly-excited configurations, Tatematsu[10] calculated the polarizabilities of several molecules according to the formula shown in Eq. (1). The calculated values were 0.504, 0.685, 0.721, and 1.128 Å^3 for N_2, CO, C_2H_2, and C_2H_4 respectively. These values are smaller than those obtained by the calculations considering only the singly-excited configurations in Ref. 1. However, the calculated anisotropies were slightly improved by considering the doubly-excited configurations, although they, as well as those in Ref. 1, are larger than the experimental ones. The electronic transition energies and the transition moments calculated by the CNDO/2-CI method are listed in Table 2 for N_2 as an example. The introduction of doubly-excited configurations reduces the transition moments in the calculation with only the singly-excited configurations and brings about new excited states which have large electronic excitation energies and small transition moments, so that the new ones contribute scarcely anything to the polarizability. The above discussions showed that the CI treatment including the doubly-excited configurations does not bring a drastic improvement in the calculation of polarizabilities, although the treatment is a powerful approach to an investigation of several lower electronic excited states.[11] In this study, therefore, calculations have been performed with the CI treatment including only the singly-excited configurations.

The polarizability and the anisotropy of C_2H_2 were calculated with various basis sets; the results are shown in Table 3. With the increase in the number of atomic orbitals in the basis set, the value of the polarizability increases and the value of the anisotropy decreases. In the investigation by Davies,[4] the 2p-orbitals of the hydrogen atom were used in the basis set for the perturbed wave functions, but the 2s-orbital was not considered. From the comparisons between the results of (D) and (F) and between those of (E) and (G) shown in Table 3, it is found that the introduction of the 2s-orbital of the hydrogen atom, in addition to the 2p-orbitals, into the basis set effectively improves the calculated results. The results in (F), (G), and (H) lead to the following discussion of the effects of the vacant orbitals of the carbon atom on the calculated results for the polarizability and the anisotropy. The value of the polarizability calculated by considering the 3s-, 3p-, and 3d-orbitals of the carbon atom, (H) in the table, is larger than the experimental one. On the other hand, the values of the polarizability in (F) and (G) are slightly smaller than the observed one. From a comparison between the results in (F) and (G), it is found that (F), including the 3s- and 3p-orbitals of the carbon arom, yields the good polarizability, while (G), including the 3d-orbitals, yields a good anisotropy.

On the basis of the above discussion of the results of C_2H_2, it is decided that two kinds of basis sets will be used in the following calculations. One of them contains the 1s-, 2s-, and 2p-orbitals of a hydrogen atom and the 2s-, 2p-, 3s-, and 3p-orbitals of first-row elements. The other one contains the 1s-, 2s-, and 2p-orbitals of a hydrogen atom and the 2s-, 2p-, and 3d-orbitals of first-row elements. The molecular orbital calculation with the former basis set will be

Table 2. The electronic transition energies and the transition moments of N_2 calculated by the CNDO-CI method.[a]

SCI[b]				DCI[b,c]			
Transition energy [eV]	Transition moment[D]			Transition energy[eV]	Transition moment[D]		
	M_x	M_y	M_z		M_x	M_y	M_z
15.253	2.2051	0	0	15.861	2.1495	0	0
15.253	0	2.2051	0	15.861	0	2.1495	0
15.598	0	0	−1.5896	17.479	0	0	−0.9867
24.257	0	0	4.6430	26.153	0	0	3.6547
				26.615	−0.1773	0	0
				26.615	0	−0.1773	0
				32.696	−0.3635	0	0
				32.696	0	−0.3635	0
				37.359	0.0356	0	0
				37.359	0	0.0356	0
				41.842	−0.0495	0	0
				41.842	0	−0.0495	0
				43.450	0.0871	0	0
				43.450	0.0	0.0871	0
				44.323	0	0	−0.2429
50.530	0	0	−2.5074	50.936	0	0	−1.2594
				51.633	−0.0339	0	0
				51.633	0	−0.0339	0

a) The z-axis is the bond axis of N_2. b) SCI means the calculation including only the singly-excited configurations while DCI does the CI calculation including all the singly- and doubly-excited configurations. c) The excited states which have the transition energies larger than 51.633 eV are omitted from the table because of their negligible contributions to the polarizability.

Table 3. The polarizabilities and the anisotropies of C_2H_2 calculated with various basis set

	N[a]	Atomic orbitals in a basis set		Polarizability (Å)	Anisotropy
		Hydrogen	Carbon		
(A)	10	1s	2s, 2p	1.052	0.671
(B)	16	1s, 2p	2s, 2p	2.006	0.701
(C)	18	1s, 2s, 2p	2s, 2p	2.549	0.462
(D)	24	1s, 2p	2s, 2p, 3s, 3p	3.039	0.428
(E)	26	1s, 2p	2s, 2p, 3d	2.950	0.363
(F)	26	1s, 2s, 2p	2s, 2p, 3s, 3p	3.438	0.343
(G)	28	1s, 2s, 2p	2s, 2p, 3d	3.292	0.280
(H)	36	1s, 2s, 2p	2s, 2p, 3s, 3p, 3d	5.968	0.136
obsd[b]				3.49	0.178

a) N is the number of atomic orbitals in the basis set. b) From Ref. 12.

Table 4. Polarizabilities calculated by several MO methods (Å^3)

	EB/sp[a]	EB/d[a]	EB/sp′[a]	RCNDO[a]	RCNDO/v[a]	CNDO/2[a]	obsd[b]
N_2	1.807	1.832	1.959	1.409	1.289	0.754	1.77
CO	2.087	2 092	2.264	1·657	1.507	0.933	1.97
CO_2	2.815	2.336	3.178	2.522	2.375	1.189	2.63
C_2H_2	3.438	3.292	4.340	2.369	1.754	1.028	3.49
C_2H_4	4.492	4.660	5.363	3.386	2.303	1.497	4.22
C_2H_6	5.402	5.840	5.965	3.290	1.859	1.376	4.47
CH_4	3.078	3.289	3.449	1.843	0.877	0.644	2.60[c]
NH_3	2.387	2.566	2.961	1.456	0.810	0.547	2.22

a) See text. b) From Ref. 12. c) From Ref. 13,

TABLE 5. ANISOTROPIES CALCULATED BY SEVERAL MO METHODS

	EB/sp[a]	EB/d[a]	EB/sp′[a]	RCNDO[a]	RCNDO/v[a]	CNDO/2[a]	obsd[b]
N_2	0.232	0.132	0.016	0.522	0.575	0.472	0.131
CO	0.229	0.082	0.052	0.329	0.362	0.236	0.090
CO_2	0.426	0.517	0.379	0.703	0.751	0.717	0.266
C_2H_2	0.343	0.280	0.135	0.528	0.715	0.683	0.178
C_2H_4	0.250	0.228	0.058	0.316	0.466	0.446	0.143
C_2H_6	0.124	0.185	0.016	0.001	0.023	0.019	0.058
CH_4	0	0	0	0	0	0	0[c]
NH_3	0.061	0.063	0.030	0.183	0.333	0.286	0.043

a) See text. b) From Ref. 12. c) From Ref. 13.

called EB/sp (Extended-basis Set containing 3s- and 3p-orbitals) method for short and the latter, the EB/d (Extended-basis Set containing 3d-orbitals) method. The calculated polarizabilities are listed in Table 4. In the table the values calculated by the use of the wave functions obtained from other molecular orbital calculations are also shown. The results calculated using the EB/sp and the EB/d methods are improved as compared with those from the CNDO method used in the previous work.[1] Also, the results from the RCNDO/v method are improved by the use of the RCNDO method; here, RCNDO/v means the RCNDO calculation without the vacant orbitals. However, the RCNDO method gives poor results for the polarizabilities in comparison with those of the EB/sp and the EB/d methods. There are differences between the orbital exponents of the vacant orbitals used in the RCNDO method and the method in this work and between the estimations of the molecular integrals in these methods. It is considered that the introduction of the different orbital exponents is not the direct cause of the inferiority of the RCNDO method, because the results from the EB/sp′ method, which is the EB/sp calculation with the same orbital exponents as those in the RCNDO method except for a hydrogen atom, are rather analogous to those calculated by the EB/sp method.

The calculated anisotropies are listed in Table 5. Most of the calculated results are larger than the experimental ones. The values calculated by the CNDO/2 method are much improved by the EB/sp and the EB/d methods. For the calculation of the anisotropies as well as the polarizabilities, the RCNDO method is inferior to both the EB/sp and the EB/d methods. The inferiority of the RCNDO method may be caused by the estimation of the bonding parameter for the valence orbital-vacant orbital interaction. In the RCNDO method, the bonding parameter, β_{AB}^{nm}, was given by the following expression:

TABLE 6. THE WEIGHTS OF THE VACANT ORBITALS IN THE GROUND STATE WAVE FUNCTIONS (%)

Molecule	EB/sp[a]	EB/d[a]	EB/sp′[a]	RCNDO[a]
CO	9.04	6.90	4.44	0.02
CO_2	7.71	13.1	3.91	0.02
CH_4	18.8	15.4	16.2	0.375

a) See text.

$$\beta_{AB}^{nm} = \eta(I_A^n + I_B^m),$$

where I_A^n is the average of the ns- and the np-ionization potentials of the A atom and where η was taken

TABLE 7. COMPARISON OF THE PRESENT RESULTS OF THE POLARIZABILITIES WITH THOSE IN THE NON-EMPIRICAL CALCULATIONS[a]

UPHF[b]				
			CO	CH_4
Ref. 13	one term			2.819
	three terms		2.384	3.171
	four terms		2.429	3.179
EB/sp			2.087	3.078
EB/d			2.092	3.289
obsd			1.97	2.60
CPHF[c]				
CH_4				
	N[d]	α	Basis Set	
Ref. 15	22	1.073	$1s_C$, $1s'_C$, $2s_C$, $2s'_C$, $3s_C$, $2p_C$, $2p'_C$, $2p''_C$, $1s_H$, $2s_H$	
	27	1.751	$1s_C$, $1s'_C$, $2s_C$, $2s'_C$, $3s_C$, $2p_C$, $2p'_C$, $2p''_C$, $3d_C$, $1s_H$, $2s_H$	
	39	1.398	$1s_C$, $1s'_C$, $2s_C$, $2s'_C$, $3s_C$, $2p_C$, $2p'_C$, $2p''_C$, $1s_H$, $2s_H$, $2p_H$	
	39	1.831	$1s_C$, $1s'_C$, $2s_C$, $2s'_C$, $3s_C$, $2p_C$, $2p'_C$, $2p''_C$, $3d_C$, $1s_H$, $2s_H$, $2p_H$	
EB/sp	28	3.078	$2s_C$, $2p_C$, $3s_C$, $3p_C$, $1s_H$, $2s_H$, $2p_H$	
EB/d	29	3.289	$2s_C$, $2p_C$, $3d_C$, $1s_H$, $2s_H$, $2p_H$	
obsd		2.60		
NH_3				
Ref. 16	8	0.624	$1s_N$, $2s_N$, $2p_N$, $1s_H$	
	16	0.930	$1s_N$, $1s'_N$, $2s_N$, $2s'_N$, $2p_N$, $2p'_N$, $1s_H$, $1s'_H$	
	31	1.386	$1s_N$, $1s'_N$, $2s_N$, $2s'_N$, $2s''_N$, $2p_N$, $2p'_N$, $3d_N$, $1s_H$, $1s'_H$, $2p_H$, $1s_{CLP}$[e]	
EB/sp	23	2.387	$2s_N$, $2p_N$, $3s_N$, $3p_N$, $1s_H$, $2s_H$, $2p_H$	
EB/d	24	2.566	$2s_N$, $2p_N$, $3d_N$, $1s_H$, $2s_H$, $2p_H$	
obsd		2.22		

a) Units in Å^3. b) The uncoupled perturbed Hartree Fock method. c) The coupled perturbed Hartree Fock method. d) The number of the atomic orbitals. e) Located upon the estimated centroid of the lone pair (0.7 a.u. from N).

as 0.4 for the valence orbital-valence orbital interaction and as 0.05 for all the others. By comparing the equation with Eq. (5), it is found that the values of the β_{AB}^{nm} for the valence orbital-vacant orbital interaction in the RCNDO method are smaller than those given by Eq. (5). The influence of the bonding parameters appears in the weights of the atomic vacant orbitals in the wave functions of the ground state. Some of the calculated results for the weights are shown in Table 6. The weights in the RCNDO method are very small in comparison with those in the other methods. The results obtained by the RCNDO method may be improved by the introduction of some other vacant orbitals, for example, 3d-orbitals of first-row elements, into the basis set, because the calcu lated values of the polarizabilities increase with the number of atomic orbitals, as has been shown in Table 3.

Finally, some results of the polarizabilities in the present work will be compared with those in the non-empirical calculations. The results are listed in Table 7. The values calculated by Liebmann and Moskowitz[13] by means of the uncoupled perturbed Hartree Fock (UPHF) method with the variation technique are larger than the experimental ones; this is the case even when the polynomial in the perturbing variable is restricted to only one term. The overestimation is not due to the zeroth-order wave function used in the calculation, because it appeared also in the results of the UPHF method using the other zeroth-order wave functions.[14] Arrighini *et al.*[15,16] used several basis sets for each molecule in the coupled perturbed Hartree Fock (CPHF) calculation in order to discuss the effect of the basis sets and concluded that their choice of the basis sets was improper for the polarizabilities because even their largest basis set yielded a small polarizability. The results obtained by the EB/sp and the EB/d methods seem to be good in comparison with those obtained by the non-empirical ones. Because of the results for C_2H_2 in Table 3, however, it can not be said that the basis sets used in the present work bring a convergence of the polarizabilities. The present work is not appropriate as the basis of a discussion of the convergence, which is rather an interesting subject for a non-empirical calculation.

From a consideration of the results in Tables 3—6, it may be said that the effect of the atomic vacant orbitals on the calculated polarizabilities is not independent of the parameter values in the molecular integrals and that good results for the polarizabilities can be obtained by the calculation with the basis set in the EB/sp or the EB/d methods if the parameter values are suitably determined. The influences of the introduction of the atomic vacant orbitals and of the parameter values on some other physical values will be investigated in future studies.

The authors would like to thank Professor Tomoo Miyazaki for his helpful advice and for his critical reading of the manuscript. They are also indebted to Mr. Hidenobu Tatematsu of the Railway Technical Research Institute, J. N. R., for permitting them to use his unpublished data in their discussion. In their calculations, they were helped by the "University Contribution" of UNIVAC Japan, Ltd.

References

1) T. Miyazaki and H. Shinoda, This Bulletin, **46**, 1216 (1973).
2) N. S. Hush and M. L. Williams, *Chem. Phys. Lett.*, **5**, 507 (1970).
3) N. S. Hush and M. L. Williams, *ibid.*, **6**, 163 (1970).
4) D. W. Davies, *Mol. Phys.*, **17**, 473 (1969).
5) D. R. Salahub and C. Sandorfy, *Theor. Chim. Acta* (Berl.), **20**, 227 (1971).
6) C. C. J. Roothaan, *Rev. Mod. Phys.*, **23**, 69 (1951).
7) J. A. Pople, D. P. Santry, and G. A. Segal, *J. Chem. Phys.*, **43**, S129 (1965); J. A. Pople and G. A. Segal, *ibid.*, **43**, S136 (1965).
8) C. Moore, "Atomic Energy Levels," Vol. 1, Circ. 467, Washington, Nat. Bureau Stand., 1949.
9) "Tables of Interatomic Distances and Configurations in Molecules and Ions," The Chemical Society, London (1958), and its Supplement (1965).
10) H. Tatematsu (private communication).
11) H. Shinoda, H. Tatematsu, and T. Miyazaki, This Bulletin, **46**, 2950 (1973).
12) N. J. Bridge and A. D. Buckingham, *Proc. Roy. Soc.*, **295A**, 334 (1966).
13) S. P. Liebmann and J. W. Moskowitz, *J. Chem. Phys.*, **54**, 3622 (1971).
14) J. M. O'Hare and R. P. Hurst, *ibid.*, **46**, 2356 (1971); A. J. Sadlej, *Theoret. Chim. Acta* (Berl.), **21**, 159 (1971).
15) G. P. Arrighini, C. Guidotti, M. Maestro, R. Moccia, and O. Salvetti, *J. Chem. Phys.*, **49**, 2224 (1968).
16) G. P. Arrighini, M. Maestro, and R. Moccia, *Chem. Phys. Lett.*, **1**, 242 (1967).

An INDO Molecular-orbital Interpretation of the NMR of Several Protonated Heteroaliphatic Compounds

Katsutoshi OHKUBO, Kohji TSUCHIHASHI, Toshiaki YOSHIDA and Masahide OKADA

Department of Synthetic Chemistry, Faculty of Engineering, Kumamoto University, Kurokami, Kumamoto 860

(Received February 14, 1975)

Several protonated alcohols, acids, and esters were investigated by means of the INDO-MO theory and in connection with their proton and carbon-13 NMR results. The relative stability of the protonated conformers as detected by the NMR spectroscopy, had a good coincidence with the MO-theory and the experimental results. The proton or carbon-13 chemical shifts and coupling constants also showed satisfactory linear correlations between the theory and the experiment; the proton and isotropic (^{13}C) chemical shifts could be well explained by the linear correlation between the diamagnetic shielding constant and the electron density on the proton of the O–H bond and between the calculated paramagnetic shielding effect and the observed isotropic chemical shifts. The observed coupling constants of the proton and carbon-13 NMR had good overall parallelisms with those evaluated by means of the Fermi contact effect.

Considerable interest has recently centered on the elucidation of the structures of protonated heteroaliphatic compounds, with particular attention being paid to the NMR results of their protons or carbonium carbons.[1] Concerning protonated aliphatic alcohols, acids, and esters, which were investigated in the present work, Olah *et al.* [2-7] and others[8-10] have extensively studied their proton or carbon-13 NMR in a superacid system and have reported that all the keto-protonated conformers except for protonated alcohols are stable species.

The protonated compounds of the above oxygenated species, however, have been the object of only limited investigation in terms of their molecular orbital treatments. Only protonated formic acid has been studied in a few *ab initio* calculations;[11-13] the small Gaussian basis sets brought about some discrepancy between theory and experiment with respect to the relative stability of the protonated isomers.[12]

In connection with the NMR observations of several protonated species, an extensive investigation of the protonated compounds seems significant and of interest. In the present study we will focus on the PMR or ^{13}C NMR chemical shifts and coupling constants of the protonated conformers of alcohols, acids, and esters from the viewpoints of both the INDO-MO theory and experiments.

Method of Calculation

The following five homologue series were investigated in this work: (a) the protonated formates, $HC(OH)OR^+$ (R=H, CH_3, and CH_3CH_2); (b) the protonated acetates, $CH_3C(OH)OR^+$ (R=H, CH_3, and CH_3CH_2); (c) the protonated methyl esters, $RC(OH)OCH_3^+$ (R=H, CH_3, and CH_3CH_2); (d) the protonated acids, $RC(OH)_2^+$ (R=H, CH_3, and CH_3CH_2), and (e) the protonated alcohols, ROH_2^+ (R=CH_3, CH_3CH_2, and $CH_3CH_2CH_2$).

Since the geometric data for the above protonated compounds (except $HC(OH)_2^+$) are not available in the literature, the geometries of the protonated compounds were assumed to be the same as those of the parent molecules, which can be found in a standard compendium,[14] except for the bond lengths of C–O, R_{CO}, in $C-OH^+=R_{CO}$ in C–OH or C–OR, $R_{OH^+}=R_{OH}$, and $\angle COH^+=\angle COH$ or $\angle COR$; they are given in Table 1. The bond lengths of R_{CC} and R_{CH} were uniformly taken to be 1.54 Å and 1.09 Å respectively, while the bond angles of C–C–C and H–C–C were

Table 1. Assumed geometries of protonated compounds

Series	No.	Molecule	R_{CO}/Å	R_{OH}/Å	∠OCO	∠COC	∠COH
Protonated formates	1	$HC(OH)OH^+$ a)	1.312	0.95	124°18′		107°48′
	2	$HC(OH)OCH_3^+$	1.334	0.96	125°52′	114°47′	114°47′
	3	$HC(OH)OC_2H_5^+$	1.334	0.96	125°52′	114°47′	114°47′
Protonated acetates	4	$CH_3C(OH)OH^+$	1.430	0.95	130°		107°48′
	5	$CH_3C(OH)OCH_3^+$	1.360	0.96	124°	113°	116°
	6	$CH_3C(OH)OC_2H_5^+$	1.334	0.96	125°52′	114°47′	114°47′
Protonated methyl esters	2	$HC(OH)OCH_3^+$	1.334	0.96	125°52′	114°47′	114°47′
	5	$CH_3C(OH)OCH_3^+$	1.360	0.96	124°	113°	116°
	7	$C_2H_5C(OH)OCH_3^+$	1.360	0.96	124°	113°	114°47′
Protonated acids	1	$HC(OH)_2^+$	1.312	0.95	124°18′		107°48′
	4	$CH_3C(OH)_2^+$	1.430	0.95	130°		107°48′
	8	$C_2H_5C(OH)_2^+$	1.430	0.95	130°		107°48′
Protonated alcohols	9	$CH_3OH_2^+$	1.421	0.958			110°15′
	10	$C_2H_5OH_2^+$	1.480	0.958			110°15′
	11	$C_3H_7OH_2^+$	1.480	0.958			110°15′

a) All geometries of the protonated compounds were assumed on the basis of those for the parent molecules (see Ref. 14).

also uniformly settled to be 109°30′ for simplicity of computation.

Results and Discussion

Geometrical Aspects. We will first discuss briefly the geometries of the protonated compounds listed in Table 1; later we will consider the NMR of protonated species. It is noteworthy here with respect to the geometries of the protonated species that the C=O distance of the parent molecule is appreciably lengthened by the protonation so as to be near the single C–O bond-distance[11–13] and that the distance between the carbonyl oxygen and the proton is somewhat longer than the O–H bond length of formic acid or methyl alcohol.[12] In order to check the plausibility of the settled geometries, we compared the stretching-force constants, K_{AB}, for the C=O and O–H bonds of the parent molecules with those for the C–O and O–H bonds of the protonated compounds, using Badger's formula[18] with the parameters of Cossee and Schachtschneider[19]:

$$K_{CO} = 1.86/(R_e - 0.658)^3 \quad (1)$$

$$K_{OH} = 1.86/(R_e - 1.335)^3 \quad (2)$$

where the equilibrium distance, R_e, was based as the settled C–O or O–H bond-distance.

In regard to the parent molecules, the K_{CO} values of 9.19—11.68 mdyn/Å and the K_{OH} values of 7.69 (alcohols) —7.99 (acids) mdyn/Å seem plausible in view of the experimental values of K_{CO}=9.7—11.2 mdyn/Å[20] and of K_{OH}=7.2 (acids)—7.6 (alcohols) mdyn/Å.[20] It is also noticeable, with respect to the geometries of the parent molecules, that the dipole moments calculated by the INDO-MO method[15,16] are satisfactorily in accordance with the observed results.[17] On the other hand, the protonated compounds showed the K_{CO} values of 4.04—6.65 mdyn/Å and the K_{OH} value of 7.62 mdyn/Å. The force constants for both the protonated compounds seem somewhat too small in view of the fact that the *ab initio* calculation on the protonated formaldehyde[11] brought about the K_{CO} value of 8.11 mdyn/Å and a somewhat longer O–H bond (R_{OH}=0.985 Å) than that of methanol[21] or formic acid.[22] It is also of interest here, with respect to the property of the protonated compounds, that the calculated first-ionization potentials[23] for all the compounds in Table 1 were higher by 0.25—0.43 a.u. than those (about five-fourths of the experimental values[17]) for their parent molecules. This trend may be explained well by the decrease in the electron densities on the oxygen lone-pair orbitals by the protonation, which causes a lowering of the highest-occupied MO localized by the said lone-pairs.

With regard to the relative stability of the keto-protonated conformers (detected by the NMR spectroscopy) of the formates, acetates, methyl esters, and acids in Fig. 1, the present INDO calculations gave a good parallelism of the stability with the NMR observations:[1,4,9,10] that is, I>II>III in the protonated formates, I>II in the protonated methyl ester, and I>II in the protonated acids. It may be deduced, therefore, that the present assumed geometries for the

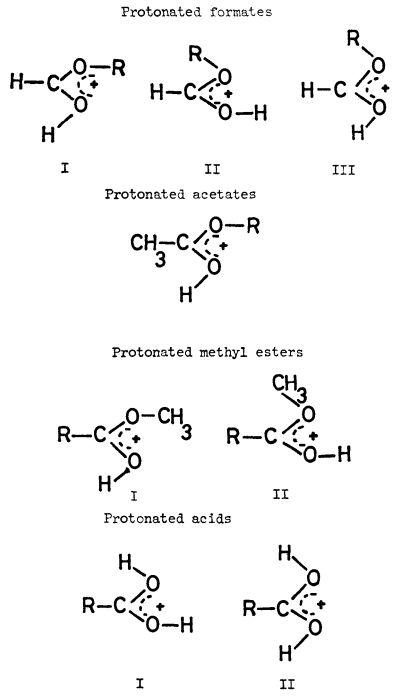

Fig. 1. Keto-protonated conformers used for the INDO calculation.

protonated compounds can be useful for discussing the NMR observations which will be developed below.

Proton Chemical Shifts and Coupling Constants. We will now investigate the correlation between the magnitude of the proton-chemical shift, δ ppm, of the protonated species and the electron density on their protons, q_H. As is shown in Fig. 2, there exist sufficient linear-correlations between the δ and q_H values for the proton of the O–H bond in all the homologue series investigated. Hence, in the proton-chemical shifts of the protonated compounds, the paramagnetic term, σ_p, and the magnetic anisotropy of the neighboring atom, σ', can be omitted from the total shielding constant, $\sigma(=\sigma_d+\sigma_p+\sigma')$, as is usual.[24] The above correlations can, then, be represented by:

$$\sigma_d(\text{ppm}) = -Aq_H \quad (A\text{: constant}) \quad (3)$$

where σ_d denotes the diamagnetic shielding constant. It is noteworthy here that the chemical shifts of the protons in the alkyl substituent, R, also have a good overall parallelism with their electron densities (q_H), as is shown in Fig. 3.

Next, let us notice the coupling constants of $J_{HH'}$, with a particular view to the correlation between the experimental and calculated constants (abbreviated as $J_{HH'}^{expt}$ and $J_{HH'}^{calcd}$ respectively). Since the proton-coupling constant depends predominantly on the Fermi-type contribution,[25] the $J_{HH'}^{calcd}$ values were evaluated by means of the following Fermi contact effect:[26]

$$J_{HH'}^{calcd} = (\hbar/2\pi)(64\pi^2/9)r_H r_{H'}\beta^2(s_H|\delta(r_H)|s_H) \times (s_{H'}|\delta(r_{H'})|(s_{H'}) \times \pi_{s_H's_H'} \quad (4a)$$

$$\pi_{s_H's_H} = 4\sum_i^{occ}\sum_j^{unocc}(\varepsilon_i-\varepsilon_j)^{-1}c_{is_H}c_{is_H'}c_{js_H}c_{js_H'} \quad (4b)$$

where the notations have the same meanings as in

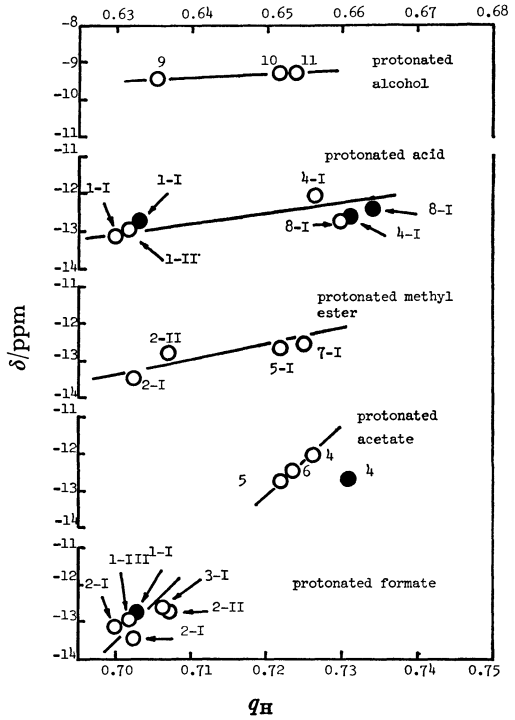

Fig. 2. Plots of δ *vs.* q_H values (remarked signs are specified in Table 1 and Fig. 1: empty circle for *cis*-proton against R; filled circle for *trans*-proton against R).

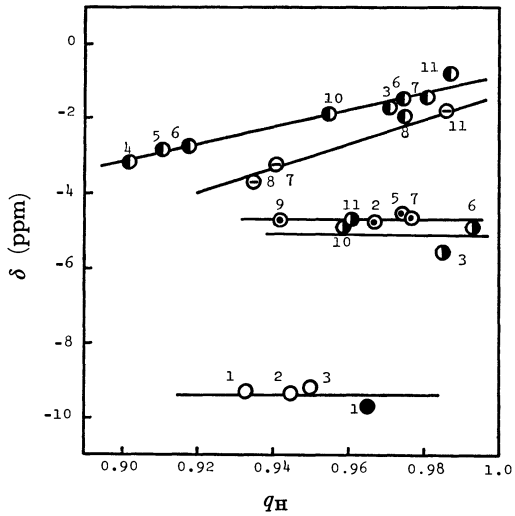

Fig. 3. The correlations between the δ values for the protons on the alkyl substituents and the q_H values (all compounds except the *cis-cis* isomer indicated by a filled circle, are the *cis-trans* protonated species specified by the compound number in Table 1).
○ or ●: H(-C); ⊖: CH_2(-C); ◑: CH_2(-O)
◐: CH_3(-CH_2); ⊙: CH_3(-O).

Ref. 26; the atomic orbital constants and the nuclear magnetogyric ratio (r_H or $r_{H'}$) were taken to be 0.5500 a.u.[27] and 2.675×10^4 $G^{-1}s^{-1}$ respectively. The $J_{HH'}^{calcd}$ and $J_{HH'}^{exptl}$ values for the protonated formic acid and methyl formate are plotted against one another in Fig. 4 (the other protonated compounds in Table 1 were not found in the NMR data). The correlation

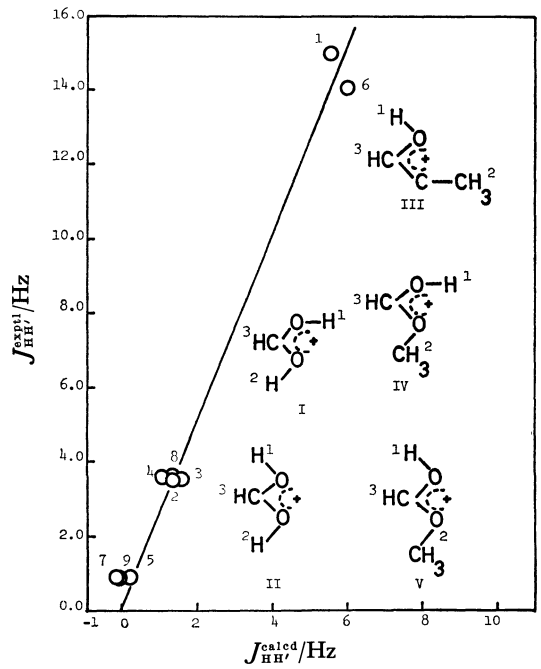

Fig. 4. Plots of $J_{HH'}^{exptl}$ *vs.* $J_{HH'}^{calcd}$ values.
1: J_{13}(I) 2: J_{23}(I) 3: J_{13}(II)=J_{23}(II) 4: J_{13}(III) 5: J_{23}(III) 6: J_{13}(IV) 7: J_{23}(IV) 8: J_{13}(V) 9: J_{23}(V).

can be shown by a straight line with an intersect of zero, but the slope of the straight line was not 45°.

Carbon-13 Chemical Shifts and Coupling Constants. We will now investigate the correlations between the calculated and observed ^{13}C-chemical shifts and coupling constants, using the ^{13}C NMR (data found only for the protonated acids) and INDO calculation results. In the calculation, the total shielding tensor, σ, was approximated by the paramagnetic shielding effect, σ_p^{AA}, without the diamagnetic contribution and the effects of the circulation on all the other atoms and of ring currents:[28]

$$\sigma_p^{AA} = ((\sigma_p)_{xx} + (\sigma_p)_{yy} + (\sigma_p)_{zz})/3 \quad (5a)$$

$$(\sigma_p)_{zz} = -(e^2\hbar^2/2m^2c^2(\Delta E))\langle r^{-3}\rangle_{2p}[(Q_{AA})_{zz}+\sum_{AB}(Q_{AB})_{zz}] \quad (5b)$$

$$(Q_{AA})_{zz} = 2-2(P_{x_Ax_A}-1)(P_{y_Ay_A}-1) + 2P_{x_Ay_A}{}^2 \quad (5c)$$

$$(Q_{AB})_{zz} = -2P_{x_Ax_B}P_{y_Ay_B} + 2P_{x_Ay_B}P_{y_Ax_B} \quad (5d)$$

where $(\sigma_p)_{xx}$ and $(\sigma_p)_{yy}$ can be given by corresponding terms and where the notations have the same meanings as in Ref. 28. The calculated and observed ^{13}C -chemical shifts (δ_{calcd} and δ_{obsd} respectively) from the reference substance of carbon disulfide are listed in Table 2. In Table 2, the average excitation energy (ΔE) for the protonated species was taken to be a number (7.9 eV) higher than that for the parent molecules (ΔE=7.7 eV), because the energies of the ground states in the former were appreciably lower than those in the latter, and because the energies of the excited states in the former were slightly higher than those in the latter. As can be seen from Table 2, there is a good overall agreement of the δ_{calcd} values with the δ_{obsd} values, and the ^{13}C-chemical shifts of

Table 2. Calculated and observed isotoropic (^{13}C)-chemical shifts eor some protonated and parent molecules

Molecule	ΔE/eV	$-\sigma_p^{AA}$/ ppm	δ_{calcd}/ ppm	δ_{exptl}/ ppm
$H^{13}COOH$	7.7	359.5	34.5	27.0[a]
$H^{13}C(OH)_2^+$(*cis-trans*)	7.9	382.8	20.9	17.0[a]
$H^{13}C(OH)_2^+$(*cis-cis*)	7.9	382.1	21.5	19.9[a]
$CH_3{}^{13}COOH$	7.7	375.1	18.9	15.6[a]
$CH_3{}^{13}C(OH)_2^+$	7.9	413.5	−9.1	−1.6[b]
$CH_3CH_2{}^{13}COOH$	7.7	375.0	19.0	14.8[a]
$CH_3CH_2{}^{13}C(OH)_2^+$	7.9	413.3	−8.8	1.6[a]
$CH_2{}^{13}COOCH_3$	7.7	374.8	19.2	23.0[c]
$CH_2{}^{13}C(OH)OCH_3^+$	7.9	393.7	0.3	
$CH_3{}^{13}COOC_2H_5$	7.7	372.8	21.2	22.9[c]
$CH_3{}^{13}C(OH)OC_2H_5^+$	7.9	390.6	3.4	
$CH_3{}^{13}COOCH_2\cdot CH_2CH_3$	7.7	373.0	21.0	22.3[c]
$CH_3{}^{13}C(OH)OCH_2\cdot CH_2CH_3^+$	7.9	390.4	3.6	
$H^{13}COOCH_2CH_3$	7.7	353.3	40.7	33.0[c]
$H^{13}C(OH)OCH_2CH_3^+$	7.9	370.3	23.7	
$^{13}CS_2$	7[d]	394.0[d]	(0)	0

a) From Ref. 6. b) From Ref. 7. c) From J. B. Stothers and P. C. Lauterbur, *Can. J. Chem.*, **42**, 1563 (1964). d) From Ref. 29.

the protonated compounds appeared in a lower magnetic field than those of the parent molecules. It is of interest here to notice the changes in the local isotropic chemical shifts ($(\sigma_p)_{xx}$, $(\sigma_p)_{yy}$, and $(\sigma_p)_{zz}$) due to the protonation, taking the formic acid and its protonated species (all the atoms on the *x-y* cross section and the C=O and C$^+$–OH bonds on the *y* axis) as examples. The *yy* element, $(\sigma_p)_{yy}$, is deshielded predominantly by the protonation from −243 ppm to about −340 ppm; the *xx* element is shielded by about 32 ppm (from −459 ppm), while the *zz* element is deshielded slightly by about −2 ppm (from −378 ppm). In this case, all the elements (*xx*, *yy*, and *zz*) of the *cis-trans* isomer, I, are not markedly different from those of the *cis-cis* isomer, III. The negative *yy* element of the multiple-bond terms ($\sum_{B\neq A} Q_{AB}$) for the protonated molecule is appreciably diminished by the protonation to be less than one half of that for the parent compound.

Table 3. Calculated and observed C^{13}-NMR coupling constants and %s character for protonated and parent molecules

Molecule	$J^{exptl}_{^{13}CH}$/Hz	$J^{calcd}_{^{13}CH}$/Hz	%s	Hybridization
$HC^{13}OOH$	225.1[a]	75.91	29.74	$sp^{2.36}$
$HC^{13}(OH)_2^+\cdot$ (*cis-trans*)	244.8	83.98	31.68	$sp^{2.16}$
$HC^{13}(OH)_2^+\cdot$ (*cis-cis*)	235.8[a]	82.06	31.59	$sp^{2.17}$
$HC^{13}OOCH_3$	226.2[b]	76.03	29.65	$sp^{2.37}$
$HC^{13}OOCH_2CH_3$	225.6[b]	75.47	29.65	$sp^{2.37}$

a) From Ref. 6. b) From N. Muller and D. E. Pritchard, *J. Chem. Phys.*, **31**, 1471 (1959).

Finally, we will discuss the carbon-13 NMR coupling constants, J^{13}_{CH}, of the protonated compounds. The J^{13}_{CH} values were calculated by means of equations similar to Eqs. (4a—4b), with the r^{13}_C value of 0.6726×10^4 G^{-1}s^{-1} and the carbon atomic orbital constant of 2.767.[27] In Table 3 we list the calculated and experimental J^{13}_{CH} values (denoted as $J^{calcd}_{^{13}CH}$ and $J^{exptl}_{^{13}CH}$ respectively) and the %s characters for the protonated formic acid and a few parent molecules. Here, the %s character was evaluated from the INDO-MO calculation results, with the following relation:

$$\%s = 100N_{C_s}/(N_{C_s}+N_{C_p}) \quad (6)$$

where N_{C_s} and N_{C_p} stand for the AO densities of the carbon-13 s- and p-orbitals respectively.

There is a satisfactorily good linear correlation between the J^{13}_{CH} values and the %s characters; this correlation can be expressed by:

$$J^{exptl}_{^{13}CH} = 7.25\%s + 14.99 \quad \text{(in Hz unit)} \quad (7a)$$

$$J^{calcd}_{^{13}CH} = 3.66\%s - 32.03 \quad \text{(in Hz unit)} \quad (7b)$$

The contribution of the %s character to the isotropic chemical shifts is different between the calculated and the experimental results, so this is reflected in the slope (not unity) of the linear correlation between the $J^{exptl}_{C^{13}H}$ and $J^{calcd}_{C^{13}H}$ values:

$$J^{exptl}_{^{13}CH} = 2.16J^{calcd}_{^{13}CH} + 61.4 \quad \text{(in Hz unit)} \quad (8)$$

The trend shown in Eqs. (7a—b and 8) may be attributed mainly to the gap between the conditions in the present calculation and those in the NMR experiment; it seems that the %s character is not completely correct in view of the approximations involved in the INDO-MO theory.

The calculations were carried out on a FACOM 230-75 computer at the Data Procession Center of Kyushu University.

References

1) The protonated heteroaliphatic compounds have been reviewed by G. A. Olah, A. M. White, and D. H. O'Brien, *Chem. Rev.*, **70**, 561 (1970).
2) G. A. Olah and E. Namanworth, *J. Amer. Chem. Soc.*, **88**, 5327 (1966).
3) G. A. Olah, J. Sommer, and E. Namanworth, *ibid.*, **89**, 3576 (1967).
4) G. A. Olah and A. M. White, *ibid.*, **89**, 3591 (1967).
5) G. A. Olah, D. H. O'Brien, and A. M. White, *ibid* **89**, 5694 (1967).
6) G. A. Olah and A. M. White, *ibid.*, **89**, 7072 (1967).
7) G. A. Olah and A. M. White, *ibid.*, **91**, 5801 (1969).
8) T. Birchall and R. J. Gillespie, *Can. J. Chem.*, **43**, 1045 (1965).
9) H. Hogeveen, A. F. Bickel, C. W. Hilbers, E. L. Mackor, and C. Maclean, *Chem. Comm.*, 898 (1966).
10) M. Brookhart, G. C. Levy, and S. Winstein, *J. Amer. Chem. Soc.*, **89**, 1735 (1967).
11) P. Ros, *J. Chem. Phys.*, **49**, 4902 (1968).
12) A. C. Hopkinson, K. Yates, and I. G. Csizmadia, *ibid.*, **52**, 1784 (1970).
13) A. C. Hopkinson and I. G. Csizmadia, *Can. J. Chem.*, **52**, 546 (1974).

14) L. E. Sutton, Editor, "Tables of Interatomic Distances," The Chemical Society, London, Special Publications No. 11 (1958) and No. 18.
15) J. A. Pople and D. L. Beveridge, "Approximate Molecular Orbital Theory," McGraw-Hill, New York, N, Y. (1970).
16) M. D. Newton, W. A. Lathan, W. J. Hegre, and J. A. Pople, *J. Chem. Phys.*, **52**, 4064 (1970).
17) K. Ohkubo, K. Tsuchihashi, and M. Okada, This Bulletin, in press.
18) R. M. Badger, *J. Chem. Phys.*, **2**, 128 (1934).
19) P. Cossee and J. H. Schachtschneider, *ibid.*, **44**, 97 (1966).
20) W. V. F. Brooks and C. M. Haas, *J. Phys. Chem.*, **71**, 650 (1967).
21) E. U. Ivash and D. M. Denison, *J. Chem. Phys.*, **21**, 1804 (1953).
22) I. L. Karle and J. Karle, *ibid.*, **22**, 43 (1954).
23) The first ionization potentials were obtained from the energy of the highest-occupied MO as a positive number, according to the Koopmans theorem (T. Koopmans, *Physica*, **1**, 104 (1933)).
24) T. Yonezawa, H. Kato, H. Saito, and K. Fukui, This Bulletin, **35**, 1814 (1962).
25) H. M. McConnel, *J. Chem. Phys.*, 23, 760 (1955); **24**, 460 (1956).
26) J. A. Pople and D. P. Santry, *Mol. Phys.*, **8**, 1 (1964).
27) J. R. Morton, J. R. Rowlands, and D. H. Whiffen, National Physical Laboratory Report BPR13 (1962).
28) J. A. Pople, *Mol. Phys.*, **7**, 301 (1964).

The Infrared Absorption Spectra of Nickel Metal Surfaces Modified with Optically Active α-Alanine from Its Aqueous Solution[1)]

Aritada HATTA, Yoshihiro MORIYA, and Wataru SUËTAKA

Laboratory of Interface Science of Metals, Faculty of Engineering, Tohoku University, Aramaki, Aoba, Sendai 980

(Received February 19, 1975)

The infrared absorption spectra of thin films of α-alanine formed on pure nickel and "Raney nickel" surfaces, modified with its aqueous solution, were measured by the high-sensitivity reflection method. From the infrared dichroism in the reflection spectra, the molecular orientations in the thin films were derived. In the thin film formed on pure nickel modified at 5 °C, the CO_2^- group of α-alanine is oriented nearly vertical to the metal surface and the O· · ·O axis is inclined to the surface. On the other hand, when the "Raney nickel" film is modified at 5 °C, the C_α–C_o(carboxylate) bond is oriented obliquely to the surface. When the "Raney nickel" film is modified at 100 °C, the Ni-alanine chelate is formed on the surface: the C_α–C_o bond and the NH_2 group are nearly parallel to the substrate surface, while the O· · ·O axis is vertical to that surface.

It is well recognized that infrared spectroscopy is one of the most powerful tools for investigating the adsorptions of a reactant or an intermediate on a catalyst. Adsorptions on metal supported on such carriers as silica and alumina are most often investigated by employing the transmission method.[2)] In this case, however, the metal particles give rise to background scattering, and the interaction of the supported metal with the carrier is also inevitable[3)]; hence, straightforward explanations of the observed spectrum are, in general, difficult to give. In addition, the transmission method can not give any direct information about the orientations. On the other hand, the high-sensitivity reflection method,[4)] which is relatively new, has been employed by a few investigators[5)] in studying the adsorptions of simple gaseous molecules to evaporated metals. In this method, the infrared radiation in the vicinity of the reflecting surface is markedly polarized normal to the mirror surface and the observed spectrum is closely correlated to the orientation of molecules existing on the metals. This technique may also be used in the investigation of the structure of thin crystal films formed on a metal substrate. In fact, it has been found that the crystal structures in thin films are often different from those in bulk materials.[6)] This result can be interpreted by taking account of the interaction of the metal substrate, which may determine the structure of the crystal nuclei on the substrate.

The asymmetric hydrogenation of the C=O double bond using Raney nickel modified with optically active amino acids or hydroxy acids has been systematically investigated by Izumi and his co-workers.[7)] In such an asymmetric synthesis, what we are interested in is the relationship between the absolute configuration of the modifying reagent and the asymmetric direction of the catalyst. In connection with this mechanism, it seemed that it might be interesting to observe the infrared dichroism arising from the preferred orientation of modifying molecules on the nickel metal surface.

Recently we have obtained results for the cases in which L-β-phenyllactic acid and L-β-phenyl-α-alanine were used as modifying reagents.[8)] In the latter case, the spectrum was in accord with an orientational model where the COO^- ion is asymmetric in alignment to the nickel surface. Recently, Groenewegen and Sachtler[9)] reported the spectrum of L-α-alanine adsorbed on silica-supported nickel; the spectrum they obtained was the same as that of a nickel chelate, but no details about the orientation were given. The objective of this paper is to obtain information about the orientation of α-alanine molecules in thin films formed on the nickel substrate. Although the direct determination of the orientation of species strongly adsorbed on the metal surface is quite desirable, the signal from the species was too weak to provide any available information, so the spectra of the thin films formed on modified nickel were observed in the present paper.

The thin films treated in this paper are probably a few hundred angstroms thick. Therefore, the reflection spectra of films with such a thickness cannot directly reveal the orientation of the species chemisorbed on the substrate. However, the orientation of the molecule in a thin film is very often determined by the orientation of the species which are adsorbed strongly on the substrate and which, consequently, act as the nuclei of the epitaxial overgrowth.[10,11)] The molecular orientation determined by the posture of the molecule at the interface is also known in liquid and liquid-crystal thin films on solid substrates.[12,13)] The orientation of the species strongly adsorbed on the substrate surface may, therefore, be deduced from the molecular orientation in the thin films.

α-Alanine was used in the present work because α-alanine is one of the simplest compounds which are practically used as modifying reagents in the asymmetric synthesis.[14)] It is, therefore, considered to be well-suited for the fundamental study of the mechanism of modification. In addition, the vibrational assignment[15)] for this molecule is almost completely established and, based on the available data, the reflection spectra can easily be analyzed.

Experimental

The infrared spectrum was obtained by means of a JASCO IR-G grating spectrophotometer with an assembly designed for use in single-beam reflection operation. Signal averaging and background-subtraction procedures were performed on a JEOL model JEC-5 spectrum computer. By using this technique, the absorptions of atmospheric water vapor was removed satisfactorily and the signal-to-noise ratios were greatly improved. The guaranteed-grade reagents of L- and D-α-alanine were obtained from the Wako Pure Chemicals Co. and were used without further purification. In

the present experiment, an electrolytical nickel (99.9% pure) plate and a thin "Raney nickel" film formed on a nickel plate were used as substrates and mirrors. The "Raney nickel" alloy was prepared, for convenience, by the vacuum deposition of aluminum onto nickel surfaces and by subsequent annealing at 550 °C for 3 hr under a nitrogen or hydrogen atmosphere.

Nickel metal plates with and without Al-Ni alloy layer were treated with a 20% aqueous sodium hydroxide solution at 80 °C and then rinsed in distilled water. The substrate, nickel or "Raney nickel," was modified with a 0.5% aqueous solution of L- or D-α-alanine at 5 °C and 100 °C. The pH-value of the solution was about 5.9 at room temperatures. The modified sample were then dried in air and subjected to the reflection measurement. Very fine crystals of the amino acids grew on the strongly adsorbed molecules, with the evaporation of water. The background spectra were obtained by using a pure nickel or thin "Raney nickel" plate just before modification.

Results and Discussion

Figure 1 shows the infrared absorption spectrum of L-α-alanine obtained as a KBr pellet in the frequency range from 1800 cm^{-1} to 900 cm^{-1}. The vibrational assignment of the infrared spectrum of DL-α-alanine was previously made on the basis of a normal coordinate treatment.[15] The high-sensitivity reflection spectra of bulk nickel plates, which were modified at

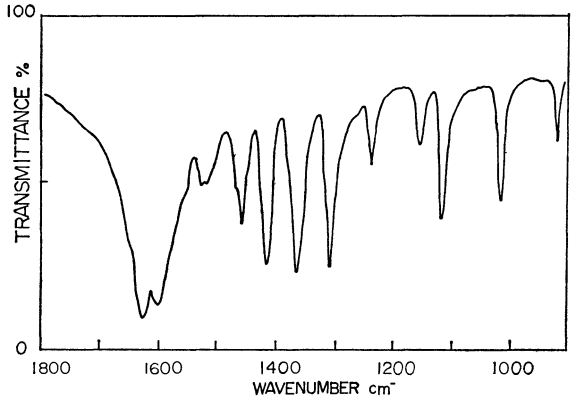

Fig. 1. Infrared transmission spectrum of L-α-alanine (KBr pellet).

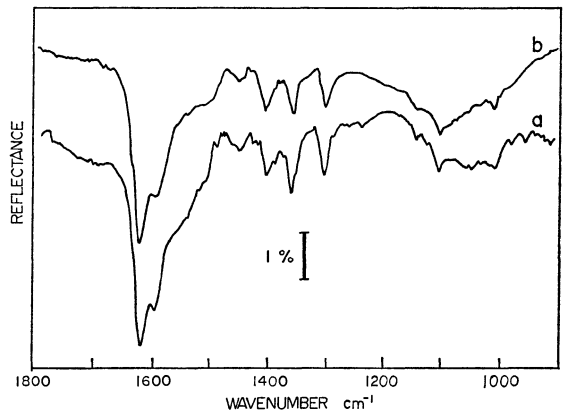

Fig. 2. High-sensitivity reflection spectra of bulk nickel plates modified at 5 °C with 0.5% aqueous solutions of L- and D-α-alanine. a: L-α-alanine; b: D-α-alanine.

5 °C over periods between a few hours and two weeks with 0.5% aqueous solutions of L-α-alanine (labeled a) and D-α-alanine (labeled b) and then covered by thin film crystals of these compounds, are shown in Fig. 2. No remarkable differences were detected in the spectra of different modifying times.

The most remarkable difference in the thin film spectra from bulk crystals, which can be clearly seen in Fig. 2, is the broad absorption with the maximum falling near 1070 cm^{-1}, probably due to the surface hydroxyl groups formed on the nickel substrate in the course of modification in an aqueous solution. Except for this band, however, the spectra of modified nickel plates with L-α-alanine and also D-α-alanine are in agreement with that of bulk L-α-alanine or D-α-alanine, except for band shifts to a slightly lower frequency, indicating that the α-alanine molecule in the film over the nickel surface is intact. Therefore, this allows us to compare the relative intensities of the bands of modified nickel with those of bulk crystals in order to determine the orientation of the α-alanine in the film on the nickel surface. As can be seen in Fig. 2, the most striking feature of the spectra of thin films on nickel is the enhanced intensity of the 1620 and 1600 cm^{-1} bands, which are assigned to NH_3^+ degenerate deformation and COO^- antisymmetric stretching respectively.[15] However, the band intensity of the COO^- antisymmetric stretching relative to that of the NH_3^+ degenerate deformation vibration somewhat decreases in comparison with the spectrum of the non-oriented sample (KBr pellet). The broad band centered at 1515 cm^{-1} in the thin film spectra, which is very weak in the spectra of Fig. 2 and which corresponds to the 1520 cm^{-1} band of bulk crystals, may be attributed to the NH_3^+ symmetric deformation. The same spectral feature was also obtained for thicker crystal films of α-alanine grown on nickel-metal surfaces during the evaporation of solvent water.

As has been mentioned above, the spectrum obtained by means of the high-sensitivity reflection method may be regarded as a polarized spectrum because it results from the interaction of molecular vibration with infrared radiation polarized normal to the reflection plane or the metal surface. Therefore, the relative intensities of the observed band in each vibrational mode depend on the orientation of the vibrational transition moments. On this basis, our attention is focused on the orientations of the CO_2^- and NH_3^+ ions, for which an approximate quantitative treatment is possible.

The transition moment of the antisymmetric CO_2^- stretching mode at 1600 cm^{-1} is parallel to the O–O direction, while that of the symmetric CO_2^- stretching mode at 1400 cm^{-1} is normal to the O–O direction. These moments are shown schematically in Fig. 3, where μ_a and μ_s refer the vibrational transition moments of antisymmetric and symmetric CO_2^- stretching vibrations respectively. The model is placed in a coordinate system where the C_α–C_0 axis lies on the yz plane, but the CO_2^- plane does not coincide with it. The rotation of the O–O axis about the C_2 axis is designated by the angle θ. The projection of μ_a on the yz plane is, therefore, given by $\mu_a \cos\theta$. Then,

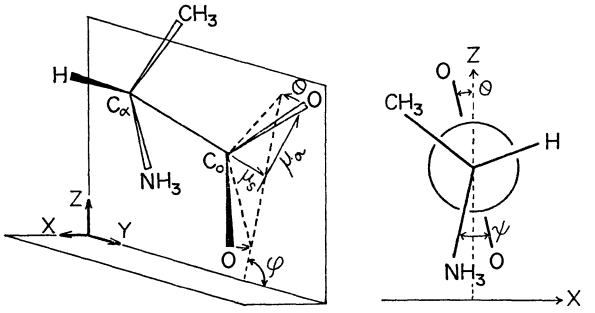

Fig. 3. Coordinates and angles for the oriented D-α-alanine. The conformation is shown as viewed along the C_α–C_o bond.

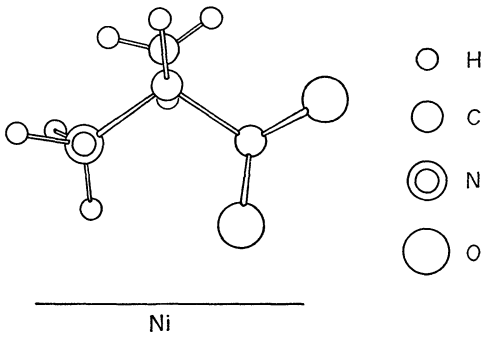

Fig. 4. Orientational model in thin D-α-alanine crystal formed on nickel metal surface at 5 °C.

the component of μ_a parallel to the radiation, polarized in the z direction, is equal to $\mu_a \cos\theta \sin\varphi$, where φ is the angle which the yz plane projection of μ_a makes with the xy plane (nickel surface). The transition moment of CO_2^- symmetric stretching, μ_s, lies along the C_α–C_o bond, regardless of the rotation of the CO_2^- group. The μ_s component parallel to the polarized radiation is, therefore, given by $\mu_s \cos\varphi$.

The electric vector of infrared radiation in the vicinity of the metal surface is practically vertical to that surface or parallel to the z axis. Accordingly, the band intensity to be observed in the high-sensitivity reflection spectra is proportional to the square of the transition moment in the z direction. Consequently, the band intensity of CO_2^- symmetric stretching relative to that of CO_2^- antisymmetric stretching can be expressed in the term: $R=(\mu_s^2/\mu_a^2)\sec^2\theta\cot^2\varphi$. The expression derived above is valid only when neither of the vibrational modes interacts with any other modes. In the present work, the coupling of the vibration is not important and so is neglected. Here, μ_s^2/μ_a^2 can be taken from the spectrum of randomly oriented α-alanine molecules. If the value is assumed to remain unchanged in the KBr matrix, the data from the spectrum shown in Fig. 1 can be used. The R value is, of course, obtained from the reflection spectrum exhibited in Fig. 2.

While the values of φ and θ can not be obtained separately, if θ is assumed, for simplicity, to be 0°, the values of φ may be calculated to be 57° and 60° for D- and L-α-alanine respectively. The difference obtained here is not significant in view of the uncertainties involved. When the θ value of 30° is used, $\varphi=61°$ is obtained from the spectrum of D-α-alanine.

The second point of special interest is the orientation of the C–NH_3^+ fragment. Information concerning the alignment of the C–N bond with respect to the CO_2^- group can be obtained from the NH_3^+ symmetric deformation band based on the assumption that the C–NH_3^+ group holds C_{3v} symmetry. The value of 110°, which is taken from the literature,[16] is used for the ∠C–C–N angle of L-α-alanine. Assuming $\theta=0°$ and $\varphi=57°$, the azimuthal angle, ψ, of the C–N bond measured from the CO_2^- plane is obtained to be 8°. If $\theta=7°$ and $\varphi=57°30'$ are chosen, the result of $\psi=16°$, which is near to the value 17° calculated by Hayashi *et al.*[17] from the X-ray data,[18] can be obtained. The orientational model of D-α-alanine is depicted in Fig. 4. The model agreed very closely with that previously obtained for L-β-phenyl-α-alanine.[8] Therefore, there seems to be no remarkable effect exerted on the molecular orientation in converting the methyl group of α-alanine to a phenyl group.

Recently Tanabe and Uyeda investigated the thin film of L-α-alanine, formed from an aqueous solution on nickel film, by electron microscopy and diffraction; they found that L-α-alanine overgrows epitaxially in a polymorphic form on the substrate surface. Different crystals were obtained according to whether or not the nickel film was treated with HCl, suggesting the occurrence of the original nucleation in a different form. However, it should be noted here that the orientation of the L-α-alanine molecule on the nickel film without HCl treatment agrees very well with that shown in Fig. 4.

The reflection spectrum of the nickel surface modified with D-α-alanine at 100 °C resembles that of the nickel surface modified at 5 °C, but several differences can be seen between them. The most noticeable are that the band intensity of the NH_3^+ degenerate deformation was much decreased on the 100 °C modified nickel surface, relative to that of the CO_2^- antisymmetric stretching band, and that the latter overcame the former, indicating a high orientation of the CO_2^- group normal to the nickel surface. In addition, the broad band centered at 1070 cm^{-1}, which was also observed with the 5 °C modified sample, was observed as a more intense band.

The reflection spectrum of the 100 °C modified nickel changed with time, showing that the thin film underwent a spontaneous change. The spectral change was complete after several hours, and the spectrum finally reached that of the 5 °C modified nickel. This fact shows that the crystal structure in the thin film, formed at 100 °C, is unstable, and that a rearrangement of the molecules to a more stable structure occurs. Although the reproducibility in band intensity was not very good, repeated experiments definitely showed that the bands due to the CO_2^- symmetric stretching as well as the NH_3^+ degenerate deformation increased in intensity with the change in the structure of thin films, whereas the CO_2^- antisymmetric stretching decreased. On the basis of the facts presented above, the orientation of the important part of the molecule

in the unstable film on the surface modified at 100 °C can be determined; the C_α–C_o bond lies approximately parallel to the nickel metal surface, with the remaining part randomly oriented. This results in an orientation which can be said to be near to that shown in Fig. 7 for the "Raney nickel" surfaces.

The reflection spectra of the unstable and the stable films can be elucidated without supposing the formation of a nickel–alanine chelate, which was found on the "Raney nickel" surface. This fact, however, does not exclude the presence of the chelate in a small amount at the interface, because the signal from the chelate must be very weak and may be masked by the bands of the molecules in the film.

The molecular orientation in the unstable film, which is similar to that in the film on the "Raney nickel" modified at 100 °C, may be determined by the orientation of chelates strongly adsorbed on nickel and acting as the nuclei of crystal growth. The chelate-nickel surface and/or chelate-alanine interaction may not be sufficiently strong, however, to maintain the unstable structure.

When a thin "Raney nickel" film was used as a substrate, the spectral behavior was different from that obtained using the bulk nickel plate mentioned above. It should be mentioned, however, that the "Raney nickel" used in this experiment contains aluminum oxide, undoubtedly developed while the vacuum-deposited aluminum film on a nickel plate was subjected to thermal treatment in order to prepare Ni–Al alloy layers on the nickel plate. The Al–O absorption band decreased upon treatment in an alkaline solution, the magnitude of the decrease depending upon the time-course of the treatment.

Figure 5 shows the high-sensitivity reflection spectrum of thin "Raney nickel" film modified with D-α-alanine at 5 °C. The most intense band, appearing at 940 cm^{-1}, is ascribed to the Al–O stretching; the intensity was unaltered despite prolonged modification at 100 °C. Except for the Al–O band, the spectrum is characterized by the strong absorption of the NH_3^+ degenerate deformation band at 1620 cm^{-1} and the weak absorption of the CO_2^- antisymmetric stretching band at 1595 cm^{-1}. Since the bands are essentially at the same frequencies as those of the bulk crystals shown in Fig. 1, the oxide layer at the substrate surface probably exerted an influence only upon the molecular orientation. The weak absorption of CO_2^- antisymmetric stretching can probably be ascribed to the molecular orientation in which the vibration has a small component of the transition moment normal to the substrate surface. The deduction regarding the orientation of the CO_2^- group can be supported by the fact that the band at 1400 cm^{-1} due to the CO_2^- symmetric stretching appears strong relative to the CO_2^- antisymmetric stretching, as is shown in Fig. 5. The orientation requires that the C_α–C_o bond should be largely tilted from the parallel direction with respect to the substrate surface. This orientation differs from that of molecules on pure nickel plates, shown in Fig. 4.

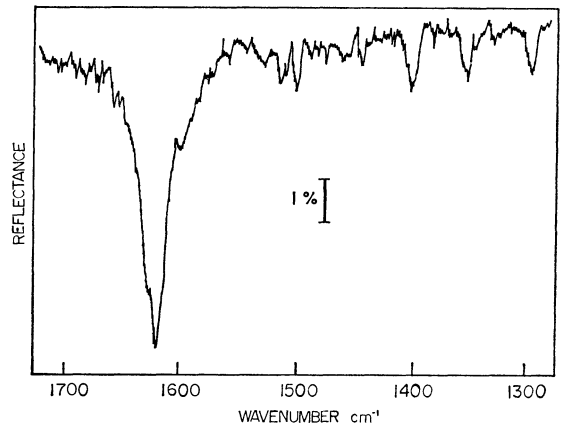

Fig. 5. High-sensitivity reflection spectrum of thin "Raney nickel" surface modified with D-α-alanine at 5 °C.

The modification of thin "Raney nickel" containing aluminum oxide with D-α-alanine at 100 °C resulted in the spectrum shown in Fig. 6. The spectrum obtained for L-β-phenyl-α-alanine is also shown in this figure for reference. The absorption at 1070 cm^{-1} is much stronger here than in the other cases mentioned above. The absorptions at 1070 and 3500 cm^{-1} (not shown in the figure) were intensified in a way parallel with each other by prolonged modification, implying that they belong to the same functional group, probably

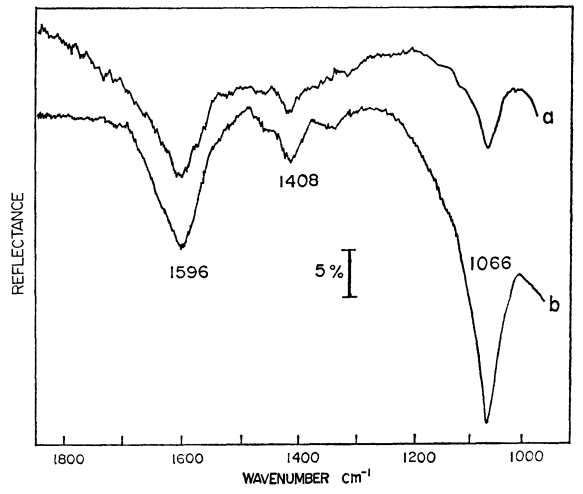

Fig. 6. High-sensitivity reflection spectra of thin "Raney nickel" surfaces modified with D-α-alanine and L-β-phenyl-α-alanine. a: D-α-alanine; b: L-β-phenyl-α-alanine.

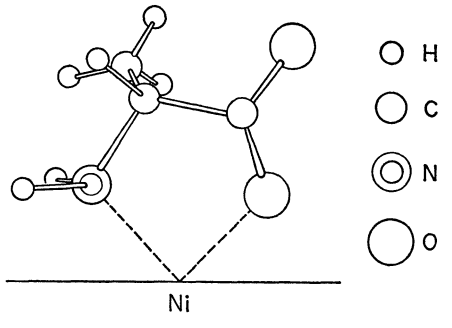

Fig. 7. Orientational model in thin D-α-alanine crystal formed on "Raney nickel" surface at 100 °C.

to the Ni–OH described above. Aside from the Ni–OH and Al–O bands, the spectrum consists of a strong CO_2^- antisymmetric stretching absorption and a weak CO_2^- symmetric stretching absorption. The absence of the NH_3^+ degenerate and symmetric deformation bands in Fig. 6 can be considered to be due to the formation of a nickel-alanine chelate on the substrate surface. It should be pointed out in this connection that this argument is valid also for the case of L-β-phenyl-α-alanine (see Fig. 6). The most probable model for molecular orientation in this case is shown in Fig. 7.

It is known that, on the chelate formation, the bands due to the NH_2 group appear instead of those of the NH_3^+ group.[19] The infrared spectrum of the nickel–alanine chelate, Ni(L-α-ala)$_2\cdot 5/2H_2O$, exhibits two intense bands, at 1600 and 1570 cm^{-1}, and two medium bands, at 1085 and 1050 cm^{-1}. Based on the band assignment given for Ni(DL-α-ala)$_2$, the former bands were assigned to the CO_2^- antisymmetric stretching and the NH_2 scissoring vibrations respectively, and one of the latter (1085 cm^{-1}), to the NH_2 wagging vibration.[19] Therefore, the orientational model shown in Fig. 7 is in accord with such a spectral feature that the NH_2 scissoring vibration is absent in Fig. 6, because its transition moment is parallel to the substrate surface and because the vibration is inactive in the reflection method employed in this experiment. On the other hand, the NH_2 wagging vibration should be observed, if the molecular orientation shown in Fig. 7 is the case, since the transition moment of the NH_2 wagging vibration lies along the direction normal to the substrate surface. However, no evidence of the NH_2 wagging band could be detected in the region where the band was expected to appear; it may be considered that the NH_2 wagging band was obscured by the overwhelming Ni–OH band, because these two bands are near in frequency. The nickel–alanine chelation observed with the "Raney nickel" modified at 100 °C is considered to be caused by its nature being more active than that of the bulk nickel plate.

Recently, Groenewegen and Sachtler[9] have examined the infrared spectra of L-α-alanine and a few amino butyric acids evaporated on Ni/SiO_2 and SiO_2. They reported that the chemisorption complex of L-α-alanine formed on Ni was very similar to the bulk complex Ni(ala)$_2$. Although it is difficult to compare the results of Groenewegen and Sachtler with ours because the experimental conditions are different, the suggestion can be made that the α-alanine reacts with the surface nickel to yield the α-alanine chelate complex at high temperatures and that this chelate formation would influence the catalytic properties of the Raney nickel.

A change in the modification temperature resulted in a change in the molecular orientation in the thin films on the bulk nickel surface as well as on the "Raney nickel" surface. This fact may correspond to the change in the optical activity of the compound obtained by the asymmetric synthesis with the modified catalyst.

References

1) Presented in part at the 29th Fall Meeting of the Chemical Society of Japan, Hiroshima, Oct., 1973.

2) L. H. Little, "Infrared Spectra of Adsorbed Species," Academic Press Inc. Ltd., London (1966).

3) For example, R. P. Eischens and W. A. Pliskin, *Advan. Catal.*, **10**, 1 (1958).

4) W. Suëtaka, *Sci. Rept. Tohoku Univ., Ser. A*, **18**, Suppl., 129 (1966); R. G. Greenler, *J. Chem. Phys.*, **44**, 310 (1966).

5) J. Pritchard and M. L. Sims, *Trans. Faraday Soc.*, **66**, 427 (1970); H. G. Tompkins and R. G. Greenler, *Surface Sci.*, **28**, 194 (1971); M. L. Kottke, R. G. Greenler, and H. G. Tompkins, *ibid.*, **32**, 231 (1972); M. Ito and W. Suëtaka, *J. Phys. Chem.*, **79**, 1190 (1975).

6) W. Suëtaka, *J. Spectroscop. Soc. Japan*, **16**, 219 (1968); K. Suzuki, A. Hatta, and W. Suëtaka, *Chem. Lett.*, **1973**, 189.

7) For example, Y. Izumi, *Yuki Gosei Kagaku Kyokai Shi*, **25**, 1013 (1967).

8) A. Hatta and W. Suëtaka, This Bulletin, **48**, 2428 (1975).

9) J. A. Groenewegen and W. M. H. Sachtler, *J. Catal.*, **33**, 176 (1974).

10) K. Tanabe and N. Uyeda, *Bull. Inst. Chem. Res., Kyoto Univ.*, **52**, 616 (1974).

11) M. Ashida, A. Hamada, and T. Watanabe, This Bulletin, **45**, 2312 (1972); N. Uyeda, Y. Murata, T. Kobayashi, and E. Suito, *J. Cryst. Growth*, **26**, 267 (1974).

12) A. Mellier and M. Léard, *J. Chim. Phys.*, **70**, 1360 (1973).

13) T. Uchida, H. Watanabe, and M. Wada, *Jap. J. Appl. Phys.*, **11**, 1559 (1972).

14) Y. Izumi, M. Imaida, H. Fukawa, and S. Akabori, This Bulletin, **36**, 155 (1963); F. Higashi, T. Ninomiya, and Y. Izumi, *ibid.*, **44**, 1333 (1971).

15) K. Fukushima, T. Onishi, T. Shimanouchi, and S. Mizushima, *Spectrochim. Acta*, **15**, 236 (1959); S. Suzuki, T. Ohshima, N. Tamiya, K. Fukushima, T. Shimanouchi, and S. Mizushima, *ibid.*, **15**, 969 (1959); R. Adamowicz and E. Fishman, *ibid.*, **28A**, 889 (1972).

16) H. J. Simpson, Jr., and R. E. Marsh, *Acta Cryst.*, **20**, 550 (1966).

17) M. Hayashi, T. Shimanouchi, and S. Mizushima, This Bulletin, **29**, 802 (1956).

18) H. A. Levy and R. B. Corey, *J. Amer. Chem. Soc.*, **63**, 2095 (1941); J. Donohue, *ibid.*, **72**, 949 (1950).

19) J. F. Jackovitz, J. A. Durkin, and J. L. Walter, *Spectrochim. Acta*, **23A**, 67 (1967).

The Adsorption of α- and β-Cyclodextrins on the Dropping Mercury Electrode in an Aqueous Solution

Yoshihisa MATSUI, Hiroshi SAWADA, Kazuo MOCHIDA, and Yoshio DATE
Department of Agricultural Chemistry, Shimane University, Nishikawazu, Matsue 690
(Received March 20, 1975)

The adsorption of α- and β-cyclodextrins on the surface of the dropping mercury electrode was examined in a phosphate buffer solution by means of voltammetry with a triangular potential sweep. The α- and β-cyclodextrins gave two capacitive peaks corresponding to the adsorption and desorption processes respectively. The α-cyclodextrin additionally gave two cathodic peaks and an anodic peak, probably due to reorientation processes. The effects on the peak heights were investigated in terms of the sweep rate, the cyclodextrin concentration, the temperature, the ionic strength, and the pH. The adsorption of both cyclodextrins followed the Langmuir isotherm, and the equilibrium constants for the adsorption were evaluated to be 1.2×10^4 M^{-1} for α-cyclodextrin and 1.0×10^5 M^{-1} for β-cyclodextrin at 25°C and pH 6.5.

The degradation of starch by the action of *Bacillus macerans* amylase yields cyclic dextrins composed of six (in α-cyclodextrin), seven (in β-cyclodextrin), or more α-D-glucopyranose units linked 1→4 as in amylose.[1] These molecules have void spaces and form 1 : 1 inclusion complexes with a variety of organic compounds in aqueous solutions.[2] In the course of a polarographic study of the inclusion complexes, we found that cyclodextrins are adsorbed on the surface of a dropping mercury electrode. This phenomenon is interesting in connection not only with the analysis, but also with the physicochemical properties of cyclodextrins. The present study was undertaken in order to examine the adsorption behavior of α- and β-cyclodextrins by means of voltammetry with a triangular potential sweep. This method is suitable for obtaining both the charging and discharging capacitive curves as functions of the applied potential,[3] although the method of differential capacity measurements with an impedance-type capacity bridge is in general use for the investigation of the electric double-layer structure and the adsorption of various organic substances.[4]

Experimental

The α- and β-cyclodextrins were prepared by the method of Lane and Pirt[5] and were purified according to the directions of Cramer and Henglein.[6]

The apparatus used for the measurement of the capacity patterns was of a Randles-Sevcik type with a triangular potential sweep (multi-sweep method). The details have been described previously.[7] A two-electrode system with a dropping mercury electrode and mercury pool electrode was used. In order to minimize the iR drop yielded across the cell, a fairly concentrated electrolyte solution (0.50 M of phosphate buffer) was used, except when the effect of the buffer concentration was examined. No test solution was degassed, since it had been found that dissolved oxygen gives no capacitive peak and has no influence on the current-potential curves of the α- and β-cyclodextrins. The dropping mercury electrode used in most experiments had the following characteristics in a 0.50 M phosphate buffer (pH 6.5): $m=0.587$ mg/s and $t=11.0$ s. The capacitive current increases with an increase in the surface area of the dropping mercury electrode. The influence of the growth of the mercury drop on the current was minimized by registering the current-potential curves immediately before the drop fell. The time interval from the moment the mercury begins to form to the time of exposure of the capacity pattern was measured by means of a stopwatch.

The DC and AC polarography were carried out with a Yanagimoto polarograph, model GA-103, which has an admittance-type capacity bridge. The superimposed sinusoidal voltage was 15 mV, 60 Hz.

Results

The adsorption of organic compounds on the mercury electrode surface causes, in general, a decrease in the surface tension of the mercury. Figure 1 shows the effects of α- and β-cyclodextrins on the electrocapillary curve of the 0.50 M phosphate buffer (pH 6.5)

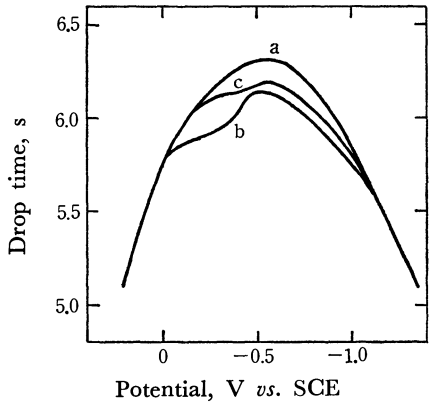

Fig. 1. Electrocapillary curves at 25 °C.
a: 0.50 M phosphate buffer (pH 6.5), b: a+5.0 mM α-cyclodextrin, c: a+5.0 mM β-cyclodextrin.

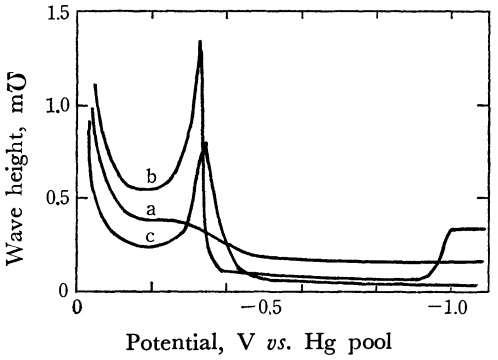

Fig. 2. AC polarograms of the cyclodextrins in 0.50 M phosphate buffer (pH 6.5) at 25 °C.
a: No cyclodextrin, b: 1.0 mM α-cyclodextrin, c: 1.0 mM β-cyclodextrin.

at 25 °C. The drop time of the mercury electrode did markedly decrease upon the addition of the cyclodextrins at potentials from 0.0 to −1.1 V *vs.* SCE for α-cyclodextrin and from −0.2 to −1.1 V *vs.* SCE for β-cyclodextrin.

Neither α- nor β-cyclodextrin gave any DC polarographic wave at these potential regions, but both did give a well-defined AC polarographic wave (Fig. 2).

Figures 3 and 4 are the current-potential curves of α- and β-cyclodextrins respectively, as determined by cyclic voltammetry. No other peaks due to the cyclodextrins were observed at any potential range not shown in these figures. A dilute solution (below 0.05 mM) of α-cyclodextrin gave two peaks (A and B) in the cathodic scan and two peaks (C and D) in the anodic scan, whereas a concentrated solution (above 0.10 mM) of the cyclodextrin gave another peak (A') on the right shoulder of the A peak. On the other hand, a solution of β-cyclodextrin gave only one cathodic peak (A) and one anodic peak (B) at all the concentrations studied (up to 1.00 mM). All the facts described above indicate that both α- and β-cyclodextrins are adsorbed on the surface of the mercury electrode and lower the differential capacity of the electrode, although the adsorption and desorption processes are not straightforward in the case of α-cyclodextrin. The potentials at which the capacitive peaks appeared are as follows (V *vs.* Hg pool): for 0.20 mM α-cyclodextrin; A, −0.44 V, A', −0.46 V, B, −1.19 V, C, −0.78 V, D, −0.36 V, for 0.01 mM β-cyclodextrin; A, −0.43 V, B, −0.37 V. The potentials of the A' and D peaks for α-cyclodextrin shifted slightly toward less negative potentials with an increase in the cyclodextrin concentration.

Since the capacitive current (i) varies in proportion to the surface area (A) of the dropping mercury electrode, the current density ($j=i/A$) was used instead of i in the following results. The value of A was calculated by means of this equation:[8]

$$A = (4\pi)^{1/3}(3mt/\rho)^{2/3} \quad (1)$$

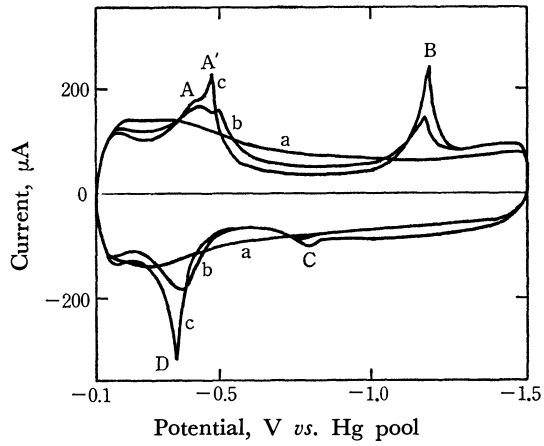

Fig. 3. Current-potential curves in the cyclic voltammetry of α-cyclodextrin in 0.50 M phosphate buffer (pH 6.5) at 25 °C.
a: 0.00 mM, b: 0.10 mM, c: 0.20 mM.
Sweep frequency: 20 Hz.

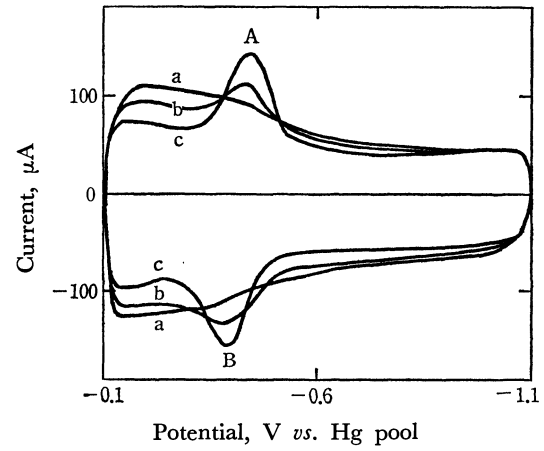

Fig. 4. Current-potential curves in cyclic voltammetry of β-cyclodextrin in 0.50 M phosphate buffer (pH 6.5) at 25 °C.
a: 0.000 mM, b: 0.005 mM, c: 0.025 mM.
Sweep frequency: 20 Hz.

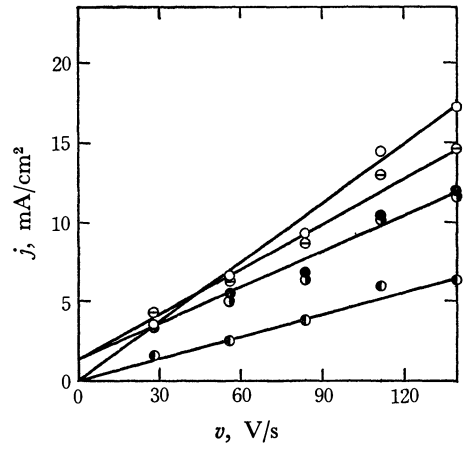

Fig. 5. The plots of j *vs.* potential sweep rate for the capacitive peaks of 0.10 mM α-cyclodextrin in 0.50 M phosphate buffer (pH 6.5) at 25 °C.
○: Peak A, ●: Peak A', ◑: Peak B, ◐: Peak C, ⊖: Peak D.

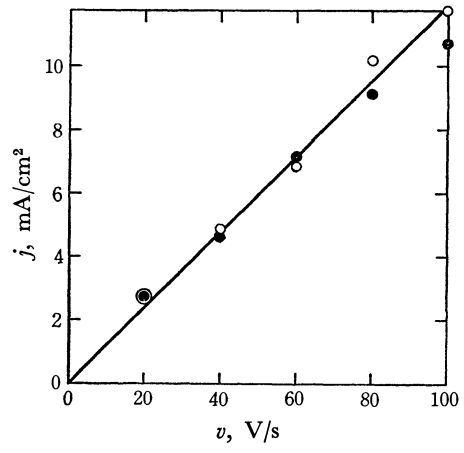

Fig. 6. The plots of j *vs.* potential sweep rate for the capacitive peaks of 0.010 mM β-cyclodextrin in 0.50 M phosphate buffer (pH 6.5) at 25 °C.
○: Peak A, ●: Peak B.

where m is the average mass of mercury flowing per unit time; t, the time interval from the moment the mercury begins to form to the time of photographic exposure, and ρ, the density of mercury. According to Loveland and Elving,[3] the value of j should be proportional to the potential sweep rate (v). Figures 5 and 6 show the plots of j *vs.* v for the 0.10 mM α- and 0.010 mM β-cyclodextrin solutions respectively in the 0.50 M phosphate buffer (pH 6.5) at 25 °C. Virtually linear plots passing the point of origin were obtained for the A and C peaks of α-cyclodextrin and for the A and B peaks of β-cyclodextrin. However, the approximately linear plots for A', B, and D peaks of α-cyclodextrin did not pass the point of origin; this suggests that these peaks involve some complex processes other than the simple adsorption-desorption processes.

Figures 7 and 8 show the plots of j *vs.* the concentrations of α- and β-cyclodextrins respectively in the 0.50 M phosphate buffer (pH 6.5) at 25 °C. Again, the plots for the A and C peaks of α-cyclodextrin and for the A and B peaks for β-cyclodextrin showed the curves characteristic of the Langmuir isotherm, but the plots for the A', B, and D peaks of α-cyclodextrin did not. On the assumption that the value of $j-j_0$ (j_0 is the value of j at a zero concentration of the adsorbate) is proportional to the amount of material adsorbed,[9] the Langmuir isotherm can be written as:

$$(j-j_0)/(j_\infty-j_0) = Kc/(1+Kc) \qquad (2)$$

where j_∞ is the maximum value of j; c, the concentration of the adsorbate, and K, the equilibrium constant for the adsorption. Eq. (2) can be rewritten as:

$$j = j_\infty - (j-j_0)/Kc \qquad (3)$$

Figure 9 shows the plots of j *vs.* $(j-j_0)/c$ for the A peaks of α- and β-cyclodextrins. Both of the plots are approximately linear. The K values were determined from the slopes of the plots to be 1.2×10^4 M^{-1} for α-cyclodextrin and 1.0×10^5 M^{-1} for β-cyclodextrin.

The dependence of j on the temperature is shown in Table 1. The j values for the A and C peaks of α-cyclodextrin and for the A and B peaks of β-cyclodextrin increased slightly with an increase in the

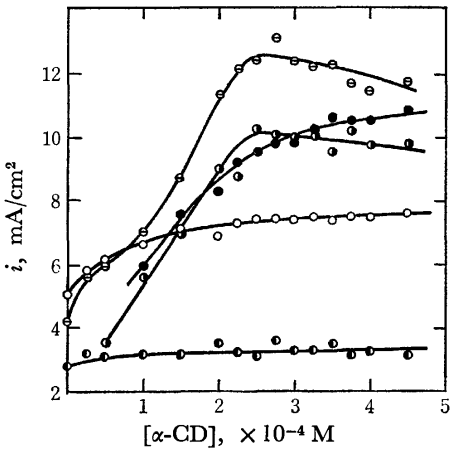

Fig. 7. The plots of j *vs.* the α-cyclodextrin concentration in 0.50 M phosphate buffer (pH 6.5) at 25 °C.
○: Peak A, ●: Peak A', ◑: Peak B, ◐: Peak C, ⊖: Peak D.
Potential sweep rate: 56 V/s.

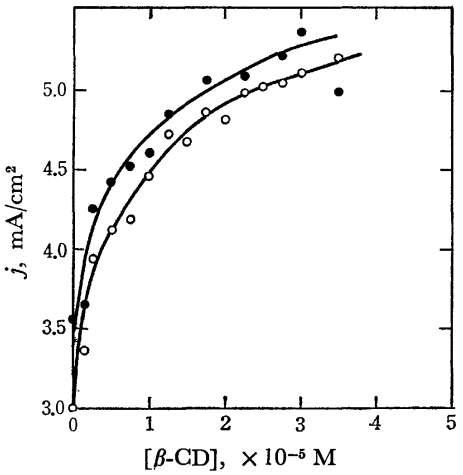

Fig. 8. The plots of j *vs.* the β-cyclodextrin concentration in 0.50 M phosphate buffer (pH 6.5) at 25 °C.
○: Peak A, ●: Peak B.
Potential sweep rate: 40 V/s.

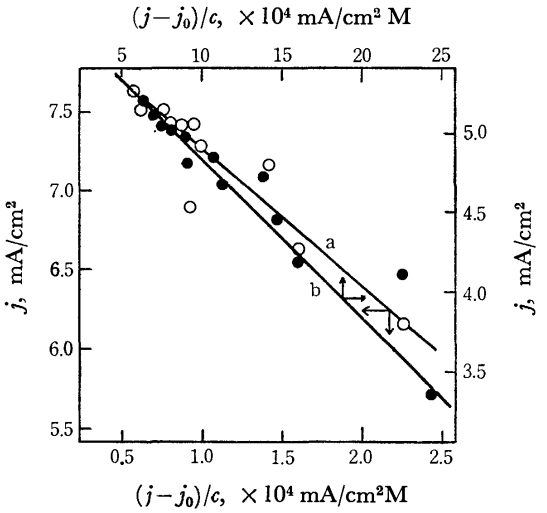

Fig. 9. The plots of j *vs.* $(j-j_0)/c$ for the A peaks of α- and β-cyclodextrins in 0.50 M phosphate buffer (pH 6.5) at 25 °C.
a: α-cyclodextrin, b: β-cyclodextrin.

TABLE 1. THE DEPENDENCE OF THE PEAK HEIGHTS ON TEMPERATURE IN 0.5 M PHOSPHATE BUFFER (pH 6.5)

Cyclodextrin	peak	$(1/j)(dj/dT)$, %
α[a]	A	+0.4
	A'	−2.1
	B	−1.0
	C	+0.5
	D	−0.9
β[b]	A	+0.1
	B	+0.1

a) [α-CD]=0.10 mM and v=56 V/s. b) [β-CD] = 0.010 mM and v = 40 V/s.

temperature. On the other hand, the other peaks of α-cyclodextrin were significantly lowered with a temperature increase. When the concentration of the phosphate buffer at pH 6.5 increased from 0.025 M to 0.50 M, the heights of the A and C peaks for α-cyclodextrin increased slightly, whereas that of the A′ peak decreased slightly. The other peaks of α- and β-cyclodextrins showed virtually no change with an increase in the ionic strength. A similar change in the heights for the A and A′ peaks of α-cyclodextrin was observed when the pH of the phosphate buffer (0.50 M) was increased from 5.0 to 8.0.

Discussion

The adsorption of α- and β-cyclodextrins on the surface of the dropping mercury electrode is apparent on the basis of the following observations: (1) a solution of α- or β-cyclodextrin gives no DC polarographic wave, but does give an AC polarographic peak and some cyclic voltammetric peaks, and (2) the surface tension of the dropping mercury electrode in a phosphate buffer is markedly depressed by the addition of α- or β-cyclodextrin.

There is no dobut that the least negative capacitive peak in the cathodic scan for each cyclodextrin (Peak A) corresponds to the adsorption process of the cyclodextrin. The dependence of the peak height for this process on the rate of the potential scan agrees with the equation presented for the capacitive current. The peak height also follows the Langmuir isotherm. The equilibrium constant (K) for the adsorption of β-cyclodextrin ($1.0\times10^5\ M^{-1}$) is about 8 times larger than that of α-cyclodextrin ($1.2\times10^4\ M^{-1}$). This result may be related to the fact that β-cyclodextrin is about 8 times less soluble in water than α-cyclodextrin.[10] According to Blomgren, Bockris, and Jesch,[11] the adsorptivity of organic substances on the mercury surface increases with a decrease in the solubility in water. Similar results have also been reported by Kaganovich *et al.*[12] who showed that the adsorption of normal aliphatic acids, alcohols, or amines is enhanced by increasing the length of the hydrocarbon chains—that is, by a decrease in the solubility in water.

The anodic peak B of β-cyclodextrin is almost symmetrical with the cathodic peak A and may be due to the desorption of the cyclodextrin. In the case of α-cyclodextrin, the behavior of the peaks other than the cathodic peak A is very complex. The A′ peak does not appear until the concentration of α-cyclodextrin exceeds 0.10 mM, in which case, according to the plot of j for peak A *vs.* the cyclodextrin concentration in Fig. 7, about half of the adsorption sites of the mercury electrode are occupied by the adsorbate. The peak height decreases with an increase in the temperature, the pH, or the ionic strength. The peak can be attributed either to the multilayer adsorption of the cyclodextrin or, more probably, to the reorientation of the adsorbed molecules on the electrode surface. However, it is not clear why the behavior of α-cyclodextrin is so different from that of β-cyclodextrin. The behavior of the B peak of α-cyclodextrin is similar to that of the A′ peak, so it is reasonable to ascribe the peak to the reverse process of the A′ peak. The anodic peaks C and D of α-cyclodextrin may also involve the adsorption-desorption and/or reorientation processes, but the details remain still unclear.

The present cyclic-voltammetric method could be applied to the determination of microquantities of the cyclodextrins. By the use of calibration curves, it is possible to determine *ca.* 20—200 μg/ml of α-cyclodextrin or *ca.* 1—20 μg/ml of β-cyclodextrin at 25 °C.

References

1) D. French, *Advan. Carbohyd. Chem.*, **12**, 189 (1957).
2) For recent reviews, see D. W. Griffiths and M. L. Bender, *Advan. Catal.*, **23**, 209 (1973); T. Kuge and K. Takeo, *Denpun Kagaku*, **21**, 151 (1974).
3) J. W. Loveland and P. J. Elving, *Chem. Rev.*, **51**, 67 (1952).
4) B. B. Damaskin and A. N. Frumkin, "Reactions of Molecules at Electrodes," ed. by N. S. Hush, Wiley-Interscience, New York, N. Y. (1971), p. 1.
5) A. G. Lane and S. J. Pirt, *J. Appl. Chem. Biotechnol.*, **21**, 330 (1971).
6) F. Cramer and F. M. Henglein, *Chem. Ber.*, **91**, 303 (1958).
7) Y. Matsui, Y. Kurosaki, and Y. Date, This Bulletin, **43**, 1707 (1970).
8) I. M. Kolthoff and J. J. Lingane, "Polarography," 2nd Ed., Interscience Publishers, New York, N. Y. (1952), p. 44.
9) S. G. Mairanovskii, "Catalytic and Kinetic Waves in Polarography," Plenum Press, New York, N. Y. (1968), p. 69.
10) D. French, M. L. Levine, J. H. Pazur, and E. Norberg, *J. Amer. Chem. Soc.*, **71**, 353 (1949).
11) E. Blomgren, J. O. M. Bockris, and C. Jesch, *J. Phys. Chem.*, **65**, 2000 (1961).
12) R. I. Kaganovich, V. M. Gerovich, and T. G. Osotova, *Dokl. Akad. Nauk SSSR*, **155**, 893 (1964); R. I. Kaganovich and V. M. Gerovich, *Elektrokhimiya*, **2**, 977 (1966).

Chemical Effects of $^{31}P(n,\gamma)^{32}P$ Reaction in Phosphate Glass—A Radiation Chemical Approach to Hot Atom Chemistry

Tsing-Ko Lin and Niro Matsuura*

Institute of Nuclear Energy Research, P.O. Box 3, Lung-Tan, Taiwan, Republic of China

**Department of Pure and Applied Sciences, College of General Education, University of Tokyo, Tokyo 153*

(Received March 25, 1975)

Sodium metaphosphate glass, with a polymerization degree of 50—100, was used as target material for the study of the chemical effects of (n, γ) reaction. Mean oxidation number of ^{32}P was introduced as a new parameter to elucidate the oxidation reaction brought on the recoil product. The mean oxidation number of ^{32}P from (n, γ) recoil in such glassy polyphosphate was about +4. More than 90% of the ^{32}P set free was reattached as an end group in the newly formed radioactive polyphosphate. The recoiled monoatomic ^{32}P species (less than 10% of the total ^{32}P) defficient in oxygen kept a low mean oxidation number *ca.* +3. Ionizing radiation produced color center (with λ_{max} at 510 nm) which seemed partially to oxidize the ^{32}P product. The effect was very weak, and could be suppressed by the hold scavengers. Thermal annealing showed that the mean oxidation number of ^{32}P rapidly attained +5 (the valence of target) by 300 °C; however, it seems very difficult to raise the mean oxidation number of ^{32}P to +5 by γ-ray annealing. The oxidation of ^{32}P through thermal annealing is considered to be a diffusion process, with an activation energy of *ca.* 7×10^3 cal/mol. Possible reaction between the hot-zone and the radiation spurs is discussed.

During the course of $^{31}P(n, \gamma)$ ^{32}P reaction in oxyphosphorus compounds, more than 90% of the recoil ^{32}P was set free from its bonding. However, most of the ^{32}P underwent recombination to form radiophosphates even in polymer skeletones.[1] Electrophoretic study of the reactor-irradiated oxyphosphates of ammonium and alkali metal salts at liquid nitrogen temperature indicates that fourteen different anions labelled with ^{32}P in the skeletones of polymer species were found.[2,3] Such ^{32}P-labelled polyphosphates were also observed in the aqueous target of varilous orthophosphate solutions.[4] Our experiments with polyphosphates as target clarified how the recoil ^{32}P was converted into the radiopolyphosphates.[5-7] Ionizing radiation seems to affect the distribution of radiophosphates. In a previous work we have thoroughly investigated the oxidation of ^{32}P species induced by γ-radiation in the tripolyphosphate solution, in which the recoil ^{32}P products were found almost in monomer forms.[9] In solid target, however, the separable ^{32}P-labelled polyphosphate products were so complicated that their chromatographic patterns provided no clue to clarify the redox reaction occurring on the recoil ^{32}P.[6,9,10] The radiopolyphosphate products can be classified into five kinds, each having one ^{32}P attached as an end group.[6,7] After acid hydrolysis they undergo the following changes quantitatively.[11,12] (Blazer's notation is used.[13])

$$\overset{3}{P}\text{-O-}\overset{3}{P}\text{-} \longrightarrow 2\overset{3}{P}, \qquad \overset{2}{P}\text{-}\overset{4}{P} \longrightarrow 2\overset{3}{P},$$

$$\overset{3}{P}\text{-O-}\overset{5}{P}\text{-} \longrightarrow \overset{3}{P} + \overset{5}{P}, \quad \overset{4}{P}\text{-}\overset{4}{P} \longrightarrow \overset{3}{P} + \overset{5}{P},$$

$$\overset{5}{P}\text{-O-}\overset{5}{P}\text{-} \longrightarrow 2\overset{5}{P}$$

The apparent oxidation unmber of ^{32}P is almost unchanged even after hydrolysis into monomers. The average of the oxidation number of the total recoil ^{32}P thus can be easily estimated from the hydrolyzed monomers. A mean oxidation number of the total ^{32}P is more available than the individual ^{32}P specimen for the study of the redox reaction occurring on the recoil ^{32}P.

In the present work, sodium metaphosphate glass, a glassy polyphosphate known as Graham's salt, was used as a target to investigate the reaction of ionizing radiation on the recoil ^{32}P, since such glass can firmly trap the reactive radicals produced by the γ-radiolysis at room temperature.[14-15] In order simplify the reaction system, all the ^{32}P precursors of low oxidation state can be represented by $\overset{3}{P}$ (phosphite species) since there are only $\overset{3}{P}$ and $\overset{5}{P}$ states after hydrolysis. The "mean oxidation number" (abbreviated as "MON") is also applied as a parameter to evaluate the effects of ionizing radiation on the chemical state of the recoil product.

Experimental

Preparation of Target Materials. Graham's salt, sodium metaphosphate glass having the chemical form $(NaPO_3)_n$ was prepared as follows:

Sodium dihydrogen phosphate dihydrate was dehydrated at 800 °C for three hours in an electric furnace. The fused salt was then quenched to give a clear glass sheet with thickness of about 2 ± 0.2 mm between two brass plates. The degree of polymerization, determined by pH titration[17] and viscosity measurement,[18] showed a value between 50 and 100. In the metal-doped Graham's slat, about 0.5—3 mol percent of MnO, Sb_2O_3, Sb_2O_5 or NiO was mixed thoroughly with sodium dihydrogen phosphate dihydrate and was then treated in the same way as in the preparation of a metal containing phosphate glass.

NaI doped Grabam's salt was prepared under nitrogen atmosphere in a specially designed quartz tube.[7] The content of iodide was determined colorimetrically after being extracted into chloroform.

Irradiation. Neutron activation was carried out with the Kyoto University Reactor (KUR), with a neutron flux of *ca.* 2×10^{13} n cm^{-2} s^{-1} and a gross γ-ray dose rate of about 4.5×10^{21} eV g^{-1} hr^{-1} in the pneumatic tube, or a neutron flux of *ca.* 4×10^{12} n cm^{-2} s^{-1} and a gross γ-ray dose rate of *ca.* 2×10^{21} eV g^{-1} hr^{-1} in a slant tube.

Gamma ray irradiation was carried out with a ^{60}Co source at the Institute for Solid State Physics of University of Tokyo.

Eight positions, with γ-ray dose rate of $(3.7\pm0.1)\times10^{18}$ eV·g^{-1} hr^{-1}, around the standard source were chosen.

Chemical Analysis. In order to prevent the redox reaction induced by dissolution, the irradiated solid sample was carefully dissolved in 6 M HCl under nitrogen atmosphere. The role of HCl is not only to hydrolyze polyphosphate into monomer forms, but also to suppress the oxidation reaction induced by the color center during the course of dissolution.[15,16]

All the samples except the isothermally annealed ones were separated by anion-exchange chromatography. A gradient elution of 0.1—0.6 M ammonium acetate solution through an acetate form Dowex 1×8 anion-exchange resin of the size of 1×15 cm ϕ was applied for the separation of the phosphoxy anions of different oxidation states.[6,8]

Separation of the annealed samples was carried out by the paper chromatographic method. Toyo Roshi No. 50 filter paper was used as paper strip, and a mixture of *n*-propanol, ammonia and water in the ratio 6 : 3 : 1 in volume was used as developer. The R_f-values of the radioactive $\overset{1}{P}$, $\overset{3}{P}$ and $\overset{5}{P}$ species, determined by automatic radioactive scanning method, were found to be 0, 0.30 and 0.66, respectively. Quantitative determination of the phosphorus species was carried out colorimetrically by the molybdenum blue method[19-22]; 1 ml from each of the separated fraction was taken prior to colorimetry for the determination of radioactivity.

Results

Distribution of Radioactive Species and the Mean Oxidation Number of ^{32}P in Pure Salt. Distribution of ^{32}P species in the forms of hypophosphite ($\overset{1}{P}$), phosphite ($\overset{3}{P}$) and phosphate ($\overset{5}{P}$), obtained from the Graham's salt after hydrolysis with 6 M HCl is given in Table 1 for two independent series of experiments, A and B. The result shows that all the ^{32}P is hydrolyzed into monomer forms. The MON ^{32}P calculated from the yields of $\overset{1}{P}$, $\overset{3}{P}$ and $\overset{5}{P}$, is given in the last column of Table 1.

The MON of ^{32}P depends predominantly upon the radioactivity ratio of $\overset{3}{P}$ and $\overset{5}{P}$ species. Since the yield of radioactive $\overset{1}{P}$ is negligibly small as compared with that of $\overset{3}{P}$ and $\overset{5}{P}$, it has little effect on the evaluation of MON. The estimated mean oxidation number of ^{32}P is *ca.* +4.0, when irradiation time is shorter than 60 s. (the absorbed energy, by referring to ^{60}Co γ-ray dose, was about 6×10^{19} eV/g).

A rise of mean oxidation number of ^{32}P was observed only when the exposure of target in the nuclear reactor is sufficiently long. For instance, the mean oxidation number of ^{32}P was found to be +4.2 by 120 s irradiation, in which the target absorbed an energy dose of about 1.2×10^{20} eV/g. Such an observation indicates that the ambient radiation in the reactor is partially effective in raising the oxidation state of ^{32}P.

A color center was formed in the glass during the course of exposure in the reactor. The absorbancy at 510 nm, which attributed to trapped hole by many workers[14,16,23] increased with the exposure time (Fig. 1).

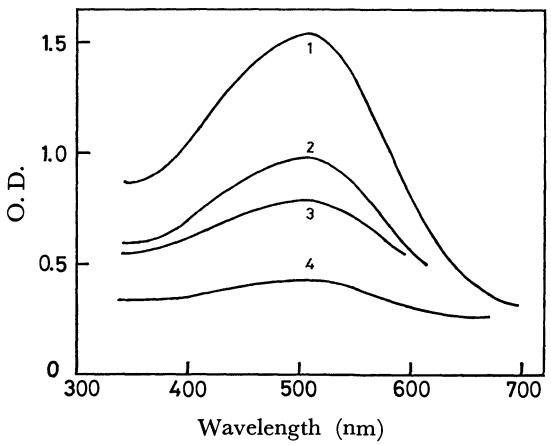

Fig. 1. Absorption spectra of reactor irradiated Graham's salts. Curves 1, 2, 3 and 4 denote irradiation times 120, 60, 30, 15 seconds in pneumatic tube.

Table 1. Distribution of radioactive hypophosphite ($\overset{1}{P}$), phosphite ($\overset{3}{P}$), and phosphate ($\overset{5}{P}$) species as well as the mean oxidation number of ^{32}P in reactor irradiated pure Graham's salt

Experiments of series A and B were carried out, independently.

Irradiation time (s)[d]	Series	Energy[a] absorbed (10^{19} eV/g)	Specific Activity (μci/g)	^{32}P yield $\overset{1}{P}$ (%)	^{32}P yield $\overset{3}{P}$ (%)	^{32}P yield $\overset{5}{P}$ (%)	$\overset{5}{P}/\overset{3}{P}$	R[b] (%)	MON[c]
5	A	0.33	1.8	0.6	47.0	52.4	1.1	—	4.0
15	A	1.3	6.0	1.2	45.8	42.6		111	4.0
	B	1.5	7.5	1.6	44.1	54.3	1.1	94.9	4.0
30	A	2.8	13.6	1.4	45.9	51.6		107	4.0
	B	3.1	14.0	1.6	44.6	53.9	1.1	101	4.0
60	A	5.5	21.5	1.8	45.7	52.5		102	4.0
	B	7.2	31.0	0.9	47.5	51.6	1.1	85.6	4.0
120	A	—	51.8	2.0	35.5	62.5		—	4.2
	B	11	56.0	1.1	39.5	59.5	1.6	91.3	4.2

a) Monitrored by phosphate glass. (*i. e.* by the optical densisy of Graham's salt)[7] b) Total recovery of radioactivity with average value of 98.9%. c) Mean oxidation number of ^{32}P. d) Irradiated in pneumatic tube.

A separate series of irradiation by ^{60}Co γ-ray shows that the optical density of the phosphate glass at 510 nm obeys Beer's law at least up to 10^{19} eV/g, which is in good agreement with Kobayashi's works[7,15,16] The optical absorbancy in a higher dose region does not seem to obey Beer's law but logarithmic one.[15,16,24] It should be emphasized that the mean oxidation number of ^{32}P increases beyond critical point, turning logarithmic.

Effect of Additives on MON of ^{32}P. In order to study the effect of ambient radiation in the reactor, hole scavengers such as Mn^{2+}, Sb^{3+} and I^- as well as electron scavengers such as Ni^{2+} and Sb^{5+} were doped individually from 0.5 to 3.0 mol% into Graham's salt. They were all irradiated in the slant tube together with a pure salt for about 6 min.

These glasses doped with hole scavenger always showed no absorption at 510 nm even after having absorbed a radiation energy *ca.* 10^{21} eV/g. The mean oxidation number of ^{32}P remained at 3.96—4.02, while that of ^{32}P in pure salt was found to be 4.25. The value on pure salt is also expected (Table 1), if we compare the energies absorbed. On the other hand the mean oxidation number of ^{32}P in these Ni^{2+}- and Sb^{5+}-doped salts were found to be +4.22 and 4.12, respectively. This value of MON for ^{32}P is very close to that observed in the pure salt which was irradiated under the same conditions. The detail of the experimental results are summarized in Table 2 (a) for both the distribution of ^{32}P species and its mean oxidation number. The results show that the oxidation of ^{32}P products might be due to the trapped hole. The reaction of electron is not clear, though electron may form oxygen center and reacts as an oxidant.[7,15,25,26]

The yields of the recoiled monoatomic ^{32}P species obtained merely by dissolving the irradiated glass into pure water without hydrolysis, are also given in the forms of $\overset{1}{P}$, $\overset{3}{P}$ and $\overset{5}{P}$ in Table 2 (b). The radioactivity involved in the monoatomic ^{32}P fractions was less than 10% except Sb^{3+}- and Sb^{5+}-doped glasses in which it was near 20%. As a matter of fact, more than 90% of the recoil ^{32}P was labelled into the polyphosphate.[6,7] The mean oxidation number of ^{32}P in such monoatomic ^{32}P product, however, kept a comparatively low value *ca.* +3.0, independent of the dopants. Both trapped hole and electron has little effect on such recoiled monoatomic ^{32}P species.

Table 2. Mean oxidation number of ^{32}P in doped Graham's salt

Irradiated samples were treated in two ways before chemical analysis:
(a) hydrolyzed with 6M HCl,
(b) dissolved in water without hydrolysis.

Ion doped (mol %)	$\overset{1}{P}$(%)	$\overset{3}{P}$(%)	$\overset{5}{P}$(%)	MON
(a) Hydrolyzed sample				
Mn^{2+} (2)	1.2	48.6	50.2	3.98
Sb^{3+} (2)	4.4	42.8	52.7	3.96
I^- (5)	0.8	47.2	52.0	4.02
Sb^{5+} (2)	—	44.0	56.0	4.12
Ni^{2+} (0.5)	1.9	37.4	61.7	4.22
pure salt	—	37.4	62.6	4.25
(b) Unhydrolyzed sample				
Mn^{2+}	0.4	4.4	1.0	3.2
Sb^{3+}	8.2	3.3	8.6	3.0
I^-	0.6	8.5	—	2.9
Sb^{5+}	5	4	5	2.9
pure salt	0.8	5.0	1.2	3.3

All samples were irradiated together in the slant tube for about 6 min. corresponding to a γ-energy of *ca.* 10^{20} eV/g.

Effects of γ-Ray Annealing on Recoil ^{32}P. Further studies of the radiation effect on ^{32}P were carried out by ^{60}Co source prior to neutron activation. After having absorbed an energy of about 10^{20} eV/g (approximately the order of energy which the target might absorb during its exposure in the reactor), the colored glasses were irradiated together with the untreated Graham's salts in the pneumatic tube. The results are illustrated in Figs. 2 (a) and (b) in terms of the radioactivity growth of $\overset{3}{P}$ and $\overset{5}{P}$ as a function of irradiated time. The yields of radioactive $\overset{1}{P}$ are always as low as 1% of the total activity, remaining virtually unchanged. The gamma ray treated samples always had higher $\overset{5}{P}$ activity and lower $\overset{3}{P}$ activity than the untreated ones. This indicates that the ionizing radiation may partially induce the oxidation of the recoil ^{32}P species and pre-neutron irradiation γ-ray treatment can enhance such a reaction. This evidence is more clearly confirmed in Fig. 3. The $\overset{5}{P}/\overset{3}{P}$ ratio and the mean oxidation number of ^{32}P for both series are shown as functions of the absorbed energy in Fig. 3 (a) and (b), respectively. The γ-ray treated sample always

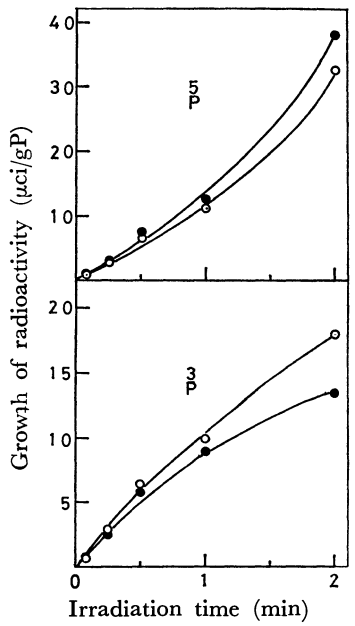

Fig. 2. Growth of the specific activities of $\overset{3}{P}$ and $\overset{5}{P}$ fractions in neutron activated Graham's salt.
-○-: Uutreated salt. -●-: Target was irradiated by ^{60}Co γ-ray with a dose of obout 10^{20} eV/g before neutron activation.

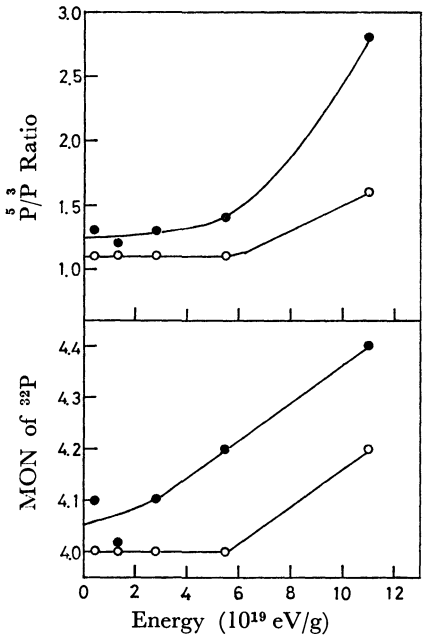

Fig. 3. Variations of MON of ^{32}P and the radioactive $^5P/^3P$ ratio as function of energy absorbed in the reactor.
-○-: Untreated sample, -●-: Target was irradiated by 10^{20} eV/g before neutron activation.

kept higher $^5P/^3P$ ratio and the mean oxidation number of ^{32}P than those of the untreated sample, the difference increasing with energy. The oxidation induced by γ-radiation seems to have a threshold of energy. From the curves of untreated sample (Fig. 3), when energy absorbed was less than 6×10^{19} eV/g, the reaction does not seem able to occur. The oxidation would occur only after the target absorbed enough energy which might exceed 6×10^{19} eV/g.

The post-neutron irradiation γ-ray annealing was studied within the γ-ray dose ranging from 1.4×10^{20} to 1.9×10^{21} eV/g. The results are given in Fig. 4 in terms of the MON of ^{32}P and the yields of radioactive ^5P and ^3P. In contrast to the pre-neutron annealing curves (Fig. 3) the post-neutron annealing curves (Fig. 4) show an opposite trend in the oxidation of ^{32}P. The reaction is rapid in the beginning, but becomes slow with the increase in radiation dose. It seems very difficult for the mean oxidation number of ^{32}P to retain the valence state +5 of the target phosphorus by the gamma ray annealing.

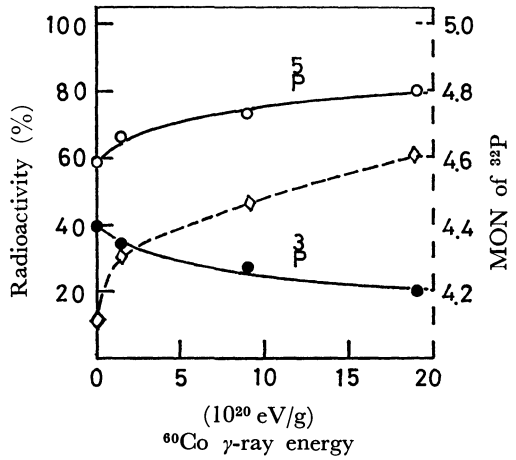

Fig. 4. Post-neutron irradiation ^{60}Co γ-ray annealing curves for radioactive ^3P and ^5P fractions. Dotted line denotes the variation of MON of ^{32}P as function of γ-ray energy.

Effects of Thermal Annealing on Recoil ^{32}P. Thermal annealing of the reactor irradiated glass was carried out at 50, 100, 200, 250, 300 and 400 °C. The results are summarized in Table 3.

The isothermal annealing curves at each temperature are given in Fig. 5. Paper chromatographic scanning was made for the two major components, ^3P and ^5P of ^{32}P products, from the hydrolyzed acidic solution (6M HCl) of the annealed sample. The detectable ^1P-activity was always less than one percent, almost completely disappearing at 300 °C. No matter what the annealing temperature was, within 2—5 min, the yield of ^{32}P components attained rapidly a fixed ratio between ^3P and ^5P. The higher the annealing

Table 3. Thermal annealing of the reactor irradiated Graham's salt

Annealing temperature (°C)	Annealing time (min)					Change of Color
51±1	5	10	20	40	60	brown
101±2	5	10	20	40	60	brown
199±3	5	10	20	40	60	colorless
250	5	10	30	60		colorless
300±2	5	10	20	20	40	colorless
396±2	2[a]	5	10	15		white

a) colorless.

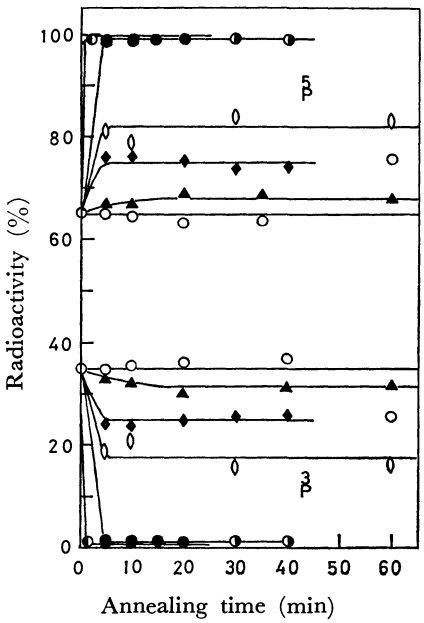

Fig. 5. Isothermal annealing curves of radioactive ^3P and ^5P fractions in reactor irradiated Graham's salt. ○: 50°, △: 100°, ◆: 200°, ○: 250°, ◑: 300° and ◐: 400 °C.

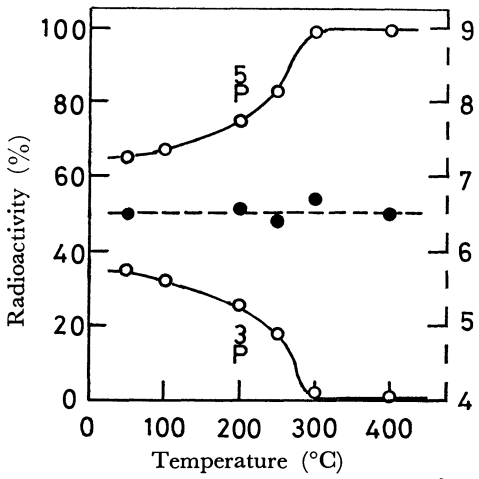

Fig. 6. Isochronic curves of radioactive ^{3}P and ^{5}P fractions. The total specific activities detected at each annealing temperature are also presented in dotted line.

temperature, the more rapidly the isothermal curves reached its equilibrium. Such stationary composition of ^{32}P products at each annealing temperature maintained some 60 min.

In Fig. 6, the radioactive yields of both ^{3}P and ^{5}P, estimated at the stationary state of each isothermal curve, are plotted against the annealing temperature along with corresponding specific activity detected at the same temperature. A rapid increase (or decrease) of ^{5}P (or ^{3}P) yield was observed from 200 °C and finally the yield of ^{5}P (or ^{3}P) became closer to hundred (or null) percent by 300 °C. This range of temperature (200—300 °C) just covers the decomposition temperature of the low oxyphosphorus compounds such as phosphite.[11] In the case that decomposition occurs, a part of the ^{32}P would escape in the gaseous phosphine species,[27,28] and thus the detectable specific activity would decrease with the temperature from 200 °C. However, the specific activity curve (Fig. 7) showed no change even

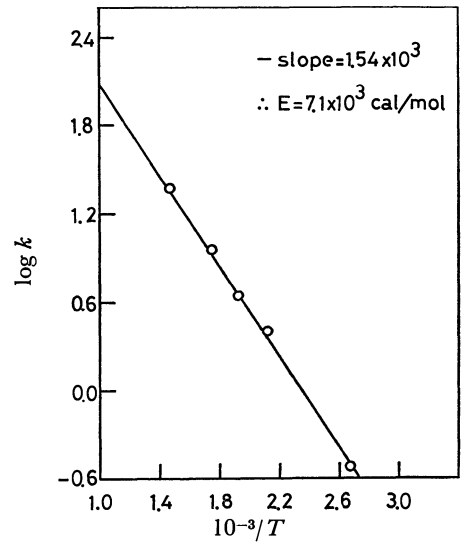

Fig. 7. An Arrhenins plot for estimation of the activation energy of the thermal annealing reaction.

when the sample was heated up to 400 °C. All the ^{32}P were converted into penta-valence by thermal annealing. The rate of conversion of ^{3}P into ^{5}P was estimated from the slope for each annealing curve (Fig. 5). This conversion rate was used for the Arrhenius plot to estimate the activation energy of this particular system. A straight line of such a plot is shown in Fig. 7, an activation energy of 7.1 kcal/mol being obtained.

A comparison was made between the fading in color and the change in mean oxidation number of ^{32}P in order to investigate the correlation between the trapped hole (the color center) and the oxidation of ^{32}P species (Fig. 8). The optical absorbancy at 510 nm attributed to the trapped hole[14,23] disappeared completely with the temperature range 100—200 °C. However, the rise of the mean oxidation number of ^{32}P between 100—200 °C was very gradual. It rose sharply from 200 °C and attained +5 by 300 °C (dotted line, Fig. 8).

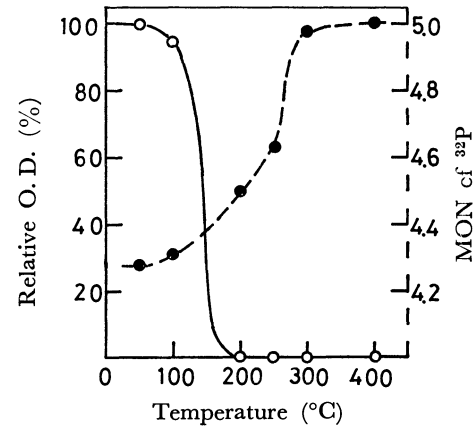

Fig. 8. Correlation between color center (trapped hole) and MON of ^{32}P at various temperature; solid line shows the fading of OD at 510 nm and dotted line denotes the variation of MON of ^{32}P.

The trapped hole might disappear through two ways; by recombination with the free electron located in the vicinity or by the reaction with the electron donor species such as ^{3}P.

The curves in Fig. 8 indicate that in glass matrix, though the oxidation of ^{32}P species by the trapped hole is not impossible, it is not a predominant reaction. Disappearance of the color center is mainly due to its recombination with electron or negative ion during thermal annealing.

Discussion

During $^{31}P(n,\gamma)$ ^{32}P recoil in polyphosphate, all the ^{32}P are freed from their bonding to become a monomer which is often deficient in oxygen.[7,29] However, in the spiral shape of polyphosphate molecule, about 90% of the recoil ^{32}P undergoes recombination to reform radioactive polyphosphate with one ^{32}P as end group which, compared with the monoatomic ^{32}P product, is fairly rich in oxygen[7]. Hence the mean oxidation number of ^{32}P in polymer forms is always higher than

that in monomer forms[30]. Ionizing radiation might cause the oxidation of the recoil ^{32}P product. Such oxidation seems to be an electronic process since it can be suppressed by the electron donor (Table 3 (a)). The γ-radiolysis of phosphate glass can be simplified as follows.

$$\underset{\text{(glass)}}{G} \rightsquigarrow \underset{\text{(trapped hole)}}{G^+} + \underset{\text{(electron)}}{e^-}$$

Subsequent reaction might occur between G^+ and hole scavenger(S):

$$G^+ + S \longrightarrow G + S^+$$

If there is no such electron donor as hole scavenger, G^+ may react with recoil ^{32}P species of lower chemical state; for instance:

$$G^+ + \overset{3}{P} \longrightarrow G + \overset{4}{P}$$

which apparently raises the mean oxidation number of ^{32}P. However, such an oxidation is partial and greatly depends on the concentrations of both the trapped holes and ^{32}P. Another possibility for raising the mean oxidation number by radiation is OH radical from water molecule[30]. In such a radiolytic achievement, phase effects play an important role. The post-neutron irradiation γ-ray annealing shows an entirely different behavior between solid and aqueous targets. The mean oxidation number of ^{32}P observed in solid target increases only from +4.1 to +4.6 by absorbing an energy even higher than 10^{21} eV/g.[7] Such discrepancy in oxidation reaction may be due to the different diffusion rates of the reactants in solid and liquid phases. The higher diffusion rate and concentration of OH radical in liquid state give rise to a more rapid and complete oxidation of the recoil ^{32}P product in aqueous target than in solid target.

The effect of diffusion phenomena on the oxidation of recoil product in the solid target can be elucidated by annealing. Isochronic curves (Fig. 6) indicate that within the temperature range 200—300 °C, all the recoil ^{32}P products are converted into $\overset{5}{P}$ state. The temperature range gives no definite correlation with the temperature for disappearance of the color center (positive defects) which disappeared completely by 100 °C (Fig. 8). The activation energy of the annealing is about 0.3 eV (7.1 kcal/mol). This value of activation energy seems to demonstrate that the thermal annealing reaction is not an electronic but a diffusion process. The potential well of the trapped hole (color center) produced by the γ-radiolysis in the glass is about 0.3 eV which is ten times as low as the optical activation energy 2.6 eV (510 nm). The following conclusion can be made for the annealing effects. In the reactor irradiation, two kinds of abnormal domains are produced and localized in the solid target, a) the recoil site (or hot zone) which involves radioactive product and many other reactive fragments, and b) the radiation spur which contains positively and negatively charged species (color centers). During the course of annealing, within the first domain, hot zone, the recoil product may react with its surrounding reactive fragments to raise the retention value.[31] Within the second domain, radiation spur, the interaction between the positive and negative defects also takes place.[32,33] Interactions between the recoil product and the color centers are possible. However, before the trapped species in the radiation spur diffuse to react with the recoil product which is considerably far away, they have already reacted one another within the domain (radiation spur). This is why the temperature of the complete disappearance of the color center and that of the oxidation of the recoil product do not coincide (Fig. 8).

References

1) L. Lindner and M. Harbottle, "Chemical Effects of Nuclear Transformation," Vol. p. 485, IAEA, Vienna (1961).
2) J. Fenger, *Radiochim. Acta*, **12**, 186 (1969).
3) J. Fenger, *ibid.*, **16**, 42 (1971).
4) J. Fenger and P. B. Pagsberg, *J. Inorg. Nucl. Chem*, **35**, 31 (1973).
5) N. Matsuura, N. Shinohara, and T. K. Lin; *ibid.*, **31**, 1251 (1969).
6) N. Matsuura and T. K. Lin, *ibid.*, **32**, 353 (1970).
7) T. K. Lin, Dissertation, The University of Tokyo. (1972).
8) N. Matsuura and T. K. Lin, *J. Inorg. Nucl. Chem.*, **33**, 2281 (1971).
9) T. Nakamura, K. Ujimoto, N. Yoza, and S. Ohashi, *ibid.*, 32, 3191 (1970).
10) M. Tominaga, T. Nakamura, and S. Ohashi, *ibid.*, 34, 1409 (1972).
11) S. Ohashi, "Topics in Phosphorus Chemistry," Vol. 1, p. 113 Interscience Pub. New York (1974).
12) Van Wazer, "Phosphorus and Its Compounds," Vol. 1, Interscience Pub., New York (1962), p. 390.
13) B. Blazer and K. H. Worms, *Z. Anorg. Allg. Chem.*, **300**, 225 (1959).
14) A. Treinin, "Radical Ions," p. 525, Interscience Pub. New York (1968).
15) Y. Kobayashi, A. Barkatt, and J. Rabani, *J. Phys. Chem.*, **78**, 752 (1974).
16) Y. Kobayashi, Dissertation, The University of Tokyo (1975).
17) Ref. 12, pp. 419, 717.
18) N. Matsuura, T. K. Lin, and Y. Kobayashi, This Bulletin, **43**, 2850 (1970).
19) N. Matsuura and Y. Kurimura, *Bunseki Kagaku*, **16**, 622 (1967).
20) F. Lucena-Conde and L. Prat, *Anal. Chim. Acta*, **16**, 473 (1957).
21) N. Yoza and S. Ohashi, This Bulletin, **37**, 33 (1964).
22) N. Yoza and S. Ohasi, *ibid.*, **37**, 37 (1964).
23) Y. Kobayashi and N. Matsuura, *ibid.*, **46**, 1346 (1973).
24) Y. Kobayashi and N. Matsuura, *Chem. Lett.*, **1975**, 1.
25) J. L. Baptista, G. W. A. Newton, and V. J. Robinson, *Trans. Faraday Soc.*, **64**, 462 (1968).
26) T. Andersen and J. L. Baptista, *ibid.*, **67**, 1213 (1971).
27) Ref. 12, p. 379.
28) Clement Duval, "Inorganic Thermogravimetric Analysis," 2nd Ed. Elsevier (1963), p. 201.
29) D. L. Bunker and G. V. Volkenburgh, *J. Phys. Chem.*, **74**, 2193 (1970).
30) T. K. Lin, *Nucl. Sci. J.*, to be published.
31) G. Harbottle and N. Sutin, *Adv. Inorg. Chem. Radiochem.*, **1**, 267 (1959).
32) J. H. Thompson and W. Miller, *J. Chem. Phys.*, **38**, 2477 (1963).
33) C. Bettinali and P. Granati, *Z. Phys. Chem. N. F.*, **70**, 24 (1970).

Kinetics of Ion Exchange in the Chelating Resin Dowex A-1

Hideo MATSUZURU and Yoshiki WADACHI

Japan Atomic Energy Research Institute, Tokai-mura, Ibaraki-ken 319-11

(Received April 1, 1975)

The kinetics of ion exchanges of Ag^+, Zn^{2+} and Cr^{3+} at extremely low concentrations on the chelating resin Dowex A-1 has been studied by means of finite volume method. The rate of exchanges for both Ag^+ and Zn^{2+} is dependent on the ionic strength, particle size of the resin and reaction temperature. At higher ionic strength (0.1—0.05) the kinetics is controlled by particle diffusion, whereas at lower ionic one (0.01—0.001) film diffusion is predominant. The apparent activation energy obtained is 3.84 kcal/mol for Ag^+ and 3.91 kcal/mol for Zn^{2+}. The exchange rate of Cr^{3+} obeys a first-order rate equation independent of the ionic strength and particle size of the resin. The apparent activation energy is 15.5 kcal/mol. These results support the view that the rate-determining step of this reaction is chelate formation reaction.

It has long been established that the ion exchange reaction in the synthetic cation exchange resin is controlled either by film or by particle diffusion.[1] Since the chelating resin with iminodiacetic acid as the functional group was prepared by Moris *et al.*,[2] increasing interest has been paid to the kinetic behavior of the resin. Upon studying the exchange kinetics of a series of cations such as Na^+, Mg^{2+}, Ca^{2+}, Co^{2+}, Ni^{2+}, Mn^{2+}, Cd^{2+} and Cu^{2+} in Dowex A-1, Turse and Rieman[3] concluded that the rate-determining step is particle diffusion for cations which do not form chelate with the functional group, while in the case of cations which chelate with it the slowest step is a second-order chemical reaction. However, Schwartz *et al.*[4] reported that ion exchanges of Na^+, Co^{2+} and Zn^{2+} in this resin are controlled by particle diffusion. Varon and Rieman[5] reinvestigate this problem and concluded that the slowest step is particle diffusion. The authors found that exchanges of Ce^{3+} and Pu^{4+} in Dowex A-1 are controlled by a first-order chemical reaction.[6,7]

In this paper, an attempt was made to establish the kinetic behavior of this resin and to elucidate the possibility of the chemical reaction, *i.e.* chelate formation reaction between the metal ion and the functional group, being the rate-determining step with the use of Ag^+, Zn^{2+} and Cr^{3+} at extremely low concentrations.

Experimental

Materials. Dowex A-1 (crosslinked polystyrene matrix with iminodiacetic acid as the functional group, DVB content; *ca.* 1%, Dow Chemical) was used. The resin was treated with 2 M NaOH and 2 M HNO_3 three times in a column. After conversion into the sodium form, the resin was washed with distilled water until the effluent came to have the same composition as that of the influent. By subjecting the resin to the wet elutriation method, resin beads of a constant particle size were obtained. The mean particle radius was determined microscopically with a calibrated eye piece ocular. The quantity of iminodiacetic acid per unit weight of the resin was determinated by putting 300 mg of the resin (in the hydrogen form) into contact with 100 ml of 0.1 M NaOH in a 200 ml flask. When ion exchange equilibrium was reached, the supernatant solution was filtered, and free hydroxide was titrated with 0.1 M HCl. The capaicty obtained was 2.29 ± 0.24 mM/g resin. Radionuclides used were $^{51}CrCl_3$(8.8×10^4 mCi/g Cr), $^{65}ZnCl_2$ (7.4×10^2 mCi/g Zn), and $^{110m}AgNO_3$(1.2×10^3 mCi/g Ag) from the Radiochemical Centre, Amersham. The radiochemical purity of these nuclides was confirmed by γ-ray spectrometer using a Ge(Li) detector, no other peaks greater than 0.1% of the expected predominant peak being observed. Cr(III) was separately purified from Cr(VI) by adsorbing Cr(III) onto the cation exchanger(Dowex 50W×8), then desorbing it from the resin by eluting with 0.5 M HNO_3. The chemical form of Zn^{2+} was converted into the nitrate by the ion exchange method. Reagent grade chemicals were used without further purification.

Procedure. The batch method was used throughout the work. A three-necked flask containing 300 mg of the resin and 400 ml of the solution adjusted to pH 4.5 and to prescribed ionic strength ($NaNO_3$), was submerged in the thermostatically controlled water bath. From the requirement in the heterogeneous reaction system, the whole reaction system was vigorously stirred (400 rpm). This rotation speed was high enough to neglect the effect of agitation on the rate of exchange reaction. After thermal equilibrium was attained, a fixed volume of the solution containing a radionuclide was added to the reaction system to initiate the reaction. At each preset time interval, 100 μl of the solution was pipetted out for measurement of radioactivity. Even though the volume of reaction system decreased gradually owing to the fact that a definite volume of it has to be removed at preset time intervals, no correction was made for this decrease since the amount of the solution taken out was negligibly small as compared with that of the reaction system.

The radioactivity of the sample was determined with a conventional scintillation counter combined with NaI(Tl) detector.

The molar concentration of each metal ion was determined by the measured radioactivity obtained with a 2π-proportional counter and the specific activity of the corresponding radionuclide.

Results and Discussion

Kinetic Equation. Since the concentration of the adsorbing ion is extremely low, the changes in composition of the resin and the external solution remain insignificant. In such a system the conventional rate law for an isotope exchange reaction is valid.[8] The kinetic equation[9] for an exchange reaction controlled by film diffusion under the conditions of finite volume is

$$U(t) = 1 - \exp\left(\frac{-3Dt(\bar{C}\bar{V}+VC)}{r\delta\bar{C}\bar{V}}\right) \quad (1)$$

where $U(t)$ is the fractional attainment of equilibrium,

D the diffusion coefficient, r the radius of resin beads, δ the thickness of the film, C and $\bar{C}$ are the equilibrium concentrations in solution of volume V and in resin of volume $\bar{V}$, respectively.

Similarly for a particle diffusion controlled exchange with the finite volume condition, the kinetic equation is given by the Paterson' equation:[10]

$$U(t) = 1 - \frac{2}{3w}\sum_{n=1}^{\infty}\frac{\exp(-S_n^2\tau)}{1+S_n^2/9w(w+1)} \quad (2)$$

where $w=\bar{C}\bar{V}/CV$, $\tau=D\,t/r^2$, S_n are the roots of equation: $S_n \cot S_n = 1+S_n^2/3w$. Under the experimental conditions, the volume of the solution is significantly larger than that of the resin, hence this system may be taken as semi-finite. Equation (2) can be approximated by:[11,12]

$$U(t) = \frac{6Q_0\sqrt{Dt}}{r(Q_0-Q_\infty)\sqrt{\pi}} \quad (3)$$

where Q_0 is the amount of functional group in the reaction system, Q_∞ is the amount of exchange at equilibrium. The deviation from the linearity between $U(t)$ and $t^{1/2}$ is less than 2%, if $U(t)$ does not exceed *ca.* 0.5.

For an exchange reaction controlled by a chemical reaction, the rate is expressed by a conventional rate equation for a chemical reaction instead of such equation as Eqs. (1), (2) and (3) derived from the Fick diffusion law. Taking into consideration the fact that the amount of functional group in the reaction system is significantly larger than that of exchanging ion, this reaction can be regarded as first-order with respect to the exchanging ion.[13] The rate equation is

$$\log\left(\frac{Q_i}{Q_i-Q_t}\right) = kt/2.303 \quad (4)$$

where Q_i is the initial amount of the exchanging ion, Q_t the amount of exchange at time t, and k the rate constant. It was assumed that the reaction in the chelating resin was controlled either by diffusion (film or particle) or by a pseudo-first-order chemical reaction.

Diffusion Controlled Kinetics. Equation (1) predicts that if the rate-determining step is film diffusion, $-\log[1-U(t)]$ is directly proportional to the reaction time, and inversely to the particle radius and the film thickness. The film thickness decreases with an increase in the ionic strength. Thus the rate of exchange reaction increases with increasing ionic strength.[14] From Eq. (3), we see that $U(t)$ in the reaction controlled by particle diffusion is proportional to the square root of the time, and inversely to the particle radius.

The kinetics of exchanges of $Ag^+(1.5\times10^{-8}\,M)$ and $Zn^{2+}(1.6\times10^{-8}\,M)$ in the solution for Na^+ in the resin was studied as a function of the ionic strength. The results are given in Figs. 1 and 2 in which $U(t)$ is plotted against $t^{1/2}$. We see that at high ionic strength (0.1—0.05) a linear relationship is obtained for both ions, while at low ionic strength (0.01—0.001) no linearity is obtained in both cases. However, when the results are plotted in the form of $-\log[1-U(t)]$ *vs.* t, straight lines passing through the origin are obtained in both cases (Fig. 3). The rate of exchange increases with increasing ionic strength.

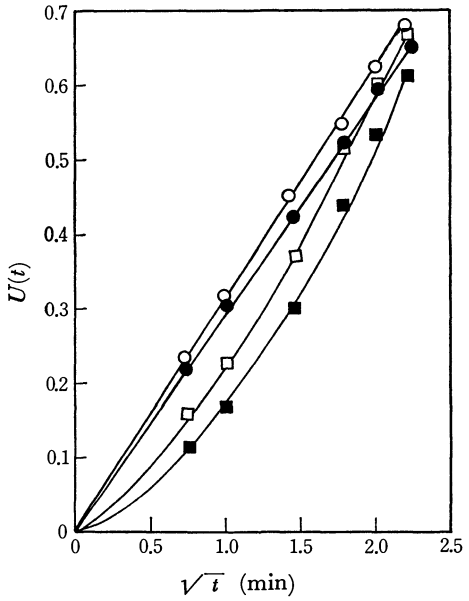

Fig. 1. Plots of $U(t)$ *vs.* $t^{1/2}$ for an ion exchange of Ag^+ on Dowex A-1 in the solutions of different ionic strength 25 °C (radius of the resin particle: 0.10 mm).
μ=○: 0.1, ●: 0.05, □: 0.01, ■: 0.001.

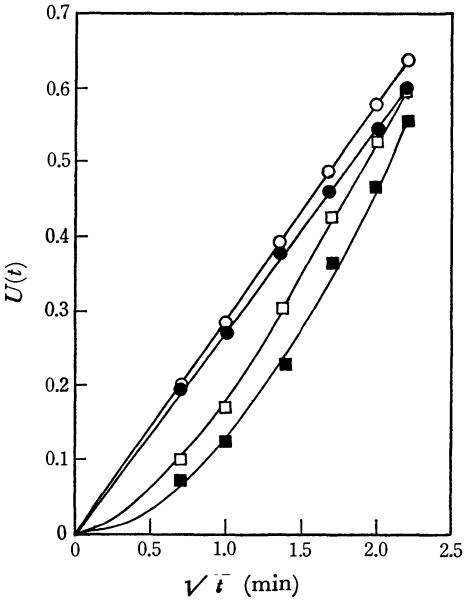

Fig. 2. Plots of $U(t)$ *vs.* $t^{1/2}$ for an ion exchange of Zn^{2+} on Dowex A-1 in the solutions of different ionic strength 25 °C (radius of the resin particle: 0.10 mm).
μ=○: 0.1, ●: 0.05, □: 0.01, ■: 0.001.

A small ionic strength effect can also be observed in the case of high ionic strength, *i.e.*, an increasing rate of exchange with an increase in the ionic strength (Figs. 1 and 2). The rate of exchange controlled by particle diffusion should also increase along with ionic strength, provided that the resin volume remains unchanged. According to Nikolaev's loose quasi-crystal model,[15,16] freely moving ions, cations and gegenions

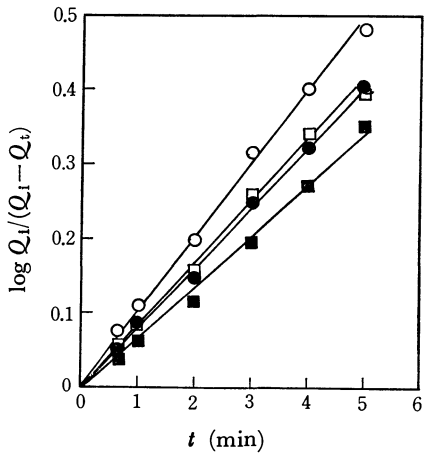

Fig. 3. Plots of $\log Q_i/(Q_i-Q_t)$ *vs.* t for ion exchanges of Ag^+ and Zn^{2+} on Dowex A-1 in the solutions of lower ionic strength, 25 °C (radius of the resin particle: 0.10 mm)
○: Ag^+, $\mu=0.01$; ●: Ag^+, $\mu=0.001$.
□: Zn^{2+}, $\mu=0.01$; ■: Zn^{2+} $\mu=0.001$.

present in the resin phase distort and diminish the depth of the potential well. The rate of diffusion of the ion which oscillates in a potential well a near the functional group, thus increases with an increase in ionic strength.

The rate-determining step of exchanges for both Ag^+ and Zn^{2+} changes from film to particle diffusion with increasing ionic strength. This may be explained as follows. In a range of lower ionic strength, the rate of diffusion through film is retarded by the Donnan exclusion, becoming significantly slow as compared with that of particle diffusion. With increasing ionic strength the Donnan potential and the film thickness might be sufficiently reduced to make the rate of diffusion through film by far greater than that of particle diffusion.

Table 1 shows the effect of the particle radius on the rate of exchange. In the cases of Ag^+ and Zn^{2+}, the half time of equilibrium increases with an increase in particle size. It seems that the effect of increasing particle radius on the exchange rate is nearly as large as that expected from Eq. (1) under the condition of low ionic strength, and from Eq. (3) under the condition of high ionic strength, within the over-all experimental error of *ca.* 10%.

Thus it could be concluded that the rates of exchange

Table 1. Effect of the radius of the resin particle (r) on the half time of equilibrium (τ)

Ion	$\mu(NaNO_3)$	r(mm)	τ(min)
Ag^+	0.1	0.10	2.6
Ag^+	0.1	0.13	4.2
Ag^+	0.001	0.10	3.3
Ag^+	0·001	0.13	4.3
Zn^{2+}	0.1	0.10	2.9
Zn^{2+}	0.1	0.13	4.7
Zn^{2+}	0.001	0.10	3.7
Zn^{2+}	0.001	0.13	4.7

for both Ag^+ and Zn^{2+} are governed by film diffusion at a low ionic strength, and by particle diffusion at a high ionic strength.

Chemical Reaction Controlled Kinetics. The kinetics of exchange of $Cr^{3+}(1.5\times10^{-8}$ M) in the solution for Na^+ in the resin was studied, and the results are given in Table 2. It can be seen that the relationship between $\log[Q_i/(Q_i-Q_t)]$ or $-\log[1-U(t)]$ and t is linear corresponding to Eq. (4) or to Eq. (1), no linearity being obtained in $U(t)$-t relation. Each value of $\log[Q_i/Q_i-Q_t)]$ at the corresponding time does not so much differ from that of $-\log[1-U(t)]$ (Table 2). This makes it difficult to determine which mechanism is operating as the rate-determining step.

Table 2. Rate of an ion exchange of Cr^{3+} on Dowex A-1 (25 °C, $\mu=0.1$, radius of the resin particle; 0.10 mm)

t(min)	$U(t)$	$\log Q_i/(Q_i-Q_t)$	$-\log[1-U(t)]$
1.00	0.109	0.049	0.050
2.00	0.193	0.091	0.093
3.00	0.306	0.155	0.159
4.00	0.370	0.196	0.201
5.00	0.433	0.238	0.246
6.00	0.505	0.297	0.305

For the sake of clarification, the effects of the ionic strength (0.1—0.0001) and the particle radius (0.10—0.13 mm) on the rate of exchange reaction were examined. The rate of exchange is independent of both the particle radius and the ionic strength over the ranges investigated. If the exchange reaction is controlled by film diffusion, the rate should depend on these factors. Thus it might be concluded that the rate of exchange of Cr^{3+} in the resin should be controlled by a pseudo-first-order chemical reaction.

The effect of temperature on the rate of exchange can also be expected to afford a criterion of mechanism, since the activation energy for an exchange controlled by diffusion is supposed to be distinctly lower than that for the chelate formation reaction. This is

Table 3. Influence of the reaction temperature on the diffusion coefficient for exchanges of Ag^+ and Zn^{2+} (particle diffusion) and the rate constants for an exchange of Cr^{3+}, $\mu=0.1$, radius of the resin particle; 0.10 mm.

Ion	Temperature (°C)	D(cm²/s)	k(s⁻¹)	E_a(kcal/mol)
Ag^+	15	1.13×10^{-8}		
	20	1.26×10^{-8}		
	25	1.41×10^{-8}		3.84
	30	1.56×10^{-8}		
Zn^{2+}	15	9.39×10^{-9}		
	20	1.07×10^{-8}		
	25	1.20×10^{-8}		3.91
	30	1.34×10^{-8}		
Cr^{3+}	15		7.68×10^{-4}	
	20		1.21×10^{-3}	
	25		1.88×10^{-3}	15.5
	30		2.89×10^{-3}	

certainly the case with such metal ions as Ce^{3+} and Pu^{4+} adsorbed onto the Dowex A-1, where the apparent activation energy is about 14—20 kcal/mol, whereas that of most ions taking part in particle diffusion is about 4—6 kcal/mol. Table 3 shows the rate constant for an exchange of Cr^{3+} and the diffusion coefficient (particle diffusion) for exchanges of Ag^{+} and Zn^{2+}, depending on the temperature, and the apparent activation energy obtained from the Arrhenius plots. The apparent activation energy for an exchange of Cr^{3+} is higher than that for exchanges of both Ag^{+} and Zn^{2+} which are controlled by particle diffusion.

From the fact that Cr^{3+} is inert in the chelate formation reaction,[17] it is reasonable to suppose that the rate of chelate formation reaction between Cr^{3+} and iminodiacetate is sufficiently smaller than that of either film or particle diffusion.

The results also support the view that the rate-determining step of this reaction is chelate formation reaction.

Conclusion. The results of kinetic studies on Dowex A-1 given by various authours might be summarized as follows.

(1) The exchange reactions of univalent and divalent metal ions are controlled either by film or particle diffusion except for the cations which are inert in the chelate formation reaction such as Ni^{2+} and V^{2+}.

(2) The exchange reactions of multivalent and other ions which are inert in the chelate formation reaction are controlled by chemical reaction.

The kinetic behavior of Dowex A-1 is similar to that of Bio-Rex 63 (containing phosphonic acid as a functional group, Bio Rad Laboratories).[18]

References

1) G. E. Boyd, A. W. Adamson, and L. S. Meyers, Jr., *J. Amer. Chem. Soc.*, **69**, 2836 (1947).
2) L. R. Moris, R. A. Mock, C. A. Marshall, and J. H. Howe, *ibid.*, **81**, 377 (1959).
3) R. Turse and W. Rieman, III, *J. Phys. Chem.*, **65**, 1821 (1961).
4) A. Schwartz, J. A. Marinsky, and K. S. Spiegler, *ibid.*, **68**, 918 (1964).
5) A. Varon and W. Rieman, III, *ibid.*, **68**, 2716 (1964).
6) H. Matsuzuru and Y. Wadachi, *Nippon Kagaku Kaishi*, **1973**, 643.
7) H. Matsuzuru and Y. Wadachi, *ibid.*, **1974**, 617.
8) F. Nelson, *J. Polym. Sci.*, **40**, 563 (1959).
9) F. Helfferich, "Ion Exchange," MaGraw-Hill, New York (1962), p. 264.
10) S, Paterson, *Proc. Phys. Soc.*, **59**, 50 (1947).
11) R. M. Barrer, *Trans. Faraday Soc.*, **45**, 358 (1949).
12) T. R. E. Kressman and J. A. Kichener, *Discuss. Faraday Soc.*, **4**, 90 (1949).
13) A. A. Frost and R. G. Pearson, "Kinetics and Mechanism," 2nd. Ed., John Wiley and Sons, New York (1961) p. 11.
14) D. Reichenberg, *J. Amer. Chem. Soc.*, **75**, 589 (1953).
15) N. Nikolaev, M. D. Kalinina, and G. G. Chuvileva, *Zh. Fiz. Khim.*, **44**, 3110 (1970).
16) N. Nikolaev, A. M. Filimonova, and N. N. Tunitskii, *ibid.*, **43**, 1249 (1969).
17) M. C. Day, Jr., and J. Selbin, "Theoretical Inorganic Chemistry," 2nd. Ed., Van Nostrand Reinhold, New York (1969) p. 473.
18) C. Heitner-Wirguim and V. Urbach, *J. Phys. Chem.*, **69**, 3400 (1965).

The Mechanism of Amine Sensitization of the Emission of Tris(dibenzoylmethano)europium(III)

Tadashi FUKUZAWA,* Nozomu EBARA, Mikio KATAYAMA, and Hideaki KOIZUMI**

College of General Education, The University of Tokyo, Komaba, Meguro-ku, Tokyo 153

(Received April 14, 1975)

The mechanism of enhancement of emission quantum yield of the methanol solution of tris(dibenzoylmethano)europium(III) by triethylamine has been investigated. Lifetime of Eu^{3+} resonance emission of the chelate did not change remarkably when triethylamine was added. The aspect of temperature dependence of the emission intensity was similar for both the chelate itself and the chelate-amine adduct under direct excitation of the metal level, but differed under excitation of the ligand. It was suggested that the sensitization is mainly due to a suppression of nonradiative process in the ligand triplet state.

Intramolecular energy transfer process in rare earth metal chelate has been studied by many investigators since Crosby *et al.*[1] suggested that the transfer of energy from ligands to excited electronic levels of metal takes place *via* the lowest triplet state of ligands. Their assumption was supported by Matsuda *et al.*[2] who observed a sensitized emission of Eu chelate in the presence of La chelate, in which an energy transfer, if any, was allowed only from the ligand triplet of the latter to the ligand triplet of the former. The time constant of energy transfer from the triplet state to the rare earth level was determined by Tanaka *et al.* to be of the order of 10 ns.[3] Their observation proved to be in good coincidence with the cascade mechanism of Crosby *et al.*[1]

On the other hand, a number of mechanisms have been proposed for the sensitization and quenching effect of the emission of rare earth metal compound.[4–6] It is well-known that there are several rare earth metals, such as europium and terbium, which give narrow emission in solutions. Their quantum yields are generally low, varying with ligand, solvent, or temperature.

In order to study the energy loss due to the solvent or other added components, it is convenient to consider the three separate processes, (I) quenching in the ligand level, (II) quenching in the upper levels of the ions, and (III) quenching in the emitting levels of the metal. Weissman[7] assumed that process (I) is important but no experimental confirmation was given. Kropp and Dawson[8] showed that process (II) is effective in methanol solution of $Eu(NO_3)$. Contribution of quenching process (III) was investigated by Dawson *et al.*[9] who showed that for terbium chelate strong temperature dependence of the emission intensity can be explained in terms of quenching of the emitting level *via* thermal excitation to the lowest triplet state of the ligand.

Sato and Wada[10] also reported that the yield of the emission of europium chelate in several solutions depends upon the energy difference between the triplet level of ligand and the emitting level of europium ion, a maximum yield being observed at a certain value of the energy difference. They interpreted the change of the quantum yield as due to the thermal deactivation process from the emitting level of rare earth ions.

In a preceeding paper[11] the effect of several amines on the yield of the emission of tris(dibenzoylmethano) europium(III) (EuD_3) was reported with emphasis on the effect of triethylamine. It was shown that the yield of the emission of EuD_3 in methanol solution increased by a factor of 11 when triethylamine was added. It was suggested that the enhancement of the yield can be ascribed to the suppression of some deactivation process in which the solvent may take part. The present paper deals with the mechanism of the sensitization of the emission of EuD_3 by triethylamine molecule.

Experimental

Materials. Tris(dibenzoylmethano)europium(III) was prepared from europium oxide and dibenzoylmethane according to the method of Charles and Perroto.[12] Mp 231 °C. Elemental analysis; found: C, 65.73; H, 3.87%; calcd for C, 65.78; H, 3.87%. Triethylamine was used after fractional distillation. Commercial fluorescence spectrograde methanol was used as a solvent without further purification.

Method of Measurement. EuD_3-triethylamine were dissolved in methanol at a concentration of 10^{-4} mol/l. Emission and excitation spectra were observed with a Hitachi MPF II fluorescence spectrometer. The emission lifetimes of the EuD_3 and EuD_3-triethylamine complex in methanol were measured as follows. Fresh solutions of the sample were introduced into 3 mm diameter quartz tube and immersed in a liquid nitrogen or other coolants in a transparent quartz dewar. An exciting light pulse from Gellar coaxial nitrogen laser,[13] 10 kW peak power with 20 ns pulse width, was focussed on the sample through an aqueous $CuSO_4$ filter solution. The emission was focused on a Canon optical fiber guide (6 mm diameter, 1000 mm length) after transmission of Toshiba filters UV-39 and VR-60, and detected by HTV-R500 red sensitive and short transit time photomultiplier placed in an electric shield room. In order to minimize stray capacitance, an output resister of the photomultiplier was directly connected with the BNC receptacle of a vertical amplifier 7A11 plug-in-unit of Tektronix oscilloscope 7904. The apparatus had overall rise time of less than 10 ns. The measurement of the temperature dependence was carried out with the same sample tube and Dewar as was used in the lifetime measurement. After being cooled with liquid nitrogen, the sample was left standing to allow the temperature to rise gradually, and the emission intensity and the temperature were measured simultaneously. The tem-

* Present address: Central Research Laboratory, Hitachi Ltd. Kokubunji, Tokyo.

** Present address: Naka Works, Hitachi Ltd. Katsuta, Ibaraki,

perature was measured with a Cu-constantan thermocouple placed in the sample solution just above the excitation volume.

First, the samples were excited by 365 nm radiation of a high pressure Hg-Xe lamp filtered through a $CuSO_4$ aqueous solution and a Toshiba UV-DIC filter, or by 465.8 nm line of an Ar ion laser Coherent Radiation model CR52G. The former radiation excited the ligand level efficiently. According to our observation of the excitation spectra of Eu^{3+} ion, 465.8 nm line of Ar laser coincides with one of the absorbing lines of Eu^{3+} ion ($^7F_0$-$^5D_2$). Since the ligand has no absorption at 465.8 nm, we can directly excite the ion which forms the chelate.

The temperature dependence of the emission intensity under 365 nm and 465.8 nm excitation was measured at 538 nm ($^5D_1$-$^7F_1$) and 612 nm ($^5D_0$-$^7F_2$), respectively. For the measurement of intensity, it is important to note that the magnetic field of Ar laser seriously affects the photomultiplier. In order to eliminate the effect, we used a long optical fiber between a monochrometer and HTV photomultiplier R 306 placed in a shield room. The output of photomultiplier and thermocouple was led into the x axis and y axis of a x-y recorder.

Results

Emission and Excitation Spectra. EuD_3 and triethylamine were mixed at 15 °C in methanol solution. The concentration of the former was kept constant (7.67×10^{-5} mol/l), and that of the latter was varied from 5.27×10^{-4} to 3.37×10^{-2} mol/l. The solutions were left standing more than 30 min, and the emission and excitation spectra were observed. At room temperature, there was no difference between the excitation and emission spectra of EuD_3 solution and those of EuD_3–amine complex solution. Even at 77 K the difference was slight.

The change of absorption spectrum of the EuD_3 solution by addition of the amine was also slight. Thus, the enhancement of emission intensity is not due to an increase in the photon uptake in the excitation process.

Lifetime of the Emission. The solution contains 4.72×10^{-4} mol/l EuD_3 and 4.25×10^{-1} mol/l triethylamine. Because of the weak intensities, lifetime measurements were made only for the strongest transition of $^5D_0$–$^7F_2$. The measured lifetimes of EuD_3 and EuD_3–triethylamine complex at several temperature are listed in Table I. Charles and Ohlman[4] showed that the lifetime of EuD_3–amine complex is 8 times as long as that of EuD_3. However, our measurement showed no remarkable difference between the lifetimes of EuD_3 and amine complex in methanol solutions.

The efficiency of the emission of the complex in methanol solution is 11 times as large as that of EuD_3. Such a striking enhancement can hardly be considered to be due to a decrease in the radiative lifetime. As the quantum yield of emission is low (0.005 in methanol)[9] it is also impossible that an increase in the radiationless lifetime of the emitting level causes the enhancement without affecting the overall lifetime. The effect should be attributed to the change in the radiationless process in the ligand levels.

Table 1. Emission lifetimes of EuD_3 and EuD_3–triethylamine complex

Materials	Lifetime		
	77 K	273 K	289 K
EuD_3 in MeOH	440 μs	384 μs	140 μs
EuD_3-TA in MeOH	439	394	136

Temperature Dependence of Emission Intensity. The solution contains 4.72×10^{14} mol/l EuD_3 and 4.25×10^{-1} mol/l triethylamine. Figure 1 shows the temperature dependence of the emission intensity at 538 nm ($^5D_1$–$^7E_1$) of EuD_3 and amine complex in methanol solution when only Eu^{3+} ions were excited by 465.8 nm of Ar ion laser. Both curves are normalized at the maximum intensities. With a rise in temperature they show sharp decrease at the temperature of phase change, presumably because of inhomogeneity of solid solution.

When the ligand was excited by 365 nm radiation, the emission intensities changed with temperature as shown in Fig. 2. In contrast to the 465.8 nm excitation, the intensity still decreased gradually with the rise of temperature in the liquid state, after a sharp decrease at melting point. This strongly suggests that the deactivation in the ligand level plays a dominant

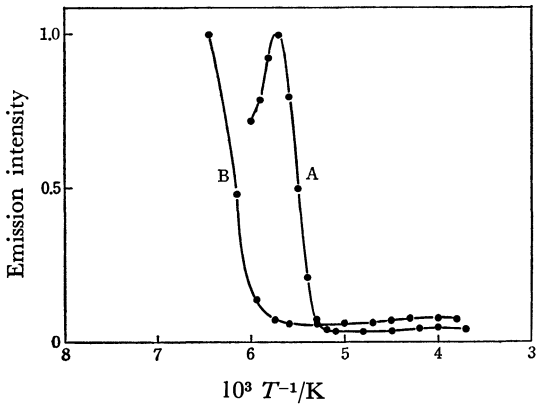

Fig. 1. Temperature dependence of the emission intensities excited by Ar ion laser. A; EuD_3, B; EuD_3–amine complex. Wave length; 538 nm ($^5D_1-{}^7F_1$).

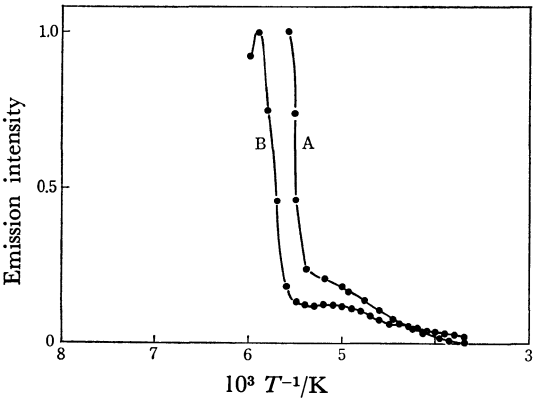

Fig. 2. Temperature dependence of the emission intensities excited by 365 nm radiation. A; EuD_3, B; EuD_2–amine complex. Wave length; 538 nm ($^5D_1-{}^7F_1$).

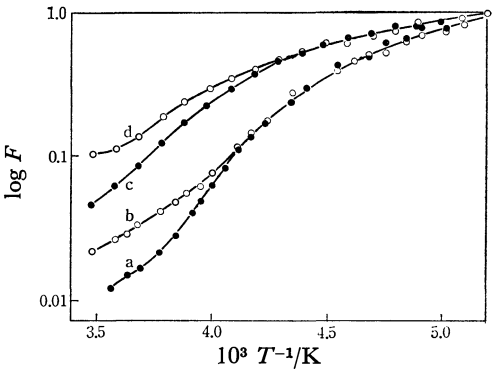

Fig. 3. Logarithm of the emission intensities measured at 612 nm and 538 nm versus $1/T$ in the case of excitation by 365 nm radiation. a; EuD_3, 612 nm, b; EuD_3, 538 nm, c; EuD_3-TA, 612 nm, d; EuD_3-TA, 538 nm.

role in the intensity change. Figure 3 shows the relation between $1/T$ and the emission intensities of 612 nm and 538 nm in logarithmic scale in the temperature range 192—294 K for both EuD_3 and the amine complex when the ligand was excited. All the curves are normalized at the value of 192 K.

The change of intensity of EuD_3 with temperature was larger than that of the complex. The intensity of 612 nm decreased much faster than that of the 538 nm radiation at temperatures above 240 K. Since the difference between a and b is similar to that between c and d (Fig. 3), the differences can be ascribed to the phonon process in $^5D_0$ level of EuD_3 in which triethylamine takes no part. The formation of EuD_3–amine complex causes the difference between a and c as well as that between b and d. It should be noted that these differences appeared only in the case of ligand excitation.

Mechanism of Thermal Quenching

Figure 4 shows the energy levels of EuD_3 and the processes involved in the excitation of emission from Eu^{3+} ion. Here, n_T, n_A and n_B denote deactivation rates from ligand triplet T and from metal levels A ($^5D_0$) and B ($^5D_1$), respectively, r_A and r_B the corresponding radiative rate constants and k_A, k_B, k_C, k_{TA}, k_{TB} and k_{BT} the internal transition rates from A to B, B to A, C to B, T to A, T to B and B to T, respectively.

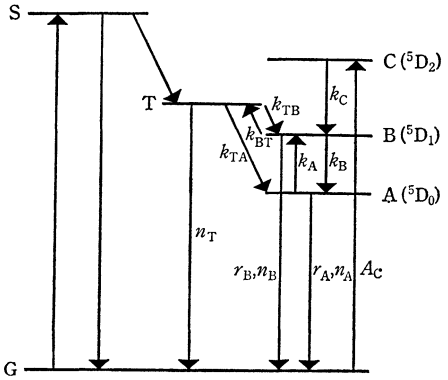

Fig. 4. Energy diagram of chelate. S and T are singlet and triplet of chelate, A, B and C are the excited states of europium ion.

To account for the thermal property of emission, the temperature dependence of radiationless process should be taken into consideration. Since the internal rates k_B, k_{TA} and k_{TB} can be regarded as temperature independent, we can assume that k_{BT}, k_A, n_A and n_T depend on temperature, because the former two are endothermic processes and the latter two are slow processes liable to external deactivation. n_A can be regarded as constant below 260 K, as the emission lifetime becomes constant. For k_{BT} and k_A, we assume that the transfer takes place *via* Boltzmann distribution, so that

$$k_{BT} = k_{TB}\exp(-E_{TB}/kT),$$

and

$$k_A = k_B\exp(-E_{BA}/kT),$$

where E_{TB} and E_{BA} are the energy differences between level T and level B and between level B and level A, respectively. Since both the values of E_{TB} and E_{BA} are nearly 1600 cm^{-1}, the Boltzmann factors amount to as 10^{-4} at room temperature.

As for the rate constant n_T, we assume that the deactivation of the triplet levels takes place by a thermalization which is established by the interaction between the vibronic levels of the triplet state of the ligand and the phonon levels of the solvent molecules; n_T is then expressed approximately as

$$n_T = k_n\exp(-E/kT),$$

where E is the average energy difference between the triplet state and some dissipative state which might be provided by weak bonded solvent molecules, and k_n is the density factor in the dissipative process in the triplet state.

The intensity of 538 nm emission ($^5D_1$-$^7F_1$) at temperature T under ligand excitation is expressed, after some manipulation, by

$$I = \frac{\alpha k_{TB}}{k_{TB}+k_{TA}+k_n\exp(-E/kT)},$$

where $\alpha = I_0 r_B/(r_B+n_B+k_B)$ and I_0 is the pumping intensity to the ligand triplet. This equation is rewritten as

$$\ln F = -E/kT + \ln(k_n/k_{TB}), \qquad (1)$$

where $F = 1/I - 1/I'$ and $I' = k_{TB}/(k_{TA}+k_{TB})$. Since I' can be assumed to be constant, we can plot in F *versus* T^{-1} by selecting an appropriate value of I' in order to obtain a straight line. The Arrhenius plots of 538 nm emissions of EuD_3 and amine complex are shown in Fig. 5, with best values of $1/I'$, 4.0 for the former and 4.5 for the latter (intensity scale is the same as in Fig. 2), from which the values of energy difference E are obtained: 2300 cm^{-1} for EuD_3 and 1400 cm^{-1} for the complex. It is to be noted that the energy values are not sensitive to the values of I'. Next, we define the radiative ratio R by

$$R = (k_{TB}+k_{TA})/k_n,$$

which can be obtained from the emission intensity ratio

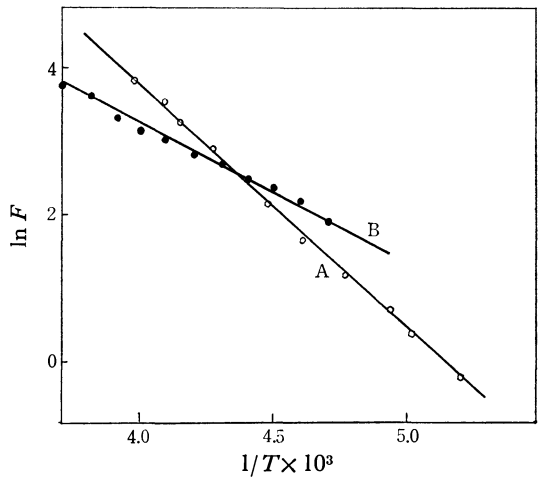

Fig. 5. Arrhenius plot of thermal quenching of emission measured at 538 nm. A; EuD_3, B; EuD_3-amine complex.

$$I_2/I_1 = \frac{k_{TB}+k_{TA}+k_n \exp(-E/kT_1)}{k_{TB}+k_{TA}+k_n \exp(-E/kT_2)} = \frac{R+\exp(-E/kT_1)}{R+\exp(-E/kT_2)}, \quad (2)$$

where I_1 and I_2 are the intensities observed at T_1 and T_2. The ratio R can be obtained from Eq. (2). Any pair of temperature T_1 and T_2 gives consistent R values, which indicates that the assumed mechanism is appropriate.

In the same way, the emission intensity of 612 nm ($^5D_0$-$^7F_2$) is represented by

$$I = \frac{(k_{TA}+\beta k_{TB})\gamma}{k_{TA}+k_{TB}+k_n \exp(-E/kT)} \quad (3)$$

where $\beta=k_B/(k_B+r_B+n_B)$ and $\gamma=I_0 r_A/(r_A+n_A)$, both of which can be assumed constant. Arrhenius plots are obtained from Eq. (3) in a similar way and we get energy difference E and the ratio R. The values of E and R for EuD_3 and amine complex calculated from both 538 and 612 nm emission are listed in Table 2.

Table 2. Energy difference between the ligand triplet level and quenching level and the ratio of the radiative to nonradiative processes

Materials	Emission Wave length	E		R
EuD_3	538 nm	2270 cm^{-1}		2×10^{-7}
			av. 2225 cm^{-1}	
EuD_3	612	2180		3×10^{-7}
EuD_3-TA complex	538	1390		8×10^{-4}
			av. 1507	
EuD_3-TA complex	612	1624		4×10^{-5}

Mechanism of Amine Sensitization

We have shown that the enhancement of emission intensity from Eu^{3+} ion is traceable to the change in the processes in the ligand levels. The values of I' for EuD_3 and the complex differ only by about 10%, which seems to circumscribe the range of the changes in k_{TB} and k_B (and possibly in k_{TA}). Table 2 shows that the ratio R of the complex is hundred to thousand times as large as that of EuD_3, although the value of E is somewhat smaller. The enhancement of the intensity in the amine complex seems to be entirely due to the large value of R, which is brought about by a marked decrease in the value of k_n. If we assume that the dissipative channel is provided by an interaction with solvent phonon state, weak bonds formed between the solvent molecules and chelate produce dense energy state near the vibronic band of the ligand to facilitate deactivation. Triethylamine forms a comparatively rigid bond with the chelate and replaces the solvent molecules, thus reducing the state density for deactivation.

It was found that at higher temperature the emission intensity of the amine complex decreased more rapidly than that of the chelate. This is presumably due to the fact that the amine molecule dissociates and is replaced by a solvent molecule. The lifetime of the 612 nm emission decrease abruptly above 273 K. This may be ascribed to the quenching in the $^5D_1$ and $^5D_0$ levels of EuD^{3+} ion.

We are grateful to Dr. A. Kuboyama of the National Chemical Laboratory for Industry of Tokyo for his stimulating discussion.

References

1) G. A. Crosby, R. E. Whan, and R. M. Alire, *J. Chem. Phys.*, **34**, 743 (1961).
2) Y. Matsuda, S. Makishima, and S. Shionoya, This Bulletin, **41**, 1513 (1968).
3) M. Tanaka, G. Yamaguchi, J. Shiokawa, and C. Yamanaka, *ibid.*, **43**, 549 (1970).
4) R. G. Charles and R. C. Ohlmann, *J. Chem. Phys.*, **40**, 3131 (1964); *J. Inorg. Nucl. Chem.*, **27**, 119 (1965).
5) F. Halverson, J. S. Brinen, and J. R. Leto, *J. Chem. Phys.*, **41**, 157 (1964).
6) L. I. Kononenko and M. A. Tishchenko, *Opt. Spectrosc*, **25**, 392 (1968).
7) S. I. Weissman, *J. Chem. Phys.*, **10**, 214 (1942).
8) J. L. Kropp and W. R. Dawson, *ibid.*, **45**, 2419 (1966).
9) W. R. Dawson, J. L. Kropp, and M. W. Windsor, *ibid.*, **45**, 2410 (1966).
10) S. Sato and M. Wada, This Bulletin, **43**, 1955 (1970).
11) T. Fukuzawa and N. Ebara, *ibid.*, **45**, 1324 (1972).
12) R. G. Charles and A. Perroto, *J. Inorg. Chem.*, **26**, 373 (1964).
13) M. Geller, D. E. Altoman and T. A. DeTemple, *J. Appl. Phys.*, **37**, 3639 (1966).

Infrared Band Shape of the C–I Stretching Vibration of Methyl Iodide in Solutions

Kenji FUJIWARA,* Kohji FUKUSHI, Shun-ichi IKAWA, and Masao KIMURA**

Department of Chemistry, Faculty of Science, Hokkaido University, Sapporo 060

(Received April 17, 1975)

The infrared band shapes of the fundamental and overtone C–I stretching vibrations of methyl iodide in solutions are well approximated by the superposition of Lorentzian functions. From a comparison of the band-widths of the $\nu_3(0\rightarrow1)$, $\nu_3(1\rightarrow2)$, and $\nu_3(0\rightarrow2)$ transitions, it is pointed out that the vibrational relaxation of the translational-diffusion type proposed by Bratos *et al.* contributes to the band-widths, in addition to reorientational relaxation. A slight deviation from the Lorentzian function was observed in the low-frequency region of the fundamental band.

The band shape of the infrared spectra of a liquid involves information about the molecular dynamics in the liquid. Shimizu[1] and Gordon[2] first showed that the band shape is given by the Fourier transformation of the time correlation function for the vibrational-transition dipole moment. They adopted a model of random reorientation of molecules in condensed phase. Since then, many studies have been carried out by means of the Fourier transformation of observed band shapes.[3–14] Meanwhile, it has been recognized that only the reorientational process is not always sufficient to provide a full account of an observed band shape. It is often necessary to take into account additional factors, such as the vibrational relaxation,[12,15] the vibration-rotation interaction,[13] the overlap of hot bands,[16] the overlap of bands of various isotopic species,[16] and the dielectric-field effect.[5,17–19]

In order to discuss band shape and molecular dynamics, it is necessary to extract the band assigned to a single transition from an observed band. Since methyl iodide is a representative of symmetric top molecules and has no isotopic species, extensive spectroscopic studies have been carried out on it. However, there are only a few studies on the band shape and on the reorientational process of this molecule in solutions.[20–22] Among the observed bands of methyl iodide, the ν_3 band of the C–I stretching vibration is appreciably deformed by the overlap of hot bands. Therefore, the half-width[23] of the ν_3 band reported in previous work must include some uncertainty. The present study has been undertaken in order to obtain the half-widths of the individual transitions, *i.e.*, the fundamental $\nu_3(0\rightarrow1)$, the hot band $\nu_3(1\rightarrow2)$, and the overtone $\nu_3(0\rightarrow2)$. For this purpose, the observed band at about 525 cm^{-1} was decomposed into the components, $\nu_3(0\rightarrow1)$ and $\nu_3(1\rightarrow2)$, by assuming a Lorentzian profile for each. A similar analysis was also applied to the overtone band, $\nu_3(0\rightarrow2)$, which appears at about 1030 cm^{-1} in the high-frequency wing of the intense ν_6 band.

Experimental

The infrared transmission was measured by a single beam method using two JASCO DS-701G Spectrophotometers at room temperature. The spectra were run at the rate of about 2.5 cm^{-1}/min. It was confirmed that no deformation of the observed band shape was induced at this scanning speed. For a band with a half-width of 10 cm^{-1} or narrower, it is very difficult to correct the observed half-width for deficiencies in the linearity of the wave number scale of the spectrophotometers. The reproducibility of the observed half-width on a spectrophotometer was good to within ±0.1 cm^{-1}, but the results from the two spectrophotometers differed from each other by about 0.3 cm^{-1}. Therefore, we estimated the error due to the uncertainty in the wave number scale to be ±0.2 cm^{-1}, although this estimate is rather arbitrary. The slit width was set to provide a resolution of about 1.5 cm^{-1}. Thus, the effect of the finite slit width on the band-width observed in the present study is insignificant.[24] Base lines were corrected for solvent absorption which exists more or less for all the solvents used. An error in the observed half-width due to uncertainties in drawing the base line and in reading the transmission on a chart was estimated to be 1%. Thus, the over-all error included in the observed half-width, ω_{obsd}, was estimated to be ±0.3 cm^{-1}.

Concentrations of methyl iodide in solutions were chosen in between 2.0 and 0.4 mol/l and the sample cells used were 0.2 to 1 mm thick. No concentration dependency of half-widths and solvent-induced frequency shifts, $\Delta\nu$, were observed for all the methyl iodide-solvent systems studied in the present work. The observed infrared absorption bands in some solutions are shown in Fig. 1.

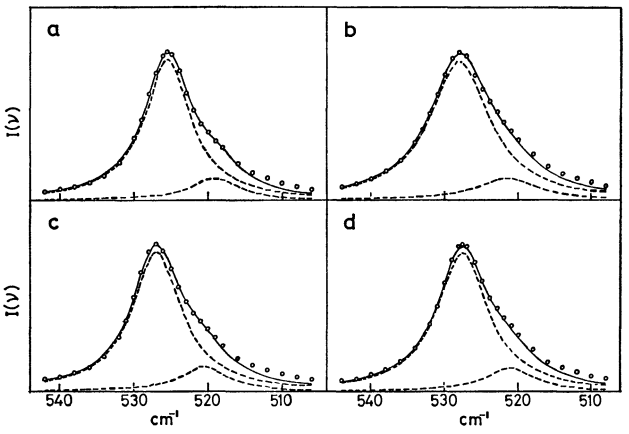

Fig. 1. The infrared ν_3 band of methyl iodide in solutions: (a) $CHCl_3$, (b) n-C_6H_{14}, (c) CS_2, and (d) CCl_4; ooo observed band, — calculated band, --- component bands; (1) $\nu(0\rightarrow1)$ and (2) $\nu(1\rightarrow2)$.

* Present address : Canon Inc., Ota, Tokyo.

** To whom correspondence should be addressed.

Table 1. The observed and calculated parameter values of the ν_3 band of methyl iodide[a)]

Solvent	Band center (cm^{-1})		Half-width (cm^{-1})				
	ν^0_{obsd}	$\nu^0(0\rightarrow1)$	ω_{obsd}	$\omega(0\rightarrow1)$	$\omega(1\rightarrow2)$		ω_{obsd} in Refs.
n-C_5H_{12}	528.8	528.7	11.9	10.8	11.9		11.5[22)]
n-C_6H_{14}	528·5	528.6	11.2	10.2	10.6		10.7[22)]
CCl_4	527.4	527.6	9.1	8.3	8.3	13[20)]	9.1[22)]
CS_2	526.8	526.8	9.2	8.3	7.7	7.8[21)]	9.7[22)]
$CHCl_3$	525.5	525.6	8.8	7.9	8.4		9.1[22)]
C_6H_5Br	525.2	525.3	9.1	8.2	8.9		9.1[22)]
C_6H_5	525.0	525.0	9.3	8.2	8.1		9.3[22)]
	ν^0_{obsd}	$\nu^0(0\rightarrow2)$		$\omega(0\rightarrow2)$			
CS_2	1046.5	1046.7		13.2			

a) Uncertainties in the observed values are $\pm0.3\ cm^{-1}$, see text.

Analysis of Bands and Results

The absorption bands of the solutions were measured at sample thicknesses of 0.2 mm or larger. For such weak bands, the deformation of the band shape by the dielectric field is negligible.[19)] The observed half-widths are shown in the fourth column of Table 1. The values reported previously[20–22)] are also entered in the last two columns. The present results agree fairly well with those of Higuchi *et al.*[22)] Except for the solutions in n-pentane and n-hexane which give rise to notably broader bands, the half-widths are identical to one another within the experimental errors. It appears to be difficult to determine a simple relation between the observed half-width and any physical quantity of the solvent, such as a relation associated with the viscosity of the solvent as proposed by Higuchi *et al.*[22)]

The band was decomposed into two components corresponding to the fundamental transition, $\nu_3(0\rightarrow1)$, and the hot-band transition, $\nu_3(1\rightarrow2)$, by the least-squares method based upon the following equation

$$I(\nu) = \frac{(\omega(0\rightarrow1)/2)^2 P(0\rightarrow1)}{(\nu-\nu^0(0\rightarrow1))^2+(\omega(0\rightarrow1)/2)^2} + \frac{(\omega(1\rightarrow2)/2)^2 P(1\rightarrow2)}{(\nu-\nu^0(1\rightarrow2))^2+(\omega(1\rightarrow2)/2)^2}$$

where $I(\nu)$ is the observed band intensity defined by $\ln(T_0/T)_\nu/\nu(1-\exp(-hc\nu/kT))$,[2)] and $\nu^0(m\rightarrow n)$, $\omega(m\rightarrow n)$, and $P(m\rightarrow n)$ are the wave number of the band center, the half-width, and the intensity of the band center for the m to n transition, respectively. The above equation contains six parameters to be adjusted. The second term is concerned with the hot band and accordingly, it makes only a small contribution to the total intensity. Since there must be a strong correlation between the parameters for the fundamental and hot bands, it was expected that the possible minor deviation of a single-transition band from a Lorentzian profile and small errors included in the observed intensity might obscure the resulting parameter values for the hot band. Indeed, it was found by a preliminary calculation that no plausible parameter values were obtained for the hot band. In such circumstances it is desirable to adjust the parameters under reasonable constraints.

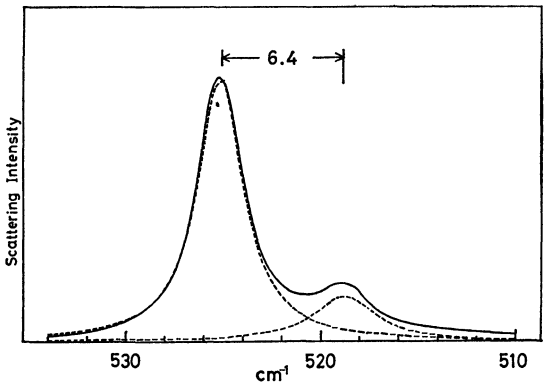

Fig. 2. The Raman ν_3 band of methyl iodide in carbon disulfide (1.8 mol/l). The band was decomposed into $\nu(0\rightarrow1)$ and $\nu(1\rightarrow2)$ using the Lorentzian functions shown by broken lines. The spectrum was recorded on a JASCO R300S Laser Raman Spectrophotometer.

The following two restrictions were then introduced into the calculations: (1) the ratio of the band areas, $[\omega(1\rightarrow2)\cdot P(1\rightarrow2)]/[\omega(0\rightarrow1)\cdot P(0\rightarrow1)]$, is equal to a theoretical value, $2\exp(-hc\nu/kT)$, which is 0.162 at $T=300$ K and $\nu=527\ cm^{-1}$, and (2), the separation between the fundamental and the first hot bands, $\nu^0(0\rightarrow1)-\nu^0(1\rightarrow2)$, is equal to the value in the gas phase, $6.6\ cm^{-1}$. This value was calculated from the fundamental and first overtone frequencies reported by Jones and Thompson[25)] by means of the relation $\nu^0(1\rightarrow2)-\nu^0(0\rightarrow1)=2x_{33}=\nu^0(0\rightarrow2)-2\nu^0(0\rightarrow1)$, where x_{33} is the anharmonicity constant for ν_3. This value is supported by the Raman spectrum of methyl iodide in carbon disulfide. As is shown in Fig. 2, the separation, $2x_{33}$, is almost the same as in the gas phase. The width of the highly-polarized Raman band is narrower than that of the infrared absorption band, so that the hot band is more conspicuous in the Raman spectrum.

The simulation was carried out over a range from 508 to $548\ cm^{-1}$ for the solutions in n-pentane, n-hexane, and carbontetrachloride, and a range from 504 to $544\ cm^{-1}$ for the solutions in carbon disulfide, chloroform, benzene, and bromobenzene. Figure 1 shows examples of the results. Good fits between the observed and calculated bands were obtained for

all the solutions except for slight discrepancies in the low-frequency wing. The higher hot-bands ignored in the above calculations are too weak to indicate this discrepancy. For the other a_1-type bands, ν_1 and ν_2, of methyl iodide, slight discrepancies were also found in the low-frequency wings,[4,21,26] although the general profile of each band was well reproduced by a Lorentzian function.[21] The deviation of the observed band from a Lorentzian function is a measure of the asymmetry of the band and will be discussed later.

The parameter values obtained are summarized in Table 1. If we take into account the fact that the values of $\omega(1\rightarrow2)$ involve more uncertainty than those of $\omega(0\rightarrow1)$, it may be said that the $\omega(0\rightarrow1)$ and $\omega(1\rightarrow2)$ values are nearly equal to each other in all the solutions studied and that they are about 10% smaller than the corresponding apparent half-widths, ω_{obsd}.

The band shape of the overtone, $\nu_3(0\rightarrow2)$, was determined from the spectrum of a solution in carbon disulfide. The overtone ν_3 band overlaps on the high-frequency wing of the strong degenerate vibrational band, ν_6. As may be seen in Fig. 3, the $\nu_3(0\rightarrow2)$ peak is well-resolved and the foot of the ν_6 band forms a strong background. Since the wing of the ν_6 band has been found to be well-reproduced by a Lorentzian function,[26] the spectrum ranging from 1010 to 1080 cm^{-1} was decomposed by means of the superposition of three Lorentzian functions. The analysis was carried out under the restriction, $\omega(0\rightarrow2)=\omega(1\rightarrow3)$, which was set referring to the results obtained for the fundamental band. The best fit parameters are as follows: $\nu^0(0\rightarrow2)=1046.7\ cm^{-1}$, $(\nu^0(1\rightarrow3)-\nu^0(0\rightarrow2))/2=-6.9\ cm^{-1}$ $(=2x_{33})$, $[\omega(1\rightarrow3)\cdot P(1\rightarrow3)]/[\omega(0\rightarrow2)\cdot P(0\rightarrow2)]=0.14$, and $\omega(0\rightarrow2)=\omega(1\rightarrow3)=13.2\ cm^{-1}$. The half-width of the hot band is larger than that of the fundamental band. The value of $2x_{33}$ obtained here agrees with the value of $-6.9\ cm^{-1}$, which is derived using the relation $2x_{33}=\nu^0(0\rightarrow2)-2\nu^0(0\rightarrow1)$. The value, $-6.6\ cm^{-1}$, assumed in the decomposition of the fundamental band is also satisfactorily close to $-6.9\ cm^{-1}$. The ratio of the band area, 0.14, is nearly the same as the ratio of 0.16, which was assumed in the analysis of the fundamental band.

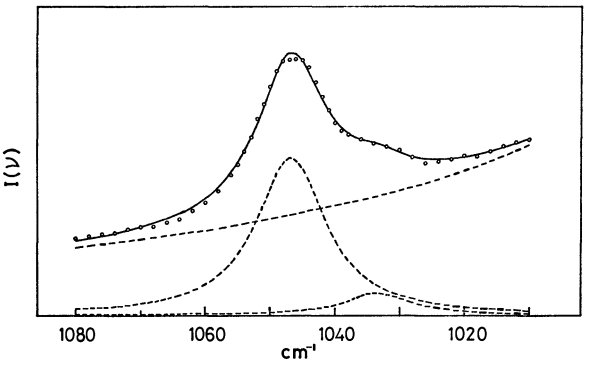

Fig. 3. The overtone $\nu_3(0\rightarrow2)$ band of methyl iodide in carbon disulfide solution (2 mol/l); ooo observed band, — calculated band, --- component bands; (1) $\nu_3(0\rightarrow2)$, (2) $\nu_3(1\rightarrow3)$, and (3) ν_6.

Discussion

An infrared band shape may be expressed by the convolution of spectral densities associated with the reorientational and vibrational relaxations of the transition dipole moment of a molecule.[15] If both of the relaxations are assumed to be characterized by exponential decays, the band width is given by the sum of the widths of the two spectral densities.[12]

The reorientational motion of a molecule should contribute equally to the band widths of the $\nu_3(0\rightarrow1)$, $\nu_3(1\rightarrow2)$, and $\nu_3(0\rightarrow2)$ transitions, for the vibration-rotation interaction, such as A_1-E type Coriolis interaction,[27] may be negligible in these transitions. Therefore, the observed difference in band-widths between the overtone and fundamental bands must be due to the difference in the vibrational relaxation for the two transitions.

According to Valiev,[28] the broadening of a quantum level due to the resonant exchange of vibrational energy between solute molecules is proportional to the square root of the product of its quantum number n and the concentration of the solution c. Then, the band broadening of the transition $n\rightarrow n'$ is given by the sum of the broadening of the n and n' vibrational levels as follows,

$$\omega_{res}(n\rightarrow n') = A\sqrt{c}(\sqrt{n}+\sqrt{n'}),$$

where A is a constant involving the dipole moment derivative with respect to the normal coordinate in question, the Stokes radius of the molecule, and the molecular weight. Accordingly, the half-widths for the $0\rightarrow1$, $1\rightarrow2$, and $0\rightarrow2$ transitions are given by $A\sqrt{c}$, $(1+\sqrt{2})A\sqrt{c}$, and $\sqrt{2}\,A\sqrt{c}$, respectively. However, the observed half-widths were independent of concentration, at least in the concentration range employed, and furthermore, $\omega(1\rightarrow2)$ and $\omega(0\rightarrow1)$ are nearly equal to each other and both are smaller than $\omega(0\rightarrow2)$. This means that the vibrational relaxation of the resonant exchange type does not contribute appreciably to the broadening of the C–I stretching band of methyl iodide in solution.

The vibrational relaxation of the translational diffusion type proposed by Bratos *et al.*[15] seems more favorable in order to interpret the present experimental results. According to their theory, the broadening of a band is related to the difference between the mean energies of the solute-solvent interaction in the two vibrational states involved in the transition. This difference is merely reflected in the solvent-induced frequency shift of the band center. The relationship between n and the frequency shift for a $0\rightarrow n$ transition, $\Delta\nu_{0n}$, was evaluated by Bratos *et al.*[15] As may be seen in Fig. 4 of Ref. 15, $\Delta\nu_{0n}$ is nearly proportional to n for a few lower vibrational states. This is obtained in the present study for the C–I stretching band of methyl iodide in carbon disulfide, *i.e.*, $\Delta\nu_{01}=6.4\ cm^{-1}$ and $\Delta\nu_{02}=13.2\ cm^{-1}$ [29]. Since $\Delta\nu_{12}=\Delta\nu_{02}-\Delta\nu_{01}$, $\Delta\nu_{12}$ is nearly equal to $\Delta\nu_{01}$. Bratos *et al.* also showed that the time scale in the decay of the vibrational relaxation function for the $n\rightarrow n'$ transition is inversely proportional to the frequency shift, $\Delta\nu_{nn'}$. Then, the

band broadening caused by vibrational relaxation of this type, $\omega_{tr}(n\rightarrow n')$, is roughly proportional to $\Delta\nu_{nn'}$. It follows that the values of $\omega_{tr}(0\rightarrow1)$ and $\omega_{tr}(1\rightarrow2)$ are nearly equal to each other and the value of $\omega_{tr}(0\rightarrow2)$ is about twice as large as those values. This is consistent with the information obtained about on the half-widths of $\omega(0\rightarrow1)$, $\omega(1\rightarrow2)$, and $\omega(0\rightarrow2)$. It has been pointed out that for a symmetric top molecule, the broadening of the isotropic component of an a_1-type Raman vibrational band arises exclusively from the vibrational relaxation of the molecules.[26,30-32] For the $\nu_3(0\rightarrow1)$ band of methyl iodide in carbon disulfide (concentration, 1.7 mol/l), the width of its isotropic component was measured to be 2.0 cm^{-1}.[33] The width due to vibrational relaxation may be the same for both the Raman and infrared absorption bands. If the observed value of 2.0 cm^{-1} is attributed to vibrational relaxation, then the contribution of the reorientational relaxation to $\omega(0\rightarrow1)$ is evaluated to be 6.3 cm^{-1} by subtracting the value of 2.0 cm^{-1} from the observed $\omega(0\rightarrow1)$ value. Moreover, if the vibrational relaxation is of the translational diffusion type, the $\omega(0\rightarrow2)$ value may be estimated by adding twice the vibrational contribution 2×2.0 cm^{-1}, to the reorientational one, 6.3 cm^{-1}. The resulting value of 10.3 cm^{-1} is smaller than the observed value of 13.2 cm^{-1} and is insufficient to interpret the observed width. Further explanation seems to be required to explain the broadening of the overtone band. Since the estimation of $\omega(0\rightarrow2)$ described above is very rough, it is inappropriate to draw any definite conclusion from the present results. However, for the time being, it appears that in addition to the reorientational relaxation, the vibrational relaxation of the translational diffusion type proposed by Bratos *et al.* contributes to the width of the ν_3 band.

A slight deviation from the Lorentzian function in the low-frequency wing was recognized in the observed band. In the band envelope of the ν_3 band of methyl iodide in the gas phase, the P branch has a longer tail than the R branch, as is shown in Fig. 4. This is due to the fact that the value of $B'-B''$ is not equal to zero because of the vibration-rotation interaction, where B is the rotational constant about the axis perpendicular to the three-fold symmetry axis, and the prime and double prime denote the excited and ground states respectively. This asymmetry of the band in the gas phase seems to correspond to that in the solution, although the latter is much less marked.[34]

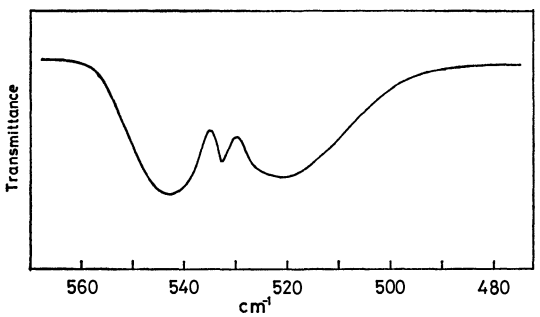

Fig. 4. The envelope of the infrared ν_3 band of methyl iodide in the gas phase.

The authors wish to thank Professors Kozo Tanabe and Osamu Yonemitsu of the Hokkaido University for permission to use the JASCO DS-701G infrared spectrophotometers. The numerical calculations were carried out on a FACOM 230—60 of the Hokkaido University Computing Center.

References

1) H. Shimizu, *J. Chem. Phys.*, **43**, 2453 (1965). This Bulletin, **39**, 2385 (1966).
2) R. G. Gordon, *J. Chem. Phys.*, **43**, 1307 (1965).
3) J. T. Shimozawa and M. K. Wilson, *Spectrochim. Acta*, **22**, 1609 (1966).
4) C. E. Favelukes, A. A. Clifford, and B. L. Crawford, Jr., *J. Phys. Chem.*, **72**, 962 (1968).
5) T. Fujiyama and B. L. Crawford, Jr., *ibid.*, **72**, 2174 (1968).
6) T. Fujiyama and B. L. Crawford, Jr., *ibid.*, **73**, 4040 (1969).
7) W. G. Rothschild, *J. Chem. Phys.*, **49**, 2250 (1968); **51**, 5187 (1969); **52**, 6453 (1970); **53**, 990, 3265 (1970); **55**, 1402 (1971); **56**, 4722 (1972); **57**, 991 (1972); *Macromolecules*, **1**, 43 (1968); *Chem. Phys. Lett.*, **9**, 149 (1971).
8) G. Lévi and M. Chalaye, *C. R. Acad. Sci. Paris, Ser. B*, **271**, 1093 (1970).
9) I. R. -Sonnichsen, J. -P. Bouanich, and N. -V. -Thani, *ibid., Ser. C*, **273**, 19 (1971).
10) R. E. D. McClung, *J. Chem. Phys.*, **55**, 3459 (1971).
11) G. Lévi, M. Chalaye, F. M. -Herail, and J. P. Marsault, *Mol. Phys.*, **24**, 1217 (1972).
12) M. Kakimoto and T. Fujiyama, This Bulletin, **45**, 2970 (1972).
13) M. Kakimoto and T. Fujiyama, *ibid.*, **45**, 3021 (1972).
14) K. Koga, Y. Kanazawa, and H. Shimizu, *J. Mol. Spectrosc.*, **47**, 107 (1973).
15) S. Bratos, J. Rios, and Y. Guissani, *J. Chem. Phys.*, **52**, 439 (1970).
16) R. V. Konynenburg and W. A. Steele, *ibid.*, **56**, 4776 (1972).
17) N. G. Bakshiev, O. P. Girin, and V. S. Libov, *Opt. Spectrosc.*, **14**, 255, 336, 395 (1963); **16**, 549 (1964).
18) R. L. Fulton, *J. Chem. Phys.*, **55**, 1386 (1971).
19) S. Ikawa, S. Takahashi, and M. Kimura, *J. Quant. Spectrosc. Rad. Trans.*, **15**, 1093 (1975).
20) W. K. Glass and A. D. E. Pullin, *Trans. Faraday Soc.*, **59**, 25 (1963).
21) M. O. Bulanin and M. V. Tonkov, *Opt. Spectrosc.*, **16**, 234 (1964).
22) S. Higuchi, S. Tanaka, and S. Kamada, *Nippon Kagaku Zasshi*, **89**, 849 (1968).
23) The full width at half maximum.
24) D. A. Ramsay, *J. Amer. Chem. Soc.*, **74**, 72 (1952).
25) E. W. Jones and H. W. Thompson, *Proc. Roy. Soc., Ser. A*, **288**, 50 (1965).
26) K. Fukushi, K. Fujiwara, S. Ikawa, and M. Kimura, unpublished data.
27) H. S. Goldberg and P. S. Pershan discussed the effect of A_1-E type Coriolis coupling on the shape of a weak band in the liquid phase; *J. Chem. Phys.*, **58**, 3816 (1973).
28) K. A. Valiev, *Opt. Spectrosc.*, **11**, 253 (1961).
29) Frequencies in the gas phase are taken from Ref. 25.

30) G. P. Buyan, I. I. Kondilenko, and V. E. Pogorelov, *Opt. Spectrosc.*, **27**, 132 (1969); I. I. Kondilenko, V. E. Pogorelov, and K. Khue, *ibid.*, **28**, 367 (1970).
31) S. Bratos and E. Marechal, *Phys. Rev.*, **A4**, 1078 (1971).
32) F. J. Bartoli and T. A. Litovitz, *J. Chem. Phys.*, **56**, 404 (1972).
33) K. Fukushi, unpublished data.
34) The value of $B'-B''$ for the $0\rightarrow2$ transition is about two times larger than that for the $0\rightarrow1$ transition. Thus, the overtone $\nu_3(0\rightarrow2)$ band should be more asymmetric than the fundamental $\nu_3(0\rightarrow1)$ band. However, such detailed character of the $\nu_3(0\rightarrow2)$ band cannot be discussed because of the uncertainty due to overlap with the intense ν_6 band.

The Triplet State of Acenaphthenequinone Crystals Studied by Means of Zeeman Spectroscopy

Mizuka SANO, Takatoshi NARISAWA, and Yasumasa J. I'HAYA

Department of Materials Science, The University of Electro-Communications, Chofu, Tokyo 182

(Received May 7, 1975)

The origin peak for the lowest singlet-triplet absorption transition of acenaphthenequinone crystals has been observed at 17981.7 cm^{-1} at 4.2 K. From the direction of the polarization and the Zeeman intensity pattern at 50 kOe, the lowest triplet-state configuration is identified as $^3B_1(n\pi^*)$. The transition to the state from the ground state gains its intensity from the z-polarized $^1A_1(\pi\pi^*)$—$^1A_1$ transition through the y-component in the spin-orbit interaction.

The phosphorescent emission of acenaphthenequinone has been reported to occur in various kinds of solvents[1,2] and in the vapor phase.[3] The spectral features, solvent effect, and lifetime are indicative of a triplet $n\pi^*$ emitting state. They, however, do not present information on the mechanism of spin-orbit coupling, through which the emission gains its intensity. If the emitting state were a pure triplet state, a radiative transition back to the ground singlet state would be forbidden by the spin-multiplicity rule. The phosphorescent emission indicates that the triplet state contains some singlet character through a spin-orbit interaction between the state and perturbing singlet states, and that the ground state contains a small admixture of a triplet character.

The transition from a ground state to a triplet state assumes a polarization of the transition to a perturbing singlet in the first-order approximation. Measurements of the polarized absorption spectra for single crystals will determine the polarization of the transition, and Zeeman spectroscopy will elucidate the mechanism of the spin-orbit interaction. In the presence of a sufficiently high, steady magnetic field, a triplet state splits into Zeeman levels which can be denoted by their magnetic quantum numbers. The relative probability for radiative transitions between the individual Zeeman levels and the ground state depends on a route effective in the spin-orbit coupling.

In this paper we will present sufficient experimental proof for the assignment of the lowest triplet-state configuration for acenaphthenequinone by determining both the polarization in absorption and an effective route in the interaction.

Experimental

Acenaphthenequinone (Tokyo Kasei Organic Chemicals) was purified by recrystallization three times from *o*-dichlorobenzene and then by repeated sublimation at 160 °C *in vacuo*. It could not be zone-refined, because it decomposed thermally upon prolonged heating at elevated temperatures. Single crystal platelets, *ca.* 30 μ thick with an area of *ca.* 6×3 mm^2, were obtained by sublimation. The platelets were found to be elongated along the c-axis, with the ac plane well developed, by X-ray diffractometry.

A crystal was mounted in an Oxford optical cryostat containing a 55 kOe superconducting magnet, and the absorption spectra were observed at 4.2 K. The spectra were analyzed with the aid of an NLM-E2M spectrometer with an Echelles grating in a 2-meter Czerny-Turner mount. The reciprocal dispersion at 550 nm was 0.068 nm mm^{-1} in the 10th order. They were photographed with Fuji spectroscopic plates and recorded with the aid of an HTV R189 photomultiplier tube and electrometer amplification. An Ushio 2 kW xenon arc was used as the light source, while a Polaroid HN-32 film placed between the crystal and the spectrometer acted as the polarizer.

The phosphorescence of a crystal immersed in liquid helium was excited by 365 nm radiation filtered from an ORC 1 kW superhigh pressure mercury arc through a $CuSO_4$ aqueous solution and Toshiba UV-DIC and UV-D25 filters.

Results and Discussion

The first peak was observed at 555.97 nm (17981.7 cm^{-1}) in the a-polarized absorption spectrum for a 30 μ thick crystal. The second peak, about 120 times stronger than the first one, was observed at 499.87 nm (19999.5 cm^{-1}). Under a magnetic field, the former was found to split into three lines, but the latter did not split, so the former could be assigned to the transition to a state of a triplet character, while the latter was assigned to a state of a singlet character. We could not find any prominent peak of a triplet character in the spectral region between these two peaks. Most of the intensity for the singlet-triplet transition lies in the first peak, which seems to show the feature of being orbitally allowed.

The phosphorescence spectrum observed at 2 K showed its first peak at 557.77 nm (17924 cm^{-1}). It is taken as the electronic origin of the phosphorescence. The spectral feature is also indicative of an orbitally allowed transition, the first peak being strongest in intensity in the spectrum. Another strong peak was found to be located at 1719 cm^{-1} from the origin. It is identified as the transition from the origin level to the ground-state vibrational level of the carbonyl stretching mode. The corresponding frequency in the Raman spectrum is 1724 cm^{-1}.[4] The good agreement between the values indicates that the phosphorescence originates not from an impurity but from crystalline acenaphthenequinone, probably from an X-trap level.

From these considerations, the first peak observed in the absorption spectrum is assigned to the origin for the lowest singlet-triplet transition. The second peak is assigned tentatively to the origin for the singlet-singlet transition.

The molecule is planar in a crystal, belonging to the C_{2v} point group. The z-axis is taken as the mole-

cular twofold axis, and the z, y-plane, as the plane of the molecule. The z-axis is approximately parallel with the crystallographic a-axis.[5] The polarization ratio for the triplet origin peak was found to be $I_a/I_c = 7.4+1.1$. The I_a/I_c ratios can be expected from the orientational data of the molecule to be 0.14, 0.24, and 6.4 for the x, y, and z polarizations respectively. The observed ratio indicates that the origin peak is predominantly z-polarized.

On the other hand, the singlet origin peak showed a polarization ratio of less than unity. This fact indicates that the peak is not z-polarized. More intense bands of a singlet character were observed around 22000 and 23000 cm^{-1} in the absorption spectrum for a crystal.

Figure 1 shows the Zeeman-absorption-intensity pattern for the triplet origin peak. The pattern was observed for a 30 μ thick crystal with the magnetic field directed along the b-axis, which is approximately perpendicular to the molecular z-axis. The single peak split into three sublines, the central line being found to be the most prominent in the magnetic-field direction mentioned above. The intensity ratio of the central line, I_0, to the wing lines, $I_{\pm 1}$, was found to be 13 at the field of 50 kOe.

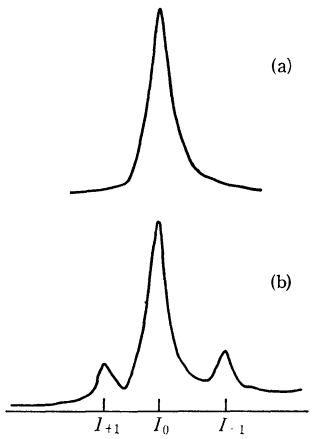

Fig. 1. Zeeman absorption pattern observed with the aid of a photomultiplier tube.
(a) $H=0$, (b) $H=50$ kOe, I_{+1}: 17985.8, I_0: 17981.7, I_{-1}: 17976.4 cm^{-1} (H//b, E//a).

If only one of the spin-orbit coupling routes is active in a spin-orbit interaction mechanism, the intensity ratio is expressed by:

$$\frac{I_0}{I_{\pm 1}} = \frac{2\rho}{1-\rho}, \tag{1}$$

where ρ is the squared direction cosine of the molecular axis with respect to the crystal axis along which a magnetic field is directed.[6] The calculated ratios are 0.29, 14.0, and 0 for the x, y, and z routes respectively, with the magnetic field directed along the b-axis of the crystal. Only when the y route is active, the central line is expected to be stronger than the wing lines. The experimental finding is consistent only with the route involved in the spin-orbit coupling being y (a B_1 representation in the C_{2v} point group).

A simple molecular orbital description of acenaphthenequinone leads to the prediction that the lowest triplet states are those corresponding to the lowest singlet $n\pi^*$ states, A_2 and B_1. Here we may conclude from the experimental results that the lowest triplet state belongs to $^3B_1(n\pi^*)$, and that the transition to this state gains its intensity mainly from the z-polarized $^1A_1(\pi\pi^*)-{}^1A_1$ transition through the y-route in the spin-orbit coupling mechanism. An intensity stealing from an allowed triplet-triplet transition is possible, but a large energy separation between a perturbing triplet and the ground state would reduce its contribution.

References

1) A. Kuboyama and S. Yabe, This Bulletin, **40**, 2475 (1967).
2) A. Kuboyama and S. Matsuzaki, *Nippon Kagaku Kaishi*, **1973**, 2249.
3) S. N. Singh, M. G. Jayswal, and R. S. Singh, This Bulletin, **42**, 2048 (1969).
4) S. N. Singh and R. S. Singh, *Current Sci.*, **36**, 624 (1967).
5) T. C. W. Mak and J. Trotter, *Acta Crystallogr.*, **16**, 811 (1963).
6) G. Castro and R. M. Hochstrasser, *Solid State Commun.*, **3**, 425 (1965).

The Additions of Acetic Acid to Limonene over Solid Acid Catalysts

Tohr YAMANAKA

Central Research Laboratory of Takasago Perfumery Co., Ltd., Kamata, Ohta-ku, Tokyo 144

(Received May 13, 1975)

The addition of acetic acid (AcOH) to limonene (IV) over 111—333 g/l of solid acid catalysts, at 28—92 °C and in an excess of AcOH (19—100 times of IV in molarity), were studied in terms of the kinetic data, at a total conversion of IV less than 10 mol%, and in terms of acid strength distributions of the catalysts. In the reaction medium, a leveling of the acid strength on solids was observed. For the formation of α- and β-terpinyl acetates (I and II) and a mixture of the isomeric *p*-menthadienes (III) as by-products, (1) the rates are proportional to the square root of the initial concentrations of IV; (2) the apparent activation energies are 18.3 kcal/mol for all the catalysts, and (3) the pre-exponential factors are roughly proportional to the square root of the highest acidity ($h_{0,max}$) of the catalyst surface in the medium. The effects of the acid properties of the catalyst on the catalytic activity and the selectivity are different from those in a homogeneous liquid acid-catalyst system.

Recently,[1] we studied the addition of AcOH to limonene (IV), with H_2SO_4 as a catalyst, in a homogeneous system with a large excess of AcOH and without solvent. Considerable amounts of *p*-menthadienes (III) and β-terpinyl acetate (II) were formed besides the desired product, α-terpinyl acetate (I). It was regarded as very difficult to suppress the formation of III by the variation in the H_2SO_4 concentration.

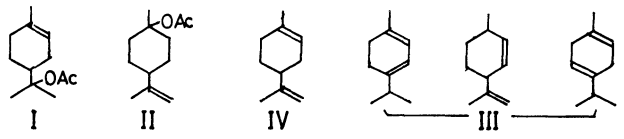

Scheme 1.

In the present study, the kinetic data of the same additions over solid acids, such as metal sulfates and silica-alumina, in an AcOH solution were obtained and related to the acid properties of the solids in order to compare them with the previous results.[1] Those catalytic mechanisms were also discussed in connection with the catalytic activities and selectivities. In general, in the liquid phase, the extrapolations of the catalytic properties of homogeneous acids to heterogeneous solid acids are still uncertain,[2] although such extrapolations are desirable for both practical and theoretical reasons. Comparing the two catalytic systems experimentally will be helpful in establishing such extrapolations. The same reaction conditions as in the previous paper[1] were taken, except that solid catalysts were used instead of H_2SO_4.

Experimental

Solid Catalysts. $MgSO_4$, $Al_2(SO_4)_3$, $NiSO_4$, and $Fe_2(SO_4)_3$ of a guaranteed reagent grade and silica-alumina (Silica-alumina-L; Nikki Chemicals Co., Ltd.; termed Si-Al-L in this study) were ground and sieved to prepare powder of a 100—200 mesh. Some of them were calcined before grinding. $NiSO_4$ was calcined at 520 °C for 3 hr; $Fe_2(SO_4)_3$, at 100 °C for 3 hr, and $MgSO_4$, at 520 °C for 2 hr, all in a dry nitrogen stream. $Al_2(SO_4)_3$ and Si-Al-L were used without calcination.

Materials. Limonene (IV) was purified in the same way as before.[1] The content of IV was 96.7 wt%. AcOH was a guaranteed reagent and was not purified further.

Analysis. The composition of the products was determined by quantitative gas-chromatographic (glc) analysis with an internal standard, using a Shimadzu GC-3AH under the same conditions as before.[1]

Procedure. The reaction was the same as before,[1] except that a solid catalyst was suspended instead of H_2SO_4. A 24.3-g portion (which corresponds to a large excess over the stoichiometric requirement) of AcOH, 0.5—3.0 g of IV, and 3.0—9.0 g of the catalyst were used. At any reaction time, a 2—3 ml sample of the suspended solution of catalyst was taken out, diluted with 70 ml of NaCl-saturated water to stop the reaction, and extracted with *n*-hexane. The extract was then concentrated and used for the glc analysis.

During the reaction, sampling was repeated at arbitrary time intervals. The reaction temperature was 28—92 °C. The reference volume of the reaction mixture used to express the concentration of components or solids was taken at 28 °C. The concentration of IV was 0.151—0.782 mol/l, while that of the catalyst was 110.8—333 g/l.

Measurement of the Acid-base Strength Distribution. During the reaction, a drop of a basic indicator in benzene (0.1 wt%) was added to a portion of the suspended reaction medium in order to examine the existence of acid sites on the solid by means of the color change. The indicators used were Neutral red (+6.8), 1-phenylazo-4-naphthylamine (+4.0), Butter yellow (+3.3), *p*-(phenylazo)diphenylamine (+1.5), and dicinnamylideneacetone (−3.0); the values in parentheses are the pK_a values of the conjugate acids. On the other hand, a modified Johnson method[3] using a set of the same indicators was used to determine the acid-base strength distributions of fresh solids.

Results

Acidities of Catalysts. The acid-base strength distributions of the fresh catalysts are shown in Table 1, together with the qualitative data in the reaction medium, where H_0 denotes the acid strength on a solid defined by Benesi[5] employing the acidity function as defined by Hammett and Deyrup[4] in the liquid phase. The acidity and basicity in the reaction medium could not be titrated because of the existence of AcOH. Therefore, in Fig. 1, the extent of the color change to an acid one in the medium is indicated to decrease in this order: ++, +, −. As may be seen in Table 1, the stronger acid sites of most catalysts disappeared upon the addition of AcOH or IV. The range of the highest H_0 value of the remaining acid sites was estimated qualitatively from

TABLE 1. ACID-BASE STRENGTH DISTRIBUTIONS OF CATALYSTS

	Range of highest-H_0[a)]	Acid amount (meq/g) at different H_0				
		+6.8	+4.0	+3.3	+1.5	−3.0
$Fe_2(SO_4)_3$		0.969	0.848	0.751	0.175	0.071
	<−3.0	++	++	++	++	++
$NiSO_4$		9.502	0.393	0.278	0.127	0.070
	−3.0—+1.5	++	++	++	+	−
$Al_2(SO_4)_3$		0.097	0.083	0.075	0.037	B
	+1.5—+3.3	++	++	+	−	−
$MgSO_4$		0.191	0.101	0.0	B (0.035)[b)]	B
	+3.3—+4.0	++	+	−	−	−
Si-Al-L		1.67	1.47	0.570	0.169	0.089
	+1.5—+3.3	++	++	+	−	−

a) Remained range of highest-H_0 during reaction. b) Basic color of an indicator and the value in parenthesis shows the base amount.

the color change. Except for $Fe_2(SO_4)_3$, each catalyst lowered the highest H_0 value in the medium. In every reaction medium, the color in the liquid phase did not change, and the color change of a catalyst was not affected by the reaction time or by the amount of the catalyst.

Reaction Order. The components of the products were the same as in the homogeneous system —*i.e.*, I, II, and III. The concentration-time curve for each product, the acetates (I and II), and isomers (III) could be taken as a straight line when the total conversion of IV was less than 10 mol%. The formation rate (r_i) of I, II, and III was defined as $dC/d\theta$, where θ denotes the reaction time (hr). The C and i terms denote the concentration; the components I, II, and III, correspond to i=1, 2, and 3 respectively. Figure 1 shows the logarithmic plots of the initial rates (at $\theta=0$) *vs.* C_0 over Si-Al-L, where C_0 denotes the initial concentration of IV. The straight lines of the slope=0.5 indicate that every rate (r_i) at $\theta=0$ is proportional to the square root of C_0: $r_{i,\theta=0}=k_iC_0^{0.5}$. k_i was defined as a rate constant for each product.

Dependency on the Catalyst Amount. In Fig. 2,

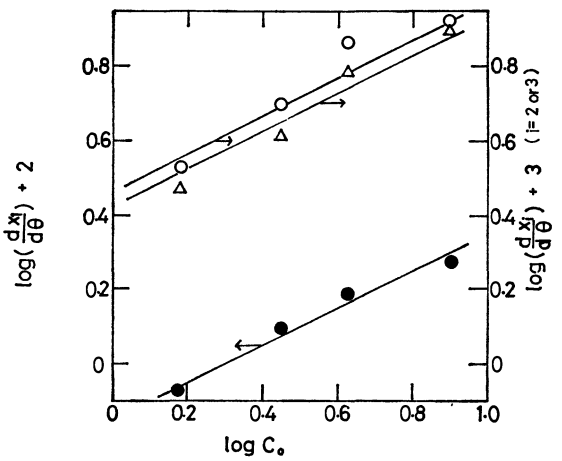

Fig. 1. Dependency of initial rates on initial concentrations of IV over Si-Al-L (166.5 g/l) at 78.5 °C. ●, I; ○, II; △, III.

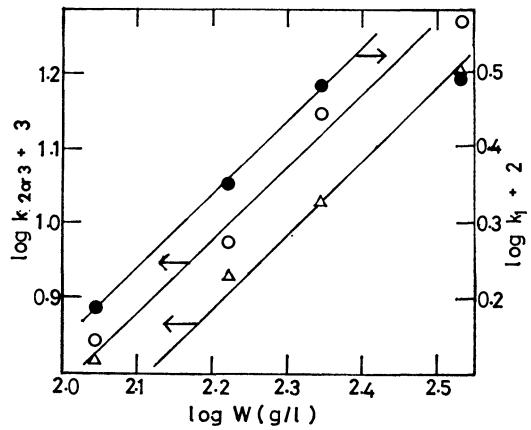

Fig. 2. Dependency of initial rates on amounts of Si-Al-L at $C_0=0.529$ mol/l and 78.5 °C. ●, I; ○, II; △, III.

the log k_i values are plotted against the log W of Si-Al-L. The linear correlation of the slope=1.0 for each product means that every k_i is proportional to W. It may be reasonable to consider that the catalytic action is restricted in the neighborhood of a solid surface in the heterogeneous catalyst system.

Temperature Dependency of k_i. In Fig. 3, the Arrhenius plots for k_i over every catalyst are shown. All the apparent activation energies (E_i) are the same in all cases, *i.e.*, 18,300 cal/mol. Therefore, the relative catalytic activity of the solids must be entirely due to the pre-exponential factors (A_i) of k_i in the equation: $k_i=A_i\exp(-E_i/RT)$. The constant activation energy in Fig. 3 suggests that all the reactions to form I, II, and III over each catalyst have equivalent rate-determinig steps and activated complexes with identical structures at the double bonds. A_i in every case was calculated to be as is shown in Table 2. In each catalyst, the A_i's are in almost the same order.

Effects of the Catalyst Acidity on the Activity and Selectivity. In Fig. 4, each log A_i is plotted against the highest H_0 value in the reaction medium. The correlations between log A_i and the highest H_0 seem to follow straight lines with a slope of ≈ 0.5. Therefore, the catalytic activities are roughly proportional

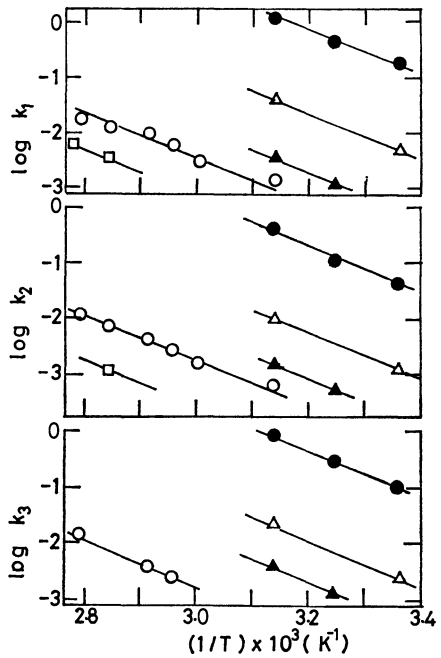

Fig. 3. Dependency of rate constants on reaction temperature over various solid acids (W=166.5 g/l).
●, $Fe_2(SO_4)_3$; △, $NiSO_4$; ▲, $Al_2(SO_4)_3$; ○, Si-Al-L; □, $MgSO_4$.

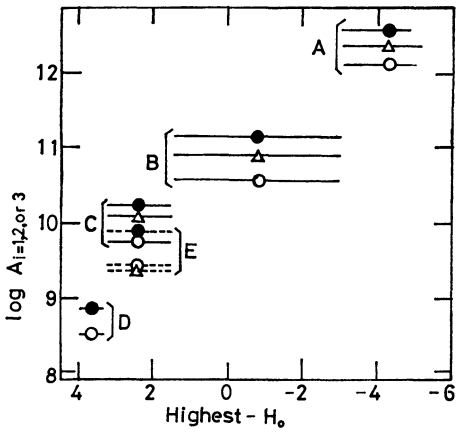

Fig. 4. Correlation between pre-exponential factors and highest-H_0 at 28 to 92.5 °C, C_0=0.529 mol/l, AcOH=15 mol/l.
A, $Fe_2(SO_4)_3$; B, $NiSO_4$; C, $Al_2(SO_4)_3$; D, $MgSO_4$; C, $Al_2(SO_4)_3$; D, $MgSO_4$; E, Si-Al-L. ●, I; ○, II; △, III.

to the square root of the maximum h_0 (termed by $h_{0,max}$; highest $H_0=-\log(h_{0,max})$; $H_0=-\log h_0$) in the medium. When are compared A_i with the acid properties of catalyst (Tables 1 and 2), it must be noted that no significant correlation can be found between the highest H_0 or the acidity at a definite H_0 on the fresh catalyst and A_i.

The selectivities of the products depend entirely on the pre-exponential factors. They are presented in Table 2. The selectivity of I against II (A_1/A_2) lies in the range from 2.09 to 3.68. These values are different from those in the homogeneous system.[1] On the other hand, the selectivities of the isomers against the two acetates $A_3/(A_1+A_2)$ fall into two groups; one consists of $Fe_2(SO_4)_3$, $NiSO_4$, and $Al_2(SO_4)_3$ with 0.44—0.55, while the other consists of Si-Al-L and $MgSO_4$ with $\leq$0.27.

Discussion

Acid Sites in the Reaction Medium. In the medium, a positive shift of the highest H_0 from the original value was observed (Table 1). This must be due to a leveling effect[7] of the medium caused by a neutralization of the acid sites with AcO^-. Although IV may also neutralize acid sites, it has little effect because of its weak basicity. Therefore, the leveling effect must consist of the following steps:

$$2AcOH \rightleftharpoons AcOH_2^+ + AcO^- \quad (1)$$

$$AcO^- + HA_s \rightleftharpoons AcOH \cdot A_s^- \quad (2)$$

$$AcO^- + A_{sL} \rightleftharpoons AcO^- \cdot A_{sL} \quad (3)$$

where HA_s and A_{sL} denote a proton-acid site and a Lewis-acid site respectively. Steps (2) and (3) are possible with an acid site having $H_0 \leq 4.76$ (=pK_a of AcOH). A decrease in the AcO^- in Steps (2) and (3) will result in an increase of $AcOH_2^+$ *via* the autoprotolysis of Step (1). $AcOH_2^+$ also orients to sites where AcO^- has been adsorbed, there to supply the unbalanced negative charge of the surface by AcO^-. However, because of the low dielectric constant of the medium, the concentration of $AcOH_2^+$ can not be increased to finish the neutralization of acid sites, and the above steps will be settled into an equilibrium before the neutralization of the acid sites is complete. The case of $Fe_2(SO_4)_3$ seems to be the most obvious. After all, the leveling effect by Eqs. (1) to (3) will enrich the surface with AcOH.

The observed highest H_0 value in the reaction

Table 2. Pre-exponential factors and selectivities

	Pre-exponential factors A_i ((mol/l)$^{0.5}\cdot$hr^{-1})			Selectivities	
	A_1	A_2	A_3	A_1/A_2	A_3/A_1+A_2
$Fe_2(SO_4)_3$	3.78×10^{12}	1.24×10^{12}	2.69×10^{12}	3.06	0.545
$NiSO_4$	1.27×10^{11}	3.44×10^{10}	7.13×10^{10}	3.68	0.443
$Al_2(SO_4)_3$	1.59×10^{10}	5.27×10^{9})	1.16×10^{10}	3.01	0.550
$MgSO_4$	6.62×10^{8}	3.16×10^{8}	—	2.09	—
Si-Al-L	6.33×10^{9}	2.60×10^{9}	2.38×10^{9}	2.44	0.266
H_2SO_4[a)]	8.90×10^{6}	6.91×10^{5}	5.24×10^{8}	12.9	0.6—1.7[b)]

a) Taken from the previous paper at $C_{H_2SO_4}$ 3.68×10^{-3} mol/l, and C_0 0.529 mol/l. In this case, A_i's are represented by hr^{-1}. b) The values in the range of 28 to 92 °C.

medium is considered to be the highest acid strength, among the remaining acid sites or some of the neutralized acid sites, capable of exchanging AcO^- with a weak base such as the indicators.

Catalytic Activity. It is clear that IV acts as a weak base to acid sites. Therefore, the following scheme can be postulated for the double bonds of IV with the remaining acid sites and AcOH on the surface:

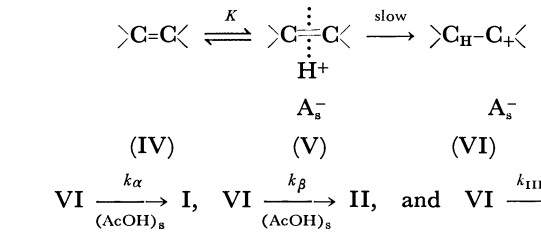

In the above scheme, Step V→VI is considered to be the rate-determining step, because the diffusion of IV and the products (I, II, and III) in AcOH will be rapid enough; the activation energy is estimated to be 2—3 kcal/mol. Steps VI→I, VI→II, and VI→III can not be rate-determining steps because the same activation energies were observed.

The reaction rates are proportional to the concentration of the chemisorbed π-complex (C_v). C_v will be represented by $K\ C_{IV}^{1/n}$, where K denotes the apparent equilibrium constant in the chemisorption step (IV→V) and where n denotes a constant; $n=1$ in a chemisorption of the Langmuir type and $n>1$ in a chemisorption of the Freundlich type.[6] From the fact that each reaction rate (r_1) is proportional to $C_0^{0.5}$, within the low conversion range (Fig. 1), n can be estimated to be 2.0. This suggests a Freundlich-type adsorption and seems consistent with the concept of "surface heterogeneity,"[6] because a solid surface is considered heterogeneous in having sites of various acid strengths, or the surface, at least, behaves as a heterogeneous one the overall acid-strength, h_0, of which varies with the coverage of the sites. On the other hand, the fact that each pre-exponential factor (A_1) is proportional to $(h_{0,max})^{0.5}$ suggests that K is proportional to $(h_{0,max})^{0.5}$.

The apparent activation energy of overall reactions is the difference between the activation energy in Step V→VI and the apparent heat of the chemisorption. The equivalent activation energy over solids of various $h_{0,max}$ values suggests that the variation in the heats of chemisorption on different solid surfaces is negligibly small. Considering that the variation depends entirely on the variation in the energy of interaction between a protonated double bond and a conjugated anion (A_s^-), the interaction must be weak enough to result in a nearly constant heat of chemisorption.

The $K \propto (h_{0,max})^{0.5}$ relation explains the efficiency or the nature of the h_0 function on a solid surface. An h_0 is considered to be a parameter which indicates the overall ability of proton donation on the surface and its neighbor, supplied by various acid sites. Limonene (IV) will enter the vicinity of acid sites with the strength of h_0 and will be protonated at a double bond. The facility of the proton addititon will depend on h_0. The protonated IV will be immediately adsorbed to the anion (A_s^-), which itself came from an acid site upon the release of the proton. The adsorbed state, V, will be kept by an electrostatic interaction; the energy of the interaction seems neither to vary very much with the strength of the original acid site nor to be affected directly by h_0.

It must be noted that the catalytic mechanism in this study is quite different from that of the homogeneous catalyst system.[1]

Selectivity. According to the above scheme, the selectivities are represented:

$$A_1/A_2 = zK_\alpha/((1-z)k_\beta)$$

$$A_3/(A_1+A_2) = k_{III}/(C_{VII}[zK_\alpha+(1-z)k_\beta])$$

where z represents a fraction of C_8-position ion in C_{VI}; k_α, k_β, and k_{III} denote the rate constants in Step VI→I, VI→II, and VI→III respectively, of the above scheme; C_{VII} denotes the concentration of the AcOH adsorbed on the surface, $(AcOH)_s$.

The selectivity (A_1/A_2) will be determined by steric effects. The chemisorption (IV→V) at the double bond in the isopropenyl group is sterically more favored; $z>(1-z)$. On the contrary, in an adsorbed state, the carbonium ion at the β-position (C_1) might be less hindered from an attack of AcOH. Consequently, such a steric effect will settle the selectivity in a narrow range, compared with the case of the homogeneous system, where the α-position (C_8) is entirely predominant.[1]

The selectivity of III ($A_3/(A_1+A_2)$) will be due to the C_{VII} on the surface. The low selectivity of III over Si-Al-L may be interpreted in terms of the fact that a large number of acid sites are consumed, resulting in a large C_{VII} on the surface; the consumed acidity may be 0.169 meq/g, while it is 0.1 meq/g, at most, on the other solids. It must also be noted that, in a solid system, the formation of the isomeric *p*-menthadienes (III) can be suppressed by the selection and design of the catalyst, and that the effects of the steric factors and the catalyst acidity on the selectivity in a heterogeneous system are different from those in a homogeneous system.

We wish to thank the Takasago Perfumery Co., Ltd., for the permission to publish this article.

References

1) T. Yamanaka, This Bulletin, to be submitted (50333, "The Addidtion of Acetic Acid to Limonene with Sulfuric Acid").

2) a) K. Tarama, *Kagaku Kogyo*, **1968**, No. 10, P. 995. b) V. A. Golodov, A. B. Fasman, and D. V. Sokolsky, Proc. 5th Int. Congr. Catal., Miami, 1972, p. 452; K. Davis, *et al.*, *ibid*, p. 491; E. Tijero, F. Castano, and E. Hermana, *ibid*, p. 505.

3) T. Yamanaka and K. Tanabe, *Shokubai*, **17**, 26p (1975); *J. Phys. Chem.*, **79**, (1975), in press.

4) L. P. Hammett and A. J. Deyrup, *J. Amer. Chem. Soc.*, **54**, 2721 (1932).

5) H. A. Benesi, *ibid.*, **78**, 5490 (1956).

6) K. J. Laidler, "Catalysis", Vol. 1, ed. by P. H. Emmett, Reinhold, New York (1954), p. 75.

7) R. P. Bell, "The Proton in Chemistry," Cornell Univ. Press, New York (1959), p. 57.

A Temperature-Jump Study of Electron-Transfer Reactions Involving Ion Radicals: Reactions of the Cation Radicals of Phenothiazine and Aromatic *p*-Diamines

Akihiko YAMAGISHI

Department of Chemistry, Faculty of Science, Hokkaido University, Sapporo 060

(Received May 16, 1975)

The reversible one-electron-transfer reactions of the following cation radicals were studied by temperature-jump and stopped-flow methods: phenothiazine (PhZ)/*N,N,N',N'*-tetramethyl-*p*-phenylenediamine cation (TMPD$^+$), PhZ/*N,N*-dimethyl-*p*-phenylenediamine cation (DMPD$^+$), DMPD/TMPD$^+$ and DMPD/*N,N,N',N'*-tetramethylbenzidine cation (TMBZ$^+$). The solvent used was either 1 : 3 ethanol–water or acetonitrile. For PhZ/TMPD$^+$, PhZ/DMPD$^+$ in ethanol–water and also for DMPD/TMPD$^+$ in acetonitrile, the backward reaction corresponding to the negative free energy change of reaction ($\Delta F^\circ < 0$) proceeds almost at the diffusion controlled rate. The backward rate constant for DMPD/TMPD$^+$ in ethanol–water, $(6\pm1)\times10^8$ M^{-1} s^{-1}, is slightly less than a diffusion controlled one even for $\Delta F^\circ < 0$. The results are discussed as compared with the previous study on 7,7,8,8-tetracyanoquinodimethane/substituted-*p*-benzoquinone anions.

In a previous paper, a study on the reversible one-electron-transfer reactions between 7,7,8,8-tetracyanoquinodimethane anion radical and substituted *p*-benzoquinones was given, attention being paid to the dependence of the rate constant on the free energy change of reaction.[1] It was revealed that the electron-transfer reaction proceeds with no activation free energy when the free energy change of reaction is negative. This result can not be interpreted by the application of the Marcus theory.[2]

The above results provide two possibilities for the mechanism of the electron-transfer; (i) there exists a non-equilibrium polarization of solvents at the activated state,[2] but the potential barrier due to it is much smaller than that expected by the theory, and (ii) the electronic interaction between electron donor and acceptor is so large as to cause an appreciable lowering of the potential surfaces. These two mechanisms could be discriminated, if it were possible to detect the relaxation process of solvent polarization before and after the electronic transition or to prove kinetically the existence of an intermediate complex as has been done in the innersphere electron-transfer reactions of metal ions.[3] At present, however, neither of these two approaches seems to be possible.

We have studied the reactions of cation radicals with the purpose of attacking the above problem from another approach. The reacting pairs studied differ from each other in molecular size, electronic structure and kind of substituent to varying extent. Accordingly the electronic interaction between an electron donor (neutral molecule) and an acceptor (cation radical) would vary a great deal from one extreme in which a stable intermediate (dimer cation) is possible, to the other extreme in which the overlap of electron clouds is hardly possible. By examining these effects on the reaction rates, we intended to see how far the electronic interaction between reactants dominates the electron-transfer rates.

Experimental

Phenothiazine (PhZ) was sublimed once. The dihydrochlorides of *N,N,N',N'*-tetramehyl-*p*-phenylenediamine (TMPD) and *N,N*-dimethyl-*p*-phenylenediamine (DMPD) were used without purification. The free base of DMPD was obtained by neutralizing it with NaOH and then extracting with diethylether. The obtained free base was sublimed once. *N,N,N',N'*-Tetramethylbenzidine(TMBZ) was used without purification.

Perchlorate salts of TMPD and DMPD (TMPD$^+$ClO$_4^-$ and DMPD$^+$ClO$_4^-$, respectively) were prepared according to the method of Michaelis and Granich.[4] Phenothiazine picrate (PhZ$^+$Pic$^-$) was supplied by Dr. Y. Iida. The cation radical of TMBZ was generated by electrolytic oxidation in acetonitrile, using a platinum electrode in 0.01 M tetra-*n*-propylammonium perchlrorate. The stability of these salts in various media was studied. Acetonitrile was distilled once using a distillating column of *ca.* 50 cm length (water content 0.5 mg/ml). Ethanol was distilled once. Water was deionized and distilled once.

The electronic spectra were measured with an EPS-3T spectrophotometer. pH was measured with a Radiometer equipped with G 200B glass electrode and K 100 reference calomel electrode. The concentration of proton in 1 : 3 ethanol–water solvent was calculated by means of the equation $p[H^+]=pH-\alpha$ ($\alpha=0.11$). This relation is obtained by measuring the pH of an ethanol–water mixture containing 10^{-2}—10^{-3} M of $HClO_4$. The variation of α with ionic strength (0—0.01 M) is neglected in calculating the proton concentration.

The rate of reaction was measured with a Union-Giken temperature-jump apparatus or a Union-Giken rapid-scan stopped-flow spectrophotometer. 0.01 M tetra-*n*-propylammonium perchlorate was added as a supporting electrolyte in measuring the rate in acetonitrile with a temperature-jump apparatus. Equilibrium and kinetic measurements were carried out at 10 °C. The effect of temperature at temperature-jump (2—5 °C) on the rate constants was considered to be negligible.

Results

A. Phenothiazine (PhZ) and N,N,N',N'-*Tetramethyl*-p-*Phenylenediamine (TMPD) Cation Radical System.* TMPD$^+$ClO$_4^-$ is stable in both water and ethanol at pH less than 8. Phenothiazine picrate (PhZ$^+$Pic$^-$) is stable in water at pH less than 3, but it decomposes rapidly in ethanol at any pH. The reaction between PhZ and TMPD$^+$ was, therefore, investigated in 1 : 3 ethanol–water solvent in the presence of more than 10^{-3} M HCl, since PhZ hardly dissolves in pure

TABLE 1. EQUILIBRIUM CONSTANT OF THE PhZ AND $TMPD^{+}$ SYSTEM

HCl/M	K_{ap}	$K_{ap}[H^+]^{-2}/M^{-2}$
4.5×10^{-3}	2.2×10^{-2}	1.1×10^{3}
9.1×10^{-3}	6.6×10^{-2}	0.80×10^{3}
18×10^{-3}	26×10^{-2}	0.80×10^{3}
35×10^{-3}	120×10^{-2}	1.0×10^{3}
67×10^{-3}	490×10^{-2}	1.1×10^{3}
		av. 0.96×10^{3}

water. The apparent equilibrium constant defined by

$$K_{ap} = [PhZ^{+}][TMPD]_t/[PhZ][TMPD^{+}]$$

is determined spectrophotometrically, adding a known amount of PhZ into a $TMPD^{+}ClO_4^{-}$ solution at a constant HCl concentration. Parenthesis $[\ ]_t$ represents the total concentration of TMPD, since TMPD is present as $TMPDH^{+}$ and $TMPDH_2^{++}$ in the pH region (1.3—2.5). $[PhZ^{+}]$ and $[TMPD^{+}]$ are determined, using the values ε_{437} (PhZ^{+}) 5.7×10^{3} and ε_{612} ($TMPD^{+}$) 1.1×10^{4}, respectively.[5,6] $[TMPD]_t$ is equated to the decrease of $TMPD^{+}$. The presence of the isosbestic point at 520 nm confirms the view that the one-electron-transfer reaction occurs between PhZ and $TMPD^{+}$.

$$PhZ + TMPD^{+} \rightleftharpoons PhZ^{+} + TMPD \quad (1)$$

K_{ap} is remarkably dependent on $[H^+]$ as seen in Table 1. The observed H^+ dependence of K_{ap} is ascribed to the protonation of TMPD in acidic media.

$$TMPD + H^+ \rightleftharpoons TMPDH^+;\ K_{a1} \quad (2)$$

$$TMPDH^+ + H^+ \rightleftharpoons TMPDH_2^{++};\ K_{a2} \quad (3)$$

Assuming that no protonation takes place on either PhZ or cation radicals, K_{ap} is expressed as

$$K_{ap} = (1+K_{a1}[H^+]+K_{a1}K_{a2}[H^+]^2)K$$

where K_{a1}, K_{a2} and K are the equilibrium constants of reactions (2), (3) and (1), respectively. K_{a1} and K_{a2} are determined by the pH titration of TMPD·2HCl with 0.02 M NaOH.

$K_{a1} = (3.3\pm1)\times10^{6}\ M^{-1}$

$K_{a2} = (3\pm2)\times10^{2}\ M^{-1}$ in 1 : 3 ethanol-water

The relations $1 \ll K_{a1}[H^+] \ll K_{a1}K_{a2}[H^+]^2$ hold in the pH range (1.3—2.5). Thus K_{ap} is reduced to

$$K_{ap} = K_{a1}K_{a2}K[H^+]^2$$

This expression agrees with the observed H^+ dependence of K_{ap} (the last column, Table 1). The true equilibrium constant K of reaction (1) is determined to be 0.96×10^{-6} at 10 °C, which leads to 7.8 kcal mol^{-1} for the free energy change of reaction (1).

The relaxation time observed by the temperature-jump experiments (*ca.* 1 s) exceeds the duration within which a raised temperature is maintained (*ca.* 0.5 s). The rate of this system is, therefore, followed with a stopped-flow apparatus. The backward rate of reaction (1) is obtained by mixing the $PhZ^{+}Pic^{-}$ solution with the TMPD·2HCl solution under the conditions of a large excess of TMPD·2HCl over $PhZ^{+}Pic^{-}$. The decrease of PhZ^{+} is exponential with time, leading to the following rate equation (Table 2),

TABLE 2. PSEUDO FIRST-ORDER RATE CONSTANT k_{obsd} OF THE REACTION BETWEEN PhZ^{+} AND TMPD

a) Dependence of k_{obsd} on [TMPD]. The initial concentrations of PhZ^{+} and HCl are $[PhZ^{+}]_0$ 3.0×10^{-6} M and $[HCl]_0$ 3.0×10^{-2} M, respectively.

TMPD/M	k_{obsd}/s^{-1}	$k_{obsd}[TMPD]^{-1}/M^{-1}\,s^{-1}$
1.4×10^{-4}	2.5	1.8×10^{4}
2.7×10^{-4}	4.2	1.6×10^{4}
4.1×10^{-4}	5.8	1.4×10^{4}
$6\cdot7\times10^{-4}$	7.8	1.2×10^{4}
		av. 1.5×10^{4}

b) Dependence of k_{obs} on $[H^+]$. $[PhZ^{+}]_0$ 1.9×10^{-6} M and $[TMPD]_0$ 3.2×10^{-4} M.

HCl/M	k_{obsd}/s^{-1}	$k_{obsd}[H^+]^{-2}/M^{-2}\,s^{-1}$
9.4×10^{-2}	0.72	3.4×10^{-3}
5.6×10^{-2}	1.7	5.2×10^{-3}
3.8×10^{-2}	2.7	3.8×10^{-3}
1.9×10^{-2}	7.9	2.7×10^{-3}
		av. 3.8×10^{-3}

$$-d[PhZ^{+}]/dt = k_b[TMPD]_t[H^+]^{-2}[PhZ^{+}], \quad (4)$$

$$k_b = 12\pm2\ M\,s^{-1}$$

where the contribution of the forward rate is neglected, since the equilibrium concentration of PhZ^{+} is zero.

The forward rate is obtained by mixing the $TMPD^{+}ClO^{-}$ solution with the PhZ solution under the conditions of a large excess of $TMPD^{+}ClO_4^{-}$ over PhZ. The pseudo first order rate constant of the decrease of $TMPD^{+}$ is plotted against $[H^+]$ in Fig. 1. Although k_{obsd} increases slightly with the increase in $[H^+]$, it approaches a constant value k_f as $[H^+]$ decreases. Thus the rate equation in the low $[H^+]$ region is given by

$$-d[PhZ]/dt = k_f[PhZ][TMPD^{+}] \quad (5)$$

$$k_f = (8\pm2)\times10^{3}\ M^{-1}\,s^{-1}$$

The ratio k_f/k_b is equal to $(0.7\pm0.2)\times10^{3}\ M^{-2}$ which agrees with the equilibrium constant $K_{ap}[H^+]^{-2} = 0.96\times10^{3}\ M^{-2}$ (Table 1).

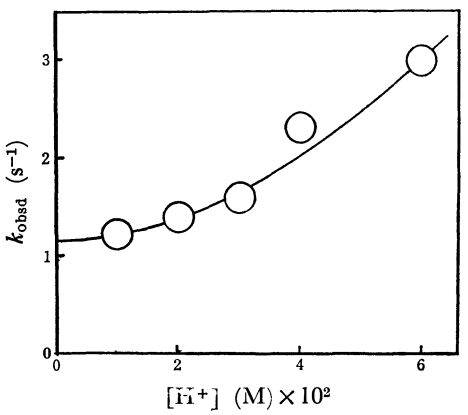

Fig. 1. The dependence of k_{obsd} on $[H^+]$ in the reaction between $TMPD^{+}$ and PhZ in 1 : 3 ethanol-water. $[TMPD^{+}]_0$ 1.7×10^{-4} M and [PhZ] 9.0×10^{-6} M.

The H^+ dependence of the backward rate could be interpreted by the assumption that the overall reaction proceeds only through the neutral form of TMPD, and through neither $TMPDH^+$ nor $TMPDH_2^{++}$. Under this assumption, k_f and k_b in Eqs. (5) and (4) are related to the forward and backward rate constants of Reaction (1), $\vec{k}$ and $\overleftarrow{k}$, respectively, as follows,

$$k_f = \vec{k} \text{ and } k_b = \overleftarrow{k}/K_{a1}K_{a2}$$

Thus

$$\vec{k} = (8\pm2) \times 10^3 \text{ M}^{-1} \text{ s}^{-1}$$

$$\overleftarrow{k} = (1.4\pm0.7) \times 10^{10} \text{ mol}^{-1} \text{ s}^{-1}.$$

The large uncertainty in $\overleftarrow{k}$ arises from the uncertainty of determining K_{a2}. The inertness of $TMPDH^+$ and $TMPDH_2^{++}$ in donating an electron was observed in both $TMPD^+$/DMPD and $TMPD^+$/TMPD systems.[7,8] The origin of the increase of k_f in the high $[H^+]$ region is uncertain.

B. Phenothiazine (PhZ) and N,N-*Dimethyl*-p-*Phenylenediamine (DMPD) Cation Radical System.* $DMPD^+ClO_4^-$ is less stable than $TMPD^+ClO_4$. It decomposes gradually in 1 : 3 ethanol–water solvents.

Table 3. Equilibrium constant of the PhZ and $DMPD^+$ system

HCl/M	K_{ap}	$K_{ap}[H^+]^{-1}/M^{-1}$
6.3×10^{-4}	6.4×10^{-2}	1.0×10^2
12×10^{-4}	12×10^{-2}	1.0×10^2
19×10^{-4}	21×10^{-2}	1.1×10^2
27×10^{-4}	54×10^{-2}	2.0×10^2
		av. 1.0×10^2

The decomposition is, however, depressed in the presence of excess TMPD. K_{ap} is determined by adding PhZ^+Pic^- to the DMPD solution (Table 3). $[DMPD^+]$ is calculated from the absorbance, using $\varepsilon_{555}=6.4\times10^3$.[6] In the $[H^+]$ range investigated, the monoprotonated form of DMPD is predominant.

$$DMPD + H^+ \rightleftharpoons DMPDH^+ ; K_{a1}$$

K_{ap} is related to K, the true equilibrium constant of the reaction, as follows.

$$PhZ + DMPD^+ \rightleftharpoons PhZ^+ + DMPD \quad (6)$$

$$K_{ap} = K K_{a1}[H^+]$$

where $K_{a1}[H^+] \gg 1$ is assumed. Using $K_{a1}=(3.3\pm0.3)\times10^6$ which is determined by the pH titration, K is calculated to be

$$K = (3\pm1) \times 10^{-5}$$

$$\Delta F^\circ = 5.9 \text{ kcal mol}^{-1}.$$

The rate of reaction (6) was studied with a temperature-jump apparatus. The pseudo first order rate constant defined by

$$d\Delta[DMPD^+]/dt = -k_{obsd}\Delta[DMPD^+]$$

is given as a function of $[H^+]$ (Fig. 2). Under the assumption that $DMPDH^+$ is inert in electron–transfer, k_{obsd} is expressed as

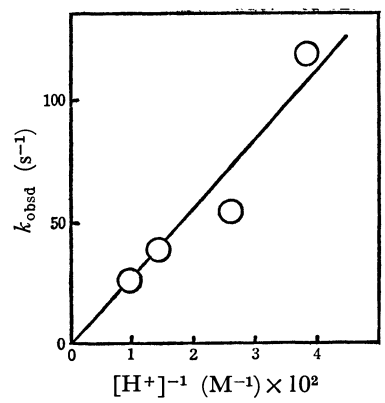

Fig. 2. The dependence of k_{obsd} on $[H^+]^{-1}$ in the reaction between PhZ and $DMPD^+$ in 1 : 3 ethanol–water. $[DMPDH^+]_e$ 2.5×10^{-4} M, $[PhZ]_e$ 3.1×10^{-5} M, $[DMPD^+]_e$ 8.9×10^{-5} M and $[PhZ^+]_e$ 8.9×10^{-5} M.

$$k_{obsd} = \vec{k}\{[PhZ]_e + [DMPD^+]_e\} + \overleftarrow{k}/(K_{a1}[H^+]) \times \{[DMPDH^+]_e + [PhZ^+]_e\}_c \quad (7)$$

where $\vec{k}$ and $\overleftarrow{k}$ are the forward and backward rate constants, respectively, of reaction (6) and $[\ ]_e$ denotes the equilibrium concentration of each species at the elevated temperature. Fig. 2 shows the linear dependence of k_{obsd} on $1/[H^+]$, the second term in Eq. (7) being taken to be predominant. From the results and the relation $K=\vec{k}/\overleftarrow{k}$, we get

$$\vec{k} = (1.0\pm0.5) \times 15^5 \text{ M}^{-1} \text{ s}^{-1}$$

$$\overleftarrow{k} = (2.8\pm1) \times 10^9 \text{ M}^{-1} \text{ s}^{-1}.$$

C. N,N-*Dimethyl*-p-*Phenylenediamine (DMPD) and* N,N,N′,N′,-*Tetramethyl*-p-*Phenylenediamine (TMPD) Cation Radical System.* A study of the TMPD/$DMPD^+$ system in water was reported previously.[7]

$$DMPD + TMPD^+ \rightleftharpoons DMPD^+ + TMPD \quad (8)$$

The forward and backward rate constants obtained are

$$\vec{k} = (4.2\pm2) \times 10^5 \text{ M}^{-1} \text{ s}^{-1},$$

$$\overleftarrow{k} = (1.5\pm0.2) \times 10^8 \text{ M}^{-1} \text{ s}^{-1}.$$

Since $\overleftarrow{k}$ which corresponds to the negative free energy change of reaction is apparently below a diffusion controlled limit in contrast to $\overleftarrow{k}$ in Reactions (1) and (6), the same system was studied in acetonitrile in order to clarify the role of solute-solvent interaction in electron-transfer.

$TMPD^+ClO_4^-$ is stable in acetonitrile. K for Reaction (8) in acetonitrile was, therefore, obtained spectrophotometrically by adding DMPD to the $TMPD^+ClO_4^-$ acetonitrile solution. The gradual decomposition of $DMPD^+$ causes about 40% error in K.

$$K = (3.8\pm1.5) \times 10^{-2}$$

$$\Delta F^\circ = 1.8 \text{ kcal mol}^{-1}$$

The rate was measured with a temperature-jump apparatus. k_{obsd} values at various concentrations are iven in Table 4. Here k_{obsd} is defined by the relation

TABLE 4. k_{obsd} OF THE TMPD AND DMPD$^+$ SYSTEM IN ACETONITRILE

C[a)]/M	k_{obsd}/s^{-1}	$k_{obsd}\,C^{-1}/M^{-1}\,s^{-1}$
1.2×10^{-5}	7.0×10^{4}	6.0×10^{9}
2.5×10^{-5}	12×10^{4}	5.0×10^{9}
6.4×10^{-5}	19×10^{4}	3.0×10^{9}
26×10^{-5}	35×10^{4}	1.3×10^{9}
		av. $4\pm2\times10^{9}$

a) C is defined as $K([TMPD^+]_e+[DMPD]_e)+[TMPD]_e+[DMPD^+]_e$. $[TMPD]_e$ $4.0-40\times10^{-5}$ M, $[DMPD]_e$ $8-25\times10^{-3}$ M, $[DMPD^+]_e$ $4.0-40\times10^{-5}$ M and $[TMPD^+]_e$ $9-25\times10^{-6}$.

$$-d\Delta[TMPD^+]/dt = k_{obsd}\Delta[TMPD^+],$$

and expressed by

$$k_{obsd} = \vec{k}\{[TMPD^+]_e+[DMPD]_e\} + \overleftarrow{k}\{[TMPD]_e+[DMPD^+]_e\},$$

or

$$= \overleftarrow{k}[K\{[TMPD^+]_e+[DMPD]_e\} + \{[TMPD]_e+[DMPD^+]_e\}],$$

where $K=\vec{k}/\overleftarrow{k}$. $\vec{k}$ and $\overleftarrow{k}$ are determined to be

$$\vec{k} = (1.5\pm1)\times10^{8}\ M^{-1}\,s^{-1},$$

$$\overleftarrow{k} = (4\pm2)\times10^{9}\ M^{-1}\,s^{-1}.$$

$\overleftarrow{k}$ is almost a diffusion controlled rate constant (*ca.* $10^{10}\ M^{-1}\,s^{-1}$) in acetonitrile. It is, therefore, concluded that the low value of $\overleftarrow{k}$ in water arises from the water-solute interaction, or most likely from the hydrogen-bonding of water on the nitrogen atoms of the amino groups in TMPD and DMPD.

D. N,N-Dimethyl-p-Phenylenediamine (DMPD) and N,N,N',N'-Tetramethylbenzidine (TMBZ) Cation Radical System. Electrolytically generated TMBZ$^+$ is stable in acetonitrile. Thus the equilibrium constant of reaction (9) is determined by adding DMPD to the solution containing TMBZ$^+$ and excess TMBZ (Fig. 3).

$$DMPD + TMBZ^+ \rightleftharpoons DMPD^+ + TMBZ \qquad (9)$$

The isosbestic point at 486 nm confirms the occurrence of the one-electron-transfer from DMPD to TMBZ$^+$. The equilibrium constant is determined to be

$$K = (3\pm1)\times10^{3}$$

and

$$\Delta F^\circ = -4.6\ \text{kcal mol}^{-1}$$

The molar extinction coefficient of TMBZ$^+$ $\varepsilon_{472}=2.5\times10^{4}$ is also obtained from the result in Fig. 3. At a large excess of DMPD over TMBZ$^+$, the isosbestic point at 472 nm disappears, showing the decomposition of cation radicals. When the temperature-jump measurements were performed, only an increase of the transmittance was observed in the time range of 50 μs at 470—550 nm, corresponding to the decrease of DMPD$^+$ at the temperature rise, no increase of TMBZ$^+$ being observed at 400—470 nm. It is not certain whether the signal obtained actually corresponds to the electron-transfer reaction (9).

We have tried to obtain the forward rate of reaction (9) with a stopped-flow apparatus, using a 1 : 3 : 0.4 ethanol–water–acetonitrile solvent. TMBZ$^+$ is stable in this solvent for $[H^+]<10^{-3}$ M. In more acidic media, the fine structure in the electronic spectra of TMBZ$^+$ in 430—480 nm is smoothed out, indicating the conversion of TMBZ$^+$ into another species. Thus the rate was measured by mixing the TMBZ$^+$ solution with the solution containing DMPD and HCl less than 10^{-3} M. The pseudo first-order rate constant of the decrease of TMBZ$^+$ depends linearly on $1/[H^+]$ (Fig. 4). Assuming that DMPDH$^+$ is inert in donating an electron, the forward rate constant of reaction (9), $\vec{k}$, is obtained from the relation

$$k_{obsd} = \vec{k}/(K_{a1}[H^+])\cdot[DMPDH^+].$$

This leads to

$$\vec{k} = (6\pm2)\times10^{8}\ M^{-1}\,s^{-1},$$

where K_{a1} is assumed to be equal to the one obtained

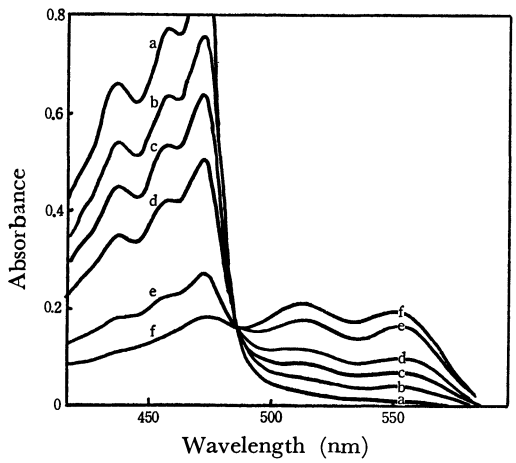

Fig. 3. The variation of the electronic spectrum of TMBZ$^+$ with the addition of DMPD in acetonitrile. a) TMBZ$^+$ only b)—e) DMPD added to the amount of 2.4×10^{-5} M f) no TMBZ$^+$ left when 3.3×10^{-5} M DMPD added.

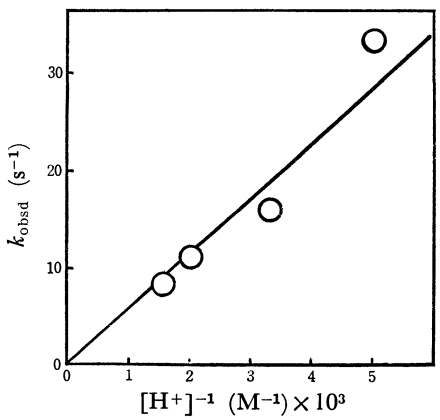

Fig. 4. The dependence of k_{obsd} on $[H^+]^{-1}$ in the reaction between TMBZ$^+$ and DMPD in 1 : 3 : 0.4 ethanol–water–acetonitrile. $[DMPD]=2.0\times10^{-5}$ M. $[TMBZ^+]_0=2.0\times10^{-6}$ M.

in 1 : 3 ethanol–water solvent. $\vec{k}$ is apparently below a diffusion controlled limit, which is analogous to the DMPD/TMPD^{+} system in water.

Discussion

The observed rate constants are plotted against the free energy change of reaction, $\Delta F°$ (Fig. 5). For the systems, PhZ/TMPD^{+}, PhZ/DMPD^{+} in ethanol–water, and DMPD/TMPD^{+} in acetonitrile, the rate constants for $\Delta F°<0$ are nearly equal to a diffusion controlled limit. The systems are quite analogous to the reactions between tetracyanoquinodimethane anion radical and substituted *p*-benzoquinones in acetonitrile.[1] In the latter systems, too, the rate constants for $\Delta F°<0$ are in the range 10^{9}—10^{10} M^{-1} s^{-1} at 25±2 °C. Thus, the results may lead us to the conclusion that the electron-transfer between a free organic ion radical and a neutral molecule takes place with no activation free energy, as long as $\Delta F°$ is less than zero, unless the rigid solvation structure or ion pairing is formed around reactants. This conclusion is consistent with the results accumulated for the electron exchanges between free organic ion radicals and their parent molecules.[8]

It should be noted that the electron-transfer from TMPD to PhZ^{+} proceeds at the same rate of magnitude as from DMPD to PhZ^{+} in spite of the increased steric hindrance of TMPD due to additional methyl groups on nitrogen atoms. As far as the dimerizations of TMPD^{+} and DMPD^{+} are concerned, the interaction between two cation fragments is appreciably diminished because of the presence of methyl groups.[9] It is concluded that the electronic interaction which operates in the electron-transfer of cation radicals is of a considerably different nature from the one operating in dimerization.

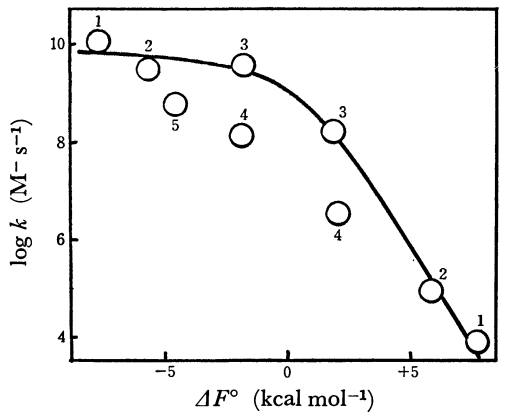

Fig. 5. The rate constants plotted against $\Delta F°$: (1) PhZ/TMPD^{+}, (2) PhZ/DMPD^{+}, (3) DMPD/TMPD^{+} (in acetonitrile) (4) DMPD/TMPD^{+} (in water), (5) DMPD/TMBZ^{+}.

In contrast to the above systems, the rate constants for the systems, DMPD/TMPD^{+} in water and DMPD/TMBZ^{+} in ethanol–water–acetonitrile, are about one order less than a diffusion controlled limit, even when $\Delta F°$ is negative. The origin for these slower rates is not certain. One possiblility is that the strong solvent-solute interaction causes an additional energy barrier to the electron-transfer as was reported for the electron exchange of nitrobenzene anion radical in acetonitrile/water.[10] In the systems showing slower rate constants, the nitrogen atoms on the amino groups of aromatic *p*-diamines seem to be hydrogen-bonded with water molecules. The difficulty in this interpretation lies in the fact that these hydrogen bonds do not slow down the rates of reactions between phenothiazine cation and TMPD or DMPD.

The author thanks Professor Masatoshi Fujimoto for his continuous encouragement, Dr. Mitsuyuki Soma for his valuable suggestions and Dr. Yoichi Iida for kindly supplying the materials. The work was supported by the Ministry of Education.

References

1) A. Yamagishi, *Chem. Lett.*, **1975**, 899. Parts of the results were presented at the 29th Annual Meeting of the Japan Chemical Society, Tokyo, April 1—4, 1975.
2) R. A. Marcus, *J. Chem. Phys.*, **24**, 966 (1956).
3) F. Basolo and R. G. Pearson, "Mechanism of Inorganic Reactions", John Wiley and Sons, Inc., New York (1967), p. 454.
4) L. Michaelis and S. Granick, *J. Amer. Chem. Soc.*, **68** 1747 (1943).
5) Y. Iida, This Bulletin, **44** 663 (1971).
6) L. Michaelis, M. P. Schubert, and S. Granick, *J. Amer. Chem. Soc.*, **61** 1981 (1939).
7) A. Yamagishi, *Chem. Lett.*, **1975**, 595.
8) N. Hirota, "Radical Ions," E. T. Kaiser and L. Kevan, Ed. Interscience, New York, N. Y. (1968), p. 35.
9) S. Nakayama and K. Suzuki, This Bulletin, **46** 3694 (1973).
10) T. Layloff, T. Miller, R. N. Adams, H. Fah, A. Horsfield, and W. Proctor, *Nature*, **205**, 382 (1965).

Nuclear Quadrupole Resonance of Tellurium Tetraiodide

Tsutomu OKUDA, Koji YAMADA, Yoshihiro FURUKAWA, and Hisao NEGITA
Department of Chemistry, Faculty of Science, Hiroshima University, Hiroshima 730
(Received May 22, 1975)

The nuclear quadrupole resonance (NQR) of ^{127}I in tellurium tetraiodide was observed, and the Zeeman effect on a single crystal was examined. Tellurium tetraiodide shows ten resonance lines in the frequency range from 195 to 260 MHz. From the analysis of the zero-splitting patterns, it has become apparent that tellurium tetraiodide crystals contain eight nonequivalent iodine atoms, two of which yield large asymmetry parameters (94.9% and 73.8%) and small quadrupole coupling constants (775.07 MHz and 929.55 MHz) at room temperature. These two may be assigned to the bridging iodine atoms, but they differ markedly from each other in the temperature dependences of e^2Qq/h and η. The other six iodine atoms have small η values and coupling constants of about 1600 MHz; they are assigned to the terminal atoms. From these results, it may be concluded that each tellurium atom has three terminal and two bridging iodine atoms.

The crystal structures of tellurium tetrachloride ($TeCl_4$)[1] and tellurium tetrabromide ($TeBr_4$)[2] are ionic and consist of tetramers $(TeX_3^+X^-)_4$ which have approximately the T_d symmetry. On the other hand, in the solid tellurium tetrafluoride (TeF_4)[3] each tellurium atom is surrounded by three terminal and two bridging atoms at the corners of a distorted square pyramid. These square pyramid units are linked by *cis* bridging into an endless chain. From the far-infrared spectrum of TeI_4,[4] it was concluded that TeI_4 has an ionic structure such as $TeI_3^+I^-$, because the spectrum is similar to those of SbI_3. According to the X-ray diffraction studies,[5] the crystal structure of TeI_4 belongs to an orthorhombic system with a space group P_{nma} or $Pn2_1a$, but its detailed structure has not been reported so far. In the NQR studies of $TeCl_4$ and $TeBr_4$,[6] six resonance lines were observed for both compounds; these lines were assigned to two species of TeX_3^+ (X=Cl, Br) ions. In this connection, we observed the ^{127}I NQR of TeI_4 and examined the Zeeman effect on a single crystal in order to determine the e^2Qq/h and η for each resonance line.

Experimental

The NQR spectrometer used in this experiment was a super-regenerative oscillator with frequency modulation, while the resonance frequencies were determined with a VHF signal generator and a frequency counter, TR-5578, from the Takeda Riken Co., Ltd. The Zeeman effect was examined by means of the zero-splitting cone method[7] on an oscilloscope at room temperature. The magnetic field of about 250 G was applied by means of a Helmholtz coil. The orientation of the magnetic field for the zero-splitting was determined by polar coordinates (Φ, Θ), where Φ and Θ are the azimuthal and polar angles respectively, in the coordinate system fixed to the sample. The single crystal of TeI_4 was grown by the Bridgman-Stockbarger method.

Results and Discussion

Zeeman Effect. As is shown in Table 1, ten resonance lines were observed in the frequency range from 195 to 260 MHz. As the nuclear spin of ^{127}I is equal to 5/2, a pair of NQR lines, ν_1 and ν_2, corresponding to the $\pm1/2\leftrightarrow\pm3/2$ and $\pm3/2\leftrightarrow\pm5/2$ transitions, are to be found for each kind of iodine atoms.[7] Therefore, the asymmetry parameter (η) and the quadrupole coupling constant (e^2Qq/h) can be derived from the frequency ratio, ν_1/ν_2. In the present compound, however, it is necessary to observe the Zeeman effect on each line in order to determine whether it is ν_1 or ν_2, and which ones form a pair, because the resonance lines distributed very widely.

In general, the zero-splitting cone can be expressed in the principal axis system of the efg tensor as follows:[7]

$$\sin^2\theta = \frac{A}{B+C\cos_2\phi} \qquad (1)$$

where θ and ϕ are, respectively the polar and azimuthal angles of the magnetic field which shows zero-splitting.

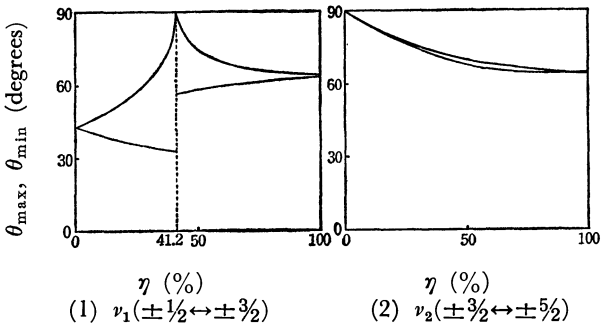

Fig. 1. Calculated maximum and minimum zero-splitting angles as a function of η for ν_1 and ν_2.

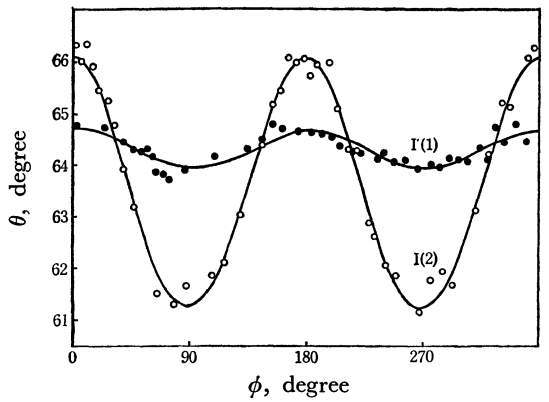

Fig. 2. Zeeman zero-splitting patterns of I'(1) and I(2) lines in the efg principal axis system.

Table 1. NQR parameters of TeI_4 (296 K and 77 K)

	ν_1 (MHz)		ν_2 (MHz)	η (%)[a]	η (%)[b]	e^2Qq/h (MHz)
I (1)	198.27 (198.67)[c]	I′ (1)	206.72 (212.78)	94.0±2.0 —	94.91 (91.70)	775.07 (793.66)
I (2)	205.23 (209.85)	I′ (2)	256.79 (259.15)	73.5±1.5 —	73.75 (75.23)	929.55 (940.44)
I (3)	228.52 (232.65)		—	3.2±0.5 —		1522.5 —
I (4)	234.82 (236.72)		—	5.6±0.5 —		1560.1 —
I (5)	242.75 (245.45)		—	5.6±0.5 —		1612.8 —
I (6)	243.27 (246.55)		—	1.2±0.5 —		1621.8 —
I (7)	250.86 (254.55)		—	1.4±0.5 —		1622.0 —
I (8)	252.35 (256.01)		—	2.9±0.5 —		1680.9 —

a) Obtained from the Zeeman effects. b) Obtained from the frequency ratio (ν_1/ν_2) using tabulated values of spin 5/2. c) The values in parentheses correspond to 77 K.

For the case of the 5/2 spin, A, B, and C can not be expressed in simple formulas when η is large. Hence, the maximum and minimum values of θ were calculated as a function of η for ν_1 and ν_2, as is shown in Fig. 1, according to the literature.[7,8] The zero-splitting patterns of I′(1) and I(2) lines are shown in Fig. 2 in the principal-axes system. The maximum and minimum values of θ for the zero-splitting patterns were obtained by the use of the least-squares method. These values were 66.1° and 61.3° for the I(2) pattern and 64.7° and 63.9° for that of I′(1). On the basis of these values, the I(2) line was assigned to ν_1, with $\eta=73.5\pm1.5\%$, and the corresponding ν_2 was observed at 256.79 MHz. On the other hand, the I′(1) pattern was assigned to ν_2, with $\eta=94.0\pm2.0\%$. The corresponding ν_1 was observed at 198.27 MHz, although this line was broad and weak compared with the others. The quadrupole coupling constants for these lines were calculated by the use of the tabulated eigenvalues of spin 5/2.

The I(3)~I(8) lines have approximately the same intensity for the powder sample, and from the zero-splitting patterns for the single crystal it becomes apparent that all these lines are ν_1 with small η values. For example, the zero-splitting patterns of the I(6) and I(7) lines are shown in Fig. 3. Therefore, η and e^2Qq/h can be calculated by means of the following equations:[7,9]

$$\eta = 17(\sin^2\theta_{max}-\sin^2\theta_{min})/24(\sin^2\theta_{max}+\sin^2\theta_{min}) \quad (2)$$

$$e^2Qq/h = 20\nu_1/3(1+1.0926\eta^2-0.6430\eta^4) \quad (3)$$

where θ_{max} and θ_{min} are the maximum and minimum zero-splitting angles. Table 1 shows the NQR parameters thus obtained. From these results it may be concluded that this crystal contains two nonequivalent TeI_4 molecules and that each tellurium atom is bonded to three terminal and two bridging iodine atoms. This configuration around the tellurium atom has a stronger resemblance to that of TeF_4 than to those of $TeCl_4$ and $TeBr_4$.

I(3) and I(6) yield two patterns of zero-splitting loci. On the other hand, for the I′(1), I(2), I(4), I(5), I(7), and I(8) lines only three patterns out of four were observed because one of the z-axis in each line was nearly parallel to the rf coil. From the symmetry of the observed patterns, three mutually perpendicular twofold axes were found within the limits

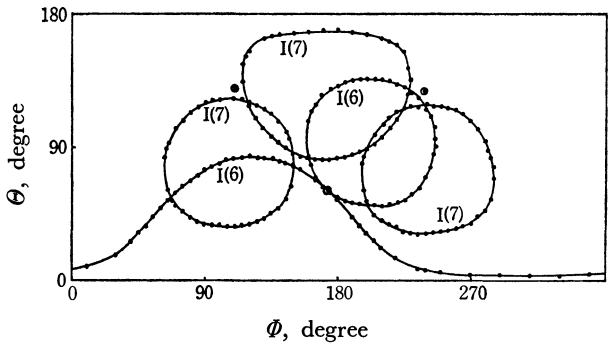

Fig. 3. Zero-splitting patterns of I(6) and I(7) lines in the coordinates fixed to the sample. Crystal axes of orthorhombic system are indicated by ⊙.

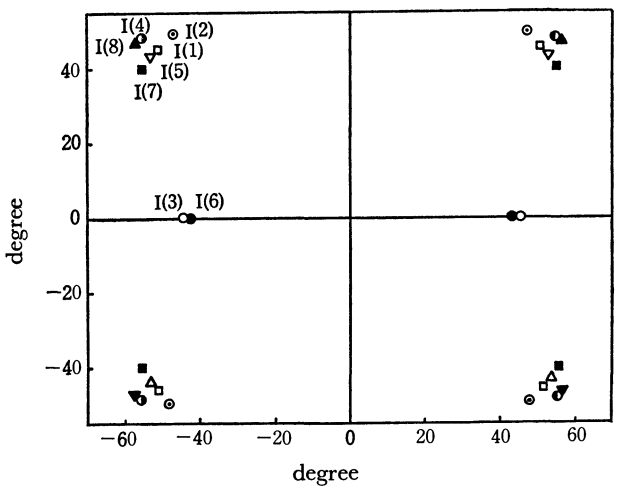

Fig. 4. Orientation of z-axes with respect to the crystal axes which are located at (0°, 0°), (90°, 0°), and (0°, 90°). In the case of I(2), y-axes are shown.

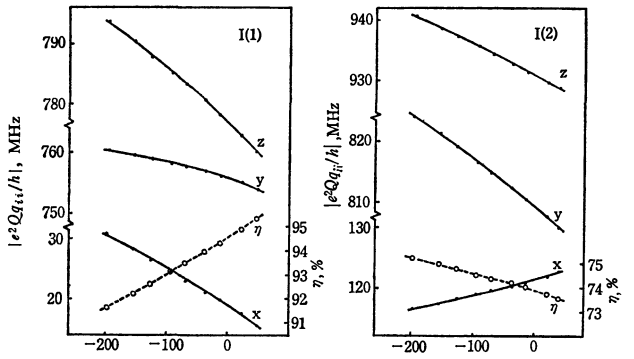

Fig. 5. Temperature dependence of quadrupole coupling constants for I(1) and I(2).

of experimental error. This finding suggests that the crystal is orthorhombic and that these three twofold axes correspond to the crystal axes.[10] Figure 4 shows the orientations of all the z-axes with respect to the crystal axes. In this figure, the three crystal axes are located at (0°, 0°), (90°, 0°), and (0°, 90°).

Temperature Dependences of the Quadrupole Coupling Constant for Bridging Iodines. Figure 5 shows the temperature dependences of $|e^2Qq_{zz}/h|$, $|e^2Qq_{yy}/h|$, and $|e^2Qq_{xx}/h|$ for I(1) and I(2). The principal values of the efg tensor can be expressed by:

$$\left.\begin{aligned} V_{zz} &= eq \\ V_{yy} &= -(1+\eta)eq/2 \\ V_{xx} &= -(1-\eta)eq/2 \end{aligned}\right\} \quad (4)$$

If the amplitudes of torsional oscillation about the x, y, and z axes are denoted by θ_x, θ_y, and θ_z respectively, the averaged principal values of the efg tensor can be expressed by the following equations:[11]

$$\left.\begin{aligned} V_{zz} &= eq_0\{1-\langle\theta_y^2\rangle(3-\eta_0)/2-\langle\theta_x^2\rangle(3+\eta_0)/2\} \\ V_{yy} &= eq_0\{-(1+\eta_0)/2+\langle\theta_z^2\rangle\eta_0+\langle\theta_x^2\rangle(3+\eta_0)/2\} \\ V_{xx} &= eq_0\{-(1-\eta_0)/2-\langle\theta_z^2\rangle\eta_0+\langle\theta_y^2\rangle(3-\eta_0)/2\} \end{aligned}\right\} \quad (5)$$

where q_0 and η_0 are the values in the static lattice and where $\langle\theta_i^2\rangle$ (i=x, y, and z) indicates the mean square amplitude of the oscillation about the i-axis. In the symmetrical bridging iodine, the principal axes of the efg tensor depend upon the bridging angle, as is shown in Fig. 6. It may be considered that the bridging iodine is more mobile in the direction perpendicular to the bridging plane than in that parallel to it. Therefore, we may assume that, in Model (a), the torsional oscillation about the y-axis contributes predominantly to the temperature dependence of the quadrupole coupling constant and the asymmetry parameter, whereas, in Model (b), the torsional oscillation about the z-axis contributes predominantly to the parameters. The temperature dependence of the I(1) atom can be interpreted satisfactorily by assuming $\langle\theta_x^2\rangle\approx\langle\theta_z^2\rangle<\langle\theta_y^2\rangle$ in Eq (5): this situation corresponds to Model (a). The positive temperature coefficient of η was also found

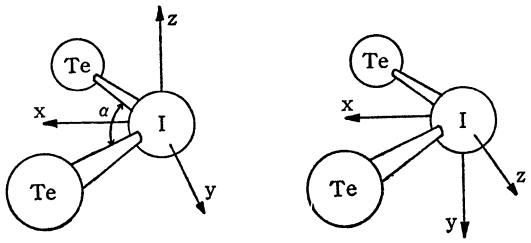

(a) $90°<\alpha<109.5°$ (b) $109.5°<\alpha<180°$

Fig. 6. Orientation of efg principal axis at a bridging iodine atom.

for the bridging iodine in Al_2I_6 and Ga_2I_6.[12] These bridging iodine atoms have been supposed to have the principal axes of Model (a) by analogy with Al_2Br_6.[13] Therefore, the temperature dependence of the I(1) atom is mainly due to the characteristic torsional oscillation of the bridging iodine atom, as in those of Al_2I_6 and Ga_2I_6. Furthermore, the I(1) atom is supposed to have bonds such as those in Model (a).

On the other hand, the tendency of the I(2) atom can be roughly interpreted on the basis of Model (b) by assuming $\langle\theta_x^2\rangle\approx\langle\theta_y^2\rangle<\langle\theta_z^2\rangle$. However, as the quadrupole coupling constant of I(2) is fairly larger than that of I(1), it may be considered that I(2) is not so symmetrical in its bridging as I(1). Therefore, the variation in the electronic structure of the bridging iodine atom may also contribute to the temperature dependence of the quadrupole coupling constant.

References

1) B. Buss and B. Krebs, *Inorg. Chem.*, **10**, 2795 (1971).
2) C. B. Shoemaker and S. C. Abrahams, *Acta Crystallogr.*, **18**, 296 (1965).
3) A. J. Edwards and F. I. Hewaidy, *J. Chem. Soc., A*, **1968**, 2977.
4) N. N. Greenwood, B. P. Straughan, and A. E. Wilson, *J. Chem. Soc., A*, **1966**, 1479.
5) W. R. Blackmore, S. C. Abrahams, and J. Kalnajs, *Acta Crystallogr.*, **9**, 259 (1956). C. B. Shoemaker and S. C. Abrahams, *ibid.*, **18**, 296 (1965).
6) A. Schmitt and W. Zeil, *Z. Naturforsch., A*, **18**, 428 (1963). T. Okuda, K. Yamada, Y. Furukawa, and H. Negita, This Bulletin, **48**, 376 (1975).
7) T. P. Das and E. L. Hahn, "Nuclear Quadrupole Resonance Spectroscopy," Solid State Physics, Suppl. 1, Academic Press, New York (1957).
8) M. H. Cohen, *Phys. Rev.*, **96**, 1278 (1954).
9) I. P. Biryukov, M. G. Voronkov, and I. A. Safin, "Tables of Nuclear Quadrupole Resonance Frequencies," Israel, IPST Press (1969).
10) K. Shimomura, *J. Phys. Soc. Japan*, **12**, 652 (1957).
11) B. L. Barton, *J. Chem. Phys.*, **46**, 1553 (1967).
12) R. Barnes and S. Segel, *J. Chem. Phys.*, **25**, 578 (1956).
13) T. Okuda, H. Terao, O. Ege, and H. Negita, *ibid.*, **52**, 5489 (1970).

Proton Hyperfine Splittings in the ESR of Some Alkylphosphine Dimeric Radicals

Masamoto IWAIZUMI, Takashi KISHI, Fumio WATARI,* and Taro ISOBE

The Chemical Research Institute of Non-Aqueous Solutions, Tohoku University, Sendai 980

**Department of Applied Science, Faculty of Engineering, Tohoku University, Sendai 980*

(Received May 29, 1975)

The triplet splittings due to protons were observed for the ESR of the dimeric cation radicals of $P(CH_3)_3$, $P(CH_2CH_3)_3$, and $PH(CH_3)_2$; they were formed by the γ irradiation of the rigid CH_2Cl_2 solutions of these alkylphosphines at 77 K. The observed proton hyperfine splittings for the dimer-cation radicals, $[(CH_3)_3P\text{-}P(CH_3)_3]^+$ and $[(CH_3CH_2)_3P\text{-}P(CH_2CH_3)_3]^+$, were assigned to the hyperfine interaction with two of the methyl and with two of the methylene protons respectively, while those for the $[(CH_3)_2HP\text{-}PH(CH_3)_2]^+$ radical were assigned to the hyperfine interaction with the two P–H protons. In the former two radicals, the rotations of the methyl and the ethyl groups are restricted. The conformations of the methyl and the ethyl groups have been estimated on the basis of the observed proton hyperfine splittings. The P–H protons of the $[(CH_3)_2HP\text{-}PH(CH_3)_2]^+$ radical have an extremely large isotropic coupling constant of 58 G; it may be attributed to the direct interaction with the unpaired electron in the anti-bonding σ^* orbital of the P–P bond.

When γ-irradiated trialkylphosphines are examined by ESR at 77K, clear parallel and perpendicular features, separated by over 1000 G, are often observed. These hyperfine patterns have been assigned by Lyons *et al.*[1] to alkylphosphine dimer-cation radicals of the $(R_3P\text{-}PR_3)^+$ type. From the observed phosphorus hyperfine interaction, they concluded that these radicals are σ^* radicals which have their unpaired electrons in anti-bonding σ^* orbitals. In these investigations, the ESR of the dimer cation radicals showed only phosphorus splittings; no proton hyperfine splittings have not been resolved. During the course of our investigations of γ-irradiated phosphorus compounds, we found the ESR of dimer-cation radicals to show further splittings due to protons for the dichloromethane solutions of trimethylphosphine, triethylphosphine, and dimethylphosphine. In this paper we will report some information of the radical structure mainly obtained through these proton hyperfine splittings.

Experimental

The dimethylphosphine $[PH(CH_3)_2]$, trimethylphosphine $[P(CH_3)_3]$, and triethylphosphine$[P(CH_2CH_3)_3]$ were obtained as has been described elsewhere.[2] The deuterated compound of dimethylphosphine $[PD(CH_3)_2]$ was prepared by the reaction of $PH(CH_3)_2$ with D_2O in the presence of DBr, while $PH(CD_3)_2$ was prepared by using CD_3I instead of CH_3I in the course of the preparation of $PH(CH_3)_2$. $P(CD_3)_3$ was prepared by dissolving $(CD_3)_3PH^+I^-$, formed from $PH(CD_3)_2$ and CD_3I, into a KOH–dimethyl sulfoxide suspension; thereafter the product was separated from the solution by vacuum distillation. The CH_2Cl_2 solutions of these compounds were irradiated by ^{60}Co γ-rays in ESR sample tubes at 77 K after they has been degassed. The ESR spectra were measured with a Hitachi 771 ESR spectrometer with 100 kHz field modulation.

Results and Discussion

Figure 1 shows the ESR spectrum obtained from the γ-irradiated CH_2Cl_2 solution of $P(CH_3)_3$ at 77K. An ESR absorption similar to the outermost features in the figure (labelled I) is observed for all the compounds treated here; it is assigned to the dimer-cation radicals of the alkylphosphines by reference to Lyons and Symons' assignment for the triethyl- and tributylphosphine dimer-cation radicals.[1] The expected central component ($M_I^{31P}=0$) is considered to be hidden under the intense absorptions due to other radical species. Though Lyons *et al.*'s assignments of the dimer-cation radicals were made by the analogy between the reaction and that of trialkylarsines to form their dimer cations, conclusive evidence for the assignment of the spectra is given by the observation of the triplet splittings due to the two P–H protons in the radical $[(CH_3)_2HP\text{-}PH(CH_3)_2]^+$ (*vide infra*). It was also observed that the relative intensity of the dimer cation to the monomer-cation radical clearly changes in proportion to the concentration of the parent phosphine in the case of the $P(CH_2CH_3)_3$ solution.

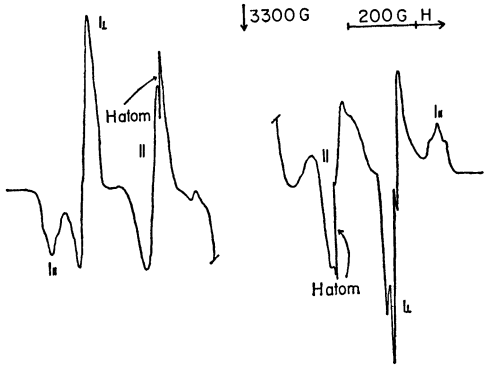

Fig. 1. ESR Spectrum of γ-irradiated $P(CH_3)_3$ at 77 K in CH_2Cl_2. ESR absorption I is assigned to $[(CH_3)_3P\text{-}P(CH_3)_3]^+$ and II to $P(CH_3)_3CH_2Cl$.[2]

The high-field-side signals for the dimer-cation radicals are shown in Figs. 2—4. The parallel and perpendicular features for the undeuterated compounds show triplet splittings. It is apparent that the triplet splittings for the $[(CH_3)_3P\text{-}P(CH_3)_3]^+$ radical arise from the hyperfine interaction with the methyl protons, since the dimer-cation radical of $P(CD_3)_3$ does not show such triplet splittings (Fig. 2). For the case

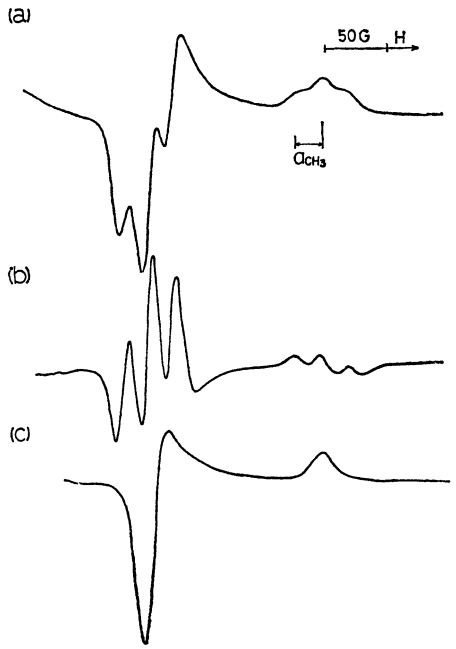

Fig. 2. High field components of ESR spectra for the radicals a) $[(CH_3)_3P\text{-}P(CH_3)_3]^+$ and c) $[(CD_3)_3P\text{-}P(CD_3)_3]^+$ at 77 K, and b) the derivative curve of (a) (2nd derivative ESR spectrum).

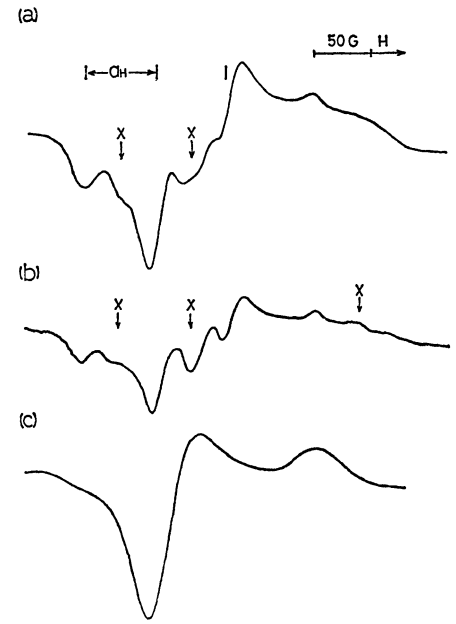

Fig. 3. High field components of ESR spectra for the radicals a) $[(CH_3)_2HP\text{-}PH(CH_3)_2]^+$, b) $[(CD_3)_2HP\text{-}PH(CD_3)_2]^+$ and c) $[(CH_3)_2DP\text{-}PD(CH_3)_2]^+$. See text for X in a) and b).

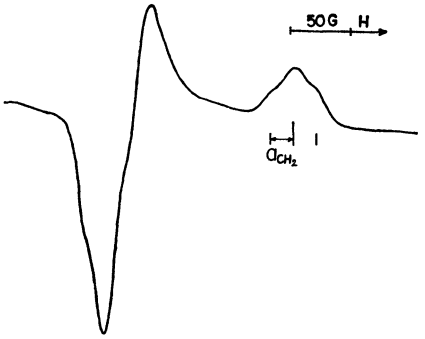

Fig. 4. High field component of the ESR spectrum for the $[(CH_3CH_2)_3P\text{-}P(CH_2CH_3)_3]^+$ radical.

of the $[(CH_3)_2HP\text{-}PH(CH_3)_2]^+$ radical, the triplet splittings were not observed when the P–H protons were deuterated, though the $[(CD_3)_2HP\text{-}PH(CD_3)_2]^+$ radical shows the same triplet splittings as the undeuterated dimer-cation radical. This apparently indicates that the triplet splittings in the $[(CH_3)_2HP\text{-}PH(CH_3)_2]^+$ radical arise from the hyperfine interaction with the P–H protons. The signals labelled "X" in Fig. 3 are probably due to the dimer-cation radical in which one of the P–H protons is replaced with the chlorine of the solvent. When diethylether was used as the solvent, the X signals were not observed. The ESR parameters obtained are summarized in Table 1, together with the orbital populations of the unpaired electron, which were determined by the use of the atomic parameters in the literature.[4]

As may be seen from the p/s ratios in Table 1, the phosphorus orbitals occupied by the unpaired electrons take the sp^3 hybridization. This indicates that Lyons *et al.*'s model[1] is reasonable for the present system also. An interesting result in the present system is the appearance of the proton hyperfine splittings. The triplet splittings due to the methyl protons in the $[(CH_3)_3P\text{-}P(CH_3)_3]^+$ radical indicate that only two among 18 methyl protons have an observable hyperfine interaction. This suggests that the rotation of the methyl groups is strongly restricted and that the radical takes a conformation where only two protons are at the positions of the maximum overlap with the anti-bonding σ^* orbital of the P–P bond containing the unpaired electron. That is, one of the three methyl groups on each phosphorus takes the Ia conformation, where one of the C–H bonds eclipses the lobe of the anti-bonding σ^* orbital, while the other two methyl groups take the Ib conformation, where the methyl group rotates about 60° from the conformation of Ia. In the latter conformation, though one of the C–H bonds is located at a position

TABLE 1. ESR PARAMETERS AND ORBITAL POPULATIONS FOR SOME DIMER-CATION RADICALS

Radical	$g_{//}$	$g_\perp$	Hyperfine coupling/G				a_s^2(%)	a_p^2(%)	p/s
			$^{31}P_{//}$	$^{31}P_\perp$	$^{31}P_{iso}$	^1H			
$[PH(CH_3)_2]_2^+$	2.003	2.014	581	442	488	58	13.4	45.1	3.3
$[P(CH_3)_3]_2^+$	1.992	2.012	569	439	482	20	13.3	42.2	3.2
$[P(CH_2CH_3)_3]_2^+$	1.990	2.009	549	415	460	18	12.6	43.2	3.4

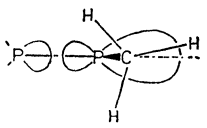

Ia

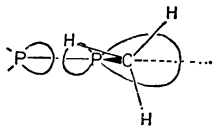

Ib

parallel to the σ^* orbital, it has no significant hyperfine interaction. It was observed that the triplet splittings smear as the temperature increases from 77 K, though the radical promptly decays above 150 K. The smearing of the proton hyperfine splittings may indicate the onset of the rotation of the methyl groups.

It may be noteworthy that the hyperfine interaction of the P–H protons in the $[(CH_3)_2HP–PH(CH_3)_2]^+$ radical has the large isotropic coupling constant of 58 G. In the case of the methyl radical, it has been shown by theoretical calculations[5] that the contribution of the direct interaction with the unpaired electron does not exceed the spin polarization effect on the isotropic hyperfine interaction, even when the radical deforms to a pyramidal structure, and that the hyperfine coupling constant of 23.04 G for the planar structure is the largest value which can be expected for the radical. In view of this fact, the hyperfine coupling constant observed in the present system is surprisingly large; it is probably due to the direct overlap of the unpaired electron orbital with the P–H protons, which are located on the same side as the big lobe of the unpaired electron orbital in the tetrahedral conformation of phosphorus (II).

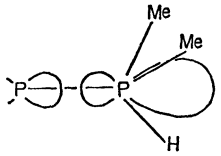

II

The triplet splittings observed for the $[(CH_3CH_2)_3P–P(CH_2CH_3)_3]^+$ radical may be attributed to the two methylene protons of the radical by analogy with the case of the $[(CH_3)_3P–P(CH_3)_3]^+$ radical. The observation of the splittings also suggests that the rotation of the ethyl groups about the P–Et bond is restricted and that the ethyl groups take a conformation where two of the methylene protons are placed near the positions of the maximum overlap with the unpaired electron orbital, as in the case of the $[(CH_3)_3P–P(CH_3)_3]^+$ radical.

References

1) a) A. R. Lyons, G. W. Neilson, and M. C. R. Symons, *Chem. Commun.*, **1972**, 507; b) A. R. Lyons and M. C. R. Symons, *J. Chem. Soc. Faraday II*, **1972**, 1589.

2) M. Iwaizumi, T. Kishi, T. Isobe, and F. Warati, *J. Chem. Soc. Faraday II*, in press.

3) To be discussed elsewhere.

4) P. W. Atkins and M. C. R. Symons, "The Structure of Inorganic Radicals," Elsevier, Amsterdam (1967).

5) D. L. Beveridge and K. Miller, *Mol. Phys.*, **14**, 401 (1968); *ibid.*, **21**, 768 (1971).

Photosolvation Reactions and Their Quantum Yields of Hexacyanocobaltate(III) in Non-aqueous Solvents

Katsumi NAKAMARU, Kazuo JIN, Atsuko TAZAWA, and Masaru KANNO

Department of Chemistry, Faculty of Science, Hirosaki University, Bunkyo, Hirosaki, Aomori 036

(Received May 31, 1975)

The photoreactions of hexacyanocobaltate(III) in non-aqueous solvents (methanol, ethanol, acetonitrile, DMF, pyridine) caused by irradiation at 365 nm or 313 nm are found to be the photosolvation

$$[Co(CN)_6]^{3-} + Solv. \xrightarrow{h\nu} [Co(CN)_5(Solv.)]^{2-} + CN^-$$

In pyridine, in addition to the photosolvation product, a fluorescent substance which is perhaps an aromatic compound is also formed by the irradiation at 365 nm. The quantum yields are almost the same as that in aqueous solution. In ethanol, the quantum yields irradiated at both 313 nm and 365 nm are the same, indicating that the quantum yield is independent of the exciting wavelength. The sensitized photosolvation using several donors failed to occur because of the solubility limitation. Interesting spectral results are also reported.

A large number of investigations have been performed on the photochemical[1,2] and photophysical[2,3] behaviors of transition metal complexes in the last decade. Most of these studies, however, have been done in aqueous solutions, except for the carbonyl complexes, and this seems to be due to the fact that most transition metal complexes have very low solubilities in non-aqueous organic solvents. It is mainly in aqueous solutions that many investigators have studied the photochemistry of transition metal complexes with great interest.

Recently several papers on the photochemistry and photophysics of transition metal complexes in non-aqueous solvents were reported. The photosolvation of tetrabutylammonium hexacyanochromate(III) in *N,N*-dimethylformamide (DMF) was studied and some evidence against the doublet hypothesis for the photoreactive state of the Cr(III) complex was obtained.[4] The same system was investigated from the standpoint of the sensitized photoaquation and photosolvation reaction and the photoreactive state was also identified as the lowest quartet excited state.[5] On the other hand, the intersystem crossing efficiency of hexacyanochromate(III) was reported from the results of the direct and $[Ru(bipy)_3]^{2+}$-sensitized phosphorescence intensities in DMF solutions.[6] Other papers dealt with the phosphorescence quenching of $[Ru(bipy)_3]^{2+}$ in ethanol–benzene,[7] and in DMF or methylformamide.[8] As for Co(III) complexes, however, neither photochemical nor photophysical studies have been made in non-aqueous solvents.

In the field of the photochemistry of transition metal complexes in aqueous solutions, it is well known that the Co(III) complexes show the photoredox reaction and/or the photoaquation and that the photoredox reaction is more likely to occur when irradiated at the shorter charge transfer band than at the longer ligand field band and that the phosphorescence cannot be seen except in a few cases even with the crystal at low temperature.[1] It is particular in the Co(III) complexes, however, that hexacyanocobaltate(III) shows only the photoaquation and does not exhibit any photoredox reaction even when the complex is irradiated at the charge transfer absorption band, 254 nm,[9] and that, moreover, it shows the phosphorescence with the crystal at low temperature (4.2 K or 77 K).[10] The reason for this unusual behavior of hexacyanocobaltate(III) has not been clarified yet. Therefore, taking account of the fact that the phosphorescence of hexacyanochromate(III) is observed in DMF but not in water,[4] photochemical and photophysical studies seem to be necessary for Co(III) complexes in non-aqueous solvents. First of all, hexacyanocobaltate(III), which shows the unusual behavior mentioned above, attracted our attention and we report in this paper the preliminary results obtained from the photochemical experiments of tetrabutylammonium hexacyanocobaltate(III) ($[Bu_4N]_3[Co(CN)_6]$) in several organic solvents.

Experimental

Materials. Tetrabutylammonium hexacyanocobaltate(III) ($[Bu_4N]_3[Co(CN)_6]$) was prepared from $K_3[Co(CN)_6]$ and tetrabutylammonium bromide.[11] The spectrum of $[Bu_4N]_3[Co(CN)_6]$ in water agreed with that of $K_3[Co(CN)_6]$.[9] Potassium pentacyanopyridinecobaltate(III) ($K_2[Co(CN)_5py]$) was prepared according to the literature.[12] Fluoranthene was purified by passing it through a column of silica gel. Michler's ketone was recrystallized twice from ethanol. Triacetylacetonatorhodium(III) ($Rh(acac)_3$) was recrystallized from chloroform. Reagent grade pyrazine and triphenylamine were used without further purification. Reagent grade methanol and ethanol were dried by the literature method.[13] Acetone, acetonitrile, and DMF were dried by the method reported.[14] Reagent grade pyridine was purified by distillation. Chloroform was of spectrograde and used without further purification. All these solvents were stocked in a desiccator in the dark.

Apparatus. The irradiation equipment was used in the usual way. The excitation wavelength 313 nm was isolated from a Toshiba SHL-100UV-2 mercury lamp by means of a combination of the chemical filter described by Murov[15] and the Toshiba UV-D25 glass filter. Light of 365 nm was isolated by using a Toshiba UV-D1C glass filter and a glass plate. Light of 436 nm was isolated by the method described.[16] The light intensity was measured by a ferrioxalate actinometer.[17] The absorption spectrum was measured with a Hitachi 124 double beam spectrophotometer and the emission spectrum was measured with a Aminco-Bowman spectrophotofluorometer.

Procedures. Although $[Co(CN)_6]^{3-}$ in organic solvents did not cause any thermal reactions, the sample solutions used for the irradiation were always prepared just before the measurements. When the organic sensitizers were added

to the solution of $[Co(CN)_6]^{3-}$, no change of the absorption of the complex was observed. The sensitization experiments were carried out under the condition that the donors absorbed most of the incident light. Degassed solutions were obtained by successive freeze-pump-thaw cycles. The quantum yields were determined spectrophotometrically using the molar extinction coefficients(ε) of the photoproducts, which were obtained by the complete photolysis of $[Co(CN)_6]^{3-}$. In the case of $[Co(CN)_5py]^{2-}$, the ε of the synthesized sample was used because the isosbestic points in the photolysis of $[Co(CN)_6]^{3-}$ in pyridine were not seen at later stages. In benzonitrile, the quantum yield could not be obtained because the reaction did not proceed with clean isosbestic points.

Results and Discussion

Absorption Spectra. $[Co(CN)_6]^{3-}$ shows three characteristic bands in the ultraviolet region which are assigned as follows, in the order of decreasing wavelength: $^1A_{1g}\rightarrow{}^1T_{1g}$ (the first absorption band), $^1A_{1g}\rightarrow{}^1T_{2g}$ (the second absorption band), and metal to ligand charge transfer(MLCT) band, respectively.[1,18,19] The first two bands are spin-allowed ligand field transitions and have rather low molar extinction coefficients (ε). The last one is an allowed $t_{2g}\rightarrow\pi^*$ transition and hence is a very intense band. The spin-forbidden, lowest energy ligand field transition, $^1A_{1g}\rightarrow{}^3T_{1g}$, is observed in the crystalline spectrum, but not in solution.[10]

The absorption data obtained in several organic solvents are summarized in Table 1, together with the values of the dielectric constants in the second column. At first sight, there seems to be no regularity in the position of the absorption maximum of $[Co(CN)_6]^{3-}$ in these solvents, but it may be seen that there are two groups of solvents: (a) one is water, methanol, ethanol, ethylenediamine, and chloroform; (b) the other is acetonitrile, benzonitrile, pyridine, and DMF. In the former group, as the values of dielectric constants decrease, the absorption maximum shifts to longer wavelengths (red shift). On the other hand, the behavior of the latter group is unusual: despite the values of the dielectric constants, they all show greater red shifts than the (a) group. For example, acetonitrile, which is next to water in the order of the dielectric constants of the solvents used, shows a longer maximum wavelength, 320 nm, than does chloroform, 318 nm, which has the smallest dielectric constant. The second absorption bands show a similar tendency to the first absorption bands. This phenomena cannot be explained only from the difference in the polarity of solvents. When we note that all the solvents in the (b) group have double or triple bonds, it can be said that the π-electrons of the solvents in the (b) group are responsible for the greater red shift in the spectra of $[Co(CN)_6]^{3-}$ in these solvents. It is known that the spectrochemical series should reflect the π-bonding properties of the various ligands and, in fact, strong π-acceptor ligands such as CN^- and NO_2^- cause larger Δ(the energy separation of the t_{2g} and e_g metal d orbitals in an octahedral complex) values. Hence, the π-electron interactions between the ligand CN^- of $[Co(CN)_6]^{3-}$ and the organic solvents in the (b) group may play an important role.

The various maximum wavelengths of the photoproducts can be reasonably explained from the standpoint of spectrochemical series. It may be noted that acetonitrile cannot coordinate at a position other than an N atom and that $[Co(CN)_5(CH_3CN)]^{2-}$ shows a peak at longer wavelengths than that of $[Co(CN)_6]^{3-}$. Thus a CN^- which coordinates at a C atom is at a higher position than CH_3CN in the spectrochemical series.

Photosolvation Reactions. The solutions of $[Co(CN)_6]^{3-}$ in ethanol, methanol, acetonitrile, DMF, pyridine, benzonitrile, acetone, chloroform, and ethylenediamine were irradiated at 365 nm (in ethanol, also at 313 nm) and the spectral changes are shown in Fig. 1 to Fig. 5.

In ethanol, upon irradiation at 365 nm, $[Co(CN)_6]^{3-}$

Table 1. Spectral data and photosolvation quantum yields of $[Co(CN)_6]^{3-}$ in water and various non-aqueous solvents

Solvent	Dielectric constant[a]	$\lambda^1_{max}(\varepsilon)$[d]	$\lambda^2_{max}(\varepsilon)$[d]	$\lambda^p_{max}(\varepsilon)$[d]	Φ_{313}[e]	Φ_{365}[e]
H_2O[f]	78.3[b]	311(199)	258(136)	382(294)	0.31	0.32
CH_3CN	38.0[c]	320(186)	264(137)	353(190)		0.28
DMF	36.1[c]	322(188)	265(135)	399(276)		0.28
CH_3OH	32.6[b]	313(191)	259(136)	391(283)		0.32
C_6H_5CN	25.2[b]	320(190)				j)
C_2H_5OH	24.3[b]	314(190)	261(136)	392(184)	0.28	0.28
en[g]	14.2[b]	317				k)
py[h]	12.3[b]	321(198)		361(271[i])		0.31
$CHCl_3$	4.81[b]	318(200)	261			k)

a) Values at 25 °C except en ($CHCl_3$ at 20 °C). b) Data from J. A. Dean (editor), "Lange's Handbook of Chemistry," McGraw-Hill, New York, (1973). c) Data from Ref. 14. d) λ^1_{max}, λ^2_{max}, and λ^p_{max} are the maximum wavelengths of the first and second absorption bands and that of the photoproduct, at room temperature, respectively. e) Φ_{313} and Φ_{365} are the photosolvation quantum yields irradiated at 313 nm and 365 nm, at 25 °C, respectively. f) Photoaquation quantum yield irradiated at 436 nm is 0.31 in aqueous solution. g) Ethylenediamine. h) Pyridine. i) Value of $K_2[Co(CN)_5py]$ in aqueous solution. j) Φ cannot be obtained. See Experimental Section. k) No reaction occurred.

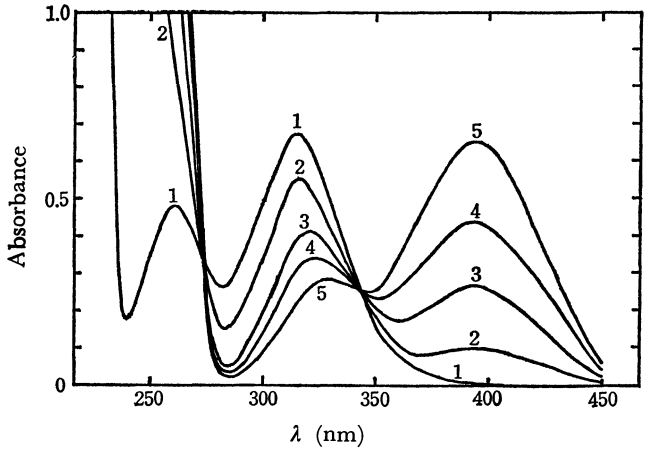

Fig. 1. Spectral change of $[Co(CN)_6]^{3-}$ in the aerated ethanol solution upon irradiation at 365 nm ([complex] 3.532×10^{-3} M, 25 °C). Time of irradiation, 1) 0, 2) 18 min, 3) 55 min, 4) 1 hr and 50 min, 5) 5 hr and 5 min.

undergoes a reaction and shows the spectral changes in Fig. 1, which are different from that in aqueous solution.[9] The peak at 314 nm decreases gradually and instead the peak at 392 nm increases. After sufficient irradiation time, this peak does not show any substantial increase. Two isosbestic points are seen at 280 nm and 342 nm, indicating that the primary photoproduct is photochemically stable. When the irradiated solution is left alone in the dark, the peak at 392 nm decreases and the peak at 314 nm recovers, but this back reaction is very slow and the recovery is not complete. Thus this thermal reaction is negligible during the irradiation. As for the photoproduct, it may be considered that ethanol has the ability to coordinate with the excited state transition metal complexes and, in fact, in the ethanol solution of $W(CO)_6$ which is studied in many coordinative organic solvents,[1] it is known that a solvent ethanol coordinates as a ligand by the irradiation.[20] Besides, we examined the effect of the addition of water to the ethanol solution. In this mixed solvent, $[Co(CN)_6]^{3-}$ undergoes a reaction also, but the isosbestic points cannot be seen cleanly. Moreover, the features of the spectral change upon irradiation become the same as that in aqueous solution[9] as the content of water increases, on the one hand, and it becomes the same as that in ethanol solution when the content of ethanol increases, on the other hand. Thus, we may consider from this preliminary result that in the dried ethanol solution, the following photosolvation reaction occurs:

$$[Co(CN)_6]^{3-} + EtOH \xrightarrow{h\nu} [Co(CN)_5(EtOH)]^{2-} + CN^- \quad (1)$$

The quantum yield of reaction (1) is 0.28 and almost the same as that in aqueous solution, 0.32 in our experimental conditions. When light of 313 nm is used for the excitation wavelength, the same reactions as described above occur and the quantum yield is also 0.28. Although, because of the solubility limitation, the photosolvation reaction irradiated at 436 nm could not be studied in ethanol as well as in other solvents, it seems that the same results obtained by the irradiation at both 313 nm and 365 nm show that the quantum yields are independent of the wavelengths and this agrees with the results in aqueous solution (we found that the quantum yield at the excitation wavelength of 436 nm was also 0.31 in aqueous solution). O_2 had no effect on the photosolvation quantum yield.

In methanol, as shown in Fig. 2, the reaction which occurs upon the irradiation at 365 nm can be regarded as a photosolvation similar to Eq. (1), for we found that when the photoproduct in methanol was redissolved in water, its spectrum had a peak at 388 nm which did not coincide with that of $[Co(CN)_5H_2O]^{2-}$ in aqueous solution, 382 nm. The quantum yield 0.32 is the same in aqueous and in ethanol solution. The back reaction is also slow and the degree of recovery is smaller than that in ethanol.

In acetonitrile and DMF, as shown in Fig. 3 and Fig. 4, respectively, the change of the spectra caused

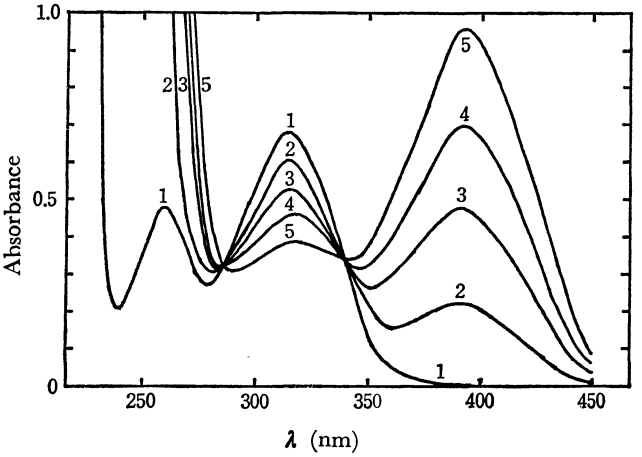

Fig. 2. Spectral change of $[Co(CN)_6]^{3-}$ in the aerated methanol solution upon irradiation at 365 nm ([complex] 3.524×10^{-3} M, 25 °C). Time of irradiation, 1) 0, 2) 35 min, 3) 1 hr and 35 min, 4) 3 hr, 5) 8 hr.

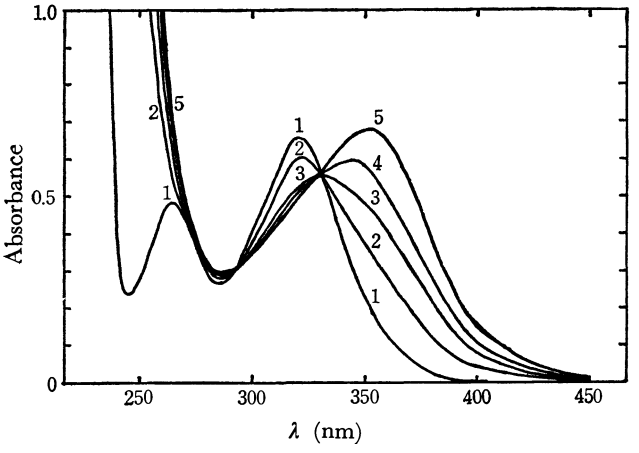

Fig. 3. Spectral change of $[Co(CN)_6]^{3-}$ in the aerated acetonitrile solution upon irradiation at 365 nm ([complex] 3.538×10^{-3} M, 25 °C). Time of irradiation, 1) 0, 2) 40 min, 3) 1 hr and 40 min, 4) 3 hr and 30 min, 5) 14 hr.

by the irradiation at 365 nm is also explained by the photosolvation

$$[Co(CN)_6]^{3-} + CH_3CN \text{ (or DMF)} \xrightarrow{h\nu} [Co(CN)_5(CH_3CN)(\text{or DMF})]^{2-} + CN^- \quad (2)$$

The quantum yield of the reaction in both solvents is 0.28. In DMF, O_2 had no effect on the quantum yield.

In pyridine solution (Fig. 5), the situation is greatly different from that in the above solvents; a fluorescent compound is formed by the irradiation at 365 nm. At the beginning, the fluorescence cannot be seen, but after about 30 minutes from the beginning of irradiation, the blue fluorescence becomes visible and the intensity increases with time. After about two hours, the intensity reaches a maximum. From this stage, however, the isosbestic points gradually disappear. The fluorescence and its excitation spectrum are given in Fig. 6. The absorption spectrum of the photoproduct shows a peak at 352 nm when

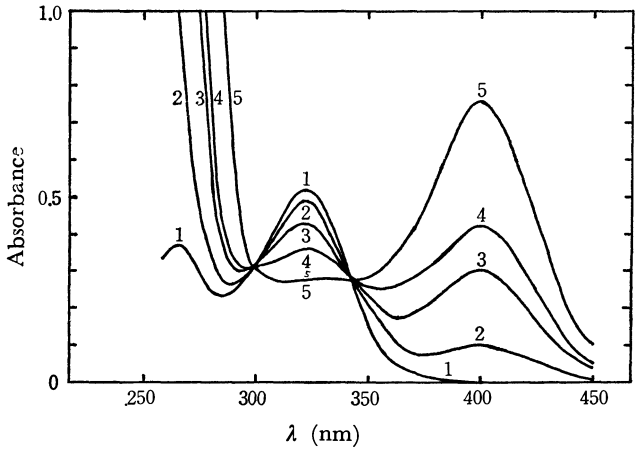

Fig. 4. Spectral change of $[Co(CN)_6]^{3-}$ in the aerated DMF solution upon irradiation at 365 nm ([complex] 2.746×10^{-3} M, 25 °C). Time of irradiation, 1) 0, 2) 10 min, 3) 40 min, 4) 1 hr, 5) 6 hr and 20 min.

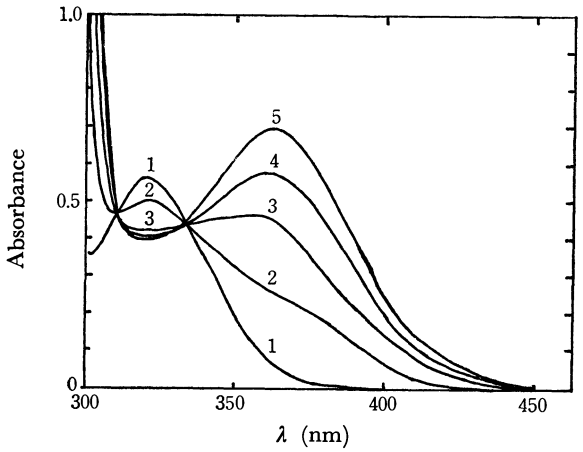

Fig. 5. Spectral change of $[Co(CN)_6]^{3-}$ in the aerated pyridine solution upon irradiation at 365 nm [(complex] 2.828×10^{-3} M, 25 °C). Time of irradiation, 1) 0, 2) 30 min, 3) 1 hr and 30 min, 4) 3 hr, 5) 6 hr.

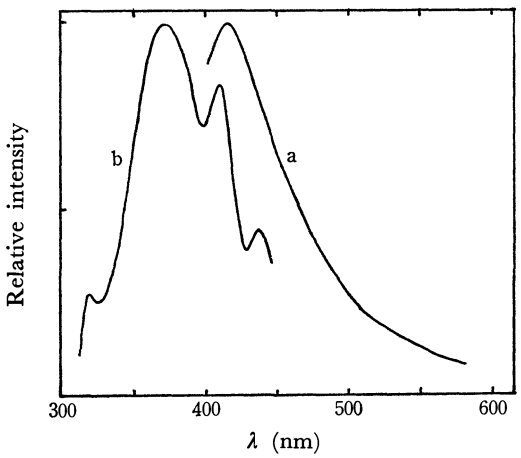

Fig. 6. Emission and excitation spectrum of the photoproduct of $[Co(CN)_6]^{3-}$ in the aerated pyridine solution produced by the irradiation at 365 nm for 6 hr at 25 °C.
a) emission spectrum, b) excitation spectrum measured at room temperature, respectively.

measured in aqueous solution. Since $K_2[Co(CN)_5py]$ which is prepared has an absorption maximum at 352 nm in water and exhibits no fluorescence at room temperature, and since the excitation spectrum of the fluorescent solution does not coincide with the absorption spectrum of $[Co(CN)_5py]^{2-}$, we can consider that the fluorescent product is not $[Co(CN)_5py]^{2-}$ but perhaps some organic compound. Therefore the total reaction is written as

$$[Co(CN)_6]^{3-} + py \xrightarrow{h\nu} [Co(CN)_5py]^{2-} + \text{fluorescent compound} \quad (3)$$

The deaerated solution causes the same reaction also and there is no difference in the quantum yield. Interestingly, the preliminary experiments show that the benzonitrile solution of $[Co(CN)_6]^{3-}$ gives rise to the fluorescent compound also (in this case the isosbestic points cannot be seen from the initial stage), whereas the acetonitrile solution does not give any product other than $[Co(CN)_5(CH_3CN)]^{2-}$. It is therefore reasonable to consider that the aromatic ligand is required in order to form the fluorescent compound. A reaction analogous to Eq. (3) is found in the case of $[Cr(CN)_6]^{3-}$ in the aerated pyridine.[21] These types of reaction involving the formation of the fluorescent compound have not been known till now and though at this stage we have not been able to determine the structure of the fluorescent compound, we will report all the features of this interesting reaction in the near future.

The quantum yields obtained in several organic solvents are also summarized in Table 1. It can be seen from this Table that the quantum yields are almost the same in our experimental conditions except those in chloroform and ethylenediamine where no reaction occurred. Thus, in these coordinative solvents, the rate-determining step may be regarded as the elimination process of CN^-.

Sensitization Experiments. The donors used are pyrazine, $Rh(acac)_3$, triphenylamine, Michler's ketone,

and fluoranthene, and the concentration of $[Co(CN)_6]^{3-}$ varies from 1×10^{-3} M to 1×10^{-2} M. Higher concentrations than this cannot be obtained because of the solubility limitation. It is found that in both the cases of using as donors the first three sensitizers irradiated at 313 nm and the latter two sensitizers irradiated at 365 nm, no sensitized photosolvation reactions in ethanol occur.

The authors are grateful to Professors C. Sato and K. Uchida for helpful discussions. This work was partly supported by the scientific research fund from the Ministry of Education.

References

1) V. Balzani and V. Carassiti, "Photochemistry of Coordination Compounds," Academic Press, London (1970).
2) P. D. Fleischauer, A. W. Adamson, and G. Sartori, *Progr. Inorg. Chem.*, **17**, 1 (1972).
3) P. D. Fleischauer and P. Fleischauer, *Chem. Rev.*, **70**, 199 (1970).
4) H. F. Wasgestian, *J. Phys. Chem.*, **76**, 1947 (1972).
5) N. Sabbatini, M. A. Scandola, and V. Carassiti, *ibid.*, **77**, 1307 (1973).
6) N. Sabbatini, M. A. Scandola, and V. Balzani, *ibid.*, **78**, 541 (1974).
7) M. Wrighton and J. Markham, *ibid.*, **77**, 3042 (1973).
8) F. Bolletta, M. Maestri, L. Moggi, and V. Balzani, *ibid.*, **78**, 1374 (1974).
9) L. Moggi, F. Bolletta, V. Balzani, and F. Scandola, *J. Inorg. Nucl. Chem.*, **28**, 2589 (1966).
10) M. Mingardi and G. B. Porter, *J. Chem. Phys.*, **44**, 4354 (1966).
11) J. J. Alexander and H. B. Gray, *J. Amer. Chem. Soc.*, **90**, 4260 (1968).
12) R. Barca, J. Ellis, M. Tsao, and W. K. Wilmart, *Inorg. Chem.*, **6**, 243 (1967).
13) H. Lund and J. Bjerrum, *Ber.*, **64**, 210 (1931).
14) K. Burger, F. Gaizer, E. Papp-Molnâr, and Tran Thi Binh, *J. Inorg. Nucl. Chem.*, **36**, 863 (1974).
15) S. L. Murov, "Handbook of Photochemistry," Marcel Dekker, New York (1973).
16) J. G. Calvert and J. N. Pitts, Jr., "Photochemistry," John Wiley and Sons, New York (1967).
17) C. G. Hatchard and C. A. Parker, *Proc. Roy. Soc., Ser. A*, **235**, 518 (1956).
18) H. B. Gray and N. A. Beach, *J. Amer. Chem. Soc.*, **85**, 2922 (1963).
19) J. J. Alexander and H. B. Gray, *Coor. Chem. Rev.*, **2**, 29 (1967).
20) I. W. Stolz, G. R. Dobson, and R. K. Sheline, *Inorg. Chem.*, **2**, 323 (1963).
21) In the deaerated pyridine solution of $[Cr(CN)_6]^{3-}$, the irradiation at 365 nm causes predominantly the photosolvation. A little formation of the fluorescent compound can be seen also. It is clear that O_2 plays an important role in this system.

Apparent Molal Volumes of *n*-Alkylammonium Chlorides and Sodium *n*-Alkanecarboxylates in Dilute Aqueous Solutions

Masao SAKURAI, Tsuyoshi KOMATSU, and Tsurutaro NAKAGAWA

Department of Polymer Science, Faculty of Science, Hokkaido University, Sapporo 060

(Received June 2, 1975)

The densities of dilute aqueous solutions of two homologous organic salts, RNH_3Cl and RCOONa, where R varies from H to *n*-octyl, have been measured at 5, 25, and 45 °C using a buoyancy technique. The apparent molal volumes, ϕ_v, of the salts and the limiting partial molal volumes, $\bar{V}°$, of the individual ions have been evaluated. The contributions of a methylene group to the partial molal volume, $\bar{V}°(CH_2)$, as estimated from the $\bar{V}°$ data for longer-chain salts, are nearly the same for both series: approximately 15.3, 15.9, and 16.5 ml/mol at 5, 25, and 45 °C respectively. Compared to these values, on the other hand, the $\bar{V}°(CH_2)$ estimated for shorter-chain RNH_3Cl is larger and that for shorter-chain RCOONa is smaller. The second derivative of the $\bar{V}°$ with respect to the temperature, $\partial^2\bar{V}°/\partial T^2$, which is often regarded as a useful measure of structural effects, is almost independent of the chain length for longer-chain homologues. The concentration dependence of ϕ_v does not always vary in a regular manner with the chain length. The present results suggest that the volumetric behavior of aqueous organic electrolyte solutions is more complicated than has previously been believed.

A careful examination of the volumetric properties of aqueous solutions can provide useful information about the nature of solute–water and solute–solute interactions. Although the partial molal volumes of simple electrolytes and alkylammonium halides have been extensively investigated,[1] little attention has been paid to other organic salts.

It is known that the hydrogen-bonded structure of water is enhanced by the introduction of a nonpolar solute molecule. Such a solute–water interaction is often called "iceberg formation,"[2] "hydrophobic hydration,"[3] or "hydration of a second kind."[4] The nature of this interaction is, however, not yet clearly understood. Furthermore, little is known about the contributions of polar groups to the structural effect. Previously we reported that the effects of NH_3^+ and COO^- groups on the hydrophobic hydration are quite different from one another.[5,6] The purpose of this paper is to supplement the earlier study[5] by presenting data on the apparent molal volumes of the organic salts recently measured in our laboratory.

Experimental

The *n*-alkylammonium chlorides, $H(CH_2)_nNH_3Cl$, and sodium *n*-alkanecarboxylates, $H(CH_2)_nCOONa$, were prepared by the neutralization of the corresponding amines and carboxylic acids with hydrochloric acid and sodium hydroxide respectively. The salts were recrystallized twice from ethanol for shorter-chain homologues and from ethanol–benzene mixtures for longer-chain salts. Each sample was then dried under vacuum at room temperature. The water used in all the measurements was deionized and further distilled using a quartz still.

The float densitometer (with a precision of 2 ppm) and the experimental procedure were previously described.[5]

The apparent molal volume, ϕ_v, was calculated by means of this equation:

$$\phi_v = \frac{1000(d_0-d)}{mdd_0} + \frac{M}{d} \qquad (1)$$

where d and d_0 are the densities of the solutions and the water respectively, M is the molecular weight of the salts, and m is the molality.

Results and Discussion

The limiting partial molal volumes, $\bar{V}°(=\phi_v^\circ)$, were obtained from this equation:

$$\phi_v = \phi_v^\circ + S_v\sqrt{c} + b_v c \qquad (2)$$

where S_v is the Debye-Hückel limiting slope, b_v is a deviation constant, and c is the molarity calculated from the observed density. The S_v values for the 1–1 electrolyte at 5, 25, and 45 °C are 1.529, 1.868, and 2.234 respectively.[7]

A few typical examples of the plots of $\phi_v - S_v\sqrt{c}$ *vs.* c are shown in Fig. 1. Good linearities were obtained over the concentration range studied, except for the octylammonium and octanecarboxylate salts (Figs. 5 and 6), which will be discussed later. The $\bar{V}°$ values estimated from these figures are summarized in Table

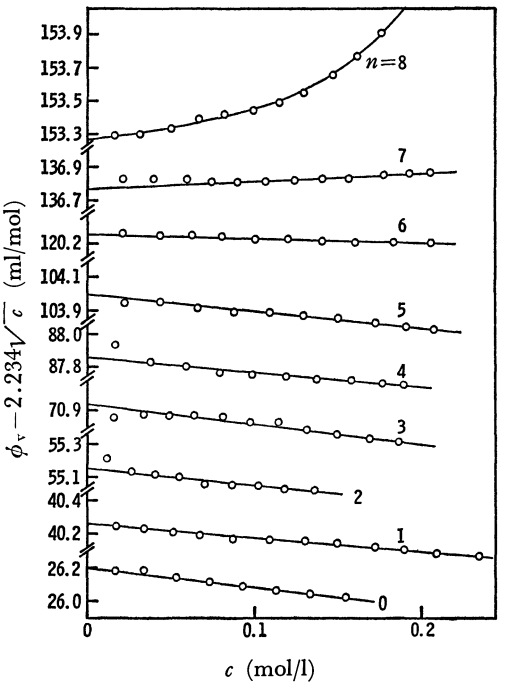

Fig. 1. Apparent molal volumes of sodium *n*-alkanecarboxylates, $H(CH_2)_nCOONa$, in water at 45 °C.

Table 1. Values of $\bar{V}°$ and b_v at 5, 25, and 45 °C

n	$\bar{V}°$ (ml/mol)			b_v (1 ml/mol²)		
	5 °C	25 °C	45 °C	5 °C	25 °C	45 °C
			$H(CH_2)_nNH_3Cl$			
0	34.51[a]	35.78[a]	36.03[a]	0.4[a]	−0.5[a]	−1.0[a]
1	52.52	53.93	54.39	0.04	−0.59	−0.89
2	70.13[a]	71.23[a]	71.86[a]	−0.7[a]	−0.8[a]	−1.3[a]
3	85.99	87.33	88.14	−1.24	−1.30	−1.56
4	101.69	103.36	104.60	−1.84	−1.79	−1.83
6	132.55[a]	135.26[a]	137.50[a]	−3.1[a]	−2.8[a]	−2.3[a]
7	147.72	151.02	153.86	−3.06	−2.33	−1.55
8	163.04	166.93	170.34	−3.91	−2.7	−1.4
			$H(CH_2)_nCOONa$			
0	22.53[a]	25.15[a]	26.20[a]	0.6[a]	0.0[a]	−1.1[a]
1	37.03	39.31[a]	40.26	0.72	0.0[a]	−0.80
2	51.19[a]	53.71[a]	55.15[a]	0.8[a]	0.0[a]	−1.0[a]
3	66.42	69.32[a]	70.93	0.48	−0.2[a]	−1.13
4	82.16	85.69	87.86	0.09	−0.81	−0.88
5	97.45	101.36	103.99	−0.28	−0.77	−0.96
6	112.59	117.05	120.25	−0.57	−0.57	−0.23
7	127.85	133.00	136.76	−0.37	−0.46	0.54
8	143.01	148.73	153.26	1.3	0.14	1.92

a) Ref. 5.

1. We could not obtain reasonable ϕ_v data for pentylammonium chloride; the value obtained by us was in disagreement with that calculated from the data of pentylammonium bromide[8] at 25 °C, and, furthermore, if the value was used in the calculation of $\bar{V}°(CH_2)$ described below, Fig. 2a gave an anomalous maximum and minimum. It was also found that our earlier ϕ_v values[5] for butane-, pentane-, and hexanecarboxylate salts were too small compared to the present results.

Partial Molal Volume of a Methylene Group. The $\bar{V}°$ increment per methylene group, $\bar{V}°(CH_2)$, was calculated as:

$$\bar{V}°(CH_2) = \frac{\bar{V}°(n_i) - \bar{V}°(n_j)}{n_i - n_j} \quad (3)$$

where n_i and n_j are the number of methylene groups in the homologous pairs considered. Figure 2 shows the $\bar{V}°(CH_2)$ as a function of $(n_i+n_j)/2$. It appears to converge toward a common $\bar{V}°(CH_2)$ value as the chain length increases; approximately 15.3, 15.9, and 16.5 ml/mol at 5, 25, and 45 °C respectively. These values are in good agreement with our previous results obtained with the *n*-alcohol series: 15.5, 15.9, and 16.4 ml/mol at the above temperatures.[9]* These values represent the limiting partial molal volumes of the methylene group free from the influences of the polar groups.

With shorter-chain homologues, on the contrary, deviations from the common $\bar{V}°(CH_2)$ value are apparent: a positive deviation was found for alkylammonium and a negative deviation for alkanecarboxylate salts. It seems likely that the deviations can be ascribed primarily to the influences of the polar groups on the hydrophobic hydration of the methylene group. This explanation may be supported by the fact that the $\bar{V}°$ of branched isomers of butylammonium and butanecarboxylate salts, in which polar groups exist very

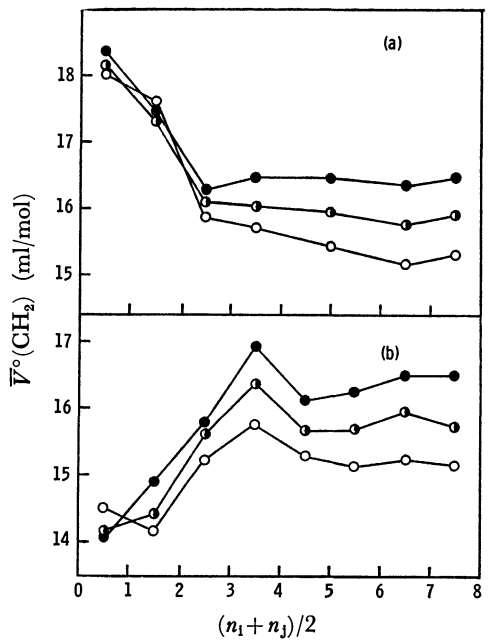

Fig. 2. Partial molal volume of a methylene group calculated from the data of *n*-alkylammonium chlorides (a) and sodium *n*-alkanecarboxylates (b).
○: 5 °C, ◑: 25 °C, ●: 45 °C.

* Misleading errata are, unfortunately, present in Ref. 9. Readers interested in this paper are kindly asked to request a corrected copy from the authors.

near to the CH_2 groups, can be well predicted on the basis of the additivity of the $\bar{V}°(CH_2)$ values.[6] The good agreement between predicted and experimental values suggests that the distance between the nonpolar part and the polar group in a solute molecule is a significant factor in determining the volumetric behavior of the organic salts. The effects of polar groups on the hydrophobic hydration have been discussed by Krishnan and Friedman[10] on the basis of their studies of the solvation enthalpies of various solutes.

Particularly to be noted in Fig. 2a is the fact that the $\bar{V}°(CH_2)$ estimated from the $\bar{V}°$ data of $MeNH_3Cl$ and $EtNH_3Cl$ at 5 °C is larger than that estimated at 25 or 45 °C. A similar phenomenon was observed with the $\bar{V}°(CH_2)$ estimated from the data of HCOONa and MeCOONa (Fig. 2b). The former is closely related to the negative expansibility of the *tert*-butylammonium ion.[6] Quite similar behavior has been accounted for[6] in the case of the negative expansibilities of *tert*-butanol[11] and the methylene group estimated from methanol and ethanol.[9] These results suggest that the negative expansibility is mainly attributable to the influence of the polar group on the hydrophobic hydration; further details have been described in a previous paper.[6]

Temperature Dependence of Partial Molal Volume. For the study of ion–water interactions, it is necessary to divide the $\bar{V}°$ values of salts into those of ions. Using $\bar{V}°(H^+) = -5.1$, -5.4, and -5.8 ml/mol at 5, 25, and 45 °C respectively,[1] and also using the $\bar{V}°$ data for HCl[12] and NaCl,[13] we calculated the ionic partial molal volumes of the organic ions under consideration.

Since the structural effect is considered to show characteristic temperature behavior, it is very useful to examine the partial molal expansibility, $\partial\bar{V}°/\partial T$, and especially its temperature dependence, $\partial^2\bar{V}°/\partial T^2$.[5,9,14-16] Figure 3 shows the $\partial\bar{V}°/\partial T$ values at 15 and 35 °C as a function of the chain length. For both the homologous ions, the expansibilities seem to increase linearly with the increase in chain length when $n>3$ or 4. Therefore, it appears that the ionic

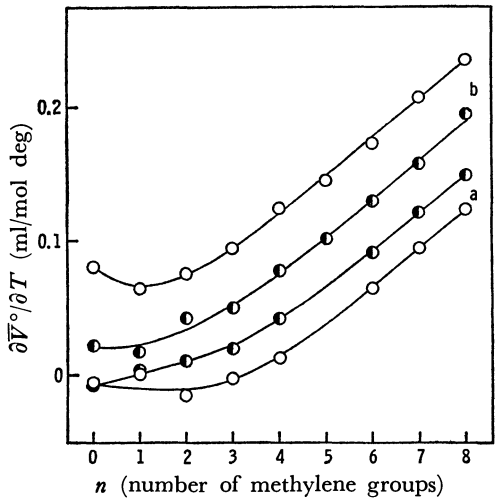

Fig. 3. Partial molal expansibilities of *n*-alkylammonium ions (a) and *n*-alkanecarboxylate ions (b). ○: 15°C, ◐: 35 °C.

hydration caused by NH_3^+ or COO^- ions affects the hydrophobic hydration up to the β- or γ-CH_2 groups. This is consistent with the results of the chain-length dependence of $\bar{V}°(CH_2)$ shown in Fig. 2.

On the basis of the thermodynamic relation, $\partial(\bar{C}_p°/\partial P)_T = -T(\partial^2\bar{V}°/\partial T^2)_p$, Hepler[14] proposed that structure-making solutes are accompanied by positive $\partial^2\bar{V}°/\partial T^2$ values, and structure-breaking solutes, by negative values. His proposal has been supported by the experimental results with tetraalkylammonium halides[15] and various nonelectrolytes.[16] Recently we have reported that, in the case of the homologous *n*-alcohol series, the $\partial^2\bar{V}°/\partial T^2$ values increase linearly with the chain length;[9] this may imply that the hydrophobic hydration becomes more significant with the increase in the chain length. It is apparent from Fig. 4 that, for the alkylammonium and alkanecarboxylate salts, on the other hand, the $\partial^2\bar{V}°/\partial T^2$ values are almost independent of the chain length, with the exception of the shorter-chain homologues. This fact may suggest either that the saturation of the hydrophobic hydration takes place with an increase in the chain length,[17] or that the $\partial^2\bar{V}°/\partial T^2$ value is governed primarily by the influence of the polar group on the hydrophobic hydration. At present, the second interpretation seems to us more likely, although the molecular aspect of the effect of the polar group is less understood. As was mentioned in the preceding section and in a previous paper,[6] we consider that the anomalous temperature behavior of the nonpolar groups, especially that of the *tert*-butyl group, which has been believed to be evidence of the hydrophobic hydration, can be mainly ascribed to the effect of the polar group.

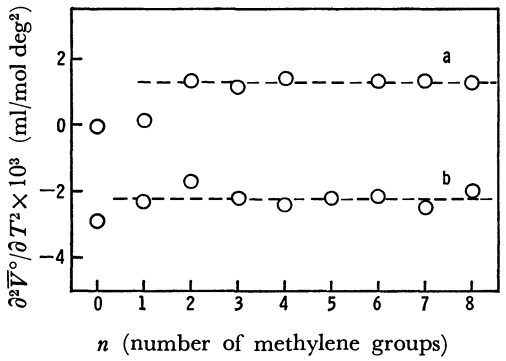

Fig. 4. The $\partial^2\bar{V}°/\partial T^2$ values of *n*-alkylammonium ions (a) and *n*-alkanecarboxylate ions (b).

It is interesting that the $\partial^2\bar{V}°/\partial T^2$ values for RNH_3^+ are positive, while those for $RCOO^-$ are negative. Based on the classification of the structural effect of solutes proposed by Hepler,[14] it may be concluded that the alkylammonium ion is a structure-maker, and the alkanecarboxylate ion, a breaker. In this connection we should note another classification of the solutes presented recently by Tamaki *et al.*[18] on the basis of viscosity measurements; the carboxylate ion is an "electrostrictive structure maker," while the ammonium ion is a "structure breaker." The apparent contradiction of the two classifications men-

tioned above may not be surprising, because it is known that the features of the structural effect vary from property to property.

Concentration Dependence of Apparent Molal Volume. We can obtain information on solute-solute interactions from a careful examination of the concentration dependence of the apparent molal volume. The b_v value in Eq. (2) reflects the solute–solute interactions other than the Coulombic force expected from the Debye-Hückel theory. A number of investigators have discussed the b_v values,[19] but, in our opinion, there still appears to be no satisfactory explanation. For the most of the alkylammonium salts,[8,20-23] the b_v values have been reported to be more or less negative; this is also the case in our study, as can be seen from Table 1. It has been known that the concentration dependence of the apparent molal volume, $\partial\phi_v/\partial m$, is negative for hydrophobic nonelectrolytes, such as alcohols[9,24] or amines,[24] and positive for hydrophilic solutes, such as glycol or urea.[16] Furthermore, it has been known that the b_v or $\partial\phi_v/\partial m$ value becomes more negative as the alkyl-chain length increases.[5,8,9,20,21] On the basis of these experimental results, the negative b_v value has been interpreted in terms of the overlap of the hydrophobic hydration accompanying the increase in concentration.

At present, however, there are two contradictory explanations for the overlapping effect: (1) the overlap results in a more efficient hydrophobic hydration because of co-operative stabilization,[5,25] and (2) the total increase in the hydrophobic hydration caused by the two solutes is less than twice that caused by the first solute alone.[8,9] The discrepancy in the above two explanations may be related in part to the model used for the explanation of the volume change associated with the mixing of water and organic solutes. Many authors believe that the hydrophobic hydration is accompanied by a net volume contraction.[8] On the other hand, some workers[9,26] have attributed the negative excess volume of mixing observed in aqueous systems to the ability of the small water molecules to fill in the free space between larger solute molecules. They have, therefore, concluded that the hydrophobic hydration results in an increase in the volume as a result of the increase in the bulky icelike structure of water.

In Table 1 we can find some interesting features of the variation of the b_v values with the solute species, with the chain length, and with the temperature. For both the homologous series, the b_v values decrease with the increase in the chain length. However, with longer-chain members, the opposite order was observed, especially in the cases of alkanecarboxylate salts and at higher temperatures. This unexpected trend for the salts with large alkyl residues has been also reported by Desnoyers *et al.*,[27,28] who proposed extra weak interactions between the solutes other than the hydrophobic hydration. Lindenbaum[29] pointed out that the positive b_v values for sodium carboxylates signify the structure-breaking effect of the salts and are, therefore, incompatible with the thermochemical results. Recently we reported that the b_v values are almost independent of the chain branching of alkyl residues,[6] although the chain branching causes some changes in the nature of the hydration layers, as can be expected from the $\bar{V}^\circ$ behavior. Considering these experimental results and the obscurity concerning the effect of the hydrophobic hydration on the volumetric behavior mentioned above, we cannot offer a plausible explanation of the concentration dependence of the apparent molal volume. Before we can do so it will be necessary to examine the b_v values as functions of various solute species, solvents, and temperatures.

Figures 5 and 6 show the concentration dependence of ϕ_v for the octylammonium and octanecarboxylate salts at 5, 25, and 45 °C. We can see upward deviations from the linearity of the $\phi_v - S_v\sqrt{c}$ *vs.* c plot. This is analogous to the sharp increase in ϕ_v at critical micelle concentration(CMC) in surfactant solutions.[28,30,31] Although the micellization is not sharp for the salts under consideration, the CMC seems to be about 0.15~0.2 mol/l for both the salts; this is in agreement with the literature value.[32] It should be

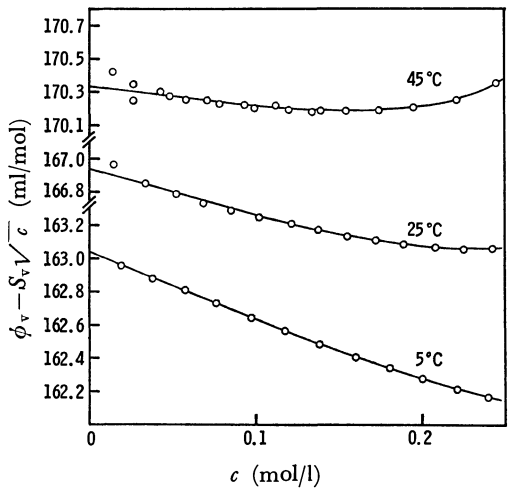

Fig. 5. Apparent molal volumes of *n*-octylammonium chloride.

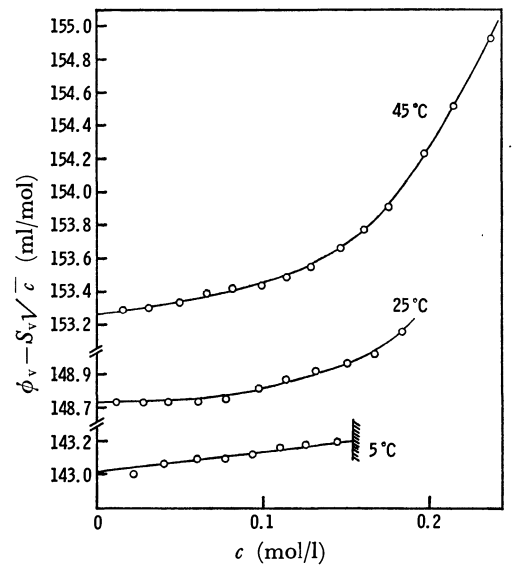

Fig. 6. Apparent molal volumes of sodium *n*-octanecarboxylate.

noted that the deviations are more remarkable at higher temperatures, whereas the CMC of typical surfactants goes through a minimum at room temperature.[28] The large increase in ϕ_v may be interpreted mainly in terms of the increase in free space associated with the micellization.[28,31]

We would like to thank Mr. Toshio Nakajima and Mr. Shigeharu Harada for their helpful discussions. The present work has been supported in part by a Grant for Scientific Research from the Ministry of Education.

References

1) F. J. Millero, "Water and Aqueous Solutions," ed. by R. A. Horne, Wiley-Interscience, New York, N. Y. (1971), Chapter 13.
2) H. S. Frank and M. W. Evans, *J. Chem. Phys.*, **13**, 507 (1945).
3) F. Franks, *Ann. New York Acad. Sci.*, **125**, 277 (1965).
4) E. Wicke, *Angew. Chem., Int. Ed.*, **5**, 106 (1966).
5) M. Sakurai, This Bulletin, **46**, 1596 (1973).
6) M. Sakurai, T. Komatsu, and T. Nakagawa, *J. Solution Chem.*, **4**, 511 (1975).
7) O. Redlich and D. M. Meyer, *Chem. Rev.*, **64**, 221 (1964).
8) J. E. Desnoyers and M. Arel, *Can. J. Chem.*, **45**, 359 (1967).
9) T. Nakajima, T. Komatsu, and T. Nakagawa, This Bulletin, **48**, 783 (1975).
10) C. V. Krishnan and H. L. Friedman, *J. Solution Chem.*, **2**, 37 (1973).
11) F. Franks and H. T. Smith, *Trans. Faraday Soc.*, **64**, 2962 (1968).
12) F. J. Millero, E. V. Hoff, and L. Kahn, *J. Solution Chem.*, **1**, 309 (1972).
13) F. J. Millero, *J. Phys. Chem.*, **74**, 356 (1970).
14) L. G. Hepler, *Can. J. Chem.*, **47**, 4613 (1969).
15) F. J. Millero, *J. Chem. Eng. Data*, **15**, 562 (1970).
16) J. L. Neal and D. A. I. Goring, *J. Phys. Chem.*, **74**, 658 (1970).
17) C. V. Krishnan and H. L. Friedman, *ibid.*, **73**, 1572 (1969).
18) K. Tamaki, Y. Ohara, H. Kurachi, M. Akiyama, and H. Odaki, This Bulletin, **47**, 384 (1974).
19) F. J. Millero, *Chem. Rev.*, **71**, 147 (1971).
20) R. E. Verrall and B. E. Conway, *J. Phys. Chem.*, **70**, 3961 (1966).
21) G. Perron and J. E. Desnoyers, *J. Chem. Eng. Data*, **17**, 136 (1972).
22) P. -A. Leduc, J. L. Fortier, and J. E. Desnoyers, *J. Phys. Chem.*, **78**, 1217 (1974).
23) S. Cabani, G. Conti, and L. Lepori, *ibid.*, **76**, 1343 (1972).
24) S. Cabani, G. Conti, and L. Lepori, *ibid.*, **78**, 1030 (1974).
25) F. Franks and H. T. Smith, *Trans. Faraday Soc.*, **63**, 2586 (1967).
26) L. Bøje and A. Hvidt, *J. Chem. Thermodyn.*, **3**, 663 (1971); *Biopolymers*, **11**, 2357 (1972).
27) P. -A. Leduc and J. E. Desnoyers, *Can. J. Chem.*, **51**, 2993 (1973).
28) G. M. Musbally, G. Perron, and J. E. Desnoyers, *J. Colloid Interface Sci.*, **48**, 494 (1974).
29) S. Lindenbaum, *J. Chem. Thermodyn.*, **3**, 625 (1971).
30) F. Franks, M. J. Quickenden, J. R. Ravenhill, and H. T. Smith, *J. Phys. Chem.*, **72**, 2668 (1968).
31) S. Harada, T. Nakajima, T. Komatsu, and T. Nakagawa, *Chem. Lett.*, **1975**, 725.
32) "Handbook of Surfactants," ed. by E. Takahashi, Y. Namba, M. Koike, and M. Kobayashi, Kogakutosho, Tokyo (1972).

Solution Properties of Phycocyanin. III. Studies of the Sedimentation Equilibrium of Phycocyanin*

Haruo MIZUNO, Takahide SAITO, and Naomichi ISO

Department of Food Science and Technology, Tokyo University of Fisheries, Konan, Minato-ku, Tokyo 108

(Received June 6, 1975)

The dissociation-association behavior of phycocyanin has been studied by sedimentation-equilibrium measurements under various pH and ionic-strength conditions. The weight-average molecular weight of phycocyanin changed according to the changes in concentration of the solute. From the concentration dependence of the molecular weight, it has been claimed that the dissociation-association equilibrium system of phycocyanin is trimer⇌monomer at pH 6.8 in the relatively low concentration region and hexamer⇌monomer at pH 5.4. However, the coexistence of the trimer⇌monomer and hexamer⇌monomer systems is in evidence in the concentration region larger than 0.06 g/dl. This dissociation-association behavior of phycocyanin is supported by the experimental results obtained from sedimentation-transportation[1] and osmotic-pressure measurements.[5]

In the course of our continuing study of the solution properties of phycocyanin, it was found, from an analysis of the sedimentation velocity data, that the dissociation-association reacting state for phycocyanin was a trimer⇌monomer system at pH 6.8 and a hexamer⇌monomer system at pH 5.4, and that the dissociation constants for the reacting systems were $0.13\sim0.15\times10^{-4}$ $(g/dl)^2$ for a trimer⇌monomer system at pH 6.8 and in the ionic-strength(μ) range of 0.1∼0.2, and $0.1\sim0.5\times10^{-13}$ $(g/dl)^5$ for a hexamer⇌monomer system at pH 5.4 and at an ionic strength of 0.1∼0.2. From the results, it was assumed that the predominant species of phycocyanin was a trimer at pH 6.8 and a hexamer at pH 5.4.[1] Since the dissociation constants described above were evaluated from the concentration dependence of the sedimentation coefficients, these constants should not considered to be thermodynamically the equillibrium values. Therefore, it is desirable to investigate the dissociation-association equilibrium of phycocyanin on the basis of sedimentation-equilibrium experiments.

The purpose of the work to be reported here is to determine the dissociation constant of phycocyanin under various conditions of pH and ionic strength by sedimentation-equilibrium measurements and to obtain information about the dissociation-association state of phycocyanin.

Experimental

Materials and Buffers. The crystalline phycocyanin used in this study was obtained from red algae *Porphyra tenera* by repeated precipitations with ammonium sulfate. The details of the purification of the protein were presented in an earlier paper.[1] Phosphate(pH 6.8, μ 0.1 and 0.2) and acetate (pH 5.4, μ 0.1 and 0.2) buffer solutions were used in this study.

Sedimentation-equilibrium Measurements. The sedimentation-equilibrium measurements were carried out using a magnetically suspended equilibrium-type ultracentrifuge with an interference optical system; a double sectorial cell was also used. The apparatus used here has been described in detail elsewhere.[2]** All the measurements were made at a given speed for approximately 24 hours so as to ensure that an equilibrium was established in an about 3-mm liquid column. The rotor speeds were set at approximately 6000∼9000 rpm, and the temperature was maintained at 25.00± 0.01 °C through all the measurements.

The apparent weight-average molecular weight, M_w^{app}, and the apparent z-average molecular weight, M_z^{app}, of phycocyanin were calculated from Eq. (1) and Eq. (2).

$$M_w^{app} = \frac{2RT}{(1-\bar{v}\rho)\omega^2}\frac{1}{(r_b^2-r_a^2)}\frac{\Delta c}{c_0} \quad (1)$$

$$M_z^{app} = \frac{RT}{(1-\bar{v}\rho)w^2}\frac{(dc/dr)_b-(dc/dr)_a}{\Delta c} \quad (2)$$

In these expressions, $\bar{v}$ is the partial specific volume of the solute; ρ, the density of the solvent; ω, the angular velocity of the rotor; r, the radial position from the center of rotation in the ultracentrifuge cell, and r_a and r_b, the position of the meniscus and the cell bottom respectively. The concentration difference, Δc, between r_a and r_b, was calculated by the use of this formula:

$$\Delta c = (\Delta N)\lambda/(dn/dc)L$$

where ΔN is the number of fringes counted from the standard fringe along the direction of the ultracentrifugal field; λ, the wavelength of light (546 nm), dn/dc, the refractive-index increment, and L, the thickness of the cell (12 mm). The refractive index increment of the protein was obtained from the schlieren pattern of a protein solution of a known concentration; the value of 0.18 ml/g was obtained at 546 nm. This value for dn/dc was used throughout this study irrespective of the aggregation state of phycocyanin. For the partial specific volume, $\bar{v}$, of phycocyanin, the literature value[3] of 0.744 ml/g was used in all the measurements. The solvent density, ρ, was determined with a pycnometer approximately 2 ml in volume.

Determination of the Dissociation Constant. The determination of the dissociation constants for each dissociation-association system with a computational method was performed by using the sedimentation-equilibrium data. The computational method used in this study is essentially an extension of the theory for a monomer-dimer self-association system published by Williams.[4] In this procedure, it is assumed that all of the systems considered here are ideal solutions. The thermodynamic ideality of phycocyanin was confirmed by the experimental results from the osmotic-pressure measurements.[5]

For the i-mer⇌monomer equilibrium system, the weight-average molecular weight, M_w, is expressed by the following formula;

$$M_w = \frac{c_1M_1+c_iM_i}{c} \quad (3)$$

* Some of the experimental results in this paper were presented at the 23rd Annual Meeting of The Socity of Polymer Science, Japan, Tokyo, June 6, 1974.

** This apparatus is in the possession of the Department of Chemistry, Tokyo Kyoiku University.

where c is the total weight concentration of the solute, c_1 and M_1 are the weight concentration and the molecular weight of the monomer, and c_i and M_i are the weight concentration and the molecular weight of i-mer respectively.

The dissociation constant for the trimer$\rightleftharpoons$monomer system, K_3, is defined as Eq. (4) by using the mass-action law;

$$K_3 = c_1^3/c_3 \tag{4}$$

$$M_3 = 3M_1$$

$$c = c_1 + c_3 \tag{5}$$

From Eqs. (3)$\sim$(4), the following expression can be derived:

$$\frac{M_1^2(M_w^{app}-M_1)}{(3M_1-M_w^{app})^3} = \left(\frac{1}{4K_3}\right)c^2 \tag{6}$$

where M_w^{app} is the apparent weight-average molecular weight at the initial concentration, c. Equation (6) may be rewritten as Eq. (7):

$$\frac{(X-1)}{(3-X)^3} = \left(\frac{1}{4K_3}\right)c^2 \tag{7}$$

where X is M_w^{app}/M_1. It is clear that the quantity, $(X-1)/(3-X)^3$, becomes zero when $c=0$. Therefore, the dissociation, constant, K_3, can be determined from the initial slope of the plot of $(X-1)/(3-X)^3$ *versus* c^2.

By a similar treatment, Eq. (8) can be derived for the hexamer$\rightleftharpoons$monomer system by the same procedure as that used for Eq. (7):

$$\frac{(X-1)}{(6-X)^6} = \left(\frac{1}{625K_6}\right)c^5 \tag{8}$$

where K_6 is the dissociation onstant.

When the apparent z-average molecular weight, M_z^{app}, is used in place of M_w^{app} in Eqs. (7) and (8), the following equations, (9) and (10), are obtained:

$$\frac{(X-1)(4-X)^2}{(3-X)^3} = \left(\frac{27}{4K_3}\right)c^2 \tag{9}$$

$$\frac{(X-1)(7-X)^5}{(6-X)^6} = \left(\frac{6^6}{5^5K_6}\right)c^5 \tag{10}$$

where X is M_z^{app}/M_1.

Results and Discussion

The apparent weight-average molecular weight and the apparent z-average molecular weight were obtained from sedimentation-equilibrium measurements performed at a number of initial concentrations of the solute. Figure 1 shows the concentration dependence of the apparent weight- or number-average molecular weight of phycocyanin and, in the inset, that dependence in the low concentration region. The lines in this figure represent the theoretical curves except for (e). The (a), (b), (c) and (d) lines were calculated by using the dissociation constant obtained from the subsequent analysis in this work. The (a) and (b) lines were computed by using the dissociation constants obtained from the weight-average and the z-average molecular weight respectively for the trimer$\rightleftharpoons$monomer system, and the (c) and (d) lines, by using those constants for the hexamer$\rightleftharpoons$monomer system. The (e) line was drawn based on the dissociation constant for the hexamer$\rightleftharpoons$monomer system which was obtained from the sedimentation coefficient.[1]

As is shown in Fig. 1, the values for the apparent weight-average molecular weight depend on the change

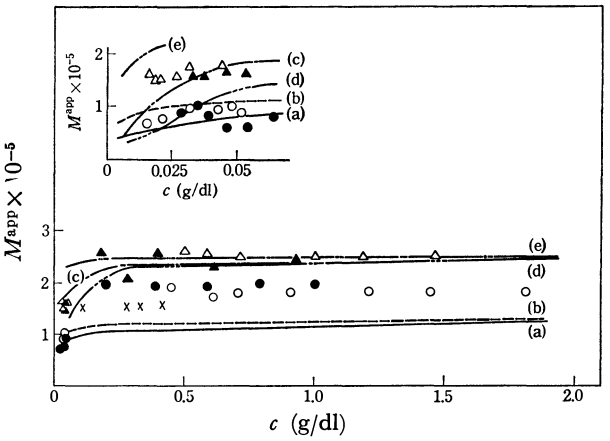

Fig. 1. Concentration dependence of apparent molecular weight of phycocyanin in various buffer solution over a wide concentration range; ○, pH 6.8 and $\mu=0.1$; ●, pH 6.8 and $\mu=0.2$; ×, pH 6.8 and $\mu=0.01$; △, pH 5.4 and $\mu=0.1$; ▲, pH 5.4 and $\mu=0.2$. Lines in this figure were obtained by using various K_3 and K_6 values; (a), $K_3=6.1\times10^{-4}$ (from M_w^{app}); (b), $K_3=1.4\times10^{-5}$ (from M_z^{app}); (c), $K_6=4.4\times10^{-10}$ (from M_w^{app}); (d), $K_6=2.4\times10^{-8}$ (from M_z^{app}); (e), $K_6=0.5\times10^{-13}$ (from s). These dissociation constants have units of $(g/dl)^2$ for K_3 and that of $(g/dl)^5$ for K_6.

in the pH of the solution. In addition, it is clear that the weight-average molecular weight in each system tends to decrease with a decrease in the concentration of the solute in the concentration region studied. The authors conclude from this evidence that phycocyanin undergoes a dissociation-association reaction in solution. The concentration dependencies of the apparent weight-average molecular weight under different pH values are independent of the ionic strength in the concentrations examined in this study. The mean values of the weight-average molecular weight were 78000 at pH 6.8 and 156000 at pH 5.4, while the values for the z-average molecular weight were 125000 at pH 6.8 and 181000 at pH 5.4.

It has been reported from the sedimentation-transportation experiment that the dissociation-association equilibrium system is trimer$\rightleftharpoons$monomer at pH 6.8 and hexamer$\rightleftharpoons$monomer at pH 5.4.[1] Therefore, these systems were assumed to be in a stable equilibrium state under each pH condition. The equilibrium constants were calculated from the experimental data by using Eqs. (7)$\sim$(10). The molecular weight of the monomeric species, M_1, is necessary for this calculation. As has been described in a previous paper[1], the phycocyanin molecule is stable in solution at pH 5.4, and the predominant species is the hexameric form under this pH condition. This conclusion receives support from the results of the osmotic-pressure measurement, which gives a value of 256000 as the number-average molecular weight of the protein.[5] It is, therefore, assumed that the molecular weight of the monomer is 42000.

Figure 2 shows the plot of the quantity, $(X-1)/(3-X)^2$, as a function of the square values of the concentration, c^2, where $X=M_w^{app}/M_1$. Since all of the

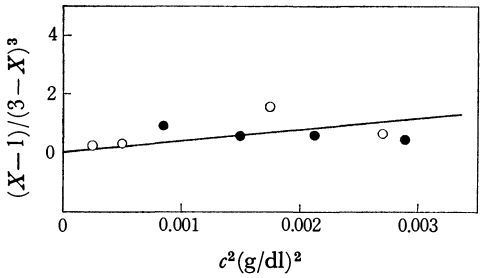

Fig. 2. Plot of $(X-1)/(3-X)^3$ with respect c^2 for phycocyanin in phosphate buffer solutions (pH 6.8); ○, $\mu=0.1$; ●, $\mu=0.2$. $X=M_w^{app}/M_1$.

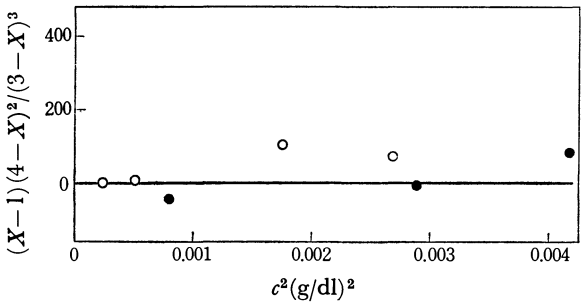

Fig. 3. Plot of $(X-1)(4-X)^2/(3-X)^3$ with respect to c^2 for phycocyanin in phosphate buffer solutions (pH 6.8); ○, $\mu=0.1$; ●, $\mu=0.2$. $X=M_z^{app}/M_1$.

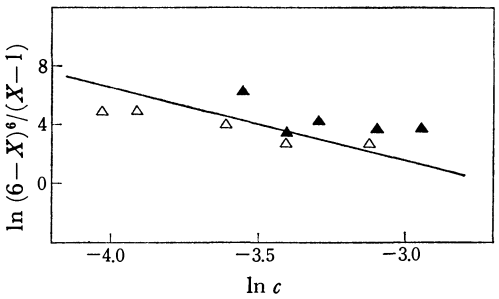

Fig. 4. Plot of $\ln(6-X)^6/(X-1)$ with respect to $\ln c$ for phycocyanin in acetate buffer solutions (pH 5.4); △, $\mu=0.1$; ▲, $\mu=0.2$. $X=M_w^{app}/M_1$.

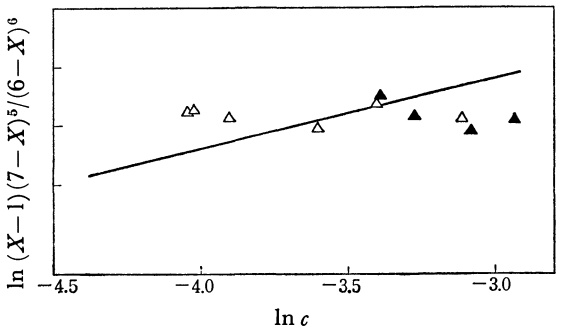

Fig. 5. Plot of $\ln(X-1)(7-X)^5/(6-X)^6$ with respect to $\ln c$ for phycocyanin in acetate buffer solutions (pH 5.4); △, $\mu=0.1$; ▲, $\mu=0.2$. $X=M_z^{app}/M_1$.

protein species in solution are expected to decompose to the monomer at an infinite dilution, the left-hand side of Eq. (7) approaches zero at an extremely low concentration. The dissociation constant, K_3, was calculated from the slope of the plot. Though there is some error in the z-average molecular weight as a result of the difficulty of making an accurate analysis of the experimental data, the dissociation constant, K_3, was calculated by using the M_z^{app} value as a trial (Fig. 3).

Figure 4 shows the plot of $\ln(6-X)^6/(X-1)$ *versus* $\ln c$. As is known from Eq. (8), the plot is a straight line with the value of slope −5. Although there are some scattering in the experimental data, the dissociation constant, K_6, was calculated from the interception of the ordinate for the straight line with the tangent value at $\ln c=0$, and was also calculated from M_z^{app} (Fig. 5).

The values for K_3 were given as 6.1×10^{-4} (g/dl)^2 from M_w^{app} and 1.4×10^{-5} (g/dl)^2 from M_z^{app}, while those for K_6 were 4.4×10^{-10} (g/dl)^5 from M_w^{app} and 2.4×10^{-8} (g/dl)^5 from M_z^{app}.

In order to ascertain the validity of the results obtained in this study, the concentration dependencies of M_w^{app} were recalculated from the K_3 and K_6 values obtained from the sedimentation-equilibrium measurement. There is another way to recalculate the concentration dependence of M_w^{app} by using the data obtained from the sedimentation-transportation method. The results obtained from these procedures are shown in Fig. 1. Although there is some difference between the numerical value for the dissociation constants obtained from the sedimentation equilibrium and those from the transportation measurements,[1] the concentration dependencies recalculated from the two procedures are essentially in accordance with the experimental results. In this figure, the molecular weights in the lower-concentration region are the weight-average values, while those at higher concentrations are the number-average values which were obtained from the osmotic-pressure experiments.[5]

As is shown in Fig. 1, the curves calculated by using the K_6 values at pH 5.4 agree with the experimental data over the whole range of concentrations. On the other hand, the curves calculated by using the K_3 values show a significant deviation from the experimental values in the concentration region larger than 0.06 g/dl. Therefore, it may be concluded from a comparison of the calculated and experimental values of M^{app} as functions of the concentration that the state of the dissociation-association equilibrium at pH 5.4 is hexamer⇌monomer over a wide concentration range. However, the equilibrium state at pH 6.8 depends on the concentration of the solute in the solution. The trimer⇌monomer system can be expected to be predominant in the concentration region less than 0.06 g/dl, and a higher-order aggregate, probably a hexamer, is formed in the concentration higher than 0.06 g/dl. It may be supposed both the trimer⇌monomer and hexamer⇌monomer systems exist in the higher-concentration region.

In the lower-concentration region, below 0.06 g/dl, the dissociation-association equilibrium is significantly shifted in one direction at both pH 6.8 and 5.4; that is, the predominant species at pH 6.8 are trimers, and those at pH 5.4, hexamers. Furthermore, the effect of the ionic strength on the equilibrium shift

in the higher-concentration region is almost negligible for the solution of pH 5.4. However, the effect of the ionic strength on the shift in the higher-concentration region is clear for the solution at pH 6.8.

The authors wish to express their gratitude to Professor Emeritus A. Kotera, of Tokyo Kyoiku University, for his interest and helpful discussion of the problem, and for permission to use the magnetically suspended equilibrium ultracentrifuge. They also wish to express their gratitude to Dr. K. Yoshizaki and Mr. K. Kanoo for their valuable assistance in the sedimentation-equilibrium measurements.

References

1) T. Saito, N. Iso, and H. Mizuno, This Bulletin, **47**, 1375 (1974).
2) Y. Goto, Y. Miyazawa, and T. Sudo, *Bull. J. S.M.E.*, **4**, 598 (1961).
3) A. Hattori, H. L. Crespi, and J. J, Katz, *Biochemistry*, **4**, 1225 (1965).
4) J. W. Williams, "Ultracentrifugation of Macromolecules," Academic Press, New York and London (1972), p. 39.
5) A. Kotera, T. Saito, N. Iso, H. Mizuno, and N. Taki, This Bulletin, **48**, 1176 (1975).

Long-range Interaction between a Hydrogen Atom and a Hydride Ion

Tokio YAMABE, Kazuyoshi TANAKA, Hiroshi UENO, and Kenichi FUKUI

Department of Hydrocarbon Chemistry, Faculty of Engineering, Kyoto University, Sakyo-ku, Kyoto 606

(Received June 20, 1975)

The long-range force between a hydrogen atom and a hydride ion has been studied by means of the second-order perturbation theory. This H–H$^-$ system has been chosen as the simplest example of a system composed of a neutral atom and an anion. The results seem to suggest that the analytical closed form of the second-order energy is desirable for any discussion of the long-range interaction between H and H$^-$ in place of the usual multipole expansion. According to the multipole expansion until the R^{-12} term, the nature of the long-range interaction operating in this system seems to be dispersive, and it seems to become inductive at a much larger R because of the existence of the leading R^{-4} term.

Generally, long-range forces among atoms and molecules are conveniently classified into two categories: the induction force and the dispersion force. The former is due to the long-range interaction energy between a neutral system and a cationic one, and the latter, to that between two neutral systems. Numerous theoretical studies have been devoted to these forces, particularly the systems composed of combinations of H$^+$, H, and He; the perturbation theory or equivalent variational methods have been used.[1] As a matter of course, the long-range interaction between a cation and an anion is Coulombic. Now, then, what kind of interaction operates between a neutral system and an anionic one? In order to clarify the nature of the interaction energy between such systems, we will try, as the first step, to investigate the long-range force between H and H$^-$ as the simplest system.

The long-range force between H and H$^-$ actually has an important role in the dissociation process of the H_2^- molecule ion into H and H$^-$ in the solar corona[2] and is referred to as considerably strong in spite of its anionic nature.[3] Theoretical investigations of the H–H$^-$ long-range force have been done only by Dalgarno and Kingston[4] and by Davison[5] using the usual multipole expansion of the second-order perturbation energy. The latter has evaluated the coefficients of the R^{-4}, R^{-6}, and R^{-8} terms in the series expansion of the inverse powers of the internuclear distance, R, between H and H$^-$ (hereafter we will briefly representthe above quantities as C_4, C_6, C_8, *etc.* and will use the atomic units for energies and distances throughout this paper). The results, however, were too poor for us to get the interaction energy by means of the multipole expansion, since the convergency of the series was bad, even in the asymptotic sense:

$$\bar{E}_2(\text{Davison}) = -\left(\frac{2.25}{R^4}+\frac{93}{R^6}+\frac{7\cdot10^3}{R^8}\right) \tag{1}$$

For instance, the values of these terms are comparable at $R=10$; hence, we need to estimate the higher-order terms at least in the region of *ca.* $R=10$.

In view of this inherent defect in the series expansion, an analytical form is desirable instead. In preceding papers,[6a–6d] we have already investigated the analytical formulae for the second-order perturbation energies with respect to the H–H$^+$, H–H, and He–He systems, neglecting exchange in the framework of the Unsöld approximation. Similarly, in this paper, we will try to obtain a closed form of the second-order perturbation energy of the interaction between H and H$^-$, both in their ground states, and afterwards, will try to show an expansion form again derived from the closed one in order to discuss the nature of the force operating in this system.

Method of Calculation

As is well known, in the framework of the Unsöld approximation,[7] neglecting the exchange for a larger R, the second-order perturbation energy caused by a perturbation, H_1, can be represented by:

$$\bar{E}_2(\text{Unsöld}) = -\frac{\langle H_1^2\rangle_{00}-\langle H_1\rangle_{00}^2}{\langle \Delta E\rangle_{\text{AV}}}, \tag{2}$$

where 0 means the eigenfunction, Φ_0, in the ground state with respect to the unperturbed Hamiltonian, H_0; $\langle \Delta E\rangle_{\text{AV}}$ is called an 'average excitation energy,' after Unsöld. In the cases of the H–H$^-$ system, neglecting the exchange, Φ_0 appears as follows:

$$\Phi_0 = \Psi_a(1)\Psi_b(2,3), \tag{3}$$

where $\Psi_a(1)$ is the 1s-function of a hydrogen atom, a, and where $\Psi_b(2,3)$ is a wavefunction of a hydride ion, b. In order to get an analytical form of $\bar{E}_2$ (Unsöld), we need a wavefunction, $\Psi_b(2,3)$, simple enough to be used for Φ_0, but also accurate enough to show the stability of H$^-$. The simplest form is one for the $1s^2\ {}^1S$ state, but it gives no stabilization of H$^-$.[8] The form we employ here is a linear combination of the product of the 1s-like functions with different orbital exponents, z and z', for different spins:

$$\Psi_b(2,3) = \frac{1}{\sqrt{2(1+s^2)}}[\Psi_b(2)\Psi_b'(3)+\Psi_b(3)\Psi_b'(2)], \tag{4}$$

where:

$$\Psi_b(i) = \frac{z^{3/2}}{\sqrt{\pi}}\exp[-zr_i], \tag{5-a}$$

and

$$\Psi_b'(j) = \frac{z'^{3/2}}{\sqrt{\pi}}\exp[-z'r_j], \tag{5-b}$$

and where:

$$s = \left(\frac{2\sqrt{zz'}}{z+z'}\right)^3. \tag{6}$$

The notations in the H–H$^-$ system are shown in Fig. 1. This wavefunction, which was first obtained by Chandrasekhar[9] and was thereafter used by Dalgarno *et al.*[3] and Fischer-Hjalmars[10] for the calculation of

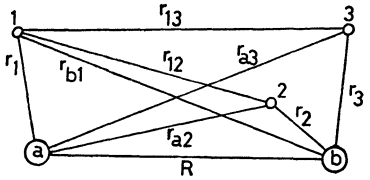

Fig. 1. Notation for distances among electrons 1, 2, and 3, and nuclei a and b in the H-H⁻ system.

the energy of H_2^-, predicts the stability of H^- when $z' \simeq z/3$; hence, we assume that this wavefunction is the correct one for H^-. Using this $\Psi_b(2,3)$, we construct an unperturbed wavefunction as follows:

$$\Phi_0 = \left(\frac{zz'}{\pi}\right)^{3/2} \cdot \frac{1}{\sqrt{2(1+s^2)}} \exp[-r_1]\{\exp[-zr_2] \times \exp[-z'r_3] + \exp[-zr_3]\exp[-z'r_2]\}. \quad (7)$$

The perturbation, H_1, between H and H^- at an internuclear distance, R, is written by:

$$H_1 = \frac{1}{R} - \frac{1}{r_{a2}} - \frac{1}{r_{a3}} - \frac{1}{r_{b1}} + \frac{1}{r_{12}} + \frac{1}{r_{13}}, \quad (8)$$

which is then rearranged into three parts:

$$H_1 = \left[\frac{1}{r_{12}} + \frac{1}{R} - \frac{1}{r_{b1}} - \frac{1}{r_{a2}}\right] + \left[\frac{1}{r_{13}} + \frac{1}{R} - \frac{1}{r_{b1}} - \frac{1}{r_{a3}}\right] - \left[\frac{1}{R} - \frac{1}{r_{b1}}\right] \equiv H_1(1,2) + H_1(1,3) - H_1(1). \quad (9)$$

It can easily be seen that the first two terms and the last term furthest to the right correspond to the interactions between H–H and that between H–H^+ respectively. Using the wavefunction in Eq. (7), $\langle H_1\rangle_{00}$ and $\langle H_1^2\rangle_{00}$ may be rewritten as:

$$\langle H_1\rangle_{00} = \langle H_1(1,2)\rangle_{00} + \langle H_1(1,3)\rangle_{00} - \langle H_1(1)\rangle_{00} = 2\langle H_1(1,2)\rangle_{00} - \langle H_1(1)\rangle_{00}, \quad (10)$$

and:

$$\langle H_1^2\rangle_{00} = \langle H_1^2(1,2)\rangle_{00} + \langle H_1^2(1,3)\rangle_{00} + \langle H_1^2(1)\rangle_{00} + 2\langle H_1(1,2)H_1(1,3)\rangle_{00} - 2\langle H_1(1,2)H_1(1)\rangle_{00} - 2\langle H_1(1,3)H_1(1)\rangle_{00} = 2\langle H_1^2(1,2)\rangle_{00} + \langle H_1^2(1)\rangle_{00} + 2\langle H_1(1,2)H_1(1,3)\rangle_{00} - 4\langle H_1(1,2)H_1(1)\rangle_{00}. \quad (11)$$

It should be noticed that only the first two terms furthest to the right in Eq. (11) contain non-exponentially decreasing terms and therefore contribute to the origin of the long-range interaction. That is, the first term, $\langle H_1^2(1,2)\rangle_{00}$, corresponds to the second-order interaction energy of H–H with the well-known R^{-6} decay, while the second term, $\langle H_1^2(1)\rangle_{00}$, corresponds to that of H–H^+ giving the first leading term of R^{-4} in the Unsöld approximation except for the factors of the 'average excitation energy.'

Using Eqs. (10) and (11), Eq. (2) can be rewritten as:

$$\bar{E}_2(\text{Unsöld}) = -\frac{1}{\langle \Delta E\rangle_{AV}}\left[-\frac{2}{R^2} + \frac{4}{R}\langle H_1(2)\rangle_{00} - \langle H_1^2(1)\rangle_{00} - 2\langle H_1^2(2)\rangle_{00} + 4\left\langle \frac{1}{r_{a2}} W(2,1)\right\rangle_{00} + 2\left\langle \frac{1}{r_{12}^2}\right\rangle_{00} + 2\langle H_1(2)H_1(3)\rangle_{00} - 2\langle H_1(2)W(1,3)\rangle_{00} - 2\langle H_1(3)W(1,2)\rangle_{00} + 2W\langle (1,2)W(1,3)\rangle_{00} - 4\langle H_1(1,2)\rangle_{00}^2 - \langle H_1(1)\rangle_{00}^2 + 4\langle H_1(1,2)\rangle_{00}\langle H_1(1)\rangle_{00}\right], \quad (12)$$

where:

$$W(1,i) = \frac{1}{r_{b1}} - \frac{1}{r_{1i}} \quad (i=2,3), \qquad W(i,1) = \frac{1}{r_{ai}} - \frac{1}{r_{1i}} \quad (i=2,3), \quad (13)$$

In order to avoid complexity arising from the presence of many terms, we will introduce some further notations. For any hermitian operator, F, the expectation value, $\langle F\rangle_{00}$, in which 0 stands for the function defined as in Eq. (7), is decomposed into three parts:

$$\langle F\rangle_{00} = \frac{1}{2(1+s^2)}[\{F|R,z,z'\} + \{F|R,z',z\} + 2s^2\{F|R,z'',z''\}], \quad (14)$$

where s is defined as in Eq. (6), where $z''=(z+z')/2$, and where:

$$\{F|R,z,z'\} = \langle \Psi_a^*(1)\Psi_b^*(2)\Psi_b'^*(3)|F|\Psi_a(1)\Psi_b(2)\Psi_b'(3)\rangle,$$
$$\{F|R,z',z\} = \langle \Psi_a^*(1)\Psi_b'^*(2)\Psi_b^*(3)|F|\Psi_a(1)\Psi_b'(2)\Psi_b(3)\rangle, \quad (15)$$

and

$$\{F|R,z'',z''\} = \langle \Psi_a^*(1)\Psi_b''^*(2)\Psi_b''^*(3)|F|\Psi_a(1)\Psi_b''(2)\Psi_b''(3)\rangle.$$

In Eq. (15), the asterisk indicates the hermitian conjugate, $\Psi_b(i)$ and $\Psi_b'(j)$ are defined by Eqs. (5-a) and (5-b), and

$$\Psi_b''(k) = \frac{z''^{3/2}}{\sqrt{\pi}} \exp[-z''r_k]. \quad (5\text{-c})$$

All the integrals used in Eq. (12) are shown in the Appendix. Thus, Eq. (12) may be evaluated exactly without resorting to a series expansion and can be given in a closed analytical form applicable to an arbitrary internuclear distance, R, and orbital exponents, z and z'.

Results and Discussion

In the calculation of $\bar{E}_2$ (Unsöld), we adopt the values of the orbital exponents following Fischer-Hjalmars[10] that is, $z=1.00$, $z'=0.30$, and hence $z''=(z+z')/2=0.65$. As to $\langle \Delta E\rangle_{AV}$, we can consider three kinds of values: 1) the sum of the first ionization potentials of H and H^-, 0.52775*, which is

* Pekeris has obtained, by concentrated numerical efforts, the ground state energy of H^- as −0.52775 (*Phys. Rev.*, **126**, 1470 (1962)). He has also thought that H^- has no more than one bound state; that is, the first ionization potential of H^- is 0.02775 to make the H+e⁻ system. Power and Somorjai have tried to prove the above fact (*ibid.*, **A5**, 2401 (1972)), but in vain (*ibid.*, **A6**, 1996 (1972)). It is very likely, however, that H^- has no more than one bound state (Ref. 2-b); hence, we assume that the first ionization potential is 0.02775.

TABLE 1. LONG-RANGE INTERACTION ENERGY ΔW BETWEEN H AND H^- IN 10^{-3} a.u.

R (a. u.)	$-E_1$	$-\bar{E}_2$ (Unsöld)[a]			$\Delta W=-E_1-\bar{E}_2$ (Unsöld)[a]			CI[b] (D)	Modified CI[c] (E)
		(A)	(B)	(C)	(A)	(B)	(C)		
4.0	5.8912	17.749	34.565	45.293	23.640	40.456	51.184	13.3	6.25
5.0	2.6218	8.4450	16.446	21.550	11.067	19.068	24.172	11.3	4.25
6.0	1.2900	4.3092	8.3919	10.996	5.5992	9.6819	12.286	9.3	2.25
7.0	0.67434	2.3220	4.5219	5.9253	2.9963	5.1962	6.5996	8.3	1.25
8.0	0.36306	1.2996	2.5309	3.3164	1.6627	2.8940	3.6795	—	—
9.0	0.19804	0.74726	1.4552	1.9069	0.94530	1.6532	2.1049	—	—
10.0	0.10863	0.43891	0.85473	1.1200	0.54754	0.96336	1.2287	—	—
11.0	0.059717	0.26288	0.51195	0.67084	0.32260	0.57167	0.73056	—	—
12.0	0.032853	0.16068	0.31292	0.41004	0.19353	0.34577	0.44289	—	—

a) $\langle\Delta E\rangle_{AV}=1.02775$, 0.52775, and 0.402775 in the cases (A), (B), and (C), respectively. b) Ref. 11. c) At $R=\infty$, $E=-1.02775$.

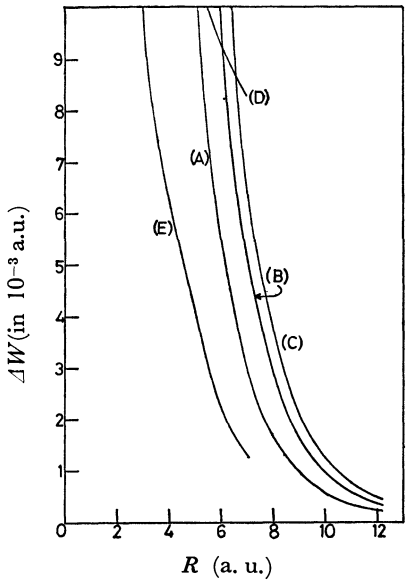

Fig. 2. Long-range interaction energy ΔW between H and H^-.

reasonable and which is usually adopted, 2) the sum of the first excitation energies, 0.40275, which gives an approximate lower bound of $\bar{E}_2$ (Unsöld), and 3) the sum of the ground state energies of H and H^-, -1.02775, which gives an approximate upper bound.[6c,6d] By substituting these values into Eq. (12), three kinds of $\bar{E}_2$ (Unsöld) values for various R values are obtained, as is shown in Table 1. The first-order perturbation energy, E_1, is equal to the expectation value, $\langle H_1\rangle_{00}$; it is also shown in Table 1 for each R.

On the other hand, Taylor and Harris have previously obtained a potential curve for the $^2\Sigma_u^+$ state of the H_2^- system using a CI method until $R=7.0$;[11] this seems to be the most reliable value at present. In Fig. 2, three kinds of total interaction energy curves, (A), (B), and (C) taken as far as the second-order between the H and H^- obtained by means of the above criterion, are compared with the results of the variational calculation done by Taylor and Harris and also with the version modified here using the exact sum of the ground state energies of H and H^-, -1.02775, as the standard of the separated system. This modified version can afford a strict lower bound of the total interaction energy.** The potential curve (A) represents almost the lower bound of the interaction energy taken up to the second-order term, and (C), almost the upper bound. The exact one would lie in the zone between (A) and (C). The result of the original variational calculation, (D), lies above the zone obtained here. However, the modified version, (E), lies below.

Now, discarding the terms attenuating exponentially with an increase in R in Eq. (12), we obtain this reduced formula:

$$\bar{E}_2(\text{Unsöld}) \simeq -\frac{1}{\langle\Delta E\rangle_{AV}}\cdot\frac{1}{2(1+s^2)}[V(R,z)+V(R,z')+2s^2V(R,z'')], \quad (16)$$

where:

$$\begin{aligned}V(R,z) &= \exp[-2R]\widetilde{Ei}[2R]\times\left\{-1+\frac{2z^4}{(1-z^2)^2}+\left(-\frac{1}{2}+\frac{z^4(5-z^2)}{(1-z^2)^3}\right)\frac{1}{R}\right\}\\ &+\exp[2R]Ei[-2R]\times\left\{-1+\frac{2z^4}{(1-z^2)^2}+\left(\frac{1}{2}-\frac{z^4(5-z^2)}{(1-z^2)^3}\right)\frac{1}{R}\right\}\\ &+\exp[-2zR]\widetilde{Ei}[2zR]\times\left\{-2z^2+\frac{2z^2}{(1-z^2)^2}+\left(-z+\frac{z(1-5z^2)}{(1-z^2)^3}\right)\frac{1}{R}\right\}\\ &+\exp[2zR]Ei[-2zR]\times\left\{-2z^2+\frac{2z^2}{(1-z^2)^2}+\left(z-\frac{z(1-5z^2)}{(1-z^2)^3}\right)\frac{1}{R}\right\}. \quad (17)\end{aligned}$$

In Eq. (17), $\widetilde{Ei}[x]$ is the usual exponential integral, defined as:

$$\widetilde{Ei}[x] = -\int_{-x}^{\infty}\frac{\exp[-t]}{t}dt,$$

and

$$Ei[-x] = -\int_{x}^{\infty}\frac{\exp[-t]}{t}dt.$$

** It should be noticed that the lower and the upper bound alternate in the case of the interaction energy, since it is defined as a positive quantity.

Using the well-known asymptotic expansion,

$$\exp[-x]\widetilde{Ei}[x] \simeq \sum_{n=1}^{\infty} \frac{(n-1)!}{x^n},$$

and

$$\exp[x]Ei[-x] \simeq \sum_{n=1}^{\infty} \frac{(-1)^n(n-1)!}{x^n},$$

we obtain:

$$V(R,z) = \frac{1}{R^4} + \frac{3(8+3z^2)}{2z^2}\cdot\frac{1}{R^6} + \frac{45(3+3z^2+z^4)}{z^4}\cdot\frac{1}{R^8} + \frac{315(16+18z^2+16z^4+5z^6)}{2z^6}\cdot\frac{1}{R^{10}} + \frac{14175(3z^8+10z^6+12z^4+12z^2+10)}{2z^8}\cdot\frac{1}{R^{12}}\cdots\cdots \quad (18)$$

Using Eqs. (16) and (18), and substituting $z=1.00$, $z'=0.30$, and $z''=0.65$, we obtain a form of series expansion with respect to the inverse powers of R, which can be compared with Davison's result using Eq. (1), as follows:

$$\bar{E}_2(\text{Unsöld}) = -\frac{1}{\langle \Delta E\rangle_{\text{AV}}}\left(\frac{1}{R^4} + \frac{65.497}{R^6} + \frac{7116.8}{R^8} + \frac{1.4302\cdot 10^6}{R^{10}} + \frac{4.4604\cdot 10^8}{R^{12}} + \cdots\cdots\right). \quad (19)$$

In this series, at $R=18$, 14, and 10, the R^{-12} term is comparable with the R^{-10} term, the R^{-10} term with the R^{-8} term, and the R^{-8} term with the R^{-6} term. Adopting $\langle \Delta E\rangle_{\text{AV}}=0.52775$, which gives the potential (B) in Fig. 2, we obtain:

$$\bar{E}_2(\text{Unsöld}) = -\left(\frac{1.8948}{R^4} + \frac{1.2411\cdot 10^2}{R^6} + \frac{1.3485\cdot 10^4}{R^8} + \frac{2.7100\cdot 10^6}{R^{10}} + \frac{8.4517\cdot 10^8}{R^{12}} + \cdots\cdots\right). \quad (20)$$

The results definitely show the divergent nature of the sequence C_{2n} ($n=2$, 3, 4, 5, 6, and so on). On the contrary, the use of the closed form obtained in this paper easily affords the value of $\bar{E}_2$ (Unsöld) at any given R. It can easily be seen that the R^{-4} term comes from the first term of the induction force in the H–H⁺ system:[12]

$$\bar{E}_2 = -\left(\frac{2.25}{R^4} + \frac{7.50}{R^6} + \frac{65.625}{R^8} + \frac{1063.125}{R^{10}} + \frac{27286.875}{R^{12}} + \cdots\cdots\right). \quad (21)$$

The other terms in Eq. (21) contribute little to Eq. (20). In order to clarify this, we have calculated another series expansion with regard to the perturbation H_1:

$$H_1 = H_1(1,2) + H_1(1,3), \quad (22)$$

which involves no H–H⁺ interaction, in contrast with Eq. (9). The results of expansion are as follows:

$$\bar{E}_2(\text{Unsöld}) = -\frac{1}{\langle \Delta E\rangle_{\text{AV}}}\left(\frac{60.998}{R^6} + \frac{7071.8}{R^8} + \frac{1.4294\cdot 10^6}{R^{10}} + \frac{4.4601\cdot 10^8}{R^{12}} + \cdots\cdots\right). \quad (23)$$

In this case, $V(R, z)$ as defined in Eq. (16) becomes:

$$V(R,z) = \frac{12}{z^2}\cdot\frac{1}{R^6} + \frac{135(1+z^2)}{z^4}\cdot\frac{1}{R^8} + \frac{2520(1+z^4)+2835z^2}{z^6}\cdot\frac{1}{R^{10}} + \frac{70875(1+z^6)+85050(z^4+z^2)}{z^8}\cdot\frac{1}{R^{12}} + \cdots\cdots. \quad (24)$$

If we subsitute unity into z, this $V(R, z)$ is clearly reduced to twice the values of the well-known H–H long-range interaction previously obtained by Dalgarno and Lewis.[13] When we compare Eq. (19) with Eq. (23), the terms of higher-order than R^{-4}, therefore, prove to be mainly due to the dispersion force.

In Fig. 3, we show some $\bar{E}_2$ (Unsöld) curves obtained by the partial summation of the series in Eq. (20), along with Davison's series expansion in Eq. (1). It should be noticed that his expansion may be rather near to our closed form at R values less than 6.0, while at larger R values there appears an underestimating tendency. On the other hand, the series expansion until the R^{-10} or R^{-12} term leads to an overestimation of the interaction energy at R values less than *ca.* 9.0.

In conclusion, it turns out that the closed form obtained above is effective for describing the long-range interaction for the H–H⁻ system. Although the values of the second-order interaction energy predicted here have some ambiguousness because of the arbitrariness of the 'average excitation energy,' the upper and lower bounds obtained are reliable to a considerable extent. The series expansion described here shows that the dispersion force contributes to the nature of the interaction: when R is much larger, the R^{-4} term comes to be dominant, and hence

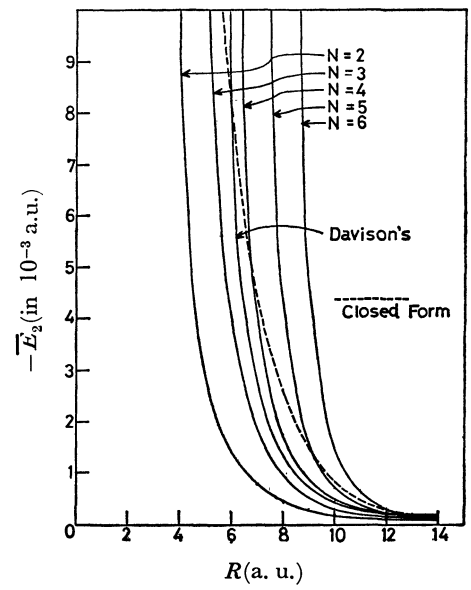

Fig. 3. Various curves of the second-order perturbation energy in the H–H⁻ system obtained by partial summations, $-\bar{E}_2(\text{Unsöld}) = \sum_{n=2}^{N} \frac{C_{2n}}{R^{2n}}$ in Eq. (20). The closed form curve corresponds to (B) in Table 1, and Davison's curve is based on the result in Ref. 5.

the induction force begins to prevail over the dispersion. The former extraordinary large magnitude of the dispersion force mainly comes from the quantity of z' in Eq. (7)—namely, the orbital exponent of the outer orbital in H^-. In other words, the weakly bound electron plays an important role in the origin of the large dispersion force in the system. Generally speaking, a weakly bound electron, which exists also in such anions as F^- or Cl^-, or the electron in frontier orbital with a similar physical nature, will maintain its importance when the system interacts with other distant species.

Appendix

The miscellaneous integrals used in Eq. (12) are shown in the form of $\{F|R,z,z'\}$ in Eq. (15).

$$\{H_1(1)\,|\,R,z,z'\} = \int_{-\infty}^{\infty}\frac{1}{\pi}\exp[-2r_1]\left(\frac{1}{R}-\frac{1}{r_{b1}}\right)d\tau(1)$$
$$= \left(1+\frac{1}{R}\right)\exp[-2R]. \quad \text{(A-1)}$$

$$\{H_1(2)\,|\,R,z,z'\} = \int_{-\infty}^{\infty}\frac{z^3}{\pi}\exp[-2zr_2]\left(\frac{1}{R}-\frac{1}{r_{a2}}\right)d\tau(2)$$
$$= \left(z+\frac{1}{R}\right)\exp[-2zR]. \quad \text{(A-2)}$$

$$\{H_1(1,2)\,|\,R,z,z'\} = \int_{-\infty}^{\infty}\frac{z^3}{\pi^2}\exp[-2(r_1+zr_2)]$$
$$\times\left(\frac{1}{R}+\frac{1}{r_{12}}-\frac{1}{r_{b1}}-\frac{1}{r_{a2}}\right)d\tau(1)d\tau(2)$$
$$= \frac{1}{(1-z^2)^3}\exp[-2R]$$
$$\times\left\{(2z^4-3z^2+1)+\frac{1}{R}(-3z^2+1)\right\}$$
$$+\frac{z^3}{(1-z^2)^3}\exp[-2zR]$$
$$\times\left\{(-z^4+3z^2-2)+\frac{z}{R}(-z^2+3)\right\}, \quad (z\neq 1) \quad \text{(A-3)}$$

if $z=1$,

$$\{H_1(1,2)\,|\,R,1,z'\} = \exp[-2R]\left(\frac{1}{R}+\frac{5}{8}-\frac{3R}{4}-\frac{R^2}{6}\right). \quad \text{(A-3')}$$

$$\{H_1^2(1)\,|\,R,z,z'\} = \int_{-\infty}^{\infty}\frac{1}{\pi}\exp[-2r_1]$$
$$\times\left(\frac{1}{R^2}-\frac{2}{r_{b1}R}+\frac{1}{r_{b1}^2}\right)d\tau(1)$$
$$= -\frac{1}{R^2}+\frac{2}{R}\left(1+\frac{1}{R}\right)\exp[-2R]$$
$$+\left(1+\frac{1}{2R}\right)\exp[-2R]\widetilde{Ei}[2R]$$
$$+\left(1-\frac{1}{2R}\right)\exp[2R]Ei[-2R]. \quad \text{(A-4)}$$

$$\{H_1^2(2)\,|\,R,z,z'\} = \int_{-\infty}^{\infty}\frac{z^3}{\pi}\exp[-2zr_2]$$
$$\times\left(\frac{1}{R^2}-\frac{2}{r_{a2}R}+\frac{1}{r_{a2}^2}\right)d\tau(2)$$
$$= -\frac{1}{R^2}+\frac{2}{R}\left(z+\frac{1}{R}\right)\exp[-2zR]$$
$$+\left(z^2+\frac{z}{2R}\right)\exp[-2zR]\widetilde{Ei}[2zR]$$
$$+\left(z^2-\frac{z}{2R}\right)\exp[2zR]Ei[-2zR]. \quad \text{(A-5)}$$

$$\left\{\frac{1}{r_{a2}}W(2,1)\,|\,R,z,z'\right\} = \int_{-\infty}^{\infty}\frac{z^3}{\pi^2}\exp[-2(r_1+zr_2)]$$
$$\times\left(\frac{1}{r_{a2}^2}-\frac{1}{r_{a2}r_{12}}\right)d\tau(1)d\tau(2)$$
$$= \exp[-2zR]\left[-z^2\log\left|\frac{z-1}{z+1}\right|+\frac{z^3}{1-z^2}\right.$$
$$\left.+\frac{1}{R}\left(\frac{-z^2}{(1-z^2)^2}-\frac{z}{2}\log\left|\frac{z-1}{z+1}\right|\right)\right]$$
$$+\frac{z^2}{(1-z^2)^2R}\exp[-2R]$$
$$+\left(z^2+\frac{z}{2R}\right)\exp[-2zR]Ei[-2(1-z)R]$$
$$+\left(z^2-\frac{z}{2R}\right)\exp[2zR]Ei[-2(1+z)R], \quad (z\neq 1) \quad \text{(A-6)}$$

if $z=1$,

$$\left\{\frac{1}{r_{a2}}W(2,1)\,|\,R,1,z'\right\} = \exp[-2R]$$
$$\times\left[-\frac{3}{4}+\frac{R}{2}+\left(1+\frac{1}{2R}\right)(\gamma+\log 4R)\right]$$
$$+\exp[2R]Ei[-4R]\left(1-\frac{1}{2R}\right), \quad \text{(A-6')}$$

where γ is Euler's constant, 0.5772156649…….

$$\left\{\frac{1}{r_{12}^2}\,|\,R,z,z'\right\} = \int_{-\infty}^{\infty}\frac{z^3}{\pi^2}\exp[-2(r_1+zr_2)]\frac{1}{r_{12}^2}d\tau(1)d\tau(2)$$
$$= \left[\frac{z^4}{(1-z^2)^2}+\frac{z^4(5-z^2)}{2(1-z^2)^3R}\right]\exp[-2R]\widetilde{Ei}[2R]$$
$$+\left[\frac{z^4}{(1-z^2)^2}-\frac{z^4(5-z^2)}{2(1-z^2)^3R}\right]\exp[2R]Ei[-2R]$$
$$+\left[\frac{z^2}{(1-z^2)^2}+\frac{z(1-5z^2)}{2(1-z^2)^3R}\right]\exp[-2zR]\widetilde{Ei}[2zR]$$
$$+\left[\frac{z^2}{(1-z^2)^2}-\frac{z(1-5z^2)}{2(1-z^2)^3R}\right]\exp[2zR]Ei[-2zR], \quad (z\neq 1) \quad \text{(A-7)}$$

if $z=1$,

$$\left\{\frac{1}{r_{12}^2}\,|\,R,1,z'\right\} = -\frac{7}{12}$$
$$+\left(\frac{5}{16R}+\frac{5}{8}+\frac{R}{2}+\frac{R^2}{6}\right)\exp[-2R]\widetilde{Ei}[2R]$$
$$+\left(-\frac{5}{16R}+\frac{5}{8}-\frac{R}{2}+\frac{R^2}{6}\right)\exp[2R]Ei[-2R]. \quad \text{(A-7')}$$

$$\{H_1(2)H_1(3)\,|\,R,z,z'\} = \int_{-\infty}^{\infty}\frac{z^3z'^3}{\pi^2}\exp[-2(zr_2+z'r_3)]$$

$$\times\left(\frac{1}{R^2}-\frac{1}{r_{a2}R}-\frac{1}{r_{a3}R}+\frac{1}{r_{a2}r_{a3}}\right)d\tau(2)d\tau(3)$$
$$=\left(\frac{1}{R^2}+\frac{z}{R}+\frac{z'}{R}+zz'\right)\exp[-2(z+z')R]. \quad \text{(A-8)}$$

$$\{H_1(2)W(1,3)\,|\,R,z,z'\}$$
$$=\{H_1(2)\,|\,R,z,z'\}\{W(1,3)\,|\,R,z,z'\}$$
$$=\frac{1}{(1-z'^2)^2}\left(z+\frac{1}{R}\right)\left[\frac{1}{R}(-1+3z'^2)+(-1+2z'^2)\right]\times\exp[-2(1+z)R]$$
$$+\frac{1}{(1-z'^2)^2}\left(z+\frac{1}{R}\right)\left[z'+\frac{1-3z'^2}{(1-z'^2)R}\right]\times\exp[-2(z+z')R], \quad (z'\neq 1) \quad \text{(A-9)}$$

if $z'=1$,

$$\{H_1(2)W(1,3)\,|\,R,z,1\}$$
$$=\exp[-2(1+z)R]\left(z+\frac{1}{R}\right)\left(\frac{R^2}{6}+\frac{3R}{4}+\frac{3}{8}\right). \quad \text{(A-9')}$$

$$\{H_1(3)W(1,2)\,|\,R,z,z'\}$$
$$=\{H_1(3)\,|\,R,z,z'\}\{W(1,2)\,|\,R,z,z'\}$$
$$=\frac{1}{(1-z^2)^2}\left(z'+\frac{1}{R}\right)\left[\frac{1}{R}(-1+3z^2)+(-1+2z^2)\right]\times\exp[-2(1+z')R]$$
$$+\frac{1}{(1-z^2)^2}\left(z'+\frac{1}{R}\right)\left[z+\frac{1-3z^2}{(1-z^2)R}\right]\times\exp[-2(z+z')R], \quad (z\neq 1) \quad \text{(A-10)}$$

if $z=1$,

$$\{H_1(3)W(1,2)\,|\,R,1,z'\}$$
$$=\exp[-2(1+z')R]\left(z'+\frac{1}{R}\right)\left(\frac{R^2}{6}+\frac{3R}{4}+\frac{3}{8}\right). \quad \text{(A-10')}$$

$$\{W(1,2)W(1,3)\,|\,R,z,z'\}$$
$$=\iiint_{-\infty}^{\infty}\frac{z^3z'^3}{\pi^3}\exp[-2(r_1+zr_2+z'r_3)]$$
$$\times\left(\frac{1}{r_{b1}}-\frac{1}{r_{12}}\right)\left(\frac{1}{r_{b1}}-\frac{1}{r_{13}}\right)d\tau(1)d\tau(2)d\tau(3)$$
$$=\exp[-2R]\left[\left[-\log\left|\frac{z+z'-1}{z+z'+1}\right|\right.\right.$$
$$+\frac{(z+z')\{(z+z')^2+zz'-1\}}{\{1-(z+z')^2\}^2}+\frac{1}{R}\left[-\frac{1}{2}\log\left|\frac{z+z'-1}{z+z'+1}\right|\right.$$
$$\left.\left.+\frac{(z+z')\{(z+z')^4-(z+z')^2+zz'(z+z')^2+zz'\}}{\{1-(z+z')^2\}^3}\right]\right]$$
$$+\exp[-2(z+z')R]\left[\frac{-zz'}{\{1-(z+z')^2\}^2}\right.$$
$$-\frac{z+z'}{\{1-(z+z')^2\}^3}\{R(z+z')^3-(z+z')^2$$
$$\left.-2(z+z')-2zz'+1\}\right]$$
$$+\exp[2R]Ei[-2(z+z'+1)R]\left(1-\frac{1}{2R}\right)$$
$$+\exp[-2R]Ei[-2(z+z'-1)R]\left(1+\frac{1}{2R}\right). \quad (|z+z'|\neq 1) \quad \text{(A-11)}$$

References

1) For example, see (a) "Intermolecular Force," in 'Advances in Chemical Physics,' ed. by J. O. Hirschfelder, Vol. 12, Interscience Publishers, New York (1967); (b) P. R. Certain and L. W. Bruch, "Intermolecular Forces," in 'MTP International Review of Science, Theoretical Chemistry,' ed. by W. B. Brown, Vol. 1, Univ. of Park Press, Baltimore (1972).

2) (a) Y. Öhman, *Arkiv. Astron.* **2**, 1 (1955); (b) H. A. Bethe and E. E. Salpeter, "Quantum Mechanics of One- and Two-Electron Atoms," Academic Press Inc., New York (1957), p. 240.

3) A. Dalgarno and M. R. C. McDowell, *Proc. Phys. Soc.* (London), **A69**, 615 (1956).

4) A Dalgarno and K. E. Kingston, *ibid.*, **A73**, 455 (1959).

5) W. D. Davison, *ibid.*, **A87**, 133 (1966).

6) (a) K. Fukui and T. Yamabe, *Int. J. Quant. Chem.*, **2**, 359 (1968); **5**, 478 (1971); (b) T. Yamabe, S. Ishimaru, and K. Fukui, This Bulletin, **43**, 2012 (1970); (c) T. Yamabe, S. Ishimaru, and K. Fukui, *ibid.*, **45**, 1384 (1972); (d) T. Yamabe, S. Ishimaru, and K. Fukui, *ibid.*, **46**, 2361 (1973).

7) A. Unsöld, *Z. Phys.*, **43**, 374 (1927).

8) H. Eyring, J. O. Hirschfelder, and H. S. Taylor, *J. Chem. Phys.*, **4**, 479 (1936).

9) S. Chandrasekhar, *Astrophys. J.*, **100**, 176 (1944).

10) I. Fischer-Hjalmars, *Ark. Fys.*, **16**, 33 (1959).

11) H. S. Taylor and F. E. Harris, *J. Chem. Phys.*, **39**, 1012 (1963).

12) A. Dalgarno and N. Lynn, *Proc. Phys. Soc.* (London), **A70**, 223 (1957).

13) A. Dalgarno and J. T. Lewis, *ibid.*, **A86**, 239 (1965).

Studies of Phase Transitions in Cholesteryl Myristate by Means of Simultaneous Measurements of Polarizing Microscopy and Thermal Analyses*

Kazuko SASAKI KUNIHISA and Takako SHINODA
National Chemical Laboratory for Industry, Shibuya-ku, Tokyo 151
(Received June 7, 1975)

An improved DTA furnace and sample cell have been used for accurate DTA measurements and clear polarizing microscopic photographs. The photographs, DTA and TTA curves were obtained simultaneously at different heating or cooling rates for solid-smectic, smectic-cholesteric and cholesteric-isotropic liquid phase transitions in cholesteryl myristate.

Polarizing microscopy has been used for observing the static state of the substance microscopically, and differential thermal analysis (DTA) and total thermal analysis (TTA) for studying the thermal behavior of a substance dynamically. With simultaneous use of the two methods, it is possible to observe the process of transition more in detail.

We have studied the solid-smectic, the smectic-cholesteric and the cholesteric-isotropic liquid phase transitions in cholesteryl $CH_3(CH_2)_{12}COOC_{27}H_{45}$.

Experimental

Apparatus. A DTA furnace and a cell were constructed for increasing the accuracy of DTA measurements and for obtaining clear polarizing microscopic photographs. The furnace is illustrated in Fig. 1. A heater ($\phi=0.3$ mm, manganin) and all the electrical lead wires are wound around A. A sectional view of the sample or reference cell, made of pyrex glass (0.6 mm thick) and a quartz plate, with an internal volume *ca.* 0.07 ml, is shown in Fig. 2. The thermocouple, a chromel *p*-constantan type, is used for the absolute or difference temperature measurements. Measurements for the calibration of the absolute temperature scale were reported previously.[1] For increasing the accuracy of DTA measurements, two differential thermocouples were connected in series. Operations for polarizing microscopy and DTA were the same as those described previously.[2]

Material. Cholesteryl myristate (Tokyo Kasei Kogyo Co., Ltd.) was recrystallized from *n*-pentanol twice, pumping being carried out for 22.5 h with a rotary pump in order to remove any trace of solvent. Cholesteryl benzoate (Tokyo Kasei Kogyo Co., Ltd.) was used as a refernce substance.

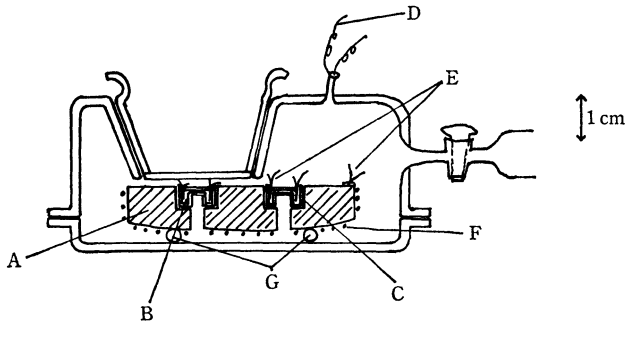

Fig. 1. Cross-section diagram of the DTA furnace.
A: copper block, B: sample cell, C: reference cell, D: lead wires, E: thermocouples, F: heater, G: O-ring.

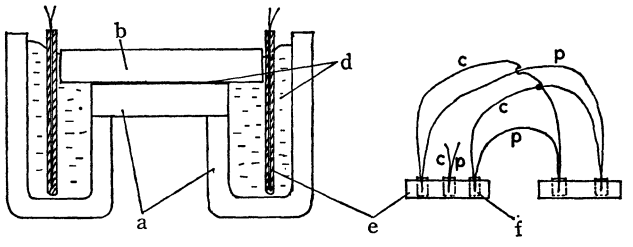

Fig. 2. Cross-section diagram of sample or reference cell and the devised thermocouple junctions.
a: pyrex glass, b: quartz plate, c: constantan wires, d: sample, e: copper plate, f: insulated paper, p: chromel-*p* wires.

Microscopic observations were carried out through crossed nicols and a color-sensitive plate, magnification being 200. A tungsten lamp (30 W) was used as a light source. The position for taking a photograph is marked on the recording paper for the DTA and TTA.

Results and Discussion

Annealing Effects. Polymorphic behavior of solid phases of substances forming liquid crystals has been reported for PAA,[3] MBBA[4] and OH-MBBA.[5] In the course of annealing the solid specimen, polymorphic behavior for cholesteryl myristate has also been observed. The results are shown in Figs. 3 and 4. The solid state established by cooling the specimen of isotropic liquid state with an average cooling rate of

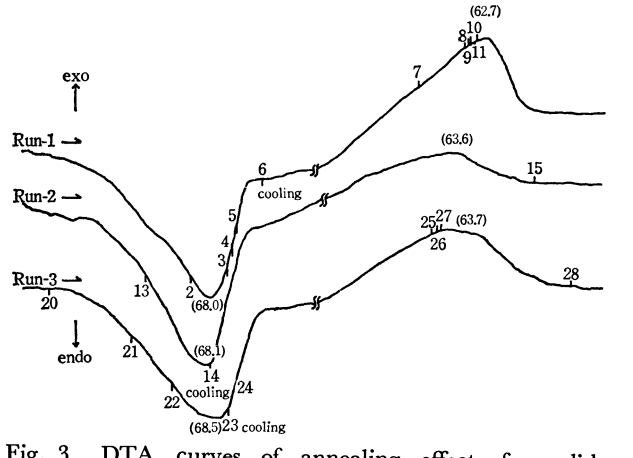

Fig. 3. DTA curves of annealing effects for solid cholesteryl myristate. Numerals in parentheses indicate T_{max} (°C).

* Presented at the 32nd Annual Meeting of the Chemical Society of Japan, Tokyo, April 1, 1975.

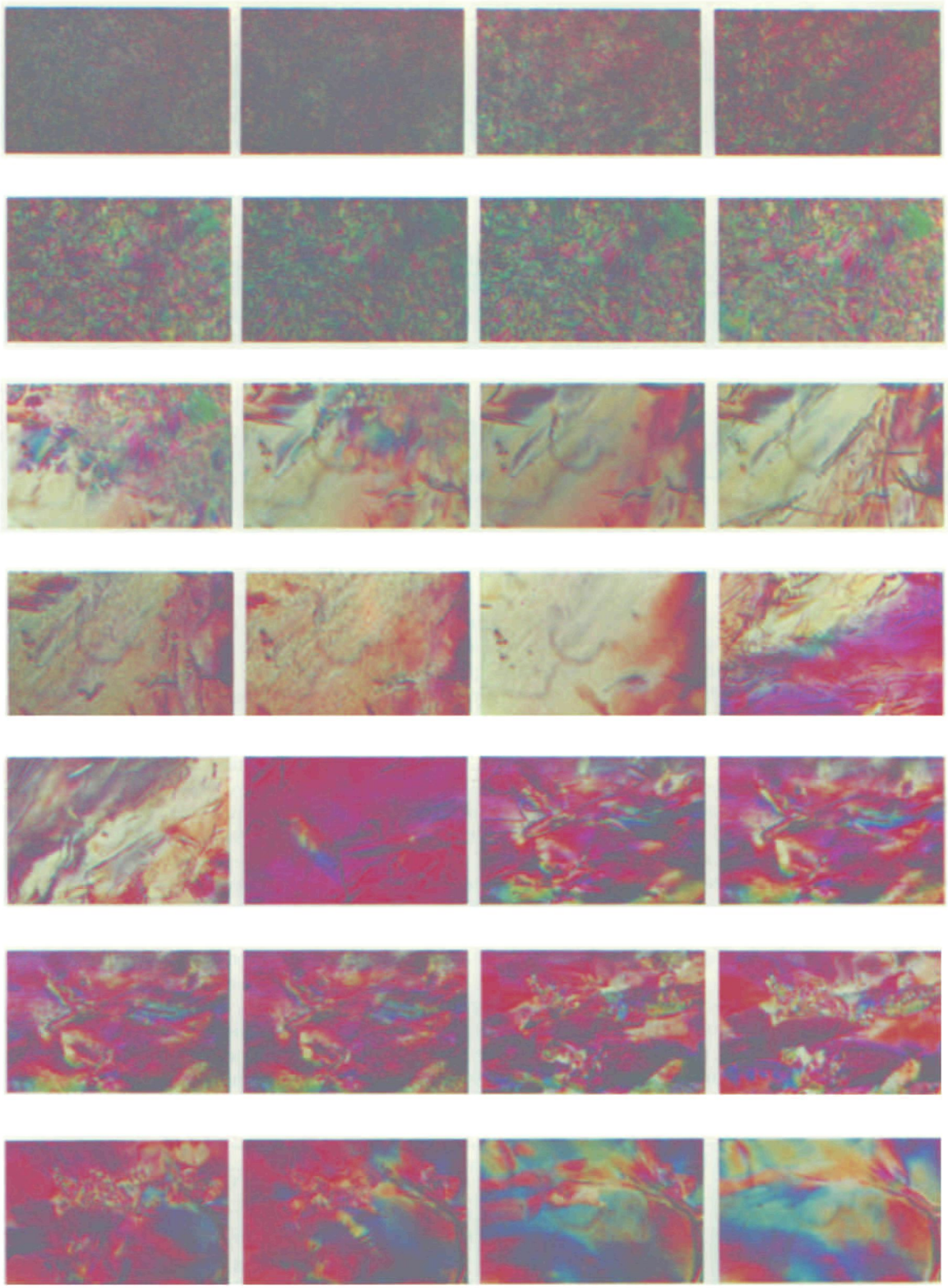

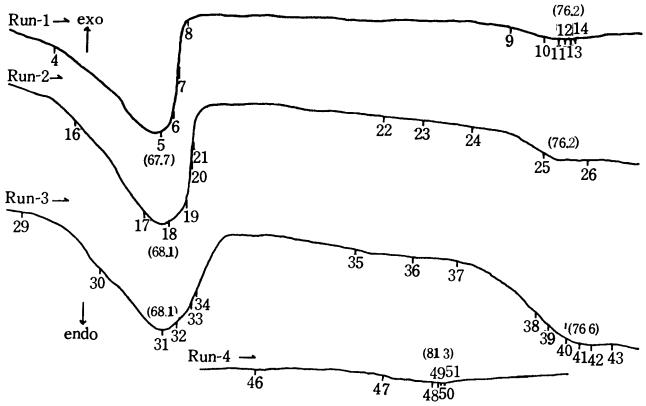

Fig. 5. DTA curves of cholesteryl myristate at heating condition. Numerals in parentheses indicate T_{max} (°C).

ca. 1.79 °C min^{-1} to room temperature, is denoted by solid-I. In Fig. 3, Run-1 represents a DTA curve obtained by heating solid-I at the rate 0.22°C min^{-1} from room temperature to point 6, and then by cooling at the rate 0.23 °C min^{-1} to room temperature. Figure 4-12 gives a photograph of the solid obtained at 32 °C after 18.5 hr. The annealing effects for this solid are shown by the DTA curve at the heating rate 0.23 °C min^{-1} and the cooling rate 0.22 °C min^{-1} for Run-2. Figs. 4-16, 4-17, 4-18 and 4-19 show the annealed solid states at room temperature after 19 hr. Run-3 gives a DTA curve obtained by annealing the specimen (Fig. 4-19) at the heating rate 0.24 °C min^{-1} and the cooling rate 0.22 °C min^{-1}. The last established solid is denoted by solid-III.

Heating Process. Another solid state denoted by solid-II (Fig. 6-15) was obtained by cooling the specimen of isotropic liquid state to 49.4 °C at the cooling rate *ca.* 0.22 °C min^{-1}. We found that the situation of the transitions from solid to smectic and then to cholesteric depends upon the starting solid-state. The DTA curves for solids-I, II and III are shown by Runs-1, 2, and 3, respectively, in Fig. 5, at heating rates of 0.21, 0.21 and 0.23 °C min^{-1}, respectively. Figs. 6-1 to 6-43 show the microscopic photographs taken during the course of transformation.

Figure 6-1 shows the microscopic photograph of solid-I at room temperature, Figs. 6-2 and 6-3 being those of partial solid-I states. Figs. 6-4 to 6-14 show photographs corresponding to the points indicated by the numbers in the DTA curve for Run-1 in Fig. 5, Fig. 6-8 giving the smectic-state obtained from solid-I state. The smectic-to-cholesteric transition takes place directly from the openings of the rod (or bunch) shaped smectic-liquid crystals, as shown in Figs. 6-12 and 6-13. Figure 6-14 shows the established cholesteric state.

Figures 6-15 to 6-26 show microscopic photographs of solid-II corresponding to the DTA curve of Run-2 in Fig. 5. Figure 6-22 shows the smectic-state obtained by heating the specimen of solid-II. The upper part on the left is similar to the smectic-state obtained from solid-III. The lower part on the right shows the rod shaped smectic-state found in solid-I. Figure 6-26 gives the cholesteric-state obtained and resembles Fig. 6-14.

We found locally the state of solid-III at room temperature as shown in Fig. 6-28. It might be a glassy solid-state. Figures 6-29 to 6-43 show the microscopic photographs for solid-III (Fig. 6-27) corresponding to the DTA curve of Run-3 in Fig. 5. The established smectic-state(Fig. 6-35) was transformed into the cholesteric-state by way of establishing the spherical-state (Figs. 6-36 to 6-40). The thermal behavior was also observed on the DTA curve in Fig. 5 (compare with Runs-1 and 3). The obtained cholesteric-state (Fig. 6-43) is much the same as shown in Figs. 6-14 and 6-26.

We see from Figs. 5 and 6 that there is some difference between the thermal behavior of solids-I, II and III not only in the solid-to-smectic transition but also in the smectic-to-cholesteric one. However, no difference was observed in the cholesteric-to-isotropic liquid transition between solids-I, II and III. The transition for solid-II is shown by the DTA curve for Run-4 in Fig. 5 and by the microscopic photographs (Figs. 6-46 to 6-51). The cholesteric-state of cholesteryl myristate (Fig. 6-46) is a state in which spherical-liqud crystals (Figs. 6-37 to 6-39) stick to each other. It might be assumed that the difference in color between the yellow part and the blue part corresponds to the molecular orientation of the block, the red part being similar to the isotropic liquid state. The red part spreads with the progress of cholesteric-to-isotropic liquid transition.

Figures 6-44 and 6-45 give microscopic photographs

Table 1. Transition temperatures and enthalpy ratios of transition for cholesteryl myristate

	Heating rate (°C min^{-1})	$t_{solid\text{-}to\text{-}smectic}$ (°C)	$t_{smectic\text{-}to\text{-}cholesteric}$ (°C)	$t_{cholesteric\text{-}to\text{-}isotropic}$ (°C)
Solid-I	1.73	68.8	77.3	82.8
	0.89	68.4	76.8	82.1
Annealed solid	1.79	70.3	78.5	83.7
	0.90	68.7	77.0	82.0
	Heating rate (°C min^{-1})	ΔH-ratio (solid-to-smectic)	ΔH-ratio (smectic-to-cholesteric)	ΔH-ratio (cholesteric-to-isotropic)
Solid-I	1.73	47.0 (95.6%)	1.2 (2.4%)	1.0 (2.0%)
	0.89	43.5 (95.1%)	1.2 (2.7%)	1.0 (2.2%)
Annealed solid	1.79	39.4 (93.7%)	1.7 (3.9%)	1.0 (2.4%)
	0.90	34.2 (91.2%)	2.3 (6.1%)	1.0 (2.7%)
Griffen and Porter[7]	—	45.4 (95.0%)	1.4 (2.9%)	1.0 (2.1%)

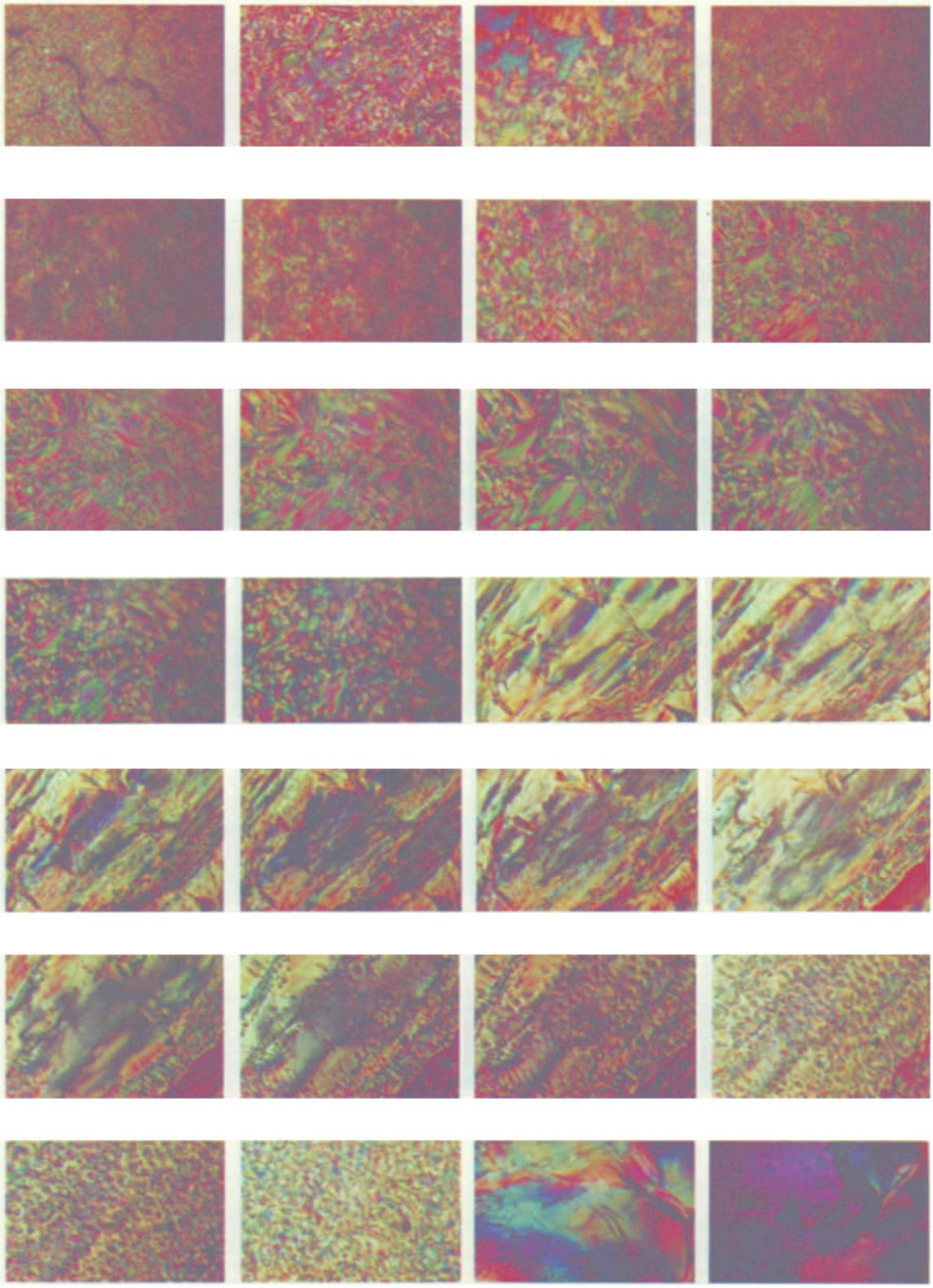

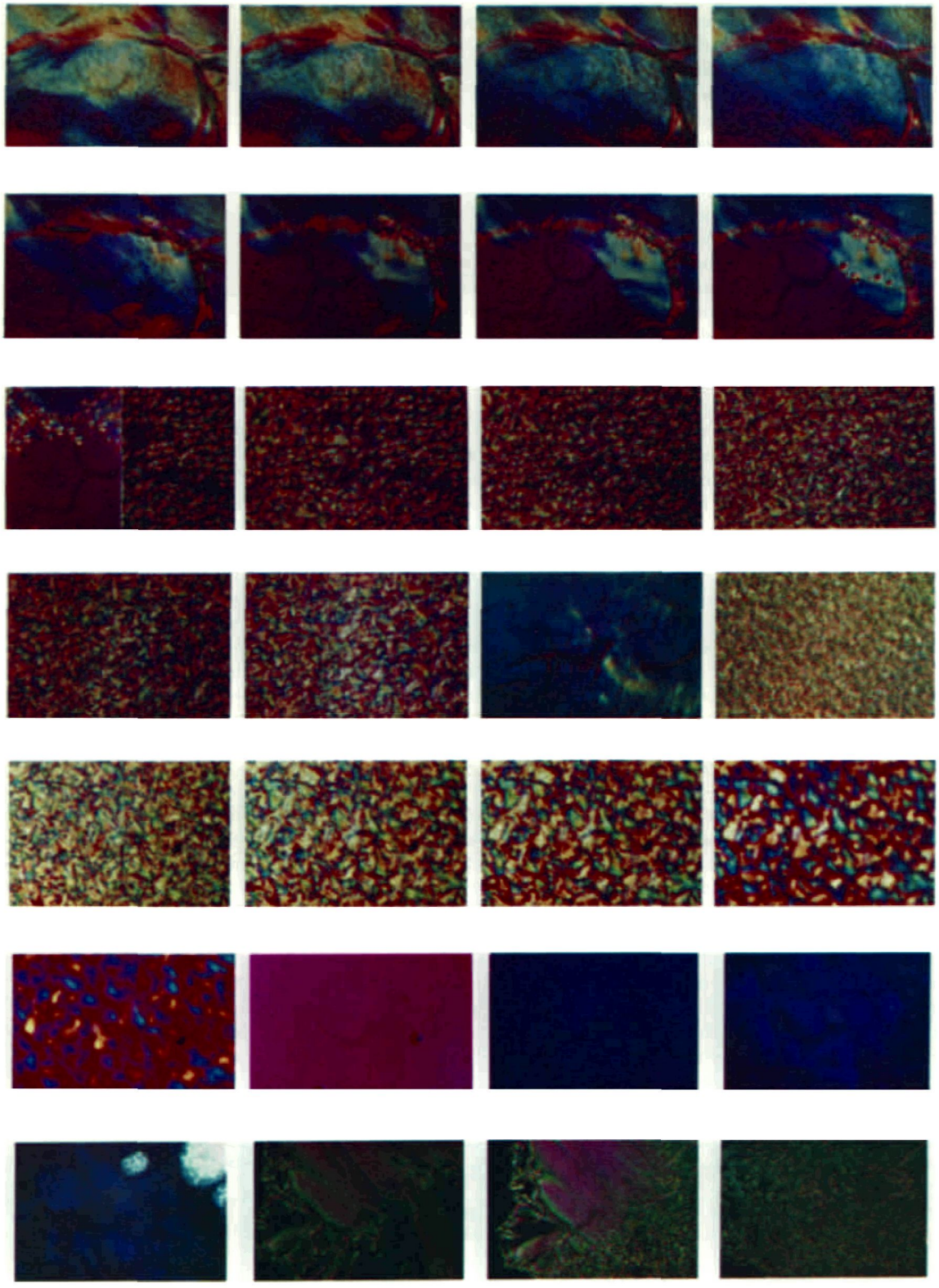

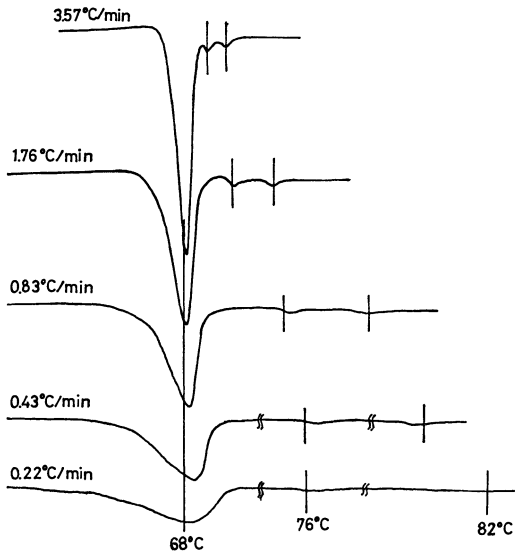

Fig. 7. DTA curves obtained at various heating rate of solid-I.

of the smectic and cholesteric states established by heating the specimen of the solid-state obtained by heating solid-I from room temperature to the maximum point of the solid-to-smectic transition and by cooling to 42.5 °C at a rate of *ca.* 0.22 °C min^{-1}. It is suggested that on the basis of molecular configuration solid-I is a frozen-in solid state of cholesteric-state(compare Figs. 4-1 and 6-45), the annealed solid (Fig. 4-12) is a frozen-in solid state of smectic-state (Fig. 6-44), and solid-II is a mixed state of these solids (compare Figs. 6-8, 6-22 and 6-44).

Cooling Process. All states obtained during the course of heating were also observed in the course of cooling the specimen from isotropic liquid-state to solid-state.

Figures 6-52 to 6-54 show the process of isotropic-to-cholesteric transition at such a slow cooling rate that no DTA curve can be observed. The blue color turns light with the thickness of the specimen, probably because of high optical-rotatory power[6] of the cholesteric state. Figures 6-52 to 6-57 were taken without color sensitive plate but with crossed nicols. Figures 6-55 to 6-57 show the microscopic photographs during the course of smectic-to-solid transition. The solid-state became wrinkled horizontally with the width of the rod shaped smectic-block.

Differential Thermal Analysis (DTA). DTA measurements at several heating rates were made for the specimen of solid-I. Figure 7 shows the DTA curves obtained. The changes in the transition temperature due to the discrepancy of heating rate were found to be considerably small. Two measurements of solid-I and annealed-solid were also made at different heating rates. The transition temperature and the enthalpy ratio* of transition are summarized in Table 1.

The transition temperatures from solid to smectic and to cholesteric for the annealed-solid are higher than those for solid-I. The transition temperature from cholesteric to isotropic liquid for the annealed-solid is much the same as that for solid-I. The enthalpy of the solid-to-smectic transition for the annealed-solid is smaller than that for solid-I, the enthalpy of the smectic-to-cholesteric transition for the annealed-solid being larger than that for solid-I.

References

1) H. Enokido, T. Shinoda, and Y. Mashiko, This Bulletin, **44**, 108 (1971).
2) K. S. Kunihisa, *ibid.*, **46**, 2862 (1973).
3) C. R. Robiner and J. C. Poisier, *J. Amer. Chem. Soc.*, **90**, 4760 (1968); L. C. Chow and D. E. Martine, *J. Phys. Chem.*, **73**, 1127 (1969).
4) J. Mayer, T. Waluga, and J. A. Janik, *Phys. Lett.*, **41A**, 102 (1972); T. Shinoda, Y. Maeda, and H. Enokido, *J. Chem. Thermodynamics*, **6**, 921 (1974).
5) M. Sorai, and S. Seki, IV Intern. Liq. Cryst. Conference, Kent State Univ. (1972).
6) G. W. Gray, *J. Chem. Soc.*, **1956**, 3733.
7) C. W. Griffen, and R. S. Porter, *Mol. Cryst. Liquid Cryst.*, **21**, 77 (1973).

* Since we cannot obtain the enthalpy of transition directly from DTA curves, the ratio of the enthalpy of each transition to that of cholesteric-to-isotropic liquid transition is given.

Topological Index as Applied to π-Electronic Systems. II. Topological Bond Order*

Haruo HOSOYA and Miyuki MURAKAMI

Department of Chemistry, Ochanomizu University, Bunkyo-ku, Tokyo 112

(Received June 24, 1975)

Topological bond order p_l^T is proposed to be defined for a bond l in the graph corresponding to the carbon atom skeleton of a hydrocarbon. This quantity is obtained by hand calculation of the topological indices of the graph and its subgraphs. The p_l^T value is linearly correlated well with the Coulson bond order p_l^C for both the chain and cyclic compounds. If the bonds with the same Pauling bond order p_l^P are compared this linear relationship is greatly improved and one gets an empirical relation as

$$p_l^C = A\,p_l^T + B\,p_l^P .$$

In order to describe the π-electronic distribution on the carbon atom skeleton of a given unsaturated hydrocarbon several bond orders have been proposed, *e.g.*, by Paluing,[1] Coulson,[2] Mulliken,[3] Ham and Ruedenberg,[4] and so on. The Coulson bond order, p_{rs}^C, is obtained from the molecular orbitals of LCAO form as

$$p_{rs}^C = 2\sum_n^m C_{nr}C_{ns} \tag{1}$$

in terms of the notations currently adopted. Because of mathematical neatness let us confine ourselves to the ground state of neutral unsaturated hydrocarbon molecules with even number $[N=2m]$ of π-electrons without any NBMO and let the term "molecular orbital" be meant by the Hückel molecular orbital. The Pauling bond order, p_l^P, is defined in the valence bond method as

$$p_l^P = \frac{K(G\ominus l)}{K(G)}, \tag{2}$$

where $K(G)$ is the number of the Kekulé structures for graph $\boldsymbol{G}$ (composed of points and lines corresponding to the carbon atom skeleton of a hydrocarbon) and the notation $\boldsymbol{G}\ominus l$ stands for the subgraph of $\boldsymbol{G}$ obtained by deleting a bond, say $l(\overline{rs})$, together with all the bonds adjacent to l. The value $K(G\ominus l)$ is equal to the number of the Kekulé structures for $\boldsymbol{G}$ such that a double bond is assigned to l. This means that the Pauling bond order is the weight of a bond in the graph with respect to a set of the Kekulé structures.

Ham has given an ingenious proof[5] that the molecular orbital (MO) and valence bond (VB) methods are rigorously connected to each other through the bond order p_{rs}^{HR} as defined by

$$p_{rs}^{HR} = 2\sum_n^m \frac{C_{nr}C_{ns}}{X_n},^{4)} \tag{3}$$

where X_n is the eigenvalue of the secular equation, or the root of the characteristic polynomial

$$P_G(X) = (-1)^N \det|\boldsymbol{A}-X\boldsymbol{E}| = \sum_{k=0}^N a_k X^{N-k}. \tag{4}$$

Here $\boldsymbol{A}$ and $\boldsymbol{E}$ are respectively the adjacency and unit matrices of graph $\boldsymbol{G}$. It was shown that for alternant hydrocarbons without any $4n$-membered ring the MO expression p_{rs}^{HR} is identical to the VB expression p_l^P,

$$p_{rs}^{HR} = p_l^P \qquad (l=\overline{rs}).^{5)} \tag{5}$$

Aside from the two main streams (MO and VB) of the electronic theory the topological or graph-theoretical approach is now being realized as a powerful and perspective tool for understanding the nature of the several properties of molecules.[6,7] In this paper a topological bond order, p_l^T, is proposed to be defined as

$$p_l^T = \frac{Z_{G\ominus l}}{Z_G}, \tag{6}$$

where Z_G is the topological index for graph $\boldsymbol{G}$. The topological index is an integer assigned to a graph for characterizing the topological nature of the graph and will be explained later in detail. It will be shown that p_l^T is correlated well with all the bond orders described above. One can roughly estimate the relative magnitudes of the bond orders quite easily with a "paper and pencil" manipulation for the graph.

Topological Index

Consider a graph ($\boldsymbol{G}$) composed of linearly connected six points, which may be the carbon atom skeleton of *n*-hexane or 1,3,5-hexatriene (I) (See Table 1). A non-adjacent number $p(G, k)$ is defined as the number of ways in which k disconnected lines are chosen from G, $p(G, 0)$ being defined as unity for all the graphs. It has been shown that for a tree graph, *i.e.*, a graph without any ring, the coefficients of the characteristic polynomial is equal to $p(G, k)$ numbers as

$$P_G(X) = \sum_{k=0}^m (-1)^k p(G,k) X^{N-2k} \quad (\boldsymbol{G}\in\text{Tree}).^{6)} \tag{7}$$

Especially for linear graph $\overline{N}$ composed of consecutive N points we have

$$P_{\overline{N}}(X) = \sum_{k=0}^m (-1)^k \binom{N-k}{k} X^{N-2k}. \tag{8}$$

These are special cases of a more general relation for non-tree graphs between the $p(G, k)$ and $P_G(X)$,

$$P_G(X) = \sum_{R_i\in G}\sum_{k=0}^{m_i} (-2)^{r_i}(-1)^k p(G\ominus R_i, k) X^{N-n_i-2k} \tag{9}$$

where R_i runs over all the sets of $r_i(\geq 0)$ disjoint rings with a total of $n_i(\geq 0)$ points.[7,8] This relation is

* The first paper of this series is, H. Hosoya, K. Hosoi, and I. Gutman, "A Topological Index for the Total π-Electron Energy. Proof of a Generalised Hückel Rule for an Arbitrary Network," *Theor. Chim. Acta*, **38**, 37 (1975).

Table 1. Physical meaning of the topological index as exemplified by graph $\bar{6}$.

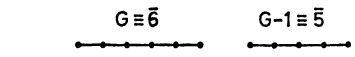

k	l 1 2 3 4 5	p(G,k)	p(G-1,k)
0	x x x x x	1	1
1	o x x x x	5	4
	x o x x x		
	x x o x x		
	x x x o x		
	x x x x o		
2	o x o x x	6	3
	o x x o x		
	o x x x o		
	x o x o x		
	x o x x o		
	x x o x o		
3	o x o x o	1	0
	5 3 4 3 5 $Z_{G\ominus l}$	13 Z_G	8 Z_{G-1}

equivalent to the more compact one derived independently by Sachs

$$P_G(X) = \sum_{n=0}^{N} \sum_{s\in S_n} (-1)^{c(s)}\, 2^{r(s)}\, X^{N-n} \tag{10}$$

where s runs over all the Sachs graph composed of n points, $c(s)$ components and $r(s)$ rings.[9-11] However, Eq. (9) has more advantage over and is more practical than Eq. (10) in that useful recursive relations which will be described later are known to get the $p(G,k)$ numbers for larger graphs.

The value $p(G, 1)$ is nothing else but the number of lines in $\boldsymbol{G}$. As illustrated in Table 1 for I ($=\bar{6}$) there are six different ways in which two disconnected lines are chosen and we have $p(G, 2)=6$. There is only a unique choice of three disconnected lines for $\boldsymbol{G}$ and one gets $p(G, 3)=1$, the maximum number m of k for I being three. This means graph I has only one Kekulé structure.

The topological index is the sum of the $p(G, k)$ numbers of a given graph as

$$Z_G = \sum_{k=0}^{m} p(G,k). \tag{11}$$

For tree graphs Z_G is the sum of the absolute values of the coefficients of the characteristic polynomial.

$$Z_G = \sum_{k=0}^{N} |a_k| = \sum_{k=0}^{m} |a_{2k}| \qquad (\boldsymbol{G}\in\text{tree}). \tag{12}$$

For later discussions it is convenient to define the Z-counting polynomial $Q_G(Y)$ as

$$Q_G(Y) = \sum_{k=0}^{m} p(G,k)\, Y^k. \tag{13}$$

With this polynomial the topological index is expressed as

$$Z_G = Q_G(1). \tag{14}$$

For graph I in Table 1 we have

$$Q_{\bar{6}}(Y) = 1 + 5Y + 6Y^2 + Y^3 \tag{15}$$

and $Z_{\bar{6}}=13$. Extensive tabulation on the quantities $p(G, k)$, Z_G, and $P_G(X)$ are given elsewhere.[12-14]

Let such a subgraph of $\boldsymbol{G}$ be denoted as $\boldsymbol{G}$-l that is derived by deleting bond l. The polynomial $Q_G(Y)$ is expressed as

$$Q_G(Y) = Q_{G-l}(Y) + Y\cdot Q_{G\ominus l}(Y). \tag{16}$$

If graph $\boldsymbol{G}$ is decomposed into fragments $\boldsymbol{L}$, $\boldsymbol{M}$, ... by the deletion of l,

$$\boldsymbol{G} - l = \boldsymbol{L} \cup \boldsymbol{M} \cup \cdots \tag{17}$$

$$\boldsymbol{L} \cap \boldsymbol{M} \cap \cdots = 0, \tag{18}$$

the polynomial $Q_{G-l}(Y)$ reduces to their product

$$Q_{G-l}(Y) = Q_L(Y)\cdot Q_M(Y)\cdots \tag{19}$$

and so does $Q_{G\ominus l}(Y)$.

For the topological index we have

$$Z_G = Z_{G-l} + Z_{G\ominus l} \tag{20}$$

$$Z_{G-l} = Z_L\cdot Z_M \cdots \tag{21}$$

Note that Eqs. (16) and (20) hold true irrespective of the choice of l.

As a special case the Z-counting polynomials $Q_G(Y)$'s of a series of graphs $\bar{N}$ recurse as

$$Q_{\bar{N}}(Y) = Q_{\bar{N-1}}(Y) + Y\cdot Q_{\bar{N-2}}(Y) \qquad (N\geq 2) \tag{22}$$

$$Q_{\bar{0}}(Y) = Q_{\bar{1}}(Y) = 1, \tag{23}$$

and their topological indices $Z_{\bar{N}}$'s form the well-known Fibonacci numbers (1,1,2,3,5,8,13 ...) as

$$Z_{\bar{N}} = Z_{\bar{N-1}} + Z_{\bar{N-2}} \qquad (N\geq 2) \tag{24}$$

$$Z_{\bar{0}} = Z_{\bar{1}} = 1. \tag{25}$$

A number of interesting mathematical relations are derived for $Q_G(Y)$ and Z_G.[6,15]

Topological Bond Order

The value Z_G may be regarded as the total number of ways in which disconnected double bonds are assigned onto the single bond skeleton of $\boldsymbol{G}$ as in Table 1, where a 13×5 matrix is constructed with elements o and x corresponding respectively to double and single bonds. Each row forms a set of disconnected double bonds and the number of rows gives the topological index Z_G. Then this number is thought to represent the degree of choice for distributing π-electrons over the molecular skeleton $\boldsymbol{G}$. The mode of π-electron population will then be dependent on the topology of molecules.

Choose any bond l from $\boldsymbol{G}$, say bond 1 from this graph. Then the Z_G sets of disconnected double bonds are divided into two groups, according to such a criterion that bond l is chosen as double (l-inclusive) or not (l-exclusive). The numbers of these two groups are denoted respectively as Z_G (l-inclusive) and Z_G (l-exclusive) and we have

$$Z_G = Z_G(l\text{-inclusive}) + Z_G(l\text{-exclusive}). \tag{26}$$

They are obtained respectively as the numbers of o and x's in the given column l. In this case ($l=1$) one gets $Z_G(l\text{-inclusive})=5$ and $Z_G(l\text{-exclusive})=8$. It is to be noted that each set of disconnected double bonds in the latter group appears once and only once in counting the value of Z_{G-l} (See the double rectangles in

Table 2. Comparison of the topological and Coulson bond orders for an isomer II of tetradecaheptaene[a)]

Bond type	Bond[a)] l	$Z_{G\ominus l}$[b)]	p_l^c approx.[c)]	p_l^c exact
Single bond	f	70	0.387	0.389
	b	75	0.400	0.400
	h	81	0.416	0.411
	d	100	0.466	0.469
	j	105	0.479	0.478
	l	109	0.489	0.488
Double bond	e	125	0.713	0.709
	k	148	0.775	0.777
	c	150	0.780	0.780
	g	162	0.813	0.818
	m	183	0.869	0.867
	i	197	0.907	0.907
	a	200	0.915	0.913

a) See Fig. 1. b) $p_l^\tau = Z_{G\ominus l}/Z_G$, $Z_G = 475$ for this graph. c) For single bonds: $0.002636\ Z_{G\ominus l} + 0.2020$, for double bonds: $0.002697\ Z_{G\ominus l} + 0.3757$.

Table 1). It means

$$Z_{G-l} = Z_G(l\text{-exclusive}). \tag{27}$$

Now by combining Eqs. (20), (26), and (27) one gets

$$\begin{aligned} Z_G(l\text{-inclusive}) &= Z_G - Z_{G-l} \\ &= Z_{G\ominus l}\,. \end{aligned} \tag{28}$$

The quantity Z_G (l-inclusive), or $Z_{G\ominus l}$, can then be considered as the weight of bond l in distributing π-electrons over G, and the topological bond order for l in G may be defined as Eq. (6).

In what follows a number of examples will be given of the good correlation between p_l^c and p_l^τ or $Z_{G\ominus l}$. In Table 2 and Fig. 1 the values of p_l^c and $Z_{G\ominus l}$ for an unsaturated hydrocarbon isomer II with 14 electrons

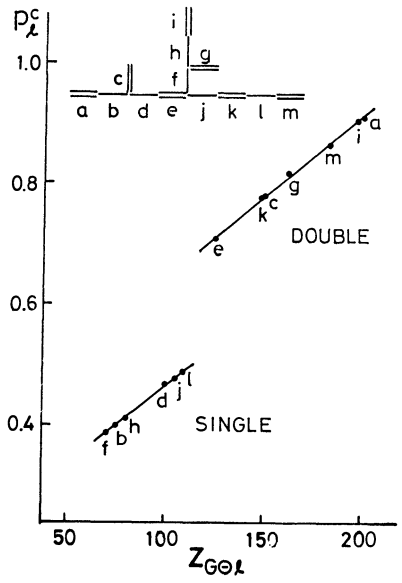

Fig. 1. Linear relationships between the Coulson bond order p_l^c and the topological bond order $p_l^\tau = Z_{G\ominus l}/Z_G$. The Z_G value for this graph (II) is 475. See also Table 2.

are compared. Note that two different sets of linear relationships are observed respectively for the bonds marked with "single" and "double" in the Kekulé structure. A procedure for obtaining the $Z_{G\ominus l}$ values with the recursive relations (20) and (21) is exempli-

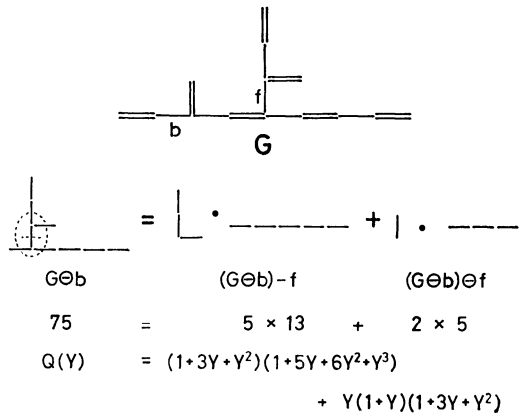

Fig. 2. The procedure for obtaining the topological index Z_G and the Z-counting polynomial $Q_G(Y)$ as exemplified by the subgraph $G\ominus b$ of the graph given in Fig. 1. Bond f is chosen to decompose the graph into fragments.

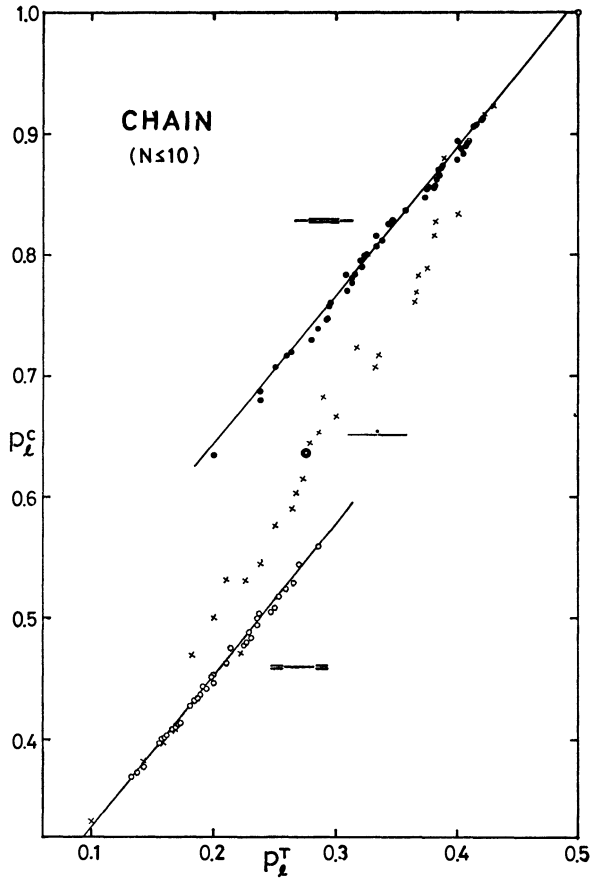

Fig. 3. Plots of p_l^c and p_l^τ values for all the possible isomers of polyenes not larger than decapentaene. ○: single bond, ●: double bond, x: bond in a radical, ◎: limiting bond order ($p_l^c = 0.6366$ and $p_l^\tau = 0.2764$) of an infinite polyene (See Eqs. (29)—(31), (40), (43)).

fied in Fig. 2 for bond b in the graph concerned, where bond f is chosen to decompose the graph into fragments. The topological indices of the fragmental graphs are given as the Fibonacci numbers or their combinations. The procedure is simple and easy enough for hand calculation but the result is surprizingly predictable.

Figure 3 gives the plots of p_l^c and p_l^τ for all the possible isomers of chain polyenes with not more than ten carbon atoms. The circles for the "single" (open) and "double" (filled) bonds in even-numbered polyenes with singlet ground states lie respectively on the two parallel lines, while for radicals (marked with crosses) the points lie on a line spanning from the "single bond line" over to the "double bond line" in Fig. 3. Two different classes of radicals are involved in this category, *i.e.*, even-numbered polyenes with a triplet ground state as III and odd-numbered polyenes with a doublet or higher multiplet ground state as IV. Thus for

III IV

chain polyenes or hydrocarbon radicals the Coulson bond order p_l^c can be estimated fairly accurately by hand calculation of p_l^τ value and bond type (single, double, or radical) classification. Tentatively from the set of points in Fig. 3 the following relations were obtained for the three classes of bonds.

$$p_l^c = 1.24\,p_l^\tau + 0.392 \quad (l=\text{double bond}) \tag{29}$$

$$p_l^c = 1.24\,p_l^\tau + 0.200 \quad (l=\text{single bond}) \tag{30}$$

$$p_l^c = 1.67\,p_l^\tau + 0.164 \quad (l=\text{bond in a radical}). \tag{31}$$

It is interesting to note that the topological bond orders of a linear polyene oscillate by going from the terminal to the center and converge to a limit as predicted by the p_l^c value. This is demonstrated in Fig. 4 for 1,3,5,7,9,11,13-tetradecaheptaene. For an infinite polyene p_l^τ and p_l^c values converge to $(5-\sqrt{5})/10=0.2764$ and $2/\pi=0.6366$ respectively (See Appendix), the speed of convergence of the former being much faster. Thus it is expected that for higher members of chain polyenes the relations (29)—(31) are getting worse as shown in Fig. 5, where p_l^τ and p_l^c values for linear polyenes larger than decapentaene are plotted. This is the limitation of the topological bond order for chain compounds.

For cyclic compounds there is no rigorous one-to-one correspondence between the coefficients of $P_G(X)$ (Eq. (7)) and $Q_G(Y)$ (Eq. (13)) polynomials as inferred from Eq. (9). Then correlation between p_l^c and p_l^τ values is not expected as good as what is

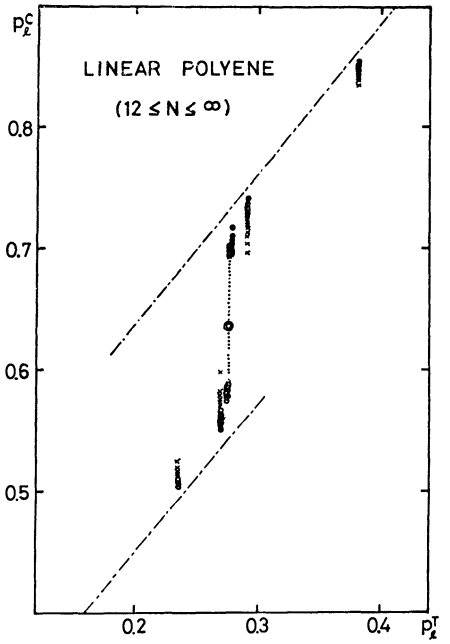

Fig. 5. Plots of p_l^c and p_l^τ values for larger linear polyenes ($N>10$). In the dotted line region a number of circles and crosses are crowded. The two parallel lines are the "single" and "double bond lines" in Fig. 3. Other marks are the same as used in Fig. 3.

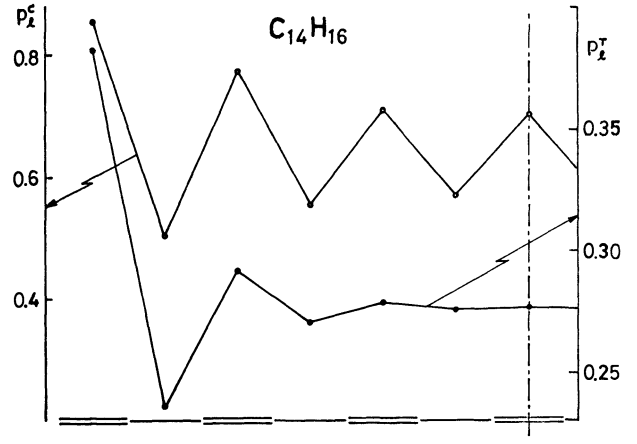

Fig. 4. Zig-zag nature of the Coulson and topological bond orders for a linear polyene (1,3,5,7,9,11,13-tetradecaheptaene).

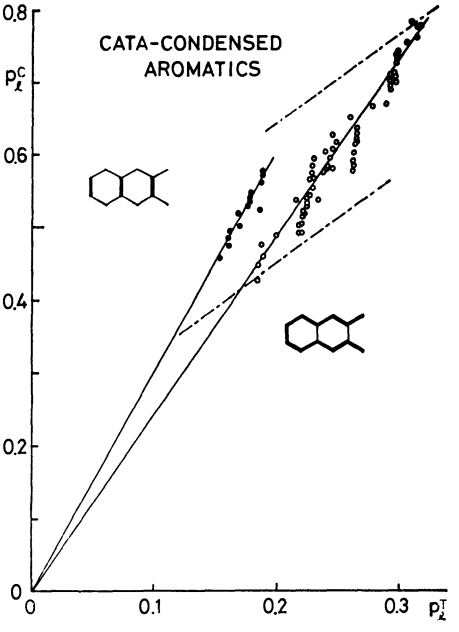

Fig. 6. Plots of p_l^c and p_l^τ values for cata-condensed aromatic hydrocarbons not larger than pentacene. ●: bridge bond, ○: peri-bond.

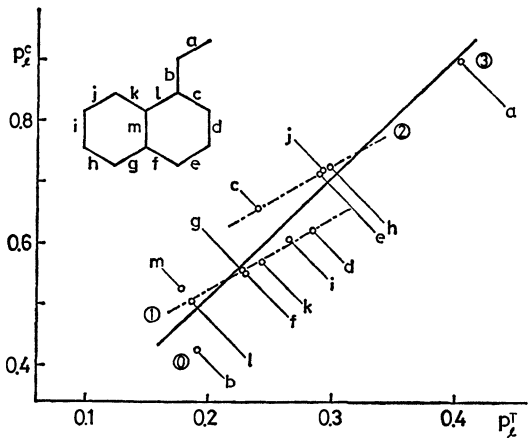

Fig. 7. Correlation between the p_l^C and p_l^T values of 1-vinylnaphthalene. The number in the circle indicates the $K(G\ominus l)$

shown in Figs. 1 and 3. In Fig. 6 are plotted the p_l^C and p_l^T values for cata-condensed aromatic hydrocarbons not larger than pentacene. Almost all the points lie within the region between the two parallel lines for single and double bonds in Fig. 3 and are grouped into two parts. The filled and open circles respectively correspond to the "bridge" and "peri-bonds". Both the classes of points lie on the respective lines passing through the origin. The linearity of these two classes of points is not so good as that of small polyenes (Fig. 3) but is unexpectedly good if one thinks of a simple procedure for getting the p_l^T values. Further, on the contrary to the chain compounds, the larger the cyclic graphs the better the correlation between p_l^C and p_l^T values as shown in Fig. 7 for 1-vinylnaphthalene. The thirteen points lie around a straight bold line. Inspection of this figure reveals an interesting feature of the correlation between p_l^C and p_l^T values. That is, the "corner bonds" (c, e, h, and j) lie perfectly on a straight line, while the "side bonds" (d, f, g, i, k, and l) lie on another line parallel to the former. The point for the "bridge bond" m is located nearby the latter line. Note that the unnormalized Pauling bond orders p_l^P's, *i.e.*, $K(G\ominus l)$ defined in Eq. (2), of these two groups of bonds are respectively two and one. The $K(G\ominus l)$ values of bonds a and b are respectively three and zero. Similar relations have been found in Eqs. (29)—(31).

Now it is empirically induced that for a certain group of molecules or for a group of bonds in a certain molecule the following relation is generally observed,

$$p_l^C = A\,p_l^T + B\,p_l^P. \tag{32}$$

This will be mathematically proved in a forthcoming paper by the use of an integration over the complex plane.[7,16]

Recently it is discussed which of the bond orders p_l^C and p_l^P is correlated better with the bond length.[17,18] However, as the aim of the present paper is to show the relation between these bond orders, much will not be discussed on this problem. Table 3 gives the comparison of the bond lengths and various bond orders for coronene. This is one of the cases where the topological bond order shows the best correlation

Table 3. Comparison of the bond lengths and various bond orders for coronene

Bond	Coulson p_l^C	Pauling p_l^P	Topological p_l^T	Bond length[a] (Å)
a	0.745	0.7	0.314	1.347
b	0.538	0.3	0.222	1.417
c	0.538	0.4	0.185	1.433
d	0.522	0.3	0.206	1.425

a) J. M. Robertson and J. G. White, *Nature*, **154**, 605 (1944); J. K. Fawcett and J. Trotter, *Proc. Roy. Soc., Ser. A*, **289**, 366 (1966).

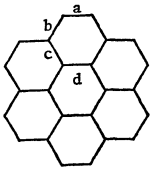

with the experimentally obtained bond lengths.

Appendix

The Limiting Values of the Topological Bond Order p_l^T.

Consider a polyene $\overline{N}$ with N consecutive points linearly connected. The topological bond order p_l^T of the l-th bond from one of the terminals is given by Eq. (6) as

$$p_l^T = \frac{Z_{\overline{N}\ominus l}}{Z_{\overline{N}}}. \tag{33}$$

Note that graph $\overline{N}\ominus l$ has two component graphs $\overline{l-1}$ and $\overline{N-l-1}$.

Then we have

$$Z_{\overline{N}\ominus l} = Z_{\overline{l-1}} \times Z_{\overline{N-l-1}}. \tag{34}$$

The $Z_{\overline{N}}$ series form the Fibonacci numbers and is expressed by the Binét's formula as

$$Z_N = (\alpha^{N+1} - \beta^{N+1})/\sqrt{5} \tag{35}$$

where

$$\alpha = (1+\sqrt{5})/2$$

and

$$\beta = (1-\sqrt{5})/2.^{6)} \tag{36}$$

From Eqs. (33)—(36) one gets

$$p_l^T = \frac{1}{\sqrt{5}\,\alpha}\,\frac{1-X^l+X^N(1-X^{-l})}{1-X^{N+1}} \tag{37}$$

where

$$X = \beta/\alpha = (\sqrt{5}-3)/2 = -0.38197. \tag{38}$$

For larger N Eq. (37) reduces to

$$p_l^T \to (1-X^l)/(\sqrt{5}\,\alpha) \tag{39}$$

which oscillates by going from the terminal ($l=1$) to the center ($l\to\infty$) and finally reaches

$$p_l^T \to 1/(\sqrt{5}\,\alpha) = (5-\sqrt{5})/10 = 0.27639. \tag{40}$$

This behavior of p_l^T corresponds to that of p_l^C as expressed by

$$p_l^C = \frac{1}{N+1}\left\{\operatorname{cosec}\frac{\pi}{2N+2} + (-1)^{l-1}\operatorname{cosec}\frac{(2l+1)\pi}{2N+2}\right\} \quad (N=\text{even}) \tag{41}$$

$$p_l^c = \frac{1}{N+1}\left\{\cot\frac{\pi}{2N+2} + (-1)^{l-1}\cot\frac{(2l+1)\pi}{2N+2}\right\}$$

$$(N=\text{odd}).^{19)} \quad (42)$$

Namely, since for larger N $\operatorname{cosec}\theta$ and $\cot\theta$ converge to θ^{-1}, one gets

$$p_l^c \to \frac{2}{\pi}\left\{1+(-1)^{l-1}\frac{1}{2l+1}\right\} \to 2/\pi = 0.63662. \quad (43)$$

References

1) L. Pauling, "The Nature of the Chemical Bond," Cornell Univ. Press, Ithaca, N. Y. (1960), p. 232.
2) C. A. Coulson, *Proc. Roy. Soc., Ser. A*, **169**, 413 (1939).
3) R. S. Mulliken, *J. Chem. Phys.*, **23**, 1833 (1955).
4) N. S. Ham and K. Ruedenberg, *J. Chem. Phys.*, **29**, 1215 (1958).
5) N. S. Ham, *J. Chem. Phys.*, **29**, 1229 (1958).
6) H. Hosoya, This Bulletin, **44**, 2332 (1971).
7) H. Hosoya, K. Hosoi, and I. Gutman, *Theor. Chim. Acta*, **38**, 37 (1975).
8) H. Hosoya, *Theor. Chim. Acta*, **25**, 215 (1972).
9) H. Sachs, *Publ. Math. Debrecen*, **11**, 199 (1963).
10) A. Graovac, I. Gutman, N. Trinajstić, and T. Živković, *Theor. Chim. Acta*, **26**, 67 (1972).
11) R. B. Mallion, N. Trinajstić, and A. J. Schwenk, *Z. Naturforsch.*, **29a**, 1481 (1974).
12) K. Mizutani, K. Kawasaki, and H. Hosoya, *Natural Science Report of Ochanomizu Univ.*, **22**, 39 (1971).
13) K. Kawasaki, K. Mizutani, and H. Hosoya, *Natural Science Report of Ochanomizu Univ.*, **22**, 181 (1971).
14) T. Yamaguchi, M. Suzuki, and H. Hosoya, *Natural Science Report of Ochanomizu Univ.*, **26**, 39 (1975).
15) H. Hosoya, *Fibonacci Quarterly*, **11**, 255 (1973).
16) C. A. Coulson and H. C. Longuet-Higgins, *Proc. Roy. Soc., Ser. A*, **191**, 39 (1947).
17) N. L. Allinger and J. T. Sprague, *J. Amer. Chem. Soc.*, **95**, 3893 (1973).
18) W. C. Herndon, *ibid.*, **96**, 7605 (1974).
19) See for example, C. A. Coulson and A. Streitwieser Jr., "Dictionary of π-Electron Calculations," Pergamon Press, Oxford (1965).

Competition of the Two Reaction Mechanisms of Maleic Anhydride Formation in Vapor-Phase Oxidation of Butadiene over Supported Molybdena Catalysts

Masamichi Akimoto and Etsuro Echigoya

Department of Chemical Engineering, Tokyo Institute of Technology, Ookayama, Meguro-ku, Tokyo 152

(Received June 25, 1975)

Vapor-phase oxidation of butadiene, 2,5-dihydrofuran and furan over supported molybdena catalysts has been investigated with reference to the reaction mechanism and the rate-determining step of maleic anhydride formation from butadiene. Formation of maleic anhydride during the oxidation of butadiene was found to follow two reaction mechanisms, (a) *via* 2,5-dihydrofuran and furan, and (b) *via* 2,5-dihydrofuran but not *via* furan. The energy barrier for the addition of oxygen species to adsorbed butadiene or furan is very high, *i.e.*, 28.9 or 21.9 kcal/g-mol, respectively, as compared to that for the oxidative dehydrogenation of the intermediate compounds such as 2,5-dihydrofuran. Formation of 2,5-dihydrofuran is rate-determining in these mechanisms during the oxidation of butadiene to maleic anhydride. The second mechanism plays a more important role in maleic anhydride formation at low temperatures, the role of the first mechanism increasing with a rise in the reaction temperature.

The increasing technical importance of maleic anhydride has strongly stimulated interest in its production by the direct oxidation of C_4-fraction obtained from petroleum. Many attempts to oxidize butane, butenes, and butadiene with gaseous oxygen, forming maleic anhydride, have been made, but most of them have been mainly devoted to the development of new catalysts.[1] In contrast, there are only a few studies on the mechanism and the rate-determining step for anhydride formation.[2] Ai, Harada, and Suzuki[3] studied extensively the vapor-phase oxidation of *n*-butenes to maleic anhydride over P_2O_5–V_2O_5 catalyst and concluded that the anhydride is formed *via* butadiene and furan. However, the exact mechanism and the rate-determining step have not yet been clarified.

In previous studies on the vapor-phase oxidation of butadiene over supported molybdena catalysts, it was shown that the selectivity for maleic anhydride formation is strongly affected not only by the kind of oxygen species formed on molybdenum ion but also by the nature of adsorbed butadiene species and that 2,5-dihydrofuran is the first intermediate compound for the anhydride formation from butadiene.[4,5] Thus, it is meaningful to study the oxidation of butadiene, 2,5-dihydrofuran, and furan over supported molybdena catalyst with reference to the reaction path for maleic anhydride formation in the oxidation of butadiene. Detailed investigation of these oxidation reactions has been made over various molybdena catalysts followed by the prediction of the reaction mechanism for anhydride formation. The reaction step for maleic anhydride formation at which the energy barrier is highest was also determined.

Experimental

The apparatus and procedure used for the oxidations were the same as those reported,[5] except that 2,5-dihydrofuran and furan were evaporated by bubbling air through the liquids cooled with ice-water followed by dilution with a large amount of air and then by introduction of the mixtures into the reactor. As reactants, very pure butadiene, reagent grade 2,5-dihydrofuran and furan were used.

Various supported molybdena catalysts and molybdena-titania modified with 5B group element were prepared by the method reported.[5,6]

The gaseous effluent from the reactor was analyzed by gas chromatography. PEG 20 M 20 wt% on Neopak 1 A (80 °C, 2,5-dihydrofuran, furan, acrolein), propylene carbonate 40 wt% on Celite 545 (room temp, butadiene, carbon dioxide) and molecular sieve 13X (room temp, carbon monoxide, nitrogen, oxygen) were used as separating columns. Since maleic anhydride was the only acid obtained, the product was absorbed into water followed by titration with an aqueous solution of sodium hydroxide using a pH meter, after boiling off carbon dioxide.

Results and Discussion

Reaction Mechanism for Maleic Anhydride Formation. Anatase-type titania is a very good carrier for molybdena catalyst in vapor-phase oxidation of butadiene to maleic anhydride, in contrast with alumina and magnesia and a maximum activity and selectivity is obtained at a molybdena content of 25 mole%.[4] In order to predict the intermediate compound for anhydride formation, the effects of the contact time on the selectivity to maleic anhydride formation and on the distribution of the reaction products were

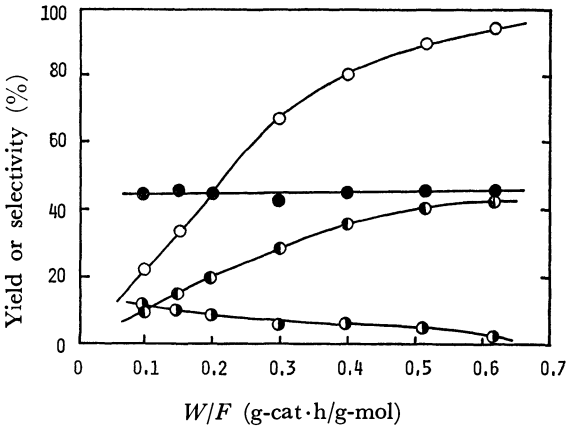

Fig. 1. Effect of the contact time on the distribution of the products in the oxidation of butadiene. Cat.: MoO_3–TiO_2–Sb_2O_3 [MoO_3/TiO_2=1/3, Sb/Mo=15 atom%], reaction temp: 380 °C, butadiene: 1.50 vol% in air, ○: conversion of butadiene, ◐: yield of (CO_2+CO), ●: selectivity to maleic anhydride, ◑: selectivity to furan

Table 1. Oxidation of furan over MoO_3–TiO_2 (1 : 3) catalyst[a)]

Temp (°C)	Conversion (%)	Yield (%)		Selectivity (%)
		CO_2+CO	Maleic anhydride	Maleic anhydride
284	negligible	0.40	0.34	—
295	6.00	1.06	1.26	21.0
313	20.9	3.42	2.93	14.0
326	32.0	9.74	5.56	17.4
338	41.2	12.1	10.4	25.3
353	54.1	15.1	16.2	29.9
369	72.0	21.1	24.2	33.6
393	89.3	25.4	31.2	35.0

a) Furan: 1.54 vol% in air, contact time: $W/F=0.376$ (g-cat·h/g-mol).

investigated with MoO_3–TiO_2 (1 : 3 mole ratio) catalyst modified with a small amount of antimony oxide at 380 °C and butadiene 1.50 vol% in air. The result obtained is graphically represented in Fig. 1. 2,5-Dihydrofuran is hardly obtained in the oxidation. Formation of a small amount of furan is observed in the reaction product. Increase in the contact time results in a decrease of selectivity for furan formation in contrast with conversion of butadiene and yield of (CO_2+CO), but the selectivity for maleic anhydride remains almost unchanged. For the sake of comparison, the oxidation of furan over MoO_3–TiO_2 (1 : 3) catalyst was carried out. The results obtained are summarized in Table 1. It seems that furan is easily converted into the anhydride at 380 °C. Thus, furan formed is possibly oxidized consecutively to the anhydride during the course of oxidation of butadiene at this temperature. However, if furan is an intermediate compound for the anhydride formation, it is expected that the selectivity for maleic anhydride is enhanced with decrease in the slectivity for furan formation. This is not in line with the results shown in Fig. 1. They suggest that furan is an intermediate compound for maleic anhydride formation from butadiene (denoted by mechanism A) in accordance with the result of earlier workers[3)] and also the presence of a reaction path through which the anhydride is formed not *via* furan (denoted by mechanism B).

As 2,5-dihydrofuran was already assumed to be the first intermediate for the anhydride formation from butadiene, it is very likely that furan is formed as a result of oxidative dehydrogenation of 2,5-dihydrofuran produced during the course of oxidation of butadiene over the molybdena catalyst. For the purpose of confirming this assumption, oxidation of 2,5-dihydrofuran was carried out over unsupported Bi_2O_3–MoO_3 (1 : 2) catalyst, *i.e.*, a typical catalyst for oxidative dehydrogenation of butenes to butadiene, and MoO_3–TiO_2 (1 : 3) catalyst with reference to the formation of furan (Table 2). The selectivity for furan formation over the Bi_2O_3–MoO_3 catalyst is very high, in contrast with that over the MoO_3–TiO_2. This can be attributed to the different nature of the catalysts, *viz.*, the latter catalyst has the ability of oxidizing 2,5-dihydrofuran to maleic anhydride in addition to oxidative dehydrogenation even at low temperatures. The results show definitely the formation of furan by oxidative dehydrogenation of 2,5-dihydrofuran produced during the oxidation of butadiene.

For the sake of clarifying the difference between mechanisms A and B, vapor-phase oxidation of 2,5-dihydrofuran was studied in detail using MoO_3–TiO_2 (1 : 3) catalyst. Figures 2 and 3 show the effect of the contact time and that of the reaction temperature on the distribution of the reaction products in the oxidation of 2,5-dihydrofuran. The selectivity for maleic anhydride formation at 320 °C is found to be

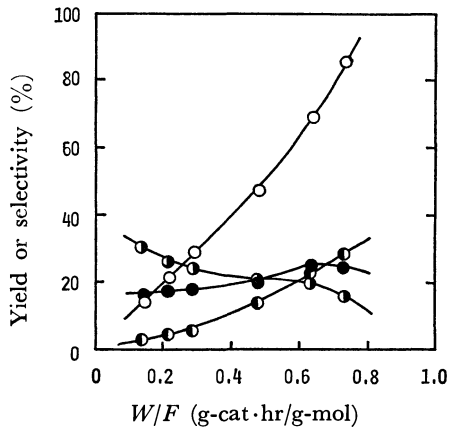

Fig. 2. Effect of the contact time in the oxidation of 2,5-dihydrofuran.
Cat.: MoO_3–TiO_2 (1 : 3), reaction temp.: 320 °C, 2,5-dihydrofuran: 1.50 vol% in air, ○: conversion of 2,5-dihydrofuran, ◐: yield of (CO_2+CO), ●: selectivity to maleic anhydride, ◑: selectivity to furan

Table 2. Oxidative dehydrogenation of 2,5-dihydrofuran

Catalyst	Temp (°C)	Conversion (%)	Yield of furan (%)	rate × 10^3 (furan g-mol/g-cat·h)	E_{all} (kcal/g-mol)
Bi_2O_3–MoO_3 (1 : 2)[a)] unsupported	256	8.9	8.21	1.683	
	273	11.4	11.2	2.285	9.5
	288	13.6	13.8	2.821	
MoO_3–TiO_2 (1 : 3)[b)]	258	8.4	2.36	0.929	
	270	10.0	2.65	1.044	6.0
	284	12.1	3.07	1.209	

a) 2,5-Dihydrofuran: 1.52 vol% in air, contact time: $W/F=0.724$ (g-cat·h/g-mol). b) 2,5-Dihydrofuran: 1.48 vol% in air, contact time: $W/F=0.377$ (g-cat·h/g-mol).

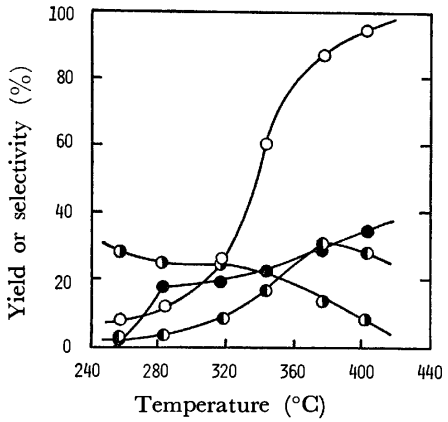

Fig. 3. Effect of the reaction temperature in the oxidation of 2,5-dihydrofuran.
Cat.: MoO_3-TiO_2 (1 : 3), 2,5-dihydrofuran: 1.49 vol% in air, contact time: $W/F=0.377$ [g-cat·h/g-mol], ○: conversion of 2,5-dihydrofuran, ◐: yield of (CO_2+CO), ●: selectivity to maleic anhydride, ◑: selectivity to furan

gradually enhanced with increase in the contact time in contrast with that to furan, which together with the results given in Table 1 give good evidence for the formation of maleic anhydride from 2,5-dihydrofuran *via* furan. A sudden enhancement of selectivity for maleic anhydride formation is observable without a large decrease in the selectivity for furan when the reaction temperature varies from 258 °C to 284 °C, though formation of maleic anhydride in the oxidation of furan is thought to be negligible at these temperatures (Table 1). Mechanism B seems to play an important role in maleic anhydride formation especially at these low temperatures, where furan is not an intermediate compound for the anhydride, being formed immediately from 2,5-dihydrofuran. Selectivity for both maleic anhydride- and furan-formations is almost unchanged at 284—320 °C though an increase in anhydride formation from furan with the rise in temperature is remarkable. This suggests formation of maleic anhydride *via* furan and at the same time not *via* furan as discussed below.

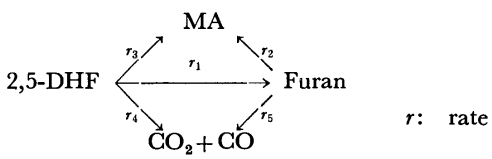

In the reaction path, the selectivities are defined by the following equations.

$$\text{select. to MA}=\frac{r_2+r_3}{r_1+r_3+r_4},\quad \text{select. to furan}=\frac{r_1-r_2-r_5}{r_1+r_3+r_4}$$

Assuming that these rates are independent of the concentration of 2,5-dihydrofuran and furan, if $r_2\fallingdotseq 0$, the overall activation energies in r_1, r_3, r_4, and r_5 are expected to be equal in order to obtain these constant selectivities. However, this condition can not be satisfied. In the case where $r_3\fallingdotseq 0$, the constant selectivities can be obtained so long as the activation energies in r_1, r_2, r_4, and r_5 are equal. The latter condition seems also not to be attained. Thus, it is impossible to deny that maleic anhydride is formed through

Table 3. Kinetic parameters for maleic anhydride formation[a)]

Reactant	Temp range (°C)	α	β	E_{all} (kcal/g-mol)
Butadiene	340—390	−0.17	0.65	28.9
Furan	340—370	0.00	0.49	21.9
2,5-Dihydrofuran	258—320	—	—	17.2

a) Cat.: MoO_3-TiO_2 (1 : 3), α,β: reaction order with respect to the reactant or oxygen, reactant: 1—2.5 vol%, oxygen: 7—20 vol%.

mechanisms A and B at these temperatures. Therefore, the anhydride appears to be formed *via* furan (mechanism A) above 284 °C in addition to the mechanism B, and the role of mechanism A seems to become important with rise in the reaction temperature.

Rate-Determining Step for Maleic Anhydride Formation

For the purpose of determining the reaction step for maleic anhydride formation from butadiene at which the energy barrier is the highest, butadiene, furan and 2,5-dihydrofuran were oxidized over the MoO_3–TiO_2 catalyst by means of a differential method. The kinetic parameters obtained are summarized in Table 3. Yield of furan is larger than that of maleic anhydride in the oxidation of 2,5-dihydrofuran (Fig. 3). It is likely because of the low reaction temperatures that the anhydride is formed mainly from 2,5-dihydrofuran and not *via* furan. Unlike the reaction orders of maleic anhydride formation, a striking difference appears between the overall activation energies for the anhydride formation from butadiene, furan, and 2,5-dihydrofuran. This suggests that the real activation energy for maleic anhydride formation from butadiene is also larger than that from furan and 2,5-dihydrofuran, the energy barrier from 2,5-dihydrofuran being the lowest.

The rates of furan formation in the oxidative dehydrogenation of 2,5-dihydrofuran over the Bi_2O_3–MoO_3 and the MoO_3–TiO_2 catalyst are included with the overall activation energy required for this reaction step in Table 2. The energy barrier for the oxidative dehydrogenation step is very low, *i.e.*, only 6.0—9.5 kcal/g-mol, as compared to that for maleic anhydride formation in the oxidation of butadiene and furan. This is presumably attributed to the larger delocalization of π-electrons even over oxygen atom in the intermediate compound formed by the abstraction of α-hydrogen from 2,5-dihydrofuran. Thus, the energy barrier for hydrogen abstraction from various oxygenated intermediate compounds is expected to be very low. The activation energy 28.9 or 21.9 kcal/g-mol is possibly required for the addition of the selective oxygen species to adsorbed butadiene or furan forming 2,5-dihydrofuran or maybe 5,6-dioxabicyclo[2.1.1]-hex-2-ene, respectively. Hence, it can be said that oxidative dehydrogenation of 2,5-dihydrofuran to furan is not rate-determining because of the very low energy barrier. This is also valid in oxidative dehydrogenation of the bicyclo-compound and other intermediate compounds. This is strongly supported by the absence of 2,5-dihydrofuran and the bicyclo-compound in the reaction product in contrast with furan during the

oxidation of butadiene. Therefore, it can be concluded that the reaction step for maleic anhydride formation from butadiene, at which the energy barrier is the highest, is an addition of the selective oxygen species to adsorbed butadiene followed by 2,5-dihydrofuran formation.

Double bond type lattice oxygen $Mo^{6+}=O$ is selective for maleic anhydride formation and its reactivity as a radical oxygen decreases with the electronegativity of molybdenum ion on which the lattice oxygen is bonded.[4,6] When the molybdena catalyst is modified with a relatively small amount of oxide of 5B group element, the reactivity of the double bond oxygen can be expected to be $Bi_2O_3>Sb_2O_3>As_2O_3>P_2O_5$ as a sequence of modifiers. The oxidation of butadiene was thus studied over MoO_3–TiO_2 (1 : 3) catalysts modified with various 5B group elements by a differential method, and the rate of maleic anhydride formation per unit surface area was carefully measured (Fig. 4). We see that the order of the activities of the catalysts for the anhydride formation is $Bi_2O_3>Sb_2O_3>P_2O_5>As_2O_3$, in line with that of the reactivities of the double bond oxygen in these modified catalysts. This provides further evidence for the above conclusion. Butadiene, furan, and 2,5-dihydrofuran were oxidized over the MoO_3–TiO_2 catalyst by means of a differential method with respect to the reaction temperature at which formation of the anhydride becomes remarkable (Fig. 5). The order in the rate of maleic anhydride formation is 2,5-dihydrofuran>furan>butadiene at 250—320 °C, in line with the sequence of the rate as judged from the height of the energy barrier. A relatively large rate of the anhydride formation is observed even at 258 °C in the oxidation of 2,5-dihydrofuran as compared to furan and butadiene oxidations. Thus, the results strongly suggest the presence of mechanism B through which maleic anhydride is produced not *via* furan.

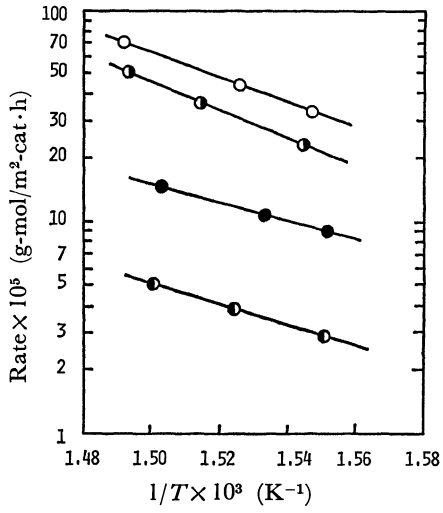

Fig. 4. Rate of maleic anhydride formation in the oxidation of butadiene over modified MoO_3–TiO_2 catalysts.
Cat.: X_mO_n–MoO_3–TiO_2 [$MoO_3/TiO_2=1/3$, X/Mo =30 atom%, X=Bi, Sb, As, or P], butadiene: 1.50 vol% in air, ○: Bi, ◑: Sb, ◐: As, ●: P

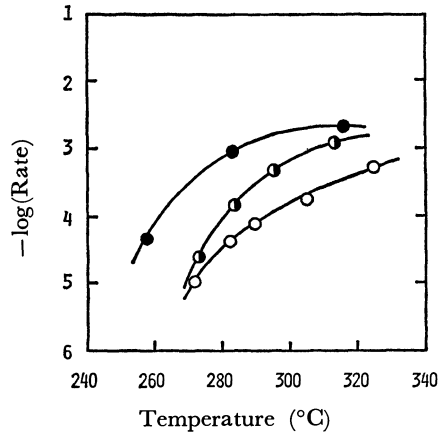

Fig. 5. Oxidation of butadiene, furan, and 2,5-dihydrofuran over MoO_3–TiO_2 catalyst.
Cat.: MoO_3–TiO_2 (1 : 3), feed: 1.50 vol% in air, rate: [g-mol MA/g-cat·h], ●: 2,5-dihydrofuran, ◑: furan, ○: butadiene

In general, the rate of catalytic reaction is proportional to the rate constant of surface reaction and the concentration of adsorbed reactant species. Determination of the surface concentration of the intermediate compounds such as 2,5-dihydrofuran, furan, and 5,6-dioxabicyclo[2.1.1]hex-2-ene during the oxidation of butadiene was not carried out. However, it is apparent that addition of the selective oxygen species to adsorbed butadiene or furan species forming 2,5-dihydrofuran or 5,6-dioxabicyclo[2.1.1]hex-2-ene is the rate-determining step for maleic anhydride formation from butadiene. Conversion of butadiene and the selectivity to furan formation are 44% and 8.5%, respectively, at $W/F=0.200$ g-cat·h/g-mol and 380 °C (Fig. 1). From this, the average concentrations of butadiene and furan in the vapor-phase along the catalyst bed are calculated to be 1.17 vol% and 0.028 vol%, respectively. The concentration of butadiene is very high relative to that of furan, but rate (butadiene→2,5-dihydrofuran), rate (2,5-dihydrofuran→furan), and rate (furan→maleic anhydride) through mechanism A are the same. This suggests the lowest reactivity of butadiene for anhydride formation. Formation of 2,5-dihydrofuran seems to be rate-determining, as previously presumed, as regards the activation energy. The reaction mechanisms are assumed as follows.

Mechanism A

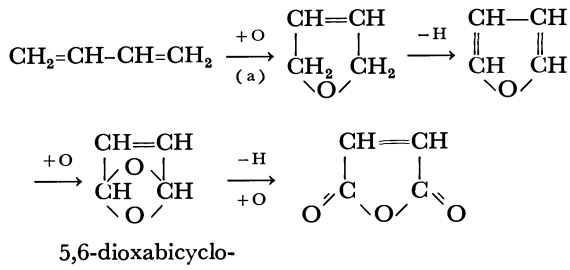

5,6-dioxabicyclo-[2.1.1]hex-2-ene

where step (a) is rate-determining.

Mechanism B

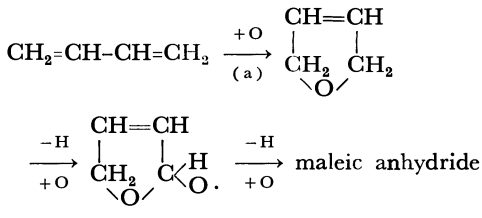

where step (a) is rate-determining.

In the case of mechanism B, since the intermediate compound formed from 2,5-dihydrofuran by the hydrogen abstraction is a radical, addition of the double bond oxygen to this compound seems to proceed more easily than that to adsorbed furan species. Thus, this path is energetically advantageous, as is evident from the oxidation of 2,5-dihydrofuran to maleic anhydride (Table 3). Consequently, it is natural that mechanism B plays the main role in anhydride formation especially at low temperatures. However, with a rise in temperature, rate of furan formation from 2,5-dihydrofuran becomes very large and thus the role of mechanism A seems to increase. It is, therefore, not unlikely that the selectivity for maleic anhydride formation is almost independent of that for furan formation (Fig. 1).

There is no direct evidence for the formation of 5,6-dioxabicyclo[2.1.1]hex-2-ene. As formation of an intermediate such as the bicyclo-compound was proposed in the vapor-phase oxidation of furfral to maleic anhydride,[7] it is probable that the anhydride is formed from butadiene *via* the bicyclo-compound in mechanism A. With the exception of 2,5-dihydrofuran and furan, formation of 5,6-dioxabicyclo[2.1.1]hex-2-ene is not really confirmed.

In conclusion, two mechanisms A and B have been found to participate in the selective oxidation of butadiene to maleic anhydride over supported molybdena catalyst. Mechanism B seems to play the main role of anhydride formation at low temperatures. Addition of the double bond oxygen to adsorbed butadiene species leading to 2,5-dihydrofuran formation is rate-determining in these mechanisms.

References

1) R. H. Bretton, S. W. Wan, and B. F. Dodge, *Ind. Eng. Chem.*, **44**, 594 (1952); N. Nagasako, M. Matsumoto, T. Ikawa, and S. Sakamoto, *Coal Tar*, **11**, 121 (1959); M. Matsumoto, T. Ikawa, and N. Nagasako, *Kogyo Kagaku Zasshi*, **63**, 734 (1960); M. Matsumoto, T. Ikawa, M. Kozai, N. Nagasako, and Y. Tsuchiya, *J. Japan. Petr. Inst.*, **3**, 394 (1960); B. L. Moldavskii and Y. D. Kernos, *Kinet. Katal.*, **1**, 267 (1960); W. A. Skinner and D. Tieszer, *Ind. Eng. Chem.*, **53**, 557 (1961); T. C. Bissot and K. A. Benson, *Ind. Eng. Chem. Prod. Res. Develop.*, **2**, 57 (1963); M. Ai, T. Niikuni, and S. Suzuki, *Kogyo Kagaku Zasshi*, **73**, 165 (1970); M. Ai, *ibid.*, **73**, 950 (1970).

2) Y. D. Kernos and B. L. Moldavskii, *Neftekhimiya*, **2**, 519 (1962); C. F. H. Tipper, "Oxidation and Combustion Reviews," vol. 1, Elsevier, Amsterdam (1965) p. 271; I. Komuro, *Shokubai*, **10**, 252 (1968).

3) M. Ai, K. Harada, and S. Suzuki, *Kogyo Kagaku Zasshi*, **73**, 524 (1970).

4) M. Akimoto and E. Echigoya, *J. Catal.*, **29**, 191 (1973).

5) M. Akimoto and E. Echigoya, *ibid.*, **31**, 278 (1973).

6) M. Akimoto and E. Echigoya, *ibid.*, **35**, 278 (1974).

7) N. A. Milas and W. L. Walsh, *J. Amer. Chem. Soc.*, **57**, 1389 (1935).

Non-empirical Calculation of the *G*-Values for the Ionization and Excitations in Diatomic Molecules Irradiated by 100 keV Electrons

Kiyoshi OKAZAKI and Shin SATO

Department of Applied Physics, Tokyo Institute of Technology, Ookayama, Meguro-ku, Tokyo 152

(Received June 26, 1975)

The binary-encounter collision theory has been applied to the calculation of the *G*-values for the ionization and excitations of diatomic molecules irradiated by 100 keV electrons. The obtained *G*-values of electrons are as follows, in the order of H_2, N_2, CO, NO, and O_2: 2.83, 2.55, 2.68, 3.61, and 2.98. These values are in fair agreement with the experimental ones. The present non-empirical method is compared with the semi-empirical ones proposed by other investigators. The *G*-values of some other products were also calculated: the excited hydrogen atoms in the radiolysis of H_2 (0.9) and the ozone formation in the radiolysis of O_2 (12.6). These *G*-values are also in fair agreement with the experimental ones.

Many investigators have measured the *W*-values ($=100/G_e$; G_e is the *G*-value of electrons) of diatomic molecules by the saturation-ion-current-method.[1-4] In the experiments of the radiolysis of carbon monoxide, nitric oxide, oxygen, and nitrogen, some of the information about the yields of the charged and excited species produced in the primary process has been obtained by measuring the final products and by considering the reaction mechanisms.[5-10] However, scarcely no theoretical treatment of the primary process in the radiolysis of these molecules has been carried out.

Recently, we have developed the non-empirical method for the estimation of the initial *G*-values by combining the binary-encounter collision theory with the theory of the degradation spectrum.[11,12] We have thus far calculated the cases of noble gases from helium to xenon and of such molecules as methane, ammonia, and water, and have shown that our calculation can provide much information for use in considering the primary processes of the radiolyses of these atoms and molecules.[13,14]

In this paper, we will apply this method to estimating the initial *G*-values of products from five diatomic molecules: H_2, N_2, CO, NO, and O_2. The most striking aspect of the present results is that the *W*-values calculated from this comparatively simple method are in reasonable agreement with the experimental values. In the discussion, we will compare the present method with the semi-empirical ones proposed by other investigators.[15-18]

Method of Calculation

The procedure for the present calculation is the same as that shown in the previous paper,[11-14] except for the treatment of the highly excited states of hydrogen to be described below; this treatment was special because the energies of these highly excited states are now available.

When the modes of the excitations of hydrogen are considered in further detail, two channels of the energy loss of electrons have to be introduced at the energy above the ionization potential. These channels are the dissociative excitation and the dissociative ionization. In the present treatment, their threshold energies are denoted by E^* and $E^\dagger$ respectively. When high-energy-electrons lose the energies between E^* and $E^\dagger$, we assume that one half of the energy gives rise to the ordinary ionization ($H_2^+ + e^-$), while the other half of this energy gives rise to the dissociative excitation ($H + H^*$). Therefore, the cross section for the dissociative excitation producing an excited hydrogen atom may be expressed in this form:

$$Q_{de}(T) = \frac{1}{2}\int_{E^*}^{E\dagger}[\sigma_{E,dir}+\sigma_{E,exc}]dE \qquad (1)$$

for $T \geq E^\dagger$. Here $\sigma_{E,dir}$ and $\sigma_{E,exc}$ denote, respectively, the differential cross sections for direct and exchange excitations.[11,12] When $E^* \leq T < E^\dagger$, the upper limit of the integral in Eq. (1) has to be replaced by T. When $T < E^*$, $Q_{di}(T)$ is set equal to zero.

Similarly, the total cross section for the dissociative ionization ($H + H^+ + e^-$) may be expressed by:

$$Q_{di}(T) = \frac{1}{4}\int_{E\dagger}^{E^{**}}[\sigma_{E,dir}+\sigma_{E,exc}]dE \qquad (2)$$

for $T \geq E^{**}$. Here E^{**} is the threshold energy for the double excitation ($H^* + H^*$). When $E^\dagger \leq T < E^{**}$, the upper limit of Eq. (2) has to be replaced by T. When $T < E^\dagger$, $Q_{di}(T)$ is set equal to zero. The factor of 1/4 in Eq. (2) has to be introduced because there are two energy-loss-processes (the ordinary ionization and dissociative ionization); also, we cannot distinguish the origin of the scattered electron and so do not know whether it is originally the incident electron or the molecular electron.

Therefore, the total cross section for the ordinary ionization can be expressed by:

$$Q_i(T) = \frac{1}{2}\int_{I_i}^{T}[\sigma_{E,dir}+\sigma_{E,exc}]dE - \frac{1}{2}Q_{de}(T) - Q_{di}(T) \qquad (3)$$

Constants Used for Calculation

The binding energies (I_i), the kinetic energies (E_i), and the lowest energies of the allowed and forbidden excitations (E_s and E_t) used in the present calculation are summarized in Table 1. Here, the I_i values are those obtained by the technique of ESCA[19] and the E_i values are those calculated from the SCF wave functions.[20-23] The E_s and E_t values in the outermost shell were those experimentally obtained,[24] and the values in the inner shells were calculated using the following equations: $E_s(\text{inner shell}) = I_i(\text{inner}) - (I_i - E_s)_{outermost}$, $E_t(\text{inner shell}) = I_i(\text{inner}) - (I_i - E_t)_{outermost}$.

Table 2 shows the constants used for the calculation

Table 1. The binding energy (I_i), the kinetic energy (E_i) and the lowest allowed (E_s) and forbidden (E_t) levels of electrons

Molecule	(orbital)		I_i	E_i	E_s	E_t
H_2	$1\sigma_g$	2	16.0	31.96	12.6	8.8
N_2	$3\sigma_g$	2	15.57	52.18	9.2	6.2
	$1\pi_u$	4	16.69	43.87	10.3	7.3
	$2\sigma_u$	2	18.75	65.57	12.4	9.4
	$2\sigma_g$	2	37.3	59.8	31.0	28.0
	$1\sigma_u$	2	409.9	600.0	404.0	401.0
	$1\sigma_g$	2	409.9	600.0	404.0	401.0
CO	5σ	2	14.5	52.52	8.4	6.2
	1π	4	17.2	50.08	11.0	9.0
	4σ	2	20.1	68.41	14.0	12.0
	3σ	2	38.3	70.93	32.0	30.0
	2σ	2	295.9	434.8	290.0	288.0
	1σ	2	542.1	792.0	536.0	534.0
NO	2π	1	9.26	70.20	6.5	3.9
	1π	4	14.0	57.42	11.0	9.0
	5σ	2	16.7	52.85	14.0	11.0
	4σ	2	21.7	73.45	19.0	16.0
	3σ	2	40.6	73.19	38.0	35.0
	2σ	2	410.3	605.7	408.0	405.0
	1σ	2	543.3	799.5	541.0	538.0
O_2	$1\pi_g$	2	13.1	82.14	8.4	1.0
	$1\pi_u$	4	17.0	72.24	12.3	4.9
	$3\sigma_g$	2	18.8	60.08	14.1	6.7
	$2\sigma_u$	2	25.3	90.40	20.6	13.2
	$2\sigma_g$	2	39.6	78.19	34.9	27.5
	$1\sigma_u$	2	543.1	795.1	538.0	531.0
	$1\sigma_g$	2	544.2	794.8	540.0	532.0

Table 2. The constants used for the calculation of the double collision

	H_2	N_2	CO	NO	O_2
n_e	2	6	6	7	8
$\bar{I}_i$ (eV)	16.0	16.3	16.3	14.1	16.5
$\bar{E}_s$	12.6	10.0	10.0	11.0	12.0
$\bar{E}_t$	8.8	7.0	8.0	9.0	4.4
E_i	31.96	46.6	51.0	58.0	72.0
I_{ii}	20.7[a)]	32.6	32.6	28.2	33.0
E^{**}	29.9	33.0	33.0	28.0	33.0
E^{+*}	33.3	41.0	41.0	35.0	41.0
$\bar{r}$ (Å)	1.06	1.094	1.128	1.15	1.208

a) Calculated by use of the equation; $I_{ii}=E^{++}-I_i$.

of the double collision. The procedure used to estimate these constants was the same as that described in a previous paper.[12)]

In the case of the hydrogen molecule, the values of E^*, E^+, and E^{++} are 17.0, 23.1, and 36.7 eV respectively. Here, E^{++} is the threshold energy of the double ionization.

Results

Figure 1 shows the degradation spectra, $y(T)$, of the electrons in H_2, N_2, CO, NO, and O_2. It is noticeable

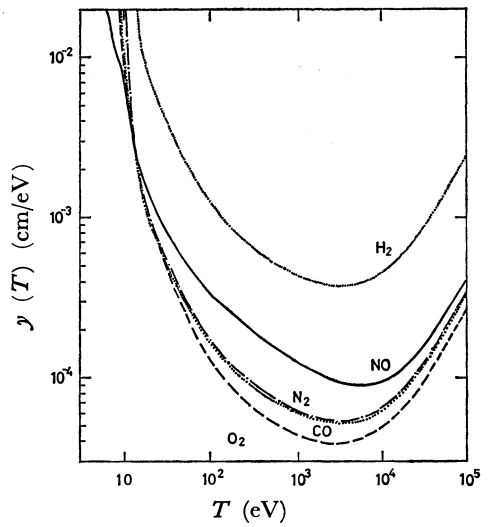

Fig. 1. The electron degradation spectra in H_2 (·····), N_2 (·—·—), CO (·····), NO (——), and O_2 (----).

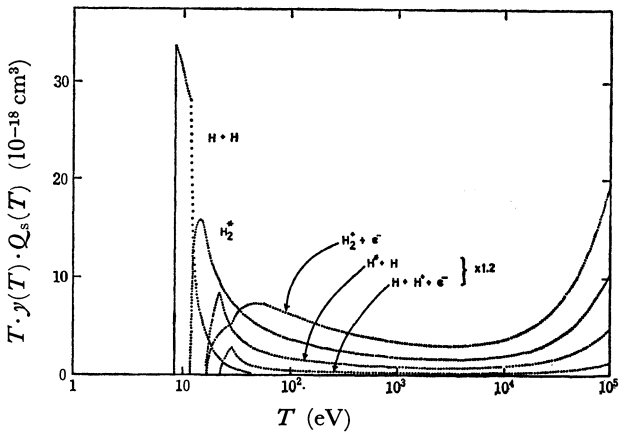

Fig. 2. Contribution of different portion of the electron degradation spectrum to the ionization and excitation in H_2.

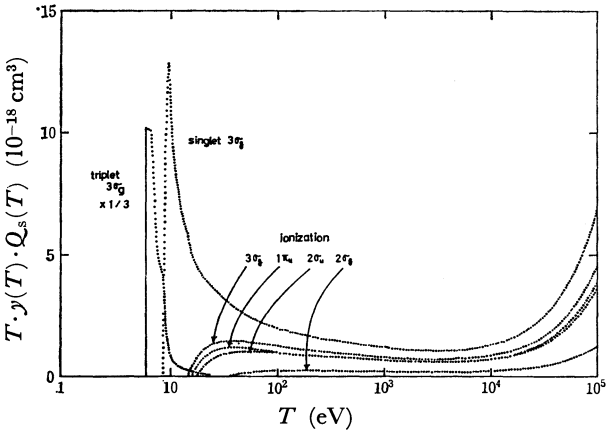

Fig. 3. Contribution of different portion of the electron degradation spectrum to the ionization and excitation in N_2.

that the $y(T)$ in N_2 nearly agrees with that of CO, probably because the construction of the molecular orbitals in the two molecules are similar. Figures 2, 3, 4, 5, and 6 show the $T\cdot y(T)\cdot Q_s(T)$ values for the

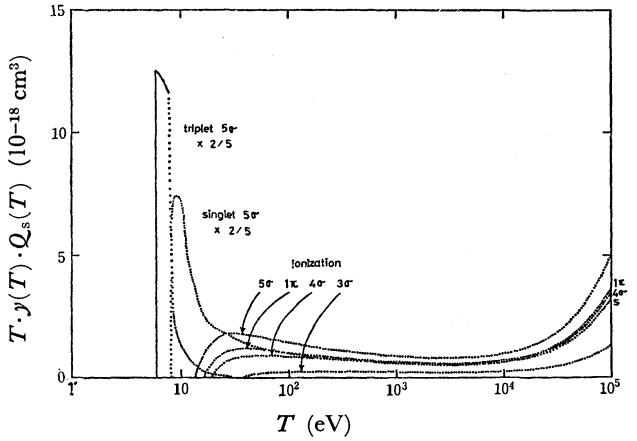

Fig. 4. Contribution of different portion of the electron degradation spectrum to the ionization and excitation in CO.

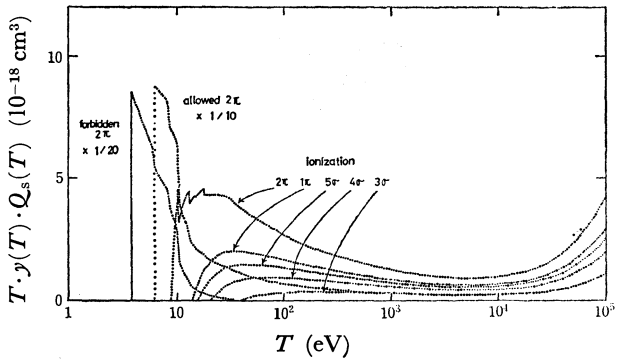

Fig. 5. Contribution of different portion of the electron degradtion spectrum to the ionization and excitation in NO.

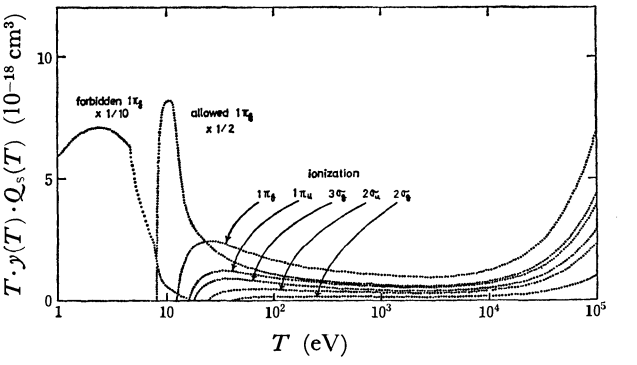

Fig. 6. Contribution of different portion of the electron degradation spectrum to the ionization and excitation in O_2.

excitations in H_2, N_2, CO, NO, and O_2 respectively as functions of In T. Figures 7 and 8 show the $T \cdot y(T) \cdot Q_s(T)$ values for the excitations from the inner shell in N_2, CO, NO, and O_2.

Tables 3 and 4 summarize the G-values for the ionization and excitations on each molecular orbital of the five diatomic molecules, and also for each double collision. Here, the values in parentheses are the G-values for autoionization in N_2 and CO. The M^{ii}, M^{ee}, M^{ie}, and M^{ie} values in Table 5 denote,

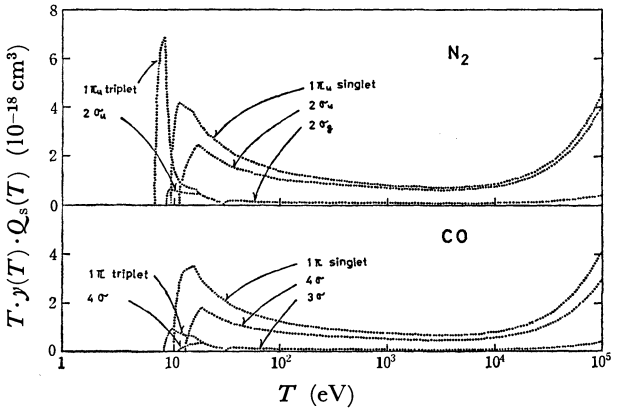

Fig. 7. Contribution of different portion of the electron degradation spectrum to the inner-shell-excitations in N_2 and CO.

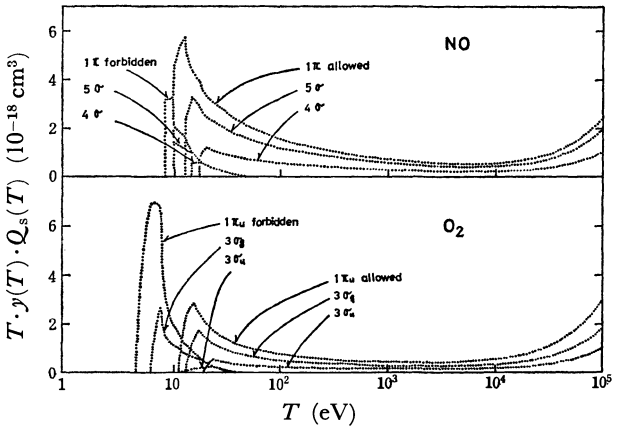

Fig. 8. Contribution of different portion of the electron degradation spectrum to the inner-shell-excitations in NO and O_2.

Table 3. The G-value of ionizations and excitations in hydrogen molecule

Mode	G-value
$H_2^* \longrightarrow H + H$	0.82
$H_2^* \longrightarrow H_2^*$	1.98
$H_2^* \longrightarrow H + H^*$	0.68
$H_2^+ \longrightarrow H_2^+$	2.62
$H_2^+ \longrightarrow H + H^+$	0.18
$H_2^{ii} \longrightarrow H^+ + H^+$	0.015
$H_2^{ee} \longrightarrow H^* + H^*$	0.031
$H_2^{ie} \longrightarrow H^+ + H^*$	0.17
$H_2^{ei} \longrightarrow H^* + H^+$	0.026

respectively, double ionization, double excitation, ionization and successive excitation, and excitation and successive ionization.

Discussion

W-Value. The calculated G-values of electrons and W-values are summarized in Table 6, along with the W-values obtained both experimentally[1-4] and theoretically.[15-18] Obviously, our W-values are in fair agreement with the experimental ones. Similar

Table 4. The G-values for the ionizations and excitations on each molecular orbital

		G_i	$G_{ex,s}$	$G_{ex,t}$
N_2	$3\sigma_g$	0.59	1.24	0.58
	$1\pi_u$	0.93	1.55	0.26
	$2\sigma_u$	0.47	0.59(0.20)	0.027(0.005)
	$2\sigma_g$	0.13	0.049	0.0017
	$1\sigma_u$	0.0072	0.00018	0.0000031
CO	5σ	0.67	1.69	0.65
	1π	0.93	1.37	0.070
	4σ	0.41	0.43(0.37)	0.014(0.008)
	3σ	0.13	0.048	0.0014
	2σ	0.010	0.00034	0.0000054
	1σ	0.0051	0.000093	0.0000014
NO	2π	0.54	2.72	2.12
	1π	1.16	1.41	0.18
	5σ	0.46	0.49	0.049
	4σ	0.32	0.22	0.022
	3σ	0.14	0.040	0.0055
	2σ	0.0085	0.00017	0.00014
	1σ	0.0061	0.000093	0.000097
O_2	$1\pi_g$	0.87	1.65	7.05
	$1\pi_u$	0.94	0.92	0.50
	$3\sigma_g$	0.34	0.27	0.076
	$2\sigma_u$	0.25	0.12	0.010
	$2\sigma_g$	0.099	0.025	0.0017
	$1\sigma_u$	0.0040	0.000061	0.0000015
	$1\sigma_g$	0.0040	0.000050	0.0000015

Table 5. The G-values for each double collision

	N_2	CO	NO	O_2
M^{ii}	0.025	0.009	0.133	0.039
M^{ee}	0.039	0.008	0.148	0.054
M^{ie}	0.081	0.065	0.388	0.143
M^{ei}	0.031	0.006	0.097	0.041

Table 6. The G-values of electrons and W-values

	H_2	N_2	CO	NO	O_2
G_e	2.83	2.55	2.68	3.61	2.98
W-value					
present	35.3	39.2	37.3	27.7	33.5
experiment	35.9[a]	34.1[a]	33.2[a]	27.5[a]	31.0[a]
		34.9[b]	33.3[c]		30.9[b]
					30.4[d]
calculation	34.9[e]	35.7[f]	35.8[g]		32.0[f]

a) Ref. 1. b) Ref. 2. c) Ref. 3. d) Ref. 4. e) Ref. 16. f) Ref. 15. g) Ref. 17.

results have been obtained previously with noble gases from He to Xe, methane, ammonia, and water.[11-14] Therefore, it may be concluded that our method is useful for estimating the G-values of the electrons for all atoms and molecules.

Recently, Green and his associates have calculated the W-values for N_2.[15] O_2,[15] H_2,[16] and CO[17] out of aeronomic interest. In order to perform the calculation, they accumulated experimental data concerning

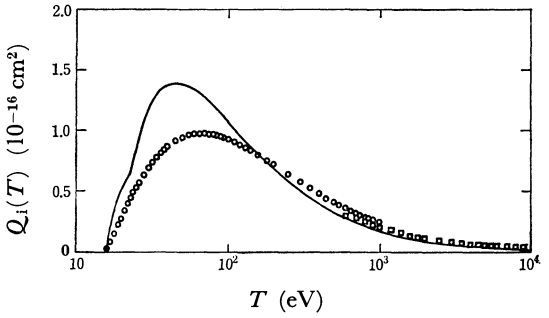

Fig. 9. The total cross section of ionization in H_2. ——, Calculated; ○, Ref. 25; □, Ref. 26.

the total cross section, the energy distribution of the secondary electrons, and the stopping power. They then determined the parameters of one equation to fit the experimental data, and finally they calculated the W-values under the assumption of a continuous slowing down. They did not use the concept of the degradation spectrum. On the other hand, Jones calculated the W-value and the yield of excitations in a hydrogen molecule out of radiation-chemical interest.[18] He did not use the assumption of a continuous slowing down either, but calculated the Fowler equation; the parameters were obtained semi-empirically. These two semi-empirical methods used to estimate the W-value both have the demerits that the method of calculation is very complex and that, if a complete set of the experimental data is not available, the estimation of any value is impossible.

On the other hand, the treatment of our non-empirical calculation is much simpler, and no experimental data on the cross sections are needed. Moreover, once the degradation spectrum of the electrons is constructed, we can estimate the G-values of any process by combining the degradation spectrum with the cross sections if they are available either theoretically or experimentally. However, since the cross sections used in our calculation are formulated only from the Coulomb interaction between two encountering species, the theoretical total cross section does not agree exactly with the experimental one. Nevertheless, the G-values calculated by our non-empirical method are in good agreement with the experimental values.

Figure 9 shows the total cross section for ionization in a hydrogen molecule as a function of ln T. The calculated cross sections at the electron energies from 10^2 to 10^4 eV are in good accordance with the experimental ones, but between the threshold energy and 10^2 eV the calculated ones are about 1.4 times the experimental ones.[25,26] Similarly, the calculated cross sections for N_2, CO, NO, and O_2 under the electron energy of 10^3 eV are much larger than the experimental ones.[25-27]

Since the calculated cross sections in N_2 is about three times the experimental one at its maximum, we tried to calculate the G-values by assuming that the differential and total cross sections were one-third of the cross sections used above; *i.e.*, the stopping power, $S(T)$, is one-third of that used above. However, the G-values thus obtained were the same as those obtained

above. This is because, when the degradation spectrum, $y(T)$, is calculated, the stopping power comes to the denominator. That is, the factor of three is cancelled during the course of the calculation. Consequently, we may conclude that, in order to estimate the G-values, it is not necessary to use the absolute cross sections, but only the relative values at each electron energy.

The Ratio of the G-Values of Excited Species to Those of Ionic Ones. We calculated the G-values for the total excitations, G_{ex}, the total loss of molecules, $G(-M)$, and the ratios of the G_{ex} to G_e. The results are shown in Table 7. Since the G_{ex}/G_e ratios of diatomic molecules are much larger than those of noble gases (0.4—0.6)[12], the excited species may play a more important role in the successive reaction than those in noble gases. This is similar to the finding in the molecules consisting of ten electrons.[14] Therefore, when we analyze the radiolyses of molecules, we must consider not only the charged species but also the excited ones. Especially, the G_{ex}/G_e of the oxygen molecule is very large because the energy of the lowest excited state ($^1\Delta$) is small.

The G-Value of Emissions. From the present calculations using the $y(T)$, the G-values for the emission of the light from highly excited species can be estimated by the use of the experimental cross sections described in the previous paper.[14] These cross sections in the hydrogen molecule and the nitrogen molecule have been reported by Vroom and de Heer[28] and by Aarts and de Heer[29] respectively. The results are shown in Tables 9 and 10. Especially, the G-value of the emission from excited hydrogen atoms (0.81) accords fairly well with the $G(H^*)$ in Table 8 (0.94). These G-values of the products of the charged and excited species in Table 8 are calculated from Table 3. The G-value of the excited nitrogen atoms in N_2 is the same amount as that of the excited hydrogen atoms in methane, ammonia, and water. However, since the G-value of the excited hydrogen atoms in H_2 is very large, the G-value of the hot hydrogen atoms in H_2 may be produced in a large amount. The G-value of the hot hydrogen atoms was estimated to be about 2.

Table 7. The ratio of the G-value for total excitation to that of electrons

	H_2	N_2	CO	NO	O_2
G_{ex}	3.45	3.97	3.85	6.73	10.38
$G(-M)$	6.27	6.49	6.52	10.21	13.32
G_{ex}/G_e	1.22	1.56	1.44	1.86	3.48

Table 8. The G-value for the products in hydrogen molecule

	G
H_2^*	1.92
H^*	0.94
H	2.49
H^+	0.40
H_2^+	2.43
e^-	2.83

Table 9. The G-values of emissions in hydrogen molecule

	G
Lyman α	0.52
H (2s)	0.25
Balmer α	0.03
β	0.006
γ	0.002
δ	0.0008
Total	0.81

Table 10. The G-values of emissions in nitrogen molecule

	Transition	λ (A)	G
NI	$3s\ ^4P-2p^3\ ^4S^\circ$	1200	0.028
	$3s\ ^2P-2p^3\ ^2D^\circ$	1494	0.011
	$3s'\ ^2P-2p^3\ ^2D^\circ$	1243	0.0098
	$3p\ ^4D^\circ-3s\ ^4P$	8680	0.012
	$2p^4\ ^4P-2p^3\ ^4S^\circ$	1134	0.0064
	$3d\ ^2D-2p^3\ ^2D^\circ$	1164	0.0026
			0.069
NII	$2p^3\ ^3D^\circ-2p^2\ ^3P$	1084	0.018
	$2p^3\ ^3P^\circ-2p^2\ ^3P$	916	0.0035
	$2p^3\ ^1D^\circ-2p^2\ ^1D$	776	0.0008
	$3s\ ^1P^\circ-2p^2\ ^1D$	747	0.0010
	$3d\ ^3F^\circ-3p\ ^3D$	5003	0.0015
			0.024
	$a\ ^1\Pi_g-X\ ^1\Sigma_g^+(2-0)$	1384	0.0033
	$p'\ ^1\Sigma_u^+-X\ ^1\Sigma_g^+(0-1)$	981	0.0056
	$p'\ ^1\Sigma_u-a\ ^1\Pi_g(0-0)$	2825	0.00016

The Radiolysis of Nitric Oxide. Hochanadel *et al.* proposed the following reaction mechanism and estimated the G-values of the products in the radiolysis at 25°C of NO irradiated by a 2 MeV electron beam:[6]

$$24.8\,NO \rightarrow 5.3\,N_2 + 7.0\,NO_2 + 3.6\,N_2O_3$$

$$NO \rightsquigarrow NO^+ + e^-$$

$$\rightarrow NO^* \rightarrow N + O$$

$$NO^+ + e^- \rightarrow NO^* \rightarrow N + O$$

$$NO + e^- \rightarrow NO^-$$

$$NO^+ + NO^- \rightarrow N + O + NO$$

$$N + NO \rightarrow N_2 + O$$

$$O + NO \rightleftarrows NO_2^*$$

$$NO_2^* + M \rightarrow NO_2 + M$$

$$NO_2 + NO \rightleftarrows N_2O_3$$

If the excited state of the outermost shell in our calculation cannot dissociate into nitrogen and oxygen atoms, the G-values of the nitrogen and oxygen atoms can be estimated to be 5.50. Therefore, the G-values of these atoms are in fair accordance with the experimental values (5.3).

The Formation of Ozone. The radiolysis of an oxygen molecule at a high dose rate has been experi-

mented with by Willis *et al.*[7,8] They reported that the *G*-value of ozone is 12.8; this value is used as a chemical dosimeter. If we assume as follows, we can estimate the *G*-value of ozone from the present results: all the nuetralization reactions give two oxygen atoms per ion pair, and all the excited oxygen molecules, except for the lowest excited one ($^1\Delta$), dissociate into two oxygen atoms. That is, one oxygen atom produces one ozone. Then, the calculated *G*-value of ozone is 12.6. This value is in reasonable agreement with the experimental one.

References

1) G. G. Meisels, *J. Chem. Phys.*, **41**, 51 (1964).
2) P. Adler and H. K. Bothe, *Z. Naturforsch.*, **20a**, 1700 (1965).
3) R. M. Leblanc and J. A. Herman, *J. Chim. Phys.*, **63**, 1055 (1966).
4) R. Cooper and R. M. Mooring, *Australian J. Chem.*, **21**, 2417 (1968).
5) C. Willis and O. A. Miller, *Can. J. Chem.*, **48**, 3029 (1970).
6) C. J. Hochanadel, J. A. Ghormley, and P. J. Ogren, *J. Chem. Phys.*, **50**, 3075 (1969).
7) A. W. Boyd, C. Willis, R. Cyr, and D. A. Armstrong, *Can. J. Chem.*, **47**, 4715 (1969).
8) C. Willis, A. W. Boyd, M. J. Young, and D. A. Armstrong, *ibid.*, **48**, 1505 (1970).
9) T. Oka, R. Kato, S. Sato, and S. Shida, This Bulletin, **41**, 2192 (1968).
10) G. M. Meaburn, D. Perner, J. LeCalve, and M. Bourene *J. Phys. Chem.*, **72**, 3920 (1968).
11) S. Sato, K. Okazaki, and S. Ohno, This Bulletin, **47**, 2174 (1974).
12) K. Okazaki, S. Sato, and S. Ohno, *ibid.*, **48**, 1411 (1975).
13) S. Ohno, H. Nagayama, K. Okazaki, and S. Sato, *ibid.*, **48**, 2153 (1975).
14) K. Okazaki, S. Sato, and S. Ohno, submitted for publication.
15) L. R. Peterson and A. E. S. Green, *J. Phys. B*, **1**, 1131 (1968).
16) W. T. Miles, R. Thompson, and A. E. S. Green, *J. Appl. Phys.*, **43**, 678 (1972).
17) T. Sawada, D. L. Sellin, and A. E. S. Green, *J. Geophys. Res.*, **77**, 4819 (1972).
18) W. M. Jones, *J. Chem. Phys.*, **59**, 5688 (1973).
19) K. Siegbahn *et al.*, "ESCA Applied to Free Molecules," North-Holland, Amsterdam (1969).
20) W. Kolos and C. C. J. Roothaan, *Rev. Mod. Phys.*, **32**, 219 (1960).
21) B. J. Ransil, *ibid.*, **32**, 239 (1960).
22) H. Brion, *J. Chem. Phys.*, **30**, 673 (1959).
23) Y. K. Kim, *Radiat. Res.*, **61**, 21 (1975).
24) G. Herzberg, "Spectra of Diatomic Molecules," Van Nostrand, Princeton, N. J. (1963).
25) D. Rapp and P. Englander-Golden, *J. Chem. Phys.*, **43**, 1464 (1965).
26) B. L. Schram, F. J. de Heer, M. J. van der Wiel, and J. Kistemaker, *Physica*, **31**, 94 (1965).
27) L. J. Kieffer and G. H. Dunn, *Rev. Mod. Phys.*, **38**, 1 (1966).
28) D. A. Vroom and F. J. de Heer, *J. Chem. Phys.*, **50**, 580 (1969).
29) J. F. M. Aarts and F. J. de Heer, *Physica*, **51**, 425 (1970); **52**, 45 (1971); **52**, 609 (1971).

Microwave Spectrum of Ethylene Oxide in Excited Vibrational States

Nobuaki YOSHIMIZU, Chiaki HIROSE, and Shiro MAEDA

Research Laboratory of Resources Utilization, Tokyo Institute of Technology, O-okayama, Meguro-ku, Tokyo 152

(Received June 26, 1975)

In the rotational spectrum of ethylene oxide, the five lowest-lying vibrational states are assigned and the vibration-rotation constants and the centrifugal distortion constants are derived. The vibrational frequencies are estimated from relative intensity measurements at $\nu_a=803\pm18$ cm^{-1} and $\nu_b=814\pm23$ cm^{-1} for the antisymmetric species (with respect to the C_2 operation) and at $\nu_c=872\pm34$ cm^{-1}, $\nu_d=1020\pm33$ cm^{-1}, and $\nu_e=1109\pm42$ cm^{-1} for the symmetric species. The intensity measurements of the remaining spectral lines showed that these lines belong to vibrational states at frequencies above about 1000 cm^{-1}. The ν_a, ν_b, and ν_c states are tentatively assigned to ν_{15}, ν_{12}, and ν_5, respectively, by taking into account the Coriolis interactions.

With a considerable number of infrared and Raman investigations carried out so far,[1-13] the assignments of certain fundamental frequencies of ethylene oxide are still subject to controversy. Namely, as shown by some examples in Table 1, different authors have proposed considerably different frequencies for ν_7 (A_2, CH_2-twisting), ν_8 (A_2, CH_2-rocking), and ν_{12} (B_1, ring deformation), for which no direct spectral evidence has been obtained. Under these circumstances, further infrared and Raman studies would seem to be ineffective in improving the situation significantly, and rather somewhat different approach is required.

Now, it is known that the intensity measurements of microwave absorption in vibrationally-excited states[14] and the analysis of the vibration-rotation interaction[15-18] provide useful information about the energy and symmetry of these vibrational states. In fact, these methods may certainly be advantageous when the vibrational transition is extremely weak or forbidden as in those described above. Thus, the present work was carried to out examine the frequencies and the assignments of the lower fundamental frequencies of ethylene oxide using microwave spectroscopy.

TABLE 1. VIBRATIONAL ASSIGNMENT OF ETHYLENE OXIDE (in cm^{-1})

Symmetry	Type of vibration	Lord and Nolin[a]	Potts[b]	Hirokawa *et al.*[c]	Cant *et al.*[d]
A_1	ν_1(CH stretch)[f]	3005	(3006)[e]	3005	3018
	ν_2(CH_2 deform)	1490	1497.5	1494	1498
	ν_3(ring breath)[f]	1266	1270.5	1270	1270
	ν_4(CH_2 wag)[f]	1120	(1130)[e]	1120	1148
	ν_5(ring deform)	877	877	877	877
A_2	ν_6(CH stretch)	3063	(3065)[e]	3065	3073[g]
	ν_7(CH_2 twist)	(1345)[e]	(1300)[e]	1030	1047[g]
	ν_8(CH_2 rock)	807	(860)[e]	807	825[g]
B_1	ν_9(CH stretch)[f]	3019	3006	3019	3006
	ν_{10}(CH_2 deform)	1470	1471.5	1470	1472
	ν_{11}(CH_2 wag)	1153	1151	1153	1151
	ν_{12}(ring deform)	892	(890)[e]	840	840
B_2	ν_{13}(CH stretch)	3079	3065	3065	3065
	ν_{14}(CH_2 twist)	1143	1142	1143	1142
	ν_{15}(CH_2 rock)	821	821.5	822	821

a) Ref. 5. b) Ref. 6. c) Ref. 12. d) Ref. 13. e) Values in parenthesis were estimated in the original papers. f) ν_1, ν_3, ν_4, and ν_9 respectively, are assigned to the bands at 3018, 1269, 1123, and 3008 cm^{-1} of the Raman spectra of gaseous C_2H_4O obtained by the present authors. g) The values from IR spectra of solids.

Experimental

Ethylene oxide was purchased from the Matheson Co. and was used without further purification. The rotational spectrum was observed with a conventional spectrometer at 300 K mainly in the frequency region from 9 to 42 GHz. Previous results[19-21] were referred to in eliminating the spectral lines of isotopic species. A double resonance experiment was performed on the $2_{11}\leftarrow2_{02}$ and $2_{20}\leftarrow2_{11}$ transitions in order to confirm the assignment of the Q-branch transitions. Spectral line intensities were measured from a chart recorded using a Hewlett-Packard MRR8460A-607 R-band spectrometer.[24] The accuracy of the measurements was checked by measuring the natural abundance ratio of $^{12}C^{13}CH_4O$ to $^{12}C_2H_4O$.

Results and Discussion

The microwave spectra of ethylene oxide and its isotopic species have been investigated in the ground state by a number of authors,[19-23] resulting in the determination of the r_0, r_s, and r_m structures,[19-21] the dipole moment,[19] the centrifugal distortion constants,[21-23] and the ^{17}O quadrupole coupling constants.[23] On the basis of these results, the rotational spectrum of the vibrationally-excited states was identified and frequencies were assigned to the transitions in five low-lying vibrational states, ν_a, ν_b, ν_c, ν_d, and ν_e in increasing order of frequency, as listed in Table 2. Since the molecular dipole moment lies along the b-axis, a rotational transition $J_{K_{-1}K_1}\leftrightarrow J_{K_{-1}'K_1'}$ is allowed only for such $K_{-1}K_1\leftrightarrow K_{-1}'K_1'$ combinations as ee↔oo and eo↔oe, where e and o signify even and odd. The calculated transition frequencies for the three lower vibrational states, ν_a, ν_b, and ν_c, were obtained using the parameters given in Table 3, which were determined by a least-squares fit including the centrifugal distortion effect to the first order.[25] For ν_d and ν_e states no R-branch transitions were identified, so that their calculated transition frequencies were derived from the observed values of $1_{10}\leftarrow1_{01}$ and $2_{20}\leftarrow2_{11}$ *via* Q-branch plots without taking account of the centrifugal distortion.

In Table 4, the intensities of the excited state lines

Table 2. Rotational transitions of ethylene oxide in excited vibrational states (in MHz)

Transition	ν_a state		ν_b state		ν_c state		ν_d state		ν_e state	
	Obsd	Obsd−Calcd[a]	Obsd	Obsd−Calcd[a]	Obsd	Obsd−Calcd[a]	Obsd	Obsd−Calcd[c]	Obsd	Obsd−Calcd[c]
$1_{11}-0_{00}$	39464.11	−0.00	38849.04	−0.00	39939.20	0.00				
$2_{02}-1_{11}$	63135.78	−0.24	62460.26	0.25	64345.03	0.18				
$2_{12}-1_{01}$	67484.20	0.47	66105.41	−0.10	68771.68	−0.36				
$2_{21}-1_{10}$	90368.44	−0.22	89292.51	−0.15	90981.28	0.18				
$1_{10}-1_{01}$	11442.82	0.01	11594.62	−0.11	11104.31	−0.13	11206.23	0 00	10746.71	0.00
$2_{11}-2_{02}$[b]	24875.38	0.04	26462.83	−0.02	23818.16	0.13	24793.06	−0.89	24795.98	8.83
$2_{21}-2_{12}$	34327.74	0.00	34781.85	−0.03	33313.46	−0.04	33618.01	−0.68	32246.05	5.92
$2_{20}-2_{11}$[b]	15790.68	−0.48	15238.77	0.21	15531.11	−0.05	15194.78	−0.02	13978.02	0.00
$3_{21}-3_{12}$	—	—	24869.12	−0.12	22693.94	−0.14	23427.70	−1.70	—	—
$3_{31}-3_{22}$	40008.99	−0.03	39634.30	−0.14	39061.58	−0.07	38864.19	−2.34	—	—
$3_{30}-3_{21}$	23561.09	−0.01	21692.29	0.26	23454.24	−0.07	22304.39	−0.67	19695.59	11.01
$4_{22}-4_{13}$	41406.58	−0.05	—	—	39439.08	0.01	41517.05	−5.06	—	—
$4_{31}-4_{22}$	25002.35	0.31	25211.15	0.31	24361.27	0.10	24395.55	−2.96	23411.99	9.81
$4_{40}-4_{31}$	34884.00	−0.06	31300.39	−0.24	34919.31	0.20	32754.56	−3.69	—	—
$5_{32}-5_{23}$	37613.44	0.15	40960.67	0.16	—	—	—	—	38658.26	31.06
$5_{41}-5_{32}$	30155.73	0.37	28511.53	−0.07	29917.02	0.06	28750.93	−5.80	26126.32	24.97
$6_{42}-6_{33}$	—	—	38061.82	−0.11	34407.62	−0.15	35560.69	−9.55	35836.07	25.12
$6_{51}-6_{42}$	39574.30	0.03	35406.37	0.29	39786.69	−0.18	37052.08	−12.10	32037.08	78.42
$7_{52}-7_{43}$	37680.97	−0.25	37669.26	0.05	36967.51	0.16	36549.65	−14.51	35080.86	33.86
$8_{62}-8_{53}$	—	—	40927.98	−0.15	—	—	41765.74	−29.90	37492.10	91.00

a) Errors in the observed values are generally within ±0.1 MHz. b) The transitions were confirmed by a double-resonance experiment. c) The calculated frequencies of the rotational transitions for the ν_d and ν_e states were derived from the $1_{10}-1_{01}$ and $2_{20}-2_{11}$ transitions using Q-branch plots without taking account of the centrifugal distortion.

Table 3. Rotational and centrifugal distortion constants in excited vibrational states (in MHz)[a]

	Ground state[b]	ν_a	ν_b	ν_c
A_s	25483.92	25453.45	25222.09	25521.92
B_s	22120.82	22003.60	22250.62	22041.25
C_s	14097.82	14010.75	13626.91	14417.47
α_s^a		30.47	261.83	−38.00
α_s^b		117.22	−109.80	79.57
α_s^c		87.07	470.91	−319.65
τ_{aaaa}'	−0.2832±0.0084	−0.29±0.27	−0.30±0.20	−0.36±0.17
τ_{bbbb}'	−0.1250±0.0085	−0.01±0.28	−0.29±0.21	−0.21±0.18
τ_{cccc}'	−0.0327±0.0086	−0.06±0.30	0.46±0.23	−0.43±0.19
t_1[c]	−0.2351±0.0110	−0.59±0.37	0.11±0.26	−0.35±0.23
t_2[c]	−0.1021±0.0144	−0.91±0.49	0.65±0.37	−0.29±0.31

	Ground state[b]	ν_d	ν_e
$2B_s-A_s-C_s$	4659.90	4799.59	5404.57
A_s-C_s	11386.10	11206.23	10749.00

a) Error limits for the rotational constants and the vibration-rotation constants (α_s^x) for ν_a, ν_b, and ν_c were estimated from 2.5 times the standard deviations to be less than ±0.5 MHz. For the ν_d and ν_e states the values of $2B_s-A_s-C_s$ and A_s-C_s were derived using Q-branch plots of the observed values of the $1_{10}\leftarrow 1_{01}$ and $2_{20}\leftarrow 2_{11}$ transitions, and the reliability intervals were estimated to be ±0.5 MHz and ±2 MHz or more, respectively, for ν_d and ν_e. The large ambiguity in ν_e is due to the Coriolis interaction. b) The values for the ground state were calculated from the observed transitions reported in Ref. 22. c) $t_1=\tau_{aabb}'+\tau_{ccaa}'(A-B)/(A-C)$, $t_2=\tau_{bbcc}'+\tau_{ccaa}'(B-C)/(A-C)$.

are given by the ratios to those of the corresponding ground state lines. The table is limited within the frequency range covered by the MRR8460A-607 R-band spectrometer, and leaves quite a few lines unlisted because of the uncertainty due to overlapping. It can be noticed, however, that in the ν_a and ν_b states the relative intensity I of eo↔oe type transitions is about three times that of ee↔oo type values, while the I is approximately equal for both types of transitions in the ν_c, ν_d, and ν_e states.

Table 4. Values of $\exp(-h\nu/kT)\cdot g^{v}(J_{K_{-1}K_1})/g^{0}(J_{K_{-1}K_1})$,[a] the Boltzmann factor, and estimated vibrational frequencies

	ν_a	ν_b	ν_c	ν_d	ν_e	$^{12}C^{13}CH_4O$
$e^{-h\nu/kT}\cdot g^{v}(J_{ee})/g^{0}(J_{ee})$ and/or $e^{-h\nu/kT}\cdot g^{v}(J_{oo})/g^{0}(J_{oo})$						
$1_{11}-0_{00}$	—	0.012_0	0.014_1	—	—	0.016_4
$3_{31}-3_{22}$	—	—	0.017_0	0.007_9	—	—
$4_{41}-4_{31}$	0.012_6	—	0.014_3	0.007_6	—	—
$6_{42}-6_{33}$	—	0.011_3	0.015_0	0.007_5	0.004_4	0.016_7
$6_{51}-6_{42}$	(0.014_4)[b]	0.012_7	0.015_4	0.007_6	0.005_0	—
Average	0.012_6	0.012_0	0.015_2	0.007_7	0.004_7	0.016_6
$e^{-h\nu/kT}\cdot g^{v}(J_{eo})/g^{0}(J_{eo})$ and/or $e^{-h\nu/kT}\cdot g^{v}(J_{oe})/g^{0}(J_{oe})$						
$2_{21}-2_{12}$	0.035_1	0.034_8	0.015_3	0.006_6	—	0.028_5
$5_{41}-5_{32}$	0.034_8	0.034_2	0.015_9	—	—	0.027_7
$5_{32}-5_{23}$	0.037_5	—	—	—	0.005_2	—
$7_{52}-7_{43}$	0.034_7	0.033_6	0.015_1	0.007_6	0.005_0	0.029_3
Average	0.035_5	0.034_2	0.015_3	0.007_1	0.005_1	0.028_5
$e^{-h\nu/kT}$	0.021_3	0.020_2	0.015_3	0.007_5	0.004_9	0.021_1
2.5σ[c]	0.001_8	0.002_1	0.002_3	0.001_1	0.000_9	0.001_5
$\nu(cm^{-1})$	803 ± 18[c]	814 ± 23[c]	872 ± 34[c]	1020 ± 33[c]	1109 ± 42[c]	

a) $g^{0}(J_{K_{-1}K_1})$ and $g^{v}(J_{K_{-1}K_1})$ denote the spin weights of the $J_{K_{-1}K_1}$ rotational level for the ground and excited vibrational states, respectively. b) Since Stark components were not fully resolved, the value was not used in the subsequent analysis. c) 2.5 times the standard deviations introduced by $\exp(-h\nu/kT)\cdot g^{v}/g^{0}$ are indicated.

Now, this fact can be understood as arising from the degeneracy of the hydrogen nuclear spin states. Namely, the symmetry requirement for the composite wave functions formed by the vibrational, rotational, and nuclear spin parts leads to the following statement for the present C_{2v} case:[26] in the vibrational states of the A_1 and A_2 species, ee and oo type rotational levels are associated with a 10-fold nuclear spin weight, while eo and oe levels are associated with a 6-fold weight, with the situation in the B_1 and B_2 vibrational states, however, being inverted, *i.e.*, ee and oo are 6-fold while eo and oe are 10-fold. Then, since the ground state is necessarily an A_1 species, the Γ of the A_1 and A_2 states should be equal to the vibrational Boltzmann factor irrespective of the type of rotational transition. In B_1 and B_2 states, however, the Γ of ee$\leftrightarrow$oo type and eo$\leftrightarrow$oe type transitions prove to be equal to 6/10 and 10/6 times the Boltzmann factor, respectively. Thus, it is evident from Table 4 that ν_a and ν_b are of the B-type species and the rest are of the A-type. The energy of each vibrational state is calculated from the Boltzmann factor obtained as is given in Table 4. Slight changes in the dipole moment, rotational energies, and line widths in different vibrational states were ignored in the above discussion, as they are not expected to influence the conclusion significantly.

Referring to Table 3, it is noted that the rotational constant C and the centrifugal distortion constant τ'_{cccc} of the ν_b and ν_c states show unusually large deviations from those of the ground state in opposite directions. This observation indicates the presence of a c-type Coriolis interaction between the ν_b and ν_c states. It can be shown that the Coriolis terms in α^c and τ'_{cccc} are approximately given by $\mp 4C^2(\zeta_{b,c}^{(c)})^2/(E_b-E_c)$ and $\mp 64C^4(\zeta_{b,c}^{(c)})^4/(E_b-E_c)^3$, where the upper and lower signs refer to the ν_b and ν_c states at the vibrational energies E_b and E_c respectively.[16,18,27] Taking the conclusion of the preceding paragraph into consideration, the Coriolis coupling constant $\zeta_{b,c}^{(c)}$ proves to vanish except when the ν_b and ν_c states belong to either B_1 and A_1 or B_2 and A_2 species. Accordingly, after comparing the ν_b and ν_c energies in Table 4 with those in Table 1, their possible assignments are reduced to the following two cases: (i) ν_b to ν_{12} (B_1, ring deform) and ν_c to ν_5 (A_1, ring deform), or (ii) ν_b to ν_{15} (B_2, CH_2 rock) and ν_c to ν_8 (A_2, CH_2 rock). A tentative calculation using the force field fitted to the assignment of Lord and Nolin gives $\zeta_{12,5}^{(c)}=0.9965$ and $\zeta_{15,8}^{(c)}=0.3689$.[28] Then, the Coriolis parts of α^c and τ'_{cccc} are calculated to be ± 454 MHz and ± 0.473 MHz in case (i), and ± 62 MHz and ± 0.009 MHz in case (ii), respectively. Comparing these results with Table 3, the assignment of case (i) appears to be more probable, though not definite because of the uncertainty in E_b-E_c value used above. Assuming case (i) above to be correct, ν_a, ν_d, and ν_e may be reasonably assigned to ν_{15} (B_2, CH_2 rock), ν_7 (A_2, CH_2 twist) and ν_4 (A_1, CH_2 wag), respectively, in view of their frequencies and symmetries (see Table 1). Then the situation arises that the present microwave results lack an assignment for the vibrational state ν_8 (A_2, CH_2 rock). As it is very unlikely that the present study should have missed a vibrational state as low as about 800 cm^{-1},[29] this means that the frequency of ν_8 should be higher than those proposed by other authors, as listed in Table 1. In fact, we observed several spectral lines in addition to those

listed in Table 4 in the same frequency region, but their intensities gave little indication of the sixth vibrational state below 1000 cm^{-1}.

This conclusion is in fair agreement with the assignments of Hirokawa *et al.*[12] and the very recent one by Cant *et al.*[13] except for the location of ν_8 (A_2). The frequency of the last mode has, so far, always been based on solid spectra obtained at low temperature,[7,10,13] for which the infrared prohibition of A_2 modes may perhaps be lifted. In solid spectra, however, the appearance of crystal field splittings has always to be taken into account in dealing with such closely lying lines as 825 and 818 cm^{-1}, which have been assigned to ν_8 and ν_{12} by Cant *et al.* The present result suggests that they are not separate fundamental frequencies but are the split components of ν_{12}, contrary to the conclusions in Ref. 13. Incidentally, Cant *et al.* assigned the corresponding C_2D_4O frequencies at 587 and 779 cm^{-1}, but the former was also very close to the 595 cm^{-1} line which they assigned to ν_{15}. In view of their observation on a dilute C_2D_4O/C_2H_4O mixture, which gave only a single evident line near 590 cm^{-1}, it seems that the lines at 587 and 595 cm^{-1} are more likely to be the crystal field doublet of ν_{15}.

Finally, the possibility for case (ii) is mentioned, though it was previously discarded on the basis of Coriolis interaction behavior. Assuming the choice of case (ii), we can conclude that the ν_5 (A_1) state is missing in the present result, instead of ν_8. Such a case is very improbable, however, because the ν_5 frequency given in Table 1 has been established quite convincingly.

The authors are grateful to Professor Robert F. Curl, Jr., for allowing them to use the spectrometer in his laboratory at the initial stage of the present study. The authors wish to express their appreciation also to Dr. Shuji Saito of Sagami Chemical Research Center for his loan of the millimeter-wave klystrons and spectrometer for observation of some of the $J=2\leftarrow1$ transitions, and to Professor Kunio Kozima for encouragement throughout the work. They also wish to thank Professors Kozo Kuchitsu and Yonezo Morino, and Drs. Charles D. LeCroix and Harold Jones for reading the draft of this paper and making critical comments.

References

1) L. G. Bonner, *J. Chem. Phys.*, **5**, 704 (1937).
2) K. W. F. Kohlrausch and A. W. Reitz, *Proc. Indian Acad. Sci.*, **8A**, 255 (1938).
3) J. W. Linnett, *J. Chem. Phys.*, **6**, 692 (1938).
4) H. W. Thompson and W. T. Cave, *Trans. Faraday Soc.*, **47**, 946 (1951).
5) R. C. Lord and B. Nolin, *J. Chem. Phys.*, **24**, 656 (1956).
6) W. J. Potts, *Spectrochim. Acta*, **21**, 511 (1965).
7) J. LeBrumant and D. Maillard, *C. R. Acad. Sci. Paris*, **264**, 1107 (1967).
8) J. LeBrumant, *ibid.*, **268**, 486 (1969).
9) J. LeBrumant, *ibid.*, **270**, 801 (1970).
10) V. T. Aleksanyan, E. R. Razumova, A. P. Kurbakova, and S. M. Shostakovskii, *Opt. Spectrosc.*, **31**, 369 (1971).
11) J. E. Bertie and D. A. Othen, *Can. J. Chem.*, **51**, 1155 (1973).
12) T. Hirokawa, M. Hayashi, and H. Murata, *J. Sci. Hiroshima Univ.*, **37A**, 283 (1973).
13) N. W. Cant and W. J. Armstead, *Spectrochim. Acta*, **31A**, 839 (1975).
14) A. P. Cox and A. S. Esbitt, *ibid.*, **38**, 1636 (1963).
15) E. Hirota, *J. Mol. Spectrosc.*, **7**, 242 (1961).
16) T. Tanaka and Y. Morino, *ibid.*, **32**, 436 (1969).
17) V. W. Laurie and D. T. Pence, *ibid.*, **10**, 155 (1963).
18) E. Hirota and M. Sahara, *ibid.*, **56**, 21 (1975).
19) G. L. Cunningham, A. W. Boyd, R. J. Myers, W. D. Gwinn, and W. I. LeVan, *J. Chem. Phys.*, **19**, 676 (1951).
20) T. E. Turner and J. A. Howe, *ibid.*, **24**, 924 (1956).
21) C. Hirose, This Bulletin, **47**, 1311 (1974).
22) C. Hirose, *Astrophys. J.*, **189**, L145 (1974).
23) R. A. Creswell and R. H. Schwendeman, *Chem. Phys. Lett.*, **27**, 521 (1974).
24) The present study was initiated by one of the authors (C. H.) during his stay in the laboratory of Professor Robert F. Curl, Jr. at the Department of Chemistry of Rice University, Houston, Texas. The intensities were measured as the line intensities of the spectral lines which were recorded under the same conditions of the sample and spectrometer except that the strength of the Stark field to resolve the Stark components varied from line to line. The preliminary spectrum recorded there was of great help in the subsequent study.
25) J. K. G. Watson, *J. Chem. Phys.*, **46**, 1935 (1967).
26) C. H. Townes and A. L. Schawlow, "Microwave Spectroscopy," McGraw-Hill, New York (1955), p. 101.
27) H. H. Nielsen, "Handbuch der Physik," Vol. 38, ed. by S. Flügge, Springer, Berlin (1959), p. 173.
28) K. Venkateswarlu and P. A. Joseph, *Indian J. Pure Appl. Phys.*, **10**, 754 (1972).
29) There are two possible causes of missing the rotational lines of a vibrational state as low as about 800 cm^{-1}: (1) overlapping of the lines with those of the ground state, or (2) extremely strong Coriolis interaction which shifts all the transitions outside of the frequency region of the present observation. For the former case, all the three rotational constants of the vibrational state have to be equal to those of the ground state to within a few megahertz, thus, case (1) is unlikely though not impossible. Although, for the latter case, such a strong Coriolis interaction requires a fifth vibrational state located very close to the fourth state, none of the ν_a, ν_b, and ν_c states is perturbed as strongly and no rotational spectra that can be assigned to the fourth and fifth vibrational states were observed in this region. Furthermore, infrared and Raman spectra do not indicate the existence of the fifth state around 800 cm^{-1}. Therefore, this case can be ruled out.

Studies of the Coagulation Flotation of Bentonite and Its Application to the Removal of Co^{2+} Ions and Fission Products, Ce and Eu

Koichi KOBAYASHI,* Hiroshi SATO,** Kosei KACHI,*** Masao NAKAMURA,**** and Tsunetaka SASAKI****

Department of Chemistry, Faculty of Science, Tokyo Metropolitan University, Setagaya, Tokyo 158

(Received July 11, 1975)

The regions of dispersion, coagulation precipitation, coagulation flotation, and redispersion were determined for aqueous bentonite-cationic surfactant and bentonite-cationic surfactant-polyacrylamide(PAA) systems. The region of coagulation flotation was markedly extended by the addition of PAA to both the lower and higher concentration regions of the cationic surfactant, hexadecyldimethylbenzylammonium chloride(HDBAC), and to the lower concentration region of bentonite. The phenomenon of coagulation flotation was investigated in detail and was applied to the removal of Co^{2+} ions and nuclear fission products, ^{144}Ce and ^{155}Eu, from an aqueous solution. The composition of the reagents for the maximum efficiency of bentonite flotation corresponded to that of the maximum efficiency of Co^{2+}-ion flotation. The effect of the pH on the flotation efficiency was studied in particular. The maximum flotation efficiency of 96% was obtained at pH 11 for Co^{2+} ions, 86% at pH 9.7 for ^{144}Ce, and 93% at pH 10.5 for ^{155}Eu. These radioactive elements were almost completely adsorbed on the surface of bentonite particles and were floated with them in the pH region of the maximum flotation efficiency. It was confirmed that Co^{2+} ions could be floated also from an extremely low concentration (10^{-9} mol/l) of Co^{2+} ions with nearly the same efficiency of flotation and with the additives in the same condition. Co^{2+} ions could also be effectively removed by using the step-by-step flotation, showing as high a flotation efficiency as 99.8%.

The importance of coagulation flotation is well known, as has already been discussed in a previous paper.[1] Coagulation flotation is of interest as a means for the rapid removal or separation of suspended particles from suspensions, since the velocity of flotation is faster than that of coagulation precipitation. Also, coagulation flotation is an effective means for the removal of coexisting ions from the solution when the coagulating particles have an ion-exchange capacity, like bentonite; this process is called adsorbing particle flotation,[2] or "piggy-back" flotation.[3] As has been pointed out in a previous paper,[4] the region of coagulation flotation is extended by the addition of PAA towards the higher and lower concentrations of the cationic surfactant and toward the lower-concentration region of bentonite. Therefore, the addition of PAA is considered to be effective for the removal of bentonite or radioactive cations.

Recently, the removal of substances from an aqueous solution has drawn increasing attention in connection with the problem of water pollution. The radioactive decontamination or the removal of radioactive elements is one of the most important problems involved in the processing of radioactive elements; it is also concerned with public health. Various methods for the removal of these contaminating elements have been employed —for instance, adsorption including ion exchange, coagulation precipitation, evaporation concentration, foam separation, and flotation.[5] Among these methods, the flotation method is considered to be the most effective and the least expensive. However, a comparatively limited number of works have reported on the ion flotation of radioactive elements.[6] For these reasons, it is of importance to investigate the basic parameters to be considered in the flotation process.

In the present study, the coagulation flotation of bentonite, the effect of PAA upon the flotation, and its application to the separation of Co^{2+} ions and some fission products were investigated in detail. The amount of bentonite, the cationic surfactant, PAA, and the effect of the pH on the flotation efficiency were studied in particular.

Experimental

Materials. The cobalt chloride used was a reagent-grade $CoCl_2 \cdot 6H_2O$, which was used without further purification. The stock solution of Co^{2+} ions (1×10^{-4} mol/l) was prepared by dissolving cobalt chloride in triply distilled water, with the addition of a small amount of ^{60}Co as a radiotracer. The ^{144}Ce and ^{155}Eu, which had been obtained by processing fission products, were supplied by the Japan Atomic Energy Research Institute. The initial activities of the aqueous ^{144}Ce and ^{155}Eu solutions were 2×10^{-2} and 1.5×10^{-2} μCi/ml respectively. The bentonite powder(Bt) used as an ion exchanger was supplied by the Wako Pure Chemical Co., Ltd.; the fraction passing through a 350-mesh sieve was collected and dried under reduced pressure. A suspension of the desired Bt content was made before each experiment and was used after shaking.

The hexadecyldimethylbenzylammonium chloride (HDBAC, 95% purity) was supplied by the Nippon Oils and Fats Co., Ltd., recrystallized from acetone, and dried under reduced pressure. The critical micelle concentration of HDBAC in an aqueous solution was found from surface-tension measurements to be about 8×10^{-5} mol/l. Polyacrylamide (PAA) with an 87% amide content was used as a coagulating agent; it was the product of the Nitto Chemical Co., Ltd., and had been dried under reduced pressure. The Bt, HDBAC, and PAA were all kept in a desiccator. The water was triply

* Address all correspondence to the present address: Laboratory of Chemistry, Musashi Institute of Technology, 1-28-1, Tamatsutsumi, Setagaya, Tokyo 158.

** Present address: Takeda Chemical Industries Ltd., 2-17-85, Jiyusouhonmachi, Yodogawa, Osaka 532.

*** Present address: Japan Automobile Research Institute, 2530, Karima, Yatabe-cho, Tsukuba, Ibaraki.

**** Present address: Department of Chemistry, Faculty of Science, Tokai University, Hiratsuka, Kanagawa 259-12.

distilled using a borosilicate glass apparatus after it had been refluxed overnight with a sulfuric acid-potassium permanganate solution.

Apparatus and Procedure. The procedure used for the measurements of the dispersion state of Bt by HDBAC was the same as that described in the previous paper.[1] The apparatus and method used for flotation were likewise the same as those described previously.[7] A humidified nitrogen gas was introduced through a sintered glass plate of No. 4 into a 10-ml sample solution held in a glass tube (1.0 cm in inner diameter and 32.0 cm in length) for 1 or 2 min at a gas-flow rate of 10 ml/min, unless otherwise specified. Experiments were run under the condition of bubble flotation—namely, flotation using only ascending bubbles, without the aid of foam formation. The concentration of Bt was determined by turbidity measurements using a photoelectric colorimeter, Spectronic 20, of Bausch and Lomb, Inc. The light absorbance was measured at 440 mμ. The concentration of the stock solution of Co^{2+} ions was determined by the chelate titration method with EDTA[8], using murexide as an indicator. For the measurement of the flotation efficiency, a constant amount of the sample was pipetted out of the solution and dried in a stainless steel planchet, and the radioactivities of ^{60}Co, ^{144}Ce, and ^{155}Eu were measured by using the Geiger-Muller counter tube. From the radioactivity of the solution before and after the flotation, the flotation efficiency was calculated.

The flotation efficiency, F, was calculated according to this equation:

$$F = (1 - C_f/C_i) \times 100\%$$

where C_i and C_f are the concentrations or radioactivities of the solution before and after the flotation respectively.

The centrifugation was carried out in a 15-ml cell at 3000 rpm for 10 min; the concentration or radioactivity of the supernatant solution was similarly determined. The efficiency of centrifugation, R, was calculated as follows:

$$R = (1 - A_f/A_i) \times 100\%$$

where A_i and A_f are the radioactivities of the solution before and after the centrifugation respectively.

The pH of the solution was adjusted by means of a sodium hydroxide solution, which had been prepared by the dilution of a saturated NaOH solution. All the experiments were carried out at room temperature (about 25 °C).

Results and Discussion

Change of Dispersion State of Bt by HDBAC and/or PAA. The coagulation-dispersion and precipitation-flotation behavior is shown in Fig. 1 as a function of the amount of HDBAC and Bt added. The regions of dispersion, coagulation precipitation, coagulation flotation, and redispersion may be seen distinctly. Especially the change from coagulation precipitation to coagulation flotation is very sensitive to the slight addition of HDBAC under a constant Bt concentration.

Figure 2 shows the effect of HDBAC on the Bt suspension in the presence of 10 ppm PAA. As may be seen in Fig. 2, the region of coagulation flotation extended towards lower and higher concentrations of HDBAC and a lower concentration of Bt compared with the case of the Bt–HDBAC system. Also, the addition of PAA markedly clarifies the turbid solution and markedly increases the floating velocity of the coagulum by increasing the size of the aggregates. The transition from the region of dispersion to that of coagulation flotation is more distinct in the presence of PAA than in the system without PAA. In Fig. 2 a second region of coagulation precipitation appears, though it is somewhat indistinct at the low-concentration regions of Bt and HDBAC.

Figure 3 shows the change in the dispersion state in the PAA–Bt system in the absence of HDBAC.

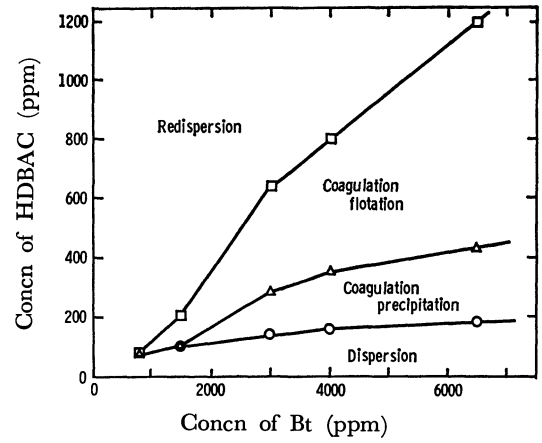

Fig. 1. Effect of HDBAC on dispersion state of Bt suspension.

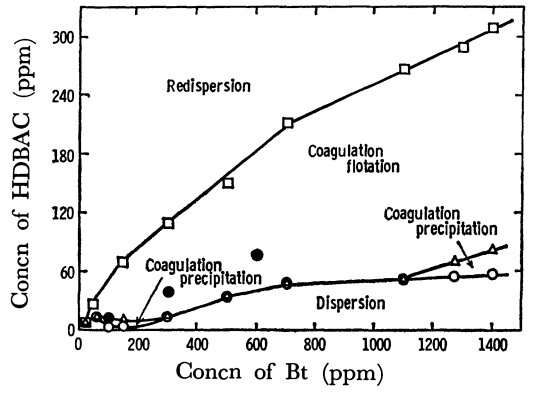

Fig. 2. Effect of HDBAC on dispersion state of Bt suspension in the presence of PAA. ●: composition of maximum flotation efficiency of Bt as shown in Fig. 4.

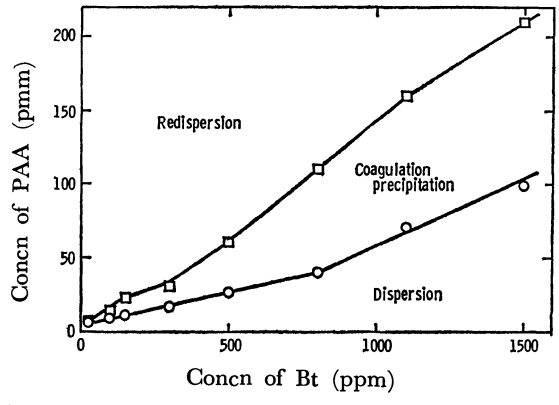

Fig. 3. Effect of PAA on dispersion state of Bt suspension.

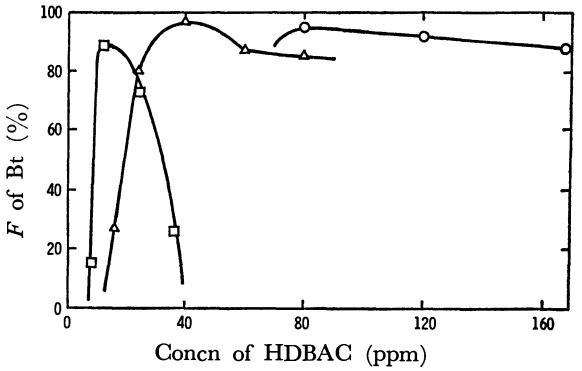

Fig. 4. Effect of HDBAC on flotation efficiency of Bt in the presence of PAA. PAA: 10 ppm, pH: 5—7, gas-flow time: 1 min, Bt: 100 ppm(□), 300 ppm(△), 600 ppm(○).

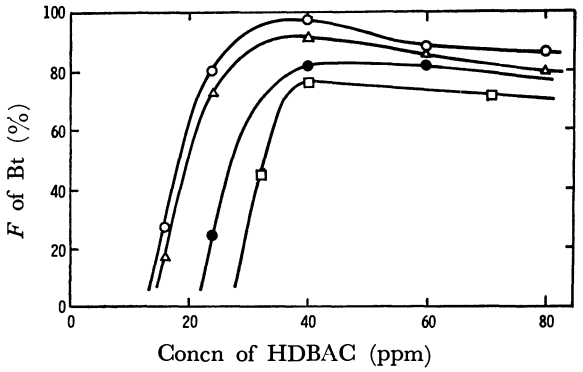

Fig. 5. Effect of PAA on flotation of Bt by HDBAC. Bt: 300 ppm, pH: 7, gas-flow time: 1 min, PAA: 0 ppm(□), 5 ppm(●), 10 ppm(○), 26 ppm(△).

As expected, the region of coagulation flotation disappears in Fig. 3. The fact that the lines separating each region are nearly linear and pass through the point of origin may suggest that the coagulation-dispersion change occurs at constant compositions of the Bt–PAA complex.

Effect of HDBAC on the Efficiency of Coagulation Flotation. In order to study the behavior of the Bt suspension in the region of coagulation flotation in detail, the efficiency of the flotation of Bt at various concentration levels of HDBAC was studied in the presence of 10 ppm of PAA. The results are shown in Fig. 4. It may be seen that the maximum efficiency of flotation appears and that the maximum becomes flatter with the increase in the concentration of Bt. The concentration ratio of Bt/HDBAC at the maximum flotation is nearly constant, as may be seen from the plots shown by filled circles in Fig. 2. This constancy may also indicate the constancy of the aggregate composition at the maximum flotation efficiency. Values of more than 90% were observed at the maximum of flotation. Beyond the maximum points of the flotation efficiency, redispersion began to occur and the supernatant become opaque or turbid. Although the composition of the floated Bt-surfactant aggregates was not determined, it must be similar to what has been reported for Bt–HTAC.[1] In the case of the low concentration of Bt, the flotation efficiency of Bt rapidly decreased beyond a sharp maximum and the region of coagulation flotation became narrow.

Effect of PAA on Efficiency of Coagulation Flotation. Figure 5 shows the effect of PAA on the relation between the coagulation-flotation efficiency and the HDBAC concentration in the system of 300 ppm Bt. As may be seen in the figure, the HDBAC concentration at the maximum efficiency of Bt flotation is nearly independent of the PAA concentration, but the flotation efficiency itself is markedly influenced by the concentration of PAA. From Fig. 5, the concentration of 10 ppm PAA was found to be optimum in the case of 300 ppm Bt. From this result, together with the results obtained from Fig. 4, it may be concluded that an optimum concentration ratio of Bt : HDBAC : PAA, and therefore an optimum composition of the aggregate, exists which gives a maximum efficiency of flotation. The concentration ratio is estimated to be 300 : 40 : 10 (in the case of 300 ppm Bt).

Effect of the Heat Treatment on the Flotation Efficiency of Bt. In Fig. 6, the flotation efficiencies of Bt are compared between two samples; one was heated at 110 °C for 48 h, while the other had no heat treatment. In the case of pH 7 (solid curves), a flat maximum appeared in the *F vs.* HDBAC concentration curve for the system of untreated Bt, while a distinct maximum of a larger value was observed for the heat-treated Bt. In the case of pH 11 (dashed curves), both curves show a flat maximum and the effect of heat treatment disappears.

Effect of the Coexistence of PAA and HDBAC on the Flotation Efficiency of Bt and Co^{2+} Ions. From the enhancement of the flotation efficiency of Bt by the simultaneous addition of HDBAC and PAA, it may be presumed that the Co^{2+} ions can also be effectively floated under such conditions. To confirm this, the flotation efficiencies of Bt and Co^{2+} ions were investigated for the Co^{2+}–Bt–HDBAC–PAA, Co^{2+}–Bt–HDBAC, and Co^{2+}–HDBAC–PAA systems. The results are shown in Table 1. As may be seen in Table 1, both Bt and Co^{2+} ions are best floated by the simultaneous addition of PAA and HDBAC, while the

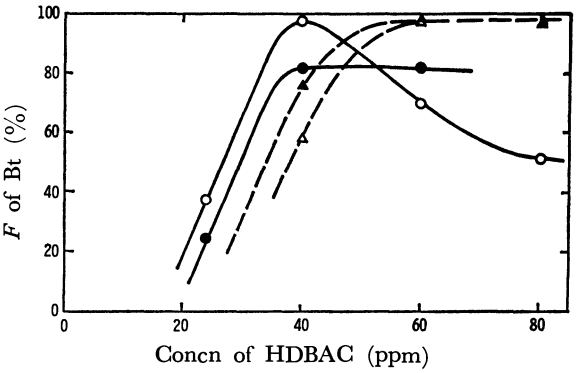

Fig. 6. Effect of heat treatment of Bt flotation.
Flotation efficiencies of untreated Bt (●, ▲) and Bt treated at 110 °C for 48 h (○, △).
Solid curves; Bt: 300 ppm, PAA: 5 ppm, pH: 7, gas-flow time: 1 min.
Dashed curves; Bt: 300 ppm, PAA: 100 ppm, pH: 11, gas-flow time: 1 min.

Table 1. Effect of PAA, HDBAC, and Bt on the flotation efficiency of Co^{2+} ions and Bt

Bt (ppm)	PAA (ppm)	HDBAC (ppm)	pH	F	
				Co^{2+}(%)	Bt(%)
200	10	20	10.9	72.6	77.5
200	0	20	10.7	56.3	38.0
0	10	20	10.8	15.6	0
750	0	88	10.9	51.3	30.1

Co^{2+}: 1×10^{-5} mol/l.

Table 2. Effect of Bt concentration on the flotation efficiency of Co^{2+} ions and Bt

Bt (ppm)	pH	F	
		Co^{2+}(%)	Bt(%)
100	9.5	87.0	86.9
100	10.1	95.0	92.7
110	10.1	97.3	94.4
130	10.0	99.2	96.0
140	9.8	97.1	89.3
130[a)]	10.0	96.2	93.9

Co^{2+}: 1×10^{-5} mol/l, HDBAC: 20 ppm, PAA: 3 ppm.
a) Heated at 110 °C for 48 h.

flotation efficiencies markedly fall for the system lacking either PAA or Bt. In particular, the flotation efficiency of Co^{2+} ions in the absence of Bt is quite poor. The decrease in flotation efficiency due to the lack of PAA does not completely recover even if the concentration of HDBAC is increased. Further, the comparision of the flotation efficiencies of the Co^{2+} ions and Bt shows that the Co^{2+} ions may be considered to float by combining with Bt at the optimum flotation, as will be shown in Table 2, while some Co^{2+} ions can float without the aid of Bt in other systems.

Relation between the Coagulation Flotation and the Concentration of Bt. The relation between the Bt concentration and the flotation efficiency was investigated under the conditions of 3 ppm PAA and 20 ppm HDBAC at pH 9. The results are shown in Table 2. It may be seen that the flotation efficiencies of 99.2% for the Co^{2+} ions and 96% for Bt are obtained at Bt : PAA= 130 : 3 (wt). Thus, the optimum conditions of Co^{2+}-ion flotation were found to be 130 ppm Bt, 20 ppm HDBAC, and 3 ppm PAA for Co^{2+} of a 1×10^{-5} mol/l concentration; these conditions are in agreement with the ratio listed in the former section.

Effect of the Time of the Gas-Flow on the Flotation Efficiency of Co^{2+} Ions and Bt. Figure 7 shows the floatation of Co^{2+} ions and Bt from the Co^{2+}–Bt–HDBAC–PAA system of the composition listed in each figure as a function of the time. The effect of the gas-flow time on the flotation efficiency of Bt closely resembles that of Co^{2+} ions, as is shown by Curve A in Fig. 7. In this case, the flotation efficiencies of both Co^{2+} and Bt increase with the gas-flow time. About 95.5% of the flotation efficiency was attained after 2—3 min. When the amount of additives is doubled, as is shown by Curve B, a maximum of F=

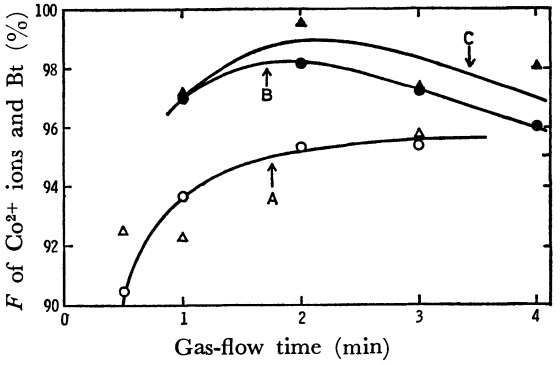

Fig. 7. Effect of gas-flow time on flotation efficiency of Co^{2+} ions and Bt. Co^{2+}: 1×10^{-5} mol/l, pH: 10—11, gas-flow rate: 10 ml/min,
(A) Bt: 130 ppm, HDBAC: 20 ppm, PAA: 3 ppm, } Co^{2+}(○), Bt(△)
(B) Bt: 260 ppm, HDBAC: 40 ppm, PAA: 6 ppm, } Co^{2+}(●)
(C) Bt: 260 ppm, HDBAC: 40 ppm, PAA: 6 ppm, } Bt(▲)

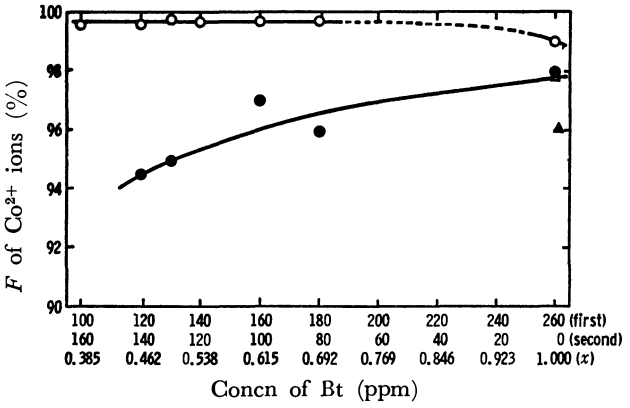

Fig. 8. Stepwise flotation of Co^{2+} ions.
Co^{2+}: 1×10^{-5} mol/l, pH: 10—11, gas-flow time: 2 min. Amount of Bt, HDBAC, and PAA are variable for the first and second flotations, but the total amount of each of these additives must sum up to 260 ppm, 40 ppm, and 6 ppm, respectively.
●: first flotation efficiency, ○: first plus second flotation efficiencies. △, ▲: results of one step flotation process under the condition of 260 ppm Bt, 40 ppm HDBAC, and 6 ppm PAA(△ is for gas-flow time of 2 min, ▲ is for gas-flow time of 4 min)

98.2% also appears after 2 min, but this gradually decreases on a further increase in the gas-flow time. The decrease is perhaps due to the partial redispersion of a scum once floated by continued bubbling. A similar curve was obtained for Bt, as is shown by Curve C. Therefore, the gas-flow time of 2 min was used as the optimum condition for all subsequent investigations.

Effect of the Step-by-step Flotation of Co^{2+} Ions. In the practice of flotation, a step-by-step method is often adopted.[9] Here, the effect of such a method will also be discussed. First, the flotation of Co^{2+} ions from a solution containing 1×10^{-5} mol/l Co^{2+}

ions, 260x ppm Bt, 40x ppm HDBAC, and 6x ppm PAA was run at pH 10—11, where $x(\leqq 1)$ is a variable. After the underlying liquid had been removed from the flotation cell as completely as possible, the second flotation of the solution was carried out with the further addition of $260(1-x)$ ppm Bt, $40(1-x)$ ppm HDBAC, and $6(1-x)$ ppm PAA. The F value for the first flotation and the sum of the F-values for the first and second flotations are plotted against the initial Bt concentration of 260x ppm in Fig. 8, together with the flotation efficiency obtained for the one-step flotation process of 260 ppm Bt with the gas-flow times of 2 and 4 min, for comparison. It is evident in Fig. 8 that the step-by-step flotation is far more effective than the simple flotation; it is especially so when we compare the open circles with the filled triangle, which indicates the F-value of the simple flotation with a total gas-flow time of 4 min. In the case of the step-by-step flotation, a flotation efficiency as high as 99.6—99.8% was obtained at pH 10—11.

Effect of the pH on the Flotation Efficiencies of Co^{2+} Ions and Bt. According to Table 2, the optimum conditions of Co^{2+} ion flotation are presumed to occur at the composition of 130 ppm Bt, 20 ppm HDBAC, and 3 ppm PAA. The subsequent flotations were carried out under these conditions and under varying pH values. Figure 9 shows the results concerning the flotation efficiencies of Co^{2+} ions and Bt from a solution containing 1×10^{-5} mol/l Co^{2+} ions. It may be seen that the flotation efficiency of Co^{2+} ions begins to increase sharply at around pH 8 and that the maximum F of 95% is recorded in the pH range from 9 to about 11. The flotation efficiency is seen to decrease gradually with a further increase in pH. The flotation efficiency of Bt shows a curve with a flat maximum which coincides with that of Co^{2+} ions in the pH region of 9—11. As the cobalt hydroxide begins to form in the vicinity of pH 9, Co^{2+} ions are considered to float as polynuclear species,[10] similar to the flotation of Cu^{2+},[7] and Cd^{2+} ions.[7] In this pH region, Co^{2+} ions are considered to combine almost completely with Bt and are floated together with Bt with the aid of a surfactant, while in other pH regions, especially in the acid region, a large amount of Bt is floated without adsorbing Co^{2+} ions. The effect of Bt is clearly shown by comparing the flotation efficiencies of Co^{2+} ions for the system containing HDBAC with and without Bt, as is shown in Figs. 9 and 10, where Fig. 10 shows the flotation efficiency of Co^{2+} ions from solutions each containing 1×10^{-5} and 7.4×10^{-9} mol/l of Co^{2+} ions and 20 ppm of HDBAC. It is evident that the flotation efficiency of Co^{2+} ions decreases from about 95% for the system with Bt to 5% for the system without Bt, although the latter system also lacks PAA. This decrease in flotation efficiency is more remarkable than in the case of Cu^{2+}-ion flotation.[7] Further, we can observe a remarkable foam formation in the case of the system lacking Bt; this renders the bubble flotation impossible.[7] From these facts, it may be concluded that the addition of Bt acts both to bridge Co^{2+} ions and HDBAC and to suppress foam, thus ensuring bubble flotation.

A similar flotation experiment was carried out for such a dilute solution of Co^{2+} as 7.4×10^{-9} mol/l. The system was studied since the behavior of Co^{2+} ions in such a dilute solution may give information concerning that of the carrier-free state or of radioactive contamination. The measurements of the flotation efficiency of the Co^{2+} ions and Bt were made for the systems with the same conditions as those listed in

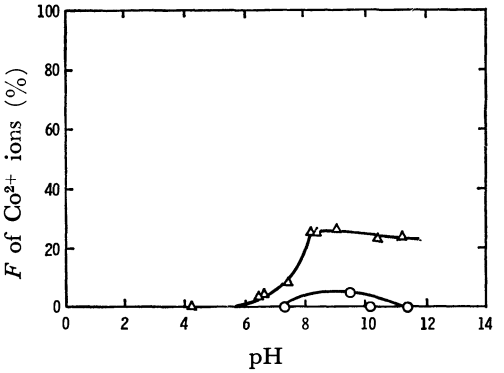

Fig. 10. Foam flotation of Co^{2+} ions.
HDBAC: 20 ppm, gas-flow time: 2 min, ○: 1×10^{-5} mol/l Co^{2+} ions, △: 7.4×10^{-9} mol/l Co^{2+} ions.

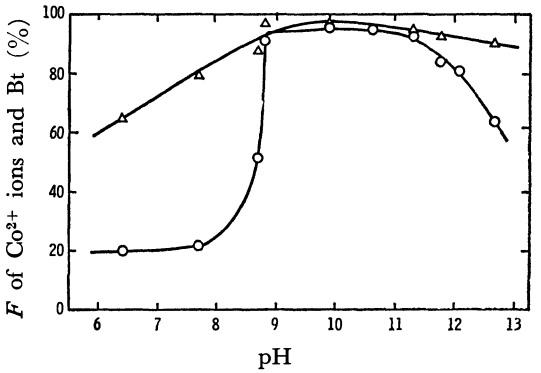

Fig. 9. Effect of pH on flotation efficiency of Co^{2+} ions and Bt.
Co^{2+}: 1×10^{-5} mol/l, Bt: 130 ppm, HDBAC: 20 ppm, PAA: 3 ppm, gas-flow time: 2 min, ○: F of Co^{2+} ions, △: F of Bt.

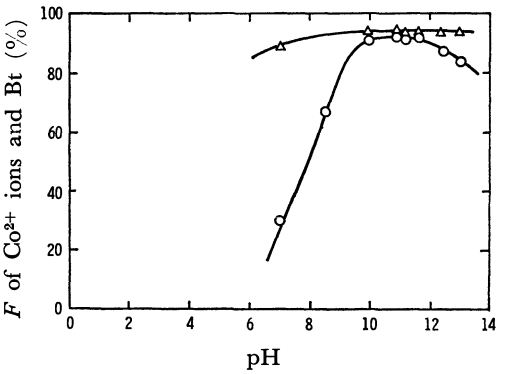

Fig. 11. Effect of pH on flotation efficiency of Co^{2+} ions and Bt.
Co^{2+}: 7.4×10^{-9} mol/l, Bt: 130 ppm, HDBAC: 20 ppm, PAA: 3 ppm, gas-flow time: 2 min.
○: F of Co^{2+} ions, △: F of Bt.

Fig. 9 except that the concentration of the Co^{2+} ions was 7.4×10^{-9} mol/l. The results are shown in Fig. 11. It may be seen that the plots are similar as a whole to those of Fig. 9, though somewhat lower maxima. Also, in this case, the coincidence of the maxima of the flotation efficiency of the Co^{2+} ions and Bt indicates that the Co^{2+} ions are adsorbed on Bt particles and are removed with them.

Removal of Co^{2+} Ions by Centrifugation. It may be considered likely, on the basis of the above observations, that Co^{2+} ions combine with Bt particles under the optimum conditions of flotation. To further confirm this mechanism, the centrifugation of the Co^{2+} ions was carried out at 3000 rpm for 10 min at varying pH values, and the efficiency of the centrifugation or efficiency of the adsorption of Co^{2+} ions on Bt was measured and was plotted against the pH (*cf.* Fig. 12).

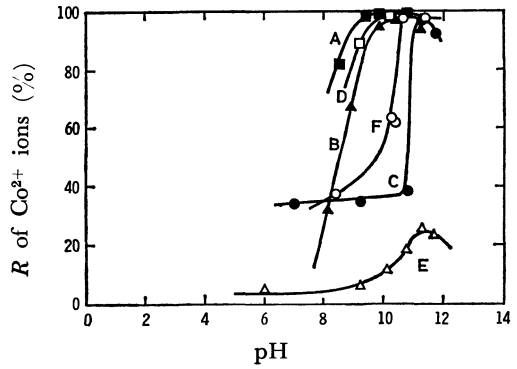

Fig. 12. Effect of pH on R or adsorption of Co^{2+} ions.
Co^{2+}: 1×10^{-5} mol/l, Bt: 130 ppm, HDBAC: 20 ppm, PAA: 3 ppm, centrifugation: 3000 rpm for 10 min.
A: Co^{2+}-Bt-HDBAC-PAA system,
B: Co^{2+}-Bt-HDBAC system,
C: Co^{2+}-Bt-PAA system,
D: Co^{2+}-Bt system,
E: Co^{2+}-PAA system,
F: Co^{2+} system.

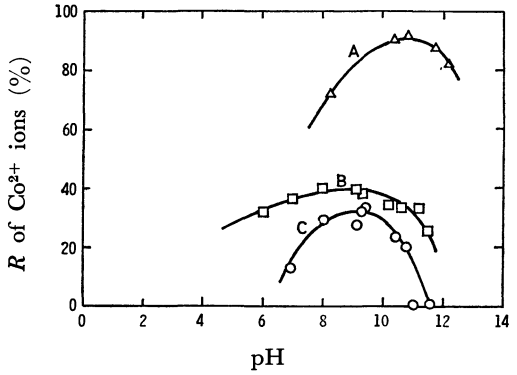

Fig. 13. Effect of pH on efficiency of centrifugation of Co^{2+} ions.
Bt: 130 ppm, HDBAC: 20 ppm, PAA: 3 ppm, centrifugation: 3000 rpm for 10 min.
A: Co^{2+}-Bt-HDBAC-PAA system, Co^{2+}: 3.1×10^{-9} mol/l,
B: Co^{2+}-Bt-PAA system, Co^{2+}: 7.4×10^{-9} mol/l,
C: Co^{2+}-PAA system, Co^{2+}: 7.4×10^{-9} mol/l.

As may be seen in Fig. 12, high R values were obtained for the Co^{2+}-Bt-HDBAC-PAA system(A), the Co^{2+}-Bt-HDBAC system(B), and the Co^{2+}-Bt system-(D). It is confirmed that the R value of the system containing PAA but lacking HDBAC is very low up to high pH values, while the system containing Co^{2+} ions alone still shows a large R value in a sufficiently high alkaline region. It seems likely that, in the absence of HDBAC, the Co^{2+} ions are protected by PAA against adsorption on Bt and hydroxide formation. The centrifugation was carried out further for solutions containing 7.4×10^{-9} mol/l of Co^{2+} ions or 3.1×10^{-9} mol/l of Co^{2+} ions, with other constituents similar to those of Systems (A), (B), and (E), shown in Fig. 12. The results are shown in Fig. 13. The tendencies are similar to those of Fig. 12, and the Co^{2+}-Bt-HDBAC-PAA system is seen to be most effective in removing the Co^{2+} ions from this dilute solution.

Application of Adsorbing Particle Flotation to the Fission Product. Figure 14 shows the results of the flotation of ^{155}Eu from a solution containing 2×10^{-2} μCi/ml of ^{155}Eu ions, 130 ppm of Bt, 20 ppm of HDBAC, and 3 ppm of PAA. The flotation efficiency of ^{155}Eu ions is plotted against the pH. As may be seen in Fig. 14, the flotation efficiency increases from pH 3 with an increase in the pH and two maxima of 85% and 93% flotation efficiencies are observed, at

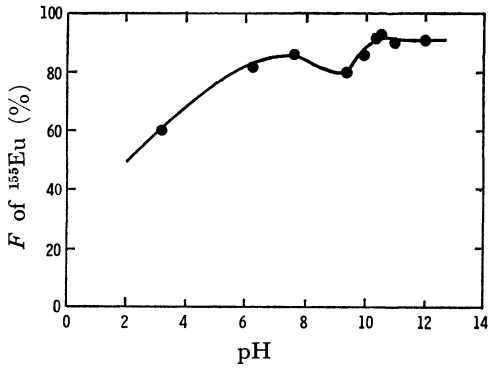

Fig. 14. Effect of pH on flotation efficiency of ^{155}Eu.
^{155}Eu: 2×10^{-2} μCi/ml, Bt: 130 ppm, HDBAC: 20 ppm, PAA: 3 ppm, gas-flow time: 2 min.

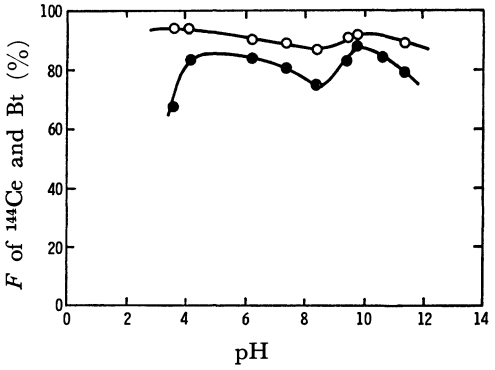

Fig. 15. Effect of pH on flotation efficiency of ^{144}Ce and Bt.
^{144}Ce: 1.5×10^{-2} μCi/ml, Bt: 130 ppm, HDBAC: 20 ppm, PAA: 3 ppm, gas-flow time: 2 min,
●: F of ^{144}Ce, ○: F of Bt.

pH 7.5 and 10.5 respectively. The former and the latter maxima may be explained by the formation of the radiocolloid of ^{155}Eu and of insoluble europium hydroxide respectively, but this requires further study.[11] Figure 15 shows the flotation efficiency of ^{144}Ce and Bt from a solution of 1.5×10^{-2} μCi/ml of ^{144}Ce ions, 130 ppm of Bt, 20 ppm of HDBAC, and 3 ppm of PAA as a function of the pH. In this case, the similar maxima of 85% at pH 5 and 80% at pH 9.7 are observed. The flotation efficiency of ^{144}Ce ions parallels that of Bt. Likewise, this may suggest that there is a relationship between the combining ratio of Bt and the cerium ion under its optimum flotation conditions.

The authors wish to thank Dr. Fujio Ichikawa of the Japan Atomic Energy Research Institute for the supply of fission products.

References

1) T. Inakazu, K. Kobayashi, and T. Sasaki, This Bulletin, **48**, 3008 (1975).
2) R. Lemlich, "Adsorptive Bubble Separation Techniques," Academic press, New York and London (1972), pp. 273—278.
3) R. Lemlich *Ind. Eng. Chem.*, **60**, 17 (1968).
4) K. Kobayashi, This Bulletin, **48**, 1750 (1975).
5) W. Rudolfs, "Industiral Waste," Reinhold, New York (1957), p. 454; J. E. Sabadell, "Traces of Heavy Metals in Water, Removal Process and Monitoring," Princeton University, Princeton, New Jersey, November 15—16 (1973).
6) B. M. Davis and F. Sebba, *J. Appl. Chem.*, **16**, 297 (1966); *ibid.*, **17**, 40 (1967); R. Lemlich, "Adsorptive Bubble Separation Techniques," Academic Press, New York and London (1972), pp. 243—248, pp. 285—288; Y. Koyanaka, *Nippon Genshiryoku Gakkaishi*, **7**, 621 (1965); Y. Koyanaka, *Radioisotopes*, 77 (1966).
7) K. Kobayashi, This Bulletin, **48**, 1180 (1975).
8) H. Flaschka, *Microchemie ver Mikorochim. Acta*, **39**, 38 (1952); K. Ueno, "Chelate Titration Method," Nankodo (1972), p. 292.
9) H. Kishimoto, *Kolloid-z.*, **192**, 66 (1963).
10) F. Sebba, "Ion Flotation," American Elsevier, New York (1966).
11) F. Ichikawa and T. Sato, *Radiochim. Acta*, **12**, 89 (1969).

Interfacial Layer between a Mercury Electrode and Dilute Aqueous Solutions of Alkali-Metal Chloride at Potentials of the Cathodic Limiting Current Plateau

Katsuo TAKAHASHI and Reita TAMAMUSHI

The Institute of Physical and Chemical Research, Hirosawa, Wako, Saitama 351

(Received June 27, 1975)

The electrochemical properties of the interfacial layer between a DME and dilute aqueous solutions of MCl (M: alkali-metal) at the cathodic limiting current plateau were studied by means of impedance measurements at relatively low frequencies ($\leq$250 Hz). From the frequency and potential dependence of the capacitive and the resistive components of the electrode impedance, the following conclusions were obtained concerning the properties of the interfacial layer under the above condition: (i) when the concentration of cations is extremely low in the vicinity of the electrode surface, the impedance behaves as if the conventional double-layer were absent: (ii) the impedance behavior of the present system can be explained by assuming an equivalent circuit which is given by a series combination of the Warburg impedance for the reduction of M^+ and the resistance of solution; and (iii) such an interfacial layer is conventionally called "the Nernst double-layer" and its formation is determined by the mass-transport of the reacting species M^+.

A conventional double-layer of the Helmholtz-Gouy-Chapman type is formed at a polarizable electrode/solution interface by some nonfaradaic interaction between the electrode and ionic species in the solution. The structure of such a double-layer has been extensively studied.[1,2] However, only a limited amount of information is available on the properties of an electrode/solution interface where the concentration of electrochemically-inactive ions is extremely low.[3-5]

The capacitance behavior of the interface between mercury and dilute electrolyte solutions was reported in previous papers.[6,7] Contrary to Grahame's model of the double-layer, the capacitance of a compact double-layer at highly negative electrode potentials was found to decrease with a decrease in the concentration of electrolytes.[6] It was observed that the capacitance of a dropping mercury electrode (DME)/TlOH system decreased markedly at electrode potentials in the region of the cathodic limiting current plateau.[7] Such a decrease in the double-layer capacitance was explained in terms of the deficiency of electrochemically-inactive cations forming the conventional double-layer.

This study deals with the impedance behavior of a DME/MCl (M: alkali-metal) system in the potential region of the cathodic limiting-current plateau. Sluyters-Rehbach *et al.*[8,9] measured the impedance of similar systems and discussed the electrode reaction of alkali-metal cations at a DME; in contrast to their study, our measurements were carried out with dilute aqueous solutions (less than a few mM) of alkali-metal chlorides in order to obtain detailed information on the structure of the interfacial layer where the concentration of cations is extremely low. From the frequency dependence of the electrode impedance, a possible equivalent circuit is proposed, and the characteristics of such an interfacial layer are discussed.

Experimental

The conductive and the susceptive components of the admittance of an electrode/solution system were measured as a function of the electrode potential by means of a phase-sensitive AC polarograph consisting of a conventional AC polarographic unit and two phase-sensitive detectors. In order to make accurate measurements with high-impedance systems, the phase-sensitive detectors were carefully adjusted and calibrated by using appropriate dummy-cells of known resistors and capacitors. The details of the measuring circuits and procedures have been reported elsewhare.[10]

The cell employed was a glass beaker of 100 cm^3 capacity with a silicon-rubber stopper. The working electrode was a conventional DME; in most cases, the rate of flow of mercury was 0.526 mg s^{-1}, and the drop-time was mechanically controlled at 4.1 s. Admittance measurements were made on a surface area of 0.0142 cm^2. A platinized-platinum spiral of large surface area was used as a counter electrode. The reference electrode was a silver-silver chloride electrode placed in the cell as shown in Fig. 1; this location of the reference electrode is not desirable from the standpoint of eliminating the ohmic *IR*-drop, but is essential for the stable performance of the potentiostat when a high-impedance system is to be measured. The correction of the electrode potential for the ohmic drop was made by calculating the *IR*-values assuming an appropriate value of the solution resistance.

The measurements were made with deaerated solutions at 25.0$\pm$0.1 °C. All solutions were prepared from analytical reagent grade chemicals and redistilled water.

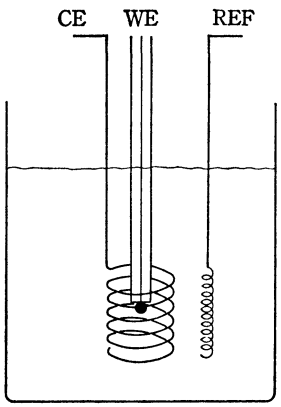

Fig. 1. Position of the electrodes; WE, dropping mercury electrode; CE, platinized-platinum counter electrode; REF, Ag-AgCl reference electrode.

Results and Discussion

Frequency Dependence of the Electrode Impedance and a Possible Equivalent Circuit. A typical DC-polarogram of a DME/1 mM KCl system is presented in Fig. 2; the potential regions F_1, P, and F_2 correspond to the reduction wave of K^+, the limiting current plateau, and the reduction of water, respectively. In this paper, the impedance behavior in the potential region P ($E=-2.7$ to -0.3 V *vs.* Ag-AgCl) will be discussed.

Figure 3 shows the potential dependence of the series capacitance C_s and the series resistance R_s of the impedance observed with a DME/1 mM KCl system at several frequencies. A remarkable frequency dispersion of C_s and R_s is observed at each electrode potential of the cathodic limiting current plateau. The value of C_s is clearly lower than that of the conventional double layer (about 16 $\mu F\ cm^{-2}$), and R_s is much higher than that corresponding to the resistance of the bulk solution.

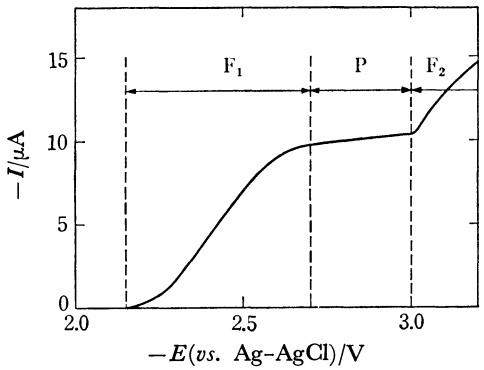

Fig. 2. Current-potential curve obtained with a DME/1 mM KCl system at 25 °C: F_1, the potential region of the reduction step of K^+; P, the limiting current plateau; F_2, the potential region of the reduction of water.

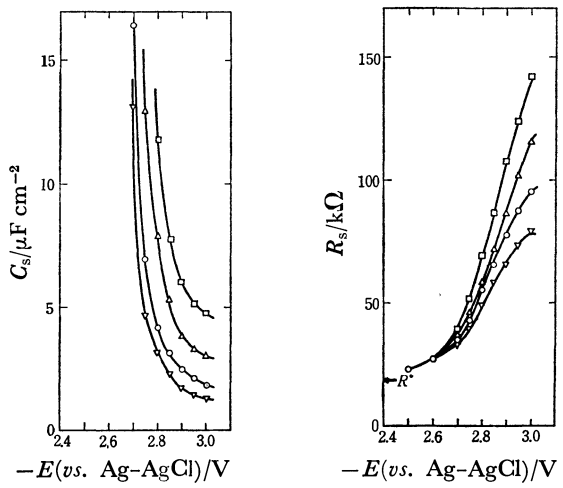

Fig. 3. Potential dependence of the series capacitance C_s and resistance R_s of a DME/1 mM KCl system (25 °C) at different frequencies: -□- 32 Hz, -△- 64 Hz, -○- 120 Hz, -▽- 250 Hz. $R°$ is the resistance of solution as defined by Eq. (12).

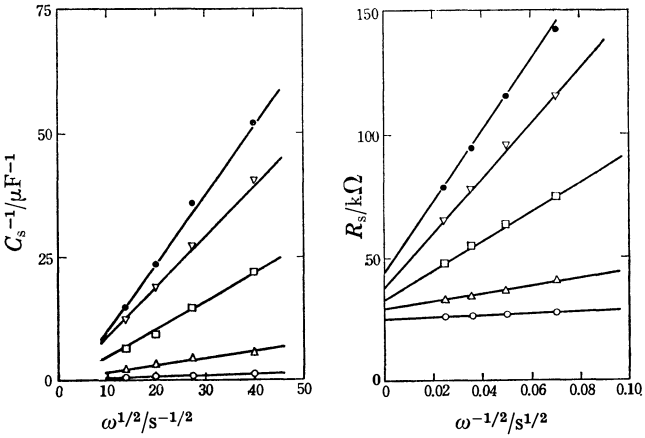

Fig. 4. Frequency dependence of the C_s- and R_s-components of a DME/1 mM KCl system (25 °C) at various electrode potentials: E(*vs.* Ag-AgCl)/V= −2.6(-○-), −2.7(-△-), −2.8(-□-), −2.9(-▽-), and −3.0(-●-).

Table 1. The intercepts and the slopes of Eqs. (1) and (2), obtained with a DME/1 mM KCl system at 25.0 °C

$-E$ (*vs.* Ag-AgCl)/V	$(C_s°)^{-1}$ / μF^{-1}	S_c / $\Omega s^{-1/2}$	$R_s°$ / kΩ	S_r / $\Omega s^{-1/2}$
2.6	~0	3.5×10^4	25	4.0×10^4
2.7	~0	1.4×10^5	29	1.6×10^5
2.8	−1	5.7×10^5	33	6.0×10^5
2.9	−1	1.04×10^6	38	1.12×10^6
3.0	−4	1.41×10^6	44	1.46×10^6

In Fig. 4, the C_s and R_s at each electrode potential are plotted as a function of the angular frequency ω. From the linear relationship observed with the C_s^{-1} *vs.* $\omega^{1/2}$ and the R_s *vs.* $\omega^{-1/2}$ plots, the frequency dependence of C_s and R_s can be represented by the following equations:

$$C_s^{-1} = (C_s°)^{-1} + S_c\omega^{1/2} \quad (1)$$

$$R_s = R_s° + S_r\omega^{-1/2} \quad (2)$$

The intercepts ($(C_s°)^{-1}$ and $R_s°$) and the slopes (S_c and S_r) as given by Eqs. (1) and (2) are summarized in Table 1. It can be assumed from this result that, at each potential, $S_c=S_r=S$ and $(C_s°)^{-1}=0$ within the limit of experimental accuracy. With this approximation, Eqs. (1) and (2) can be reduced to

$$C_s^{-1} = S\omega^{1/2} \quad (3)$$

$$R_s = R_s° + S\omega^{-1/2} \quad (4)$$

Figure 5(a) shows the simplest electrical equivalent circuit which satisfies the impedance behavior represented by Eqs. (3) and (4). The impedance Z_w is a Warburg-type impedance given by

$$Z_w = R_w + jX_w \quad (5)$$

with

$$R_w = -X_w = S\omega^{-1/2} \quad (6)$$

The magnitude of Z_w is equal to $\sqrt{2}S\omega^{-1/2}$, and the phase angle between R_w and X_w is equal to $\pi/4$.

Consider a simple electrode reaction,

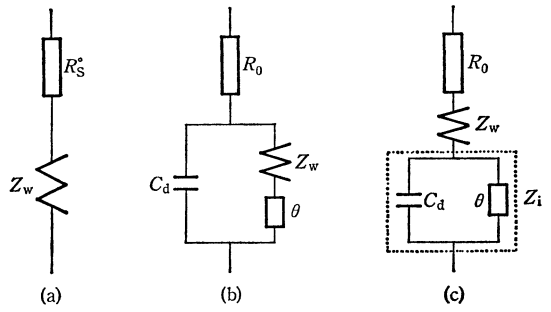

Fig. 5. Electrical equivalent circuits of the electrode impedance.

$$M^+ + e(Hg) \rightleftharpoons M\text{-}Hg \quad (M: \text{alkali-metal}) \qquad (7)$$

in which the mass-transport of M^+ and M in mercury is controlled by diffusion. According to the theory of electrode processes,[11,12] the equivalent circuit for the electrode reaction (7) in solutions containing an excess of supporting electrolytes is represented by Fig. 5(b), where C_d is the conventional double-layer capacitance; θ, the polarization resistance; and R_0, the resistance of solution. This equivalent circuit implicitly involves the assumption that different kinds of ions are responsible for the faradaic and the double-layer charging processes, *i.e.*, the faradaic process is controlled by the depolarizer flux, while the charging process is controlled by the supporting electrolyte flux.

In solutions containing no supporting electrolytes, however, both the faradaic and charging processes may be controlled by the flux of the same ionic species—alkali-metal cations, in the present systems. When alkali-metal cations reach the electrode surface by mass-transport, they will contribute to both faradaic and charging currents. In such cases, the equivalent circuit is considered to be represented by Fig. 5(c), where the Warburg impedance of the depolarizer is in series with the impedance of electrode interface, Z_I, which involves θ and C_d. If the flux of the depolarizer contributes mainly to the charging process, the impedance Z_I should be capacitive, while, if the flux contributes mainly to the faradaic process, Z_I should be resistive.

The equivalent circuit (Fig. 5(a)) determined by the impedance measurements shows that the impedance Z_I in Fig. 5(c) should be resistive, *i.e.*, the condition

$$\theta \ll 1/\omega C_d \qquad (8)$$

is satisfied at the frequencies used in the present study. This relationship is reasonable, because the electrode reaction (7) is known to be polarographically reversible and the polarization resistance θ is very small. In this case, the Warburg-type impedance in Fig. 5(a) can be considered to be due to the mass-transport of the depolarizer, and the resistance R_s° is assumed to be practically equal to the resistance, R_0, of the solution.

Resistance Component R_s°. It should be mentioned that the resistance component R_s° observed with the DME/KCl system depends on the electrode potential as shown in Fig. 6. Such a potential-dependence

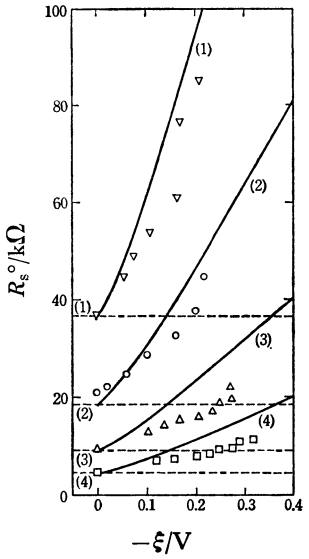

Fig. 6. Potential dependence of resistance R_s° of a DME/x mM KCl system (25 °C): x=0.5(1, ▽), 1.0 (2, ○), 2.0(3, △), and 4.0(4, □). Solid lines are theoretical curves, and broken lines represent the R°-values for each concentration. Potential axis $\xi = E_{cor} - E_{1/2}{}^r$ (see text).

of R_s° can be explained by taking into account the contribution from the resistance R_m of a mass-transport layer where the concentration of depolarizer changes with the distance from the electrode surface. The resistance component R_s° is then given by

$$R_s^\circ \simeq R_o = R_m + R_b \qquad (9)$$

R_b being the resistance of the bulk solution where the composition of the solution is uniform.

In the present systems containing no supporting electrolytes, the resistance R_m is expected to increase with an increase in the negative electrode potential because of the decrease in the concentration of depolarizer at the electrode surface. In the following calculation, we assume that the concentration change of the depolarizer is linear in the mass-transport layer (the Nernst-type layer) as shown in Fig. 7 and that the ionic mobilities are constant throughout the solution phase.

With these approximations, the resistance of the mass-transport layer R_m and that of the bulk solution R_b are given by the following equations:

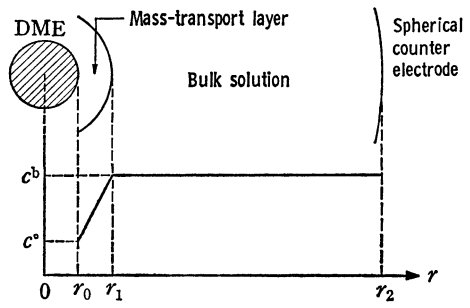

Fig. 7. A model of the mass-transport layer.

$$R_m = R^\circ c_M^b\left(\frac{1}{r_0}-\frac{1}{r_2}\right)^{-1}\frac{r_1-r_0}{r_1c_M^\circ - r_0c_b^M} \times\left[\left(\frac{1}{r_0}-\frac{1}{r_1}\right)+\frac{c_M^b-c_M^\circ}{r_1c_M^\circ-r_0c_M^b}\ln\frac{r_0c_M^b}{r_1c_M^\circ}\right] \quad (10)$$

and

$$R_b = R^\circ\left(\frac{1}{r_0}-\frac{1}{r_2}\right)^{-1}\left(\frac{1}{r_1}-\frac{1}{r_2}\right) \quad (11)$$

with

$$R^\circ = \frac{1000}{4\pi\Lambda c_M^b}\left(\frac{1}{r_0}-\frac{1}{r_2}\right) \quad (12)$$

where c_M^b and c_M° are the concentrations of M^+ in the bulk solution ($r_1 \leq r \leq r_2$) and at the electrode surface ($r=r_0$), respectively, and Λ is the molar conductivity of the solution. The value of R° corresponds to the resistance of the solution phase when the composition of the solution is uniform from r_0 to r_2; R° can be determined from the measurement at potentials where no electrode reaction occurs.

In the calculation of R_s° using Eqs. (9)—(12) as a function of the electrode potential, the following two assumptions are introduced:

$$\delta = r_1 - r_0 = \left(\frac{3}{7}\pi D_M t\right)^{1/2} \quad (13)$$

and

$$\frac{c_M^b - c_M^\circ}{c_M^\circ} = \exp\left(\frac{-F}{RT}\xi\right) \quad (14)$$

with

$$\xi = E_{cor} - E_{1/2}{}^r \quad (15)$$

where δ is the thickness of the mass-transport layer, D_M the diffusion coefficient of the depolarizer M^+, t the time of electrolysis, $E_{1/2}{}^r$ the reversible half-wave potential, and E_{cor} the electrode potential corrected for the ohmic IR-drop. Relation (13) is obtained from the theory of the polarographic limiting current, and relation (14) is based upon the Nernstian behavior of the electrode reaction.[13]

In Fig. 6, the experimental relationship between R_s° and ξ is compared with the theoretical curves (solid lines) obtained with the numerical values: $r_0=0.0339$ cm, $r_2=0.5$ cm, $t=4.0$ s, and $D_M=1\times10^{-5}$ cm^2 s^{-1}. The agreement between the experimental and the theoretical curve is sufficiently good to support the assumption that R_s° is the resistance of the solution phase from r_0 to r_2 as represented by the simplified model shown in Fig. 7.

Warburg-type Impedance Z_w. Let us assume that the Warburg-type impedance in our present system is given by an expression[12] similar to that derived for the electrode reaction in the supporting electrolyte solutions. Then, the coefficient σ of the Warburg impedance for electrode reaction (7) may be given by the equation,

$$\sigma = SA = \frac{RT}{\sqrt{2}F^2}\left[\frac{1}{\sqrt{D_A^*}}\exp\left(\frac{\alpha_aF}{RT}\xi\right)+\frac{1}{\sqrt{D_M^*}}\times\exp\left(-\frac{\alpha_cF}{RT}\xi\right)\right]\left[\alpha_ac_a^\circ\exp\left(\frac{\alpha_aF}{RT}\xi\right)+\alpha_cc_M^\circ\exp\left(-\frac{\alpha_cF}{RT}\xi\right)\right]^{-1} \quad (16)$$

where A is the surface area of the electrode, $\alpha_{a(c)}$ the anodic (cathodic) transfer coefficient, $D_{a(M)}^*$ the apparent diffusion coefficient of M-Hg (M^+), $c_{a(M)}^\circ$ the concentration of M-Hg (M^+) at the electrode surface, and other symbols have their usual meanings.

At sufficiently negative potentials where the cathodic limiting current is observed, the following conditions can be satisfied:

$$c_a^\circ \simeq c_M^b \quad (17)$$

and

$$\exp\left(\frac{\alpha_aF}{RT}\xi\right) \ll \exp\left(-\frac{\alpha_cF}{RT}\xi\right) \quad (18)$$

Then, assuming the relation, $\alpha_a+\alpha_c=1$, we obtain the expression:

$$\sigma = \frac{RT}{(2D_M^*)^{1/2}F^2}\left[\alpha_ac_M^b\exp\left(\frac{F}{RT}\xi\right)+\alpha_cc_M^\circ\right]^{-1} \quad (19)$$

Equation (19) shows that the experimental values of σ provide information on the surface concentration c_M° of the depolarizer at each potential ξ. If the surface concentration is determined by the Nernstian relation, expression (20) can be obtained from Eqs. (14) and (19):

$$\sigma = \frac{RT}{(2D_M^*)^{1/2}F^2c_M^b}\exp\left(-\frac{F}{RT}\xi\right) \quad (20)$$

In Fig. 8, the experimental values of σc_M^b obtained with several alkali-metal chlorides are plotted against the electrode potential ξ; the theoretical line with the slope given by Eq. (20) is also shown. Considering the accuracy of the measurements and the rough approximations involved in the theoretical calculation, we can conclude that the agreement between the

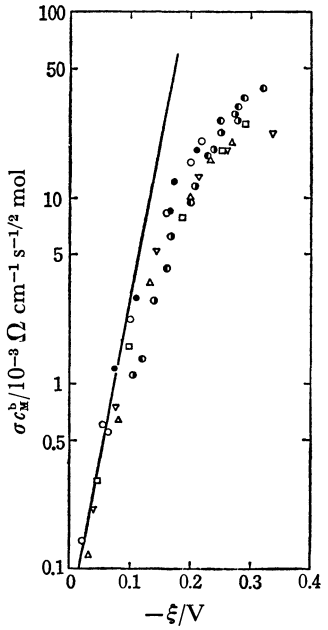

Fig. 8. Potential dependence of the Warburg-parameter σc_M^b of DME/alkali-metal chloride systems (25 °C): 0.5 mM KCl(-●-); 1.0 mM KCl(-○-); 2.0 mM KCl(-◑-); 4.0 mM KCl(-◐-); 1.0 mM NaCl (-□-); 1.0 mM RbCl(-△-); 1.0 mM CsCl(-▽-). Solid line shows the theoretical curve as calculated with $D_M^*=1\times10^{-5}$ cm^2 s^{-1} by means of Eq. (20).

experiments and the theory is satisfactory unless $|\xi|$ exceeds 150 mV.

Conclusion

The present results show that the impedance behavior of the DME/MCl (M: alkali-metal) system at the potentials of the limiting current plateau (region P in Fig. 2) can be represented by the equivalent circuit as shown in Fig. 5(a); the Warburg impedance Z_w for electrode reaction (7) is in series with resistance $R_s°$ of the solution from the surface of the working electrode to the counter electrode. It is interesting that, at relatively low frequencies ($\leq$250 Hz), the impedance in the potential region P behaves as if the conventional double-layer were absent. For this situation, the interfacial layer between the electrode and the solution phase may be called "the Nernst double-layer"; the potential difference across the Nernst double-layer is determined by the electrode reaction, and the formation of the layer is controlled by the mass-transport of the reacting species.

References

1) D. C. Grahame, *Chem. Rev.*, **41**, 441 (1947).
2) M. J. Sparnaay, "The Electrical Double Layer," The International Encyclopedia of Physical Chemistry and Chemical Physics 4/14, Pergamon Press, Oxford (1972).
3) P. Delahay, R. de Levie, and A. M. Giuliani, *Electrochim. Acta*, **11**, 1141 (1966).
4) R. D. Armstrong and W. P. Race, *J. Electroanal. Chem.*, **33**, 285 (1971).
5) F. C. Anson, R. F. Martin, and C. Yarintzky, *J. Phys. Chem.*, **73**, 1835 (1969).
6) K. Takahashi and R. Tamamushi, *Electrochim. Acta*, **16**, 875 (1971).
7) K. Takahashi and R. Tamamushi, *ibid.*, **16**, 1157 (1971).
8) M. Sluyters-Rehbach and J. H. Sluyters, *J. Electroanal. Chem.*, **34**, 55, 69 (1972); **36**, 101, 287 (1972).
10) K. Matsuda, K. Takahashi, and R. Tamamushi, *Sci. Papers Inst. Phys. Chem. Res.*, **64**, 62 (1970).
11) P. Delahay, "New Instrumental Methods in Electrochemistry," Chap. 7, Interscience Publishers, Inc., New York (1954).
12) M. Sluyters-Rehbach and J. H. Sluyters, "Electroanalytical Chemistry", Vol. 4 (Allen J. Bard, ed.), Marcel Dekker, Inc., New York (1970), pp. 16—18.
13) See for example: G. W. C. Milner, "The Principles and Applications of Polarography and other Electroanalytical Processes", Chap. 3 and 4, Longmans, Green and Co., London (1957).

The Inductive Susceptance Observed with Electrode Reaction of Water at Far Negative Potentials

Katsuo TAKAHASHI, Kiyoshi MATSUDA, and Reita TAMAMUSHI
The Institute of Physical and Chemical Research, Hirosawa, Wako, Saitama 351

(Received July 16, 1975)

The admittance of various electrodes/dilute aqueous electrolyte solution systems was measured at far negative potentials in the frequency range of 22—500 Hz, and the experimental results were discussed in terms of the mechanism of the electrochemical reduction of water molecules. The frequency dependence of the conductance- and susceptance-components was analyzed by assuming possible equivalent circuits. It was concluded that, in the systems which give inductive susceptances at low frequencies, the reduction of water proceeds according to the electrochemical mechanisms;

$$H_2O + e \longrightarrow H_{ad} + OH^-, \quad H_{ad} + H_2O + e \longrightarrow H_2 + OH^-$$

where the current density due to the second reaction path is proportional to the product of θ and $(1-\theta)$, θ being the coverage of the electrode surface by adsorbed hydrogen atoms, H_{ad}. At some metal electrodes in solutions of alkali-metal cations, no inductive susceptance was observed; this suggests that the hydrogen evolution proceeds according to other mechanisms.

The faradaic admittance of usual electrode reactions involves a positive conductance and a capacitive susceptance. In some electrode reactions, however, unusual faradaic admittances with negative conductances and/or inductive susceptances have been observed under certain experimental conditions. A typical example with a negative conductance is the reduction of In(III) at a dropping mercury electrode (DME) in thiocyanate solutions,[1] while an example with an inductive susceptance is the electrochemical dissolution of iron and nickel in alkaline solutions.[2] The theoretical interpretation of these unusual faradaic admittances has been made by several authors[1-6] in connexion with the mechanisms of electrode reactions; in particular, a recent study of Smith and Sobel[5] clearly demonstrates the possibility of some ECE mechanisms giving inductive susceptances.

In the cathodic evolution of hydrogen, the appearance of an inductive susceptance was suggested on a theoretical basis by Gerischer and Mehl,[3] by Batrakov and Iofa,[7] and by Novosel'skii and Gudina.[8] In a previous paper,[9] the present authors reported the experimental observation that the susceptance components of DME/dilute aqueous electrolyte solutions become inductive at far negative potentials, where the reduction of water molecules is supposed to proceed. This paper will present the details of the admittance behavior of the above-mentioned systems and will discuss the possible mechanism of the electrochemical reduction of water molecules.

Experimental

The electrolytic currents (DC-components), conductances, and susceptances due to the electrode process were measured as functions of the electrode potential by using an apparatus whose block diagram is shown in Fig. 1; the instrumental details of the apparatus were reported previously.[10] The readings of each output-signal of the instrument were carefully calibrated by using appropriate dummy cells consisting of known resistors and capacitors. The output-signal of the 90°-phase-sensitive-detector at the stage before a low-pass filter, when observed with a cathode-ray oscilloscope, gives the patterns shown in Fig. 2 according to the nature of the admittance to be measured; this difference in the oscilloscopic patterns was used to determine whether the susceptance component was capacitive or inductive.

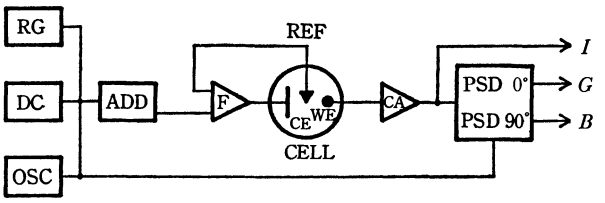

Fig. 1. Block diagram of the measuring instrument. RG: ramp-generator; DC: DC-voltage source; OSC: oscillator; ADD: adder; F: follower-type potentiostat; CA: current amplifier; PSD: phase-sensitive detector.

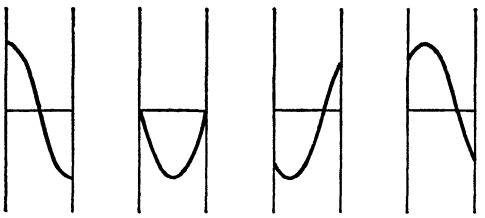

Fig. 2. Typical oscilloscopic patterns observed at the output of the 90°-PSD (before the low-pass filter) when the admittance to be measured (a) pure resistance, (b) pure capacitance, (c) capacitive admittance, (d) inductive admittance.

The arrangement of electrodes (working, counter, and reference electrodes) in a cell was the same as that described in a previous paper.[11] Conventional DME and microelectrodes (both rotating and stationary) of various metals were used as the working electrodes; in the case of the DME, the rate of the flow of the mercury was 0.526 mg s^{-1}, the drop time was mechanically controlled at 4.1 s, and admittance measurements were made at a surface area of 0.0142 cm^2. The counter electrode was a Pt–Pt spiral with large dimensions. In most solutions a Pt–Pt spiral was employed as the reference electrode; in chloride solutions, however, a Ag–AgCl electrode was also used as the reference. In this paper, the electrode potential is not corrected for the ohmic *IR*-drop.

All the solutions were prepared from analytical reagent-

grade chemicals by using redistilled water. The measurements were carried out with deaerated solutions at 25.0± 0.1 °C.

Results

The direct current (I)-potential (E), conductance (G)-E, and susceptance (B)-E curves observed with a DME/0.5 mM $Cd(NO_3)_2$ system were given in a previous paper;[9] the B-E curve clearly shows the inductive susceptance ($B<0$) at very negative potentials, where the cathodic current, which is considered to be due to the reduction of water molecules,[12] increases almost linearly with the electrode potential. Similar inductive susceptances were also observed at the DME in solutions containing various cations and at many solid electrodes in dilute aqueous solutions of strong acids; the systems examined in this work are summarized in Table 1.

Figures 3, 4, and 5 present typical examples of the I-E, G-E, and B-E curves obtained with the DME/1 mM KNO_3, Pt/2 mM HCl, and Pt/1 mM NaCl systems

Table 1. Appearance of the inductive susceptance in various electrode/solution systems at far negative potentials

Electrode	Inductive susceptance ($B<0$)	
	Observed in solutions containing	Not observed in solutions containing
Hg (DME)	Ag(I), Hg(I), Cd(II), Pb(II), Zn(II), Ni(II), In(III), H^+, Li^+, Na^+, K^+, Ca^{2+}, Al^{3+}	Mg^{2+}, tetraalkylammonium ions
Pt, Cu, Cd, Pb, Sn, Ni, Ti, W, graphite	H^+ (strong acids)	alkali metal cations, NH_4^+, Mg^{2+}
Ag	H^+ ($HClO_4$)	H^+ (HCl)

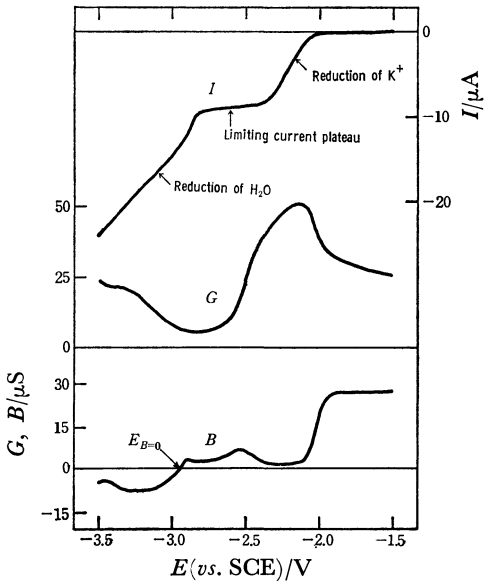

Fig. 3. I-E, G-E, and B-E curves observed at a DME in a 1 mM KNO_3 solution of 25 °C; the admittance being measured at 31 Hz.

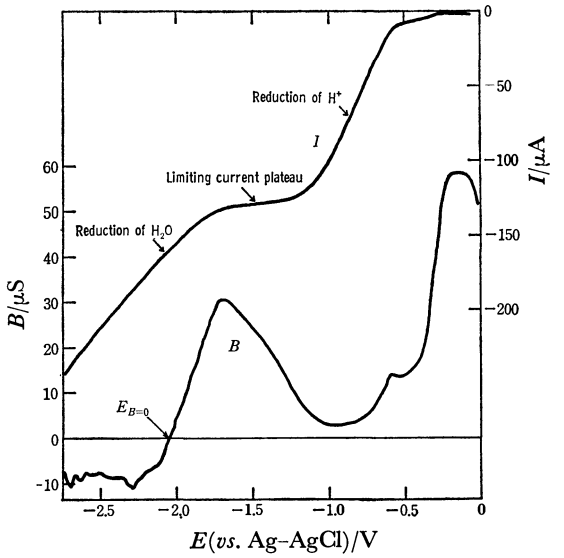

Fig. 4. I-E and B-E curves observed at a Pt-electrode in a 2 mM HCl solution of 25 °C; admittance being measured at 64 Hz.

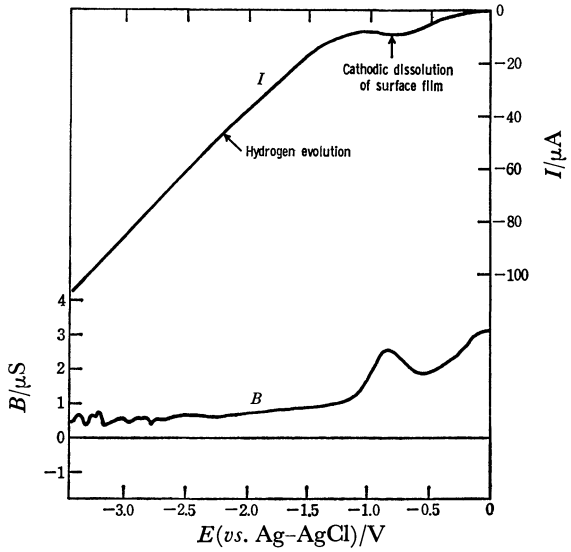

Fig. 5. I-E and B-E curves observed at a Pt-electrode in a 1 mM NaCl solution of 25 °C; admittance being measured at 64 Hz.

respectively. In the systems which give inductive susceptances at far negative potentials, the cathodic limiting-current plateau due to the reduction of the cations in the solution is clearly observed on the I-E curve, and the final rise in the cathodic current is well separated from the previous reduction step of the cation (see Figs. 3 and 4). On the other hand, no inductive susceptances could be observed at many solid electrodes in aqueous solutions containing alkali-metal cations; in these systems, the cathodic current increases monotonously without reaching a limiting-current plateau (see Fig. 5). The following part of this paper will be concerned mainly with the inductive susceptances observed with the DME systems.

The electrode potentials, $E_{B=0}$, where the susceptance, B, changes from capacitive ($B>0$) to inductive ($B<0$),

Table 2. Electrode potential, $E_{B=0}$, observed with DME/nitrate solutions of various cations; measured at 31 Hz and at 25 °C

Cation	$E_{B=0}$ V(*vs.* SCE)	$E_{1/2}$[a] V(*vs.* SCE)
Pb(II)	−1.9	−0.4
Cd(II)	−1.9	−0.6
Zn(II)	−1.9	−1.1
Ni(II)	−1.9	−1.1
Ag^+	−2.3	>0
Hg(I)	−2.3[b]	>0
In(III)	−2.3	−1.0
H^+	−2.5	−1.6
Al^{3+}	−2.6	−1.7
Na^+	−2.8	−2.1
K^+	−3.0	−2.1
Li^+	−3.1	−2.3
Ca^{2+}	−3.2	−2.2

a) Approximate values. b) In a perchlorate solution.

are summarized in Table 2. As may be seen from this table, the cations can be classified into two groups according to the correlation between their $E_{B=0}$ and their polarographic half-wave potentials, $E_{1/2}$: Group (A) includes the cations (Pb^{2+}, Cd^{2+}, Zn^{2+}, Ni^{2+}, Ag^+, Hg_2^{2+}, and In^{3+}), whose half-wave potentials are less negative than that of H^+; Group (B) includes the cations (Li^+, Na^+, K^+, Ca^{2+}, and Al^{3+}), whose half-wave potentials are more negative than that of H^+. The $E_{B=0}$ values for the cations in Group (A) do not show any particular correlation with the half-wave potentials, while the $E_{B=0}$ values for the cations in Group (B) become more negative in the same order as their half-wave potentials.

The effect of the frequency on the inductive susceptance was studied mainly with DME/KNO_3 (or KCl) solutions. The electrode potential, $E_{B=0}$, for a DME/1 mM KNO_3 system shifted to more negative potentials almost linearly with the increasing frequency, as is shown in Fig. 6. The $E_{B=0}$ value extrapolated to zero frequency was found to be equal to the electrode potential, E_D, where the polarographic cathodic current begins to increase linearly with the electrode potential (see Fig. 6).

The frequency dependence of the admittance measured with a DME/1 mM KNO_3 system at several electrode potentials is shown in Fig. 7 by plotting B against G on a complex admittance plane. Similar diagrams were also obtained with DME/KCl solutions of different concentrations at $E=-3.2$ V (*vs.* SCE) (see Fig. 8). The *B-G* plots for these systems suggest that the electric properties of the systems can be represented by assuming some resonance circuits which involve capacitive and inductive elements.

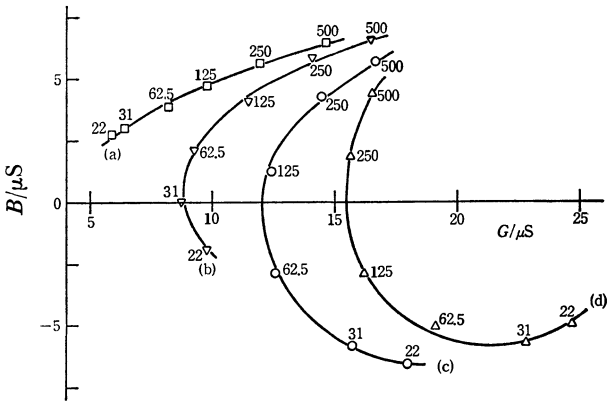

Fig. 7. Frequency dependence of the admittance measured with a DME/1 mM KNO_3 system at different electrode potentials; E/V(*vs.* SCE) = −2.8(a), −3.0 (b), −3.2(c), and −3.4(d). The figure beside each experimental point represents the frequency in Hz.

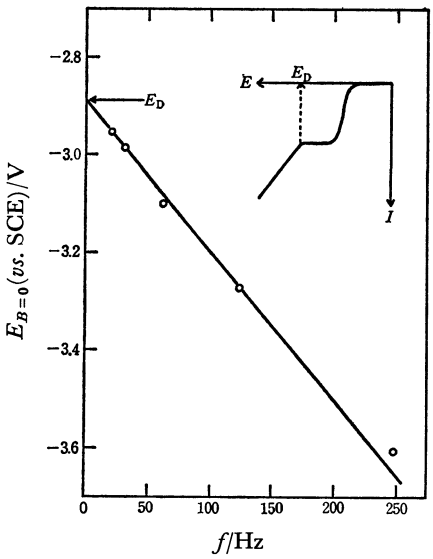

Fig. 6. Frequency dependence of $E_{B=0}$ of a DME/1 mM KNO_3 system at 25 °C.

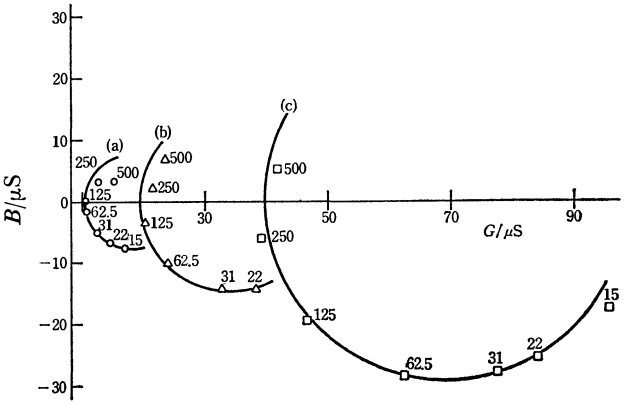

Fig. 8. Frequency dependence of the admittance measured with a DME/KCl system at different concentrations of KCl and at $E=-3.2$ V(*vs.* SCE): (a) 1 mM, (b) 2 mM, and (c) 4 mM KCl. The figure beside each experimental point represents the frequency in Hz.

Discussion

The experimental results presented in the previous section suggest that the appearance of the inductive susceptance is related to the mechanism of the reduction process of water molecules at the electrodes.

In analogy with the mechanisms proposed for the hydrogen overvoltage,[13] water molecules are considered to be reduced electrochemically through either one of the following reaction schemes: the recombination (EC) mechanism (I):

$$H_2O + e \rightarrow H_{ad} + OH^- \quad \text{(I-1)}$$

$$H_{ad} + H_{ad} \rightarrow H_2 \quad \text{(I-2)}$$

or the electrochemical (EE′ or ECE′) mechanism (II):

$$H_2O + e \rightarrow H_{ad} + OH^- \quad \text{(II-1)}$$

$$H_{ad} + H_2O + e \rightarrow H_2 + OH^- \quad \text{(II-2)}$$

where H_{ad} indicates the hydrogen atom adsorbed on the electrode surface. In solutions containing alkali-metal cations, a third (catalytic) mechanism (III) can be considered, in which the reduction of water molecules proceeds *via* an intermediate discharge of alkali-metal cations:

$$M^+ + e(Me) \rightarrow M(Me) \quad \text{(III-1)}$$

$$M(Me) + H_2O \rightarrow M^+ + H_{ad} + OH^- + (Me) \quad \text{(III-2)}$$

$$H_{ad} + H_{ad} \rightarrow H_2 \quad \text{(III-3)}$$

where M^+ is an alkali-metal cation and Me represents a metal of the electrode.

According to the theoretical analysis of the faradaic admittance by Smith and Sobel,[5] no faradaic susceptance of the inductive nature can be expected for the electrode reactions with the following mechanisms: a simple charge-transfer process, the CE and EC mechanisms, and a catalytic mechanism, unless negative transfer-coefficients are assumed. In the cases of the ECE′ and $(EC)_nE'$ mechanisms, however, the theory shows that inductive susceptances can be observed under certain conditions. This theoretical result suggests that the inductive susceptance in our present systems can be explained more reasonably by assuming the electrochemical mechanism (II) than by assuming the recombination mechanism (I) or the mechanism (III) for the reduction of water molecules.

Theoretical Expressions for the Faradaic Admittance. In this paper, the theoretical expressions of the faradaic admittance for the reaction mechanism (II) are derived on the basis of the following assumptions*:

(a) In the negative potential region where the cathodic current due to the reduction of water molecules is observed, the partial anodic current can be neglected in comparison with the partial cathodic current. Thus, the overall faradaic current density (c.d.), j, due to the reaction (II) is given by:

$$j = j_{c1} + j_{c2} \quad (1)$$

where j_{c1} and j_{c2} are the partial cathodic c.d. for the reaction steps (II-1) and (II-2) respectively.

(b) The partial cathodic c.d., j_{c1}, is represented by:

$$j_{c1}/F = -k_1(1-\theta)\exp(-\beta_1 E) \quad (2)$$

with

$$\beta_1 = \frac{\alpha_{c1}F}{RT} \quad (3)$$

where θ is that fraction of the electrode surface which is covered with H_{ad}; E, the electrode potential referred to a given reference electrode; α_{c1}, the cathodic transfer-coefficient for the step (II-1); k_1, a positive constant which is independent of E, and θ but a function of the concentration of H_2O at the electrode surface. The other symbols have their usual meanings. In this paper, the sign of the cathodic current is taken as negative.

(c) The partial cathodic c.d., j_{c2}, is given by:

$$j_{c2}/F = -k_2\,\theta(1-\theta)\exp(-\beta_2 E) \quad (4)$$

with

$$\beta_2 = \frac{\alpha_{c2}F}{RT} \quad (5)$$

where α_{c2} is the cathodic transfer-coefficient for the step (II-2), and k_2, a positive constant similar to k_1.

Some authors[2,7,8] have used the expression:

$$j_{c2}/F = -k_2\,\theta\exp(-\beta_2 E) \quad (4')$$

As will be discussed later, however, Eq. (4′) cannot explain the present experimental results. Therefore, the following analysis will be made primarily on the basis of Eq. (4).

(d) Under the experimental conditions of the admittance measurement, the electrode potential, E, is equal to the sum of a DC-component, $\bar{E}$, and an AC-component, $\tilde{E}$:

$$E = \bar{E} + \tilde{E} \quad (6)$$

The AC-component is assumed to be sufficiently small, so that the condition:

$$\exp(-\beta_{1(2)}\tilde{E}) = 1-\beta_{1(2)}\tilde{E} \quad (7)$$

is satisfied.

For the faradaic c.d. and for the coverage, we assume the following relations, respectively:

$$j = \bar{j} + \tilde{j} = (\bar{j}_{c1}+\bar{j}_{c2}) + (\tilde{j}_{c1}+\tilde{j}_{c2}) \quad (8)$$

and

$$\theta = \bar{\theta} + \tilde{\theta} \quad (9)$$

where $\bar{j}$ and $\bar{\theta}$ are the DC-components, and $\tilde{j}$ and $\tilde{\theta}$, the AC-components.

(e) When $\tilde{E}$ is given by

$$\tilde{E} = \Delta E\exp(j\omega t) \quad (10)$$

$\tilde{\theta}$ is represented by

$$\tilde{\theta} = \Delta\theta\exp(j\omega t+\phi) \quad (11)$$

where ΔE and $\Delta\theta$ are the amplitudes; ω, the angular frequency; ϕ, the phase-angle between $\tilde{E}$ and $\tilde{\theta}$, and t, the time.

(f) The contribution of the time-dependence of the H_2O-concentration at the electrode surface to the

* Similar treatments of the faradaic admittance have been reported by Batrakov and Iofa,[7] by Novosel'skii and Gudina,[8] and by Epelboin *et al.*[2]

faradaic admittance can be ignored, because a large amount of H_2O is available for the reaction.

By using these assumptions and by neglecting the terms involving a product of the AC-components (*e.g.*, $\tilde{\theta}\tilde{E}$), we obtain the following expressions for $\bar{j}$ and $\tilde{j}$:

$$-\bar{j}/F = (1-\bar{\theta})(\bar{k}_1+\bar{k}_2\bar{\theta}) \tag{12}$$

and

$$\tilde{j}/F = \{\bar{k}_1+\bar{k}_2(2\bar{\theta}-1)\}\tilde{\theta} + (1-\bar{v})(k_1\beta_1+k_2\bar{\theta}\beta_2)\tilde{E} \tag{13}$$

where

$$\bar{k}_1 = k_1\exp(-\beta_1\bar{E}) \text{ and } \bar{k}_2 = k_2\exp(-\beta_2\bar{E}) \tag{14}$$

The faradaic admittance, Y_F, is then given by the equation:

$$Y_F = G_F + jB_F = \frac{d\bar{j}}{d\tilde{E}} = F(1-\bar{\theta})(\bar{k}_1\beta_1+\bar{k}_2\bar{\theta}\beta_2) + F\{\bar{k}_1+\bar{k}_2(2\bar{\theta}-1)\}\frac{d\tilde{\theta}}{d\tilde{E}} \tag{15}$$

where G_F is the faradaic conductance, and B_F, the faradaic susceptance.

The time-dependence of the coverage, θ, follows the relation:

$$[H_{ad}]_s\frac{d\theta}{dt} = k_1(1-\theta)\exp(-\beta_1E) - k_2\theta(1-\theta)\exp(-\beta_2E) \tag{16}$$

where $[H_{ad}]_s$ is the maximum amount of H_{ad} divided by the surface area of the electrode when the surface is saturated with H_{ad}. Similarly to the faradaic c.d., $d\theta/dt$ can be divided into the DC- and AC-components:

$$[H_{ad}]_s\frac{d\bar{\theta}}{dt} = (1-\bar{\theta})(\bar{k}_1-\bar{k}_2\bar{\theta}) \tag{17}$$

and

$$[H_{ad}]_s\frac{d\tilde{\theta}}{dt} = -\{\bar{k}_1+\bar{k}_2(1-2\bar{\theta})\}\tilde{\theta} - (1-\bar{\theta})(\bar{k}_1\beta_1-\bar{k}_2\bar{\theta}\beta_2)\tilde{E} \tag{18}$$

The introduction of Eq. (11) into Eq. (18) gives the equation for $d\tilde{\theta}/d\tilde{E}$:

$$\frac{d\tilde{\theta}}{d\tilde{E}} = -\frac{(1-\bar{\theta})(\bar{k}_1\beta_1-\bar{k}_2\bar{\theta}\beta_2)}{\bar{k}_1+\bar{k}_2(1-2\bar{\theta})+j\omega[H_{ad}]_s} \tag{19}$$

From Eqs. (15) and (19), the following expressions are derived for the faradaic conductance and susceptance respectively:

$$G_F = G_F' + G_F'' \tag{20}$$

$$G_F' = F(1-\bar{\theta})(\bar{k}_1\beta_1+\bar{k}_2\bar{\theta}\beta_2) \tag{21}$$

$$G_F'' = \frac{q}{1+\omega^2p^2} \tag{22}$$

$$B_F = \frac{-\omega pq}{1+\omega^2p^2} \tag{23}$$

where

$$p = \frac{[H_{ad}]_s}{\bar{k}_1+\bar{k}_2(1-2\bar{\theta})} \tag{24}$$

and

$$q = -F\frac{\bar{k}_1-\bar{k}_2(1-2\bar{\theta})}{\bar{k}_1+\bar{k}_2(1-2\bar{\theta})}(1-\bar{\theta})(\bar{k}_1\beta_1-\bar{k}_2\bar{\theta}\beta_2) \tag{25}$$

The conductance, G_F', being independent of the frequency, is equivalent to the reciprocal of the charge-transfer resistance, while the conductance, G_F'', and the susceptance, B_F, both being dependent on the frequency, are due to the concentration polarization.

Equation (21) shows that G_F' is always positive if both the transfer-coefficients, α_{c1} and α_{c2}, are positive (*i.e.*, $\beta_1>0$ and $\beta_2>0$). In our present systems, the possibility of negative transfer-coefficients may be excluded because of the normal behavior of the DC *I-E* curves (if the transfer-coefficient were negative, some abnormal decrease in the cathodic current could be observed with the increase in the negative potentials).

In order to discuss the conditions under which the faradaic susceptance becomes inductive ($B_F<0$), the stationary-state assumption is introduced with respect to the DC-component of the coverage: $d\bar{\theta}/dt=0$. By using this assumption, we obtain the relation:

$$\bar{k}_1 = \bar{k}_2\bar{\theta} \tag{26}$$

from Eq. (17) unless $(1-\bar{\theta})=0$.

From Eqs. (21), (24), (25), and (26), the following expressions are derived for p and a dimensionless parameter, r, which is the ratio of q to G_F':

$$p = \frac{[H_{ad}]_s}{\bar{k}_2(1-\bar{\theta})} \tag{27}$$

and

$$r \equiv \frac{q}{G_F'} = \frac{(3\bar{\theta}-1)(1-b)}{(1-\bar{\theta})(1+b)} \tag{28}$$

where b is a dimensionless quantity as defined by

$$b \equiv \frac{\beta_1}{\beta_2} = \frac{\alpha_{c1}}{\alpha_{c2}} \tag{29}$$

When $r>0$, q must be positive and the faradaic susceptance, B_F, becomes inductive ($B_F<0$), because p should be positive according to Eq. (27). On the other hand, if $r<0$, q must be negative and the faradaic susceptance becomes capacitive ($B_F>0$). By means of Eq. (28), the relationship between b and $\bar{\theta}$ can be drawn for different values of r, as is shown in Fig. 9; (a) represents the b-$\bar{\theta}$ diagram for $r>0$ (inductive susceptance), and (b), the b-$\bar{\theta}$ diagram for $r<0$ (capacitive susceptance). In Fig. 9(a), the combination of b and $\bar{\theta}$ which will result in an inductive susceptance under the condition, $b>0$, is shown by solid lines.

The above theoretical treatment of the faradaic admittance, although not very rigorous, clearly demonstrates that the susceptance, B_F, for the electrochemical mechanism (II) can be either capacitive or inductive according to the conditions determined by the r, b, and $\bar{\theta}$ parameters (see Fig. 9(a) and (b)).

Complex Admittance Plane Diagram and the Equivalent Circuit. Equations (20)—(23) for the faradaic conductance and susceptance show that, when $q>0$,

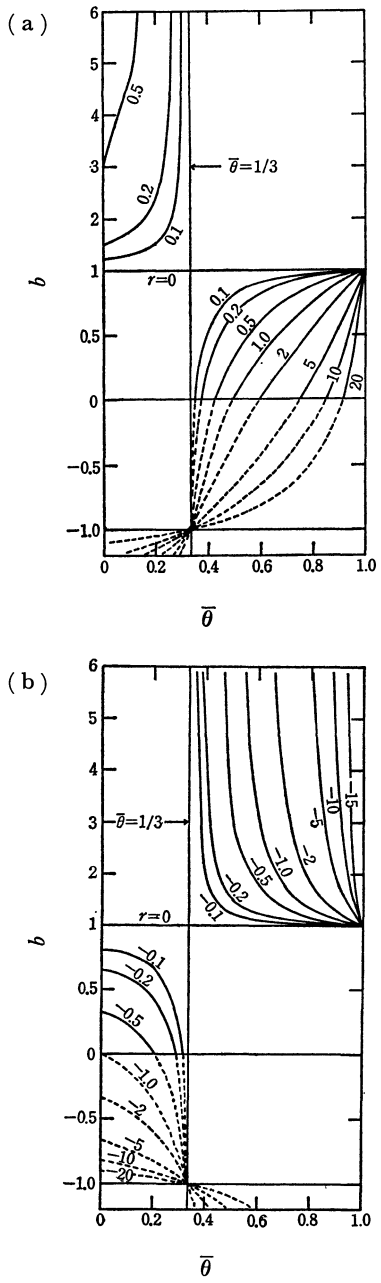

Fig. 9. Theoretical b-$\bar{\theta}$ curves for various values of the parameter, r, as calculated by means of Eq. (28): (a), b-$\bar{\theta}$ curves for $r>0$ (inductive susceptance); (b), b-$\bar{\theta}$ curves for $r<0$ (capacitive susceptance). Solid lines correspond to the condition, $b>0$, and broken lines to the condition, $b<0$.
The figure beside each curve represents the r-value.

a plot of B_F against G_F on a complex admittance plane gives a semi-circle with its center at $[(G_F')+(q/2)]$ and a radius of $q/2$, as is shown in Fig. 10. This admittance behavior can be represented by assuming an equivalent circuit which consists of two resistances, R_1 and R_2, and an inductance, L, as is presented in Fig. 10(a), where $R_1=(G_F')^{-1}$, $R_2=q^{-1}$, $r=R_1/R_2$, $L=p/q$, and the time-constant of the circuit is equal to L/R_2 $(=p)$.

The conductance and the susceptance of an electrode/solution system, which can be measured experimentally,

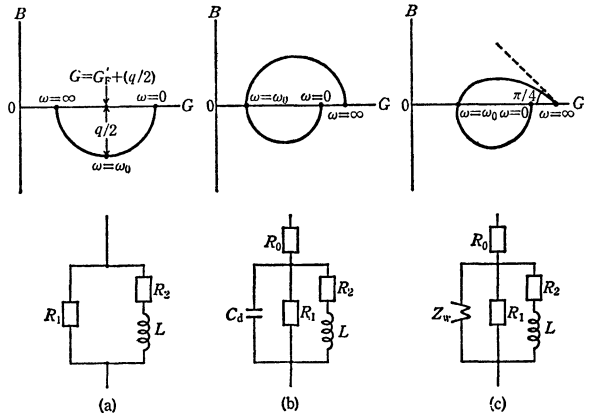

Fig. 10. Theoretical B-G plots (schematic) on a complex admittance plane and the corresponding equivalent circuits.

involve not only the faradaic components, but also the solution resistance, R_0, and the double-layer capacity, C_d. It has been shown by our previous studies[11,14] that, in the far negative potential region where the reduction of all the cations present in the solution gives the cathodic limiting-current plateau, the double-layer capacity of the Helmholtz-Gouy-Chapmann type becomes very small and the admittance behavior of the electrode surface is practically determined by the Warburg-type impedance, Z_w, due to the mass-transport of the depolarizable cations. Consequently, the actual equivalent circuit for the system which gives inductive susceptances may be considered to be represented either by (b) or (c) in Fig. 10; the schematical B-G plots corresponding to the equivalent circuits are presented in the same figure. The expressions for the characteristic points on the complex admittance plane are summarized in Table 3.

Both the equivalent circuits, (b) and (c), can reproduce the experimental observation that the B-G plot starts from the fourth quadrant of the complex admittance plane at lower frequencies and then passes into the first quadrant with the increase in the frequency (see Figs. 7 and 8). In Fig. 11, one of the best experimental results is compared with the B-G diagrams obtained by means of simulation using the equivalent circuits (b) and (c) in Fig. 10; the values of each element, as determined by simulation, are summarized in Table 4. The values of r thus obtained are relatively large, suggesting that the possible values of $\bar{\theta}$ should be in the range of $0.8<\bar{\theta}<1$ (see Fig. 9(a)); in other words, $\bar{k}_2$ is close to $\bar{k}_1$, according to relation (26).

Finally, let us discuss the possibility that the current density due to the reaction path (II-2) is given by Eq. (4'). In this case, too, inductive susceptances can be expected when $r>0$; by following a similar treatment, we obtain the b-$\bar{\theta}$ diagram shown in Fig. 12 for various positive values of r. Figure 12 suggests that the values of r cannot be larger than unity $(r<1)$ for the appearance of inductive susceptances. This result is not in agreement with the r-values ($r=15$ or 25) evaluated by means of simulation (see Table 4).

Table 3. Expressions for the characteristic points on the *B-G* plot in terms of the equivalent circuits given in Fig. 10

Characteristic point	Expression in terms of the equivalent circuit (a)	(b)	(c)[a]
$G(\omega=0)$	$\frac{1}{R_1}+\frac{1}{R_2}$	$\frac{1}{R_0+\left(\frac{1}{R_1}+\frac{1}{R_2}\right)^{-1}}$	$\frac{1}{R_0+\left(\frac{1}{R_1}+\frac{1}{R_2}\right)^{-1}}$
$G(\omega=\infty)$	$\frac{1}{R_1}$	$\frac{1}{R_0}$	$\frac{1}{R_0}$
$G(\omega=\omega_0)$	$\frac{1}{R_1}+\frac{1}{2R_2}$	$\frac{1}{R_0+\left\{\frac{1}{R_1}+\frac{1}{R_2}\left(1+\frac{\omega_0^2L^2}{R_2^2}\right)^{-1}\right\}^{-1}}$	$\frac{1}{R_0+\left\{\frac{1}{R_1}+\frac{1}{2S\left(\frac{R_2}{L\sqrt{\omega_0}}+\sqrt{\omega_0}\right)}\right\}^{-1}}$
ω_0	$\omega_0=\frac{R_2}{L}$	$\omega_0^2=\frac{1}{LC_d}-\left(\frac{R_2}{L}\right)^2$	$\omega_0^2L^2-2SL\sqrt{\omega_0}+R_2^2=0$

a) The Warburg impedance is assumed to be given by $Z_w=S\omega^{-1/2}(1-j)$.

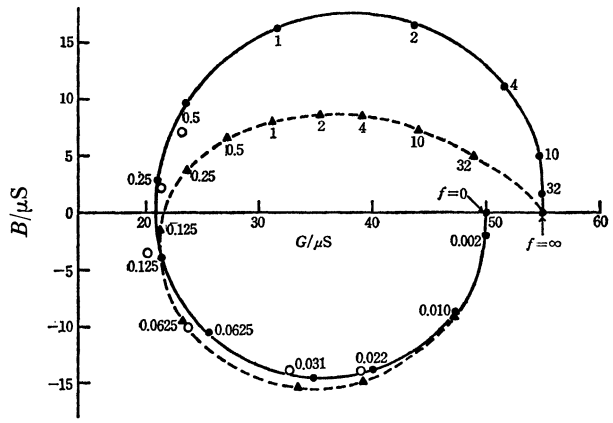

Fig. 11. Comparison of the simulated *B-G* diagrams with the experimental results obtained with a DME/2 mM KCl system at $E=-3.2$ V(*vs.* SCE): -●- and -▲-, simulated curves by using the equivalent circuits (b) and (c), respectively, in Fig. 10; ○, experimental points. The figure beside each point represents the frequency in kHz.

Table 4. The values of each element in the equivalent circuits given in Fig. 10, as determined by simulation (see Fig. 11)

System: DME/2 mM KCl; $E=-3.2$ V(*vs.* SCE); surface area of the DME, 0.0142 cm².

Equivalent circuit	R_0 / kΩ	R_1 / kΩ	R_2 / kΩ	r	L / H	C_d / μF	S[a] / kΩ s$^{-1/2}$
Fig. 10(b)	18	30	2	15	70	0.01	—
Fig. 10(c)	18	50	2	25	70	—	10^3

a) The Warburg impedance is assumed to be given by $Z_w=S\omega^{-1/2}(1-j)$; an approximate value of $S(S=10^3$ kΩ s$^{-1/2}$) was estimated from our previous work.[11]

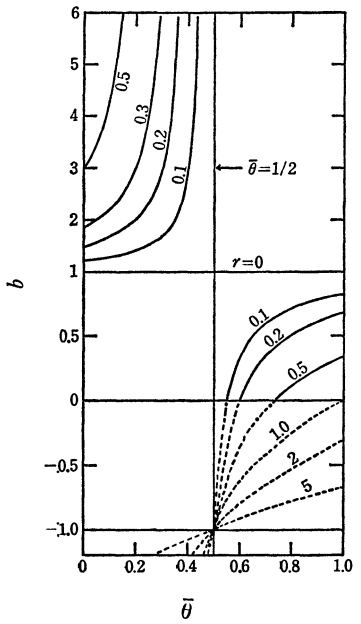

Fig. 12. Theoretical b-$\bar{\theta}$ curves for various positive values of r, as calculated by means of an equation which is derived on the basis of Eq. (4′). Solid lines correspond to the condition, $b>0$, and broken lines to the condition, $b<0$.

Conclusion

The discussion above has been made on the basis of the assumption that the inductive susceptance is related to the mechanism of the faradaic processes. There may exist some other mechanisms of the non-faradaic nature which also give inductive susceptances at an electrode/solution interface. However, so long as we accept the above assumption, we can conclude that, in the electrode systems which show the inductive susceptance at far negative potentials, water molecules are reduced through the electrochemical mechanism (II), in which the rate of reaction path (II-2) is proportional to the product of θ and $(1-\theta)$.

The experimental fact that no inductive susceptance is observed at some metal electrodes in solutions containing alkali-metal cations (see Table 1) suggests the possibility that the hydrogen evolution proceeds according to the other mechanisms, such as (I) or (III), in such systems.

References

1) N. Tanaka, T. Takeuchi, and R. Tamamushi, This Bulletin, **37**, 1435 (1964); R. Tamamushi and K. Matsuda, *J. Electroanal. Chem.*, **12**, 436 (1966); B. Timmer and M. Sluyters-Rehbach, *ibid.*, **19**, 73 (1968); R. de Levie and A. A. Husovsky, *ibid.*, **22**, 29 (1969).

2) I. Epelboin, M. Keddam, and J. -C. Lestrade, *Revue Generale de l'electricite*, **76**, 777 (1967); R. Wiart, *Oberflach-Surface*, **9**, 213, 241, 275 (1968); I. Epelboin, and M. Keddam, *J. Electrochem. Soc.*, **117**, 1052 (1970).

3) H. Gerischer and W. Mehl, *Z. Elektrochem.*, **59**, 1049 (1955).

4) D. Schumann, *J. Electroanal. Chem.*, **17**, 45 (1968).

5) D. E. Smith and H. R. Sobel, *Anal. Chem.*, **42**, 1018 (1970).

6) R. de Levie, J. C. Kreuser, and H. Moreira, *ibid.*, **43**, 784 (1971).

7) V. V. Batrakov and Z. A. Iofa, *Elektrokhim.*, **1**, 123 (1965).

8) I. M. Novosel'skii and N. N. Gudina, *ibid.*, **5**, 820 (1969).

9) K. Matsuda, K. Takahashi, and R. Tamamushi, This Bulletin, **44**, 2880 (1971).

10) K. Matsuda, K. Takahashi, and R. Tamamushi, *Sci. Papers IPCR*, **64**, 62 (1970).

11) K. Takahashi and R. Tamamushi, This Bulletin, **48**, 3540 (1975).

12) D. Ilkovič, *Collection Czechoslov. Chem. Commun.*, **4**, 480 (1932); T. Okada and S. Yoshizawa, This Bulletin, **49**, 183 (1946); H. Imai and P. Delahay, *J. Phys. Chem.*, **66**, 1683 (1962).

13) A. N. Frumkin, "Advances in Electrochemistry and Electrochemical Engineering," Vol. 1 (P. Delahay, ed.) Interscience Publishers, New York (1961), pp. 65—121; A. Frumkin, V. Korshunov, and I. Bagozkaya, *Electrochim. Acta*, **15**, 289 (1970).

14) K. Takahashi and R. Tamamushi, *Electrochim. Acta*, **16**, 875, 1157 (1971).

Partition Coefficients of Alkanols and Polyoxyethylene Alkyl Ethers in the Dodecane–Water System at 25 °C

Masahiro MANABE, Masaharu KODA, and Keishiro SHIRAHAMA*

Department of Technical Chemistry, Niihama Technical College, Niihama, Ehime 792

**Department of Chemistry, Faculty of Science and Engineering, Saga University, Saga 804*

(Received July 19, 1975)

The partition coefficients of normal alkanols (R_mOH, m=2 to 6) and a number of polyoxyethylene normal alkyl ethers (R_mE_nOH, n=1,2 m=2 to 5; n=3,4 m=4,5) in the dodecane–water system have been determined at a high dilution at 25 °C. From the finding that the standard free energies of the transfer of the solutes from water to the dodecane phase show a linear relation with the number of methylene and oxyethylene groups, the contribution of the groups to the free energy was obtained as −0.858 for alkanols and −0.808 kcal/mol methylene group for ethers, and 0.655 kcal/mol oxyethylene group respectively. Extrapolation to zero oxyethylene in the linear relationship for the normal alkylethers gave standard free energies of transfer less than those for normal alkanols with the same alkyl chain length. Thus, the alkanol is more hydrophilic than the hypothetical "ether" with no oxyethylene group. The difference in the free energies is discussed from the viewpoint of intramolecular hydrogen-bond formation in the polyoxyethylene chain in the dodecane phase.

In spite of the importance and usefulness of the data of the partition coefficient for amphiphiles between water and the nonpolar phase for the study of colloid chemistry, only a few systematic investigations[1,2] have ever been made. The process of the transfer of amphiphiles from an aqueous to a nonpolar phase seems of much interest in many respects. Davies[3] proposed a relation of the hydrophile-lipophile balance (HLB) with the partition coefficenet, and further estimated the "group number". The solubilization and micelle formation are regarded as a partition process, especially in the treatment by the phase-separation model for micell formation.[4] The solubilities of alkanols[5] and hydrocarbons[6] in water are also a measure of a similar process of transfer.

The standard free energy of transfer obtained from the partition coefficients can be applied to such transfer processes in colloid chemistry, and the comparison of the free energies for different processes yields useful information about the environment around a solute molecule. It is well known that the physicochemical properties of the alkyl[7] or polyoxyethylene derivatives[8] show a linear dependence on the number of methylene or oxyethylene groups. In the present investigation, the contribution of each group contained in the solute molecules to the standard free-energy changes of transfer was tentatively estimated. Dodecane is chosen as the nonpolar phase because of its low mutual solubility with water as well as because of the possibility of disregarding a specific interaction with solute molecules. Normal alkanols and polyoxyethylene alkyl ethers are chosen for the solutes; the former are simple amphiphilic compounds, and the later, model compounds for nonionic surfactants.

Experimental

Materials. The normal alkanols (R_mOH, m=2 to 6) and some (m=2 to 4, n=1,2) of the polyoxyethylene normal alkyl ethers (R_mE_nOH) used as solutes were commercially available (Tolyo Kasei, G.R. and E.P. grade). They were dehydrated and distilled prior to use. The other ethers (m=4, n=3, 4; m=5, n=1 to 4) were prepared by the Williamson reaction of the corresponding glycol and alkyl bromide.[9] Their purification was carried out by the following procedure. After the addition of a large amount of water to the reaction mixture, the ether was repeatedly extracted with a small amount of hexane. Each hexane fraction was analyzed by g-l chromatography, whereupon diether was found to be rich in the earlier fractions, and glycol, in the later ones. The middle fractions, being rich in monoether, were collected and evaporated. The extract was distilled to obtain monoether under reduced pressure. The purities of the compounds were confirmed to be above 98% by g-l chromatography. The dodecane (Tokyo Kasei, G. R. grade) was first distilled and used once as a nonpolar phase for the measurement of the partition coefficient; it was then repeatedly washed with an amount of water sufficiently large to remove a solute, and used in the next run.

Procedure. Aqueous solutions of a desired solute were prepared at concentration of *ca.* 10^{-3} to 10^{-2} mol/kg. A sample prepared from a known weight of the aqueous solution and of dodecane was maintained for a day at room temperature; then the sample was stirred in a thermostat and kept at 25±0.05 °C for about seven hours. This operation was performed for at least six aqueous solutions with different concentrations of a given solute. Then the sample was allowed to stand and a quantity of the aqueous phase was pipetted out. The solute concentration of the aqueous phase in equilibrium was determined at 25±0.005 °C by using a Ostwald-type viscometer the flow time of which was *ca.* 9 min. The solute concentration in the dodecane phase was obtained from the material balance relation.

Results and Discussion

Figure 1 shows the logarithmic relations between the solute concentrations in the dodecane and water phases for R_mE_nOH (m=5, n=2 to 4) as illustrative examples. All the plots dropped on a straight line, with a unity slope for each solute; therefore, we can conclude that the solute is dissolved in the monomeric state in each phase, as may be seen from the spectroscopic data for alkanols,[1] and the partition coefficient does not depend on the concentration within the region studied.

The partition coefficient is expressed as:

$$K_x = x_o/x_w \quad (1)$$

where x_o and x_w are the mole fractions of solute in

TABLE 1. PARTITION COEFFICIENTS IN *n* DODECANE-WATER SYSTEM AT 25 °C

Compound	K_x	Compound	K_x	Compound	K_x
R_2OH	$8.67(\pm0.09)\times10^{-2}$	R_2E_1OH	$9.95(\pm0.58)\times10^{-2}$	R_2E_2OH	$3.30(\pm0.04)\times10^{-2}$
R_3OH	$3.74(\pm0.10)\times10^{-1}$	R_3E_1OH	$5.94(\pm0.48)\times10^{-1}$	R_3E_2OH	$1.88(\pm0.08)\times10^{-1}$
R_4OH	$1.70(\pm0.07$	R_4E_1OH	$2.37(\pm0.10)$	R_4E_2OH	$8.56(\pm0.32)\times10^{-1}$
R_5OH	$7.24(\pm0.11)$	R_5E_1OH	$9.38(\pm0.23)$	R_5E_2OH	$3.16(\pm0.01)$
R_6OH	$2.74(\pm0.16)\times10$				
		R_4E_3OH	$2.84(\pm0.06)\times10^{-1}$	R_4E_4OH	$9.40(\pm0.11)\times10^{-2}$
		R_5E_3OH	$1.06(\pm0.006)$	R_5E_4OH	$3.61(\pm0.08)\times10^{-1}$

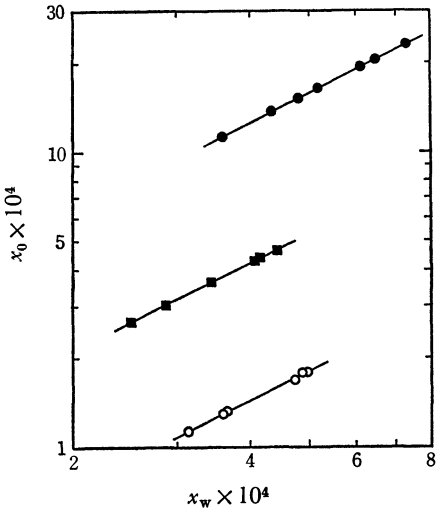

Fig. 1. The relation between the solute concentrations in *n*-dodecane and water phase.
●: R_5E_2OH, ■: R_5E_3OH, ○: R_5E_4OH.

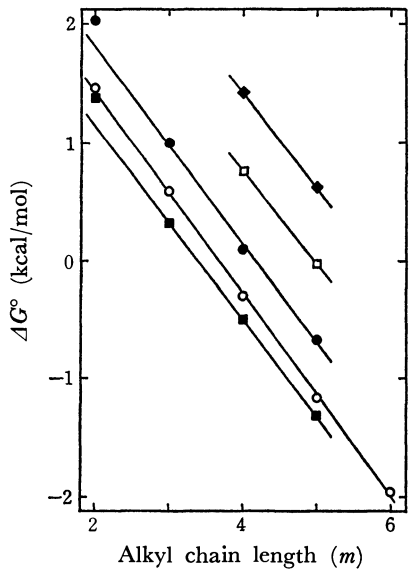

Fig. 2. The dependence of ΔG° on the alkyl chain length (m).
○: R_mOH, ■: R_mE_1OH, ●: R_mE_2OH, □: R_mE_3OH, ◆: R_mE_4OH.

dodecan and in the water phase, respectively. The partition coefficients for each solute were determined for at least six samples with different concentrations of the solute; the mean values for a given solute are listed in Table 1, along with their standard deviations. The expression of the partition coefficient in the mole fraction is convenient not only for the thermodynamic discussion of the transfer phenomena between different phases, but also for indicating the independence of the kind of nonpolar-phase substances (normal hydrocarbons containing different chain lengths), although the partition coefficient in molarity depends on the kind of nonpolar-phase substance, as may be supposed from the results for alkanols reported by Aveyard and Mitchell.[1]

The standard free energy of the transfer of a solute from the water to the dodecane phase can be calculated from the K_x value assuming ideality, because it is a value at a high dilution;

$$\Delta G^\circ = -RT\ln K_x \qquad (2)$$

The ΔG° value is plotted against the chain length in the alkyl group in Fig. 2, and the plot for a homologous series shows a linear relation except for R_mE_nOH with $m=2$. We can now assume that ΔG° is divisible into independent additive contributions from each group constituting the solute molecule:

$$\Delta G^\circ = \Delta G^\circ_{CH_2}(m-1) + \Delta G^\circ_{CH_3} + \Delta G^\circ_g \qquad (3)$$

where $\Delta G^\circ_{CH_2}$, $\Delta G^\circ_{CH_3}$, and ΔG°_g are the contributions from the methylene, terminal methyl, and polar groups respectively. A least-squares treatment gives the $\Delta G^\circ_{CH_2}$ and $(\Delta G^\circ_{CH_3}+\Delta G^\circ_g)$, as may be seen for $\Delta G^\circ_{CH_2}$ in Table 2. The $\Delta G^\circ_{CH_2}$ values are −0.858 and −0.808 kcal/mol for R_mOH and R_mE_nOH respectively in the table; they are numerically comparable with the corresponding values for alkyl derivatives in the related processes.[5-7] The standard free energy of the transfer of one mole of the methylene group from water to micelle or to an air-water interface is about −0.65 kcal/mol, a little less negative than the present value.

The estimation of ΔG°_g in Eq. (3) requires $\Delta G^\circ_{CH_3}$;

TABLE 2. STANDARD FREE ENERGY CONTRIBUTIONS FROM METHYLENE AND POLAR GROUPS

Compound	m[a]	$-\Delta G^\circ_{CH_2}$ (kcal/mol)	ΔG°_g (kcal/mol)
R_mOH	2—6	0.858	4.39
R_mE_1OH	3—5	0.818	4.05
R_mE_2OH	3—5	0.837	4.75
R_mE_3OH	4—5	0.781	5.19
R_mE_4OH	4—5	0.799	5.89
		0.808[b]	

a) Range of alkyl chain length for least-squres treatment. b) Mean value of $\Delta G^\circ_{CH_2}$ for ethers alone.

therefore, the value is estimated as −2.10 kcal/mol from the available data for the solubility[6] of liquid alkanes (m=5 to 8) in water at 25 °C, from the assumption of an additive contribution[11] such as:

$$\Delta G^\circ = \Delta G^\circ_{CH_2}(m-2) + 2\Delta G^\circ_{CH_3} \quad (4)$$

Assuming that, in the present solutes, the terminal methyl group in the alkyl group makes the same contribution to ΔG° as that in the normal alkanes, the ΔG°_g values can be calculated by means of Eq. (3); they are tabulated in Table 2. Those are not an intrinsic value for the polar group itself, but an apparent value (extrapolated value) of the standard free energy of the transfer of the polar group from water to dodecane, for the property of the methylene group proximal to the polar group may differ from that of the separate one, as may be seen from Fig. 2. The value is, however, useful, considering the hydrophilic properties of whole of the solute molecule, which consists of a long alkyl chain and a polar group. The ΔG°_g value for R_mOH, *i.e.*, for the OH group (denoted by ΔG°_{OH}), is 4.39 kcal/mol; this value is comparable to the standard free energy of transfer, about 4 kcal/mol, of water from liquid water into hydrocarbons obtained from the data for solubility of water in hydrocarbons.[12] This implies that the most important factor govering ΔG°_{OH} is the dehydration of the group.

The relation between ΔG° for R_mE_nOH and the number of the oxyethylene group in the ethers is shown in Fig. 3, together with ΔG°_g; the ΔG° value for R_mOH is also plotted at n=0 for comparison. It is evident from the linear relation for each ether containing the same alkyl-chain length that the contribution of an oxyethylene group to ΔG°, denoted by ΔG°_E, is additive. A similar relation is also seen for ΔG°_g in Fig. 3. Therefore, Eq. (3) may be rewritten as follows for R_mE_nOH:

$$\Delta G^\circ = \Delta G^\circ_{CH_2}(m-1) + \Delta G^\circ_{CH_3} + \Delta G^\circ_E n + \Delta G^\circ_{\langle OH\rangle} \quad (5)$$

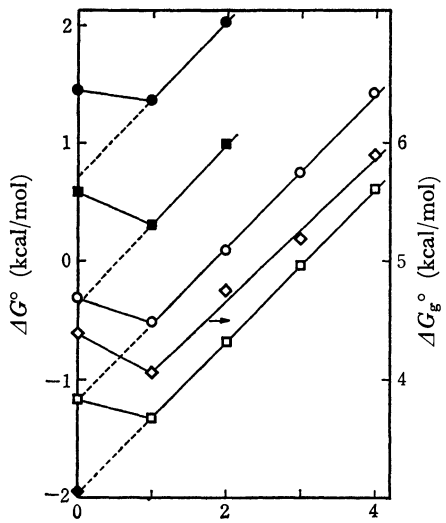

Fig. 3. The dependence of ΔG° and ΔG_g° on the number of oxyethylene groups (n), ΔG° for R_mOH is plotted at n=0.
●: R_2E_nOH, ■: R_3E_nOH, ○: R_4E_nOH,
□: R_5E_nOH, ◇: ΔG_g°, ◆: R_6OH.
For dotted line, see in text.

Table 3. Values of ΔG°_E, $\Delta G^\circ_{\langle ROH\rangle}$, and ΔG°_{HB}

Compound	n[a]	ΔG°_E (kcal/mol)	$\Delta G^\circ_{\langle ROH\rangle}$ (kcal/mol)	$-\Delta G^\circ_{HB}$ (kcal/mol)
R_2E_nOH	1—2	0.654	0.714	0.736
R_3E_nOH	1—2	0.682	−0.373	0.956
R_4E_nOH	1—4	0.639	−1.17	0.852
R_5E_nOH	1—4	0.644	−1.97	0.797
mean value		0.655		0.835
polar group[b]	1—4	0.596	3.48	0.91

a) Range the number of oxyethylene groups for least-squares treatment. b) Obtained from ΔG°_g.

where $\Delta G^\circ_{\langle OH\rangle}$ is the apparent contribution of the OH group in the ether molecule to the ΔG°, distinct from the contribution of that in R_mOH. The ΔG°_E listed in Table 3 can be obtained by the least-squares treatment of R_mE_nOH. The mean value for all of the ethers studied is 0.655 kcal/mol, which is comparable with the value of 0.60 kcal/mol obtained from the partition coefficients of homogeneous octylphenoxypolyethoxyethanols in the *iso*-octane–water system investigated by Crook *et al.*[2] The positive value of ΔG°_E may result from a positive change in the enthalpy of dehydration exceeding a positive change in entropy; this shows that the oxyethylene group behaves as a hydrophilic group, as is usual for nonionic surfactants, *e.g.*, the CMC of a surfactant, polyoxyethylene alkyl ether, increases with the increase in the number of the groups.[8]

The infercept of the line for R_mE_nOH in Fig. 3 is more negative than the ΔG° for R_mOH with the same alkyl-chain length. This means that the OH group situated in the terminal portion of the polyoxyethylene chain is not in the same state as that in R_mOH; *i.e.*, the former is less hydrophilic than the latter. Yamaguchi *et al.*[13] deduced, from their calorimetric study, that, for polyoxyethylene dodecylethers in dodecane, intramolecular hydrogen-bond formation occurs between the terminal OH group and an oxygen atom in the polyoxyethylene chain; this is unlike the results for normal dodecanol. The ΔG° at n=0 in Eq. (5) is expressed as $\Delta G^\circ_{\langle ROH\rangle}$, which is distinct from the value for R_mOH (denoted by ΔG°_{ROH}). If the OH group in R_mE_nOH in the monomeric and non-hydrogen bonding state behaves thermodynamically in the same way as that in R_mOH in dodecane, it may be considered that the difference between $\Delta G^\circ_{\langle ROH\rangle}$ and ΔG°_{ROH} is a standard free energy change (ΔG°_{HB}) for hydrogen-bond formation in the dodecane phase, *i.e.*:

$$\Delta G^\circ_{HB} = \Delta G^\circ_{\langle ROH\rangle} - \Delta G^\circ_{ROH} \quad (6)$$

The calculated ΔG°_{HB} values for the present ethers containing different alkyl-chain lengths are in good agreement with each other; their mean value is −0.835 kcal/mol, as is shown in Table 3. A similar value corresponding to ΔG°_{HB} can be obtained as the difference between $\Delta G^\circ_{\langle OH\rangle}$ and ΔG°_{OH}, −0.91 kcal/mol, but this value is less reliable because of the scattering of the ΔG°_g values, as may be seen from Fig. 3. It happens that this value is numerically coincident with

$\Delta G^{\circ}_{CH_2}$; ΔG° for R_mE_nOH becomes equal to that for $R_{m+1}OH$, as may be seen from Fig. 3. From the ΔG°_{HB} obtained here and the enthalpy of hydrogen-bond formation, -5.19 kcal/mol, for alkanol in alkanes, as was established in the calorimetric study by Aveyard and Mitchell,[1] we can evaluate the corresponding entropy, -14.5 eu., by assuming that the enthalpy for the intermolecular hydrogen-bond formation of alkanol is the same as for the intramolecular one in the polyoxyethylene chain. These thermodynamic parameters for hydrogen-bond formation seem reasonable compared with the published values.[14,15]

We would like to thank Professor Ryohei Matsuura and Assistant Professor Shoji Kaneshina of Kyushu University for their helpful suggestions and observations.

References

1) R. Aveyard and R. W. Mitchell, *Trans. Faraday Soc.*, **65**, 2645 (1969).
2) E. H. Crook, D. B. Fordyce, and C. F. Trebii, *J. Colloid Sci.*, **20**, 191 (1965).
3) J. T. Davies and E. K. Rideal, "Interfacial Phenomena," Academic Press, New York (1963), p. 371.
4) K. Shinoda, T. Nakagawa, B. Tamamushi, and T. Isemura, "Colloidal Surfactants," Academic Press, New York (1963), p. 25.
5) K. Kinoshita, H. Ishikawa, and K. Shinoda, This Bulletin, **31**, 1081 (1958).
6) C. McAuliffe, *Nature*, **200**, 1092 (1963).
7) I. J. Lin and P. Somasundaran, *J. Colloid Interface Sci.*, **37**, 731 (1971).
8) J. M. Corkill, J. F. Goodman, and S. P. Harrold, *Trans. Faraday Soc.*, **60**, 202 (1971).
9) F. C. Cooper and M. W. Partridge, *J. Chem. Soc.*, **1950**, 459.
10) I. Mandru, *J. Colloid Interface Sci.*, **41**, 430 (1972).
11) C. Tanford, "The Hydrophobic Effect," Wiley-Interscience Publication, Tronto (1973), p. 6.
12) C. Black, G. G. Joris, and H. S. Taylor, *J. Chem. Phys.*, **16**, 537 (1948).
13) M. Yamaguchi, T. Miura, and M. Nakamura, The Proceeding of the 26th Colloid and Interface Chemistry, Fukui, Japan (1973), p. 96.
14) G. C. Pimental and A. L. McClellan, "The Hydrogen Bond," Freeman, San Francisco (1960), p. 206 and p. 348.
15) S. N. Vinogradov and R. H. Linnell, "Hydrogen Bonding," Van Nostrand Reinfold Co., New York (1971), p. 114.

Infrared and Raman Spectra and Rotational Isomerism of 1,4-Pentadiene

Fuyuhiko INAGAKI, Masaaki SAKAKIBARA, Issei HARADA, and Takehiko SHIMANOUCHI
Department of Chemistry, Faculty of Science, The University of Tokyo, Hongo, Bunkyo-ku, Tokyo 113
(Received July 23, 1975)

Rotational isomerism of 1,4-pentadiene has been studied. Normal frequencies have been calculated for the low frequency vibrations of four possible rotational isomers. From the change in the spectra in the gaseous, liquid, glassy, and solid states, it has been concluded that the two skew-skew forms (SS and SS′) and the *cis*-skew form (CS) are stable in the liquid and gaseous states, the SS and SS′ forms coexist in the glassy state, and only the SS form remains in the solid state. It has also been found that the energy difference among the three isomers in liquid state is not appreciably large.

The rotational isomerism about the C–C bond adjacent to the C=C double bond has been studied by several authors. Harrah and Mayo suggested the existence of rotational isomers of 1-olefins from the infrared spectra.[1] Kondo, Hirota, and Morino analyzed the rotational spectra of 1-butene and determined the structures of the *cis* and skew isomers, the latter being obtained from the *cis* form by an internal rotation of about 120°.[2] Shimanouchi, Abe, and Alaki studied the skeletal deformation vibrations of 1-olefins in relation to the stable conformations of 1,4-polybutadiene chains. They concluded that the *cis* and skew conformations are stable for the C–C bond neighbouring the *trans* C=C bond, whereas only the skew conformation is stable for the C–C bond adjacent to the *cis* C=C bond.[3]

As an extension of such a work, we have studied the molecular conformations of 1,4-pentadiene in the gaseous, liquid, and solid states by analyzing the infrared and Raman spectra. After our work had been completed, we found a paper by Gallinella and Cadioli, which treated the same subject by means of Raman spectroscopy and *ab initio* MO calculations.[4] Although their conclusion about the conformations of the stable isomers in liquid is consistent with ours, there seems to be significant differences regarding the assignments of bands to each isomer. In this paper we will describe the band assignments based on our experimental results and normal vibration calculations.

Experimental

1,4-Pentadiene(Tokyo Chemical Industry Co.) was used without further purification for the measurement of the infrared spectra. The sample was distilled *in vacuo* prior to measurement of the Raman spectra. The infrared spectra were recorded on a Hitachi EPI-L double beam grating spectrometer in the region 700—300 cm^{-1}, and on a Hitachi FIS-1 double beam vacuum grating spectrometer in the region 500—200 cm^{-1}. The spectra in the gaseous state were taken with a 10 cm cell in the region 700—200 cm^{-1} and a 4.9 m multireflection cell with polyethylene windows in the region 400—200 cm^{-1}. We measured the spectrum in the liquid state for the thin film obtained by warming up the solid film deposited on a cooled KRS-5 plate just above the melting point. The glassy solid was obtained by the deposition of the sample on a cooled window of KRS-5 or silicon. For the spectrum in the crystalline state, the sample was repeatedly annealed until no further spectral change was observed. The Raman spectra were measured on a JRS-400D spectrophotometer with a Coherent Radiation CR-3 argon ion laser as the light source. A multireflection accessary was used for the measurement of the spectrum of gaseous state.

Results and Discussion

Infrared and Raman Spectra and Rotational Isomerism. The infrared and Raman spectra of 1,4-pentadiene in the gaseous, liquid, and solid states are shown in Figs. 1 and 2. The Raman spectra in the liquid and solid states are just the same as those reported by Gallinella and Cadioli.[4] The results so far obtained for the rotational isomerism about the C–C axis adjacent to the C=C bond show that the stable conformations are always *cis* and skew.[2,3] Since 1,4-pentadiene has two C–C axes, four isomers, SS, SS′, CS, and CC (Fig. 3) are considered to exist. Because of the steric repulsion between the terminal CH_2 groups in the CC form, the existence of this isomer is unlikely. Thus, the SS, SS′, and CS forms are the possible stable isomers. For each isomer, two CH out-of-plane vibrations and three skeletal deformation vibrations are expected in the regions 700—500 cm^{-1} and 500—200 cm^{-1}, respectively.[3] Thus the five Raman lines observed at 672, 618, 457, 376, and 318 cm^{-1} in the crystalline state (Fig. 2d) are reasonably assigned to one isomer. In the infrared spectra, the bands at 444 and 306 cm^{-1}

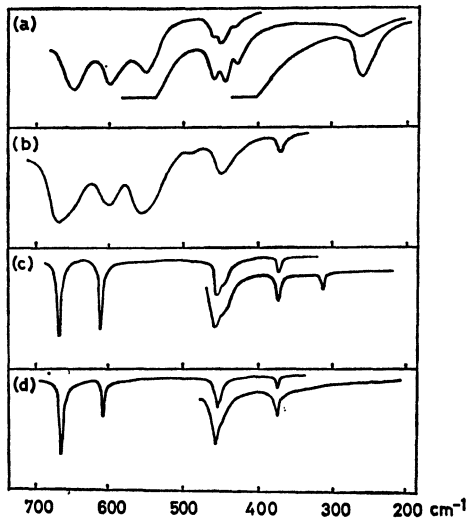

Fig. 1. Infrared spectra of 1,4-pentadiene.
(a) gas, (b) liquid, (c) glassy solid, (d) annealed solid.

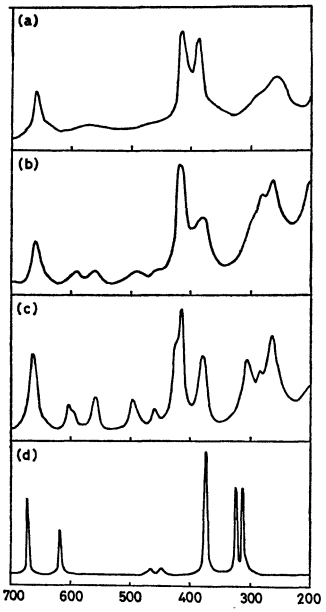

Fig. 2. Raman spectra of 1,4-pentadiene.
(a) gas (550 Torr), 296 K, (b) liquid, 273 K
(c) liquid, 163 K, (d) solid, 77 K.

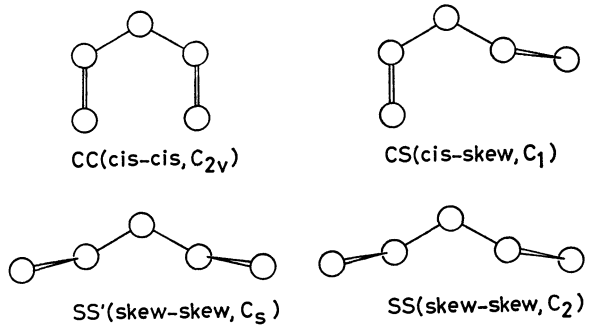

Fig. 3. Possible conformations of 1,4-pentadiene.

in the glassy state (Fig. 1c) which disappear in the spectrum in the crystalline state (Fig. 1d) are evidently assigned to another isomer. A third isomer is clearly identified by the bands at 555 and 268 cm^{-1} newly appearing in the spectra in the gaseous and liquid states (Figs. 1a and 1b). Gallinella and Cadioli misassigned these two bands to two different isomers.[4]

Normal Vibration Calculations. Normal frequencies were calculated for the purpose of the assignment of the observed bands to the rotational isomers. For the calculation of normal frequencies and normal modes, a Hitachi 5020E computer at the Computer Centre of the University of Tokyo and the programs BGLZ and LSMB prepared in our laboratory were used.[5] The values of the bond lengths and angles were taken from the corresponding values of 1-butene and are listed in Table 1.[2] The torsion angles were assumed as 0° for the *cis* form and 120° for the skew form.

The wagging constants, the torsional constants, wagging-torsion interaction constants and the *cis* C· · ·C repulsive constant were introduced in addition to the simple Urey Bradley force field. The values of the force constants were transferred from those of olefins[3] and used without further modification (Table 2). The calculated frequencies below 700 cm^{-1} are compared with the observed in Table 3 and Fig. 4. Assignments based on the potential energy distribution are also given in Table 3.

Shimanouchi, Abe, and Alaki showed that the CH out-of-plane vibration consisting of the C=C torsion and CH wagging modes is a good key band for the study of the rotational isomerism of 1-olefins.[3] When CH_2=CH–CH_2–C group takes the skew conformation, the CH out-of-plane vibration couples with the skeletal

Table 1. Molecular parameters used in the normal vibration calculation

Bond lengths (Å)		
C-C	1.507	
C=C	1.336	
C-H(methylene)	1.095	
C-H(vinyl)	1.09	
Bond angles	(a)	(b)
∠CCC	114.8°	112.1°
∠C=CC	126.7°	125.4°
∠HC=C	120.0°	120.0°
∠HC-C(vinyl)	115.1°	117.1°
∠HCH(vinyl)	120.0°	120.0°
∠HCH(methylene)	105.2°	105.7°
∠HCC(methylene)	109.1°	109.6°

(a) For the CC form. (b) For the CS, SS, and SS' forms.

Table 2. Force constants used in the normal vibration calculation[a]

Strtching (md/Å)			
K(=C-H)	4.39		
K(C-H)	4.23		
K(C=C*)	7.42		
K(C-C*)	3.24		
Bending (md/Å)		Repulsive (md/Å)	
H(HCH)	0.365	F(HCH)	0.21
H(HC=C)	0.16	F(HC=C)	0.45
H(HC*C')	0.21	F(HC*C')	0.38
H(HC'H)	0.37	F(HC'H)	0.21
H(HC'C*)	0.23	F(HC'C*)	0.51
H(C=C*C')	0.287	F(C=C*C')	0.40
H(C*C'C*)	0.26	F(C*C'C*)	0.40
Wagging (md·Å)		Torsion (md·Å)	
W(=CH_2)	0.30	Y(C=C*)	0.485
W(=CH)	0.359	Y(C'-C*)	0.1
Wagging-torsion interaction (md·Å)			
WT(CH wag, C=C tor)	0.063		
Intramolecular tension (md·Å)			
κ	0.015		
Cis repulsive constant (md/Å)			
R(C†=C-C-C†)[b]	0.169		

a) C, C*, and C' are the carbons in =CH_2, =CH–, and –CH_2– parts of the molecule, CH_2=C*H-C'H_2-C*H=CH_2. b) Force constant between C†'s in the *cis* form.

Table 3. Observed and calculated frequencies of 1,4-pentadiene in cm^{-1}

Observed							Calculated				
gas		liq.		glass	solid						
IR	R	IR	R	IR	IR	R	C-C	C-S	S-S′	S-S	P. E. D. (%)
650	662	666	665	664	664	672				643	CH wag(36) C=C tor(22) CCC def(9)
							642				C=CC def(41) CCC def(28) $=CH_2$ rock(22)
									637		CH wag(30) C=C tor(25) CCC def(7)
590		600	604	610	610	618				609	CH wag(49) C=C tor(25)
			597						605		CH wag(55) C=C tor(25)
								603			CH wag(20) C=C tor(20) CCC def(19)
555	580[a]	555	560					585			CH wag(46) C=C tor(16)
							550				CH wag(61) C=C tor(43)
							522				CH wag(61) C=C tor(28)
	475[a]		494					486			C=CC def(34) CH wag(29) C=C tor(22)
457		450	457	455	455	457				470	C=CC def(77)
446				444					437		C=CC def(89)
425			421					425			C=CC def(76)
	415		418						419		C=CC def(56)
							412				CCC def(68)
	387	370	380	375	375	376				367	C=CC def(67)
			305			318				325	CCC def(57) C=CC def(14)
			285	306					310		CCC def(62) C=CC def(17)
268	260[b]		265					264			CCC def(34) C=CC def(19)
							226				C-C tor(92)
							206				C=CC def(30) CCC def(30)

a) Weak broad band. b) Broad band.

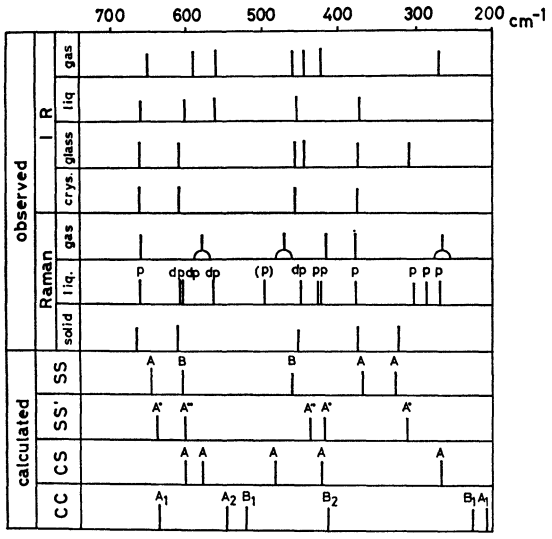

Fig. 4. Observed and calculated frequency patterns of 1,4-pentadiene.

deformation vibrations and gives a frequency near 640 cm^{-1}, while this coupling does not occur for the *cis* conformation the former giving a frequency near 580 cm^{-1}. There are two such vibrations for each isomer in the case of 1,4-pentadiene. These vibrations of the CC form do not couple with the skeletal deformation by symmetry requirement and give frequencies, 550 and 522 cm^{-1}. For the SS and SS′ forms, the symmetric CH out-of-plane vibration couples with C–C–C deformation and gives a frequency near 640 cm^{-1} and the antisymmetric CH out-of-plane vibration gives a frequency of about 610 cm^{-1}. The skew and *cis* parts of the CS form have the frequencies 603 and 585 cm^{-1}, respectively. Therefore, the frequency of the CH out-of-plane vibration can also be a clue to the assignment of rotational isomers in the case of 1,4-pentadiene. The difference in frequency of C–C–C deformations may be useful for the discrimination of the SS form from the SS′ form.

Stable Conformations. From the results given in Table 3 and Fig. 4, it can be concluded that the conformation in the crystalline state is the SS form. The frequencies calculated for this form are 643, 609, 470, 367, and 325 cm^{-1}. They correspond to the five Raman lines at 672, 618, 457, 376, and 318 cm^{-1}. The calculated values for the CC and CS forms differ greatly from the observed in the crystalline state. There is a possibility that the SS′ form exists in the crystalline state. However, it is not probable since the frequencies 437 and 419 cm^{-1} calculated for the SS′ form do not correspond to the observed.

The appearance of two frequencies at 444 and 306 cm^{-1} in the spectrum of glassy state in addition to the bands observed in the crystalline state is explained by the coexistence of the SS and SS′ forms. These two bands are assigned to the calculated frequencies, 437 and 310 cm^{-1}, of the SS′ form. Moreover, the change of the relative intensities of the infrared bands at 664 and 610 cm^{-1} on going from the crystalline state to the glassy state can be explained by the overlap of the two CH out-of-plane vibrations of the SS′ form with those of the SS form. Thus, the third isomer corresponds to the CS form. Actually, the Raman lines (infrared bands) at 560 (555), 494, ~420 (425),

and 265 (268) cm^{-1} are in good agreement with the frequencies calculated for the CS form, 585, 486, 425, and 264 cm^{-1}. No corresponding bands to the calculated frequencies of the CC form were found in the spectra.

Now, the stable isomers of 1,4-pentadiene are proved to be the SS, SS′, and CS forms. It is noteworthy that these forms are in accord with those of the stable isomers predicted by *ab initio* MO calculations.[4] It is to be noted that the band broadening and the frequency shifts are distinctly observed by the change in the temperature in the liquid state. This tendency is also observed in the spectrum in the gaseous state. The spectral changes are far more pronounced than in the case of 1,2-dichloroethane[6] and other molecules[7] with the usual C–C torsion axis. This suggests that the barrier to internal rotation is low except for the *cis-cis* barrier and the anharmonicity in the potential function causes the band broadening and frequency shifts.

Conclusion

It is shown that 1,4-pentadiene exists in the SS form in the crystalline state. The SS and SS′ forms coexist in the glassy state while three forms, the SS, SS′, and CS, are found in the liquid and gaseous states. Although the intensities of the Raman lines at 560 and 494 cm^{-1} decreased slightly and the line at 305 cm^{-1} broadened and shifted toward lower frequency at a higher temperature (Figs. 2b and 2c), no significant intensity change due to the temperature change was observed. This shows that the energy difference among the three isomers is not very large and the stability of the SS form in the crystal can be ascribed to the possible close packing of the molecules.

References

1) L. A. Harrah and D. W. Mayo, *J. Chem. Phys.*, **33**, 299 (1960).

2) S. Kondo, E. Hirota, and Y. Morino, *J. Mol. Spectrosc.*, **28**, 471 (1968).

3) T. Shimanouchi, Y. Abe, and Y. Alaki, *Polymer J.*, **2**, 199 (1971).

4) E. Gallinella and B. Cadioli, *J. Chem. Soc. Faraday II*, **4**, 781 (1975).

5) T. Shimanouchi, Computer Programs for Normal Coordinate Treatment of Polyatomic Molecules, Department of Chemistry, Faculty of Science, University of Tokyo, Tokyo, 1968.

6) S. Mizushima, T. Shimanouchi, I. Harada, Y. Abe, and H. Takeuchi, *Can. J. Phys.*, in press.

7) T. Shimanouchi, Y. Abe, and M. Mikami, *Spectrochim. Acta*, **24A**, 1037 (1968).

Effect of the Viscosity Ratio, μ_d/μ_c, on the Particle-size Distribution in Emulsions

Shun'ichi TSUKIYAMA, Akira TAKAMURA, Yasuko FUKUDA, and Masumi KOISHI*

Meiji College of Pharmacy, 1-22-1, Yato-chō, Tanashi-shi, Tokyo 188

**Faculty of Pharmaceutical Sciences, Science University of Tokyo, Ichigaya Funakawara-machi, Shinjuku-ku, Tokyo 162*

(Received August 4, 1975)

The object of this paper is to investigate the effect of the ratio of the viscosities of dispersed and continuous phases, μ_d/μ_c, on the particle-size distribution in o/w-type emulsions. The viscosity ratios (μ_d/μ_c) used were 0.836 : 1, 0.271 : 1, 0.0992 : 1, 0.0280 : 1, and 0.00133 : 1. The size of the dispersed liquid droplets was measured by the microphotographic method. The mean diameter and the particle-size distribution were determined, and, further, the specific interfacial energy was evaluated. When the viscosity ratio was much smaller than unity, the particle-size distribution showed a skewed curve. On the contrary, the specific interfacial energy increased remarkably as the viscosity ratio approached unity.

Emulsion formation has, in general, been discussed from two different points of view[1] from the point of view of surface chemical[2] and from that of chemical engineering.[3] There are many factors which affect emulsion formation; the combination of two liquids, the mode of mixing two liquid phases, the concentration of the dispersed phase, the kind of emulsifying agent, the viscosity ratio of the two phases, the temperature, the equipment, the method of agitation, the impeller velocity, the agitation time, and so on.

In our previous papers,[4-6] statistical considerations of the experimental results were presented in connection with emulsion formation under various conditions. In those considerations, attempts were made to obtain the effects on emulsion formation of the kind and concentration of emulsifying agents, the energy efficiency of agitation,[5] and the agitation time. However, these studies were all undertaken without taking the viscosity factor into account.

In this paper, therefore, the effect of the ratio of the viscosities of the dispersed and continuous phases, μ_d/μ_c, on emulsion formation will be examined in relation to the particle-size distribution, the mean diameter of the dispersed phase, and the specific interfacial energy.

Experimental

Equipment. A sketch of the apparatus employed is shown in Fig. 1. The clear acrylate resin agitation tank with 4-baffles was 150 mmϕ in diameter and 210 mm deep. A stainless-steel agitation impeller of 49.00 mmϕ was of the standard Rushton type with 6-blades.[7] The tank was surrounded by a water jacket in order to keep the temperature of the liquid within it at 20.0 °C.

Measurement of Physical Properties. Mixtures of sodium silicate (Kishida Chemical Co.) and distilled water in varying ratios were used as the continuous phase. The total concentration of sodium silicate in the mixtures was varied from 17.0 to 88.0% (w/w). The dispersed phase was made up by mixing *n*-C_7H_{16} and CCl_4 in various volume ratios; the density was adjusted so as to be the same as that of the continuous phase (1.000—1.567 g/cm^3).

Tween-20 (Tōhō Chemical Industry Co.) was employed as the emulsifying agent; its concentration was 0.1% (w/w). The interfacial tensions were measured by the ring method,[8] and the viscosities of liquids, by the rotating viscometer[9] at

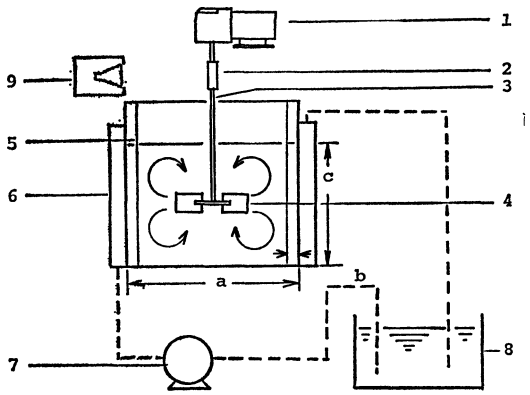

Fig. 1. Apparatus.

1 : motor 2 : toruqe meter 3 : shaft 4 : impeller
5 : baffle 6 : tank 7 : pump 8 : thermostat
9 : storobo scope.

TABLE 1. PHYSICAL PROPERTIES OF EACH CONTINUOUS PHASE

Concentration of Sodium Silicate (%, w/w)	Concentration of Tween-20 (%, w/w)	Density of continuous phase ρ_c (g/cm^3)	Density ratio ρ_d/ρ_c (—)	Viscosity of continuous phase μ_c (g/cm·s)	Viscosity ratio μ_d/μ_c (—)	Interfacial tension $\lvert\gamma_d-\gamma_c\rvert$ (dyn/cm)
0.0	0.1	1.000	1.000	1.005	8.36×10^{-1}	22.85
17.5	0.1	1.290	1.000	4.000	2.71×10^{-1}	15.50
58.0	0.1	1.400	1.000	12.20	9.92×10^{-2}	15.82
70.5	0.1	1.482	1.000	47.00	2.80×10^{-2}	18.03
88.0	0.1	1.567	1.000	1100	1.33×10^{-3}	21.58

Impeller diameter: 49.0 mm, Tank diameter: 150 mm, Revolution number: 330, 400, and 660 rpm.

20.0±0.1 °C.

The viscosity ratio, μ_d/μ_c, was widely varied from 0.836 : 1 to 0.00133 : 1. The concentration of sodium silicate, the density of the continuous phase, the density ratio, the viscosity of the continuous phase, the viscosity ratio, and the interfacial tension are summarized in Table 1.

Experimental Procedure. The experiments were carried out under the following conditions:

(1) The viscosity ratios, μ_d/μ_c, used were 0.836 : 1, 0.271 : 1, 0.0992 : 1, 0.0280 : 1, and 0.00133 : 1.

(2) The revolution rates were 330, 400, and 660 rpm.

(3) Samplings were made 5, 10, 20, 35, and 60 min after agitation has started.

The agitation tank was filled with 1960 ml of an aqueous sodium silicate solution, a continuous phase, containing Tween-20 as an emulsifying agent. The impeller was set in the center of the tank. On the middle of the impeller was gently placed 40 ml of a mixed solvent, a dispersed phase, as an almost perfect globule. The concentration of the dispersed phase was kept at 2.0% (v/v). The total liquid volume was, therefore, 2000 ml. After agitation has started, the liquid was sampled with a glass tube (5 mmϕ) at regular time intervals. Each sample was photographed with a Nikon AFM camera under a microscope. The diameters of the droplets were measured by a micrometer scale which has been photographed and enlarged under the same conditions. The number of droplets measured was one thousand[10] in all cases. The mean length diameter, the mean surface diameter, the mean volume diameter, the standard deviation, and the particle-size distribution were calculated by means of a SEIKO-301 computer.

Results and Discussion

Effect of the Viscosity Ratio, μ_d/μ_c, on the Particle-size Distribution. The particle-size distributions, calculated based on the length diameters measured at different revolution number and after 60 min of agitation, are shown in Fig. 2. In these cases, the viscosity ratio was 0.271 : 1, and the revolution rates were 330, 400, and 660 rpm. Although sufficient agitation was undertaken, the size distribution was broad and had two peaks at the revolution number of 330 and 400 rpm. The size distribution at 660 rpm, however, was normal and had only one peak.

Changes in the particle-size distribution, calculated using the length diameter measured in the course of agitation, are shown in Fig. 3. The viscosity ratio and the revolution number were 0.271 and 400 rpm respectively. The size distribution at an agitation time of 5 min spread over a wide range of particle-sizes and had three peaks. After 20 min of agitation, the size distribution had two peaks, because large particles were subdivided into small ones. The size distribution at an agitation time of 60 min was narrower than that at a shorter agitation time, but it still had two peaks.

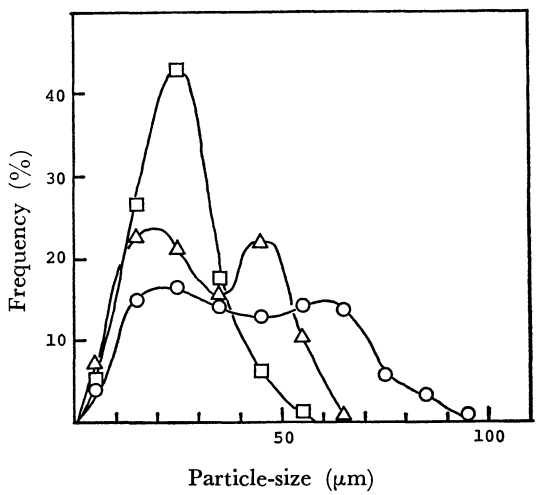

Fig. 2. Particle-size distributions at different revolution number.
D_I: 49.0 mm, D_T: 150 mm, θ: 60 min, T-20: 0.1% (w/w), μ_d/μ_c: 0.271.
○: 330 rpm, △: 400 rpm, □: 660 rpm.

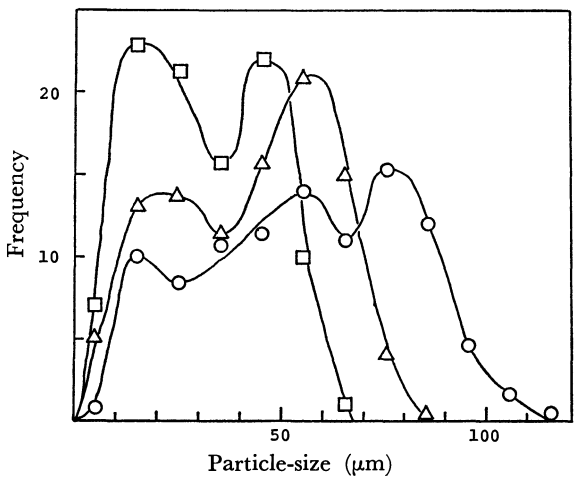

Fig. 3. Particle-size distributions at different agitation times.
D_I: 49.0 mm, D_T: 150 mm, N': 400 rpm, T-20: 0.1% (w/w), μ_d/μ_c: 0.271.
○: 5 min, △: 20 min, □: 60 min.

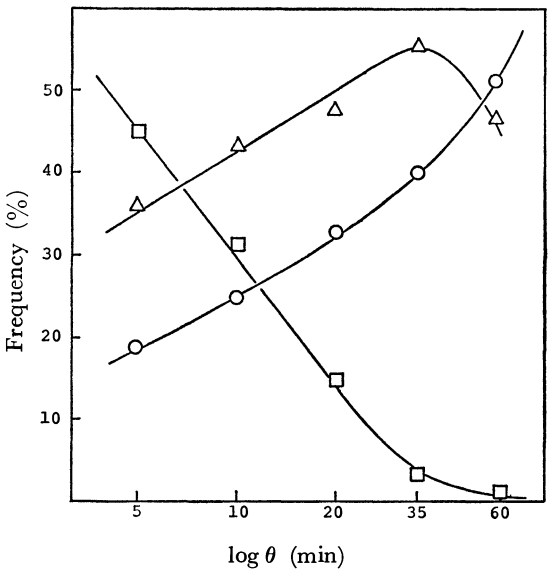

Fig. 4. Variation of frequency in the three particle-size subranges in the course of agitation.
D_I: 49.0 mm, D_T: 150 mm, N': 400 rpm, T-20: 0.1% (w/w).
○: 0—30 μm, △: 30—60 μm, □: 60 μm.

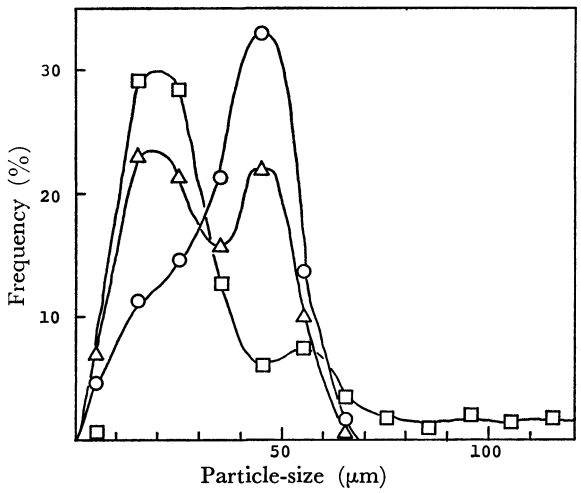

Fig. 5. Particle-size distributions at various viscosity ratios.
D_I: 49.0 mm, D_T: 150 mm, θ: 60 min, N': 400 rpm, T-20: 0.1% (w/w).
○: μ_d/μ_c=0.836, △: μ_d/μ_c=0.271, □: μ_d/μ_c= 0.00133.

In order to analyze the above results, we divided the observed particle-size range of droplets into the following three subranges: 60 μm and larger, 60 μm to 30 μm, and 30 μm and smaller. Variations in the frequency of the three subranges in the course of agitation are plotted in Fig. 4. It can clearly be observed that the frequency of droplets larger than 60 μm decreased slowly with an increase in the agitation time. On the contrary, the frequency in the middle and low subranges increased with an increase in the agitation time. However, in the middle subrange, it showed a maximum value at an agitation time of about 35 min, and then decreased.

Particle-size distributions calculated using the length diameters measured at three different viscosity ratios are shown in Fig. 5. The revolution number and the agitation time were 400 rpm and 60 μm respectively. When the continuous phase consisted of distilled water (μ_d/μ_c=0.836 : 1) alone, the size-distribution curve had only one peak. When the continuous phase consisted of a mixture of distilled water and sodium silicate (μ_d/μ_c=0.271 : 1 or 0.0133 : 1), however, the size distribution showed two peaks. On the other hand, as the viscosity ratio got smaller than unity, a broadening tendency of the size distribution was obtained. In particular, when the viscosity ratio was 0.00133 : 1, there appeared a very broad size distribution extending to the range from 70 μm to 150 μm.

Effect of the Viscosity Ratio, μ_d/μ_c, on the Mean Length Diameter. As has already been described in the section on the experimental procedure, 40 ml of an aqueous solution, a dispersed phase, was gently placed on the middle of the impeller as a globule (d_1=4.4 cm) before agitation. As soon as the agitation started, the globule was subjected to a strong shear stress in and around the impeller. Then, the globule was broken up into a number of droplets of some hundreds of microns within a few seconds. The mean length diameter of the broken-down droplets in the course of agitation at each of four different viscosity ratios was found to decrease linearly on a log-log plot, as is shown in Fig. 6. The mean length diameter was found to have the smallest value when the viscosity ratio was 0.271 : 1. In Fig. 6, the straight lines are drawn by the least-squares method. From these results, the relation between the average diameter, d_1, and the agitation time, θ, may be experimentally formulated as:

$$\log d_1 = \log \beta + \alpha \log \theta \quad (1)$$

Furthermore, the effect of the viscosity ratio on the mean length diameter at three revolution number after 60 min of agitation is given in Fig. 7. At each revolution number, the plot of the data gave a concave curve with a minimum at a viscosity ratio of 0.271 : 1. Consequently, the optimum condition for preparing an emulsion of the minimum mean length diameter would be when the viscosity of the continuous phase is slightly higher than that of water, as in Table 1. Table 3 summarizes the results of the calculations of the standard deviation, σ, of the mean length diameter and the maximum diameter of the droplets, d_m, under various conditions. As the viscosity ratio at each revolution number decreased, both σ and d_m increased. However, this trend was not observed when the continuous phase consisted of distilled water (μ_d/μ_c= 0.836 : 1) alone.

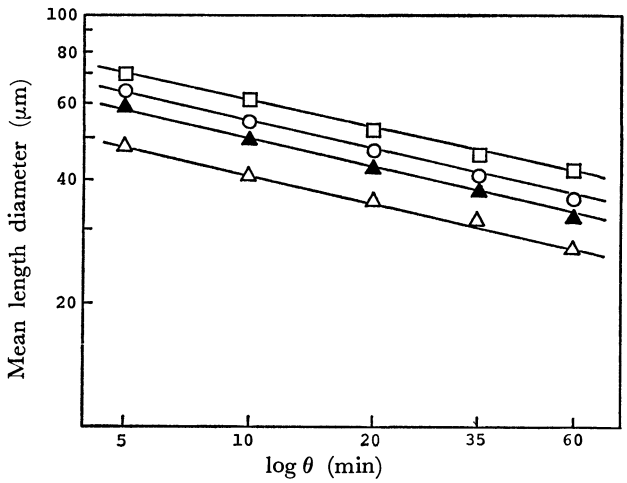

Fig. 6. Changes of the mean length diameter in the course of agitation.
D_I: 49.0 mm, D_T: 150 mm, N': 400 ppm, T-20: 0.1% (w/w).
○: μ_d/μ_c=0.836, △: μ_d/μ_c=0.271, ▲: μ_d/μ_c= 0.0280, □: μ_d/μ_c=0.00133.

Table 2. Calculated values from the plots of Fig. 6

Viscosity ratio μ_d/μ_c	Slope α	Intercept at 1 min β	Interrelation coefficient
0.836	−0.2634	2.000	0.9845
0.271	−0.1943	1.813	0.4962
0.0280	−0.2433	1.948	0.9987
0.00133	−0.2340	2.019	0.9865

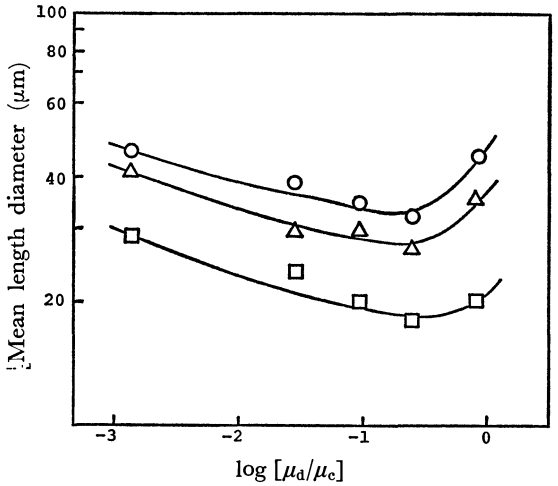

Fig. 7. Relation between the mean length diameter and the viscosity ratio.
D_I: 49.0 mm, D_T: 150 mm, θ: 60 min, T-20: 0.1% (w/w).
○: 330 rpm, △: 400 rpm, □: 660 rpm.

Table 3. Effect of experimental conditions on standard deviation and maximum diameter

Experimental conditions			Standard deviation	Maximum diameter
Viscosity ratio μ_d/μ_c	Revolution number N' (rpm)	Agitation time θ (min)	σ	d_m (μm)
0.836	330	60	13.8	200.0
0.836	400	60	10.8	100.5
0.836	600	60	5.62	53.1
0.271	330	60	20.0	84.2
0.271	400	60	12.9	59.6
0.271	660	60	6.46	32.6
0.0992	330	60	18.2	80.0
0.0992	400	60	12.7	70.2
0.0992	660	60	8.23	49.0
0.0280	330	60	20.3	93.4
0.0280	400	60	15.9	80.0
0.0280	660	60	10.0	32.4
0.00133	330	60	50.3	113.0
0.00133	400	60	41.0	195.0
0.00133	660	60	21.4	246.0

The Relation between the Specific Interfacial Energy and the Viscosity Ratio. The mean surface-volume diameter of droplets is generally represented by;

$$d_{sv} = \frac{\sum d_i^3}{\sum d_i^2} = \frac{\sum d_i^3/n}{\sum d_i^2/n} = \frac{d_v^3}{d_s^2} \quad (2)$$

where d_i is the length diameter; n, the number of droplets measured; d_s, the mean surface diameter (cm), and d_v, the mean volume diameter (cm). The specific interfacial area per 1 cm³ of the dispersed phase is given by;

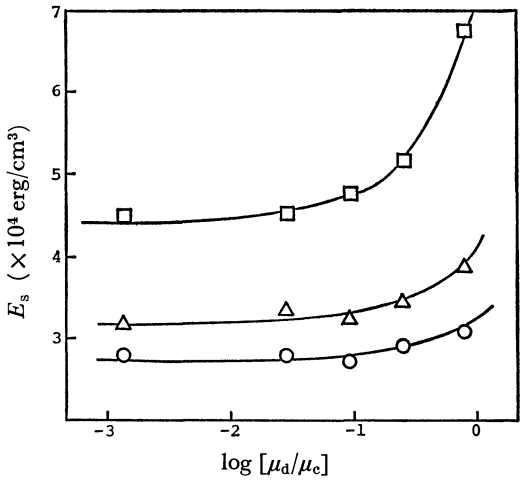

Fig. 8. Relation between the specific interfacial energy and the viscosity ratio.
D_I: 49.0 mm, D_T: 150 mm, θ: 60 min, T-20: 0.1% (w/w).
○: 330 rpm, △: 400 rpm, □: 660 rpm.

$$S = \frac{\pi \sum d_i^2}{\pi/6 \cdot \sum d_i^3} = \frac{6 d_s^2}{d_v^3} = \frac{6}{d_{sv}} \quad (3)$$

Further, the specific interfacial energy is defined as:

$$E_s = \gamma \cdot S = 6 \cdot \gamma / d_{sv} \quad (4)$$

where E_s is the specific interfacial energy (erg/cm³) and where γ is the interfacial tension (dyn/cm).

The relation between the specific interfacial energy and the viscosity ratio is shown in Fig. 8. At each revolution number, the specific interfacial energy increases remarkably as the viscosity ratio approached unity. This trend was especially notable at a high revolution number (660 rpm). Accordingly, the probability of the droplets breaking-up during agitation will increase as the viscosity ratio approaches unity.

References

1) K. J. Valentas, *I. & E. C. Fundamentals*, **5**, 271 (1966).
2) K. Shinoda and H. Arai, *J. Phys. Chem.*, **68**, 385 (1964).
3) W. A. Rodgen, V. G. Trice, and J. H. Rushton, *Chem. Eng. Progr.*, **52**, 515 (1956).
4) S. Tsukiyama and A. Takamura, *Chem. Pharm. Bull.* (Tokyo), **23**, 616 (1975).
5) S. Tsukiyama and A. Takamura, *ibid.*, **22**, 2607 (1974).
6) S. Tsukiyama, H. Takahashi, I. Takashima, and S. Hatano, *Yakugaku Zasshi*, **91**, 305 (1971).
7) S. Tsukiyama, A. Takamura, and N. Nakura, *ibid.*, **94**, 490 (1974).
8) S. Tsukiyama, A. Takamura, and M. Nakano, *ibid.*, **93**, 231 (1973).
9) S. Tsukiyama, A. Takamura, and Y. Moronuki, *ibid.*, **94**, 471 (1974).
10) H. G. Jellinek, *J. Soc. Chem. Ind.* (London), **69**, 225 225 (1950).

Anharmonic Potential Functions of Simple Molecules. II. Direct Numerical Diagonalization of Vibratinal Hamiltonian Matrix and Its Application to CO_2 and CS_2

Isao SUZUKI

Educational Computer Centre, The University of Tokyo, Hongo, Bunkyo-ku, Tokyo 113

(Received August 9, 1975)

A general formalism is presented for the calculation of the vibration-rotation energy levels of linear symmetrical XY_2 type molecules through direct numerical diagonalization of the vibrational hamiltonian matrix. This method is applied to the CO_2 and CS_2 molecules, of which the general quartic force fields have been known accurately. The results are compared with those obtained by an ordinary perturbation treatment, and the truncation effects of the matrix sizes as well as of the expansions of the potential functions are discussed. Special attention is paid to the peculiarities in the potential function of CO_2 for which very strong mixings of the basis harmonic oscillator wave functions are observed. The general formula for evaluating the matrix elements of the transition moment are also discussed and its applicability to the problems of vibrational intensities and the dipole moment functions is discussed.

In Part I,[1] a method was presented in which the vibration or vibration-rotation energy levels of a diatomic molecule are calculated from the harmonic and anharmonic force constants by solving the vibrational hamiltonian numerically. This method has an advantage over the conventional contact transformation approach,[2] since a true (perturbed) orthonormal wave function is readily obtained for a given vibrational level through numerical diagonalization. Two basic physical properties of a molecule, *i.e.* the potential and dipole moment functions may be handled simultaneously by this method.[3]

As pointed out in I, the numerical diagonalization method is very attractive in handling the polyatomic molecules, since no special treatment is required for the anharmonic resonances. Efforts have been made to extend this method to a linear symmetrical triatomic molecule. This extension is not altogether simple, since the vibration-rotation hamiltonians of polyatomic molecules are complex and possess extra terms which are not present in diatomic molecules. The basic algorithms to compute vibration and vibration-rotation energy levels have been established for this type of molecule, and they are applied to the cases of the CO_2 and CS_2 molecules. The results are reported in the present paper.

Hamiltonian

The general form of vibration-rotation hamiltonian of a polyatomic molecule is given by Goldsmith, Amat, and Nielsen.[4] The form is greatly simplified in the specific case of a linear symmetrical molecule XY_2.[5] The vibration-rotation hamiltonian may be expressed as the sum of vibrational, rotational, and Coriolis hamiltonians. With replacement of a degenerate pair of bending coordinates q_{2x} and q_{2y} by cylindrical coordinates r_2 and χ_2, it has the following form.[6]

$$\mathbf{H} = \mathbf{H}_{\mathrm{vib}} + \mathbf{H}_{\mathrm{rot}} + \mathbf{H}_{\mathrm{Cor}}, \tag{1}$$

$$\begin{aligned}\mathbf{H}_{\mathrm{vib}} = {} & (1/2)\sum_{s=1,3}\omega_s(q_s^2+p_s^2)+(\omega_2/2)(r_2^2+p_{r_2}^2) \\ & + (k_{111}q_1^2+k_{122}r_2^2+k_{133}q_3^2)q_1 \\ & + k_{1111}q_1^4+k_{1133}q_1^2q_3^2+k_{3333}q_3^4 \\ & + (k_{1122}q_1^2+k_{2222}r_2^2+k_{2233}q_3^2)r_2^2 \\ & + \mathbf{H}_{\mathrm{vib}'},\end{aligned} \tag{2}$$

$$\mathbf{H}_{\mathrm{vib}'} = B_e(j_x^2+j_y^2)\sum_{k=0} R_k q_1^k, \tag{3}$$

$$\mathbf{H}_{\mathrm{rot}} = B_e(J_x^2+J_y^2)\sum_{k=0} R_k q_1^k, \tag{4}$$

$$\mathbf{H}_{\mathrm{Cor}} = -2B_e(j_xJ_x+j_yJ_y)\sum_{k=0} R_k q_1^k, \tag{5}$$

where $R_k=(-1)^k(k+1)\gamma_1^{(k/2)}$, $\gamma_1=(2B_e/\omega_1)$, j_x and j_y are the dimensionless vibrational angular momenta ($j_x=p_x/\hbar$ and $j_y=p_y/\hbar$). The totally symmetric q_1 normal coordinate plays essentially the same role as q in diatomic molecules, and each hamiltonian is expressed as a power series expansion of q_1. This is suited for numerical treatment and the hamiltonians may be truncated at a desired order of approximation. The normal coordinates q_{2x}, q_{2y}, and q_3 do not appear in the expressions in Eqs. (3)—(5). The molecular vibrations affect the moments of inertia through the shift of the average nuclear positions as well as by the anisotropy of the mean square amplitude of vibration. The former effect is linear in normal coordinates and vanishes unless $\langle\bar{q}_r\rangle\neq 0$, which holds only for $r=1$ in linear XY_2. The latter effect is quadratic in normal coordinates, and there are, indeed, non-vanishing terms for q_{2x}^2, q_{2y}^2, and q_3^2, but they are all cancelled out when the Eckart condition is imposed to separate vibration and rotation. This problem has been discussed by Oka[6a] in greater detail.

The term designated $\mathbf{H}_{\mathrm{vib}}'$ arises from the squared vibrational angular momentum and contributes only to the vibrational energies of a molecule, it is treated as a part of vibrational hamiltonian. The general quartic potential function is used in Eq. (2). If higher-order force constants are included, another term,

$$(B_e/2)\sum_{k=1}\gamma^{(k/2)}q_1^k, \tag{6}$$

which is originated from pseudo-potential $U(q's)$[2,7] must also be considered in $\mathbf{H}_{\mathrm{vib}}'$.

Energy Levels

Vibrational Energy Levels. As diatomic molecules, the vibrational hamiltonian matrix elements may be evaluated from the harmonic oscillator basis functions,

$$\langle n|\mathbf{H}_{\mathrm{vib}}|n'\rangle$$

where $|n>$ represents $|n_1, n_2, l_2, n_3>$.[8] The vibrational energy levels are calculated by diagonalizing the vibrational hamiltonian matrix numerically. For a given vibrational level v, the corresponding wave function is evaluated as a linear combination of the basis harmonic oscillator wave functions, and may be expressed as

$$|v> = \sum_n a_{vn}|n>, \tag{7}$$

where the coefficients a_{vn}'s are the corresponding elements of eigen vectors. The basis functions may be arranged according to their symmetry so that the resultant vibrational hamiltonian matrix is divided into symmetry blocks, each of which may be treated separately. Therefore, Eq. (7) holds in each symmetry block. It is readily seen that the wave functions $|v>$ also form an orthonormal set.

Vibration-Rotation Energy Levels. The rotational energy levels in a given vibrational state v are given as

$$E_v(J) = B_v[J(J+1)-l_2^2]-D_v[J(J+1)-l_2^2]^2 \tag{8}$$

Both $\mathbf{H}_{\rm rot}$ and $\mathbf{H}_{\rm Cor}$ must be considered to obtain the rotational constants B_v. The contribution from $\mathbf{H}_{\rm rot}$ is simpler to evaluate, and the procedure is essentially similar to the evaluation of B_v in diatomic molecules. By applying the first order perturbation treatment, the contribution from $\mathbf{H}_{\rm rot}$ to $E_v(J)$ is given as

$$\begin{aligned} E_v(J)^r &= \langle v,J|\mathbf{H}_{\rm rot}|v,J\rangle \\ &= B_e[J(J+1)-l_2^2]\sum_{k=0} R_k\langle v|q_1^k|v\rangle, \end{aligned} \tag{9}$$

which is further reduced to

$$\begin{aligned} E_v(J)^r &= B_e[J(J+1)-l_2^2]\sum_{k=0}\sum_n\sum_{n'} a_{vn}a_{vn'}R_k\langle n|q_1^k|n'\rangle \\ &= B_e[J(J+1)-l_2^2] \\ &\quad\times[1+\sum_{k=1}\sum_n\sum_{n'} a_{vn}a_{vn'}R_k\langle n|q_1^k|n'\rangle]. \end{aligned} \tag{10}$$

TABLE 1. NON-VANISHING MATRIX ELEMENTS FOR J_+, J_-, j_+, AND j_-

(a) J_+ and J_-

$$\langle J, l_2|J_+|J, l_2+1\rangle = \langle J, l_2+1|J_-|J, l_2\rangle = [J(J+1)-l_2(l_2+1)]^{1/2}$$
$$\langle J, l_2|J_-|J, l_2-1\rangle = \langle J, l_2-1|J_+|J, l_2\rangle = [J(J+1)-l_2(l_2-1)]^{1/2}$$

(b) j_+ and j_-

$\langle n_2, l_2, n_3|j_+|n_2', l_2', n_3'\rangle = \langle n_2', l_2', n_3'|j_-|n_2, l_2, n_3\rangle$

	n_2'	l_2'	n_3'	Matrix element
j_+	n_2-1	l_2-1	n_3+1	$\Omega_{23}[(n_2+l_2)(n_3+1)]^{1/2}$
	n_2+1	l_2-1	n_3-1	$\Omega_{23}[(n_2-l_2+2)n_3]^{1/2}$
	n_2-1	l_2-1	n_3-1	$\Phi_{23}[(n_2+l_2)n_3]^{1/2}$
	n_2+1	l_2-1	n_3+1	$\Phi_{23}[(n_2-l_2+2)(n_3+1)]^{1/2}$
j_-	n_2+1	l_2+1	n_3-1	$\Omega_{23}[(n_2+l_2+2)n_3]^{1/2}$
	n_2-1	l_2+1	n_3+1	$\Omega_{23}[(n_2-l_2)(n_3+1)]^{1/2}$
	n_2+1	l_2+1	n_3+1	$\Phi_{23}[(n_2+l_2+2)(n_3+1)]^{1/2}$
	n_2-1	l_2+1	n_3-1	$\Phi_{23}[(n_2-l_2)n_3]^{1/2}$

$\Omega_{23}=(1/2)[(\omega_2/\omega_3)^{1/2}+(\omega_3/\omega_2)^{1/2}]$
$\Phi_{23}=[(\omega_2/\omega_3)^{1/2}-(\omega_3/\omega_2)^{1/2}]$

R_k, a_{vn}, and the matrix element $\langle n|q_1^k|n'\rangle$ are all known. The contribution from $\mathbf{H}_{\rm Cor}$ to the rotational energy is more complex. Obviously, the diagonal matrix element $\langle v, J|\mathbf{H}_{\rm Cor}|v, J\rangle$ vanishes, and the second-order contribution must be considered,

$$E_v(J)^C = \sum H_{vv'}{}^{(1)}H_{v'v}{}^{(1)}/(E_v^\circ - E_{v'}^\circ) \tag{11}$$

$\mathbf{H}_{\rm Cor}$ may be expressed in more convenient form by using ladder operators $J_\pm = J_x \pm iJ_y$ and $j_\pm = j_y \pm ij_x$,

$$\mathbf{H}_{\rm Cor} = -B_e(j_+J_- + j_-J_+)\sum_{k=0} R_k q_1^k. \tag{12}$$

The relevant non-vanishing matrix elements are listed in Table 1. Again, $|v>$ and $|v'>$ may be expressed in terms of the harmonic oscillator wave functions, $|v>=\sum_n a_{vn}|n>$ and $|v'>=\sum_m a_{v'm}|m>$. As expected from the nature of Coriolis force, $H_{vv'}$ vanishes unless the direct product of v and v' contains the π_g representation to which the rotations around the x- and y- axes (R_x, R_y) belong. For example, if v belongs to the σ_g^+ species, v' should be the π_g state, and if v belongs to the π_u state, v' should be either in the σ_u^+ or Δ_u state. $H_{vv'}{}^{(1)}$ is given as

$$\begin{aligned} H_{vv'}{}^{(1)} &= \sum_n\sum_m a_{vn}a_{v'm}\langle n,J|\mathbf{H}_{\rm Cor}|m,J\rangle \\ &= -B_e[J(J+1)-l_2(l_2-1)]^{1/2}\sum_n\sum_m a_{vn}a_{v'm}\langle n|j_+|m\rangle \\ &\quad -B_e[J(J+1)-l_2(l_2+1)]^{1/2}\sum_n\sum_m a_{vn}a_{v'm}\langle n|j_-|m\rangle. \end{aligned} \tag{13}$$

It is readily seen from Table 1 that $H_{vv'}{}^{(1)}=H_{v'v}{}^{(1)}$ holds and that either $\langle n|j_+|m\rangle$ or $\langle n|j_-|m\rangle$ vanishes.[9] In the latter case, the leading term of $E_v(J)^C$ is given as

$$\begin{aligned} E_v(J)^C &= B_e^2[J(J+1)-l_2(l_2-1)] \\ &\quad\times\sum_{v'}[\sum_n\sum_m a_{vn}a_{v'm}\langle n|j_+|m\rangle]^2/(E_v^\circ - E_{v'}^\circ)] \end{aligned} \tag{14}$$

The final expression for B_v is, therefore,

$$\begin{aligned} B_v &= B_e\sum_{k=0}[R_k\sum_n\sum_m a_{vn}a_{vn'}\langle n|q_1^k|n'\rangle \\ &\quad + B_eR_k\sum_{v'}\{\sum_n\sum_m a_{vn}a_{v'm}\langle n|q_1^k\cdot j_+|m\rangle\}^2/(E_v^\circ - E_{v'}^\circ)]. \end{aligned} \tag{15}$$

The higher-order term in $\mathbf{H}_{\rm Cor}$ is included in Eq. (15). The wave functions designated with n and n' belong to the same symmetry species, while those with n and m do not. The last integral Eq. (15) may be rewritten as $\langle n|q_1^k\cdot j_+|m\rangle = \langle n_2, l_2, n_3|j_+|m_2, l_2', m_3\rangle\cdot\langle n_1|q_1^k|m_1\rangle$, since j_+ (or j_-) does not involve q_1. When the σ_g^+ or σ_u^+ state ($l_2=0$) is considered, the Coriolis contributions from the $l_2=-1$ states as well as those from the $l_2=+1$ states must be considered, and this doubles the value given in Eq. (15). Since $E_v(J)^C$ is derived by the ordinary second-order perturbation method, it breaks down for a case of accidental degeneracy in which a (v,J) level locates close to another (v', J') level with proper symmetry. Such a case must be handled separately.

l-Type Doubling in XY_2. So far it is implicitly assumed that the levels with the positive and negative l_2 values have identical energy. This holds for rotationless case. There is also no vibration-rotation hamiltonian which directly connects, for example, the 01^10 and $01^{-1}0$ states. However, these levels couple with each

other through the third states (001 or 02^01 in the above example) by $\mathbf{H}_{Cor}$. For illustration, the 01^10, 001, and $01^{-1}0$ levels are chosen and the vibration-rotation hamiltonian matrix for a given J is expressed,

$$\begin{matrix}\phi(01^1\ 0,J)\\ \phi(00\ \ 1,J)\\ \phi(01^{-1}0,J)\end{matrix}\begin{bmatrix}E_{vJ}^{\circ} & a & 0\\ a & E_{v'J}^{\circ} & a\\ 0 & a & E_{vJ}^{\circ}\end{bmatrix}$$

with $a=[J(J+1)]^{1/2}\langle 1^10|j_+|01\rangle=[J(J+1)]^{1/2}\langle 01|j_-|1^{-1}0\rangle=\sqrt{2}\,\Omega_{23}[J(J+1)]^{1/2}$. By using the linear combinations ϕ_c and ϕ_d given below, the matrix is reduced to

$$\begin{matrix}\phi_c=(1/\sqrt{2})[\phi(01^10,J)+\phi(01^{-1}0,J)]\\ \phi(001,J)\\ \phi_d=(1/\sqrt{2})[\phi(01^10,J)-\phi(01^{-1}0,J)]\end{matrix}\begin{bmatrix}E_{vJ}^{\circ} & \sqrt{2}\,a & 0\\ \sqrt{2}\,a & E_{v'J}^{\circ} & 0\\ 0 & 0 & E_{vJ}^{\circ}\end{bmatrix}$$

This indicates that in calculating the rotational constants of the c and 001 levels, the contributions from H_{vv}[2] must be doubled, while the d state is free from Coriolis type interaction. This causes the well-known l-type doubling: A given J level of the 010 state splits into two sub-levels with slightly different energies. Since ν_3 is larger than ν_2, the rotational constant of the c sub-level is expected to be smaller than that of the d sub-level. It must be noted, however, the Eq. (15) still holds for evaluating the average rotational constant of the c and d levels. In the present calculation this average rotational constant is usually computed, and calculation of the l-type doubling constants is installed as option.

Higher Order Force Constants. The present method is not limited to the treatment of the general quartic force field, and any higher order terms may be included without disturbing the general procedure. This is an advantage of the direct diagonalization method over the contact transformation approach, since the latter requires at least the twice transformed hamiltonians to go beyond the quartic force field. It has already been pointed out[10,11] that some third-order parameters λ_1, λ_2, λ_3, and δ, which appear in Fermi resonance off-diagonal matrix elements are necessary to elucidate the vibration and vibration-rotation levels of most linear triatomic molecules, particularly those in CO_2. In the present treatment this is equivalent to including the quintic force constants k_{11112}, k_{12222}, and k_{12233}, and this has been done very easily.

Computational Methods

Most of numerical computations have been carried out on a MELCOM 7700 system in Educational Computer Centre in the University of Tokyo. A HITAC 8800/8700 system in Computer Centre in the University of Tokyo has also been used for eigenvalue problems of large matrices. Programs written in FORTRAN IV are compatible in both systems: only the sizes of a certain arrays are changed.

Generation of Basis Functions and Matrix Elements. In actual calculations, the harmonic oscillator basis functions are specified by a set of four integers corresponding to n_1, n_2, l_2, and n_3 ($l_2=n_2, n_2-2, \ldots,$ 1 or 0). A desired number of the basis functions are systematically generated with the condition of $n_1+n_2+n_3<n$, where n is a suitable interger. The following simple rule has been applied to identify the symmetry species of a given basis function:

(i) n_2+n_3 (even, odd) $\leftrightarrow$ (g, u)

(ii) l_2 $(0, 1, 2, 3, \cdots) \leftrightarrow (\sigma^+, \pi, \delta, \phi, \cdots)$

The matrix elements of the vibrational hamiltonian are generated by using the subroutines OPERQ and OPERR. The former was described in I, and the latter is written to evaluate the radial part matrix elements $\langle n,l|r^m|n',l'\rangle$. The diagonal part of vibrational hamiltonian matrix has a familiar form of

$$\langle n|\mathbf{H}_{v1b}|n\rangle=\sum_i \omega_i(n_i+d_i/2)+\sum_{i,j} x^*_{ij}(n_i+d_i/2)(n_j+d_j/2)+x^*_{l_2l_2}l_2^2 \qquad (16)$$

where $d_1=d_3=1$ and $d_2=2$. The asterisks indicate that they differ from the x_{ij}'s defined by Nielsen,[2] and if the general quartic force field is employed, $x^*_{ii}=(3/2)k_{iiii}$, $x^*_{l_2l_2}=k_{2222}/2$, and $x_{ij}{}^*=k_{iijj}$ with an exception of $x^*_{23}=k_{2233}+B_e[(\omega_2/\omega_3)+(\omega_3/\omega_2)]$. The last term in x^*_{23} arises from $\mathbf{H}_{v1b}{}'$. The contributions from $\mathbf{H}_{v1b}{}'$ are also considered for the evaluation of off-diagonal matrix elements which involve $\langle n_2,\ l_2,\ n_3|n_2\pm 2,\ l_2,\ n_3\rangle$, $\langle n_2,\ l_2,\ n_3|n_2,\ l_2,\ n_3\pm 2\rangle$, $\langle n_2,\ l_2,\ n_3|n_2\pm 2,\ l_2,\ n_3\pm 2\rangle$, and $\langle n_2,\ l_2,\ n_3|n_2\pm 2,\ l_2,\ n_3\mp 2\rangle$. The resultant vibrational hamiltonian matrix is divided into symmetry blocks, which can be treated separately. The correction of the zero-point energy, however, should be done to each level.

Just as in the case of diatomic molecules, the vibrational hamiltonian matrix is obtained as the form of matrix sum:

$$\mathbf{H}_{v1b}=\sum k^{(i)}\mathbf{A}^{(i)} \qquad (17)$$

The harmonic and anharmonic force constants are numbered consecutively; $i=1,2\ldots,f$. $\mathbf{A}^{(1)}$ represents the contribution of the i-th force constant to the vibrational hamiltonian matrix, the elements of which may be evaluated once for all if the set of basis functions has been determined. Non-vanishing matrix elements $a_{ij}^{(k)}$ may be stored in magnetic tapes or discs. The contribution from the $\mathbf{H}_{v1b}{}'$ term may also be included in Eq. (17) by formally setting $k^{(0)}\equiv 1$. The elements of $\mathbf{A}^{(0)}$ are easily obtained from Eq. (3). Also time-consuming is the process to calculate the second term in Eq. (15). The computing time is considerably abridged, however, by storing the non-vanishing elements of $\langle n|q_1^k\cdot j_+|m\rangle$ and $\langle n|q_1^k\cdot j_-|m\rangle$ for $k=0$ to 4.

Eigenvalue Problems. In the present calculations it is necessary to solve real $n\times n$ symmetric matrices, where n ranges from 30 to 200. Usually 30 lowest eigenvalues and eigenvectors are obtained for each symmetry block. The Givens-Householder method for symmetric matrices[12] is satisfactory in most cases. In HITAC 8700/8800 system it takes eight seconds to solve 100×100 matrix (30 seconds for a 200×200 matrix). Double precision arithmetics are used to retain the desired accuracy.

As seen from Eq. (2), the present calculation is primarily based on the force constants in dimensionless normal coordinates. However, the force constants

in curvilinear internal coordinates are more convenient for the systematic handling of various isotopic molecules, since the latters are independent to isotopic substitutions. Therefore, a subprogram is implemented which handles the transformation from the internal to the normal coordinate systems. Either the general valence force constants or the force constants in dimensionless normal coordinates are allowed as input.

Results and Discussion

Application to CO_2 and CS_2. The present method has been applied to two XY_2 type linear molecules, *i.e.* CO_2 and CS_2. They are probably only molecules of this type, of which the general quartic force fields have been studied extensively.[10,13-16] The force constants of CO_2 and CS_2 used in the present calculations have been taken from Refs. 10 and 16, respectively, they are listed in Table 2. It is clearly seen in Table 2 that the both sets of force constants show markedly similar trend. In terms of the Nielsen-Amat's perturbation scheme,[2,4] however, these molecules differ considerably in Fermi resonance of the $v_1 \simeq 2v_2$ type. It is known that the unperturbed v_1° and $2v_2^\circ$ levels are almost coincident in CO_2, while they are apart by about 130 cm^{-1} in CS_2.[16] It is, therefore, interesting to see how they differ in the numerical diagonalization method.

Table 2. General quartic force constants of CO_2 and CS_2

	General valence[a] representation			Dimensionless normal representation (cm^{-1})	
	CO_2[b]	CS_2[c]		CO_2	CS_2
K_{11}(md/Å)	8.0112	3.9383	ω_1	1354.31	672.57
K_{13}(md/Å)	1.2613	0.6441	ω_2	672.85	398.21
K_{22}(md·Å/rad²)	0.3925	0.2846	ω_3	2396.32	1558.85
K_{111}(md/Å²)	−18.989	−7.478	k_{111}	−45.78	−18.39
K_{113}(md/Å²)	−1.955	−0.842	k_{122}	74.72	43.15
K_{122}(md/rad²)	−0.609	−0.369	k_{133}	−249.14	−130.30
K_{1111}(md/Å³)	26.251	8.697	k_{1111}	1.92	0.59
K_{1113}(md/Å³)	3.676	0.643	k_{1122}	−11.15	−5.39
K_{1133}(md/Å³)	3.022	0.479	k_{1133}	19.52	8.74
K_{1122}(md/Å·rad²)	0.504	0.111	k_{2222}	2.45	1.70
K_{1223}(md/Å·rad²)	1.870	0.461	k_{2233}	−27.56	−15.26
K_{2222}(md·Å/rad⁴)	0.046	0.044	k_{3333}	6.30	3.83

a) $R_1=\Delta r_{CX}$, $R_2=\Delta\phi$, and $R_3=\Delta r_{CX'}$. b) Set (iv) of Table 2 in Ref. 10. c) Set (i) of Table 2 in Ref. 1.

Truncation Effect. Presicion of the present calculations is determined, at least in part, from the number of basis functions taken for a symmetry block: the more basis functions are used, the more accurate results are usually expected. In the treatment of diatomic CO and HCl in I, 20 to 30 harmonic oscillator wave functions must be taken as basis to elucidate the vibrational levels up to $v=6$. As mentioned earlier, a set of three quantum numbers must be considered in XY_2,[17] and the sum of these quantum numbers $n=\sum n_s$ may be regarded as the measure corresponding to n in diatomic molecules. The value of n is in the ranges of 13—14 and 18—20 in the respective cases of 100 and 200 basis functions, the latter may be a practical limit in the present treatment. Therefore, the truncation effect of the matrix sizes has first been examined by varying the number of basis functions from 30 to 200 for each of eight symmetry blocks ($l_2=0$, 1, 2, 3). Parts of the results are given in Tables 3—6. In each table the results for the Σ_g^+, Σ_u^+, and Π_g blocks are given, the latter two blocks are chosen because relatively large number of corresponding experimental data is available. The calculated values for the 200×200 problem are given in the first column in each table and the differences from the 200×200 case are entered in the remaining columns. The entry of zero or small numbers indicates that the convergence is completed at that stage. For the lowest two or three levels 100 basis functions are sufficient, but 200 basis functions are needed to account for the lowest six to ten levels in a given symmetry block. The convergence in CS_2 is somewhat faster than that in CO_2, which is in accordance with our results in diatomic molecules (I). The off-diagonal matrix elements of CS_2 are relatively smaller than those of CO_2.

In order to calculate the rotational constants, the terms up to $k=4$ in Eqs. (4) and (5) have been retained just as in the case of diatomic molecules. Fewer terms may be used, since the values for $\gamma_1=(2B_e/\omega_1)$, which represent 'order of smallness', are 5.8×10^{-4} and 3.2×10^{-4} for CO_2 and CS_2, respectively, which are considerably smaller than the corresponding values of $(2B_e/\omega_e)$ in CO and HCl (1.7×10^{-3} and 7.0×10^{-3}) we have adopted the following values: $B_e=0.391600$ cm^{-1} for CO_2 and $B_e=0.108859$ cm^{-1} for CS_2.

Comparison with Contact Transformation Method. One of the primary purposes of the present study is to compare the results of the numerical diagonalization method with those in Refs. 10 and 18 which utilized the 2nd-order perturbation treatment with 3rd-order Fermi resonance corrections. The differences between the two calculated quantities are given in the columns designated as δ_{cal} in Tables 3—6. The differences are much larger than expected particularly for the higher levels of CO_2 which are involved in strong Fermi resonance. The general quartic force field is used in the both methods, the only difference is the inclusion of the third-order parameters λ's and δ in the treatment of Fermi resonances. These third-order parameters are rather complicated functions of force constants and geometrical parameters.[18] However, the contributions of force constants quadratic through quartic terms are considered to infinite order of approximation in the numerical diagonalization method, and the only extra terms which have to be considered are three quintic force constants, k_{11122}, k_{12222}, and k_{12233}. These quintic force constants may be evaluated from the values of the three λ's as well as those of the lower order force constants, but this requires the rather lengthy calculations. Fortunately, the sextic potential function of CO_2 has been explored by Cihla and Chedin[19] who reported the values of 0.665, −1.052, and 5.4 cm^{-1} respectively for k_{11122}, k_{12222}, and

Table 3. Calculated vibrational levels of CO_2 and their variations with the number of basis functions[a,b]

Species	Level n_1	n_2	n_3	$\nu_{calcd}(200)$	$\delta(150)$	$\delta(100)$	$\delta(50)$	$\delta(30)$	δ_{calcd}[c]	δ'_{calcd}
Σ_g^+ ($l_2=0$)	0	2	0	1285.36	0	1	2	14	24	−44
	1	0	0	1386.84	0	1	3	19	117	95
Σ_u^+ ($l_2=0$)	0	0	1	2349.01	0	0	3	6	16	−179
	0	2	1	3615.49	1	7	24	162	−268	−207
	1	0	1	3708.80	1	11	38	250	582	−150
	0	4	1	4855.06	1	14	189	1505	−148	−293
	1	2	1	4977.27	7	34	637	2423	56	−242
	2	0	1	5084.90	2	31	378	2211	1452	161
	0	6	1	6071.02	4	38	927	2312	467	−630
	1	4	1	6228.21	28	136	2396	4131	−6	−313
	2	2	1	6337.93	41	197	3017	4982	1033	−312
	3	0	1	6479.10	10	119	1356	3736	2375	744
	0	0	3	6978.88	41	241	3684	4112	−616	−2276
Π_g ($l_2=1$)	0	1	1	3002.08	0	1	5	68	224	−84
	0	3	1	4247.76	0	7	24	136	26	−99
	1	1	1	4380.96	0	8	40	209	975	154
	0	5	1	5472.44	2	15	179	1593	—	—
	1	3	1	5625.28	7	39	539	2423	—	—
	2	1	1	5771.94	3	32	377	2362	—	—
	0	7	1	6676.55	5	37	1159	2554	1141	−722
	1	5	1	6854.70	34	134	2422	4294	956	219
	2	3	1	7004.07	46	201	3021	4932	2045	482
	3	1	1	7176.26	16	118	1556	4188	2765	1364
	0	1	3	7599.06	54	227	4146	4708	423	−2155

a) $\nu_{calcd}(n)$ in cm^{-1}: obtained by solving $n\times n$ secular equation. b) $\delta(n)=[\nu_{calcd}(n)-\nu_{calcd}(200)]\times 100$. c) $\delta_{calcd}=\nu_{calcd}-\nu_{calcd}(200)$, where ν_{calcd} was obtained by an ordinary perturbation method (Ref. 10 for CO_2 and Ref. 18 for CS_2).

Table 4. Calculated vibrational levels of CS_2 and their variations with the number of basis functions[a]

Species	Level n_1	n_2	n_3	$\nu_{calcd}(200)$	$\delta(150)$	$\delta(100)$	$\delta(50)$	$\delta(30)$	δ_{calcd}	δ'_{calcd}
Σ_g^+ ($l_2=0$)	1	0	0	657.90	0	1	2	9	9	−22
	0	2	0	800.97	0	0	0	9	81	55
	2	0	0	1313.64	0	1	26	330	−1	−62
	1	2	0	1443.58	0	1	9	235	339	62
	0	4	0	1617.79	0	1	8	198	197	153
Σ_u^+ ($l_2=0$)	0	0	1	1535.34	0	1	2	32	8	−87
	1	0	1	2186.65	0	4	14	708	−113	−201
	0	2	1	2321.87	0	2	5	88	265	58
	2	0	1	2835.98	2	17	281	1107	−275	−351
	1	2	1	2958.17	0	8	103	818	356	−13
	0	4	1	3124.11	0	4	32	697	586	364
	3	0	1	3483.17	14	48	1478	2291	−475	−539
	2	2	1	3592.81	9	30	1167	1654	420	−115
	1	4	1	3746.69	7	24	901	1260	1507	409
	0	5	1	3938.55	4	17	645	1451	962	829
Π_g ($l_2=1$)	0	1	1	1924.07	0	0	2	4	96	−43
	1	1	1	2567.12	0	4	12	96	34	−144
	0	3	1	2719.31	0	2	8	435	401	190
	2	1	1	3208.05	2	10	203	1108	−57	−279
	1	3	1	3348.55	1	8	103	934	661	172
	0	5	1	3528.15	1	7	40	829	754	576

a) See Footnotes to Table 3.

Table 5. Calculated rotational constants of CO_2 and their variations with the number of basis functions[a,b]

Species	Level n_1	n_2	n_3	$B(200)$	$\delta(150)$	$\delta(100)$	$\delta(50)$	$\delta(30)$	δ_{calcd}[c]	δ'_{calcd}
Σ_g^+ ($l_2=0$)	0	2	0	3.19	0	1	2	24	59	13
	1	0	0	−0.66	0	0	1	22	−76	−65
Σ_u^+ ($l_2=0$)	0	0	1	−30.22	0	0	3	9	37	49
	0	2	1	−25.98	0	3	37	191	137	29
	1	0	1	−32.44	1	3	41	181	−98	115
	0	4	1	−17.70	3	9	256	438	285	291
	1	2	1	−37.09	6	24	486	612	6	−401
	2	0	1	−28.79	2	17	240	248	−189	15
	0	6	1	−8.25	5	50	501	1599	521	300
	1	4	1	−31.80	24	100	733	2413	377	788
	2	2	1	−41.71	17	103	639	1963	−444	267
	3	0	1	−23.03	13	64	273	2377	−131	−66
	0	0	3	−88.84	20	205	855	1746	386	848
Π_g ($l_2=1$)	0	1	1	−23.56	0	0	12	17	36	−133
	0	3	1	−19.36	0	5	46	192	64	227
	1	1	1	−25.40	1	4	71	225	−139	130
	0	5	1	−11.70	3	20	124	712	—	—
	1	3	1	−27.82	8	47	490	949	—	—
	2	1	1	−23.33	6	35	387	1068	—	—
	0	7	1	−2.36	9	77	660	2797	621	251
	1	5	1	−40.37	574	684	2701	4604	−1550	135
	2	3	1	−31.35	45	165	1105	3190	−271	574
	3	1	1	−16.70	40	268	441	7705	−266	−236
	0	1	3	−83.45	52	259	1737	3441	−115	855

a) $B(n)=[B_v^{calcd}(n)-B_{000}^{calcd}(n)]\times 10^4\ cm^{-1}$, where $B_v^{calcd}(n)$ is obtained from the eigen vectors of the $n\times n$ problem. b) $\delta(n)=[B(200)-B(n)]\times 100$; Note that the definition is reversed to make most of $\delta(n)$ positive. c) $\delta_{calcd}=B(200)-B_{calcd}$, where B_{calcd} is obtained by an ordinary perturbation method (Ref. 10 for CO_2 and Ref. 18 for CS_2).

Table 6. Calculated rotational constants of CS_2 and their variations with the number of basis functions[a]

Species	Level n_1	n_2	n_3	$B(200)$	$\delta(150)$	$\delta(100)$	$\delta(50)$	$\delta(30)$	δ_{calcd}	δ'_{calcd}
Σ_g^+ ($l_2=0$)	1	0	0	−1.62	0	0	0	6	−3	0
	0	2	0	3.79	0	0	0	0	9	1
	2	0	0	−3.11	0	1	15	15	−6	−4
	1	2	0	2.65	0	0	2	8	6	−6
	0	4	0	7.18	0	0	1	7	37	2
Σ_u^+ ($l_2=0$)	0	0	1	−7.07	0	0	0	13	6	22
	1	0	1	−8.63	0	0	7	41	6	31
	0	2	1	−3.53	0	0	3	9	−7	34
	2	0	1	−10.05	1	3	89	85	5	34
	1	2	1	−4.68	0	2	38	70	−13	39
	0	4	1	−0.36	0	1	18	126	2	47
	3	0	1	−11.26	3	12	105	136	9	36
	2	2	1	−5.76	2	10	84	122	−15	41
	1	4	1	−1.27	1	9	69	302	−2	53
	0	6	1	2.63	1	11	53	447	22	60
Π_g ($l_2=1$)	0	1	1	−5.07	0	0	1	1	−5	26
	1	1	1	−6.29	0	1	7	42	−10	26
	0	3	1	−1.81	0	1	6	60	−7	41
	2	1	1	−7.32	0	4	82	114	−23	22
	1	3	1	−2.79	0	5	41	164	−14	47
	0	5	1	1.25	0	5	25	311	11	55

a) See Footnotes of Table 5.

k_{12233}. Another calculation has been proceeded by including the matrix elements originated from these three quintic force constants. In the last columns designated as δ_{cal}' in Tables 3 and 5, the corresponding differences are entered. Significant changes (most of them are improvements) are observed upon the inclusion of the three quintic force constants.

As mentioned earlier, the numerical diagonalization method has an advantage that in that process anharmonic resonances are automatically taken care of. As shown in I, however, this method is not free from the truncation effects of the potential functions. This effect is magnified in the special case of CO_2 in which an ordinary separation of higher-order force constants from the general quartic force constants does not work properly. Since a number of smaller anharmonic resonances are considered in the present process, the discrepancies in calculated vibrational levels and rotational constants are still expected, and the fit to the experimental data may be improved by slightly adjusting the 15 force constants including the three quintic force constants.

The inclusion of other quintic as well as sextic force constants has also been tested, the changes of calculated vibrational levels and rotational constants are far smaller than those induced by the three quintic force constants above, but they are not negligible. This encourages us to proceed the least-squares fit of higher-order force constants to experimental data. This will be our project in near future.

l-Type Doubling Constants. The l-type doubling constants for a given pair of the $l_2=\pm1$ states may be evaluated through the procedure given earlier. In harmonic approximation the separation of the levels is expressed as

$$\Delta\nu = q^e_{harm}(v_2+1)J(J+1), \tag{18}$$

where

$$q^e_{harm} = (B_e^2/\omega_2)[1+4\omega_2^2/(\omega_3^2-\omega_2^2)]. \tag{19}$$

From the harmonic frequencies listed in Table 1 as well as the equilibrium rotational constants, the following values are obtained: q^e_{harm} $(CO_2)=5.27\times10^{-4}$ cm^{-1} and q^e_{harm} $(CS_2)=7.63\times10^{-5}$ cm^{-1}. Deviations from the above values may be regarded as anharmonic effects. For a few vibrational levels of CO_2 and CS_2 the l-type doubling constants have been measured accurately[20-22]. In Table 7 the observed l-type doubling constants are listed along with the corresponding calculated values. The isotopically consistent set of force constants is used to evaluate the constants of $^{13}CS_2$ species. The agreements between the calculated and observed values are quite satisfactory.

Vibrational Wave Functions and Their Application to Intensity Problem. Another useful feature in the numerical diagonalization method is its readiness to obtain an orthonormal set of perturbed vibrational wave functions, $|v\rangle=\sum_n a_{vn}|n\rangle$. The six lowest levels in the Σ_u^+-block are chosen as examples for both CO_2 and CS_2, and the coefficients which make major contributions to the above levels are listed in Table 8. The mixings of the basis harmonic oscillator wave functions are so complete in CO_2, it is senseless to label a certain level in terms of a single basis function. The mixings are not so strong in CS_2 for which the labeling is much simpler. There also exists a considerable mixing between the wave functions $|n_1, n_2, l_2, n_3\rangle$ and $|n_1\pm1, n_2, l_2, n_3\rangle$ probably through the cubic force constant k_{111}.

The usefulness of the coefficient a_{vn} may be demonstrated in its application to the calculation of the transition moment from v to v' states, $R_v^{v'}$, the square of which is related to the total integrated intensity of the band:

$$R_v^{v'} = \langle v'|M|v\rangle, \tag{20}$$

where M is the dipole moment function $M=M(q_1, q_2, q_3)$, which may be expressed as the sum of the $M_{/\!/}$ and $M_\perp$ components for linear symmetrical XY_2 molecule. The former is parallel to the molecular axis (z-axis) and has the same symmetry property as $T_z(\sigma_u^+)$, whereas the latter is perpendicular to the z-axis and has the Π_u symmetry to which T_x and T_y belong. The both components are expanded as

$$M_{/\!/} = \mu_3 q_3 + \mu_{13}q_1q_3 + \sum_{i=1}^{3}\mu_{ii3}q_i^2q_3 + \cdots \tag{21}$$

and

$$M_\perp = \mu_2 q_2 + \mu_{12}q_1q_2 + \sum_{i=1}^{3}\mu_{ii2}q_i^2q_2 + \cdots \tag{22}$$

For simplicity q_2 is used instead of r_2. The zeroth order term vanishes because of the molecular symmetry ($D_{\infty h}$). If $v\times v'\ni\sigma_u^+$, Eq. (20) is rewritten as

$$R_v^{v'} = \langle v'|M|v\rangle = \mu_3\sum_n\sum_m a_{vn}a_{v'm}\langle n|q_3|m\rangle + \mu_{13}\sum_n\sum_m a_{vn}a_{v'm}\langle n|q_1q_3|m\rangle + \cdots \tag{23}$$

Similar expression may be written for the case of $v\times v'\ni\Pi_u$. In Eq. (23), the first term vanishes unless $m_1=n_1$, $m_2=n_2$ $(l'_2=l_2)$ and $m_3=n_3\pm1$, while the second term vanishes unless $m_1=n_1\pm1$, $m_2=n_2(l'_2=l_2)$, and $m_3=n_3\pm1$. Such requirements considerably simplify the practical calculations.

TABLE 7. OBSERVED AND CALCULATED l-TYPE DOUBLING CONSTANTS FOR CO_2 AND CS_2

i) $^{12}C^{16}O_2$ Level	q_{obsd}[a]	q_{calcd}	ii) $^{12}C^{32}S_2$ Level	q_{obsd}[b]	q_{calcd}	iii) $^{13}C^{32}S_2$ Level	q_{obsd}[c]	q_{calcd}
0 1^1 0	6.10	6.16	0 1^1 0	7.82	7.65	0 1^1 0	8.52	7.92
1 1^1 0	9.64	9.61	1 1^1 0	9.05	8.63	0 1^1 1	8.68	7.83
0 3^1 0	9.19	9.12	0 3^1 1	14.65	14.38	1 1^1 1	9.75	9.05
1 1^1 1	8.59	9.39	1 3^1 1	15.78	15.57	0 3^1 1	15.19	14.59
						2 1^1 1	11.60	10.57

a) Ref. 20; unit 10^{-4} cm^{-1}. b) Ref. 21; unit 10^{-5} cm^{-1}. c) Ref. 22; unit 10^{-5} cm^{-1}.

Table 8. Some examples of eigenvector coefficients a_{vn}'s in CO_2 and CS_2[a)]

Level	CO_2 Σ_u^+-block				$\sum a^2_{vn}$
2349.01	0.980 (001)	0.188 (101)			0.996
3615.49	0.724 (021)	0.639 (101)	0.201 (201)		0.973
3708.80	0.675 (021)	0.671*(101)	0.227*(201)		0.957
4855.06	0.711 (121)	0.565 (041)	0.333 (201)		0.936
4977.27	0.699 (201)	0.553*(041)	0.335 (301)	0.256*(101)	0.972
5084.90	0.648 (121)	0.601*(041)	0.330*(201)		0.890
Level	CS_2 Σ_u^+-block				$\sum a^2_{vn}$
1535.34	0.980 (001)	0.184 (101)			0.994
2186.65	0.912 (101)	0.282 (201)	0.211 (021)		0.956
2321.87	0.969 (021)	0.190*(101)			0.975
2835.98	0.821 (201)	0.359 (301)	0.305 (121)		0.896
2958.17	0.861 (121)	0.347 (041)	0.254*(201)		0.895
3124.11	0.929 (041)	0.332*(121)			0.973

a) Asterisks indicate negative coefficients.

It is emphasized here that Eq. (23) is valid for any transitions satisfying the relation $v \times v' \ni \sigma_u^+$. This contrasts with the expressions derived from the perturbation method[23)] or those derived from the contact transformation method as has been applied to the intensity problem of the bent XY_2 molecules.[24)] Actually the numerical diagonalization method was used by Foord and Whiffen[25)] for the treatment of the dipole moment function of OCS. They obtained the vibrational wave functions by solving a 30×30 vibrational hamiltonian matrix.

Conclusions. In the present paper it has been shown that the direct diagonalization method is applicable to the treatment of vibration and vibration-rotation problem of linear symmetrical XY_2 molecules. This method has a certain merits over the conventional perturbation method: Exact solutions are usually secured if the number of basis functions is taken large enough, the quintic and higher-order force constants are easily accomodated and the method may be extended to handle with the general sextic potential function. A set of orthonormal vibrational wave functions may be obtained regardless of the potential functions employed. Eq. (23) holds whatever potential functions may be used. The obvious demerit of the present method is that it involves the eigenvalue problem for large martices to avoid the truncation effect of the vibrational hamiltonian matrix. In addition, the calculation of vibration-rotation constants is not simple and rather time consuming. However, the rapid progress of existing computers as well as of computational technique has made the above calculations quite manageable, and its application to the determination of more precise force field or to the intensity problem through dipole moment functions seems very promising.

This research has been supported by the grant from the Ministry of Education.

References

1) Part I: I. Suzuki, This Bulletin, **44**, 3277 (1971). Hereafter referred to as I.

2) H. H. Nielsen *Rev. Mod. Phys.*, **23**, 90 (1951); G. Amat, H. H. Nielsen, and G. Tarrago, "Rotation-Vibration of Polyatomic Molecules," Marcel Decker, New York (1971).

3) I. Suzuki, This Bulletin, **45**, 2429 (1972).

4) M. Goldsmith, G. Amat, and H. H. Nielsen, *J. Chem. Phys.*, **24**, 1178 (1956); **27**, 838 (1957).

5) Aliew gave an equivalent but a little more complicated formula for linear molecules: M. R. Aliew, *Opt. Spectrosc.*, **26**, 463 (1969).

6) Throughout this paper, hamiltonians are given in cm^{-1} (equivalent to H/hc), and operators are dimensionless (J_x, j_x, q, p). 6a) T. Oka, *J. Chem. Phys.*, **47**, 5410 (1967). Discussion given in Section IIA of this paper is especially pertinent to the present problem.

7) J. K. G. Watson, *Mol. Phys.*, **15**, 479 (1968).

8) The indices n and m are used to indicate the harmonic oscillator wave functions. More strictly n represents the four quantum numbers (n_1, n_2, l_2, n_3) and $|n\rangle = |n_1, n_2, l_2, n_3\rangle = \phi^\circ_{n_1}(q_1)\Phi^\circ_{n_2 l_2}(r_2, \chi_2)\phi^\circ_{n_3}(q_3)$, where Φ° is the wave function for two-dimensional harmonic oscillator. The indices v and v' refer to the true (perturbed) vibrational states.

9) In the preceding example of $v \ni \pi_u$, $\langle v|j_+|v'\rangle = 0$ if $v' \ni \Delta_u$ and $\langle v|j_-|v'\rangle = 0$ if $v' \ni \sigma_u^+$.

10) I. Suzuki, *J. Mol. Spectrosc.*, **25**, 479 (1968).

11) I. Suzuki, *ibid.*, **32**, 54 (1969).

12) J. Ortega, "The Givens-Housholder Method for Symmetric Matrices," pp. 94～115 in "Mathematical Method for Digital Computers," Vol. 2. ed. by A. Ralston and H. S. Wilf, John Wiley (1967).

13) M. A. Pariseau, I. Suzuki, and J. Overend, *J. Chem. Phys.*, **42**, 2335 (1965).

14) D. F. Smith, Jr., and J. Overend, *ibid.* **54**, 3632 (1971).

15) J. Giguere, V. K. Wang, J. Overrnd, and A. Cabana, *Spectrochim. Acta*, **29A**, 1197 (1973).

16) I. Suzuki, This Bulletin, **48**, 1685 (1975).

17) The quantum number l_2 may be excluded, since it is a constant in a symmetry block.

18) S. Maes, *Cahier Phys.*, **14**, 125 (1960); *J. Mol. Spectrosc.*, **9**, 204 (1962).

19) Z. Cihla and A. Chedin, *ibid.*, **40**, 337 (1971).

20) F. R. Gordon and T. K. McCubbin, Jr., *ibid.*, **19**, 137 (1966).

21) A. G. Maki, *ibid.*, **47**, 217 (1973).

22) G. Blanquet and C. P. Courtoy, *ibid.*, **54**, 350 (1975).

23) D. F. Eggers, Jr. and B. L. Crawford, Jr. *J. Chem. Phys.*, **19**, 1554 (1951).

24) C. Secroun, A. Barbe, and P. Jouve, *J. Mol. Spectrosc.*, **45**, 1 (1973).

25) A. Cunnington and D. H. Whiffen, *Chem. Commun.*, **1971**, 981; A. Foord and D. H. Whiffen, *J. Mol. Phys.*, **26**, 959 (1973).

Vibrational Spectra and Molecular Structure of Ethyl Methyl Sulfide

Norimasa NOGAMI,* Hiromu SUGETA, and Tatsuo MIYAZAWA[1)]

*Department of Chemistry, Faculty of Science, The University of Tokyo, Hongo, Bunkyo-ku, Tokyo 113
Institute for Protein Research, Osaka University, Yamada-kami, Suita, Osaka 565

(Received September 4, 1975)

The Raman spectra of the liquid, unannealed solid and annealed solid, and the infrared spectra of the gas, liquid, and annealed solid of ethyl methyl sulfide were measured. Normal vibrations were treated of the *trans* and *gauche* isomers. C–S stretching, CH_2 rocking and skeletal deformation vibrations were discussed in relation with molecular structures. Only the *gauche* isomer was found to exist in the annealed solid. In the liquid state, the *gauche* isomer was found to be more stable, by 0.14±0.05 kcal/mol, than the *trans* isomer. The vibrational assignment made of ethyl methyl sulfide is consistent with those of related sulfides and disulfides.

The vibrational spectra and molecular structure of ethyl methyl sulfide have been extensively studied,[2)] and it has been concluded that the *trans* isomer exists in the crystalline state. In our previous studies, however, the molecules of dialkyl sulfides[3,4)] and dialkyl disulfides[5,6)] were taken up as models of methionine and cystine groups of protein side-chains. The Raman spectra of ethyl methyl sulfide, methyl propyl sulfide, and isobutyl methyl sulfide were analyzed in the region 800—600 cm^{-1}. A systematic assignment was made of the normal vibrations of these three molecules, and the Raman lines of the annealed solid of ethyl methyl sulfide were assigned to the *gauche* isomer rather than the *trans* isomer.[3)]

In the present study, a normal coordinate treatment was made of the *trans* and *gauche* isomers of ethyl methyl sulfide and the vibrational spectra (C–S stretching, CH_2 rocking, and skeletal deformation vibrations) were analyzed for establishing the molecular conformation of ethyl methyl sulfide in the crystalline state.

Experimental

The sample of ethyl methyl sulfide was obtained from commercial sources and was purified by fractional distillation. Raman spectra were recorded with a JEOL Raman Spectrometer (Model JRS-02AS) with an argon-ion laser. Infrared spectra were recorded with a Hitachi EPI-G3 Infrared Spectrophotometer.

Normal Coordinate Treatment

As an aid for analyzing the vibrational spectra in the low frequency region, normal vibrations were treated for the *trans* (C_s) and *gauche* (C_1) isomers of ethyl methyl sulfide. The structural parameters used in the calculations were the bond lengths of r(C–S)=1.81 Å, r(C–C)=1.54 Å, and r(C–H)=1.09 Å, bond angles of ϕ(C–S–C)=98.67° and the tetrahedral angles for carbon atoms. The internal-rotation angles were taken as 180° and 60° for the *trans* and *gauche* forms, respectively. The force constants of the Urey-Bradley type were mostly transferred from dialkyl disulfides,[7)] except that the bending constant H(C–S–C) [=0.244 mdyn/Å·rad²] and repulsion constant F(C–S–C) [=0.210 mdyn/Å] were transferred from dimethyl sulfide.[8)]

C–S Stretching Vibrations

The Raman spectra of ethyl methyl sulfide in the 800~200 cm^{-1} region are shown in Fig. 1. The top spectrum (a) was observed for the liquid at room temperature. The second spectrum (b) was observed after freezing the sample rapidly. Then the frozen solid sample was readily annealed and the third spectrum (c) was observed. The infrared spectra of the liquid and annealed solid of ethyl methyl sulfide are shown in Figs. 2(b) and (c).

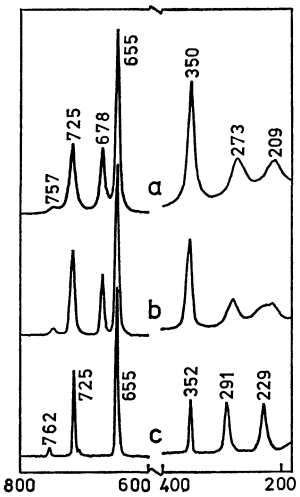

Fig. 1. The Raman spectra of ethyl methyl sulfide; (a) liquid at 300 K, (b) unannealed solid at 150 K, and (c) annealed solid at 130 K.

For each of the *trans* and *gauche* isomers of ethyl methyl sulfide, three fundamental vibrations are expected to lie in the 800—600 cm^{-1} region, including two C–S stretching and one CH_2 rocking vibrations. In fact, the Raman [Fig. 1(c)] and infrared [Fig. 2(c)] spectra of the annealed solid exhibit only three bands, indicating the presence of only one isomer. The band observed at 762 cm^{-1} (weak in Raman scattering but strong in infrared absorption) is assigned to the CH_2 rocking vibration while the bands at 725 and 655 cm^{-1} are assigned to the CH_3–S and CH_2–S stretching vibrations, respectively. For the liquid or unannealed solid, an additional band is observed at 678 cm^{-1} and is assigned to the CH_2–S stretching vibration of the other isomer. From the comparison of these C–S stretching frequencies with those of methyl propyl sulfide and isobutyl methyl sulfide,[3,4)] the Raman lines of ethyl methyl sulfide at 725 and 655 cm^{-1} are assigned to the *gauche* isomer and the Raman line at 678 cm^{-1} is assigned to the *trans* isomer.

Energy Difference between Rotational Isomers. Relative intensities of the Raman lines at 678 cm^{-1} (*trans*) and 655 cm^{-1} (*gauche*) were measured over the temperature range from 290 K to 180 K. Thus, the *gauche* isomer was found to be slightly more stable than the *trans* isomer, with the energy difference of 0.14±0.05 kcal/mol.

The temperature dependence of the relative intensities of the Raman lines at 725 and 655 cm^{-1} was also measured. The apparent energy difference of 0.05±0.05 kcal/mol is consistent with the assignment of the liquid Raman line at 725 cm^{-1} to the overlap of the CH_3–S stretching vibrations of the *trans* and *gauche* isomers.[4]

Skeletal Deformation Vibrations

For each isomer of ethyl methyl sulfide, two skeletal deformation vibrations and one CH_3–CH_2 torsional vibration are expected to lie in the 400—200 cm^{-1} region. Generally in the Raman scattering, skeletal vibrations are strongly observed but CH_3–CH_2 torsional vibrations are hardly observed. However, if the CH_3–CH_2 torsional mode is extensively hybridized with skeletal deformation modes, "CH_3–CH_2 torsional" vibration may well be observed in Raman spectra.

Such hybridization was found to be the case for the *gauche* isomer of ethyl methyl sulfide. The potential energy distribution calculated for the *gauche* isomer indicates that the skeletal deformation modes and CH_3–CH_2 torsional mode are appreciably hybridized to yield the normal vibrations at 291 and 229 cm^{-1}. Indeed, three well-defined Raman lines were observed for the annealed solid [Fig. 1(c)]. This observation is consistent with the presence of the *gauche* isomer in the annealed solid, since such hybridization is not expected to occur for the *trans* isomer belonging to the point group C_s.

CH_2 Rocking Vibrations

In our previous studies on dialkyl disulfides, the correlations were found between the CH_2 rocking frequencies and internal rotation about the CH_2–S bond of CH_3–CH_2–S–S group.[6] For the case of ethyl methyl disulfide [Fig. 2(d)], the infrared bands of the liquid at 781 and 761 cm^{-1} were assigned to the *trans* and *gauche* forms, respectively, of the CH_3–CH_2–S–S group. Similarly for diethyl disulfide, the infrared bands at 781 and 762 cm^{-1} were found to be due to the *trans* and *gauche* forms, respectively. Thus, the CH_2 rocking frequency of the *trans* form is higher, by about 20 cm^{-1}, than that of the *gauche* form. This correlation may now be applied to the case of ethyl methyl sulfide. The infrared bands of the liquid at 785 and 760 cm^{-1} are assigned to the *trans* and *gauche* isomers respectively. The observation of the infrared band at 764 cm^{-1} indicates that the *gauche* isomer exists in the annealed solid.

CH_2 rocking frequencies were also observed for the rotational isomers of isobutyl methyl sulfide, $(CH_3)_2$-CH–CH_2–S–CH_3. The infrared bands of the liquid at 813 and 803 cm^{-1} are due to the P_C-T and P_C-G

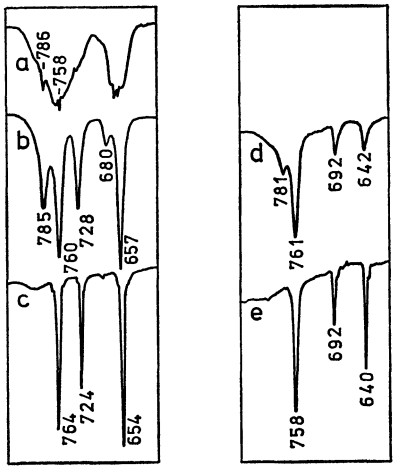

Fig. 2. Left: the infrared spectra of ethyl methyl sulfide; (a) vapor at 130 Torr and 300 K, (b) liquid at 300 K, and (c) annealed solid at 80 K. Right: the infrared spectra of ethyl methyl disulfide; (d) liquid at 300 K and (e) annealed solid at 80 K.[6]

forms, where the second symbol (T or G) refers to the internal rotation about the CH_2–S bond.[4] In the case of methyl propyl sulfide CH_3CH_2–CH_2–S–CH_3, there are two CH_2 rocking vibrations for each isomer and the lower frequency vibration lies in the 800—700 cm^{-1} region. The infrared bands (see Fig. 1 of Ref. 3) observed at 751 and 731 cm^{-1} are assigned to the P_C-T and P_C-G forms and those at 793 and 785 cm^{-1} to the P_H-T and P_H-G forms, respectively.[3] In all these cases, the CH_2 rocking frequency of the *trans* form (P_C-T or P_H-T) is higher, by 8∼25 cm^{-1}, than that of the *gauche* form (P_C-G or P_H-G).

Gas Phase. The electron diffraction of ethyl methyl sulfide was studied by Oyanagi *et al.*,[9] and the *gauche* isomer was found to be more abundant than the *trans* isomer in the gas phase. In our present study, the infrared spectrum of the gas phase was measured at the gas pressure of 130 Torr and room temperature [Fig. 2(a)]. The infrared bands due to CH_2 rocking vibrations were observed at 786 cm^{-1} (*trans*) and 758 cm^{-1} (*gauche*). The absorption band of the *gauche* isomer is stronger than that of the *trans* isomer. This observation is consistent with the result of the electron diffraction study.

To summarize, the present analyses of the Raman and infrared spectra (C–S stretching, CH_2 rocking and skeletal deformation vibrations) indicate that the *gauche* isomer of ethyl methyl sulfide exists in the annealed solid.

The authors wish to thank Prof. K. Kuchitsu, Dr. T. Fukuyama and Miss K. Oyanagi of the University of Tokyo for making available the results of the gas electron diffraction studies prior to publication.

References

1) To whom correspondences may be addressed; present address: Department of Biophysics and Biochemistry, Faculty of Science, The University of Tokyo, Hongo, Bunkyo-ku, Tokyo 113.

2) D. W. Scott, H. L. Finke, J. P. McCullough, M. E. Gross, K. D. Williamson, G. Waddington, and H. M. Huffman, *J. Amer. Chem. Soc.*, **73**, 261 (1951); M. Hayashi, *Nippon Kagaku Zasshi*, **77**, 1692 (1956), **78**, 627 (1957); M. Hayashi, T. Shimanouchi, and S. Mizushima, *J. Chem. Phys.*, **26**, 608 (1957); M. Ohsaku, Y. Shiro, and H. Murata, This Bulletin, **45**, 954 (1972), **46**, 1399 (1973).

3) N. Nogami, H. Sugeta, and T. Miyazawa, *Chem. Lett.*, **1975**, 147.

4) N. Nogami, H. Sugeta, and T. Miyazawa, This Bulletin, **48**, 2417 (1975).

5) H. Sugeta, A. Go, and T. Miyazawa, *Chem. Lett.*, **1972**, 83.

6) H. Sugeta, A. Go, and T. Miyazawa, This Bulletin, **46**, 3407 (1973).

7) H. Sugeta, *Spectrochim. Acta*, **31A**, 1729 (1975); K(C–H)=4.30, K(C–C)=2.53, K(C–S)=1.75 mdyn/Å, H(H–C–H)=0.35, H(H–C–C)=0.31, H(H–C–S)=0.18, H(C–C–C)=0.32, H(C–C–S)=0.19 mdyn·Å/rad², Y(C–C)=0.09, Y(C–S)=0.045 mdyn·Å/rad², F(H–C–H)=0.20, F(H–C–C)=0.36, F(H–C–S)=0.39, F(C–C–C)=0.23, F(C–C–S)=0.43 mdyn/Å, $\kappa(CH_3C)=-0.06$, $\kappa(CH_3S)=-0.03$, $\kappa(CH_2S)=-0.07$, $l(CH_2S)=-0.02$ mdyn·Å/rad², and p(H–C–H)=−0.10 mdyn/Å.

8) Y. Shiro, M. Ohsaku, M. Hayashi, and H. Murata, This Bulletin, **43**, 609 (1970).

9) K. Oyanagi, T. Fukuyama, and K. Kuchitsu, 32nd Annual Meeting of the Chemical Society of Japan, Tokyo (1975), 1I26.

Direct Measurement of Interaction Energy between Solids and Gases. I. Heat of Adsorption of Ammonia on Zeolite

Kazuo TSUTSUMI, Hong Qui KOH, Seiichi HAGIWARA*, and Hiroshi TAKAHASHI

Institute of Industrial Science, The University of Tokyo, Roppongi, Minato-ku, Tokyo 106

**Tokyo Riko Co. Ltd., 3-2-16 Kita-machi, Hoya-shi, Tokyo 188*

(Received October 23, 1973)

The differential heat of adsorption of ammonia on synthetic zeolites was calorimetrically measured and the distribution of the surface acidity was discussed in relation to the catalytic activity for cumene-cracking as a function of zeolite compositions. A newly designed apparatus, a twin-conduction-type calorimeter equipped with a semiconductor thermoelement and an adsorption apparatus, was used for the direct measurement of the differential heat of adsorption. The differential heat of adsorption of ammonia decreased with the increase in surface coverage, the acid site on the surface becoming stronger up to 27 kcal/mol for ammonia-adsorption when the ratio of silica to alumina was higher and the content of exchanged ammonium ions was higher. The cumene-cracking reaction was effectively catalyzed by zeolites having such sites with heat of adsorption of ammonia exceeding 25 kcal/mol.

Calorimetric studies on the interaction between solids and gases or liquids provide significant information on the surface state of the solids. For this purpose, the heats of adsorption of gas and the heats of immersion of solid into liquids are the important quantities to be measured. The heat of immersion of solids into liquids has been extensively measured calorimetrically for the past two decades.[1] It is difficult, however, to measure the heat of adsorption calorimetrically and it was usually calculated from the isotherm of adsorption[2] or from the temperature dependence of the retention volume in gas-chromatography.[3] The calculation of heat of adsorption is based on the assumptions that a reversible adsorption mechanism holds and the surface state is invariable during measurement. However, these assumptions are not necessarily applicable to the practical systems.

The difficulty in the calorimetric measurement of the interaction energy between solids and gases lies in the accurate measurement of the heat evolved. A few authors reported the results on evaporated metal films using metallic thermometers[4-6] and some other dealt with Dewar-type calorimeters.[7-11] Recently, Gravelle measured the heat of adsorption on heterogeneous catalysts by means of a heat-flow calorimeter.[12] Several other studies have also appeared.[13-16]

This paper reports a newly designed calorimeter for the measurements of the interaction energy between solids and gases, and the measurements of differential heat of adsorption of ammonia on zeolites, the results being discussed in relation to the cracking of cumene catalyzed by the zeolites.

Experimental

The calorimeter used is of a twin-conduction-type, the main cell of which is illustrated in Fig. 1. The cell is made of stainless steel and Pyrex glass which are joined by Kovar glass. The calorimeter has a second cell as a reference, which is of the same structure as that of the sample cell and serves to eliminate the effect of external disturbance. The two cells and the gas storage tank are connected to each other by a Pyrex glass tube having a stopcock connected to a vacuum line and a manometer. The sample in the cell was pretreated at various temperatures and pressures. The two cells and the gas storage tank were set in a thermostated

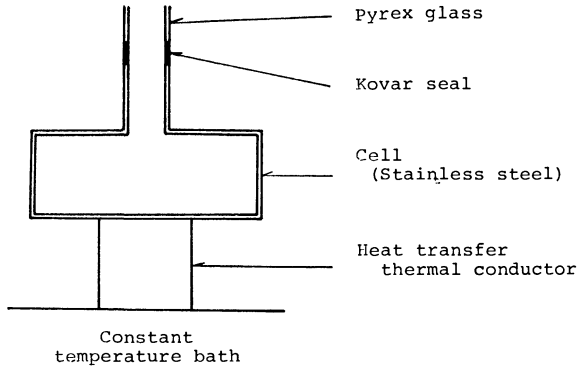

Fig. 1. Calorimetric cell.

bath. After the whole system reached thermal equilibrium, the gas storage tank was opened and the gas was led to the cell. The heat evolved in the sample cell caused the thermoelectromotive force in the thermoelement, which was amplified and recorded as shown in Fig. 2. When the thermal equilibrium was again established after completion of adsorption, the amount of heat was calibrated by flowing a given amount of electrical energy through a standard electric heater which was set in contact to the cell. An example of the cooling curve and the calibration curve is shown in Fig. 2. The ordinate, ΔT, indicates the temperature difference between the sample cell and the thermostated bath. When the heat, q, is generated in a unit of time within the cell, the following equation can be derived for the

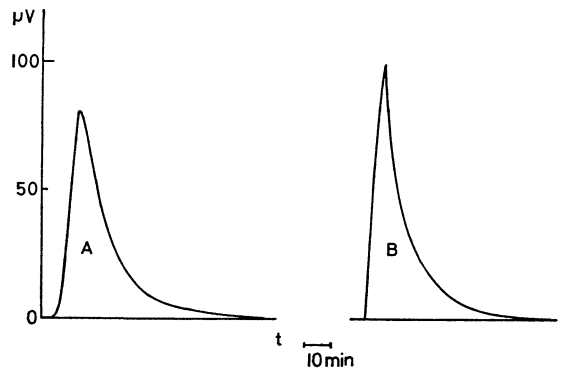

Fig. 2. Representation of $\Delta T-t$ curve (500 mcal)
A: curve recorded at the measurement
B: calibration curve by a standard electric heater

Table 1. Chemical composition and extent of exchange of zeolites

Zeolite	Composition	Extent of exchange (%)
NH_4-$Y_{10.29}$	$0.67(NH_4)_2O \cdot 0.15Na_2O \cdot 10.29SiO_2 \cdot Al_2O_3$	80.7
NH_4-$Y_{7.38}$	$0.67(NH_4)_2O \cdot 0.16Na_2O \cdot 7.38SiO_2 \cdot Al_2O_3$	78.1
NH_4-$Y_{4.8}$	$0.78(NH_4)_2O \cdot 0.15Na_2O \cdot 4.8SiO_2 \cdot Al_2O_3$	83.9
NH_4-$Y_{3.47}$	$0.70(NH_4)_2O \cdot 0.10Na_2O \cdot 3.47SiO_2 \cdot Al_2O_3$	87.5
NH_4-$X_{2.5}$	$0.41(NH_4)_2O \cdot 0.36Na_2O \cdot 2.5SiO_2 \cdot Al_2O_3$	53.3
La-$Y_{4.71}$	$0.66La_2O_3 \cdot 0.27Na_2O \cdot 4.71SiO_2 \cdot Al_2O_3$	71.0
Ca-$Y_{5.0}$	$0.80CaO \cdot 0.10Na_2O \cdot 5.0SiO_2 \cdot Al_2O_3$	88.9

relation between the amount of q and the temperature change of the cell by assuming a uniform temperature distribution in the cell.

$$q = C \cdot d(\Delta T)/dt + \sigma \Delta T \quad (1)$$

where C is the heat capacity of the cell with the sample and the thermoelement, and σ the heat transfer coefficient. The total heat released, Q, can be obtained by integrating q with respect to time t:

$$Q = \int_{-\infty}^{+\infty} q \cdot dt = C(\Delta T)_{-\infty}^{+\infty} + \sigma \int_{-\infty}^{+\infty} \Delta T \cdot dt \quad (2)$$

Since the thermal equilibrium is established in the cell before and after the adsorption, the first term on the right side of Eq. 2 is reduced to zero. Thus the total heat should be proportional to the area under the ΔT–t curve.

The amount of adsorbed gas was determined as the difference between the amount introduced to the adsorption vessel and that of the residual gas. In most initial doses, no gas remained in the gas phase. In these runs, the relation between the heat of adsorption and the adsorbed amount of gas gave the differential heat of adsorption. After the adsorption of the first dose had been accomplished, the second dose of gas was introduced; the same procedure was repeated until the differential heat of adsorption became constant.

The heat of adsorption of ammonia was measured at 25 °C. Ammonia was condensed in a liquid nitrogen trap and then allowed to evaporate into the vacuum system. The pretreatment of zeolites was carried out at 400 °C and 10^{-5} Torr for 8 hr. The catalytic activity for the cumene-cracking reaction was measured in a microreactor, the details of which were described in a previous paper.[17]

Materials. The original zeolites were the commercial Linde Molecular Sieve 13X, SX-40 and Na-$Y_{3.47}$ synthesized from silica-alumina gel and sodium hydroxide. The calcium-, lanthanum- and ammonium-form zeolites were prepared by treating Na-form zeolite with an 0.1 M solution of the corresponding chloride (guaranteed-grade reagents of Wako Pure Chemicals Industries, Ltd.). The treatment was repeated several times in order to obtain a high extent of exchange. The remaining salts were removed by washing the samples with distilled water until no chloride ions detected in washing solutions with silver nitrate. The samples were then dried and stored over the saturated sodium chloride solution. Zeolites with silica-to-alumina ratios greater than 5 were prepared by extracting aluminum atoms in NH_4-$Y_{4.8}$ zeolite with EDTA.[18] Decationated zeolites were obtained by heat treatment of the ammonium-form zeolite at 400 °C. The compositions of zeolites were measured by chemical analysis and flame photometry. The results are summarized in Table 1.

Results and Discussion

The accuracy of the calorimeter was confirmed by comparing the areas under the ΔT–t curve for the standard electric heater. The constant current supplied to the heater buried in the solid yielded a typical ΔT–t curve as shown in Fig. 2A. The ΔT–t curve for the calibration heat is also shown in Fig. 2B The ratio of the integrated area of the former ($S_{samp.}$) to that of the latter ($S_{calib.}$) is given in Table 2. We see that the ratio is equal to unity. The integrated area changes linearly with the amount of the supplied heat, the lower limit of the detected heat being a few milli-calories. The results on the heat of adsorption of ammonia on the ammonium-form zeolites with various ratios of silica-to-alumina (H-$Y_{10.29}$, H-$Y_{7.38}$, H-$Y_{4.8}$, H-$Y_{3.47}$ and H-$X_{2.5}$) are shown in Fig. 3. Since the initial stages of adsorption below 2 mmol/g are considered to be important for the catalytic activity, the results in these ranges are shown in Fig. 4 in a larger scale. Except the case of H-$X_{2.5}$, the initial heats of adsorption of ammonia on the

Table 2. Calibration of a standard electric heater

Heat supplied	$S_{samp.}/S_{calib.}$
7.0 mcal	0.96
41.6 mcal	0.98
62.5 mcal	1.01
83.2 mcal	0.99
250.0 mcal	1.01
500.0 mcal	1.01
1.0 cal	1.00
2.0 cal	1.01
5.0 cal	1.00

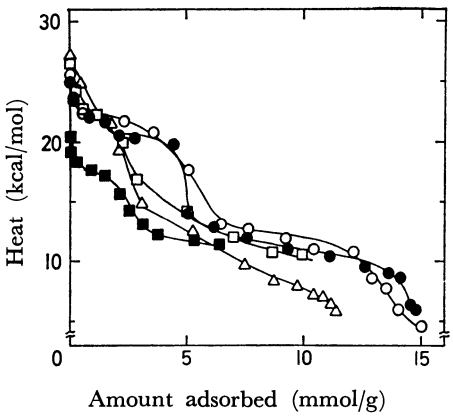

Fig. 3. Variation of differential heat of adsorption of ammonia with amount adsorbed on zeolites.
△: H-$Y_{10.29}$ □: H-$Y_{7.38}$ ○: H-$Y_{4.8}$ ●: H-$Y_{3.47}$
■: H-$X_{2.5}$

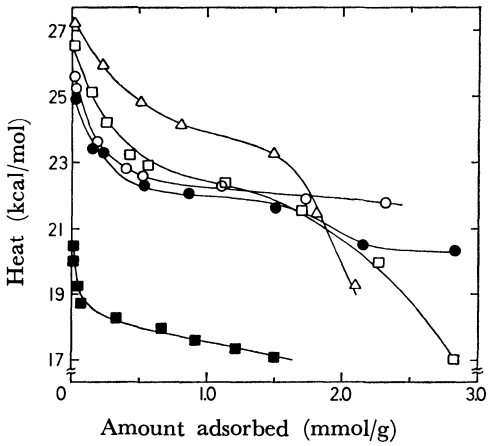

Fig. 4. Variation of differential heat of adsorption of ammonia with amount adsorbed on zeolites.
△: H-$Y_{10.29}$ □: H-$Y_{7.38}$ ○: H-$Y_{4.8}$ ●: H-$Y_{3.47}$
■: H-$X_{2.5}$

zeolites were larger than 24 kcal/mol in the coverage range less than 3×10^{-2} mmol/g. The heats, then, decrease sharply to about 21.5 kcal/mol, where the four curves intersect at 1.75 mmol/g. The abrupt decrease of the heat of adsorption at the coverage of 3×10^{-2} mmol/g suggests that the selective adsorption of ammonia molecules on the strongest acid sites takes place at a lower coverage.

It is interesting to note that the number of sites with the heat of adsorption of ammonia above 23 kcal/mol on the surface of H-$Y_{10.29}$ is larger than those of other specimens (Fig. 4). As the adsorbed amount increases to about 1.7 mmol/g, the heats of adsorption H-$Y_{10.29}$ and on H-$Y_{7.38}$ fall off steeply to about 15 kcal/mol, whereas the heats of adsorption on H-$Y_{4.8}$ and H-$Y_{3.47}$ decrease gradually to about 19.5 kcal/mol in the coverage range up to 4.5 and 5.0 mmol/g, respectively.

It is known that the thermal treatment of ammonium-form zeolites at 400 °C generates Brönsted acid sites. The initial heats of adsorption of ammonia on H-$Y_{7.38}$ and H-$Y_{10.29}$ are larger than those on H-$Y_{4.8}$ and H-$Y_{3.47}$ (Fig. 3 and 4). However, the total number of acidic sites with heats of adsorption larger than 20 kcal/mol on H-$Y_{4.8}$ and H-$Y_{3.47}$ is greater than those on H-$Y_{10.29}$ and H-$Y_{7.38}$. Since H-$Y_{10.29}$ and H-$Y_{7.38}$ were prepared by extracting aluminum atoms from the alumino-silicate frame-work with EDTA, the treatment would bring about a decrease in the total number of sites to which protons could combine. On the other hand a decrease in the aluminum content reduces the number of negative sites and lowers the electric shielding for the cations in the zeolitic cavity. Thus, the protons with weaker electrostatic shielding should be more mobile and form stronger acidic sites.

The total number of protons contained in the zeolites could be calculated by assuming that ammonium ions were converted into protons during the course of heat treatment at 400 °C. The numbers of protons thus calculated for H-$Y_{10.29}$, H-$Y_{7.38}$, H-$Y_{4.8}$ and H-$Y_{3.47}$ are 1.76, 2.26, 3.79 and 4.76 mmol/g, respectively. If one ammonia molecule is chemisorbed on one acidic site, the chemisorption of ammonia on H-$Y_{10.29}$ would amount to 1.76 mmol/g. The heat of adsorption of ammonia on H-$Y_{10.29}$ falls steeply from 22 kcal/mol to 14 kcal/mol at the coverage of 1.76 mmol/g, in accordance with the prediction (Fig. 3). A similar coincidence occurs also in the other cases. The heats of adsorption of ammonia on H-$Y_{7.38}$, H-$Y_{4.8}$ and H-$Y_{3.47}$ steeply decrease at the adsorbed amounts of 2.3, 3.4, 4.5 mmol/g, respectively, which are also consistent with the values calculated above. The heat values at these amounts are about 19.5 kcal/mol in all three cases. We can conclude that the minimum value of the chemical interaction energy between ammonia molecules and Brönsted acid sites is greater than 19.5 kcal/mol. It is likely that the acidic sites of H-$Y_{10.29}$ and H-$Y_{7.38}$ are more homogeneous in energetic character than those of H-$Y_{4.8}$ and H-$Y_{3.47}$.

By comparing with the results of infrared spectroscopy, pyridine molecules are supposed to be chemisorbed on the acidic sites of zeolites, where the heat of adsorption is greater than 20 kcal/mol.[18] Since ammonia is chemisorbed on both Brönsted and Lewis acid sites and the steric factor in adsorption of ammonia differs from that of pyridine, no quantitative coincidence was found between the adsorption of pyridine and that of ammonia.

After stepwise decrease, the heats of adsorption attain the nearly plateau region of *ca.* 10 kcal/mol and then decrease to *ca.* 5 kcal/mol. In the cases where the molecules adsorbed exceed the monolayer, the interaction between ammonia molecules and ammonium ions should be considered. According to Hsiesh[14], newly adsorbed ammonia molecules interact with the ammonium ions formed by ammonia molecules adsorbed on Brönsted acid sites. The ammonium ions polarize the ammonia molecule; the ammonia molecules also interact with the catalyst surface by the van der Waals force. In these regions, the differential heat of adsorption continues to decrease gradually until four ammonia molecules "co-ordinate" with each ammonium ion on the surface, which is in accordance with the present observations. The differential heat of adsorption finally drops to *ca.* 6 kcal/mol, which is quite close to the value of the heat of liquefaction of ammonia, 5.2 kcal/mol.

The initial heat of adsorption of H-$X_{2.5}$ is *ca.* 20.5 kcal/mol. The differential heat of adsorption gradually decreases to *ca.* 12 kcal/mol at 4 mmol/g, and then becomes constant at about 11 kcal/mol. The number of the acid sites with heats of adsorption over 19.5 kcal/mol is *ca.* 0.4 mmol/g. The value is very low as compared with that of the zeolites with higher silica-to-alumina molar ratios. Some authors[19,20] reported that the faujasite zeolite with the silica-to-alumina molar ratio of 2.5 is unstable under heat treatment. The remarkable decrease in the heat of adsorption of ammonia on H-$X_{2.5}$ might be due to the destruction of the crystalline structure by the pretreatment at 400 °C.

Figure 5 shows the plots of the heat of adsorption of ammonia *vs.* the adsorbed amount on faujasite Y with various exchange ions (Na-, Ca-, La-, and H-). The heat of adsorption of ammonia on both Ca-$Y_{5.0}$

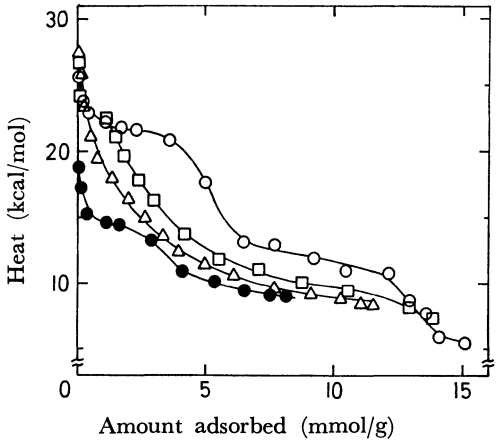

Fig. 5. Variation of differential heat of adsorption of ammonia with amount adsorbed on zeolites.
●: $Na\text{-}Y_{5.0}$ □: $Ca\text{-}Y_{5.0}$ △: $La\text{-}Y_{4.71}$ ○: $H\text{-}Y_{4.8}$

Table 3. Conversion of cumene-cracking on zeolite catalysts

Zeolite	Conversion %
$H\text{-}Y_{10.29}$	91
$H\text{-}Y_{7.38}$	95
$H\text{-}Y_{4.8}$	62
$H\text{-}Y_{3.47}$	44
$H\text{-}X_{2.5}$	0
$La\text{-}Y_{4.71}$	89
$Ca\text{-}Y_{5.0}$	71
$Na\text{-}Y_{4.8}$	0

and $La\text{-}Y_{4.71}$ falls sharply at first from a high initial value and then gradually to *ca.* 6 kcal/mol, which is nearly equal to the heat of liquefaction of ammonia. As compared with the case of the multi-valent ion-exchange zeolites, the initial heat of adsorption on the original $Na\text{-}Y_{4.8}$ is very low (about 19 kcal/mol), and decreases slowly. This indicates that the $Na\text{-}Y_{4.8}$ has a rather homogeneous surface. The conversion of the cumene-cracking on the zeolites is listed in Table 3. We see that the conversion of the cumene-cracking on ammonium-form zeolites increases in the order $H\text{-}X_{2.5}<H\text{-}Y_{3.85}<H\text{-}Y_{4.8}<H\text{-}Y_{7.38}$; it increases with the increase in the silica-to-alumina molar ratio. The conversion activity of $H\text{-}Y_{10.29}$ is somewhat lower than that of $H\text{-}Y_{7.38}$. $La\text{-}Y_{4.71}$ has a higher activity than $Ca\text{-}Y_{5.0}$, while $Na\text{-}Y_{4.8}$ has no cracking ability. In the cracking reaction of cumene, the carbonium ion is formed on the Brönsted acid site of the catalyst.[21] A site having stronger acidity will show larger activity of the formation of carbonium ions and consequently a larger cracking ability. Decrease in aluminum content makes the proton active, and increases the catalytic activity.

Morita *et al.*[22] reported that the sites effective for the cracking of cumene have the acid strengths of $H_0 \leq -3.0$, as measured by the butylamine titration with Hammett indicators. By using the same method, we found that the amount of acid sites of $H\text{-}Y_{4.8}$ with an acid strength of $H_0 \leq -3.0$ is *ca.* 2 mmol/g.[23] The heat of adsorption of ammonia at this surface coverage is found to be *ca.* 22 kcal/mol (Fig. 4). If sites on which the heat of adsorption is more than 22 kcal/mol were available for the cracking reaction of cumene, the activities of $H\text{-}Y_{3.47}$, $H\text{-}Y_{4.8}$ and $H\text{-}Y_{7.38}$ should be nearly equal to each other and lower than that of $H\text{-}Y_{10.38}$. But this is apparently not the case.

The $H\text{-}Y_{10.29}$ sample has a higher heat of adsorption of ammonia than other samples in the region of coverage 0.2—1.7 mmol/g. However, the cumene-cracking activity of $H\text{-}Y_{10.29}$ is lower than that of $H\text{-}Y_{7.38}$. Beaumont and Barthomeuf[19] reported that the crystalline structure of zeolite was partially destroyed if the content of aluminum was below 28 atoms per unit cell. The zeolite with 28 atoms per unit cell corresponds to that with a silica-to-alumina molar ratio of 9.8. In fact, the X-ray diffraction pattern of $H\text{-}Y_{10.29}$ shows a decrease in intensity.[18] The decrease in activity of cumene-cracking and the high initial heat of adsorption of $H\text{-}Y_{10.29}$ might be attributed to the partial destruction of the lattice structure.

The $H\text{-}Y_{4.8}$ and $H\text{-}Y_{3.47}$ samples, which have the same values of the initial heat of adsorption, show a remarkable difference in the activity of cumene-cracking. This is probably owing to the difference in the number of strong sites. The initial heat of adsorption on $H\text{-}Y_{3.47}$ is larger than 25.5 kcal/mol. On the other hand, the number of adsorption sites for this energy region on $H\text{-}Y_{4.8}$ is three times as much as that of $H\text{-}Y_{3.47}$. A possible reason for the difference in the activity of cumene-cracking between the two zeolites may lie in the difference in the degree of change of the Brönsted acid site to the Lewis one. Since the catalyst was treated at 550 °C before activity measurement, its number of Brönsted acid sites should be smaller than that of the sample treated at 400 °C. Dehydration occurs easily at higher temperatures on $H\text{-}Y_{3.47}$, since it possesses a larger amount of hydroxyl groups.

The present evidence is not yet conclusive as to which sites are effective in cumene-cracking reaction. However, all the data about the heat of adsorption and the cracking activity seem to be compatible with the suggestion that the sites with the heat of adsorption of ammonia of more than 25 kcal/mol are effective in cumene-cracking reaction and that the sites of stronger acidity show a greater activity. The total number of such strong acid sites also affects the activity.

References

1) K. Tsutsumi and H. Takahashi, *Seisan Kenkyu*, **23**, 368 (1971).
2) For example; Y. -Y. Huang, *J. Catal.*, 24, 183 (1972).
3) For example; P. A. Elkington and G. Curthoys, *J. Phys. Chem.*, **73**, 2321 (1969).
4) O. Beeck, W. A. Cole and A. Wheeler, *Discuss. Faraday. Soc.*, **8**, 159 (1950).
5) D. F. Kemperer and F. S. Stone, *Proc. Roy. Soc. Ser.* A, **243**, 375 (1957).
6) D. Brennan, D. O. Hayward, and B. M. W. Trapnell, *ibid.*, **256**, 81 (1960).
7) R. L. Gale, J. Haber, and F. S. Stone, *J. Catal.*, **1**, 32 (1962).

8) R. A. Beebe and E. R. Camplin, *J. Phys. Chem.*, **63**, 480 (1959).
9) M. E. Dry, T. Shingles, L. J. Boshoff, and G. J. Ooshuizen, *J. Catal.*, **15**, 190 (1969).
10) A. Clark and J. R. Harris, *ibid.*, **21**, 179 (1971).
11) M. Breysse, M. Guenin, B. Claudel, and T. Veron, *ibid.*, **28**, 54 (1973).
12) P. C. Gravelle, *Adv. Catal.*, **22**, 191 (1971).
13) S. Cerny and V. Ponec, *Catal. Rev.*, **2**, 249 (1968).
14) P. Y. Hsiesh, *J. Catal.*, **2**, 211 (1963).
15) V. Kevorkian and R. O. Steiner, *J. Phys. Chem.*, **67**, 545 (1963).
16) F. S. Stone and L. Whalley, *J. Catal.*, **8**, 173 (1967).
17) K. Tsutsumi and H. Takahashi, *ibid.*, **24**, 1 (1972).
18) K. Tsutsumi, H. Kajiwara, and H. Takahashi, This Bulletin, **47**, 801 (1974).
19) R. Beaumont and D. J. Barthomeuf, *J. Catal.*, **26**, 218 (1972).
20) H. Ito, Y. Nogata, S. Matsuzaki, and A. Kuboyama, This Bulletin, **42**, 2453 (1969).
21) J. W. Ward, *J. Catal.*, **11**, 259 (1968).
22) Y. Morita, T. Kimura, F. Kato, and M. Tamagawa, *Bull. Japan Petro. Inst.*, **14**, 192 (1972).
23) M. Ikemoto, K. Tsutsumi, and H. Takahashi, This Bulletin, **45**, 1330 (1972).

Multidentate Ligand Kinetics. I. The Ligand Substitution Reaction between Ethylenediaminetetraacetatocuprate(II) and Triethylenetetraminezinc(II)

Tetsuo KATSUYAMA and Toshihiko KUMAI

Department of Basic Technology, Faculty of Engineering, Yamagata University, Yonezawa, Yamagata 992

(Received January 24, 1975)

The kinetics and the mechanism of the ligand substitution reaction between ethylenediaminetetraacetatocuprate(II)(CuY^{2-}) and triethylenetetraminezinc(II)(ZnT^{2+}) were studied spectrophotometrically in the pH range 7.0—10.5 at I=0.2($NaClO_4$) and 25.0 °C. The exchange reaction was accelerated by traces of either EDTA or triethylenetetramine(Trien). The exchange reaction was shown to proceed by the chain reaction mechanism where the chain-propagating steps are the reaction of CuY^{2-} with Trien and the reaction of ZnT^{2+} with EDTA. Each chain-propagating step was investigated. The apparent rate constant of the reaction of CuY^{2-} with Trien increases with pH, while that of ZnT^{2+} with EDTA decreases with pH.

Ligand substitution reactions between two multidentate ligand complexes have been studied by Margerum *et al.*[1-4] The exchange reactions were found to be accelerated by the addition of small numbers of free ligands and to be inhibited by the addition of small numbers of metal ions. A coordination chain reaction mechanism was proposed for the exchange reactions, where the chain-propagating steps are the reactions of metal complexes with free ligands.

These catalytic exchange reactions are useful for analysis.[5-7] In analytical applications, rapid coordination chain reactions are of interest for several reasons. (1) In coordination chain reactions, a metal impurity reacts very rapidly with ligands and the resulting complexes may influence the chain reaction. In rapid coordination chain reactions, this influence may be eliminated if the main chain reaction takes place rapidly. (2) In rapid coordination chain reactions, kinetic measurements can be easily repeated using the stopped-flow technique. Therefore, rapid analysis may be achieved by handling the results statistically with an on-line computer.

It seemed worthwhile to find rapid coordination chain reaction systems. In the present study, the kinetics and mechanism of the ligand substitution reaction between ethylenediaminetetraacetatocuprate(II)(CuY^{2-}) and triethylenetetraminezinc(II)(ZnT^{2+}) were studied.

$$CuY^{2-} + ZnT^{2+} \rightleftharpoons CuT^{2+} + ZnY^{2-} \quad (1)$$

The reaction of this system was greatly accelerated by the addition of free ligands.

Experimental

Reagents. Reagent grade zinc(II) and copper(II) perchlorates, and guaranteed reagent grade sodium perchlorate were recrystallized from their aqueous solutions. Guaranteed reagent grade triethylenetetramine(Trien) was purified by distillation at reduced pressure. EDTA used was a Dotite reagent. Water used was distilled with an all quartz distillation apparatus after passing through a column of mixed-bed ion exchange resin. A standard copper nitrate solution was prepared from copper plate, and used to standardize the Trien and EDTA solutions.

Solutions of CuY^{2-} and ZnT^{2+} were prepared by the following procedure. The ligand was dissolved in water and standardized. Metal perchlorate was added stoichiometrically to the ligand solution and also a slight excess of the metal perchlorate was added to the solution. The excess metal was precipitated as hydroxide at about pH 9. The resulting precipitate was filtered off and the solution prepared was adjusted to about pH 7 for storage. The concentrations of the solutions prepared were standardized by the following procedure. CuY^{2-}: a large excess of Trien was added to the CuY^{2-} solution and the concentration of the CuT^{2+} formed was measured spectrophotometrically. ZnT^{2+} : a slight excess of the copper(II) ion was added to the ZnT^{2+} solution. The zinc(II) ion liberated and the excess of copper(II) ion were precipitated at pH 9, because the reaction of ZnT^{2+} with the copper(II) ion proceeds essentially to completion. Then the concentration of the CuT^{2+} formed was measured spectrophotometrically.

Other reagents were of guaranteed reagent grade.

Kinetic Measurements and Apparatus. The kinetics of the double ligand-exchange reaction between CuY^{2-} and ZnT^{2+} was studied in the presence of a large excess of CuY^{2-} and small amounts of EDTA over a pH range 7.0—10.5. In the kinetic measurements, a stopped-flow technique was employed with a Hitachi Model RSP2 Rapid Scanning Spectrophotometer which was equipped with two syringes used as reactant containers. One of the syringes was filled with a CuY^{2-} solution containing small amounts of EDTA, and the other, with a ZnT^{2+} solution containing a buffer and sodium perchlorate. After the two reactant solutions were mixed, the change in the transmittance at 550 nm was recorded on a storage-type oscilloscope as a function of time. Molar absorption coefficients of CuT^{2+} and CuY^{2-} at 550 nm are 138 and 5, respectively, which were measured with a Hitachi 139 spectrophotometer. ZnT^{2+} and ZnY^{2-} do not absorb light at 550 nm.

A mannitol—boric acid—sodium borate or sodium borate—sodium hydroxide buffer system was used to control the pH of the solutions. All pH values were measured with a Toa-Electronics Model HM-15A digital pH-meter. The temperature was controlled at 25.0 °C and the ionic strength was adjusted to 0.2 with sodium perchlorate. In this study, several calculations were performed with the aid of an electronic computer (TOSBAC 40).

Results

Equilibrium reaction (1) is highly favored to proceed to the right so that the ligand exchange reaction between CuY^{2-} and ZnT^{2+} goes to completion and the reverse reaction can be neglected in the kinetic study.

At high pH(9.5—10.5), the rate equation can be expressed as

$$-\frac{d[ZnT^{2+}]}{dt} = k_1'[ZnT^{2+}] \quad (2)$$

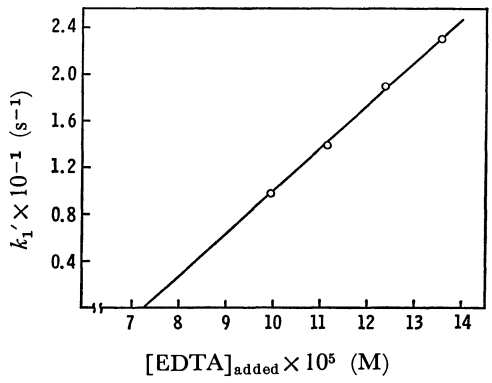

Fig. 1. Dependence of the conditional rate constant k_1' on concentration of added EDTA.
Conditions: $[CuY^{2-}]=2.40\times10^{-2}$ mol/l, $[ZnT^{2+}]=1.60\times10^{-3}$ mol/l, pH=10.12, $I=0.2(NaClO_4)$, 25.0 °C.

where k_1' is the conditional rate constant involving the added EDTA and hydrogen ion concentrations. The rate plots of $\log(A_\infty - A)$ *vs.* t were linear for over 80% of the reaction. The conditional rate constant k'_1 was determined from the slope of the straight line. In Fig. 1, the values of k_1' determined at pH 10.12 are plotted against the added EDTA concentration. It is evident from Fig. 1 that k_1' is linearly related to the added EDTA concentration [Ya] in the region above a threshold value b, and thus, the following relation is obtained:

$$k_1' = k_1([Ya]-b) \tag{3}$$

where k_1 is the slope of the straight line. The values of k_1 were obtained at various pH values.

On the other hand, for low pH (7.0—8.5), reaction (1) was of pseudo-zero-order with respect to ZnT^{2+}. Thus, the rate equation is given by

$$-\frac{d[ZnT^{2+}]}{dt} = k_0' \tag{4}$$

where k_0' is the conditional zero-order rate constant involving the CuY^{2-}, added EDTA and hydrogen ion concentrations. Integration of Eq. (4) yields

$$A = \Delta\varepsilon k_0' t + A_\infty - a\Delta\varepsilon \tag{5}$$

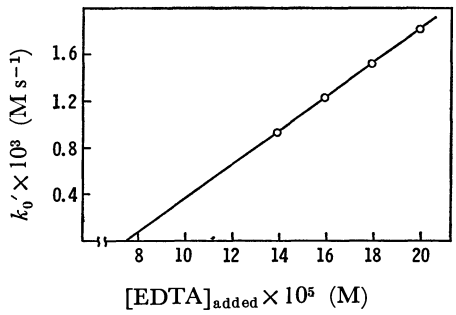

Fig. 2. Dependence of the conditional rate constant k_0' on concentration of added EDTA.
Conditions: $[CuY^{2-}]=2.40\times10^{-2}$ mol/l, $[ZnT^{2+}]=1.60\times10^{-3}$ mol/l, pH=7.55, $I=0.2(NaClO_4)$, 25.0 °C.

where A_∞ and A are the absorbance of the reaction system at $t=\infty$ and t, respectively, $\Delta\varepsilon$ is the difference in molar absorption coefficient between CuT^{2+} and CuY^{2-}, and a is the initial concentration of ZnT^{2+}. The plots of A *vs* t are linear for over 80% of the reaction. The conditional zero-order rate constant k_0' was calculated from the slope of the straight line. In Fig. 2, the values of k_0' determined at pH 7.55 are plotted against the added EDTA concentration. k_0' is linearly related to the added EDTA concentration, thus

$$k_0' = k_0([Ya]-b') \tag{6}$$

The values of the slope k_0 were obtained at various pH values.

Discussion

Reaction Mechanism. The ligand-exchange reaction between CuY^{2-} and ZnT^{2+} can be shown to proceed by the chain reaction mechanism:

$$CuY^{2-} + T' \underset{k_{-2}}{\overset{k_2}{\rightleftharpoons}} CuT^{2+} + Y' \tag{7}$$

$$ZnT^{2+} + Y' \underset{k_{-3}}{\overset{k_3}{\rightleftharpoons}} ZnY^{2-} + T' \tag{8}$$

where Y′ and T′ represent the sum of the uncomplexed species of EDTA and Trien, respectively. The equilibrium constants of reactions (1), (7) and (8) at an ionic strength $I=0.2$ were calculated from the stability constants of the related complexes and the protonation constants of the related ligands. The stability constants and the protonation constants at an ionic strength $I=0.2$ were estimated from the constants[8] at $I=0.1$ on the basis of the diagram of Ringbom.[9] The equilibrium constants calculated are plotted against pH in Fig. 3.

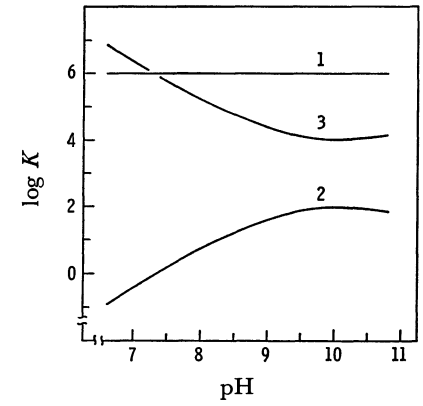

Fig. 3. Dependence of the conditional equilibrium constants of Eqs. (1), (7) and (8) on pH at 25 °C and $I=0.2$.
1: Eq. (1), 2: Eq. (7), 3: Eq. (8).

Steady-State Treatment. The rate expression derived from a steady-state treatment with the assumptions that all of the exchange is carried by reactions (7) and (8), and that the concentration of the free ligand remains constant throughout the exchange is

$$-\frac{d[ZnT^{2+}]}{dt} = \frac{(k_2k_3[CuY^{2-}][ZnT^{2+}]-k_{-2}k_{-3}[ZnY^{2-}][CuT^{2+}])[L]}{k_2[CuY^{2-}]+k_{-2}[CuT^{2+}]+k_3[ZnT^{2+}]+k_{-3}[ZnY^{2-}]} \quad (9)$$

where [L] is the total concentration of free ligands, EDTA and Trien. Because the value of the equilibrium constant of reaction (8) shows $k_3 \gg k_{-3}$, Eq. (9) can be simplified to

$$-\frac{d[ZnT^{2+}]}{dt} = \frac{(k_2k_3[CuY^{2-}][ZnT^{2+}])[L]}{k_2[CuY^{2-}]+k_{-2}[CuT^{2+}]+k_3[ZnT^{2+}]} \quad (10)$$

In the denominator of Eq. (10), term $k_2[CuY^{2-}]$ becomes predominant and the other terms may be neglected at pH 9.5—10.5, which will be shown later. Equation (10) then becomes

$$-\frac{d[ZnT^{2+}]}{dt} = k_3[L][ZnT^{2+}] \quad (11)$$

Since the metal impurity reacts very rapidly with added EDTA, the total concentration of free ligands in the solution is written as

$$[L] = [Ya] - [M] \quad (12)$$

where [Ya] and [M] are the concentrations of the added EDTA and metal impurity, respectively. Thus Eq. (11) becomes

$$-\frac{d[ZnT^{2+}]}{dt} = k_3([Ya]-[M])[ZnT^{2+}] \quad (13)$$

Equation (3) can be rewritten as

$$k_1' = k_1([Ya]-b) = k_1([Ya]-[M]) \quad (14)$$

where b equals [M]. Therefore, Eq. (13) agrees with the rate equation derived experimentally at high pH. Thus k_3 is equal to k_1.

On the other hand, in the denominator of Eq. (10), term $k_3[ZnT^{2+}]$ becomes predominant and the other terms may be neglected for pH 7.0—8.5, which will also be shown later. Equation (10) then becomes

$$-\frac{d[ZnT^{2+}]}{dt} = k_2[L][CuY^{2-}] \quad (15)$$

For a large excess of CuY^{2-}, $k_2[CuY^{2-}]$ can be constant during the reaction so that Eq. (15) becomes

$$-\frac{d[ZnT^{2+}]}{dt} = (\text{const.})[L] = (\text{const.})([Ya]-[M]) \quad (16)$$

Therefore, Eq. (16) agrees with the rate equation derived experimentally at low pH, because Eq. (6) can be rewritten as

$$k_0' = k_0([Ya]-[M]) \quad (17)$$

Thus k_2 can be calculated from the value of k_0. The values of k_2 and k_3 obtained are plotted against pH in Fig. 4. The approximations used in this discussion can be shown to be valid from Figs. 3 and 4, and the experimental conditions.

Several possible reactions excepting the chain-propagating steps may be eliminated from the exchange reaction mechanism by adding either EDTA or Trien to the reaction system, because the chain reaction pathway becomes predominant with the addition of the ligand.

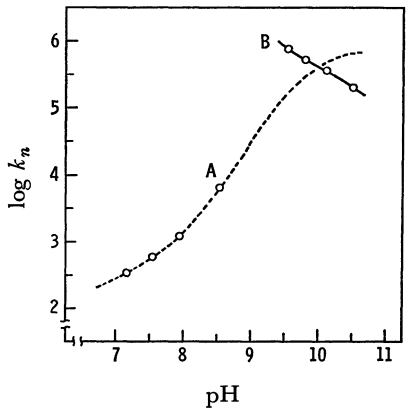

Fig. 4. Dependence of the apparent rate constants k_2 and k_3 on pH at 25.0 °C and $I=0.2$($NaClO_4$).
A: k_2, B: k_3. The dotted line(A) is the theoretical curve calculated with the aid of the individual rate constants.

Resolution of the Apparent Rate Constant k_2. From a steady-state consideration of reactions (7) and (8) with the assumption that the concentration of the free ligand remains constant, the following relation is derived

$$\frac{[Y']}{[T']} = \frac{k_2[CuY^{2-}]+k_{-3}[ZnY^{2-}]}{k_{-2}[CuT^{2+}]+k_3[ZnT^{2+}]} \approx \frac{k_2[CuY^{2-}]}{k_3[ZnT^{2+}]} \quad (18)$$

At low pH, the form k_3 $[ZnT^{2+}] \gg k_2[CuY^{2-}]$ holds, as mentioned above, so that the total free ligand concentration in the solution becomes equal to the Trien concentration.

At low pH (7.0—8.5), the total uncomplexed Trien concentration is expressed as

$$[T'] = [T] + [HT^+] + [H_2T^{2+}] + [H_3T^{3+}] \quad (19)$$

Thus, the following relationship can be derived:

$$\begin{aligned} k_2[L][CuY^{2-}] &= k_2[T'][CuY^{2-}] \\ &= k_T[T][CuY^{2-}] + k_{HT}[HT^+][CuY^{2-}] \\ &\quad + k_{H_2T}[H_2T^{2+}][CuY^{2-}] + k_{H_3T}[H_3T^{3+}][CuY^{2-}] \end{aligned} \quad (20)$$

where k_T, k_{HT}, k_{H_2T} and k_{H_3T} are the resolved rate constants. With the protonation constants of Trien species, Eq. (20) is written as

$$\begin{aligned} k_2(1+K_1[H^+]+K_1K_2[H^+]^2+K_1K_2K_3[H^+]^3) &= k_T + K_1[H^+]k_{HT} + K_1K_2[H^+]^2k_{H_2T} \\ &\quad + K_1K_2K_3[H^+]^3k_{H_3T} \end{aligned} \quad (21)$$

where K_1, K_2 and K_3 are the successive protonation constants of HT^+, H_2T^{2+} and H_3T^{3+}, respectively. The apparent rate constant k_2 was resolved into the individual proton dependent terms, k_T, k_{HT}, k_{H_2T} and k_{H_3T}, satisfying Eq. (21) with the aid of a computer. The rate constants k_T, k_{HT}, k_{H_2T} and k_{H_3T} determined in this investigation are 9.1×10^5, 1.8×10^4, 3.6×10^2 and 4.4×10 $M^{-1}s^{-1}$, respectively.

The resolved rate constants at $I=0.1$, which were estimated from those of this investigation ($I=0.2$) by evaluating the influence of the primary salt effect, agree approximately with the rate constants of the reaction of CuY^{2-} with Trien at $I=0.1$ which were determined by Margerum *et al.*[10] Using the resolved

rate constants, the apparent rate constant k_2 can be calculated. The calculated values are shown in Fig. 4.

Characteristics of the Present System. The coordination chain reactions studied by Margerum *et al.* are slow. In analytical applications, their customary reaction time is about 10 min or longer. However, the reaction of the present system takes place rapidly. The reaction time is about 1 s at low pH and about 0.2 s at high pH.

The ligand substitution reaction of ZnT^{2+} with EDTA cannot be investigated by the usual spectrophotometric method as the spectral data of ZnT^{2+} and ZnY^{2-} are essentially identical. In this paper it was shown that the coordination chain reaction of the present system provides a useful method for the study of the ligand substitution reaction of ZnT^{2+} with EDTA.

References

1) D. C. Olson and D. W. Margerum, *J. Amer. Chem. Soc.*, **84**, 680 (1962).
2) D. C. Olson and D. W. Margerum, *ibid.*, **85**, 297 (1963).
3) D. W. Margerum and J. D. Carr, *ibid.*, **88**, 1639 (1966).
4) J. D. Carr and D. W. Margerum, *ibid.*, **88**, 1645 (1966).
5) D. W. Margerum and R. K. Steinhaus, *Anal. Chem.*, **37**, 222 (1965).
6) R. H. Stehl, D. W. Margerum, and J. J. Latterll, *ibid.*, **39**, 1346 (1967).
7) D. W. Margerum and R. H. Stehl, *ibid.*, **39**, 1351 (1967).
8) L. G. Sillén and A. E. Martell, "Stability Constants of Metal-ion Complexes," The Chemical Society, London (1964).
9) A. Ringbom, "Complexation in Analytical Chemistry," Interscience Publishers Inc., New York, N.Y. (1963), p. 24.
10) J. D. Carr, R. A. Libby, and D. W. Margerum, *Inorg. Chem.*, **6**, 1083 (1967).

Presumptive Structures of Activated Complexes of Polarographic Redox Reactions of Unsaturated Organic Compounds. I.[1] Polarographic Reductions of Aromatic Hydrocarbons, Aromatic Aldehydes, and Quinones

Yo UEDA and Yukio ONO

Faculty of Pharmaceutical Sciences, Kyushu University, Maedashi, Higashi-ku, Fukuoka 812

(Received February 10, 1975)

Activated complexes of the polarographic reductions of unsaturated organic compounds were assumed to be formed by the interaction of the π-molecular orbital of each compound with a hypothetical atomic orbital of the electrode employed. Linear correlations were obtained between the mutual differences in the polarographic half-wave reduction potentials of a series of unsaturated organic compounds and the respective differences in the π-stabilization energies calculated on the basis of the presumed structures of activated complexes. These linear relationships were considered to lend experimental support to the propriety of the presumed structures of the activated complexes of the polarographic reductions of unsaturated organic compounds.

The electron-transfer phenomenon in electrochemical reactions has become rather clearer as a result of several theoretical investigations. However, the structures of the activated complexes in the electrochemical reaction are still ambiguous. For example, Marcus[2] developed a unified theory of homogeneous and electrochemical electron-transfer rates; he also gave a basis for the quantitative correlations among the chemical and electrochemical rate constants. There have been several papers[3] describing satisfactory results obtained by the application of Marcus's theory to each subject. Hush[4] also developed a theory accounting for the activation process in electrochemical reactions.

With regard to the structures of activated complexes in electrochemical reactions, it may be said that no concrete figure of an activated complex has yet been presented. For example, Vlček[5] reported that an initial activated complex ($*D \cdot E^-$) is formed by the contact of a depolarizer, *D, having an excited electronic state with the electrode, E^-, in the polarographic reduction reaction. However, this structure may not be considered to be concrete, because no definite explanation of either the mechanism of the contact of *D with E^- or the mechanism of electronic excitation was given.

By the way, it is known that mutual reactivity differences in the chemical reactions of a homologous series of organic compounds with the same reagent and under the same reaction conditions must be explained in terms of the differences in the potential energy changes of their possible reaction paths calculated theoretically. However, this kind of calculation is almost impossible except for simple reactions of small molecules. Therefore, such differences are usually explained in terms of the differences in the activation energies of the reactions. If a profile of the potential energy surface of an electrochemical reaction is very similar to that of the homogeneous chemical reaction, as in Marcus's theory, the mutual differences in the electrode potentials required for polarographic reactions of organic compounds having analogous chemical structures with the same electrode in the same solvent to proceed may also have to be explained in terms of the differences in their activation energies.

It is known that the stabilization energy of an activated complex of a chemical reaction can be estimated by a simple quantum-chemical method.[6] It has also been known that the mutual reactivity differences of a homologous series of organic compounds in the same kind of chemical reaction can be correlated rather roughly with the differences in their stabilization energies. This roughness may be assumed to be due to the complex reaction mechanisms involved and to the consequent difficulty of making presumptions as to the structures of the activated complexes.

However, in the case of polarographic reactions, many reactions proceed by means of rather simple reaction mechanisms. Moreover, the reagent in a usual chemical reaction is nothing else than the electron(s) on the electrode.[7] Therefore, the presumption of the structures of activated complexes is expected to be rather easy. If this presumption can be made a mutual difference in the energies necessary for the reversible electrochemical oxidation-reduction reactions of two analogous compounds with the same electrode under the same condition to proceed, it may be expected to be correlated linearly with the difference in the stabilization energies of their activated complexes.

In this paper, the structures of activated complexes of the diffusion-controlled reversible polarographic reductions, employing a dropping mercury electrode, of unsaturated organic compounds are presumed. Moreover, an expected linear correlation between the mutual differences in the half-wave reduction potentials of a series of compounds and the differences in their stabilization energies calculated on the basis of the presumed structures of activated complexes is derived. Lastly, the proprieties of the presumed structures of activated complexes are examined on the basis of the experimental results.

Results and Discussion

Presumption of the Structure of Activated Complexes. The comparisons of the half-wave potentials ($E_{1/2}$) of a series of diffusion-controlled reversible polarographic one-electron reactions, employing a dropping mercury electrode, of a homologous series of unsaturated organic

compounds (R) in the same solvent are considered. If these reactions are assumed to proceed *via* the respective activated complexes (Eq. (1)), the standard free-energy change (ΔG°) of the reaction of a compound, R, is equal to the difference in the free energies of the activation of its forward and reverse reactions ($\vec{\Delta G}^{\neq} - \overleftarrow{\Delta G}^{\neq}$):

$$R + e^-(Hg) \rightleftharpoons [\text{activated complex}] \rightleftharpoons R^- + (Hg) \quad (1)$$

Moreover, the difference in the standard free-energy changes of two analogous compounds, R_A and R_B, is expressed by Eq. (2). The polarographic half-wave reduction potential of a reversible

$$\begin{aligned}\Delta G^\circ_A - \Delta G^\circ_B &= (\vec{\Delta G}^{\neq}_A - \overleftarrow{\Delta G}^{\neq}_A) - (\vec{\Delta G}^{\neq}_B - \overleftarrow{\Delta G}^{\neq}_B) \\ &= (\vec{\Delta G}^{\neq}_A - \vec{\Delta G}^{\neq}_B) - (\overleftarrow{\Delta G}^{\neq}_A - \overleftarrow{\Delta G}^{\neq}_B) \quad (2)\end{aligned}$$

reaction system such as Eq. (1) is known to be a linear function of the free-energy change (Eq. (3)).[8] Moreover, according to the law of linear free-energy relation, ($\Delta G^\circ_A - \Delta G^\circ_B$) can be considered to be proportional to ($\vec{\Delta G}^{\neq}_A - \vec{\Delta G}^{\neq}_B$) (Eq. (4)). Here, a is the proportional constant determined by the nature of the reaction. Therefore, the difference in the polarographic half-wave potentials of two compounds can be correlated with the difference in their free energies of activation (Eq. (5)).

$$E_{1/2} = -\frac{\Delta G^\circ}{F} + \frac{RT}{F}\ln\left(\frac{D_{R^-}}{D_R}\right)^{1/2}\left(\frac{f_R}{f_{R^-}}\right) \quad (3)$$

D: diffusion coefficient; R: gas const.;
F: Faradays const.; f: activity coefficient; T: K

$$\vec{\Delta G}^{\neq}_A - \vec{\Delta G}^{\neq}_B = a(\Delta G^\circ_A - \Delta G^\circ_B) \quad (4)$$

$$\begin{aligned}E^A_{1/2} - E^B_{1/2} &= -\frac{(\Delta G^\circ_A - \Delta G^\circ_B)}{F} \\ &\quad + \frac{RT}{F}\ln\left(\frac{D_{R_A}\text{-}D_{R_B}}{D_{R_A}D_{R_B^-}}\right)^{1/2}\left(\frac{f_{R_A}f_{R_B^-}}{f_{R_A^-}f_{R_B}}\right) \\ &= -\frac{(\vec{\Delta G}^{\neq}_A - \vec{\Delta G}^{\neq}_B)}{aF} \\ &\quad + \frac{RT}{F}\ln\left(\frac{D_{R_A}\text{-}D_{R_B}}{D_{R_A}D_{R_B^-}}\right)^{1/2}\left(\frac{f_{R_A}f_{R_B^-}}{f_{R_A^-}f_{R_B}}\right) \quad (5)\end{aligned}$$

$$E^A_{1/2} - E^B_{1/2} \simeq -\frac{(\vec{\Delta G}^{\neq}_A - \vec{\Delta G}^{\neq}_B)}{aF} \quad (6)$$

Because R_A and R_B were supposed to have similar chemical structures, the contribution of the second term on the right-hand side of Eq. (5) to the left-hand side seems insignificant. Therefore, Eq. (5) is simplified to Eq. (6).

In order to estimate the free energy of activation of R, a presumption as to the structure of its activated complex is necessary. In the forward reaction of Eq. (1), the electron (e^-) on a dropping mercury electrode [(Hg)] may be considered to be supplied from the Fermi level of liquid mercury, whose energy is known to be -6.84 eV.[9] Since only one electron participates in the reaction, while innumerable electrons on (Hg) do not, it might be thought that the electron is the true reagent of the forward reaction, while (Hg) is its carrier. Therefore, the electron is assumed to occupy a hypothetical atomic orbital of liquid mercury [$\chi_{(Hg)}$][10] with the orbital energy of -6.84 eV. The magnitude of the energy of this hypothetical atomic orbital is not much different from that of the Coulomb integral (α) of a carbon atom forming part of a π-electronic system of organic compounds, because the Coulomb integral is generally considered to be about -7 to -9 eV. Therefore, the hypothetical atomic orbital of the electrode is considered to be able to interact with the π-molecular orbital of a compound, R. Therefore, when the compound is going to collide with the electrode, the hypothetical atomic orbital of the electrode and the π-molecular orbital of R may begin to overlap each other; at the moment of collision, this overlap may become complete. In this state, of course, it cannot be considered that the electron and R are bound rigidly, but it may be considered that the π-electronic cloud of R spreads not only over the molecule, but also over the hypothetical atom of the electrode. In other words, the electron localized initially on the hypothetical atomic orbital of the electrode is considered to be delocalized on the π-electronic system newly formed. Therefore, the transference of an electron from the electrode to R may occur. This state may be presumed to be the activated complex, and its structure may be expressed by $[R\cdots e^-\cdots(Hg)]^{\neq}$. Just after the collision, the electron may be localized on the original π-electronic system of R, and an activated complex of the reaction may begin to decompose. This decomposition may produce the products (an anion radical and the electrode with a vacant hypothetical atomic orbital).

In the reverse reaction of Eq. (1), a vacant hypothetical atomic orbital of the electrode of the same kind as that of the forward reaction may be assumed. Much as in the case of the forward reaction, the formation of an activated complex, $[R\cdots e^-\cdots(Hg)]^{\neq}$, may be considered.

Therefore, the process of the reversible one-electron polarographic reductions of a series of unsaturated organic compounds may be assumed to be as follows (Eq. (7)):

$$R + e^-(Hg) \rightleftharpoons [R\cdots e^-\cdots(Hg)]^{\neq} \rightleftharpoons R^- + (Hg) \quad (7)$$

The presumed structure of the activated complexes of one-electron reactions may be applicable, with a slight modification, to the structure of the activated complexes of two-electron reactions. That is, in a reversible reaction of an unsaturated organic compound, R(Eq. (8)), a hypothetical atomic orbital of the electrode occupied by two electrons may be assumed. These two electrons may then be assumed to be transferred to the π-molecular orbital of R. The formation of an activated complex, $[R\cdots 2e^-\cdots(Hg)]^{\neq}$, may also be assumed:

$$R + 2e^-(Hg) \rightleftharpoons [R\cdots 2e^-\cdots(Hg)]^{\neq} \rightleftharpoons R^{2-} + (Hg) \quad (8)$$

π-Stabilization Energy of the Presumed Activated Complex. According to the transition-state theory, the $\vec{\Delta G}^{\neq}$ of a forward reaction of Eq. (7) can be correlated with its equilibrium constant $K^{\neq}$ (Eq. (9)), and $K^{\neq}$ can be expressed by Eq. (10). Here, Q is the parti-

tion function, and $\vec{E}_0$ is the activation energy, defined by the difference between the zero-point energy of the reactant and that of the activated complex.

$$\vec{\Delta G}^{\neq} = -RT\ln K^{\neq} \tag{9}$$

$$K^{\neq} = \frac{Q_{[R\cdots e^-\cdots(Hg)]^{\neq}}}{Q_R Q_{e^-(Hg)}} \exp\left(-\frac{\vec{E}_0}{RT}\right) \tag{10}$$

$$\vec{\Delta G}^{\neq} = -RT\ln\left(\frac{Q_{[R\cdots e^-\cdots(Hg)]^{\neq}}}{Q_R Q_{e^-(Hg)}}\right) + \vec{E}_0 \tag{11}$$

$$\vec{\Delta G}^{\neq}_A - \vec{\Delta G}^{\neq}_B = -RT\ln\left(\frac{Q_{R_B}}{Q_{R_A}}\right) + (\vec{E}^A_0 - \vec{E}^B_0) \tag{12}$$

$$\vec{\Delta G}^{\neq}_A - \vec{\Delta G}^{\neq}_B \simeq (\vec{E}^A_0 - \vec{E}^B_0) \tag{13}$$

$$E^A_{1/2} - E^B_{1/2} \simeq -\frac{(\vec{E}^A_0 - \vec{E}^B_0)}{aF} \tag{14}$$

Because the partition functions of two activated complexes, $[R_A\cdots e^-\cdots(Hg)]^{\neq}$ and $[R_B\cdots e^-\cdots(Hg)]^{\neq}$, formed from two compounds, R_A and R_B, with analogous chemical structures and the same electrode can be assumed to be very similar, the difference in their free energies of activation, $\vec{\Delta G}^{\neq}_A - \vec{\Delta G}^{\neq}_B$, can be correlated with the difference in their activation energies, $\vec{E}^A_0 - \vec{E}^B_0$ (Eq. (12)). Moreover, Q_{R_A} and Q_{R_B} may also be regarded as very similar. Equations (13) and (14) can thus be obtained.

The activation energy of a molecule is considered to be contributed by five energy changes[11]: the vibrational energy change ($\Delta\varepsilon^{\neq}_v$), the energy change of localized bonds ($\Delta\varepsilon^{\neq}_l$), the energy change of delocalized system ($\Delta\varepsilon^{\neq}_d$), the energy change of interaction between nonbonded atoms ($\Delta\varepsilon^{\neq}_{n,t}$) and the energy change of solvation ($\Delta\varepsilon^{\neq}_s(T)$) (Eq. (15)). When the differences $(\vec{E}^A_0 - \vec{E}^B_0)$ between two unsaturated organic

$$\vec{E}_0 = \Delta\varepsilon^{\neq}_v + \Delta\varepsilon^{\neq}_l + \Delta\varepsilon^{\neq}_d + \Delta\varepsilon^{\neq}_{n,t} + \Delta\varepsilon^{\neq}_s(T) \tag{15}$$

compounds with analogous chemical structures in the same solvent is considered, the following approximations may be considered to be reasonable. The vibrational energies of their activated complexes may not be much different each other. Not only the magnitude of $\Delta\varepsilon^{\neq}_l$ itself, but also the difference in $\Delta\varepsilon^{\neq}_l$ between two compounds may be insignificant, because the formation of an activated complex is presumed to be based on the interaction of the π-electronic system of a compound and a hypothetical atomic orbital of the electrode. For the same reason, both $\Delta\varepsilon^{\neq}_{n,t}$, and its difference between two compounds may also be insignificant. Because the overlap of two orbitals is considered to occur very rapidly, the value of $\Delta\varepsilon^{\neq}_s(T)$ may be rather small and its difference between two compounds may be insignificant. If these approximations are made, the difference $(\vec{E}^A_0 - \vec{E}^B_0)$ may become a function of the difference in $(\Delta\varepsilon^{\neq}_d)_A$ and $(\Delta\varepsilon^{\neq}_d)_B$ (Eq. (16)).

In the activated complex, the original π-electronic system of R is considered to be perturbed slightly by the interaction with a hypothetical atomic orbital of the electrode. The energy change of the π-electronic system of R due to this kind of perturbation is called the π-stabilization energy (ΔE_{rs}). Here, r and s denote the atoms of the two reactants where the interaction occurs. In the present case, one of the reactants is the electron on the electrode, so it may be expressed as $\Delta E_{r(Hg)}$. It is known that the larger the ΔE_{rs}, the smaller the π-activation energy. Therefore, it may be said that the larger the $\Delta E_{r(Hg)}$, the smaller the $(\Delta\varepsilon^{\neq}_d)$ (Eq. (17)).

$$(\vec{E}^A_0 - \vec{E}^B_0) \simeq (\Delta\varepsilon^{\neq}_d)_A - (\Delta\varepsilon^{\neq}_d)_B \tag{16}$$

$$\Delta\varepsilon^{\neq}_d = b - c\cdot\Delta E_{r(Hg)} \tag{17}$$

Equation (17) is known to be useful not only in predicting the specific position, r, of a molecule where a reaction is expected to occur preferentially, but also in predicting the difference in the reactivities of the molecules of a series of compounds with analogous chemical structures in the same kind of chemical reaction. Therefore, both b and c can be assumed to keep nearly constant throughout a series of reactions employing analogous compounds. Therefore, it might be possible to expect that the difference in the activation energies of the reversible polarographic reactions of R_A and R_B can be correlated linearly with the difference in their maximum π-stabilization energies (Eq. (18)):

$$\vec{E}^A_0 - \vec{E}^B_0 \simeq (\Delta\varepsilon^{\neq}_d)^A_{min} - (\varepsilon^{\neq}_d)^B_{min} \simeq -c[(\Delta E_{r(Hg)})^A_{max} - (\Delta E_{r(Hg)})^B_{max}] \tag{18}$$

From the viewpoint of chemical reactions, a polarographic reduction may be considered to fall in the category of addition reactions. Also, it is known that the π-stabilization energy of the addition reaction of a neutral molecule (R_m) with a radical molecule (R_n) or with an ionic molecule (R_t) at their rth and sth atom can be calculated by means of Eq. (19) or Eq. (20) respectively:

$$\Delta E_{rs} = 2\left(\sum_m^{occ}\sum_n^{unocc} - \sum_n^{occ\text{-}N}\sum_m^{unocc}\right)\frac{(C^m_r)^2(d^n_s)^2}{\lambda_n - \eta_m}(\gamma^2\beta) + \left(\sum_m^{occ} - \sum_m^{unocc}\right)\frac{(C^m_r)^2(d^N_s)^2}{\lambda_N - \eta_m}(\gamma^2\beta) \tag{19}$$

$$\Delta E_{rs} = 2\left(\sum_m^{occ}\sum_i^{unocc} - \sum_m^{unocc}\sum_i^{occ}\right)\frac{(C^m_r)^2(d^t_s)^2}{\lambda_t - \eta_m}(\gamma^2\beta) \tag{20}$$

Here, C^m_r, d^n_s, and d^t_s denote the coefficient of the rth atomic orbital of the mth molecular orbital of R_m and the coefficient of the sth atomic orbital of nth (or ith) molecular orbital of R_n (or R_t) as calculated by the HMO method, respectively. γ_n, γ_t, and η_m denote the coefficients of the resonance-energy parts of the energy levels of R_n, R_t, and R_m respectively. N denotes the half-occupied orbital of R_n. $\gamma\beta$ denotes the resonance integral of the π-electronic system newly formed between R_m and R_n (or R_t).

In the case of the calculation of the $\Delta E_{r(Hg)}$ of a one-electron reduction, R_n has only one half-occupied orbital and d^N_s is unity. Moreover, λ_n has already been assumed to be approximately equal to 0. Equa-

tion (19) is, therefore, simplified to Eq. (21),* and, in the case of two-electron reductions, Eq. (22)* is derived:

$$\Delta E_{rs} = \left(\sum_{m}^{occ} - \sum_{m}^{unocc}\right) \frac{(C_r^m)^2}{-\eta_m} (\gamma^2\beta) \tag{21}$$

$$\Delta E_{rs} = \sum_{m}^{unocc} \frac{(C_r^m)^2}{\eta_m} (\gamma^2\beta) \tag{22}$$

Now, the difference in the half-wave reduction potentials of two analogous compounds, R_A and R_B, can be correlated with the difference in their π-stabilization energies (Eq. (23)):

$$F(E_{1/2}^A - E_{1/2}^B) \simeq \frac{c}{a}[(\Delta E_{r(Hg)})_{max}^A - (\Delta E_{r(Hg)})_{max}^B] \tag{23}$$

If the presumption of the structures of activated complexes is proper, the linear relationship expressed by Eq. (23) can be expected to hold. Therefore, the validity of this equation was examined by using the values of both the diffusion-controlled reversible polarographic half-wave reduction potentials and the calculated π-stabilization energies of several types of organic compounds.

Examination of the Validity of Eq. (23). Maccoll[8] indicated that the polarographic half-wave potentials of the reversible one-electron reductions of eight unsaturated hydrocarbons can be linearly correlated with the magnitudes of the energies of the lowest vacant π-molecular orbitals (E_{LVMO}^{π}) of these compounds, as calculated by the HMO method. This indication has also been recognized to hold in many hydrocarbons by several groups of researchers, such as Hoijtink *et al.*[12] and Pullman *et al.*[13] Since this kind of quantum chemical approach to the interpretation of the $E_{1/2}$'s of organic compounds has been widely accepted as relevant, parallel examinations of the validity of Maccoll's indication and that of Eq. (23) by means of the same experimental results were thought to be significant.

a) Aromatic Hydrocarbons: According to the conclusion of Wawzonek *et al.*,[14] the first reduction waves of these compounds, determined in 75% dioxane–water, correspond to the addition of either one or two electrons to the compounds. Later, Hoijtink *et al.*[15] clarified the reduction mechanism of unsaturated hydrocarbons in a protic solvent (75% and 96% dioxane–water) as follows: (i) At first, an anion radical (R^-) is formed by the reversible addition of one electron to the compound, regardless of the solvent employed, and (ii) the number of electrons corresponding to the first wave is decided according to whether the rate of the proton addition to R^- is lower or higher than the rate of the diffusion of R^- from the electrode surface layer to the bulk of the solution. The latter mechanism means that, if the former rate is lower than the latter one, as it is so in many unsaturated hydrocarbons, the first wave corresponds to the addition of one electron.

The first wave of the polarographic reduction of unsaturated hydrocarbons, such as stilbene, styrene, and 1,1-diphenylethylene, as determined in an aprotic solvent, has also been reported[16] to correspond to the addition of either one or two electrons to the compounds. However, Bergman[17] concluded that the first reduction wave of many aromatic hydrocarbons, as determined in ethylene glycol monomethyl ether, corresponds to the addition of one electron. Bergman's investigation not only included seventy-two aromatic polynuclear hydrocarbons of a variety of chemical structures, but also all of the $E_{1/2}$ of these compounds were determined in the same solvent. Therefore, the $E_{1/2}$ values of the present study were taken from this literature. He classified these compounds into several classes with respect to the similarities in their chemical structures. In this study, at first sixty-nine compounds were classified into four classes (a, b, c, and d) in accordance with Bergman's classification, as is shown below. However, the three compounds which form the class e in Bergman's report were omitted, because one of them, diindeno[1,2,3-*fg*: 1′,2′,3′-*op*]naphthacene, has a nonbonding orbital which makes the calculation of $\Delta E_{r(Hg)}$ impossible. Consequently, the remainder was insufficient for the investigation. Also, it was considered that four compounds (No. 42, 43, 57, and 58) should be classified into a new class, c′, because they are related not only to both perylene and pyrene, but also to *p*-terphenyl.

a) the *cata*-condensed aromatic hydrocarbons (No. 1—31)

b) the *peri*-condensed aromatic hydrocarbons related to perylene (No. 32—41)

c) the *peri*-condensed aromatic hydrocarbons related to pyrene (No. 44—61(except 57 and 58))

c′) the *peri*-condensed aromatic hydrocarbons related to perylene, pyrene, and *p*-terphenyl(No. 42, 43, 57, and 58)

d) the non-alternant hydrocarbons related to fluoranthene (No. 62—69)

Unlike the case of the aromatic carbonyl compounds to be discussed later, each aromatic hydrocarbon can be expected to be reduced simply at the position bearing the maximum π-stabilization energy. Then, the π-stabilization energies at all positions of all compounds were calculated.

The differences in both $E_{1/2}$ and $(\Delta E_{r(Hg)})_{max}$, and the values of both $E_{1/2}$ and E_{LVMO}^{π}, are shown in Tables 1—4. The standard deviations and correlation coefficients are also shown in these tables. The correlation between the differences in the values of $(\Delta E_{r(Hg)})_{max}$ and the differences in the $E_{1/2}$ values of compounds of Group a is shown in Fig. 1. This figure indicates that the linear relationship given by Eq. (23) is satisfactorily fullfilled.

b) Aromatic Aldehydes: Schmidt *et al.*[18] described how, in a strong alkaline solution, the polarographic half-wave reduction potential of aromatic aldehydes is independent of the pH value of the solution employed, and how the diffusion current corresponds to the addition of one electron to the oxygen atom of a molecule (Eq. (24)). They also showed that the $E_{1/2}$ of six aromatic aldehydes determined in a strong alkaline solution are linearly correlated with the E_{LVMO}^{π}'s expressed by the unit of γ. Streitwieser[19] confirmed the

* These equations are also known to be equations giving the superdelocalizabilities of a radical substitution and a nucleophilic substitution reaction respectively.

Table 1. Values of $E_{1/2}(V)$, $\Delta E_{1/2}(V)$, $\Delta(\Delta E_{r(Hg)})_{max}$-$(-\gamma^2\beta)$ and $E^{\pi}_{LVMO}(\alpha-m\beta)$ of a group aromatic hydrocarbonns

Compound	$-\Delta E_{1/2}$ [a]	$-\Delta(\Delta E_{r(Hg)})_{max}$ [b]	$-E_{1/2}$	m
1	0.0	0.0	1.98	0.6180
2	0.52	0.3192	1.46	0.4142
3	0.845	0.5108	1.135	0.2950
4	1.12	0.8006	0.86	0.2197
5	0.045	0.0034	1.935	0.6052
6	0.45	0.2574	1.53	0.4523
7	0.79	0.4515	1.19	0.3271
8	1.035	0.7006	0.945	0.2436
9	0.01	−0.0656	1.97	0.6840
10	0.44	0.1592	1.54	0.4991
11	0.775	0.3920	1.205	0.3557
12	1.05	0.6124	0.93	0.2621
13	0.435	0.1518	1.545	0.4735
14	0.73	0.3385	1.25	0.3584
15	1.13	0.5849	0.85	0.2691
16	0.175	0.0497	1.805	0.5201
17	0.545	0.2949	1.435	0.4048
18	0.65	0.3144	1.33	0.3482
19	0.235	0.0046	1.745	0.5676
20	0.41	0.2061	1.57	0.4918
21	0.335	0.0378	1.645	0.5319
22	0.41	0.1226	1.57	0.5224
23	0.39	−0.0288	1.59	0.5115
24	0.25	0.0343	1.73	0.5498
25	0.58	0.2771	1.40	0.4186
26	0.19	0.0491	1.79	0.5019
27	0.455	0.2517	0.525	0.4372
28	0.76	0.4363	1.22	0.3358
29	0.485	0.2603	1.495	0.4287
30	0.465	0.1558	1.515	0.4321
31	0.515	0.2655	1.465	0.3940
Standard Deviation		0.0901		0.0764
Correlation Coefficient		0.9553		0.9681

a) $\Delta E_{1/2}=(E_{1/2})^{Naphthalene}-(E_{1/2})^{Compound}$
b) $\Delta(\Delta E_{r(Hg)})_{max}=(\Delta E_{r(Hg)})^{Naphthalene}_{max}-(\Delta E_{r(Hg)})^{Compound}_{max}$
$(\Delta E_{r(Hg)})^{Naphthalene}_{max}=0.9940$

Table 2. Values of $E_{1/2}(V)$, $\Delta E_{1/2}(V)$, $\Delta(\Delta E_{r(Hg)})_{max}$-$(-\gamma^2\beta)$ and $E^{\pi}_{LVMO}(\alpha-m\beta)$ of b group aromatic hydrocarbons

Compound	$-\Delta E_{1/2}$ [a]	$-\Delta(\Delta E_{r(Hg)})_{max}$ [b]	$-E_{1/2}$	m
32	0.0	0.0	1.25	0.3473
33	0.285	0.4592	0.965	0.2648
34	0.37	0.6015	0.88	0.2135
35	0.25	0.4531	1.00	0.2673
36	−0.235	−0.1000	1.485	0.4392
37	−0.265	−0.1111	1.515	0.4631
38	−0.10	0.0843	1.35	0.4114
39	−0.39	−0.2036	1.64	0.5392
40	−0.03	0.1227	1.28	0.3557
41	0.335	0.4241	0.915	0.2539
Standard deviation		0.0593		0.0378
Correlation coeffieient		0.9737		0.9894

a) $\Delta E_{1/2}=(E_{1/2})^{Perylene}-(E_{1/2})^{Compound}$
b) $\Delta(\Delta E_{r(Hg)})_{max}=(\Delta E_{r(Hg)})^{Perylene}_{max}-(\Delta E_{r(Hg)})^{Compound}_{max}$
$(\Delta E_{r(Hg)})^{Perylene}_{max}=1.1949$

Table 3. Values of $E_{1/2}(V)$, $\Delta E_{1/2}(V)$, $\Delta(\Delta E_{r(Hg)})_{max}$-$(-\gamma^2\beta)$ and $E^{\pi}_{LVMO}(\alpha-m\beta)$ of c group aromatic hydrocarbons

Compound	$-\Delta E_{1/2}$ [a]	$-\Delta(\Delta E_{r(Hg)})_{max}$ [b]	$-E_{1/2}$	m
44	0.0	0.0	1.61	0.4450
45	−0.06	−0.0508	1.67	0.4970
46	0.25	0.2930	1.36	0.3711
47	0.53	0.2416	1.08	0.3983
48	0.165	0.1476	1.445	0.4216
49	−0.075	−0.1177	1.685	0.5550
50	0.45	0.4214	1.16	0.3027
51	0.295	0.3234	1.315	0.3420
52	0.105	0.0420	1.505	0.5053
53	0.46	0.4182	1.15	0.3026
54	0.83	0.7111	0.78	0.2130
55	0.46	0.4752	1.15	0.2734
56	0.27	0.1594	1.34	0.3957
59	0.42	0.3896	1.19	0.2910
60	0.55	0.5282	1.06	0.2580
61	0.81	0.8832	0.80	0.1891
Standard Deviation		0.0805		0.1034
Correlation Coefficient		0.9533		0.9212

a) $\Delta E_{1/2}=(E_{1/2})^{Pyrene}-(E_{1/2})^{Compound}$
b) $\Delta(\Delta E_{r(Hg)})_{max}=(\Delta E_{r(Hg)})^{Pyrene}_{max}-(\Delta E_{r(Hg)})^{Compound}_{max}$
$(\Delta E_{r(Hg)})^{Pyrene}_{max}=1.1149$

Table 4. Values of $E_{1/2}(V)$, $\Delta E_{1/2}(V)$, $\Delta(\Delta E_{r(Hg)})_{max}$-$(-\gamma^2\beta)$ and $E^{\pi}_{LVMO}(\alpha-m\beta)$ of c′ and d groups aromatic hydrocarbons

Compound	$-\Delta E_{1/2}$ [a]	$-\Delta(\Delta E_{r(Hg)max})$ [b]	$-E_{1/2}$	m
42	0.0	0.0	0.675	0.1826
43	−0.020	−0.0368	0.695	0.1916
57	−0.500	−0.2516	1.175	0.2847
58	−0.475	−0.3885	1.15	0.3445
Standard deviation		0.0821		0.0836
Correlation coefficient		0.9391		0.9368
62	0.0	0.0	1.345	0.3709
63	0.370	0.4525	0.975	0.2521
64	0.695	0.8777	0.65	0.1604
65	−0.030	0.0957	1.375	0.3770
66	0.180	0.0661	1.165	0.3116
67	−0.045	0.0095	1.39	0.4007
68	0.290	0.2036	1.055	0.2666
69	−0.030	0.2229	1.375	0.3966
Standard deviation		0.1051		0.0287
Correlation coefficient		0.9042		0.9932

a) $\Delta E_{1/2}=(E_{1/2})^{X}-(E_{1/2})^{Compound}$
b) $\Delta(\Delta E_{r(Hg)})_{max}=(\Delta E_{r(Hg)})^{X}_{max}-(E_{r(Hg)})^{Compound}_{max}$
c′ group: X=Tetrabenzo[*de,h,kl,rst*]pentaphene (42)
d group: X=Fluoranthene (62)
$(\Delta E_{r(Hg)})_{max}$ of (42)=1.5117 and that of (62)=1.1370.

Table 5. Values of $\Delta E_{1/2}(V)$ and $\Delta(\Delta E_{o(Hg)})(-\gamma^2\beta)$ of aromatic aldehydes

Parameter		1[c]	2[d]	3[e]
Compound	$-\Delta E_{1/2}$[a]	$-\Delta(\Delta E_{o(Hg)})$[b]	$-\Delta(\Delta E_{o(Hg)})$[b]	$-\Delta(\Delta E_{o(Hg)})$[b]
70	0.0	0.0	0.0	0.0
71	0.257	0.0394	0.0746	0.1517
72	0.116	0.0163	0.0366	0.0728
73	0.087	0.0043	0.0108	0.0213
74	0.385	0.0498	0.1090	0.2182
75	0.143	0.0167	0.0377	0.0750
Standard deviation		0.0251	0.0185	0.0188
Correlation coefficient		0.9795	0.9889	0.9885

a) $\Delta E_{1/2}=(E_{1/2})^{\text{Benzaldehyde}}-(E_{1/2})^{\text{Compound}}$. b) $\Delta(\Delta E_{o(Hg)})=(\Delta E_{o(Hg)})^{\text{Benzaldehyde}}-(\Delta E_{o(Hg)})^{\text{Compound}}$.
c) Ref. 20. d) Ref. 18. e) Ref. 19.
$(\Delta E_{o(Hg)})^{\text{Benzaldehyde}}$ values are 0.5260 (parameter 1), 0.6753 (parameter 2), and 1.0783 (parameter 3).

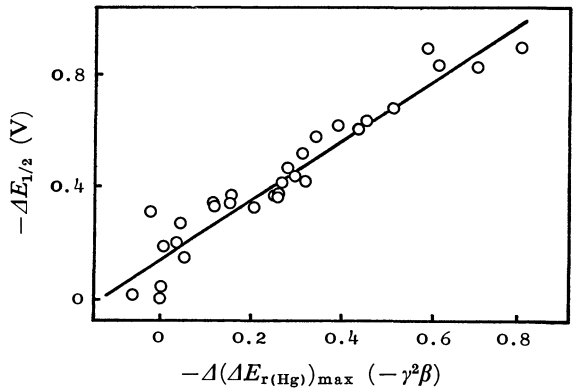

Fig. 1. Correlation between mutual differences of $E_{1/2}$ values and the respective differences of $(\Delta E_{r(Hg)})_{max}$ values of a group aromatic hydrocarbons.

same linear relationship between the very same value of every one of the $E_{1/2}$ values determined by Schmidt *et al.* and the E^{π}_{LVMO} value expressed by the unit of β.

$$R\text{-}CHO + e^- \rightleftharpoons R\text{-}\dot{C}HO^- \quad (24)$$

In this case, the activated complex $[(R\text{-}C(H)=O\cdots e^-\cdots(Hg))^{\neq}]$ is assumed to be formed by the interaction of a hypothetical atomic orbital occupied by one electron of the electrode with the π-molecular orbital of a molecule at the oxygen atom of the carbonyl group. Then the linear relationship between the differences in $E_{1/2}$ values and the differences in the π-stabilization energies $(\Delta E_{O(Hg)})$ of the same series of six aromatic aldehydes was investigated.

Although neither Schmidt *et al.* nor Streitwieser described anything about the influence of the change in the hetero-atomic parameters of the carbonyl group on the linearity between $E_{1/2}$ and E^{π}_{LVMO}, this influence ought not to be ignored. Also, the $\Delta E_{O(Hg)}$ values should be dependent on the same change. Therefore, the $\Delta E_{O(Hg)}$ values were calculated repeatedly by the HMO method with the employment of three sets of parameters proposed in the literature.[18-20] The results, the differences in the two $E_{1/2}$ values determined by Schmidt *et al.*, and the $\Delta E_{O(Hg)}$ values calculated by three kinds of parameters are listed in Table 5. The $E_{1/2}$ values and three kinds of E^{π}_{LVMO} values are shown in Table 6. The standard deviations and correlation coefficients of each set of parameters are also listed in these tables. These tables indicate that all three sets of hetero-atomic parameters gave the comparable linear relationships expected by Eq. (23).

Table 6. Values of $E_{1/2}(V)$ and $E^{\pi}_{LVMO}(\alpha-m\beta)$ of aromatic aldehydes

Parameter		1[a]	2[b]	3[c]
Compound	$-E_{1/2}$	m	m	m
70	1.553	0.8561	0.4251	0.3859
71	1.296	0.5656	0.2776	0.2602
72	1.437	0.5654	0.3245	0.3028
73	1.466	0.5946	0.3789	0.3500
74	1.168	0.3720	0.2081	0.1993
75	1.410	0.5553	0.3211	0.3000
Standard Deviation		0.0607	0.0254	0.0237
Correlation Coefficient		0.8733	0.9789	0.9818

a) Ref. 20. b) Ref. 18. c) Ref. 19.

c) Quinones: With regard to the polarographic reduction of quinones in an aprotic solvent, Wawzonek *et al.*[21] made it clear that the first wave corresponds to the formation of semiquinone anion radicals (Eq. (25)), while the succeeding reduction of these anions to dianions (Eq. (26)) is the second step:

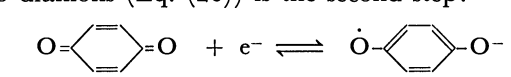

(25)

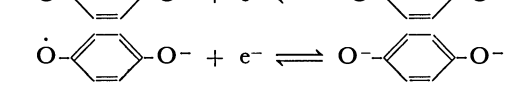

(26)

Then the linear relationship between the differences between the $E_{1/2}$ values taken from the literature[22] and the differences between the $\Delta E_{O(Hg)}$ values corresponding to the structure $\left[\left(O=\bigcirc=O\cdots e^-\cdots(Hg)\right)^{\neq}\right]$ of the four *p*-quinones was investigated. *p*-Quinones with substituents in their molecule and *o*-quinones were omitted from this investigation, because it was considered that the usefulness of the hetero-atomic parameters employed in this work has not yet been examined for the calculation of compounds with an *ortho* di-substituted structure.

In the preceding example it was clarified that all three sets of hetero-atomic parameters gave comparable

Table 7. Values of $E_{1/2}(V)$, $\Delta E_{1/2}(V)$, $\Delta(\Delta E_{o(Hg)})$-$(-\gamma^2\beta)$ and $E^{\pi}_{LVMO}(\alpha-m\beta)$ of quinones

Compound	$-\Delta E_{1/2}$ [a]	$-\Delta(\Delta E_{o(Hg)})$ [b]	$-E_{1/2}$	m
76	0.0	0.0	0.51	0.4827
77	−0.20	−0.0388	0.71	0.5570
78	−0.24	−0.0400	0.75	0.5772
79	−0.43	−0.0685	0.94	0.6452
Standard deviation		0.0178		0.0050
Correlation coefficient		0.9932		0.9995

a) $\Delta E_{1/2}=(E_{1/2})^{1,4\text{-Benzoquinone}}-(E_{1/2})^{\text{Compound}}$.
b) $\Delta(\Delta E_{o(Hg)})=\Delta(\Delta E_{o(Hg)})^{1,4\text{-Benzoquinone}}-(\Delta E_{o(Hg)})^{\text{Compound}}$.
$(\Delta E_{o(Hg)})^{1,4\text{-Benzoquinone}}=0.6524$.

results. Therefore, only one set of the hetero-atomic parameters, one which had previously been proposed by us,[20] was employed.

The differences between the two $E_{1/2}$ values taken from the literature[22] and $\Delta E_{O(Hg)}$, and the values of both $E_{1/2}$ and E^{π}_{LVMO} are shown in Table 7. The standard deviations and correlation coefficients obtained are also listed in the same table.

The standard deviations and correlation coefficients shown in Tables 1—7 indicate that, in all the cases examined, the differences in the $E_{1/2}$'s can be correlated linearly with the differences in the π-stabilization energies as satisfactorily as the linear relationship observed between $E_{1/2}$'s and E^{π}_{LVMO}'s. Since no investigation of the systematic polarographic reduction reaction of unsaturated organic compounds with no substituent other than that of these three groups of compounds has yet been reported in the literature, this examination can be considered to include all of the cases. Therefore, the results of these examinations may be considered to be experimental support to the presumed structures of the activated complexes of the reversible polarographic reductions of unsaturated organic compounds are proper.

Experimental

The molecular orbital calculations were carried out on a FACOM 230-60 computer at the Computation Center of Kyushu University.

The names of all the compounds employed in this study are listed below. The basic structures of many aromatic polynuclear hydrocarbons are shown in Chart 1.

1. Naphthalene
2. Anthracene
3. Naphthacene
4. Pentacene
5. Phenanthrene
6. Benzo[*a*]anthracene
7. Benzo[*a*]naphthacene
8. Benzo[*a*]pentacene
9. Triphenylene
10. Benzo[*b*]triphenylene
11. Dibenzo[*a*, *c*]naphthacene
12. Dibenzo[*a*, *c*]pentacene
13. Dibenzo[*a*, *h*]anthracene
14. Dibenzo[*a*, *j*]naphthacene

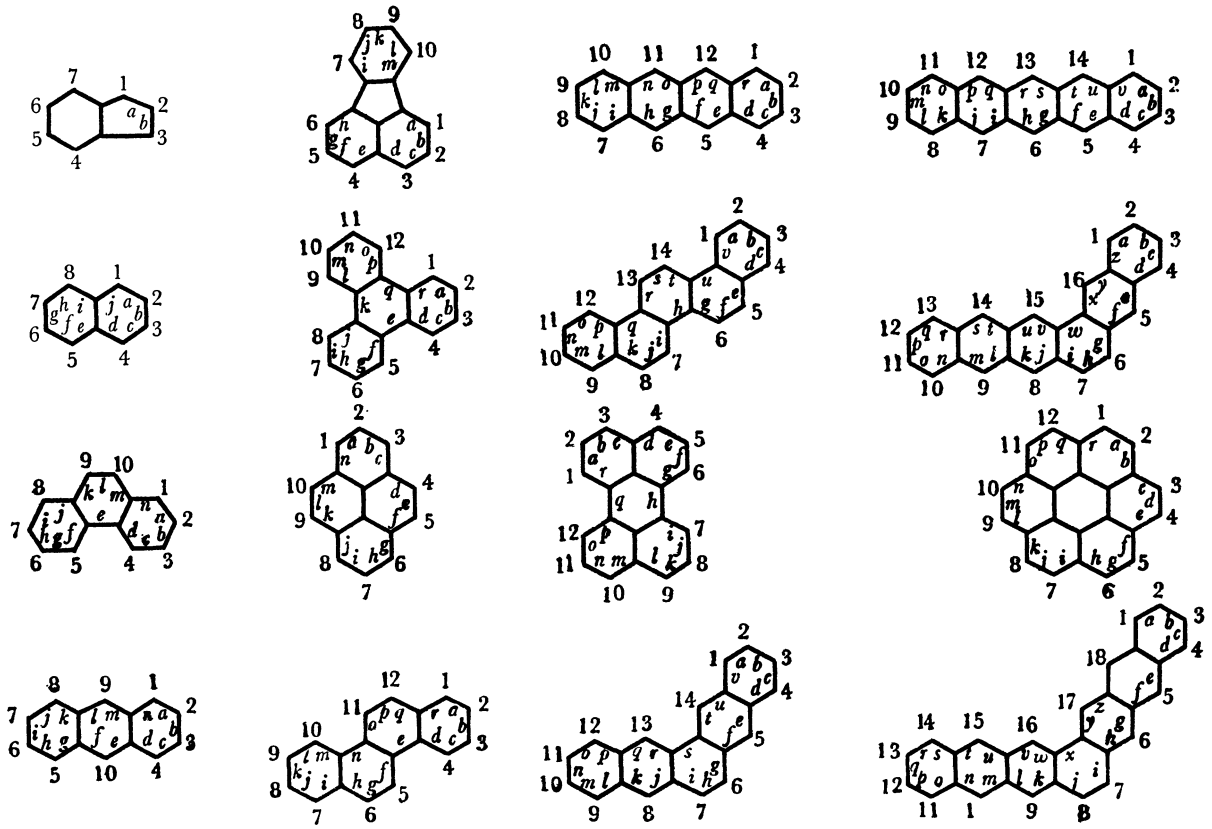

Chart 1.

15. Dibenzo[*a*, *l*]pentacene
16. Chrysene
17. Benzo[*b*]chrysene
18. Dibenzo[*b*, *k*]chrysene
19. Benzo[*c*]phenanthrene
20. Dibenzo[*a*,*j*]anthracene
21. Benzo[*g*]chrysene
22. Tribenzo[*a*, *c*, *h*]anthracene
23. Dibenzo[*g*, *p*]chrysene
24. Benzo[*c*]chrysene
25. Dibenzo[*b*, *g*]phenanthrene
26. Picene
27. Pentaphene
28. Hexaphene
29. Benzo[*c*]pentaphene
30. Dibenzo[*c*, *m*]pentaphene
31. Naphtho[2,3-*c*]pentaphene
32. Perylene
33. Benzo[*a*]perylene
34. Dibenzo[*a*, *j*]perylene
35. Dibenzo[*a*, *n*]perylene
36. Benzo[*ghi*]perylene
37. Dibenzo[*b*, *pqr*]perylene
38. Tribenzo[*b*,*ghi*,*k*]perylene
39. Coronene
40. Dibenzo[*fg*, *qr*]pentacene
41. Dibenzo[*bc*, *ef*]coronene
42. Tetrabenzo[*de*, *h*, *kl*, *rst*]pentaphene
43. Tetrabenzo[*de*, *hi*, *op*, *st*]pentacene
44. Pyrene
45. Benzo[*e*]pyrene
46. Benzo[*a*]pyrene
47. Bibenzo[*a*, *l*]pyrene
48. Dibenzo[*a*, *e*]pyrene
49. Dibenzo[*fg*, *op*]naphthacene
50. Dibenzo[*a*, *h*]pyrene
51. Benzo[*rst*]pentaphene
52. Dibenzo[*de*, *qr*]naphthacene
53. Naphtho[2,3-*a*]pyrene
54. Dinaphtho[2,3-*a*,2′,3′-*h*]pyrene
55. Benzo[*xyz*]heptaphene
56. Dibenzo[*h*,*rst*]pentaphene
57. Dibenzo[*cd*,*lm*]perylene
58. Tetrabenzo[*a*,*cd*,*j*,*lm*]perylene
59. Dibenzo[*def*,*mno*]chrysene
60. Tribenzo[*ghi*,*m*,*pqr*]picene
61. Tetrabenzo[*b*,*def*,*k*,*mno*]chrysene
62. Fluoranthene
63. Benzo[*a*]fluoranthene
64. Dibenzo[*b*,*g*]fluoranthene
65. Benzo[*b*]fluoranthene
66. Benzo[*j*]fluoranthene
67. Benzo[*k*]fluoranthene
68. Naphtho[2,3-*j*]fluoranthene
69. Naphtho[2,3-*k*]fluoranthene
70. Benzaldehyde
71. Cinnamaldehyde
72. 1-Naphthalenealdehyde
73. 2-Naphthalenealdehyde
74. 9-Anthracenealdehyde
75. 9-Phenanthrenealdehyde
76. 1,4-Benzoquinone
77. 1,4-Naphthoquinone
78. 1,4-Anthraquinone
79. 9,10-Anthraquinone

References

1) This paper forms Part V of "The Application of Molecular Orbital Method," Part IV: Y. Ueda, Y. Ono, K. Ogawa, Y. Ohkura, and K. Kohashi, *Yakugaku Zasshi*, **95**, 470 (1975), "X-Ray Photoelectron Spectra of σ Complexes of 1,3,5-Trinitrobenzene and Picric Acid." A part of this paper was presented at the Meeting of the Kyushu Branch of the Pharmaceutical Society of Japan, Fukuoka, February, 1973.

2) R. A. Marcus, *Ann. Rev. Phys. Chem.*, **15**, 155 (1964); R. A. Marcus, *J. Chem. Phys.*, **43**, 679 (1965).

3) *e.g.*, H. Bartelt, *J. Electroanal. Chem.*, **27**, 447 (1970); F. C. Anson, N. Rathjen, and R. D. Frisbee, *J. Electrochem. Soc.*, **117**, 477 (1970); J. L. Huntington and D. G. Davis, *ibid.*, **118**, 57 (1971).

4) N. S. Hush, *J. Chem. Phys.*, **28**, 962 (1958).

5) A. A. Vlček, "Progress in Polarography," Vol. I, ed. by P. Zuman and I. M. Kolthoff, Interscience Publishers, New York (1962); A. A. Vlček, "Progress in Inorganic Complexes," Vol. V, ed. by F. A. Cotton, Interscience Publishers, New York (1963), p. 211.

6) T. Yonezawa, K. Hayashi, C. Nagata, S. Okamura, and K. Fukui, *J. Polymer Sci.*, **14**, 312 (1954); K. Hayashi, T. Yonezawa, C. Nagata, S. Okamura, and K. Fukui, *ibid.*, **20**, 537 (1956); K. Fukui, T. Yonezawa, and C. Nagata, This Bulletin, **27**, 423 (1954); K. Fukui, K. Morokuma, T. Yonezawa, and C. Nagata, *ibid.*, **33**, 963 (1960).

7) P. Zuman, *Rev. Polarography* (Kyoto), **11**, 102 (1963).

8) A. Maccoll, *Nature*, **163**, 178 (1949).

9) E. G. Wilson and S. A. Rice, "Optical Properties and Electronic Structure of Metals and Alloys," ed. by F. Abeles, North-Holland, Amsterdam (1966), p. 271.

10) E. Heilbronner, "Hückel Bunshi Kido Ho 1 (Translated edition of "Das HMO-Model und seine Anwendung" by H. Sakurai and T. Takeuchi)," Hirokawa Publ. Co., Tokyo (1973), p. 335.

11) R. Daudel, "Kagaku Hanno no Ryoshiron (Translated edition of "Theorie Quantique de la Reactivite Chimique" by J. Souma, K. Hayashi, and M. Shiotani)," Baifukan, Tokyo (1972), p. 102.

12) G. J. Hoijtink and J. Van Schooten, *Rec. Trav. Chim.*, **71**, 1089 (1952).

13) A. Pullman, B. Pullman, and G. Berthier, *Bull. Soc. Chim. Fr.*, **17**, 591 (1950).

14) H. A. Laitinen and S. Wawzonek, *J. Amer. Chem. Soc.*, **64**, 1765 (1942); S. Wawzonek and H. A. Laitinen, *ibid.*, **64**, 2365 (1942).

15) G. J. Hoijtink, J. Van Schooten, E. De Boer, and W. I. Aalbersberg, *Rec. Trav. Chim.*, **73**, 355 (1954).

16) S. Wawzonek and E. W. Blaha, *J. Electrochem. Soc.*, **102**, 235 (1956); S. Wawzonek and D. Wearring, *J. Amer. Chem. Soc.*, **81**, 2067 (1959).

17) I. Bergman, *Trans. Faraday Soc.*, **50**, 829 (1954).

18) R. W. Schmidt and E. Heilbronner, *Helv. Chim. Acta*, **37**, 1453 (1954).

19) A. Streitwieser Jr., "Molecular Orbital Theory for Organic Chemists," John Wiley & Sons, New York (1961).

20) Y. Ono and Y. Ueda, *Chem. Pharm. Bull.* (Tokyo), **18**, 2013 (1970).

21) S. Wawzonek, R. Berkey, E. W. Blaha, and M. E. Runner, *J. Electrochem. Soc.*, **103**, 456 (1956).

22) M. E. Peover, *J. Chem. Soc.*, **1962**, 4540.

The Mechanism of the Hydrolysis of Condensed Phosphates. III. The Mechanism of the Hydrolysis of Trimeta- and Tetrametaphosphates

Makoto WATANABE, Shoji SATO, and Hajime SAITO*

Department of Industrial Chemistry, Chubu Institute of Technology, Matsumoto-cho, Kasugai-shi, Aichi 487

**Department of Applied Chemistry, Faculty of Engineering, Nagoya University, Chigusa-ku, Nagoya-shi 464*

(Received March 3, 1975)

The hydrolysis of sodium trimeta- and tetrametaphosphates was run in water, dioxane–water, and formic acid–water solvents with an initial concentration of 0.025 mol/l at various pH values and temperatures. The hydrolysis of both the metaphosphates followed first-order kinetics with respect to the concentration of the phosphate under all the conditions studied and was an acid- and base-catalyzed reaction. In acidic solutions, the rate of hydrolysis of both the metaphosphates in water is faster than that in formic acid–water and slower than that in dioxane–water. Therefore, it is concluded that, in the formic acid–water solvent, the nucleophilicity of the water molecule may decrease on account of the solvation of the water molecule with the acid, while, in the dioxane–water solvent, since the scission of the hydrogen bond between water molecules may occur by the interaction of dioxane and water molecules, the nucleophilicity of the water molecule may increase. The hydrolysis of both metaphosphates in acidic solutions is considered to be an S_N2 reaction, because the overall-reaction rate is highly dependent upon the nucleophilicity of the water molecule. In basic solutions, the rate of hydrolysis of sodium trimeta- and tetrametaphosphates in water is faster than or almost the same as that in dioxane–water. Consequently, the mechanism of the hydrolysis of both the metaphosphates in basic solutions seems to differ from that in acidic solutions. The increase in the rate of hydrolysis of small-ring phosphates in acidic solutions depends upon the activation energy and frequency factor, while that in basic solutions depends significantly upon the frequency factor. This may cause the difference in the solvent effect on the rate of hydrolysis of small-ring phosphates between acidic and basic solutions. The activation energy of the hydrolysis of both ring phosphates was 20—40 kcal/mol in the pH range of 1.0—12.5. The rate of hydrolysis of the metaphosphates in an aqueous sodium hydroxide solution is faster than that in an aqueous tetramethyl ammonium hydroxide solution and this can be attributed to catalysis by a sodium ion. The hydrolysis of sodium tripolyphosphate was also carried out in basic water and dioxane–water solvents. The solvent effect on the rate of hydrolysis of tripolyphosphate in basic solutions was the same as that in acidic solutions.

The solvent effect on organic reactions has been studied by many investigators.[1,2] An S_N1 reaction is generally accelerated in an ionizing solvent, while the solvent effect on an S_N2 reaction is complex. The hydrolysis of condensed phosphates has never been considered from the viewpoint of the exact interaction between a phosphate and a water molecule. In previous works[3,4] by the present authors, the hydrolysis of sodium pyro-, tripoly-, and long-chain polyphosphates was carried out in water, formic acid–water, acetic acid–water, and dioxane–water solvents. Formic acid and acetic acid are so-called protic solvents and dioxane is a dipolar aprotic solvent.[5] It was concluded from the kinetic data that the nucleophilic attack of a water molecule on a phosphorus atom of pyro-, tripoly- (in acidic solution), and long-chain polyphosphates (in basic solution) plays an important role in the hydrolytic degradation of the phosphates. It is well known that the hydrolysis of short-chain phosphates is an acid-catalyzed reaction and that of small-ring phosphates is an acid- and base-catalyzed reaction.[6] The reason for the different hydrolytic reactivity between the short-chain and small-ring phosphates has never been discussed. In the present paper, the hydrolysis of sodium trimeta- and tetrametaphosphates will be accomplished in the same types of solvent mentioned above in order to obtain some information about the hydrolytic mechanism of the small-ring phosphates.

Experimental

Materials and Procedure. All the materials used other than the sodium trimeta-, tetrameta-, and tripolyphosphates were of commercial grade. Sodium trimetaphosphate hexahydrate, sodium tripolyphosphate hexahydrate, and sodium tetrametaphosphate tetrahydrate were prepared by the method described in Refs. 7 and 8. The solvents used in this experiment are listed in Table 1. The pH's of the phosphate solutions with water and dioxane–water solvents were controlled with nitric acid and/or aqueous tetramethyl ammonium hydroxide at reaction temperature by using a Hitachi-Horiba pH meter, F-5. The pH of the phosphate solution with formic acid–water did not change at any time, while those of the solutions with water and dioxane–water changed with the reaction time elapsed. Therefore, aqueous tetramethyl ammonium hydroxide or nitric acid was added to restore them to the proper pH. The pH adjustment was made to within ±0.1 unit of the desired pH value. For the hydrolysis of sodium trimeta- and tetrametaphosphates in basic water and dioxane–water solvents, aqueous sodium hydroxide was also used to obtain the required pH value in order to compare the hydrolysis of the phosphates with that in an aqueous tetramethyl ammonium hydroxide solution. Since a sodium ion is considered to act as a catalyzer for the hydrolysis of polyphosphates,[9-11] an equal volume of aqueous sodium hydroxide was added to each solvent in all conditions studied and the pH adjustment was made by using nitric acid; the concentration of the sodium ion was

TABLE 1. SOLVENTS USED FOR THE HYDROLYSIS OF TRIMETA- AND TETRAMETAPHOSPHATES

Solvent	Symbol
35 vol% aqueous dioxane	S_1
21 vol% aqueous dioxane	S_2
Water	S_3
Formic acid–water	S_4

Table 2. Composition of the solvents used for paper-chromatography[12]

Acidic solvent		Basic solvent	
isopropyl alcohol	70 ml	isopropyl alcohol	20 ml
25% aqueous trichroloacetic acid	20 ml	dimethylfolmamide	20 ml
water	10 ml	methyl ethyl ketone	20 ml
28% aqueous ammonia	0.3 ml	water	39.1 ml
		28% aqueous ammonia	0.9 ml

1.11 mol/l. The initial concentration of the phosphates was 0.025 mol/l. This concentration is suitable for analysis. The 0.025 mol/l concentration of the phosphates in the acidic S_1 solvent having pH values smaller than 2 and that in the basic S_2 solvent produced nearly saturated concentration. After the pH adjustment of a sample solution was completed at the reaction temperature, 10 μl of the sample solution was spotted on Toyo No. 51A filter paper (2×50 cm) for the paper-chromatographic separation of the phosphates. At measured time intervals, further samples were similarly taken for quantitative chromatographic analysis. When the pH of the sample solution was larger than 11, the separation of each phosphate on the chromatagram is not complete. Therefore, after the basic sample solution was acidified with nitric acid, the acidified solution was spotted on the filter paper. Development was made by using an acidic (for the separation of polyphosphates) and basic (for the separation of metaphosphates) solvents[12] at 3 °C. The composition of the solvents is listed in Table 2. Each band of the phosphates on the filter paper was identified by the same treatment of a reference solution of known phosphates. The colorimetric determination of each band on the filter paper was carried out by using the method of a previous paper.[3]

Results and Discussion

Order of Reaction and the pH Dependence of the Reaction Rate. The rate of the hydrolysis of sodium tri-

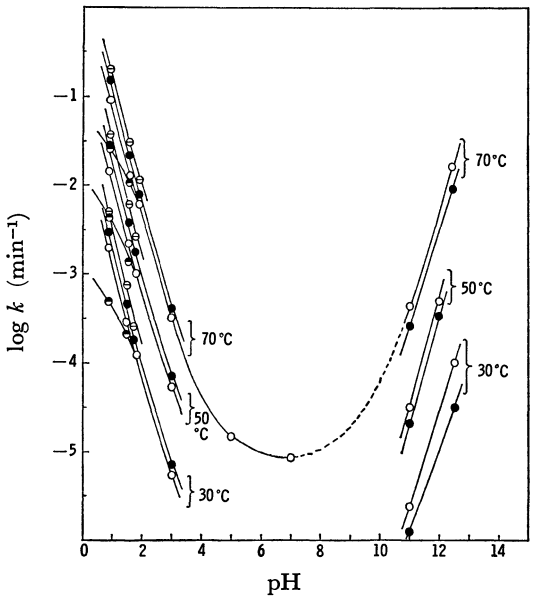

Fig. 1. pH dependence of rate constant of the hydrolysis of trimetaphosphate.[a]
⊖: S_1,[b] ●: S_2, ○: S_3, ◓: S_4
a) pH adjustment was made by aqueous tetramethyl ammonium hydroxide and nitric acid.
b) The symbol refers to Table 1.

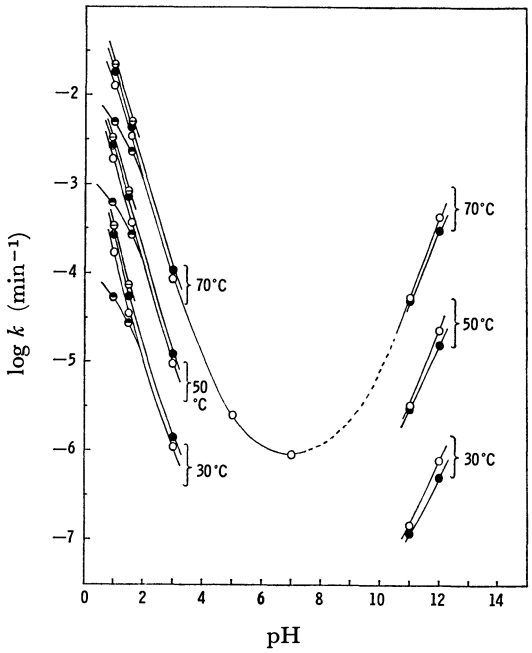

Fig. 2. pH dependence of rate constant of the hydrolysis of tetrametaphosphate.[a]
⊖: S_1,[b] ●: S_2, ○: S_3, ◓: S_4
a) pH adjustment was made by aqueous tetramethyl ammonium hydroxide and nitric acid.
b) The symbol refers to Table 1.

meta-, tetrameta-, and tripolyphosphates follows first-order kinetics with respect to the concentration of the phosphates under all conditions studied. The pH dependences of the rate constant for trimeta- and tetrametaphosphates are shown in Figs. 1 and 2, respectively. In all solvents, the rates of hydrolysis of both the metaphosphates decreases in acidic solutions and increases in basic solutions with an increase in the pH value. The rate is slowest in a neutral solution. Therefore, the hydrolysis of both the metaphosphates is an acid- and base-catalyzed reaction. The results agree well with those reported in previous papers.[6] To obtain information concerning the mechanism of the hydrolysis of trimeta- and tetrametaphosphates, the activation energy and log A (A: frequency factor) of the hydrolysis of both the phosphates were calculated by means of an Arrhenius plot and are listed in Table 3. In all acidic solutions, the activation energy of the hydrolysis of both the metaphosphates increases and the log A of the hydrolysis of both the metaphosphates decreases with an increase in the pH value. Accordingly, the increase in the rate of hydrolysis of both the metaphosphates in acidic solutions depends on the

Table 3. Activation energies, ΔE_A (kcal·mol^{-1}), and log A (A: frequency factor) of the hydrolysis of trimeta- and tetrametaphosphates

pH[a]	Solvent[b]	Phosphate[c]	ΔE_A	log A
1.0	S_1	M_3	19.8	11.8
		M_4	22.8	12.9
	S_2	M_3	20.2	12.0
		M_4	23.1	12.9
	S_3	M_3	20.7	12.1
		M_4	23.6	12.9
	S_4	M_3	21.2	11.9
		M_4	23.9	12.9
2.0	S_1	M_3	20.1	11.1
		M_4	23.0	11.9
	S_2	M_3	20.3	10.8
		M_4	24.2	12.6
	S_3	M_3	21.8	11.6
		M_4	24.8	12.9
11.0	S_2	M_3	27.6	14.0
		M_4	30.6	13.2
	S_3	M_3	27.3	14.0
		M_4	30.6	13.6
12.0	S_2	M_3	29.3	16.2
		M_4	33.0	17.5
	S_3	M_3	27.5	15.3
		M_4	32.6	17.4

a) pH adjustment was made by using aqueous tetramethyl ammonium hydroxide and nitric acid. b) Solvents refer to Table 1. c) M_3 and M_4 stand for sodium trimeta- and tetrametaphosphates, respectively.

activation energy and frequency factor. In basic solutions, as the pH rises, the rate and activation energy of the hydrolysis of both the metaphosphates increase. Therefore, the increase in the rate of hydrolysis of both the metaphosphates in basic solutions is strongly dependent on the frequency factor.

The Stability of Tetrametaphosphate. The rate of hydrolysis of trimetaphosphate is about 4—30 times faster than that of tetrametaphosphate under all the conditions studied. The results agree well with those obtained by other investigators.[6] In the case of the hydrolysis of short-chain polyphosphates, generally, the longer the chain of the phosphate, the faster is the reaction rate. The stability of tetrametaphosphate against hydrolysis is explained by Van Wazer as follows; a tetrametaphosphate ring exhibits a greater number of possible atomic configurations and modes of internal motion than does a trimetaphosphate ion, so that the latter is essentially more rigid and hence more subject to scission.[6] According to Griffith and Rutt,[13] a trimetaphosphate ion has a D_{3h} symmetry (planer form) and a tetrametaphosphate ion has a C_{2h} symmetry (chair form) in an aqueous solution. The former may be more rigid than the latter. By quantum-chemical consideration, the stability of a system generally proceeds with an increase in the number of obtainable states of the system. It can reasonably be concluded from the data in Table 3 that the stability of tetrametaphosphate against hydrolytic scission depends mainly on the activation energy.

The Solvent Effect on the Rate of Hydrolysis. As is shown in Figs. 1 and 2, in acidic solutions, the rate of hydrolysis of trimeta- and tetrametaphosphates in water is slower than that in dioxane–water and faster than that in formic acid–water at the same pH value. In an acidic dioxane–water solvent, as the content of dioxane increases, the rate constants of both the phosphates increase for all pH values. The rates of hydrolysis of both the metaphosphates in the acidic S_1 and S_2 solvents are about 2.1—2.6 and 1.6—2.0 times faster, respectively, than that in the acidic S_3 solvent for all pH values. While the rates of hydrolysis of both the metaphosphates in the S_4 solvent are about 3.3—3.6 and 1.3—1.6 times slower, respectively, than that in the S_3 solvent at respective pH values of 0.9 and 1.5 (the concentrations of formic acid at the pH values of 0.9 and 1.5 are about 30 and 10%, respectively), that is, the difference in the rate constants for the S_3 and S_4 solvents is larger at smaller pH values. This can reasonably be explained in terms of the difference in the nucleophilicity of the water molecule in each solution as follows; since formic acid (protic solvent) combines with a water molecule by means of a hydrogen bond (solvation), the nucleophilicity of the water molecule for the phosphorus atom of the phosphates may decrease, and since the oxygen atom of dioxane forms a hydrogen bond with the hydrogen atom of the water molecule and since, consequently, the hydrogen bond between water molecules may be broken, the nucleophilicity of the water molecule for the phosphorus atom of the phosphates may increase in the S_1 and S_2 solvents. When the nucleophilicity of the water molecule decreases through the hydrogen bond with the acid, the hydrolysis of the phosphate may become energetically disadvantageous and the approach of the water molecule to the phosphorus atom of the phosphates may also be prevented. The results given in Table 3 seem to support this contention, because the activation energy of hydrolysis of both the metaphosphates in the S_3 solvent is larger than those in the S_1 and S_2 solvents and is smaller than that in the S_4 solvent at pH 1 and 2. These results are in good agreement with those for the hydrolysis of pyro- and tripolyphosphates.[3] Since the overall-reaction rate of the hydrolysis of both the metaphosphates is highly dependent upon the nucleophilicity of a water molecule in the acidic solution, the rate-determining step of the hydrolysis of both the metaphosphates in an acidic solution may be the nucleophilic attack of a water molecule on the phosphorus atom of the phosphates and the reaction may be of the S_N2 type.[3,4]

In basic solutions, as is seen in Figs. 1 and 2, the rate of hydrolysis of both the metaphosphates in the S_3 solvent is faster than that in the S_2 solvent at all temperatures and pH values, and the activation energy of hydrolysis of both the metaphosphates in the S_3 solvent is smaller than or the same as that in the S_2 solvent at pH 11 and 12. This tendency is completely contrary to that in an acidic solution. The hydrolysis of sodium tripolyphosphate was also studied at 50 °C in the S_2 and S_3 solvents at pH 11.0, in order to compare the behavior of polyphosphate with that of trimeta- and tetrametaphosphates in basic solutions. The pH ad-

justment of the tripolyphosphate solutions was made by using nitric acid and aqueous tetramethyl ammonium hydroxide. The rate constants of the hydrolysis of tripolyphosphate in the S_2 and S_3 solvents at pH 11.0 are 3.27×10^{-6} and 1.54×10^{-6} min^{-1}, respectively. This tendency of the solvent effect on the rate of the hydrolysis of tripolyphosphate is the same as that in acidic solutions[3] and it can be concluded that the mechanism of the hydrolysis of short chain polyphosphates in basic solutions is analogous to that in acidic solutions. However, according to the above results, the mechanism of the hydrolysis of trimeta- and tetrametaphosphates in basic solutions differs from that in acidic solutions. The difference in the rates of hydrolysis of both the metaphosphates in the basic S_2 and S_3 solvents cannot be reduced to the difference in the nucleophilicities of the water molecule in each solvent. Therefore, it can hardly be considered that the nucleophilic attack of a water molecule on the phosphorus atom of the metaphosphates has the most important influence on the overall-reaction rate of the hydrolysis of trimeta- and tetrametaphosphates in basic solutions. As mentioned above, the acceleration of the rate of hydrolysis of both the metaphosphates in basic solutions depends very much upon the entropy term (as is clearly seen by comparing the results in Tables 3 and 4, the increase in the rate of hydrolysis of both the metaphosphates by a sodium ion is also highly dependent upon the frequency factor), while the increase in the rate of hydrolysis of both the metaphosphates in acidic solutions depends upon both the activation energy and frequency factor. This may be the reason for the difference in the solvent effects on the rate of hydrolysis of both the metaphosphates in acidic and basic solutions.

The Effect of the Sodium Ion. The hydrolysis of sodium trimeta- and tetrametaphosphates was also carried out in the S_2 and S_3 solvents at pH 12.5 and at 30, 40, 50, and 60 °C by adjusting the pH of the solutions with aqueous sodium hydroxide and nitric acid. The kinetic data are listed in Table 4. As is seen by comparing the data in Table 4 and those in Figs. 1 and 2, the rate of hydrolysis of both the metaphosphates in aqueous sodium hydroxide is very much faster than that in aqueous tetramethyl ammonium hydroxide in any solvent, and at all temperatures, and pH values. This can be attributed to catalysis by a sodium ion, because, excluding the concentration of sodium ions, the other conditions of the trimeta- and tetrametaphosphate solutions of aqueous sodium hydroxide are the same as those of aqueous tetramethyl ammonium hydroxide. The activation energies of the hydrolysis of both the metaphosphates in aqueous tetramethyl ammonium hydroxide at pH 12.5 were calculated by using an Arrhenius plot on the basis of the data obtained by extrapolating the lines in Figs. 1 and 2. The activation energy of the hydrolysis of trimetaphosphate was 34 kcal/mol in the S_2 solvent and 33 kcal/mol in the S_3 solvent, and that of tetrametaphosphate was 30 kcal/mol in the S_2 solvent and 27 kcal/mol in the S_3 solvent. The rate of hydrolysis of both the metaphosphates in all aqueous sodium hydroxide solutions is nevertheless very much faster than that in any aqueous tetramethyl ammonium hydroxide solution, the activation energy of the hydrolysis in the faster solutions being larger than in the latter solutions. Therefore, the increase in the rate of the hydrolysis of both trimeta- and tetrametaphosphates in basic solutions by a sodium ion depends entirely upon the frequency factor. As Table 4 shows, the rate of hydrolysis of trimetaphosphate in the S_3 solvent is about 1.5—1.7 times faster than that in the S_2 solvent, and the rate of hydrolysis of tetrametaphosphate in the S_3 solvent is the same as that in the S_2 solvent. The solvent effect on the rate of hydrolysis of both the metaphosphates in alkaline solutions differs from that in acidic solutions. Therefore, the nucleophilic attack of a water molecule on the phosphorus atom of the metaphosphates has little influence on the overall-reaction rate of the hydrolysis of both the phosphates in alkaline solutions. As stated above, the increase in the rate of hydrolysis of both the metaphosphates in alkaline solutions depends significantly upon the entropy term, and this may cause the solvent effect on the rate of hydrolysis of both the small-ring metaphosphates in alkaline solutions.

References

1) I. Moriya, "Kayobai Chikan Hanno", Kagaku Dojin, Tokyo (1966), p. 12.
2) K. Okamoto, "Kyukaku Chikan Hanno S_N2 Hanno," Kagaku Dojin, Tokyo (1969), p. 202.
3) M. Watanabe, This Bulletin, **47**, 2048 (1974).
4) M. Watanabe, S. Sato, and H. Saito, *ibid.*, **48**, 896 (1975).
5) A. J. Parker, *Quart. Rev. (London)*, **16**, 163 (1962).
6) J. R. Van Wazer, "Phosphorus and its Compounds," Vol. 1, Interscience Publishers, New York (1958), p. 452

TABLE 4. RATE CONSTANTS (min^{-1}), ACTIVATION ENERGIES, ΔE_A($kcal\cdot mol^{-1}$), AND $\log A$(A: FREQUENCY FACTOR) OF THE HYDROLYSIS OF TRIMETA- AND TETRAMETAPHOSPHATES AT pH 12.5[a]

Phosphate	Solvent[b]	Temp. (°C) 30	40	50	60	ΔE_A	$\log A$
Trimeta	S_2	4.29×10^{-4}	3.40×10^{-3}	2.39×10^{-2}	1.53×10^{-1}	39.2	24.9
	S_3	7.30×10^{-4}	5.60×10^{-3}	3.78×10^{-2}	2.30×10^{-1}	38.5	24.6
Tetrameta	S_2	3.78×10^{-5}	2.45×10^{-4}	1.52×10^{-3}	8.58×10^{-3}	36.3	21.8
	S_3	3.92×10^{-5}	2.52×10^{-4}	1.43×10^{-3}	8.37×10^{-3}	36.3	21.7

a) pH adjustment was made by using aqueous sodium hydroxide and nitric acid. The concentration of sodium ion is 1.11 mol/l. b) Solvents refer to Table 1.

and 679, and the references therein.
7) L. F. Audrieth, "Inorganic Synthesis," Vol. III, McGraw-Hill, New York (1950), p. 101 and 104.
8) R. N. Bell, L. F. Audrieth, and O. F. Hill, *Ind. Eng. Chem.*, **44**, 568 (1952).
9) D. O. Campbell and M. L. Kilpatrick, *J. Amer. Chem. Soc.*, **76**, 893 (1954).
10) W. Wieker and E. Thilo, *Z. Anorg. Allg. Chem.*, **313**, 296 (1961).
11) E. J. Griffith and R. L. Buxton, *J. Amer. Chem. Soc.*, **89**, 2884 (1967).
12) S. Ohashi, *Kagaku to Kogyo*, **21**, 878 (1968), and the references therein.
13) W. P. Griffith and K. J. Rutt, *J. Chem. Soc. (A)*, **1968**, 2331.

The Amperometric Titration of Metal(II) Ions with *trans*-1,2-Cyclohexanediamine-*N*,*N*,*N*′,*N*′-tetraacetate (CyDTA)

Mutsuo KODAMA

Department of Chemistry, College of General Education, Hirosaki University, Bunkyo, Hirosaki 036

(Received March 22, 1975)

The use of CyDTA in the amperometric determination of metal-ion mixtures was studied systematically. Because of the sluggishness of the nickel(II)-EDMA~CyDTA substitution reaction, the nickel(II) ion in the EDMA solution could be masked completely in respect to the CyDTA. Therefore, even in the presence of an excess of nickel(II)ions, the copper(II), lead(II), cobalt(II), cadmium(II), and zinc(II) ions in the EDMA solution at about pH=6.50 could be determined accurately with CyDTA. In the amperometric titration of binary mixture of copper(II) and zinc(II), lead(II), cadmium(II), or cobalt(II) ions in the EDMA solution, titration curves with two sharp breaks could be obtained by following the change in the diffusion current due to the reduction of the copper(II)-EDMA complex. The first and second breaks correspond, respectively, to the equivalence point of zinc(II), lead(II), cadmium(II), or cobalt(II) and to that of copper(II).

Chelatometric titrations play an increasingly important role in the analysis of metal-ion mixtures. To widen the scope of these applications, a great number of methods of selective titrations have been proposed. However, the selectivity in the chelatometric titration of a mixture of metal ions has very often been discussed only from the thermodynamic point of view,[1] and the reaction rate effect on the titration has been disregarded. Therefore, it seems worthwhile to discuss this phenomenon from both thermodynamic and kinetic points of view in predicting the optimum conditions necessary for selective titrations. In this paper, the amperometric titration of metal-ion mixtures in an EDMA solution will be studied by using CyDTA as a titrant and will be discussed from both thermodynamic and kinetic points of view.

Experimental

Reagents. The CyDTA and diethylenetriaminepentaacetate (DTPA) used in this study were recrystallized from their aqueous solutions as their acids. The preparation and purification of the acid form of ethylenediaminemonoacetate (EDMA) were described in a previous paper.[2] All the other chemicals used were of an analytical-reagent grade and were used without further purification.

Apparatus and Experimental Procedures. All the DC current-voltage curves were measured with a Yanagimoto pen-recording polarograph P-8 or with a manual polarograph similar to Kolthof and Lingane's. The characteristic features of the dropping mercury electrode used were described previously.[3] All the other apparatus and the experimental procedures were the same as those in that paper. In this study, no buffer reagent was used, because the sample solutions contained a large excess of uncomplexed EDMA and had a sufficient buffer capacity in its pH ranges ($5.80<$ pH <7.70 and $8.50<$pH<10.50).

Results and Discussion

Let us consider the amperometric titration of the complexed metal ion, M, existing in the forms of MX and MX_2, with the chelon Z. If the reaction is rapid enough so that the equilibrium with respect to the formation reaction of MZ is practically maintained at every stage of the titration, the successful determination of M with Z is possible only when the conditional formation constant of MZ, K'_{MZ}, defined as $K'_{MZ}=[MZ]/([MX]+[MX_2])\cdot[Z]_f=K_{MZ}/(\alpha_H)_Z\cdot(K'_1\cdot[X]_f+K'_1\cdot K'_2\cdot[X]_f^2)$, is larger than $1\times10^4/C$, where C means the total concentration of the metal ion; $[X]_f$, the concentration of the uncomplexed X; K'_i, the i-th conditional successive formation constant of the M–X complex, and $(\alpha_H)_Z$, the (α_H) value of Z $(=1+[H^+]/K_n+\cdots+[H^+]^n/K_n\cdots K_1)$. Here, the charges are omitted for the sake of simplicity. Table 1 lists the K'_{MZ} values calculated for the reaction of CyDTA with metal ions in a 20 mM EDMA solution using the related equilibrium constants previously reported.[4,5] The K'_{MZ} values given in Table 1 show that if the reactions of CyDTA with metal ions in the EDMA solution are sufficiently rapid, 1.0 mM copper(II), nickel(II), cobalt(II), zinc(II), lead(II), and cadmium(II) ions in the 20 mM EDMA solution of pH=6.00 can be titrated successfully with CyDTA. In all cases other than the cobalt(II) system, the equivalence point was determined by following the change in the diffusion current of the metal(II)–EDMA complex, because the negative shift in the reduction potential at DME due to the complexation with CyDTA is sufficient. In the case of the cobalt(II) system, the course of the titration was followed by measuring the change in the oxidation wave-height of the cobalt(II)–EDMA complex at the DME. Typical titration curves obtained for the copper(II) and lead(II) ions are reproduced in Fig. 1. All the metal ions other than nickel(II) ion could be titrated accurately with CyDTA. In the case of the nickel(II) system, no end point could

TABLE 1. $\log K_e'$ FOR VARIOUS METAL(II)-IONS
$\mu=0.30$, 25 °C, $[EDMA]_f=20.0$ mM
$\log K'_{MZ}$ $(=K_{MZ}/(\alpha_H)_Z(K_1'\cdot[X]_f+K_1'\cdot K_2'\cdot[X]_f^2))$

Metal(II) ion	pH	
	6.00	6.50
Cu(II)	7.15	6.24
Ni(II)	9.30	8.84
Co(II)	11.10	10.95
Zn(II)	11.00	10.97
Pb(II)	11.98	11.87
Cd(II)	10.23	10.09

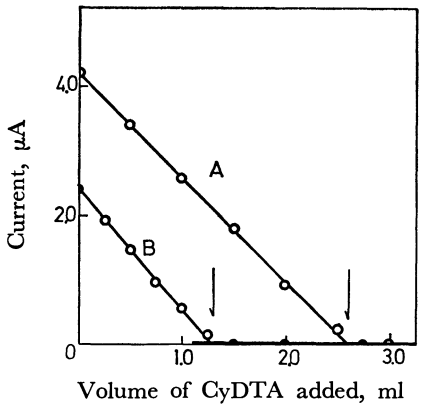

Fig. 1. Amperometric titration curves for the titration of 50 ml metal(II) solution with 19.2 mM CyDTA.
$[EDMA]_f=20.0$ mM, $\mu=0.30$, 25 °C
Equivalence points are indicated by arrows
A) 1.02 mM copper(II), B) 0.50_0 mM lead(II).

Table 2. Amperometric determination of metal(II) ions in the EDMA solution using CyDTA as a titrant
$\mu=0.30$, 25 °C, $[EDMA]_f=20.0$ mM
sample solution: 50 ml

Metal(II)	Metal(II) concn., mM	CyDTA concn., mM	Equivalence point, ml	
			Obsd	Calcd
Cu(II)	2.04	38.4	2.64	2.65
	1.02	19.2	2.65	2.65
	0.51_0	19.2	1.34	1.33
	0.20_4	3.84	2.68	2.65
Zn(II)	2.15	38.4	2.77	2.80
	1.07_5	19.2	2.79	2.80
	0.53_8	19.2	1.41	1.40
	0.21_5	3.84	2.82	2.80
Cd(II)	2.04	38.4	2.66	2.65
	1.02	19.2	2.64	2.65
	0.20_4	3.84	2.63	2.65
Pb(II)	2.00	38.4	2.62	2.60
	1.00	19.2	2.63	2.60
	0.20_0	3.84	2.57	2.60
Co(II)	1.82	38.4	2.38	2.38
	0.91_1	19.2	2.37	2.38
	0.18_2	3.84	2.40	2.38

be obtained. This can be ascribed to the slow reaction of CyDTA with the nickel(II)-EDMA complex in the EDMA solution. Some typical results are given in Table 2.

In the titration of a binary metal-ion mixture solution of M and M′ containing an excess of X and using Z as a titrant, when the equilibria with respect to the formation reactions of metal-Z complexes are always maintained, the optimum conditions for the selective titration can be easily predicted only from a theoretical consideration of the chemical equilibria involved. In this case, if the K'_{MZ} value for the M system is 1×10^4 times larger than that of the M′ system, M in the solution containing an equal amount of M′ will react preferentially with Z, hence, a titration curve with two sharp breaks, the first and second of which correspond to the equivalence points of M and M′ respectively, can be obtained by following the change in the concentration of M′. On the other hand, in cases where the reactions of Z with the metal complexes of X are rapid, while those of the metal-Z complexes formed during the course of the titration are very slow, the situation is complicated, because M, with a larger K'_{MZ} value, does not always react with Z at a rate larger than M′, which has a smaller K'_{MZ} value; hence, the formation of MZ may proceed not only through the direct reaction of the M-X complex with Z, but also through the exchange reaction of M′Z with the M-X complex. Therefore, if M′Z, with a smaller K'_{MZ} value, is substitution-inert, M can be titrated preferentially with Z only when the reaction of Z with M in the solution containing X proceeds much faster than that with M′. However, when the reaction of Z with M in the solution of X is much slower than that with M′, M′ will react first and can be titrated first with Z, irrespective of its smaller K'_{MZ} value. Thus, in the amperometric titration of the above binary mixture, when the course of titration is followed by determining the change in the limiting current of M′, the shape of the titration curve will depend on the relative rate constants of the reactions of Z with M and M′. The amperometric titration curves for such system can be calculated by using the following relation (1) for various reaction rates, assuming that the reaction of M′Z is completely substitution-inert:

$$r_{M'}=\frac{k_{M'}\cdot[M']_f}{k_{M'}\cdot[M']_f+k_M\cdot[M]_f}\times f_t \qquad (1)$$

where f_t is the total fraction titrated ($=C_Z/(C_M+C_{M'})$); $r_{M'}$, the fraction of M′ reacted with Z; k_M and $k_{M'}$, the relative apparent rate constants, and $[M]_f$ and $[M']_f$, the metal-ion concentration at a given f_t value. The titration curves calculated for the equimolar mixture of M and M′ are reproduced in Fig. 2. The results shown in Fig. 2 clearly indicate that, if the rate constant ratio, $k_M/k_{M'}$, is smaller than 0.02, the

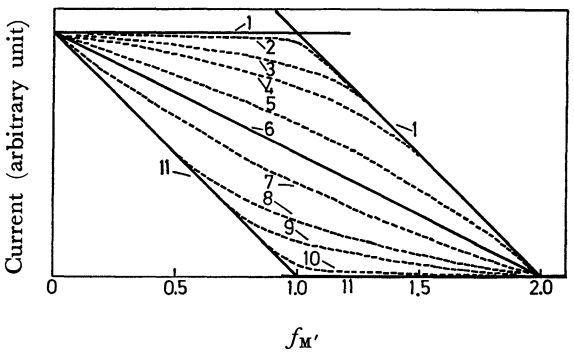

Fig. 2. Amperometric titration of an equimolar binary metal(II)-ion mixture of M and M′ with Z in the solution of X.
Titration curves were calculated at various rate constant ratio's, $R=k_M/k_{M'}$, under the conditions where $K'_{MZ}>K'_{M'Z}$, M′Z is substitution-inert, and the rate of the reaction of Z with M′-X complex is large sufficiently for the successful determination of M′.
$R=k_M/k_{M'}$ $f_{M'}=C_Z/C_{M'}$
1: >500, 2: 50, 3: 10, 4: 5, 5: 2, 6: 1, 7: 0.5, 8: 0.2, 9: 0.1, 10: 0.02, 11: <0.002.

titration curve shows only one break, corresponding to the equivalence point of M′, whereas if the $k_M/k_{M'}$ value is larger than 50, two break points occur, the former corresponding to the equivalence point of M, and the latter, to that of M′. Furthermore, if the $k_M/k_{M'}$ ratio is nearly identical to unity, the titration with Z will give only one break point, corresponding to the sum of M and M′.

The K'_{Mz} values in Table 1 show that all the EDMA complexes studied in this paper other than the copper(II) complex can replace the CyDTA anion thermodynamically from the copper(II)–CyDTA complex in the EDMA solution of pH=6.00 to 6.50. The kinetics of the reaction of the copper(II)–CyDTA complex with the EDMA complexes of zinc(II), lead(II), cadmium(II), cobalt(II), and nickel(II) ions in the EDMA solution was studied by observing the increase in the reduction wave-height of the copper(II)–EDMA complex in the pH range from 5.60 to 7.00. The reaction proceeds so slowly that the rate could not be determined accurately. However, the following results could be obtained in the preliminary experiments. In all the reactions studied except in the nickel(II) system, the rates 1) were independent of the concentrations of the zinc(II), lead(II), cadmium(II), and cobalt(II) ions and 2) were exactly proportional to the concentration of the copper(II)–CyDTA complex and that of the uncomplexed EDMA. Furthermore, 3) the plot of the product of the initial rate and $(\alpha_H)_{edma}/[H^+]$ against the hydrogen-ion concentration, $[H^+]$, gave a linear relation passing through the point of origin, provided that the other experimental conditions were kept constant (Fig. 3). In the nickel(II) system, no reduction step due to the copper(II)–EDMA complex could be observed. The above findings suggest the following reaction mechanism for the reaction of the copper(II)–CyDTA complex with the EDMA complexes of zinc(II), lead(II), cadmium(II), and cobalt(II) ions in the EDMA solution:

$$Cucydta^{2-} + H_2edma^+ \overset{k_{2H}}{\rightleftharpoons} Cu(edma)^+ + H_2cydta^{2-} \quad \text{rds} \qquad (2a)$$

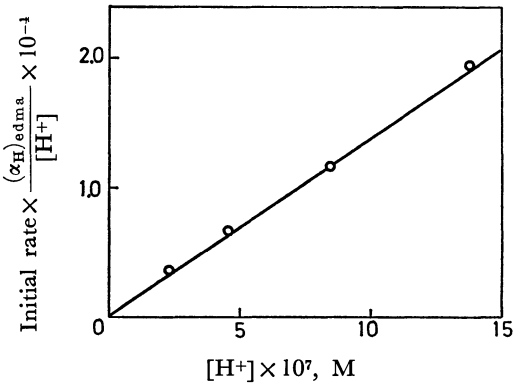

Fig. 3. The effect of the solution pH on the rate of the substitution reaction of copper(II)–CyDTA complex with zinc(II) ion in the EDMA solution.
μ=0.30, 25 °C, $[Cucydta^{2-}]$=1.0 mM
$[EDMA]_f$=30.0 mM, $[Zn(II)]_t$=10.0 mM
pH ranged from 5.80 to 6.80

$$M(edma)^+ + H_2cydta^{2-} \rightleftharpoons Mcydta^{2-} + H_2edma^+ \qquad (2b)$$
$$\downarrow\uparrow \quad \text{in a rapid equilibrium}$$
$$M(edma)_2^0$$

corresponding to the following relation:

$$\text{initial rate} = \frac{k_{2H}\cdot[Cucydta^{2-}]\cdot[edma]_f}{(\alpha_H)_{edma}\cdot K_3\cdot K_2}\times[H^+]^2 \qquad (3)$$

where K_i denotes the i-th deprotonation constant of H_3edma^{2+}. The k_{2H} value was determined to be $6.7\times10^{-3}\ M^{-1}\cdot s^{-1}$ from the slope of the above linear relation. The k_{2H} value thus determined suggests that only the 0.5% of the CyDTA anion coordinated to the copper(II) (1 mM) can be replaced by the 1 mM metal(II) ion in the 10 mM EDMA solution within an hour. As is clear from the above kinetic consideration of the titration of a binary mixture, this fact obviously suggests that the conditions for the titration of a binary mixture involving the copper(II) ion with CyDTA using the EDMA solution should be discussed from the kinetic point of view. As has been mentioned by Olson and Margerum,[6] the exchange reaction of two metal complexes generally proceeds by means of a chain-reaction mechanism. Therefore, the above reaction mechanism proposed for the reaction of the copper(II)–CyDTA complex with the metal–EDMA complex in the EDMA solution must be reasonable. Since the reactions of CyDTA with the EDMA complexes of metal(II) ions other than the nickel(II) ion in the EDMA solution proceed very rapidly, one cannot determine their reaction rates by a conventional method. Previously, the present author studied the kinetics of the substitution reaction of the nickel(II)–EDMA complex with the aminopolycarboxylate anion,[7,5b] and proposed the following reaction mechanism:

$$Ni(edma)_2^0 \rightleftharpoons Ni(edma)^+ + edma^- \qquad (4a)\ \text{rapid}$$

$$Ni(edma)^+ + H_nZ^{n-m} \underset{k_{b'}}{\overset{k_{f'}}{\rightleftharpoons}} NiZ^{2-m} + H_iedma^{i-1} + (n-i)H^+ \qquad (4b)$$

He also studied the kinetics of the dissociation reaction of the nickel(II)–EDMA complex.[8] From the magnitude of their reaction rates, it was concluded that the rates of the substition and formation reactions of the nickel(II)–EDMA complex can be understood by assuming the ethylenediamine reaction mechanism[9] and the water-exchange mechanism[10,11] respectively. Furthermore, there are several features which support the conclusion that the reactions of the cadmium(II), lead(II), zinc(II), and cobalt(II) complexes also have a reaction mechanism similar to that of the corresponding reaction of the nickel(II) complex.[11,12] Therefore, it is not unreasonable to assume the ethylenediamine reaction mechanism for the CyDTA reactions of the EDMA complexes of the zinc(II), lead(II), cadmium(II), and cobalt(II) ions and the water-exchange mechanism for the formation reactions of these EDMA complexes. Thus, the relative rates for the CyDTA reactions with the EDMA complexes were calculated by assuming the ethylenediamine-reaction mechanism for the CyDTA reactions and the water-exchange mechanism for the formation reactions

of the EDMA complexes, with the aid of Eq. (5):

$$k_M = \frac{k_f'}{(1+K_2'\cdot[X]_f)} = \frac{k_M^{-H_2O}\cdot K_{os}\cdot K_{M-gly}}{K_1\cdot(1+K_2'\cdot[X]_f)} \quad (5)$$

where all the symbols have their usual meanings.[5,11] The estimated relative k_M values for the EDMA concentration of 20 mM and the solution pH of 6.50 are listed in Table 3. Here, the steric effects of the CyDTA anion on the reaction rates are all assumed to be the same. As is shown in Table 3, the k_M values calculated for the zinc(II), cadmium(II), and lead(II) systems are much larger than that of the copper(II) system. This suggests that the equilibrium for the formation reaction of the zinc(II)-, cadmium(II)-, or lead(II)-CyDTA complex will be ensured even in the presence of the copper(II) ion. Therefore, the titration of a mixture of copper(II) and zinc(II), cadmim(II), or lead(II) can safely be discussed from the thermodynamic point of view.

Table 3. Relative rate constants for the reactions of CyDTA with metal(II)-EDMA complexes, k_M*
$[EDMA]_f = 20.0$ mM, pH=6.50

System	$\log k_M$	$\log k_M^{-H_2O}$	$\log K_{M-gly}$
Cu(II)	2.61	9.9	7.85
Ni(II)	−0.86	4.5	5.71
Cd(II)	5.47	8.3	4.65
Zn(II)	5.87	7.7	5.37
Pb(II)	6.09	8.0	5.32
Co(II)	3.72	6.0	5.08

* Rate = $k_M\cdot$[Metal(II)-EDMA]$_t\cdot$[CyDTA]

Thus, the amperometric titration (the course of which is followed by measuring the change in the concentration of the copper(II)-EDMA complex) of a mixture of copper(II) and zinc(II), cadmium(II), or lead(II) in the EDMA solution with CyDTA can be expected to give two sharp breaks. The first break corresponds to the equivalence point of zinc(II), cadmium(II), or lead(II), and the second, to that of the copper(II) ion. On the other hand, in the light of the above kinetic consideration, the k_M values for the copper(II) and nickel(II) systems evidently show that the titration of a mixture of copper(II) and nickel(II) ions in the EDMA solution will give only one end-point break, corresponding to the equivalence point of the copper(II) even when the concentration of the nickel(II) ion is 20 times higher than that of the copper(II) ion. Furthermore, as is shown by the titration curve (3) in Fig. 2, the titration of cobalt(II) in the presence of the copper(II) ion will probably give a positive error for the cobalt(II) and a negative error for the copper(II). Since the copper(II)-EDMA complex is reduced at much less negative potentials than its CyDTA complex and the EDMA and CyDTA complexes of other metal(II) ions, the above prediction was examined experimentally by following the change in the reduction wave-height of the copper(II)-EDMA complex. Some typical titration curves obtained for the Cu(II)~Zn(II) and Cu(II)~Ni(II) systems are reproduced in Fig. 4. In full accordance with the theoretical prediction, the equimolar mixture of copper(II) and zinc(II), cadmium(II), or lead(II) ions in the EDMA solution could be titrated successfully with CyDTA, and the

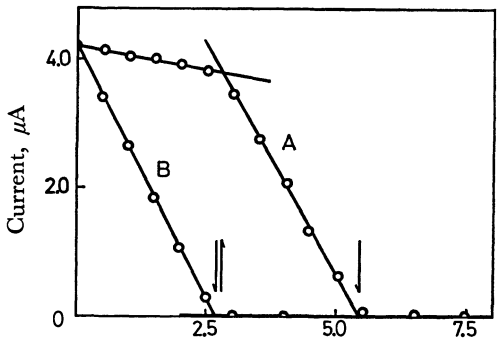

Fig. 4. Amperometric titration curves of 50 ml binary metal(II)-ion mixture with CyDTA.
$[EDMA]_f = 20.0$ mM, 25 °C, $\mu = 0.30$
[CyDTA] = 19.2 mM, pH=6.30
A) [Cu(II)] = 1.02 mM, [Zn(II)] = 1.07_5 mM
B) [Cu(II)] = 1.02 mM, [Ni(II)] = 20.0 mM

Table 4. Amperometric titration of a binary metal-ion mixture with CyDTA
$\mu = 0.30$, 25 °C, $[EDMA]_f = 20$ mM
sample solution: 50.0 ml

A) Cu(II)~Zn(II) mixture

[Cu(II)] mM	[Zn(II)] mM	[CyDTA] mM	Equivalence point, ml Zn(II) Obsd	Zn(II) Calcd	Cu(II) Obsd	Cu(II) Calcd
1.02	4.30	76.8	2.76	2.80	0.67	0.66_5
1.02	2.15	38.4	2.78	2.80	1.33	1.33
1.02	0.53_8	19.2	2.76	2.80	2.66	2.65
2.04	1.07_5	38.4	1.39	1.40	2.66	2.65
1.02	1.07_5	19.2	2.78	2.80	2.66	2.65
0.51_0	1.07_5	19.2	2.81	2.80	1.32	1.33

B) Cu(II)~Ni(II) mixture

[Cu(II)] mM	[Ni(II)] mM	[CyDTA] mM	Equivalence point, ml Cu(II) Obsd	Cu(II) Calcd
1.02	22.0	19.2	2.63	2.65
1.02	5.50	19.2	2.64	2.65
1.02	1.10	19.2	2.64	2.65
1.02	0.55	19.2	2.65	2.65
0.20_4	11.0	3.84	2.68	2.65

C) Cu(II)~Co(II) mixture

[Cu(II)] mM	[Co(II)] mM	[CyDTA] mM	Equivalence point, ml Cu(II) Obsd	Cu(II) Calcd	Co(II) Obsd	Co(II) Calcd
0.51_0	3.73	38.4	0.43	0.44_4	3.60	3.57
1.02	0.91_1	19.2	2.60	2.65	2.43	2.38
1.02	0.91_1	9.60	5.14	5.30	2.54	2.38
2.04	0.45_6	19.2	5.22	5.30	1.27	1.19

nickel(II) ion had no effect on the amperometric determination of copper(II) (Table 4). The amperometric titration of a binary mixture of the nickel(II) ion and the lead(II), cadmium(II), or cobalt(II) ion with CyDTA was also carried out in the EDMA solution. The nickel(II) had no effect on the determination of lead(II), cadmium(II), or cobalt(II) with CyDTA. This can be also be ascribable to the inertness of the CyDTA reaction of the nickel(II)–EDMA complex. As is shown by the data in Table 4, the CyDTA titration of a mixture of copper(II) and cobalt(II) ions, especially when the concentration of copper(II) ions is high, gave a positive error for the cobalt(II) determination. This is in good accordance with the theoretical prediction made from the kinetic point of view. The K'_{MZ} values in Table 1 evidently show that, thermodynamically, the successful determination of cobalt(II) in the presence of copper(II) is possible.

The present author also investigated the amperometric titration of a mixture of copper(II) and nickel(II) ions in the EDMA solution, using DTPA as a titrant. As in the case of the CyDTA system, the K'_{MZ} value for the nickel(II) ion is much larger than that of the copper(II) ion, but the k_M value for the copper(II)–EDMA∼DTPA reaction can be expected to be much larger than that of the nickel(II)–EDMA∼DTPA reaction, suggesting the possibility of the successful performance of the selective titration of copper(II). However, no distinct end break could be obtained. This can probably be ascribed to the fact that the reaction of the copper(II)–DTPA complex with the nickel(II)–EDMA complex in the EDMA solution proceeds to an appreciable extent.

This paper has been concerned only with the amperometric titration of binary metal-ion mixtures in an EDMA solution with CyDTA, because the kinetics of this system could be fully investigated. However, many other systems can probably be submitted to the titration of multicomponent mixtures.

References

1) C. N. Reilley and R. W. Schmid, *Anal. Chem.*, **31**, 887 (1959).
2) Y. Fujii, E. Kyuno, and R. Tsuchiya, This Bulletin, **43**, 786 (1970).
3) M. Kodama, *ibid.*, **47**, 1434 (1974).
4) L. G. Sillen and A. E. Martell, "Stability Constants of Metal-Ion Complexes," 2nd Ed., The Chemical Society, London (1964).
5) a) Y. Fujii and M. Kodama, This Bulletin, **42**, 3172 (1969). b) M. Kodama, Y. Fujii, and T. Ueda, *ibid.*, **43**, 2085 (1970). c) M. Kodama, Y. Fujii, and T. Ueda, *ibid.*, **43**, 409 (1970). d) M. Kodama, *ibid.*, **47**, 1430 (1974). e) M. Kodama, unpublished result.
6) D. C. Olson and D. W. Margerum, *J. Amer. Chem. Soc.*, **85**, 297 (1963).
7) M. Kodama, M. Hashimoto, and T. Watanabe, This Bulletin, **45**, 2761 (1972).
8) M. Kodama and N. Oyama, *ibid.*, **44**, 2849 (1971).
9) The reaction which proceeds through the reaction intermediate where the leaving EDMA and entering aminopolycarboxylate anion respectively are bonded through the ethylenediamine and glycinate chelate rings, and the dissociation of EDMA anion from the reaction intermediate is the rate-determining step.
10) M. Eigen, *Pure Appl. Chem.*, **6**, 97 (1963).
11) M. Kodama, K. Namekawa, and T. Horiuchi, This Bulletin, **47**, 2011 (1974).
12) M. Kodama, *ibid.*, **47**, 2490 (1974).

Analysis of the Elution Curve in Eluting Lutetium from Cation-Exchanger with α-Hydroxyisobutyric Acid

Masumitsu KUBOTA

Japan Atomic Energy Research Institute, Tokai, Naka, Ibaraki 319-11

(Received April 28, 1975)

The elution behavior of lutetium from a cation-exchange column with α-hydroxyisobutyric acid solution (pH 3.77) was studied as a function of column distribution ratio of lutetium, flow rate, temperature and amount of lutetium. The elution curve fitted the normal distribution when the flow rate was smaller than 40 cm hr^{-1} for 0.14 M of the eluant, 60 cm h^{-1} for 0.12 M and 120 cm h^{-1} for 0.10 M. However, the normal distribution and constancy of the peak position could not be maintained when the amount of lutetium exceeded 200 μg cm^{-2}. Within the range 15—35 °C, the peak position appeared late and the elution curve became sharper with temperature rise, but the diffusion coefficients remained constant. The value of the height equivalent to the theoretical plate was determined from the position and width of the elution peak which varied as a function of the flow rate. The diffusion coefficients of lutetium ions in the ion-exchange resin and the solution were calculated to be 2.6×10^{-7}—$6.4\times10^{-9}\ \lambda''$ cm^2s^{-1} and $4.2\times10^{-5}\ \lambda''$ $cm^2\,s^{-1}$, respectively, according to Glueckauf's theoretical equation, where λ'' is the column distribution ratio of lutetium ions. The experimental results make it possible to construct an elution curve for any column distribution ratio of lutetium in the range 2—20, temperature and flow rate.

In the cation-exchange separation of trace amounts of rare earths, α-hydroxyisobutyric acid has been used as the most prominent eluant. However, there are few reports on quantitative discussion of the elution behavior in connection with such factors as compositions of the eluant, operating temperatures, amounts of rare earths, *etc.* Only Seyb,[1] Massart and Hoste[2] have reported that yttrium and terbium can be separated successfully only by using eluant solutions containing sufficient amounts of undissociated hydroxy acid, and that the operating temperature and the amount of lutetium absorbed on the resin bed affect the appearance and shape of the elution peak. Although the flow rate of the eluant is an important factor influencing the separation, no one has ever discussed quantitatively the effect of flow rate on elution behavior of rare earths.

According to Glueckauf,[3] the elution curve can be expressed as follows with the assumption that the ion-exchange reaction is reversible:

$$C_i(V) = C_{i\max}\exp\left[-\frac{N(V_i-V)^2}{2V_iV}\right] \qquad (1)$$

where C_i=concentration of species i in the effluent
N=plate number
V=effluent volume—dead volume of the column
V_i=effluent volume at which the concentration of the given ion reaches its maximum—dead volume of the column.

The shape of the elution curve apparently depends on V_i and N obtained by dividing the bed length (L) by the height equivalent to the theoretical plate (HETP). The value of HETP can be calculated by the theoretical formula:[3]

$$\mathrm{HETP} = 1.64\,r_0 + \frac{\lambda_i''0.14r_0^2u}{(\lambda_i''+\beta)^2\overline{D}} + \left(\frac{\lambda_i''}{\lambda_i''+\beta}\right)^2\frac{0.266\,r_0^2u}{D(1+70\,r_0u)} + \frac{D\beta\sqrt{2}}{u} \qquad (2)$$

where r_0=radius of spherical ion-exchange resin particle
λ_i''=column distribution ratio of species i
$$=\frac{\text{amount of species } i \text{ per ml of the resin bed}}{\text{amount of species } i \text{ per ml of the solution}}$$
β=fractional void volume of the resin bed
u=linear flow rate of the eluant
$\overline{D}$=interdiffusion coefficient in the ion-exchange resin
D=diffusion coefficient in the solution

Of the right hand terms of the equation, the first is due to finite particle size, the second to slow particle diffusion, the third to slow film diffusion, and the last to longitudinal diffusion. This equation indicates that the HETP varies with the flow rate of the eluant. If Eq. (2) is applicable to the elution of lutetium with α-hydroxyisobutyric acid, and the diffusion coefficients are known, the equation enables us, in combination with Eq. (1), to construct an elution curve for any flow rate at a given column distribution ratio.

This paper deals with the effect of the flow rate as the main subject in the study of the elution behavior of lutetium from cation-exchange resin bed with α-hydroxyisobutyric acid solution having pH 3.77, the most suitable for the separation of thulium and lutetium at a lutetium distribution coefficient of around 10 $ml\cdot g^{-1}$. The temperature dependence of the diffusion coefficients as well as the column distribution ratio and the variation of elution curve with the amount of lutetium were also studied.

The elution curves obtained under various conditions were analyzed to get HETP, and the diffusion coefficients $\overline{D}$ and D were determined as a function of λ'' so as to satisfy Eq. (2). The results enabled us to construct an elution curve under arbitrary conditions.

Experimental

Reagent and Apparatus. Ion-exchange Resin: Cation-exchange resin (Diaion SK-1, 100~200 mesh) was digested with a mixture of 30% hydrogen peroxide, ethylendiaminetetraacetic acid and ammonium hydroxide, and washed with distilled water. This ion-exchange resin was successively treated in a glass column with a large excess of 3 M hydrochloric acid and 3 M ammonium chloride. After being washed with distilled water, the resin was suspended in distilled water in a large glass column to collect particles

of uniform size. Over 95% of the particles thus obtained had a diameter between 100~150 μm in 0.10 M α-hydroxyisobutyric acid solution, as confirmed by microscopic examination. The resin was stored in distilled water.

Column: A glass column of 0.8 cm in diameter and 25.0 cm in length with a water jacket was used. Water was circulated through the jacket to keep the column temperature at 15.0± 0.1 °C unless otherwise stated.

Eluant: α-Hydroxyisobutyric acid (HB), supplied by Wako Chem. Co., was dissolved in redistilled water to give a 2.5 M solution, and in redistilled water and concentrated ammonia solution to give a 2.5 M solution having pH 6.97. The acid solution (2.5 M) was mixed with a salt solution (2.5 M NH_4B) in a volume ratio of 3 : 2. Finally, eluants were prepared simply by diluting this mixed solution with redistilled water.

Lutetium Tracer: Lutetium-177 was produced by neutron irradiation of "spec pure" lutetium oxide, which had been spectrographically guaranteed by Johnson Matthey Co., in the JRR-2 reactor with a thermal neutron flux of 3×10^{13}n $cm^{-2}s^{-1}$. The irradiated oxide (5 mg Lu_2O_3) was dissolved in concentrated hydrochloric acid, dried under an infrared lamp and finally dissolved in 50 ml of 0.1 M hydrochloric acid.

Procedure. A resin slurry was poured into the column to make a resin bed of 21.9 cm long. Before each experiment, the bed was washed with eluant until the pH of the effiuent became the same as that of the eluant. The lutetium tracer solution was introduced into the column. The column was then washed successively with 2 ml of distilled water, 0.5 ml of 0.5 M ammonium chloride solution and 1.5 ml of distilled water. Lutetium absorbed was eluted with the α-hydroxyisobutyric acid solution. The effluent from the column was passed through a thin polyethylene tube connected to the column and wound into a spiral to record its radioactivity counting rate continuously with an end-window GM counter. The flow rate was controlled by varying the height of the exit of the tube. One drop was taken from every one ml of the effluent onto a glass plate and evaporated to dryness with an infrared lamp. The radioactivity was counted with a GM counter to make an elution curve. The fractional void volume of the resin bed was determined with $^{131}I^-$ by the eqution

$$\beta = \frac{V_{^{131}I^-}}{V_b} \tag{3}$$

where V_b=bed volume of the column and $V_{^{131}I^-}$=effluent volume at which the first appearance of $^{131}I^-$ is confirmed in the effluent solution−dead volume of the column. The column distribution ratio of lutetium was determined from the peak position of lutetium activity by the equation

$$\frac{V_i}{V_b} = \lambda_i'' + \beta \tag{4}$$

Results and Discussion

Effect of Flow Rate on Elution Curve. Elution curves are shown in Figs. 1, 2 and 3 as a function of the flow rate and concentration of the eluant. At the elution with 0.10 M solution with a flow rate up to 120 cm h^{-1}, elution curves were symmetrical within 5% with respect to the vertical line passing the maximum of the peak. However, as the eluant concentration increases, the maximum flow rate at which a symmetrical elution curve is obtained, becomes small, *i.e.*, up to 60 cm h^{-1} for 0.12 M and 40 cm h^{-1} for

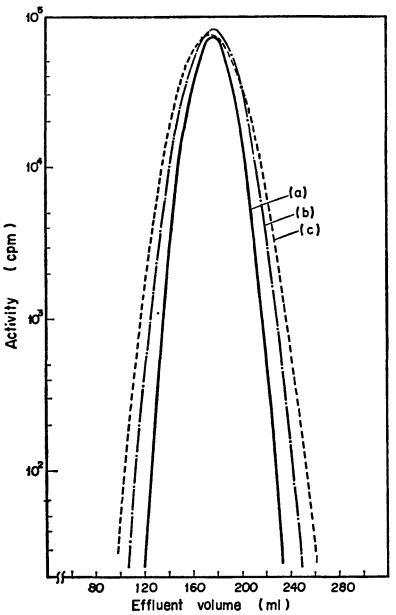

Fig. 1. Effect of the flow rate on the elution curve at the eluant concentration of 0.10 M.
(a): 21.9 cm h^{-1}, (b): 69.0 cm h^{-1}, (c): 116 cm h^{-1}.

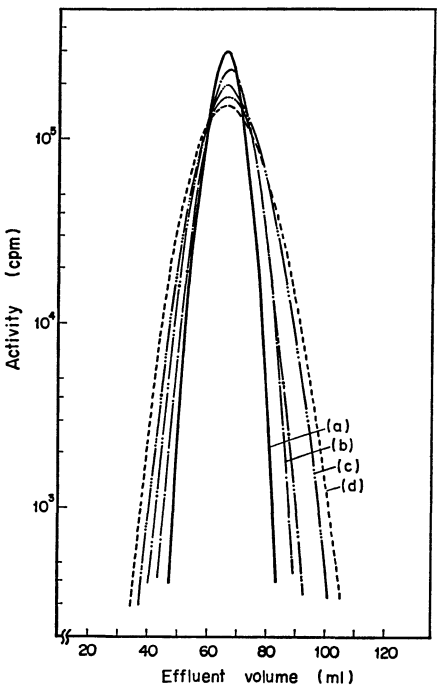

Fig. 2. Effect of the flow rate on the elution curve at the eluant concentration of 0.12 M.
(a): 16.8 cm h^{-1}, (b): 34.8 cm h^{-1}, (c): 53.1 cm h^{-1}, (d): 90.5 cm h^{-1}, (e): 118 cm h^{-1}.

0.14 M (Figs. 2 and 3). Variations of the widths at 1/2, 1/10, $1/10^2$, and $1/10^3$ peak height of the elution curves are shown in Fig. 4 as a function of the flow rate for 0.12 M eluant. Apparently a linear relation holds between the flow rate and the width of the elution peak within the symmetrical flow rate region (0~60 cm h^{-1}). This differs from the elution with citric acid,[4] where the width of the elution peak is

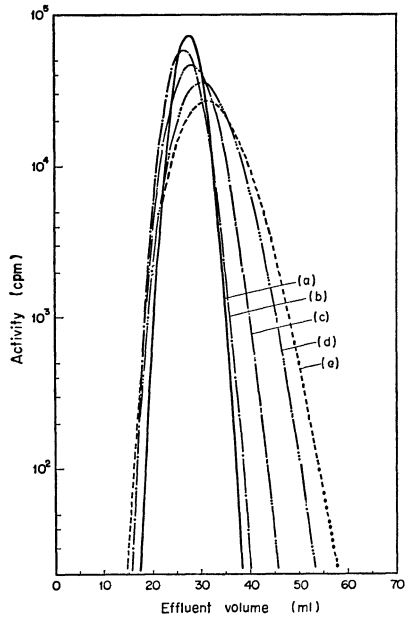

Fig. 3. Effect of the flow rate on the elution curve at the eluant concentration of 0.14 M.
(a): 15.9 cm h^{-1}, (b): 29.8 cm h^{-1}, (c): 47.2 cm h^{-1}, (d): 83.6 cm h^{-1}, (e): 109 cm h^{-1}.

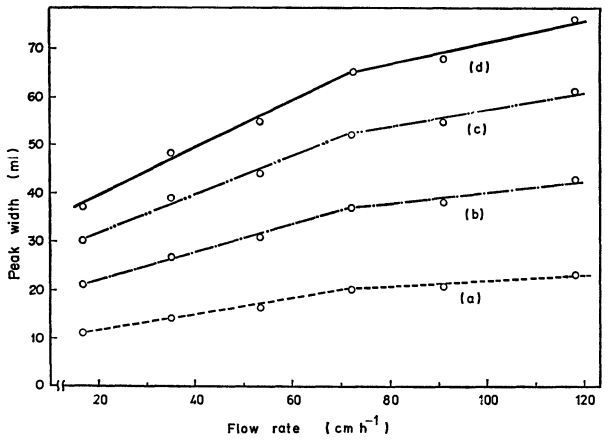

Fig. 4. Relation between the peak widths and the flow rate at the eluant concentration of 0.12 M.
(a): peak width at 1/2 peak height, (b): peak width at 1/10 peak height, (c): peak width at $1/10^2$ peak height, (d): peak width at $1/10^3$ peak height.

nearly independent of the flow rate below 30 cm h^{-1}. Ratios of the widths at 1/2, $1/10^2$ and $1/10^3$ peak height to that at 1/10 peak height do not vary with the flow rate and consist of those of the normal distribution curve.

For the symmetrical flow rate region in which the ion-exchange is considered to proceed reversibly, HETP can be calculated from the elution curve by the simplified equation[3]

$$\mathrm{HETP} = \frac{L}{16}\left(\frac{\Delta V_i}{V_i}\right)^2 \qquad (5)$$

where the bandwidth ΔV_i of species i is defined as the number of solution-volume units in the effluent between the intercepts of the tangents to the front and rear flanks of the peak with the abscissa.[3] The values of HETP calculated from Eq. (5) show linear increase with the flow rate (Fig. 5). The increase in the concentration of the eluant, or the decrease in the distribution coefficient makes the slope steeper. However, the change of the slope can not be explained only by the variation of the column distribution ratio λ_1'' in Eq. (2). The variation of the diffusion coefficients with the eluant concentration should be taken into consideration.

The diffusion coefficients $\overline{D}$ and D, which satisfy the relation of Eq. (2), were calculated by means of Eq. (2) and experimental values of $r_0 = 1.31 \times 10^{-2}$ cm, $\beta = 0.33$, and $\lambda_1'' = 17.3$ for 0.1 M α-hydroxyisobutyric acid solution, 6.26 for 0.12 M and 2.29 for 0.14 M. The results are shown in Fig. 6. The interdiffusion coefficient in the ion-exhcanger $\overline{D}$ increases with the concentration of the eluant, contrary to the view that the diffusion coefficient decreases with increase of salt concentration. The diffusion coefficient in solution D decreased as the concentration of the eluant increases.

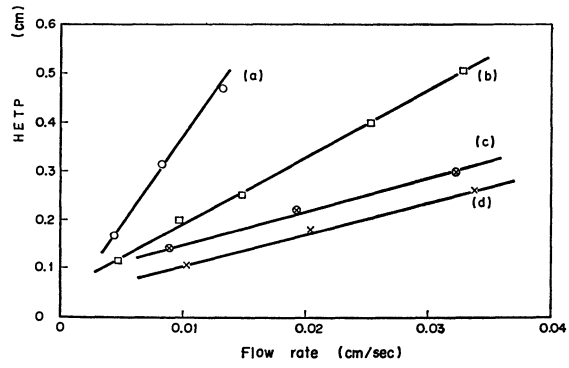

Fig. 5. Relation between HETP and the flow rate under the condition of various eluant concentrations and different column temperatures.
(a): 0.14 M, 15 °C, $\lambda'' = 2.29$, (b): 0.12 M, 15 °C, $\lambda'' = 6.26$, (c): 0.10 M, 15 °C, $\lambda'' = 17.3$, (d): 0.12 M, 33.8 °C, $\lambda'' = 15.7$.

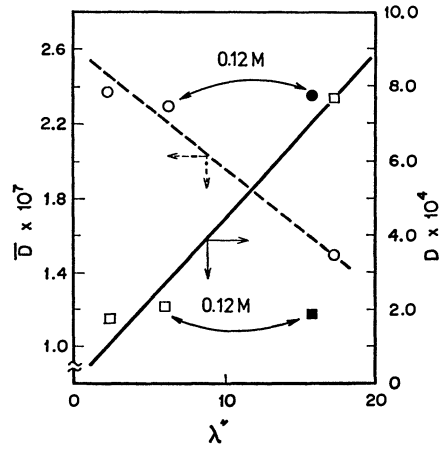

Fig. 6. Relations between the column distribution ratio and the diffusion coefficients $\overline{D}$ and D.
○: $\overline{D}$ at 15 °C, □: D at 15°C, ●: $\overline{D}$ at 33.8 °C, ■: D at 33.8 °C.

Brücher and Szarvas[5] recognized a similar phenomenon, *viz.*, the interdiffusion coefficients of cerium and promethium ions in the ion-exchanger increase with the concentration of ammonium lactate. They explained the phenomenon to be due to the decrease of the charge from 3 to a value around 2 of the rare earth ions diffusing in the resin phase owing to the formation of lactate complex above a certain ammonium lactate concentration. By applying their explanation to the present work, the increase of $\overline{D}$ with the eluant concentration can be connected to the increase in the contribution of LuB^{2+} ions to the ion-exchange reaction, where B is α-hydroxyisobutyrate ion. The assumption of the absorption of lutetium as LuB^{2+} ions is consistent with the view of Holm[6] and Powell.[7] However, the contribution of LuB^{2+} ions is thought to be smaller than that of Lu^{3+} ions, since the interdiffusion coefficient obtained in this work is almost consistent with that of Lu^{3+} ions.[8]

The linear relationships between $\overline{D}$ and D, and λ_1'' in Fig. 7 can be expressed as $\overline{D}=2.6\times10^{-7}-6.4\times10^{-9}\ \lambda_1''$ and $D=4.2\times10^{-5}\ \lambda_1''$, respectively. Consequently, in the case of separating lutetium with the eluant of pH 3.77, HETP at an arbitrary column distribution ratio and a flow rate can be calculated by substituting the above expressions for $\overline{D}$ and D into Eq. (2).

Effect of Temperature on Elution Curve. The elution curves of lutetium (Fig. 7) were obtained when the operating temperature varied within the range 15—35 °C. The peak position or the column distribution ratio varies greatly with temperature. There is a linear relationship between the column distribution ratio and the reciprocal of absolute temperature (Fig. 8). A similar linear relation was observed by Seyb[1] for terbium and yttrium except that his temperature dependence is rather small.

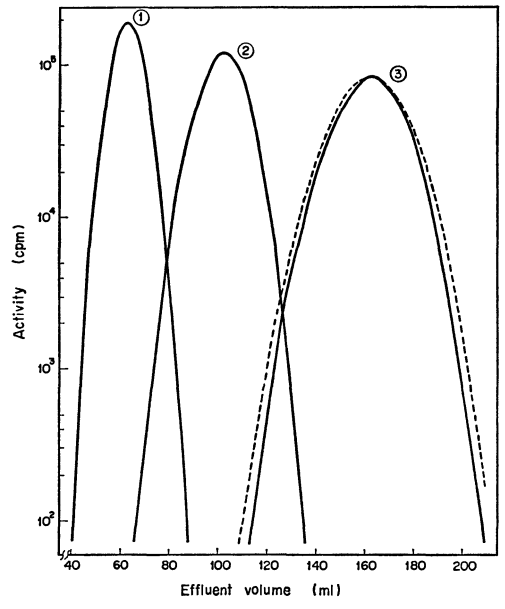

Fig. 7. Variation of the elution curve with column temperature at the eluant concentration of 0.12 M.
①: 15 °C, 33.6 cm h^{-1}, ②: 25 °C, 44.4 cm h^{-1}, ③: 34.8 °C, 50.1 cm h^{-1}.
The dotted line represents the calculated elution curve obtained at the column temperature of 15 °C by changing the eluant concentration so as to fit the peak position to that of case ③.

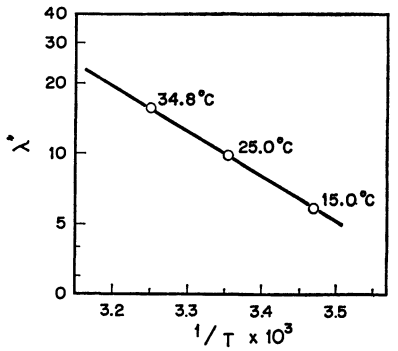

Fig. 8. Relation between the column distribution ratio and the reciprocal of absolute temperature (T).

From a direct comparision of the elution curves in Fig. 7, it is not clear whether a sharper elution peak can be obtained or not with temperature rise, since the peak position of lutetium is not kept constant. The effect of temperature on the shape of the elution peak can be analyzed by taking the variation of the diffusion coefficients due to the rise of temperature into consideration.

The values of HETP and the diffusion coefficients $\overline{D}$ and D at 33.8 °C were calculated in the same way as described above. The results are plotted in Figs. 5 and 6, respectively. The $\overline{D}$ and D values are equal to those obtained for the same concentration of the eluant at the operating temperature 15 °C (Fig. 6). The decrease of HETP with the increase of the column distribution ratio due to the rise of the operating temperature from 15 °C to 33.8 °C (compare b and d

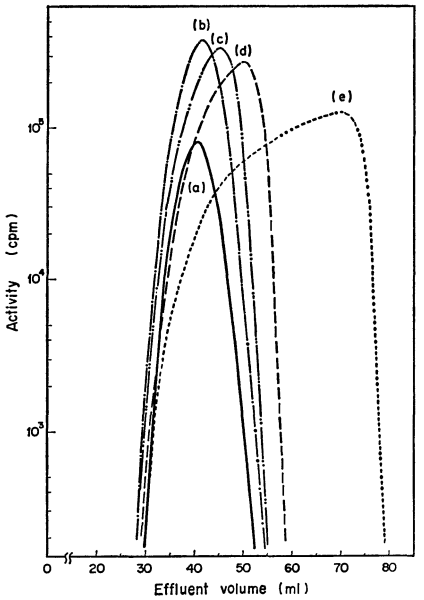

Fig. 9. Variation of the elution curve with the amounts of lutetium.
(a) 16 μg cm^{-2}, (b) 200 μg cm^{-2}, (c) 1.00 mg cm^{-2}, (d) 2.00 mg cm^{-2}, (e) 10.0 mg cm^{-2}.

in Fig. 5) exceeds the decrease of HETP by the increase of the column distribution ratio due to the decrease of the concentration of the eluant from 0.12 M to 0.10 M at 15 °C (compare b and c in Fig. 5), since the decrease of the concentration of the eluant results in the decrease of $\bar{D}$ and the increase of D as well as the increase of the column distribution ratio.

When the concentration of the eluant at 15 °C is selected so as to give the same column distribution ratio as obtained with 0.12 M of the eluant at 34.8 °C, the calculated elution curve of lutetium becomes as shown by the dotted line in Fig. 7. Obviously a sharper elution curve can be obtained by raising the operating temperature from 15 °C to 34.8 °C.

Effect of Lutetium Amount on Elution Curve. The shape of the elution curve of lutetium varies as shown in Fig. 9 as the amount of lutetium increases. The peak positions of the elution curves are the same in a deviation of 5% up to 200 μg cm^{-2} of lutetium. The result differs from that of Massart and Hoste.[2] Over 200 μg cm^{-2}, however, the symmetric elution curve is deformed rapidly with the increase of lutetium amount, simultaneously with the delay of the appearance of the position of the elution curve.

References

1) K. E. Seyb, *Z. Anal. Chem.*, **226**, 159 (1967).
2) D. L. Massart and J. Hoste, *Anal. Chim. Acta*, **28**, 378 (1963).
3) E. Glueckauf, "Ion Exchange and Its Applications," Society of Chemical Industry, London (1955); F. Helfferich, "Ion Exchange," McGraw-Hill Book Company, Inc., New York (1962).
4) E. R. Tompkins, D. H. Harris, and J. X. Khym, *J. Amer. Chem. Soc.*, **71**, 2504 (1949).
5) E. Brücher and P. Szarvas, *J. Inorg. Nucl. Chem.*, **28**, 2361 (1966).
6) L. W. Holm, G. R. Choppin, and D. Moy, *ibid.*, **19**, 251 (1961).
7) J. E. Powell, *ibid.*, **30**, 1331 (1968).
8) H. D. Sharma, R. E. Jervis, and L. W. McMillen, *J. Phys. Chem.*, **74**, 969 (1970).

Mixed Complexes with Bulky Ligands. I. Cobalt(II) Complexes Containing *N,N*-Bis[2-(dimethylamino)ethyl]methylamine

Shunji UTSUNO

Department of Chemistry, Faculty of Science, Shizuoka University, Oya, Shizuoka 422

(Received May 12, 1975)

Nine new cobalt(II) complexes were prepared which contained *N,N*-bis[2-(dimethylamino)ethyl]methylamine (dienMe) and some unidentate or bidentate ligands, such as acetonitrile, ammonia, ethylenediamine (en), trimethylenediamine (tn), the acetylacetonate ion (acac), or the oxalate ion. The solid-reflectance spectra revealed that six complexes of the $[Co(XX)dienMe](ClO_4)_n$ formula ($XX=2CH_3CN$, $2NH_3$, en, tn, acac, or $1/2C_2O_4$; $n=1$ or 2) are five-coordinated, whereas three complexes, $[Co(C_2O_4)(H_2O)dienMe]$ and $Co(C_2O_4)_{1/2}(solv)(dienMe)ClO_4$ ($solv=CH_3CN$ or CH_3OH), are six-coordinated. On the basis of their electronic spectra, most of the five-coordinated complexes were supposed to have a trigonal-bipyramidal structure in the solid state and in solution. The IR spectra of three hemioxalato complexes revealed the presence of quadridentate oxalate-ion bridging between two cobalt ions, regardless of their coordination number.

In recent years, five-coordinated complexes have been extensively studied. From this laboratory, it has been reported that the bulky ligand, 6-methyl-2-aminomethylpyridine (mepic), reacts with the bivalent metal salts to form five-coordinated complexes $[MX(mepic)_2]ClO_4$ (M=Cu, Ni, or Co; X=Cl, Br, or I).[1] However, six-coordinated complexes were also obtained when the halo-ligand was replaced with relatively small ligands, such as two isothiocyanate ions, a bidentate nitrate ion, or two molecules of water.

N,N-Bis[2-(dimethylamino)ethyl]methylamine (dienMe) is also a bulky ligand reported to form high-spin complexes with the bivalent transition metals from manganese to zinc, these complexes have the general formula of $[MX_2dienMe]$ (X=Cl, Br, or I).[2] We have attempted to study the preparation and the properties of a mixed complex containing a simple bidentate ligand or unidentate ones in place of the two halo-ligands. This paper will report a study of the mixed complexes with cobalt(II).

Experimental

Reagents. *N,N*-Bis[2-(dimethylamino)ethyl]methylamine was prepared by the method in the literature.[3] Cobalt(II) perchlorate was obtained from perchloric acid and cobalt(III) hydroxide, which had itself been prepared by the reaction of chloropentaamminecobalt(III) chloride and sodium hydroxide. Nitromethane was purified by the fractional distillation of the water azeotrope, followed by dehydration with calcium chloride and by distillation under a nitrogen atmosphere using a 50-cm column packed with glass helices. All the other reagents were reagent-grade chemicals.

Preparation of the Complexes. Because of the unstability of the complexes toward moisture and carbon dioxide, all the complexes were prepared in a dry box in the presence of solid potassium hydroxide and silica gel. The ethylenediamine and the trimethylenediamine complexes were prepared under nitrogen.

$[Co(CH_3CN)_2dienMe](ClO_4)_2$. An acetonitrile solution of cobalt(II) perchlorate hexahydrate (18.3 g : 50 mmol in 100 dm^3 of the solvent) was evaporated with stirring almost to dryness. An additional 100 dm^3 of acetonitrile was then added to the residue, and the mixture was evaporated repeatedly to a volume of about 30 dm^3. After the solution had cooled to room temperature, 8.67 g (50 mmol) of dienMe was added. The crystals thus formed were collected on a sintered glass filter and washed with ethanol. The crude product was recrystallized by the addition of ethanol to the acetonitrile solution. In the open air, the complex turned from purple to green in only a few minutes.

$[Co(XX)dienMe](ClO_4)_2$ ($XX=2NH_3$, en, or tn). Into a filtered solution of 2 mmol of $[Co(CH_3CN)_2dienMe](ClO_4)_2$ in 30 dm^3 of methanol, an equimolar quantity of ammonia or diamine in methanol was stirred. The complex thus precipitated was collected on a filter, washed with ethanol, and dried over phosphorus pentoxide. It was then recrystallized from hot methanol.

$[Co(acac)dienMe]ClO_4$. In to a solution of 2 mmol of bis(acetylacetonato)cobalt(II) in ethanol, a drop of acetylacetone, 4 mmol of dienMe and 2 mmol of cobalt(II) perchlorate hexahydrate were stirred successively. The resulting solution was evaporated to dryness under a reduced pressure at room temperature. The residue was treated with chloroform, filtered, and evaporated to dryness. It was then recrystallized from small amount of hot ethanol and washed with 1 : 1 ethanol and diethyl ether.

$[Co(C_2O_4)(H_2O)dienMe]$. Freshly precipitated cobalt(II) oxalate was treated with equimolar quantities of dienMe in the presence of a small amount of water. The resulting solution was filtered and allowed to evaporate to dryness under a reduced pressure. The residue was dissolved in chloroform and was precipitated by the addition of diethyl ether to the filtrate.

$Co(C_2O_4)_{1/2}(dienMe)ClO_4$ and $Co(C_2O_4)_{1/2}(solv)(dienMe)ClO_4$ ($solv=CH_3CN$ or CH_3OH). To a slurry of 5.132 g (10 mmol) of $[Co(CH_3CN)_2dienMe](ClO_4)_2$ in 50 dm^3 of ethanol, 0.670 g (5 mmol) of sodium oxalate was added, after which the mixture was stirred overnight. The resulting crystals were collected on a glass filter and washed with hot ethanol. Recrystallization from hot methanol gave the methanol adduct, which yielded $Co(C_2O_4)_{1/2}(dienMe)ClO_4$ when washed with hot ethanol. The acetonitrile adduct was obtained by the addition of dry diethyl ether to the acetonitrile solution of the crude product.

Physical Measurements. The absorption spectra of the solutions were recorded at room temperature with a Shimadzu MPS-5000 recording spectrophotometer and silica cells with a path length of 1 cm. The reflectance spectra were obtained using the reflectance attachments and using potassium perchlorate as the reference. For the moisture-sensitive complexes, finely ground samples, prepared in a dry box, were covered with a glass plate. The IR spectra were measured over the range of 400—4000 cm^{-1} with a Hitachi EPI-G3 grating spectrophotometer. The samples were prepared as Nujol and hexachlorobutadiene mulls. The

magnetic moments were determined by the Gouy method at room temperature, using water as the standard. The molar susceptibility in each case was corrected for the diamagnetism of the ligands and perchlorate ions.

Analysis. The cobalt was determined volumetrically with an EDTA solution, using Xylenol Orange as the indicator. The sample solutions were prepared after decomposing the complexes with a mixture of sulfuric acid and perchloric acid. The organic elements were analyzed by Wako Pure Chemical Ind., Ltd., Osaka.

Results and Discussion

Table 1 shows the colors, the magnetic moments, and the analytical data for the complexes prepared. The analytical values of C, H, and N for $Co(C_2O_4)_{1/2}$(solv)-(dienMe)ClO_4 (solv=CH_3CN and CH_3OH) indicate that some of the solvent molecules were lost or displaced by water, however, the results of the metal analysis and the physical measurements, which were carried out in this laboratory with particular care taken to avoid moisture, show no signs of any loss of the solvent molecules or any adsorption of water.

The magnetic moments of $Co(C_2O_4)_{1/2}$(solv) (dienMe)ClO_4 (solv=CH_3CN and CH_3OH) and [$Co(C_2O_4)$(H_2O)dienMe] lie in the range of the six-coordinated cobalt(II) complexes (4.7—5.2 B.M.), whereas those of the others, which are identified from the electronic spectra as five-coordinated ones, are low, as Table 1 shows. The magnetic moments of most of the five-coordinated cobalt(II) complexes previously reported seem to lie in the range of the tetrahedral complexes (4.4—4.7 B.M.).[1b,2,4]

The IR spectra were measured for all the complexes studied. Because of their complex spectra, however, the assignment of each band was not possible. Thus, the configuration of the ligand was not determined. However, some information can be obtained from the characteristic bands due to anions or ligands: 1) The possibility of the coordination of a perchlorate ion can be rejected, because the bands at 1100 and 625 cm^{-1} are not appreciably split for any of the complexes containing the perchlorate ions. 2) As for the complexes with acetonitrile, *i.e.*, [$Co(CH_3CN)_2$dienMe]-(ClO_4)$_2$ and $Co(C_2O_4)_{1/2}(CH_3CN)$(dienMe)ClO_4, the sharp bands due to C≡N stretching were observed at 2280 and 2300 cm^{-1}, which are slightly higher than those of free acetonitrile, 2233 and 2282 cm^{-1}, in a neat solvent. No bands due to the presence of uncoordinated acetonitrile were observed in either complex. 3) In the 1600—1700 cm^{-1} region, the antisymmetric (O–C–O) stretching bands of the oxalato and the hemioxalato complexes are markedly different; *i.e.*, the former exhibits the splitted bands at 1614 and 1670 cm^{-1}, whereas the latter exhibit a sharp band at *ca.* 1660 cm^{-1}. The single peak found for the hemioxalato complexes seems to indicate that the four carbon-oxygen bonds of the oxalate ion are equivalent with each other. Thus, it may be inferred that the oxalate ion is bidentate in [$Co(C_2O_4)(H_2O)$-dienMe], whereas quadridentate in three hemioxalato complexes. It has been reported that an oxalate ion can bridge two metal ions, using all the oxygens as the ligand atoms.[5] This may also be the case for the present hemioxalato complexes.

The electronic spectra of these complexes were measured both in the solid state and in solution. Table 2 shows the positions and the molar absorptivities of the observed maxima.

The solid-reflectance spectra reveal that [$Co(C_2O_4)$-(H_2O)dienMe] and $Co(C_2O_4)_{1/2}$(solv) (dineMe)ClO_4 (solv=CH_3CN and CH_3OH) are six-coordinated, whereas the others are five-coordinated. The spectra of these five-coordinated complexes resemble that of [CoCl(trenMe)]Cl (trenMe=tris[2-(dimethylamino)-ethyl]amine) rather than that of [$CoCl_2$(dienMe)].[2,6] It has been reported that the former has essentially a trigonal-bipyramidal structure,[6,7] whereas the latter has a structure intermediate between a trigonal-bipyramidal one and a tetragonal-pyramidal one.[8] The similarlity of the spectra is the most remarkable in the acetylacetonato complex, the most probable structure of which is shown in Fig. 1. It may be supposed that the en, tn, and diammine complexes also take this structure.

In solution, most of the complex ions seem to maintain their structure in the solid state, because the absorption spectrum of the solution is essentially the same as the reflectance spectrum of the solid. An exception is the hemioxalato complex, $Co(C_2O_4)_{1/2}$-(dienMe)ClO_4. As Fig. 2 shows, the absorption spectra of this complex in nitromethane, in acetonitrile, and in methanol are different from each other,

Table 1. Color, magnetic moments, and chemical analyses of the dienMe complexes

Complex[a]	Color	μ_{eff} (B.M.)	Temp. (°C)	Found (%)				Calcd (%)			
				Co	C	H	N	Co	C	H	N
$2CH_3CN$, $2ClO_4$	purple	4.43	15.1	11.56	30.38	5.76	13.12	11.48	30.42	5.70	13.65
$2NH_3$, $2ClO_4$	purple	4.51	13.7	12.41	23.40	6.34	14.47	12.67	23.24	6.28	15.05
en, $2ClO_4$	violet	4.42	17.3	12.07	26.61	6.14	14.27	12.00	26.90	6.36	14.26
tn, $2ClO_4$	violet	4.50	19.8	11.54	28.31	6.51	13.81	11.66	28.53	6.58	13.86
acac, ClO_4	olive	4.45	15.7	13.45	39.17	7.14	9.92	13.68	39.03	7.02	9.75
C_2O_4, H_2O	red	4.96	15.7	17.08	40.13	7.14	12.56	17.42	39.06	7.45	12.42
$\frac{1}{2}C_2O_4$, ClO_4	violet	4.41	15.7	15.53	31.50	6.12	11.07	15.69	31.97	6.17	11.18
$\frac{1}{2}C_2O_4$, CH_3OH, ClO_4	purple	4.94	22.2	14.44	31.66	6.42	10.39	14.45	32.40	6.67	10.31
$\frac{1}{2}C_2O_4$, CH_3CN, ClO_4	purple	4.78	21.8	14.08	33.35	6.08	12.81	14.14	34.58	6.29	13.44

a) All the species contained in the complex per one cobalt ion are indicated but a dienMe molecule.

Table 2. Absorption maxima of the dienMe complexes

Complex[a]	State	ν_{max}, 10^3 cm^{-1} (ε_{max} for the solution)
$2CH_3CN$, $2ClO_4$	solid	*ca.* 5.6, 15.2, 18.1, 20 sh., 21.5
	CH_3CN soln.	6.0(10.0), 15.0(15.2), 17 sh., 17.9(47.1), 20 sh., 21.6(35.2)
$2NH_3$, $2ClO_4$	solid	*ca.* 5.6, 13.7, 17.5, 19.5 sh., 20.0, 21 sh.
	CH_3CN soln.	*ca.* 5.5(10.0), 14.0(14.5), 17.9(27.6), 19.2 sh., 20.2(31.8), 21 sh.
en, $2ClO_4$	solid	*ca.* 5.6, 14.3, 17.1, 20.2, 20 sh.
	CH_3CN soln.	*ca.* 5.0(10.0), 14.0(15.5), 17.3(16.6), 20.1(41.5), 21 sh.
tn, $2ClO_4$	solid	*ca.* 5.6, 13.9, 17.2, 20.2, 21 sh.
	CH_3CN soln.	5.0(10.1), 13.9(15.2), 17.5(20.5), 20.0(45.2), 21 sh.
acac, ClO_4	solid	5.9, 14.3, 17.0, 20.5, 21.3 sh.
	soln.[b]	5.8(12.4), 14.5(21.0), 17.1(29.0), 20.5(47.6), 21.5 sh.
C_2O_4, H_2O	solid	8.6, 19 sh., 19.5, 20 sh., 21 sh.
	soln.[b]	8.8(6.1), 19.0 sh., 19.8(26.7)
$\frac{1}{2}C_2O_4$, ClO_4	solid	*ca.* 4.5, 13.3, 17.3, 18.7, 19.5, 21.5 sh.
	CH_3NO_2 soln.	*ca.* 5.2(8.9), 13.7(11.2), 17.3(17.6), 18.9 sh., 19.5(23.3). 23 sh.
	CH_3CN soln.	8.8(5.9), *ca.* 14(2.0), 17 sh., 18.5 sh., 19.4(25.2), 20.3(24.2)
	CH_3OH soln.	8.5(4.6), *ca.* 14(2.5), 17 sh., 18.5 sh., 19.7(22.5), 21 sh.

a) All the species contained in the complex per one cobalt ion are indicated but a dienMe molecule. b) The chloroform, nitromethane, and the acetonitrile solutions give rise to practically the same spectra with each other.

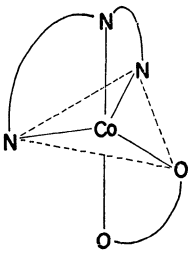

Fig. 1. The plausible coordination in $[Co(acac)dienMe]ClO_4$.

but are quite similar to the reflectance spectra of $Co(C_2O_4)_{1/2}(dienMe)ClO_4$, $Co(C_2O_4)_{1/2}(CH_3CN)(dienMe)ClO_4$, and $Co(C_2O_4)_{1/2}(CH_3OH)(dienMe)ClO_4$ respectively. The fact implies that solvolysis occurs both in acetonitrile and in methanol to form six-coordinated complexes. The coordination structure of this complex in a solid appears not to change only in nitromethane. No signs of the formation of six-coordinated complex were found in the nitromethane solution in the range of 9000—11000 cm^{-1}.

Both in the solid state and in solution, the ν_{max} values of the acac complex are slightly higher than those of the complexes containing en, tn, or ammonia. This is curious because the spectrochemical series of these ligands are generally in this order: en>tn> $NH_3 \gg$ acac. This fact may be ascribed to the stereochemical nature of the dienMe ligand, which has bulky methyl groups at the terminal nitrogen atoms. The steric repulsion between the methyl groups and the amine or ammine hydrogens may make the field around the cobalt(II) ion weaker than that in the acac complex.

The author is indepted to Miss Mitsue Futagi for her help in part of the measurements and the preparation of the complexes. This work was partly supported by the Scientific Research Grant from the Ministry of Education.

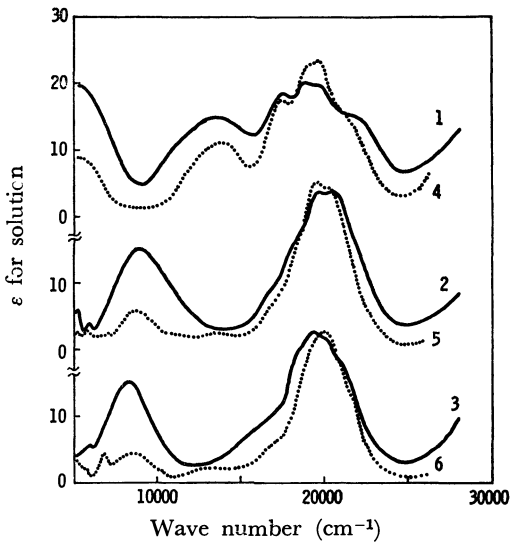

Fig. 2. The electronic spectra of the hemioxalato complexes in the solid state (——) and in solution (·····): the reflectance spectra of 1) $Co(C_2O_4)_{1/2}(dienMe)ClO_4$, 2) $Co(C_2O_4)_{1/2}(CH_3CN)(dienMe)ClO_4$, and 3) $Co(C_2O_4)_{1/2}(CH_3OH)(dienMe)ClO_4$; and the absorption spectra of $Co(C_2O_4)_{1/2}(dienMe)ClO_4$ in 4) nitromethane, 5) acetonitrile, and 6) methanol.

References

1) S. Ustuno, *J. Inorg. Nucl. Chem.*, **32**, 1631 (1970); b) S. Ustuno, *ibid.*, **32**, 183 (1970); c) S. Ustuno and K. Sone, *ibid.*, **28**, 2647 (1966).
2) M. Ciampolini and G. P. Speroni, *Inorg. Chem.*, **5**, 45 (1966).
3) A. Marxer and K. Miesher, *Helv. Chim. Acta*, **34**, 924 (1951).
4) R. L. Carlin, "Transition Metal Chemistry," Vol. 1, ed. by R. L. Carlin, Marcel Dekker, New York (1965), p. 20.
5) N. F. Curtis, *J. Chem. Soc.*, **1963**, 4109.
6) M. Ciampolini and N. Nardi, *Inorg. Chem.*, **5**, 41 (1966).
7) M. Di Vaira and P. L. Orioli, *ibid.*, **6**, 955 (1967).
8) M. Di Vaira and P. L. Orioli, *Chem. Commun.*, **1965**, 590.

Circular Dichroism of Chromium(III) Complexes. V. Circular Dichroism of *trans*-Dihalogenobis(diamine) Complexes with Optically Active Diamines

Sumio KAIZAKI and Yoichi SHIMURA

Department of Chemistry, Faculty of Science, Osaka University, Toyonaka, Osaka 560

(Received June 19, 1975)

Nine chromium(III) complexes of *trans*-$[CrX_2(N)_4]$ type with three kinds of optically active diamines (*R*-propylenediamine, *S,S*-stilbenediamine and *S,S*-2,4-pentanediamine) were prepared and the absorption and circular dichroism spectra were measured in the region of their d–d transitions. The CD behaviors in the spin-allowed transitions were discussed in comparison with the corresponding cobalt(III) complexes and their bands were assigned to the tetragonal components. On the basis of the theoretical correlation between the rotational strengths for the spin-forbidden transitions and for the spin-allowed transitions, the CD peaks in the spin-forbidden transitions were discussed and assigned.

In the previous paper,[1] circular dichroism (CD) spectra of optically active tris-chelate chromium(III) complexes in the spin-forbidden transitions have been reported and analyzed in connection with the CD in the spin-allowed transitions in terms of the theoretical correlation between the rotational strengths in the spin-forbidden and the spin-allowed transitions. Since there have remained some ambiguities about the assignment of the trigonal splitting CD components in the spin-allowed transitions, alternative assignments may be possible. On the other hand, it has been well known that for so-called praseo type complexes the first spin-allowed bands of octahedral parantage split largely enough to resolve the tetragonal components in solution absorption spectra at room temperature and this allows to make the band assignment feasible. On the basis of analyses of absorption spectra as well as crystal field approximation treatments,[2–7] the assignments of spin-allowed d-d transitions of chromium(III) complexes in tetragonal field have been made rigorously, and the tetragonal crystal field parameters, *Dt* and *Ds*, and/or the angular overlap model (AOM) parameters, $\delta\sigma$ and $\delta\pi$,[8] have been derived and discussed.[2–7,9] By using these parameters, the positions and the splittings of the doublet states can also be estimated.[10] Thus, the observation of the spin-forbidden bands provides a criterion for testing the crystal field or AOM parameters. Some absorption and emission data in the spin-forbidden transitions have been reported[11–15] and their peaks have been assigned according to the crystal field theory. The CD in the spin-forbidden transitions will be expected to offer more detailed information, because the rotational strengths for these transitions are theoretically related to those for the spin-allowed transitions. Nevertheless, there has been no report on the CD spectra of tetragonal complexes with optically active diamines not only in the spin-allowed transitions but also in the spin-forbidden transitions, though optical activity of the corresponding Co(III) complexes has been intensively studied in the spin-allowed transitions.[16–19]

In this paper, nine *trans*-$[CrX_2(N)_4]$ type complexes with three kinds of optically active diamines (*R*-propylenediamine=*R*-pn, *S,S*-stilbenediamine=*S,S*-stien and *S,S*-2,4-pentanediamine=*S,S*-2,4-ptn) have been prepared and their absorption and CD spectra have been measured in their spin-allowed and spin-forbidden transition regions. The theoretical correlation between the rotational strengths for the spin-forbidden and spin-allowed transitions will be presented in a manner similar to the trigonal complexes, but in a more refined form including the configuration interaction and molecular orbital extension to the spin-orbit coupling effect on axial ligands.

Experimental

Preparation of Optically Active Diamines. *1)* R-*Propylenediamine*: This was resolved through its tartrate and isolated as free diamine.

2) S,S-*Stilbenediamine*: The racemic diamine was prepared by the method of Williams and Bailar,[20] and resolved into the enantiomer through its tartrate by the method of Lifschitz and Bos.[21]

3) R,R- *or* S,S-*2,4-Pentanediamine*: This was prepared and resolved by the method of Bosnich,[19] and isolated as its dihydrogen dichloride.

Preparation of the Complexes. The fluoro complexes were prepared by the method analogous to Glerup *et al.*'s.[22] The conversion of the fluoro complexes to the chloro and bromo complexes was carried out by the modified method of Fee *et al.*[23]

The R-*Propylenediamine Complexes.* *1)* trans-$[CrF_2(R\text{-}pn)_2]ClO_4\cdot H_2O$: This complex was obtained by the method of Glerup *et al.*[22] Found: C, 19.97; H, 6.35; N, 15.39%. Calcd for *trans*-$[CrF_2(R\text{-pn})_2]ClO_4\cdot H_2O$: C, 20.26; H,6.23; N, 15.75%.

2) trans-$[CrCl_2(R\text{-}pn)_2]ClO_4$: *trans*-$[CrF_2(R\text{-pn})_2]ClO_4\cdot H_2O$ (12 g) was dissolved in 15 cm³ of 40—44% hydrochloric acid, which was obtained by bubbling hydrogen chloride to concentrated hydrochloric acid at 0 °C. The dark red solution obtained was kept with stirring for a while at room temperature; then red crystals were precipitated. The color of the separated crystals was grayish green with a reddish tint. The yield was about 8 g. Recrystallization was carried out from methanol–ether. Found: C, 18.91; H, 5.66; N, 15.10%. Calcd for *trans*-$[CrCl_2(R\text{-pn})_2]ClO_4$: C, 19.45; H, 5.44; N, 15.12%.

3) trans-$[CrBr_2(R\text{-}pn)_2]Br\cdot H_2O$: One gram of *trans*-$[CrF_2(R\text{-pn})_2]ClO_4\cdot H_2O$ was dissolved in 3 cm³ of 48% hydrobromic acid, and the mixture was stirred for a while at room temperature. The complex was obtained as a green precipitate; the yield was about 0.3 g. This was recrystallized from methanol–ether. This complex was also obtained in good yield from the reaction in 3.5 M methanolic hydrogen bromide solution. Found: C, 15.70; H, 4.83; N, 11.98%. Calcd for *trans*-$[CrBr_2(R\text{-pn})_2]Br\cdot H_2O$: C, 15.74; H, 4.84; N, 12.23%.

The S,S-Stilbenediamine Complexes. *1)* trans-[CrF_2(S,S-*stien*)$_2$]$ClO_4 \cdot H_2O$: *trans*-[CrF_2(py)$_4$]ClO_4[22] (17.5 g) was dissolved in 100 cm^3 of hot 2-methoxyethanol. To the resulting violet solution was added 14 g *S,S*-stilbenediamine, and then the solution was refluxed for a while. The red solution obtained was condensed by a vacuum rotary evaporator. The red orange precipitate was obtained by adding the condensed solution to water. This was dissolved in methanol, filtered and the pinkish orange crystals were precipitated by adding ether. The color of the filtrate was red. The pinkish orange compound was insoluble in acetone, while the red one was soluble in acetone. The purification of this pinkish orange complex was performed by adding the methanolic solution to acetone. Found: C, 53.49; H, 5.49; N, 8.90%. Calcd for *trans*-[CrF_2(*S,S*-stien)$_2$]$ClO_4 \cdot H_2O$: C, 53.20; H, 5.42; N, 8.86%.

2) trans-[$CrCl_2$(S,S-*stien*)$_2$]$Cl \cdot 2H_2O$: To 47% methanolic hydrogen chloride solution was added 0.55 g of *trans*-[CrF_2(*S,S*-stien)$_2$]$ClO_4 \cdot H_2O$. The color of the solution changed to dark red. Then the reaction mixture was poured into water. The pale green powder was obtained. This was recrystallized from methanol–ether. Found: C, 54.27; H, 5.87; N, 9.03%. Calcd for *trans*-[$CrCl_2$(*S,S*-stien)$_2$]$Cl \cdot 2H_2O$: C, 54.33; H, 5.86; N, 9.05%.

3) trans-[$CrBr_2$(S,S-*stien*)$_2$]$Br \cdot CH_3OH$: *trans*-[CrF_2(*S,S*-stien)$_2$]$ClO_4 \cdot H_2O$ (1 g) was suspended in 20 cm^3 of 3.5 M methanolic hydrogen bromide solution. The starting complex was gradually dissolved during about one hour. After stirring for about two hours, the color of the solution turned to green. The resulting solution was poured into water. Then the desired complex was obtained as a green precipitate. This was recrystallized from methanol–ether. Found: C, 46.34; H, 4.83; N, 7.62%. Calcd for *trans*-[$CrBr_2$(*S,S*-stien)$_2$]$Br \cdot CH_3OH$: C, 46.55; H, 4.85; N, 7.49%.

The S,S-2,4-pentanediamine complexes. *1)* trans-[CrF_2(S,S-*2,4-ptn*)$_2$]ClO_4: Pure sodium (1.1 g) was dissolved in 30 cm^3 of 2-methoxyethanol. To this solution was added 4 g of *S,S*-2,4-ptn·2HCl by portions; then white powder of sodium chloride was precipitated. During this procedure, dry nitrogen gas was bubbled into the solution in order to protect from carbon dioxide and moisture. The sodium chloride was removed by filtration, and washed with a small amount of 2-methoxyethanol. To the combined filtrate and washings was added 5 g of *trans*-[CrF_2(py)$_4$]ClO_4. The mixture was heated on a steam bath and then orange crystals were precipitated. This product was contaminated by a small amount of impurities such as chromium(III) hydroxide. The recrystallization was carried out from the aqueous solution which was slightly acidified with a small amount of $HClO_4$. The yield was about 2.3 g. Found: C, 30.42; H, 7.24; N, 14.20%. Calcd for *trans*-[CrF_2(*S,S*-2,4-ptn)$_2$]ClO_4: C, 30.50; H, 7.17; N, 14.23%.

2) trans-[$CrCl_2$(S,S-*2,4-ptn*)$_2$]ClO_4: In a 5 cm^3 portion of concentrated hydrochloric acid was dissolved 0.7 g of *trans*-[CrF_2(*S,S*-2,4-ptn)$_2$]ClO_4, and the mixture was allowed to stand for 3—4 hr. Green needles were precipitated. They were recrystallized from methanol–ether. Found: C, 28.19; H, 6.67; N, 13.34%. Calcd for *trans*-[$CrCl_2$(*S,S*-2,4-ptn)$_2$]ClO_4: C, 28.21; H, 6.63; N, 13.16%.

3) trans-[$CrBr_2$(S,S-*2,4-ptn*)$_2$]Br: *trans*-[CrF_2(*S,S*-2,4-ptn)$_2$]ClO_4 (1 g) was dissolved in a small amount of 4 M ethanolic hydrogen bromide. The solution was allowed to stand over night in a refrigerator. Then light green leaflets were obtained. They were recrystallized from methanol–ether. Found: C, 24.03; H, 5.77; N, 11.30%. Calcd for *trans*-[$CrBr_2$(*S,S*-2,4-ptn)$_2$]Br: C, 24.21; H, 5.68; N, 11.29%.

Measurements. The electronic absorption spectra were measured by a Shimadzu spectrophotometer UV-200. The CD spectra were recorded with a Jasco MOE-1 spectropolarimeter. The CD measurements were carried out with the wavelength expansion of 4 nm/cm and 10 nm/cm in the spin-forbidden and spin-allowed transition regions, respectively. Therefore, four significant figures were used in expressing wave numbers in the spin-forbidden transition region, whereas three significant figures were used in the spin-allowed transition region. The concentrations of the complexes for the CD measurements in the spin-forbidden transition region were 10^{-1} to 10^{-2} mol dm^{-3}, and the cell lengths employed were 5 and 10 cm. The absorption and CD spectra of the fluoro complexes with *R*-pn and *S,S*-ptn were measured in water, while those of the other complexes in methanol.

Results and Discussion

1) Absorption Spectra. The ligand field absorption spectra of the nine complexes concerned are given in Figs. 1—3, and their characteristics are listed in Table 1. It is noted that their absorption patterns are similar, on the whole, to those of the corresponding *trans*-dihalogenobis(ethylenediamine)chromium(III) complexes, being independent of the optically active diamines and only dependent on the axial ligands. That is, for the fluoro complexes, two split components are observed in both the first $^4T_2 \leftarrow {}^4A_2$ and the second $^4T_1 \leftarrow {}^4A_2$ spin-allowed octahedral transition regions, whereas the other complexes show two largely split components in the first band region and only one in the second band region as in Figs. 1—3. The higher frequency component in the first band region shifts scarcely for any halogeno complexes and lies at about 22000 cm^{-1}, where the first absorption band of [Cr(N)$_6$] type complex is expected. While the lower frequency component shifts to the lower frequency side in the order of fluoro, chloro and bromo complexes. This order is in coincidence with spectrochemical series of the axial halogeno ligands.[21]

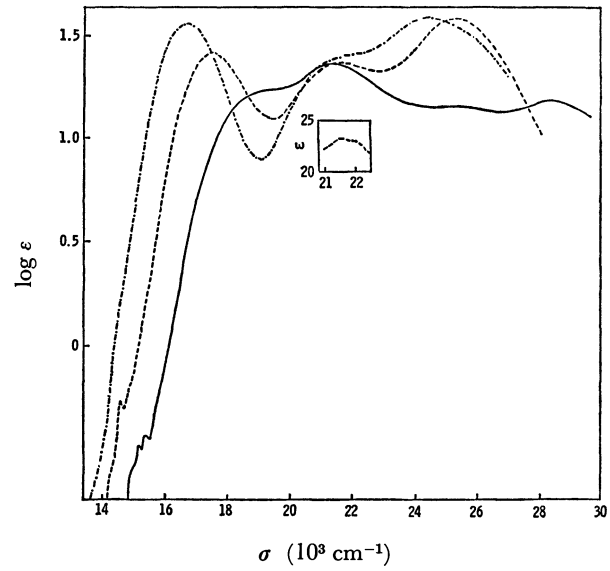

Fig. 1. Absorption curves of *trans*-[CrX_2(*R*-pn)$_2$]$^+$, X=F (——) in water; X=Cl (----) in methanol; X=Br (—·—·—) in methanol.

TABLE 1. ABSORPTION (AB) AND CD DATA FOR TETRAGONAL CHROMIUM(III) COMPLEXES IN THE d-d TRANSITIONS (Wave numbers are in 10^3 cm^{-1}; CD intensities asterisked are multiplied by 10^3)

AB ($\log \varepsilon_{max}$)		CD ($\Delta\varepsilon_{ext}$)		Assignment
trans-[CrF_2(*R*-pn)$_2$]$ClO_4 \cdot H_2O$				
		13.33	(+0.67*)	$^2E(^2T_1)$
		14.50	(+0.93*)	
14.92[a]		14.73	(+1.35*)	$^2B_1(^2E)$
15.08	($\bar{1}$.52)	15.03	(+9.96*)	$^2A_1(^2E)$
15.33	($\bar{1}$.56)	15.30[a]	(+2.4*)	$^2A_2(^2T_1)$
		15.55	(+4.49*)	
		15.68	(−0.56*)	
		15.79	(+5.08*)	
19.3[a]	(1.24)	18.8	(+0.41)	$^4E(^4T_2)$
21.5	(1.36)	22.0	(−0.15)	$^4B_2(^4T_2)$
25.0	(1.16)			$^4E(^4T_1)$
28.5	(1.18)	29.7	(−0.0043)	$^4A_2(^4T_1)$
trans-[$CrCl_2$(*R*-pn)$_2$]ClO_4				
		14.08	(+0.71*)	
		14.33	(+2.78*)	$^2A_1(^2E)$
14.52	($\bar{1}$.73)	14.58	(+0.45*)	$^2B_1(^2E)$
		14.70	(−0.13*)	$^2E(^2T_1)$
		14.90[a]	(+0.30*)	
		15.02	(+1.11*)	$^2A_2(^2T_1)$
		15.19	(−0.73*)	
		15.36	(−0.21*)	
17.5	(1.43)	17.7	(+0.37)	$^4E(^4T_2)$
21.7	(1.39)	21.7	(−0.09)	$^4B_2(^4T_2)$
25.3	(1.60)	25.7	(+0.11)	$^4E(^4T_1)$
trans-[$CrBr_2$(*R*-pn)$_2$]Br				
		14.08	(−1.26*)	$^2E(^2T_1)$
		14.29	(+0.28*)	$^2A_1(^2E)$
		14.39	(−0.98*)	$^2B_1(^2E)$
		14.55	(−0.49*)	
		14.65	(+0.53*)	$^2A_2(^2T_1)$
		14.88	(−0.50*)	
16.7	(1.57)	17.0	(+0.35)	$^4E(^4T_2)$
22.0	(1.40)	21.3	(−0.06)	$^4B_2(^4T_2)$
24.6	(1.58)	26.0	(+0.13)	$^4E(^4T_1)$
trans-[CrF_2(*S,S*-stien)$_2$]$ClO_4 \cdot H_2O$				
		12.71	(−0.50*)	$^2E(^2T_1)$
		13.58	(−1.14*)	
14.12	(0.00)	13.92	(−1.81*)	
15.00	(0.005)	14.65	(−6.54*)	$^2B_1(^2E)$
15.29	(0.037)	14.95	(−22.9*)	$^2A_1(^2E)$
		15.21	(−5.20*)	$^2A_2(^2T_1)$
		15.44	(−8.60*)	
19.0[a]		18.9	(−0.80)	$^4E(^4T_2)$
21.2	(1.61)	20.7[a]	(−0.52)	$^4B_2(^4T_2)$
25.0[a]		25.0	(+0.13)	$^4E(^4T_1)$
29.5	(1.36)			$^4A_2(^4T_1)$
trans-[$CrCl_2$(*S,S*-stien)$_2$]$Cl \cdot H_2O$				
		14.27	(−9.95*)	$^2A_1(^2E)$
14.50	(0.16)	14.50	(−3.32*)	$^2B_1(^2E)$
		14.81	(−0.97*)	$^2E(^2T_1)$
		15.07	(−2.75*)	$^2A_2(^2T_1)$
		15.33	(−3.44*)	
17.7	(1.50)	17.6	(−0.60)	$^4E(^4T_2)$
22.1	(1.62)	21.7	(−0.58)	$^4B_2(^4T_2)$
		22.0	(−0.60)	
25.5	(1.80)	25.7	(−0.35)	$^4E(^4T_1)$
trans-[$CrBr_2$(*S,S*-stien)$_2$]$Br \cdot CH_3OH$				
		14.26	(−5.58*)	$^2A_1(^2E)$
		14.43	(−2.65*)	$^2B_1(^2E)$
		14.57	(−3.50*)	$^2A_2(^2T_1)$
16.9	(1.74)	17.0	(−0.52)	$^4E(^4T_2)$
22.0	(1.67)	21.5[a]	(−0,59)	$^4B_2(^4T_2)$
		21.8	(−0.60)	
24.5	(1.77)	24.0[a]	(−0.40)	$^4E(^4T_1)$
trans-[CrF_2(*S,S*-2,4-ptn)$_2$]ClO_4				
		13.95	(−0.99*)	$^2E(^2T_1)$
14.95	($\bar{1}$.84)	14.85	(+6.30*)	$^2B_1(^2E)$
15.11	($\bar{1}$.94)	15.08	(−4.92*)	$^2A_1(^2E)$
15.33	($\bar{1}$.96)	15.50	(+6.10*)	
		15.73	(+16.5*)	
		16.42	(+23.8*)	
18.5	(1.28)	18.7	(−0.31)	$^4E(^4T_2)$
21.3	(1.36)	21.7	(+0.53)	$^4B_2(^4T_2)$
25.0	(1.26)			$^4E(^4T_1)$
27.8	(1.26)	28.3	(+0.016)	$^4A_2(^4T_1)$
trans-[$CrCl_2$(*S,S*-2,4-ptn)$_2$]ClO_4				
		13.75[a]	(+0.5*)	
		14.00[a]	(+2.0*)	
		14.26	(+3.74*)	
14.45		14.41	(−1.65*)	$^2A_1(^2E)$
		14.59	(+7.10*)	$^2B_1(^2E)$
		14.88[a]	(+8.85*)	$^2E(^2T_1)$
		15.07	(+15.0*)	
		15.31	(+18.9*)	
		15·53	(+18.4*)	
17.0	(1.44)	17.3	(−0.31)	$^4E(^4T_2)$
21.3	(1.37)	21.2	(+0.33)	$^4B_2(^4T_2)$
		22.2[a]		
25.0	(1.66)	25.7	(−0.32)	$^4E(^4T_1)$
trans-[$CrBr_2$(*S,S*-2,4-ptn)$_2$]Br				
		14.33	(+14.8*)	
		14.51	(+19.8*)	
		14.64	(+25.7*)	
		14.77[a]	(+22.6*)	
		15.00[a]	(+20.0*)	
16.3	(1.53)	16.7	(−0.20)	$^4E(^4T_2)$
21.0[a]	(1.33)	21.1	(+0.20)	$^4B_2(^4T_2)$
		21.8	(+0.19)	
24.7	(1.55)	25.7	(−0.47)	$^4E(^4T_1)$

a) shoulder.

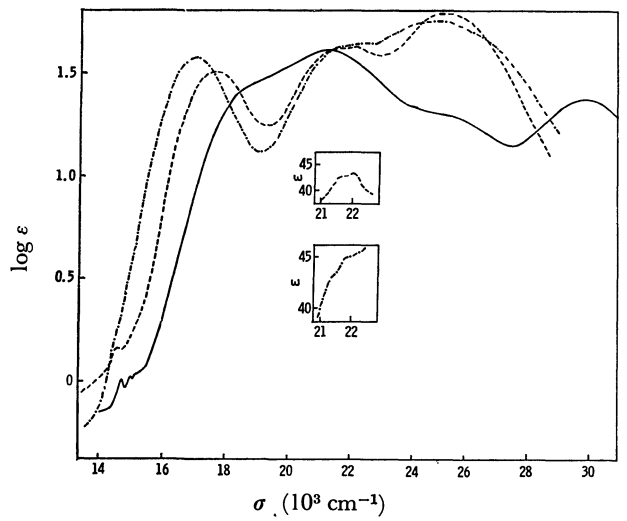

Fig. 2. Absorption curves of *trans*-$[CrX_2(S,S\text{-stien})_2]^+$ X=F (——); X=Cl (----); X=Br (—·—·—) in methanol.

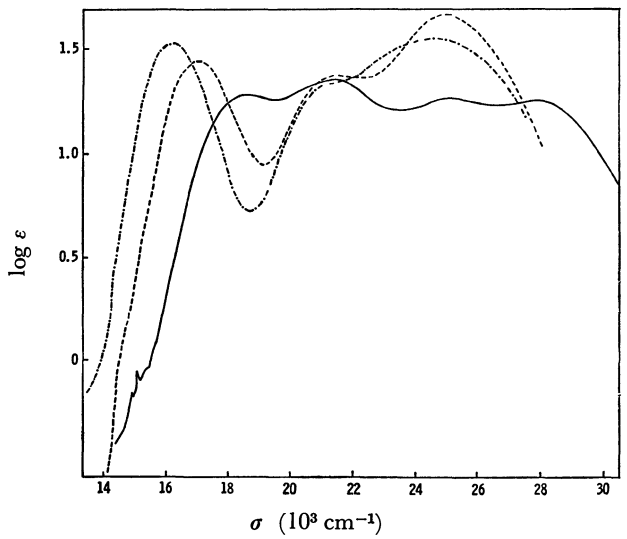

Fig. 3. Absorption curves of *trans*-$[CrX_2(S,S\text{-2,4-ptn})_2]^+$, X=F (——) in water; X=Cl (----) in methanol; X=Br (—·—·—) in methanol.

Since these absorption behavior agrees with the expectation from the ligand field theory[2] and the angular overlap model[6] for tetragonal chromium(III) complexes, the higher frequency and the lower frequency components in the first band region are due to the $^4E\leftarrow$ and $^4B_2\leftarrow{}^4B_1$ transition, respectively. This assignment has been unequivocally confirmed from single crystal polarized absorption spectra of *trans*-dihalogenobis(ethylenediamine)Cr(III) complexes.[4]

Both the split components, ^4E and $^4B_2$, in the first band region of the dichloro and dibromo complexes are found to shift to the lower frequency side in the order of *S,S*-stien, *R*-pn and *S,S*-2,4-ptn complexes. This fact suggests that the ligand field of the diamines decreases in this order as found in the case of the corresponding cobalt(III) complexes.[18,19]

The molar absorptivities of the $^4B_2$ components for the fluoro, chloro, and bromo complexes with a given diamine are close to each other, whereas those of the ^4E components increase in the order of the fluoro, chloro, and bromo complexes. This order is consistent with the hyperchromic series of the axial ligands.[25] The $^4B_2$ components of *trans*-$[CrCl]_2(R\text{-pn})_2]^+$ and *trans*-$[CrX_2(S,S\text{-stien})_2]^+$ (X=Cl, Br) split by some 500—800 cm^{-1}. This splitting may result from a strong spin-orbit coupling between the $^2\Gamma(^2T_2)$ and $^4B_2$ states as discussed later.

In the lower frequency region, where the doublet← quartet spin-forbidden transitions occur, some weak but sharp peaks or inflections are observed for the fluoro and chloro complexes, but none for the bromo complexes as shown in Figs. 1—3. The absorption intensities of spin-forbidden bands are found to be one twentieth to one fiftieth times as weak as those of the spin-allowed bands. The spin-forbidden transitions of the fluoro complexes are shifted to the lower frequency than those of the chloro complexes.

2) CD Spectra in the First Spin-allowed Transitions. Two CD components associated with the first $^4E\leftarrow$ and $^4B_2\leftarrow{}^4B_1$ spin-allowed transitions are observed for all the complexes concerned in Figs. 4—6. The CD patterns depend largely on the optically active diamines and independent of the axial ligands. That is, for the *R*-pn complexes, a large positive and a small negative CD component is observed in the region corresponding to the lower frequency ^4E and the higher frequency $^4B_2$ absorption band, respectively. For

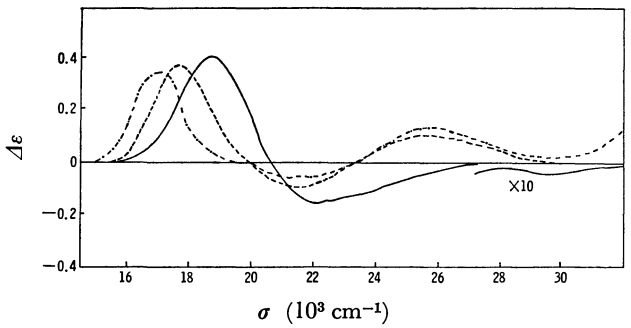

Fig. 4. CD curves in the spin-allowed transitions of *trans*-$[CrX_2(R\text{-pn})_2]^+$, X=F (——) in water; X=Cl (----) in methanol; X=Br (—·—·—) in methanol.

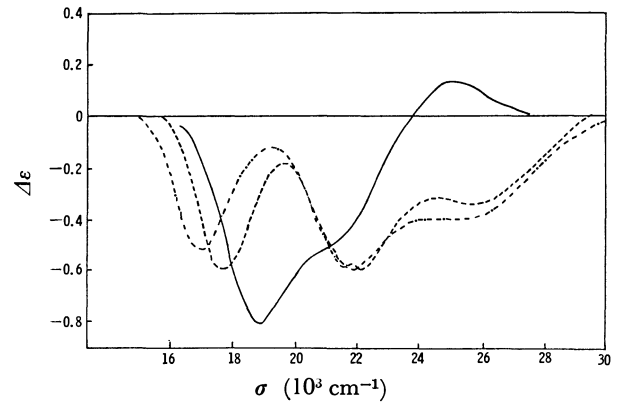

Fig. 5. CD curves in the spin-allowed transitions of *trans*-$[CrX_2(S,S\text{-stien})_2]^+$, X=F (——); X=Cl (----); X=Br (—·—·—) in methanol.

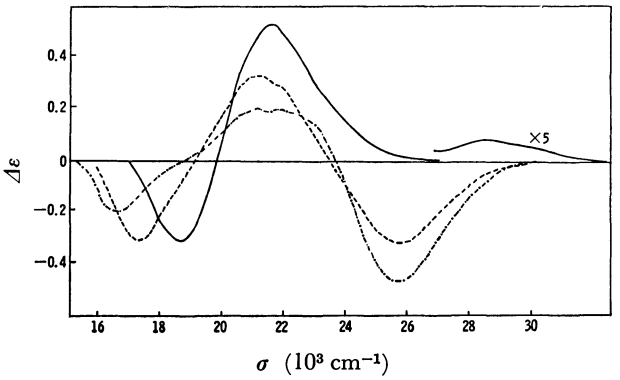

Fig. 6. CD curves in the spin-allowed transitions of *trans*-$[CrX_2(S,S\text{-2,4-ptn})_2]^+$, X=F (——) in water; X=Cl (----) in methanol; X=Br (—·—·—) in methanol.

the *S,S*-stien complexes, two negative CD bands are observed in this region. The *S,S*-2,4-ptn complexes show two CD components with opposite signs, (−) and (+) from the longer wavelength side, having nearly equal area. Such CD behavior of chromium(III) complexes is quite similar to the corresponding cobalt(III) complexes.[18,19,26] Therefore, it seems reasonable that the coordinated optically active diamines in the chromium(III) complexes take the same conformations as those in the cobalt(III) complexes. That is, the conformation of the *R*-pn, *S,S*-stien and *S,S*-2,4-ptn is assigned to *λ*-,[27] *δ-gauche*[26b] and *δ*-twist[18] form, respectively.

The CD intensities of the chromium(III) complexes are found to be about half as compared with those of the corresponding cobalt(III) complexes, as predicted by a general theory on CD of metal complexes.[28]

3) CD Spectra in the Second Spin-allowed Transitions. One CD component associated with the second $^4T_1 \leftarrow {}^4A_2$ octahedral transition of the chloro or bromo complex is observed at the higher frequency side than the absorption band, as in Figs. 4—6 and Table 1, indicating that the CD band is ascribed to the $^4E_b(^4T_1)$ component which lies at the higher frequency than the $^4A_2(^4T_1)$ component as is predicted theoretically and confirmed by single crystal polarized absorption spectra.[4] These CD bands are of the same signs as those of the $^4E_a(^4T_2)$ components. The CD band of the fluoro complexes with *R*-pn and *S,S*-2,4-ptn observed in the second band region lies rather closely to the $^4A_2$ absorption component, and therefore this band is assigned to the $^4A_2 \leftarrow {}^4B_1$ transition which may be vibronically allowed by lowering symmetry through the mixing with the $^4B_2$ component, as has been observed for *trans*-$[CoCl]_2(R\text{-pn})_2]^+$.[30] The CD intensities of these bands are found to be much weaker than those of the $^4E_b(^4T_1)$ components. The CD band of the fluoro complex with *S,S*-stien in the second band region corresponds to the ^4E_b absorption component, and is of opposite sign to the ^4E_a component. The fact that the ^4E_b CD component are not observed for the fluoro complexes with *R*-pn and *S,S*-2,4-ptn may be responsible for the overlapping with the $^4B_2$ component which may have the same sign as the ^4E_b one. Thus, it is seen that the CD sign of the ^4E_b component for the fluoro complexes in the second band region is opposite to those for the chloro and bromo complexes. This fact may be elucidated by taking into consideration of the configuration interaction between the ^4E_a and ^4E_b states. The magnetic dipole forbidden $^4E_b \leftarrow {}^4B_1$ transition borrows its magnetic transition dipole moment from that for the magnetic dipole allowed $^4E_a \leftarrow {}^4B_1$ transition through the configuration interaction between the ^4E_a and ^4E_b states in tetragonal field, of which the off-diagonal element, $\langle {}^4E_a | V(D_{4h}) | {}^4E_b \rangle$, is given as $(\sqrt{3}/2)\delta\sigma$.[30] The AOM parameter, $\delta\sigma$, is defined as the splitting of one electron level of the $e_g(d)$ orbital in tetragonal field and can be estimated from the observed splittings of the first and second octahedral bands. Thus, the rotational strength for the $^4E_b \leftarrow {}^4B_1$ transition is expressed as follows.

$$R(^4E_b) = (\sqrt{3}/2)\delta\sigma/\{E(^4E_b) - E(^4E_a)\} \cdot \mathrm{Im}\langle {}^4E_a | M | {}^4B_1 \rangle \cdot \langle {}^4B_1 | P | {}^4E_b \rangle$$

where M and P are magnetic and electric dipole operator, respectively, and Im means the "imaginary part of". Since the energy denominator, $E(^4E_b) - E(^4E_a) = 36B + \delta\sigma$, is usually positive, the sign of the $R(^4E_b)$ is governed by that of $\delta\sigma$. According to the measurements of single crystal polarized absorption spectra as well as theoretical crystal field calculations,[4] the $\delta\sigma$ value for *trans*-$[CrX_2(en)_2]^+$ complex has been estimated to be +600, −1240 and −1780 cm^{-1}, for the fluoro, chloro and bromo complex, respectively. The $\delta\sigma$ values for the present complexes do not seem to differ largely from those for the ethylenediamine complexes, for the ligand field strengths of these complexes are close to each other. Therefore, the sign inversion of the ^4E_b CD component from the fluoro to the chloro and bromo complexes is responsible for that of the $\delta\sigma$ parameter. A similar formulation can be also applied to the CD behaviors of the corresponding Co(III) complexes. It has been found that all the *trans*-difluoro, dichloro and dibromo(*l*-cyclohexanediamine)cobalt(III) complexes give the positive CD sign in the $^1E_b(^1T_2)$ component.[31] This finding is in accordance with the $\delta\sigma$ parameters for the three complexes having the same sign (negative).[31]

4) CD Spectra in the Spin-forbidden Transitions. a) General Considerations: The splitting of the doublet excited states in tetragonal field occurs as shown in Fig. 7. Although each the $^2E(^2T_1)$ and the ground $^4B_1(^4A_2)$ state is split into two Kramers doublets by a spin-orbit coupling, these splittings are estimated to be too small to be resolved spectroscopically at room temperature.[8b] Thus, in this case, these will be ignored and only four electronic spin-forbidden transitions, $^2A_1(^2E)$, $^2B_1(^2E)$, $^2E(^2T_1)$ and $^2A_2(^2T_1) \leftarrow {}^4B_1(^4A_2)$, will be taken into account throughout the following discussion. Contrary to the expectation, however, more than four sharp but weak CD peaks are observed for the present complexes. This fact indicates the appearance of vibronic structures as discussed later.

The Rotational Strengths for the Spin-forbidden Transitions. For tetragonal chromium(III) complexes,

TABLE 2. ROTATIONAL STRENGTHS FOR THE SPIN-FORBIDDEN $^2\Gamma \leftarrow {}^4B_1$ TRANSITIONS IN TETRAGONAL CHROMIUM(III) COMPLEXES

		in unit of $\zeta'^2/18\{\Delta E(^2\Gamma)\}^2$	
^2E	$^2A_1$	$24R(^4E)$	$(1/3)(3\zeta_3'^2+\zeta_4'^2)\varepsilon_1^{-2}\cdot R(^4E)$
	$^2B_1$	$8\{R(^4E)+4R(^4B_2)\}$	$(1/9)(3\zeta_3'^2+\zeta_4'^2)\varepsilon_1^{-2}\cdot R(^4E)+(16/9)\zeta_1'^2\varepsilon_2^{-2}\cdot R(^4B_2)$
$^2T_1$	^2E	$6\{R(^4E)+2R(^4B_2)\}$	$(1/12)(3\zeta_2'^2+\zeta_1'^2)\varepsilon_1^{-2}\cdot R(^4E)+(2/3)\zeta_4'^2\varepsilon_2^{-2}\cdot R(^4B_2)$
	$^2A_2$	$6R(^4E)$	$(1/12)(3\zeta_3'^2+\zeta_4'^2)\varepsilon_1^{-2}\cdot R(^4E)$

$\Delta E(^2\Gamma) = E(^2\Gamma)-E(^4\Gamma)$; ζ_1', ζ_2', ζ_3' and ζ_4' are the effective spin-orbit coupling constants as defined in the text. ε_1 and ε_2 are the energy interval between the $^2\Gamma$ and ^4E and between the $^2\Gamma$ and $^4B_2$, respectively.

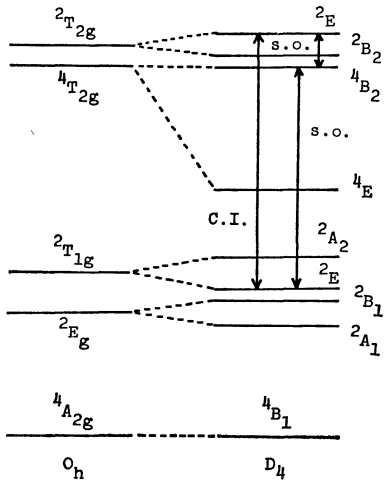

Fig. 7. Energy levels of a tetragonal chromium(III) ion. The vertical lines indicate the configuration interaction (C. I.) among the ^2E states or the spin-orbit coupling (s. o.) between the ^2E and the quartet state.

the spin-forbidden $^2\Gamma(t_2^3)\leftarrow{}^4B_1(t_2^3)$ transitions attain their rotational strengths by aquiring a small part, $(k\zeta'/\Delta E)^2$, of the rotational strengths for the nearby spin-allowed and magnetic dipole allowed $^4E(t_2^2e)$, $^4B_2(t_2^2e)\leftarrow{}^4B_1(t_2^3)$ transitions, as given by

$$R(^2\Gamma) = (k\zeta'/\Delta E)^2 R(^4\Gamma) \qquad (1)$$

where k is a numerical coefficient, and ζ' is a spin-orbit coupling constant, $\zeta'=(\sqrt{2}/6)i\langle t_2|H_{so}|e\rangle$, and ΔE refers to the energy interval between the $^2\Gamma$ and $^4\Gamma$, and $R(^4\Gamma)$ is the rotational strengths for the tetragonal splitting components of the $^4T_2$, $R(^4E)=2\mathrm{Im}\langle{}^4E|P|{}^4B_1\rangle\cdot\langle{}^4B_1|M|{}^4E\rangle$ and $R(^4B_2)=\mathrm{Im}\langle{}^4B_2|P|{}^4B_1\rangle\cdot\langle{}^4B_1|M|{}^4B_2\rangle$. The $k^2R(^4\Gamma)$ in the Eq. (1) are obtained by using the Wigner and Clebsh-Gordan coefficients with tetragonal field in the absence of vibronic contribution[32,33] as in the case of trigonal complexes[1] as shown in the third column of Table 2. This approximation seems to be valid, since it is inferred that CD intensity is static in origin for the corresponding tetragonal Co(III) complexes.[29] This Table shows that the $^2A_2\leftarrow{}^4B_1$ and $^2A_1\leftarrow{}^4B_1$ transitions borrow their rotational strengths only from the $R(^4E)$ and hence they should have the same sign. In the cases of the $R(^2B_1)$ and $R(^2E)$ to which both the $R(^4E)$ and $R(^4B_2)$ contribute, however, more exact examinations of $\zeta'/\Delta E$ are required. As seen in section *1)*, the energy separation between the $^4B_2$ and ^4E states is so large that the differencc between $\varepsilon_1=E(^2\Gamma)-E(^4E)$ and $\varepsilon_2=E(^2\Gamma)-E(^4B_2)$ needs to be taken into consideration. For the complexes concerned, ε_1 depends on axial ligands, increasing in the order of the fluoro, chloro and bromo complexes and ε_2 is almost constant. Assuming no spin-orbit effect on ligands, the terms involving the $R(^4E)$ give larger contribution to the $R(^2\Gamma)$ by a factor of $(\varepsilon_2/\varepsilon_1)^2$ than those involving the $R(^4B_2)$, for the $(\varepsilon_2/\varepsilon_1)^2$ is found to be ~3 for the fluoro, ~4—~5 for the chloro and ~7—~8 for the bromo complexes. In addition, the ratio between the contribution of the $R(^4E)$ to that of the $R(^4B_2)$ is governed by the kinds of optically active diamines. That is, it is found that the $|R(^4E)/R(^4B_2)|$ obtained from the observed CD spectra is about 3 to 6 for the *R*-pn complexes and about 1 for the *S,S*-stien and *S,S*-2,4-ptn complexes. Consequently, it is expected that the $R(^2\Gamma)$ increase in the order of the fluoro, chloro and bromo complexes and that the contribution from the terms involving the $R(^4E)$ is large in comparison with those involving the $R(^4B_2)$. These are contrary to the findings. That is, the CD intensities in the spin-forbidden transitions decrease in the order of the fluoro, chloro and bromo complexes and they do not always exhibit the same sign as that of the ^4E component, as in Figs. 8—10 and Table 1. These facts suggest the importance of a spin-orbit effect on the ligands.

According to a simple molecular orbital treatment, it has been shown that the spin-orbit effects on the halogeno ligands in $[CoX(NH_3)_5]^{2+}$ play an important role in gaining the spin-forbidden absorption band intensities.[34,35] The application of this MO treatment to the tetragonal Cr(III) complexes leads to four nonequivalent effective spin-orbit coupling constants. Assuming no π bonding between the metal and amine ligands, one electron antibonding LCAO-MO for the *trans*-$[CrX_2(N)_4]$ type complexes is given as follows.[4]

$$\left.\begin{aligned} a_1(e) &= N_{\sigma X}[a_1(d_{z^2})-\lambda_{\sigma X}\Sigma p_{zi}(X)] \\ b_1(e) &= N_{\sigma N}[b_1(d_{x^2-y^2})-\lambda_{\sigma N}\Sigma p_{zi}(N)] \\ a_2(t_2) &= a_2(d_{xy}) \\ e(t_2) &= N_{\pi X}[e(d_{xz})-\lambda_{\pi X}\Sigma\{p_{xi}(X)-p_{xj}(X)\}] \\ e(t_2) &= N_{\pi X}[e(d_{yz})-\lambda_{\pi X}\Sigma\{p_{yi}(X)-p_{yj}(X)\}] \end{aligned}\right\} \qquad (2)$$

where $N_{\sigma N}$, $N_{\sigma X}$, $N_{\pi X}$ and $\lambda_{\sigma N}$, $\lambda_{\sigma X}$, $\lambda_{\pi X}$ are normalizing and admixture coefficients, respectively, $\Sigma p(N)$ and $\Sigma p(X)$ stand for symmetry adapted linear combinations of p orbitals of nitrogens and halogens, respectively, and $a_1(d_{z^2})$ *etc.* are pure d orbitals. The

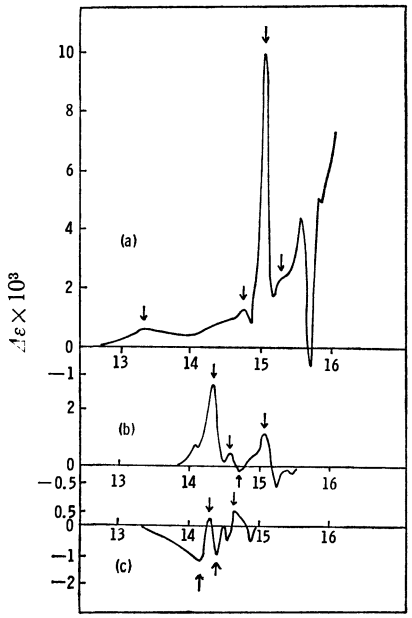

Fig. 8. CD curves in the spin-forbidden transitions of *trans*-$[CrX_2(R\text{-pn})_2]^+$ (a) X=F, (b) X=Cl, (c) X=Br. The arrows indicate the electronic states assigned in the text.

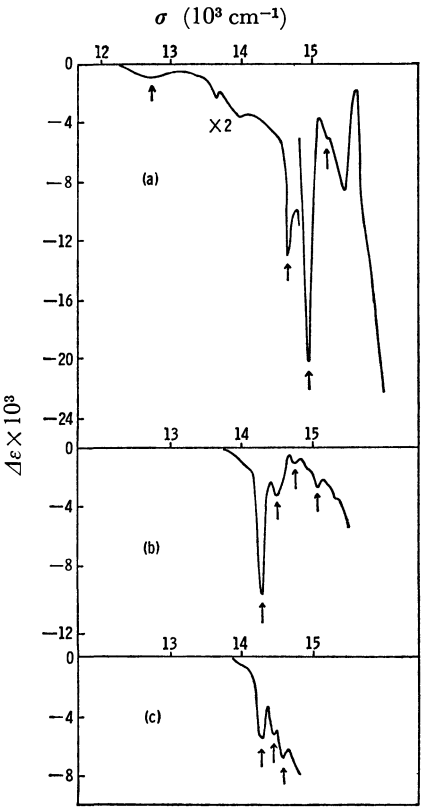

Fig. 9. CD curves in the spin-forbidden transitions of *trans*-$[CrX_2(S,S\text{-stien})_2]^+$ (a) X=F, (b) X=Cl, (c) X=Br. The arrows as in Fig. 8.

upper two e orbitals and lower two t_2 orbitals are σ- and π-antibonding MO's, respectively. By using these molecular orbitals, the molecular orbital matrix elements, $\langle t_2|H_{so}|e\rangle$, are evaluated as,[33]

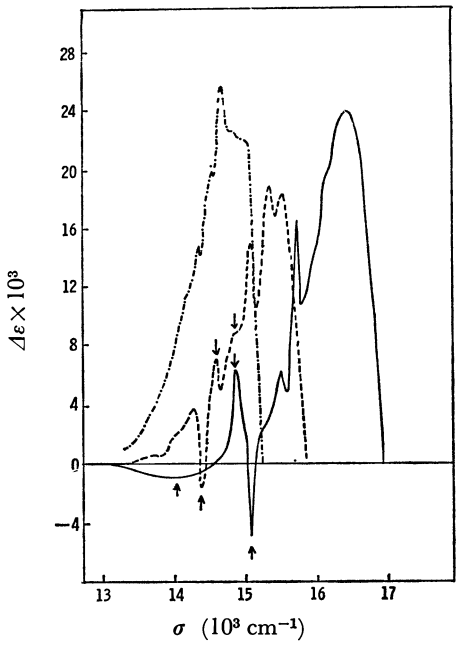

Fig. 10. CD curves in the spin-forbidden transitions of *trans*-$[CrX_2(S,S\text{-2,4-ptn})_2]^+$, X=F (——) in water; X=Cl (----) in methanol; X=Br (—·—·—) in methanol. The arrows as in Fig. 8.

$$\left.\begin{aligned}
\zeta_1' &= (\sqrt{2}/6)i\langle a_2(t_2)|H_{so}|b_1(e)\rangle = N_{\sigma N}\zeta_d' \\
\zeta_2' &= (\sqrt{2}/6)i\langle a_2(t_2)|H_{so}|a_1(e)\rangle = N_{\sigma X}\zeta_d' \\
\zeta_3' &= (\sqrt{2}/6)i\langle e(t_2)|H_{so}|a_1(e)\rangle \\
&= N_{\pi X}N_{\sigma X}\{\zeta_d' - (1/2)\lambda_{\pi X}\lambda_{\sigma X}\zeta_p\} \\
\zeta_4' &= (\sqrt{2}/6)i\langle e(t_2)|H_{so}|b_1(e)\rangle \\
&= N_{\pi X}N_{\sigma N}\zeta_d'
\end{aligned}\right\} \quad (3)$$

where ζ_d' and ζ_p are the spin-orbit coupling constants of pure 3d orbitals of Cr(III) ion and of p orbitals of halogen, respectively. It is noted that the ζ_1' and ζ_3' correspond to the effective spin orbit coupling constant for $Cr(N)_6^{3+}$ and $Cr(X)_6^{3-}$, respectively. Since the ζ_3' is given as a linear combination of ζ_d' and ζ_p, the value of ζ_3' varies with the halogen ligands. The Eq. (3) may be rewritten in terms of the relativistic nephelauxetic ratios, β^*(N) for the amine ligand and β^*(X) for the halogen ligands as follows. $\zeta_1'=\beta_{55}^*(N)\zeta_d'$, $\zeta_2'=\sqrt{\beta_{33}^*(X)\,\beta_{55}^*(N)}\,\zeta_d'$, $\zeta_3'=\beta_{55}^*(X)\,\zeta_d'$, $\zeta_4'=\sqrt{\beta_{33}^*(N)\,\beta_{55}^*(X)}\,\zeta_d'$, where ζ_p in ζ_3' is ignored. The $\beta_{55}^*(N)$ is mainly due to the relativistic nephelauxetic effect caused by the central field covalency.[36] Using these correlations, the ζ_2' and ζ_4' are connected with the ζ_3' and ζ_1' through the $\beta_{55}^*(N)$ and $\beta_{55}^*(X)$, as shown in the following. $\zeta_4'=\sqrt{\beta_{55}^*(X)/\beta_{55}^*(N)}\,\zeta_1'$; $\zeta_2'=\sqrt{\beta_{55}^*(N)/\beta_{55}^*(X)}\,\zeta_3'$, hence $\zeta_4'/\zeta_3'=\zeta_1'/\zeta_2'$, where it is assumed that $\beta_{55}^*=\sqrt{\beta_{33}^*\,\beta_{55}^*}$.[36] In this case, the values of the four constants seem close each other. In the case of the complexes having heavy ligands with large ζ_p, however, the substantial decrease in ζ_3' may be expected owing to the subtractive contribution of the terms involving the ζ_p to the ζ_3', assuming appropriate values of the ligand admixture coefficient, $\lambda_{\pi X}\lambda_{\sigma X}$.[37] Therefore, the difference between the ligand-dependent spin-orbit coupling constant ζ_3' and the other constants must be taken into consideration.

By introducing four different effective spin-orbit coupling constants in terms of the strong field wave functions of d^3 configurations in tetragonal field,[2] together with two kinds of the energy denominator, ε_1^{-1} and ε_2^{-1}, the refined rotational strengths for the spin-forbidden transitions can be represented as in the fourth column of Table 2. It is seen that most of the $R(^2\Gamma)$'s are rather sensitive to the ζ_3' and decrease with increasing ζ_p in the order of the fluoro, chloro and bromo complexes. This order is consistent with the observation.* As for the sign of the CD components, in either case of the complexes with vanishingly small ζ_3', or the complexes having $(\varepsilon_2/\varepsilon_1)^2<4$ and almost equal effective spin-orbit coupling constants, only the $R(^2B_1)$ among the four $R(^2\Gamma)$'s may be expected to exhibit the same sign as the $R(^4B_2)$, and the rotational strengths for the remaining spin-forbidden transitions are predicted to be of the same sign as the $R(^4E)$ for any axial ligands. It appears that this prediction holds for the *S,S*-stien complexes, though these complexes show two same signed CD bands in the first spin-allowed transition region. For the complexes with oppositely signed CD bands in the first spin-allowed transitions, some oppositely signed CD components are observed also in the spin-forbidden transitions as shown in Figs. 8 and 10. Such a CD behavior, however, was not elucidated by the spin-orbit coupling mechanism, only between the ^2E, $^2T_1$ and the $^4E(^4T_2)$, $^4B_2(^4T_2)$ states. Thus some additional contributions from the terms involvong the $R(^4B_2)$ become needed in terms of another mechanism.

More exact consideration including the configuration interaction accounts for the large mixing of the $^4B_2$ state into the doublet states. Of the doublet states, the $^2E(^2T_2)$ is strongly mixed with the $^4B_2$ state through a spin-orbit coupling, because these states lie very closely in the crystal field approximation. This strong coupling is substantiated from the fact that the $^4B_2$ component is split into double peaks in the absorption and CD spectra as in Figs. 1—2 and 4—6. In addition, the configuration interaction between the $^2E(^2T_2)$ and $^2E(^2T_1)$ occurs in tetragonal field. The off-diagonal matrix element is obtained as $3Ds-5Dt=2\delta\pi$, where Ds, Dt and $\delta\pi$ are the crystal field and AOM parameter, respectively.[2] The consequence of this configuration interaction has been discussed in photochemical implication for chromium(III) complexes[39] and in relation to the lower frequency shift of the $^2E(^2T_1)$ state.[14] The spin-orbit coupling gives rise to large admixture of the $^4B_2$ into the $^2E(^2T_2)$, and the $^4B_2$ mixes with the $^2E(^2T_1)$ through the configuration interaction with the $^2E(^2T_2)$ as in Fig. 7. The operation of these interactions gives additional rotational strengths for the $^2E(^2T_1)\leftarrow{}^4B_1(^4A_2)$ spin-forbidden transition by $(2/3)\varepsilon_4^{-2}\cdot\varepsilon_3^{-2}\cdot\zeta_4'^2\cdot4(\delta\pi)^2\cdot R(^4B_2)$, where ε_4 and ε_3 are the energy interval between the $^2E(^2T_2)$ and $^4B_2$ $(=10Dq-15B-5C)$ and between the $^2E(^2T_1)$ and $^2E(^2T_2)$ $(=6B+2C)$, respectively. Then the contribution of the terms involving the $R(^4B_2)$ to the $R(^2E(^2T_1))$ becomes $(2/3)\zeta_4'^2\varepsilon_3^{-2}\{1+4\varepsilon_4^{-2}(\delta\pi)^2\}\cdot R(^4B_2)$, assuming $\varepsilon_3\simeq\varepsilon_2$. The value of $\delta\pi$ is found to be of the order of 1000 cm^{-1} from the crystal field approximations and single crystal polarized absorption spectra of *trans*-$[CrX_2(en)_2]^+$. The ε_4 seems to be of the order of 1000 cm^{-1} or less. In the strong coupling case of $E(^4B_2)\simeq E(^2E(^2T_2))$ with zero spin-orbit coupling, the ε_4 is equal to $(\sqrt{3}/2)\zeta_4'$ and thus being estimated to be 100—200 cm^{-1}. Then the additional rotational strengths are sensitive to the ε_4 and in some cases, are expected to be so large that the term involving the $R(^4B_2)$ overwhelms that involving the $R(^4E)$.**

From these considerations, it may be summarized that the $R(^2A_1)$ should be the most intense and four times as large as the $R(^2A_2)$, and they should have the same sign as the $R(^4E)$. Further, the $R(^2E)$ and $R(^2B_1)$ are not always of the same sign as the $R(^4E)$.

b) The Assignments of the CD Components. The Fluoro Complexes with R-*pn and* S,S-*stien.* The crystal field theory predicts the positions and the splittings of the doublet states. In general, the ^2E cubic parent component lies at the lower frequency by about 700 cm^{-1} than the $^2T_1$ one. According to Macfarlane's approximation,[10a] the splitting of the ^2E cubic state into $^2A_1$ and $^2B_1$ in tetragonal field may be calculated in terms of the parameters, $\delta\sigma$, $\delta\pi$, $10Dq$, B and C; *i.e.*,

$$E(^2A_1)-E(^2B_1)=192B^2/(10Dq+14B+3C)\times\{\delta\pi/(10Dq+14B+3C)+\delta\sigma/(10Dq+5B)\} \quad (4)$$

On the other hand, owing to the configuration interaction between the $^2E(^2T_1)$ and $^2E(^2T_2)$ states, the $^2E(^2T_1)$ state is shifted by $4(\delta\pi)^2/\varepsilon_3$ to the lower frequency side. The former Eq. (4) leads to the expectation that the $^2B_1$ state for the fluoro complexes always locates at the lower frequency side than the $^2A_1$ because of positive sign of both the $\delta\pi$ and $\delta\sigma$.[3-6] The shift of the $^2E(^2T_1)$ state is sensitive to the value

* In the case of Co(III) complexes, the molecular spin-orbit coupling constants corresponding to the ζ_3', $\zeta=(-i/3)\langle t_2|H_{so}|t_2\rangle$, are given as an additive contribution of the terms involving ζ_p of halogeno ligands.[33] Thus, this constants increase with increasing ζ_p and in the order of the fluoro, chloro and bromo complexes. This order agrees with that obtained from the spin-forbidden absorption intensities.[38] On the other hand, for the Cr(III) complexes, the intensity order of the spin-forbidden absorption bands is contrary to that of CD intensities in the spin-forbidden transitions. This finding can not be interpreted in the course of the present discussion, since the sharp spin-forbidden bands are overlapped with the lower frequency envelope of the broad first spin-allowed bands to increasing extent in the order of the fluoro, chloro and bromo complexes.

** In the case of $[Cr(en)_3]^{3+}$, the similar configuration interaction between the $^2E(^2T_1)$ and $^2E(^2T_2)$ state and/or $^2E(^2E)$ and $^2E(^2T_2)$ state and the strong spin-orbit coupling between the $^2E(^2T_2)$ and $^4E(^4T_2)$ or $^4A_1(^4T_2)$ state can occur. The off-diagonal elements of these configuration interactions are proportional to the trigonal splitting parameter K. [S. Sugano and M. Peter, *Phys. Rev.*, **122**, 381 (1961).] In this case, however, the mixing of the $^2E(^2T_2)$ state with the $^2E(^2E)$ and $^2E(^2T_1)$ state seems to be negligible owing to small K value. [A. J. McCaffery, S. F. Mason, and B. J. Ballard, *J. Chem. Soc.*, **1965**, 5094.] In the trigonal case, therefore, these interactions may be ignored.

of $\delta\pi$, because ε_3 includes only the Racah electronic repulsion parameters, and hence almost independent on the ligand field. Thus, the $^2E(^2T_1)$ state for the fluoro complexes seems to be shifted to the lower frequency than that for the other aniono complexes, because the $\delta\pi$ value of the fluoro complexes is largest in the three halogeno complexes.[4] Then the $^2A_2(^2T_1)$ state locates at the highest frequency. In fact, from the luminescence and absorption spectra of *trans*-$[CrF_2(en)_2]ClO_4$ and its iodide, Flint *et al.*[14] have revealed that the lowest frequency phosphorescence band at 13098 cm^{-1} is assigned to the $^2E(^2T_1)$ state and the $^2B_1$, $^2A_1$ and $^2A_2$ states locate at 14860, 15052 and 15270 cm^{-1}, respectively, in spite of a number of observed vibronic structures. This assignment is also consistent with the prediction based on the crystal field theory. By collating this assignment with the CD components of the present fluoro complexes, the peaks are assigned on the assumption that the crystal field parameter values of the optically active diamine complexes are close to those of the ethylenediamine complex. For the *R*-pn complex, the lowest frequency positive CD peak at 13330 cm^{-1} is due to the $^2E(^2T_1)$ state, and the weak positive peak at 14730 cm^{-1} and the strongest positive peak at 15030 cm^{-1} are due to the $^2B_1$ and $^2A_1$ state, respectively, as in Fig. 8 a). The $^2A_2$ state may correspond to the shoulder near 15300 cm^{-1} of positive sign. The theoretical correlation between the rotational strengths in the spin-forbidden transitions and those in the spin-allowed transitions can account for the CD behaviors of these peaks semi-quantitatively. That is, the $^2A_1$ peak is the strongest and about four times as strong as the $^2A_2$ one as mentioned before. The weak intensities of the ^2E and $^2B_1$ peaks may be responsible for the increasing contribution of the terms involving the $R(^4B_2)$. That the ^2E peak of the fluoro complex is of the same sign as the ^4E one suggests a weak spin-orbit coupling between the $^2E(^2T_2)$ and $^4B_2$ state. In fact, no double peaks of the $^4B_2$ component is observed in absorption and CD spectra of the fluoro *R*-pn complex. Although a negative peak is observed at 15680 cm^{-1}, no negative sign is expected in this region. The vibronic CD theory for electric dipole forbidden and magnetic dipole allowed transitions which are spin-allowed either in zeroth order or in first order *via* a spin-orbit coupling expects the mixed signs of CD and that vibrational progressions of totally symmetric modes on electronic origins should contribute to CD spectra.[40] Therefore, this CD peak with negative sign together with other positive peaks unassigned may be due to the vibronic bands.*** The strong intensities of vibronic bands observed in CD are compatible with those in absorption spectra.[14]

For the *S,S*-stien complex (Fig. 9 a), the 12700 cm^{-1} peak with negative sign may be assigned to the $^2E(^2T_1)$ state. It appears that the $^2B_1$ and $^2A_1$ state correspond to a weak 14650 cm^{-1} and a strong 14950 cm^{-1} peak, respectively. The 15210 cm^{-1} peak is due to the $^2A_2(^2T_1)$ state, of which the CD intensity is about one fourth of that of the $^2A_1$ peak. The remaining peaks may be ascribed to the vibronic origins. It seems plausible that the CD signs of these peaks agree with those of the CD bands in the first spin-allowed transitions.

The Chloro Complexes with R-*pn and* S,S-*stien.* The luminescence spectrum of *trans*-$[CrCl_2(en)_2]^+$ has shown that the lowest frequency doublet state locates at 14380 cm^{-1}.[11] For the *S,S*-stien complex, the lowest frequency negative CD peak at 14270 cm^{-1} is the most intense and hence this peak is assigned to the $^2A_1$ state. The next-neighbouring peak at 14500 cm^{-1} may be due to the $^2B_1$ state. The CD peak at 15070 cm^{-1} may be assigned to the $^2A_2$ state, because the CD intensity of this peak is about one fourth of that of the $^2A_1$ component, as theoretically expected. Further, since the ^2E state is expected to lie at the lower frequency than the $^2A_2$ state, the CD peak at 14810 cm^{-1} may be assigned to the ^2E state.

The most intense CD peak of the *R*-pn complex at 14340 cm^{-1} may be due to the $^2A_1$, and it seems that the $^2B_1$, ^2E and $^2A_2$ state correspond to the 14580, 14700 and 15020 cm^{-1} peaks, respectively, although the lowest frequency peak at 14080 cm^{-1} can not be identified. In this complex also the $^2A_2$ peak is weaker than the $^2A_1$ one. It needs to be noted that the $^2E(^2T_1)$ component is negative and of the same sign as the $^4B_2$ one. This sign inversion may be attributed to that a spin-orbit coupling between the $^2E(^2T_2)$ and $^4B_2$ state is strong enough to cause the additional contribution of the term involving the $R(^4B_2)$, $(2/3)\zeta_4'^2\varepsilon_2^{-2}\{1+4\varepsilon_4^{-2}(\delta\pi)^2\}\cdot R(^4B_2)$, and to overcome the term involving the $R(^4E)$, $(1/12)(3\zeta_2'^2+\zeta_1'^2)\varepsilon_1^{-2}\cdot R(^4E)$, as discussed in the previous section. In fact, such a strong spin-orbit coupling gives rise to the splitting of the $^4B_2$ component in absorption spectra by about 400 cm^{-1} as in Fig. 1. The positions and the splitting of the doublet states of this complex is in accordance with the crystal field calculation for the corresponding ethylenediamine complex.[2,3] The remaining CD peaks may be due to the vibronic bands, though some negative peaks are observed.

The Bromo Complexes with R-*pn and* S,S-*stien.* The *R*-pn complex gives only two positive CD peaks at 14290 cm^{-1} and 14650 cm^{-1} (Fig. 8c). Thus, the lower frequency 14290 cm^{-1} peak and the higher frequency 14650 cm^{-1} peak are assigned to the $^2A_1$ and $^2A_2$ state, respectively, because their rotational strengths should have the same sign as the $R(^4E)$ and the $^2A_1$ state should lie at the lower frequency than the $^2A_2$ state from a theoretical point of view. Contrary to the other complexes mentioned before, however, the $^2A_2$ peak is more intense than the $^2A_1$ one. This may be due to the large mutual cancellation among the neighbouring CD peaks with alternate signs. For the bromo complexes, the crystal field approximation predicts the lowest frequency shift of the $^2E(^2T_1)$ state.[2,3] Therefore, a negative CD peak at 14080 cm^{-1} may be due to the ^2E state. The negative sign of this

*** The influences of the methyl group of *R*-pn in the present complex on the vibronic CD bands are disregarded, since the CD pattern in the spin-forbidden transitions of the fluoro complex with *R*-pn is found to be quite identical with that of the fluoro complex with *R,R*-cyclohexanediamine which was prepared by the method of Glerup *et al.*[22]

peak implies a strong spin-orbit coupling between the $^2E(^2T_2)$ and $^4B_2$ state, which may give rise to the splitting of the $^4B_2$ component in CD spectrum of this complex as in Fig. 4. The $^2B_1$ state may correspond to a negative peak at 14390 cm^{-1}. The negative sign of the $^2B_1$ state is caused by the vanishing decrease in ζ_3' owing to the large ζ_p of the axial ligand, in which case the term involving the $R(^4B_2)$ is $16(\zeta_1'/\zeta_4')^2$-$(\varepsilon_1/\varepsilon_2)^2$ times as large as that involving the $R(^4E)$ and, assuming $(\varepsilon_1/\varepsilon_2)^2 \simeq 1/8$ and $(\zeta_1'/\zeta_4')^2 = \beta^*_{55}(N)/\beta^*_{55}(Br) \gg 1$, thus overwhelming the $R(^4E)$.

From comparison with the *R*-pn complex, three CD peaks observed for the *S,S*-stien complex are assigned to the $^2A_1$, $^2B_1$ and $^2A_2$ state from the lower frequency side, respectively, though the ^2E component is missing.

The S,S-*2,4-ptn Complexes.* The *S,S*-2,4-ptn complexes show anomalous CD patterns in the spin-forbidden band region, compared with the *R*-pn and *S,S*-stien complexes as in Fig. 10. That is, relatively intense structural CD bands with positive sign are observed in the region of 16500—14500 cm^{-1}. Although the shift pattern with varying the axial ligands is similar to that of the ^4E component, suggesting that these bands seem to be associated with the spin-allowed transitions, they can not be assigned at the present. The spin-forbidden transitions may occur at the lower frequency side than these anomalous CD bands, but overlapping of some of them with the anomalous bands makes their assignments difficult. The tentative assignments are made as follows. For the fluoro complex, the lowest frequency CD peak at 13950 cm^{-1} with negative sign may be due to the ^2E state, and the 14850 cm^{-1} and 15080 cm^{-1} peaks to the $^2B_1$ and $^2A_1$ states, respectively, as in the case of the other fluoro complexes. It seems plausible that the $^2A_1$ peak exhibits the same sign as the ^4E one. The $^2B_1$ peak is of the same sign as the $^4B_2$ one. This is because of the $(\varepsilon_2/\varepsilon_1)^2 \simeq 3$ and $R(^4E)/R(^4B_2) \simeq -1$ and hence $R(^2B_1) = (4/9)\zeta_1'^2\varepsilon_1^{-2}\{R(^4E) + 4/3R(^4B_2)\} \simeq (4/27)\zeta_1'^2\varepsilon_1^{-2}$-$R(^4B_2)$ where $\zeta_1' \simeq \zeta_2' \simeq \zeta_3' \simeq \zeta_4'$ for the fluoro complex with *S,S*-2,4-ptn. The $^2A_2$ peak is obscured by the rather intense positive band. For the chloro complex, only one negative CD peak was observed at 14410 cm^{-1} and this may be due to the $^2A_1$ state. The 14590 cm^{-1} peak with positive sign may be assigned to the $^2B_1$ state, since the crystal field calculation predicts that the $^2B_1$ state lies at the higher frequency side of the $^2A_1$ state. The positive sign of the $^2B_1$ state may be caused by the considerable decrease in ζ_3' owing to the large ζ_p and the increasing contribution of the term involving the $R(^4B_2)$, as in the case of the bromo complex with *R*-pn. The $^2E(^2T_1)$ state may correspond to a positive peak observed at 14880 cm^{-1}. This positive sign may be attributed to a strong spin-orbit coupling as found for the chloro complex with *R*-pn. For the bromo complex, only in view of the transition energies, the 14330, 14510, and 14640 cm^{-1} CD peaks may be due to the $^2A_1$, $^2B_1$ and $^2A_2$ state, respectively, although their signs are all positive.

Conclusion. On the basis of the assignments thus obtained for the three series of complexes as in Table 1, it has been found that the positions of the $^2A_1$ state are shifted to the lower frequency in the order of the fluoro, chloro and bromo complexes, demonstrating the nephelauxetic effect.[37] The splitting of the ^2E cubic state, $E(^2A_1) - E(^2B_1)$, is found to be about +300 cm^{-1} for the fluoro, about −250 cm^{-1} for the chloro and −100 to −150 cm^{-1} for the bromo complexes, although the *S,S*-2,4-ptn complexes give somewhat smaller splittings. The splitting obtained for the chloro and bromo complexes is in an order of magnitude larger than the theoretical value estimated from Macfarlane's approximation on the crystal field calculation. That is, the theoretical splittings are obtained as +180, −41 and −11 cm^{-1} for the fluoro, chloro and bromo complexes, respectively, by using the parameter values estimated by Dubicki *et al.*[4] As observed[12,13] and discussed for the pentaammine aniono Cr(III) complexes by Flint and Matthews,[13] such a large splitting of the ^2E cubic state can not be elucidated by the crystal field theory. The positions of the $^2E(^2T_1)$ state vary with the coordinated diamines, *i.e.*, 13098 cm^{-1} for the en complex,[14] 13330 cm^{-1} for the *R*-pn complex, 12710 cm^{-1} for the *S,S*-stien complex, and 13950 cm^{-1} for the *S,S*-2,4-ptn complex. This is probably caused by variation of the parameters $\delta\pi$ and ε_3 for the diamines.

References

1) S. Kaizaki, J. Hidaka, and Y. Shimura, *Inorg. Chem.*, **12**, 142 (1973).
2) J. R. Perumareddi, *Coord. Chem. Rev.*, **4**, 73 (1969); J. R. Perumareddi, *J. Phys. Chem.*, **71**, 3155 (1967).
3) L. Dubicki and R. L. Martin, *Austral. J. Chem.*, **22**, 839 (1969).
4) L. Dubicki, M. A. Hitchman, and P. Day, *Inorg. Chem.*, **9**, 188 (1969); L. Dubicki and P. Day, *ibid.*, **10**, 2043 (1971).
5) R. L. Klein, Jr., N. C. Miller, and J. R. Perumareddi, *Inorg. Chim. Acta*, **7**, 685 (1973).
6) J. Glerup and C. E. Schäffer, Prog. Coord. Chem., Proceed. 11th ICCC (1968), p. 500.
7) W. W. Fee and J. N. MacB. Harrowfield, *Austral. J. Chem.*, **23**, 1049 (1969).
8) H. Yamatera, This Bulletin, **31**, 95 (1958); D. S. McClure, "Advances in the Chemistry of the Coordination Compounds," S. Kirschner, Ed., Macmillan, New York, N.Y., (1961), p. 498; C. E. Schäffer and C. K. Jørgensen, *Kgl. Danske Videnskab. Mat. -fys. Medd.*, **34**, No. 13 (1965).
9) J. C. Donini, B. R. Hollebone, G. London, A. B. P. Lever, and J. C. Hempel, *Inorg. Chem.*, **14**, 455 (1975); T. J. Barton and R. C. Slade, *J. Chem. Soc., Dalton*, **1975**, 650.
10) a) R. M. Macfarlane, *J. Chem. Phys.*, **47**, 2066 (1967); b) W. M. Fairbank, Jr. and G. K. Klauminzer, *Phys. Rev., B*, **7**, 500 (1973).
11) G. B. Porter and H. L. Schläfer, *Z. Phys. Chem.*, **40**, 280 (1964).
12) W. N. Shepard and L. S. Forster, *Theoret. Chim. Acta*, **20**, 135 (1971).
13) C. D. Flint and A. P. Matthews, *J. Chem. Soc., Faraday Trans. II*, **69**, 419 (1973).
14) C. D. Flint and A. P. Matthews, *ibid.*, **70**, 1307 (1974).
15) R. K. Rowry, Jr. and J. R. Perumaredii, *J. Phys. Chem.*, **74**, 1371 (1970).
16) C. J. Hawkins, E. Larsen, and I. Olsen, *Acta Chem. Scand.*, **19**, 1915 (1965).

17) S. F. Mason, *J. Chem. Soc. A*, **1971**, 667.
18) F. Mizukami, H. Ito, J. Fujita, and K. Saito, This Bulletin, **45**, 2129 (1972).
19) B. Bosnich and J. MacB. Harrowfield, *J. Amer. Chem. Soc.*, **94**, 3425 (1972).
20) O. F. Williams and J. C. Bailar, Jr., *ibid.*, **81**, 4464 (1959).
21) I. Lifschitz and J. G. Bos, *Rec. Trav. Chim.*, **59**, 173 (1940).
22) J. Glerup, J. Josephsen, K. Michelsen, E. Pedersen, and C. E. Schäffer, *Acta Chem. Scand.*, **24**, 247 (1970).
23) W. W. Fee, J. N. MacB. Harrowfield, and W. G. Jackson, *J. Chem. Soc., A*, **1970**, 2612.
24) Y. Shimura and R. Tsuchida, This Bulletin, **29**, 311 (1956).
25) C. K. Jørgensen, "Modern Aspects of Ligand Field Theory", North-Holland Publishing Company, Amsterdam, (1971), p. 339; S. Yamada and R. Tsuchida, This Bulletin, **26**, 15 (1953).
26) a. P. L. Fereday and S. F. Mason, *Chem. Commun.*, **1971**, 1314; b. S. F. Mason and R. H. Seal, *ibid.*, **1973**, 422. The absolute configuration of $(-)_{589}$-stilbenediamine used here is consistent with that determined by Mason *et al.* in 1973; *i.e.*, the $(-)_{589}$-isomer takes (*S*,*S*)-configuration.
27) Y. Saito and H. Iwasaki, This Bulletin, **35**, 1131 (1962).
28) F. S. Richardson, *J. Chem. Phys.*, **54**, 2453 (1971).
29) R. Dingle, *ibid.*, **46**, 1 (1967).
30) R. A. D. Wentworth and T. S. Piper, *Inorg. Chem.*, **4**, 202 (1965).
31) R. S. Treptow, *ibid.*, **5**, 1593 (1966).
32) S. Sugano and Y. Tanabe, *J. Phys. Soc., Japan*, **13**, 880 (1958); S. Sugano, A. L. Schawlow, and F. Varsanyi, *Phys. Rev.*, **120**, 2045 (1960).
33) S. Sugano, Y. Tanabe, and H. Kamimura, "Multiplets in Transition Metal Ions in Crystals", Academic Press, New York, N. Y. (1970), p. 273.
34) C. K. Jørgensen, *Structure and Bonding*, **1**, 3 (1966).
35) C. J. Ballhausen, *Mol. Phys.*, **5**, 461 (1963).
36) C. K. Jørgensen, "Absorption Spectra and Chemical Bonding in Complexes", Pergamon Press, Oxford, (1962), p. 134; "Oxidation Number and Oxidation State," Springer-Verlag, Berlin (1969), p. 72.
37) From the electron spin resonance studies for tetragonal Cr(III) complexes [E. Pedersen and S. Kallesoe, *Inorg. Chem.*, **13**, 1603 (1974); E. Pedersen and S. Kallesoe, *ibid.*, **14**, 85 (1975).], Pedersen *et al.* have required such a spin-orbit effect on ligands in terms of a simple molecular orbital treatment in order to elucidate the large zero field splittings of bromo and iodo complexes. Although the ESR results are apparently contrary to the present CD results, the manifold origins of the zero field splittings may be taken into consideration. [L. E. Mohrmann and B. B. Garrett, *ibid.*, **13**, 357 (1974).]
38) M. Linhard and M. Weigel, *Z. Phys. Chem, N. F.*, **11**, 308 (1957); J. Fujita and Y. Shimura, This Bulletin, **36**, 1281 (1963); T. Yasui and Y. Shimura, *ibid.*, **36**, 1286 (1963).
39) J. I. Zink, *Inorg. Chem.*, **12**, 1957 (1973).
40) W. Moffitt and A. Moscowitz, *J. Chem. Phys.*, **30**, 648 (1959); O. E. Weigang, Jr., *ibid.*, **43**, 3609 (1965); S. E. Harnung, E. C. Ong, and O. E. Weigang, Jr., *ibid.*, **55**, 5711 (1971); M. J. Harding, *J. Chem. Soc., Faraday Trans. II*, **68**, 234 (1972).

Transition-metal Complexes of Pyrrole Pigments. XII. Optical and Magnetic Resonance Spectra of the Cobalt(II) and Nickel(II) Complexes of 1,19-Disubstituted Tetradehydrocorrins†

Yukito MURAKAMI, Kazunori SAKATA, Yasuhiro TANAKA, and Tadashi MATSUO

Department of Organic Synthesis, Faculty of Engineering, Kyushu University, Hakozaki, Higashi-ku, Fukuoka 812

(Received July 10, 1975)

The cobalt(II) and nickel(II) complexes of 1,19-dimethyl- and 1,19-diethoxycarbonyltetradehydrocorrins were prepared by the template reaction as functioned by metal ions from the corresponding 1,19-disubstituted 1,19-dideoxybiladiene-ac's. The absorption bands appearing in the energy region greater than 15000 cm^{-1} were attributed to the $\pi \rightarrow \pi^*$ transitions within a ligand molecule. The ligand-field bands were observed in the lower energy region ($<15000\ cm^{-1}$) for the cobalt(II) complexes in which cobalt(II) assumes the C_{2v} coordination symmetry: $^2A_1 \leftarrow {}^2A_1$, $^2A_2 \leftarrow {}^2A_1$, $^2B_2 \leftarrow {}^2A_1$, and $^2B_1 \leftarrow {}^2A_1$ in an increasing order of energy. The vibrational spectra provided evidences for the formation of the tetradehydrocorrin complexes with perchlorate ion as the counter ion. The angular methyl groups placed at the 1- and 19-positions of tetradehydrocorrins showed the abnormally large up-field shift (2.0 ppm) of their proton signal relative to the parent biladiene-ac's due to the magnetic anisotropy of the adjacent pyrrole rings A and D. For a 1,19-diethyoxycarbonyltetradehydrocorrin complex, the 1,19-substituents were also placed in the shielding zone of the neighboring pyrrole rings. In the case of the cyclized 2,8,12,18-tetra(2-ethoxycarbonylethyl) derivative, the ethyl ester groups of the 2,18-substituents were presumably placed in a conformational space different from that occupied by those of the 8,12-substituents according to the proton NMR behaviors. The parent biladiene-ac which carries ethoxycarbonyl groups at the 1,19-positions caused a up-field shift of its methine (at bridge positions) proton signal upon cyclization due to the loss of electronic conjugation of carbonyl groups with pyrrole rings, in consistent with the vibrational data. The ESR spectra were measured in chloroform–benzene (2 : 1) at 77 K in the presence and absence of pyridine. The cobalt(II) complexes were identified as of low-spin square-planar type with the unpaired electron in the cobalt d_{z^2} orbital. The coordination capability of 2-ethoxycarbonylethyl groups, which are directly bound to the pyrrole rings in the cyclized metal complex system, was also suggested.

Much work has been carried out on vitamin B_{12} model compounds of the cobaloxime type to obtain some information which may throw light on the chemistry of vitamin B_{12} itself.[1,2] On the other hand, 1,19-disubstituted tetradehydrocorrins have a ring structure which is closely related to the corrin ring of vitamin B_{12}. The cobalt complexes are of particular interest since these are the direct analogs of the vitamin B_{12} complexes. Hush and Woolsey studied the electronic and ESR spectra of the cobalt(II) and nickel(II) complexes of 1,19-diethoxycarbonyltetradehydrocorrins[3,4] without assignments of ligand-field bands observable in the electronic spectra.

On account of the increasing interest in the chemistry and structural feature of vitamin B_{12}, we report in this paper the results of electronic spectra of the cobalt(II) and nickel(II) complexes of 1,19-dimethyl- and 1,19-diethoxycarbonyltetradehydrocorrins with ligand-field interpretations as well as vibrational spectra of the complexes. The detailed NMR studies for the nickel(II) complexes and the ESR data for the cobalt(II) are also provided. The metal complexes of 1,19-disubstituted tetradehydrocorrins (**2**) were prepared by the template reaction as functioned by metal ions from the corresponding 1,19-disubstituted 1,19-dideoxybiladiene-ac's (**1**).

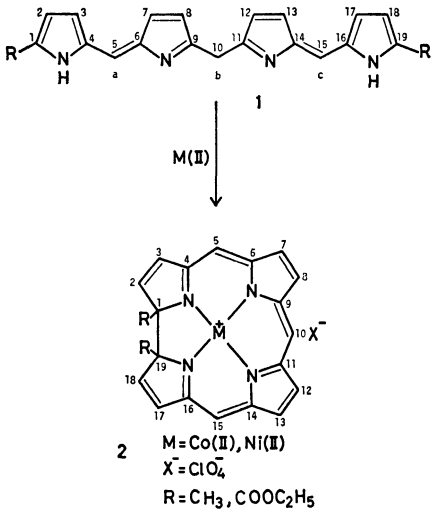

1 2

Chart 1.

Experimental

1,19-Dideoxy-1,3,7,8,12,13,17,19-octamethylbiladiene-ac Dihydrobromide (3). Prepared after Johnson *et al.*[5] from 3,3′,4,4′-tetramethyl-5,5′-dicarboxydipyrromethane[6,7] (14.0 g) and 2-formyl-3,5-dimethylpyrrole[8] (11.5 g) in methanol (1150 ml) and aqueous ammonia (3.3 ml, 28%), the resulting solution being treated with aqueous hydrobromic acid (33 ml, 47%). The product was recrystallized from chloroform as red prisms with a green luster; yield 18.1 g (66%). UV($CHCl_3$): 19200(ε 2.05×10^5), 20400 sh(ε 3.58×10^4), 22100(ε 2.10×10^4), 23500 sh(ε 9.20×10^3), 27100(ε 1.37×10^4), and 34400 cm^{-1}(ε 2.73×10^3). IR(Nujol mull): 1611 cm^{-1}(biladiene skeletal str.). Found: C, 56.41; H, 6.05; N, 9.49%. Calcd for $C_{27}H_{34}Br_2N_4$: C, 56.46; H, 5.97; N, 9.75%.

1,19-Dideoxy-1,2,3,7,8,12,13,17,18,19-decamethylbiladiene-ac Dihydrobromide (4). Prepared as above[9] from 3,3′,4,4′-tetramethyl-5,5′-dicarboxydipyrromethane (1.5 g) and 2-

† Contribution No. 377 from this Department. Part XI: Y. Murakami and K. Sakata, This Bulletin, **47**, 3025 (1974).

formyl-3,4,5-trimethylpyrrole[10,11] (0.75 g) in methanol (150 ml) and aqueous ammonia (0.2 ml, 28%). The resulting solution was treated with aqueous hydrobromic acid (3 ml, 47%) and the product was recrystallized from chloroform–light petroleum as red prisms; yield 1.4 g (67%).

1,19-Dideoxy-8,12-di(2-ethoxycarbonylethyl)-1,2,3,7,13,17,18,19-octamethylbiladiene-ac Dihydrobromide (5). 3,3′-Di(2-ethoxycarbonylethyl)-4,4′-dimethyldipyrromethane-5,5′-dicarboxylic acid (**6**) was first prepared as follows. Dibenzyl 3,3′-di(2-ethoxycarbonylethyl)-4,4′-dimethyldipyrromethane-5,5′-dicarboxylate[12] (10 g) was hydrogenated in dry tetrahydrofuran (250 ml) and triethylamine (0.5 g) over 10% palladium–carbon (1.25 g) for 2 h. Saturated aqueous sodium hydrogen carbonate was added to the resulting mixture and tetrahydrofuran was removed *in vacuo* from the filtrate. The precipitates obtained by the addition of acetic acid were recovered and washed repeatedly with water; white powder, yield 6.1 g (85%), mp>300 °C. IR(KBr disk): 1710 (ester C=O str.), and 1656 cm^{-1} (carboxyl C=O str.). NMR (H_2O-KOH, tetramethylammonium chloride): δ 1.56 (2H, s, $-CH_2-$(bridge)), 0.64 (4H, q J=7.0 Hz, 3,3′-CH_3CH_2-$OCOCH_2CH_2-$), −0.18—−0.46 (8H, m, 3,3′-CH_3CH_2 $OCOCH_2CH_2-$), −0.75 (6H, s, 4,4′-CH_3), and −1.85 (6H, t J=7.0 Hz, 3,3′-$CH_3CH_2OCOCH_2CH_2-$).

The biladiene-ac dihydrobromide (**5**) was prepared[13] from **6** (1.51 g) and 2-formyl-3,4,5-trimethylpyrrole (0.68 g) in ethanol (7 ml) and aqueous hydrobromic acid (1 ml, 47%). The product was washed and recrystallized from chloroform–light petroleum (bp 80—100 °C) as red needles; yield 1.03 g (40%), mp>300 °C. IR(KBr disk): 1732 (ester C=O str.), 1616 (biladiene skeletal str.), and 1245 cm^{-1} (C–O–C str.). Found: C, 56.90; H, 6.41; N, 7.09%. Calcd for $C_{37}H_{50}Br_2N_4O_4$: C, 57.37; H, 6.51; N, 7.23%.

1,19-Dideoxy-2,8,12,18-tetra(2-ethoxycarbonylethyl)-1,3,7,13,17,19-hexamethylbiladiene-ac Dihydrobromide[13] (7). A mixture of 3,3′-di(2-ethoxycarbonylethyl)-4,4′-dimethyldipyrromethane-5,5′-dicarboxylic acid (2.31 g), aqueous ammonia (0.4 ml, 28%), and methanol (50 ml) was refluxed with stirring. After addition of 3-(2-ethoxycarbonylethyl)-5-formyl-2,4-dimethylpyrrole[13] (2.23 g) dissolved in methanol (20 ml) and aqueous hydrobromic acid (3.5 ml, 47%) subsequently, the reaction mixture was refluxed for another 15 min with stirring. Upon cooling the mixture in a refrigerator overnight, the crystalline solid was recrystallized from chloroform–acetone to give red needles; yield 2.8 g (59%), mp>300 °C. IR(KBr disk): 1728 (ester C=O str.), 1610 (biladiene skeletal str.), and 1237 cm^{-1} (C–O–C str.).

1,19-Dideoxy-1,19-diethoxycarbonyl-2,3,7,8,12,13,17,18-octamethylbiladiene-ac Dihydrobromide[14] (8). A mixture of phosphorus oxychloride (13 ml) and *N,N*-dimethylformamide (100 ml) was added dropwise into 3,4-dimethyl-2-ethoxycarbonylpyrrole[6] (20.8 g) which was dissolved in *N,N*-dimethylformamide (200 ml) and cooled with ice-water. An aqueous solution (700 ml) of anhydrous sodium acetate (44 g) was added into the reaction mixture, which was heated at 70—80 °C for 1 h subsequently. After being allowed to stand overnight in a refrigerator, the crystalline solid was recovered and recrystallized from *i*-octane to give colorless plates of 3,4-dimethyl-2-ethoxycarbonyl-5-formylpyrrole; yield 19.4 g (79.8%), mp 107.5—108.0 °C (lit,[15] mp 106—108 °C). IR(Nujol mull): 3320 (N–H str.), 1692, 1656 (C=O str.), and 1265 cm^{-1} (C–O–C str.). NMR(CCl_4, TMS): δ 1.39 (3H, t J=7.0 Hz, 2-CH_3CH_2OCO-), 2.23, 2.27 (6H, each s, 3-CH_3 and 4-CH_3), 4.38 (2H, q J=7.0 Hz, 2-CH_3CH_2-$OCO-$), 9.77 (1H, s, 5-CHO), and 10.03 (1H, s, 1-H).

Into a mixture of 3,4-dimethyl-2-ethoxycarbonyl-5-formylpyrrole (2.05 g), 3,3′,4,4′-tetramethyldipyrromethane-5,5′-dicarboxylic acid (1.3 g) and glacial acetic acid (25 ml) was added aqueous hydrobromic acid (5.5 ml, 47%) with stirring. The mixture was warmed at 40—43 °C for 40 min and allowed to stand in a refrigerator overnight. The crystalline solid was washed with acetic acid and ethyl ether subsequently to give reddish brown needles; yield 2.35 g (72.4%), mp>300 °C. IR(Nujol mull): 1705, 1712 (ester C=O str.), and 1604 cm^{-1} (biladiene skeletal str.).

1,3,7,8,12,13,17,19-Octamethyltetradehydrocorrinatocobalt(II) Perchlorate. Air was bubbled through a mixture of biladiene-ac dihydrobromide (**3**) (0.5 g), cobalt acetate tetrahydrate (0.5 g), and ethanol (30 ml) at room temperature for 6 h. The mixture was concentrated to *ca.* 10 ml *in vacuo*, and subsequently an aqueous solution (10 ml) of sodium perchlorate monohydrate (0.5 g) was added into it. The precipitates were separated and recrystallized from methanol–acetone to give dark brown needles; yield 0.29 g (59%), mp>300 °C. Found: C, 56.82; H, 5.12; N, 9.84%. Calcd for $C_{27}H_{29}ClCoN_4O_4$: C, 57.10; H, 5.15; N, 9.87%.

1,3,7,8,12,13,17,19-Octamethyltetradehydrocorrinatonickel(II) Perchlorate. A mixture of biladiene-ac dihydrobromide (**3**) (0.5 g), nickel acetate tetrahydrate (0.5 g), and ethanol (7 ml) was heated at 60 °C for 30 min. The stream of air was bubbled through the reaction mixture into which anhydrous sodium acetate (0.5 g) was added in advance. An aqueous solution (7.5 ml) of sodium perchlorate monohydrate (1 g) was added in the reaction mixture which was subsequently kept in a refrigerator overnight. The recovered crystalline solid was recrystallized from chloroform to give dark violet needles; yield 0.135 g (68%). Found: C, 56.90; H, 5.24; N, 10.00%. Calcd for $C_{27}H_{29}ClN_4NiO_4$; C, 57.12; H, 5.15; N, 9.87%.

1,2,3,7,8,12,13,17,18,19-Decamethyltetradehydrocorrinatocobalt-(II) Perchlorate. Prepared from biladiene-ac dihydrobromide (**4**) (2.3 g) and cobalt acetate tetrahydrate (2.3 g) in ethanol (200 ml) after Melent'eva *et al.*[9] The product was recrystallized from methanol–acetone to give dark brown prisms of golden luster; yield 1.42 g (62%). Found: C, 58.27; H, 5.62; N, 9.53%. Calcd for $C_{29}H_{33}ClCoN_4O_4$: C, 58.44; H, 5.58; N, 9.40%.

1,2,3,7,8,12,13,17,18,19-Decamethyltetradehydrocorrinatonickel-(II) Perchlorate. Prepared from biladiene-ac dihydrobromide (**4**) (1.4 g) and nickel acetate tetrahydrate (1.4 g) in the presence of anhydrous sodium acetate (1.4 g) and ethanol (200 ml) after Melent'eva *et al.*[9] The product was recrystallized from methanol–acetone to give dark brown needles; yield 0.83 g (60%). Found: C, 58.77; H, 5.73; N, 9.52%. Calcd for $C_{29}H_{33}ClN_4NiO_4$: C, 58.47; H, 5.58; N, 9.40%.

8,12-Di(2-ethoxycarbonylethyl)-1,2,3,7,13,17,18,19-octamethyltetradehydrocorrinatocobalt(II) Perchlorate. Prepared from biladiene-ac dihydrobromide (**5**) (0.287 g) and cobalt acetate tetrahydrate (0.30 g in 3 ml H_2O) in ethanol (100 ml) after Johnson *et al.*[13] The crystalline solid was washed with ethyl ether (100 ml) and *n*-hexane (40 ml) successively and recrystallized from dichloromethane–*n*-hexane to give reddish brown needles; yield 0.075 g (27%), mp 225.0—225.2 °C (lit.,[13] mp 181—183 °C). Found: C, 58.15; H, 5.96; N, 6.98%. Calcd for $C_{37}H_{45}ClCoN_4O_8$: C, 57.85; H, 5.91; N, 7.29%.

8,12-Di(2-ethoxycarbonylethyl)-1,2,3,7,13,17,18,19-octamethyltetradehydrocorrinatonickel(II) Perchlorate. Prepared from biladiene-ac dihydrobromide (**5**) (0.52 g) and nickel acetate tetrahydrate (0.60 g) in the presence of anhydrous sodium acetate (0.60 g) and ethanol (15 ml) after Johnson *et al.*[13] The product was recrystallized from ethanol–light petroleum

(bp 80—100 °C) to give violet needles; yield 0.37 g (71%), mp 243.2—244.3 °C (lit.,[13] mp 243—244 °C). Found: C, 58.08; H, 5.83; N, 7.21%. Calcd for $C_{37}H_{45}ClN_4NiO_8$: C, 57.87; H, 5.91; N, 7.30%.

2,8,12,18 - Tetra(2 - ethoxycarbonylethyl) - 1,3,7,13,17,19 - hexamethyltetradehydrocorrinatocobalt(II) Perchlorate. Prepared from biladiene-ac dihydrobromide (**7**) (1.0 g) and cobalt acetate tetrahydrate (1.0 g in 10 ml H_2O) in ethanol (200 ml) after Johnson *et al.*[13] The crystalline solid was washed with ethyl ether (100 ml) and recrystallized from ethanol–light petroleum (bp 80—100 °C) to give dark reddish needles; yield 0.50 g (48%), mp 139.9—141.7 °C (lit.,[13] mp 175 °C). Found: C, 56.85; H, 6.03; N, 5.89%. Calcd for $C_{45}H_{57}ClCON_4O_{12}$: C, 57.48; H, 6.11; N, 5.96%.

2,8,12,18 - Tetra(2 - ethoxycarbonylethyl) - 1,3,7,13,17,19 - hexamethyltetradehydrocorrinatonickel(II) Perchlorate. Prepared from biladiene-ac dihydrobromide (**7**) (1.0 g) and nickel acetate tetrahydrate (1.0 g) in the presence of anhydrous sodium acetate (1.0 g) and ethanol (50 ml) after Johnson *et al.*[13] The product was recrystallized from ethanol–light petroleum (bp 80—100 °C) to give reddish violet needles; yield 0.56 g (56%), mp 162.4—165.6 °C (lit.,[13] mp 169—170 °C). Found: C, 57.70; H, 5.97; N, 6.16%. Calcd for $C_{45}H_{57}ClN_4NiO_{12}$: C, 57.49; H, 6.11; N, 5.96%.

1,19 - Diethoxycarbonyl - 2,3,7,8,12,13,17,18 - octamethyltetradehydrocorrinatocobalt(II) Perchlorate.[14] An aqueous solution (25 ml) of cobalt acetate tetrahydrate (5.0 g) was added into an ethanol suspension (500 ml) of biladiene-ac dihydrobromide (**8**) (5.0 g). Air was introduced into the reaction mixture at room temperature for 2 hr with continuous stirring, which was subsequently concentrated to a half volume. After addition of an aqueous solution (30 ml) of sodium perchlorate monohydrate (5.0 g), the reaction mixture was allowed to stand in a refrigerator for 3 hr. The crystalline solid was washed with ethyl ether and recrystallized from acetone–*n*-hexane to give brown pillar-like crystals of golden luster; yield 4.2 g (85%), mp> 300 °C. Found: C, 55.89; H, 5.46; N, 7.92%. Calcd for $C_{33}H_{37}ClCoN_4O_8$: C, 55.67; H, 5.24; N, 7.87%.

1,19 - Diethoxycarbonyl - 2,3,7,8,12,13,17,18 - octamethyltetradehydrocorrinatonickel(II) Perchlorate.[14] A methanol solution (10 ml) of nickel acetate tetrahydrate (2.0 g) was added into a methanol suspension (200 ml) of biladiene-ac dihydrobromide (**8**) (2.0 g). The mixture was refluxed for 2 hr while air was continuously bubbled through it, and then concentrated to a half volume. After addition of an aqueous solution (100 ml) of sodium perchlorate monohydrate (2.0 g), the reaction mixture was allowed to stand overnight in a refrigerator. The crystalline product was recrystallized from acetone–*n*-hexane to give brown pillar-like crystals; yield 1.7 g (86%), mp> 300 °C. Found: C, 55.53; H, 5.20; N, 7.76%. Calcd for $C_{33}H_{37}ClN_4NiO_8$: C, 55.67; H, 5.24; N, 7.89%.

Spectral Measurements. Electronic spectra covering the 5000—40000 cm^{-1} region were recorded on a Hitachi EPS-2 spectrophotometer for chloroform solutions at room temperature. Vibrational spectra were measured with a JASCO DS-403G spectrophotometer by Nujol mull and KBr disk methods. A Varian A-60 spectrometer was used to obtain NMR spectra in trifluoroacetic acid at room temperature. Chemical shifts were reported in ppm from internal TMS and calibrated by the use of chloroform signal as the external reference. ESR spectra were recorded on a JEOL JES-ME-3 X-band spectrometer equipped with a 100K Hz field modulation unit. All samples were measured in chloroform–benzene (2 : 1) at 77 K, concentrations being maintained in the 10^{-2} M range. The manganese ion diffused into magnesium oxide was used to obtain the standard reference signals for measurements.

Results and Discussion

Electronic Spectra. The electronic spectra of the cobalt(II) and nickel(II) complexes are shown in Figs. 1 and 2, respectively, and the absorption bands appearing in the energy region greater than 15000 cm^{-1} are reasonably attributed to the $\pi\rightarrow\pi^*$ transitions within a ligand molecule. The general features of the spectra arising from the $\pi\rightarrow\pi^*$ transitions are similar to those observed for metal porphyrins[16,17] and corrins.[18] An extremely intense band is observed around 28000 cm^{-1} analogous to the Soret band of porphyrins, with a weaker series of bands in the 15000—25000 cm^{-1} region comparable with the α and β bands of metal porphyrins. Hush and his associates have established on the basis of PPP-SCF π-electron calculations [4,19] that the absorption bands of metal corroles appearing in the similar energy region arise from the $\pi\rightarrow\pi^*$ transitions of the corrole ligand. The $\pi\rightarrow\pi^*$ transition energies for the present cobalt(II) and nickel(II) complexes are summarized together in Table 1.

The nickel(II) complexes do not show any significant absorption in the region lying below 15000 cm^{-1}. This spectral behavior is consistent with the square planar coordination of nickel(II).[20] Due to the presence of intense $\pi\rightarrow\pi^*$ absorption bands in the higher energy region, we failed to assign ligand-field transition bands for the nickel(II) complexes.

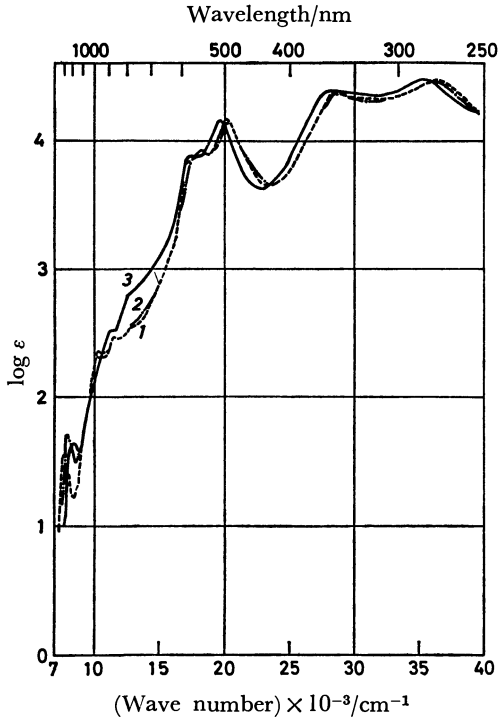

Fig. 1. Electronic absorption spectra of the tetradehydrocorrinatocobalt(II) perchlorates in chloroform at room temperature. Ligands: **1**, 1,2,3,7,8,12,13,17,18,19-decamethyltetradehydrocorrin; **2**, 8,12-di(2-ethoxycarbonylethyl) - 1,2,3,7,13,17,18,19 - octamethyltetradehydrocorrin; **3**, 1,19-diethoxycarbonyl-2,3,7,8,12,13,17,18-octamethyltetradehydrocorrin.

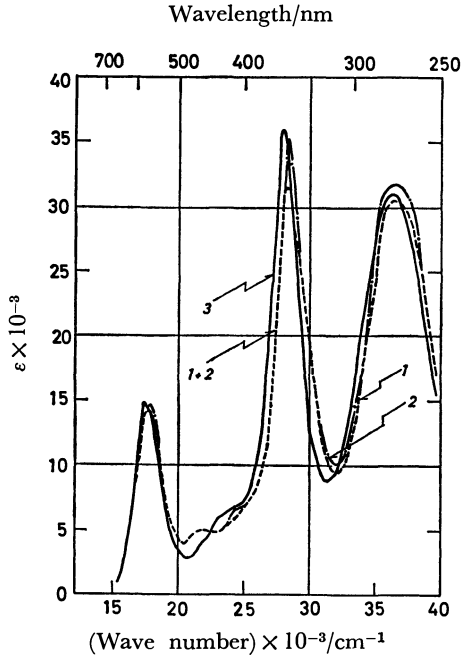

Fig. 2. Electronic absorption spectra of the tetradehydrocorrinatonickel(II) perchlorates in chloroform at room temperature. See Fig. 1 for numbering of the ligands.

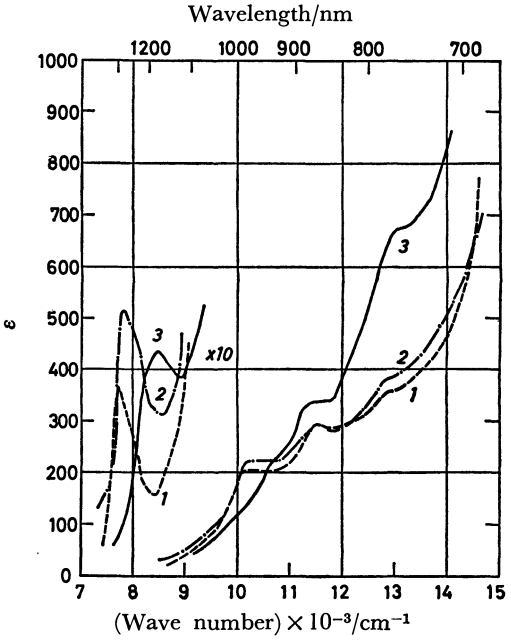

Fig. 3. Ligand-field spectra of the tetradehydrocorrinatocobalt(II) perchlorates in chloroform at room temperature. See Fig. 1 for numbering of the ligands.

The absorption spectra of the cobalt(II) complexes in the lower energy region (below 15000 cm^{-1}) are shown in Fig. 3. Nishikawa and Yamada pointed out that the ligand-field band appeared at around 8000 cm^{-1} is characteristic of the square planar low-spin cobalt(II) complexes.[21] The present cobalt(II) complexes show a distinct absorption band in the similar energy region. Meanwhile, Nishida and Kida[22] and Engelhardt and Green[23] as well have carried out ligand-field calculations for tetragonal low-spin d^7 complexes using a d^3 hole ligand-field model. We employed a energy level correlation different from these proposed by the former investigators on the basis of band-splitting behavior of the present spectra, and the ligand-field bands are assigned under the assumption of C_{2v} coordination

Table 1. Electronic absorption bands due to $\pi \rightarrow \pi^*$ transitions for the cobalt(II) and nickel(II) complexes of 1,19-disubstituted tetradehydrocorrins[a]

Ligand[b]	Transition energy in cm^{-1} (ε)			
	Co(II)		Ni(II)	
I	17600 sh (6590)	18400 (7950)	18200 (14400)	22200 (5070)
	20400 (13500)	28600 (20300)	25000 sh (6290)	28500 (27600)
	36100 (27600)		36500 (27700)	
II	17500 sh (7080)	18200 (8190)	17900 (14200)	21700 (4990)
	20100 (14400)	28400 (23400)	25000 sh (6520)	28300 (31400)
	36100 (29400)		36500 (30500)	
III	17500 sh (7420)	18300 (8230)	17900 (14500)	21700 (4990)
	20200 (13800)	28400 (23900)	24400 sh (6490)	28400 (34100)
	35700 (29300)		36400 (31700)	
IV	17500 sh (7650)	18200 (8190)	17700 (14300)	21700 sh (5900)
	20100 (13000)	28400 (23100)	25000 sh (9160)	28200 (32300)
	35300 (29900)		36000 (32100)	
V	17400 (7670)	18200 sh (7580)	17400 (14600)	21700 sh (3810)
	19700 (14300)	28200 (23700)	23300 sh (6000)	27900 (34900)
	35200 (29700)		36200 (31000)	

a) Measured in chloroform at room temperature. All the metal complexes are in the perchlorate salt form. b) I, 1,3,7,8,12,13,17,19-octamethyltetradehydrocorrin; II, 1,2,3,7,8,12,13,17,18,19-decamethyltetradehydrocorrin; III, 8,12-di(2-ethoxycarbonylethyl)-1,2,3,7,13,17,18,19-octamethyltetradehydrocorrin; IV, 2,8,12,18-tetra(2-ethoxycarbonylethyl)-1,3,7,13,17,19-hexamethyltetradehydrocorrin; V, 1,19-diethoxycarbonyl-2,3,7,8,12,13,17,18-octamethyltetradehydrocorrin.

Table 2. Ligand-field bands for the tetradehydrocorrinatocobalt(II) perchlorates[a,b]

Ligand[c]					Assignment	
I	II	III	IV	V	C_{2v}	D_{4h}
7840(49.0)	7700(36.2)	7800(51.0)	8000(111)	8500(43.4)	$^2A_1 \leftarrow {}^2A_1$	$^2B_{2g} \leftarrow {}^2A_{1g}$
10400(238)	10200(202)	10200(221)	10200 sh (390)	10600 sh (217)	$^2A_2 \leftarrow {}^2A_1$	$^2E_g \leftarrow {}^2A_{1g}$
11800 sh (361)	11500(291)	11500(293)	11500 sh (620)	11300 sh (327)	$^2B_2 \leftarrow {}^2A_1$	
12800 sh (432)	12800 sh (351)	12800 sh (377)	12800 sh (921)	13000 sh (670)	$^2B_1 \leftarrow {}^2A_1$	$^2B_{1g} \leftarrow {}^2A_{1g}$

a) Band positions are expressed in cm^{-1} and molar extinction coefficients are given in parentheses after the band positions. b) Measured in chloroform at room temperature. c) See Table 1 for numbering of the ligands.

symmetry in consistent with the spectral feature shown in Fig. 3, as listed in Table 2.

Vibrational Spectra. The characteristic IR bands, which are meaningful for the present discussion, are summarized in Table 3 for metal-free biladiene-ac's and tetradehydrocorrin complexes. A strong absorption band observed at around 1600 cm^{-1} for a biladiene-ac dihydrobromide can be attributed to the stretching mode of the dipyrromethene skeleton. The similar spectral feature has been observed for dipyrromethenes,[24-29] tripyrrene-b, and bilene-b.[30] This characteristic band loses its intensity to a large extent as seen in Fig. 4 upon formation of the tetradehydrocorrin macrocycle in a manner as observed for the porphyrin system.[31] The change in absorption intensity may be due to the structural nature of the macrocycle which is nearly fixed in one plane. This structural effect would inhibit the independent skeletal vibration of each pyrrole ring and consequently diminish its IR activity.

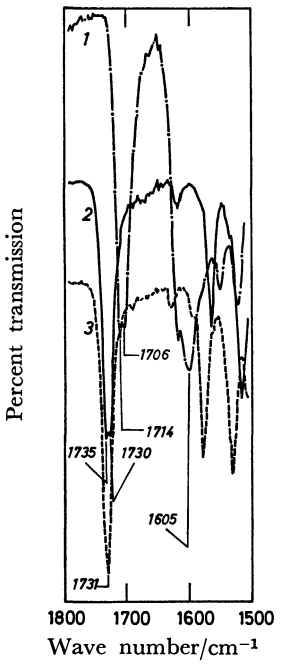

Fig. 4. Infrared spectra of biladiene-ac dihydrobromide and tetradehydrocorrin complexes by a Nujol mull technique: **1**, 1,9-dideoxy-1,19-diethoxycarbonyl-2,3,7,8,12,13,17,18-octamethylbiladiene-ac dihydrobromide; **2**, 1,19-diethoxycarbonyl-2,3,7,8,12,13,17,18-octamethyltetradehydrocorrinatocobalt(II) perchlorate; **3**, 1,19-diethoxycarbonyl-2,3,7,8,12,13,17,18-octamethyltetradehydrocorrinatonickel(II) perchlorate.

Since the carbonyl group of 2-ethoxycarbonylethyl in the biladiene-ac's does not have any electronic interaction with the pyrrole rings due to the structural reasons, the corresponding stretching mode is not affected by metal coordination as seen in spectra for the corresponding metal tetradehydrocorrins (III and IV in Table 3). On the other hand, the ethoxycarbonyl groups of 1,19-dideoxy-1,19-diethoxycarbonyl-2,3,7,8,12,13,17,18-octamethylbiladiene-ac lose their electronic conjugation with the pyrrole rings upon formation of the tetradehydrocorrin ring. Consequently, the C=O stretching band due to these carbonyl groups, which is observed in a relatively low frequency region for the biladiene-ac, is shifted to higher frequency upon metal coordination (V is Table 3).

A strong broad absorption at around 1080 cm^{-1} was observed for all the metal complexes and attributed to the stretching vibrational mode of perchlorate ion.[32] Since no splitting of this characteristic band was detected, the perchlorate group in the present metal complexes may be present not as a coordinated group but as a simple isolated ion.[33] Another peak due to the perchlorate group was observed at about 620 cm^{-1}, which may be attributed to its bending vibration.[33]

NMR Spectra. The NMR data for the 1,19-dideoxybiladiene-ac's and the corresponding tetradehydrocorrinatonickel(II) complexes are summarized in Table 4. The methyl-proton peak observed in the lowest field (2.72—2.77 ppm) for the biladiene-ac's is shifted to up-field by about 2.0 ppm upon cyclization along with nickel(II)-coordination (I—IV in Table 4). The abnormally large up-field shift is most likely associated with the angular methyl groups of the 1- and 19-positions.[15] The angular methyl groups placed at the 1- and 19-positions of tetradehydrocorrin are subjected to the shielding effect caused by the magnetic anisotropy of the adjacent pyrrole rings A and D. The proton signals for other methyl groups directly bound to the pyrrole rings show the down-field shift upon cyclization to form the tetradehydrocorrin macrocycle. These down-field shifts can be attributed to the deshielding effect due to positive charge provided by nickel(II) as well as to the additional anisotropy by the macrocyclic ring system. A similar behavior of methyl resonances has been observed for the zinc(II) chelates of dipyrromethenes.[29]

In the case of the cyclized 1,19-diethoxycarbonyl derivative, the 1,19-substituents are also placed in the shielding zone of the neighboring pyrrole rings as

Table 3. Characteristic IR absorption bands for the cobalt(II) and nickel(II) complexes of 1,19-disubstituted tetradehydrocorrins and the parent biladiene-ac's[a,b]

Ligand[c]	Form	IR band (cm^{-1})	Assignment
I′	2 HBr	1613 (s)	$\nu_{C=C,\ C=N}$ (dipyrromethene skeletal)
I	Co^{II} chelate	1614 (w)	$\nu_{C=C,\ C=N}$ (macrocyclic skeletal)
		1095 (s br)	$\nu_{ClO_4^-}$
		622 (s)	$\delta_{ClO_4^-}$
I	Ni^{II} chelate	1621 (w)	$\nu_{C=C,\ C=N}$ (macrocyclic skeletal)
		1085 (s br)	$\nu_{ClO_4^-}$
		622 (s)	$\delta_{ClO_4^-}$
II′	2 HBr	1613 (s)	$\nu_{C=C,\ C=N}$ (dipyrromethene skeletal)
II	Co^{II} chelate	1622 (w)	$\nu_{C=C,\ C=N}$ (macrocyclic skeletal)
		1088 (s br)	$\nu_{ClO_4^-}$
		621 (s)	$\delta_{ClO_4^-}$
II	Ni^{II} chelate	1625 (w)	$\nu_{C=C,\ C=N}$ (macrocyclic skeletal)
		1092 (s br)	$\nu_{ClO_4^-}$
		622 (s)	$\delta_{ClO_4^-}$
III′	2 HBr	1730 (s)	$\nu_{C=O}$ (ester)
		1618 (s)	$\nu_{C=C,\ C=N}$ (dipyrromethene skeletal)
III	Co^{II} chelate	1726 (s)	$\nu_{C=O}$ (ester)
		1623 (w)	$\nu_{C=C,\ C=N}$ (macrocyclic skeletal)
		1086 (s br)	$\nu_{ClO_4^-}$
		622 (s)	$\delta_{ClO_4^-}$
III	Ni^{II} chelate	1727 (s)	$\nu_{C=O}$ (ester)
		1630 (w)	$\nu_{C=C,\ C=N}$ (macrocyclic skeletal)
		1079 (s br)	$\nu_{ClO_4^-}$
		622 (s)	$\delta_{ClO_4^-}$
IV′	2 HBr	1728 (s)	$\nu_{C=O}$ (ester)
		1611 (s)	$\nu_{C=C,\ C=N}$ (dipyrromethene skeletal)
IV	Co^{II} chelate	1725 (s)	$\nu_{C=O}$ (ester)
		1622 (w)	$\nu_{C=C,\ C=N}$ (macrocyclic skeletal)
		1090 (s br)	$\nu_{ClO_4^-}$
		621 (s)	$\delta_{ClO_4^-}$
IV	Ni^{II} chelate	1726 (s)	$\nu_{C=O}$ (ester)
		1632 (w)	$\nu_{C=C,\ C=N}$ (macrocyclic skeletal)
		1088 (s br)	$\nu_{ClO_4^-}$
		622 (s)	$\delta_{ClO_4^-}$
V′	2 HBr	1714 (s), 1706 (s)	$\nu_{C=O}$ (ester)
		1605 (s)	$\nu_{C=C,\ C=N}$ (dipyrromethene skeletal)
V	Co^{II} chelate	1735 (s), 1730 (s)	$\nu_{C=O}$ (ester)
		1623 (w)	$\nu_{C=C,\ C=N}$ (macrocyclic skeletal)
		1080 (s br)	$\nu_{ClO_4^-}$
		621 (s)	$\delta_{ClO_4^-}$
V	Ni^{II} chelate	1731 (s)	$\nu_{C=O}$ (ester)
		1631 (w)	$\nu_{C=C,\ C=N}$ (macrocyclic skeletal)
		1084 (s br)	$\nu_{ClO_4^-}$
		621 (s)	$\delta_{ClO_4^-}$

a) Measured by the Nujol mull method at room temperature. b) Relative intensities: s, strong; w, weak; br, broad. c) See Table 1 for numbering of the ligands I through V.
I′, 1,19-dideoxy-1,3,7,8,12,13,17,19-octamethylbiladiene-ac; II′, 1,19-dideoxy-1,2,3,7,8,12,13,17,18,19-decamethylbiladiene-ac; III′, 1,19-dideoxy-8,12-di(2-ethoxycarbonylethyl)-1,2,3,7,13,17,18,19-octamethylbiladiene-ac; IV′, 1,19-dideoxy-2,8,12,18-tetra(2-ethoxycarbonylethyl)-1,3,7,13,17,19-hexamethylbiladiene-ac; V′ 1,19-dideoxy-1,19-diethoxycarbonyl-2,3,7,8,12,13,17,18-octamethylbiladiene-ac.

Table 4. Proton NMR data for the nickel(II) complexes of 1,19-disubstituted tetradehydrocorrirs and the parent biladiene-ac's[a,b]

Ligand[c]	Form	$-C\underline{H}_3$ (ester)	$-C\underline{H}_3$ 1,19	$-C\underline{H}_3$ 2,18	$-C\underline{H}_3$ 3,17	$-C\underline{H}_3$ 7,13	$-C\underline{H}_3$ 8,12	$-C\underline{H}_2-$ (ester)	$-C\underline{H}_2-$	$-C\underline{H}_2C\underline{H}_2-$	$-C\underline{H}=$ 5,15	$-C\underline{H}=$ 10	$\underline{H}$
I	2 HBr		2.74		2.38	2.46	2.25		4.53		7.48		6.43
I	Ni^{II} chelate		0.80		2.65	2.71	2.61				7.60	7.65	7.80
													7.81
II′	2 HBr		2.73	2.12	2.36	2.36	2.24		4.47		7.43		
II	Ni^{II} chelate		0.81	2.55	2.61	2.66	2.61				7.55	7.49	
III′	2 HBr	1.39(3)	2.72	2.12	2.40	2.40		4.36(4)	4.64	3.00(m)	7.46		
III	Ni^{II} chelate	1.37(3)	0.77	2.59	2.65	2.72		4.38(4)		3.10(3)	7.62	7.74	
										3.59(3)			
IV′	2 HBr	1.38(3)	2.77		2.44	2.44		4.36(4)	4.68	3.00(m)	7.51		
IV	Ni^{II} chelate	1.35(3)	0.79		2.65	2.71		4.30(4)		3.07(3)	7.63	7.79	
		1.46(3)						4.53(4)		3.46(3)			
V′	2 HBr	1.52(3)		2.50	2.43	2.43	2.18	4.60(4)	4.87		7.85		
V	Ni^{II} chelate	1.10(3)		2.58	2.63	2.83	2.63	4.07(4)			7.55	7.77	

a) Measured in trifluoroacetic acid with TMS as an internal reference; chemical shifts are given in ppm. b) Multiplicity of a proton signal is given in parentheses after δ-value ($J=7.0$ Hz). c) See Tables 1 and 3 for numbering of the ligands.

observed for the angular methyl groups mentioned above. Thus, the methylene-proton peaks ($CH_3C\underline{H}_2$-OCO–) and the methyl-proton signals ($C\underline{H}_3CH_2OCO$–) show up-field shifts by 0.5 and 0.4 ppm, respectively, upon cyclization. The magnitude of up-field shifts for these ethyl groups is much smaller than those observed for the angular methyl groups. This is primarily due to the fact that the ethyl ester groups are placed further from the adjacent pyrrole rings, which provide magnetic anisotropy, relative to the angular methyls.

In the case of the cyclized 2,8,12,18-tetra(2-ethoxycarbonylethyl) derivative (IV in Table 4), the proton signals for ester-methylene ($CH_3C\underline{H}_2OCOCH_2CH_2$–) and ester-methyl ($C\underline{H}_3CH_2OCOCH_2CH_2$–) of the 2-ethoxycarbonylethyl group were observed as quintet and quartet, respectively. These peaks were analyzed as the overlaps of two quartet and of two triplet, respectively, for the quintet and quartet signals. This seems to indicate that the ethyl ester groups of the 2,18-substituents are placed in a conformational space different from that occupied by those of the 8,12-substituents. Consequently, one type of these ethyl ester groups secures the magnetic anisotropy effect due to the macrocyclic ring system in a manner different from the other.

The cyclization of biladiene-ac's, which do not carry any carbonyl group in conjugation with the pyrrole rings, causes a down-field shift of the proton signal due to the 5- and 15-methine groups. Another proton peak was observed in a lower field relative to the above one for the same tetradehydrocorrins along with the disappearance of the proton signal due to the 10-methylene group of the biladiene-ac precursors. Only exception is noticed in the case of tetradehydrocorrin complex II (see Table 4): the reversed relation of these proton signals is observed although the reason for this is not obvious at present. These down-field shifts may be attributed to the presence of aromaticity in the chelate rings as well as the electron-withdrawing effect of nickel(II) as observed previously for the zinc(II) complexes of dipyrromethenes[29] and bilene-b.[30] Meanwhile, the biladiene-ac precursor which carries ethoxycarbonyl groups at the 1,19-positions causes an up-field shift of its methine proton signal upon cyclization (V′ and V in Table 4) on the contrary. Since the strong electronic conjugation of carbonyl groups placed at the 1- and 19-positions is lost upon formation of the tetradehydrocorrin ring, the electron density at the 5- and 10-carbons is increased significantly as a whole. This result is consistent with the corresponding IR spectral behavior.

ESR Spectra. The ESR spectrum of 1,19-diethoxycarbonyl-2,3,7,8,12,13,17,18-octamethyltetradehydrocorrinatocobalt(II) perchlorate observed in chloroform–benzene at 77 K is shown in Fig. 5 as an example for those of the cobalt(II) complexes of 1,19-disubstituted tetradehydrocorrins. In this spectrum, a set of eight cobalt hyperfine lines on the parallel component of the g-tensor ($g_{\parallel}$), which lie at higher fields, with a g-value close to spin free. The low-field set of hyperfine lines that belongs to the perpendicular component of the g-tensor ($g_{\perp}$) is not clearly resolved. Thus, unambiguous analysis of these low-field lines is difficult and the evaluated $g_{\perp}$ values would involve some minor errors. In any case, the ESR spectra indicate that the present cobalt(II) complexes are of low-spin square-planar type with an unpaired electron in the cobalt d_{z^2} orbital. The similar spectral features have also been observed for the complexes derived from porphyrins,[34,35] phthalocyanin,[36] vitamin B_{12} and related compounds,[37–39] and Schiff bases.[40]

In the presence of a few drops of pyridine in the chloroform–benzene solution, the spectrum shown in Fig. 5 is transformed into that in Fig. 6. Since a triplet nitrogen superfine coupling due to axial coordination of a pyridine molecule is observed on the parallel cobalt hyperfine lines, it may be concluded that the unpaired electron of cobalt(II) is certainly in the d_{z^2}

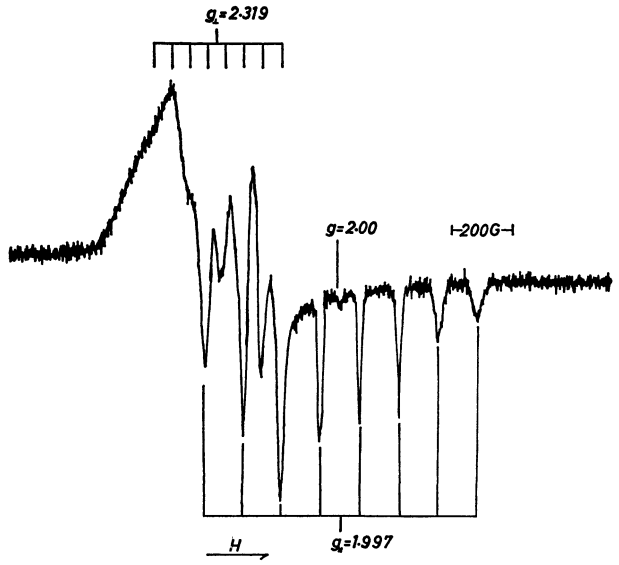

Fig. 5. ESR spectrum of 1,19-diethoxycarbonyl-2,3,7, 8,12,13,17,18-octamethyltetradehydrocorrinatocobalt-(II) perchlorate in chloroform-benzene(2 : 1) at 77 K.

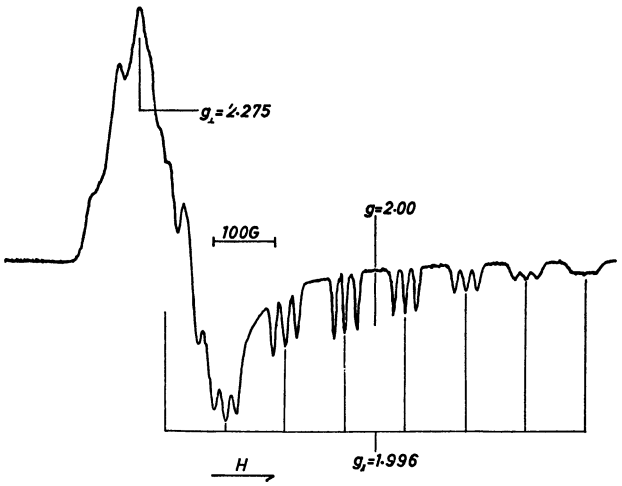

Fig. 6. ESR spectrum of 1,19-diethoxycarbonyl-2,3,7, 8,12,13,17,18 - octamethyltetradehydrocorrinatocobalt-(II) perchlorate in chloroform-benzene (2 : 1) at 77 K upon addition of pyridine.

orbital.

The ESR spectra were analyzed in terms of the spin Hamiltonian given by Eq. (1).

$$\mathscr{H}_s = \beta_e[g_{\parallel}H_zS_z + g_{\perp}(H_xS_x + H_yS_y)] + A_{\parallel}S_zI_z + A_{\perp}(S_xI_x + S_yI_y) \quad (1)$$

For the unpaired electron in the d_{z^2} orbital, the g factors of second-order calculations are[34]

$$g_{\parallel} = 2.0023 - 3(\lambda/\Delta)^2 \quad (2)$$

$$g_{\perp} = 2.0023 + 6(\lambda/\Delta) - 6(\lambda/\Delta)^2 \quad (3)$$

where λ is the spin-orbit coupling for Co(II), and Δ is the excitation energy from the degenerated d_{xz} and d_{yz} orbitals to the d_{z^2} orbital. The first-order $A_{\parallel}$ and $A_{\perp}$ components of hyperfine interaction are given as:[4]

$$A_{\parallel} = P[4/7 - K + 6/7(\lambda/\Delta)] \quad (4)$$

$$A_{\perp} = P[-2/7 - K + 45/7(\lambda/\Delta)] \quad (5)$$

where $P = g_e\beta_e g_n\beta_n\langle d_{z^2}|1/r^3|d_{z^2}\rangle$ and K is the Fermi contact interaction term. The spin Hamiltonian parameters evaluated according to Eqs. (2) through (5) are summarized in Table 5. The $g_{\parallel}$ values are quite similar in magnitude to those reported by Hush and Woolsey[3,4] for 1,19-diethoxycarbonyltetradehydrocorrinatocobalt(II) complexes, but the $g_{\perp}$ components are somewhat different from those evaluated by them and seem to be quite sensitive to the solvent environment. The decrease in A-tensor components along with the coordination of a pyridine molecule suggests that an unpaired electron in the d_{z^2} orbital of cobalt(II) is delocalized through the coordinate bond formed between cobalt(II) and pyridine nitrogen. The formation of similar penta-coordinated cobalt(II) complexes of square pyramidal structure with axial coordination of pyridine has been reported for the $\alpha,\beta,\gamma,\delta$-tetra($p$-methoxyphenyl)porphine complex, and the vitamine B_{12} and related complexes.[37-39] On the other hand, the cobalt(II) complexes derived from phthalocyanin,[36] and dimethylglyoxime[39] were found to take up two pyridine molecules at their axial positions. The reason for the difference in coordination

Table 5. Spin hamiltonian parameters for the cobalt(II) complexes of 1,19-disubstituted tetradehydrocorrins[a,b]

Ligand	Added base	$g_{\parallel}$	$g_{\perp}$	$A_{\parallel}^{Co}\times10^4$ (cm^{-1})	$A_{\perp}^{Co}\times10^4$ (cm^{-1})	$A_{\parallel}^{N}\times10^4$ (cm^{-1})	λ/Δ	$P\times10^4$ (cm^{-1})	K	$(P/P_0)\times100$[c] (%)
I		1.998	2.286	126	69		0.0379	98.1	−0.746	38.6
I	pyridine	1.995	2.270	93.2	45[d]	18.9	0.0493	96.8	−0.421	38.1
II		1.999	2.295	128	70		0.0332	94.3	−0.817	37.1
II	pyridine	1.995	2.274	97.9	48[d]	19.2	0.0493	100	−0.449	39.3
III		1.991	2.259	135	69		0.0614	161	−0.320	63.4
III	pyridine	1.989	2.267	91.5	48[d]	17.3	0.0666	117	−0.268	46.1
IV		1.992	2.278	133	72		0.0586	142	−0.416	55.9
IV	pyridine	1.990	2.263	89.7	49[d]	17.5	0.0640	104	−0.345	40.9
V		1.997	2.319	120	70		0.0420	90.7	−0.783	35.7
V	pyridine	1.996	2.275	98.2	46[d]	19.2	0.0458	100	−0.451	39.3

a) Measured in chloroform-benzene (2 : 1) at 77 K; concentration, 10^{-2}—10^{-3} M. b) Maximum possible errors: g, ±0.005; $A_{\parallel}^{Co}$, $\pm0.5\times10^{-4}$ cm^{-1}; $A_{\perp}^{C}$, $\pm5\times10^{-4}$ cm^{-1}, $A_{\parallel}^{N}$, $\pm0.05\times10^{-4}$ cm^{-1}. c) P_0 for the free cobalt(II) ion, 2.54×10^{-2} cm^{-1}. d) Estimated from line width.

behavior of pyridine molecule is not clear at present.

The P/P_0 values listed in Table 5 may be referred to as a measure for the degree of covalency of coordinate bonds, P_0 being as for the free cobalt(II) ion (254×10^{-4} cm^{-1} [41]). When the tetradehydrocorrin carries more than two groups of 2-ethoxycarbonylethyl (III and IV in Table 5), the P/P_0 value becomes relatively large compared to other analogous complexes given in Table 5. This seems to suggest that the 2-ethoxycarbonylethyl groups have a coordination interaction with cobalt(II) at the axial positions and can be replaced by a pyridine molecule along with the formation of the corresponding penta-coordinated complex.

Meanwhile, the present tetradehydrocorrinatocobalt(II) complexes which underwent reaction with $NaBH_4$ in dimethylformamide did not show any ESR signal, most likely due to the formation of the diamagnetic cobalt(I) complexes.

References

1) A. Bigotto, *et al.*, *Inorg. Chim. Acta Rev.*, **4**, 41 (1970).
2) (a) G. N. Schrauzer, *Accounts Chem. Res.*, **1**, 97 (1968). (b) G. N. Schrauzer, "Bioinorganic Chemistry," ed. by R. F. Gould, Advances in Chemistry Series No. 100, Amer. Chem. Soc. (1971), pp 1—20.
3) N. S. Hush and I. S. Woolsey, *J. Amer. Chem. Soc.*, **94**, 4107 (1972).
4) N. S. Hush and I. S. Woolsey, *J. Chem. Soc., Dalton*, **1974**, 24.
5) I. D. Dicker, R. Grigg, A. W. Johnson, H. Pinnock, K. Richardson, and P. van den Broek, *J. Chem. Soc., C*, **1971**, 536.
6) G. G. Kleinsphen, *J. Amer. Chem. Soc.*, **77**, 1546 (1955).
7) E. Bullock, R. Grigg, A. W. Johnson, and J. W. F. Wasley, *J. Chem. Soc.*, **1963**, 2326.
8) Y. Murakami, Y. Kohno, and Y. Matsuda, *Inorg. Chim. Acta*, **3**, 671 (1969).
9) T. A. Melent'eva, N. D. Pekel', and V. M. Berezovskii, *J. Gen. Chem., U.S.S.R.*, **40**, 150 (1970).
10) A. Treibs and H. Derra-Scherer, *Justus Liebigs Ann. Chem.*, **589**, 196 (1954).
11) A. W. Johnson, N. Shaw, and J. W. F. Wasley, *J. Chem. Soc.*, **1962**, 2556.
12) A. W. Johnson, I. T. Kay, E. Markham, R. Price, and K. B. Shaw, *J. Chem. Soc.*, **1959**, 3416.
13) R. Grigg, A. W. Johnson, R. Kenyon, V. B. Math, and K. Richardson, *J. Chem. Soc., C*, **1969**, 176.
14) Preparation of these compounds was aided by Mr. Hidetaka Iwamoto of these laboratories.
15) D. Dolphin, R. L. N. Harris, J. L. Huppatz, A. W. Johnson, and I. T. Kay, *J. Chem. Soc., C*, **1966**, 30.
16) L. Edwards, D. H. Dolphin, and M. Gouterman, *J. Mol. Spectrosc.*, **35**, 90 (1970).
17) C. Weiss, H. Kobayashi, and M. Gouterman, *ibid.*, **16**, 415 (1965).
18) P. O. Offenhartz, B. H. Offenhartz, and M.M.Fung, *J. Amer. Chem. Soc.*, **92**, 2966 (1970).
19) N. S. Hush, J. M. Dyke, M. L. Williams, and I. A. Woolsey, *J. Chem. Soc., Dalton*, **1974**, 395.
20) A. B. P. Lever, "Inorganic Electronic Spectroscopy," Elsevier Publishing Co., Amsterdam (1968), Chapter 9.
21) Y. Nishikawa and S. Yamada, This Bulletin, **37**, 8 (1964).
22) Y. Nishida and S. Kida, *ibid.*, **45**, 461 (1972).
23) L. M. Engelhardt and M. Green, *J. Chem. Soc., Dalton*, **1972**, 724.
24) Y. Murakami and K. Sakata, *Inorg. Chim. Acta*, **2**, 273 (1968).
25) Y. Murakami, Y. Matsuda, and K. Sakata, *Inorg. Chem.*, **10**, 1728 (1971).
26) Y. Murakami, Y. Matsuda, K. Sakata, and A. E. Martell, *J. Chem. Soc., Dalton*, **1973**, 1729.
27) Y. Murakami, Y. Matsuda, K. Sakata, and K. Harada, This Bulletin, **47**, 458 (1974).
28) Y. Murakami, K. Sakata, K. Harada, and Y. Matsuda, *ibid.*, **47**, 3021 (1974).
29) Y. Murakami and K. Sakata, *ibid.*, **47**, 3025 (1974).
30) Y. Murakami, Y. Matsuda, and S. Kobayashi, *J. Chem. Soc., Dalton*, **1973**, 1734.
31) L. J. Boucher and J. J. Katz, *J. Amer. Chem. Soc.*, **89**, 1340 (1967).
32) K. Nakamoto, "Infrared Spectra of Inorganic and Coordination Compounds," John Wiley & Sons, Inc., New York (1963), p. 107.
33) B. J. Hathaway and A. E. Underhill, *J. Chem. Soc.*, **1961**, 3091.
34) J. M. Assour, *J. Chem. Phys.*, **43**, 2477 (1965).
35) F. A. Walker, *J. Amer. Chem. Soc.*, **92**, 4235 (1970).
36) J. M. Assour, *ibid.*, **87**, 4701 (1965).
37) J. H. Bayston, F. D. Looney, J. R. Pilbrow, and M. E. Winfield, *Biochemistry*, **9**, 2164 (1970).
38) S. Cockle, H. A. O. Hill, S. Ridsdale, and R. J. P. Williams, *J. Chem. Soc., Dalton*, **1972**, 297.
39) G. N. Schrauzer and L. P. Lee, *J. Amer. Chem. Soc.*, **90**, 6541 (1968).
40) B. M. Hoffman, D. L. Diemente, and F. Basolo, *ibid.*, **92**, 61 (1970).
41) B. R. McGarvey, *J. Phys. Chem.*, **71**, 51 (1967).

Isolation and Circular Dichroism of the Isomers of Dicyanobis[(*R*,*R*)-1,2-cyclohexanediamine] and bis[(*S*)-propylenediamine]cobalt(III) Complexes

Kazuo KASHIWABARA (née KONYA), Toshimasa YAMANAKA, and Kazuo SAITO
Department of Chemistry, Faculty of Science, Tohoku University, Aramaki, Sendai 980
Naoto KOMATSU, Nobuhiro HAMADA, Hiroaki NISHIKAWA, and Muraji SHIBATA
Department of Chemistry, Faculty of Science, Kanazawa University, Marunouchi, Kanazawa 920
(Received July 31, 1975)

Three isomers of *trans*- and *cis*-$[Co(CN)_2\{(R,R)\text{-}1,2\text{-cyclohexanediamine}\}_2]^+$ and five isomers of the corresponding (*S*)-propylenediamine complexes have been isolated by chromatography with Dowex 50W-X8 and SP-Sephadex columns, their geometrical structures being assigned on the basis of the ligand field absorption and PMR spectra. Isomers of *cis*-$[Co(CN)_2\{(S)\text{-propylenediamine}\}_2]Cl$, which have different placement of methyl groups of (*S*)-propylenediamine, gave different methyl PMR resonances with different chemical shifts. The absolute configuration of the isomers was determined from the circular dichroism in the first spin-allowed d-d and the charge transfer band region. The configurational and the vicinal effect have been discussed.

Although several methods have been developed for the preparation of mixed cyano-diamine and cyano-ammine cobalt(III) complexes,[1-7] only a few studies[8,9] have been reported on the optically active complexes. The cyanide ion is the ligand which gives the strongest ligand field and a π-back donating character. It is interesting to compare the circular dichroism (CD) of the cyano-diamine complexes with those which have been extensively studied so far.[10] McCaffery *et al.*[8] showed that CD spectra of *cis*-$[CoL_2(en)_2]^{n+}$ have different patterns from the corresponding tris(diamine) complexes whenever the ligand L is well separated from neutral nitrogen donors in the spectrochemical series. When $L=CN^-$, two peaks with the same sign were observed in the region of the octahedral T_{1g} absorption.

The purpose of this study is to investigate the CD behavior more extensively for a variety of mixed cyano complexes of cobalt(III). We report preparation and characterization of the isomers of $[Co(CN)_2(R,R\text{-chxn})_2]^+$ and $[Co(CN)_2(S\text{-pn})_2]^+$ (chxn=1,2-cyclohexanediamine, pn=propylenediamine). Their visible and ultraviolet absorption, CD and PMR spectra are discussed for assigning the geometrical and optical isomers.

Experimental

Preparation and Separation of the Isomers of Dicyanobis[(R,R)-1,2-cyclohexanediamine]cobalt(III) Complexes. One gram of potassium cyanide was dissolved in 150 ml of dimethyl sulfoxide (DMSO) at 60 °C. To this solution was added 2 g of *trans*-$[CoCl_2(R,R\text{-chxn})_2]Cl\cdot 1/2H_2O$ in portions with stirring. The color of the solution turned from green to orange instantly. The solution was allowed to stand at 60 °C for 30 min., cooled to room temperature and poured into a column (120×4 cm) of an SP-Sephadex C-25 ion exchanger. The column was washed with water in order to remove DMSO. When the adsorbed band was eluted with a 0.05 M aqueous solution of sodium perchlorate at a rate 2 ml/min, one orange yellow and then two light yellow bands were eluted. The first orange yellow eluate was evaporated to dryness at 40 °C in a rotary evaporator under reduced pressure. Thirty ml of acetone was added to dissolve sodium perchlorate, leaving orange yellow residues which were then dissolved in a minimum amount of hot water and filtered. The filtrate was kept in a refrigerator overnight to obtain orange yellow crystals, C-1. Yield about 400 mg. Found: C, 37.53; H, 6.40; N, 18.89%. Calcd for $[Co(CN)_2\text{-}(R,R\text{-chxn})_2]ClO_4\cdot 1/2H_2O$: C, 37.56; H, 6.53; N, 18.77%.

The second and the third light yellow eluates were evaporated at 40 °C in rotary evaporators to dryness. Five ml portions of ethanol were added to extract the light yellow precipitates and the ethanol solutions were evaporated to dryness. The residues were dissolved in minimum amounts of hot water and the solutions were cooled in a refrigerator. Light yellow needlelike crystals were obtained from the two lots, C-2 and C-3. The yield was about 100 mg for both C-2 and C-3. These products were much more soluble than C-1. Found for C-2: C, 37.08; H, 6.60; N, 19.00%. Found for C-3: C, 37.41; H, 6.56; N, 18.79%. Calcd for $[Co(CN)_2(R,R\text{-chxn})_2]ClO_4\cdot 1/2H_2O$: C, 37.56; H, 6.53; N, 18.77%.

Preparation and Separation of the Isomers of Dicyanobis[(S)-propylenediamine]cobalt(III) Complexes. Method 1): To a cold solution (*ca.* 0 °C) of 10 g of $[Co(S\text{-pn})_3]Cl_3$[11] in 800 ml of water was added dropwise 2.5 g of potassium cyanide in 10 ml of cold water with stirring. Activated charcoal (2 g) was added and the solution was allowed to stand at room temperature for several days. The orange yellow solution was filtered and the filtrate was added at a rate 0.3 ml/min to a column (4×40 cm) of the ion exchanger (Dowex 50W-X8, 100—200 mesh) in the sodium form. After the column was washed with water the adsorbed band was eluted with a 0.2 M aqueous sodium chloride solution at a 0.15 ml/min rate. This procedure separated the adsorbed band into four bands. The first orange yellow band gave only one kind of crystal (P-1), which was assigned to *trans*-$[Co(CN)_2(S\text{-pn}_2)]Cl$ from the visible absorption spectrum (*vide infra*). The fourth band which remained at the top of the column consisted mainly of $[Co(S\text{-pn})_3]^{3+}$. During the progress of elution with the same eluent, both the second and the third band were separated into three bands. The six portions of eluates were individually concentrated under reduced pressure at 40 °C and treated with ethanol to precipitate sodium chloride, which was filtered off. Addition of ethanol, evaporation and filtration were repeated several times to remove sodium chloride as far as possible. Diethyl ether was added to the ethanol solutions to precipitate crude products, which were recrystallized by dissolving them in minimum amounts of water at 40 °C and keeping the solutions in a refrigerator. The six portions of light yellow crystals were named P-2, P-3, P-4, P-5, P-6 and P-7 in the order of elution and assigned to geometrical isomers of *cis*-$[Co(CN)_2(S\text{-pn})_2]Cl$ on the basis of the visible absorption spectra. P-2, P-3, P-4 and P-6 were in good crystalline state and gave satisfactory results

on elemental analysis. The yields of P-5 and P-7 were os poor that only spectral measurements were made and satisfactory elemental analysis was not carried out. Found for P-1: C, 29,77; H, 7.54; N, 26.66%. Calcd for $[Co(CN)_2(S\text{-pn})_2]Cl\cdot 3/2H_2O$: C, 29.96; H, 7.23; N, 26.21%. Found for P-2: C, 30.46; H, 7.32; N, 26.40%. Calcd for $[Co(CN)_2(S\text{-pn})_2]Cl\cdot H_2O$: C, 30.73; H, 7.09; N, 26.88%. Found for P-3: C, 31.57; H, 7.51; N, 27.27%. Calcd for $[Co(CN)_2(S\text{-pn})_2]Cl\cdot 1/2H_2O$: C, 31.75; H, 6.99; N, 27.77%. Found for P-4: C, 32.24; H, 7.43; N, 28.07%. Calcd for $[Co(CN)_2(S\text{-pn})_2]Cl$: C, 32.61; H, 6.84; N, 28.51%. Found for P-6: C, 30.06; H, 7.17: N, 26.46%. Calcd for $[Co(CN)_2(S\text{-pn})_2]Cl\cdot 3/2H_2O$: C, 29.96; H, 7.23; N, 26.21%.

Method 2) The same method as for the corresponding (*R,R*)-1,2-cyclohexanediamine complexes was applied, using *trans*-$[CoCl_2(R\text{-pn})_2]Cl$ in DMSO. One orange band and two light yellow bands were separated in an SP-Sephadex column. The orange one was assigned to the *trans* isomer of $[Co(CN)_2(R\text{-pn})_2]^+$, and the light yellow ones were to the *cis* isomers, on the basis of the visible absorption spectra. However, the two light yellow bands could not be separated further even on elution at a very small elution rate. The elemental analysis for these three isomers gave satisfactory results.

Measurement. The electronic absorption spectra were obtained with a Hitachi EPU-2A spectrophotometer and a Hitachi 323 recording spectrophotometer. The CD spectra were recorded on a JASCO Model ORD/UV-5 and J-20 spectropolarimeter. The PMR spectra were measured with a JEOL Model JNM MH 60 II spectrometer in deuterium oxide using sodium 2,2-dimethyl-2-silapentane-5-sulfonate (DSS) as an internal reference. Infrared spectra were measured as KBr disk with a DS 301 infrared spectrometer of Japan Spectroscopic Company.

Results and Discussion

Preparation, Separation and Characterization of the Isomers. The preparation of mixed cyano cobalt(III) complexes has been known to be difficult because of the strong tendency of cyanide ions to coordinate to a central cobalt(III) ion. In recent years, however, some preparative studies on the mixed complexes have been developed by several groups.[1-7] In the present work, two methods have been adopted to prepare the optically active dicyanobis(diamine)cobalt(III) complexes. One is the reaction of *trans*-$[CoCl_2(diamine)_2]^+$ with KCN in DMSO.[5] The other is based on the reaction of $[Co(diamine)_3]^{3+}$ with KCN in an aqueous solution in the presence of activated charcoal.[4] The former method is effective for preparing the *trans* dicyano isomers, the formation ratio *trans*/*cis* being about 2. In the latter method, the yields of the *trans* isomer were very poor as compared with those of the corresponding *cis* isomers. The yields for each isomer are very similar to those of the corresponding ethylenediamine complexes. The geometrical structure, *trans* or *cis*, was determined on the basis of the visible absorption spectra which are almost identical with those of the corresponding ethylenediamine complexes respectively; *i.e.* the *trans* isomer is well characterized by the splitting of its first absorption band, but the *cis* isomers show no splitting in the same region.

The bidentate ligand, propylenediamine, is unsymmetrical due to the placement of a methyl group on the chelate ring so that five geometrical isomers are possible for the $[Co(CN)_2(S\text{-pn})_2]^+$ complex as shown in Fig. 1. When the configuration (Δ and Λ) around the cobalt ion is considered, six isomers are possible for the *cis* dicyano complexes. The isomers would be expected to be nearly energetically equivalent because of the nearly symmetrical nature of pn. Several workers have studied such a geometrical isomerism. Most of them could observe no distinct differences in the chemical and spectroscopic properties.

For the tris(*R*-pn)cobalt(III) complexes, MacDermott[12] and Kojima *et al.*[13] separated the geometrical isomers (*facial* and *meridional*), although they could not observe any distinguishable differences in the visible and ultraviolet absorption, CD and PMR spectra. Sudmeier *et al.*[14] observed nonequivalent methyl resonances only in the 251 MHz PMR spectrum of *N*-deuterated Δ-$[Co(R\text{-pn})_3]^{3+}$ with Co-59 decoupling. Recently, the Co-59 NMR was successfully applied to this system.[15-17] For the bis(*R*-pn) complexes, MacDermott[18] tried to separate the isomers of $[Co(NO_2)_2(R\text{-pn})_2]^+$ and isolated three isomers. However, assignment of the structure only distinguished the *trans*(dinitro) and *cis*(dinitro) isomer. For the mono(*R*-pn) complexes, Lewis and Alexander[19] isolated the two isomers of $\Delta(C_3)$-*cis*β-$[Co(R\text{-pn})(2,3,2\text{-tet})]^{3+}$ (2,3,2-tet : 3,7-diaza-1,9-nonanediamine), which differ only in the placement of the methyl group of the *R*-pn. They could not observe, however, distinct differences in the visible absorption, CD and PMR spectra. On the other hand, Halloran and Legg[20] isolated the four isomers of *uns-cis*-$[Co(R\text{-pn})(edda)]^+$(edda : ethylenediamine-*N,N'*-diacetate) and observed a shift by 0.13 ppm for the methyl resonances between *cis*, *cis* (N–O) and *cis*,*trans*(N–O) isomers, which differ only in the placement of the methyl group of the *R*-pn.

In a previous paper,[21] some isomers of bis(L-hydrogenaspartato)(*R*-pn) and (L-aspartato)bis(*R*-pn)cobalt(III) complexes were isolated and characterized on the basis of the visible absorption, CD and PMR spectra. In the present work, we could separate all the isomers of *cis*-$[Co(CN)_2(S\text{-pn})_2]^+$ using a Dowex 50W-X8 ion exchange resin. This is useful for the separation of low charge complexes in contrast to an SP-Sephadex ion exchanger which is very good for high charge complexes.

Only one band was observed on the chromatographic separation of *trans*-$[Co(CN)_2(S\text{-pn})_2]^+$. The PMR spectrum of the isomer exhibits a doublet (J= 6 Hz) due to the CH_3 group of the coordinated *S*-pn at 1.23 ppm. Since the chemical environments of the methyl protons of the coordinated two *S*-pn are equivalent in the *trans* isomer, it is impossible to determine whether the obtained isomer is *trans-cis* or *trans-trans* isomer, or a mixture of the two (Fig. 1). However, the *trans-trans* isomer seems to be most predominant as in the corresponding dichloro complexes.[22]

For the *cis* dicyano complexes, P-2, P-3 and P-4 are assigned to Δ configuration around the cobalt ion and P-5, P-6 and P-7 to Λ on the basis of the CD spectra. Crystals P-5 and P-7 gave identical visible and ultraviolet absorption spectrum with those of P-2, P-3, P-4 and P-6, and the *cis* structure is verified although satisfactory elemental analysis was not obtained. The

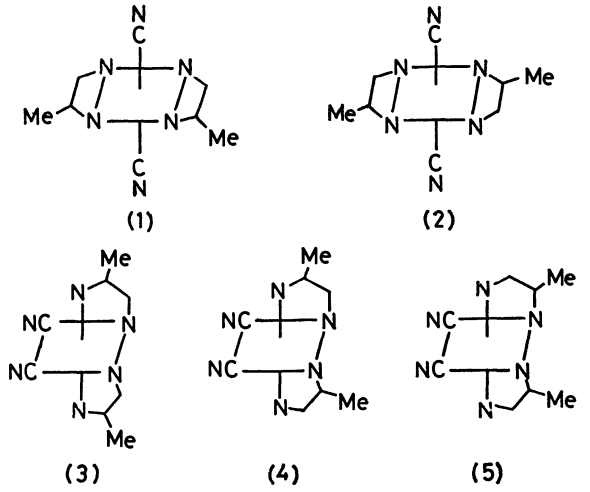

Fig. 1. Geometrical isomers of $[Co(CN)_2(S\text{-pn})_2]^+$. (1) *trans-cis*, (2) *trans-trans*, (3) *cis-trans*, (4) *cis*(C_1), (5) *cis-cis*.

cis-trans and *cis-cis* isomers (Fig. 1) have a C_2 symmetry axis and the *cis*(C_1) isomer has only a C_1 symmetry axis. The PMR spectra of P-2 and P-4 exhibit a doublet (J=6 Hz) due to the methyl groups of *S*-pn at 1.19 ppm and 1.34 ppm, respectively. P-3 showed two doublets at 1.19 ppm and 1.34 ppm and was assigned to the *cis*(C_1) isomer (Fig. 1). P-2 and P-4 isomers exhibit a significant difference in the methyl resonance. The absorption of P-4 isomer is shifted downfield relative to that of P-2. Assuming that the major environmental factor contributing to this shift is the relative position of the methyl group in the complex, such a difference in the chemical shift might arise from the intramolecular nonbonding interactions and the influence of ligating atoms, specifically the arrangement of ligating atoms in the other coordination sites. In a series of mixed en-pn and tris(pn) complexes of cobalt(III), the chemical shift hardly differs at all. The great chemical shift difference between P-2 and P-4 isomers seems to be due to the arrangement of cyanide ions. The chemical shift of the methyl group in $[Co(pn)_3]^{3+}$ is at about 1.37 ppm,[14] while in $[Co(CN)_4(R\text{-pn})]^-$ it is at about 1.25 ppm.[23] The methyl groups in the *cis-trans* isomer in Fig. 1 are nearer the cyanide ions than those in the *cis-cis* isomer. Thus we tentatively assigned P-2 isomer to *cis-trans* and P-4 to *cis-cis*. P-5, P-6 and P-7 showed a similar PMR behavior to P-2, P-3 and P-4, respectively. Hence we tentatively assigned P-5 to *cis-trans*, P-6 to *cis*(C_1) and P-7 to *cis-cis*.

The infrared absorption of these isomers was measured in the 4000—400 cm^{-1} region. Coordinated cyanide ions in each isomer showed a strong stretching $\nu(C{\equiv}N)$ band at *ca.* 2200 cm^{-1} which exhibited no splitting.

Circular Dichroism and Absolute Configuration. The observed absorption and CD spectral data for $[Co(CN)_2(R,R\text{-chxn})_2]^+$ and $[Co(CN)_2(S\text{-pn})_2]^+$ are summarized in Table 1.

Figure 2 shows the visible and ultraviolet absorption and CD spectra of *trans*-$[Co(CN)_2L_2]^+$ (L=*R*,*R*-chxn or *R*-pn) in water and of *trans*-$[CoCl_2(R,R\text{-chxn})_2]^+$ in methanol. The first absorption band, $^1T_{1g}{\leftarrow}^1A_{1g}$, of cobalt(III) complexes in an octahedral field splits into $^1A_{2g}+{}^1E_g{\leftarrow}^1A_{1g}$ in a tetragonal field. Yamatera[24] showed that the $^1A_{2g}$ band for *trans*-$CoN_4X_2^+$ should have roughly the same energy as the $^1T_{1g}$ band of CoN_6^{3+}. Furthermore, for axial ligand, X, which is lower than N in the spectrochemical series, ^1E_g should be lower in energy than $^1A_{2g}$. The first two peaks in the CD spectra of *trans*-dihalobis(diamine)cobalt(III) complexes are generally assigned to the ^1E_g and $^1A_{2g}$ levels in the order of increasing energy.[25,26] For the *trans*-$[Co(CN)_2(R,R\text{-chxn})_2]^+$ complexes, the axial ligands, CN^-, lie higher in the spectrochemical series than the basal cyclohexanediamine, so that the crystal field

Table 1. Absorption and CD spectral data for the dicyano complexes ($\tilde{\nu}$ in 10^3 cm^{-1})

Complex	I Band		II Band	
	$\tilde{\nu}_{max}$ (log ε)	$\tilde{\nu}_{ext}^{CD}$ ($\Delta\varepsilon_{ext}$)	$\tilde{\nu}_{max}$ (log ε_{max})	$\tilde{\nu}_{ext}^{CD}$ ($\Delta\varepsilon_{ext}$)
$[Co(CN)_2(R,R\text{-chxn})_2]ClO_4$				
C-1 (*trans*)	22 (sh)	20.85 (−0.28)	32.00 (1.84)	30.60 (−0.36)
	24.40 (1.83)	24.50 (+2.28)		
C-2 (*cis-Λ*)	24.80 (1.97)	25.50 (+2.24)	32.26 (2.00)	32.40 (−0.20)
C-3 (*cis-Δ*)	24.90 (2.00)	21.60 (−0.38)	32.30 (1.99)	32.60 (+0.06)
		24.30 (+1.06)		
		28.60 (−0.14)		
$[Co(CN)_2(S\text{-pn})_2]Cl$				
P-1 (*trans*)	22 (sh)	21.00 (+0.25)	32.10 (1.80)	31.35 (+0.14)
	24.51 (1.80)	24.66 (−1.07)		
P-2 (*cis-trans-Δ*)	24.60 (1.98)	25.80 (−1.39)	32.27 (1.96)	32.68 (+0.18)
P-3 (*cis*(C_1)-*Δ*)	24.83 (1.91)	25.64 (−1.10)	32.20 (1.90)	32.77 (+0.15)
P-4 (*cis-cis-Δ*)	25.10 (1.92)	26.00 (−0.98)	32.27 (1.93)	33.00 (+0.19)
P-6 (*cis*(C_1)-*Λ*)	25.21 (1.94)	22.00 (+0.42)	32.22 (1.96)	33.30 (−0.02)
		25.00 (−0.58)		35.33 (+0.01)
		30.00 (+0.12)		

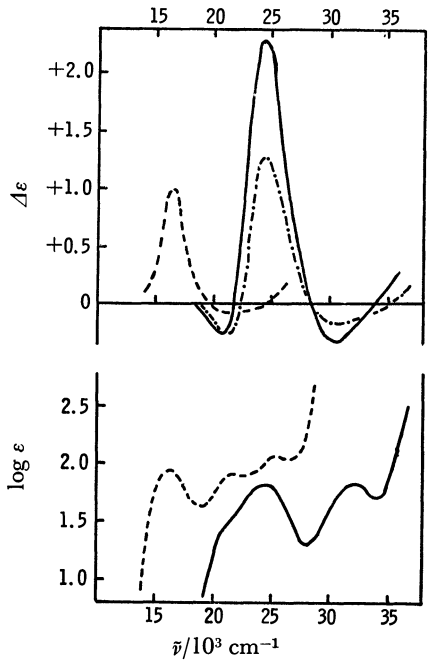

Fig. 2. Absorption and CD spectra of *trans*-$[Co(CN)_2(R,R\text{-chxn})_2]^+$ in H_2O (——), *trans*-$[Co(CN)_2(S\text{-pn})_2]^+$ in H_2O (—·—·—) and *trans*-$[CoCl_2(R,R\text{-chxn})_2]^+$ in methanol (— — —).

model expects the ^1E_g band to be at a higher energy than the $^1A_{2g}$ band. In the visible absorption spectra in Fig. 2, two components are observed in the first absorption band region. On the other hand, for the CD spectra two components, a small negative and a strong positive band, are observed in the first absorption band region, which we assign to $^1A_{2g}$ and ^1E_g component, respectively, in the order of increasing energy. The sign of the Cotton effect for each component is consistent for the dihalo and dicyano complexes, and related to the conformation of the chelate rings. The intensity of the Cotton effect for the dicyano complexes is much stronger than expected, as compared with the corresponding dihalo complexes. It seems that the conformation of the chelates is almost the same as for the dihalo and the dicyano complexes. A more complete molecular orbital treatment would be necessary to interpret the spectroscopic properties. However, quite recently similar differences in CD intensity were observed for *trans*-*R,R*-$[CoX_2(3,2,3\text{-tet})]^+$, *trans*-*S,S*-$[CoX_2(S,R,R,S\text{-}sk\text{-}3,2,3\text{-tet})]^+$ and *trans*-*S,S*-$[CoX_2(R,R\text{-}R,R\text{-}sk\text{-}3,2,3\text{-tet})]^+$ ($X=Cl^-$, CN^-).[27]

Figure 3 shows the CD spectra for the complexes obtained from the second(C-2) and the third (C-3) fraction of *cis*-$[Co(CN)_2(R,R\text{-chxn})_2]^+$ in H_2O. The CD spectrum of C-2 shows a very strong positive band in the first absorption band region which suggests a *Λ* configuration on the basis of an empirical rule.[10] C-3 shows two small negative bands and a strong positive band in the first absorption band region, which are rather complicated for the assignment of the absolute configuration. In the ultraviolet region, however, these two isomers gave very contrasting CD spectra; the CD spectrum of C-2 is similar to that of *cis*-*Λ*-$[Co(CN)_2(en)_2]Cl\cdot H_2O$, the absolute configuration of

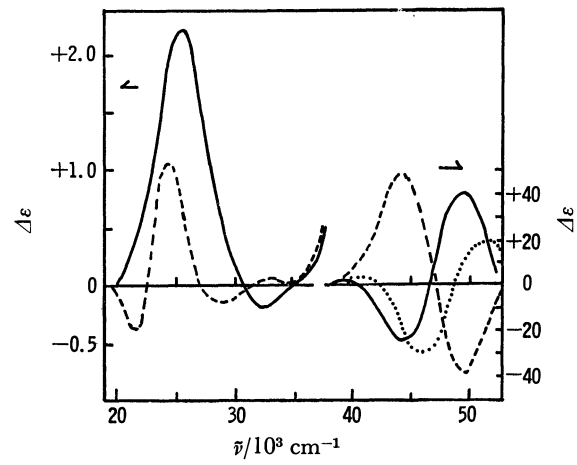

Fig. 3. CD spectra of *cis*-$[Co(CN)_2(R,R\text{-chxn})_2]^+$ in H_2O. C-2 (——), C-3 (— — —) and *cis*-*Λ*-$[Co(CN)_2(en)_2]Cl\cdot H_2O$ (·····).

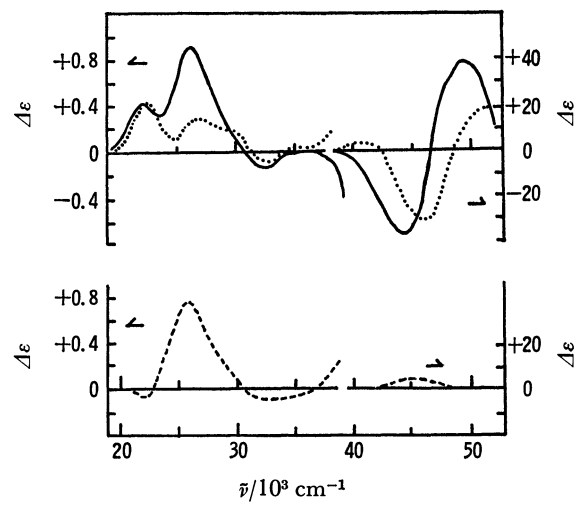

Fig. 4. Calculated configurational and vicinal CD curves of *cis*-$[Co(CN)_2(R,R\text{-chxn})_2]^+$. (C-2−C-3)/2 (——), (C-2+C-3)/4 (— — —) and *cis*-*Λ*-$[Co(CN)_2(en)_2]^+$ (·····).

which was determined by X-ray analysis.[28] Ogino *et al.*[29] suggested that in tris(diamine)cobalt(III) ions the configurational and the vicinal effect are also additive for the CD in the charge transfer region. This empirical rule would be useful for assigning the absolute configuration of dicyanobis(diamine) complexes. We have thus assigned the C-2 isomer to be *Λ* form.

The configurational and vicinal curves of *cis*-$[Co(CN)_2(R,R\text{-chxn})_2]^+$ are shown in Fig. 4. They were derived from the observed curves by use of the following relations.

$$\Delta\varepsilon(L) = 1/4\cdot[\Delta\varepsilon(\Lambda_{2L})+\Delta\varepsilon(\Delta_{2L})]$$
$$\Delta\varepsilon(\Delta) = 1/2\cdot[\Delta\varepsilon(\Delta_{2L})-\Delta\varepsilon(\Lambda_{2L})]$$
$$\Delta\varepsilon(\Lambda) = 1/2\cdot[\Delta\varepsilon(\Lambda_{2L})-\Delta\varepsilon(\Delta_{2L})]$$

where $\Delta\varepsilon(\Delta_{2L})$ and $\Delta\varepsilon(\Lambda_{2L})$ are the observed CD for the *Δ* and the *Λ* diastereoisomer, respectively, of *cis*-$[Co(CN)_2(R,R\text{-chxn})_2]^+$ complex and $\Delta\varepsilon(\Delta)$ and $\Delta\varepsilon(\Lambda)$ are the configurational CD, and $\Delta\varepsilon(L)$ is the vicinal CD for (*R,R*)-1,2-cyclohexanediamine ligand. The pattern of configurational CD curves agrees with the

observed CD of the corresponding ethylenediamine complex, except that the intensity of the peak at 2.62 $\times 10^4$ cm^{-1} (assigned to B_1 transition in C_{2v} symmetry by McCaffery *et al.*[8]) is strong in the cyclohexanediamine complex. The pattern of derived vicinal CD curves is similar to the observed CD spectrum of *trans*-$[Co(CN)_2(R,R\text{-chxn})_2]^+$.

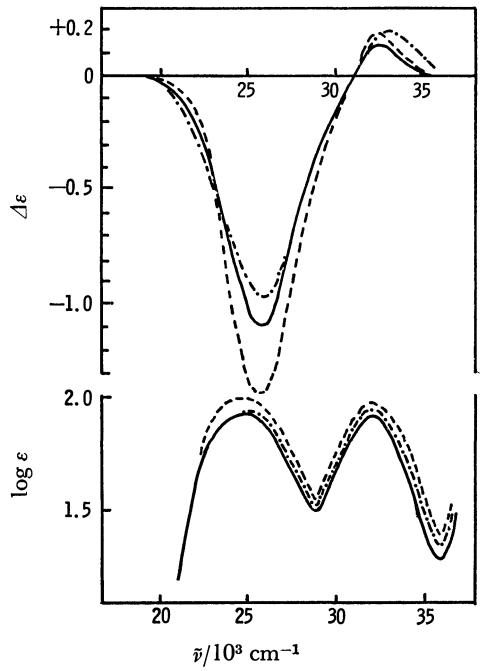

Fig. 5. Absorption and CD spectra of *cis*-$[Co(CN)_2(S\text{-pn})_2]^+$ in H_2O. P-2 (— — —), P-3 (——) and P-4 (—·—·—).

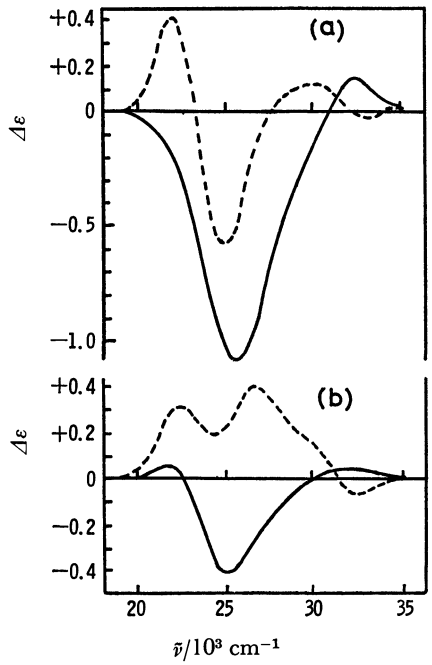

Fig. 6. (a) CD spectra of *cis*-$[Co(CN)_2(S\text{-pn})_2]^+$ in H_2O. P-3 (——) and P-6 (— — —). (b) Calculated configurational and vicinal CD curves of *cis*-$[Co(CN)_2(S\text{-pn})_2]^+$. (P-6−P-3)/2 (— — —) and (P-6+P-3)/4 (——).

Figure 5 shows the visible absorption and CD spectra of P-2, P-3 and P-4 isomer of $[Co(CN)_2(S\text{-pn})_2]^+$. The absorption and CD behavior are similar to those of the corresponding cyclohexanediamine complexes. The absorption maximum for each complex is slightly shifted, the intensity differing slightly from each other. However, the pattern is typical of *cis*-dicyanobis(diamine) complexes. The CD spectra of P-2, P-3 and P-4 are in contrast to that of *cis*-*Λ*-$[Co(CN)_2(R,R\text{-chxn})_2]^+$ in Fig. 3. When configurational and vicinal contribution are taken into consideration, these complexes are assigned to isomers of *cis*-*Λ*-$[Co(CN)_2(S\text{-pn})_2]^+$. Although the CD strength of these isomers in the first absorption band region differs somewhat from each other, geometrical isomers due to the placement of the methyl groups of propylenediamine give no difference in CD behavior.

Figure 6 shows the CD spectra of P-3 and P-6 isomer of $[Co(CN)_2(S\text{-pn})_2]^+$, the geometrical structure of which seems to be *cis*(C_1) (Fig. 1). The calculated configurational and vicinal curves are almost the same as those calculated for the cyclohexanediamine complexes. On the basis of these CD data, P-2, P-3 and P-4 are assigned to *Δ*-configuration and P-5, P-6 and P-7 to *Λ*-configuration.

References

1) P. R. Ray and B. Sarma, *J. Indian Chem. Soc.*, **28**, 59 (1951).
2) H. Siebert, *Z. Anorg. Allgem. Chem.*, **327**, 63 (1964).
3) M. Shibata, M. Mori, and E. Kyuno, *Inorg. Chem.*, **3**, 1573 (1964).
4) K. Konya, H. Nishikawa, and M. Shibata, *ibid.*, **7**, 1165 (1968).
5) M. Muto, T. Baba, and H. Yoneda, This Bulletin, **41**, 2918 (1968).
6) K. Kuroda, *Nippon Kagaku Zasshi*, **89**, 720 (1968).
7) N. Maki and S. Sakuraba, This Bulletin, **42**, 1908 (1969).
8) A. J. McCaffery, S. F. Mason, and B. J. Norman, *Chem. Commun.*, **1965**, 132; *J. Chem. Soc.*, **1965**, 5094.
9) K. Ohkawa, J. Hidaka, and Y. Shimura, This Bulletin, **40**, 2830 (1967).
10) C. J. Hawkins, "Absolute Configuration of Metal Complexes," Interscience, New York, 1971, Ch. 5.
11) F. P. Dwyer, F. L. Garvan, and A. Schulman, *J. Amer. Chem. Soc.*, **75**, 1526 (1959).
12) T. E. MacDermott, *Inorg. Chim. Acta*, **2**, 81 (1968).
13) a) M. Kojima, Y. Yoshikawa, and K. Yamasaki, *Inorg. Nucl. Chem. Lett.*, **9**, 689 (1973). b) M. Kojima and K. Yamasaki, This Bulletin, **48**, 1093 (1975).
14) J. L. Sudmeier, G. L. Blackmer, C. H. Bradley, and F. A. L. Anet, *J. Amer. Chem. Soc.*, **94**, 757 (1972).
15) A. Johnson and G. W. Everett, Jr., *Inorg. Chem.*, **12**, 2801 (1973).
16) K. L. Craighead, *J. Amer. Chem. Soc.*, **95**, 4434 (1973).
17) Y. Koike, F. Yajima, A. Yamasaki, and S. Fujiwara, *Chem. Lett.*, **1974**, 177.
18) T. E. MacDermott, *Inorg. Chim. Acta*, **3**, 246 (1969).
19) R. H. Lewis and M. D. Alexander, *ibid.*, **5**, 86 (1971).
20) L. J. Halloran and J. I. Legg, *Inorg. Chem.*, **13**, 2193 (1974).
21) Y. Kojima and M. Shibata, *ibid.* **10**, 2382 (1971).

22) C. J. Hawkins, E. Larsen, and I. Olsen, *Acta Chem. Scand.*, **19**, 1915 (1965).
23) S. Yano, H. Ito, Y. Koike, J. Fujita, and K. Saito, This Bulletin, **42**, 3184 (1969).
24) H. Yamatera, *ibid.*, **31**, 95 (1958).
25) R. A. D. Wentworth and T. S. Piper, *Inorg. Chem.*, **4**, 202 (1965).
26) R. S. Treptow, *ibid.*, **5**, 1593 (1966).
27) B. Bosnich and J. MacB. Harrowfield, *Inorg. Chem.*, **14**, 828, 847, 861 (1975).
28) K. Matsumoto, S. Ooi, and H. Kuroya, *ibid.*, **44**, 2721 (1971).
29) K. Ogino, K. Murano, and J. Fujita, *Inorg. Nucl. Chem. Lett.*, **4**, 351 (1968).

The Resonance Energies of Polyacenes and Related Compounds

Jun-ichi AIHARA

Department of Chemistry, Faculty of Science, Hokkaido University, Sapporo 060

(Received August 1, 1974)

The resonance energies of polyacenes were determined on the basis of the additive principle of π-bond energies in nonaromatic compounds. The additive components in the total π-energies for these compounds were reasonably estimated from the infinitely large polyacene. The calculated resonance energies appear to be much improved as compared with those calculated by Hess and Schaad.

In 1965, Dewar and Gleicher, using the semi-empirical SCF-MO method, found that the bond energies of acyclic polyenes are additive.[1-3] Therefore, we can readily calculate the total energy of any acyclic polyene by summing the energies of all its bonds. Using these additive bond energies, we can also calculate the reference energies of cyclic polyenes, and hence obtain their resonance energies. Here, the reference energy is defined as the energy which the compound in question would possess if it were absolutely olefinic in nature. These resonance energies were the first aromaticity indices which correlated very well with the experimental stability for a wide range of conjugated hydrocarbons.[4,5]

Subsequent HMO calculations, carried out by Hess and Schaad,[6-8] have produced results which nicely parallel the corresponding results of the SCF-MO approach. They classified the carbon-carbon bonds of acyclic polyenes into eight types, five types of double bonds and three types of single bonds, depending upon the number of attached hydrogens. The additive π-bond energies were then assigned to these types of π-bonds. These energies were used to calculate the reference energies of cyclic polyenes.

However, it must be noted that the additive bond energies have been, in all cases, somewhat arbitrarily determined from some groups of acyclic polyenes. Although the agreement between the calculated resonance energies and the experimental stabilities is generally good, the use of these fixed bond energies might sometimes cause a considerable ambiguity in the obtained resonance energies, especially for the larger conjugated systems.[9,10] With this in view, we reexamined the reference energies for the linear polyacenes within the framework of the HMO theory; we would now like to point out that the HMO resonance energies hitherto published for the polyacenes[6,7] appear to be considerably larger than what they should be. The classification of π-bonds made by Hess and Schaad[6] is assumed throughout this article.

Results and Discussion

It is widely known that the linear annellation of unsaturated six-membered rings yields a series of hydrocarbons (polyacenes) which show a decreasing stability as the number of rings is increased.[11,12] According to Clar,[11,12] every polyacene is stabilized primarily by a single aromatic sextet. One sextet is shared among all the rings by migrating from one ring to the other. This means a dilution of the sextet. The benzenoid character decreases with the length of polyacene. Such an aspect of polyacenes can be adequately visualized with the help of Herndon's resonance theory.[13,14]

In 1973, Herndon succeeded in applying the resonance-theoretical approach to the evaluation of Dewar-type resonance energies. According to his theory, the resonance energy (E_R) for [N]acene, which contains N six-membered rings, is expressed as follows:

$$E_R([N]\text{acene}) = \frac{2[N\gamma_1 + (N-1)\gamma_2]}{N+1}\ , \qquad (1)$$

where γ_1 denotes the resonance interaction between two Kekulé structures related by a permutation of three double bonds within a six-membered ring, and where γ_2 denotes the resonance interaction related by a permutation of five double bonds within a periphery of two annellated rings.

On this basis, the resonance energy for an infinitely large polyacene (I) can readily be given as:

$$E_R(\text{I}) = 2(\gamma_1 + \gamma_2)\ . \qquad (2)$$

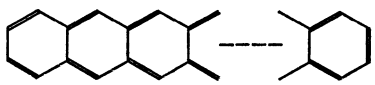

(I)

The limiting resonance energy of polyacene is thus a finite quantity, *i.e.*, twice the sum of the resonance energy of benzene and that of the ten-membered ring. It is, hence, assumed with little difficulty that the reference energy of any polyacene can be estimated from the infinitely large polyacene because the resonance energy per π-electron (REPE) is considered to be zero. The use of an infinitely large species as a reference compound has been successfully demonstrated for the monocyclic conjugated systems.[10,15]

The unit energy (E_U) of polyacene is defined as the increment of the π-energy of the reference structure associated with every additional six-membered ring. All the energies will hereafter be given in units of β. The total π-energy (E_{HMO}) of [N]acene is analytically expressed in this form:[16,17]

$$E_{HMO}([N]\text{acene}) = 2 + 2\sum_{m=1}^{N}\sqrt{9+8\cos\frac{m\pi}{N+1}}\ . \qquad (3)$$

With the use of this expression, the unit energy of polyacene is given by the following expression:

$$\begin{aligned} E_U(\text{polyacene}) &= \lim_{N\to\infty}\frac{2}{N}\sum_{m=1}^{N}\sqrt{9+8\cos\frac{m\pi}{N+1}} \\ &= 2\int_0^1\sqrt{9+8\cos\pi x}\ dx \\ &= 5.6113421\ \ldots\ldots\ . \end{aligned} \qquad (4)$$

In this connection, it is noteworthy that the unit

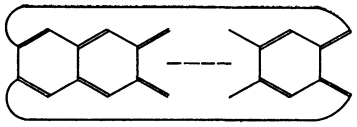

(II)

energy of polyacene does not necessarily depend upon the boundary conditions of the infinitely large polyacene. The hypothetical cyclic polyacene (II) has the same unit energy as that of the linear polyacene. It is clear that there is no aromatic sextet in any Kekulé structure of the cyclic polyacene. All six-membered rings in it are "empty" in Clar's sense.[11,12] According to Herndon's resonance theory,[13,14] the cyclic polyacene of any size must have zero resonance energy because neither γ_1-type nor γ_2-type interactions are present in it. This fact strongly suggests that the E_U(polyacene)-value, obtained in this manner, is free from aromaticity.

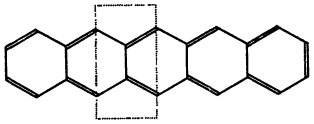

(III)

The unit structure corresponding to the unit energy of polyacene is illustrated in III as the portion of pentacene enclosed in the dotted line. As in the case of the cyclic polyacene, the unit structure of the infinitely large polyacene is considered to be a combination of two CH=C bonds, two CH–C bonds, and one C–C bond. In other words, the unit energy of polyacene is written as:

$$E_U(\text{polyacene}) = 2E_{CH=C} + 2E_{CH-C} + E_{C-C}, \quad (5)$$

where $E_{CH=C}$ is the additive π-bond energy of the CH=C bond, E_{CH-C} is that of the CH–C bond, and E_{C-C} is that of the C–C bond.

For this reason, the use of Kekulé structure of Type I is recommended for estimating the resonance energy for any polyacene. If it is employed as a reference structure, all the polyacene unit structures in it are structurally the same and are expressed by Eq. (5). Although there are N other Kekulé structures for [N]-acene, they are disregarded in the following calculations. It appears safe to arbitrarily adopt one Kekulé structure as a representative of all, as it has been reported that in no cases were the additive energies of the resonance structures of the same compound significantly different.[6]

The actual polyacene cannot, however, be constructed with the unit structures of the above type only. For example, pentacene is composed of four polyacene unit structures and the residual parts on both edges. If the residual parts are combined, they form a geometry of benzene. Therefore, the canonical structure of Type I for [N]acene corresponds to the sum of the $N-1$ polyacene unit structures and the reference structure of benzene. The π-energy of the reference structure (E_A) of benzene has already been calculated from the unit energy of the infinitely large annulene,[10] that is:

$$E_A(\text{benzene}) = 3(E_{CH=CH} + E_{CH-CH}) = 7.6394373\ldots\ldots, \quad (6)$$

where $E_{CH=CH}$ is the additive π-bond energy of the CH=CH bond and where E_{CH-CH} is that of the CH–CH bond. Accordingly, the additive energy, *i.e.*, the reference energy, of [N]acene is written in this form:

$$E_A([N]\text{acene}) = (N-1)E_U(\text{polyacene}) + E_A(\text{benzene}). \quad (7)$$

Using this expression for the reference energy, the resonance energy of [N]acene is given by:

$$E_R([N]\text{acene}) = E_{HMO}([N]\text{acene}) - E_A([N]\text{acene}). \quad (8)$$

The obtained resonance energies of polyacenes and related compounds are all listed in Table 1.

As may easily be seen, the total resonance energy of polyacene is a slowly varying function of N, and it appears to converge to some value near 0.460. These

TABLE 1. RESONANCE ENERGIES OF POLYACENES AND RELATED CONPOUNDS IN UNITS OF β

Species	E_{HMO}	E_A	E_R	REPE
Benzene	8.0000	7.6394	0.3606 (0.39)	0.0601 (0.065)
Naphthalene	13.6832	13.2508	0.4325 (0.55)	0.0432 (0.055)
Anthracene	19.3137	18.8621	0.4516 (0.66)	0.0323 (0.047)
Tetracene	24.9308	24.4735	0.4574 (0.75)	0.0254 (0.042)
Pentacene (III)	30.5440	30.0848	0.4592 (0.84)	0.0209 (0.038)
Hexacene	36.1560	35.6961	0.4598	0.0177
Heptacene	41.7675	41.3075	0.4600	0.0153
Octacene	47.3789	46.9188	0.4601	0.0135
Nonacene	52.9903	52.5302	0.4601	0.0121
Decacene	58.6017	58.1415	0.4601	0.0110
Compound IV	30.0785	30.0848	−0.0063 (0.37)	−0.0003 (0.017)
Azulene	13.3635	13.2508	0.1127 (0.23)	0.0113 (0.023)
Naphthalene-2,3-quinododimethide	15.532*	15.525	0.007 (0.093)	
Anthracene-2,3-quinododimethide	21.133*	21.137	−0.004 (0.169)	
Tetracene-2,3-quinododimethide	26.741*	26.748	−0.007 (0.253)	
Pentacene-2,3-quinododimethide (V)	32.351*	32.359	−0.008 (0.338)	

Total HMO π-energies marked with asterisks were taken from Ref. 19.

resonance energies are in marked contrast to those determined by Hess and Schaad,[6,7] which are placed in parentheses in Table 1. The latter resonance energies increase with an increase in the number of six-membered rings. This discrepancy between the two sets of resonance energies correspondingly expands on going to higher polyacenes. As a result, our resonance energy of pentacene (0.4592) is about a half of theirs (0.84), although the resonance energies of benzene are similar to each other.

This discrepancy in energy is mainly due to the difference between the π-energies of the polyacene unit structure as estimated by them and by us. The π-energy of the unit structure is calculated to be 5.5248 with the use of the π-bond energies determined by Hess and Schaad.[6] For reference, their additive π-bond energies are 2.1083 for the CH=C bond, 0.4362 for the CH–C bond, and 0.4358 for the C–C bond. Since the π-energy of the same unit structure is 5.6113 according to Eq. (4), the energy difference of 0.0865 is every time added to their resonance energy of polyacene. The most important point is that, if their π-bond energies are used, the limiting REPE amounts to as much as 0.0216; any higher polyacene must be as stable as azulene (REPE=0.023).

On the contrary, it is noticeable that the resonance energies determined by us are approximately constant from anthracene to decacene. Such a tendency of the resonance energies is in good accord with Clar's aromatic sextet theory.[11,12] The constancy of the total resonance energies apparently reflects the presence of a single aromatic sextet in every polyacene. The increment in the resonance energy from benzene to decacene is only 27.6 percent of the resonance energy of benzene. Such a small increment might be attributed to the resonance interactions among all possible Kekulé structures.

In this relation, it is interesting to see that the limiting resonance energy estimated by Herndon's method [Eq. (2)] is about twice as much as ours. Although we premised Herndon's resonance theory in evaluating the polyacene unit energy, the HMO resonance energies for the individual polyacenes are considerably different from the predictions of his theory. However, we might say that the two series of resonance energies of polyacenes are fairly consistent with each other in the sense that the REPE-values, which are closely associated with the stability of the compounds, rapidly converge to zero on going to higher polyacenes.

The validity of the polyacene unit energy, as estimated by us, is further supported by the plausible estimate of the resonance energies of some other polyacene analogues. Compound IV is one of the structural isomers of pentacene. This not-yet-isolated compound has been of theoretical interest, because its lowest energy state is supposedly a triplet.[18] As long as the spin states are disregarded, this compound possesses the same reference energy as pentacene. It can, then, be predicted to have the resonance energy of 0.3716 by using the π-bond energies of Hess and Schaad,[6] while it is much reduced to −0.0063 by using the present reference energy of pentacene. According to the PMO method,[3] when the essentially single bond is introduced between carbon atoms of a like parity in an alternant annulene, it leads to no first-order change in π-energy. In this sense, Compound IV should have the resonance energy similar to that of [22]annulene (0.0954).[10] In addition, there is no aromatic sextet in any of the resonance structures of this compound. These facts are evidently favorable to our resonance energy for this compound.

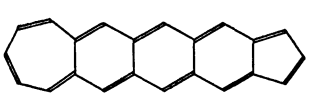

(IV)

The resonance energy ratio of azulene to benzene is 0.59 according to the calculations made by Hess and Schaad.[6] It is reduced by our treatment to 0.3127, which is in good agreement with Herndon's prediction (0.38).[13] The SCF-MO calculations performed by Dewar and de Llano[2] also favor our resonance energy of azulene. They showed azulene to have 19.4 percent of the resonance energy of benzene. Non-alternant hydrocarbons, such as Compound IV and azulene, are thus found to possess much less aromatic character than the isomeric benzenoid species. At the same time, it is suggested that the aromatic sextet in the classical resonance structure is the main origin of the aromaticity.

On the other hand, Gleicher *et al.* showed that the overall results of HMO calculations for quinododimethides with the use of the method and π-bond energies of Hess and Schaad are gratifying.[19] Nevertheless, the results concerning the series of polyacene-2,3-quinododimethides were disturbing. Although only a single classical structure can be written for each of these compounds, there is a steady increase in the REPE. Thus, pentacene-2,3-quinododimethide (V) is predicted to possess half the aromatic character associated with pentacene itself.

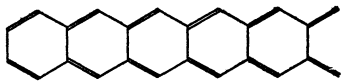

(V)

This problem can also be solved with the present unit energy of pentacene as follows. Note that there are $N-1$ polyacene unit structures in [N]acene-2,3-quinododimethide ([N]AQDM). Therefore, a correction must be made, at least, for the additive energy of this portion. As was mentioned above, the additive energy of the polyacene unit structure determined with the use of the π-bond energies of Hess and Schaad[6] differs by 0.0865 from that determined from Eq. (4). With this unit-energy difference, the reference energy of the entire compound can be approximately modified to this form:

$$E_A([N]\text{AQDM}) = E_{HS}([N]\text{AQDM}) - 0.0865(N-1). \quad (9)$$

Here, E_{HS} signifies the reference energy determined according to the method of Hess and Schaad. The resonance energies refined with Eq. (9) are much more acceptable, because the corresponding REPE values are all negligibly small. This is in good accord with

the fact that there is no aromatic sextet in the resonance structure of any polyacene-2,3-quinododimethide. Furthermore, the present resonance energies parallel fairly well the results of the SCF-MO calculations carried out by Gleicher *et al.*[19]

In conclusion, the well-established additivity of the π-bond energies of nonaromatic polyenes allowed us to take an infinitely large polyacene as a reference compound in estimating the aromatic character of a given polyacene. The present approach appears to be superior to the original method of Hess and Schaad when both are applied to polyacenes and related compounds. As has been pointed out in previous papers,[10,15] the discrepancy between the resonance energies of Hess and Schaad and ours is attributable to the differently determined π-bond energies. They determined the π-bond energies from acyclic polyenes of a medium size. Slight energy deviations from ours have been magnified in larger compounds, and have sometimes become comparable to the resonance energies themselves. The polyacene series is a good example of how small errors in the π-bond energies can easily produce spurious results by a cumulative effect. Our simplified model neglected all effects arising from bond alternation. It is hoped that the gross features of the aromatic character of these compounds are not changed by them.

We are grateful to the Hokkaido University Computing Center for the use of their FACOM 230-60, on which all the calculations were performed.

References

1) M. J. S. Dewar and G. J. Gleicher, *J. Amer. Chem. Soc.*, **87**, 685, 692 (1965).
2) M. J. S. Dewar and C. de Llano, *ibid.*, **91**, 789 (1969).
3) M. J. S. Dewar, "The Molecular Orbital Theory of Organic Chemistry," McGaw-Hill, New York, N.Y. (1969), Ch. 5.
4) L. J. Schaad and B. A. Hess, Jr., *J. Amer. Chem. Soc.*, **94**, 3068 (1972).
5) I. Gutman, M. Milun, and N. Trinajstić, *Chem. Phys. Lett.*, **23**, 284 (1973).
6) B. A. Hess, Jr. and L. J. Schaad, *J. Amer. Chem. Soc.*, **93**, 305 (1971).
7) B. A. Hess, Jr. and L. J. Schaad, *ibid.*, **93**, 2413 (1971).
8) B. A. Hess, Jr. and L. J. Schaad, *J. Org. Chem.*, **36**, 3418 (1971).
9) J. Aihara, This Bulletin, **47**, 3169 (1974).
10) J. Aihara, *ibid.*, **48**, 517 (1975).
11) E. Clar, "Polycyclic Hydrocarbons," Vols. I and II, Academic Press, London (1964).
12) E. Clar, "The Aromatic Sextet," John Wiley and Sons, London (1972).
13) W. C. Herndon, *J. Amer. Chem. Soc.*, **95**, 2404 (1973).
14) W. C. Herndon, *J. Chem. Educ.*, **51**, 10 (1974).
15) J. Aihara, This Bulletin, **48**, 1501 (1975).
16) C. A. Coulson and A. Streitwieser, Jr., "Dictionary of π-Electron Calculations," Pergamon, Oxford (1965).
17) W. England and K. Ruedenberg, *J. Amer. Chem. Soc.*, **95**, 8769 (1973).
18) P. Hochmann, R. Zahradník, and V. Kvasnicka, *Coll. Czech. Chem. Commun.*, **33**, 3478 (1968).
19) G. J. Gleicher, D. D. Newkirk, and J. C. Arnold, *J. Amer. Chem. Soc.*, **95**, 2526 (1973).

An Investigation of the *endo* Product Selectivity in the Diels-Alder Reaction[1]

Kazuyoshi SEGUCHI, Akira SERA, Yoshinobu OTSUKI, and Kazuhiro MARUYAMA
Department of Chemistry, Faculty of Science, Kyoto University, Kyoto 606

(Received February 26, 1975)

The Diels-Alder reactions of cyclopentadienes with a variety of substituted ethylenes were carried out, and their reaction rates and the *endo* : *exo* isomer ratios of the products were determined. It was shown that the faster reaction is characterized by a higher *endo* isomer distribution and the existence of a linear correlation between the reaction rate and the *endo* isomer distribution. The results were interpreted in terms of the concept of secondary orbital interaction in the transition state.

Many investigators have been interested in the *endo* addition rule of the Diels-Alder reaction[2] since Alder expressed it as the "maximum accumulation of unsaturation."[3] The *endo* selectivity of the reaction has been discussed mainly in terms of dipole—dipole[4] or secondary orbital[5] interactions, steric[2a] and electronic[6] effects, dispersion force,[7] and favorable geometry for interacting orbitals[8] on both experimental and theoretical grounds. There have been a large number of studies of the *endo* selectivity of the reaction, but little has been done to investigate it from the viewpoint of the reactivity of dienophiles.

In the some Lewis acid-catalyzed Diels-Alder reactions, it has been reported that the dienophiles complexed with the catalysts show an enhanced *endo* selectivity in comparison with that of the uncomplexed ones in spite of the higher reactivities of the formers.[9,10] There seems to be a particular parallelism between the enhanced selectivity and the higher reactivity in the Diels-Alder reaction. In order to get a better insight into the mechanism of the Diels-Alder reaction, a detailed examination of this phenomenon is essential. Therefore, this work will be concerned with an investigation of the correlation between the *endo* selectivity and the reaction rate of the Diels-Alder reaction. For this purpose, the reactions of cyclopentadienes with various substituted ethylenes were examined (Scheme 1).

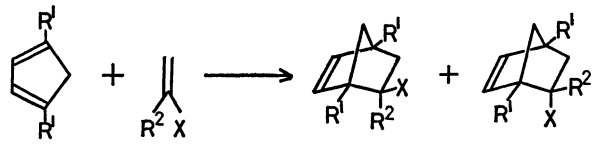

(1) Diene Dienophile *exo* (**2x**) *endo* (**2n**)

(**1a**) R^1=H R^2=H, Me, Et, *n*-Bu
(**1b**) R^1=C_6H_5 X=CO_2Me, CHO, COMe, COEt, CO-*n*-Pr, CO-*iso*-Pr, COCl, COBr, maleic anhydride and *N*-phenylmaleimide.
(**1c**) R^1=*p*-Cl-C_6H_4

Scheme 1.

Results and Discussion

The following sets of Diels-Alder reactions were carried out: Dienes; cyclopentadiene (**1a**), diphenyl- and di-*p*-chlorophenylcyclopentadiene (**1b**, **1c**): Dienophiles; acrylic acid derivatives, vinyl ketones, acrolein, and maleic acid derivatives. All the reactions were carried out at 25° C and 35 °C. The second-order rate constants were determined by following the reaction by means of glpc and spectrophotometry. A competitive reaction method was employed for the estimation of the rate constants of **1a** with vinyl ketones and methyl 2-alkylacrylates. The results are tabulated in Tables 1 and 2. The isomer distributions of the reactions were analyzed by means of glpc and NMR. Control experiments showed that no *endo-exo* interconversion operated under the present reaction conditions and during the analytical procedure.

The isomeric adducts were isolated by means of glpc and tlc, and their configurations were confirmed by means of NMR analysis, taking into account the fact that the shielding effect of the double bond in 5-substituted 2-norbornene leads the signal of the *endo*-5-methyl proton to a higher field than that of the *exo*-5-methyl proton. The chemical shifts and the splitting patterns of the adducts were similar to those

TABLE 1. SECOND-ORDER RATE CONSTANTS FOR THE REACTIONS OF CYCLOPENTADIENES WITH VARIOUS DIENOPHILES AT 35 °C

No.	Diene	Dienophile	Solvent	k_2 (l mol^{-1} s^{-1})[a]
1	cyclopentadiene	*N*-phenylmaleimide	dioxane	1.30×10^{-1} [b]
2	cyclopentadiene	maleic anhydride	dioxane	1.22×10^{-1} [b]
3	cyclopentadiene	acryloyl bromide	benzene	3.09×10^{-2} [c]
4	cyclopentadiene	acryloyl chloride	benzene	2.00×10^{-2} [c]
10	cyclopentadiene	methyl acrylate	*n*-butyl chloride	5.30×10^{-5} [c]
11	1,4-diphenylcyclopentadiene	methyl acrylate	chloroform	6.94×10^{-6} [d]
12	1,4-di-*p*-chlorophenyl-cyclopentadiene	methyl acrylate	chloroform	2.55×10^{-6} [d]

a) Values are average of two or more runs. Estimated errors are about 10% for the reactions 3 and 4, and about 5% for the reactions 10—12. b) Calculated from the reported data, see ref. 21. c) Determined by means of glpc. d) Determined by spectrophotometry.

Table 2. Relative rates and *endo*-isomer distributions in the Diels-Alder reactions of cyclopentadienes with various dienophiles in benzene

No.	Diene[a] R^1	Dienophile[a] R^2	X	Relative rate[b]	*endo*-Adduct[c] (%)
1	H	*N*-phenylmaleimide		2.45×10^{3}	>99.5[d]
2	H	maleic anhydride		2.30×10^{3}	99.5
3	H	H	COBr	5.83×10^{2}	92.2
4	H	H	COCl	3.77×10^{2}	90.7
5	H	H	CO-*iso*-Pr	3.20	82.1
6	H	H	CO-*n*-Pr	2.40	80.5
7	H	H	COEt	2.28	82.8
8	H	H	COMe	2.28	82.3
9	H	H	CHO	2.00	75.0
10	H	H	CO_2Me	1.00	73.7
11	Ph	H	CO_2Me	1.30×10^{-1}	51[d]
12	*p*-Cl-Ph	H	CO_2Me	4.81×10^{-2}	50[d]
13	H	Me	CO_2Me	1.65×10^{-2}	35.3[e]
14	H	Et	CO_2Me	1.62×10^{-2}	37.0[e]
15	H	*n*-Bu	CO_2Me	7.78×10^{-3}	30.6[e]

a) See Scheme 1. b) Relative to the reaction 10. The values for the reactions 1, 4, 11, and 12 were calculated from Table 1. The others were determined by competitive reactions with methyl acrylates. Analysis based on glpc. c) Determined by glpc. The values are accurate to within 0.2%. d) Determined by NMR. The values are accurate to within 1%. e) In methylene chloride.

reported for related compounds.[11]

Cyclopentadienes were employed as the diene components in order to avoid the uncertainty which is unavoidable in the reactions of acyclic dienes because of their *cis-trans* isomerization. The dienophiles employed were characterized by their carbonyl function so that the reactions to be compared would have similar character.

As may be seen in Table 2, a higher *endo* isomer distribution appeared when a more reactive dienophile was used. Although it is difficult to treat the reactivity of a dienophile in a quantitative sense, the logarithms of the apparent relative rate constants were employed as a provisional measure of the reactivity of the dienophile. In Fig. 1, the logarithms of the *endo* : *exo* isomer ratios, a measure of the *endo* selectivity, are plotted against the logarithms of the relative rates of the reactions. A fair correlation is found between the rates and the *endo* selectivity.

The fact that a more reactive addend has a higher *endo* selectivity seems to be contrary to the so-called selectivity-reactivity relationship in polar reactions.[12] Kojima and Inukai[13] have observed a similar phenomenon in the aluminum chloride-catalyzed Diels-Alder reactions. They have also pointed out the major role of the electrophilicity of dienophiles for the observed inter- and intramolecular selectivities.

Recently we ourselves reported on the pressure effect of the Diels-Alder reaction.[14] From an examination of the activation volumes of the reactions, it was deduced that a faster Diels-Alder reaction proceeds through a tighter transition state. The tighter transition state implies the existence of a stronger secondary orbital interaction as well as a closer proximity of the reacting species. The extent of stabilization due to secondary orbital interaction must be responsible

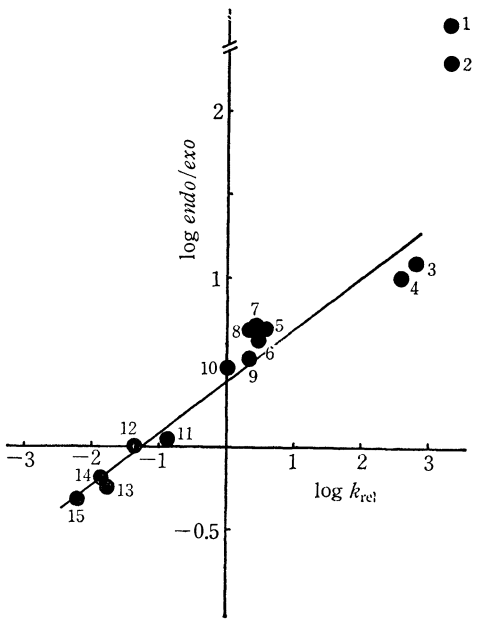

Fig. 1. A correlation of log (*endo*/*exo*) with log k_{rel}. The numerals correspond to the reaction number in Table 2.

for the determination of the *endo*: *exo* isomer ratio. The correlation shown in Fig. 1 indicates that the more reactive dienophile is characterized by the possibility of the stronger secondary orbital interaction.

The introduction of an alkyl group into the dienophile resulted in a decrease in the *endo* isomer distribution to less than 50%. However, even in these cases the correlation still holds, as is shown in Fig. 1.[15] Naturally, the alkyl group in the dienophile may depress its reactivity for electronic (inductive) and steric reasons.

A steric repulsion can operate between the alkyl group and the methylene group of cyclopentadiene in the *endo* transition state. These effects will make the *endo* transition state looser, and will result in a decrease in the amount of the *endo* isomer.

Thus, Fig. 1 substantiates the existence of a correlation between the *endo* selectivity and the relative rates in a given set of Diels-Alder reactions. Although it has been well-known in the field of synthetic organic chemistry that the faster Diels-Alder reactions preferentially yield a large amount of *endo* isomers, it should be emphasized that the linear correlation holds over a wide range of the reactivities of dienophiles.

Some anomalous deviation is seen in Fig. 1. That is, in the reactions of maleic anhydride or maleimide with cyclopentadiene, higher selectivities were observed than those expected from their relative rates. This possibly results from the two-fold interaction between the π-orbits of carbonyl groups and cyclopentadiene, as was pointed out in our previous report.[14] In the reaction of cyclopentadiene with maleic anhydride and maleimide, the transition-state geometry is quite favorable for secondary orbital interaction because of the cyclic feature of the dienophile. This must also be responsible for the observed higher *endo* selectivity in these two cases.

Experimental

All the NMR spectra were recorded on a JEOL PS-100 spectrometer, using TMS as the internal standard. The chemical shifts were expressed in δ-values. The analytical determination by glpc was performed by means of JEOL JGC-20K and Perkin-Elmer model 800 gas-chromatographs. The preparative glpc was performed by means of JEOL JGC-1100 gas-chromatograph. The UV spectra were recorded on a Shimadzu UV-200 spectrometer.

Materials. Methyl vinyl ketone[16] (bp 81 °C); ethyl vinyl ketone[17] (bp 102—103 °C); *n*-propyl vinyl ketone[17] (bp 35—36 °C/22 mmHg); isopropyl vinyl ketone[17] (33—35 °C/30 mmHg); acryloyl chloride[18] (bp 74—75 °C); acryloyl bromide[18] (bp 99—100 °C); methyl 2-*n*-butyl acrylate[19] (bp 69—70 °C/25 mmHg) and 1,4-diphenylcyclopentadiene-1,3 (**1b**)[20] (mp 161—162 °C) were prepared by the methods reported in the literature. 1,4-Di-(*p*-chlorophenyl)cyclopentadiene-1,3 (**1c**) was prepared from ethyl 3-(*p*-chlorophenyl)-propionate and *p*-chloroacetophenone[20]; mp 167—168 °C. Found: C, 71.37; H, 4.15%. Calcd for $C_{21}H_{12}O_2Cl_2$: C, 71.09; H, 4.21%. The other dienophiles were commercially available and were redistilled when necessary.

Product Analysis. In a typical run, a mixture of 2.5×10^{-3} M of a dienophile, 2.5×10^{-3} M of a diene, and 2 ml of a solvent was sealed in a glass ampoule and immersed in a thermostatted bath. The reaction time was changed from three hours to several days according to the reactivity of the addends and the temperature. The Diels-Alder adducts were analyzed by means of glpc and NMR. Stainless steel columns (2 m) packed with 5% PEG (column A), 5% TCPE (column B), 5% PEGS (column C), and 5% Silicon SE-30 (column D) on Diasolid L were used.

*Reactions of **1a** with Alkyl Vinyl Ketones.* The Diels-Alder adducts were separated by means of glpc (column A). All the adducts were colorless liquids. Retention times: 5-*endo*-acetylbicyclo[2.2.1]hept-2-ene (**3n**), 5.2 min; 5-*exo*-acetylbicyclo[2.2.1]hept-2-ene (**3x**), 4.0 min at 130 °C: 5-*endo*-propionylbicyclo[2.2.1]hept-2-ene (**4n**), 6.8 min; 5-*exo*-propionylbicyclo[2.2.1]hept-2-ene (**4x**), 5.2 min at 130 °C: 5-*endo*-*n*-butyrylcyclo[2.2.1]hept-2-ene (**5n**), 3.8 min; 5-*exo*-*n*-butyrylbicyclo[2.2.1]hept-2-ene (**5x**), 3.0 min at 160 °C: 5-*endo*-isobutyrylbicyclo[2.2.1]hept-2-ene (**6n**), 4.0 min; 5-*exo*-isobutyrylbicyclo[2.2.1]hept-2-ene (**6x**), 3.0 min at 160 °C.

NMR spectra (characteristic signals): **3n**, 2.00(CH_3); **3x**, 2.10 (CH_3); **4n**, 1.01 (CH_3CH_2-), 2.44(CH_3CH_2-); **4x**, 1.06(CH_3CH_2-), 2.50(CH_3CH_2-): **5n**, 0.88($CH_3CH_2CH_2$-), 2.30($CH_3CH_2CH_2$-); **5x**, 0.90 ($CH_3CH_2CH_2$-), 2.34($CH_3CH_2CH_2$-): **6n**, 0.98, 1.04 ((CH_3)$_2$CH-); **6x**, 1.06, 1.18 ((CH_3)$_2$CH-).

Elementary analysis: Found: **5n**, C, 80.24; H, 9.76%; **5x**, C, 80.24; H, 10.03%: **6n**, C, 80.38; H, 9.91%; **6x**, 80.18; H, 9.66%. Calcd for $C_{10}H_{16}O$: C, 80.44; H, 9.83%.

*Reactions of **1a** with Methyl Acrylate and Methyl 2-Alkylacrylates.* The Diels-Alder adducts were separated by means of glpc (columns A and B). All the adducts were colorless liquids. Retention times: 5-*endo*-carbomethoxybicyclo[2.2.1] hept-2-ene (**7n**), 3.1 min; 5-*exo*-carbomethoxybicyclo[2.2.1]hep -2-ene (**7x**), 2.7 min at 150 °C (column A): 5-*endo*-carbomethoxy-5-*exo*-methylbicyclo[2.2.1] hept-2-ene (**8n**), 2.9 min; 5-*exo*-carbomethoxy-5-*endo*-methylbicyclo-[2.2.1]hept-2-ene, (**8x**), 2.6 min at 110 °C (column B): 5-*endo*-carbomethoxy-5-*exo*-ethylbicyclo[2.2.1]hept-2-ene (**9n**), 3.2 min; 5-*exo*-carbomethoxy-5-*endo*-ethylbicyclo[2.2.1]-2-ene (**9x**), 2.7 min at 120 °C (column B): 5-*endo*-carbomethoxy-5-*exo*-*n*-butylbicyclo[2.2.1]hept-2-ene (**10n**), 4.3 min; 5-*exo*-carbomethoxy-5-*endo*-*n*-butylbicyclo[2.2.1]hept-2-ene (**10x**), 3.7 min at 126 °C (column B).

NMR spectra (characteristic signals): **7n**, 3.57 (CO_2CH_3); **7x**, 3.63 (CO_2CH_3): **8n**, 3.56 (CO_2CH_3), 1.38 (CH_3); **8x**, 3.65 (CO_2CH_3), 1.08 (CH_3): **9n**, 3.55 (CO_2CH_3), 0.82 (CH_3CH_2-); **9x**, 3.65 (CO_2CH_3), 0.72 (CH_3CH_2-): **10n**, 3.56 (CO_2CH_3), 0.90 ($CH_3(CH_2)_3$-); **10x**, 3.68 (CO_2CH_3), 0.88 ($CH_3(CH_2)_3$-).

Elementary analysis: Found: **10n**, C, 74.73; H, 9.72%; **10x**, C, 75.23; H, 9.77%. Calcd for $C_{13}H_{20}O_2$: C, 74.96; H, 9.68%.

*Reaction of **1a** with Acrolein.* The Diels-Alder adducts, 5-*endo*-formylbicyclo[2.2.1]hept-2-ene (**11n**) and 5-*exo*-formylbicyclo[2.2.1]hept-2-ene (**11x**), were separated by means of glpc (column A, at 125 °C; retention times: **11n**, 2.7 min; **11x**, 2.3 min). These are colorless liquids. NMR spectra (characteristic signals); **11n**, 9.32 (CHO): **11x**, 9.76 (CHO).

*Reactions of **1a** with Acryloyl Halides.* After the reactions were completed, the products were esterified with methanol containing lutidine in a sealed ampoule at room temperature, and subsequently analyzed by glpc (column A). The added litidine had no effect on the *endo* : *exo* isomer ratios. The esterified products were identified as **7n** and **7x** by comparing the retention time and the NMR spectra with those of authentic samples.

*Reactions of **1b** and **1c** with Methyl Acrylate.* The Diels-Alder adducts, 1,4-diphenyl-5-*endo*-carbomethoxybicyclo-[2.2.1]hept-2-ene (**12n**) and 1,4-diphenyl-5-*exo*-carbomethoxybicyclo[2.2.1]hept-2-ene (**12x**); 1,4-di(*p*-chlorophenyl)-5-*endo*-carbomethoxybicyclo[2.2.1]-hept-2-ene (**13n**) and 1,4-di-(*p*-chlorophenyl)-5-*exo*-carbomethoxybicyclo[2.2.1]hept-2-ene (**13x**) were separated by means of preparative tlc. The *endo* : *exo* isomer ratios were determined by integration on the NMR spectra. **12n**, oily liquid, NMR: 7.28 (Ph), 6.35 (CH=CH), 3.37(CO_2CH_3), 3.24(5-*exo*-H), 2.40(6-*endo*-H), 2.00(6-*exo*-H), 1.96(7-*anti*- and 7-*syn*-H): **12x**, mp 63—65 °C, NMR; 7.30(Ph), 6.35(CH=CH), 3.08(CO_2CH_3), 2.76(7-*anti*-H), 2.68(5-*endo*-H), 2.40(6-*exo*-H), 1.88(7-*syn*-H), 1.80(6-*endo*-H): **13n**, mp 88 °C, NMR; 7.28(Ph), 6.28(CH=CH), 3.48

(CO_2CH_3), 3.32(5-*exo*-H), 2.36(6-*exo*-H), 2.04—1.72 (other protons): **13x**, mp 96—97 °C, NMR; 7.30(Ph), 6.30(CH=CH), 3.20(CO_2CH_3), 2.75(7-*anti*-H), 2.72(5-*endo*-H), 2.38(6-*exo*-H), 1.96—1.70 (6-*endo*- and 7-*syn*-H).

Elementary analysis: Found: **12n**, C, 83.02; H, 6.69%: **12x**, C, 82.78; H, 6.62%. Calcd for $C_{21}H_{20}O_2$: C, 82.86; H, 6.62%. Found: **13n**, C, 67.41; H, 4.68%: **13x**, C, 67.38; H, 5.02%. Calcd for $C_{21}H_{18}Cl_2O_2$: C, 67.57; H, 4.86%.

Reactions of ***1a*** *with Maleic Anhydride and* N-*Phenylmaleimide.* The isomer distribution of the reaction of **1a** with maleic anhydride was determined by means of glpc (column D). Retention time: bicyclo[2.2.1]hept-5-ene-*endo*-2,3-dicarboxylic anhydride (**14n**), 3.9 min; bicyclo[2.2.1]hept-5-ene-*exo*-2,3-dicarboxylic anhydride (**14x**), 3.2 min at 150 °C. However, a small portion (0.15%) of **14n** was isomerized to **14x** in the glpc condition. Accordingly, the value of the isomer ratio was corrected by this figure. **14n**, mp 163—164 °C; NMR, 6.32(CH=CH), 3.40—3.70 (1—4-H's), 1.30—1.90 (other protons). **14x**; although no attempt to isolate **14x** was made, the structure of **14x** was confirmed by an isomerization experiment according to Craig's method.[22] NMR (including 70% of **14n**), 2.92 (2- and 3-H).

The adduct of **1a** with *N*-phenylmaleimide (**15n**), mp 144 °C; NMR, 7.10—7.64 (Ph), 6.28 (CH=CH), 3.28—3.64 (1—4-H's), 1.50—1.90 (other protons). The isomer distribution was determined by means of comparing the NMR data with those of **14**. An inspection of the NMR of the adduct with *N*-phenylmaleimide showed an *endo* isomer distribution of more than 99.5%.

Kinetic Experiments (a) The Reactions of ***1a*** *with Acryloyl Halides.* The initial concentrations were 0.0620—0.0842 M for the acryloyl halides, 0.0442 M for **1a**, and 0.0178 M for the internal standard (2,4-dichlorotoluene). The reaction mixture was maintained at 35±0.02 °C. Portions of the sample were withdrawn at appropriate time intervals and quenched with a large excess of methanol containing lutidine. After three hours, the solutions were analyzed by means of glpc. By following the amount of the esters, **7n** and **7x**, the second-order rate constants were calculated.

(b) The Reactions of ***1b*** *and* ***1c*** *with Methyl Acrylate.* The initial concentrations were $5.11—5.81\times10^{-4}$ M for the dienes and $7.07—10.1\times10^{-2}$ M for the dienophile. By following the disappearance of **1b** (or **1c**) spectrophotometrically, the pseudo-first-order rate constants were calculated (λ_{max}=353 nm for **1b** and 360 nm for **1c**).

The competitive reaction technique employed was the same as that used in the aromatic substitution reactions. The relative rates were calculated using the following formula:

$$k_1/k_2 = \{\log C_1^\circ - \log (C_1^\circ - X_1)\}/\{\log C_2^\circ - \log (C_2^\circ - X_2)\}$$

where C_1° and C_2° refer to the initial concentrations of dienophiles and where X_1 and X_2 refer to the final concentrations of the products. Analysis was performed by means of glpc, using appropriate internal standards. In most of the experiments, the competitive reaction of cyclopentadiene with the methyl acrylate—other dienophile pair was employed. However, the relative rate of methyl methacrylate was not obtained because of the coincidental overlap of the glpc peaks of the two reaction products. The relative rate of methyl methacrylate was calculated from the rate of methyl methacrylate relative to that of acrylonitrile and the rate of the latter relative to that of methyl acrylate. The results are shown in Table 3.

Table 3. Relative rates of the Diels-Alder reactions of cyclopentadiene with methyl acrylate (MeA), methyl methacrylate (MeMA), and acrylonitrile (AN)

Diene (mmol/l)	MeA (MeMA)[a] (mmol/l)	AN (mmol/l)	Relative rate
214	74.4	145	1.07[b]
325	46.9	136	1.02[b]
354	46.9	136	1.00[b]
627	(441)[a]	204	1.58×10^{-2}[c]
710	(430)[a]	192	1.63×10^{-2}[c]
720	(291)[a]	187	1.66×10^{-2}[c]

a) The values in parenthese are the concentration of MeMA. b) k_{AN}/k_{MeA}. c) k_{MeMA}/k_{AN}.

The authors wish to express their gratitude to Professor William J. leNoble for his valuable discussion. The financial support from the Ministry of Education is gratefully acknowledged.

References

1) Presented at the 30th Annual Meeting of the Chemical Society of Japan, Osaka (1974).
2) a) J. G. Martin, and R. K. Hill, *Chem. Rev.*, **61**, 537 (1961). b) J. Sauer, *Angew. Chem.*, **79**, 76 (1967).
3) K. Alder and G. Stein, *ibid.*, **50**, 510 (1937).
4) a) J. A. Benson, Z. Hamlet, and W. A. Mueller, *J. Amer. Chem. Soc.*, **84**, 297 (1962). b) P. B. Sargent, *ibid.*, **91**, 3061 (1969).
5) a) R. B. Woodward and R. Hoffmann, "The Conservation of Orbital Symmetry," Academic Press, New York (1970), p. 145. b) K. N. Houk, *Tetrahedron Lett.*, **1970**, 2621. c) K. N. Houk and L. J. Luskus, *J. Amer. Chem. Soc.*, **93**, 4606 (1971).
6) M. Charton, *J. Org. Chem.*, **31**, 3745 (1966); and references cited therein.
7) a) Y. Kobuke, T. Fueno, and J. Furukawa, *J. Amer. Chem. Soc.*, **92**, 6548 (1970). b) Y. Kobuke, T. Sugimoto, J. Furukawa, and T. Fueno, *ibid.*, **94**, 3633 (1972).
8) W. C. Herndon and L. H. Hall, *Tetrahedron Lett.*, **1967**, 3095.
9) J. Sauer and J. Kredel, *ibid.*, **1966**, 731.
10) T. Inukai and T. Kojima, *J. Org. Chem.*, **31**, 2032 (1966).
11) a) J. C. Davis and T. V. van Auken, *J. Amer. Chem. Soc.*, **87**, 3900 (1965). b) P. Laszlo and P. von R. Schleyer, *ibid.*, **85**, 2709 (1963).
12) J. E. Leffler and E. Grunwald, "Rates and Equilibria of Organic Reactions," John Wiley and Sons, Inc., New York (1963), p. 162.
13) T. Kojima and T. Inukai, *J. Org. Chem.*, **35**, 1342 (1970).
14) K. Seguchi, A. Sera, and K. Maruyama, This Bulletin, **47**, 2242 (1974).
15) A similar correlation was observed in the reactions of cyclopentadiene with 2-alkylacrylonitriles; unpublished results.
16) S. Archer, W. B. Dickinson, and M. J. Unser, *J. Org. Chem.*, **22**, 92 (1957).
17) R. B. Woodward, F. Sondheimer, D. Taub, K. Heusler, and W. M. McLamore, *J. Amer. Chem. Soc.*, **74**, 4239 (1952).
18) H. C. Brown, *ibid.*, **60**, 1325 (1938).
19) T. Tsuruta and K. Chikanishi, *Kogyo Kagaku Zasshi*, **67**, 150 (1964).
20) N. L. Drake and J. R. Adams, Jr., *J. Amer. Chem. Soc.*, **61**, 1326 (1939).
21) a) J. Sauer, H. Wiest, and A. Mielert, *Ber.*, **97**, 3183 (1964). b) J. Sauer, H. Wiest, and D. Lang, *ibid.*, **97**, 3208 (1964).
22) D. Craig, *J. Amer. Chem. Soc.*, **73**, 4889 (1951).

The Retardation of the Benzidine Rearrangement of Hydrazobenzene by Cyclodextrins

Yoshihisa MATSUI, Kazuo MOCHIDA, Osamu FUKUMOTO, and Yoshio DATE

Department of Agricultural Chemistry, Shimane University, Nishikawazu, Matsue 690

(Received March 7, 1975)

The benzidine rearrangement of hydrazobenzene is retarded by the addition of α-, β-, and γ-cyclodextrins. The effects on the rate of the cyclodextrins are decreased by the addition of cyclohexanol. The deceleration of the reaction by the cyclodextrins was attributed to the equilibrium complexation of the substrate in the cavities of the cyclodextrins, which may either restrict the large conformational change of the substrate necessary for reaching a sandwich-type transition state or lower the concentration of the diprotonated hydrazobenzene by means of the space alkalinity of cyclodextrins.

Cyclodextrins form monomolecular inclusion complexes with a variety of substrates in aqueous solutions and affect the reactivity of the substrates. Griffiths and Bender[1] have explained the catalytic actions of cyclodextrins in terms of the nucleophilic catalysis, the microsolvent effect, and/or the conformational effect. However, there are relatively few examples in which the accelerations or decelerations of reactions are derived from the conformational effect of cyclodextrins. The present study will deal with the effects of cyclodextrins on the benzidine rearrangement of hydrazobenzene. It has been proven that the rearrangement requires a large conformational change to reach the transition state.

Experimental

Materials. The α-, β-, and γ-cyclodextrins were prepared by the method of Lane and Pirt.[2] They were separated and purified according to the directions of Cramer and Henglein.[3] The hydrazobenzene was prepared by the reduction of nitrobenzene with zinc dust and alkali in the presence of ethanol.[4] Mp 125.5—127.0 °C (lit, mp 125 °C[4]). Bindschedler's Green, used as an analytical reagent in following the rate of the rearrangement of hydrazobenzene, was prepared by the directions of Shine, Snell, and Trisler.[5] A solution of Bindschedler's Green was standardized against a standardized solution of titanium trichloride.[5] Reagent-grade cyclohexanol, methanol, citric acid, potassium citrate, and potassium sulfate were used without further purification.

Procedures. The reaction medium, generally 25 ml of a citrate buffer with a pH of 2.94 and with an ionic strength of 0.50 M adjusted by the use of potassium sulfate, was thermostated and degassed with N_2. To the solution we then added 3 ml of a 0.5 mM solution of hydrazobenzene in 60% methanol. Aliquots (2.0 ml) were pipetted out at regular time intervals and added to 10-ml standardized solutions of Bindschedler's Green. The residual amounts of Bindschedler's Green were colorimetrically determined at 712 nm with a Hitachi spectrophotometer, Model 124. The error in the determination of the hydrazobenzene concentration up to 1.00×10^{-4} M was about 0.01×10^{-4} M. The addition of cyclodextrins had virtually no effect either on the molar absorbance of Bindschedler's Green at 712 nm or on the determination of the hydrazobenzene contained in the solution. Therefore, the observed rate for the reaction of hydrazobenzene in the presence of cyclodextrins corresponds to the sum of the rate for the free hydrazobenzene and that for the complexed hydrazobenzene.

Results and Discussion

Hammond and Shine[6] have shown that the rate of the benzidine rearrangement of hydrazobenzene increases in proportion to the hydrazobenzene concentration and to the square of the hydrogen-ion concentration. Similar results were also obtained in the present study in both the absence and the presence of 8.97 mM β-cyclodextrin. Since the reaction rate is very sensitive to the pH of the medium, the effects of carbohydrates were examined at a constant pH. The first-order rate constants in the presence of methyl α-D-glucopyranoside or α-, β-, or γ-cyclodextrin are summarized in Table 1.

The reaction of hydrazobenzene was little influenced by the addition of methyl α-D-glucopyranoside, whereas it was markedly retarded by cyclodextrins, especially

TABLE 1. FIRST-ORDER RATE CONSTANTS FOR THE BENZIDINE REARRANGEMENT OF HYDRAZOBENZENE IN THE PRESENCE OF CARBOHYDRATES AT 25 °C

Carbohydrate	(mM)	pH[a]	$k_{obsd}\times10^2$min^{-1}	k_{obsd}/k_{un}[b]
None		2.94	1.51±0.02	1.00
Methyl α-D-gulcopyranoside	62.5	2.94	1.60±0.02	1.06
α-Cyclodextrin	8.97	2.94	1.19±0.02	0.79
	17.9	2.94	1.01±0.01	0.67
	26.8	2.94	0.89±0.01	0.59
	35.9	2.94	0.74±0.02	0.49
	44.6	2.94	0.69±0.03	0.46
β-Cyclodextrin	0.90	2.94	1.04±0.01	0.69
	1.79	2.94	0.83±0.01	0.55
	3.59	2.94	0.56±0.02	0.37
	5.38	2.94	0.43±0.02	0.28
	7.18	2.94	0.32±0.02	0.21
	8.97	2.94	0.29±0.02	0.19
γ-Cyclodextrin	0.00	2.91	2.03±0.02	1.00
	4.59	2.91	1.63±0.02	0.80
	9.30	2.91	1.37±0.03	0.67
	13.6	2.91	1.16±0.01	0.57

a) Citrate buffer with the ionic strength of 0.50 M.
b) k_{un}: The first-orde rater constants in the absence of the carbohydrates.

Table 2. Effect of cyclohexanol on the rate of the rearrangement of hydrazobenzene in the presence of 8.97 mM β-cyclodextrin at 25 °C and pH 2.91

[Cyclohexanol], mM	$k_{obsd} \times 10^2$, min^{-1}	k_{obsd}/k_{un} [a]
0	0.46±0.01	0.23
11	0.75±0.03	0.37
21	0.95±0.01	0.47
32	1.29±0.03	0.64
53	1.60±0.02	0.79
106	1.72±0.01	0.85

a) $k_{un} = (2.03 \pm 0.02) \times 10^{-2}$ min^{-1}.

by β-cyclodextrin. This fact suggests that the retardation of the reaction by cyclodextrins is not due to the action of the glucopyranose groups, but to the inclusion of the substrate in the cavities of cyclodextrins. This presumption was substantiated by the examination of the effect of cyclohexanol on the rate-constants in the presence of 8.97 mM β-cyclodextrin at pH 2.91 (Table 2). It has been known that cyclohexanol is included in the cyclodextrin cavity[7,8] and that it competitively retards the catalytic action of cyclodextrins on substrates. As anticipated, the effect of the cyclodextrin on the reaction rate decreased with an increase in the concentration of cyclohexanol.

In order to evaluate the dissociation constant (K_{diss}) and the rate constant (k_c) for the inclusion complex between cyclodextrin and hydrazobenzene, the effect of the cyclodextrin concentration on the rate constant was examined and analyzed in the standard way on the basis of the Michaelis-Menten kinetics.[9] On the assumption of the formation of the 1 : 1 cyclodextrin–hydrazobenzene complex, the observed first-order rate constant (k_{obsd}) may be represented by Eq. (1), if the concentration of the cyclodextrin is much higher than that of hydrazobenzene:

$$k_{obsd} = K_{diss}(k_{un} - k_{obsd})/[CD]_0 + k_c \quad (1)$$

where $[CD]_0$ is the total concentration of the cyclodextrin. Figure 1 shows the plot of k_{obsd} *vs.* $(k_{un} - k_{obsd})/[CD]_0$ for the reaction in the presence of β-cyclodextrin. The plot was virtually linear with a slope ($=K_{diss}$) of $(2.0 \pm 0.2) \times 10^{-3}$ M and with an

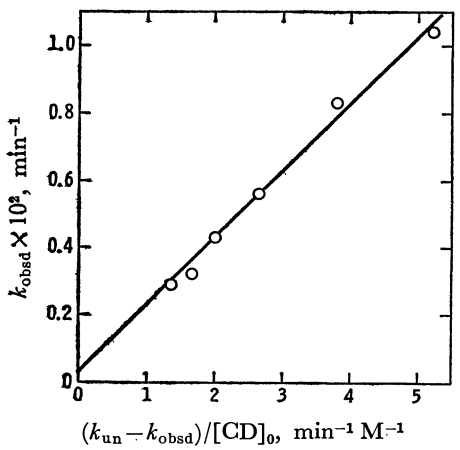

Fig. 1. The plot of k_{obsd} *vs.* $(k_{un} - k_{obsd})/[CD]_0$ for the reaction in the presence of β-cyclodextrin.

Table 3. The dissociation constant (K_{diss}) and the rate constant (k_c) of the cyclodextrin–hydrazobenzene complex at 25 °C

Cyclodextrin	pH	K_{diss}, mM	$k_c \times 10^2$ min^{-1}
α	2.94	30 ± 8	0.15±0.21
β	2.94	2.0± 0.2	0.02±0.03
γ	2.91	20 ±11	−0.10±0.84

intercept ($=k_c$) of $(0.02 \pm 0.03) \times 10^{-2}$ min^{-1}.[10] Although it might be possible that hydrazobenzene combines with two cyclodextrin molecules in a manner much like methyl orange,[11] the linearity of the above plot suggests that such complex formation, if present, is negligible. Similar linear plots were obtained for the reactions in the presence of α- and γ-cyclodextrins. The K_{diss} and k_c values determined are summarized in Table 3. It is apparent that the benzidine rearrangement of hydrazobenzene is virtually inhibited by the formation of the inclusion complexes with the cyclodextrins, although the K_{diss} values for α-, β-, and γ-cyclodextrins, were significantly different from one another.

It has been proven that the rearrangement is intramolecular, proceeding through a sandwich-type transition state in which the two benzene rings lie over each other. Recently, Olah *et al.*[12] has suggested that the folded structure, **1**, is the most likely diprotonated intermediate.

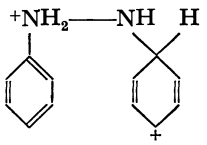

1

When hydrazobenzene is included in the cavity of cyclodextrin, this large conformational change, accompanied by the rearrangement, may be suppressed by the rigid structure of the cyclodextrin. That is, the cyclodextrin may restrict the conformation of the diprotonated hydrazobenzene to the unfolded one. The importance of the conformational restrictions of substrates has often been reported in enzymatic reactions, too.

Another explanation, which is less probable, of the effect of the cyclodextrins is that they depress the protonation of hydrazobenzene. Cramer[13] has shown that the acid-catalyzed hydrolysis of indican is depressed by the formation of the inclusion complex with β-cyclodextrin. The author explained the effect of the cyclodextrin in terms of the "space alkalinity" of the cavity of the cyclodextrin. However, cyclodextrin generally acts as a weak acid[14] rather than as a base, and the concept of space alkalinity is itself rather doubtful. Thus, Broser and Lautsch[15] have shown that, although cyclodextrins do facilitate the acid dissociation of various indicator molecules, they do not actually act as proton acceptors, but, rather, act as electrophiles on the dissociated indicator molecules to stabilize them.

In order to examine the driving force for the interaction of hydrazobenzene with cyclodextrin, the

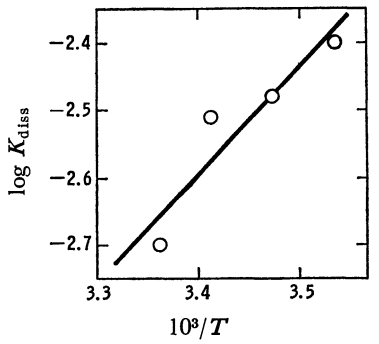

Fig. 2. The plot of log K_{diss} *vs.* the reciprocal of the temperature for the complex of hydrazobenzene with β-cyclodextrin.

thermodynamic parameters were determined for the complex formation. Figure 2 shows the plot of log K_{diss} *vs.* the reciprocal of the temperature for the complex of hydrazobenzene with β-cyclodextrin. The plot is approximately linear; the ΔH and ΔS for the dissociation of the complex were evaluated from the slope and the intercept to be -7.3 ± 6.0 kcal/mol and -36 ± 20 e.u. respectively.[10] It is evident that the driving force for the complex formation is entropic rather than enthalpic.

References

1) D. W. Griffiths and M. L. Bender, *Advan. Catal.*, **23**, 209 (1973).
2) A. G. Lane and S. J. Pirt, *J. Appl. Chem. Biotechnol.*, **21**, 330 (1971).
3) F. Cramer and F. M. Henglein, *Chem. Ber.*, **91**, 308 (1958).
4) W. J. Hickinbottom, "Reactions of Organic Compounds," 3rd Ed., Longmans, Green, London (1957), p. 462.
5) H. J. Shine, R. L. Snell, and J. C. Trisler, *Anal. Chem.*, **30**, 383 (1958).
6) G. S. Hammond and H. J. Shine, *J. Amer. Chem. Soc.*, **72**, 220 (1950).
7) R. Breslow and L. E. Overman, *ibid.*, **92**, 1075 (1970).
8) W. B. Gruhn and M. L. Bender, *Bioorg. Chem.*, **3**, 324 (1974).
9) G. S. Eadie, *J. Biol. Chem.*, **146**, 85 (1942).
10) These values were obtained by the method of least-squares with the aid of a computer.
11) F. Cramer, W. Saenger, and H. -Ch. Spatz. *J. Amer. Chem. Soc.*, **89**, 14 (1967).
12) G. A. Olah, K. Dunne, D. P. Kelly, and Y. K. Mo, *ibid.*, **94**, 7438 (1972).
13) F. Cramer, *Ann. Chem.*, **579**, 17 (1953).
14) R. L. VanEtten, G. A. Clowes, J. F. Sebastian, and M. L. Bender, *J. Amer. Chem. Soc.*, **89**, 3253 (1967).
15) W. Broser and W. Lautsch, *Z. Naturforsch.*, **B8**, 711 (1953).

Hydrogenation and Hydrogenolysis. XV.[1] Hydrogenation of Isomeric Anisidines with Platinum Metal Catalysts in Acetic Acid

Shigeo NISHIMURA, Takeaki TAKAOKA, and Yoshihiro MAEKAWA

Department of Industrial Chemistry, Tokyo University of Agriculture and Technology, Koganei, Tokyo 184

(Received March 31, 1975)

m-Anisidine was hydrogenolyzed to an extent of 92.5% in hydrogenation with a palladium catalyst in acetic acid at 60 °C and 90 kg/cm². The amount of hydrogenolysis in *o*- and *p*-anisidine was only 2.1 and 2.5%, respectively. This great difference in hydrogenolysis between the isomers was not observed with rhodium and platinum catalysts. With *m*- and *p*-anisidines, selectivity at the initiation of hydrogenation was studied for the formation of *N*-cyclohexylanisidine intermediates and for other products by an extrapolation method. Extensive hydrogenolysis of *m*-anisidine and slight hydrogenolysis of *o*- and *p*-anisidines over palladium result from a high selectivity in the formation of the enamine or imine intermediates. The hydrogenation pathways leading to hydrogenolysis and secondary amine formation over the three platinum metals are discussed.

In a previous paper,[2] it was shown that *m*-anisidine and *m*-phenetidine are hydrogenolyzed with a ruthenium catalyst to greater extents than the corresponding *ortho* and *para* isomers. With a rhodium catalyst, however, no appreciable difference in the amount of hydrogenolysis was observed among the isomers.[3] The ease of hydrogenolysis in the *meta* isomer over the *ortho* and *para* isomers was also observed in the hydrogenation of isomeric dimethoxybenzenes with platinum metal catalysts.[4] It has been suggested that the ready hydrogenolysis of methoxyl group in the *meta* isomers is due to the presence of electron releasing methoxy or amino group located *meta* to the methoxyl group to be hydrogenolyzed. The allyl-type ethers, formed as intermediates, have been assumed to hydrogenolyze readily, since the electron releasing groups would stabilize the transition states of carbonium ion character when the allyl ether intermediates are hydrogenolyzed. On the other hand, the electron releasing groups such as methoxy and amino might influence the distribution of various dihydro and tetrahydro intermediates in hydrogenation of aromatic compounds and thus cause differences in the amount of hydrogenolysis among the isomers.

In view of the pronounced effects of some electron releasing groups on the distribution of intermediates, as observed in the palladium-catalyzed hydrogenation of isomeric cresols[5] and ethyl tolyl ethers,[1,6] we have been interested in the hydrogenation of isomeric anisidines with a palladium catalyst. The presence of the amino group might lead to preferential formation of enamine or imine intermediate, which is expected to cause a great difference in the extent of hydrogenolysis among the isomers. In this investigation, acetic acid was chosen as the solvent, since anilines are hydrogenated most readily with palladium in this solvent,[7,8] and extensive formation of *N*-cyclohexylaniline as an intermediate allows to estimate the amount of the enamine or imine intermediate.[8] Anisidines were also hydrogenated using rhodium and platinum as catalysts under the same conditions in order to compare their selectivities with those of palladium.

The hydrogenation of anisidines with platinum metal catalysts was previously studied by Freifelder, Ng, and Helgren,[7] using ethanol–acetic acid and acetic acid as solvents. However, neither detailed analyses of high boiling products nor investigation of intermediates were made.

Results

Products of the hydrogenation of isomeric anisidines with 5% palladium-carbon, rhodium and 5% platinum-carbon catalysts in acetic acid at 60 °C under a hydro-

TABLE 1. HYDROGENATION OF ANISIDINES WITH PALLADIUM, RHODIUM AND PLATINUM CATALYSTS IN ACETIC ACID[a]

Anisidine	Catalyst	Composition of reac. mixture (%)[b]							
		1	**2**	**3**	**4**	**5**	**6**	**7**	**8**
Ortho	Pd/C	0.0	0.9	46.2	0.1	2.2	50.6	0.0	0.0
Meta	Pd/C	0.0	50.8	2.4	36.5	10.3	0.0	0.0	0.0
Para	Pd/C	0.0	1.0	34.8	0.3	2.4	61.5	0.0	0.0
Ortho	Rh[c]	0.0	4.4	62.7	0.8	5.0	22.3	0.0	0.0
Meta	Rh	0.0	10.1	72.4	5.3	12.2	0.0	0.0	0.0
Para	Rh	0.0	11.4	71.0	0.2	4.6	12.8	0.0	0.0
Meta	Pt/C	33.4	12.8	14.2	12.2	14.2	0.0	13.2	0.0
Para	Pt/C	16.8	8.7	8.1	17.1	27.2	7.5	9.1	5.5

a) The anisidine (0.03 mol) was hydrogenated in 15 ml acetic acid at 60 °C under 90±10 kg/cm² hydrogen pressure. b) Values are based on mol% of anisidine consumed for the formation of each compound. **1**: anisidine; **2**: cyclohexylamine; **3**: methoxycyclohexylamine; **4**: dicyclohexylamine; **5**: methoxydicyclohexylamine; **6**: dimethoxydicyclohexylamine; **7**: *N*-cyclohexylanisidine; **8**: *N*-(methoxycyclohexyl)anisidine. Trace amounts of cyclohexane, cyclohexanol, methoxycyclohexane and methoxycyclohexanol were formed besides the compounds given in the table. c) 4.8% of 2-methoxycyclohexanol was found in the products.

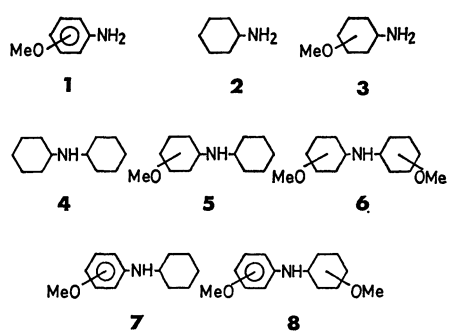

[The letters **a**, **b** and **c** attached to the compound numbers refer to the products from *o*-, *m*- and *p*-anisidine, respectively]

gen pressure of 90±10 kg/cm² are summarized in Table 1. Acetylation of anisidines always occurs to 2—23% extent under these conditions, the hydrogenation of the acetylation products being very slow. It was confirmed that neither the acetylation of saturated amines nor the transformation of 2 mol of saturated primary amine into secondary amine occurs under these conditions. The acetylation products are excluded from the composition of the reaction mixture in Table 1.

The proportion of hydrogenolysis was calculated according to

$$\frac{\%\ \text{yield}\ (\mathbf{2}+\mathbf{4}+(1/2)\times\mathbf{5}+(1/2)\times\mathbf{7})}{\%\ \text{of}\ \mathbf{1}\ \text{hydrogenated}}\times 100 \qquad (1)$$

using the data in Table 1. The results are given in Table 2.

The proportion of secondary amines in the product was calculated according to:

Table 2. Proportion of hydrogenolysis in hydrogenation of isomeric anisidines (%)

Catalyst	Anisidine		
	Ortho	*Meta*	*Para*
Pd/C	2.1	92.5	2.5
Rh	7.7	21.5	13.9
Pt/C	—	64.5[a)]	57.9[b)]

a) At 60.0% ring hydrogenation. b) At 75.9% ring hydrogenation.

Table 3. Proportion of secondary amines in the product from hydrogenation of isomeric anisidines (%)[a)].

Catalyst	Anisidine		
	Ortho	*Meta*	*Para*
Pd/C	52.9(36.0)	46.8(30.5)	64.2(47.3)
Rh	28.1(16.3)	17.5(9.60)	17.6(9.65)
Pt/C	—	59.5(42.3)[b)]	79.8(66.4)[c)]

a) Calculated according to Formula (2). Selectivity in mol% calculated according to Formula (3) is given in parentheses. b) At 66.6% conversion of *m*-anisidine. c) At 83.2% conversion of *p*-anisidine.

$$\frac{\%\ \text{yield}\ (\mathbf{4}+\mathbf{5}+\mathbf{6}+\mathbf{7}+\mathbf{8})}{\%\ \text{of}\ \mathbf{1}\ \text{converted}}\times 100 \qquad (2)$$

using the data in Table 1. The results are given in Table 3. The selectivity for secondary amine formation in mol% is given by

$$\frac{\%\ \text{yield}\ [(1/2)(\mathbf{4}+\mathbf{5}+\mathbf{6}+\mathbf{7}+\mathbf{8})]}{\%\ \text{yield}\ [\mathbf{2}+\mathbf{3}+(1/2)(\mathbf{4}+\mathbf{5}+\mathbf{6}+\mathbf{7}+\mathbf{8})]}\times 100 \qquad (3)$$

The effects of hydrogen pressure on hydrogenolysis and secondary amine formation in the hydrogenation with palladium and rhodium catalysts are shown in Figs. 1 and 2. In accord with the results obtained previously,[9)] the amount of hydrogenolysis always decreased with increasing hydrogen pressure. The effect of hydrogen pressure on secondary amine formation is not so straightforward. Formation of secondary amines increases with increasing pressure with a palladium catalyst, whereas a reverse trend was observed with a rhodium catalyst.

In order to obtain information on intermediates, the variation in the composition of reaction mixture with hydrogenation was studied with *m*- and *p*-anisidines. The results are shown in Figs. 3—8. By extrapolating the selectivity for saturated primary

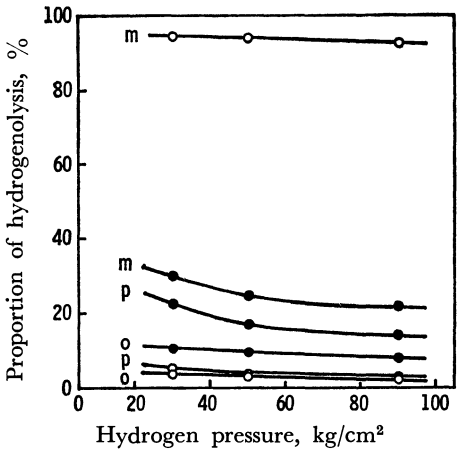

Fig. 1. Effect of hydrogen pressure on hydrogenolysis in hydrogenation of anisidines with Pd-C and Rh catalysts (AcOH, 60 °C). ○ Pd-C; ● Rh.

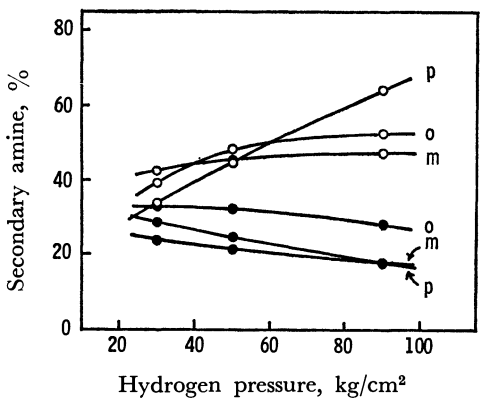

Fig. 2. Effect of hydrogen pressure on secondary amine formation in hydrogenation of anisidines with Pd-C and Rh catalysts (AcOH, 60 °C). ○ Pd-C; ● Rh.

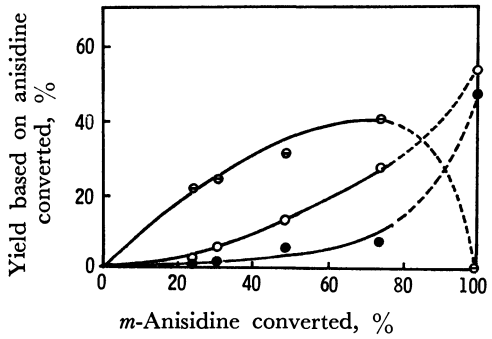

Fig. 3. Hydrogenation of *m*-anisidine with Pd–C catalyst in acetic acid. ⊖ *N*-Cyclohexyl-*m*-anisidine; ○ saturated primary amines; ● saturated secondary amines.

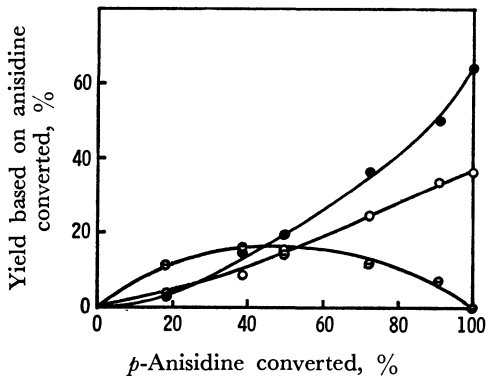

Fig. 4. Hydrogenation of *p*-anisidine with Pd–C catalyst in acetic acid. ⊖ *N*-(4-Methoxycyclohexyl)-*p*-anisidine. For other indications, see Fig. 3.

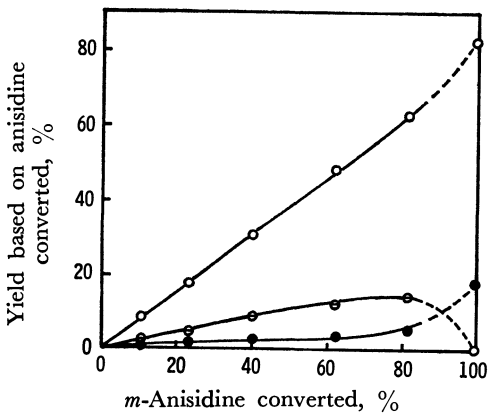

Fig. 5. Hydrogenation of *m*-anisidine with Rh catalyst in acetic acid. For indications, see Fig. 3.

amines, saturated secondary amines, and *N*-cyclohexylanisidines, together with the composition of reaction mixtures, the selectivity for individual products at the initiation of hydrogenation was obtained. The results are summarized in Table 4.

In order to know the behavior of *N*-cyclohexylanisidines, *N*-cyclohexyl-*m*-anisidine (**7b**) and *N*-(4-methoxycyclohexyl)-*p*-anisidine (**8c**) were hydrogenated in the presence of an equimolar amount of ammonium acetate (Table 5). Ammonia is formed together with *N*-cyclohexylanisidines in the hydrogenation of

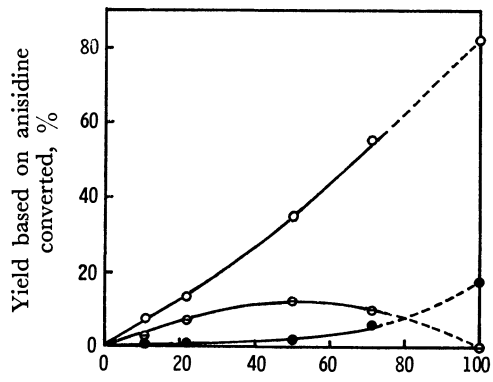

Fig. 6. Hydrogenation of *p*-anisidine with Rh catalyst in acetic acid. ⊖ *N*-Cyclohexyl- and *N*-(4-methoxycyclohexyl)-*p*-anisidine. For other indications see Fig. 3.

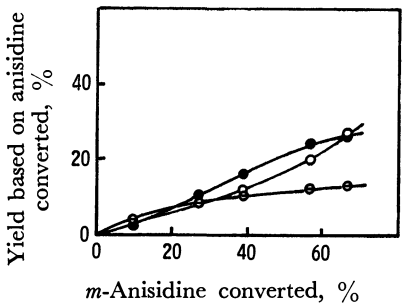

Fig. 7. Hydrogenation of *m*-anisidine with Pt–C catalyst in acetic acid. For indications, see Fig. 3.

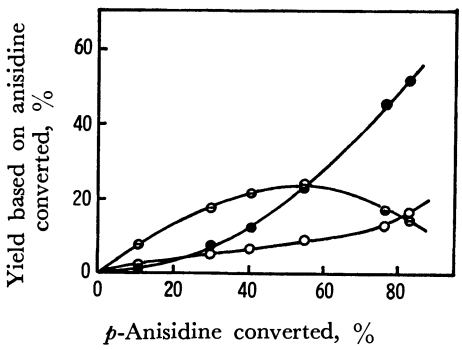

Fig. 8. Hydrogenation of *p*-anisidine with Pt–C catalyst in acetic acid. For indications, see Fig. 6.

anisidines. Its presence may have considerable influence on the course of the hydrogenation of the *N*-cyclohexylanisidines.[8]

Discussion

We see from Table 2 that the ease of hydrogenolysis in the *meta* isomer over the *ortho* and *para* isomers is most pronounced in the palladium-catalyzed hydrogenation. The amount of hydrogenolysis is as large as 92.5% in the *meta* isomer, whereas in the *ortho* and *para* isomers it is only 2.1 and 2.5%, respectively. The same trend is also seen over rhodium and platinum catalysts, although the difference in the amount of hydrogenolysis between the isomers is much smaller.

an increase in primary amine formation as seen in Fig. 2.

Very slight hydrogenolyses in *o*- and *p*-anisidines over palladium are noteworthy and could be understood in terms of high selectivity for enamine or imine formation over this metal. As in the case of *m*-anisidine, the selectivity for formation of *N*-cyclohexyl-*p*-anisidine intermediate is very high (70.1 mol%) (Table 4). However, in sharp contrast to the hydrogenation of *m*-anisidine, no loss of the methoxyl group was observed in the formation of this intermediate. Hydrogenation of the intermediate **8c** also gave only a small amount of hydrogenolysis (2.6%) (Table 5). The hydrogenation of *o*-anisidine appears very similar to that of *p*-anisidine. The results indicate that hydrogenolysis scarcely occurs at all in the course of the formation of enamine or imine intermediates as well as in their further hydrogenation in the cases of *o*- and *p*-anisidines. A probable course of hydrogenation leading to selective formation of the enamine or imine intermediate over palladium is suggested to be as shown in Scheme 2 for the hydrogenation of *p*-anisidine.

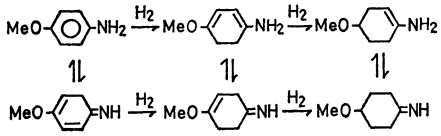

Scheme 2. Hydrogenation pathways leading to selective formation of the enamine or imine intermediate in *p*-anisidine.

The characteristic feature of the palladium-catalyzed hydrogenation of anisidines probably results from the selective hydrogenation of the enol ether moiety over the enamine moiety. This would lead to readily hydrogenolyzable enamines **9**, **11** or imine **10** in a high selectivity in the case of the *meta* isomer. Very poor tendency of palladium toward the hydrogenolysis of an enol ether,[1,11] might explain the occurrence of only slight hydrogenolysis in the course of the formation of enamines or imines in the case of *o*- and *p*-anisidines.

The primary amines formed at an initial stage of hydrogenation (Table 4) might arise through enamine or imine or through other unsaturated amines as intermediates. However, extensive hydrogenolysis at the primary amines from *m*-anisidine and slight hydrogenolysis at those from *p*-anisidine (Table 4) suggest that most of the primary amines is also formed through enamine or imine as an intermediate in the palladium-catalyzed hydrogenation.

On the basis of the results shown in Tables 4 and 5, the hydrogenation pathways of *m*- and *p*-anisidines over palladium are estimated to be those shown in Schemes 3 and 4. It is seen that the compositions of the products thus obtained are in good agreement with those in Table 1. They are also shown in parentheses theses in the Schemes.

In the rhodium-catalyzed hydrogenation, the formation of secondary amines is at low level and the formation of *N*-cyclohexylanisidines is not conspicuous. The selectivity for formation of secondary amines, however,

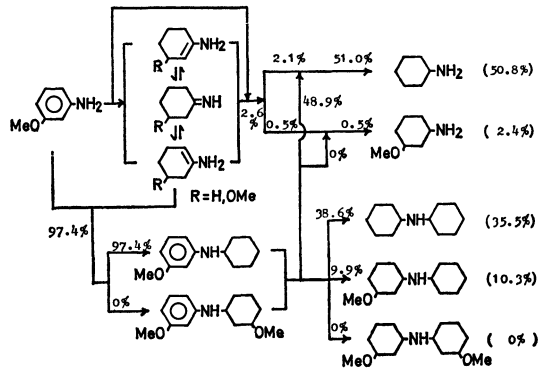

Scheme 3. Hydrogenation pathways of *m*-anisidine over a Pd-C catalyst in acetic acid (60 °C, 90±10 kg/cm² H_2).

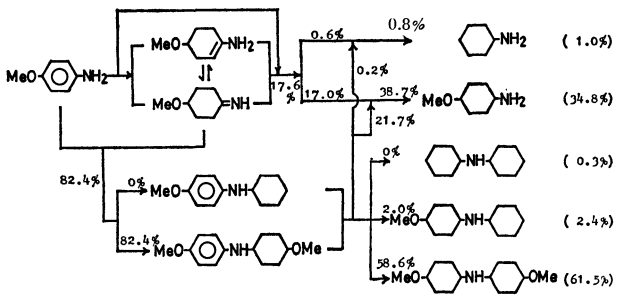

Scheme 4. Hydrogenation pathways of *p*-anisidine over a Pd-C catalyst in acetic acid (60 °C, 90±10 kg/cm² H_2).

is larger at initiation than at complete hydrogenation, particularly in the case of *p*-anisidine. Since *N*-cyclohexylanisidines are mostly hydrogenated over rhodium catalyst to saturated secondary amines even in the presence of ammonium acetate (Table 5),[12] the result suggests that the selectivity for formation of *N*-cyclohexylanisidines decreases with decreasing concentration of anisidine in the course of hydrogenation. Accordingly the proportion of enamine or imine, formed from anisidine and hydrogenated directly to primary amine, might increase at a later stage of hydrogenation. This course of primary amine formation [step (2), Scheme 1] was suggested by Ikedate and Suzuki to be significant in the rhodium-catalyzed hydrogenation of aniline.[13] However, a great difference in the proportion of hydrogenolysis between the primary amines (9.6%) and *N*-cyclohexyl-*m*-anisidine (100%) found in the hydrogenation of *m*-anisidine (Table 4) suggests that most of the primary amines is formed in the rhodium-catalyzed hydrogenation through unsaturated amines as intermediates rather than through enamines or imines. A high degree of hydrogenolysis in the primary amines formed from the hydrogenation of **7b** (90%) (Table 5) might support the view, since it suggests that the formation of primary amines through enamines **9**, **11** or imine **10** would also result in extensive hydrogenolysis. It is of interest to note that, in line with the results with anisidines, 45—48% of cresol is hydrogenated to methylcyclohexanol through other intermediates

than methylcyclohexanone over a rhodium catalyst.[5] With palladium as a catalyst, however, all cresol is hydrogenated through the ketone as the intermediate.[5]

In the hydrogenation of anisidines with platinum, hydrogenolysis of the methoxy group as well as the formation of secondary amines occurred extensively. However, unlike the palladium-catalyzed hydrogenation, no great difference in the extent of hydrogenolysis was observed between *meta* and *para* isomers. An extensive loss of methoxyl group in *N*-cyclohexyl-*p*-anisidines (76%) (Table 4) indicates that hydrogenolysis has occurred extensively during the course of formation of enamine or imine intermediate. This result is plausible if we consider that platinum shows very high activity toward the hydrogenolysis of an enol ether.[1,11] The selectivity for formation of secondary amines does not differ much between the initiation and later stage of hydrogenation. With platinum considerable amounts of saturated secondary amines are formed together with *N*-cyclohexylanisidines (Figs. 7 and 8). However, when the selectivity for the formation of the saturated secondary amines is extrapolated to initiation, it is reduced to only a few percent (Table 4). Thus most of the secondary amines seems to be formed through *N*-cyclohexylanisidines as intermediates. Probably, in this case hydrogenation of the intermediates is fast as compared with that of anisidine. The same conclusion was also reached by Ikedate and Suzuki in the platinum-catalyzed hydrogenation of aniline.[13] Fairly large amounts of secondary amines formed over platinum indicate that the selectivity for the formation of enamine or imine intermediates is rather high over this metal.

Experimental

Materials. *o*-, *m*- and *p*-Anisidines (G. R. grade, Tokyo Kasei Kogyo) were used after distillation before use. *N*-cyclohexyl-*m*-anisidine (**7b**) and *N*-(4-methoxycyclohexyl)-*p*-anisidine (**8c**) were prepared by reductive condensation of the corresponding anisidine and cyclohexanone in isopropyl alcohol with 5% palladium-carbon at 35 °C and 3—7 kg/cm² pressure. **7b**: bp 175 °C/9 mmHg; **8c**: bp 175 °C/4 mmHg. The structures of **7b** and **8c** were confirmed by their NMR spectra (Table 6).

Catalysts. 5% Palladium-carbon and 5% platinum-carbon were obtained from Nippon Engelhard Co. Rhodium oxide was prepared by heating the rhodium hydroxide, precipitated from a hot rhodium chloride solution with an aqueous lithium hydroxide,[14] at 350 °C for 8 hr.

Solvent. The S. S. G. acetic acid (Wako Pure Chemical Ind.) was used without further purification.

Hydrogenations. All hydrogenations were carried out in a 40 ml stainless steel autoclave with a stirrer driven magnetically. The catalyst (0.2—3.2 g of the supported catalyst or 0.01—0.12 g of the oxide catalyst), the substrate (0.03 mol anisidine or 0.015 mol *N*-cyclohexylanisidine) and 15 ml acetic acid were put into the autoclave. After the air had been replaced by hydrogen, the autoclave was charged with hydrogen to the required pressure. The autoclave was then immersed in an oil bath maintained at 60±0.5 °C, hydrogenation being allowed to start after 20 min. The hydrogen pressure was kept constant within±10 kg/cm² during hydrogenation. The amount of catalyst used was adjusted to complete hydrogenation within a reasonable time (2—6 hr). Hydrogenation with the platinum catalyst became very

Table 6. Methoxy- and dimethoxydicyclohexylamines and *N*-cyclohexylanisidines

Compound	Bp (°C/mmHg)	n_D	NMR spectral data, δ[a]						
			Benzene ring protons	CH_3O (Benzene ring)	CH_3O (Cyclohexane ring)	>CHO–	>CHNH–	–NH–	Cyclohexane ring protons
5a	143.5/17	1.4811	—	—	3.24, 3H, s	3.1—3.4, 1H, m	2.2—2.8, 2H, m	0.7—2.1, 19H, bm	
6a	150/16	1.4808	—	—	3.24, 6H, s	3.1—3.4, 2H, m	2.6—2.9, 2H, m	0.8—2.2, 17H, bm	
5b	164/28	1.4833	—	—	3.30, 3H, s	3.2—3.4, 1H, m	2.2—2.8, 2H, m	0.8—2.2, 19H, bm	
5c	114—6/2	1.4824[b]	—	—	3.20, 3H, s	3.1—3.4, 1H, m	2.2—2.8, 2H, m	0.8—2.1, 19H, bm	
6c	181/17	1.4834[b]	—	—	3.20, 6H, s	3.1—3.4, 2H, m	2.4—2.9, 2H, m	0.8—2.2, 17H, bm	
7b	175/9	1.5568	6.8—7.2, 1H, t[$H_{(5)}$] 6.0—6.3, 3H, m[$H_{(3)}$,$H_{(4)}$,$H_{(6)}$]	3.67, 3H, s	—	—	2.8—3.3, 1H, m	3.33, 1H, s	0.8—2.3, 10H, bm
7c[c]	185/17[d]	—	6.7, 2H, d[$H_{(3)}$, $H_{(5)}$] 6.5, 2H, d[$H_{(2)}$, $H_{(6)}$]	3.53, 3H, s	—	—	2.8—3.3, 1H, m	3.20, 1H, s	0.7—2.2, 10H, bm
8c[c]	175/4[e]	—	6.7, 2H, d[$H_{(3)}$, $H_{(5)}$] 6.5, 2H, d[$H_{(2)}$, $H_{(6)}$]	3.50, 3H, s	3.10 3H, s	2.7—3.2, 2H, m		3.37, 1H, s	0.7—2.1, 8H, bm

a) Unless otherwise noted, the NMR spectra were obtained on a JEOL C-60HL spectrometer at 60 MHz using TMS as an internal standard at 25 °C in CCl_4 solution. b) n_D^{25}. c) The NMR spectra obtained at 50 °C in neat. d) Mp 42—43 °C. e) Solid at room temperature.

slow during the course of reaction and could not be completed by prolonging the reaction time (over 20 hr).

Analysis of Product. The reaction mixture was analyzed directly by gas chromatography. For low boiling products, a 3 mm×2.25 m column containing 10% PEG 6000—10% KOH on Chromosorb W was used in the temperature range 170—200 °C programmed at 4 °C/min. For high boiling products, a 3 mm×0.75 m column containing 30% PEG 20 M on Celite 545 was used at a temperature initially kept at 200 °C for 6 min and then programmed at 6 °C/min to 250 °C. For the separation of *N*-acetylanisidines and *N*-(methoxycyclohexyl)anisidines a combined column containing PEG 20M (3 mm×0.75 m) and OV-17 (3 mm×3 m) was used at 250 °C.

The secondary amines required for identification of the product peaks on gas chromatography were synthesized by the reductive condensation of the corresponding amines and cyclohexanones under the conditions described above for the preparation of **7b** and **8c**. Methoxycyclohexlamines for this condensation were prepared by hydrogenating the corresponding anisidines with ruthenium hydroxide as a catalyst in the presence of lithium hydroxide in isopropyl alcohol at 80 °C under 80—100 kg/cm².[2] The characteristics of the compounds synthesized are summarized in Table 6. The synthesis of 3,3'-dimethoxydicyclohexylamine (**6b**) and *N*-(3-methoxycyclohexyl)-*m*-anisidine (**8b**) was unsuccessful because of complete loss of the methoxyl group of the cyclohexanone component during the course of reductive condensation. Probable peaks of **6b** and **8b**, as inferred from the peaks of **6a**, **6c** and **8a**, **8c**, respectively, could not be found in the gas chromatograms of the products from hydrogenation of *m*-anisidine. A peak located around a probable peak region of **8b** was proved to be that of *N*-acetyl-*m*-anisidine by isolation with a gas chromatograph and measurement of its NMR spectrum. The gas chromatograms of the products at intermediate stages of hydrogenation often showed small peaks of *N*-cyclohexylideneanisidines in amounts less than 1%. They were added to the corresponding *N*-cyclohexylanisidines. *N*-Cyclohexylidenecyclohexylamines seem to undergo decomposition when subjected to gas chromatography in acetic acid solution. Their behavior on gas chromatography was not investigated further, but they can be neglected when we obtain the results in Table 4 by an extrapolation method. The peak areas were standardized by the mixtures of known compositions. This was done with *p*-anisidine and its hydrogenation products. The standardization for *o*- and *m*-anisidines and their hydrogenation products was approximated by applying that obtained with the *p*-anisidine series compounds.

The authors are indebted to Asst. Prof. Michiko Tsuchimoto for her helpful discussions concerning the NMR spectra and to Mr. Yoshiyuki Tomiyama for his assistance in glpc analyses.

References

1) Part XIV: S. Nishimura, M. Uramoto, and T. Watanabe, This Bulletin, **45**, 216 (1972).
2) S. Nishimura and H. Yoshino, *ibid.*, **42**, 499 (1969).
3) S. Nishimura, H. Uchino, and H. Yoshino, *ibid.*, **41**, 2194 (1968).
4) Y. Takagi, S. Ishii, and S. Nishimura, *ibid.*, **43**, 917 (1970).
5) Y. Takagi, S. Nishimura, and K. Hirota, *ibid.*, **43**, 1846 (1970).
6) S. Nishimura, T. Watanabe, and M. Uramoto, Abstracts of the 23rd Annual Meeting of the Chemical Society of Japan, Tokyo, April, 1970, I, p. 88; S. Nishimura, T. Ozawa, and Y. Kano, Abstracts of the 27th Annual Meeting of the Chemical Society of Japan, Nagoya, October, 1972, II, p. 325.
7) M. Freifelder, Y. H. Ng, and P. F. Helgren, *J. Org. Chem.*, **30**, 2485 (1965).
8) K. Ikedate, T. Suzuki, and S. Suzuki, *Nippon Kagaku Zasshi*, **89**, 304 (1968).
9) S. Nishimura and H. Taguchi, This Bulletin, **36**, 353 (1963).
10) For the reactivity of this type compounds, see D. J. Hupe, M. C. R. Kendall, and T. A. Spencer, *J. Amer. Chem. Soc.*, **95**, 2271 (1973) and references cited therein.
11) S. Nishimura, M. Katagiri, T. Watanabe, and M. Uramoto, This Bulletin, **44**, 166 (1971).
12) The presence of primary amine depresses the primary amine formation through *N*-cyclohexylanisidines (unpublished results). This might have considerable influence on the rhodium-catalyzed hydrogenation, where *N*-cyclohexylanisidines are hydrogenated in the presence of considerable amounts of primary amines.
13) K. Ikedate and S. Suzuki, *Nippon Kagaku Zasshi*, **90**, 91 (1969).
14) Y. Takagi, T. Naito, and S. Nishimura, This Bulletin, **38**, 2119 (1965); S. Nishimura and M. Hama, *ibid.*, **39**, 2467 (1966).

Über die Feststellung der Wanderung des Äthoxycarbonyl-Restes bei der Dienon-Phenol-Umlagerung

Tadashi SUEHIRO und Shozo YAMAZAKI

Chemisches Institut der Gakushuin Universität, Toshima-ku, Mejiro, Tokyo 171

(Eingegangen am 11. 4. 1975)

3,4-Dimethyl-4-äthoxycarbonyl-cyclohexa-2,5-dienon-4-^{14}C (**9**) lagert sich bei 60—70 °C in 60% Schwefelsäure zu 2,3-Dimethyl-5-hydroxybenzoesäure-äthylester-2-^{14}C (**10**, 99.8%) und -1-^{14}C (**10b**, 0.2%) insgesammt in *ca.* 50% Ausbeute um, unter Nebenbildung von 3,4-Xylenol (**11**, 12%) und 2,3-Dimethyl-5-hydroxybenzoesäure (**12**, 5%). Dass **10** die Struktur von 2,3-Dimethylbenzoesäure-Derivat hat, wurde durch Mischprobe mit der authentischen Verbindung festgestellt.

Wir baben früher mitgeteilt, dass bei der durch Säure katalysierten Umlagerung von 3,4-Dimethyl-4-äthoxycarbonyl-cyclohexa-2,5-dienon (**9**) 2,3-Dimethyl-5-hydroxy-benzoesäure-äthylester (**10**) entsteht.[1,2] Die struktur des Ester **10** wurde unterstützt durch dessen chemische Eigenschaften, wie die schwierige Decarboxylierung der von **10** geleiteten Dimethyl-hydroxy-benzoesäure **12**[1] und auch durch die spektroskopischen Eigenschaften wie UV-Spektren von **12**, die der der *m*-Hydroxybenzoesäure ähnlich sind und wie die KMR-Spektren von **10**, die zwei Doubletts aromatischer Wasserstoffe und zwei Singuletts von Methyl-Wasserstoffen zeigen.[2] Wir haben diesmal die Struktur, die die nebeneinander stehenden CH_3-CH_3-COOR-Reste enthält, durch die Mischprobe von der aus **12** überführten 2,3-Dimethyl-cyclohexancarbonsäure (**14**) mit der aus *o*-Xylidin hergestellten Verbindung nachgewiesen, und weiter haben wir die Wanderung des Äthoxycarbonyl-Restes durch die ^{14}C-Markierungstechnik festgestellt, worüber wir hier berichten wollen.

Die Dienon-Phenol-Umlagerung ist viel untersucht worden, darunter findet man einige merkwürdige Ergebnisse, wie die 1,3-Wanderung des CCl_3-Restes[3] und die bevorzugte 1,2-Wanderung des Äthoxycarbonyl-Restes.[1] Weil der Rest COOR einen Elektronen anziehenden Charakter hat, ist die Wanderung von COOR zum Kation-Zentrum schneller als die der Elektronen liefernden Methyl-Gruppe schwierig zu verstehen.*

Es ist noch ein anderer Weg ohne die COOR-Wanderung denkbar, und zwar ein Weg von **9** zu **10** über die Bicyclo[3.1.0]hexen-Derivate **A** und **B** unter Umbau des aromatischen Ringes und mit anschliessender Umlagerung der Methyl-Gruppe zum Kation-Zentrum (Schema 1). Die Umlagerung unter Umbau des aromatischen Ringes dieser Art sieht man bei der photochemischen Dienon-Phenol-Umlagerung wie von 4-Methyl-4-dichlormethyl-cyclohexa-2,5-dienon in säurer Lösung.[4] Die kationische disrotatorische 5-Ring-Elektrocyclisierung und die kationische suprafaciale 1,4-sigmatropische Umlagerung sind nach der Woodward-Hoffmann-Regel** photochemisch erlaubt und die antarafaciale thermische Wanderung **A**→**B**

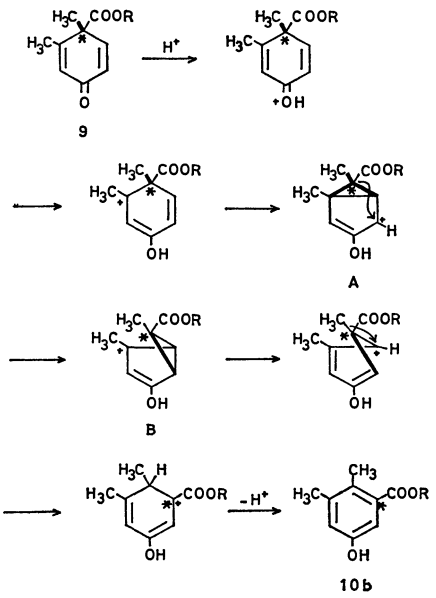

Schema 1.

müsste bei den Kleinring-Verbindungen schwierig sein, trotzdem ist es vom Wert, chemisch festzustellen, wie es bei **9** wirklich ist.

Ergebnisse und Diskussion

Wir haben 3,4-Dimethyl-4-äthoxycarbonyl-cyclohexa-2,5-dienon-4-^{14}C nach dem Schema 2 synthetisiert. Man führt Bromessigester-2-^{14}C (**2**) durch die Reformatsky-Reaktion mit Acetnitril nach der Methode von Dahn und Hauth[5] in mässiger Ausbeute in Acetessigester-^{14}C (**3**) über. α-Methyl-acetessigester-^{14}C (**4**) unterwirft man in Toluol der Michael-Addition bei −10 °C in Gegenwart katalytischer Mengen von Kalium *t*-Butoxid und cyclisiert das Produkt durch Erhitzen mit Piperidin-Acetat in 3,4-Dimethyl-4-äthoxycarbonyl-cyclohex-2-enon-4-^{14}C (**6**). Man verwandelt Cyclohexenon in festen Semicarbazon **7** zur Reinigung des flüssigen Ketons **6** und gewinnt das Keton durch säure Hydrolyse wieder. Dehydrierung von Cyclohexenon **8** zu Cyclohexadienon **9** gelang durch Kochen mit Selendioxid in *t*-Butanol. Die totale Ausbeute aus Eisessig in Cyclohexadienon **9** betrug 2.1% des theoretischen Wertes.

Bei der Behandlung von **9** mit 60% Schwefelsäure 30 Min. bei 60—70 °C erhält man 2,3-Dimethyl-5-hydroxy-benzoesäure-äthylester (**10**) vom Schmp.

* Siehe auch den Artikel von R. M. Acheson, *Accounts Chem. Res.* **4**, 177 (1971) über Umlagerung des COOR-Restes.

** R. B. Woodward und R. Hoffmann, "The Conservation of Orbital Symmetry" Verlag Chemie—Academic Press Inc (1970), Seite 45 und 118.

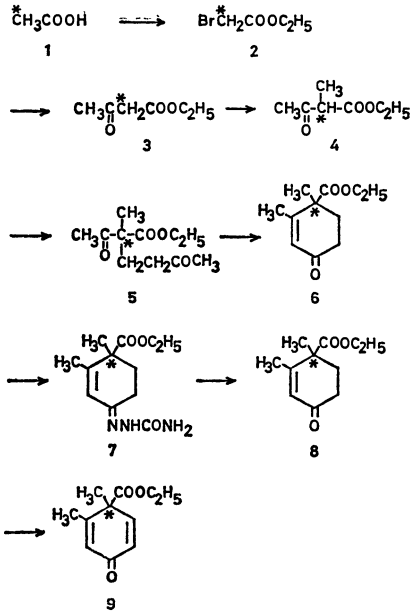

Schema 2.

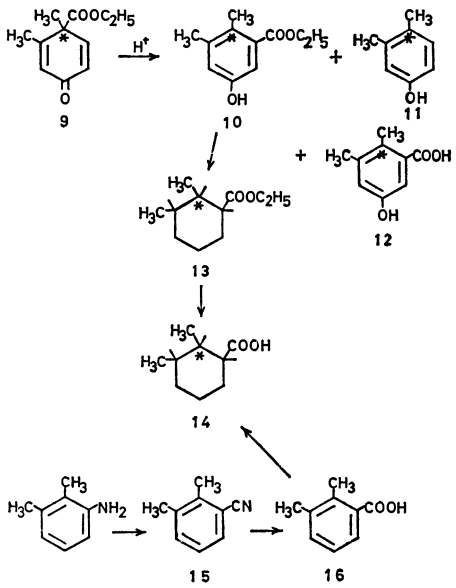

Schema 3.

67.5—68.0 °C, 3,4-Xylenol (**11**) vom Schmp. 64—65 °C und 2,3-Dimethyl-5-hydroxy-benzoesäure (**12**) vom Schmp. 186—187 °C je in Ausbeute *ca.* 50, 12 und 5%. Die Umlagerung geschah also sehr sauber, und es war keine bemerkenswerte Nebenreaktion zu finden. Bei der Hydrierung von **10** bei Raumtemperatur in Eisessig auf Platinoxid nimmt **10** 4 Mole Wasserstoff auf und gibt in quantitativer Ausbeute 2,3-Dimethyl-cyclohexan-carbonsäure-ester-^{14}C (**13**) unter Hydroxyl-Abspaltung. Man erhält aus **13** durch Verseifen Dimethyl-cyclohexancarbonsäure-^{14}C (**14**) vom Schmp. 59—60 °C. Diese Carbonsäure kann man auch ausgehend von *o*-Xylidin über Dimethylbenzonitril **15**, Dimethylbenzoesäure **16** und durch anschliessende Hydrierung herstellen. Die Umsetzung von *o*-Xylidin in Nitril **15** geht sehr schlecht (18%), wahrscheinlich durch sterische Behinderung unter Nebenbildung von *o*-Xylenol vom Schmp. 75 °C. Die Hydrolyse von **15** gelang in mässiger Ausbeute erst durch Erhitzen von **15** mit Polyphosphorsäure auf 165 °C. Die Hydrierung von Dimethylbenzoesäure **16** verlief genau so gut wie bei **10** und man erhält Dimethylcyclohexancarbonsäure vom Schmp. 59—60.5 °C in 97% Ausbeute. Die beiden Dimethylcyclohexancarbonsäuren zeigten keine Schmelzpunkterniedrigung bei der Mischprobe, damit wurde klar, dass **10** die Struktur von 2,3-Dimethyl-benzoesäure-Derivat hat (Schema 3).

Wenn die Dienon-Phenol-Umlagerung von **9** nach dem Schema 1 verläuft, dann musste die 4-^{14}C-Markierung von **9** in die 1-Stellung von **10** wandern. Zur Bestimmung der Stellung der ^{14}C-Markierung in **10** haben wir **10** in Dimethyl-oxo-hexamethylenimin überführt und durch dessen Schmidt-Reaktion in Kohlendioxid und Dimethyl-pentamethylendiamin abgebaut. Um **14** in **19** oder **20** zu verwandeln, versetzt man **14** zuerst mit Thionylchlorid und das entstandene Säurechlorid **17** verwendet man direkt für die Friedel-Crafts-Reaktion in Benzol mit Aluminiumchlorid, wobei man in 62% Ausbeute Dimethylcyclohexyl-phenyl-keton **18** erhält. Wenn man das Keton **18** bei 65 °C in 90% Schwefelsäure-Natriumnitrit behandelt[6], so gewinnt man in 81% Ausbeute rohe Dimethyl-oxo-hexamethylenimine (**19**+**20**) vom Schmp. *ca.* 90 °C, woraus man nach mehrmaligem Umkristallisieren aus *n*-Hexan Nadeln vom Schmp. 123—125 °C (**19**, 28%) isoliert. Zur Analyse brachte man ein Produkt vom Schmp. 124.5—126 °C nach dem weiteren Umkristallisieren. Aufgrund der KMR-Spektren[7] von **19** in Tetrachlorkohlenstoff, δ 3.15 ppm (2H, m) und 2.7 ppm (1H, quartett) hat **19** wahrscheinlich die Struktur 3,4-Dimethyl-2-oxo-hexamethylenimin. Aus der Mutterlauge der Umkristallisierung vom Produkt Schmp. *ca.* 90 °C ohne ^{14}C-Markierung erhält man noch ein isomeres 2,3-Dimethyl-7-oxo-hexamethylenimin (**20**) vom Schmp. 65.5—67.5 °C mit KMR-Spektrum in Tetrachlorkohlenstoff, δ 2.3 ppm (2H, m) und 3.6 ppm (1H, quintett).

Die Schmidt-Reaktion von **19** mit anschliessender Benzoylierung gab glatt Dimethyl-pentamethylendiamin-dibenzamid vom Schmp. 151—153 °C (**21**, 69%) und Bariumcarbonat (**22**, 76%). Die Grignard-Reaktion mit dem aus **22** entwickelten Kohlendioxid und 3-fachen Mengen Phenylmagnesiumbromid in einem Einschlussrohr gab direkt Triphenylcarbinol (**23**) vom Schmp. 161—162.5 °C in 84% Ausbeute, dessen Struktur durch Mischprobe mit der authentischen Verbindung festgestellt wurde (Schema 4).

Die Ergebnisse der Radioaktivitäts-Bestimmung von **19**, **21** und **23** sind in Tabelle 1 aufgestellt, daraus ersieht man, dass das Ring-Gerüst von **10** während der Umlagerung 99.8% unverändert bleibt: Während der Umlagerung wandert der Äthoxycarbonyl-Rest schneller als der Methyl-Rest zum Kation-Zentrum. Dies stimmt genau mit den Ergebnissen der Blaise-Umlagerung überein[8]: Die Behandlung von α,α-Dimethyl-β-hydroxy-β-phenylpropionsäure-ester in Benzol mit Phosphorpentoxid ergab Dimethyl-atropasäure-ester unter COOR-Wanderung. Andere ähnliche Um-

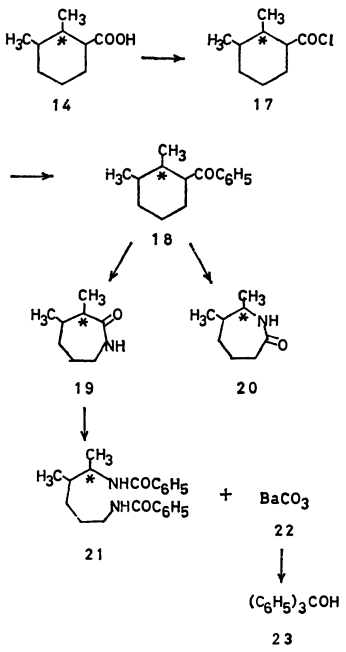

Schema 4.

Tabelle 1. Radioaktivitäts-bestimmung[a] von **19**, **21** und **23**

Verbindung	mg	Molgew.	dpm/mg	Mittelwert	dpm/mMol	Aktivität %
19	10.50	141	1269.4			
	10.74	141	1265.0	1267	$1786 \cdot 10^2$	100
21	10.81	338	526.7			
	9.80	338	528.1	527.4	$1783 \cdot 10^2$	99.8
23	10.38	260	1.21			
	9.43	260	1.51	1.36	$3.54 \cdot 10^2$	0.2

a) Die Bestimmung erfolgte mit dem Gerät Packard Tri-Carb Spektrophotometer mit einer Dioxan/PPO-DMPOPOP-Naphthalin Lösung.

lagerungen wurden auch bei den verwandten Verbindungen ausfindig gemacht.[9]

Wir finden zugleich eine kleine aber doch deutliche Radioaktivität (0.2%) in Kohlendioxid im Carbonat **22**: Thermische kationische 1,4-sigmatropische Umlagerung bei Kleinring-Verbindung findet anscheinend innerhalb 0.2% der ganzen Umlagerung statt und führt zur Bildung von **10b** (Schema 1).

Zum Mechanismus der Umlagerung haben Marx und andere[10] aufgrund ihrer kinetischen Untersuchung vorgeschlagen, dass die Geschwindigkeitsbestimmende Stufe der Umlagerung in der Stufe der Wanderung der Substituenten des protonisierten Dienons **24** liege und der Übergangszustand der Wanderung eher Produkt-ähnlich als Ausgangssubstanz-ähnlich sei: Die schnelle Wanderung des Äthoxycarbonyl-Restes werde durch die höhere Stabilität des Carboniumions **25** nach der COOR-Umlagerung als die des Ions **26** nach der Methyl-Umlagerung kontrolliert.

Es ist aber schlecht verständlich, warum sich 4,4-Dimethyl-cyclohexa-2,5-dienon mit nur ein Fünftel der Geschwindigkeit von 4-Methyl-4-äthoxycarbonyl-

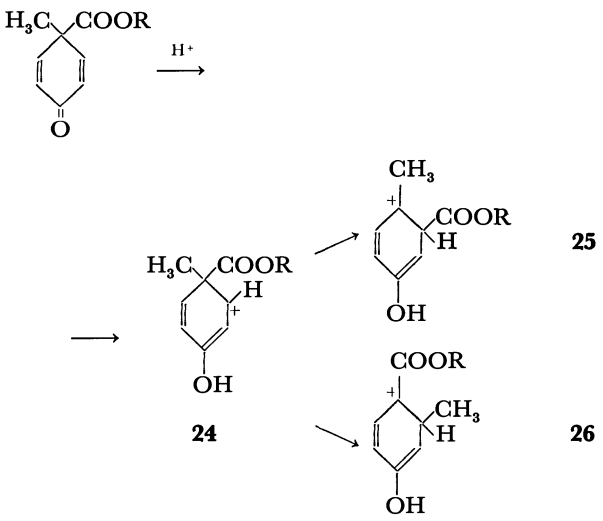

cyclohexa-2,5-dienon umlagert[10]: Die beiden Dienone sollten eigentlich mit derselben Geschwindigkeit umgesetzt werden.

Wir wissen noch nicht genau, wie die Umlagerung des Äthoxycarbonyl-Restes vor sich geht. Eine ähnliche NO_2-Wanderung findet man bei der Säure-katalysierten Umlagerung von 1-Acetoxy-3,4-dimethyl-4-nitro-cyclohexa-2,5-dien[11] und von 1-Acetoxy-1-isopropyl-4-methyl-4-nitro-cyclohexa-2,5-dien.[12] Die Doppelbindung im COOR-Rest könnte für dessen bevorzugte Wanderung viel beitragen wie z. B. bei den homoallylischen Systemen der Bicyclo[2.2.1]hepten-Verbindungen[13]: Die C=O Gruppe könnte durch einfach Überschirmung auf dem Kation-Zentrum oder durch teilweise Verknüpfung an das Kation-Zentrum in der homoallylischen Stellung den Methyl-Rest vom Reaktionsbereich herausschliessen.

Herrn Dr. N. Morikawa an der Universität Tokyo danken wir herzlichst für die Bestimmung der Radioaktivität.

Beschreibung der Versuche

Die Synthese von 3,4-Dimethyl-4-äthoxycarbonyl-cyclohexa-2,5-dienon-4-^{14}C (**9**) wurde im Prinzip nach der Vorschrift von Plieninger und Suehiro[1] ausgehend von Eisessig-2-^{14}C durchgeführt, ausser der Überführung von Cyclohexenon **8** in Cyclohexadienon **9**.

3,4-Dimethyl-4-äthoxycarbonyl-cyclohexa-2,5-dienon-4-^{14}C (***9***): Nach der Method von Mystre und anderen[14] kocht man 25.31 g (0.128 Mol) **8** 7 Stunden lang mit 15 g (0.135 Mol) Selendioxid in 250 ml *t*-Butanol–2 ml Eisessig. Man dampft unter vermindertem Druck *t*-Butanol ab, nimmt den Rückstand in Dichlormethan auf, filtriert den Überschuss Selendioxid ab, lässt die Lösung durch eine Kolonne von Aluminiumoxid laufen, eluiert mit weiterem 800 ml Dichlormethan, dampft die Dichlormethan-Lösung ab und destilliert den Rückstand unter 2 Torr. Das Produkt geht bei 105—107 °C über. Ausbeute 7.51 g (38.4 mMol, 30%). KMR in Tetrachlorkohlenstoff, δ 6.83 ppm (1H, d, J=10 Hz, 6-C-H), 6.22 ppm (1H, doppelte d, J=10 Hz und 2 Hz, 5-C-H), 6.12 ppm (1H, breites s, 3-C-H).

Umlagerung von ***9***: Man erhitzt 7.51 g (38.4 mMol) von **9** in 100 ml 60% Schwefelsäure 25 Min. bei 60 °C. Die Mischung verdünnt man mit 300 ml Eiswasser und schüttelt mit Äther aus. Die äther. Lösung gibt nach dem Waschen

mit Natriumhydrogencarbonat und Abdampfen und Umkristallisieren aus Benzol–*n*-Hexan (1 : 5) **10** in Nadeln 3.64 g (18.5 mMol, 48%) vom Schmp. 66—68 °C (Schmp. in der Literatur[1] 69 °C). Gef. C 68.26, H. 7.30%. Ber. für $C_{11}H_{14}O_3$, C 68.02, H. 7.27%. KMR in Chloroform-*d*, δ 7.23 ppm (1H, d, J=3 Hz, 6-C-H), 7.07 ppm (breites s, O-H), 6.88 ppm (1H, d, J=3 Hz, 4-C-H), 2.25 ppm (3H, s, 2-CH_3), 2.10 ppm (3H, s, 3-CH_3).

Bei der Behandlung von nicht markiertem **9** isoliert man durch Schütteln mit Natriumcarbonat und fraktionierende Destillation ausser **10** noch 3,4-Xylenol vom Schmp. 64—65 °C in 12% Ausbeute, dessen Struktur durch Mischprobe mit der authentischen Verbindung und durch Schmp. von dem 3,5-Dinitrobenzoesäure-ester 180—181 °C festgestellt wurde, und auch 2,3-Dimethyl-5-hydroxybenzoesäure vom Schmp. 186—187 °C in 5% Ausbeute. Gef. C 64.87, H 6.09%. Ber. für $C_9H_{10}O_3$, C 65.05, H 6.07%. UV-Spektrum in Methanol, λ_{max} 301 nm (log ε=4.18), λ_{min} 267 nm.

2,3-Dimethyl-cyclohexancarbonsäure-äthylester-^{14}C ***(13)***: Man hydriert 3.64 g radioaktiven und 1.63 g nicht radioactiven Dimethyl-hydroxy-benzoesäure-ester (insgesammt 27.2 mMol) **10** in 30 ml Eisessig bei atmosphärem Druck und bei Raumtemp. über 0.4 g Platinoxid. Die Wasserstoff-Aufnahme betrug 2.75 Liter (25 °C, Th. 2.65 Liter). Nach dem Abtrennen vom Katalysator erhält man beim Destillieren unter 0.2 Torr. ein Produkt, das bei 48—50 °C überght. Ausbeute 4.67 g (25.4 mMol, 93%). KMR in Tetrachlorkohlenstoff, δ 0.93 ppm (3H, d, J=6.5 Hz, CH_3), 0.74 ppm (3H, J=6.5 Hz, CH_3).

2,3-Dimethyl-cyclohexancarbonsäure-^{14}C ***(14)***: Man kocht 4.67 g (25.4 mMol) von **13** 2 Stunden in 20 ml Äthanol—4 ml Wasser mit 4.0 g Natriumhydroxid. Man destilliert Äthanol ab, verdünnt den Rückstand mit Wasser, behandelt mit Teirkohle und säuert mit verd. Salzsäure an, dabei fallen Kristalle aus. Rohprodukt 2.84 g (18.2 mMol, 72%) vom Schmp. 52—57 °C. Umkristallisieren aus *n*-Hexan gibt ein Produkt vom Schmp. 59—60 °C. IR(KBr) 3300—2500 (breit), 1700 (breit), 1250 und 930 cm^{-1}. KMR in Tetrachlorkohlenstoff, δ 12.13 ppm (1H, s, COO-H), 2.5—1.0 ppm (breites m, 9H), 0.87 ppm (3H, d, J=7 Hz, CH_3), 0.76 ppm (3H, d, J=7 Hz, CH_3). Dieses Produkt zeigte keine Schmelzpunkterniedrigung bei der Mischprobe mit dem Produkt aus 2,3-Dimethylbenzoesäure durch Hydrierung vom Schmp. 60.5—61.5 °C. UV- und KMR-Spektren stimmten vollkommen mit denen des letzteren Pruduktes überein.

Hydrierung von 2,3-Dimethyl-benzoesäure zu 2,3-Dimethyl-cyclohexancarbosäure: Die aus *o*-Xylidin hergestellte 2,3-Dimethyl-benzoesäure vom Schmp. 144—145 °C (Literatur-Angabe, Schmp. 145 °C[15]) 8.90 g (59.3 mMol) hydriert man in 75 ml Eisessig bei atmosphärem Druck und Raumtemp. über 0.7 g Platinoxid. Die Hydrierung verläuft glatt und nimmt 4.94 Liter Wasserstoff auf (30 °C. Th. 4.47 Liter). Nach dem Trennen vom Katalysator erhält man bei Destillation unter 0.2 Torr. ein kristallines Produkt, das bei 91—96 °C übergeht. Umkristallisieren aus *n*-Hexan bei −5 °C gibt ein Produkt vom Schmp. 60.5—61.5 °C. Ausbeute 8.94 g (57.3 mMol. 97%). Gef. C 69.41, H 10.08%. Ber. für $C_9H_{16}O_2$, C 69.19, H 10.32%.

2,3-Dimethylcyclohexyl-phenyl-keton-^{14}C ***(18)***: Zu einer Lösung von 1.71 g radioaktiver und 2.61 g nicht radioaktiver 2,3-Dimethylcyclohexancarbonsäure **14** (insgesammt 27.7 mMol) in 15 ml Benzol gibt man 10.8 g (90 mMol) Thionylchlorid und kocht 2 Stunden unter Rückfluss. Man destilliert den Überschuss Thionylchlorid und Benzol ab und erhält bei der Destillation unter 25 Torr. ein Öl vom Siedep. 106—108 °C. Ausbeute 3.60 g (20.5 mMol, 74%). Zu einer Mischung von 3.60 g Säurechlorid **17** in 30 ml trocknem Benzol gibt man bei 20 °C unter Umrühren portionsweise 3.10 g (23 mMol) Aluminiumchlorid und erwärmt in einer Stunde bis auf 70 °C und lässt gleich danach die Mischung bis auf Raumtemp. abkühlen und über Nacht stehen. Man giesst die Mischung aufs Eis, schüttelt die Benzol-Lösung mit verd. Salzsäure, dann mit Natriumhydroxid. Aus der Benzol-Lösung erhält man bei Destillation under 0.05 Torr. ein Öl vom Siedep. 94—95 °C. Ausbeute 2.73 g (12.6 mMol, 62%). KMR in Tetrachlorkohlenstoff, δ 7.8 und 7.3 ppm (5H, m, aromatische H), 3.32 ppm (1H, m, cyclohexyl-1-C-H), 2.5—1.0 ppm (8H, m), 0.85 ppm (3H, d, J=6 Hz, CH_3), 0.56 ppm (3H, d, J=7 Hz, CH_3).

3,4-Dimethyl-2-oxo-hexamethylenimin-^{14}C ***(19)***: Nach der Methode von SNIA VISCOSA[6] löst man unter Umrühren 2.73 g (12.6 mMol) von **18** bei *ca.* 10 °C in 14 ml 90% Schwefelsäure, darauf gibt man bei 10—20 °C 1.05 g (15.1 mMol) Natriumnitrit in festem Zustand. Man erwärmt die Mischung allmählich bis auf 65 °C und hält 5 Stunden bei dieser Temp. Man giesst die Reaktionsmischung aufs Eis, zieht mit Äther die Carbonsäure und ebenso die schwerlösliche neutrale Substanz aus. Man neutralisiert die schwefelsäure-sauere wässer. Lösung mit Natriumhydroxid (*ca.* 18 g) bis zu pH 7.8 mit Kresolrot und gibt dazu ein Paar Tropfen 2 M Natriumcarbonat und schüttelt 6-mal mit je 30 ml Chloroform aus.

Der äther. Auszug gibt nach dem Waschen mit Soda-Lösung ein festes neutrales Produkt, ein rohes Laktam. Dieses rohes Produkt destilliert man zusammen mit dem aus der Chloroform-Lösung bei 0.2 Torr. und man bekommt ein Öl, das bei *ca.* 90 °C übergeht. Das Öl wird bald fest und schmilzt bei *ca.* 95 °C. Ausbeute 1.44 g (10.2 mMol, 81%). Nach mehrmaligem Umkristallisieren aus *n*-Hexan erhält man ein Produkt vom Schmp. 123—125 °C, 498 mg, wovon 463 mg zur weiteren Umsetzung gebracht wurde. Eine Analyse-Substanz gewinnt man nach weiterem Umkristallisieren, 19 mg vom Schmp. 124.5—126 °C. Gef. C 67.93, H 10.67, N 10.15%. Ber. für $C_8H_{15}ON$, C 68.04, H 10.71, N 9.92%. KMR in Tetrachlorkohlenstoff, δ 3.15 ppm (2H, m, CONHC-H_2), 2.7 ppm (1H, quartett, NHCOC-H).

2,3-Dimethyl-7-oxo-hexamethylenimin ***(20)***: Beim Umsetzen mit 3.61 g (16.8 mMol) von nicht radioaktivem Keton **18** wie oben beschrieben isoliert man 1.45 g rohes Produkt vom Schmp. 93—105 °C (**19**+**20**). Aus der Mutterlauge des Produktes erhält man nach mehrmaligem Umkristallisieren aus *n*-Hexan ein isomers Laktam vom Schmp. 65—67 °C, 57 mg. Gef. C 68.27, H 10.93, N 9.71%. Ber. für $C_8H_{15}ON$, C 68.04, H 10.71, N 9.92%. KMR in Tetrachlorkohlenstoff, δ 3.6 ppm (1H, quintett, CONHC-H), 2.3 ppm (2H, m, NHCOC-H_2).

1,2-Dimethyl-pentamethylendiamin-dibenzamid-^{14}C ***(21)*** *und Bariumcarbonat-*^{14}C ***(22)***: Man kocht 463 mg (3.27 mMol) von **19** mit 10 ml 5 M Salzsäure 7 Stunden unter Rückfluss (Dünnschicht-Chromatographie an Aluminiumoxid mit Essigester zeigte freie Aminosäure und deren HCl-Salz, aber kein Laktam). Nach dem Abdampfen unter vermindertem Druck versetzt man den Rückstand mit 3.2 g (32 mMol) Schwefelsäure und vertreibt Chlorwasserstoff bei 60 °C in Vak.

Man stellt eine Stickstoffwasserstoffsäure-Lösung in 10 ml Chloroform–5 ml Benzol her, durch Zutropfen von 1.00 g konz. Schwefelsäure (10 mMol) auf 1.3 g (20 mMol) Natriumazid–1.5 ml Wasser in Chloroform–Benzol-Mischung unter Ümrühren bei −5—+3 °C innerhalb 15 Min. Der Gehalt an Stickstoffwasserstoffsäure betrug 16 mMol.

Die Stickstoffwasserstoffsäure-Lösung wird bei 30—44 °C unter Ümrühren im Laufe von 40 Min. auf die Aminosäure-Schwefelsäure zugetropft, und die Mischung wird über Nacht bei 44 °C erwärmt. Das entwickelte Kohlendioxid leitet man durch eine Lösung 0.5 g Kaliumpermanganat—10 ml 0.5 M Schwefelsäure in die Alkali aus 4 ml 50% Natriumhydroxid-16 ml Kohlendioxid-freiem Wasser. Aus der alkali schen Lösung fällt man durch Zugabe von 100 ml 0.5 M Bariumchlorid-1.5 M Ammoniumchlorid 487 mg (2.47 mMol, 76%) Bariumcarbonat (**22**).

Die saure Reaktionsmischung wird in Vak. abgedampft und mit Wasser verdünnt. Durch Versetzen mit 3.45 g (86 mMol) Natriumhydroxid in 5 ml Wasser macht man alkalisch. Bei der Zugabe von 1.98 g (14 mMol) Benzoylchlorid bei 50 °C erhält man 0.76 g (2.25 mMol, 69%) rohes Dibenzamid vom Schmp. 141—146 °C, nach dem Umkristallisieren aus 40 ml Benzol-Essigester (1 : 2). Durch mehrmaliges Umkristallisieren gewinnt man eine Analyse-Substanz vom Schmp. 151—153 °C. Gef. C 74.31, H 7.66, N 8.43%. Ber. für $C_{21}H_{26}O_2N_2$, C 74.52, H 7.74, N 8.24%.

Triphenylcarbinol-^{14}C (***23***): In eine am Vakuum-System angeschlossene Ampulle fügt man 5 ml Phenylmagnesiumbromid-Lösung (7.38 mMol), dazu destilliert man Kohlendioxide aus 487 mg von **22** (2.47 mMol) und 5 ml konz. Schwefelsäure unter 0.01 Torr. ein, und schliesst die Ampulle in Vak. ab. Nach Stehenlassen über Nacht bei Raumtemp. versetzt man die Mischung mit verd. Salzsäure. Aus dem Soda-Auszug beim Ansäuern erhält man nur wenig Benzoesäure, aber aus dem neutralen Produkt isoliert man 532 mg (2.05 mMol, 84%) Triphenylcarbinol vom Schmp. 159—161 °C. Umkristallisieren aus Methanol gibt eine Analyse-Substanz vom Schmp. 161—162.5 °C. Sie zeigt bei der Mischprobe mit dem authentischen Triphenylcarbinol keine Schmelzpunkterniedrigung.

Literaturen

1) H. Plieninger und T. Suehiro, *Chem. Ber.*, **89**, 2789 (1956).
2) H. Plieninger, L. Arnold und W. Hoffmann, *Chem. Ber.*, **101**, 981 (1968).
3) J. G. Miller, *J. Org. Chem.*, **27**, 1549 (1962).
4) N. Fillpescu und J. W. Pavlic, *J. Amer. Chem. Soc.*, **92**, 6062 (1972).
5) H. Dahn und H. Hauth, *Helv. Chim. Acta*, **42**, 1214 (1959).
6) SNIA VISCOSA Ital. Pat. 604,795 (Mai 14. 1960), *Chem. Abstr.*, **55**, 19797f (1961).
7) Ref. R. M. Silverstein und G. C. Bassler, "Spectrophotometric Identification of Org. Compounds" 2nd Ed. John Wily & Sons, N. Y. (1967), NMR Spectroscopy Apendix B; K. Nakamura, O. Yamamoto, T. Suzuki, M. Takeuchi, und M. Ohnishi, *Anal. Chem.*, **35**, 1892 (1963).
8) E. E. Blaise und A. Courtor, *Bull. Soc. Chim. Fr.*, (3) **35**, 360, 589 (1906); Y. Yukawa und Y. Yokoyama, *J. Chem. Soc. Japan, Pure Chem. Sect.*, **82**, 259 (1961).
9) J. Kagan, D. A. Agdeppa, Jr. und S. P. Singh, *Helv. Chim. Acta*, **55**, 2252 (1972); J. Kagan und D. A. Agdeppa, Jr., *ibid.*, **55**, 2255 (1972).
10) J. N. Marx, J. C. Argyle und L. R. Norman, *J. Amer. Chem. Soc.*, **96**, 2121 (1974).
11) P. C. Hyhre, *J. Amer. Chem. Soc.*, **94**, 7921 (1972).
12) R. C. Hahn und D. L. Strack, *J. Amer. Chem. Soc.*, **96**, 4335 (1974).
13) J. D. Roberts, C. C. Lee und W. H. Saunders, Jr., *J. Amer. Chem. Soc.*, **77**, 3034 (1955) und ihre frühere Arbeiten.
14) C. Mystre, H. Frey, W. Voser und A. Wettstein, *Helv. Chim. Acta*, **39**, 734 (1956).
15) E. D. Bergman und R. Ikan, *J. Amer. Chem. Soc.*, **80**, 5803 (1958).

Photochemical Reactions between Dibromomaleic Anhydride and *N*-Phenylpyrrole[1]

Taku MATSUO and Satoru MIHARA

Department of Organic Synthesis, Faculty of Engineering, Kyushu University, Fukuoka 812

(Received April 28, 1975)

With the irradiation of dibromomaleic anhydride and *N*-phenylpyrrole, photosubstitution and photocyclization took place in succession to yield pyrrolo[1,2-a]quinoline-4,5-dicarboxylic anhydride as the final product. On the basis of energy-transfer experiments, both of the reactions were concluded to proceed *via* triplet species. Solvent effects were carefully examined and the presence of polar reaction intermediates was proposed to account for the solvent-dependent deactivation process.

The photoinduced addition between maleic anhydride and benzene is a well known example where charge-transfer complexes determine the course of photochemical reactions.[2] In the case of dibromomaleic anhydride and benzene homologues closely related to the above system, the irradiation of charge-transfer bands induced successive substitution of the two bromine atoms with phenyl groups, and further irradiation afforded phenanthrene-9,10-dicarboxylic anhydride as the final product.[3] Since the photochemical characteristic of dibromomaleic anhydride has not been reported, the mechanistic details of the reaction were investigated here by the use of *N*-phenylpyrrole, whose ionization potential is much lower than other benzene homologues.[4]

Results

Identification of the Reaction Products. After irradiation of dibromomaleic anhydride (**1**) and *N*-phenylpyrrole (**2**) with a high-pressure mercury lamp, the reaction mixture was treated with silica-gel column chromatography, and a crystalline material was obtained. On the basis of the spectroscopic data, the crystalline material was suggested to be 3-bromo-4-(*N*-phenyl-2-pyrryl)-2,5-furandione (**3**). On further irradiation, **3** was quantitatively converted to pyrrolo-[1,2-a]quinoline-4,5-dicarboxylic anhydride (**4**). The structure of **4** was deduced from the spectroscopic data and was verified by the fact that 5,6-benzopyrocholine (**5**) was obtained after the thermal decarboxylation. The overall reactions are summarized as follows:

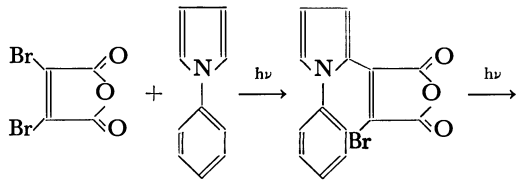

1 **2** **3**

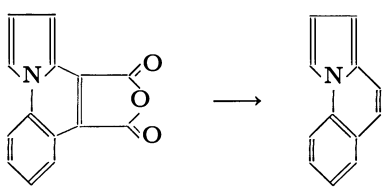

4 **5**

Quantum Yields. The absolute quantum yields for the formation of **3** (called photosubstitution hereafter) in benzene solution on direct excitation were determined by irradiating the sample solution with a collimated beam of monochromatic light (334 nm). The light intensity was determined by the use of a potassium ferrioxalate actinometer. Relative quantum yields in the presence of various additives were determined by the use of a modified merry-go-round irradiation apparatus. The irradiating light from a high-pressure mercury lamp was filtered through two layers of solutions around the lamp. The growth of **3** was monitored in each case by the change in optical density at the characteristic absorption band in the electronic spectra. The total conversion was never allowed to exceed 5%. The results are summarized in Table 1, where the triplet energy of each additive is also included. Biacetyl (E_T=55 kcal/mol) also was found to sensitize the reaction, although the quantum yield was not accurately determined due to the small extinction coefficient of biacetyl. No sensitization was observed with either pyrene (E_T=49 kcal/mol) or anthracene (E_T=42 kcal/mol). In the absence of additives, the quantum yields (Φ_p) depend on the concentration of **2**. A linear correlation between the inverse of the two quantities was observed, as discussed later (Fig. 1). In the case of photocyclization from **3** to **4**, the quantum yield on the direct excitation of **3** was strongly affected by the change in solvents, as shown in Table 2. The effect of additives on the photocyclization was also investigated. The reaction was sensitized in the presence of xanthone (E_T=74), benzophenone (E_T=69), phenanthrene (E_T=62), and pyrene (E_T=49 kcal/mol). Quenching of the reaction was observed, on the other hand, when acridine (E_T=

TABLE 1. QUANTUM YIELDS OF THE PHOTOSUBSTITUTION (Φ_p) IN THE PRESENCE OF VARIOUS ADDITIVES[a]

Additive	Triplet energy (kcal/mol)	Φ_p
None	53.5[b]	0.050
Sensitizer		
Xanthone	74[c]	0.064
Benzophenone	69[c]	0.065
Quencher		
Cyclooctatetraene[e]	<39[d]	0.042
Oxygen[f]	23[c]	0.039

a) The benzene solution containing **1** and **2** in equal amounts (5×10^{-3} M) was irradiated with 334 nm-light. b) See Ref. 5. c) See Ref. 6. d) See Ref. 7. e) 5×10^{-4} M. f) Air-saturated solution.

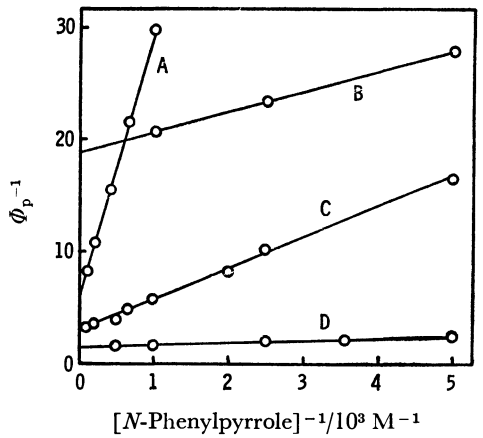

Fig. 1. Relationship between the quantum yield of **3** and the concentration of **2** in various solvents. A: Chlorobezene. B: Dichloromethane C: Diethyl ether. D: Carbon tetrachloride.

Table 2. Solvent effects on the quantum yield of the photocyclization of **3**[a] under irradiation with 436 nm-light

Solvent	Φ_p	Polarity parameter[b]
Carbon tetrachloride	0.23	32.5
Toluene	0.072	33.9
Benzene	0.070	34.5
Chlorobenzene	0.042	37.5
Diethyl ether	0.025	34.6
Dioxane	0.021	36.0
Ethylene chloride	0.009	41.9
Dichloromethane	0.007	41.1
Acetone	0.001	42.2
Acetonitrile	0.001	46.0

a) 6×10^{-5} M solutions. b) Dimroth's E_T-value. See Ref. 8.

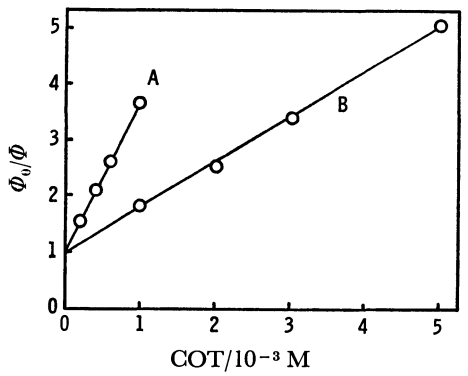

Fig. 2. Stern-Volmer plots of the reaction between **1** and **2** in dichloromethane. A: [**2**]$=2\times10^{-4}$ M. B: [**2**]$=1\times10^{-3}$ M.

45), anthracene ($E_T=42$), COT ($E_T<39$) and oxygen ($E_T=23$ kcal/mol) were present in the solution.

Quenching Studies. Since the photosubstitution reaction was quenched either by COT or oxygen as described above, the variation of the quantum yield was studied as a function of COT concentration. A typical example of a Stern-Volmer plot is shown in Fig. 2. The Stern-Volmer plot was invariably linear out to Φ_0/Φ values greater than 5. The quenching constant (K) was found to depend both on the concentration of **2** and also on the solvent, as summarized in Table 3. The photocyclization from **3** to **4** also gave nice Stern-Volmer plots, as shown in Fig. 3, for three different quenchers in benzene solutions. The lifetimes of the triplet state of **3** thus obtained in various solvents are summarized in Table 4.

Table 3. Quenching constants (K) for photosubstitution reaction under irradiation with 313 nm-light

Solvent	[**2**] (mM)	K (M^{-1})
Carbon tetrachloride	0.2	2600
	1.0	670
Diethyl ether	0.3	700
	3.0	220
Chlorobenzene	3.0	120
	10	60
Dichloromethane	0.2	2700
	1.0	620

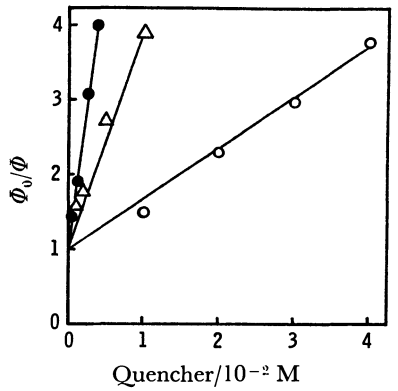

Fig. 3. Stern-Volmer plots of the photocyclization of **3** in the benzene solution (6×10^{-5} M). The reactions were quenched by the following additives (Q): COT (—●—), anthracene (—△—), and acridine (—○—).

Table 4. Quenching constants (K) and lifetimes (τ_0)[a] of the triplet species in the photocyclization of **3**[b] under irradiation with 436 nm light, when the reaction was quenched with COT

Solvent	K, M^{-1}	τ_0, s
Carbon tetrachloride	1.3×10^4	2.0×10^{-6}
Benzene	8.6×10^3	8.0×10^{-7}
Diethyl ether	5.2×10^3	9.0×10^{-8}
Dichloromethane	3.2×10^3	3.5×10^{-7}

a) The lifetime ($\tau_0=K/k_q$) is defined as the inverse of the sum of the rate constants for the radiationless decay and for the photocyclization of **3**. The k_q-value was estimated on the assumption that the quenching process is diffusion-controlled ($k_q=k_{diff}$), where the value for k_{diff} was obtained by the use of the following equation:

$$k_{diff}=\frac{8RT}{3000\,\eta}\ M^{-1}\,s^{-1}\ (20\ ^\circ C)$$

b) 6×10^{-5} M solutions.

Discussion

Photosubstitution Reaction. On the basis of both sensitization and quenching studies, the photosubstitution reaction is clearly concluded to proceed *via* a triplet state. Results of the sensitization experiment in Table 1 suggest that the energy of the triplet state lies between 49 and 55 kcal/mol. The triplet energy of **1**, on the other hand, has been estimated to be 53.5 kcal/mol by studying the phosphorescence spectra.[5] The experimental condition for the irradiation without any additive was adjusted so that **1** alone was selectively excited. Then, it is quite reasonable to suggest that the reactive species is the triplet state of **1**. One may suggest that a charge-transfer complex between **1** and **2** would be involved in the excitation. It is true that a charge-transfer band is observed on mixing **1** and **2**, and also irradiation of the charge-transfer band induces the same reaction as above.[9] On the basis of the equilibrium constant (0.1 m^{-1}), however, it is concluded that the concentration of the charge-transfer complex is too small to make any contribution to the excitation under the present experimental conditions. When the reaction was sensitized by benzophenone, the Φ_p-value is raised by 30% (Table 1). The experimental conditions were adjusted so that neither spontaneous decay or self-quenching of excited benzophenone effectively competed with the rate of quenching induced by **1**. In other words, the excitation energy of benzophenone is expected to be transferred to **1** without any loss. Then, the difference in Φ_p-values is taken to correspond to that in the intersystem-crossing efficiency between **1** and benzophenone. On the basis of these arguments, the intersystem-crossing efficiency in **1** is estimated to be close to 0.8. Then, the following reaction scheme is suggested to explain the above experimental observations. The presence of an associated species C is assumed here in order to take into consideration the deactivation process after the reactive triplet **1** encountered **2**. Essentially the same reaction schemes have been adopted to account for the photoreaction between acenaphthylene and 1,3-pentadiene,[10] and photodimerization of 2-cyclopentenone *etc.*[11] The relevant species, **1**, **2**, **3**, sensitizer, and quencher are denoted by A, D, P, S, and Q, respectively. Under the usual steady state assumption, the quantum yield for the photosubstitution is given by Eq. (10). In the absence of Q, a linear correlation between Φ_p^{-1} and $[D]^{-1}$ is expected to hold. This expectation was fulfilled, as shown in Fig. 1. The intercept and slope correspond to $(k_p+k_{-r})/(\Phi_{isc}\cdot k_p)$ and $k_{d-3}\cdot(k_p+k_{-r})/(\Phi_{isc}\cdot k_r\cdot k_p)$, respectively. Assuming the above estimated intersystem-crossing efficiency (0.8), one can evaluate a quotient, k_p/k_{-r}, as summarized in Table 5. Equations (12) and (13) indicate that the quenching constant (K) obtained from Stern-Volmer plots depends on the concentration of D. The lifetime of ^3A ($\tau_0=1/k_{d-3}$) and the rate constant k_r can be estimated from the K-values obtained at two different concentration of D. These results are summarized in Table 6, where k_{d-3}/k_r is also included. The values for k_{d-3}/k_r in Table 6 are in good agreement with those in Table 5. The agreement between the values obtained with two different methods may be taken to substantiate the proposed reaction scheme. The most important point in the reaction scheme is the presence of a deactivation step (Eq. (8)), which is suggested to take place after ^3A collides with D. The following argument affords

	Rate	
$A \xrightarrow{h\nu} {}^1A$	I_a	(1)
${}^1A \xrightarrow{k_{d-1}} A$	$k_{d-1}[{}^1A]$	(2)
${}^1A \xrightarrow{k_{isc}} {}^3A$	$k_{isc}[{}^1A]$	(3)
${}^3S + A \xrightarrow{k_e} S + {}^3A$	$k_e[{}^3S][A]$	(4)
${}^3A \xrightarrow{k_{d-3}} A$	$k_{d-3}[{}^3A]$	(5)
${}^3A + Q \xrightarrow{k_q} A + {}^3Q$	$k_q[{}^3A][Q]$	(6)
${}^3A + D \xrightarrow{k_r} C$	$k_r[{}^3A][D]$	(7)
$C \xrightarrow{k_{-r}} A + D$	$k_{-r}[C]$	(8)
$C \xrightarrow{k_p} P$	$k_p[C]$	(9)
$\frac{1}{\Phi_p} = \frac{1}{\Phi_{isc}}\cdot\frac{k_p+k_{-r}}{k_p}\cdot\left(1+\frac{k_{d-3}+k_q[Q]}{k_r[D]}\right)$		(10)
$\Phi_{isc} = k_{isc}/(k_{isc}+k_{d-1})$		(11)
$(\Phi_p)_0/(\Phi_p) = 1 + K[Q]$		(12)
$K = k_q/(k_{d-3}+k_r[D])$		(13)
$\tau_0 = 1/K_{d-3}$		(14)

Reaction scheme.

Table 5. Kinetic parameters for the photosubstitution estimated from the concentration dependence of the quantum yields in various solvents

Parameter	Solvents: Carbon tetrachloride	Diethyl ether	Chlorobenzene	Dichloromethane
k_{d-3}/k_r, M	8.2×10^{-5}	7.9×10^{-4}	4.6×10^{-3}	9.6×10^{-5}
k_p/k_{-r} [a]	2.9	0.57	0.31	0.07
Polarity parameter [b]	32.5	34.7	37.5	41.1

a) The intersystem crossing efficiency (0.8) was assumed in order to evaluate k_p/k_{-r} by the use of Eq. 10. b) Dimroth's E_T-value. See Ref. 8.

Table 6. Kinetic parameters for the photosubstitution obtained from the data of quenching experiments in various solvents

Parameters	Solvents: Carbon tetrachloride	Diethyl ether	Chlorobenzene	Dichloromethane
k_{d-3}, s^{-1}	7.0×10^5	4.0×10^7	4.2×10^7	1.0×10^6
k_r, $(M\cdot s)^{-1}$	9.3×10^9	4.3×10^{10}	9.3×10^9	2.3×10^{10}
k_{d-3}/k_r, M	7.5×10^{-5}	9.3×10^{-4}	4.5×10^{-3}	4.4×10^{-5}
τ_0, s	1.4×10^{-6}	2.5×10^{-8}	2.4×10^{-8}	1.0×10^{-6}
k_{diff}, $(M\cdot s)^{-1}$	6.7×10^9	3.7×10^{10}	8.1×10^9	1.5×10^{10}

further evidence in favor of the presence of C. The quantum yield of **3** in dichloromethane is less than that in carbon tetrachloride by a factor of 10. It is quite unlikely that Φ_{isc} for ^1A is appreciably different for the two solvents. The lifetime (τ_0) of ^3A is also practically the same for the two cases (Table 6). Then, it is most reasonable to suggest that deactivation takes place after the collision of ^3A and D but before the formation of P. The associated species C is thus included in the reaction schemes. The k_r-value in Table 6 is found to be practically the same as k_{diff} in each solvent. The corresponding value in the photoreaction of the 1,3-pentadiene-acenaphthylene system has been reported to be of the order of 10^4 M^{-1} sec^{-1}.[10] The k_r-values obtained in the photodimerizations of both 2-cyclopentenone and 2-cyclohexene also are of the order of 10^8 $M^{-1}sec^{-1}$.[11] This comparison in k_r clearly indicates that the collision between ^3A and D is extraordinarily effective for producing C. It should also be noted that the quotient k_p/k_{-r} decreases with the increase in solvent polarity, as estimated by Dimroth's E_T-values (Table 5). The associated species C is expected to be a type of donor-acceptor complex, since charge-transfer absorption is observed for the system containing **1** and **2** even in their ground states. It is well known that radiationless transitions of excited DA complexes are strongly enhanced in polar solvents.[12] Then, the decrease in the quotient k_p/k_{-r} is suggested to be due to the increase in k_{-r} in the polar solvent rather than to a decrease in k_p. In this connection, it should also be noted that the lifetime (τ_0) of ^3A in both diethyl ether and chlorobenzene is shorter than that in either dichloromethane or carbon tetrachloride (Table 5). This is also explained as due to the contribution of donor-acceptor interactions, since the former two solvent molecules are much better electron donors than the latter. In short, it is concluded that the photosubstition reaction proceeds *via* an associated species C, which is characterized as an electron donor-acceptor complex between **1** in the triplet state and **2** in the ground state.

Photocyclization. In the presence of COT as a quencher, Stern-Volmer plots of the photocyclization reaction from **3** to **4** followed a nice straight line until more than 75% of the reaction was quenched (Fig. 3). This reaction is sensitized by the additives with $E_T>$ 49 kcal/mol, but quenched by those with $E_T<45$ kcal/mol. Thus the reactive species in this reaction is concluded to be a triplet species with energy between 45 and 49 kcal/mol. The slope of Stern-Volmer plot decreased considerably when either anthracene ($E_T=$ 42 kcal/mol) or acridine ($E_T=45$ kcal/mol) was used as a quencher. The reduction in quenching efficiency may be explained as due to the contribution of back energy-transfer from these particular quenchers to **3**. On the basis of these observation, the energy of the reactive triplet is estimated to be close to 44 kcal/mol. The quantum yield for the formation of **4** varies considerably with the change in solvents, as summarized in Table 2. Two properties of the solvents appear to be effective in reducing the quantum yield: one is the polarity as given by Dimroth's E_T-value and the other is the electron-donating ability, as can be noticed in comparing Φ_p-values between carbon tetrachloride and toluene (or benzene) solutions. A similar trend was also observed for the lifetime of **3** in various solvents (Table 4). Then, the solvent effects on these two quantities are compared in Table 7, where the values in carbon tetrachloride are taken as the reference. Fairly good correspondence is observed as far as the values for the first three solvents are concerned. The values in dichloromethane indicate, however, that the effect on the cyclization is much larger than that on the lifetime. It is rather unlikely that either the intersystem-crossing efficiency or the rate of photocyclization of **3** is so strongly reduced as to explain sufficiently the large decrease in Φ_p in polar solvents given in Table 2. A better explanation will be that the photocyclization from **3** to **4** proceeds *via* a metastable intermediate, which may revert to **3** with a strongly solvent-dependent rate constant.

Table 7. Solvent effects on the photocyclization of **3**[a]

Solvent	Relative life-time of **3**	Relative Quantum Yield of **4**
Carbon tetrachloride	1.00	1.00
Benzene	0.40	0.31
Diethyl ether	0.05	0.11
Dichloromethane	0.18	0.03

a) 6×10^{-5} M solutions.

Experimental

Materials and Equipment. Solvents and sensitizers of guaranteed grade were each purified before use. The following compounds were synthesized according to the methods given in the references in parentheses: **1** (Ref. 13, mp 115—116 °C) and **2** (Ref. 14, mp 61—62 °C). The photoproducts were isolated by the use of column chromatography on silica gel (Mallinckrot, silic acid 100 mesh). The IR, NMR, mass, and electronic spectra were recorded on a JASCO DS-301, Varian A-60, JEOL JES-01SG, and Shimadzu UV-200 spectrometer, respectively.

*Photoreaction between **1** and **2** in Preparative Scale.* A dioxane solution (100 ml) containing **1** (1.3 g) and **2** (1.4 g) was internally irradiated with a high-pressure mercury lamp (Riko-Sha UVL-700P) equipped with a pyrex water jacket in nitrogen atmosphere for 8 hr. After the solvent, **1** and **2** were almost completely removed under reduced pressure, and then the residue was subjected to column chromatography. Elution with benzene–hexane mixture afforded **3** (670 mg) and **4** (10 mg). 3-Bromo-4-(*N*-phenyl-2-pyrryl)-2,5-furandione (**3**): mp 140—141 °C; IR (KBr) 1826 and 1759 (C=O), 1248 and 1237 (COC) cm^{-1}; UV (Dioxane): λ_{max} 233 (ε 14700) and 402 nm (11400); Mass, *m/e* 319 (M^+) and 317; NMR (Acetone): δ 6.57 (1H, q, 4-H), 7.16 (1H, q, 5-H), 7.44 (5H, m, C_6H_5), and 7.58 (1H, q, 3-H), $J_{3,4}=2.8$, $J_{3,5}=1.8$ and $J_{4,5}=4.0$ Hz. Found: C, 53.24; H, 2.58; N, 4.40%. Calcd for $C_{12}H_8BrNO_3$: C, 52.87; H, 2.54; N, 4.40%. Pyrrolo[1,2-a]-quinoline-4,5-dicarboxylic anhydride (**4**): mp 251—251.5 °C; IR (KBr): 1835 and 1769 (C=O), 1185 and 1190 (COC) cm^{-1}; UV(Dioxane): λ_{max} 241 (ε 26400), 288 (9210), 381 (4350) and 440 nm (5960); Mass, *m/e*

237 (M^+); NMR (DMSO): 6.6—8.6(m). Found: C, 70.39; H, 3.05; N, 5.74%. Calcd for $C_{12}H_7NO_3$: C, 70.89; H, 2.97; N, 5.90%.

Decarboxylation of **4**. Fifteen mg of **4** was dissolved into 0.5 ml of 5 M NaOH solution, and the solution was placed in a glass tube. Small amounts (0.1 g) of soda lime was added and the tube was heated above 300 °C under reduced pressure. Yellow crystal sublimed out of the tube and was identified as 5,6-benzopyrocholine (**5**)[15]: mp 107—108 °C; UV (acetonitrile): λ_{max} 226 (ε 31000), 242 (20000), 249 (22000), 263 (9800), 275 (7900), and 348 nm (6,400).

Determination of Quantum Yields. (A) Irradiation with a Collimated Beam: This method was used to determine the absolute quantum yield of both the photosubstitution (at 313 and 334 nm in benzene, and at 313 nm in carbon tetrachloride) and the photocyclization reactions (at 436 nm in benzene) without any sensitizer. The light source was a Ushio 500-W super-pressure mercury arc lamp (Ushio HB-5001B). Each monochromatic light was isolated by the use of the following combined filters: (1) 313 nm: Toshiba UV-D25 glass filter, window glass (1.5 mm), and a layer (5 cm) of nickel sulfate solution (1.05 M); (2) 334 nm: Toshiba UV-D25 glass filter, a layer (5 cm) of aqueous cupric nitrate (0.05 M), and a layer (5 cm) of aqueous solution containing nickel sulfate (0.19 M) and potassium chromic sulfate (0.015 M); (3) 436 nm: A layer (5 cm) of aqueous potassium nitrate solution (2.8 M) and a layer (5 cm) of cupric sulfate(0. 035 M) in 10% aqueous ammonium hydroxide solution. The sample solution was degassed and was placed in a cylindrical cell, which was irradiated with a collimated beam of the above described monochromatic light. After the irradiation, the amounts of photoproducts (**3** or **4**) were spectrophotometrically evaluated. The intensity of the monochromatic light was determined by the use of a potassium ferrioxalate actinometer.

(B) Irradiation of Sample Tubes Assembled on a Rotating Cylinder: The relative quantum yields in the energy-transfer experiments, the concentration dependence of the quantum yields, and the solvent effects were studied by the use of the following experimental set up. Sample solutions were appropriately prepared in each experiment, and were placed in a pyrex tube (10 mm inner diameter). The required number of sample tubes were fixed on the surface of a rotating cylinder (7.5 cm diameter), which rotated at a speed of approximately 100 rpm. The center of the rotating cylinder was located 13 cm away from the center of a 400 W high-pressure mercury arc lamp (Riko-Sha UVL-400 HA). The lamp was equipped with two coaxial, Pyrex jackets, which provided two layers of filter solutions (1 cm path length for each) surrounding the light source. The following filter solutions were used in order to irradiate the samples with the lights shown below: (1) 313 nm: An aqueous solution of potassium chromate (0.0025 M) and an aqueous solution containing nickel sulfate (0.95 M) and potassium chromic sulfate (0.075 M); (2) 334 nm: An aqueous solution of cupric nitrate (0.25 M) and an aqueous solution containing nickel sulfate (0.95 M) and potassium chromic sulfate (0.075 M); (3) 436 nm: An aqueous solution of potassium nitrite (14 M). The amount of photoproducts was determined by the use of the electronic absorption spectra.

References

1) Contribution No. 368 from the Department of Organic Synthesis, Faculty of Engineering, Kyushu University.
2) D. Brice-Smith, R. Deshpande, A. Gilbert, and J. Grzonka, *Chem. Commun.*, **1970**, 562.
3) T. Matsuo, Y. Tanoue, T. Matsunaga, and K. Nagatoshi, *Chem. Lett.*, **1972**, 709.
4) T. Matsuo and H. Shosenji, This Bulletin, **41**, 1068 (1968).
5) H. -D. Scharf, H. Leismann, and H. Lechner, *Chem. Ber.*, **104**, 847 (1971).
6) N. J. Turro, "Molecular Photochemistry," W. A. Benjamin, Inc., New York, N. Y. (1967), p. 132.
7) W. I. Ferree Jr. and B. F. Plummer, *J. Amer. Chem. Soc.*, **95**, 6709 (1973).
8) K. Dimroth, C. Reichardt, T. Siepmann, and F. Bohlmann, *Ann. Chem.*, **661**, 1 (1963); *ibid.*, **669**, 95 (1965).
9) The reaction kinetics could not be studied because the absorption band of the product overlapped with the charge-transfer absorption of the unreacted species.
10) W. I. Ferree Jr. and B. F. Plummer, *J. Amer. Chem. Soc.*, **95**, 6709 (1973).
11) P. J. Wagner and D. J. Buckeck, *ibid.*, **91**, 509 (1969).
12) R. M. Bowman, T. R. Chamberlain, C. W. Huang, and J. J. McCullough, *ibid.*, **96**, 692 (1974).
13) H. Shimonis, *Ber.*, **32**, 2084 (1899); B. Diels and M. Reinbeck, *ibid.*, **43**, 1271 (1910).
14) L. Lichtenstein, *ibid.*, **14**, 933 (1881); A. Truchan, U. S. 2809988 (1957); *Chem. Abstr.*, **52**, 4683c (1958).
15) E. M. Roberts, M. Gates, and V. Boekelheide, *J. Org. Chem.*, **20**, 1443 (1955).

Oxygen-accelerated Generation of the Bromocarbenoid Reagent of Zinc from Diethylzinc and Bromoform. Bromocyclopropanes from Olefins

Sotaro MIYANO and Harukichi HASHIMOTO

Department of Applied Chemistry, Faculty of Engineering, Tohoku University, Aramaki, Sendai 980

(Received May 6, 1975)

Oxygen greatly accelerates the generation of the bromocarbenoid reagent of zinc from diethylzinc and bromoform. Olefins, including cyclohexene, cyclooctene, 1-hexene, *cis*- and *trans*-2-butene, isobutene, and 2-methyl-2-butene were bromocyclopropanated in yields of *ca.* 60—85% using a diethylzinc–bromoform–oxygen system. The bromocarbenoid showed high *syn*-selectivity for the addition to cyclooctene and *cis*-2-butene. 9-Bromo-9-deutero[6.1.0]nonane was obtained from cyclooctene using $CDBr_3$. Styrene inhibited the formation of the bromocarbenoid reagent and polymerized under the reaction conditions, suggesting a free radical chain mechanism for the formation of the carbenoid reagent.

Monobromocyclopropanes have usually been obtained *via* the reduction of *gem*-dibromocyclopropanes, and numerous reducing agents have effectively been employed in the conversion.[1,2] Several bromocarbene[3] or bromocarbenoid[4] reagents have been reported, but useful methods for the direct synthesis of monobromocyclopropanes from olefins are only limited to those with less available reagents.[5,6] The Furukawa procedure for the cyclopropanation of olefins using the diethylzinc–polyhalomethane system[7] is applicable only to the polyhalomethanes which contain at least one iodine atom. Thus, dibromoiodoform was used for the synthesis of 7-bromonorcaranes from cyclohexene, but the preparation of the mixed haloform is not efficient.[8]

In the course of our investigation of the zinc-carbenoid reaction, we found that oxygen greatly accelerates the formation of the bromocarbenoid reagent of zinc from diethylzinc and bromoform.[9] In this report, a convenient synthesis of monobromocyclopropanes from olefins by means of the bromocarbenoid reagent is described.

Results and Discussion

Accelerating Effect of Oxygen on the Formation of 7-Bromonorcarane from Cyclohexene, Diethylzinc, and Bromoform. Table 1 shows the results of the reaction of diethylzinc and bromoform with cyclohexene. When the reaction was carried out in a nitrogen atmosphere, no apparent changes of the reaction mixture were observed after 6 hr at a reaction temperature of 50 °C, and a large amount of unchanged bromoform was recovered with the formation of 7-bromobicyclo[4.1.0]-heptanes (7-bromonorcaranes, **1**) in a poor yield (Run 1). On the other hand, by passing dry air at a rate of 10 ml/min into a space above the reaction mixture at room temperature, fuming occurred accompanying an exothermic reaction with the precipitation of white solids, and the reaction terminated within one hour with the complete consumption of the bromoform affording **1** in a fairly good yield (Run 3). The dilution of cyclohexene with *n*-hexane reduced the yield of **1** (Runs 4—8). Besides 3-ethylcycloheptene, small amounts of norcarane, cycloheptene, and 1,3-cycloheptadiene were also detected in the reaction mixture in a combined yield of less than 5%. In a previous paper, the authors reported the formation of these by-products during the iodocyclopropanation of cyclohexene with iodoform and diethylzinc.[10] The ratio of *syn*-**1** to *anti*-**1** decreased as the molar ratio of diethylzinc to bromoform increased, and *syn*-**1** appeared to react with the excess ethylzinc bromide present in the reaction mixture *via* a ring opening producing 3-ethylcycloheptene.[10] The reaction temperature is one of the important reaction variables. When the reaction was carried out in cyclohexene, a satisfactory yield of **1** was obtained with a $CHBr_3$/Et_2Zn molar ratio of *ca.* 1.2 at reaction temperatures from 0 to 10 °C (Table 2).

TABLE 1. REACTION OF DIETHYLZINC AND BROMOFORM WITH CYCLOHEXENE[a]

Run	Cyclohexene ml	Et_2Zn mmol	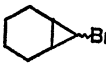 Yield[b], %	*syn*/*anti* ratio	Yield[b], %
1[c]	50	50	9.4	2.6	0
2[d]	50	50	52	1.3	6.1
3[e]	50	50	59	1.6	5.1
4[d]	10	14	18	1.8	0.2
5[d]	10	26	30	1.6	2.0
6[d]	10	37	36	1.6	3.5
7[d]	10	50	39	1.4	6.7
8[d]	10	70	32	1.1	12

a) Reactions were carried out in cyclohexene (Runs 1—3) and in 40 ml of *n*-hexane (Runs 4—8); $CHBr_3$, 50 mmol; 50 °C, 1—1.5 hr. b) Glc yield based on $CHBr_3$. c) In a nitrogen atmosphere, 6 hr. d) Dry air was introduced into the space above the reaction mixture at a rate of 10 ml/min during the reaction. e) The reaction was started at room temperature, and the temperature of the reaction mixture increased to 35—40 °C upon contact with air.

Bromocyclopropanation of Several Olefins. The accelerating effect of oxygen on the zinc-carbenoid reaction with diethylzinc and bromoform was utilized for the bromocyclopropanation of several olefins (Table 2). The yields of the products were determined by glc, and the reaction conditions were not necessarily optimum. Bromocylopropanes were separated by distillation and, if necessary, by preparative glc, and were confirmed by NMR spectral studies and elemental analyses. The results show that the $CHBr_3$–Et_2Zn–oxygen system provides a convenient route to mono-

Table 2. Bromocyclopropanation of several olefins with $CHBr_3$-Et_2Zn-oxygen[a]

Olefin	ml(or g)	$CHBr_3$ mmol	Et_2Zn mmol	Temp. °C	Bromocyclopropane yield[b], %	*syn*/*anti* ratio
Cyclohexene	35	35	28	0—10	84	1.9
1-Hexene	30	31	20	0—10	68	2.5
	50	50	50	50	42	2.4
Cyclooctene	30	31	20	0—10	75	7.1
	50	50	50	50	63	6.4
	20	12[c]	8	0—10	79[d]	6.9
2-Methyl-2-butene	20	30	20	0—10	61	e)
cis-2-Butene	15 g	30	20	0—10	85	*syn*[f]
trans-2-Butene	12 g	30	20	0—10	84	—
Isobutene	11 g	30	20	0—10	85	—
Styrene[g]	50	50	50	50	trace	e)

a) Reactions were carried out in olefins for 1—2 hr. b) Glc yield based on $CHBr_3$. c) $CDBr_3$. d) 9-Bromo-9-deuterobicyclo[6.1.0]nonane. e) Not determined. f) *anti* <1.5%. g) Reaction time, 8 hr.

bromocyclopropanes from some olefins (reaction 1).

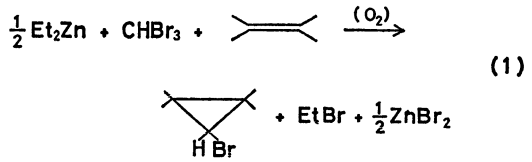

(1)

It is known that asymmetrical carbenes and carbenoids tend to add to substituted olefins producing sterically more hindered cyclopropanes (*syn*-isomer).[11] For example, Martel and Hiriart have reported that a *syn*/*anti* ratio of as high as 50 was obtained with the addition of the bromocarbenoid reagent formed from methylene bromide and potassium bis(trimethylsilyl)-amide to cyclooctene.[6b] The bromocarbenoid reagent of zinc also preferentially produced *syn*-isomers, and high *syn*-selectivity of the bromocarbenoid to *cis*-2-butene is noteworthy. The glc study showed the presence of less than 2% of the *anti*-isomer in the zinc-carbenoid reaction mixture. For comparison, the *anti*-isomer was obtained *via* the reduction of *gem*-dibromo-*cis*-2,3-dimethylcyclopropane with sodium bis-(2-methoxyethoxy)aluminum hydride (SAH) according to the method described by Sydnes and Skatteböl[12] (reaction 2).

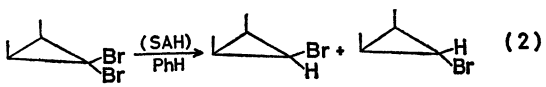

(2)

syn/*anti*=0.14

Deuterium labeling of the cyclopropane ring can easily be accomplished with $CDBr_3$ (reaction 3). It is obvious that higher isotopic purity is obtained and the deuterium source is utilized more effectively by this procedure than by conventional methods.[13]

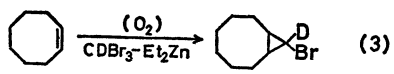

(3)

Reaction of Diethylzinc and Bromoform in Styrene. Upon treatment of diethylzinc and bromoform in styrene for 8 hr at 50 °C in a nitrogen atmosphere, no product ascribed to the carbenoid reaction was detected on the glc, and 91% of the bromoform was recovered unchanged. Even in the presence of oxygen, the carbenoid reaction scarcely occurred and the polymerization of styrene preceded (Table 2).

A free radical chain mechanism for the formation of the zinc-carbenoid reagent from diethylzinc and CH_2IX (X=Cl, I) is proposed.[14] Similar reaction paths may also occur for the diethylzinc–bromoform system on the basis of the accelerating effect of oxygen and the inhibiting effect of styrene on the formation of the bromocarbenoid reagent of zinc from diethylzinc and bromoform (reactions 4—7).

$$EtZnR \xrightarrow{\text{initiator}} \rightarrow Et\cdot \quad (4)$$

$$Et\cdot + CHBr_3 \longrightarrow EtBr + \cdot CHBr_2 \quad (5)$$

$$\cdot CHBr_2 + EtZnR \longrightarrow Et\cdot + Br_2HCZnR \quad (6)$$

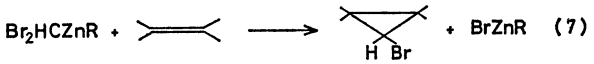

(7)

(R=Et or Br)

Experimental

The glc analysis was carried out on a Shimadzu GC 3AF apparatus equipped with hydrogen-flame detectors; three different stainless steel columns (3 m×3 mm) were used, packed with Diasolid M coated with Silicone DC 550, Silicone DC 410, and Apiezon Grease L, respectively. Preparative glc was carried out on a Shimadzu GC 2C apparatus with an Apiezon Grease L or Silicone DC 550 filled column. The infrared spectra were obtained with a JASCO Model IR-E spectrophotometer. The proton NMR data were obtained at 60 MHz with a Hitachi R-24A spectrometer or at 100 MHz with a Varian AHA-100 spectrometer. All the chemical shifts are given in units of δ relative to the internal TMS reference (*ca.* 1—5 wt% solution in CCl_4). Elemental analysis was performed at the Elemental Analysis Center, Chemical Research Institute of Nonaqueous Solutions, Tohoku University.

Materials. The bromoform was washed successively with water, dil. sodium hydrogen sulfite, and water, dried

over calcium chloride, and distilled twice in a nitrogen atmosphere (bp 69—70 °C/50 mmHg). Reagent grade commercial olefins were distilled over calcium hydride. The diethylzinc was distilled under reduced pressure. The materials were stored in nitrogen. The deuterobromoform (Merck Co., deuterium content>99%) containing no stabilizer was used without further purification. The nitrogen was purified by passage through a column packed with an activated Ni catalyst (Nikki Kagaku Co., Ltd., N 111 cat.) in a furnace at 130—140 °C followed by drying with silica gel.

Bromocyclopropanation of Olefins. The bromocyclopropanation of cyclohexene and *cis*-2-butene are representative. The reaction rate depended somewhat on the rate of the introduction of air and the stirring speed of the reaction mixture, but the yields of bromocyclopropanes and the *syn/anti* ratio were not so sensitive to these reaction variables as long as the reaction temperature was maintained within a given range.

*7-Bromonorcaranes (**1**)*: The reaction was carried out in a 200 ml round-bottomed flask equipped with a magnetic stirrer, a reflux condenser, a pressure-equilibrating dropping funnel topped with a gas inlet cock, and a thermometer. The flask was flushed with prepurified nitrogen. In the flask, 40 ml of cyclohexene and 5 ml (50 mmol) of diethylzinc were placed. The mixture was stirred, and then warmed to 50 °C. Bromoform (12.6 g, 50 mmol) dissolved in 10 ml of cyclohexene was dropped from the dropping funnel to the solution over a 10 min period in a nitrogen atmosphere. Dry air was introduced *via* the gas inlet cock into the space above the reaction mixture at a rate of 10 ml/min. Fuming was observed accompanying an exothermic reaction, and white solids precipitated for 0.5 hr, with the reaction continuing for another 0.5 hr. The reaction mixture was hydrolyzed with dil. hydrogen chloride, extracted with ether, and washed successively with dil. hydrogen chloride, dil. sodium hydrogen sulfite, dil. sodium hydrogen carbonate, and water. An aliquot of the solution was used for glc analysis. After the solution had been dried over anhydrous magnesium sulfate, ether and cyclohexene were removed by distillation *in vacuo*. The residue was fractionated through a short Vigreux column. A portion boiling at 70.5—71.3 °C/13 mmHg was collected (3.4 g) as a mixture of *syn*-**1** and *anti*-**1** in a *syn/anti* ratio of 1.5 (lit,[15] bp 78 °C/16 mmHg, *syn/anti*=2.5). The assignment of the *syn*- and *anti*-isomer was based on the assumptions described before.[10] Found: C, 48.29; H, 6.42%. Calcd for $C_7H_{11}Br$: C, 48.02; H, 6.33; Br, 45.65%. The NMR spectra were consistent with those of **1**:[16] H_7[17] for the *syn*-**1**, δ 3.24 (t, A_2X system, $J_{1,7}=7.5$ Hz); H_7 for the *anti*-**1**, δ 2.51 (t, A_2X system, $J_{1,7}=3.4$ Hz). The glc analysis of the reaction mixture indicated the presence of several by-products in small amounts, among which cycloheptene, norcarane, 1,3-cycloheptadiene, and 3-ethylcycloheptene were confirmed by a comparison of the retention times with those of authentic samples.[10]

*9-Bromobicyclo[6.1.0]nonanes (**2**)*: A mixture of diethylzinc (5 ml, 50 mmol) and bromoform (12.7 g, 50.4 mmol) was treated in 50 ml of cyclooctene at 50 °C. Distillation gave a portion boiling at 87—89 °C/4.5 mmHg (5.2 g) as a mixture of *syn*-**2** and *anti*-**2** in a *syn/anti* ratio of 5.1 (lit,[15] 40—42 °C/0.13 mmHg for *syn*-**2**[18]). Found: C, 53.23; H, 7.44%. Calcd for $C_9H_{15}Br$: C, 53.22; H, 7.44; Br, 39.34%. NMR: H_9 for the *syn*-**2**[19]; δ 3.20 (t, A_2X system, $J_{1,9}=7.3$ Hz). The *anti*-**2** showed an identical retention time on the glc with a freshly packed Silicone DC 550 or Silicone DC 410 column with that of authentic sample (*vide infra*), but it decomposed on preparative glc under the conditions necessary to resolve isomeric **2**.

9-Bromo-9-deuterobicyclo[6.1.0]nonanes: A portion boiling at 82—83 °C/4 mmHg (1.8 g) indicated a *syn/anti* ratio of 5.0. Found: C, 53.40; H+D, 7.51%. Calcd for C_9H_{14}-DBr: C, 52.95; H, 6.91; D, 0.99; Br, 39.15%. The NMR spectrum showed no absorption assigned to H_9.

*1-Bromo-2-*n*-butylcyclopropanes (**3**)*: A mixture of diethylzinc (5 ml, 50 mmol) and bromoform (12.6 g, 50 mmol) was treated in 50 ml of 1-hexene at 50 °C. Distillation gave a portion boiling at 73.5—74.2 °C/28.5 mmHg (2.4 g) as a mixture of *syn*-**3** and *anti*-**3** in a *syn/anti* ratio of 2.2. Found: C, 47.24; H, 7.38%. Calcd for $C_7H_{13}Br$: C, 47.48; H, 7.40; Br, 45.13%. Each isomer was separated by preparative glc. NMR for *syn*-**3**: δ 2.96 (1H, H_1, sextet-like, ABMX system, $J_{1,2}\approx J_{1,3(cis)}=7.4$ Hz,[20] $J_{1,3(trans)}=4.3$ Hz), 1.55—1.25 (6H, 3-CH_2-, br,), 1.15 (1H, $H_{3(cis)}$, octet-like), 1.0—0.7 (4H, Me+H_2, m), 0.48 (1H, $H_{3(trans)}$, octet-like, $J_{2,3(trans)}=5.6$ Hz, $J_{3(gem)}=6.1$ Hz. NMR for *anti*-**3**: δ 2.7—2.4 (1H, H_1, m), 1.5—1.1 (6H, 3-CH_2-, br), 1.1—0.8 (5H, Me+H_2+$H_{3(trans)}$, m), 0.8—0.6 (1H, $H_{3(cis)}$, m).

syn-*1-Bromo*-cis-*2,3-dimethylcyclopropane (**4**)*: The reaction was carried out in a pressure bottle of 100 ml inner volume equipped with a pressure-equilibrating dropping funnel of 50 ml volume. Into the bottle, 15 g of *cis*-2-butene was distilled, into which 2 ml (20 mmol) of diethylzinc was dissolved. The bottle was cooled in an ice-water bath, and bromoform (2.6 ml, 30 mmol) was added from the dropping funnel to the solution. Another pressure bottle of 140 ml volume containing oxygen at *ca.* 1.5 kg/cm^2 was connected to the reaction bottle through a needle valve and the reaction mixture was stirred for 2 hr. After the usual work-up, distillation gave a 2.7 g portion boiling at 124—125 °C which was composed of *syn*-**4** at a purity of *ca.* 90% contaminated with several unidentified impurities (lit,[3] bp 119—120 °C, *syn/anti*=30). Some decomposition was observed during distillation. Pure **4** was obtained by preparative glc. Found: C, 40.38; H, 6.22%. Calcd for C_5H_9Br: C, 40.29; H, 6.09; Br, 53.62%. NMR:[3] δ 3.25—3.05 (1H, H_1, m), 1.10—0.95 (8H, 2Me+H_2+H_3, m, rather sharp peak at δ 1.05). Detailed glc analysis showed he presence of only trace amounts of *anti*-**4** (*ca.* 1.5%) (*vide infra*) in the reaction mixture.

1-Bromo-trans-*2,3-dimethylcyclopropane*: Bp 64 °C/122 mmHg, yield 2.3 g. Found: C, 40.36; H, 6.35%. Calcd for C_5H_9Br: C, 40.29; H, 6.09; Br, 53.62%. NMR:[3] δ 2.66 (1H, H_1, dd, ABX system, $J_{1,2(trans)}=3.9$ Hz, $J_{1,3(cis)}=6.7$ Hz), 1.3—1.1 (6H, 2Me, t-like), 1.1—0.3 (2H, H_2+H_3, m).

1-Bromo-2,2-dimethylcyclopropane: Bp 55—55.5 °C/120 mmHg, yield 1.52 g. Found: C, 40.39; H, 6.20%. Calcd for C_5H_9Br: C, 40.29; H, 6.09; Br, 53.62%. NMR:[21] δ 2.74 (1H, H_1, dd, ABX system, $J_{1,3(trans)}=4.4$ Hz, $J_{1,3(cis)}=7.9$ Hz), 1.26 (3H, Me, s), 1.13 (3H, Me, s), 0.95 (1H, H_3, dd, $J_{3(gem)}=6.2$ Hz), 0.60 (1H, $H_{3(trans)}$, dd).

syn-*1-Bromo-2,2,3-trimethylcyclopropane (**5**)*: A portion boiling at 66.5—68 °C/70 mmHg contained *ca.* 15% complex by-products, and the *syn*-**5** was purified by preparative glc. Found: C, 44.45; H, 6.48%. Calcd for $C_6H_{11}Br$: C, 44.19; H, 6.80; Br, 49.01%. NMR:[3] δ 2.86 (1H, H_1, d, AX system, $J_{1,3}=7.2$ Hz), 1.3—0.9 (9H, 3Me, t-like), 0.9—0.3 (1H, H_3, m).

Reaction of Bromoform and Diethylzinc in Styrene. Dry air was introduced at a rate of 10 ml/min for 8 hr to a mixture of diethylzinc (5 ml, 50 mmol) and bromoform (12.6 g, 50 mmol) in 50 ml of styrene at 50 °C. The reaction mixture was worked up as usual. Glc analysis showed the presence of 74% of unchanged $CHBr_3$ and only traces of the carbenoid

reaction products. After the bulk of the styrene and unchanged $CHBr_3$ were distilled off *in vacuo*, 18.0 g of a pale yellow resinous material remained, which was dissolved in 20 ml of benzene and precipitated with 700 ml of methanol affording 12.4 g of polystyrene as a white powder. The IR absorption spectra (KBr pellet) of the precipitate was identical with those of polystyrene film. NMR: δ 7.4—6.8 (br) and 6.8—6.2 (br) (5H, benzene ring), 2.3—0.6 (br) (3.18H).

*Reduction of 9,9-Dibromobicyclo[6.1.0]nonane (**6**) with Sodium Bis(2-methoxyethoxy)aluminum Hydride (SAH).*[12] The **6** was prepared by a method analogous to that described by Dale and Swartzentruber[22] (bp, 109.5—111.5 °C/3.5 mmHg, lit,[23] bp 45 °C/0.15 mmHg). To a solution of **6** (5.64 g, 20 mmol) in 10 ml of benzene was added a 2 molar amount of SAH as a 70% solution in benzene (12 ml) which was refluxed for 3 hr. After the usual work-up, distillation of the reaction mixture gave a portion boiling at 78 °C/3 mmHg (0.9 g) which consisted of a mixture of *syn*-**2** and *anti*-**2** in a *syn*/*anti* ratio of 0.24. The NMR spectrum of the H_9 of *anti*-**2** appeared at δ 2.5—2.0 as a multiplet.[16]

*Reduction of 1,1-Dibromo-*cis*-2,3-dimethylcyclopropane (**7**) with SAH.* The **7** was prepared by a treatment of bromoform (9.0 ml, 0.104 mol) and *tert*-BuOK (prepared from 4 g of K) in *cis*-2-butene (*ca.* 30 ml) and *n*-hexane (30 ml) in a pressure bottle at 0—5 °C overnight, bp 55 °C/20.5 mmHg, yield 13.8 g. Treatment of **7** (7.3 g, 31 mmol) with a 2 molar amount of SAH in benzene gave 0.9 g of a mixture of *syn*-**4** and *anti*-**4** in a *syn*/*anti* ratio of 0.16, bp 63.5 °C/122.5 mmHg. NMR for the *anti*-**4**:[3] δ 2.3—2.1 (1H, H_1, m), 1.3—1.0 (8H, $2Me+H_2+H_3$, m).

References

1) J. T. Groves and K. W. Ma, *J. Amer. Chem. Soc.*, **96**, 6527 (1974), and references cited therein.

2) R. M. Blankenship, K. A. Burdett, and J. S. Swenton, *J. Org. Chem.*, **39**, 2300 (1974).

3) G. L. Closs and J. J. Coyle, *J. Amer. Chem. Soc.*, **87**, 4270 (1965).

4) a) M. E. Volpin, D. N. Kursanov, and V. G. Dulova, *Tetrahedron*, **8**, 33 (1960); b) W. L. Dilling and F. Y. Edamura, *J. Org. Chem.*, **32**, 3492 (1967); c) W. L. Dilling and F. Y. Edamura, *Tetrahedron Lett.*, **1967**, 587; d) O. M. Nefedof, A. A. Ivashenko, M. N. Manakov, V. I. Shiryaev, and A. D. Petrov, *Izv. Akad. Nauk SSSR, Otd. Kim. Nauk*, **1962**, 367; *Chem. Abstr.*, **57**, 11041 g (1962).

5) D. Seyferth, H. D. Simmons, Jr., and G. Singh, *J. Organometal. Chem.*, **3**, 337 (1965).

6) a) B. Martel and J. M. Hiriart, *Angew. Chem. Internat. Edit. Engl.*, **11**, 326 (1972); b) B. Martel and J. M. Hiriart, *Synthesis*, **1972**, 201.

7) N. Kawabata, S. Noda, and S. Yamashita, This Bulletin, **45**, 2580 (1972), and references cited therein.

8) J. Nishimura and J. Furukawa, *Chem. Commun.*, **1971**, 1375.

9) A preliminary account: S. Miyano, Y. Matsumoto, and H. Hashimoto, *Chem. Commun.*, **1975**, 364.

10) S. Miyano and H. Hashimoto, This Bulletin, **47**, 1500 (1974).

11) a) R. Hoffmann, C. C. Levin, and R. A. Moss, *J. Amer. Chem. Soc.*, **95**, 629 (1973); b) T. Fueno and S. Nagase, *Kagaku no Ryoiki*, **26**, 441 (1972).

12) L. Sydness and L. Skatteböl, *Tetrahedron Lett.*, **1974**, 3703.

13) *cf.* Ref. 2.

14) S. Miyano and H. Hashimoto, This Bulletin, **46**, 892 (1973); **46**, 1895 (1973).

15) D. Seyferth, H. Yamazaki, and D. L. Alleston, *J. Org. Chem.*, **28**, 703 (1963).

16) C. L. Osborn, T. C. Shields, B. A. Shoulders, C. G. Cardenas, and P. D. Gardner, *Chem. Ind.* (London), **1965**, 766.

17) H_n indicates a proton attaching to the carbon at the *n*-position.

18) *cf.* Sydness and Skatteböl have claimed that the tributyltin hydride reduction of **6** afforded a mixture of **2** in a *syn*/*anti* ratio of 6.7.[12]

19) M. S. Baird and C. B. Reese, *J. Chem., Soc. C*, **1969**, 1803.

20) $H_{3(cis)}$ and $H_{3(trans)}$ indicate the protons *cis* and *trans* to H_1, respectively.

21) *cf.* Closs and Coyle assigned the $H_{3(cis)}$ to the signal at τ 9.39 and the $H_{3(trans)}$ to that at τ 9.05.[3]

22) W. J. Dale and P. E. Swartzentruber, *J. Org. Chem.*, **24**, 955 (1959).

23) P. D. Gardner and M. Narayana, *ibid.*, **26**, 3518 (1961).

Photochemical *cis-trans* Isomerization of 2,4,5-Triphenylimidazolines[1]

Teruo MATSUURA and Yoshikatsu ITO

Department of Synthetic Chemistry, Faculty of Engineering, Kyoto University, Sakyo-ku, Kyoto 606

(Received May 16, 1975)

Irradiation of *cis-* (amarine; I) and *trans-* (isoamarine; II) 2,4,5-triphenylimidazolines in acetonitrile or benzene gave a photostationary mixture of *cis-* and *trans*-isomers, the latter predominating over the former. On irradiation in a dilute acetone solution under the conditions that acetone absorbed most of the incident light, *cis-trans* isomerization occurred only with isoamarine but not with amarine. In acetone, 2,4,5-triphenylimidazole (III) was also formed. Two kinds of intermediate species for the *cis-trans* isomerization were proposed; imidazolinyl radicals IV and/or V formed by hydrogen abstraction with the excited state of acetone (in acetone) and a biradical or a zwitterionic species VIa formed by cleavage from the excited state of I or II (in acetonitrile or benzene). Evidences for the intermediacy of VIa are presented.

In a previous paper,[2] it has been shown that imidazolines, on irradiation in acetone solutions, are dehydrogenated to give the corresponding imidazoles *via* imidazolinyl radicals which are formed by hydrogen abstraction with excited acetone. In the course of this investigation 2,4,5-triphenylimidazolines, amarine (I; *cis*) and isoamarine(II; *trans*), were found to undergo *cis-trans* isomerization simultaneously with dehydrogenation to 2,4,5-triphenylimidazole(III; lophine). Since such a type of *cis-trans* isomerization in heterocyclic systems appeared relatively rare,[3] the photochemical *cis-trans* isomerization of I and II was examined in some details.

Results and Discussion

cis-trans *Isomerization of I and II under Various Conditions.* Amarine(I) and isoamarine(II) were irradiated with a 100 W high-pressure mercury lamp (Pyrex) or a 10 W low-pressure mercury lamp (Vycor, mainly 2537 Å) under bubbling nitrogen in various solvents at different concentrations. The results are summarized in Table 1. The material balance of the photoreaction induced by Pyrex-filtered light was considerably good, and products other than I, II and lophine (III) were obtained only in small yields (*vide infra*).

In acetonitrile, no lophine (III) was formed and a photostationary mixture of I and II with predominance of the thermodynamically more stable isomer II was obtained from either I or II. Piperylene, a triplet quencher, failed to quench the *cis-trans* isomerization at various concentrations (Table 2), indicating that the excited state responsible for the isomerization may be singlet or short-lived triplet, provided that the triplet energies of I and II exceed that of piperylene.

In benzene, which is known as a triplet sensitizer except a few exceptional cases,[4] only a trace of III was detected and the photostationary mixture of I and II was obtained in the similar ratio to that in acetonitrile. Both I and II were found to isomerize at such a low concentration (0.17×10^{-2} M) that more than 99% of the incident light was absorbed by benzene. It was also found that the II/I ratio in the isomerization of I in benzene decreased with increase in the amount of added piperylene (Table 3), possibly due to partial quenching of the benzene triplet. These results suggest that the *cis-trans* isomerization of I and II may take place at least partly from their short-lived triplet state.

In acetone, lophine (III) was always formed to a

TABLE 1. PHOTOCHEMICAL *cis-trans* ISOMERIZATION OF AMARINE AND ISOAMARINE IN VARIOUS SOLVENTS

Solvent	Starting material	Concn ($\times10^2$ M)	Light source[a]	Irradn time (hr)	II/I ratio	Yield (%) III	Yield (%) I+II
MeCN	I	3.14	B	24	1.8	0	61
	II	3.12	B	24	1.6	0	63
	I	1.77	A	8	2.3	0	96
	II	1.71	A	8	2.3	0	93
C_6H_6	I	3.45	A	15	1.6	trace	96
	I	0.172	B	3	1.6	trace	n. d.[b]
	II	0.168	B	3	1.4	trace	n. d.
Me_2CO	I	3.55	B	24	0.60	35	41
	I	3.27	A	15	0.46	21	74
	I	0.0282	A	1	0	29[c]	n. d.
	II	3.62	B	24	0.59	28	43
	II	0.0302	A	1	~0[d]	19[c]	n. d.
Me_2CHOH	I	3.54	A	15	3.0	0	95
Et_2O	I	1.36	A	15	1.8	trace	n. d.

a) A: high-pressure mercury lamp (Pyrex), B: low-pressure mercury lamp (2537 Å). b) Not determined.
c) Determined after 30 min irradiation. d) II/I ratio is 0.43 after 0.5 hr, 0.083 after 1 hr.

Table 2. Quenching of excited I with piperylene in acetonitrile[a)]

Piperylene added(M)	0	0.0604	0.12	0.179	0.237	0.295	0.573
III/I ratio[b)]	0.24	0.31	0.33	0.30	0.27	0.26	0.27

a) Initial concentration of I: 2.05×10^{-2} M. Light source, irradiation time, and temperature: 450-W high pressure mercury lamp (Pyrex), 3 hr, and 30±1 °C, respectively. b) Irradiation of I without piperylene showed that the value of II/I ratio increased almost linearly with increased irradiation time in the earlier stage of photolysis.

Table 3. Quenching experiment with piperylene in benezene[a)]

Initial concentrations[b)] of I ($\times10^3$ M)	1.71	1.87	1.72
Piperylene added(M)	0	0.0421	0.633
II/I ratio	1.6	1.4	0.8

a) Light source: 10-W low pressure mercury lamp (Vycor). Irradiation time: 3 hr b) At these concentrations of I, more than 99% of the incident light is absorbed by benzene.

considerable extent regardless of the light sources, and the *cis-trans* isomerization was found to be dependent on the initial concentration of I and II. At low concentrations (*ca.* 3×10^{-4} M), at which more than 99% of the incident light was absorbed by acetone, the isomerization occurred only from isoamarine(II) toward amarine(I) but not from I toward II. At high concentrations (*ca.* 3.5×10^{-2} M), at which about 50% of the incident light was absorbed by acetone, either I or II afforded a photostationary mixture of I and II with predominance of I over II in contrast to the case in acetonitrile and in benzene. These results obviously indicate that the mechanism of the *cis-trans* isomerization in acetone solution is different from that in acetonitrile or benzene solution.

In the course of our study on the photochemical dehydrogenation of imidazolines to imidazoles in acetone,[2)] it has been shown that excited acetone can abstract a hydrogen atom at 4- or 5-position of imidazolines to yield imidazolinyl radicals IV and/or V and the acetone ketyl radical, and that the resultant imidazolinyl radical can be led either to the original imidazolines, a hydrogen atom being supplied by the acetone ketyl radical, or to the corresponding imidazoles. It is, therefore, quite reasonable to suppose that the photochemical *cis-trans* isomerization of I and II in dilute acetone solutions accompanied with dehydrogenation of both I and II to III proceeds through the imidazolinyl radicals IV and/or V as depicted in Scheme 1 (A).[2)] The completely stereoselective isomerization toward I in dilute acetone solutions must require that the hydrogen transfer from the acetone ketyl radical to the imidazolinyl radicals IV and/or V occurs only in the direction toward the thermodynamically less stable isomer I but not toward II. The result implies that the *cis-trans* isomerization of I or II from their excited states does not sensitized by acetone; in other words the acetone triplet acts only as a hydrogen

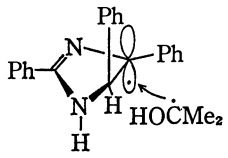

IV

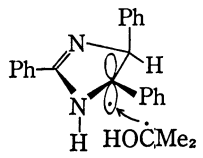

V

A (in dilute acetone solution)

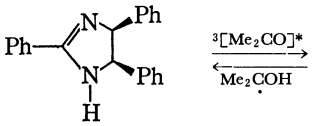

I

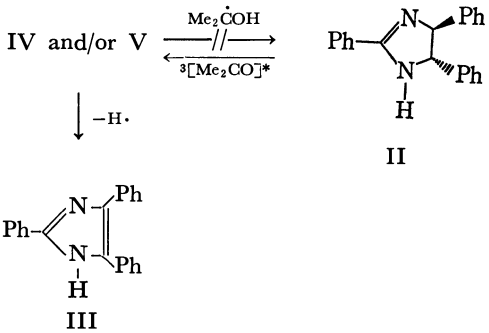

II

III

B (in acetonitrile or benzene)

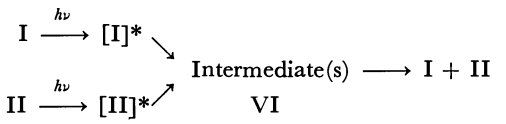

VI

Scheme 1.

transfer agent but not as a donor of excitation energy. The acetone ketyl radical may attack IV and/or V predominantly from the opposite side of a bulky phenyl group as shown below. At high concentrations of I and II in acetone, *cis-trans* isomerization through a common intermediate(s) (VI) from their excited states as in acetonitrile or benzene [Scheme 1 (B)] is possibly competing with *cis-trans* isomerization *via* the imidazolinyl radicals. Thus, it is reasonably explained that the II/I ratio observed at higher concentrations in acetone is smaller than that observed in acetonitrile or benzene. It should be noticed that these two processes shown in Scheme 1 provide a typical example of kinetically (A) and thermodynamically (B) controlled *cis-trans* isomerizations, and that reaction A provides an additional example of the so-called chemical sensitization.[4a)]

Irradiation of I in isopropyl alcohol or ether under the similar conditions also resulted in the *cis-trans* isomerization with predominance of II over I.

The Nature of the Intermediate VI. It seems reasonable to assume a homolytic or a heterolytic bond cleavage of ring bonds (VIa, VIb, VIc or VId) as the intermediate step of *cis-trans* isomerization in acetonitrile or benzene. Other pathways involving migration of 4-hydrogen (VIe or VIf[5)]) are also possible

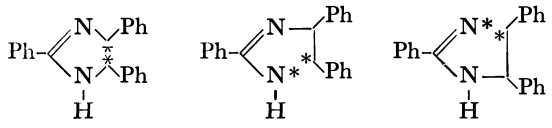

VIa VIb VIc

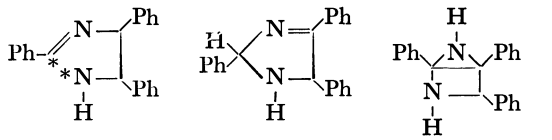

VId VIe VIf

*=· or +, −

although less probable because of the following reasons. If 1,3-hydrogen shift occurs stepwise and homolytically in the process, I (or II)⇌VIe, the imidazolinyl radical IV must be transiently formed and consequently lophine (III) must be formed concurrently. Since III was unable to be detected among the products at least in acetonitrile, the 1,3-hydrogen shift, if it occurs, should proceed concertedly in a suprafacial manner[6] and should not result in *cis-trans* isomerization *via* the intermediary formation of VIe. The intermediate VIf also has the difficulty in explaining the results that deuterium incorporation is very inefficient during irradiation of I in acetonitrile–D_2O (below 1.9% after over the half of I employed isomerized into II).

Among possible biradical or zwitterionic intermediates (VIa—VId), VIa is the most plausible one in view of bond dissociation energy data for similar types of bonds : $PhCH_2$—CH_2Ph (45—48 kcal/mol)[7] and $PhCH_2$—$NHCH_3$ (58 kcal/mol).[8] The bond dissociation energy data for –C=N—C< and –N—C=N– bonds are not available, but they may have a higher value than those for other bonds in the imidazoline ring considering the less resonance-stabilized nature of >C=N· or ·C=N– radical. The photochemical homolytic cleavage of C–C bonds has been recently reported.[3,9] Furthermore, the hetrolytic cleavage to generate VIa has some analogy to that of azirines[10] and 2,3-dihydropyrazines.[11]

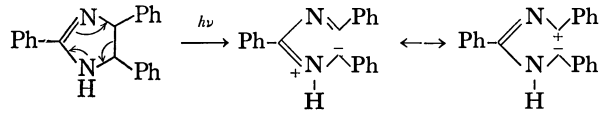

I or II VIa

Compare with

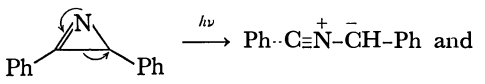

and

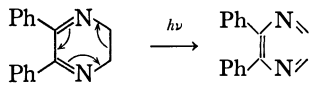

In order to see whether the rupture of C_4–C_5 bond of I or II (VIa) occurs, it was attempted to isolate by-products, which may be formed from the plausible intermediate VIa, and also to trap VIa by radical scavengers such as *n*-butyl mercaptan,[12] oxygen, and 2,2,6,6-tetramethylpiperidine-1-oxyl[13] and by the solvent isopropyl alcohol.[9a]

Amarine (I) was irradiated in acetonitrile with light through Pyrex to give a mixture of products from which *trans*-2,3,5,6-tetraphenyl-2,3-dihydropyrazine (VII, 2%) was isolated by chromatography. In addition, 2,3,5,6-tetraphenylpyrazine (VIII), which was probably formed by autoxidation of VII[14b] during work-up, was detected on tlc. A small amount (1—2%) of lophine (III) was also obtained in this case. Since VII and VIII are known to be formed photochemically from 2,3-diphenyl-2*H*-azirine (IX),[14] it is reasonably assumed that IX is an intermediate in the transformation of I into VII. The formation of IX can be rationalized by fragmentation of I or II through the intermediate

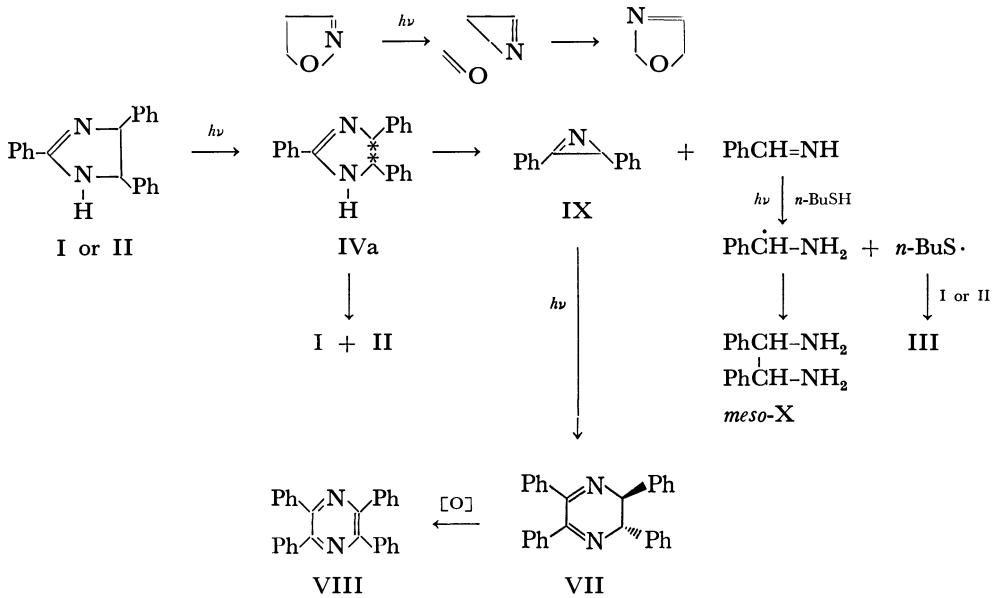

Scheme 2.

VIa (Scheme 2), similar to that of 2-isoxazolines to give an azirine and a carbonyl compound which recombine to form 3-oxazoline.[15]

Attempts for trapping VIa with 1-butanethiol (0.38 M in acetonitrile), 2,2,6,6-tetramethylpiperidine-1-oxyl (0.127 M in benzene), and the solvent isopropyl alcohol were unsuccessful. However, irradiation (Pyrex) of I in acetonitrile in the presence of 1-butanethiol afforded VII(2%), VIII (3%), III(48%), I(17%), II(9%) and *meso*-stilbenediamine (X, 2%). The last compound X appears to be a product derived from benzaldimine, the counterpart of IX (Scheme 2). Photoreductive dimerization of imines with a suitable hydrogen donor is well-known.[16] The formation of a large amount of III may be attributed at least partly to hydrogen abstraction with the 1-butanethiyl radical.[17]

It is worthwhile to mention about the preliminary results of photolysis of *cis*-2,4,5-triphenyloxazoline(*cis*-XI). Upon photolysis (2537 Å) *cis*-XI afforded its *trans*-isomer (14%) and benzaldehyde. It should be noticed that this reaction is also explained by cleavage of the C_4–C_5 bond in the first step. If the O_1–C_2 bond is first broken, benzonitrile must be formed considering the photofragmentation of 2-isoxazolines.[15]

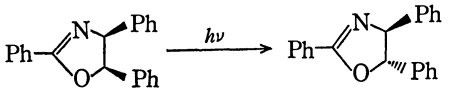

cis-XI *trans*-XI

+ PhCHO + unidentified product(s)

The formation of VII may be rationalized by other mechanisms (Scheme 3). The pathways a and b were eliminated by the fact that photolysis of lophine(III) or a mixture of III and *dl*-stilbenediamine did not yield even a trace of VII and VIII. The pathway c, which must involve complex reactions, is also improbable, because the photolysis of I in acetonitrile in the presence of a small amount of benzaldehyde resulted in the decrease (less than 1%) of yields of VII and VIII. And a new product, which was assigned as oxaziridine XII (2% yield) on the basis of spectral data and an independent synthesis, was obtained in addition to I and II.

Irradiation (Pyrex) of I in acetonitrile under bubbling oxygen gave *N*,*N*′-dibenzoylbenzamidine (XIII, 43%),

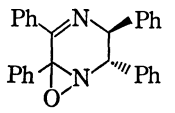

XII

N-benzoylbenzamidine (XIV), dibenzamide (XV) (the total yield of XIV and XV is 16%) and II (13%). At first glance, the oxidation of I to XIII appeared to proceed *via* trapping of the intermediate VIa by oxygen. It is, however, known[18,19] that the photochemical oxidation of III produces a lophine hydroperoxide (XVI), which decomposes gradually to XIII. In the present photooxidation of I, neither III nor XVI could be detected (tlc). But, at low temperature (−78 °C) at which the intermediate XVI is known to be stable and to be accumulated as the primary photooxidation product of III,[18] I resisted to photooxidation and only underwent *cis-trans* isomerization. Therefore, it can not be unambiguously known whether XIII, XIV, and XV were formed *via* VIa.

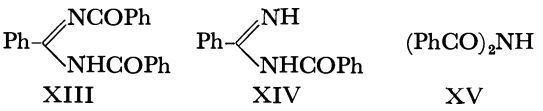

XIII XIV XV

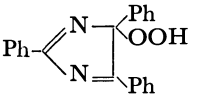

XVI

In conclusion, the *cis-trans* isomerization of I and II, the bond energy data, the isolation of VII and X, and the photoproducts of *cis*-XI are well accommodated by a mechanism involving the scission of C_4–C_5 bond. The result of photochemical oxidation of I is not inconsistent with this mechanism.

Experimental

All the melting points are uncorrected. NMR spectra were taken on an NEVA T-60 spectrometer with tetramethylsilane as the internal standard. IR and UV spectra were measured on a JASCO IRS spectrophotometer, and on a MODEL ORD/UV-5 Japan Spectrometer, respectively. Column chromatography was carried out with Mallinckrodt silica gel (100 mesh) as the adsorber. Thin layer chromatography (tlc) was carried out with Merck Kieselgel GF_{254} using UV

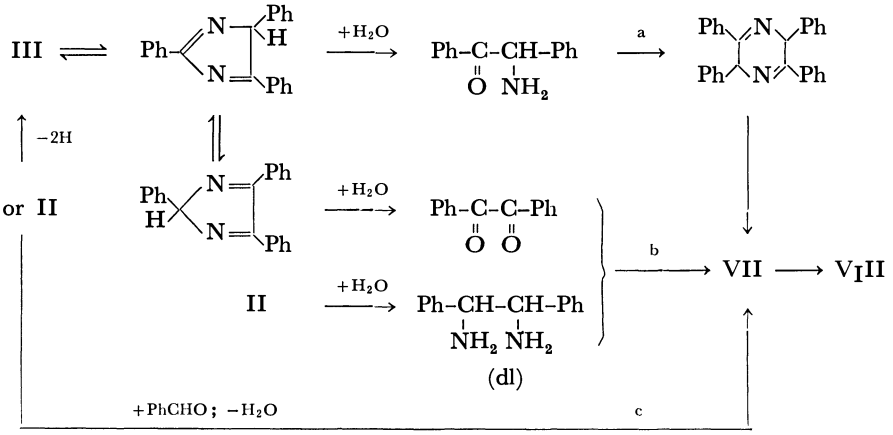

Scheme 3.

light and iodine for compound detection. Synthesis of amarine (I) and isoamarine (II) has been described.[2] All the solvents were distilled before use.

cis-trans *Isomerization of I and II under Various Conditions (Table 1).* A solution of I or II dissolved in a solvent, 110 ml when a 100-W highpressure mercury lamp (Pyrex filter) was used, 220 ml when a 10-W lowpressure mercury lamp (Vycor filter, mainly 2537 Å) was used, and 500 ml (acetone) for low concentration experiments, was irradiated several hours under bubbling nitrogen. After evaporation of the solvent under reduced pressure, the residue was subjected to NMR analysis (CCl_4–DMSO-d_6) and the II/I ratio was determined from the peak intensities of singlets at τ 4.55 for I and τ 5.10 for II. The yields of lophine (III) and recovered imidazolines (I+II) were determined by UV analysis (EtOH) and NMR analysis (CCl_4+DMSO-d_6; pinacol or 2-methylimidazoline as the internal standard), respectively. In solvents except acetone, none or a trace of III was detected by careful tlc analysis.

Quenching of the cis-trans *Isomerization of I.* Pyrex tubes (volume 20 ml) containing a fixed amount of I and freshly distilled piperylene (bp 45—47 °C) in acetonitrile were sealed after bubbling nitrogen through the solution and irradiated externally on a merry-go-round apparatus. After removing the solvent and the piperylene under reduced pressure, the II/I ratio was determined by NMR technique (Table 2).

The results of Table 3 were obtained by irradiating a fixed amount of I and piperylene in benzene (220 ml) under bubbling nitrogen and then by determining the II/I ratio by NMR spectroscopy.

Isolation of Byproducts and Experiments to Trap VIa in the cis-trans *Isomerization of I.* All irradiations were done with a 100-W high pressure mercury lamp (Pyrex filter) under bubbling nitrogen, unless otherwise specified. The photoproducts obtained after removing the solvent under reduced pressure were separated and characterized in the following way.

A) Isolation of Byproducts. The product mixture (after 17 hr irradiation)[20] from a solution of I (1.17 g) in acetonitrile (110 ml) was chromatographed on silica gel (40 g). Elution with 200 ml of 1 : 1 benzene–chloroform gave 12 mg of a solid which contained a trace of 2,3,5,6-tetraphenylpyrazine (VIII) (tlc). Further elution with 400 ml of the same solvent, followed by preparative tlc, afforded 35 mg (2%) of VII identified by IR, NMR, and tlc and 15 mg (1—2%) of III identified by IR and tlc. Further elution with the same solvent and finally with acetone gave 760 mg of II and 350 mg of I, respectively (total yield of I and II, 95%).

B) Irradiation of I with Trapping Reagents. i) 1-Butanethiol: A chloroform-insoluble part of the product mixture (after 15 hr irradiation) from a mixture of I (2.33 g; 0.035 M) and 1-butanethiol (9.0 ml; 0.38 M) in acetonitrile (220 ml) was recrystallized from acetone and 135 mg of III was obtained. The residue from the mother liquor was chromatographed on silica gel (70 g). Elution with 700 ml of chloroform afforded a yellow solid, which after preparative tlc (benzene) yielded 60 mg (3%) of 2,3,5,6-tetraphenylpyrazine (VIII) mp 260—261 °C (acetone–chloroform) (lit. mp 252 °C[21]) and 40 mg (2%) of *trans*-2,3,5,6-tetraphenyl-2,3-dihydropyrazine(VII), mp 205—206 °C (chloroform–ethanol) (lit. mp 199.5—200.5 °C[22]). The IR spectrum of VII were identical with that of an authentic sample.[22] The IR sepctrum of VIII was identical with that in the Sadtler Standard Spectra. Further elution with 800 ml of chloroform yielded 990 mg of III (the total yield of III, 48%). Further elution with chloroform and acetone, followed by preparative tlc (1 : 1 chloroform–acetone), yielded I (380 mg) and II (210 mg) and 40 mg (2%) of *meso*-stilbenediamine(X), mp 121—123 °C (ligroin–ether) (lit. mp 118—120 °C[23]) which was identical with an authentic sample.[24]

ii) Oxygen: The product mixture obtained from photolysis (15 hr) of a solution of I (1.07 g) in acetonitrile (110 ml) under bubbling oxygen instead of nitrogen was separated by preparative tlc (30—50 : 1 chloroform–acetone). Following products, in the order of increasing R_f values, were isolated: (1) *N,N'*-Dibenzoylbenzamidine(XIII); 460 mg (43%), which was unstable on silica gel (Kieselgel GF_{254}) or alumina (Aluminiumoxide GF_{254}) and decomposed to a mixture of XIII, XIV, and XV as reported earlier[18,19] but could be obtained in a sufficiently pure state for IR and NMR measurements. Its identity was confirmed by comparison with an authentic sample.[19] (2) *N*-Benzoylbenzamidine (XIV) and (3) dibenzamide(XV); combined yield, 165 mg (16%). These two compounds had the same R_f value of tlc ($CHCl_3$) and XIV decomposed on tlc to give XV. Recrystallization of the mixture from 3 : 1 ligroin–acetone, however, could yield pure XV, mp 152—154 °C (lit. mp 147—148 °C[25]) which was identified by NMR and IR spectra and had UV spectrum identical to the published data.[26] The residue from the mother liquor consisted of mainly XIV, whose NMR and IR spectral data were in accord with those of an authentic sample.[19] (4) Isoamarine (II); 140 mg (13%). Amarine (I) was not detected. Low-temperature (−78 °C) oxidation of I was also carried out in the same manner and the reaction was followed by tlc, giving results that only I and II were detected, but III, XIII, XIV, XV and XVI[18] could not be detected.

iii) 2,2,6,6-Tetramethylpiperidine-1-oxyl.[27] A mixture of I (1.14 g, 0.0191 M) and this free radical (3.96 g, 0.127 M) in benzene (200 ml) was irradiated under nitrogen with light at 313 nm isolated from a 100-W mercury lamp with a chromate–carbonate filter.[28] The reaction was followed by tlc confirming the occurrence of *cis-trans* isomerization. In addition, a small amount of III was detected.[29] However, products expected from the trapping of VIa by the nitroxyl radical could not be observed until 52 hr of irradiation. At this point an aliquot of the photolysate was submitted to preparative tlc (30 : 1 chloroform–ethanol) and an almost equal amount of I and II and a small amount of III were isolated. The nitroxyl radical was fairly stable under these conditions and was largely recovered unchanged (*ca.* 72%).

iv) Isopropyl Alcohol. After 70 hr of irradiation, the photolysate from I (1.01 g) in isopropyl alcohol (100 ml) contained no significant product except I and II as the main product and traces of III, VII and VIII by tlc analysis.

Photolysis of I in the Presence of Benzaldehyde. The mixture obtained by the photolysis (15 hr) of a solution containing 1.01 g (3.41×10^{-2} M) of I and 50 μl (4.81×10^{-3} M) of benzaldehyde in acetonitrile (110 ml) with a 100-W high pressure mercury lamp (Pyrex) under bubbling nitrogen was evaporated and the residue was chromatographed on silica gel (30 g). Elution with chloroform, followed by preparative tlc (benzene or 20—50 : 1 chloroform–acetone) of the eluates, yielded 3 mg (<0.5%) of VIII, 5 mg (<0.5%) of VII, 20 mg (2%) of III and 23 mg (2%) of XII. Further elution with chloroform and acetone afforded 530 mg (52%) of II and 435 mg (43%) of I. The structure of XII, mp 184—185 °C (petroleum ether–methanol), was assigned from its spectral and analytical data; ν (film) 1665, 1325 cm^{-1}; τ (CCl_4) 2.17—3.17 (20H, m, arom), 4.88 (1H, d, J=3 Hz) and 4.98 (1H, d, J=3 Hz); λ_{max}(EtOH) 242 (ε 18400) nm.

Found: C, 83.48; H, 5.65; N, 6.82%. Calcd for $C_{28}H_{22}N_2O$: C, 83.55; H, 5.51; N, 6.96%.

Synthesis of XII. To a solution of 90 mg (2.33×10^{-4} M) of VII in 1 ml of chloroform was added dropwise 450 mg (2.93×10^{-4} M) of perbenzoic acid (9% chloroform solution) with stirring. The mixture was stirred for further 1 hr at room temperature, and evaporated to dryness. The residue was separated by preparative tlc (chloroform) and 15 mg (23%) of XII was isolated as the main product which showed an IR spectrum identical with that of XII obtained photochemically. The method to prepare oxaziridines by the action of peracids or aerated aldehydes on Schiff's bases is well-known.[30]

Photolysis of III in the Presence or Absence of dl-*Stilbenediamine.* Two Pyrex tubes, each containing a solution of III (10 mg) in acetonitrile (20 ml) and a solution of III (11 mg) and *dl*-stilbenediamine (5 mg) in acetonitrile (20 ml), were irradiated externally with a 400-W high pressure mercury lamp (Pyrex) under bubbling nitrogen for 8 hr. By careful examination of the photolysate by tlc VII and VIII were not detected at all.

Deuterium Incorporation Experiment. A solution of 94 mg of I in a mixture of acetonitrile (15 ml) and D_2O (5 ml) placed in a Pyrex tube was sealed after bubbling nitrogen and irradiated externally with a 450-W high pressure mercury lamp for 16 hr. After evaporation of the photolysate under reduced pressure, the residue (II/I=1.2 by NMR) was dissolved in chloroform (20 ml) and washed four times with 20 ml of water to remove deuterium bound to nitrogen. The solution was evaporated after drying over Na_2SO_4 and was separated by preparative tlc (3 : 2 chloroform–acetone) to give I (25 mg) and II (34 mg). The latter was recrystallized from ether–ethanol and analyzed by mass spectroscopy (Hitachi RMU-6C) to determine deuterium content. It was estimated as less than 1.9% from comparison with the mass spectrum of the nondeuterated II.

Photolysis of cis-*2,4,5-Triphenyloxazoline (XI).* A solution of XI[31] (1.03 g) in acetonitrile (220 ml) was irradiated with a 10-W low pressure mercury lamp (Vycor) under bubbling nitrogen for 15 hr. After removing the solvent under reduced pressure, the residue (1.03 g) was chromatographed on silica gel (50 g). Elution with benzene (400 ml) afforded 35 mg of a yellow oil which contained *ca.* 1 mg of benzaldehyde (IR) by vpc analysis. Further elution with benzene (400 ml), followed by preparative tlc (2 : 1 chloroform–benzene), afforded 144 mg of *trans*-2,4,5-triphenyloxazoline, mp 86—87.5 °C (from petroleum ether) (lit. mp 83—85 °C[31]), which gave satisfactory spectral and analytical data. Further elution with benzene (1600 ml), followed by preparative tlc (5 : 1 chloroform–benzene), afforded a white solid (345 mg); mp 122—135 °C (from petroleum ether–acetone), which was unidentified.

References

1) Photoinduced Reactions. LXXXVIII. Part LXXXVII: I. Saito, Y. Chujo, H. Shimazu, M. Yamane, T. Matsuura, and H. J. Cahnmann, *J. Amer. Chem. Soc.*, **97**, 5272 (1975). A preliminary communication of the present paper appeared: T. Matsuura and Y. Ito, *Chem. Lett.*, **1972**, 431.

2) T. Matsuura, Y. Ito, and I. Saito, This Bulletin, **46**, 3805 (1973).

3) A photochemical *cis-trans* isomerization of *N*-substituted 2,3-diphenylaziridine *via* homolytic cleavage of C–C bond [A.G. Anastassiou and R. B. Hammer, *J. Amer. Chem. Soc.*, **94**, 303 (1972)] and a photochemical transformation of *trans*-2,3-dihydro-2,3,5,6-tetraphenylpyrazine to *cis*-isomer [A. Padwa and E. Glazer, *J. Amer. Chem. Soc.*, **94**, 7788 (1972)] have been reported.

4) a) P. S. Engel and B. M. Monroe, *Advan. Photochem.*, **8**, 245 (1971); b) J. P. Ferris and F. R. Antonucci, *J. Amer. Chem. Soc.*, **96**, 2014 (1974).

5) A similar rearrangement has been found with *N*-diphenylmethylidenediphenylmethylamine [K. N. Mehrotra and T. V. Singh, *Tetrahedron Lett.*, **1972**, 4949].

6) R. B. Woodward and R. Hoffmann, "The Conservation of Orbital Symmetry," Verlag Chemie GmbH, Academic Press, New York (1970).

7) M. Szwarc, *Chem. Rev.*, **47**, 75 (1950).

8) J. A. Kerr, *ibid.*, **66**, 496 (1966).

9) a) M. H. Delton and D. J. Cram, *J. Amer. Chem. Soc.*, **94**, 2471 (1972). b) T. Shirafuji, Y. Yamamoto and H. Nozaki, This Bulletin, **45**, 2574 (1972).

10) A. Padwa and S. I. Wetmore, Jr., *J. Amer. Chem. Soc.*, **96**, 2414 (1974) and references cited therein.

11) P. Beck and J. L. Miesch, *J. Amer. Chem. Soc.*, **89**, 2375 (1967).

12) P. J. Wagner and R. G. Zepp, *ibid.*, **94**, 287 (1972).

13) W. K. Robbins and R. H. Eastmann, *ibid.*, **92**, 6077 (1970).

14) a) N. Gakis, M. Märky, H. -J. Hansen and H. Schmid, *Helv. Chim. Acta*, **55**, 748 (1972). b) A. Padwa, S. Clough, M. Dharan, J. Smolanoff and S. I. Wetmore, *J. Amer. Chem. Soc.*, **94**, 1395 (1972).

15) T. Matsuura and Y. Ito, *Tetrahedron Lett.*, **1973**, 2283; Y. Ito and T. Matsuura, *Tetrahedron*, **31**, 1373 (1975).

16) a) A. Padwa, W. Bergmark and D. Pashayan, *J. Amer. Chem. Soc.*, **91**, 2654 (1969). b) N. Toshima, H. Hirai and S. Makishima, *Kogyo Kagaku Zashi*, **72**, 184 (1969).

17) S. G. Cohen and C. H. Wang, *J. Amer. Chem. Soc.*, **77**, 4435 (1955).

18) E. H. White and M. J. C. Harding, *Photochem. Photobiol.*, **4**, 1129 (1965).

19) C. Dufraisse and J. Martel, *C. R. Acad. Sci. Paris*, **244**, 3106 (1957).

20) In this photoproduct a trace of III was detected by tlc, although it was not detected in the experiments in Table 1.

21) H. H. Strain, *J. Amer. Chem. Soc.*, **51**, 272 (1929).

22) T. Hayashi, *Sci. Pap. Inst. Phys. Chem. Res.* (Tokyo), **39**, 89 (1941).

23) "Beilstein Handbuch der Organischen Chemie," E II, XIII, p. 114.

24) F. Feist, *Ber.*, **27**, 214 (1894). He isolated only *dl*-stilbenediamine, but in our case a mixture of *dl*- and *meso*-isomers was obtained (*dl*/*meso*=4.1/4.9 (NMR)). Each isomer was separated by preparative tlc (5 : 1 benzene–ethanol), and the reaction with benzyl according to the previous method[22] produced the corresponding dihydropyrazine.

25) "Beilsteins Handbuch der Organischen Chemie," EI, IX, p. 104.

26) "Organic Electronic Spectral Data," Volume II, Interscience Publishers, New York, London (1953—1955), p. 390.

27) R. Brière, H. Lemaire and A. Rassat, *Bull. Soc. Chim. Fr.*, **1965**, 3273.

28) P. J. Wagner, *J. Amer. Chem. Soc.*, **89**, 5898 (1967).

29) A trace of III was also detected in the mixture kept in the dark.

30) "Advan. Heterocyclic Chem.", Vol. 2, ed. by A. R. Katritzky and A. J. Boulton, Academic Press, New York (1963), p. 85.

31) M. Svoboda, J. Sicher, J. Farkaš and M. Pánková, *Collect. Czech. Chem. Commun.*, **20**, 1426 (1955).

The Addition Reaction of Benzenesulfinic Acid to *N*-Substituted Maleimides

Itsuo MATSUDA, Keiichi AKIYAMA, Takaaki TOYOSHIMA*, Shinji KATO*, and Masateru MIZUTA*

General Engineering Group, Toshiba Chemical Co., Ltd., c/o Toshiba Research and Development Center, Komukai Toshiba-cho, Saiwai-ku, Kawasaki, Kanagawa 210

**Department of Industrial Chemistry, Faculty of Engineering, Gifu University, Kagamigahara, Gifu 504*

(Received May 26, 1975)

It was found that benzenesulfinic acid reacted with *N*-substituted maleimides in aqueous ethanol to give sulfoneimides in good yields. The rate for the reaction was determined by the use of the neutralization titration, the effect of a substituent in *N*-substituted maleimides on the rate was studied, and the reaction route of benzenesulfinic acid with *N*-substituted maleimide was deduced.

The facile addition of nucleophiles to the double bond of maleimide compounds is well known and has been extensively studied.[1-6] The analogous reaction employing sulfinic acid has, however, received little attention. Therefore, this study was conducted in order to determine the course of the maleimide-sulfinic acid reaction and its potential adaptability to the preparation of polymers.

Although the nucleophilic property of sulfinic acid has been considered interesting, the nucleophilic addition reaction of sulfinic acid with maleimide has not yet been reported.

It is well known that the acidity of sulfinic acid is stronger than that of carboxylic acid and that sulfinic acid is unstable;[7] it easily disproportionates, and it decomposes. Sulfinic acid is known to react with α, β-unsaturated compounds in a buffer solution or in the presence of weak acids, such as boric or acetic acid.[8]

TABLE 1. ANALYTICAL DATA AND PHYSICAL PROPERTIES OF ADDUCTS (**3**)

Compd. No.	X	Mp °C	Yield %	Found (Calcd) % C	H	N	S	Cl	IR (KBr wafer, cm^{-1}) $\nu_{C=O}$	ν_{C-N}	$\nu_{C=C}$	ν_{SO_2}
3a	*p*-C_2H_5O	139.5—141.0	97	59.91 (60.15)	4.74 (4.77)	3.90 (3.90)	8.96 (8.92)		1713	1403	1518 1590	1330 1170
3b	*p*-CH_3O	116.0—117.0	97	59.10 (59.12)	4.25 (4.38)	4.11 (4.06)	9.06 (9.28)		1713	1395	1514 1585	1332 1159
3c	*p*-CH_3	159.0—160.0	96	61.83 (61.99)	4.44 (4.59)	4.20 (4.25)	9.63 (9.74)		1713	1393	1515 1585	1325 1165
3d	H	194.0—196.0	96	60.75 (60.94)	4.13 (4.15)	4.38 (4.44)	10.01 (10.17)		1710	1393	1502 1585	1335 1163
3e	*p*-Cl	200.0—202.0	98	54.66 (54.94)	3.35 (3.46)	3.98 (4.00)	9.17 (9.17)	10.25 (10.14)	1717	1395	1500 1585	1319 1149
3f	*m*-Cl	187.0—188.0	98	54.84 (54.94)	3.45 (3.46)	4.05 (4.00)	9.12 (9.17)	10.20 (10.14)	1720	1396	1484 1580	1328 1156
3g	*m*-NO_2	169.0—170.5	98	53.12 (53.33)	3.28 (3.36)	7.69 (7.77)	8.85 (8.90)		1723	1385	1533 1586	1316 1155

Compd. No.	UV (ethanol) λ_{max} (nm)	(ε_{max})		NMR ($CDCl_3$) δ (ppm) Aromatic (4*H*)	Aromatic (5*H*)	CH	CH_2	CH_2	CH_3
3a	273 (17400)	266 (21400)	—	8.07—7.55	7.15—6.90	4.50	4.07	3.37	1.40
3b	273 (8200)	266 (10400)	259 (10200)						
3c	273 (7500)	266 (11200)	—	8.07—7.55	7.35—6.85	4.42		3.32	2.33
3d	273 (5300)	266 (7400)	260 (7500)	8.07—7.52	7.42—7.02	4.50		3.40	
3e	273 (6600)	266 (9600)	—						
3f	273 (7700)	266 (9400)	260 (8500)						
3g	—	—	260 (36400)						

The present paper will deal with the addition reaction of benzenesulfinic acid to seven *N*-substituted maleimides, conducted in aqueous ethanol. By measuring the unreacted benzenesulfinic acid by means of neutralization titration, the rate constants of the reaction were calculated; the effect of the substituent in *N*-substituted maleimides on the reaction is discussed, and the course of the reaction is deduced.

Experimental

Materials. The benzenesulfinic acid was extracted, by means of diethyl ether (40 ml) in a separating funnel, from a mixture of sodium benzenesulfinate (16.4 g, 0.1 mol) dissolved in chilled water and concd HCl (7.9 ml, 0.095 mol). By removing the diethyl ether, benzenesulfinic acid (10 g, mp 74—76.0 °C) was obtained in a 70% yield; it was then preserved below 0 °C before use. The structure was confirmed by comparison with the spectral data in the literature.[8,10]

Seven *N*-substituted maleimides were prepared by the usual method[9] and recrystallized from ethanol; the following materials were used: *N*-phenylmaleimide, 87.5—88.5 °C; *N*-(*p*-ethoxyphenyl)maleimide, 133.0—135.0 °C; *N*-(*p*-methoxyphenyl)maleimide, 146.0—148.0 °C; *N*-(*p*-methylphenyl)maleimide, 147.0—150.0 °C; *N*-(*p*-chlorophenyl)-maleimide, 115.0—117.0 °C; *N*-(*m*-chlorophenyl)maleimide, 93.0—95.0 °C; *N*-(*m*-nitrophenyl)maleimide, 132.0—133.0 °C.

Preparation of Adducts of Benzenesulfinic Acid with N-Substituted Maleimides. A typical preparation is presented. The yields and physical properties and elemental analyses are summarized in Table 1.

*N-Phenyl-2-phenylsulfonylsuccinimide (**3d**).* A solution of benzensulfinic acid (0.002 mol) in water (100 ml) was added to a solution of *N*-phenylmaleimide (0.002 mol) in ethanol (100 ml) at 15 °C, after which the mixture was stirred for 10 hours. The recrystallization of the separated precipitates from ethanol gave 0.605 g (yield 96%) of **3d** as white needles.

Measurement of the Reaction Rate. Since a reaction product precipitates soon after the mixing of a benzenesulfinic acid aqueous solution with an *N*-substituted maleimide alcoholic solution, the conventional method for measuring a reaction rate was inapplicable. Therefore, the procedures used were as follows. *N*-substituted maleimide was dissolved to 0.02 mol/l with ethanol, and benzenesulfinic acid was dissolved to 0.02 mol/l with water. After aliquot portions (10 ml) of the *N*-substituted maleimide solution had been pipetted into several 50-ml glass-stoppered flasks for one run and put in a water bath kept at a prescribed temperature (accuracy±0.1 °C), just as much (10 ml) of the benzenesulfinic acid solution was added to each flask. The time of the mixing-in of the benzenesulfinic acid solution was considered the starting point of the reaction. After the glass-stoppered flasks containing the reaction mixture (20 ml) had then been taken out at regular time intervals, the reaction mixture put in the flasks was immediately subjected to the measurement of the remaining unreacted benzenesulfinic acid by means of neutralization titration with 0.1 M KOH alcoholic solution, using phenolphthalein as the indicator. All the kinetic runs were followed as above. All the rate constants were determined from the second-rate equation as follows:

$$k_2 t = \frac{1}{A_0}\left(\frac{a}{a_0-a}\right) = \frac{1}{A_0}\left(\frac{a_0}{a_0-a}-1\right)$$

a_0-a: The titre of the 0.1 M KOH alcoholic solution at

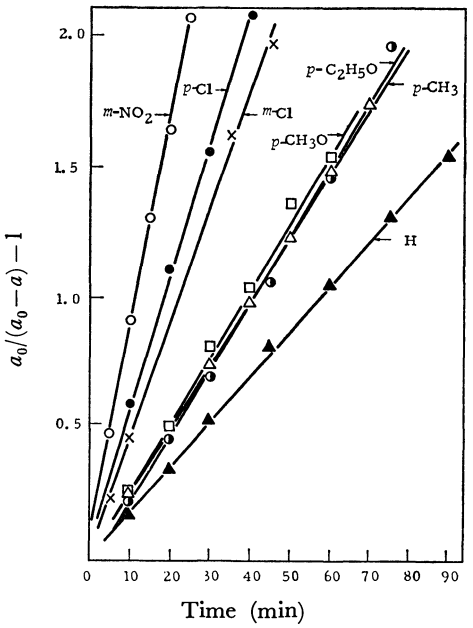

Fig. 1. The second order plots of the reactions of benzenesulfinic acid with *N*-substituted maleimides at 15 °C.

TABLE 2. THE SECOND ORDER RATE CONSTANTS OF ADDITION REACTION OF BENZENESULFINIC ACID TO *N*-SUBSTITUTED MALEIMIDES IN ETHANOL/WATER (1/1)

Maleimides	Temp. (°C)	$k_2\times10^2$ ($mol^{-1}\cdot l\cdot s^{-1}$)	
p-C_2H_5O	15.0	4.40	
	20.0	5.85	
	25.0	7.31	
	30.0	9.10	
p-CH_3O	15.0	4.28	
	20.0	6.01	
	25.0	7.73	
	30.0	9.70	
p-CH_3	15.0	4.14	
	20.0	5.75	
	25.0	7.30	
	30.0	9.49	
H	0.3	1.41	
	5.0	1.73	
	10.0	2.23	
	14.6	2.85	
p-Cl	5.0	4.41	
	10.0	5.80	
	15.0	7.67	
	20.0	11.2	
m-Cl	0.5	3.87	
	5.0	4.63	
	10.0	5.66	
	15.0	6.90	
m-NO_2	0.3	6.11[a]	9.17[b]
	5.0	8.54[a]	12.8[b]
	10.0	10.9[a]	16.4[b]
	15.0	14.1[a]	21.2[b]

a) In ethanol/water (2/1). b) The calculated value in ethanol/water (1/1) on the data in Table 3.

a time (t).

a_0: The initial titre of the 0.1 M KOH alcoholic solution.

A_0: The initial concentration (mol/l) of *N*-substituted maleimide.

Plots of some typical runs are shown in Fig. 1. All the rate constants are shown in Table 2.

Results and Discussion

The addition reaction of benzenesulfinic acid to *N*-substituted maleimide is shown in the following scheme.

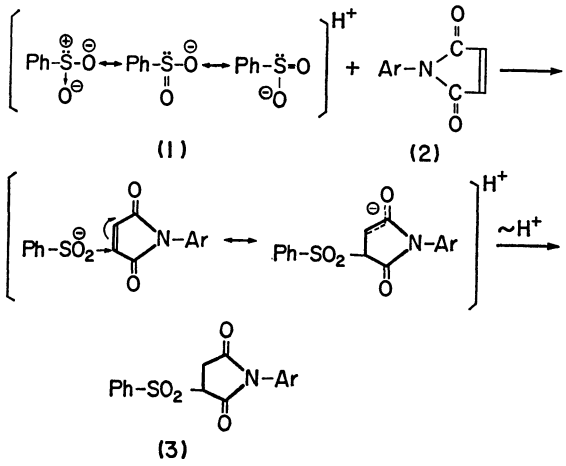

Although the reaction of benzenesulfinic acid with *N*-phenylmaleimide was attempted in ethanol or acetone at room temperature, no adduct could be detected. When a strong acid such as HCl or H_2SO_4 was used as the catalyst in ethanol or acetone, no adduct could be detected, either. However, when aqueous ethanol or aqueous acetone was used as the solvent, the adduct, *i.e.*, *N*-phenyl-2-phenylsulfonyl-succinimide (**3d**), was obtained in a good yield.

This is evidently because, as is shown in Table 3, as the polarity of the solvent increases with an increase in the water content, the reaction rate also increases; *i.e.*, the polarity of the solvent is important for the addition of benzenesulfinic acid to *N*-substituted maleimide.

All the *N*-substituted maleimides react smoothly with benzenesulfinic acid in aqueous ethanol at room temperature and gave readily isolable products; these products are summarized in Table 1. The structures

Table 3. Solvent effect for addition reaction of benzenesulfinic acid to *N*-phenylmaleimide

EtOH (%)	$k_2 \times 10^2$ ($mol^{-1} \cdot l \cdot s^{-1}$)
75	1.75
67	2.32
50	2.85
40	4.79
35	6.11

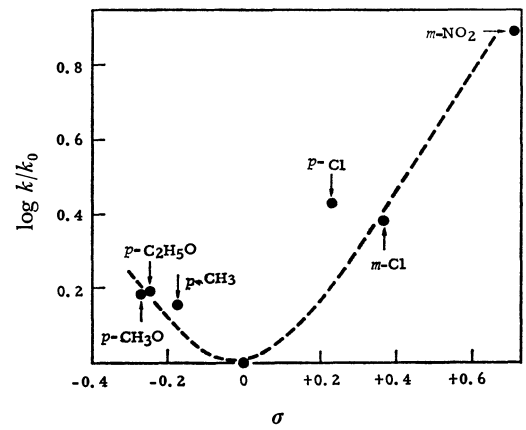

Fig. 2. Hammett plots (at 15.0 °C).

of the reaction products were determined on the basis of the spectral data and elemental analyses, the details of which have been given in the Experimental section. These results undoubtedly indicate that the nucleophilic addition of benzenesulfinic acid takes place only at the carbon-carbon double bond of *N*-substituted maleimide, thus forming sulfon-imide.

The kinetic measurements were carried out by following the remaining unreacted benzenesulfinic acid by means of neutralization titration.

Figure 2 shows Hammett's plot of log k/k_0 *vs.* the σ value at 15 °C. As a result, the introduction of all the substituents was found to accelerate the rate of addition reaction.

The above results suggest that the reaction mechanism involves a charged intermediate or transition state which is stabilized by the medium. The course shown above, involving considerable charge separation, may be concluded to be a reasonable mechanism for the reaction; it is in agreement with the observed kinetic order.

References

1) M. K. Hargreaves, J. G. Pritehard, and H. R. Dave, *Chem. Rev.*, **70**, 451 (1970).
2) T. V. Shetemeteva, G. N. Larina, M. G. Zhenevskaya, and V. A. Gusinsaya, *J. Polym. Sci.*, **C16**, 1631 (1967).
3) P. Kovacic and R. W. Hein, *J. Amer. Chem. Soc.*, **81**, 1187 and 1190 (1959).
4) J. V. Orivello, *J. Polym. Sci.*, *A*-1, **11**, 1185 (1973).
5) N. Kardush and M. P. Stevens, *ibid.*, **10**, 1093 (1972).
6) I. Matsuda, A. Yoshizumi, and K. Akiyama, *Kobunshi Ronbunshu*, **31**, 47 (1974).
7) W. E. Truce and M. M. Murphy, *Chem. Rev.*, **48**, 69 (1951).
8) S. Oae, "Yuki Iou Kagoobutsu No Kagaku," Ge, Kagaku Doojin, Kyoto (1969), p. 358.
9) H. N. Cole and W. F. Gruber, U.S.P., 3127414 (Jan. 12, 1962); *Chem. Abstr.*, **60**, 14444b (1964).
10) M. Kobayashi and N. Koga, This Bulletin, **39**, 1788 (1966).

Nonenzymatic Hydrolysis of Adenosine 5′-Triphosphate in Micellar and Reversed Micellar Systems

Manabu Senō, Shinsaku Shiraishi, Koji Araki, and Hideo Kise
Institute of Industrial Science, The University of Tokyo, Roppongi, Minato-ku, Tokyo 106
(Received June 9, 1975)

The nonenzymatic hydrolysis of adenosine 5′-triphosphate (ATP) in micellar and reversed micellar system was examined as an approach to elucidate the function of ATPase. In aqueous micellar systems an anionic surfactant does not affect the hydrolysis rate, but a cationic surfactant, cetyltrimethylammonium bromide(CTAB), retards the hydrolysis. This deceleration effect is interpreted to be owing to the pH change or accumulation of hydroxide ions at the cationic micellar-water interface which serves as reaction site. In the reversed micellar system where aqueous ATP phase is solubilized in *n*-hexane by dodecylammonium propionate(DAP), the hydrolysis rate of ATP is enhanced by several times as compared with that in an aqueous system. Addition of Mg^{2+} or Ca^{2+} enhances the hydrolysis rate markedly only in the DAP reversed micellar system. The catalytic effect of the DAP reversed micellar system is discussed with respect to the polarity of water phase solubilized in the core of reversed micelles.

Adenosine 5′-triphosphate(ATP) plays an important role in repository and transfer of chemical energy in many enzymatic processes in living systems. Energy transfer in these systems usually involves the reactions of ATP into adenosine 5′-diphosphate (ADP). Though many studies have been made as to the structure and function of ATPase, the mechanism of its catalytic action is not yet clear. To improve this situation, some nonenzymatic model reactions have also been examined, and it has been observed that the hydrolysis reaction of ATP is enhanced either by the addition of metal ions or polyamines,[1,2] or in the presence of aprotic polar solvent.[3]

On the other hand, surfactant micelles affect rates of various reactions and are noticed as a model for enzymatic action. Recently, Fendler *et al* observed that reversed micelles in nonpolar solvents showed a significant rate enhancement in several reactions and pointed out that reversed micelles could provide a favorable model for the micro-environment of enzyme active sites.[4]

In the present investigation, we carried out the nonenzymatic hydrolysis of ATP both in an aqueous micellar system and in a reversed micellar system, and examined the micellar effect on hydrolysis rate to shed light on the function of ATPase.

Experimental

Materials. Disodium salt of ATP was purchased from Sigma Chemical Co. and was used without further purification. Cetyltrimethylammonium bromide(CTAB) and sodium dodecylsulfate(SDS) were recrystallized three times from methanol–ether. Dodecylammonium propionate(DAP) was prepared by Kitahara's method and purified three times by recrystallization from *n*-hexane;[5] mp 55—56 °C (lit, 54—56 °C)[5]. Found (Calcd): C, 69.68(69.44), H, 12.38 (12.82), N, 5.32(5.40)%. Magnesium chloride and calcium chloride of analytical grade were used after dried.

Reactions. *Reaction in Aqueous Micellar System*: A sample solution, pH of which was adjusted by using a buffer solution or addition of small amount of a *dil* NaOH solution, was prepared by dissolving ATP and surfactant *etc.* The solution was maintained at 50 °C with stirring. A pH meter of Toa HM-5A was used for pH measurement. The mixture was heterogeneous at low CTAB concentration (below about 6×10^{-3} M when ATP concentration was 2×10^{-3} M at 50 °C) because of the precipitation of CTAB–ATP salt, but at higher CTAB concentration the precipitate was dissolved to form a homogeneous solution. Reactions were carried out only when the mixture was homogeneous.

Reaction in Non-aqueous Reversed Micellar System: A sample solution was prepared by solubilizing an aqueous ATP solution in *n*-hexane using DAP (Fig. 1). When the amount of the aqueous solution added is too large for the DAP concentration, the aqueous solution is not solubilized completely, and when too small, DAP does not dissolve completely. The solubilized system was obtained in a range of $[H_2O]$/[DAP] ratio of 0.55—2.2 at DAP concentration of 0.2 M at 50 °C, and reactions were carried out only under these conditions at 50 °C.

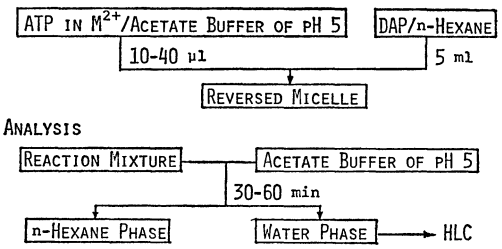

Fig. 1. Experimental procedure for the reversed micellar system.

Analysis. ATP and its hydrolysis products, *i.e.* ADP, adenosine 5′-monophosphate(AMP) and adenosine, were determined by a high speed liquid chromatography (hlc) under following conditions: column, Hitachi anion exchanger #2630; column temprature, 45 °C; mobile phase, 0.25 M NaCl in 0.01 M HCl solution; flow rate, 1.2 ml·min^{-1}; detector, Iatron UV photometer LC-1 at 254 nm. When *n*-hexane was used as a solvent, ATP and its hydrolysis products were extracted from the reaction mixture with water prior to hlc analysis. Under the condition that less than 10 per cent of initial amount of ATP was hydrolyzed, the hydrolysis product was mainly ADP, and the amount of AMP or adenosine produced was negligibly small. Therefore, the hydrolysis rate of ATP was determined from the change in ADP concentration in this range.

Other Measurements. UV spectra of pyridine 1-oxide were observed by a Hitachi spectrophotometer model EPS-3T using a thermostated cell. Aggregation numbers of DAP

in the reversed micellar system were estimated from the average molecular weights of micelles, which were measured by a Hewlett-Packard vapour pressure osmometer model 302B at 37 °C.

Results and Discussion

The rate of hydrolysis reaction of ATP in an aqueous solution obeys a pseudo first order rate kinetics for ATP concentration (Eq. (1));

$$\mathrm{ATP} + \mathrm{H_2O} \xrightarrow{k_{app}} \mathrm{ADP} + \text{phosphoric acid}$$

$$-\frac{d[ATP]}{dt} = k^{\circ}_{app}[ATP] \quad (1)$$

where k°_{app} is a pseudo first order rate constant. The hydrolysis rate in the micellar system shows also a first order dependence on ATP concentration, and the pseudo first order rate constants, k^{m}_{app} in an aqueous micellar system and k^{r}_{app} in a reversed micellar system were determined experimentally.

ATP Hydrolysis in Aqueous Micellar Solutions. Effects of surfactants on k^{m}_{app} are shown in Table 1. The addition of an anionic surfactant, SDS, has little or no effect on k_{app}, but the addition of a cationic surfactant, CTAB, reduces it. Since the addition of tetramethylammonium bromide (TMAB) which does not form micelles shows no effect on the hydrolysis rate, the deceleration effect of CTAB is thought to be caused by the formation of its cationic micelles. Figure 2 shows the effect of CATB concentration on k^{m}_{app}. When the CTAB concentration is higher than 8×10^{-3} M, the value of k^{m}_{app} is reduced by half compared to k°_{app} and is almost independent of CTAB concentration.

Table 1. Hydrolysis rate constants of ATP in aqueous micellar solutions at 50 °C

Surfactant or salt added	$k_{app}\times10^{6}$ (s^{-1})	$k_{rel.}$
None	1.12	=1
SDS	1.04	0.92
CTAB	0.676	0.60
TMAB	1.09	0.97

ATP=2×10^{-3} M; Surfactant or salt=2×10^{-2} M; in pH 4.1 acetate buffer.

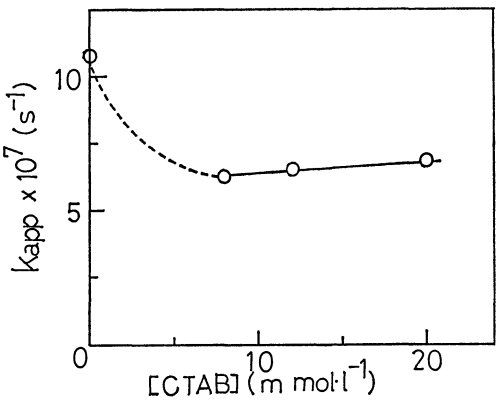

Fig. 2. Effect of CTAB concentration on the hydrolysis rate of ATP(2×10^{-3} M) at 50 °C in pH 4.1 acetate buffer.

The rate of hydrolysis could not be measured at lower CTAB concentration, where ATP did not dissolve uniformly.

The effect of addition of methanol to the reaction mixture with or without CTAB was examined, and result is shown in Fig. 3. With an increase in methanol content, the value of k^{m}_{app} in micellar solution becomes close to that of k°_{app}, and both the values are almost the same at methanol contents higher than about 50 v/v%, where CTAB micelles were destroyed almost completely.[6] This fact ensures that the effect of CTAB on hydrolysis rate is caused by its cationic micelles.

The effect of pH on hydrolysis rate both in aqueous and in CTAB micellar systems is given in Fig. 4. The value of pH of these solutions was adjusted by addition of a *dil* NaOH solution and determined by a glass electrode pH meter. Both of k°_{app} and k^{m}_{app} decrease as pH increases, and abrupt decreases are observed around pH 7 for k°_{app} and pH 6 for k^{m}_{app}. These pH values are nearly equal to those of the second dissociation of γ-phosphate of ATP in these systems (pk°_{2}= 7.1 and pk^{m}_{2}=6.1), which were determined from titration curves shown in the same figure. This result indicates that the hydrolysis rate is closely related with

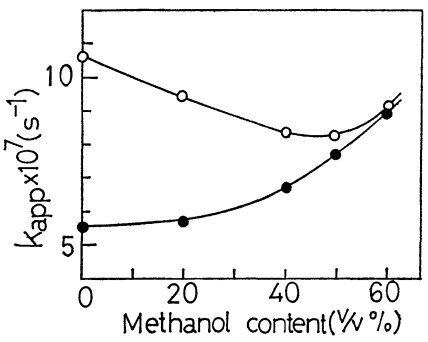

Fig. 3. Effect of methanol on the hydrolysis rate of ATP (2×10^{-3} M) both in aqueous (○), and in CTAB (1.2×10^{-2} M) micellar (●) solutions at 50 °C.

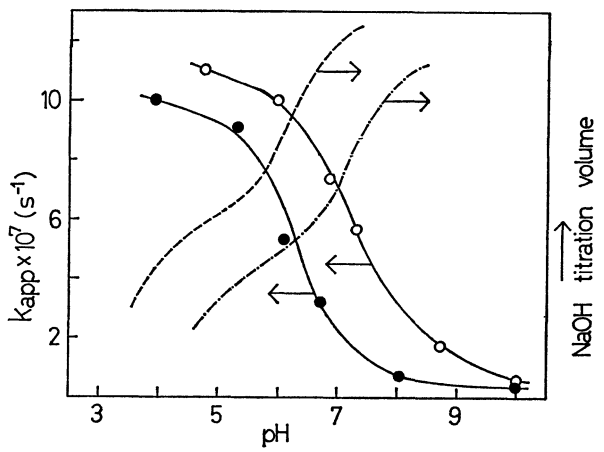

Fig. 4. Effect of pH on the hydrolysis rate of ATP (2×10^{-3} M) in aqueous (○), and in CTAB (1.2×10^{-2} M) micellar (●) solutions; and titration curves of ATP in aqueous (·—·), and in CTAB (1.2×10^{-2} M) micellar (----) solutions; at 50 °C.

the near environment of ATP or the dissociation state of ATP. Furthermore, it is to be noted that shifting the curve of k^{o}_{app} *vs.* pH to the lower pH side by about 1 makes it similar to that of k^{m}_{app} *vs.* pH. This result might imply that the pH value at the reaction site in micellar solution is higher by about 1 than that determined by a pH meter, which measures the pH value in the bulk aqueous phase.[7] This leads to the following interpretation of the result. ATP molecules exist at the interface between water and micelle, where hydroxide ions are accumulated by its cationic character to give a rise in pH. The deceleration effect of CTAB micellar system on hydrolysis rate of ATP is owing to this accumulation effect at micellar interface.

ATP Hydrolysis in Reversed Micellar Systems. The hydrolysis of ATP was also examined in a reversed micellar system in nonpolar medium. *n*-Hexane was used as a nonpolar solvent and DAP as an oil-soluble surfactant. ATP, which is insoluble in organic solvents, could be solubilized in *n*-hexane by addition of a small amount of water in the presence of DAP to form a reversed micellar system. By assuming that ATP molecules would exist in the core of reversed micelle or, in other words, in the water phase dispersed in *n*-hexane, the rate constant k^{r}_{app} in this system was obtained by a similar procedure to that in aqueous systems. The value of k^{r}_{app} thus obtained was proportional to the DAP concentration and inversely proportional to the water concentration in the range examined; the result could be represented by the expression;

$$-\frac{d[ATP]}{dt} = k^{r}_{app}[ATP] = k'\frac{[DAP]}{[H_2O]}[ATP] \qquad (2)$$

as shown in Fig. 5. The value of k^{r}_{app} is 1—5 times larger than that of k^{o}_{app}; that is, ATP hydrolysis is enhanced in the reversed micellar system.

Effects of Metal Ions. It is known that Mg^{2+} and Ca^{2+} play an important role in the enzymatic hydrolysis of ATP in living systems. In this respect, the effects of these ions on hydrolysis of ATP in aqueous micellar and reversed micellar systems were examined by adding these chlorides into the systems. The values of k^{o}_{app} and k^{m}_{app} are little affected, but that of

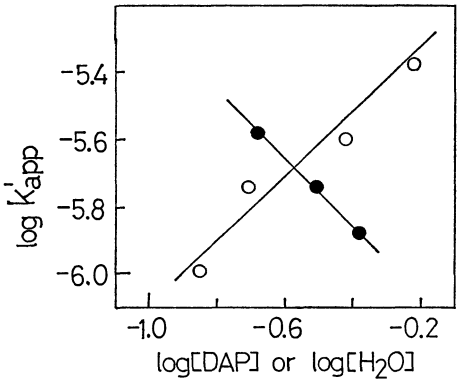

Fig. 5. Dependences of the hydrolysis rate of ATP (6×10^{-4} M) both on DAP concentration (○) where water concentration was 3.33×10^{-1} M, and on water concentration (●) where DAP concentration was 2×10^{-1} M; in *n*-hexane at 50 °C.

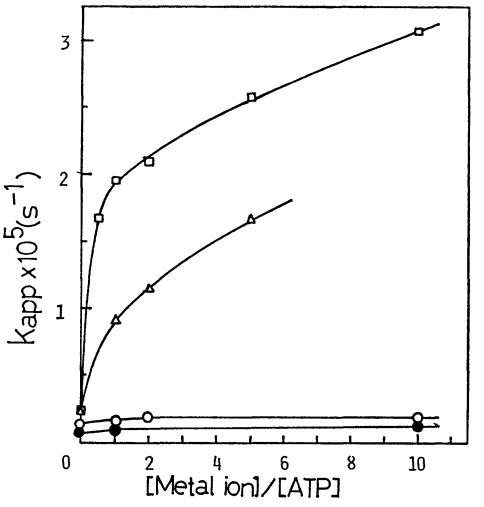

Fig. 6. Effect of divalent metal ions on hydrolysis rate of ATP (6×10^{-4} or 2×10^{-3} M) at 50 °C; (□): M^{2+}, reversed micellar system in *n*-hexane (DAP= 2×10^{-1} M, $H_2O=3.33\times10^{-1}$ M); (△): Ca^{2+}, reversed micellar system in *n*-hexane (DAP=2×10^{-1} M, $H_2O=3.33\times10^{-1}$ M); (○): Mg^{2+}, aqueous solution (pH=4.1); (●): Mg^{2+}, aqueous micellar system (CTAB=1.2×10^{-2} M, pH=4.1).

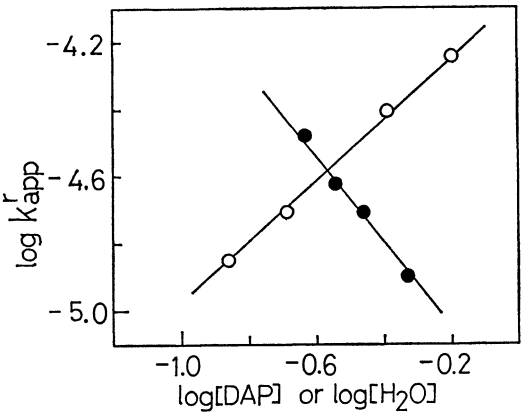

Fig. 7. Dependences of the hydrolysis rate of ATP (6×10^{-4} M) in the presence of Mg^{2+} (1.2×10^{-3} M) both on DAP concentration (○) where water concentration was 3.33×10^{-1} M, and on water concentration (●) where DAP concentration was 2×10^{-1} M; in *n*-hexane at 50 °C.

k^{r}_{app} markedly increases with an increase in the amount of Mg^{2+} added, and the value of k^{r}_{app} levels off at about $Mg^{2+}/ATP=1$ as are shown in Fig. 6. This indicates that the hydrolysis rate is enhanced by the formation of 1 : 1 complex of Mg^{2+}–ATP. Addition of Ca^{2+} also shows a rate enhancement in the reversed micellar system though its effect is smaller than that of Mg^{2+}.

The effect of amounts of DAP and water on k^{r}_{app} was examined at $Mg^{2+}/ATP=2$. The result shows that the hydrolysis rate obeys Eq. (2) as is shown in Fig. 7.

Rate Enhancement in Reversed Micellar System. The hydrolysis reaction of ATP is enhanced in reversed micellar system, and especially when Mg^{2+} or Ca^{2+} is added. The hydrolysis rate is followed by Eq. (2)

whether the divalent cation is added or not. This result suggests that the micellar reaction mechanism itself is not affected by the presence of divalent cation.

The aggregation number of DAP in the reversed micellar system was measured by a vapor pressure osmometer and the result is shown in Table 2. The aggregation number is small and therefore the number of water molecules solubilized in the core of the reversed micelle is very small. So, it is hard to consider the ion condensation at the interface as being observed in the aqueous cationic micellar system. Some other factors must contribute to the rate enhancement.

It is important to note that k^{r}_{app} depends on [DAP]/[H_2O] ratio. Menger *et al.* measured the Z value of water phase solubilized in octane by an anionic surfactant, di-2-ethylhexyl sodium sulfosuccinate, by using pyridine 1-oxide and 2-toluidinylnaphthalene-6-sulfonate as probes, and observed that the value depends on [H_2O]/[Surfactant] ratio.[8] We also measured the polarity of water solubilized in DAP reversed micelles in *n*-hexane by using pyridine 1-oxide as a probe. The change in absorbance maxima of pyridine 1-oxide near 260 nm is given in Fig. 8 as a function of [H_2O]/[DAP] ratio. The polarity of water in the core of the reversed micelle shows a good linear dependence on [H_2O]/[DAP] ratio, and lies midway between those of ethanol and chloroform at [H_2O]/[DAP]=0.55. On the other hand, Nelson *et al.* observed that the hydrolysis rate of ATP was enhanced in aqueous solution of aprotic polar solvent such as dimethyl sulfoxide, dioxane or formamide.[3] Considering them altogether, the rate enhancement of ATP hydrolysis in the DAP reversed micellar system is supposed to be caused by lowering in the polarity of water phase in the core of the reversed micelle, and the [DAP]/[H_2O] term in Eq. (2) may represent the degree of lowering in the polarity.

Table 2. Aggregation number of DAP in the reversed micellar solutions at 37 °C

[H_2O]/[DAP] ratio	Aggregation number
0.55	4.56
1.10	4.53
1.75	4.61
2.20	4.66
2.75	5.23

DAP=2×10^{-1} M; in *n*-hexane.

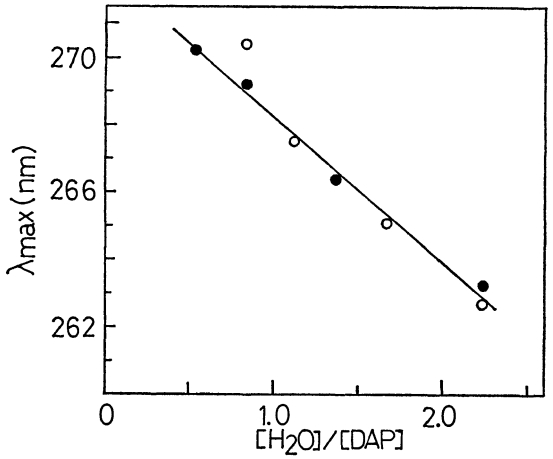

Fig. 8. Dependences of the absorbance maxima (λ_{max}) of pyridine 1-oxide (7.7×10^{-5} M) on [H_2O]/[DAP] ratio in reversed micellar system in *n*-hexane at 50 °C; (○): DAP concentration was 2×10^{-1} M at various water concentrations; (●): water concentration was 3.33×10^{-1} M at various DAP concentrations. λ_{max} of pyridine 1-oxide in various solvents was reported; 254.4 nm in water, 263.3 nm in methanol, 265.1 nm in ethanol, and 276.1 nm in chloroform.[9]

It is well known that a divalent cation, most often Mg^{2+} or Ca^{2+}, is required to activate ATPase in living system, but these metal ions show low or almost no activity in aqueous nonenzymatic hydrolysis of ATP. It is interesting that these metal ions are effective only in the reversed micellar system. Nelson *et al.* also observed that Mg^{2+} was much effective on ATP hydrolysis and Tagaki *et al.* on hydrolysis of phenyl phosphosulfate both in less polar media.[3,10]

Mg^{2+} and Ca^{2+} are hard acids and, therefore, have a stronger interaction with phosphate, which is a base harder than adenine ring. Moreover, it was found that Mg^{2+} ion, a harder acid than Ca^{2+}, is more effective than Ca^{2+} in the reversed micellar system. It was suggested from this consideration that the effect of these ions on ATP hydrolysis is caused by the neutralization of negative charges on phsophate part of ATP. By supposing that the hydrolysis of ATP proceeds *via* nucleophilic mechanism, this reasoning would be plausible. On this respect, it is interesting to note that the mechanism of γ-phosphate splitting of ATP by ATPase is nucleophilic.

References

1) M. Tetas and J. M. Lowenstein, *Biochemistry*, **2**, 350 (1963); P. W. Schneider and H. Brintzinger, *Helv. Chim. Acta*, **47**, 1717 (1964).
2) S. Suzuki, T. Higashimura, and A. Nakahara, *Bioorg. Chem.*, **2**, 145 (1973).
3) N. Nelson and E. Racker, *Biochemistry*, **12**, 563 (1973).
4) E. J. Fendler, S. A. Chang, J. H. Fendler, R. T. Medary, O. A. El Sound, and V. A. Woods, "Reaction Kinetics in Micelles," ed. by E. H. Cordes, Plenum Press, New York, N. Y. (1973), p. 127.
5) A. Kitahara, This Bulletin, **28**, 234 (1955).
6) A. W. Ralston and C. W. Hoerr, *J. Amer. Chem. Soc.*, **68**, 851 (1946).
7) C. A. Bunton and B. Wolfe, *ibid.*, **95**, 3742 (1973).
8) F. M. Menger, J. A. Donohue, and R. F. Williams, *ibid.*, **95**, 288 (1973).
9) E. M. Kosower, *ibid.*, **80**, 3253 (1958).
10) W. Tagaki, Y. Asai, and T. Eiki, *ibid.*, **95**, 3037 (1973).

Reaction of Organoboranes with Lithium Aldimines. A New Procedure for the Synthesis of Unsymmetrical Ketones[1]

Yoshinori YAMAMOTO,* Kaoru KONDO, and Ichiro MORITANI[2]

Department of Chemistry, Faculty of Engineering Science, Osaka University, Toyonaka, Osaka 560

(Received June 26, 1975)

Unsymmetrical ketones are obtained in good yields *via* the reaction of dialkylchloroboranes with lithium aldimines followed by treatment with (i) thioglycolic acid and (ii) H_2O_2–NaOH. The reaction permits the introduction of both primary and secondary alkyl groups into R and R′ substituents of ketones (RR′C=O), and can even be extended to the accommodation of a functional group. The reaction of B-*n*-hexyl-9-borabicyclo[3.3.1]-nonane with lithium aldimine derived from *n*-butyllithium also gives unsymmetrical ketone, 5-undecanone, upon treatment with H_2O_2–NaOH.

In recent years, various procedures for the synthesis of ketones *via* organometallics have been developed.[3] The synthesis through organoboranes is the most useful and convenient. Symmetrical ketones are obtained from the reaction of trialkylboranes with carbon monoxide in the presence of water[4] or with sodium cyanide and trifluoroacetic anhydride,[5] or *via* the reaction of dialkylborinates with α,α-dichloromethyl methyl ether and lithium triethylcarboxide.[6] Unsymmetrical ketones are available *via* the reaction of thexyldialkylboranes with carbon monoxide[7] or with sodium cyanide,[8] *via* the reaction of trialkylboranes with α,β-unsaturated carbonyl derivatives,[9] α-bromoketones,[10] diazoketones,[11] α-lithio derivative of 1,1-bis(phenylthio)pentane,[12] or α-azidostyrene,[13] or *via* the reaction of lithium alkynyltrialkylborates with electrophilic reagents.[14] Although thexylborane can combine two different olefins with a different reactivity toward the B–H bonds, union of two different olefins with similar reactivity such as 1-hexene and 1-butene is unsuccessful.[15] This causes an unsatisfactory result for the union of two primary alkyl groups such as *n*-hexyl and *n*-butyl in the unsymmetrical ketone synthesis.[15] We report a new synthesis of unsymmetrical ketones *via* the reaction of organoboranes with lithium aldimines.

Results and Discussion

Lithium aldimines (**1**) are obtained by addition of alkyllithiums to isocyanides which do not contain α-hydrogens[16] (Scheme 1). The reaction of dialkylchloroboranes (**2**) with **1** gives the corresponding adduct (**3**) (Scheme 2).

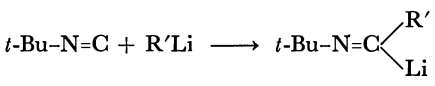

$$t\text{-Bu-N=C} + \text{R'Li} \longrightarrow t\text{-Bu-N=C}\begin{matrix}\text{R'}\\ \text{Li}\end{matrix} \quad (1)$$

1

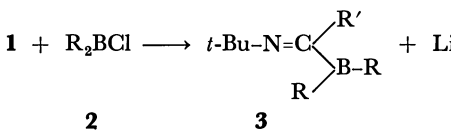

$$\mathbf{1} + \text{R}_2\text{BCl} \longrightarrow t\text{-Bu-N=C}\begin{matrix}\text{R'}\\ \text{B-R}\\ \text{R}\end{matrix} + \text{LiCl} \quad (2)$$

2 **3**

It was anticipated that such a compound as **3** can react with an electrophile to induce alkyl transfer from boron to carbon,[17] in which case alkaline hydrogen peroxide oxidation of **4** might give ketone (**5**), where the one alkyl group (R) arises from **2** and the other (R′) from alkyllithium (Scheme 3).

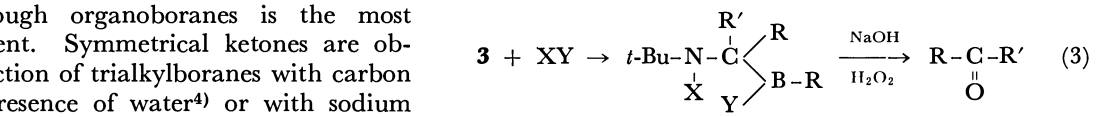

$$\mathbf{3} + \text{XY} \rightarrow t\text{-Bu-N-C}\begin{matrix}\text{R'}\\ \text{X}\\ \text{Y}\\ \text{B-R}\\ \text{R}\end{matrix} \xrightarrow[\text{H}_2\text{O}_2]{\text{NaOH}} \text{R-C(=O)-R'} \quad (3)$$

4 **5**

As a typical case we examined the reaction of di-*n*-hexylchloroborane (10 mmol) with lithium aldimine derived from *n*-butyllithium (10 mmol) and *t*-butylisocyanide (10 mmol). The borane was added to the lithium aldimine at 0 °C, trifluoroacetic anhydride (20 mmol) then being added to the resultant mixture as an electrophile. After being stirred for 1 hr at room temperature, the mixture was subjected to alkaline hydrogen peroxide oxidation, giving 5-undecanone. However, it was obtained in a relatively low 56% yield. This was apparently due to the improper choice of reaction temperature since boranes similar to **3** undergo dimerization.[18] When the reaction was performed at −78 °C, the ketone was obtained in a remarkably improved 95% yield. Various ketones prepared are listed in Table 1.

Unsymmetrical ketones can be prepared by utilizing olefins and alkyl halides as building blocks that can be varied independently. There appears no difficulty in introducing a primary alkyl group containing a functional substituent. However, isopropyl cyclopentyl ketone (**12**) is obtained in only 44% yield, suggesting that the combination of two secondary alkyl groups proceeds with some difficulty under the reaction conditions. This might be due to the difficulty for the transfer of sterically bulky alkyl groups. The relative migratory aptitudes of alkyl groups in the related boranes are in the order primary>secondary>tertiary.[19] We selected several electrophiles and examined the yield of **12** in order to find the best reagent in the present reaction system. The results are summarized in Table 2.

Thioglycolic acid is recommended as a reagent inducing the migration. The present procedure offers the following advantages over the previous methods;[7,8] (i) accommodation of an alkyl group such as isopropyl which can not be introduced *via* the hydroboration methods, (ii) the combination of two different alkyl groups such as *n*-hexyl and *n*-butyl which is not attainable through thexylborane. The only disadvantage is the loss of one alkyl group (R) (Scheme 3). This

* To whom correspondence should be addressed.

Table 1. Synthesis of unsymmetrical ketones *via* the reaction of **1** with **2**

Olefin	Alkyllithium	Ketone	Yield, %
1-Hexene	*n*-Butyllithium	5-Undecanone (**6**)	95
1-Hexene	3-Methylbutyllithium	2-Methyl-5-undecanone (**7**)	92
1-Hexene	Ethyllithium	3-Nonanone (**8**)	86
1-Hexene	*iso*-Propyllithium	2-Methyl-3-nonanone (**9**)	71
5-Bromo-1-pentene	*n*-Butyllithium	10-Bromo-5-undecanone (**10**)	61
Cyclopentene	*n*-Butyllithium	*n*-Butyl cyclopentyl ketone (**11**)	63
Cyclopentene	*iso*-Propyllithium	*iso*-Propyl cyclopentyl ketone (**12**)	44

Table 2. Effectiveness of electrophiles in the synthesis of unsymmetrical ketones

Electrophile	$PhSO_3H$	CH_3SOCl	$(CF_3CO)_2O$	H_2S	CF_3CO_2H	$(CH_3)_2SO_4$	PhSH	$HSCH_2CO_2H$
12 (Yield, %)	26	44	44	45	54	58	64	91

Table 3. Effectiveness of additives in the reaction of *n*-hexyldichloroborane with *n*-butyllithium aldimine

Additive	$PhNH_2$	$(CF_3CO)_2O$	PhSH	C_2H_5SH	C_2H_5SNa-C_2H_5SH	$HSCH_2CO_2H$
6 (Yield, %)	28	29	45	49	49	50

may be overcome by utilizing $RBCl_2$ instead of R_2BCl.

We examined the reaction of *n*-hexyldichloroborane with lithium aldimine derived from *n*-butyllithium (Scheme 4).

$$CH_3(CH_2)_5BCl_2 + t\text{-Bu-N=C}\begin{matrix}(CH_2)_3CH_3\\ Li\end{matrix} \xrightarrow[2)\ H_2O_2\text{-NaOH}]{1)\ HSCH_2CO_2H} CH_3(CH_2)_5\overset{\overset{O}{\|}}{C}(CH_2)_3CH_3 \quad (4)$$

6 50%

The yield of product (**6**) depends upon the additive (Table 3), thioglycolic acid giving the best result. However, the yield never exceeded 50%, the reason not being clarified.

Additives such as $HSCH_2CO_2H$, C_2H_5SH, PhSH, and $(CF_3CO)_2O$ may act as electrophiles in the manner described above (Scheme 3). The other additives ($PhNH_2$ and C_2H_5SNa–C_2H_5SH) are not electrophilic, but nucleophilic. It seems that these reagents attack the electron deficient boron atom, inducing the migration of hexyl group *via* the borate complex. We might conclude that such a borane as **3** undergoes rearrangement under the influence of both electrophilic and nucleophilic reagents, though the latter agents are less effective. In fact, such rearrangement under electrophilic and nucleophilic conditions is observed in the case of α-bromoboranes.[20]

We then tried the reaction of *n*-hexyl-9-borabicyclo-[3.3.1]nonane (*n*-hexyl-9-BBN) (**13**) with lithium aldimine derived from *n*-butyllithium (Scheme 5).

The simple oxidation of reaction mixture gave **6** in 69% yield. When thioglycolic acid was employed before the oxidation, **6** was produced in only 4% yield. Instead, a large amount of diol was detected by glpc analysis, which presumably arose from the migration of 9-BBN ring. This suggests that the borate intermediate (**14**) undergoes rearrangement more easily than the borane intermediate (**3**); presumably the migration in **14** proceeds without assistance of electrophilic or nucleophilic reagents to produce the borane intermediate.[21]

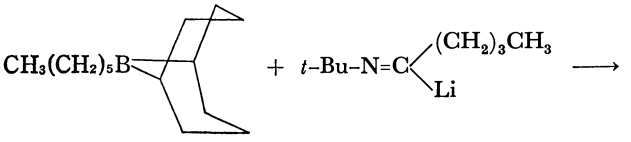

13

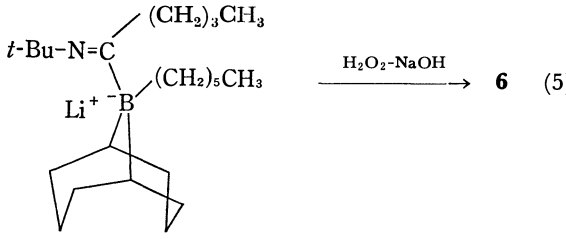

14

The reaction of trialkylboranes with lithium aldimines was in sharp contrast with that of dialkylchloroboranes. In the case of R_2BCl, the migration of second alkyl group (R) was very difficult under the conditions (i) $HSCH_2CO_2H$–(ii) H_2O_2–NaOH (Scheme 3). On the other hand, in the case of R_3B, the migration was very facile, leading to the trialkylcarbinylborane ($R_2R'C$–B<). [22] However, this was avoided by the removal of thioglycolic acid as shown in Scheme 5. In contrast to **13**, the reaction with tri-*n*-hexylborane with *n*-butyllithium aldimine followed by treatment with H_2O_2–NaOH gave 7-*n*-butyl-7-tridecanol in 19% yield along with **6**.[22] This can be explained by the fact that the ease of migration of the primary alkyl group (*e.g.* *n*-hexyl) is greater than that of the secondary one (*e.g.* 9-BBN ring).

In conclusion, the reaction of dialkylchloroboranes with lithium aldimines is recommended for the syn-

thesis of unsymmetrical ketones. When the loss of one alkyl group in R_2BCl causes a serious problem, the utilization of 9-borabicyclo[3.3.1]nonane derivatives might remove the difficulty.

Experimental

All boiling points are uncorrected. The IR spectra were obtained on a Hitachi 215 spectrophotometer. The NMR spectra were obtained on a JEOL JNM-MH-60 spectrometer, TMS being chosen as an internal standard. The elemental analysis was performed by Mr. Y. Harada in our Department. Glpc analyses were carried out on a Yanagimoto GCG 550T using a 2 m column packed with Carbowax 20 M or SE-30 10 wt% on Celite 545 AW.

Materials. Reagent grade solvents were purified by standard techniques and kept over a drying agent. B_2H_6: THF, $BH_2Cl : OEt_2$, $BHCl_2 : OEt_2$, dialkylchloroboranes, tri-*n*-hexylborane, *n*-hexyl-9-borabicyclo[3.3.1]nonane, and *n*-hexyldichloroborane were prepared according to the known procedures.[23] Commercial 1-hexene, cyclopentene, the electrophiles, and *n*-butyllithium in hexane were used. Other alkyllithiums were prepared by standard procedures (ethyllithium in ether,[24] isoamyllithium in ether,[24] and isopropyllithium in pentane[25]). Titration was performed according to the method of Gilman and Haubein[26] or that of Watson and Eastham.[27] 5-Bromo-1-pentene[28] and *t*-butylisonitrile[29] were prepared according to the methods previously reported.

Reaction of Lithium Aldimine with Dialkylchloroborane. General Procedure: In a 200-ml flask maintained under N_2 and fitted with a septum inlet, magnetic stirrer, and reflux condenser, were placed *t*-butylisonitrile (3.6 ml, 30 mmol) and dry ether (60 ml). The solution was cooled to 0 °C and a solution of alkyllithium (30 mmol) was added dropwise. The mixture was stirred for 30 min at 0 °C and then cooled to −78 °C with a dry-ice acetone bath. Dialkylchloroborane (30 mmol) was added, and the resulting mixture was kept at −78 °C for 30 min. Thioglycolic acid (4.2 ml, 60 mmol) or trifluoroacetic anhydride (8.4 ml, 60 mmol) was then added, the temperature being regulated to reach room temperature over 1 hr. Oxidation was accomplished by the addition of 6 M aqueous NaOH (10 ml)–30% H_2O_2 (10 ml). The organic phase was separated and the aqueous layer was extracted with ether. The combined organic layer was dried over anhydrous K_2CO_3. The solvent was removed under reduced pressure and the product was filtered through the column of silica (*ca.* 200 g). The ketones were eluted with benzene in substantially pure form. The ketones were then distilled under reduced pressure and/or subjected to a preparative glpc to obtain analytically pure materials. Alcohols were removed from the column with ether. No attempt was made to attain optimum yields of individual ketones, but all were subjected to the general procedure described above. The spectral data, boiling points and n_D are summarized in Table 4. Authentic samples of **6** and **8**, commercially available, were used. The other authentic samples (**7**, **9**, **11**, and **12**) were independently prepared by the reported procedures (Table 4). Elemental analysis was performed on the unknown compound (**10**); (Found: C, 51.40; H, 8.33; Br, 33.00%. Calcd for $C_{10}H_{19}BrO$: C, 51.07; H, 8.14; Br, 33.98%). For the synthesis of **6**—**11** except **12**, trifluoroacetic anhydride was utilized as an electrophile, satisfactory results being obtained. Utilization of thioglycolic acid in these cases improved the yields. Pronounced effect of this reagent was observed in the preparation of **12** (Table 2).

*Reaction of Di-*n*-hexylchloroborane with* n*-Butyllithium Aldimine. Temperature Effect.* Lithium aldimine was prepared as described above. Di-*n*-hexylchloroborane (10 mmol, 2.4 ml) was added at 0 °C to the solution of lithium aldimine. The resulting mixture was stirred for 30 min at 0 °C. Trifluoroacetic anhydride (20 mmol, 2.8 ml) was then added. The mixture was allowed to reach room temperature over 1 hr. Oxidation was accomplished in the normal way. The aqueous layer was saturated with K_2CO_3 and the organic layer was analyzed by glpc with *n*-dodecane as an internal standard. The reaction at −78 °C was carried out according to the general procedure.

Check for the Effectiveness of Electrophiles in the Preparation of ***12***. All reactions (10 mmol scale) were carried out according to the general procedure. Neat electrophiles (20 mmol) (Table 2) were added directly to the reaction mixture, except that H_2S dissolved in ether was added. After oxidation, the aqueous layer was saturated with K_2CO_3 and the organic layer was analyzed by glpc with *n*-dodecane as an internal standard. Increase in the amount of electrophiles did not significantly improve the yield of **12**, though a decrease in the amount lowered the yield.

Table 4. Spectral and physical data of products

Compd No.	Bp, °C/mmHg (lit)	n_D^{20} (lit)	IR (neat) (ν_{max}, cm^{-1})	NMR (δ in CCl_4, J=Hz)
6	82—83/5 (227/760)[30]	1.4287 (n_D^{18} 1.4275)[30]	1710	0.90 (t, 6H, J=6), 1.26 (broad s, 12H), 2.30 (t, 4H, J=7)
7	84—85/4 (126—128/23.5)[31]	1.4308 (1.4307)[31]	1710	0.88 (d, 6H, J=6), 0.88 (t, 3H, J=6), 1.10—1.70 (m, 11H), 2.29 (t, 4H, J=7)
8	67—68/10 (187/751)[32]	1.4210 (1.4208)[32]	1710	0.88 (t, 3H, J=6), 0.97 (t, 3H, J=6), 1.30 (broad s, 8H), 2.33—2.50 (m, 4H)
9	50—51/2 (77/4)[33]	1.4228 (1.4226)[33]	1716	0.88 (t, 3H, J=6), 1.03 (d, 6H, J=7), 1.22—1.65 (m, 8H), 1.96—2.78 (m, 3H)
10	90—91/1	1.4667	1710	0.90 (t, 3H, J=6), 1.11—2.01 (m, 10H), 2.34 (t, 4H, J=7), 3.33 (t, 2H, J=6)
11	77—78/4 (104—106/25)[34]	1.4477 (n_D^{23} 1.4479)[34]	1710	0.89 (t, 3H, J=6), 1.15—1.90 (m, 12H), 2.35 (t, 2H, J=7), 2.65—2.90 (m, 1H)
12	50—52/3 (84/30)[35]	1.4444	1714	1.03 (d, 6H, J=7), 1.61 (broad s, 8H), 2.32—3.16 (m, 2H)

Reaction of n-*Hexyldichloroborane with* n-*Butyllithium Aldimine.* The reaction (10 mmol scale) was carried out according to the general procedure, except for the utilization of *n*-hexyldichloroborane (10 mmol, 1.8 ml) and of pentane as the solvent. Various additives (20 mmol) to induce the migration were examined (Table 3). Analyses were performed by glpc.

Reaction of n-*Hexyl-9-borabicyclo[3.3.1]nonane with* n-*Butyllithium Aldimine.* Lithium aldimine (10 mmol) was prepared as described above. To this solution was added *n*-hexyl-9-borabicyclo[3.3.1]nonane (**13**) prepared from 1-hexene (10 mmol, 1.25 ml) and 9-borabicyclo[3.3.1]nonane (10 mmol) at −78 °C and the resulting mixture was kept at this temperature for 30 min. Oxidation was accomplished after the reaction was allowed to reach room temperature over 1 hr. Analysis was carried out by glpc. Ketone (**6**) was produced in 69% yield.

Thioglycolic acid (20 mmol, 1.4 ml) was added at −78 °C before oxidation. Oxidation and subsequent analysis were performed according to the general procedure. Along with the minor product (**6**, 4%), a large peak with longer retention time was detected in glpc, the precise structure of which was not determined.

References

1) For a preliminary communication, see Y. Yamamoto, K. Kondo, and I. Moritani, *Tetrahedron Lett.*, **1974**, 793.

2) Present address, Kuraray Co. Ltd., Osaka.

3) D. T. Thompson and R. Whyman, "Transition Metals in Homogeneous Catalysis," ed. by G. N. Schrauzer, Marcel Dekker, New York (1971), p. 149.

4) H. C. Brown and M. W. Rathke, *J. Amer. Chem. Soc.*, **89**, 2738 (1967).

5) A. Pelter, M. G. Hutchings, and K. Smith, *Chem. Commun.*, **1970**, 1529; A. Pelter, K. Smith, M. G. Hutchings, and K. Rowe, *J. Chem. Soc. Perkin I*, **1975**, 129.

6) B. A. Carlson and H. C. Brown, *J. Amer. Chem. Soc.*, **95**, 6876 (1973).

7) H. C. Brown, G. W. Kabalka, and M. W. Rathke, *ibid.*, **89**, 4530 (1967); H. C. Brown and E. Negishi, *ibid.*, **89**, 5285 (1967).

8) A. Pelter, M. G. Hutchings, and K. Smith, *Chem. Commun.*, **1971**, 1048.

9) A. Suzuki, A. Arase, H. Matsumoto, M. Itoh, H. C. Brown, M. M. Rogić, and M. W. Rathke, *J. Amer. Chem. Soc.*, **89**, 5708 (1967); G. W. Kabalka, H. C. Brown, A. Suzuki, S. Homma, A. Arase, and M. Itoh, *ibid.*, **92**, 710 (1970); H. C. Brown and G. W. Kabalka, *ibid.*, **92**, 712 (1970); A. Suzuki, S. Nozawa, M. Itoh, H. C. Brown, G. W. Kabalka, and G. W. Holland, *ibid.*, **92**, 3503 (1970); H. C. Brown and E. Negishi, *ibid.*, **93**, 3777 (1971); A. Suzuki, S. Nozawa, M. Itoh, H. C. Brown, E. Negishi, and S. K. Gupta, *Chem. Commun.*, **1969**, 1009.

10) H. C. Brown, M. M. Rogić, and M. W. Rathke, *J. Amer. Chem. Soc.*, **90**, 6218 (1968); H. C. Brown, M. M. Rogić, H. Nambu, and M. W. Rathke, *ibid.*, **91**, 2147 (1969); H. C. Brown and M. M. Rogić, *ibid.*, **91**, 4304 (1969); H. C. Brown, H. Nambu, and M. M. Rogić, *ibid.*, **91**, 6852 (1969).

11) J. Hooz and S. Linke, *ibid.*, **90**, 5936 (1968); J. Hooz and D. M. Gunn, *Chem. Commun.*, **1969**, 139; J. Hooz, D. M. Gunn, and H. Kono, *ibid.*, **49**, 2371 (1971); D. J. Pasto and P. W. Wojikowski, *J. Org. Chem.*, **36**, 1790 (1971); D. J. Pasto and K. McReynolds, *Tetrahedron Lett.*, **1971**, 801.

12) S. Yamamoto, M. Shiono, and T. Mukaiyama, *Chem. Lett.*, **1973**, 961.

13) A. Suzuki, M. Tabata, and M. Ueda, *Tetrahedron Lett.*, **1975**, 2195.

14) a) M. Naruse, T. Tomita, K. Utimoto, and H. Nozaki, *Tetrahedron Lett.*, **1973**, 795; *Tetrahedron*, **30**, 835 (1974); M. Naruse, K. Utimoto, and H. Nozaki, *Tetrahedron Lett.*, **1973**, 2741; *Tetrahedron*, **30**, 3037 (1974). b) A. Pelter, C. R. Harrison, and D. Kirkpatrick, *Chem. Commun.*, **1973**, 544; *Tetrahedron Lett.*, **1973**, 4491; A. Pelter, K. J. Gould, and L. A. P. K-Maguire, *Chem. Commun.*, **1974**, 1029. c) *via* other borate complexes, E. Negishi, A. Abramovitch, and R. E. Merrill, *ibid.*, **1975**, 138; E. Negishi, K-W. Chiu, and T. Yoshida, *J. Org. Chem.*, **40**, 1676 (1975); see also, E. Negishi and T. Yoshida, *Chem. Commun.*, **1973**, 606.

15) E. Negishi and H. C. Brown, *Synthesis*, **1974**, 77.

16) H. M. Walborsky and G. E. Niznik, *J. Amer. Chem. Soc.*, **91**, 7778 (1969); G. E. Niznik, W. H. Morrison, III, and H. M. Walborsky, *J. Org. Chem.*, **39**, 600 (1974).

17) G. Hesse, H. Witte, W. Gulden, *Angew. Chem.*, **77**, 591 (1965); *Tetrahedron Lett.*, **1966**, 2707.

18) J. Casanova, Jr., "Isonitrile Chemistry," ed. by I. Ugi, Academic, New York (1971), p. 109.

19) A. Pelter, M. G. Hutchings, K. Smith, and D. J. Williams, *J. Chem. Soc. Perkin I*, **1975**, 145.

20) H. C. Brown and Y. Yamamoto, *J. Amer. Chem. Soc.*, **93**, 2796 (1971); *Chem. Commun.*, **1972**, 71.

21) We assume that a borane intermediate such as **15** is involved in the reaction. The oxidation leads to the formation of **6**. The treatment with $HSCH_2CO_2H$ presumably induces the migration of 9-BBN ring. However, these are assumptions, and no evidence has so far been obtained.

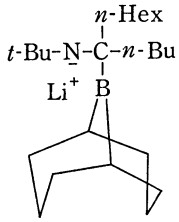

15

22) Y. Yamamoto, K. Kondo, and I. Moritani, *J. Org. Chem.*, in press.

23) H. C. Brown, "Organic Syntheses *via* Boranes," Wiley, New York (1975).

24) The same procedure as that for the preparation of *n*-butyllithium was employed ("Organic Reactions," Vol. 6 (1951), p. 352).

25) H. Gilman, F. W. Moore, and O. Baine, *J. Amer. Chem. Soc.*, **63**, 2479 (1941).

26) H. Gilman and A. H. Haubein, *ibid.*, **66**, 1515 (1944).

27) S. C. Watson and J. F. Eastham, *J. Organometal. Chem.*, **9**, 165 (1967).

28) J. I. G. Cadogan, D. H. Hey, and S. H. Ong, *J. Chem. Soc.*, **1965**, 1932.

29) The same method as that for the preparation of 1,1,3,3-tetramethylbutylisonitrile was employed "Organic Syntheses," Vol. 51 (1971), p. 31).

30) "Handbook of Chemistry and Physics," 53rd ed., The Chemical Rubber Company, Cleveland ,1973.

31) S. G. Powell and F. Hagemann, *J. Amer. Chem. Soc.*, **66**, 374 (1944).

32) E. Vogel, *J. Chem. Soc.*, **1948**, 613.

33) H. H. Morris and R. H. Young, Jr., *J. Amer. Chem. Soc.*, **77**, 6678 (1955).

34) G. Vavon and A. Guedon, *Bull. Soc. Chim.*, **47**, 901 (1930).

35) J. Crouzet, L. Giral, G. Cauquil, and J. Rouzaud, *Bull. Soc. Chim. Fr.*, **1967**, 3722.

Restricted Rotation Involving the Tetrahedral Carbon. XVII. Isolation of Three "Diastereomeric" Rotamers of a Triptycene Type Compound and Stereoselectivity in the Synthesis[1]

Gaku YAMAMOTO and Michinori ŌKI*

Department of Chemistry, Faculty of Science, The University of Tokyo, Tokyo 113

(Received July 4, 1975)

Three rotameric forms of 2,3-dichloro-9-(1,1-dimethyl-2-phenylethyl)-11,12-bis(methoxycarbonyl)-9,10-dihydro-9,10-ethenoanthracene (**3**) were isolated as stable entities at room temperature. The structural assignment of the rotamers based on the PMR characteristics. Since the synthesis of **3** produced only the *ap* form, another reaction involving benzyne was carried out to test the generality of the stereoselectivity. Thus the *ap* form and the *sc* form of 2,3-dichloro-9-(1,1-dimethyl-2-phenylethyl)triptycene (**4**) were prepared separately. Equilibration of isomers of **4** was carried out and the barrier to isomerization was obtained as 36.6 kcal/mol.

A triptycene type compound (**1**) was found to possess an extremely high barrier to rotation about the bond between the *t*-butyl group and the skeleton.[2] As an extention, racemic and *meso* forms of **2** were isolated[3] and the racemic form was resolved into enantiomers.[1]

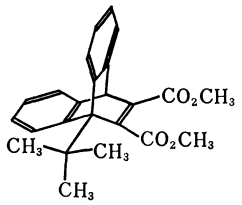

(**1**)

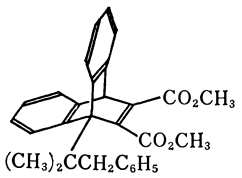

(**2**)

Since **2** has no asymmetric carbon atom, optical resolution was necessary to isolate all the possible rotational isomers. However, if a like compound has a center of asymmetry, the frozen rotation should result in the formation of stable diastereomers, although the compound has only one asymmetric center. If this is the case, the three isomers should be separated by physical means such as chromatography. We wish to report, in the first half of this paper, the realization of such expectation: three isomers of 2,3-dichloro-9-(1,1-dimethyl-2-phenylethyl)-11,12-bis(methoxycarbonyl)-9,10-dihydro-9,10-ethenoanthracene (**3**) were isolated by chromatography.[4]

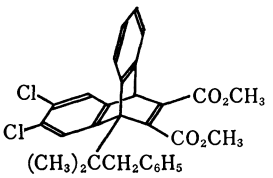

(**3**)

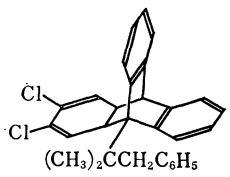

(**4**)

The second half of this paper is mainly concerned with the stereoselectivity in the Diels-Alder type reaction of 9-(1,1-dimethyl-2-phenylethyl)anthracene (**5**) and its 2,3-dichloro derivative (**6**). Since the reaction of **5** with dimethyl acetylenedicarboxylate is known to produce the *meso* form almost exclusively[1,3] and **6** was found to react similarly, it must be interesting to see the generality of the stereoselectivity. We wish to report that the Diels-Alder reaction of **6** as well as **5** is really stereoselective and rotameric *sc* (*dl*) and *ap* (*meso*) forms of a triptycene derivative can be prepared separately.[5]

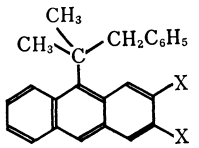

X=H (**5**)
X=Cl (**6**)

Results and Discussion

The required anthracene **6** was prepared by Grignard reaction between 2,3-dichloroanthrone (**7**) and 1,1-dimethyl-2-phenylethylmagnesium chloride followed by dehydration.

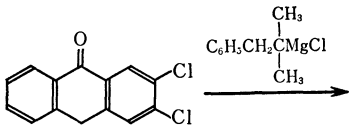

(**7**)

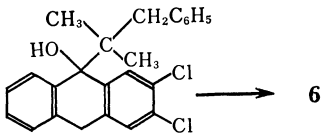

6

Diels-Alder reaction between **6** and dimethyl acetylenedicarboxylate was carried out by heating the substrates in toluene. Chromatography of the product followed by recrystallization gave pure compound in 42% yield which was a sole isomer, as judged from the PMR data (see Table 1). If one considers the mechanical loss during the purification processes this yield must be taken as an indication of high selectivity of the reaction.

The assignment of the structure caused trouble, because there are three possible isomers and only one

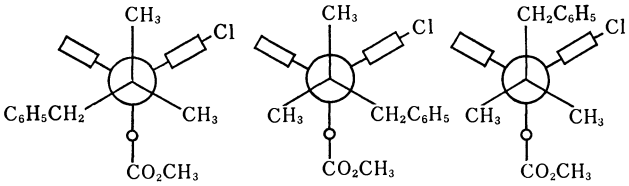

(**3a**) *M-sc* Form (**3b**) *P-sc* Form (**3c**) *ap* Form

(only the 9-(*R*) forms are shown)

was isolated. Thus, in order to obtain other isomers, thermal equilibration was carried out.

The equilibration of rotational isomers (**3a**, **3b**, and **3c**) was reached within 8 hr by heating an *o*-dichlorobenzene solution of **3** at 150 °C. A half-life of **3** under these conditions was *ca.* 2 hr, although it was not possible to run the kinetic study due to the heavy overlap of the signals concerned. The isomer ratio at the equilibrium was estimated to be 3 : 3 : 2.

The equilibrated mixture was chromatographed on silica gel, benzene being used as an eluent. Separation of the least populated isomer was not difficult by this means, because it was eluted most sluggishly among the isomers. This isomer gave identical spectral data with the one obtained by the Diels-Alder reaction and is named Isomer C. Separation of the remaining two isomers was tedious but spectroscopically pure isomers were obtained by repeating the chromatographic operations ten times.* These were named Isomers A and B, respectively, according to the ease of elution. Heating these isomers in *o*-dichlorobenzene caused redistribution of the isomers and afforded the equilibrium mixtures with the identical composition, as judged from the PMR spectra. Thus the rotational isomers could be separated by physical means, because they correspond to diastereomers with each other in spite of the fact that they have only one asymmetric carbon atom.

The PMR data are summarized in Table 1. Theoretically two methyls and two benzyl methylene protons should be nonequivalent because they are located closely to the chiral center. Some peaks showed coincidence of the chemical shifts in one solvent, although they appeared as two different ones in another solvent.

Having all the possible isomers in hand, we may proceed to the assignment of the structures. The PMR spectral data in Table 1 did not seem to be helpful because the differences in chemical shifts of various corresponding signals were too small to draw a definite conclusion. Fortunately however, examination of the whole region of the PMR spectra indicated that there were typical differences in the patterns of signals at the lowest part of the aromatic region. Since the severe steric effect is given by the 9-*t*-alkyl group, the peri protons are expected to give signals at the low field due to the compression effect. The integrated areas (2H) correspond well to the number of the peri protons also.

For the assignment of the structure, comparison of

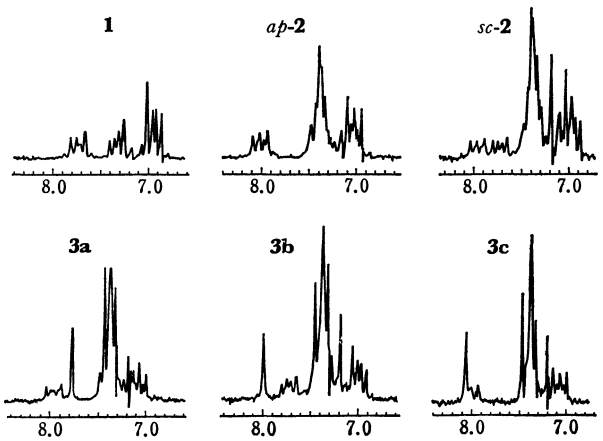

Fig. 1. Shapes of the peri proton signals.

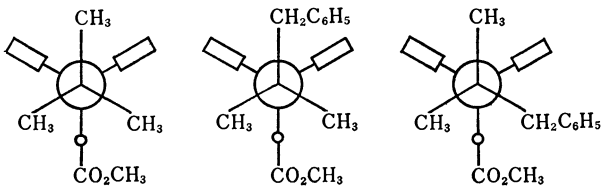

(**1'**) (*ap*-**2**) (*sc*-**2**)

* The PMR spectral charts of these compounds are given in a short communication.[4]

Table 1. Physical properties and PMR data of the isomers of **3**

Isomer	A	B	C
Assignment	**3a**	**3b**	**3c**
Mp (°C)	oil	oil	215.5—216.5
Chromatographic behavior	eluted first	eluted second closely behind the first	eluted last
Relative population at equilibrium (152 °C)	3	3	2
PMR data			
Solvent / Assignment	$CDCl_3$ / C_6D_6	$CDCl_3$ / C_6D_6	$CDCl_3$ / C_6D_6
C-CH_3	1.80 / 1.63	1.77 / 1.67	1.71 / 1.72
	/ 1.80	1.88 / 1.94	1.80 / 1.89
O-CH_3	3.74 / 3.33	3.74 / 3.33	3.68 / 3.28
	3.77 / 3.47	3.77 / 3.47	3.75 / 3.40
C-CH_2	3.60 q / 3.80	3.50 q / 3.77	3.69 q / 3.49 q
	J=14.1 Hz, $\Delta\nu$=15.6 Hz	J=14.1 Hz, $\Delta\nu$=12.1 Hz	J=14.6 Hz, $\Delta\nu$= 8.7 Hz / J=14.4 Hz, $\Delta\nu$=11.8 Hz
10-H	5.49 / 5.44	5.49 / 5.44	5.49 / 5.44
1-H	7.76 / 7.75	7.99 / 8.04	8.05 / 8.05
8-H	7.9 m / 7.9 m	7.7 m / 7.7 m	8.0 / 8.0 m

the chemical shifts and/or shapes of the signals with the model compounds may be helpful. Thus the peri proton signal shapes of the isomers are shown in Fig. 1 together with those of **1**, *ap*-**2**, and *sc*-**2**.

Inspection of the Newman-type projections of **1** and **2** reveals that the peri protons in **1** are equivalent because they are both located between two methyls, and those in *ap*-**2** are also equivalent because they are both placed between a methyl and a benzyl group. On the other hand, peri protons in *sc*-**2** are not equivalent: one is placed between two methyls and the other between a methyl and a benzyl group. The spectra in Fig. 1 conform with this expectation and it can now be concluded that the multiplet signal centered at δ 7.7 corresponds to a peri proton placed between two methyl groups and the multiplet centered at δ 8.0 to a peri proton placed between a methyl and a benzyl groups.

Now that the isomers in question have a chlorine atom ortho to the peri proton, the assignment may be possible by taking advantage of the substituent. Fortunately a chloro substituent in the aromatic ring is known to give little effect on the chemical shift of the protons ortho to it.[6] The chloro substituents in **3** will cause the appearance of an apparent singlet of the peri proton because they erase the ortho and meta couplings and the para coupling is small. Thus it may be assumed that a peri proton ortho to the chloro group gives a singlet at about the same chemical shift with the corresponding protons in **1** and **2**.

Since Isomer A, which is eluted first, gives a sharp signal at δ 7.7 and a multiplet centered at δ 8.0, it should have two kinds of peri protons: one is ortho to a chloro group and placed between two methyl groups and the other is placed between a methyl and a benzyl group. **3a**, which is the *M-sc* form, is qualified to meet the above conditions. Thus Isomer A is the *M-sc* form. Likewise, Isomer B which is eluted closely behind Isomer A is concluded to have a peri proton which is ortho to a chloro substituent and placed between a methyl and a benzyl group and another peri proton which is placed between two methyl groups. Thus isomer B is **3b** which is the *P-sc* form. Isomer C should possess both peri protons placed between a benzyl and a methyl group and thus is the *ap* form (**3c**).

After the establishment of the structural assignment, the composition of the equilibrium mixture may be compared with the data of **1** which gave $K=3.0$ at various temperatures in favor of the *sc* form.[3,4] Since **3a** and **3b** are the *sc* forms and **3c** the *ap*, the sum of **3a** and **3b** may be taken in discussing the thermal stability of the isomers. Then the ratio is obtained as *sc* : *ap* $=3:1$ which coincides with the equilibrium constant of **1**. From these data, it may be concluded that the two chloro groups in compound **3** play little role in determining the thermodynamic stability. This is so probably because the chloro groups are located distantly from the *t*-alkyl group. The same population of the *M-sc* and *P-sc* forms is another indication that the remote chloro groups have scarce effect on the stability.

The almost exclusive formation of the *ap* form in the Diels-Alder reaction is interesting. This stereoselectivity matches that obtained in the reaction of **5** with dimethyl acetylenedicarboxylate, in which *ca.* 85% of the product was the one formed by the attack from the least hindered side. A possible explanation was described in a preceding paper.[1] Although it may be possible to postulate that the rotation about the C_9–C_{alkyl} bond is frozen, the postulate is not consistent with the facts that no anomaly is found in PMR spectra and the selectivity is not exclusive in the case of **5**. Some steric and electronic effects may be responsible in causing the results.

It is then tempting to investigate the scope of the selectivity. Accordingly Diels-Alder reaction between **6** and benzyne was carried out. If the reaction is really stereoselective, an expected product is the *sc* form (*dl* form), because the attack of benzyne from the

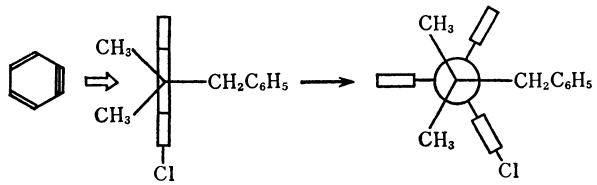

(*sc*-**4**)

Scheme 1.

least hindered side will proceed as depicted in scheme 1. Only one product was isolated indeed. A PMR spectrum of the product shows the presence of a non-equivalent set of methyls and that of benzyl methylene protons to indicate that it is really an *sc*-form. The peri proton signals are also consistent with this assignment and the following signals are found: a multiplet centered at δ 7.73 corresponding to 1 H which is placed between two methyl groups, a multiplet centered at δ 7.95 corresponding to 1 H which is placed between a methyl and a benzyl group, and a sharp singlet at δ 8.03 corresponding to 1 H which is ortho to a chloro substituent and placed between a methyl and benzyl group.

The stereoselectivity discussed above seemed to open up a way for the synthesis of individual rotational isomers. If the combination of **6** and benzyne gives the *sc* (or *dl*) isomer, the combination of **5** and 4,5-dichlorobenzyne should give the *ap* (or *meso*) form (Scheme 2). The actual synthesis proceeded as expected and a sole product was obtained, of which structure was evident from the PMR data: one methyl signal (δ 2.02, 6H), a sharp singlet (δ 3.86) for the benzyl methylene, two peri protons (a multiplet centered at δ 7.95) placed between a methyl and a benzyl group, and one peri proton (δ 7.78) which is ortho to a chloro substituent and placed between two methyl groups.

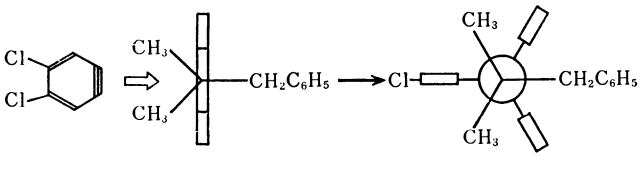

(*ap*-**4**)

Scheme 2.

The equilibration between *ap*-**4** and *sc*-**4** proceeded sluggishly: no isomer was detected after heating either *ap*-**4** or *sc*-**4** in *o*-dichlorobenzene at the boiling point for 60 hr. Apparently, the higher temperature was needed to cause equilibration in the practical rate. The choice of a solvent caused trouble, however. A high boiling solvent tends to have the higher viscosity at room temperature, causing the difficulty in PMR spectroscopy. 1-Chloronaphthalene was chosen as a solvent from these aspects.

In principle, the population of each isomer can be determined by careful integration of the methyl or other signals. In practice, however, due to the heavy overlap of the signals, it was not possible to obtain the population directly from the simple integration. Thus calibration curves were drawn by the procedure described in the experimental section and first order rate constants k_1 (*ap*→*sc*) and equilibrium constants K were obtained at four temperatures in the range of 211—259 °C. The results are given in Table 2.

Table 2. Rates of isomerization of *ap*-**4** and the equilibrium constants for *ap*-**4** ⇌ *sc*-**4**

T °C	k_1 (s^{-1})	K
259	4.1×10^{-4}	2.0
245	1.6×10^{-4}	2.0
232	7.5×10^{-5}	2.0
211	1.3×10^{-5}	2.0

Table 3. Kinetic parameters for isomerization *ap*-**4** → *sc*-**4**

E_a=36.6 kcal/mol	ΔH=35.7 kcal/mol
log A=11.7	ΔS=−7.9 eu

Arrhenius and Eyring plots of k_1's gave the good linear relationship and thermodynamic parameters were obtained as shown in Table 3. The Arrhenius activation energy of 36.6 kcal/mol is one of the highest barriers to the isomerization of this type.[7] Interconversions of the atropisomers may be most reasonably assumed to proceed through rotation about the axis bond, although other possibilities such as a retro-Diels-Alder reaction and ionic or radical type fission-recombination mechanisms cannot be ruled out. Then this barrier is one of the highest to rotation about a C_{sp^3}–C_{sp^3} bond.

The equilibrium constant remained constant throughout the temperature range examined. Thus the equilibrium is controlled by the entropy factor. Indeed there are two enantiomeric *sc* forms which are energetically identical. In this case also, two chloro groups in a benzo group seems to give little effect on the enthalpy of the atropisomers.

Finally we wish to comment on the conformation of the benzyl group in the compounds studied here. The typical features of the PMR spectra are that 1) a peri proton gauche to the benzyl group gives the signal at *ca.* δ 8.0 which is lower by *ca.* 0.3 ppm than a peri proton *trans* to the benzyl and 2) the coupling constants of the benzyl methylenes are *ca.* 14 Hz. These features are best explained if one assumes the conformation such as **8**, because, in this conformation, the peri protons gauche to the benzyl group are located in the deshielding region of the benzene ring and the coupling constants agree with the theoretical value of this conformation.[9] Molecular models support this conformation on the ground of the steric effect and a fact that the chemical shifts of the methyl groups in *ap*-**4** are close to that of the methyl groups of 9-*t*-butyltriptycene may be another support, because the methyls are located in the region where little anisotropy effect of the benzene ring is expected.

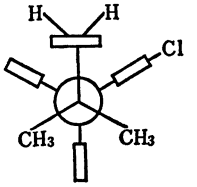

(**8**)

Experimental

2,3-Dichloroanthrone. A suspension of 39 g (0.14 mol) of 2,3-dichloroanthraquinone[9] and 8 g of red phosphorus in 1.5 l of acetic acid and 66 ml of hydriodic acid was heated under reflux for 5 hr. The resulted mixture was concentrated by removal of *ca.* 700 ml of the solvent by distillation and the concentrate was cooled to room temperature. The solid was collected by filtration and extracted with 300 ml of boiling benzene. The benzene extract was cooled to give 26 g (70%) of yellow crystals, mp 198—200 °C. This compound was directly used for the next synthesis.

2,3-Dichloro-9-(1,1-dimethyl-2-phenylethyl)anthracene (**6**). To a chilled solution of a Grignard reagent prepared from 42 g (0.25 mol) of 1,1-dimethyl-2-phenylethyl chloride, was added 22.8 g (0.1 mol) of 2,3-dichloroanthrone powder in small portions during the course of 1 hr. The reaction mixture was decomposed with aqueous ammonium chloride. The ethereal solution was filtered and evaporated. The resulting oil was dissolved in 200 ml of carbon tetrachloride and heated with *ca.* 30 g of phosphorus pentoxide under reflux for 5 hr. The carbon tetrachloride solution was decanted and evaporated. The residue was chromatographed on alumina. Elution with 9 : 1 hexane-benzene gave 2.95 g (7.9%) of yellow fluorescent crystals, mp 121—123 °C. PMR (δ, CCl_4): 1.73 (6H, s), 3.63 (2H, s), 6.9—8.3 (12H, m). Found: C, 76.68; H, 5.11; Cl, 18.48%. Calcd for $C_{24}H_{20}Cl_2$: C, 75.99; H, 5.31; Cl, 18.69%.

ap-*2,3-Dichloro-9-(1,1-dimethyl-2-phenylethyl)-11,12-bis(methoxycarbonyl)-9,10-dihydro-9,10-ethenoanthracene* (**3c**). A solution of 1.53 g (4.0 mmol) of the anthracene (**6**) and 1 ml of dimethyl acetylenedicarboxylate in toluene was heated under reflux for 5 hr. The reaction mixture was chromatographed on silica gel with benzene as an eluent. Recrystallization of the product from benzene-methanol gave 0.87 g (42%) of colorless crystals, mp 215.5—216.5 °C. Found: C, 69.24; H, 5.07; Cl, 13.68%. Calcd for $C_{30}H_{26}O_4Cl_2$: C, 69.10; H, 5.03; Cl, 13.60%.

Isomerization of **3c** *and Separation of the Isomers.* Heating a solution of **3c** in *o*-dichlorobenzene at 152 °C for 10 hr caused equilibration of the rotamers, the composition being 3 : 3 : 2. The least populated isomer was the *ap* form. The solvent was evaporated *in vacuo* and the residue was taken up in benzene. The chromatographic behavior of the *ap* form was different enough to separate it from other two but those of *M-sc* and *P-sc* forms were quite close to

cause the heavy overlap of the chromatographic bands. Nonetheless it was possible to isolate pure *M-sc* and *P-sc* forms after repeated chromatographies. The *M-sc* form and *P-sc* form resisted crystallization but they showed no peaks attributable to impurities in PMR spectra. Heating either the *M-sc* or the *P-sc* form in *o*-dichlorobenzene at 152 °C caused isomerization and gave the equilibrium mixture of the identical composition with the one obtained from the *ap* form. This can be taken as another piece of evidence for the structures of the *sc* forms.

sc-*2,3-Dichloro-9-(1,1-dimethyl-2-phenylethyl)triptycene* (sc-**4**). To a boiling solution of 1.30 g (3.43 mmol) of **6** and 2 ml of isoamyl nitrite in *ca.* 20 ml of methylene chloride, was added a solution of 600 mg (4.4 mmol) of anthranilic acid in 10 ml of tetrahydrofuran over a period of 1 hr. The mixture was heated for another hour and then the solvent was evaporated. The residue was chromatographed on alumina with the use of 9 : 1 hexane–benzene as an eluent. Recrystallization of the product from tetrahydrofuran–methanol gave 1.29 g (83%) of colorless crystals, mp 215.5—216.5 °C. Found: C, 79.40; H, 5.47: Cl, 15.65%. Calcd for $C_{30}H_{24}Cl_2$: C, 79.12; H, 5.31; Cl, 15.57%. PMR (δ, $CDCl_3$): 1.99 (3H, s), 2.08 (3H, s), 3.75 and 3.89 (2H, q, J=14.6 Hz), 5.17 (1H, s), 6.7—7.6 (12H, m), 7.73 (1H, m), 7.95 (1H, m), 8.03 (1H, s).

4,5-Dichloroanthranilic acid was obtained by hydrogenation of 4,5-dichloro-2-nitrobenzoic acid[10] and used for generation of dichlorobenzyne.

ap-*2,3-Dichloro-9-(1,1-dimethyl-2-phenylethyl)triptycene* (ap-**4**). Treatment of the anthracene (**6**) with 3,4-dichloroanthranilic acid and isoamyl nitrite in boiling methylene chloride–tetrahydrofuran, as described in the preparation of the *sc* form, caused precipitation of reddish brown solid which was found to be the corresponding diazonium carboxylate from the IR spectrum ($N^+{\equiv}N$, 2280 cm^{-1}). The solution contained *ca.* 7 : 3 mixture of the anthracene and the triptycene. Thus the decomposition of the diazonium salt seemed to require the higher temperature.

A mixture of 3.10 g (10 mmol) of the anthracene and 2.38 g of the diazonium salt (*ca.* 11 mmol) in 80 ml of chlorobenzene was heated at 100 °C for 1 hr. Evolution of gas and disappearance of the solid were observed. The solvent was evaporated and the residue was taken up in hexane. Chromatagraphy on alumina with the use of 9 : 1 hexane–benzene gave colorless crystals which were recrystallized from tetrahydrofuran–methanol. The *ap* form was obtained as colorless crystals, mp 200—201 °C, in 3.97 g (88%) yield. Found: C, 79.29; H, 5.53; Cl, 15.68%. Calcd for $C_{30}H_{24}Cl_2$: C, 79.12; H, 5.31; Cl, 15.57%. PMR (δ, $CDCl_3$): 2.02 (6H, s), 3.86 (2H, s); 5.17 (1H, s), 6.8—7.6 (12H, m), 7.78 (1H, s), 7.96 (2H, m).

Equilibration and Determination of Rates of Isomerization. *ap*-**4** was dissolved in 1-chloronaphthalene to make up 4.8 (w/w)% solution and sealed in an NMR sample tube. The sample tube was immersed in a boiling solvent bath and PMR spectra were determined at 34 °C with appropriate intervals. The solvents used for the bath and the boiling points were as follows: diphenyl ether 259 °C, diethylene glycol 245 °C, *m*-nitrotoluene 232 °C, nitrobenzene 211 °C.

A calibration curve was drawn by the following procedure. A 4.8 (w/w)% solution in 1-chloronaphthalene was prepared for each of the *ap* and the *sc* form. These two solutions were mixed in various ratios to make up solutions of which concentration remained 4.8 (w/w)% when the sum of both forms was taken. For each solution thus made up, the ratio of the apparent height of the methyl signals of the *ap* form to that of the lower field methyl signal of the *sc* form was observed and plotted against

$$-\log\left\{1-\left(1+\frac{1}{K}\right)\frac{[sc]}{[sc]+[ap]}\right\}$$

which was calculated from the known $[sc]/[ap]$ values. Using this calibration curve, the apparent height ratios observed in the kinetic run directly gave the

$$-\log\left\{1-\left(1+\frac{1}{K}\right)\frac{[sc]}{[sc]+[ap]}\right\}$$

values which were necessary for kinetic analysis. These values were plotted against time and the slope of the straight line produced the desired rate constants. The equilibrium constants at various temperatures were found to be constant, 2.0, within the experimental error.

Measurement of the Spectra. The PMR spectra were recorded on a Hitachi R-20B spectrometer operating at 60 MHz. Samples were dissolved either in $CDCl_3$ or in C_6D_6 to make up *ca.* 10 (w/w)% solutions, unless otherwise stated.

References

1) Preceding paper: G. Yamamoto, N. Nakamura, and M. Ōki, This Bulletin, **48**, 2592 (1975).
2) M. Ōki and M. Suda, *ibid.*, **44**, 1876 (1971).
3) M. Ōki and G. Yamamoto, *Chem. Lett.*, **1972**, 45.
4) A preliminary paper has been published: G. Yamamoto and M. Ōki, *Chem. Lett.*, **1974**, 67.
5) A preliminary paper has been published: G. Yamamoto and M. Ōki, *Chem. Commun.*, **1974**, 713.
6) H. Spiesecke and W. G. Schneider, *J. Chem. Phys.*, **33**, 731 (1961).
7) H. Iwamura, *Chem. Commun.*, **1973**, 232.
8) J. A. Pople and A. A. Bothner-By, *J. Chem. Phys.*, **42**, 1339 (1965): M. Barfield and D. M. Grant, *J. Amer. Chem. Soc.*, **85**, 1899 (1963).
9) M. Hida, *Yuki Kagobutsu Gosei Ho* (*Methods of Organic Syntheses*), **16**, 25 (1965).
10) P. Ruggli and H. Zaeslin, *Helv. Chim. Acta*, **19**, 434 (1936).

Studies on Interaction of Isocyanide with Transition Metal Complexes. XIII.[1] Preparation of Carbene Complexes of Nickel, Iron, and Cobalt through Protonation of Monoimino and Polyimino Type Complexes

Yasuhiro YAMAMOTO and Hiroshi YAMAZAKI

The Institute of Physical and Chemical Research, Wako-shi, Saitama 351

(Received July 7, 1975)

Reactions of η-$C_5H_5Ni(CNR^1)[C(R)=NR^1]$ ($R=CH_3$, p-ClC_6H_4; $R^1=C_6H_{11}$, $(CH_3)_3C$) and η-$C_5H_5Fe(CO)_2$-$[C(CH_2C_6H_4X\text{-}p)=NC_6H_{11}]$ (X=H, Cl) with HBF_4 gave the cationic carbene complexes, η-$C_5H_5Ni(CNR^1)$-$[C(R)NHR^1]BF_4$ and η-$C_5H_5Fe(CO)_2[C(CH_2C_6H_4X\text{-}p)$ $NHC_6H_{11}]BF_4$. η-$C_5H_5Co[-C(=NR)-CPh=CPh-C(=NR)-]$ (**1a**; $R=2,6\text{-}(CH_3)_2C_6H_3$: **1b**; $R=p\text{-}CH_3C_6H_4$) reacted with HBF_4 to give η-$C_5H_5Co[-C(NHR)-CPh=CPh-C(=NR)-]BF_4$ (**2a, b**). Compound **2a** exists as two isomers, induced by the restricted rotation about the C–N bond. Treatment of **1a** with HCl gave η-$C_5H_5Co[-C(NHR)-CPh=CPh-C(=NR)-]Cl$ (**3b**). The H(N) proton showed some fluxional behavior in its proton NMR spectrum. Reaction of **1b** with CF_3COOH gave the dicationic complex η-$C_5H_5Co[-C(NHR)-CPh=CPh-C(NHR)-](CF_3COO)_2$ **4b**. Compound **2** reacted with R^1NC ($R^1=(CH_3)_3C$, $2,6\text{-}(CH_3)_2C_6H_3$) to give η-$C_5H_5Co(CNR^1)[-C(=NR)-CPh=CPh-C(=NR)-]$**5**. Reaction of **5** with HBF_4 gave again the cationic carbene complex η-$C_5H_5Co(CNR^1)[-C(NHR)-CPh=CPh-C(=NR)-]BF_4$.

Since the current interest of the metal-stabilized carbene complexes started with the preparation of $W[C(OCH_3)Ph](CO)_5$,[2] several preparative methods of the carbene complexes have been reported.[3–5] Among them, the acetyl complexes of iron, molybdenum, and ruthenium are known to take up a proton or a carbonium ion to give the corresponding cationic carbene complexes, when reacted with protic acids or trialkyloxonium salt (Eq. (1)).[6,7]

$$M\text{—}\underset{\underset{O}{\|}}{C}\text{—}R + R^{1+} \longrightarrow [M\leftarrow\underset{\underset{OR^1}{|}}{C}\text{—}R]^+ \qquad (1)$$

One would expect that more facile protonation of the imino type complex in comparison with the acetyl derivative may occur because of the higher inherent basicity of nitrogen over oxygen. Treichel *et al.* reported briefly that the reaction of $Pt(PPh_3)_2I[C(Ph)=NCH_3]$ with NH_4^+ produced $Pt(PPh_3)_2I[C(Ph)NH\text{-}CH_3]^+$.[8] Lappart and coworkers reported recently that treatment of rhodium complexes with imidoyl chloride in the presence of hydrogen chloride gave the carbene complexes.[9,10] This reaction has been believed to proceed with protonation of the imino complex formed as the unstable intermediate.

We report in this paper that the imino type compounds of nickel,[11] iron,[12,13] and cobalt[14] react readily with protic acids to give stable cationic carbene complexes.

Experimental

All reactions were carried out under an atmosphere of nitrogen. Melting points were taken on a Mitamura capillary melting point apparatus, and are uncorrected. Infrared spectra were recorded on a Shimadzu IR-27G spectrophotometer. Proton magnetic resonance spectra were obtained on JEOL C-60HL or Varian HA-100B spectrometers, using tetramethylsilane as an internal reference. Isocyanides[15] were prepared by procedures described in the literature. The organometallic complexes, η-C_5H_5Ni-$(CNR^1)[C(R)=NR^1]$ ($R=CH_3$, Ph or p-ClC_6H_4; $R^1=C_6H_{11}$ or $(CH_3)_3C$),[11] η-$C_5H_5Fe(CO)_2[C(CH_2C_6H_4X\text{-}p)=NC_6H_{11}]$ (X=H or Cl)[12], η-$C_5H_5Fe(CO)[-C(=NC_6H_{11})$-$C(NHR^1)-C(R)-C(NHR^2)]$ ($R=H$ or Ph; $R^1=C_6H_{11}$ or $CH_3)_3C$; $R^2=(CH_3)_3C$ or C_6H_{11})[13] and η-$C_5H_5Co[-C(=NR)-CPh=CPh-C(=NR)-]$ ($R=(CH_3)_3C$, p-$CH_3C_6H_4$ or $2,6\text{-}(CH_3)_2C_6H_3$)[14], were prepared according to the published methods.

Preparation of Carbene Complexes. *(a)* η-$C_5H_5Ni(CNC_6H_{11})[C(C_6H_4Cl\text{-}p)NHC_6H_{11}]BF_4$. A mixture of η-C_5H_5-$Ni(CNC_6H_{11})[C(C_6H_4Cl\text{-}p)=NC_6H_{11}]$ [0.22 g, 0.5 mmol), 42% HBF_4 (3 ml) and benzene (15 ml) was stirred for 1 hr at room temperature. The reddish orange solution changed to dark yellow. The benzene layer was separated and the aqueous layer was extracted twice with CH_2Cl_2 (5 ml). The combined extracts were washed with water and dried over anhydrous magnesium sulfate. The solvent was evaporated almost to dryness under reduced pressure, and the residue was crystallized from CH_2Cl_2–*n*-hexane at −30 °C to give the dark yellow crystalline material (0.22 g, 82%). Other nickel carbene complexes were also prepared according to procedures similar to those described above.

(b) η-$C_5H_5Fe(CO)_2[C(CH_2Ph)NHC_6H_{11}]BF_4$. A mixture of η-$C_5H_5Fe(CO)_2[C(CH_2Ph)=NC_6H_{11}]$ (0.7 g, 1.9 mmol), 42% HBF_4 (2 ml) and benzene (15 ml) was stirred for 2 hr at room temperature. Yellow crystalline material was separated. Methylene chloride was added to dissolve the crystals. The organic layer was washed with water and dried over $MgSO_4$. The solvent was removed *in vacuo* and the residue was crystallized from CH_2Cl_2–*n*-hexane at −30 °C to give yellow crystals (0.77 g, 85%). Other iron carbene complexes were also prepared according to procedures similar to those described above.

(c) η-$C_5H_5Co[-C\{=NC_6H_3(CH_3)_2\text{-}2,6\}-CPh=CPh-C\{NHC_6$-$H_3(CH_3)_2\text{-}2,6-\}-]BF_4$. A mixture of η-$C_5H_5Co[-C\{=NC_6H_3(CH_3)_2\text{-}2,6\}-CPh=CPh-C\{=NC_6H_3(CH_3)_2\text{-}2,6\}-]$ (0.18 g, 0.32 mmol), 42% HBF_4 (1 ml) and benzene was stirred at room temperature for 1 hr. The resulting orange crystals were filtered and washed with ether (0.18 g, 86%).[16]

(d) η-$C_5H_5Co[-C(=NC_6H_4CH_3\text{-}p)-CPh=CPh-C(NHC_6H_4$-$CH_3\text{-}p)-]Cl$. A mixture of η-$C_5H_5Co[-C(=NC_6H_4CH_3$-$p)-CPh=CPh-C(=NC_6H_4CH_3\text{-}p)-]$ (0.16 g, 0.3 mmol) and 6M-HCl (4 ml) was kept at room temperature for 2 hr. The orange layer changed to pale yellow. The resulting brown crystalline solid was filtered off, washed with water, and then extracted with benzene. After drying over Na_2SO_4, the solvent was removed under reduced pressure, and the residue was crystallized from *n*-hexane to give the title compound (0.095 g, 56%) as brown crystals.

(e) η-$C_5H_5Co[-C(NHC_6H_4CH_3$-p$)$-CPh=CPh-C(NHC_6H_4$-$CH_3$-p$)-](CF_3COO)_2$. To a solution of **1b** (0.12 g, 0.22 mmol) in CH_2Cl_2 (2 ml) was added CF_3COOH (0.2 ml) at room temperature. The resulting dark brown solution was concentrated to 1 ml under reduced pressure, and *n*-hexane was added. The dark brown crystals (0.17 g, 85%) were filtered off.

Reaction of η-$C_5H_5Ni(CNC_6H_{11})[C(Ph)NHC_6H_{11}]BF_4$ *with* CH_3ONa. A mixture of the carbene complex (0.075 g, 0.13 mmol), CH_3ONa (0.1 g), and CH_3OH (10 ml) was stirred at room temperature for 30 min. The solution changed rapidly from dark yellow to reddish brown. The solvent was evaporated, and the residue was dissolved with CH_2Cl_2. The solution was washed with water and dried over Na_2SO_4. Removal of the solvent and crystallization of the residue from benzene–*n*-hexane gave η-$C_5H_5Ni(CNC_6H_{11})$ [C(Ph)$=$NC$_6$H$_{11}$] (0.84 g, 83%).

Analogous procedures were applied for the deprotonation reactions of the iron and cobalt carbene complexes.

Reaction of **2a** *with* $(CH_3)_3CNC$. A mixture of **2a** (0.25 g, 0.38 mmol) and *tert*-butyl isocyanide (0.83 g, 1.0 mmol) in THF (15 ml) was kept at room temperature for 20 hr, followed by removal of the solvent and dark orange crystals of **5a** (0.19 g, 73%; mp 234—236 °C (decomp. with melting)). The infrared spectrum consisted of 2153-(N≡C), 1623(C=N), and 1584 cm^{-1}(C–N). The proton NMR spectrum in $CDCl_3$ showed four singlets at 1.48(s, $(CH_3)_3$), 2.17(CH_3), 2.23(CH_3), and 4.41(C_5H_5) ppm, and a complex signal at *ca.* 7.00 (C_6H_5 and C_6H_3) ppm. Found: C, 77.65; H, 6.41; N, 6.34%. Calcd for $C_{42}H_{42}N_3Co$: C, 77.88; H, 6.54; N, 6.49%.

Kinetic Analysis. The methods developed by Gutowsky and Holm was applicable for the determination of the kinetic parameters.[17] The difference between the chemical shifts of the methyl protons of the two isomers at various temperatures are listed in Table 1.

TABLE 1. CHEMICAL SHIFT DIFFERENCES FOR METHYL PROTONS IN **2a** AT VARIOUS TEMPERATURES

Temp. (°C)	$\delta\omega_e$ (cycles s^{-1})
−10	43
28	37
36	33
45	30
48	26.5
52	22
59	14

Results and Discussion

Nickel Carbene Complexes. Imino type complexes of nickel react with an excess of HBF_4 in benzene or CH_2Cl_2 at room temperature to produce the cationic carbene complexes (Eq. (2)), which undergo deprotonation by alkyllithium or CH_3ONa to recover the parent imino type complexes.

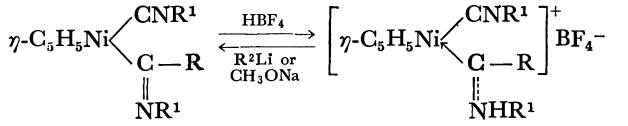

(2)

These compounds are freely soluble in methylene chloride and acetone, but less soluble in benzene. The infrared spectra show the strong NH-stretching bands at 3300—3100 cm^{-1}, which shift to 2700—2500 cm^{-1} on deuteration. The isocyanide absorptions are observed in the range of 2200—2500 cm^{-1}, which are 40—70 cm^{-1} higher than those for the neutral parent compounds.

The proton NMR spectra of these complexes indicate the presence of isomers. The spectrum of η-C_5H_5Ni-[CNC$(CH_3)_3$][C(Ph)NHC$(CH_3)_3$]BF_4 shows a pair of signals for each of the following: C_5H_5, $(CH_3)_3CN$=, and $(CH_3)_3CNH$– protons (the isomer ratio 3 : 1). This is reasonably explained in terms of the orientation of the N–H group. The hydrogen atom could assume either a *cis* or a *trans* orientation to the metal group with respect to the C–N bond, as follows:

M$=\eta$-$C_5H_5Ni(CNR^1)$

Analogous isomerism was observed in the [(*p*-chlorophenyl)(*N*-*tert*-butylamino)]carbene complex (the isomer ratio 1.7 : 1). The [(alkyl or aryl)(*N*-cyclohexylamino)]carbene complexes, however, do not show the presence of isomers. This may arise from the bulkiness of the *N*-substituted group.

We have no direct means to distinguish between the two isomers. However, it is known that the predominant isomer in the metal carbene complexes is generally the one with the least steric interaction within the carbene groups.[4,5] Examination of molecular models of the carbene complexes suggested that the *cis* isomer had less steric interaction than the *trans* isomer.

The ratio between *cis* and *trans* isomers does not depend on the solvents and temperatures ($\lesssim$100 °C), showing restricted rotation about the C_{carb}–nitrogen bond (Table 3). Evidence of restricted rotation about C_{carb}–heteroatom bonds has also been obtained, *e.g.*, in the series *trans*-[MX{C(NHR)Q}L_2]ClO_4 (where M$=$Pt or Pd; R$=$Ph or *p*-$CH_3C_6H_4$; Q$=$PhNH, EtNH, CH_3O or EtO; L$=$$PEt_3$, $PPhMe_2$, or $AsMe_3$; X$=$Cl or Br).[18,19]

Iron Carbene Complexes. The reaction of η-$C_5H_5Fe(CO)_2$[C$(CH_2C_6H_4X$-*p*$)$=NC$_6$H$_{11}$] (X=H or Cl) with HBF_4 proceeds with protonation at the imino nitrogen atom to give the cationic carbene complex in nearly quantitative yield, which was characterized by the infrared N–H stretching frequency. The reaction of this compound with CH_3ONa or PhLi occurs readily with deprotonation to regenerate the parent imino type complex (Eq. (3)).

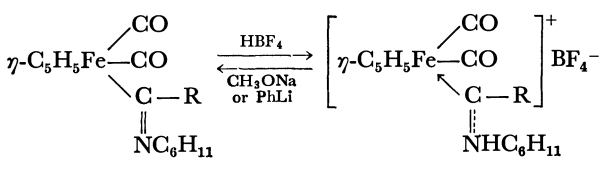

(3)

The proton NMR spectra of the carbene complexes at room and low temperatures ($\geq$−60 °C) do not

TABLE 2. ANALYTICAL AND SPECTROSCOPIC DATA OF NICKEL CARBENE COMPLEXES, η-$C_5H_5Ni(CNR)[C(R^1)NHR]BF_4$

R	R^1	Yield (%)	Mp[a] (°C)	Analyses, Found (Calcd) C	H	N	IR (cm^{-1})[b] N-H	C≡N	C-N
C_6H_{11}	Ph	78	113—115	60.98 (60.83)	6.40 (6.62)	5.14[c] (5.25)	3246 3146	2199	1572
C_6H_{11}	*p*-ClC_6H_4	82	151—153	57.25 (57.14)	5.83 (6.04)	5.06[c] (4.94)	3246 3148	2200	1577
C_6H_{11}	CH_3	78			h)		3235 3143	2231	1575
$(CH_3)_3C$	Ph	69	135—138	55.54 (55.44)	6.31 (6.42)	6.20 (6.16)	3233 3143	2175	
$(CH_3)_3C$	*p*-ClC_6H_4	61	157—159	51.56 (51.54)	5.66 (5.77)	5.63 (5.72)	3248 3152	2171	1578

R	NMR (ppm) in $CDCl_3$[d] C_5H_5	Other signals
C_6H_{11}	5.38	2.22—1.05(c, C_6H_{10}), 4.02—3.70(b, C_6H), 4.80—4.44(b, C_6H) 7.6—7.3(c, *m*-, *p*-H), 8.0—7.78(c, *o*-H), 10.18—9.7(b, NH)
C_6H_{11}	5.37	2.30—1.1(c, C_6H_{10}), 4.03—3.6(b, C_6H), 4.89—4.45(b, C_6H) 7.64(q, J_{AB}=8.4 Hz, C_6H_4)[e], 10.3—9.8(b, NH)
C_6H_{11}	5.42	2.16—1.2(c, C_6H_{10}), 2.63(s, CH_3), 4.0—3.7(b, C_6H) 4.54—4.07(b, C_6H), 10.7—9.4(b, NH)
$(CH_3)_3C$	5.37[f]	1.42(s, $(CH_3)_3CN$), 1.77(s, $(CH_3)_3CN(H)$), 8.04—7.30(c, Ph)
	5.26	1.46(s, $(CH_3)_3CN$), 1.53(s, $(CH_3)_3CN(H)$), 10.35—9.4(b, NH)
$(CH_3)_3C$	5.36[g]	1.43(s, $(CH_3)_3CN$), 1.76(s, $(CH_3)_3CN(H)$), 7.64(q, J_{AB}=9 Hz, C_6H_4)[e]
	5.24	1.45(s, $(CH_3)_3CN$), 1.52(s, $(CH_3)_3CN(H)$), 10.8—9.74(b, NH)

a) Decomposed on melting. b) KBr disk. c) 1/3 C_6H_6 is contained. d) c=complex, b=broad, s=singlet, q=quartet. e) Center of AB quartet. f) Isomer ratio (in $CDCl_3$); 3 : 1. g) Isomer ratio; 1.74 : 1 (in $CDCl_3$), 1.7 : 1 (in DMSO). h) Pure product was not obtained.

TABLE 3. ISOMER RATIO OF η-$C_5H_5Ni[CNC(CH_3)_3]$-$[C(R)NHC(CH_3)_3]BF_4$

R	Temp. (°C)	Solvent[a]	Isomer ratio
Ph	25	$CDCl_3$	3 : 1
Ph	25	DMSO	2.9 : 1
Ph	63	DMSO	3 : 1
p-ClC_6H_4	25	$CDCl_3$	1.74 : 1
p-ClC_6H_4	25	DMSO	1.7 : 1
p-ClC_6H_4	56	DMSO	1.8 : 1
p-ClC_6H_4	84	DMSO	1.8 : 1

a) DMSO=$(CD_3)_2SO$.

show the presence of any isomers. Consideration of molecular models indicates that the predominant isomer is the *cis* form similar to the above mentioned nickel complexes.

The two C–O stretching frequencies appear within the range 1958—2043 cm^{-1}, 43—26 cm^{-1} higher than the value of ν(CO) of the parent complexes. They decrease in the order CO, RNC, PPh_3, and $C(CH_2Ph)$-NHC_6H_{11} for L in the complexes $[\eta$-$C_5H_5Fe(CO)_2L]X$ (X=BF_4 or PF_6), as shown in Table 5. The decrease is probably comparable with the order of the enhanced donor property of L.

The cyclic neutral monoamino carbene complexes react also with HBF_4 to give the cationic bisamino carbene derivatives (Eq. 4).

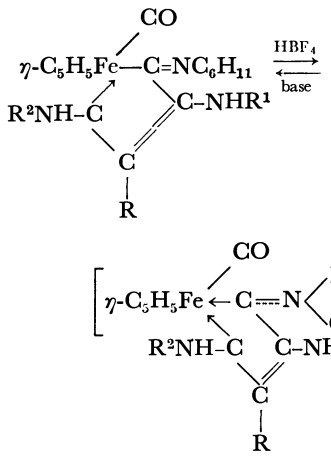

(4)

The infrared spectra show the NH-stretching frequencies in the range 3654—3097 cm^{-1}. In the proton NMR spectra the resonances due to the NH groups appear at *ca.* 6.7 (2H) and 9.8 (1H) ppm as two broad signals.

Diamino carbene complexes lose a proton again to regenerate the parent complexes by treatment with

TABLE 4. ANALYTICAL AND SPECTROSCOPIC DATA OF IRON CARBENE COMPLEXES $[\eta\text{-}C_5H_5Fe(CO)(L)]BF_4$

L	Yield (%)	Mp (°C)	Analysis Found (Calcd) C	H	N	IR (cm^{-1})[a] N-H	C≡O
$(CO)\{C(CH_2Ph)NHC_6H_{11}\}$	85	122—123	54.45 (54.23)	5.26 (5.20)	3.08 (3.01)	3275 3180	2042 1959
$(CO)\{C(CH_2C_6H_4Cl\text{-}p)NHC_6H_{11}\}$	92	134—136	50.67 (50.49)	4.61 (4.64)	2.92 (2.80)	3226 3118	2043 1958
$[(CNHC_6H_{11})\{CNHC(CH_3)_3\}(CPh)(CNHC_6H_{11})]$	63	151—153	59.42 (61.06)	7.01 (7.05)	6.53 (6.68)	3654 3540 3215 3097	1923
$[(CNHC_6H_{11})(CNHC_6H_{11})(CH)\{CNHC(CH_3)_3\}]$	70	207—209	56.38 (56.45)	7.25 (7.29)	7.38 (7.60)	3418 3374 3283	1928

L	NMR (ppm)[b] C_5H_5	Other signal
$(CO)\{C(CH_2Ph)NHC_6H_{11}\}$	4.77	2.3—1.0(b, C_6H_{10}), 4.55—4.05(b, C_6H), 4.43(s, CH_2), 7.6—7.16(c, Ph)
$(CO)\{C(CH_2C_6H_4Cl\text{-}p)NHC_6H_{11}\}$	4.67	2.3—1.0(b, C_6H_{10}), 4.55—4.0(b, C_6H_4), 4.45(s, CH_2), 7.55—7.1(c, C_6H_4)
$[(CNHC_6H_{11})\{CNHC(CH_3)_3\}(CPh)(CNHC_6H_{11})]$	5.30	1.05(s, $(CH_3)_3$), 2.3—0.8(b, C_6H_{10}), 4.35—3.8(b, C_6H), 7.7—7.4 and 7.25—7.05(c, Ph), 8.1—7.8(b, NH, 2 H), 10.2—9.85(b, NH)
$[(CNHC_6H_{11})(CNHC_6H_{11})(CH)\{CNHC(CH_3)_3\}]$	5.48	1.47(s, $CH_3)_3$), 2.3—1.0(b, C_6H_{10}), 3.6—2.88(C_6H), 4.32—3.9(b, C_6H), 6.02(s, CH_3), 6.86—6.57(b, NH), 7.50—7.22(b, NH), 10.06—9.67(b, NH)

a) KBr disk. b) Measured in CD_3COCD_3. b=broad. s=singlet. c=complex.

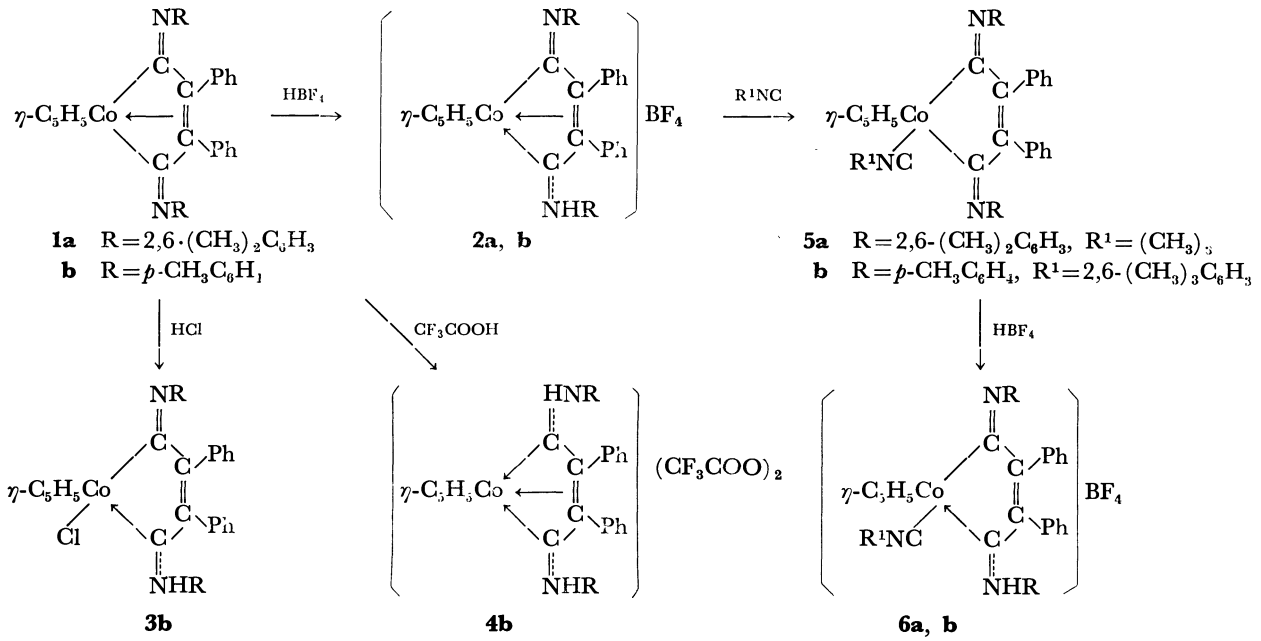

Scheme 1. Reaction of cobalt complexes.

Table 5. Infrared spectra of $[\eta\text{-}C_5H_5Fe(CO)_2L]X$

L	X	$\nu_{C=O}$ (cm^{-1})[a]	Ref.[b]
CO	PF_6	2120, 2070	1
CH_3NC	PF_6	2079, 2037	2
PPh_3	PF_6	2055, 2010	1
PPh_3	BF_4	2057, 2014	3
$C(CH_2R)NHC_6H_{11}$	BF_4	2043, 1958	This paper

a) Measured in CH_2Cl_2. b) 1) P. M. Treichel, R. L. Shubkin, K. W. Barnett, and D. Reichard, *Inorg. Chem.*, **5**, 1177 (1966). 2) R. J. Angelici, P. A. Christian, B. D. Dombek, and G. A. Pfeffer, *J. Organometal. Chem.* **67**, 287 (1974). 3) B. D. Dombek and R. J. Dombek and R. J. Angelici, *Inorg. Chim. Acta*, **7**, 345 (1973).

CH_3ONa or NaOH.

Cobalt Carbene Complexes. The reaction of organocobalt complexes are summarized in Scheme I. η-Cyclopentadienyl-2,5-di(*N*-2,6-dimethylphenylimino)-3,4-diphenylcobaltacyclopentene (**1a**) takes up readily a proton to give the cationic carbene complex (**2a**), when reacted with a large excess of HBF_4 in benzene or NH_2Cl_2 at room temperature. The infrared spectrum shows three bands at 1769 (C=N), 1630 (C=O), and 1587 (O–N) cm^{-1}, higher than those for the parent complex (**1a**). In addition to these, a new weak absorption due to the NH stretching frequency appears at 3203 cm^{-1}. The high frequency due to the C–N double bond suggests the highly strained five-membered

Table 6. Analytical and spectroscopic data of cobalt complexes

$\eta\text{-}C_5H_5Co[\text{-}C(=NR)\text{-}PhC=CPh\text{-}C(NHR)\text{-}]BF_4$ (Type I), $\eta\text{-}C_5H_5Co[\text{-}C(=NR)\text{-}PhC=CPh\text{-}C(NHR)\text{-}]Cl$ (Type II), $\eta\text{-}C_5H_5Co[\text{-}C(NHR)\text{-}PhC=CPh\text{-}C(NHR)\text{-}](CF_3COO)_2$ (Type III), and $\eta\text{-}C_5H_5Co[\text{-}C(=NR)\text{-}PhC=CPh\text{-}C(NHR)\text{-}](CNR^1)BF_4$ (Type IV)

	R	R^1	Yield (%)	Mp[a] (°C)	Analyses Found (Calcd) C	H	N
	Type I						
2a	2,6-$(CH_3)_2C_6H_3$		85	210—212	67.37 (68.12)	5.01 (5.25)	4.37 (4.23)
2b	*p*-$CH_3C_6H_4$		92	—167	67.39 (67.33)	4.83 (4.84)	4.37 (4.49)
	Type II						
3b	*p*-$CH_3C_6H_4$		56	159—161	73.67 (73.36)	5.02 (5.28)	5.01 (4.89)
	Type III						
4b	*p*-$CH_3C_6H_4$		85	167—170	55.95 (56.05)	3.59 (3.67)	3.14[c] (3.19)
	Type IV						
6a	2,6-$(CH_3)_2C_6H_3$	$(CH_3)_3C$	73	123—126	69.75 (69.95)	5.20 (5.20)	5.43 (5.56)
6b	*p*-$CH_3C_6H_4$	2.6-$(CH_3)_2C_6H_3$	78	105—107	68.43 (68.58)	5.72 (5.89)	5.82 (5.71)

	IR (cm^{-1})[b] N–H	C=N	C=C	N≡C	NMR (ppm) in $CDCl_3$[d] C_5H_5	Other signals
	Type I					
2a	3203	1769	1630		5.35(s)	2.16(s, CH_3), 1.78(bs, CH_3), 2.36(bs, CH_3), 7.80—6.5(c, Ph, C_6H_3), 12.2—11.84(b, NH)
2b	3261	1758	1639		5.34(s)	2.16(bs, *p*-CH_3), 2.40(bs, *p*-CH_3), 8.00—6.8(c, Ph, C_6H_4), 12.6(b, NH)
	Type II					
3b	3260	1628	1594		4.49(s)	7.61(s, CH_3), 8.0—6.9(Ph, C_6H_4)
	Type III					
4b	3273	1772	1691		4.82(s)	2.50(s, *p*-CH_3), 7.7—7.0(c, Ph, C_6H_4), 11.2—10.8(b, NH)
	Type IV					
6a	3247	1632	1587	2192	4.73(s)	1.68(s, CH_3), 2.26(b, CH_3), 7.36—6.6(c, Ph, C_6H_3)
6b	3260	1632	1591	2152	4.47(s)	2.25(s, CH_3), 2.39(s, CH_3), 7.28—6.57(c, C_6H_3, C_6H_4)

a) Decomposed on melting. b) KBr disk. c) One mole of CF_3COOH is contained. d) s=singlet. bs=broad singlet. c=complex.

ring structure, resulting from the coordination of the C–C double bond to the cobalt atom as well as **1a**.[14] The proton NMR spectrum shows the presence of the two isomers in the ratio 2 : 1. The resonances due to the *ortho*-methyl groups occur at 2.16(s), 1.78(bs), and 2.36(bs) ppm in the relative intensity of 6 : 4 : 2, respectively. The first resonance is assignable to the methyl groups of the *N*-substituted imino group, and the latter two to those of the isomeric *N*-substituted amino one. The four structures for the compound (**2a**) are illustrated as follows:

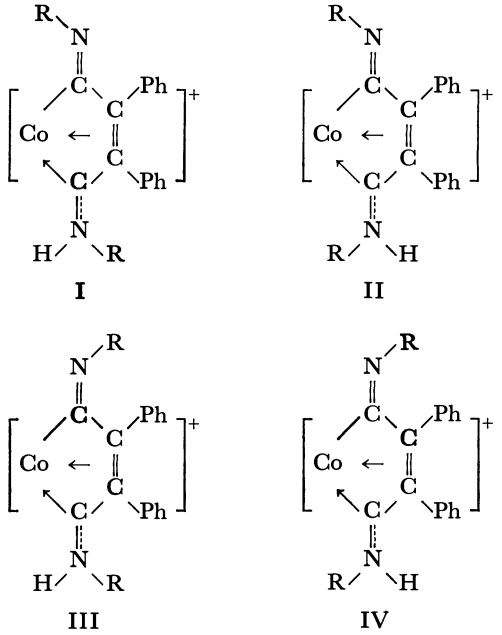

Fig. 1. Possible structures of **2a**. η-C_5H_5 and BF_4^- groups are omitted for clarity, where R is 2,6-dimethylphenyl group.

An X-ray crystallographic examination of η-C_5H_5Co-[–C(=NPh)–CPh=CPh–C(=NPh)–][14] as an analog of **1a** has shown that the *N*-phenyl group has the *cis* orientation to cobalt with respect to the C–N double bond. Accordingly, we tentatively assign two isomers to I and II. The interconversion between I and II was observed by various temperature PMR spectra. The *ortho*-methyl protons of the *N*-2,6-dimethylphenylimino group of two isomers appear at 1.78 and 2.36 ppm as relatively broad singlet at 17 °C. They became broader and their chemical shift difference became smaller on heating. At 63 °C, the spectrum consisted of one single broad signal. Finally the broad signal turned into a sharp singlet (2.06 ppm) above *ca.* 75 °C. These changes in PMR patterns are reversible.

Kinetic parameters for the rotation barrier about the C_{carb}–N bond[20] were determined by PMR line-broading technique of variable temperature PMR spectra. The approximate activation energy was 4.8 kcal/mol, and frequency factor, 1.5×10^5 s^{-1}; the former value is lower than that of C_{carb}–O bond (11.5—13.8 kcal/mol) for $Cr[C(OCH_3)(C_6H_4X)](CO)_5$.[21] The relatively low activation energy, in comaprison with those of rotation barriers of organic amides (6.8—7.8 kcal/mol),[22] may be ascribed to the presence of a labile amino-proton, which leads to facile deprotonation on successive treatment with H_2O.

η-Cyclopentadienyl-2,5-di(*N*-*p*-tolylimino)-3,4-diphenylcobaltacyclopentene (**1b**) also undergoes protonation with HBF_4 to give the carbene complex (**2b**), which however shows an absence of isomers. When **1b** was allowed to react with aqueous HCl, a neutral carbene complex (**3b**) is formed. The infrared spectrum of **3b** shows three significant absorptions at 3260(NH), 1628(C=N), and 1594(C=C) cm^{-1}. The absorption due to the C–N double bond is 102 cm^{-1} lower than that (1730 cm^{-1}) for the parent compound, suggesting the absence of intramolecular coordination of the double bond to the cobalt atom. The proton NMR spectrum in $CDCl_3$ shows a sharp singlet at 2.39 ppm due to two *para*-methyl groups. The origin for this singlet may arise either (1) from an accidental degeneracy of two chemical shifts or (2) from the fluxional behavior of hydrogen in the PMR time scale. The *para*-methyl groups in the PMR spectrum of this complex in CD_3COCD_3 retain a sharp singlet resonance, whereas **2b** shows two respective singlets at 2.16 and 2.40 ppm for the two *para*-methyl groups. In the temperature variations of the PMR spectra of **3b**, a sharp singlet changes to a relatively broad singlet at *ca.* −35 °C, which is converted to a doublet at *ca.* −60 °C. These changes are reversible. These observations are consistent with predictions for the fluxional behavior of hydrogen. Similar behavior has been observed in the carbene complex of platinum.[23]

The compound **1b** reacts readily with CF_3COOH in CH_2Cl_2 to give **4b**. The infrared spectrum shows two bands at 3170 and 3125 cm^{-1} (NH) and three peaks at 1772, 1707, and 1691 cm^{-1} (C=O). The PMR spectrum in $CDCl_3$ shows two sharp singlets at 2.50 and 4.83 ppm due to the *para*-methyl and cyclopentadienyl groups, respectively.

When **2a** was treated with *t*-butyl isocyanide, both deprotonation and release of the coordinated double bond occur to give **5a**, characterized by the absence of ν(NH) and the presence of ν(N≡C) at 2152 cm^{-1}. The compound **5a** takes up a proton again to give the cationic carbene complex (**6a**), when treated with HBF_4. The analogous type of complex (**6b**) is obtained by the reaction of **5b** with HBF_4. The infrared spectra of these compounds (**6a** and **6b**) show the absorption at 3267 (for **6a**) and 3260 cm^{-1} (for **6b**) due to the N–H stretching frequency. The C=N stretching frequencies appear at 1632 and 1634 cm^{-1}, respectively. They are within the range of the normal carbon–nitrgon double bonds, suggesting the absence of coordination of the carbon–carbon double bond to the cobalt atom.

In their PMR spectra the four *ortho*-methyl groups for **6a** and the two *para*-metnyl ones for **6b** show a broad singlet at 2.26 ppm and a sharp singlet at 2.38 ppm, respectively. The respective singlets are converted to doublets consisting of the relative intensity of 1 : 1 in the low temperature PMR spectra, again showing the proton exchange in the PMR time scale as well as that in the neutral complex (**3b**). The observation of the fluxional behavior arising from rapid migration of a proton seems to originate from the planarity of the five-membered ring system containing cobalt.

References

1) Part XII. K. Aoki and Y. Yamamoto, *Inorg. Chem.* in press.

2) E. O. Fischer and Maasböl, *Angew. Chem., Int. Ed. Engl.*, **3**, 580 (1964).

3) E. O. Fischer, *Pure Appl. Chem.*, **24**, 407 (1970).

4) F. A. Cotton and C. M. Lukehart, *Progr. Inorg. Chem.*, **16**, 487 (1972).

5) D. J. Cardin, B. Cetinkaya, and M. F. Lappert, *Chem. Rev.*, **72**, 545 (1972).

6) M. L. H. Green, L. C. Mitchard, and M. G. Swanwick, *J. Chem. Soc. A*, **1971**, 794.

7) E. O. Fischer and A. Riedel, *Chem. Ber.*, **101**, 156 (1968).

8) P. M. Treichel, J. J. Benedict, R. W. Hess, and J. P. Stenson, *J. Chem. Soc. D*, **1970**, 1627.

9) M. F. Lappert and A. J. Oliver, *J. Chem. Soc. Dalton*, **1974**, 65.

10) P. B. Hitchcock, M. F. Lappert, G. M. McLaughlin, and A. Oliver, *ibid.*, **1974**, 68.

11) Y. Yamamoto, H. Yamazaki, and N. Hagihara, This Bulletin, **41**, 532 (1968); *J. Organometal. Chem.*, **18**, 189 (1969).

12) Y. Yamamoto and H. Yamazaki, *Inorg. Chem.*, **13**, 2145 (1974).

13) Y. Yamamoto, K. Aoki, and H. Yamazaki, *J. Amer. Chem. Soc.*, **96**, 2647 (1974).

14) H. Yamazaki, K. Aoki, Y. Yamamoto, and Y. Wakatsuki, *ibid.*, **97**, 3546 (1975)., 22nd Symposium on Organometal. Chem. Japan. October 16—18, 1974. Preceeding p. 67.

15) I. Ugi and R. Meyer, *Chem. Ber.*, **93**, 239 (1960).

16) When the reaction mixture was washed several times with water, the resulting carbene complex was reformed to the parent one.

17) H. S. Gutowsky and R. H. Holm, *J. Chem. Phys.*, **25**, 1228 (1956).

18) M. H. Chisholm and H. C. Clark, *Chem. Commun.*, **1971**, 809.

19) B. Crociani and R. L. Richards, *J. Chem. Soc. Dalton*, **1974**, 693.

20) The chelating carbene ligand of **2a** has the advantage of eliminating ambiguities or complications arising from rotation about the M–C (carb) bond.

21) J. W. Emsley, J. Feeney, and L. H. Sutcliffe, "High Resolution Nuclear Magnetic Resonance Spectrscopy," Vol. 1, Pergamon Press, p. 556.

22) E. O. Fischer, C. G. Kreiter, H. J. Kollmeier, J. Muller, and R. D. Fischer, *J. Organometal. Chem.*, **28**, 237 (1971).

23) W. M. Butler, J. H. Enemark, J. Parks, and A. Balch, *Inorg. Chem.*, **12**, 451 (1973).

Kinetics and Stereochemistry of Alkaline Cleavage of 1,1-Diacetyl-2-arylcyclopropane[1]

Osamu Itoh, Nobuyuki Yamamoto, Katsuyuki Nakano, Toshio Sugita, and Katsuhiko Ichikawa*

Department of Hydrocarbon Chemistry, Faculty of Engineering, Kyoto University, Yoshida, Kyoto 606

(Received July 10, 1975)

The kinetics and the stereochemistry of alkaline cleavage of several 1,1-diacetyl-2-arylcyclopropanes (**1**) in ethanol–water mixture are reported. The rates can be expressed approximately by a third order equation, rate= k_2[**1**][OH^-]^2. With *para*-substituted derivatives (*p*-CH_3, H, *p*-Cl and *p*-Br) of 2-phenyl ring, the reaction constant ρ was obtained as +4.3 by plotting log k_2 against normal Hammett σ. At 0 °C, the main products were thermodynamically unstable *cis*-1-acetyl-2-arylcyclopropanes. The *cis* to *trans* ratio in the products decreased with increasing reaction temperature. The reaction mechanism has been discussed in relation to the cleavage reaction of unenolizable acyclic β-diketone. The large ρ value and preferred formation of *cis* product suggest that the substituent effects of 2-aryl group are transmitted through cyclopropane ring much more effectively to *trans* direction than to *cis* direction.

Pearson and Mayerle showed that the alkaline cleavage of dimethylacetylacetone, which belongs to unenolizable β-diketone, is second-order (rate=k_1-[ketone] [OH^-]).[2] The same kinetics and mechanism might be expected in the same cleavage of 1,1-diacetyl-2-arylcyclopropanes with hydroxide ion, since they are also unenolizable β-diketone, and the effects of the substituents at phenyl ring on the cleavage rates appear to provide a convenient tool to study the transmitting ability of the effects through cyclopropane ring. The present paper describes the stereochemistry and kinetics of alkaline cleavage of several 1,1-diacetyl-2-arylcyclopropanes in ethanol–water (75 : 25 by volume) mixture containing potassium hydroxide.

Cleavage of 1,1-diacetyl-2-phenylcyclopropane (**1**-H) with potassium hydroxide (0.05—0.6 M) gave *cis*- and *trans*-1-acetyl-2-phenylcyclopropane (**2**-H) with no detectable amount of by-product. Gas-chromatographic analysis showed that the *cis* to *trans* ratio in the products at 0 °C (concn of KOH=0.4 M) was 90 : 10, while the value decreased with increasing reaction temperature (40—60 °C) to 50 : 50. Considering that the *cis*-isomer should be thermodynamically much more unstable than *trans* isomer, it appears that the cleavage at lower temperatures predominantly gives kinetically controlled products. With *p*-methylphenyl (**1**-CH_3), *p*-chlorophenyl (**1**-Cl) and *p*-bromophenyl (**1**-Br) derivatives, almost the same results were obtained. Although the detailed analysis to determine whether the *trans* isomer was formed through the rearrangement of *cis*-isomer or directly from **1** was not performed, the change of *cis* : *trans* ratio with time appears to show that the *trans*-isomer resulted partly through rearrangement and in part directly, even at higher temperature (Fig. 1).

Curve IV in Fig. 1 was obtained by the estimation from the isomerization rate of *cis*-**2**-H to *trans*-**2**-H which will be reported in a succeeding paper.[3]

The rates of cleavage were determined by following the concentrations of potassium hydroxide. Quantitative analysis by gas chromatography could be applied to determine the *cis-trans* ratio of the products but not to the reaction mixture because of the partial decomposition of **1**-H.

In contrast to the reported case of 3,3-dimethyl-2,4-pentanedione,[2] the rates can be expressed approximately by a third-order equation, rate=k_2[**1**][OH^-]^2. The results are shown in Table 1.

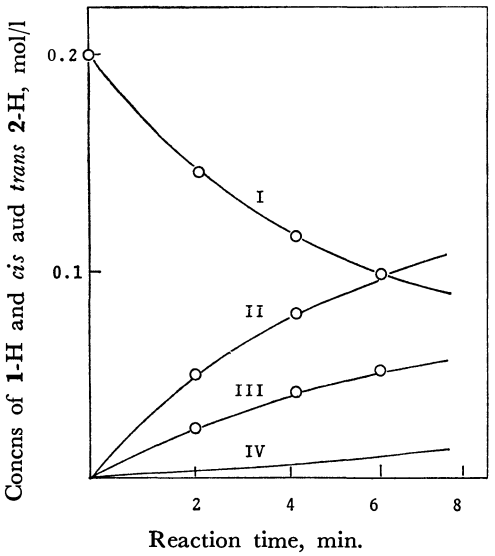

Fig. 1. Plot of the cleavage reaction of **1**-H in 75% ethanol at 25 °C. The initial concentrations of **1**-H and potassium hydroxide were 0.200 and 2.00 M, respectively. Curve I, II and III show the observed concentrations of **1**-H, sum of *cis* and *trans*-**2**-H, and *trans*-**2**-H, respectively.

Deviations from the third-order equation in lower concentration ranges of potassium hydroxide cannot be neglected and is considered to be due to the second-order term k_1[**1**] [OH^-] which must be added to the main term of the third-order.

The substituents at the *para* position of phenyl ring in **1** showed profound effects on the cleavage rates. Data with the substituents of methyl, chloro and bromo are given in the following table.

Hammett plot of the rates against normal σ values gave a straight line with a ρ value of +4.3. This large value shows that the substituent effect can be transmitted effectively through cyclopropane ring.

Pearson and Mayerle showed that the cleavage rates of acetylacetones by hydroxide ion consist of two terms; one is associated with one mole of ketone and

Table 1. Kinetical data of the cleavage reaction of **1**-H with potassium hydroxide in 75% ethanol[a)]

Initial concn of **1**-H (mol/l)	Initial concn of KOH (mol/l)	$k_2\times10^3$ (l^2/mol^2·s)	$k_1\times10^5$ (l/mol·s)
At 25.0°			
0.100	0.105	0.60	6.2
0.100	0.215	0.47	9.4
0.100	0.375	0.54	19.5
0.100	0.375	0.57	19.6[b)]
0.100	0.545	0.66	33.5
0.025	0.102	0.62	6.0
0.045	0.165	0.61	9.0
		mean 0.58	
At 30.0°			
0.100	0.112	1.7	
0.100	0.215	1.2	
0.100	0.400	1.2	
0.100	0.560	1.4	
		mean 1.4	
At 40.0°			
0.116	0.058	6.6	
0.116	0.111	3.7	
0.116	0.239	2.8	
0.116	0.474	2.5	
0.116	0.708	2.6	
0.035	0.071	6.0	
0.224	0.214	2.7	
		mean 2.9	
At 60.0°			
0.116	0.058	31	
0.117	0.116	16	
0.105	0.225	12	
0.036	0.073	21	
0.037	0.146	13	
0.030	0.178	12	
0.223	0.210	13	
		mean 15	

a) $\Delta H^{\neq}=13$ kcal/mol and $\Delta S^{\neq}=-18$ e. u. b) NaOAc (0.100 M) was added.

Table 2. Substituent effects on the cleavage rates at 40 °C

	$k_2\times10^3$ (l^2/mol^2·s)	Rel. rate	σ[4)]
1-CH_3	1.5	0.557	−0.170
1-H	2.82	1.00	0
1-Cl	8.12	2.88	+0.227
1-Br	8.78	3.11	+0.237

one mole of hydroxide ion (k_1, splitting of acetic acid from the monoanion formed by the addition of hydroxide ion to carbonyl) and the other with one mole of ketone and two moles of hydroxide ion (k_2, splitting of acetate ion from the dianion formed by proton abstraction from hydroxyl group of the monoanion with hydroxide ion), and the ratio of k_2/k_1 decreases by methyl substitution and becomes almost zero in the case of 3,3-dimethyl-2,4-pentanedione.[2)] The explanation for the changes of the ratio is not easy and they mentioned simply that this may be due to a weakening of carbon–carbon bond which renders less necessary the helping effect of double charged anion in cleaving. The difference of the reaction-order of the cleavage of 3,3-dimethyl-2,4-pentanedione and that of the present case is also difficult to explain. Binding the carbons of the two methyl groups in dimethylacetylacetone makes the carbon between the carbonyls a ring member of cyclopropane, reduces the steric requirement, and changes the character of the carbon. How it works in the reaction mechanism is difficult to predict, and remains unsolved.

One of the special features of the present cleavage is the formation of thermodynamically unstable *cis* product. A straightforward explanation may be as follows. First addition of hydroxide ion must occur at the *trans* acetyl group of **1** because of a larger steric hindrance of the adduct at *cis* acetyl group. Second attack of hydroxide ion forms dianion C (Fig. 2). Splitting of acetate anion from C forms carbanion F which gives *cis*-product through proton abstraction from the solvent.[4)]

If the addition of hydroxide ion to carbonyl is reversible and faster than the cleavage of C, as was pointed out by Pearson and Mayerle, other reaction pathways must be examined. Possible ones are depicted in Fig. 2. Equilibrium concentrations of A and C are higher than those of B and E, respectively,

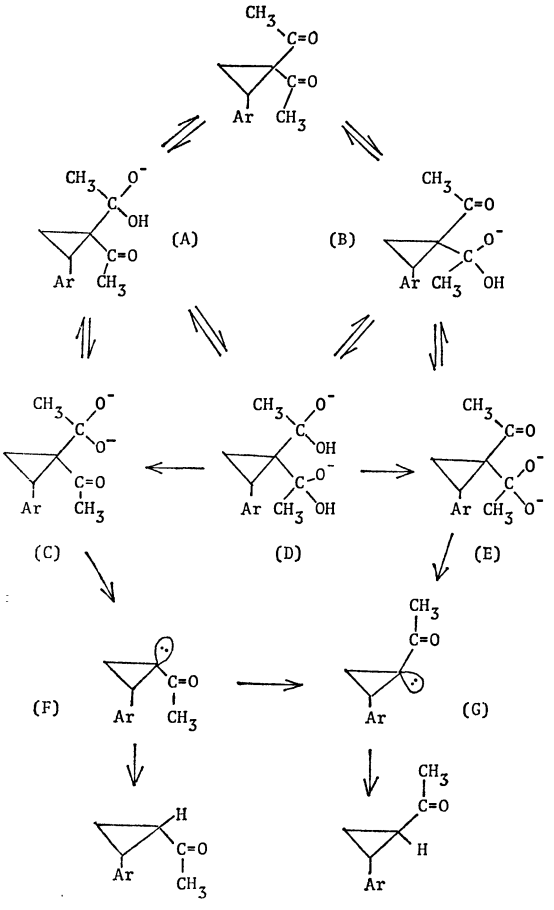

Fig. 2. Possible pathways of the cleavage of **1**.

because of the steric effects. The cleavage rate of E, however, must be faster than that of C because of the same effects. If the equilibria shown in Fig. 2 are attained rapidly, the relative rates of the cleavage of C and E determine the stereochemistry and the *trans* product must be obtained. To explain why the *cis* is the main product, at least at 0 °C, some other kind of factor than the steric which is more effective to accelerate the cleavage of C must be considered. An assumption that the substituent effects are transmitted more effectively to *trans* direction than to *cis* through cyclopropane ring may explain the present results. Although they may not be enough to rationalize the assumption, the fact that the carbanion formation by proton abstraction from ring methylene of *cis*-**2**-H with hydroxide ion proceeded much more rapidly than that from *trans*-**2**-H[3] appears to support the proposal.

The substrates **1** have been prepared by demercurations of 3,3-diacetyl-2-arylpropylmercuric acetates (**3**-H, **3**-Cl, **3**-Br and **3**-CH_3 for phenyl, *p*-chlorophenyl, *p*-bromophenyl and *p*-tolyl, respectively). Although **1**-H can be obtained by the demercuration of the corresponding chloride of **3**-H with potassium hydroxide as was reported previously,[5] applications of the same method to the others gave only poor yields. It was found, however, that the demercuration of **3** proceeded smoothly in dimethyl sulfoxide (DMSO) at about 120 °C and gave much better yields of **1**. At higher temperatures than 120 °C, the yields of **1** became low because of the formation of isomeric dihydrofurans. **3** were prepared by the reactions of acetylacetone with β-acetoxy-β-arylethylmercuric acetates (**4**-H, **4**-Cl, **4**-Br and **4**-CH_3 for phenyl, *p*-chlorophenyl, *p*-bromophenyl and *p*-tolyl, respectively), which were obtained by acetoxymercuration of styrenes, in acetic acid containing perchloric acid or boron trifluoride.[5] Typical examples of the results are shown in Table 3.

Table 3. Preparation of **1** by the demercuration of **3**

	Temp. °C	Time min	Yield of **1** %[a]	Mp, °C
1-H	120	30	35	57.5—59.0
1-CH_3	111—120	15	34	57.6—59.0
1-Cl	110—115	35	57	74.6—75.5
1-Br	120	10	33	72.2—73.2

a) After recrystallization from *n*-heptane.

Experimental

*Preparation of **1** through **4** and **3**.* The following example shows the typical experimental procedure for the preparation of **1**. Into a mixture of acetic acid (300 ml) and mercuric acetate (1.0 mol), styrene (1.0 mol) was added and stirred at room temperature for 1 hr, and then acetylacetone (2.0 mol) was added. Under keeping the mixture below 40 °C, 60% perchloric acid (160 g) was added dropwise and stirred for 2 hr. The reaction mixture was poured into 20% aqueous solution of sodium acetate (1000 g). Crystals of **3**-H formed were collected, washed with ether, and recrystallized from ethanol (1.2 l), 370 g (0.80 mol). Purified **3**-H (0.80 mol) was dissolved into hot DMSO (660 ml) and kept at 120 °C for 30 min. After removing metallic mercury formed, the reaction mixture was poured into saturated aqueous solution of sodium chloride (1.5 l). Brownish raw crystals were collected and recrystallized from *n*-heptane (1.8 l) to give pure **1**-H (56 g, 35% yield), mp 57.5—59.0 °C.

Starting from *p*-substituted styrenes, which were prepared by reduction of the corresponding acetophenones and subsequent dehydration,[6] **3** were obtained in 75—80% yields and then **1** in 33—57% yields. Purifications of **3** were essential to get better yields of **1** (Table 4).

Table 4. Analyses of **1**

	Found (%)			Calcd (%)		
	C	H	X	C	H	X
1-H	76.85	7.17		77.20	6.98	
1-Cl	65.87	5.48	14.86	65.91	5.54	14.98
1-Br	55.27	4.76	28.67	55.54	4.66	28.42

Because of the lack of the sufficient amount of the material, **1**-CH_3 was not analyzed.

IR spectra were recorded on HITACHI EPI-G2. IR of **1**-H (KBr): $\nu_{C=O}$, 1700(s) and 1680(s); δ_{C-H} of CH_3, 1370(s) and 1360(s); $\delta_{C=O}$, 1260(s); δ C-H of benzene ring, 780(s), 740(m), and 700(s). NMR spectra (in deuteriochloroform with TMS as an internal standard) were recorded on a Varian Associates HR-220 at 220 MHz at room temperature. δ values are summarized in Table 5.

*Alkaline Cleavage of **1**.* Into 100 ml volumetric flask, **1**-H (2.02 g, 0.01 mol), ethanol-water (75 : 25 by volume) mixture and potassium hydroxide dissolved in the same mixture (25 ml of 1.6 M solution) were added. After keeping the flask at 20 °C for 5 hr, the mixture was neutralized with hydrochloric acid (32.6 ml of 1 M). This result showed that 74% of the theoretical amount of potassium hydroxide were consumed. After ethanol was removed by distillation, the mixture was extracted with ether and dried over sodium sulfate. After removing ether, the product was analyzed by gas chromatography (YANACO GC-550 TPH, 1.5 m of 3 mmφ, Apiezon-L grease, helium). No other peak than **1**-H and *cis*- and *trans*-**2**-H was observed. The product was distilled *in vacuo*, bp 107—110 °C/7 mmHg. By column chromatography (Wakogel C-200, 30 mmφ × 40 cm, hexane-ethyl acetate (90: 10 by volume)), *cis*- and *trans*-**2**-H were isolated. Repeating the same procedure, pure *cis*- and *trans*-**2**-H were obtained. IR of *trans*-**2**-H was identical with that reported by Pierre *et al.*[7] IR of *cis*-**2**-H (bp 123—124 °C/11 mmHg) showed no absorption at 1358(m) and 1190(m) cm^{-1} which were observed in *trans*-**2**-H. IR (liq. film): $\nu_{C=O}$, 1703(s) and 1698(s); $\delta_{CH\ of\ CH_3}$, 1388(s); $\delta_{C=O}$, 1170(s); $\delta_{CH\ of\ benzene\ ring}$, 770(m), 720(w), and 695(m). Found: C, 82.61; H, 7.81%. Calcd for $C_{11}H_{12}O$: C, 82.46; H, 7.55%.

The cleavage products of *para*-substituted **1** gave the same pattern of gas chromatograms as that of **1**-H, showing that the reaction proceeded as in the case of **1**-H. Since sufficient amounts of pure *trans* products could not be isolated, NMR spectra were obtained for only *cis*-products and are shown in the following table. The differences of the chemical shift of **1**-H due to the anisotropy of aromatic ring made possible the discrimination of *cis*- and *trans*-**2**.

Kinetics. The rates were determined by following the potassium hydroxide concentrations by the titration

Table 5. δ Values

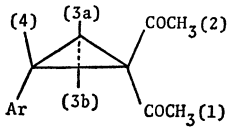

	H-1	H-2	H-3a	H-3b	H-4
1-H	1.77 s	2.27 s	1.57 d. of d. J=5.2 and 9.1	2.22 d. of d. J=5.2 and 7.8	3.24 d. of d. J=7.8 and 9.1
1-Br	1.80 s	2.20 s	1.57 d. of d. J=9 and 4	2.22 d. of d. J=8 and 4	3.13 d. of d. J=9 and 8
1-CH_3	1.80 s	2.27 s	1.65 d. of d. J=9 and 4	2.22 d. of d. J=8 and 4	3.23 d. of d. J=9 and 8

Table 6. NMR spectra

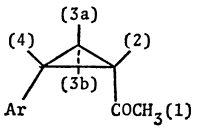

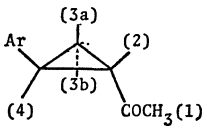

	H-1	H-2	H-3a	H-3b	H-4
cis-**2**-H	2.01 (s)	2.43 (m)	1.30 (m)	1.83 (m)	2.69 (m)
2-Cl	2.04 (s)	2.1—2.7	1.32 (m)	1.79 (m)	2.2—2.8
2-Br	2.05 (s)	2.44 (m)	1.30 (m)	1.79 (m)	2.61 (m)
2-CH_3	2.00 (s)	2.39 (m)	1.26 (m)	1.80 (m)	2.64 (m)
trans-**2**-H	2.30 (s)	2.21 (m)	1.38 (m)	1.67 (m)	2.52 (m)

with hydrochloric acid as usual. By plotting log of initial rates at constant concentrations of **1**-H against log[KOH], straight lines were obtained. The slopes of the lines were 1.99, 2.17 and 2.21 at 40, 30 and 20 °C. The third-order rate constants were obtained by the usual method of calculation.

This work was partially supported by a Grant-in-Aid for Scientific Research from the Ministry of Education, Japan (No. 911503).

References

1) Partly reported at the annual meeting of the Chemical Society of Japan, March 31, 1969.

2) R. G. Pearson and E. Mayerle, *J. Amer. Chem. Soc.*, **73**, 925 (1951).

3) O. Itoh, N. Yamamoto, and K. Ichikawa, unpublished results. See, for a partial reference, This Bulletin, **42**, 3045 1969).

4) H. M. Walborsky and J. M. Motes, *J. Amer. Chem. Soc.*, **92**, 2445 (1970).

5) K. Ichikawa, O. Itoh, T. Kawamura, M. Fujiwara, and T. Ueno, *J. Org. Chem.*, **31**, 447 (1966).

6) K. Ichikawa, K. Nishimura, and S. Takayama, *ibid.*, **30**, 1593 (1965).

7) J. L. Pierre, R. Barlet, and P. Arnaud, *Spectrochim. Acta*, **23A**, 2297 (1967).

The Chlorination of Norbornene by Metal Chlorides and the Product Isomerization

Sakae UEMURA,* Akira ONOE, and Masaya OKANO
Institute for Chemical Research, Kyoto University, Uji, Kyoto 611
(Received July 15, 1975)

The reaction of norbornene with $CuCl_2$, $TlCl_3 \cdot 4H_2O$, $PbCl_4$, $SeCl_4$, $SbCl_5$, and VCl_4 in CCl_4, CH_2Cl_2, or CH_3CN gave a mixture of nortricyclyl chloride (**1**), and six isomeric dichloronorbornanes [*trans*-2,3-(**2**), *exo*-2-*anti*-7-(**3**), *trans*-2,5-(**4**), *exo-cis*-2,5-(**5**), *exo-cis*-2,3-(**6**), and *exo*-2-*syn*-7-(**7**)], the product distribution depending very much on metal chlorides and reaction conditions. The reactions did not show any participation of a chlorine molecule which may be released from metal chlorides. The ability of $SeCl_4$ and VCl_4 to chlorinate olefins was found for the first time. From a synthetic viewpoint $CuCl_2$ was a good reagent for obtaining **2**, while $TlCl_3 \cdot 4H_2O$ and $SbCl_5$ were recommended for either **3** or **7**. The reactions with the following metal chlorides did not give any dichloronorbornanes; $SnCl_4$, $BiCl_3$, $TiCl_4$, $FeCl_3$, $NbCl_5$, $TaCl_5$, and WCl_6. It was revealed that isomerization of **2** or **7** to a mixture of **3**, **4**, and **5** occurred very rapidly by $SbCl_5$ and smoothly by $TlCl_3 \cdot 4H_2O$. The chlorination of norbornene and their products isomerization were mainly explained by assuming a chloronorbornyl cation as an intermediate.

Recently we have shown that the chlorination of norbornene by $SbCl_5$[1] and $MoCl_5$[2] gave a quite different distribution of the products with that by Cl_2[3] and (dichloroiodo)benzene.[4] Namely, *exo*-2-*anti*-7-(**3**), *trans*-2,5-(**4**), and *exo-cis*-2,5-dichloronorbornane(**5**) were the main products in the case of $SbCl_5$, while *exo-cis*-2,3-isomer(**6**) was mainly obtained in the case of $MoCl_5$. On the other hand, a mixture of nortricyclyl chloride(**1**) and *exo*-2-*syn*-7-isomer(**7**) (ionic condition) and a mixture of *trans*-2,3-iosmer(**2**) and **6** (radical condition) were mainly obtained in chlorination by Cl_2 or $PhICl_2$. In the chlorination of olefin by metal chloride it is sometimes difficult to distinguish whether it is a specific reaction by metal chloride itself or it involves a chlorine molecule released from metal chloride. The clear-cut different product distribution described above, however, suggests that norbornene is a good olefinic substrate to study whether the reaction involves a chlorine molecule. Therefore we carried out its chlorination by various metal chlorides with the intentions of giving a further insight on the nature of metal chloride chlorination and also of finding any metal chlorides for selective formation of each of **1**–**7** if possible.

Results and Discussion

Reaction conditions, the yields of the products, and the isomer distributions are summarized in Table together with the reported data of $MoCl_5$[2] and $AuCl_3$[5] (Scheme 1). The data of typical ionic and radical chlorination by Cl_2[3] were also added for comparison. All reactions were carried out by addition of norbornene to a solution of metal chloride in the presence of atomospheric amounts of oxygen unless otherwise stated.

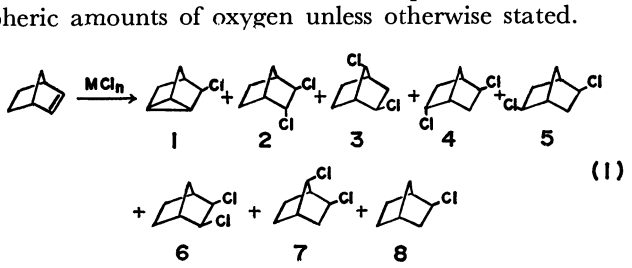

(1)

* To whom all correspondence should be addressed.

$CuCl_2$. The reaction proceeded smoothly in CH_3CN where LiCl was added to increase the reaction rate and the solubility of copper(II) salt to give **2** and **6** almost selectively (Run 1), while no reaction occurred in CCl_4, CH_2Cl_2, and $CHCl_3$ as solvents. Although the isomer distribution in the products, which was shown to be kinetically controlled one, was similar to that in radical chlorination by Cl_2[3] or $PhICl_2$,[4] the reaction was not affected by addition of *m*-dinitrobenzene (Run 2) and no change in the product distribution was observed even when the reactions were conducted under bubbling oxygen or nitrogen. Therefore it is clear that the chlorinating species is not a chlorine molecule which may be released from $CuCl_2$, but $CuCl_2$ itself or its LiCl complex.

$TlCl_3 \cdot 4H_2O$. Chlorination by this salt in CCl_4 at refluxing temperature afforded a mixture of **3**, **4**, **5**, and **7**, the ratio of a mixture of **3**—**5** to **7** being increased by prolonging the reaction time (Runs 3 and 4). The reaction proceeded even at −10 °C where the compounds other than **3** and **7** were scarcely obtained (Run 5). We showed in separate experiments that **7** isomerized smoothly to a mixture of **3**—**5** in CCl_4 at 5—76 °C in the presence of $TlCl_3 \cdot 4H_2O$, while no isomerization occurred at −10 °C (See Experimental). Therefore it can be concluded that the isomer distribution in Run 5 is kinetically controlled. The formation of *exo*-2-chloronorbornane(**8**), HCl addition product to norbornene, was observed in Runs 3 and 4. The evolution of HCl by interaction of $TlCl_3 \cdot 4H_2O$ with CCl_4 at refluxing temperature has been known.[6]

$PbCl_4$. Chlorination by this salt was carried out by addition of olefin to a yellow CH_2Cl_2 solution of $PbCl_4$[7] which was produced *in situ* by action of HCl on $Pb(OAc)_4$ at −60 °C. The characteristic feature of this reaction was found in selective formation of **3** and **7** without any other isomers when the reaction was conducted at −40 °C (Run 6). It was shown in separate experiments that neither interconversion between **3** and **7** nor isomerization of other isomers to **3** and **7** occurred in CH_2Cl_2 at −30——40 °C in the presence of $PbCl_4$ and/or $PbCl_2$. Therefore the isomer distribution in Run 6 is kinetically cotnrolled. The reaction also proceeded in CCl_4 at −10 °C (Run 7),

though the formation of **1** was observed in this case probably because of the slight release of a chlorine molecule from $PbCl_4$ at this temperature. Since excess HCl is present in solution, **8** was always formed as a side-product.

$SbCl_5$. We have reported previously that the chlorination of norbornene by this chloride in CCl_4 gave mainly **3**, **4**, and **5** in good yields.[1] In view of the observation that **7** was isomerized to a mixture of **3**—**5** by $TlCl_3 \cdot 4H_2O$, we reexamined the product distributions under various conditions. When norbornene was added drop by drop in a period of *ca.* 0.5—3 min to a CCl_4 solution of $SbCl_5$ (Run 8), none of **7** was obtained and the main products were **3**—**5** as shown in our previous report.[1] However, when norbornene was added all at once (Runs 9—11), **3** and **7** were obtained as the main products, while the amounts of **4** and **5** in the products were very small. In these cases the product distribution appeared to be nearly constant irrespective of the total reaction time and its temperature. When the reverse addition was employed (Run 12), namely addition of a CCl_4 solution of $SbCl_5$ to a CCl_4 solution of norbornene, the product distribution was nearly the same as those in Runs 9—11 almost irrespective of the speed of the addition. In separate experiments we observed that $SbCl_5$ was a very effective catalyst for isomerization of **2** and **7** to a mixture of **3**—**5**, while $SbCl_3$ showed no effectiveness for such isomerization. For example, almost all of **2** or **7** were converted to a mixture of **3**—**5** by treating with $SbCl_5$ at 20 °C in only 10 min (See Experimental). The chlorination of norbornene by $SbCl_5$ occurs very rapidly under the conditions we employed and it was nearly complete as soon as norbornene was added to a solution of $SbCl_5$ (Run 9). Thus we can conclude that in Run 8 initially formed **7** was isomerized to a mixture of **3**—**5** by excess $SbCl_5$ present in a solution, while in Runs 9—11 and also in Run 12 $SbCl_5$ did not exist in such extent as making the isomerization of **7** complete, because $SbCl_5$ turned to $SbCl_3$ as soon as chlorination took place. Since there have been no convenient methods of preparing **4** and **5**, the method described here (Run 8) seems to be useful for this purpose.

$SeCl_4$ and VCl_4. We have tried to chlorinate norbornene by several other commercial metal chlorides with which chlorination of olefin has never been reported. As a result both $SeCl_4$ and VCl_4 were revealed to chlorinate olefins. The following metal chlorides did not give any dichloroalkanes under the conditions we have employed (cyclohexene and norbornene as substrates; at 20—76 °C in CCl_4); $SnCl_4$, $BiCl_3$, $TiCl_4$, $FeCl_3$, $NbCl_5$, $TaCl_5$, and WCl_6.

As to chlorination by $SeCl_4$, there have been no reports on direct chlorination of olefins, although the reaction of $SeCl_4$ with unsaturated linkages to produce organoselenium dichlorides has been well known.[8] However, chlorination occurred with norbornene in CCl_4 to give several dichloronorbornanes in which **7** was the main product (Runs 13 and 14). Since we

Table. Chlorination of norbornene

Run	Norbornene (mmol)	Chlorinating agent	(mmol)	Solvent (50 ml)	React. Temp. (°C)	React. Time (hr)	Addendum (mmol)	Products: Isomer distribution 1	2	3	4	5	6	7	Yield[a] (%)	By-product 8 (mmol)
1	12.5	$CuCl_2$	25	CH_3CN	82	3	LiCl 25	0	80	0	0	0	18	2	90	
2	12.5	$CuCl_2$	25	CH_3CN	82	3	LiCl 25 *m*-DNB[b] 5	0	82	0	0	0	15	3	87	
3	12.5	$TlCl_3 4H_2O$	6.3	CCl_4	76	0.1		s.[c]	2	34	5	5	0	54	23	0.7
4	12.5	$TlCl_3 4H_2O$	6.3	CCl_4	76	2		s.	2	45	11	10	0	32	62	3.1
5	12.5	$TlCl_3 4H_2O$	6.3	CCl_4	−10	3		s.	1	31	1	1	0	66	48	
6	11	$PbCl_4$	5	CH_2Cl_2	−40	3		0	0	41	0	0	0	59	57	7.8
7	11	$PbCl_4$	5	CCl_4	−10	2		30	0	13	0	0	0	57	58	0.7
8	5	$SbCl_5$	3	CCl_4[d]	20	0.17[e]		0	3	35	31	31	0	0	81	
9	5	$SbCl_5$	3	CCl_4[d]	20	5 sec[f]		0	1	52	9	7	0	31	84	
10	5	$SbCl_5$	3	CCl_4[d]	20	0.17[f]		0	s.	50	7	6	0	37	91	
11	5	$SbCl_5$	3	CCl_4[d]	−30	0.17[f]		0	s.	52	6	6	0	36	91	
12	5	$SbCl_5$	3	CCl_4[d]	20	0.17[g]		0	1	49	3	2	0	45	85	
13	5	$SeCl_4$	3	CCl_4	76	2		0	s.	20	2	3	0	75	31	
14	5	$SeCl_4$	3	CCl_4	25	12		0	s.	22	3	2	0	73	22	
15	20	VCl_4	7	CCl_4	76	2		4	11	7	6	4	64	4	67	1.7
16	5	VCl_4	3.5	CCl_4	27	12		1	14	5	1	s.	71	8	32	0.3
17[h]	4	$MoCl_5$	1.3	CCl_4	25	2		0	1	7	13	11	68	0	42	0.7
18[i]	6—15	$AuCl_3$	3—5	C_6H_{12}[j]	20	—[k]		0	0	←—66—→			0	34	77	
19	—[k]	Cl_2	—[k]	CCl_4	25	0.5	O_2	65	6	0	0	0	4	25	95	
20	—[k]	Cl_2	—[k]	CCl_4	25	0.5	N_2, $h\nu$	19	37	0	0	0	35	0	—[k,l]	

a) Based on MCl_n charged. Determined by glc. b) *m*-Dinitrobenzene. c) <0.5%. d) 10 ml. e) Olefin was added in *ca.* 20—30 sec. f) Olefin was added all at once. g) $SbCl_5$ was added to olefin. h) Ref. 2. i) Ref. 5. j) Cyclohexane. k) No description. l) Other products; *exo*- and *endo*-5-chloro-2-norbornenes, 6% and 3% respectively.

showed in separate experiments that **7** did not isomerize to other isomers under the reaction conditions, the isomer ratios in Runs 13 and 14 seem to be kinetically controlled. The reaction of cyclohexene with $SeCl_4$ gave *trans*-dichlorocyclohexane in a 44% yield together with chlorocyclohexane by stirring at 20 °C for 2 hr. In order to see whether these dichloroalkanes were produced *via* organoselenium compounds, we prepared separately bis(2-chlorocyclohexyl)selenium dichloride by the reported method[8] (mp 142 °C; lit,[8] mp 141—142 °C) and heated it to reflux in CCl_4 for 2 hr in the presence or absence of $SeCl_4$. As a result none of dichlorocyclohexane was obtained. This shows that chlorination by $SeCl_4$ does not proceed through the formation of organoselenium compounds at least in CCl_4 solvent.

The chlorination of norbornene by VCl_4 proceeded smoothly in CCl_4 to give all of **1**—**7** in which the main product was the *cis*-dichlorinated isomer **6** (Runs 15 and 16). Although the chlorinating action of VCl_4 has been noted in the chlorination of aromatic hydrocarbons,[9] there have so far been no reports on the direct chlorination of olefins. Since we showed that no isomerization occurred between each isomer under the conditions of Runs 15 and 16 and also that the isomer distribution was nearly the same even when the reaction was stopped in a shorter time, the isomer ratios shown in Table are clearly kinetically controlled. Although a preferential formation of **6** is quite characteristic, chlorination of norbornadiene and cyclohexene gave hardly any *cis*-dichloroalkanes. Therefore, the molecular *cis*-addition mechanism which was proposed in the chlorination by $MoCl_5$[2] does not seem to be applicable in this case. It should be added that radical scheme can be excluded because no change in the isomer distribution and the yields of the products was observed when the reactions were conducted under the presence of *m*-dinitrobenzene or bubbling oxygen.

By considering the product distribution in each reaction described above, we can conclude that chlorination by any metal chlorides does not involve a chlorine molecule which may be released from metal chlorides. Since a fractional distillation can nearly separate **2** from **6** and also **3** from **7**, additional useful conclusion can be drawn from a synthetic viewpoint. For obtaining **2** chlorination by $CuCl_2$ (Run 1) is recommended, while for either **3** or **7** the reactions with $TlCl_3 \cdot 4H_2O$ (Run 5) and $SbCl_5$ (Run 12) should be employed because of its simplicity, high selectivity, and high yields of the products. In order to obtain **4** and **5**, the method of Run 8 by the use of $SbCl_5$ is applicable, though it is necessary to use preparative glc for the separation of each isomer.

Reaction Scheme and Product Isomerization. The results that chlorinations by $TlCl_3 \cdot 4H_2O$, $PbCl_4$, $SbCl_5$, and $SeCl_4$ gave mainly **3** and **7** as kinetically controlled products (usually **7**>**3**) seem to be explained by Scheme 2. Namely, at first a chloronorbornyl cation **A** may be formed as an intimate ion-pair with gegen-ion MCl_{n+1}^- because of low polarity of solvent. In some extent the cation may be converted to another isomeric bridged ion **B** through 2,6-hydride shift. As noted earlier,[10] the low cationic character

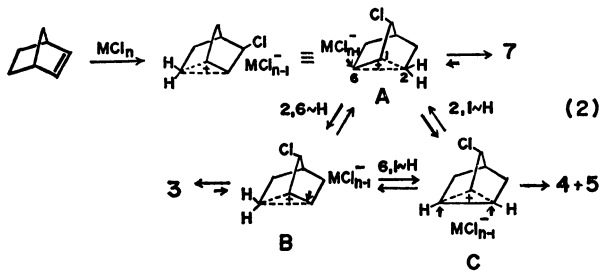

at C_1 in **A** and **B** due to the inductive effect of the adjacent chlorine atom probably prevents the attack of MCl_{n+1}^- on C_1, and makes the almost exclusive attack on C_6 and C_2 possible, leading to the formation of **7** and **3** respectively. It is also apparent by similar reason that 6,1- or 2,1-hydride shift to give **C** would be less important than 2,6-shift, and hence **4** and **5** are minor products. Such equilibrium as shown in Scheme 2 has been assumed to explain the result of the acetolysis and isomerization of *syn*- and *anti*-7-chloro-*exo*-norbornyl *p*-toluenesulfonate.[11]

In the chlorination by VCl_4, the reaction scheme for the formation of **2** and **6** is not yet clear. The isomer distribution in the minor products, however, suggests that the reaction proceeded through Scheme 2 to some extent.

Chlorination by $CuCl_2$ which gave 2,3-dichloronorbornanes almost selectively and only a small amount of carbon skeleton rearranged product, on the contrary, does not seem to proceed through Scheme 2. Coordination of copper salt on double bond may be one of the determining factors for such selective formation.

Isomerization of **2** or **7** to a mixture of **3**—**5** by rather strong Lewis acids such as $SbCl_5$ and $TlCl_3 \cdot 4H_2O$ in CCl_4 may be explained by Scheme 2. Thus, the abstraction of *exo*-Cl (on C_2) by MCl_n gives the cations **A** and **B** from **7** and **2** respectively which then afford **3**—**5** by recombination with Cl^- of MCl_{n+1}^-. We also observed the slow isomerization of **3** to **4** and **5** by $SbCl_5$ and $TlCl_3 \cdot 4H_2O$ at 20 °C and 76 °C respectively. This isomerization may involve the abstraction of *exo*-Cl from **3**. It should also be noted that no isomerization of **6** by $SbCl_5$ was observed at 20 °C for 10 min in CCl_4. The reason why **6** is so stable compared to **2** is not yet clear.

Experimental

All materials except $PbCl_4$[7] were commercial products and used without further purification. The identification of each product was described in previous papers.[1,2] The product distributions were analyzed by glc by the use of Shimadzu apparatus 5APTF and 4BMPF on both EGSS-X(15%)-Chromosorb-W (3 m) and PEG 6000 (25%)-Chromosorb-W (3 m) columns (carrier gas, N_2; bromobenzene or *trans*-dichlorocyclohexane as internal standard). In the reaction with VCl_4 or $SeCl_4$, **6** or **7** was isolated respectively by a fractional distillation in almost pure state and analyzed by NMR to ascertain the structure (Varian A-60 spectrometer; in CCl_4).

Synthesis of **2**. A homogeneous mixture of $CuCl_2$ (26.8 g, 200 mmol), LiCl (8.4 g, 200 mmol), CH_3CN (200 ml) and norbornene (4.7 g, 50 mmol) was stirred for 5 hr under reflux. After being cooled down to room temperature the

mixture was concentrated to *ca.* 50 ml by evaporation of solvent, added by water (300 ml), and then extracted with benzene. Distillation of the extract through a fractionating column (30 cm) with glass packings afforded two fractions leaving only a small amount of residue; D_1 5.0 g (bp 89—94 °C/19 mmHg) and D_2 0.86 g (bp 88—92 °C/10 mmHg). The fraction D_1 was shown by glc to contain **2** (95%) and small amounts of **6** and **7**. The fraction D_2 was revealed to be a mixture of **2**(15%), **6**(75%), and **7**(10%).

*Synthesis of **3** and **7**.* To a CCl_4 (170 ml) solution of norbornene (4.7 g, 50 mmol) was slowly added a yellow homogeneous CCl_4 (30 ml) solution of $SbCl_5$ (10.0 g, 33.4 mmol) at 20 °C for 5 min. After 5 min, water was added to the reaction mixture and the precipitated SbOCl was filtered off. Similar fractional distillation of the filtrate as described above afforded three fractions; D_1 2.1 g (bp 95—98 °C/18 mmHg), D_2 1.2 g (bp 102—109 °C/18 mmHg), and D_3 0.43 g (bp 75—77 °C/5 mmHg). The fraction D_1 was shown by glc to contain **3**(90%) and small amounts of **2**, **4**, **5**, and **7**. The fraction D_3 was shown to be a mixture of **3**(13%), **7**(84%) and small amounts of **4** and **5**.

*Isomerization of **7** or **2** to a Mixture of **3**—**5** by $TlCl_3 \cdot 4H_2O$.* A CCl_4 (25 ml) solution containing **7** (0.22 g, 1.33 mmol) and $TlCl_3 \cdot 4H_2O$ (0.80 g, 2.09 mmol) was stirred at 76 °C for 2 hr. After being cooled down to room temperature, organic layer was washed with water and analyzed by glc. The products were **2**(3.6%), **3**(27.6%), **4**(28.8%), **5**(34.6%), and **7**(5.4%); recovered yield of dichloronorbornanes was 90%. Similar treatment of **7** at 5 °C for 3 hr gave a mixture of **2**(0.4%), **3**(39.4%), **4**(19.8%), **5**(1.6%), and **7**(38.8%); yield, 91%. When **2**(1.04 mmol) was stirred in CCl_4 (25 ml) with $TlCl_3 \cdot 4H_2O$ (1.68 mmol) at 76 °C for 2 hr, it isomerized to a mixture of **2**(6.9%), **3**(21.3%), **4**(36.6%), and **5**(35.2%); yield, 89%. No isomerization of **2** or **7** to other isomers was observed at −10 °C.

*Isomerization of **7** or **2** to a Mixture of **3**—**5** by $SbCl_5$.* A CCl_4 (25 ml) solution containing **7** (1.47 mmol) and $SbCl_5$ (1.67 mmol) was kept at 20 °C for 10 min. Glc analysis of CCl_4 layer after usual work-up procedure revealed the presence of a mixture of **2**(5.4%), **3**(40.7%), **4**(24.3%), **5**(29.4%), and **7**(0.2%); yield of a mixture, 96%. Similar treatment of **2**(1.12 mmol) with $SbCl_5$ (1.69 mmol) gave a mixture of **2**(4.2%). **3**(17.6%), **4**(36.3%), and **5**(41.9%); yield, 98%.

References

1) S. Uemura, A. Onoe, and M. Okano, This Bulletin, **47**, 692 (1974).
2) S. Uemura, A. Onoe, and M. Okano, *ibid.*, **47**, 3121 (1974).
3) M. L. Poutsma, *J. Amer. Chem. Soc.*, **87**, 4293 (1965).
4) D. D. Tanner and G. C. Gidley, *J. Org. Chem.*, **33**, 38 (1968).
5) R. Hüttel, H. Reinheimer, and K. Nowak, *Chem. Ber.*, **101**, 3761 (1968).
6) S. Uemura, F. Tanaka, O. Sasaki, and M. Okano, *Bull. Inst. Chem. Res. Kyoto Univ.*, **49**, 97 (1971).
7) P. W. Henniger, L. J. Dukker, and E. Havinga, *Rec. Trav. Chim. Pays-Bas*, **85**, 1177 (1966).
8) R. F. Riley, J. Flato, and D. Bengels, *J. Org. Chem.*, **27**, 2651 (1962) and references therein.
9) P. Kovacic and R. M. Lange, *ibid.*, **30**, 4251 (1965).
10) W. G. Woods, R. A. Carboni, and J. D. Roberts, *J. Amer. Chem. Soc.*, **78**, 5653 (1956).
11) H. L. Goering and M. J. Degani, *ibid.*, **91**, 4506 (1969).

(−)-(1*S*,4*R*,5*R*)-Guaia-6,9-diene from Geranium Bourbon

Yoko NAGAHAMA, Hideo NAOKI, and Yoko NAYA

The Institute of Food Chemistry, Shimamoto-cho, Mishima-gun, Osaka 618

(Received July 28, 1975)

A sesquiterpene from Geranium Bourbon has been found to be guaia-6,9-diene in accordance with the report of Pesnelle *et al.*; it had previously been erroneously assigned as 3,7-diene by Herout *et al.* The details of the evidence on the structure, along with its stereochemistry, are described.

In the course of the study of Geranium oil[1] (Geranium Bourbon), we have isolated guaia-6,9-diene (I), which was identical with the compound previously reported[2] as "guaia-3,7-diene." This had been pointed out by Pesnelle *et al.*[3] In this paper, we wish to report the evidence for the correction of the structure, together with its stereochemistry, since we have not yet seen any detailed publication relating to the revised structure, I.

Commercial Geranium oil* was subjected to separation by column chromatography and preparative glc to obtain Compound I. Compound I, $[\alpha]_D$ −50.9°, was a colorless oil which exhibited its molecular ion peak at *m/e* 204 ($C_{15}H_{24}$) in its mass spectrum. Its IR spectrum revealed the absorptions of the isolated double bond and the trisubstituted ethylenes. In addition, no UV absorption maxima were observed in the region of 215—280 nm. The PMR spectrum exhibited two doublets, at δ 0.93 (6H, J=6.0) and at 1.02 (3H, J=6.0), which were assignable to an isopropyl and a secondary methyl group respectively; a broad singlet at 1.53 (3H) and a complex signal at around 5.35 (1H), accounting for the CH_3C=CH− system, as was confirmed by spin-spin decoupling, and a broad signal at around 5.16 (1H) coupled with a broad signal around 2.86 (1H), which was attributable to a vinyl proton adjacent to a methine.

The catalytic hydrogenation of I over PtO_2 in acetic acid afforded a mixture of two tetrahydro derivatives in the ratio of three to one. The IR spectrum of the major product (II), $[\alpha]_D$ +40.6°; M^+, *m/e* 208 ($C_{15}H_{28}$), was identical with that of Šorm's "guaiane."[4] On the other hand, in methanol over the same catalyst, I was reduced to a complex mixture of the dihydro isomers, accompanied by a small amount of II. The examination of the PMR spectrum of the main dihydro compound (III), M^+, *m/e* 206 ($C_{15}H_{26}$), revealed that CH_3C=CH had been reduced and that another trisubstituted double bond remained.

I was ozonized in ethyl acetate at −40 °C, followed by oxidative degradation. Its acidic fraction was treated with diazomethane-etherate. The methyl esters thus obtained were determined to be (IV) and (V) by an examination of their physical data. Compound IV exhibited the molecular ion peak at *m/e* 184 ($C_{10}H_{16}O_3$) in its mass spectrum. Its IR spectrum revealed the absorptions arising from nonconjugated C=O vibrations and the C–O bands of the methyl ester. The PMR spectrum exhibited a doublet at δ 0.9 (3H, J=6.5), indicating a secondary methyl; a singlet at 2.19 (3H) corresponding to $-COC\underline{H}_3$, and a signal at 3.69 (3H) which was assigned to $-COOC\underline{H}_3$. From all the above data, it seems that IV should contain a cyclopentane skeleton. Compound V, M^+, *m/e* 144 ($C_7H_{12}O_3$), obtained in a small amount, exhibited the absorption bands of carbonyl and methyl ester in its IR spectrum. Its PMR spectrum exhibited a doublet at δ 1.18 (6H, J=6.0), accounting for an isopropyl group, and a singlet at 3.67 (3H) which was assigned to a methyl ester group. Therefore, V should be methyl 4-methyl-3-oxopentanoate.

Now, in order to obtain the physical data of "guaiane" with definitely established stereochemistry, it was prepared from (−)-guaiol[5] (VI) *via* crystalline (−)-dihydroguaiol[6] (VII), with its known stereochemistry. VII was dehydrated by thionyl chloride–pyridine to afford two hydrocarbons, with isopropenyl (VIII) and isopropylidene (IX) groups respectively, in the ratio of three to two. The major hydrocarbon, VIII, was reduced to a saturated hydrocarbon (II *bis*), $[\alpha]_D$ −58°, which was found to be identical with "guaiane"[4] by a comparison of their IR spectra.

Hydrogenation of IX afforded a mixture of (II *bis*) and its isomer at C_7 (X) in the same ratio. On the other hand, oily (+)-dihydroguaiol[7] (XI), with a known stereochemistry, prepared from (−)-guaiol, afforded saturated (+)-hydrocarbon isomers (XII) and (XIII) in a similar manner. The IR spectra of X, XII, and XIII differed from that of (II *bis*), though

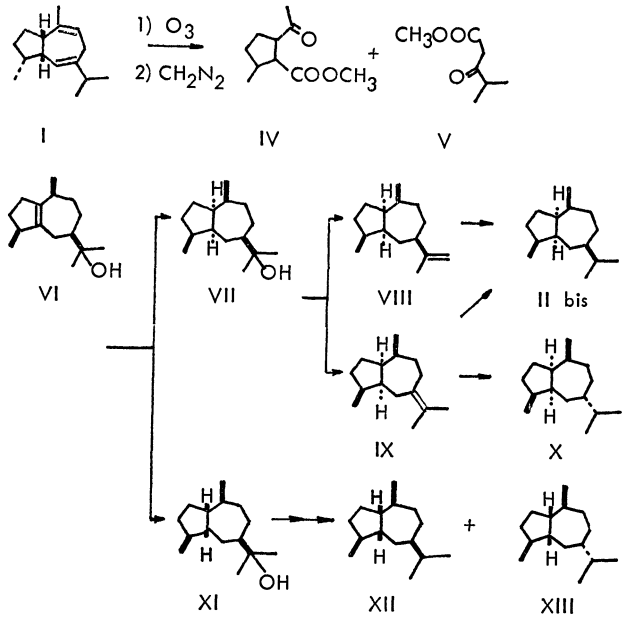

* Commercial Geranium oil was produced by Soda Aromatic Co., Ltd., in the Shodo island in 1974.

they exhibited quite similar mass spectra. Consequently, the structure including the absolute configuration of I was concluded to be (−)-(1*S*,4*R*,5*R*)-guaia-6,9-diene.

Experimental

The IR spectra were measured using a Hitachi EPI-G2 spectrometer. The UV spectra were taken on a Jasco Model ORD/UV-5 spectrometer. Measurements of optical rotation were carried out with a Perkin-Elmer 141 polarimeter. The mass spectra were measured using a Hitachi RMU-6 spectrometer with a indirect-inlet system operating at 80 eV. The PMR spectra were taken by a Hitachi R-20 B spectrometer at 60 MHz in CCl_4. The chemical shifts were expressed in δ downfield from TMS as an internal standard and coupling constants in Hz. The preparative glc conditions, using a model 920 Varian Aerograph fitted with a thermal-conductivity detector, were as follows: a 10-ft×3/8 in. aluminum column containing 20% Carbowax 20M on 60—80 mesh Diasolid-L. Nitrogen was used as the carrier gas, and the column temperature was set at 170—200 °C. All the melting points are uncorrected.

Isolation of I. Commercial geranium oil* (400 g) was successively chromatographed on SiO_2 and $AgNO_3$-SiO_2 (15%) columns and then eluted with *n*-hexane. On further purification by preparative glc, Compound (I) (400 mg) was obtained. Compound I was a colorless oil; $[\alpha]_D$ −50.9° (*c* 1.49, EtOH); IR (liq.) 1658 (C=C), 1360, 1375 (-$\underset{\underset{CH_3}{|}}{CH}$-$CH_3$), 854, 828 cm^{-1} (-C=C-); PMR (CCl_4) δ 0.93 (6H, d, J=6.0, an isopropyl group), 1.02 (3H, d, J=6.0: 4-CH_3), 1.53 (3H, br. s) and 5.35 (1H, m): a system of CH_3C=CH, 2.23 (1H, m) and 2.98 (1H, br. signal): protons at 8-C, 2.86 (1H, br. signal) coupled with 5.16 (1H, br. signal): protons at 5-C and 6-C, and 1.0—2.4 (7H, complex signals: methines and methylenes); mass spectrum *m/e* 204(38%, M^+, $C_{15}H_{24}$), 105(100%), 119(62%), and 161(52%).

Hydrogenation of I in Acetic Acid. I was reduced catalytically (PtO_2) in acetic acid at room temperature. After the filtration of the catalyst, the filtrate was diluted with water and extracted with ether. The evaporation of the ether gave a residue, which was purified on preparative glc (CW-20M, at 180 °C) to afford two compounds, (II) and (II′), in the ratio of three to one. The major product, II, was a colorless oil; $[\alpha]_D$ +40.6° (*c* 1.45, EtOH); δ 0.82 (6H, d, J=6.0), 0.83 (3H, d, J=6.0), 0.90 (3H, d, J=6.0), 1.0—2.3 (16H, complex signals); *m/e* 208 (9%, M^+, $C_{15}H_{28}$), 109(100%), 95(70%), 81(60%); the IR spectrum agreed with that of "guaiane."[4] The minor product, II′, was a colorless oil; δ 0.85 (6H, d, J=6.0), 0.88 (3H, d, J=6.0), 0.94 (3H, d, J=6.0), and 1.0—2.2 (16H, complex signals). Its IR spectrum was identical with that of the (X) prepared from guaiol (VI).

Hydrogenation of I in Methanol. A solution of I in methanol was hydrogenated in the presence of PtO_2 at room temperature. The filtration of the catalyst and the evaporation of the solvent left a residue, which was purified by preparative glc (CW-20M, at 180 °C) to afford (III), accompanied by a small amount of II. III was a colorless oil; ν_{max} 1655 cm^{-1} (C=C); δ 0.86 (3H, d, J=6.0), 0.95 (6H, d, J=6.0), 1.02 (3H, d, J=6.0), 1.1—2.5 (13H, complex signals), and 5.13 (1H, br. d, J=3.5); *m/e* 206 (5%, M^+, $C_{15}H_{26}$), 107(100%), 163(76%), 81(76%), 93(50%), and 121(22%).

Ozonolysis of I. A solution of I in ethyl acetate was ozonized at −40 °C. When the reaction was completed, hydrogen peroxide (30%) and a potassium bicarbonate solution (5%) were added to the ozonide for degradation. The solution was then allowed to stand overnight at 0 °C. The organic layer was further treated as usual to obtain acidic compounds. The acids thus obtained were treated with diazomethane-etherate to give the methyl esters, (IV) and (V). Compound IV was a colorless oil; ν_{max} 1710, 1725 (sh) (C=O), 1200, 1170 cm^{-1} (C-O); δ 0.9 (3H, d, J=6.5), 2.19 (3H, s), 3.69 (3H, s), 3.0—3.5 (2H, m), and 1.3—2.5 (5H, m); *m/e* 184 (3%, M^+, $C_{10}H_{16}O_3$), 81 (100%), 43(96%).

Compound V was obtained in a very small amount as a colorless oil; ν_{max} 1730 (C=O), 1200, 1170 cm^{-1} (C-O); δ 1.18 (6H, d, J=6.0), 3.67 (3H, s), 2.0—3.5 (3H, complex signals); *m/e* 144 (4%, M^+, $C_7H_{12}O_3$), 143(21%), 55(100%).

Hydrogenation of Guaiol VI.[8] A solution of 1.86 g of (−)-guaiol (VI)** in 30 ml of ethanol and 0.69 g of a Raney nickel catalyst was shaken for 20 hr at 100 °C under a hydrogen pressure of 100 atm. The filtration of the catalyst and the evaporation of the solvent yielded a mixture of dihydroguaiols. They were both diastereomers at the ring juncture and were revealed on the gas chromatogram in the ratio of 2 : 3. Separation by preparative glc (CW-20M, at 200 °C) led to the dihydroguaiol (VII)[6] (major) and (XI),[7] with known stereochemistries. VII was a colorless needle; mp 76—76.5 °C; $[\alpha]_D$ −44.8° (*c* 1.06, acetone); ν_{max} 3325 (-OH), 1166, 1134 cm^{-1} (C-O); δ 0.86 (3H, d, J=6.0), 0.95 (3H, d, J=6.0), 1.07 (3H, s), 1.10 (3H, s), and 1.2—2.4 (16H, m, including -OH); *m/e* 224 (M^+, trace, $C_{15}H_{28}O$), 206 (2%, M^+-18), 164(10%), 81(19%), and 59(100%). XI was a colorless oil; $[\alpha]_D$ +73.5° (*c* 0.93, acetone); ν_{max} 3380 (-OH), 1158, 1120 cm^{-1} (C-O); δ 0.95 (6H, br. d, J=9.5), 1.10 (6H, s), 1.2—2.0 (15H, complex signals), and 2.51 (1H, s, -OH); *m/e* 224 (M^+, trace, $C_{15}H_{28}O$), 206 (3%, M^+-18), 163(7%), 81(22%), and 59 (100%).

Dehydration of (−)-Dihydroguaiol VII with Thionyl Chloride-Pyridine. Thionyl chloride (1.38 equiv) was stirred, drop by drop into a solution of (−)-dihydroguaiol VII in pyridine at 5—10 °C. After observation by tlc of the completion of the reaction, the mixture was poured over ice and then extracted with pet. ether. The extract was washed with water, dried (Na_2SO_4), and evaporated to give a brown oil, which was purified on preparative glc to afford (VIII) and (IX). Compound VIII was a colorless oil; $[\alpha]_D$ −47.0° (*c* 0.57, EtOH); ν_{max} 3070, 888 cm^{-1} (=CH_2); *m/e* 206 (M^+, 14%, $C_{15}H_{26}$), 163(52%), 81(100%). Compound IX was a colorless oil; *m/e* 206 (M^+, 12%, $C_{15}H_{26}$), 163(44%), 81(100%).

Dehydration of (+)-Dihydroguaiol XI with Thionyl Chloride-Pyridine. (+)-Dihydroguaiol XI was worked up with thionyl chloride (1.38 equiv.) and pyridine as has been described above, affording two products, (VIII′) and (IX′). Compound VIII′ was a colorless oil; ν_{max} 3070, 888 cm^{-1} (=CH_2); *m/e* 206 (M^+, 25%, $C_{15}H_{26}$), 163(60%), 81(100%). Compound IX′ was a colorless oil; *m/e* 206 (M^+, 22%, $C_{15}H_{26}$), 163(48%), and 81(100%).

Hydrogenation of VIII in Ethanol. VIII in ethanol was hydrogenated over PtO_2 at room temperature. After the completion of the reaction, the catalyst and the solvent were removed. (II *bis*) was obtained as the sole product and identified with II by a comparison of their IR spectra;

** (−)-Guaiol was kindly presented by Inabata Koryo Co., Ltd.

a colorless oil; $[\alpha]_D$ −58.1° (*c* 0.74, EtOH); δ 0.82 (6H, d, J=6.0), 0.83 (3H, d, J=6.0), 0.90 (3H, d, J=6.0), and 1.0—2.3 (16H, complex signals); *m/e* 208 (M^+, 12%, $C_{15}H_{28}$), 109 (100%).

Hydrogenation of IX in Acetic Acid. IX was hydrogenated in acetic acid over PtO_2 at room temperature. After the filtration of the catalyst, water was added to the reaction mixture, extracting with *n*-pentane. The evaporation of the solvent left a mixture of (II *bis*) and X, in the ratio of 1 : 1; those substances were separated by preparative glc (CW-20M, at 170 °C). Compound X was a colorless oil; $[\alpha]_D \fallingdotseq 0°$ (*c* 0.13, EtOH); δ 0.85 (6H, d, J=6.0) 0.88 (3H, d, J=6.0), 0.94 (3H, d, J=6.0), 1.0—2.2 (16H, complex signals); *m/e* 208 (M^+, 14%, $C_{15}H_{28}$), 109 (100%).

Hydrogenation of VIII′ in Ethanol and IX′ in Acetic Acid. VIII′ was hydrogenated over the PtO_2 catalyst in ethanol in a way similar to that as in the case of VIII to afford a colorless oil (XII); $[\alpha]_D$ +58.1° (*c* 0.91, EtOH); δ 0.86 (6H, d, J=6.0), 0.92 (3H, d, J=6.0), 0.95 (3H, d, J=6.0), 1.1—2.0 (16H, complex signals); *m/e* 208 (M^+, 10%, $C_{15}H_{28}$), 109(100%). IX′ was reduced over the PtO_2 catalyst in acetic acid in a way similar to that in the case of IX to give XII and (XIII) on purification by preparative glc (CW-20M, at 180 °C). Compound XIII was a colorless oil; $[\alpha]_D$ +34.7° (*c* 0.23, EtOH); δ 0.84 (6H, d, J=6.0), 0.92 (3H, d, J=6.0), 0.97 (3H, d, J=6.0), 1.1—2.0 (16H, complex signals); *m/e* 208 (M^+, 12%, $C_{15}H_{28}$), 109(100%).

The authors wish to thank Dr. Yoshihiro Hirotsu of the university of Osaka for the hydrogenation under high pressure.

References

1) H. Naoki, T. Sakai, Y. Naya, and Y. Hirose, The 18th TEAC Meeting at Chiba Pref., Abst. p. 12 (1974).

2) V. Benešová, P. N. Chou, V. Herout, Y. R. Naves, and D. Lamparsky, *Coll. Czech. Chem. Commun.*, **29**, 1042 (1964). Dr. Herout kindly sent us IR and PMR spectra of "guaia-3,7-diene" for the comparison and informed us the structure had been corrected by Pesnelle *et al.*[3]

3) P. Pesnelle, B. Corbier, and P. Teisseire, *Recherches*, No. 18, 45 (1971). *idem*, *Riv. Ital. Essenze, Profumi, Piante Off., Aromi, Saponi, Cosmet., Aerosol*, **54**, 92 (1972).

4) J. Plíva, M. Horák, V. Herout, and F. Šorm, Die Terpene "Sammlung der Spektren nnd physikalischen Konstanten," Teil 1, Akademie-Verlag, Berlin (1960) S. 133.

5) H. Minato, *Tetrahedron*, **18**, 365 (1962); K. Takeda and H. Minato, *Tetrahedron Lett.*, **1960**, 33.

6) L. Dolejš, A. Mironov, and F. Šorm, *Coll. Czech. Chem. Commun.*, **26**, 1015 (1961).

7) E. J. Eisenbraun, T. George, B. Riniker, and C. Djerassi, *J. Amer. Chem. Soc.*, **82**, 3648 (1960).

8) Pl. A. Plattner and L. Lemay, *Helv. Chim. Acta*, **23**, 897 (1940).

Formations and Reactions of *o*-Benzoquinone Mono- and Di-imines. I.

Takashi NOGAMI, Tadanori HISHIDA,* Masakazu YAMADA, Hiroshi MIKAWA, and Yasuhiko SHIROTA

Department of Applied Chemistry, Faculty of Engineering, Osaka University, Yamadakami, Suita, Osaka 565

(Received August 6, 1975)

We have succeeded in obtaining *o*-benzoquinone monoimine (*o*-BQMI) and *o*-benzoquinone diimine (*o*-BQDI) by oxidizing *o*-aminophenol (*o*-AP) and *o*-phenylenediamine (*o*-PD), respectively, with freshly prepared lead dioxide at −10 °C in several organic solvents, and also with potassium hexacyanoferrate (III) in an aqueous buffer solution. The formations and reactions of *o*-BQMI and *o*-BQDI in aqueous buffer solution were investigated by a stopped flow technique together with a conventional electronic absorption measurements. Both *o*-BQMI and *o*-BQDI were formed in the pH range 8—12, and the hydrolysis of *o*-BQMI to produce *o*-benzoquinone was found in the pH range 6—8. Both *o*-BQMI and *o*-BQDI were found to be unstable at a room temperature to produce 2-aminophenoxazin-3-one (APZ) and 2,3-diaminophenazine (DAP), respectively, as the main products. The formation reactions of APZ and DAP were investigated by observing the spectroscopic course of the reactions in *o*-BQMI- *o*-AP and *o*-BQDI- *o*-PD system in diethyl ether.

p-Benzoquinone monoimine (*p*-BQMI) and *p*-benzoquinone diimine (*p*-BQDI) have long been considered as the intermediates in the oxidative coupling reactions of *p*-aminophenol and of *p*-phenylenediamine with aromatic amines and phenols.[1]

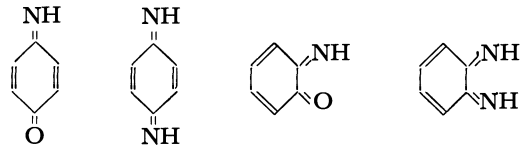

p-BQMI *p*-BQDI *o*-BQMI *o*-BQDI

Their derivatives have also been used as the developers in color photography.[2] Recently, J. F. Corbett investigated many dye formation reactions between *p*-BQMI and *p*-BQDI with several aromatic amines and phenols.[3] Inspite of the extensive studies on *p*-benzoquinone imines, investigations on the isomeric *o*-benzoquinone imines are scanty. Although *o*-BQDI has been obtained about seventy years ago,[4] instability of this compound prevented further work. Without direct evidence, *o*-BQMI and *o*-BQDI have been considered as the reaction intermediates in the oxidation reactions of *o*-aminophenol (*o*-AP)[5] and *o*-phenylenediamine (*o*-PD),[6] respectively. Recently, the intermediacy of *o*-BQDI was demonstrated for the first time in the dehydrogenation reaction of *o*-phenylenediamine with chloranil.[7]

In the present paper, we report that *o*-BQMI and *o*-BQDI were obtained by the oxidations of *o*-AP and *o*-PD, respectively, with active PbO_2 in several organic solvents and also with potassium hexacyanoferrate (III) in an aqueous buffer solution for the first time. As expected, these imines were found to be reactive, and the reactions of *o*-BQMI with *o*-AP and of *o*-BQDI with *o*-PD were investigated spectrophotometrically in diethyl ether.[8]

Experimental

Materials. *o*-Aminophenol and *o*-phenylenediamine were purified by repeated sublimations. Commercially available NaH_2PO_4, Na_2HPO_4, Na_3PO_4, $K_3Fe(CN)_6$, Ag_2O, and catechol were used without further purification. Active PbO_2 was prepared according to the literature.[9] The solvents diethyl ether, methyl alcohol, ethyl alcohol, toluene, acetone, acetonitrile, and chloroform were purified by the usual procedures.

Buffer Solutions. Buffer solutions were prepared by appropriate mixtures of 0.1 M aqueous solutions of NaH_2PO_4, Na_2HPO_4 and Na_3PO_4.

Syntheses of o-Benzoquinone Mono- and Di-imines. Freshly prepared PbO_2[9] (350 mg) and anhydrous sodium sulfate (100 mg) baked beforehand for 30 min were added to an organic solution (chloroform, diethyl ether, toluene, acetone, and acetonitrile) of *o*-aminophenol or *o*-phenylenediamine (2 mg in 25 ml solvent) under cooling with ice-salt (−10 °C) and vigorously stirred for five min. The solution was filtered, and the yellow colored filtrate was used directly for further investigations. All procedures were performed under anhydrous conditions. Both *o*-BQMI and *o*-BQDI were fairly stable only when kept below 0 °C in a dilute solution, and unstable at a room temperature or in a concentrated solution. This prevented us from carrying out their isolations.

Separation of Reaction Products. The reaction products in diethyl ether and aqueous buffer solutions were separated as follows. In the case of ether solutions, the reaction mixtures of *o*-AP–*o*-BQMI and *o*-PD– *o*-BQDI systems were kept overnight, and the ether was removed by distillation. The residue thus obtained was chromatographed on alumina (benzene–acetone mixed solvent as an elute) and the main reaction products were purified further by a Liquid Chromatograph LC-07 (Japan Analytical Industry Co. Ltd.). In the case of the buffer solutions, the mixtures of $K_3Fe(CN)_6$ and amines were also kept overnight, and the precipitate was collected by filtration. After the precipitate was dried completely, it was purified by the same manner as described above. The identifications of the reaction products as 2-aminophenoxazin-3-one (APZ), 2,3-diaminophenazine (DAP) and 2,2′-diaminoazobenzene (AB) were made by comparing their UV, VIS, IR and mass spectra with those of the authentic samples.[7,8] The yields of APZ, DAP and AB are: APZ, 1.57% (pH 4.5); 18.9% (pH 7); 16% (in diethyl ether); DAP, 4.76% (pH 4.5); 11.11% (pH 7); AB, 26.6% (in diethyl ether), respectively. Many byproducts other than APZ, DAP and AB were also obtained. Most of them may be such polymers as shown below.[10]

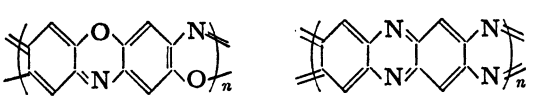

However, they could not be identified well because of the difficulties in their purifications.

* Present address: Sharp, Co. Ltd., Nagaike-cho, Abeno-ku, Osaka 545

Measurements. The electronic absorption spectra were measured by a Stopped Flow Rapid Reaction Analyser RA 1100 (Union Giken) in the cases of rapid reaction and by a Hitachi 124 spectrophotometer in the cases of slow reaction. Infrared spectra were measured by an IR-G Spectrometer (Japan Spectroscopic Co. Ltd.).

Results and Discussion

Formations of o-Benzoquinone Mono- and Di-imines in Organic Solvents. We tried to obtain *o*-BQMI and *o*-BQDI by oxidizing *o*-AP and *o*-PD, respectively, with active PbO_2[9] in several organic solvents. As a typical example, the experimental results in diethyl ether will be described below. Yellow colored solutions were obtained after the oxidations of *o*-AP and *o*-PD as described in the experimental section. Since the yellow compound obtained could not be isolated because of their instabilities, they were identified as *o*-BQMI and *o*-BQDI from their reactivities and electronic absorption spectra in diethyl ether, the latter of which are similar to that of the isoelectronic *o*-benzoquinone. Figure 1 shows the electronic absorption spectra of *o*-AP–PbO_2 and *o*-PD–PbO_2 systems and of *o*-benzoquinone (*o*-BQ) obtained by the oxidation of catechol with Ag_2O.[11] The close similarity of the absorption spectra of *o*-AP–PbO_2 and *o*-PD–PbO_2 systems to *o*-BQ (λ_{max} 365 nm, 350 nm and 372 nm, respectively) shows that the yellow compound obtained in the solution would be *o*-BQMI and *o*-BQDI. These identifications seem to be reasonable also when the reactions of these compounds with aromatic amines are considered as to be described later. The formation schemes of *o*-BQMI and *o*-BQDI are as follows.

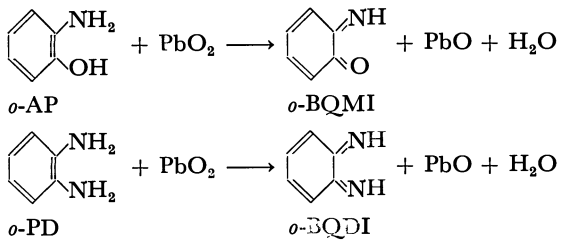

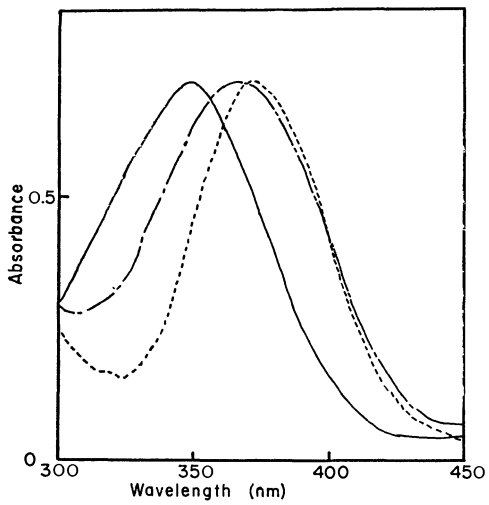

Fig. 1. Absorption spectra of *o*-BQ, *o*-BOMI, and *o*-BQDI. Concentration: 7.4×10^{-4} M.
····· *o*-BQ, ---- *o*-BQMI, —— *o*-BQDI.

The formations of *o*-benzoquinone imines in solution seem to be quantitative, since no starting amine was detected after the reaction. Thus, the extinction coefficients of *o*-BQMI and *o*-BQDI at absorption peaks were estimated as [12]: *o*-BQMI, λ_{max}=365 nm, ε=1100; *o*-BQDI, λ_{max}=350 nm, ε-1300.

Both *o*-BQMI and *o*-BQDI could be obtained also in toluene, chloroform, acetone, and acetonitrile, but not in methyl alcohol and ethyl alcohol, since their reactivities in these solvents are too large. Table 1 shows the absorption peaks of *o*-BQMI and *o*-BQDI in several solvents. The absorption peak tends to shift to the shorter wavelength region with increasing solvent polarity, being characteristic to $n\pi^*$ transition. We have also succeeded in obtaining the absorption spectra of *o*-BQMI and *o*-BQDI or their protonated species[13] in water by the following manner: An ether solution of *o*-BQMI or *o*-BQDI was poured into an aqueous buffer solution (pH 4.35), and the absorption spectra of the water phase was measured immediately. The results are also shown in Table 1.

Table 1. Absorption peaks of *o*-BQMI and *o*-BQDI in several solvents

	Toluene	Chloroform	Ether	Acetone	Aceto-nitrile	Buffer solution (pH 4.35)
o-BQMI	374	372	365	370	370	390
o-BQDI	358	352	350	346	338	382

Formations and Reactions of o-BQMI and o-BQDI in Aqueous Buffer Solution. J. F. Corbett studied the formations and reactions of *p*-BQMI and *p*-BQDI by oxidizing *p*-aminophenol (*p*-AP) and *p*-phenylenediamine (*p*-PD), respectively, with potassium hexacyanoferrate (III).[3,14] In *p*-AP–$K_3Fe(CN)_6$ and *p*-PD–$K_3Fe(CN)_6$ systems, no reaction occurs at pH<4, but the formations of dyes (unknown in the former system and Bandrowski's base in the latter system) occurred by the reaction of *p*-benzoquinone imines once formed with amines in the pH range 4—8. He also reported that the hydrolyses of *p*-BQMI and *p*-BQDI occurred to produce *p*-benzoquinone as shown below.[14]

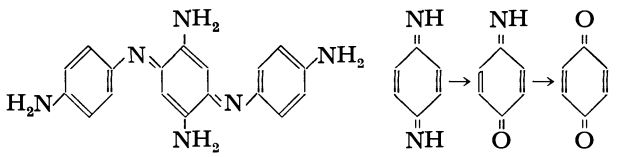

Bandrowski's base *p*-BQDI *p*-BQMI *p*-BQ

In order to compare the reactivities of the isomeric *o*-benzoquinone imines, we have carried out the analogous studies of the reactions in *o*-AP–$K_3Fe(CN)_6$ and *o*-PD–$K_3Fe(CN)_6$ systems at pH 4.5, 6, 7, 8, 9, 10, 11, and 12. The initial fast reactions were followed by a stopped flow technique to obtain the spectral change from zero to a few seconds after mixing. The succeeding slow reactions were followed by a conventional electronic absorption measurements. The main features of the reactions and absorption peaks of various species

Table 2. Formations and reactions of *o*-BQMI and *o*-BQDI in aqueous buffer solution

pH	*o*-AP–$K_3Fe(CN)_6$			*o*-PD–$K_3Fe(CN)_6$		
	o-BQMI[a]	Hydrolysis[b]	APZ[c]	*o*-BQDI[a]	Hydrolysis[b]	DAP[c]
4.5	−	−	+	−	−	+
6	−	+	+	−	−	+
7	−	+	+	−	−	+
8	+	+	+	−	−	+
9	+	−	+	+	−	+
10	+	−	+	+	−	+
11	+	−	−	+	−	+
12	+	−	−	+	−	+

a) The signs + and − mean that *o*-benzoquinone imines are formed and not formed, respectively. b) The signs + and − mean that hydrolysis of *o*-benzoquinone imines occurs and does not occur, respectively. c) The signs + and − mean that the reaction products, APZ and DAP, are produced and not produced, respectively.

Table 3. Absorption peaks of the species involved in the reaction

	In water (nm)	In diethyl ether (nm)
o-BQ	415	380
o-BQMI	390	365
o-BQDI	382	350
APZ	435	405 425
DAP	445 (pH 4.5)	430
	423 (pH 6)	
	418 (pH 7—12)	
$K_3Fe(CN)_6$	420	
AIP		495
AB		470

involved in the reactions are summarized in Table 2 and Table 3, respectively.

(1) o-AP–$K_3Fe(CN)_6$ System. In the pH range 4.5—6, no distinct change of the absorption spectra was observed for a few seconds, but a gradual formation of 2-aminophenoxazin-3-one (APZ) peaking at 435 nm for observed was several hours. In the pH range 7—8, *o*-BQMI was observed together with *o*-benzoquinone (*o*-BQ) and APZ. The typical results at pH 7 is shown in Figs. 2(a), 2(b), and 2(c) ($[o\text{-AP}]=2.0\times10^{-4}$ M, $[K_3Fe(CN)_6]=4.0\times10^{-4}$ M). The increase of the *o*-BQMI band at 390 nm together with the decrease of $K_3Fe(CN)_6$ band at 420 nm was observed for 0.1 s with an isosbestic point at 395 nm. Thereafter, the *o*-BQ band at 415 nm increased from 0.1—0.9 s, the assignment being made from the comparison of this band with the spectrum of *o*-BQ in aqueous solution which was obtained by extracting the ether solution of *o*-BQ with the buffer solution. APZ band increased gradually after 0.9 s. In the pH range 9—12, the

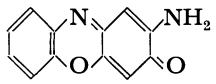

APZ

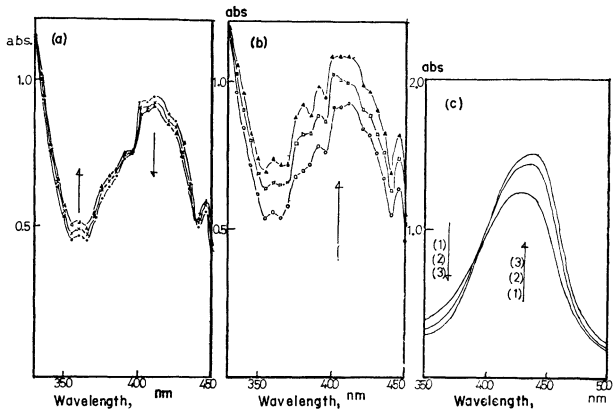

Fig. 2. Spectroscopic course of the reaction in *o*-AP–$K_3Fe(CN)_6$ system at pH 8. $[o\text{-AP}]=2.0\times10^{-4}$ M, $[K_3Fe(CN)_6]=4.0\times10^{-4}$ M.
(a) Formation process of *o*-BQMI.
—·— 0 s, —×— 50 ms, —△— 100 ms.
(b) Hydrolysis process of *o*-BQMI.
—○— 200 ms, —□— 500 ms, —▲— 900 ms.
(c) Formation process of APZ.
(1) 1 min, (2) 6 min, (3) 19 min.

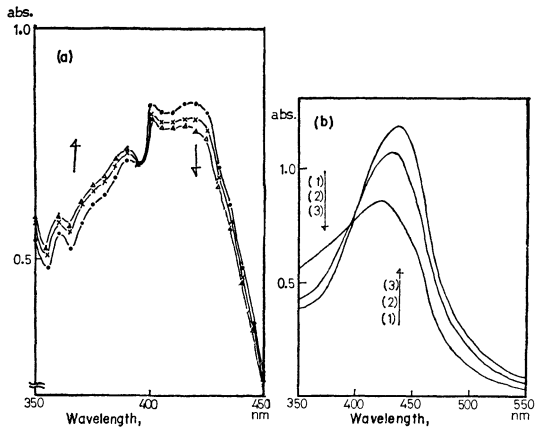

Fig. 3. Spectroscopic course of the reaction in *o*-AP–$K_3Fe(CN)_6$ system at pH 9. $[o\text{-AP}]=2.0\times10^{-4}$ M, $[K_3Fe(CN)_6]=4.0\times10^{-4}$ M.
(a) Formation process of *o*-BQMI.
—·— 0 s, —×— 50 ms, —△— 100 ms.
(b) Formation process of APZ.
(1) 1 min, (2) 7 min, (3) 30 min.

formation of *o*-BQMI was clearly found at 390 nm with the decrease of $K_3Fe(CN)_6$. At the later stage of the reaction, APZ was found to be formed at pH 9 and 10, but the final reaction product at pH 11 and 12 could not be identified well. The spectral change at pH 9 is shown in Figs. 3(a) and 3(b) as a typical example ($[o\text{-AP}]=2.0\times10^{-4}$ M, $[K_3Fe(CN)_6]=4.0\times10^{-4}$ M).

The above mentioned reactions of this system may lead us to the following conclusion. (1) the results in the pH range 4.5—10 show that APZ is the final reaction product of the oxidation of *o*-AP. (2) *o*-BQ observed in the pH range 6—8 is produced by the hydrolysis of *o*-BQMI. This is supported by the fact that *p*-benzoquinone is produced by the hydrolysis of *p*-BQMI or *p*-BQDI.[14] (3) The results in the pH

range 8—9 suggest that *o*-BQMI is a precursor to the APZ formation. This point may be made more conclusive later in this paper. The discussions (1)—(3) lead to the following reaction scheme:

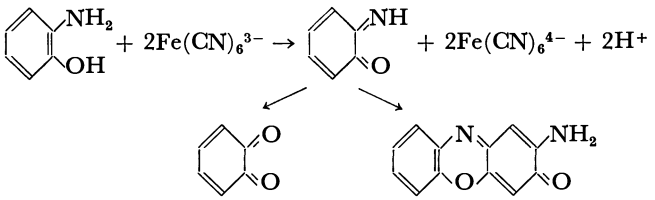

The formation scheme of APZ from *o*-BQMI will be discussed later.

(2) o-PD–$K_3Fe(CN)_6$ System. In the pH range 4.5—8, no distinct spectral change was observed by a stopped flow method at the initial stage of the reaction, but 2,3-diaminophenazine (DAP) (λ_{max}=445 nm (pH 4.5), 423 nm (pH 6), 418 nm (pH 7—12)) was found to be formed slowly with the decrease of $K_3Fe(CN)_6$.

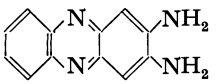

DAP

The red-shift of the absorption spectrum of DAP in acidic solution is probably due to the protonation of the amino group. The spectroscopic course of the reactions in the pH range 9—12 can be explained by a typical example at pH 12 (Figs. 4(a) and 4(b), [*o*-PD]=2.0×10^{-4} M, [$K_3Fe(CN)_6$]=4.0×10^{-4} M). Formation of *o*-BQDI was clearly observed with the decrease of $K_3Fe(CN)_6$ for about 0.35 s, the yield of *o*-BQDI being higher with increasing pH values. After the formation of *o*-BQDI, the increase of the absorption band around at 500 nm was observed, which then decreased to produce DAP with an isosbestic point at 478 nm. The compound peaking at 500 nm seems to be the precursor to the DAP formation, but could not be isolated because of its instability. We assigned it as 2-amino-*N*-(2-aminophenyl)-*p*-benzoquinone diimine (AABI) from the following reasons: (1) It is reasonable that cyclization of AABI produces DAP, which was clarified recently by J. F. Corbett *et al.*[15]

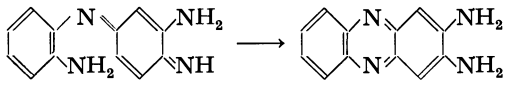

AABI DAP

(2) Absorption peak around 500 nm is reasonable in view of the fact that many *p*-indamine derivatives have their absorption peaks between 450—550 nm.[15,16]

These experimental results, especially of pH 9—12, show that *o*-BQDI may be a precursor to the DAP formation, and lead us to the following reaction scheme:

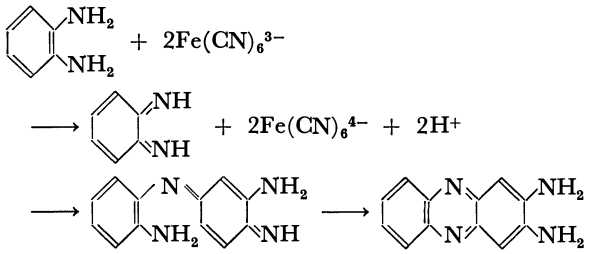

The formation scheme of AABI from *o*-BQDI will be discussed later. The high yield of *o*-BQDI at high pH range may be due to the efficient neutralization of the proton in the above oxidation process. The hydrolysis of *o*-BQDI was not observed, being in striking contrast to the cases of *o*-BQMI, *p*-BQMI and *p*-BQDI.

Reaction of o-BQMI and o-BQDI in Diethyl Ether.[8] As shown previously, oxidations of *o*-AP and *o*-PD with $K_3Fe(CN)_6$ in an aqueous buffer solution produce APZ and DAP, respectively, but the reaction rate in the initial stage is too fast to make clear the reaction scheme. Since in these reactions *o*-BQMI or *o*-BQDI is formed initially and APZ or DAP is produced thereafter as a main reaction product, *o*-benzoquinone imines are considered to be the intermediate for the products. To make clear the reaction scheme, the reactions of *o*-BQMI with *o*-AP and that of *o*-BQDI with *o*-PD were investigated in diethyl ether by measuring the change of the absorption spectra with time, because the reaction rate is considerably reduced in this solvent.

(1) o-BQMI–o-AP System. When a diethyl ether solution of *o*-BQMI was kept at a room temperature, some amount of APZ was produced slowly, *o*-BQMI being thus somewhat unstable in the solution. When *o*-AP was added to the *o*-BQMI solution, however, APZ was produced much faster. The fact shows that APZ is produced mainly by the reaction between *o*-BQMI and *o*-AP. Figs. 5(a) and 5(b) show the spectroscopic course of the reaction in *o*-BQMI- *o*-AP system ([*o*-BQMI]=3.1×10^{-4} M, [*o*-AP]=2.8×10^{-4}M) at a room temperature (Fig. 5(a), 0—5 hr after mixing; Fig. 5(b), 5—10 hr after mixing). The *o*-BQMI band at 365 nm decreased and a new band at 495 nm increased for the first five hr with an isosbestic point at 336 nm,[17] but thereafter the latter band decreased. Apparent induction period was observed for the increase of the characteristic APZ band at 405 and 425 nm (Fig. 5(a)), and isosbestic points appeared again at 465 and 336 nm in the later half of the reaction (Fig.

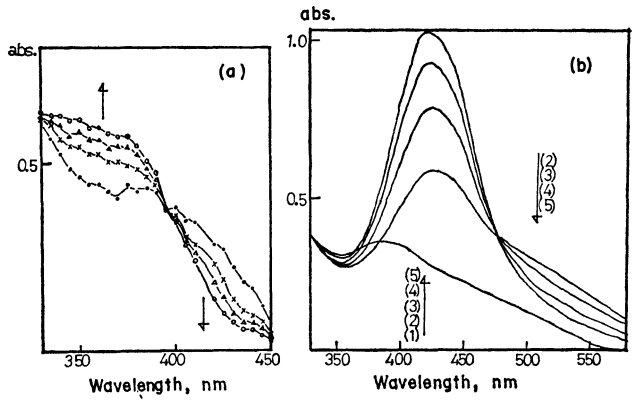

Fig. 4. Spectroscopic course of the reaction in *o*-PD–$K_3Fe(CN)_6$ system at pH 12. [*o*-PD]=2.0×10^{-4} M, [$K_3Fe(CN)_6$]=4.0×10^{-4} M.
(a) Formation process of *o*-BQDI.
—·— 0 s, —×— 50 ms, —△— 100 ms, —○— 300 ms.
(b) Formation process of DAP.
(1) 1 min, (2) 6 min, (3) 12 min, (4) 18 min, (5) 23 min.

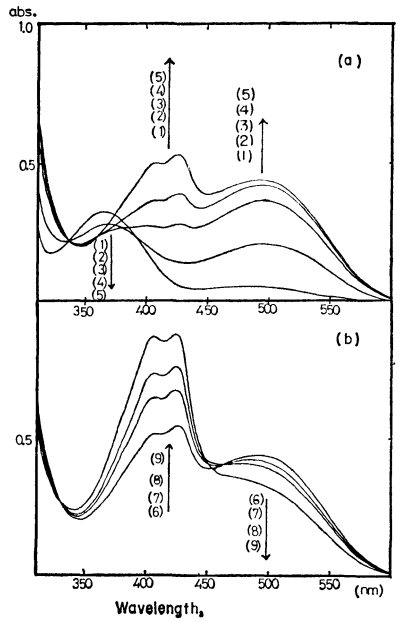

Fig. 5. Spectroscopic course of the reaction in *o*-BQMI–*o*-AP system in diethyl ether. [*o*-AP]$=2.8\times10^{-4}$ M, [*o*-BQMI]$=3.1\times10^{-4}$ M, estimated from the initial concentration of *o*-AP in the preparation of *o*-BQMI. (a) (1) 1 min, (2) 28 min, (3) 102 min, (4) 180 min, (5) 300 min. (b) (6) 312 min, (7) 417 min, (8) 462 min, (9) 567 min.

5 (b)). Fig. 5 (b) shows that the species peaking at 495 nm is a precursor to the APZ formation, but we could not isolate it because of its easy conversion into APZ during the isolation. We assigned this intermediate as 2-amino-*o*-indophenol (AIP) from the following

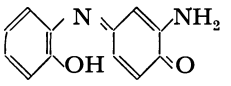

AIP

reasons: (1) It is quite reasonable that AIP has its absorption peak at 495 nm in view of the facts that many *p*-indophenol derivatives are reported to have their absorption peaks between 470 and 510 nm.[18] (2) As hydroxyindamine derivatives, for example, cyclize easily into phenoxazine-3-imine derivatives as shown below,[18] cyclization reaction of AIP to produce APZ is reasonable.[19]

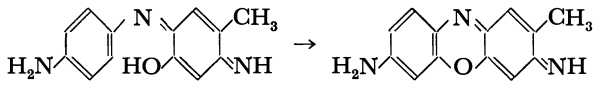

AIP itself may be produced by the addition reaction of *o*-BQMI with *o*-AP. Namely, by this reaction a leuco base of AIP, though not detected, may be formed in the initial stage of the reaction, followed by the oxidation of this leuco compound with *o*-BQMI.[20] Thus, the reaction mechanism in the present system is expected to be as follows.

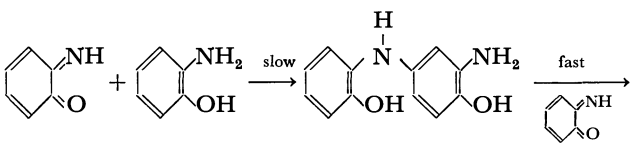

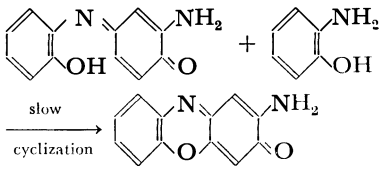

We believe that this scheme also holds in the reaction of *o*-AP–$K_3Fe(CN)_6$ system, although not clarified yet.

(2) o-BQDI– o-PD System. When diethyl ether solution of *o*-BQDI was kept at a room temperature, some amount of 2,2′-diaminoazobenzene (AB) was produced slowly, *o*-BQDI being thus somewhat unstable in the solution. When *o*-PD was added to the *o*-BQDI solution, however, AB was produced much faster. This fact shows that AB is produced mainly by the reaction between *o*-BQDI with *o*-PD. Figure 6 shows the spectroscopic course of the reaction in *o*-BQDI–*o*-PD system ([*o*-BQDI]$=3.8\times10^{-3}$ M, [*o*-PD]$=9.5\times10^{-4}$ M) at a room temperature. This figure shows that with decreasing intensity of the *o*-BQDI band at 352 nm, the intensity of AB band at 470 nm increased

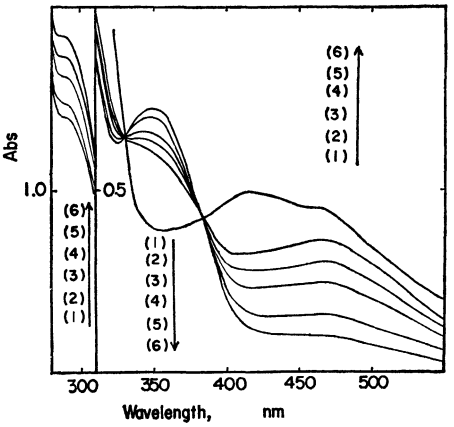

Fig. 6. Spectroscopic course of the reaction in *o*-BQDI–*o*-PD system in diethyl ether. [*o*-PD]$=9.5\times10^{-4}$ M, [*o*-BQDI]$=3.8\times10^{-3}$ M, estimated from the initial concentration of *o*-PD in the preparation of *o*-BQDI.
(1) 1 min, (2) 8 min, (3) 41 min, (4) 85 min, (5) 164 min, (6) 24 hr.

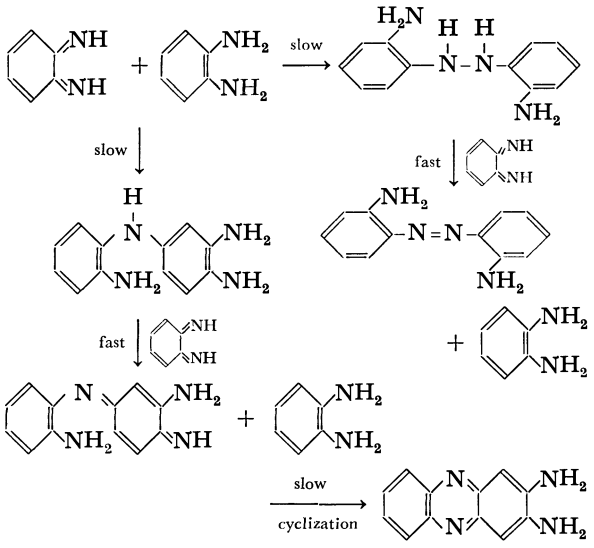

with an isosbestic point at 380 nm, followed by the formation of DAP (λ_{max} 430 nm) in the later stage of the reaction. The reaction scheme for the formations of AB and DAP in *o*-BQDI–*o*-PD system is supposed to be as shown below: DAP is probably produced through AABI[21] as in the case of *o*-PD–$K_3Fe(CN)_6$ system in water, and AABI itself may be produced by the oxidation of its leuco base with *o*-BQDI. The formation of AB through 2,2′-diaminohydrazobenzene is suggested from the similarity of the reaction to those of *p*-BQDI with several aromatic amines.[20]
Unfortunately, the intermediate AABI could not be detected clearly in diethyl ether, probably because the absorption band of AABI is covered with that of AB. The reason why AB is not produced sufficiently in aqueous buffer solution has not been clarified yet.

o-Benzoquinone imines have long been considered as the possible intermediates in the oxidation reactions of *o*-AP and *o*-PD,[5,6] and this has been demonstrated for the first time in the present study.

We express our sincere gratitudes to Professor T. Tanaka and his collaborators in Osaka University for affording facilities for the stopped flow measurements.

References

1) R. Willstätter and E. Mayer, *Ber.*, **37**, 1496 (1904); E. Erdman, *ibid.*, **37**, 2906 (1904).
2) L. K. J. Tong and M. C. Glesmann, *J. Amer. Chem. Soc.*, **79**, 583, 592, 4310 (1957); L. K. J. Tong and M. C. Glesmann, *ibid.*, **90**, 5164 (1968).
3) J. F. Corbett, *J. Chem. Soc., B*, **1969**, 818; J. F. Corbett and E. P. Gamson, *J. Chem. Soc., Perkin II*, **1972**, 1531 and papers cited therein.
4) R. Willstätter and A. Pfannenstiel, *Ber.*, **38**, 2350 (1905).
5) H. T. Nagasawa and H. R. Gutmann, *J. Biol. Chem.*, **234**, 1593 (1959); H. T. Nagasawa, H. R. Gutmann, and M. R. Morgan, *ibid.*, **234**, 1600 (1959); P. M. Nair and C. S. Vaidyanathen, *Biochim. Biophys. Acta*, **81**, 507 (1964).
6) L. H. Piette, P. Ludwig, and R. H. Adams, *Anal. Chem.*, **30**, 916 (1958); P. J. Elving and A. F. Krivis, *ibid.*, **30**, 1648 (1958); H. Y. Lee and R. N. Adams, *ibid.*, **34**, 1587 (1962).
7) T. Nogami, T. Hishida, Y. Shirota, H. Mikawa, and S. Nagakura, This Bulletin, **47**, 2103 (1974).
8) T. Nogami, T. Hishida, Y. Shirota, and H. Mikawa, *Chem. Lett.*, **1973**, 1019; T. Hishida, T. Nogami, Y. Shirota, and H. Mikawa, *ibid.* **1974**, 293.
9) L. C. Newell and R. W. Maxon, *Inorg. Syn.*, **1**, 45 (1939). We could not obtain *o*-BQMI and *o*-BQDI with the use of commercially available lead dioxide. Both imines were obtained with the use of excess amount of lead dioxide prepared freshly.
10) "Chemistry of Carbon Compounds," ed. by E. H. Rodd, Elsevier Publishing Company, Amsterdam, Houston, London, New York, Vol. III, p. 451; Vol. IV, p. 1500, 1541, 1549 (1954).
11) H. Mason, *J. Amer. Chem. Soc.*, **70**, 138 (1948).
12) Estimated from the initial concentrations of *o*-AP and *o*-PD in the syntheses of *o*-BQMI and *o*-BQDI, respectively.
13) The observed spectra are due to *o*-benzoquinone imines or such protonated species as
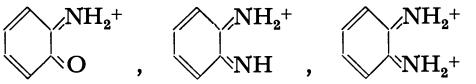
14) J. F. Corbett, *J. Chem. Soc., B*, **1969** 213.
15) J. F. Corbett, S. Pohl, and I, Rodriguez, *J. Chem. Soc., Perkin II*, **1975**, 728.
16) J. F. Corbett, *J. Chem. Soc., B*, **1969**, 827.
17) The increase of the absorption band in the shorter wavelength region than 336 nm is mainly due to the same species peaking at 495 nm.
18) J. F. Corbett, *J. Chem. Soc., B*, **1970**, 1502.
19) *o*-BQMI or oxygen may take part in the cyclization reaction of AIP, but the detailed mechanism is unknown.
20) Similar reaction mechanisms have been postulated in the reactions of *p*-BQMI and *p*-BQDI with several aromatic amines, in which the leuco bases produced by the addition reactions were oxidized with *p*-benzoquinone imines to produce dyes such as Bandrowski's base, indophenol and indamine, see Refs, 3, 13, and 16.
21) *o*-BQDI or oxygen may take part in the cyclization reaction of AABI, but the detailed mechanism is unknown.

Optical Activation of α-Substituted Carbonyl Compounds by Asymmetric Transformation

Hajime MATSUSHITA, Masao NOGUCHI, Masahiko SABURI*, and Sadao YOSHIKAWA*

Central Research Institute, The Japan Tobacco and Salt Public Corporation, 6-2 Umegaoka, Midori-ku, Yokohama, Kanagawa 227

**Department of Synthetic Chemistry, Faculty of Engineering, The University of Tokyo, Hongo, Bunkyo-ku, Tokyo 113*

(Received August 11, 1975)

Immonium salts of enamines of racemic α-substituted carbonyl compounds with optically active acids gave, on hydrolysis with water, the corresponding optically active carbonyl compounds. Several reaction conditions were examined and a plausible reaction mechanism, an asymmetric transformation, was proposed. Rates of racemization for the (+)-α-phenylpropionaldehyde were also determined.

The synthesis of optically active carbonyl compounds has been considered of interest in the field of terpenoids, steroids and alkaloids.[1] Resolutions of racemic carbonyl compounds (chemical and biochemical),[2,3] asymmetric destruction,[4] asymmetric synthesis[5] and asymmetric transformation[6] have been reported. In the resolution and asymmetric destruction, the maximum theoretical yield of either pure enantiomer based on the original weight of the racemic material is obviously 50%. In an asymmetric synthesis, there are many restrictions and higher yields in optical activity usually give lower yields of the product. On the other hand, in the asymmetric transformation, although a resolution method, the theoretical yield of one pure enantiomer exceeds 50%. One enantiomer was obtained in nearly 100% yield by this method.[7]

This paper deals with a phenomenon which can be accounted for by the asymmetric transformation. The enamines of racemic α-substituted carbonyl compounds were treated with optically active acids. Hydrolysis of the salts gave the optically active carbonyl compounds. This is a new method to get optically active α-substituted carbonyl compounds from their racemic forms.

Seven carbonyl compounds, α-phenylpropionaldehyde(**1**), 2-ethylhexanal(**2**), 2-methylcyclohexanone(**3**), 2-(2-cyanoethyl)cyclohexanone(**4**), methyl 3-(2-oxocyclohexyl)propionate(**5**), 2-(2-cyanoethyl)cyclopentanone(**6**) and methyl 3-(2-oxocyclopentyl)-propionate(**7**) were examined.

Pyrrolidine, piperidine and 2-methylpiperidine were used as the amine components of the enamines.

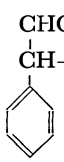

(**1**)

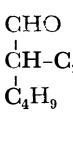

(**2**)

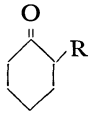

(**3**) R=CH_3
(**4**) R=CH_2CH_2CN
(**5**) R=$CH_2CH_2COOCH_3$

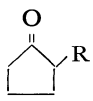

(**6**) R=CH_2CH_2CN
(**7**) R=$CH_2CH_2COOCH_3$

Experimental

Optical activities were determined with a JASCO Digital Automatic Polarimeter Model DIP 181. Gas chromatographic analyses were carried out on a 2 m column of 5% Carbowax 20M on Chromosorb W with a Hitachi Gas Chromatograph, Model K53.

Preparation of Enamines. Enamines of **1**, **2** and **3** were prepared by the usual azeotropic procedures with benzene as a solvent. Pyrrolidine enamines of **4**, **5**, **6** and **7** were synthesized according to the method of Stork *et al.*[8] The enamines obtained were directly subjected to the subsequent procedures without further purification.

Pyrrolidine enamine of **1**: bp 108—109 °C (6.5 mmHg), 91% yield; IR 1635 cm^{-1} ($\nu_{C=C}$). Piperidine enamine of **1**: bp 84—109 °C (7 mmHg), 85.9% yield; Mass *m/e* 201 (M^+, Parent); IR 1637 cm^{-1} ($\nu_{C=C}$); NMR($CDCl_3$) mixture of two geometrical isomers, 1.97 and 2.09 (C=C–CH_3, s), 5.82 and 6.11 (N–CH=C, s). 2-Methylpiperidine enamine of **1**: bp 129—130 °C (5 mmHg), 71.2% yield; Mass *m/e* 215 (M^+), 200 (Parent); IR 1638 cm^{-1} ($\nu_{C=C}$); NMR($CDCl_3$) mixture of two geometrical isomers though one isomer existed in a trace amount, 1.03 (N–C–CH_3, d, *J* 6.7 Hz), 2.09 (C=C–CH_3, s), 6.40 (N–CH=C, s).

Pyrrolidine enamine of **2**: bp 95—96.5 °C (9 mmHg), 92.3% yield; Mass *m/e* 181 (M^+), 138 (Parent); IR 1658 cm^{-1} ($\nu_{C=C}$).

Piperidine enamine of **2**: This was reported by Opitz *et al.*[9] 2-Methylpiperidine enamine of **2**: bp 97—99 °C (6 mmHg), 93.8% yield; Mass *m/e* 209 (M^+), 166 (Parent); IR 1664 cm^{-1} ($\nu_{C=C}$); NMR($CDCl_3$) 5.12 (N–CH=C, s). Pyrrolidine enamine of **3**: This was reported by House and Schellenbaum.[10]

Piperidine enamine of **3**: This was reported by Gurowitz and Jaseph.[11] 2-Methylpiperidine enamine of **3**: bp 136 °C (8.5 mmHg), 65% yield; Mass *m/e* 193 (M^+), 178 (Parent); IR 1634 cm^{-1} ($\nu_{C=C}$): NMR($CDCl_3$) 0.83 (N–C–CH_3, d, *J* 6.0 Hz), 1.70 (CH_3–C–C–N, s).

Salt of Enamines and Their Hydrolysis. The preparation and hydrolysis of the salt of piperidine enamine of **1** with D-10-camphorsulfonic acid (**8**) were carried out as follows.

Acid **8** (0.02 mmol) was added to a benzene solution (30 ml) of **1** (0.02 mmol), and the mixture was stirred until **8** was completely dissolved. Water (15 ml) was added dropwise to the solution in an ice bath with vigorous stirring. The reaction was continued until completion of the hydrolysis which was confirmed by gas chromatography. The benzene layer was separated, successively washed with water, 5% aqueous sodium carbonate and water, dried over anhydrous sodium sulfate; the optical activity was then measured.

Recovery of the carbonyl compound was determined with

a gas chromatograph. The same procedure was applied to the other enamines except for those of **4**, **5**, **6** and **7**. These were subjected to synthesis, after which the solvent (dioxane) was replaced with benzene, and the benzene solutions were then subjected to the same procedure as that for the enamine of **1**. The liberated carbonyl compounds were isolated by vacuum distillation, and the optical rotation of the distillates were measured.

Examination of the Solvent Effect. The immonium salt of **1** with **8** in several solvents was similarly hydrolyzed. The solvent was distilled off *in vacuo* and the residue was dissolved in benzene. The solution was washed and dried as in the case of the enamine of **1** and its optical activity was measured.

Rapid racemization took place when a few drops of 0.05 M KOH alcoholic solution were added to the solution.

Results and Discussions

Hydrolysis of the Immonium Salts. The results of the hydrolysis of the immonium salts are summarized in Table 1. Fairly optically active carbonyl compounds were obtained in all the cases examined. No by-products other than each carbonyl compounds were detected in the benzene solution. As blank experiments, phenylacetaldehyde and cyclohexanone, which have no asymmetric carbons, were examined. The immonium salts of *N*-(2-phenyl-1-propenyl)-piperidine[12] and *N*-(1-cyclohexenyl)piperidine[12] were treated according to the same procedure. Contamination of **8** was found to be negligible. The optical rotations of the α-phenylpropionaldehyde recovered were the most active ones of all, although that of the pure enantiomer is still unknown.

Investigation of Racemization. Optically active **1** was easily racemized with acid or base at 23 °C. The racemization rates in the presence of 12.5% CH_3COOH or $N(C_2H_5)_3$ in benzene, and 0.7% *p*-toluenesulfonic acid or 0.25% D-10-camphorsulfonic acid in benzene–ethanol (1 : 1) were measured. In every case, a plot of log α_0/α *vs.* time gives a straight line. The half-life period for each case was 200.7, 18.8, 21.8 and 19.9 min. Optically active **3** was racemized very quickly with a strong base, such as KOH. On the other hand, the racemization of **8** could not be detected under these conditions. This shows that the observed optical rotations were not due to the contamination of **8**. The rate of racemization of **1** was fairly high in the presence of **8**, which indicates that the real optical activity attained would have been larger than the observed activity.

Table 1.

Carbonyl compounds	Amines	$[\alpha]_D^{23}$	Recovery (%)
1	Piperidine	+16.2 (*c* 3.67)	89.6
	Pyrrolidine	+13.8 (*c* 7.10)	84.1
	2-Methyl-piperidine	+15.9 (*c* 1.15)	92.0
2	Piperidine	+0.22 (*c* 55.1)	82.5
	Pyrrolidine	+0.18 (*c* 20.5)	62.8
	2-Methyl-piperidine	+0.11 (*c* 28.8)	78.0
3	Piperidine	+0.63 (*c* 2.30)	73.1
	Pyrrolidine	+0.39 (*c* 10.8)	88.8
	2-Methyl-piperidine	+0.89 (*c* 20.1)	80.0
4	Pyrrolidine	+0.058 (neat)	51.5
5	Pyrrolidine	+0.085 (neat)	39.1
6	Pyrrolidine	+0.018 (neat)	42.2
7	Pyrrolidine	+0.011 (neat)	38.8
Phenyl-acetaldehyde	Piperidine	+0.000 (*c* 11.5)	80.7
	Pyrrolidine	+0.000 (*c* 22.4)	68.9
Cyclohexanone	Piperidine	+0.000 (*c* 18.1)	62.3
	Pyrrolidine	+0.000 (*c* 57.1)	71.2

The Effect of Acid Component. The piperidine enamine of **1** was treated with each of several optically active acids in benzene solution, and the resulting mixture was hydrolyzed in an ice bath. The rate and the end point of the hydrolysis were measured by gas chromatography. The results are shown in Table 2. The salt with **8** was hydrolyzed rapidly, and gave high active **1**. On the other hand, the rates of hydrolysis of those with the other acids were slow, and the activities of the products were low. This tendency was also observed with other immonium salts. The most suitable acid among the acids examined was **8**. Its strong acidity as well as its steric factor might largely contribute to the introduction of optical activity.

Table 2. Effect of acid component

Acids	Time (min)	$[\alpha]_D^{23}$	Recovery (%)
L-Tartaric acid	80	−0.93 (*c* 7.3)	97.8
D-Camphoric acid	75	+2.61 (*c* 3.4)	53.3
D-Quinic acid	80	+0.56 (*c* 3.2)	29.8
8	35	+16.2 (*c* 3.67)	89.6

Solvent Effect. The immonium salts of the enamines of **1** with **8** were prepared in several solvents and subjected to hydrolysis. The amount of water used for the hydrolysis did not affect the activity. In non-polar aprotic solvents, such as benzene, high optically active **1** was obtained (Table 3). It is known that strong acid components and non-polar solvents are preferable for the stability of immonium salts.[13] The result of the solvent effects as well as the acid components suggests that the stability of an immonium salt is an important factor for the introduction of optical activity.

Mechanism of Introduction of Optical Activity. Enamines have been studied and applied by many workers since they were first described by Mannich and Davidsen.[12] The structure of enamines and their salts,[13] and mechanism of the hydrolysis[8] have been subjects of great interest.

It was found that formation of an enamine causes deprotonation from the α-carbon of the carbonyl compound, and formation of the immonium salt causes protonation to the carbon, which is the first step of hydrolysis. We found no evidence of the formation of immonium salts. However, the above mechanism seems to be appropriate to account for the observed stereospecificity. When the enamine of a racemic α-substituted carbonyl compound is

Table 3. Solvent effect on optical activity

		Benzene	Dioxane	CH_3CN	EtOH	MeOH	H_2O
Piperidine enamine	$[\alpha]_D^{23}$	+16.2 (*c* 3.67)	+10.0 (*c* 1.81)	+2.81 (*c* 2.10)	+0.091 (*c* 23.3)	+0.100 (*c* 31.9)	+0.000 (*c* 50.8)
	Recovery (%)	89.6	28.0	42.3	61.7	78.0	89.7
Pyrrolidine enamine	$[\alpha]_D^{23}$	+18.3 (*c* 6.77)	+11.8 (*c* 3.88)	+1.08 (*c* 11.3)	+0.026 (*c* 35.5)	+0.082 (*c* 41.3)	+0.000 (*c* 67.1)
	Recovery (%)	84.1	32.7	38.1	49.9	58.9	92.3

formed by the removal of the α-hydrogen atom, such an enamine has an enantiotropic plane but no asymmetric α-carbon atom.

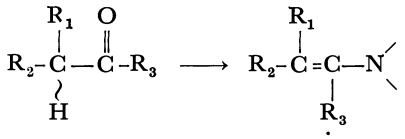

Racemic form Enamine

Addition of an optically active acid causes the protonation of the α-carbon to form the immonium salt. The immonium salt would exist as an equilibrium mixture of two diastereomeric isomers. The enamine could be considered to be an intermediate of the isomers in the solution.

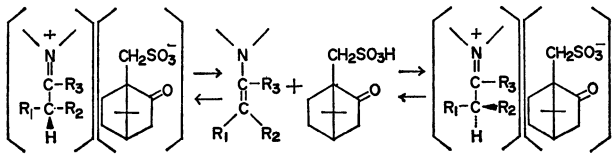

Displacement of the balance of the interconversion reactions in favor of one diastereomeric isomer results in an optically active carbonyl compound. The lability of the enamine is shown by the equilibrium of the two geometrical isomers of the piperidine enamine of **1**. The proportion of the two isomers depends on temperature. Attainment of the equilibrium was fairly rapid, and accelerated by the use of some acid.

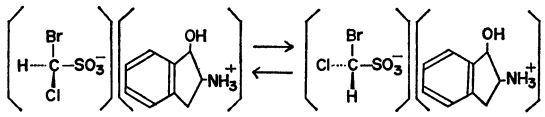

The mechanism mentioned above seems to be an asymmetric transformation reported by Read and McMath.[14] They reported the equilibrium of the two diastereomeric chlorobromomethanesulfonic acid with an equivalent of active 1-hydroxy-2-aminoindan in a dilute acetone solution, the resulting solution exhibit mutarotation. An examination of the rotation at equilibrium shows that the solution contains 81% of the salt of one isomer and 19% of that of the other one. Attempts to liberate the active acid from the solution were not successful.

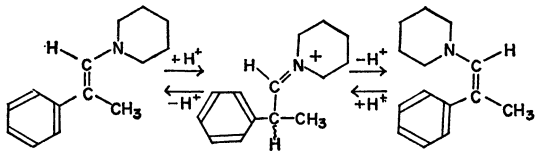

From the mechanism of the asymmetric transformation, the factor which determines the degree of optical activity is considered to be the stability of diastereomeric immonium salts.

References

1) K. Hiroi and S. Yamada, *Chem. Pharm. Bull.*, **23**, 1103 (1975); K. Nagasawa, H. Takahashi, K. Hiroi and S. Yamada, *Yakugaku Zasshi*, **95**, 33 (1975)

2) J. W. Scott, R. Borer, and G. Saucy, *J. Org. Chem.*, **37**, 1659 (1972); H. Nohira and H. Miura, *Nippon Kagaku Kai Shi*, **1975**, 1122.

3) L. M. Kogan, V. E. Gulaya and I. V. Torgov, *Tetrahedron Lett.*, **1967**, 4673.

4) G. Bredig and K. Fajas, *Chem. Ber.*, **41**, 752 (1908).

5) R. Kuhn, H. E. Driesen and H. J. Haas, *Ann.*, **718**, 78 (1968); G. Otani and S. Yamada, *Chem. Pharm. Bull.*, **21**, 2130 (1973).

6) N. Marckwald and A. McKenzie, *Chem. Ber.*, **32**, 2120 (1899).

7) H. Leuchs, *ibid.*, **54**, 830 (1921).

8) G. Stork, A. Brizzolara, H. Landesman, J. Szmuzkovicz and R. Terrell, *J. Amer. Chem. Soc.*, **85**, 207 (1963).

9) G. Opitz, H. Hellmann, and H. W. Schubert, *Ann.*, **623**, 442 (1959).

10) H. O. House and M. Schellenbaum, *J. Org. Chem.*, **28**, 34 (1963).

11) W. D. Gurowitz and M. A. Jaseph, *ibid.*, **32**, 3289 (1967).

12) C. Mannich and H. Davidsen, *Chem. Ber.*, **69**, 2106 (1936).

13) G. Opitz, H. Hellmann, and H. W. Schubert, *Ann.*, **623**, 447 (1959); M. E. Herr, M. E. Heyl, J. C. Babcock, A. E. Fonken, J. E. Stafford, and F. W. Heyl, *J. Amer. Chem. Soc.*, **78**, 430 (1956).

14) J. Read and A. M. McMath, *J. Chem. Soc.*, **1925**, 1572.

Charge-transfer Intermediate in The Reaction of Thioketone with Nucleophiles

Atsuyoshi OHNO, Kaoru NAKAMURA, Misao UOHAMA, Shinzaburo OKA, Tokio YAMABE*, and Shinichi NAGATA*

Institute for Chemical Research, Kyoto University, Uji, Kyoto 611

**Department of Hydrocarbon Chemistry, Faculty of Engineering, Kyoto University, Sakyo-ku, Kyoto 606*

(Received August 14, 1975)

Thiobenzophenone reacts with butyllithium, phenyllithium, and sodium ethoxide in ethanol giving benzhydryl butyl sulfide, benzhydryl phenyl sulfide, and dibenzhydryl disulfide, respectively. On the other hand di-*t*-butyl thioketone affords 2,2,4,4-tetramethylpentane-3-thiol, 2,2,4,4-tetramethyl-3-phenylpentane-3-thiol, and 2,2,4,4-tetramethylpentane-3-thiol by the reaction with butyllithium, phenyllithium, and sodium ethoxide in ethanol, respectively. Product analyses and tracer experiments with deuteriums have revealed that these reactions proceed through a charge-transfer mechanism.

Thiophilic addition of nucleophiles to thiocarbonyl compounds has been reported by several groups.[1-4] Namely, Beak and Worley proposed three possible mechanisms for thiophilic reaction of thiocarbonyl groups (thiobenzophenone and phenyl trithiocarbonate) with phenyllithium.[1b] One of those is based on the concept that the bonding electrons of the thiocarbonyl group are intrinsically polarized with carbon negative relative to sulfur. Dipole moment[5] and SCF-LCAO-MO calculation[6] support the intrinsic polarity of the thiocarbonyl group proposed. Second mechanism involves the formation of a charge-transfer (CT) complex between a thiocarbonyl compound and a nucleophile followed by an in-cage radical combination giving an ion-pair, **1**. The presence of the thioketyl

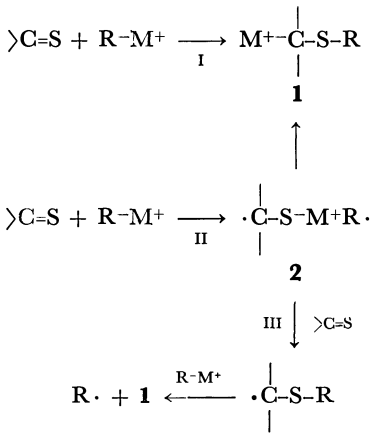

radicals in the reacting solution has been confirmed by ESR spectroscopy.[1b,7] This mechanism, however, cannot explain why the free-radical R· in **2** attacks on the sulfur instead of attacking on the carbon, on which locates an unshared electron. The third mechanism consists of free-radical chain reactions. That the thiocarbonyl-sulfur is a good acceptor of a carbon free-radical has been proved.[8,9]

In this paper, we wish to report unequivocal evidence to support the CT-intermediate—radical-combination mechanism (Process II) for the reaction of thioketones with nucleophiles.

Results

Thiobenzophenone reacts with butyllithium affording benzhydryl butyl sulfide (**3**) in 70% yield as previously reported.[1,10] On the other hand, di-*t*-butyl thioketone[11] is reduced quantitatively by this reagent to the corresponding thiol, **4**, under the same condition.[10]

$$Ph_2C{=}S + Bu^nLi \longrightarrow Ph_2\overset{Li^+}{\overline{C}}{-}SBu^n \xrightarrow{H^+/H_2O} \underset{\mathbf{3}}{Ph_2CHSBu^n} \quad (1)$$

$$Bu^t_2C{=}S + Bu^nLi \longrightarrow Bu^t_2CH{-}S^-Li^+ + C_2H_5CH{=}CH_2$$
$$\downarrow H^+/H_2O \quad (2)$$
$$\underset{\mathbf{4}}{Bu^t_2CHSH}$$

That butyllithium-β,β-d_2 transfers the deuterium onto the thiocarbonyl-carbon and that the reaction with butyllithium gives **4**-*S*-*d* after the treatment of the reaction mixture with deuterium oxide prove the reaction scheme shown in Eq. 2. It is noteworthy that, in general, organolithium compounds are less susceptible to the reduction of carbonyl compounds than Grignard reagents.[12]

The reaction of thiobenzophenone with phenyllithium affords benzhydryl phenyl sulfide (**5**),[1] whereas the same reaction with di-*t*-butyl thioketone results in the formation of **6** and **7** in 25 and 35% yields, respectively.[10]

$$Ph_2C{=}S + PhLi \longrightarrow Ph_2\overset{Li^+}{\overline{C}}{-}SPh \xrightarrow{H^+/H_2O} \underset{\mathbf{5}}{Ph_2CHSPh} \quad (3)$$

$$Bu^t_2C{=}S + PhLi \longrightarrow Bu^t_2C\langle^{S^-Li^+}_{Ph} + Bu^t_2\overset{Li^+}{\overline{C}}{-}SPh$$
$$\xrightarrow{H^+/H_2O} \underset{\mathbf{6}}{Bu^t_2C\langle^{SH}_{Ph}} + \underset{\mathbf{7}}{Bu^t_2CHSPh} \quad (4)$$

Essentially the same result was obtained when the organolithium compound was substituted by the corresponding Grignard reagent.

The reaction of thiobenzophenone with ethanol in the presence of sodium ethoxide at room temperature *in vacuo* ($\sim 10^{-6}$ Torr) in the dark resulted in the quantitative formation of dibenzhydryl disulfide (**8**)[13] immediately. A similar reaction with di-*t*-butyl thioketone gave **4** in quantitative yield after a day at 60 °C. The

Table 1. Reactions of thioketones in deuterated alcohols

Starting material	Product	Alcohol (D-Content, %)	D-Content in product, %	D-Transfered, %
$Ph_2C=S$	**8**-α,α′-d_2	Ethanol-*O*-*d* (99.9)	85±5	89±3
		1-Butanol-α,α-d_2 (91.8)	4	4
I $t_2C=S$	**4**-α-*d*	Ethanol-*O*-*d* (99.9)	14.3	14.3
		1-Bntanol-α,α-d_2 (91.8)	65.4	71.2
4[a]	**4**-α-*d*	Ethanol-*O*-*d* (99.9)	0	0
8[a]	**8**-α,α′-d_2	Ethanol-*O*-*d* (99.9)	0	0

a) A controlled experiment to confirm the absence of isotope-exchange in products.

Table 2. Charge and spin density distributions in radical anions of thioacetone and thiobenzaldehyde[a,b]

	Thioacetone		Thiobenzaldehyde	
	on C	on S	on C	on S
Charge density	+0.2192	−0.9490	−0.0154	−0.7594
	(+0.2115)	(−0.9896)	(−0.0407)	(−0.7843)
Spin density	+0.8264	+0.1547	+0.6041	+0.1987
	(+0.7692)	(+0.2073)	(+0.5409)	(+0.2683)

a) Numbers out of and in parentheses are results of calculations excluding and including d orbitals on sulfur, respectively. b) Geometries of molecules are shown in Table 3 and Fig. 1.

$$Ph_2C=S + C_2H_5OH/C_2H_5O^-Na^+ \longrightarrow Ph_2CHSSCHPh_2 \quad (5)$$
8

$$Bu^t_2C=S + C_2H_5OH/C_2H_5O^-Na^+ \longrightarrow Bu^t_2CHS^-Na^+ \xrightarrow{H^+/H_2O} \mathbf{4} \quad (6)$$

results listed in Table 1 were obtained from the reactions with deuterated alcohols, which indicate that thiobenzophenone abstracts a proton from the solvent whereas di-*t*-butyl thioketone abstracts a hydrogen atom.

All reactions in Eqs. (1)—(6) were not affected by the presence of equimolar (to the thioketone) amount of hydroquinone, or the presence of air except for the reaction in Eq. (6), which afforded the corresponding disulfide under an aerobic condition. In other words, the formation of **8** cannot be accounted for by the oxidation of benzhydryl mercaptan. Instead, it might be formed by the combination of benzhydryl mercapto radicals.

Discussion

Since the phenyl group, or even the *t*-butyl group,[14] is bound to the carbonyl-carbon in di-*t*-butyl ketone, the difference of the reaction mode cannot be attributed to the steric effect in the reactants. The present result is best interpreted by assuming CT-intermediates for each reactions. Preliminary INDO-type molecular orbital calculations on anion radicals of thioacetone and thiobenzaldehyde, models for di-*t*-butyl thioketone and thiobenzophenone, respectively, indicate that a phenyl group attached to the thiocarbonyl group increases intrinsic negative charge on carbon and spin density on sulfur, respectively, in comparison to an aliphatic substituent (Table 2). That is, structures (or the most important canonical forms, i. not exclusive) for the radical anions of thiobenzophenone and di-*t*-butyl thioketone may be represented by **9** and **10**, respectively.

$$Ph_2\bar{C}-S\cdot \qquad Bu^t_2\dot{C}-S^-$$
9 **10**

Consequently, thiobenzophenone and di-*t*-butyl thioketone are expected to form CT-intermediates, **11** and **12**, respectively, in reactions with nucleophiles.

$$Ph_2C=S + R^-M^+ \longrightarrow \overset{M^+\ R\cdot}{Ph_2\bar{C}-S\cdot} \quad (7)$$
11

$$Bu^t_2C=S + R^-M^+ \longrightarrow \overset{R\cdot\quad M^+}{Bu^t_2\dot{C}-\bar{S}} \quad (8)$$
12

Under an aprotic condition, **11** is stabilized by radical-combination, whereas **12** is stabilized by either radical-combination or hydrogen-transfer, when possible.

$$\mathbf{11} \xrightarrow{M^+} Ph_2\bar{C}-SR \xrightarrow{H^+} \mathbf{3}\ (R=Bu^n) \text{ or } \mathbf{5}\ (R=Ph) \quad (9)$$

$$\mathbf{12} \begin{cases} \xrightarrow{R=Ph} Bu^t_2C\langle^{S^-M^+}_{Ph} \xrightarrow{H^+} \mathbf{6} \\ \xrightarrow[R=R'CH_2Z]{} Bu^t_2CHS^-M^+ \xrightarrow{H^+} \mathbf{4} + R'CH=Z \end{cases} \quad (10)$$

(Z=CH_2, O)

Note that a thiyl radical has less ability than a carbon radical to abstract a hydrogen atom.[15]

Under a protic condition, on the other hand, **11** abstracts a proton from the solvent to form a stable thiyl radical rather than to form relatively unstable carbanion. The fate

$$\mathbf{11} + C_2H_5OH \longrightarrow Ph_2CHS\cdot + C_2H_5O^-Na^+ + C_2H_5O\cdot \quad (11a)$$
$$\downarrow$$
$$\mathbf{8}$$

and/or

$$\mathbf{11} \longrightarrow Ph_2\bar{C}SS\bar{C}Ph_2\ ^{Na^+Na^+} \xrightarrow{C_2H_5OH} \mathbf{8} + C_2H_5O^-Na^+ \quad (11b)$$
$$+$$
$$C_2H_5O\cdot$$

$$C_2H_5O\cdot + C_2H_5OH \longrightarrow C_2H_5OH + CH_3\dot{C}HOH \quad (12)$$

$$CH_3\dot{C}HOH \xrightarrow{-H\cdot} CH_3CH{=}O \quad (13)$$
$$(R^-M^+ = C_2H_5O^-Na^+)$$

of ethoxy radical is well known.[16] The reaction in Eq. (12) explains the scrambling of deuterium.

Similarly, **12** affords a stable thiolate anion by hydrogen-abstraction instead of forming an unstable carbon radical.

$$\mathbf{12} \longrightarrow Bu^t{}_2CHS^-Na^+ + CH_3CH{=}O \quad (14)$$
$$(R^-M^+ = C_2H_5O^-Na^+)$$

About 20% of scrambling in the last reaction indicates that not all of the radical-ion pairs, **12**, undergo the spontaneous reaction shown in Eq. (14). Instead some of them dissociate and the ethoxy radical abstracts a hydrogen from ethanol (Eq. (12)). Note that the reaction with di-*t*-butyl thioketone is much slower than that of thiobenzophenone, which may describe larger scrambling in the reaction of di-*t*-butyl thioketon than in the reaction of thiobenzophenone.

The proposed mechanism is supported by the fact that the reaction of thiobenzophenone with sodium ethoxide in an aprotic solvent such as tetrahydrofuran or diglyme affords benzhydryl mercaptan in 79% yield together with small amount (10% yield) of the disulfide, **8**. Since there is no proton in the system and the sulfenate, expected to be formed by radical combination, is an unstable compound, **11** has to be stabilized by hydrogen-atom-transfer.

$$\mathbf{11} \xrightarrow{+H\cdot} Ph_2\bar{C}(^{Na^+})\text{-}SH \xrightarrow{\text{disproportionation}} Ph_2CHS^-Na^+$$
$$\downarrow H^+/H_2O \qquad\qquad \downarrow H^+/H_2O$$
$$Ph_2CHSH \qquad\qquad Ph_2CHSH$$

Experimental

Materials. Di-*t*-butyl thioketone,[11] thiobenzophenone,[17] hexyllithium,[18] and phenyllithium[19] were prepared according to literatures. Butyllithium was purchased from Merck & Co., Inc. Solvents were dried and purified by distillation prior to use. 1-Butanol-α,α-d_2 was obtained by reduction of methyl butyrate with lithium aluminium deuteride. Ethanol-*O*-*d* was purchased from Merck & Co., Inc. Butyllithium-β,β-d_2 was prepared according to the following scheme:

$$CH_3CH_2CO_2CH_3 \xrightarrow[2)\ H^+/H_2O]{1)\ LiAlD_4} CH_3CH_2CD_2OH \xrightarrow[H_2SO_4]{NaBr}$$

$$CH_3CH_2CD_2Br \xrightarrow[2)\ HCHO]{1)\ Mg} CH_3CH_2CD_2CH_2OH \xrightarrow[H_2SO_4]{NaBr}$$

$$CH_3CH_2CD_2CH_2Br \xrightarrow{Li} CH_3CH_2CD_2CH_2Li$$

General Procedure. All reactions were run both under nitrogen atmosphere with stirring and under high vacuum of about 10^{-6} Torr. For the latter reactions a solution of thioketone, a solution of organometallic reagent, and water were respectively vacuum-sealed in ampoules, which were connected with break-seals. The thioketone and organometallic reagent were mixed through a break-seal and, at the end of the reaction, water was added to the reaction mixture through the other break-seal. The apparatus was wrapped by aluminium foil to avoid unnecessary photoreactions.

Reaction of Di-t-butyl Thioketone with Butyllithium. In to 1.2 g of 20% hexane solution of butyllithium (4 mmol), was added 316 mg (2 mmol) of di-*t*-butyl thioketone at room temperature. The color of the thioketone disappeared immediately. Water (5 ml) was added to the reaction mixture and the organic materials were extracted with ether. The ether layer was dried over Drierite and the solvent was evaporated *in vacuo*. The residue was subjected to column chromatography over silica gel with benzene eluent, yielding 2,2,4,4-tetramethylpentane-3-thiol (**4**)[10] quantitatively.

Reaction of Di-t-butyl Thioketone with Phenyllithium. Into 7 ml of ether solution containing 420 mg (5 mmol) of phenyllithium was added 574 mg (3 mmol) of di-*t*-butyl thioketone at 0 °C. Usual work-up and column chromatography over silica gel with hexane eluent gave 210 mg (25% yield) of 2,2,4,4-tetramethyl-3-phenylpentane-3-thiol (**6**)[10] and 280 mg (35% yield) of di-*t*-butylmethyl phenyl sulfide (**7**).[10]

The sulfide, **7**, was oxidized with 30% hydrogen peroxide in acetic acid by keeping the solution in a refrigerator for 2 days. The solution was neutralized with sodium bicarbonate and the product was extracted with ether. The ether layer was dried over Drierite and the solvent was evaporated *in vacuo*. The white crystals thus obtained were recrystallized from hexane giving the corresponding sulfone: mp 138 °C. NMR $\delta^{TMS}_{CCl_4}$ 1.33 (s, 18H), 3.20 (s, 1H), and 7.33—7.90 (m, 5H). ν_{SO_2} 1130 and 1290 cm^{-1}. Found: C, 66.86; H, 9.22; S, 12.11%. Calcd for $C_{15}H_{24}O_2S$: C, 67.17; H, 8.92; S, 11.94%.

Reaction of Di-t-butyl Thioketone with Sodium Ethoxide in Ethanol. Into 5 ml of ethanol, 50 mg of metallic sodium was added. This ethanol solution was mixed with a solution of di-*t*-butyl thioketone (500 mg, 3.4 mmol) in 5 ml of ethanol. The whole mixture was kept at 60 °C for a day.

The reaction under nitrogen atmosphere, after work-up and column chromatography on silica gel with an eluent of a mixture of hexane–benzene (1 : 1), gave 250 mg (50% yield) of di(di-*t*-butyl)methyl disulfide: mp 74 °C. NMR $\delta^{TMS}_{CDCl_3}$ 1.15 (s, 18H) and 2.54 (s, 1H). IR 1215, 1362, 1387, 1475, and 2950 cm^{-1}. Found: C, 67.67; H, 12.13; S, 20.02%. Calcd for $C_{18}H_{38}S_2$: C, 67.85; H, 12.02; S, 20.13%. Mass spectrum M^+: *m/e* 318.

The reaction under high vacuum yielded, after work-up and column chromatography, 490 mg (98% yield) of **4**.

Reaction of Thiobenzophenone with Sodium Ethoxide in Ethanol. Into 1 ml of ethanol was dissolved 50 mg of metallic sodium and the solution was mixed with 2 ml of ethanol solution of thiobenzophenone (480 mg, 2.4 mmol) at room temperature. The reaction took place immediately. After addition of 2 ml of water, the precipitate was filtered off and recrystallized from a mixture of benzene and ethanol giving 480 mg (99% yield) of dibenzhydryl disulfide: mp 151—152 °C (lit,[20] 151—152 °C).

Reaction of Thiobenzophenone with Sodium Ethoxide in Tetrahydrofuran. Into 10 ml of tetrahydrofuran were dissolved 198 mg (1 mmol) of thiobenzophenone and 500 mg (7.35 mmol) of sodium ethoxide at room temperature. The reaction took place immediately. After addition of 10 ml of water, the organic materials were extracted with ether. The ether layer was dried over sodium sulfate and the solvent was removed *in vacuo*. The residue was chromatographed on a column of silicic acid and eluted with a hexane–benzene (8 : 2) mixture affording 157 mg of benzhydryl mercaptan[13] and 20 mg of dibenzhydryl disulfide.

Reaction of Di-t-butyl Thioketone with Sodium Ethoxide in Tetrahydrofuran. The reaction with di-*t*-butyl thioketone was similarly run as menthioned above and **4** was isolated in quantitative yield.

2,2,4,4-Tetramethylpentane-3-thiol. Into 10 ml of solution containing 40 mg of lithium aluminium hydride was added dropwise a solution of di-*t*-butyl thioketone (158 mg, 1 mmol) in 5 ml of ether under nitrogen atmosphere at 0 °C. After usual work-up, **4** was obtained in 72% yield (115 mg).[10]

Identification of Oxidized Products. An ether solution obtained from the reaction of di-*t*-butyl thioketone with hexyllithium was subjected to vpc analysis on Yanagimoto G-1800 (5% SD-200, 2 m, 27 °C, N_2 0.4 kg/cm^2, FID). Quantitative formation of hexene was thus confirmed. Another ether solution obtained form the reaction of di-*t*-butyl thioketone or thiobenzophenone with sodium isopropoxide in 2-propanol was quantitatively analyzed on vpc (Yanagimoto G-1800: 15% PEG, 1 m, 76 °C, N_2 0.4 kg/cm^2, FID). The formation of acetone was thus confirmed.

Table 3. Cartesian coordinates of thiocarbonyl compounds[a]

Atom	x	y	z
	Thioacetone		
S	1.600000	0.000000	0.000000
C1	0.000000	0.000000	0.000000
C2	−0.775000	1.342339	0.000000
C3	−0.775000	−1.342339	0.000000
H1	−0.956707	1.657066	−1.027633
H2	−0.185983	2.102044	0.513816
H3	−1.727432	1.212088	0.513816
H4	−0.956707	−1.657066	1.027633
H5	−0.185983	−2.102044	−0.513816
H6	−1.727432	−1.212088	−0.513816
	Thiobenzaldehyde		
S	0.000000	1.610000	0.000000
C1	0.000000	0.000000	0.000000
C2	1.316359	−0.760000	0.000000
C3	1.316359	−2.150000	0.000000
C4	2.520134	−2.845000	0.000000
C5	3.723909	−2.150000	0.000000
C6	3.723909	−0.760000	0.000000
C7	2.520134	−0.065000	0.000000
H1	0.381052	−2.690000	0.000000
H2	2.520134	−3.925000	0.000000
H3	4.659216	−2.690000	0.000000
H4	4.659216	−0.220000	0.000000
H5	2.520134	1.015000	0.000000
H6	−0.540000	−0.935307	0.000000

a) Atom-numbers are shown in Fig. 1.

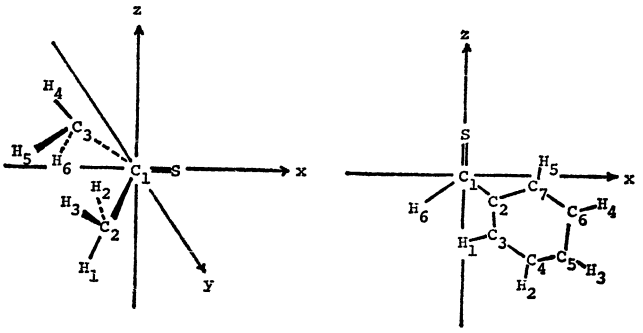

Fig. 1. Cartesian coordinates of thiocarbonyl compounds.

Into this ether solution was added ethanol solution of 2,4-dinitrophenylhydrazine. The isolated 2,4-dinitrophenylhydrazone (98% yield) melted at 128 °C (lit,[21] mp 128 °C).

Analyses of Deuterium Contents. Deuterium contents were analyzed on Varian T-60 NMR Spectrometer and Shimadzu LKB-9000S GC-MS Spectrometer attached by a MID-PM peak matcher.

Method of Calculation. Semi-empirical MO calculations were carried out with the usual unrestricted Hartree-Fock (UHF) method[22] using the INDO-type approximation. To evaluate the core resonance integrals, the Wolfsberg-Helmholz equation,[23] $H_{rs}=-KS(I_r+I_s)/2$, was used, where the value of the parameter K was taken to be 0.85. The two-center Coulomb repulsion integrals were calculated according to the Ohno's approximation.[24] The exponent of sulfur 3d orbitals and one-center Coulomb integrals between d orbitals were adopted to be 1.0 and 7.19, respectively, as reported by Nanda and Narasimhan.[25]

Other parameters including one-center exchange repulsion integrals were the same as those employed by Yonezawa and co-workers.[26] Furthermore, we discussed on the calculated results after a single annihilation proposed by Amos and Snyder.[27] The expectation values of the spin angular momentum operator S^2 from UHF method, $\langle S^2\rangle_{UHF}$, were near 0.75, which is the eigenvalue of the pure doublet state.

References

1) (a) P. Beak and J. W. Worley, *J. Amer. Chem. Soc.*, **92**, 4142 (1970); (b) P. Beak and J. W. Worley, *ibid.*, **94**, 597 (1972) and references cited therein.

2) M. Dagonneau and J. Vialle, *Tetrahedron*, **30**, 3119 (1974).

3) S. Tamagaki, K. Sakai, and S. Oae, This Bulletin, **46**, 2608 (1973).

4) D. Horton and C. G. Tindall, Jr., *J. Org. Chem.*, **35** 3558 (1970).

5) R. H. Lumbroso and C. Andrieu, *Bull. Soc. Chim. Fr.*, 3201 (1966).

6) C. Baid and J. R. Swenson, *J. Phys. Chem.*, **77**, 277 (1973).

7) Cf. also A. Ohno and N. Kito, *Chem. Lett.*, **1972**, 369.

8) (a) A. Ohno, Y. Ohnishi, M. Fukuyama, and G. Tsuchihashi, *J. Amer. Chem. Soc.*, **90**, 7038 (1968); (b) A. Ohno, Y. Ohnishi, and G. Tsuchihashi, *ibid.*, **91**, 5038 (1969).

9) G. Tsuchihashi, M. Yamauchi, and A. Ohno, This Bulletin, **43**, 969 (1970).

10) A. Ohno, K. Nakamura, M. Uohama, and S. Oka, *Chem. Lett.*, **1975**, 983.

11) A. Ohno, K. Nakamura, Y. Nakazima, and S. Oka, This Bulletin, **48**, 2403 (1975).

12) B. J. Wakefield, "The Chemistry of Organolithium Compounds," Pergamon Press, New York, N. Y. (1974), p. 129.
13) A. Ohno and N. Kito, *Int. J. Sulfur Chem., A*, **1**, 26 (1971).
14) P. D. Bartlett and M. Stiles, *J. Amer. Chem. Soc.*, **77**, 2804 (1955).
15) W. A. Pryor, "Mechanisms of Sulfur Reactions," McGraw-Hill Book, Co., New York, N. Y. (1962), pp. 89—93.
16) For example, see A. Ledwith, P. J. Russell, and L. H. Sutcliffe, *Proc. Roy. Soc. London, A*, **332**, 151 (1973).
17) B. F. Gofton and E. A. Braude, "Organic Syntheses," Coll. Vol. 4, p. 927 (1963).
18) H. Gilman, F. W. Moore, and O. Baine, *J. Amer. Chem. Soc.*, **63**, 2479 (1941).
19) L. A. Walter, "Organic Syntheses," Coll. Vol. 3, p. 757 (1955).
20) G. Oster, L. Citarel, and M. Goodman, *J. Amer. Chem. Soc.*, **84**, 703 (1962).
21) Th. Curtius and G. M. Dedichen, *J. Prakt. Chem.*, **50**, [2], 266 (1894).
22) J. A. Pople and R. Nesbet, *J. Chem. Phys.*, **22**, 571 (1954).
23) M. Wolfsberg and L. Helmholz, *ibid.*, **20**, 837 (1952).
24) K. Ohno, *Theoret. Chim. Acta*, **2**, 219 (1964).
25) D. N. Nanda and P. T. Narasimhan, *Mol. Phys.*, **24**, 1341 (1972).
26) T. Yonezawa, H. Konishi, and H. Kato, This Bulletin, **42**, 933 (1969).
27) T. Amos and L. C. Synder, *J. Chem. Phys.*, **41**, 1773 (1964).

An Alternative Synthesis of (+)-1,7-Dimethyl-4-*endo*-isopropyl-8-*syn*-(2-hydroxyethyl)bicyclo[3.2.1]oct-6-ene, the Key Intermediate for the Synthesis of (+)-Sativene and (+)-Cyclosativene[1)]

Hisahiro HAGIWARA, Masaaki MIYASHITA, Hisashi UDA, and Akira YOSHIKOSHI

Chemical Research Institute of Non-Aqueous Solutions, Tohoku University, Katahira-2, Sendai 980

(Received August 14, 1975)

The title compound, the key intermediate for the synthesis of (+)-sativene and (+)-cyclosativene, has been synthesized through the alternative route starting with (−)-carvone.

Recently Piers and co-workers[2)] reported the stereoselective total synthesis of (+)-sativene (**1**)[3,4)] and (+)-cyclosativene (**2**)[5,6)] through the common intermediate, (+)-1,7-dimethyl-4-*endo*-isopropyl-8-*syn*-(2-hydroxyethyl)bicyclo[3.2.1]oct-6-ene (**3**). We have independently investigated an approach to the synthesis of these sesquiterpenes in the optically active forms using the compound **3** as the key intermediate and wish to report our synthetic route of **3** starting from (−)-carvone in this paper.

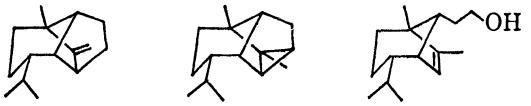

1 **2** **3**

Introduction of a suitable substituent at the α-methylene of carvomenthone (**4**) for the construction of a five-membered ring was accomplished *via* alkylation of a β-ketoester **5**. Thus, the reaction of **4**, prepared from (−)-carvone[7)], with sodium hydride–dimethyl carbonate in dioxane gave **5**, which was allylated to **6** in an excellent overall yield. Demethoxycarbonylation of **6** was achieved by heating in dimethyl sulfoxide in the presence of an equimolar amount of sodium cyanide[8)] to produce **7** in 92% yield. It should be noted that decarboxylation of **6** under the usual alkaline conditions was unsatisfactory, resulting in opening of the ring.

Attempts to transform directly the allylic side chain into the acetonyl one, **7**→**8**, by employing oxymercuration-demercuration procedure did not give clear result, even if the various derivatives (alcohol, acetate, or tetrahydropyranyl ether) were used. The modified Lemieux-Johnson oxidation[9)] of **7** produced an aldehyde **9** which, without purification, was cyclized to a mixture of bicyclic aldols **10** (50% from **7**) by treating with 20% potassium hydroxide–methanol. The products **10**, which were separable into the crystalline, mp 80—82 °C, and oily isomers by chromatography on silica gel, are epimeric as shown from the close resemblance of the physical properties (IR, NMR, and ORD) and the conversion into a diketone **11**. But the actual configuration of the hydroxyl group in each epimer has not been determined at present and, fortunately, this ambiguity is not essential to our purpose. Then, a choice between the *endo* and *exo* isopropyl structures **10** and **12** can be made by the following consideration and finally on the basis of ORD of the compound **13**. The thermodynamically more stable carbon-framework, having the equatorial isopropyl group on the chair

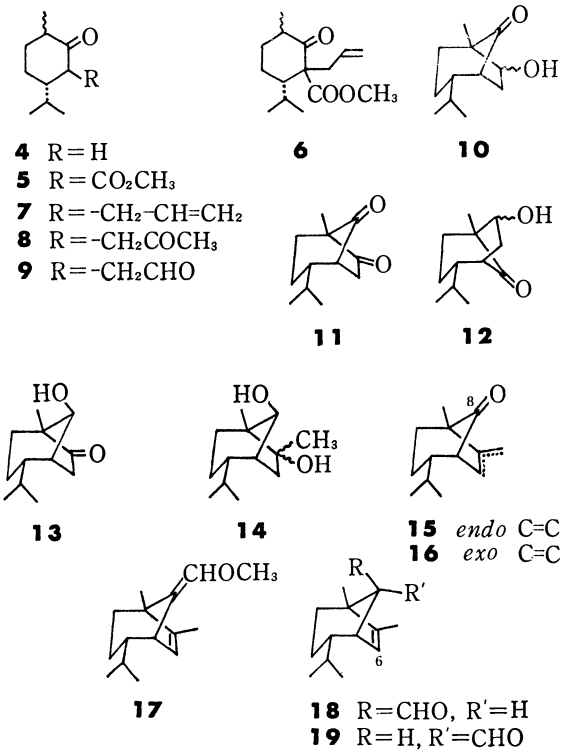

4 R=H
5 R=CO_2CH_3
7 R=$-CH_2-CH=CH_2$
8 R=$-CH_2COCH_3$
9 R=$-CH_2CHO$

6 **10** **11** **12** **13** **14**

15 *endo* C=C
16 *exo* C=C

17 **18** R=CHO, R'=H
19 R=H, R'=CHO

cyclohexane ring as **10**, would be formed preferentially in such an equilibrium (reversible) reaction.

The mixture **10** was transformed into the isomeric aldol **13** in 50% overall yield by sequential application of the following procedures: (1) acetylation of the hydroxyl group in **10**, (2) reduction of the ketone with sodium borohydride, (3) protection of the newly formed hydroxyl group with dihydropyrane, (4) reduction of the acetate function with lithium aluminum hydride, (5) oxidation of the resulting alcohol with Collins' reagent[10)], and finally (6) hydrolytic removal of the pyranyl ether group. Aldol **13** thus obtained was a single crystalline compound, mp 80—81 °C, which shows the negative Cotton effect in ORD. This ORD property establishes the assigned absolute stereochemistry **13** having α (*endo*-equatorial) isopropyl group at C-4 as shown.[11)] The configuration of the hydroxyl group was tentatively assigned to be *anti* from the fact that hydride ion would be expected to attack the bridge ketone of **10** from the less hindered side (five-membered ring side) in such a ring system. Treatment of **13** with excess methyl lithium gave a methylated diol **14**. Oxidation of **14** with Collins' reagent followed by dehydration of the resulting ketol with phosphorous oxychloride–pyridine produced a mixture

of the *endo* and *exo* olefinic ketones **15** and **16** in roughly equal amounts, and iodine-catalyzed isomerization of the mixture in refluxing xylene[12] gave exclusively the desired isomer **15**.

Elongation of a two-carbon unit with the appropriate configuration, being *syn* with respect to the five-membered ring, at the C-8 position of **15** was accomplished by applying doubly the Wittig reaction using methoxymethylenetriphenylphosphorane. Reaction of **15** with methoxymethylenetriphenylphosphorane in dimethyl sulfoxide[13] gave **17** which was then hydrolyzed by treating with perchloric acid in ether to give a single aldehyde **18**. This substance must have the thermodynamically unfavorable *anti* (axial on the six-membered ring) formyl group since upon treatment with potassium carbonate in methanol it was changed exclusively to the isomeric *syn* aldehyde **19**. The assignment of the configuration of the formyl group was further supported by NMR spectrum; the signal of the olefinic proton at C-6 in **19** appeared at a higher field (0.1 ppm) than that in **18**, presumably due to the anisotropic effect of the *syn* formyl group. Again, **19** was subjected to the Wittig reaction followed by hydrolysis in the same manner as in the case of **15** to yield a homologous aldehyde, which was reduced to the desired alcohol **3** with lithium aluminum hydride.

The pure sample of **3** collected by preparative glpc, $[\alpha]_D = +133°$, was identical with the sample prepared by Piers, *et al.*[2]

Experimental

All melting points and boiling points are uncorrected. IR spectra were taken on a Hitachi EPI-S2 or a G2 spectrometer. NMR spectra were obtained on a JEOL Model C-60HL instrument using TMS as an internal standard and CCl_4 as the solvent unless otherwise indicated, and chemical shifts are given in δ and coupling constants in Hz. Mass spectra were taken on a Hitachi RMU-6D spectrometer. Specific rotations and ORD curves were recorded on a JASCO Model ORD/UV-5 spectrometer. Glpc analyses were performed on a JEOL Model JGC-1100 instrument. Elemental analyses were performed in the microanalytical laboratory of this institute.

*Methoxycarbonylation of (−)-Carvomenthone (**4**).* To a stirred mixture of sodium hydride (12.5 g, 0.52 mol) and dimethyl carbonate (50 g, 0.55 mol) in dry dioxane (100 ml) was added dropwise over 5 hr a solution of (−)-carvomenthone (**4**) (42 g, 0.27 mol) in dry dioxane (100 ml) at 85—95 °C under nitrogen. Stirring was continued at the same temperature overnight; the mixture turned to wine-red. The cooled mixture was poured into ice-water, acidified with dilute hydrochloric acid to pH 3, and extracted with ether three times. The combined extracts were washed with water twice and then saturated salt solution, and dried over anhydrous sodium sulfate. After removal of the solvent, distillation of the residual liquid gave 50 g (86%) of 3-isopropyl-2-methoxycarbonyl-6-methylcyclohexanone (**5**) as colorless liquid, bp 96—108 °C/3 mmHg, which gave a purple color with alcoholic ferric chloride. IR (neat) 1745, 1710 cm^{-1}; NMR 0.90—1.10 (m, 9H), 1.20—2.50 (m, 8H), 3.70 (s, 3H).

*2-Allyl-3-isopropyl-2-methoxycarbonyl-6-methylcyclohexanone (**6**).* To a suspension of sodium hydride (6.5 g, 0.25 mol) in dry dioxane (100 ml) was added dropwise over 1 hr a solution of **5** (49 g, 0.23 mol) in dry dioxane (100 ml) at 85—90 °C under nitrogen. After the evolution of hydrogen ceased, freshly distilled allyl bromide (30 ml, 0.35 mol) was added over a period of 1 hr, and the mixture was stirred at 80—85 °C overnight. After cooling to room temperature, the reaction mixture was poured into ice-water, neutralized with dilute hydrochloric acid to Congo Red, and extracted with ether three times. The combined extracts were washed with water and saturated salt solution, dried over anhydrous sodium sulfate, and freed from the ether. Distillation of the residual liquid gave 51.3 g (88%) of **6** as colorless oil, bp 110—120 °C/3 mmHg; IR (neat) 3070, 1740, 1715, 1645, 928, 880 cm^{-1}. Found: C, 71.99; H, 9.72%. Calcd for $C_{15}H_{24}O_3$: C, 71.39; H, 9.59%.

*2-Allyl-3-isopropyl-6-methylcyclohexanone (**7**).* Finely powdered sodium cyanide (10 g, 0.2 mol) was added to a solution of **6** (51 g, 0.2 mol) in dimethyl sulfoxide (200 ml), and the mixture was heated at 160 °C for 2 hr with vigorous stirring. The cooled reaction mixture was poured into ice-water and extracted with petroleum ether twice. The extracts were washed thoroughly with water and then saturated salt solution, dried over anhydrous sodium sulfate, and freed from the solvent. Distillation of the residual liquid gave 36 g (92%) of **7** as colorless oil, bp 80—90 °C/0.6 mmHg: IR (neat) 3070, 1705, 1640, 920 cm^{-1}; NMR 0.90—1.00 (m, 9H), 1.50—1.80 (m, 8H), 2.20—2.40 (m, 4H), 4.80—5.10 (m, 3H). Found: C, 80.53; H, 11.38%. Calcd for $C_{13}H_{22}O$: C, 80.35; H, 11.41%.

*7-Hydroxy-4-isopropyl-1-methylbicyclo[3.2.1]octan-8-one (**10**).* To a mechanically stirred solution of **7** (35 g, 0.17 mol) in dioxane (1000 ml) was added osmium tetroxide (1 g, 4 mmol) in the dark with cooling in an ice-bath and then a solution of sodium metaperiodate (50 g, 0.23 mol) in water (1.5 l) over a period of 6 hr. The stirring was continued in the dark overnight. Inorganic salt was removed by filtration and the filtrate was thoroughly extracted with ether. The combined extracts were washed with 10% sodium sulfide solution until the water layer became colorless, and then with water and saturated salt solution. Evaporation of the ether at room temperature under reduced pressure gave 32 g (91%) of the keto aldehyde **9**: IR ($CHCl_3$) 2700, 1715, 1120, 870 cm^{-1}, which was subjected to aldol cyclization without further purification.

To a solution of potassium hydroxide (225 g) in methanol (2.5 l) was added dropwise a solution of **9** (32 g) in methanol (500 ml) with cooling in an ice-bath. The mixture was allowed to stir at room temperature for 36 hr, neutralized with 10% hydrochloric acid, and thoroughly extracted with ether. After removal of the solvent, distillation of the residue gave 15 g of an epimeric mixture of **10**, bp 130—140 °C/0.25 mmHg, which partially crystallized on standing. Crystalline substance was collected and recrystallized from *n*-hexane–ether to afford 5.23 g of an epimer of **10**, mp 80—81 °C. The residual part was chromatographed on silica gel (500 g) using 3 : 1 petroleum ether–ether as eluent to give additional crystals (4.77 g) and a colorless oily epimer (7.23 g). Total yield was 52%. Crystalline epimer: IR ($CHCl_3$) 3600, 3450, 2900, 1735, 1200, 1040 cm^{-1}; NMR ($CDCl_3$) 0.90—1.00 (m, 9H), 1.30—1.90 (m, 7H), 2.20—2.60 (m, 2H), 2.50 (s, 1H, exchangeable with D_2O), 4.08 (m, 1H, changed to q by D_2O addition); ORD (EtOH) $[\phi]_{309}$ $+8.24\times10^3$, $[\phi]_{272}$ -9.02×10^3. Found: C, 73.29; H, 10.33%. Calcd for $C_{12}H_{20}O_2$: C, 73.43; H, 10.27%. Oily epimer: IR ($CHCl_3$) 3600, 3400, 2900, 1735 cm^{-1}; NMR 0.90—1.00 (m, 9H), 1.40—2.50 (m, 9H), 3.65 (s, 1H), 4.00 (m, 1H); ORD (EtOH) $[\phi]_{309}$ $+6.06\times10^3$, $[\phi]_{272}$ -8.20×10^3. Found: C, 72.69 H, 10.22%. MS *m/e* 196

(M^+). Calcd mol wt 196.

Jones oxidation of each epimer in the usual manner gave the same diketone **11** as a viscous oil: IR (CCl_4) 2900, 1770, 1745 (sh), 1730, 1045 cm^{-1}.

*4-Isopropyl-8-hydroxy-1-methylbicyclo[3.2.1]octan-7-one (**13**).* A solution of **10** (7.53 g) in pyridine (30 ml) was treated with acetic anhydride (10 ml) at room temperature for 15 hr. Usual work-up gave 9.24 g (100%) of a mixture of the keto acetate. Analytical sample was purified by evaporative distillation, bp 130 °C (bath temp)/2 mmHg. IR (neat) 1740, 1250, 1030 cm^{-1}; NMR 1.99 (s, 3H), 5.00 (m, 1H). Found: C, 70.49; H, 9.68%. Calcd for $C_{14}H_{22}O_3$: C, 70.55; H, 9.31%.

To a solution of the acetate (9.2 g) in methanol (120 ml) was added sodium borohydride (1.48 g) and one pellet of potassium hydroxide, and the mixture was stirred at room temperature for 2 hr. Usual work-up gave 9.03 g (97%) of a mixture of the oily hydroxy acetate. From the pure oily epimer of **10** the crystalline hydroxy acetate was obtained. Recrystallized sample from *n*-hexane had mp 32 °C. IR ($CHCl_3$) 3550, 3400, 1710, 1250, 1100 cm^{-1}; NMR 2.00 (s, 3H), 3.85 (d, J=6.0, 1H), 4.77 (q, J=3.8 and 8.3, 1H). Found: C, 70.18; H, 9.93%. Calcd for $C_{14}H_{24}O_3$: C, 69.96; H, 10.07%.

A solution of the hydroxy acetate (5.18 g) and dihydropyrane (5 ml) in dry ether (100 ml) containing a catalytic amount of *p*-toluenesulfonic acid was allowed to stir at room temperature for 3 hr. Usual work-up gave 8.2 g of the pyranyl ether. IR ($CHCl_3$) 1720, 1260, 1125, 1020, 970 cm^{-1}; NMR 1.60 (m, 6H), 2.00 (s, 3H), 4.60 (m, 2H).

To a cold suspension of lithium aluminum hydride (1.10 g) in anhydrous ether (150 ml) was added dropwise a solution of the pyranyl ether (8.30 g) in anhydrous ether (20 ml), and the mixture was stirred at room temperature for 4 hr. Usual work-up gave 7.33 g (88%) of the alcohol. IR ($CHCl_3$) 3600, 3400, 1120, 1070, 970 cm^{-1}; NMR 1.70 (m, 6H), 3.30—3.37 (m, 4H), 4.70 (m, 1H).

A solution of the above alcohol (7.33 g) in dichloromethane (500 ml) was treated with the Collins' reagent (31.0 g) at room temperature for 30 min. Usual work-up gave 7.03 g (96%) of the ketone. IR ($CHCl_3$) 1735, 1124, 1075, 1030, 970 cm^{-1}; NMR 1.70 (m, 6H), 3.50—3.90 (m, 3H), 4.75 (m, 1H).

A solution of the above product (212 mg) in 20% aqueous dioxane (5 ml) containing a catalytic amount of *p*-toluenesulfonic acid was heated at 70 °C for 1 hr. The mixture was diluted with water and extracted with ether twice. The combined extracts were washed with water and saturated salt solution, and evaporated to give 105 mg (71%) of crystalline **13**, mp 80—81 °C, recrystallized from *n*-hexane. IR (CCl_4) 3600, 3400, 1740 cm^{-1}; NMR 0.80—1.00 (m, 9H), 1.10—2.20 (m, 8H), 2.30—2.70 (m, 2H, 1H exchangeable with D_2O) 3.85 (d, J=6.0, 1H). ORD (EtOH) $[\phi]_{316}$ -1.99×10^3, $[\phi]_{275}$ $+2.50\times10^3$. Found: C, 73.37; H, 10.35%. Calcd for $C_{12}H_{20}O_2$: C, 73.43; H, 10.27%.

*7,8-Dihydroxy-1,7-dimethyl-4-isopropylbicyclo[3.2.1]octane (**14**).* A solution of **13** (105 mg) in ether (2 ml) was added dropwise to an ethereal solution of methyl lithium, prepared from lithium (400 mg) and methyl iodide (3 ml) in ether (20 ml), with cooling in an ice-bath, and the mixture was stirred overnight at room temperature under nitrogen. The mixture was carefully poured into ice-water and the water layer was extracted with two 30 ml portions of ether. Evaporation of the ether and recrystallization of the residual crystals from *n*-hexane–ether gave 60 mg (53%) of **14**, mp 116—117 °C: IR ($CHCl_3$) 3600, 3400, 1050 cm^{-1}; NMR ($CDCl_3$) 0.75—0.95 (m, 9H), 1.15 (s, 3H), 1.20—1.75 (m, 8H), 2.17 (m, 1H), 3.65 (d, J=6.0, 1H). Found: C, 73.72; H, 11.95%. Calcd for $C_{13}H_{24}O_2$: C, 73.53; H, 11.39%.

*1,7-Dimethyl-4-isopropylbicyclo[3.2.1]oct-6-en-8-one (**15**).* To a stirred slurry of the Collins' reagent (1.0 g) in dichloromethane (10 ml) was added a solution of **14** (123 mg) in dichloromethane (10 ml) at room temperature, and the mixture was stirred for 15 min. After the usual work-up, recrystallization of the residue from *n*-hexane gave 110 mg (90%) of the keto alcohol, mp 124 °C. IR (CCl_4) 3600, 3400, 1730 cm^{-1}; NMR 0.80—1.00 (m, 9H), 1.12 (s, 3H), 1.50—2.50 (m, 10H). Found: C, 74.10; H, 10.30%. Calcd for $C_{13}H_{22}O_2$: C, 74.24; H, 10.54%.

To a solution of the above keto alcohol (64 mg) in pyridine (0.5 ml) was added phosphorous oxychloride (0.04 ml), and the resulting mixture was heated gradually in an oil-bath until the bath temperature reached to 90 °C (30 min) and maintained at that temperature for 15 min. After cooling, the mixture was poured into ice-water in a separatory funnel with the aid of ether and the water layer was extracted with ether. The combined ether layers were successively washed with dilute hydrochloric acid, sodium bicarbonate solution, water, and saturated salt solution. Evaporation of the ether gave 46 mg of a *ca.* 1 : 1 mixture of **15** and the *exo*-isomer **16**, as indicated by glpc on a column of Carbowax 20M (2 m, 155 °C, He 1.4 kg/cm^2, retention times: 5.4 min and 6.3 min). IR (neat) 1755, 1655 cm^{-1}; NMR 1.70 (br. s), 4.90 (m), 5.75 (m).

A solution of the above mixture (550 mg) and a catalytic amount of iodine in anhydrous xylene (20 ml) was heated under reflux for 8 hr under nitrogen. The cooled reaction mixture was successively washed with dilute sodium thiosulfate solution, water, and saturated salt solution. Evaporation of the xylene followed by evaporative distillation of the residual liquid gave 470 mg of pure **15**, bp 100 °C (bath temp)/2 mmHg. IR (neat) 1755 cm^{-1}; NMR 0.80—1.20 (m, 9H), 1.75 (d, J=1.5, 3H), 1.20—2.40 (m, 6H), 2.75 (m, 1H), 5.75 (m, 1H). Found: C, 80.93; H, 10.29%. Calcd for $C_{13}H_{20}O$: C, 81.20; H, 10.48.%

*Wittig Reaction of **15** and Hydrolysis of the Product **17**.* A solution of methoxymethylenetriphenylphosphorane in dimethyl sulfoxide was prepared according to the literature using sodium hydride (0.66 g) and methoxymethyltriphenylphosphonium chloride (9.25 g) in dimethyl sulfoxide (57 ml). To this red solution was added a solution of **15** (1.10 g) in dimethyl sulfoxide (14 ml); and the resulting mixture was stirred at 53 °C overnight under nitrogen. Then, the reaction mixture was poured into ice-water and extracted with petroleum ether three times. The combined extracts were washed with 50% aqueous dimethyl sulfoxide, water (five times), and saturated salt solution, and freed from the solvent.

The crude oily product thus obtained was dissolved in ether and a few drops of 30% hydrogen peroxide was added with cooling in an ice-bath. After stirring for 30 min at room temperature, a large amount of petroleum ether was added and the resulting organic layer was passed through a short column of neutral alumina (Woelm V). Evaporation of the solvent gave 1.03 g (87%) of the oily methoxymethylene compound **17**. IR (CCl_4) 3060, 1705, 1430 cm^{-1}; NMR 1.60 (m, 3H), 2.70 (m, 1H), 3.42 (s, 3H), 5.35 (m, 1H), 5.50 (s, 1H). MS *m/e* 222 (M^+). Calcd for $C_{15}H_{24}O$: mol wt 222.

Compound **17** (213 mg) was dissolved in ether saturated with perchloric acid (5 ml). The reaction mixture was allowed to stand for 2 hr at room temperature and then washed with dilute sodium bicarbonate solution, water, and finally saturated salt solution. Evaporation of the ether gave

200 mg (100%) of the *anti*-aldehyde **18**: IR (CCl_4) 2740, 1725 cm^{-1}; NMR 1.65 (m, 3H), 5.50 (m, 1H), 10.10 (d, J=6.0, 1H).

Isomerization of ***18*** *to the* syn-*Isomer* ***19***. A solution of **18** (150 mg) in ether (3 ml) was added to a saturated methanolic solution of potassium carbonate (2 ml), and the mixture was stirred overnight at room temperature. Then, the mixture was diluted with water and extracted with ether. The extract was washed with water and saturated salt solution, dried, and freed from the ether, giving 128 mg (85%) of an oil, which consisted mainly of the desired compound, 1,7-dimethyl-8-*syn*-formyl-4-isopropylbicyclo[3.2.1]oct-6-ene (**19**): IR (neat) 2700, 1718, 1436, 1120 cm^{-1}; NMR 1.65 (br. s, 3H), 2.75 (m. 1H), 5.40 (m, 1H), 9.50 (d, J=4.0, 1H).

*(+)-1,7-Dimethyl-4-*endo-*isopropyl-8-*syn-*(2-hydroxyethyl)bicyclo[3.2.1]oct-7-ene* (***3***). A solution of **19** (430 mg) in dimethyl sulfoxide (10 ml) was treated with a solution of an excess methoxymethylenetriphenylphosphorane (4 equiv.) in dimethyl sulfoxide (10 ml) at room temperature overnight under nitrogen. The mixture was worked up as before to give 403 mg (87%) of the enol ether as a colorless oil: IR (CCl_4) 3050, 1650, 1430, 1100 cm^{-1}; NMR 1.62 (br. s, 3H), 3.50 (s, 3H), 5.25 (m, 1H), 5.80 (q, J=12.0 and 6.0, 1H), 6.25 (d, J=12.0, 1H).

A solution of the above product (112 mg) in ether (5 ml) was added to cold ether saturated with perchloric acid (5 ml). After stirring for 30 min at room temperature, the mixture was successively washed with dilute sodium bicarbonate solution, water and saturated salt solution, dried over anhydrous sodium sulfate, and freed from the ether, giving 106 mg (89%) of the aldehyde: IR ($CHCl_3$) 2700, 1725, 1450, 1370, 1120 cm^{-1}.

To a stirred suspension of lithium aluminum hydride (21 mg, 4 equiv) in anhydrous ether (5 ml) was added a solution of the above aldehyde (106 mg) in anhydrous ether (3 ml) at 0 °C, and the mixture was stirred for 1 hr at room temperature. Usual work-up gave 101 mg of an oil, which consisted of two components as indicated by glpc analysis (20% Carbowax 20M, 2 m×3 mm, 160 °C, He 0.95 kg/cm^2): the major peak with 77% of area at 7.8 min and the minor one with 23% of area at 9.4 min. The collected sample of the major product was identical with the authentic sample of **3**. IR (CCl_4) 3620, 3040, 1460, 1440, 1380, 1365, 1050 cm^{-1}; NMR 0.80—0.95 (m, 9H), 1.60 (br. s, 3H), 1.00—2.00 (m, 10H, 1H exchangeable with D_2O), 2.55 (m, 1H), 3.65 (d, J=7.5, 2H), 5.45 (m, 1H). $[\alpha]_D$=+133° (c, 1.52×10^{-2}, EtOH). Found: C, 80.46; H, 11.55%. Calcd for $C_{15}H_{26}O$: C, 81.02; H, 11.79%.

Minor product was assigned to be 8-*anti*-isomer from the following spectral data: IR (CCl_4) 3620, 3040, 1460, 1440, 1380, 1120, 1045, 1010 cm^{-1}, NMR 0.75—0.95 (m, 9H), 1.55 (br. s, 3H), 1.00—1.90 (m, 9H), 2.45 (m, 1H), 3.50 (m, 3H), 5.20 (m, 1H).

We thank Professor E. Piers and Dr. M. Soucy (University of British Columbia) for generous gift and the identification of the compound **3**.

References

1) Presented in part at the 24th Annual Meeting of the Chemical Society of Japan, April 1971, Suita, Osaka Pref.

2) E. Piers, M. B. Geraghly, and M. Soucy, *Synth. Commun.*, **3**, 401 (1973) and references cited therein.

3) The naturally occurring hydrocarbon is the (−)-enantiomer. P. de Mayo and R. E. Williams, *J. Amer. Chem. Soc.*, **87**, 3275 (1965); P. de Mayo, J. R. Robinson, E. Y. Spencer, and R. W. White, *Experientia*, **18**, 359 (1962).

4) For two alternatives of the total synthesis of the racemic **1**, see J. E. McMurry, *J. Amer. Chem. Soc.*, **90**, 6821 (1968); G. L. Hodgson, D. F. MacSweeney, and T. Money, *J. Chem. Soc., Perkin I*, **1973**, 2113.

5) L. Smedman and E. Zavarin, *Tetrahedron Lett.*, **1968**, 3833; L. Smedman, E. Zavarin, and R. Teranishi, *Phytochem.*, **8**, 1457 (1969).

6) (a) For the structural relation of cyclosativene to sativene and cyclocopacamphene, see J. E. McMurry, *Tetrahedron Lett.*, **1969**, 55; *J. Org. Chem.*, **36**, 2826 (1971); F. Kido, R. Sakuma, H. Uda, and A. Yoshikoshi, *Tetrahedron Lett.*, **1969**, 3169. (b) Very recently an alternative synthesis of the racemic **2** has been reported. S. W. Baldwin and J. C. Tomesch, *Tetrahedron Lett.*, **1975**, 1055.

7) E. S. Rothman and A. R. Day, *J. Amer. Chem. Soc.*, **76**, 111 (1954).

8) A. P. Krapcho, G. A. Glynn, and B. J. Grenon, *Tetrahedron Lett.*, **1967**, 215; J. Harley-Mason and Att-Ur-Rahman, *Chem. Ind.*, **1968**, 1845.

9) M. Shamma and H. R. Rodoriguez, *Tetrahedron*, **24**, 6583 (1968).

10) J. C. Collins, W. W. Hess, and F. J. Frank, *Tetrahedron Lett.*, **1968**, 3363.

11) C. Djerassi, R. Riniker, and B. Riniker, *J. Amer. Chem. Soc.*, **78**, 6362 (1956).

12) A. Yoshikoshi, M. Kitadani, and Y. Kitahara, *Tetrahedron*, **23**, 1175 (1967).

13) R. Greenwald, M. Chaykovsky, and E. J. Corey, *J. Org. Chem.*, **28**, 1128 (1963).

Reaction of 2,4,6-Tri-*t*-butylnitrobenzene with Alkyl Grignard Reagents

Yoshio INAGAKI, Renji OKAZAKI, and Naoki INAMOTO

Department of Chemistry, Faculty of Science, The University of Tokyo, Hongo, Bunkyo-ku, Tokyo 113

(Received August 20, 1975)

Reactions of 2,4,6-tri-*t*-butylnitrobenzene (**1**) with alkylmagnesium halides afforded 2,4,6-tri-*t*-butylaniline (**2**), *N*-alkyl-2,4,6-tri-*t*-butylanilines (**3**), 6-alkyl-2,4-di-*t*-butylanilines (**4**), 4-alkyl-1-hydroxyimino-2,4,6-tri-*t*-butyl-2,5-cyclohexadienes (**5**), and 6-alkyl-1-hydroxyimino-2,4,6-tri-*t*-butyl-2,4-cyclohexadienes (**6**) depending on the Grignard reagents used. Reduction of the oxime **6** proved to be responsible for the formation of the aniline **4**. Comparison of the present reactions with those of 2,4,6-tri-*t*-butylnitrosobenzene (**7**) with Grignard reagent, *syn-anti*-isomers of the oxime **6**, and the formation mechanisms of the products have been discussed.

Only a few studies have been reported on the reaction between Grignard reagents and nitroarenes.[1-3] Grignard reagents have been reported to attack nitroarenes usually on the nitro group resulting in its reduction; for example, reactions of ethylmagnesium bromide with nitrobenzene and nitrotoluenes merely afforded the corresponding *N*-ethylanilines and azobenzenes.[3] The only one exception is an abnormal addition of a Grignard reagent to 1,3,5-trinitrobenzene leading to 1,3,5-trinitro-2,4,6-trialkylcyclohexanes.[2]

We describe here the reaction of 2,4,6-tri-*t*-butylnitrobenzene (**1**) with Grignard reagents giving some abnormal products,[4] and discuss the mechanism of their formation. This reaction was carried out with the intention of obtaining cyclohexadienone oximes (6-alkyl-1-hydroxyimino-2,4,6-tri-*t*-butyl-2,5-cyclohexadienes and 4-alkyl-1-hydroxyimino-2,4,6-tri-*t*-butyl-2,4-cyclohexadienes) whose properties we are interested in:[5] the only one route to the oximes is the reaction of 2,4,6-tri-*t*-butylnitrosobenzene (**7**) with Grignard reagents.[6] However, considering reducing ability of Grignard reagents, it seemed to be possible to prepare the oximes using the nitrobenzene **1** instead of the nitrosobenzene **7**, and such reaction is more convenient because **1** is the starting material in the preparation of **7**.[7]

Results and Discussion

Reaction Products. Reactions of **1** with a large excess of alkylmagnesium halides in ether at 0 °C afforded some of the following compounds: 2,4,6-tri-*t*-butylanilines(**2**), *N*-alkyl-2,4,6-tri-*t*-butylanilines (**3**), 6-alkyl-2,4-di-*t*-butylanilines (**4**), 4-alkyl-1-hydroxyimino-2,4,6-tri-*t*-butyl-2,5-cyclohexadienes (**5**), and 6-alkyl-1-hydroxyimino-2,4,6-tri-*t*-butyl-2,4-cyclohexadienes (**6**).

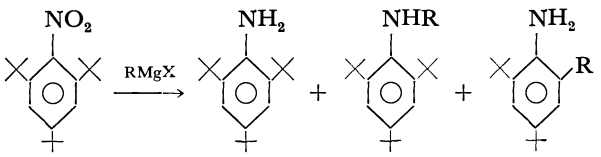

R	
a	Me
b	Et
c	*i*-Pr
d	*t*-Bu
e	$PhCH_2$
f	1-Ad*

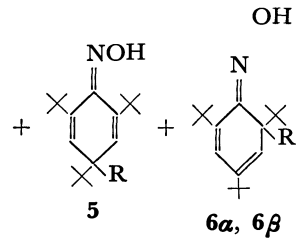

* Ad represents adamantyl group.

The yields of the products and the reaction conditions are summarized in Table 1. The structures of the products were confirmed by the analytical and spectral data. Compound **6α** which was obtained also in the reactions of Grignard reagents with 2,4,6-tri-*t*-butylnitrosobenzene (**7**)[6] is one of the *syn*- and *anti*-isomers, and **6β** is the other. These two isomers could easily be distinguished from each other by the NMR spectra and separated by chromatography: R_f value of **6α** was smaller than that of **6β**. The NMR spectra of **6αa** showed two olefinic protons at δ 5.42 and 6.15, whereas **6βa** at 5.17 and 6.10, similarly **6αb** at 5.33 and 6.22, but **6βb**

Table 1. Reaction conditions and yields (%) of the products

No.[a]		RMgX	Reaction time (hr)	Yields (%)					
				2	**3**	**4**	**5**	**6α**	**6β**
1		MeMgI	3.7	40	2	17	—	—	—
2[b,c]	**a**	MeMgI	5	5	—	—	5	19	2
3[b]		MeMgI	20	5	—	—	15	43	7
4	**b**	EtMgBr	1.5	41	4	7	14	—	8
5	**c**	*i*-PrMgBr	4.8	40	16	6	21	—	—
6	**d**	*t*-BuMgCl	5.9	49	28	—	—	—	—
7	**e**	$PhCH_2MgCl$	3.4	12	—	—	25	38	—
8[d]	**f**	1-AdMgBr	5	12	—	—	4	—	—

a) Excess amount of magnesium was used in preparation of Grignard reagents except for Nos. 2 and 3. b) Excess amount of methyl iodide was used in preparation of Grignard reagent. c) 51% of **1** was recovered. d) A considerable amount of **1** was recovered.

at 5.13 and 6.12. The difference in the chemical shifts of the two olefinic protons of **6β** is larger than that of **6α**. There are other features on the NMR spectra: the signals due to the methyl group on the 6-position of **6αa** appeared at δ 1.32, but that of **6βa** at 1.61, similarly the methylene protons of the 6-ethyl group of **6αb** appeared at δ 1.4—2.3, but that of **6βb** at 3.00. Thus the signals of 6-alkyl group on **6β** appeared at a lower field than those of **6α**. This difference makes it possible to evaluate the isomer ratio.

Absorption maxima of **6αa**, **6αb**, **6βa**, and **6βb** are listed in Table 2. The isomers **6β** are characterized by the absorption maxima at longer wavelength by a few nm than those of **6α**.

Table 2. Absorption maxima of **6α** and **6β** in hexane

6	λ_{max} (nm)	ε
6αa	304	4400
6βa	308.5	4370
6αb	308	4400
6βb	310.5	3690

Although these data are insufficient to establish their configuration, we tentatively assign **6α** to structure (A) and **6β** to (B) on the following basis: (1) the protons *syn* to the hydroxyl group of the oximes have lower chemical shifts (δ) than those of the other isomer,[8] (2) the slight hypsochromic shift in the UV absorption of α-isomer is consistent with the larger twisting of the hydroxyimino group from the molecular plane, because the 2-*t*-butyl group is in the molecular plane but the 6-*t*-butyl and the 6-alkyl groups are out of the molecular plane, and (3) the larger R_f value of **6β** than that of **6α** in thin layer chromatography (tlc) is consistent with structure (B), in which the hydroxyl group is more thickly covered with two alkyl groups than that of (A).

(A)≡**6α** (B)≡**6β**

The formation of **5**, **6α**, and **6β**, which seemingly shows that the Grignard reagents attacked to *ortho*- and the *para*-positions of the nitro group, is unprecedented in the reactions of the Grignard reagents with nitro arenes,[1-3] though a similar compound, 1-hydroxyimino-2,4,6-tri-*t*-butyl-2,4-cyclohexadiene (**6**, R=H), could be obtained by the reduction of **1** with sodium-bis(2-methoxyethoxy)aluminum hydride (Vitride).[9] The direct formation of **3c** and **3d** from the readily available nitrobenzene **1** is of synthetic significance, considering the difficulties reported for alkylation of **2**.[10] The only alternative route to these compounds is the reaction of 2,4,6-tri-*t*-butylnitrosobenzene (**7**) with Grignard reagents,[6] but the present reaction seems to provide a more convenient method for preparation of these compounds.

Reaction Mechanism. Although a possibility of direct addition of Grignard reagents to **1** cannot be ruled out, reducing ability of Grignard reagents suggests that oximes **5** and **6**, and secondary amines **3** are probably produced by addition of Grignard reagents to the nitrosobenzene **7** formed by reduction of **1**, for the reaction rate depends on the amount of magnesium metal which was found to play an important role in the reduction process as discussed below: in the reaction with methylmagnesium iodide prepared by use of excess magnesium, **1** was consumed completely in 3.5 hr, but the reaction with methylmagnesium iodide prepared by use of an excess of methyl iodide resulted in 51% recovery of **1** even after 5 hr.

However, in Nos. 1, 4, and 5 in Table 1, the reaction products were different from those of the reaction with **7**; the reactions of **7** afforded the cyclohexadienone oximes (R=Me, Et, *i*-Pr, $PhCH_2$, 1-Ad) or **3a** (R=*t*-Bu) mainly but reduction products **2** and **4** only in small amounts.[6] This difference is ascribed to some secondary reactions discussed below.

The yields of **4** were decreased in the following order:

Me>Et>*i*-Pr

The yields of **6α** obtained in the reactions of **7** with Grignard reagents were also in the same order.[6] These facts suggest that **4** was formed *via* **6α**. Since a longer reaction time is required in the reaction with **1**, it is considered that further reaction of **6α** into **4** is effected in the case of **1**. In order to prove this pathway, reaction of **6αa** with methylmagnesium iodide in the absence of magnesium was carried out, and **6αa** was recovered quantitatively. However, reaction of **6αa** with methylmagnesium iodide in the presence of excess magnesium at room temperature for 3 hr afforded 32% of **4a** and 30% of **6βa** besides 38% recovery of **6αa** based on the NMR spectrum, and they were isolated by tlc in 18, 13, and 12% yields, respectively. This result suggests that magnesium metal in combination with magnesium halide is responsible for the reduction of **6α** into **4**.

In fact, the reaction mixture of **6αa**, magnesium, and magnesium bromide (at room temperature for 2.8 hr) showed NMR signals due to **4a** and **6αa**. The molar ratio was found to be 8 : 3 (73 and 27% respectively) from the NMR spectrum, and the chromatographic separation afforded 27% of **4a** and 9% of **6αa**, which seemed to be contaminated by a trace of **6βa** according to the NMR spectrum.

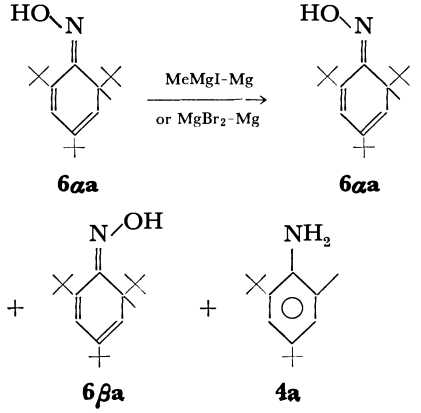

6αa **6αa**

6βa **4a**

Therefore, the formation of **4** is interpreted as follows:

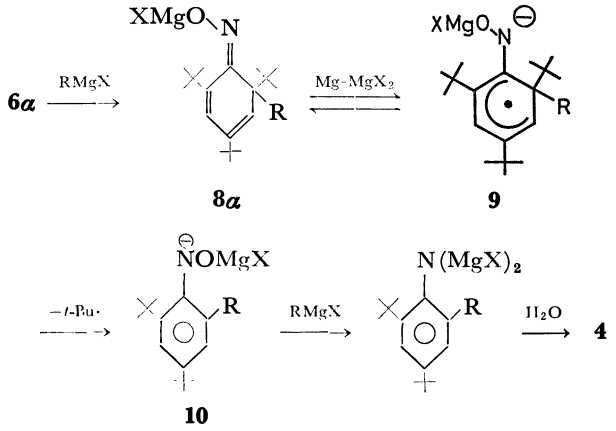

The isomerization of the oxime **6** may be ascribed to the reversibility between **8** and **9**.

This interpretation may explain a reason why **4** was not produced in the case of benzylmagnesium chloride despite of the presence of excess magnesium,

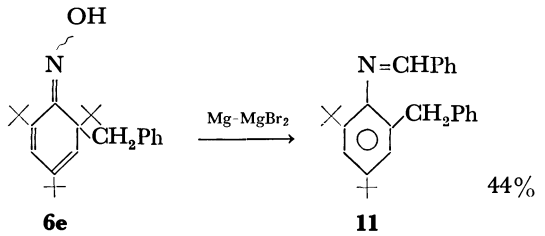

because the reducing ability of Mg–$MgCl_2$ system may be weaker than that of Mg–$MgBr_2$ system. However, **6e** afforded an unusual product, 2-benzyl-4,6-di-*t*-butyl-*N*-benzylideneaniline (**11**) by reaction with Mg–$MgBr_2$. The formation mechanism is obscure.

In contrast to these lines of evidence suggesting that **4** was formed *via* **6**, any proof for reduction of the oxime **5** into 4-alkyl-2,6-di-*t*-butylaniline was not obtained. Actually, the reaction of **5c** with isopropylmagnesium bromide in the presence of magnesium metal resulted in complete recovery of **5c**. This selectivity in reduction is probably because an electron affinity of **5** is less than that of **6** as a simple HMO calculation demonstrates that the orbital energy (-0.445β)for the LUMO of 1,3,5-hexatriene has a lower value than that (-0.581β) of 2-vinyl-1,3-butadiene.[11] Namely, the single electron transfer into the

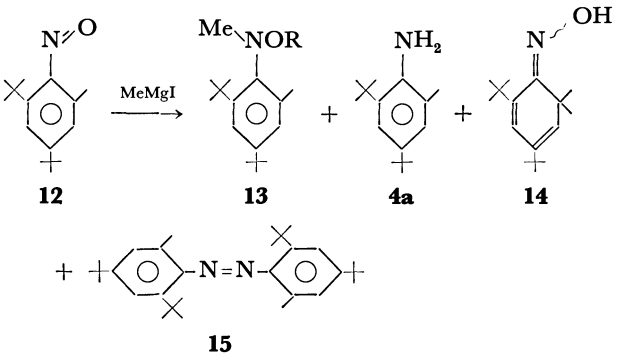

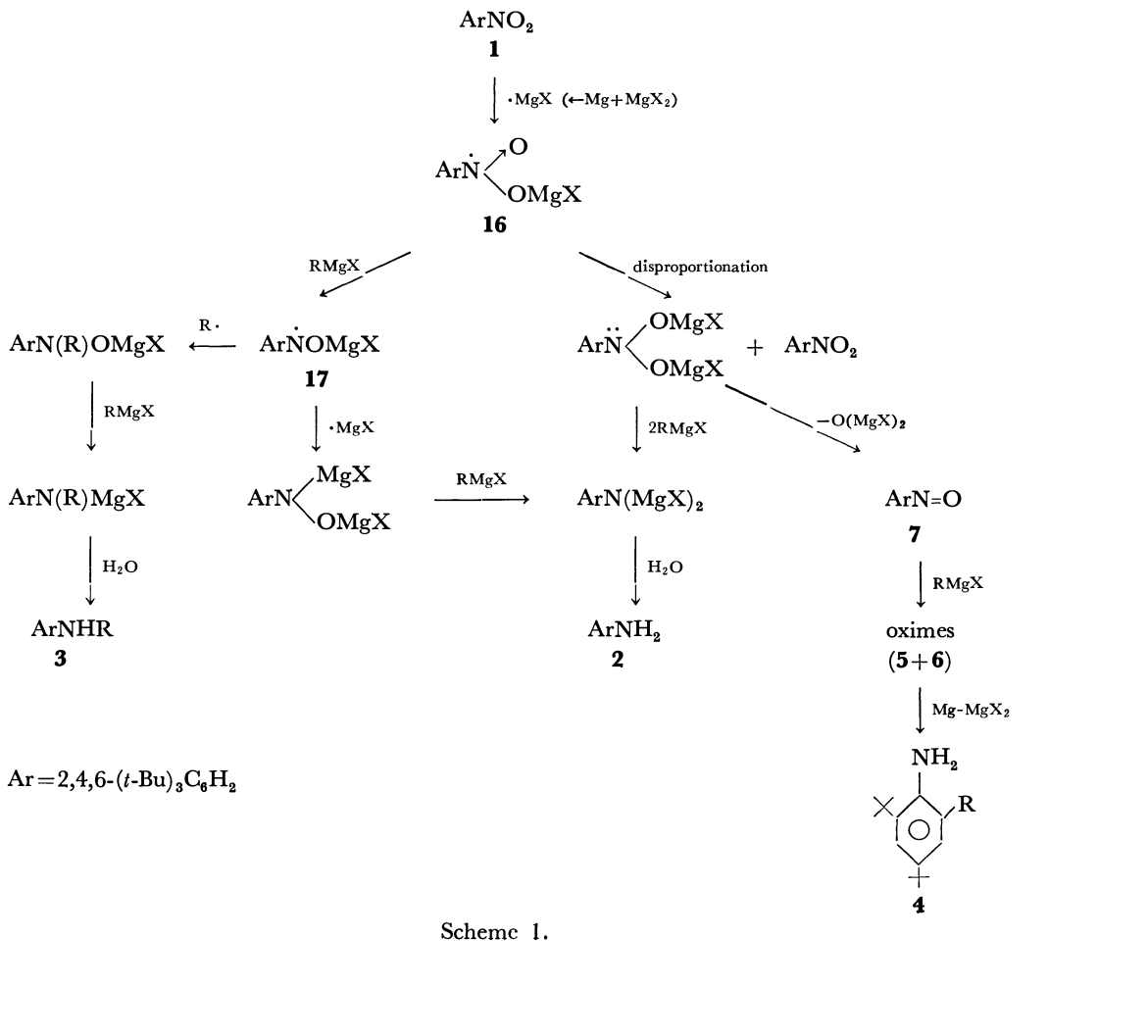

Scheme 1.

LUMO of **6** leading to the radical anion **9** is energetically more advantageous than that of **5**.

A route to **4** *via* 2,4-di-*t*-butyl-6-methylnitrosobenzene (**12**) can be ruled out: reaction of **12** with methylmagnesium iodide afforded **4a** only in a 22% yield besides 44% of *N*-(2,4-di-*t*-butyl-6-methylphenyl)-*N*-methylhydroxylamine (**13**), 17% of 1-hydroxyimino-2,4-di-*t*-butyl-6,6-dimethyl-2,4-cyclohexadiene (**14**), and 0.6% of 2,4,2′,4′-tetra-*t*-butyl-6,6′-dimethylazobenzene (**15**). The formation of considerable amounts of **13** and **14** was inconsistent with the result of the reaction of **1** with methylmagnesium iodide.

The formation of a large amount of **2** remains unresolved. The reduction of intermediary nitrosobenzene **7** might be possible but not be predominant, because the addition of Grignard reagents to **7** is faster than the reduction of **7** as suggested by the fact that only a small amount of **2** was obtained in the reaction of **7** with Grignard reagents.[6] Two processes may be possible: the one is a process involving a disproportionation of the radical anion **16**.[12] The other pathway involves reduction of **1** into an anion radical **17** which is considered to be the common intermediate for **2** and **3** as described in a previous paper,[6] and this route might explain the increased yield of the secondary amine **3** in the present reaction compared with the reaction of **7**.[6]

The probable reaction mechanism is summarized in Scheme 1.

It is concluded that the higher yields of oximes (**5** and **6**) can be obtained by the reaction of **1** with Grignard reagents in the absence of magnesium. Actually, the oxime **6αa** was obtained as a main product in No. 3 in Table 1 where an excess amount of methyl iodide was used in preparation of the Grignard reagent.

Experimental

All melting points were not corrected. The IR and UV spectra were recorded with Hitachi EPI-G2 and EPS-3 spectrophotometers respectively. The NMR spectra were measured with a Hitachi R-24 spectrometer using tetramethylsilane as an internal standard. The mass spectra were recorded with a Hitachi RMU-6L mass spectrometer. All reactions were carried out under nitrogen.

Materials. 2,4,6-Tri-*t*-butylnitrobenzene[10] (**1**) (mp 202.5—203.5 °C), 2,4-di-*t*-butyl-6-methylnitrosobenzene[7] (**12**) (mp 31.5—33.5 °C), 2,4-di-*t*-butyl-6-methylaniline[13] (**4a**) (mp 31.5—32.5 °C), 2,4,6-tri-*t*-butyl-*N*-methylaniline[10] (**3a**) (mp 109.5—111.0 °C), and 2,4,6-tri-*t*-butyl-*N*-ethylaniline[10] (**3b**) (mp 79.5—81.0 °C) were prepared by the reported methods. 2,4,6-Tri-*t*-butyl-*N*-isopropylaniline (**3c**), 2,4,6,*N*-tetra-*t*-butylaniline (**3d**), 6-alkyl-1-hydroxyimino-2,4,6-tri-*t*-butyl-2,4-cyclohexadienes (**6α**), and 4-alkyl-2,4,6-tri-*t*-butyl-2,5-cyclohexadienes (**5**) were prepared as described previously.[6]

Reaction of 2,4,6-Tri-t-butylnitrobenzene (1) with Methylmagnesium Iodide. To an ice-cold Grignard solution prepared from 2.02 g (83.1 mmol) of magnesium and 9.77 g (68.8 mmol) of methyl iodide in 25 ml of ether, a solution of 2.00 g (6.87 mmol) of **1** in 30 ml of ether was added dropwise with stirring over 1.7 hr. After additional stirring at 0 °C for 2 hr, the reaction mixture was poured into aqueous ammonium chloride and extracted with ether. The extract was washed with water and dried over anhydrous magnesium sulfate. After removal of the solvent, the residue was chromatographed on a silica gel dry column with carbon tetrachloride to be devided into nine fractions, each of which was eluted with ether. The first fraction gave 12 mg of orange crystals, which could not be purified. The third fraction afforded 45 mg of pale yellow crystals. The fourth fraction gave 111 mg of colorless crystals, which recrystallized from methanol to give the same material as that obtained from the third fraction by the spectral data, mp 143—145 °C; IR (KBr): 3000, 2950, 1625, 1600, 1455, 1420, 1390, 1360, 1240, and 1210 cm^{-1}; NMR (CCl_4): δ 0.78 (s, 9H), 1.18 (s, 9H), 1.27 (s, 27H), 1.54 (s, 9H), 6.50 (broad s, 1H), 6.60 (broad s, 1H), and 7.05 (s, 2H); λ_{max}(hexane): 241 and 260 nm (the absorbances of a solution (28.5 mg/l) were 1.09 and 0.61 respectively); Mass: *m/e* 260 (22%), 245 (100), and 231 (64). These data were insufficient to elucidate the structure. From the mother liquor 40 mg (2%) of 2,4,6-tri-*t*-butyl-*N*-methylaniline (**3a**) was isolated, and identified by the IR and NMR spectra. The sixth fraction afforded 720 mg (40%) of 2,4,6-tri-*t*-butylaniline (**2**) (by NMR and IR). The eighth fraction afforded 330 mg of tarry material, which was rechromatographed on alumina with carbon tetrachloride as eluent to give 262 mg (17%) of 2,4-di-*t*-butyl-6-methylaniline (**4a**) (by NMR and IR) and 60 mg of unidentified crystalline material. The other fractions afforded small amounts of unidentified materials.

Reaction of 1 with Methylmagnesium Iodide Prepared Using Excess of Methyl Iodide. Reaction of a Grignard solution prepared from 5.25 g (37 mmol) of methyl iodide and 816 mg (33.6 mmol) of magnesium in 15 ml of ether with 1.00 g (3.44 mmol) of **1** in 19 ml of ether for 5 hr at 0 °C afforded 507 mg (50.7%) of recovered **1**, 102 mg of a mixture of **2** and the oxime **6βa** (molar ratio 7 : 4 based on the NMR signal intensity), 54 mg (5%) of **5a**, and 190 mg (19%) of **6αa**, after a similar treatment. The mixture of **2** and **6βa** was rechromatographed on an alumina dry column with hexane to give 43 mg (5%) of **2** and 21 mg (2%) of **6βa**·**6βa**: mp 103—105 °C; IR (KBr): 3300, 3180 (νOH), 980, and 960 cm^{-1} (νNO); NMR (CCl_4): δ 0.89 (s, 9H), 1.09 (s, 9H), 1.24 (s, 9H), 1.61 (s, 3H), 5.17 (d, J=2 Hz, 1H), 6.10 (d, J=2 Hz, 1H), and 7.10 (broad s, 1H), λ_{max} (hexane): 305 nm (ε 4520); Mass: *m/e* 291 (M^+, trace) and 57 (100%).

Reaction of 1 with Ethylmagnesium Bromide. Reaction of a Grignard solution prepared from 2.03 g (83.5 mmol) of magnesium and 7.94 g (68.7 mmol) of ethyl bromide in 26 ml of ether with 2.00 g (6.87 mmol) of **1** in 30 ml of ether for 1.5 hr at 0 °C gave 80 mg (4%) of 2,4,6-tri-*t*-butyl-*N*-ethylaniline (**3b**) (by IR and NMR), 35 mg of white crystals, which failed to be purified (NMR (CCl_4): δ 0.91 (s, 9H), 1.11 (s, 9H), 1.28 (s, 9H), 5.15 (d, J=2 Hz, 1H), 6.15 (d, J=2 Hz, 1H), and the signals of the ethyl group were not resolved clearly), 169 mg of **2** (by IR and NMR), 871 mg of a mixture of **2** (570 mg) and 1-hydroxyimino-2,4,6-tri-*t*-butyl-4-ethyl-2,5-cyclohexadiene (**5b**, 301 mg, 14%) (by NMR), and 428 mg of tarry material. The mixture of **2** and **5b** was rechromatographed on an alumina dry column with hexane to give 508 mg of **2** and 228 mg (11%) of **5b**. Therefore, the total amount of **2** was 677 mg (38%, isolated), and 739 mg (41%) from NMR. The last tarry material was again chromatographed on a silica gel dry column with carbon tetrachloride to divide into A and B fractions. Fraction A gave 160 mg (8%) of an isomer of 1-hydroxyimino-2,4,6-tri-*t*-butyl-6-ethyl-2,4-cyclohexadiene (**6βb**) as white crystals, which were recrystallized three times from aqueous methanol, mp 122—123.5 °C; IR (KBr): 3300, 3170 (νOH), and 975 cm^{-1} (νNO); NMR (CCl_4): δ 0.74 (t, J=

7 Hz, 3H), 0.91 (s, 9H), 1.10 (s, 9H), 1.26 (s, 9H), 3.00 (q, J=7 Hz, 2H), 5.13 (d, J=2 Hz, 1H), 6.12 (d, J=2 Hz, 1H), and 6.95 (broad s, 1H); λ_{max} (hexane): 310.5 nm (ε 3690); Mass: *m/e* 305 (M^+, 0.8%) and 57 (100).

Found: C, 78.58, H. 11.25; N, 4.45%. Calcd for $C_{20}H_{35}NO$: C, 78.63; H, 11.55; N, 4.58%.

Fraction B afforded 113 mg (7%) of 2,4-di-*t*-butyl-6-ethylaniline (**4b**) as tarry material, which was treated twice with tlc (silica gel, benzene) and distilled twice molecularly to give white crystals, mp 34.5—37 °C; IR (neat): 3490 and 3405 cm^{-1} (νNH_2); NMR (CCl_4): δ 1.23 (t, J=7 Hz, 3H), 1.26 (s, 9H), 1.42 (s, 9H), 2.50 (q, J=7 Hz, 2H), 3.57 (broad s, 2H), and 6.95 (ABq, $\Delta\delta$=0.16, J=2 Hz, 2H), λ_{max} (hexane): 240 (ε 8620) and 289 nm (2490); Mass: *m/e* 233 (M^+, 21%) and 218 (100).

Found: C, 82.29; H, 11.74; N, 6.06%. Calcd for $C_{16}H_{27}N$: C, 82.35; H, 11.66; N, 6.00%.

Reaction of ***1*** *with Isopropylmagnesium Bromide.* Reaction of a Grignard solution prepared from 2.02 g (83.1 mmol) of magnesium and 9.30 g (75.6 mmol) of isopropyl bromide in 25 ml of ether with 2.00 g (6.87 mmol) of **1** in 29 ml of ether for 4.8 hr at 0 °C produced 330 mg (16%) of 2,4,6-tri-*t*-butyl-*N*-isopropylaniline (**3c**) (by NMR and IR), 1.23 g of white crystals, and 100 mg (6%) of 2,4-di-*t*-butyl-6-isopropylaniline (**4c**), which was recrystallized eight times from methanol, mp 86.0—87.5 °C; IR (KBr): 3485 and 3405 cm^{-1} (νNH_2); NMR (CCl_4): δ 1.20 (d, J=7 Hz, 6H), 1.26 (s, 9H), 1.43 (s, 9H), 2.89 (sep, J=7 Hz, 1H), 3.54 (broad s, 2H), and 7.00 (ABq, J=2 Hz, $\Delta\delta$=0.08, 2H); Mass: *m/e* 247 (M^+, 23%) and 232 (100).

Found: C, 82.77; H, 11.81; N, 5.87%. Calcd for $C_{17}H_{29}N$: C, 82.52; H, 11.82; N, 5.66%.

The white crystals were rechromatographed on an alumina dry column with hexane to give 449 mg (21%) of 1-hydroxyimino-2,4,6-tri-*t*-butyl-4-isopropyl-2,5-cyclohexadiene (**5c**) and 710 mg (40%) of **2**, which were identified by the spectral data.

Reaction of ***1*** *with* t-*Butylmagnesium Chloride.* Reaction of a Grignard solution prepared from 2.02 g (83.1 mmol) of magnesium and 6.34 g (68.5 mmol) of *t*-butyl chloride in 20 ml of ether with 2.00 g (6.87 mmol) of **1** in 27 ml of ether for 5.9 hr at 0 °C afforded 646 mg (28% based on consumed **1**) of 2,4,6,*N*-tetra-*t*-butylaniline (**3d**) (by NMR), 113 mg (5.7%) of recovered **1**, and 833 mg (49%) of **2** (by IR and NMR).

Reaction of ***1*** *with Benzylmagnesium Chloride.* Reaction of a Grignard solution prepared from 3.47 g (151 mmol) of magnesium and 9.59 g (75.5 mmol) of benzyl chloride in 25 ml of ether with 2.00 g (6.87 mmol) of **1** in 22 ml of ether for 3.5 hr at 0 °C gave 1.86 g of bibenzyl contaminated with a small amount of impurities, 535 mg of white crystals, 460 mg 1-hydroxyimino-4-benzyl-2,4,6-tri-*t*-butyl-2,5-cyclohexadiene (**5e**), 961 mg (38%) of 1-hydroxyimino-6-benzyl-2,4,6-tri-*t*-butyl-2,4-cyclohexadiene (**6e**) (by IR and NMR), and 594 mg of brown oil, which seemed to be mainly benzyl alcohol according to the IR and NMR spectra. The white crystals were treated with hexane. The insoluble part (100 mg) was identified as **5e** by IR and NMR. The soluble part was chromatographed on an alumina dry column with hexane to give 222 mg (12%) of **2** and 78 mg of **5e**, the total amount of which was 638 mg (25%).

Reaction of ***1*** *with* 1-*Adamantylmagnesium Bromide.* The Grignard reagent was prepared from 586 mg (24.2 mmol) of magnesium and 4.34 g (20.2 mmol) of 1-adamantyl bromide in 24 ml of ether over 2 hr. An ethereal solution (14 ml) of **1** (1.00 g, 3.44 mmol) was added to the Grignard reagent dropwise with stirring at 0 °C over 1 hr. After additional stirring for 4 hr, the reaction mixture was treated with aqueous ammonium chloride, extracted with ether and filtered to give 943 mg of light gray crystals, mp>220 °C (lit,[14] 288—290 °C); Mass: *m/e* 270 (M^+, 11%) and 135 (100). This compound was considered to be biadamantane. The filtrate was dried over anhydrous magnesium sulfate. After the solvent was removed, the residue was chromatographed on a silica gel dry column with carbon tetrachloride.

The first fraction (R_f=1.0—0.4) gave 2.153 g of pale yellow crystalline material, which seemed to contain **1** according to the NMR spectrum but the accurate amount could not be determined, NMR (CCl_4): δ 1.33 (s), 1.38 (s), 7.46 (s) [these three signals are due to **1**], and broad signals at 1.62, 1.79, and 1.81. The second fraction (R_f=0.4—0.2) afforded 352 mg of tarry material, which was rechromatographed on an alumina dry column with hexane to give 110 mg (12.2%) of **2** and 59 mg (4.2%) of 1-hydroxyimino-4-(1-adamantyl)-2,4,6-tri-*t*-butyl-2,5-cyclohexadiene (**5f**) as colorless tar, which showed the identical IR and NMR spectra with those of an authentic sample.[6] The other fractions gave unidentified materials.

*Reaction of 1-Hydroxyimino-2,4,6-tri-*t*-butyl-6-methyl-2,4-cyclohexadiene (**6αa**) with Methylmagnesium Iodide in the Presence of Excess Magnesium.* The Grignard reagent was prepared from 2.4 g (16.9 mmol) of methyl iodide and 530 mg (21.8 mmol) of magnesium in 9 ml of ether. Into a reaction tube containing an ethereal solution (0.5 ml) of **6αa** (50.0 mg, 0.171 mmol), 2 ml of the Grignard reagent with excess of magnesium metal was pipetted. After being stirred for 3 hr at room temperature, the reaction mixture was worked up as usual to give 36.1 mg of tarry material, which was a mixture of **6αa**, **6βa**, and 2,4-di-*t*-butyl-6-methylaniline (**4a**) (molar ratio: 19 : 15 : 16 ; 38, 30, and 32%, respectively, according to the signal intensity on the NMR spectrum). The separation of the products was carried out by tlc (silica gel, benzene) to afford 8.8 mg (17.6%) of an isomer of 1-hydroxyimino-2,4,6-tri-*t*-butyl-6-methyl-2,4-cyclohexadiene (**6βa**), 6.1 mg (12%) of **6αa**, and 5.0 mg (13%) of **4a**.

Reaction of ***6αa*** *with Magnesium and Magnesium Dibromide.* Anhydrous magnesium dibromide was prepared by the reaction of 1,2-dibromoethane (3.88 g, 20.7 mmol) with magnesium (624 mg, 26.4 mmol) in ether (14 ml).[15] The mixture separated into colorless upper layer and gray lower layer. The lower layer was pipetted with excess magnesium remaining therein into a reaction tube containing an ethereal solution (1 ml) of **6αa** (50.5 mg, 0.174 mmol). The mixture was stirred for 2.8 hr at room temperature and worked up as usual to give 46.5 mg of tarry material, whose NMR spectrum exhibited two sets of the signals due to **6αa** and **4a** in a molar ratio of 3 : 8 (27 and 73% respectively). The residue was subjected to preparative tlc (silica gel, benzene). The first fraction (R_f=0.68) gave 4.6 mg (9%) of **6αa**, which was identified by the NMR and IR spectra but contamination of a small amount of **6βa** was suggested by the following weak signals, NMR (CCl_4): δ 0.91 (s), 1.28 (s), 1.63 (s), and 5.25 (weak). The second fraction (R_f=0.24) afforded 18.9 mg of tarry material, whose NMR spectrum was nearly identical with that of **4a** but some other peaks were observed in the aromatic region. The purification by further tlc (silica gel, dichloromethane) gave 10.3 mg (27%) of **4a** (by IR and NMR).

Reaction of ***6e*** *with Magnesium and Magnesium Dibromide.* An ethereal solution (5 ml) of **6e** (203 mg, 0.55 mmol) and magnesium-containing 3 ml portion of an ethereal solution of magnesium dibromide prepared from magnesium (1 g, 41.2 mmol), 1,2-dibromoethane (5 g, 26.6 mmol), and ether (20 ml) were stirred for 3.5 hr at 0 °C. After hydrolysis, the

reaction mixture was chromatographed on an alumina dry column to give 29.4 mg (14.5%) of **6e** and 90 mg of tarry material, which was again chromatographed on a silica gel dry column with hexane–benzene (4 : 1) as eluent to give 46 mg (44%) of 2-benzyl-4,6-di-*t*-butyl-*N*-benzylideneaniline (**11**) as a yellow tar, which crystallized on standing and was recrystallized three times from aqueous ethanol to give pale yellow crystals, mp 92—93 °C; IR (KBr): 1625 (νC=N), 875 (1,2,4,6-substituted phenyl), 728, 695, and 685 cm^{-1} (two phenyls); NMR (CCl_4): δ 1.35 (s, 18H), 3.76 (s, 2H), and 7.0—7.7 (m, 13H); λ_{max} (hexane): 253 (ε 14300) and 349 nm (1730); Mass: *m/e* 383 (M^+, 38%), 368 (M^+-15, 100), 292 (M^+-PhCH_2, 11), 91 (33), and 57 (26).

Found: C, 87.60; H, 8.81; N, 3.64%. Calcd for $C_{28}N_{33}N$: C, 87.68; H, 8.67; N, 3.65%.

Reaction of 2,4-Di-t-butyl-6-methylnitrosobenzene (12) with Methylmagnesium Iodide. 1) To an ice-cold Grignard solution prepared from 9.47 g (71.8 mmol) of methyl iodide and 1.78 g 73.2 mmol) of magnesium in 30 ml of ether, an ethereal solution (20 ml) of 1.55 g (6.65 mmol) of **12** was added dropwise with stirring over 20 min. After additional stirring for 50 min at 0 °C and usual work-up, the residue was chromatographed on a silica gel dry column with carbon tetrachloride. The first fraction (R_f=1—0.81) gave 18 mg (0.6%) of 2,4,2′,4′-tetra-*t*-butyl-6,6′-dimethylazobenzene (**15**) as orange crystals, mp 156—158 °C; NMR (CCl_4): δ 1.37 (s, 36H), 2.24 (s, 6H), 7.04 (d, J=2 Hz, 2H), and 7.32 (d, J=2 Hz, 2H); λ_{max} (hexane): 238 (ε 9040), 247 (sh) (8750), 311.5 (15650), and 486 nm (1750); Mass: *m/e* 434 (M^+, 5.4%), 217 (35), and 57 (100).

The second fraction (R_f=0.81—0.48) gave 281 mg (17%) of 1-hydroxyimino-2,4-di-*t*-butyl-6,6-dimethyl-2,4-cyclohexadiene (**14**) as white crystals, which were recrystallized four times from methanol, mp 144.5—146 °C; IR (KBr): 3295, 3170 (νOH), and 965 cm^{-1} (νNO); NMR (CCl_4): δ 1.06 (s, 9H), 1.22 (s, 9H), 1.46 (s, 6H), 5.10 (d, J=2 Hz, 1H), 6.12 (d, J=2 Hz, 1H), and 6.96 (s, 1H); λ_{max} (hexane): 300 (sh) (ε 6510), 308.5 (7250), and 319 (sh) nm (4700); Mass: *m/e* 249 (M^+, 14%), 176 (100), and 57 (80).

Found: C, 77.34; H, 11.14; N, 5.33%. Calcd for $C_{16}H_{27}NO$: C, 77.06; H, 10.92; N, 5.62%.

The third fraction (R_f=0.48—0.36) gave 975 mg of pale yellow tarry material, which was a mixture of **13** (44%) and **4a** (22%) (molar ratio by NMR; 2 : 1). When 50 mg portion of the mixture was treated with tlc (silica gel, benzene), **13** and **4a** were isolated. The IR and NMR spectra of **4a** were identical with those of an authentic sample.[13] The compound **13** was tentatively identified as *N*-(2,4-di-*t*-butyl-6-methylphenyl)-*N*-methylhydroxylamine by the spectral data. **13**; pale yellow oil; IR (neat): 3560 and 3400 cm^{-1} (broad, νOH); NMR (CCl_4): δ 1.27 (s, 9H), 1.39 (s, 9H), 2.55 (s, 3H), 3.09 (s, 3H), 4.95 (broad s, 1H), and 6.98 (ABq, $\Delta\delta$=0.15, J=2 Hz, 2H). This compound changed into a crystalline material on standing, which seemed to be a mixture of many components because of the complexity of the NMR and mass spectra.

2) Reaction of a Grignard solution prepared from 1.16 g (47.7 mmol) of magnesium and 6.09 g (42.9 mmol) of methyl iodide in 15 ml of ether with 998 mg (4.28 mmol) of **12** in 12 ml of ether for 3.7 hr at 0 °C gave a small amount of **15**, 224 mg (21%) of **14**, and 620 mg of a mixture of **13** and **4a** (molar ratio: 1.7 : 1, which was calculated on the base of the intensity of the NMR signals due to the methyl group; a singlet at δ 3.09 of **13** and a singlet at 2.12 of **4a**).

References

1) M. S. Kharasch and O. Reinmuth, "Grignard Reagents with Nonmetallic Substances," Prentice-Hall, Engelwood Chliffs, N. J. (1954).
2) T. Severin and R. Schmitz, *Chem. Ber.*, **96**, 3081 (1963).
3) H. Hepworth, *J. Chem. Soc.*, **117**, 1004 (1920).
4) Preliminary report: R. Okazaki, Y. Inagaki, and N. Inamoto, *Chem. Lett.*, **1974**, 1503.
5) R. Okazaki, Y. Inagaki, and N. Inamoto, *Chem. Lett.*, **1974**, 1543.
6) Y. Inagaki, R. Okazaki, and N. Inamoto, This Bulletin, **48**, 621 (1975).
7) R. Okazaki, T. Hosogai, E. Iwadare, M. Hashimoto, and N. Inamoto, This Bulletin, **42**, 3611 (1969).
8) C. G. McCarty, in "The Chemistry of the Carbon-Nitrogen Double Bond," ed. by S. Patai, Interscience Publishers, New York, p. 363 (1970).
9) L. R. C. Barclay, I. T. McMaster, and J. K. Burgess, *Tetrahedron Lett.*, **1973**, 3947.
10) J. Burgers, M. A. Hoefnagel, P. E. Verkade, H. Visser, and B. M. Wepster, *Rec. Trav. Chim. Pays-Bas*, **77**, 491 (1958).
11) E. Heilbronner and H. Bock, "Das HMO-Modell und seine Anwendung; Tabellen berechneter und experimenteller Größen," Verlag Chemie, GmbH, Weinheim/Bergstr. (1970).
12) G. A. Russell, E. G. Janzen, and E. T. Strom, *J. Amer. Chem. Soc.*, **86**, 1807 (1964); G. A. Russell, E. J. Geels, F. J. Smentowski, K. -Y. Chang, J. Reynolds, and Gerd Kaupp, *ibid.*, **89**, 3821 (1967).
13) J. Geuze, C. Ruinard, J. Soeterbroek, P. E. Verkade, and B. M. Wepster, *Rec. Trav. Chim. Pays-Bas*, **77**, 491 (1958).
14) H. F. Reinhardt, *J. Org. Chem.*, **27**, 3258 (1962).
15) E. C. Ashby and R. C. Arnott, *J. Organometal. Chem.*, **14**, 1 (1968).

Phosphinidenes and Related Intermediates. IV.[1] Reactions of Phosphinothioylidenes with *cis*- and *trans*-Stilbene Oxides

Shigenobu NAKAYAMA, Masaaki YOSHIFUJI, Renji OKAZAKI, and Naoki INAMOTO
Department of Chemistry, Faculty of Science, The University of Tokyo, Hongo, Tokyo 113

(Received September 28, 1974)

Phosphinothioylidenes were generated by the reaction of phosphonothioic dichlorides with magnesium. Reactions of phosphinothioylidenes with *cis*- and *trans*-stilbene oxides gave 1,3,2-oxathiaphospholane 2-sulfide derivatives (**6**, **7**, **9**, and **11**) stereospecifically, except for the reaction of phenylphosphinothioylidene with *trans*-stilbene oxide, along with *cis*- and/or *trans*-stilbenes. The formation mechanisms, which involve phenylphosphinothioylidene coordinated by the ethereal oxygen atom, and the conformation of 1,3,2-oxathiaphospholane 2-sulfides were discussed.

There is no report on reactions of phosphinidenes, phosphinylidenes, and phosphinothioylidenes with cyclic ethers, but reaction of phenylphosphinylidene with ketene acetal[2] and reaction of phenylphosphinidene with allyl ethyl sulfide[3] have been reported. In the previous paper,[1] it has been reported that phenylphosphinothioylidene generated by the reaction of phenylphosphonothioic dichloride (**1**) with magnesium reacted with tetrahydrofuran (THF) to give 2-phenyl-1,3,2-oxathiaphosphepane 2-sulfide (**2**), but phenylphosphinylidene generated from phenylphosphonic dichloride and magnesium gave no identified product with THF.

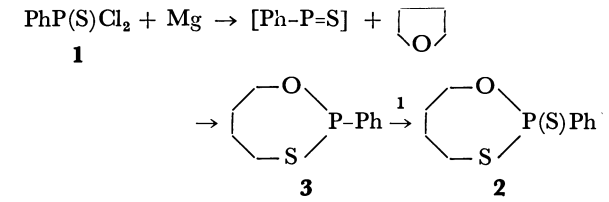

1 **3** **2**

This paper describes the reactions of phosphinothioylidenes with *cis*- and *trans*-stilbene oxides, which are more reactive than THF, to afford insertion products into the C–O bond of the epoxides and deoxygenation products of the epoxides.

Phenylphosphinothioylidene generated from **1** and magnesium reacted with *trans*-stilbene oxide to give *trans*-stilbene (**4**), benzyl phenyl ketone (**5**), 2,*trans*-4,5-triphenyl- (**6**), and 2,*cis*-4, 5-triphenyl-1,3,2-oxathiaphospholane 2-sulfides (**7**) in 65, 9, 8, and 17% yields, respectively, based on *trans*-stilbene oxide consumed. Among the isomers of **6** and **7**, 2,*c*-4, *t*-5- (**6a**), 2, *t*-4,*t*-5- (**7a**), and 2,*c*-4, *c*-5-triphenyl-1,3,2-oxathiaphospholane *r*-2-sulfides could be isolated in a pure state.

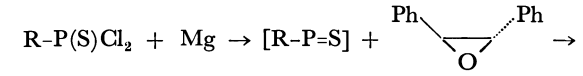

1, R=Ph
8, R=*c*-C_6H_{11}

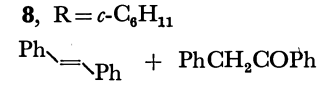

4 **5**

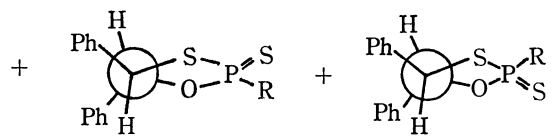

6a, R=Ph **6b**, R=Ph

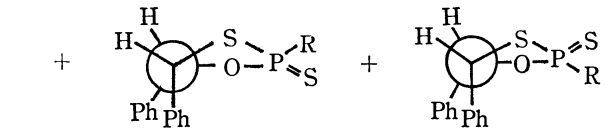

7b, R=Ph **7a**, R=Ph
9b, R=*c*-C_6H_{11} **9a**, R=*c*-C_6H_{11}

Cyclohexylphosphonothioic dichloride (**8**) reacted similarly with *trans*-stilbene oxide in the presence of magnesium to give **4**, 2-cyclohexyl-*t*-4, *t*-5-diphenyl- (**9a**), and 2-cyclohexyl-*c*-4, *c*-5-diphenyl-1,3,2-oxathiaphospholane *r*-2-sulfides (**9b**) in 34, 6, and 9% yields, respectively.

The structures of **6**, **7**, and **9** were confirmed by elemental analyses and spectral data. The assignment of *cis* or *trans* configuration between 4- and 5-phenyl groups in **6** and **7** was done by comparison of their spectral data with those of authentic samples synthesized by unequivocal routes. In the case of **9**, the assignment was done based on the similarity of the coupling constants of the methine protons to those of **7**.

A mixture of **6a** and **6b** was synthesized from *threo*-2-mercapto-1,2-diphenylethan-1-ol[4] and **1** using triethylamine as a base. Reaction of the *erythro* derivative[4] and **1** gave a mixture of **7a** and **7b** by use of pyridine as a base, but the use of triethylamine afforded only **7b**.

The assignment of *cis* or *trans* between 2- and 4-substituents in **6**, **7**, and **9** was done based on chemical shifts and coupling constants of the methine protons by use of molecular models as will be discussed later.

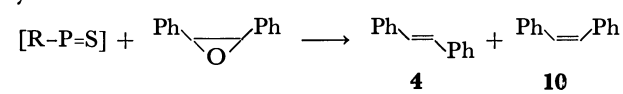

4 **10**

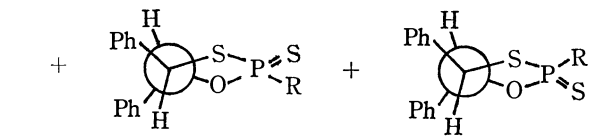

6a, R=Ph **6b**, R=Ph
11a, R=*c*-C_6H_{11} **11b**, R=*c*-C_6H_{11}

cis-Stilbene oxide reacted with **1** in the presence of magnesium to afford *trans*- (**4**), *cis*-stilbenes (**10**), and **6** in 28, 2, and 31% yields, respectively. Similarly the reaction of *cis*-stilbene oxide with **8** in the presence of magnesium gave **4**, **10**, and 2-cyclohexyl-*trans*-4,5-diphenyl-1,3,2-oxathiaphospholane 2-sulfides (**11**) in 16, 14, and 32% yields, respectively, based on *cis*-

stilbene oxide consumed. In these reactions, **7** and **9** could not be detected by NMR.

In the presence of magnesium(II) chloride, the reaction of **1** with magnesium and *trans*-stilbene oxide gave **4**, **5**, **6**, and **7** in 39, 5, 18, and 1% yields, respectively, based on *trans*-stilbene oxide consumed. The product ratio of **6** and **7** in this reaction is remarkably different from that in the absence of magnesium(II) chloride.

Reaction of *trans*-stilbene oxide with magnesium and magnesium(II) chloride gave no stilbenes but benzyl phenyl ketone (**5**) and *erythro*-2-chloro-1,2-diphenylethan-1-ol (**12**) in 53 and 43% yields, respectively, based on *trans*-stilbene oxide consumed. It is known that **5** is formed in the reaction of stilbene oxide with magnesium chloride.[5]

Reactions of phosphinylidenes with stilbene oxides gave different and complicated products, except for the formation of stilbenes. These results will be reported in near future.

Reaction Mechanism. Only the reaction of **1** with *trans*-stilbene oxide and magnesium gave **5** and a mixture of inverted and retained 1,3,2-oxathiaphospholane 2-sulfide derivatives, indicating a contribution of S_N1 pathway, but the other reactions gave only the inverted derivatives stereospecifically, suggesting the S_N2 character. Moreover, in the reaction of **1** with magnesium and *trans*-stilbene oxide, the presence of magnesium(II) chloride increased the formation of retention products (**6**) and decreased that of inversion products (**7**), supporting an increase of a contribution of S_N1 pathway by the epoxide coordinating to magnesium(II) chloride, because **6** is more thermodynamically stable than **7**.

Mechanism for the formation of **6** and **7** is considered as follows, though participation of Grignard type species, $[PhClPS]^-$ ^+MgCl, could not be ruled out completely.

The mechanism involves phenylphosphinothioylidene coordinated by the oxygen atom of *trans*-stilbene oxide (**13**) as an intermediate.

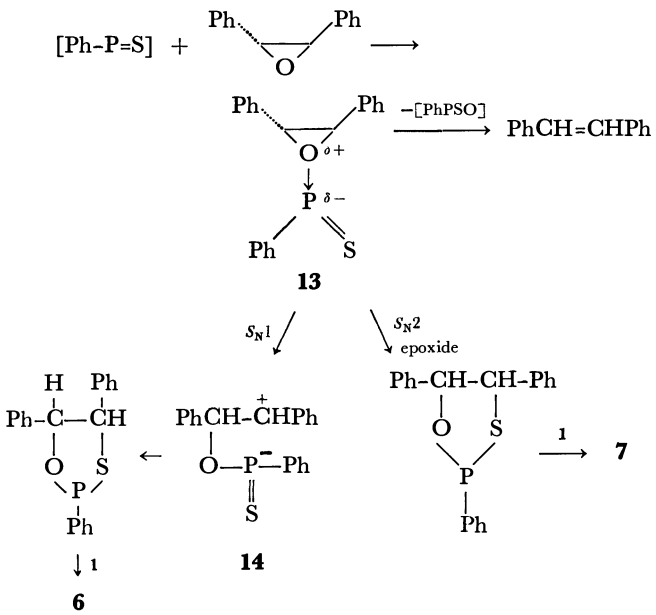

Stilbenes are considered to be produced by the decomposition of the intermediate (**13**), but isolation of the expected phosphonothioic acid was not tried.

The intermediate (**13**) attacks *trans*-stilbene oxide as sulfide anion in a S_N2 fashion or cleavages in a S_N1 manner to give **14**. Since the S_N2 attack suffers a steric hindrance by the phenyl groups in the *trans* relation and the anionic center of the zwitterion (**14**) is stabilized by the *P*-phenyl group, the S_N1 pathway becomes possible.

In the reaction with **8**, the S_N2 attack suffers a similar steric hindrance by the phenyl groups, but the cyclohexyl group does not stabilize the zwitterion analogous to **14**. Thus, the S_N1 pathway does not occur and the reaction becomes stereospecific.

In the case of *cis*-stilbene oxide, the reactions are stereospecific in the reactions with both **1** and **8**, because of almost no steric hindrance for the S_N2 attack.

The formation of **2** in the reaction of THF with phenylphosphinothioylidene[1] is explained by a similar mechanism. The following reaction has been reported to afford an analogous compound.[6]

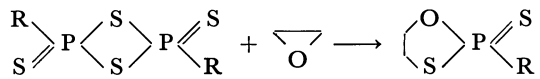

Conformation of ***6***, ***7***, ***9***, *and* ***11***. Their conformations were determined by consideration of NMR data and molecular models. The NMR data of the methine protons of **6**, **7**, **9**, and **11** are summarized in Table 1.

In the following discussion, it was assumed that protons in a 1,3-*cis* relation to a P=S group are deshielded, because protons in a 1,3-*cis* relation to a P=O group are deshielded in a five-membered ring[7] and it has been reported that P=O and P=S groups show a similar tendency in the case of six-membered rings.[8,9]

At first, the conformations of **6** and **11** are discussed.

The values of J_{HCCH}, J_{PSCH}, and J_{POCH} for all possible conformations were estimated using dihedral angles obtained from the molecular models. For J_{POCH}, a relationship proposed by Bergesen and Albriktsen[10] was used, but, for J_{PSCH}, a similar relationship was assumed considering that J_{PSCH} is usually larger than the corresponding J_{POCH}.[11]

From these considerations, the most plausible conformation is that such as (I), in which four atoms of C–S–P–O bonds form one plane. To determine the full conformation, the chemical shifts of two methine protons were taken into account.

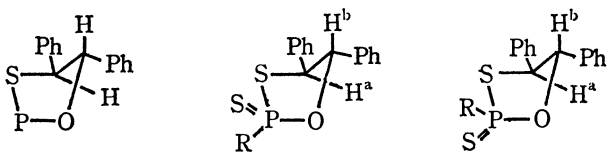

(I) (Ia) R=Ph≡**6a** (Ib) R=Ph≡**6b**
(Ia′) R=*c*-C_6H_{11}≡**11a** (Ib′) R=*c*-C_6H_{11}≡**11b**

In the case of (Ia′), H^b should be deshielded by the P=S group, whereas, in the case of (Ib′), H^a should be deshielded. Thus, the $\delta_{H^b}-\delta_{H^a}$ value in (Ia′) becomes larger than that in (Ib′). Therefore, it is

Table 1. NMR data of methine protons of **6**, **7**, **9**, and **11** (in $CDCl_3$)

		6a	6b	7a	7b	9a	9b	11a	11b
δ	SCH<	5.08	5.17	5.3	5.07	5.2	5.00	4.77	4.93
(ppm)	OCH<	5.83	5.52	6.38	5.72	6.23	5.77	5.62	5.32
J_{HCCH} (Hz)		10.6	10.6	5	5	5	5.3	10.6	10.0
J_{PSCH}		0	0	14	12	12	12	0	0
J_{POCH}		1.5	2	5	8	5	7.3	1.6	0

reasonable to consider that **11a** and **11b** have the conformations such as (Ia') and (Ib'), respectively. Since it has been known that the effects on H^a and H^b are analogous, even though an alkyl group on the phosphorus atom is substituted by a phenyl group,[7,8] it may be reasonable to consider that **6a** and **6b** have the conformations such as (Ia) and (Ib), respectively.

Next, the conformations of **7** and **9** are discussed. On the basis of a similar consideration, the partial conformation (II) is the most reasonable for these compounds.

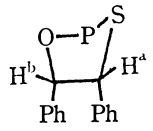

(II)

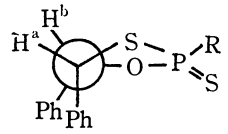

(IIa) R=Ph≡**7b** (IIb) R=Ph≡**7a**
(IIa') R=*c*-C_6H_{11}≡**9b** (IIb') R=*c*-C_6H_{11}≡**9a**

In the case of (IIa'), H^a and H^b should be shielded by the P=S group. In the case of (IIb'), H^a and H^b should be deshielded. Thus, it may be reasonable to consider that **9a** and **9b** have the full conformations such as (IIb') and (IIa'), respectively. In the cases of (IIa) and (IIb), it may be reasonable to consider that **7a** and **7b** have the full conformation such as (IIb) and (IIa), respectively.

Experimental

All melting and boiling points are uncorrected. The instruments used for spectral measurements were the same as those described in the previous paper.[1] All reactions were carried out under nitrogen.

Materials. The following compounds were prepared by the methods reported in the literature: phenylphosphonothioic (**1**)[12] (bp 134—138 °C/14 mmHg), cyclohexylphosphonothioic dichlorides (**8**)[13] (bp 96—97 °C/0.95 mmHg), *cis*-[14] (mp 37.3—37.6 °C), and *trans*-stilbene oxides[15] (mp 69.5—71 °C).

Reaction of **1** *in the Presence of* trans-*Stilbene Oxide.* *a) With Magnesium.* A solution of **1** (5.32 g, 25.2 mmol) in THF (7 ml) was added dropwise to a stirred mixture of magnesium (0.66 g, 27.5 mg-atom) and *trans*-stilbene oxide (2.47 g, 12.6 mmol) in THF (43 ml) under cooling with water occasionally, initiating by addition of a small amount of iodine. After the exothermal reaction ceased (about 1 hr), the mixture was refluxed with stirring for additional 2 hr. The solvent was removed *in vacuo*, and the residue was extracted with chloroform. The extract was washed with water, and dried with anhydrous magnesium sulfate. After evaporation, the residue was chromatographed using a silica gel dry column to give 0.45 g (2.3 mmol) of unchanged *trans*-stilbene oxide, 1.21 g (6.7 mmol) of **4**, 0.17 g (0.9 mmol) of **5**, mp 56—57 °C (from *n*-hexane) (lit,[16] 57 °C), 0.29 g (0.8 mmol) of a mixture of **6a** and **6b** (18 : 1 by NMR), and 0.62 g (1.7 mmol) of a mixture of **7a** and **7b** (1.1 : 1 by NMR). The yields of **4**, **5**, **6**, and **7** were 65, 9, 8, and 17%, respectively, based on *trans*-stilbene oxide consumed.

Recrystallization of the mixture of **6a** and **6b** from methanol gave pure **6a**, mp 112.5—113.5 °C. IR (KBr): 1107 (P-Ph) and 975 cm^{-1} (P-O-C); NMR ($CDCl_3$): δ 5.08 (d, J_{HCCH} 10.6 Hz, 1H, S-CH<), 5.83 (dd, J_{HCCH} 10.6. J_{POCH} 1.5 Hz, 1H, O-CH<), 7.0—7.4 (m, 10 H, 2Ph), 7.4—7.9 (m, 3H, $2H^m$ and H^p of P-Ph), and 7.9—8.45 (m, J_{PH^o} 16 Hz, 2H, $2H^o$ of P-Ph); Mass: *m/e* 368 (M^+).

Found: C, 65.36;, H, 4.43; S, 17.12%. Calcd for $C_{20}H_{17}OPS_2$: C, 65.20; H, 4.65; S, 17.40%.

Compound **6b** could not be isolated from the mixture in the pure state. NMR ($CDCl_3$): δ 5.17 (d, J_{HCCH} 10.6 Hz, 1H, S-CH<) and 5.52 (dd, J_{POCH} 2, J_{HCCH} 10.6 Hz, 1H, O-CH<). The signal of the three phenyl groups were not clearly distinguished from those of **6a**.

Recrystallization of the mixture of **7a** and **7b** from methanol gave pure **7a** and **7b**.

7a: mp 154—155 °C; IR (KBr): 1115 (P-Ph) and 955 cm^{-1} (P-O-C); NMR ($CDCl_3$): δ 5.3 (dd, J_{HCCH} 5, J_{PSCH} 14 Hz, 1H, S-CH<), 6.38 (t, $J_{HCCH}=J_{POCH}$ 5 Hz, 1H, O-CH<), 6.85-7.45 (m, 10 H, 2Ph), 7.45—7.8 (m, 3H, $2H^m$ and H^p of P-Ph), and 7.95—8.4(m, J_{PH^o} 16 Hz, 2H, $2H^o$ of P-Ph); Mass: *m/e* 368 (M^+).

7b: mp 129—131 °C; IR (KBr): 1102 (P-Ph) and 950 cm^{-1} (P-O-C); NMR ($CDCl_3$): δ 5.07 (dd, J_{HCCH} 5, J_{PSCH} 12 Hz, 1H, S-CH<), 5.72 (dd, J_{HCOCH} 5, J_{POCH} 8 Hz, 1H, O-CH<), 7.0—7.3 (m, 10 H, 2Ph), 7.3—7.65 (m, 3H, $2H^m$ and H^p of P-Ph), and 7.9—8.4 (m, J_{PH^o} 16 Hz, 2H, $2H^o$ of P-Ph); Mass: *m/e* 368 (M^+).

Found: C, 65.17; H, 4.66; S, 17.35%. Calcd for $C_{20}H_{17}OPS_2$: C, 65.20; H, 4.65; S, 17.40%.

b) With Magnesium-Magnesium(II) Chloride. A suspended mixture of magnesium (0.66 g, 27.5 mg-atom), magnesium-(II) chloride (2.61 g, 27.5 mmol), and *trans*-stilbene oxide (2.47 g, 12.6 mmol) in THF (45 ml) was stirred under reflux until magnesium(II) chloride had almost dissolved. At room temperature, a solution of **1** (5.30 g, 25.1 mmol) in THF (5 ml) was added drop by drop with stirring to the above mixture. A small amount of iodine was added to start the reaction. The reaction was so exothermic that the mixture was cooled with water occasionally. The reaction mixture was stirred until the exothermal reaction had ceased (about 1 hr), and then further stirred under reflux for 2 hr. After a similar work-up, the residue was chromatographed using

a silica gel dry column to give 0.17 g (0.9 mmol) of unchanged oxide, 0.82 g (4.6 mmol) of **4**, 0.11 g (0.6 mmol) of **5**, 0.76 g (2.1 mmol) of a mixture of **6a** and **6b**, and 0.04 g (0.1 mmol) of a mixture of **7a** and **7b**. They yields of **4**, **5**, **6**, and **7** were 39, 5, 18 and 1%, respectively, based on *trans*-stilbene oxide consumed.

*Reaction of **8** with Magnesium and* trans-*Stilbene Oxide.* A solution of **8** (4.34 g, 20.0 mmol) in THF (5 ml) was added drop by drop to a stirred suspension containing magnesium (0.53 g, 21.8 mg-atom), *trans*-stilbene oxide (2.00 g, 10.3 mmol), and THF (40 ml). When a small amount of iodine was added, an exothermal reaction occurred, and ended in about 1 hr. The mixture was stirred at room temperature for 14 hr. After a similar work-up, the residue was chromatographed using a silica gel dry column to give 0.63 g (3.5 mmol) of **4**, 0.23 g (0.6 mmol) of **9a**, and 0.33 g (0.9 mmol) of **9b**. The yields of **4**, **9a**, and **9b** were 34, 6, and 9%, respectively, based on *trans*-stilbene oxide used.

9a: mp 162.3—163.3 °C (from hexane); NMR ($CDCl_3$): δ 1.0—3.0 (m, 11H, *c*-C_6H_{11}), 5.2 (dd, J_{HCCH} 5, J_{PSCH} 12 Hz, 1H, S–CH〈), 6.23 (t, $J_{HCCH}=J_{POCH}$ 5 Hz, 1H, O–CH〈), and 7.08 (m, 10 H, 2Ph); Mass: *m/e* 374 (M^+).

Found: C, 64.28; H, 6.24; S, 17.13%. Calcd for $C_{20}H_{23}OPS_2$: C, 64.14; H, 6.19; S, 17.12%.

9b: mp 167—168 °C (from hexane); NMR ($CDCl_3$): δ 1.0—2.6 (m, 11H, *c*-C_6H_{11}), 5.00 (dd, J_{HCCH} 5.3, J_{PSCH} 12 Hz, 1H, S–CH〈), 5.77 (dd, J_{HCCH} 5.3, J_{POCH} 7.3 Hz, 1H, O–CH〈), and 7.12 (s, 10 H, 2Ph); Mass: *m/e* 374 (M^+).

Found: C, 64.37; H, 6.30; S, 17.04%. Calcd for $C_{20}H_{23}OPS_2$: C, 64.14; H, 6.19; S, 17.12%.

*Reaction of **1** with Magnesium and* cis-*Stilbene Oxide.* A solution of **1** (2.49 g, 11.8 mmol) in THF (5 ml) was added dropwise to a stirring mixture containing magnesium (0.30 g, 12.5 mg-atom), *cis*-stilbene oxide (1.15 g, 5.9 mmol), and THF (20 ml). To activate magnesium was added a small amount of iodine. After the exothermal reaction ceased, the mixture was further stirred under reflux for 2 hr. After a similar treatment, the residue was chromatographed using a silica gel dry column to give 0.10 g (0.5 mmol) of unchanged oxide, 0.27 g (1.5 mmol) of **4**, 0.02 g (0.1 mmol) of **10**, and 0.62 g (1.7 mmol) of a mixture of **6a** and **6b** (1.8 : 1 by NMR), but **7a** and **7b** were not detected by tlc and NMR. The yields of **4**, **10**, and **6** were 28, 2, and 31%, respectively, based on the *cis*-stilbene oxide consumed.

*Reaction of **8** with Magnesium and* cis-*Stilbene Oxide.* A solution of **8** (1.95 g, 9.0 mmol) in THF (5 ml) was added dropwise with stirring to a mixture of magnesium (0.23 g, 9.5 mg-atom) and *cis*-stilbene oxide (0.89 g, 4.5 mmol) in THF (18 ml). A small amount of iodine was added to start the reaction. After exothermal reaction ended, the mixture was refluxed for 2 hr. After a similar treatment, the residue was chromatographed using a silica gel dry column to give 0.02 g (0.1 mmol) of unchanged oxide, 0.12 g (0.7 mmol) of **4**, 0.11 g (0.6 mmol) of **10**, and 0.54 g (1.4 mmol) of a mixture of **11a** and **11b** (1.7 : 1 by NMR). However, **9a** and **9b** were not detected by NMR. The yields of **4**, **10**, and **11** were 16, 14, and 32%, respectively, based on *cis*-stilbene oxide consumed. The mixture of **11a** and **11b** could not be separated by tlc and fractional recrystallization. The following data are those of the mixture, mp 139—160 °C (from methanol or hexane); NMR ($CDCl_3$): δ 1.0—2.8 (m, *c*-C_6H_{11}), 4.77 (d, J_{HCCH} 10.6 Hz, S–CH〈 of **11a**), 4.93 (d, J_{HCCH} 10 Hz, S–CH〈 of **11b**), 5.32 (d, J_{HCCH} 10 Hz, O–CH〈 of **11b**), 5.62 (dd, J_{HCCH} 10.6, J_{POCH} 1.6 Hz, O–CH〈 of **11a**), and 7.25 (s, Ph); Mass: *m/e* 374 (M^+).

Found: C, 64.44; H, 6.21; S, 16.98%. Calcd for $C_{20}H_{23}OPS_2$: C, 64.14; H, 6.19; S, 17.12%.

*Preparation of **7a** and **7b**.* *a) Using Pyridine as Base.* A solution of *erythro*-2-mercapto-1,2-diphenylethan-1-ol[4] (0.23 g, 1 mmol) and pyridine (0.4 ml) in dry benzene (10 ml) was added with stirring to a solution of **1** (0.23 g, 1.1 mmol) in dry benzene (40 ml) over 6 hr. Stirring was continued at room temperature for 17 hr and then under reflux for 9 hr. After filtration of pyridinium chloride and similar work-up, the residue was chromatographed using a silica gel dry column to give 0.07 g (0.19 mmol, 19%) of a mixture of **7a** and **7b** (1 : 1).

b) Using Triethylamine as Base. A solution of *erythro*-diphenylethane derivative (0.42 g, 1.8 mmol) and triethylamine (1.2 ml) in dry benzene (10 ml) was added to a stirring solution of **1** (0.38 g, 1.8 mmol) in dry benzene (40 ml) over 9 hr. The mixture was further stirred at room temperature for 15 hr. Similar treatment gave 0.12 g (0.32 mmol, 18%) of **7b**, mp 129—131 °C (from methanol), but **7a** could not be detected by NMR.

*Preparation of **6a** and **6b**.* A solution of *threo*-2-mercapto-1,2-diphenylethan-1-ol[4] (0.55 g, 2.4 mmol) and triethylamine (1.6 ml) in dry benzene (10 ml) was added to a stirring solution of **1** (0.51 g, 2.4 mmol) in dry benzene (40 ml) over 8 hr, and the mixture was further stirred at room temperature for 16 hr. Similar treatment gave 0.05 g (0.15 mmol) of a mixture of **6a** and **6b**, and 0.24 g (1.0 mmol) of the starting ethane. The yield was 12% based on the diphenylethane derivative consumed.

Reaction of trans-*Stilbene Oxide with Magnesium–Magnesium(II) Chloride.* A mixture of magnesium (0.22 g, 9.3 mg-atom) and magnesium(II) chloride (0.86 g, 9.1 mmol) in THF (40 ml) was stirred under reflux for 2 hr until magnesium(II) chloride had dissolved. A few drops of carbon tetrachloride were added to activate magnesium, and the mixture was stirred under reflux. A solution of *trans*-stilbene oxide (1.57 g, 8.0 mmol) in THF (10 ml) was added dropwise to the above mixture, and the mixture was further stirred under reflux for 96 hr. Similar treatment gave 0.98 g (5.0 mmol) of unchanged oxide, 0.32 g (1.6 mmol) of **5**, 0.31 g (1.3 mmol) of *erythro*-2-chloro-1,2-diphenylethan-1-ol (**12**), mp 81—82 °C (from hexane) (lit,[17] 76—77 °C); Mass: *m/e* 196 (M^+-HCl). The yields of **5** and **12** were 53 and 43%, respectively, based on *trans*-stilbene oxide consumed.

This work was supported by a grant from the Ministry of Education.

References

1) For Part III see: S. Nakayama, M. Yoshifuji, R. Okazaki, and N. Inamoto, This Bulletin, **48**, 546 (1975).

2) J. K. Stille, J. L. Eichelberger, J. Higgins, and M. E. Freeburger, *J. Amer. Chem. Soc.*, **94**, 4761 (1972).

3) A. Ecker and U. Schmidt, *Chem. Ber.*, **106**, 1453 (1973).

4) J. M. Lalancette and A. Frêche, *Can. J. Chem.*, **49**, 4047 (1971).

5) H. O. House, *J. Amer. Chem. Soc.*, **77**, 3070 (1955).

6) G. Schrader, Ger. 1,104,520; *Chem. Abstr.*, **56**, 14328e (1962).

7) D. B. Cooper, J. M. Harrison, and T. D. Inch, *Tetrahedron Lett.*, **1974**, 2697.

8) J. P. Dutasta, A. Grand, J. B. Robert, and M. Taieb, *ibid.*, **1974**, 2659.

9) W. G. Bentrude and H. -W. Tan, *J. Amer. Chem. Soc.*, **95**, 4666 (1973).

10) K. Bergesen and P. Albriktsen, *Acta Chem. Scand.*, **25**, 2261 (1971).

11) M. Yoshifuji, *Yuki Gosei Kagaku Kyokai Shi*, **28**, 192, 201 (1971).
12) W. L. Jensen, U. S. 2,662,917 (1953); *Chem. Abstr.*, **48**, 13711h (1954).
13) M. I. Kabachnik and N. N. Godovikov, *Dokl. Akad. Nauk SSSR*, **110**, 217 (1956); *Chem. Abstr.*, **51**, 4982h (1957).
14) D. Y. Curtin and D. B. Kellom, *J. Amer. Chem. Soc.*, **75**, 6011 (1953).
15) D. J. Reif and H. O. House, "Organic Syntheses," Coll. Vol. 4, p. 860 (1963).
16) C. Graebe and H. Bungener, *Ber.*, **12**, 1079 (1879).
17) G. Berti, F. Bottari, P. L. Ferrarini, and B. Macchia, *J. Org. Chem.*, **30**, 4091 (1965).

Penetration-depth Dependence of Photochemical Conversions in the Dye-sensitized Heterogeneous Photopolymerization of Acrylamide

Toshihiro YAMASE and Tsuneo IKAWA

Research Laboratory of Resources Utilization, Tokyo Institute of Technology, Ookayama, Meguro-ku, Tokyo 152

(Received March 22, 1975)

The Amethyst violet-sensitized photolysis of *p*-tolyl *p*-anilinobenzenediazo sulfone initiated the polymerization of acrylamide in ethanol–water (9.3 : 0.7, v/v) to yield insoluble polymers. The polymer particles formed scattered the incident 546 nm light, leading to a change in the rate of photopolymerization. Using a 632.8 nm laser beam for viewing the sample at various penetration depths normal to the 546 nm light beam, a new method of determining the penetration-depth dependence of the yield of polymers was presented on the basis of the approximately linear relationship between the optical density at 632.8 nm and the polymer concentration. The method had the advantage that the progress of the photopolymerization, which takes place rapidly, can be easily followed with a high sensitivity below a 2.2% monomer conversion. From an evaluation of the magnitude of both the shadowing and forward scattering arising from the increasing number of polymer particles at various depths, it was confirmed that 546 nm light scattered by polymer particles brought about an effective photopolymerization over a wide range of the depths as a forward-scattering effect. Furthermore, the exposure to the 546 nm beam intensity range from 142 μW/cm^2 to 15.6 μW/cm^2 at sample depths up to 10 mm exhibited equal contributions of shadowing and forward scattering at the depth of $\sim$1.5 mm.

In photochemical experiments, the photoabsorbing properties of a sample vary with the irradiation time. This behavior may be due to change in the fraction of the photoexcited molecules during such photochemical reactions as the photobleaching of dye and photolysis. It is conceivable that the rate of the photochemical reaction varies as a function of the penetration depth as a result of the attenuation of the light transmitted through. In the photochemistry of solutions, most of the experimental data obtained by means of continuous irradiation have been concerned with the apparent reactions over the entire penetration depths in the sample solution, although the dependence of the rate on the incident light intensity has been measured. Unfortunately, there are very few published data on the penetration-depth dependence of photochemical reactions in samples, presumably because of the difficulty of measurements. We, therefore, undertook the evalution of the photochemical conversions at various penetration depths, using the dye-sensitized heterogeneous photopolymerization of acrylamide which was initiated by the amethyst violet (AV)-sensitized photolysis of the *p*-tolyl *p*-anilinobenzenediazo sulfone (TABS) formed by a reaction between sodium *p*-toluenesulfinate and *p*-anilinobenzendiazonium sulfate in ethanol–water (9.3 : 0.7, v/v). This report will describe the experimental techniques and presents the depth-dependence of photochemical conversions in the heterogeneous polymerization of acrylamide.

Experimental

Materials. The ethanol (Tokyo Kasei Co. GR grade) was used without further purification. The other materials, obtained from the Tokyo Kasei Co., were used after purification. The *p*-anilinobenzenediazonium sulfate was dissolved in a mixture of 100 ml of glacial acetic acid and 150 ml of acetone and reprecipitated with 250 ml of ether. This salt was dried in a vacuum desiccator with phosphorus pentoxide. The sodium *p*-toluenesulfinate and AV were purified by recrystallizations from a water–ethanol mixture. The acrylamide was purified by recrystallization from ethanol.

Sample Preparations. Sample solutions were prepared in the dark by mixing 2 ml of a 2.1×10^{-3} M *p*-anilinobenzenediazonium sulfate aqueous solution, 5 ml of a 5×10^{-2} M sodium *p*-toluenesulfinate aqueous solution, and 4 ml of a 10^{-3} M AV ethanol solution, by adding 7.1 g acrylamide to the mixture, and by, then diluting it with ethanol to a total volume of 100 ml. It was confirmed that 4×10^{-5} M TABS was formed with an equilibrium constant[1] of 5.2×10^{3} M^{-1} in the resulting solution; stock solutions during the experimental procedure showed no change in the absorbance at the absorption maxima of 450 and 546 nm for TABS and AV respectively. AV dye was found to obey Beer's law at the range of dye concentration employed ($\leq4\times10^{-5}$ M).

Methods. The absorption spectra were recorded on a Hitachi 624 spectrophotometer. Unless specified otherwise, all the results were obtained with quartz cells (10 mm internal path length) containing oxygen-free solutions obtained by the usual freeze-pump-thaw cycles. The molecular weights of the polyacrylamide obtained were measured by viscosity measurements at 29.4 °C in 1 M NaCl using the following relationship:[2] $[\eta]=3.73\times10^{-4}\times(\mathrm{Mw})^{0.66}$. The schematic diagram of the apparatus used for the depth-distribution experiments is given in Figure 1. The 546 nm and 632.8 nm

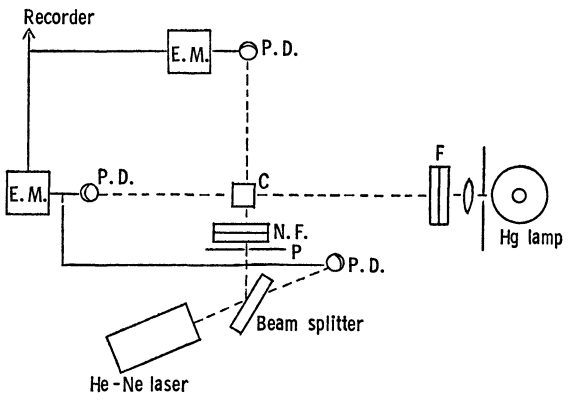

Fig. 1. Apparatus used for the depth distribution experiments.
F: 546 nm filters, N.F.: neutral density filters, P.D.: photodiode, E.M.: electrometer, C: sample cell, P: pinhole.

beam intensities were measured by means of a Coherent Radiation Laboratories Power Meter, Model 212. A 500-W super high-pressure Hg lamp was the source of the 546 nm light beam. A 2-mm aperture, a lens, and Toshiba Interference filters (KL-54+VO-52) were placed in the optical path before the cell to obtain the 546 nm light beam, which was focused at the range of the cell position with a beam diameter of 3 mm. The sample cell was positioned ~50 cm from the Hg lamp. The 632.8 nm beam from a He-Ne laser (Nippon Electric Co. GLB 2026B 1.2 mW output) was used as the analyzing light beam; its beam intensity was reduced by a beamsplitter (1 : 1), a 0.2 mm pinhole, and neutral density filters before entering the sample to prevent the photopolymerization of the sample. It was confirmed that the reduced 632.8 nm beam intensity of 0.32—0.40 μW (1.0—1.3 mW/cm²) brought about no chemical change in the sample during the experimental procedure. The intensities of the 546 and 632.8 nm light beams transmitted through the cell were monitored by means of Sharp SBC-102 photodiodes, and photocurrent signals obtained by the use of a Takeda Riken Co. electrometer TR-8651 were read out simultaneously on a Riken Denshi Co. Sp-H recorder. The calibration of the photodiode was accomplished with neutral density filters relating the electrical output of the photodiode to the fraction of light transmitted across the gap. The photocurrent output of each photodiode was directly proportional to each light-beam power. The reference beam passing through the beam splitter was converted to a signal in order to monitor the fluctuation in the beam intensity. Figure 2 shows the coordinate system for the sample. The 632.8 nm-analyzing-light beam interesects the 546 nm light beam at 90° in the sample solution. Various penetration depths up to 10 mm can be obtained by translating the sample cell in steps of 1 mm in the x direction in the stage of microscopy. When the 632.8 or 546 nm light beam is passed through the dispersion of the polymerizing medium, the beam is attenuated by diffraction, reflection, and refraction. If one polymer particle is considered, each of the three scattering mechanisms prevents the rays from maintaining their original direction. If the photodiode as a light detector is placed at a large distance from the dispersion so that it receives only parallel light, the refractive index will have little effect on the amount of light received. Thus, each photodiode was positioned ~30 cm from the sample cell. Multiple scattering occurs when light which has been scattered by one polymer particle is scattered again by another particle. This causes the photodiode to receive an excess amount of light. However, the error introduced by multiple scattering will be minimized if the photodiode has a high angular resolution and if the diameters of the light beams are small-3 mm and 0.2 mm for 546 and 632.8 nm respectively. The above possibility was confirmed by the following result: during the photopolymerization, a 632.8 nm beam detector may receive the 546 nm light scattered by the sample dispersions, too. However, the error due to the multiple scattering could be made negligible for the sample dispersions under the present experimental conditions, since no photocurrent arising from 546 nm scattered light was detected in the range of 10^{-8}—10^{-7} A corresponding to the 632.8 nm-analyzing-light-beam signal.

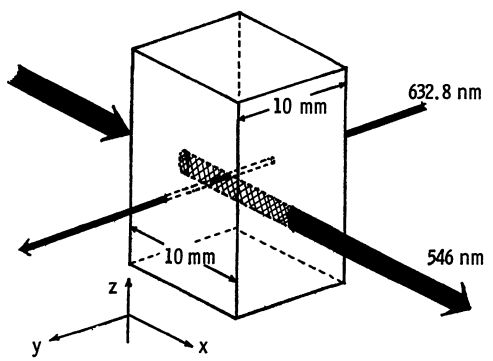

Fig. 2. Sample orientation.

Results

Fraction of 632.8 nm Laser Beam Transmission. While the deaerated sample solution was being continuously irradiated, the formation of the insoluble polyacrylamide produced a scattering of the incident light and resulted in a decrease in the fraction of the light transmitted. During the photopolymerization of acrylamide, no significant change occurred in the AV concentration. The polyacrylamide particles obtained seemed to be immovable during the irradiation (≤10 min) unless the solution was agitated. This result may be ascribed to equal specific gravities (~0.80) between the polymer particle and the solution. A long duration of the 546 nm light irradiation caused the polyacrylamide zone to bend down at the deep penetration depth in the cell. After the separation of the polymer particles produced in the 4-ml sample solution on a fine sintered glass filter, the filtrate was dumped into 200 ml of methanol, but no more polymers were precipitated as long as the monomer conversion was within 15%. This result confirmed that the amount of insoluble polymers observed in the irradiated sample cell covered sufficiently most of the polymers formed by dye sensitization, at least within a monomer conversion of 15%. The dependences of the molecular weight of the polyacrylamide on the monomer conversion and the incident 546 nm light intensity were also investigated. The experimental results are listed in Table 1. The molecular weight of 7—11 × 10^3 was slightly affected by both the monomer conversion (within 15%) and the incident 546 nm light intensity in the range from 17.5 to 350 μW/cm².

To prepare dispersions consisting of various polymer concentrations, dispersed solutions obtained by the above irradiation were diluted with ethanol. As-

Table 1. Dependences of molecular weight of polymer on monomer conversion and incident 546 nm light intensity[a)]

546 nm light intensity (μW/cm²)	Monomer conversion (%)	Molecular weight of polyer
350	14.1	7×10^3
350	11.2	9×10^3
350	6.3	$8—10\times10^3$
87.5	13.5	$7—11\times10^3$
35.0	15.4	$9—10\times10^3$
17.5	8.6	9×10^3

a) All systems contain 4×10^{-5} M AV, 4×10^{-5} M TABS, and 1 M acrylamide in ethanol-water (9.3 : 0.7, v/v).

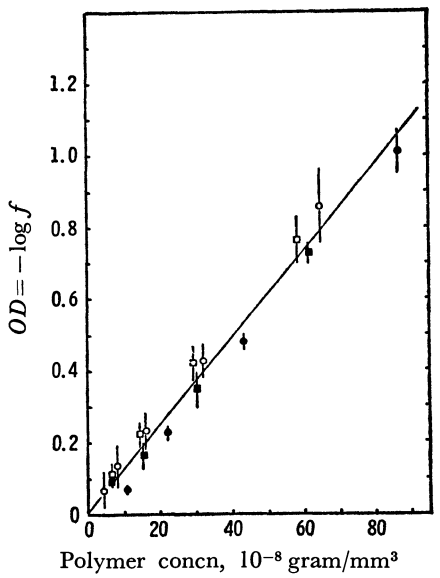

Fig. 3. Optical density ($OD=-\log f$) at 632.8 nm *vs.* concentration of polymer (10^{-8} gram/mm^3) in the dispersion obtained under various incident 546 nm light intensities. Cell thickness corresponding to the optical path length of the dispersion is 5 mm.
○: 350, ●: 87.5, □: 35.0, ■: 17.5 μW/cm^2.

suming uniform polymer concentrations in the resultant dispersions, the fraction (f) of the 632.8 nm laser beam transmitted through a dispersion (5-mm internal optical-path length) was measured. The attenuation of the incident 632.8 nm light was related to the polymer amount per unit volume of dispersion, since the AV absorption of 632.8 nm light could be neglected at low AV concentrations (below 4×10^{-5} M). The concentration of polyacrylamide, C, in 10^{-8} gram per cubic millimeter is plotted against the optical density OD ($=-\log f$) in Fig. 3. The error (vertical bars) in Fig. 3 was reflected in the fluctuation in the laser-beam intensity. An approximate linearity was shown by the curve up to $OD\approx1.1$. Above this value the experimental error was at its maximum because of the small photo-to-dark current signal ratio. The fact that the values corresponding to four different incident 546 nm light intensities seemed to lie on the same line may be explained in terms of the similar distribution of the polymer-particle size for all the dispersions, as was also suggested by the small effects of both the conversion and the incident-light intensity on the molecular weight. The slope of the rectilinear portion of the curve implied that OD was given by:

$$OD = -\log f = 2.4\times10^{-3}\,Cl = 0.17\,C'l \qquad (1)$$

where l and C' were an optical path length of the dispersion in mm and a monomer conversion in % respectively.

Recently, the light-transmission theory has been applied to non-uniform dispersions in an attempt to determine the relationship between the transmitted light and the characteristics of the dispersion. According to studies of liquid-liquid dispersions by McLaughlin and Rushton,[3] and fraction (f) of the parallel light transmitted through the liquid-liquid dispersion was independent of the drop-size distribution for all the cases studied and was expressed by the exponential relationship: $f=\exp(-al/4)$ (a is the interfacial area per unit of volume of dispersion).

It is interesting to note that Eq. (1) for our dispersions may be connected with the mathematical model simulating light transmission through liquid-liquid dispersions which was developed by McLaughlin and Rushton[3] although we have little information about the sizes and shapes of the polymer particles obtained.[4] At any rate, Eq. (1) allowed us to determine the penetration-depth dependence of the monomer conversion in the sample cell.

Photopolymerization at Various Depths. A 546 nm light beam with a diameter of 3 mm was used as an exciting light to measure monomer conversions at various penetration depths. The fraction (f) of the 632.8 nm laser beam passing through the sample at various depths normal to the 546 nm light beam was assumed to provide a one-dimensional representation of the optical-path variations in the sample as a function of x. The optical density ($=-\log f$) near the irradiated cell surface at $x\approx0.1$ mm was considered to provide the amount of the polymers obtained under a constant fraction of the incident 546 nm light beam, since there was no scattering medium in front of the cell surface during the irradiation. Figure 4 represents the variation in the optical densities at the depth of $x\approx0.1$ mm for various 546 nm light-beam intensities.

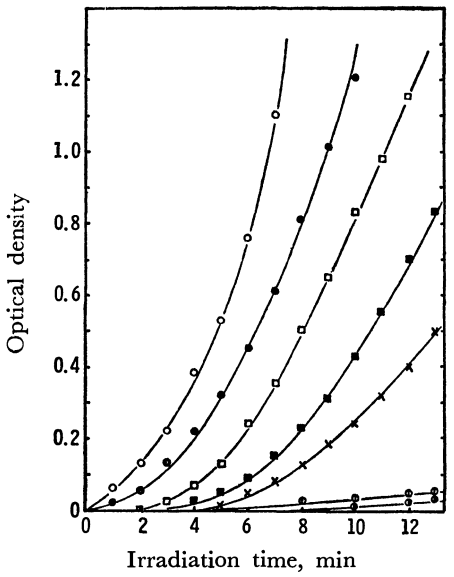

Fig. 4. Optical density at $x\approx0.1$ as a function of incident 546 nm beam intensity and irradiation time.
○: 142, ●: 99, □: 35.5, ×: 14.2, ⊕: 9.9 ◑: 7.1 μW/cm^2.

Figure 4 shows that the rate of the photopolymerization increased with the irradiation time up to the optical density of about 1.1, corresponding to a ~2.2% monomer conversion, and increased with an increase in the 546 nm-light-beam intensity. The results of the depth dependence of the optical density are shown in Fig. 5, where optical densities expressing the monomer conversions (Eq. (1)) are plotted against the irradi-

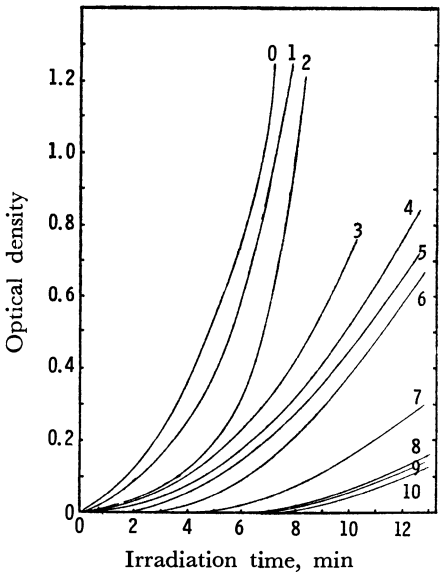

Fig. 5. Optical density as a function of irradiation time and the depth.
Numbers indicate the depth, x in mm. 546 nm light beam intensity incident on the sample is 142 μW/cm².

ation time or the corresponding values of the depth parameters. The plots show that the rate of photopolymerization decreases with an increase in the depth, x. The acceleration of the polymerization rate with the irradiation time at each depth may result from the accumulation of solid polyacrylamide in the system, as was discussed in connection with the heterogeneous thermal polymerization of acrylonitrile and vinyl chloride by Bamford and Jenkins[5] and Bengough and Norrish[6] respectively. When the exciting 546 nm light beam was turned on and off, the optical density at each depth showed a tendency to increase in the dark, but this dark reaction due to an after-effect was sluggish in comparison with the previous photo-reaction rate. The after-effect may be explained in terms of the occluded radicals observed in polyacrylamide particles, which induce continued polymerization and an increase in the optical density. The increase in the optical density during a period ($\leq$10 min) measured from the end of the 546 nm-light irradiation excluded the possibility of the significance of the diffusion of polymer particles to the outside of the 546 nm-light-beam path, since the optical density should decrease with an increase in the standing time after irradiation if the above possibility is operative. Therefore, most of the polyacrylamide particles may be considered to remain within the pathway of the exciting 546 nm light, at least during the irradiation time ($\leq$10 min). This implies that the dispersion length for the 632.8 nm laser beam is kept constant during the irradiation and that it is equal to a 546 nm-light-beam diameter of 3 mm.

Discussion

During the photopolymerization of acrylamide, the formation of insoluble polymers produced a scattering of the incident light, leading to a change in the rate of photopolymerization. The rate of the photopolymerization obviously increases when light which has been scattered by praticles induces the polymerization again ("scattering effect"). However, scattering by particles prevents a part of the exciting beam from maintaining its original direction, resulting in a less effective photopolymerization in the background ("shadowing effect"). To evaluate the magnitude of these effects of scattering and shadowing from the increasing number of polymer particles at various penetration depths, we first undertook an evaluation of the optical densities derived on the basis of the assumption that neither scattering nor shadowing occurred during the photopolymerization. This optical density will be represented by $d_1(x, t)$ as a function of the penetration depth (x) and the irradiation time (t); the optical densities without subscripts $d(x, t)$ represent the experimental values, as is shown in Fig. 5. We observed no significant permanent AV bleaching during the photopolymerization. Therefore, the 546 nm light intensity absorbed was assumed to be independent of t. Thus, the local 546 nm-light-beam intensity could be calculated, based on Beer's law, as a function of the x into the sample. When an aerobic sample solution[7] was exposed to the 546 nm light beam with its diameter of 3 mm, which would establish a beam-intensity range from 142 to 15.6 μW/cm² at sample depths up to 10 mm, the local 546 nm-light-beam intensity was given by Eq. (2):

$$\log I(x) = 2.152 - 0.096\,x \qquad (2)$$

where $I(x)$ was the beam power in μW/cm² at a certain depth, x mm.

By reference to the experimental conditions for the data acquisition of Fig. 4, the optical density in Fig. 4, $d(x\approx0.1, t)$ was assumed to represent $d_1(x\approx 0.1, t)$. When the 546 nm light-beam intensity incident on the sample was 142 μW/cm², the $d_1(x, t)$ estimation was made by calculating $I(x)$ for each depth, x, by Eq. (2) and by using the optical density-beam intensity curves obtained by replotting the optical densities in Fig. 4 against the incident-beam intensities for different times. A typical set of $d_1(x, t)$

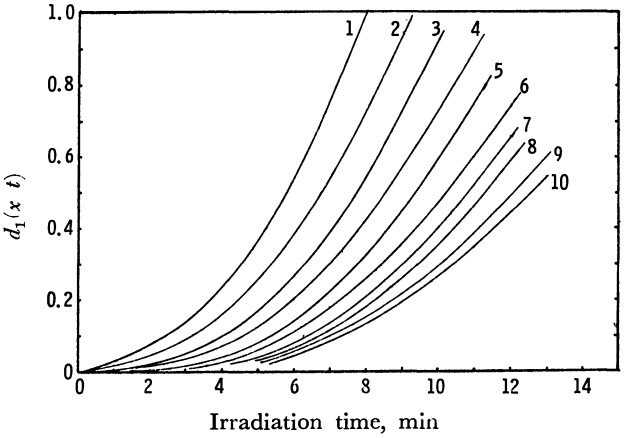

Fig. 6. $d_1(x, t)$ estimated as a function of irradiation time and depth.
Numbers indicate the depth, x in mm.

curves is shown in Fig. 6. It should be noted that the estimated set, $d_1(x, t)$, includes the contribution of the photopolymerization induced by the backscattered light from the dispersion layer with a thickness of 9.8 mm (=10−0.2), as represented by the experimental conditions in Fig. 4; therefore, the estimated set, $d_1(x, t)$, in Fig. 6 denotes the optical density derived on the basis of the assumption that neither forward scattering nor shadowing occurred. Actually, the thickness $(10-x)$ of the dispersion layer which induces a backscattering effect decreases with an increase in x. This may imply that the $d_1(x, t)$ estimated in Fig. 6 includes an excess contribution of backscattering as the x increases. However, the error introduced by this excess of backscattering becomes negligible if the backscattering effect is considered to decrease with an increase in x, since $d_1(x, t)$ decreases with an increase in x. The $d_1(x, t)$ data obtained provided the information necessary to determine the $d_{sh}(x, t)$, denoting the optical density which would be derived using the assumption that backscattering and shadowing, but not forward scattering, occurred during the photopolymerization. $d_{sh}(x, t)$ was given by Eq. (3) on the basis of the assumption of equal 546 nm light-energy densities at x:

$$d_{sh}(x, t) = -\int_0^t d_1(x, t')\frac{\partial F_1(x, t')}{\partial t'}dt' + d_1(x, t)F_1(x, t) \tag{3}$$

with $$F_1(x, 0) = 1 \tag{4}$$

where $F_1(x,t)$ was the fraction of the 546 nm light beam entering x. It should be noted that, in the estimation of $d_{sh}(x,t)$, forward scattering by polymer particles was left out of consideration. For the purpose of the approximate calculations of $d_{sh}(x,t)$, it was assumed that $dt \approx 1$(min), so Eq. (3) became:

$$\begin{aligned} d_{sh}(x, t) \approx\ & d_1(x, 0)\{F_1(x, 0) - F_1(x, 1)\} \\ & + d_1(x, 1)\{F_1(x, 1) - F_1(x, 2)\} \\ & + d_1(x, t-1)\{F_1(x, t-1) - F_1(x, t)\} \\ & \cdots\cdots\cdots\cdots \\ & \cdots\cdots\cdots\cdots \\ & + d_1(x, t)F_1(x, t) \end{aligned} \tag{5}$$

Assuming equal optical densities at the depth range from $x-0.5$ to $x+0.5$ mm (x=*integral*), $F_1(x,t)$ was given by:

$$F_1(x, t) = f_1(0, t)^{1/2l} \cdot f_1(1, t)^{1/l} \cdot f_1(2, t)^{1/l} \cdots\cdots f_1(x-1, t)^{1/l} \quad (l=3 \text{ and } x=0, 1, \cdots\cdots, 10) \tag{6}$$

with: $$F_1(0, t) = 1 \tag{7}$$

$$f_1(x, 0) = 1 \tag{8}$$

and:

$$d_1(x, t) = -\log f_1(x, t) = 2.4 \times 10^{-3} Cl = 0.17\, C'l \tag{9}$$

where $F_1(x,t)$ denoted the fraction of the 546 nm light beam entering the sample layer from $x-0.5$ to $x+0.5$ (x=*integral*) with a thickness of 1 mm (for x=0 and 10, entering the sample layer with a thickness of 0.5 mm), $f_1(x,t)$ was the fraction of the 632.8 nm laser beam transmitted through the dispersion of

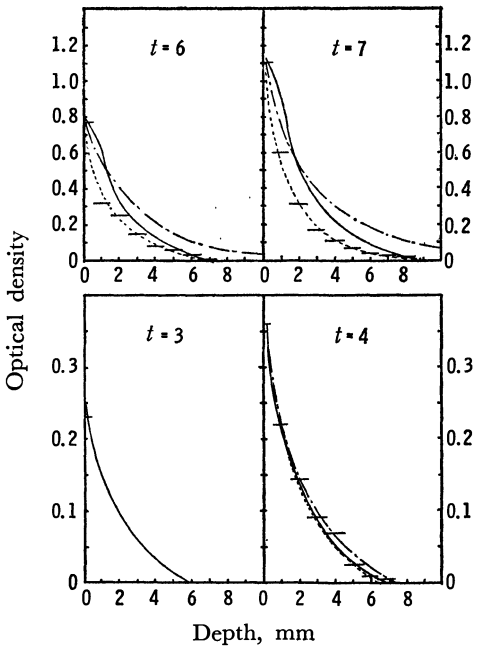

Fig. 7. Depth distribution of optical density for each of irradiation time t, in min.
—— $d(x, t)$, ——— $d_1(x, t)$, ---- $d_{sh}(x, t)$
For $t \leq 3$ three curves were identical.

$d_1(x,t)$ at x, and l was the dispersion length in the y direction and was assumed to be independent of x and t. From this assumption l should be equal to the 546 nm light-beam diameter of 3 mm. We computed $d_{sh}(x,t)$ using Eqs. (5)—(9). The results of these calculations for $d_{sh}(x,3)$, $d_{sh}(x,4)$, $d_{sh}(x,6)$ and $d_{sh}(x,7)$ are shown in Fig. 7, along with $d_1(x,t)$ and $d(x,t)$ for each t value. The horizontal hash marks for $d_{sh}(x,t)$ represent the equal values of this quantity, arising from the approximate calculation of $F_1(x,t)$ by means of Eq. (6). Figure 7 represents both the shadowing and forward-scattering effects on the photopolymerization as a function of x for each t value. The decrease in the optical density arising from the shadowing effect was represented by $d_1(x,t) - d_{sh}(x,t)$, while the increase in the optical density by the forward scattering was given by $d(x,t) - d_{sh}(x,t)$. For $t \leq 3$, neither significant shadowing nor forward scattering was apparently observed, as was represented by $d(x,t) \approx d_{sh}(x,t) \approx d_1(x,t)$, while for $t \geq 4$ both shadowing and forward-scattering effects on the photopolymerization were observed at various depths where the photopolymerization occurred and their magnitudes at each of the depth increased with an increase in t. Some values of the optical densities for $t \leq 3$ were larger than that for $t \geq 4$, as represented by $d(x \leq 1,3) \geq d(x \geq 4,6)$ or $d(x \geq 5,7)$. If the forward-scattering effect at each value of $x \geq 4$ for t=6 arose from polymer particles produced at the neighboring depth, the observation of the forward-scattering effect should be expected also at $x \leq 1$ for t=3, because of $d(x \leq 1,3) \geq d(x \geq 4,6)$. The observation of small effects of shadowing and forward scattering for $t \leq 3$ led us to the conclusion that the 546 nm scattered light due to the increasing number of polymer particles in the foregrounds brought about the forward-scattering effect

at deep penetrations. When the monomer conversion at $x\approx0$ became higher than 0.8% corresponding to $d(0,4)=0.4$, both shadowing and forward-scattering effects were apparently observed and increased with an increase in the monomer conversion, at least up to 2.2% corresponding to $d(0,7)=1.1$. $d(x,t)\approx d_1(x,t)$ at $x\approx1.5$ for $t=6$ or 7 could be explained by equal contributions of the shadowing and forward-scattering effects.

The observation of photopolymerization by the scattered light caused us to question whether the length of the dispersions in the y direction was unchanged during the irradiation, since the polymer particles in the 546 nm-light-beam path radiated 546 nm light in the form of scattered radiation to all directions, with angular distributions of its intensity, so that polymer particles might be formed also outside the original pathway of the transmitted light beam. To see if the assumption of an unchangeable length (l) of the dispersion in the y direction was realistic during the photopolymerization, the values of l were estimated for each t value. Assuming that the optical density was nearly uniform in the range from $x-0.5$ to $x+0.5$ ($x=integral$) in the x direction, the fraction of 546 nm light transmitted through the dispersion up to 10 mm in the x direction, $F(t)$, was given by Eq. (10):

$$F(t) \approx f(0,t)^{1/2l}\cdot f(10,t)^{1/2l}\cdot f(1,t)^{1/l}\cdots\cdots f(9,t)^{1/l} \quad (10)$$

with

$$d(x,t) = -\log f(x,t) \quad (11)$$

where $f(x,t)$ represented the measured fraction of the 632.8 nm laser beam transmitted through the dispersion, with a length of l mm in the y direction. It must be noted that the estimation of $F(t)$ in Eq. (10) is based on the assumption that equal dispersion densities exist at the position of the dispersion in the y direction. For data analysis, Eq. (10) was written in optical density forms:

$$\begin{aligned}-\log F(t) = D(t) &= \{d(0,t)/2 + d(10,t)/2 + d(1,t) \\ &\quad + \cdots\cdots + d(9,t)\}/l \\ &= d(t)/l \end{aligned} \quad (12)$$

with

$$d(t) = d(0,t)/2 + d(10,t)/2 + d(1,t) + \cdots\cdots d(9,t) \quad (13)$$

Eq. (12) predicted that a plot of $D(t)$ *vs.* $d(t)$ should be a straight line whose slope is related to $1/l$. Figure 8 is a plot of the experimental data of $D(t)$ and $d(t)$ for each t value. This figure shows that an approximate linear relation ($l=3$) was obtained up to $t\leq3$. Furthermore, it was pointed that, for $t\geq4$, l increased with an increase in t (for example, $l=6$ for $t=7$). The linear relationship up to $t\leq3$ seemed to be ascribable to no significant observation of the effects of shadowing and forward scattering, as is shown in Fig. 7. The

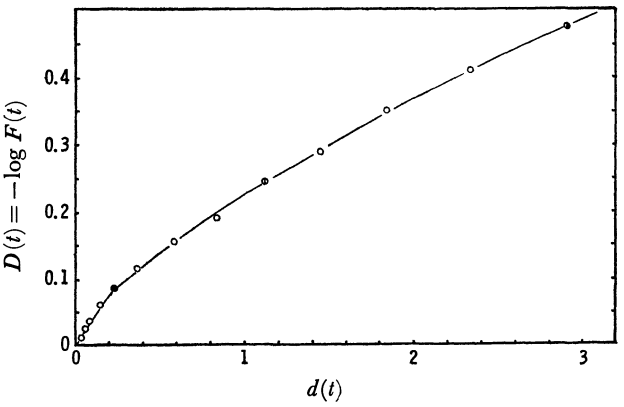

Fig. 8. $D(t)$ *vs.* $d(t)$ for each irradiation time (Ex. ● 3, ⓘ 5, ◑ 7 min).

observation of $d(x\leq1.5,\ t\geq6)>d_1(x\leq1.5,\ t\geq6)$ (Fig. 7) seemed to be evidence for the enlargement of l due to the forward-scattering effect from the increasing number of polymer particles at $x\approx0$, although the assumption that l was independent of x during the photopolymerization was not realistic. It is clear that the scattered light from the polymer particles which were positioned within the pathway of the 546 nm light beam (with a diameter of 3 mm) propagating in the x direction through the dispersion induced the polymer formation outside the original pathway of the 546 nm light beam transmitted. Therefore, it does not matter if the measured optical density $d(x,t)$ is regarded as an amount corresponding to the dispersion of $l=3$, no matter how the dispersion lengthened in the y direction during the photopolymerization.

References

1) T. Yamase, H. Hisada, S. Suzuki, and T. Ikawa, This Bulletin, to be submitted.

2) J. D. Margerum, A. M. Lackner, M. J. Little, and C. T. Petrusis, *J. Phys. Chem.*, **75**, 3066 (1971).

3) C. M. McLaughlin and J. H. Rushton, *AIChE J.*, **19**, 317 (1973).

4) The microscopic examination showed that our dispersions consisted of particles of various sizes smaller than 0.1 mm in diameter. According to studies of the heterogeneous polymerization by Bamford and Jenkins[5] a growing polymer radical becomes insoluble at a relatively low degree of polymerization, and the aggregation of polymer molecules by coiling leads to the formation of polymer particles.

5) C. H. Bamford and A. D. Jenkins, *Proc. Roy. Soc., Ser. A*, **216**, 515 (1953).

6) W. I. Bengough and R. G. W. Norrish, *ibid.*, **200**, 301 (1950).

7) The exposure of the aerobic sample to 546 nm light induced no observable polymerization of acrylamide, although the sensitized photolysis of TABS was observed without any of the permanent bleaching of AV previously reported[1].

NOTES

BULLETIN OF THE CHEMICAL SOCIETY OF JAPAN, VOL. 48(12), 3744 (1975)

Absolute Configuration of 3-Amino-1-phenylbutane

Yukio YAMAMOTO, Jun'ichi ODA, and Yuzo INOUYE
Institute for Chemical Research, Kyoto University, Uji, Kyoto 611

(Received July 26, 1975)

Synopsis. The absolute configuration of (−)-3-amino-1-phenylbutane was established by the correlation to (*R*)-(−)-*N*-benzoylalanine methylester *via* (+)-*trans*-3-amino-1-phenylbut-1-ene.

As regards the chirality of 3-amino-1-phenylbutane (**1**), two conflicting assignments have been made. Červinka[1] inferred the *R*-configuration to (+)-**1** by converting it into (+)-γ-*N*-benzoylaminovaleric acid whose configurational correlation had been achieved by the homologation of (*R*)-(−)-alanine.[2] In contrast, the opposite *S*-configuration was claimed for the same enantiomer (+)-(**1**) by Terent'ev based on chiroptical data.[3]

We were therefore inextricably confused by this situation and did not know which of these assignments should be relied upon as the correct one. Since the binary nature of chirality dictates *a priori* a 50 : 50 chance of predicting the correct configuration to a given chiral compound no matter what means one may employ, great caution must be exercised in drawing any conclusion on chirality. This is even more true because the deduced configuration may possibly divert one to an erroneous stereochemistry of asymmetric synthesis.[4]

In connection with the studies on self-immolative asymmetric synthesis, we established the absolute configuration of (+)-*trans*-3-amino-1-phenylbut-1-ene (+)-(**2**) by means of the independent chemical transformations[5] and, by virtue of this assignment, settled the disputed problem of the chirality of 3-amino-1-phenylbutane. (+)-3-Amino-1-phenylbut-1-ene (+)-(**2**) was converted to the *N*-benzoyl derivative and then was oxidized by the use of barium permanganate eventually to give (−)-*N*-benzoylalanine methylester (−)-(**3**). Since the *R*-configuration of the latter has been unequivocally established,[6] the parent amine (+)-(**2**) can be assigned the same configuration in view of the present conversion process, which does not jeopardize the chiral center.

Since the unsaturated amine (−)-(**2**) afforded the corresponding saturated amine with dextrorotation (+)-(**1**) on catalytic hydrogenation over palladium carbon[4], which is generally accepted to proceed without disturbing the chiral center, (−)-3-amino-1-phenylbutane (−)-(**1**) should be allotted the *R*-configuration in support of Terent'ev.[3]

The present transformations, when linked to those by Červinka,[1] Fischer,[7] and Balenović,[2] constitute a triligostatic stereochemical cycle[8] which involves (−)-*N*-benzoylalanine as one of the chiromers. The ligand metathesis is *a priori* ruled out for a triligostatic cycle and all the unit reactions involved in the cycle are of such a nature that no inversion of configuration occurs, so that this cycle is podal. In consequence, the disagreement between Červinka's configurational assignment and ours to **1** suggests a probable experimental fault committed in either the Červinka, Fischer, or Balenović process, inasmuch as the present chemical transformations are convincingly faultless.

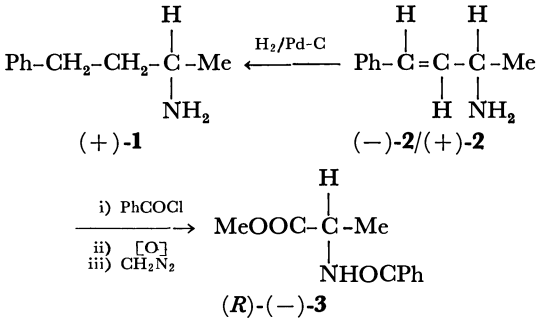

Experimental

(+)-3-Amino-1-phenylbutane (+)-(**1**). (*S*)-(−)-*trans*-3-Amino-1-phenylbut-1-ene[5] (−)-(**2**) (5.0 g, $[\alpha]_D^{25}$ −8.9° (*c*, 10.0, benzene) was hydrogenated over palladium carbon in ethanol and an equivalent amount of hydrogen (830 ml at 25 °C) was absorbed. The resulted amine (**1**) distilled at 108—109 °C/18 Torr.; n_D^{27} 1.5081, $[\alpha]_D^{27}$ 10.1° (neat), (lit,[1] bp 110—115 °C/14 Torr., (lit,[9] bp 101—102 °C/14 Torr., n_D^{20} 1.5152 for the racemate). The acetylation of (+)-**1** (4.6 g) with acetic anhydride in pyridine afforded (−)-3-acetamido-1-phenylbutane (5.6 g, 95%); bp 149 °C/2 Torr., mp 68—69 °C, $[\alpha]_D^{26}$ −35.2° (*c*, 0.7, ethanol), (lit,[1] bp 142—150 °C/3 Torr., mp 55 °C). Found: C, 75.33; H, 9.11; N, 7.38%. Calcd for $C_{12}H_{17}NO$: C, 75.35; H, 8.96; N, 7.32%.

References

1) O. Červinka, E. Kroupová, and O. Bělovský, *Coll. Czech. Chem. Commun.*, **33**, 3551 (1968).
2) K. Balenović and D. Cerar, *J. Chem. Soc.*, **1955**, 1631.
3) A. P. Terent'ev, *Zh, Obshch. Khim.*, **35**, 1538 (1965); *Chem. Abstr.*, **63**, 17854 h (1965).
4) Y. Yamamoto, J. Oda, and Y. Inouye, *Chem. Commun.*, **1973**, 848.
5) Y. Yamamoto, J. Oda, and Y. Inouye, *J. Org. Chem.*, in press.
6) K. Freudenberg and F. Rhino, *Ber.*, **57**, 1547 (1924).
7) E. Fischer and R. Groh, *Liebigs Ann.*, **383**, 363 (1911).
8) D. C. Garwood and D. J. Cram, *J. Amer. Chem. Soc.*, **92**, 4575 (1970).
9) C. Harries and A. S. de Osa, *Ber.*, **36**, 2997 (1903).

BULLETIN OF THE CHEMICAL SOCIETY OF JAPAN, VOL. 48(12), 3745—3746 (1975)

Hyperconjugative Deuterium Isotope Effects on the Redox Decomposition of Hydroxymercurated 2-Butenes in an Aqueous Solution

Miharu KOSAKI, Sumio SHINODA, and Yasukazu SAITO

Dapertment of Synthetic Chemistry, Faculty of Engineering, University of Tokyo, Hongo, Bunkyo-ku, Tokyo 113

(Received March 14, 1975)

Synopsis. The relative magnitude of the isotope effects of the deuterium atoms at the positions hyperconjugative to α- and β-carbons has been determined for the title reaction by monitoring the reaction of 2-butene-1,1,1,3-d_4 by PMR. On the basis of our results, the cation character in the transition state is concluded for both of the carbons, in support of the structure proposed previously.

The oxidation of olefins by aqueous mercuric salts is known to produce unsaturated aldehydes, saturated aldehydes, or allylic alcohols.[1] It has been found, however, that, under certain reaction conditions, saturated ketones are formed exclusively[2] by the redox decomposition of intermediate hydroxymercurated-olefins, which involves both an intramolecular hydrogen shift[3] and a two-electron transfer.[4] Recently an investigation from the viewpoint of kinetic deuterium isotope effects[5] was performed in order to elucidate the transition-state structure; the cation character was suggested on the basis of the secondary deuterium isotope effect for α-carbon, $CH_3CHOHCH-CH_3Hg^+$, which receives the migrating hydrogen and repels the reduced mercury during the reaction.[6]

With regard to β-carbon, $CH_3CHOHCHCH_3Hg^+$, however, it has no hydrogen other than the migrating one. In order to obtain complementary information about this carbon, 2-butene-1,1,1,3-d_4 is used in the present study, since the hyperconjugative isotope effects also reflect the cation character of the carbon at the reaction center.

Results and Discussion

Since the oxymercuration reaction of 2-butenes proceeds stereospecifically,[7] *cis*- and *trans*-2-butenes are hydroxymercurated into *threo*- and *erythro*-oxymercurials respectively. When unsymmetrically deuterated 2-butenes are used, two regio isomers are formed with respect to the position of the deuterium substituents.

The process of the formation of 2-butanone-d_4 from a mixture of the hydroxymercurated 2-butene-d_4's was followed by PMR *in situ*:

$$CH_3CDOHCHCD_3Hg^+ \longrightarrow CH_3COCHDCD_3 + Hg(0) + H^+ \quad (1)$$

$$CD_3CHOHCDCH_3Hg^+ \longrightarrow CD_3COCHDCH_3 + Hg(0) + H^+ \quad (2)$$

Some representative spectra taken in a time sequence are shown in Fig. 1. The methyl protons of *threo*- and *erythro*-$CD_3CHOHCDCH_3Hg^+$ were observed at δ 1.38 and δ 1.30 respectively, whereas those of *threo*- and *erythro*-$CH_3CDOHCHCD_3Hg^+$ coincidentally both appeared at δ 1.19. The singlet peak observed at δ 2.13 was assigned to the methyl protons of 2-butanone-3,4,4,4-d_4.[2]

Peak-area analyses were made for the mixture of the reactants in a manner reported previously.[6] By comparing each spectrum with preceeding ones, it was ascertained that the peak decrease at δ 1.19 was equal to the peak increase at δ 2.13; this feature can be expected from the stoichiometry of Reaction (1). From the semi-logarithmic time dependence of the peak-height at δ 1.19, the first-order[4] rate constant was obtained as $(6.23\pm0.21)\times10^{-5}$ s^{-1} for Reaction (1). By using the sum of the peaks at δ 1.38 and δ 1.30, the first-order rate constant was obtained as $(6.14\pm0.24)\times10^{-5}$ s^{-1} for Reaction (2). Since all the reactants were present in the same solution, these rate constants could be obtained under completely identical reaction conditions. Therefore, it was confirmed that the relative magnitudes of isotope effects had been determined accurately.[6]

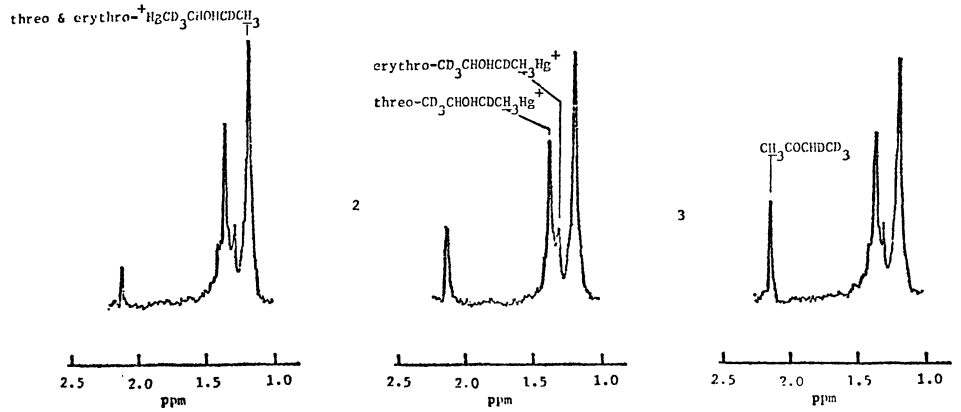

Fig. 1. The time sequential PMR spectra obtained *in situ* for the redox decomposition of the mixture of *threo*- and *erythro*-$CH_3CDOHCHCD_3Hg^+$ and -$CD_3CHOHCDCH_3Hg^+$ at 3.0 °C in an aqueous solution. These spectra were recorded after (1) 0.0 min, (2) 30.9 min and (3) 49.3 min.

Kinetic deuterium isotope effects have been considered to be almost precisely multiplicative. The mechanisms of the retro-Diels-Alder reaction of 9,10-dihydro-9,10-ethanoanthracene[8] and the base-induced dehydrotosylation and dehydrobromination of cyclohexyl derivatives[9] were discussed accordingly. With respect to the present reaction, the rate constant of Reaction (1) should be affected cumulatively by both migrating deuterium and the methyl deuterium of CD_3CHg; their effects are expressed in terms of the primary deuterium isotope effect, $(k_H/k_D)^{prim}$, and the hyperconjugative deuterium isotope effect, $(k_H/k_D)^{hyp(Hg)}$, respectively. As for Reaction (2), the effects of both α-deuterium (CDHg) and the other methyl deuterium (CD_3COH) should also be imposed on the rate cumulatively; the rate is affected by both the α-secondary deuterium isotope effect, $(k_H/k_D)^{\alpha}$, and the hyperconjugative deuterium isotope effect, $(k_H/k_D)^{hyp(OH)}$.

The ratio of the rate constants for Reactions (1) and (2) is, therefore, given as follows:

$$\frac{k(1)}{k(2)} = \frac{k_H/k(2)}{k_H/k(1)} = \frac{(k_H/k_D)^{\alpha}}{(k_H/k_D)^{prim}} \times \frac{(k_H/k_D)^{hyp(OH)}}{(k_H/k_D)^{hyp(Hg)}} \quad (3)$$

where k_H is the rate constant of $CH_3CHOHCHCH_3Hg^+$.

As far as the value of $(k_H/k_D)^{prim}/(k_H/k_D)^{\alpha}$ is concerned, the value of 1.15 was previously obtained for *cis*- and *trans*-2-butene.[6] By substituting the observed value of both $k(1)/k(2)$ and $(k_H/k_D)^{prim}/(k_H/k_D)^{\alpha}$ into Eq. (3), the ratio of the hyperconjugative isotope effects concerning the α- and β-carbons, $(k_H/k_D)^{hyp(OH)}/(k_H/k_D)^{hyp(Hg)}$, was calculated to be 1.17 ± 0.10, where the error limit was determined in view of those for both the rate constants and the isotope effects.

As is well known, the magnitude of the hyperconjugative deuterium isotope effect increases proportionally to the extent of the positive charge on the reacting carbon in the transition state.[10] With regard to the S_N1 solvolysis reactions, such magnitudes have been reported as 1.33[11], 1.34[12], and 1.40[12] per CD_3 at 25 °C. In contrast, values as small as 1.05 per CD_3 were found at 60.56 °C[13], 73.88 °C[13], and 105.02 °C[14] for the radical decomposition reactions.

Taking into account the considerable cation character of the α-carbon ($CH_3CHOHCHCH_3Hg^+$) in the present reaction,[6] it is now possible to estimate the extent of the β-carbon ($CH_3CHOHCHCH_3Hg^+$) by using the ratio of the hyperconjugative isotope effects, since it represents the relative extent of the cation character of these carbons. If the β-carbon had no cation character at all in the transition state, the ratio would be less than unity (*e.g.*, 1/1.3). The observed ratio of 1.17 ± 0.10, therefore, strongly suggests that the cation character of the β-carbon (COH) is almost comparable to, or rather larger than, that of the α-carbon (CHg).

The transition-state structure for the redox decomposition reaction of hydroxymercurated 2-butene proposed previously[6] is thus supported from the point of view of the hyperconjugative deuterium isotope effects.

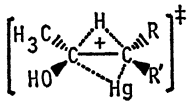

(R, R′=H, CH_3)

Experimental

All the reagents and solvents were of a G. R. grade. The diglyme was dried by refluxing it with lithium aluminum hydride before use. The alumina catalyst (spherical, 1/8 mesh) was supplied by ALCOA (F-110). The BET surface area (N_2 adsorption) was 190 m^2/g. The catalyst (20.0 g) was loaded in a flow reactor, evacuated at 350 °C for 2 hr, and then exposed to the vapor of deuterium oxide (Merck, 99.75 atom % deuterated) at 200 °C.

Preparation of 2-Butene-1,1,1,3-d_4. 2-Butanone-1,1,1,-3,3-d_5 was obtained by the hydrogen-deuterium exchange of 2-butanone by a keto-enol equilibrium in a deuterium-oxide solution of potassium carbonate at 80 °C. Isotopic purities of 98% were ascertained by PMR analysis for both methyl and methylene groups. The hydrogenation of 2-butanone-1,1,1,3,3-d_5 by lithium aluminum hydride was effected in diglyme at 50 °C to obtain 2-butanol-1,1,1,3,3-d_5, which was then dehydrated into deuterated *n*-butenes catalytically at 170 °C by the use of the flow reactor, with a nitrogen-gas carrier. The analysis of the product by glpc (20% dimethylsulfolane on Celite) confirmed the composition of *cis*-2-butene (54.1%), *trans*-2-butene (14.6%) and 1-butene (31.3%).

Kinetic Studies of the Redox Decomposition. The gaseous olefin was introduced *via* a vacumm line into an aqueous solution consisting of 3.00 M of mercuric perchlorate at 0 °C until all the mercuric ions had been consumed by hydroxymercuration. The solution of hydroxymercurated *n*-butenes was diluted with identical amounts of a 3.00 M aqueous mercuric perchlorate solution. A part of the solution was transferred into a PMR sample tube and kept in a Dry Ice–ethanol trap. The reaction was started by inserting the tube into the probe of the PMR spectrometer. By this means the solution temperature was raised up to the probe temperature (3.0 °C; calibrated by the relative shifts of ethylene glycol); the reaction was then pursued for 60 min, with fifteen spectrum charts taken in sequence. During the reaction, no evolution of gas due to olefin formation by deoxymercuration was observed.

The authors wish to express their gratitude to Professor Yukio Yoneda for his helpful discussion and encouragement. This work was supported by a Grant-in-aid for Scientific Research from the Ministry of Education, Japan (No. 011013).

References

1) H. Arzoumanian and J. Metzger, *Synthesis*, **1971**, 527.
2) Y. Saito and M. Matsuo, *J. Organometal. Chem.*, **10**, 524 (1967).
3) M. Matsuo and Y. Saito, *J. Org. Chem.*, **37**, 3350 (1972).
4) M. Matsuo and Y. Saito, This Bulletin, **44**, 2889 (1971).
5) S. E. Schepple, *Chem. Rev.*, **72**, 511 (1972) and references therein.
6) S. Shinoda and Y. Saito, This Bulletin, **47**, 2948 (1974).
7) P. L. Goggin and L. A. Woodward, *Trans. Faraday Soc.*, **58**, 1495 (1962).
8) M. Taagepera and E. R. Thornton, *J. Amer. Chem. Soc.*, **94**, 1168 (1972).
9) D. Cook, R. E. J. Hutchinson, and A. J. Parker, *J. Org. Chem.*, **39**, 3029 (1974).
10) V. J. Shiner, Jr., W. E. Buddenbaum, B. L. Murr, and G. Lamaty, *J. Amer. Chem. Soc.*, **90**, 418 (1968).
11) V. J. Shiner, Jr., B. L. Murr, and G. Heinemann, *ibid.*, **85**, 2413 (1963).
12) V. J. Shiner, Jr., *ibid.*, **78**, 2653 (1956).
13) T. Koenig and R. Wolf, *ibid.*, **91**, 2574 (1969).
14) S. Seltzer and E. J. Hamilton, Jr., *ibid.*, **88**, 3775 (1966).

BULLETIN OF THE CHEMICAL SOCIETY OF JAPAN, VOL. 48(12), 3747—3748 (1975)

Complex Cation-radical Salts Derived from Phenothiazine and Related Compounds

Susumu Doi* and Yoshio Matsunaga**

Department of Chemistry, Faculty of Science, Hokkaido University, Sapporo 060

(Received May 29, 1975)

Synopsis A new class of complex cation-radical salts is formed by the reaction of phenothiazine bromide with phenoxazine, phenothiazine, its benzo derivatives, and phenoselenazine.

Phenothiazine has been known to form a number of cation-radical salts.[1,2] However, the incorporation of formally neutral molecules has been established in no case. We have now discovered the formation of complex phenothiazine and phenoselenazine cation-radical bromides and also of some mixed complex bromides.

Simple phenothiazine cation-radical bromide was prepared by the oxidation of the parent organic compound dissolved in ether with bromine, as has been described by Kehrmann and Diserens.[2] The bromine content was a little higher than that corresponding to the 1 : 1 salt. Found: C, 48.82; H, 3.07; N, 4.71; Br, 31.54%. Calcd for $C_{12}H_9NS \cdot Br_{1.18}$: C, 49.10; H, 3.09; N, 4.77; Br, 32.12%. We earlier noted that the vibrational spectra exhibited by the bromide samples thus prepared are often superpositions of the spectra of the A and B types in various ratios.[3] The present sample showed the spectrum of the B type. When the salt was ground with an equimolar amount of phenothiazine wetted with benzene, drastic changes in both the vibrational and electronic spectra were observed. In Fig. 1, the electronic spectrum of the product is compared with that of the starting bromide. The former salt retains the spectral pattern of the latter. In addition, a broad band appears at 5.2×10^3 cm^{-1}. The resulting electronic spectrum and also the vibrational spectrum coincide with those of the A type in the previous work. It must be realized that the spectrum of the A type is not of the polymorphic form of the simple cation-radical salt suggested earlier, but of the complex salt, $(C_{12}H_{19}NS)^+(C_{12}H_9NS)^0 \cdot X^-$, in which the positive charge may be equally shared by the two molecules of phenothiazine. The low-energy absorption band newly appearing in the complex salt may be a manifestation of such a delocalization of the positive charge.

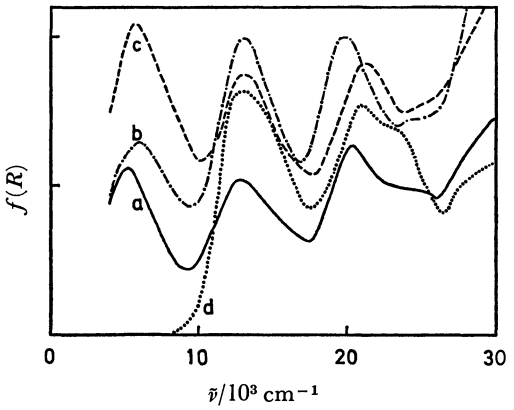

Fig. 1. Diffuse reflection spectra of the combinations of the phenothiazine bromide and a) phenothiazine, b) phenoxazine, and c) phenoselenazine, and d) the phenothiazine bromide alone.

The frequent superposition of the vibrational spectra of the A and B types in the bromide samples with an apparent composition of 1 : 1 implies that the simple cation-radical bromide, the complex cation-radical bromide, and polybromide (possibly tribromide) are all formed under similar conditions. Such complexity was further demonstrated by the transformation of the spectrum of the B type to that of the A type by storage. When the samples prepared over six years before were reexamined, only the spectrum of the A type could be detected. The following analytical results indicate a loss of bromine during the storage; nevertheless, the contents are still appreciably higher than that of the complex (2 : 1) bromide. Found: C, 53.16, 53.06; H, 3.25, 3.32; N, 4.98, 5.15; Br, 25.58, 25.54% for two independent samples. Calcd for $C_{12}H_9NS \cdot Br_{0.88}$: C, 53.46; H, 3.36; N, 5.20; Br, 26.08%. The rearrangement of the simple cation-radical bromide to a mixture of the complex cation-radical bromide and tribromide may account for the constitution of the product.

Additional evidence for the formation of the complex cation-radical salt was provided by the examination of the electrical resistivity and the Seebeck coefficient. Mixtures of the bromide and phenothiazine in five different mole ratios were heated to 80 °C in a short time to complete the reaction and also to remove all traces of the solvent. The vibrational spectra of the mixtures after the treatment were essentially the same as those made at room temperature except at a ratio of 4 : 1. Thus, the complex cation-radical bromide appeared to be more stable than the simple bromide.

The measurements were carried out on pressed pellets in the range from −90 to +50 °C by procedures described elsewhere.[4] The plot of the logarithm of resistivity against the reciprocal temperature gives a straight line. The resistivity values at 20 °C and the activation energies for semiconduction calculated on the basis of $\rho = \rho_0 \exp(\Delta E/kT)$ are presented in Table 1. The sharp maximum of the resistivity located at the 1 : 1 mole ratio supports the complex (2 : 1) salt formation. The Seebeck coefficient at 20 °C

* Present address: Central Research Laboratory, Showa Denko K. K., Tamagawa, Tokyo.

** To whom inquiries may be addressed.

is negative for all the samples, but the temperature-dependence is sensitive to the composition. As is shown in Fig. 2, the value is nearly constant at the 4 : 1 mole ratio. On the further addition of phenothiazine, the slope against the reciprocal temperature becomes negative and is exceptionally steep at the composition of the complex salt. In the presence of an excess of phenothiazine, the slope changes its sign.

Table 1. Electrical properties of the mixtures of the phenothiazine bromide and phenothiazine

Mole ratio	Resistivity at 20°C (ohm cm)	Activation energy (eV)	Seebeck coeff. at 20°C ($\mu V°C^{-1}$)
4 : 1	1600	0.27	−24
3 : 2	90	0.19	− 5
1 : 1	770	0.23	− 6
2 : 3	100	0.23	− 9
1 : 4	370	0.17	−15

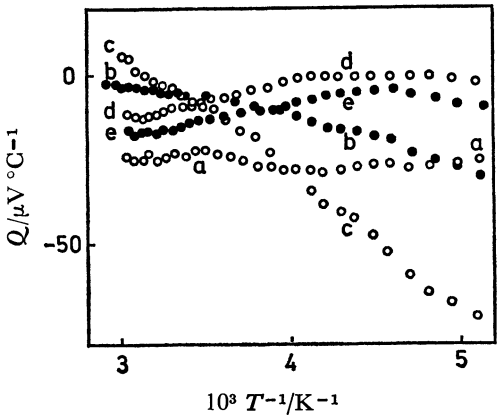

Fig. 2. Seebeck coefficients (Q) of the mixtures of the phenothiazine bromide and phenothiazine, a) 4 : 1, b) 3 : 2, c) 1 : 1, d) 2 : 3, and e) 1 : 4 (mole ratio).

On the basis of the close similarity between the vibrational spectrum of the A type and that of the phenothiazine-iodine complex, we were previously led to conclude that every phenothiazine molecule in the iodine complex bears an approximate unit-positive charge.[3] This conclusion must be revised in the light of the new findings presented above. It is now apparent that the iodine complex is a kind of complex cation-radical salt. The complex phenoselenazine cation-radical bromide was also prepared. The vibrational spectrum of this salt resembles that of the corresponding iodine complex reported previously.[5] The maximum of the low-energy electronic band appears at 6.4×10^3 cm^{-1}.

Figure 1 shows also the electronic spectra produced by the reaction of the phenothiazine bromide with phenoxazine and phenoselenazine in a mole ratio of 1 : 1. The maxima of the low-energy bands in these products are at 6.0 and 5.7×10^3 cm^{-1} respectively. The disagreement between the latter spectrum and the superposition of those of the two complex cation-radical salts suggests the formation of a complex salt containing both the thiazine and the selenazine. Similar spectral changes were observed in the combinations of the phenothiazine bromide and benzo[*a*]- and benzo[*c*]-phenothiazines. As the absorption bands in the phenothiazine bromide are overlapped by those of the benzophenothiazine bromides, the spectra of the products are dominated by the latter. The low-energy bands are located at about 4.5×10^3 cm^{-1}.

Although *p*-phenylenediamine and benzidine may be expected to have ionization potentials a little higher than the thiazines,[6] the reaction with the phenothiazine bromide resulted in the electron-transfer from the diamine to the thiazine. The dark blue products showed the spectra of the diamine cation-radical bromides.[7]

References

1) R. Pummerer and S. Gassner, *Ber.*, **46**, 2310 (1913).
2) F. Kehrmann and L. Diserens, *ibid.*, **48**, 318 (1915).
3) Y. Matsunaga and K. Shono, This Bulletin, **43**, 2007 (1970).
4) K. Kan and Y. Matsunaga, *ibid.*, **45**, 2096 (1972).
5) Y. Matsunaga and Y. Suzuki, *ibid.*, **45**, 3375 (1972).
6) G. Saito and Y. Matsunaga, *ibid.*, **44**, 1788 (1971).
7) Y. Iida and Y. Matsunaga, *ibid.*, **41**, 2615 (1968).

BULLETIN OF THE CHEMICAL SOCIETY OF JAPAN, VOL. 48(12), 3749—3750 (1975)

Enthalpies of Combustion of Organic Compounds. III.* D-, L- and DL-Alanines

Akeji KAMAGUCHI, Tomoko SATO, Minoru SAKIYAMA, and Syûzô SEKI
Department of Chemistry, Faculty of Science, Osaka University, Toyonaka, Osaka 560

(Received April 8, 1975)

Synopsis. Enthalpies of combustion of D-, L- and DL-alanines were measured by oxygen static bomb calorimetry. Derived thermodynamic quantities at 298.15 K for D-, L- and DL-isomers are as follows: $\Delta E_c^\circ = -1619.24 \pm 0.58$, -1620.26 ± 0.63 and -1617.97 ± 0.50 kJ mol^{-1}; $\Delta H_c^\circ = -1619.86 \pm 0.58$, -1620.88 ± 0.63 and -1618.59 ± 0.50 kJ mol^{-1}; $\Delta H_f^\circ(c) = -561.08 \pm 0.71$, -560.06 ± 0.76 and -562.35 ± 0.65 kJ mol^{-1}, respectively.

Measurements of heats of combustion of alanine, one of the fundamental amino acids, have been made on L-isomer by Tsuzuki *et al.*[1] and on L- and DL-isomers by Huffman *et al.*[2,3] On L-isomer, the value of ΔH_c° by Tsuzuki *et al.*[1] differs significantly from that by Huffman *et al.*[2] up to about 3%. On D-isomer there appeared no report hitherto. In this paper the enthalpies of combustion of D-, L- and DL-alanines in their crystalline states are reported. The idealized combustion reaction to which the energies and enthalpies of combustion given in this paper refer is the following one at 25 °C:

$$C_3H_7O_2N(c) + (3.75)O_2(g) = 3CO_2(g) + (3.5)H_2O(l) + (0.5)N_2(g).$$

Experimental

Materials. L-Alanine (Takara Kôsan Co., Ltd.), D-alanine (Ajinomoto Co., Ltd.) and DL-alanine (Nakarai Chemicals, Ltd.) were purified by recrystallization from aqueous solutions, twice, twice and four times, respectively. After the samples were first dried under vacuum (~0.1 kPa), they were pelletted and then stored for 6 months in a desiccator over anhydrous magnesium perchlorate. Specific rotatory power of the solutions ($c = 0.022$ mol dm^{-3} in 2.0 M HCl) was as follows: $[\alpha]_D^{20} = +14.3°$ (L-isomer), $-14.4°$ (D-isomer) and $-0.2°$ (DL-isomer), respectively. Each peak in the X-ray diffraction patterns obtained by using Cu-Kα radiation coincided with that calculated from the crystallographic data.[4,5]

Apparatus, Procedures and Calculation. An isoperibol rotating precision bomb-calorimeter reported previously[6] was used without rotation. It was pointed out, however, by Huffman *et al.*[2,3] that alanine was very troublesome to burn as it had a decided tendency to jump out of the crucible when burned partially. So, we designed a special deep crucible with a baffle (Pt-10% Rh), having the density and the specific heat capacity of 20.50 g cm^{-3} and 0.1464 J K^{-1} g^{-1} at 25 °C, respectively, (Fig. 1) and used it to facilitate complete combustion by keeping off such a jumping-out as described above. The energy equivalent was defined for the system made up of an empty bomb and a gimbal as before and was found from 13 calibration-experiments with benzoic acid (Standard Reference Material 39i, National Bureau of Standards, U.S.A.) to be 15159.78 ± 0.57 J K^{-1}, where uncertainty is the standard deviation of the mean. To make the combustion of the alanine sample more perfect, *ca.* 0.15 g of liquid paraffin (Wakô Pure Chemical Co., Ltd.) was used as promotor in each experiment. In this way we succeeded in performing perfect combustion. In order to make the ignition procedure reproducible in every run, we used two electrical timers: one for timing the begining and the other for timing the ending of ignition, respectively. Calculation was carried out as before. NEAC 2200 electronic computor of Osaka University was used to calculate Washburn corrections and to obtain the final data of energy of combustion.

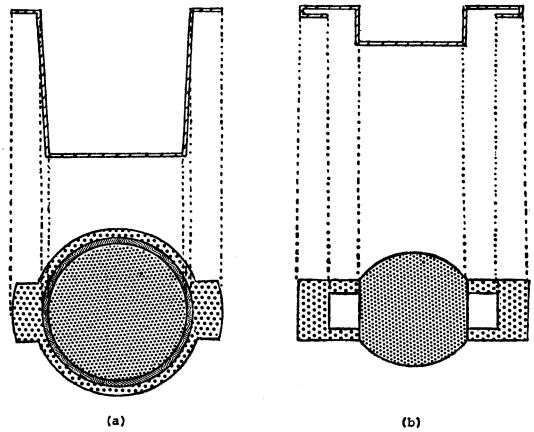

Fig. 1. (a) Crucible, (b) Baffle. (Scale, 14/17)

Auxiliary Quantities. Auxiliary data adopted in the calculation of ΔE_c°, *i.e.* the composition formula and the values (for 25 °C) of density, ρ, of specific heat capacity, c_p, and of $(\partial E/\partial P)_T$ for the combustible substances, are given in Table 1. Other auxiliary data used are as follows: M(compd.) = 89.0947 g mol^{-1}, m(Pt) = 29.511 g, V(bomb) = 0.3458 dm^3, $\Delta E_c^\circ/M$(fuse) = -16507 J g^{-1}, $\Delta E_c^\circ/M$(oil) = 45909.3 ± 4.1 J g^{-1}, where uncertainty is standard deviation of the mean. Six combustion experiments were carried out for D-, L- and DL-alanines, respectively. Data from combustions selected as typical are given in Table 2. Notations in Table 2 follow those by Hubbard *et al.*[7] except for the followings: Δm(H_2O cal.), excess water in the calorimeter can; ΔE (std. state), sum of items 81—85, 87—89, 93 and 94 in Ref. 7. The results of the individual combustion experiment in terms of ΔE_c° at 298.15 K are summarized as follows: -1618.83, -1619.90, -1619.43, -1619.68, -1619.04, -1618.54, mean and standard deviation of the mean -1619.24 ± 0.21 kJ mol^{-1} for L-alanine; -1620.55,

Table 1. Auxiliary data for the calculation of energy of combustion

		ρ/g cm^{-3}	c_p/J K^{-1} g^{-1}	$(\partial E/\partial P)_T$/ J kPa^{-1} g^{-1}
Alanine	$C_3H_7O_2N$	1.37	1.372	(-0.957)[a]
Fuse	$CH_{1.860}O_{0.930}$	1.5	1.70	-2.94
Auxiliary oil	$CH_{1.885}$	0.8824	2.22	-2.60
Pt-10% Rh	——	20.50	0.1464	——

a) The value in bracket is estimated one.

* This paper was read before the 10-th Japanese Calorimetry Conference, Tokyo (1974).

−1620.38, −1619.66, −1620.07, −1621.25, −1619.65, mean and standard deviation of the mean −1620.26± 0.25 kJ mol^{-1} for D-alanine; −1617.55, −1617.88, −1618.09, −1618.46, −1618.27, −1617. 57, mean and standard deviation of the mean −1617.97±0.15 kJ mol^{-1} for DL-alanine. Thermochemical quantities were calculated from those results and given in Table 3. In the calculation of the standard enthalpies of formation of the present samples, CODATA key values[8] for the standard enthalpies of formation at 298.15 K of $H_2O(l)$ and $CO_2(g)$; $\Delta H_f^\circ(H_2O, l) = -285.30\pm0.042$ kJ mol^{-1}, $\Delta H_c^\circ(CO_2, g) = -393.51\pm0.13$ kJ mol^{-1} were employed, where uncertainties represent the Task Group's estimates of the overall uncertainties at a 95 per cent confidence level. The standard enthalpy of formation of L-isomer in the gaseous state was calculated by using a enthalpy of vaporization reported by Svec *et al.*[9] All the uncertainties in this paper are uncertainty interval recommended by Rossini,[10] *i.e.* twice the final overall standard deviation of the mean, unless specified.

Discussion

In Table 4 our data are compared with those of Huffman *et al*[2,3] and Tsuzuki *et al.*[1] The difference between the ΔH_c° values of Huffman *et al.*[2] and of the present work for L-alanine is well within the sum of each uncertainty interval. But these values are quite far from that of Tsuzuki *et al.*,[1] the descrepancy being no less than 3%. The value of ΔH_c° of D-alanine observed in this work also coincides with those of L-alanine by Huffman *et al.*[2] and by the author within the sum of each uncertainty interval. Thus, as in the case of glutamic acid, previously described by two of the authors,[11] it is also concluded that the ΔH° values of different optical isomers of alanine coincide with each other. The ΔH_c° value of DL-alanine of this work is in good agreement with that of Huffman *et al.*[3] within the uncertainty interval.

The authors would like to express their hearty thanks to Dr. K. Toi of Ajinomoto Co., Ltd., and Dr. F. Sakiyama of the Institute for Protein Research, Osaka University, for their cooperation in obtaining the samples.

Table 2. Typical results in combustion experiments

Compound Exp. No.	L-Alanine L-5	D-Alanine D-5	DL-Alanine DL-4
m^i(compd.)/g	1.19068	1.18150	1.17692
m^i(fuse)/g	0.00298	0.00320	0.00293
m^i(oil)/g	0.11281	0.15223	0.13143
$m^i(H_2O$ tot.)/g	1.226	1.204	1.191
$\Delta m(H_2O$ cal.)/g	0.027	−0.014	0.032
p^i(gas)/MPa	3.047	3.040	3.045
T_i/°C	23.19657	23.13588	23.17551
T_f/°C	24.99832	25.04563	25.01457
ΔT_{corr}/°C	0.02867	0.02630	0.02657
$n^f(HNO_3)$/mol	0.000595	0.000696	0.000634
ΔE_{ign}/J	3.3	5.9	2.9
ΔE(std. state)†/J	14.0	14.5	14.1
$\Delta E_{dil_n}(HNO_3)$/J	−0.1	−0.1	−0.1
$\Delta E_{decomp}(HNO_3)$/J	35.0	41.0	37.3
ε^i(cont.)/J K^{-1}	21.48	21.44	21.36
ε^f(cont.)/J K^{-1}	23.95	24.00	23.84
ΔE_c°/kJ mol^{-1}	−1619.04	−1620.55	−1618.46

† items 81-85, 87-89, 93, 94 in Ref. 7.

Table 3. Results and derived quantities at 298.15 K

	L-Alanine	D-Alanine	DL-Alanine
ΔE_c°/kJ mol^{-1}	−1619.24±0.58	−1620.26±0.63	−1617.97±0.50
ΔH_c°/kJ mol^{-1}	−1619.86±0.58	−1620.88±0.63	−1618.59±0.50
ΔH_f° (c)/kJ mol^{-1}	− 561.08±0.71	− 560.06±0.76	− 562.35±0.65
ΔH_f° (g)/kJ mol^{-1}	− 433.0 ±1.8	——	——

Table 4. The comparison of ΔH_c° value obtained by different investigators

	L-Alanine	D-Alanine	DL-Alanine
This work	−1619.86±0.58	−1620.88±0.63	−1618.59±0.50
Huffman *et al.*[2,3]	−1619.71±0.54	——	−1617.37±0.57
Tsuzuki *et al.*[1]	−1577.0 ±2.1	——	——

The values of Huffman *et al.*[2,3] and of Tsuzuki *et al.*[1] were taken from Ref. 12.

References

1) T. Tsuzuki, D. O. Harper, and H. Hunt, *J. Phys. Chem.*, **62**, 1594 (1958).
2) H. M. Huffman, E. L. Ellis, and S. W. Fox, *J. Amer. Chem. Soc.*, **58**, 1728 (1936).
3) H. M. Huffman, S. W. Fox, and E. L. Ellis, *ibid.*, **59**, 2144 (1937).
4) H. J. Simpson, Jr. and R. E. Marsh, *Acta Crystallogr.*, **20**, 550 (1966).
5) J. Donohue, *J. Amer. Chem. Soc.*, **72**, 949 (1950).
6) M. Sakiyama, T. Nakano, and S. Seik, This Bulletin, **84**, 1705 (1975).
7) W. N. Hubbard, D. W. Scott, and G. Waddington, "Experimental Thermochemistry," ed. by F. D. Rossini Interscience Publishers, New York and London (1956), p. 75.
8) *J. Chem. Thermodynamics*, **4**, 331 (1972).
9) H. J. Svec and D. D. Clyde, *J. Chem. Eng. Data*, **10**, 151 (1965).
10) F. D. Rossini, *ibid.*, p. 297.
11) M. Sakiyama and S. Seki, This Bulletin, in press.
12) J. D. Cox and G. Pilcher, "Thermochemistry of Organic and Organometallic Compounds", Academic Press, London and New York (1970). In this monograph, the data of Huffman *et al.*[2] on D-alanine seems to be erroneously cited as that of L-alanine.

BULLETIN OF THE CHEMICAL SOCIETY OF JAPAN, VOL. 48(12), 3751—3752 (1975)

Solvent Extraction Equilibria of Thallium(III) from Weakly Acidic Chloride Solutions into 4-Methyl-2-pentanone

Yuko HASEGAWA, Shinji KURIHARA, Naohito MASUI, and Tatsuya SEKINE

Department of Chemistry, Science University of Tokyo, Kagurazaka, Shinjuku-ku, Tokyo 162

(Received July 4, 1975)

Synopsis. From the distribution data of thallium (III) between 4-methyl-2-pentanone and 4 mol dm^{-3} sodium perchlorate solutions containing chloride ions at pH 2, the $Na^+TlCl_4^-$ species in the organic phase and the $TlCl_2^+$, $TlCl_3$, and $TlCl_4^-$ species in the aqueous phase were recognized. The equilibrium constants for the formation and extraction of these complexes were determined.

The solvent extraction of thallium(III) chloride complexes for various analytical purposes has been carried out in most cases from hydrochloric acid solutions, and the chemical form of the extracted species is known to be $HTlCl_4$.[1] When the acidity of the aqueous phase is not high and/or the solvent is nonpolar, however, the extraction of thallium(III) chloride species containing no hydrogen ions can be expected. Walters and Dodson[2] demonstrated that, with 0.0365 mol dm^{-3} tributylphosphate (TPB) in hexane, thallium(III) was extracted as the $TlCl_3(TBP)_2$ species from aqueous solutions containing perchloric and hydrochloric acid at an ionic strength of 0.5 mol dm^{-3}, but Widmer and Dodson[3] showed that, with 0.730 mol dm^{-3} TBP in octane, the $HTlCl_4$ species was also extracted from the same solutions.

Since the thallium(III) tetrachloride complex anion can be well extracted, along with the hydrogen ion, from acid chloride solutions, the present authors considered that this complex anion might also be extracted with cations other than the hydrogen ion from weakly acid chloride solutions into solvating-type polar organic solvents. Therefore, they measured the extraction of thallium(III) from 4 mol dm^{-3} Na(Cl, ClO_4) solutions at pH 2 with 4-methyl-2-pentanone and with hexane containing 0.03 mol dm^{-3} TBP at 298 K and compared the results of these two series of experiments.

Experimental

All of the reagents were of an analytical grade. The sodium perchlorate was recrystallized three times from water. Both the 4-methyl-2-pentanone and TBP were washed with 0.1 mol dm^{-3} perchloric acid, water, and a 0.1 mol dm^{-3} sodium hydroxide solution successively, and then several times with water. Thallium(III) nitrate was dissolved in 4 mol dm^{-3} of a sodium perchlorate solution containing 0.1 mol dm^{-3} perchloric acid and a small amount of sodium chloride; a stock solution containing 1.0×10^{-2} mol dm^{-3} of thallium(III) was thus prepared. The metal concentration was checked by a colorimetric method using 8-quinolinol.[4] All of the procedures were carried out at 298 K. A portion of an aqueous 4 mol dm^{-3} Na(Cl,ClO_4) solution containing 1×10^{-6} to 1×10^{-3} mol dm^{-3} of thallium (III) and the same volume of 4-methyl-2-pentanone or hexane containing TBP was placed in a stoppered glass tube. The two phases were agitated vigorously for 30 s. After they had then been centrifuged, a portion of the aqueous phase was transferred into another glass tube and hydrochloric acid and a solution of Malachite Green were added. The concentrations of hydrochloric acid and Malachite Green in the resulting solution were 3×10^{-1} and 1×10^{-4} mol dm^{-3} respectively. This solution was shaken with benzene. The organic phase was then transferred into another tube and shaken with a solution containing hydrochloric acid and Malachite Green at the same concentrations as above in order to wash off the perchlorate ions coextracted with the metal complex. The thallium(III) in the sample was determined from the absorption of this organic solution at 635 nm. The molar extinction coefficient was 5.5×10^4. The distribution ratio of thallium(III) was defined as:

$$D = [\mathrm{Tl(III)}]_{\mathrm{org,total}}/[\mathrm{Tl(III)}]_{\mathrm{total}}$$

where 'org' denotes the chemical species in the organic phase and where a lack of a subscript denotes those in the aqueous phase. The total thallium(III) concentration in the organic phase was determined from the difference between its initial and equilibrium concentrations in the aqueous phase. When the metal concentration in the initial aqueous phase was high, a correction was made for the decrease in the free-chloride concentration due to the extraction of the chloride complex.

Results

The distribution ratio may generally be expressed by the following equation;

$$D = ([TlCl_3]_{org} + [Na^+TlCl_4^-]_{org})/\sum [TlCl_n^{3-n}] \quad (1)$$

Extraction with 4-Methyl-2-pentanone. The distribution ratio was found to be independent of the hydrogen-ion concentration, at least between pH 1 and 2.5. The open circles in Fig. 1 give the extraction data with 4-methyl-2-pentanone at pH 2. It was found that these extraction data could be analyzed by using the following equation, derived from Eq. (1):

$$D = K\mathrm{ex}_4[Na^+][Cl^-](K_3^{-1}[Cl^-]^{-1} + 1 + K_4[Cl^-])^{-1} \quad (2)$$

where

$$K_n = [TlCl_n^{3-n}][TlCl_{n-1}^{4-n}]^{-1}[Cl^-]^{-1} \quad (3)$$

$$K\mathrm{ex}_4 = [Na^+TlCl_4^-]_{org}[TlCl_3]^{-1}[Cl^-]^{-1}[Na^+]^{-1} \quad (4)$$

The values for the constants in Eq. (2) were determined by a curve-fitting method.[5] The solid curve for the open circles in Fig. 1 was calculated by introducing these values into Eq. (2). It is possible that a part of the $Na^+TlCl_4^-$ ion-pair undergoes dissociation in this polar organic solvent, but, for the reasons already presented in a previous paper,[6] this effect should be negligible under the conditions employed in the present study.

Extraction with TBP in Hexane. The distribution

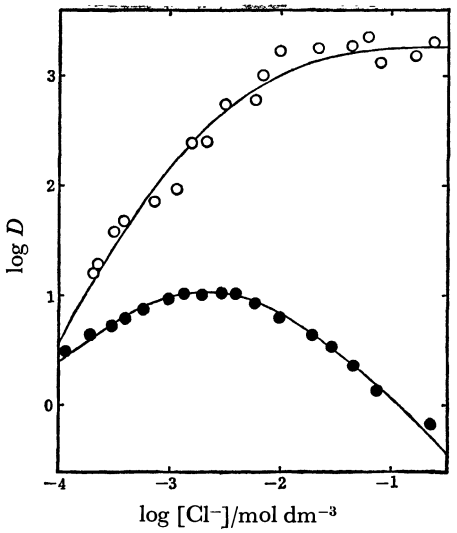

Fig. 1. Distribution ratio of thallium(III) as a function of chloride concentration. Org. phase: closed circles hexane containing 3.0×10^{-2} mol dm^{-3} of TBP and open circles 4-methyl-2-pentanone. Aq. phase: 4 mol dm^{-3} Na(Cl, ClO_4) at pH 2. Temperature 298 K.

Table 1. Equilibrium constants for the complexes

Org. phase: 4-methyl-2-pentanon for $K\text{ex}_4$ and hexane containing TBP for $K\text{ex}_3$.
Aq. phase: 4 mol dm^{-4} Na(Cl, ClO_4) at pH 2.
Temperature: 298 K.

log K_3	log K_4	log $K\text{ex}_3$	log $K\text{ex}_4$
3.22	2.12	4.26	4.79

ratio was found to be second-order dependent on the TBP concentration in its concentration range between 5×10^{-3} to 5×10^{-2} mol dm^{-3} and independent of the hydrogen ion concentration, at least between pH 0.6 and 2.5. The closed circles in Fig. 1 give the extraction data when the TBP concentration was 3×10^{-2} mol dm^{-3} at pH 2. It was found that the extraction data could be analyzed by using the following equation:

$$D = K\text{ex}_3[\text{TBP}]_{org}^2(K_3^{-1}[\text{Cl}^-]^{-1}+1+K_4[\text{Cl}^-])^{-1} \quad (5)$$

where:

$$K\text{ex}_3 = [\text{TlCl}_3(\text{TBP})_2]_{org}[\text{TlCl}_3]^{-1}[\text{TBP}]_{org}^{-2} \quad (6)$$

The data were also analyzed by the curve-fitting method. The stability constants of the aqueous complexes were found to be identical with those obtained by the 4-methyl-2-pentanone extraction. The values for the constants in Eq. (5) are listed in Table 1. The solid curve for the closed circles in Fig. 1 was calculated by introducing these values into Eq. (5).

Discussion

Since the data at the chloride concentrations lower than 1×10^{-4} mol dm^{-3} could not be obtained by the method employed in this study, the formation constants, K_1 and K_2, could not be determined. However, the Tl^{3+} and $TlCl^{2+}$ species should be negligible in the chloride-concentration range of the present study. The reported stability constants for the thallium(III) chloride complexes[2,7-9] are, for all practical purposes, in agreement with the present values; the values reported for log k_3 are 2.75 (0.4), 2.68 and 2.74 (0.5), 3.10 (1.2), 3.08, 3.15, and 3.55 (3), and 3.41 (4) and for log K_4 are 2.25 (0.4), 1.60 and 1.81 (0.5), 2.5 (1.2), 2.17, 2.22, and 2.36 (3), and 2.79 (4) respectively, when the ionic concentration in the solution is at the value in the parentheses. No evidence for the higher complexes was observed in the chloride-concentration range of the present study.

The extraction curve with TBP reported by Walters and Dodson[2] is quite similar to that in Fig. 1. However, the $K\text{ex}_3$ value given by the previous authors is 9.7×10^2 when the diluent was octane;[3] this is probably due to the difference in the salting-out effect. Such a large difference in the partition coefficient of metal complexes in TBP extraction when the electrolyte concentration in the aqueous phase was different was also found in a previous work on the extraction of the $In(SCN)_3$ species.[10]

It is marked that only the neutral complex, $TlCl_3$, was extracted into hexane containing a small amount of TBP, even from the aqueous phase of the high sodium-ion concentration, while only the anionic complex as an ion-pair was extracted into the polar solvent, 4-methyl-2-pentanone.

It is obvious that the chloride complexes of thallium(III) are much more stable than the corresponding complexes of indium(III) because, for the latter metal ion, only the first and second chloride complexes were found in the chloride concentration range from 10^{-4} to 10^{-1} mol dm^{-3}, and the extractability of the thallium(III) as chloride complex is much higher than that of indium(III), because the latter was not extracted into those solvents under conditions identical with those of the present study.[6,11]

References

1) E. B. Sandell, "*Colorimetric Determination of Traces of Metals*," 3rd Ed. Interscience, New York (1959) p. 826.
2) R. M. Walters and R. W. Dodson, "Solvent Extraction Chemistry," ed. by D. Dyrssen, J.-O. Liljenzin, and J. Rydberg, North Holland, Amsterdam (1967), p. 71.
3) H. M. Widmer and R. W. Dodson, *J. Phys. Chem.*, **74**, 4289 (1970).
4) H. Goto, Y. Kakita, and N. Ichinose, *Nippon Kagaku Zasshi*, **88**, 640 (1967).
5) D. Dyrssen and T. Sekine, *J. Inorg. Nucl. Chem.* **26**, 981 (1964).
6) Y. Hasegawa, H. Takeuchi, and T. Sekine, This Bulletin, **45**, 1388 (1972).
7) A. E. Martell and L. G. Sillén, "Stability Constants" The Chemical Society, London, *Spec. Pub.*, No. 17 (1964).
8) S. Ahrland, I. Grenthe, L. Johansson, and B. Norén, *Acta Chem. Scand.*, **17**, 1567 (1963).
9) M. J. M. Woods, P. K. Gallagher, Z. Z. Hugus, Jr., and E. L. King, *Inorg. Chem.*, **3**, 1313 (1964).
10) Y. Hasegawa and T. Sekine, *J. Inorg. Nucl. Chem.*, **36**, 421 (1974).
11) Y. Hasegawa, This Bulletin, **43**, 2665, (1970).

BULLETIN OF THE CHEMICAL SOCIETY OF JAPAN, VOL. 48(12), 3753—3754 (1975)

Determination of Silver in Sea Water after Flotation with 2-Mercaptobenzothiazole

Masataka HIRAIDE and Atsushi MIZUIKE

Faculty of Engineering, Nagoya University, Chikusa-ku, Nagoya 464

(Received August 4, 1975)

Synopsis. Nanogram quantities of silver in 3000 ml of acidified sea water were quantitatively coprecipitated with 2-mercaptobenzothiazole. The precipitate was then floated with the aid of small nitrogen bubbles, and the silver determined by atomic-absorption spectrophotometry after wet oxidation. The silver concentration was 0.09 μg per liter.

Since the silver content of sea water is low (reported values: 0.0—2.9 μg per liter),[1,2] it must be concentrated from a large volume of sample before atomic-absorption spectrophotometric determination. Traces of silver ions in aqueous solutions can be collected on the precipitate formed by adding an acetone solution of 2-mercaptobenzothiazole,[3] but filtration of this amorphous precipitate is difficult. Centrifugation also is not applicable because of incomplete sedimentation. In the present work, the flotation technique[4] was successfully applied. The precipitate is readily separated from the main liquor without surfactants, and then the silver in it is determined by atomic-absorption spectrophotometry. Commercial 2-mercaptobenzothiazole contained appreciable amounts of silver, but it was easily purified by the amalgamation method.[5]

Experimental

Apparatus. A Nippon Jarrell-Ash model AA-1 Mark II atomic-absorption spectrophotometer with an SA-61 slit burner and a Hitachi model QPD53 recorder, and a Fujitsu well-type NaI(Tl) scintillation counter were employed. The flotation cell consisted of a 120 mm i.d. × 700 mm or 45 mm i.d. × 250 mm glass tubing tapered at the lower end with a sintered-glass disc (No. 4, 110 mm or 40 mm diam.) near the lower end.

Reagents. A 2-mercaptobenzothiazole solution (40 mg/ml) was prepared and purified as follows: 4 g of 2-mercaptobenzothiazole was dissolved in 90 ml of acetone in a 200-ml tall beaker, 2 ml of mercury was added, and the solution was stirred vigorously for 10 min with a magnetic stirrer. The mercury was separated by centrifugation, another 2 ml of mercury was added to the solution, and the above treatment was repeated once more. The solution was diluted to 100 ml with acetone. Standard silver solutions were prepared from silver nitrate. Water was purified by distillation and ion-exchange. All reagents used were of reagent grade. ^{110m}Ag was used as a tracer.

Recommended Procedure. Place 3000 ml of sea water (acidified to 0.1 M with nitric acid) in a 5000-ml beaker, and add 50 ml of 2-mercaptobenzothiazole solution in small portions while stirring with a magnetic stirrer. Stir the solution vigorously for 30 min. Transfer the contents of the beaker (excluding the stirring bar) to a flotation cell (120 mm i.d. × 700 mm), and wash the beaker with 50 ml of 1 M nitric acid. Pass nitrogen from the lower end of the cell for 1—2 min to effect complete agitation followed by flotation of the precipitate with small bubbles (*ca.* 0.1 mm diam.). Suck off the main liquor through the sintered-glass disc, and wash the precipitate with two 100-ml portions of 1 M nitric acid followed by two 100-ml portions of water (to remove the nitric acid). Discard the filtrate and washing solutions. Add 50 ml of acetone to the cell to dissolve the precipitate, collect the filtrate by suction in a 200-ml beaker, and wash the sintered-glass disc with 20 ml of acetone. Evaporate the solution to dryness on a water bath, cautiously add 20 ml of 13.8 M nitric acid, heat gently to dissolve the residue, and evaporate to 5 ml. Transfer the solution to a 50-ml beaker, and wash the 200-ml beaker with 15-ml of 13.8 M nitric acid. Evaporate the solution to near dryness and cool. Add 4 ml of 30% hydrogen peroxide in small portions (the residue becomes colorless) and evaporate to near dryness. Wash the walls of the beaker with 3 ml of 30% hydrogen peroxide and evaporate again to near dryness. Dissolve the residue in 3 ml of 13.8 M nitric acid, transfer the solution to a 5-ml volumetric flask, wash the beaker with water, and dilute to the mark. Determine the silver in the solution by atomic-absorption spectrophotometry under the following operating conditions: wavelength 328.1 nm, lamp current 10 mA, air 8.0 l/min, acetylene 2.5 l/min, slit-widths 0.10 (entrance) and 0.15 mm (exit). Construct a calibration curve by taking 1 ml of standard silver solutions containing 0—5.0 μg of silver and 3 ml of 13.8 M nitric acid in a 5-ml volumetric flask and diluting to the mark with water. Run a blank through the whole procedure using 3000 ml of 0.5 M nitric acid.

Tracer Experiments. The recovery of silver from 3000 or 100 ml of artificial sea water[6] or diluted nitric acid was examined radiochemically. For the 3000-ml samples, the gamma-activity of a 2-ml aliquot of the final 5-ml solution obtained by the recommended procedure was measured. For 100-ml samples, the separation of silver was carried out as follows. A hundred ml of artificial sea water or diluted nitric acid containing 0.05 μg of labeled silver was placed in a 200-ml beaker, 2.5 ml of 2-mercaptobenzothiazole solution was added, and the solution was stirred for 30 min. The contents of he beaker were transferred to a flotation cell (45 mm i.d. × 250 mm), the beaker was washed with 10 ml of water, and nitrogen was passed for 15 s. The main liquor was sucked off and discarded. Six ml of acetone was added to the cell to dissolve the precipitate, the filtrate was collected in a 10-ml volumetric flask, and diluted to the mark with acetone. The gamma-activity of a 2-ml aliquot was measured.

Results and Discussion

Purification of 2-Mercaptobenzothiazole. 2-Mercaptobenzothiazole is a readily available and inexpensive reagent, but containing 0.15—0.30 ppm of silver. Tracer experiments showed that more than 95% of silver was removed by the amalgamation method (80% removed by a single treatment). Silver in 50 ml of purified 2-mercaptobenzothiazole solution was less than 0.1 μg (from atomic-absorption spectro-

photometry).

Reaction Conditions. Tracer experiments were carried out on 100-ml samples to determine the optimal acidity for the separation of silver. The results are shown in Fig. 1. Silver, 0.05 μg, was recovered in yields greater than 95% from artificial sea water acidified to 0.04—1.5 M with nitric acid and from 0.3—1.5 M nitric acid. The low recoveries in nitric acid below 0.2 M were due to the passage of the precipitate through the sintered-glass disc (resulting from incomplete coagulation).

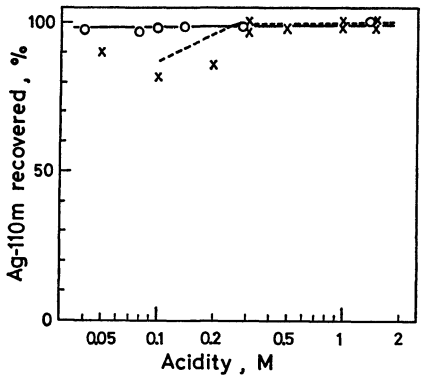

Fig. 1. Effect of acidity on silver recovery.
Solution volume: 100 ml; Ag: 0.05 μg;
2-mercaptobenzothiazole solution: 2.5 ml.
—○—: Artificial sea water, --×--: Diluted nitric acid.

Table 1. Determination of silver in sea water

Sample	Ag found (μg)	Ag in sample (μg/l)
1	0.30	0.10
2	0.28	0.09
3	0.28	0.09
4[a)]	0.30	0.10
5[b)]	0.57	0.09
6[c)]	0.72	0.07
		Av. 0.09

Solution volume: 3000 ml; Salinity: 35.16 ‰;
Location: 22°01'N, 152°00'E.
a) An acidic sample was filtered through a Millipore filter HA (0.45 μm). b) 0.30 μg of silver was added. c) 0.50 μg of silver was added.

From 3000 ml of artificial sea water (acidified to 0.1 M with nitric acid) and 0.5 M nitric acid, 0.05—5 μg of labeled silver was separated by the recommended procedure with the following recoveries: 96, 97% for 0.05 μg of silver, 96, 96, 96, 97, 97% for 1 μg, 97, 98% for 5 μg (in artificial sea water); 95, 95% for 0.05 μg, and 96% for 5 μg (in 0.5 M nitric acid).

Atomic-Absorption Measurements. The calibration curve was linear up to at least 5 μg of silver with a maximum deviation of 0.05 μg, and passed through the origin. The lower limit of determination was 0.1 μg. Fifty mg each of sodium, magnesium, potassium, and strontium, and 2.5 mg of calcium did not interfere with the determination of silver. The residue from evaporation of the final 5-ml solution weighed 25—35 mg, and the calcium in it was less than 1 mg (determined by EDTA titration).

Determination of Silver in Sea Water. The analyses were carried out on 3000-ml aliquots of a sample of surface sea water acidified to 0.1 M with nitric acid immediately after collection. The results are shown in Table 1. The blank through the whole procedure was less than 0.1 μg of silver. The time required for a determination was about 4 hr.

The authors wish to express their gratitude to Dr. Satoru Kanamori of Nagoya University for providing a sample of sea water. Their thanks are also due to Teruo Matsui for technical assistance.

References

1) J. P. Riley and R. Chester, "Introduction to Marine Chemistry," Academic Press, London and New York (1971), p. 65.
2) J. P. Riley and G. Skirrow, "Chemical Oceanography," Academic Press, London and New York (1965), p. 295.
3) Y. Ujihira, *Nippon Kagaku Zasshi*, **84**, 642 (1963).
4) M. Hiraide and A. Mizuike, *Talanta*, **22**, 539 (1975).
5) A. Mizuike, T. Sakamoto and K. Sugishima, *Mikrochim. Acta*, **1973**, 291.
6) H. U. Sverdrup, M. W. Johnson, and R. H. Fleming, "The Oceans: Their Physics, Chemistry, and General Biology," Prentice-Hall, Englewood Cliffs, N. J. (1942), p. 186.

BULLETIN OF THE CHEMICAL SOCIETY OF JAPAN, VOL. 48(12), 3755—3756 (1975)

An X-Ray Diffraction Study of a Concentrated Aqueous Sodium Iodide Solution

Masunobu MAEDA and Hitoshi OHTAKI

Laboratory of Solution Chemistry, Tokyo Institute of Technology, O-okayama, Meguro, Tokyo 152

(Received August 6, 1975)

Synopsis. X-Ray diffraction measurements of a 7 M NaI aqueous solution showed that iodide ion is surrounded by approximately six water molecules, the I^-–H_2O distance being 3.60 Å and that sodium ion is bonded to about four water molecules at the distance of 2.4 Å.

According to the results so far reported, halide–water distances in the first hydration sphere are about 3.2 Å for Cl^-, 3.4 Å for Br^-, and 3.7 Å for I^-.[1-3] These distances for Cl^- and Br^- ions are in good agreement with the sums of the respective crystal ionic radii and the molecular radius of water. For I^- ion, the anion–water bond length is more than 0.1 Å longer compared with the sum of the crystal radius of iodide ion and the radius of a water molecule. The halide ions are reported to be surrounded by seven to ten water molecules as their closest neighbors.[1-3] However, the number of water molecules around halide ions and the structural arrangement were not definitely determined. The recent X-ray and neutron scattering measurements of LiCl solutions by Narten *et al.*[4] revealed the six-coordinated structure for the hydrated Cl^- ion, although the bond is estimated to be rather weak. Then, questions arise how many water molecules are really coordinated to one iodide ion and if the I^-–H_2O bond is longer by 0.1 Å than the sum of the crystal radius of iodide and the radius of a water molecule.

Lithium and potassium ions were reported to be bonded to four water molecules in the first hydration sphere, their ion-water distances being 2.0 Å[4] and 2.9 Å,[1] respectively. For Na^+ ion, on the contrary, it was suggested that the cation is surrounded by six water molecules, 2.4 Å distant from the central ion.[5] In view of the previous results it seems unlikely that Na^+ ion has a different hydration number from Li^+ and K^+ ions.

In order to reconfirm these points, we have carried out X-ray diffraction measurements of a concentrated sodium iodide solution.

Experimental and Treatment of Data

The NaI aqueous solution was prepared by dissolving recrystallized sodium iodide in water. The concentration of NaI in the solution was found to be 7.009 M from the gravimetric analysis of I^- as AgI.

X-Ray scattering data were obtained at 25 °C on a θ–θ diffractometer (JEOL Co., Tokyo) equipped with a Philips Mo X-ray tube; the details of the measurements are described elsewhere.[6] The measured scattering angle range (2θ) was between 2° and 140°. The intensity data were corrected for background and polarization, and then scaled to absolute intensities $I(\theta)$ according to the ordinary procedures.[6-8] Reduced intensities $i(\theta)$ were extracted by subtraction of independent coherent and incoherent scatterings from the scaled intensities $I(\theta)$.[6]

The radial distribution function $D(r)$ was calculated by means of the Fourier transform of the reduced intensities $i(\theta)$ on the basis of the following equation.

$$D(r) = 4\pi r^2\rho_0 + 2r\pi^{-1}\int_0^{s_{max}} s\cdot i(s)\cdot M(s)\cdot\sin(rs)\mathrm{d}s \qquad (1)$$

Here ρ_0 is the average scattering density in electron units and $s=4\pi\sin\theta/\lambda$ ($\lambda=0.7107$ Å). The modification function $M(s)$ used is $(f_I^2(0)/f_I^2(s))\cdot\exp(-0.01s^2)$, where $f_I(s)$ is the coherent scattering factor of iodine atom at "angle" s. s_{max} is the maximum value of s ($\simeq 16.5$ Å^{-1}) reached in the experiments.

Results and Discussion

Figure 1 draws the radial distribution curve $D(r)$ and the differential curve $(D(r)-4\pi r^2\rho_0)$. These curves show three peaks at around 2.4 Å, 3.6 Å, and 4.8 Å. It is readily deduced from the previous results[2,3,5] that the first peak at 2.4 Å is due to the Na^+–OH_2 bond in the first hydration sphere and the second

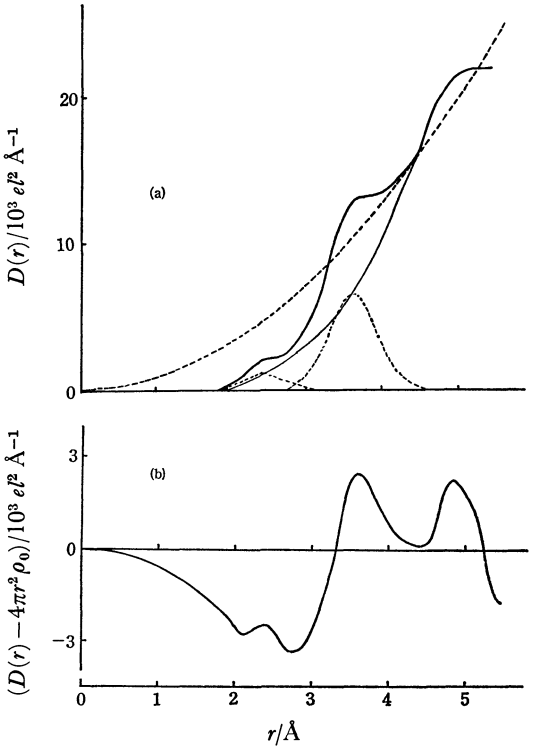

Fig. 1(a). Comparison between the $D(r)$ curve (thick solid line) and the peak shapes calculated for the Na^+–OH_2 and I^-–H_2O bonds.
The curve $4\pi r^2\rho_0$ is shown by the thick solid line, the calculated peak shapes by the fine dashed line, and the residual curve by the fine solid line.
(b) Differential curve, $D(r)-4\pi r^2\rho_0$.

peak at 3.6 Å represents the I^-–H_2O bond within the hydrated iodide ion.

The distances for sodium– and iodide–water bonds, and the hydration numbers were evaluated by the trial and error method in such a way that the residual curve brought about by subtraction of the theoretical peaks for the ion–water bonds from the $D(r)$ curve led to a smooth background curve.[6-8] The theoretical peak shapes were produced by the Fourier transform (Eq. (1)) of the theoretical intensities for a given structure calculated by Eq. (2).

$$i_{calc}(s) = \sum_i \sum_j n_{ij} f_i(s) f_j(s) \frac{\sin(r_{ij}s)}{r_{ij}s} \exp(-b_{ij}s^2) \qquad (2)$$

where $f_i(s)$ and $f_j(s)$ denote the scattering factors of atoms i and j, respectively, and n_{ij}, r_{ij}, and b_{ij} represent the frequency factor, the distance and the temperature factor of the interaction between any atoms i and j, respectively.

In Fig. 1a are illustrated the theoretical peak shapes (fine dashed line) for the Na^+–OH_2 and I^-–H_2O bonds and the resultant residual curve (fine solid line), together with the $D(r)$ curve. The values $r=2.40\pm0.03$ Å, $b=0.004\pm0.002$ Å^2, and n (hydration number)$=4\pm1.5$ for the hydrated Na^+ ion, and $r=3.60\pm0.02$ Å, $b=0.025\pm0.005$ Å^2, and $n=6\pm1$ for the hydrated I^- ion brought about a smooth remainder curve (fine solid line) with no indication of other residual peaks (Fig. 1a). These values were refined by direct comparison of the reduced intensities $s\cdot i(s)$ and the theoretical ones calculated from Eq. (2). The satisfactory agreement was obtained between the observed and calculated intensities in the s region larger than 3.5 Å^{-1}.

In conclusion, the distance (2.4 Å) for the Na^+–OH_2 bond is in good agreement with that reported previously.[5] On the contrary, the I^-–H_2O distance of 3.60 Å found in this work is shorter than that reported by Lawrence and Kruh in concentrated alkali iodide solutions.[2] Our I^-–H_2O bond length corresponds to the sum of the crystalline radius of I^- ion (2.16 Å)[9] and the radius of a water molecule (1.4 Å), as is true for the distances of the Cl^-–H_2O and Br^-–H_2O bonds.[2-4] The hydration number of I^- ion found in this work was a little smaller than that reported previously,[2,3] but the same as that of Cl^- ion.[4] Although the number of water molecules coordinated to Na^+ ion was not definitely determined because of the small scattering power of Na, our result showed that $n=4$ is more probable than 6.

It was difficult to clearly identify the asymmetric peak ranging from 4.5 Å to 5.2 Å; the peak may be ascribed to the Na^+–OH_2 and I^-–H_2O interactions in their second hydration spheres and H_2O–H_2O interactions within the hydrated I^- ion.

References

1) G. W. Brady and J. T. Krause, *J. Chem. Phys.*, **27**, 304 (1957).
2) R. M. Lawrence and R. F. Kruh, *ibid.*, **47**, 4758 (1967).
3) G. Licheri, G. Piccaluga, and G. Pinna, *J. Appl. Cryst.*, **6**, 392 (1973).
4) A. H. Narten, F. Vaslow, and H. A. Levy, *J. Chem. Phys.*, **58**, 5017 (1973).
5) O. Devik, C. Finbak, and O. Rönning, *Tidsskr. Kjemi. Bergvesen Met.*, **4**, 50 (1944).
6) H. Ohtaki, M. Maeda, and S. Ito, This Bulletin, **47**, 2217 (1974).
7) H. Ohtaki and M. Maeda, *ibid.*, **47**, 2197 (1974).
8) M. Maeda, H. Ohtaki, and G. Johansson, *ibid.*, **47**, 2229 (1974).
9) L. Pauling, "General Chemistry," 2nd Ed., Freeman, San Francisco and London (1953), p. 217.

BULLETIN OF THE CHEMICAL SOCIETY OF JAPAN, VOL. 48(12), 3757—3758 (1975)

Phenylations of β-Nitrostyrene Derivatives with Benzene by the Use of Palladium(II) Acetate

Kimiaki YAMAMURA and Setsuo WATARAI

Institute of Chemistry, College of General Education, Kobe University, Tsurukabuto, Nada, Kobe, Hyogo 657

(Received November 13, 1974)

Synopsis. The phenylations of several β-nitrostyrene derivatives with benzene in the presence of palladium(II) acetate have been studied. The nitro group of the β-nitrostyrenes investigated affects the phenylations very strongly, because of its powerful electron-withdrawing nature, and a high reactivity and regiospecificity were observed.

Nucleophilic addition reactions to a carbon-carbon double bond conjugated with electron-withdrawing groups are well-known. We have ourselves previously reported the nucleophilic addition of ethanol to β-nitrostyrenes under very mild conditions.[1] Recently, Moritani and Fujiwara *et al.* reported a novel aromatic substitution reaction with olefins in the presence of palladium salts,[2] and also reported that an electron-withdrawing group on the olefinic carbon atom assists the phenylation reaction.[3] This prompted us to examine the phenylation reaction of β-nitrostyrenes by the use of palladium acetate.

A mixture of a β-nitrostyrene derivative and palladium acetate in a large excess of benzene and acetic acid was refluxed under stirring until the precipitation of black metallic palladium ceased. The results are summarized in Table 1. From β-nitrostyrene(I), 1,1-diphenyl-2-nitroethylene(III) was obtained predominantly; no α-nitrostilbene(II) was produced under the present reaction conditions. The selective formation of III from I in a good yield is interesting, since the treatment of *trans*-1-phenyl-1-propene under the same conditions gave *trans*-methylstilbene in a lower yield (24%) and *trans*-stilbene yielded triphenylethylene in a 28% yield on treatment with palladium acetate under similar conditions.[4] These facts indicate that, in this reaction, an electronic factor of the nitro group in I plays an important role. Both α-nitrostilbene (II) and 1,1-diphenyl-2-nitroethylene(III) reacted with benzene to give 1,1,2-triphenyl-2-nitroethylene(VII) (14.4 and 2.2% yields respectively), accompanied by considerable amounts of biphenyl and unidentified carbonyl compounds. The low yields of the phenylated compounds and the formation of appreciable amounts of by-products may be due to the steric hindrance of two phenyl groups and the nitro group. In fact, in their study of the phenylations of a series of phenyl-substituted ethylenes, Fujiwara *et al.* reported that the reactivity in olefin arylation using palladium salts was markedly influenced by a steric factor and that 1,1,2-triphenylethylene gave tetraphenylethylene in a 13% yield under similar conditions.[4] That the yield of VII from III was lower than those in the cases of II and triphenylethylene is interesting. This fact indicates that, in III, the nitro group on the carbon atom carrying the hydrogen which undergoes substitution interferes with the phenylation reaction.

Ethyl α-nitrocinnamate(IV) reacted with benzene under similar conditions to afford the corresponding phenylated product, VIII, in a 47.3% yield; here the steric factor does not seem to be as important as had been expected. This is presumably due to the powerful electron-withdrawing nature of the nitro and carboethoxy groups on the same ethylenic carbon atom. With β-bromo-β-nitrostyrene(V), the expected phenylated compound, 1,1-diphenyl-2-bromo-2-nitroethylene, was not obtained; instead, III was obtained as the main product, together with small amounts of VII and (*Z*)-α-nitrostilbene(IX).

Heck proposed a reaction mechanism for the arylation using palladium salts and an arylmercury compound, in which the first step is the *cis*-addition of arylpalladium acetate to the olefinic double bond, followed by the *cis*-elimination of hydridopalladium acetate.[5] When this mechanism is applied to the case of V, the following reaction pathway is considered. The yield of IX was very slight compared with that of III. This can be explained by considering that the initial complex, XI, was produced in preference to XII, because the phenyl group would tend to be introduced at the carbon atom adjacent to that bearing the nitro group. VII might be derived *via* III and

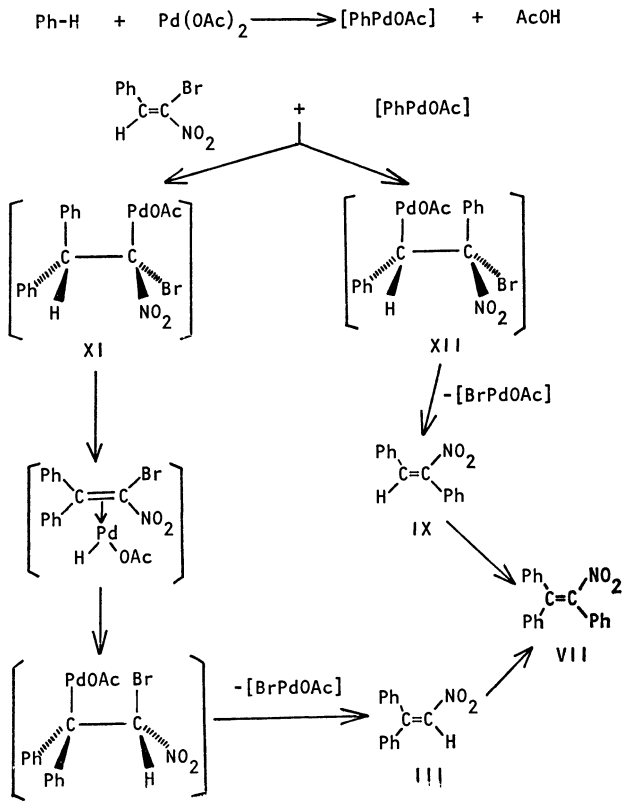

Table 1. Results of phenylation of β-nitrostyrenes

Starting β-nitrostyrene		Reaction time (hr)	Phenylated Product		Yield (%)[a]
$PhCH=CHNO_2$	I[b]	20	$Ph_2C=CHNO_2$	III	70.0
$PhCH=CPhNO_2$	II[b]	50	$Ph_2C=CPhNO_2$	VII	14.4
$Ph_2C=CHNO_2$	III	250	$Ph_2C=CPhNO_2$	VII	2.2
$PhCH=C(COOEt)NO_2$	IV[c]	20	$Ph_2C=C(COOEt)NO_2$	VIII	47.3
$PhCH=CBrNO_2$	V[b]	30	$Ph_2C=CHNO_2$	III	20.0[d]
$PhCH=C(CH_2Ph)NO_2$	VI[b]	20	$PhCH=C(CHPh_2)NO_2$	X	66.0[e]

a) Yields are of isolated and purified products. b) (*E*)-isomer. c) (*Z*)-isomer. d) Small amounts of (*Z*)-α-nitrostilbene(IX) and VII were also isolated. e) Total yield; (*E*)-: 34.0, (*Z*)-: 32.0 %.

IX. From 1,3-diphenyl-2-nitro-1-propene(VI), two unexpected compounds, (*E*)- and (*Z*)-1,3,3-triphenyl-2-nitro-1-propene(X), were obtained as the main products,[6] and at the end of reaction considerable amounts of the starting VI were recovered. When VI was treated with a 2-mol equiv. of palladium acetate under similar conditions, (*E*)- and (*Z*)-X were obtained in 34.0 and 32.0% yields respectively. The usual phenylated compound, 1,1,3-triphenyl-2-nitro-1-propene, was not obtained. The formation of X from VI may also be explained by the addition-elimination mechanism.[5]

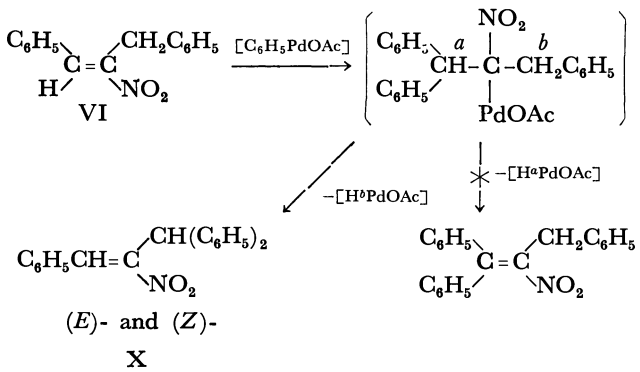

(*E*)- and (*Z*)-X

In all of the β-nitrostyrenes investigated in this study, the reactivity and the direction of the introduction of the phenyl group are markedly influenced by the electronic factor of the nitro group. This finding is interesting because it has previously been reported that the direction of the introduction of an aromatic group to unsymmetrical olefins is influenced by the steric factor rather than by the electronic one.[7]

Experimental

Materials. Palladium acetate was prepared according to the method of Stephenson *et al.*[8] All the β-nitrostyrene derivatives except 1,3-diphenyl-2-nitro-1-propene(VI) were prepared by the method described in a previous paper.[1]

Preparation of VI. A mixture of freshly distilled benzaldehyde (0.05 mol), 1-phenyl-2-nitroethane (0.05 mol), and butylamine(0.02 mol) in 100 ml of toluene was refluxed for 16 hr. After the evaporation of the solvent, the residue was chromatographed over silica gel. Pale yellow crystals of VI were thus obtained in a 51% yield; mp 52 °C. IR (KBr), 1639, 1514, 1495, 1447, 1325, 767, 740, 695 cm^{-1}; NMR ($CDCl_3$), δ 8.30(s 1H, vinyl), 7.42 (s 5H, phenyl), 7.27 (s 5H, phenyl), 4.27 (s 2H, methylene). Found: C, 75.37; H, 5.44: N, 5.90%.

General Procedure for the Phenylation of β-Nitrostyrenes. A mixture of the β-nitrostyrene derivative (0.01 mol) and palladium acetate (0.01 mol) in 150 ml of benzene and 40 ml of acetic acid was refluxed until the precipitation of palladium metal ceased. After the filteration of palladium metal, the reaction mixture was poured into water. The organic layer was separated, and the aqueous layer was extracted with benzene. The combined extract was washed with water, and then the solvent was evaporated. The residue was chromatographed over silica gel, using a mixture of hexane-benzene (1 : 1) as the eluent. The first elution gave biphenyl, while subsequent fractions gave the phenylated products. The structures of the products were determined by means of their IR, UV, and NMR spectra and by elemental analyses. The following results were obtained:

a) The phenylation of I afforded III in a 70.0% yield.

b) The phenylations of II and III afforded VII in 14.4 and 2.2% yields respectively; mp 175 °C (lit,[9] 175 °C).

c) The phenylation of IV afforded VIII in a 47.3% yield; yellow crystals, mp 74 °C. NMR ($CDCl_3$) δ 7.47—7.09 (m, 10H, phenyl), 4.13 (q 2H, methylene, J=8 Hz), 1.05 (t 3H, methyl). Found: C, 68.63; H, 4.95; N, 4.68%.

d) The phenylation of V afforded III in a 20.0% yield, accompanied by small amounts of VII and XI.

e) The phenylation of VI with a 2-mol equiv. of palladium acetate afforded a mixture of (*E*)- and (*Z*)-isomers of X in a 66.0% yield. The physical data have been reported in a previous paper.[6]

Phenylation of trans-1-*Phenyl*-1-*propene.* Under conditions similar to those described above, *trans*-1-phenyl-1-propene gave *trans*-methylstilbene in a 24% yield.

The authors are indebted to Miss Masuko Nishinaka for her IR spectra measurements and elemental analyses and to Mrs. Kazuko Azumi for her technical assistance. Thanks are also due to Mr. Yasuo Morimoto for his skillful collaboration.

References

1) K. Yamamura, S. Watarai, and T. Kinugasa, This Bulletin, **44**, 2440 (1971).

2) M. Watanabe, M. Yamamura, I. Moritani, Y. Fujiwara, and A. Sonoda, *ibid.*, **47**, 1035 (1974), and references therein.

3) S. Danno, I. Moritani, and Y. Fujiwara, *Tetrahedron*, **25**, 4819 (1969).

4) Y. Fujiwara, I. Moritani, R. Asano, and S. Teranishi, *Tetrahedron Lett.*, **1968**, 6015.

5) R. F. Heck, *J. Amer. Chem. Soc.*, **91**, 6707 (1969).

6) (*E*)- and (*Z*)-X were also obtained from β-methyl-β-nitrostyrene in the presence of 3 mol equiv. of palladium acetate under the similar conditions; K. Yamamura, *J. Chem. Soc., Perkin I*, **1975**, 988.

7) R. F. Heck, *J. Amer. Chem. Soc.*, **90**, 5518 (1969).

8) T. A. Stephenson, S. M. Morehouse, A. R. Powell, J. P. Heffer, and G. Wilkinson, *J. Chem. Soc.*, **1965**, 3632.

9) F. Bergmann, *J. Amer. Chem. Soc.*, **70**, 1618 (1948).

BULLETIN OF THE CHEMICAL SOCIETY OF JAPAN, VOL. 48(12), 3759—3760 (1975)

Reaction of *N*-Aroyl-*N*-arylhydroxylamines with *o*-Nitrobenzenesulfenyl Chloride

Shigeru OAE*, and Tadamitsu SAKURAI**

**Institute of Chemistry, The University of Tsukuba, Niihari-gun, Ibaraki 300-31*

***Department of Applied Chemistry, Faculty of Engineering, Osaka City University, Sugimoto-cho, Osaka 558*

(Received April 8, 1975)

Synopsis. Reactions of *N*-aroyl-*N*-arylhydroxylamines with *o*-nitrobenzenesulfenyl chloride were found to afford the corresponding *N*-aroylarylamines and *S*-(*o*-nitrophenyl) *o*-nitrobenzenethiosulfonate in good yields, respectively. Both the product distributions and the effect of substituents on the amount of reduction product suggest these reactions to proceed *via* homolytic cleavage of the N–O bond.

The rearrangement of allylic sulfenates to the corresponding sulfoxides with no allylic shift has been known to proceed *via* the homolytic scission of C–O bonds.[1] A similar mode of C–O bond scission has been observed in the rearrangements of both benzyl *p*-toluenesulfenate[2] and cyclohexenyl benzenesulfenate.[3]

However, the reaction of *N*,*N*-disubstituted hydroxylamines with the sulfenyl chloride could also lead to the formation of sulfinamide (III) by rearrangement as in the case of the allylic sulfenates as shown below. However, no such reaction has yet been investigated.

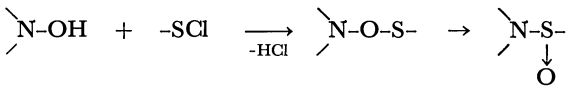

(I) (II) (III)

This paper describes the reaction of *N*-aroyl-*N*-arylhydroxylamines with *o*-nitrobenzenesulfenyl chloride, comparing the reaction route of the hydroxylamine with that of the corresponding alcohol.

Results and Discussion

The *N*-aroyl-*N*-arylhydroxylamines (Ia—e) were allowed to react with an equimolar amount of *o*-nitrobenzenesulfenyl chloride, and *S*-(*o*-nitrophenyl) *o*-nitrobenzenethiosulfonate and the corresponding *N*-aroylarylamines were obtained in good yields along with small amounts of *o*,*o*'-dinitrodiphenyl disulfide as shown in the Table. No rearrangement product (III) was found among the products.

Apparently, the more polar the solvent used, the greater was the yield of the unexpected reduction products, the *N*-aroylaryamines, while the introduction of an electron-releasing *p*-methyl group into the phenyl ring of the hydroxylamines resulted in an increase of the amount of the reduction product. Futhermore, the yield of the reduction product was not affected very much by the functional group (R) directly attached to the nitrogen atom of the hydroxylamines.

The *p*-nitrobenzenesulfinyl radical is known to be quite stable due to the electron-sharing 3d-orbital resonance, and to dimerize readily eventually yielding *S*-(*p*-nitrophenyl) *p*-nitrobenzenethiosulfonate.[4,5] Therefore, one may safely assume that the hydroxylamines (Ia—e) react with the sulfenyl chloride to give the intermediate (IIa—e), which undergoes homolytic scission of the N-O bond in (IIa—e) as shown below. The resulting acylamino radical undoubtedly affords the *N*-aroylarylamine by hydrogen abstraction and the *S*-(*o*-nitrophenyl) *o*-nitrobenzenethiosulfonate is formed by the dimerization of *o*-nitrobenzenesulfinyl radical, like the *p*-nitrobenzenesulfinyl radical.

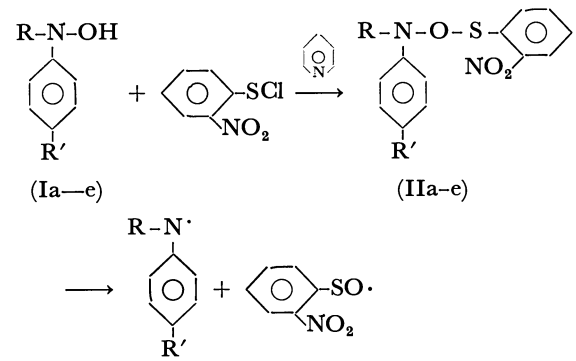

(Ia—e) (IIa—e)

R=PhCO, R'=H (Ia); R=PhCO, R'=CH_3 (Ib); R=PhCO, R'=Cl (Ic); R=CH_3CO, R'=H (Id); R=Ts, R'=H (Ie)

If the N–O bond of (IIa—e) is assumed to cleave heterolytically, there are the following two possibilities for heterolysis.

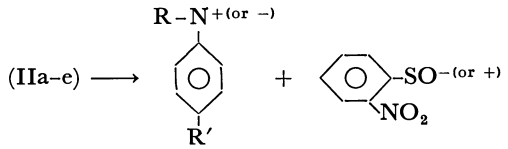

These possibilities, however, may be ruled out by the following observations: (1) no substantial formation of the disulfide whose amount must be comparable to that of the thiosulfonate[5a,6] and (2) little influence by any polar functional group (R) on the yield of the reduction product was observed, unlike the reduction of *O*-(3,5-dinitrobenzoyl)-*N*-aroyl-*N*-arylhydroxylamines by cyanide ions in a dipolar aprotic solvent.[7] If the N–O bond of (IIa—e) were cleaved heterolytically, the nucleophilic attack of the chloride ion on the sulfenate-sulfur atom of (IIa—e) should give *o*-nitrobenzenesulfinyl chloride and the anilide anion. Thus, the alternative mechanism involving the homolysis of the N–O bond remains the most plausible possibility.

The lone-pair electron of the acylamino radical has been suggested to be extensively delocalized into the carbonyl group as shown by (b) in preference to the allylic resonance (c), placing the odd electron on the oxygen atom, being quite unimportant.[8]

TABLE 1. THE PRODUCTS OF THE REACTION OF R-N(OH)-C$_6$H$_4$-R′ WITH *o*-NITROBENZENESULFENYL CHLORIDE AT ROOM TEMPERATURE[a,b]

Substituents		Reaction Condition		Products and Yields, %	
R	R′	Solvent	Time (hr)	$(O_2N)(NO_2)C_6H_3$-S-SO$_2$-C$_6$H$_4$ [c]	R-NH-C$_6$H$_4$-R′ [d]
PhCO	H	CH_2Cl_2	24	41	57
PhCO	H	CH_3CN	24	60	76
PhCO	CH_3	CH_2Cl_2	24	57	86
PhCO	Cl	CH_2Cl_2	24	50	57
CH_3CO	H	CH_2Cl_2	24	46	53
Ts	H	CH_2Cl_2	24	46	57

Ts=*p*-$CH_3C_6H_4SO_2$-

a) The reactions were carried out in the presence of dissolved oxygen. b) A small amount of *o*, *o*′-dinitrodiphenyl disulfide was obtained in each run. c) Yield based on the sulfenyl chloride used. d) Yield based on the hydroxylamine used.

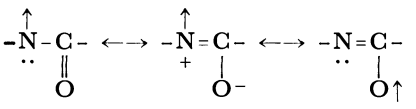

(a) (b) (c)

In addition, ESR spectroscopy revealed the electronic ground state of the acylamino radical to possess not a σ-, but a π-character. The π-radical is stabilized by the π-delocalization of an odd electron on the nitrogen atom in the phenyl ring. Consequently, the effects of the solvent and the substituent R′ on the amount of the reduction product can be interpreted in terms of the enhanced stability of the acylamino radical, formed by the homolytic scission of the N–O bond. The absence of any appreciable effect of the substituent R may be due to the negligible contribution of the allylic resonance (c) in the acylamino radical.

Thus, the different behaviors of the hydroxylamine and the alcohol in the reaction with the sulfenyl chloride appears to be attributable to the difference in the thermodynamical stabilities of the sulfinamide and the sulfoxide.

Experimental

Materials and Solvent. *N*-Aroyl-*N*-arylhydroxylamines (Ia—e) were prepared by the reactions of the corresponding *N*-arylhydroxylamines (2 mol) with aroyl chloride (1 mol) in dry ether at 0 °C. Repeated recrystallization from benzene-hexane gave mp, 121.5—122.0 °C (Ia), 110—111 °C (Ib), 156—157 °C (Ic), 68.5—69.5 °C (Id), and 145—146 °C (Ie; Found; C, 59.06; H, 4.98; N, 5.38%. Calcd for $C_{13}H_{13}NO_3S$: C, 59.30; H, 4.97; N, 5.32%). *o*-Nitrobenzenesulfenyl chloride was synthesized by the chlorination of *o*,*o*′-dinitrodiphenyl disulfide with dry chlorine gas in chloroform at room temperature. Repeated recrystallization from hexane gave light yellow needles, mp 74—75 °C (lit, 73—74.5 °C)[10]. All the solvents used were purified by the usual methods.

General Procedure for the Reactions of (Ia—e) with o-Nitrobenzenesulfenyl Chloride. Solutions of *o*-nitrobenzenesulfenyl chloride (4.58—6.62 mmol) in 20 ml of methylene chloride were dropped for 10 min with stirring into solutions of *N*-aroly-*N*-arylhydroxylamines (4.58—6.62 mmol) and pyridine (4.58—6.62 mmol) in 30 ml of methylene chloride at 0 °C. After keeping the mixtures at room temp. for 24 hr, the solutions were washed with water and dried over anhyd. sodium sulfate. Evaporation of the solvent afforded residual solids, which were then separated by column chromatography packed with silica gel using methylene chloride as the eluent. The structures of the products (shown in the Table) were identified by comparing their melting points and IR spectra with those of authentic compounds.

References

1) S. Braverman and Y. Stabinsky, *Chem. Commun.*, **1967**, 720; S. Braverman, *Int. J. Sulfur Chem.*, Part C, **6**, 149 (1971).

2) E. G. Miller, D. R. Rayner, and K. Mislow, *J. Amer. Chem. Soc.*, **88**, 3139 (1966).

3) N. S. Zefirov and F. A. Abdulaveeva, *Zh. Org. Khim.*, **7**, 947 (1971).

4) S. Oae and K. Ikura, This Bulletin, **38**, 58 (1965).

5) a) S. Oae and S. Kawamura, *ibid.*, **35**, 1156 (1962). b) H. J. Backer and H. Kloosterziel, *Rec. Trav. Chim. Pays-Bas*, **1954**,129. c) R. N. Topping and N. Kharasch, *Chem. Ind.* (London), **1961**, 178.

6) E. Kuhle, "The Chemistry of the Sulfenic Acids," Georg Thieme Publishers, Stuttgart (1973); F. A. Davis, A. J. Friedman, and E. W. Kluger, *J. Amer. Chem. Soc.*, **96**, 5000 (1974).

7) S. Oae and T. Sakurai, This Bulletin, **48**, 1071 (1975).

8) Y. L. Chow and T. C. Joseph, *Chem. Commun.*, **1969**, 490; H. J. Dauben and L. L. McCoy, *J. Amer. Chem. Soc.*, **81**, 4869 (1959); T. R. Beebe and F. H. Howard, *ibid.*, **91**, 3379 (1969); E. Hedaya, R. L. Hinman, V. Schomaker, S. Theodoropulos, and L. M. Kyle, *ibid.*, **89**, 4875 (1967).

9) P. Tord, E. Flesia, G. Labrot, and J. M. Surzur, *Tetrahedron Lett.*, **1972**, 1413; T. Koenig, J. A. Hoobler, and W. R. Mabey, *J. Amer. Chem. Soc.*, **94**, 2514 (1972); W. C. Danen and R. W. Gellert, *ibid.*, **94**, 6853 (1972).

10) M. H. Hubacher, *Org. Syn.*, Coll. Vol. II, p. 455 (1953).

BULLETIN OF THE CHEMICAL SOCIETY OF JAPAN, VOL. 48(12), 3761—3762 (1975)

Synthesis of Sugar Derivatives of *N*-Alkyl-*N*-nitrosourea

Tomoya MACHINAMI, Kazuki KOBAYASHI, Yoshiki HAYAKAWA and Tetsuo SUAMI

Department of Applied Chemistry, Faculty of Engineering, Keio University, Hiyoshi, Yokohama 223

(Received May 29, 1975)

Synopsis. Thirteen sugar derivatives of *N*-alkyl-*N*-nitrosourea have been prepared as follows. The reaction of a sugar amine with alkyl isocyanate gives a sugar derivative of *N*-alkylurea. When the product is treated with sodium nitrite in aqueous acetic acid, it gives the *N*-alkyl-*N*-nitrosourea derivative.

Streptozotocin is a broad spectrum antibiotic and possesses antitumor[1] and mutagenic activities.[2] The antibiotic was isolated from a fermentation broth of Streptomyces achromogenes var. streptozoticus by the Upjohn research group[3] and its structure was established to be *N*-carbamoyl-*N'*-methyl-*N'*-nitroso-D-glucosamine.[4] An undesirable side effect of the antibiotic, its diabetogenic property, was removed by methylating an anomeric hydroxyl group of the D-glucosamine moiety.[5] Later an attempt was made to prepare its analogs,[6] since the nitrosoureido group seems to be an essential group for the appearance of an antitumor activity.[7]

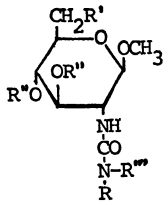

Derivatives of methyl β-D-glucosaminide

We have been working on the preparation of carbohydrate derivatives of *N*-alkyl-*N*-nitrosourea, and we wish to report a synthesis of methyl glycosides of *N*-alkyl analogs of the antibiotic and *N'*-alkyl-*N*-carbamoyl-*N'*-nitroso derivatives of glycosylamines. All the compounds show remarkable antitumor activities.

Experimental

Melting points were determined in a capillary tube in a liquid bath and are uncorrected. Optical rotations were measured on a JASCO DIP-SL polarimeter. IR spectra were measured on potassium bromide disks with a JASCO IR-E spectrometer. PMR spectra were determined at 60 MHz on a Varian A-60D spectrometer in deuteriochloroform with reference to tetramethylsilane as an internal standard. Solutions were evaporated under reduced pressure at 25—30 °C. Catalytic hydrogenation was carried out under hydrogen atomosphere (3.4 kg/cm²) with a Parr apparatus in the presence of Raney nickel. Acetylation was carried out in a mixture of acetic anhydride and pyridine in the usual manner. De-*O*-acylation was performed by dissolving a compound in methanolic ammonia or in 0.01～0.06 M methanolic sodium metoxide.

General Procedure for N-*Alkylurea Derivatives.* Alky isocyanate was added to a solution of carbohydrate amine in methanol and the mixture was stirred for 20 min at 10 °C to give crystalline precipitates. The mixture was settled in a refrigerator and the crystals were collected by filtration.

General Procedure for N-*Alkyl*-N-*nitrosourea Derivatives.* The carbamoyl derivative was dissolved in aqueous acetic acid. Sodium nitrite was added to the solution under ice cooling with agitation to give crystals. The crystals were

TABLE 1. *N*-ALKYLUREAS

R	R'	No.	Yield %	Mp °C	$[\alpha]_D^a$	Molecular Formula	C % Calcd	C % Found	H % Calcd	H % Found	N % Calcd	N % Found
A. Derivatives of Methyl β-D-glucosaminide R"=OH, R"'=H												
Ethyl	OH	1	98	239-240	-29	$C_{10}H_{20}N_2O_6$	45.44	45.68	7.63	7.46	10.60	10.65
Propyl	OH	4	95	227-229	-29	$C_{11}H_{22}N_2O_6$	47.47	47.23	7.97	7.73	10.09	10.13
Butyl	OH	7	89	227-228	-26	$C_{12}H_{24}N_2O_6$	49.30	49.50	8.28	8.17	9.58	9.56
Methyl	OMs	10	52	178-179	-34	$C_{10}H_{20}N_2O_8S$[b]	36.58	36.81	6.13	6.18	8.53	8.29
Methyl	H	13	67	237(dec)	-55	$C_9H_{18}N_2O_5$	46.14	45.98	7.74	7.43	11.96	11.75
Methyl	-NHCONHCH$_3$	16	37	265-266	-24	$C_{11}H_{22}N_4O_6$	43.13	42.96	7.24	6.98	18.29	17.99
B. N-Alkyl-N'-(poly-O-acyl-D-glycosyl)ureas RNH-CO-NHR'												
Tetra-O-acetyl-β-D-glucopyranosyl	Ethyl	21	90	171-172	+5*	$C_{17}H_{26}N_2O_{10}$	48.80	48.88	6.26	6.25	6.70	6.56
Tetra-O-acetyl-β-D-glucopyranosyl	Propyl	24	81	144-145	+1*	$C_{18}H_{28}N_2O_{10}$	49.99	49.87	6.53	6.46	6.48	6.35
Tetra-O-acetyl-β-D-glucopyranosyl	Butyl	28	95	109-110	+2*	$C_{19}H_{30}N_2O_{10}$	51.11	50.85	6.79	6.83	6.09	6.09
Tetra-O-acetyl-β-D-mannopyranosyl	Methyl	31	86	210-211	-24*	$C_{16}H_{24}N_2O_{10}$	47.52	47.54	5.98	5.92	6.93	6.85
Tri-O-acetyl-β-D-xylopyranosyl	Methyl	34	71	170-172	+4*	$C_{13}H_{20}N_2O_8$	46.98	47.08	6.07	6.15	8.43	8.22
Tri-O-benzoyl-β-D-ribofuranosyl	Methyl	38	29	168-169	-31*	$C_{28}H_{26}N_2O_8$	64.86	64.58	5.05	5.06	5.40	5.09
C. N-Alkyl-N'-(D-glycosyl)ureas RNH-CO-NHR'												
β-D-Glucopyranosyl	Propyl	25	80	191-193	-26	$C_{10}H_{20}N_2O_6$	45.44	45.47	7.64	7.39	10.60	10.31
β-D-Mannopyranosyl	Methyl	32	88	120-122	-27**	$C_8H_{16}N_2O_6$	40.67	40.90	6.83	6.80	11.86	11.63
β-D-Xylopyranosyl	Methyl	35	62	197-198	-27	$C_7H_{14}N_2O_5$	40.77	40.50	6.84	6.63	13.59	13.26
β-D-Ribofuranosyl	Methyl	39	21	184-185	-26**	$C_7H_{14}N_2O_5$	40.77	40.83	6.84	6.73	13.59	13.32

a Optical rotation was measured at 20-33°C in water, chloroform(*) and methanol(**). *b* Compound 10: Found: S, 9.45%. Calcd: S, 9.76%.

TABLE 2. *N*-ALKYL-*N*-NITROSOUREAS

R	R'	No.	Yield %	Mp °C	$[\alpha]_D^{\alpha}$	Molecular Formula	C % Calcd	C % Found	H % Calcd	H % Found	N % Calcd	N % Found
D. Derivatives of Methyl β-D-glucosaminide						R''=OH, R'''=NO						
Ethyl	OH	2	92	113(dec)	-30	$C_{10}H_{19}N_3O_7$	40.95	40.66	6.53	6.35	14.33	14.04
Propyl	OH	5	90	126(dec)	-26	$C_{11}H_{21}N_3O_7$	42.99	42.55	6.89	6.64	13.67	13.36
Butyl	OH	8	93	125(dec)	-26	$C_{12}H_{23}N_3O_7$	44.85	44.60	7.21	6.99	13.08	12.83
Methyl	OMs	11	80	129(dec)	-14	$C_{10}H_{19}N_3O_9S$ [c]	33.61	33.87	5.35	5.36	11.75	11.44
Methyl	H	14	90	135(dec)	-13	$C_9H_{17}N_3O_6$	41.06	41.03	6.51	6.42	15.96	16.00
Methyl	-NHCON(NO)CH_3	17	80	159(dec)	-14	$C_{11}H_{20}N_6O_8$	36.26	36.50	5.49	5.58	23.08	22.89
E. Derivatives of Methyl 3,4-di-O-acetyl-β-D-glucosaminide						R''=OAc, R'''=NO						
Ethyl	OAc	3	92	130-131	+39*	$C_{16}H_{25}N_3O_{10}$	45.82	45.92	6.01	5.98	10.02	10.02
Propyl	OAc	6	89	112-114	+19*	$C_{17}H_{27}N_3O_{10}$	47.11	47.16	6.28	6.50	9.70	10.04
Butyl	OAc	9	80	126-127	+18*	$C_{18}H_{29}N_3O_{10}$	48.32	48.46	6.53	6.54	9.39	9.49
Methyl	OMs	12	80	136-137	+35*	$C_{14}H_{23}N_3O_{11}S$ [d]	38.09	38.29	5.25	5.31	9.52	9.27
Methyl	H	15	76	115-117	+65*	$C_{13}H_{21}N_3O_8$	44.96	45.12	6.28	6.41	12.10	11.98
Methyl	-NHCON(NO)CH_3	18	76	121	+22*	$C_{15}H_{24}N_6O_{10}$	40.18	40.05	5.40	5.34	18.74	18.40
F. N-Alkyl-N'-(D-glycosyl)-N-nitrosoureas						RNH-CO-N(NO)R'						
β-D-Glucopyranosyl	Methyl	19 [e]	90	184(dec)	-19	$C_8H_{15}N_3O_7$	36.23	36.12	5.70	5.69	15.84	15.46
β-D-Glucopyranosyl	Ethyl	22	96	hygroscopic	-2	$C_9H_{17}N_3O_7$ [f]						
β-D-Glucopyranosyl	Propyl	26	80	112(dec)	-6	$C_{10}H_{19}N_3O_7$	40.95	40.77	6.54	6.69	14.33	13.93
β-D-Glucopyranosyl	Butyl	29	90	hygroscopic	-1.5	$C_{11}H_{21}N_3O_7$ [f]						
β-D-Mannopyranosyl	Methyl	33	78	103(dec)	-13	$C_8H_{15}N_3O_7$	36.23	35.92	5.70	5.70	15.84	15.67
β-D-Xylopyranosyl	Methyl	36	63	109(dec)	-27	$C_7H_{13}N_3O_6$	35.74	35.92	5.57	5.54	17.87	17.65
β-D-Ribofuranosyl	Methyl	40	75	105(dec)	-31	$C_7H_{13}N_3O_6$	35.74	36.04	5.57	5.56	17.87	18.14
G. N-Alkyl-N'-(poly-O-acetyl-D-glycosyl)-N-nitrosoureas						RNH-CO-N(NO)R'						
Tetra-O-acetyl-β-D-glucopyranosyl	Methyl	20 [g]	89	125-126	-13*	$C_{16}H_{23}N_3O_{11}$	44.34	44.50	5.35	5.18	9.70	9.58
Tetra-O-acetyl-β-D-glucopyranosyl	Ethyl	23	65	118-120	-8*	$C_{17}H_{25}N_3O_{11}$	45.63	45.89	5.64	5.60	9.39	9.34
Tetra-O-acetyl-β-D-glucopyranosyl	Propyl	27	76	111	-10*	$C_{18}H_{27}N_3O_{11}$	46.84	46.66	5.91	5.85	9.11	8.89
Tetra-O-acetyl-β-D-glucopyranosyl	Butyl	30	80	124-125	-12*	$C_{19}H_{29}N_3O_{11}$	47.99	48.17	6.16	6.07	8.84	8.82
Tri-O-acetyl-β-D-xylopyranosyl	Methyl	37	87	127-128	-25*	$C_{13}H_{19}N_3O_9$	43.21	42.96	5.26	5.32	11.63	11.51

c Compound 11: Found: S, 8.73%. Calcd: S, 8.97%. d Compound 12: Found: S, 7.08%. Calcd: S, 7.26%. e Lit.[11] mp 177-180°C(dec), $[\alpha]_D$ -12° (water). f Compounds did not give correct analyses. g Lit.[11] mp 89-90°C, $[\alpha]_D$ -8° (chloroform).

collected by filtration and another crop of the product was obtained from the filtrate by evaporation.

Starting Materials. Compounds: **1, 4** and **7** were synthesized from methyl β-D-glucosaminide.[8] Compound **10** was prepared by selective mesylation of methyl 2-deoxy-2-(*N'*-methylureido)-β-D-glucopyranoside.[6a] Compound **13** was prepared from **10** by the four step reaction in 70% yield. Compound **16** was synthesized from methyl 2-*N*-benzyloxycarbonyl-β-D-glucosaminide[9] by the four step reaction in 37% yield. Compound **19** was prepared from 1-(β-D-glucopyranosyl)-3-methylurea[10] in 90% yield. Compounds: **21, 24** and **28** were synthesized from 2,3,4,6-tetra-*O*-acetyl-β-D-glucopyranosylamine.[12] Compound **31** was prepared from 2,3,4,6-tetra-*O*-acetyl-β-D-aminopyranosylamine which was obtained by azidolysis and subsequent catalytic hydrogenation of 2,3,4,6-tetra-*O*-acetyl-α-D-mannopyranosyl bromide.[13,14] Compound **34** was prepared from 2,3,4-tri-*O*-acetyl-β-D-xylopyranosyl azide.[15] Compound **38** was prepared from 1-*O*-acetyl-2,3,5-tri-*O*-benzoyl-D-ribofuranosyl chloride.[16,17]

The *N*-alkyl-*N*-nitrosourea derivatives revealed a characteristic absorption for *N*-nitroso group at 1480—1495 cm^{-1} in their ir spectra. The position of the nitroso group was deduced from their PMR spectra by ascertaining the absence of a proton on the nitrogen atom possessing an alkyl group.

We wish to express our thanks to Mr. Saburo Nakada for the elemental analyses. We are also indebted to Mr. Shigeru Nishiyama, Mr. Kazuo Kikuchi and Mr. Yasuhiro Nagamatsu for assistance in the preparation of the compounds.

References

1) F. R. White, *Cancer Chemother. Rep.*, **30**, 49 (1963); J. S. Evans, G. C. Gerritsen, K. M. Mann, and S. P. Owen, *ibid.*, **48**, 1 (1965).
2) F. Reusser, *J. Bacteriol.*, **105**, 580 (1971).
3) J. J. Vavra, C. DeBoer, A. Dietz, L. J. Hanka, and W. T. Sokolski, *Antibio. Ann.*, **1959—1960**, 230 (1960).
4) R. R. Herr, H. K. Jahnke, and A. D. Argoudelis, *J. Amer. Chem. Soc.*, **89**, 4808 (1967).
5) T. Suami and T. Machinami, This Bulletin, **43**, 3013 (1970); Biological data will be reported elesewhere.
6) T. Machinami and T. Suami, *ibid.*, **46**, 1013 (1973).
7) T. Suami and T. Machinami, *ibid.*, **43**, 2953 (1970); ditto., *ibid.*, **48**, 1333 (1975).
8) Y. Matsushima and T. Miyazaki, *ibid.*, **38**, 1325 (1965).
9) A. Neuberger and R. T. Rivers, *J. Chem. Soc.*, **1939**, 122.
10) B. Helferich and W. Kosche, *Ber.*, **59**, 69 (1929).
11) B. Bannister, *J. Antibiotics*, **25**, 377 (1972).
12) A. Bertho and D. Aures, *Ann. Chem.*, **512**, 54 (1955).
13) P. A. Levene and S. Tipson, *J. Biol. Chem.*, **90**, 89 (1931).
14) E. A. Talley, D. D. Reynolds, and W. L. Evans, *J. Amer. Chem. Soc.*, **65**, 575 (1943).
15) A. Bertho, *Ann. Chem.*, **562**, 229 (1949).
16) E. F. Recond and H. Rinderknecht, *Helv. Chim. Acta.*, **42**, 1171 (1959).
17) N. Yung and J. J. Fox, "Methods in Carbohydrate Chemistry," Vol. 2, Academic Press, New York (1963), p. 109.

BULLETIN OF THE CHEMICAL SOCIETY OF JAPAN, VOL. 48(12), 3763—3764 (1975)

Synthesis of (2-Chloroethyl)-nitrosourea Derivatives of Carbohydrate

Tomoya MACHINAMI, Shigeru NISHIYAMA, Kazuo KIKUCHI, and Tetsuo SUAMI*

Department of Applied Chemistry, Faculty of Engineering, Keio University, Hiyoshi, Yokohama 223

(Received June 7, 1975)

Synopsis. Six antileukemic carbohydrate derivatives which have a (2-chloroethyl)-nitrosoureido group have been prepared by a reaction between amino sugars and 2-chloroethyl isocyanate, followed by nitrosation.

It has been suggested by Johnston *et al.*[1] that the replacement of a methyl group with a 2-chloroethyl group in numerous congeners of methyl-nitrosoureas increased antitumor activities against leukemia L1210, as was demonstrated with BCNU: 1,3-bis(2-chloroethyl)-1-nitrosourea and CCNU: 1-(2-chloroethyl)-3-cyclohexyl-1-nitrosourea.[1] More recently, two papers[2,3] have described a preparation of 2-chloroethyl analog of antitumor antibiotic streptozotocin.[4] In our laboratory, a synthesis of methyl glycoside of streptozotocin was initiated[5] and afterward, several nitrosourea derivatives of carbohydrate have been prepared by a reaction between amino sugars and alkyl isocyanate, followed by nitrosation.[6-8] In connection with the previous papers, we have attempted to prepare (2-chloroethyl)-nitrosourea derivatives, and in the present note, we wish to report a preparation of the derivatives of D-glycosylamines and polyhydroxycyclohexylamines by the analogous reaction sequence employed in the previous papers.[5-8] The position of the nitroso group in each compound has been established by PMR spectroscopy by demonstrating a spectral symmetry of the $ClCH_2CH_2N(NO)$ group (A_2B_2 system).[1]

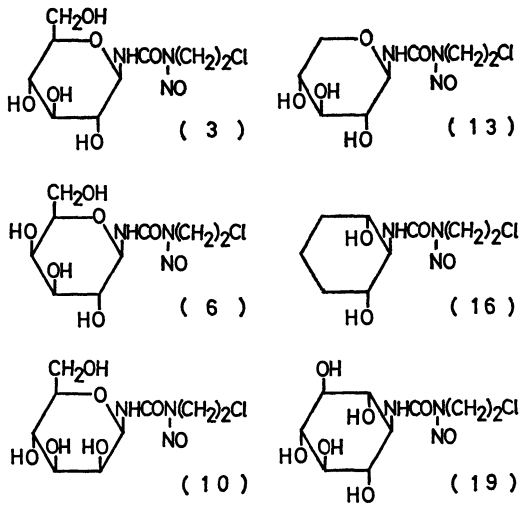

All the six compounds showed a remarkable antitumor activity against L1210 leukemia in mice, which will be reported in a near future.

Experimental

Melting points were determined in a capillary tube in a liquid bath and are uncorrected. Solutions were evaporated under diminished pressure. Acetylation was carried out with acetic anhydride and pyridine in the usual manner. Optical rotations were measured on a Japan Spectroscopic

TABLE 1. 1-(2-CHLOROETHYL)UREAS

$$R\text{-}NH\text{-}\underset{\underset{O}{\|}}{C}\text{-}NHCH_2CH_2Cl$$

R	No.	Yield %	Mp °C	$[\alpha]_D$†	Molecular Formula	C% Calcd (Found)	H% Calcd (Found)	N% Calcd (Found)	Cl % Calcd (Found)
A. 1-(2-Chloroethyl)-3-(poly-*O*-acetyl-D-glycosyl)ureas									
Tetra-*O*-acetyl-β-D-glucopyranosyl	**1**	88	154—155	−7*	$C_{17}H_{25}N_2ClO_{10}$	45.09 (45.23)	5.56 (5.56)	6.19 (6.22)	7.83 (7.85)
Tetra-*O*-acetyl-β-D-mannopyranosyl	**8**	80	140—141	−14*	$C_{17}H_{25}N_2ClO_{10}$	45.09 (44.83)	5.56 (5.44)	6.19 (5.95)	7.83 (7.93)
B. 1-(2-Chloroethyl)-3-(D-glycosyl) ureas and -3-(polyhydroxycyclohexyl) ureas									
β-D-Glucopyranosyl	**2**	95	153 (dec)	−8	$C_9H_{17}N_2ClO_6$	37.97 (37.69)	6.02 (5.82)	9.84 (9.62)	12.45 (12.20)
β-D-Galactopyranosyl	**5**	85	116 (dec)	+9.5	$C_9H_{17}N_2ClO_6$	37.97 (37.86)	6.02 (6.18)	9.84 (9.57)	12.45 (12.25)
β-D-Mannopyranosyl	**9**	78	158—159 (dec)	−34	$C_9H_{17}N_2ClO_6$	37.97 (37.96)	6.02 (5.84)	9.84 (9.81)	12.45 (12.21)
β-D-Xylopyranosyl	**12**	47	159—160 (dec)	−13	$C_8H_{15}N_2ClO_5$	37.73 (37.49)	5.94 (6.00)	11.00 (10.79)	13.92 (13.89)
1, 3/2N-Dihydroxycyclohexyl	**15**	66	125—127		$C_9H_{17}N_2ClO_3$	45.67 (45.73)	7.24 (7.11)	11.83 (12.09)	14.98 (15.02)
1N, 3, 5/2, 4, 6-Pentahydroxycyclohexyl	**18**	90	195—197		$C_9H_{17}N_2ClO_6$	37.97 (37.96)	6.02 (5.78)	9.84 (9.76)	12.45 (12.71)

† Opitical rotations were measured at 14—30°C in water and chloroform(*).

Table 2. 1-(2-Chloroethyl)-1-nitrosoureas

$$R\text{-}NH\text{-}\underset{\underset{O}{\|}}{C}\text{-}\underset{\underset{NO}{|}}{N}\text{-}CH_2CH_2Cl$$

R	No.	Yield %	Mp °C	$[\alpha]_D$†	Molecular Formula	C% Calcd (Found)	H% Calcd (Found)	N% Calcd (Found)	Cl % Calcd (Found)
A. 1-(2-Chloroethyl)-3-(D-glycosyl)-1-nitrosoureas and -3-(polyhydroxycyclohexyl)-1-nitrosoureas									
β-D-Glucopyranosyl	**3**	97	85 (dec)	−14	$C_9H_{16}N_3ClO_7$	34.46 (34.36)	5.14 (5.09)	13.40 (13.20)	11.30 (11.33)
β-D-Galactopyranosyl	**6**	64	145 (dec)	+13	$C_9H_{16}N_3ClO_7$	34.46 (34.58)	5.14 (5.09)	13.40 (13.12)	11.30 (11.22)
β-D-Mannopyranosyl	**10**	67	104 (dec)	−10	$C_9H_{16}N_3ClO_7$††				
β-D-Xylopyranosyl	**13**	76	84—85 (dec)	−8	$C_8H_{14}N_3ClO_6$	33.87 (34.17)	4.97 (5.10)	14.81 (14.44)	12.50 (12.80)
1, 3/2N-Dihydroxycyclohexyl	**16**	58	125—126 (dec)		$C_9H_{16}N_3ClO_4$	40.68 (40.51)	6.07 (5.87)	15.82 (15.70)	13.34 (13.13)
1N, 3, 5/2, 4, 6-Pentahydroxy-cyclohexyl	**19**	78	140—142 (dec)		$C_9H_{16}N_3ClO_7$	34.46 (34.58)	5.14 (5.13)	13.40 (13.10)	11.30 (11.50)
B. 1-(2-Chloroethyl)-3-(poly-*O*-acetyl-D-glycosyl)-1-nitrosoureas and -3-(polyacetoxycyclohexyl)-1-nitrosoureas									
Tetra-*O*-acetyl-β-D-glucopyra-nosyl	**4**	55	88—90	−14*	$C_{17}H_{24}N_3ClO_{11}$	42.38 (42.55)	5.02 (5.06)	8.72 (8.44)	7.36 (7.44)
Tetra-*O*-acetyl-β-D-galactopyra-nosyl	**7**	76	69—70	+5*	$C_{17}H_{24}N_3ClO_{11}$	42.38 (42.59)	5.02 (5.02)	8.72 (8.61)	7.36 (7.38)
Tetra-*O*-acetyl-β-D-mannopyra-nosyl	**11**	87	78 (dec)	−20*	$C_{17}H_{24}N_3ClO_{11}$	42.38 (42.68)	5.02 (5.05)	8.72 (8.47)	7.36 (7.50)
Tri-*O*-acetyl-β-D-xylopyranosyl	**14**	40	124—125	−19*	$C_{14}H_{20}N_3ClO_9$	41.03 (41.32)	4.92 (5.06)	10.25 (10.23)	8.65 (8.80)
1, 3/2N-Diacetoxycyclohexyl	**17**	82	151—152		$C_{13}H_{20}N_3ClO_9$	44.64 (44.52)	5.76 (5.74)	12.01 (11.81)	10.14 (10.09)
1N, 3, 5/2, 4, 6-Pentaacetoxy-cyclohexyl	**20**	85	206—209		$C_{19}H_{26}N_3ClO_{12}$	43.56 (43.58)	5.00 (4.97)	8.02 (7.79)	6.77 (6.75)

† See, Table 1. †† Compound did not give a correct analysis.

DIP-SL polarimeter. Elementary analyses were performed by Mr. Saburo Nakada to whom our thanks are due.

General Procedure for 1-(2-Chloroethyl)-3-(D-glycopyranosyl)urea and -3-(polyhydroxycyclohexyl)urea. *O*-Acetyl-D-glycosylamine or aminocyclitol was treated with 2-chloroethyl isocyanate (1.1—2.2 mol. equiv.) in a solvent. The reaction mixture was agitated for 1—2.5 hr under ice cooling and then evaporated. The residue was recrystallized from an appropriate solvent. The product was de-*O*-acetylated in methanolic ammonia or 0.1 M methanolic sodium methoxide.

General Procedure of Nitrosation. The carbamoyl derivative was treated with sodium nitrite (2 mol. equiv.) in 99% formic acid. After agitated for 1—2 hr under ice cooling, the solution was diluted with ice cold water and deionized with Amberlite IR-120(H^+). The solution was evaporated or lyophilized to give the product.

Starting Materials. Compound **1** was prepared from 2,3,4,6-tetra-*O*-acetyl-β-D-glucopyranosylamine,[9] compound **5** was from 2,3,4,6-tetra-O-acetyl-β-D-galactopyranosylamine,[9] and compound **8** was from 2,3,4,6-tetra-*O*-acetyl-β-D-mannopyranosylamine.[8] Starting from 2,3,4-tri-*O*-acetyl-1-azido-1-deoxy-β-D-xylopyranose,[10] compound **12** was prepared. Compound **15** was synthesized from 1,3/2N-aminocyclohexanediol[11] and compound **18** was from *scyllo*-inosamine.[12]

References

1) T. P. Johnston, G. S. McCaleb, P. S. Opliger, and J. A. Montgomery, *J. Med. Chem.*, **9**, 892 (1966).

2) T. P. Johnston, G. S. McCaleb, and J. A. Montgomery, *ibid.*, **18**, 104 (1975).

3) J. L. Montero and J. L. Imbach, *Compt. Rend.*, **18**, 809 (1974).

4) J. J. Vavra, C. Deboer, A. Dietz, L. J. Hanka, and W. T. Sokolski, *Antibiot. Ann.*, **1959—1960**, 230 (1960); W. T. Sokolski, J. J. Vavra, and L. J. Hanka, *ibid.*, **1959—1960**, 241 (1960); C. Lewis and A. R. Barbiers, *ibid.*, **1959—1960**, 247 (1960); R. R. Herr, T. E. Ebler, M. E. Bergy, and H. K. Jahnke, *ibid.*, **1959—1960**, 236 (1960); R. R. Herr, H. K. Janke, and A. D. Argoudelis, *J. Amer. Chem. Soc.*, **89**, 4808 (1967).

5) T. Suami and T. Machinami, This Bulletin, **43**, 3013 (1970).

6) T. Suami and T. Machinami, *ibid.*, **43**, 2953 (1970).

7) T. Machinami and T. Suami, *ibid.*, **46**, 1013 (1973).

8) T. Machinami, K. Kobayashi, Y. Hayakawa, and T. Suami, *ibid.*, in press.

9) A. Bertho and J. Maier, *Ann. Chem.*, **498**, 50 (1932).

10) A. Bertho, *ibid.*, **562**, 229 (1949).

11) F. W. Lichtenthaler, *Chem. Ber.*, **96**, 845 (1963); T. Suami and S. Ogawa, This Bulletin, **37**, 194 (1964).

12) B. Bannister and A. D. Argoudelis, *J. Amer. Chem. Soc.*, **85**, 119 (1963); T. Suami, F. W. Lichtenthaler, and S. Ogawa, This Bulletin, **39**, 170 (1966).

BULLETIN OF THE CHEMICAL SOCIETY OF JAPAN, VOL. 48(12), 3765—3766 (1975)

Reaction of a Stable Free Nitrogen-Centered Radical, 3,4-Dihydro-2,4,6-triphenyl-2*H*-1,2,4,5-tetrazin-1-yl, with Organoaluminum Compounds

Yozo MIURA, Yuzo MORIMOTO, and Masayoshi KINOSHITA

Department of Applied Chemistry, Faculty of Engineering, Osaka City University, Sumiyoshi-ku, Osaka 558

(Received June 26, 1975)

Synopsis. Reactions of 3,4-dihydro-2,4,6-triphenyl-2*H*-1,2,4,5-tetrazin-1-yl (**1**) with triethylaluminum, triisobutylaluminum, and diethylaluminum chloride were examined, and from the product analysis, these reactions are proposed to proceed by means of a homolytic substitution process.

In previous reports,[1,2] the reactions of 3,4-dihydro-2,4,6-triphenyl-2*H*-1,2,4,5-tetrazin-1-yl (**1**)[3] with Grignard reagents or alkyllithiums have been described, and these reactions have been proposed to proceed by means of a homolytic substitution process.

The extension of this investigation to organoaluminum compounds is of interest, because these reactions of the reagents with oxygen-centered radicals have been widely investigated,[4] and have been demonstrated to proceed through homolytic processes. However, reactions of organoaluminum compounds with nitrogen-centered radicals have been little investigated, and thus, no unambiguous examples of homolytic substitution reactions with nitrogen-centered radicals have been found,[4] thus

$$AlR_3 + R'O\cdot \longrightarrow AlR_2OR' + R\cdot$$

From this point of view, the reaction of **1** with organoaluminum compounds have been examined, and in this paper the results are described and the mechanism is discussed.

Experimental

All the melting points were uncorrected. Triethylaluminum, triisobutylaluminum, and diethylaluminum chloride were used as heptane solutions of 24, 26, and 22 w/w %, respectively. 3, 4-Dihydro-2,4,6-triphenyl-2*H*-1,2,4,5-tetrazin-1-yl (**1**) was prepared according to the procedure of Kuhn and Trischmann, and which was recrystallized from methanol, mp 141—142 °C (lit,[3] 139—140 °C).

The reactions of **1** with the organoaluminum compounds were carried out according to the similar procedure described in a previous report.[2] The amounts of regenerated **1** and of isolated coupling compounds (**2**) were determined similarly. The compounds (**2**) were recrystallized from methanol.

1-Ethyl-2,4,6-triphenyl-1,2,3,4-tetrahydro-1,2,4,5-tetrazine: 0.21 g (0.62 mmol), mp 133—134 °C (isolated from the reaction mixture with triethylaluminum); 0.23 g (0.67 mmol), mp 134—136 °C (with diethylaluminum chloride, lit,[2] 133—134 °C).

1-Isobutyl-2,4,6-triphenyl-1,2,3,4-tetrahydro-1,2,4,5-tetrazine: 0.22 g (0.59 mmol), mp 161—163 °C (lit,[2] 158—160 °C).

Results and Discussion

In the general procedure, when an organoaluminum compound is added to a degassed toluene solution of **1** at 0 °C, the characteristic green color of **1** (λ_{max} 720 nm, ε 4330 in benzene)[3] turned immediately to light brown, indicating that **1** reacted rapidly and completely with the reagent. The color remained when the solution was not exposed to moisture but, when it was poured into water, the original green color reappeared immediately, this coloration showing that **1** was regenerated. The organic layer was extracted with benzene and dried over sodium sulfate.

The benzene solution was examined by thin-layer chromatography (tlc, silica gel : benzene), and three spots were detected. Two spots were easily identified to correspond to **1** and a leuco compound (**4**), respectively, from the green color and by comparison with authentic samples in tlc. **4** is known to oxidize easily to **1** even when subjected to atmospheric oxygen,[3] thus the **1** detected was certainly formed from the oxidation of **4** in air. Therefore, the amount of regenerated **1** was determined, after **4** had been confirmed by tlc to be oxidized thoroughly to **1** on standing in air (for *ca.* two days), by optical density measurements at 720 nm in a benzene solution. The results are summarized in Table.

The residual unidentified spot is probably a coupling compound of **1** with an alkyl radical originally attached to the organoaluminum compound from its R_f value. The green benzene solution was concentrated under reduced pressure and the residue was subjected to columnchromatography (silica gel : benzene), resulting in the expected coupling compound, 1-alkyl-2,4,6-triphenyl-1,2,3,4-tetrahydro-1,2,4,5-tetrazine (**2**). Their structures were confirmed by mps, and

TABLE. THE RESULTS OF THE REACTION OF 3,4-DIHYDRO-2,4,6-TRIPHENYL-2*H*-1,2,4,5-TETRAZIN-1-YL (**1**) WITH ORGANOALUMINUM COMPOUNDS[a]

Aluminum compound	mmol	Regenerated **1** %	Isolated coupling compound (**2**)	
			R in **2**	%[b]
Triethylaluminum	1.5	39	Ethyl	45
Triisobutylaluminum	1.6	37	Isobutyl	47
Diethylaluminum chloride	1.5	42	Ethyl	41

a) **1** : 0.50 g (1.6 mmol), toluene : 20 ml, 0°C. b) : based on **1** used.

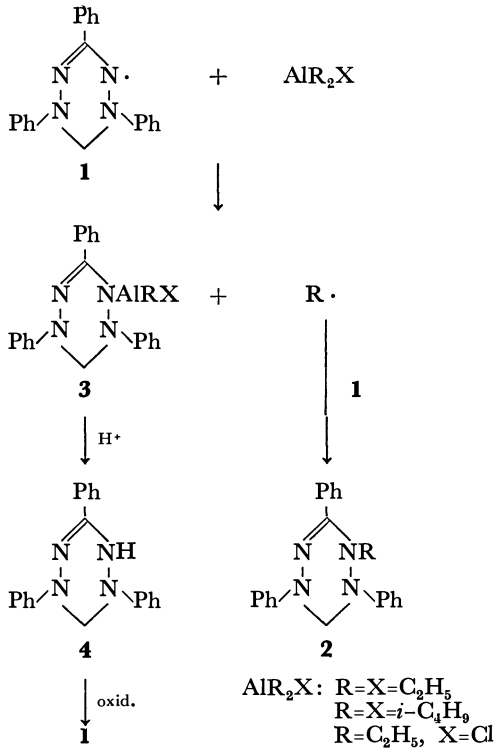

Scheme.

IR and MNR spectra, and the results are given in Table.

On the basis of these results, a reasonable reaction mechanism may be illustrated as shown in Scheme; **1** and an organoaluminum compound are converted into compound (**3**) and an alkyl radical, and the alkyl radical formed is captured exclusively by another unreacted **1** to give the coupling compound **2**. However, **3** is hydrolyzed immediately to a leuco compound (**4**) in contact with water, which is oxidized to **1** gradually by atmospheric oxygen.

References

1) Y. Miura, Y. Morimoto, and M. Kinoshita, *Makromol. Chem.*, **175**, 3487 (1974).

2) Y. Miura, Y. Morimoto, and M. Kinoshita, This Bulletin, in press.

3) R. Kuhn and H. Trischmann, *Monatsh. Chem.*, **95**, 457 (1964).

4) a) E. Muller, P. Ziemek, and A. Rieker, *Tetrahedron Lett.*, **1964**, 457; b) A. G. Davies and B. P. Roberts, *J. Chem. Soc. B*, **1968**, 1074; c) A. G. Davies and B. P. Roberts, *J. Organometal. Chem.*, **19**, 17 (1969); d) P. J. Krusic and J. K. Kochi, *J. Amer. Chem. Soc.*, **91**, 3942 (1969); e) G. W. Kabalka and R. F. Daley, *ibid.*, **95**, 4428 (1973).

5) A. G. Davies, S. C. W. Hook, and B. P. Roberts, *J. Organometal. Chem.*, **22**, C37 (1970).

BULLETIN OF THE CHEMICAL SOCIETY OF JAPAN, VOL. 48(12), 3767—3768 (1975)

The Convenient Syntheses of Biopterin and Its Three Opitical Isomers

Takashi SUGIMOTO and Sadao MATSUURA

College of General Education, Nagoya University, Chikusa Nagoya 464

(Received August 8, 1975)

Synopsis. Simple syntheses of biopterin (**4a**) and its three optical isomers (**4b, c, d**) are described. The condensation of 2,4,5-triaminopyrimidin-6(1*H*)-one (**1**) with each of the 5-deoxypentose phenylhydrazones (**2a, b, c, d**), followed by oxidation with $K_3[Fe(CN)_6]$ and H_2O_2 in the presence of KI, gives biopterin (**4a**) and the isomers (**4b, c, d**) respectively.

Biopterin [2-amino-6-(L-*erythro*-1,2-dihydroxypropyl)-pteridin-4(3*H*)-one] (**4a**), first isolated from human urine,[1,2] has attracted considerable interest because of its biological activities: biopterin is a growth factor for *Crithidia fasciculata*[1,2] and its tetrahydro derivative has been found to be a potent cofactor for phenylalanine,[3] tyrosine,[4] and tryptophan hydroxylases.[5] Because of this importance, much effort has been expended on the synthesis of biopterin (**4a**)[2,6,7,8] and its optical isomers (**4b, c, d**).[6c] The resulting methods, however, all suffer from difficulties, *e.g.*, in separating the biopterin (**4a**) from its isomer, isobiopterin (**5a**),[2,6,8] or in making appropriate starting materials.[7,8b,c] Accordingly, we sought a more general simple synthesis.

In 1970, Viscontini *et al.*[9] synthesized D-*erythro*-neopterin (**4e**) by the condensation of 2,4,5-triaminopyrimidin-6(1*H*)-one (**1**) with D-arabinose phenylhydrazone (**2e**). In this reaction, a tetrahydropteridine (**3e**) was formed which, on aerial oxidation at pH 7, gave neopterin (**4e**) unaccompanied by the 7-isomer (**5e**).

When we applied this method to the synthesis of biopterin (**4a**), though, using 5-deoxy-L-arabinose phenylhydrazone (**2a**) instead of **2e**, we obtained no biopterin. The only isolable product was the 6-unsubstituted pteridine (**4f**), apparently formed by the loss of the 6-dihydroxypropyl group during the oxidation step. A similar reaction was also observed by Viscontini and Provenzale.[8a] We investigated further the conditions of oxidation and found that the use of a mixture of $K_3[Fe(CN)_6]$ and H_2O_2 in the presence of KI in an acidic solution gave biopterin as the main product.

We synthesized 5-deoxy-L-arabinose by the method Hough and Taylor,[10] involving the oxidative degradation of L-rhamnose diethyl dithioacetal. 5-Deoxy-D-arabinose and 5-deoxy-L (and D)-xylose were made from the corresponding pentose by the procedures of Zinner, Wessely, and Kristen.[11] Heating 5-deoxy-L-arabinose phenylhydrazone (**2a**) with 2,4,5-triaminopyrimidin-6(1*H*)-one (**1**) in 50% aqueous methanol under nitrogen gave a compound unstable to oxidation, probably the tetrahydropteridine (**3a**), by analogy with **3e**.[9] When the intermediate was oxidized by air in a neutral or weakly alkaline solution, only the 6-unsubstituted pteridine (**4f**) was formed. However, when the same oxidation was carried out under acidic conditions, a small amount of biopterin (**4a**) was formed, together with **4f**. Eventually, we found that the intermediate (**3a**) was oxidized effectively to biopterin (**4a**) in an acidic solution using a mixture of $K_3[Fe(CN)_6]$ and H_2O_2 in the presence of a little KI. A small amount (*ca.* 20%) of the unsubstituted pteridine (**4f**) was formed, but no 7-isomer (**5a**) was detected. The separation of biopterin from **4f** and several other minor components was achieved easily by chromatography, first on a Florisil column using 2M-hydrochloric acid as the developer, then on another Florisil column by gradient elution using 0—1% ammonia,[12] and finally on a P-Cellulose column[6b,c] eluted by water. The structure of the product was confirmed by its UV spectra.

The three optical isomers (**4b, c, d**) were made similarly by the condensation of the pyrimidine (**1**) with the appropriate phenylhydrazone (**2b, c,** or **d**).

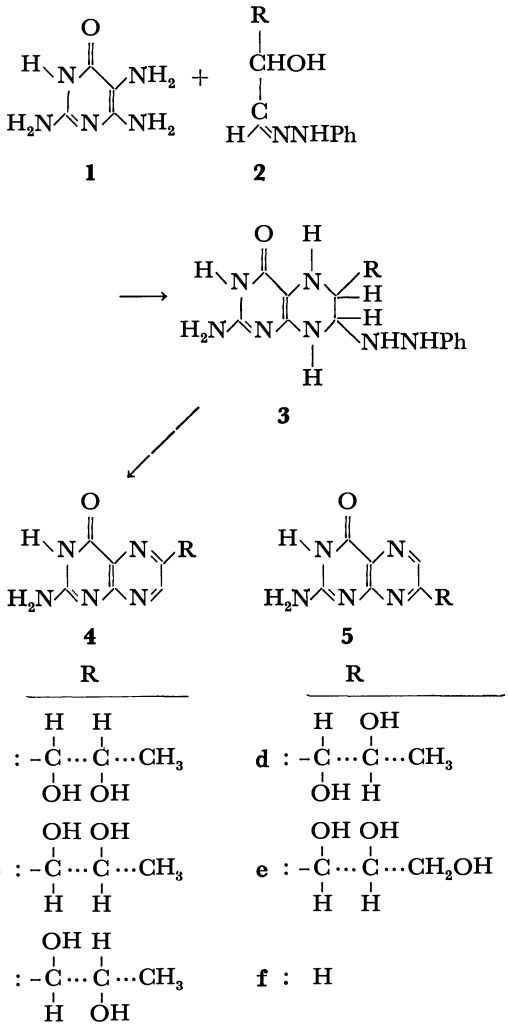

Table 1. pK_a Values and UV spectra of biopterin and its opitical isomers

	pK_a	pH Ionic species[a]	λ_{max} (log ε)[b]			
4a	2.23±0.02	0.0 +	212 (4.21),	248 (4.09),	321 (3.94)	
	7.89±0.01	5.0 ○	*223* (*4.07*),	235.5(4.10),	274.5(4.18),	345 (3.82)
		10.0 −	221.5(3.92),	254.5(4.38),	364 (3.84)	
4d	2.23±0.02	0.0 +	212 (4.20),	248 (4.07),	321 (3.93)	
	7.90±0.01	5.0 ○	*223* (*4.09*),	235.5(4.10),	274 (4.17),	345 (3.82)
		10.0 −	224 (3.97),	255 (4.37),	364 (3.89)	
4c	2.24±0.02	0.0 +	213 (4.18),	248 (4.07),	322.5(3.93)	
	7.87±0.02	5.0 ○	*222* (*4.05*),	236 (4.09),	274 (4.17),	346 (3.81)
		10.0 −	224 (3.94),	254 (4.37),	364 (3.89)	
4d	2.20±0.02	0.0 +	213 (4.19),	248 (4.07),	321.5(3.94)	
	7.92±0.02	5.0 ○	223 (4.04),	236 (4.07),	274.5(4.15),	345.5(3.78)
		10.0 −	223 (3.94),	255.5(4.38),	364 (3.89)	

a) +; cation, ○; neutal molecule, −; anion. b) Shoulders are in italics.

Experimental

The analyses were done by the Analytical Section, Meijo University, Nagoya; the UV spectra were measured with a Shimadzu model UV-210 spectrophotometer.

L-Erythro-*biopterin (4a)*. Phenylhydrazine (3.6 g) and one drop of acetic acid were added to 5-deoxy-L-arabinose[10] (4.0 g) in ethanol (5 ml). After stirring at 20 °C for 30 min, the mixture was diluted with ether (5 ml) and chilled to give fine needles (3.6 g) of the phenylhydrazone (**2a**), which were then collected by filtration and washed with ether. A solution of this product (3.6 g) and 2,4,5-triaminopyrimidin-6(1H)-one dihydrochloride (3.0 g) in 50% aqueous methanol (400 ml) was stirred under nitrogen at 20 °C for 2 hr, and then under reflux for 4 hr. After cooling to *ca.* 20 °C, potassium ferricyanide (5.0 g), potassium iodie (0.10 g), and hydrogen peroxide (35%, 5 ml) were added quickly to the solution, and the mixture was stirred by introducing air at 20—25 °C for 12 hr. The mixture was concentrated under reduced pressure to *ca.* 50 ml and then chilled. The dark solid was collected by filtration, washed with a little cold water, and then extracted with 1% ammonia (2×100 ml). The extracts were combined and evaporated to dryness under reduced pressure. The residue was dissolved in 2M hydrochloric acid (100 ml) and fractionated on a Florisil column[12] (4×40 cm), using 2M hydrochloric acid as the developer. Biopterin was well separated from several minor by-products, including **4f**, during this procedure. The fractions containing biopterin were evaporated to dryness under reduced pressure, and the residue was extracted again with 1% ammonia (200 ml); a considerable amount of an inorganic material remained undissolved. The extract was evaporated to dryness and chromatographed on a Florisil column (4×30 cm), and then developed by gradient elution with water (1.0 l) and 1% ammonia (1.0 l). The biopterin fractions were finally purified on P-Cellulose[11] (acid form; 3×30 cm; eluted with water) to remove a small amount of colored impurities. The evaporation of the final eluate gave a solid, which was dissolved in 1% ammonia (50 ml) and then added drop by drop into vigorously stirred boiling formic acid (1M, 50 ml). Chilling gave almost colorless needles (270 mg) of L-*erythro*-biopterin (**4a**); mp>300 °C (Found: C, 43.9; H, 4.5; N, 28.3%. Calcd for $C_9H_{11}N_5O_3 \cdot 1/2H_2O$: C, 43.9; H, 4.9; N, 28.4%).

Synthesis of the Optical Isomers (4b, c, d). 5-Deoxy-L-xylose (2.5 g), phenylhydrazine (2.0 g), and 6M-HCl (5 drops) were stirred in methanol (30 ml) at 40—45 °C for 15 min. Without isolating the phenylhydrazone (**2c**), the solution was treated with the pyrimidine dihydrochloride (5.0 g) as above. Chromatographic purification as before afforded colorless needles (495 mg) of L-*threo*-biopterin (**4c**);[6c] mp>300 °C (Found: C, 44.1; H, 4.5; N, 28.0%. Calcd for $C_9H_{11}N_5O_3 \cdot 1/2H_2O$: C, 43.9; H, 4.9; N, 28.4%).

Replacing the 5-deoxy-L-xylose in the foregoing condensation by 5-deoxy-D-arabinose and 5-deoxy-D-xylose gave 205 mg of D-*eryhtro*-biopterin(**4b**)[6c] (mp>300 °C) (Found: C, 42.5; H, 4.6; N, 27.9%. Calcd for $C_9H_{11}N_5O_3 \cdot H_2O$: C, 42.35; H, 5.1; N, 27.4%) and 250 mg of D-*threo*-biopterin (**4d**)[6c] (mp>300 °C) (Found: C, 43.75; H, 4.6; N, 28.4%. Calcd for $C_9H_{11}N_5O_3 \cdot 1/2H_2O$: C, 43.9; H, 4.9; N, 28.4%) respectively.

We thank Miss Noriko Itoh for her technical help and Dr. D. J. Brown of Australian National University for his help in preparation of this manuscript.

References

1) E. L. Patterson, H. P. Broquist, A. M. Albrecht, M. H. von Saltza, and E. L. R. Stokstad, *J. Amer. Chem. Soc.*, **77**, 3167 (1955).

2) E. L. Patterson, R. Milstrey, and E. L. R. Stokstad, *ibid.*, **78**, 5868 (1956).

3) S. Kaufman, *Pharmcol. Rev.*, **18**, 61 (1966).

4) a) A. R. Brenneman and S. Kaufman, *Biochem. Biophys. Res. Commun.*, **17**, 177 (1964); b) T. Nagatsu, K. Mizutani, I. Nagatsu, S. Matsuura, and T. Sugimoto, *Biochem. Pharm.*, **21**, 1945 (1972).

5) T. Nukiwa, C. Tohyama, C. Okita, T. Takaoka, and A. Ichiyama, *Biochem. Biophys. Res. Commun.*, **60**, 1029 (1974).

6) a) R. Tschesche, B. Hess, I. Ziegler, and H. Macheidt, *Ann. Chem.*, **653**, 193 (1962); b) H. Rembold and H. Metzyer, *Chem. Ber.*, **96**, 1395 (1963); c) C. B. Green and H. Rembold, *ibid.*, **99**, 2162 (1966).

7) K. J. M. Andrews, W. E. Baker, and B. P. Tong, *J. Chem. Soc. C*, 928 (1969).

8) a) M. Viscontini and R. Provenzale, *Helv. Chim. Acta*, **52**, 1225 (1969); b) M. Viscontini, R. Provenzale, and W. F. Frei, *ibid.*, **55**, 570 (1972); c) M. Viscontini and W. F. Frei, *ibid.*, **55**, 574 (1972).

9) M. Viscontini, R. Provenzale, S. Ohlgart, and J. Mallevialle, *ibid.*, **53**, 1202 (1972).

10) L. Hough and T. J. Taylor, *J. Chem. Soc.*, 3544 (1955).

11) H. Zinner, K. Wessely, and H. Kristen, *Chem. Ber.*, **92**, 1618 (1959).

12) S. Matsuura, M. Yamamoto, and Y. Kaneko, This Bulletin, **45**, 492 (1972).

BULLETIN OF THE CHEMICAL SOCIETY OF JAPAN, VOL. 48(12), 3769—3770 (1975)

Michael Reactions of α-Phenylthio and α-Phenylsulfinyl Crotonic Esters with Cyclic Enones

Hisahiro HAGIWARA, Kiyoshi NAKAYAMA, and Hisashi UDA

Chemical Research Institute of Non-Aqueous Solutions, Tohoku University, Katahira-2, Sendai 980

(Received August 12, 1975)

Synopsis. The Michael reactivities of ethyl α-phenylthio- and α-phenylsulfinylcrotonates with 2-cyclohexenone, 3-methyl-2-cyclohexenone, and 3-methyl-2-cyclopentenone have been investigated.

In connection with the study of α-phenylthio or α-phenylsulfinyl α,β-unsaturated esters[1] for synthetic utility, we have examined the reactivities of ethyl α-phenylthiocrotonate **1** and ethyl α-phenylsulfinylcrotonate **2** to cyclic enones as the Michael acceptor and addend.[2]

Compound **1** easily underwent the sequential Michael additions with the enolates of 2-cyclohexenone and 3-methyl-2-cyclohexenone, generated by treatment with lithium diisopropylamide in the presence of HMPA, to give the bicyclo[2.2.2]octane derivatives **3** and **4** in 70 and 77% yields, respectively.[3] (Table 1).

TABLE 1. MICHAEL ADDITION PRODUCTS OF **1** AND **2** WITH CYCLIC ENONES*

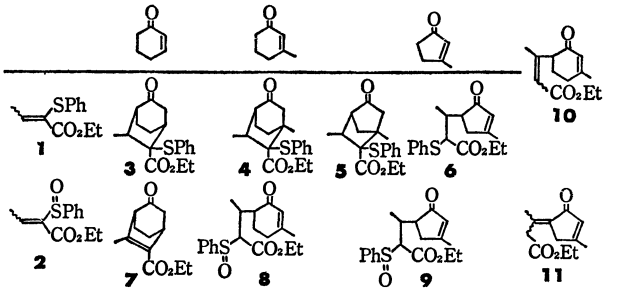

* All the products except **7** were mixtures of diastereoisomers.

In the reactions the addition of HMPA was essential, since an intractable mixture was produced when the reaction of **1** with 2-cyclohexenone was conducted in the absence of HMPA. On the other hand, in the reaction with 3-methyl-2-cyclopentenone the double Michael product **5** was the minor component (17%), the major one (58%) being the first Michael adduct **6**. Such a difference in the second Michael addition process between the six and five membered enones may be attributed to the difference of ring strain in the enolates of the bicyclo[2.2.2]octanone system in **4** and bicyclo[2.2.1]heptanone one in **5**; in the latter the ring-opened enolate, the first Michael adduct, appears to be more favorable in the equilibrium condition.

The sequential Michael addition was also observed in the reaction of **2** with 2-cyclohexenone, accompanied by desulfenylation during the work-up, giving rise to the bicyclo[2.2.2]octene derivative **7**. The reaction of **2** with 3-methyl-2-cyclohexenone and 3-methyl-2-cyclopentenone afforded only the first Michael adducts **8** and **9** in low yields. Failure for the second Michael additions of **8** and **9** would be ascribed to the stability of the anion, $-\bar{C}(SOPh)COOEt$, and the steric effect of the ring methyl group.

The structures of **3**, **8**, and **9** were further confirmed by transformation into the desulfenylated compounds **7**, **10**, and **11**, respectively.

Experimental

IR spectra were taken on a Hitachi EPI-S2 spectrophotometer using CCl_4 as a solvent. NMR spectra were obtained on a JEOL C-60HL instrument using TMS as an internal standard and CCl_4 as a solvent. The results are given in terms of the δ scale, the values of ester ethyl and phenyl protons except **1** and **2** being omitted. Analytical samples were purified by evaporative distillation and bath temperatures are given as the boiling points. Elemental analyses were carried out in the microanalytical laboratory of this institute.

Ethyl α-Phenylthio- and α-Phenylsulfinylcrotonates ***1*** *and* ***2***. Ethyl α-phenylsulfinylbutyrate (3.07 g, 12.8 mmol) was prepared by the reaction of ethyl α-bromobutyrate with sodium thiophenolate followed by oxidation with $NaIO_4$ in the usual manner. To this was added dropwise trifluoroacetic anhydride (4.2 g, 20 mmol) with stirring and ice-cooling (the Pummerer rearrangement and subsequent elimination of trifluoroacetic acid took place). The mixture was stirred at room temperature for 1.5 hr and then evaporated to dryness *in vacuo*. The residual liquid was dissolved in ether, passed through Woelm neutral alumina activity III, and freed from ether to give spectroscopically single ethyl α-phenylthiocrotonate **1** (2.34 g, 82%): bp 120—130 °C (3.5 mmHg, large scale distillation caused decomposition to produce a considerable amount of a substance with lower-boiling point, reducing the yield of **1**, *ca.* 52%); IR 1730, 1620 cm^{-1}; NMR 1.02 (3H, t, J=7.5), 2.05 (3H, d, J=6.8), 4.05 (2H, q, J=7.5), 7.15—7.50 (5H, m), 7.45 (1H, q, J=6.8); Anal. Found: C, 65.11; H, 6.62%. Calcd for $C_{12}H_{14}O_2S$: C, 64.85; H, 6.35%. The geometry of the double bond has not been determined.

Ethyl α-phenylsulfinylcrotonate **2** was prepared from **1** by oxidation with an equivalent amount of *m*-chloroperbenzoic acid in CH_2Cl_2 (0 °C, 10 min) in the usual manner and purified by chromatography on SiO_2. Yield: 67%. IR 1720, 1627 cm^{-1}; NMR 1.07 (3H, t, J=7.5), 2.26 (3H, d, J=7.5), 4.06 (2H, q, J=7.5), 7.25—7.80 (6H, q and m).

General Procedure for Michael Reactions of ***1*** *and* ***2*** *with Cyclic Enones.* To a solution of lithium diisopropylamide (1.20—1.30 mmol) in anhydrous THF (2 ml) and ether (1 ml) was added dropwise at −60 °C a solution of a cyclic enone (1.00 mmol) and then a solution of HMPA (1.00 mmol) in anhydrous THF (2 ml each). After being stirred at −60 °C for 1 hr, the solution was cooled at −75 °C and a solution of **1** or **2** (1.10 mmol) in anhydrous THF (2 ml)

was added. The operation was carried out under nitrogen. The progress of the reaction was followed by tlc. The reaction mixture was stirred at an appropriate temperature for an appropriate time, and then acidified with dil. HCl and thoroughly extracted with CH_2Cl_2. The extract was washed with saturated salt solution, dried, and freed from the solvent. The product was separated by preparative tlc on SiO_2 with 1 : 1 petroleum ether-ether for **3**—**6** and with 1 : 10 or ether alone for **8** and **9**. The reaction conditions (temperature and time) and the yields of products are shown for each case.

Ethyl 3-Methyl-5-oxo-2-(phenylthio)bicyclo[2.2.2]*octane-2-carboxylate* ***3*** *and its Conversion into* ***7***. Reaction conditions: −75——55 °C for 2 hr. Yield: 70%. IR 1725 (br.) cm^{-1}; NMR 0.80—1.50 (6H, complex d and t), 1.50—3.20 (9H, m).

To a cold solution of **3** (230 mg, 0.72 mmol) in CH_2Cl_2 (4 ml) was added dropwise a solution of *m*-chloroperbenzoic acid (85%, 147 mg, 0.72 mmol) in CH_2Cl_2 (4 ml), and the mixture was stirred at 0 °C for 30 min. Aqueous saturated $NaHSO_3$ was added and the water layer was extracted with CH_2Cl_2. The combined organic layers were washed with saturated $NaHCO_3$ and salt solution, dried, and evaporated. The residue was dissolved in toluene (5 ml) and heated under reflux for 30 min. Evaporation of toluene, followed by preparative tlc of the residue (SiO_2, 2 : 1 petroleum ether-ether) afforded **7** (41 mg, 27%): bp 120 °C (4 mmHg); IR 1725, 1700, 1632 cm^{-1}; NMR 1.50—3.37 (8H, m), 2.23 (3H, s); Anal. Found: C, 69.31; H, 7.63%. Calcd for $C_{12}H_{16}O_3$: C, 69.21; H. 7.74%.

Ethyl 1,3-Dimethyl-5-oxo-2-(phenylthio)bicyclo[2.2.2]*octane-2-carboxylate* ***4*** *and Desulfurization.* Reaction conditions: −75——50 °C for 1.5 hr. Yield: 77%. Bp 120—130 °C (5 mmHg); IR 1725 (br) cm^{-1}; NMR 0.80—1.45 (9H, complex s, d, and t), 1.50—3.50 (8H, m); Anal. Found: C, 68.80; H, 7.28%. Calcd for $C_{19}H_{24}O_3S$: C, 68.65; H, 7.28%.

A mixture of **4** (102 mg), Raney-Ni (pest, 0.5 ml), and acetone (3 ml) was heated under reflux for 20 min. The reaction mixture was passed through SiO_2 and evaporated. The residue was purified by preparative tlc (SiO_2, 1 : 1 petroleum ether-ether) to give ethyl 1,3-dimethyl-5-oxobicyclo[2.2.2]octane-2-carboxylate (**4**, PhS group = H) (33 mg, 42%): IR 1730 (br.) cm^{-1}; NMR 0.90—1.15 (6H, s and d), 1.40—3.00 (9H, m). Attempt to apply oxidation-desulfenylation procedure to **4** failed.

Ethyl 1,3-Dimethyl-5-oxo-2-(phenylthio)bicyclo[2.2.1]*heptane-2-carboxylate* ***5*** *and Ethyl α-Phenylthio-β-(2-oxo-4-methyl-3-cyclopentenyl)butyrate* ***6***. Reaction conditions: −75——70 °C for 30 min. Yield: 17% for **5** and 58% for **6**. **5**: bp 110—120 °C (2.5 mmHg); IR 1755, 1725 cm^{-1}; NMR 1.35 (3H, d, J=7.5) 1.62 (3H, s), 1.19—2.40 (5H, m), 2.99 (1H, m); Anal. Found: C, 67.95; H, 7.16%. Calcd for $C_{18}H_{22}O_3S$: C, 67.91; H, 6.97%. **6**: bp 130—140 °C (3 mmHg); IR 1725, 1693, 1627 cm^{-1}; NMR 0.74—1.35 (6H, complex d and t), 2.05 (3H, br. s), 1.50—3.90 (5H, m), 5.83 (1H, br.); Anal. Found: C, 67.86; H, 6.92%. Calcd for $C_{18}H_{22}O_3S$: C, 67.91; H, 6.97%.

When the reaction mixture was warmed up above −50 °C, **6** was the sole product.

Ethyl 3-Methyl-5-oxobicyclo[2.2.2]*oct-2-ene-2-carboxylate* ***7***. Reaction conditions: −75 °C for 1 hr and 20 °C for 1.5 hr. Yield: 48%. The IR and NMR spectra were identical with those of the sample derived from **3**.

Ethyl α-Phenylsulfinyl-β-(2-oxo-4-methyl-3-cyclohexenyl)butyrate ***8*** *and Pyrolysis.* Reaction conditions: −60—20 °C for 4 hr. Yield: 46%. IR 1730, 1670 cm^{-1}; NMR 0.75—1.42 (6H, complex d and t), 1.93 (3H, br. s), 1.80—4.42 (7H, m), 5.83 (1H, br.)

Pyrolysis of **8** in toluene was carried out in the same manner as described above to give ethyl β-(2-oxo-4-methyl-3-cyclohexenyl)crotonate **10** (70% yield): bp 120—130 °C (5 mmHg): IR 1715, 1670, 1640 cm^{-1}; NMR 1.96 (3H, s), 2.08 (3H, s), 1.78—3.10 (5H, m), 5.58—5.90 (2H, br.); Anal. Found: C, 70.51; H, 8.34%. Calcd for $C_{13}H_{18}O_3$: C, 70.24; H, 8.16%.

Ethyl α-Phenylsulfinyl-β-(2-oxo-4-methyl-3-cyclopentenyl)butyrate ***9*** *and Pyrolysis.* Reaction conditions: −60—20 °C for 2 hr. Yield: 23%. IR 1730, 1695, 1625 cm^{-1}; NMR 0.73—1.32 (6H, complex d and t), 2.16 (3H, br. s), 2.30—4.30 (5H, m), 5.92 (1H, br.).

Pyrolysis of **9** in toluene was carried out in the same manner as described above to give ethyl β-(2-oxo-4-methyl-3-cyclopentylidene)butyrate **11** (73% yield): bp 110—120 °C (5 mmHg); IR 1735, 1693, 1650, 1625 cm^{-1}; NMR 1.85 (3H, s), 2.10 (3H, s), 3.10 (2H, br. s), 3.87 (2H, s), 6.00 (1H, br. s); Anal. Found: C, 68.98; H, 7.40%. Calcd for $C_{12}H_{16}O_3$: C, 69.21; H, 7.74%.

References

1) H. Kosugi, H. Uda, and S. Yamagiwa, *Chem. Commun.*, **1975**, 192.

2) For the reaction of methyl α-methylthioacrylate as the Michael acceptor, see R. J. Cregge, J. L. Herrmann, and R. H. Schlessinger, *Tetrahedron Lett.*, **1973**, 2603; J. L. Herrmann, J. E. Richman, and R. H. Schlessinger, *ibid.*, **1973**, 3271; J. L. Herrmann, R. J. Cregge, J. E. Richman, C. L. Semmelhack, and R. H. Schlessinger, *J. Amer. Chem. Soc.*, **96**, 3702 (1974).

3) There have been two precedents of this type sequential Michael addition. R. A. Lee, *Tetrahedron Lett.*, **1973**, 3333; T. Ohnuma, T. Oishi, and Y. Ban, *Chem. Commun.*, **1973**, 301.